TRANSACTIONS

OF THE

AMERICAN SOCIETY

OF

MECHANICAL ENGINEERS

1946

VOLUME 68

PUBLISHED BY
THE AMERICAN SOCIETY OF MECHANICAL ENGINEERS
29 WEST THIRTY-NINTH STREET, NEW YORK, N. Y.

Copyright, 1947, by
THE AMERICAN SOCIETY OF MECHANICAL ENGINEERS

Printed in the United States of America by
The Mack Printing Co., Easton, Pa.

Engineering Library
The American Society of Mechanical
Engineers
6-28-47

Foreword

VOLUME 68 of the Transactions of The American Society of Mechanical Engineers contains the individual papers published during 1946 under the sponsorship of the Society's professional divisions and technical committees, including the contributions of the Applied Mechanics Division, issued originally in a quarterly known as *Journal of Applied Mechanics*, and the 1946 Society Records and Index. The technical papers and reports that make up this volume represent the Society's annual contribution to the permanent record of mechanical-engineering achievement. Most of these papers and reports were presented at meetings of the Society and its professional divisions and sections and were published in monthly issues, eight being distributed as the Transactions of The American Society of Mechanical Engineers and four as the *Journal of Applied Mechanics*. Indexes to other A.S.M.E. papers and publications will be found on page RI-51 at the end of this volume.

In view of the fact that the material of which this volume is composed was originally issued periodically as the Transactions, *Journal of Applied Mechanics*, and Society Records, three sets of page numbers will be found. Numbers without letter symbols are those of the eight issues of Transactions, those with letter symbol A preceding the number refer to the pages of the *Journal of Applied Mechanics*, which follow, and those with letter symbol RI to the Society Records and Index section, which concludes the volume.

All sections of the Transactions are bound together at the end of the year for the convenience of libraries and of engineers who wish all of the papers in permanent form. Copies of the bound Transactions will be found in depositories located in selected engineering, university, and public libraries throughout the world. A complete list of these depositories will be found on pages RI-47 to RI-50 of the Society Records and Index. Copies of the Transactions have also been set aside for sale.

The Society Records of the A.S.M.E. for 1946, which form a part of these Transactions, are the permanent records of the Society's activities for the year, including lists of committees. The Index provides a means of locating special A.S.M.E. publications and articles in *Mechanical Engineering*, as well as in the Transactions.

THE COMMITTEE ON PUBLICATIONS

Rate of Temperature Change in Short-Length Round Timbers

By J. D. MacLEAN,[1] MADISON, WIS.

This paper discusses factors affecting the rate of temperature change in wood and includes time-temperature curves for use in determining the temperature obtained at different points in short-length log sections when heated in steam or hot water. One group of curves shows the temperature distribution from the ends to the mid-length and at different points between the circumference and axis, of logs 12, 24, 36, 48, and 60 in. in diameter. Other charts show the time-temperature distribution at various points between the circumference and axis at the mid-length of log sections of any diameter between 12 and 60 in. Examples are given illustrating the procedure for using the charts in finding the temperature at a parcular point, under different heating conditions.

Introduction

GREEN logs of various species are often heated in steam or in hot water to condition them for veneer-cutting. These logs are relatively short, and the ratio of diameter to length is large in comparison with round timbers in the form of posts, poles, and piling. In timbers in which the ratio of diameter to length is small, the effect of longitudinal heating can extend only a limited distance, while the portion between the end regions is raised to any desired temperature. Because of the comparatively short length of veneer logs, however, it is necessary to consider the effect of heat transfer in the longitudinal as well as in the transverse direction. The relative amount of heating that takes place in these two directions depends upon a number of variables, such as cross-sectional dimensions, length, heating period, and temperature of the heating medium.

The purpose of this paper is to discuss methods of finding the rate of temperature change in timbers of this kind. No attempt is made to discuss the temperatures needed for satisfactory results in veneer-cutting, for some woods apparently require less heating than others. When the optimum temperature is known, however, the data presented provide a guide for selecting the required heating period for logs of different species and of different dimensions. The data also furnish a useful aid in studying the effect of different heating conditions on veneer-cutting operations.

A large amount of experimental work has been done at the Forest Products Laboratory to study the rate of temperature change in wood when heated in different mediums and to investigate the effect of variables, such as species, moisture content, density, or specific gravity, and variation in the rate of heating in the radial, tangential, and longitudinal directions. A number of papers have been published which discuss the results of these experiments (1 through 10).[2]

[1] Engineer, Forest Products Laboratory, Forest Service, U. S. Department of Agriculture. (The Forest Products Laboratory is maintained in co-operation with the University of Wisconsin.)

Contributed by the Wood Industries Division of The American Society of Mechanical Engineers.

Note: Statements and opinions advanced in papers are to be understood as individual expressions of their authors and not those of the Society.

Effect of Variables on Rate of Temperature Change

Heating Medium. Experiments with different heating mediums show that for the same heating period and the same temperature conditions, steam heats wood faster than water, and water heats faster than such liquids as preservative oils (6). In general, water heated wood about 5 to 10 per cent more slowly than steam. All of the liquids, however, heated the wood somewhat faster than hot plates (6, 8). The slowest rate of heating was obtained in air at a low humidity, but the rate was increased as the humidity of the air was increased (10).

Variation in the rate at which wood heats in different mediums is apparently caused by such variables as type of surface contact, rate of circulation when liquids and gases are used, specific heat of the heating substance, and heat of vaporization as in the case of steam.

Differences in Moisture Content. Wood seasoned well below 30 per cent moisture content, which is about the fiber saturation point, was found to heat more slowly than green wood. Results obtained in heating green wood nevertheless indicate that differences in moisture content above the fiber saturation point have no significant effect on the rate of heating in the range of temperatures commonly employed (4). For practical purposes, therefore, it may be assumed that green timbers of any given species will heat at about the same rate at any moisture content above the fiber saturation point.

Direction of Grain. Studies made of the relative rate of heating in the radial and tangential directions (at right angles and parallel to the rings, respectively) showed there was no important difference in the rate of temperature change for these two directions, but the rate of heating in the longitudinal direction or along the fibers was found to be from $2^1/_4$ to $2^3/_4$ times faster than in the transverse direction (2, 6, 7). For practical purposes it should be sufficiently accurate to assume that on the average the rate of temperature change longitudinally is about $2^1/_2$ times faster than it is across the grain or in a plane at right angles to the axis of the tree. This ratio has been used in the calculation of temperature data that will be discussed later.

Density or Specific Gravity and Species. Experiments on specimens of the same species and on those of different species having different specific gravities showed that with any given heating medium, the rate of heating varied inversely with the specific gravity (6). The rate of temperature change is apparently influenced by the density of the wood rather than by the species, which affects the results merely to the extent that different species may vary in density.

The specific gravity of wood is usually based upon the volume at current moisture content and weight when oven-dry.

Table 1 shows the average specific-gravity values for various species of hardwoods and softwoods. These values are based upon volume when green and weight when oven-dry and are convenient to use when employing the time-temperature curves

[2] Numbers in parentheses refer to the Bibliography at the end of the paper.

TABLE 1 AVERAGE SPECIFIC GRAVITY OF VARIOUS SPECIES OF SOFTWOODS AND HARDWOODS[a]

Species	Average specific gravity (based on volume when green, and weight when oven-dry)
Hardwoods:	
Ash, white (Fraxinus americana)	0.55
Aspen, bigtooth (Populus grandidentata)	0.35
Basswood, American (Tilia americana)	0.32
Beech, American (Fagus grandifolia)	0.56
Birch, yellow (Betula lutea)	0.55
Chestnut, American (Castanea dentata)	0.40
Elm, American (Ulmus americana)	0.46
Elm, rock (Ulmus thomasii)	0.57
Hackberry (Celtis occidentalis)	0.49
Hickory, mockernut (Hicoria alba)	0.64
Maple, silver (Acer saccharinum)	0.44
Maple, sugar (Acer saccharum)	0.56
Oak, red (commercial) (Quercus sp.)	0.56
Oak, white (commercial) (Quercus sp.)	0.59
Pecan (Hicoria pecan)	0.60
Sweetgum (Liquidambar styraciflua)	0.44
Sycamore, American (Platanus occidentalis)	0.46
Tupelo, black (Nyssa sylvatica)	0.46
Tupelo, water (Nyssa aquatica)	0.46
Walnut, black (Juglans nigra)	0.51
Yellow poplar (Liriodendron tulipifera)	0.38
Softwoods:	
Baldcypress (Taxodium distichum)	0.42
Douglas fir, coast (Pseudotsuga taxifolia)	0.45
Douglas fir, Rocky Mountain (Pseudotsuga taxifolia)	0.40
Fir, white (Abies sp.)	0.37
Hemlock, Eastern (Tsuga canadensis)	0.38
Hemlock, Western (Tsuga heterophylla)	0.38
Larch, Western (Larix occidentalis)	0.48
Pine, Eastern white (Pinus strobus)	0.34
Pine, jack (Pinus banksiana)	0.39
Pine, loblolly (Pinus taeda)	0.47
Pine, longleaf (Pinus palustris)	0.54
Pine, ponderosa (Pinus ponderosa)	0.38
Pine, red (Pinus resinosa)	0.44
Pine, shore (Pinus contorta)	0.38
Pine, shortleaf (Pinus echinata)	0.46
Pine, slash (Pinus caribaea)	0.56
Pine, sugar (Pinus lambertiana)	0.35
Pine, Western white (Pinus monticola)	0.36
Red cedar, Eastern (Juniperus virginiana)	0.44
Red cedar, Western (Thuja plicata)	0.31
Redwood (Sequoia sempervirens)	0.38
Spruce, Engelmann (Picea engelmanni)	0.31
Spruce, Sitka (Picea sitchensis)	0.37
Spruce, white (Picea glauca)	0.37
Tamarack (Larix laricina)	0.49
White-cedar, Northern (Thuja occidentalis)	0.29

[a] Data for other species can be found in "Strength and Related Properties of Woods Grown in the United States," U. S. Dept. of Agriculture, technical Bulletin 479.

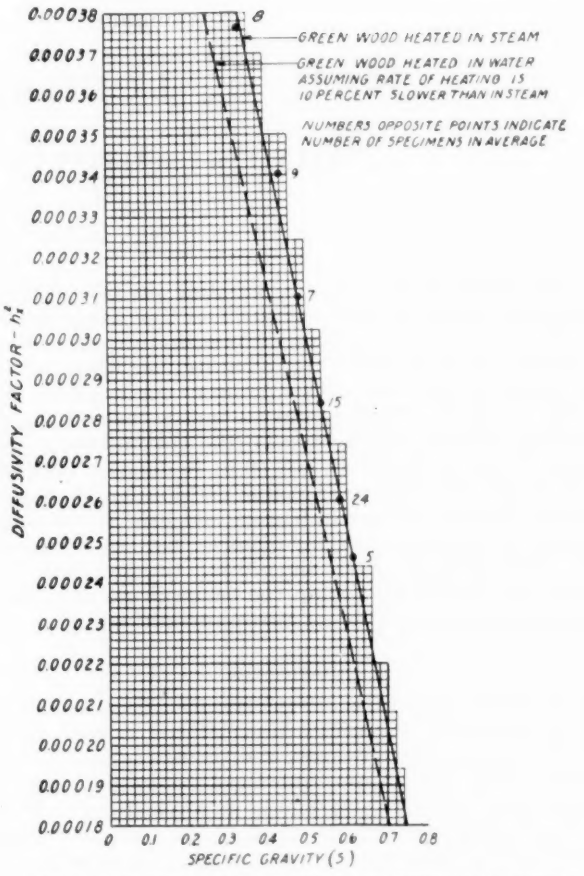


FIG. 1 RELATION OF DIFFUSIVITY AND SPECIFIC GRAVITY

shown in the figures. The method of using the data on density, or specific gravity, is discussed in the following section.

COMPUTATION OF TEMPERATURE

The rate of temperature change in any solid depends upon the diffusivity which, like conductivity, may be considered a constant for normal ranges of temperature. This factor is a measure of the rate of temperature change and may be defined as the change in temperature produced in a unit volume of the substance by the quantity of heat that passes in unit time through unit area of a layer of unit thickness and having unit difference of temperature between the faces. If the diffusivity is represented by the symbol h^2, the specific heat by c, the density by ρ, and the conductivity by K, the relation of these variables is shown by the algebraic expression, $h^2 = \frac{K}{c\rho}$. Thus the diffusivity varies inversely as the product of specific heat and density, and directly as the conductivity.

Fig. 1 shows the relation of diffusivity and the specific gravity of wood determined from tests made on green material heated in steam. As previously mentioned, water was found to heat a little more slowly than steam, and for the purpose of calculation it should be satisfactory to assume that the rate of heating in water is about 90 per cent as fast as in steam. On this basis the dotted line in Fig. 1 represents the relation of diffusivity and specific gravity for green wood heated in water. If, for example, green wood having a specific gravity of about 0.5 were heated in steam, the diffusivity would be determined from Fig. 1 as about 0.000302, while the corresponding diffusivity for heating in water would be about 0.000272. These diffusivity factors are in inch-second units.

Since the rate of temperature change depends to a certain extent upon the method of heating, the diffusivity values determined from experimental tests may be considered as values which apply for the heating medium used.

Wood is a substance that is naturally more or less variable in structure; hence temperature calculations cannot be made with the same precision that would be possible if it were a homogeneous material or a substance having the same physical properties in all directions. Nevertheless, the calculated temperature values, which are based upon average results from experimental tests, are sufficiently accurate for practical purposes, and whatever differences there may be between the computed temperatures and those actually obtained in a given timber will be small provided care is taken to maintain the heating conditions assumed.

In the early part of the heating period a variable amount of time is usually needed to bring the heating medium to the desired maximum temperature. A gradual change in the surface temperature is therefore obtained during this period, while the temperature calculations are necessarily based upon the assumption that the surfaces of the timbers are maintained at a constant temperature from the time the heating period is started.

If the temperature rise is fairly uniform, a convenient way to make an adjustment for the lower average temperature to which the wood is exposed during the early period of heating is to assume that the full temperature is applied for one half of this period. For example, if 2 hr were taken to bring the heating medium to the maximum temperature, the 2-hr period would be

counted as 1 hr at the maximum temperature. While this is an approximate method of adjusting for the period of variable temperature, it is generally satisfactory for moderate periods of changing surface temperature when the rate of temperature rise of the heating medium is reasonably uniform. A consideration of this lower average temperature at the beginning of the heating period naturally becomes of less importance as the total time of heating is increased. When the heating conditions are not controlled so that they are approximately uniform over most of the heating period, individual judgment must be exercised in determining the total time the timbers should be heated to compensate for the variable conditions.

Factors Involved in Temperature Calculations

Equation [4] in the Appendix was derived for computing the temperature data shown in Figs. 4 to 16, inclusive. Definitions of the symbols used and a brief outline of the development of this equation are also given in the Appendix.

An examination shows that the following factors are included in the fundamental equation:

1 Initial wood temperature = U_0
2 Temperature of heating medium = U_1
3 Diffusivity factor for radial heating = h^2
4 Diffusivity factor for longitudinal heating = q^2
5 Heating period = T (sec)
6 Radius of timber = a (in.)
7 Length of timber = L (in.)
8 Distance from nearest end surface, of point at which temperature is to be computed = Z (in.)
9 Distance from axis, of point at which temperature is to be computed = r (in.)
10 Temperature at the point (r, Z) under consideration = U

Fig. 2 shows the distance from the end surface and the distance from the circumference at which temperatures were computed for plotting the time-temperature curves. Fig. 3 is a chart for finding the corresponding wood temperatures when the heating conditions are different from those assumed in computing the temperature data plotted.

In the preparation of the time-temperature curves shown in Figs. 4 to 16, inclusive, the initial wood temperature U_0 was taken as 70 F, the heating-medium temperature U_1 as 212 F, the diffusivity factor for radial heating h^2 as 0.000270 (in-sec), and the diffusivity factor q^2 for longitudinal heating as about 2.5 times h^2, in round figures 0.000680, making the ratio slightly over 2.5, or about 2.52. It may be noted in Fig. 1 that the diffusivity factor of 0.000270 corresponds to about that for green wood having a specific gravity of 0.5, when heated in water.

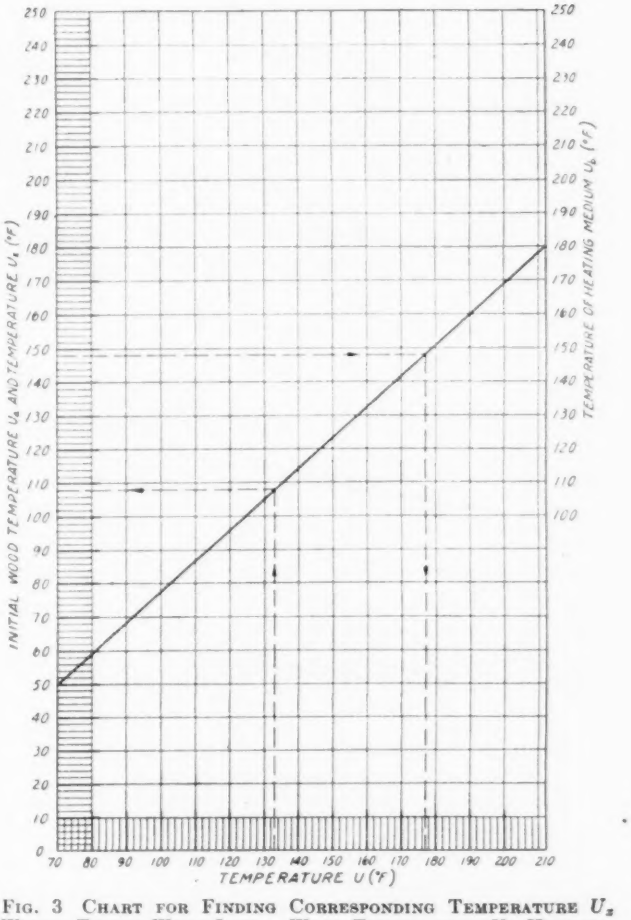
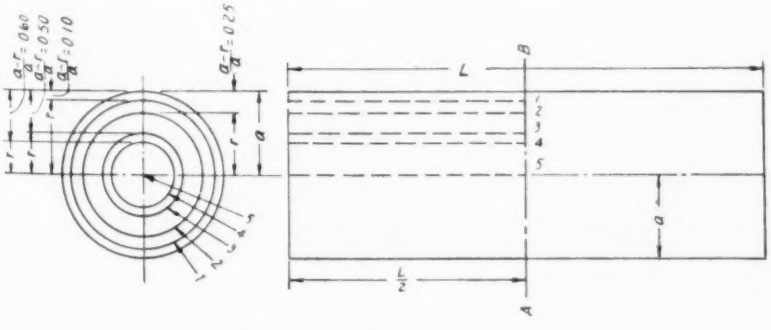


Fig. 3 Chart for Finding Corresponding Temperature U_x Within Timber When Initial Wood Temperature U_0, Heating-Medium Temperature U_b, or Both, Are Different From Those Assumed in Computing Plotted Temperatures

(Dotted lines illustrate examples.)



TEMPERATURE CURVES IN GROUP 1 ARE TEMPERATURES FROM END SURFACE TO MID-SECTION A-B AT DIFFERENT DISTANCES FROM THE CIRCUMFERENCE, NUMBERED 1, 2, 3, 4, AND 5
TEMPERATURE CURVES IN GROUP 2 SHOW TEMPERATURE DISTRIBUTION FROM CIRCUMFERENCE TO CENTER OF MID-SECTION A-B, AND TEMPERATURE CURVES IN GROUP 3 SHOW TEMPERATURES IN MID-SECTION AT DISTANCES OF 0.25a, 0.50a, 0.75a, AND a INCHES FROM THE CIRCUMFERENCE WHERE a=RADIUS IN INCHES

Fig. 2 Sketch Showing Distance From End Surface and Distance From Circumference at Which Temperatures Are Computed

Since the diffusivity for the longitudinal direction q^2 is taken as $2.52h^2$, the exponential function

$$e^{-T\left(h^2\lambda_n^2 + \frac{\pi^2 q^2 m^2}{L^2}\right)}$$

in the general Equation [3] can be written in the form

$$e^{-h^2T\left(\lambda_n^2 + \frac{2.52\pi^2 m^2}{L^2}\right)}$$

and a similar substitution can be made for q^2 in the terms of Equation [4] (Appendix). A change in the diffusivity factor for radial heating will therefore represent a proportional change in the longitudinal diffusivity factor q^2.

Although the temperature curves given in the various charts were computed by assuming the particular diffusivities and temperature conditions cited, these curves may be used for any predetermined conditions of temperature and for any species having diffusivities different

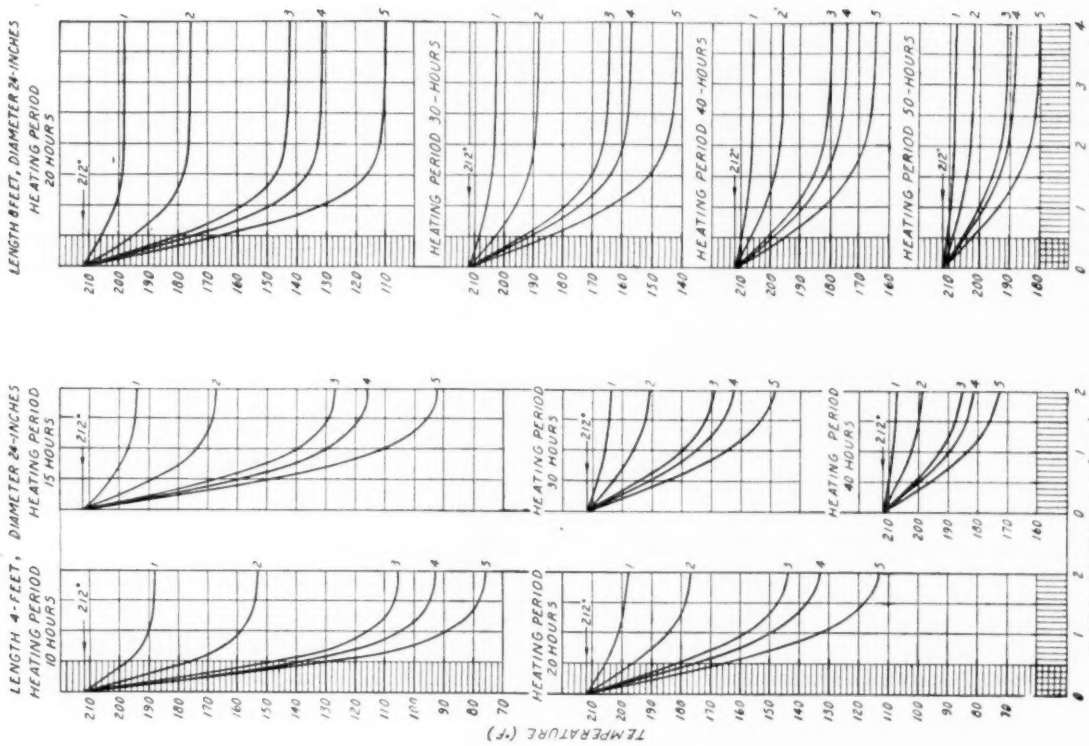


FIG. 5 TEMPERATURES OBTAINED AT DIFFERENT DISTANCES FROM END OF LOGS 4 AND 8 FT LONG AND 24 IN. DIAM

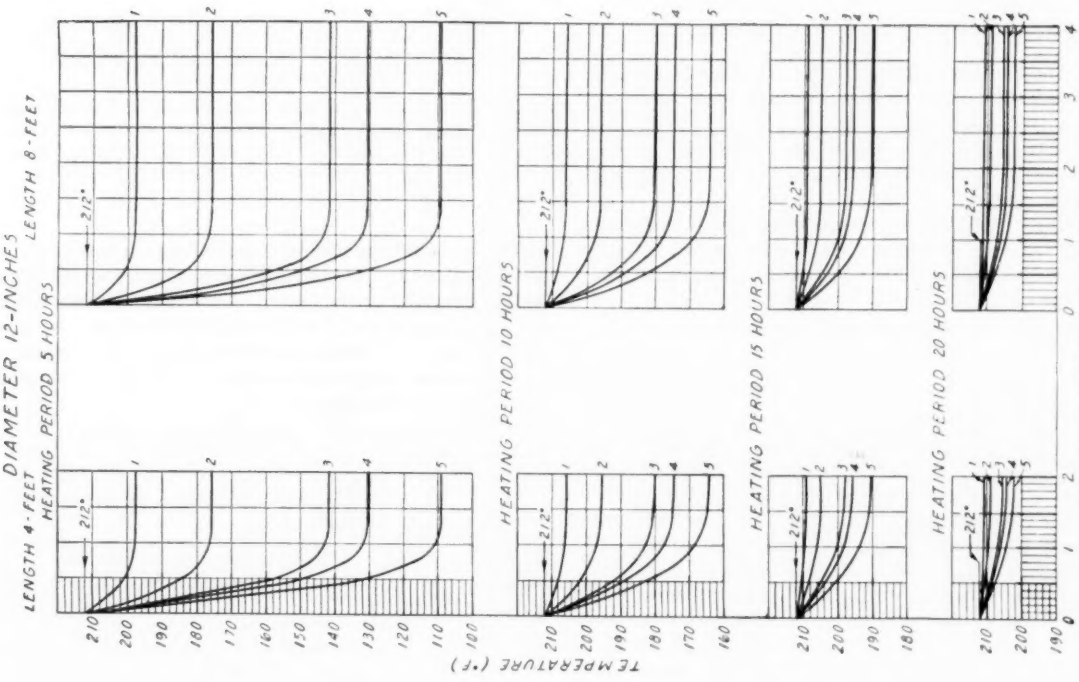


FIG. 4 TEMPERATURES OBTAINED AT DIFFERENT DISTANCES FROM END OF LOGS 4 AND 8 FT LONG AND 12 IN. DIAM

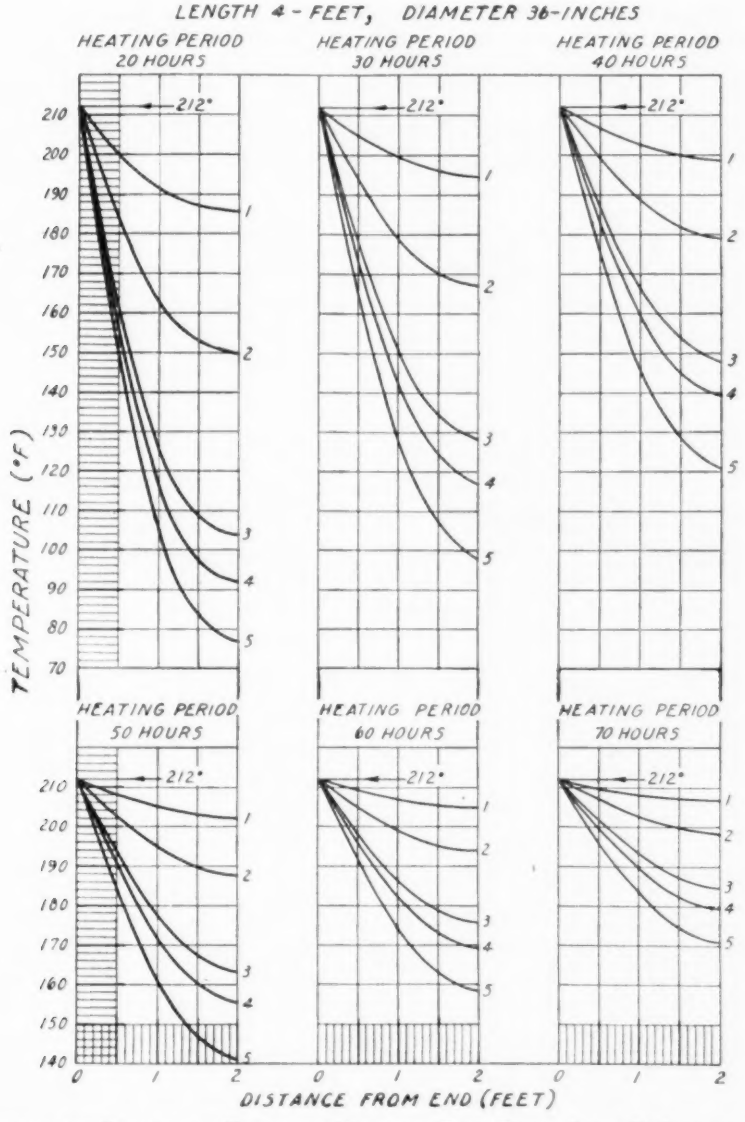


FIG. 6 TEMPERATURES OBTAINED AT DIFFERENT DISTANCES FROM END OF LOG 4 FT LONG AND 36 IN. DIAM

from those assumed. The method of doing this is explained in the Appendix under the heading, "Method of Using the Figures When the Diffusivity, Heating Conditions, or Both Are Different From Those Assumed in Computing the Time-Temperature Curves." Examples illustrating the use of the curves under different conditions will be given later.

DATA PLOTTED IN TEMPERATURE CURVES

The temperature curves comprise three groups in which the initial wood temperature was taken as 70 F and the heating-medium temperature as 212 F.

Group 1. Figs. 4 to 11, inclusive, show the computed temperature distribution from the end to the mid-length of logs 4 and 8 ft long and having diameters of 1, 2, 3, 4, and 5 ft. Each set of curves is for a different heating period, in most cases varying in intervals of 5 to 10 hr, depending upon the diameter.

Five temperature curves showing the temperature at the different distances from the circumference shown in Fig. 2 are given for each heating period. The top curve in Figs. 4 to 11, inclusive, shows the temperature in the zone or isothermal region at a distance from the circumference equal to $^1/_{10}$ (a) where a is the radius. The second, third, fourth, and fifth curves from the top show the corresponding temperatures in the zones that are at distances of $^1/_4$ (a), $^1/_2$ (a), $^3/_5$ (a), and a, respectively, from the circumference. In other words, if a is the radius of the log and r is the distance from the center or axis to the isothermal region at which the temperature is computed, then $(a - r)$ is the distance from the surface to the point at which the temperature is given. The ratio $\left(\frac{a-r}{a}\right)$ is therefore equal to 0.10, 0.25, 0.50, 0.60, and 1.0 for the curves shown. In the last case, $r = 0$; hence the curve for this distance from the circumference shows the temperature variation along the axis from the end to the mid-length of the timber. The distance from the circumference to the point on the radius at which the temperature is computed is evidently equal to the numerical value of $\left(\frac{a-r}{a}\right)$ multiplied by the radius. For example, if the radius is 12 in. and $\left(\frac{a-r}{a}\right) =$

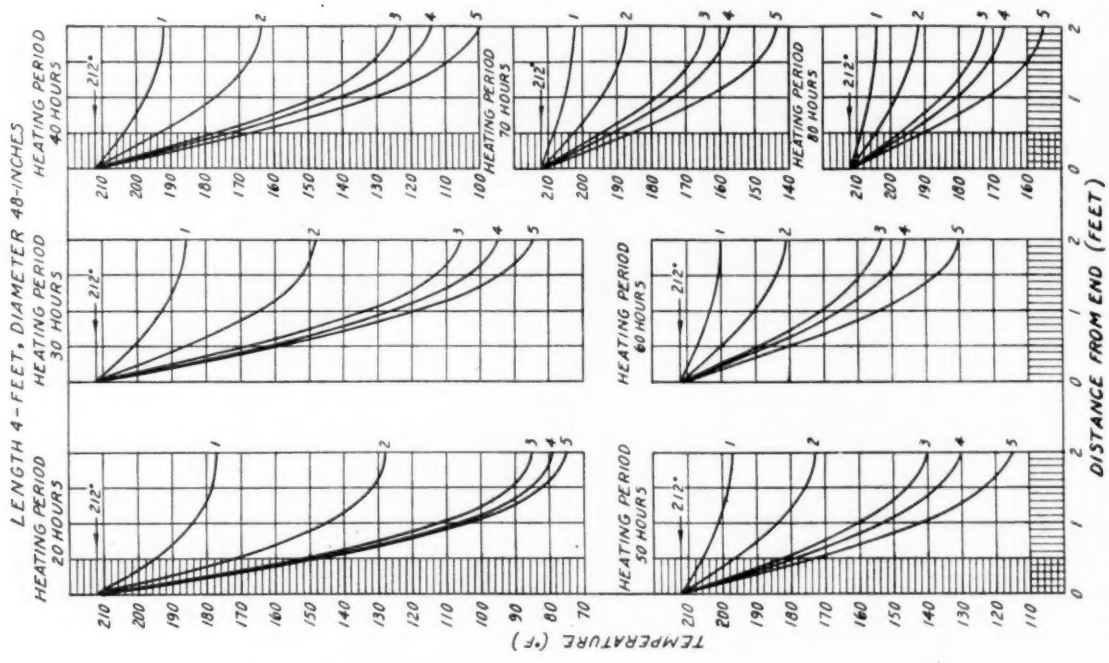


FIG. 8 TEMPERATURES OBTAINED AT DIFFERENT DISTANCES FROM END OF LOG 4 FT LONG AND 48 IN. DIAM

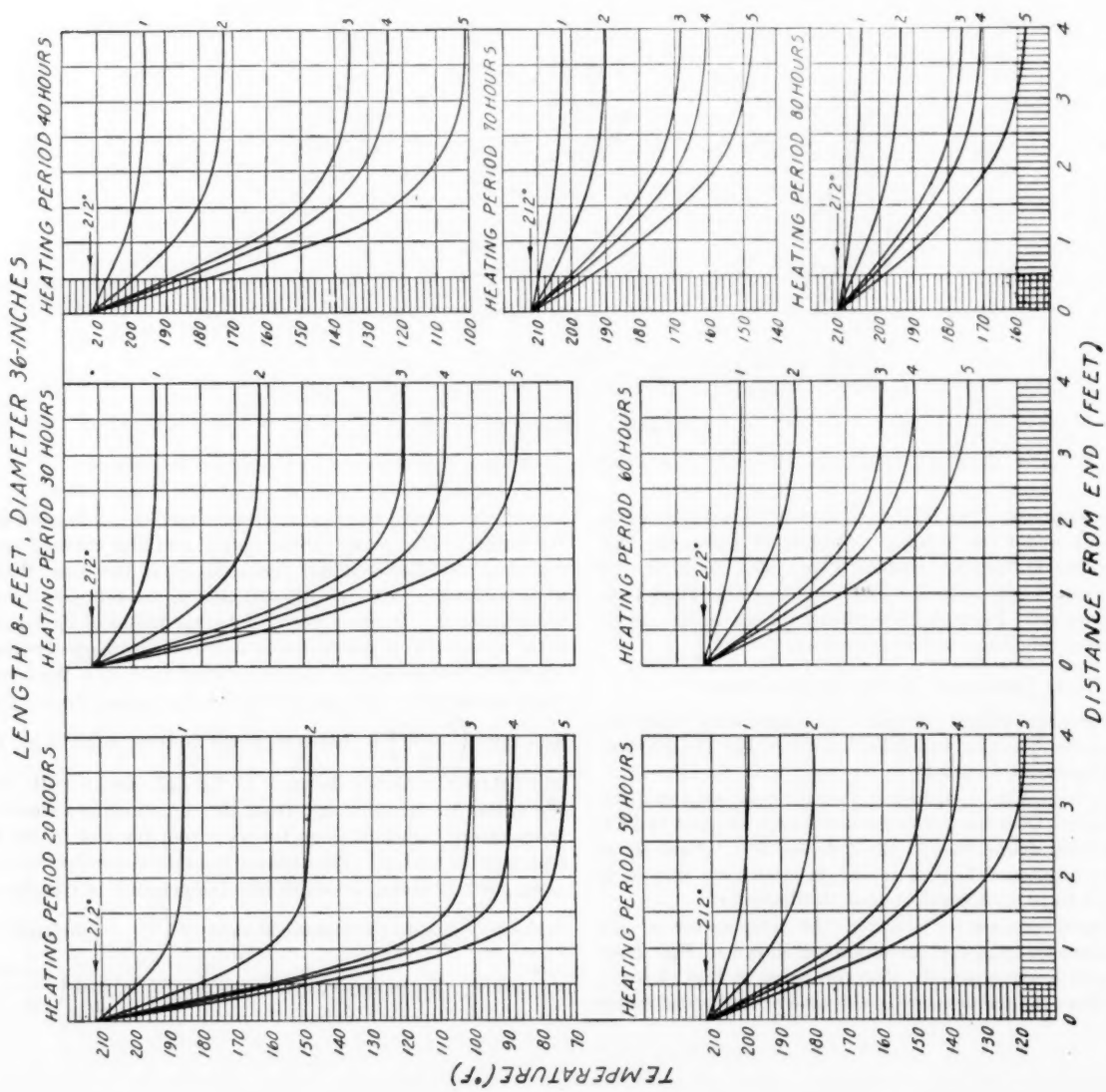


FIG. 7 TEMPERATURES OBTAINED AT DIFFERENT DISTANCES FROM END OF LOG 8 FT LONG AND 36 IN. DIAM

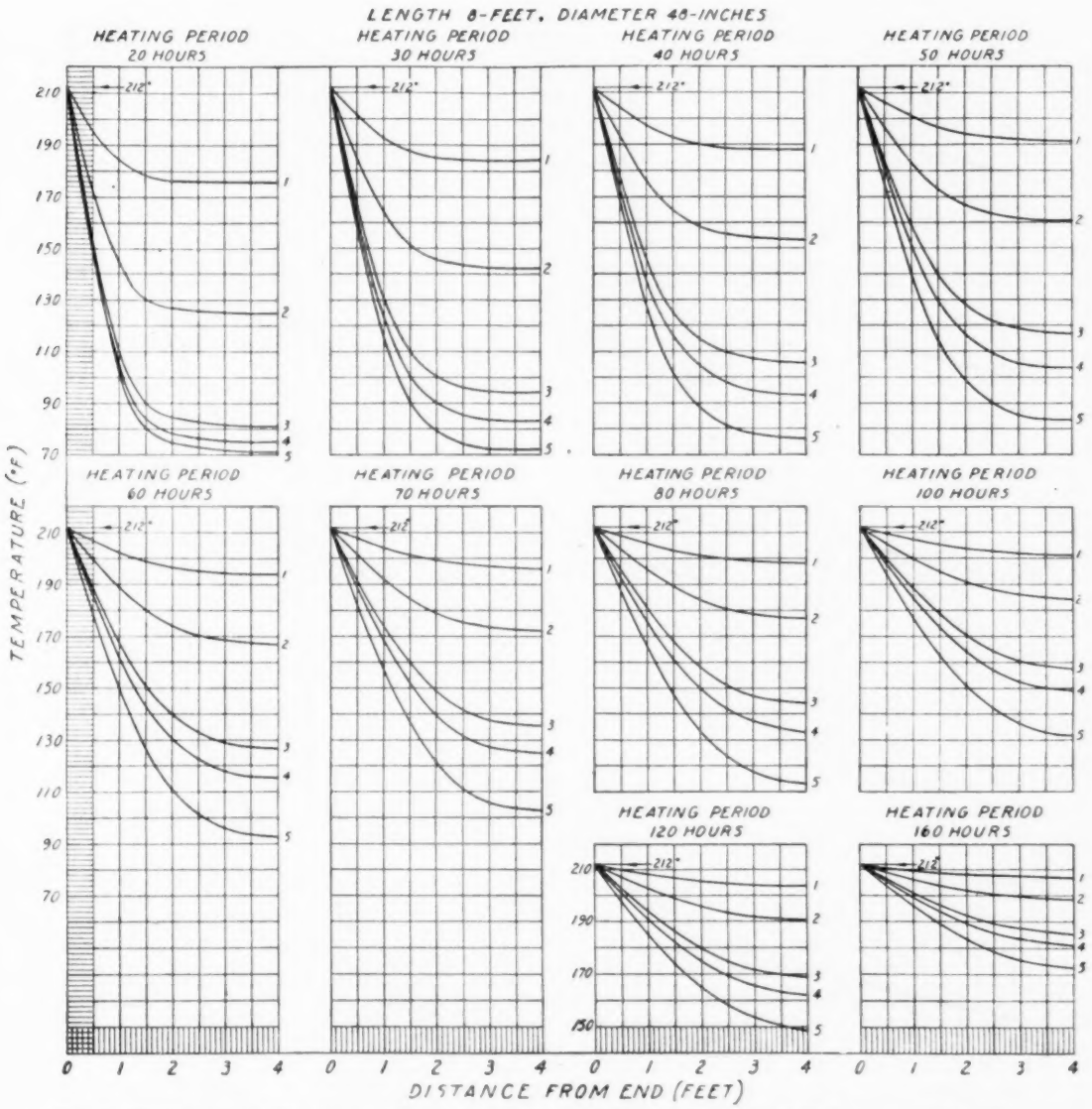


FIG. 9 TEMPERATURES OBTAINED AT DIFFERENT DISTANCES FROM END OF LOG 8 FT LONG AND 48 IN. DIAM

0.10, the distance from the surface is 12(0.10) or 1.2 in. The curves are shown for only one half the length since the rate of temperature change is assumed to be the same from either end.

Group 2. Figs. 12 to 14, inclusive, show the computed temperature distribution for various heating periods at all distances from the circumference to the center at the transverse mid-section of logs 4 and 8 ft long, for diameters of 1, 2, 3, 4, and 5 ft. Similar curves could be prepared for a transverse section at any distance from the end surface by plotting the temperature data from the curves shown in group 1 as was done in preparing the curves in group 2. The temperature at the transverse mid-section, however, is generally of most interest, since the lowest temperatures are obtained in this region. The curves given in group 2 (Figs. 12 to 14, inclusive) show the temperatures obtained at the end of 5- to 10-hr heating periods, except for particularly long heating periods or when the rate of temperature change was very slow. Under conditions in which this rate was unusually slow, somewhat longer time differences were used.

The time required to obtain a given temperature (which is found between any two time-temperature curves) can be determined with sufficient accuracy for practical purposes from the proportional distance on the vertical line intersecting the two curves between which the temperature is found. This assumes that the change in temperature between any two time-temperature curves is directly proportional to the time heat is applied during this time interval. For example, assume the required temperature is 170 F at 8 in. from the surface of a log 36 in. diam and 8 ft long. In this case $\left(\frac{a-r}{a}\right) = \frac{8}{18}$ or approximately 0.45. The vertical line from 0.45, Fig. 13*B*, intersects the horizontal line from 170 F at a point between the temperature curves for heating periods of 60 and 70 hr. The temperature after heating for 60 hr is 164 F, and that after heating for 70 hr is about 173 F, or an increase of 9 deg in 10 hr. When the proportional change in temperature is assumed to be the same as the proportional change in time of heating the temperature ratio is $\frac{170-164}{173-164} = \frac{6}{9}$ or $\frac{2}{3}$. Since the time interval is 10 hr, the time is found from the relation, $2:3 = x:10$ and x (the time that is required to in-

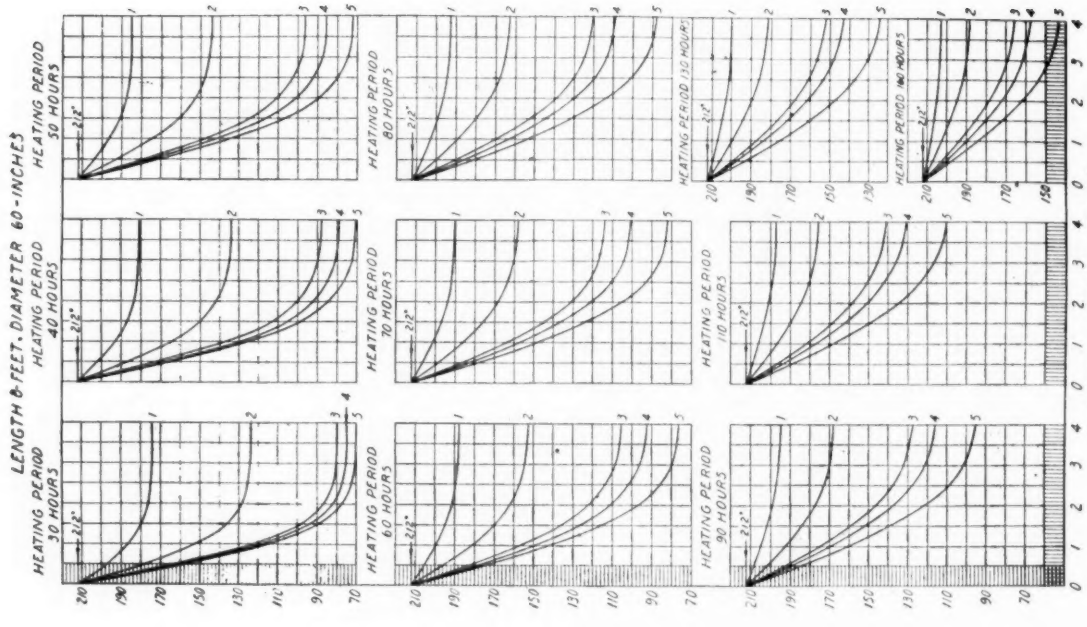


FIG. 11 TEMPERATURES OBTAINED AT DIFFERENT DISTANCES FROM END OF LOG 8 FT LONG AND 60 IN. DIAM

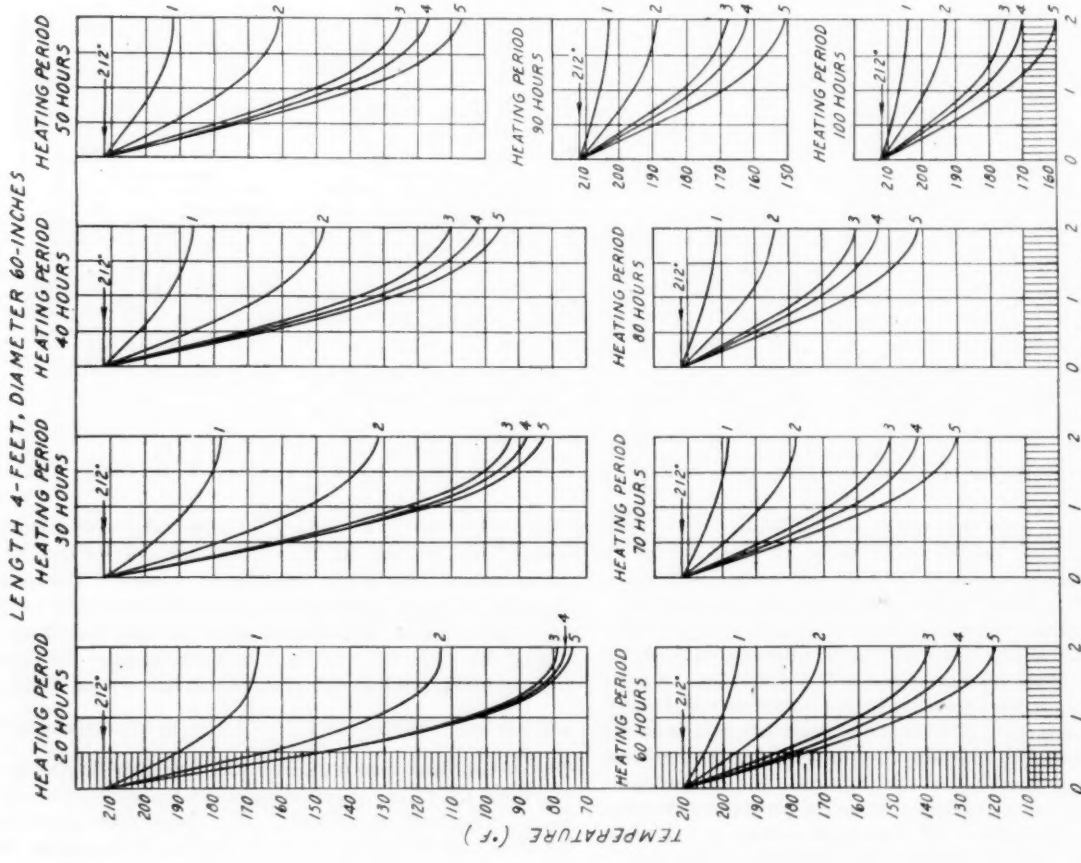


FIG. 10 TEMPERATURES OBTAINED AT DIFFERENT DISTANCES FROM END OF LOG 4 FT LONG AND 60 IN. DIAM

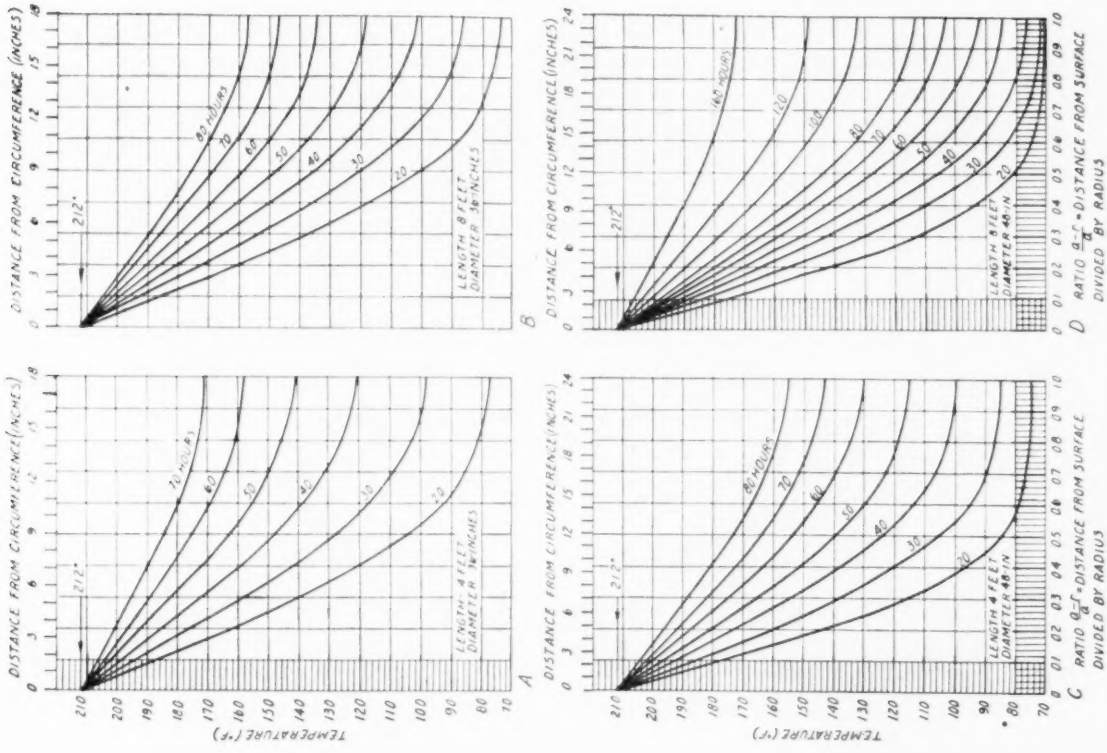


FIG. 13 TEMPERATURE DISTRIBUTION FROM CIRCUMFERENCE TO CENTER OF MID-SECTION; LOGS 4 AND 8 FT LONG AND 36 AND 48 IN. DIAM

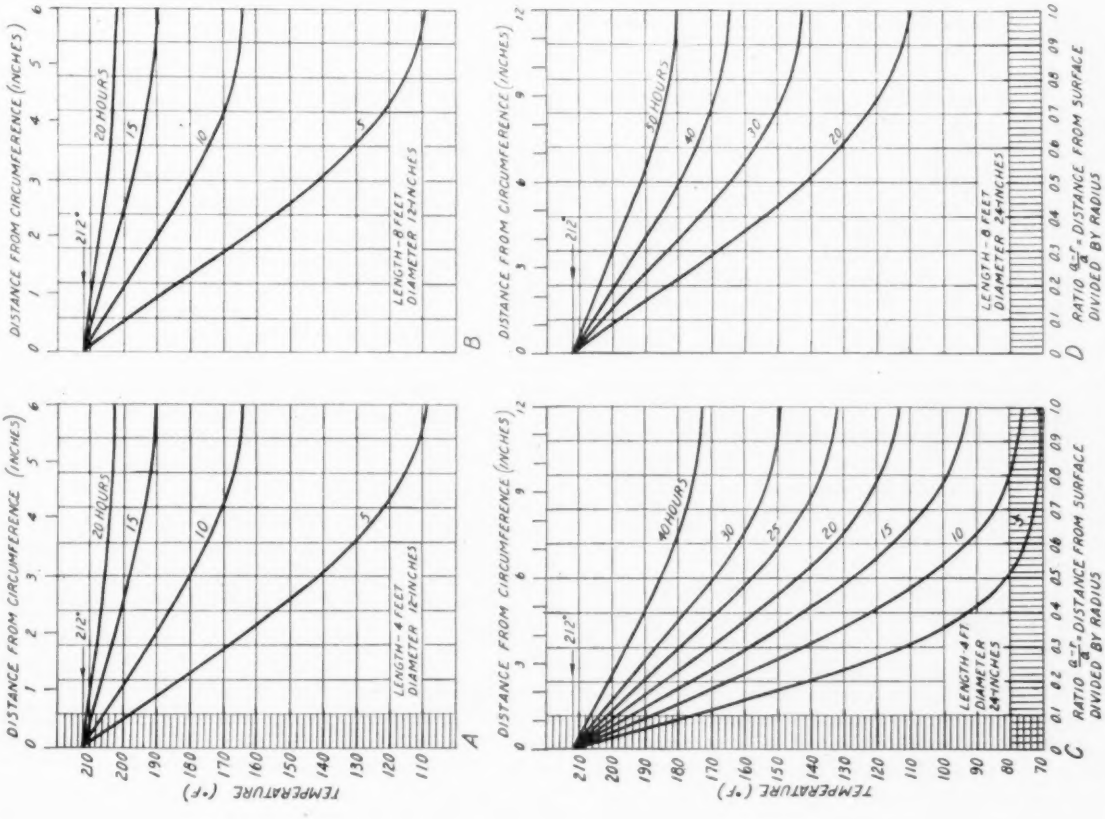


FIG. 12 TEMPERATURE DISTRIBUTION FROM CIRCUMFERENCE TO CENTER OF MID-SECTION; LOGS 4 AND 8 FT LONG AND 12 AND 24 IN. DIAM

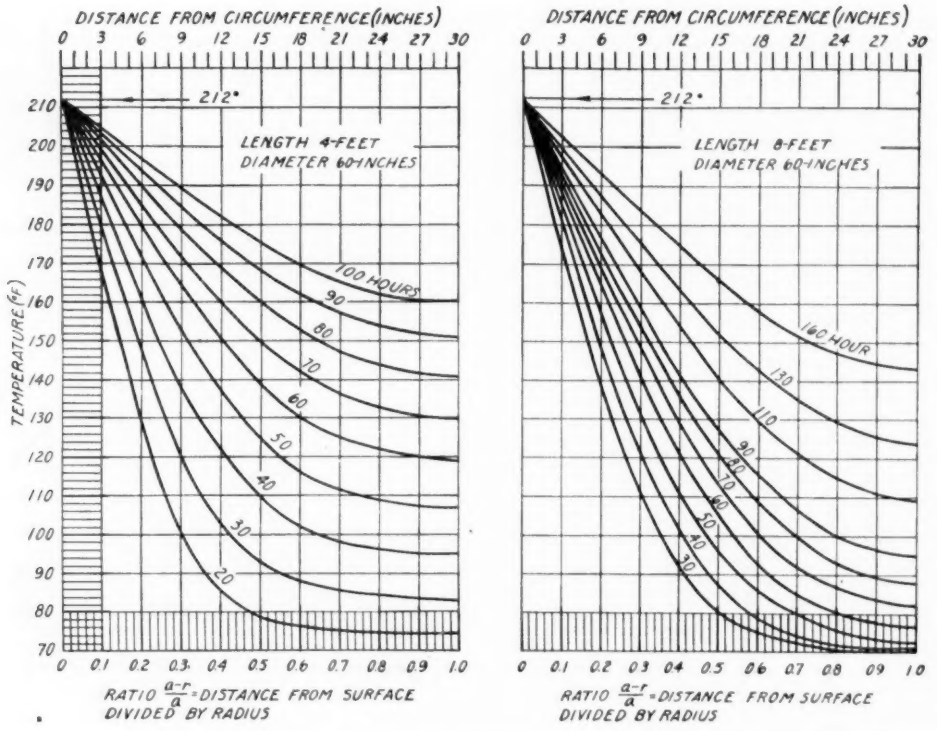


FIG. 14 TEMPERATURE DISTRIBUTION FROM CIRCUMFERENCE TO CENTER OF MID-SECTION; LOGS 4 AND 8 FT LONG AND 60 IN. DIAM

crease the temperature from 164 F to 170 F) is (2/3) 10 or 6 2/3 hr. The total time necessary to reach a temperature of 170 F is then 60 + 6.7 = 66.7 hr.

The same method would be used in finding the corresponding temperature when the heating period is known. If, for example, the heating period is 23.5 hr, and it is desired to find from Fig. 12*D* the temperature obtained at a point in the log half way between the axis and circumference, the figure shows that after 20 hr heating the temperature is 142 F, and after 30 hr heating it is 164 F, or an increase of 22 deg in 10 hr. The temperature increase above 142 F is then computed by the proportion (23.5 — 20):10 = x:22, from which it is found that the temperature change $x = \left(\frac{3.5}{10}\right) 22 = 7.7$ deg F. The temperature obtained after heating for 23.5 hr is then obtained by adding 7.7 deg to 142 F and is approximately 150 F.

If desired, the temperatures can be plotted against heating periods for any particular point in the timber, as for example at the center. Such curves would furnish a convenient method for reading directly the temperature obtained in a given time, or the corresponding heating period required to reach a definite temperature.

Group 3. In order to obtain curves that would show the temperature at various distances from the circumference at the mid-length of logs of any diameter between 12 and 60 in., data used in plotting the curves in group 2 were also used in preparing the curves shown in Figs. 15 and 16. Each curve in Figs. 15 and 16 was prepared by plotting the temperatures for each heating period for the logs of different diameters. Curves were then drawn through these plotted points for the same heating period. For heating periods over 50 hr, data were plotted only for timbers 36 in. or more in diameter.

Temperatures plotted in group 3, Figs. 15 and 16, are for points at distances from the circumferential surface of 1/4, 1/3, and 3/4 the radius, and for the center or where $\frac{a-r}{a} = 1$. When the required heating period or temperature is found between two time-temperature curves, the heating period or temperature can be found by using the proportional relation as explained for the curves in group 2.

The data show that it is not feasible to heat the large-diameter timbers at a considerable distance from the surface because of the extremely long heating periods required. For example, under the conditions assumed in making the temperature computations, Fig. 15*B* shows that if a temperature of 150 F is desired at a distance of 12 in. from the circumference of a log 4 ft diam, the heating period would be nearly 58 hr or 2.4 days. In such cases it would probably be better to heat to the minimum required temperature at a shorter distance from the circumference. After cutting to this depth the log could be reheated and with the reduced diameter the rate of heating would be much faster. This procedure would also avoid overheating the wood near the surface and at the ends.

The temperature curves shown in group 3 will be particularly useful for general purposes, since they show the relation of temperature and heating period for all diameters between 12 and 60 in. If it is desired to find the temperature at distances from the circumference that are intermediate between $\frac{a-r}{a} = 0.25, 0.50,$ 0.75, and 1.0, which are the distances shown in this group of curves, the data for any distance required may be found in the figures for group 2. These temperatures can then be plotted for the different diameter timbers as was done in preparing the curves for group 3. Temperatures for these four points can also be plotted against the proportional distance from the surface (as in Figs. 12 to 14, inclusive) for any diameter and any heating period. Smooth curves drawn through these plotted points will

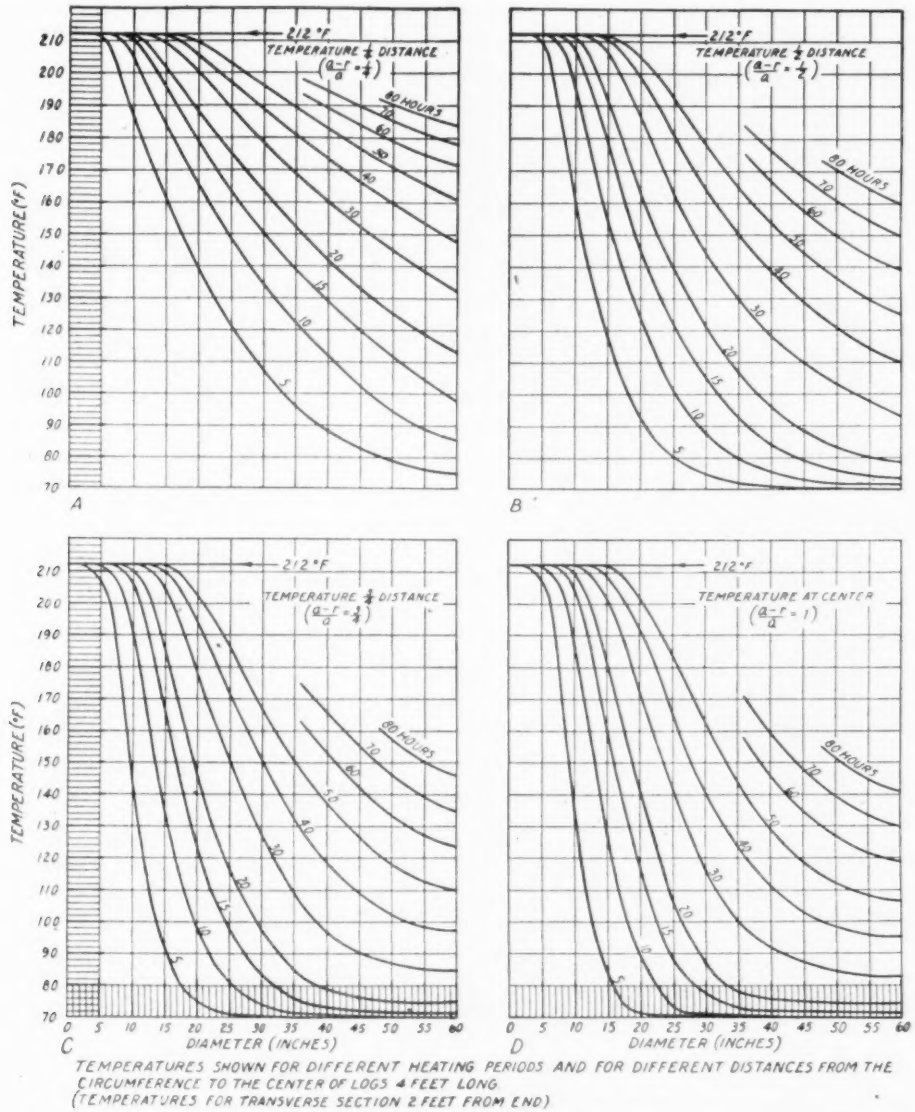


FIG. 15 TEMPERATURES OBTAINED AT DISTANCES OF 1/4, 1/2, AND 3/4 RADIUS AND AT CENTER OF LOGS 4 FT LONG

then show the approximate temperature for all distances from the surface to the center or axis of the timber.

Method of Using Fig. 3. Fig. 3 is a chart that furnishes a convenient method for finding the corresponding wood temperature when the heating conditions are different from those assumed in computing the temperature curves shown in the different groups.

The initial wood temperature U_a and the temperature U_x obtained in the wood after any given heating period are read on the left vertical scale, while the heating-medium temperature U_b is read on the right vertical scale. Values of U, the corresponding computed wood temperatures found from the figures, are given on the bottom scale.

In using Fig. 3, it is merely necessary to place a straightedge connecting the initial wood temperature U_a on the left scale with the heating-medium temperature U_b on the right scale. This is illustrated by the line connecting the initial wood temperature U_a = 50 F on the left scale with the heating temperature U_b = 180 F on the right scale. Assume, for example, that with the foregoing temperature conditions it is desired to find the corresponding computed temperature U (see Appendix for definition of symbols) at a point in the timber when the required temperature U_x is 148 F. This is found as follows:

Pass horizontally from 148 F on the left scale to the point of intersection with the line joining 50 and 180 F. Directly below this point of intersection U is found on the horizontal scale to be 177 F. The procedure is shown by the dotted line from 148 F. Again, let it be assumed that data from one of the charts shows that a temperature U of 133 F is obtained after heating for a period of T hr, and it is desired to find the temperature U_x that would be obtained at the same point, in the same time, and in the same timber when the initial wood temperature U_a is 50 F and the heating-medium temperature U_b is 180 F, instead of 70 and 212 F, the temperatures assumed in computing the data used in plotting the curves.

The temperature U_x is found in this case by passing vertically from U = 133 F on the horizontal scale to the line connecting 50 and 180 F. Directly across on the left scale U_x is found to be 108 F. These steps are shown in Fig. 3 by a dotted line connecting the temperature U = 133 F, and U_x = 108 F. This, is simply reversing the procedure for finding $U$when U_x is known.

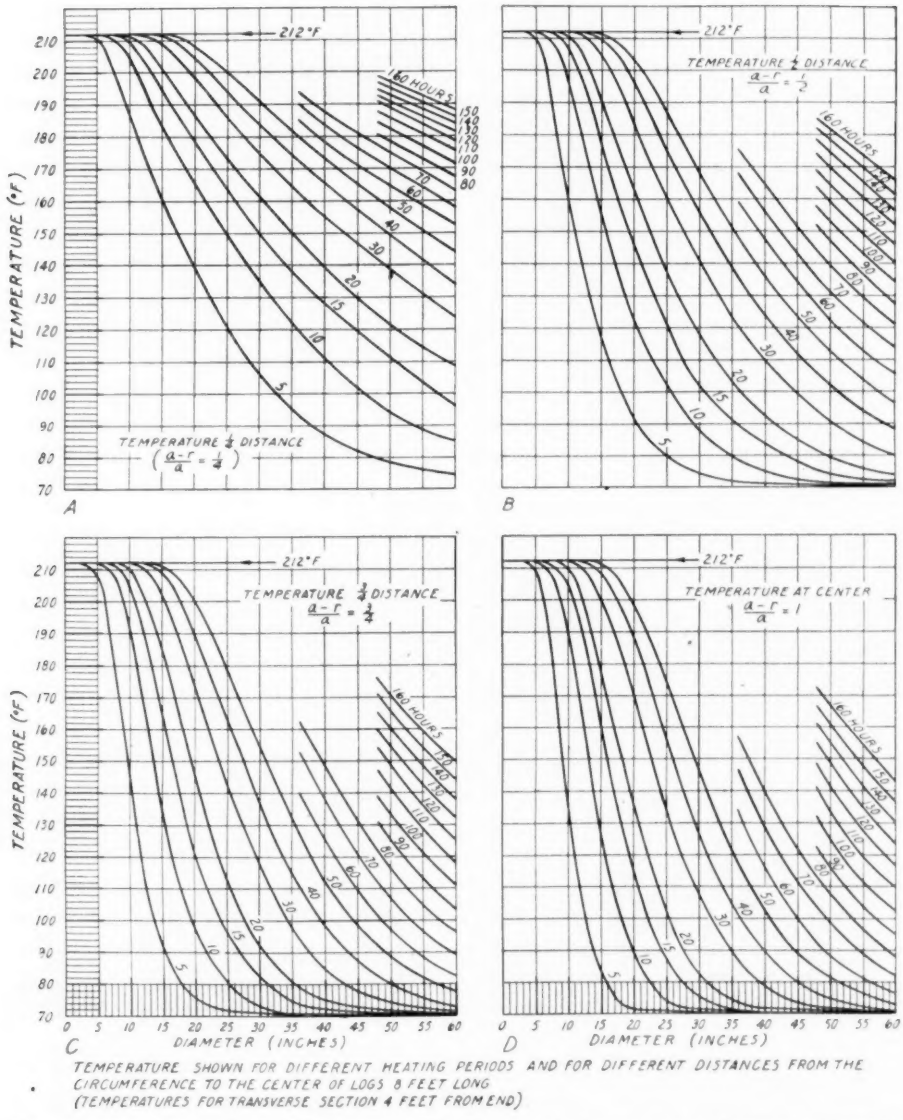


FIG. 16 TEMPERATURES OBTAINED AT DISTANCES OF 1/4, 1/2, AND 3/4 RADIUS AND AT CENTER OF LOGS 8 FT LONG

Fig. 3 is convenient to use in finding how the wood temperatures vary when different heating conditions are employed. For example, in the illustrations given, heating under the lower temperatures assumed for U_a and U_b the wood temperature will be (177 — 148) or 29 deg F lower at the point under consideration, than if the initial wood temperature had been 70 F, and the heating-medium temperature had been 212 F, which were the temperatures assumed in computing the curves. Similarly when any point is at a temperature U of 133 F (with the temperature conditions assumed in computing the curves), when heating under the lower temperature with U_a = 50 F and U_b = 180 F, the same point would be at a temperature of 108 F or 25 deg F lower. This chart can be used for finding either U_x or U instead of computing these temperatures from Equations $[B_1]$ and $[C_1]$ in the Appendix.

In general, problems relating to temperature changes will be either:

1 To find the time T_b required to obtain a specified temperature U_x at some particular point in a timber; or

2 To determine the temperature U_x that will be obtained when the time T_b and temperature U are known. In any problem the following variables are involved: Variables found by means of the temperature charts are U and T, and variables relating to the timber in question are U_a, U_b, U_x, and T_b. The relation between T and T_b is shown by Equation $[A]$ (Appendix), which is $T_b h_x^2 = T(0.00027)$

When U_a, U_b, and U_x are assumed, U is found from Equation $[C_1]$ (Appendix) or from Fig. 3. The corresponding time T required to obtain the temperature U can then be found from the proper chart, and the time T_b can be determined from Equation $[A]$.

When T_b, U_a, and U_b are given, T is found from Equation $[A]$, and the corresponding temperature U can be found from the proper chart. The temperature U_x can then be determined by means of Equation $[B_1]$ (Appendix) or from Fig. 3.

EXAMPLES SHOWING HOW CHARTS ARE USED[3]

Example 1. Data are as follows: Diameter of log = 22 in.;

[3] Refer to Appendix for definitions of symbols used.

length of log = 8 ft; species, yellow birch; heating medium, water; water temperature during heating period = 180 F = U_b; and initial wood temperature = 50 F = U_a.

Required to find the heating period (T_b) needed to obtain a temperature of 140 F (U_x) halfway between the circumference and center at the mid-length. In this case $\frac{a-r}{a} = \frac{1}{2}$. Therefore, for a log of this diameter, the distance from the surface = $^1/_2$ (11) = 5.5 in.

From Table 1 the average specific gravity of yellow birch (based on weight when oven-dry and volume when green) is found to be 0.55, and the diffusivity h_x^2 found in Fig. 1 for this specific gravity is about 0.000249 when the heating medium is water. In this example U_a, U_b, and U_x are given, while U, T, and T_b are to be determined.

The first step is to find U, using Equation [C_1] (Appendix), or Fig. 3. From Equation [C_1]

$$U = 212 - \left[\frac{(180-140)(142)}{(180-50)}\right] = 168 \text{ F}$$

This can be found readily from Fig. 3 by placing a straightedge connecting 50 F on the left scale with 180 F on the right scale, as shown by the straight line on this figure. Passing horizontally from 140 F on the left scale to this line the temperature U is found directly below on the lower scale to be 168 F, which is the temperature found by using Equation [C_1].

The second step is to find from Fig. 16(B) the time T required to reach a temperature of 168 F in a timber 22 in. diam and 8 ft long. Passing from 168 F in Fig. 16(B) to a point directly over the diameter of 22 in. shown on the abscissa, it is found that this point is between the curves for heating periods of 20 and 30 hr. The temperature after heating for 20 hr is found to be 153 F, and after heating for 30 hr is 174 F, or a temperature difference of 21 deg F. The proportion of the vertical distance between the two curves for the temperature of 168 F is then computed as $\frac{168-153}{174-153} = \frac{15}{21}$; and since the time interval is 10 hr, the time T is computed as $\left[20 + \frac{15}{21}(10)\right]$ or about 27.1 hr.

This is the time that would be required if the diffusivity were the same as that assumed in computing the temperature curves; but since the diffusivity for yellow birch was found to be about 0.000249, the time T_b must be computed from the relation shown by Equation [A] (Appendix) that gives

$$T_b = \frac{T(0.00027)}{0.000249} = (27.1)(1.084)$$

or 29.4 hr, which is the time to be determined.

If steam at 212 F were used as the heating medium, the diffusivity as indicated in Fig. 1, would be about 0.000276. With U_a = 50 F, U_b = 212 F, and the required temperature U_x = 140 F, the corresponding temperature U is determined from Equation [C_1] (Appendix) or from Fig. 3 to be 149 F. From Fig. 16(B), the time T required to reach a temperature of 149 F in a log 22 in. diam is found to be about 19 hr, and the required heating period T_b is $\frac{19(0.00027)}{0.000276} = 18.6$ hr.

Example 2. With the same data as given for example 1 find the temperature that would be obtained at $^1/_4$ the distance from the circumference to the center when the heating period T_b is 25 hr. In this example, $\frac{a-r}{a} = {}^1/_4$, and the distance from the circumference = $^1/_4$ (11) = $2^3/_4$ in. instead of $5^1/_2$ in. as in example 1. In this example U_a, U_b, and T_b are given, and T, U, and U_x are to be found.

First, find T from Equation [A] (Appendix). In this case

$$T = \frac{T_b(h_x^2)}{h^2} = \frac{25(0.000249)}{0.00027} = 23 \text{ hr, approximately}$$

Next, find U for this heating period. From Fig. 16(A) the temperature U is found to be about 185 F, after heating for 23 hr.

Then find the temperature U_x from Equation [B_1] (Appendix), or from Fig. 3.

Using Equation [B_1]

$$U_x = 180 - \left[\frac{(180-50)(212-185)}{142}\right] = 155 \text{ F}$$

which is the temperature to be determined. This temperature U_x can also be found from Fig. 3 by placing a straightedge on 50 F on the left scale and on 180 F, right scale. Reading up from 185 F on the bottom scale to the line connecting 50 F and 180 F, and directly across to the left scale, the temperature U_x is found to be about 155 F as computed from Equation [B_1] (Appendix).

If steam at 212 F were used as the heating medium the diffusivity would be 0.000276 (as found for example 1), and T would be $\frac{25(0.000276)}{0.00027}$ = 25.6 hr. The temperature U for this heating period is found from Fig. 16(A) to be about 188 F. When U_a = 50 F, and U_b = 212 F, the corresponding temperature U_x is found from Equation [B_1], or from Fig. 3, to be about 185 F.

Example 3. Data are as follows: Diameter of log = 48 in.; length of log = 8 ft; species, Coast Douglas fir; heating medium, water; water temperature during heating period = 190 F = U_b; and initial wood temperature = 60 F = U_a.

Required to find the temperature U_x obtained at a distance of 15 in. (Z) from the end surface and at a distance from the circumference equal to $^1/_4$ the radius when the log section has been heated for 30 hr (T_b). In this example $\frac{a-r}{a} = {}^1/_4$; hence the distance from the circumference = $^1/_4$ of 24 or 6 in. In this example U_a, U_b, and T_b are given, and T, U, and U_x are to be determined.

From Table 1 the average specific gravity of green Coast Douglas fir is found to be 0.45, and from Fig. 1 the corresponding diffusivity for heating in water is found to be about 0.000293 = h_x^2.

The first step is to find the heating period T using Equation [A] (Appendix)

$$T = \frac{T_b(h_x^2)}{0.00027} = \frac{30(0.000293)}{0.00027} = 32.6 \text{ hr}$$

Because of the higher diffusivity of the Douglas fir, in comparison with the diffusivity of 0.00027 used in computing the temperature curves, the Douglas fir heats $\frac{(0.000293-0.00027)}{0.00027}100 = 8.5$ per cent faster, and the temperature attained in 30 hr at the point under consideration would be the same (for the same heating conditions) as that reached after 32.6 hr heating when the wood has a diffusivity of 0.00027.

The second step is to find the temperature U in Fig. 9. From this figure the temperature U is found to be 155 F $\left(\text{for } Z = 15 \text{ in. and } \frac{a-r}{a} = \frac{1}{4}\right)$ after a heating period of 30 hr, and to be 169 F when the heating period is 40 hr. After 30 hr heating, the temperature at the point given would then be computed as

$$\left[155 + \left(\frac{32.6 - 30}{10}\right)(169 - 155)\right] = 159 \text{ F approximately}$$

This is the temperature U, or the temperature that would be obtained if $U_a = U_0 = 70$ F and $U_b = U_1 = 212$ F; but since U_a is assumed as 60 F, and U_b as 190 F, U_x is determined by using Equation [B_1] (Appendix), or from Fig. 3, and is found to be about 141 F which is the temperature to be determined.

This is similar to example 2, except that the point under consideration is between the end surface and the transverse mid-section, and the data are obtained from temperature curves shown in group 1.

Example 4. With the data given in example 3 find the heating period T_b required to obtain a temperature of $U_x = 160$ F for the same point in the log. In this example U_a, U_b, and U_x are given, and U, T, and T_b are to be determined.

The first step is to find the corresponding temperature U when $U_a = 60$ F, $U_b = 190$ F, and $U_x = 160$ F. From Equation [C_1] (Appendix), or from Fig. 3, U is found to be about 179 F.

Fig. 9 shows that when the distance from the end = 15 in. and the distance from the circumference $(a - r) = 6$ in. or $^1/_4$ the radius, the temperature of 179 F is between the temperature curves for heating periods of 50 and 60 hr. After heating for 50 hr, the temperature is 177.5 F, and after heating for 60 hr, it is about 184 F. The heating period required to reach 179 F would then be computed as

$$\left[\left(\frac{179 - 177.5}{184 - 177.5}\right)10 + 50\right] = 52.3 \text{ hr}$$

Since this is the time T required when the diffusivity is 0.00027 the time T_b is as follows

$$T_b = \frac{52.3(0.00027)}{0.000293} = 48.2 \text{ hr}$$

This is similar to example 1 except that the point at which the temperature is to be determined is between the end surface and transverse mid-section.

BIBLIOGRAPHY

1 "Studies of Heat Conduction in Wood—Results of Steaming Green Round Southern Pine Timbers," by J. D. MacLean, Proceedings of the American Wood Preservers' Association, 1930, pp. 197–217.

2 "Studies of Heat Conduction in Wood—Part II—Results of Steaming Green Sawed Southern Pine Timber," by J. D. MacLean, Proc. American Wood Preservers' Association, 1932, pp. 303–329.

3 "Temperatures in Green Southern Pine Timbers After Various Steaming Periods," by J. D. MacLean, Proc. American Wood Preservers' Association, 1934, pp. 355–373.

4 "Temperature and Moisture Changes in Coast Douglas Fir," by J. D. MacLean, Proc. American Wood Preservers' Association, 1935, pp. 77–103.

5 "Average Temperature and Moisture Reduction Calculations for Steamed Round Southern Pine Timbers," by J. D. MacLean, Proceedings of the American Wood Preservers' Association, 1936, pp. 256–279.

6 "Relation of Wood Density to Rate of Temperature Change in Wood in Different Heating Mediums," by J. D. MacLean, Proc. American Wood Preservers' Association, 1940, pp. 220–248.

7 "Thermal Conductivity of Wood," by J. D. MacLean, *Heating, Piping and Air Conditioning*, vol. 13, 1941, pp. 380–391. Same in Trans. American Society of Heating and Ventilating Engineers, vol. 47, 1941, pp. 323–354. Abstract in *Mechanical Engineering*, vol. 63, 1941, pp. 734–736.

8 "Rate of Temperature Change in Wood Panels Heated Between Hot Plates," by J. D. MacLean, Forest Products Laboratory Mimeo. No. R1299, 1942.

9 "Method of Computing the Rate of Temperature Change in Wood and Plywood Panels When the Two Opposite Surfaces Are Maintained at Different Temperatures," by J. D. MacLean, Forest Products Laboratory Mimeo. No. R1406, 1943.

10 "Rate of Temperature Change in Laminated Timbers Heated in Air Under Controlled Relative Humidity Conditions," by J. D. MacLean, Forest Products Laboratory Mimeo. No. R1434, 1943.

Appendix

Method of Computing Temperatures in Round Timbers of Short Length Where End Heating as Well as Heating in the Radial Direction Must Be Taken Into Consideration

In order to derive an equation for computing the temperature U at any point r inches from the axis and Z inches from one of the end surfaces, it is necessary to solve the following partial differential equation

$$\frac{\delta U}{\delta T} = \left[h^2\left\{\frac{\delta^2 U}{\delta r^2} + \frac{1}{r}\frac{\delta U}{\delta r}\right\} + q^2\frac{\delta^2 U}{\delta Z^2}\right] \quad \ldots\ldots\ldots [1]$$

In this equation h^2 is the diffusivity factor for heating in the radial direction and q^2 is the diffusivity factor for heating in the longitudinal direction.

Equation [1] must be solved, subject to the following boundary conditions: Let $\theta = (U - U_1)$, where U_1 is the temperature of the heating medium and U is the temperature at the point under consideration at any time T.

Let U_0 = initial wood temperature; a = average radius of log, and L = length in inches.

If $\theta = (U - U_1)$, $U = U_0$ and $\theta = (U_0 - U_1)$ when $T = 0$

$$\left.\begin{aligned} \theta &= 0 \text{ when } r = a \\ Z &= 0 \\ Z &= L \end{aligned}\right\} \quad \text{and } T > 0$$

$\theta = f(r,Z)$ when $T = 0$

Substituting θ in Equation [1]

$$\frac{\delta\theta}{\delta T} = \left[h^2\left\{\frac{\delta^2\theta}{\delta r^2} + \frac{1}{r}\frac{\delta\theta}{\delta r}\right\} + q^2\frac{\delta^2\theta}{\delta Z^2}\right] \quad \ldots\ldots\ldots [1a]$$

A solution of differential Equation [1a] to meet the boundary conditions gives

$$\theta = \sum_{m=1}^{m=\infty}\sum_{n=1}^{n=\infty} A_{m,n} e^{-T\left(h^2\lambda_n^2 + \frac{q^2\pi^2m^2}{L^2}\right)} \sin\frac{m\pi Z}{L} J_0(\lambda_n r) \quad [2]$$

where

$$A_{m,n} = \frac{4}{a^2L[J_1(\lambda_n a)]^2}\int_0^a dr\int_0^L rf(r,\mu)J_0(\lambda_n r)\sin\frac{m\pi\mu}{L}\,d\mu$$

When $f(r,\mu)$ is a constant and equal to $(U_0 - U_1)$, as in this case

$$A_{m,n} = \frac{4(U_0 - U_1)}{a^2L[J_1(\lambda_n a)]^2}\int_0^a dr\int_0^L rJ_0(\lambda_n r)\sin\frac{m\pi\mu}{L}\,d\mu$$

$$= \left[\frac{4(U_0 - U_1)}{L\lambda_n a J_1(\lambda_n a)}\right]\left(\frac{L}{m\pi}\right)(1 - \cos m\pi)$$

$$= \frac{8(U_0 - U_1)}{m\pi\lambda_n a J_1(\lambda_n a)} \text{ when } m \text{ is odd, and } = 0 \text{ when } m \text{ is even}$$

Substituting the value

$$\frac{8(U_0 - U_1)}{m\pi\lambda_n a J_1(\lambda_n a)}$$

for Am,n and the temperature difference $(U - U_1)$ for θ, Equation [2] may be written

$$U - U_1 = 8(U_0 - U_1) \sum_{m=1}^{m=\infty} \sum_{n=1}^{n=\infty} \frac{1}{m\pi\lambda_n a J_1(\lambda_n)} \sin \frac{m\pi Z}{L} J_0(\lambda_n r) e^{-T\left(h^2\lambda_n^2 + \frac{\pi^2 q^2 m^2}{L^2}\right)} \quad \ldots\ldots\ldots [3]$$

In the foregoing equations T is the time in seconds, $J_0(\lambda_n r)$ and $J_1(\lambda_n a)$ are Bessel functions of the zeroth and first order, respectively, and $(\lambda_n r) = x$ in $J_0(x)$ and $J_1(x)$.[4] Term λ_n is a root of $J_0(\lambda_n a) = 0$ and e is the base of the Napierian logarithms.

Writing the first few terms of Equation [3]

$$\begin{aligned} U = U_1 + (U_0 - U_1)\frac{8}{\pi}\Bigg[& \frac{1}{\lambda_1 a J_1(\lambda_1 a)} \sin \frac{\pi Z}{L} J_0(\lambda_1 r) e^{-T\left(h^2\lambda_1^2 + \frac{\pi^2 q^2}{L^2}\right)} \\ & + \frac{1}{\lambda_1 a J_1(\lambda_1 a)} \frac{1}{3} \sin \frac{3\pi Z}{L} J_0(\lambda_1 r) e^{-T\left(h^2\lambda_1^2 + \frac{9\pi^2 q^2}{L^2}\right)} \\ & + \frac{1}{\lambda_1 a J_1(\lambda_1 a)} \frac{1}{5} \sin \frac{5\pi Z}{L} J_0(\lambda_1 r) e^{-T\left(h^2\lambda_1^2 + \frac{25\pi^2 q^2}{L^2}\right)} + \ldots \\ & + \frac{1}{\lambda_2 a J_1(\lambda_2 a)} \sin \frac{\pi Z}{L} J_0(\lambda_2 r) e^{-T\left(h^2\lambda_2^2 + \frac{\pi^2 q^2}{L^2}\right)} \\ & + \frac{1}{\lambda_2 a J_1(\lambda_2 a)} \frac{1}{3} \sin \frac{3\pi Z}{L} J_0(\lambda_2 r) e^{-T\left(h^2\lambda_2^2 + \frac{9\pi^2 q^2}{L^2}\right)} + \ldots \\ & + \frac{1}{\lambda_3 a J_1(\lambda_3 a)} \sin \frac{\pi Z}{L} J_0(\lambda_3 r) e^{-T\left(h^2\lambda_3^2 + \frac{\pi^2 q^2}{L^2}\right)} \\ & + \frac{1}{\lambda_3 a J_1(\lambda_3 a)} \frac{1}{3} \sin \frac{3\pi Z}{L} J_0(\lambda_3 r) e^{-T\left(h^2\lambda_3^2 + \frac{9\pi^2 q^2}{L^2}\right)} + \ldots \\ & + \frac{1}{\lambda_4 a J_1(\lambda_4 a)} \sin \frac{\pi Z}{L} J_0(\lambda_4 r) e^{-T\left(h^2\lambda_4^2 + \frac{\pi^2 q^2}{L^2}\right)} \\ & + \frac{1}{\lambda_4 a J_1(\lambda_4 a)} \frac{1}{3} \sin \frac{3\pi Z}{L} J_0(\lambda_4 r) e^{-T\left(h^2\lambda_4^2 + \frac{9\pi^2 q^2}{L^2}\right)} + \ldots \Bigg]. \quad [4] \end{aligned}$$

The number of terms that must be used in making temperature calculations will depend to a considerable extent upon the value of the negative exponent of the Napierian log base e. Since this exponent involves the time T and the dimensions of the timber (as well as the diffusivity factors h^2 and q^2), the series converges more rapidly as the time T increases, and as the diameter and length of the timber decrease, since the values of λ vary inversely with the radius, and the second term of the negative exponent varies inversely as the square of the length L.

[4] Tables of Bessel's functions for different values of x and roots of $J_n(x) = 0$ are given in "Smithsonian Physical Tables," Smithsonian Institute, Washington, D. C., and in "Fourier Series and Spherical Harmonics," by W. E. Byerly, Ginn and Co., 1893, New York, N. Y.

METHOD OF USING FIGURES WHEN DIFFUSIVITY, HEATING CONDITIONS, OR BOTH, ARE DIFFERENT FROM THOSE ASSUMED IN COMPUTING THE TIME-TEMPERATURE CURVES

Equation [A] which follows, shows the relation of time and diffusivity, and Equations [B] and [C] show the method of finding the corresponding wood temperatures when the heating conditions are different from those assumed in computing the data for the temperature curves shown in the figures.

Symbols applying to computed data in figures are as follows:

U_0 = initial wood temperature, assumed as 70 F
U_1 = heating-medium temperature, assumed as 212 F
h^2 = diffusivity in radial direction = 0.00027 sq in. per sec
q^2 = diffusivity in longitudinal direction = $2.52(h^2) = 0.00068$
U = temperature obtained in given time T at some particular distance from surface. Values of U are temperatures within wood at distance from surface shown by figure
T = time of heating (in hours) necessary to obtain temperature U. This period is found from figure for diameter and length under consideration

Symbols, applying to temperature computations when the diffusivity, heating conditions, or both, are different from those used in computing the data plotted in the figures, are as follows:

U_a = any initial wood temperature
U_b = any heating-medium temperature
h_x^2 = any value of diffusivity for transverse direction, sq in. per sec

Since the diffusivity in the longitudinal direction (q^2) is taken as approximately $2^1/_2$ times the diffusivity in the transverse direction for the calculated temperatures, only values of h_x^2 need to be considered.

U_x = temperature obtained at definite point in timber when initial wood temperature U_a, heating temperature U_b, or both, are different from $U_0 = 70$ F, and $U_1 = 212$ F, the initial wood and heating-medium temperatures assumed in computing curves shown in figure
T_b = time of heating (in hours) required to obtain temperature U_x when either diffusivity h_x^2, initial wood temperature U_a, the heating-medium temperature U_b, or all three variables are different from corresponding values used in computing data for curves

Relation of Heating Period and Diffusivity. The relation of the heating period T and the heating period T_b is shown by the equation

$$T_b(h_x^2) = T(0.00027) \ldots\ldots\ldots\ldots\ldots [A]$$

In this equation T_b is the heating period assumed or to be determined when the wood has a diffusivity h_x^2, and T is the heating period found from the figure for the timber in question. Values of h_x^2 for green wood of any given specific gravity can be found in Fig. 1, when either water or steam is used as the heating medium. Specific-gravity values for different woods, based on weight when oven-dry and volume when green, are given in Table 1.

Relation of Initial Wood Temperature, Heating-Medium Temperature, and Temperatures Obtained in Wood. A simple proportional relation exists between the temperatures obtained under any given heating conditions. For example, the relation of the temperatures obtained when the initial wood temperature U_a, the heating-medium temperature U_b, or both, are different from those assumed in making temperature computations are expressed by the equation

$$\frac{(U_b - U_x)}{(U_b - U_a)} = \frac{(U_1 - U)}{(U_1 - U_0)}$$

When U_a, U_b, and U are known it is necessary to determine U_x, the wood temperature obtained when U_a, U_b, or both are different from U_0 and U_1. Solving for U_x in terms of U_b, U_a, U_1, U_0, and U gives

$$U_x = U_b - \left[\frac{(U_b - U_a)(U_1 - U)}{(U_1 - U_0)}\right] \ldots\ldots\ldots [B]$$

When U_x, U_a, and U_b are known it is necessary to solve for U to find the heating period T from the proper figure. Solving for U in terms of U_a, U_b, U_x, U_0, and U_1 gives

$$U = U_1 - \left[\frac{(U_b - U_x)(U_1 - U_0)}{(U_b - U_a)}\right] \ldots\ldots\ldots [C]$$

If the values of $U_0 = 70$ F and $U_1 = 212$ F (the initial wood and heating-medium temperatures assumed in making the computations) are substituted in Equations [B] and [C]

$$U_x = U_b - \left[\frac{(U_b - U_a)(212 - U)}{142}\right] \ldots\ldots\ldots [B_1]$$

$$U = 212 - \left[\frac{(U_b - U_x)(142)}{(U_b - U_a)}\right] \ldots\ldots\ldots [C_1]$$

Values of U_x and U can also be determined by means of Fig. 3, as explained in the text.

(Owing to travel emergency conditions existing when this paper was presented, discussion will be accepted until February 10, 1946)

Flame-Temperature Measurements in Internal-Combustion Engines

By O. A. UYEHARA,[1] P. S. MYERS,[2] K. M. WATSON,[3] and L. A. WILSON[4]

The theory, development, and calibration of an electro-optical pyrometer, capable of determining instantaneous true temperatures of luminous flames, are described. A description is also given of auxiliary apparatus used with the electro-optical pyrometer to obtain simultaneous values of pressure, temperature, and crank position in an internal-combustion engine. Typical data obtained with this instrumentation as applied to a Diesel engine are included.

THE need for instantaneous and continuous temperature data throughout the combustion process in internal-combustion engines has long been recognized. Combustion rates, chemical equilibria, fuel vaporization, ignition lag, and heat transfer are all affected by temperature. Measurement of high temperatures in internal-combustion engines is complicated by the rapidity of temperature fluctuations and by variations in flame thickness and emissivity.

About two years ago the chemical-engineering and mechanical-engineering departments of the University of Wisconsin initiated a co-operative Diesel-fuel research program, the objectives of which could best be achieved if precise combustion temperature and pressure data were obtainable. A study of methods used by previous investigators to measure combustion temperatures showed that thermocouples (1, 2, 3),[5] the sodium-line reversal method (4, 5, 6), the total-radiation method (7, 8), and the "two-wire" method (9) are obviously not adaptable to instantaneous and continuous measurements. The "additive" method, as reported by Graff (10), is instantaneous, but it is useless when radiation from carbon particles becomes appreciable; and, in addition, the transformation of radiation to temperature is laborious and involves the use of some questionable assumptions.

Hottel and Broughton (11) employed an optical pyrometer with filters, using two different wave lengths of radiation to measure the temperature of a steady luminous flame, and established the validity of the two-color principle. Although the Hottel-Broughton pyrometer was not directly applicable to the proposed combustion-engine research, the two-color principle appeared to be feasible. This led to the development of an electro-optical pyrometer which is instantaneous in response to flame-temperature variations and will determine the temperature at every point in the combustion process for an individual cycle of the engine. Auxiliary instruments were also developed for the measurement of combustion-chamber pressures, injection-nozzle opening, and the indication of completion of combustion, all in relation to crank position. It is believed that this instrumentation may prove useful in a variety of applications, particularly where rapidly fluctuating high temperatures and pressures are encountered.

The Electro-Optical Pyrometer

The relationship between the intensity of monochromatic radiation from a black body, the wave length of the radiation, and the temperature of the black body is expressed by Wien's law

$$J = C_1 \lambda^{-5} e^{\frac{-C_2}{\lambda T}} \quad \ldots\ldots\ldots\ldots\ldots\ldots [1]$$

where

J = intensity of radiation at wave length λ
C_1, C_2 = known constants
λ = monochromatic wave length
e = base for Naperian logarithms
T = absolute black-body temperature

A graphical representation of Equation [1] is shown in Fig. 1.

For a nonblack body, it is necessary to introduce a new factor (E_λ) called the monochromatic emissivity, which is defined as the ratio of the intensity of radiation from a nonblack body to that from a black body at the particular temperature and wave length involved. Thus, for a nonblack body

$$J = E_\lambda C_1 \lambda^{-5} e^{\frac{-C_2}{\lambda T}} \quad \ldots\ldots\ldots\ldots\ldots\ldots [2]$$

The intensity of radiation from a nonblack body may also be represented mathematically by

$$J = C_1 \lambda^{-5} e^{\frac{-C_2}{\lambda T_A}} \quad \ldots\ldots\ldots\ldots\ldots\ldots [3]$$

where T_A is the apparent temperature and is defined as the temperature at which a black body would have the same monochromatic intensity of radiation as the nonblack body.

Equating [2] and [3]

$$E^\lambda = e^{\frac{-C_2}{\lambda}\left(\frac{1}{T_A} - \frac{1}{T}\right)} \quad \ldots\ldots\ldots\ldots\ldots [4]$$

or

$$\ln E_\lambda = -\frac{C_2}{\lambda}\left(\frac{1}{T_A} - \frac{1}{T}\right) \quad \ldots\ldots\ldots\ldots [4a]$$

This is the form of equation that is generally used to correct optical pyrometers for departure from black-body conditions where the monochromatic emissivity is known. These relations are shown graphically in Fig. 1, where the dotted line represents a nonblack body at 4000 deg R. The apparent temperature at λ_A would be 3000 deg R, and at λ_B 2500 deg R. If the monochromatic emissivity E_λ were the same at all wave lengths, Equation [4a] might be written for each of two different wave lengths, λ_A and λ_B, and the monochromatic emissivities equated. Then, by determining the apparent temperatures at λ_A and λ_B,

---

[1] Department of Chemical Engineering, University of Wisconsin, Madison, Wis.
[2] Department of Mechanical Engineering, University of Wisconsin, Madison, Wis. Jun. A.S.M.E.
[3] Professor of Chemical Engineering, University of Wisconsin, Madison, Wis.
[4] Professor of Mechanical Engineering, and Chairman, Department of Mechanical Engineering, University of Wisconsin, Madison, Wis. Mem. A.S.M E.

[5] Numbers in parentheses refer to the Bibliography at the end of the paper.

Contributed by the Oil and Gas Power Division and presented at a meeting of the Cleveland Section, Cleveland, Ohio, May, 1945, of The American Society of Mechanical Engineers.

Note: Statements and opinions advanced in papers are to be understood as individual expressions of their authors and not those of the Society.

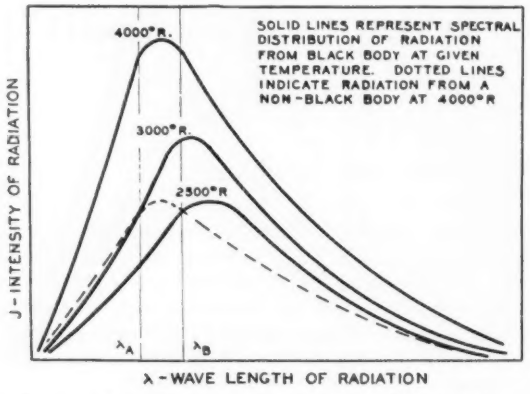


FIG. 1 GRAPHICAL REPRESENTATION OF WIEN'S LAW

the true temperature of a nonblack body might be calculated without knowing its emissivity.

In general, monochromatic emissivities are not equal at different wave lengths. It has been shown by Hottel and Broughton (11) that the monochromatic emissivity of a luminous flame is expressed by an equation of the form

$$E_\lambda = 1 - e^{\frac{-KL}{(\lambda)^\alpha}} \quad \ldots\ldots\ldots\ldots\ldots\ldots [5]$$

where

K = absorption constant per unit flame thickness and is independent of wave length
L = flame thickness
α = constant for limited wave-length range

It was also shown by Hottel and Broughton (11) that the true temperature of a flame could be determined by using this relationship between the monochromatic emissivities and measuring the apparent temperature at the two wave lengths involved. Following the development of Hottel and Broughton, substitution of Equation [5] into Equation [4*a*] gives

$$\ln\left(1 - e^{\frac{-KL}{\lambda^\alpha}}\right) = \frac{-C_2}{\lambda}\left(\frac{1}{T_A} - \frac{1}{T}\right) \quad \ldots\ldots\ldots [6]$$

Writing Equation [6] in exponential form and rearranging

$$e^{\frac{-KL}{(\lambda)^\alpha}} = 1 - e^{\frac{-C_2}{\lambda}\left(\frac{1}{T_A} - \frac{1}{T}\right)} \quad \ldots\ldots\ldots\ldots [7]$$

Taking the logarithm of each side and rearranging

$$-KL = (\lambda)^\alpha \ln\left[1 - e^{\frac{-C_2}{\lambda}\left(\frac{1}{T_A} - \frac{1}{T}\right)}\right] \quad \ldots\ldots\ldots [8]$$

Two such equations may be written for two different wave lengths, denoted by the subscripts 1 and 2. Equating the two KL terms, which are equal over a limited wave-length range, and rearranging, gives the following

$$\left[1 - e^{\frac{-C_2}{\lambda_1}\left(\frac{1}{T_{A1}} - \frac{1}{T}\right)}\right]^{\frac{(\lambda_1)^{\alpha_1}}{(\lambda_2)^{\alpha_2}}} = \left[1 - e^{\frac{-C_2}{\lambda_2}\left(\frac{1}{T_{A2}} - \frac{1}{T}\right)}\right] \quad [9]$$

If λ_1, λ_2, α_1, and α_2 are known, and the two apparent temperatures are measured, the true flame temperature T is the only unknown in Equation [9]. Once the true temperature is determined the term KL may be evaluated, thus giving an indication of the flame emissivity. Thus true flame temperatures may be obtained from two optical pyrometers which simultaneously record apparent temperatures corresponding to different wave lengths of radiation.

Apparatus. In the use of this method for measuring true flame temperatures, substantially monochromatic radiation of two different wave lengths must be obtained. Although filters have generally been used, a system of lenses and prisms was adopted in this work. This method does not require a division of the radiation as would the use of filters. Furthermore, the lenses and prisms are not affected by temperature and humidity changes. To obtain sufficient dispersion two prisms were used.

A schematic diagram of the electro-optical pyrometer is shown in Fig. 2. The radiation from the combustion chamber is focused by a lens system on a limiting diaphragm which has an opening somewhat smaller than the image of the source of radiation. Thus vibration or other small movements of the source of radiation do not cause a variation in the light permitted to pass through the limiting diaphragm. After the radiation passes the diaphragm it is paralleled by a lens, dispersed by the two prisms, and again focused by another lens. A barrier containing two slits is situated at the focal point of this lens. A phototube is located behind each slit in such a position that it is actuated by the radiation passing through the slit. A vacuum-type phototube with a caesium-oxide-silver surface was chosen because of its instantaneous response, its electrical stability, and its spectral response curve. The outputs from the phototubes are amplified and impressed on the vertical plates of two single-beam cathode-ray tubes. For this particular application the cathode rays are displaced horizontally in proportion to the engine crank position. In this manner a graph of apparent temperature as ordinates and crank angle as abscissas is repeatedly traced on each cathode-ray screen.

The amplifiers are of the direct-coupled type designed for use with vacuum-type phototubes and have a practically flat frequency response curve from 0 to approximately 15,000 cycles per sec. Two stages of amplification are required for the desired sensitivity. Batteries are used in the first-stage amplifiers to insure stability of operation. Voltage for the second-stage push-pull amplifiers is supplied from a voltage-regulated power pack.

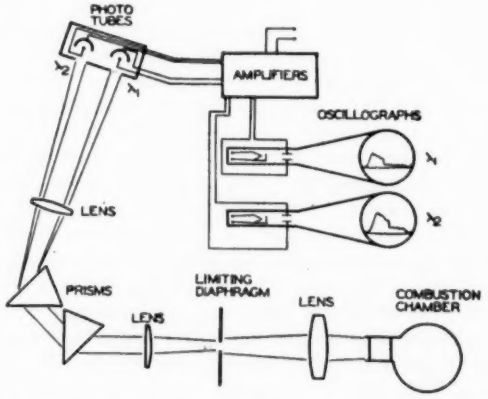


FIG. 2 SCHEMATIC DIAGRAM OF ELECTRO-OPTICAL PYROMETER

Black-Body Calibration. Care was necessary to insure an accurate calibration of the electro-optical pyrometer since the method depends on the measurement of two apparent temperatures of nearly equal values and the use of this small temperature difference in calculating the true temperature. Two methods of calibration were considered; (*a*) calibration by the use of a broad-ribbon tungsten lamp with known emissivity values and, (*b*) calibration by sighting directly upon a black body.

A search of the literature on the emissivity of tungsten (12, 13, 14) revealed wide disagreement both as to the values to be used for emissivities and as to their variation with temperature and with wave length. Accordingly, the black body was used for

calibration purposes and the broad-ribbon tungsten lamp was retained as a secondary standard. Its use in this connection is described later.

Black-body conditions were established by drilling a hole with a conical bottom in a graphite block. The graphite block was heated in the crucible of an induction furnace, and an optical pyrometer with a lamp calibrated by the Bureau of Standards was used to determine the black-body temperature.

Above 2800 F, the formation of smoke from impurities in the graphite began to cause a departure from black-body conditions. In order to eliminate this difficulty the graphite block was blanketed with an atmosphere of inert nitrogen. This prevented the formation of smoke until a temperature of about 3100 F was reached.

The procedure during the calibration process was as follows: The current to the induction furnace was adjusted and when the black body had reached a constant temperature a reading was then taken with the standard optical pyrometer. The electro-optical pyrometer was then placed in position viewing the black body. The corresponding cathode-ray deflections at the two wave lengths were measured by means of dividers and a steel scale graduated in hundredths of an inch. The electro-optical pyrometer was then removed from its position viewing the black body, and another reading of the black-body temperature was taken with the standard optical pyrometer. The average of the temperatures as measured by the standard optical pyrometer was taken as the correct temperature corresponding to the deflections noted. The foregoing procedure was repeated at various temperatures until the entire temperature range, representing zero to maximum deflection on the cathode-ray tubes had been covered. These data are shown in Fig. 3.

After the final calibration of the electro-optical pyrometer had been completed, it was used to calibrate the broad-ribbon tungsten lamp which was to be employed as a secondary standard. A rigid holder for the tungsten lamp was necessary to obtain reproducible results since the temperature of the filament was not uniform over its various portions. The resulting graph of deflection versus current is shown in Fig. 4. Since these data are from several different runs, the reproducibility of results is clearly established.

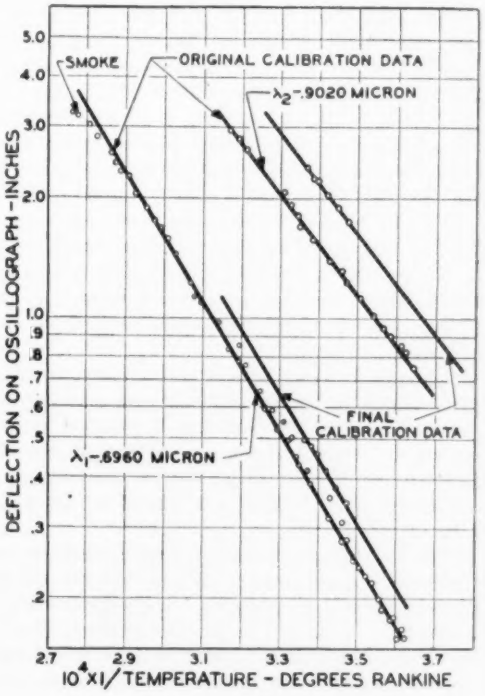


FIG. 3 BLACK-BODY CALIBRATION DATA

The original tungsten lamp proved defective and the filament broke after a short period of use. Consequently, it was necessary to repeat the black-body calibration at a few temperatures in order to standardize a second tungsten lamp. No effort was made to reproduce the original calibration and since the calibration data plot as straight lines in Fig. 3, the entire temperature range was not covered.

Determination of Equation Constants. In order to calculate true temperatures from Equation [9] it was necessary that λ_1 and λ_2 and the constants α_1 and α_2 be evaluated.

Two factors had to be considered in choosing the wave lengths to be used. Approximately equal oscillograph deflections were desired for accuracy in scaling. Assuming equal electronic amplification, the deflection is a function of the spectral sensitivity of the phototube and the intensity of radiation at the temperature and wave length involved. Rassweiler and Withrow have shown (15, 16) that in the range of wave lengths below 0.5 micron a small amount of spectral energy from intermediate products of combustion is present and might cause a departure from the relationships established between the monochromatic emissivities of a luminous flame. There is also a number of strong water-vapor absorption and emission bands (17, 18, 19) from 0.190 micron to 0.36 micron, and from 0.95 micron to 314 microns, and strong CO_2 bands (18, 19) in the region of 14 to 16 microns. However, Rassweiler and Withrow (15, 16), Graff (10), and Landen and Blanc (20) found that black-body spectral distribution existed in the flames studied at wave lengths above 0.6 micron. Accordingly, the phototubes were placed in the region of 0.6 to 1.0 micron and experimentally shifted in this region to obtain approximately equal responses under engine operating conditions.

It was first attempted to determine the values of the wave lengths used by means of a sodium-vapor lamp and a mercury-vapor lamp. The locations of the sodium and mercury lines were easily identified in the visible region of the spectrum by inspection and by the response of the phototube. However, one of the phototubes was located in the infrared region of the spectrum where it was necessary to identify the spectral lines by the response of the phototube alone. Difficulty was experienced in identifying positively the reference lines because of the fact that the response of the phototube varied considerably in the infrared region. Hence, the wave lengths determined by the phototube alone were considered unreliable.

A second method of wave-length determination utilized data obtained during the black-body calibration of the electro-optical pyrometer. Assuming constant amplification from the electronic equipment, the calibration data, when plotted as in Fig. 3, should plot as a straight line of slope $\frac{C_2}{\lambda}$, where C_2 is a known constant. From the slope of the calibration curve a value of 0.696 micron was obtained for the shorter wave length. This is in close agreement with the value of 0.699 micron determined by the use of the sodium and mercury lines. However, the value for the longer wave length of 0.902 micron was not in agreement with 0.860 micron estimated by the use of the mercury and sodium lines. Since the latter value was in doubt, and since the values obtained during the black-body calibration are "effective" wave lengths, the black-body values were taken as correct.

The range and relative intensities of the wave lengths permitted to pass through each of the two barrier slits, Fig. 2, to the phototubes are of interest since the narrowness of the peaks of the relative-intensity curves are an indication of the monochromacity of the radiation reaching the phototubes. The

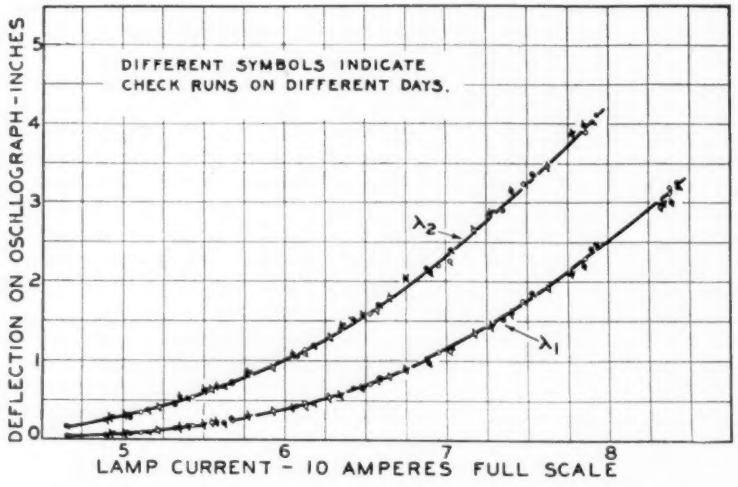


FIG. 4 CALIBRATION DATA FOR SECONDARY-STANDARD TUNGSTEN LAMP

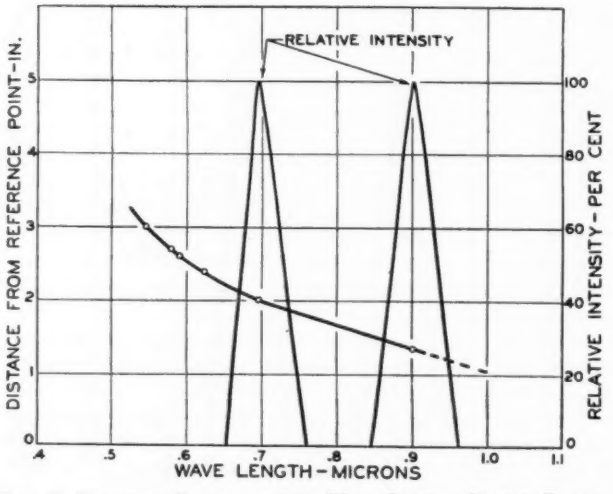


FIG. 5 RELATIVE INTENSITY AND WAVE-LENGTH RANGE DETERMINATION

following method was used to construct the relative-intensity curves shown in Fig. 5:

Data obtained during the wave-length determination were plotted showing the distances from a reference point to the points where known wave lengths were intercepted by the barrier. By measuring the distance from the two edges of the slit to the reference point, and using the curve of Fig. 5, the range of wave lengths permitted to pass through each barrier slit was obtained.

To obtain the relative intensity of the wave lengths passing through the barrier slits, the size of the image of the limiting diaphragm was measured at the barrier with monochromatic radiation entering the electro-optical pyrometer. The wave length at the center of each slit was determined from Fig. 5, and that portion of the radiation at this wave length permitted to pass through the barrier slit was calculated from the width of the slit and the dimensions of the limiting-diaphragm image. This procedure was then repeated for thirteen equidistant points across the width of each barrier slit. If the intensity of radiation is assumed to be the same for the wave lengths represented at the various points taken, the relative intensities for the wave lengths passing through each barrier slit are then given by the ratio of the respective portions of the monochromatic radiation passing through each barrier slit. The results of the analysis outlined are shown graphically by the relative-intensity curves in Fig. 5. The accuracy of the equal-intensity assumption is discussed in the next section.

The values to be used for α_1 and α_2 in Equation [9] depend on the wave lengths λ_1 and λ_2. It was suggested by Hottel and Broughton (11) that the range of wave lengths ordinarily used might be covered by two constant values of α. The values recommended are 1.39 for the range from 0.3 to 0.8 micron, and 0.95 for the range from 0.8 to 10 micron. These values were obtained by plotting experimental transmissivity data in such a manner that the slope of the line represented α. Inspection of the data indicated that each of the recommended values corresponds to the average slope of a portion of the transmissivity curve. Inasmuch as the wave lengths employed in the electro optical pyrometer had been evaluated, it was considered more accurate to determine α values by measuring the slope of the curve at the points corresponding to these particular wave lengths. The values so determined are $\alpha_1 = 1.32$ and $\alpha_2 = 1.05$. The effect of any error in these constants is discussed in the following section.

Accuracy. Since this method requires very accurate measurements of two apparent temperatures, the effect of all possible experimental errors must be minimized. One possible source of error is the electronic equipment. Direct-coupled amplifiers with two stages of amplification, batteries, and a voltage-regulated power pack were used. At first, slight inconsistencies were observed, but after waxing resistors and connections, "burning-in" resistors, etc., reproducible results were obtained as shown by the close agreement of the data in Fig. 4.

A small error is possible in measuring deflections on the cathode-ray tubes since the spot is of finite size. Measurements taken by various individuals differed by a maximum of only 0.02 in. on a 5-in. cathode-ray tube. This error was minimized by measuring each time from a given point on the spot, and by using the average of several readings.

In measuring the black-body temperature with the standard optical pyrometer observations by various individuals differed by a maximum of 15 F. Maximum deviation of the final calibration data from a straight line when plotted, Fig. 3, was only 10 F.

The effect of errors in evaluating α is discussed in reference (11), where calculations are presented showing that the error in true temperature due to a change in α from 1.7 to 1.39 is only 13.7 deg F for moderately thick flames. Thus a small error in determining α will not seriously affect the calculated temperature.

Forsythe (21) discusses the magnitude of the errors involved in assuming that the effective wave length of radiation used remains constant with changes in temperature, and he states that for most work the correction to be applied is negligible, amounting approximately to 4 deg at 5400 deg R.

The fundamental accuracy of this method of determining true flame temperatures has been demonstrated convincingly by Hottel and Broughton (11). However, in order to verify both the calibration and the calculations, a steady high-temperature flame was set up so that its temperature as determined by the electro-optical pyrometer might be compared to that measured by a standard method.

In order that the required high temperatures might be reached a burner was constructed to use acetylene, with air and oxygen supplied in any desired proportions. The experimental flame was approximately $^1/_4$ in. $\times$ 1 in. in cross section. The burner was set up inside a water-cooled jacket in order to simulate the conditions in the engine. Two peepholes were provided through which the flame might be observed.

The method used to determine the true temperature of the experimental flame was as follows: A broad-ribbon tungsten lamp of controllable brightness was placed behind the flame in the line of sight of the standard optical pyrometer. Due to the partial transparency of the flame, the standard pyrometer could "see" the tungsten lamp. The temperature of the tungsten lamp was adjusted until there was only a small difference between the reading of the standard optical pyrometer when sighted through the flame onto the tungsten lamp and when sighted directly on the tungsten lamp. Graphical interpolation of the readings taken in this manner permitted estimation of the temperature at which the apparent temperature of the tungsten lamp and the true temperature of the flame were equal.

The results of the determination of the true flame temperatures are given in Table 1. It was found that the flame temperature varied as much as 100 F over various portions of the flame visible through the peepholes; therefore, care was exercised to sight on the same portion of the flame with the standard optical pyrometer as with the electro-optical pyrometer.

To determine the effect of flame thickness on the electro-optical pyrometer temperature readings, the burner was rotated 90 deg so that the flame thickness was approximately 1 in. The lens aperture opening in the electro-optical pyrometer was stopped down so that the oscillograph deflections were not more than full scale. The data in Table 2 were then obtained.

The foregoing experimental evidence was accepted as satisfactory proof of the accuracy of the method and apparatus for the proposed internal-combustion-engine studies.

Working Charts. Since the solution of Equation [9] is a tedious process, a chart was constructed to express true temperature as a function of cathode-ray deflections. This chart was derived from the following rearrangement of Equation [9]

$$\frac{1}{T_{A1}} = \frac{1}{T} - \frac{\lambda_1}{C_2} \ln \left\{ 1 - \left[1 - e^{\frac{-C_2}{\lambda_2}\left(\frac{1}{T_{A2}} - \frac{1}{T}\right)} \right]^{\frac{(\lambda_2)\omega}{(\lambda_1)\omega}} \right\} \quad \ldots [10]$$

In the solution of this equation values were selected for T and for T_{A2} and the equation was solved for T_{A1}. By means of Fig. 3,

TABLE 1 DETERMINATION OF TRUE FLAME TEMPERATURES

I	First Comparison	
	Standard Optical Pyrometer (thin axis of flame):	
	Temperature of lamp through flame (average of two readings), deg R	4025
	Temperature of lamp (average of two readings), deg R	4025
	Electro-optical pyrometer readings (thin axis of flame):	
	Deflection at λ_1, in.	1.84
	Deflection at λ_2, in.	2.84
	True temperature, deg R	4020
II	Second Comparison	
	Standard Optical Pyrometer (thin axis of flame):	
	First trial:	
	Temperature of lamp through flame (average of three readings), deg R	4075
	Temperature of lamp, deg R	4145
	Second trial (lower lamp current):	
	Temperature of lamp through flame (average of three readings), deg R	4025
	Temperature of lamp, deg R	4005
	Using a graphical interpolation, the temperature of the lamp when sighted through the flame equals the temperature of the lamp at 4035 deg R	
	Electro-Optical Pyrometer Readings (thin axis of flame):	
	Deflection at λ_1, in.	1.86
	Deflection at λ_2, in.	2.85
	True temperature, deg R	4020

TABLE 2 ELECTRO-OPTICAL PYROMETER READINGS (THICK AXIS OF FLAME)

Deflection at λ_1, in.	2.3
Deflection at λ_2, in.	3.6
True temperature, deg R	4020

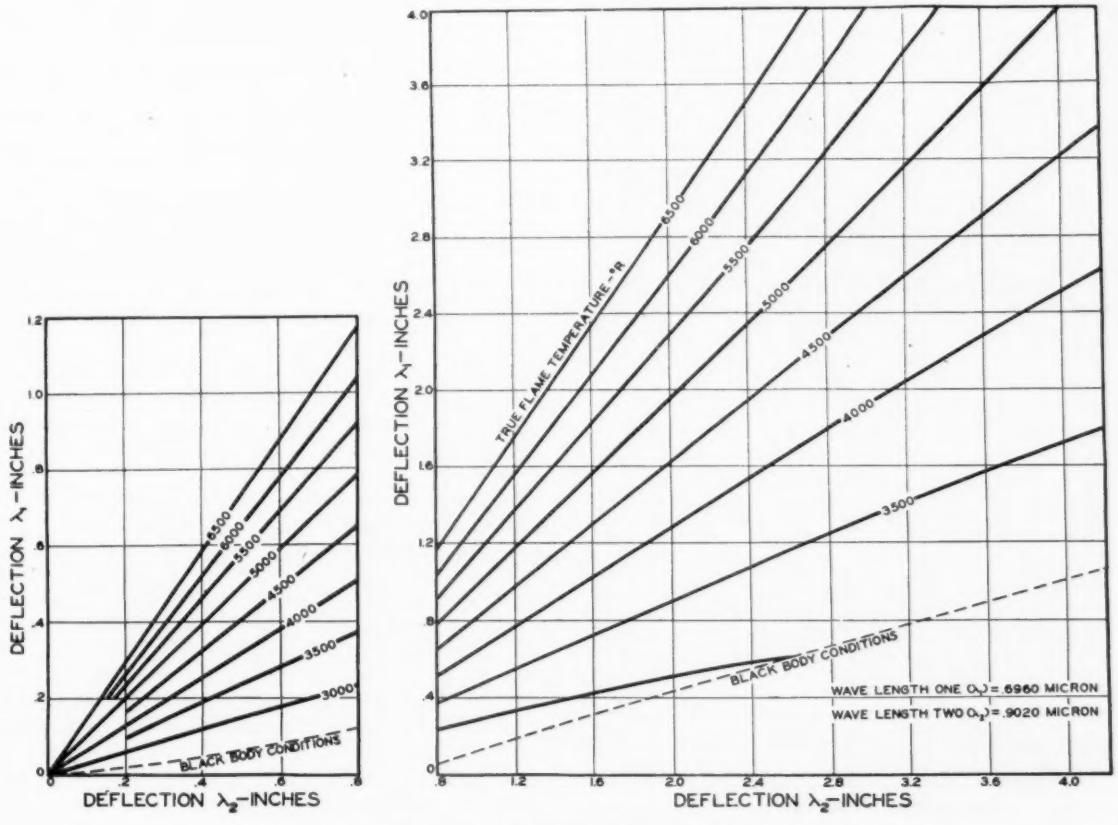


Fig. 6 True Temperature Working Chart

values of T_{A1} and T_{A2} were translated into inches of deflection on the oscillographs. The completed chart is shown in Fig. 6.

Since a knowledge of the variations in the KL factor is of interest, a similar chart, Fig. 7, was constructed, showing lines of constant KL factor.

Quartz Windows. Quartz was chosen as a suitable material to transmit combustion radiation because of the uniformity of its transmissivity over the range of wave lengths used in the electro-optical pyrometer (22). A polished quartz rod is fitted into a cylindrical steel holder which screws into one of the openings to the combustion chamber. To hold the rod against explosion pressures, a shoulder, forming a hole slightly smaller than the quartz rod, was machined at the outer end of the holder. The quartz was cemented in with litharge and glycerine to prevent leakage.

Periodically it is necessary to remove carbon deposits from the inner end of the quartz rod because the vertical deflections of the cathode rays vary with the intensity of the radiation transmitted through the quartz window. However, since the presence of a coating of carbon has the same effect as a reduction in flame emissivity, the true temperature value obtained is affected only to the extent that the scaling accuracy is impaired by the reduction in deflection.

Auxiliary Equipment Used With Electro-Optical Pyrometer

Sweep and Timing Arrangement. The two apparent temperatures to be used in calculating the instantaneous true temperature of a rapidly fluctuating flame must of necessity be measured at precisely the same instant. In the conventional internal-combustion engine this is best accomplished by an arrangement whereby the rotation of the engine controls the horizontal motion of the cathode rays and simultaneously provides timing marks at frequent intervals corresponding to known crank positions. In addition, it should be readily adjustable so that any small portion of the combustion process can be expanded to reveal minute details which are not clearly discernible when the entire process is shown on the cathode-ray screen, and it should function equally well at all engine speeds without alteration. These features were incorporated in the sweep and timing arrangement designed for use with the electro-optical pyrometer.

The sweep and timing arrangement was built as a separate unit and coupled to the end of the dynamometer shaft by an Oldham-type coupling. The characteristics of this type of coupling are such that the angular velocity of the driven shaft is the same at every instant as that of the driving shaft, even if the shafts are not in perfect alignment.

The arrangement of the working parts of the unit is shown in Fig. 8. Secured to the shaft are two cam-shaped disks, H and I. One of these disks has a constant increase in radius per degree for 330 deg, while the other has the same total increase in 90 deg. The remainder of the periphery in each case is at a constant radius until finally a radial decrease in diameter reduces the radius to the minimum value. Using either disk, light from a source A is projected through a radial slit C, behind which the edge of the rotating disk gradually cuts off the beam of light. A mirror E reflects the remaining light into a phototube D. Thus the amount of light reaching the phototube at any instant is directly related to the position of the disk at that instant. The phototube is connected to a direct-coupled two-stage amplifier, and the output voltage is impressed on the horizontal plates of all the cathode-ray tubes. Inasmuch as the voltage required to sweep the cathode rays a given distance is not the same for all tubes, potentiometers were installed as a means of making compensatory adjustments. Since the horizontal movement of the cathode rays is controlled by the variation in radius of a disk, the sweep is directly related to engine rotation during the period corresponding to K in Fig. 8. After a pause occasioned by the

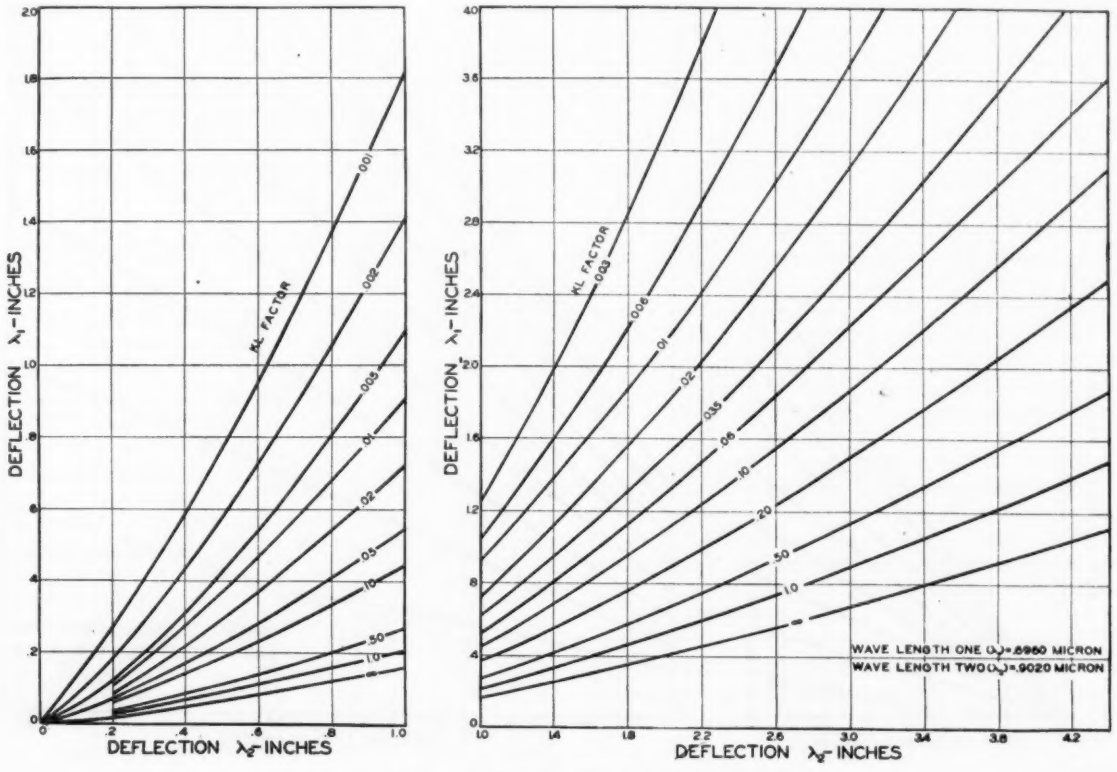


Fig. 7 *KL* Factor Working Chart

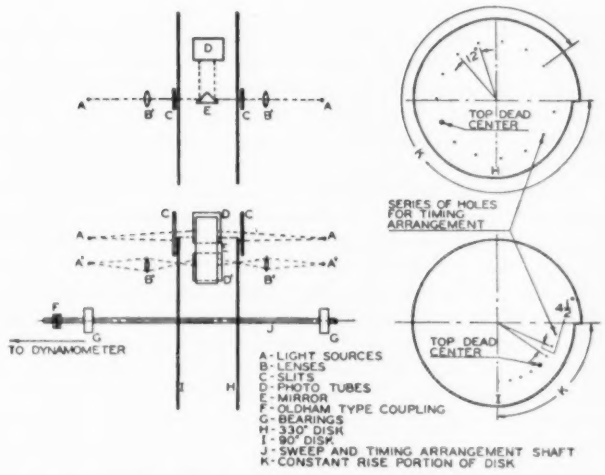


FIG. 8 SCHEMATIC DRAWING OF SWEEP-AND-TIMING ARRANGEMENT

constant-radius part of the disk, the abrupt decrease in radius instantaneously returns each ray to the opposite side of its screen to begin another sweep cycle.

The portion of the combustion process viewed on the cathode-ray screen can be varied, either by changing from one disk to the other by switching lights A, or by varying the intensity of the light. Using the first method, the horizontal sweep of the cathode rays can be made to correspond either to 330 deg of crank rotation, or to 90 deg, depending on which of the lights A is illuminated. With equal ease, the total sweep of the cathode rays can be adjusted at will by varying the intensity of the light source A by means of a rheostat. These adjustments permit as much or as little of the combustion process as desired to be spread across the fluorescent screens of the cathode-ray tubes. The range, in degrees of crankshaft rotation, may be any amount from 9 to 330 deg. The 9-deg range is particularly advantageous where pressure and temperature changes occur most rapidly.

The timing device is integral with the sweep arrangement. Using a milling-machine head, small holes were drilled in each disk on an arc 5 in. from the center of rotation and extending over that portion of the disk where the constant increase in radius occurs. The holes are $4^1/_2$ deg apart in the 90-deg disk, and 12 deg apart in the 330-deg disk. The center hole of the series was drilled slightly larger than the others.

A light source A', a lens B', the mirror E, and a phototube D', Fig. 8, are so placed that light reaches the phototube intermittently through the holes in the disk as the disk rotates. The phototube is connected through amplifiers to the vertical plates of one of the cathode-ray tubes. This arrangement causes the cathode ray to be deflected vertically at intervals corresponding to the spacing of the holes in the disk. The position of each disk on the shaft was fixed in assembling so that the large hole passes light to the phototube when the engine is exactly at top center, causing a higher deflection which clearly marks the top-center position.

In order to bring into view portions of the cycle outside the normal range, the holder for the lights, lenses, mirror, and phototubes was made movable about the axis of the shaft, and a ring graduated in degrees was mounted adjacent to the holder. When the holder is shifted from its normal position the long timing mark on the screen no longer corresponds to the top-center position. However, since all the timing marks are shifted the same number of degrees as the holder, the position on the screen corresponding to top center can readily be found by means of the graduated ring.

It was found necessary to balance the disk-and-shaft assembly dynamically and to mount the entire assembly on a heavy cast-iron block insulated from floor vibration. It was also found necessary to use bronze bearings rather than ball bearings since the latter, when tried, set up vibrations of a magnitude sufficient to cau e noticeable distortion of the cathode-ray diagrams. The entire unit is painted black and inclosed in a lightproof housing to prevent stray light from reaching the two phototubes. The unit is shown in Fig. 9.

Pressure Indicator. An electro-optic pressure indicator developed by Robertson (23) at the University of Wisconsin is employed to obtain pressure data. A schematic diagram of the pressure pickup unit is shown in Fig. 10, in which light from source A is made parallel by lens B, then is reflected by a mirror C through a limiting diaphragm D onto a highly polished pressure diaphragm E, which is screwed into an opening in the wall of the combustion chamber. Pressure variations in the combustion chamber cause the diaphragm E to change shape, dispersing the light reflected back by the polished surface. A portion of this light passes through perforations in the reflecting surface of the mirror C, and through a limiting diaphragm F to a phototube G. The output of the phototube is amplified and impressed on the vertical plates of a cathode-ray tube. The cathode ray is actuated horizontally by the sweep circuit previously described. Since the intensity of the light reaching the phototube is varied by changes in pressure, the cathode ray traces a pressure versus crank-angle diagram on the tube screen.

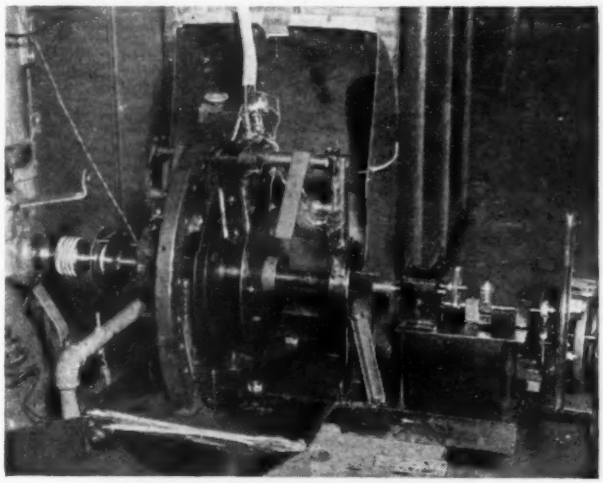


FIG. 9 THE SWEEP-AND-TIMING ARRANGEMENT

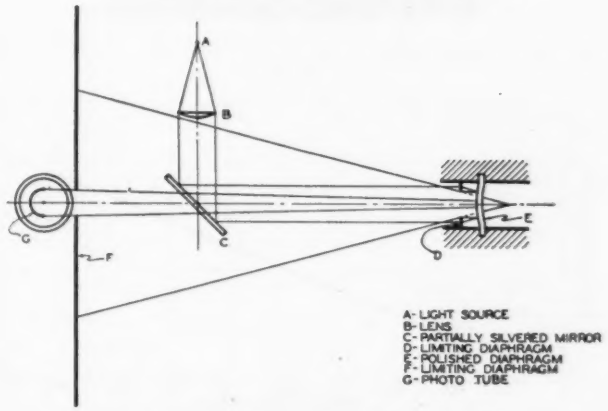


FIG. 10 SCHEMATIC DRAWING OF PRESSURE INDICATOR

The electro-optic pressure indicator was calibrated in place on the engine under actual operating conditions by using a supplementary balanced-diaphragm indicator. This method eliminates the possibility of errors due to changes in the modulus of elasticity of the polished diaphragm, or in the reflectivity of its surface, when exposed to high-temperature conditions. The balanced-diaphragm indicator was similar to one developed by the Bureau of Standards, but was modified slightly to avoid any change in the engine-clearance volume when it was screwed into an opening normally occupied by a quartz window. A tank of compressed nitrogen was connected to the outer side of the diaphragm to balance the engine pressure, and a calibrated pressure gage was used to measure the applied pressure. When the engine pressure exceeded the nitrogen pressure, the diaphragm moved outward, making contact with the electrically insulated center portion of the indicator which was coupled electrically, by a condenser, to the grid of the first-stage amplifier used to amplify the output of the phototube of the electro-optic pressure indicator. Whenever this contact was made or broken, the cathode ray was temporarily displaced, producing a jog in the pressure diagram. A reproduction of a pressure diagram taken with the balanced-diaphragm indicator in operation is shown in Fig. 11. The effect of engine vibration on the condenser coupling is visible in this picture. Nevertheless, the point at which the diaphragm made contact is clearly indicated. By varying the pressure supplied to the outside of the balanced diaphragm and measuring the corresponding deflections, a calibration curve of deflection versus pressure was obtained as shown in Fig. 12. The intake pressure was taken as atmospheric since the error in this assumption was negligible.

Since the magnitude of the deflections obtained depended on the light intensity as well as the pressure variations, it was found necessary to supply closely regulated direct current to the light source. This was accomplished by the use of storage batteries which were constantly charged at a rate slightly higher than the current required for the light source. By the use of this method to obtain constant light intensity, results reproducible within the limits of measuring accuracy were obtained.

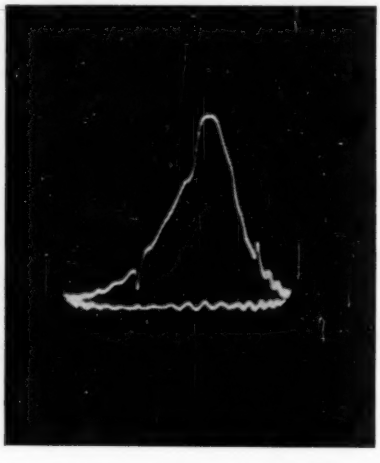


FIG. 11 PRESSURE-INDICATOR DIAGRAM SHOWING CALIBRATION MARKS

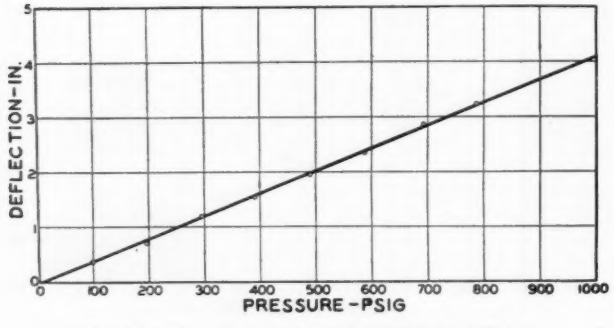


FIG. 12 PRESSURE-INDICATOR CALIBRATION DATA

Injection Indicator. The engine is equipped with a Bosch solid-injection system with the conventional commercial method of varying the time of injection. A shutter is attached to the nozzle plunger so that when the nozzle valve is lifted from its seat and injection started, the amount of shutter opening is increased. A light on one side of the shutter actuates a phototube on the other side whenever the shutter opening changes. The output of the phototube is amplified and impressed on the vertical plates of one of the cathode-ray tubes. This cathode ray is actuated horizontally by the sweep circuit previously described. Thus the beginning of injection is indicated by a vertical deflection of the cathode ray, and the end of injection is indicated by the return of the cathode ray to its original position. In addition, any pressure waves of sufficient magnitude to move the nozzle plunger and shutter are shown.

End-of-Combustion Indicator. The end of combustion occurs either in the precombustion chamber or in the main chamber, depending on the load on the engine and the point at which injection occurs. One of the quartz windows is located in the cylinder head so that combustion in the main chamber can be viewed through it. By observation, it was found that at light engine loads combustion apparently does not carry over from the precombustion chamber into the main chamber. Therefore, at light loads, the end of combustion is indicated by the electro-optical pyrometer. Under heavy-load conditions combustion carries over into the main chamber. Accordingly, a phototube was placed in such a position that it is actuated by the radiation from the quartz window viewing the main chamber. The output of this phototube is amplified and impressed on the vertical plates of one of the cathode-ray tubes. This cathode ray is actuated horizontally by the sweep circuit. Thus the end of combustion can be determined regardless of where combustion ceases.

Camera-Shutter Synchronizer. A permanent record of the data is obtained by photographing simultaneously all of the oscillographs while all the devices which activate the cathode rays are in operation. In order that single cycles with their cyclic pressure and temperature fluctuations can be studied, as well as general trends of numerous cycles, photographs of single cycles are desired.

In order to photograph these single cycles, a shutter synchronizer is required which will open and close the shutter at the proper crank position regardless of engine speed, and which will do so one time only without being reset.

The device, shown in Fig. 13, was developed to meet these requirements. A wooden disk *I* is coupled to the end of the sweep-and-timing mechanism shaft through reduction gears having a ratio of 40 to 1. Two small blocks *A* are attached to one side of the disk to form an adjustable cam. This cam actuates a follower *C* which closes the breaker points *D*, permitting current to flow through the solenoid *F* which opens the camera shutter. When the cam leaves the follower the breaker points open the solenoid circuit and the camera shutter closes. The combined length of the two blocks forming the adjustable cam corresponds to one engine cycle. Therefore the camera shutter remains open for one cycle, the point at which it opens and closes being determined by the location of the adjustable blocks on the disk. A manually operated switch *H* in the solenoid circuit is closed when a picture is desired and opened immediately after the shutter closes. Thus one combustion cycle is photographed at a time,

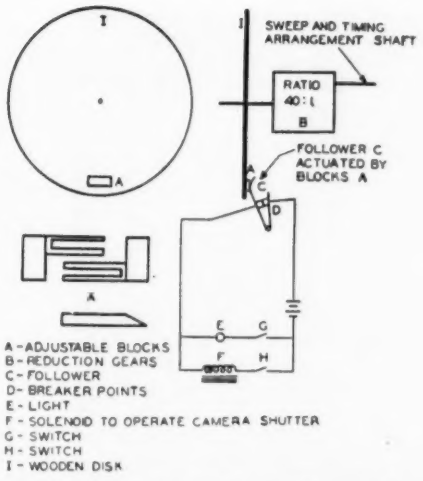


FIG. 13 SCHEMATIC DIAGRAM OF CAMERA-SHUTTER SYNCHRONIZER

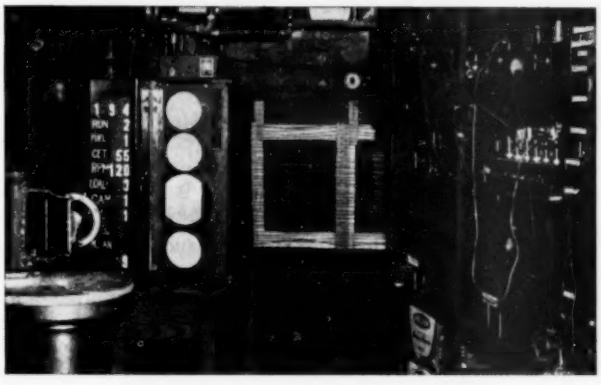


FIG. 14 CATHODE-RAY TUBES, ASSOCIATED ELECTRONIC EQUIPMENT AND CAMERA

and as many additional photographs as desired can be taken by repeating the operation with fresh film. To prevent the inadvertent closing of this switch when the breaker points are already closed, a light E is connected in parallel with the solenoid.

In order to obtain compact and complete photographic records of original data, the cathode-ray tubes were placed in a vertical row beside a black title board on which pertinent identifying data are shown by white letters. A view of this arrangement is shown in Fig. 14. The board is illuminated when taking photographs. Also, two small illuminated holes, 10 in. apart, to be used for alignment and enlargement purposes, were provided adjacent to the bank of cathode-ray tubes and are photographed simultaneously with the oscillographs. Before photographs are taken, the horizontal travel of the cathode rays is adjusted by means of the potentiometers so that, at any time, a vertical line through all the cathode-ray "spots" is parallel to the two illuminated holes. When the image of the oscillographs is projected onto a ground-glass screen with the proper enlargement, the alignment "dots" are 10 in. apart. The deflections corresponding to particular crank positions are determined by projecting lines from the corresponding timing marks parallel to the two dots. A 35-mm camera fitted with an f 1.9 lens is used to photograph the oscillographs.

Engine and Auxiliary Apparatus. The engine to which the previously described apparatus is attached is a commercial-model Diesel engine, the specifications of which appear in Table 3. It has a high-turbulence precombustion-chamber type of head which has openings as shown in Fig. 15. The engine is coupled to an electric dynamometer. A view of the engine with the electro-optical pyrometer, the pressure indicator, the injection indicator, and the end-of-combustion indicator in position is shown in Fig. 16.

The length of time necessary for the engine to consume a predetermined amount of fuel, and the total revolutions during that time, are automatically measured by means of an electromagnetic tripping device.

As part of the energy balance, the heat loss to the jacket cooling water is measured by means of calibrated thermometers, a direct-connected positive-displacement pump, and a calibrated $^3/_8$-in. sharp-edged stainless-steel orifice.

In order to determine the average air-fuel ratio, the air consumption is measured by means of a thin-plate orifice constructed according to the A.S.M.E. Code. Air pulsations are smoothed out by volumes and pressure drops as recommended by the Code.

Two smoke meters are attached to the exhaust line, one a continuous-flow type and the other a sampling type.

A Bureau of Mines gas-analysis apparatus is used to analyze the exhaust gases for oxygen, carbon dioxide, and carbon monoxide. The remainder is assumed to be nitrogen.

PRELIMINARY RESULTS

The engine head, as shown in Fig. 15, has a radial opening and a tangential opening in the precombustion chamber through

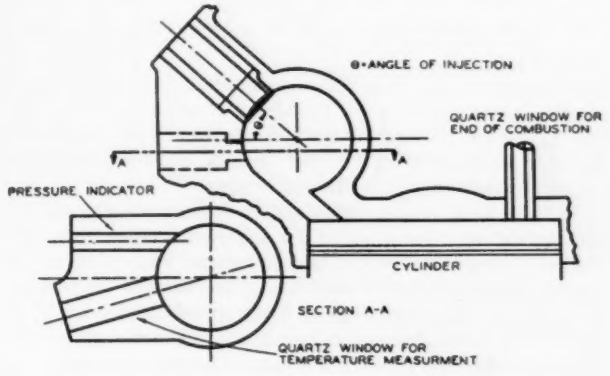


FIG. 15 SCHEMATIC DRAWING OF ENGINE HEAD

which temperature observations could be made. In order to determine which one would be best suited for temperature measurements, quartz windows were installed and observations were made through each of these openings. The procedure for obtaining comparative data for the two openings was as follows: The engine was run at rated speed and load until equilibrium conditions were reached. Then the engine was momentarily stopped, the quartz windows cleaned and reinserted, and the engine started and allowed to run for about 5 min in order to again reach equilibrium conditions. Temperature observations were then made by sighting alternately the electro-optical pyrometer through the two windows, and photographing the oscillographs of apparent temperature variations.

The temperatures determined through the tangential window

TABLE 3 SPECIFICATIONS OF TEST DIESEL ENGINE

Manufacturer	Fairbanks-Morse & Co.
Model no.	36A
Number of cylinders	1
Bore, in.	$4^1/_4$
Stroke, in.	6
Rated rpm	1200
Rated bhp	10
Compression ratio	14.5
Strokes per cycle	4

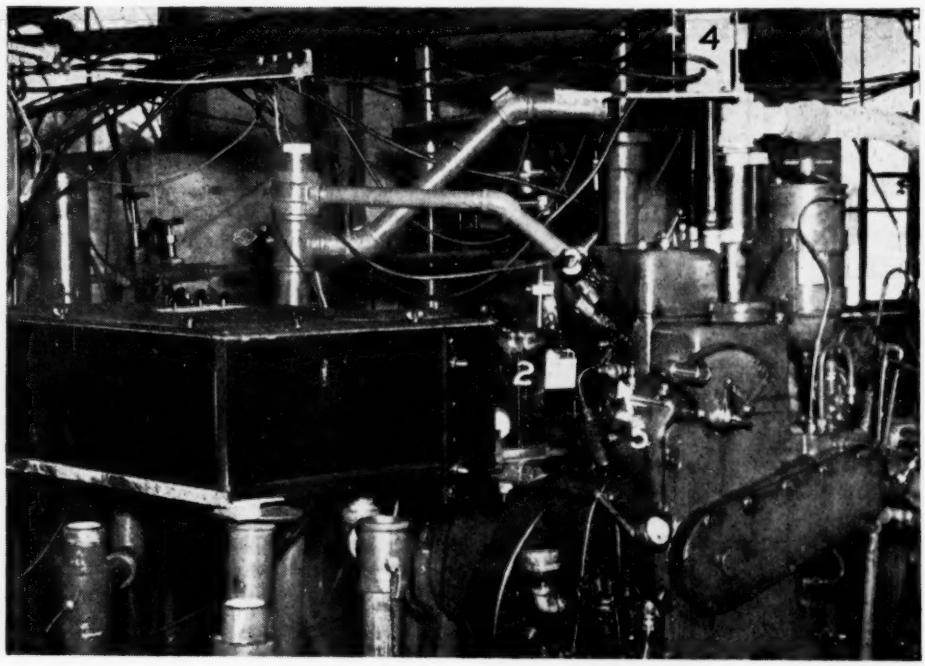


FIG. 16 DIESEL ENGINE AND ASSOCIATED EQUIPMENT
(1 Electro-optical pyrometer; 2 Pressure indicator; 3 Injection indicator; 4 End-of-combustion indicator; 5 Quartz window.)

were slightly lower than those determined through the radial window, particularly during the first part of combustion. This was undoubtedly a result of the cooling effect of the combustion-chamber walls. During the last half of combustion the two temperatures were found to be nearly equal.

At light loads, rapid variations in flame emissivity, with a consequent rapid variation in the apparent temperatures, were observed when the electro-optical pyrometer was sighted on the opening which views the precombustion chamber tangentially. At full load these variations in flame emissivity tended to decrease both in rapidity and in magnitude. The flame-emissivity variations observed through the radial opening were always less rapid and of smaller magnitude than those viewed through the tangential opening.

The analysis of the photographic records from the two openings failed to show any appreciable difference in ignition lag.

After consideration of these factors, the quartz window for temperature measurements was left in the radial opening and the pressure indicator was inserted in the tangential opening, as indicated in Fig. 15.

Having settled on a suitable location for the quartz window, and having previously established the reproducibility of temperatures measured with the electro-optical pyrometer, Fig. 4, the cyclic reproducibility of engine temperatures under constant operating conditions was next investigated. Some of the results of this investigation are shown in Fig. 17. These data show that the average trend is reproduced, but the temperature at any particular point in the cycle is not necessarily reproduced from cycle to cycle. Data taken on different days under the same operating conditions showed similar temperature fluctuations, but the average trend was the same as shown in Fig. 17. The pressure measurements showed closer agreement.

As a preliminary to investigating the effects of fuel composition on the combustion process, tests were in progress at the time this paper was prepared to establish for a single fuel the effect of different operating conditions on the temperatures during the combustion process. Operating variables such as engine speed, engine load, point of injection, jacket-water temperature, etc., are individually varied while the other operating variables are maintained constant.

For the preliminary tests reported in this paper, the operating variable was the point of injection, which was adjusted to occur at top center, at 18 deg before top center, and at 24 deg before top center, rated speed and load being maintained in each case. Photographs were taken with the horizontal scale expanded different amounts, so that particular portions of the combustion process might be studied in detail. The photographs were analyzed in the manner previously described.

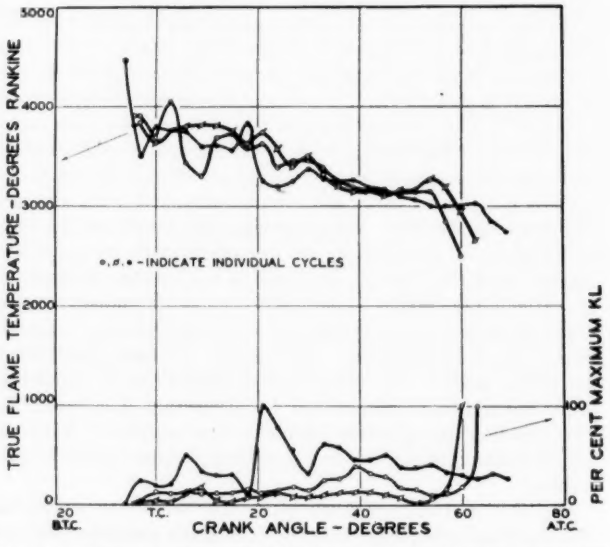


FIG. 17 TEMPERATURE AND *KL* FLUCTUATIONS UNDER CONSTANT OPERATING CONDITIONS

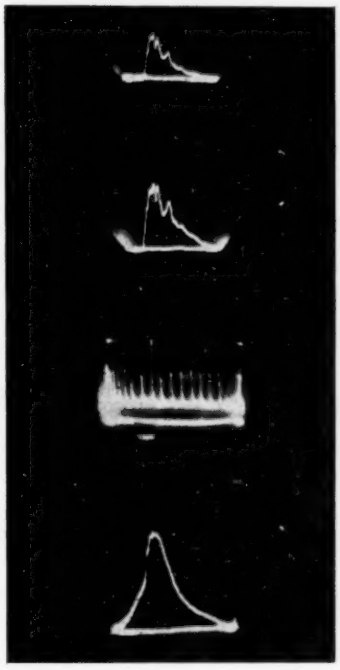


FIG. 18 OSCILLOGRAM OF ENTIRE COMBUSTION PROCESS WITH INJECTION AT 24 DEG BEFORE TOP CENTER

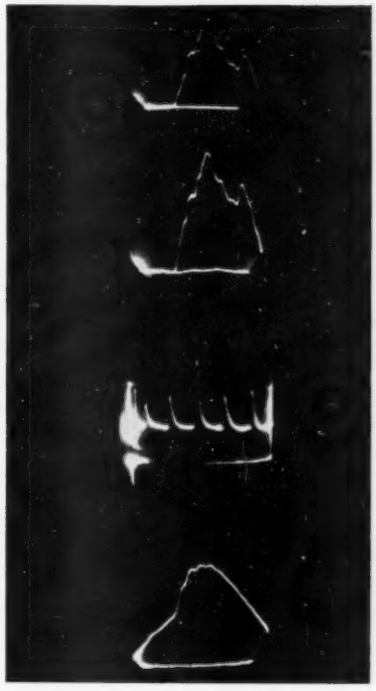


FIG. 19 OSCILLOGRAM WITH INJECTION AT 24 DEG BEFORE TOP CENTER AND HORIZONTAL SCALE EXPANDED



FIG. 20 OSCILLOGRAM WITH INJECTION AT 24 DEG BEFORE TOP CENTER AND HORIZONTAL SCALE EXPANDED

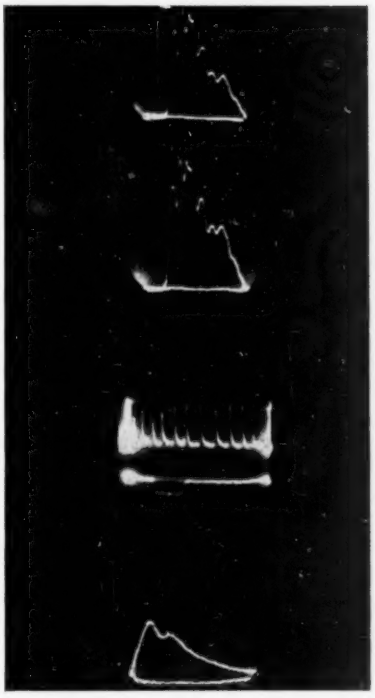


FIG. 21 OSCILLOGRAM OF ENTIRE COMBUSTION PROCESS WITH INJECTION AT TOP CENTER

Views taken during the run with injection occurring at 24 deg before top center are shown in Figs. 18, 19, and 20. In Fig. 18 the horizontal scale is compressed so that the whole combustion process is shown. The timing marks are 12 deg apart, the high mark indicating top center. The effect of expanding the horizontal scale by increasing the light intensity passing through the slit is shown in Fig. 19. The timing marks are still 12 deg apart. The 90-deg disk was in use when the photograph reproduced in Fig. 20 was taken, consequently the timing marks in this picture are $4^1/_2$ deg apart. Fig. 21 shows the effect of late injection. The alignment dots are visible on the right-hand side of all the photographs.

The true temperature, pressure, and KL factor fluctuations, as recorded on the illustrations Figs. 18 and 21, are shown in Fig. 22, together with data for a single cycle with injection occurring at 18 deg before top center. Each of the dotted lines in Fig. 22 was obtained by analyzing 10 cycles, similar to Figs. 18, 19, and 20, for each point of injection and drawing average curves for these data.

The data in Fig. 22 are presented at this time primarily to show that the electro-optical pyrometer is capable of following and recording the temperature variations inside the cylinder of an internal-combustion engine. Not enough data have been obtained to explain the cyclic temperature fluctuations or the variations in temperature with point of injection. However, additional tests are now in progress to establish more completely the effect upon the temperature of varying the point of injection, as well as the effect of the other operating variables and the fuel composition. The results of these tests will be reported at some future time.

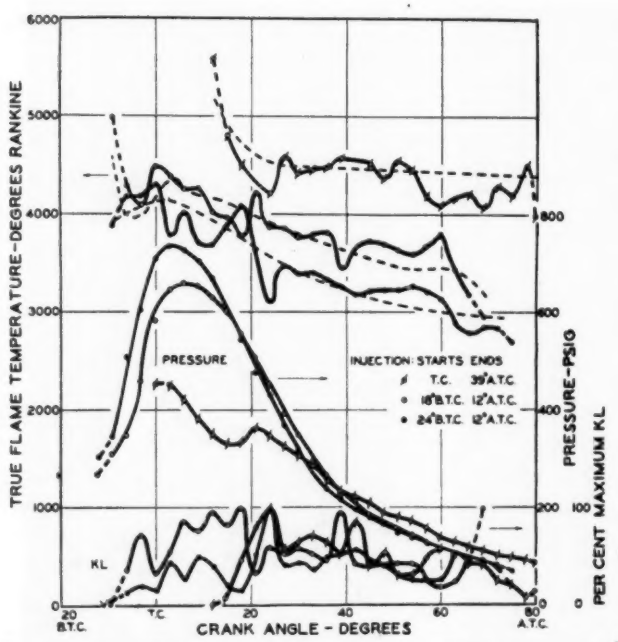


FIG. 22 TRUE TEMPERATURE, PRESSURE, AND *KL* FLUCTUATIONS WHEN POINT OF INJECTION IS VARIED

ACKNOWLEDGMENT

The work reported herein was made possible by financial support granted by the Wisconsin Alumni Research Foundation and by the University of Wisconsin College of Engineering. To these organizations, and to the many students and members of the faculty who have rendered valuable assistance and encouragement, the authors desire to express their sincere gratitude.

BIBLIOGRAPHY

1 "Second Report to the Gas-Engine Research Committee," by F. W. Burstall, Proceedings of The Institution of Mechanical Engineers, parts 3–5, 1901, pp. 1031–1154.

2 "On the Measurement of Temperatures in the Cylinder of a Gas Engine," by H. L. Callendar and W. E. Dalby, Proceedings of the Royal Society of London, England, vol. 80, series A, 1907–1908, pp. 57–74.

3 "Cyclical Changes of Temperature in a Gas-Engine Cylinder," by E. G. Coker and W. A. Scoble, Proceedings of The Institution of Civil Engineers, vol. 196, Part 2, 1913–1914, pp. 1–74.

4 "Flame Temperatures in an Internal-Combustion Engine, Measured by Spectral Line Reversal," by A. E. Hershey and R. F. Paton, University of Illinois, Engineering Experiment Station, Bulletin No. 262, Urbana, Ill., Oct., 1933.

5 "Flame Temperatures Vary With Knock and Combustion-Chamber Position," by G. M. Rassweiler and L. Withrow, *S.A.E Journal*, vol. 36, 1935, Trans. section, pp. 125–133.

6 "The Measurement of Flame Temperatures in a Petrol Engine by the Spectral Line-Reversal Method," by S. S. Watts and B. J. Lloyd-Evans Proceedings of the Physical Society, vol. 46, 1934, pp. 444–449.

7 "Flame Radiation and Temperature Measurements on an Internal-Combustion Engine," by A. E. Hershey, *Industrial and Engineering Chemistry*, vol. 24, 1932, pp. 867–870.

8 "Measurement of Gas Temperatures in an Internal-Combustion Engine," by A. E. Hershey, Trans. A.S.M.E., vol. 58, 1936, paper PRO-58-2, pp. 195–201.

9 "Measurement of Fluctuating Temperature of Working Gas in Internal-Combustion Engines," by A. Kobayashi, Trans. Society of Mechanical Engineers of Japan, vol. 3, no. 11, May, 1937, pp. 192–197.

10 "Gas Temperature Measurements in Internal-Combustion Engines," by. H. Graff, *Zeitschrift des Vereines deutscher Ingenieure*, vol. 86, no. 29–30, July 25, 1942, pp. 461–466.

11 "Determination of True Temperature and Total Radiation From Luminous Gas Flames," by H. C. Hottel and F. P. Broughton, *Industrial and Engineering Chemistry*, Analytical Edition, vol. 4, 1932, pp. 166–175.

12 "Spectral Radiant Intensities of Some Tungsten Filament Incandescent Lamps," by W. E. Forsythe and B. T. Barnes, *Journal of the Optical Society of America*, vol. 26, 1936, pp. 313–315.

13 "The Properties of Tungsten and the Characteristics of Tungsten Lamps," by W. E. Forsythe and A. G. Worthing, Abstract, Bulletin of Lamp Development Laboratory, Incandescent Lamp Department of General Electric Company, vol. 2, January, 1930, pp 6–12.

14 "Positive and Negative Thermionic Emission From Tungsten," by H. B. Wahlin and L. V. Whitney, *Physical Review*, vol. 50, 1936, pp. 735–738.

15 "Emission Spectra of Engine Flames," by G. M. Rassweiler and L. Withrow, *Industrial and Engineering Chemistry*, vol. 24, 1932, pp. 528–538.

16 "Spectroscopic Studies of Engine Combustion," by L. Withrow and G. M. Rassweiler, *Industrial and Engineering Chemistry*, vol. 23, 1931, pp. 769–776.

17 "Properties of Ordinary Water-Substance," by N. Ernest Dorsey, Reinhold Publishing Corporation, New York, N. Y., 1940, pp. 128–130 and 150.

18 "Measurement of Radiant Energy," by W E. Forsythe, McGraw-Hill Book Company, Inc., New York, N. Y., 1937, pp. 181–182.

19 "Infrared Radiation From Explosions in a Spark-Ignition Engine," by C. F. Marvin, Jr., F. R. Caldwell, and S. Steele, Report no. 486, National Advisory Committee for Aeronautics, 1934, pp. 223–234.

20 "Instrumentation in the Study of Diesel Combustion," by E. W. Landen and L. A. Blanc, Trans. A.S.M.E., vol. 65, 1943, pp. 121–125.

21 Ref. (18), pp. 382–383.

22 "Sapphire and Other New Combustion-Chamber Window Materials," by George Calingaert, S. D. Heron, and Ralph Stair, *S.A.E. Journal*, vol. 39, 1936,Trans. section, pp. 448–450.

23 "An Electro-Optic Pressure Indicator," by A. F. Robertson, *Review of Scientific Instruments*, vol. 12, 1941, pp. 142–148.

Discussion

H. B. NOTTAGE.[6] As a tribute to experimental ingenuity and skill in tackling a difficult problem of practical interest, this paper is of outstanding merit. Even with slight imperfections, just so they would be consistent and recognized, the results of a comprehensive engine study with the author's equipment should fundamentally advance our recognition of the perverse idiosyncracies of combustion in an engine.

It is admittedly difficult to make a paper of this nature complete in its coverage of all details of technique. A further word from the authors would be appreciated concerning the extent to which this equipment is independent of the diagnostic and manipulative sensitivities of the individuals who have made it work. What pitfalls would await the uninitiated adventurer following in their path?

Is the present form of the equipment the first one assembled? What further improvements are needed or expected? What is the useful life of the mechanical parts? How quickly do the photocells deteriorate? How frequently must the photocells be recalibrated? Are separate means advisable to check on the interchangeability of the photocells? How high an engine speed would this equipment stand with maintained accuracy? What maximum and minimum pressure and temperature limits can be handled? Will this equipment show up detonating frequencies independent of "hash?"

Is it worth while to consider building in a differentiating circuit to determine the rates of pressure and temperature variations?

How much of the lack of reproducibility between cycles might be due to the engine-operating controls themselves? How long is the engine run in before data are taken? Is ordinary commercial injection equipment believed to be satisfactory here? An-

[6] Project Engineer, Pratt & Whitney Aircraft, East Hartford, Conn. Jun. A.S.M.E.

other oscillogram of fuel injections rate versus time might be imagined as an additional complication.

Then, from an analytical viewpoint, are there believed to be any limitations on Equation [5], as applied to an engine combustion chamber? What is the magnitude of the monochromatic transmissivity of the flame? What would be the corresponding reflectivity and absorptivity of the combustion-chamber surfaces in operation? What kind of temperature does one measure along a radiant beam passing through a gas mass in violent physical and chemical agitation? Has this temperature been employed to calculate the radiant component of the heat transfer to the combustion-chamber walls?

Further data are most certainly awaited with keen interest.

J. P. Megroot.[7] In studies such as the author has made, the apparatus involves a small window inset in a cylinder. Beyond doubt the coolest part of the cylinder is the wall. The question then arises, can a really good idea of the temperature inside the cylinder be obtained from measurement through such a window?

Why was the measurement of pressure taken with the presented method instead of with the piezo-electric crystal method in which the indicating parts are inertia-free and therefore more correct?

Hans Bohuslav.[8] How many pictures could be taken before the window had to be removed and cleaned? Were the measurements influenced by the radiation of the combustion-chamber walls? Was it possible to measure the combustion-chamber-wall temperature and determine the effect of an increase in such temperatures on the cleanliness of combustion and flame temperature? It is commonly known that after an engine has run for a while and is properly warmed up, the combustion becomes cleaner; therefore, the temperature of the combustion-chamber wall would have an influence on the speed of combustion and temperature of the flame.

L. R. Turner.[9] What is the possibility of using this method to measure the temperature of gases which have no radiant particles in them? In their experiments, have the authors used additives in sufficient quantities such that the radiation is along one wave length? It is the writer's understanding that a method has been worked out but he is unfamiliar with the quantities required to get black-body conditions at one wave length.

Leopold Strauss.[10] The authors' illustrations show the precombustion chamber as spherical. What would be the effect of a differently shaped chamber on the temperature measurements? Also, what effect does turbulence within the chamber have on temperature measurement?

Authors' Closure

The discussion submitted by H. B. Nottage includes several pertinent questions which one thoroughly conversant with the technical theories and principles involved might naturally raise. The authors welcome the opportunity to discuss these questions at this time but not all of them can be answered conclusively until after further experience and experimentation.

The authors believe that the equipment is quite independent of the personal element, once the operators become familiar with the basic principles and technique. The equipment is still in its original form except for a few minor changes. Simplification is possible and certainly would be necessary before it could be used successfully by nontechnical operators.

Probably the most desirable improvement in the electro-optical temperature indicator would be realized if the equations involved were solved electronically so as to produce true temperatures directly on a single oscillograph screen. This would eliminate the laborious, time-consuming routine inherent in the present arrangement and should improve the accuracy. Needless to say, some means of attaining this objective is vigorously being sought.

The mechanical parts are few and not subject to rapid wear or deterioration. The phototubes are used at low light levels, and at moderate voltages, consequently they should be usable for a long period of time. The original phototubes are still in use and show no appreciable deterioration after many hours of service. Any change that might occur in the characteristics of the phototubes, occasioned by deterioration or replacement, is taken care of by strict adherence to the practice of checking the calibration of the apparatus each time it is used.

The authors are of the opinion that the instrumentation will operate successfully at any speeds employed in present-day reciprocating engine practice if proper precautions are observed in designing the electrical circuits and the mechanical auxiliaries. Since there are no mechanical connections between the engine and the electronic indicators, these instruments should follow accurately, without interference from engine vibrations, any frequency up to the limit of frequency response of the amplifiers.

As a matter of possible interest, the electro-optical temperature indicator was once sighted toward the sun and the temperature thus obtained checked the generally accepted value very closely.

If, as is hoped, the true flame temperature can be indicated directly on a single oscillograph screen as a function of crank angle, temperature rate curves will definitely be of interest. With the present equipment, however, apparent temperature rate curves do not seem to be in order as both flame emissivity and temperature variation affect the rate.

Lack of cycle reproducibility is believed to be inherent in the combustion process, since the injector rack is usually locked in a fixed position while data are being obtained. This conclusion seems reasonable because of the manner in which ignition originates and combustion is propagated in a Diesel engine, and more particularly so in the high turbulence, precombustion-chamber type used in the present investigation.

The engine is run at the desired operating conditions for a period of approximately one hour before data are taken. Special injection equipment may prove useful, but the final answer to this question must await further experimental work. The use of injection rate diagrams has been considered. While such additional data would undoubtedly contribute useful information, the necessary equipment has not been developed as far as the authors are aware and consequently this improvement must await future development work.

The authors consider that Equation [5] is just as applicable to luminous flames in engine combustion chambers as it is to open flames. The equation must fail, however, when a luminous flame becomes nonluminous and the radiation becomes discontinuous with respect to wave length. In the present experiments the luminosity of the Diesel flame is of such magnitude that the equation is considered applicable. Further experimental work will be necessary to establish its validity in the case of the less luminous Otto-cycle flames.

The monochromatic transmissivity varies between wide limits. As yet, the authors have made no attempt to separate the transmissivity of the flame and that of the sooty quartz window. KL values for the flame-window combination range from 0.001 to 1.0. The corresponding absorptivity of the combustion-chamber

---

[7] Engineer Consultant, Cleveland, Ohio.

[8] Vice-President in Charge of Engineering, Sterling Engine Company, Buffalo, N. Y. Mem. A.S.M.E.

[9] National Advisory Committee for Aeronautics, Cleveland Airport, Cleveland, Ohio.

[10] Sterling Engine Company, Buffalo, N. Y. Jun. A.S.M.E.

walls is unknown but must be quite high due to the surface coating of soot. It should be noted that the temperature obtained with the electro-optical pyrometer is exponentially weighted toward the highest temperature existing in the radiant particles visible to the instrument. This fact, together with the high turbulence and the suspected lack of thermal equilibrium, may be largely responsible for the lack of reproducibility.

Separation of the flame absorptivity and the window absorptivity would be necessary before the radiant heat transfer could be calculated. A new type of quartz window is now being employed which may make such separation feasible.

With respect to Mr. Megroot's question concerning the effect of window temperature, it is unlikely that radiation from the window itself can appreciably alter the electro-optical pyrometer readings because the window temperature is far less than the flame temperatures, and the exponential averaging previously mentioned tends to nullify minor radiation effects.

Experience with the piezo-electric pressure indicator in previous combustion studies at the University of Wisconsin indicated that it does not hold to its calibration well. The electro-optical pressure indicator has proved entirely satisfactory in that respect. Furthermore, the natural frequency of the diaphragm used in the electro-optical pressure indicator is approximately 200,000 cycles. Since the ability of the diaphragm to respond to rapid changes in pressure is determined by its natural frequency, the response is satisfactory up to the limit of the frequency response of the amplifiers used.

Replying to Hans Bohuslav's questions, the frequency with which the quartz window must be cleaned is a function of the engine-operating conditions, with a minimum of about 15 minutes. Since the paper was presented, a self-cleaning window has been developed which apparently remains clean indefinitely. No attempt has been made in the present investigation to measure combustion-wall temperatures. In view of the exponential averaging, previously mentioned, radiation from the relatively cool wall is negligible as far as flame-temperature measurement is concerned.

Concerning the discussion submitted by Mr. Turner, since the method in question measures the temperature of the soot particles in the flame it is not applicable to nonluminous flames. Inasmuch as the Diesel flame is luminous, there has been no occasion to employ additives in the present investigation. The possibility of additives affecting the combustion characteristics would seem to make their use undesirable if it can be avoided. The authors have not experimented with the amount of additives required to approach black-body conditions, nor do they know of any reference to experiments of this nature. Reference (10) describes a method whereby the spectral radiation of an additive was used to measure flame temperatures, but black-body conditions were not approximated.

The question by Leopold Strauss concerning the effect of combustion-chamber shape must await further experimentation because, as yet, the apparatus has been employed on only one type of combustion chamber. Turbulence should have no effect upon the temperature measurements if thermal equilibrium exists. Lacking thermal equilibrium, however, temperature variations would be indicated if "hot" and "cold" masses were swept alternately in front of the combustion-chamber window.

The authors wish to express their appreciation to those who contributed to the discussion of the paper.

Polar Diagram for Tuning of Exhaust Pipes

By TROELS WARMING,[1] MILWAUKEE, WIS.

In this paper is shown how a simple polar diagram, not requiring any higher mathematics, can be used for calculation of the natural frequency of the exhaust system on a Diesel engine. In general this diagram can be used for determination of all the natural frequencies of any system consisting of gases or fluids in containers of complex form.

CURRENTLY there seems to be an increasing interest in tuning of exhaust pipes on Diesel engines, see, for instance, a paper by P. H. Schweitzer;[2] and it may therefore be of advantage to have an easy method to determine the natural frequencies of such systems. A polar diagram, similar to the diagram developed some years ago by F. M. Lewis[3] for calculation of crankshaft systems, may be used for this purpose. It will be found, however, that gas systems are much simpler to deal with than shaft systems.

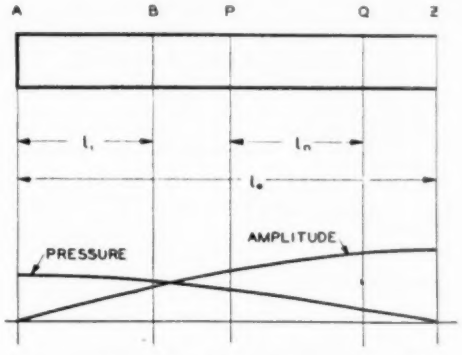


FIG. 1 OSCILLATION IN PIPE OPEN AT ONE END

Consider first the system shown in Fig. 1, consisting of a pipe with constant area and open at one end. The natural frequency of this system is

$$N = \frac{v}{4\,l_0} \cdot 60 = \frac{15\,v}{l_0} \text{ vibrations per min} \quad \ldots\ldots [1]$$

where l_0 is the length of the pipe in inches, and v the sound velocity in inches per second. The exhaust from a Diesel engine may with good approximation be considered as atmospheric air for which the sound velocity is

$$v = 585\sqrt{t + 460} \text{ in. per sec} \quad \ldots\ldots [2]$$

where t is the temperature in degrees F.

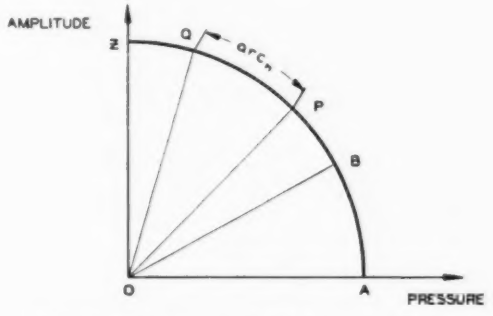


FIG. 2 POLAR DIAGRAM FOR SYSTEM IN FIG. 1

When the air in this pipe oscillates, amplitude and pressure at the various points are given by a sine and a cosine curve, Fig. 1. Amplitude and pressure at a point B in the pipe are therefore the co-ordinates for the corresponding point B on the circle shown in Fig. 2, where

$$\text{arc } AB = \frac{l_1}{l_0} \cdot 90 \text{ deg}$$

The scales used in this polar diagram are of no importance for the determination of natural frequencies since only the relative values are needed. Amplitude and pressure are therefore both measured in inches on the diagram. It is of importance, however, that these scales are not influenced by the area of the pipe.

Consider now length $PQ = l_n$ of the pipe. The corresponding circle arc $PQ = \text{arc}_n$ is

$$\text{arc}_n = \frac{l_n}{l_0} \cdot 90 \text{ deg} \quad \ldots\ldots [3]$$

Substituting l_0 from Equation [1]

$$\text{arc}_n = \frac{6\,N\,l_n}{v} \text{ deg} \quad \ldots\ldots [4]$$

The air particles between P and Q oscillate independently of what takes place in the rest of the pipe, with the exception that at P and Q certain pulsating pressures are supplied and certain volumes of air are pumped in and out. If these pressures and volumes were provided by oscillation at the same frequency but in pipes of different diameter, the oscillations between P and Q would not be affected.

This makes it possible to treat more complicated systems, Figs. 3 and 4. Each length of pipe with constant area will have a corresponding arc of a circle determined by Equation [4]. Where two pipes of different area are connected, the pressure does not change, but the two amplitudes, a_n and a_{n+1}, at the point of connection are inversely proportional to the areas, S_n and S_{n+1}

$$\frac{a_{n+1}}{a_n} = \frac{S_n}{S_{n+1}} \quad \ldots\ldots [5]$$

It may be added that the condition is different from that of constant flow, in which case the pressure changes where the area changes. This pressure change is necessary to accelerate the air passing to a different velocity. In a vibratory system, as con-

[1] Mechanical Engineer, Nordberg Manufacturing Company. Jun. A.S.M.E.

[2] "Improving Engine Performance by Exhaust-Pipe Tuning," by P. H. Schweitzer, *Journal of the American Society of Naval Engineers*, vol. 56, May, 1944, p. 185.

[3] "Torsional Vibration in the Diesel Engine," by F. M. Lewis, Trans. Society of Naval Architects and Marine Engineers, vol. 33, 1925, p. 109.

Contributed by the Oil and Gas Power Division and presented at a meeting of the Cleveland Section, Cleveland, Ohio, May, 1945, of THE AMERICAN SOCIETY OF MECHANICAL ENGINEERS.

NOTE: Statements and opinions advanced in papers are to be understood as individual expressions of their authors and not those of the Society.

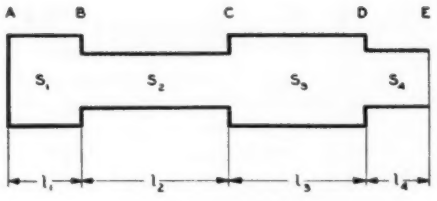


FIG. 3 MORE COMPLICATED SYSTEM
(Letters S indicate pipe areas.)

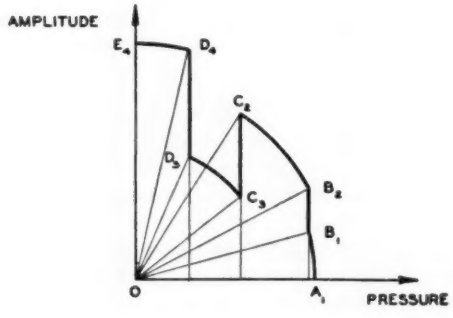


FIG. 4 POLAR DIAGRAM FOR SYSTEM IN FIG. 3

sidered here, the air in the whole pipe is accelerated simultaneously, thus not causing any sudden pressure changes at any point in the system.

CONSTRUCTION OF POLAR DIAGRAM

In order to explain the construction of the polar diagram in Fig. 4, it is first assumed that the natural frequency N of the system is known. The first point A_1 of the diagram is chosen arbitrarily on the abscissa axis because it gives the condition at the closed end A of the system where the amplitude is zero. Point B_1, which gives the condition at the end B of the first pipe, is located on a circle arc through A_1 determined by Equation [4] and with center in point O. Point B_2 gives the condition at the beginning of the second pipe, where the pressure is the same as at B_1, while the amplitude is determined by Equation [5]. Point B_2 is therefore found by simply multiplying the ordinate for B_1, as measured on the diagram, by this proportion. The circle arc B_2C_2 has center in point O and is determined by Equation [4].

The construction is continued through all the steps of the system, but, with atmospheric pressure at the open end, the last point must fall on the ordinate axis. However, if the diagram had been drawn for a frequency different from the natural frequency of the system, the last point would not have fallen on this axis. We have therefore in the polar diagram a method of checking whether a given frequency is the natural frequency.

It is added that the diagram may be drawn just as well by first choosing point E_4 arbitrarily on the ordinate axis and then proceeding the other way through the system. If point A_1 then falls on the abscissa axis, the frequency used was the natural frequency.

So far only the fundamental vibration of the system has been considered, but for higher frequencies the polar diagram, instead of 90 deg, will go through 270 deg, 450 deg, etc. For a system closed at both ends, the diagram will go through 180 deg (or 360 deg, 540 deg, etc.) thus beginning and ending on the abscissa axis. If the system is open at both ends, the diagram will begin and end on the ordinate axis.

Before calculating the natural frequency of an actual exhaust system, it must be simplified to a system of pipes with constant area, see, for instance, Figs. 3, 5, or 7. Parts of complicated shape are changed so that they keep the same volume and the same length, the length being measured as the distance the gases flow. Exhaust pots and mufflers are thus considered as short pipes with large area. At the open end of a pipe is added a length equal to 0.4 times the pipe diameter in order to provide for the fact that the air particles just outside the pipe take some part in the vibration.

A frequently used exhaust system has a pipe, with constant area S and length l, and some additional volume V as, for instance, valves or exhaust pots, near the closed end. If $V/S < l/2$, the system may be calculated as one straight pipe, Fig. 1, of length $l_0 = V/S + l$. The error involved is less than 3 per cent.

CALCULATING NATURAL FREQUENCY

As an example, the natural frequency will be calculated of the system shown in Fig. 5, assumed filled with exhaust gas at an average temperature of 500 F. The sound velocity, Equation [2], then is

$$v = 585\sqrt{500 + 460} = 18{,}100 \text{ in. per sec}$$

A rough estimate of the natural frequency is obtained from Equation [1] by considering the system as one straight pipe

$$= \frac{15v}{l} = \frac{15 \cdot 18{,}100}{160} = 1700 \text{ vibrations per min}$$

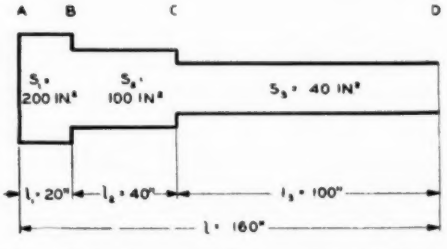


FIG. 5 EXHAUST SYSTEM CALCULATED IN EXAMPLE

The first polar diagram in Fig. 6 is drawn for this frequency. The angle of the circle arcs, all of which have center in point O, is from Equation [4]

$$\text{arc}_n = \frac{6Nl_n}{v} = \frac{6 \cdot 1700 \cdot l_n}{18{,}100} = 0.564 \cdot l_n \text{ deg}$$

where l_n is the corresponding pipe length.

Point A_1 is chosen somewhere on the abscissa axis. Point B_1 is found by

$$\text{arc } A_1B_1 = 0.564 \cdot l_1 = 0.564 \cdot 20 = 11.28 \text{ deg}$$

Point B_2 is found by multiplying the ordinate for B_1 by

$$\frac{S_1}{S_2} = \frac{200}{100} = 2$$

Point C_2 is found by

$$\text{arc } B_2C_2 = 0.564 \cdot l_2 = 0.564 \cdot 40 = 22.56 \text{ deg}$$

Point C_3 is found by multiplying the ordinate for C_2 by

$$\frac{S_2}{S_3} = \frac{100}{40} = 2.5$$

Point D_3 is found by

$$\text{arc } C_3D_3 = 0.564 \cdot l_3 = 0.564 \cdot 100 = 56.4 \text{ deg}$$

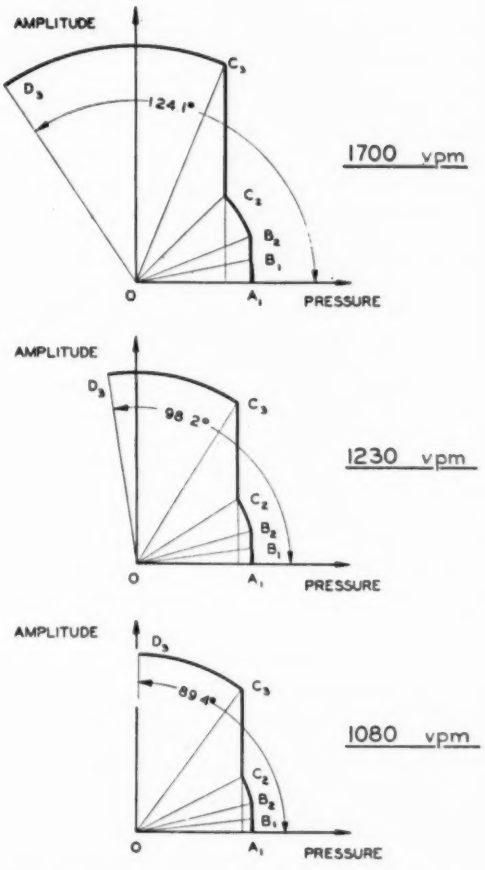


FIG. 6 POLAR DIAGRAMS FOR SYSTEM IN FIG. 5

The diagram shows that the estimate of 1700 vibrations per min was too high since the total angle described is 124.1 deg instead of 90 deg. A second estimate is therefore made

$$N = \frac{90}{124.1} \cdot 1700 = 1230 \text{ vibrations per min}$$

For this frequency a new polar diagram is constructed with the angle of the circle arcs

$$\text{arc}_n = \frac{6 \cdot 1230 \cdot l_n}{18{,}100} = 0.407 \cdot l_n \text{ deg}$$

The procedure is the same as before and the result this time is a total described angle of 98.2 deg.

By extrapolation from the first two estimates is found

$$N = 1230 - \frac{1700 - 1230}{124.1 - 98.2}(98.2 - 90)$$

$$= 1080 \text{ vibrations per min}$$

A polar diagram for this frequency has a total described angle of 89.4 deg which is quite close to 90 deg. However, by interpolation between the last two tries will be found

$$N = 1080 + \frac{1230 - 1080}{98.2 - 89.4}(90 - 89.4) = 1090 \text{ vibrations per min}$$

which is the natural frequency of the system with good accuracy.

During the construction of the polar diagram, difficulties may arise with points falling either outside the paper or too close to the center to give an accurate construction. The following rule will then be helpful: Any point in the diagram may be moved on a radius, closer to or away from the center, and the construction may then be continued from the new location.

BRANCHED SYSTEMS

Branched systems need a separate polar diagram for each branch and for the main pipe, all diagrams using the same frequency, Figs. 7 and 8. The diagrams for the branches are begun at the end of the branch and worked toward the junction. At this point the pressure p must be the same in both branches so the diagram for one of them, in this case branch II, is reduced accordingly. The diagram for the main pipe now can be drawn beginning at the junction point. The pressure p must be the same as in the branches, and the amplitude a_7 is determined by

$$a_7 \cdot S_7 = a_4 \cdot S_4 + a_6 \cdot S_6$$

where a_4, a_6, and a_7 are measured in inches on the diagram, and S_4, S_6, and S_7 are pipe areas. The diagram is then completed and, if the last point falls on the ordinate axis, we have the natural frequency of the branched system.

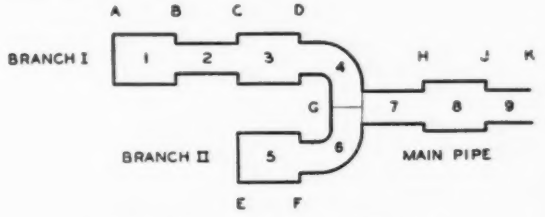


FIG. 7 BRANCHED EXHAUST SYSTEM

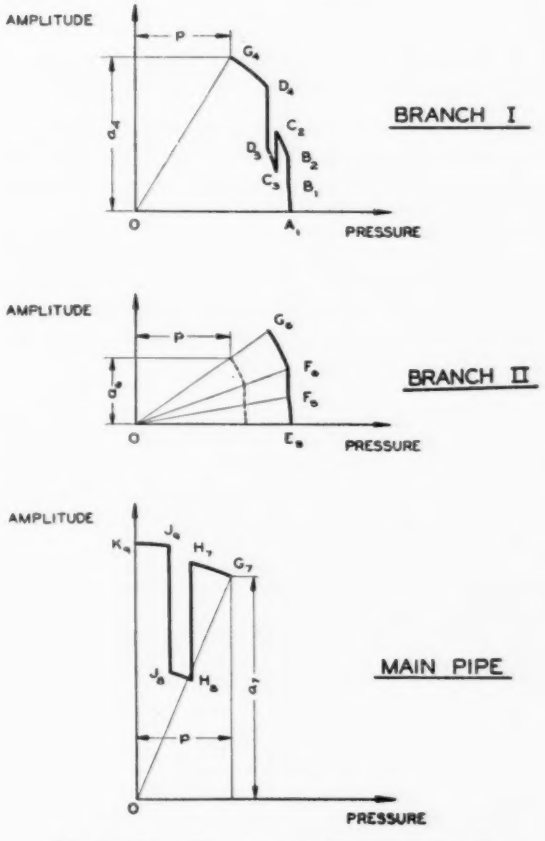


FIG. 8 POLAR DIAGRAMS FOR SYSTEM IN FIG. 7

Discussion

T. M. Robie.[4] What is the effect of discharging into a concrete pit and taking the exhaust pipe out somewhere before the end of the pit? In other words, supposing the exhaust pipe enters the pit horizontally at one end and leaves the pit vertically at some point before the other end of the pit. Would the vibrations in the pit, due to the exhaust gases hitting the end wall and bouncing back, affect the calculations and if so, what correction should be made?

R. O. Bernauer.[5] The author has been a co-worker with the writer at Nordberg for the past 5 or 6 years and in that time has worked on the critical speeds of crankshafts, parallel operation of synchronous generators, and various other vibration problems. He has always had a way of presenting anything very simply and has used polar diagrams a great deal in solving problems. This paper is his latest application of the polar diagram.

The writer is not going into a technical discussion regarding the use of it. In 1925, Professor Lewis used the polar diagram in the determination of critical speeds of crankshafts and the author is using it in an analogous manner in this paper. In parallel-operations problems he uses vector diagrams which are closely related. The writer congratulates the author on his unique and simple paper and thinks it should be of great value to engineers because of its simplicity. The paper deals with relative lengths from which pressures and amplitudes in any system may be secured.

In his presentation the author did not go into branch or network systems at any length but did give examples in his paper. These are obtained by the confluence of pipes and are very difficult to handle by other methods. His method is important in that it presents a simple way of solving branch or networks problems.

L. R. Turner.[6] In connection with the polar diagrams, what happens where there is a restriction at the end of the pipe?

L. M. Tichvinsky.[7] The determination of natural frequencies even of simple members of a Diesel engine is required in order to obviate a possible condition of resonance. Their calculations are rather lengthy and require accurate procedures.

The simple and elegant method presented by the author for the same purpose invites a question as to its accuracy. It is believed that the method is practical for designers; however, it would be interesting to know the error when comparing the calculated and the graphically obtained values of natural frequencies of a system such as shown in Fig. 7 of the paper.

V. L. Maleev.[8] The writer checked the method described in this paper for an exhaust system connecting several Diesel engines to a common muffler with a long tail pipe. The system contains chambers of various volumes and pipes of various diameters and lengths and it was a tedious job to find by usual calculations the natural frequency of the gases in this system. The polar-diagram method gave a great saving of time without any sacrifice of accuracy. In addition, this method shows very clearly what changes should be made in a system if a certain natural frequency is to be obtained.

The writer believes that, where due to the difficulty of calculating the natural frequency, the latter was often only estimated, with the polar-diagram method available the natural frequency actually will be computed and this will lead to better design. Furthermore, the writer believes that this method will be very helpful not only for tuning exhaust pipes of internal-combustion engines, but also for designing exhaust mufflers which up to date are not too satisfactory, and possibly in designing injection systems of compression-ignition engines.

The only criticism which pertains, however, not to the content of the paper, is in respect to the use of the designation "arc" instead of the word "angle;" 90 deg multiplied by a ratio gives a certain number of degrees and not an arc. In laying out the diagrams, again one uses angles on the protractor and not arcs. The polar diagram itself deals with angles, not arcs.

The paper is written very clearly and will be appreciated by all who have to deal with natural frequencies of gases or fluids in various systems. It constitutes a valuable contribution to the engineering literature.

Author's Closure

Mr. Robie asks about a concrete pit. Usually it will be sufficient to substitute a straight pipe, of the same length as the average path of the gases through the pit, and with an area giving same volume as the pit. If the part of the pit beyond the vertical outlet is very long, it may be necessary to consider it as a branch to the system. This also should be done if higher orders of vibration are considered.

Mr. Bernauer's kind remarks are very much appreciated. The association with him, through the past years, has always been very pleasant.

In reply to Mr. Turner, it can be said that if the open end of a pipe is restricted by a plate with a hole, this hole is considered as the open end. We then must add a pipe, of same diameter d as the hole, and of length $0.4\,d$, on both sides of the plate. It will be found this way, that the smaller the hole, the more effective is the mass in the added pipe, and consequently the lower is the natural frequency.

Mr. Tichvinsky questions whether the simplicity of the polar diagram is at the expense of accuracy. This is not the case. With a careful graphical construction the error should be less than 1 per cent and if that is not satisfactory, it is quite simple to calculate the steps of the diagram, if necessary with logarithms. Usually that does not serve any purpose, however, because the engine does not behave that accurately.

Compared to other published methods, the polar diagram is more accurate because it takes account of the inertia and the compressibility of the air throughout the system. In other methods, the inertia in exhaust pots or other large volumes is disregarded. The error involved is small, but the polar diagram takes care of the inertia automatically.

It is interesting that Professor Maleev has found the polar diagram useful and time-saving. That is what the author hoped to accomplish with this paper.

---

[4] General Diesel Sales Division, Fairbanks Morse & Company, Chicago, Ill. Mem. A.S.M.E.

[5] Nordberg Manufacturing Company, Milwaukee, Wis.

[6] National Advisory Committee for Aeronautics, Cleveland Airport, Cleveland, Ohio.

[7] Vice-President in Charge of Engineering, American Bearing Corporation, St. Louis, Mo., and Indianapolis, Ind. Mem. A.S.M.E.

[8] Aviation Division, Harvey Machine Company, Inc., Los Angeles, Calif.

Substitution of Lower-Quality Industrial Diamonds in Diamond Dresser Tools

By H. WHITTAKER,[1] CRANFORD, N. J.

A shortage of grinding-wheel dresser diamonds, which threatened the war effort early in 1942, led to an investigation of lower-quality diamonds hitherto not used for dresser tools. According to estimates made available by the British Ministry of Supply to the War Production Board, the supply of those qualities and sizes of industrial diamonds preferred and used in large quantities for truing and dressing abrasive grinding wheels was expected to be critical. The War Metallurgy Committee on the recommendation of the Office of Production Research and Development of the War Production Board undertook a study, as "restricted" Project NRC-507, to determine if lower-quality, more plentiful stones could be substituted for the preferred qualities and sizes for some or all wheel-truing and dressing operations. The investigation was carried out in the Research and Development Laboratories of the Crane Company, Chicago. This paper, based on that work, has been released for publication by the OPRD. In the first part of this investigation, a survey of users of diamond dresser tools established definitely that the higher qualities were preferred and used almost exclusively for dressing grinding wheels. The results of this survey and a review of the literature on the practices and the factors which influence the use of dresser tools were reported in a previous paper.[2] In order to provide positive information on the possibilities of using lower-quality stones, it was necessary to classify the seemingly infinite variety of industrial diamonds according to distinguishing characteristics and to test each type under controlled conditions which simulated grinding practices.

Examination and Classification of Industrial Diamonds

PRACTICALLY the entire production of industrial diamonds is distributed in bulk by the Diamond Trading Company, London, in the form of six general classified assortments. These assortments, from highest to lowest in value, are known commercially as "industrial serie," "finest industrials," "industrial smalls and mine rejections," "industrial cleavages and chips," "better bort" (not distributed in quantity at present), and "crushing bort."

The "industrial serie" contains the better, whole, mostly transparent stones from all producing areas. The stones are classified according to size, color, shape, and quality, and range in size from about 0.25 carat to 7 carat.

The assortment known as "finest industrials" is made up from the production of Consolidated African Selection Trust and Gold Coast fields. It contains whole stones, twinned crystals, called macles, flats, and a fairly large number of chips, or fragmented stones all in small sizes averaging about 0.05 carat, with some stones as large as 0.25 to 0.5 carat.

"Industrial smalls and mine rejections" is roughly 70 per cent C.A.S.T. production with the balance from Forminiere and Angola. The stones are all under 0.1 carat in size down to fine "sand" 60 per carat. Over one half the assortment is made up of chips and fragments dark in color, and the remainder is whole stones transparent to dark colored.

"Industrial cleavages" range from transparent to colored fragments, as opposed to single, whole stones, in all sizes. Darkest colors and frosted and coated fragments are usually not included.

All of the remaining materials from all producing areas not included in the foregoing assortments are lumped together in "crushing bort," which is intended for crushing to powder. The dark-colored coated fragments and stones characteristic of the Belgian Congo predominate in crushing bort; and for this reason the term crushing bort is often used synonymously with Belgian Congo. "Better bort" consists of the single, whole, and sound stones selected from crushing bort.

The main source of dresser-tool stones is the industrial serie. The most plentiful sources, and practically the only sources, of substitutes for dresser-tool stones over 0.25 carat in size to supplement the supply are crushing-bort and better-bort assortments. Samples representing the preferred types of dresser stones and the possible substitutes were obtained for testing. Stones were selected from 15 of the 32 categories in the industrial serie. These categories were second yellow, first and second colored, first gray, first brown, dark and darkest brown, first and second gray brown, second river, and common gray colored rounds, first yellow, first brown, first gray, and second gray shapes. A few samples of "cleavages" were obtained, representative of the classifications known as colored, first and common gray cleavages. A 5000-carat parcel of bort completed the sampling of materials. It was made up of selections from crushing bort and better bort and it covered most of the varieties found in these assortments, such as common coated stones, common coated cleavages, black-bort stones, and colored-bort stones.

Representative samples of each of the different categories were examined with a binocular microscope, a petrographic microscope, and other methods for soundness and distinguishing characteristics. The higher-quality stones in the industrial serie were transparent whole stones of definite crystal habit. Most of the stones contained small inclusions and several stones were fractured internally. The lower-quality stones in the serie were darker in color, of low transparency, and they contained inclusions in fairly large amounts. The crystal habit of the lower qualities was not so well defined, and these stones had more striated and irregular surfaces than had the other qualities. Three quarters of the transparent stones showed fluorescence, which varied in degree from vivid to pale shades of blue and yellow, when the stones were exposed to the light of a mercury-vapor lamp. About one half of the stones exhibited phosphorescence. A majority of the diamonds examined under polarized light showed the presence of internal strain. Density measurements made by the immersion method using carbon tetrachloride on about 50

---

[1] Consulting Engineer. Mem. A.S.M.E.

[2] "Substitution of Lower Quality Diamonds," War Metallurgy Committee Progress Report W-57, Nov. 6, 1943.

Contributed by Special Research Committees on Cutting Fluids and Metal Cutting Data and Bibliography and presented at a Meeting of the Chicago Section, Chicago, Ill., June 18–19, 1945, of The American Society of Mechanical Engineers.

Note: Statements and opinions advanced in papers are to be understood as individual expressions of their authors and not those of the Society.

of the larger stones gave values of density ranging from 3.510 to 3.526 on the basis of water at 4 C.

In contrast with the samples from the serie, a majority of the stones examined from the bort assortment were translucent to opaque; the degree of opacity appearing to vary with structure and crystal habit. Most of the stones were well defined in crystal habit. A considerable number of the stones consisted of cleavages, fragments, and aggregated crystal masses. Those stones that were sufficiently translucent to enable internal inspection were observed to contain large areas of inclusions. Only about one fifth of the opaque coated stones examined showed fluorescence of dull intensity, and a few showed phosphorescence. A few of the more opaque stones were radiographed to determine whether internal defects could be detected by this method. The stones were immersed in Russian mineral oil in cellophane containers and exposed for 5 sec at 5 in. focal distance to unfiltered X rays produced by a molybdenum target operated at 20 kv and 18 ma. The resulting shadowgraphs, several of which are given in Fig. 1, indicated that it may be possible to detect flaws and inclusions in opaque stones by this method. However, the detection of small inclusions of foreign elements having low absorption coefficients comparable to carbon is not possible; and thus limitations may be placed on the usefulness of radiography.

It was desirable to supplement the present commercial classification, which is rather loose, with a classification which would make possible closer distinctions among the various types of diamonds for testing purposes. While the physical properties of diamond establish its suitability for wheel dressers, variations in structural characteristics and soundness are the criteria for selection of individual stones.

The structural characteristics and factors to be considered are as follows:

1 Wholeness; whole stones or fragments.
2 Crystal habit; largely determines shape.
3 Opacity; degree of impurities.
4 Homogeneity; continuity of structure.
5 Soundness; number of fractures and cracks.
6 Size.

Compared with the present loose classification, crystal habit is analogous to shape, quality is a combination of wholeness, opacity, homogeneity, and soundness, and color is partially analogous to opacity. Practically all of the industrial serie stones were whole single crystals of definite crystal habit. Of the 5000 carats of better and crushing bort available for this investigation, about 3000 carats were whole stones. Well over 90 per cent of the bort exhibited definite crystal habit. One half of the whole stones were single crystals, 17 per cent were twinned crystals, 30 per cent were aggregated crystal masses, and 3 per cent were of no discernible crystal habit.

It was observed that the stones occurred in one of three crystal forms: Octahedron, dodecahedron, and cube, and combinations of these forms. No other crystal forms were evident except modification to tetrahexahedron. Thirteen classes, grouped under five general headings, illustrated in Figs. 2 and 3, were defined which served to include all of the observed forms and combinations, as follows:

Dodecahedron. Class No. 1, "distorted dodecahedron:" Elliptical, dodecahedron crystals lengthened in the direction of trigonal axis of symmetry with faces more or less modified to tetrahexahedron.

Class No. 2, "normal dodecahedron:" Symmetrical dodecahedron crystals with or without curved faces resulting from tetrahexahedral influence.

Octahedron. Class No. 3, "octahedron - dodecahedron:" Twenty-faced combination octa-dodec crystals with octahedron faces usually curved and shieldlike.

Classes No. 4 and No. 5, "octahedron:" Octahedron crystals with or without rounded faces caused by transparent or glassy growth plates, and giving rise to striated edges. No. 5 is same except growth plates are translucent.

Combination Octahedron, Dodecahedron, and Cube. Classes Nos. 6 to 9 constitute a series between an octahedron and a cube with the sizes of the octahedron faces decreasing as the cube faces increase, the dodecahedron faces varying accordingly: No. 6 octahedron faces large, others small; No. 7 octahedron faces large, other faces larger, but not as large as the octahedron faces; No. 8 equal-sized octa-dodec-cube faces, which configuration produces a spheroidal stone; No. 9 minor octahedron and dodecahedron faces relative to cube faces.

Cube. Class No. 10 and No. 11, "cube:" Six-sided crystals with rough terraced growths on faces. No. 11 has convex, concave, pyramidal, or flat faces.

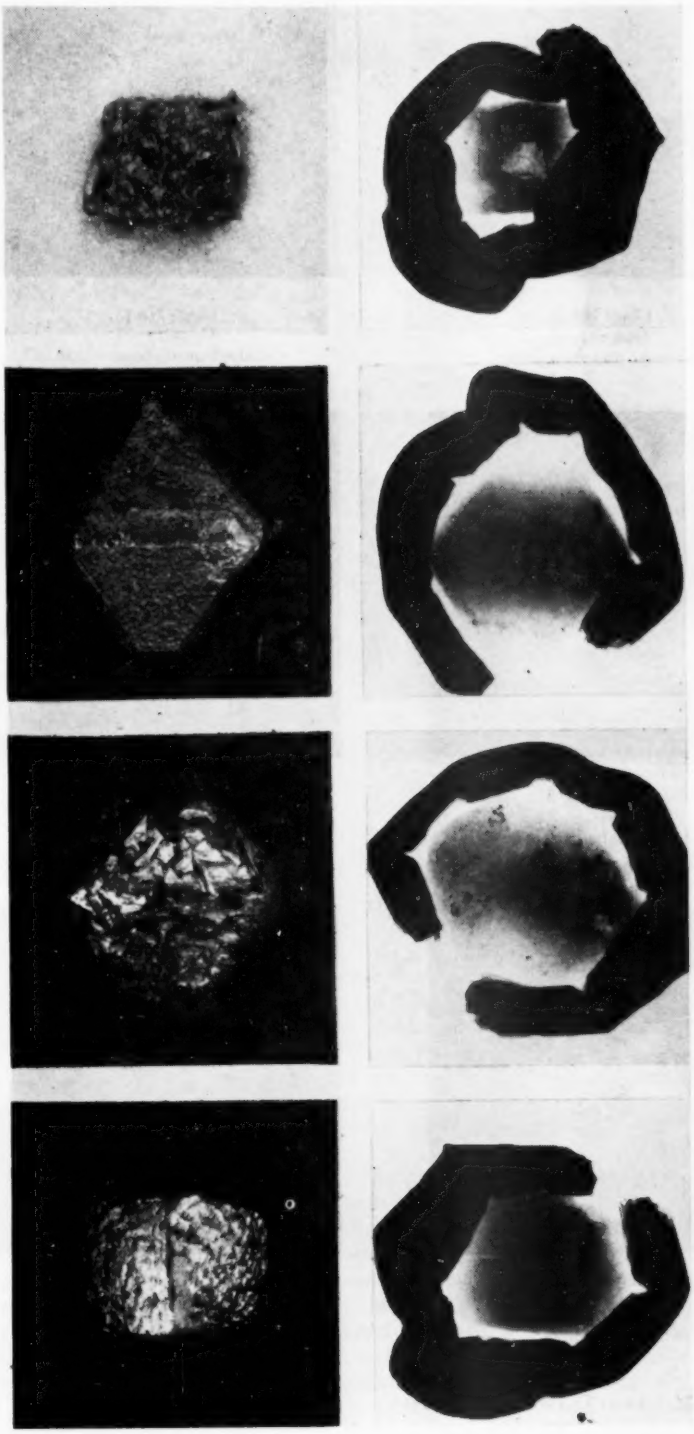
No Definite Crystal Habit. Classes No. 12 and No. 13, no habit: Crystal habit not evident with glassy or transparent rind. No. 13 has translucent to opaque coating or rind.

Opacity, degree of diaphaneity or ability to transmit light, is a measure of the amount of impurities in the form of dispersed included matter. A scale was set up based on the amount of light transmitted through a stone using a 10-w Mazda lamp contained in a white-walled box covered with a $^1/_8$-in-thick sheet of opal glass. An opaque stone that did not transmit any light under these conditions was assigned a value of 7 and a water-white stone was assigned a value of 1. Five other stones having equal intermediate steps of increasing opacity were selected to serve as standards of comparison to give a complete graded range of opacities.

Homogeneity, or continuity of structure was observed to be related somewhat to crystal habit and opacity. A large number of stones which fell in classes 6 to 9, "combination octahedron-dodecahedron-cube," and which had high opacities 4 to 7, consisted of a transparent octahedron crystal nucleus surrounded by a secondary growth containing large amounts of inclusions, thus giving rise to a discontinuity in structure at the interface between core and rind. The thickness of the secondary growth appeared to be rather definitely related to the width of the dodecahedron face in the ratio of 0.4–0.7 to 1, depending on the extent of rounding of the face. Transparent crystals, classes 1 to 5 in particular, appeared to be built up of layers on a basic octahedron form. The interfacial boundaries in this case do not result in as marked a discontinuity in structure because the primary and secondary growths are about equal in composition.

During the detailed examination of over 5000 carats of bort and higher-quality material, a great deal of evidence was found in support of the theory of diamond-crystal formation stated by Polinard, "one might explain that all forms of diamonds are due to the development and to the piling up of octahedron plates which superimpose themselves on the faces of an octahedral nucleus."

Soundness is used to indicate the number of weaknesses which may be contained in a stone as a result of cracks, fractures, and fissures. The soundness of transparent stones can be judged by inspection with a microscope using suitable lighting. Radiography may be of some assistance in detecting flaws in opaque stones which cannot be inspected by ordinary means. The Norton Company has used an impact test to grade bort for suitability for dresser tools with fair success. That firm has tested samples of most of the classes herein described. According to the results of these tests, the impact resistance of single crystals averaged higher than either twinned or aggregated stones in like classes. Discernible differences in impact resistance were ob-



Class No. 11
Opacity—7
Opaque Cube
Diamond inclusion
shown

Class No. 6
Opacity—4
Opaque Combination

Class No. 4
Opacity—5
Opaque Octahedron
Inclusions shown

Class No. 11
Opacity—3
Translucent Cube
No inclusions

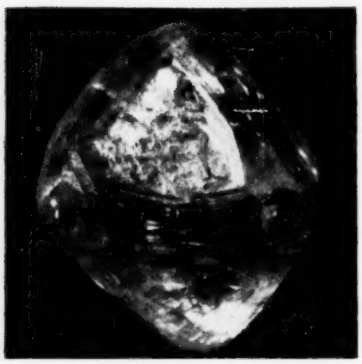
FIG. 1 RADIOGRAPHS OF OPAQUE DIAMONDS
(The black outline which surrounds the radiographs is caused by aluminum foil which was used to support the stones.)



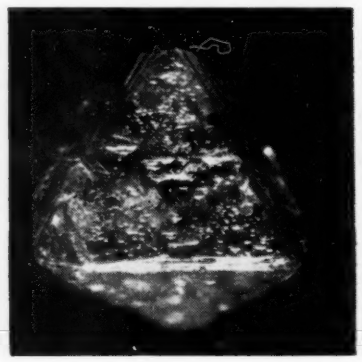
Class No. 1
Opacity—1
Distorted dodecahedron



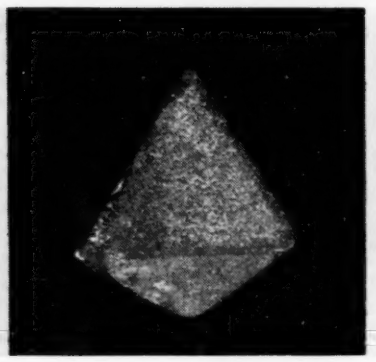
Class No. 2
Opacity—1
Normal dodecahedron



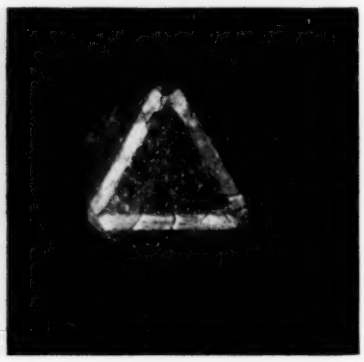
Class No. 3
Opacity—1
Octahedron-dodecahedron



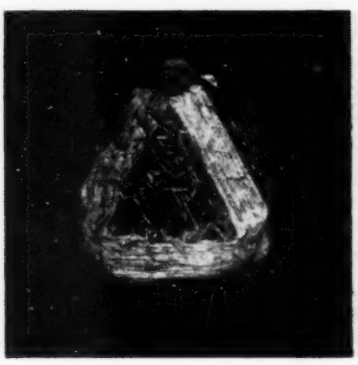
Class No. 4
Opacity—2
Octahedron
Transparent growth



Class No. 5
Opacity—3
Octahedron



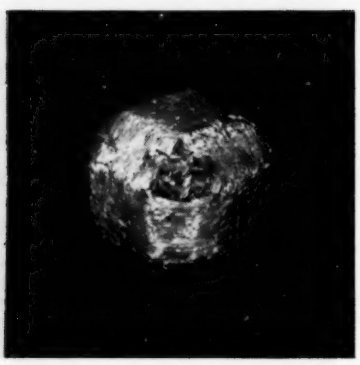
Class No. 6
Opacity—4
Combination habit



Class No. 7
Opacity—4
Combination habit

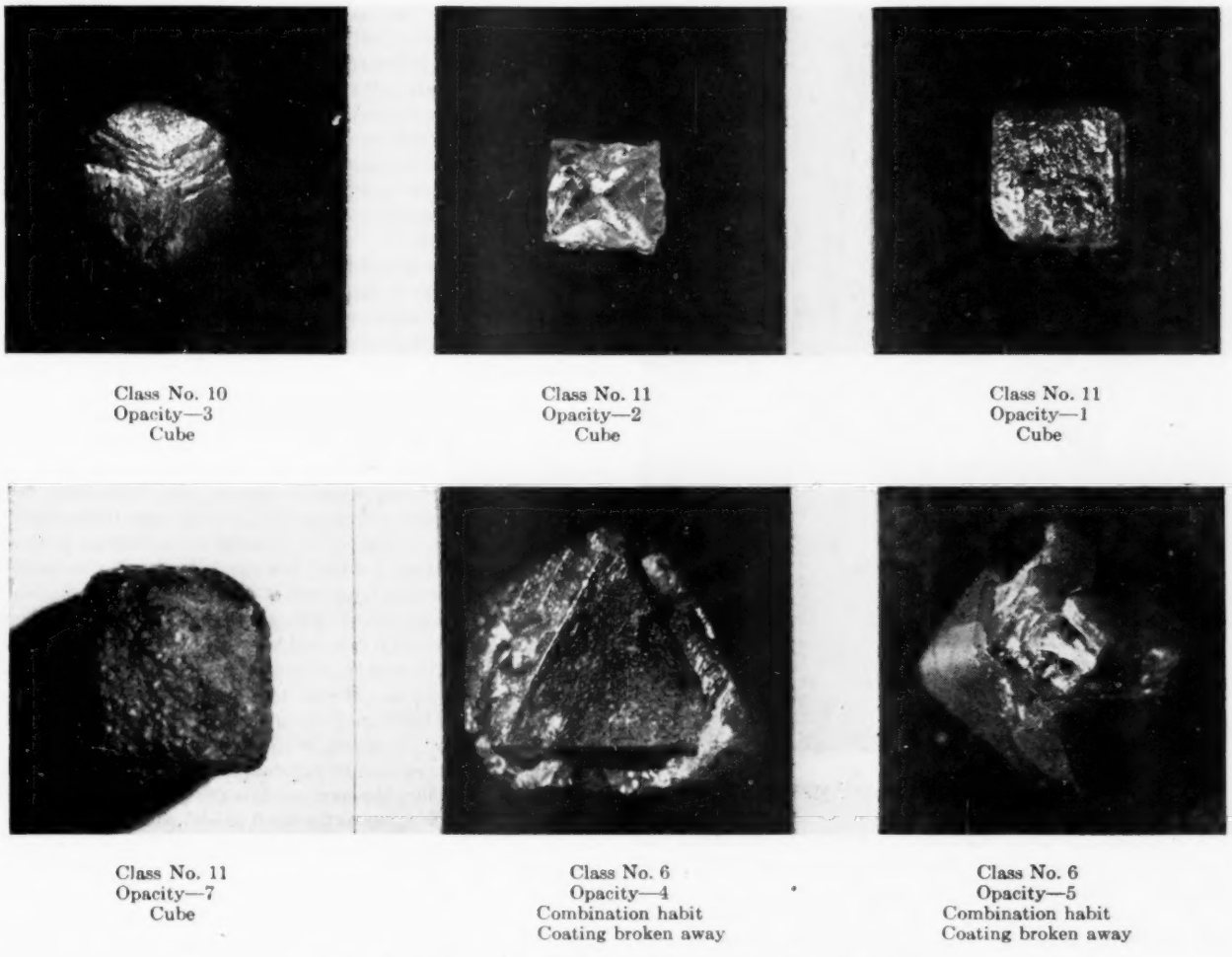


Class No. 8
Opacity—3
Combination habit



Class No. 9
Opacity—4
Combination habit

FIG. 2 ILLUSTRATIONS OF CLASSES OF DIAMONDS



Class No. 10
Opacity—3
Cube

Class No. 11
Opacity—2
Cube

Class No. 11
Opacity—1
Cube

Class No. 11
Opacity—7
Cube

Class No. 6
Opacity—4
Combination habit
Coating broken away

Class No. 6
Opacity—5
Combination habit
Coating broken away

FIG. 3 ILLUSTRATIONS OF CLASSES OF DIAMONDS AND COATED STONES

tained for six classes tested. The more rounded stones exhibited greater resistance to impact than did stones having sharp corners. The classes fell in the following order: Classes Nos. 9, 8, 7, 6, 10, and 11, from 92 per cent unbroken grain to a low of 50 per cent unbroken grain. It may be possible to adjust the impacting force to just destroy flawed and weak stones without damaging sound stones and thus produce a sharper and more efficient separation.

The classification herein proposed and used experimentally on over 5000 carats of industrial diamonds accounts for the most important factors which are thought to influence the utility of industrial diamonds for dressing purposes. Whereas, further refinements may be needed, it is flexible and allows for all possible types and combinations of crystal form, structural differences, and degrees of impurities. The author has examined, in addition to the materials herein described, original parcels of all assortments among which he has not found any stones that could not be fitted into this classification, in particular with respect to crystal habit.

A stone may be completely defined for the purpose by designating (1) the class number, from 1 to 13, which defines its crystal habit and shape; (2) the opacity number, from 1 to 7, which indicates degree of impurities; (3) the extent of flaws; and in addition, (4) by indicating whether a whole stone, a fragment, a twin or an aggregated crystal mass. Industrial-serie materials fall in classes 1 to 4 in the lower opacities, numbers from 1 to 3, with some exceptions; for example, dark-brown rounds having an opacity of 5. The major portion of material in crushing bort falls in classes 6 to 9 and higher opacities, numbers from 3 to 7. Minor amounts fall in classes 3 to 5 and 10 to 13.

GRINDING-WHEEL DRESSER-TOOL TEST METHOD

To compare the different varieties of diamonds as to their relative suitability for dressing grinding wheels, a test method was developed for the rapid quantitative determination of the rate of wear under simulated shop-dressing conditions. The test consisted of the continuous dressing of a 1-in. face-grinding wheel, the periodic measurement of the amounts worn off the diamond and the abrasive wheel, and careful observations of changes in shape and chipping of the diamond point. The essential parts of the test apparatus, shown in Fig. 4, were a heavy tool holder, specially designed to allow for any desired setting of drag, rotation, and traverse angles, mounted on the table of a Brown and Sharpe No. 2 cylindrical grinder with automatic feed, counter, speed control, and fluid system for wet dressing. The diamonds, which ranged from $^1/_2$ to 1 carat, were set by the powder hot-press method in a large-head steel shank. The shank was $^7/_8$ in. long, $^1/_2$ in. diam at the head, and $^1/_4$-in-diam shaft.

To save time and also to enable an inspection of the stone as wear took place, the loss on the diamond was measured by means

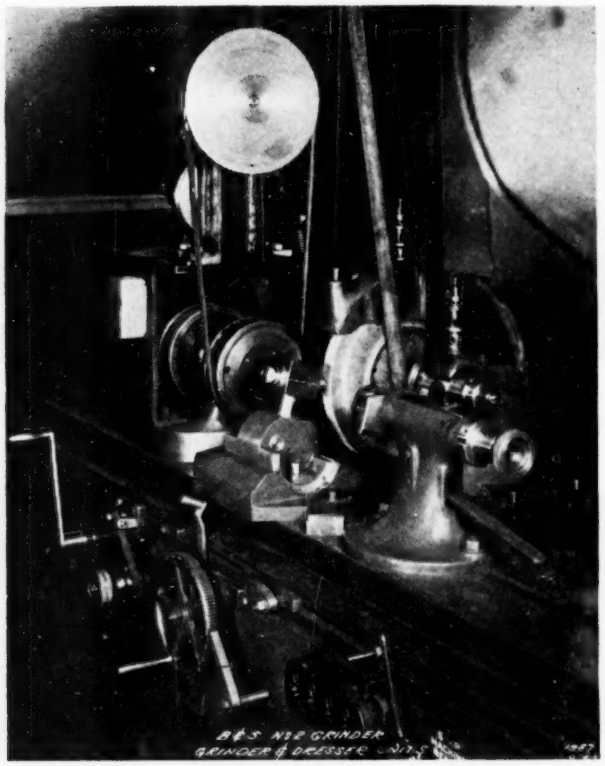


FIG. 4 WEAR-TEST APPARATUS

of a graphical method. The diamond point in its shank was projected on a screen at ×100 magnification and the profile recorded. After testing, a second profile was made in the same position over the first projection. The difference between the two profiles was a measure of the loss in height because of wear. The area of the flat generated on the diamond point was traced at ×100 magnification using a reflection microscope and a reflex camera and was measured with a planimeter. Height loss and area measurements are all that are needed to compute the volume loss, provided the shape of the removed portion is known. The volume loss was then converted to weight loss using 3.52 for the specific gravity of the diamond. The computed weight loss of the diamond in carats was divided by the volume in cubic inches removed from the grinding wheel to give the "unit of wear rate." Since the order of magnitude of the unit of wear rate was ten hundred thousandths of a carat per cubic inch, the notation ct. $\times 10^{-5}$/cu in. was used, that is, the unit was multiplied by 100,000 in order to express the result in terms of whole numbers.

The test procedure had the advantage of savings in time and materials, but precision was sacrificed to some extent. By means of this testing procedure a diamond could be tested under almost any combination of conditions that might be encountered in practice in about a day and a half. To do the same job by weighing would consume 5 times as many test wheels and would take a week, because of the larger amount of diamond that must be worn off to enable an accurate weight determination. The greatest source of error was in the assumption of the shape of the solid removed in making the volume-loss computation.

Since the actual shape of the solid figure removed from the point of the diamond would be some shape between that of a sharp-sided pyramid and a segment of a sphere of equal heights and base areas, depending on how close the assumed shape is to the actual shape, the error can be as great as 20 per cent. This was checked experimentally by testing a number of stones sufficiently to enable accurate weight-loss determinations, and in most cases the wear rates determined by weight and by computed volume were well within the possible error of 20 per cent. Therefore, for purposes of comparison in this investigation, differences less than 25 per cent, roughly 5×10^{-5} ct./cu in. (0.00005) were not considered significant; two stones of 15 and 20 $\times$ 10^{-5} ct./cu in., respectively, would be considered alike in so far as could be determined.

Of interest in the establishment of a set of standard test conditions for comparison of diamonds and also of practical value were the tests that were made to learn the effects of the many factors which may influence the rate of wear of diamond dressers in the dressing operation. These factors had to be controlled in order to place the test results on a comparable basis:

1 One set of factors is determined by the conditions of operation, such as loading of the wheel with metal, wheel speed, rate of traverse, feed, and use of a coolant. In practical grinding operations the grinding wheel is dressed and trued after the wheel has been loaded with metal and the edges are broken down from the grinding of work. No appreciable difference in wear rates was found when a wheel was dressed after it was loaded with metal by grinding a number of pieces of hard tool steel and when the wheel was dressed without loading. Changing wheel speed from 4000 to 6000 fpm had very little effect on wear rate. Nor did varying the rate of traverse between 0.001 and 0.003 in. per revolution affect rate of wear to any great extent. Contrary to expectations, a 0.001-in. feed caused $1^1/_2$ times the wear rate of a 0.005-in. feed. However, it will be noted that for each pass a 5 times greater volume of grinding wheel is removed with a 0.005-in. feed. Thus the average loss per pass was 3 times as great for the 0.005-in. cut as for the 0.001-in. cut. Observations on the durability of diamond dressers in the shop are usually based on the number of dressings. The feed used would have an important bearing on the comparisons. A considerable difference in wear rate was observed between wet and dry dressing. The average rate of wear on nine stones when the wheel was dressed dry was 20×10^{-5} ct./cu in. and was only one fifth as great, 4×10^{-5} ct./cu in., when the tools were flooded with water at the rate of 7200 cc/min. The difference tended to become slightly greater as grit size was decreased. Average values obtained for 36, 60, and 120-grit vitreous wheels were 27, 18, and 8 for dry dressing and 6, 4, and less than 1 for wet dressing, respectively (all $\times$ 10^{-5} ct./cu in.).

2 Another set of factors is introduced by the variations in types of grinding wheels. The grinding-wheel factors are grit size, grade, type of bond, type of abrasive, and size. The rate of wear may be affected as much as tenfold over the range of types of grinding wheel. The rate of wear increased as grit size increased. A soft grade (Norton 60I5BE) wheel abraded the test diamond at the rate of 7; a medium grade (Norton 60M-5BE) at 11; and a hard grade (Norton 60P5BE) at 13, $\times$ 10^{-5} ct./cu in. Of all factors in the wheel, the type of bond had the greatest effect on wear rate; for example, vitreous-bonded wheels are up to 10 times as abrasive to the diamond as are resin-bonded wheels. The effect is less marked for fine grits, soft grades, and wet dressing, but is still of the order of fivefold. The two types of abrasive aluminum oxide and silicon carbide have similar effects on wear rate. That the size of the grinding wheel influences wear on the diamond was apparent from the results of tests on a 20-in. × 6-in. wheel. The average wear rate of 10 stones was 19×10^{-5} ct./cu in. as opposed to 4×10^{-5} ct./cu in. obtained on a 12-in. × 1-in. wheel, both dressed wet. The increase in wear rate with size of wheel is due, possibly, to the increased time of continuous contact of the wearing surfaces, and the

TABLE 1 DIAMOND-DRESSER SHOP TESTS ON HEAVY AND LIGHT GRINDERS

Tests made by	Crane Company		Buick Aviation Plant	
Tool no.	6689	6690	103	72
Initial weight, carats	3.1	3.9	0.725	0.688
Final weight, carats	2.59	3.83	0.720	0.685
Loss in weight, carats	0.51	0.07	0.005	0.003
Make of grinder	Cincinnati	Mattson	Heald	Heald
Type of grinder	Centerless	Surface	Internal	Internal
Wheel size, in.	20 × 6	20 × 3	3½ × 2	3½ × 2
Wheel grit size	36	36	60–	60–
Number of dressings	1532	243	810	516
Passes per dressing	2	2	3 and 1	3 and 1
Depth of cut, in.	0.0025	0.002	0.003 and 0.001	0.003 and 0.001
Volume of wheel removed	2514	184	141	90
Wear rate, ct. × 10^{-5}/cu in.	20.1	38	3.6	3.3
Work ground	Valve stems	Toggle-valve links	6-In. gears	6-In. gears

tendency of the area of the wearing surface of the diamond to increase, both resulting in higher temperatures on the stone. The effect of wheel size was further demonstrated in results of shop tests given in Table 1. These results also served to indicate that the order of magnitude of wear rate under the test conditions was the same as under shop conditions.

Thus it appears that the rate of wear of diamond dressers is considerably influenced by the conditions of use. The tests, while preliminary, served to establish in a general way the wide range of wear rates that may be encountered. The wear rate may vary between 1 and 40 × 10^{-5} ct./cu in. depending upon the combination of conditions and may be as high as 100 × 10^{-5} ct./cu in. under particularly severe conditions. For most dressing operations the average combination of conditions produces a wear rate of 15–25 × 10^{-5} ct./cu in., and this would be a good figure to keep in mind, or about 20 × 10^{-5} carat per dressing, since between ½ to 1 cu in. is removed per dressing from medium-sized wheels. Consumption of one half of a 1-carat stone should produce about 2500 dressings. To produce a reasonable number of dressings per tool, the size of the stone must bear some relation to the rate of wear for the conditions of use. This does not mean that for double the rate of wear, the stone should necessarily be doubled in size, but a certain minimum size is required. However, factors other than the rate of wear must be considered in determining the proper size to be used.

Another factor which has received very little attention is the effect of the shape and size of the stone on the finish imparted to the wheel for different classes of grinding wheels and work. Also, the size and shape of the stone are important in connection with form-grinding. When these effects are known more precisely, size and shape specifications can be developed which should lead to more efficient and economical use of diamond dressers. Of interest in this connection was the observation that in the dressing operation the wear on the diamond progresses across the flat in the form of a ridge as the diamond is traversed across the wheel, starting at the point of first contact with the wheel (see Fig. 5). The ridge may be compared with the broad cutting edge of a chipping tool. Thus the main working area of diamond is roughly the length of the developed ridge, which extends across the flat, × the width of the ridge, which usually measures less than 1 mm. The remaining areas do, however, maintain some rubbing contact. Recognition of this mechanism of cutting and wear involved may lead to improved designs of dresser tools.

Wear Tests on Varieties of Industrial Diamonds

Representative samples of the various classes of industrial diamonds were tested under controlled standard conditions designed in conformity with the foregoing findings to reproduce average shop conditions. A 1-in-wide by 12 in. to 7-in-diam, 60-mesh-grit medium-grade vitreous-bonded aluminum-oxide grinding wheel was dressed dry; the speed of the wheel was maintained at 5000 fpm; and the tools were traversed, with a

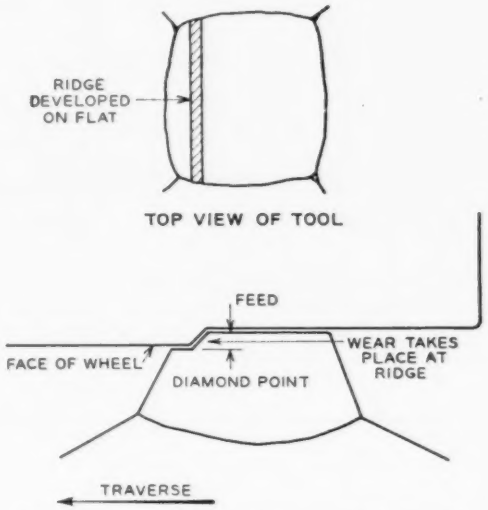


Fig. 5 Diagram Showing Contact Between Diamond Point and Grinding Wheel

drag angle of 15 deg across the 1-in. face of the wheel at a rate of 0.0015 in. per revolution for six to eight runs of 50 passes each. The amount of wear was measured after each 50 passes, and the tool was rotated to a new position for each run.

The results of the tests on 60 diamonds are listed in Table 2 on an "adjusted" basis and on an "over-all" basis. The "adjusted" value of wear rate is derived by excluding values of runs in which chipping occurred and in which "soft" directions happened to be struck to give abrupt increases in wear. This latter effect was an indication that the variation in hardness of diamond influences the performance of dresser tools; for, when the orientation of the stone during a run happened to coincide roughly with the so-called soft direction, almost invariably the wear rate for the run was high and the flat usually had a polished or shiny appearance. The soft directions are crystallographically the same directions that the gem cutter uses in lapping on the facets of a cut stone. Analysis of a large number of runs on a large number of stones indicated that the rate of wear on the soft directions was on the order of 3 times as high as on the other or "hard" directions.

Incidentally, when a slight drag angle is used in the dressing operation, setting of the diamond with a crystallographic axis parallel with the axis of the tool would tend to avoid the possibility of striking soft directions as the tool is rotated to new positions; and thus the best results would be obtained.

Reference to Table 2 will indicate that the results on the "adjusted" basis show definitely that many of the lower-quality diamonds are as resistant to abrasion by grinding wheels as are the higher-quality stones. Taking each class as a whole, there were no distinct differences among the classes. The wear rates

TABLE 2 WEAR RATE OF DIFFERENT TYPES OF INDUSTRIAL DIAMONDS

GROUP	CRYSTAL CLASS NO.	OPACITY NO.	D.T.C. CATEGORY	STONE NO.	WEAR RATE ADJ.[1]	WEAR RATE OVERALL[2]	CHIPPING
A. Dodecahedron	1	1	1st Brown Round	102	20	49	None
	1	2	1st Yellow Shape	111	36	38	None
	1	2	Common Grey	141	31	37	None
	2	2	1st Grey Round	93	14	12	None
	2	2	1st Colored Round	1	13	11	None
	2	2	1st Colored Round	9	10	10	None
	2	2	Common Coated	271	11	17	None
	2	2	2nd Grey Brown	63	11	16	None
	2	2	2nd River Round	70	16	20	Chip
	2	4	Darkest Brown Round	43	15	14	None
B. Octahedron	3	1	2nd Yellow Round	126	24	41	Small Chip
	3	1	2nd Grey Shape	78	11	46	None
	3	1	1st Grey Round	97	24		None
	3	2	2nd Yellow Round	84	12	32	None
	3	2	1st Cleavage	139	16	50	None
	3	2	Dark Brown Round	37	21	19	None
	3	3	Black Rejection	273	10	5	Chip
	4	1	1st Brown Shape	129	18	23	Chip
	4	1	Colored Cleavage	136	14	108	Many chips
	4	1	Cut Gem Stone	158	12	18	Chip
	4	2	1st Grey Shape	120	32	34	Crumbled
	4	2	1st Grey Brown	52	16	20	Chips
	4	2	2nd Grey Brown	61	12	21	None
	4	5	Black Rejection	283	11	8	None
	4	6	Black Rejection	284	12	30	Chip
	5	5	Common Grey Colored	28	15	31	Large Chip
	5	5	Black Bort Stone	156	36	52	Large Chip
C. Combination Octa-Dodec-Cube	6	2	Common Coated	272	--	--	Large Chip
	6	3	Common Coated	275	12	18	None
	6	4	Colored Bort Stone	281	18	42	None
	6	4	Common Coated	154	18	10	None
	6	4	Colored Bort	250	20	--	None
	6	6	Colored Bort Stone	164	13	24	None
	6	7	Black Bort Stone	286	9	9	None
	7	2	2nd Colored Round	16	10	9	None
	7	4	Common Coated	160	10	37	Crumble
	7	4	Common Coated	276	13	15	Chip
	7	4	Common Coated	152	30	53	Chipping
	7	5	Common Coated	169	13	38	Crumble
	7	5	Colored Bort Stone	144	9	12	Small Chip
	7	5	Black Rejection	279	26	26	None
	7	5	Common Coated	282	29	356	Chipping
	7	5	Common Coated	174	11	--	None
	7	7	Black Rejection	148	22	160	Large Chip
	8	4	Black Bort Stone	277	31	78	Chip
	8	7	Black Bort Stone	150	11	290	Large Chip
	8	7	Black Bort Stone	287	47	353	None
	9	5	Colored Bort Stone	278	22	22	None
D. Cube	11	2	1st Colored Round	7	36	42	Large Chip
	11	2	Common Coated	270	13	15	None
	11	2	Common Coated	269	14	29	None
	11	2	Common Coated	163	18	--	None
	11	3	Common Coated	167	23	41	Many Chips
	11	3	Common Coated	274	21	59	Chips
	11	4	Colored Bort	162	22	--	None
	11	6	Black Rejection	285	24	24	Chip
	11	6	Colored Bort	280	25	37	None
	11	7	Black Rejection	289	18	38	Chips
E.	12	3	Common Coated	143	14	15	None
	12	6	Black Rejection	290	11	54	Crumble
	13	7	Black Rejection	288	24	69	None

[1] Adjusted wear rate in carats loss per cubic inch of wheel removed $\times 10^{-5}$. Values are adjusted to exclude high individual values due to wear on soft directions, chipping, crumbling, etc.

[2] Over-all wear rates in carats loss per cubic inch of wheel removed $\times 10^{-5}$. Values are actual over-all wear based on weighing stones before and after testing.

adjusted basis, in each group varied from about 10 to 25 and averaged 18 × 10^{-6} ct./cu in., with a few scattered values above 30 × 10^{-6} ct./cu in. in each group.

The "over-all" wear rate differs from the adjusted wear rate in that it was based on the total amount of diamond lost and included loss due to wear in all positions, chipping, and crumbling. The difference in rate between over-all and adjusted wear rates might be thought of as a measure of the structural failure which takes place. Excessive over-all losses, values over 40 × 10^{-6} ct./cu in. in Table 2, shown by a number of stones in all classes, were caused in most cases by chipping and crumbling of localized areas. This excessive over-all rate was more prevalent among the lower qualities, classes 4 to 11, than among other qualities. On the other hand, many of the lower qualities did not exhibit chipping or localized increases in wear, and the over-all wear rates were essentially equal to the adjusted wear rates.

In the progress of this research it became more and more apparent that the chief factor involved in the use of diamonds for wheel-dressing purposes is the ability of the stone to withstand fracture. Structural weaknesses of diamonds which may be potential sources of failure are the same as those for other crystalline materials, such as cleavage planes, twinning planes, internal fractures, incipient cracks, inclusions which act as loci of stress concentrations. To this list should be added the interface between the interior crystal and the exterior, or later growth, which is often of a dissimilar color, characteristic of coated stones. Relatively easy parting in the octahedron plane known as cleavage follows from the diamond structure. All that is needed is a sufficient force applied in the proper direction to cause cleavage. Incipient cracks in the cleavage directions increase the tendency to cleave and are potential sources of failure. Large inclusions of dissimilar material may be causes of failure, in particular, under thermal stresses. Flaws and internal fractures are potential starting points of failure.

What has been said of cleavage planes is also true of twinning planes. Diamond twins are common with the twinning plane parallel to the octahedron face. These are known as contact or spinel twins. In the trade the stones are called macles. Judging from the structure of the so-called coated stones, the interface between the interior crystal and the coating, or secondary growth, may be a plane of weakness. Pieces of the coating are likely to be pulled out when the stone is worn to expose the interior crystal. It would be expected that the position of the plane of weakness in the stone would be important. The further from the working point that the flaw, or plane of weakness, is removed, the less should be its influence. The setting metal and method is important in that a stone well supported at all points is less apt to fail through a plane of weakness.

To test for strength, in particular, the effect of weaknesses in structure, a large number of runs must be made to wear the stone down and expose the planes of weakness; and also, long use may develop cracks from continuous shocking. While the laboratory test was quite severe in that no coolant was used, the amount of abrasive wheel removed was small, and very little of the diamond was consumed in a test. In the life of a tool in the shop the number of passes is far greater by 50 to 100 times. Hence the chances of striking a plane of weakness in a stone are increased proportionately. In order to approach the requirement of a large number of dressings, tests were made with ten tools representing the most important classes of stones on a Cincinnati centerless grinder. The conditions of test were essentially the same as those of the standard laboratory test except that a coolant was used and the wheel was much larger. Each tool was given at least 850 passes over the wheel, removing between 250 to 270 cu in. of the wheel in a test. The amount of diamond consumed in each case was between 0.05 and 0.1 carat which amounted to 5 to 20 per cent of the stone, depending on the initial size. The results are listed in Table 3.

TABLE 3 WEAR RATE ON VARIOUS CLASSES OF STONES WHEN TESTED ON CINCINNATI CENTERLESS GRINDER USING 20-IN. × 6-IN. WHEEL, WET DRESSING

	Wear rate—carat loss × 10^{-6} per cu in. wheel removed			
		Cincinnati centerless grinder test, 20-in. × 6-in. wheel		
Class no.	Standard laboratory test 12-in. × 1-in., wheel	Computed from volume loss	Weight-loss check	Remarks
2.2	12.5	11.1	8.4	
4.2	10.3	17.5	16.1	
4.3A	9.8	25.5	19.7	Some chipping
4.5	10.5	23.4	17.6	Some chipping
6.7	9.4	23.8	22.3	Slight chip at interface
7.4	12.9	15.8	94.2[a]	Large chip — 0.14 carat
7.5A	25.8	14.0	30.4[b]	Small chip at interface
10.5	21.8	15.5	15.7	
10.6T	24.5	14.7	12.2	Fissure opened
11.6	24.1	32.4	26.9	Some chipping
Average	16.2	19.4	18.8	

[a] Large chips caused by high infeed on last run accounts for high wear rate on weight check. If chip of 0.14 carat is allowed for, wear rate is about 25.

[b] Difference between computed and weight check can be accounted for with 0.03-carat chip.

Here again, there was very little difference in wear rate, chipping excluded, between the types of stones tested. Two out of the eight lower-quality stones chipped quite badly. The chipping occurred when the stones were worn sufficiently to expose the core under the coating. Fig. 6 shows the chipping progressively. Other coated stones were worn down to the point of exposing the plane between the primary and secondary growth but did not chip. Aside from failure by chipping it was observed that the wear rate did not change as the stones were penetrated from their exterior natural skins inward to depths equal to 50 per cent of the radius. This observation is contrary to the opinion of the trade, which has maintained that the natural skin of the diamond is harder than its interior.

Thus it appears that the performance of coated bort stones may be influenced by the thickness of the coating. When the coating is very thick in relation to the diameter of the stone, a large number of dressings at normal wear may be made before the interface is penetrated at which point chipping may or may not occur. Such chipping as may occur would then reduce the life of a stone by only a small amount. When the coating is relatively thin, flaking may occur after only a few dressings, but the life is not materially shortened since the chipping consumes only a small portion of the stone.

The practicability of bort for dressing purposes was further demonstrated by the results of tests which were made by Norton Company. These results were especially helpful in providing practical confirmation of the laboratory tests, which confirmation would have entailed considerable time and effort to obtain. Forty-eight tools made with selected bort, similar to classes 6 to 9, were used under regular shop conditions on most types of grinders in general use for over a year. The tools were used to the limit of the setting, no attempt being made to obtain maximum use by resetting. Thus the tools were worn down until the stone dropped out of the setting. In one half of the tools, the residual stone was lost. The results of these tests are compiled in Table 4 and are analyzed in Table 5.

The average size of stone used in the tools was 1.28 carats. An average of 0.6 carat was consumed which produced an average of 2000 dressings. In all, upward of 100,000 dressings were made with the forty-eight tools and six are still in use, with about 20 to be reset. Fifty per cent of the tools performed as well as first-quality stones to give over-all wear rates of less than 40 × 10^{-6} ct./cu in., and an average of 26 × 10^{-6} ct./cu in. Chipping proba-

TABLE 4 RESULTS OF SHOP TESTS ON DIAMOND DRESSERS USING SELECTED BORT BY NORTON CO.

Tool No.	Weights in Carats			No. Dressings	Weight Loss Carats x 10^{-5} per Dressing	Wear[2] Rate	Remarks
	Initial	Final	Loss				
1	1.52	.53*	.99	3000	33	44	Pulled out
2	1.46			6608	Still in use		
3	1.00	.22	.88	996	88	118	Fragment
4	1.67	.53	1.14	3587	31.8	42.5	Pulled out
5	1.21	.74	.47	3787	12.4	16.6	Normal wear
6	1.04	.44	.60	1382	43.5	58.0	High wear
7	1.08	.21*	.87	1692	51.3	68.5	Pulled out
8	1.66	1.12	.54	1120	48.4	64.5	High wear
9	1.44			5841	Still in use		
10	1.34	.98	.36	1056	34.2	45.6	High wear
11	1.47	.68*	.79	1699	46.5	62	Pulled out
12	1.16	.70*	.46	354	131	175	Fragment
13	1.25	.46*	.79	967	82	110	
14	1.30	.77*	.53	3049	17.3	23	Normal wear
15	1.18	.63	.55	504	109	146	Fragment
16	1.62	.94	.68	1942	35	46.8	High wear
17	1.46			1116	Still in use		
18	1.01	.22*	.79	3460	23	31	Pulled out
19	1.10	.84*	.26	1060	24.5	32.8	Normal wear
20		.95		560	Failed Setting		
21	1.42	.70	.72	3270	22	29.4	Normal wear
22	1.14	.64*	.50	2616	19.3	25.8	Normal wear
23	1.31	.60*	.71	2927	23.9	32	Normal wear
24	1.14	.21*	.93	3231	29.0	39	Pulled out
25	1.22	.60*	.62	2945	20.0	27	Normal wear
26	1.54	.42*	1.12	1451	77.4	103	Pulled out
27	1.50	.53	.97	2730	35.6	47.5	Pulled out
28	1.25	1.15	.10	1467	6.8	9.1	Normal wear
29	1.19	.51*	.68	1371	50	67	Pulled out
30	1.06			4458	Still in use		
31	1.02	.47*	.55	1452	37.8	50.5	High wear
32		.64		333	Failed Setting		
33	1.28	.96	.32	2062	15.5	20.8	Normal wear
34	1.68	1.23	.45	1250	36.4	48.6	High wear
36	1.16	.09	1.07	1240	86.7	116	Fragment
37	1.21	1.11	.10	1691	6.2	8.3	Normal wear
38	1.14	.37*	.77	2747	28.1	37.4	Pulled out
39	1.00	.39*	.61	1070	57.5	76.6	Pulled out
40	1.20	.54*	.66	1237	53.0	71	Pulled out
41		1.36		791	Failed Setting		
42	1.34	.48*	.86	2335	36.8	49	Pulled out
43	1.02	.53*	.49	2335	21.0	28	Normal wear
44	1.05	.34*	.71	1599	44.5	59.5	Pulled out
45	1.59			5552	Still in use		
46	1.27	.25	1.02	670	153	205	Fragment
47	1.27	.35*	.92	1886	49.0	65.5	Pulled out
48	1.53			2430	Still in use		

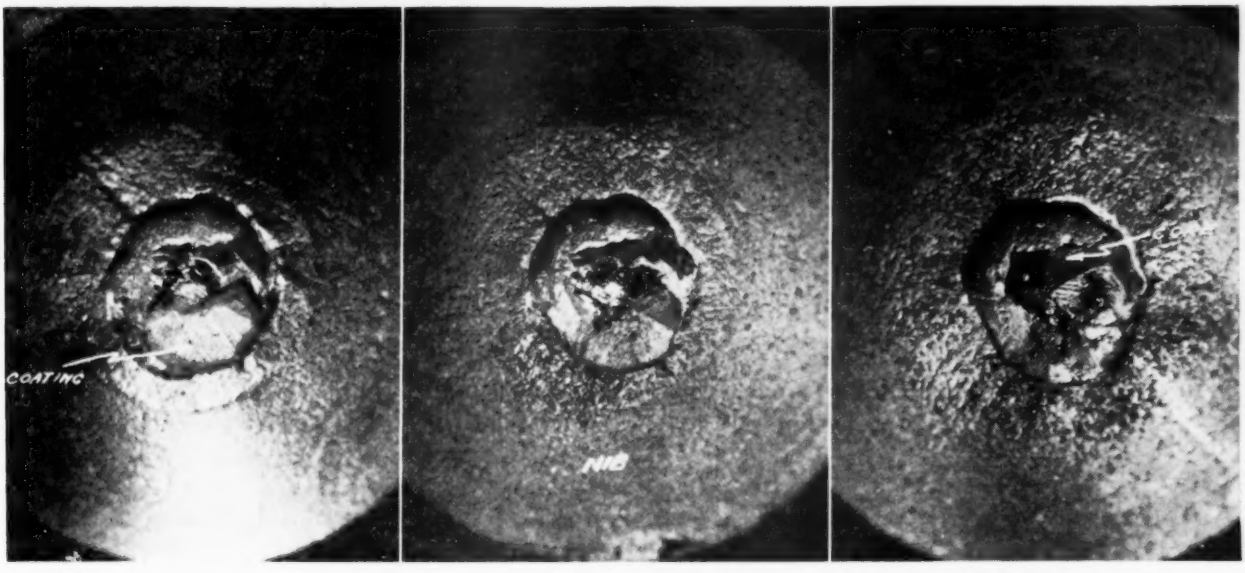
* Final weight estimated from cavity in tool nib since tool was used to the limit of the setting and the residual stone was pulled out and lost. All other values are weights of residual stone.

[2] Wear rate in carats lost $\times 10^{-5}$ per cubic inch of wheel removed. Wear per dressing divided by 0.75 cu. in., the average amount of wheel removed per dressing as estimated by Norton Company.

bly accounted for most of the high losses obtained with 30 per cent of the tools. Ten per cent of the tools exhibited the exceptionally high average loss of 152×10^{-5} ct./cu in. because the stones broke up into fragments. In all cases a fair number of dressings was obtained before failure occurred. All things considered, the coated Congo stones which were tested in the Norton shops performed exceptionally well. Costwise, the comparison is in favor of bort many times over.

TABLE 5 ANALYSIS OF NORTON CO. SHOP TESTS ON SELECTED BORT

	No. of tools	Per cent	Average wear rate $\times 10^{-5}$ ct./in.[3]	Average number of dressings
Setting failed	4	8	...	420
Fractured to fragments	5	10	152	750
Wear rate above 40, indicating chipping and fracturing	14	30	53	1450
Wear rate below 40, indicating normal wear	25	52	26	3000



After 637 passes After 756 passes After 900 pastes

FIG. 6 TOOL WITH COATED STONE, SHOWING PROGRESSIVE FRACTURING OF COATING IN USE; ABOUT ×6

(Test conditions: Cincinnati centerless grinder, wet dressing, 20-in. × 6-in., 60M30 Carborundum Company wheel, 0.001 in. feed, 15-deg drag angle.)

CONCLUSIONS

The order of magnitude of the rate at which diamond wears when used to dress grinding wheels was established over the range of conditions encountered in dressing operations. A dressing of the average size and type of grinding wheel in the shop consumes about 0.0002 carat of diamond. A tremendous quantity of grinding wheel can be removed with a very small consumption of diamond; the ratio is on the order of 1 part diamond to 1,000,000 parts grinding wheel by weight. The consumption of diamond may vary between less than 0.00001 to 0.0004 carat per cu in. of wheel removed, depending on the combination of conditions. Fine-grained wheels and resin-bonded wheels abrade diamond at a much lower rate than coarse-grained wheels and vitreous-bonded wheels. To obtain the best and most economical performance with diamond dressers, particular attention should be given to the selection of the most efficient feed consistent with requirements and the adjustment of the coolant in wet dressings, since these two factors have the greatest effect on wear.

Grinding wheels can be dressed satisfactorily with lower-quality industrial diamonds. Results of laboratory and practical shop tests indicated that many of the so-called lower-quality types of stones, of which large quantities are available in better-bort and crushing-bort assortments, may perform as well as the higher-quality stones of the industrial-serie variety in a majority of standard dressing operations. The different varieties and types of diamond have essentially the same resistance to wear by abrasion of grinding wheels, when all factors are considered.

Factors other than the resistance to wear are of greater importance in determining the suitability of individual stones for dressing purposes. Soundness and structural strength and the ability of individual stones to withstand chipping and crumbling appear to be the limiting factors in their utilization.

The selection of sound stones from bort is difficult, because of the wide variation and the opacity of bort. The uncertainty in performance usually associated with bort arises from this difficulty in selection, and this difficulty probably accounts for the preference in the trade for the so-called higher qualities which can be more readily inspected because they are transparent. Even so, it should be possible to select sufficient quantities of single-coated stones from bort categories to make up shortages which may occur in the thirty-two categories of the industrial serie.

Care is necessary in the selection of suitable stones from better bort and crushing bort. Solid appearing more or less symmetrical whole stones, free from surface flaws, fissures, and granulated areas, octahedron to cubic in shape, may be expected to produce consistent results. Aggregated crystal masses, fractured stones, fragments and cleavages, can be used to dress grinding wheels, but their performance may not be entirely satisfactory because of a tendency to chip.

ACKNOWLEDGMENTS

The author wishes to express his appreciation for the assistance and co-operation in this investigation given by the following organizations: Buick Motor Division, Aviation Engine Plant, Chicago, Ill.; Carboloy Company, Detroit, Mich.; Arthur A. Crafts Company, Boston, Mass.; Ex-Cell-O Corporation, Detroit, Mich.; General Motors Corporation, Electromotive Division; LaGrange, Ill.; F. F. Gilmore and Company, Boston, Mass., Koebel Diamond Tool Company, Detroit, Mich.; J. Montezines, New York, N. Y.; Norton Company, Worcester, Mass.; Rough Diamond Company, New York, N. Y.; J. K. Smit and Sons, Inc., New York, N. Y.; H. R. Spandel, Inc., New York, N. Y.; Studebaker Aviation Engine Plant, Chicago, Ill.; United States Industrial Diamond Corporation, New York, N. Y.; Wheel Trueing Tool Company, Detroit, Mich.

Thanks are also due many others in the industrial-diamond and metalworking industries.

(Owing to travel emergency conditions existing when this paper was presented, discussion will be accepted until February 10, 1946)

Measurements of Temperatures in Metal Cutting

By A. O. SCHMIDT,[1] O. W. BOSTON,[2] AND W. W. GILBERT[3]

Measurements of the heat developed in a metal-cutting operation, as well as investigation of cutting and chip temperatures by the authors have brought out that the chip temperature is uniform at the higher cutting speeds when all other conditions are kept constant. The temperature of the tool increases with the cutting speed, and the amount of metal removed before tool failure will generally be inversely proportional to the cutting speed.

Review and Discussion of Previous Investigations

IN a previous paper (1)[4] by the present authors, it was shown that the work done by a metal-cutting tool is transformed into heat which is carried away by the tool, workpiece, and chips. When the time of cutting is very short, the losses due to radiation, convection, and conduction are so small that they can be disregarded in most metal-cutting tests in which the calorimetric principle is applied. A comparison of the horsepower values in drilling, as computed from torque and thrust with those computed from the heat generated during cutting, showed that the calorimetric method gives results comparable to those of a well-calibrated dynamometer.

When the quantity of heat in the chips only is measured with a calorimeter (2), the average temperature increase of the chip resulting from a cutting operation can be computed by the thermal-balance method:

(ΔT_c) (chip weight) (specific heat) = (ΔT) (water equivalent of calorimeter, chips, and water)

where ΔT_c = average temperature rise of chips, deg F; and
ΔT = temperature rise in calorimeter, deg F.

The foregoing formula does not take into account the change of specific heat with increasing temperatures. With the specific-heat values of gamma iron, a corrected maximum average chip-temperature value was computed for cutting tests in which the test-bar material was S.A.E. 1055.

Boston and Kraus (3) evaluated cutting temperatures when machining an annealed low-carbon steel in a lathe at cutting speeds between 20 and 320 fpm. A constant depth of cut of 0.150 in. and a constant feed of 0.030 in. were used. The cutting temperatures were measured with a thermocouple arrangement in which one element was the tool and the other the workpiece. These were calibrated in a furnace and the temperatures evaluated in millivolts. The temperatures obtained during cutting operations at different speeds are plotted in their paper and indicate an increase in temperature from 650 to 900 F between 56 and 115 fpm cutting speed.[5] For the cutting speeds between 115 and 320 fpm, the cutting temperatures are reported as varying between 900 and 1000 F, the maximum temperature of 1000 F being obtained at a cutting speed of 210 fpm.

Plotted on the same co-ordinates are chip temperatures determined from temper colors. Very little variation could be detected for the cutting speeds between 100 and 320 fpm, and the authors state in their conclusions: "The temperature of the chip as determined by temper colors was changed less than 5 per cent in the range of cutting speed from 90 to 320 fpm."

This finding is supported by the measurements of chip temperatures with the calorimeter. The temperatures were determined as almost constant for the higher cutting speeds. This is not the case at the lower cutting speeds. Even though the work to remove the chip is the same, at a low cutting speed the workpiece and tool will conduct a higher percentage of the heat generated in the chip because of the slow separation of the chip from the workpiece.

Even though work, which is transformed into heat, must be done in metal cutting, it is possible to remove metal at extremely low speeds with a relatively low temperature increase in the chip. This is because the chip is separated slowly, and the heat in the chip is given a chance to flow into the tool and workpiece. It is recognized that at the low cutting speeds less heat per unit time is generated, although a larger proportion of this smaller amount of heat generated at low speeds goes by conduction into the tool and workpiece. At higher speeds the work done is nearly proportional to the increased cutting speed, and most of the heat developed is carried away with the chip because of the short time the chip is in contact with the workpiece and tool. Assuming that the energy or work required to remove a given amount of metal is the same regardless of the time involved in removing it, it follows that for a longer period of time, that is, at low cutting speeds, the heat per unit time is less. At higher cutting speeds the time to remove the chip is reduced, and the amount of heat developed at any one instant is higher. It is therefore held that the temperature of the tool is much higher at higher speeds than at low speeds because the work done per unit time is much greater. For this reason a tool will generally remove a greater amount of metal at low cutting speeds before failure than at high cutting speeds.

The average chip temperature measured at higher cutting speeds is more uniform because there is less chance for the heat to travel into the tool and workpiece. On the other hand, as soon as the temperature at the cutting edge is equal to that in the chip, there will be no heat flow from the chip into the tool. The higher amount of work which is done per unit time at higher cutting speeds and the resulting greater amount of heat is also carried by a correspondingly larger weight of chips.

When the cutting speed is increased, the tool will have to do a proportionately greater amount of work. This results in a temperature increase in the tool material. The heat will not be uniform in the tool, but most intense near the point at which the cutting takes place. The zone which is near the cutting edge

[1] Research Engineer in Charge of Metal Cutting Research, Kearney & Trecker Corporation, Milwaukee, Wis. Mem. A.S.M.E.

[2] Professor of Metal Processing, Chairman of Department, University of Michigan, Ann Arbor, Mich. Mem. A.S.M.E.

[3] Associate Professor, Metal Processing, University of Michigan, Ann Arbor, Mich. Mem. A.S.M.E.

[4] Numbers in parentheses refer to the Bibliography at the end of the paper.

Contributed by the A.S.M.E. Research Committees on Cutting Fluids, and on Metal Cutting Data and Bibliography and presented at the meeting of the Chicago Section, Chicago, Ill., June 16–19, 1945, of The American Society of Mechanical Engineers.

Note: Statements and opinions advanced in papers are to be understood as individual expressions of their authors and not those of the Society.

[5] Bibliography (3), Fig. 12.

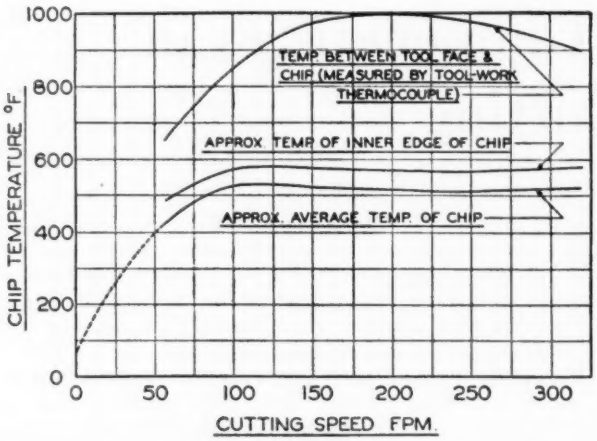


FIG. 1 CURVES OF CHIP TEMPERATURE VS. CUTTING SPEED

(From diagram by Boston and Kraus, reference 3, Fig. 12. The upper temperature line was determined by the tool-work thermocouple while the lower ones were estimated from the temper colors of the chips. Annealed 0.21C steel, depth of cut 0.150 in., feed 0.030 in. per revolution. The dotted line indicates average temperature values at the low speeds.)

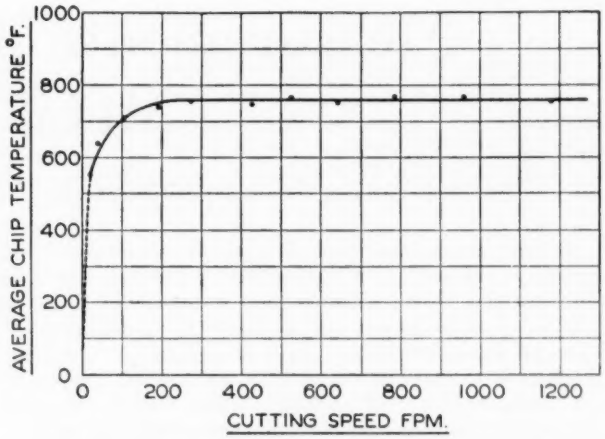


FIG. 2 AVERAGE CHIP TEMPERATURE IN RELATION TO CUTTING SPEED

(These chip temperatures were measured with a calorimeter when machining 1-in-diam test bars of S.A.E. 1055, normalized, with a face mill which had two tungsten-carbide tips of 6-deg negative radial rake. Depth of cut 0.125 in., feed per tooth 0.008 in. The dotted line indicates estimated temperature values at lower cutting speeds.)

will reach the highest temperature and will break down first.

When using the tool-work thermocouple, Boston and Gilbert (4) came to the conclusion that the temperatures measured may be affected by changed electrical properties of the metal in the test log which is compressed and deformed by the tool point. However, this change of electrical properties is brought about not only by the changes in the test log but also by those in the tool. Because the thermocouple was calibrated with the tool and workpiece at the same temperature, the calibration was not made under the condition which generally exists in a metal-cutting operation. During cutting, tool and workpiece temperatures will vary, and at the higher cutting speeds the temperature of the tool will be higher than that of the chip. This is a condition which can hardly be obtained during the calibration of the tool-work thermocouple, and its readings in an actual test will not reveal true cutting temperatures.

MEASUREMENTS OF CHIP TEMPERATURES

From the investigation carried out on the calorimetric principle, it was found that the cutting force for a particular radial rake angle and chip cross section has substantially the same value at any cutting speed (5). In the foregoing tests the cutting speed was varied between 100 and 800 fpm.

At a cutting speed of 300 fpm, the tool forces were the same as those at 600 fpm. Since the maximum volume of metal removed with any test cutter was 0.6 cu in., the cutters could be considered sharp. Therefore, any error introduced by a change in the cutting edge could be disregarded entirely. However, when cutting at 600 fpm, twice as much metal is removed per unit time as at 300 fpm and, consequently, the power required for cutting is doubled. In computing the chip temperature with the formula given, the same value was obtained for both cutting speeds. Although twice as much work was done per unit time when cutting at a speed of 600 fpm as compared with 300 fpm, the temperature of the chips remained the same because the work was done in removing twice the amount of metal. This means there is twice as much chip material to carry away twice as much heat. (The amount of heat per unit weight of chips remains constant.)

Most of the work expended in a metal-cutting operation is carried away as heat in the chips. The remainder of the heat is absorbed by the tool and workpiece.

The heat in the tool is of greatest importance because it is the

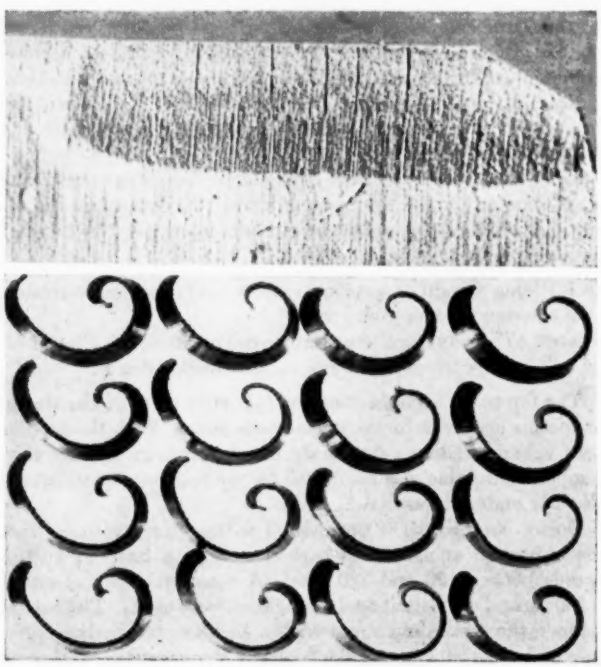


FIG. 3 CEMENTED CARBIDE CUTTING TOOL AFTER MACHINING 10.8 CU IN. OF STEEL AT 580 FPM CUTTING SPEED, DEPTH OF CUT 0.150 IN., FEED 0.010 IN. PER TOOTH

(Two passes were taken over the workpiece and the chips are arranged in columns in the order in which they were removed. Chip formation is uniform throughout the cut. Abrasive action of chips on blade face has formed a shallow crater 0.006 in. deep.)

accumulation and concentration of intense heat at the cutting edge of the tool which hastens failure. Comparing tool life with cutting speed, as brought out in numerous investigations (6), it is evident that the amount of metal removed before tool failure will generally be inversely proportional to the cutting speed when the chip cross section is kept constant. This happens despite the fact that the chip temperature will remain substantially the same. Assuming an ideal case in which the tool does not wear and thus change the cutting forces, the same volume of

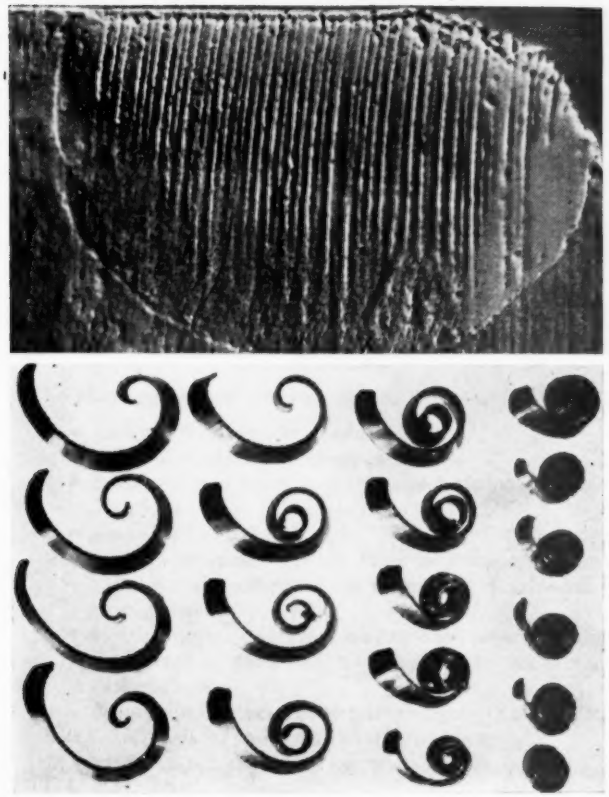


FIG. 4 CEMENTED CARBIDE CUTTING TOOL AFTER MACHINING 10.8 CU IN. OF STEEL UNDER CONDITIONS IDENTICAL WITH THOSE IN FIG. 3 EXCEPT THAT THE CUTTING SPEED WAS 2650 FPM

(Note that at the start the chip formation is similar to Fig. 3 but, due to the rapid increase in heat at the cutting edge, wear of the tip has made a crater 0.050 in. deep through which the chip formation is affected.)

tool metal has to dissipate twice the amount of heat per unit time when the cutting speed is doubled. For this reason, a tool will break down faster at higher cutting speeds, and remove a smaller volume of metal than at a lower cutting speed. There is only a small zone including the cutting edge of the tool which will have a high heat increase with an increase in cutting speed. It is in this zone also that most of the friction between the chip and the tool occurs (7).

The temperature of the workpiece is affected mainly by its size, its heat conductivity, and specific heat. Other factors which also influence the workpiece temperature include cutting speed, cross section of chip, tool design, and wear at the cutting edge. All these must be taken into consideration.

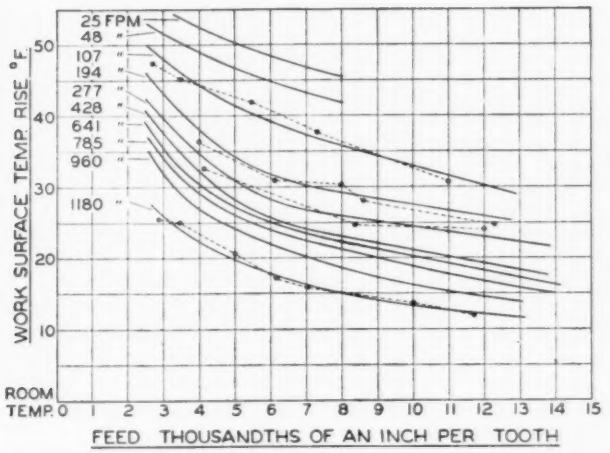


FIG. 5 SURFACE TEMPERATURE RISE OF WORKPIECE

(This graph is based on the evaluation of 500 readings taken with an Alnor low-range thermocouple when machining workpieces of S.A.E. 1055 of identical properties and dimensions at speeds and feeds as indicated and a constant depth of cut of 0.125 in. The cutter was the same as the one used in tests plotted in Fig. 2.)

However, if all conditions except cutting speed are kept constant, the following can be stated with regard to the chips, tool, and workpiece.

1 The temperature of chips of uniform cross section remains approximately the same in the high range of cutting speeds.

2 The temperature at the cutting edge of a tool increases with the cutting speed.

3 The temperature of the workpiece is lower at the higher cutting speeds.

BIBLIOGRAPHY

1 "A Thermal-Balance Method and Mechanical Investigation for Evaluating Machinability," by A. O. Schmidt, W. W. Gilbert, and O. W. Boston, Trans. A.S.M.E., vol. 67, 1945, pp. 225–232.

2 "Determining Tool Forces in High-Speed Milling by Thermo-analysis," by A. O. Schmidt, *Mechanical Engineering*, vol. 66, 1944, pp. 439–442; *Mechanical World*, Sept. 15, 1944, pp. 301–303.

3 "A Study of the Turning of Steel Employing a New-Type Three-Component Dynamometer," by O. W. Boston and C. E. Kraus, Trans. A.S.M.E., vol. 58, 1936, pp. 47–53.

4 "Cutting Temperatures Developed by Single-Point Turning Tools," O. W. Boston and W. W. Gilbert, Trans. American Society for Metals, vol. 23, 1935, pp. 703–726.

5 "An Investigation of Radial Rake Angles in Face Milling," by J. B. Armitage and A. O. Schmidt, Trans. A.S.M.E., vol. 66, 1944, pp. 633–643; *Western Metals*, July and August, 1945.

6 "Influence of Applying Cutting Fluids at Different Temperatures When Turning Steel," by O. W. Boston, W. W. Gilbert, and R. E. McKee, Trans. A.S.M.E. vol. 67, 1945, pp. 217–224.

7 "Radial Rake Angles in Face Milling," by J. B. Armitage and A. O. Schmidt, *Mechanical Engineering*, vol. 67, 1945, pp. 453–456.

(Owing to travel emergency conditions existing when this paper was presented, discussion will be accepted until February 10, 1946)

Charts for Fuselage Torsion Versus Control-Surface Flutter

By W. T. THOMSON,[1] SAN DIEGO, CALIF.

Charts for evaluating the allowable unbalance in the control-surface product of inertia for tail flutter involving fuselage torsion are presented. The basic theory, assumptions, and limitations are fully discussed.

Nomenclature

The following nomenclature is used in the paper:

θ = torsional displacement of tail, radians
θ_w = torsional displacement of wings, radians
β = control-surface rotation with respect to fixed surface, radians
b = semi-chord of tail surface, in.
c = location of control-surface hinge axis measured from tail-surface mid-chord, as a fraction of tail-surface semi-chord
e = location of control-surface leading edge, measured from tail-surface mid-chord, as a fraction of tail surface semi-chord
x_β = distance from hinge line to center of gravity of the control surface (positive if CG is behind hinge), in.
y = span distance measured from torsional axis, in.
L = control-surface span, in.
J_w = mass moment of inertia of wings with respect to torsional axis, lb-in. sec^2
J_T = mass moment of inertia of tail with respect to torsional axis, lb-in. sec^2
$J_\theta = J_T + \left(\frac{\theta_w}{\theta}\right)^2 J_w$ = effective torsional moment of inertia, lb-in. sec^2
J_β = mass moment of inertia of control surface with respect to hinge line (rudder or two elevators), lb-in. sec^2
m_β = mass of rudder or two elevators, lb-in.$^{-1}$ sec^2
ρ = mass density of air, lb-in.$^{-4}$ sec^2
v = flight velocity, in. sec^{-1}
ω = circular frequency of flutter, radians sec^{-1}
ω_θ = natural torsional frequency of fuselage, radians sec^{-1}
ω_β = natural circular frequency of control-surface system, radians sec^{-1}
g = structural damping coefficient $\left(\frac{1}{\pi}\right.$ times logarithmtic decrement$\left.\right)$

Introduction

Flutter of control surfaces may be avoided by balancing. The complete balancing of control surfaces, however, is costly in weight and often unnecessary in avoiding flutter.

The study of varying the amount of balance by flutter calculations is long and tedious. To avoid such calculations, charts enabling the determination of the allowable static unbalance of the control surfaces have been presented by the Army Air Force (1)[2] for flutter modes involving fuselage bending. The purpose of this paper is to present a similar type of labor-saving device for the flutter modes involving fuselage torsion.

Development of Equations

In the following analysis with two degrees of freedom, Lagrange's equation

$$\frac{d}{dt}\left(\frac{\partial T}{\partial \dot{q}_s}\right) + \frac{\partial U}{\partial q_s} = Q_s \quad \ldots\ldots [1]$$

will be used, where T and U are kinetic and potential energies, respectively, Q_s the generalized force associated with the work done in a virtual displacement δq_s, and q_s the generalized co-ordinate for the particular mode.

The kinetic energy of the airplane in the torsional oscillation then becomes

$$T = \frac{1}{2} J_\theta \dot{\theta}^2 + \frac{1}{2}\int_0^L [(y\dot{\theta} + x_\beta \dot{\beta})^2 - (y\dot{\theta})^2] dm_\beta + \frac{1}{2}\int_0^L \dot{\beta}^2 (dJ_\beta - x_\beta^2 dm_\beta) \quad \ldots\ldots [2]$$

Differentiating with respect to the generalized co-ordinates and time, and assuming harmonic motion, the Lagrangian inertia forces become

$$\left.\begin{aligned} \frac{d}{dt}\left(\frac{\partial T}{\partial \dot{\theta}}\right) &= -\omega^2 (J_\theta \theta + \int x_\beta y dm_\beta \cdot \beta) \\ \frac{d}{dt}\left(\frac{\partial T}{\partial \dot{\beta}}\right) &= -\omega^2 (\int x_\beta y dm_\beta \cdot \theta + J_\beta \cdot \beta) \end{aligned}\right\} \quad \ldots\ldots [3]$$

The potential energy represents the strain energy stored in the structure. Assuming Hooke's law, it may be written as

$$U = \frac{1}{2} K_{\theta\theta}\theta^2 + \frac{1}{2} K_{\beta\beta}\beta^2 \quad \ldots\ldots [4]$$

The Lagrangian elastic forces then become

$$\left.\begin{aligned} \frac{\partial U}{\partial \theta} &= K_{\theta\theta}\theta = \omega_\theta^2 J_\theta \theta \\ \frac{\partial U}{\partial \beta} &= K_{\beta\beta}\beta = \omega^2_\beta \int x_\beta y dm_\beta \cdot \beta \end{aligned}\right\} \quad \ldots\ldots [5]$$

where the K coefficients have been replaced by the inertia coefficients by considering uncoupled motion in each co-ordinate.

For terms which remove energy from the system, structural damping which is nearly independent of frequency and proportional to the amplitude must be considered. This can be accomplished by multiplying the elastic coefficients K by $(1 + ig)$.

---

[1] Design Specialist in Charge of Vibration and Flutter Analysis, Ryan Aeronautical Company.

Presented at a meeting of the Aviation Division, Los Angeles, Calif., June 11–14, 1945, of The American Society of Mechanical Engineers.

Note: Statements and opinions advanced in papers are to be understood as individual expressions of their authors and not those of the Society

[2] Numbers in parentheses refer to the Bibliography at the end of the paper.

The aerodynamic forces and moments supplying the energy for flutter are defined by Theodorsen (2) and Kussner and Schwarz (3), for the two-dimensional flow. These equations have been organized in a form convenient for flutter analysis by B. Smilg (4).

The expressions applicable to this analysis are ones for the lift per unit span and the torque about the control-surface hinge per unit span, and may be written as follows

$$\left.\begin{aligned} L' &= \pi\rho b^3\omega^2\left(A_{\theta\theta}\frac{y}{b}\theta + A_{\theta\beta}\cdot\beta\right) \\ T' &= \pi\rho b^4\omega^2\left(A_{\beta\theta}\frac{y}{b}\theta + A_{\beta\beta}\cdot\beta\right) \end{aligned}\right\} \quad \ldots\ldots\ldots [6]$$

where the aerodynamic coefficients A are complex functions of $\frac{v}{b\omega}$ and have been evaluated in terms of the following coefficients appearing in reference (4)

$$\left.\begin{aligned} A_{\theta\theta} &= L_h \\ A_{\theta\beta} &= L_\beta - L_z(c-e) \\ A_{\beta\theta} &= T_h - P_h(c-e) \\ A_{\beta\beta} &= T_\beta - P_\beta(c-e) - T_z(c-e) + P_z(c-e)^2 \end{aligned}\right\} \quad \ldots [7]$$

The generalized forces Q are determined from the work associated with the virtual displacements as follows

$$\left.\begin{aligned} \delta W &= \int_0^L L'\delta(y\theta)dy + \int_0^L T'\delta(\beta)dy \\ Q_\theta &= \frac{\delta W}{\delta\theta} = \int_0^L L'ydy = \pi\rho b^2\omega^2\left(A_{\theta\theta}\frac{L^2}{3}\theta + A_{\theta\beta}\frac{bL^2}{2}\beta\right) \\ Q_\beta &= \frac{\delta W}{\delta\beta} = \int_0^L T'dy = \pi\rho b^2\omega^2\left(A_{\beta\theta}\frac{bL^2}{2}\theta + A_{\beta\beta}b^2L\beta\right) \end{aligned}\right\} \quad \ldots [8]$$

The Stability Equation

Substituting the expressions of the previous section into Equation [1], the following two equations are obtained

$$\left.\begin{aligned} E\theta + F\beta &= 0 \\ G\theta + H\beta &= 0 \end{aligned}\right\} \quad \ldots\ldots\ldots\ldots [9]$$

where

$$E = -J_\theta[\omega^2 - \omega_\theta^2(1 + ig_\theta)] - \pi\rho b^2\omega^2 A_{\theta\theta}\frac{L^2}{3}$$

$$F = -\omega^2\int_0^L x_\beta ydm_\beta - \pi\rho b^2\omega^2 A_{\theta\beta}\frac{bL^2}{2}$$

$$G = -\omega^2\int_0^L x_\beta ydm_\beta - \pi\rho b^2\omega^2 A_{\beta\theta}\frac{bL^2}{2}$$

$$H = -J_\beta[\omega^2 - \omega_\beta^2(1 + ig_\beta)] - \pi\rho b^2\omega^2 A_{\beta\beta}b^2L$$

Dividing each term by $-\pi\rho b^2\omega^2L^2$ and equating the determinant to zero, the stability equation becomes

$$\left\{\frac{\left(\frac{J_\theta}{L}\right)}{(\pi\rho b^2)L^2}\left[1 - \left(\frac{\omega_\theta}{\omega}\right)^2(1 + ig_\theta)\right] + \frac{1}{3}A_{\theta\theta}\right\}\left\{\frac{\left(\frac{J_\beta}{L}\right)}{(\pi\rho b^2)b^2}\left[1 - \left(\frac{\omega_\beta}{\omega}\right)^2(1 + ig_\beta)\right] + A_{\beta\beta}\right\} - \left\{\frac{\int_0^L \frac{x_\beta ydm_\beta}{L}}{(\pi\rho b^2)bL} + \frac{1}{2}A_{\beta\theta}\right\}$$

$$\left\{\frac{\int_0^L \frac{x_\beta ydm_\beta}{L}}{(\pi\rho b^2)bL} + \frac{1}{2}A_{\beta\theta}\right\} = 0 \ldots\ldots [10]$$

Equation [10] is a quadratic in ω^2, resulting in two roots corresponding to the two flutter modes. The equation is nondimensional, the three parameters being as follows

$$A = \frac{\left(\frac{J_\theta}{L}\right)}{(\pi\rho b^2)L^2}$$

which involves the moment of inertia of the airplane about the torsional axis.

$$B = \frac{\left(\frac{J_\theta}{L}\right)}{(\pi\rho b^2)b^2}$$

which involves the moment of inertia of the control surface about its hinge line.

$$P = \frac{\int_0^L \frac{x_\beta ydm_\beta}{L}}{(\pi\rho b^2)bL}$$

which involves the product of inertia of the control surface about the hinge and torsional axis.

Considerable simplification results from assuming the control-surface natural frequency to be zero, under which condition the solution of the foregoing equation results in a real and an imaginary part as follows

$$\left.\begin{aligned} \text{Real} &= \frac{\left(\frac{J_\theta}{L}\right)}{(\pi\rho b^2)L^2}\left[1 - \left(\frac{\omega_\theta}{\omega}\right)^2\right] \\ \text{Imaginary} &= -\frac{\left(\frac{J_\theta}{L}\right)}{(\pi\rho b^2)L^2}\left(\frac{\omega_\theta}{\omega}\right)^2 g \end{aligned}\right\} \quad \ldots\ldots\ldots [11]$$

Since $\left(\frac{\omega_\theta}{\omega}\right)$ is near unity in the critical-flutter ranges, the value of the structural damping g, necessary to sustain steady-state oscillation, may be determined from the imaginary part.

Charts for Allowable Product of Inertia

The numerical evaluation of Equation [10] was carried out under the following assumptions:

1 The natural frequency of the control surface at zero air speed equals zero ($\omega_\beta = 0$).

2 The leading edge of the control surface is at mid-chord ($e = 0$). The effect of varying the leading-edge position is indicated by one set of calculations for 40 per cent control surface ($e = 0.2$).

3 The effective torsional axis of the airplane is along the center line of the fuselage.

4 The control-surface aerodynamic balance equals 20 per cent or 33 per cent (chosen arbitrarily).

5 Aerodynamic vectors for infinite aspect ratio are applicable.

The real and imaginary parts of Equation [10], as indicated by Equations [11], are tabulated as shown herewith. The charts, Figs. 1 to 9, represent the imaginary part of the solution as function of $\frac{v}{b\omega}$. Since the ordinate is proportional to the structural damping, while the abscissa is proportional to the true

FUSELAGE TORSION VERSUS CONTROL-SURFACE FLUTTER ($\omega\beta = 0$) COMPUTATION FORM

$$\frac{1}{3}\begin{bmatrix} (A_{\alpha\alpha})_R \\ (A_{\alpha\alpha})_I \end{bmatrix} \boxtimes \begin{bmatrix} B + (A_{\beta\beta})_R \\ (A_{\beta\beta})_I \end{bmatrix} = \begin{bmatrix} a \end{bmatrix}$$

$$\begin{bmatrix} P \end{bmatrix}^2 = \begin{bmatrix} b \end{bmatrix}$$

$$\frac{1}{2}\begin{bmatrix} P \end{bmatrix} \cdot \begin{bmatrix} (A_{\alpha\beta})_R + (A_{\beta\alpha})_R \\ (A_{\alpha\beta})_I + (A_{\beta\alpha})_I \end{bmatrix} = \begin{bmatrix} c \end{bmatrix}$$

$$\frac{1}{4}\begin{bmatrix} (A_{\alpha\beta})_R \\ (A_{\alpha\beta})_I \end{bmatrix} \boxtimes \begin{bmatrix} (A_{\beta\alpha})_R \\ (A_{\beta\alpha})_I \end{bmatrix} = \begin{bmatrix} d \end{bmatrix}$$

$$\begin{bmatrix} B + (A_{\beta\beta})_R \end{bmatrix}^2 + \begin{bmatrix} (A_{\beta\beta})_I \end{bmatrix}^2 = \begin{bmatrix} e \end{bmatrix}$$

$$\begin{bmatrix} B + (A_{\beta\beta})_R \\ -(A_{\beta\beta})_I \end{bmatrix} \boxtimes \begin{bmatrix} a - b - c - d \end{bmatrix} = \begin{bmatrix} f \end{bmatrix}$$

$$A\left[1-\left(\frac{\omega_\beta}{\omega}\right)^2\right] = \frac{(f)_R}{e} = _____$$

$$A\left(\frac{\omega_\beta}{\omega}\right)^2 g = \frac{(f)_I}{e} = _____$$

$\frac{V}{b\omega}$ = _____
c = _____
e = _____
B = _____
P = _____

B = .30 C = .20 e = 0

P	.10		.20		.50		1.0	
$\frac{V}{b\omega}$	R	I	R	I	R	I	R	I
.83	.31	-.12	.24	-.032	-.29	.07		
2.00	.47	.014	.22	.65	.51	1.74	.06	2.7
3.33	-.13	.25	-.67	1.20	-2.2	3.80	-4.4	7.5
4.17	-.52	-.04	-1.40	.78	-3.8	3.13	-7.4	6.7
6.25	-.91	-.90	-2.0	-.38	-5.1	1.18	-10.2	3.7

B = .40 C = .20 e = 0

P	.10		.20		.50		1.0	
$\frac{V}{b\omega}$	R	I	R	I	R	I	R	I
.83								
2.00	.59	-.18	.73	.25	.98	1.28	.79	2.2
3.33	.19	.37	-.22	1.50	-1.3	4.5	-3.0	8.84
4.17	-.37	.16	-1.20	1.10	-3.6	3.9	-7.3	8.20
6.25	-.89	-.79	-2.00	-.22	-5.3	1.5	-10.5	4.2

B = .50 C = .20 e = 0

P	.10		.20		.50		1.0	
$\frac{V}{b\omega}$	R	I	R	I	R	I	R	I
.83								
2.00	.61	-.35	.79	-.01	1.16	.82	1.1	1.6
3.33	.57	.37	.38	1.6	-.16	4.9	-.95	9.7
4.17	-.14	.36	-.94	1.5	-3.2	4.8	-6.7	9.9
6.25	-.86	-.66	-2.01	-.04	-5.4	1.8	-10.9	4.8

B = .60 e = .20 e = 0

P	.10		.20		.50		1.0	
$\frac{V}{b\omega}$	R	I	R	I	R	I	R	I
.83					.02	-.04	-1.05	.003
2.00	.59	-.47	.78	-.20	1.18	.46	1.25	1.1
3.33	.94	.20	1.0	1.4	1.17	4.8	1.37	9.7
4.17	.16	.54	-.54	1.9	-2.6	5.7	-5.6	11.6
6.25	-.82	-.52	-2.02	.16	-5.5	2.2	-11.2	5.4

B = .50 e = .33 e = 0

P	.10		.20		.50		1.0	
$\frac{V}{b\omega}$	R	I	R	I	R	I	R	I
.83					.05	-.03	-1.15	.08
2.00					1.43	-.04	1.76	.43
3.33			2.06	-.64	4.61	.62	8.25	2.42
4.17			3.16	-.56	7.33	1.71	13.70	5.12
6.25	3.94	-1.68	6.94	.67	15.81	7.60	30.14	18.71
10.00	10.32	.22	15.17	8.58				

B = .30 C = .33 e = 0

P	.10		.20		.30		1.0	
$\frac{V}{b\omega}$	R	I	R	I	R	I	R	I
.83					-.13	.09	-2.07	.11
2.00			1.27	-.13	1.86	.67	2.24	1.46
3.33			2.57	-.33	5.66	2.88	10.08	6.49
4.17	1.699	-.53	3.75	.97	8.44	5.31	15.62	11.87
6.25	4.262	.06	7.03	3.85	5.01	12.51		
10.0	8.962	3.75	11.46	13.84				

B = .60 e = .33 e = 0

P	.10		.20		.50		1.0	
$\frac{V}{b\omega}$	R	I	R	I	R	I	R	I
.83					.09	-.07	-.92	.05
2.00					1.26	-.21	1.57	.18
3.33					4.09	.06	7.34	1.38
4.17			2.84	-.97	6.62	.72	12.41	3.25
6.25			6.49	-.40	15.01	5.01	28.79	12.66
10.00			15.75	5.82	32.14	27.45		

B = .40 C = .33 e = 0

P	.10		.20		.50		1.0	
$\frac{V}{b\omega}$	R	I	R	I	R	I	R	I
.83					.012	.025	-1.51	.11
2.00					1.63	.22	1.99	.82
3.33			2.33	-.26	5.17	1.50	9.84	4.40
4.17	1.96	-1.03	3.52	.055	8.02	3.17	14.93	7.87
6.25	4.20	-.92	7.20	2.09	16.06	10.96	30.40	25.21
10.00	11.33	1.62	15.18	10.98			45.61	84.81

B = .60 C = .36 e = .20

P	.10		.20		.50		1.0	
$\frac{V}{b\omega}$	R	I	R	I	R	I	R	I
2.00	.56	-.67	.82	-.52	1.39	-.15		
3.33	1.80	-.57	2.87	.49	5.98	3.54	10.32	7.72
4.17	1.91	1.54	2.28	4.57	3.36	13.25	5.12	26.37
5.00	-.54	1.80	-2.28	4.52	-7.31	12.29	-15.10	24.82
6.25	-1.66	.21	-3.79	1.57	-10.08	5.59	-20.15	12.10

	e = .20		e = 0	
$\frac{v}{b\omega}$	$A_{\beta\beta}$	$A_{\beta\theta}$	$A_{\theta\beta}$	$A_{\theta\theta}$
.83	.8538 -.8833 i	-.5493 -.6744 i	.1075 -.02824 i	-.000864 -.1402 i
2.0	.3972 -2.3916 i	-4.0459 -.9812 i	.09293 -.07646 i	-.1699 -.3161 i
3.33	-.1950 -4.433 i	-12.4643 -.2001 i	.0740 -.1417 i	-.5620 -.4809 i
4.17	-.5520 -5.8242 i	-20.3737 .8505 i	.06259 -.18621 i	-.9230 -.56592 i
6.25	-1.3450 -9.5350 i	-49.6014 5.0190 i	.03724 -.3049 i	-2.2330 -.7295 i
10.0	-2.4460 -16.6400 i	-137.4490 16.4656 i	.00203 -.5320 i	-6.0960 -.8970 i

	e = .33		e = 0	
$\frac{v}{b\omega}$	$A_{\beta\beta}$	$A_{\beta\theta}$	$A_{\theta\beta}$	$A_{\theta\theta}$
.83	.8538 -.8833 i	-.5988 -.5805 i	.045988 -.007378 i	.01601 -.0724 i
2.0	.3972 -2.3916 i	-4.0467 -.7268 i	.04217 -.01998 i	.01709 -.1682 i
3.33	-.1950 -4.433 i	-12.4022 .2715 i	.0372 -.03703 i	.0116 -.2679
4.17	-.5520 -5.8242 i	-20.2736 1.4701 i	.0342 -.0487 i	.00238 -.3255 i
6.25	-1.3450 -9.5350 i	-49.4170 6.0244 i	.0276 -.0796 i	-.0448 -.4564 i
10.0	-2.4460 -16.6400 i	-137.1474 18.2358 i	.0184 -.1390 i	-.2266 -.6584 i

	e = .36	e = .20		
$\frac{v}{b\omega}$	$A_{\beta\beta}$	$A_{\beta\theta}$	$A_{\theta\beta}$	$A_{\theta\theta}$
2.0	.3972 -2.3916 i	-3.6876 -.5434 i	.05426 -.04325 i	-.1157 -.1606 i
3.33	-.1950 -4.433 i	-11.334 .4407 i	.04352 -.08018 i	-.3628 -.2499 i
4.17	-.5520 -5.824 i	-18.534 1.578 i	.03706 -.1053 i	-.5887 -.2938 i
5.00	-.8860 -7.276 i	-27.689 3.0608 i	.03102 -.1316 i	-.8712 -.3315 i
6.25	-1.3450 -9.5350 i	-45.1814 5.8428 i	.02272 -.1724 i	-1.4027 -.3779 i

air speed, the charts represent a series of flutter-stability curves. The real part of the solution presented in the tabulation may be used to determine the flutter frequency if this information is desired. All computations were carried out in the tabular form shown.

Effect of Finite-Control-Surface Frequency

Examination of Equation [10] indicates that the effect of finite-control-surface frequency may be readily determined from the charts presented by assuming $g = 0$, and using

$$B' = B\left\{1 - \left(\frac{\omega\beta}{\omega}\right)^2\right\} \cong B\left\{1 - \left(\frac{\omega\beta}{\omega\theta}\right)^2\right\}$$

Due to neglecting the friction in the control-surface system, the results will be on the conservative side.

Illustrative Example. Determine the allowable rudder product of inertia from the following data:

Average rudder chord = 22 in.

Average fin chord = 22 in. (i.e., $e = 0$)

Aerodynamic balance $\dfrac{c - e}{1 - e} = 0.20$

Moment of inertia of rudder $J_\beta = 3.0$ lb-in. sec^2

Rudder span = fin span = $L = 80$ in.

Moment of inertia of tail about torsional axis = 1500 lb-in. sec^2

Moment of inertia of wings about torsional axis = 50,000 lb-in. sec^2

Ratio of torsional deflections $\left(\dfrac{\theta_w}{\theta}\right) = 0.20$

Torsional natural frequency of airplane = 1000 cycles per min

Maximum flight speed of airplane = 500 mph

The calculation of the nondimensional parameters are as follows:

$\pi\rho b^2 = \pi(8.45 \times 10^{-8})22^2 = 0.0001285$ (10,000 ft altitude assumed)

$J_\theta = 1500 + (0.20)^2\,50{,}000 = 3500$ lb-in. sec^2

$Ag = \dfrac{3500 \times 0.03}{0.0001285 \times 80^3} = 53.2 \times .03 = 1.60$ (3 per cent damping assumed)

$B = \dfrac{3.0}{0.0001285 \times 80 \times 22^2} = 0.603$

$$\frac{v}{b\omega} = \frac{500 \times \dfrac{88}{60} \times 12}{22 \times \dfrac{1000}{60} \times 2\pi} = 3.82$$

From the stability curve for $B = 0.6$ find $P = 0.18$ corresponding to $Ag = 1.60$. The allowable product of inertia is then

$$\int x_\beta y dm_\beta = 0.18 \times 0.0001285 \times 22 \times 80^2 = 32.6 \text{ lb-in. sec}^2$$

From the real part of the solution $R \cong 0.2$ corresponds to the foregoing values. The frequency ratio then becomes

$$\left(\frac{\omega\theta}{\omega}\right) = \sqrt{1 - \frac{R}{A}} = \sqrt{1 - \frac{0.2}{53.2}} = 0.998$$

and the error in neglecting this correction is less than 1 per cent.

Summary and Conclusions

Control-surface flutter involving fuselage torsion has been investigated in terms of nondimensional parameters and presented in chart form. The results are applicable to conventional tail surfaces with 20 or 33 per cent aerodynamic balance. The effect of fin or stabilizer bending was not included in the investigation since this mode is generally covered in the three-dimensional analysis involving fuselage bending. The real part of the solution was included in the tabulation as an indication of the frequency ratio $\left(\dfrac{\omega\theta}{\omega}\right)$ which was assumed to be unity.

Several conclusions may be drawn by examination of the charts, as follows:

1 The stability of the control surface for this form of flutter is mainly a function of its product of inertia and aerodynamic balance.

2 For a given product of inertia, the flutter speed will be higher for a control surface with larger aerodynamic balance.

3 Large aerodynamic balance increases the explosiveness of flutter, as indicated by higher peaks of the stability curves.

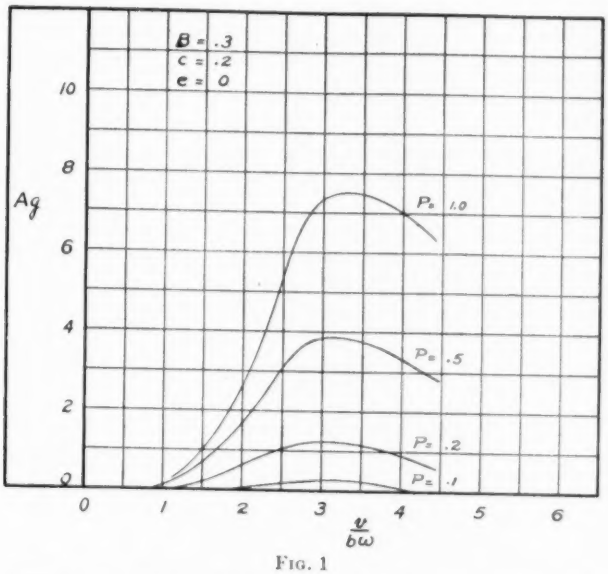


FIG. 1

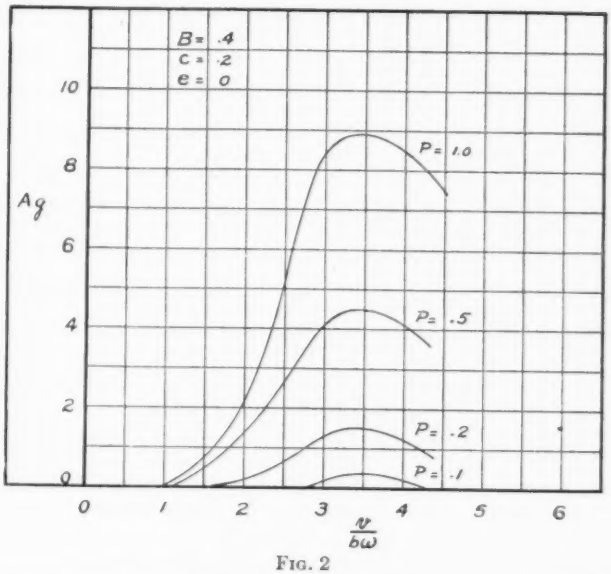


FIG. 2

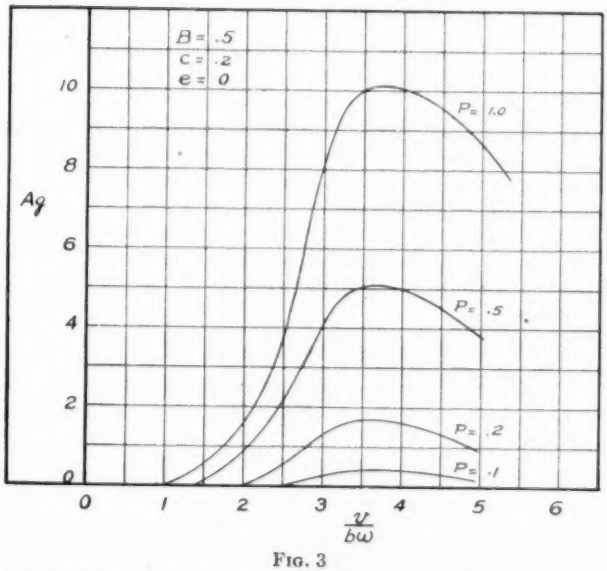


FIG. 3

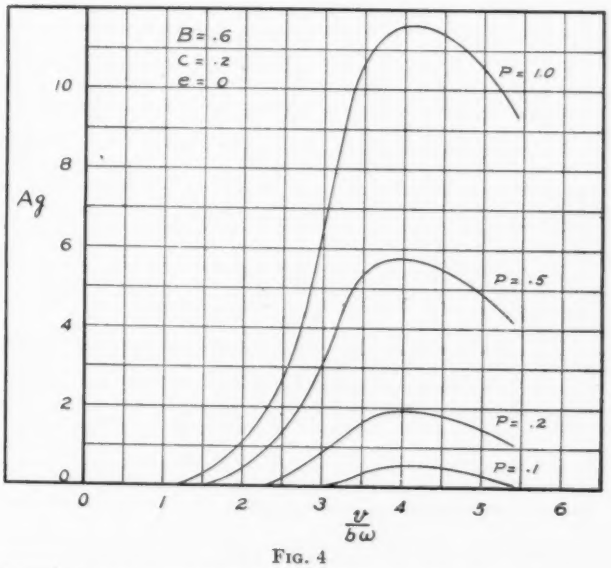


FIG. 4

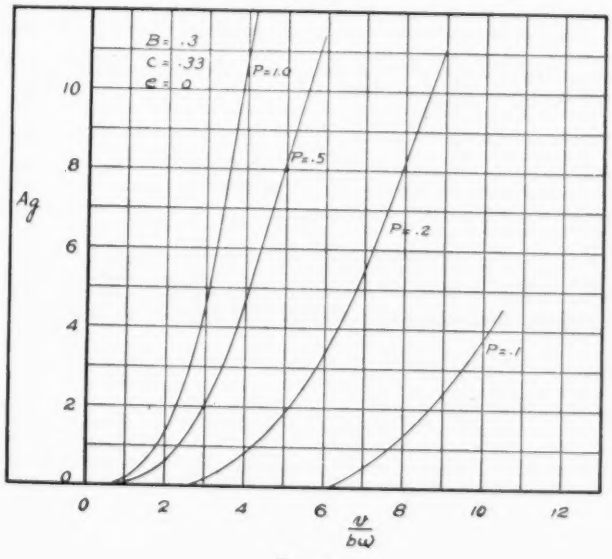


FIG. 5

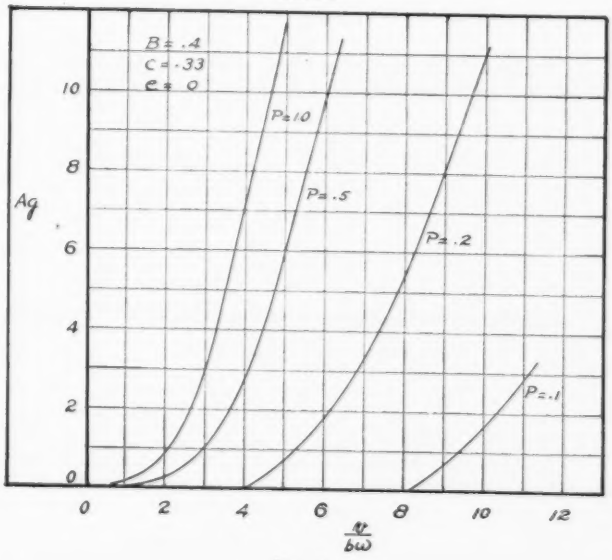


FIG. 6

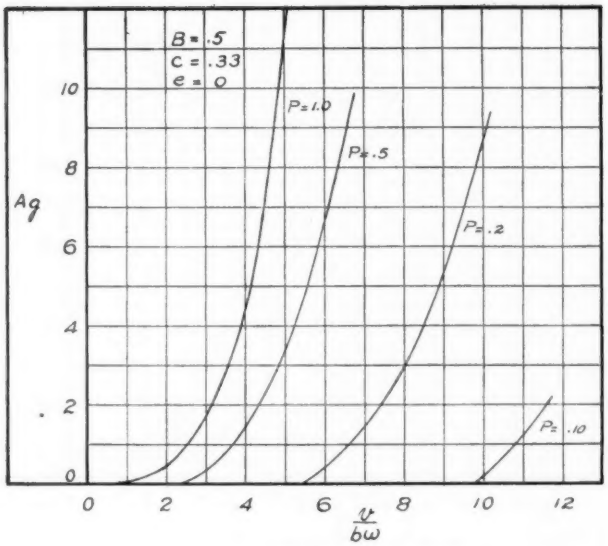


FIG. 7

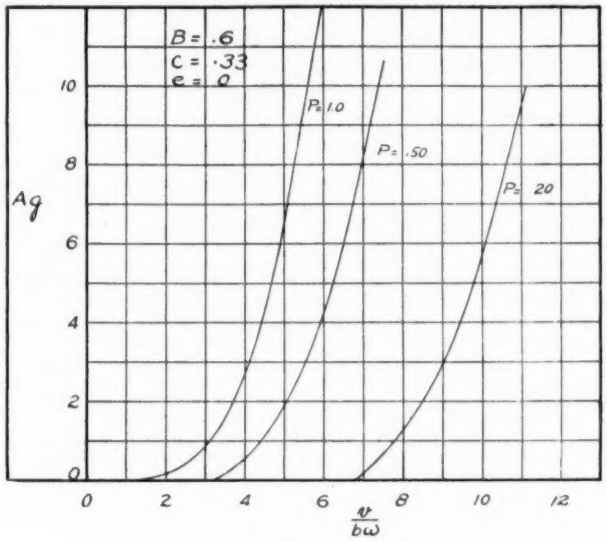


FIG. 8

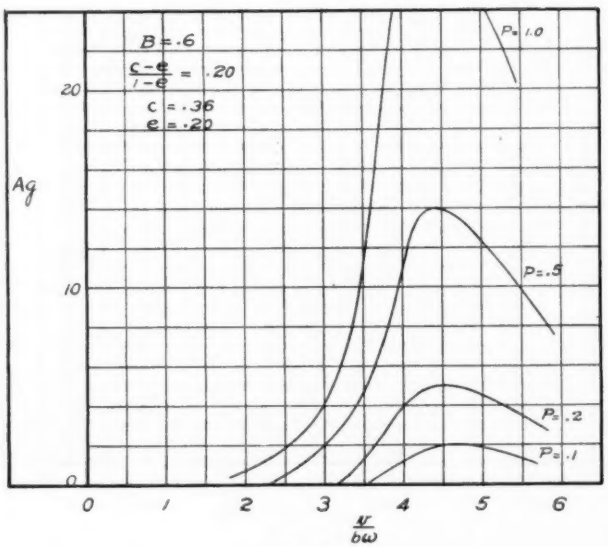


FIG. 9

4 Reducing the control-surface chord for the same aerodynamic balance increases the flutter speed and its explosiveness, as indicated by the shift of the stability peak to higher values of $\frac{v}{b\omega}$ and Ag.

5 The effect of the finite-control-surface frequency is to shift the stability curve to a lower value of B, the main effect of which is to decrease the stability peaks to lower values. The flutter speed is also lowered slightly.

The charts presented are intended to aid in the preliminary determination of the required product of inertia. They also enable a study to be made of the effect of varying the design parameters.

ACKNOWLEDGMENT

The author wishes to acknowledge his appreciation to Miss C. L. Dick who carried out the numerical work for the charts.

BIBLIOGRAPHY

1 "Charts for Fuselage Bending Vs. Control Surface Flutter," by L. S. Tolve, A.A.F. TR. 5107, April, 1944.

2 "General Theory of Aerodynamic Instability and Mechanism of Flutter," by T. Theodorsen, N.A.C.A. TR. 496, 1935.

3 "The Oscillating Wing With Aerodynamically Balanced Elevators," by H. G. Kussner and I. Schwarz, N.A.C.A. TM. 991, 1941.

4 "Application of Three Dimensional Flutter Analysis," by B. Smilg, A.A.F. TR. 4798, 1942.

(Owing to travel emergency conditions existing when this paper was presented, discussion will be accepted until February 10, 1946)

Thermal Accommodation Coefficients[1]

By M. L. WIEDMANN[2] AND P. R. TRUMPLER[3]

This investigation deals with the conduction of heat through a gas at low pressure. The theoretical work of M. Knudsen is extended to cover the case of conduction between two infinite concentric cylindrical surfaces of different properties. Experiments to determine the accommodation coefficients of air on flat black lacquer and nine metal surfaces indicate that the values lie between 0.87 and 0.97.

Nomenclature

The following nomenclature is used in the paper:

- A = surface area, sq ft
- a = radiant emissivity
- E_1 = energy of a gas stream in equilibrium with surface 1
- E_1' = energy of a gas stream after collision at surface 1
- $F = \frac{r_1}{r_2}$
- L = length of cylindrical test section, ft
- M = molecular weight of the gas (O_2 is 32)
- p = gas pressure, mm mercury
- Q_c = net conduction heat transfer, Btu per hr
- Q_R = net radiation heat transfer, Btu per hr
- r = radius, ft
- T = gas temperature, deg F abs
- T_1 = temperature of surface 1, deg F abs
- α = accommodation coefficient
- $\gamma = \frac{c_p}{c_v}$ = ratio of specific heats of the gas
- ρ = length of a path between inner and outer surfaces, ft
- σ = Boltzmann constant = 0.172×10^{-8} Btu per hr per sq ft per (deg F)[4]
- β, δ, θ = angles

Subscript 1 refers to inner surface, subscript 2 to outer surface.

Introduction

In a sense there are only two methods by which heat may be transferred between solids separated by a gas, i.e., radiation and molecular collision. Collisions may take place between the gas molecules themselves or between gas molecules and the surface of the containing vessel. The latter type of collision is the subject of this investigation.

At ordinary pressures the effect of surface collisions is lost in the large number of collisions involving only gas molecules. But if the pressure is reduced far enough there will be only a comparatively small number of gas molecules in the containing vessel, and most of the collisions will be made at the bounding surfaces. These collisions will then exert a controlling influence on the heat transfer.

Kinetic theory predicts that the conductivity of a perfect gas far from a solid surface is independent of the pressure. If certain dimensions of the containing vessel are of the order of magnitude of the mean free path,[4] the heat conduction is a function of the pressure and the surface characteristics. For the special case of gas pressure so low that collisions between gas molecules are infrequent compared with surface collisions, the heat conduction is proportional to the pressure (1, 2, 3).[5] The theoretical treatment to be presented applies to a perfect gas at this low pressure, hereafter called a "rarefied gas," and the experimental work was conducted with air in or near this pressure region.

Air at 32 F and 0.000001 atm pressure has a mean free path of 2.3 in. (4). It is apparent that the results here presented are applicable primarily to problems of heat conduction through a gas at very low pressure or in a very small space.

The characteristic properties of a surface which determine the radiation are the emissivity and the absorptivity. In heat transfer by surface collisions the characteristic property is the accommodation coefficient, which expresses the extent to which a particle stream impinging upon a solid surface comes to thermal equilibrium with the solid.

If a particle stream approaches a surface at energy E_2' and leaves at energy E_1', and if the energy of the stream at thermal equilibrium with the solid would be E_1, then the accommodation coefficient is defined as

$$\alpha = \operatorname*{Limit}_{E_2' \to E_1} \left[\frac{E_2' - E_1'}{E_2' - E_1} \right] \quad \ldots\ldots\ldots\ldots [1]$$

If only kinetic-energy changes are considered and the particle stream has a maxwellian velocity distribution before and after collision, the accommodation coefficient may be expressed in terms of temperatures

$$\alpha = \operatorname*{Limit}_{T_2' \to T_1} \left[\frac{T_2' - T_1'}{T_2' - T_1} \right] \quad \ldots\ldots\ldots\ldots [2]$$

Values of accommodation coefficient reported in the literature range from less than 0.1 to unity.

Results of Tests

The equation for heat conduction between two infinite concentric cylinders separated by a rarefied gas is

$$\frac{Q_c}{L} = 3600\, r_1 \frac{\gamma + 1}{\gamma - 1} \frac{p(T_1 - T_2)}{\sqrt{MT}} \frac{1}{\frac{r_1}{r_2}\left(\frac{1}{\alpha_2} - 1\right) + \frac{1}{\alpha_1}} \quad \ldots [3]$$

where

- $\frac{Q_c}{L}$ = heat transfer by conduction, per unit cylinder length, Btu hr^{-1} ft^{-1}
- $\gamma = \frac{c_p}{c_v}$ = ratio of specific heats of the gas
- p = gas pressure, mm mercury

---

[1] This paper summarizes a dissertation submitted by one of the authors[3] to Yale University in partial fulfillment of requirements for the degree of Doctor of Philosophy.

[2] Associate Professor of Mechanical Engineering, Yale University, New Haven, Conn.

[3] Development Engineer, M. W. Kellogg Company, New York, N. Y. Jun. A.S.M.E.

Contributed by the Heat Transfer Division and presented at the Annual Meeting, New York, N. Y., Nov. 29–Dec. 3, 1943, of The American Society of Mechanical Engineers.

Note: Statements and opinions advanced in papers are to be understood as individual expressions of their authors and not those of the Society.

[4] The mean free path may be defined as the average distance a gas molecule travels between collisions with other gas molecules.

[5] Numbers in parentheses refer to the Bibliography at the end of the paper.

T = gas temperature at place where the pressure is p, deg FA
M = molecular weight of the gas (O_2 is 32)
T_1, T_2 = temperatures of inner and outer cylinders, respectively, deg FA
r = radius, ft
α = accommodation coefficient

Subscripts 1 and 2 refer to inner and outer cylindrical surfaces respectively.

Experiments were made to determine the accommodation coefficients and emissivities of aluminum, cast iron, and bronze. Polished, machined, and etched surfaces of each metal were tested. The values of $\frac{Q_c\sqrt{T}}{T_1 - T_2}$ are plotted against pressure for nine metallic surfaces and a reference surface of flat black lacquer in Figs. 1–3, inclusive. Maximum and minimum values of accommodation coefficients were taken from a plot of $\frac{Q_c\sqrt{T}}{p(T_1 - T_2)}$ as a function of pressure p, Fig. 4, and are tabulated with the emissivities in Table 1.

TABLE 1 SUMMARY OF RESULTS

Surface	Description	Emissivity	Accommodation coefficient — Minimum	Accommodation coefficient — Maximum
X	Flat black lacquer on bronze	0.932	0.881	0.894
A	Bronze, polished	0.103	0.91	0.94
F	Bronze, machined	0.110	0.89	0.93
D	Bronze, etched	0.192	0.93	0.95
B	Cast iron, polished	0.184	0.87	0.93
E	Cast iron, machined	0.391	0.87	0.88
G	Cast iron, etched	0.697	0.89	0.96
C	Aluminum, polished	0.221	0.87	0.95
J	Aluminum, machined	0.0909	0.95	0.97
H	Aluminum, etched	0.775	(0.89)	(0.97)

Two general conclusions may be drawn as follows:

1 The values of all measured accommodation coefficients lie between 0.87 and 0.97.

2 The effect of different technical surfaces on the accommodation coefficient, if such an effect exists, is small and is not shown by the present tests.

In evaluating the experimental results the abnormal behavior of two of the surfaces should be noted. The emissivities of the etched aluminum dropped from 0.833 to 0.753 during the tests, and the value of the accommodation coefficient is therefore unreliable. In testing the etched cast-iron surface *G* it was observed that the air pressure in the sealed system decreased appreciably in the course of each conduction test. The emissivity remained unchanged.

It is undoubtedly true that all the metallic surfaces were oxidized to some extent. The appearance of each surface was the same before and after the tests, and, except for the etched aluminum, the emissivity was constant. But even if the oxide coatings were stable their influence on the properties of the metallic surfaces must be considered in interpreting the data.

The values of accommodation coefficient found by the authors are of the same magnitude as those given by Knudsen (1) for oxygen in contact with polished platinum, platinum coated lightly and then heavily with platinum black. His values are 0.808, 0.910, and 0.934, respectively.

Theory

The apparatus employed by the authors for determining accommodation coefficient requires the heat-transfer equations for radiation and for rarefied-gas conduction between two infinite concentric cylinders having different surface properties. The radiation equation, assuming diffuse reflection, is well known (5) as

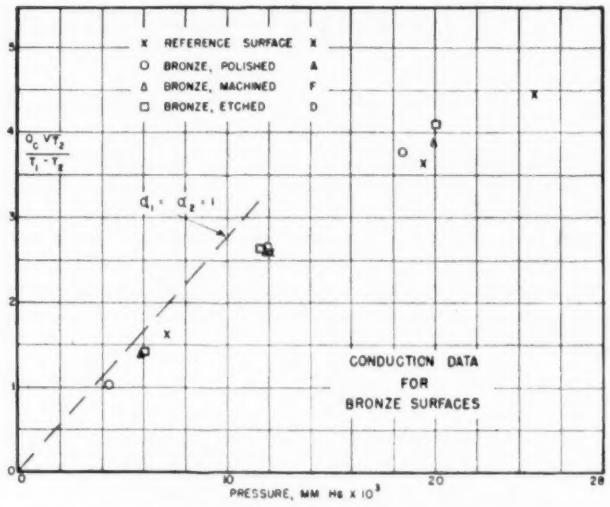


FIG. 1 CONDUCTION DATA FOR BRONZE SURFACES

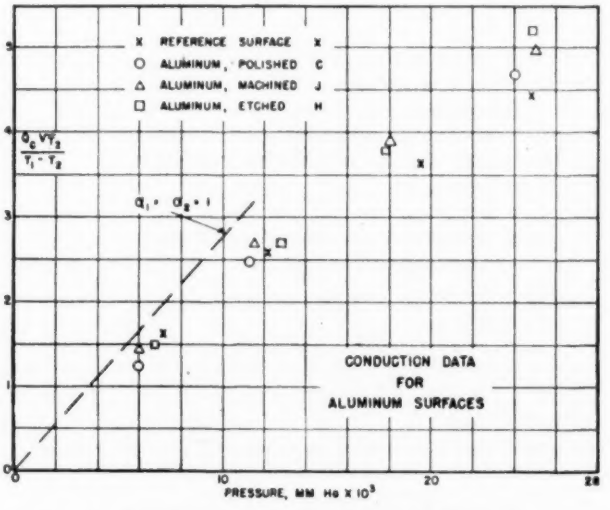


FIG. 2 CONDUCTION DATA FOR ALUMINUM SURFACES

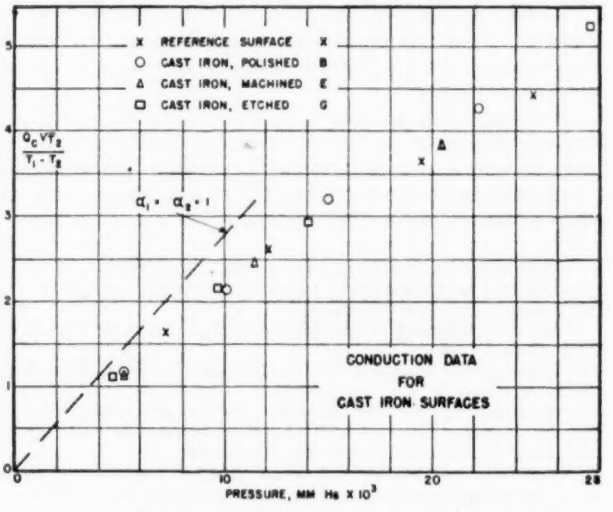


FIG. 3 CONDUCTION DATA FOR CAST IRON SURFACES

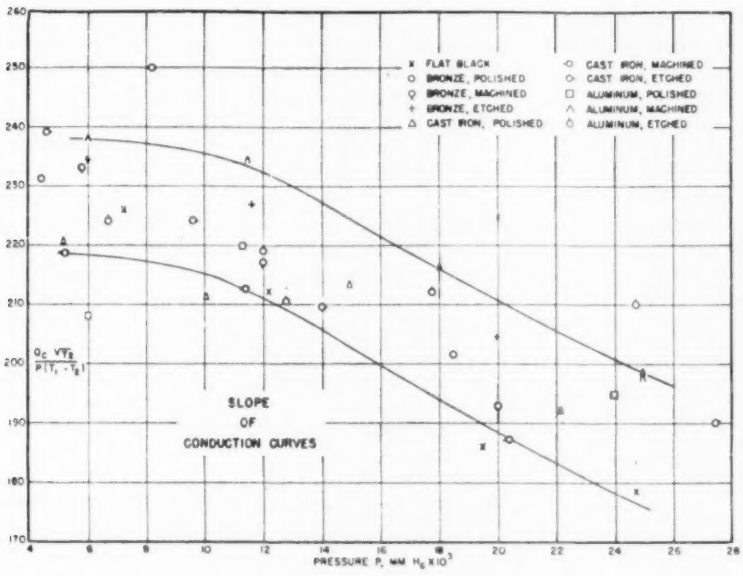


FIG. 4 SLOPE OF CONDUCTION CURVES

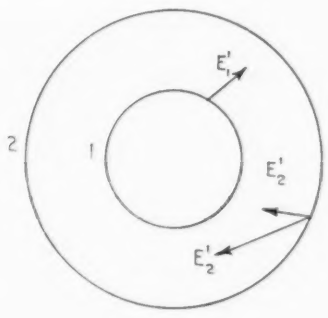


FIG. 5

$$Q_R = \frac{\sigma A_1 (T_1^4 - T_2^4)}{\frac{A_1}{A_2}\left(\frac{1}{a_2} - 1\right) + \frac{1}{a_1}} \quad \ldots\ldots [4]$$

or

$$\frac{Q_R}{L} = \frac{2\pi r_1 \sigma (T_1^4 - T_2^4)}{\frac{r_1}{r_2}\left(\frac{1}{a_2} - 1\right) + \frac{1}{a_1}} \quad \ldots\ldots [5]$$

$\frac{Q_R}{L}$ = heat transfer by radiation, per unit cylinder length, Btu $hr^{-1} ft^{-1}$
A = area of cylindrical surface, sq ft
a = radiant emissivity
σ = Boltzmann constant = 0.172×10^{-8}

Although Equation [5] applies only to gray bodies, its use with metallic surfaces is justified as a means of separating radiation from conduction in the authors' experiments. Emissivities calculated from Equation [5] are not accurate if the surfaces differ appreciably from those of gray bodies.

The equation for the conduction through a rarefied gas (almost all particle collisions at the solid surfaces) may be derived by extending the work of M. Knudsen (1), the validity of which has been fairly well established (6, 7, 8, 9). His equation for maximum conduction between two concentric infinite cylinders (accommodation coefficients unity) is

$$\frac{Q_c}{L} = 3600\, r_1 \frac{\gamma + 1}{\gamma - 1} \frac{p(T_1 - T_2)}{\sqrt{MT}} \quad \ldots\ldots [6]$$

With reference to Fig. 5, consider a large number of gas molecules striking a unit area of surface 1 per unit time having a total energy E_2' before, and E_1' after collision. Then the energy transferred from surface 1 is $E_1' - E_2'$ per unit area per unit time and the accommodation coefficient is

$$\alpha_1 = \frac{E_2' - E_1'}{E_2' - E_1} \quad \ldots\ldots [7]$$

After collision with surface 2, a particle stream has energy E_2'. The same particle stream does not, however, approach the outer surface with energy E_1', for only a fraction F of the particles comes from the inner surface. The remainder $(1 - F)$ come from the outer surface at energy E_2'; therefore

$$\alpha_2 = \frac{FE_1' + (1 - F)E_2' - E_2'}{FE_1' + (1 - F)E_2' - E_2} \quad \ldots\ldots [8]$$

or

$$\alpha_2 = \frac{F(E_1' - E_2')}{FE_1' + (1 - F)E_2' - E_2} \quad \ldots\ldots [9]$$

From Equations [7] and [9]

$$E_1' - E_2' = \frac{E_1 - E_2}{F\left(\frac{1}{\alpha_2} - 1\right) + \frac{1}{\alpha_1}} \quad \ldots\ldots [10]$$

The symbol F is defined as the fraction of particles leaving the outer surface taking direct paths to the inner. Its value can be calculated on the basis of Knudsen's cosine law (7), which may be stated as follows: The probability that a gas molecule leaves a surface on a path making an angle θ with the normal to the surface is proportional to $\cos\theta$.[6]

For a given path between the surfaces if β and δ represent the angles made by the path with the normals to the surfaces at the points of contact, and if ρ is the path length, then

$$F = \frac{1}{\pi} \int_{A_1} \frac{\cos\beta \cos\delta}{\rho^2}\, dA_1 = \frac{r_1}{r_2} \quad \ldots\ldots [11]$$

Returning to Equation [10], since $E_1 - E_2$ represents maximum energy transfer as given by Equation [6], the general equation for heat conduction between two infinite concentric cylinders separated by a rarefied gas is

$$\frac{Q_c}{L} = 3600\, r_1 \frac{\gamma + 1}{\gamma - 1} \frac{p(T_1 - T_2)}{\sqrt{MT}} \frac{1}{\frac{r_1}{r_2}\left(\frac{1}{\alpha_2} - 1\right) + \frac{1}{\alpha_1}} \quad \ldots [12]$$

Using $M = 29.0$ and $\gamma = 1.404$ for air

$$\left(\frac{Q_c}{L}\right)_{air} = 3980\, r_1 \frac{p(T_1 - T_2)}{\sqrt{T}} \frac{1}{\frac{r_1}{r_2}\left(\frac{1}{\alpha_2} - 1\right) + \frac{1}{\alpha_1}} \quad \ldots [13]$$

In the experiments, r_1 varied from 0.1040 to 0.1042, $r_2 = 0.1094$, and $L = 0.667$. For this case

$$Q_c = 276 \frac{p(T_1 - T_2)}{\sqrt{T}} \frac{1}{0.952\left(\frac{1}{\alpha_2} - 1\right) + \frac{1}{\alpha_1}} \quad \ldots\ldots [14]$$

[6] This law is analogous to Lambert's cosine law for diffuse reflection of radiation.

Although Equation [14] should be used only with small values of $T_1 - T_2$, Knudsen's experiments show (1) that the maximum value of 60 F in the present experiments is well within the range of application.

Experimental Procedure

The apparatus generally used for the measurement of accommodation coefficients (1, 2, 10) is not well adapted to an investigation of various types of surfaces. This objection is overcome in the new design, shown in Fig. 6, which has the additional advantage of a center, or test cylinder of simple construction which can be easily changed without duplication of test equipment. With the exception of the disk washers at the ends of the test cylinder, which were designed for a press fit, all other parts were used interchangeably for all ten inner cylinders.

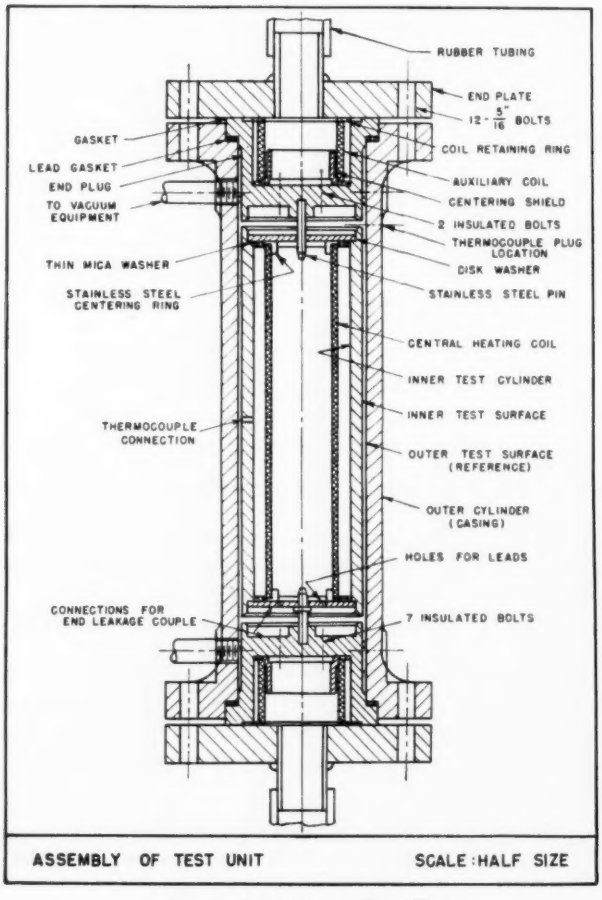


Fig. 6 Assembly of Test Unit

Heat supplied by the central heating coil flows outward between the two test surfaces approximately 2.50 and 2.62 in. diam. The test length is 8.00 in. Energy input to the auxiliary coil at each end is regulated to maintain a very small temperature differential between the disk washer and the inner face of the end plug. Therefore, substantially all the heat input to the central coil flows through the test surface.

The outer test surface was used as a reference and was given a double coat of flat black paint in order to make it nearly "gray" in response to radiation. Its properties were determined by testing a similarly prepared surface on an inner cylinder. The emissivity was 0.932 and the accommodation coefficient 0.89. The five radiation tests on this surface for temperature differences from 40 to 80 F checked the Stefan-Boltzmann law with an average deviation of 0.25 per cent. To prevent damage to the reference surface while changing test cylinders, a special fixture, not shown in the illustration, was designed.

Energy to the heating coils was supplied by a direct-current generator driven by a synchronous motor. Heat loss from the central coil leads was experimentally measured and a correction established.

The test section was evacuated by a Cenco Megavac pump, and the pressure was measured by a McLeod gage with a dry-ice trap. The system included a phosphorus pentoxide drier. The pressure was corrected for thermal diffusion between air at water temperature entering the test casing and air between the test cylinders. No correction was made for pressure drop in the piping from gage to casing because the correction is less than 4 per cent at the lowest conduction test pressures. The diffusion correction is actually applied by substituting T_2 for gas temperature T in Equation [3].

Temperatures inside the test unit were measured with calibrated copper-constantan thermocouples of 24 B&S gage wire, with arc-welded junctions. A Leeds and Northrup Type K potentiometer served to measure the temperature difference between the test cylinders, and a galvanometer sensitive to 0.05 deg F was used for the end-loss couples.

The thermocouple installations should be noted. Contact between the couple junction and the inner test cylinder was established mechanically by a set screw, Fig. 9(*c*). The junction on the reference cylinder, being electrically insulated from the casing, provides poor thermal contact and therefore conduction through the leads should be held to a minimum. The plug containing the element is shown in Fig. 7, its assembly in the cylindrical shell extending from the casing in Fig. 9(*a*), and the position of the shell on the casing in Fig. 10. Installation of the end-loss couples is shown in Fig. 9(*d*), and Fig. 8 shows them connected to the end plugs but detached from the disk washers.

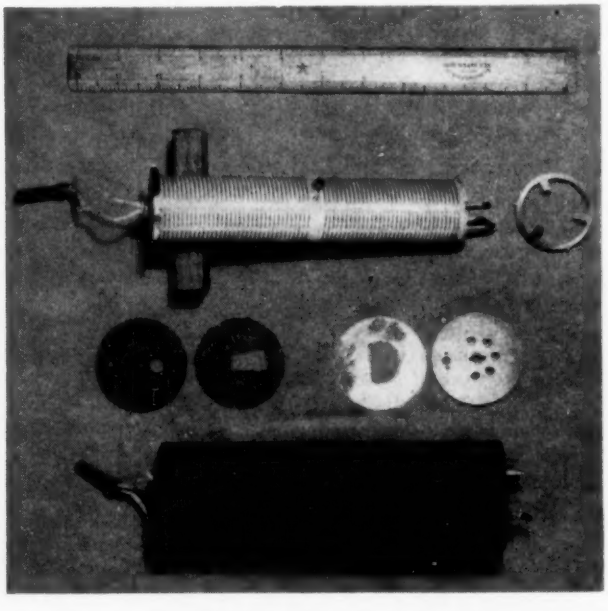


Fig. 7 Units Composing Inner Cylinder Assembly

To draw leads out of the test section, stainless-steel bolts, Figs. 8 and 9(*b*), were made part of each thermocouple circuit. An emf correction for the copper-to-steel junctions in each cir-

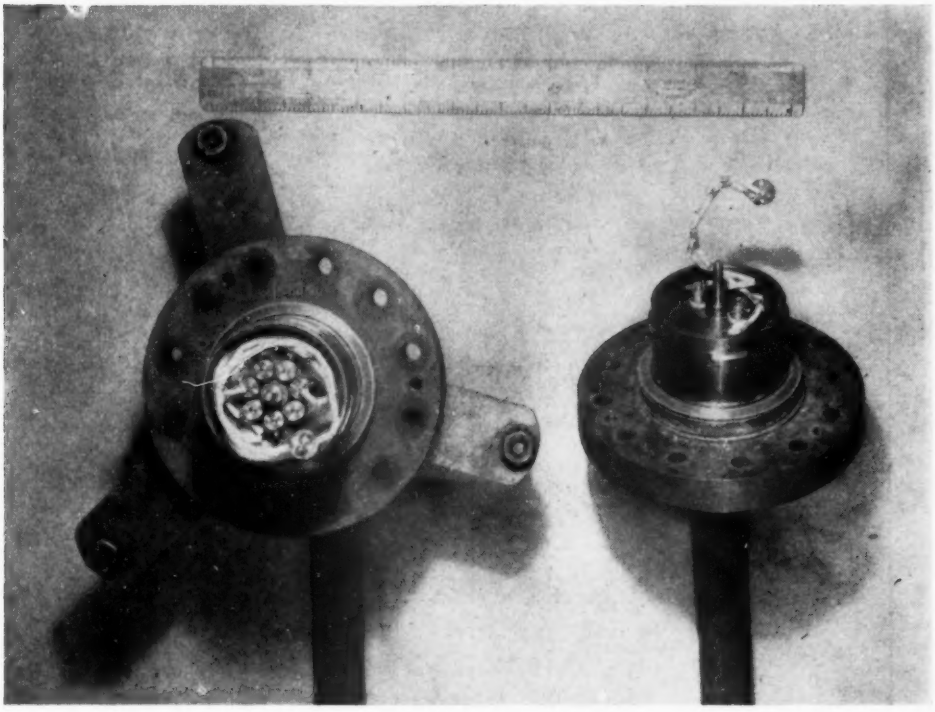


FIG. 8 END PLUGS AND END-LEAKAGE COUPLES

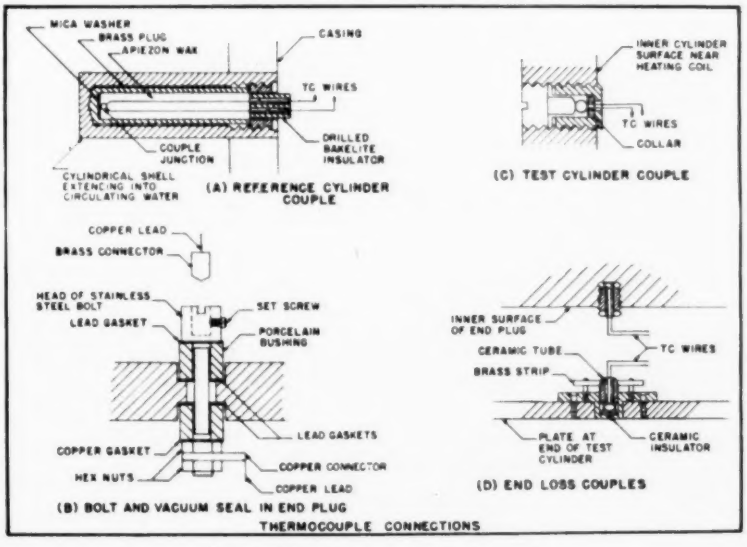


FIG. 9 THERMOCOUPLE CONNECTIONS

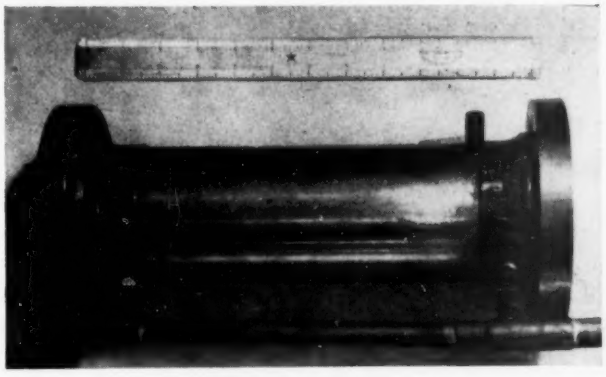


FIG. 10 CASING OF TEST UNIT

cuit was determined by joining the bolt heads with copper wire and operating the equipment under previously established conditions. The correction in no instance exceeded 2 deg.

Preparation of Test Surfaces. The test cylinders were machined from castings made by commercial foundries in Connecticut. The bronze was an alloy of 85 per cent copper, 5 per cent each of tin, lead, and zinc by weight; the cast iron was actually a semisteel, since steel scrap had been added; the aluminum was alloyed with traces of other elements to provide free machining and corrosion resistance. All castings of one metal came from the same lot. Only cylinders without flaws on the finished test surface were used.

Test cylinders were machined without lubrication. Before the final lathe cuts were made the cylinder and the plugs which supported it between centers were removed from the lathe and cleaned with soap solution, dioxane, and distilled water. After this cleaning the cylinder was not touched by hand. No further cleaning of any kind was given the machined or polished surface.

Polishing, except for cast iron, was done on a lathe with five grades of polishing paper ending with 4/0. Because of metal porosity cast iron was finished only to 1/0 paper. On aluminum the finer papers produced a dull finish on which the many fine surface pits were entirely covered up. Polishing at various speeds and pressures was tried without obtaining a brighter finish. The machined aluminum, on the other hand, was bright but clearly showed the porosity of the casting. The fact that the emissivity of the machined surface was found to be less than that of the polished was not entirely unexpected.

Etching was done with nitric acid, reducing the over-all diameter of a cylinder 0.004 to 0.005 in. Upon removal from the acid bath, the cylinders were washed and scrubbed in tap water, a dilute ammonium hydroxide solution, more tap water, and finally distilled water.

TABLE 2 TEST DATA

Run No.	r_1 inches	Pressure mm Hg x 10^3	T_2 °FA	T_1 °FA	Energy Input I amp.	E volts	Q watts	a_1	Q_r watts	Q_c Btu/hr	$\frac{Q_c\sqrt{T_2}}{T_1 - T_2}$	$\frac{Q_c\sqrt{T_2}}{p(T_1 - T_2)}$
X-1	1.2505	0.1	535.8	597.9	0.801	10.96	8.779	0.932	8.761	0.061		
X-1a		0.1	535.3	598.8	.808	11.06	8.936	.929	8.918	.061		
X-2		0.1	536.9	585.8	.704	9.63	6.780	.938	6.766	.048		
X-3		0.1	536.5	578.7	.644	8.79	5.661	.931	5.649	.041		
X-4		0.09	536.3	618.1	.936	13.05	12.215	.931	12.194	.072		
X-5		7.2	537.9	585.2	.734	10.15	7.450	.932	6.480	3.312	1.62	226
X-6		12.2	538.3	587.0	.774	10.73	8.305	.932	6.711	5.440	2.59	212
X-7		19.5	537.4	586.4	.804	11.16	8.973	.932	6.726	7.669	3.63	186
X-8		24.8	536.8	588.2	.847	11.76	9.961	.932	7.079	9.836	4.43	178
X-9		111.	536.0	582.8	.990	13.77	13.63	.932	6.338	24.88	12.31	111
X-10		25,500	537.4	569.4	.990	13.71	13.57	.932	4.191	32.01	23.19	0.91
A-1	1.2495	0.06	538.1	606.2	.296	3.97	1.175	.104	1.164	.038		
A-2		0.09	536.9	606.8	.296	4.00	1.184	.102	1.166	.061		
A-3		4.4	536.2	579.9	.304	4.11	1.249	.103	0.686	1.922	1.02	231
A-4		8.2	537.8	582.4	.371	5.01	1.859	.103	0.708	3.932	2.04	250
A-5		12.0	536.9	588.2	.434	5.83	2.530	.103	0.825	5.819	2.63	219
A-6		18.5	536.6	590.6	.505	6.82	3.444	.103	0.874	8.771	3.76	202
B-1	1.2490	0.1	538.1	604.9	.391	5.26	2.057	.187	2.040	.061		
B-2		5.2	537.8	592.6	.421	5.66	2.383	.184	1.588	2.713	1.15	220
B-3		10.1	537.5	587.5	.455	6.10	2.776	.184	1.428	4.601	2.13	211
B-4		15.0	538.6	588.1	.504	6.78	3.417	.184	1.420	6.816	3.20	213
B-5		22.2	539.0	591.4	.568	7.63	4.334	.184	1.518	9.611	4.26	192
B-6		0.1	537.6	594.0	.348	4.69	1.632	.181	1.616	.055		
C-1	1.2490	0.06	532.5	593.4	.400	5.28	2.112					
C-2		0.09	533.0	594.6	.404	5.34	2.157	.223	2.142	.051		
C-3		0.07	531.8	569.8	.303	4.01	1.215	.219	1.208	.024		
C-4		6.0	531.6	571.3	.380	5.02	1.908	.221	1.279	2.147	1.25	208
C-5		11.3	532.6	576.2	.460	6.09	2.801	.221	1.427	4.689	2.48	220
C-6		24.0	532.6	583.6	.599	7.91	4.738	.221	1.704	10.36	4.69	195
C-7		92.0	531.9	580.6	.816	10.89	8.89	.221	1.611	24.85	11.77	128
D-1	1.2480	0.06	535.8	614.8	.441	5.81	2.562	.194	2.549	.044		
D-2		0.05	536.2	580.1	.310	4.11	1.274	.191	1.268	.020		
D-3		6.0	536.8	586.0	.421	5.53	2.328	.192	1.455	2.980	1.40	234
D-4		11.6	537.4	589.7	.501	6.59	3.302	.192	1.565	5.928	2.63	226
D-5		20.0	536.4	592.6	.589	7.81	4.600	.192	1.691	9.928	4.09	204
D-6		91.	537.0	585.4	.808	10.74	8.68	.192	1.430	24.74	11.85	130
E-1	1.2500	0.1	537.6	592.9	.507	6.71	3.402	.394	3.387	.051		
E-2		0.09	536.1	575.2	.412	5.45	2.245	.387	2.235	.034		
E-3		5.2	536.6	578.6	.480	6.36	3.052	.391	2.448	2.061	1.14	218
E-4		11.4	536.5	582.4	.556	7.39	4.109	.391	2.703	4.799	2.42	212
E-5		20.4	535.6	584.1	.627	8.31	5.210	.391	2.863	8.010	3.82	187
E-6		90.5	536.7	581.4	.826	11.04	9.12	.391	2.626	22.15	11.48	127

TABLE 2 (*Continued*)

Run No.	r_1 inches	Pressure mm Hg x 10^3	T_2 °FA	T_1 °FA	Energy Input I amp.	E volts	Q watts	a_1	Q_T watts	Q_c Btu/hr	$\frac{Q_c\sqrt{T_2}}{T_1 - T_2}$	$\frac{Q_c\sqrt{T_2}}{p(T_1 - T_2)}$
F-1	1.2500	0.09	535.7	603.9	0.310	4.09	1.268	.113	1.251	.058		
F-2		0.1	534.3	583.3	.250	3.30	0.825	.108	0.811	.048		
F-3		5.8	535.8	584.5	.354	4.69	1.660	.110	0.826	2.846	1.35	233
F-4		12.0	534.6	585.0	.436	5.77	2.516	.110	0.853	5.676	2.60	217
F-5		20.0	536.0	587.9	.518	6.85	3.548	.110	0.889	9.075	3.86	193
F-6		38.0	535.2	596.4	.682	9.06	6.179	.110	1.070	17.44	6.59	173
G-1	1.2480	0.1	534.3	583.3	.619	8.19	5.070	.702	5.057	.044		
G-2		0.09	534.0	596.9	.705	9.44	6.655	.693	6.640	.051		
G-3		4.6	534.3	586.9	.679	9.09	6.172	.697	5.438	2.505	1.10	239
G-4		9.6	533.8	584.2	.700	9.34	6.538	.697	5.165	4.686	2.15	224
G-5		14.0	535.7	583.2	.705	9.42	6.641	.697	4.878	6.017	2.93	210
G-6		27.5	535.6	578.2	.729	9.78	7.130	.697	4.314	9.612	5.22	190
G-7		0.09	534.5	581.8	.604	8.01	4.838	.697	4.826	.041		
H-1	1.2495	0.11	536.7	575.4	.592	7.84	4.641	.833	4.629	.041		
H-2		0.11	537.2	595.8	.725	9.78	7.091	.792	7.073	.061		
H-3		6.7	534.9	589.0	.734	9.90	7.267	.775	6.239	3.509	1.50	224
H-4		12.8	534.4	584.1	.739	9.94	7.346	.775	5.647	5.799	2.70	210
H-5		17.8	535.3	585.9	.780	10.53	8.213	.775	5.792	8.263	3.78	212
H-6		24.8	535.8	584.0	.801	10.83	8.675	.775	5.495	10.85	5.21	210
H-7		0.1	534.4	586.0	.655	8.84	5.790	.758	5.776	.048		
H-7a		0.1	535.7	586.4	.649	8.75	5.679	.753	5.665	.048		
J-1	1.2495	0.1	537.8	608.7	.283	3.81	1.078	.0908	1.058	.068		
J-2		0.06	534.8	609.0	.289	3.89	1.124	.0911	1.112	.041		
J-3		6.0	537.9	575.4	.297	4.01	1.191	.0909	0.516	2.304	1.42	238
J-4		11.5	536.4	583.3	.409	5.50	2.250	.0909	0.657	5.437	2.68	234
J-5		18.0	537.8	586.8	.480	6.46	3.102	.0909	0.695	8.215	3.89	216
J-6		25.0	537.8	590.5	.550	7.37	4.053	.0909	0.755	11.26	4.95	198
J-6a		25.0	537.1	590.4	.553	7.43	4.108	.0909	0.762	11.42	4.96	198

Remarks: r_2 = 1.3125 inches; L = 8.00 inches.
C-1 Mica washers omitted
C-6 Fluctuation of 1% in I
E-6 Fluctuation of 1.5% in E
F-3,4,5 Pressure rise about 1% per hour
G-3,4,5,6 Pressure drop observed, about 5% per test
H-1 to 7 Fluctuation in E as much as 2%
J-6 Fluctuation of 3% in I

Method of Testing. All metallic surfaces subjected to low pressures were cleaned so as to be free of volatile impurities. Degassing was done at test-cylinder temperatures not exceeding 160 F. During radiation tests the vacuum pump was run continuously, but in conduction tests the system was closed at the desired pressure. The pressure rise for an 8- to 12-hr test was usually negligible. The one exception was cylinder *F*, machined bronze, for which the pressure increased as much as 1 per cent per hr.

For each surface at least two radiation tests (air pressure about 10^{-4} mm of mercury) and four conduction tests were made. The conduction tests were in or near the rarefied-gas region, the upper limit of which is about 0.01 mm of mercury for the apparatus. Each test was continued until the temperature change was within 0.1 deg F per hr. The temperature of the inner cylinder ranged from 109.5 to 158 F, and the water temperature, assumed to be the same as that of the reference surface, from 71.6 to 79 F.

ACKNOWLEDGMENT

The authors wish to express their appreciation to Prof. W. J. Wohlenberg of Yale University for general direction of the investigation and for his invaluable advice concerning many of the details.

BIBLIOGRAPHY

1 "Die Moleculare Wärmeleitung der Gase und der Akkommodationskoeffizient," by M. Knudsen, *Annalen der Physik*, vol. 34, 1911, p. 593.

2 "The Exchange of Energy Between a Platinum Surface and Gas Molecules," by W. B. Mann, Proceedings of the Royal Society of London, Eng., vol. A146, 1934, p. 776.

3 "Conduction of Heat Through Rarefied Gases," by F. Soddy and A. J. Berry, Proceedings of the Royal Society of London, Eng., vol. A83, 1910, p. 254; also vol. A84, 1911, p. 576.

4 "The Dynamical Theory of Gases," by J. H. Jeans, University Press, Cambridge, England, fourth edition, 1925.

5 "Heat Transmission," by W. H. McAdams, McGraw-Hill Book Company, Inc., New York, N. Y., second edition, 1942.

6 "Researches on Heat Conduction by Rarefied Gases," by W. H. Keesom and G. Schmidt, *Physica*, vol. 3, 1936, pp. 590 and 1085; also vol. 4, 1937, p. 828.

7 "Das Cosinusgesetz in der kinetischen Gastheorie," by M. Knudsen, *Annalen der Physik*, vol. 48, 1915, p. 1113.

8 "Radiometerdruck und Akkommodationskoeffizient," by M. Knudsen, *Annalen der Physik*, vol. 6, 1930, p. 129.

9 "Optische Untersuchung des Akkommodationskoeffizienten der Moleculartranslation und dessen Verteilungsfunktion in einem verdünnten Gase," by L. S. Ornstein and W. R. van Wyk, *Zeitschrift der Physik*, vol. 78, 1932, p. 734.

10 "Exchange of Energy Between Gas Atoms and Solid Surfaces," by J. K. Roberts, Proceedings of the Royal Society of London, Eng., vol. A129, 1930, p. 146; also vol. A135, 1932, p. 192, and vol. A142, 1933, p. 518.

11 "The Accommodation Coefficient of Helium on Nickel," by B. Raines, *Physical Review*, vol. 56, 1939, p. 691.

Certain Aspects of High-Pressure Centrifugal Pumping Cycles

By I. J. KARASSIK,[1] HARRISON, N. J.

The author discusses the hydraulic and mechanical limitations imposed upon centrifugal boiler feed pumps by certain features of the modern regenerative feedwater heating cycles, as well as the influence of the practical limitations of pump design on the cycles themselves.

REDUCED to its essential elements, a power plant is composed of a boiler feed pump, a boiler, and a heat engine such as a turbine. All other equipment represents refinements which supplement the functions of these three elements and which are directed at improving the over-all efficiency of the power plant.

As the size and number of steam-generating stations grew, the desire for improvements in operating economy dictated many refinements in the steam cycle. These refinements lay in two separate directions. The first of these refinements involved a steady increase in operating pressures and temperatures, in order to provide for a greater heat drop between boiler and condenser.

Operating pressures grew until at the present time 1250-psi boilers are quite common, and a few plants are operating at even higher pressures. Temperatures rose from a conservative 600 and 750 F, until today 900 to 950 F is not considered radical practice. Wartime experience with superchargers and gas turbines promises to lead to even higher steam temperatures. The direct effect of this rise in steam-plant operating conditions will be discussed later.

The second refinement was directed toward greater utilization of heat through increased feed heating. The problem presented by the introduction of multiple heaters centered in the choice between direct-contact heaters and closed heat exchangers. From the thermodynamic point of view, the former have certain definite advantages. It must be considered, however, that a separate boiler feed pump is required after each direct-contact heater, as shown in Fig. 1, while the use of a group of closed heaters permits the application of a single boiler feed pump discharging through these heaters and into the boiler, Fig. 2.

Multiple Direct-Contact Heaters

The first of the problems introduced by a feed cycle with multiple direct-contact heaters is the requirement of separate feed pumps for each of the heaters. This of course may be partially circumvented by the use of a multistage boiler feed pump with multiple inlets and discharge connections, each stage or group of stages serving an individual heater, and each such group operating at a successively elevated temperature.

The most difficult problem, however, resides in the control of the boiler feed pump or pumps. A centrifugal pump will always operate at those conditions of head and capacity which correspond to the intersection between its head-capacity characteristic at its operating speed and the system-head curve. Thus in order to alter the operating conditions, it becomes necessary to alter the shape either of the head characteristic by varying the operating speed, or of the system-head curve by varying one of its components. In a boiler-feed cycle this variation is provided by the feedwater-level regulator, as illustrated in Fig. 3, where curves (*a*) to (*d*), inclusive, correspond to various positions of the feedwater-regulator valve. Thus, depending on the boiler load and consequently on the position of the feedwater-regulator throttling valve, the pump-discharge capacity will correspond to the intersection of the H-Q curve with curves (*a*) to (*d*), or with any intermediate curve.

In the case of a feed cycle with multiple direct-contact heaters, as in Fig. 1, it becomes necessary to interpose a feedwater regulator in the discharge of each individual boiler feed pump. The controlling impulse would be the boiler-drum level in the case of the last discharge and the level in the storage space of the direct-contact heaters in the intermediate units. This multiplication

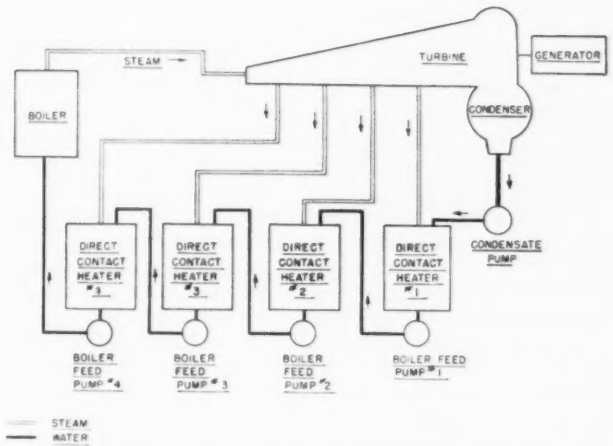


FIG. 1 FEED CYCLE WITH MULTIPLE DIRECT-CONTACT HEATERS

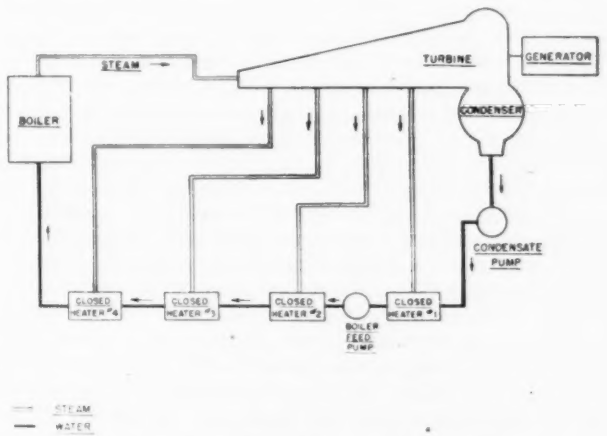


FIG. 2 FEED CYCLE WITH MULTIPLE CLOSED HEATERS

[1] Application Engineer, Worthington Pump & Machinery Corporation. Mem. A.S.M.E.

Contributed by the Hydraulic Division and presented at the Spring Meeting, Birmingham, Ala., April 3–5, 1944, of THE AMERICAN SOCIETY OF MECHANICAL ENGINEERS.

NOTE: Statements and opinions advanced in papers are to be understood as individual expressions of their authors and not those of the Society.

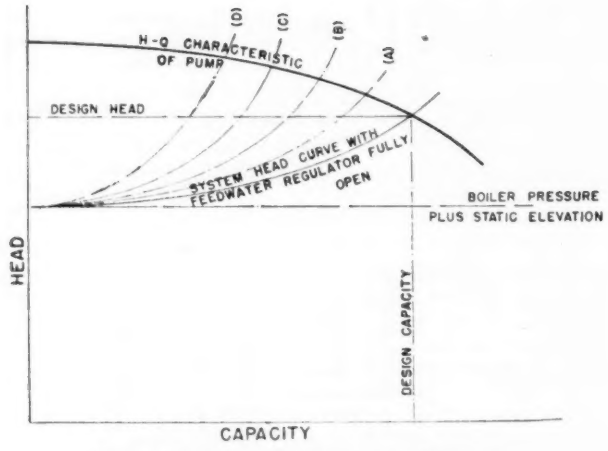


FIG. 3 OPERATION OF FEEDWATER REGULATOR

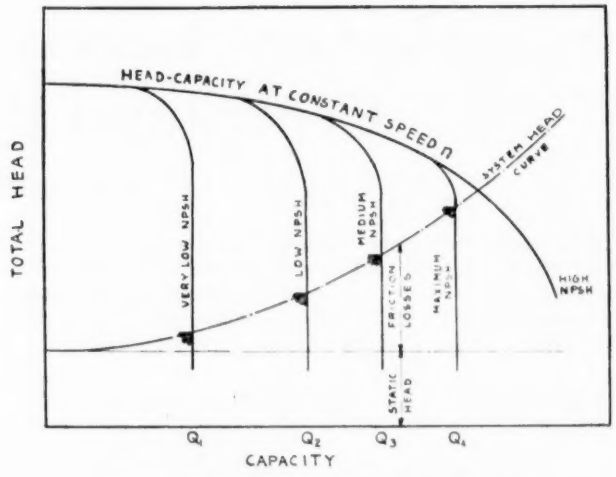


FIG. 4 OPERATION OF A CONDENSATE PUMP

of controls introduces additional expense as well as an increase in the source of potential maintenance troubles.

Of course, any centrifugal pump is, to a certain extent, self-regulating as regards delivery through the effect of suction conditions on the pump head-capacity curve. A typical example of a self-regulating installation is that of a hot well or condensate-removal pump. In this particular case, the delivery of the pump is generally controlled by the submergence over the pump center line, this submergence representing the net positive suction head available over and above the vapor pressure. If the inflow to the condenser hot well is reduced, the pump will withdraw more water than is returned to the condenser with a resultant change in the level of the hot well, a reduction in the available net positive suction head, and a consequent reduction in the delivery of the condensate pump. This operation is illustrated in Fig. 4.

In theory the same principle of operation could be applied to a feed cycle with multiple direct-contact heaters. The delivery of the last boiler feed pump would be controlled by a feedwater regulator while the intermediate units would be subjected solely to the control of the available net positive suction head, that is, of the submergence from the storage space of the direct-contact heater. As the boiler load would be reduced, each pump in turn would continue for a short period of time to handle more feedwater than was being returned into the direct-contact heater at the head of the system, with the result that levels in the storage space would fall and reduce the pump capacity through the reduction of the net positive suction head.

In practice, however, this would prove to be a difficult undertaking. It must be considered, in the first place, that in order to obtain satisfactory capacity variations through level control, the available net positive suction head itself must undergo variations of as much as 80 per cent or even more of its maximum value. This is entirely feasible in the case of a condenser hot well, where the available net positive suction head may vary between 4 ft and 1 ft. Condensate pumps are properly proportioned and designed to avoid excessive inlet and rotative speeds and are provided with special condensate-type impellers. The application of such designs to high-head boiler feed pumps would not be practical, as the latter operate at high speeds and require net positive suction heads of 15 to 20 ft or even more. Even if it were possible to provide suction-level control to the operation of boiler feed pumps, the storage space of the direct-contact heaters would have to extend to within 2 or 3 ft of the pump center line, increasing the cost of the heaters quite appreciably.

There is, finally, one more factor which presents difficulties in the application of a feed cycle with multiple direct-contact heaters. Operation of boiler feed pumps at extremely reduced capacities is conducive to a variety of undesirable effects due to the temperature rise experienced within the boiler feed pump at light flows. In the normal case, the boiler feed pump is provided with a by-pass in its discharge, leading to some region of lower pressure in the feed cycle where the excess heat in the by-passed feedwater may be dissipated without harmful effects. This by-pass is operated either manually or automatically whenever the flow through the pump falls to some predetermined minimum or whenever such a reduction in capacity is expected. A boiler-feed cycle such as illustrated in Fig. 1 would require the installation of an individual by-pass beyond each separate boiler feed pump, and each by-pass would require its own piping and its own individual control. An automatic-control system would be quite feasible but, again, would add to the initial investment and probable maintenance expense.

We have not touched upon the problem of heater construction because this analysis is concerned strictly with the effect of various feed cycles on the centrifugal pumping equipment involved. There is little doubt, however, that certain problems must arise in the design and operation of direct-contact heaters at the elevated pressures and temperatures imposed by the application of a feed cycle with multiple direct-contact heaters.

MULTIPLE CLOSED HEATERS

It cannot be said that the application of a feed cycle with multiple closed heaters is entirely devoid of problems. As a matter of fact, the average power-plant cycle is based on a modified system; one direct-contact heater fulfills the function of feedwater deaeration, while several additional heaters of the closed type are located upstream as well as downstream of the direct-contact heater and its boiler feed pump.

The condensate drains from the closed heaters must be returned to the cycle in order to avoid a waste of treated feedwater and of its heat and pressure energy. Two basic methods are available for the reintroduction of the heater drains into the feed cycle:

1 Pumping the drains into the feedwater cycle at some higher pressure point, as in Fig. 5.

2 Flashing the drains into the steam space of a lower-pressure portion of the feed cycle, as in Fig. 6. (When this is done successively with several closed heaters, the process is referred to as "cascading.")

Thermal-balance calculations indicate that the first method shows a gain in over-all plant economy over the straight cascading

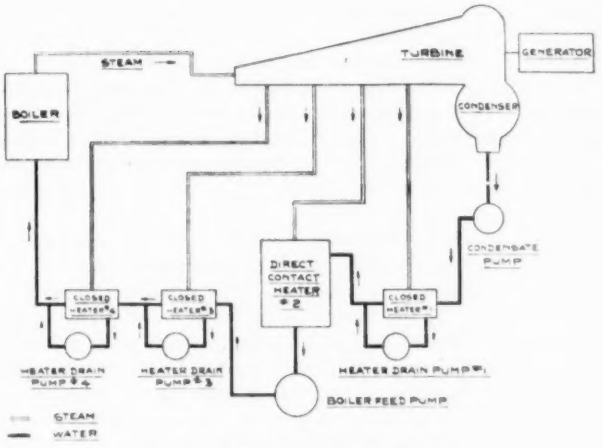


FIG. 5 STRAIGHT PUMPING SYSTEM

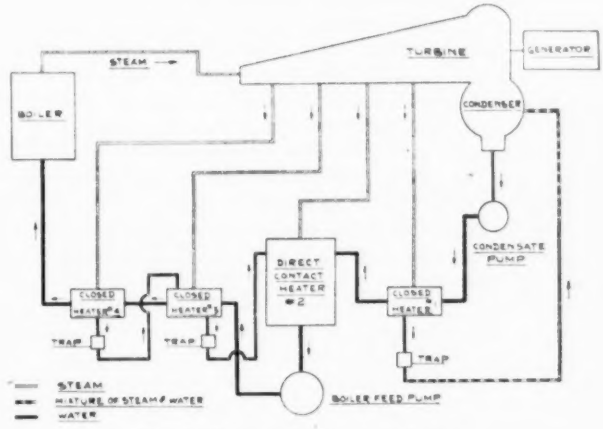


FIG. 6 STRAIGHT CASCADING SYSTEM

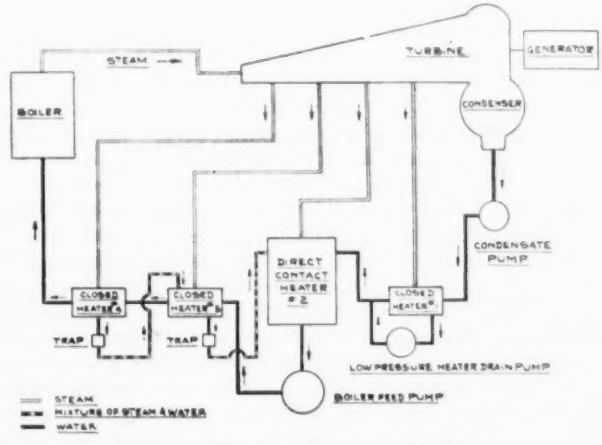


FIG. 7 MODIFIED CASCADING SYSTEM

system. However, the economy to be gained by the inclusion of individual heater drain pumps at each closed heater is hardly justifiable in view of the added initial expense and greater maintenance required. As a matter of fact, pumping from the closed heaters on the discharge side of the boiler feed pump in a high-pressure installation is quite impractical. The capacity of the heater drain pumps is but a fraction of the design capacity of the feed pump itself, while the discharge pressures of the two are of an equivalent order or magnitude. As a result, it may become impossible to apply a centrifugal pump for the service strictly because of hydraulic-design considerations.

A compromise between these two basic methods is illustrated in Fig. 7. It consists of cascading the heater drains of all closed heaters located on the discharge side of the boiler feed pump back into the direct-contact heater and of pumping the drains of the low-pressure heater into the discharge from the condensate pump. The over-all losses in plant economy brought about by this modified cascading system, when compared to the straight pumping system, are negligible.

EFFECTS OF RISE IN OPERATING PRESSURES

It has been mentioned that the rise in power-plant operating pressures had a very definite effect on centrifugal boiler-feed-pump construction and operation. The pump of some 20 or 30 years ago seldom operated at speeds in excess of 1800 rpm. While boiler pressures hovered around 200 to 250 psi, there was relatively little advantage to be gained from the introduction of higher operating speeds for any but the smallest-capacity boiler feed pumps. However, as soon as boiler pressures started on their upward climb, the lower operating speed of 1800 rpm became no longer practical and the modern practice of 3600 rpm for boiler feed pumps was launched.

It is interesting to note that high-pressure installations of the central stations have distinctly showed the way for the smaller units which started on a parallel growth toward 300, 600, and now even 1200 psi. What 3600 rpm did for the medium- and large-capacity boiler feed pump, it could no longer do for the smaller-capacity unit, until today there is a definite growing trend toward operating speeds in excess of 3600 rpm.

This might serve, incidentally, as a logical occasion to discuss the oft-quoted technical superiority of our European counterpart in the field of centrifugal-pump design. The more frequent use of high operating speeds in Europe stems not from the greater talent and ingenuity of their engineers but rather from a series of economic and geographical circumstances.

The first and probably least important of these circumstances is the fact that European electric-distribution practice is based on 50-cycle current, permitting a maximum synchronous speed of only 3000 rpm, compared to a possible 3600 rpm in the United States. This lower limit handicapped European designers sufficiently to make it desirable to exceed the 3000-rpm speed, either through greater use of turbine drive or through the application of stepup gears. Once the natural speed limit of motor-driven pumps was exceeded and abandoned, there was little reason to carry the increase to only 3600 rpm, and higher-speed pumps were widely introduced.

The more important reason, however, is the fact that, while raw-material costs are generally higher in Europe, labor costs were always abysmally low. The European designer has through necessity learned to spare materials even at the cost of increasing labor man-hours, both in production and in maintenance. Where an American engineer will use a safety factor of 5, European training dictates the choice of lighter structures, close figuring, and safety factors of 2 or even less.

Even after the advent of 3600 rpm as standard practice in this country, the rise in boiler pressures kept pace. Soon, discharge pressures in excess of 1200 psi became a common requirement and even the use of cast steel for the pump casings proved an insufficient barrier to internal leakage of the then common axially split casing boiler feed pump. The next step was the introduction of radially split casing designs, culminating in the well-known forged-steel-barrel double-casing construction of today for the higher-pressure range. It is interesting to note, incidentally, that the dividing line of approximately 1250 psi between axially

and radially split casings appears due for a slight upward revision, probably to 1350 or 1400 psi.

Damage to pump stationary parts was found to be the most troublesome item standing in the way of such upward increases in operating pressures, and it is being overcome now by the use of stainless-steel alloys of similar grade to those already in use for the rotating pump parts, such as impellers, impeller rings, and shaft sleeves. Thus the old dividing line will be greatly affected by a more general adaptation of erosion-resisting material in all the parts of the pump. Part of this revision may be said to derive from greater accumulated experience with axially split casings operating near the old dividing line; part may be ascribed to the availability of better materials than heretofore used.

Once the general principles of design for this higher pressure range had become more or less stabilized, there still remained the question of the limiting stage pressures. From a strictly hydraulic point of view, there was much to be gained from maintaining low- or medium-stage pressures, at the cost of multiplying the required number of stages. The lower heads per stage kept disk-horsepower losses to a minimum and avoided possible reduction of pump efficiencies. It also became necessary to reconsider the effects of the higher velocities brought by higher stage pressures on the erosion problems in the pump casings. The use of extremely low heads per stage, however, leads to a greatly increased number of stages, greater shaft spans and shaft deflections, and greater stresses on the pump casings. The increased number of running joints in a pump designed with too great a number of stages added seriously to its disadvantages. A satisfying compromise had to be reached, taking into account available materials, the optimum number of stages, and the required operating speed, the main consideration being to obtain a pump design which can be maintained in service with the least expenditure of cost, effort, and expert knowledge.

As a result of the availability of better materials, it has been the practice lately to increase stage pressures and keep the number of stages to an absolute minimum. Six stages are considered today the best possible combination for most pressures in excess of 1000 psi, although in the case of relatively low-capacity pumps it becomes necessary once in a while to provide seven or even eight stages. Assuming a net pressure of 1800 psi, a six-stage pump would develop 300 psi per stage (or about 725 ft). Once thought excessive and even impossible, 725 ft per stage can be considered as a very safe and reliable figure today.

High Suction Temperatures

Along with rising discharge pressures, boiler feed pump designers have had to contend with a trend toward higher suction temperatures and higher suction pressures. This trend can be traced to two separate power-plant developments. In certain cases, the desire to improve the station heat balance dictates the choice of a higher pressure stage in the main turbine for feed heating at the direct-contact heater. As a result, instead of 3 to 15 psig, direct-contact heaters are being more frequently designed for 65 psia, and even higher. In other cases, the pumping temperatures are increased through the application of two boiler feed pumps operating in series with one or more closed heaters being located between the primary and main feed pumps. This frequently occurs in topping installations, where the pumps which fed the low-pressure boilers are retained and serve as booster pumps to the higher-pressure addition.

When the direct-contact heater is fed with steam from a relatively high pressure stage of the main turbine, special attention must be given to the boiler feed pump suction conditions if the heater pressure is not held at a constant value regardless of bleed-pressure fluctuations, because there exists a danger of flashing in the pump suction whenever a severe and sudden drop is experienced in the station load.

As the generator dumps its electric load, the first tendency of the main turbine is to overspeed, because it is receiving an excess of steam over the requirements of the lighter load. However, since turbogenerators are so arranged in their controls as to prevent asynchronous operation, the turbine governor immediately acts to throttle the steam supply to the turbine and holds the turbine speed at its rated value.

The consequence of this reduction in pressure at the steam inlet is a proportionate reduction at all the successive stages of the turbine and of course at the bleed stage supplying the direct-contact heater. In the meantime, the water in the storage space of the heater, which was at a temperature corresponding to the pressure in the heater, is suddenly subjected to a severe decrease in pressure without a corresponding decrease in temperature. The net result of this situation is severe flashing which occurs in the heater as well as in the feedwater in the suction piping to the boiler feed pump.

The time element involved in again bringing the pressure and temperature within the heater to a correlated value will of course vary with each individual case. The variation in the time component is due to the great variation in the size and shape of the storage space, since these two elements are important factors in the rate of flashing at the free surface of the feedwater.

It must also be considered that the downward velocity of the feedwater in the suction piping is too high to permit the vapor bubbles generated by flashing, to rise up to the heater and thus to clear the boiler feed pump suction of the flashing steam. A safety factor must be provided to take care of the time lag which exists between a certain reduction of pressure in the heater and the ultimate reduction of temperature at the pump suction. It is therefore necessary either to provide an excessive factor of safety in the installation of the boiler feed pump through the addition of an empirical percentage to the calculated net positive suction head or else some means whereby any appreciable pressure reduction in the heater would be accompanied immediately by a temperature reduction at the pump suction.

The latter solution is obviously predicated upon the injection of colder water into the pump suction. While the design of a control for such injection is not an insurmountable problem, the practicability of this solution is governed by circumstances peculiar to each individual installation. The cooler injection water must be taken from the downstream side of the cycle, that is, either from the discharge of the condensate pump or from the drains of a low-pressure closed heater ahead of the direct-contact heater. To introduce nondeaerated condensate into the boiler feed pump suction is not recommended, especially in the case of high-pressure boilers where the possible effects of contamination are severe. It must be considered, however, that a high-pressure installation, including a direct-contact heater operating at high temperature, will probably also include a low-pressure closed heater between the condensate discharge and the direct-contact heater itself. It must be further considered that the drains from this heater, generally pumped by a separate pump into the direct-contact heater, are to all intents and purposes pure deaerated condensate, and that their injection into the feedwater suction stream will cause no harmful effects.

A logical precaution, therefore, might consist in the installation of a by-pass line from the low-pressure heater drain pump discharge into the boiler feed pump suction. This by-pass line would be properly valved and controlled by some means such as the difference between the suction pressure and the vapor pressure at the suction, any decrease of this difference below a predetermined minimum causing the by-pass valve to operate and inject colder water into the suction of the feed pump. Two charts

have been prepared to illustrate the effect of colder water injection on the available net positive suction head. Fig. 8 shows the temperature depression resulting from the injection, plotted against the difference in temperature between the feedwater and the injection stream and given for varying ratios of injection. Fig. 9 illustrates the effect of temperature depression on the available net positive suction head at various feedwater temperatures.

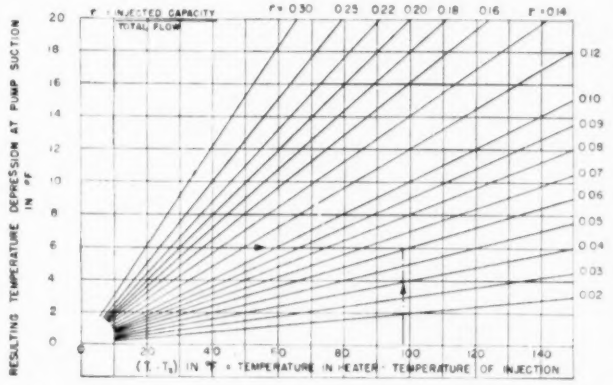


FIG. 8 EFFECT OF INJECTION OF COOLER FEEDWATER ON TEMPERATURE OF MIXTURE

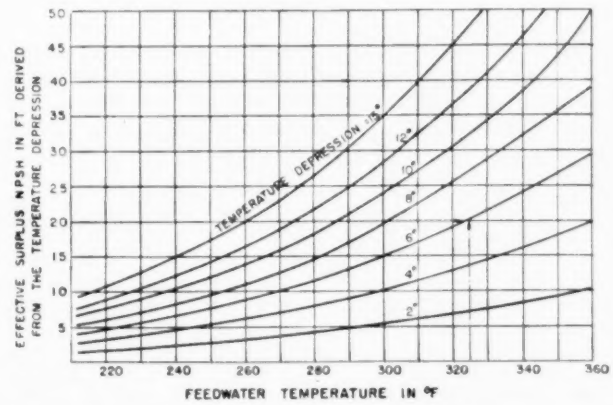


FIG. 9 EFFECT OF TEMPERATURE DEPRESSION ON AVAILABLE NET POSITIVE SUCTION HEAD

Thus, for instance, if it is desired to provide 20 ft surplus net positive suction head at the boiler feed pump suction and if the feedwater temperature is 325 F, the required temperature depression is 6 deg F. Assuming that the temperature of the heater drains is 227 F, allowing a 98-deg difference between feedwater and injection water, the by-pass line must be proportioned to pass 0.062 of the maximum boiler feed pump capacity, or 6.2 per cent.

Another serious problem introduced by high feedwater temperatures, especially when coupled to high suction pressures, resides in the operation of the stuffing boxes. The design of the pump interior parts can be accommodated to these conditions without undue difficulties, now that high-grade alloy stainless steels are readily available. The practice of shrinking impellers on the shaft in high-pressure applications has further helped solve some of the earlier problems. Finally, the design of the pump casing itself, through the application of materials such as forged steel and in some cases even stainless alloys, as well as through certain mechanical improvements, has likewise eliminated some of the earlier temperature limitations.

There remains, however, the problem of providing a reliable and economical stuffing-box design. Certain objectives may be said to have been attained even in this field. For instance, within the last few years a more thorough understanding of the interrelation of stuffing-box pressures, rubbing speeds, and leakage temperatures has led to an improved style of water-cooled stuffing-box design. Such stuffing boxes have been built suitable to withstand feedwater temperatures up to 400 F and stuffing-box pressures up to 500 psi, without recourse to pressure-reducing labyrinths. The construction of such a stuffing box is illustrated in Fig. 10. It will be noted that one of the outstanding features of this design is that the stuffing-box leakage is precooled before it reaches the packing proper. Operating records in excess of 6 months have been obtained with this construction without renewing the packing.

While this combination of pressures and temperatures does not necessarily represent the ultimate limit, further increases will probably be reached more slowly and after much careful laboratory and field experimentation. Furthermore, it may be noted that, at the present time and with very few exceptions, this range of pressures and temperatures represents the maximum conditions which might have to be imposed on boiler feed pump stuffing boxes.

Whenever boiler feed cycle requirements are such that these limits have to be exceeded, the only solution resides in the application of pressure-reducing devices ahead of the stuffing box proper. Since the design of such devices has now reached a high degree of proficiency, the only remaining drawback to their application is the necessity of bleeding a part of the effective capacity back to a lower pressure level and the attendant reduction in efficiency.

PRESSURE AND TEMPERATURE CONTROL IN CLOSED FEED CYCLES

There is a certain interesting although little known phase in the control problem of the so-called closed feed cycle, where

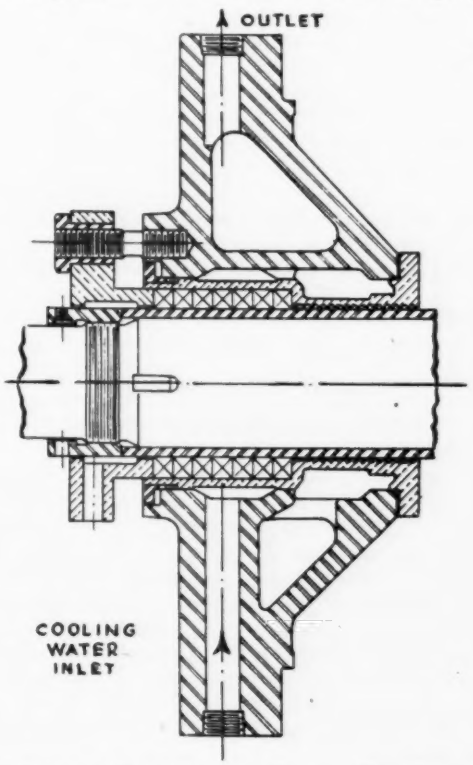


FIG. 10 IMPROVED STYLE STUFFING BOX FOR HIGH SUCTION PRESSURES AND TEMPERATURES

several boiler feed pumps are operated in series with closed heaters interposed between successive pumps, and where one or more of these pumps is operated at variable speed, as illustrated in Fig. 11.

Normally, the variable-speed operation is restricted to the low-pressure unit of the combination, the controlling mechanism being either an excess-pressure or a constant-pressure regulator. This regulator is used to vary the speed of the centrifugal pump in question, which is driven by a steam turbine, a wound-rotor motor, or even through a variable-speed coupling.

This control is obviously unaffected by the relationship between the temperature and the pressure at the suction of any one of the pumps so that conditions might arise where the speed regulation on one pump lowers the suction pressure of the following pump dangerously close to or even below the vapor pressure of the feedwater at the suction.

While at full load the temperature of the feedwater leaving the individual pumps is for practical purposes equivalent to the temperature at the pump suction, this does not hold true at light loads, and for that reason the illustration indicates this by using different subscripts for the temperatures at the suction and discharge of each pump. It is obvious that the margin between the pressure at the suction of the secondary feed pump (P_4) and the vapor pressure corresponding to the temperature T_4 must never be allowed to fall below a certain predetermined value which depends on the pump design.

The selection of the individual pump-discharge pressures is a relatively complex problem which is affected by the amount of required pressure regulation, that is, by the system head curve of the boiler feed cycle, by the head-capacity characteristics of the individual pumps, the maximum temperatures of the feedwater at the outlet of the various heaters, the permissible speed variation of the variable-speed drivers, and finally by the desired maximum hydraulic pressure to be imposed on the intermediate closed heaters.

Fig. 12 illustrates qualitatively the characteristics of a typical closed system such as in Fig. 11. For purposes of simplification, frictional losses between the pumps have been neglected. It will be seen that the pressure at the discharge of the secondary pump considerably exceeds the required system head pressure at light loads if all the pumps are operated at constant speed, and that even if the primary feed pump is by-passed altogether, the secondary feed pump can develop sufficient pressure from shut-off to capacity "A." In other words, the speed variation required of the driver of the primary pump ranges all the way from 0 to 100 per cent. This, obviously, is impractical for a great many reasons, especially if the pump is driven by a wound-rotor motor where reduction of speed below 50 per cent of design speed is seldom practiced. As a result, the operation of such a cycle at variable speed generally takes place along the lines illustrated in Fig. 13. Whatever excess pressure remains is throttled by the feedwater regulator.

The important feature of a proper selection of primary feed pump conditions and of a suitable variable-speed control is that means must be made available to prevent the discharge pressure of the primary feed pump (P_3 in Fig. 11), from falling below a certain minimum determined by the relationship between P_4 (P_3 less losses through the closed heater), and the vapor pressure corresponding to the temperature T_4. Should certain operating conditions arise which might lead to a dangerous reduction of the difference between P_4 and the vapor pressure at T_4, some control must be instituted, actuated by this difference and arranged to set a definite limit to the speed reduction called for by the excess-pressure regulator.

Fig. 13 indicates the introduction of such a speed-reduction limiting control, whereby the discharge pressure of the primary

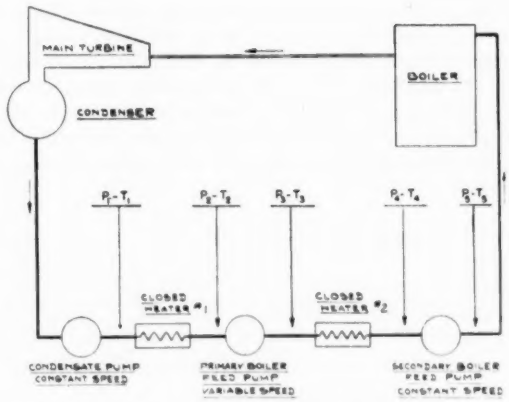


FIG. 11 CLOSED FEED CYCLE WITH VARIABLE-SPEED PRIMARY FEED PUMP

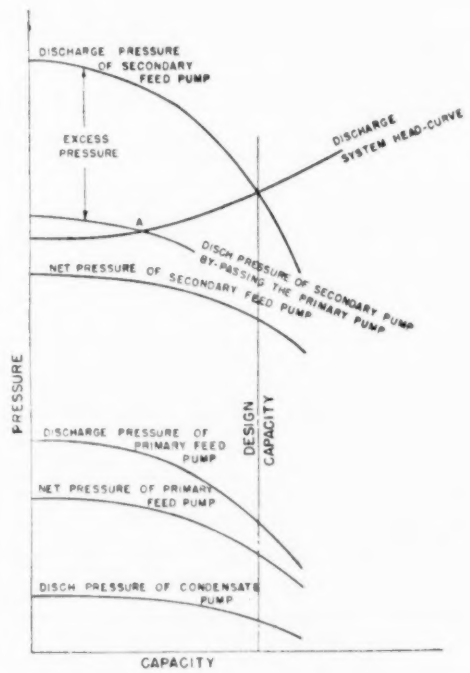


FIG. 12 CHARACTERISTICS OF A CLOSED FEED CYCLE AT CONSTANT SPEED

feed pump is not permitted to fall below a predetermined minimum. For the sake of simplification, it has been assumed that the value of T_4 is constant at all loads, and therefore that the minimum permissible value of P_3 is likewise constant. Actually, the closed heaters are fed with steam bled from some given stage of the main turbine and the pressure and temperature of this steam are reduced as the load is reduced. Thus in an actual installation, the process of checking the minimum permissible primary feed pump discharge pressures may be a little more tedious than indicated here.

CONCLUSIONS

The foregoing discussion of boiler feed cycles has been presented not as an attempt to catalogue in an exhaustive manner all the possible variations and ramifications which can be found in these cycles, but rather with the desire to illustrate the close relationship between cycle and pump design. There is no ques-

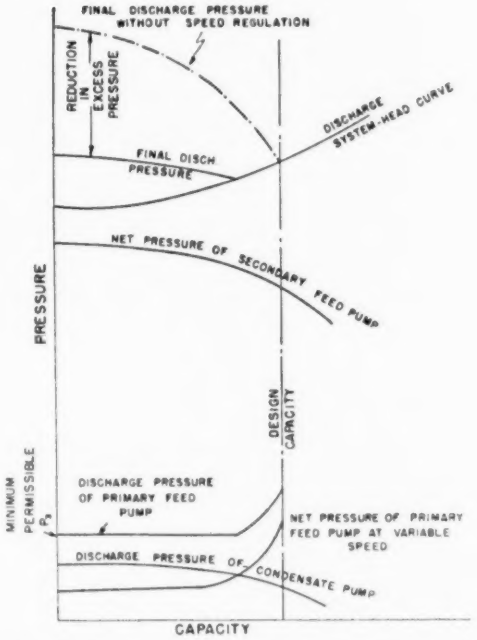


FIG. 13 CHARACTERISTICS OF A CLOSED FEED CYCLE WITH VARIABLE-SPEED REGULATION

tion that the degree of integration of the pump into the pumping cycle itself is a direct criterion of the ultimate success of the entire installation. It is toward such complete integration that the pump designer, the application engineer, and the technical operating personnel have had to apply their efforts, and it is through this integration that modern centrifugal-pump designs have achieved their relative success.

It is hoped that the present analysis will give rise to more studies of all the factors connected with high-pressure cycles, and thus the seed will be sown for further improvements based upon mutual understanding and co-operation between designer and operating personnel. The problems which high-pressure pumping cycles have presented have not grown easier with time. But it may be said, with a certain pardonable pride, that the centrifugal-pump designer has so far fully met the challenge.

Discussion

R. P. MOORE.[2] The author describes a clever means of preventing loss of the suction pressure on boiler feed pumps drawing water from direct-contact deaerating heaters when the load on the turbine is reduced. This scheme includes some automatic valving. Experience has proved, in certain cases at least, that it is possible to accomplish the same result without any automatic valves or other moving equipment. Proper design of the deaerating heater, as is described in an article by the writer,[3] accomplishes the desired result. The scheme consists of placing baffles in the heater so as to guide the freshly deaerated water directly to the boiler feed pump suction and to allow any flash steam which forms in the water in the heater to rise to the steam space without interference with this flow.

Fig. 14 of this discussion shows the baffles and vents added to the bleeder deaerating heater of standard design in use in Huntley Station No. 2 of the Buffalo Niagara Electric Corporation. The results accomplished by this addition are shown in curve form in

[2] Mechanical Engineering Department, Buffalo Niagara Electric Corp., Buffalo, N. Y. Mem. A.S.M.E.

[3] *Electrical World*, October 14, 1944.

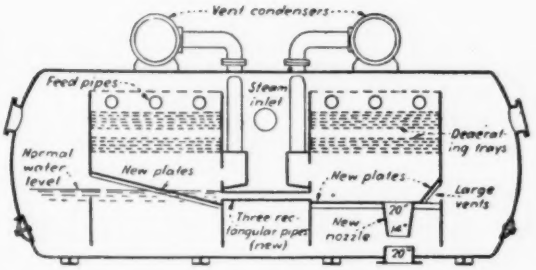
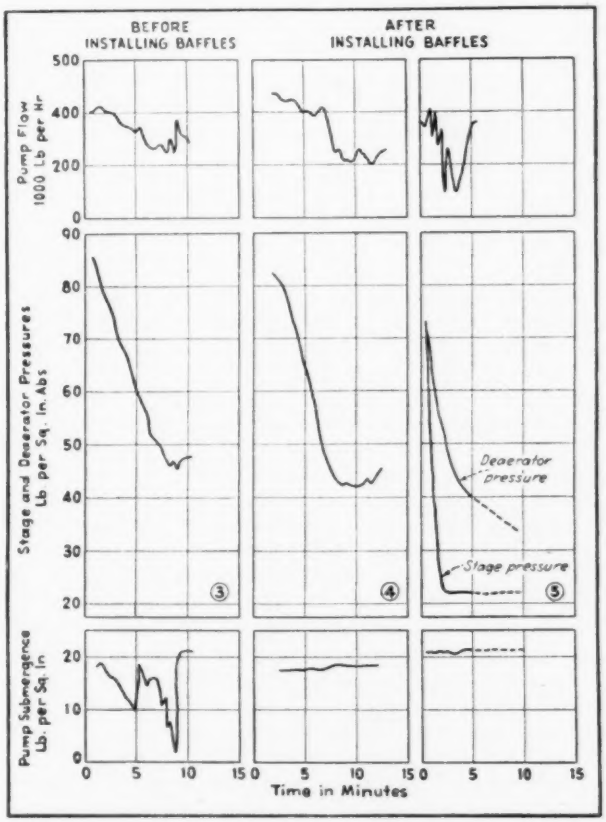


FIG. 14 LONGITUDINAL SECTION OF DEAERATOR, SHOWING NEW PARTS



FIGS. 15, 16, AND 17 (*Left to Right*): AFTER INSTALLING BAFFLES, LOAD COULD BE REDUCED RAPIDLY, I.E., 10 PSI PER MIN IN FIG. 16, AND 20,000 KW PER MIN IN FIG. 17, WITHOUT OCCASIONING LOSS OF PUMP SUBMERGENCE THAT OCCURRED BEFORE THEY WERE INSTALLED, FIG. 15

Figs. 16 and 17, taken from the article referred to,[3] compared to the conditions prior to the change, Fig. 15. In Fig. 16, the rate of pressure drop was such that deaerator and stage pressures remained the same. In Fig. 17 the stage pressure dropped so rapidly that the bleeder nonreturn valve closed, and the deaerator pressure could not follow. Not only has loss of pump suction been eliminated when the turbine load drops, even if instantaneously, but the water continues to pass through the deaerator and is deaerated under all conditions.

R. M. SEAGO.[4] In connection with higher boiler feed pump

[4] Efficiency Engineer, New Orleans Public Service, Inc., New Orleans, La. Mem. A.S.M.E.

suction temperatures, the author states that in the event of a severe and sudden drop in station load, turbine-stage pressures will quickly drop resulting in severe flashing in the direct-contact heater serving as boiler feed storage tank and also in suction piping to the boiler feed pump. While drop in pressure of bleed steam to the boiler feed heater undoubtedly contributes to the condition of severe flashing, it is not, in the writer's opinion, the only factor involved.

To illustrate, let us follow the train of events resulting from a severe and sudden drop in station load:

1 Due to sudden decrease in load on the electric generator, the turbine tends to overspeed, resulting in a rapid throttling of control valves by the governor.

2 As a result of control valves throttling, stage pressures drop rapidly and throttle pressure rises rapidly.

3 Sudden rise in throttle pressure may result in one of two effects, in so far as the boiler is concerned, depending on the severity of the load drop, that is, depending on whether it is within or without the capability of combustion control.

If the drop is too severe for combustion control to handle, one or more safety valves will lift, causing an instantaneous rise in boiler-drum water level. The feedwater regulator might close completely, and if automatic recirculation is provided the boiler feed pump will be subjected to minimum flow as determined by its recirculating orifice capacity. If manual recirculation control is provided, under these conditions, the pump will probably be subjected to zero flow, resulting in severe flashing and probable damage to its internal parts.

On the other hand, if the load drop is within the capability of combustion control to prevent popping of safety valves, another train of events, detrimental to boiler feed pump operation, will be started. Rise in throttle steam pressure will result in an initial rise in boiler-drum pressure causing a drop in drum water level, followed by a more severe drop in water level as the firing rate is rapidly decreased. If the feedwater regulator is of the single-element type, it will open rapidly, placing a sudden demand on the boiler feed pump and also on the boiler-feed tank. If the regulator is of the multiple-element type, the water-level effect will probably override the effect of diminished steam flow to result in a similar though less pronounced increase in feeding rate. This will result in a rapid decrease in boiler feed pump npsh over and above the decrease imposed by drop in turbine stage pressure.

Further aggravation will also be imposed in some installations by quenching of vapor in the boiler feed tank by make-up water supplied from an auxiliary storage or surge tank.

If return of turbine loading is rapid, as in the case of a short-duration electrical interruption, similar hardships will be placed on the boiler feed pump. Rapid increase in boiler firing rate will result in almost instantaneous swelling of water within the boiler, often causing the feed regulator to close completely. Again the boiler feed pump will be subjected to minimum flow conditions followed by a gradual return to normal flow.

The foregoing is certainly not intended as a criticism of the author's analysis of causes of erratic boiler feed pump suction conditions, but rather is intended as an amplification of this analysis in line with a personal opinion that correction of such conditions should be, in the majority of cases, thrown back in the lap of engineers responsible for the heater, piping, and pump layout. Obviously, sufficient submergence of boiler feed pumps to provide ample static suction head in excess of any reductions imposed by normal surges would remedy the situation without recourse to injection of colder water into the boiler feed pump suction. For the majority of cases where space or operating pressure limitations will not allow provision of sufficient static suction head, the injection of colder water offers definite possibilities.

The use of low-pressure heater condensate as injection water presents another problem in connection with many existing systems. In a typical installation, for example, at full turbine load, low-pressure heater condensate represents 8 per cent of throttle steam flow (or boiler feed pump flow). However, at one half load, low-pressure heater condensate is only 5 per cent of throttle flow. This may or may not provide sufficient injection water to insure adequate temperature depression at the boiler feed pump suction.

In line with these possible restrictions, it might be well to re-examine the possibility of using condensate direct from main condensate pumps. It has been our experience, based on numerous tests on two modern condensers designed for de-aeration of hot-well water, that condensate leaving condensate pumps is oxygen-free within limits of detection, by the modified Winkler test, and consequently, from this standpoint, is suitable for injection directly into the boiler.

Papers of this type, together with the discussions which they evoke, are of tangible benefit to the engineer faced with similar problems. Encouragement should be given to preparation of more papers in which the equipment designer freely discusses the limitations as well as the capabilities of the apparatus.

A. J. Stepanoff.[5] The writer will call attention to a few problems in high-pressure boiler feed practice not mentioned in the paper, which are not caused directly by the high pressure, high temperatures, or pump high operating speed. One of them is the wear of internal parts resulting from corrosion and erosion commonly referred to as "cutting." The pH value of the pumped water does not indicate the corrosiveness of water when applied to pure water. A definite trend to purer feedwater in central-station application will demand wider use of stainless steels for pump parts than has been the case in the past.

Mechanical problems connected with high-pressure high-temperature boiler feed pumps were not different from those encountered with the hot-oil charging pumps. A number of these were in service some 10 to 15 years ago, pumping oils at 800 F, maximum pressures from 1000 to 1500 psi (2300 psi was used at one refinery) and 4000 rpm pump speed. Even with the most corrosive (sour) oils, pump-casing cutting was practically unknown with hot-oil pumps.

Pressure "surges," accompanied by the capacity, speed, and power fluctuations, presented another problem in boiler feed pump operation not previously encountered in hot-oil or any other pumping service. Such surges are of the same nature as those observed in hydroelectric power plants frankly and completely discussed in a paper by Rheingans.[6] Both systems have a mass of water suspended between the free surfaces at their ends. This is free to oscillate if some impulses appear at a frequency synchronous with that of the natural frequency of the system. As a result of such fluctuations, in the case of boiler feed pumps, the piping may require additional bracing, and some pumps cannot be operated at low capacities. R. Dziallas[7] has studied the surges and was able to reproduce those in a laboratory setup.

It should be noted that condensate-pump cycle presents another swinging system with two free water surfaces at the ends, but no surges are observed on this system as long as the condensate pumps operate beyond the breakdown point on the head-

[5] Engineer, Cameron Engineering Department, Ingersoll-Rand Company, Phillipsburg, N. J. Mem. A.S.M.E.

[6] "Power Swings in Hydroelectric Power Plants," by W. J. Rheingans, Trans. A.S.M.E., vol. 62, 1940, pp. 171–184.

[7] "Schwingungen bei Kreiselpumpen mit labiler Kennlinie," by R. Dziallas, *Archiv für Wärmewirtschaft und Dampfkesselwesen*, March, 1941, pp. 63–66.

capacity curve, Fig. 4 of the paper, because cavitation destroys the regularity of impulses in the system. Similarly, surges can be stopped on any boiler feed pump by throttling the pump discharge slightly (sometimes as little as 20 psi), thus destroying the regularity of the water mass oscillation.

The writer does not believe that the author's criticism of European engineering or training is justified. The high-pressure-boiler development is only one example of European engineering achievement.

In so far as pump speeds are concerned, the general trend toward higher speeds is very definite in this country too. While 3600 rpm was a top speed only recently, 6000 to 7000 rpm is quite common now. Cost is only secondary to weight and space saving, and hydraulic advantages in the advance in the operating speeds of boiler feed pumps.

G. H. Van Hengel.[8] The paper gives a good detailed description of the difficulties encountered when operating centrifugal pumps with net positive suction heads close to their guarantee. These pitfalls are generally not realized when the layout of a plant is made and are difficult to correct afterward because they are dependent on the elevations which have been fixed by the structure of the building.

In large power stations where bleeding is used, a change of load will change the pressures in all the turbine stages practically proportionally to the load. Thus in case 20 per cent of the turbine load is dropped, the stage pressures will also drop 20 per cent, and with them the heater pressures. All the pumps extracting from these bleeding heaters will therefore be suddenly robbed of 20 per cent of their suction pressure.

The stage temperatures, however, because of the heat storage in the condensate present in the heater, will not drop as rapidly. It is this phenomenon of the lag in temperature with respect to pressure that causes a difficult condition for the heater pumps. Because this lag depends on various conditions of the layout and the rate change of load, it differs for each individual case. The whole matter reduces to the question of how fast the load on the turbine drops in comparison to the ensuing rate of temperature changes in the heater.

This comment is intended to emphasize the severity of the condition of pump operation caused by the persistence of this lag, and to show a ready method of calculation to provide for any condition that may occur.

Let us now consider different cases of installation and required operation. For all cases, we assume: That no undercooling of the condensate leaving the heaters exists in regard to the steam entering the heaters or that the pump is running with a net positive suction head at the least value required for its operation.

The following cases are discussed:

1 Instantaneous load drop.
2 Very gradual load drop.
3 Decrease of load throughout a given period.
  (*a*) With no storage capacity.
  (*b*) With storage capacity.

Case 1. Instantaneous Load Drop. As a basis of calculation, let us assume that the load change on the turbine is instantaneous and that the temperature in the heater does not change, a case which corresponds to infinite storage capacity. For safe operation, an excess suction head has to be available to provide a corresponding pressure drop. To calculate this excess suction head, we can readily determine the head equivalent of the assumed sudden pressure drop by using the conservative formula, 1 psi pressure = 2.6 ft head. Thus a sudden drop of 10 psi on a heater would demand an excess net positive suction head of 26 ft on the pump to prevent unsafe operation.

Example: A condensing 80,000-kw turbine with 17 stages has a main steam pressure and temperature of 800 psia and 900 F. It has four direct-contact heaters supplied with steam bled from the 4th, 7th, 10th, and 13th stages at full-load stage pressures of 250, 100, 40, and 8 psia, respectively. If there is a sudden load drop of 20 per cent, the conditions which result are as listed in Table 1 of this discussion.

TABLE 1 CONDITIONS RESULTING FROM 20 PER CENT LOAD DROP

		Heater stages				Condenser
		4th	7th	10th	13th	
1	Full-load pressure, psia	250	100	40	8	0.50
2	80 per cent load pressure, 0.80 × (1), psia	200	80	32	6.4	0.47
3	Sat. temp corr. to (1), deg F	401	327	267	183	80
4	Sat. temp corr. to (2), deg F	382	312	254	173	28
5	Temp diff. due to load, (3–4), deg F	19	15	13	10	2
6	Head increment needed on heater pumps [2.6 (1–2)], ft water	130	52	21	4	0.08

Table 1 shows that with an instantaneous drop of load of 20 per cent and with the greatest possible temperature lag in the heaters, we would have to provide 130, 52, 21, 4 ft additional head on the pumps if this instantaneous drop in load is to be provided for.

For a hot-well pump on a condenser with automatic level control, however, the table shows that the sudden 20 per cent drop of turbine load demands only 0.08 ft excess suction head. Therefore, for the condenser hot-well pump, sudden drops of turbine load can never be a serious factor to be considered in design.

For the heaters this is somewhat different. It must be noted here that for the heaters the additional net positive suction head required is proportional to the absolute heater pressure. The higher the heater pressure, the more probability there is for losing the suction of the heater pump and the more margin in suction head we should have on the pump.

Case 2. Gradual Load Drop. At the other extreme is the case of dropping the load over a very long period which will cause the heater condensate temperature to follow the bled-steam temperature with no lag.

The suction head which must be provided on the pumps in excess of the manufacturer's guarantee would then be zero feet for this case.

The actual provision of suction head to be made must lie between the two extreme Cases 1 and 2.

Case 3(a). Decrease in Load Throughout a Given Period of Time—No Storage Capacity. Now assume that the load drops not instantaneously, but 20 per cent in 5 min; furthermore, that the condensate level is not in the heater but in the suction pipe; a case with practically no storage capacity. Then for the 4th-stage heater in the example, the condensate should increase its pressure by flowing downward at a rate of at least 130 ft in 5 min, or 0.43 fps if we want to prevent flashing. This 0.43 fps will thus determine the maximum size of our pump suction line.

If we have an existing installation, then our suction velocity should be greater than 0.43 fps for successful operation.

Case 3(b). Decrease in Load Throughout a Given Period of Time—With Storage Capacity. Assume again 20 per cent load drop in 5 min. The case can be considered first as Case 3(*a*), but the hot-well cross section replaces the suction-line area. In addition, the colder condensate flow will mix with the hot-well storage, reducing the required suction head. This problem has to be solved mathematically and is dependent on heater hot-well capacity and rate of steam going to the heater. Space limitations prevent treating this case.

All cases so far treated assumed no undercooling or no addi-

[8] The Detroit Edison Company, Detroit, Mich. Mem. A.S.M.E.

tional net positive suction head. In direct-contact heaters, the undercooling will be practically zero. In closed heaters some undercooling always exists. Assume a 5-deg F undercooling for a closed heater on the 4th stage of the example given. The net positive suction head needed would be reduced by

$$\frac{5}{19} \times 130 = 34 \text{ ft}$$

Also, if regulation of the pump discharge is taking place, it may be possible that additional suction head is available at the time the load is dropped.

For safe operation of the heater pump, with time for load drop as in Cases 3(*a*) and (*b*), the undercooling and the additional suction head available during operation reduce the maximum head required under Case 1.

Conclusion. Power stations should be designed not only to meet maximum load conditions, but also certain rate changes in load. For instance, the requirements for the net positive suction head on heater extraction pumps (boiler feed or heater drain pumps), due to sudden load drops, are not sufficiently recognized. Oversight of this fact often leads to dangerous operation which is difficult to correct because of the limitations of the building structure. The problem of variability in load during operation must therefore be thoroughly investigated during the preliminary layout of the station.

Author's Closure

The author wishes to acknowledge with appreciation the contributions of the discussers.

Mr. Moore's solution of the problems introduced by sudden load fluctuations is an extremely valuable contribution to satisfactory heater operation and, the author believes, should be well studied by feedwater heater designers. While the possibility remains that this solution may not meet all cases, it is gratifying to see that it attacks the problem exactly where it arises, that is in the feedwater heater. One of the features of this solution which remain to be investigated resides in the effect of the baffling arrangement described on installations embodying very large feedwater storage volumes, where such baffling may lead to excessive subcooling of that portion of the stored feedwater which is farthest removed from the heater outlet. The author is confident, however, that even this problem is not unsurmountable.

The additional effect of boiler controls on the phenomena which take place at a boiler feed-pump suction on a sudden drop of main turbine load are very well brought out by Mr. Seago. While a sudden increase in boiler feedwater demand may or may not impose additional difficulties, depending upon the margin available over the minimum npsh at maximum pump flow, the reverse case—that of complete closure of the feedwater regulator—introduces very serious possibilities.

If we were to assume that the sudden load drop occurs when operation was taking place between 50 and 100 per cent full load and that the by-pass is manually controlled, it is logical to expect that all by-passes are closed at the time of the load drop and the pumps may be severely damaged. This, incidentally, is quite independent of the suction pressure and temperature and could occur even if the pressure in the heater was pegged to a definite value. Much as it may be desired to avoid the introduction of additional controls, the sequence of events outlined by Mr. Seago shows the advantages and the added protection afforded by an automatically controlled by-pass.

If, as Mr. Seago states, the low pressure heater condensate at one-half load corresponds to but 5 per cent of the throttle flow, its injection into the feed pump suction may or may not be sufficient to afford the required protection against flashing. Assuming the conditions outlined in the paper, that is, 325 F feedwater, 227 F heater drains, and a required margin of 20 feet—the injected condensate must be 6.2 per cent of the boiler feed pump capacity and in accordance with Mr. Seago's statement, the available condensate is insufficient. On the other hand, assuming the same temperature conditions, a 5 per cent injection will provide about 17 ft surplus npsh (see Figs. 8 and 9) and may be sufficient in some cases. Obviously, where it is possible to use the discharge from the condensate pumps, the available flow is fully ample and because of the greater temperature differential, the percentage of injected feedwater appreciably reduced. It must be remembered that the injection is an emergency measure and that the slight danger of feedwater contamination is justifiable, especially since the emergency is not a frequent one.

The problems of corrosion and erosion of internal boiler feed-pump parts mentioned by Mr. Stepanoff have been purposely omitted from this paper as their importance merits a complete and separate study, while their inclusion would have lengthened the present paper unnecessarily without exhausting the subject matter. It may be of some interest to mention, however, that very serious studies have been carried out on these problems within the past twelve months. The preliminary results seem to justify the growing trend toward stainless steels mentioned in Mr. Stepanoff's discussion as well as in the author's paper. It is already becoming apparent that stainless steel casings in a range from a minimum of 4 per cent chromium content to the 25 per cent chromium-20 per cent nickel type, will be utilized to a much greater extent than heretofore. Coupled to the already prevalent use of stainless steel fittings, this trend gives definite indications of solving the twin problems of corrosion and erosion, even at the higher stage pressures predicted.

No criticism of European engineering or training was voiced or even implied by the author. The comparison of practices was brought out to illustrate the possible effect of economic and geographical circumstances on engineering designs and no issue can be taken with the fact that European labor is cheaper than in the U. S. A. and raw materials less available.

Mr. Van Hengel's calculations illustrate very forcefully the theoretical head increment needed on pumps taking suction from direct contract heaters operating at high pressures, both with instantaneous and gradual load drop. Fortunately for the power-plant designer, the usual case corresponds to Mr. Van Hengel's Case No. 3 and the entire theoretical increment in npsh need not be provided for. The determination of the minimum permissible safety margin in npsh is rather complex but can be carried out fairly accurately by the feedwater heater designer, once all the contributory factors and component data have been made available. It is highly important, however, that power stations be designed, as Mr. Van Hengel states, not only to meet maximum load conditions, but also the expected range of load changes.

The Behavior of a Hot-Wire Anemometer Subjected to a Periodic Velocity

By R. C. MARTINELLI[1] and R. D. RANDALL,[2] BERKELEY, CAL.

A method is presented which allows a rapid graphical prediction of the response of the constant-current hot-wire anemometer to a periodic velocity. From such a prediction the suitability of the hot-wire anemometer for any particular application can be readily determined. The method is demonstrated by several illustrative examples.

Nomenclature

The following nomenclature is used in the paper:

A = surface area of wire, sq ft
α = temperature coefficient of resistance, deg F^{-1}
c = constant of integration
C_p = heat capacity of wire, Btu/(lb)(deg F)
ϵ = base of Napierian logarithms
E = voltage across hot-wire anemometer at any temperature, t, volts
E_∞ = Voltage across hot-wire anemometer when wire is at room temperature, τ_∞, volts
$e = E - E_\infty$, voltage across hot wire referred to room-temperature voltage, volts
e_m = voltage across hot wire, referred to room-temperature voltage, corresponding to mean velocity, volts
e_0 = voltage across hot wire, referred to room-temperature voltage, corresponding to conditions of zero thermal lag, volts
f = unit thermal conductance between hot wire and air, Btu/(hr)(sq ft)(deg F) (actually f includes convection, radiation, and conduction to anemometer supports)
i = current through hot wire, amperes
$P(\theta)$ = function of time defined in text
$P(v)$ = function of velocity defined in text
Q = "characteristic" of hot wire, defined in text, volts per hr or volts per sec
R = resistance of wire at any temperature, t, ohms
R_∞ = resistance of wire at room temperature, ohms
$S = \frac{de}{d\theta}$ = rate of change of voltage with time, volts per hr or volts per sec
t = temperature of hot wire, deg F
τ_∞ = temperature of air around hot wire, deg F
W = weight of hot wire, lb
θ = time, hr
3.413 = number of Btu per hr in 1 watt

Introduction

The hot-wire anemometer, as normally operated, consists of a small wire (usually of platinum) suspended between supports in a fluid stream and heated by an electric current. Variations of the velocity of the fluid flowing past the hot wire produce corresponding variations in the heat lost from the wire and thus vary the wire temperature, which in turn alters its electrical resistance. By proper calibration, the wire resistance can be correlated with the velocity of the fluid flowing past the wire, and therefore the hot wire can be used for the measurement of fluid velocities.

The application of the hot wire to the measurement of steady velocities or to small velocity fluctuations about a large mean has been the subject of many studies (1 to 11).[3] Some work has also been done on the behavior of the hot wire when subjected to small velocity fluctuations about a zero mean, mainly in conjunction with the hot-wire "microphone" (12 to 15). The hot wire has also been utilized to measure fluctuating wind velocities, which are usually relatively large variations in velocity of rather low frequency (16, 17).

In all these applications the lag of the response of the hot wire to velocity variations, due to the heat capacity of the wire, has been given considerable attention. However, no complete analysis of the problem has been presented which would allow the prediction of the hot-wire behavior when subjected to large velocity variations of relatively high frequency. It is the purpose of this paper to present such an analysis.

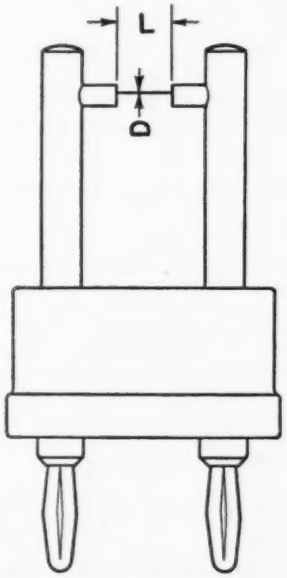


Fig. 1 Hot-Wire Anemometer

Description of Ideal System

In the following discussion a hot wire of length L and diameter D is considered suspended between two supports, Fig. 1. The actual system will be idealized as follows:

1 The temperature of the wire is considered uniform at all

[1] Assistant Professor of Mechanical Engineering, University of California. Jun. A.S.M.E.

[2] Research Engineer, Department of Engineering, University of California. Mem. A.S.M.E.

Contributed by the Heat Transfer Division and presented at the Aviation War Conference, Los Angeles, Cal., June 11–14, 1945, of The American Society of Mechanical Engineers.

Note: Statements and opinions advanced in papers are to be understood as individual expressions of their authors and not those of the Society.

[3] Numbers in parentheses refer to the Bibliography at the end of the paper.

times. This is not strictly true because of the cooling of the ends of the wire by the supports, and the radial temperature distribution existing in the wire during transient operation.

2 The wire operates at constant current. This requirement is easily met in the actual system.

3 All heat losses from the wire are proportional to the difference in temperature between the wire and the ambient air.

4 The heat loss from the wire at any fluid velocity during transient operation is exactly equal to the heat loss at the same velocity during steady-state operation.

Basic Equations

Since the operation of the hot wire depends upon its heat loss to the surrounding fluid, the basic equation describing the operation of the anemometer is a heat balance on the wire. During transient operation, the energy supplied to the wire by the electric current appears in two places; part of it is lost to the surroundings, and the remainder is used to heat the wire from one temperature to another. Thus the heat balance becomes

$$WC_p \frac{dt}{d\theta} + fA(t - \tau_\infty) = 3.413\, i^2 R \ldots\ldots\ldots [1]$$

The first term represents the heat required to change the temperature of the wire, by an amount dt in a time $d\theta$; the second term represents the heat lost to the surroundings; and the last term the heat supplied by the electric current. All term sare in Btu per hour. Equation [1] is the basic equation for the idealized hot-wire anemometer.

In practice it is more convenient to measure the voltage drop across the wire than to measure the wire temperature. The temperature and voltage are simply related, as shown below.

The resistance of the hot wire R, at any temperature t, may be written as

$$R = R_\infty [1 + \alpha(t - \tau_\infty)] \ldots\ldots\ldots\ldots [2]$$

where R_∞ is the resistance of the wire at the temperature of the ambient air τ_∞. The voltage across the wire at constant current is

$$E = iR = iR_\infty [1 + \alpha(t - \tau_\infty)] = E_\infty [1 + \alpha(t - \tau_\infty)] \ldots [3]$$

Thus

$$dt = \frac{dE}{i\alpha R_\infty} \ldots\ldots\ldots\ldots\ldots\ldots [4]$$

and

$$(t - \tau_\infty) = \frac{E - E_\infty}{i\alpha R_\infty} \ldots\ldots\ldots\ldots\ldots [5]$$

Substituting in Equation [1] yields

$$\frac{dE}{d\theta} + \frac{fA}{WC_p}(E - E_\infty) = \left(\frac{3.413\, i^2 R_\infty \alpha}{WC_p}\right) E \ldots\ldots [6]$$

For simplicity, a new variable $e = E - E_\infty$ may be defined. Then Equation [6] becomes

$$\frac{de}{d\theta} + \left(\frac{fA - 3.413\, i^2 R_\infty \alpha}{WC_p}\right) e = \left(\frac{3.413\, i^2 R_\infty \alpha E_\infty}{WC_p}\right) \ldots [7]$$

The problem of determining the behavior of the hot-wire anemometer subjected to a periodic (or fluctuating) velocity is then to solve Equation [7], obtaining e as a function of time, corresponding to a given variation of the velocity as a function of time. Although the velocity, per se, does not appear in Equation [7], variations in velocity cause definite variations of the unit thermal conductance f, and thus the coefficient of e in Equation [7] is a function of velocity, and finally of time, since the velocity depends upon time. An idea of the variation of f with time can be obtained as follows:

If the frequency of velocity variation is not too great, it may be postulated that, during a cycle of velocity variation, the value of f at any instantaneous velocity v is equal to the value of f which would have been obtained at an equal steady velocity. With a given current flowing through the wire, values of f versus v may be obtained at various steady velocities. A typical plot of f versus v is shown in Fig. 2. The variation of f with v is complex because at zero velocity, free convection, radiation, and conduction are important; while at high velocities forced convection controls. Now, assuming the data for Fig. 2 are applicable at each instant of a cycle of variable velocity, the construction of Fig. 3 would yield the corresponding variations of f with θ.

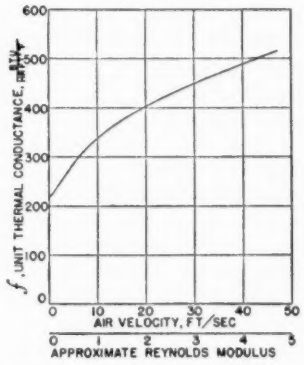


Fig. 2 Unit Thermal Conductance for 0.0005-In. Wire Suspended in Air

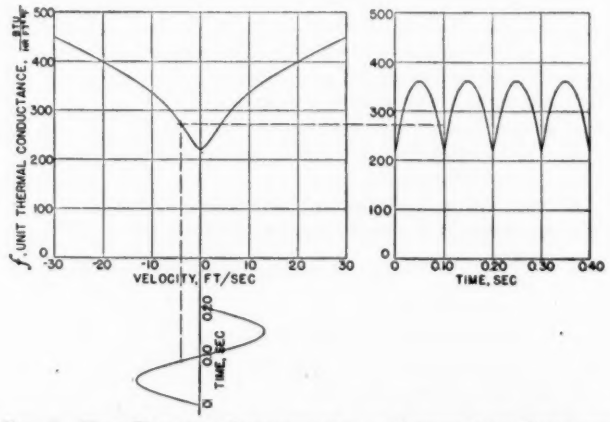


Fig. 3 Unit Thermal Conductance as Function of Time for 0.0005-In. Hot Wire Being Subjected to a Periodic Velocity of 13-Fps Amplitude About Zero Mean

It is noted that although the velocity v becomes negative, the value of f is, of course, always positive since heat is transferred regardless of the direction of air velocity. At the point $v = 0$ the curve of f versus v may not be exactly symmetrical due to free convection effects (2, 9, 12, 14).

Since f varies with time, the coefficient of e in Equation [7] is a function of time, and Equation [8] may be formally written as

$$\frac{de}{d\theta} + P(\theta)\, e = Q \ldots\ldots\ldots\ldots\ldots [8]$$

where

$$P(\theta) = \left(\frac{fA - 3.413\, i^2 R_\infty \alpha}{WC_p}\right)$$

and

$$Q = \left(\frac{3.413\, i^2 R_\infty \alpha E_\infty}{WC_p}\right)$$

The formal solution of Equation [9] is (18)

$$e = \epsilon^{-\int P d\theta}\left[\int Q \epsilon^{\int P d\theta}\, d\theta + c\right] \ldots\ldots\ldots\ldots [9]$$

Unfortunately, this formal solution is of little use, since the analytical expression for $P(\theta)$ is of such a nature that direct integration is impossible. Maxwell (15) has solved Equation [8] for small periodic-velocity variations about a zero mean by expanding the voltage e in a Fourier series. This method, however, is laborious and not practical for engineering purposes. Fortunately, another method of solution of Equation [8] is available, namely, the method of isoclines (19), which in this particular case leads quickly to an engineering answer.

In the isocline method, Equation [8] is plotted on the e-θ plane, using constant values of $(de/d\theta)$ as a parameter. Having established loci along which $de/d\theta$ is constant, short lines are drawn with a slope of $de/d\theta$ on these loci. The plane therefore becomes covered with these "direction" lines. Having the initial condition given locates a point in the plane, and the desired solution is found by drawing a curve from this initial point, always tangent to the direction lines. This curve will, of course, satisfy Equation [8] and also the initial condition and therefore is a solution of the equation.

A difficulty still remains, however, since the function $P(\theta)$ is not known. Inspection of Equation [8] reveals a method of obtaining this function by a simple graphical method.

When the steady-velocity calibration curve of the anemometer is obtained, since $\frac{de}{d\theta} = 0$, Equation [8] reduces to

$$P(v)e_0 = Q \ldots\ldots\ldots\ldots [10]$$

where P is now a function of v rather than θ, since f depends on v. The subscript 0 denotes a condition of zero thermal lag. A plot of e_0 versus v obtained experimentally then yields

$$e_0 = \frac{Q}{P(v)} \ldots\ldots\ldots\ldots [11]$$

A typical calibration curve, which can be readily obtained experimentally, is shown in Fig. 4. It is noted that Fig. 4 is closely akin to Fig. 2.

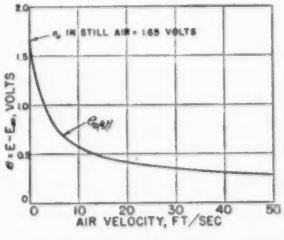


FIG. 4 STEADY-VELOCITY CALIBRATION OF A 0.0005-IN. HOT WIRE

Now if a periodic velocity of very low frequency, $\frac{de}{d\theta} \to 0$, is applied to the hot wire, the construction shown in Fig. 5 can be made. Projecting the instantaneous velocities on the steady-velocity calibration yields the voltage e_0, existing across the wire

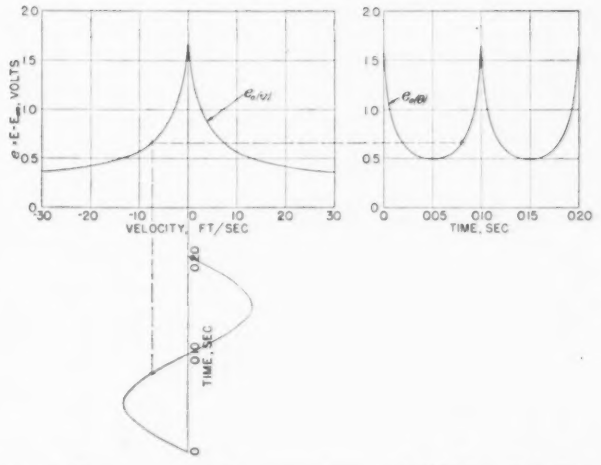


FIG. 5 VARIATION OF VOLTAGE ACROSS 0.0005-IN. HOT-WIRE ANEMOMETER SUBJECTED TO PERIODIC VELOCITY OF LOW FREQUENCY, $\frac{de}{d\theta} \to 0$, WITH NO THERMAL LAG

at each instant of time. Thus on the right of Fig. 5, the curve plotted represents the voltage-time variation across the anemometer if there is no thermal lag. The curve therefore represents

$$e_0(\theta) = \frac{Q}{P(\theta)} \ldots\ldots\ldots\ldots [12]$$

and is the locus of the isoclines $\frac{de}{d\theta} = 0$. Equation [12] allows the evaluation of the function $P(\theta)$. Returning to Equation [8] and substituting the foregoing relation

$$\frac{de}{d\theta} + \frac{Q}{e_0(\theta)} e = Q \ldots\ldots\ldots\ldots [13]$$

Thus curves of constant $\frac{de}{d\theta} = S$ become

$$e = \left(\frac{Q - S}{Q}\right) e_0(\theta) = e_0(\theta)\left(1 - \frac{S}{Q}\right) \ldots\ldots\ldots [14]$$

Equation [14] represents the locus of isoclines of value S and is immediately known once $e_0(\theta)$ and Q are known.

It should be remembered that this method is based on the postulate that the heat loss at any velocity v, during a cycle of periodic velocity variation, is exactly equal to the heat loss at the same velocity during steady-flow operation. This postulate may not be exactly true because of the difference in the hydrodynamic conditions about the wire in the two cases. Experimental work needs to be performed to check this point.

If the method is experimentally verified, it may be possible to correct an experimental response curve by means of Equation [14] to obtain $e_0(\theta)$, from which the true velocity existing at any instant may be determined.

NUMERICAL EXAMPLES

Two numerical examples, illustrating the application of the isocline method of solution, will be presented. The first example shows the prediction of the response of the hot-wire anemometer subjected to a periodic velocity of 13 fps about a zero mean, with a frequency of 5 cycles per sec. The second example shows the response of the hot wire to a periodic velocity with an amplitude of 8 fps about a mean of 20 fps, with a frequency of 5 cycles per sec, and also 50 cycles per sec.

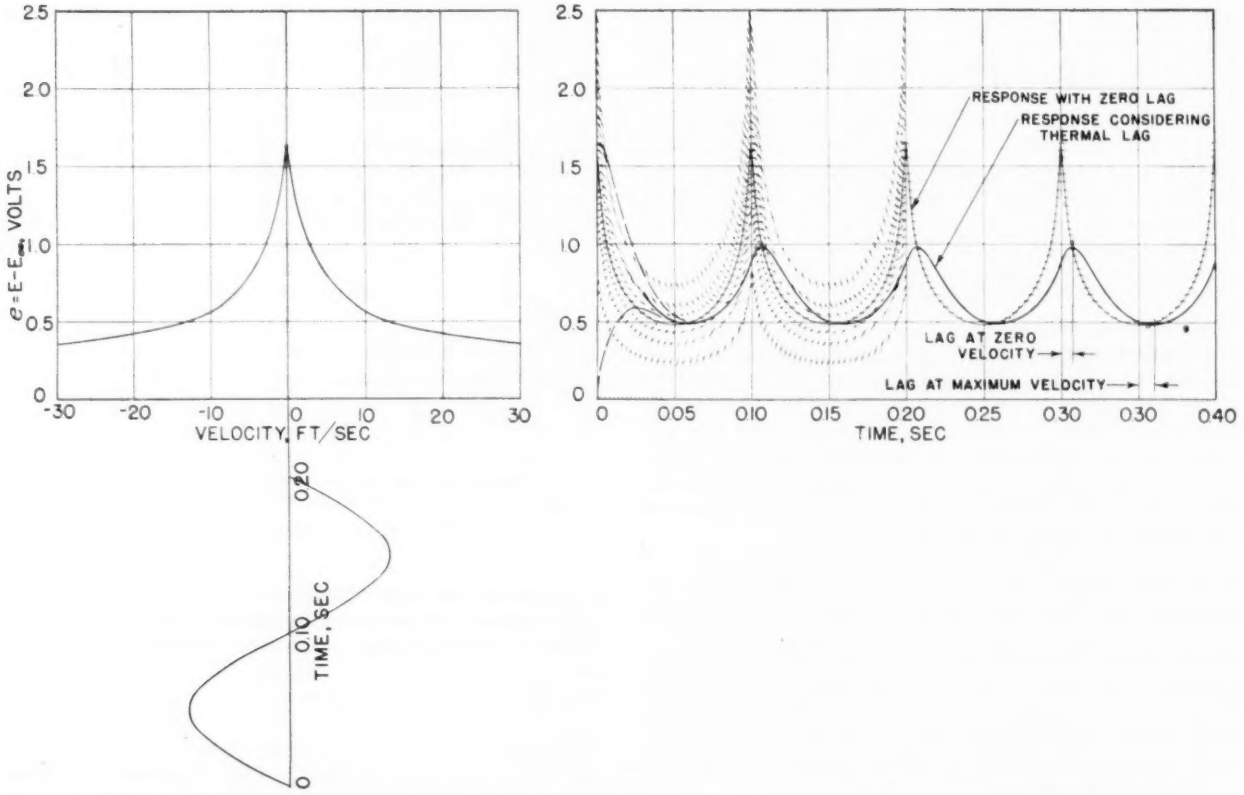


FIG. 6 ISOCLINE SOLUTION FOR RESPONSE OF HOT WIRE TO PERIODIC VELOCITY OF 13-FPS AMPLITUDE ABOUT ZERO MEAN

The following data are available for both examples:

1 Steady-velocity calibration curve of the wire operating with a constant current of 0.140 amp.

2 The properties of the hot wire as follows:

(*a*) Material = platinum
(*b*) Diameter = 0.000532 in. (may be calculated from resistance and resistivity of wire)
(*c*) Length of wire = 0.285 in.
(*d*) Resistance at room temperature = 4.60 ohms

The following properties of platinum are used in the calculations:

(*a*) Density = 1340 lb per cu ft
(*b*) Heat capacity = 0.032 Btu/(lb)(deg F)

From these data the quantity Q can be calculated

$$Q = 2.12 \times 10^5 \text{ volts per hr} = 59 \text{ volts per sec}$$

Example 1. The velocity cycle shown in Fig. 6, which has an amplitude of 13 fps and a frequency of 5 cycles per sec, is projected on the steady-state calibration curve, and the zero lag response determined. This curve is also the locus of the isocline $S = 0$. To determine the loci of other isoclines, the values of e_0 at each instant are multiplied by $\left(1 - \frac{S}{59}\right)$, where S is measured in volts per second. These loci, for several values of S, are shown in Fig. 6. Having established the isocline field, the response of the anemometer can be determined by starting at any point and following the isoclines until the resulting curve becomes periodic. The periodic curve represents the steady-state behavior of the hot wire. The initial point at which the curve is started is of no consequence, since the steady-state solution is independent

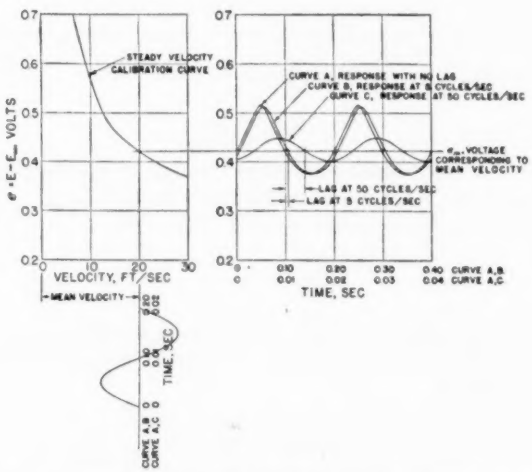


FIG. 7 RESPONSE OF HOT WIRE TO PERIODIC VELOCITY OF 8-FPS AMPLITUDE ABOUT MEAN VELOCITY OF 20 FPS, FOR FREQUENCIES OF 5 AND 50 CYCLES PER SEC

of the initial conditions. The response of the hot wire in the first cycle or so represents the transient behavior of the wire before reaching steady state. Two initial conditions are shown in Fig. 6, both, of course, leading to the same steady-state solution. Fig. 6 reveals clearly the effect of the heat capacity on the hot-wire response. It is interesting to note that due to the nonlinearity of the steady-state calibration curve, the lag differs at various parts of the cycle. Also the wire never heats up to its "still-air" temperature even when the velocity cycle passes through zero. Thus

the voltage across the wire never exceeds 1.0 volts, although the still-air voltage is 1.65 volts.

Example 2. In example 2, shown in Fig. 7, the wire is subjected to a periodic velocity of 8 fps. The isocline method is again used to predict the behavior of the hot wire for frequencies of 5 and 50 cycles per sec. For simplicity, the construction lines are not shown. The figure reveals that for a frequency of 5 cycles per sec, the lag and the reduction in amplitude are very small, but for 50 cycles per sec, they have become appreciable. It is also noted that at higher frequencies the higher harmonics in the response curve are damped out and the response curve approaches a pure sine wave. A comparison of the lags and reductions in amplitude obtained by the isocline method, with the approximate equation of Dryden and Keuthe (6), reveals a good check for the low-frequency response, and considerable divergence for the high-frequency curve.

Conclusions

A method has been presented which allows a rapid graphical prediction of the response of a hot-wire anemometer to periodic velocities. From such a prediction, the suitability of the hot wire for any particular application can be readily determined.

Acknowledgments

The authors wish to thank Prof. L. M. K. Boelter, F. A. Ryder, A. E. Harrison, and T. F. Reinhardt for providing them with a background for this paper.

BIBLIOGRAPHY

1 "On the Convection of Heat From Small Cylinders in a Stream of Fluid: Determination of the Convection Constants of Small Platinum Wires With Applications to Hot-Wire Anemometry," by L. V. King, Philosophical Transactions of the Royal Society of London, vol. A214, 1914, pp. 373–432.

2 "On the Precision Measurement of Air Velocity by Means of the Linear, Hot-Wire Anemometer," by L. V. King, *Philosophical Magazine*, series 6, vol. 29, 1915, pp. 556–577.

3 "The Hot-Wire Anemometer: Its Application to the Investigations of Velocity of Gases in Pipes," by J. S. G. Thomas, *Philosophical Magazine*, series 6, vol. 39, 1920, pp. 505–534.

4 "A Method for the Quantitative Measurement of Quick Changes in the Outflow of Liquids," by G. V. Anrep, A. C. Downing, *Journal of Scientific Instruments*, vol. 3, 1925–1926, pp. 221–224.

5 "Experiments on the Fluctuation of the Velocity in a Current of Air," by J. M. Burgers, Koninklijke Akademie v. Wetenschappen, Amsterdam, Proceedings of the Section of Sciences, vol. 29, 1926, pp. 547–558.

6 "The Measurement of Fluctuations of Air Speed by the Hot-Wire Anemometer," by H. L. Dryden, A. M. Keuthe, N.A.C.A. Technical Report no. 320, 1929.

7 "Effect of Turbulence on Wind Tunnel Measurements," by H. L. Dryden and A. M. Keuthe, N.A.C.A. Report no. 342, 1930.

8 "Improved Apparatus for the Measurement of Fluctuations of Air Speed in Turbulent Flow," by W. C. Mock, Jr., and H. L. Dryden, N.A.C.A. Report no. 448, 1932.

9 "Note on the Use of Hot Wire Anemometers," by D. LeB. Cooper, E. P. Linton, Nova Scotian Institute Science Proceedings, vol. 19, part 1, 1934–1935, pp. 119–120.

10 "Alternating-Current Equipment for the Measurement of Fluctuations of Air-Speed in Turbulent Flow," by W. C. Mock, Jr., N.A.C.A. Technical Report no. 598, 1937.

11 "A Note on a Hot Wire Speed and Direction Meter," by L. F. G. Simmons and A. Bailey, British Aeronautical Research Committee Reports and Memoranda No. 1019, 1926.

12 "A Selective Hot-Wire Microphone," by W. S. Tucker, E. T. Paris, Philosophical Trans. of the Royal Society of London, vol. A221, 1920–1921, pp. 389–430.

13 "The Resistance of a Hot Wire in an Alternating Air Current," by R. C. Richards, *Philosophical Magazine*, series 6, vol. 45, 1923, pp. 926–934.

14 "Die Theorie des Thermomikrophons," by Arthur Hippel, *Annalen der Physik*, vol. 75, 1924, pp. 521–548.

15 "The Escape of Heat From a Harmonically Oscillating Hot Wire," by R. S. Maxwell, *Philosophical Magazine*, series 7, vol. 6, 1928, pp. 945–964.

16 "A Method for the Instantaneous Determination of the Direction and Velocity of the Wind," by E. Huguenard, A. Magnan, A. Planiol, N.A.C.A. Technical Memo. No. 264, 1924.

17 "Method of Recording Rapid Wind Changes," by A. Magnan, N.A.C.A. Tech. Memo. No. 692, Nov., 1932.

18 "Mathematical Methods in Engineering," Th. von Kármán and M. A. Biot, McGraw-Hill Book Company, New York, N. Y., 1940, p. 11.

19 Ibid. ref. 17, p. 7.

(Owing to travel emergency conditions existing when this paper was presented, discussion will be accepted until February 10, 1946)



FIG. 1 NORTH AMERICAN AT-6C AIRPLANE

The Practicability of Vibration Control in Light Aircraft

BY DWIGHT C. KENNARD, JR.,[1] DAYTON, OHIO

The approach of the Air Technical Service Command to the problem of developing and evaluating a new engine-mount design is outlined, including a description of instrumentation, methods of vibration analysis, and presentation of natural-frequency formulas for elastically mounted power plants. The results of flight-vibration tests are presented for the standard engine mount, and an improved experimental engine mount installed in the North American AT-6C airplane. The results are discussed in detail showing the relative merits of the two engine installations. The test results show that the experimental engine mount, by providing natural frequencies of the mounted power plant which fall within the frequency range specified by the Air Technical Service Command, reduces appreciably the vibration of the engine and airplane structure.

INTRODUCTION

THE development of successful antivibration mountings for aircraft radial engines of 1800 or more cu in. displacement has not been paralleled in the field of smaller aircraft engines. This development apparently has lagged owing to the understandable reluctance on the part of airplane manufacturers to accept what was considered to be a penalty in weight and cost in light airplane designs incorporating antivibration engine mountings. Pilots came to regard many of the light airplanes as uncomfortably "rough," and maintenance problems due to excessive vibration were looked upon as an inherent evil in such airplanes. However, the benefits of vibration control in airplanes equipped with larger engines was proving so successful that the Air Technical Service Command undertook a program of research and development directed toward attaining like benefits in light airplanes. Efforts were directed toward realizing an effective yet practical antivibration engine-mounting system for such light engine installations as are used in training, cargo, liaison, and other types of Army aircraft.

As a first step in this program, the Air Technical Service Command issued a design specification,[2] defining requirements for the antivibration provisions to be incorporated in an experimental engine mount for the Pratt and Whitney R-985 engine. Such a mount was subsequently procured[3] and thoroughly tested with an R-985 engine installed on a test stand. Upon satisfactory completion of these tests, the second step was to procure a similar engine mount for the Pratt and Whitney R-1340 engine to be installed in an AT-6C airplane.

This paper concerns the vibration tests which were conducted by the Air Technical Service Command on the AT-6C standard and experimental engine-mount installations in flight (1).[4]

DESCRIPTION OF THE AT-6C AIRPLANE

The North American AT-6C airplane which was chosen for the test program is a two-place all-metal low-wing monoplane with monocoque fuselage and full cantilever wings, Fig. 1. The landing gear is the conventional type and is retractable. The tactical mission of the airplane is to provide a means for the advanced training of student pilots and their transition flying training to combat-type airplanes. The airplane is equipped

[1] Aeronautical Engineer, Dynamics Branch, Aircraft Laboratory, Engineering Division, Air Technical Service Command, Wright Field. Jun. A.S.M.E.

Contributed by the Aviation Division of THE AMERICAN SOCIETY OF MECHANICAL ENGINEERS.

NOTE: Statements and opinions advanced in papers are to be understood as individual expressions of their authors and not those of the Society.

[2] This specification embodied the standard AAF requirements which restrict the natural frequencies of the mounted power plant to a lower limit of 400 cycles per min and an upper limit corresponding to 45 per cent normal rated engine rpm, or 75 per cent normal rated propeller rpm, whichever has the lower value.

[3] This engine mount was designed and manufactured by the United Aircraft Corporation, Pratt and Whitney Engine Division, and the Goodyear Tire and Rubber Corporation.

[4] Numbers in parentheses refer to the Bibliography at the end of the paper.

with a Pratt and Whitney nine-cylinder single-row air-cooled radial R-1340-AN-1 engine, which drives directly a Hamilton Standard two-blade controllable-pitch constant-speed aluminum-alloy propeller, 9 ft diam. The engine has a power rating of 550 bhp at 2200 rpm and produces a maximum power for take-off amounting to 600 bhp at 2250 rpm.

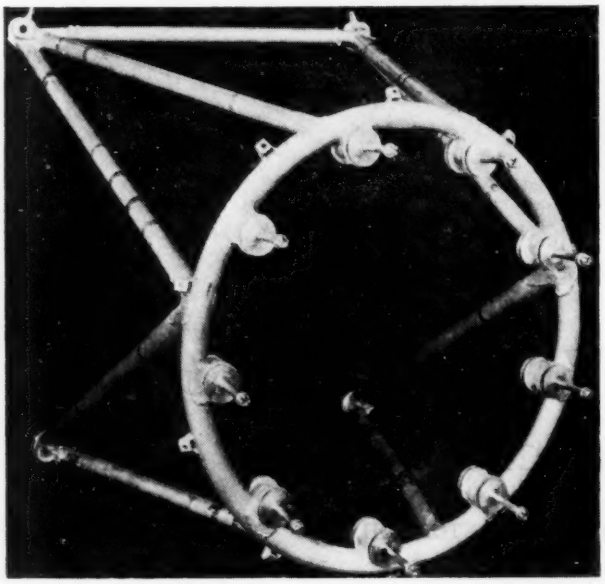


FIG. 2 STANDARD ENGINE-MOUNT ASSEMBLY FOR AT-6C AIRPLANE

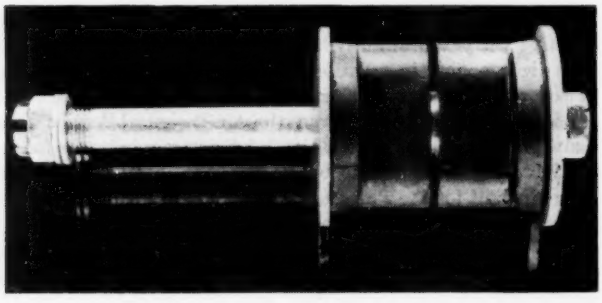


FIG. 3 STANDARD ENGINE MOUNTING UNIT FOR AT-6C AIRPLANE

ENGINE MOUNTS TESTED

The engine mounting structure is the conventional welded-steel tubular-truss construction, embodying a circular ring, around the periphery of which are welded the engine attaching bosses. The nine equally spaced bosses of the standard mount are provided with elliptically shaped recesses which accommodate compression-type rubber blocks interposed between the mounting structure and the crankcase attaching bolts, Figs. 2 and 3. Experience has shown that this type of elastic mounting is not generally effective because the rubber affords insufficient elasticity when forced to act in compression.

The experimental mount tested utilizes six engine attaching points (attaching points behind cylinders Nos. 1, 4, and 7 are omitted). This arrangement provides symmetrical elastic restraint by virtue of the fact that three pairs of mounting units are equidistantly spaced about the periphery of the mounting ring, Fig. 4. The engine-mount bosses are set at an angle with circular shear type sandwich rubber bushings located on each side of the bosses. The bushings are much stiffer in a compressionwise direction than in the shear direction so that they act as directional springs tending to deflect mainly in the shear plane which is parallel to the bonded steel facing plates, Fig. 5. The bushings are held in place on each side of the mounting-ring bosses by forged angle bolts so that no metal-to-metal contact is allowed between the bolts and the bosses. The directional stiffness of the bushings is utilized by arranging the faces of the mounting-ring bosses to bear an angular relationship to the thrust line in such a way that the elastic center of the mount coincides with the center of gravity of the power-plant mass. This arrangement is termed "virtual center of gravity suspension" of the power plant. The outer bonded steel facings of the rubber bushings are eccentric with respect to each other so that when they are deflected by full engine torque, they become approximately concentric. The inner steel faces of the rubber bushings are locked to the mounting-ring bosses by mating dowel pins. The flanges of the inner faces also mate with the mounting-ring boss so as to effect a journal bearing. Shoulders on the forged angle bolt space the outer steel facings when the nut is tightened. Torque arms join adjacent angle bolts so that they cannot twist. Table 1 presents a weight breakdown for the two engine-mount assemblies tested, which shows that the experimental assembly entails an increased weight over the standard assembly amounting to only 4.5 lb.

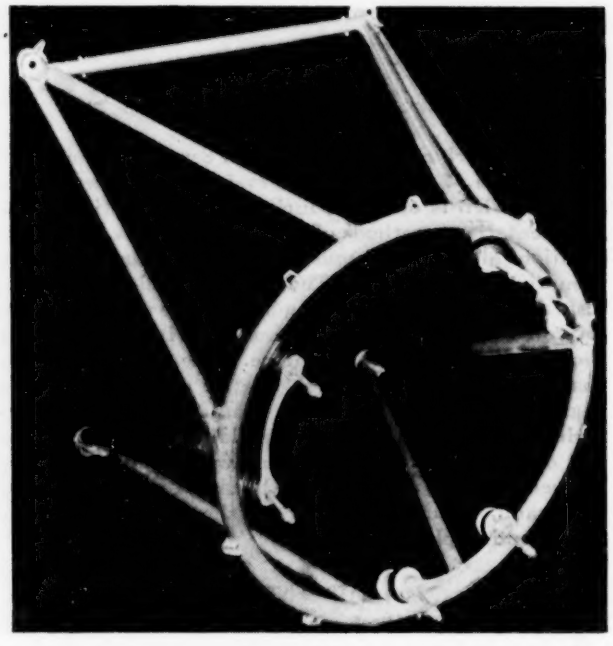


FIG. 4 EXPERIMENTAL ENGINE-MOUNT ASSEMBLY FOR AT-6C AIRPLANE

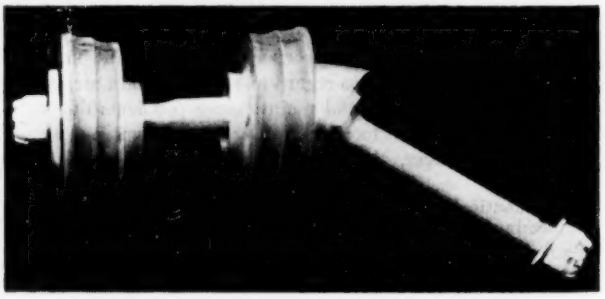


FIG. 5 EXPERIMENTAL ENGINE MOUNTING UNIT FOR AT-6C AIRPLANE

TABLE 1 WEIGHT BREAKDOWN FOR STANDARD AND EXPERIMENTAL MOUNTING ASSEMBLIES

	Weight, lb
Experimental mounting assembly, shown in Fig. 4	43.75
Standard mounting assembly, shown in Fig. 2	39.25
Experimental mounting units, total	9.48
Rubber sandwiches, 12 required	4.02
Angle bolts, 6 required	3.96
Nuts and washers	0.50
Torque arms, 3 required	1.00
Standard mounting units, total	5.09
Rubber bushings, 18 required	0.92
Engine mount bolts, 9 required	2.52
Nuts and washers	1.10
Bushings, 9 required	0.55

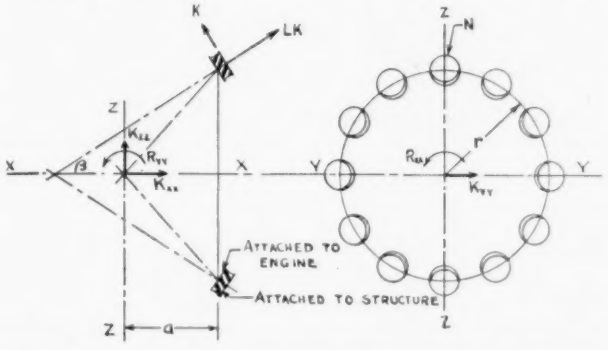


FIG. 6 SCHEMATIC ARRANGEMENT OF VIRTUAL-CENTER-OF-GRAVITY POWER-PLANT SUSPENSION

ESTIMATION OF POWER-PLANT NATURAL FREQUENCIES

It has been shown that the stiffnesses of a virtual-center-of-gravity type power-plant suspension may be expressed as follows, referring to Fig. 6 (2):

Roll about the crankshaft axis

$$R_{xx} = Nkr^2 \text{ in-lb per radian}$$

Pitching or yawing about the lateral or vertical axis

$$R_{yy} = R_{zz} = \frac{Nkr^2}{2}\left[\frac{a^2}{r^2} + L\left(\frac{a}{r}\sin\beta - \cos\beta\right)^2 + \left(\frac{a}{r}\cos\beta + \sin\beta\right)^2\right] \text{ in-lb per radian}$$

Thrustwise along the crankshaft axis

$$K_{xx} = Nk(\sin^2\beta + L\cos^2\beta) \text{ lb per in.}$$

Along the lateral or vertical axis

$$K_{yy} = K_{zz} = \frac{Nk}{2}\left[1 + (\cos^2\beta + L\sin^2\beta)\right] \text{ lb per in.}$$

where N = number of equally spaced mounting units
k = shear rate of each mounting unit, lb per in.
L = ratio of compressionwise rate to shear rate of each unit
r = radius of mounting units, in.
a = distance between plane of mounting units and virtual point of suspension, in.
β = angle made by the compression axis of mounting units with respect to thrust line, deg

It can be shown that the point of virtual suspension may be expressed as

$$a = \frac{1}{2}\,\frac{r\sin 2\beta}{\frac{2}{L-1} + \sin^2\beta} \text{ in.}$$

Neglecting the effect of gyroscopic forces and structural coupling, the natural frequencies may be determined by the well-known relationships

$$F = \frac{60}{2\pi}\sqrt{\frac{\text{Angular stiffness}}{\text{Moment of inertia}}} = \frac{60}{2\pi}\sqrt{\frac{R}{I}} \text{ cycles per min.}$$

or

$$F = \frac{60}{2\pi}\sqrt{\frac{\text{Translational stiffness}}{\text{Mass}}} = \frac{60}{2\pi}\sqrt{\frac{K}{M}} \text{ cycles per min.}$$

Applying these equations to the experimental mount under consideration

$N = 3 \times 2 = 6$
$k = 1250$ lb per in.
$L = 12.7$
$r = 12.2$ in.
$a = 10.75$ in.
$\beta = 35$ deg

Power-plant moment of inertia about the thrust axis (minus propeller inertia) = 240 lb-in. sec²
Power-plant moment of inertia about the vertical or lateral axis (including maximum propeller inertia) = 355 lb-in. sec²
Weight of power plant (including propeller) = 996 lb

Roll about the crankshaft axis

Stiffness $= 6 \times 1250 \times 12.2^2 = 1{,}120{,}000$ in-lb per radian

$$\text{Natural frequency} = \frac{60}{2\pi}\sqrt{\frac{1{,}120{,}000}{240}} = 645 \text{ cycles per min}$$

Pitching or yawing about lateral or vertical axis

$$\text{Stiffness} = \frac{6 \times 12.2^2 \times 1250}{2}\left[\frac{10.75^2}{12.2^2} + 12.7\left(\frac{10.75}{12.2}\sin 35° - \cos 35°\right)^2 + \left(\frac{10.75}{12.2}\cos 35° + \sin 35°\right)^2\right]$$

$$= 1{,}170{,}000 \text{ in-lb per radian}$$

$$\text{Natural frequency} = \frac{60}{2\pi}\sqrt{\frac{1{,}170{,}000}{355}} = 547 \text{ cycles per min}$$

Thrustwise along the crankshaft axis

Stiffness $= 6 \times 1250\ (\sin^2 35° + 12.7\cos^2 35°) = 66{,}500$ lb per in.

$$\text{Natural frequency} = \frac{60}{2\pi}\sqrt{\frac{66{,}500}{996} \times 386} = 1520 \text{ cycles per min}$$

Laterally or vertically

$$\text{Stiffness} = \frac{6 \times 1250}{2}\left[1 + (\cos^2 35° + 12.7\sin^2 35°)\right]$$

$$= 21{,}750 \text{ lb per in.}$$

$$\text{Natural frequency} = \frac{60}{2\pi}\sqrt{\frac{21{,}750}{996} \times 386} = 876 \text{ cycles per min}$$

Distance of elastic center from plane of mounts

$$a = \frac{1}{2}\,\frac{12.2\sin 70°}{\frac{2}{12.7-1} + \sin^2 35°} = 11.5 \text{ in.}$$

Distance of elastic center ahead of center of gravity = 11.5 − 10.75 = 0.75 in.

INSTRUMENTATION FOR FLIGHT TESTS

The Air Technical Service Command has standardized on the use of Sperry-M.I.T. instrumentation for flight measurements of engine vibration and associated vibration of the aircraft structure. This equipment comprises velocity-type vibration pickups

which are fed into integrating amplifiers. The amplifier outputs actuate a four-element recording oscillograph, the traces of which indicate amplitudes which are proportional to vibratory displacement through a useful frequency range of 7 to 1500 cycles per sec.

The bridge network shown in Fig. 7 was used on the amplifier outputs so as to produce simultaneous traces on the four strings of the oscillograph which would correspond to addition, subtraction, and individual voltage outputs of a given pickup pair. The addition and subtraction traces indicated the translational and rotation components of power-plant vibratory motion.

Six pickups were suitably located to measure vibratory motion of the power plant in translation along and rotation about its three principal central axes as shown in Fig. 8. The pickup pair which measured power-plant vertical and pitching motion could not be located symmetrically with respect to the center of gravity. Hence a correction factor was applied to the vertical motion at the power-plant center of gravity. The pickup pair which

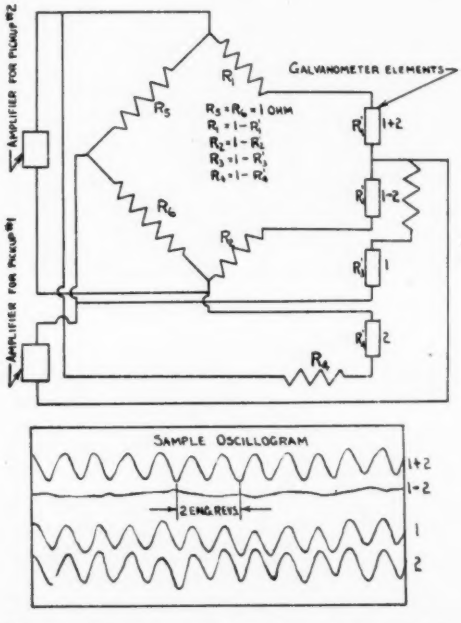
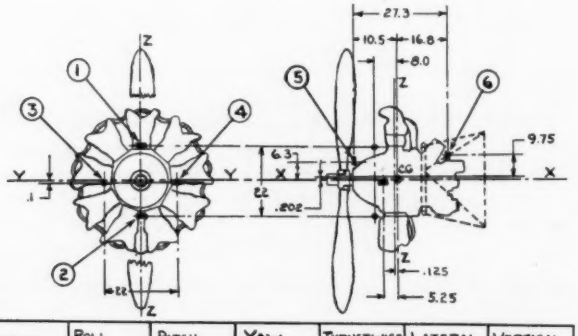


FIG. 7 BRIDGE NETWORK FOR OBTAINING SIMULTANEOUS INDICATION OF ADDITION, SUBTRACTION, AND INDIVIDUAL VOLTAGE OUTPUTS OF PAIRED PICKUPS

(Sample oscillogram first-order translational vibratory motion.)



MODE	ROLL ABOUT X-X	PITCH ABOUT Y-Y	YAW ABOUT Z-Z	THRUSTWISE ALONG X-X	LATERAL ALONG Y-Y	VERTICAL ALONG Z-Z
PICKUPS	1 − 2	5 − 6	3 − 4	3 + 4	1 + 2	5 + 6

FIG. 8 PICKUP LOCATIONS AND MODES OF POWER-PLANT VIBRATION MEASURED

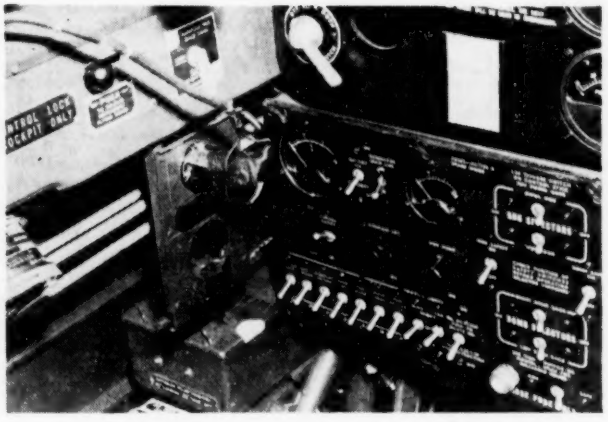


FIG. 9 VIBRATION PICKUP INSTALLATION IN FRONT COCKPIT OF AT-6C AIRPLANE

measured lateral and rolling vibration was located in a plane 8 in. ahead of the center of gravity so that the lateral motion indicated contained components due to yawing vibration of the power plant about its center of gravity. A pickup was located in each cockpit to measure lateral vibration of the fuselage structure, Fig. 9. Selection of pickups was accomplished by means of a hand-operated rotary switch which fed the outputs of two pickups at a time into the amplifiers. Pickups were calibrated before and after tests by means of a mechanically driven calibrator which produces sinusoidal vibratory motion at a predetermined amplitude.

In order to correlate the vibration frequencies with engine speeds, a pickup coil was installed on one of the spark-plug cables. The voltage induced in this coil was fed into the second stage of one of the amplifiers. This produced a mark superimposed on the vibration traces each instant the corresponding cylinder fired.

The amplifying and recording equipment was located in the rear cockpit where it could be controlled by the operator, Fig. 10. The amplifiers and oscillograph were powered by the 12-v electrical system of the airplane. The voltage input to the equipment was maintained at 12 v by means of a rheostat in series.

"Scratch plates" were installed on the three unused crankcase mounting bosses in the experimental engine-mount installation for the purpose of measuring over-all deflections of the mounted power plant. Stylii were held against the plates by means of springs in such a way that relative motion between the engine mount and crankcase resulted in scratches on the plates.

Test Procedure. The following tests were conducted in consecutive order:

1 Vibration records for the standard AT-6C engine-mount installation were taken in level flight at 8000 ft altitude throughout the operating range of engine speeds. Upon completion of this test, the standard engine mount was removed from the airplane and the experimental mount installed.

2 The test just outlined was repeated with the experimental engine-mount installation.

3 Vibration records for the experimental engine-mount installation were taken at various engine speeds while the airplane was in a 20-deg bank both to the right and to the left.

4 A series of ground tests were conducted for the purpose of checking the natural modes and frequencies of the power plant elastically suspended on the experimental mount. The natural mode in roll about the crankshaft axis was excited by running the engine on one magneto with one spark plug disconnected. This caused an excitation about the crankshaft axis at a frequency corresponding to one-half engine speed. The engine speed was

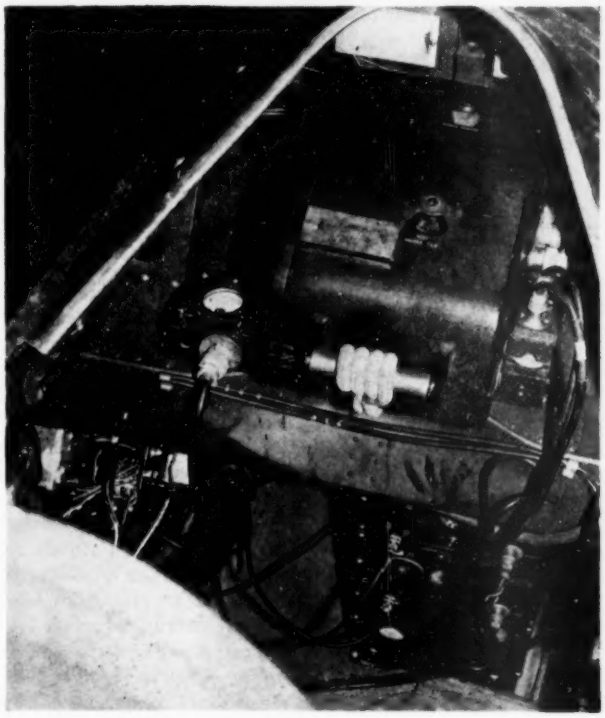


FIG. 10 INSTALLATION OF VIBRATION-RECORDING EQUIPMENT IN AT-6C AIRPLANE

increased to 2200 rpm on both magnetos, at which speed the engine was switched over to the magneto having one spark plug disconnected. A vibration record of the rolling mode was then taken as the engine was throttled back to idling speed in a period of approximately 25 seconds. The spark plug was reconnected and sufficient masking tape was applied to a propeller blade to cause an unbalance of approximately 1.05 in-lb rotating at crankshaft speed. The engine speed was again raised to 2200 rpm and lowered to idling speed while vibration records of the pitching, vertical, yawing, and lateral modes were being taken.

5 A series of tests were conducted to determine the maximum movement of the engine relative to the supporting structure under various conditions by means of stylii bearing on scratch plates. The first condition investigated was that of cold idling of the engine. Stylii were allowed to bear on the scratch plates for approximately 1 min while the engine was idling in a cold condition. For the second condition, the stylii were allowed to bear on the plates while the engine was started, held at idling speed for a short time, and then shut down. The third condition consisted of an entire flight including starting, "warming up" the engine, taking off, climbing to an altitude of 8500 ft, making $4^1/_2$ turns of a right-hand spin, landing, and shutting off the engine. The stylii were allowed to bear against the plates for the entire flight.

6 In order to determine the durability of the experimental mount in service, the airplane was assigned to Headquarters, Air Technical Service Command, for postadministrative and flying duties.

ANALYSIS OF VIBRATION RECORDS

Vibration records were prepared for harmonic analysis by enlarging to a 40-cm base line a section of each vibration trace included between two spark indications which mark an interval corresponding to four engine revolutions. The enlarged vibration traces were then analyzed for the five largest harmonics by means of a Coradi-type five-element rolling-sphere harmonic analyzer, Fig. 11.

The principle underlying the operation of the Coradi-type harmonic analyzer can be understood by considering the mathematical properties of the Fourier series (3). It can be shown that any periodic curve $f(t)$ can be expressed as a Fourier series, that is

$$f(t) = a_0 + a_1 \sin \omega t + a_2 \sin 2\omega t + \ldots + a_n \sin n\omega t \ldots + b_1 \cos \omega t + b_2 \cos 2\omega t + \ldots + b_n \cos n\omega t \ldots$$

where the function repeats itself in a period $T = \frac{2\pi}{\omega}$. The frequency of the fundamental or first harmonic is represented by ω and the frequency of the nth harmonic by $n\omega$. It can be shown, furthermore, that the amplitudes may be expressed as

$$a_n = \frac{\omega}{\pi} \int_0^{\frac{2\pi}{\omega}} f(t) \sin n\omega t dt$$

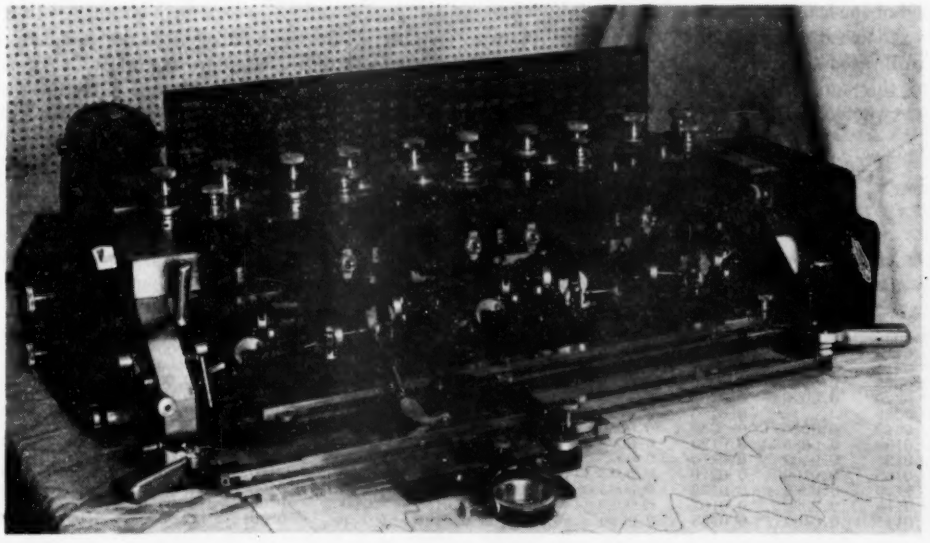


FIG. 11 AIR TECHNICAL SERVICE COMMAND FIVE-ELEMENT ROLLNG SPHERE HARMONIC ANALYZER

$$b_n = \frac{\omega}{\pi}\int_0^{\frac{2\pi}{\omega}} f(t)\cos n\omega t dt$$

These definite integrals can be evaluated for a particular harmonic by determining the area included between the harmonic curve and the neutral axis. The Coradi-type harmonic analyzer measures these areas by applying the principles utilized in the ordinary planimeter. Each integrator head is geared to revolve about a vertical axis n times as the curve follower moves on a lead screw across a span of 40 cm which represents the period of the first harmonic $\frac{2\pi}{\omega}$. On each integrator head are two planimeter wheels in vertical planes at right angles to each other, Fig. 12.

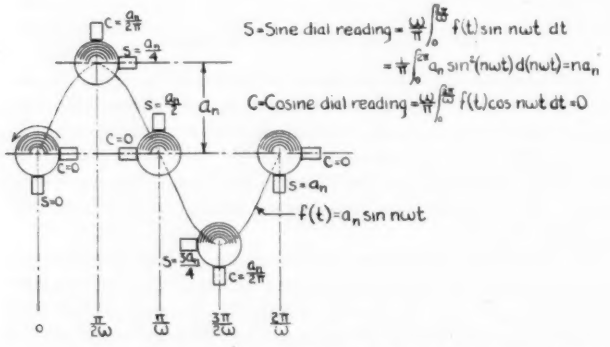


FIG. 12 ILLUSTRATION OF THE WAY IN WHICH THE CORADI-TYPE HARMONIC ANALYZER OPERATES UPON THE PERIODIC CURVE $f(t) = a_n \sin n\omega t$

(The sphere makes one complete revolution about a vertical axis in the period included between 0 and $\frac{2\pi}{\omega}$. At the end of the revolution, the sine dial registers a_n and the cosine dial registers 0, hence the amplitude $A_n = \sqrt{a_n^2 + b_n^2} = a_n$. In n periods the sine dial will read na_n.)

The planimeter wheels bear against a ground-glass sphere. The sphere in turn rides on a wheel which revolves in accordance with back-and-forth motion of the entire machine. The machine is constrained to back-and-forth motion only, and this motion is controlled by the operator in keeping the curve follower on the vibration trace as the lead screw advances the follower across the carriage. The speed of the lead screw can be controlled by a foot pedal which varies the speed of the driving motor. The planimeter wheels are calibrated to read Σa_n and Σb_n. In order to determine a_n and b_n, the planimeter readings must be divided by the harmonic being extracted, that is

$$a_n = \frac{\Sigma a_n}{n} \quad \text{and} \quad b_n = \frac{\Sigma b_n}{n}$$

The resultant amplitude is

$$A_n = \sqrt{a_n^2 + b_n^2}$$

and the phase angle may be found as

$$\tan \phi_n = \frac{b_n}{a_n}$$

The property of the analyzer which enables it to exclude all harmonics other than the nth harmonic being extracted can be understood by considering a harmonic amplitude h_0 having a frequency $m\omega$. Then

$$f(t) = h_0 \sin (m\omega t + \phi)$$

and

$$a_n = \frac{\omega}{\pi}\int_0^{\frac{2\pi}{\omega}} h_0 \sin (m\omega t + \phi)\sin n\omega t dt$$

but

$$\sin (m\omega t + \phi) = \sin m\omega t \cos \phi + \cos m\omega t \sin \phi$$

$$a_n = \frac{\omega h_0 \cos \phi}{\pi}\int_0^{\frac{2\pi}{\omega}} \sin m\omega t \sin n\omega t dt + \frac{\omega h_0 \sin \phi}{\pi}\int_0^{\frac{2\pi}{\omega}} \cos m\omega t \sin n\omega t dt = 0$$

Similarly $b_n = 0$, showing that the planimeter dials produce a zero reading over the complete cycle except for the nth harmonic.

DISCUSSION OF TEST RESULTS

The test results presented in Table 2 indicate that the experimental engine mount was very effective in attenuating that vibratory response of the power plant due to first-order forcing functions. These forcing functions, which correspond to the rotational speed of the engine crankshaft, arise from the inherent inertia forces of the articulated connecting-rod system, gas-pressure forces in the cylinders, and static, dynamic, and aerodynamic unbalances in the directly driven propeller.

On the other hand, the natural frequencies of the power plant on the standard mount were in a range where they could be excited by the first-order forcing functions, that is, the inertia and gas-pressure forces which produce alternating first-order couples about the crankshaft axis, induced resonance of the power plant on the standard mount at 1440 rpm. Inertia forces and propeller unbalances excited angular and translational modes about and along the vertical and lateral axes of the power plant. Resonances occurred in pitch about the lateral axis at 1460 and 2020 engine rpm. These peaks were reflected slightly in the measured vertical vibration and thus indicate appreciable cou-

TABLE 2 FIRST-ORDER POWER-PLANT VIBRATION FOR STANDARD AND EXPERIMENTAL MOUNTINGS

Nominal engine speed settings, rpm	Roll about X-X		Pitch about Y-Y		Yaw about Z-Z		Thrustwise along X-X		Lateral along Y-Y		Vertical along Z-Z	
	Std	Exp	Std	Exp	Std	Exp	Std	Exp	Std	Exp	Std	Exp
1100	0.0035	....	0.0045	0.0080	0.0055	....	0	....	0.0025	....	0.0020	....
1200	0.0115	0.0070	0.0070	0.0095	0.0055	0.0095	0.0005	0.0010	0.0045	0.0025	0.0010	0.0010
1300	0.0315	0.0065	0.0090	0.0090	0.0100	0.0135	0.0005	0.0010	0.0070	0.0035	0.0010	0.0010
1400	0.0375	0.0060	0.0300	0.0110	0.0245	0.0055	0.0025	0.0005	0.0040	0.0025	0.0030	0.0005
1500	0.0320	0.0090	0.0165	0.0125	0.0445	0.0045	0.0035	0.0005	0.0030	0.0025	0.0035	0.0015
1600	0.0280	....	0.0160	0.0120	0.0380	0.0085	0.0025	0.0005	0.0040	....	0.0035	0.0010
1700	0.0240	0.0085	0.0080	0.0050	0.0240	0.0115	0.0015	0.0010	0.0040	0.0030	0.0020	0.0010
1800	0.0150	0.0085	0.0120	0.0065	0.0150	0.0150	0.0015	0.0020	0.0040	0.0030	0.0020	0.0010
1900	0.0125	0.0100	0.0110	0.0055	0.0250	0.0140	0.0020	0.0010	0.0040	0.0030	0	0.0010
2000	0.0165	0.0100	0.0270	0.0055	0.0220	0.0155	0.0010	0.0015	0.0045	0.0030	0.0025	0.0010
2100	0.0110	0.0090	0.0135	0.0035	0.0235	0.0155	0.0010	0.0010	0.0040	0.0030	0.0005	0.0010
2200	0.0115	0.0090	0.0165	0.0080	0.0175	0.0180	0.0005	0.0005	0.0050	0.0035	0.0010	0.0010
2250	0.0145	0.0100	0.0155	0.0080	0.0110	0.0105	....	0.0010	0.0040	0.0030	0.0015	0.0010

NOTE: Double amplitudes in degrees for rotation, in inches for translation.

pling between the two modes. A resonance also occurred in yaw about the vertical axis at 1540 engine rpm which exhibited slight coupling with thrustwise vibration. A first-order lateral resonance of the power plant was measured at 1320 engine rpm.

The experimental mount eliminated all first-order resonances experienced with the standard mount. Reductions of power-plant response were attained amounting to as much as 76 per cent in roll about the crankshaft axis; 58 per cent in pitch about the lateral axis; and 84 per cent in yaw about the vertical axis. First-order lateral motion in the front cockpit also was reduced 40 to 75 per cent throughout the operating range of engine speeds. Lateral motion in the rear cockpit was not reduced but was very small for both engine-mount installations (0.0025 in. or less).

Since the natural frequencies of the power plant on the standard mount were well above the range where they can be excited by one-half order forcing functions (arising from irregularities in ignition and air-fuel induction) the corresponding power-plant responses indicated were largely due to excitation of a combined bending-torsion mode of the fuselage. This was confirmed by a lateral response in the rear cockpit which corresponded to the power-plant yawing response about the vertical axis at 2040 rpm (1020 cycles per min). A variation of this mode apparently was responsible for the magnified vertical power-plant response, coupled with roll about the crankshaft axis at 1780 to 1830 rpm (890 to 915 cycles per min).

The experimental mount did not alter appreciably the magnitude of one-half order power-plant response. Lateral response of the rear cockpit followed very closely that measured for the standard mount.

First-order crankshaft unbalance forces are largely compensated by the counterweight in a radial engine but this compensation introduces transverse second-order forces of appreciable magnitude because the center of mass of the rotating and articulating system travels in an oval rather than in a circular path, as does the center of mass of the counterweight. The frequency of the second-order forces is above the natural frequencies of the mounted power plant by a sufficient amount to result in approximately the same power-plant and cockpit response for either the standard or the experimental mount. Since the second-order unbalance forces act in the transverse plane, a comparatively low magnitude of vibration was measured in all modes of power-plant motion other than lateral or vertical. The second-order response of the cockpits probably was largely due to propeller-blade-passage impulses in the slip stream which impinged upon the canopy.

Because the moment of inertia of the power plant about a given transverse axis varies from a maximum to a minimum twice during each revolution of a two-blade propeller, second-order gyroscopic couples result during a bank and turn due to rotation of the airplane about its vertical axis. In order to check this effect for the experimental engine-mount installation, vibration records were taken at various engine speeds during a 20-deg bank and turn both to the right and to the left. Examination of the records revealed no important increase of second-order response of the power plant or the cockpit structure.

Two $3^1/_2$-order peak responses were indicated in the angular modes about the vertical and lateral axes at 1430 rpm (5000 cycles per min) and 1830 rpm (6410 cycles per min) which were the result of so called "conical whirls." In this particular case the whirls were largely independent of the dynamics of both engine mounts because they were generated by $4^1/_2$-order (frequency of cylinder firing) torsional vibration of the crankshaft combined with crankshaft bending. This mode of crankshaft vibration energized a propeller-bending mode which was symmetrical in the plane of rotation but asymmetrical perpendicular to the plane of rotation, that is, the propeller tips were moving out of phase in a thrustwise direction but in phase in the transverse plane. In such a condition, transverse reactions are imposed upon the thrust bearing due to the symmetrical vibration of the propeller blades in the plane of rotation, and moments about transverse axes are imposed upon the propeller shaft due to asymmetrical propeller-blade vibration perpendicular to the plane of rotation. These forces and moments cause a conical whirl of the engine at a frequency of $\left(n - \frac{P}{N}\right)$, where n is the harmonic order of propeller vibration, N is the engine speed, and P is the propeller speed (4).

In the case under consideration, the whirling frequency was $3^1/_2$-order ($4^1/_2$—1) although $4^1/_2$-order vibration of the power plant was negligible. This mode was also apparent in the indication of the lateral pickups which were located in a plane ahead of the power-plant center of gravity so that they responded to a yawing component of motion. Since there was no $3^1/_2$-order response vertically, it is apparent that the power plant underwent a conical whirl with a node in the vicinity of the power-plant center of gravity.

The engine run-down tests with one cylinder not firing, as conducted on the experimental engine mount, indicated that the power-plant natural frequency in roll about the crankshaft axis was 680 cycles per min (645 cycles per min calculated). The natural frequencies excited by unbalancing the propeller 1.05 in. lb were 850 cycles per min for the vertical-pitching mode and 865 cycles per min for the lateral-yawing mode. The calculated natural frequency for the vertical and lateral modes was 875 cycles per min and for the pitching and yawing modes, 547 cycles per min. The engine could not be run slow enough to produce a satisfactory excitation of the pitching-yawing natural modes, however. The foregoing natural frequencies are sufficiently low to provide adequate vibration isolation for the important forcing functions. Resonance with one-half order couples about the crankshaft axis is possible at 1360 rpm (680 cycles per min), but under the conditions of the flight tests, the response indicated was small.

The results of scratch-plate records indicating relative motion between the crankcase and mounting ring for the experimental mount are given in Table 3. The mounting elements are manufactured 0.140 in. eccentric in order to offset engine torque. The scratch-plate records show a deflection of 0.156 in. at take-off power. This means that full engine torque deflects the mounting elements 0.016 in. beyond the concentric configuration which is not considered to be excessive. No metal-to-metal contact in the mounts is likely to occur.

TABLE 3 SCRATCH-PLATE RECORDS OF RELATIVE MOTION BETWEEN CRANKCASE AND MOUNTING RING

Condition	Indicated deflection, in. Right	Left	Top	Remarks
Engine idling prior to warm-up	1/8	1/8	—	Deflection on clockwise side of neutral position due to torque reaction
Engine started, idled at 550 rpm, shut off	9/64	13/64	—	
Engine started, airplane taken off and climbed to 8500 ft, $4^1/_2$ turns of a spin made, airplane landed and engine shut off	5/32	5/32	5/32	Deflection due to torque reaction at take-off power
	1/16	1/16	1/16	Diameter of circular trace resulting from spin

Conclusion

The principles embodied in the design of the experimental engine mount herein described are applicable for the control of vibration in many types of aircraft where lightweight and simplicity of design are important factors. Vibration control need be limited no longer to the larger aircraft-engine installations.

On the contrary, development of this type of engine mount suggests new opportunities for attaining greater flying comfort and added serviceability in light airplanes without attendant design penalties. It will be an increased pleasure to fly in the light airplanes of tomorrow!

ACKNOWLEDGMENT

The writer is indebted to Ensign Paul V. Roberts for his valuable assistance in carrying out the flight-test program and the reduction of data which form the basis of this paper.

BIBLIOGRAPHY

1 "Effectiveness of the Goodyear Six-Point Power Plant Mounting in Controlling Vibration in the North American AT-6C Airplane," Army Air Forces Technical Report No. 5165.

2 "Vibration Isolation of Aircraft Power Plants," by E. S. Taylor and K. A. Browne, *Journal of the Aeronautical Sciences*, vol. 6, December, 1938, pp. 43–49.

3 "Mechanical Vibrations," by J. P. den Hartog, second edition, McGraw-Hill Book Company, Inc., New York, N. Y., 1940.

4 "Vibration Characteristics of Aircraft Engine-Propeller Systems," by Charles M. Kearns, S.A.E. Transactions, vol. 34, 1939, pp. 540–548.

(Owing to travel emergency conditions existing when this paper was presented, discussion will be accepted until March 11, 1946)

Gasoline Explosion Pressures

By M. S. PLESSET[1] and F. R. GILMORE,[2] SANTA MONICA, CALIF.

A numerical method is outlined which permits the calculation of the temperatures and pressures obtained when mixtures of air and aviation-gasoline vapor are exploded in a closed chamber. The calculations use basic thermodynamic data to determine the final equilibrium state of the air and gasoline mixtures after combustion. Similar calculations have been carried out previously by other investigators, but only for a limited range of mixture ratios. Experimental measurements of the explosion pressures were made using an explosion bomb with a strain-gage pressure pickup. The measured pressures were of the same order of magnitude as the calculated pressures, but in general were somewhat above the theoretical values. Some possible explanations for this trend are discussed in the text.

Introduction

THE investigation covered by this paper was initiated so that some conception could be formed of the temperatures and pressures developed in aviation combustion heaters under the assumption that an explosion takes place. No general solution of the problem applicable to all mixture ratios was found so that an analysis based on fundamental physico-chemical principles was necessary.

An estimate was also desired of the ignition limits of gasoline-air mixtures at various temperatures and pressures. These limits have an important bearing on the problem of combustion-heater ignition.

Theoretical Considerations

The pressures which are produced when a mixture of air and fuel vapor explodes in a closed chamber can be calculated from basic chemical principles, provided the assumption is made that all chemical reactions reach equilibrium at the high explosion temperature, and provided that sufficient thermodynamic data on the reaction products are available.

If aviation gasoline is assumed to have the average molecular composition, C_8H_{16}, the combustion of 1 mole of a gasoline-air mixture can be represented by the following total reaction:

$$X\,C_8H_{16} + 0.2095\,(1-X)\,O_2 + 0.7809\,(1-X)\,N_2 + 0.0093\,(1-X)\,A + 0.0003\,(1-X)\,CO_2 \rightarrow a\,CO_2 + b\,CO + c\,H_2O + d\,H_2 + e\,O_2 + f\,N_2 + g\,NO + h\,NO_2 + i\,CH_4 + j\,OH + k\,H + m\,O + n\,O_3 + q\,C\,(\text{graphite}) + r\,C_2\,(\text{gas}) + s\,C(\text{gas}) + t\,NH_3 + 0.0093\,(1-X)\,A$$

In this X is the mole fraction of gasoline vapor present before the explosion. The composition of dry air, according to Humphreys (1)[3] is used. Although argon does not take part in the chemical reaction, it has been included in the equation because its thermal capacity enters into the heat-balance equation. The seventeen letters a to t represent unknown coefficients which are to be determined. Some possible products of the reaction, such as CH and CH_2, have been omitted because thermodynamic data on these compounds are not available; it is believed that this omission should not appreciably affect the results. Other possible products, such as C_2H_8, C_2N_2, etc., can be shown to be entirely negligible.

The requirement that the foregoing reaction equation be balanced yields four equations for the unknown coefficients

$$a + b + i + q + 2r + s = 8X + 0.0003\,(1-X) \quad [1]$$

$$2c + 2d + 4i + j + k + 3t = 16X \quad [2]$$

$$2a + b + c + 2e + g + 2h + j + m + 3n = 0.4196\,(1-X) \quad [3]$$

$$2f + g + h + t = 1.5618\,(1-X) \quad [4]$$

The remaining thirteen equations necessary for the evaluation of the seventeen constants are derived from a consideration of the various reactions which are assumed to be in equilibrium at the explosion temperature; for example, the carbon monoxide can react with the oxygen to form carbon dioxide

$$CO + {}^1/_2O_2 \rightleftharpoons CO_2$$

For this reaction, there is a certain equilibrium constant

$$K_1 = \frac{p_{CO}\sqrt{p_{O_2}}}{p_{CO_2}}$$

where p_{CO}, p_{O_2}, and p_{CO_2} are the partial pressures of the carbon monoxide, oxygen, and carbon dioxide, respectively. If the explosion has taken place at constant volume, then b moles of carbon monoxide, e moles of oxygen, and a moles of carbon dioxide are occupying the same volume at the explosion temperature T_m that one mole of the mixed gases occupied at the initial temperature T_0 and pressure P_0. From the perfect-gas law, it follows that

$$p_{CO} = b\,\frac{T_m}{T_0}\,P_0$$

$$p_{O_2} = e\,\frac{T_m}{T_0}\,P_0$$

$$p_{CO_2} = a\,\frac{T_m}{T_0}\,P_0$$

The expression for the equilibrium constant then becomes

$$K_1 = \frac{p_{CO}\sqrt{p_{O_2}}}{p_{CO_2}} = \frac{b}{a}\sqrt{e\left[\frac{T_m}{T_0}\,P_0\right]} \quad [5]$$

In a similar manner, twelve other equations can be derived

$$K_2 = \frac{p_{H_2}\sqrt{p_{O_2}}}{p_{H_2O}} = \frac{d}{c}\sqrt{e\left[\frac{T_m}{T_0}\,P_0\right]} \quad [6]$$

$$K_3 = \frac{p_{NO}}{\sqrt{p_{N_2}p_{O_2}}} = \frac{g}{\sqrt{fe}} \quad [7]$$

---

[1] Analytical Group Engineer, Douglas Research Laboratories, Douglas Aircraft Company.

[2] Analytical Group, Douglas Research Laboratories, Douglas Aircraft Company.

[3] Numbers in parentheses refer to the Bibliography at the end of the paper.

Contributed by the Aviation Division and presented at the Aviation War Conference, Los Angeles, Calif., June 11–14, 1945, of The American Society of Mechanical Engineers.

Note: Statements and opinions advanced in papers are to be understood as individual expressions of their authors and not those of the Society.

$$K_4 = \frac{p_{NO}\sqrt{p_{O2}}}{p_{NO2}} = \frac{g}{h}\sqrt{e\left[\frac{T_m}{T_0}P_0\right]} \quad [8]$$

$$K_5 = \frac{\sqrt{p_{H2}{}^3 p_{N2}}}{p_{NH3}} = \frac{\sqrt{d^3 f}}{t}\left[\frac{T_m}{T_0}P_0\right] \quad [9]$$

$$K_6 = \frac{p_{OH}\sqrt{p_{H2}}}{p_{H2O}} = \frac{j}{c}\sqrt{d\left[\frac{T_m}{T_0}P_0\right]} \quad [10]$$

$$K_7 = \frac{p_H{}^2}{p_{H2}} = \frac{k^2}{d}\left[\frac{T_m}{T_0}P_0\right] \quad [11]$$

$$K_8 = \frac{p_O{}^2}{p_{O2}} = \frac{m^2}{e}\left[\frac{T_m}{T_0}P_0\right] \quad [12]$$

$$K_9 = \frac{p_{O3}}{\sqrt{p_{O2}{}^3}} = \frac{n}{\sqrt{e^3}}\sqrt{\frac{T_0}{T_m P_0}} \quad [13]$$

$$K_{10} = \frac{\sqrt{p_{O2}}}{p_{CO}} = \frac{1}{b}\sqrt{e\left[\frac{T_0}{T_m P_0}\right]}, (q > 0) \quad [14]$$

$$K_{11} = \sqrt{p_{C2\ (gas)}} = \sqrt{r\left[\frac{T_m}{T_0}P_0\right]}, (q > 0) \quad [15]$$

$$K_{12} = \frac{p_{H2}{}^2}{p_{CH4}} = \frac{d^2}{i}\left[\frac{T_m}{T_0}P_0\right], (q > 0) \quad [16]$$

$$K_{13} = p_{C(gas)} = s\left[\frac{T_m}{T_0}P_0\right], (q > 0) \quad [17]$$

The values of these equilibrium constants at various temperatures are given in Appendix 1 (Table 3). A sufficient number of algebraic relations have now been obtained to permit the calculation of the amount of each gas present after combustion, provided the temperature can be determined.

The explosion temperature T_m is calculated by equating the energy of combustion of the fuel at constant volume to the energy required to heat the products of combustion to the temperature T_m plus the energy required to cause the dissociation which occurs at this temperature. The energy of complete combustion of 100-octane gasoline vapor can be taken to be 18,700 Btu per lb (for the liquid) plus 140 Btu per lb (energy of vaporization; see Appendix 1). The internal energies of various gases at different temperatures, using as base values (zero internal energy) the energy of CO_2, H_2O, O_2, and N_2, and A, are given in Table 2.

The solution of these relations to obtain the explosion temperature and pressure involves successive approximation. For a particular mole-fraction of fuel vapor X, and particular initial temperature and pressure T_0 and P_0, a value for the explosion temperature T_m is guessed, and the values for the equilibrium constants, $K_1, \ldots, K_{13}$, at the temperature T_m are interpolated from the table in Appendix 1. The values for T_0, T_m, P_0, K_1, . . ., K_{13} can now be substituted in the equilibrium equations. These equations are then solved for the unknown coefficients, a, . . ., t, by the method of successive approximation. Thus, the chemical composition of the mixture after combustion has been calculated. The energy balance is then checked by comparing the energy evolved in the complete combustion of the fuel with the energy change associated with the heating of the reaction products from T_0 to T_m accompanied by the change in chemical composition from CO_2, H_2O, N_2, and O_2 to the composition just calculated. If the energy does not balance, a new value of T_m must be estimated and the whole process repeated.

After the temperature and composition of the mixture after explosion are found in this manner, the explosion pressure is readily calculated from the formula

$$P_m = P_0 N_m \frac{T_m}{T_0} \quad [18]$$

where N_m is the number of final moles of gas per unit initial mole and is therefore equal to $a + b + c + \ldots + t$.

An example of the calculation of explosion temperatures and pressures by this method is given in Appendix 2.

For five particular mixture ratios, corresponding to five values of X, thermodynamic charts were available which greatly simplified the problem of calculating the explosion temperatures and pressures. These charts are not reproduced here because they are as yet restricted in distribution.

Apparatus and Tests

In order to check the calculations of explosion pressures experimentally, a spherical explosion bomb was constructed by modifying a 9-in. aluminum pressure accumulator. A pair of strain gages was cemented to the outside surface of the bomb. The pressure pickup system is shown in Fig. 1, and a block diagram of the electrical circuit is given in Fig. 2.

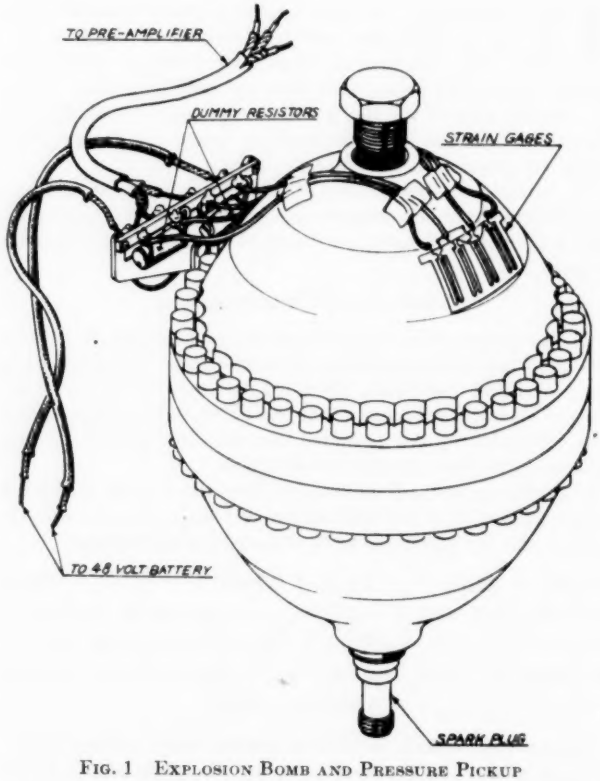


Fig. 1 Explosion Bomb and Pressure Pickup

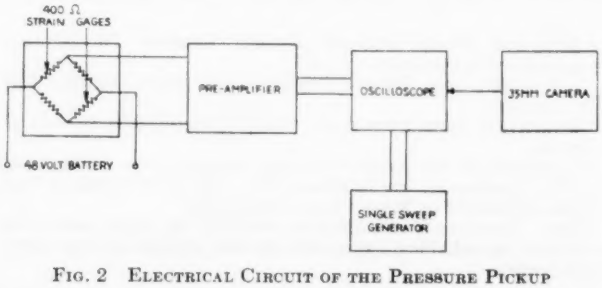


Fig. 2 Electrical Circuit of the Pressure Pickup

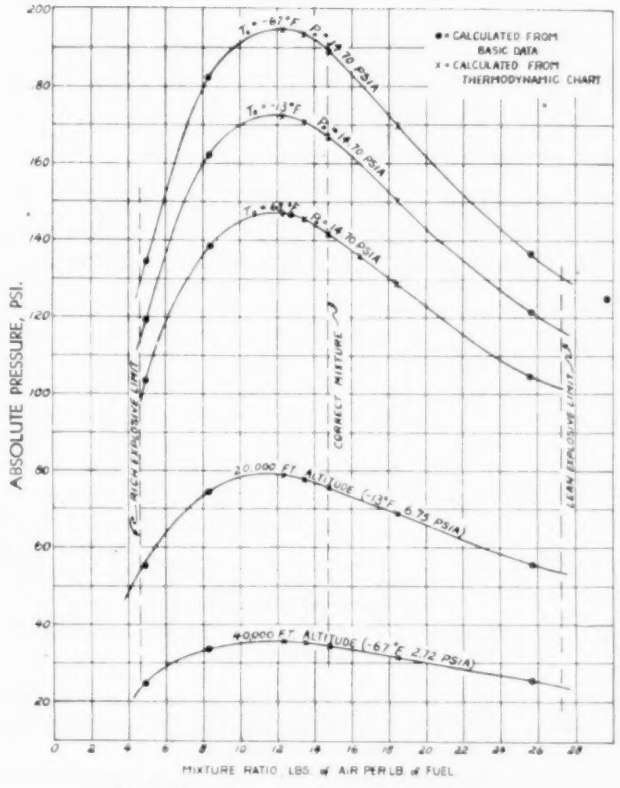


FIG. 3 THEORETICAL EXPLOSION PRESSURES

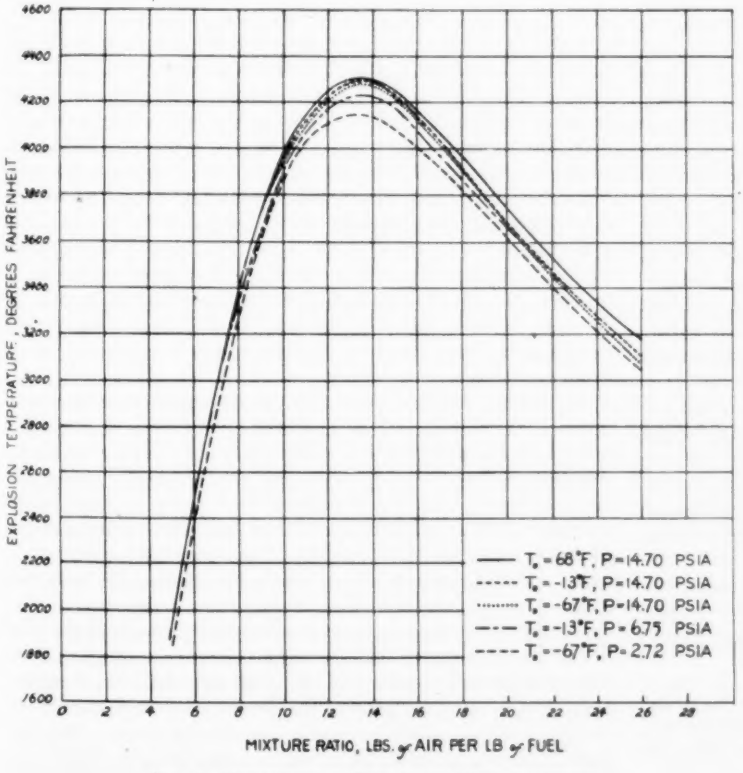


FIG. 4 THEORETICAL EXPLOSION TEMPERATURES

The two strain gages used to measure the pressure were made opposite legs of a balanced Wheatstone bridge. Pressure inside the bomb caused the surface of the bomb, and hence the gages, to be strained, which increased the resistance of the gages and produced a voltage difference across the vertical plates of an oscilloscope. A single-sweep voltage pulse was simultaneously applied to the horizontal plates.

In the tests, the bomb was charged by injecting measured amounts of 100-octane gasoline into it. The bomb was agitated manually, then allowed to stand for 15 or 20 min to permit complete vaporization. The pressure of the gasoline-air mixture immediately before the explosion was therefore 1 atm plus the partial pressure of the gasoline vapor. The mixture was exploded by a spark, and the pressure rise was shown visually by the oscilloscope. The oscilloscope trace was simultaneously photographed. To determine the actual explosion pressure, the oscilloscope trace deflection shown on the photographic film was measured and compared with the deflections produced by charging the bomb with compressed air under known pressures.

RESULTS OBTAINED

Theoretical. The temperatures and pressures that should result when various mixtures of air and 100-octane gasoline are exploded in a closed chamber, at various initial temperatures and pressures, have been calculated by the method described in the section discussing theory. Sample calculations are given in Appendix 2. The results are presented graphically in Figs. 3 and 4.

The results have been related to the conventional mixture ratio M_R, which is defined as the ratio of the weight of air to the weight of gasoline vapor. It should be noted that

$$M_R = \frac{\text{Vol per cent of air}}{\text{Vol per cent of gasoline vapor}} \times \frac{28.98}{112.2} = 0.2583\,(1 - X)/X$$

Experimental. The results of the explosion pressure measurements made with the spherical bomb are given in Table 1. These results are also compared graphically with the theoretical curve in Fig. 5.

DISCUSSION OF RESULTS

Theoretical. It can be seen from Figs. 3 and 4, that very good agreement is obtained between the algebraic method of calculation developed in this paper and the method based on thermodynamic charts.

Except for very rich mixtures, these theoretical calculations should be quite accurate. The gasoline has been rather arbitrarily assigned the average composition C_8H_{16}, which is equivalent to specifying a hydrogen-carbon ratio of 2, and an average molecular weight of 112. The hydrogen-carbon ratios for aviation gasolines are known to be very close to 2; moreover, a considerable variation of the ratio affects the calculated pressures only slightly (for example, use of the charts of reference (2) calculated for a hydrogen-carbon ratio of 2.25, gives for M_R = 14.76 a pressure 0.7 per cent lower). The molecular weight enters into the problem only in the determination of the amount of air displaced by the fuel vapor. A 10 per cent error in the estimated molecular weight would change the final results by only 0.5 per cent for X = 0.05.

TABLE 1 EXPERIMENTAL MEASUREMENTS OF EXPLOSION PRESSURES

M_R	Time Allowed for Vaporiz. min.	T_o °F	Time, Spark to Max. Press. sec*	P_o (calc.) psia**	ΔP psi	P_m psia
4.6	16	70	0.15	15.5	158	174
4.6	15	72	0.22	"	130	146
5.2	15	91	0.40	15.4	112	127
5.2	15	91	0.65	"	102	117
5.2	15	87	0.35	"	107	112
5.2	975	41	0.15	"	165	180
6	17	66	0.12	15.3	168	183
6	18	70	0.12	"	162	177
6	17	49	0.22	"	146	161
6	26	56	0.12	"	141	156
6	16	61	0.12	"	146	161
7	16	70	0.09	15.2	170	185
7	16	70	0.09	"	170	185
7	16		0.09	"	165	180
8	15	70	0.11	"	130	145
8	15		0.13	"	187	202 (1†)
8	25		0.12	"	182	197 (2)
11	16	80	0.09	15.1	168	183
11	17	84	0.09	"	168	183
11	16	87	0.09	"	162	177
15	20	90	0.12	14.9	161	176 (3)
15	15	92	0.12	"	153	168 (4)
15	15	92	0.17	"	147	162 (5)
18	15	86	0.21	"	120	135
18	17	80	0.23	"	112	127
18	17	80	0.26	"	112	127
18	15	75	0.23	"	112	127
18	15	75	0.35	"	95	110
22	27	84	0.40	"	103	118
22	16	84	0.45	"	95	110

* Tabulated times may all be short by about the same amount.

** Initial pressure equals one atmosphere plus the partial pressure of the gasoline vapor.

† Numbers indicate first five explosions in the bomb, showing decrease of pressure readings as inside of bomb becomes coated with carbon and other explosion products.

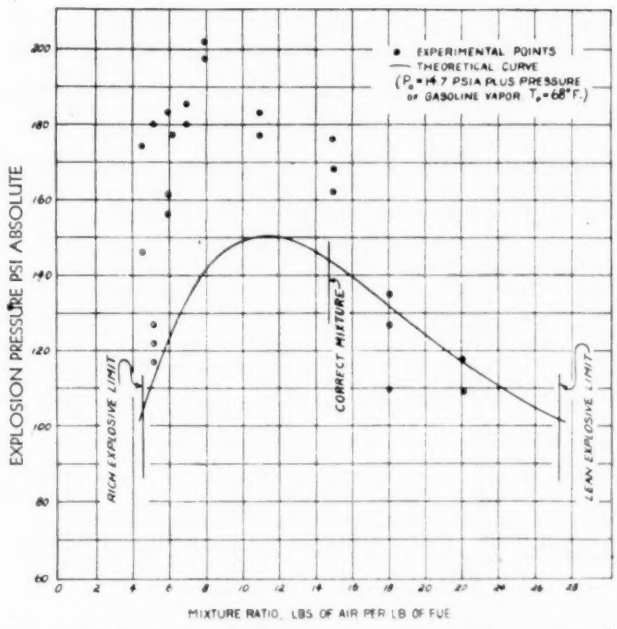


FIG. 5 COMPARISON OF THEORETICAL AND EXPERIMENTAL EXPLOSION PRESSURES

The error due to inaccuracies in the values for the internal energy of the gases (Appendix 1) should be less than 0.5 per cent. Inaccuracies in the values of the equilibrium constants would probably affect the results by less than 1 per cent. The possible errors caused by nonequilibrium conditions, radiation losses, and other minor effects[4] are presumably small, since calculations by Lewis and von Elbe[5] for explosion pressures of lighter gases (H_2, CO, C_2H_2) agree with the experimentally measured pressures within 3 per cent. (These lighter gases contain the same elements as gasoline, and the composition of the hot burned mixture depends only on the elements present and the temperature, not on the original compounds present.)

When very rich mixtures are exploded, radicals such as CH and CH_2 can be expected to take part in the reaction. No thermodynamic data on such radicals are available, so their presence has been perforce neglected in the calculations for this paper. The error thus introduced is probably not large, since the calculations show that the related molecule CH_4 is present only in a minor amount. However, at the lower explosion temperatures which occur with rich mixtures, the assumption that all chemical reactions reach equilibrium may be in appreciable error. Moreover, the presence of finely divided free carbon may greatly increase the radiation losses. For these reasons, that part of the theoretical curves to the left of $M_R = 8$ should be considered as approximate only.

Experimental. A graphical comparison of the explosion-pressure calculations with the experimental measurements is presented in Fig. 5. As was explained in the "Apparatus and Tests" section, the initial pressures for the bomb explosions were slightly higher than 1 atm, and the initial temperature assumed in the calculation of the theoretical curve was 68 F.

The experimental points fall generally above the theoretical curve and also show much scatter among themselves. A number of factors probably contribute to these discrepancies. Perhaps the most important factor is the incomplete vaporization and mixing of the fuel. The theoretical calculations assume that the gasoline is completely vaporized and the vapor uniformly mixed with the air. Under the conditions of the tests, it is very possible that the heavier fractions of the gasoline remained unvaporized. Since the lighter hydrocarbons in the gasoline have hi her heats of combustion, the actual explosion pressures would be above the calculated values. This agrees with the experimental measurements. Furthermore, for mixtures richer than the maximum-pressure mixture, the experimentally measured pressures would appear to be too high because the mixtures are actually leaner than would be supposed from the amount of gasoline injected. The large variations in pressures for repeated explosions of mixtures having supposedly the same mixture ratio can be attributed to variations in the degree of vaporization of the fuel and in the homogeneity of the explosive mixture.

A possible cause of error in the strain-gage pressure measurements is the thermal strain produced by the contact of the hot gases with the inner surface of the bomb wall. If the wall were uniformly heated, the temperature of the gages would rise simultaneously, and the error introduced would be small, since the gages are practically temperature-compensated for aluminum. However, only the inside surface of the bomb is heated by the gases. If the temperature at the outer surface remains constant, while the temperature increases toward the inner surface such that the average temperature increase throughout the shell is 1 C, it can be shown that the thermal strain causes a rise in the apparent pressure reading of about 85 psi, while the heat loss from the gas mixture reduces the actual pressure about 30 psi, leaving a net apparent increase in pressure of 55 psi. It is difficult to determine how high a temperature rise in the shell of the bomb should be expected during the short time between sparking

[4] Such as the nonuniform final temperature distribution (reference (3), pp. 167, 175–176, 293–299), and the "excitation lag" due to the greater rapidity with which energy flows into the translational and rotational rather than the vibrational degrees of freedom (reference (3), p. 306).

[5] Reference (3). pp. 301–308.

and attainment of maximum pressure, but a 1-deg C average rise might not be unreasonable. It might be expected that the layer of carbon and other materials deposited on the inner surface of the bomb after several charges have been exploded would reduce the amount of heat conducted to the walls and therefore reduce the apparent pressure readings. The experimental data, which designate the first five charges fired, appear to confirm this hypothesis (see Table 1).

An estimate has been made of the gasoline temperature as a function of air pressure which gives the lean-explosive-limit mixture with gasoline vapor saturation. This estimate is shown in Fig. 6, where air pressure has been converted into altitude by the standard atmospheric table. The gasoline vapor pressure as a function of temperature was taken from work of the Cooperative Fuel Research Committee.[6] As long as the rich explosive limit is not exceeded, the region above this curve is the region of true ignitibility, assuming that the lean-limit-mixture ratio is a constant independent of temperature and pressure. The latter assumption implies that the kinetics of the chain reactions involved in ignition do not change appreciably within the temperature and pressure range. Such an assumption can only represent an approximation and most likely is optimistic in that the air-gasoline lean-limit mixture will tend to decrease with temperature. The true ignition-limit curve would thus most likely be above the curve in Fig. 6.

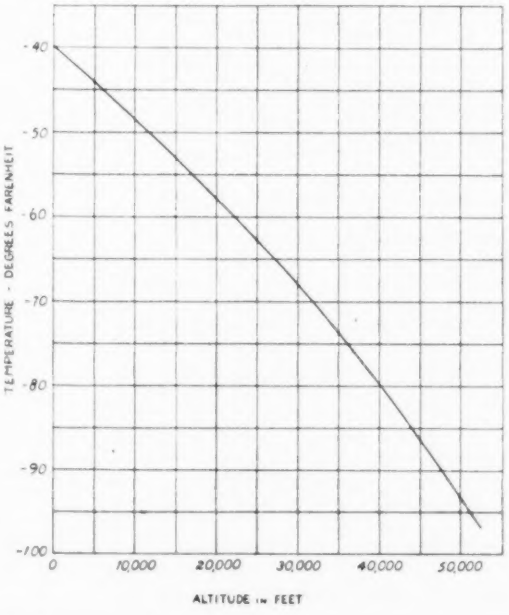


FIG. 6 ESTIMATED LEAN-EXPLOSIVE-LIMIT TEMPERATURES FOR SATURATED GASOLINE-AIR MIXTURES
(Standard atmospheric conditions assumed.)

CONCLUSIONS

A method is developed which permits the calculation of the temperatures and pressures attained when mixtures of air and aviation-gasoline vapor are exploded in a closed chamber. For a few mixture ratios, calculations may be made by the use of thermodynamic charts. Calculations by the two methods show close agreement. The results for various initial temperatures and pressures are presented graphically.

Experimental measurements of the explosion pressures were made using an explosion bomb with a strain-gage pressure pickup. The measured pressures were of the same order of magnitude as the calculated pressures, but in general were somewhat higher than the theoretical values. Possible explanations for this trend are incomplete vaporization of the fuel, incomplete attainment of chemical equilibrium at the explosion temperature, and errors in the pressure measurements caused by temperature gradients.

An estimate of the lower ignition-temperature limit as a function of altitude, for standard atmospheric conditions, is also given.

[6] Reference (4), p. 44.

Appendix 1

THERMODYNAMIC DATA

The internal energy of combustion (i.e., heat of combustion at constant volume) of gasoline vapor is equal to the energy of combustion of liquid gasoline plus the energy of vaporization of gasoline. A minimum net calorific value of 18,700 Btu per lb is specified[7] for 100-octane gasoline (liquid). No data have been found for the energy of vaporization of 100-octane gasoline, but Holcomb and Brown (5) give the heat of vaporization of normal octane at room temperature as 140 Btu per lb. Since this figure does not affect the total greatly, the approximation that the energy of vaporization of aviation gasoline equals 140 Btu per lb will be used. The energy of combustion of the gasoline vapor is therefore 18,700 + 140 = 18,840 Btu per lb. If the gasoline has an average molecular weight of 112.21, this value is equivalent to 1,174,400 cal per g-mole.

Values for the thirteen pertinent equilibrium constants at various temperatures are given in Table 2 and plotted in Fig 7. The values are taken from Lewis and von Elbe (3), except the values for log K_5, which are derived from an expression for the free energy of NH_3 given by Thacker, Folkins, and Miller (6).

Table 3 shows the internal energy per gram-mole of the various gases present after combustion, as a function of temperature. For the gases usually present in large amounts, exact energy values at various temperatures, taken from (2), are given. For gases present only in small amounts, approximate equations for the energy as a function of the absolute temperature are given. These expressions have been derived[8] from values of C_p; and from values of the energies of reaction.[9] The quantities are expressed in terms of gram-moles and degrees Kelvin (deg C + 273.2) rather than in the usual engineering units. In all cases, the zero energy level is taken as the internal energy of CO_2, H_2O, O_2, N_2, and A at 300 K, but corrections are given for changing to a base level of 20 C (68 F), —25 C (—13 F), or —55 C (—67 F)

Appendix 2

EXAMPLE OF ALGEBRAIC CALCULATION OF EXPLOSION PRESSURES

As an example of the method of calculating explosion pressures and temperatures as described in the section, "Theoretical Considerations," consider the problem with the particular initial conditions $P_0 = 1$ atm, $T_0 = 68$ F (20 C), and $X = 0.0300$.

Substitution of this value of X in Equations [1] to [4], inclusive, yields

$$a + b + i + q + 2r + s = 0.2403 \quad [19]$$

$$2c + 2d + 4i + j + k + 3t = 0.4800 \quad [20]$$

$$2a + b + c + 2e + g + 2h + j + m + 3n = 0.4070 \quad [21]$$

$$2f + g + h + t = 1.5150 \quad [22]$$

[7] Reference (4), p. 12.
[8] Reference (6), p. 586; and (7), p. 75.
[9] Reference (3), pp. 378–385.

TABLE 2 COMMON LOGARITHMS OF THE EQUILIBRIUM CONSTANTS AT VARIOUS TEMPERATURES
(Pressure units: atmospheres)

Temp °K	log K_1	log K_2	log K_3	log K_4	log K_5	log K_6	log K_7	log K_8	log K_9	log K_{10}	log K_{11}	log K_{12}	log K_{13}
300	-44.72	-39.77	-15.04	-6.42	. .	-43.3	-70.23	-80.2	-28.29	-24.08	. .	-8.935	. .
400	-32.43	-29.26	-11.13	-3.94	. .	-31.7	-51-35	-58.6	-22.15	-19.23	. .	-5.580	. .
600	-20.07	-18.64	-7.194	-1.44	. .	-20.0	-32.41	-36.9	-15.98	-14.41	. .	-2.047	. .
800	-13.89	-13.28	-5.231	-0.18	. .	-14.07	-22.88	-26.1	-12.89	-11.98	. .	-0.180	. .
1000	-10.20	-10.05	-4.052	+0.57	+3.26	-10.53	-17.13	-19.48	-11.03	-10.52	. .	+0.985	. .
1200	-7.755	-7.90	-3.267	+1.08	+3.72	-8.17	-13.28	-15.10	-9.79	-9.530	. .	+1.779	. .
1400	-5.999	-6.34	-2.706	+1.43	+4.08	-6.47	-10.51	-11.97	-8.89	-8.817	. .	+2.354	. .
1600	-4.715	-5.20	-2.285	+1.69	+4.36	-5.20	-8.429	-9.61	-8.22	-8.277	. .	+2.790	. .
1800	-3.690	-4.27	-1.959	+1.89	+4.56	-4.19	-6.803	-7.772	-7.70	-7.850	. .	+3.129	. .
2000	-2.862	-3.52	-1.695	+2.07	+4.72	-3.40	-5.496	-6.298	-7.29	-7.504	-1.695	+3.397	-5.455
2200	-2.193	-2.91	-1.479	+2.18	+4.84	-2.74	-4.424	-5.091	-6.95	-7.221	-1.10*	+3.616	-4.212
2400	-1.648	-2.41	-1.300	+2.29	+4.93	-2.19	-3.529	-4.078	-6.66	-6.980	-0.60*	+3.801	-3.187
2600	-1.206	-2.00	-1.150	+2.39	+5.01	-1.74	-2.759	-3.228	-6.42	-6.777	. .	+3.960	-2.315
2800	-0.811	-1.63	-1.019	+2.48	+5.07	-1.34	-2.115	-2.495	-6.21	-6.595	. .	+4.098	-1.573
3000	-0.470	-1.31	-0.907	+2.56	+5.12	-0.999	-1.548	-1.858	-6.03	-6.440	+0.474	+4.218	-0.926

* Interpolated values.

NOTE: These equilibrium constants are defined in the Theory section. All pressures are in standard atmospheres.

These values are derived from Ref. (2), Table 2, p. 382, except the values for log K_3, which are derived from the values of free energy for NH_3 given in Ref. (6), p. 587.

Some of these values are plotted in Fig. 7, for convenience in interpolation.

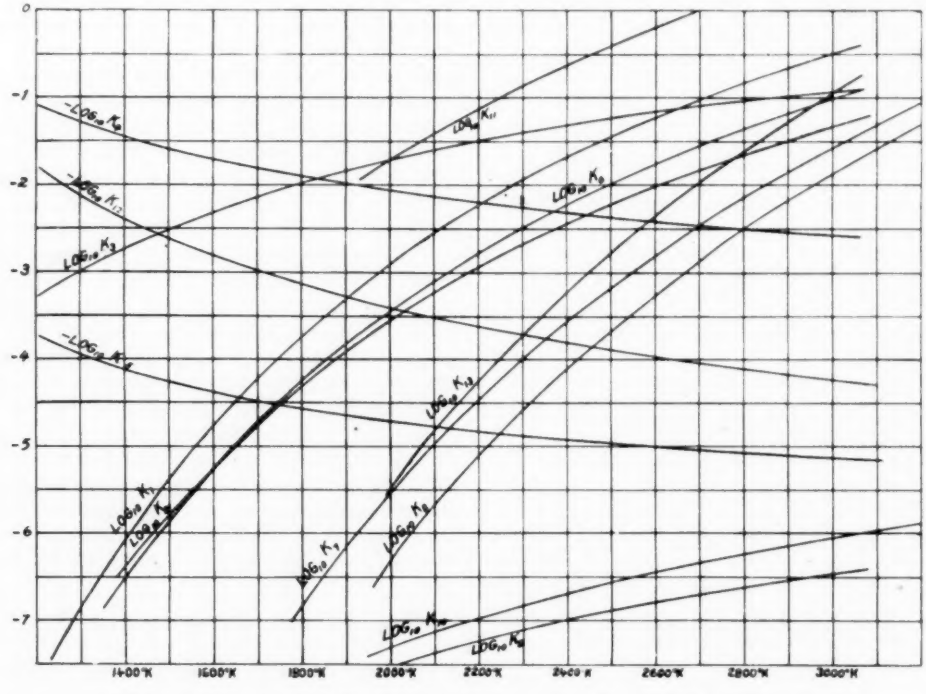


FIG. 7 LOGARITHMS OF EQUILIBRIUM CONSTANTS AT VARIOUS TEMPERATURES
(From Table 2.)

The next step in the calculation is to guess a value for the explosion temperature T_m, which value will be checked at the conclusion of the calculations. Suppose the value $T_m = 2200$ deg K is chosen. The values of the pertinent equilibrium constants $K_1, K_2, \ldots, K_{13}$, are found in Table 2. When these values and the values of T_0 and T_m are substituted in Equations [5] to [17], inclusive, the following equations result

$$\frac{b}{a}\sqrt{e} = 2.34 \times 10^{-3} \quad [23]$$

$$\frac{d}{c}\sqrt{e} = 4.49 \times 10^{-4} \quad [24]$$

$$\frac{g}{\sqrt{fe}} = 0.0332 \quad [25]$$

$$\frac{g}{h}\sqrt{e} = 55.5 \quad [26]$$

$$\frac{\sqrt{d^2 f}}{t} = 9{,}220 \quad [27]$$

$$\frac{j}{c}\sqrt{d} = 6.64 \times 10^{-4} \quad [28]$$

$$\frac{k^2}{d} = 5.02 \times 10^{-6} \quad [29]$$

TABLE 3 INTERNAL ENERGY OF VARIOUS GASES AT T DEG

(Base values at 300 deg equal internal energy of formation from CO_2, H_2O, O_2, N_2, A; units, calories per gram-mole)

Gas	Temperature, Degrees Kelvin														Correction to be Added for Change of Base Temperature to:		
	300	600	800	1000	1200	1400	1600	1800	2000	2200	2400	2600	2800	3000	20°C	-25°C	-55°C
CO_2	0	2,475	4,447	6,587	8,843	11,184	13,586	16,038	18,527	21,043	23,588	26,159	28,746	31,352	46	353	557
H_2O	0	1,896	3,282	4,786	6,409	8,129	9,949	11,864	13,859	15,909	18,009	20,154	22,334	24,539	41	312	492
N_2	0	1,517	2,589	3,727	4,921	6,157	7,423	8,718	10,039	11,368	12,711	14,061	15,425	16,798	34	257	405
O_2	0	1,602	2,779	4,025	5,316	6,637	7,990	9,366	10,762	12,181	13,624	15,084	16,563	18,058	34	261	413
CO	67,329	68,657	69,950	71,110	72,325	73,581	74,865	76,174	77,505	78,851	80,205	81,565	82,936	84,316	29	223	351
H_2	57,503	58,999	60,010	61,041	62,106	63,214	64,356	65,540	66,763	68,017	69,297	70,608	71,944	73,293	24	182	286
OH	34,700	36,225	37,246	38,295	39,377	40,517	41,702	42,917	44,162	45,432	46,742	48,067	49,412	50,784	29	221	349
H	80,326	81,220	81,815	82,411	83,007	83,603	84,199	84,795	85,390	85,986	86,582	87,178	87,773	88,368	12	91	143
O	58,801	59,695	60,290	60,886	61,482	62,078	62,674	63,270	63,865	64,461	65,057	65,653	66,248	66,843	17	130	206
NO	21,528	23,108	24,244	25,446	26,698	27,986	29,301	30,636	31,987	33,351	34,726	36,109	37,500	38,897	34	259	409

A	$-894 + 2.979\ T$				20	154	244
NO_2	$6190 + 5.0\ T + 3.5 \times 10^{-3}\ T^2 - 6.2 \times 10^{-7}\ T^3$				41	389	615
NH_3	$73,910 + 6.05\ T + 3.5 \times 10^{-4}\ T^2 + 1.7 \times 10^{-6}\ T^3$				53	401	631
O_3	$32,440 + 5.0\ T + 3.5 \times 10^{-3}\ T^2 - 6.2 \times 10^{-7}\ T^3$				41	391	619
CH_4	$189,500 + 4.74\ T + 5.1 \times 10^{-3}\ T^2 + 1.12 \times 10^{5}\ T^{-1}$				60	456	716
C (graphite)	$93,071 + 2.673\ T + 1.308 \times 10^{-3}\ T^2 + 1.17 \times 10^{5}\ T^{-1}$				12	92	144
C (gas)	$217,000 + 3.0\ T$				12	92	144
C_2(gas)	$309,000 + 4.5\ T + 5 \times 10^{-4}\ T^2$				12	92	144

NOTE: Precise energy values (in upper part of Table) taken from Ref. (2), Table 5A, p. 423. Approximate expressions in lower part of table (for gases present in small amounts) derived from values of C_p given in Ref. (6), p. 586, and Ref. (7), p. 75, and values of thermal energies and energies of reaction given in Ref. (3), pp. 378–385. T = temperature in degrees Kelvin (°C + 273.2).

$$\frac{m^2}{e} = 1.08 \times 10^{-6} \quad [30]$$

$$\frac{n}{e^{3/2}} = 3.07 \times 10^{-7} \quad [31]$$

$$\frac{1}{b}\sqrt{e} = 1.65 \times 10^{-7}, (q > 0) \quad [32]$$

$$\sqrt{r} = 2.9 \times 10^{-2}, (q > 0) \quad [33]$$

$$\frac{d^2}{i} = 550, (q > 0) \quad [34]$$

$$s = 8.18 \times 10^{-6}, (q > 0) \quad [35]$$

It should be noted that the last four equalities hold only when q is greater than zero, that is, when solid carbon is present. Although, with this particular gasoline-air mixture, not enough oxygen is present for complete combustion of the fuel to CO_2 and H_2O, more than sufficient oxygen is present to burn the fuel to CO and H_2O. Therefore, it might be supposed that the carbon atoms in the mixture are so completely oxidized that the free carbon remaining is so small in amount as to be completely vaporized, or, in other words, $q = 0$. In working the problem, this assumption will be made and then checked before the calculation is completed.

If $q = 0$, Equations [32] to [35], inclusive, must be replaced by the corresponding inequalities

$$\sqrt{e} > 1.65 \times 10^{-7}\, b, \quad (q = 0) \quad [36]$$

$$\sqrt{r} < 2.9 \times 10^{-2}, \quad (q = 0) \quad [37]$$

$$i < d^2/550, \quad (q = 0) \quad [38]$$

$$s < 8.18 \times 10^{-6}, \quad (q = 0) \quad [39]$$

These inequalities permit only upper limits to be set on the values of r, i, and s. However, in many instances, these upper limits are sufficiently small to show that r, i, and s are negligible. For mixture ratios which give moderately large upper limits, the exact values of r, i, and s can be calculated by transforming Equations [32], [33], [34], and [35] for equilibriums involving solid carbon into similar equations involving gaseous carbon, by the fundamental chemical principle that, in equilibriums involving a solid, the solid may be replaced by the corresponding vapor, at a pressure equal to the vapor pressure of the solid, without disturbing the equilibrium.

If it is assumed that $q = 0$ and that r, i, and s can be neglected, the problem is reduced to the solution of thirteen nonlinear simultaneous equations, Equations [19] through [31], in thirteen unknowns. These simultaneous equations cannot be solved explicitly, so the method of successive approximation must be used. Perhaps the simplest way to begin is to guess a value of a and follow through the evaluation of the other unknowns until all the equations check. Suppose the value $a = 0.0416$ is tried. Since i, q, r, and s are assumed negligible, Equation [19], becomes

$$a + b = 0.2403$$
$$b = 0.2403 - a = 0.1987 \quad [40]$$

From Equation [23]

$$e = (2.34 \times 10^{-3}\, a/b)^2$$
$$= 2.40 \times 10^{-7} \quad [41]$$

From Equation [24]

$$c = \frac{d\sqrt{e}}{4.49 \times 10^{-4}}$$
$$= 1.092\, d \quad [42]$$

From Equation [28]

$$j = 6.64 \times 10^{-4}\, \frac{c}{\sqrt{d}}$$
$$= 7.25 \times 10^{-4}\sqrt{d} \quad [43]$$

From Equation [29]

$$k = 2.24 \times 10^{-3}\sqrt{d} \quad [44]$$

From Equation [27]

$$t = 1.085 \times 10^{-4}\sqrt{d^3 f} \quad [45]$$

If the assumption is made that g, h, and t are fairly small, it follows from Equation [22] that $f = 0.757$. Therefore, from Equation [45]

$$t = 9.44 \times 10^{-5}\sqrt{d^3} \quad [46]$$

If the values of c, j, k and t from Equations [42], [43], [44], and [46] are substituted in Equation [20] that equation becomes

$$4.184d + 2.97 \times 10^{-3}\sqrt{d} + 2.83 \times 10^{-4}\sqrt{d^3} = 0.4800$$

whence

$$d = 0.1144 \quad [47]$$

It follows, from Equations [42], [43], and [44], that

$$c = 0.1249$$
$$j = 2.45 \times 10^{-4}$$
$$k = 7.58 \times 10^{-4}$$

Equation [25] can be rewritten

$$g = 0.0322\sqrt{fe}$$
$$= 1.63 \times 10^{-8}\sqrt{f} \quad [48]$$

If Equation [25] is divided by Equation [26], the result is

$$\frac{h}{e\sqrt{f}} = 5.98 \times 10^{-4}$$
$$h = 5.98 \times 10^{-4}\, e\sqrt{f}$$
$$= 1.44 \times 10^{-10}\sqrt{f} \quad [49]$$

The value of d from Equation [47] can be substituted in Equation [45] to give

$$t = 4.20 \times 10^{-6}\sqrt{f} \quad [50]$$

An equation for f results when the values for g, h, and t from Equations [48], [49], and [50] are substituted in Equation [22]

$$2f + 2.05 \times 10^{-5}\sqrt{f} = 1.5150$$
$$f = 0.7575$$

whence

$$g = 1.42 \times 10^{-5}$$
$$h = 1.25 \times 10^{-12}$$
$$t = 3.66 \times 10^{-6}$$

From Equations [30] and [31], using the value of e from Equation [41]

$$m = \sqrt{1.08 \times 10^{-6}\, e}$$
$$= 5.11 \times 10^{-10}$$

$$n = 3.07 \times 10^{-7}\, e^{3/2}$$
$$= 3.66 \times 10^{-17}$$

All of the unknowns have now been evaluated using an estimated value of a, and twelve of the thirteen equations. To check the estimated value of a, use is made of the remaining equation, Equation [21]. Substitution of the values of the unknowns in the left side of Equation [21] yields the near equality

$$0.4071 = 0.4070$$

It remains to confirm the initial assumption that q, r, i, and s are negligible. The values of b and e calculated previously are such that

$$\sqrt{e} = 2.48 \times 10^{-3}\, b$$

Comparison of this with inequality [36]

$$\sqrt{e} > 1.65 \times 10^{-7}\, b, \quad (q = 0)$$

shows that q does equal zero. The ratio of the pressure of the carbon vapor actually present to the vapor pressure of carbon at the explosion temperature is $1.65 \times 10^{-7}/2.48 \times 10^{-3} = 6.65 \times 10^{-5}$. Inequalities [37], [38], and [39] can then be converted into the following equations

$$\sqrt{r} = (6.65 \times 10^{-5})\,(2.9 \times 10^{-2}) = 1.9 \times 10^{-6}$$

$$i = \frac{6.65 \times 10^{-5}\, d^2}{550} = 1.21 \times 10^{-7}\, d^2$$

$$s = (6.65 \times 10^{-5})\,(8.18 \times 10^{-6}) = 5.44 \times 10^{-10}$$

Evaluation of r and i yields

$$r = 3.6 \times 10^{-12}$$
$$i = 1.58 \times 10^{-9}$$

Thus the assumption that q, r, i, and s can be neglected is verified.

The calculations thus far have shown the equilibrium composition of the gasoline-air mixture at 2200 K. It must still be demonstrated that the heat evolved by the reaction is just sufficient to raise the temperature of the gas mixture to the assumed value of 2200 K.

The heat energy evolved at room temperature by the complete constant-volume combustion of 0.030 mole of gasoline vapor to H_2O (vapor) and CO_2 is (1,174,400) (0.030) = 35,232 cal (see Appendix 1).

The energy required to raise the temperature from 293 K to 2200 K and cause the dissociation which occurs at the latter temperature is calculated by using the coefficients a, b, . . ., t already calculated, and the internal energy per mole of the various gases at 2200 K above the energy of O_2, N_2, H_2O, and CO_2 at 293 K, values of which are given in Table 2.

The calculation may be conveniently presented as in Table 4.

The last two columns of Table 4 show the rate of change of energy with temperature and will be used to estimate how much the actual explosion temperature differs from 2200 K. The

TABLE 4

Gas	No. moles	ΔE per mole[a]	ΔE per react.	$\frac{d(\Delta E \text{ per mole})}{dT}$	$\frac{d(\Delta E \text{ per react.})}{dT}$
a CO_2	0.0416	21089	878	12.2	0.51
b CO	0.1987	78880	15670	6.8	1.35
c H_2O	0.1249	15950	1991	10.5	1.31
d H_2	0.1144	68041	7783	6.4	0.73
f N_2	0.7575	11402	8630	6.71	5.14
j OH	0.00025	45461	11	....	....
k H	0.00076	85998	65	....	....
A	0.0090	5680	51	....	....
Total	1.2471		35079		9.04

[a] Refer to Table 3.

difference between the energy evolved and the energy at 2200 K is 35,232 — 35,079 = 153 cal. The actual temperature is, therefore, approximately 153/9.04 = 16.9 deg above 2200 K. This is not different enough from 2200 K to change the equilibrium constants significantly, so the value T_m = 2217 K (1944 C) may be taken as accurate. The explosion pressure P_m can be calculated from Equation [18]

$$P_m = P_0 N_m T_m / T_0$$
$$= (1.000)\,(1.2471)\,(2217)/293.2$$
$$= 9.42 \text{ atm} = 138.5 \text{ psia}$$

It should be noted that if the energy-balance calculation shows that the temperature is considerably different from the estimated temperature which was used to calculate the unknown coefficients, the entire calculations must be repeated using the equilibrium constants at the newly estimated temperature. However, if the difference between the two temperatures is not too great, the recalculation may be greatly simplified by neglecting the coefficients which the previous calculation has shown are negligible. In fact, for all mixture ratios, more than one half of the seventeen coefficients can be neglected; however, the coefficients which may be neglected are different for different mixture ratios. In the calculations presented, the precise value of every coefficient has been given so that there will be no question as to which coefficients are negligible.

BIBLIOGRAPHY

1 "Physics of the Air," by W. J. Humphreys, McGraw-Hill Book Company, Inc., New York, N. Y., 1940, p. 67.

2 "Thermodynamic Properties of the Working Fluid in Internal-Combustion Engines," by R. L. Hershey, J. E. Eberhardt, and H. C. Hottel, S.A.E. Transactions, vol. 31, 1936, pp. 409–424.

3 "Combustion, Flames, and Explosions of Gases," by B. Lewis and G. von Elbe, Cambridge University Press, London, England, 1938.

4 "Test Procedures and General Information in Current Use in the Development and Utilization of Aviation, Motor and Automotive Diesel Fuels," Co-operative Fuel Research Committee, 1941.

5 "Thermodynamic Properties of Light Hydrocarbons," by D. E. Holcomb and G. G. Brown, *Industrial and Engineering Chemistry*, vol. 34, 1942, pp. 590–601.

6 "Free Energies of Formation of Gaseous Hydrocarbons and Related Substances," by C. M. Thacker, H. O. Folkins, and E. L. Miller, *Industrial and Engineering Chemistry*, vol. 33, 1941, pp. 584–590.

7 "A Course of Study in Chemical Principles," by A. A. Noyes and M. S. Sherrill, second edition, The Macmillan Company, New York, N. Y., 1938.

(Owing to travel emergency conditions existing when this paper was presented, discussion will be accepted until March 11, 1946)

Heat Transfer in Annuli

By C. Y. CHEN,[1] G. A. HAWKINS,[2] AND H. L. SOLBERG[3]

A survey of the literature reveals that few data are available relative to heat transfer in annular spaces for the case of laminar flow. This paper presents data acquired in an experimental study[4] of the heat-transfer coefficients at the inner wall of four different annuli for the case of laminar flow of water. Both heating and cooling tests were conducted. The experiments were performed over a range of Reynolds numbers from 200 to 2000. The accompanying dimensionless equation was

$$\frac{hD}{k} = 1.02\left(\frac{VD\rho}{\mu_a}\right)^{0.45}\left(\frac{c_p\mu_a}{k}\right)^{1/3}\left(\frac{\mu_a}{\mu_w}\right)^{0.14}\left(\frac{D}{L}\right)^{0.4}\left(\frac{D_1}{D_2}\right)^{0.8} \cdot \left(\frac{D^3\rho^2\beta g\Delta t}{\mu_a^2}\right)^{0.05}$$

found to correlate both the heating and the cooling data for all four annuli with an average deviation of ±6.6 per cent and a maximum deviation of ±14.1 per cent. This equation may be used for computing the heat-transfer coefficient on the inner wall of an annulus for laminar flow of water for Reynolds numbers in the range of 200 to 2000.

Nomenclature

The following nomenclature is used in the paper:

a = constant
A = area, sq ft
b = constant
c_p = heat capacity at constant pressure, Btu/(lb_{mass})(deg F)
d = constant
D_1 = outer diameter of annulus, ft
D_2 = inner diameter of annulus, ft
D = equivalent diameter of annulus, ft
D_e = characteristic dimension of annulus, ft
e = constant
f = constant
g = gravitational acceleration, ft/hr²
h = surface coefficient of heat transfer, Btu/(hr)(sq ft)(deg F)
k = thermal conductivity, Btu/(hr)(ft)(deg F)
L = characteristic linear dimension, ft
L = heating or cooling length of an annular section, ft
m = constant
m = hydraulic radius, ft
q_r = heat transferred by radiation, Btu/hr
t = temperature, deg F
T = absolute temperature, deg R
V = velocity, fph
α = constant
ϵ = emissivity of surface for radiation
β = coefficient of cubical expansion, (deg F)$^{-1}$
ρ = density, (lb_{mass})/cu ft
μ = dynamic (absolute) viscosity, (lb_{mass})/(hr)(ft)
μ_w = dynamic (absolute) viscosity at the surface temperature, (lb_{mass})/(hr)(ft)
μ_a = dynamic (absolute) viscosity evaluated at bulk-fluid temperature, (lb_{mass})/(hr)(ft)
Δ = difference

Introduction

The double-pipe heat exchanger is frequently used in engineering work to transmit heat from one fluid to another. The design of this type of heat exchanger requires a knowledge of the heat-transfer coefficient in the annular space. Designing engineers have long felt the need for a single heat-transfer correlation which could be used for determining the coefficient for the case of an annular space for either a heating or a cooling process. In an annular space, heat transfer may take place either at the inner surface of the annulus or at the outer surface or both.

A survey of the literature reveals that in the last decade a number of successful investigations have been made on the heat transfer in annular spaces for the case of turbulent flow. However, very little has been done for the case of laminar flow in annular spaces. Jakob and Rees (1)[5] presented a mathematical theory of heat transfer between the walls of an annulus and a fluid passing through it in laminar flow for the cases of uniform heating or cooling from outside, inside, or from both sides at the same time.

In a recent paper, Davis (2) suggested a tentative dimensionless equation for determining heat-transfer coefficients in annuli for the case of laminar flow. Since there were no experimental data available, the constants of the equation were left as unknowns.

The criterion of flow is the Reynolds number $\frac{VD\rho}{\mu}$. In case of flow in an annular space, usually an equivalent diameter is used for D. There are two methods of calculating the equivalent diameter of an annulus. In the first of these methods, a value of 4 times the hydraulic radius m is used for the equivalent diameter. The hydraulic radius may be expressed as follows

$$m = \frac{\frac{\pi}{4}(D_1^2 - D_2^2)}{\pi(D_1 + D_2)} = \frac{D_1 - D_2}{4}$$

The equivalent diameter in this case is therefore $(D_1 - D_2)$.

In the second method, the heated perimeter is used. Where heat transfer takes place at the inner wall the equivalent diameter is

$$D = \frac{4 \times \frac{\pi}{4}(D_1^2 - D_2^2)}{\pi D_2} = \frac{D_1^2 - D_2^2}{D_2}$$

This was the first suggested by Jordan (3) and later by Nusselt (4).

---

[1] Research Foundation Fellow, Purdue University, Lafayette, Ind. Jun. A.S.M.E.

[2] Westinghouse Research Professor of Heat Transfer, Purdue University. Mem. A.S.M.E.

[3] Head, School of Mechanical and Aeronautical Engineering, Purdue University. Mem. A.S.M.E.

[4] Based on a doctoral thesis, Purdue University, 1943, by one of the authors.[1]

Contributed by the Heat Transfer Division of The American Society of Mechanical Engineers.

Note: Statements and opinions advanced in papers are to be understood as individual expressions of their authors and not those of the Society.

[5] Numbers in parentheses refer to the Bibliography at the end of the paper.

Although both of these equivalent diameters have been used for correlating data dealing with heat transfer in annular spaces, the one based on 4 times the hydraulic radius was used in this investigation to compute the Reynolds number.

For flow in a round pipe, it has been established that the lower critical Reynolds number occurs at about 2300. The lower critical Reynolds number for flow in an annular space has not been completely ascertained. Using an annular cylinder having a ratio of radii of 0.818 to 1, Page (5) found a value of 2400 as the lower critical Reynolds number. Researchers (6, 7) on fluid friction in annular spaces have shown that there is no abrupt change in friction factor for Reynolds number below 2000. It is therefore believed that the lower critical Reynolds number for flow in annular spaces must be about 2000.

In the present experiments, the range of Reynolds number investigated was from 200 to 2000. A few cases of abrupt increase in the heat-transfer coefficient occurred near a Reynolds number of 2000. This was taken as an indication that the critical Reynolds number had been reached and these data were discarded. None of the tests were conducted at a Reynolds number less than 200, owing to the difficulty of regulating the flow with the available equipment.

Theoretical Considerations

The problem of forced convection has long defied mathematical solution. Only for the simplest cases and corresponding simplified assumptions has the mathematical solution been successful. In the present cases, because of geometrical complications, variable temperature gradients, and heat exchange, dimensional analysis was used to correlate the test data. By using general dimensionless groups which have been used in other correlations, the following equation was selected as a first approximation

$$\frac{hD_e}{k} = \alpha \left(\frac{VD_e\rho}{\mu_a}\right)^a \left(\frac{c_p\mu_a}{k}\right)^b \left(\frac{L}{D_e}\right)^d \left(\frac{D_1}{D_e}\right)^e \left(\frac{\mu_w}{\mu_a}\right)^f \quad \ldots\ldots [1]$$

where D_e is some characteristic dimension of the annulus. Since the criterion of flow is the Reynolds number based on the equivalent diameter D, it is logical to use this equivalent diameter for D_e throughout the correlation.

The factor $(D_1/D_e)^e$ expresses the effect of geometric proportion of different annuli. Inasmuch as the equivalent diameter D is a function of D_1 and D_2, it will simplify computations to use the factor $(D_1/D_2)^e$ directly rather than to use an equivalent or some other form.

For the case of laminar flow of fluids of low viscosities such as water, natural convection sometimes plays a prominent part. When dimensional analysis is applied to problems dealing with natural convection, the Grashof number, $\frac{L^3\rho^2\Delta t\beta g}{\mu^2}$ appears. Introducing the Grashof number, Colburn (8) has correlated the data for water, air, and petroleum oil for the case of laminar flow in round pipes by use of the following multiplying factor:

$$(1 + 0.015\mathbf{G}^{1/3})$$

It has been pointed out by Martinelli and his associates (9) that for fluids of low viscosities the Grashof number appears in the general equation as a constant multiplier. Thus the effect of free convection which is represented by the Grashof number does not decrease as the Reynolds number becomes larger, but remains a constant multiplier.

In this work attempts were made to express the free convection effect as a function of the Reynolds number, the product of the Grashof and Prandtl numbers, and other dimensionless groupings. However, for the data obtained in these experiments the most satisfactory correlation was found using the factor $K(\mathbf{G}/\mathbf{R})^r$, where K is a constant. By use of this relation in Equation [1], it is possible to combine the equation constant and K and the various Reynolds numbers. Hence in the final equation the Grashof number appears as a multiplying factor.

It is recognized that this procedure is open to question. Other correlations may be possible, which would make the equation suitable for use beyond the range of the experimental data reported.

Since D, the equivalent diameter, is to be used in Equation [1], in the Reynolds number, it is desirable to use this same D as the characteristic dimension L in the Grashof number. There seems to be no universally accepted method of evaluating viscosity in the Grashof number. Colburn (8, 10) used the viscosity at the film temperature but there is some uncertainty as to how this film temperature should be computed. The viscosity at the bulk fluid temperature μ_a therefore was used in the computation of the Grashof number in this correlation.

Hence Equation [1] becomes

$$\frac{hD}{k} = \alpha' \left(\frac{VD\rho}{\mu_a}\right)^{a'} \left(\frac{c_p\mu_a}{k}\right)^b \left(\frac{L}{D}\right)^d \left(\frac{D_1}{D_2}\right)^e \left(\frac{\mu_w}{\mu_a}\right)^f \left(\frac{D^3\rho^2\Delta t\beta g}{\mu_a^2}\right)^m \quad [2]$$

For both the laminar and the turbulent flow in round pipes, Sieder and Tate (11) and Colburn (8, 10) used an exponent for the Prandtl number equal to $^1/_3$. For heat transfer at the inner wall of the annuli with turbulent flow, Monrad and Pelton (12), and Davis (2) correlated the data with a dimensionless equation, in which the exponent of $^1/_3$ was used for the Prandtl number. Based on these results, a value of $b = {}^1/_3$ was used in correlating the experimental data.

The use of $(\mu_w/\mu_a)^f$ in the heat-transfer correlation was first introduced by Sieder and Tate (11). For flow inside round pipes they used —0.14 for f. This factor accounts for the effect of the increased or decreased velocity gradients at a heated or cooled wall and may hold even if another wall is placed opposite to it as in an annulus. The 0.14 power is valid in crossflow according to Sieder. It seems probable that the presence of another wall would not affect appreciably the velocity gradient at the heated or cooled wall. Davis (2) used this power to correlate the data for heat transfer at the inner wall of the annuli with turbulent flow, and f = —0.14 was also used to correlate the data in this investigation. All of these assumptions can be justified only in the light of additional experimental data.

Description of Apparatus

Fig. 1 is a schematic diagram of the complete setup of the equipment. Letter A designates a large water tank equipped with a suitable overflow. The heating device consisted of copper coils connected to a steam pipe. A mechanical stirrer was used to maintain a uniform temperature.

From tank A water was pumped to the test section. A valve and a by-pass were inserted to control the flow. The inlet temperature to the annular section was measured by a thermometer inserted through a cork plug at one end of a tee. The temperature was measured at a point where the leading pipe made a turn which was located at a considerable distance from the entrance to the test section. The location of the thermometer was selected in order to eliminate unnecessary turbulence near the entrance. The leading pipe was suitably insulated.

Water flowed through the annular section into the mixing chamber where the outlet temperature was measured by means of thermometers. From the mixing chamber, the water flowed either to the weighing tank or to the drain. Water flowing in the inner pipe followed a somewhat similar path, as shown in Fig. 1.

The test section consisted of two brass pipes, one inside the other. Fig. 2 shows a part of the test section. The inner pipe

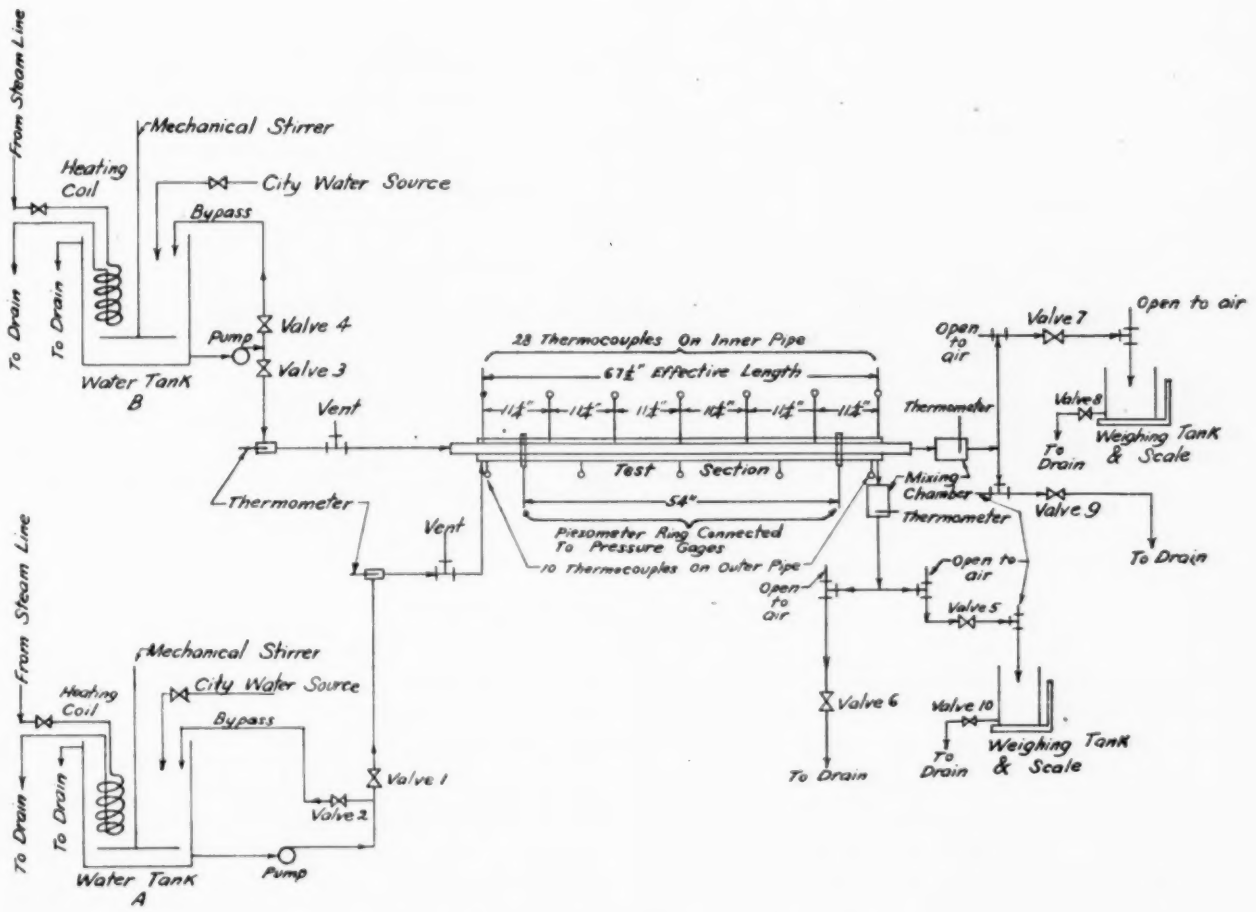


FIG. 1 SCHEMATIC DIAGRAM OF COMPLETE SETUP

was 7 ft in length. It was connected to the inlet pipe by a bronze sleeve, threaded on one end and soldered to the inner pipe at the other end. The outer pipe was 66½ in. long. Both of its ends were slipped into the ends of two cast-iron pieces and the joints soldered. These two cast-iron pieces served as the entrance and exit pieces and were designed to have the flow area in the section leading to the inlet and outlet of the annular section approximately equal to the cross-sectional area of the annular space, thus eliminating rapid changes in the flow areas. Wooden plugs screwed into these cast-iron pieces were designed to permit smooth entrance to and from the annulus, and to serve as heat insulation. Steel packing glands were used to prevent leakage.

A total of 67½ in. effective internal heating or cooling length was used in all tests. No calming section was used owing to construction difficulties. Water was led into and out of the test section in a horizontal direction.

The following brass pipes were used:

Pipe	Outside diameter, in.	Inside diameter, in.
A	2¼	2
B	1⅓	1⅜
C	1	⅞
D	¾	⅝

Four combinations were tested. These were *A-C*, *A-D*, *B-C*, and *B-D*. The inner pipe was centered inside the outer pipe by the wooden plugs and steel packing glands, and was strong enough to prevent sagging.

The temperatures of the outside surface of the inner pipe were measured along the pipe by calibrated 28-gage copper-constantan thermocouples. Seven sets of couples located 11¼ in. apart were spaced over the effective length. Each set of couples consisted of 4 pairs of couples placed around the section at 90-deg intervals so as to give an average temperature of the section. The first and last sets were placed near the ends of the wooden plugs.

The thermocouples were attached to the pipe wall by a modified method suggested by Colburn and Hougen (13). Longitudinal slots 3 in. long, 1/16 in. wide, and 1/16 in. deep were cut on the outside surface of the inner pipe. The cotton-covered insulation on the wires was first impregnated with a water-resistant varnish. After welding the junction, the insulated wires were twisted together and pressed into the slot. A drop of solder was placed over the welded ends of wires to form a rigid connection between the thermocouple and the pipe. The soldered joint was then polished with fine emery cloth in order to get a surface flush with the pipe surface. Waterproof varnish was applied to the wires in the slots in order to make the surface of the slot flush with the pipe surface.

The thermocouples were led out vertically from the inner pipe surface through 1/8-in. holes drilled in the outer pipe and through a small packing gland to the outside. These small packing glands were screwed into seats which were soldered to the outside surface of the outer pipe. All the thermocouple wires were led downstream except the last group which was brought upstream because of space limitations. In this case a fine copper wire was

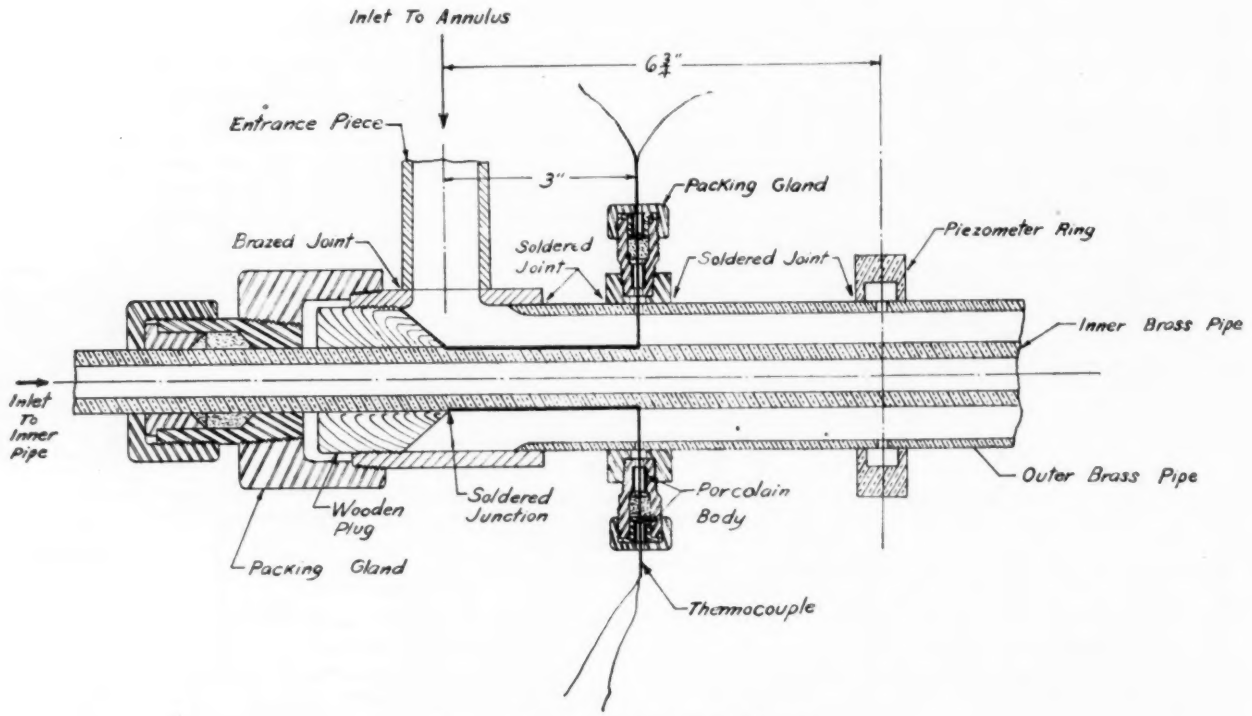


FIG. 2 ENTRANCE SIDE OF TEST SECTION

wound around the ends to prevent them from becoming loose. This prevented the couples from being moved out of the slot by the flowing fluid. After the tests the couples were all inspected and were found to be practically in the same condition as they were when first placed in the slots.

The outer pipe was cut into three sections to simplify the operation of installing the thermocouple wires. After all the couples were installed and checked, the outer pipe sections were joined by two sleeves and soldered. The surfaces at the sections were faced smoothly so that when the sections were joined together in the sleeve, they would closely match each other and thus prevent turbulence.

The short lengths of thermocouple wire leading from the inner pipe surface through the holes in the outer pipe surface and through the glands, were impregnated with waterproof varnish. Since 28-gage thermocouple wires were used, it is believed that the wires caused very little disturbance to the flow. The accuracy obtained from averaging the temperatures around the section should more than offset the small additional turbulence caused by the thermocouples.

Five sets of thermocouples were soldered on the outside surface of the outer pipe. Each set consisted of two pairs of couples, one at the top and the other at the bottom. These gave the outer-wall temperature gradient along the pipe.

Piezometer holes $^1/_8$ in. diam were drilled at two sections on the outer pipe 54 in. apart, spaced equally from the two ends. At each section the four openings were connected to a brass piezometer ring. The pressure readings from a Wahlen gage and an inclined draft gage served as a check as to whether laminar flow existed in the annular space.

The mixing chambers, Fig. 3, were made of 4-in. standard galvanized pipe and were fitted with half-moon baffles on the inside to promote mixing. In order to obtain the outlet temperature, two thermometers were inserted through the rubber stoppers at the top of the mixing chamber with their bulbs widely spaced at two different heights in the chamber. The exact check of the two thermometer readings indicated the efficiency of the mixing chamber. A short glass tube inserted through one of the rubber stoppers and connected to a glass stopcock served as a vent for the air to escape from the chamber when the fluid started to flow. The results of temperature measurements made on the mixing chamber during preliminary calibration tests did not show any evidence of stratification.

The outside surface of the outer pipe and the mixing chambers were heavily insulated.

The test section was mounted horizontally with a slight inclination to enable air to escape from the vent at the exit end.

From the mixing chamber, water was led to the weighing tank and the drain through separate pipe lines and valves. As shown in Fig. 1, two tees were placed in the flow paths before the valves. The tees were open to the atmosphere at one end to stabilize the flow.

After the tests had been completed on each combination of pipes, the inner pipe was taken out and examined. The outer wall of the inner pipe was found to be slightly fouled. When the inner pipe was used again, in a different combination, its outer surface was carefully polished.

TEST PROCEDURE

All thermometers were calibrated. The thermocouples were checked against each other by running water at the same temperature through both the inner pipe and the annular section. Only parallel flow was employed and both heating and cooling runs were made. Water was used in both the annulus and the inner pipe.

To start a test, the sources of water were turned on and the mechanical stirrer set into operation. Cooling tests were conducted first. Valves nos. 1 and 2, Fig. 1, were adjusted to give the flow corresponding to the Reynolds number. Valves nos. 3 and 4 on the inner pipe side were adjusted to give a flow such that

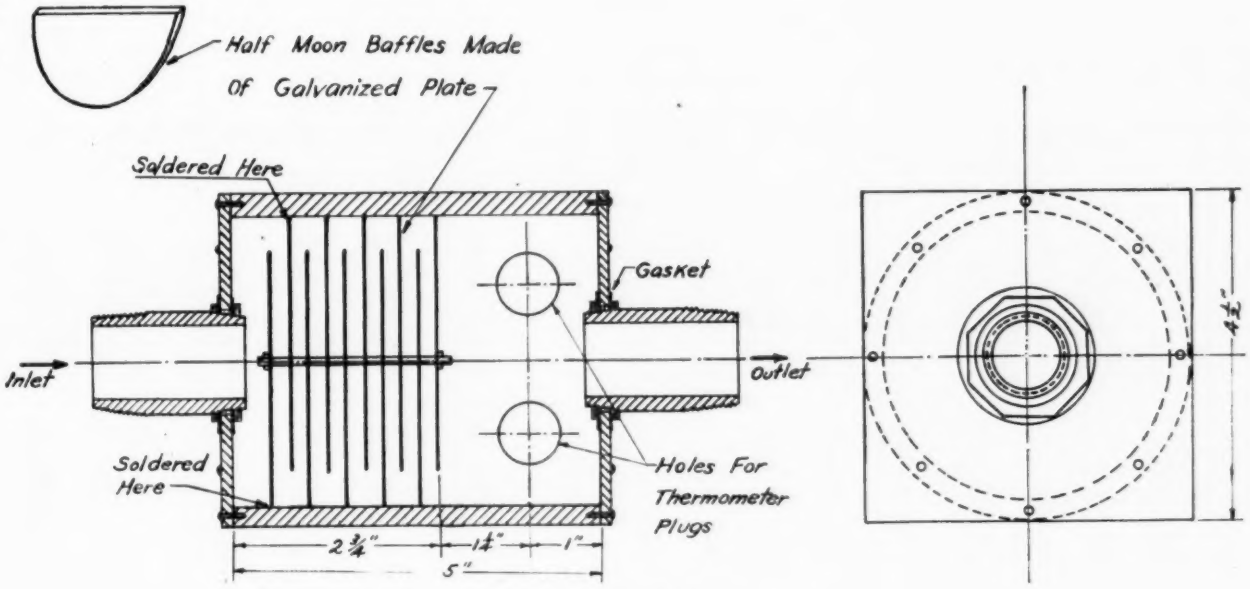


FIG. 3 MIXING CHAMBER

the drop in temperature of the fluid in the annular section would be as small as practical but large enough to give a suitable temperature between water flowing out from the annulus and water flowing out from the inner pipe. Valves nos. 5 and 7 were kept open while valves nos. 6 and 9 were closed. Water flowed into the two weighing tanks during the test except for a brief instant when the initial tank readings were taken.

The various temperature and pressure readings were taken at regular intervals. After these readings had remained constant for about 1 hr, thermal equilibrium was reached and a set of readings was taken, which included the inlet and outlet temperatures of water in both the annulus and the inner pipe, the pipe-wall temperatures, and the weight rate of flow in both the annulus and the inner pipe.

Check tests were conducted on different days to ascertain whether or not the surfaces were becoming contaminated by dirt or other substances. In every case these test results agreed.

EXPERIMENTAL RESULTS AND CONCLUSIONS

The original experimental data together with computations are presented in Tables 1, 2, 3, and 4. In computing the data the average fluid temperature in the annulus was taken as the arithmetic average of the inlet and outlet temperatures. The heat transferred was based on readings on the inner pipe. The heat-transfer coefficient was based on the arithmetic-mean temperature difference. The inner pipe-wall temperature was the average of the 28 thermocouple readings. Values of μ, c_p, and k were based on those given by Dorsey (14). The coefficients of cubical expansion of water at different temperatures were based on Kopp's data on the relative volumes of water at different

TABLE 1

D_1 = 2 in. D_2 = 1 in. $\frac{D_1}{D_2}$ = 2 D = 1 in.

Heating or cooling length, L = 67 1/2 in. $\frac{L}{D}$ = 67.5

Cooling Tests: Water in the Annulus Being Cooled

Run No.	Water Temp. °F Annulus Out	Annulus In	Inner Pipe Out	Inner Pipe In	Aver. Water Temp. In Annulus, °F	Aver. Inner Pipe Wall Temp. °F	Temp. Diff. t °F	Water Rate in Annulus lb hr^{-1}	Water Rate in Inner Pipe lb hr^{-1}	Heat Transferred (Based on readings on Inner Pipe B hr^{-1}	Heat Transfer Coefficient h Btu hr^{-1} ft^{-2} °F	Nu $(\frac{hD}{k})$	Pr $(\frac{c_p \mu_a}{k})$	$(\frac{D^3 \rho^2 g}{\mu_a^2} \beta \Delta t)$	$\frac{\mu_a}{\mu_w}$	Re $(\frac{nD\rho}{\mu_a})$
1	106.3	126.1	98.3	62.7	116.2	103.9	12.3	67.5	28.5	1013	56.0	12.60	3.79	1,425,000	0.885	245
2	112.2	126.0	108.9	61.7	119.1	106.3	12.8	95.7	26.7	1260	66.6	14.97	3.68	1,624,000	0.870	358
3	108.9	120.7	93.0	61.9	114.8	98.9	15.9	170.3	61.3	1906	81.5	18.4	3.85	1,770,000	0.850	810
4	106.8	121.0	83.9	60.5	113.9	94.1	19.8	202	113.6	2660	91.2	20.6	3.88	2,150,000	0.811	719
5	114.3	121.8	102.1	64.0	118.1	105.9	12.2	238	42.5	1620	90.1	20.3	3.72	1,595,000	0.887	881
6	121.8	121.4	92.4	60.7	116.8	101.2	15.6	316	83.1	2640	115.0	25.9	3.76	1,848,000	0.832	1156
7	113.0	122.7	85.6	62.0	117.9	98.9	19.0	367	143.1	3380	120.9	27.2	3.72	2,310,000	0.825	1356
8	112.8	121.3	80.6	61.0	117.1	97.5	19.6	480	202	3960	137.2	30.9	3.75	2,330,000	0.817	1760
9	114.3	120.2	90.9	60.9	117.3	100.7	16.6	539	102.3	3070	125.7	28.3	3.74	1,985,000	0.847	1980
Heating Tests: Water in the Annulus Being Heated																
10	71.0	64.8	73.1	113.6	67.9	75.2	7.8	113.0	16.9	683	64.0	15.43	7.05	128,500	1.100	236
11	71.3	64.7	76.6	114.1	68.0	77.4	9.4	166.6	27.6	1037	74.7	18.00	7.04	167,000	1.133	348
12	70.3	63.2	79.1	118.1	66.8	78.5	11.7	205	36.0	1403	81.5	19.65	7.19	194,200	1.168	421
13	69.2	64.0	81.2	117.1	66.6	78.6	12.0	312	47.2	1693	95.9	23.2	7.20	196,100	1.173	638
14	69.6	63.1	96.1	119.0	66.4	82.9	16.5	428	124.5	2850	117.0	28.1	7.22	270,000	1.239	876
15	70.8	63.9	101.4	115.8	67.4	86.1	18.7	483	232	3340	121.5	29.3	7.12	320,000	1.271	1000
16	68.8	64.2	99.3	117.1	66.5	83.1	16.6	666	165.3	2940	120.5	29.1	7.21	272,000	1.198	1360
17	67.6	62.9	100.3	114.9	65.3	85.2	19.9	885	288	4200	143.1	34.7	7.35	304,000	1.293	1780
18	67.8	63.3	100.7	115.4	65.6	84.8	19.2	964	290	4260	150.5	36.4	7.32	300,000	1.282	1945

TABLE 2

L_1 = 1.375 in. L_2 = 0.750 in. $\frac{D_1}{D_2}$ = 1.833 D = 0.625 in.

Heating or cooling length, L = 67 1/2 in. $\frac{L}{D}$ = 108.0

Cooling Tests: Water in the Annulus being Cooled

Run No.	Water Temp. F Annulus Out	Annulus In	Inner Pipe Out	Inner Pipe In	Aver. Water Temp. in Annulus, F	Aver. Inner Pipe Wall Temp. F	Temp. Diff. t F	Water Rate in Annulus lb hr^{-1}	Water Rate in Inner Pipe lb hr^{-1}	Heat Transferred (Based on readings on Inner Pipe) $(Q)_1$ B hr^{-1}	Heat Transfer Coefficient h $Bhr^{-1}ft^{-2}F$	Nu $(\frac{hD}{k})$	Pr $(\frac{c_p\mu_a}{k})$	$(\frac{D^3\rho^2 g\beta\Delta t}{\mu_a^2})(\frac{Q_T}{Q})$	$\frac{\mu_a}{\mu_w}$	Re $(\frac{\mu D\rho}{\mu_a})$
19	106.4	113.2	100.4	63.2	109.8	104.8	5.0	69.3	10.8	414	74.5	10.58	4.06	117,800	0.952	334
20	107.8	118.2	102.4	61.1	113.0	103.5	9.5	81.8	19.5	805	76.4	10.80	4.05	244,000	0.907	408
21	109.4	128.1	99.8	63.0	117.8	103.5	14.3	85.5	35.5	1305	82.8	11.63	3.72	425,000	0.866	446
22	111.0	121.9	100.5	61.1	116.5	103.5	13.0	135.9	34.5	1369	94.9	13.36	3.77	370,000	0.880	699
23	109.2	118.8	97.4	62.3	114.0	99.7	14.3	187.3	48.2	1690	107.0	15.10	3.88	381,000	0.865	942
24	107.7	118.1	92.9	61.3	112.9	97.4	15.5	227	68.8	2170	126.4	17.82	3.92	399,000	0.848	1180
25	111.0	120.9	92.3	62.7	116.0	98.6	17.4	255	80.8	2390	124.2	17.50	3.80	491,000	0.837	1310
26	116.8	121.9	107.1	61.9	119.4	109.5	9.9	310	33.5	1511	137.7	19.32	3.66	307,000	0.910	1640
27	112.8	121.6	95.2	61.5	117.2	99.0	18.2	352	86.8	2920	145.0	20.3	3.75	531,000	0.831	1823
28	114.2	123.9	95.1	61.8	119.1	99.5	19.6	383	101.6	3380	156.3	21.9	3.66	604,000	0.820	2020
					Heating Tests: Water in the Annulus Being Heated											
29	74.2	64.9	79.1	112.8	69.8	80.0	10.4	91.8	27.3	925	80.1	12.00	6.88	49,400	1.147	276
30	71.5	64.8	75.8	110.4	68.2	73.4	9.2	126.3	24.1	834	81.6	12.27	7.02	39,800	1.128	374
31	69.7	64.8	73.5	110.8	67.3	74.9	7.6	158.8	19.5	728	86.5	13.21	7.12	31,800	1.104	482
32	73.9	66.2	85.9	111.3	70.1	82.1	12.0	178.8	50.3	1278	96.1	14.41	6.83	58,300	1.168	542
33	71.7	65.9	85.1	113.3	68.8	82.3	13.5	252	52.7	1486	99.6	14.97	6.95	61,300	1.190	751
34	71.4	65.8	89.7	111.0	68.6	82.8	14.2	303	82.5	1760	112.0	16.83	6.97	64,000	1.200	902
35	71.3	66.1	94.0	112.0	68.7	83.8	15.1	388	112.9	2030	122.0	18.33	6.97	68,400	1.212	1156
36	70.4	64.5	95.4	113.4	67.5	85.3	17.8	440	146.0	2630	133.5	20.2	7.10	75,000	1.260	1288
37	70.0	63.5	96.1	110.2	66.8	87.4	20.6	543	246	3460	152.0	22.9	7.18	83,500	1.302	1575
38	69.6	63.7	95.6	109.7	66.7	87.2	20.5	650	265	3730	164.5	24.8	7.20	82,800	1.302	1881

TABLE 3

L_1 = 1.375 in. L_2 = 1 in. $\frac{D_1}{D_2}$ = 1.375 D = 0.375 in.

Heating or cooling length, L = 67 1/2 in. $\frac{L}{D}$ = 179.8

Cooling Tests: Water in the Annulus Being Cooled

Run No.	Water Temp. F Annulus Out	Annulus In	Inner Pipe Out	Inner Pipe In	Aver. Water Temp. in Annulus, F	Aver. Inner Pipe Wall Temp. F	Temp. Diff. t F	Water Rate in Annulus lb hr^{-1}	Water Rate in Inner Pipe lb hr^{-1}	Heat Transferred (Based on Readings on Inner Pipe B hr^{-1}	Heat Transfer Coefficient h $Bhr^{-1}ft^{-2}F$	Nu $(\frac{hL}{k})$	Pr $(\frac{c_p\mu_a}{k})$	$(\frac{D^3\rho^2 g\beta\Delta t}{\mu_a^2})(\frac{Q_T}{Q})\sqrt{\frac{\mu_a}{\mu_w}}$	Re $(\frac{\mu D\rho}{\mu_a})$
39	95.9	117.5	84.2	60.0	106.7	91.8	14.9	68.1	56.1	1360	62.0	5.30	4.20	68,500	0.848	285
40	99.3	120.8	85.7	59.0	110.5	92.3	18.2	86.7	69.1	1844	68.8	5.86	4.05	93,100	0.825	375
41	105.3	123.7	90.8	59.7	114.5	97.6	16.9	110.0	59.3	1843	74.1	6.27	3.85	98,200	0.840	497
42	98.8	115.4	76.9	58.9	107.1	90.4	16.7	158.9	137.4	2440	99.0	8.47	4.18	77,000	0.830	669
43	99.5	115.5	73.6	58.9	107.5	87.7	19.8	282	289	4250	145.3	12.41	4.16	93,100	0.801	1191
44	105.7	116.6	82.4	58.8	111.2	95.6	15.6	340	151.3	3570	156.0	13.06	3.93	80,000	0.845	1490
45	110.0	121.1	84.9	59.0	115.6	99.1	16.5	382	157.5	4080	168.5	14.30	3.82	98,500	0.848	1650
46	113.2	122.2	82.2	60.5	117.7	104.3	13.4	400	155.1	3370	171.0	14.41	3.73	85,600	0.876	1863
47	109.9	120.1	80.0	59.5	115.0	98.4	16.6	443	211	4320	176.2	14.92	3.84	98,200	0.843	2010
					Heating Tests: Water in the Annulus Being Heated											
48	72.2	61.1	75.5	112.1	66.7	75.7	9.0	78.4	22.1	810	60.8	5.51	7.18	7,860	1.126	202
49	75.6	64.9	91.2	111.2	70.3	82.6	12.3	111.2	85.6	1265	69.8	6.29	6.80	13,200	1.171	302
50	70.8	63.2	85.5	112.4	67.0	78.4	11.4	185	58.3	1520	90.7	8.21	7.16	10,070	1.161	482
51	71.2	63.5	96.1	112.1	67.4	80.6	13.2	235	120.6	1935	99.0	8.96	7.12	11,980	1.190	615
52	69.6	62.6	94.1	109.5	66.1	79.7	13.6	269	132.0	2030	101.7	9.22	7.23	11,490	1.195	693
53	68.3	62.6	93.9	110.0	65.4	77.6	12.2	339	127.3	2050	114.3	10.40	7.35	9,890	1.175	864
54	68.8	61.7	97.4	112.5	65.3	79.6	14.3	486	223	3350	159.0	14.45	7.36	11,500	1.210	1235
55	67.2	61.7	96.2	112.0	64.5	77.5	13.0	705	232	3680	192.0	17.48	7.48	11,890	1.190	1780
56	65.6	61.2	96.1	113.4	63.4	75.8	12.4	840	208	3650	197.1	18.00	7.57	8,970	1.180	2080

TABLE 4

D_1 = 2 in. D_2 = 0.750 in. $\frac{D_1}{D_2}$ = 2.66 D = 1.25 in.

Heating or cooling length, L = 67 1/2 in. $\frac{L}{D}$ = 54.0

Cooling Tests: Water in the Annulus Being Cooled

Run No.	Water Temp. F Annulus Out	Annulus In	Inner Pipe Out	Inner Pipe In	Aver. Water Temp. in Annulus, F	Aver. Inner Pipe Wall Temp. F	Temp. Diff. t F	Water Rate in Annulus lb hr^{-1}	Water Rate in Inner pipe lb hr^{-1}	Heat Transferred (Based on Inner Pipe B hr^{-1}	Heat Transfer Coefficient h $Bhr^{-1}ft^{-2}F$	Nu $(\frac{hD}{k})$	Pr $(\frac{c_p\mu_a}{k})$	$(\frac{D^3\rho^2 g\beta\Delta t}{\mu_a^2})(\frac{Q_T}{Q})\frac{\mu_a}{\mu_w}$	Re $(\frac{\mu D\rho}{\mu_a})$
57	103.3	118.0	96.9	62.7	110.6	97.1	13.5	57.3	22.9	785	52.6	14.92	4.02	2,610,000	0.865	216
58	107.6	114.6	99.5	64.0	111.1	103.5	7.6	81.2	15.0	532	53.0	17.88	4.00	1,492,000	0.925	307
59	107.0	115.3	95.5	63.1	111.1	100.4	10.7	129.0	31.1	1006	85.1	24.1	4.00	2,100,000	0.897	488
60	107.5	117.9	91.7	61.8	112.7	97.6	15.1	140.3	46.1	1380	82.8	23.5	3.93	3,100,000	0.852	540
61	109.9	119.2	93.7	61.7	114.5	100.7	13.8	191.0	51.0	1630	107.0	30.2	3.85	2,980,000	0.871	747
62	113.1	119.8	97.5	62.6	116.4	103.7	12.7	258	45.0	1570	111.8	31.4	3.78	2,910,000	0.881	1027
63	113.3	120.2	92.9	62.5	116.7	101.4	15.3	326	69.5	2110	124.7	35.1	3.76	3,550,000	0.857	1303
64	114.1	120.2	93.3	63.0	117.2	102.1	15.1	416	77.5	2350	140.9	39.6	3.75	3,520,000	0.860	1668
65	113.8	120.5	89.9	62.8	117.2	98.8	18.4	460	107.6	2920	144.1	40.6	3.75	4,270,000	0.830	1842
					Heating Tests: Water in the Annulus Being Heated											
66	74.9	64.1	85.6	109.6	69.5	82.4	12.9	108.0	44.1	1060	74.6	22.4	6.89	484,000	1.182	251
67	71.7	64.1	83.9	107.5	67.9	80.5	12.6	154.7	50.5	1192	85.9	25.8	7.05	437,000	1.178	352
68	68.9	63.3	80.1	108.9	66.6	78.0	11.4	182.0	39.2	1135	90.5	27.3	7.20	368,000	1.162	407
69	70.7	62.7	88.3	110.8	66.7	81.1	14.4	216	72.5	1632	103.0	31.1	7.19	465,000	1.206	484
70	68.3	62.8	83.8	110.4	65.5	78.2	12.7	294	55.0	1461	104.6	31.6	7.33	384,000	1.182	648
71	69.3	61.2	96.2	110.7	65.2	87.2	22.0	377	211	3060	126.1	38.1	7.34	656,000	1.329	829
72	70.5	63.7	100.5	118.9	67.1	90.3	23.2	512	186.8	3440	134.6	40.6	7.16	765,000	1.342	1150
73	66.0	63.5	95.0	110.8	65.8	85.2	19.4	692	188.9	2980	139.1	42.1	7.30	597,000	1.284	1530
74	69.0	64.0	99.6	113.4	66.5	90.9	24.4	844	305	4210	156.0	47.1	7.22	782,000	1.362	1882

temperatures as listed in Kent's Mechanical Engineers' Handbook.

In making the correlation, an exponent of $-1/3$ was assumed for the L/D factor in Equation [2], and four sets of cooling-test data for the different annular combinations were selected with approximately equal Reynolds numbers. The function

$$\left(\frac{hD}{k}\right)\left(\frac{c_p\mu_a}{k}\right)^{-1/3}\left(\frac{\mu_a}{\mu_w}\right)^{-0.14}\left(\frac{D}{L}\right)^{-1/3}$$

was plotted against (D_1/D_2) values for these four sets on logarithmic paper. Different straight lines were drawn to join the four points. The slopes of the lines were found to vary from 0.8 to 1, the majority being in the neighborhood of 0.8. As a result, it was decided to use a value of 0.8.

The function

$$\left(\frac{hD}{k}\right)\left(\frac{c_p\mu_a}{k}\right)^{-1/3}\left(\frac{\mu_a}{\mu_w}\right)^{-0.14}\left(\frac{D}{L}\right)^{-1/3}\left(\frac{D_1}{D_2}\right)^{-0.8}$$

was plotted against

$$\left(\frac{D^3\rho^2\beta g\,\Delta t}{\mu_a^2}\right)\left(\frac{\mu_a}{VD\rho}\right)$$

on logarithmic paper for eight sets of cooling and heating tests on the four combinations with approximately equal Reynolds numbers. A straight line was drawn to join the points and a slope of 0.05 was found for the line.

The function

$$\left(\frac{hD}{k}\right)\left(\frac{c_p\mu_a}{k}\right)^{-1/3}\left(\frac{\mu_a}{\mu_w}\right)^{-0.14}\left(\frac{D}{L}\right)^{-1/3}\left(\frac{D_1}{D_2}\right)^{-0.8}\left[\left(\frac{D^3\rho^2\beta g\,\Delta t}{\mu_a^2}\right)\left(\frac{\mu_a}{VD\rho}\right)\right]^{-0.05}$$

was plotted against $\dfrac{VD\rho}{\mu}$ on logarithmic paper for all 74 runs. The plotted points fell within a strip on the graph, showing the definite existence of a correlation; however, the spread of the data was rather large.

Finally the exponent of (D/L) was changed to -0.4 and the function

$$\left(\frac{hD}{k}\right)\left(\frac{c_p\mu_a}{k}\right)^{-1/3}\left(\frac{\mu_a}{\mu_w}\right)^{-0.14}\left(\frac{D_1}{D_2}\right)^{-0.8}\left[\left(\frac{D^3\rho^2\beta g\,\Delta t}{\mu_a^2}\right)\left(\frac{\mu_a}{VD\rho}\right)\right]^{-0.05}$$

was plotted against $\dfrac{VD\rho}{\mu}$. A satisfactory correlation resulted.

Combining the Reynolds number, the function

$$\left(\frac{hD}{k}\right)\left(\frac{c_p\mu_a}{k}\right)^{-1/3}\left(\frac{\mu_a}{\mu_w}\right)^{-0.14}\left(\frac{D}{L}\right)^{-0.4}\left(\frac{D_1}{D_2}\right)^{-0.8}\left(\frac{D^3\rho^2\beta g\,\Delta t}{\mu_a^2}\right)^{-0.05}$$

was plotted against the Reynolds number as shown in Fig. 4.

A close examination shows that the slope of a line drawn through the cooling data is slightly steeper than a similar line for the heating data. The difference between the two is so small that it can be neglected.

The equation of the single line in Fig. 4 was found to be

$$\left(\frac{hD}{k}\right)\left(\frac{c_p\mu_a}{k}\right)^{-1/3}\left(\frac{\mu_a}{\mu_w}\right)^{-0.14}\left(\frac{D}{L}\right)^{-0.4}\left(\frac{D_1}{D_2}\right)^{-0.8}\left(\frac{D^3\rho^2\beta g\,\Delta t}{\mu_a^2}\right)^{-0.05} = 1.02\left(\frac{VD\rho}{\mu_a^2}\right)^{0.45}$$

Solving for the Nusselt number gives

$$\frac{hD}{k} = 1.02\left(\frac{VD\rho}{\mu_a}\right)^{0.45}\left(\frac{c_p\mu_a}{k}\right)^{1/3}\left(\frac{\mu_a}{\mu_w}\right)^{0.14}\left(\frac{D}{L}\right)^{0.4}\left(\frac{D_1}{D_2}\right)^{0.8}\left(\frac{D^3\rho^2\beta g\,\Delta t}{\mu_a^2}\right)^{0.05}$$

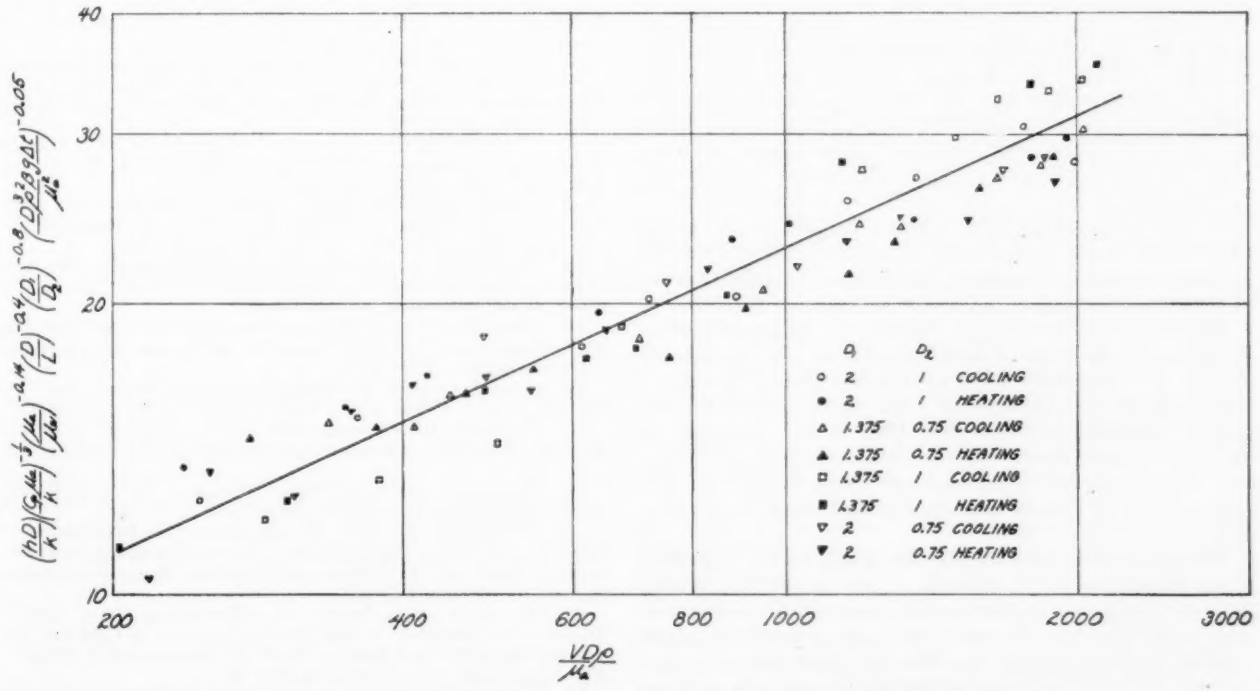


FIG. 4 RECOMMENDED CORRELATION OF DATA FOR HEATING AND COOLING TESTS

Equation: $\left(\frac{hD}{k}\right)\left(\frac{C_p\mu_a}{k}\right)^{-1/3}\left(\frac{\mu_a}{\mu_w}\right)^{-0.14}\left(\frac{D_1}{D_2}\right)^{-0.8}\left(\frac{D}{L}\right)^{-0.4}\left(\frac{D^3\rho^2\beta g\,\Delta t}{\mu_a^2}\right)^{-0.05} = 1.02\left(\frac{DV\rho}{\mu_a}\right)^{0.45}$

Discussion and Conclusion

The following equation

$$\frac{hD}{k} = 1.02\left(\frac{VD\rho}{\mu_a}\right)^{0.45}\left(\frac{c_p\mu_a}{k}\right)^{1/3}\left(\frac{\mu_a}{\mu_w}\right)^{0.14}\left(\frac{D}{L}\right)^{0.4}\left(\frac{D_1}{D_2}\right)^{0.8}\left(\frac{D^3\rho^2\beta g\,\Delta t}{\mu_a^2}\right)^{0.05} \quad \ldots\ldots [3]$$

was found to correlate the test data with an average deviation of ±6.6 per cent and a maximum deviation of +14.1 per cent. In view of the variables encountered in such a problem and the difficulty of making precise temperature measurements, it is considered satisfactory and is recommended for computing the heat-transfer coefficient at the inner wall of an annulus for laminar flow. Since the tests were conducted over a range of Reynolds number from 200 to 2000, the relation is only valid for this range of Reynolds number. However, as the effects on heat transfer in the laminar region should be the same for all Reynolds numbers below the lower critical value, as is the case for flow in round pipes, it can be reasonably expected that the equation may also hold for Reynolds numbers smaller than 200.

It should be noted that the exponent for (**P**) was assumed to be $^1/_3$. The Prandtl number is connected solely with the properties of the fluid. As water was the only fluid used, the exponent for (**P**) was not verified for all fluids. Nevertheless, it is safe to presume that this exponent should be somewhere around $^1/_3$, as this was the exponent used successfully in the correlation of the heat-transfer data for both laminar and turbulent flow in round pipes, and for turbulent flow in annuli.

The Grashof number (**G**) in Equation [3] accounts for the effect of natural convection. This effect should decrease with an increase in the flow rates or Reynolds number. This was proved qualitatively by the temperature-distribution data.

The temperature at any section was found to be the highest at the top and the lowest at the bottom. In 1931 Drew and Ryan (15) studied the distribution of heat about the circumference of a pipe in a stream of fluid flowing across the pipe. Baker and Mueller (16) investigated the temperature variation around the perimeter of a tube when pure and mixed vapors were condensing. They found that the top surface attained the highest temperature and the bottom the lowest. Since only four temperature readings were obtained at each section, no quantitative analysis can be made.

The percentage of difference between temperatures at the top and bottom of any one section decreased with an increase in the Reynolds number. This means that the effect of natural convection decreased for a given increase of the Reynolds number.

The end effect constitutes a variable, the influence of which could not be determined quantitatively from the experimental results. It is felt that the end effect on the heat-transfer rate is very small for these experiments. The (L/D) ratio for the four annular combinations varies from 179.8 to 54. However, the test data fell into a satisfactory correlation. This should indicate that the end effect for different (L/D) ratios within this range were of the same order of magnitude at the same Reynolds number.

The difference between the heat loss or gain for the water flowing in the annulus and the heat loss or gain for the water flowing in the inner pipe was used as a relative index of the heat balance. Due to the facts that the area of the external insulation surface was not known accurately, and that the temperature differences between the outer insulation surface and the air were small, no effort was made to compute the heat-transfer loss by convection and radiation from the insulation surface. Approximate computations could be made for this loss, which when taken into account would decrease the difference between the heat gained or lost by the fluid in the annular space and the heat gained or lost by the fluid in the inner pipe. It was felt that the difference between the heat gained or lost by the water in the annular space and that in the pipe would serve as an index of the reliability of the tests. The average difference for all of the tests was approximately 5.8 per cent. The results obtained on the first test conducted showed a difference of 31.6 per cent. The data for one other test checked to within 16.9 per cent. The differences for seventy-two tests were less than 11 per cent, the average for these tests being 5.22 per cent.

The heat-transfer coefficients for the inner pipe were computed in order to check the experimental values. These data correlated in a satisfactory manner with those already published.

Acknowledgment

The authors are indebted to the Purdue Research Foundation for making funds available for carrying out this work.

BIBLIOGRAPHY

1 "Heat Transfer to a Fluid in Laminar Flow Through an Annular Space," by Max Jakob and K. A. Rees, Trans. A.I.Ch.E., vol. 37, 1941, pp. 619–648.

2 "Heat Transfer and Pressure Drop in Annuli," by E. S. Davis, Trans. A.S.M.E., vol. 65, 1943, pp. 755–760.

3 "On the Rate of Heat Transmission Between Fluids and Metal Surfaces," by H. P. Jordan, Proceedings of The Institution of Mechanical Engineers, London, England, 1909, part 4, pp. 1317–1357.

4 "Über Wärmeübergang auf ruhige oder bewegte Luft," by W. Nusselt, *Zeitschrift des Vereines deutscher Ingenieure*, vol. 57, 1913, pp. 197–199.

5 "The Influence of Wall Oscillations, Wall Rotation, and Entry Eddies, on the Breakdown of Laminar Flow in an Annular Pipe," by A. Page, Proceedings of the Royal Society of London, England, series A, vol. 165, 1938, pp. 501–529.

6 "Strömungsvorgänge in ringförmigen Spalten (Labyrinthdichtungen)," by E. Becker, *Zeitschrift des Vereines deutscher Ingenieure*, vol. 51, 1907, pp. 1133–1141.

7 "Der Durchfluss von Wasser durch konzentrische und exzentrische zylindrische Drosselspalte mit und ohne Ringnuten," by E. Schneckenberg, *Zeitschrift für Angewandte Mathematik und Mechanik*, vol. 11, 1931, pp. 27–40.

8 "A Method of Correlating Forced-Convection Heat Transfer Data and a Comparison With Fluid Friction," by A. P. Colburn, Trans. A.I.Ch.E., vol. 29, 1933, pp. 174–210.

9 "Heat Transfer and Pressure Drop for a Fluid Flowing in the Viscous Region Through a Vertical Pipe," by R. C. Martinelli and colleagues, Trans. A.I.Ch.E., vol. 38, 1942, pp. 493–530.

10 "Heat Transfer by Natural and Forced Convection," by A. P. Colburn, Purdue University, Engineering Experiment Station, Research Series, Bulletin no. 84, Jan., 1942.

11 "Heat Transfer and Pressure Drop of Liquids in Tubes," by E. N. Sieder and G. E. Tate, *Industrial and Engineering Chemistry*, vol. 28, 1936, pp. 1429–1435.

12 "Heat Transfer by Convection in Annular Spaces," by C. C. Monrad and J. F. Pelton, Trans. A.I.Ch.E., vol. 38, 1942, pp. 593–611.

13 "Studies in Heat Transmission," by A. P. Colburn and O. A. Hougen, *Industrial and Engineering Chemistry*, vol. 22, 1930, pp. 522–539.

14 "Properties of Ordinary Water-Substance," by N. E. Dorsey, Reinhold Publishing Corporation, New York, N. Y., 1940.

15 "Mechanism of Heat Transmission: I. Distribution of Heat Flow About the Circumference of a Pipe in a Stream of Fluid," by T. B. Drew and W. P. Ryan, *Industrial and Engineering Chemistry*, vol. 23, 1931, pp. 945–953.

16 "Condensation of Vapors on a Horizontal Tube. Part I. Temperature Variation Around the Perimeter of a Tube on Condensing Pure and Mixed Vapors," by E. M. Baker and A. C. Mueller, Trans. A.I.Ch.E., vol. 33, 1937, pp. 531–561.

17 "Transfer Processes in Annuli," by J. H. Wiegand and E. M. Baker, Trans. A.I.Ch.E., vol. 38, 1942, pp. 569–592.

(Owing to emergency travel conditions existing when this paper was presented, discussion will be accepted until March 11, 1946)

Heat Transfer in the Locomotive Boiler

By LAWFORD H. FRY,[1] NEW YORK, N. Y.

It is shown that the total heat absorption in a locomotive boiler for any assumed rate of heat release and weight of gases of combustion can be predicted with all of the accuracy practically necessary. The over-all heat transfer is considered as taking place in two separate operations which can be represented by two formulas, a fourth-power equation of the usual type for the radiation in the firebox, and a double logarithmic equation for the convection in the flues. This form of equation was suggested by Fessenden (1),[2] and its usefulness has been extended by the coefficients developed by the present author. It may not represent the exact physical reactions of the process of heat transfer, but it has the pragmatic sanction of giving practically accurate results under many different conditions. Actually that is all that can be claimed for any other heat-transfer formula even if it uses the Reynolds number. Fessenden pointed out, "It should be noted that the apparently rational idea that the rate of heat transfer is directly proportional to the temperature difference is, after all, only an assumption that has been accepted for so long that it has come to be regarded as an axiomatic statement of fact."

THE locomotive boiler with its water-enclosed firebox and its fire-tube barrel still follows the lines laid down by George and Robert Stephenson when they built the *Rocket* in 1829. This survival is sometimes criticized by advocates of other forms of motive power who think that we should be modern at all costs. Actually the retention of the locomotive-type boiler is the result of hard common sense supported by the inherent advantages of the arrangement. Change in design is not necessarily good engineering. Retention of a circular form for a wheel is still good practice.

Study of the details of operation of the locomotive boiler leads inevitably to recognition of the fact that in its modern form the locomotive boiler is an extremely compact and effective mechanism for the production of steam. Some efficiency of combustion is deliberately sacrificed to obtain the high rate of heat release necessary. It must be remembered that the boiler is part of a mobile power plant capable of running at 100 mph and able to pass through the restricted limits of a railroad loading gage. Evaporative capacities of over 100,000 lb of superheated steam per hr are obtained, and heat-release rates up to 300,000 Btu per hr per cu ft of firebox volume may be reached at maximum outputs. It is obvious that such rates of heat release are not compatible with high combustion efficiencies. The efficiency of heat absorption with which this paper is chiefly concerned is, however, generally satisfactory.

In studying the processes by which part of the heat released in the firebox is transferred to the boiler heating surfaces and taken up by the water and steam, the action may be considered as taking place in two major and individual operations. In the firebox, part of the heat released is taken up by direct radiation, while the remainder is carried into the tubes and flues by the gases of combustion. Of this gas-carried heat, part is transferred to the evaporative and to the superheating surfaces by convection while the remainder is lost through the smokebox as sensible and latent heat in the gases of combustion.

The purpose of this paper is to present formulas which represent the two processes of heat transfer and to show how they can be combined for use in estimating the amount of heat that will be taken up by a boiler of given dimensions under any known or assumed operating conditions.

In applying the formulas the boiler design is characterized by the area of the firebox heating surface, and by the number, diameters, and lengths of the flues, tubes, and superheater pipes. The operating conditions are characterized by the rate of heat release and by the weight of gases of combustion produced per hour. These dimensions and conditions are necessary and sufficient for determining the rate at which the boiler will take up heat to be used in producing and superheating the steam.

Over-All Heat Transfer

Computation of the over-all heat transfer falls into two parts. In the first the rate of heat release, the rate of gas production, and the area of the firebox surface are used to find the so-called "equilibrium temperature" of the firebox. This is the temperature at which the sum of the heat radiated direct to the firebox surface and of the sensible heat carried by the gases at that temperature is just equal to the total available heat released by combustion.

In the second part of the computation the gases are assumed to enter the flue bundle at the equilibrium temperature and to lose temperature at a rate given by the double logarithmic formula, Equation [2]. This equation takes into account the rate of gas flow, the gas-swept perimeter and the free gas area of the flue bundle, the temperature of the receiving surface, and the length of the flues.

Details of the formulas and of their application in practice are given later. Attention is here directed to the results obtained by applying the formulas to four different locomotive boilers of the dimensions shown in Table 1, for which extensive boiler test results are available. Outlines of two of the boilers are shown in Fig. 1. Two boilers have Type A superheaters with 4 pipes in each flue, while the other two boilers have Type E superheaters

TABLE 1 PRINCIPAL DIMENSIONS OF BOILERS

Test series	A	B	C	D
Flues, number, and OD in in.	69—5½	198—3½	170—3½	40—5½
Tubes, number, and OD in in.	184—2¼	50—2¼	120—2¼	236—2¼
Length between flue sheets, ft	17.9	20.4	18.9	19.1
Superheater type	AS	ED	E	A
Superheater pipes OD, in	1½	1⅜	1⅜	1½
Superheater pipes, number in flue	4	2	2	4
Evaporative surface (fireside), sq ft	3719	3986	3908	3686
Superheater surface (fireside), sq ft	2029	2640	2052	1205
Gas-swept perimeter (p), in	3477	3820	3750	3068
Free gas area (a), sq in	1522	1368	1389	1382
Ratio P/a	2.28	2.80	2.70	2.22
Firebox volume (net), cu ft	613	391	475	410
Firebox heating surface, sq ft	490	373	406	311
Grate area, sq ft	92.0	75.8	70.0	69.3

[1] Director of Research, Steam Locomotive Research Institute, Inc. Fellow A.S.M.E.

[2] Numbers in parentheses refer to the Bibliography at the end of the paper.

Contributed by the Railroad and Heat Transfer Divisions of The American Society of Mechanical Engineers.

Note: Statements and opinions advanced in papers are to be understood as individual expressions of their authors and not those of the Society.

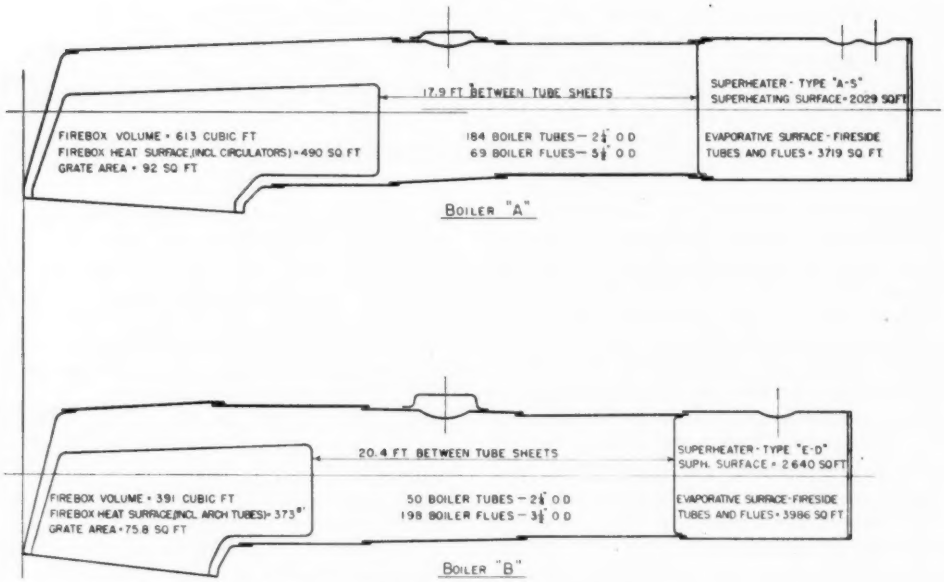
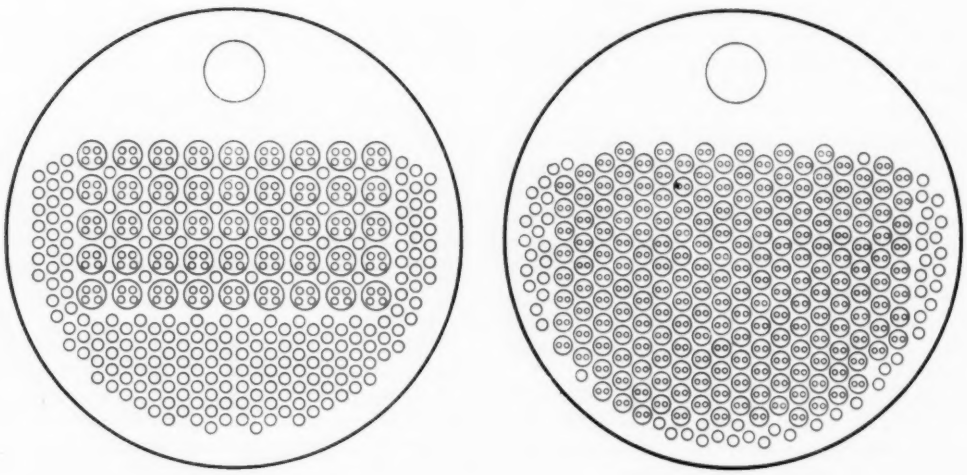


FIG. 1 COMPARISON OF BOILER DIMENSIONS



Boiler "A" Boiler "B"

FIG. 2 REPRESENTATIVE ARRANGEMENTS OF SUPERHEATER FLUES AND TUBES
(Boiler "A," equipped with Type A superheater with 4 pipes in each flue; boiler "B," equipped with Type E superheater with 2 superheater pipes in each flue.)

with 2 superheater pipes in each flue. Representative arrangements of the superheater flues and the tubes are shown in Fig. 2. Computations for heat transfer have been carried out for twenty-seven tests taken largely at random. The test data for rate of heat release and weight of gases of combustion have been used, and the rates of heat transfer in firebox and in flues and the resulting smokebox temperatures have been computed by means of the formulas. The results are given in Tables 2 and 3 for comparison with the measured values. Agreement between measured and computed values is generally satisfactory, as the greatest divergence is hardly greater than the element of uncertainty in the measured values.

HEAT DISTRIBUTION

Table 2 includes the experimental data to which the formulas are applied and gives the computed and measured firebox and smokebox temperatures. The relation between measured and computed temperatures is also shown in Figs. 3 and 4.

Table 3 is based on the same data, measured and computed, that are contained in Table 1, but the data are organized to show how the heat released in the firebox is distributed. It may be noted that rates of firing range from the low rate of 35 lb of dry coal per sq ft of grate area per hr up to the high rate of 242 lb per sq ft per hr. Column 4 gives the computed equilibrium temperature, and column 5 the corresponding rate of radiation per square foot of firebox heating surface. This rate of radiation is given in column 5 in terms of Btu per hour and in column 6 is translated into equivalent evaporation in pounds of water per hour from and at 212 F per square foot of firebox surface. These values run up to 126 lb per sq ft per hr at the maximum firing rates. At normal working rates they are about 90 to 100 lb per sq ft per hr. There is no direct method of checking these

TABLE 2 EXPERIMENTAL DATA AND COMPARISON OF COMPUTED VALUES WITH MEASURED VALUES FOR FIREBOX AND SMOKEBOX TEMPERATURES

Series	Test no.	Firing rate, lb DCF per SFG per hr	Firebox temperature, F — Measured — Center	Flue sheet	Computed equilibrium temperature	Smokebox temperature, F — Measured	Computed	Per sq ft firebox heating surface — Heat released, Btu per hr	Weight gases of combustion, lb per hr
1	2	3	4	5	6	7	8	9	10
A	1441	47	2491	1530	1840	576	570	109 500	126
	1440	68	2476	1579	1950	617	605	140 000	153
	1436	102	2643	2083	2090	686	664	208 000	235
	1437	123	2630	2163	2075	713	683	219 000	254
	1439	151	2566	1858	2230	741	721	271 000	288
	1438	182	2734	2058	2300	768	760	312 000	324
	1444	207	2642	2058	2380	775	760	334 000	324
	1442	242	2703	2150	2490	807	780	367 000	328
B	4F	56	..	1540	1915	526	515	147 000	175
	4D	62	..	1530	1970	562	525	161 000	188
	7F	85	..	1600	2120	604	557	223 000	250
	7H	97	..	1750	2190	607	562	237 000	251
	10C	114	..	1710	2260	655	595	285 000	300
	10D	115	..	1780	2260	628	585	274 000	282
	10E	134	..	1940	2320	642	590	304 000	307
	13G	139	..	1940	2410	660	600	314 000	290
	13M	161	..	2160	2400	667	607	344 000	334
	13F	182	..	2040	2480	693	620	394 000	374
	13K	208	..	2350	2500	660	634	405 000	376
C	517A	58	2173	1647	1700	507	540	104 500	148
	510A	81	2123	1692	1900	549	565	150 000	185
	519A	122	2067	1762	2015	590	612	204 000	248
	527A	175	2369	1669	2320	647	660	274 000	327
D	607A	35	1750	..	1715	500	505	86 500	106
	623A	107	2324	1646	2070	632	645	242 000	298
	651A	139	2466	1895	2310	676	690	312 000	323
	610A	173	..	..	2485	698	715	378 000	351

NOTE: DCF = dry coal fired. SFG = square feet grate area.

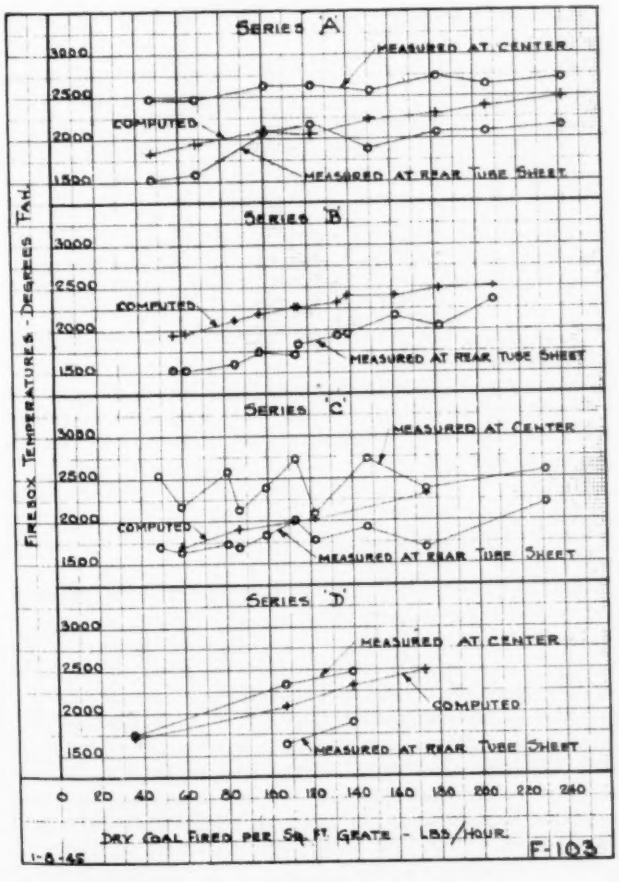


FIG. 3 RELATION BETWEEN MEASURED AND COMPUTED TEMPERATURES

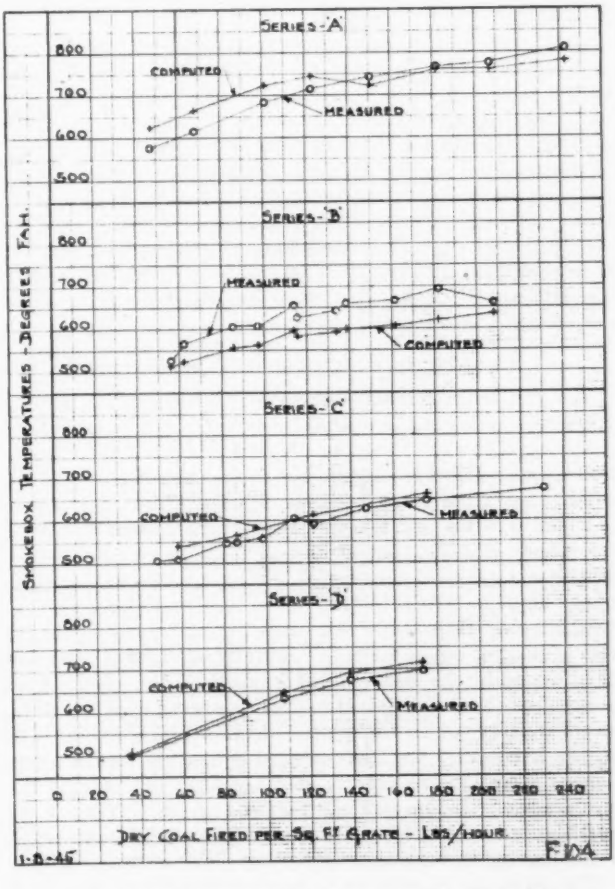


FIG. 4 RELATION BETWEEN MEASURED AND COMPUTED TEMPERATURES

TABLE 3 COMPUTED RADIATION AND EQUIVALENT EVAPORATION IN FIREBOX TOGETHER WITH PERCENTAGE DISTRIBUTION OF HEAT RELEASED

Series	Test no.	Firing rate, lb DCF per SFG per hr	Computed equilibrium temperature, F	Heat radiated, equilibrium temperature, Btu per hr per sq ft	Equivalent firebox evaporation, lb per sq ft per hr	Heat distribution in per cent of heat released: Absorbed: Firebox	Absorbed: Flues, tubes, superheater	Lost in smokebox: Sensible heat	Lost in smokebox: Latent heat
1	2	3	4	5	6	7	8	9	10
A	1441	47	1840	44 000	45	40.0	41.0	15.5	3.5
	1440	68	1950	53 000	55	38.0	42.0	15.7	4.3
	1436	102	2090	67 000	69	32.2	45.2	18.8	3.8
	1437	123	2075	65 000	67	30.0	45.5	20.0	4.5
	1439	151	2230	83 000	86	30.6	45.4	19.2	4.8
	1438	182	2300	92 000	95	29.6	45.1	20.5	4.8
	1444	207	2380	103 000	106	30.8	45.8	18.3	5.1
	1442	242	2490	120 000	123	32.6	44.1	17.8	5.5
B	4F	56	1915	51 000	52	34.6	47.0	15.0	3.4
	4D	62	1970	55 000	57	34.2	46.6	15.5	3.7
	7F	85	2120	70 000	72	31.4	48.9	15.1	3.6
	7H	97	2190	78 000	80	32.9	48.1	15.2	3.8
	10C	114	2260	87 000	90	30.5	49.0	16.5	4.0
	10D	115	2260	87 000	90	31.7	49.0	15.3	4.0
	10E	134	2320	95 000	98	31.2	49.4	15.5	3.9
	13G	139	2410	108 000	110	34.4	46.8	14.7	4.1
	13M	161	2400	106 000	109	30.8	49.0	15.7	4.5
	13F	182	2480	119 000	123	30.2	49.8	15.7	4.3
	13K	208	2500	122 000	126	30.2	50.4	14.6	4.8
C	517A	58	1700	33 000	34	31.6	47.4	16.7	4.3
	510A	81	1900	49 000	50	32.6	47.3	16.0	4.1
	519A	122	2015	59 500	61	29.2	49.2	17.2	4.4
	527A	175	2320	95 000	98	34.6	42.4	18.2	4.8
D	607A	35	1715	35 000	36	40.7	41.0	14.2	4.1
	623A	107	2070	65 000	67	26.8	50.5	18.6	4.1
	651A	139	2310	93 000	96	29.8	49.0	17.0	4.2
	610A	173	2485	120 000	124	31.7	48.2	15.6	4.5

NOTE: DCF = dry coal fired. SFG = square foot grate area.

figures with evaporations actually obtained, but they are in line with values usually accepted.

Columns 7, 8, 9, 10 split up heat released into percentages representing, respectively, in column 7 the heat radiated to the firebox at equilibrium temperature, in column 8 the heat taken up by the evaporative and superheater surface of the tube bundle in cooling the gases from equilibrium to smokebox temperature, in column 9 the heat lost in sensible heat of gases at smokebox temperature, and in column 10 the heat lost in latent heat of the vapor. Except for high values at the very low firing rates, the distribution of the heat shows no great variation with the rate of firing and is very similar for the boilers of Series B, C, and D. The boiler of Series A with shorter flues shows a slightly lower percentage of heat absorbed in the flues.

MEAN FIREBOX EQUILIBRIUM TEMPERATURE

The "mean equilibrium temperature" is defined as the temperature at which the amount of heat carried by the combustion gases, together with the amount radiated to the firebox surface, is just equal to the quantity of heat released by combustion. Its value in any given case can be found by using Table 4 or Fig. 5, provided that the experimental data furnish information as to the rate of available heat released in the firebox as well as the weight of the gases of combustion. Table 4 covers temperatures from 1400 F to 2800 F by steps of 10 deg F and for each temperature gives the sensible heat carried by the gas as well as the rate in Btu per square foot per hour at which radiated heat will be taken up by the firebox heating surface. The sensible heat in Btu above 32 F carried by 1 lb of gas is derived from the values given by Heck (6) for the products of combustion of coal with 20 per cent excess air. The original data show that the percentage of excess air has little effect on the specific heat of the mixed gases of combustion and that the figures of Table 4 are satisfactory in practice for any gas composition encountered in a coal-burning locomotive.

The values for radiated heat absorbed by the firebox heating surface are derived from the so-called Stefan-Boltzmann fourth-power equation

$$H_R = 1600\ [(T/1000)^4 - (t/1000)^4] \quad \ldots\ldots\ldots [1]$$

where

H_R is heat absorbed by radiation, in Btu per hour per square foot of firebox surface

T is absolute temperature of flame in firebox, in degrees Rankine

t is absolute temperature of receiving surface, in degrees Rankine. The temperature of the firebox surface is taken to be the temperature of the water back of the firebox surface.

Table 4 is computed for a water temperature of 380 F (200 psi) and can be used for any pressures normally encountered in locomotive practice. An increase of temperature to 600 F (1600 psi) would reduce the tabular values by 1000 Btu per sq ft per hr, which is negligible except for the lowest transmitting temperatures.

The Stefan-Boltzmann fourth-power relation is generally accepted as representative of radiation heat transfer and the factor 1600 has been found to give satisfactory results for the conditions encountered in locomotive fireboxes.

Fig. 5 has been plotted to answer graphically any question as to the mean equilibrium temperature for any combination of heat available and weight of gas per square foot of heating surface per hour.

In using Table 4 and Fig. 5, computations must be based not on total heat released, but on heat available, exclusive of the latent heat of the vapor. Usually the value given in the experimental data for heat released will be based on the upper calorific value of the fuel and will therefore include the heat involved in vaporizing the H_2O produced by combustion. The latent heat of this vapor is not available for radiation and is not included in the values for gas-carried heat in Table 4. It must therefore be deducted from the heat released to find the "heat available." Each pound of hydrogen burned produces 9 lb of vapor which will account for 8730 Btu of latent heat. Consequently, for each per cent of hydrogen in the fuel, 87.3 Btu must be deducted from the total heat released per pound of fuel to find the "net available heat" to be used in computing the equilibrium temperature.

For example, in test No. 1439 in Series A with 288 lb of gas pro-

TABLE 4 RADIATION AND HEAT-CONTENT FACTORS FOR DETERMINING FIREBOX TEMPERATURE WITH COAL FUEL AND A RECEIVING SURFACE TEMPERATURE OF 380 F[a]

	Rad. factor	Heat cont.	Rad. factor	Heat cont.	Rad. factor	Heat cont.	Rad. factor	Heat cont.	Rad. factor	Heat cont.	Rad. factor	Heat cont.	Rad. factor	Heat cont.
	1400 F		1500 F		1600 F		1700 F		1800 F		1900 F		2000 F	
0F	18200	363.3	22800	392.5	28000	421.9	34000	451.6	40890	481.5	48800	511.6	57800	541.9
10F	18700	366.2	23300	395.4	28500	424.9	34700	454.6	41600	484.5	49600	514.6	58700	545.0
20F	19200	369.1	23800	398.3	29100	427.8	35300	457.5	42400	487.5	50500	517.7	59700	548.0
30F	19600	372.0	24300	401.3	29700	431.1	36000	460.5	43200	490.5	51400	520.7	60700	551.1
40F	20000	374.9	24800	404.2	30300	433.7	36700	463.5	44000	493.5	52200	523.7	61700	554.1
50F	20500	377.8	25300	407.1	30900	436.7	37300	466.5	44700	496.5	53100	526.7	62700	557.2
60F	20900	380.8	25800	410.1	31500	439.7	38000	469.5	45500	499.5	54000	529.8	63700	560.2
70F	21400	383.7	26300	413.1	32100	442.6	38700	472.5	46300	502.6	54900	532.8	64700	563.3
80F	21800	386.6	26900	416.0	32700	445.6	39400	475.5	47100	505.6	55900	535.9	65800	566.3
90F	22300	389.5	27400	418.9	33300	448.6	40200	478.5	47900	508.6	56800	538.9	66800	569.4
100F	22800	392.5	28000	421.9	34000	451.6	40890	481.5	48800	511.6	57800	541.9	67900	572.5
	2100 F		2200 F		2300 F		2400 F		2500 F		2600 F		2700 F	
0F	67900	572.5	79300	603.2	92000	634.1	106200	665.2	122000	696.3	139500	727.6	158700	759.1
10F	69000	575.5	80500	606.3	93400	637.2	107700	668.3	123600	699.4	141300	730.8	160700	762.3
20F	70100	578.6	81700	609.3	94700	640.3	109200	671.4	125400	702.6	143200	733.9	162800	765.4
30F	71200	581.6	83000	612.4	96100	643.4	110800	674.5	127100	705.7	145100	737.1	164900	768.5
40F	72300	584.7	84200	615.5	97500	646.5	112300	677.6	128800	708.8	147000	740.2	167000	771.7
50F	73400	587.8	85500	618.6	98900	649.6	113900	680.7	130500	711.9	148900	743.3	169100	774.9
60F	74600	590.9	86800	621.7	100400	652.7	115500	683.8	132300	715.1	150800	746.5	171200	778.0
70F	75700	593.9	88000	624.8	101800	655.8	117100	687.0	134100	718.2	152700	749.7	173300	781.2
80F	76900	597.0	89300	627.9	103300	658.9	118700	690.1	135900	721.4	154700	752.8	175500	784.3
90F	78100	600.1	90700	631.0	104700	662.1	120400	693.2	137700	724.5	156700	755.9	177700	787.5
100F	79300	603.2	92000	634.1	106200	665.2	122000	696.3	139500	727.6	158700	759.1	....	790.7

[a] If the temperature of the receiving surface is increased to 600 F, the tabulated figures should be reduced by 1000 Btu.

NOTE: The "radiation factor" represents, for each temperature, the rate at which heat measured in Btu per hour is taken up by each square foot of firebox surface.

The "heat-content factor" gives the amount of sensible heat carried by each pound of the mixed gases of combustion. Latent heat is not included.

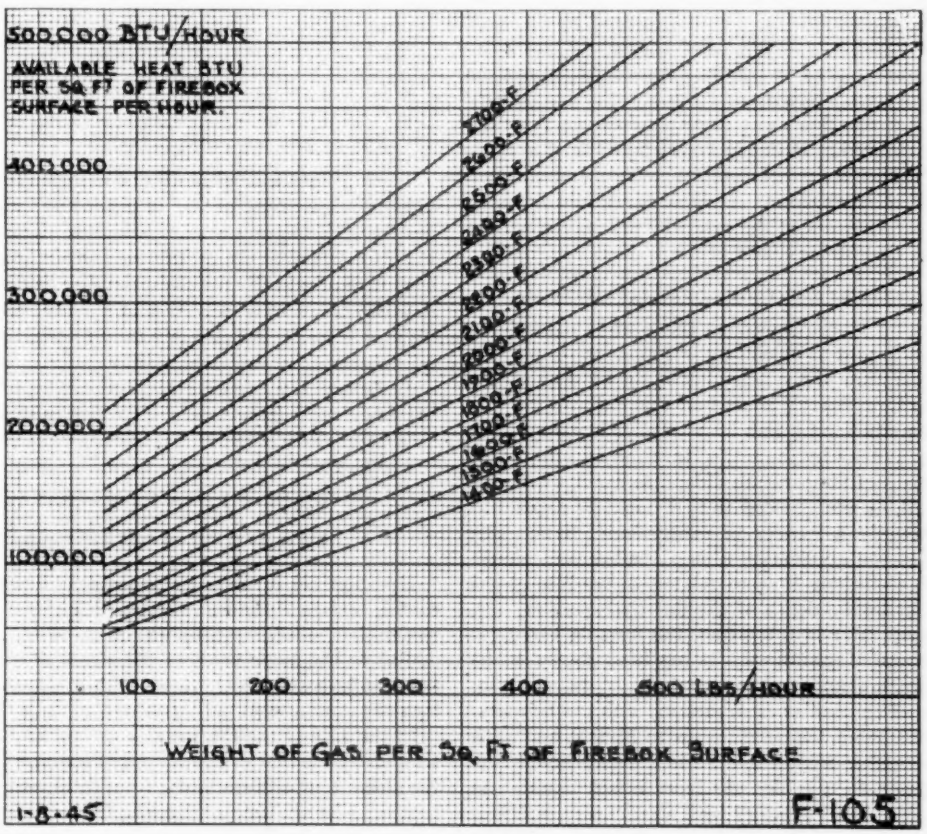


FIG. 5 EQUILIBRIUM TEMPERATURE IN RELATION TO HEAT AVAILABLE AND WEIGHT OF GAS

duced and 271,000 Btu released per sq ft of firebox heating surface per hr, the latent heat accounts for 13,000 Btu per sq ft per hr, leaving 258,000 Btu available. Inspection of Fig. 5, followed by check with Table 4, shows that at a temperature of 2230 F the heat released per hour per square foot of firebox surface will be accounted for as follows:

	Btu
Heat radiated at 2230 F	83000
Sensible heat in 288 lb of gas at 612 Btu per lb	175000
Heat available	258000
Latent heat	13000
Heat released	271000

On this basis the mean equilibrium temperature is taken to be 2230 F. It may be noted that the experimental data and the type of computation do not justify an attempt to determine the equilibrium temperature to a value closer than the nearest 10 deg F.

In test No. 1439 just quoted, the measured firebox temperatures were 2566 F at the center and 1858 F at the flue sheet. On the basis of radiation proportional to the fourth power of the absolute temperature, the mean between 2566 F and 1858 F is 2280 F, which is close to the computed mean equilibrium temperature of 2230 F. The measured values for the firebox temperatures are not sufficiently reliable to allow any final conclusions to be drawn, but it is of interest to note that where the measured values seem to be most consistent there is quite close agreement between the mean fourth-power absolute temperature and the computed equilibrium temperature. This supports the view that radiation at the mean equilibrium temperature, as given in Table 4, corresponds to the heat actually taken up by the firebox. It should be noted that the drop in firebox temperature between center and flue sheet is not due in any large degree to transfer of heat by convection. The hydraulic depth of the firebox is too large to provide any effective rate of heat transfer. The lower final temperature is due to the lower rate of heat release. With a firing rate of 100 lb of dry coal per hr, the hourly supply of combustible may be represented by 78 lb of carbon, 5 lb of hydrogen, and 248 lb of oxygen. These combustible elements are diluted by 920 lb, which is 2.8 times their weight, of inert nitrogen. As they pass through the firebox they combine until when the flue sheet is reached the combustible elements may be reduced to 16 lb of carbon and 63 lb of oxygen, diluted by 14 times their weight of inert gas consisting of nitrogen and the products of combustion. It is obvious that as these final conditions are approached the rate of heat release will be much slower than that at the center of the firebox.

Heat Transfer by Convection in Flue Bundle

The heat taken up by the flues from the gases of combustion as they pass from firebox to smokebox is found by computing the drop in temperature of the gases. The double logarithmic formula shown as Equation [2] is used for this purpose.

This form of equation, by which heat transfer is measured in temperature drop and not by the rate of transfer per square foot of surface per degree of temperature difference per hour, is due to Fessenden (1, 3, 4) who showed that it could be applied to represent satisfactorily a variety of experimental data. The author has carried the application a step further and shown (2, 5) that if the coefficient M were related to the rate of gas flow and to the hydraulic depth of the flue by Equations [3], [4a], and [4b], given later in this paper, the formula had a remarkably wide range of usefulness. It has been shown to be applicable to flues ranging in diameter from $^1/_2$ in. to 4 in. and of circular and of annular cross section, with gas temperatures ranging from room temperature up to 2500 F, and with heat transmission either from a hot gas to a cooler liquid surrounding the flue or to a cooler gas from a hot liquid. As the formula covers a broad territory with an accuracy sufficient for all practical purposes, it has useful possibilities even if its pedigree is not entirely unimpeachable from the standpoint of theoretical physics.

Fessenden pointed out that the real justification of the formula rests not so much upon the rationality of its development, as upon the manner in which it satisfies the experimental data gathered from many different sources. The fundamental assumption leading to Equation [2] might be stated in a number of ways, but the simplest is that the loss of heat from an element of gas passing along a tube takes place in accordance with the exponential formula for a damped process. This leads to the equation

$$dQ = C \cdot e^{-m.x} \quad \ldots\ldots [1]$$

where

dQ is heat lost by element of gas traversing flue length x.

Hedrick and Fessenden (1) show that this can be developed into the form

$$\text{lolog } (T_2/t) = \text{lolog } (T_1/t) - M_x \quad \ldots\ldots [2]$$

where

lolog means "the logarithm of the logarithm of"
T_1 is absolute equilibrium temperature in degrees Rankine
T_2 is absolute smokebox temperature in degrees Rankine
t is absolute mean effective temperature of receiving surface in degrees Rankine
x is length of flues in feet
M is coefficient depending only on mean hydraulic depth of tube bundle and on rate of gas flow per inch of perimeter of receiving surface

Using data from many sources, the author has found that the coefficient M is linked with the rate of gas flow and with the flue dimensions by the equation

$$\log M = B - m \log W/p \quad \ldots\ldots [3]$$

where

W is total weight of gases of combustion in pounds per hour
p is total perimeter of receiving surface, including flues, tubes and superheater pipes, in inches

The auxiliary coefficients B and m depend only upon the ratio of (p), the gas-swept perimeter of the flue through which the gas flows to (a), the free area of this flue. The ratio of perimeter to area is of course the reciprocal of the hydraulic depth. It has been used as a parameter instead of the hydraulic depth because it varies in the same direction as the heat-absorbing value of a flue. A high value of the p/a ratio corresponds to a flue with a high capacity for heat absorption.

With values of p in inches and of a in square inches, values of the coefficients B and m, corresponding to the various values of the ratio p/a, are given in Table 5. These values are derived from the equations

$$\log (B - 1.3) = 9.384 - 0.54 \log (p/a) \quad \ldots\ldots [4a]$$

$$\log m = 9.583 - 0.37 \log (p/a) \quad \ldots\ldots [4b]$$

Equation [2] involves t the absolute temperature of the receiving surface of the flue. Experience shows that for work with locomotive boilers a satisfactory mean value can be obtained by adding to the mean value of the steam or water surface of the flue a differential which varies with the heat offered per linear inch of the gas-swept perimeter of the flue, as shown in Fig. 6.

In the case of the evaporative surface of the flues, the water temperature is that of the saturated steam. In the superheater the steam temperature varies from saturated to the final superheat, and for the whole superheater surface an arithmetic mean may be taken. When evaporative and superheater surfaces are taken together a weighted mean is taken, allowing for the surface and temperature of both surfaces. In the present work both surfaces have been taken together and only the final smokebox temperature has been computed. The earlier paper referred to shows that the equations can be applied to the evaporative and superheating surfaces separately and a step-by-step computation used to find the progressive temperature drop along the flue, and to determine separately the respective amounts of heat taken up by the evaporative and by the superheating surface.

TABLE 5 COEFFICIENTS FOR COMPUTING HEAT TRANSFER IN FLUES

(p/a = perimeter/area; B and m are coefficients)

p/a	B	m	p/a	B	m	p/a	B	m
0.50	8.867	0.494	2.00	9.053	0.296	6.20	9.350	0.194
0.51	8.868	0.491	2.10	9.062	0.291	6.40	9.362	0.192
0.52	8.870	0.487	2.20	9.071	0.286	6.60	9.373	0.190
0.53	8.872	0.483	2.30	9.080	0.281	6.80	9.384	0.188
0.54	8.874	0.480	2.40	9.089	0.277	7.00	9.394	0.186
0.55	8.876	0.477	2.50	9.098	0.273	7.20	9.404	0.184
0.56	8.878	0.474	2.60	9.108	0.269	7.40	9.414	0.183
0.57	8.880	0.471	2.70	9.116	0.265	7.60	9.423	0.181
0.58	8.881	0.467	2.80	9.124	0.261	7.80	9.433	0.179
0.59	8.883	0.464	2.90	9.132	0.258	8.00	9.444	0.177
0.60	8.884	0.461	3.00	9.140	0.255	8.20	9.455	0.176
0.65	8.892	0.449	3.20	9.154	0.249	8.40	9.465	0.174
0.70	8.900	0.437	3.40	9.170	0.242	8.60	9.474	0.172
0.75	8.908	0.426	3.60	9.185	0.237	8.80	9.484	0.170
0.80	8.915	0.416	3.70	9.199	0.233	9.00	9.494	0.169
0.85	8.922	0.406	4.00	9.213	0.229	9.20	9.504	0.168
0.90	8.929	0.390	4.20	9.227	0.225	9.40	9.513	0.166
1.00	8.942	0.383	4.40	9.241	0.221	9.60	9.522	0.165
1.10	8.955	0.370	4.60	9.254	0.217	9.80	9.532	0.164
1.20	8.968	0.358	4.80	9.266	0.214	10.00	9.542	0.163
1.30	8.980	0.347	5.00	9.278	0.211	10.20	9.550	0.162
1.40	8.991	0.337	5.20	9.290	0.208	10.40	9.557	0.161
1.50	9.002	0.329	5.40	9.303	0.205	10.50	9.553	0.160
1.60	9.013	0.322	5.60	9.315	0.203			
1.70	9.023	0.315	5.80	9.329	0.200			
1.80	9.034	0.308	6.00	9.338	0.197			
1.90	9.044	0.302						

The smokebox temperatures reported in Table 2 have been obtained by taking the combined perimeter and area and the mean temperature for evaporative and superheating surface, and by assuming that the gases entered the flues at the equilibrium temperature. Agreement between the computed and the measured values meets practical requirements.

The widest deviation is found in test No. 13 F, Series B, with a smokebox temperature of 620 F computed and 693 F measured. This represents a difference of 19 Btu of sensible heat per lb of gas, and as the gas flow is 374 lb for a heat release of 394,000 Btu per hr per sq ft of firebox surface, the difference amounts to 1.8 per cent of the heat released. This is hardly greater than the factor of uncertainty in the measured values. Agreement in the three other series of tests is considerably closer so it is felt that the proposed method can be used with confidence in predicting the over-all heat-absorbing capacity of a locomotive boiler. It should be noted that in the computation the gases of combustion are assumed to leave the firebox and to enter the flues at the equilibrium temperature, while in reality the gases at the flue sheet are probably from 100 to 200 deg F below the equilibrium temperature. The justification for this is that the formula as set up gives satisfactory results and that, in estimating the heat transfer, the equilibrium temperature can be computed while the actual flue-sheet temperature is not known.

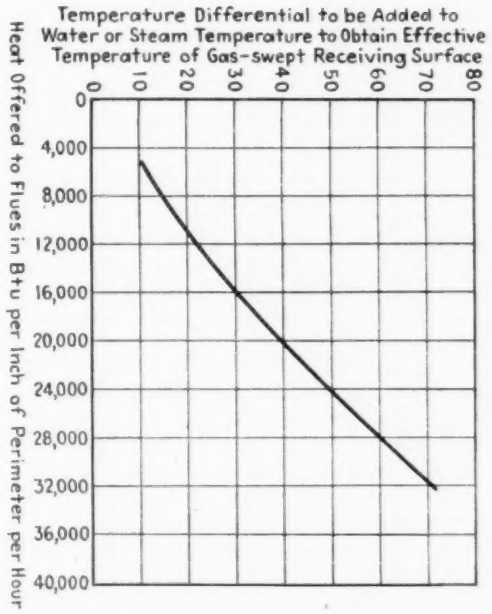


FIG. 6 TEMPERATURE DIFFERENTIAL FOR FULL LENGTH FLUES

If a close study of the heat transfer in the flues were to be made, it would be desirable to adjust the differential given in Fig. 6, so that it would correspond to heat transfer from the exact initial flue-gas temperature. This would require an increase of about 60 per cent in the values of the temperature differential given in Fig. 6.

BIBLIOGRAPHY

1 "Transmission of Heat in Boilers," by E. R. Hedrick and E. A. Fessenden, Trans. A.S.M.E., vol. 38, 1916, p. 412.

2 "The Transfer of Heat Between a Flowing Gas and a Containing Flue," by L. H. Fry, Trans. A.S.M.E., vol. 39, 1917, pp. 709–756.

3 "Heat Transmission Through Boiler Tubes," by E. A. Fessenden and J. W. Haney, University of Missouri, Engineering Experiment Station, Bulletin No. 18, October, 1916.

4 "Heat Transmission and Efficiency of Boiler Tubes," by E. A. Fessenden, Pennsylvania State College, Engineering Experiment Station, Bulletin No. 32, September, 1924.

5 "Heat Transfer in the Locomotive Superheater," by L. H. Fry, Trans. A.S.M.E., vol. 52, 1930, paper RR-52-3.

6 "The New Specific Heats," by R. C. H. Heck, *Mechanical Engineering*, vol. 62, 1940; pp. 9–12; vol. 63, 1941, pp. 126–128, 134.

(Owing to travel emergency conditions existing when this paper was presented, discussion will be accepted until March 11, 1946)

The Influence of Tube Shape on Heat-Transfer Coefficients in Air to Air Heat Exchangers

By F. H. GREEN[1] and L. S. KING,[1] LOS ANGELES, CALIF.

Heat-transfer coefficients are reported for air passing through round tubes, through partially flattened tubes, and through partially flattened tubes which have also been dimpled. It was found that flattened tubes maintained fully turbulent flow and, consequently, a higher heat-transfer coefficient at lower Reynolds number values than did round tubes. The addition of dimples to the flattened tubes maintained fully turbulent flow from the transition point and increased the heat-transfer coefficient substantially. The addition of the dimples also improved the relation between heat transfer and pressure drop in the flattened tubes.

Nomenclature

The following nomenclature is used in the paper:

A = tube internal cross section area, sq ft
A_i = total area of inside surface of tubes in unit, sq ft
A_o = total area of outside surface of tubes in unit, sq ft
D_H = hydraulic diameter, ft
D_o = outside diameter of tube, ft
E_i = effectiveness on air inside tubes = $\frac{t_1 - t_2}{t_1 - t_3}$
E_o = effectiveness on air outside tubes = $\frac{t_4 - t_3}{t_1 - t_3}$
G = mass velocity, lb/(hr)(sq ft)
h_i = coefficient of heat transfer inside tubes, Btu/(hr)(sq ft)(deg F)
h_o = coefficient of heat transfer outside tubes, Btu/(hr)(sq ft)(deg F)
i_1 = enthalpy of steam, Btu per lb
i_2 = enthalpy of condensate, Btu per lb
k = thermal conductivity of fluid, Btu/(hr)(sq ft)(deg F per ft)
L = length of tube or tube section, ft
N = Nusselt number = $\frac{hD_H}{k_{avg}}$
R = Reynolds number = $\frac{D_H G_{max}}{\mu_{avg}}$
$\sigma \Delta P$ = air pressure drop corrected to standard conditions at center of unit, in. H_2O
q = rate of heat transfer, Btu per min
T = absolute temperature, deg F + 460
Δt = temperature change, deg F
Δt_m = log-mean temperature difference, deg F
t_1 = inlet temperature of air inside tubes, deg F
t_2 = outlet temperature of air inside tubes, deg F
t_3 = inlet temperature of air outside tubes, deg F
t_4 = outlet temperature of air outside tubes, deg F
U = over-all heat-transfer coefficient, Btu/(hr)(sq ft)(deg F)
w_a = mass rate of air flow, lb per min
w_s = mass rate of steam flow, lb per min
μ = absolute viscosity, lb/(hr)(ft)

[1] Heat Transfer Engineer, AiResearch Manufacturing Company.

Contributed by the Heat Transfer Division and presented at the Aviation War Conference held under the auspices of the Southern California Section, Los Angeles, Calif., June 11–14, 1945, of The American Society of Mechanical Engineers.

Note: Statements and opinions advanced in papers are to be understood as individual expressions of their authors and not those of the Society.

Introduction

Aircraft-engine supercharger intercoolers are designed to reduce the temperature of the air leaving the supercharger before it enters the carburetor. These intercoolers use cooling air obtained from the outside air and forced through the intercooler by the ram pressure created by the forward motion of the airplane. The first units manufactured by the authors' company were constructed with round aluminum tubes about 1/4 in. diam with the supercharged air flowing through the tubes while the cooling air flowed across the tubes. This type is satisfactory, however, only for certain limited types of installations. In order to maintain a sufficient temperature difference between the average cooling air and the average supercharged air, it is necessary to have a fairly high rate of flow of cooling air. The actual amount of cooling air required for a given intercooler effectiveness of course depends also on the over-all heat-transfer coefficient. However, at high air flows, the pressure drop outside the tubes becomes excessive in a round-tube unit. Since the drag imposed on the airplane by the intercooler is a function of the product of the pressure drop of the cooling air by the amount of cooling air required and since the drag which is required for operating the intercooler increases substantially at high altitudes, it became necessary to develop an improved form of low-drag intercooler for modern high-altitude high-speed airplanes.

The first step in this development was to partially flatten the tubes so that their axes would be parallel to the cooling-air-flow direction. This permitted a greater flow of cooling air at the same pressure drop and reduced the cooling-air drag. Although the outside film coefficient was probably reduced in many cases, the inside coefficient, which with round tubes had been smaller than the outside coefficient, was raised by the decrease in the internal cross section of the tube. The net result was an increase in over-all heat-transfer coefficient for a given horsepower without reduction in surface per tube. Also, flattening the tubes allowed them to be placed closer together, thus forming a lighter-weight and more compact unit.

In an attempt to reduce still further the cooling-air drag horsepower, the flattened tubes were dimpled with small creases about 1/2 in. apart running crosswise on the flattened portion of the tubes. At the same time, the outside dimension perpendicular to the flattened portion of the tube was increased to avoid increasing the pressure drop of the supercharged air inside the tubes too greatly by the introduction of the dimples.

The net result of this dimpling was greater than anticipated. In one typical case the cooling-air flow was reduced 30 per cent at an increase in pressure drop of only 25 per cent, resulting in a net saving of 12.5 per cent in horsepower required. Since the reduced cooling-air flow required resulted in a log-mean temperature difference only 87 per cent as great as before, it was apparent that this change had made a substantial increase in heat-transfer coefficient, most of which was estimated to be an increase in the coefficient for the air flowing inside the tube, since the air flow



FIG. 1 LONGITUDINAL CROSS SECTION OF DIMPLED TUBE

outside had been reduced. The tests to be described were performed in an attempt to obtain information which would correlate these results with the usual methods of computing heat-transfer coefficients.

APPARATUS USED IN TESTS

The apparatus tested consisted of three tubular-type aircraft-engine intercoolers of approximately the same external dimensions. One unit was constructed with round tubes, one with partially flattened tubes, and one with partially flattened and dimpled tubes. The flattened and flattened dimpled tubes had the same flattening dimension and were placed with a no-flow clearance or cooling-air passage which was the same clearance as the diagonal clearance used in the round-tube unit. Major dimensions of the test units are given in Table 1. A longitudinal cross section of a portion of a dimpled tube is shown in Fig. 1.

TABLE 1 MAJOR DIMENSIONS OF TEST UNITS

	Round	Flattened	Dimpled
Tube length, net, in.	12	12	12
Tube outside diameter at headers, in.	0.247	0.247	0.247
Dimension perpendicular to flats, in.	....	0.1215	0.1215
Depth of dimple, in.	....	....	0.030
Dimple spacing, in.	....	....	0.5
Minimum space outside tubes, in.	0.0885	0.0885	0.0885
Hydraulic diameter inside, ft	0.0192	0.0136	0.0105
Hydraulic diameter outside, ft	0.0144	0.0144	0.0144
Number of active tubes	567	659	652
Surface area inside tubes, sq ft	34.3	39.8	39.4
Surface area outside tubes, sq ft	36.7	42.6	42.1

For the first tests the units were mounted as shown in Figs. 2 and 3, with air being blown through the tubes while steam condensed around the tubes. The steam was fed at low pressure and slightly superheated to provide complete dryness and allow determination of its enthalpy from measurements of temperature and pressure alone. A small portion of the steam was bled off the bell at the bottom of the unit in order to keep a steady flow of steam past the tubes and prevent the accumulation of water in the lower passages. The condensate ran to a pipe coil in which it was subcooled slightly and then passed to the weighing bucket. A sight glass was used to keep a constant water level in the lower part of the apparatus and thus prevent loss of steam. The inlet steam temperature and pressure were measured with a mercury-in-glass thermometer and a mercury manometer.

The air inlet temperature was measured with two thermometers in the inlet duct just ahead of the unit. The outlet temperature was measured with four thermometers in the outlet duct just beyond the unit. The outlet air temperature was also measured after the air had passed through a baffled mixing box. It was found that when the temperature at the outlet of the mixing box was corrected for the experimentally determined drop of temperature in the mixing box, this corrected temperature agreed very well with the average of the four outlet thermometers placed immediately after the unit.

Most of the air flows were measured with a flat-plate sharp-edged orifice in a duct following the mixing box. The largest air flows were computed from the pressure drop across the unit under test by extrapolation of the pressure drop versus flow curve drawn from the runs where the flow was determined by the orifice. The apparatus was thoroughly insulated with glass wool at all parts where needed.

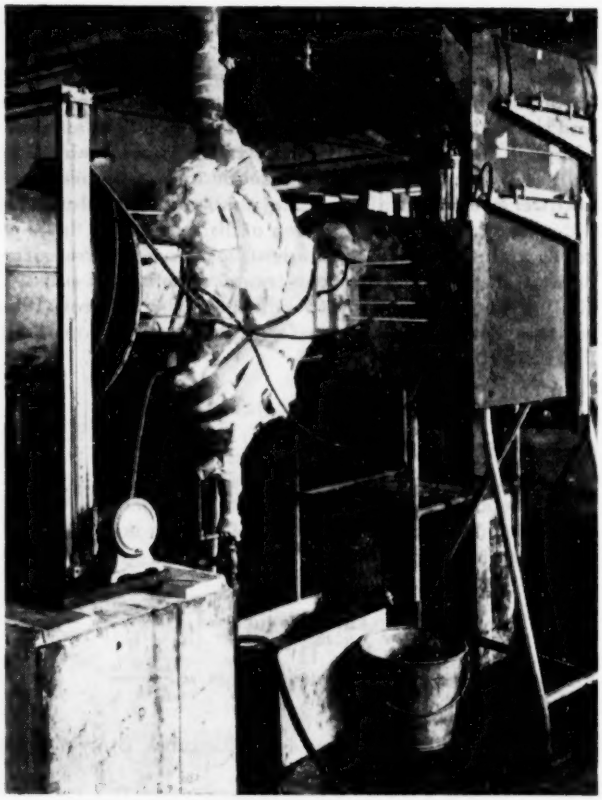


FIG. 2 SETUP FOR STEAM-AIR TEST

For the other series of tests the units were mounted as shown in Fig. 4. Hot air was used inside the tubes while room-temperature air was passed outside the tubes. Inlet air temperatures were measured with one thermometer on the cooling-air side and with three thermometers on the hot-air side. Outlet air temperatures were measured after the air had passed through the mixing boxes, and the temperatures were corrected for the known loss in the boxes. The air flows were measured with orifice plates for the lower air flows and were determined from unit pressure drops for the higher air flows. Because of the relatively high resistance of the unit as compared with that of the duct, a uniform flow distribution was obtained in both the cooling air and the hot paths.

EXPERIMENTAL PROCEDURE

The first series of tests was run to determine the heat-transfer coefficient to air passing inside the tubes. Each of the three units was treated in the same manner. Air was passed through the tubes at a range of velocity to give values of **R** ranging from approximately 1400 to the highest available with the fan used as shown in Table 2. Steam was supplied to the unit under approximately 2 psig pressure and with approximately 10 deg F superheat. The air flow and steam temperature and pressure were kept constant within very close limits, and the system was allowed to balance thoroughly before readings were taken. Readings of all quantities except condensate flow rate were then

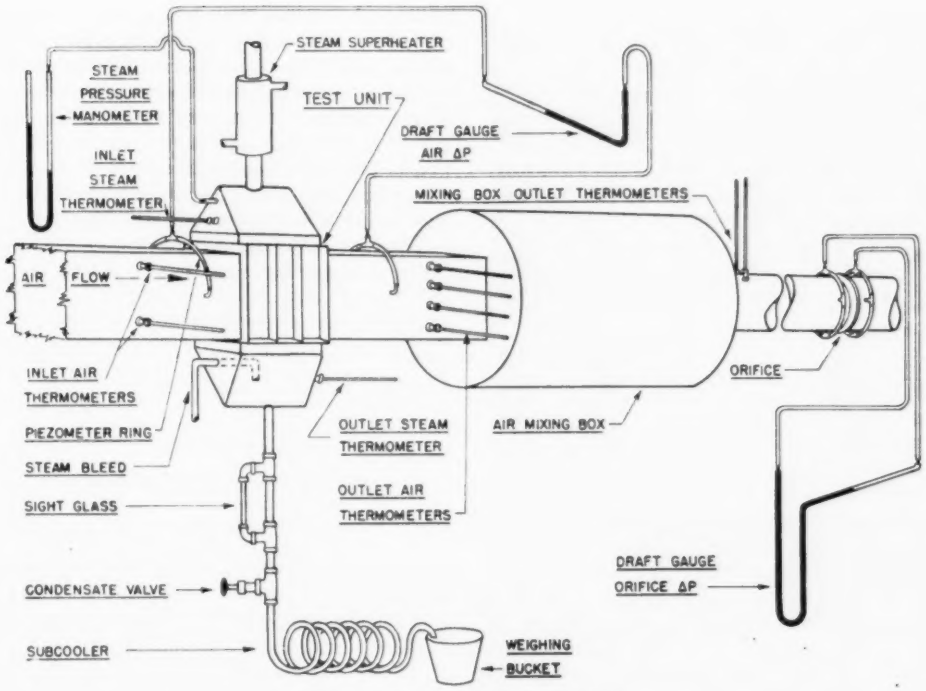


FIG. 3 SETUP FOR STEAM-AIR TEST

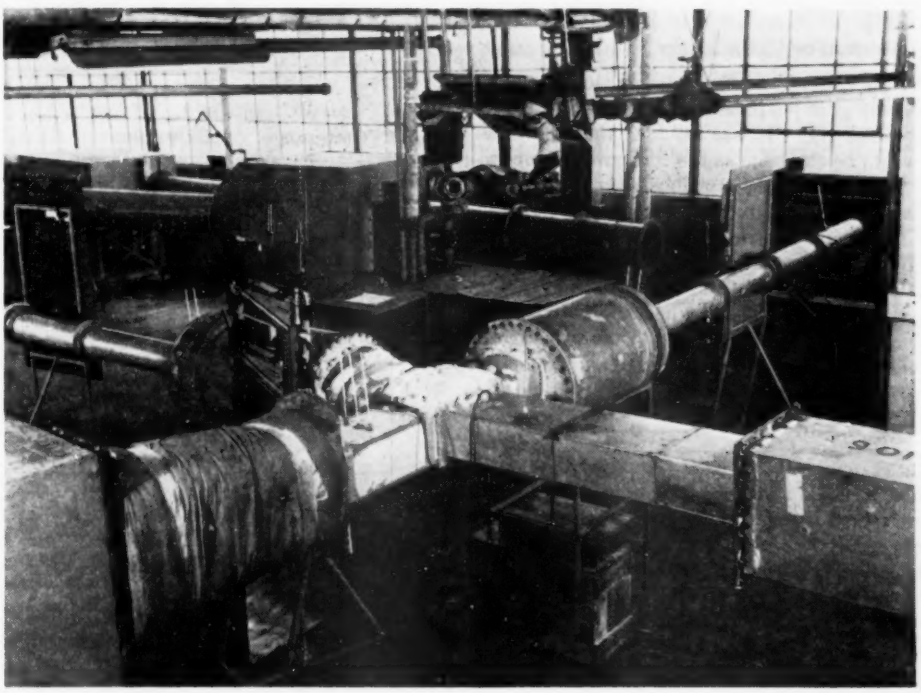


FIG. 4 SETUP FOR AIR-AIR TEST

taken every 2 min for a period of 10 min. At the end of this period, the condensate was weighed. Since the condensate level was kept constant in the sight glass during the run, it was possible to determine from the amount of adjustment necessary in the condensate valve whether the condensate rate was constant. The heat balances obtained on the higher air-flow points show some discrepancies due to the necessity for bleeding steam from the outlet header at these points in order to keep the condensate blown off the tubes and to obtain the highest heat transfer to the air inside the tubes. The extensive experience of the laboratory of the authors' company in measuring air heat gains and losses indicates that the errors involved in these measurements did not exceed 3 per cent. For this reason, all computations of heat-transfer coefficients have been based on the air-side heat gains.

TABLE 2 RANGE OF PRINCIPAL VARIABLES

	Round tubes Max	Round tubes Min	Flattened tubes Max	Flattened tubes Min	Dimpled tubes Max	Dimpled tubes Min
Air-Steam Test—Inside Tubes						
w_s	117.5	9.65	90.0	9.5	76.5	9.6
R	17600	1450	11600	1230	9870	1239
t_1	111.4	70.3	113.3	79.5	119.2	71.0
t_2	173.8	150.7	193.6	182.3	209.1	196.9
Δt_m	93.2	71.7	72.5	58.0	52.1	41.0
h_i	39.1	4.61	38.1	6.09	55.1	9.62
G	42900	3520	40000	4230	44200	5650
q	2245	224	1635	264	2320	302
Air-Air Test—Inside Tubes						
w_s	97.0	16.2	...	...	44.5	10.1
R	14550	2430	...	...	5740	1305
t_1	257.8	240.5	...	...	256.7	246.0
t_2	239.1	155.6	...	...	205.0	118.2
E_i	0.486	0.111	...	...	0.901	0.253
Air-Air Test—Outside Tubes						
w_s	39.1	7.4	...	...	112.0	14.3
R	4650	880	...	...	9300	1185
t_3	109.1	83.3	...	...	103.0	86.0
t_4	243.0	125.9	...	...	202.4	124.6
E_0	0.918	0.206	...	...	0.705	0.083
Δt_m	93.7	44.8	...	...	75.5	51.3
h_i	33.0	5.1	...	...	35.1	10.1
h_0	62.0	15.5	...	...	74.0	10.9
U	23.3	4.1	...	...	21.4	5.8

To determine heat-transfer coefficients to air outside the tubes, the units were operated as intercoolers with hot air inside the tubes and cool air outside the tubes. The air flows were varied throughout the range of the apparatus as shown in Table 2. The flows were maintained until steady conditions were observed at all points and then all instruments were read as rapidly as possible by three observers. This procedure was repeated until there were two sets of readings at each point which agreed within an effectiveness of 0.01 with each other. At least 30 such points were taken on each unit.

Method of Calculation

In the steam test the enthalpy of the entering steam was determined from the readings of temperature and pressure by reference to the steam tables (1).[2] It was assumed that the tube-wall temperature would be the same as the condensing temperature of the steam. This assumption probably leads to much less error than would have been introduced if thermocouples had been used to determine tube-wall temperatures in the small thin-wall tubes. The enthalpy of the condensate was determined from the condensing temperature of the steam and the steam tables. By experiment it was determined that the heat loss through the insulation of the unit in the steam tests was approximately 7 Btu per min, therefore the net heat loss of the steam was determined as

$$q = w_s(i_1 - i_2 - 7) \quad [1]$$

Air inlet and outlet temperatures were computed by taking the arithmetic average of the respective thermometer readings. Air flows were determined from pressure-drop and temperature readings at the orifice and were computed from graphs based on reference (2). The air-side heat gained was therefore

$$q = 0.244\, w_a \Delta t \quad [2]$$

The over-all heat-transfer coefficient U was determined from the inside surface area of the tubes, from the log-mean temperature difference based on the condensing temperature of steam at the observed pressure and the inlet- and outlet-air temperatures and from the air-side heat gain as determined from Equation [2]. The over-all heat-transfer coefficient was therefore

$$U = \frac{60\, q}{A_i \times \Delta T_m} \quad [3]$$

[2] Numbers in parentheses refer to the Bibliography at the end of the paper.

Since the steam-side coefficient was probably of the order of 2000 Btu/(hr)(sq ft)(deg F) very slight error was introduced by assuming that the air-side coefficient was equal to the over-all coefficient. Also this error had the effect of giving a slightly lower inside coefficient which was desirable for design purposes. A plot of the air-side coefficient inside the tubes of the three units versus Reynolds number is shown in Fig. 5. A plot of the Nusselt number versus Reynolds number for the three units is shown in Fig. 6. In computing Reynolds number and Nusselt number the hydraulic diameters were based on the minimum cross section of the tube, that is, in the dimpled-tube unit the

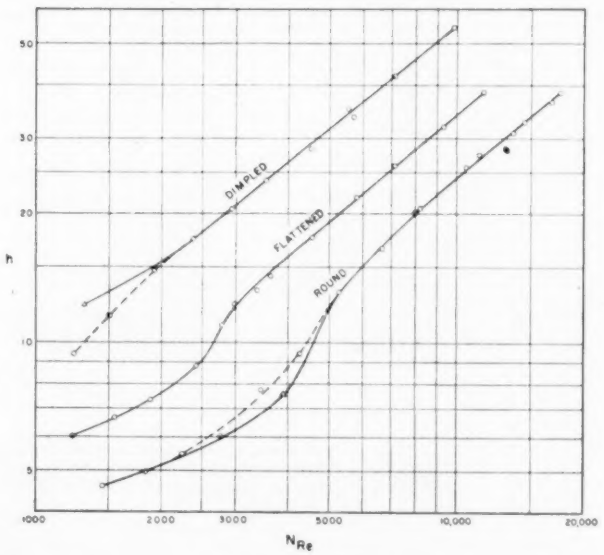


Fig. 5 Comparison of Experimental Heat-Transfer Coefficients for Air Inside Tubes

(Dashed lines show steam-air test results which were modified by air-air test results shown by triangles.)

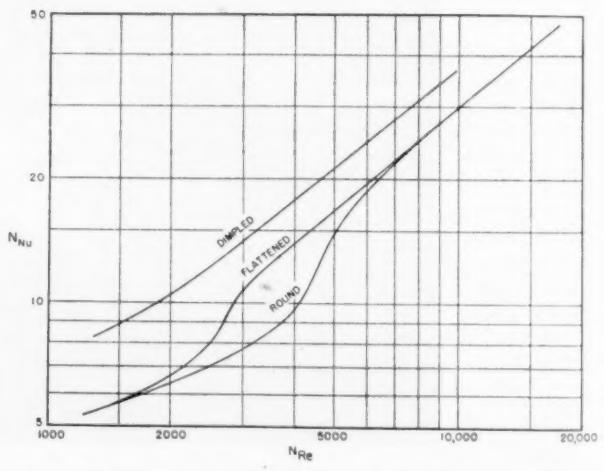


Fig. 6 Comparison of Experimental Values of Nusselt Number for Air Inside Tubes

internal cross section was determined under the dimple. The hydraulic diameter was then computed as

$$D_H = \frac{4A}{P} \quad [4]$$

The mass velocity G was computed from the same minimum cross section and the conductivity and viscosity of the air were taken as 0.0155 Btu/(hr)(sq ft)(deg F/ft) and 0.047 lb/(hr)(sq ft), respectively, at an assumed average temperature of 140 F.

In the intercooler test the air temperatures and air flows were measured in the same manner as in the steam test. The air heat gains and losses were also determined in a similar manner in order to check the heat balance. The over-all heat-transfer coefficient in the intercooler test was determined from the log-mean temperature difference corrected for crossflow (4). The amount of heat transfer was assumed to be the average of the computed heat gained and heat lost. The surface area used was the average of the internal and external surfaces. The external heat-transfer coefficients were then determined from the following equation

$$\frac{1}{h_o A_o} = \frac{2}{U(A_i + A_o)} - \frac{1}{h_i A_i} \quad [5]$$

These outside coefficients are plotted in Figs. 7 and 8.

Correlation of Test Results

Fig. 6, which shows Nusselt number versus Reynolds number for flow inside the tubes, indicates that for the round tubes fully turbulent flow is not established until the Reynolds number

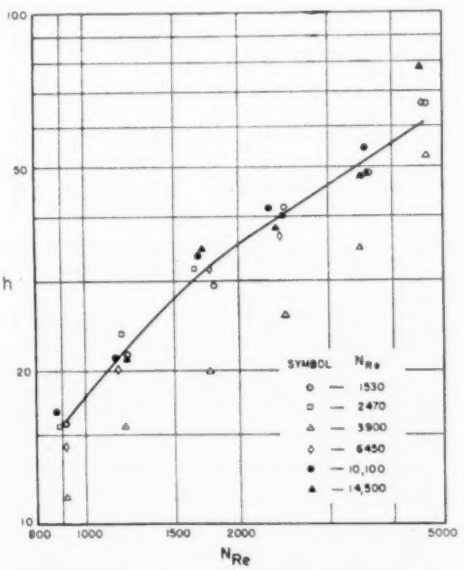


Fig. 7 Experimental Heat-Transfer Coefficients for Air Outside Round Tubes, Showing Results With Various Values of Reynolds Number Inside the Tubes

reaches 8000 and that laminar flow appears to continue up to a Reynolds number of about 2500. In contrast, it is noted that turbulent flow in the flattened tubes starts at approximately 3500 Reynolds number. The dimpled tubes appear to maintain fully turbulent flow from a Reynolds number of 2000.

The graph shows good correlation between the round tubes and flattened tubes tested in both the fully turbulent and fully laminar flow regions. This curve lies only slightly below the average curve given by McAdams (3). The position of this curve seems confirmed by other experiments with very small hydraulic diameters (5).

Both the dimpled-tube curve and the common curve for round and flattened tubes have approximately the same slope in the fully turbulent-flow regions, namely, 0.82.

It will be noted that the curve for dimpled tubes lies 26 per cent above the curve for flattened tubes. A suggested explanation of this is as follows:

Schack (6) states that the heat-transfer coefficient should vary with the length of the pipe, the exponent expressing this variation being —0.05. A recalculation of his figures shows that this exponent should have been stated as —0.07. Now, a dimpled tube might be considered as consisting of a series of short tubes with a new one starting at each dimple. Since, in the unit tested there are 21 dimples per tube, therefore 22 short tubes are represented. The Nusselt number for the dimpled-tube unit was found to be 26 per cent higher than for nondimpled tubes, thus

$$\left(\frac{1}{22}\right)^n = 1.26 \quad [6]$$

where n is the exponent expressing the effect of tube length. Solving, n equals —0.07 which checks with the recalculation of Schack's result. Thus a logical justification may be established for use of the minimum cross-sectional area in determination of hydraulic diameter and mass velocity in dimpled tubes.

Fig. 5 shows the film coefficient inside the tubes for all three units. In drawing Fig. 6, the lines in Fig. 5 which pass through the points marked by triangles were used to determine the Nusselt number. The method of obtaining these points is explained as follows:

Fig. 7 shows the heat-transfer coefficients outside of round tubes. In this plot Reynolds number has been based on the hydraulic diameter of the diagonal passes between the tubes instead of on the tube diameter, in order to provide a more direct comparison with the results of the tests on the dimpled-tube unit in which the Reynolds number is also based on the passage available. It may be noted that the points plotted for a value of **R** of 3900 inside the tubes fall consistently below the average of all the other test points. It was therefore assumed that the steam-test points at values of **R** of 3450 and 4300 inside the tubes were in error since these were based on two runs, whereas the intercooler result is based on ten runs. By assuming outside coefficients at each of the cooling-air flows as read from the average line in Fig. 7, the inside coefficients were recalculated and averaged, and this average was plotted as the intercooler test point at a value of **R** of 3900 shown in Fig. 5. The same procedure was used in obtaining the intercooler test

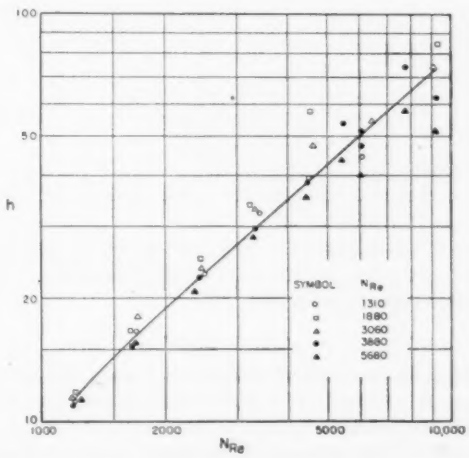


Fig. 8 Experimental Heat-Transfer Coefficients for Air Outside Dimpled Tubes, Showing Results With Various Values of Reynolds Number Inside the Tubes

point for the dimpled-tube unit shown at a value of **R** of 1300 in Fig. 5.

For heat-transfer coefficients outside round tubes, Fig. 7, extrapolation of Grimison's (7) values gives the following estimated equation for a no-flow spacing of 2.4 D_0 and a cooling-air spacing of 0.6 D_0 as used in the test unit

$$h = \frac{0.296\ k\ G_{max}^{0.61}}{\mu^{0.61}\ D_0^{0.39}} \qquad [7]$$

The test results in Fig. 7 average 27 per cent above the values given by Equation [7] in the region where **R** is greater than 2000.

Fig. 8 shows heat-transfer coefficients versus Reynolds number for air outside the dimpled-tube unit. In this case the arrangement of the dimpled tubes is such that an approximately straight passage of rectangular cross section is provided for air outside the tubes. The hydraulic diameter of this passage was determined from Equation [4]. It will be noted that the slope of the line in the turbulent-flow region is approximately 0.8 as compared to a slope of approximately 0.6 with the round-tube unit. This would seem to indicate that with this type of construction heat-transfer coefficients outside the tubes should be computed on the same basis as for flow inside the tubes.

There is seen to be a rather large spread of points in the higher values of **R** in Fig. 8. However, this spread does not indicate a very large experimental error. If heat-transfer coefficients outside the tubes are read from the curve in Fig. 8, and heat-transfer coefficients inside the tubes are read from Fig. 5, and the over-all coefficient U is computed for each of the test points, it is found that the computed U has an average variation of ±5 per cent from the values of U obtained in the intercooler test. It is probable that these coefficients for air outside dimpled tubes are too high and it is hoped that further work can be done on this subject.

Fig. 9 shows heat-transfer coefficients inside the tubes plotted against the air pressure drop corrected to a standard density of 0.07651 pcf at the center of the unit. This air pressure drop is

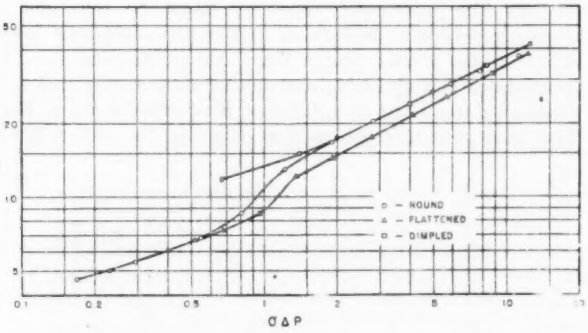


FIG. 9 COMPARISON OF EXPERIMENTAL HEAT-TRANSFER COEFFICIENTS AND PRESSURE DROP FOR AIR INSIDE TUBES

the over-all pressure drop as measured by static fittings located on the sides of the ducts 4 in. upstream and 4 in. downstream of the test unit, as shown in Fig. 3.

CONCLUSIONS

1 The transition from laminar to turbulent flow extends over the range **R** = 2000 to **R** = 8000 for small round tubes. If the tubes are flattened the transition region extends only from **R** = 2000 to **R** = 3500 while if the flattened tubes are dimpled the transition takes place at **R** = 2000.

2 For any given Reynolds number, flattening a round tube increases the heat-transfer coefficient substantially, while dim-

TABLE 3 ROUND TUBE AIR-STEAM TEST DATA

Run number	1	2	3	4	5	6	7	8	9	10	11	12	13	14	15	16
STEAM																
Inlet temperature, (avg) deg F	227.5	229.1	228.1	229.3	229.2	230.7	232.5	231.5	228.8	229.1	230.4	224.0	224.0	231.5	217.8	229.8
Pressure, psia	16.6	15.0	16.5	15.0	16.6	16.5	16.5	16.5	16.7	16.7	16.7	16.7	16.5	16.7	16.4	16.7
Condensing temperature, deg F	218.2	213.0	218.0	213.0	218.1	218.0	218.0	218.0	218.4	218.4	218.4	218.4	218.0	218.4	217.5	218.4
Enthalpy, Btu per lb	1161	1161	1161	1161	1161	1161	1162	1162	1161	1161	1161	1160	1160	1162	1158	1161
Enthalpy condensate, Btu per lb	186	181	186	180	186	186	186	186	186	186	186	186	185	186	185	186
Enthalpy change, Btu per lb	975	980	975	981	975	975	976	976	975	975	975	974	975	976	973	975
Condensate flow, lb per min	0.238	0.263	0.297	0.323	0.407	0.510	0.641	0.733	1.053	0.975	1.081	1.520	1.566	1.84	1.81	2.20
Heat loss of steam, Btu per min	232	258	289	317	397	497	626	735	1028	950	1053	1480	1525	1795	1757	2142
Insulation loss, Btu per min	7	7	7	7	7	7	7	7	7	7	7	7	7	7	7	7
Net heat loss of steam, Btu per min	225	251	282	310	390	490	619	728	1021	943	1046	1473	1518	1788	1750	2135
AIR																
Outlet temperature, (avg) deg F	172.0	160.2	159.0	153.5	161.3	157.4	165.9	169.6	159.1	168.7	173.0	156.0	162.3	153.2	164.6	152.0
Inlet temperature, (avg) deg F	76.8	76.2	78.7	84.7	91.4	85.7	92.7	102.0	76.2	97.6	111.4	72.7	94.2	74.0	103.9	73.7
Temperature rise, deg F	95.2	84.0	80.3	68.8	69.9	71.7	73.2	67.6	82.9	71.1	61.6	83.3	68.1	79.2	60.7	78.3
Air flow, lb per min	9.65	12.2	14.9	18.4	23.0	28.5	35.1	44.5	53.9	54.7	70.3	75.5	91.0	96.5	112	117.5
Air heat gain, Btu per min	224	250	290	309	386	491	616	734	1090	959	1070	1533	1513	1865	1660	2245
Discrepancy, per cent	0.4	0.4	3.4	0.3	0.5	1.6	1.3	0.8	6.3	0.7	0.9	3.9	0.3	4.1	5.4	4.9
Air pressure drop, $\sigma\Delta P$, in. H_2O	0.17	0.23	0.30	0.40	0.55	0.81	1.22	1.91	...	2.79	...	4.94	...	7.74	...	...
Log-mean temperature difference, deg F	85.0	88.2	93.2	89.3	87.3	91.8	83.4	77.4	94.7	80.2	71.7	98.2	85.4	99.5	79.5	100.6
Over-all coefficient, Btu/hr(sq ft)(deg F)	4.61	4.96	5.48	6.06	7.73	9.49	13.2	16.6	20.1	20.7	25.7	27.4	31.0	32.7	36.6	39.1
Nusselt number, dimensionless	5.71	6.15	6.80	7.51	9.58	11.8	16.3	20.6	24.9	25.7	31.8	34.0	38.4	40.5	45.4	48.5
Reynolds number, dimensionless	1450	1830	2240	2760	3450	4270	5260	6670	8100	8200	10500	11300	13650	14500	16800	17600

TABLE 4 FLATTENED TUBE AIR-STEAM TEST DATA

Run number	1	2	3	4	5	6	7	8	9	10	11	12	13
STEAM													
Inlet temperature, (avg) deg F	228.7	228.7	228.3	229.2	228.1	229.1	228.4	228.7	227.7	228.0	226.9	226.9	226.4
Pressure, psia	16.6	16.6	16.6	16.6	16.6	16.6	16.6	16.6	16.6	16.6	16.6	16.6	16.6
Condensing temperature, deg F	218.1	218.1	218.1	218.1	218.1	218.1	218.1	218.1	218.1	218.1	218.1	218.1	218.1
Enthalpy, Btu per lb	1161	1161	1161	1161	1161	1161	1161	1161	1161	1161	1160	1160	1160
Enthalpy condensate, Btu per lb	186	186	186	186	186	186	186	186	186	186	186	186	186
Enthalpy change, Btu per lb	975	975	975	975	975	975	975	975	975	975	974	974	974
Condensate flow, lb per min	0.285	0.328	0.369	0.438	0.495	0.516	0.562	0.678	0.788	0.873	1.068	1.438	1.581
Heat loss of steam, Btu per min	278	320	360	427	482	503	548	660	768	851	1029	1400	1540
Insulation loss, Btu per min	7	7	7	7	7	7	7	7	7	7	7	7	7
Net heat loss of steam, Btu per min	271	313	353	420	475	496	541	653	761	844	1022	1393	1533
AIR													
Outlet temperature, (avg) deg F	193.6	188.2	184.2	182.3	187.6	190.7	191.7	186.8	187.6	190.3	188.0	182.5	184.1
Inlet temperature, (avg) deg F	79.5	81.3	84.9	89.8	95.6	101.5	106.5	92.0	100.0	113.3	109.5	99.7	109.7
Temperature rise, deg F	114.1	106.9	99.3	92.5	92.0	89.2	85.2	94.8	87.6	77.0	78.5	82.8	74.4
Air flow, lb per min	9.5	12.0	14.6	18.7	21.5	23.1	26.2	28.1	35.5	45.0	55.2	72.4	90.0
Air heat gain, Btu per min	264	313	353	422	482	503	524	650	760	845	1057	1462	1635
Discrepancy, per cent	2.6	0.0	0.0	0.5	1.5	1.4	3.2	0.5	0.1	0.1	3.3	4.7	6.2
Air pressure drop, $\sigma \Delta P$, in. H_2O	0.40	0.52	0.68	0.96	1.20	1.36	1.67	1.92	2.78	4.10	5.64	8.70	12.3
Log-mean temperature difference, deg F	65.9	70.3	72.5	72.3	66.1	61.6	59.1	68.0	64.5	58.0	61.2	68.8	64.1
Over-all coefficient, Btu/hr(sq ft)(deg F)	6.03	6.70	7.33	8.79	11.0	12.3	13.3	14.4	17.7	21.9	25.9	32.0	38.3
Nusselt number, dimensionless	5.29	5.88	6.43	7.71	9.63	10.8	11.7	12.6	15.6	19.2	22.7	28.1	33.6
Reynolds number, dimensionless	1230	1550	1880	2420	2780	2980	3380	3620	4580	5800	7130	9340	11600

TABLE 5 DIMPLED TUBE AIR-STEAM TEST DATA

Run number	1	2	3	4	5	6	7	8	9	10	11	12	13
STEAM													
Inlet temperature, (avg) deg F	226.5	226.8	226.4	227.2	226.9	226.3	226.0	229.9	225.7	229.2	229.3	228.8	227.2
Pressure, psia	16.6	16.6	16.6	16.6	16.6	16.6	16.6	16.8	16.6	16.7	16.7	16.7	16.6
Condensing temperature, deg F	218.1	218.1	218.1	218.1	218.1	218.1	218.1	218.8	218.1	218.6	218.6	218.6	218.1
Enthalpy, Btu per lb	1160	1160	1160	1161	1160	1160	1160	1161	1160	1161	1161	1161	1161
Enthalpy condensate, Btu per lb	187	186	186	186	186	186	186	187	186	187	186	187	186
Enthalpy change, Btu per lb	973	974	974	975	974	974	974	974	974	974	975	974	975
Condensate flow, lb per min	0.317	0.380	0.473	0.520	0.588	0.747	0.836	1.36	0.964	1.69	1.65	2.20	2.20
Heat loss of steam, Btu per min	309	370	460	507	572	728	813	1323	938	1645	1610	2142	2144
Insulation loss, Btu per min	7	7	7	7	7	7	7	7	7	7	7	7	7
Net heat loss of steam, Btu per min	302	363	453	500	565	720	806	1316	931	1638	1603	2135	2137
AIR													
Outlet temperature, (avg) deg F	208.6	208.9	209.1	208.8	208.6	207.1	206.5	202.5	205.7	199.9	200.3	196.9	197.4
Inlet temperature, (avg) deg F	79.7	82.5	87.7	96.3	108.0	99.8	113.0	71.0	119.1	71.4	74.3	73.1	73.2
Temperature rise, deg F	128.9	126.4	121.4	112.5	100.6	107.3	93.5	131.5	86.6	128.5	126.0	123.8	124.2
Air flow, lb per min	9.6	11.7	14.9	18.5	22.8	27.3	35.1	43.1	44.2	55.2	55.2	76.2	76.5
Air heat gain, Btu per min	302	361	442	508	559	716	800	1382	935	1730	1697	2297	2320
Discrepancy, per cent	0.0	0.8	2.5	1.6	1.1	0.7	0.8	4.8	0.4	5.3	5.5	7.0	8.0
Air pressure drop, $\sigma \Delta P$, in. H_2O	0.67	0.95	1.40	1.99	2.82	3.97	5.89	8.25	8.62	12.5	12.5	21.4	21.3
Log-mean temperature difference, deg F	48.2	47.0	45.4	43.7	41.0	45.1	42.4	59.6	41.7	62.2	61.0	64.7	63.9
Over-all coefficient, Btu/hr(sq ft)(deg F)	9.41	11.6	14.7	17.5	20.5	23.9	28.4	35.3	33.7	42.3	42.4	54.0	55.3
Nusselt number, dimensionless	6.38	7.83	9.96	11.9	13.9	16.2	19.3	23.9	22.8	28.5	28.5	36.8	37.4
Reynolds number, dimensionless	1240	1510	1920	2380	2940	3520	4530	5560	5700	7120	7120	9830	9870

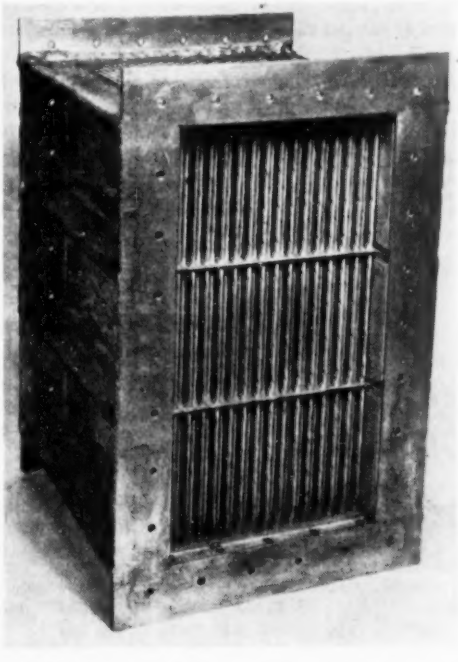


FIG. 10 TEST UNIT WITH DIMPLED TUBES

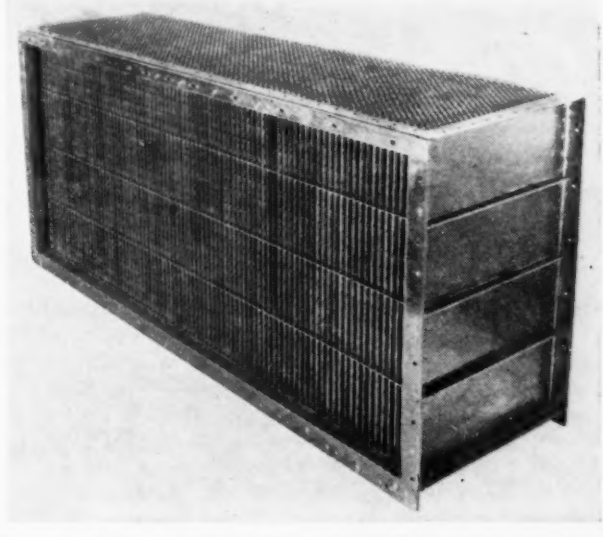


FIG. 11 LARGE AIRCRAFT INTERCOOLER WITH DIMPLED TUBES

pling the flattened tube increases the heat-transfer coefficient to an even higher value. This statement also applies to equal weight flows of air, since the Reynolds number for a tube of given perimeter at a given weight flow is not varied by flattening the tube or by dimpling it.

3 For the same air-pressure drop, dimpled tubes have the same or higher heat-transfer coefficient than round tubes, while plain flattened tubes have a lower heat-transfer coefficient, except at very low air-pressure drops.

4 The use of dimpled tubes in intercoolers permits a reduction in the amount of cooling air required and therefore leads to a lower drag on the airplane.

ACKNOWLEDGMENTS

The authors express their appreciation to Mr. Robert W. Wagner and Mr. Harry H. Beckwith of their company for assistance in the performance of the tests and in the compilation of the report.

BIBLIOGRAPHY

1 "Steam Tables and Mollier Diagram," by Joseph H. Keenan, The American Society of Mechanical Engineers, New York, N. Y., 1930.

2 "Fluid Meters, Their Theory and Application," Part 1, The American Society of Mechanical Engineers, New York, N. Y., 1937.

3 "Heat Transmission," by W. H. McAdams, McGraw-Hill Book Company, Inc., New York, N. Y., 1942.

4 "Mean Temperature Difference in Design," by R. A. Bowman, A. C. Mueller, and W. M. Nagle, Trans. A.S.M.E., vol. 62, 1940, p. 288.

5 "Heat Transfer and Pressure Drop in Rectangular Air Passages," by Lawrence Washington and W. M. Marks, *Industrial and Engineering Chemistry*, vol. 29, 1937, p. 341.

6 "Industrial Heat Transfer," by Alfred Schack, translated by Goldschmidt and Partridge, John Wiley & Sons, Inc., New York, N. Y., 1933, p. 101.

7 "Correlation and Utilization of New Data on Flow Resistance and Heat Transfer for Cross flow of Gases Over Tube Banks," by E. D. Grimison, Trans. A.S.M.E., vol. 59, 1937, p. 583.

(Owing to travel emergency conditions existing when this paper was presented, discussion will be accepted until March 11, 1946)

Heat Transfer From a Cylindrical Surface to Air in Parallel Flow With and Without Unheated Starting Sections[1]

By MAX JAKOB[2] AND W. M. DOW,[3] CHICAGO, ILL.

The present investigation sponsored by the Illinois Institute of Technology, Armour Research Foundation, and Institute of Gas Technology, deals with the heat transfer of air in parallel flow to a surface, a process of great practical importance which, for instance, occurs with all kinds of fins or on the skin of an airplane in flight. Previous knowledge of that process was based on a few sets of experiments which were performed with plane surfaces and led to a considerably higher heat transfer than a reliable theory, due to H. Latzko. In particular, the influence of nonheated starting sections seemed to require a new investigation. Compared with the use of plane plates by previous investigators, the use of an electrically heated cylindrical specimen has the following advantages: A cylinder can be easily placed in the center of an air jet and is free of the edge losses of a plate; for both reasons, air jets of moderate diameter can be used. Uniform heating is easier to provide, heat losses to the back are easier to control, and noses of different shape and cylindrical starting sections can readily be used for studying the behavior of the so-called boundary layer of the fluid which is developing along the surface, first streamlined and then turbulent, and in which all resistance against heat transfer is concentrated. The experiments were performed with specimens of 1.3 in. diam and 9 to 20 in. total length, the ratio of the heated length to the total length being varied from 40 to 90 per cent. Spherical, ellipsoidal, and conical nosepieces were used. The air velocity was varied from 10 to 150 fps and it is assumed that the results can be theoretically extrapolated above sound velocity, using the principle of similarity.

Nomenclature

The following nomenclature is used in the paper:

A = area of heating surface, sq ft
b = thickness of boundary layer, ft
C, C_0, C_1, C_2, C_3 are constant factors
c_p = specific heat at constant pressure of air, B lb_m^{-1} F^{-1}
$F = N/M$ = correction factor
H = velocity head in feet of air, ft
H_w = velocity head, in. of water
h = coefficient of heat transfer by convection (mean taken over heating length, L_{th},) B hr^{-1} ft^{-2} F^{-1}
h_x = local coefficient of heat transfer by convection at distance x from leading edge, B hr^{-1} ft^{-2} F^{-1}
$h_{x,m}$ = mean of h_x, taken from $x = x_1$ to $x = x$, B hr^{-1} ft^{-2} F^{-1}
J = mechanical equivalent of heat, ft lb/B
k = thermal conductivity of air, B hr^{-1} ft^{-1} F^{-1}
L_{st} = hydrodynamic starting length, ft
L_{th} = thermal or heating length, ft
L_{tot} = total length, ft
M, N are integrals, defined in text, sq ft/sec
m and n are constant exponents

$N_{Nu} = \dfrac{hL_{tot}}{k}$ = Nusselt number (total mean)

$(N_{Nu})_{max}$ = Nusselt number, corresponding to q_{max}
$(N_{Nu})_{min}$ = Nusselt number, corresponding to q_{min}
$(N_{Nu})_0$ = Nusselt number for $L_{st}/L_{tot} = 0$

$(N_{Nu})_x = \dfrac{h_x x}{k}$ = local Nusselt number

$(N_{Nu})_{x,m} = \dfrac{h_{x,m} x}{k}$ = mean Nusselt number for distance x from leading edge

$N_{Nu'} = \dfrac{h(L_{tot} - x_0)}{k}$

$N_{Pr} = \dfrac{\rho c_p \nu}{k}$ = Prandtl number

$N_{Re} = \dfrac{v_a L_{tot}}{\nu}$ = Reynolds number with L_{tot} as characteristic length

$(N_{Re})_{cr}$ = critical Reynolds number

$(N_{Re})_x = \dfrac{v_a x}{\nu}$ = Reynolds number with x as characteristic length

$N_{Re'} = \dfrac{v_a (L_{tot} - x_0)}{\nu}$

$(N_{Re'})_x' = \dfrac{v_a x'}{\nu}$

q = rate of heat flow, B/hr
q' = rate of heat transferred by convection over length $x - x_1$ and unit width, B/hr
q_c = rate of heat transferred by convection from cylindrical surface, B/hr
q_i = rate of heat input, B/hr
q_l = sum of heat losses, B/hr
q_{max} = rate of heat transferred for certain values of L_{tot} and L_{st}, B/hr
q_{min} = rate of heat transferred for the same L_{tot}, but $L_{st} = 0$, B/hr

---

[1] Based partly on a thesis submitted by W. M. Dow to the Graduate School, Illinois Institute of Technology, in partial fulfillment of the requirement for the degree of Master of Science, for studies completed in the Institute of Gas Technology.

[2] Research Professor of Mechanical Engineering, Illinois Institute of Technology; Consultant in Heat Research, Armour Research Foundation, Chicago, Ill. Mem. A.S.M.E.

[3] Fellow of the Institute of Gas Technology, Chicago, Ill., now Ensign, U. S. Navy.

Contributed by the Heat Transfer Division and presented at a meeting of the Chicago Section, Chicago, Ill., June 17–19, 1945, of The American Society of Mechanical Engineers.

Note: Statements and opinions advanced in papers are to be understood as individual expressions of their authors and not those of the Society.

q_p = rate of heat transferred by convection from plane surface, B/hr
r = radius of cylinder, ft
t = air temperature at distance y from surface, °F
t_a = temperature of bulk of air stream, °F
t_f = $(t_a + t_s)/2$ = film temperature, °F
t_i = $t_a + \theta_i$ = impressed temperature of unheated surface, °F
t_s = average surface temperature, °F
v = air velocity at distance y from surface, ft/sec
v_a = velocity of bulk of fluid (air), ft/sec
v_b = air velocity at distance b from surface, ft/sec
W = width of flat surface, ft
x = distance from leading edge, general, ft
x_0 = distance from leading edge, defined by Fig. 1, ft
x_1 = L_{st} (see this symbol), ft
x_{cr} = distance from leading edge where critical Reynolds number occurs, ft
x' = $x - x_0$, ft
y = perpendicular distance from surface, ft
θ = $t - t_a$ = temperature excess at distance y from surface, F
θ_{ad} = temperature increment by frictionless adiabatic stopping of flow, F
θ_i = temperature increment by adiabatic stopping of flow, including effect of friction, F
θ_s = $t_s - t_a$ = temperature difference between heating surface and bulk of air stream, F
ν = kinematic viscosity of fluid (air) at bulk temperature t_a, sq ft/sec
ν_f = kinematic viscosity of air at film temperature t_f, sq ft/hr
ρ = density of air, lb_m/cu ft
$\varphi(N_{Pr})$ = function of N_{Pr}

Introduction

While the heat transfer between a cylindrical surface and a fluid has been abundantly studied for the flow in a tube and across a cylinder, no experiments seem to have been done for the parallel flow on the surface of a cylinder on the outside of a tube, and only a few sets of experiments have been performed concerning the free stream parallel to a plane heating surface. As a consequence, the numerous correlations of heat transfer for flow inside of tubes and channels and across cylinders have a much better foundation than the few correlations known for the flow parallel to a heating or cooling surface when the fluid is not bounded by the walls of a tube or channel.

The present experimental investigation was undertaken to secure and correlate data of heat transfer for this sort of flow, including transition-state conditions and the influence of hydrodynamic starting sections.

Referring to Fig. 1, it may be remembered that at the leading edge the fluid is suddenly caused to adhere to the solid surface. As a result a thin layer is formed in which the viscosity forces of the fluid bring about a change of velocity. As the stream moves over the surface, the retarding effect of the viscosity forces gradually penetrates deeper and deeper into the surrounding fluid so that the boundary layer increases in thickness. For some distance the flow in that layer is laminar; in a transition range it gradually becomes turbulent; in the turbulent stage, finally, the thickness of the layer increases more rapidly than it did in the laminar range. Within the boundary layer, however, still a very thin laminar film exists next the surface, being a permanent feature of any fully established flow.

The boundary layer of a free stream parallel to a surface can be characterized by a dimensionless Reynolds number xv_a/ν,

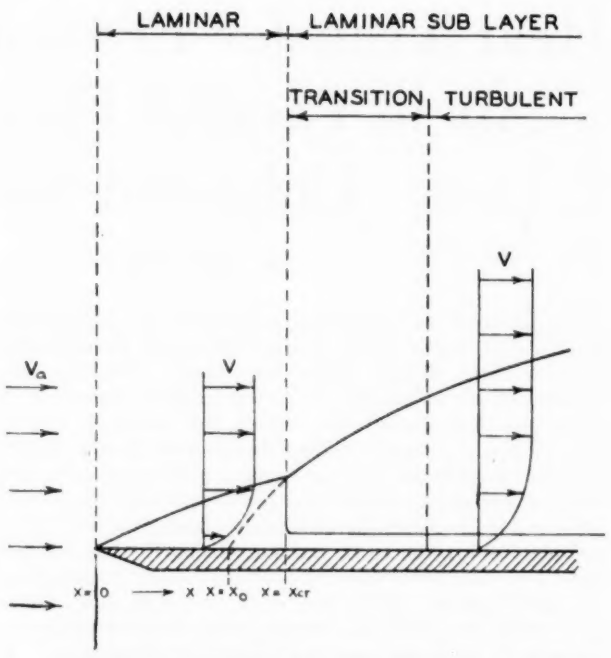


Fig. 1 Boundary-Layer Development Along a Flat Plate

where x is the distance from the leading edge ($x = 0$ in Fig. 1), v_a is the unaltered velocity, and ν is the kinematic viscosity of the fluid. The transition from laminar to turbulent flow is not sharp; it depends on original disturbances in the turbulent stream ahead of the surface, the shape of the leading edge, and the roughness of the surface. Critical Reynolds numbers, determining the place, $x = x_{cr}$, where laminar flow ceases in the layer, have been measured from 100,000 to 500,000, depending on the starting conditions, 300,000 being the ordinary value according to van der Hegge Zijnen (1)[4] and Hansen (2). With blunt leading edges, however, turbulent boundary layers have been obtained straight from the start (3),[5] $x = 0$.

Due to the well-known analogy between momentum transfer and heat transfer, the mode of heat transmission depends on whether the flow in the boundary layer is laminar or turbulent. A difference in the coefficient of heat transfer by convection can also be expected if heating does not begin at the leading edge, but is preceded by a hydrodynamic starting length. Whereas the development of the boundary layer and its effect on heat transfer will not necessarily be the same for cylindrical and plane surfaces, the difference will be considerable only if the radius of the surface curvature is relatively small (4).[6]

Considering the described features of flow and heat transfer along a surface, the objectives of the investigation are as follows:

1 To determine the heat transfer between a cylindrical surface and air in parallel flow, laminar or turbulent, under conditions where only a small influence of the surface curvature is to be expected.

2 To determine the effect of different hydrodynamic starting lengths on the heat-transfer coefficient.

3 To compare the results with theoretical and experimental results for plane surfaces reported in the literature.

Compared with the use of plane plates by previous investiga-

[4] Numbers in parentheses refer to the Bibliography at the end of the paper.
[5] Loc. cit., p. 139.
[6] Loc. cit., p. 249.

tors the use of a cylindrical specimen has the following advantages:

1 A cylinder can be easily placed in the center of an air jet without disturbing the uniform velocity field ahead of the apparatus.

2 With a plane plate, heat losses to the side have to be considered, and for this reason the plate must be rather wide. Such losses do not exist in a cylinder and therefore its diameter can be relatively small so that an air jet of moderate diameter can be used.

3 Uniform heating is easier to provide and losses to the backside of the heater are smaller and easier to control than with plane plates.

4 A cylindrical specimen is particularly convenient for studying the influence of the hydrodynamic starting length.

With these objectives and advantages in mind a cylindrical specimen was designed with an electric heating coil inside and thermocouples just below the outer surface to insure accurate temperature measurements without interference with the air stream. Wooden nosepieces of different shape and length served to close the upstream end of the specimen and to vary the hydrodynamic starting conditions.

In the experiments air was pressed through a channel by a blower and discharged by a nozzle into the room and against the nose of the specimen which was placed in the air stream with its axis parallel to the flow lines. Under these conditions the main air-stream velocity was measured with a Pitot tube; the heat input to the specimen was determined from the wattage of the heating coil by electric instruments; and the temperatures of the main air stream and the specimen surface were measured by thermocouples. These are the data necessary for calculating the coefficient of heat transfer by convection. Experimental runs were made at various velocities and under different hydrodynamic starting conditions. The results were correlated in graphs and formulas, discussed and compared with those of previous investigators.

Description of Apparatus

For the time being the experiments had to be restricted to one heating cylinder. In order that the results might be applicable to the case of a plane surface with reasonable approximation, a diameter of 1.3 in. seemed to be appropriate, considering the range of Reynolds numbers which could be covered by the experimental arrangement.

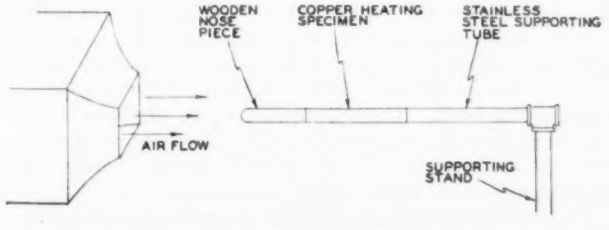


Fig. 2 General Arrangement of Apparatus

Fig. 2 is a self-explanatory sketch of the general setup of the apparatus. The nozzle indicated in this sketch had a square throat, 10 in. × 10 in. Details of the specimen with supporting assembly are given in Figs. 3 and 4. The main parts are a copper tube 8 in. long, 1.300 in. OD, 0.950 in. ID, and a stainless-steel tube 0.840 in. OD, 0.622 in. ID, on which nichrome wire, B and S gage No. 24 B (0.0201 in. diam) was wound. This heating coil was insulated by glass cloth and placed inside the copper tube.

Extreme care was taken to insure a smooth and continuous surface junction between the wooden nosepiece and the copper tube, as irregularities at this point would greatly influence the character of the boundary layer. The surface junctions were made with paper rings inserted in grooves as shown in Figs. 3 and 4. Melted paraffin was then painted on the junction and carefully scraped flush with the surface of the copper tube and the wooden nosepiece. A Pitot tube constructed according to Prandtl's design (5),[7] in connection with an inclined manometer, was provided for the velocity-head measurements.

All thermocouples used in the investigation were made of copper and constantan, B & S gage No. 28 (0.0126 in. diam). The cold junctions were placed in melting ice at 32 deg F. By means of a mercury-contact selector switch, each thermocouple could be connected to a Leeds and Northrup portable precision potentiometer which allowed readings of 0.001 mv.

One thermocouple served to the measurement of the air-flow temperature. It was inserted into a $^1/_8$-in-diam copper tube which was placed parallel to the air flow for a distance of 2 in. and was sealed at the upstream end.

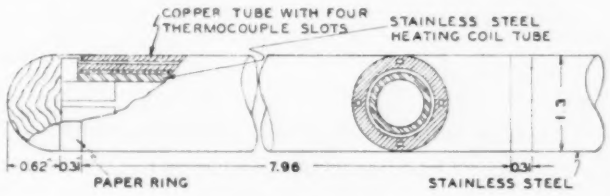


Fig. 3 Details of Copper Heating Specimen

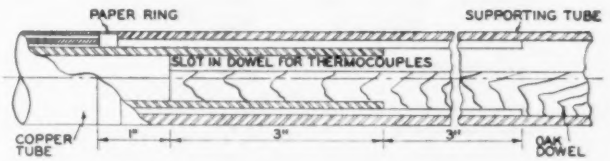


Fig. 4 Details of Supporting Assembly

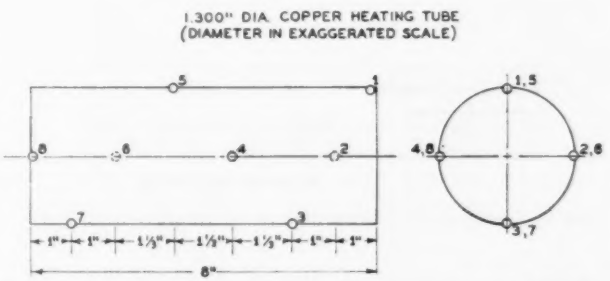
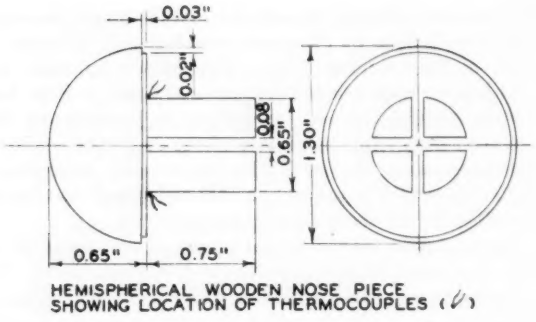


Fig. 5 Locations of Surface Thermocouples in Copper Heating Specimen

In order to avoid disturbances on the surface, the eight thermocouples serving for the measurement of the surface temperature were placed in, and brought out axially through four slots of square cross section (0.080 in. side length) in the wall of the heating tube as shown in Fig. 3. The thermocouples fitted snugly in the axial slots but were removable for ease of calibration and manipulation. Locations of the hot joints of the thermocouples are shown in Fig. 5.

Thermocouples for secondary temperature measurements were placed in the wooden nosepieces, Fig. 6, and on the rear part of the heating-coil tube, Fig. 7. Each of the latter thermocouples was wrapped around the tube once so that the wires were in an

[7] Loc. cit., p. 170.



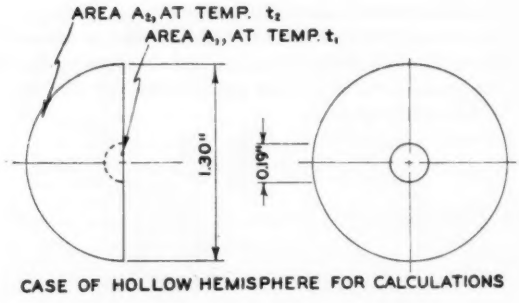


FIG. 6 HEMISPHERICAL WOODEN NOSE PIECE

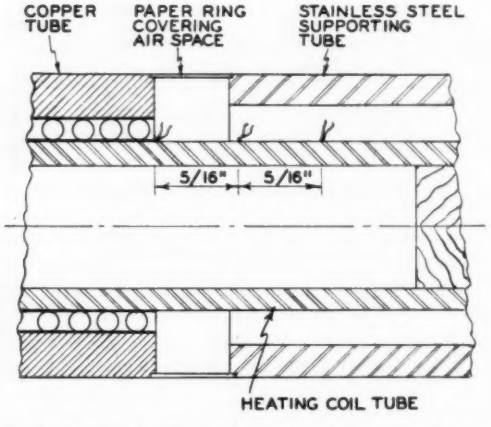


FIG. 7 LOCATION OF THERMOCOUPLE ON HEATING COIL TUBE

isothermal zone for about 1 in. from the joint. The purpose of these thermocouples will be explained in the following section.

A hemispherical nosepiece of 0.65 in. diam is shown in Fig. 3. The six different starting pieces used in the experiments are described in Table 1.

TABLE 1 STARTING PIECES

Specification	L_{st} ft	L_{tot} ft	L_{st}/L_{tot}
Cylinder with hemispherical nose	1.026	1.693	0.606
Cylinder with hemispherical nose	0.689	1.356	0.508
Cylinder with hemispherical nose	0.354	1.021	0.347
Conical piece (4 in. long)	0.187	0.854	0.220
Ellipsoidal nose	0.092	0.759	0.122
Hemispherical nose	0.075	0.742	0.101

In this table L_{st} is the hydrodynamic starting length of the specimen, defined as the ratio of the surface area of the starting piece to the perimeter of the heating cylinder. The total length, L_{tot}, is defined as the sum of the starting length L_{st}, and the thermal or heating length L_{th}, of 8 in.[8]

TEST PROCEDURES

The velocities were measured by the Pitot tube, using the equation

$$v_a = \sqrt{2gH} = 18.275 \sqrt{H_w/\rho} \quad \ldots\ldots\ldots\ldots [1]$$

where

v_a = velocity, ft/sec
H = velocity head as used in test, ft of air
H_w = velocity head, in. of water
ρ = density of air, lb_m/cu ft

H_w was read directly on the inclined manometer.

Preliminary velocity traverses through the air jet, conducted in horizontal and vertical direction, revealed that for a distance of 2 ft downstream from the nozzle, the air velocity varied less than 1 per cent within an 8-in. core. Therefore, in the main experiments the velocity of the air stream was determined at one point only, midway between the ends of the heating coil and 2 in. from the surface of the specimen.

The electromotive force of the thermocouples was checked at the water boiling point. The indications of the couples, when placed in saturated steam, were compared with the values of Keenan and Keyes's steam tables (6). The deviations from the manufacturer's calibration table were less than 0.1 F at 212°F.[9]

As the velocity of the air, also its temperature, were always taken at a point midway between the ends of, and 2 in. from the heating surface. No correction was applied for the influence of velocity on temperature measurement, which may have reached 0.7 F at the highest velocities, corresponding to about 1 per cent in the measured coefficient of heat transfer.

The measurement of the temperature of the exposed surface is a delicate operation in any heat-transfer experiment. The thermocouple wires in the axial slots below the surface parted from the junctions virtually along isothermal lines, the maximum variation of the surface temperature in axial direction being generally below and only exceptionally slightly above 1 F/in. Therefore the junctions were not sensibly affected by conduction in the axial direction. On the other hand, the influence of the slots in the copper wall on the cross-sectional temperature field had to be studied. Obviously, the length of the heat-flow path near the slots was increased and the distribution of the surface temperature around the tube was not uniform any more. In order to find the surface temperatures from the indications of the thermocouples in the slots, the temperature field in a cross section of the copper tube was determined by Lehmann's graphical method (7).[10] Fig. 8 shows the temperature field in the tube wall for the most drastic conditions encountered in the experimental work. The maximum possible deviation of the thermocouple indication from the undisturbed surface temperature was less than 0.1 F and consequently the thermocouple readings were taken as the surface temperatures.

The heat input was determined by electric-resistance and current measurements. Direct current was used in the heating coil. Its resistance was measured by a Wheatstone bridge, the slight increase of the resistance of the nichrome wire with temperature being taken from Knowlton's handbook (8). A millivoltmeter

[8] The slight difference between the sixth ratio given in Table 1, and L_{st}/L_{tot}, as calculated from the lengths given in Fig. 3, is due to some details in design not indicated in the figure.

[9] In order to distinguish temperature differences from temperatures the unit symbols F and °F, respectively, are employed in this paper. A similar procedure is recommended when the centigrade temperature scale or an absolute temperature scale is used.

[10] Loc. cit., p. 187.

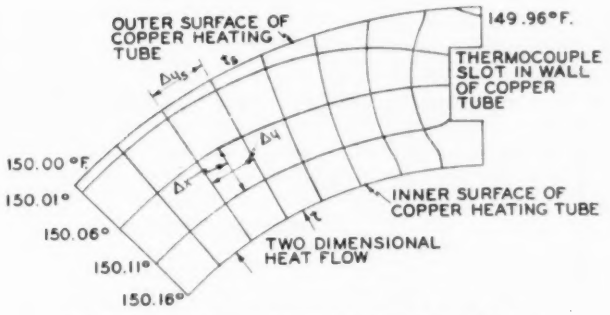


FIG. 8 TEMPERATURE FIELD IN COPPER TUBE WALL

with shunt served to determine the heating current. Voltmeter readings were also taken for each run as a check.

Any portions of the heat input which are not given up from the heating surface to the flowing air by convection will be called heat losses. They might be due to the following:

(*a*) Radiation from the heating surface of the specimen to the room.

(*b*) Conduction and convection from the paper rings at both ends of the specimen.

(*c*) Conduction through the wooden nosepiece.

(*d*) Conduction through the downstream end of the heating-coil tube.

(*e*) Conduction and convection through the air space at the downstream end of the specimen.

Loss (*a*) was calculated by Kirchhoff's and Stefan-Boltzmann's laws. Loss (*b*) was found, considering the paper rings as straight sheets protruding from a copper base at known temperature and exposed to the same air flow and at the same coefficient of heat transfer as the heating surface of the specimen. The calculation of the heat loss (*c*) was reduced to the problem of radial heat conduction in a hollow hemisphere with the inner surface area equal to the cross-sectional areas of the wooden prongs holding the nosepiece in the heating-coil tube. The inner temperature was measured for several representative runs by means of the thermocouples indicated in Fig. 6.

The heat loss (*d*) down the heating-coil tube was calculated from the temperature gradient, measured by the three thermocouples, shown in Fig. 7, the cross-sectional area of that tube and the thermal conductivity of the stainless steel. From the decrease of the temperature gradient the loss (*e*) was found.

The four losses, (*a*), (*b*), (*c*), and (*e*) together were less than 1.5 per cent of the total heat input. They were calculated for several representative runs throughout the entire velocity range of the experiments, and an average correction of 1.4 per cent was applied to each run.

The heat loss (*d*) was the only one of some weight. It amounted from 1.4 to 5.3 per cent of the heat input and had to be determined individually for each run.

Denoting the area of the heating surface by A, the rate of heat input by q_i, and the sum of the heat losses by q_j, the average surface temperature by t_s, and the temperature of the bulk of the air stream by t_a, the coefficient of heat transfer by convection is found from the equation

$$h = \frac{q_i - q_j}{A(t_s - t_a)} \quad \ldots\ldots\ldots\ldots\ldots\ldots [2]$$

EXPERIMENTAL RESULTS

The experimental results are represented in Figs. 9 to 13, inclusive. They comprise 92 experiments under seven different starting conditions. Six of these were obtained by using the different starting pieces described in Table 1, and the seventh occurred when no particular care was taken to insure a continuous surface in gluing the paper ring in place. Sixteen runs were taken with this somewhat rough junction and twelve when the junction had been carefully smoothed with wax.

The range of the experiments is shown in Table 2.

TABLE 2 RANGE OF EXPERIMENTS

Item	Symbol	Units	Minimum	Maximum
Lengths ratio	L_{st}/L_{tot}		0.101	0.606
Air velocity	v_a	ft/sec	9.8	148.0
Air temperature	t_a	°F	43.0	83.5
Reynolds number	N_{Re}		45300	1450000
Heat input	q_i	B/hr	42.9	362.0
Heat losses	q_j	B/hr	2.0	9.0
Heat transferred by convection	q_s	B/hr	39.5	353.5
Surface temperature	t_s	°F	110.8	146.9
Temperature difference	$t_s - t_a$	F	55.8	86.6
Coefficient of heat transfer by convection	h	$Bhr^{-1}ft^{-2}F^{-1}$	2.55	26.2
Nusselt number	N_{Nu}		126	2660
Nusselt number for $L_{st}/L_{tot} = 0$	$(N_{Nu})_0$		146	2420

For each run the Reynolds number, N_{Re}, and Nusselt number, N_{Nu}, were calculated from the following equations of definition

$$N_{Re} = \frac{v_a L_{tot}}{\nu} \quad \ldots\ldots\ldots\ldots\ldots\ldots [3]$$

and

$$N_{Nu} = \frac{hL_{tot}}{k} \quad \ldots\ldots\ldots\ldots\ldots\ldots [4]$$

where ν is the kinematic viscosity and k the thermal conductivity of the air.

Since the characteristics of the boundary layer at any point depend on the total length from the start of hydrodynamic action to the point under consideration, the two dimensionless groups were formed with L_{tot} and not L_{th} as characteristic length. The former has been previously defined as $L_{tot} = L_{st} + L_{th}$. The definition of the starting length L_{st} is based on the fiction that every surface element of the starting piece was placed on a cylindrical surface having the radius of the heating cylinder. This is correct for the cylindrical sections of the starting pieces, but somewhat arbitrary, though reasonable for the nose portions. It can be assumed that L_{st} is a fair equivalent of the starting length of a plane surface.

Also the choice of temperatures at which ν in Equation [3] and k in Equation [4] should be taken is rather arbitrary. However, it is of secondary importance only because the temperature differences used were not too high (see Table 2). Since the Reynolds number is influenced by no other temperature but t_s in the starting section and partly by the same in the heating section, the kinematic viscosity ν was taken at this temperature. The thermal conductivity k, on the other hand, enters the process only in the heating section and depends a good deal on the film temperature $t_f = (t_a + t_s)/2$. Therefore it was taken at this temperature.

Figs. 9 to 13, inclusive, show plots of N_{Nu} versus N_{Re} for the various cases of a constant ratio, L_{st}/L_{tot}. The influence of the Prandtl number does not appear since all runs were made with air at virtually the same Prandtl number.

According to these figures the transition to turbulence was generally finished at $N_{Re} = 300{,}000$, with the rough junction, however, already at $N_{Re} = 100{,}000$ (see Fig. 12). It is striking that the relatively small roughness of the joint was sufficient to increase N_{Nu} by almost 10 per cent.

Fig. 13 shows the thermal behavior of the specimen in the laminar range and the starting of the transition in the runs where the ellipsoidal and the long conical nosepieces were used.

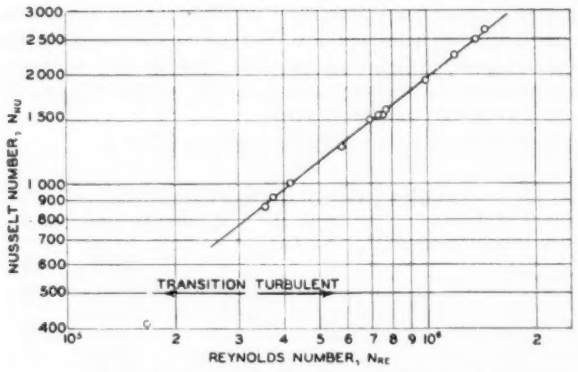


FIG. 9 EXPERIMENTAL DATA FOR $L_{st}/L_{tot} = 0.606$

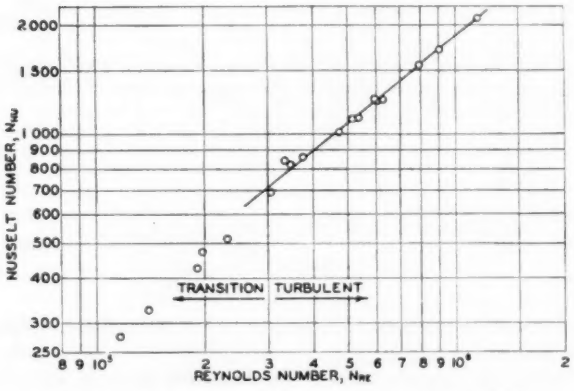


FIG. 10 EXPERIMENTAL DATA FOR $L_{st}/L_{tot} = 0.508$

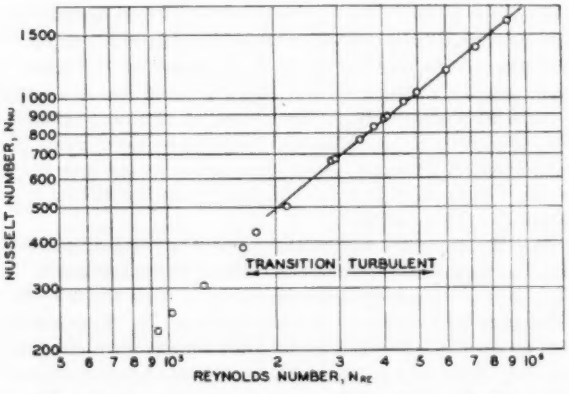


FIG. 11 EXPERIMENTAL DATA FOR $L_{st}/L_{tot} = 0.347$

CORRELATION AND ANALYSIS OF THE RESULTS

Mean Heat Transfer. In Fig. 14 the Nusselt number is plotted versus L_{st}/L_{tot} for two constant values of N_{Re} in the turbulent range. These curves can be represented by an equation of the type

$$N_{Nu} = C_0(N_{Re})^m[1 + C_1(L_{st}/L_{tot})^n] = C(N_{Re})^m \ldots [5]$$

or for N_{Re} = const

$$N_{Nu} = C_2 + C_3(L_{st}/L_{tot})^n \ldots [6]$$

Determining the constants from the experimental data, the following equation for the turbulent region of the boundary layer was obtained

$$N_{Nu} = 0.0280(N_{Re})^{0.80}[1 + 0.40(L_{st}/L_{tot})^{2.75}] \ldots [7]$$

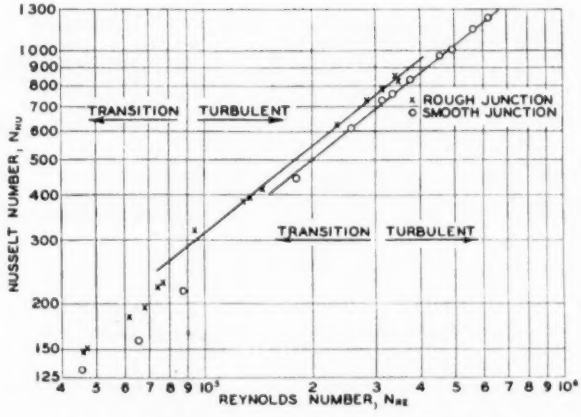


FIG. 12 EXPERIMENTAL DATA FOR $L_{st}/L_{tot} = 0.101$

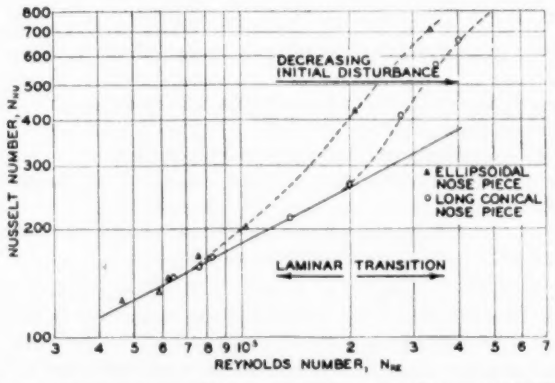


FIG. 13 EXPERIMENTAL DATA FOR $L_{st}/L_{tot} = 0.122$ AND 0.220 WITH ELLIPSOIDAL AND CONICAL NOSEPIECES

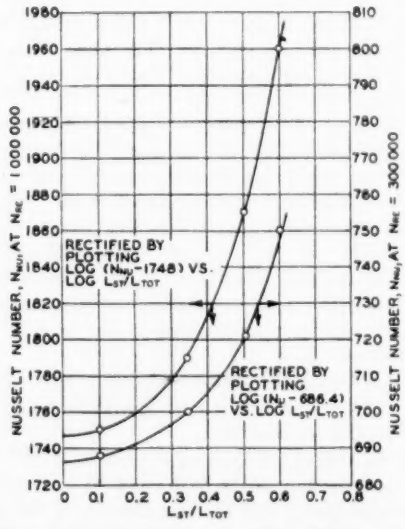


FIG. 14 EXPERIMENTAL DATA AT TWO CONSTANT REYNOLDS NUMBERS FOR HEMISPHERICAL NOSEPIECES

If the thermal and hydrodynamic actions start at the same point, Equation [7] reduces to

$$N_{Nu} = 0.0280(N_{Re})^{0.80} \ldots [8]$$

Fig. 15 shows a correlation of the experimental data based on these equations.

Whereas Equations [5] to [8], inclusive, hold only for fully established turbulence, there will also be an influence of the hydrodynamic starting length on the heat transfer for a laminar boundary layer. However, the present experimental arrangement allowed going back to Reynolds numbers in the streamline range only when $L_{st}/L_{tot} \geqq 0.220$. In this range the influence upon the turbulent layer would be only 0.6 per cent as a maximum, according to Equation [7]; no influence could be

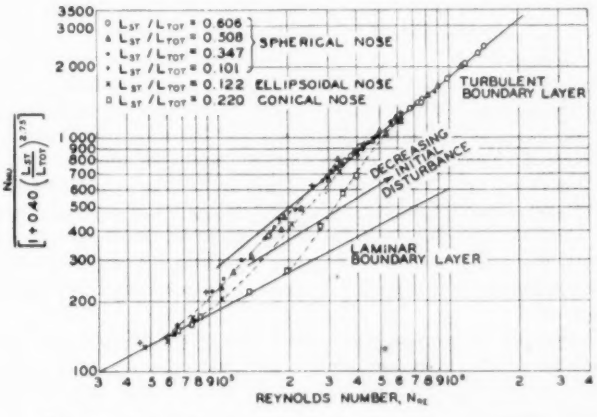


FIG. 15 FINAL CORRELATIONS OF EXPERIMENTAL DATA

observed in the mentioned range of laminar layers. The results of these tests were represented by the equation

$$N_{Nu} = 0.590(N_{Re})^{0.5} \quad \ldots\ldots [9]$$

Fig. 15 shows clearly the effect of the laminar and turbulent layers on the heat transfer. As could be predicted from the theory of boundary layers, there is no sharp critical Reynolds number but a transition, depending on the initial disturbances and the shape of the nosepieces. Increasing N_{Re}, the transition starts and ends earlier with spherical than with ellipsoidal nose and last with the long conical nosepiece. The cylindrical part of the starting length had no appreciable influence on the transition when the nosepiece was the same (spherical). In the fully developed turbulent range the points for all starting pieces fall into one line.

Local Heat Transfer. Information about the influence of hydrodynamic starting sections on the local coefficients of heat transfer is of considerable interest[11] and can be obtained from Equations [5] and [7]. However, since differentiation of an empirical equation is a delicate matter, the accuracy of the result should not be overestimated.

Considering a surface of arbitrary total length, L_{tot}, and constant starting length, L_{st}, and referring to the denotations in Fig. 16, Equation [5] can be written as

$$(N_{Nu})_{x,m} = C_0 (N_{Re})_x^m \left[1 + C_1 \left(\frac{x_1}{x}\right)^n\right] \quad \ldots\ldots [10]$$

where x is an arbitrary distance from the leading edge in the range from $x = x_1 = L_{st}$ to $x = L_{tot}$, the subscript x stands for this distance, the subscript x, m for the mean between $x = x_1$ and $x = x$.

Hence Equation [10] can be written as

$$\frac{h_{x,m}\, x}{k} = C_0 \left(\frac{v_a x}{\nu}\right)^m \left[1 + C_1 \left(\frac{x_1}{x}\right)^n\right] \quad \ldots\ldots [11]$$

[11] Capt. M. Tribus, Air Technical Service Command, Wright Field, Dayton, Ohio, directed our attention to this fact.

Let q' be the rate of heat transferred over the length $x - x_1$, from a surface of unit width, by virtue of the temperature difference $\theta_s = t_s - t_a$; then

$$q'/\theta_s = h_{x,m}\,(x - x_1) \quad \ldots\ldots [12]$$

Substituting $h_{x,m}$ from Equation [11] and differentiating with respect to x

$$h_x = \frac{dq'}{\theta_s dx} = kC_0 \left(\frac{v_a}{\nu}\right)^m x^{m-1} \left[m + (1-m)\frac{x_1}{x} - (n-m)C_1 \left(\frac{x_1}{x}\right)^n + (1+n-m)C_1 \left(\frac{x_1}{x}\right)^{n+1}\right] \quad \ldots\ldots [13]$$

q' is a function of x and $h_{x,m}$; but $h_{x,m}$, for given x_1, is a function of x only. Hence q' is a function of x and dq' is a perfect differential.

Substituting the numerical values of C_1, m, and n from Equation [7]

$$(N_{Nu})_x = \frac{h_x \cdot x}{k} = C_0 (N_{Re})_x^{0.8} \left[0.8 + 0.2\frac{x_1}{x} - 0.78\left(\frac{x_1}{x}\right)^{2.75} + 1.18\left(\frac{x_1}{x}\right)^{3.75}\right] \quad \ldots\ldots [14]$$

The local Nusselt number at the start of the heating section is obtained by taking $x = x_1 = L_{st}$. Substituting this in Equation [14]

$$(N_{Nu})_{x=L_{st}} = 1.4\, C_0 (N_{Re})_{x=L_{st}}^{0.8} \equiv (N_{Nu})_{L_{st}/L_{tot}\,=\,1} = 0.0392\,(N_{Re})_{x=L_{st}}^{0.8}$$

as could be expected, considering the form and figures of Equation [7]

For $L_{st} = 0$ or $L_{tot} = \infty$, that is, $x_1/x = 0$

$$(N_{Nu})_{x=\infty} = 0.8\, C_0 (N_{Re})_{x=\infty}^{0.8} \equiv 0.8\,(N_{Nu})_{L_{st}/L_{tot}\,=\,0} = 0.0224 (N_{Re})_{x=\infty}^{0.8}$$

These are the limits in which $(N_{Nu})_x$ may vary owing to the influence of starting length.

The local Nusselt number at the end of the heating length is obtained by taking $x = L_{tot}$. In the present experiments L_{st}/L_{tot} was varied from 0.101 to 0.606. For these two cases Equation [14] yields the local Nusselt numbers

$$(N_{Nu})_{x=L_{tot}} = 0.819\, C_0 (N_{Re})^{0.8} \text{ and } 0.905\, C_0 (N_{Re})^{0.8}$$

respectively, to be compared with the mean Nusselt numbers $N_{Nu} = 1.0007\, C_0 (N_{Re})^{0.8}$ and $1.1005\, C_0 (N_{Re})^{0.8}$, respectively.

The latter value is still considerably below the highest possible maximum $1.4\, C_0 (N_{Re})^{0.8}$, whereas the lower limit $C_0 (N_{Re})^{0.8}$ has virtually been reached in the present experiments.

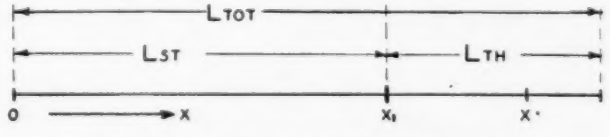


FIG. 16 DENOTATIONS OF LENGTH SECTIONS

Influence of Surface Curvature in General. It will have to be proved by further experiments how far the present results can be applied to surfaces of other curvatures and especially to plane plates. However, an estimate of the influence of curvature on the heat transfer can be obtained in the following way:

It is known that the temperature field and velocity field in a fluid flowing along a surface are almost similar. This had been assumed already by Osborne Reynolds and has been proved ex-

perimentally for the flow in a tube by Pannell (9) and on a plane surface by Éliás (10). Let y be the co-ordinate in the direction perpendicular to the surface, with $y = 0$ at the surface and $y = b$ at the imagined interface between boundary layer and bulk of the flow. The velocities and temperatures at those limits may be $v = 0$ and $v = v_b$, $t = t_s$ and $t = t_a$, respectively. Then because of the existing analogy

$$\frac{\theta}{\theta_s} = \frac{t - t_a}{t_s - t_a} = \frac{v_a - v}{v_a}$$

The rate of heat given up from a plane surface of width W to air in parallel flow between the limits $x = L_{at}$ and $x = x$ is

$$q_p = \int_0^b W\rho c_p v(t - t_a)dy = \int_0^b W\rho c_p \theta_s (v - v^2/v_a)dy \quad [15]$$

The corresponding rate of heat given up by a cylindrical surface of circumference $W = 2\pi r$ to air in parallel flow is

$$q_c = \int_0^b \rho c_p 2\pi(r + y)v(t - t_a)dy = \int_0^b W\rho c_p \theta_s (1 + y/r)(v - v^2/v_a)dy \quad [16]$$

Using the same symbols for v and b in both equations involves the assumption that these quantities are not different for flow parallel to a cylinder or to a plane plate. This assumption seems to give a fair approximation, even for relatively thick boundary layers, according to an observation of Eckert and Weise which will be discussed later on.

Then, according to Equations [15] and [16], the coefficient of heat transfer on a cylinder can be found by multiplying the coefficient for a plane surface by the factor

$$F = 1 + \frac{N - M}{M} = \frac{N}{M} \quad [17]$$

where

$$M = \int_0^b (v - v^2/v_a)dy \text{ and } N = \int^b (1 + y/r)(v - v^2/v_a)dy$$

Influence of Surface Curvature in the Laminar Range. For the laminar section of the boundary layer, the velocity distribution is exactly known from the calculations of Blasius. According to Pohlhausen (11) a close approximation is obtained by the equations

$$v = \left(\frac{2y}{b} - \frac{2y^3}{b^3} + \frac{y^4}{b^4}\right) v_a \quad [18]$$

and

$$b = 5.83\, x(N_{Re})_x^{-0.5} \quad [19]$$

Equation [19] represents the true thickness of the boundary layer and not the so-called displacement thickness for which, according to Pohlhausen, the factor 1.75 instead of 5.83 would have to be entered.

Substituting from Equation [18] in [17] and integrating yields

$$M = \frac{142}{315} bv_a$$

$$N - M = \frac{5}{126} \frac{b^2}{r} v_a$$

and

$$F = 1 + \frac{25}{284} \frac{b}{r} \quad [20]$$

where r is the radius of the surface, 0.054 ft in our case.

According to Equations [19] and [20], the correction factor F increases linearly with x and inverse linearly with $\sqrt{(N_{Re})_x}$. The extreme case in our experiments occurred with $L_{tot} = 0.759$ ft (ellipsoidal nosepiece) at $N_{Re} = 46{,}200$ (see Fig. 13). By susbstitution in Equations [19] and [20] $b = 0.0207$ ft and $F = 1.0338$ were found. Hence in our most extreme case a 3.4 per cent higher value had to be expected for the cylinder than for the plane plate.

From Fig. 13 it is seen that this is just the order of magnitude of scattering of our data. So, the differences of the coefficients of heat transfer for cylindrical and plane surfaces, if any, are in the limits of our accuracy. Should, however, really no difference exist in our range, then this would have the following consequence:

A layer of the bulk flow of unit thickness adjacent to the surface of the boundary layer at $y = b$ has a greater volume on the cylinder than on the plane surface of equal area. Hence its wiping capacity will also be greater and the thickness b may be reduced. Therefore, b in Equation [16] would be smaller than in Equation [15]. However, if Equation [18] were still holding for the velocity distribution, $(dv/dy)_{y=0}$ and, consequently, also $-(dt/dy)_{y=0}$ would become steeper which would mean a greater heat transfer. Hence in this case Equation [18] would have to be replaced by an equation giving a less steep velocity slope at $y = 0$.

Influence of Surface Curvature in the Turbulent Range. Referring to the turbulent section of the boundary layer, again Equations [15], [16], and [17] can be used. Equation [18] may be replaced by

$$v = (y/b)^{1/7} v_a \quad [21]$$

This is von Kármán's well-known equation which, notwithstanding its approximative character, may be used here, for the following reason: According to experiments about the flow in cylindrical tubes by Nikuradse (12), the exponent in Equation [21] decreases from $1/6$ to less than $1/10$ with increasing Reynolds number (13). However, it is not known how the Reynolds numbers for unbounded flow on surfaces are correlated to those for the flow in tubes. The range of turbulent flow covered in the present experiments ($N_{Re} \approx 300{,}000$ to $1{,}500{,}000$) may correspond to the range between the so-called upper critical number in tubes, $N_{Re} \approx 10{,}000$ or $20{,}000$ (see (14)[12] and (15)[13]) to $N_{Re} \approx 75{,}000$, in which range the exponent of Equation [21] equals about $1/7$.

Applying an equation of von Kármán (16), the thickness of the boundary layer can be expressed by

$$b = 0.366\, x'(N_{Re'})_{x'}^{-0.2} \quad [22]$$

where

$$x' = x - x_0$$

$$(N_{Re'})_{x'} = \frac{v_a x'}{\nu}$$

and $x = x_0$ is defined as that distance from the leading edge at which fully established turbulence should start in order to bring the boundary layer to the same thickness b at $x = x_{cr}$ which it actually attains in the laminar range (see Fig. 1). In other words, extending the turbulence curve in Fig. 1 to the left, would lead to $b = 0$ at a fictitious distance $x = x_0$.

Hence for $x = x_{cr}$ Equations [19] and [22] would yield the same b so that

$$5.83\, x_{cr} \left(\frac{v_a x_{cr}}{\nu}\right)^{-0.5} = 0.366\,(x_{cr} - x_0)\left[\frac{v_a(x_{cr} - x_0)}{\nu}\right]^{-0.2}$$

Solving for x_0 yields

[12] Loc. cit., p. 34.
[13] Loc. cit., p. 172.

$$x_0 = x_{cr}\left[1 - 31.82\left(\frac{v_a x_{cr}}{\nu}\right)^{-3/8}\right] \quad [23]$$

From Equations [22] and [23] by some transformation

$$b = 0.366\, x \left\{1 - \frac{x_{cr}}{x}\left[1 - 31.82\left(\frac{v_a x_{cr}}{\nu}\right)^{-3/8}\right]\right\}^{0.8}\left(\frac{v_a x}{\nu}\right)^{-0.2}$$

or

$$b = 0.366\, x \left\{1 - \frac{(N_{Re})_{cr}}{(N_{Re})_x}\left[1 - 31.82\,(N_{Re})_{cr}^{-3/8}\right]\right\}^{0.8}(N_{Re})_x^{-0.2} \quad [24]$$

The thickness b increases with increasing x and with decreasing $(N_{Re})_{cr}$ up to a maximum which would occur at $(N_{Re})_{cr} = 2908$.

One extreme case in our experiments occurred with a cylindrical starting piece having a hemispherical nose ($L_{tot} = 1.69$ ft) and with $(N_{Re})_{cr} \approx 50{,}000$ and $N_{Re} \approx 1{,}500{,}000$ (see Fig. 15). Using these values in Equation [24], $b = 0.0353$ ft was found.[14]

Substituting now from Equation [21] in [17] and integrating

$$M = \frac{7}{72}\, b v_a$$

$$N - M = \frac{7}{240}\,\frac{b^2}{r}\, v_a$$

and

$$F = 1 + \frac{3}{10}\,\frac{b}{r} \quad [25]$$

With $b = 0.0353$ and $r = 0.054$, $F = 1.196$ was obtained.

The other extreme occurred with the spherical nose without cylindrical starting piece ($L_{tot} = 0.74$ ft) and with $N_{Re} = (N_{Re})_{cr} = 50{,}000$. Here $b = 0.01347$ ft and $F = 1.075$ were found.

This means that for the used cylindrical surface, heat-transfer coefficients, 7.5 to 19.6 per cent higher than for a plane surface may be expected. Should actually no differences exist, then the same consequences would have to be considered as drawn when dealing with the corresponding differences for a laminar boundary layer.

Comparison With Previous Work

The present results will be compared with theoretical and experimental results of previous investigators. Most of them can be reduced to starting length zero and represented by the form

$$N_{Nu} = C_0 (N_{Re})^m \quad [26]$$

Values of C_0 and m, according to different workers, are shown in Tables 3 and 4, each in chronological sequence. For comparison it may first be noted that the present experiments led to $C_0 = 0.590$ and $m = 0.50$ for laminar boundary layer, and to $C_0 = 0.0280$ and $m = 0.80$ for turbulent layer.

Strangely enough, the first notable investigations on this subject date less than 25 years back and are purely theoretical.

For the laminar range Pohlhausen (17) in 1921 derived the following equation

$$N_{Nu} = 0.664 (N_{Re})^{1/2} (N_{Pr})^{1/3} \quad [27]$$

Substituting $N_{Pr} = 0.71$ which holds for the average temperature of the present experiments, Equation [27] takes the form of Equation [26] with $C_0 = 0.592$ and $m = 0.50$ in excellent agreement with the result of the present experiments. Incidentally, Pohlhausen's derivation is one of the few existing direct solutions of Stokes's equations of viscous flow in combination with the equation of thermal conduction in moving fluids. The attempts made by Boussinesq, King, and Aichi before Pohlhausen, and by Lévêque afterward, failed because of oversimplified assumption. Lévêque, for instance, assumed a linear velocity distribution, instead of Equation [18]. These mathematical attacks of the problem have been thoroughly described by Drew (18).

For turbulent flow, Latzko (19), also in 1921, derived the following equation for the rate of heat flow:

$$q_{L_{st}/L_{tot}=0} = 0.0356\, L_{tot} W \rho c_p \nu \theta_s (N_{Re})^{-0.2}$$

which can readily be converted to

$$N_{Nu} = 0.0356\, (N_{Re})^{0.80} N_{Pr} \quad [28]$$

This equation has the same exponent as was found in our experiments. Since Latzko's derivation is restricted to $N_{Pr} = 1$, it holds only approximately when $N_{Pr} \neq 1$. However, substituting $N_{Pr} = 0.71$, $C_0 = 0.0253$ was obtained, our experimental value of C_0 being about 11 per cent higher, in satisfactory agreement with the presented theoretical analysis concerning the influence of surface curvature to the results.

Latzko's derivation is based on von Kármán's form of Equation [24], that is, $(N_{Re})_{cr}/(N_{Re})_x$ is neglected compared to 1. Instead of this, the fictitious point $x = x_0$ (see Fig. 1) may be taken as zero point of a system, denoted by prime signs; then

$$N_{Nu} = \frac{h L_{tot}}{k} = \frac{h(L_{tot} - x_0)}{k}\,\frac{L_{tot}}{L_{tot} - x_0} = N_{Nu}'\,\frac{L_{tot}}{L_{tot} - x_0}$$

and from Equation [28], using $N_{Pr} = 0.71$

$$N_{Nu}' = 0.0253\,(N_{Re}')^{0.8}$$

After some transformations

$$N_{Nu} = 0.0253\left\{1 - \frac{(N_{Re})_{cr}}{N_{Re}}\left[1 - 31.82(N_{Re})_{cr}^{-3/8}\right]\right\}^{-0.2} N_{Re}^{0.8} = C_0 N_{Re}^{0.8} \quad [29]$$

The expression in curved brackets increases with N_{Re} and with decreasing $(N_{Re})_{cr}$ up to the previously mentioned maximum. Hence again the extreme occurred with $N_{Re} = 1{,}500{,}000$ and $(N_{Re})_{cr} = 50{,}000$. The calculation yields $C_0 = 0.0254$, compared to Latzko's value 0.0253. Hence $C_0 = 0.0280$, observed with our cylindrical surface, is about 10 per cent higher than the theoretical value for a plane surface, in satisfactory agreement with the average (13.5 per cent) of the theoretical values, calculated at the end of the preceding section.

TABLE 3 CONSTANT C_0 AND EXPONENT m OF EQUATION [26] FOR LAMINAR BOUNDARY LAYER

Authors	Kind of work	Surface	C_0	m
Pohlhausen	Theoretical	Plane	0.592	0.50
Fage and Falkner	Experimental	Plane	0.750	0.50
Jakob and Dow	Experimental	Cylindrical, diam, 1.3 in.	0.590	0.50

TABLE 4 CONSTANT C_0 AND EXPONENT m OF EQUATION [26] FOR TURBULENT BOUNDARY LAYER

Authors	Kind of work	Surface	C_0	m
Latzko	Theoretical	Plane	0.0253	0.80
Juerges	Experimental	Plane	0.0452	0.775
Juerges	Experimental[a]	Plane	0.0322	0.80
Colburn	Correlation	Plane	0.0320	0.80
Seibert	Theoretical	Plane	0.0423	0.786
Seibert	Theoretical[a]	Plane	0.0349	0.80
Jakob and Dow	Experimental	Cylindrical, diam, 1.3 in.	0.0280	0.80

[a] Results reduced to $m = 0.80$.

[14] This procedure involves the assumption that Equation [22] can be used through and past the transition region (see Fig. 1); the same assumption will be made in deriving Equation [29]. Within the transition region, however, it yields only approximation results.

Only one year after these two papers the first publication of Juerges' experiments appeared (20), followed in 1924 by a detailed report (21). He measured the heat transfer from a vertical plane copper plate, 1.64 ft × 1.64 ft, to air flowing parallel to the surface at velocities up to 100 ft/sec, surface temperatures from 115 to 140 deg F, and air temperature of 68 deg F. The hydrodynamic starting length in these experiments was 1.02 ft. For a polished plate Juerges found

$$h = 0.4997\, v^{0.775} \quad \ldots\ldots\ldots\ldots\ldots\ldots [30]$$

which can be generalized into our standard form, Equation [26], by using the term in square brackets of Equation [7]. In this way $C_0 = 0.0452$ and $m = 0.775$ were obtained. In order to simplify the comparison with our values, Juerges' results were also represented with $m = 0.80$. This led to $C_0 = 0.0322$ and to values of N_{Nu} which differ less than ±2 per cent from the values obtained by Equation [30] between $N_{Re} = 300{,}000$ and 1,500,000, but are 15 per cent higher than our values based on $C_0 = 0.0280$.

Much of this difference is probably due to a blunt leading edge of the starting surface.[15] As mentioned in the first section of this paper, turbulence will start immediately past such an edge with the effect that considerably more heat is transferred in the thermal section. Therefore, Juerges' results cannot be directly compared with the present ones in which a laminar boundary layer preceded the turbulent layer. Reference is made to Fig. 12 which shows that even a small roughness in the starting section can have an effect on the Nusselt number of similar order of magnitude as was observed between Juerges' and the authors' experiments.

In the experiments of Éliás (10) which covered almost the same range of v_a and θ_a as those of Juerges, a starting piece 3.94 in. long, with sharpened leading edge and heating lengths of 3.94 to 15.76 in. were used.

Éliás represented his experimental results by curves of the velocity and temperature distribution in the boundary layer and used these curves to determine the heat carried past in the air stream by graphical integration, according to the first part of Equation [15].

From Éliás' reported values we calculated the heat-transfer coefficients and the Reynolds and Nusselt numbers with L_{tot} as characteristic length. Again the starting length was considered by means of Equation [7].

Éliás' and Juerges' data, reduced to $L_{st} = 0$, are compared with the present results in Fig. 17. It is seen that most of Éliás' points fall in between Juerges' and our line. They show an unusual steep increase with Reynolds number ($m > 0.9$). Seibert (22) considers this as evidence of not yet finished transitions and in fact, the points of Fig. 17 fit rather well with our observations in the state of transition shown in Fig. 15. The instability due to transition and the indirect determination of heat convection from flow and temperature measurements in the boundary layer may account for the considerable scattering of the points.[16]

In contrast to the steep increase of Éliás' values, Taylor and Rehbock (23) arrived at an improbably small exponent ($m = 0.725$), using Juerges' data and their own experiments, performed on a 6-in-sq copper plate at 75 to 235 ft/sec air velocity. Unfortunately, they did not indicate the value of the hydrodynamic starting length in their experiments. For this reason a comparison with present results is not possible.

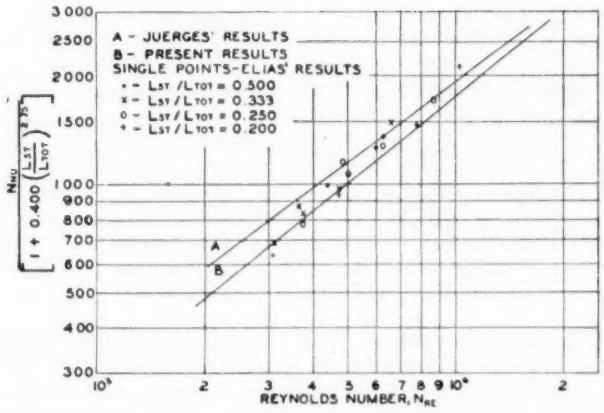


FIG. 17 COMPARISON OF PRESENT RESULTS FOR A TURBULENT BOUNDARY LAYER WITH PREVIOUS EXPERIMENTS WITH FLAT PLATES

Fage and Falkner (24) determined the heat transfer to air from platinum foils, 0.00127 cm thick, 1.27 cm wide, and from 0.333 to 1.27 cm long, in the laminar-boundary range. The air velocity was varied from 20 to 70 ft/sec, the air temperature was 72° F, the foil temperature was about 340°F. For the exponent m the usual value of 0.5 was found, for the constant C_0, however, the high value 0.750. This may be ascribed to the fact that with such short heating surfaces, the starting-section conditions prevail. Latzko (19)[17] analyzing an analogous case in the turbulent range found that in the starting section the constant C_0 should be higher than in established turbulence, whereas the exponent would remain unchanged. The same may hold for the laminar range.

Colburn (25) accepted Pohlhausen's equation and made a correlation according to which Fage and Falkner's results would be in agreement with this equation. Because we had found their values to be 27 per cent too high, we asked Dr. Colburn for an explanation of this discrepancy, and he found that due to a slide-rule error, all points representing Fage and Falkner's values in his Fig. 20 should be raised by 21 per cent. This explains the greatest part of the mentioned difference.

Colburn further correlated the experimental results of Juerges and Éliás in the turbulent region and expressed them by the following equation

$$\frac{h\,L_{th}}{k} = 0.0321 \left(\frac{v_a L_{th}}{\nu}\right)^{0.80}$$

Using[18] Juerges' $L_{st}/L_{tot} = 0.383$ and converting from ν_f at film temperature (about 98°F) as used by Colburn, to ν at bulk temperature (about 68°F), correcting also for the influence of the starting length, according to Equation [7], Colburn's equation is reduced to our standard form with $m = 0.80$ and

$$C_0 = 0.0321(L_{tot}/L_{th})^{0.2}[1 + 0.40(L_{st}/L_{tot})^{2.75}]^{-1}(\nu/\nu_f)^{0.8} = 0.0320$$

Seibert (22) also adopted Pohlhausen's theory in the laminar range. For turbulence he used the modification by which Prandtl had extended his original theory to the case of $N_{Pr} \neq 1$ and in particular, ten Bosch's (3) extensions of this theory. Employing

[15] In Fig. 2 of Juerges' paper no sharpening or smoothing of the edge is indicated. Since many minor details are dealt with in the paper, the author would certainly have mentioned any sort of treatment of the leading edge.

[16] The accuracy of the experiments is unfavorably influenced by the difficulty to co-ordinate a considerable number of measured local velocities and temperatures to the exact values of y in a total range of boundary thickness of about 1/2 in. only. Moreover, the surface temperature was measured by thermocouples placed on the back side of the heating box. It is very questionable whether sufficient symmetry existed on both sides; the surface thermocouples themselves may have disturbed such symmetry.

[17] Loc. cit., p. 283, Fig. 7A.

[18] Éliás' range of ratios was $L_{st}/L_{tot} = 0.2$ to 0.5.

Seibert's exponent $m = 0.786$, but correcting[19] for the difference in N_{Pr}, the value $C_0 = 0.0423$ was obtained. His results can be covered also by using $m = 0.80$ and $C_0 = 0.0349$. Comparison then shows that Seibert's theoretical values of N_{Nu} for plane plates are 25 per cent higher than those measured on a cylinder in the present work. This is at variance with Latzko's theoretical results which cannot be expected to be seriously in error at a Prandtl number so close to unity. However, Seibert's relation is based on different assumptions which would need to be checked, as he states himself.

Seibert also indicated the following formula for the transition state

$$N_{Nu} = 0.00178\ (N_{Re})^{0.956} \quad [31]$$

It yields too low values compared to the transition lines in Fig. 15.

Also his method of inserting Éliás' results between a maximum and minimum of Nusselt numbers is questionable. The heating section gives up more heat (q_{max}) in actual measurements if an unheated starting length exists, than would be the case if the same total length were held at the same temperature excess θ_s as the heating section was in the actual experiments (q_{min}). Seibert, however, uses a sort of mixing rule for Nusselt numbers in his Equation [20], which is not correct.

Using Equation [7], the following is obtained

$$\frac{q_{min}}{q_{max}} = \frac{[1 - (L_{st}/L_{tot})^{0.8}](1 - L_{st}/L_{tot})}{1 + 0.4(L_{st}/L_{tot})^{2.75}} \quad [32]$$

For the extreme ratios, employed by Éliás, $L_{st}/L_{tot} = 0.2$ and 0.5, Equation [32] yields $q_{min}/q_{max} = 0.901$ and 0.804, respectively, compared to the ratios $(N_{Nu})_{min}/(N_{Nu})_{max} = 0.945$ and 0.713, respectively, calculated according to Seibert, assuming the same exponent, $m = 0.8$. In general, much insight in the mechanism is not obtained by Seibert's method of asking what the heat transfer in a heated section would have been if the starting length had also been heated, whereas Equation [7], rough and improvable as it may be, considers the influence of the starting length in a straightforward way.

Finally, some theoretical and experimental papers may be mentioned which deal with the laminar part of the boundary layer at very high fluid velocity. The authors are Crocco (26), Hilton (27), Eckert and Weise (28), and Eckert and Drewitz (29). The result of these investigations is that Pohlhausen's equation can be applied up to as high speeds as twice the velocity of sound, provided that the temperature of the gas t_a is replaced by the temperature t_i which the unheated and perfectly insulated surface would assume in the gas stream. This temperature may be called "impressed temperature." For $N_{Pr} = 1$, it is found by adding to the ordinary surface temperature the temperature increment due to adiabatic stopping of the gas stream, $\theta_{ad} = v_a^2/(64.4\ Jc_p)$, where J is the mechanical equivalent of heat.[20] For $N_{Pr} \neq 1$, $\theta_i = \theta_{ad}$. $\varphi(N_{Pr})$ is to be added to t_a; values of the function φ are given in Table 5. They are calculated by means of Pohlhausen's theory; the first nine values have been taken from his original paper (17), the last two from Eckert and Weise's paper (28).

Also the heat transfer in the range of turbulent layer can be calculated with the formulas developed for small velocities if t_i is employed instead of t_a.

Hence it may be assumed that the results of the present paper also can be approximately used for high velocities and for other fluids than air if t_a is replaced by t_i.

[19] Seibert's Equation [17] has been used for this slight correction.

[20] For convenience J and c_p are expressed in the dimensions given in the "nomenclature;" the number 64.4, then, is not dimensionless.

TABLE 5 VALUES OF THE FUNCTION (φN_{Pr})

N_{Pr}	0.6	0.7	0.8	0.9	1.0	1.1	Gases
$\varphi(N_{Pr})$	0.77	0.835	0.895	0.95	1.00	1.05	Gases
N_{Pr}	7.0	10.0	15.0	100	1000		Liquids
$\varphi(N_{Pr})$	2.515	2.965	3.535	6.7	12.9		Liquids

Concerning the influence of curvature of the surface in a plane perpendicular to the main flow direction, Eckert and Weise made some tests on wires with 0.2 to 2 mm diam in the range of v_a = 400 to 1000 ft per sec air velocity, corresponding to N_{Re} = 50,000 to 500,000. Denoting the temperature excess of the unheated wire by θ_i, it was found that the ratio θ_i/θ_{ad} depended only slightly on the ratio b/r which was varied from 0.1 to 1. In the same range, Hilton measured θ_i/θ_{ad} for a plane plate and found only about 3 per cent higher values than Eckert and Weise on the thin wires. This is in good agreement with the deviation of 3.4 per cent calculated by the present authors for $b/r = 0.384$ in the fourth part of the previous section of this paper.

Summary and Conclusions

1 Systematic measurements of the heat transfer by convection from a cylinder to a fluid flowing parallel to its axis allow a simpler technique than measurements with plane surfaces. They should yield results which can be applied to plane surfaces up to rather high Reynolds numbers when cylinders with reasonably large diameters are used.

2 The present experiments were performed with air flowing parallel to an electrically heated smooth cylinder, 8 in. long, 1.3 in. diam. Wooden nosepieces of different shapes and cylindrical pieces of different lengths served as unheated starting sections. The heated lengths were varied from 40 to 90 per cent of the total length, air velocities from 10 to 150 ft per sec, corresponding to Reynolds numbers from 45,000 to 1,500,000, based on the total length as a characteristic dimension.

3 The results of the measurements could be expressed by the equations

$$N_{Nu} = 0.590\ (N_{Re})^{0.50} \quad [9]$$

and

$$N_{Nu} = 0.0280\ (N_{Re})^{0.80}[1 + 0.40\ (L_{st}/L_{tot})^{2.75}] \quad [7]$$

for laminar and turbulent boundary layers, respectively, where N_{Nu} and N_{Re} are Nusselt and Reynolds numbers with the total length L_{tot} as characteristic length, and L_{st} as the starting length. Transition to turbulence started between N_{Re} = 50,000 and 200,000 and was virtually finished between 250,000 and 600,000 (see Fig. 15). The start and end of transition depended mainly on the shape of the nose. Even a slight roughness in the starting section caused a considerable increase of the heat transfer.

4 An equation for the local Nusselt number was derived from Equation [7] by differentiation.

5 The influence of the cylinder curvature has been studied theoretically, considering similarity between velocity and temperature distribution and assuming that the velocity distribution in curved boundary layers is the same as for plane layers. Under these assumptions 8.8 b/r and 30 b/r would be the percentages by which the Nusselt numbers for cylinders would exceed those for plane plates in the ranges of laminar and turbulent layers, respectively, where r is the cylinder radius and the thickness of the boundary layer b is taken from Equations [19] and [24], respectively. It was further shown what changes in the theory might be advisable if such differences should not actually occur.

6 Using these differences in the laminar range of the present experiments, the heat transfer should be higher by 0 to 3 per cent than for a plane boundary layer. This seems to be in agreement with some recent experiments which Hilton and Eckert and Weise performed at much higher air velocities and smaller lengths. Fage and Falkner, however, obtained 25 per cent higher

values in tests on short platinum foils. No difference was found between the present experimental data on cylindrical layers and those from Pohlhausen's generally recognized theory for plane boundary layers.

7 Applying the theory to the turbulent range of the present experiments, a 7 to 20 per cent larger heat transfer would be expected than for plane plates. Actually the present experimental data are about 10 per cent higher than those obtained from Latzko's theory for a plane surface. On the other hand, they are 20 per cent lower than those according to a theory of Seibert which is based on different and not yet proved assumptions. Experiments in the range of turbulent boundary layers on plane surfaces have been performed by Juerges and Éliás. A blunt leading edge seems to have caused relatively high heat-transfer values in Juerges' experiments 15 per cent above the present data. Éliás' results are between Juerges' and the present data.

8 A recent paper of Eckert and Drewitz shows that Pohlhausen's theory holds up to twice the velocity of sound if the fluid temperature is replaced by a temperature impressed on the surface because of adiabatic stopping and friction of the stream. The same is claimed for the turbulent boundary layer.

It may be concluded also that the results of the present investigation can be approximately employed up to much higher than the experimental velocities and applied to other fluids when the equilibrium fluid temperature is replaced by the "impressed temperature" of the surface. However, it is planned to extend the experiments to velocities higher than those used in the present experiments.

9 According to the authors' theoretical reasoning, the heat transfer on plane surfaces should be somewhat smaller than given by Equation [7]. This would be in agreement with Latzko's theory. Seibert's theory for plane surfaces, however, leads to higher values of heat transfer than observed on the cylinder. It is intended to decide this controversial question by experiments with cylinders of different diameters, varying also the starting and heating lengths. For the time being it seems to be safe to use Equation [7] tentatively for any convex smooth surface with arbitrary starting section when the radius of curvature in a plane perpendicular to the main flow direction is more than $^1/_2$ in. The influence of the starting length, in particular, should be nearly the same for cylinders and plane surfaces.

BIBLIOGRAPHY

1 "Measurements of the Velocity Distribution in the Boundary Layer Along a Plane Surface," by B. C. van der Hegge Zijnen, Thesis, Delft, Holland, 1924; also Mededeeling no. 6, Lab. voor Aerodynamica en hydrodynamica, Tech. Hoogeschool, Delft, Holland

2 "Die Geschwindigkeitsverteilung in der Grenzschicht an einer Eingetauchten Platte," by M. Hansen, *Zeitschrift für angewandte Mathematik und Mechanik*, vol. 8, 1929, p. 185.

3 "Die Waermeuebertragung," by M. ten Bosch, third edition, Julius Springer, Berlin, Germany, 1936.

4 "Grenzschichtentheorie," by W. Tollmien; in Handbuch der Experimentalphysik, W. Wien and F. Harms, vol. 4, part 1, Leipzig, Germany, 1931.

5 "Hydraulics," by R. L. Daugherty, fourth edition, McGraw-Hill Book Company, Inc., New York, N. Y., 1937.

6 "Thermodynamic Properties of Steam," by J. H. Keenan and F. G. Keyes, John Wiley & Sons, Inc., New York, N. Y., 1936.

7 "Allgemeine Grundlagen der Waermeuebertragung," by M. Jakob, in *Der Chemie-Ingenieur*, A. Eucken and M. Jakob, vol. 1, part 1, Berlin, Germany, 1933; reprinted by Edwards Brothers, Ann Arbor, Mich., 1943.

8 "Standard Handbook for Electrical Engineers," by A. E. Knowlton, seventh edition, McGraw-Hill Book Company, Inc., New York, N. Y., 1941.

9 "Experiments in Heat Transmission in the Case of Air Blowing Through a Heated Pipe," by J. R. Pannell, Great Britain Advisory Committee for Aeronautics, London, England, Technical Reports 1916–1917 (R. & M. No. 243); also see "Elements of Heat Transfer and Insulation," by M. Jakob and G. A. Hawkins, John Wiley & Sons, Inc., New York, N. Y., 1942, Fig. 15–1.

10 "Die Waermeuebertragung einer geheizten Platte an strömende Luft," by Franz Éliás, *Zeitschrift für angewandte Mathematik und Mechanik*, vol. 9, 1929, pp. 434–453; vol. 10, 1930, pp. 1–14; also Abhandlungen aus dem Aerodynam. Institut an der Techn. Hochschule Aachen, no. 9, 1930, pp. 10–39; (translated in U. S., N.A.C.A. Technical Memorandum No. 614, Washington, D. C., April, 1931.)

11 "Zur naeherungsweisen Integration der Differentialgleichung der laminaren Grenzschicht," by K. Pohlhausen, *Zeitschrift für angewandte Mathematik und Mechanik*, vol. 1, 1921, pp. 252–268.

12 "Gesetzmaessigkeiten der turbulenten Stroemung in glatten Rohren," by J. Nikuradse, *V.D.I. Forschungsheft*, no. 356, Berlin, Germany, 1932.

13 "Velocity Distribution of Fluids in Turbulent Flow," discussion by M. Jakob, Trans. A.I.C.E., vol. 36, 1940, pp. 657–662.

14 "Applied Hydro- and Aeromechanics Based on Lectures of L. Prandtl," by O. G. Tietjens, McGraw-Hill Book Company, Inc., New York, N. Y., 1934.

15 "Fluid Mechanics for Hydraulic Engineers," by H. Rouse, first edition, second impr., McGraw-Hill Book Company, Inc., New York, N. Y., 1938.

16 "Ueber laminare und turbulente Reibung," by Th. von Kármán, *Zeitschrift für angewandte Mathematik und Mechanik*, vol. 1, 1921, pp. 234–252.

17 "Der Waermeaustausch zwischen festen Koerpern und Fluessigkeiten mit kleiner Reibung und kleiner Waermeleitung," by E. Pohlhausen, *Zeitschrift für angewandte Mathematik und Mechanik*, vol. 1, 1921, pp. 115–121.

18 "Mathematical Attacks on Forced-Convection Problems: A Review," by Th. B. Drew, Massachusetts Institute of Technology, vol. 67, no. 59, Pub. serial no. 869 (Department of Chemical Engineering, serial no. 282), 1931.

19 "Der Waermeuebergang an einen turbulenten Fluessigkeits- oder Gasstrom," by H. Latzko, *Zeitschrift für angewandte Mathematik und Mechanik*, vol. 1, 1921, pp. 268–290 (translated in U. S., N.A.C.A. Technical Memorandum No. 1068, Washington, D.C., 1944).

20 "Die Kuehlung einer ebenen Wand durch einen Luftstrom," by W. Nusselt and W. Juerges, *Gesundheits-Ignenieur*, vol. 45, 1922, p. 641.

21 "Der Waermeuebergang an einer ebenen Wand," by W. Juerges, Beihefte zum Gesundheits-Ingenieur, Reihe 1, Beiheft 19, Munich and Berlin, Germany, 1924.

22 "Waermeuebertragung von Profilen und Platten," by O. Seibert, Jahrbuch 1938 der deutschen Luftfahrtforschung, pp. II245–II256 (translated in U. S., N.A.C.A. Technical Memorandum No. 1044, Washington, D. C., 1943).

23 "Rate of Heat Transfer From Finned Metal Surfaces," by C. F. Taylor and A. Rehbock, U. S., N.A.C.A., Technical Note No. 331, Washington, D. C., 1930.

24 "On the Relation Between Heat Transfer and Surface Friction for Laminar Flow," by A. Fage and V. M. Falkner, Great Britain Advisory Committee for Aeronautics, Report and Memorandum No. 1408, 1931.

25 "A Method of Correlating Forced-Convection Heat Transfer Data and a Comparison With Fluid Friction," by A. P. Colburn, Trans. A.I.C.E., vol. 29, 1933, pp. 174–209.

26 "Sulla trasmissione del calore da una lamina piana a un fluido scorrente ad alta velocita," by L. Crocco, *L'Aerotecnica*, 1932, pp. 181–197 (translated in U. S., N.A.C.A., Technical Memorandum No. 690, Washington, D. C., 1932).

27 "Thermal Effects on Bodies in an Air Stream," by W. F. Hilton, Proceedings of the Royal Society of London, England, series A, vol. 168, 1938, pp. 43–56.

28 "Die Temperatur unbeheizter Koerper in einem Gasstrom hoher Geschwindigkeit," by E. Eckert and W. Weise, *Forschung aus dem Gebiete des Ingenieurwesens*, vol. 12, 1941, pp. 40–50.

29 "Der Waermeuebergang an eine mit grosser Geschwindigkeit laengs angestroemte Platte," by E. Eckert and O. Drewitz, *Forschung aus dem Gebiete des Ingenieurwesens*, vol. 11, 1940, pp. 116–124 (translated in U. S., N.A.C.A. Technical Memorandum No. 1045, Washington, D. C., 1943).

(Owing to travel emergency conditions existing when this paper was presented, discussion will be accepted until March 11, 1946)

Temperature-Time Distribution in Rectangular Bars

By W. M. ROHSENOW,[1] M. J. ARONSTEIN,[2] AND A. C. FRANK[2]

Charts for determining temperature-time distribution in flat plates, infinite cylinders, and spheres have been published previously. The purpose of this paper is to amplify the lower end of the curves thus presented, and to give the results in graphical and in tabular form. In addition, the rapid convergence of the series solution is shown, and combined curve sheets for rectangular bars are presented.

Nomenclature

The following nomenclature is used in the paper:

t = temperature
t_i = initial temperature of bar
t_a = temperature of surrounding atmosphere
θ = time
k = coefficient of thermal conductivity
ρ = density
c_p = specific heat at constant pressure
w = half-width of bar in x-direction
u = half-width of bar in y-direction
$a = k/(\rho c_p)$ — thermal diffusivity
h = film coefficient of heat transfer
$b = h/k$
$T = (t - t_a)/(t_i - t_a)$
$T_x = \sum_{n=1}^{\infty} X_n$
X_n = defined in Equation [6]

Note: Any consistent set of dimensions may be used.

Introduction

When a homogeneous solid body at a uniform temperature is suddenly exposed to an atmosphere which is held at some constant temperature different from that of the body itself, heat is exchanged between the body and the atmosphere through a film on the surface of the body. The outer parts of the body approach the temperature of the atmosphere more rapidly than do the inner parts. Heat is transferred between the inner and outer parts of the body by conduction. After an infinite amount of time the solid body is uniformly at the temperature of the surrounding atmosphere.

In engineering applications the useful information concerning this transient-state heat-transfer process is of two forms. In one case it may be desirable to know the temperature distribution existing in a solid body at any instant of time; in the other case it may be desirable to know the temperature-time curve for any point in the body. An example of these cases is the hardening of a solid steel body. The solid body is heated to a uniform high temperature; then it is suddenly quenched in oil or water. The inner parts cool more slowly than the outer parts; hence there results a body of varying degrees of hardness throughout its volume. In order to determine the stresses produced in the bar by this unequal cooling, it is necessary to know the temperature distribution at any instant of time; and, in order to determine the degree of hardness at any point in the bar, it is necessary to know the temperature-time curve at that point.

Charts for determining temperature-time distribution in infinite flat plates, infinite cylinders, and spheres have been published by Gurney and Lurie (1, 2),[3] Hottel (3) and Newman (4). The purpose of this paper is to enlarge the lower end of these curves presenting the results in graphical and in tabular form; to show the rapid convergence of the series solution; and to present combined curve sheets for rectangular bars.

Since the number of variables is large and the calculations are laborious when applying the equations resulting from the mathematical solution of the problem to any given case, the series of charts constructed permits a convenient solution under any set of given conditions. From these charts the temperature-time-position relationship for two specific cases, namely, the square bar and the 2 × 1 rectangular bar, was found as a method of illustrating the procedure. It is hoped that these specific solutions along with the solution for the infinite flat plate will give a general idea of the range of values to be encountered.

Infinite Flat Plate

Consider an infinite flat plate (infinite in the Y- and Z-directions) of thickness $2w$, as shown in Fig. 1. The plate is initially at a uniform temperature t_i and is suddenly exposed to an atmos-

[1] Instructor in Mechanical Engineering, Yale University. Jun. A.S.M.E.

[2] Senior, Navy V-12 College Training Program, School of Engineering, Yale University. Student Mem., A.S.M.E.

Contributed by the Heat Transfer Division of The American Society of Mechanical Engineers.

Discussion of this paper should be addressed to the Secretary, A.S.M.E., 29 West 39th Street, New York, N. Y., and will be accepted until March 11, 1946. Discussion received after the closing date will be returned.

Note: Statements and opinions advanced in papers are to be understood as individual expressions of their authors and not those of the Society, or the U. S. Navy, or Naval Service at large.

[3] Numbers in parentheses refer to the Bibliography at the end of the paper.

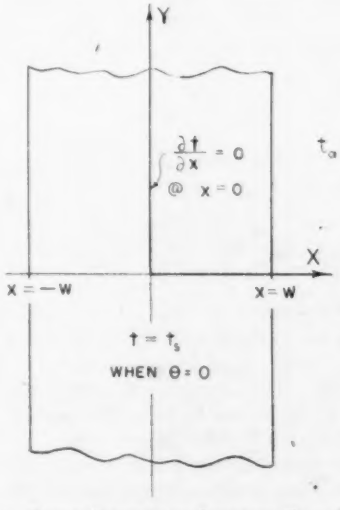


Fig. 1 Cross Section of Infinite Flat Plate

phere of temperature t_a, which may be colder or hotter than t_s. The heat-conduction equation for this case is

$$\frac{\partial t}{\partial \theta} = a \frac{\partial^2 t}{\partial x^2} \quad \ldots\ldots [1]$$

where

$$a = k/(\rho c_p) \quad \ldots\ldots [2]$$

The term a is called the thermal "diffusivity" of the material and is considered to be constant for any given solid material.

The solution of Equation [1] may be found in applied mathematics and in heat-conduction texts such as Carslaw (5). The solution is

$$\frac{t - t_a}{t_s - t_a} = \sum_{n=1}^{\infty} 2e^{-(a\theta/w^2)\delta_n^2} \cdot \frac{\cos \delta_n(x/w)}{\delta_n \csc \delta_n + \cos \delta_n} \quad \ldots\ldots [3]$$

where δ_n, called "eigenwerte," are roots of the equation

$$bw \cot \delta_n = \delta_n \quad \ldots\ldots [4]$$

The first five roots of Equation [4] are shown as a function of bw in Fig. 2. Note that since all are shown on the same ordinate scale, π must be added to the scaled value of δ_2, 2π to δ_3, etc. This arises from the fact that δ_1 varies from 0 to $\pi/2$, δ_2 from $\pi/2$ to $3\pi/2$, etc. Tabular values of these roots may be found in Gröber and Erk (6) and in Jahnke and Emde (7).

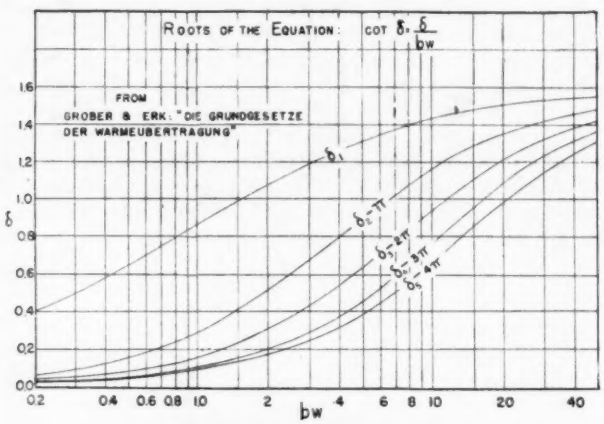


FIG. 2 VALUES OF EIGENWERTE, δ

In order to simplify the series notation of Equation [3], let it be written in the form

$$T_x = \sum_{n=1}^{\infty} X_n \quad \ldots\ldots [5]$$

where

$$X_n = 2e^{-(a\theta/w^2)\delta_n^2} \frac{\cos \delta_n(x/w)}{\delta_n \csc \delta_n + \cos \delta_n} \quad \ldots\ldots [6]$$

The first three terms of the series, X_1, X_2, and X_3 are shown in Fig. 3. The term X_3 is insignificant for values of $a\theta/w^2$ greater than 0.05, and term X_2 is insignificant for values of $a\theta/w^2$ greater than 0.20. The sum of the first three terms of the series Equation [5], T_x, is plotted in Figs. 4 through 8, for values of x/w = 0, 0.25, 0.50, 0.75, and 1, respectively.

These charts represent the solution of Equation [3] to determine the temperature-time distribution at 5 planes in one half of the infinite flat plate. The computed values obtained by adding

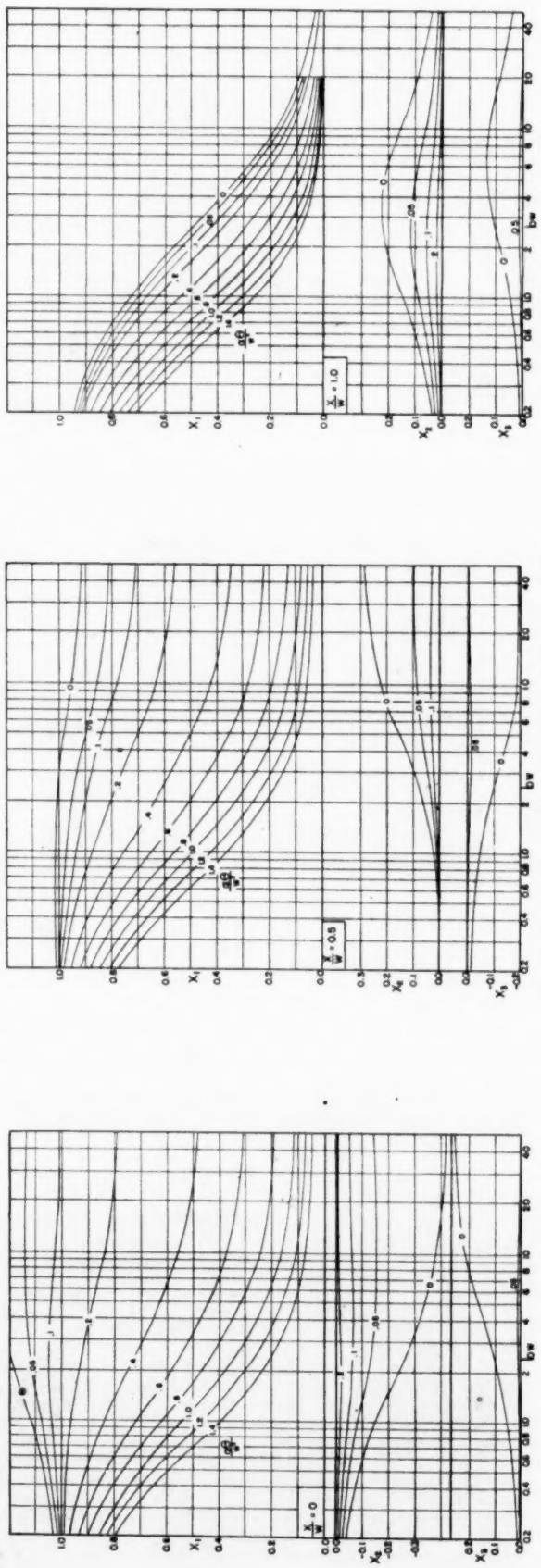


FIG. 3 FIRST THREE TERMS OF SERIES SOLUTION, T_x

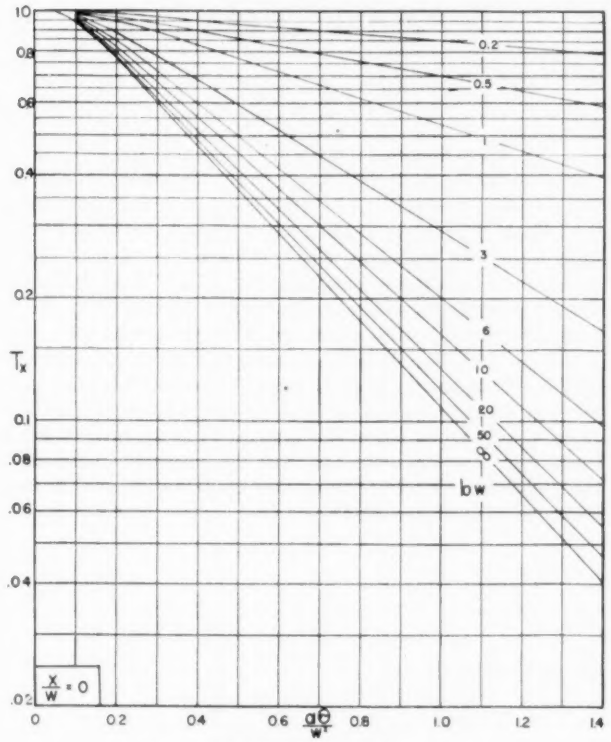


FIG. 4 T_x VERSUS $a\theta/w^2$ FOR $x = 0$

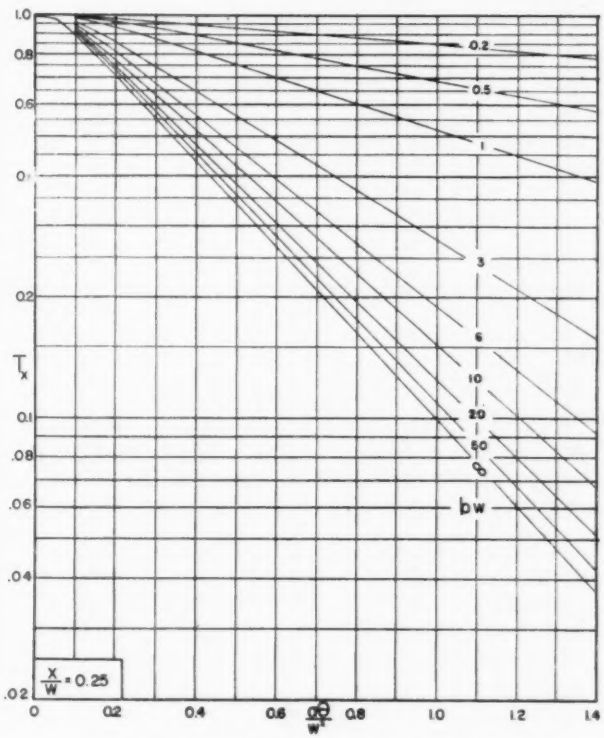


FIG. 5 T_x VERSUS $a\theta/w^2$ FOR $x = 0.25$

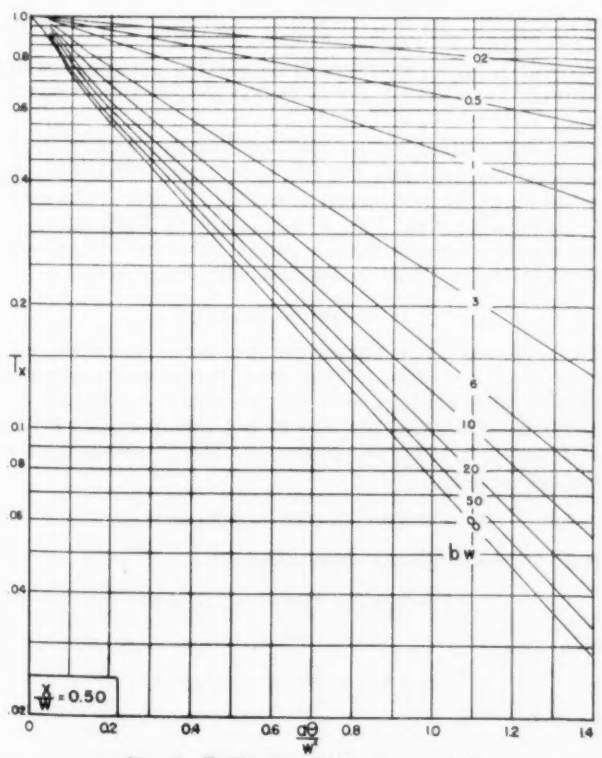


FIG. 6 T_x VERSUS $a\theta/w^2$ FOR $x = 0.50$

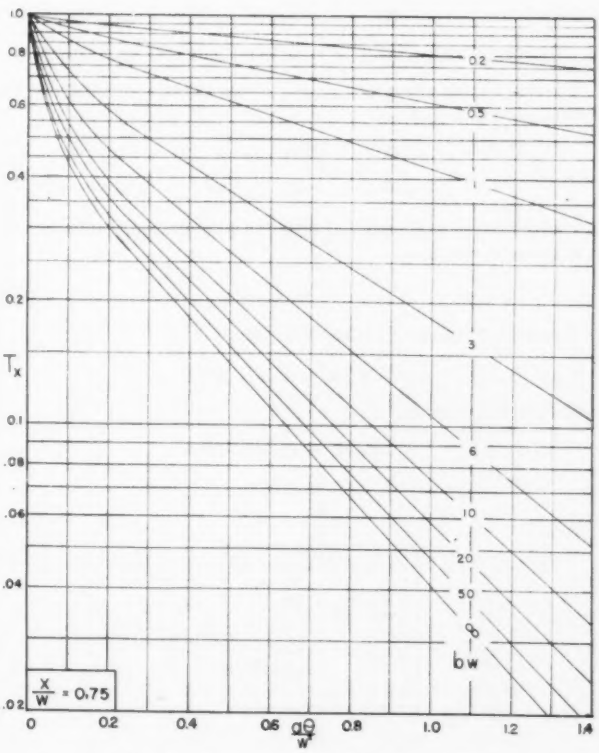


FIG. 7 T_x VERSUS $a\theta/w^2$ FOR $x = 0.75$

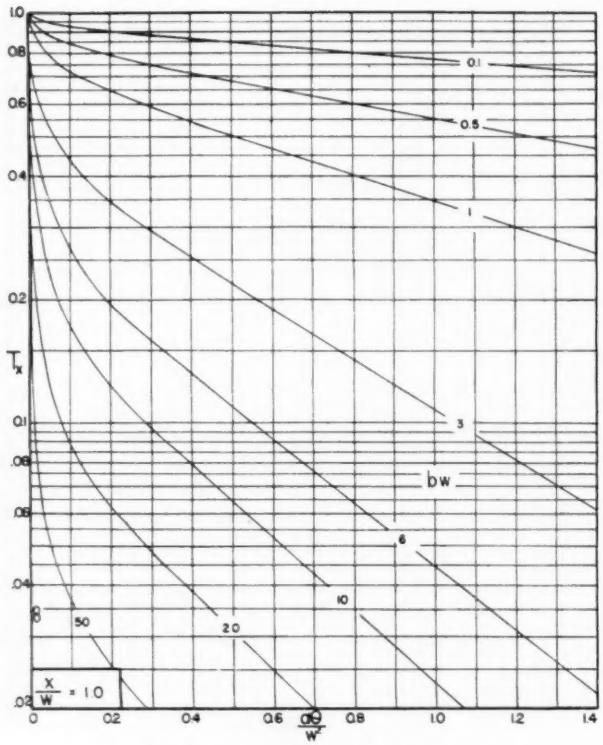


FIG. 8 T_x VERSUS $a\theta/w^2$ FOR $x = 1.0$

the first three terms of the series in Equation [5] are tabulated in Tables 1 to 5, inclusive.

INFINITE RECTANGULAR BAR AND RECTANGULAR BLOCK

The heat-conduction equation for the infinite rectangular bar represented in Fig. 9 is

$$\frac{\partial t}{\partial \theta} = a\left(\frac{\partial^2 t}{\partial x^2} + \frac{\partial^2 t}{\partial y^2}\right) \quad [7]$$

By substituting in the partial differential equation, Equation [7], it may be shown that

$$T = T_x \cdot T_y \quad [8]$$

is its solution, where T_x is the solution of

$$\partial t/\partial \theta = a(\partial^2 t/\partial x^2)$$

and T_y is the solution of

$$\partial t/\partial \theta = a(\partial^2 t/\partial y^2)$$

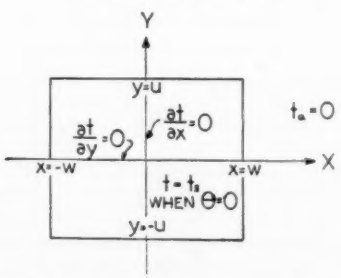


FIG. 9 QUARTER-CROSS SECTION OF INFINITE RECTANGULAR BAR

This is known as Newman's rule (4). Similarly, for a cube the differential equation is

$$\partial t/\partial \theta = a\left(\frac{\partial^2 t}{\partial x^2} + \frac{\partial^2 t}{\partial y^2} + \frac{\partial^2 t}{\partial Z^2}\right) \quad [9]$$

the solution of which is

$$T = T_x \cdot T_y \cdot T_z \quad [10]$$

where the T functions are defined as in Equation [8].

The functions T_x, T_y, T_z are given by Equations [3] and [5], and are plotted in Figs. 4 to 8, inclusive. In order to determine the solution T for any point in a bar or a block, evaluate T_x from Equation [5] (or from Figs. 4 to 8, inclusive) for each of the coordinate directions, thus obtaining T_x, T_y, T_z. The product of these three is the solution as indicated in Equation [10]. For an infinite rectangular bar, only T_x and T_y need be obtained.

A set of curves has been constructed in Figs. 11 and 12 for the solution of Equation [8] at the inner points of the infinite rectangular bar shown in Fig. 10. Fig. 11 is for a square bar, and Fig. 12, for a rectangular bar of side dimensions in the ratio of 2 to 1. In the case of a square bar, only 6 of the 9 positions indicated in Fig. 10 need be considered since there are three identical pairs of points because of symmetry.

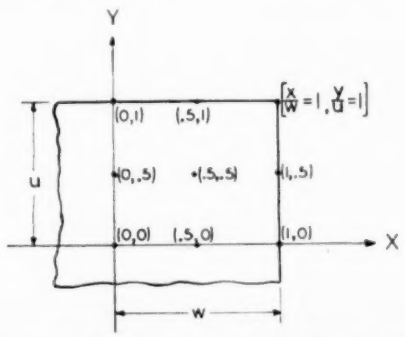


FIG. 10 QUARTER CROSS SECTION OF INFINITE RECTANGULAR BAR SHOWING POINTS FOR WHICH COMBINED SOLUTION IS PRESENTED

It will be noticed that for positions along the x-axis, the curves for the rectangular bar, Fig. 12, lie approximately midway between the curves for the square bar, Fig. 11, and the curves for the infinite flat plate, Figs. 4 to 8, inclusive. These curves are intended to indicate the range of possible values in rectangular-bar problems and to indicate a graphical method of procedure.

ILLUSTRATIVE EXAMPLE

Consider an infinite rectangular steel bar of dimensions $w = 0.125$ ft and $u = 0.250$ ft. Determine the value of temperature ratio t/t_a at the point $x/w = 0.5$, $y/u = 0.5$ at the time $\theta = 0.0271$ hr. For a steel bar, $k = 25$ Btu/(hr)(sq ft) (deg F/ft), $\rho = 493$ lb/cu ft, and $c_p = 0.11$ Btu/(lb) (deg F); hence the thermal diffusivity is

$$a = 25/(0.11 \times 493) = 0.461 \text{ sq ft/hr}$$

If the film coefficient of heat transfer is

$$h = 200 \text{ Btu/(hr) (sq ft) (deg F)}$$

then

$$b = h/k = 200/25 = 8.0 \text{ ft}^{-1}$$

and

$$bw = 1.0,\ bu = 2.0,\ a\theta/w^2 = 0.8,\ a\theta/u^2 = 0.2$$

From Fig. 6 or Table 3 for

$$a\theta/w^2 = 0.8 \text{ and } bw = 1.0,\ T_x = 0.564$$

TABLE 1 VALUES OF T_x FOR $x/w = 0$

$a\theta/w^2$ / bw	0	.05	.1	.2	.4	.6	.8	1.0	1.2	1.4
.2	1.007	1.001	.999	.988	.956	.922	.888	.856	.824	.794
.5	1.010	1.001	.997	.974	.903	.830	.762	.700	.642	.590
1	1.016	1.001	.994	.952	.832	.719	.620	.535	.461	.398
3	1.038	.998	.982	.894	.684	.516	.388	.292	.220	.166
6	1.074	.999	.974	.855	.602	.418	.290	.202	.140	.0973
10	1.078	.998	.968	.829	.558	.371	.246	.164	.109	.0724
20	1.090	.997	.960	.804	.518	.331	.212	.135	.0857	.0558
50	1.098	.996	.954	.785	.492	.306	.192	.119	.0738	.0459
∞	1.103	.996	.949	.773	.475	.290	1.77	.108	.0660	.0404

TABLE 2 VALUES OF T_x FOR $x/w = 0.25$

$a\theta/w^2$ / bw	0	.05	.1	.2	.4	.6	.8	1.0	1.2	1.4
.2	1.000	1.000	.998	.984	.952	.916	.883	.851	.819	.790
.5	.997	1.000	.994	.964	.892	.819	.752	.691	.634	.582
1	.995	1.000	.986	.935	.814	.702	.606	.523	.450	.389
3	.976	.994	.964	.861	.655	.493	.371	.279	.210	.159
6	.961	.992	.946	.812	.568	.394	.274	.191	.132	.0918
10	.948	.989	.935	.781	.523	.348	.231	.154	.102	.0678
20	.931	.986	.920	.752	.482	.308	.197	.126	.0798	.0520
50	.920	.983	.910	.732	.456	.284	.178	.110	.0674	.0425
∞	.916	.982	.900	.717	.439	.268	.164	.100	.0611	.0373

TABLE 3 VALUES OF T_x FOR $x/w = 0.50$

$a\theta/w^2$ / bw	0	.05	.1	.2	.4	.6	.8	1.0	1.2	1.4
.2	.996	.997	.989	.970	.935	.901	.868	.836	.805	.776
.5	.998	.994	.975	.933	.856	.786	.722	.663	.608	.559
1	.995	.986	.950	.880	.757	.654	.564	.486	.419	.362
3	.980	.966	.888	.757	.566	.427	.321	.241	.182	.137
6	.975	.946	.842	.682	.470	.326	.226	.158	.109	.0760
10	.983	.932	.810	.640	.421	.280	.186	.124	.0823	.0547
20	.995	.913	.776	.598	.378	.243	.155	.0990	.0628	.0409
50	1.010	.898	.753	.572	.353	.220	.138	.0854	.0530	.0330
∞	1.020	.886	.735	.553	.336	.205	.125	.0764	.0467	.0314

TABLE 4 VALUES OF T_x FOR $x/w = 0.75$

$a\theta/w^2$ / bw	0	.05	.1	.2	.4	.6	.8	1.0	1.2	1.4
.2	1.0054	.984	.961	.946	.909	.874	.842	.812	.781	.753
.5	1.015	.966	.930	.877	.799	.733	.673	.618	.567	.521
1	1.026	.933	.870	.784	.667	.574	.495	.428	.368	.318
3	1.072	.844	.722	.585	.430	.323	.243	.183	.138	.104
6	1.107	.767	.619	.471	.319	.221	.154	.107	.0742	.0516
10	1.105	.686	.533	.393	.255	.169	.112	.0749	.0498	.0331
20	1.142	.650	.495	.359	.225	.144	.0919	.0586	.0372	.0242
50	1.136	.604	.453	.325	.198	.123	.0774	.0480	.0298	.0185
∞	1.114	.570	.424	.303	.182	.111	.0677	.0413	.0253	.0155

TABLE 5 VALUES OF T_x FOR $x/w = 1.0$

$a\theta/w^2$ / bw	0	.05	.1	.2	.4	.6	.8	1.0	1.2	1.4
.2	.987	.952	.933	.907	.870	.838	.806	.778	.748	.721
.5	.963	.886	.846	.792	.719	.659	.605	.556	.510	.469
1	.923	.791	.724	.655	.545	.470	.405	.349	.301	.260
3	.780	.538	.442	.349	.254	.191	.143	.108	.0814	.0614
6	.610	.350	.265	.197	.132	.0916	.0635	.0440	.0313	.0219
10	.457	.232	.171	.123	.0789	.0525	.0348	.0232	.0154	.0102
20	.272	.124	.0881	.0622	.0387	.0248	.0159	.0101	.0064	.0042
50	.116	.050	.0363	.0252	.0152	.0094	.0059	.0037	.0023	.0014
∞	0	0	0	0	0	0	0	0	0	0

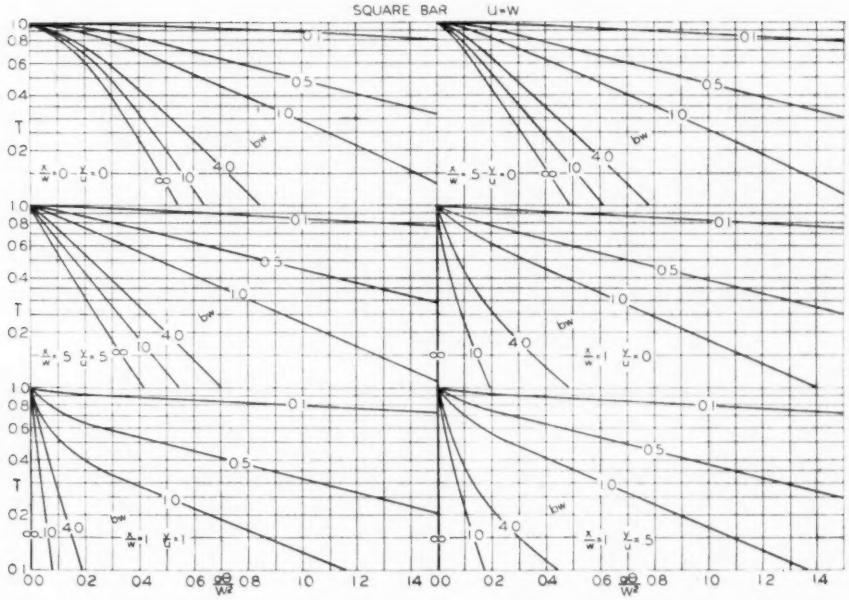


FIG. 11 COMBINED SOLUTION T, FOR POINTS IN INTERIOR OF AN INFINITE SQUARE BAR; ($u = w$)

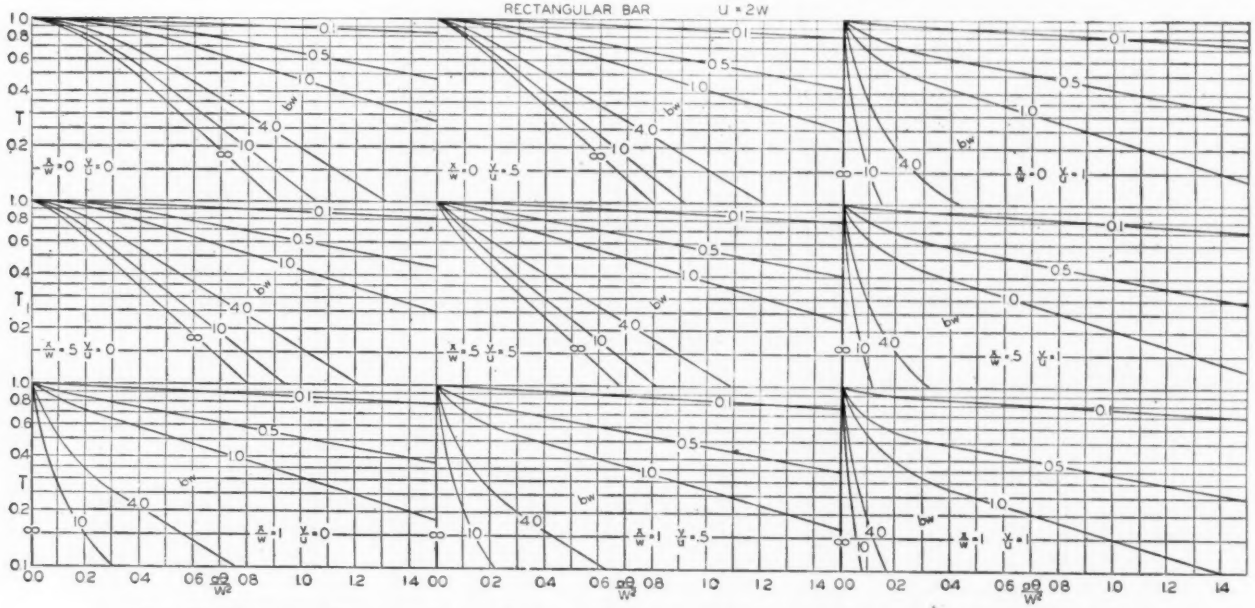


FIG. 12 COMBINED SOLUTION T, FOR POINTS IN INTERIOR OF AN INFINITE RECTANGULAR BAR; ($u = 2w$)

and for

$a\theta/u^2 = 0.2$ and $bu = 2.0$, $T_y = 0.80$ (estimated by interpolation).

Then

$$T = T_x \cdot T_y = 0.564 \times 0.80 = 0.451$$

This same result is obtained directly from curves for $x/w = 0.5$ and $y/u = 0.5$ in Fig. 12. For $a\theta/w^2 = 0.8$ and $bw = 1.0$, the value of T is seen to be 0.45, which is a close check.

CONCLUSIONS

Solutions to two-place accuracy may be obtained by interpolating in the curve sheets Figs. 4 to 8, inclusive, and Figs. 11 and 12, which were constructed from the values of T_x in Tables 1 to 5, inclusive.

More accurate solutions are obtained by solving Equation [3] directly. The first term of the series in Equation [3] is sufficient for three-place accuracy when $a\theta/w^2$ is greater than 0.3. The first two terms should be used for three-place accuracy when $0.1 < a\theta/w^2 < 0.3$.

ACKNOWLEDGMENT

The authors are gratefully indebted to Prof. T. B. Drew and Prof. W. J. Wohlenberg for many helpful suggestions in this work.

BIBLIOGRAPHY

1 "Heating and Cooling of Solid Shapes," by H. P. Gurney;

unpublished monograph, Massachusetts Institute of Technology Library.

2 "Charts for Estimating Temperature Distributions in Heating or Cooling Solid Shapes," by H. P. Gurney and J. Lurie, *Industrial and Engineering Chemistry*, vol. 15, 1923, pp. 1170–1172.

3 "Heat Transmission," by W. H. McAdams, McGraw-Hill Book Company, Inc., New York, N. Y., Chapter 2, second edition, 1942.

4 "Heating and Cooling Rectangular and Cylindrical Solids," by A. B. Newman, *Industrial and Engineering Chemistry*, vol. 28, 1936, pp. 545–548.

5 "Mathematical Theory of Conduction of Heat in Solids," by H. S. Carslaw, Dover Publications, New York, N. Y., 1945.

6 "Die Grundgesetze Der Wärmeübertragung," by H. Gröber and S. Erk, J. Springer, Berlin, Germany, second edition, 1933.

7 "Funktionentafeln," by E. Jahnke and F. Emde, Dover Publications, New York, N. Y., 1943.

8 "Heat Transfer," Supplementary Notes (unpublished), by L. M. K. Boelter, V. H. Cherry, and H. S. Johnson, University of California Press, 1942.

9 "Temperature Distribution in Solids During Heating and Cooling," by E. D. Williamson and L. H. Adams, *Physical Review*, vol. 14, 1919, pp. 99–114.

10 "Applied Mathematics in Chemical Engineering," by T. K. Sherwood and C. W. Reed, McGraw-Hill Book Company, Inc., New York, N. Y., 1939.

(Owing to travel emergency conditions existing when this paper was presented, discussion will be accepted until March 11, 1946)

Logographs

By R. S. TOUR[1]

A different type of chart[2] is presented for graphical solution of equations of the form $T^pU^qV^rW^s = K$. The charts are called "logographs" as distinct from nomographs and depend basically on the addition of logarithms. Logograph charts develop from the fact that a straight line drawn on semilog paper represents a function of the form: $\log y = a + bx$, or $x = c + n \log y$. The construction of logographs is explained and exemplified in the development of a chart for the calculation of heat-transfer coefficients in turbulent flow. As examples of more elaborate logographs, charts are also offered for the turbulent flow of fluids in pipes and for the flow of fluids through sharp-edged orifices. The equations underlying the last two charts represent new forms of the standard expressions and are briefly discussed and their limitations indicated.

TO those who have constructed or used alignment charts involving four or more variables, the attendant difficulties are evident. The reference or blank scales that become part of such nomographs, the length of the scales for wide ranges in the values of the variables, the obliqueness of the intersecting lines that must sometimes be used with resultant inaccuracy, serve to multiply the difficulties. The construction of such alignment charts is also no simple matter since each of the lines requires a special scale laboriously laid out by hand.

These difficulties are particularly evident in nomographs for evaluating heat-transfer expressions wherein the variables may number seven, eight, or more, covering ranges for some of perhaps 10^6. In addition to special scales for each variable there will also be "dummy" scales (or their equivalent) numbering three less than the number of variables. The progressive series of alignments that must be made between the scales, taken in proper order, may make the use of the nomograph so tedious and confusing as to neutralize its value for rapid computations. Especially is this the case if a solution is desired for one of the variables other than that for which the nomograph was originally designed.

A fundamentally different type of chart eliminating most of the objectionable features of nomographs is described in this paper. It is applicable in general to functions expressible in the form

$$T^pU^qV^rW^s = K \quad \ldots\ldots [1a]$$

$$p \log T + q \log U + r \log V + s \log W = \log K \quad \ldots [1b]$$

The T, U, V, W terms represent variables, with p, q, r, s as constant exponents which may be either positive or negative, integers or fractions. The K is a constant, dependent on the function and on the dimensions ascribed to the individual variables. Expressions such as Equation [1a] arise frequently in engineering design and practice, especially in the fields of heat transfer and fluid flow. They lend themselves neatly to a graphical solution based on the addition of logarithms.

The principle involved in the computation charts offered here is based on the fact that the equation of any straight line drawn on semilog co-ordinate paper is of the form

$$\log y = a + bx$$

or

$$x = c + n \log y$$

The location of the line determines the constants c (or a) and the slope of the line defines n (or b). If each of the variables in Equation [1b] be plotted as a straight line on semilog paper with the c and n properly chosen, the linear (x) co-ordinates for any true set of values of the variables may be numerically added to accord with Equation [1b]. It is to be noted that a numerical addition is here substituted for the progressive series of graphical alignments used in nomographs. The process of addition is the quicker for such functions and is not subject to the manipulative errors of a series of alignments. But the chart used in this way is obviously not an alignment chart (i.e., nomograph); it is here descriptively titled a "logograph."

Logograph for Heat Transfer in Turbulent Flow

Recently a nomograph was published (1)[3] for the Dittus-Boelter equation for determining heat-transfer film coefficients with turbulent flow in smooth pipes. The equation used to determine these coefficients is of the Nusselt type and is generally given in any consistent units as

$$h = 0.0243 \frac{k}{D} \left(\frac{Du\rho}{Z}\right)^{0.8} \left(\frac{ZC}{k}\right)^{0.4} \quad \ldots\ldots [2a]$$

This may be rewritten in an alternative form to eliminate fractional exponents

$$\frac{C^2k^3\rho^4u^4}{DZ^2h^5} = 1.18 \times 10^8 \quad \ldots\ldots [2b]$$

In the usual mixed engineering units (specified) this becomes

$$\frac{C^2k^3\rho^4u^4}{DZ^2h^5} = 3.43 \times 10^{-3} \quad \ldots\ldots [2c]$$

C = specific heat, Btu/(lb)(deg F)
k = thermal conductivity, Btu/(sq ft)(hr)(deg F/ft)
ρ = density, pcf
u = linear fluid velocity, fps
D = pipe diameter, in.
Z = viscosity, poises
h = heat-transfer coefficient, Btu/(sq ft)(hr)(deg F)

This equation with its seven variables, six independent, is an example of an expression for which a nomograph is not entirely satisfactory.

---

[1] Department of Chemical Engineering, University of Cincinnati.

[2] The charts (Figs. 1, 2, 3, 4) offered in this paper are simplified tracings from originals made on standard 11-in. × 17-in. three-cycle semilog paper. For convenience in size reduction and in printing, the tracings for this publication carry a minimum of co-ordinate lines. They are thus not satisfactory for computation purposes, but serve here merely to show the construction methods and use of logograph charts. If desired, the reader may transfer the lines shown to standard semi-log paper for more accurate computations. Full-size (11-in. × 17-in.) lithoprinted copies of the original charts are in use at the University of Cincinnati, and a limited number of these lithoprints will be available for distribution on request.

Contributed by the Heat Transfer Division and presented at the Cincinnati Section Meeting, Cincinnati, Ohio, Oct. 2–3, 1945, and at the Annual Meeting, New York, N. Y., Nov. 26–29, 1945, of The American Society of Mechanical Engineers.

Note: Statements and opinions advanced in papers are to be understood as individual expressions of their authors and not those of the Society.

[3] Numbers in parentheses refer to the Bibliography at the end of the paper.

A logograph for making computations from Equation [2c] is shown in Fig. 1. The illustrative example given on the chart shows the general method of using logographs. It is the same example used by Ryant (1) for his alignment chart, wherein it is desired to find the heat-transfer coefficient (h) for hot water flowing at a velocity (u) of 8 fps through 1-in-diameter (D) tubes, the specific heat (C), conductivity (k), density (ρ), and viscosity (Z) of the water being specified. Each of the known variables is in turn located on the logarithmic scale (ordinates) and from the appropriate line for that variable, a reading R (abscissa) is determined. The six R's are numerically added and the sum subtracted from the chart constant A. The result is the R (abscissa) for the remaining variable, in this case the heat-transfer coefficient (h), which is then determined from its line on the chart. Six R's are read, an addition and subtraction made, and the unknown variable (which can be any one of the seven) is determined.

Construction of Logographs

To construct a logograph for some specified function, it is first necessary to rewrite the function in the form of Equation [1a]. Having done this, the following procedure is suggested:

1 Choose semilog paper with N logarithmic cycles to cover some selected range in the magnitude of the variables. This choice is flexible since the range for any variable can be increased from 10^N to 10^{2N} to 10^{3N} by the addition of successive constants to the reading for that variable (see Fig. 1). In general, three-cycle semilog paper is quite satisfactory.

2 Select dimensions of suitable magnitude for each of the variables in Equation [1] so that the same logarithmic scale may serve for all variables. This avoids confusion in the use of the scales. Then modify the value of the constant K in original Equation [1a] to agree with the dimensions which are selected.

3 Transform the modified Equation [1a] into the logarithmic form of Equation [1b]

$$(p \log T) + (q \log U) + (r \log V) + (s \log W) = \log K \quad [3]$$

Although as written here the signs are positive, it should be remembered that some of the exponents (p, q, r, s) may be inherently negative. In the general case, a negative sign can be applied throughout in Equation [3]. The use of the + or — is a matter of convenience; a negative sign throughout leads to a logograph which is a mirror image of that with a positive sign.

4 A scale factor or modulus M for the linear co-ordinates (abcissas) is selected so that the linear divisions will cover some desirable range in the value of the logarithms of the variables. The factor M is used as a multiplier in Equation [3].

$$(Mp \log T) + (Mq \log U) + (Mr \log V) + (Ms \log W) = M \log K \quad [4]$$

The modulus M may be positive or negative and its magnitude is a matter of judgment. Its value controls the slope of all the lines and the relative accuracy of the readings of ordinates versus abscissas. The size of M is limited by the ranges to be covered by the various lines on the chart.

5 Added convenience in using the chart is obtained if all the linear co-ordinates (abscissas) are positive. Accordingly, add some specific positive constant of sufficient magnitude (e, f, g, h) to each of the variable terms of Equation [4]

$$(e + Mp \log T) + (f + Mq \log U) + (g + Mr \log V) + (h + Ms \log W) = e + f + g + h + (M \log K) = A \quad [5]$$

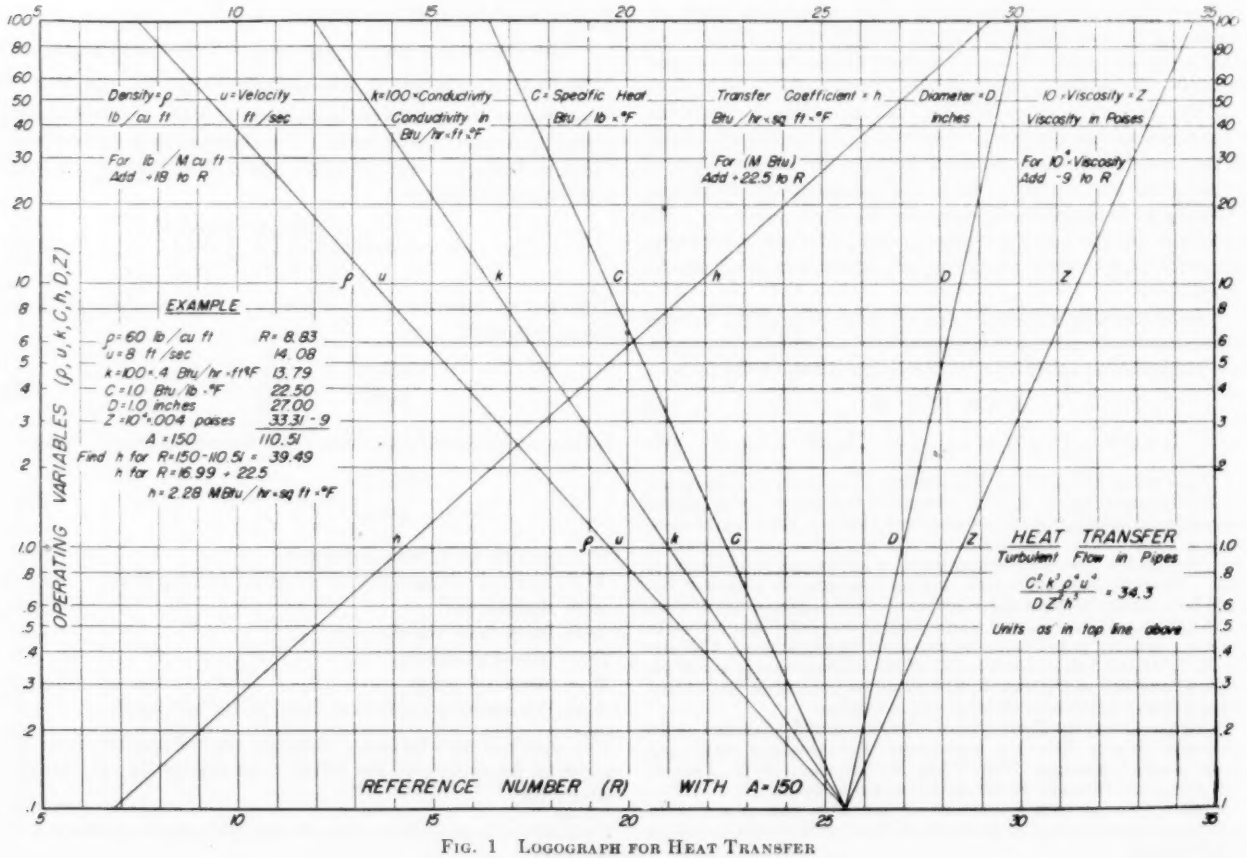


Fig. 1 Logograph for Heat Transfer

A wide choice exists for these addition constants. Their values control the relative locations of the lines on the chart. The constants should be selected so that the lines cross each other as seldom as possible and then not at too small an angle. The sum total A of the constants in Equation [5] should be some round number easily kept in mind, e.g., 150 (as in Fig. 1), and the value of A must be specified on the chart.

6 Each of the separated terms in parentheses in Equation [5] may now be plotted against the linear scale R, each plot resulting in a straight line on the semilog paper, all represented by the generalized expression

$$R_y = C + Mn \log Y$$

Here R_y refers to the abscissa readings for any one of the variables (T, U, V, or W) represented by Y, with n indicating its power (p, q, r, or s), and C the corresponding addition constant (e, f, g, or h). The lines for R_y may be located on the chart as follows: If the logarithmic scale ranges from 10^b at the bottom to 10^t at the top, then the intercepts at the bottom and top of the logograph for each of the variables Y are, respectively

$$R_y = C + (Mn)b \text{ (at bottom)}$$
$$= C + (Mn)t \text{ (at top)}$$

A line joining the bottom and top intercepts for each variable completes the chart.

7 If it is desired to increase the size of the units (or dimensions) of any one of the variables by a factor k, it is only necessary to add to reading R for that variable a quantity $+Mn \log k$. For example, a quantity expressed in inches on the chart may be read as feet by adding $+Mn \log 12 = +1.079Mn$ to the R_y obtained. Conversely, feet may be read as inches if the addition is $+Mn \log (1/12) = -1.079\,Mn$. The signs of M and n must not be neglected. A similar device may be used to change the range for any of the variables, which is equivalent to changing the size of the units for that variable by some power of 10.

8 Some expressions for which a logograph is desired may have one or more variables stated as a function of some more specific variable, e.g., $Y = F(y)$. In such cases the logograph is first designed for Y as described, but the straight line is replaced by a curve, the points for which are calculated so that a reading of y on the logarithmic scale calls for an R_y as determined by $Y = F(y)$, i.e., $R_y = M \log F(y)$.

Construction of Fig. 1. The foregoing directions, as applied specifically to the construction of the logograph in Fig. 1, may serve to clarify the procedure. The function for which the chart is to be designed has been given and the units specified under Equation [2c] as follows

$$\frac{C^2k^3\rho^4u^4}{DZ^2h^5} = 3.43 \times 10^{-3} \quad [6]$$

The working range desired for each of the variables is

C: 10^{-1} to $10^{1} = (10^{-1}$ to $10^{1})$
k: 10^{-3} to $10^{0} = (10^{-1}$ to $10^{2}) \times (10^{-2})$
ρ: 10^{-4} to $10^{2} = (10^{-1}$ to $10^{2}) \times (10^{-3})$ and $(10^{-1}$ to $10^{2})$
u: 10^{-1} to $10^{2} = (10^{-1}$ to $10^{2})$
D: 10^{-1} to $10^{2} = (10^{-1}$ to $10^{2})$
Z: 10^{-5} to $10^{1} = (10^{-1}$ to $10^{2}) \times (10^{-4})$ and $(10^{-1}$ to $10^{3}) \times (10^{-1})$
h: 10^{-1} to $10^{5} = (10^{-1}$ to $10^{2})$ and $(10^{-1}$ to $10^{2}) \times (10^{3})$

Three-cycle ($N = 3$) semilog paper is suitable for these ranges, with double ranges required for ρ, Z, and h. For the log scale it seems best to take $b = -1$, $t = 2$, $N = t - b = 3$. To use the same ordinate readings (log scale) for all the variables it is necessary to express k as 100 times the conductivity (standard units) and Z as 10 times the viscosity (in poises), i.e., viscosity in decipoises. Further modifying Equation [6] to allow for this change in the units of k and Z

$$\frac{C^2k^3\rho^4u^4}{DZ^2h^5} = 34.3 \quad [7]$$

Expressing Equation [7] in logarithmic form and applying a modulus $M = -1.5$

$$-3 \log C - 4.5 \log k - 6 \log \rho - 6 \log u$$
$$+1.5 \log D + 3 \log Z + 7.5 \log h = -2.30$$

To hold the number of intersections of the lines of the logograph to a minimum (see Fig. 1), the following addition constants have been chosen

Variable	Term	Bottom intercept	Top intercept
C	$22.5 - 3 \log C$	$22.5 + 3.0 = 25.5$	$22.5 - 6.0 = 16.5$
k	$21.0 - 4.5 \log k$	$21.0 + 4.5 = 25.5$	$21.0 - 9.0 = 12.0$
ρ	$19.5 - 6 \log \rho$	$19.5 + 6.0 = 25.5$	$19.5 - 12.0 = 7.5$
u	$19.5 - 6 \log u$	$19.5 + 6.0 = 25.5$	$19.5 - 12.0 = 7.5$
D	$27.0 + 1.5 \log D$	$27.0 - 1.5 = 25.5$	$27.0 + 3.0 = 30.0$
Z	$28.5 + 3 \log Z$	$28.5 - 3.0 = 25.5$	$28.5 + 6.0 = 34.5$
h	$14.3 + 7.5 \log h$	$14.3 - 7.5 = 6.8$	$14.3 + 15.0 = 29.3$
Add	152.3	Chart constant, A, $= 152.3 - 2.3 = 150$	

It remains only to construct the logograph and indicate the units applicable to each line (see Fig. 1). The reason for choosing the apparently haphazard constants, such as 22.5, 21.0, etc., is that crossing of lines has been largely avoided with six of the lines having a common bottom intercept at 25.5. The sum, A, of the constants is 150; hence to evaluate any one variable in Equation [7] in terms of the other six

$$R_1 = 150 - (R_2 + R_3 + R_4 + R_5 + R_6 + R_7)$$

The extended (doubled) scales with the range increased by 10^3 in each case for ρ, Z, and h are calculated by adding $+Mn \log 10^3 = -1.5 \times 3n = -4.5n$ for enlarging the unit 10^3 times and adding $+4.5n$ for reducing the unit 10^3 times. Applying the appropriate values of n

For ρ: add $+4.5 \times (+4) = +18$ (smaller unit, factor $= 10^{-3}$)
For Z: add $+4.4 \times (-2) = -9$ (smaller unit, factor $= (10^{-3})$
For h: add $-4.5 \times (-5) = +22.5$ (larger unit, factor $= 10^3$)

An example illustrating how the lines on a logograph may be moved relative to each other by changing the addition constants is shown in Fig. 2, a logograph for the same Equation [2c]. Here, $b = -1$ and $t = 2$ both as before, $M = -2$, and the sum of the constants, A, totals 100. The distribution of the constants is such as to give a chart entirely different in appearance and probably less desirable than that in Fig. 1.

Application of Logographs

Graphical solutions become desirable for application in engineering design in so far as they simultaneously offer the qualities of simplicity, speed, and accuracy. Charts should be versatile in the matter of range of the variables included and if possible in the units in which those variables are measured, and they should visually reveal the comparative effects of changes in magnitude of the individual variables. They should require a minimum of instruments or special facilities for their use. Some of these criteria of good charts may be incompatible and must therefore be foregone in special applications. Thus there are conditions under which the standard nomograph is most desirable, others for which the logograph is definitely called for, and still others where specialized diagrams are particularly suited.

The simplicity of the logograph chart for functions of the form

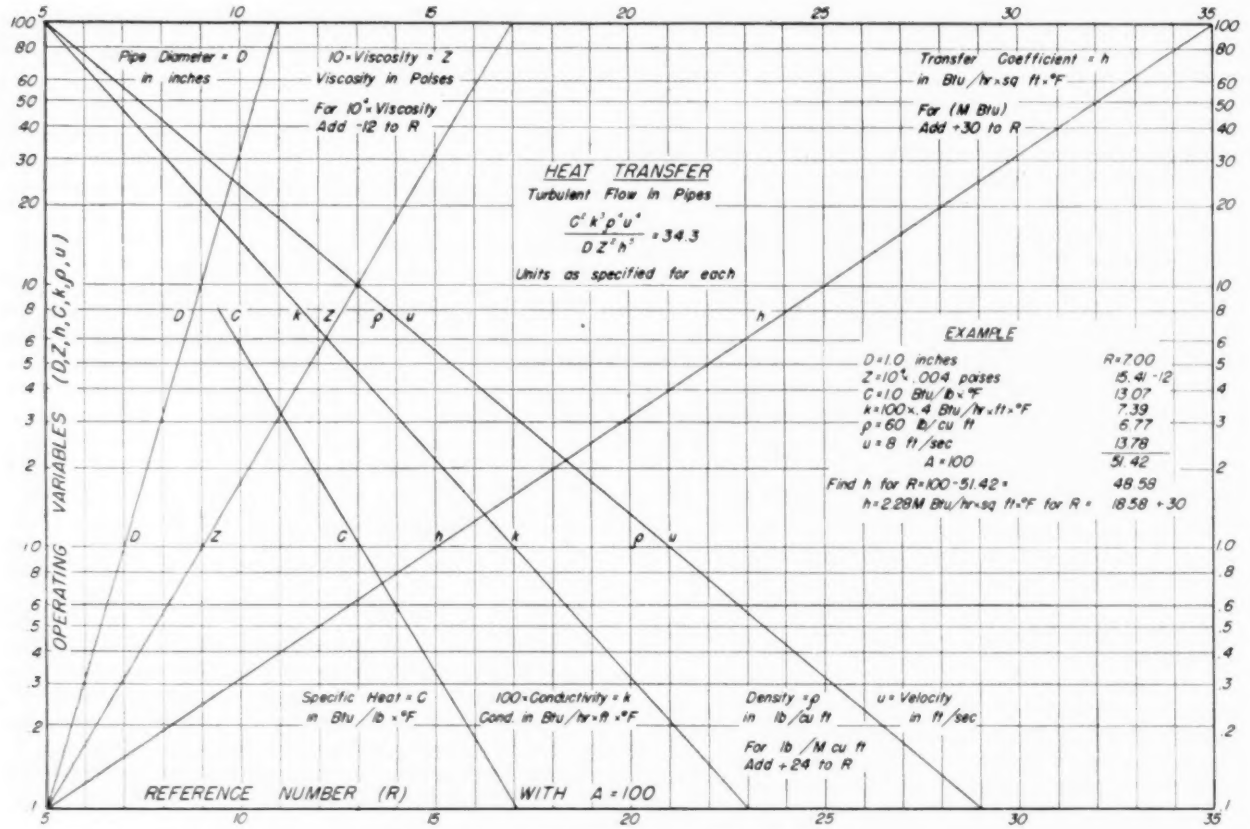


FIG. 2 MODIFIED LOGOGRAPH FOR HEAT TRANSFER

of Equation [1a] is evident. Practically unlimited ranges (10^6 in Fig. 1) are possible for any of the variables, a change in the units for any one of the quantities may be obtained simply by the addition of a constant, and uniform accuracy is available for all the variables in any combination of ranges. The order in which the readings for the variables are taken from the chart is of no importance, and any one of the variables may be the unknown. In constructing the ordinary logograph, the plot for each variable is a straight line and no special scales need be drawn on or applied to any of the lines.

Various departures from the construction and use of logograph charts as here described may be found desirable or necessary in special applications. For example, instead of using logarithmic scaled paper, the lines of the chart may have their scales plotted directly on them. The location of the lines may become unimportant if they are considered merely as logarithmic vectors, with lengths taken off each of the lines from some point of reference, the various lengths then being added vectorially. Such a procedure may be accomplished wholly graphically by using a pair of triangles to lay off vectors parallel to those specified on the chart, and transposing the proper lengths with a pair of dividers. This method of addition is practical only when not too many vectors are to be so added and when the ranges for the individual vectors are comparatively small. It may be used to accomplish results not possible by numerical addition, e.g., in the Eiffel diagrams for airplane-propeller design (2). Eiffel charts have their scaled vectors so sloped that the addition of abscissa components develops one function of the variables while the ordinate addition determines another, the interrelation of the two functions being defined by some charted line intersected by the graphical vectorial addition.

Special purpose diagrams notwithstanding, numerical addition logographs plotted on semilog paper, as here described, will best serve for repetitive computations of functions of the form of $T^p U^q V^r W^s = K$, which so often arise in engineering design. Logographs cannot, however, replace nomographs where the equation to be solved involves an addition operation as well as a multiplication.

Two more logograph charts are offered in this paper not only as examples of somewhat more complicated logograph construction with appropriate explanation, but also for their intrinsic value in the calculation of industrial problems. For each of the two subsequent logographs, "turbulent flow of fluids in pipes," Fig. 3, and "fluid flow through orifices," Fig. 4, the basic equations are given and their source or development explained.

TURBULENT FLOW IN PIPES

Although Equation [2] involves seven variables, it represents in form a simple type of logograph. One involving a curve develops from Fanning's equation for turbulent flow of fluids in pipes. Before presenting the logograph, a brief explanation is given of the underlying equation since it has not appeared in the literature in the form used here.

The variables involved in turbulent flow in pipes with units modified where necessary to suit the range of a three-cycle logograph are as follows:

Q = mass flow rate, M lb per min
P_1, P_2 = initial and final pressures, psia
ρ = density of the fluid, pcf
D = diameter of pipe, in.
f = friction coefficient $\approx 0.00759(DZ/Q)^{0.2}$

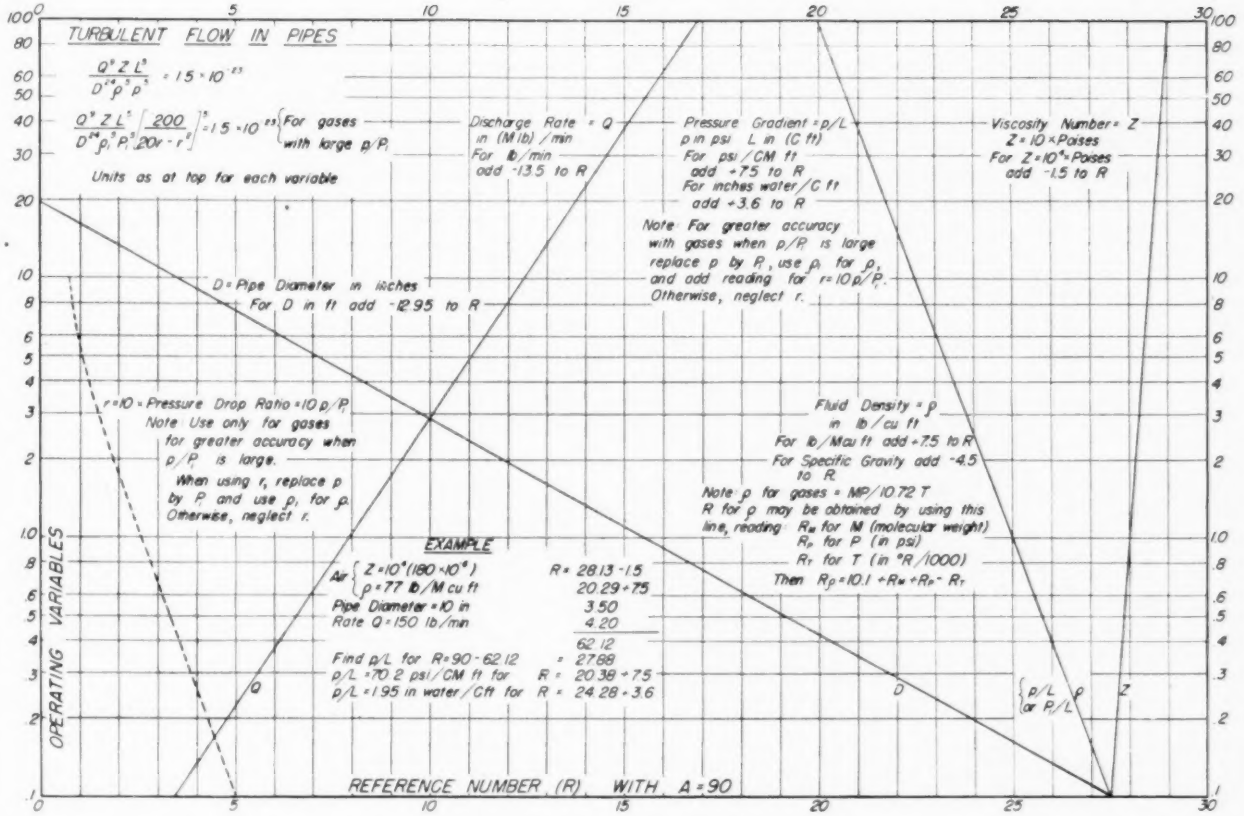


FIG. 3 LOGOGRAPH FOR TURBULENT FLOW IN PIPES

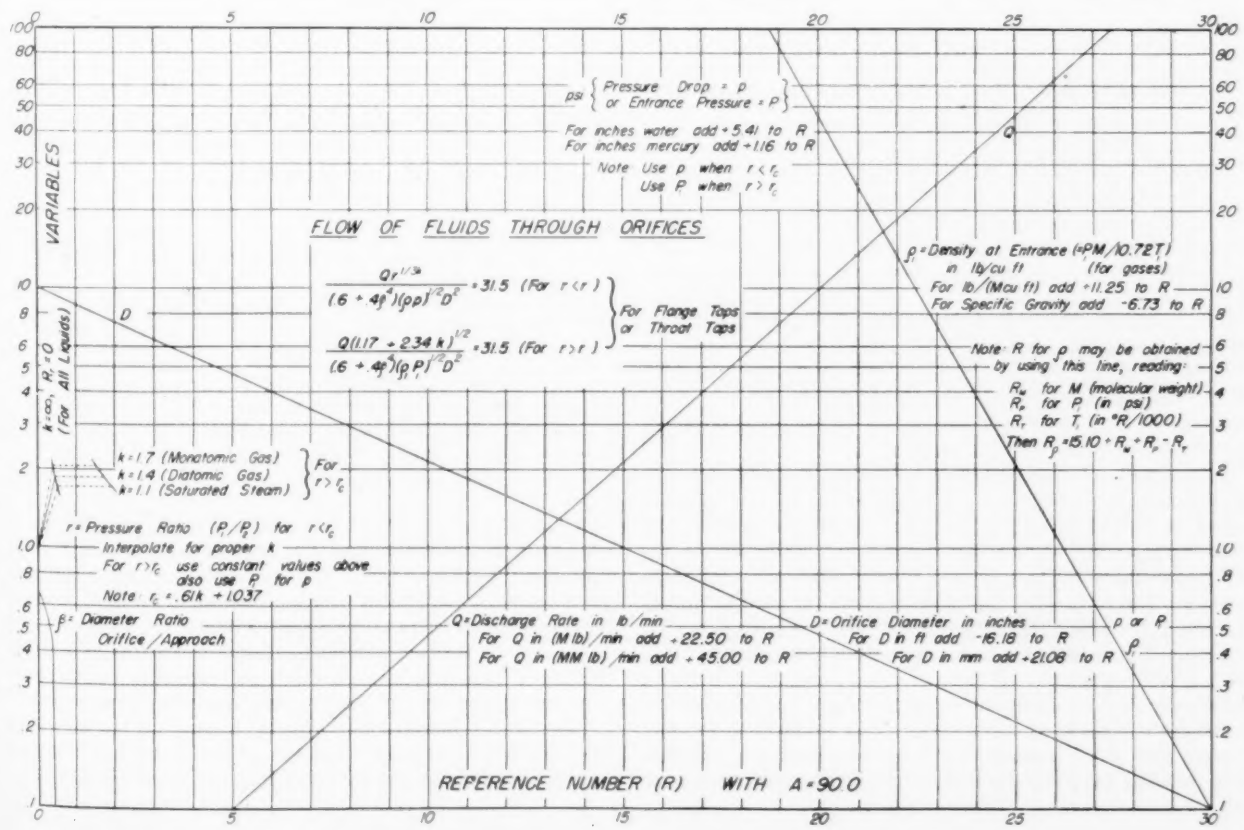


FIG. 4 LOGOGRAPH FOR FLOW OF FLUIDS THROUGH ORIFICES

L = length of pipe, ft in units of 100
p = pressure drop, psi
p/L = pressure gradient in the pipe line, psi/Cft
r = pressure drop ratio = $10p/P_1$
Z = viscosity of the fluid, decipoises
N = Reynolds number = $37{,}900\ Q/DZ$

In the foregoing units, assuming isothermal expansion and neglecting a logarithmic term which arises, Fanning's equation for turbulent flow leads to

$$Q = 3.215 \times 10^{-4} \sqrt{\frac{(P_1^2 - P_2^2)\rho_1 D^5}{fLP_1}}$$

This may be expressed by

$$\frac{fQ^2}{\rho D^5}\left(\frac{L}{p}\right) = 2.067 \times 10^{-7} \left\{\begin{matrix}\text{For all liquid flow or for} \\ \text{gases with small } p/L\end{matrix}\right\}$$

$$\frac{fQ^2}{\rho_1 D^5}\left(\frac{L}{P_1}\right)\left(\frac{200}{20r - r^2}\right) = 2.067 \times 10^{-7} \left\{\begin{matrix}\text{for gas flow} \\ \text{with large } p/L\end{matrix}\right\}$$

The coefficient of friction f is now expressed according to $1/f = 16(N)^{0.2} = 131.8\,(Q/DZ)^{0.2}$. The use of a constant exponent on N in any expression for f is not acceptable for smooth pipe or for pipe with specified roughness, but is nevertheless supported experimentally for industrial piping with its relative roughness decreasing (though its absolute roughness increases) for the larger pipe diameters. Inserting this expression for $1/f$ leads to

$$\frac{Q^2 Z}{\rho^5 D^{24}}\left(\frac{L}{p}\right)^5 = 1.5 \times 10^{-23} \left\{\begin{matrix}\text{for all liquid flow or for} \\ \text{gases with small } p/L\end{matrix}\right\} \quad \ldots\ldots [8a]$$

$$\frac{Q^2 Z}{\rho_1^5 D^{24}}\left(\frac{L}{P_1}\right)^5\left(\frac{200}{20r - r^2}\right)^5 = 1.5 \times 10^{-23} \left\{\begin{matrix}\text{gas flow with} \\ \text{large } p/L\end{matrix}\right\}$$

$\ldots\ldots\ldots [8b]$

Equations [8] are quite satisfactory for industrial piping up to Reynolds numbers of several million and offer an accuracy within a few per cent for Q. Greater precision is not required in ordinary practice since corrections for variations in original roughness of the pipe, for the effect of scaling or corrosion, and for the equivalent length of installed fittings are at best but approximate.

It must be remembered that Fanning's equation is in itself inaccurate in that it assumes isothermal gas expansion and also omits a logarithmic term. The equation may show considerable error for gas flow with large proportionate pressure drops and small frictional resistance. The inaccuracy increases nearly directly with pD/fLP_m where P_m is the logarithmic mean of P_1 and P_2; it becomes objectionable (depending on the accuracy desired) when the pressure gradient p/L exceeds some 100 times fP_m/D for gases, the error in Q then being 2 per cent (with units for p, L, P, D as previously specified). Fortunately this situation seldom arises in industrial practice.

A logograph for Equations [8] (a or b) is given in Fig. 3. The [8a] portion of the equation is a simple logograph covering five variables. The [8b] portion, used when greater accuracy is desired for gases and vapors that expand appreciably during the flow, substitutes P_1 for p in p/L with ρ taken as ρ_1 (compare Equation [8a] with [8b]) and adds a curve for the function of $r(=10p/P_1)$. This chart illustrates the use of a curved line.

An innovation, included in Fig. 3, further indicates the versatility of the logograph: R for ρ of the gas can be determined graphically from its molecular weight, pressure, and temperature if the gas is considered to be ideal. This auxiliary use of any straight line of a logograph is a direct consequence of the fact that for each variable, the line on the chart reads a value of $R_y = C + Mn \log Y$. The line can thus be used as a slide rule for calculation by logarithms.

Some sample computations from Fig. 3 may not be amiss. Air, for which the viscosity is 180×10^{-6} poises, is to be transmitted through a 10-in-diam flue at nearly atmospheric conditions (60 F, 30 in. Hg) with $\rho = 77$ lb per 1000 cu ft. For a flow of 150 lb per min (1950 cfm), the pressure gradient is desired. The solution for this problem is outlined in Fig. 3 and need not be repeated here. The p/L in this case is small and no consideration need be given to the expansion ($r = 10p/P_1$) during the flow.

Another example will show the use of r. Here high-pressure air (60 F, $P_1 = 100$ psia) is being delivered through a 2-in pipe at a rate of 150 lb per min. The pressure gradient is desired. The solution is shown both neglecting r and including r. If desired, the $\rho_1(=0.524$ pcf) can be obtained from the chart with $R_\rho = 10.07 + 21.34 + 20.0 - 25.71 = 25.70$.

	Neglecting r	*Including r*
Air $\left\{\begin{matrix}Z = 10^4(180 \times 10^{-6}) \\ \rho_1 = 0.524 \text{ pcf}\end{matrix}\right.$	$R = 28.13 - 1.5$ 25.70	28.13 — 1.5 25.70
Pipe diameter = 2 in.	11.89	11.89
Rate = 0.15 M lb per min	4.20	4.20
$P_1/L = 100$ (for 100 ft pipe)		20.0
	68.42	88.42
Find p/L for $R = 90 - 68.42 =$ p/L without r correction =	21.58 23.3 psi/Cft	
Find $r = 10p/P_1$ for $R = 90 - 88.42 =$ $r = 2.70$ or p/L corrected =		1.58 27.0 psi/Cft

Fluid Flow Through Orifices

An example of a more elaborate logograph is shown in Fig. 4. Again the equation applying is first discussed since it has not been given previously. The basic equation for the flow of fluids through a standard sharp-edged thin-plate orifice is given in hydraulic form by

$$Q = 31.5 D^2 KY\sqrt{\rho_1 p} \quad \ldots\ldots\ldots\ldots [9]$$

where

Q = mass discharge rate, lb per min
D = diameter of orifice, in.
K = orifice coefficient (approach factor included)
Y = expansion factor for the gas
ρ_1 = entrance density, pcf
p = pressure drop, psi
P_1, P_2 = initial and final pressures, psia
β = diameter ratio; orifice/approach
r = pressure ratio: $P_1/P_2 > 1.0$
k = specific-heat ratio

A series of experiments conducted by the U. S. Bureau of Standards (3) has determined KY in the hydraulic form of flow, Equation [9], for β up to 0.6, and for expansion ratios r from 1.0 to critical r_c (r_c corresponds to sonic velocities in the fluid stream). The experimental data are very well correlated (to 1 per cent) by $KY = (0.6 + 0.4\beta^4)r^{-1/3k}$ for flange-tap or throat-tap pressure readings. This expression is sufficiently accurate for the purposes of this paper and will serve for liquids by taking $k = \infty$.

More recent and elaborate experimentation (4) has indicated that the coefficient is also a function of the actual pipe diameter and of Reynolds number, but this refinement is unnecessary here.

The simple expression for KY is substituted in Equation [9] for flows at pressure drops below critical r_c. For flows with drop greater than indicated by r_c, the effective r equals r_c, the KY for the orifice becomes constant, and the effective pressure drop p is $P_1(r_c - 1)/r_c$. Thus

$$\frac{Qr^{1/2k}}{(0.6 + 0.4\beta^4)D^2(\rho_1 p)^{1/2}} = 31.5 \text{ (for gases with } r < r_c) \ldots\ldots [10a]$$

Take $k = \infty$ and $r_c = \infty$ in Equation [10a] $\left\{\begin{matrix}\text{for liquids at}\\ \text{all values of } r\end{matrix}\right\}$

$$\frac{Qr_c^{1/2k}}{(0.6 + 0.4\beta^4)D^2(\rho_1 P_1)^{1/2}}\left(\frac{r_c}{r_c - 1}\right)^{1/2} = 31.5 \left\{\begin{matrix}\text{for gases with}\\ r > r_c\end{matrix}\right\} \ldots\ldots [10b]$$

The development of the logograph for Equation [10a] gives the usual straight lines for Q, D, ρ_1, and p. A curve is calculated for the term $(0.6 + 0.4\beta^4)$ up to $\beta = {}^2/_3$; measurements are undependable beyond that value.

The principal limitation of the logograph arises in plotting the term $r^{1/2k}$. As in nomographs, functions with mixed variables cannot be represented except by a family of scales or lines. In Fig. 4 lines for r (up to r_c) are given, respectively, for $k = \infty$ (all liquids), and for $k = 1.7$, 1.4, 1.1, allowing for interpolation of k between these values. It is evident from the chart that the effect of the value of k for gases is small and a rough interpolation is satisfactory. No addition constant is included in the logarithm of the r function, hence for liquids with $k = \infty$, the R_r is zero, i.e., r and k are both neglected in using the chart for liquids.

The logograph for Equation [10b] is the same as for [10a] except that p is replaced by P_1 and the function of r_c becomes a constant depending only on k for the particular gas involved. It can be shown that

$$r_c = \left(\frac{k+1}{2}\right)^{\frac{k}{k-1}}$$

Although calculations for the logograph may be made directly from the foregoing expression for r_c, simpler empirical relations are suggested for extended calculations as follows

$$r_c \approx 0.61k + 1.037 \text{ (to 0.1 per cent)}$$

$$r_c^{1/2k}\left(\frac{r_c}{r_c - 1}\right)^{1/2} \approx \sqrt{1.17 + \frac{2.34}{k}} \text{ (to 0.1 per cent)}$$

In using Equation [10b] or the chart for gas flow with r far into the supercritical range, it must be remembered that the orifice calibration has not been experimentally determined in that region. The assumption that KY is constant for $r > r_c$ seems logical but may lead to some inaccuracy if carried too far. Orifices should not be used under conditions where r is much larger than r_c.

The logographs for Equation [10a] and [10b] may be combined into one if proper directions are given for its use. In this way Fig. 4 covers fluid flow through orifices for all cases and conditions: Liquids or gases for their complete range from $r = 1.0$ to $r = r_c$, and for $r > r_c$.

No example appears in Fig. 4, but two are given as follows: The simplest case is for liquid flow where $r(= P_1/P_2)$ is not involved. A sharp-edged orifice of 1 in. diam is being used in a 2-in. pipe line ($\beta = 0.5$) with water ($\rho = 62.4$ pcf). The pressure drop (p) is 10 in. Hg. Find rate of discharge (Q).

Orifice	$D = 1$ in.	$R = 15.00$
	$\beta = 0.5$	0.29
Water:	$\rho = 62.4$ pcf	19.41
Drop:	$p = 10$ in. Hg	22.50 + 1.16
		58.36
Find Q for $R = 90 - 58.36 =$		31.64
$Q = 360$ lb per min for $R =$		9.14 + 22.50

Using the same orifice as before for air ($k = 1.4$) with $P_1 = 100$ psia at 60 F ($\rho_1 = 0.524$ pcf) and $P_2 = 80$ psia in Case 1 (for $r < r_c$) or $P_2 < 53$ psia in Case 2 (for $r > r_c$), find the rate of discharge (Q).

		$r < r_c$	$r > r_c$
Orifice	$D = 1$ in.	$R = 15.00$	15.00
	$\beta = 0.5$	0.29	0.29
Air:	$\rho_1 = 0.524$ pcf	27.30	27.30
	$p = 20$ psi	21.37	
	$r = P_1/P_2 = 1.25$	0.17	
	$P_1 = 100$ psia		18.75
	$r > r_c$ for $k = 1.4$		1.70
		64.13	63.04
Find Q for $R = 90 - 64.13 =$		25.87	
	Q for P_2 at 80 psia =	60.6 lb per min	
Find Q for $R = 90 - 63.04 =$			26.96
	Q for $P_2 < 53$ psia =		84.7 lb per min

ACKNOWLEDGMENT

The author wishes to express his gratitude to Prof. H. J. Garber and Prof. W. Licht of the University of Cincinnati for their invaluable assistance in offering suggestions, drawing the logographs, and checking the manuscript for this paper.

BIBLIOGRAPHY

1 "Nomograph of Dittus-Boelter Equation," by C. J. Ryant, *Industrial and Engineering Chemistry*, vol. 35, 1943, pp. 1187–1188.

2 "Aircraft Propeller Design," by F. E. Weick, McGraw-Hill Book Company, Inc., New York, N. Y., 1930, pp. 97–101.

3 "Discharge Coefficients for Orifices," by H. S. Bean, E. Buckingham, and P. S. Murphy, U. S. Bureau of Standards, *Journal of Research*, vol. 2, RP-49-29, 1929, pp. 561–658.

4 "Fluid Meters," The American Society of Mechanical Engineers. Fourth edition, 1937, pp. 107–124.

(Owing to travel emergency conditions existing when this paper was presented, discussion will be accepted until March 11, 1946)

Some Effects of Work Positioning When Face-Milling Steel

By FRED W. LUCHT,[1] DETROIT, MICH.

All of the work that has been done and all of the observations which have been made to date on the subject of face-milling steel with carbide cutters have indicated clearly that the longest cutter life is obtained when (1) the cutters have double negative rake angles, and (2) the full depth of cut is taken along some definite corner angle. Until recently, not much thought had been given to the positioning of the work in relation to the cutter, and only in limited cases has any consideration been given to the fact that the radial engagement angle between the face of the tooth and the edge of the work where the cutting edge enters it should be negative. Milling operations are frequently found where the diameter of the face mill is too small to permit the proper positioning of the work to a setting which gives longest cutter life. Under such a condition, there seems to be no definite means available which will assist in determining the diameter of a face mill capable of producing the maximum number of pieces per grind. This problem of determining optimum cutter diameter for a given face-milling job, and the proper positioning of the workpiece in relation to the cutter, led to a series of studies, the results of which are reported in this paper.

Introduction

ALL of the work that has been done and all of the observations which have been made to date on the subject of face-milling steel with carbide cutters have indicated clearly that the longest cutter life is obtained when (1) the cutters have double negative rake angles, and (2) the full depth of cut is taken along some definite corner angle.

There are certain operating conditions in every milling-machine setup which should at all times be maintained as nearly ideal as possible. These objectives are design, manufacture, and sharpening of the cutter; power capacity, feed and speed of the machine; and a flywheel to smooth out the roughness obtained from the necessarily coarser-tooth cutters removing stock at increased table travel. But even after all this has been done, the cutter performance and the number of pieces obtained per cutter grind still will show noticeable variations as the work position is shifted at right angles to the direction of feed of the work past the cutter.

Until recently, not much thought had been given to the positioning of the work in relation to the cutter, and only in limited cases has any consideration been given to the fact that the radial engagement angle D, Fig. 1, between the face of the tooth and the edge of the work where the cutting edge enters it, should be negative. It is interesting to note that when this angle has been negative, the number of pieces per grind has at least been more consistent than when no attention at all was paid to it, even though the cutter may not have produced its maximum number of workpieces per grind.

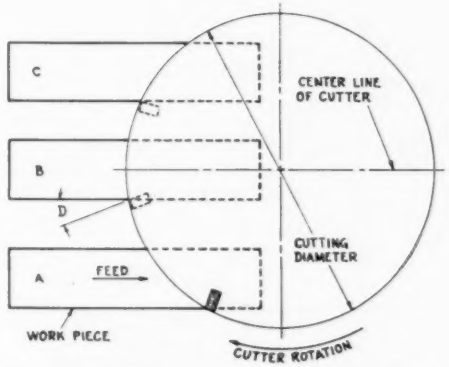


Fig. 1 Work Position Influences Face-Mill Life

It has also been found that a face-milling cutter usually gives a smooth cutting action together with the maximum number of pieces per grind when the workpiece is positioned about as shown at B. Position C generally rates second as to the number of pieces per grind, with quite consistent results. Position A rates third, with somewhat erratic results. This difference in results has been noticed for years while observing the face-milling of steel with high-speed steel cutters, but it has become more pronounced when milling steel with carbides.

Milling operations are frequently found where the diameter of the face mill is too small to permit the proper positioning of the work to a setting which gives longest cutter life. Under such a condition, there seems to be no definite means available which will assist in determining the diameter of a face mill capable of producing the maximum number of pieces per grind.

This problem of determining optimum cutter diameter for a given face-milling job, and the proper positioning of the workpiece in relation to the cutter, resulted in the investigation to be discussed.

Details of Test Procedure

Milling Machine. A No. 5-HM vertical milling machine in the engineering department of the author's company was used.

Power available:	
Main spindle, hp	20
Feed and rapid traverse, hp	5
Wattmeter:	
Main spindle, kw	30
Feed and rapid traverse, kw	12

Face-Milling Cutter. An 8-in-diam single-tooth face-milling cutter, enshrouded with an 18-in-diam × 4-in-thick steel flywheel, was used, Fig. 2. The tool-bit slot is parallel to the axis and the tool bits are clamped in place by setscrews. The combined weight of the cutter head flywheel tool unit was 255 lb.

Tool Bit. A total of twelve tool bits, as shown in Fig. 3, was used for this test. These tools were tipped with Carboloy Grade 78B, a general steel-milling grade.

[1] Development Engineer, Carboloy Company, Inc. Mem. A.S.M.E. Contributed by the Research Committee on Metal Cutting and Bibliography and presented at the Fall Meeting of the Cincinnati Section, Cincinnati, Ohio, Oct. 2–3, 1945, of The American Society of Mechanical Engineers.

Note: Statements and opinions advanced in papers are to be understood as individual expressions of their authors and not those of the Society.

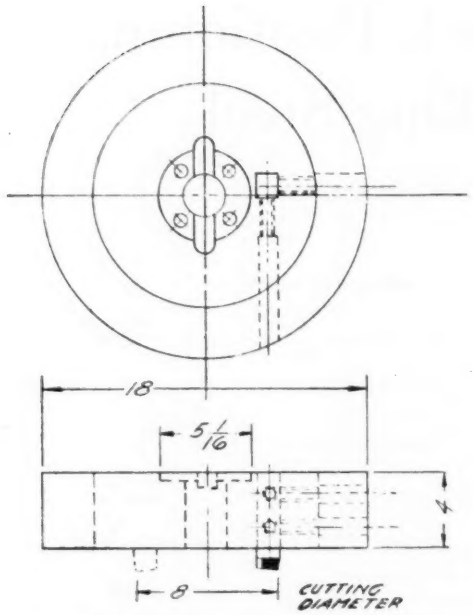


FIG. 2 TO ELIMINATE VIBRATION, CUTTER WAS ENSHROUDED IN A FLYWHEEL

Both carbide and steel on all tools were rough-ground on a single-point tool grinder using a 60-grit silicon-carbide wheel. A 220-grit resinoid-bond diamond wheel was used for the final sharpening of the carbide only.

The cutting edges on all tools were inspected at 20 magnifications. Each edge along the corner angle and the chamfer was

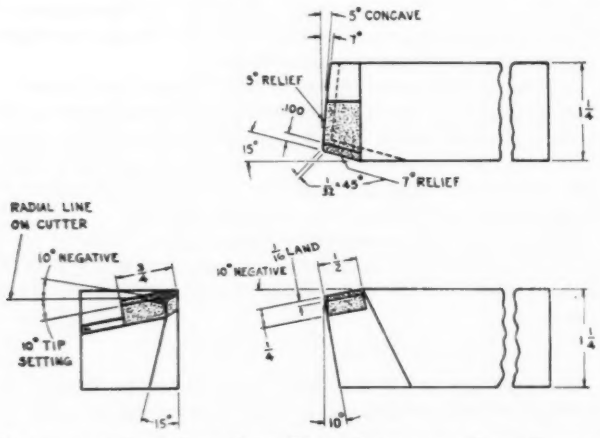


FIG. 3 ALL TOOL BITS USED WERE GROUND TO SAME CUTTING ANGLES

brushed lightly with a 320-grit silicon-carbide stone at an angle of about 45 deg to the face of the tool. This hand-honing removed any slight irregularities before the tool was assembled in the cutter head.

Positioning Tool in Cutter Head. Fig. 4 shows the method used to position the tool bit accurately in the tool-bit slot in the cutter head. Two sets of shims were required; one set, 0.100 to 0.200 in. thick, was used to maintain the 4-in. radius which gave the 8-in. cutting diameter; the second set, 0.180 to 0.310 in. thick, was used to maintain the 10-deg negative radial rake. This arrangement eliminated holding the corner location on the tool to close limits and facilitated correction for the stock which was

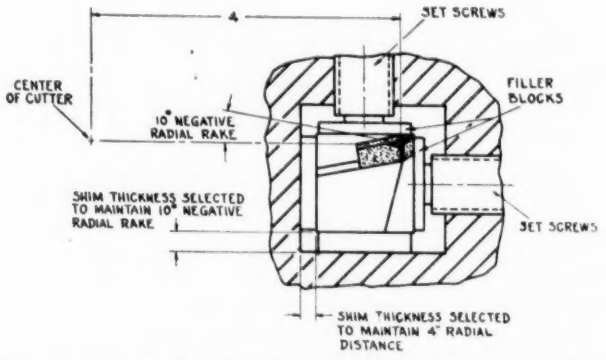


FIG. 4 ALL TOOL BITS WERE ACCURATELY POSITIONED IN CUTTER HEAD BY AID OF SHIMS

ground from the face of the tooth, the corner angle (side cutting-edge angle on the tool), and the face of the cutter (end cutting-edge angle on the tool) every time the tool bit was sharpened.

Work. For all face-milling runs, S.A.E.-1045 forged-steel billets were used. These billets were $1\frac{1}{2} \times 3 \times 12$ in. in size. They were heat-treated and drawn to a Brinell hardness of 190 to 200.

Machine Setup. Fig. 5 shows the machine setup that was used while making all milling runs. In this setup the steel billet, or workpiece, was held rigidly in a plain vise in relation to the cutter, as shown.

Speed. The 8-in. face mill was operated at 238 rpm (498 sfpm) because previous runs had indicated that this speed gave the longest cutter life when milling S.A.E. 1045 steel having a Brinell hardness of 190 to 200.

Feed. The following feeds were used to permit exploration of a wide range of face-milling activity:

Table travel, ipm	Feed per tooth, in.
2	0.0084
$2\frac{1}{2}$	0.0105
3	0.0126
$3\frac{1}{2}$	0.0147

Depth of Cut. A depth of cut of 0.150 in. was taken on all runs. This is an average depth of cut which shows wear similar to that caused by deeper cuts, yet which does not involve the machining of excessive amounts of steel as would the deeper cuts.

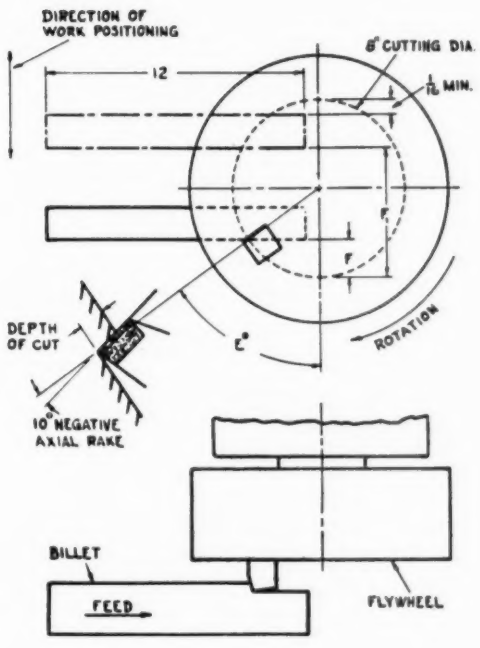
Operating Detail and Observations. In order to determine the effect of work positioning in relation to the face mill while all other conditions were kept constant, as has been outlined, the following runs were made with the work:

1 Shifted horizontally.
2 Shifted in a direction perpendicular to the table travel.
3 Shifted to each one of the positions listed in Table 1.

The "angular position *E*" represents the position where the cutting edge on the 8-in-diam tool first contacts the work.

The dimension *F* gives the distance from the point at which the cutting edge on the 8-in-diam tool first contacts the work, to the 8 in. diam measured perpendicularly to the direction of feed. During the milling runs, the work was shifted through a series of positions as listed from one extreme position where *E* equaled 10 deg and *F* was 0.061, to the other extreme position where *E* equaled 127 deg 33 min and *F* was 6.437. At each of these two extreme positions, the outside diameter of the face mill overlapped the workpiece $\frac{1}{16}$ in.

Each tool was run until the cutting edge showed the first sign of breakout. This was detected either from the marking on the inner side of the chip which came from the cut; from the lines left on the work surface by the corner angle; or from the change



WORK POSITION	
ANGULAR POSITION E (Degrees)	DISTANCE F (Inches)
10	.061
20	.241
30	.536
35	.723
40	.936
45	1.169
50	1.429
55	1.706
60	2.000
65	2.310
70	2.632
75	2.965
80	3.305
90	4.000
95	4.349
100	4.695
105	5.035
110	5.368
120	6.000
127°-33′	6.437

FIG. 5 CUTTER SETUP AND TABLE SHOWING WORK POSITIONS USED

TABLE 1 DIMENSIONS USED FOR POSITIONING WORK IN RELATION TO FACE MILL

Angular position *E*, deg	Distance *F*, in.	Angular position *E*, deg	Distance *F*, in.
10	0.061	70	2.632
20	0.241	75	2.965
30	0.536	80	3.305
35	0.723	90	4.000
40	0.936	95	4.349
45	1.169	100	4.695
50	1.429	105	5.035
55	1.706	110	5.368
60	2.000	120	6.000
65	2.310	127–33[a]	6.437

[a] Reported in deg-min.

in sound made by the milling operation. The distance traveled by the cutter, and the power readings, were recorded for analysis.

The cutting edge was inspected under a 20-power microscope and a record made in the form of an enlarged (to scale) freehand sketch showing the development of the cutting edge along the corner angle, the chamfer, and the face of the cutter. This sketch showed the width of the wear land behind the cutting edge along each of these three edges. It also showed the distance the cutting edge had worn back from the original corner-angle outline, and the width of the crater on the face of the tooth behind the cutting edge. All unusual signs of breakdown of the cutting edge were recorded on this sketch to serve as an aid in determining why the tool failed.

Using the twenty different work positions and the four different feed rates, a total of 190 runs was distributed as evenly as possible over the 12 tools. This gave 16 runs for each of 10 tools and 15 runs for each of the remaining two tools.

An average of the distances traveled up until the time of tool failure was plotted, Fig. 6, with its work position for each feed used. An average of all the runs made, irrespective of the feeds used for each work position, was also plotted.

The runs were made first at 2 ipm feed, i.e., 0.0084 in. feed per tooth. It was soon found that the various points arranged themselves in an irregular outline and also that the length of runs seemed to be somewhat erratic. Later, many additional runs were made at 0.0105, 0.0126, and 0.0147 in. feed per tooth, and it was found that not only did each set of runs follow the same general pattern but also that the lengths of runs were much more consistent than were those for the 0.0084-in. feed per tooth.

Analysis of How Tooth Contact Affects Cutter Life. To assist in determining why all the curves followed a definite general pattern, an enlarged wooden model, as shown in Fig. 7, was made of the cutter-work setup.

The model is shown in outline in Fig. 8 and is 10 times actual size. The base of the model is divided into angular spacing about a pivot point *C*. The block *D*, representing an exact 10-times enlargement of the cutting portion of the tool, is mounted on the end of the arm so that the intersection of the 15-deg corner angle and the 5-deg concavity angle is at a 40-in. radius.

Ten work blocks were made, as shown in Fig. 9, to the forms given in Table 2. This represents the exact contour cut by the cutter tooth when the entrance portion of the work is located at each one of the respective angular work positions.

To determine the type of contact for any given angular position of the cutter tooth, the work block for that angular position was placed against the guide block and slid past the 40-in. radius for a distance comparable to the feed per tooth, i.e., 0.105 in. for a 0.0105-in. feed per tooth. The cutter tooth was then swung in the direction shown until it contacted the workpiece. The type of tooth contact was observed. This procedure was repeated for each angular position. The results were compiled and the proper sequence of tooth contact for each position was recorded.

Figs. 10 to 18, inclusive, are close-up views of the various possible types of initial contacts between the cutter tooth and the

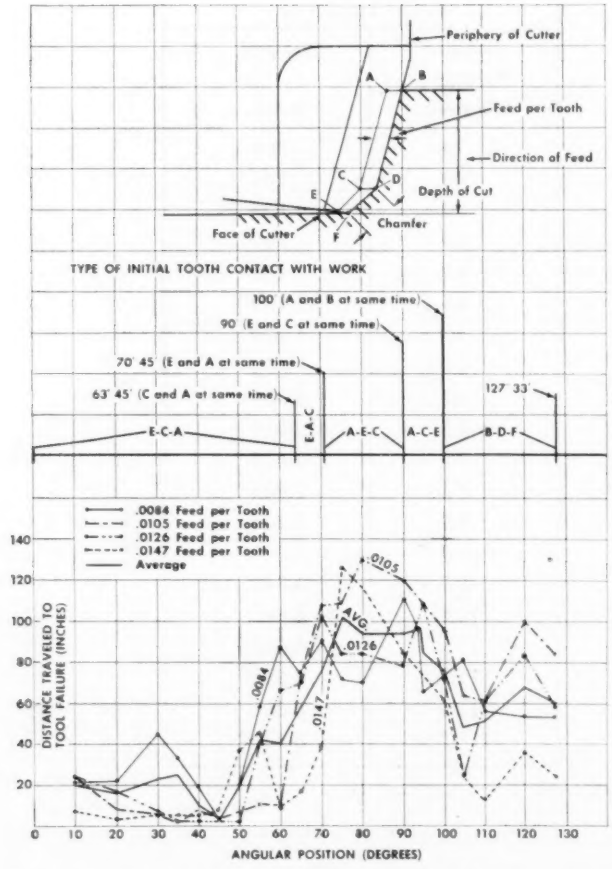


FIG. 6 CUTTER-LIFE CURVES FOR VARIOUS WORK POSITIONS AND FEEDS PER TOOTH

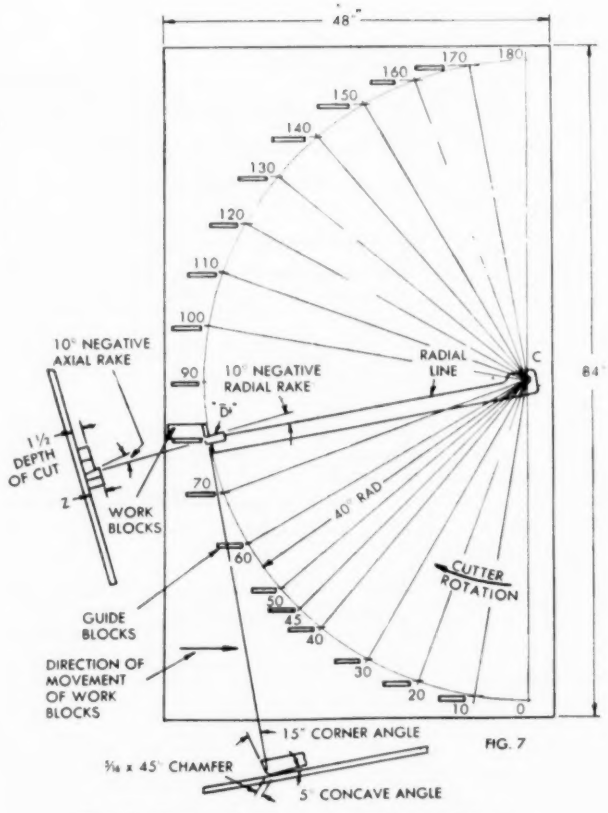


FIG. 8 DETAIL DIMENSIONS OF WOODEN MODEL

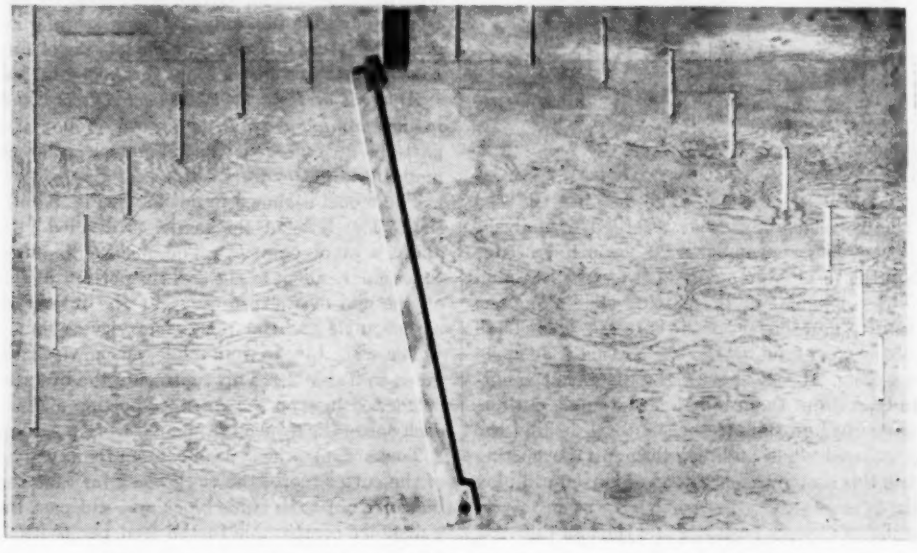


FIG. 7 ENLARGED WOODEN MODEL SHOWING TOOTH APPROACHING A WORK BLOCK

work. All of the original photographs were taken looking outward from the center of the cutter in a direction along the 10-deg negative radial rake angle on the face of the tooth.

Fig. 10 covers the conditions which exist when the point of initial tooth contact with the work is at *E* on the face of the tooth where it intersects the face of the cutter and is at a distance from the cutting edge on the chamfer equal to the feed per tooth. This is followed by point *C*, and finally by point *A*, contacting the work. This occurs when the tooth enters the cut anywhere from the zero position up to the 63-deg 45-min position.

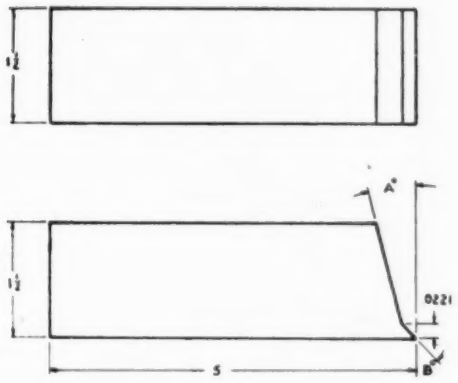


FIG. 9 WORK BLOCKS USED WHILE DETERMINING TYPE OF TOOTH CONTACT

TABLE 2 OUTLINE OF FORM MILLED ON ENTRANCE EDGE OF WORK FOR EACH WORK POSITION USED

Angular position, deg	Angle on edge of work, deg-min	
	A	B
10–170	53–32	80–36
20–160	37–06	71–18
30–150	27–50	63–32
40–140	22–30	57–19
45–135	20–39	54–46
50–130	19–13	52–35
60–120	17–09	49–07
70–110	15–55	46–47
80–100	15–13	45–27
90	15–00	45–00

At the 63-deg 45-min position, the initial contact point of the face of the tooth with the work still remains at *E*, as is shown in Fig. 11. However, as the cut progresses, the entire face of the tooth along the corner angle gives a line contact from *A* to *C*. This line contact is at a distance from the cutting edge equal to the feed per tooth.

In Fig. 12 we can see that between the 63-deg 45-min position and the 70-deg 45-min position, the face of the tooth makes contact with the work in the order of points *E* at the face of the cutter; *A* at the top of the cut; and *C* at the intersection of the corner angle and the chamfer.

Fig. 13 shows the set of conditions which obtain at the 70-deg 45-min position where both *A* and *E* on the face of the tooth contact the work at the same time. This is followed by point *C*, also on the face of the tooth, and making the final contact. The point *A* is located at a 0.150-in. distance, which is the depth of cut from *E* at the face of the cutter. This marks the beginning of the true double-negative cutting action, which extends up to the 100-deg position.

Between the 70-deg 45-min position and the 90-deg position, the initial point of contact is at *A*. This is followed by contact at *E*, and finally by contact at *C*. Fig. 14 clearly illustrates this set of conditions.

When the cutter tooth contacts the work at the 90-deg position, the initial contact is still at *A*. This is on the face of the tooth, as illustrated in Fig. 14. This is, however, followed by a line contact which is along the face of the tooth extending from *C* to *E*. This is parallel to the chamfer and is shown in Fig. 15.

Fig. 16 shows the initial tooth contact being made on the face

TABLE II

ANGULAR POSITION	ANGLE ON EDGE OF WORK A	B
10-170	53°-32′	80°-36′
20-160	37°-06′	71°-18′
30-150	27°-50′	63°-32′
40-140	22°-30′	57°-19′
45-135	20°-39′	54°-46′
50-130	19°-13′	52°-35′
60-120	17°-09′	49°-07′
70-110	15°-55′	46°-47′
80-100	15°-13′	45°-27′
90	15°-00′	45°-00′

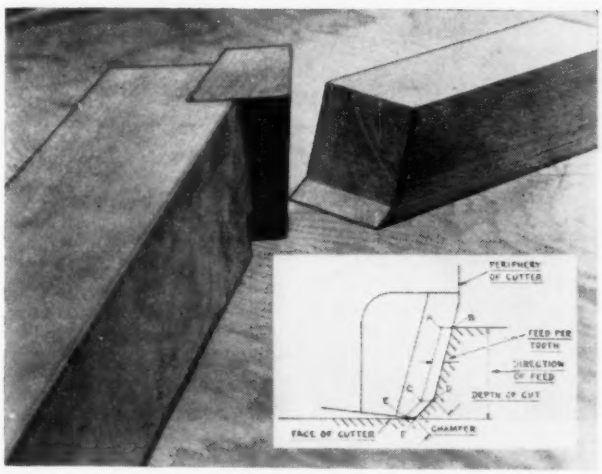


FIG. 10 SEQUENCE OF INITIAL CONTACT, *E-C-A;* POOR OPERATING CONDITION

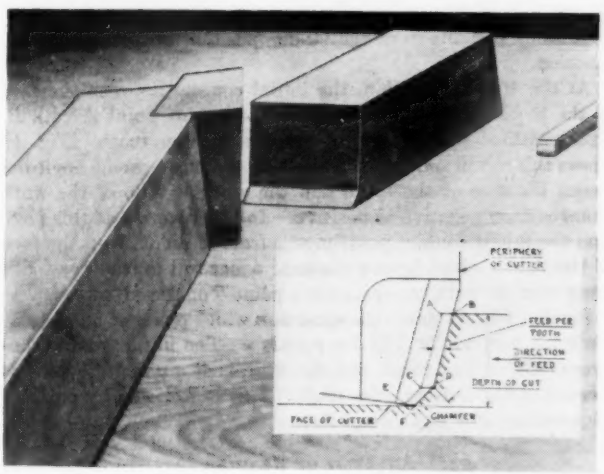


FIG. 11 SEQUENCE OF INITIAL CONTACT, *E-(CA)*; POOR OPERATING CONDITION

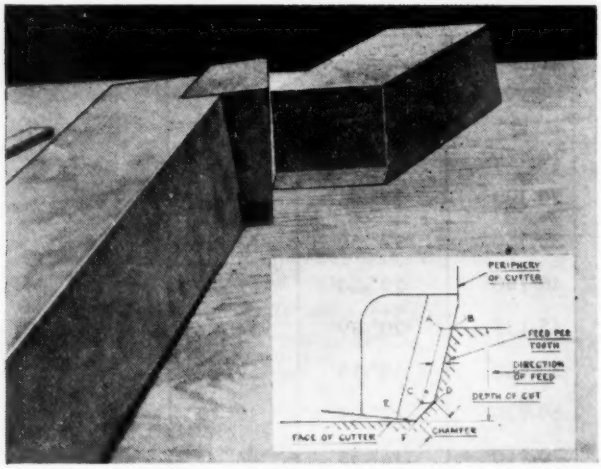


FIG. 12 SEQUENCE OF INITIAL CONTACT, *E-A-C;* POOR OPERATING CONDITION, SLIGHT IMPROVEMENT

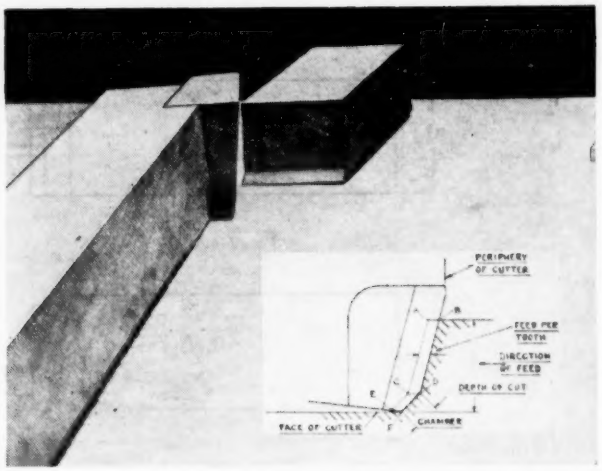


FIG. 14 SEQUENCE OF INITIAL CONTACT, *A-E-C;* GOOD OPERATING CONDITION

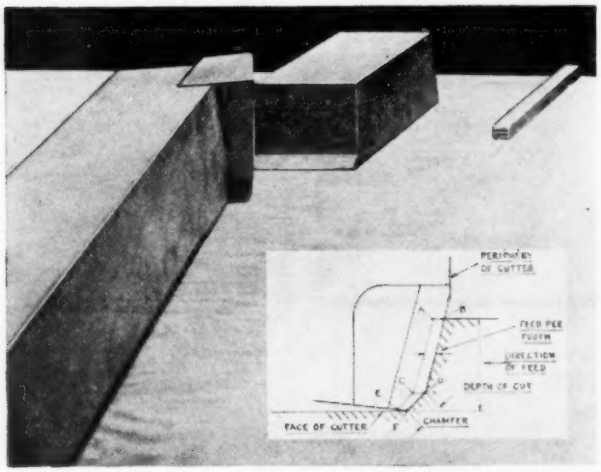


FIG. 13 SEQUENCE OF INITIAL CONTACT, *(EA)-C;* START OF DOUBLE-NEGATIVE ACTION AND GOOD PERFORMANCE

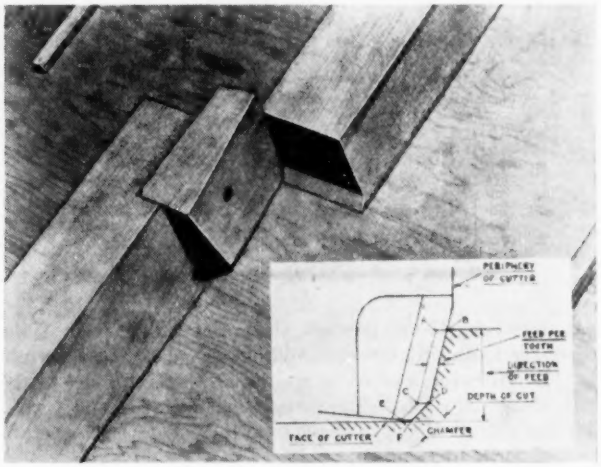


FIG. 15 SEQUENCE OF INITIAL CONTACT, *A-(EC);* GOOD OPERATING CONDITION, SLIGHTLY RETARDED

of the tooth at *A*, as illustrated in both Figs. 14 and 15. This is followed by contact at *C* and finally at *E*. This set of conditions prevails from the 90-deg position up to the 100-deg position.

At the 100-deg position, the initial contact between the face of the tooth and the work is a line connecting point *A* with *B*. The length of this line represents the feed per tooth. Fig. 17 shows this condition. At this position the engagement angle between the face of the tooth and the entering side of the work changes from negative to positive. In other words, at this position the initial contact point moves from a point *A* on the face of the tooth, which is at a distance equal to the feed per tooth away from the cutting edge, up to a point *B* on the edge itself.

Finally, Fig. 18 shows the condition which exists at all angular positions beyond the 100-deg position. The initial contact between the cutting tooth and the work is at a point *B*, which is located at the cutting edge itself. This is followed by cutting-edge contact at *D* and then at *F*.

ANALYSIS OF RESULTS

The data, compiled in Fig. 6, quickly indicate that a face-milling cutter having a 10-deg negative axial rake; a 10-deg nega-

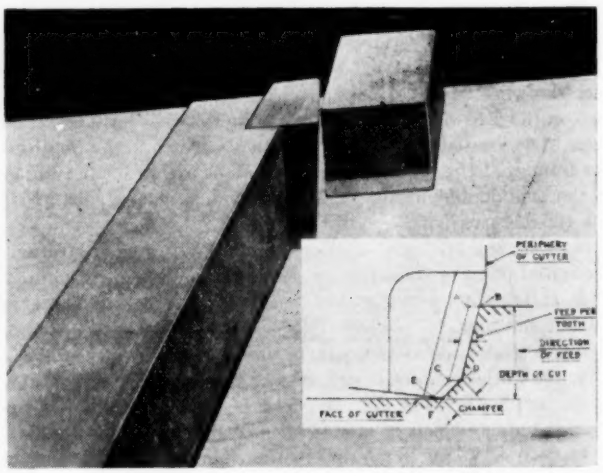


FIG. 16 SEQUENCE OF INITIAL CONTACT, *A-C-E;* EXCELLENT OPERATING CONDITION

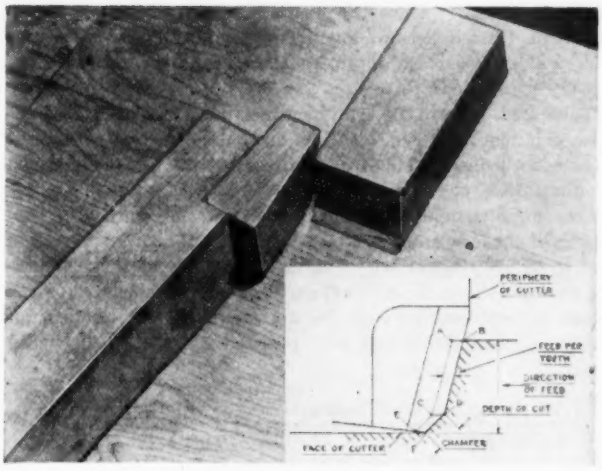


FIG. 17 SEQUENCE OF INITIAL CONTACT, (*AB*)-*D*-*F*; END OF DOUBLE-NEGATIVE ACTION AND EXCELLENT OPERATING CONDITION

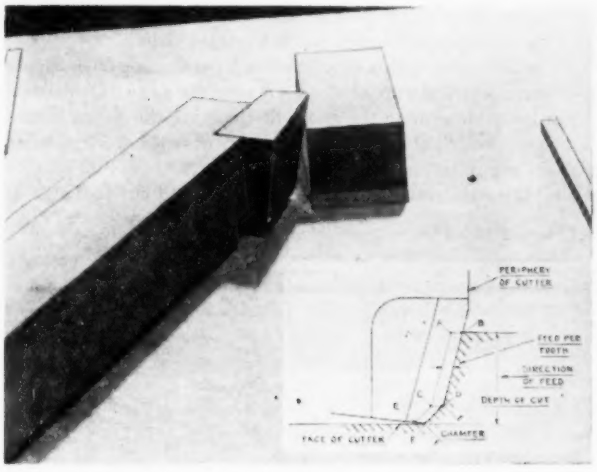


FIG. 18 SEQUENCE OF INITIAL CONTACT, *B*-*D*-*F*; FAIR TO POOR OPERATING CONDITION

tive radial rake; a 15-deg corner angle, and a $^1/_{32}$-in. × 45-deg chamfer:

1 Gives the longest cutter life when the nose or corner on the cutter enters the cut anywhere between the 70-deg 45-min and 100-deg work positions. The reason for this is the point *A* on the face of the tooth which contacts the work first.

(*a*) A 0.0105-in. feed per tooth gives the longest as well as the most uniformly consistent cutter life between the 70-deg 45-min and 100-deg work positions.

(*b*) A 0.0084-in. feed per tooth gives the shortest cutter life but has a tendency to cover a wider range of work positioning between 63 deg 45 min and 100 deg. Evidently the reason for this is the second point of contact with the work, which happens to be at *A* even though its initial point of contact is at *E*.

(*c*) The longest cutter life for a 0.0147-in. feed per tooth is confined within the narrowest range of work positioning for the four feeds used.

(*d*) At about the 90-deg tooth-entry position, the cutting edge along the 45-deg chamfer contacts the entry edge of the work broadside. This actually tends to decrease the length of run by a slight amount. An analysis of all tools run at this position shows that the initial breakdown occurs along the chamfer.

2 The life of the cutter is short and erratic when the cutter nose enters the work first anywhere between zero position and the 63-deg 45-min angular work position. This is due to the fact that the point *E* on the face of the tooth, which is below the point where the chamfer intersects the face of the cutter, contacts the work first.

This is substantiated by an analysis of the wear record of all the tools run at these positions, which indicates that a chip out of the cutting edge at *E* is followed by a complete collapse of the chamfer.

(*a*) It will be noted that an 0.0084-in. feed per tooth shows the longest cutter life, and that the 0.0126, 0.0106, and 0.0147-in. feeds per tooth, in the order given, show the shortest cutter life between the zero-deg and 55-deg work positions.

(*b*) At the 45-deg angular position, all of the feeds per tooth gave practically a zero cutter life. Plenty of runs were made at this work position to verify the results. There is no indication that this is the result of a change in the type of tooth contact because the same type of contact exists all the way from the zero-deg to the 63-deg 45-min angular position.

An analysis of the wear record of all the tools which were run at the 45-deg position showed that the cutting edge in the vicinity of the intersection of the corner angle and the chamfer consistently failed by spalling off in the same manner. It was assumed that this was due to the direction of, and also the intensity of, the impact load at the time the tooth hit the work. To verify this, an analysis was made of the major cutting forces at the time of the initial tooth impact, using the assumption that the longitudinal force (in the direction of feed) is 30 per cent of the tangential force, as outlined in Fig. 19.

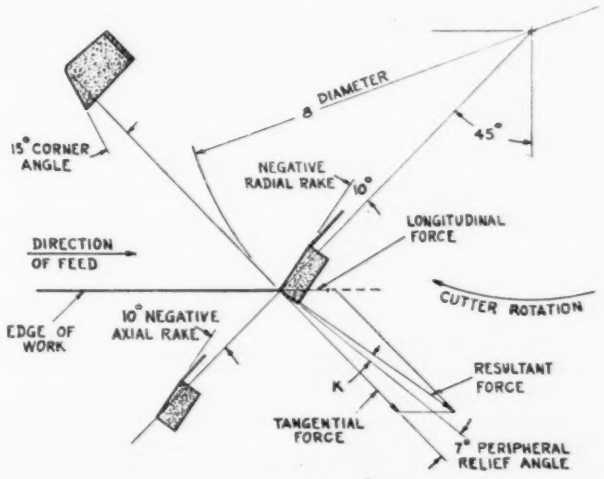


FIG. 19 GRAPHICAL ANALYSIS OF DIRECTION OF RESULTANT TOOTH-IMPACT FORCE, AT 45-DEG POSITION

This type of analysis was applied to each work position from the zero position to the 90-deg position. The angle *K*, which gives the relationship of the resultant force to the peripheral relief angle behind the cutting edge for each one of the various work positions, was determined graphically and then plotted as shown in Fig. 20.

It will be noticed that for the 45-deg position, which is shown in Fig. 19, the resultant-force line lies 3 deg 30 min within the peripheral-relief-angle line. It will also be noted that the angle *K* is zero for a work position of 32 deg. This means that the direction of the resultant force coincides with the peripheral relief angle behind the cutting edge. This also means that for all work-position angles which are less than 32 deg, the direction of

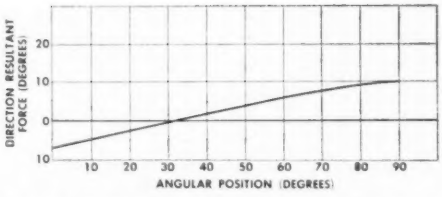


FIG. 20 GRAPH SHOWING HOW DIRECTION K OF RESULTANT IMPACT FORCE VARIES WITH WORK POSITION

the resultant force lies outside the peripheral relief angle, and shows why there is an inclination to spall off behind the cutting edge.

(*c*) There is a tendency for cutter life to decrease slightly at the 63-deg 45-min work position. This is apparently owing to the fact that at this position the entire cutting edge along the corner angle enters the work at the same time. This causes a momentary increased shock, which tends to break down the cutting edge.

(*d*) At the 70-deg 45-min work position, the face of the cutter tooth contacts the work at both A and E at exactly the same time. This momentarily increased contact also has a tendency to reduce cutter life by a slight amount.

RATING WORK POSITION BY TOTAL DISTANCE CUTTER IS IN CONTACT WITH WORK

It is a known fact that when work is so positioned in relation to a face mill that the center line of the work and the center line of the cutter, measured in the direction of the feed, actually coincide, the arc of contact B between the cutter tooth and the work is at its minimum, Fig. 21. This arc of contact increases gradually as the work position is shifted to either side of this central position. It is at its maximum under the present set of conditions, either where E equals 10 deg and F equals 0.061, or where E equals 127 deg 33 min and F equals 6.437, as we saw listed in Table 1.

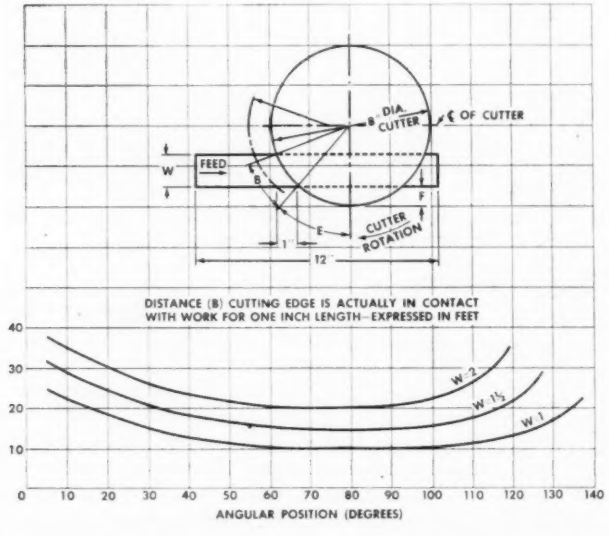


FIG. 21 ANALYSIS OF LENGTH OF TOOTH PATH THROUGH WORK WHEN CONSIDERING WORK WIDTH AND WORK POSITION

Table 3 shows the length of this arc of contact B, expressed in inches, for the various work positions for the $1^1/_2$-in. width of cut which was used in the test runs. This arc of contact (tooth path) has been called by the mathematical term "an arc of a looped trochoid." Since the width of cut is narrow, however, it will be treated here as an arc of the cutter circumference. This will give a close approximation to the theoretical curve already mentioned.

Table 3 also shows the total length of these arcs of contact expressed in feet for a 1-in. length of cut for the various work positions when using an 0.0084-in. feed per tooth. This is obtained by multiplying the length of the arc of contact for one tooth pass by the number of tooth engagements, with the work in a 1-in. length of cut for the given feed per tooth. (This is expressed in feet to reduce the number of digits in the figures.) The following example shows the method used to arrive at the total length of arc of tooth contact with the work for each inch of length of cut when using the 80-deg work position and the $1^1/_2$-in. width of cut

$$\frac{1.509\,(\text{Length of arc of contact}) \times 238\ (\text{rpm})}{2\,(\text{Inches per minute}) \times 12\ (\text{inches to feet})} = 14.96\ \text{ft}$$

The lengths, given in Table 3, were compiled for the several work positions, and the graph shown in Fig. 21 was plotted from them. This graph shows that there is a marked difference in the distance which a cutter tooth has to travel as the work position changes from either side of the central position where the center line of cutter and center line of work coincide.

This information is also expressed on a percentage basis, using the position where the arc of contact is shortest, as at 100 per cent.

In order to determine the effect of changing the width of the work on the length of arc of tooth contact with the work, similar data were compiled for both 1-in. and 2-in. cuts.

Using the data compiled for the $1^1/_2$-in-width cut in Table 3,

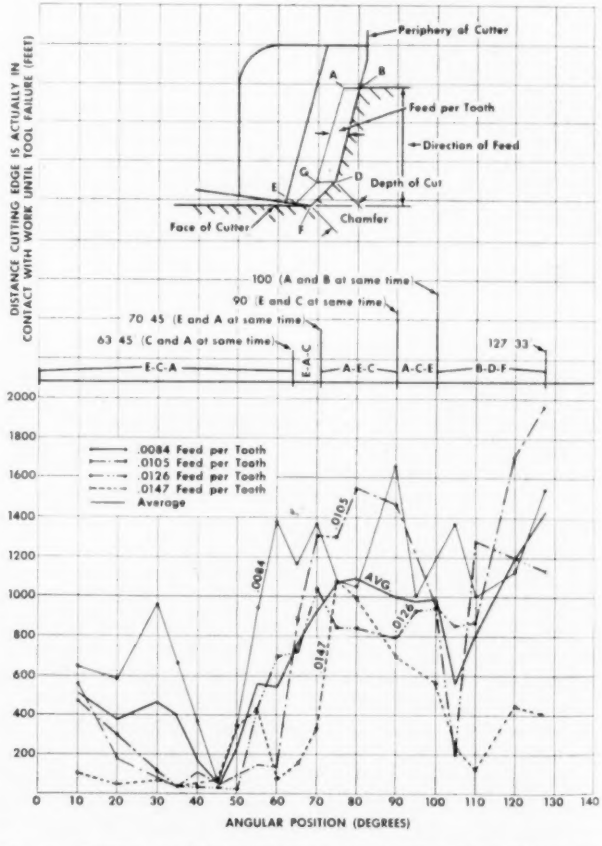


FIG. 22 EFFECT OF WORK POSITION ON CUTTER LIFE BASED ON LENGTH OF TOOTH PATH THROUGH THE WORK

TABLE 3 EFFECT OF WORK POSITIONING AND WIDTH OF CUT ON LENGTH OF TOOTH

Angular position of entrance point on work, E	Length arc-of-contact tooth makes with work, B, in.			Total length arc-of-contact tooth makes with work for each inch length of cut, ft			Per cent total length of arc-of-contact with work using position of minimum contact as 100 per cent		
	W =	W =	W =	W =	W =	W =	W =	W =	W =
deg	1 in.	1½ in.	2 in.	1 in.	1½ in.	2 in.	1 in.	1½ in.	2 in.
5	2.565	3.253	3.857	25.43	32.20	38.25	256	215	191
10	2.278	2.960	3.560	22.59	29.40	35.31	227	197	177
20	1.843	2.487	3.066	18.27	24.66	30.40	184	165	152
30	1.534	2.136	2.690	15.21	21.15	26.67	153	142	133
40	1.322	1.884	2.414	13.11	18.65	23.93	132	125	119
50	1.178	1.708	2.219	11.68	16.90	22.01	117	113	110
60	1.065	1.593	2.094	10.56	15.83	20.77	106	106	104
70	1.028	1.528	2.031	10.19	15.16	20.14	102	101	100
75–31–22	...	...	2.021	...	...	20.04	...	...	100
79–11–35	...	1.509	...	...	14.96	...	...	100	...
80	1.004	1.509	2.028	9.95	14.96	20.11	100	100	100
82–49–09	1.002	...	...	9.94	...	...	100	...	...
90	1.011	1.538	2.094	10.02	15.24	20.77	101	102	104
100	1.052	1.625	2.258	10.43	16.06	22.40	105	107	112
110	1.138	1.802	2.608	11.28	17.83	25.86	113	119	129
118–58–17	...	...	3.552	...	...	35.23	...	...	176
120	1.298	2.167	...	12.87	21.50	...	130	144	...
127–32–39	...	2.954	...	...	29.25	...	...	195	...
130	1.621	...	...	16.08	...	...	162	...	...
137–15–15	2.276	...	...	22.57	...	...	227	...	...

and shown in the graph in Fig. 21, a new set of tool curves as shown in Fig. 22 was developed to take the place of those shown in Fig. 6. This was done by multiplying "the distance traveled to tool failure," expressed in inches, by the "total length of arc of contact with the work for each inch length of cut," expressed in feet, and plotting the result against the various work positions.

This set of curves follows the same general pattern as those shown before in Fig. 6, and these curves:

1 Amplify the point that at both the low and the high angular work positions, the rapid failure of the cutting edge on the cutter tooth is accentuated by the increased distance that it is actually in contact with the cut.

2 Clearly show that there are critical work positions at 45 and 105 deg.

3 Also show the effect of the tooth engagement with the work at the 63-deg 45-min, 70-deg 45-min, 90-deg, and the 100-deg work positions in about the same manner as when rated on the actual distance traveled to point of tooth failure.

Effect of Changing Corner Angle on Work Positioning

It frequently happens that the outline of the workpiece, where the cutting edge first contacts it, is of such a shape that a corner angle other than 15 deg is required to keep the corner of the cutter from hitting the work first.

Fig. 23 (*a*) shows a condition where a cutter tooth having a 15-deg corner angle and a small chamfer contacts the work first next to the face of the cutter. This naturally results in short cutter life because the intersection M of the chamfer at the face of the cutter usually chips out first.

Fig. 23 (*b*) shows the same work outline. However, the cutter tooth has been reground to an increased corner angle of 45 deg, which takes the initial contact with the work at some point N at a distance from the intersection of the corner angle and the chamfer. This slight change of conditions prolongs the life of the cutter.

When all the data from the test runs made with a face mill having a 15-deg corner angle used on work with a square corner (90-deg included angle) had been compiled, it was learned that the best work-position angles were between 70 deg 45 min and 100 deg. The analysis of the $^1/_{32}$-in. × 45-deg chamfer angle showed that the best work-position angles for a 45-deg angle were between 90 and 100 deg.

The same analysis also showed that the high limit of this range of best work-position angles was always a constant for a given negative radial rake angle on a cutter, and was equal to 90 deg plus the negative radial rake angle on the cutter, irrespective of the corner angle.

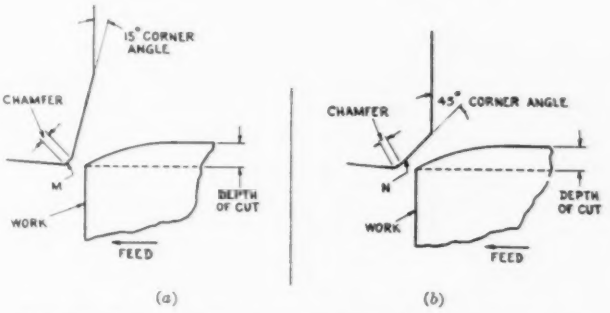


Fig. 23 Effect of Changing Corner Angle to Suit Work Contour

The analyses showed that the low limit of this range of the best angular work positions is at the work-position angle where the initial point of contact of the face of the cutter tooth and the work begins at M, in Fig. 23. A change in the corner angle on the cutter changes the angular work position where the initial contact at the point A, which was shown previously in Fig. 6, actually begins. For a 15-deg corner angle, the work position is 70 deg 45 min. For a 45-deg corner angle, the angular work position is 90 deg.

The curve X shown in Fig. 24 was developed as an aid in obtaining the best angular work positionings for other corner angles. This curve covers the work positions shown previously in Fig. 11, where points A and C contact the work at the same time. This curve shows that as the corner angle is increased with all other conditions identical, the range of operation of the best angular work position decreases, and vice versa.

Curve Y shows a similar line plotted to indicate where the face of the tooth makes initial contact at A and E at the same time, which is followed by contact at C. This set of conditions was shown in Fig. 13. The location is important because it tends to reduce cutter life. It also tends to decrease the width of range of longest cutter life as the corner angle increases.

All tests made while using the cutting angles of 15 deg corner angle, 10 deg negative radial rake, and 10 deg negative axial rake clearly indicated that the cutter life would tend to be at its lowest whenever the initial tooth contact with work would be at an angular position of 70 deg 45 min or less. This forces the work positions which gave the longest cutter life into the narrow operating band between 70-deg 45-min and 100-deg angular positions, as indicated by the curve marked 0.0105, which was previously shown in Fig. 6. This same curve also shows practically no cutter life for all angular positions of 60 deg or less.

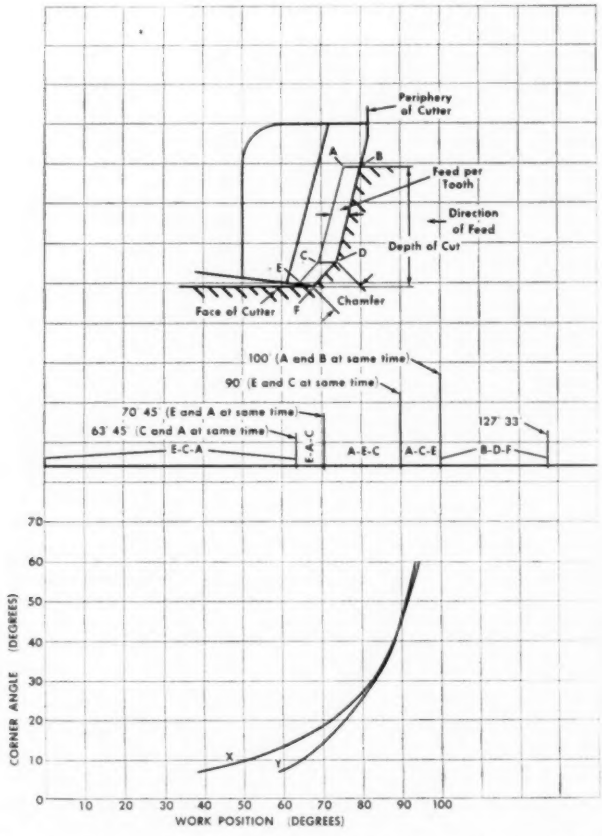


FIG. 24 GRAPHS SHOWING HOW CRITICAL-POINT POSITIONS VARY WITH CORNER ANGLE

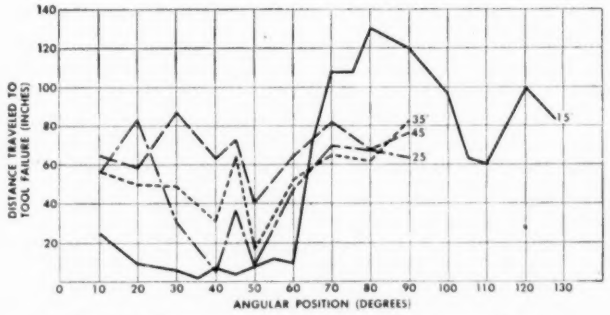


FIG. 25 EFFECT OF CORNER ANGLE ON CUTTER LIFE

The last-mentioned conditions offer a real challenge, and so a series of 60 runs was made with 40 tools while using increased corner angles to determine some means whereby the cutter life in general could be improved. The tools used were ground as follows: 14 tools to a 25-deg corner angle, 13 to a 35-deg, and 13 to a 45-deg corner angle. All other tool angles were kept the same as were ground on the tools which had the 15-deg corner angle, except for those tools with the 45-deg corner angle. In this case no chamfer was ground between the corner angle and the face of the cutter. Instead, it was broken lightly with a 320-grit silicon-carbide stone. A total of 20 runs were made for each set of tools which had the same corner angle, while using the work positions ranging between the 10 and 90 deg.

All the operating conditions were duplicated while using a table travel of $2^1/_2$ ipm (0.0105 in. feed per tooth). The distance traveled in inches per minute up to the time of tool failure was plotted for each one of the various work positions and corner angles, as shown in Fig. 25. The tool-life curve, previously shown as Fig. 6, for the same feed per tooth when using a 15-deg corner angle was also duplicated.

GENERAL CONCLUSIONS

A comparison of the four curves shows that for a face mill having a 10-deg negative radial rake and a 10-deg negative axial rake and operated under the conditions as already outlined:

1 Cutter life reaches maximum when a 15-deg corner angle is used. The only way this maximum cutter life can be obtained is by using special care to see that the initial point where the tooth enters the work lies between the 70-deg 45-min and the 100-deg work positions.

2 The limited long-life working range between the 70-deg 45-min and the 100-deg positions, when using a 15-deg corner angle, makes it necessary for the face mill to overhang the entrance side of the work by an increased amount. This results in the use of face mills slightly larger in diameter than have been ordinarily used on most face-milling jobs.

3 Cutter life is at its minimum with a 15-deg corner angle when the initial point where the tooth enters the work lies between the zero-deg and the 70-deg 45-min work positions.

4 Cutter life can be improved by using corner angles greater than 15 deg when it becomes necessary to operate a face mill within the zero-deg to 70-deg 45-min work positions.

5 When a 25, 35, or 45-deg corner angle is used, the cutter life for the 70-deg 45-min to 100-deg work position is only from 50 per cent to 60 per cent of that obtained from a face mill which has a 15-deg corner angle.

6 Any face mill with a 45-deg corner angle will produce the maximum cutter life when practically no attention at all is given to work positioning. The 35-deg and then the 25-deg corner angles rate next in the order given.

7 Mediocre but somewhat consistent results can be obtained with a face mill having a diameter slightly larger than the work width, provided that it has a 45-deg corner angle.

8 The face mill can be adapted to various face-milling operations by grinding an appropriate corner angle on it and then properly positioning the cutter entry edge of the work to the cutter. This indicates the possibility of standardizing carbide-tipped face mills and adapting them to a large number of jobs.

9 Cutter life was shortest for the 45-deg work position when operating a face mill with a 15-deg corner angle at all feeds per tooth. When the corner angle was changed to either 25, or 35, or 45 deg, the cutter life was considerably longer for the same position. However, the one work position which gave the reduced cutter life was transferred to two positions, one at 40 deg and the other at 50 deg, on either side of the 45-deg position. This set of conditions is worth further analysis. It must be kept in mind that all conclusions were reached as a result of using a face mill on work having a $1^1/_2$-in-width cut.

While these tests were being run, it was observed that when runs were made at the critical 45-deg work-entry position the cutter life could be increased many times for some cuts wider than $1^1/_2$ in., even though the stock removal was much greater. This seems to indicate that the position where a cutter tooth leaves the work or a possible variation in cutter-flywheel-spindle momentum may affect cutter life. This is another phase of work positioning which will be given extensive study in the future.

(Owing to travel emergency conditions existing when this paper was presented, discussion will be accepted until March 11, 1946)

Circular Bulging of Aluminum-Alloy Sheet at Room and Elevated Temperatures[1]

By GEORGE SACHS,[2] GEORGE ESPEY,[3] AND G. B. KASIK[3]

In this paper preliminary results are reported on the strength characteristics and forming limits of various aluminum-alloy sheet, when subjected to hydraulic pressure over a circular area at temperatures up to 500 F. The strain distributions were analyzed by means of a photogrid, after these bulges failed. The bulges exhibited a practically balanced biaxial strain state over most of the contour with the exception of a very narrow range of local deformation in the vicinity of the fractures. The maximum meridional strain outside the necked area observed at the pole of a bulge, in spite of its biaxial nature, generally exceeded the uniform elongation known from tensile tests. The forming limits for all annealed conditions increased considerably with increasing temperature if the temperature exceeded a certain critical value, between 250 and 400 F, depending upon the alloy. The heat-treated conditions of the alloys 24S and 61S were only slightly affected by the testing temperature, while the forming limits (uniform stretch) of 75S-T, R301W, and R301T were materially increased at elevated temperatures. The reduction of thickness, which is a measure of the ductility of an alloy, followed approximately the same trend as the forming limit.

THE use of a fluid as a pressure medium has been restricted in the past primarily to testing purposes and to such minor cold-forming operations as the bulging of recesses in tubular parts. However, various shapes can be formed by bulging or hydraulic application of uniform pressure to one side of a sheet over a confined area. This process has found a restricted commercial application for the forming of letters and other shapes on signs.

Temperatures in the vicinity of 400 F (200 C) are, to a small extent, being used in the bending, joggling, and dimpling of high-strength aluminum-alloy sheet. The application of temperatures in this range presumably does not impair the properties of high-strength alloys.

Hydraulic bulging at elevated temperatures has been used successfully for the fabrication of magnesium-alloy parts. On the contrary, this method has previously not been found useful for the hot-forming of aluminum alloys, as an excessive temperature was considered necessary, 850 F (450 C), approximately.

The test results obtained on this project, however, indicate that temperatures between 250 and 400 F (120 to 200 C) substantially improve some forming characteristics of a number of high-strength aluminum alloys.[4] This fact, if substantiated by further experimentation, may render forming by means of hydraulic pressure at elevated temperatures a valuable addition to the various commercial methods of aluminum-alloy-sheet forming.

Examples of specimens bulged for this investigation are shown in Fig. 1.

The metal at the crown or pole of a circular bulge is subjected to a practically uniform tensile stress, and tensile strain in all directions parallel to the metal surface. This applies throughout the test until the "forming limit" is reached when failure by local necking or fracturing occurs. Such a "balanced biaxiality" constitutes a fundamental stress-and-strain state, for it is a borderline case which many types of actual forming operations approach and which is present in aircraft and other structures in service. Therefore, rather than measure the depth of the cup or bulge at the moment of failure, the unit strains (in the vicinity of the break) which the metal exhibits after failure, were determined. These are considered as important metal characteristics.

No attempt will be made, at present, to evaluate the fundamental significance of the data discussed here. Further reports will cover various other phases of cold- and hot-forming aluminum alloys, and their fundamental analysis.

MATERIAL, EQUIPMENT, AND PROCEDURE

Materials Tested

Twenty-one different conditions of seven aluminum alloys (3S, 52S, 61S, 24S, 75S, R301, and R303) were tested. The alloys 3S, 52S, and 61S are supplied in bare (unclad) sheets, and only bare R303 was tested. 75S and R301 were available only as clad sheet, and alloy 24S was tested both bare and clad.

For the general tests on circular bulges, sheet of the same thickness for all alloys, $0.040\ ^{+0.002}_{-0.0015}$ in., was selected. For any particular alloy condition, specimens were cut from a single sheet for which the thickness variations were within ±0.001 in.

The yield strength, tensile strength, and elongation (2 in. gage length) in both the transverse and longitudinal (rolling) directions are assembled in Table 1.

The various alloy conditions are assembled into two main groups and four subgroups as follows:

Group I Annealed Sheet	Group II Heat-Treated Sheet
(A) Nonaging alloys	(A) Room-temperature-aged alloys
(B) Heat treatable alloys	(B) Artificially aged alloys

[1] This paper is the first published report on the research program on hot-forming of aluminum alloys conducted at Case School of Applied Science under contract with the Office of Production Research and Development of the War Production Board. This research, which was supervised by the War Metallurgy Committee under the "restricted" Project NRC-547, is the basis of this paper which has been released for publication by the O.P.R.D.

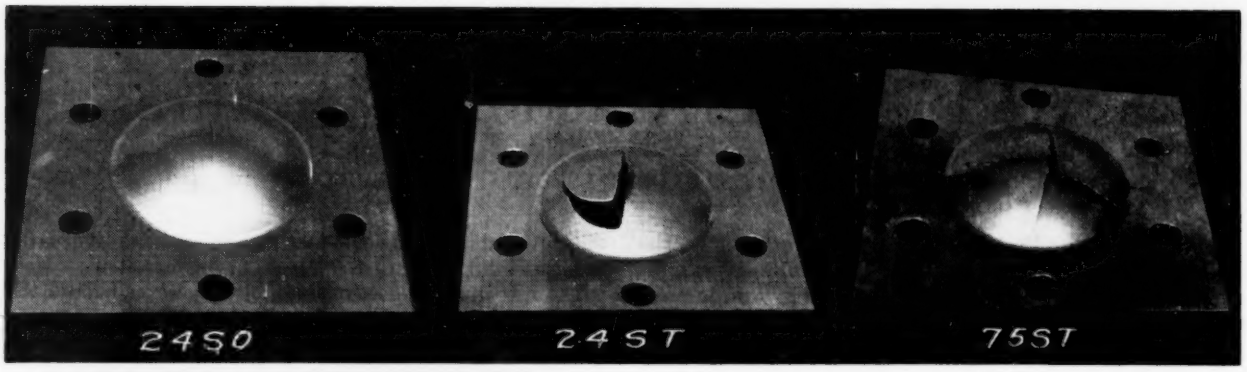
[2] Professor of Physical Metallurgy, Case School of Applied Science, Cleveland, Ohio. Mem. A.S.M.E.

[3] Department of Metallurgical Engineering, Case School of Applied Science.

Contributed by the Metals Engineering Division of The American Society of Mechanical Engineers.

Note: Statements and opinions advanced in papers are to be understood as individual expressions of their authors and not those of the Society.

[4] A particularly valuable application of hot-forming, at these temperatures, has been found to be the roll-forming of sections in the rather brittle high-strength alloys, suggested recently by an unpublished report on another phase of this W.P.B. research investigation.



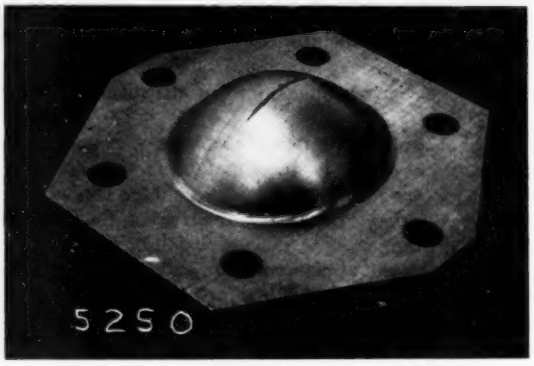


FIG. 1 TYPICAL HYDRAULIC CIRCULAR BULGES

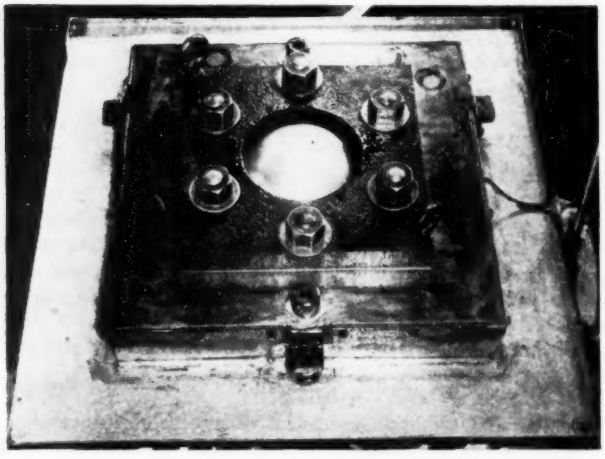
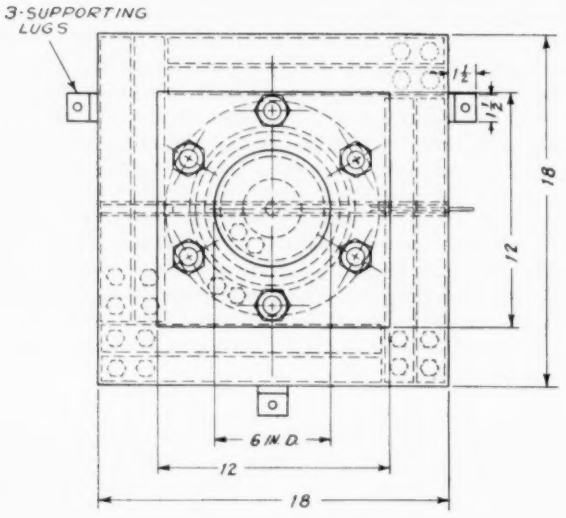


FIG. 2 HEAD FOR HOT HYDRAULIC CIRCULAR BULGING WITH SPECIMEN IN PLACE



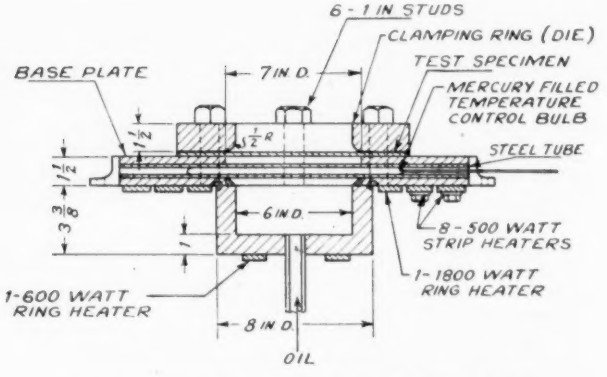


FIG. 3 DETAIL OF HOT HYDRAULIC BULGING HEAD

The alloys investigated represent all conditions for the structural alloys of high strength available at present for production and a few additional alloys which are also used in aircraft fabrication, because of their superior forming properties.

DETAILS OF EQUIPMENT

The equipment[5] consisted of a bulging head and a hot-oil displacement cylinder capable of furnishing oil under pressure up to 3000 psi to the head on which the specimen was clamped, Figs. 2 and 3. The clamping ring (die) had a $^1/_2$ in. radius to prevent tearing of the specimen at the edge of the die contour. Originally, an as-machined surface of both the base plate and clamping-ring interfaces provided satisfactory gripping surfaces. As the die became nicked it was necessary to serrate the surface with four buttress teeth per inch ($^1/_8$ in. deep $\times$ $^1/_4$ in. long).

Oil pressure for the bulging was supplied from a displacement

[5] The equipment for these tests was developed by E. J. R. Hudec and C. L. Bennett, Instructors under the supervision of G. B. Carson, Associate Professor of Mechanical Engineering, Case School of Applied Science.

TABLE 1 TENSILE PROPERTIES OF SHEET USED IN HOT HYDRAULIC CIRCULAR BULGING

(Each Value represents average from two tests)

SHEET ALLOY	TRANSVERSE SHEET THICK. IN.	TRANSVERSE YIELD STR. PSI	TRANSVERSE TENSILE STR. PSI	TRANSVERSE ELONG. IN 2" %	LONGITUDINAL YIELD STR. PSI	LONGITUDINAL TENSILE STR. PSI	LONGITUDINAL ELONG. IN 2" %
GROUP I-A							
3S0	.041	7520	17100	31.5	7400	17200	32.0
52S0	.039	13800	26300	25.0	13700	27900	24.0
GROUP I-B							
24S0 Bare	.0415	14500	33400	17.0	14400	34500	17.5
24S0 Clad	.039	12500	28200	17.5	12800	39100	16.0
R3010(Clad)	.0395	10400	23700	19.5	10600	25500	23.0
75S0 (Clad)	.040	16100	32300	14.0	16700	33100	14.0
61S0	.040	7800	17300	24.5	8220	17800	26.0
GROUP II-A							
24ST Bare	.0395	43700	67400	17.5	48400	69500	19.5
24ST Clad	.0395	41300	64700	17.0	47200	65700	17.0
24SRT Bare	.0395	55000	71000	13.5	60200	72400	13.5
24SRT Clad	.0385	51600	67500	13.0	59200	69300	11.5
R301W(Clad)	.038	36200	61300	19.5	40700	63600	21.5
61SW	.038	29700	41300	15.5	33000	42000	17.0
GROUP II-B							
24ST81 Bare	.040	60400	68900	5.0	62600	70800	7.0
24ST81 Clad	.040	59500	66500	5.5	62300	68000	6.5
24ST86 Bare	.041	65900*	72800	4.5	66400*	72800*	5.5
24ST86 Clad	.040	63400	69400	5.0	65100	70200	6.0
R301T (Clad)	.0375	57600	69100	10.5	60900	70100	10.5
75ST (Clad)	.041	64400	78000	12.0	70700	80500	12.0
61ST	.039	38100	46000	13.0	39800	46600	13.5
R303T315 (Bare)	.041	67100	75500	9.5	70000	76200	9.0

*Does not meet minimum specified by the Army Air Force Specification, No. 11354.

cylinder, the piston of which was actuated by the lead screw of a broaching machine that was driven from a variable-speed drive, Figs. 4 and 5. The total volume-displacement capacity of the cylinder was 95 cu in.

The bulging pressure was recorded by a helical-type 3000-psi recording pressure gage tapped into the oil line connecting the bulging head and displacement cylinder. A synchronous-motor drive for the recording chart permitted the recording of a pressure-time (stroke) curve for any desired test.

The elevated temperatures were obtained by heating the lower plate, the reservoir, and the oil-displacement cylinder by means of resistance heaters. A mercury-tube temperature-control switch, sensitive within ±5 deg F, inserted into the base plate, controlled the temperature of the bulging head and the oil in the head. Two manually adjusted thermoswitches (50–600 F) were used for controlling the temperature of the oil in the displacement cylinder. The actual temperature was indicated by a thermometer set in a well in the exhaust end of the cylinder, Fig. 5.

The temperature of the specimens and various parts of the bulging fixture was determined (within ±3 deg F) with a Cambridge surface pyrometer, mold type, 50–600 F range, having a minimum accuracy of 2 per cent of full scale.

To protect the operators from the danger of hot oil at high pressure, a safety-glass cover was constructed to fit over the bulging head, Fig. 4. The cover was built of $^1/_4$-in. heat-tempered plate glass set in a $^1/_8 \times$ 1-in. angle-iron frame.

For the low-temperature (30–50 F) tests, a small 3-gpm rotary gear pump was employed by which refrigerated oil was pumped from a 5-gal sump, containing dry ice as a coolant, to the reservoir of the bulging fixture, and thence circulated through the displacement cylinder. Dry ice was placed around the bulging head to maintain it at testing temperature.

Testing Procedure

A 20-line-to-the-inch orthogonal grid was applied to one side of each test specimen by a modification of the photogrid process



FIG. 4 EQUIPMENT FOR EXPERIMENTAL HYDRAULIC BULGING

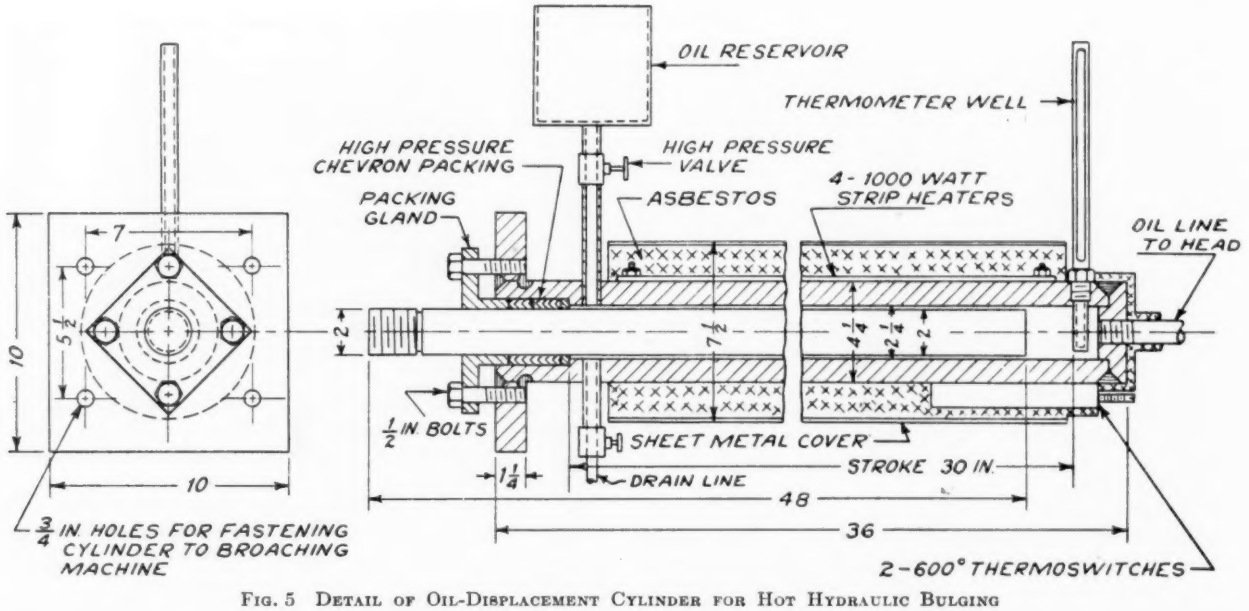


FIG. 5 DETAIL OF OIL-DISPLACEMENT CYLINDER FOR HOT HYDRAULIC BULGING

(1, 2).[6] The grid lines were applied parallel to the transverse and longitudinal directions of the sheet. The maximum variation of the grid for $^1/_2$ in. gage lengths was 0.5 per cent.

The 12-in-sq test specimens were set in a jig and drilled with six $1^1/_{16}$-in-diam holes to accommodate the 1-in. studs in the base plate.

The bulging head, with the clamping ring in place, and the displacement cylinder were held at the predetermined testing temperature for at least 15 min prior to the start of a given run. To minimize the temperature gradient across the bulge and to insure the absence of air in the head, care was exercised to have the oil level in the reservoir flush with the surface of the base plate before placing a test specimen on this fixture.

The general testing procedure was to place the test specimen on the bulging head, set the preheated die loosely in place and allow 10 min time in which to take several temperature determinations around the bulge, and then tighten the clamping ring onto the specimen. It was found that the sheet reached a constant temperature within 2 min after being placed on the bulging head. The circular edge of the sheet next to the die was generally above the temperature of the center of the sheet by 5 to 10 deg F in the vicinity of 250 F and 10 to 20 deg F in the vicinity of 500 F.

The tightening of the die, which took a few minutes, was deferred until near the end of the 10-min period (after 7 min of preheating), for it was found that premature tightening favored heat-warping of the restrained sheet specimen. After the 10-min heating period the safety cover was placed over the head and the actual bulging was started and proceeded without interruption until failure. The forward speed of the piston was held constant throughout these tests at $5^3/_8$ ipm; this gave a displacement volume of 17.7 cu in. per min. Each test required approximately 2 min for the actual bulging operation. The time required to remove the clamping plate brought the total time for each test, during which the sheet specimens were exposed to the elevated temperature, to between 14 and 16 min.

For the purpose of comparing the properties of the various alloys at different testing temperatures, the maximum bulging pressure or "bursting pressure" has been used as a measure of the metal strength. In addition, the strain distributions along the "principal axes" after failure of the specimens were determined, and the ductility characteristics were obtained, as discussed in the following section.

Measurement of Strains

The over-all investigation, of which this paper is a part, entails the consideration of the effects of various degrees of stress biaxiality. For a better understanding of the forming limits, this necessitates the theoretical consideration of various geometrical shapes, which include the border cases of a flat sheet, a tube, and a sphere. It has been found necessary to deviate from general practice and adopt a different and comprehensive system of co-ordinates and directions which will permit an unambiguous description of any stress or strain in any given part.

A system of co-ordinates which will fit those cases having two perpendicular planes of symmetry for which the strains are measured along the "principal axes" has been selected as follows: The intersection of the two planes of symmetry and surface will be designated as the "pole." For any point on the surface, the "normal direction" N is readily recognized as the direction perpendicular to the surface at that point, Fig. 6. A "meridian line" is taken to be the intersection between the part surface and a plane passing through the pole and the line normal to the surface at the point under consideration. At the given point, the "meridian direction" M is determined by the line of tangency to the meridian line. The "latitude direction" L is defined as the perpendicular to both the normal and meridian directions at the point under consideration. The relation of these terms to those used for a plane, a tube, and a sphere are readily recognized; they are assembled in Table 2.

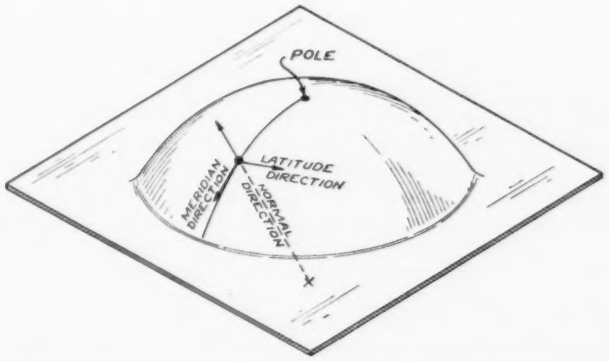


Fig. 6 Diagrammatic Representation of Co-Ordinate Designations

TABLE 2 TERMS USED IN STUDIES

Adopted terms	Common terms		
	Plane	Tube	Sphere
Normal N	Normal	Normal or radial	Normal or radial
Meridian M	(In the surface, longitudinal or transverse)	Axial or longitudinal	Circumferential or tangential
Latitude L		Circumferential or tangential	Circumferential or tangential

In the case of an extended part, the "principal axes" will be defined by the intersections between the part surface and the two symmetry planes. The axis in the direction of the larger dimension will be designated by the letter a, and that of the smaller dimension by the letter b. Even in the case of a circular bulge such axes are also necessary to designate the grain direction.

For the circular bulge the a-axis has been chosen as parallel and the b-axis as perpendicular to the rolling direction of the sheet. The strains have been designated as "meridional" e_{aM} or e_{bM}, if measured along the axes a and b, respectively, and "latitudinal" e_{aL} or e_{bL} if measured perpendicular to the axes, where the subscripts a and b refer to points along the a- and b-axes, respectively. Strains not measured at points on one of the principal axes will be referred to a special set of co-ordinates for the particular case in question.

It was observed in the tests, as discussed later, that the strain distributions were usually characterized by a rather flat maximum at the pole of the bulge, disregarding a very narrow range containing the failure. These maxima in the principal meridional directions of the sheet were considered as the "forming limits" for the bulging processes, Figs. 9 to 12, inclusive, and represent the maximum amount of strain which the metal permits without failure by local necking or fracture. The strain at the forming limit for a bulged part could not be obtained in the same manner as for a regular tensile test specimen, i.e., by measuring a value of strain some distance away from the fracture. The measurements of the strain along the two major axes of the specimen, Fig. 7, with w, and cross-grain x, however, revealed that the strain values both parallel to the direction of each axis or "meridional," and perpendicular to the direction of each axis or "latitudinal," increased continuously from a zero value somewhere at the radius of the die to a maximum value at the crown of the bulge; a few representative plots are illustrated in Figs. 7 and 8.

For a rapid determination of the forming limits, the strains occurring in an area approximately 3 in. sq and in the proximity

[6] Numbers in parentheses refer to the Bibliography at the end of the paper.

of the pole of the bulge were measured along and in the direction of the principal axes by means of a strip of orthogonal co-ordinate paper to within $^1/_2$ per cent (stretch). A gage length of $^1/_2$ in. was generally used, although in some cases a gage length of $^1/_4$ in. was necessary for measurements near the break and in directions intersecting the failure on both sides (these values of $^1/_4$ in. gage length are distinguished by parentheses in the curves). No such measurements were made closer than $^1/_8$ in. to the fracture, nor across the fracture, i.e., including the fracture. A number of curves obtained in this manner are represented in Figs. 9 to 12, inclusive. That these measurements do not include the necked regions is shown by the thickness distribution perpendicular to the locus of failure, Fig. 13. From the figure it can be seen that for the very ductile alloy 52S-O, the necked region does not extend more than 0.01 in. on either side of the fracture.

The "reduction in thickness," at the point of failure constitutes another metal characteristic, corresponding to the contraction in area (reduction of area) of a regular tensile test presumably measuring the ductility of the metal. This value was determined by measuring the thickness of the sheet at the fracture by means of a measuring microscope at ×10 magnification. Three readings approximately evenly spaced over a total distance of $^1/_2$ to 1 in. at the center of the primary fracture yielded values which could be readily reproduced.

In order to obtain the local (normal) strain distribution in the circular bulge in the vicinity of failure, thickness measurements were made with a measuring microscope at appropriate intervals on specimens sectioned in a plane perpendicular to the locus of failure. Reduction in thickness values thus obtained for two alloys yielded quite smooth strain-distribution curves, Fig. 13.

General Characteristics of Strain Distribution

The agreement between the meridional strains along the two principal axes was rather close. The maximum was flat and quite definite for all specimens yielding uniform stretch values of less than 25 per cent, Figs. 7 to 12, inclusive. The maximum was sharper for more ductile materials and differed slightly in position and value along the two axes, a difference of up to 3 per cent for temperatures below 375 F, and of up to 6 per cent for the tests at higher temperatures being observed. Less regular curves were occasionally obtained at the highest testing temperatures, probably because of slight variations in temperature. It appeared that if the temperature differences over the surface of the bulge exceeded 10 deg F during the test, such irregularities resulted.

The values of both the meridional and latitudinal strains measured along any one meridional axis, showed a variation up to $\pm 2^1/_2$ per cent (stretch) for a meridian distance within 2 in. from the crown or pole of the bulges; this change was greatest for the soft alloys and/or tests at high testing temperatures, Figs. 7 to 12, inclusive.

The depth of a bulge within an accuracy of ±10 per cent was primarily a function of the forming limit. The depth corresponding to various values of uniform stretch was approximately as follows:

Stretch, per cent	10	20	30	40	50	60
Depth, In.	1	$1^1/_2$	2	$2^3/_8$	$2^5/_8$	$2^7/_8$

The measured values for reduction in thickness generally exceeded those calculated from the meridional strains. The meaning of these values which should measure the local ductility of the metal is rather obscure, as a radical change of stress state from balanced biaxiality to plane strain occurs as soon as local necking begins. No attempts have been made, as yet, to evaluate the significance of the reduction-in-thickness measurements.

Some thickness measurements in a plane perpendicular to the

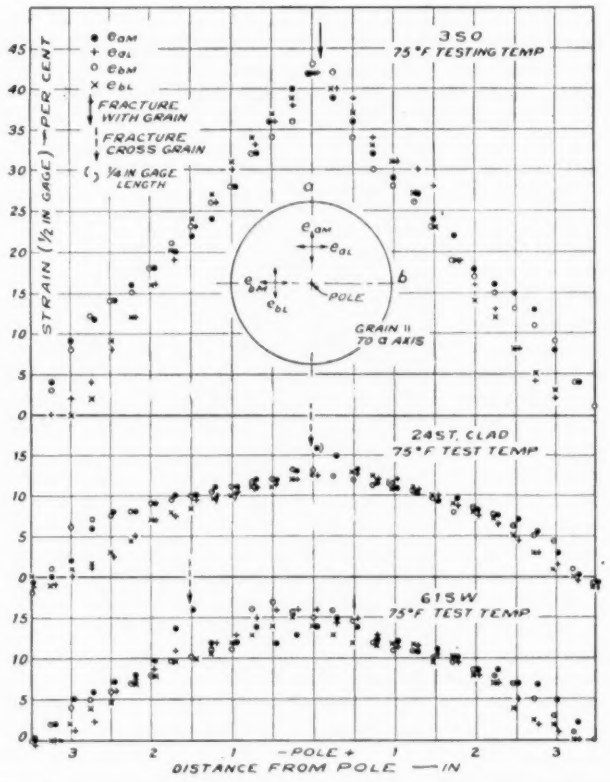


Fig. 7 Latitudinal and Meridional Stretch Distribution for Hydraulic Circular Bulges of Various Alloys Tested at Room Temperature

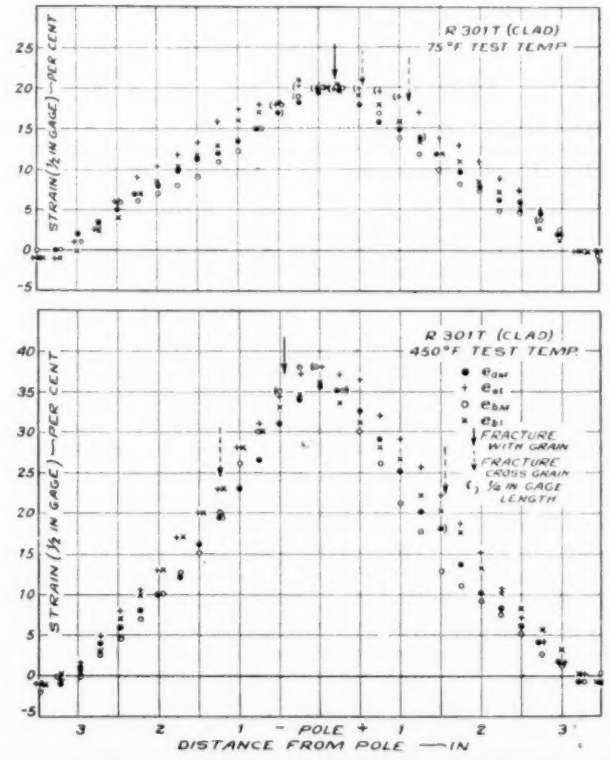


Fig. 8 Effect of Testing Temperature on Distrubution of Latiudinal and Meridional Stretch for R301T Clad, Hydraulically Bulged

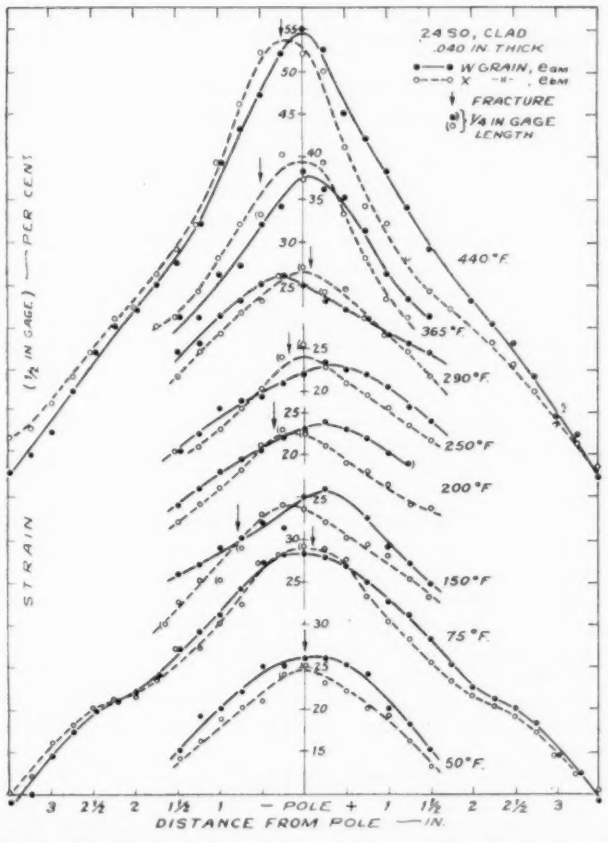


FIG. 9 MERIDIONAL STRETCH DISTRIBUTION FOR CIRCULAR BULGES OF 24S-O CLAD, HYDRAULICALLY BULGED AT VARIOUS TEMPERATURES

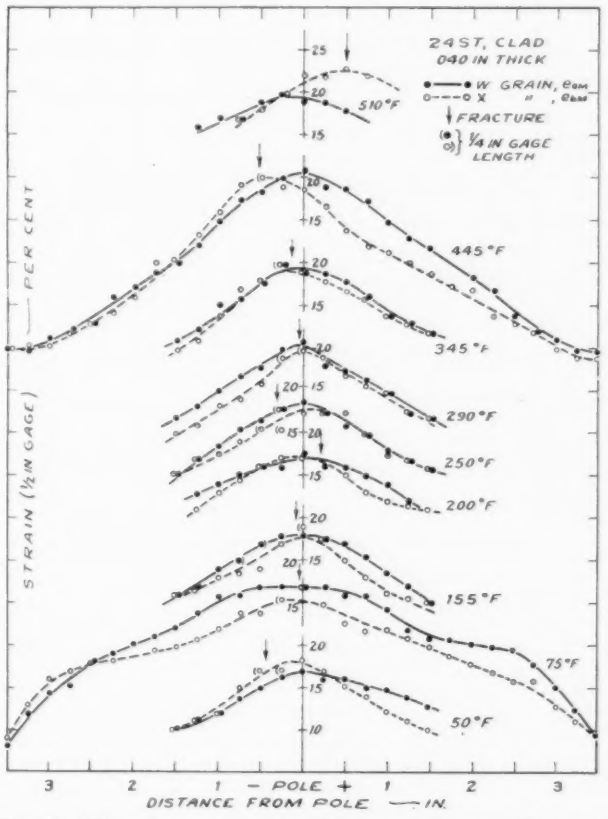


FIG. 10 MERIDIONAL STRETCH DISTRIBUTION FOR CIRCULAR BULGES OF 24S-T CLAD, HYDRAULICALLY BULGED AT VARIOUS TEMPERATURES

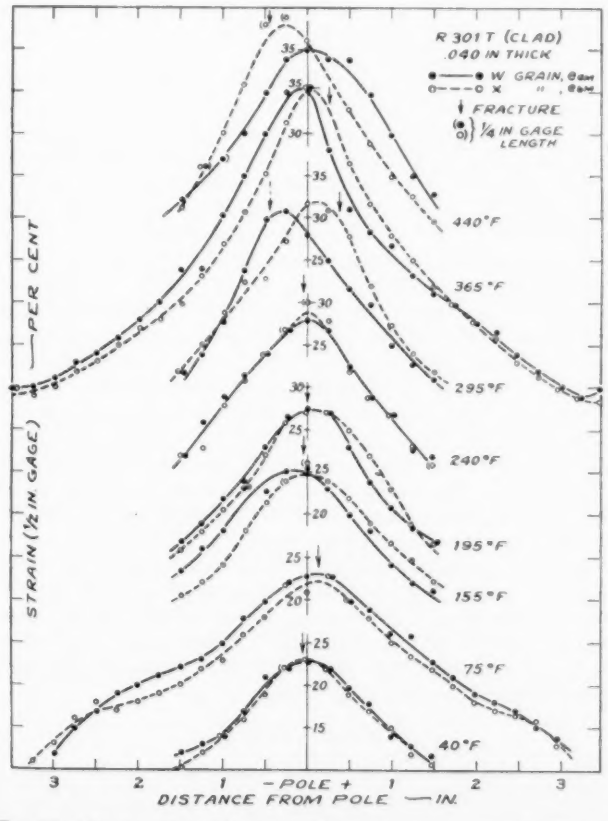


FIG. 11 MERIDIONAL STRETCH DISTRIBUTION FOR CIRCULAR BULGES OF R301T CLAD, HYDRAULICALLY BULGED AT VARIOUS TEMPERATURES

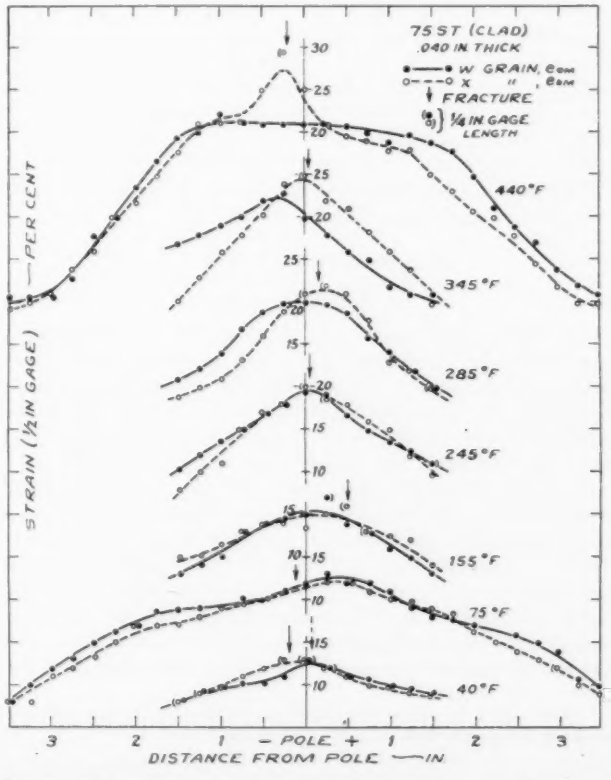


FIG. 12 MERIDIONAL STRETCH DISTRIBUTION FOR CIRCULAR BULGES OF 75S-T CLAD, HYDRAULICALLY BULGED AT VARIOUS TEMPERATURES

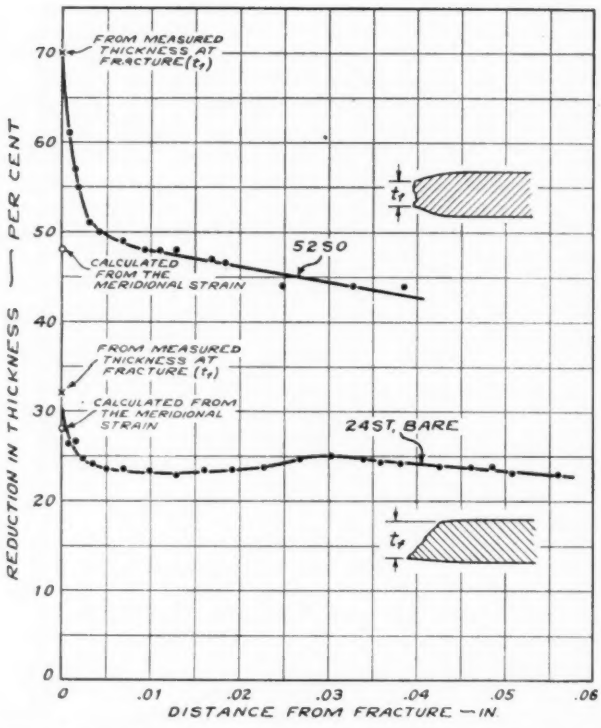


FIG. 13 REDUCTION IN THICKNESS IN VICINITY OF FRACTURE FOR TWO REPRESENTATIVE ALLOYS TESTED AT ROOM TEMPERATURE

locus of failure show that the strain gradually increases toward the locus of failure and that the larger fracture strain only affects a very narrow region,[7] Fig. 13. A very ductile alloy, 52S-O, yielded practically the same forming limits from such measurements extrapolated to the fracture, as from the grid measurements. The more brittle alloys, such as 24S-T, exhibited some irregularities in the immediate vicinity of the failure. However, disregarding this range of irregularity the curve of thickness change extrapolates to practically an identical value, as calculated from the average of two meridional-strain values at the pole, as shown in Fig. 13.

The more tedious thickness measurements, therefore, would yield practically the same average value of forming limit as the rather simple grid measurements of the strains.

RESULTS OF TESTS

BURSTING PRESSURE

The bursting pressure can be considered as a semiquantitative measure of the ultimate strength of the metal, under conditions of biaxial tension. While the ratio of bursting pressure to strength is affected by the amount of strain, or rather the curvature of the sheet, at the point of failure, this effect is apparently considerably smaller than that of the testing temperature.

As a general rule, the bursting pressure decreased continuously with increasing temperature above room temperature. Such a behavior is normal for any metal or alloy in a stable condition.

Of the alloys investigated, Figs. 14 to 24, inclusive, those of Group II-A, or the room-temperature-aged conditions, might have been expected to deviate from the general rule if artificial aging had taken place to such an extent that this change exceeded the reverse temperature effect. Obviously, this aging effect was not very pronounced, but a slight hump in the curves of all room-temperature-aged alloys, Figs. 18 to 20, inclusive, can be taken as such an effect.

A comparison of the two investigated nonaging alloys of Group I-A, showed 3S-O to be somewhat more respondent to the effect of temperature on the bursting pressure up to 200 F, while the per cent loss in this property was the same for both alloys at 400 F.

Of the alloys of Group I-B, or the annealed conditions of the age-hardenable alloys, Figs. 15 to 17, inclusive, 24S-O, both bare and clad, was least affected (10 per cent approximately) of all alloys investigated by testing temperatures up to 300 F. On the contrary, the strength of R301-0, 75S-O, and 61S-O, decreased noticeably at rather low testing temperatures, and to a considerable extent, 25 to 30 per cent, at 300 F. Alloy 75S-O suffered the largest decrease of the bursting pressure at still higher temperatures.

In the Groups II-A and II-B, Figs. 18 to 24, inclusive, i.e., room-temperature-aged and artificially aged alloys, respectively, again all 24S conditions exhibited considerably less reduction in strength on increasing the testing temperature than the other alloys, R301, 61S, and R303. At the highest temperatures investigated, 400 F and higher, the reduction of the bursting strength was largest for the alloys 75S and R303.

The absolute values of bursting pressure, of course, varied within wide limits for the different alloys and conditions, ranging between 350 and 1400 psi at room temperature, and between approximately 200 and 800 psi at 400 F. Thus, at 400 F the strength and forming resistance of the high-strength alloys are reduced almost to the values of the softest alloy investigated, 3S-O, at room temperature.

Of the alloys in Group II-A, 24S-T clad and R301-W clad, possessed approximately the same bursting strength at room temperature, while the bursting strength of 61S-W at the same temperature was only 60 per cent of 24S-T clad; 24S-T bare, was the strongest alloy of this group. At 400 F, however, the alloy R301-W required only approximately 70 per cent of the bursting pressure for 24S-T clad and at 450 F was not appreciably stronger than 61SW bare.

Of the heat-treated alloys, 75S-T clad, and R303-T315 bare, were the strongest up to 250 F, and 24S-T81 clad, and 24S-T86 clad, were the weakest at temperatures up to 300 F, while 24S-T bare and clad, R301-W and R301-T, were intermediate, Figs. 20 to 24, inclusive. At temperatures between 300 and 450 F, however, 24S-T required considerably larger bursting pressures than either 75S-T or R301-W, R301-T, and R303-T315.

At the lowest temperature investigated, approximately 35 F, the bursting pressure was usually equal to or slightly higher than at room temperature. Exceptions were 24S-T86 bare and, less pronounced, 24S-T86 clad. The decrease of the bursting strength of these alloys with decreasing temperatures, in the range below room temperature, is explained by the corresponding loss in ductility, which is apparent in both the reduction in thickness and the uniform stretch. The alloys 24S-RT both bare and clad, also exhibited irregular and low strength, and low ductility properties in a temperature range close to room temperature, and up to 250 F. Alloy 24S-T bare and clad yielded rather uniform results on specimens taken from a single sheet.

Artificial aging had very little effect on the alloy R301, while both cold-rolling (RT) and, even more, artificial aging (81 and 86), considerably reduced the bursting strength of 24S, up to a temperature of 400 F. At still higher temperatures, the different aged alloys of either 24S clad, or 24S bare, appeared to possess practically the same bursting strength.

FORMING LIMITS

Regarding the effect of testing temperature on the forming

[7] This region is extremely small as compared with the region of necking in tension tests on 0.50-in-wide specimens.

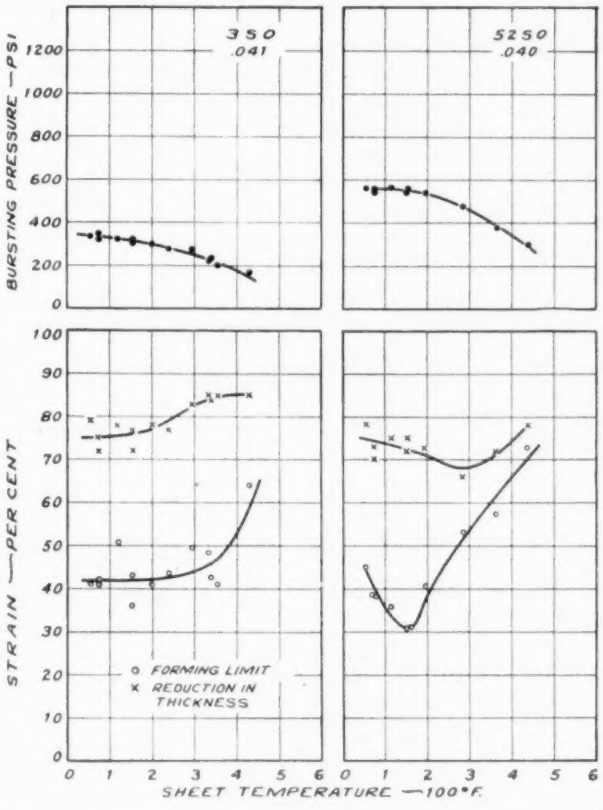


FIG. 14 RESULTS OF HOT HYDRAULIC CIRCULAR BULGING FOR 3S-O AND 52S-O

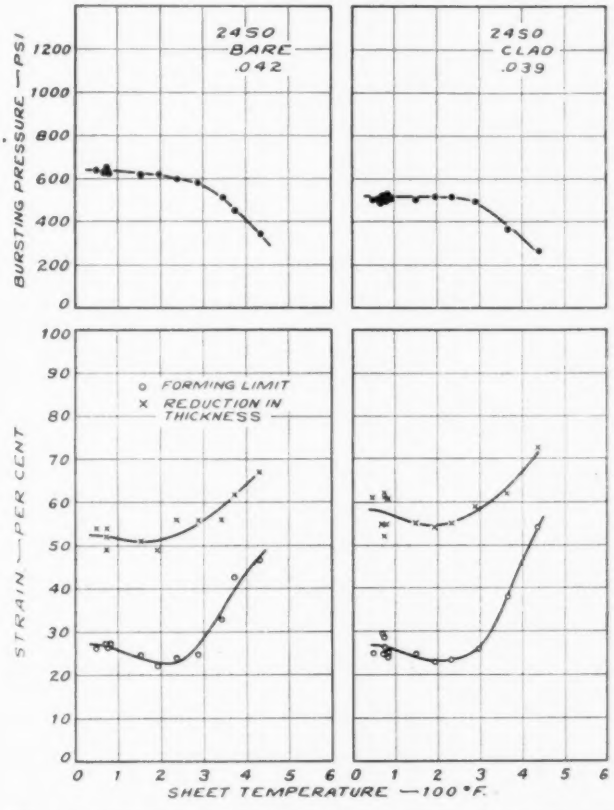


FIG. 15 RESULTS OF HOT HYDRAULIC CIRCULAR BULGING FOR 24S-O, BARE AND CLAD

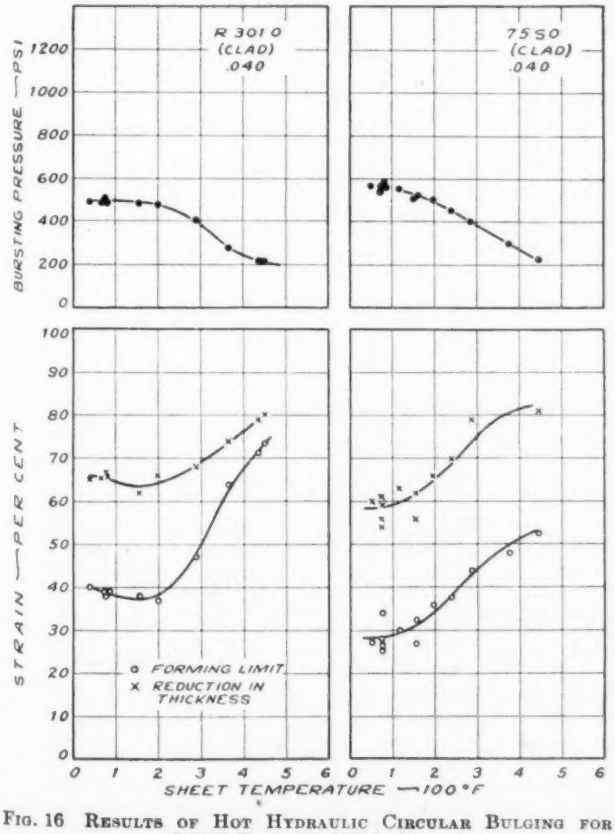


FIG. 16 RESULTS OF HOT HYDRAULIC CIRCULAR BULGING FOR R3010 CLAD AND 75S-O CLAD

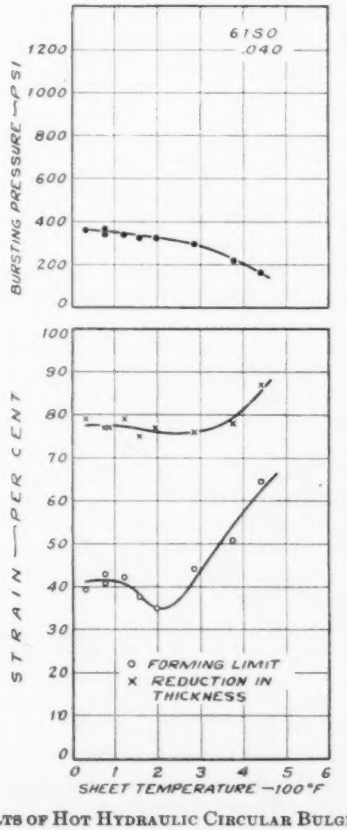


FIG. 17 RESULTS OF HOT HYDRAULIC CIRCULAR BULGING FOR 61S-O

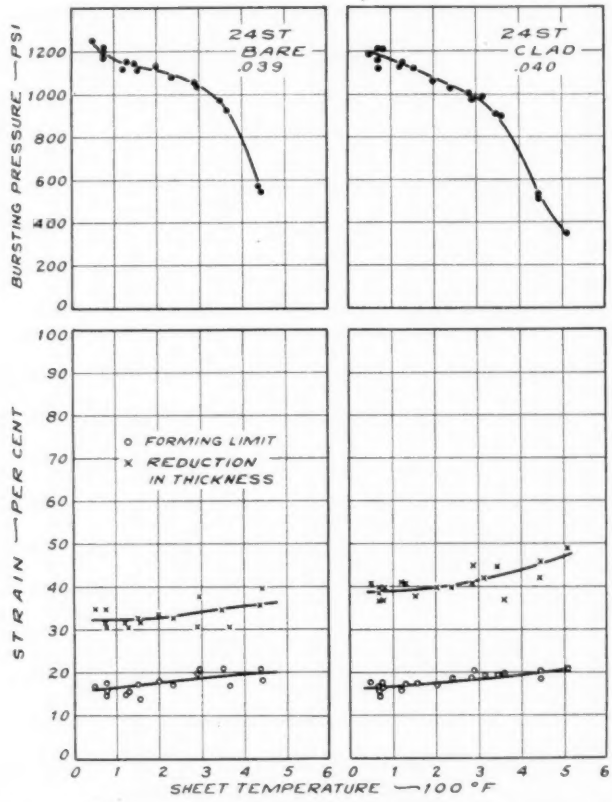


FIG. 18 RESULTS OF HOT HYDRAULIC CIRCULAR BULGING FOR 24S-T, BARE AND CLAD

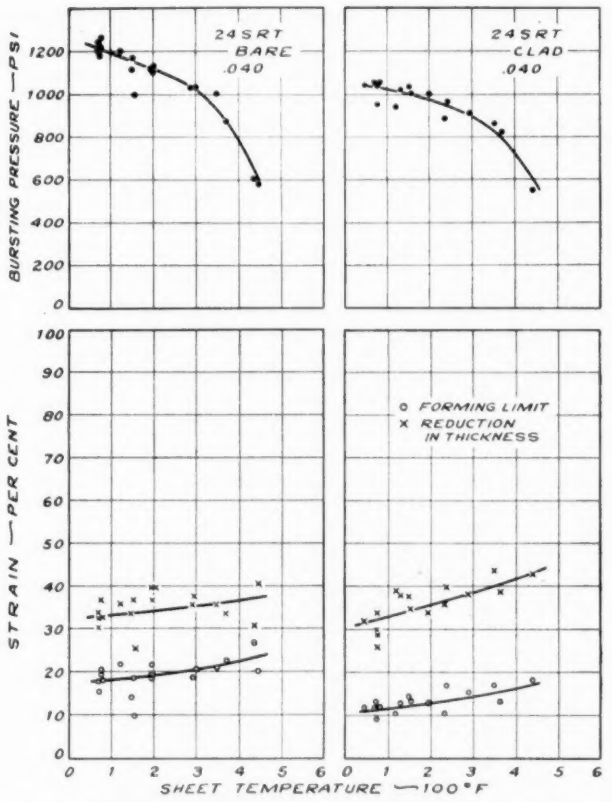


FIG. 19 RESULTS OF HOT HYDRAULIC CIRCULAR BULGING FOR 24S-RT, BARE AND CLAD

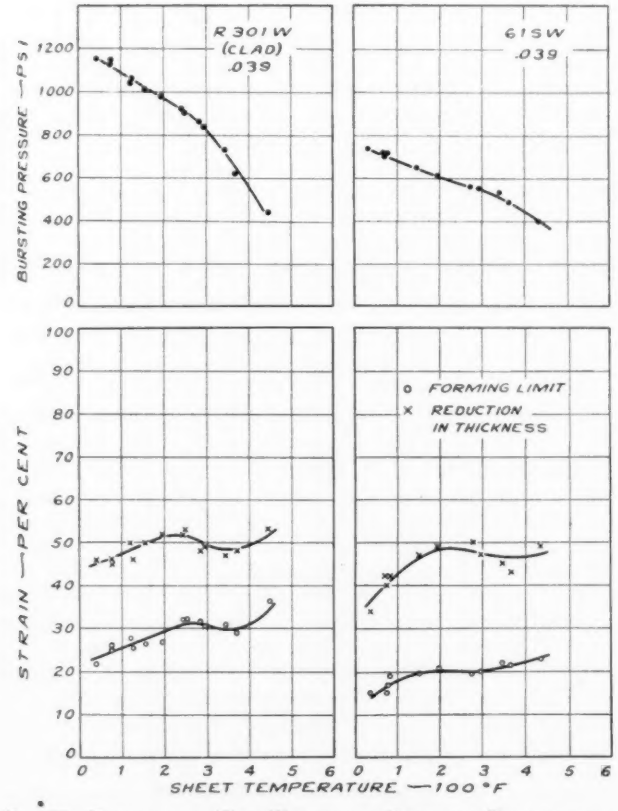


FIG. 20 RESULTS OF HOT HYDRAULIC CIRCULAR BULGING FOR R301-W CLAD AND 61S-W

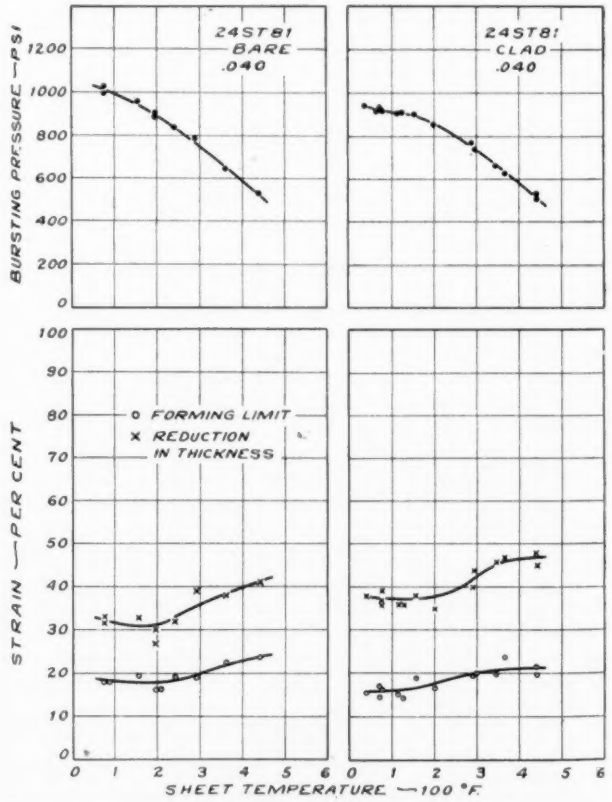


FIG. 21 RESULTS OF HOT HYDRAULIC CIRCULAR BULGING FOR 24S-T81, BARE AND CLAD

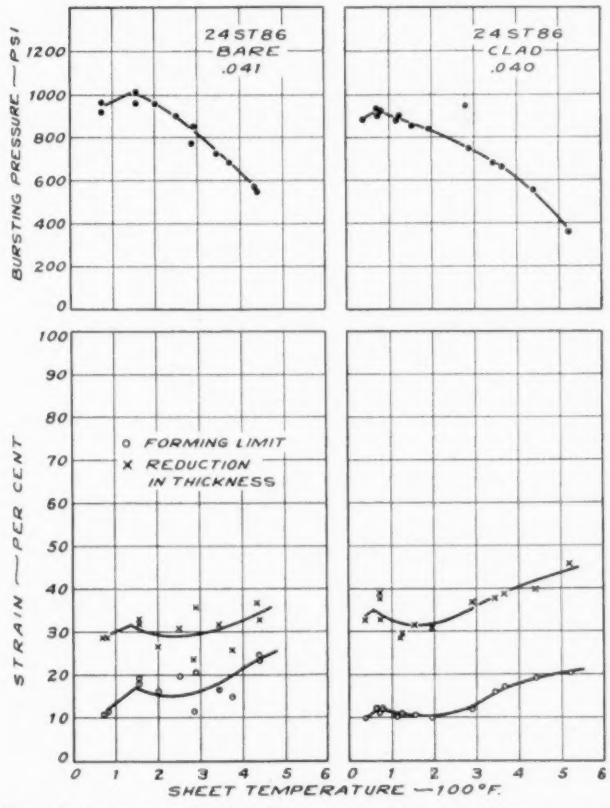


FIG. 22 RESULTS OF HOT HYDRAULIC CIRCULAR BULGING FOR 24S-T86, BARE AND CLAD

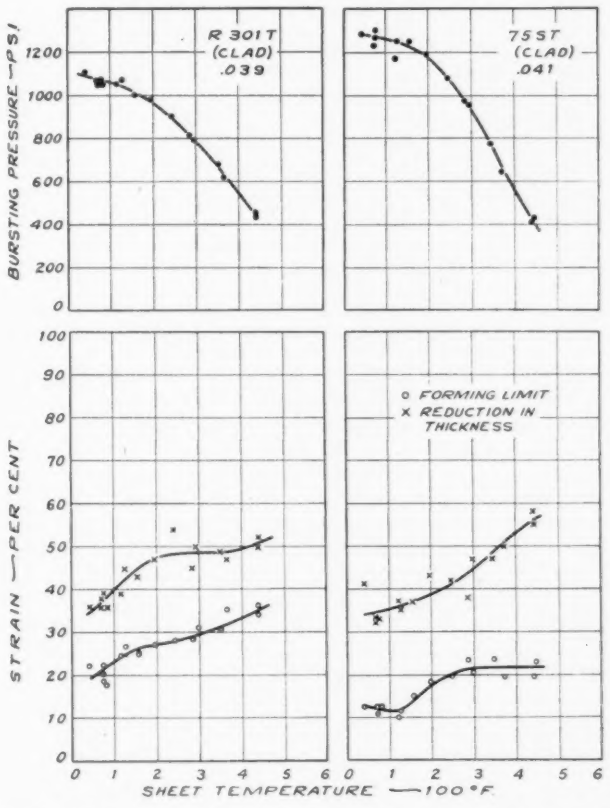


FIG. 23 RESULTS OF HOT HYDRAULIC CIRCULAR BULGING FOR R301-T CLAD AND 75S-T CLAD

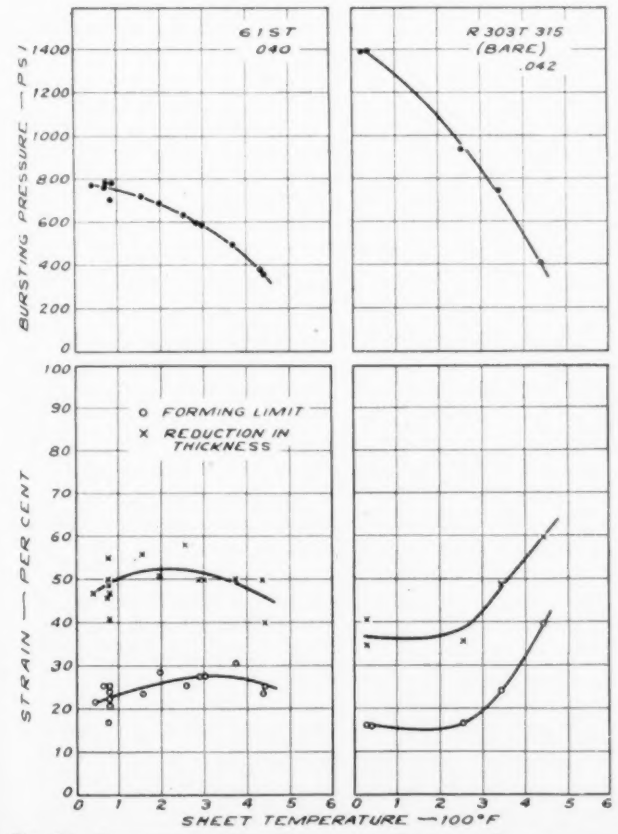


FIG. 24 RESULTS OF HOT HYDRAULIC CIRCULAR BULGING FOR 61S-T AND R303-T315 BARE

limits, the annealed alloys, Group I, may be considered together, whereas it is advantageous to discuss individually the room-temperature-aged conditions, Group II-A, the various conditions of 24S, and the artificially aged alloys Group II-B.

It appears that the forming limits of all the annealed alloys except 3S-O and 75S-O were slightly reduced by raising the temperature up to a certain limit which varied for the different alloys between 100 and 250 F (24S-O), Figs. 14 to 17, inclusive. With further increasing temperature, the forming limit of all these alloys increased continuously by as much as 35 to 40 per cent (stretch) at the testing temperature of 450 F. The magnitude of this effect probably depended considerably upon the rate of loading and was rather large for these tests because of the slow speed.

The forming limits (for the annealed conditions) at room temperature were highest for the alloys of Group I-A, 3S-O and 52S-O, and for two alloys of Group I-B, 61S-O and R3010, while 75S-O and 24S-O, both bare and clad, exhibited only approximately 70 per cent of the forming capacity of the other alloys. With increasing temperature the difference between 24S-O and the other alloys was retained, while 75S-O showed almost as high strain values as the more ductile alloys, and markedly higher strain values than 24S-O, at temperatures between 200 and 350 F. The alloys of Group II-A, Figs. 18 to 20, inclusive, aged at room temperature, were in general more responsive to the effect of temperature in the lower temperature range, but at the higher testing temperatures did not increase to definitely higher strain values than the respective artificially aged conditions.

The forming limits for the aged conditions were highest for the alloys R301-W, 61S-T, and surprisingly also R301-T, for practically the entire range of temperatures investigated.

The alloy 61S-W showed rather low strain values in comparison to the other alloys of this group, and were not appreciably higher than 24S-T.

Testing temperatures up to 250 F caused practically no change in the forming limits for all aged conditions of the alloy 24S, but slight improvement in formability was observed for all these alloys at still higher temperatures.

The lowest strain values occurred in 24S-T86 and 24S-RT, while 24S-T and 24S-T81 were intermediate.

Artificial aging of 24S-T and 24S-RT to 24S-T81 and 24S-T86, respectively, caused a surprisingly small reduction in the forming limits by not more than 1 to 2 per cent, when tested at room temperature, Figs. 18, 19, 21, and 22. However, the results at testing temperatures in excess of 200 to 300 F revealed that the artificially aged alloys have the higher forming limits after passing through a minimum at 200 F.

The cold-rolling of 24S-T clad, resulting in 24S-RT clad, Figs. 18 and 20, caused the expected reduction in strains by approximately 5 per cent, but this effect could not be recognized for 24S-RT bare, the strain values of which scattered within wide limits; with increasing temperatures this difference between the forming limits for 24S-T clad and 24S-RT clad, gradually decreased.

The alloys of Group II-B, the artificially aged conditions, Figs. 21 to 24, inclusive, were markedly affected by testing at higher temperatures, and between 300 and 400 F their forming limits exceeded those of the room-temperature-aged conditions.

The forming limit for R301-T, and to a smaller extent for R301-W, 61S-W, and 61S-T, materially increased with increasing temperature, particularly at slightly elevated temperatures. The alloys 75S-T and R303-T, possessed very low forming limits at room temperature; however, the strain values for these alloys at temperatures above 200 and 300 F, respectively, exceeded those of 24S-T. Alloy R301-T values were not appreciably different from R301-W, except that the latter showed a slight minimum in the forming-limit curve for the tests in the range 300 to 400 F. Both alloys had identical forming limits at 450 F.

Regarding the absolute strain values, some recent results show these values to be appreciably increased by increasing the sheet thickness using the same die diameter.

Reduction in Thickness at Failure

The rather large variations of the values of reduction in thickness do not permit a clear evaluation of this metal property, which measures the (local) ductility, Figs. 14 to 24, inclusive.

Of the two nonaging alloys of Group I-A, 3S-O was slightly superior and more affected by elevated temperature than was 52SO.

Of the annealed conditions of the age-hardenable alloys, Group I-B, 61S-O possessed by far the highest ductility at lower temperatures, even better than 52S-O. However, the other alloys approached such a high ductility with increasing temperatures: 75S-O above 250 F, R3010 above 400 F, and 24SO, both bare and clad, apparently above 450 to 500 F, Figs. 15 to 17, inclusive.

The forming temperature up to 450 F had only a comparatively slight effect on the ductility of the room-temperature-aged alloys, Group II-A, Figs. 18 to 20, inclusive. The reduction in thickness of the various conditions of 24ST increased continuously with increasing temperature, at a rate of 2 to 3 per cent (ductility) per 100 deg F, up to a value which was approximately 1/3 higher at 450 F than at room temperature. The other two alloys investigated, 61S-W and R301W, showed a peculiar maximum in the range of 200 to 250 F, followed by a minimum at 350 F. Both of these alloys exhibited slightly higher values of reduction in thickness than 24S-T clad, over the whole range of temperatures tested, while 24S-T bare, 24S-RT clad, and 24S-RT bare, were inferior to 24S-T, by approximately 5 to 10 per cent (ductility).

Of the alloys of Group II-B, the artificially aged conditions of 24S-T were only slightly affected regarding their ductility at temperatures up to 250 F, while their ductility increased considerably between 250 and 350 F, and then approached or even exceeded that of the corresponding room-temperature-aged condition, Figs. 21 and 22. The ductility of R301-T improved markedly at temperatures slightly above room temperature, and then continued to increase at a slow rate with further increasing temperature. On the contrary, the ductility of 75S-T and R303-T appeared to increase at a steadily increasing rate, at temperatures exceeding 150 and 200 F, respectively. Both at room temperature and at approximately 400 F, the ductility of the alloys 24S-T81 clad, R301-T, 75S-T and R303-T, was approximately the same and considerably higher than that of 24S-T86 clad, 24S-T81 bare, and 24S-T86 bare. At temperatures between 200 and 300 F, however, the ductility of the alloys R301-T and 75S-T exceeded that of 24S-T81 clad, and also that of 24S-T clad.

Effects of Cladding

A comparison of the respective clad and bare aged conditions of the alloy 24S revealed a rather pronounced effect of the cladding on the forming limits and local ductility (reduction in thickness). These values were considerably more uniform for the clad than for the bare alloys. In particular, quite uniform strain values could be obtained for 24S-T clad, 24S-T81 clad, 24S-T86 clad, and 24S-RT clad, while extreme variations were encountered in 24S-RT bare, and 24S-T86 bare.

The reduction in thickness of the clad alloys was slightly larger than that of the bare conditions, on the average, by 5 per cent (0 to 10 per cent ductility).

On the contrary, the forming limits were frequently higher for the bare alloys, and very high values were occasionally encountered in both 24S-RT bare, and 24S-T86 bare. No explanation can be given for these peculiar findings. The higher stretching ability of bare alloys, however, cannot be utilized because of their larger variations, and the minimum values of the bare and clad conditions usually differed only slightly.

Alloys 24S-O clad, and 24S-O bare possessed almost identical forming limits, while the reduction in thickness was slightly higher for 24S-O clad.

As was to be expected, the bursting pressures were, on the average, approximately 10 per cent higher for the bare alloys than for the clad alloys, other factors being equal.

Types of Fracture and Defects

While most of the blanks tested failed by splitting close to the crown in the longitudinal direction, the final appearance of a bulge after the test appeared to be determined primarily by the ductility of the alloy, Fig. 1. The various types of failures observed are diagrammatically illustrated by plan views in Fig. 25. The ductile alloys generally formed several variations of single cracks, without branches, which were designated by "D-1" and "D-2." The brittle alloys ruptured in various manners, types "B-1" to "B-4" exhibiting a well-defined straight primary crack with several secondary branches which appeared to be caused by rather violent failure of the bulge.

Two variations of ductile failures were observed. The one consisted of a straight crack, running, without exception, in the longitudinal direction, type "D-1," Figs. 1 and 25. The other, type "D-2," apparently started as a short crack but continued circumferentially to one side of the crack, forming a more or less C-shaped flap rather than a straight split. While the straight split was found to occur always in the longitudinal direction, not more than 1/2 in. away from the crown, the center of the flap-type crack ran longitudinally with some alloys, but with others (R301 and 75S) in various directions; however, it also approached

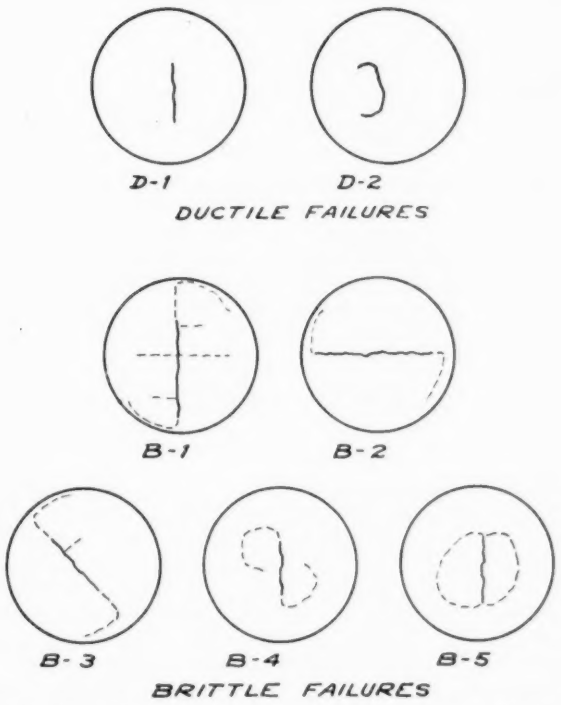


FIG. 25 DIAGRAMMATIC SKETCH OF REPRESENTATIVE TYPES OF FAILURES

the crown within a distance of less than 1/2 in.[5] Only in three instances (24S-O bare, at 345 and 375 F, and 52S-O at 285 F), a branch in the fracture was observed for a ductile alloy.

The type of failure of the heat-treated alloys, Groups II-A and II-B, differed for the various specimens of each alloy. Most of the specimens exhibited a longitudinal primary crack, while a smaller number showed a pronounced transverse crack, and a still smaller number possessed a center crack at different angles to the rolling direction. Apparently, the more brittle the specimen, the more violent was the bursting and the more branched was the fracture.

With increasing temperature, the cracks usually became shorter and more regular, and in some instances, degenerated into a pinhole at the highest temperature used.

Rather pronounced orange peel was also encountered in the alloy 61S-W, and slight orange peel in the alloys R301-0, 75S-O, 24S-RT clad, 24S-T81 clad, 24S-T86 clad, 75S-T (at higher temperatures). The results of the investigation do not appear to be markedly affected by this condition.

The heat-treated alloys, with the exception of 61S-W and 61S-T, exhibited pronounced heat warping ("oil-canning") after the tests.

[5] Only at the highest temperatures some fractures occurred farther apart from the pole of the bulge associated with a rather irregular strain distribution. This is explained by temperature variations as previously mentioned.

Tests in which some draw-in occurred because of insufficient hold-down pressure were discarded, as were the results for a few specimens which yielded pinhole fractures because of slight irregularities in the sheet. The strain values of these specimens were generally lower than those of perfect specimens.

Little difficulty was caused by failure at the radius. A few specimens of the alloy, 24S-T86 bare broke at the radius at low pressures and exhibited a peculiar small fold extending toward the inside of the bulge into the oil. Also, one specimen of 24S-T clad failed at the radius when tested at a temperature of 525 F.

CONCLUSIONS

The pressure required to burst a sheet with a circular area exposed to gradually increasing hydraulic pressure on one side is, according to the theory of strength, a function of the tensile strength of the metal, and the thickness and curvature of the part at the moment of failure. However, as far as the effect of increasing temperature is concerned, the bursting pressure follows much the same trend as the tensile strength, according to previous investigation (3). On the contrary, the relation between different alloys is clearly different in the bursting test than in the tensile test. Of the artificially aged alloys of very high strength, only 75S-T exceeded 24S-T in bursting strength at room temperature, while 24S-RT, 24S-T81, 24S-T86, and R301-T exhibited a lower bursting strength than 24S-T. No explanation can be given for this phenomenon, at present.

The general significance of the two strain values, namely, the forming limit and reduction in thickness (area), used as metal characteristics and supplied by the tests on circular bulges, and their relation to the corresponding strain values supplied by the tensile test, is also obscure at present. In a tensile test the forming limit is the uniform strain or "infinite gage length elongation" and is entirely independent of the contraction in area at failure, or "zero gage length elongation." On the contrary, the bursting tests yielded forming limits, which always apparently paralleled the reduction in thickness (or area) at failure.

This also conforms to the fact that the forming limits of the bulges considerably exceeded the uniform tensile strain, and in most instances the conventional 2-in-gage-length elongation (3). No exception to this rule was observed in these tests. However, if the metal should possess an extremely low ductility, i.e., contraction in area, this should be exhausted in a bulge test earlier than in a tensile test, and a forming limit in bulging below that in tension could be expected.

BIBLIOGRAPHY

1 "Determination of Strain Distribution by Photo-Grid Processes," by G. A. Brewer and R. B. Glassco, *Journal of the Aeronautical Sciences*, vol. 9, 1941, pp. 1–7.

2 "The Photo-Grid Printing Process," by K. Cornell, *American Photography*, Nov., 1942, pp. 16–17.

3 "Final Report on Study of the Forming Properties of Aluminum Alloy Sheet at Elevated Temperatures: Part I—Elevated Temperature Variable Speed Tensile Tests," by A. E. Flanigan, L. F. Tedson, and J. E. Dorn, War Metallurgy Committee, Report Serial No. W-122, 1944.

(Owing to travel emergency conditions existing when this paper was presented, discussion will be accepted until March 11, 1946)

Discussion

In 1945, when there was a ban on national meetings, some papers originally scheduled for these meetings were presented before local groups. In the case of these papers the Commitee on Publications suspended its rule, which requires simultaneous publication of paper and discussion, and accepted discussion based on the published paper.

Aceleration Damper: Development, Design, and Some Applications[1]

B. S. Cain.[2] This interesting paper develops the mathematical theory of the acceleration damper by analytical methods. The authors wish "to give a clear step-by-step picture of the mechanism of the acceleration damper and thereby facilitate handling of transient cases, effect of rebound, and extension of theory to modified cases." A graphical method, however, seems also to be effective in these cases. If we plot the two limits of motion of the mass particle against time, then, in any steady motion, it can easily be seen that the particle stays at one limit until this passes through a point of inflection, after which the particle moves freely until it again reaches a limit.

Taking the case of sinusoidal motion, the kinetic-energy loss per cycle is easily obtained for any conditions. It can also be seen at once that the maximum damping is obtained when the free path of the particle is π times the semiamplitude of the motion, as given in the paper. This simple graphical method lends itself to a clear picture of the operation, with easy calculation of the results. It is easy to introduce the effects of any wave-shape, of transients, of rebound, and of friction.

The graphical method is particularly adapted to practical design and analysis of behavior, because the whole picture can be seen at once, and it is not necessary to use Dirac functions or even the calculus to obtain practical results. The results of graphical analysis can be used for correlation with viscous damping without difficulty. In view of the advantages of the graphical method, it would be interesting to know if the authors have used it and what disadvantages they have found in comparison with the methods which they describe.

The experimental results and the application to flutter analysis show that a simple and easily understood theory of the acceleration damper is of real value, and the authors are to be congratulated on their contribution.

Harry Frissel.[3] The authors state that theoretical calculations show the acceleration damper to be effective in raising the flutter speed, but this had not been confirmed by experiment. In an earlier paper,[4] H. Voight mentions briefly the results of model experiments using this same device in an aileron.

In the latter case it was called a "disturbance damper." A plot of vibration amplitude versus dynamic pressure shows that for an aileron mass, balanced with a disturbance damper, the critical dynamic pressure is 4 times that for an aileron with damper inoperative. Also, if cork plates were used for the bottom of the container holding the balls, the critical dynamic pressure was approximately twice that of an aileron with damper inoperative. When the damper is inoperative, the vibration amplitude increases rapidly as the velocity approaches the critical value. With the damper acting, the vibrations at first commence in the same way. The balls then break away from their support when $1g$ acceleration is exceeded, and the amplitude is constant with increasing velocity. The function of the damper is to upset the phase relations necessary for flutter. When the impact energy of the damper can no longer upset the phase agreement sufficiently, the amplitude again rises sharply.

Authors' Closure

The authors appreciate that Mr. Cain has brought to their attention an interesting graphical method for determining the characteristics of the acceleration damper. It is believed that the graphical method proposed by Mr. Cain will prove especially useful when the effects of viscosity, friction, etc., on the motion of the particle are considered. It is noted that in spite of the involved mathematical treatment contained in the theory, the essential formulas used in the design of an acceleration damper for a specific application are simple algebraic equations and therefore the authors have not given consideration to graphical analysis.

The authors wish to bring to Mr. Frissel's attention that the type of acceleration damper considered in the theoretical investigation of its effect on the flutter characteristics of an airplane embodies a structural feature which is essential to its efficient operation and which is not contained in the disturbance damper described by H. Voight.[4] It is noted that the theory of the acceleration damper assumes that a gravitational or any other constant field does not act on the moving mass. Therefore this theory does not describe the behavior of a disturbance damper in which the motion of the particle perpendicular to the earth is acted upon by an acceleration of g. Since this paper has been submitted for publication, the authors have embodied in their acceleration damping device a structural means for realizing in practice a physical configuration treated by the theory. This feature ascertains the functioning of the damper and its effective operation for all accelerations however small, which is essential in order that the damper operate effectively in controlling flutter. The device described by Mr. Voight is not effective until accelerations of g or greater are attained. It is also noted that the disturbance damper cannot be designed to operate as effectively as the acceleration damper even when accelerations of g are exceeded, since the effect of the gravitational field changes the phase angle between the mass particle and the motion of the configuration which is being damped. As demonstrated by the theory, the selection of a suitable phase angle and its maintenance are especially important for the efficient operation of the acceleration damper. Herein lies one of the essential differences between the acceleration damper and the disturbance damper described.[4]

Another significant consideration embodied in the design of an acceleration damper is that the length of the free path of the mov-

---

[1] By Paul Lieber and D. P. Jensen, published in the October, 1945, issue of Trans. A.S.M.E., vol. 67, pp. 523–530.

[2] Assistant Engineer, Locomotive Division, General Electric Company, Erie, Pa. Mem. A.S.M.E.

[3] Research Engineer, Curtiss-Wright Corporation, Airplane Division, Research Laboratory, Buffalo, N. Y.

[4] "Weitere Versuche über Tragflügelschwingungen," by H. Voight, Jahrbuch der Deutschen Luftfahrtforschung, part 1, 1938, pp. 249–258 ("Further Experiments on Wing Vibration," R.T.P. Translation no. 874).

ing mass is definite and is determined by Equation [13] of the paper. This dimension determines the phase angle such that the damper can operate at maximum efficiency. This design criterion is not included in the description of the disturbance damper given by Mr. Voight.

Figs. 4, 5, and 6, in which the effect of the gravitational field is not considered, were intended to describe the structure of the acceleration damper schematically.

The authors regret that this was not given more emphasis in the original paper.

Jet Propulsion and Rockets for Assisted Take-Off[1]

By M. J. ZUCROW,[2] AZUSA, CALIF.

This paper discusses the two kinds of jets which may be used for propelling bodies through the atmosphere: (*a*) Highly heated compressed atmospheric air admixed with products of combustion formed by burning a fuel in the air; the thermal energy of the fuel being employed to raise the air temperature. This type is known as a "thermal-jet engine." (*b*) A jet formed by generating large quantities of gases by chemical reaction. The equipment in which such a jet is produced is known as a "rocket motor." Operating principles and estimated performance characteristics of thermal-jet engines are treated, and certain unrestricted information on the use of rocket motors or "Jato" units for assisted take-off of aircraft is presented.

Nomenclature

The following nomenclature is used in the paper:

T = propulsion thrust, lb
G = weight flow, lb per sec
g = acceleration due to gravity, ft per sec per sec
w = relative exit velocity of jet, fps
V = flight speed, fps
c = absolute exit velocity of jet, fps
a = acoustic velocity, fps
$m = \frac{G}{g}$ = mass flow, slug per sec
P_T = thrust power (TV), ft-lb per sec
P_L = exit loss, ft-lb per sec
P = propulsion power, ft-lb per sec
c_p = specific heat, Btu per lb per deg F
D = diameter, ft
$\mathbf{M}$ = Mach number
T_1 = temperature of entering air, deg R
T_2 = temperature at entrance to compressor, deg R
T_3 = temperature at end of isentropic compression, deg R
T_4 = temperature at end of actual compression, deg R
T_5 = temperature of air entering turbine, deg R
T_6 = temperature at end of isentropic expansion from turbine inlet pressure to turbine back pressure, deg R
T_7 = temperature at end of actual expansion in turbine, deg R
T_8 = temperature at end of isentropic expansion from turbine back pressure to atmospheric pressure, deg R
$\phi = T_2/T_1 = 1 + 0.2\mathbf{M}^2$ for air
$\theta = (P_3/P_2)^{\frac{k-1}{k}} = T_3/T_2$
$\alpha = T_5/T_1$
$\nu = V/w$ = velocity ratio
ρ = density, slug per cu ft
η = over-all efficiency = $\eta_i\eta_P$
η_i = internal efficiency
η_P = propulsion efficiency
η_c = compressor efficiency
η_t = turbine efficiency

$$\Sigma = \left(1 - \phi\frac{\theta - 1}{\eta_c\eta_t\alpha} - \frac{1}{\phi\theta}\right)\left[\frac{1 - \phi\dfrac{\theta - 1}{\eta_c\alpha}}{1 - \phi\dfrac{\theta - 1}{\eta_c\eta_t\alpha}}\right]$$

Subscripts:

a = air
f = fuel

Introduction

In its broadest sense, the term jet propulsion refers to the art of propelling a body by the reaction or thrust of a fluid jet. There is no limitation, in general, upon the conceivable means which may be employed to produce the jet. Furthermore, the working fluid may be a liquid, vapor, heated air, the gaseous products of a chemical reaction, or combinations of these. However, when it comes to propelling bodies through the atmosphere by jet propulsion, the jet may be one of two kinds.

1 There is the jet consisting of highly heated, compressed, atmospheric air admixed with the products of the combustion formed by burning a fuel in the air; the thermal energy of the fuel being employed to raise the air temperature. A jet of this type will be termed a "thermal jet," and the equipment utilized for producing it will be termed a "thermal-jet engine."

2 There is also the jet formed by generating large quantities of gases by a chemical reaction. These gases are usually produced by reacting a fuel with a chemical oxidizer, but reducing reactions are not ruled out. The significant thing is that atmospheric oxygen does not enter into the chemical reaction, which is therefore independent of the atmospheric surroundings. A jet produced in this manner will be termed a "rocket jet," and the equipment wherein the chemical reaction takes place, including the discharge nozzle, will be called a "rocket motor."

This paper discusses certain basic features of jet propulsion as a mode of propelling bodies through the air. In this connection, the comments on thermal-jet engines will be restricted to operating principles and estimated performance characteristics. Another purpose of this paper is to present certain unrestricted information on the rocket motors used for the assisted take-off of aircraft, commonly referred to as "Jato" units.

Reaction and Momentum Principles

The fundamental operating principle of any jet-propulsion device is the "action-equals-reaction" principle known as Newton's third law of motion. This states: "To every action there is an equal and opposite reaction." This principle is exceedingly common in Nature, and is so well known to engineers that it merits little discussion here. It should be noted, however, that where motion of a body through a fluid medium is concerned, the

[1] Based on parts of Chapters 4 and 8 of the book, "Principles of Jet Propulsion," by the author, to be published in 1946, by John Wiley & Sons, Inc., New York, N. Y.

[2] Aerojet Engineering Corporation. Mem. A.S.M.E.

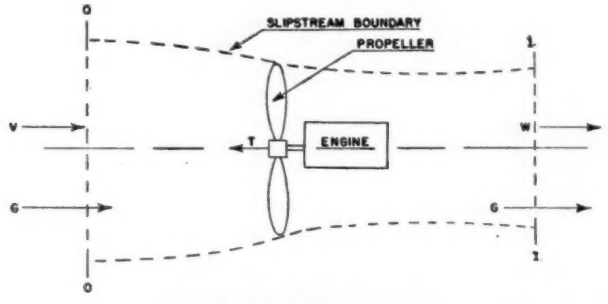
Contributed by the Aviation Division and presented at the Aviation War Conference, Los Angeles, Calif., June 11–14, 1945, of The American Society of Mechanical Engineers.

Note: Statements and opinions advanced in papers are to be understood as individual expressions of their authors and not those of the Society.

reaction principle predominates.[3] Thus the screw employed for propelling a ship, the propeller for moving an airplane, and jet propulsion all operate by virtue of this principle. In every one of these cases a fluid is accelerated in the direction opposite to that of the desired motion for the body, and the reaction due to the acceleration produces a propulsion force or thrust in the direction of motion. The magnitude of the propulsion force is determined by applying the momentum principle, "the rate of change of the momentum of a bounded mass system of discrete particles (body of fluid) is equal to the sum of the external forces acting on the system."[4]

Thrust Equations for Propulsion Systems

Fig. 1 illustrates the application of the foregoing principles to the engine-driven propeller. Since the air reactions on a body



(1) MOMENTUM ENTERING SECTION 0-0

$$M_0 = \frac{G}{g} V = \rho V$$

(2) MOMENTUM LEAVING SECTION 1-1

$$M_1 = \frac{G}{g} w$$

(3) CHANGE IN MOMENTUM PER. SEC.

$$T = M_1 - M_0 = \frac{G}{g}(w-V) \text{ LB}$$

AND $$\frac{T}{G} = \frac{w}{g}\left(1 - \frac{v}{w}\right) = \frac{w}{g}(1-v)$$

(4) THRUST POWER

$$P_T = TV = \frac{G}{g} w^2 (1-v) v$$

Fig. 1 Momentum Principle Applied to Propeller

depend only upon the relative velocity between it and the air, the body may be assumed to be stationary and the air to approach it with the actual speed of the body. In the ideal case the propeller creates a slip stream as indicated in the figure. The air enters the slip stream with the linear velocity V feet per second relative to the propeller and leaves it with the exit relative velocity w feet per second. If the air flow through the slip stream is G pounds per second, then the thrust developed is

$$T = \frac{G}{g}(w - V) \quad \ldots\ldots\ldots\ldots\ldots\ldots [1]$$

It will be seen that the difference between the characteristics of propeller propulsion and jet propulsion is not as great as might be assumed. Thus if the propeller and engine are enclosed in a duct, so that the propeller acts as a blower or compressor, and the air of the slip stream is heated by burning a fuel in it, the resulting thermal-jet engine is that originally ascribed to S. Campini. This arrangement is illustrated in Fig. 2. The essential difference between this system and the propeller is that the relative

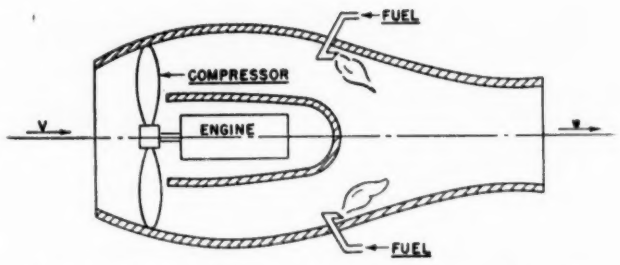


Fig. 2 Momentum Principle Applied to Campini System

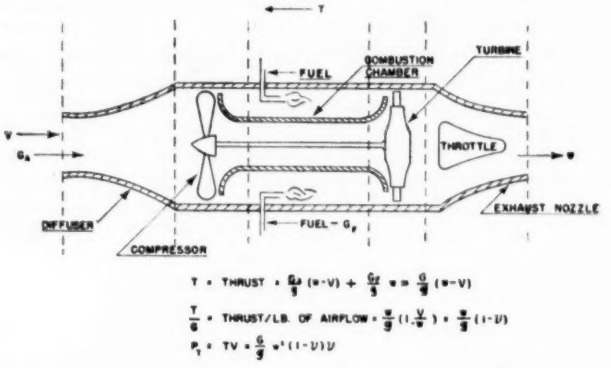


Fig. 3 Momentum Principle Applied to Thermal-Jet Engine

exit velocity of the gases (mainly air) has been increased by virtue of the addition of thermal energy. The thrust equation has the same form, but the thrust per unit mass of air flow is larger owing to the increased exit velocity. It should be noted, however, that the absolute exit velocity of the gases $c = (w - V)$ has also been increased so that the kinetic energy lost in the exit gases is also larger.

Fig. 3 illustrates the type of thermal-jet engine currently the most popular. The major difference between this and the Campini system is that the air compressor is driven by a gas turbine instead of an internal-combustion engine. The patent literature discloses many different arrangements for this type of thermal-jet engine. Their apparent differences, however, are not basic, but are confined to such features as the type of air compressor, the type of turbine, the combustion-chamber arrangement, and construction details. All of them have the same objective, i.e., to compress air, heat it, drive a turbine, and

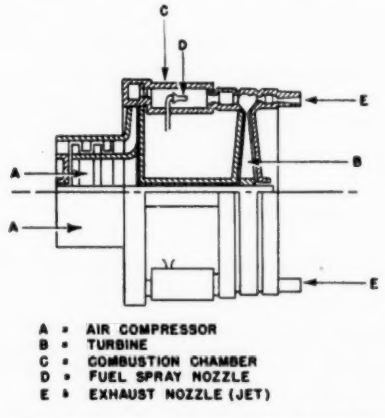


Fig. 4 Patent Application of Air Commodore Frank Whittle (British Patent No. 347,206; filed January 16, 1930.)

[3] "Raketenflugtechnik," by E. Sänger, R. Oldenbourg, Munich, Germany, 1935.

[4] "Fundamentals of Hydro- and Aeromechanics," by L. Prandtl and O. G. Tietjens, McGraw-Hill Book Company, Inc., New York, N. Y., 1944, p. 233.

discharge heated gases through some form of nozzle. The most successful pioneer in this field has been Air Commodore Frank Whittle of the R.A.F. It is interesting to note that his British Patent Application, No. 347,206, filed January 16, 1930, illustrated in Fig. 4, embraced all of the necessary elements.[5] For a review of the patent literature, the reader is referred to a text by G. Geoffrey Smith.[6]

It is seen by reference to Fig. 3 that the equation for the thrust developed by this type of thermal-jet engine is given by

$$T = \frac{G_a}{g}(w - V) + \frac{G_f}{g} w \quad \ldots\ldots\ldots\ldots [2]$$

Let $G = G_a + G_f$ which is approximately equal to G_a; since G_f can be neglected because it is ordinarily less than 3 per cent of G_a. The equation for the thermal-jet engine then becomes

$$T = \frac{G}{g}(w - V)$$

which is identical with Equation [1].

The thrust equations for the propeller and thermal-jet propulsion systems can be transformed to show the relation between the thrust and the velocity ratio ν; the latter being the ratio of the velocity of the moving body (V) to the exit relative velocity of the fluid (w). Thus for these two propulsion systems

$$T = \frac{G}{g} w (1 - \nu) \quad \ldots\ldots\ldots\ldots\ldots [3]$$

or the thrust per pound of air flow per second is

$$\frac{T}{G} = \frac{w}{g}(1 - \nu) \quad \ldots\ldots\ldots\ldots\ldots [4]$$

Equation [4] indicates how thrust developed, per pound of fluid flowing through the propulsion system per second, varies with the exit velocity (w) and the velocity ratio (ν).

It is seen that as the velocity ratio approaches unity, the thrust per pound of air flow per second approaches zero. Consequently, to develop thrust under conditions close to unity velocity ratio, the quantity of working fluid required becomes very large: hence a large exit area would be needed for passing the fluid. For a fixed velocity ratio the size of the required exit area increases as the speed of the airplane decreases; hence the propeller, with its ability to handle extremely large quantities of air at velocity ratios close to unity, is well adapted to the propulsion of bodies at moderate and low speeds. This is particularly true since, as will be seen later, operation close to unity velocity ratio gives high propulsion efficiency.

Fig. 5 is a plot of the thrust per pound of air flow per second as a function of the velocity ratio for different flight speeds. In the same figure is plotted the ideal propulsion efficiency as a function of the velocity ratio.

Fig. 6 illustrates the jet-propulsion action of the rocket system. The arrangement illustrated utilizes the chemical reaction between a liquid fuel and a liquid oxidizer; each liquid is termed a propellant. The propellants are removed from the supply tanks at the constant rate of G pounds per second. They may be, for example, gasoline and a sufficient quantity of liquid oxygen to burn it completely. At (1) the pressure of the liquids is increased by a suitable pressurizing means, and at (2) the propellants are injected into the combustion chamber. As the propellants flow through the combustion chamber they react at substantially constant pressure, producing large quantities of hot combustion gases. The combustion is completed by the time the gases reach the entrance to the exhaust nozzle through which they expand adiabatically and from which the gases are discharged with supersonic velocity.

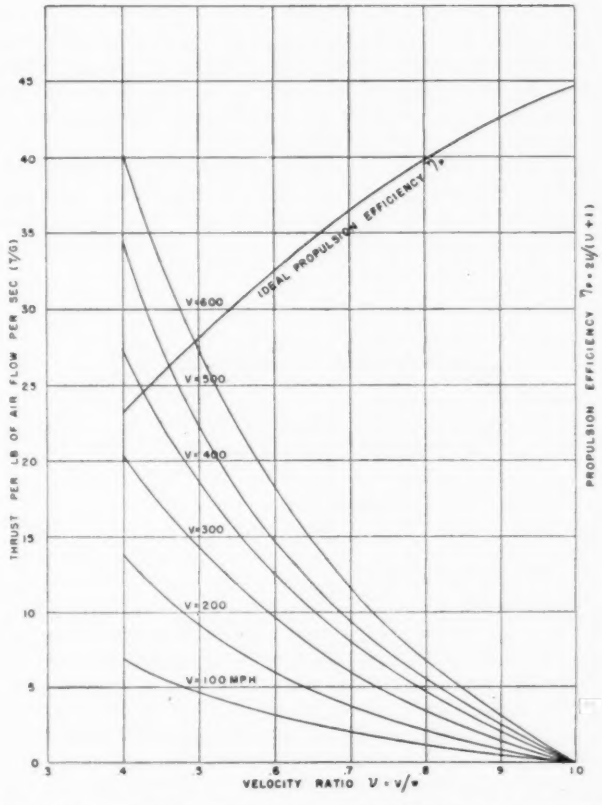


FIG. 5 THRUST PER POUND OF AIR FLOW PER SECOND AS A FUNCTION OF THE VELOCITY RATIO

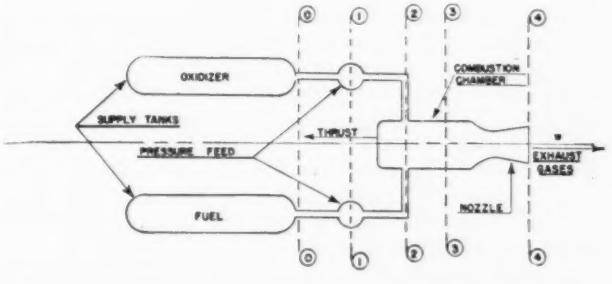


FIG. 6 JET-PROPULSION ACTION OF LIQUID ROCKET SYSTEM

If the area ratio for the nozzle is selected so that the gases are expanded to the pressure of the atmosphere surrounding the nozzle-exit section, then with a constant pressure in the combustion chamber, the thrust is given by

$$T = \frac{G}{g} w = mw \quad \ldots\ldots\ldots\ldots\ldots [5]$$

where w is the velocity of the exhaust gases relative to the nozzle, and is called the "effective exhaust velocity."[7]

[5] Thirty-second Wilbur Wright Memorial Lecture, by Sir A. H. Roy Fedden, *Journal of The Royal Aeronautical Society*, London, Eng., May 26, 1944.

[6] "Gas Turbines and Jet Propulsion for Aircraft," by G. G. Smith, published in the United States by Aerosphere, Inc., 370 Lexington Ave., New York, N. Y., 1944.

[7] "Characteristics of the Rocket Motor Unit Based on the Theory of Perfect Gases," by F. J. Malina, *Journal of The Franklin Institute*, vol. 230, 1940, pp. 433–454.

It should be noted that whereas the thrust developed by the propeller and the thermal-jet engine depends upon the difference between the relative exit velocity of the gases and the speed of the propelled body, the thrust of the rocket motor is independent of the motion of the rocket system; it depends only upon the effective exhaust velocity of the rocket jet.

Fig. 7 illustrates a rocket motor utilizing a solid propellant, fuel plus oxidizer. This is the type of rocket motor used most extensively for Jato. To obtain the desired action the propellant characteristics must be such that the propellant burns at a

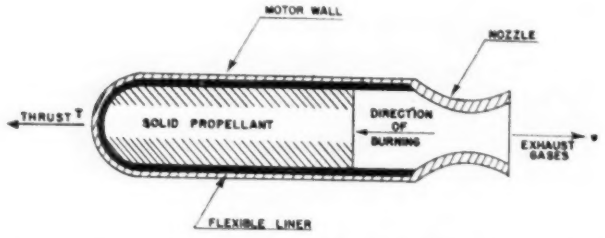


FIG. 7 JET-PROPULSION ACTION OF SOLID-PROPELLANT ROCKET MOTOR

uniform rate in layers perpendicular to the motor axis, that is, the burning is restricted to take place in one direction. One way of accomplishing this is by bonding the propellant stick and the steel walls of the motor with a special flexible sealing material, or liner, which allows the propellant stick the freedom of motion it requires for adapting its shape to the deformations produced by the gas pressure, thermal expansion, and internal stresses. The thrust equation for the solid-propellant rocket motor is, of course, identical with that for the liquid-propellant system.

PROPULSION POWER AND PROPULSION EFFICIENCY

By propulsion power is meant the total power furnished the propulsion system. A portion of this power is converted into the thrust power required to maintain motion; the thrust power being the product of the thrust developed and the speed of the propelled body. The difference between the propulsion and thrust powers depends on the energy losses associated with the propulsion system. The ratio of the thrust power to the propulsion power is termed the propulsion efficiency and is denoted by η_P. Obviously, to obtain high values of propulsion efficiency the energy losses must be kept small.

The propulsion power P of the engine-driven propeller is the power supplied to it by the engine. In the thermal-jet engine the propulsion power is derived from the thermal energy of the fuel burned in the combustion chamber. For the rocket motor, the propulsion power comes from the heat of reaction of the fuel with the particular oxidizer employed. For all of these systems the energy loss, in the ideal case, is that associated with the kinetic energy of the fluid being ejected from the propulsion system. This is called the leaving or exit loss P_L and is given by

$$P_L = {}^1/_2 \frac{G}{g} c^2 = {}^1/_2 \frac{G}{g} (w - V)^2 \quad \ldots\ldots [6]$$

Obviously, the prerequisite for a small exit loss is a low value for the absolute exit velocity of the propulsion fluid.

For all three propulsion systems, if it is assumed that the only energy loss is the exit loss, the propulsion power must be equal to the thrust power TV, plus the exit loss P_L. The ideal propulsion efficiency for each system is given by a general equation of the form

$$\eta_P = \frac{TV}{P} = \frac{TV}{TV + P_L} \quad \ldots\ldots [7]$$

By substituting for the thrust and the exit loss from the preceding equations, the ideal propulsion-efficiency equations for each system are obtained; thus

(*a*) *Ideal Propeller:*[8]

$$\eta_P = \frac{TV}{P} = \frac{2V}{V + w} = \frac{2\nu}{\nu + 1} \quad \ldots\ldots [8]$$

(*b*) *Ideal Thermal-Jet Engine:*

$$\eta_P = \frac{2V\,[(G_a + G_f)\,w - G_a V]}{(G_a + G_f)w^2 - (G_a - G_f)V^2}$$

If G_f is neglected so that $G = G_a = G_f$, then

$$\eta_P = \frac{2\nu}{\nu + 1}$$

(*c*) *Rocket Motor:*

$$\eta_P = \frac{TV}{TV + \frac{G}{2g}(w - V)^2} = \frac{2V}{w^2 + V^2} = \frac{2\nu}{1 + \nu^2} \quad \ldots\ldots [9]$$

It is seen from the foregoing that the propeller and the thermal-jet engine have identical ideal propulsion-efficiency equations and that their efficiencies depend upon the velocity ratio. It should be noted, however, that for these propulsion devices operation at unity velocity ratio is impossible because the thrust then falls to zero. For these two propulsion systems the relation between the thrust power and the velocity ratio is

$$P_T = TV = \frac{G}{g} w^2 (1 - \nu)\nu \quad \ldots\ldots [10]$$

This equation shows that for a constant rate of fluid flow G, the thrust power is a quadratic function of the velocity ratio. The maximum value for the thrust power is obtained under these conditions when the velocity ratio is $\nu = 0.5$. The corresponding value of the propulsion efficiency is then $\eta_P = 0.667$. It is seen therefore that the velocity ratio for maximum thrust power and maximum propulsion efficiency are different.

In the case of the rocket jet, the thrust depends directly on the exhaust-gas velocity w. Consequently, operation at unity velocity ratio or higher is a possibility. Thus assume that $w = 6000$ fps, then at unity velocity ratio the body propelled by the rocket-jet motor must be traveling at a speed of 4100 mph. Fig. 8 shows the effect of flight speed on the propulsion efficiency of a rocket jet, based on $w = 6000$ fps. Obviously, the rocket jet is an extremely inefficient propulsion device at travel speeds comparable to those attained by the fastest fighter aircraft.

Fig. 9 presents the estimated propulsion-efficiency curves for the propeller, thermal jet, and rocket jet at 20,000 ft altitude.[9] The propeller and thermal-jet curves intersecting at 550 mph indicate that the propeller is the more efficient at speeds below that value. These two efficiency curves intersect at lower speeds with increasing altitude. At 30,000 ft, for example, the intersection point is at 450 mph. The rocket jet has a very low propulsion efficiency except at extremely high speeds of travel.

The over-all efficiency η, of any of these propulsion systems is, of course, the product of the thermal efficiency of the power plant (or the internal efficiency η_i) and the propulsion efficiency

[8] "The Elements of Aerofoil and Airscrew Theory," by H. Glauert, The Macmillan Company, New York, N. Y., 1943, p. 203.

[9] "Aircraft Power Plant; Past and Future," by Sir A. H. Roy Fedden, *Journal of The Royal Aeronautical Society*, vol. 48, 1944, pp. 443–457.

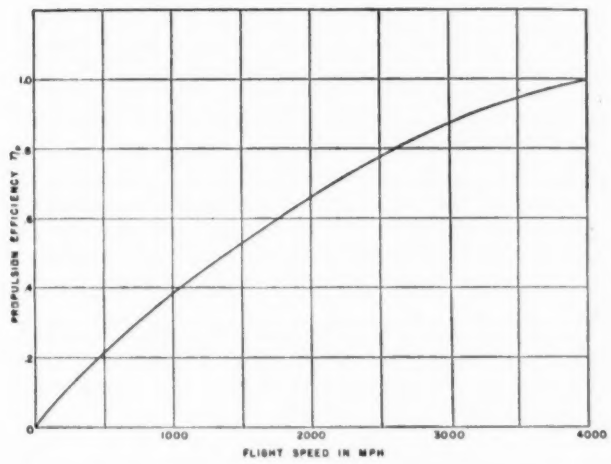


FIG. 8 EFFECT OF FLIGHT SPEED ON PROPULSION EFFICIENCY OF ROCKET MOTOR
(Based on w = 6000 fps.)

η_P); thus $\eta = \eta_i \eta_P$. Table 1 summarizes the relationships just discussed.

TABLE 1 THRUST AND POWER RELATIONSHIPS

	Propeller and thermal jet	Rocket jet
Thrust = T =	$\frac{G}{g}(w - V) = \frac{G}{g} w \left(1 - \frac{V}{w}\right)$	$T = \frac{G}{g} w$
$\frac{\text{Thrust}}{\text{Pounds fluid flow per second}}$ =	$\frac{T}{G} = \frac{w}{g}\left(1 - \frac{V}{w}\right) = \frac{w}{g}(1 - \nu)$	$\frac{T}{G} = \frac{w}{g}$
Exit loss = P_L =	$\frac{G}{2g} c^2 = \frac{G}{2g}(w - V)^2$	$P_L = \frac{G}{g} c^2 = \frac{G}{2g}(w - V)^2$
Thrust power =	$TV = P_T$	$P_T = TV$
P_T =	$\frac{G}{g} w^2 \left(1 - \frac{V}{w}\right)\frac{V}{w} = \frac{G}{g} w^2 (1 - \nu)\nu$	
Propulsion power = P =	$TV + P_L$	$P = TV + P_L$
P =	$\frac{G}{2g}(w^2 - V^2) = \frac{G}{2g} w^2 \left[1 - \left(\frac{V}{w}\right)^2\right]$	
Ideal propulsion efficiency =	η_P	η_P
η_P =	$\frac{TV}{P} = \frac{TV}{P_T + P_L} = \frac{TV}{TV + P_L} = \frac{2V}{w + V} = \frac{2(V/w)}{1 + (V/w)} = \frac{2\nu}{1 + \nu}$	$\frac{TV}{TV + P_L} = \frac{2(V/w)}{1 - (V/w)^2} = \frac{2\nu}{1 + \nu^2}$

G = fluid flow, lb per sec
V = true air speed, fps
w = relative exit velocity of propulsion fluid, fps

PROPULSION POWER AND DISCHARGE AREA

Fig. 10 is a plot of the so-called propulsion parameter $V\sqrt[3]{D^2\rho/P}$, as a function of the ideal propulsion efficiency. This curve is applicable to the engine-driven propeller and the thermal-jet engine. When applied to the propeller, D is its diameter, ρ is the atmospheric density,[10] V is the airplane speed, and P is the power furnished by the engine. For the thermal-jet engine, D is the diameter of the discharge jet, ρ is the density of the jet gases, and the propulsion power P is calculated from the increase in the kinetic energy of the gases entering and leaving the system; thus

$$P = \frac{G}{2g}(w^2 - V^2)$$

[10] It has been assumed that the density of the air is increased 15 per cent in passing through the actuator disk.

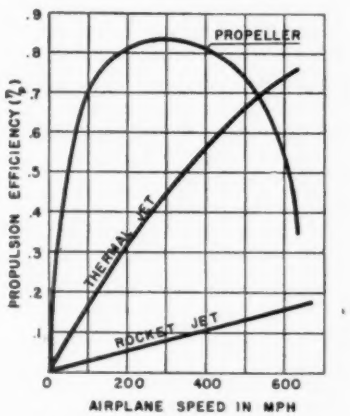


FIG. 9 COMPARISON OF PROPULSION EFFICIENCIES OF PROPELLER, THERMAL JET, AND ROCKET

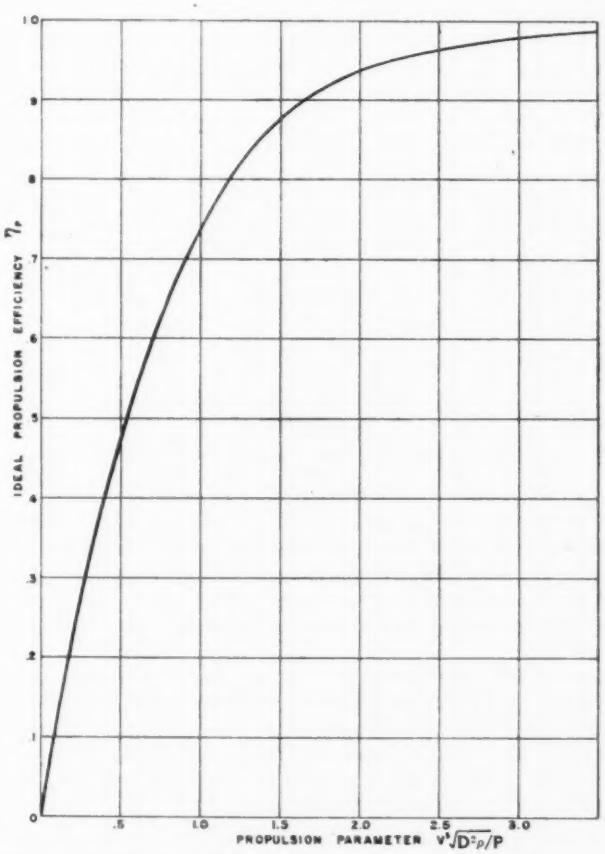


FIG. 10 PROPULSION EFFICIENCY VERSUS PROPULSION PARAMETER FOR PROPELLER AND THERMAL JET

The equations relating the propulsion parameter and the ideal propulsion efficiency are presented for reference as follows:

$$V\sqrt[3]{D^2\rho/P} = \frac{0.82\eta_P}{\sqrt[3]{1 - \eta_P}} \approx \frac{1.364\,\eta_P}{\sqrt[3]{8 - 12\eta_P + 4(\eta_P)^2}} \quad \text{[11]}$$

Propeller[11] *Thermal Jet*[12]

[11] Reference 8, p. 204.

[12] "The Modern Gas Turbine," by T. Sawyer, Prentice Hall, Inc., New York, N. Y., 1945, p. 178.

The curve gives the maximum attainable propulsion efficiency for either type of propulsion system. It is seen that to obtain high values of efficiency with low airplane speeds, D must be large, assuming the other factors constant. This operating condition is most readily met with propeller propulsion.

When flight speeds in excess of 500 mph are considered, there arise problems connected with the engine size, as well as those due to the effect of compressibility of the air upon the propeller efficiency, for the power requirements increase as the cube of the airplane speed. Thus if it takes 1200 hp to propel a given airplane at 360 mph at a given altitude, it would require an engine developing approximately 3200 hp to propel it at 500 mph, assuming all other factors remained unchanged. This calls for a heavy and complex power plant, even if this power can be furnished by a single engine. On the other hand, the thrust power for attaining this speed can be obtained from a thermal-jet engine of relatively light weight, with a jet diameter of 1 ft and an exhaust velocity of approximately 1500 fps.

Reciprocating internal-combustion engines for large power outputs require a multiplicity of accessories which result in an increase in their specific weights. Furthermore, they introduce complicated installation and maintenance problems. The probable trend in the specific weight of large internal-combustion engines, as estimated by Sir A. H. Roy Fedden, is presented in Fig. 11.

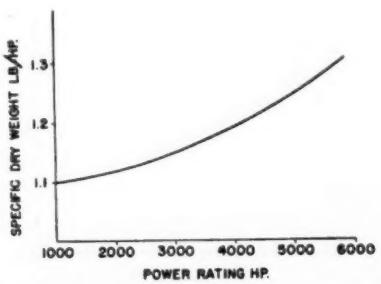


FIG. 11 TREND IN RECIPROCATING-ENGINE WEIGHTS WITH POWER RATING

The efficiency of an actual propeller will be approximately 0.85 of the ideal propulsion efficiency, or 0.833. This is due to various factors neglected by the momentum theory, such as whirl energy imparted to the slip stream, nonuniformity of the thrust distribution over the blades, blade-profile drag, and periodicity of the flow.

It was shown previously that to obtain the maximum propulsion power from a thermal-jet engine, the velocity ratio should be approximately 0.5. The propulsion efficiency for this condition is 0.667. Assuming the operating data used for the propeller previously discussed, and the discharge temperature for the jet at 1200 deg R, so that $\rho = 0.00102$ slug per cu ft, then the propulsion efficiency is about 68 per cent of that obtainable with an ideal propeller; the further assumption being made that the propeller is unaffected by compressibility. To obtain the same ideal propulsion efficiency as that for the propeller, the velocity ratio must be decreased, with the consequence that the required diameter of the jet becomes very large.

THERMODYNAMIC ANALYSIS OF THERMAL-JET ENGINE

The analysis presented here is based on the following simplified assumptions:

(*a*) There is full recovery of the dynamic pressure of the entering air (100 per cent ram).

(*b*) There is no change in the mass rate of flow of fluid passing through the engine.

(*c*) There is no change in the chemical composition of the working fluid, it being assumed to be air at all sections of the flow path.

(*d*) The working fluid (air) behaves in accordance with the laws of perfect gases; the effect of temperature on the specific heat of the air is neglected.

The inaccuracies introduced by the foregoing assumptions are so small that for the practical purpose of obtaining a general insight into the behavior of the thermal-jet engine they are well justified. The advantage of this form of analysis is that general equations for the various performance characteristics can be derived.

Fig. 12 illustrates the thermodynamic process involved on the temperature-entropy (T-S) plane. The processes have been explained in the foregoing and are denoted on the diagram.

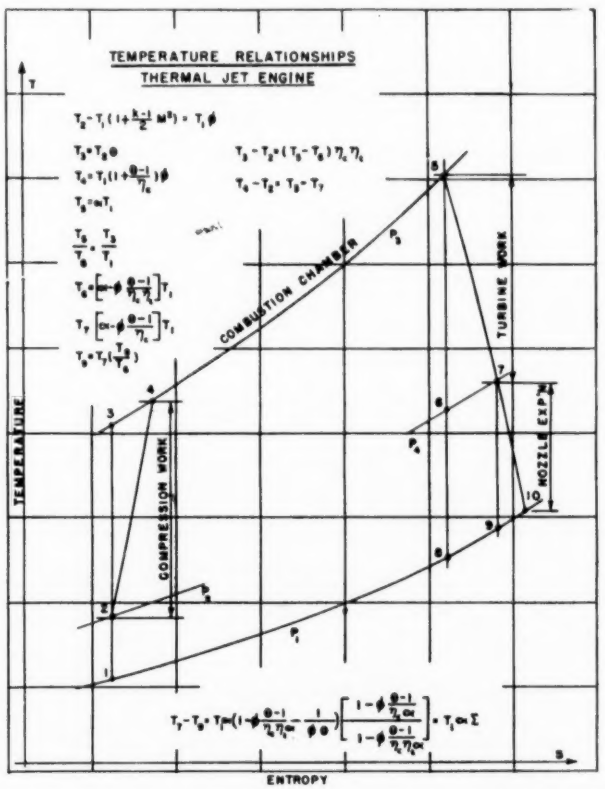


FIG. 12 THERMAL-JET ENGINE CYCLE ON TEMPERATURE-ENTROPY PLANE

The object of the analysis is to obtain equations for the temperatures at the state points indicated on the diagram in terms of the temperature of the entering air and its Mach number. These equations are listed in the diagram. From them the equation for the temperature difference $(T_7 - T_9)$, corresponding to an isentropic expansion through the nozzle, is readily obtained. Fig. 13 presents values of this temperature difference as a function of Mach number for five different altitudes ranging from sea level to 40,000 ft.

Since the temperature difference $(T_7 - T_9)$ is proportional to the isentropic enthalpy change for the expansion in the nozzle, the exhaust velocity of the jet is readily calculated; thus

$$w = 223.7 \sqrt{c_p (T_7 - T_9)} \times \text{nozzle coefficient} \quad \ldots \quad [12]$$

where $c_p = 0.24$ Btu per lb per deg F.

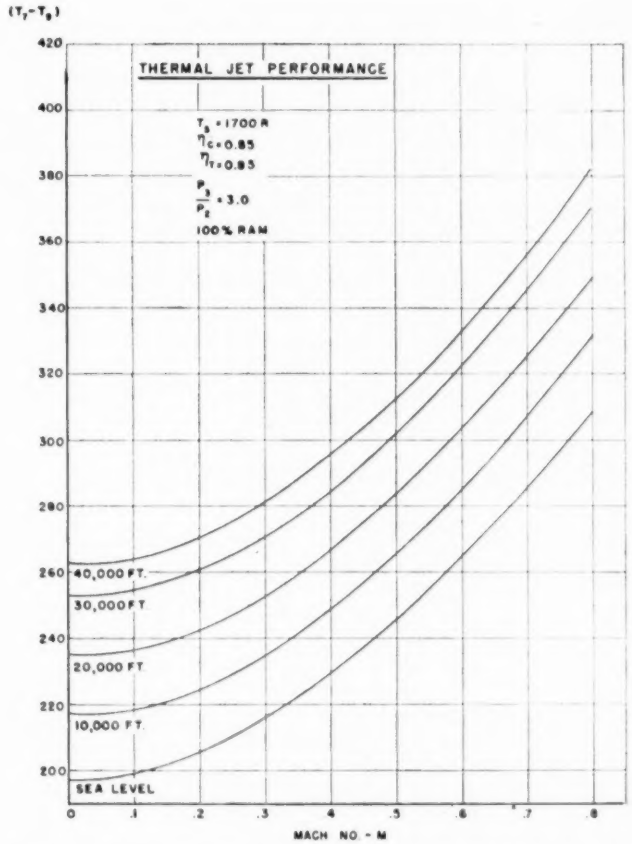


FIG. 13 TEMPERATURE DIFFERENCE (T_7 — T_0) AS A FUNCTION OF MACH NUMBER

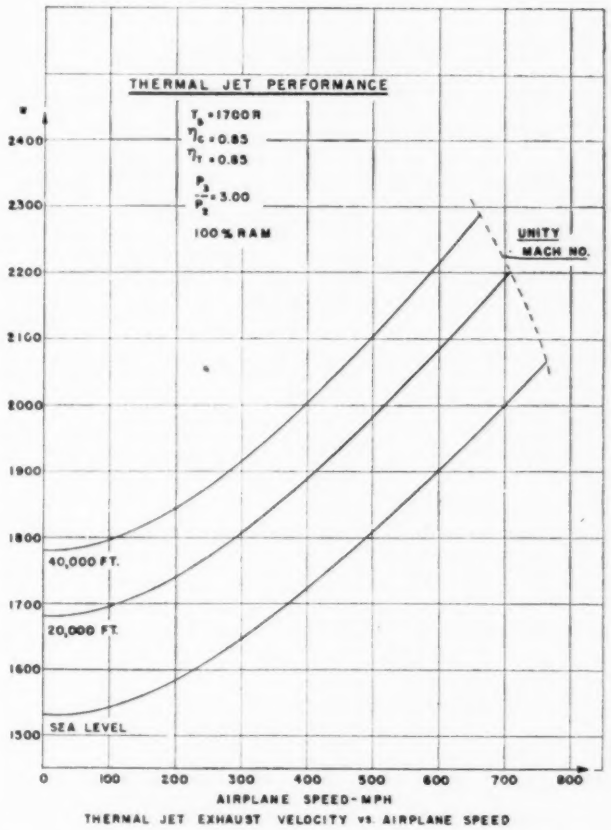


FIG. 14 THERMAL-JET VELOCITY VERSUS TRUE AIR SPEED IN MILES PER HOUR

In calculating the performance characteristics the nozzle velocity coefficient was assumed to be unity.

PERFORMANCE CHARACTERISTICS OF THERMAL-JET ENGINE

Fig. 14 illustrates how the jet velocity varies with the true air speed, in miles per hour, at different altitudes. The rapid increase in jet velocity with higher air speed is due to full recovery of the dynamic pressure of the air. Since the thrust developed by the engine depends upon the velocity difference (w — V), it is important to design the intake system so that the ram recovery is high.

Fig. 15 illustrates how the weight rate of air flow through the system varies with Mach number, with the compressor running at constant speed.

Fig. 16 shows the effect of true air speed on the thrust and the fuel consumption per pound of thrust. Assuming that the fuel has a calorific value of 18,000 Btu per lb, it is seen that the ratio of the static thrust to flight thrust is considerably less than it is for a variable-pitch, constant-speed, engine-driven propeller. As a result of the ram effect, the thrust increases at higher air speeds after passing through a minimum point. The fuel consumption per pound of thrust increases with flight velocity at all altitudes. Its rate of increase, however, diminishes somewhat with increasing altitude at speeds in excess of 250 mph.

Fig. 17 compares the thrust characteristics of the adjustable-pitch propeller with that of a thermal-jet engine. The basis of comparison is the fact that both propulsion systems provide equal thrusts at 375 mph.[13]

[13] "Gas Turbines in Aircraft," by C. D. Flagle and F. W. Godsey, Jr., *Western Flying*, June, 1945, p. 58.

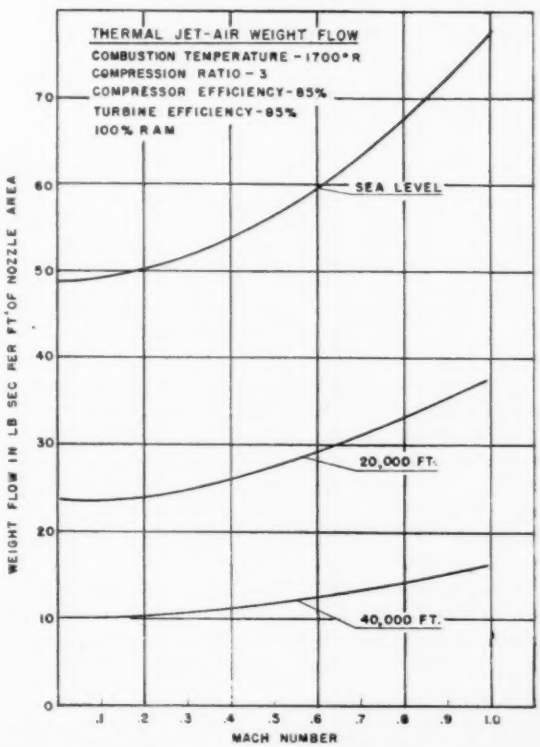


FIG. 15 WEIGHT RATE OF AIR FLOW VERSUS MACH NUMBER

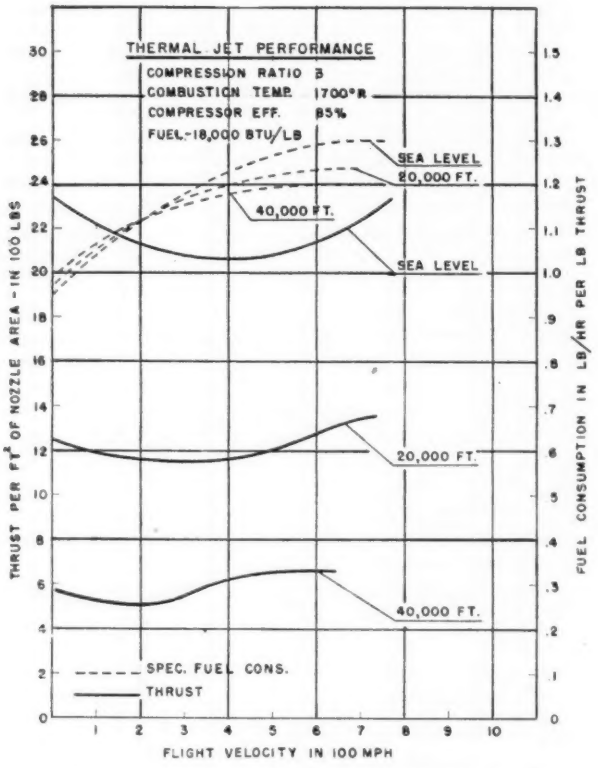


FIG. 16 THRUST AND FUEL CONSUMPTION OF THERMAL-JET ENGINE VERSUS TRUE AIR SPEED

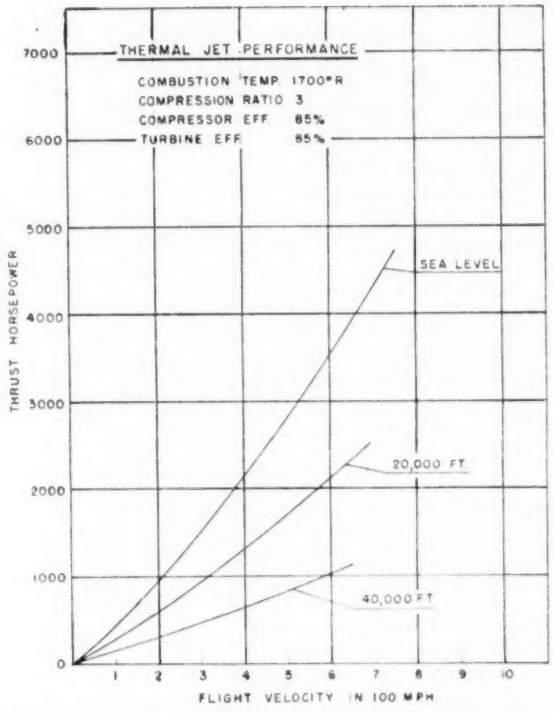


FIG. 18 THRUST HORSEPOWER OF THERMAL-JET ENGINE VERSUS FLIGHT SPEED

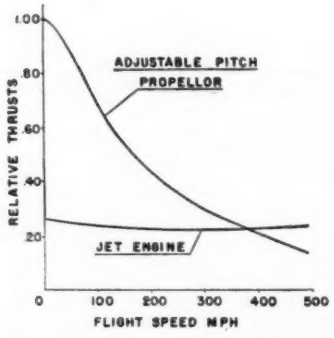


FIG. 17 COMPARISON OF PROPELLER AND THERMAL-JET THRUSTS VERSUS TRUE AIR SPEED

Fig. 18 shows how the thrust horsepower developed by the thermal jet varies with flight velocity and altitude.

Fig. 19 shows how increasing temperature of air leaving the combustion chamber affects static thrust and fuel consumption per pound of thrust. It is seen that raising the temperature greatly increases the static thrust at sea level but this is only at the expense of a slightly higher rate of fuel consumption per pound of thrust.

In the present state of the metallurgical art, operating temperatures as high as 1750 F are possible. If the present rate of improvement of refractory metals continues, operating temperatures as high as 2000 F appear to be probable.[14] As in the case of

[14] "The Gas Turbine in Aviation—Its Past and Future," by S. R. Puffer and J. S. Alford, presented at the Aviation War Conference, Los Angeles, Calif., June 11–14, 1945, of THE AMERICAN SOCIETY OF MECHANICAL ENGINEERS.

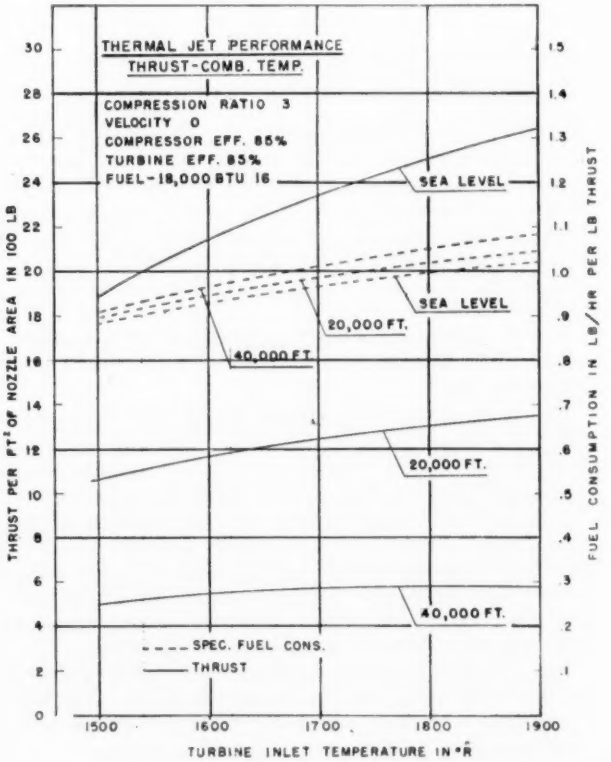


FIG. 19 EFFECT OF TEMPERATURE ON STATIC THRUST AND FUEL CONSUMPTION OF THERMAL-JET ENGINE

gas-turbine propulsion plants, the maximum benefits derivable from higher operating temperatures will necessitate using higher pressure ratios.[15]

Fig. 20 presents the static thrust and fuel consumption as functions of the pressure ratio of the air compressor for a constant temperature at the entrance to the turbine. Increasing the pressure ratio is effective in increasing the thrust and decreasing the fuel consumption.

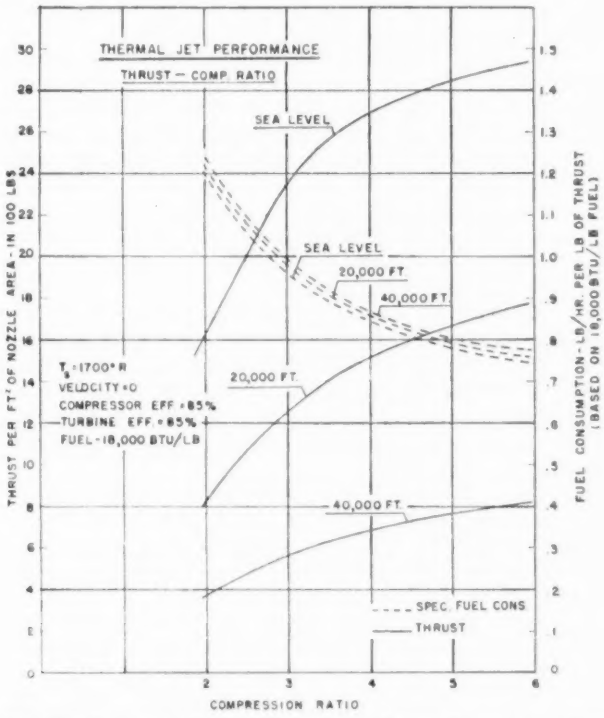


Fig. 20 Effect of Pressure Ratio on Static Thrust and Fuel Consumption of Thermal-Jet Engine

The efficiency of the unit, defined as the ratio of the thrust horsepower to the fuel supplied, is given by

$$\eta = \frac{2(\phi - 1)}{\alpha - \phi\left(1 + \frac{\theta - 1}{\eta_c}\right)}\left[\sqrt{\frac{\alpha\Sigma}{\phi - 1}} - 1\right] \quad \ldots\ldots [13]$$

With the assumed machine efficiencies, $\eta_c = \eta_t = 0.85$, and a pressure of 3, the efficiency at 500 mph and 20,000 ft altitude is approximately 15 per cent. An engine-driven propeller with a propulsion efficiency of approximately 60 per cent would give the same over-all efficiency. The efficiency, as a function of true air speed for different altitudes, is presented in Fig. 21.

Fig. 22 illustrates the effect of the efficiency of the compressor upon the static thrust developed and the corresponding fuel consumption. It is seen that with a turbine efficiency of 0.85 and a pressure ratio of 3, no thrust is developed if the compressor efficiency is less than 49 per cent. Increasing the efficiency of the compressor greatly reduces the fuel consumption and increases the thrust output. As a matter of fact, the efficiency of the system is improved by making the ratio of the compression work to the available energy of combustion as small as possible.[16]

[15] "Combustion Gas Turbine," by F. K. Fischer and C. A. Meyer, *Electrical Engineering*, vol. 63, 1944, pp. 163–169.

[16] "Reaction of Fluids and Jets," by R. Eksergian, *Journal of The Franklin Institute*, vol. 237, 1944, pp. 385–410.

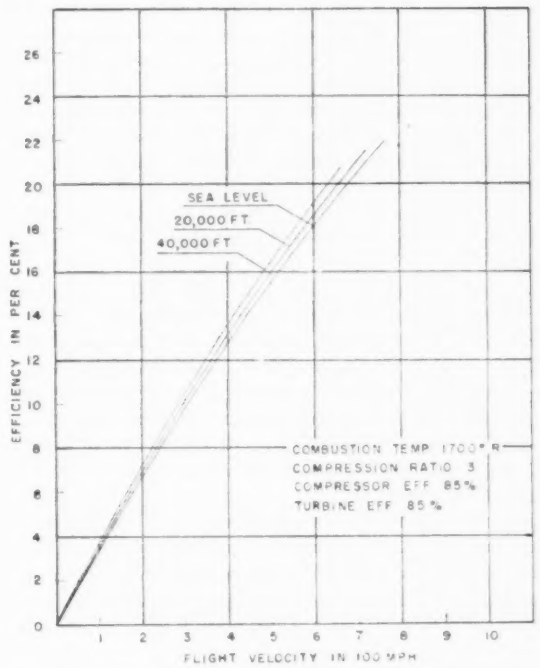


Fig. 21 Over-All Efficiency of Thermal-Jet Engine Versus True Air Speed

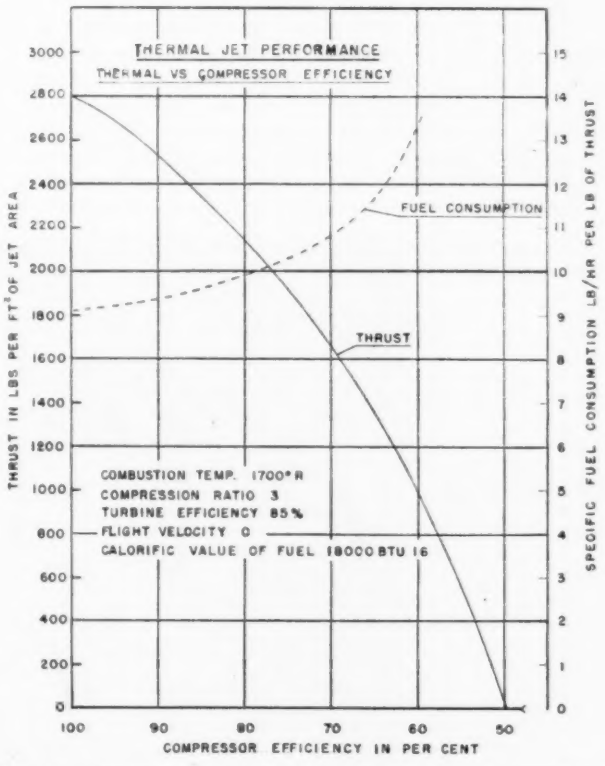


Fig. 22 Effect of Compressor Efficiency on Static Thrust and Fuel Consumption of Thermal-Jet Engine

The thermal-jet engine has made it possible to attain flight speeds higher than those obtainable with propeller propulsion. Because of its high fuel consumption, it has been widely held that its application will be restricted to short-endurance military

aircraft. Analyses of its commercial possibilities,[17] based on certain assumptions which have to be made at this stage in its development, indicate, however, that the jet-propelled transport should find a place in the postwar commercial field. These analyses indicate that for flights of the order of 500 miles, the jet-propelled transport provides economical transportation at high cruising speeds.[14] Until more of the operating data and actual performance characteristics of aircraft equipped with this form of power plant become available, the limits of the application of the thermal-jet engine to civilian aircraft cannot be stated with certainty.

Too much attention has been focused upon the apparent limitations of the thermal-jet engine, particularly upon its high fuel consumption; but these limitations appear to be related, to some extent at least, to the present state of the developments in the field of aerodynamics of high-speed flight. Thermal-jet propulsion imposes fewer restrictions upon the airplane designer. The commercial future of this method of propulsion depends to a large extent on the ability of airplane designers to produce airplanes with lower drag.

Perhaps the most attractive feature of the thermal-jet engine, apart from its ability to provide propulsion at high speeds, is its simplicity and low weight. Furthermore, this power plant is relatively free from vibration, permits using cheaper fuels than high-octane gasoline, and should require less frequent major overhauls.

Many problems are presented by the high operating temperatures required to obtain even fair fuel economy. Since weight and space are major considerations, the rate of heat liberation per cubic foot of combustion chamber has to be extremely high. For it to have reasonable life, its design must be arranged to give clean and reliable combustion, and the walls must be kept at safe operating temperatures. There are still metallurgical problems to be solved if higher operating temperatures are to be realized. In addition, there are problems in compensating for differences in thermal expansion. The fact that thermal-jet propulsion has become a practical reality is an indication, however, that great progress has been made in solving these problems.

[17] "Postwar Transport Aircraft," by E. P. Warner, *Aeronautical Engineering Review*, 1943, p. 7.

Rocket-Jet Application to Aircraft; Jato Units

The rocket has been developed to the stage where it should find a place as the power plant for short-duration high-speed aircraft (German ME 163); for long-range missiles (German V2 bomb); for superperformance at altitude, for torpedo drive, and for the assisted take-off of aircraft. Furthermore, the high-temperature high-pressure gas-producing capability of the rocket system should find application for short-duration turbine drives, or for any service where a temporary generation of such a gas can be employed for useful purposes.

In this country the principal application of rockets to aircraft apart from their use as weapons, is in the field of assisted take-off. Most of the applications have been to flying boats where the added thrust of the Jato units has made it possible to take off under conditions such that without them successful take-off would be problematical. This has increased the usefulness of such aircraft for rescue work in forward combat areas. Jato units have also been applied to carrier and land-based aircraft. As is to be expected, reductions in take-off time and/or distance have resulted from their use.[18]

Fig. 23 illustrates graphically the improvement in the sea level take-off characteristics of a DC-3 transport when equipped with a 1000-lb Jato unit having a duration of 14 sec. Fig. 24 is a similar comparison made at 6000 ft altitude. It is seen that the reduction in the distance to clear a 50-ft obstacle is from 4600 ft to 3250 ft at sea level and from 5800 ft to 3850 ft at 6000 ft altitude.

Two types of units have been applied; those employing liquid propellants, and those employing a solid propellant. To the author's knowledge, the solid-propellant units have found the greatest favor, owing to the ease of their installation, and the fewer logistic problems introduced by their use.

A liquid-propellant rocket system is ordinarily controlled from a single electric switch operated by the pilot. The switch actuates an electric control valve, thereby causing an inert pressurizing gas to communicate with the propellant tanks. The pressurizing gas passes through a regulating valve which main-

[18] "Take-Off Analysis for Flying Boats and Seaplanes," by E. G. Stout, *Aviation*, Oct., 1945, pp. 137–141; Nov., 1945, pp. 140–146, and Dec., 1945, pp. 163–166.

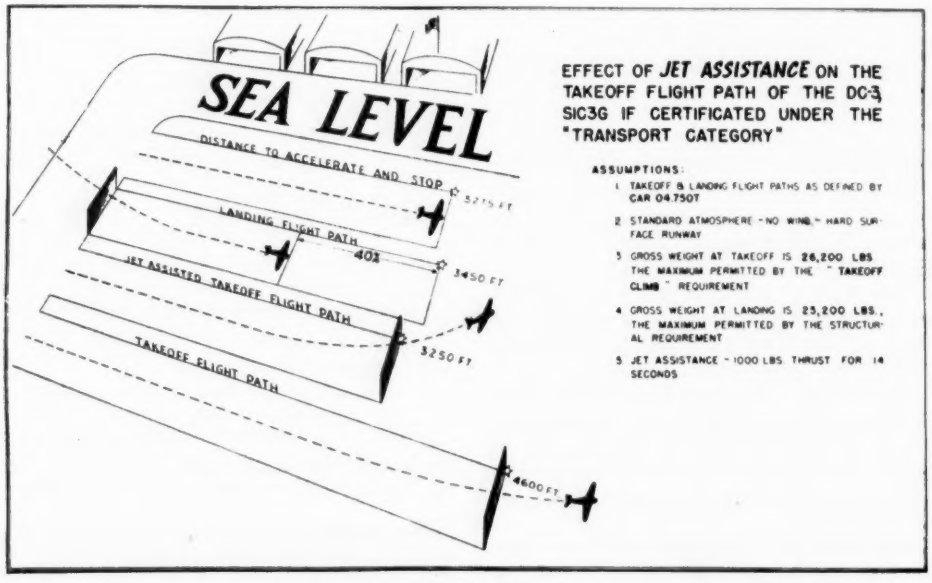


Fig. 23 Effect of Rocket-Jet Assistance on Take-Off Characteristics of DC-3 at Sea Level

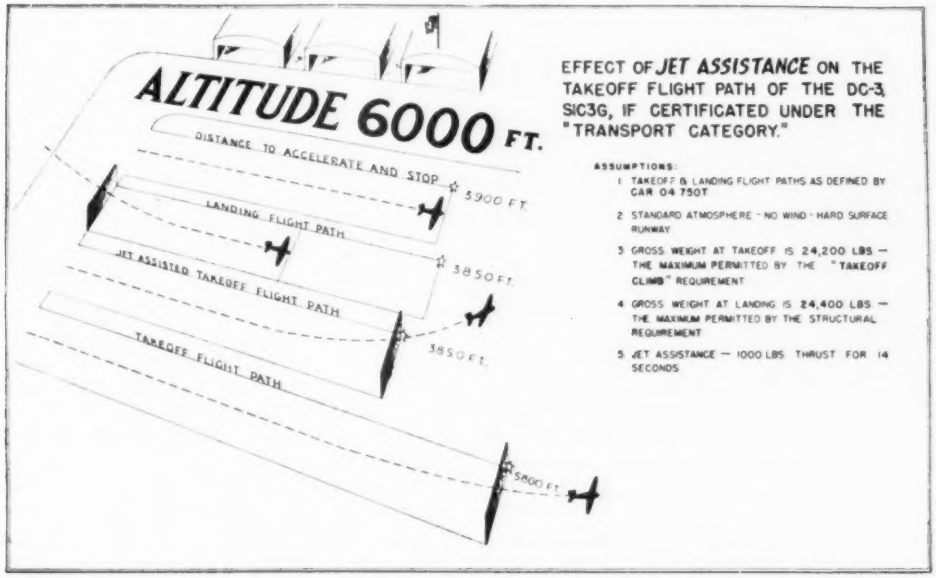


FIG. 24 EFFECT OF AUXILIARY ROCKET-JET ASSISTANCE ON TAKE-OFF CHARACTERISTICS OF DC-3 AT 6000 FT ALTITUDE

tains the gas pressure on each propellant tank at a constant value. This gas is also utilized for actuating the propellant flow control valves located upstream relative to the injector which introduces the propellants into the motor. No ignition system is employed, since the propellants used with this unit react spontaneously upon contact with each other.

Liquid-propellant Jato units have been constructed so that they can be mounted either as fixed installations in the aircraft, or so that they can be dropped by parachute after use. Reliable liquid-propellant rocket motors have been developed that have operated without difficulty for continuous periods of several minutes. These motors are light in weight and are cooled by circulating one of the propellants around the combustion chamber and nozzle. For example, a rocket motor of this type developing 1500 to 2000 lb thrust can be built to weigh less than 45 lb. For security reasons, the design details of this type of motor cannot be released, nor can information be presented regarding the developments concerned with propellants or means for injecting the propellants into the motor.

Fig. 25 shows a typical solid-propellant Jato unit which delivers 1000 lb thrust for 12 sec. It is put into operation by means of the igniter which is fired electrically. Once the unit has been



FIG. 25 TYPICAL SOLID-PROPELLANT JATO UNIT FOR 1000 LB THRUST, 12-SEC DURATION

started it cannot be stopped and restarted, as can the liquid-propellant units.

Fig. 26 shows a PB2Y3 flying boat taking off with these units installed to supply additional thrust.

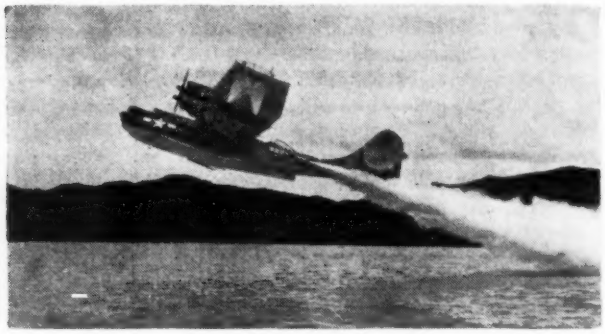


FIG. 26 FLYING BOAT TAKING OFF WITH JATO ASSISTANCE

CONCLUSIONS

Jet-propulsion devices have reached the development stage where they must be given serious consideration as a propulsion means. Where high-speed flight is of paramount importance, the thermal-jet engine has demonstrated its ability to accomplish that result. For shorter-duration high-speed flight, the rocket jet has potentialities.

In general, it appears that the future of jet propulsion in the postwar commercial field depends upon the success of the co-operative endeavors of airplane designers and jet-propulsion engineers in securing the maximum benefits offered by this mode of propulsion.

ACKNOWLEDGMENTS

The author expresses his thanks to Mr. R. Sabersky, Aerojet Engineering Corporation, for his assistance in making some of the calculations for the performance characteristics of the thermal-jet engine.

(Owing to travel emergency conditions existing when this paper was presented, discussion will be accepted until May 10, 1946)

Free Heat Convection Through Enclosed Plane Gas Layers

By MAX JAKOB,[1] CHICAGO, ILL.

Fifteen years ago, Mull and Reiher published elaborate experiments on heat convection through enclosed plane air layers. In the present paper it is shown that the representation and evaluation of the results of these experiments can be simplified, improved, and generalized when, as for a single surface in an extended medium, a laminar and turbulent range are distinguished. Defining slightly modified Nusselt and Grashof numbers with the layer thickness L as characteristic length, the experimental results for horizontal and vertical layers can be expressed by $(N_{Nu})_L = C_h(N_{Gr})_L^n$, or $C_v(N_{Gr})_L^n(L/H)^{1/9}$, respectively, where $n = 1/4$ and $1/3$ for the laminar and turbulent ranges, respectively, and H is the height of vertical layer. Comparison with tests of other authors indicates that, due to the experimental elimination of any influences from the edge of the enclosed layer, Mull and Reiher obtained relatively low values of the constants C_h and C_v, whereas without particular precaution these influences may considerably increase the heat transfer.

Nomenclature

The following nomenclature is used in the paper:

$A = H \cdot W$ = area of gas layer
C = constant
D = diameter
g = gravitational acceleration
H = height of vertical gas layer
h = coefficient of heat transfer by convection
k = thermal conductivity of gas
k_c = equivalent thermal conductivity, including conduction and convection
k_r = equivalent thermal conductivity, superseding radiation
$k_e = k_c + k_r$ = equivalent thermal conductivity
L = thickness of gas layer
N_{Gr} = Grashof number
N_{Nu} = Nusselt number
n = constant
q = rate of heat flow
$q'' = q/A$
t = temperature
W = width of gas layer
β = coefficient of thermal expansion
ν = kinematic viscosity
Φ, Ψ = functions

Subscripts:

c = convection
D = diameter as characteristic length
d = heat flow downward
H = height as characteristic length
h = horizontal gas layer
L = thickness of gas layer as characteristic length
m = mean
u = heat flow upward
v = vertical gas layer
1 = warmer surface
2 = colder surface

1 Introduction

In his excellent survey on heat transmission, presented in 1932, King (1)[2] dealt only briefly with the subject of heat transfer in air layers as "too involved to allow a complete discussion here." In particular, he had in mind the experimental results for plane air layers, published by Mull and Reiher in a not widely known supplement to a German magazine (2). It will be seen that these results are less involved than they appear in the original paper. The present paper will bring them to a more general and simpler representation and show their close relation to equations for free convection on horizontal and vertical surfaces.

2 Mull and Reiher's Procedure and Results

As a measure for the heat exchange in a gas layer, Mull and Reiher used an equivalent thermal conductivity k_e, which combines the effect of convection and radiation and is defined by

$$k_e = k_c + k_r \quad \ldots\ldots\ldots\ldots\ldots\ldots [1]$$

where k_c and k_r are themselves equivalent thermal conductivities, the first one including the effect of conduction and convection and the second one superseding the effect of radiation.

Whereas k_r can be simply calculated, using the laws of radiation, it requires special experiments to determine k_c. Mull and Reiher employed two parallel plates, each 40 in. long and 24 in. wide, which were separated by air layers. These could be divided in different ways so that it was possible to study enclosed air layers having areas of 30 to 960 sq in. Air layers of seven different thicknesses from $1/2$ to $7\,3/4$ in. were employed. One of the two plates was an electrical heating plate composed of five separate sections and surrounded by an electrical ring heater. A secondary heating plate at the rear side, insulated from the front plate and ring, was held at the same temperature as these. Thus the main heat flow was confined to the front side from where it first crossed the air layer under consideration and then a cork plate which served as an auxiliary heat flowmeter. Strips of poorly conducting balsa wood, only 80/1000 in. thick, separated the air layers from each other and from the surrounding air which was in contact with the ring heater. Zinc was the material of the heating and cooling surfaces (zinc-plated steel sheets). The whole system of plates was surrounded by granulated cork and fixed in a wooden frame. This was turnable in a horizontal bearing so that the air layer could be brought into horizontal, vertical, or oblique position.

[1] Consultant in Heat Research, Armour Research Foundation; Research Professor of Mechanical Engineering, Illinois Institute of Technology; Nonresident Research Professor of Heat Transfer, Purdue University. Mem. A.S.M.E.

Contributed by the Heat Transfer Division and presented at the Annual Meeting, New York, N. Y., Nov. 26–29, 1945, of The American Society of Mechanical Engineers.

Note: Statements and opinions advanced in papers are to be understood as individual expressions of their authors and not those of the Society.

[2] Numbers in parentheses refer to the Bibliography at the end of the paper.

The rate of heat flow by convection between a warmer surface (subscript 1) and a cooler surface (subscript 2) can be expressed by

$$q_c = k_c \frac{A}{L}(t_1 - t_2) \text{ or } q_c'' = \frac{k_c}{L}(t_1 - t_2) \quad [2]$$

where

L = the thickness of gas layer
A = $H \cdot W$, area of this layer
H = height of rectangular area A (when brought into vertical position)
W = width of this area
t_1 and t_2 are surface temperatures
$q_c'' = q_c/A$

Further, from the theory of similarity for air and probably also for any other diatomic gases (except under extreme conditions of state)

$$(N_{Nu})_L = \Phi[(N_{Gr})_L, H/L, W/L] \quad [3]$$

where slightly modified Nusselt and Grashof numbers are defined by

$$(N_{Nu})_L = \frac{q_c''}{(t_1 - t_2)} \cdot \frac{L}{k} = \frac{k_c}{k} \quad [4]$$

and

$$(N_{Gr})_L = \frac{\beta g}{\nu^2} L^3(t_1 - t_2) \quad [5]$$

with

g = gravitational acceleration
β = coefficient of thermal expansion of gas
k = its thermal conductivity
ν = its kinematic viscosity

the last two properties being taken at the mean temperature

$$t_m = {}^1/_2(t_1 + t_2)$$

From Equations [3] and [4]

$$k_c/k = \Phi[(N_{Gr})_L, H/L, W/L] \quad [6]$$

First considering horizontal layers (subscript h), the experiments, with heat flow upward, showed that $k_{c,h}/k$ is virtually independent of H and W. Then, from reasons of similitude, it will also be independent of H/L and W/L. Hence Equation [6] simplifies to

$$k_{c,h}/k = \Phi(N_{Gr})_L \quad [7]$$

Mull and Reiher represented their results by plotting $k_{c,h}/k$ versus log $(N_{Gr})_L$; obviously

$$k_{c,h}/k \longrightarrow 1 \text{ when } (N_{Gr})_L \longrightarrow 0$$

In the experimental range of $(N_{Gr})_L$ = 2112 to 8,890,000, a smooth curve of increasing steepness was obtained. Representation in bilogarithmic co-ordinates, however, will reveal that the curve has at least one bend in close relationship to other cases of free convection.

For vertical air layers (subscript v), the conditions are less simple than for horizontal layers because $k_{c,v}/k$ may not be independent of H and W. Mull and Reiher, in one of their tests, kept H/L and $(N_{Gr})_L$ constant, but reduced W/L from 25.7 to 12.8, that is, by 50 per cent. The term $(k_{c,v}/k)$ (H/L), however, changed only by 1.3 per cent. Hence, omitting W/L as independent variable and modifying Equation [6] slightly

$$\frac{k_{c,v}}{k} \cdot \frac{H}{L} = \Psi\left[(N_{Gr})_L \frac{H}{L}\right] \quad [8]$$

Similarly as for horizontal gas layers

$$k_{c,v}/k \longrightarrow 1 \quad \text{when } (N_{Gr})_L \longrightarrow 0$$

The problem also simplifies for very large Grashof numbers due to the vanishing of the frictional resistance between two parallel vertical surfaces with increasing distance; obviously

$$t_1 - t_m = t_m - t_2$$

and

$$q_{c,v}'' = h(t_1 - t_m) = h(t_m - t_2)$$

or

$$q_{c,v}'' = {}^1/_2 h(t_1 - t_2) \quad [9]$$

where h is the coefficient of convection for a single vertical surface. From Equations [2] and [9]

$$k_{c,v} = \frac{hL}{2} \text{ or } \frac{k_{c,v}}{k} \cdot \frac{H}{L} = \frac{h}{k} \cdot \frac{H}{2} = \frac{1}{2} \cdot \frac{h}{k} \cdot \frac{H}{L} \cdot L \ldots \quad [10]$$

Hence, $k_{c,v}$ becomes proportional to L for very thick air layers and the resistance against thermal convection, $L/(k_{c,v}A)$ becomes constant. Since the resistance against heat transfer by radiation is also constant for given temperatures, it follows that the insulating power of an air layer cannot be increased infinitely by increasing the layer thickness as it would be with a solid layer, but is limited.

For layers of finite thickness, Mull and Reiher plotted $(k_{c,v}/k)$ (H/L), as measured, versus log $(N_{Gr})_L$ and built up 27 curves with H/L as parameter, making ample use of interpolation and extrapolation since a total of only 21 points from their own, and 3 from other experiments were available. Again, bilogarithmic representation will give a very much simpler and more reliable picture and will lead to simple equations for the laminar and turbulent ranges, analogous to those for single plane surfaces.

3 Dimensionless Equations for Free Convection on Vertical and Horizontal Surfaces

As already indicated, the heat convection on a plane plate is an extreme case of convection through a plane fluid layer.

The Nusselt and Grashof numbers for the free convection on a vertical surface of height H and temperature t_1 to a fluid of temperature t_m is usually defined by

$$(N_{Nu})_H = \frac{hH}{k} \quad [11]$$

and

$$(N_{Gr})_H = \frac{\beta g}{\nu^2} H^3(t_1 - t_m) \quad [12]$$

where arithmetic means, taken over the temperature difference $(t_1 - t_m)$, may be used for the properties of the fluid.

Employing the principle of similarity, Nusselt (3) showed that $(N_{Nu})_H$ is proportional to $H^{3/4}$, a result which had already been obtained analytically by Lorenz (4), 34 years before. This, however, is only a fair approximation to the actual much more complicated relation between h and H, as has been demonstrated later on by different workers, particularly by Schmidt and Beckmann (5) in a theoretical and experimental investigation. Moreover, Griffiths and Davis (6) had shown by experiments that above a certain height (about 2 ft for air) the coefficient h becomes independent of H and proportional to $(t_1 - t_m)$. They correctly

concluded that turbulence occurs above that height. It is worth noting that Nusselt (3) had already predicted an analogous phenomenon for horizontal cylinders placed in cooler air when $(N_{Gr})_D > 10^7$, the diameter D being used as characteristic length.

The occurrence of an exponent $n = 1/3$ in the equation

$$N_{Nu} = C(N_{Gr} \cdot N_{Pr})^n \quad [13]$$

was later verified by a correlation of King (1) and by Jakob and Linke (7) in representing their own and Jakob and Fritz's experimental results (8) for not too vehemently boiling water. According to these investigations, the following equations can be used for vertical surfaces in an unrestricted fluid

$$(N_{Nu})_H = 0.555\,[(N_{Gr})_H N_{Pr}]^{1/4} \quad [14]$$

for the laminar range and

$$(N_{Nu})_H = 0.129\,[(N_{Gr})_H N_{Pr}]^{1/3} \quad [15]$$

for the turbulent range.

Jakob and Linke further showed that Equation [13] with $n = 1/3$ may also be used for the convection on the upper side of a horizontal plate (subscript u) on which water is boiling, and they concluded that in the range of their experiments, $q_{c,u}'' = 7$ to 5200 B hr^{-1} ft^{-2}, the coefficient of convection on a horizontal plate is independent of the size of the plate except for a possible effect of the edges. In fact, this had to be expected because it would not be understandable why the heat transfer on one place of a large horizontal plate should be different from that at any other place.

In other words, if Equation [13] is valid, then $n = 1/3$ must necessarily occur in all cases where no reason exists why h should depend upon a characteristic length. In a subsequent paper, Jakob and Linke (9) found by experiments with boiling water and carbon tetrachloride that the constant C of Equation [13] sensibly exceeds the values given in Equations [14] and [15]. For vertical surface, in the range where $n = 1/4$, $C_v = 0.61$ was found, compared to $C_v = 0.555$ in Equation [14]. This difference may be due to the action of the steam bubbles which is rather mild in the considered range, but increases rapidly at higher load (9, 10). With horizontal surface facing upward, $n = 1/3$ and $C_u = 0.16$ were observed to be compared with $C_v = 0.129$ for vertical surfaces according to Equation [15]. Here, in addition to the effect just mentioned, the difference of surface orientation seems to play a role. In fact, such an effect had previously been observed by Griffiths and Davis (6). From their tests on horizontal heating plates in air facing upward, the following equation can be derived

$$q_{c,u}'' = 0.275(t_1 - t_m)^{4/3} \quad [16]$$

with

$q_{c,u}''$ in B hr^{-1} ft^{-2} and $(t_1 - t_m)$ in Fahrenheit units.

Combining this with their original values for vertical plates, 2 and 8 2/3 ft high

$$q_{c,u}''/q_{c,v}'' \approx 1.28 \quad [17]$$

to be compared with $C_u/C_v = 0.16/0.129 = 1.24$.

For horizontal plates, facing downward (subscript d) where theoretically only conduction would be expected, Griffiths and Davis' measurements can be represented by

$$q_{c,d}'' = 0.50\, q_{c,u}'' \approx 0.64\, q_{c,v}'' \quad [18]$$

It may be noted that

$$\frac{q_{c,u}'' + q_{c,d}''}{2} \approx \frac{1.28 + 0.64}{2} q_{c,v}'' = 0.96\, q_{c,v}'' \approx q_{c,v}'' \quad [19]$$

Wilkes and Peterson (11), however, obtained about 1.6 instead of 1.28 (Equation [17]) and about 0.35 instead of 0.50 (Equation [18]). Their data are based on experiments with only 10 F temperature difference and therefore probably less exact.

4 New Equations for Free Convection Through Enclosed Plane Gas Layers

In the range of $(N_{Gr})_L = 10{,}000$ to 10,000,000, Mull and Reiher's experimental data for horizontal air layers can be represented by two straight lines in bilogarithmic co-ordinates, Fig. 1. Intersection of these lines occurs at log $(N_{Gr})_L \approx 5.57$, corresponding to $(N_{Gr})_L \approx 370{,}000$. However, a state of transition may exist between $(N_{Gr})_L \approx 200{,}000$ and 800,000. In the

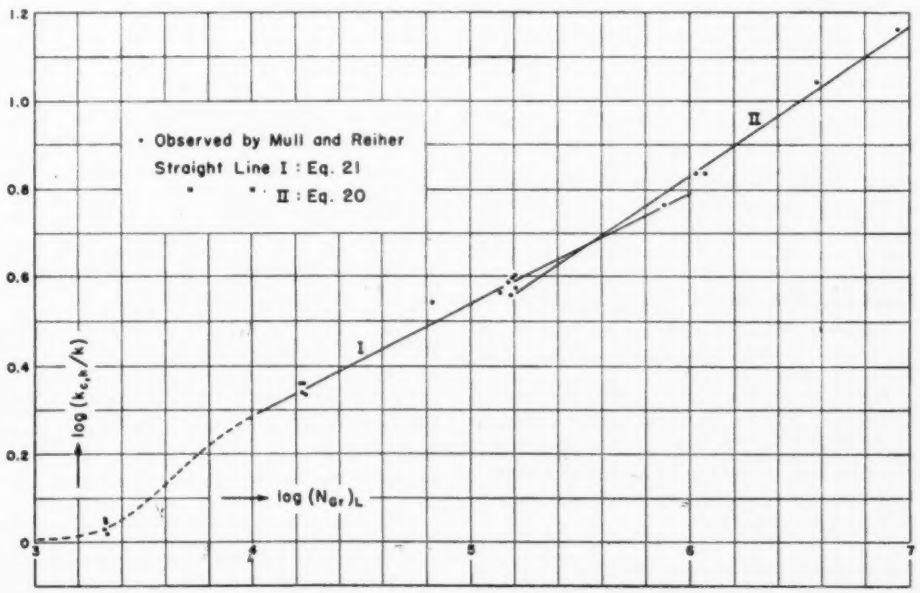


Fig. 1 Correlation for Horizontal Air Layers

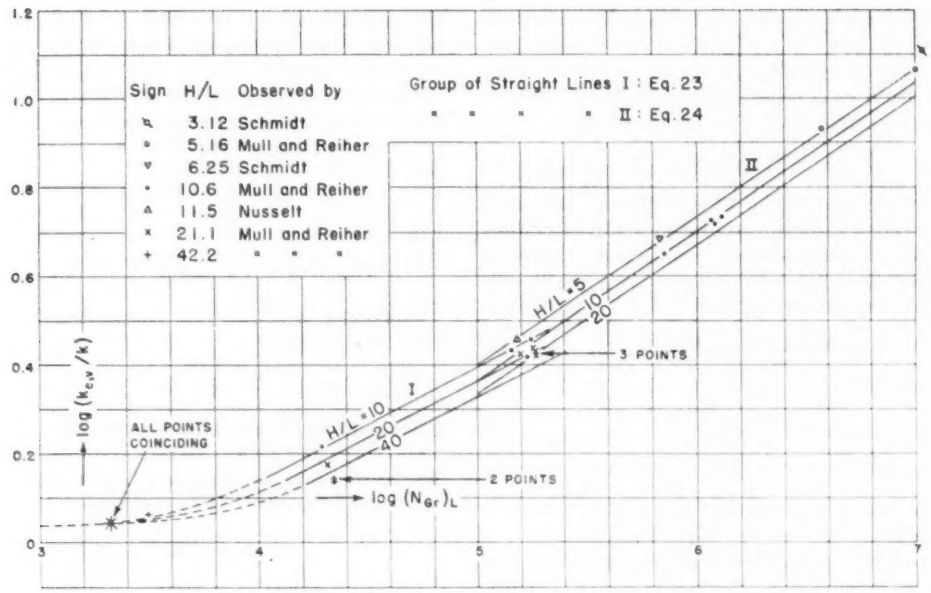


FIG. 2 CORRELATION FOR VERTICAL AIR LAYERS

upper range,[3] similarly as for a heated surface, facing upward, or for a vertical surface

$$k_{c,h}/k = 0.068(N_{Gr})_L^{1/3} \quad \ldots\ldots [20]$$

In the lower range, in analogy to the behavior of vertical surfaces in a medium range of Grashof numbers

$$k_{c,h}/k = 0.195(N_{Gr})_L^{1/4} \quad \ldots\ldots [21]$$

For $(N_{Gr})_L \longrightarrow 0$, finally

$$k_{c,h}/k \longrightarrow 1 \quad \text{or} \quad \log (k_{c,h}/k) \longrightarrow 0 \quad \ldots\ldots [22]$$

as indicated by a dotted line in Fig. 1.

The meaning of Equation [20], obviously, is that above a certain thickness L the coefficient of heat transfer does not change any more, but should be the same as for a single horizontal plate, facing upward.

This may be checked by calculating an example: According to Equation [20]

$$q_{c,h}'' = 0.068k\left(\frac{\beta g}{\nu^2}\right)^{1/3}(t_1 - t_2)^{4/3}$$

For $t_1 = 75°$ C, $t_2 = 52°$ C, and 730 mm Hg atmospheric pressure, Mull and Reiher took $\beta g/\nu^2 = 0.110$ (10^9) m^{-3} C^{-1} and $k = 23.0$ (10^{-3}) kcal hr^{-1}m^{-1}C^{-1}. Using these values and converting to British technical units

$$q_{c,h}'' = 0.068(23.0)10^{-3}(0.673)(0.110)^{1/3}(10^3)0.3048(1.8)(t_1 - t_2)^{4/3} = 0.277(t_1 - t_2)^{4/3}$$

in excellent agreement with Equation [16].

For vertical air layers, employing again bilogarithmic representation, all experimental points of Mull and Reiher and three points of other authors which they also used are plotted in Fig. 2.

At Grashof numbers as small as 2000, in analogy to Equation [7], no influence of H/L upon $k_{c,v}/k$ seems to exist in the range of the experiments ($H/L = 10.6$ to 42.2).

[3] Particularly after correcting the highest point, at $(N_{Gr})_L = 8{,}890{,}000$, for which Mull and Reiher erroneously have entered $k_{c,h}/k = 13.5$ (instead of 14.5) in their original graph.

For still smaller Grashof numbers, the ratio $k_{c,v}/k$ approaches unity in analogy to Equation [22].

In the range of $(N_{Gr})_L = 20{,}000$ to 200,000, the following equation represents the experimental data

$$k_{c,v}/k = 0.18(N_{Gr})_L^{1/4}(H/L)^{-1/9} \quad \ldots\ldots [23]$$

and in the range of $(N_{Gr})_L = 200{,}000$ to 10,000,000

$$k_{c,v}/k = 0.065(N_{Gr})_L^{1/3}(H/L)^{-1/9} \quad \ldots\ldots [24]$$

Again the exponents, $1/4$ and $1/3$, of $(N_{Gr})_L$ are significant for laminar and turbulent flow. The exponent $-1/9$ of H/L, however, has been found empirically. The increase of $k_{c,v}/k$ with decreasing H/L is probably an effect of the lower and upper edge of the gas layer.

It is questionable how far beyond the range of the experiments Equations [23] and [24] are valid and, in particular, down to which smallest value of H/L Equation [24] can be used; certainly not down to $H/L = 0$, where it would yield an infinitely large heat transfer whereas the behavior of single vertical plates should be approached. However, the experimental point for $H/L = 3.12$ at $N_{Gr} = 10{,}820{,}000$ in Fig. 2 is in excellent agreement with the value calculated from Equation [24] ($\log[k_{c,v}/k] = 1.105$, observed and 1.103, calculated) so that Equation [24] actually seems to be valid down to the ratio of $H/L \approx 3$.

Lines for $H/L = 5$; 10; 20; and 40 are drawn in Fig. 2, to facilitate interpolation. It is seen that they are in good agreement with the experimental points.

Mull and Reiher's paper includes one measurement for 45 deg inclination of the air layer. At $H/L = 10.5$ and $(N_{Gr})_L = 1{,}050{,}000$ they obtained $k_c/k = 6.13$. Under the same conditions Equations [20] and [24] yield $k_{c,h}/k = 6.92$ and $k_{c,v}/k = 5.09$, the mean of which is 6.005. This result suggests that for angles from 0 to 90 deg linear interpolation between these equations may give reasonable results.

5 DISCUSSION OF DIFFERENT EXPERIMENTAL RESULTS

It must be mentioned that experiments, performed by Wilkes and Peterson (12), led to about 50 per cent higher values of q_c'' for vertical layers. An air layer with $L = 0.302$ and $H = W =$

2.667 ft was used, and it seems that the temperatures (t_1 = 60 deg F and t_2 = 40 deg F) were not varied either, so that the result would refer to $(N_{Gr})_L \approx 1{,}700{,}000$ only. The data given in the authors' paper do not allow one to check the accuracy of the results. The higher heat transfer obtained by them may be due to inclusion of the flow of heat through the studs confining the air layer and to the lack of a ring heater with air layer. Griffiths and Davis (6), employing a vertical layer with $L = 1/6$ ft and $H/L = 24.8$, arrived at almost 40 per cent higher heat transfer than Mull and Reiher, assumedly for the same reason. Experiments of Schmidt (13), on the other hand, performed with vertical layers, 0.263 or 0.526 ft thick, led to results in good agreement with those of Mull and Reiher (see Fig. 2). In these experiments a layer of 5-ft height was divided into three layers, each $1^2/_3$ ft high, by means of thin, horizontal strips of plywood, the adjacent layers giving some heat protection to each other. A test by Nusselt (14), on a vertical layer (L = 0.13 ft, H = 1.5 ft) led also to satisfactory agreement with our representation (see Fig. 2); this, however, may be accidental, considering the not too accurate experimental procedure.

With their air layer in horizontal position, Wilkes and Peterson, again at $(N_{Gr})_L \approx 1{,}700{,}000$, obtained a 40 per cent higher value than according to Mull and Reiher, whereas an experiment of Schmidt (13), at $(N_{Gr})_L \approx 30{,}000$, led to a 33 per cent smaller value than according to Mull and Reiher. This experiment was performed on a twin-plate device for measuring thermal conductivities, using a 1-in. air layer.

Considering the results of Wilkes and Peterson, and of Griffiths and Davis, the author looked for reasons why Mull and Reiher might have obtained too small values of convection. Referring to Equation [1], the value k_r was 27 to 49 per cent of k_e in their experiments. They determined k_r individually in each test by bringing the plates in horizontal position, heating the upper one, and assuming that no convection at all occurred in this case. According to Equation [20] or Fig. 1, this would mean that at $(N_{Gr})_L = 1{,}700{,}000$, after deduction of the radiated heat, the heat flow downward would amount to 12.3 per cent of that upward. This is not an unreasonable result, considering that Wilkes and Peterson found 23 per cent, without taking such precautions as the use of a heated air ring and thin balsa-wood strips to secure a strictly vertical heat flow downward. Anyway, k_r may have been found only a few per cent too large and k_c some per cent too small in Mull and Reiher's procedure. Incidentally, the emissivity of the zinc-plated steel sheet determined by them was rather too small than too large, according to the known values from literature, and there was no systematic influence of L on the measured value of that emissivity as would have been if convection had played a role.

Hence the only explanation for the mentioned differences is that, as just given, the Mull and Reiher values belong to the case of an enclosed partition, cut out somewhere in the middle of an extended gas layer between two parallel surfaces, each at uniform temperature, and with a practically nonconducting border strip, whereas in Griffiths' and Davis' results, as well as in those of Wilkes and Peterson, conduction effects on the edge of the layer are included. Therefore Equations [20], [21], [23], and [24] and Figs. 1 and 2 of the present paper yield values which may have to be increased by empirical factors if less ideal conditions exist at the edge of the air layer.

6 Free Convection Through Enclosed Plane Liquid Layers

According to the theory of similarity, Equations [20], [21], [23], and [24] should hold for any diatomic gases, except in such extreme ranges where the Prandtl number appreciably differs from $N_{Pr} = 0.72$, as assumed for air. Since for horizontal and vertical surfaces Equation [13] has been found to hold for gases and for liquids, even in the state of not too vehement boiling, with only moderately different values of C, the equations mentioned for confined layers may tentatively be used for other than diatomic gases and for liquids by multiplying the right sides by $(N_{Pr}/0.72)^n$, with $n = 1/4$ and $1/3$, respectively.

BIBLIOGRAPHY

1 "The Basic Laws and Data of Heat Transmission. III—Free Convection," by W. J. King, *Mechanical Engineering*, vol. 54, 1932, pp 347–353.

2 "Der Wärmeschutz von Luftschichten," by W. Mull and H. Reiher, Beihefte zum *Gesundheits-Ingenieur*, Reihe 1, Heft 28, Munich and Berlin, Germany, 1930.

3 "Das Grundgesetz des Wärmeueberganges," by W. Nusselt, *Gesundheits-Ingenieur*, vol. 38, 1915, p. 477.

4 "Über das Leitungsvermoegen der Metalle fuer Wärme und Electricität," by L. Lorenz, *Wiedemanns Annalender Physik und Chemie*, vol. 13, 1881, p. 582.

5 "Das Temperatur-und Geschwindigkeitsfeld vor einer Wärme abgebenden senkrechten Platte bei natuerlicher Konvektion," by E. Schmidt und W. Beckmann, *Techn. Mech. und Thermodyn.*, vol. 1, 1930, pp. 341–349 and 391–406.

6 "The Transmission of Heat by Radiation and Convection," by E. Griffiths and A. H. Davis, Department of Scientific and Industrial Research, Special Report No. 9, London, England, 1922.

7 "Der Wärmeuebergang von einer waagerechten Platte an siedendes Wasser," by M. Jakob and W. Linke, *Forschung auf dem Gebiete des Ingenieurwesens*, vol. 4, 1933, pp. 75–81.

8 "Versuche über dn Verdampfungsvorgang," by M. Jakob and W. Fritz, *Forschung auf dem Gebiete des Ingenieurwesens*, vol. 2, 1931, pp. 435–447.

9 "Der Wärmeuebergang beim Verdampfen von Fluessigkeiten an senkrechten und waagerechten Flächen," by M. Jakob and W. Linke, *Physikalische Zeitschrift*, vol. 36, 1935, pp. 267–280.

10 "Heat Transfer in Evaporation and Condensation—I," by M. Jakob, *Mechanical Engineering*, vol. 58, 1936, pp. 643–660.

11 "Radiation and Convection From Surfaces in Various Positions," by G. B. Wilkes and C. M. F. Peterson, *Heating, Piping and Air Conditioning*, vol. 10, 1938, pp. 477–480.

12 "Radiation and Convection Across Air Spaces in Frame Construction," by G. B. Wilkes and C. M. F. Peterson, *Heating, Piping and Air Conditioning*, vol. 9, 1937, pp. 505–510.

13 "Wärmeschutz durch Aluminiumfolie," by E. Schmidt, *Zeit. V.D.I.*, vol. 71, 1937, pp. 1395–1400.

14 "Die Waermeleitfaehigkeit von Waermeisolierstoffen," by W. Nusselt, V.D.I.-Forschungsarbeiten, nos. 63 and 64, 1909.

Discussion

W. J. King.[4] This paper constitutes a useful contribution to the literature of heat transmission, by making the data of Mull and Reiher available to American engineers in the form of a convenient and significant correlation.

The use of an "equivalent conductivity," k_e, has the advantage of expressing heat transfer through air spaces in the same units as for solid insulation or building materials, which may be convenient for combining terms. On the other hand, there is a disadvantage in that the conductivity of an air space is by no means a constant property of the material, as in the case of cork or brick, so that the actual relationship between heat transfer and thickness of the air space is somewhat obscured.

For example, it is shown that for certain conditions the conductivity is proportional to the $^3/_4$ power of the thickness. Actually, since the heat-transfer coefficient h (heat flow per unit time per unit area per degree temperature difference), is equal to the conductivity divided by the thickness, i.e.

$$h = \frac{k}{L}$$

[4] Research Engineer, Battelle Memorial Institute, Columbus, Ohio. Mem. A.S.M.E.

it turns out that the heat flow varies inversely with the $^1/_4$ power, or 4th root of the thickness, in this region.

It is also important to understand that for the wider air spaces or higher Grashof's numbers, where the conductivity is directly proportional to the thickness, the actual heat-transfer rate, as Btu per hour per square foot per degree temperature difference, is independent of the thickness.

Probably the most questionable feature of this correlation is the effect of height upon heat transfer across vertical air layers, as expressed by the term $(H/L)^{-1/}$ in Equations [23] and [24] of the paper. As the author points out, for the higher values of Grashof's number, to which Equation [24] applies, the heat transfer should be similar to free convection from exposed plane surfaces, in which case the effect of height is sometimes more pronounced. In fact, for vertical surfaces about 1 ft high, the effect of the height H, may be represented by the $-^1/_4$ exponent, under ordinary conditions.

Tests on enclosed air spaces made by E. R. Queer[5] in this country showed that the heat transfer across an air layer $4^1/_2$ in. high was about 80 per cent greater than for a height of 35 in. For a height ratio of 1 to 8, as in this case, the $-^1/_9$ exponent would give a 1.27 ratio of heat-transfer rates, instead of the 1.8 ratio observed by Queer. It is very likely that the effect of height becomes more pronounced as the height is decreased.

The author recognizes the fact that this exponent is not constant, pointing out that Equation [24] would give infinitely large heat-transfer rates for $H/L = 0$. This brings out the danger of applying such equations as these to conditions too far removed from those under which the original data were obtained.

Author's Closure

In discussing the concept of "equivalent conductivity," Mr. W. J. King uses the word "equivalent" only once and then omits it for brevity. Then, of course, all statements concerning that quantity become odd, as, for instance, the one that the conductivity be proportional to the 3/4 power of the thickness. The sense of introducing an "equivalent" conductivity, however, is only to show how much more heat is actually transferred than would be by conduction alone. The ratio $k_e/k = 1.5$, for instance, means that the heat transfer by convection is 50 per cent larger than the heat transfer by mere conduction.

This sort of representation is neither novel nor unique. The rate of heat exchange by radiation q_r, for instance, is often expressed by means of an "equivalent" coefficient of radiation, h_r. For black surfaces h_r is defined by the equation

$$q_r = \sigma A(T_1^4 - T_2^4) = h_r A(T_1 - T_2)$$

wherein

T = absolute temperature
σ = constant of Stefan-Boltzmann's law

It is seen that h_r is not a constant as σ, but depends upon T_1 and T_2 in a rather odd way. However, when convection and radiation occur in the same field, it is practical to use h_r, because the total coefficient of heat transfer simply becomes

$$h = h_c + h_r$$

Also the ratio k_e/k should just be considered as a practical form or as a Nusselt number (see Equation [4] of the paper).

The term $(H/L)^{-1/9}$ of Equations [23] and [24] was chosen empirically as best representing the points in Fig. 2 of the paper. However, its influence is small and it would have been possible to neglect it entirely and to represent each of the point groups I and II of Fig. 2, by a single straight line, yielding values of $k_{e.v}$ with extreme deviations of ± 10 per cent from the measured values. Doing so, Equation [23] would contain only the exponent $^1/_4$, in analogy to Equation [14].

Mr. King has further directed the author's attention to a paper of E. R. Queer,[5] who observed a much larger increase in heat transmission when the height H was reduced than did Mull and Reiher. This seems to be partly due to the heat conduction through the wooden strips which confined the air layers and the thick plates extending over the top and bottom of the apparatus. According to Fig. 2 of Queer's paper, these probably were thick enough to cause the large heat transfer observed by him for small ratios H/L. A part of the discrepancy, however, is due to the difference in the absolute values of heat transfer, observed in the two investigations for great ratios of H/L. For example, at $L = 1/12$ ft, $t_m \backsimeq 75$ deg F, $t_1 - t_2 = 50$ F, the author's Equation [23] yields $q_{c.v}'' = 21.5$ Bhr^{-1} ft^{-2} for $H = 4.5/12$ ft, and $q_{c.v}'' = 17.2$ for $H = 35/12$ ft, in agreement with Mull and Reiher's experiments, whereas Queer obtained $q_{c.v}'' = 27.5$ and 15.3, respectively.

When the author by illness was prevented from presenting his paper personally, Mr. King kindly presented it for him, adding some interesting comments which form the subject of his discussion. The author wishes to express his appreciation for Mr. King's co-operation and valuable contribution.

[5] "Importance of Radiation in Heat Transfer Through Air Spaces," by E. R. Queer, *Heating, Piping and Air Conditioning*, vol. 3, 1931, pp. 960–965.

A Graphical Determination of Unshielded-Thermocouple Thermal Correction

By W. M. ROHSENOW,[1] ANNAPOLIS, MD.

This paper presents a simple and rapid method for determining the thermal error of an unshielded thermocouple, with slide-rule precision.

Nomenclature

The following nomenclature is used in the paper:

Q = rate of heat transfer by convection
R = rate of heat transfer by radiation
C = rate of heat transfer by conduction
T_N = absolute temperature of N, deg R
t_N = temperature of N, deg F
h = film coefficient of heat transfer, Btu hr^{-1} ft^{-2} F^{-1}
k = thermal conductivity of thermocouple wire, Btu hr^{-1} ft^{-2} $(F/ft)^{-1}$
σ_b = Stefan-Boltzmann constant = 1.723×10^{-9} Btu hr^{-1} ft^{-2} R^{-4}
ϵ = emissivity
η = transmissivity
α = absorptivity
G = mass flow per unit cross section of duct area, lb ft^{-2} sec^{-1}
A = thermocouple bulb surface area, ft^2
D = thermocouple wire diameter, ft
d_0 = thermocouple bulb diameter, in.
b = exposed length of thermocouple, ft
T_m = $[(T_T^4 - T_W^4)/4(T_T - T_W)]^{1/3}$
T_a = average temperature between T_T and T_W = $\frac{1}{2}(T_T + T_W)$
θ = $(T_G - T_T)/(T_T - T_W)$

Subscripts:

G = gas
T = thermocouple
W = wall
S = thermocouple surface
GT = gas to thermocouple
TW = thermocouple to wall

Introduction

The problem of measuring the temperature of a gas stream by employing a thermocouple has been well treated by King (4),[2] Fishenden and Saunders (6), Bennett and Pirani (7), and Bosanquet (8). The accurate measurement of the temperature of a hot gas flowing in a duct is more difficult than the accurate measurement of the temperature of a solid or liquid. The temperature indicated by a thermocouple placed in the gas stream, Fig. 1, will always lie between the temperature of the gas itself and of the surrounding walls.

The thermocouple reading is in error because heat is exchanged between the thermocouple and the wall by radiation, and heat is transferred along the thermocouple wires by conduction. The analyses for the cases in which the gas is hotter than the wall and in which the wall is hotter than the gas are identical. When the gas is hotter than the wall, the thermocouple temperature is such that the rate of heat transfer by convection from the gas to the thermocouple plus the radiation from gas to thermocouple is equal to the radiation from the thermocouple to wall plus the conduction along the thermocouple wires. This may be stated in equation form

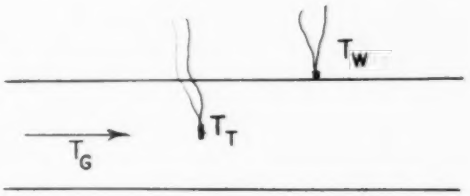


Fig. 1 Sketch of Duct With Temperatures Involved

$$Q_{GT} + R_{GT} = R_{TW} + C \quad \ldots\ldots\ldots\ldots [1]$$

The purpose of this paper is to present a simple and rapid solution of this equation in mathematical form and in chart form. The solution of Equation [1] involves solving a fourth-degree algebraic equation which is quite cumbersome to manipulate. The method of solution presented in this paper is simple and greatly reduces the time necessary to determine the thermocouple error. This method has slide-rule precision, which is more than sufficient when one realizes the inability to predict accurately emissivities and film coefficients of heat transfer.

Analysis

From the laws of convection and radiation, which may be found in McAdams (1), Equation [1] may be written in the form

$$Ah(T_G - T_T) + A\sigma\epsilon_g\left(\frac{1+\epsilon_s}{2}\right)(T_G^4 - T_T^4) = A\sigma\eta_G\epsilon_s(T_T^4 - T_W^4) \quad \ldots\ldots\ldots [2]$$

in which the conduction term is neglected. The conduction term is usually small; so it is neglected in the development of the equation from which the charts are constructed. Later a solution will be obtained for determining the magnitude of this conduction error.

The gaseous radiation term R_{GT}, and the gaseous emissivity ϵ_G of Equation [2] may be evaluated as indicated by McAdams,[3] and the thermocouple surface emissivity ϵ_s may be estimated as indicated by McAdams.[4]

If it is assumed that $\epsilon_G = \alpha_G$, then the transmissivity of the gas is

$$\eta_G = 1 - \epsilon_G$$

Dividing Equation [2] by $h(T_T - T_W)$ and simplifying

[1] Ensign, U.S.N.R., U. S. Naval Engineering Experiment Station. June A.S.M.E.

[2] Numbers in parentheses refer to the Bibliography at the end of the paper.

Contributed by the Heat Transfer Division for publication in the Transactions of The American Society of Mechanical Engineers.

Note: Statements and opinions advanced in this paper are to be understood as individual expressions of the author and are not to be construed as official nor reflecting the views of the Navy Department or naval service at large.

[3] Reference (1), p. 68.

[4] Reference (1), p. 393.

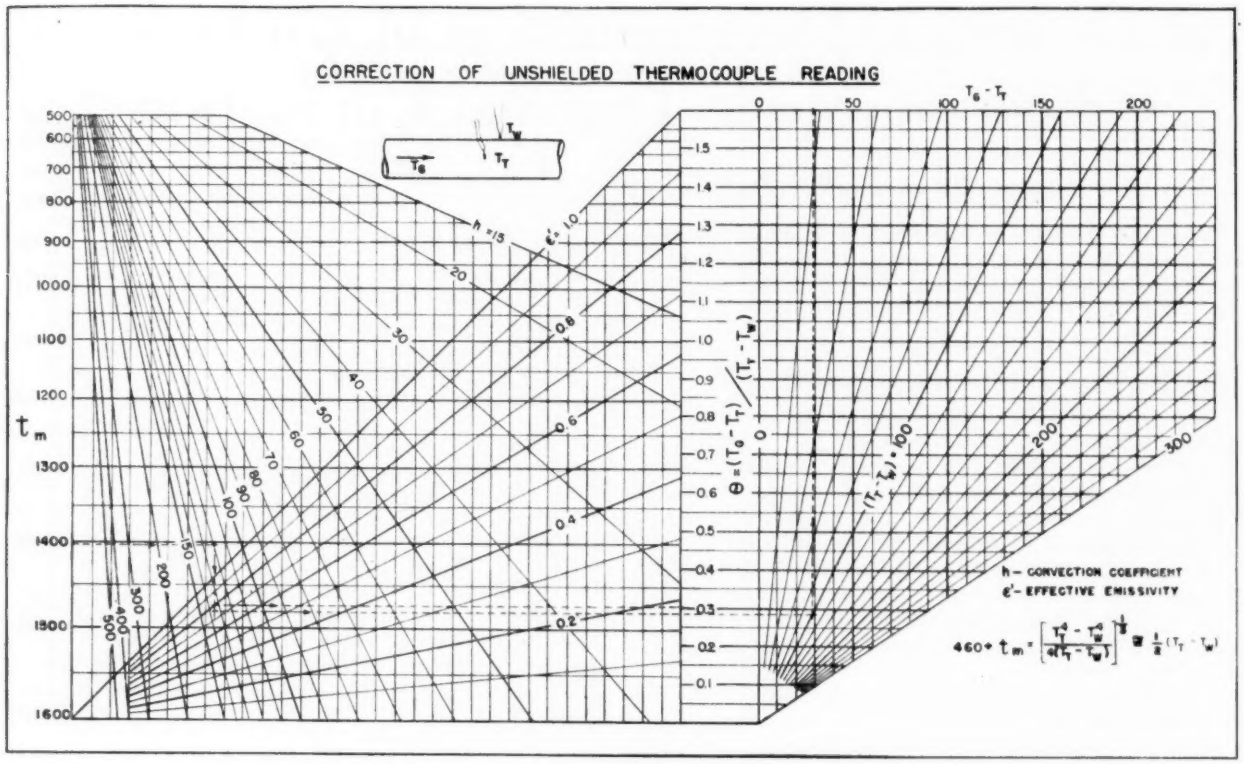


FIG. 2 DIAGRAM FOR UNSHIELDED-THERMOCOUPLE CORRECTION

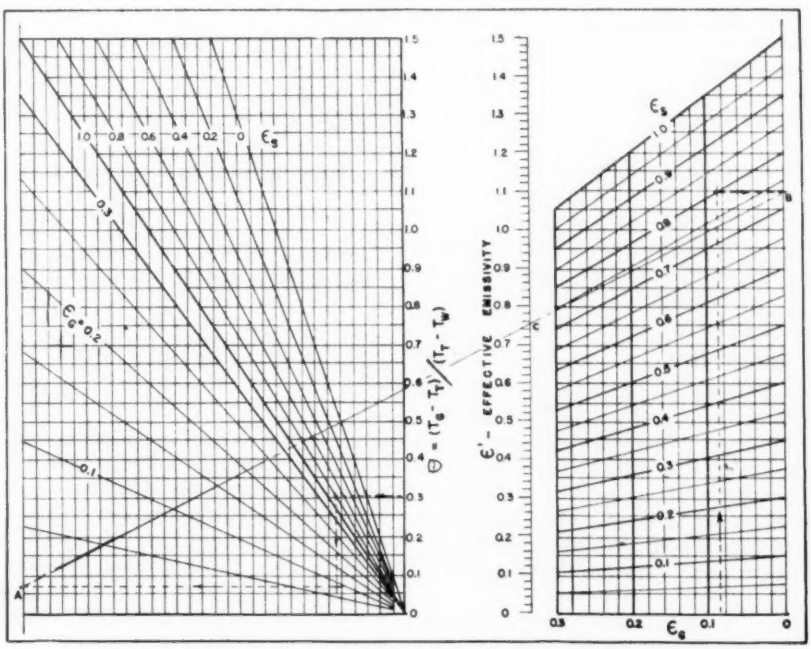


FIG. 3 DIAGRAM FOR DETERMINING EFFECTIVE EMISSIVITY

$$\frac{T_G - T_T}{T_T - T_W} = \frac{\sigma}{h} \cdot \frac{T_T^4 - T_W^4}{T_T - T_W} \left\{ \epsilon_s(1 - \epsilon_G) + \tfrac{1}{2}(1 + \epsilon_s) \cdot \epsilon_G \cdot \frac{T_G^4 - T_T^4}{T_T^4 - T_W^4} \right\} \quad [3]$$

Now

$$\frac{T_G^4 - T_T^4}{T_T^4 - T_W^4} \equiv \frac{T_G - T_T}{T_T - T_W} \cdot \frac{T_G + T_T}{T_T + T_W} \cdot \frac{T_G^2 + T_T^2}{T_T^2 + T_W^2} \quad [4]$$

Since T_G, T_T, and T_W are all large and of the same order of magnitude and their differences are small compared with the absolute magnitudes, the last two terms of the identity [4] are approximately equal to unity; hence

$$\frac{T_G^4 - T_T^4}{T_T^4 - T_W^4} \cong \frac{T_G - T_T}{T_T - T_W} \quad [5]$$

This approximation does not produce a serious error because it appears in the second term, in braces, of Equation [3]; and since ϵ_G is small compared with ϵ_s, the second term is much smaller than the first term.

Substituting Equation [5] in Equation [3]

$$\theta = 4 \frac{\sigma}{h} T_m^3 \epsilon' \quad [6]$$

where the terms are defined in the nomenclature and where

$$\epsilon' = \left\{ \epsilon_s(1 - \epsilon_G) + \tfrac{1}{2}(1 + \epsilon_s)\epsilon_G \frac{T_G - T_T}{T_T - T_W} \right\} \quad [7]$$

in which ϵ' is called the effective emissivity.

The solution of Equation [6] may be obtained from the diagram in Fig. 2, and ϵ' may be obtained from the diagram in Fig. 3.

Expand T_m as defined in the nomenclature

$$T_m^3 = \frac{T_T^4 - T_W^4}{4(T_T - T_W)} = \frac{T_T + T_W}{2} \cdot \frac{T_T^2 + T_W^2}{2} \quad [8]$$

Since $\frac{1}{2}(T_T + T_W) = T_a$ and $\frac{1}{2}(T_T^2 + T_W^2) \cong T_a^2$, where T_a is the average temperature between T_T and T_W, Equation [8] indicates that

$$T_m \cong T_a \quad [9]$$

The error in the assumption that $T_m = T_a$ is found in Fig. 4. Usually this error is less than 10 deg F and may be neglected.

If $\epsilon_G = 0$ then $\epsilon' = \epsilon_s$ and if T_m is assumed equal to T_a, Equation [6] becomes

$$\theta = 4 \frac{\sigma}{h} T_a^3 \epsilon_s \quad [10]$$

For all practical purposes

$$\sigma = \sigma_b = 1.723 \times 10^{-9} \quad [11]$$

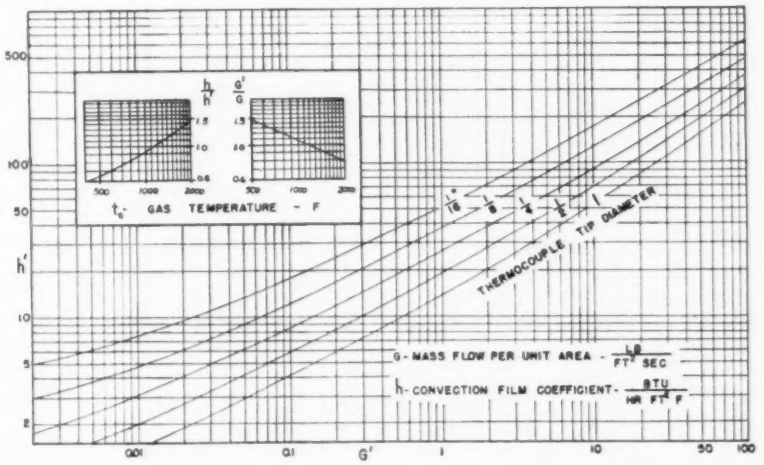


FIG. 5 DIAGRAM FOR DETERMINING FILM COEFFICIENT OF HEAT TRANSFER FOR SINGLE CYLINDERS NORMAL TO GAS STREAM
(Computed from Fig. 111, p. 221 of McAdams, Bibliography reference 1.)

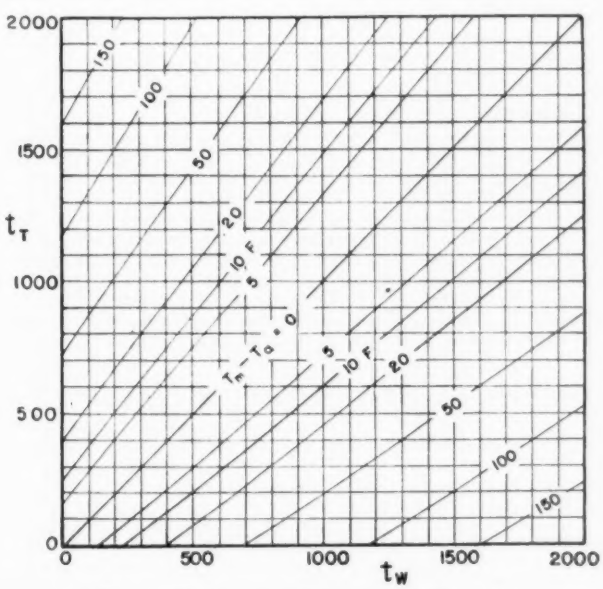


FIG. 4 DIAGRAM FOR DETERMINING $T_m - T_a$

USE OF THE DIAGRAMS

It is noted that a value of T is necessary to evaluate ϵ' in Fig. 3; hence the solution is of the trial-and-error type. First, solve for θ from Fig. 2, assuming $\epsilon' = \epsilon_s$. Then with this value of θ determine ϵ' from Fig. 3. This new value of ϵ' will be sufficiently close to the true value to obtain a solution. Now return to Fig. 2, with the new value of ϵ' and solve for θ and for $(T_G - T_W)$.

In order to obtain a solution of Equation [3] from Fig. 2, it is necessary to know h, the film coefficient of heat transfer between the flowing gas and the thermocouple. If the thermocouple approximates a cylinder normal to the gas stream, the curves in Fig. 5 may be used to estimate the value of h. For a given gas temperature, obtain from Fig. 5 the ratios G'/G and h/h'; then for any gas flow G, the value of G' is known. Now determine the value of h' for a given thermocouple tip diameter; then h is the product of h' and h/h'. The curves in Fig. 3 are computed from data presented by McAdams[5] for air flowing normal to a single cylinder. If this condition is not approximated, some other data must be used for estimating the value of h.

CONDUCTION ALONG THE LEADS

In the foregoing analysis the conduction heat-transfer term C of Equation [1] has been neglected. This term is usually small, but in order to determine its effect consider the conduction of heat to the cold wall along the two wires of the thermocouple in a gas stream as shown in Fig. 6. The differential equation is

$$\frac{d^2t}{d^2x} = \frac{4h}{kD}(t - t_G) \quad [12]$$

[5] Reference (1), Fig. 111, p. 221.

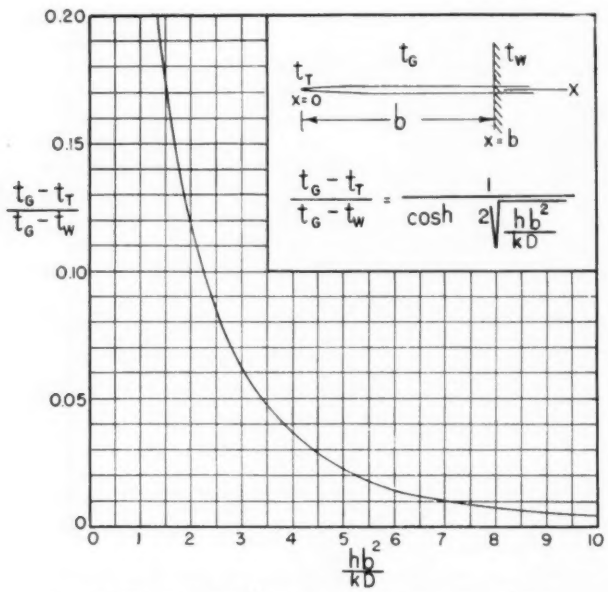


FIG. 6 DIAGRAM FOR DETERMINING CONDUCTION ERROR

whose solution[6] at $x = 0$ is

$$\frac{t_G - t_T}{t_G - t_W} = \frac{1}{\cosh 2\sqrt{\frac{hb^2}{kD}}} \quad \ldots\ldots\ldots\ldots\ldots [13]$$

This equation is shown graphically in Fig. 6.

ILLUSTRATIVE EXAMPLE

Determine the gas temperature of a gas flowing through a duct with the following conditions:

$G = 7.2$ lb sec^{-1} ft^{-2}
$t_T = 1450$ F
$t_W = 1350$ F
$D = 0.0675$ in. $= 0.005625$ ft
$d_0 = 1/8$ in.
$b = 6$ in. $= 0.5$ ft
$k = 220$ (assuming copper)
$\epsilon_G = 0.085$
$\epsilon_s = 0.80$

Solution: From Fig. 5, $G'/G = 0.90$ and $h/h' = 1.20$ for a temperature of 1450 F; then $G' = 0.90 \times 7.2 = 6.48$ lb sec^{-1} ft^{-2}. For a 1/8-in. tip diam, $h' = 100$ from Fig. 5, and $h = 1.2 \times 100$ or 120 Btu hr^{-1} ft^{-2} F^{-1}.

Now $t_a = 1/2(t_T + t_W) = 1400$ F, and from Fig. 4, $(t_m - t_a) = 1\,1/2$ F; so $t_m = 1400 + 1\,1/2 = 1402$ F.

As a first approximation determine T from Fig. 2 by assuming $\epsilon' = \epsilon_s = 0.8$; enter the diagram in Fig. 2 at the left with $t_m = 1402$; then follow the dotted line in the direction of the arrows to $h = 120$, $\epsilon' = 0.8$, and to $\theta = 0.305$. Use this value of θ to determine ϵ' from Fig. 3. Enter Fig. 3 with $\theta = 0.305$; follow the arrows to $\epsilon_s = 0.80$, $\epsilon_G = 0.085$ and then to the left alignment line to locate point A. Locate point B by following the arrows from $\epsilon_G = 0.085$ to $\epsilon_s = 0.80$ to the right alignment line. Connect points A and B with a straight line to locate point C, reading $\epsilon' = 0.755$.

Return to Fig. 2 with the new value of ϵ' to obtain the new value of $\theta = 0.285$. Continue to $(t_T - t_W) = 1450 - 1350 = 100$ F and up to obtain the thermocouple correction $(t_G - t_T) = 28$ deg F; hence $t_G = 1450 + 28 = 1478$ F.

If gaseous radiation is neglected, $\epsilon_G = 0$ and $\epsilon' = \epsilon_s$, and if t_m is assumed to be equal to t_a, the solution from Fig. 2 yields $(t_G - t_T) = 30$ F, and $t_G = 1450 + 30 = 1480$ F.

An estimate of the effect of conduction along the thermocouple wires is obtained from Fig. 6. For this example

$$\frac{hb^2}{kD} = \frac{(120)(0.5)^2}{(220)(0.005625)} = 24.2$$

then from Fig. 6, the error term due to conduction alone is

$$\frac{t_G - t_T}{t_G - t_W} = \frac{t_G - 1450}{t_G - 1350} < 0.001$$

from which $t_G < 1451$ F. Hence the error due to conduction alone is less than 1 deg F in this case.

CONCLUSIONS

To determine the gas temperature solve Equation [6] mathematically or graphically by using the diagrams in Figs. 2, 3, and 4.

For a less precise solution solve Equation [10] mathematically or graphically by using only Fig. 2, with $\epsilon' = \epsilon_s$ and $t_m = t_a$.

Either of these methods will yield results which are better than our knowledge of surface and gaseous emissivities and heat-transfer film coefficients warrants.

BIBLIOGRAPHY

1 "Heat Transmission," by W. H. McAdams, second edition, McGraw-Hill Book Company, Inc., New York, N. Y., 1942.

2 "Heat Transfer Notes," by L. M. K. Boelter, B. H. Cherry, and H. A. Johnson, third edition, University of California Press, Berkeley, Calif., 1942, chapt. 2.

3 "Measurement of the Temperature of a Flowing Gas," by R. T. Haslam and E. L. Chappell, *Industrial and Engineering Chemistry*, vol. 17, 1925, pp. 402–408.

4 "Measurement of High Temperatures in High Velocity Gas Streams," by W. J. King, Trans. A.S.M.E., vol. 65, 1943, pp. 421–431.

5 "Instruments and Apparatus," A.S.M.E. Power Test Codes, part 3, chaps. 1 and 3; *Journal of the Institute of Fuel*, vol. 12, March, 1939, pp. S1–S107.

6 "Errors in Gas Temperature Measurement and Their Calculation," by M. Fishenden and O. A. Saunders, Symposium on Gas Temperature Measurement, *Journal of the Institute of Fuel*, vol. 12, March, 1939, pp. S5–S15.

7 "Temperature of Gas—Its Meaning and Measurement," by J. G. Bennett and M. Pirani, Symposium on Gas Temperature Measurement, *Journal of the Institute of Fuel*, vol. 12, March, 1939, pp. S1–S4.

8 "Wall Effect in Gas Temperature Measurement," by C. H. Bosanquet, Symposium or Gas Temperature Measurement, *Journal of the Institute of Fuel*, vol. 12, March, 1939, pp. S14–S17.

[6] See reference (6) or (2).

(Owing to travel emergency conditions existing when this paper was contributed, discussion will be accepted until May 10, 1946)

Coaster Gate and Handling Equipment for River Outlet Conduits in Shasta Dam

By J. E. WARNOCK[1] and H. J. POUND,[2] DENVER, COLO.

At Shasta Dam, a coaster gate is used to close the intake of any one of the eighteen 102-in. conduits in the spillway section of the dam. Each conduit is provided with a control valve. The coaster gate is used to close the intake of each conduit whenever required for inspection and servicing of the control valve and conduit. It may also be used for emergency closure in the event of failure of a control valve. Since the gate design is predicated on emergency conditions of maximum head, when it is subjected to large unbalanced pressures, hydraulic model studies were conducted to determine the best shape of gate to minimize the downpull force to which it might be subjected in an emergency closing. The procedure followed in conducting the studies and the final installations are treated in this paper.

Introduction

SHASTA Dam, one of the major features of the Central Valley Project, is located on the Sacramento River, 9 miles above Redding, Calif. It is designed as a multipurpose dam with facilities for flood control, river regulation, and power generation.

Release of stored water for river regulation in excess of the capacity of the powerhouse turbines is accomplished by eighteen 102-in-diam conduits in the spillway section of the dam. Each of these conduits is provided with a control valve. A coaster gate is used to close the intake of any one of the 18 conduits whenever required for inspection and servicing of the control valves and conduits. The gate may also be used for emergency closure in the event of failure of a control valve.

Normally the gate is operated under balanced hydrostatic pressures with no flow in the conduits. However, design conditions were taken as those which exist during emergency closure under maximum head when the gate is subjected to large unbalanced pressures.

As the gate is lowered under emergency conditions, the increase in velocity under the gate acts to decrease the pressures on the downstream face while those on the upstream face remain substantially constant. The frame of the gate must resist the resultant force which pushes it against the face of the dam, and the rollers supporting the gate must have a low frictional resistance or the gate cannot be lowered into the closed position by its own weight. Another effect of the high-velocity flow is the reduction in pressure on the bottom of the gate which creates an additional force, referred to as downpull. Consideration of this force is important as it may be equal to or greater than the weight of the gate.

The hydrostatic pressures on the top of the gate can be calculated readily; but unfortunately, calculations of the downpull force can be only approximate without detailed hydraulic-laboratory studies. The pressures on the bottom of the gate are a function of the flow velocity under the gate, the shape of the gate bottom, and the gate opening, and they may vary from full hydrostatic pressure to the vapor tension of water. The value of the downpull force is therefore dependent upon the velocity distribution and flow pattern beneath the gate, since the pressure reduction at any point on the gate bottom is equal to the velocity head at that point.

In previous designs an approximation of the downpull force was considered satisfactory, but at Shasta Dam the estimated downpull on the coaster gate was so large that the total load on the handling equipment was about 60,000 lb in excess of the permissible load. The gate was to be handled by a 125-ton gantry crane, operating on the bridge across the spillway section of the dam. The capacity of this bridge was the limiting factor. Such a circumstance arose from the fact that the original plan was to handle the coaster gates from a barge and the bridge was designed for normal traffic load. When later in the design the handling equipment was transferred from the barge to the bridge, it was necessary to determine more accurately the downpull force and to reduce it, if possible, to avoid a drastic change in the design of the bridge across the spillway.

Hydraulic Model Studies

Hydraulic model studies were made to check the computed downpull and to develop a new shape for the gate bottom. Various shapes were tested and a satisfactory design was developed. A combination of this design and a properly proportioned recess in the face of the dam above the inlet reduced the downpull from the original value of 260,000 pounds to 70,000 lb.

The studies were made with a model of the conduit and coaster gate built to a scale of 1 to 17. Test data included pressure measurements on the gate and in the outlet for several heads and gate openings. The downpull was determined by integrating the pressure curves shown in Fig. 1. In the tests of the final design, the value obtained by pressure integration was verified by direct measurement with a spring scale.

With the gate of the original design in the full-open position, and a head representing the maximum of 323 ft, the downpull was approximately 75,000 lb. As the gate was lowered the downpull gradually increased to a maximum of 260,000 lb at an opening of about 8 ft 6 in. and then decreased gradually to zero for the closed position.

The typical variation of downpull with gate opening, which is shown graphically in Fig. 3, may be explained by a consideration of the variation in magnitude and distribution of velocity under the gate. When the gate was fully opened the discharge was a function of the size of the outlet conduit and its frictional resistance. As the gate was lowered it created a restriction in conduit cross section; and since the discharge was not reduced in the same proportion, there was an increase in velocity and a reduction in pressure under the gate and for a short distance downstream. The decrease in pressure caused an increase in downpull.

Since the conduit was vented downstream from the gate, air re-

---

[1] Chief, Hydraulic Laboratory, Branch of Design and Construction, Bureau of Reclamation.

[2] Chief, High-Head Gate Section, Branch of Design and Construction, Bureau of Reclamation.

Contributed by the Hydraulic Division and presented at the Annual Meeting, New York, N. Y., Nov. 26–29, 1945, of The American Society of Mechanical Engineers.

Note: Statements and opinions advanced in papers are to be understood as individual expressions of their authors and not those of the Society.

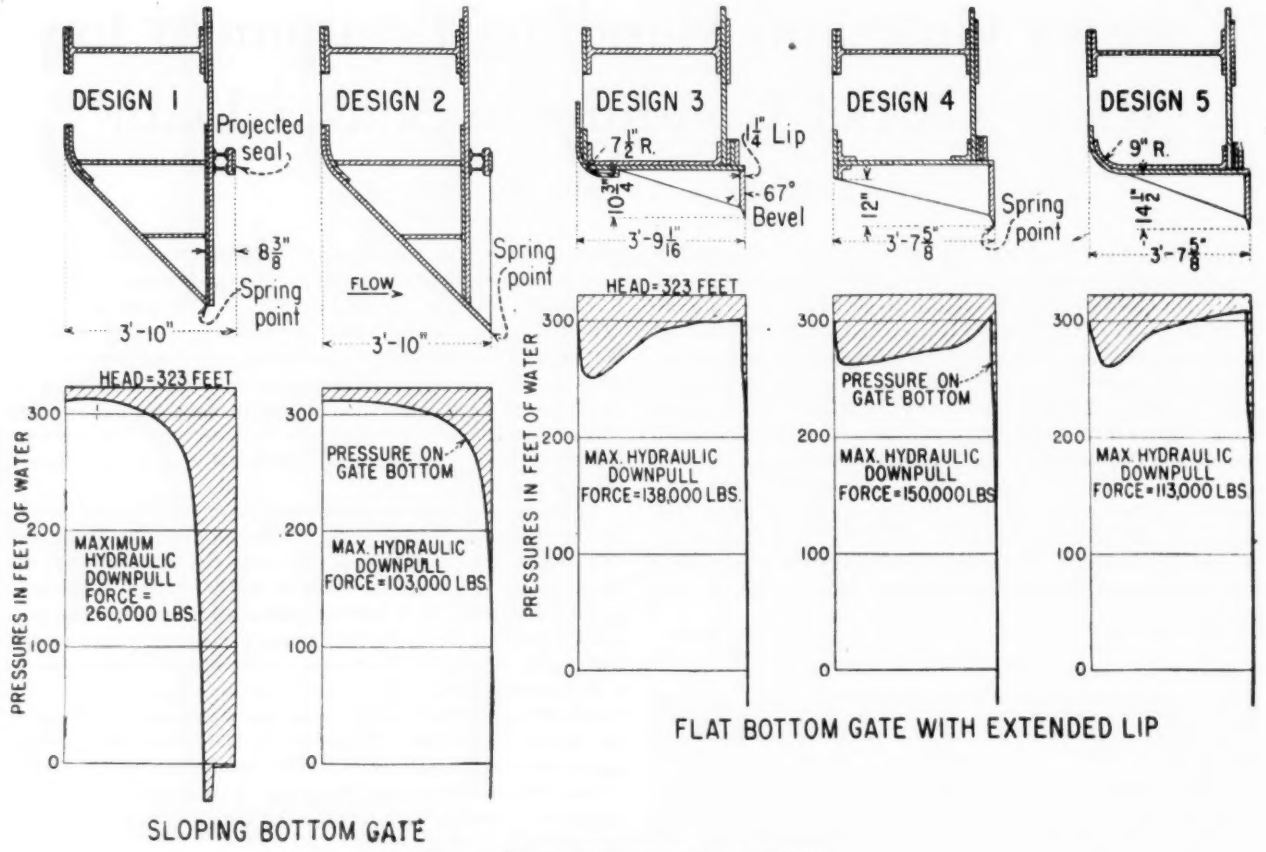


FIG. 1 PRESSURE STUDIES OF GATE BOTTOM

lief was obtained when the restriction in area was sufficient to lower the pressure at that point to atmospheric pressure. When the pressure downstream from the gate was restrained from decreasing to any appreciable extent by the presence of air relief, it may be said that the gate became a control. The discharge under this condition became a function of gate opening and head and was not affected by the conduit. At the gate opening corresponding to maximum downpull, the gate became a control and the velocity along its bottom reached its maximum value. For lesser gate openings, the velocity at the downstream edge of the bottom was increased slightly by a minor decrease in pressure downstream from the gate. However, at these openings the proportions and shape of the gate bottom relative to the size of the opening changed in such a manner that the velocity along it actually decreased and pressures increased enough to lower the value of downpull.

At small openings on the original design the jet under the gate impinged on the top of the conduit and interfered with proper action of the vent.

REDUCTION OF DOWNPULL IN ORIGINAL DESIGN

The hydraulic downpull force of 260,000 lb, as determined by the pressure tests, did not agree with the original analytical estimate of 160,000 lb. A review of the original calculations indicated that the estimate of 160,000 lb considered only the pressure reduction on the sloping portion of the gate bottom and assumed that a recess in the face of the dam above the outlet entrance would balance the pressures on the projected seals. The model test was made without a recess, and the unbalanced pressures on the top seal contributed at least 100,000 lb to the total downpull of 260,000 lb. A recess in the model of the original design would have tended to balance the pressures on the top seal, and it was possible that a closer agreement might have been obtained. However, the downpull would still have been excessive; therefore consideration was given to reduction of the force by revision of the shape of the gate bottom. The effectiveness of a recess in the face of the dam was determined only for the most satisfactory gate bottom and will be discussed subsequently.

Studies of the flow under the gate and the pressure on its bottom indicated that a large reduction of downpull could be obtained by a simple revision of the bottom. The flow under the gate and into the outlet was studied by observing the movements of paper particles in the head tank through a window. The particles approached the outlet from all directions, moving slowly until they were within a few inches of the outlet, where they appeared to be drawn instantaneously into it, indicating a rapid increase in velocity close to the outlet entrance. This rapid increase in velocity was also shown by the pressure gradient across the 45-deg sloping portion of the bottom of the gate, Fig. 1, design 1. At the upstream edge the pressures were practically hydrostatic. On approaching the outlet the pressure reduction was gradual at first, but it became rapid close to the downstream edge. At the point where the 45-deg slope ended, the pressure reached a minimum. This was the spring point of the gate, that is, the point where the water normally sprang free of the gate bottom to form a jet in the conduit.

The face of the gate projected a distance of $8^3/_8$ in. beyond the spring point as shown in Fig. 1. The pressure forces acting upward on this projection were much lower than those acting downward so that it contributed an excessively large part of the downpull when its relatively narrow width was considered. By comparison, the much larger area of the 45-deg sloping bottom played

only a minor role because the low pressure prevailed only in the vicinity of the spring point. The original bottom design was revised by extending the sloping portion until it underlay the projecting seal, as shown in Fig. 1, design 2. This change placed the spring point close to the face of the dam and eliminated the undesirable projecting area. The pressure distribution on the revised gate bottom is shown in Fig. 1, design 2. The shape of the pressure curve remained the same but the elimination of the projection and its unbalanced loading reduced the downpull from 260,000 to 103,000 lb.

In contrast to the original design, where the maximum downpull occurred when the conduit was not completely filled with water, the maximum value with the revised gate occurred while the conduit was filled with water, just before a slight additional closure would lower the pressures so that the conduit would take some air through the vent. In addition to reducing the downpull, this revised design changed the shape of the jet flowing into the outlet so that the jet at no time impinged on top of the conduit to restrict the air vent, as was the case in the original design when the gate was open between 2 and $3^1/_2$ ft.

Effect of Extended Lip Below Downstream Edge of Flat-Bottom Gate

Although the revision of the bottom accomplished the desired reduction in downpull, the gate was not satisfactory structurally. The sloping bottom would have been difficult to fabricate and heavy plates would have been required to withstand the loads on its downstream edge. Thus it was necessary to make further tests to develop some other type of gate which would have even less downpull or at least a more acceptable structural design for the bottom.

The original tests indicated that a gate having a minimum downpull would be one with a lip placed at the downstream edge of the bottom and extended vertically below the gate. This would place the spring point at a greater distance from the bottom and the effect of the rapid drop in pressure which occurs near the spring point would be exerted on the vertical plane of the extended lip and would not contribute to downpull. To verify these indications, tests were made with an extended lip. The length of the lip was varied in successive steps, from zero to a length nearly equal to the thickness of the gate.

The complete shape of the gate bottom which will be referred to hereafter as the basic shape is shown in Fig. 2. The bottom was faired into the upstream plate on a 9-in. radius, to minimize the local reduction of pressure on the bottom where the flow down the upstream face of the gate changes direction below the gate. The extended lip was $^3/_4$ in. thick, and its bottom was beveled at 45 deg to place the spring point at the downstream edge of the lip and reduce the effect of the thickness on the downpull. The extended lip was supported by gusset plates attached to the bottom of the gate. These plates were in the plane of flow so that their effect on the downpull would be small and could be ignored.

The pressure gradients, as determined in what will be referred to as general tests, were similar to those of design 5, Fig. 1, except that negative pressures occurred on the bottom of the lip. There was some reduction of pressure near the upstream plane, as was anticipated, since the flow down the upstream face of the gate had to change its direction. However, the pressure increased rapidly, becoming a maximum at the downstream corner where the lip joins the gate bottom. This effect indicated that not only does the extended lip keep the rapid reduction in pressure near the spring point on the vertical plane of the lip where it cannot cause downpull, but it also tends to form a stagnation point which increases in the downstream corner.

Although the bottom of the lip was beveled at 45 deg to place the spring point on its downstream edge, the spring point actually occurred at the upstream edge of the lip. The resulting negative pressures on the bottom of the lip would cause a downpull of approximately 15,000 lb when the lip was $^3/_4$ in. thick, as indicated in Fig. 2.

The variation of maximum downpull force with length of lip extension is shown graphically in Fig. 2. The longest extension considered was approximately equal to the thickness of the gate,

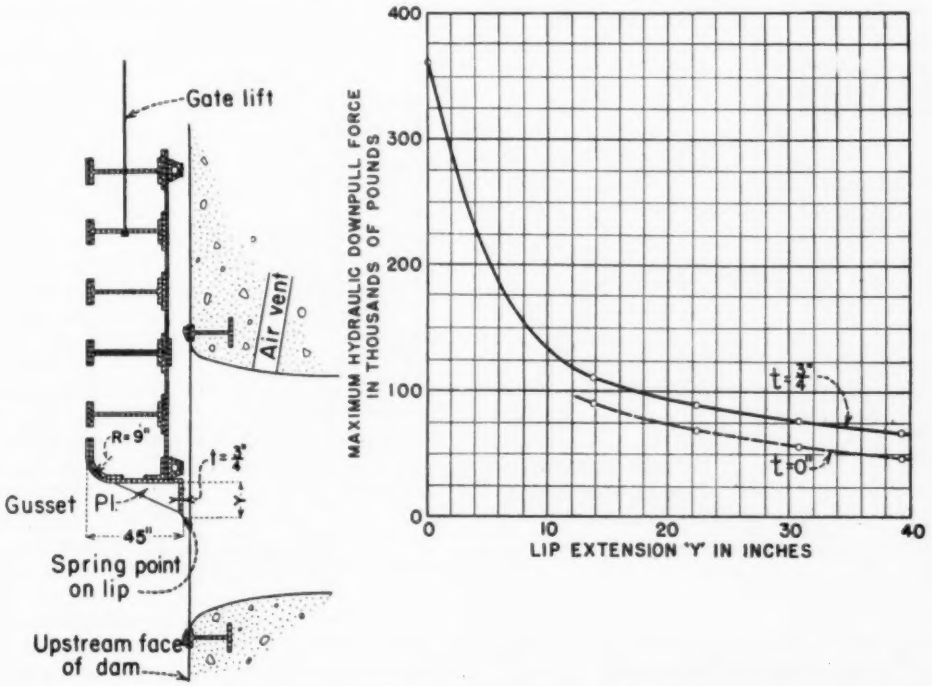


Fig. 2 Effect of Lip Extension on Hydraulic Downpull

as a greater extension would be impractical structurally. The graph shows that an extension of 40 in. would reduce the downpull to approximately 65,000 lb. As the extension was decreased, the downpull increased gradually until, at a lip extension of 14 in., the value was 110,000 lb. A further decrease in the extension caused a more rapid increase in downpull which finally became 360,000 lb when there was no extension.

Structural Designs of Flat-Bottom Gate With Extended Lip

A flat-bottom gate with an extended lip below its downstream edge, which would develop a downpull equal to that of the sloping-bottom gate of design 2, Fig. 1, or about 100,000 lb, would require a lip extension of 17 in. This was not practical, since the horizontal forces on it would be excessive. Nevertheless, a flat-bottom gate having an extended lip was a simple design compared with the sloping bottom of design 2.

Design 3 was more acceptable than the basic shape from a structural viewpoint, having a lip extension of $10^{3}/_{4}$ in. which, from the curve in Fig. 2, corresponds to a downpull of approximately 130,000 lb. The radius of the curved portion of the bottom was made $7^{1}/_{2}$ in. instead of 9 in., and the thickness of the lip was made $1^{1}/_{4}$ instead of $^{3}/_{4}$ in. It was anticipated that the smaller radius would increase the downpull a small amount. The bottom of the lip was beveled at a steeper angle, 67 deg, which placed the spring point at its downstream edge and reduced the downpull on the lip, Fig. 1. The tests showed that the downpull would be approximately 138,000 lb. Piezometers placed on the lip to determine pressures indicated that the portion of the downpull due to the $1^{1}/_{4}$-in. lip was nearly equal to that of the $^{3}/_{4}$-in. lip of the general test in which the spring point was at its upstream edge. Accordingly, the curve in Fig. 2 was used to predict the downpull of a gate having $1^{1}/_{4}$-in. lip with a 67-deg bevel at its bottom.

In design 4, Fig. 1, a simplification of the structural details was made by using flat plates and angles to eliminate the curved section of the gate bottom. The end of the plate at the upstream edge was rounded to avoid a sharp corner at that point. A $1^{1}/_{4}$-in. lip having a steep bevel, similar to design 3, was extended 12 in. below the upstream edge. The downpull was 150,000 lb, which represented a 25 per cent increase over that obtained in the general test with a 9-in. radius and a 12-in. lip extension. Neither design 3 nor 4 was satisfactory for the Shasta Dam outlet coaster gates because their downpulls, of 138,000 and 150,000 lb, respectively, exceeded the allowable limit.

A new analysis of the stresses on the bottom of a gate with the basic shape used in the general test, Fig. 2, revealed that it would be structurally sound if the lip extension did not exceed $14^{1}/_{2}$ in. Fig. 2 indicated that such a design would develop a downpull of 110,000 lb. Since this value was not excessive, design 5 was constructed and tested, Fig. 1. It differed from the gate of the general test in that a $1^{1}/_{4}$-in. lip with a 67-deg bevel at its bottom was used instead of $^{3}/_{4}$-in. lip with a 45-deg bevel. The measured downpull of 112,000 lb checked the predicted value of 110,000 lb.

The final design of the Shasta outlet coaster gate was developed from design 5. The width was increased from $43^{5}/_{8}$ to $44^{11}/_{16}$ in. for structural reasons, and a clearance of $^{1}/_{2}$ in. between the lip and the seal seats was introduced to facilitate operation of the gate. The maximum downpull as determined by pressure measurements was increased to 122,000 lb by these changes. An independent check of the downpull by direct measurement with a spring scale indicated that a slightly larger downpull of 131,000 lb occurred at a gate opening of 55 per cent. The latter value was accepted as the more accurate one as it was impractical to take the number of pressure measurements required for a comparable accuracy.

The over-all effect of the gusset plates was determined by a test with the plates removed. No appreciable difference in downpull could be detected. If plates were terminated at the point where the bevel of the lip begins as shown in Fig. 1, their effect on downpull was negligible.

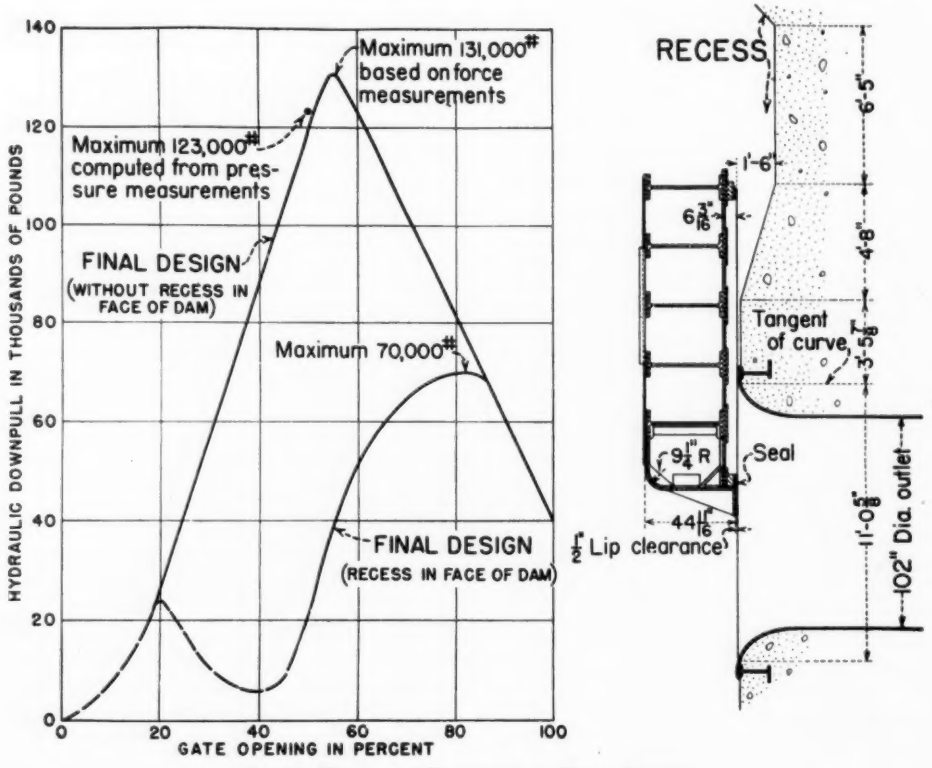


Fig. 3 Hydraulic Downpull of Final Design

Effect of Recess in Face of Dam

It had been appreciated that any one of the various designs of the gate could have been improved from the standpoint of downpull by introducing a recess in the face of the dam. This improvement was deliberately withheld until the best shape of gate bottom was determined.

To understand the action of the recess, it must be noted that the seals of the gate project beyond the skin plate. With no recess, the pressures on the top seal were unbalanced when the gate was partially closed. The full reservoir head acted on the outside, or topside, while the low

pressure which prevailed downstream from the gate was exerted on the inside, or lower side. The resulting downward force, which at times was as large as 100,000 lb, depending on the pressure in the outlet entrance downstream from the gate, contributed a large portion of the downpull on the gate. With a recess, starting a short distance above the gate seat, the increase in the clearance between the seal and the face of the recess lessened the velocity of flow around the seal and reduced the pressure differential.

Tests showed that the recess performed its desired function of reducing the maximum downpull if its depth was made several times larger than the seal extension. At all openings the pressures on the upper seal were nearly balanced. For gate openings less than 40 per cent, the presence of a recess with a uniform depth introduced an undesirable complication. With the downpull force on the top seal eliminated by the recess, the increase in pressure which occurred at small gate openings over that portion of the bottom which underlay the seal was large enough to reverse the direction of the net hydraulic load. The gate was actually subjected to an uplift force large enough to offset its weight.

The effectiveness of the recess in balancing the pressures on the top seal was directly proportional to its depth. By varying the depth in the manner shown in Fig. 3, the reversal of net force on the gate was eliminated and the downpull varied as shown in Fig. 3. The maximum downpull of 70,000 lb occurred at a gate opening of 80 per cent.

Since the dead weight of the gate and lifting mechanism is 90,000, and 10,000 lb, respectively, the maximum total load on the gantry crane, including a downpull of 70,000 lb, will be 170,000 pounds. This is less than the permissible load on the bridge, so the design was accepted as being satisfactory.

The Coaster Gate

The coaster gate is mounted on endless roller trains and is lowered by its own weight in structural guides provided in the face of the dam to an accurate position over the intakes, Fig. 4. The gate consists primarily of a downstream skin plate mounted on horizontal beams which are supported by vertical girders at the sides.

The roller trains around each vertical girder transmit the water load on the gate to tracks on the face of the dam at the inlet. The tracks are fastened to large CB-sections embedded in blockouts provided in the original concrete of the dam, Fig. 5. A rectangular steel framework embedded in the concrete around the circular inlet supports accurately finished seal seats which project slightly from the face of the dam.

When the gate is used to close one of the conduits on the lower tier, it is subjected to a head of some 330 ft, equivalent to 22,000 psf or a total load of approximately 2,750,000 lb. As the gate weighs only 90,000 lb, roller trains were selected to minimize the friction forces so that the gate would close under its own dead weight.

Metal-covered rubber "music-note" seals, Fig. 5, are provided on the downstream face of the skin plate. The design utilizes the flexibility of a rubber hinge which permits close local adjustment but retains the rigidity of metal to support the load of approximately 125 lb per linear in. to which the seals are subjected when the gate is in the closed position. The rubber core also permits simple butt and miter joints to be used in the seal as the load on the seal is converted to axial compression which acts to seal the joints.

Advantage is taken of the pressure differential across the gate to retract the seals when the gate is closing under flow. This eliminates drag on the seals and materially reduces the force resisting closure just as the gate is seated. To accomplish retraction the area immediately back of the seals is closed at the sides. This forms a continuous watertight rectangular chamber having the movable portion of the rubber seal for one of the sides. Pipes connect this chamber, through a two-way valve, to either the reservoir pressure on the upstream side of the gate or to the reduced pressure on the downstream side of the gate.

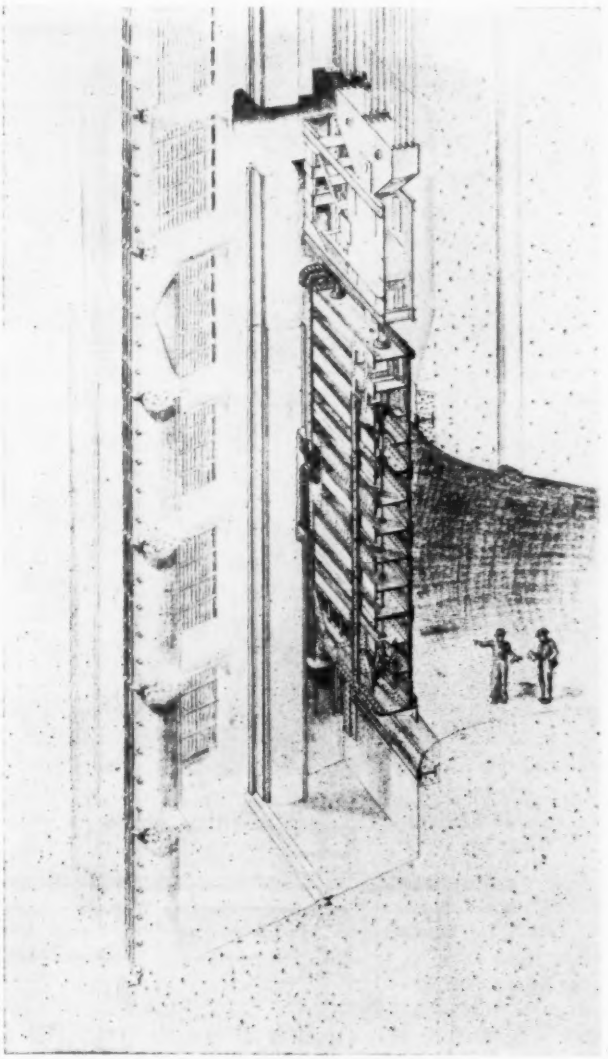


Fig. 4 Typical Coaster-Gate Installation

The valve is operated by the overtravel of the relatively heavy gate-lifting stem. While the gate is supported by the lifting stem, the valve position admits the downstream pressure to the seal chamber and the seal retracts approximately $^{3}/_{16}$ in. As soon as the gate is seated in the closed position over the inlet, a 4-in. overtravel of the lifting stem reverses the valve to admit reservoir pressure to the seal chamber and the seals are forced into contact with the seat.

Channel-shaped guide shoes at each corner of the gate engage tongues on the guides in the face of the dam, Fig. 5. The distance, face to face, of the guide tongues is held accurately during installation to a clearance of $^{1}/_{4}$ in. in each shoe, except for a short distance near the conduit opening. Below an elevation slightly greater than one gate height above the top of the conduit opening the clearance is reduced practically to zero by making longer tongues on the guides. This causes the gate to be squared

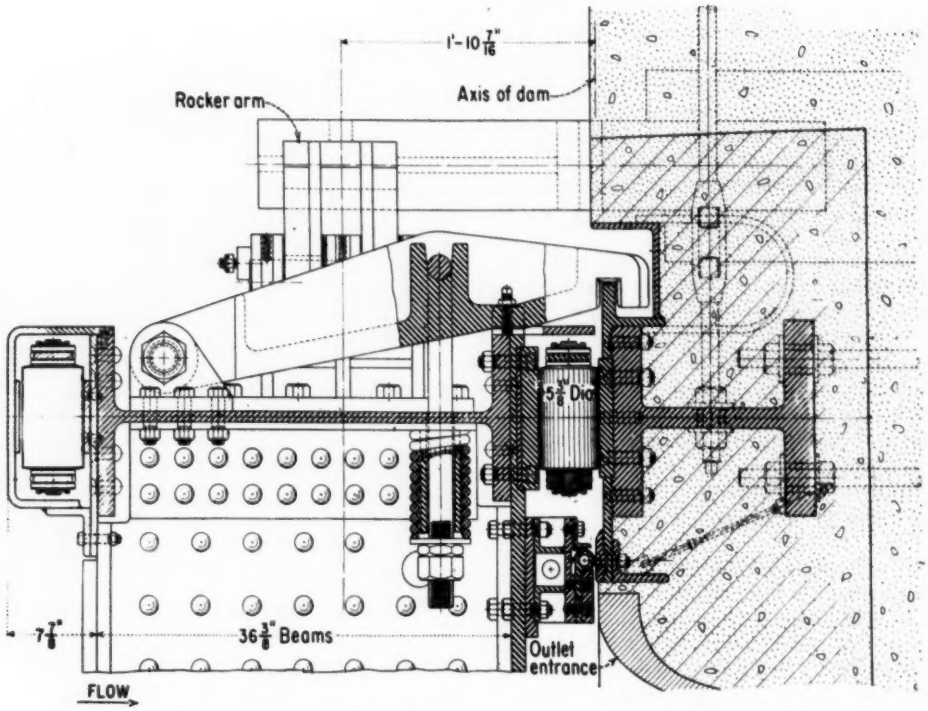


FIG. 5 SHASTA DAM OUTLET COASTER GATE SLOT SECTION

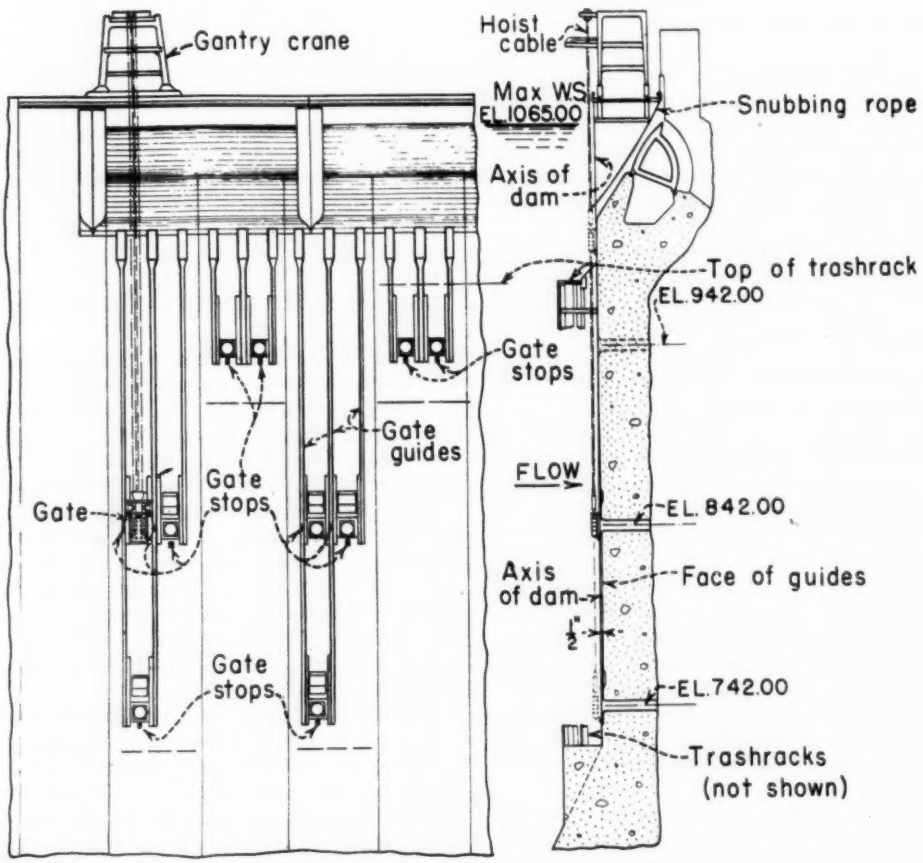


FIG. 6 LOCATION OF OUTLETS AND GUIDES ON UPSTREAM FACE OF DAM

as accurately as possible with the tracks just before it receives the water load when closing under emergency-flow conditions. The shoes are spring-loaded with snubbed springs set with an initial compression sufficient to prevent deflection during this operation.

After the gate receives water load, it is practically impossible to guide the rollers or the gate, because of the extremely high unit contact pressure between the rollers and the track. The spring-loading of the shoes allows the gate to move laterally as much as $^1/_2$ in, in either direction, while closing under load, without excessive binding or probable breaking of the shoes. When the load on the gate is removed, the capacity of the springs is sufficient to square it again.

Operation of Gate

The gate is stored in a covered pit in the top of the dam. Except in case of emergency, it is used only during a few months of the year, when conditions are most favorable for inspection and servicing of the control valves and conduits.

The inlets to the conduits through the dam are arranged so that fourteen sets of guides serve the eighteen conduits. The four conduits of the lower tier, which are 335 ft below the spillway bridge, are served by the same set of guides as four of the conduits of the intermediate tier, which are 235 ft below the spillway bridge, Fig. 6. The other ten conduits are served by individual sets of guides.

The placing of the gate in the guides on the face of the dam requires careful handling. The gate must be lowered approximately 90 ft below the bridge, and 75 ft below the normal water surface before engaging the guides. The upper ends of each set of guides are tapered in the plane parallel to the face of the dam in such a way that in the event the gate is lowered slightly off-center, it is forced to correct itself and allow the channel-shaped shoes on the gate to engage the tongues on the vertical guides.

Engagement of the shoes in the direction normal to the face of the dam is provided for in the following manner:

The gate is lowered in a plane slightly upstream from the face of the dam until it is below the sloping face of the spillway crest. It is then snubbed back into contact with the face of the dam by snubbing ropes, Fig. 6, from the downstream edge of the bridge structure. Continued lowering will then cause the gate shoes to engage the guides and the operation can continue.

A gate-lifting frame, Fig. 7, with a semiautomatic grappling mechanism is used to handle the gate. After the gate is seated in front of a conduit, the lifting frame may be released from the gate and hoisted to the bridge. This arrangement is necessary as the gate is required to remain in place in front of a conduit for several weeks at a time and the crane must be free to perform its other functions.

The position of the gate cannot be observed after it is lowered into the water. Consequently, a safety device is provided to indicate proper engagement of the gate shoes. This device consists of ropes attached to a tripping mechanism at each lower corner of the gate. When the shoes engage the tongues of the guides, the rope is released by the tripping mechanism. Two men are stationed on the bridge to pay out the telltale ropes as the gate is lowered. If both ropes are released after lowering the gate a reasonable distance below the top of the guides, it is evident that the guides have been engaged properly.

Lowering is continued until the gate is supported by stops on the guides at the inlet of the conduit. The stops are located so that the gate comes to rest exactly in the closed position in front of the inlet. The lifting frame continues downward approximately 4 in. until it comes to rest on the top of the gate. The 4-in. travel of the lifting stem down into the gate causes the gate seals to close. The same motion causes the grappling mechanism in the lifting frame to release and a slack-cable limit switch, located on the crane, stops the lowering motion of the hoist.

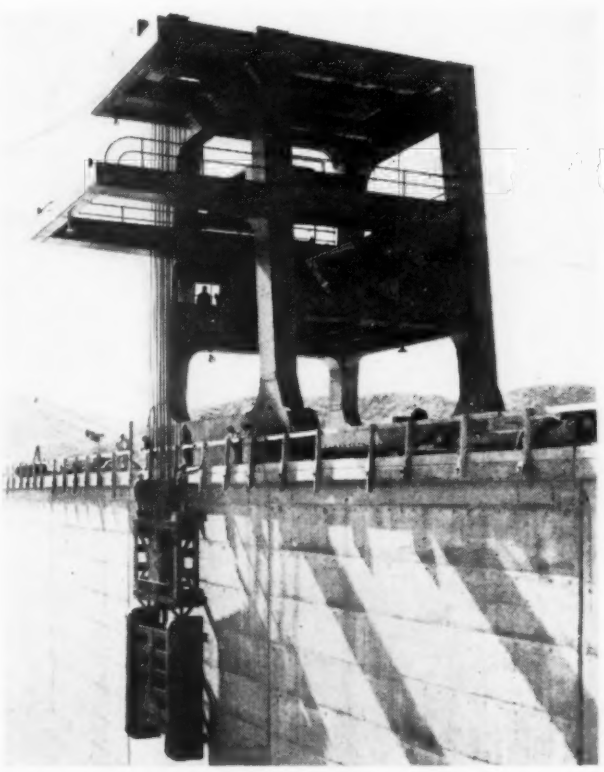


Fig. 7 Outlet Conduit Coaster Gate and Gate-Lifting Frame With Semiautomatic Grappling Mechanism

If only one conduit is served by a set of guides, a single stop is provided in the face of the dam directly below the conduit opening. Where two conduits are served by the same set of guides, that is, where one conduit is located above the other, a single stop is provided directly under the lower one. Stops for the upper one are located at the sides of the conduit, Fig. 6. Rocker arms, or pawls, are provided at each side of the gate and are interconnected by a linked tension bar. When it is desired to close the upper conduit, the bar is extended and the rocker arms are pushed outward to a position where they will contact the stops at the sides of the upper conduit and act as an equalizer as the gate comes to rest. If the lower conduit is to be closed, the bar is retracted so that the rocker arms, Fig. 7, will clear the stops at the side of the upper conduit, and the gate comes to rest on the signal stop below the lower conduit.

To remove the gate the operations described are reversed, except that the telltale ropes are attached to the tripping mechanism at each lower corner of the lifting frame.

Gantry Crane

The crane, an outdoor, traveling, gantry type, Fig. 8, is electrically operated and is provided with a 125-ton fixed hoist which handles the gates, and a 25-ton trolley hoist which handles parts of gates during assembly. The latter is also used infrequently to install stop logs in front of the power penstocks. The 125-ton capacity was determined by the installation and servicing conditions of the coaster gates for the main power-penstock inlets. These inlets are located in the curved portion of the dam, where the solid construction will support practically any crane load.

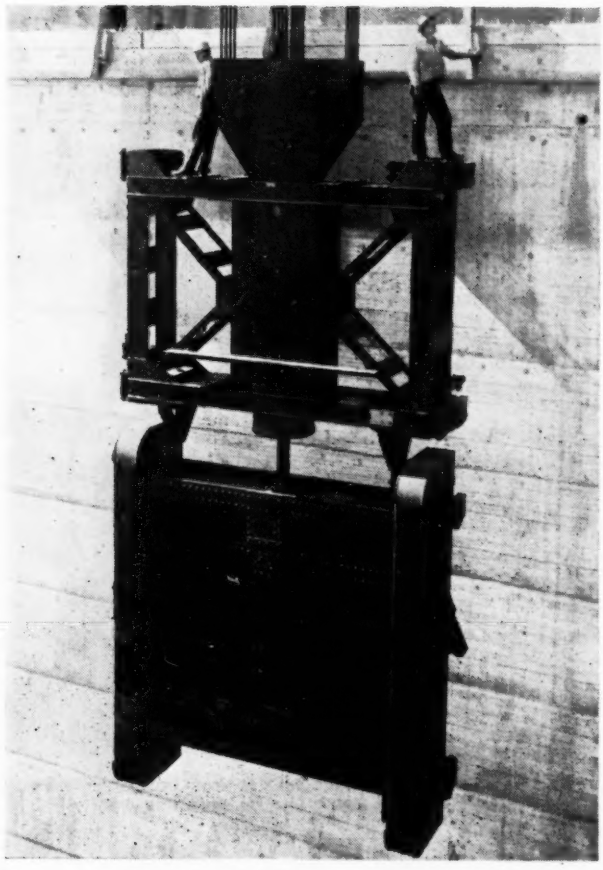


FIG. 8 GANTRY CRANE IN USE WITH LIFTING MECHANISM AND OUTLET CONDUIT COASTER GATE SUSPENDED FROM 125-TON FIXED HOIST

As previously mentioned, the bridge structure over the spillway portion of the dam in which the river outlets are located made it economically desirable to limit the crane load at this point to only a fraction of the hoist capacity in order to avoid a heavy and expensive structure which would not be otherwise required. The crane can transfer a load from any point on the dam to the overhung position upstream from the face of the dam. All gates are installed and operated from the overhung position.

The crane operates on 27-ft-gage tracks. The tracks are straight for approximately 375 ft on the bridge structure over the spillway section at the center of the dam. The remainder of the track has a 2500 ft radius of curvature for a distance of 1425 ft along the roadway on top of the right abutment.

The combination of straight and curved track made it impractical to use the conventional drive with one motor driving a shaft leading to the trucks on either side. Instead, separate motors were mounted on each of four trucks with 50 per cent of the track wheels driving. Direct current for operation of the four 8-hp shunt-wound motors is provided by a generator set. The use of direct current was made necessary by the unequal loading of the motors.

Accurate spotting of the gates is provided by direct-current-motor-operated hoists and Maxspeed control. In case the gate should encounter some obstruction in the guides, a special type of control was provided for the hoist. This control limits the maximum lifting effort when the crane is located on the bridge. If a conventional hoist with alternating-current motor and standard control had been provided, the maximum lifting effort on the crane hook under a 275 per cent breakdown torque of the motor would have been approximately 350 tons. The modified Maxspeed control limits the lifting effort at the hook to 175 tons. The control is the full-magnetic, reversing, master type. It has definite time-limit acceleration relays and six speeds in each direction of operation. Due to the extremely long lift of 360 ft, a mechanical load brake was not considered feasible and direct-current dynamic braking was provided.

A panel of indicating lights in the operator's cage warns him when the gate is approximately 16 ft above the closed position in front of any conduit. A lighting system, including floodlights, was installed on the crane so that the gates could be operated at night.

Speed and Feed Selection in Carbide Milling With Respect to Production, Cost, and Accuracy

By HANS ERNST[1] and MICHAEL FIELD[2]

The present paper reports findings of a research on milling cast iron with carbide-tipped cutters in addition to those presented previously in 1945 by Michael Field and W. E. Bullock.[3] An important finding of the earlier work was the existence of a definite maximum tool-life point, i.e., at 290 fpm, in relationship of cutting speed to tool life, when milling a cast iron of medium hardness (Bhn 190). Subsequently, it was found that a similar maximum tool-life point, i.e., 200 fpm, occurs when milling a considerably harder and less machinable cast iron (Bhn 240). An important outcome of the earlier phases of the research was the development of a combination of tool angles which gave much greater tool life and a considerably higher production rate. The original work was done with single-point tools, whereas a multitooth cutter was subsequently developed, details of which and the results obtained are included in the paper. A comprehensive account is given of the recent studies, illustrated by numerous test curves, and a practical analysis of milling costs.

IN a previous paper[3] by Michael Field and W. E. Bullock, results were given in part of a research on the milling of cast iron with carbide-tipped cutters, which had been conducted at the University of Cincinnati. The present paper covers certain subsequent findings of this research, together with a further elaboration and application of earlier findings.

One of the important findings reported in the previous paper was the existence of a definite maximum tool-life point in the relationship of cutting speed to tool life, when milling a cast iron of medium hardness (190 Bhn), designated as Meehanite A. This relationship is reproduced in the upper curve of Fig. 1. Here it will be seen that the average of the tool-life values for 210 fpm falls well to the left of the average of the values for 290 fpm. At higher cutting speeds all the values of tool life are also to the left of the value for 290 fpm and fall approximately on a line representing the equation $VL^{0.55} = 7800$, where V = cutting speed (ft per min) and L = tool life (cu in. of metal removed).

In a subsequent series of tests, it has now been found that a similar maximum tool-life point occurs when milling a considerably harder and much less readily machinable special grade of alloy cast iron, designated as Meehanite C-304B. The Brinell hardness of this material was 240; its chemical composition is given in Table 1, together with that of Meehanite A.

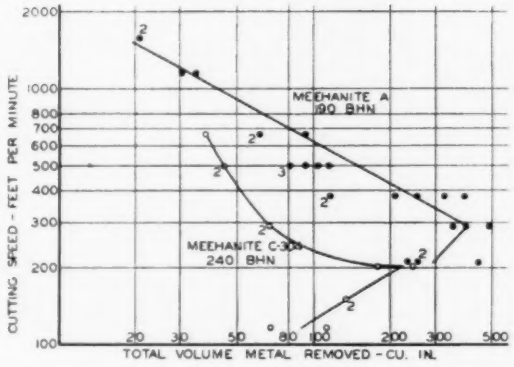


FIG. 1 CUTTING SPEED VERSUS TOTAL VOLUME OF METAL REMOVED TO DULL TOOTH WITH AXIAL RAKE OF +3 DEG, RADIAL RAKE OF +3 DEG, AND CORNER ANGLE OF 30 DEG
(Width of cut = 6 in.; depth of cut = 0.187 in.; feed per tooth = 0.015 in.; carbide, 44A.)

TABLE 1 CHEMICAL PROPERTIES OF CAST IRONS USED IN CUTTING TESTS

	Meehanite A, per cent	Meehanite C-304B, per cent
Total carbon	2.85–3.15	2.90–3.20
Silicon	1.20–1.50	2.45–3.00
Phosphorus	0.12 Max	0.18 Max
Sulphur	0.20 Max	0.20 Max
Manganese	0.80–1.20	0.75–1.00
Chromium	....	1.00
Copper	....	....
Molybdenum	....	0.50

The tool-life values for Meehanite C-304B, expressed in cubic inches per tool grind, are shown by the lower curve in Fig. 1. The maximum tool-life point here occurs at about 200 fpm in contrast to 290 fpm for the softer Meehanite A. The portion of the line to the left of this point is quite definitely curved, again in contrast to the straight line of Meehanite A.

The existence of a rather critical maximum tool-life point (which has now been found in a considerable number of tests) is a matter of real importance in practical milling. It indicates clearly the impossibility of predicting tool-life values in the normal speed range by extrapolation from the results of tests above 500 fpm.

Another important outcome of the work[3] previously reported, was the development of a combination of tool angles which gave a much greater tool life (in terms of metal removed per grind), and a considerably higher production rate, than could be obtained with the angles used in conventional practice. The initial work was done with single-point tools in which the effective angles could be readily changed. In later work a multitooth cutter was used. One such cutter is shown in Fig. 2.

The basis for this development was established in 1937, in an investigation covering the performance of face-milling cutters with very large corner angles. In a report of this investigation by M. Kronenberg,[4] it was shown that very large corner angles had

[1] Research Director, The Cincinnati Milling Machine Company, Cincinnati, Ohio. Fellow A.S.M.E.

[2] Research Fellow, University of Cincinnati, Cincinnati, Ohio. Jun. A.S.M.E.

[3] "Milling Cast Iron With Carbides," by Michael Field and W. E. Bullock, *Mechanical Engineering*, vol. 67, Oct., 1945, pp. 647–658.

Contributed by the Research Committee on Metal Cutting Data and Bibliography and presented at the Fall Meeting of the Cincinnati Section, Cincinnati, Ohio, Oct. 2–3, 1945, of THE AMERICAN SOCIETY OF MECHANICAL ENGINEERS.

NOTE: Statements and opinions advanced in papers are to be understood as individual expressions of their authors and not those of the Society.

[4] Research Department, Cincinnati Milling Machine Company (confidential report).

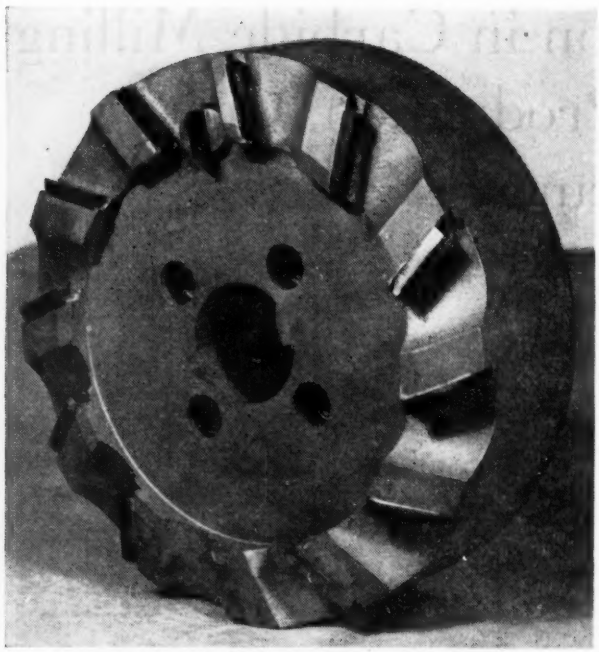


FIG. 2 CUTTER DEVELOPED IN RESEARCH, CAPABLE OF OPERATING AT EXTREMELY HIGH FEED RATES

(The 12 major teeth have an axial rake of +15 deg, a radial rake of —30 deg, a 75 deg corner angle, a true rake of +6 deg, and a face angle of 5 deg. The finished surface is produced by a separate tooth which has a face 3/4 in. long and extends axially several thousandths of an inch beyond the roughing teeth.)

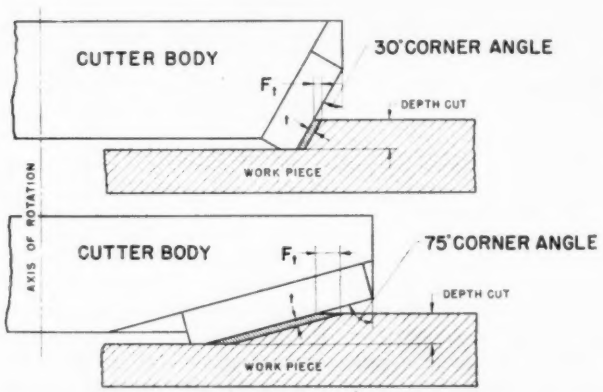


FIG. 3 EFFECT OF CORNER ANGLE ON FEED PER TOOTH FOR A CONSTANT VALUE OF UNDEFORMED CHIP THICKNESS

the unique property of distributing the work of chip removal over a much greater length of cutting edge than conventional corner angles of zero to 45 deg, thus permitting the use of a very high feed per tooth, and a consequent high rate of metal removal.

The upper view in Fig. 3 shows in diagrammatic fashion a face-milling cutter with a conventional 30 deg corner angle. In this figure the workpiece is assumed to be feeding to the left, and the small cross-hatched area represents the cross section of the metal which will be removed by the next tooth. Thus for a given feed per tooth F_t, the thickness of the undeformed chip will have the value t.

In the lower view in Fig. 3 the corner angle of the cutter is 75 deg. For the same value of the undeformed chip thickness t, it is evident that in this case the feed per tooth F_t must have a much larger value. It is also clear that the length of cutting edge engaged with the work is here much greater, even though the depth of cut is the same as in the upper view. Thus for a given value of t, the cross-sectional area of metal removed per tooth will be much greater even though the load on each element of length of the cutting edge remains virtually unchanged.

In the numerical example, illustrated in Fig. 4, it is shown that for a constant value of 0.013 in. for the undeformed chip thickness, the feed per tooth with the 30 deg corner angle cutter is 0.015 in., while with the 75 deg corner angle it is 0.050 in. This represents a rate of production 333 per cent that of the lower corner angle.

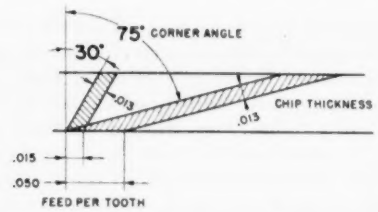


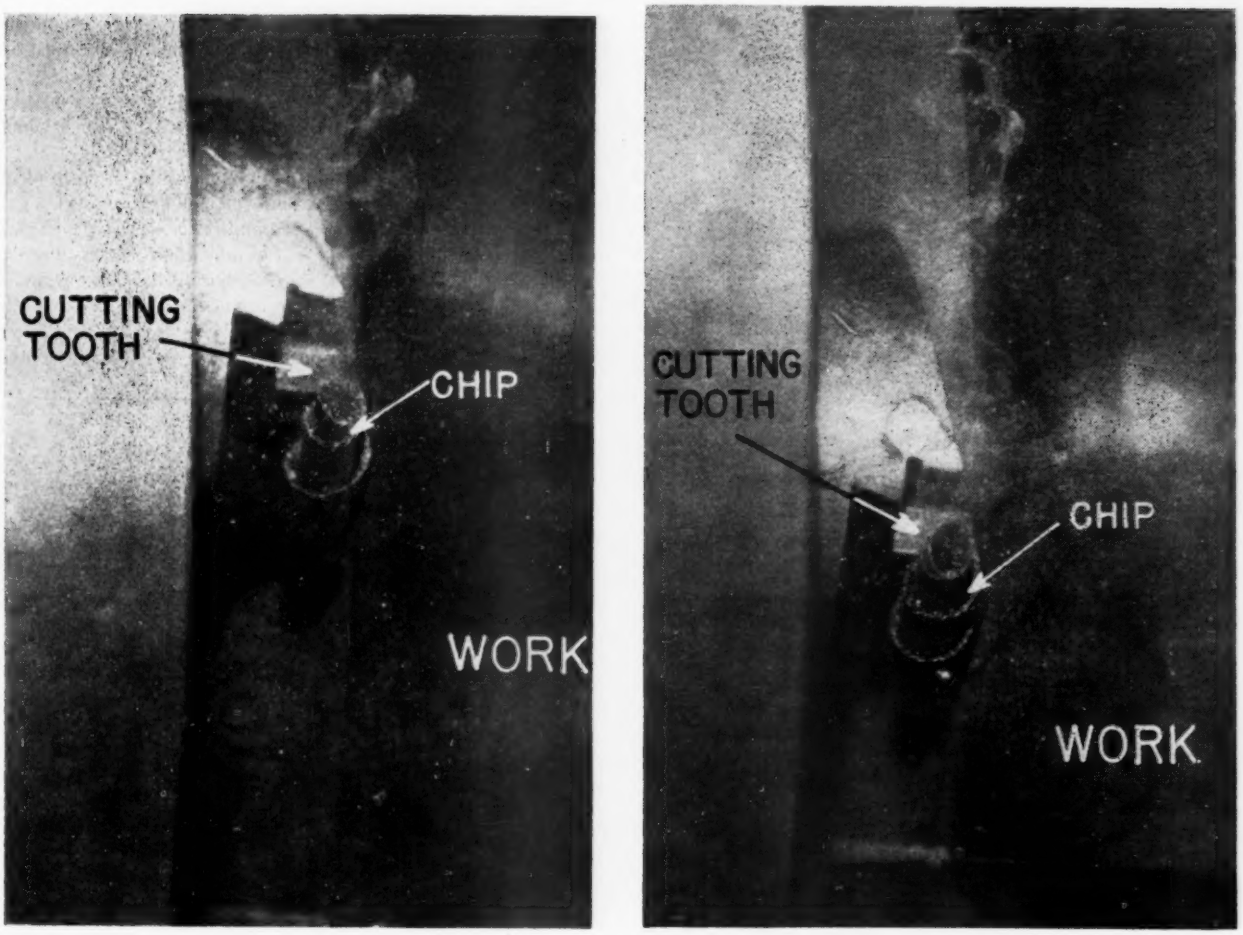
FIG. 4 EXAMPLE SHOWING INCREASE OF FEED PER TOOTH FROM 0.015 IN. TO 0.050 IN. AS CORNER ANGLE IS INCREASED FROM 30 TO 75 DEG FOR A CONSTANT UNDEFORMED CHIP THICKNESS OF 0.013 IN.

In practice it is difficult to utilize such large corner angles and high potential feed rates with the present commercially used numerically small values of axial and radial rake angle (either positive-positive, negative-negative, or positive-negative). Problems of chip disposal, high impact loads, smoothness of finish, flatness, etc., are all limiting factors. These difficulties have been overcome to a high degree of satisfaction with the combination of angles and arrangement developed in this investigation; viz., large negative radial rake (—30 deg to —45 deg); large positive axial rake (+15 deg to +20 deg), and large corner angle (70 deg to 80 deg). In the 12-tooth cutter, shown in Fig. 2, the values used are axial rake, +15 deg; radial rake, —30 deg; and corner angle 75 deg, giving a true (or resultant) rake of +6 deg. This designation may be abbreviated, +15, —30, 75, +6 (a, r, c, t).

The very large feed per revolution obtainable with such a cutter (1/2 in. to 1 in. or more, depending on number of teeth and material cut) presents a difficult problem in surface finish. This is particularly true with large carbide-tipped cutters owing to the difficulty of grinding the ends of all teeth exactly alike. This problem has been solved in the present instance by providing a separate finishing tooth with fine axial adjustment and a face sufficiently broad to cover at least the feed per revolution; it is set so as to extend a few thousandths of an inch beyond the "highest" of the roughing teeth. This separate finishing tooth is shown at the top in Fig. 2.

With this arrangement, the main teeth are ground so as to cut on their angularly disposed edges only. The adjacent edges do not lie in a radial plane but are sharply relieved so as to clear the finished surface, the latter being produced entirely by the separate finishing tooth. By separating the functions of roughing and finishing, it is also possible to use for the finishing tooth a very hard and abrasion-resistant grade of carbide; and if desired, a large positive axial rake angle, as this tooth does not have to withstand an impact load.

A characteristic feature of this cutter is the large positive angle of inclination (32 deg in the cutter shown in Fig. 2). The angle of inclination is the angle between the cutting edge and a plane normal to the path of motion. This large positive angle produces a helically curled chip which flows radially out of the cutter body, even with very high values of feed per tooth. The electronic flash photographs of a single-tooth cutter with this



(*a*) (*b*)

FIG. 5 FLASH PHOTOS SHOWING UNUSUAL HELICAL CHIP FORMATION IN CAST IRON, WITH CUTTER HAVING AXIAL RAKE OF +15 DEG, RADIAL RAKE OF —30 DEG, AND CORNER ANGLE OF 75 DEG
(In *b*, the chip is somewhat further developed than in *a*.)

angle combination, Figs. 5 (*a*) and 5 (*b*), made with an exposure time of about 0.000004 sec, clearly show this helical chip formation.

In early tests with the multitooth cutter, cast-iron test blocks were milled at feed rates of over 100 ipm. Such a cut is shown by the high-speed flash photograph, Fig. 6.

SELECTION OF FEED AND SPEED IN PRODUCTION MILLING

In practical applications of carbide milling, the question naturally arises as to what factors actually determine the speeds and feeds which can properly be used. The performance illustrated in Fig. 6, although spectacular, may not be possible, or desirable, on a given job. In any milling operation certain quality specifications such as flatness, breakout, and surface finish must first be satisfied; any of these requirements may limit the feed rate to a value appreciably lower than the maximum capacity of the machine or cutter.

In order to study the quality of surface obtainable when milling with the cutter shown in Fig. 2, the head and pan surfaces of an automobile cylinder block were milled on a special fixed-bed milling machine, Fig. 7. This machine was provided with a hydraulic feeding mechanism by means of which the table could be operated at feed rates up to 300 ipm. The spindle was driven by a separate 40-hp motor. The cylinder block was held in a fabricated fixture. The cylinder-block head surface was $7^1/_4$ in. wide × $23^1/_2$ in. long, while the pan sur-



FIG. 6 CAST-IRON BLOCK BEING MILLED AT FEED RATE OF 100 IPM
(Width of cut = 6 in.; depth of cut = 0.150 in.; cutter, $9^1/_2$ in. diam, 12 teeth, +15, —30, 75, +6; cutting speed, 350 fpm.)

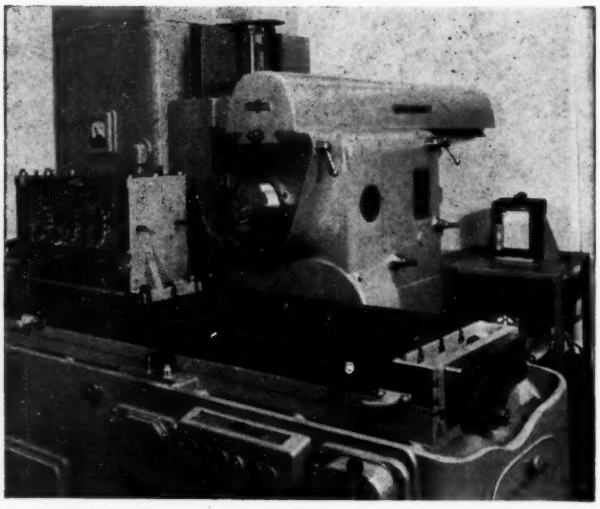


FIG. 7 FIXED-BED MILLING MACHINE USED FOR MILLING TESTS ON CYLINDER BLOCKS WITH SPECIAL CUTTER SHOWN IN FIG. 2

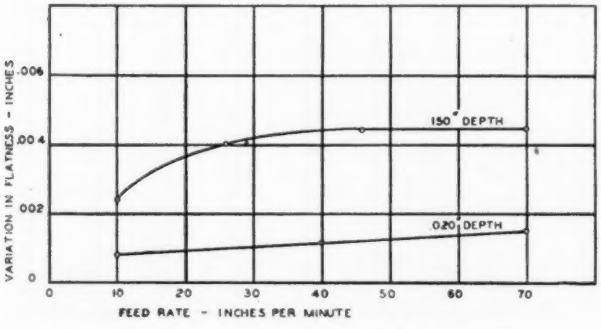


FIG. 8 VARIATION IN FLATNESS VERSUS FEED RATE
(Milling head surface of cast-iron cylinder block with special cutter shown in Fig. 2.)

face was $11\frac{1}{4}$ in. wide × 25 in. long. Cuts were made at 280 fpm, at feed rates up to 70 ipm. The thin wall sections and cored openings in the block presented a difficult test for these high feed rates.

Flatness. The variations in flatness obtained in milling the head surface of the block at both 0.150-in. and 0.020-in. depths are shown in Fig. 8. Taking a roughing cut 0.150 in. deep, the departure from surface flatness was 0.0044 in. at a feed rate of 70 ipm. This may be considered satisfactory, since such a heavy cut would always be followed by a finishing cut. At 0.020 in. depth, the flatness error never exceeded 0.0015 in. at any feed rate up to 70 ipm.

Breakout. In milling cast iron, the breakout on the work at the side where the cutter teeth emerge from the cut may possibly limit the maximum feed. The relation of breakout to feed rate, measured at the cylinder bores while taking a 0.150-in-depth cut, is shown in Fig. 9. The cylinder bores had 0.125-in. finishing stock, so that the 0.070-in. breakout at 70 ipm left a comfortable margin of safety.

Surface Finish. The surface finish obtained in milling the pan surface of the cylinder block is shown in Fig. 10. The surface finish improved somewhat as the feed rate was reduced. However, even the worst surface finish (230 microinches at 70 ipm, with a depth of 0.150 in.) would be satisfactory as a roughing cut. Figs. 11 (*a*) and (*b*) are reproductions of Faxfilm replicas showing the finish obtained at 70 and 26 ipm, respectively. By careful attention to the shape and smoothness of the cutting edge on the finishing tooth, a very high quality of surface can be obtained on finishing cuts.

Tool Life. There are, of course, other factors than quality specifications that influence the choice of speed and feed. Chief among these is tool life.

Fig. 12 shows the relationship between tool life (measured in terms of cubic inches of metal removed per sharpening) for a single-tooth cutter having the combination of angles developed in this investigation, and used in the multitooth cutter, Fig. 2. In this case the work material was Meehanite A. Here again a definite maximum tool-life point occurs at about 300 fpm; both above and below this speed the tool life rapidly decreases. Higher cutting speeds permit higher feed rates, and, conse-

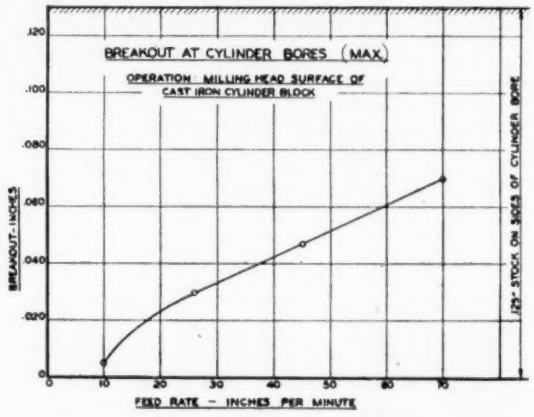


FIG. 9 MAXIMUM BREAKOUT AT CYLINDER BORES VERSUS FEED RATE
(Milling head surface of cast-iron cylinder block with special cutter shown in Fig. 2. Depth of cut, 0.150 in.)

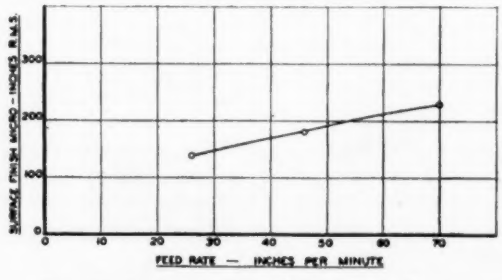
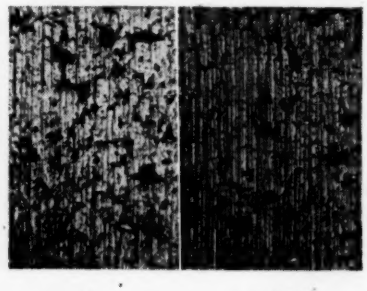


FIG. 10 SURFACE FINISH VERSUS FEED RATE
(Milling pan surface of cast-iron cylinder block with special cutter shown in Fig. 2. Depth of cut, 0.150 in.)



(*a*) (*b*)

FIG. 11 SURFACE FINISH OBTAINED ON CAST-IRON CYLINDER BLOCK WITH SPECIAL CUTTER SHOWN IN FIG. 2
(Depth of cut, 0.150 in. Fig. *a*: 70 ipm feed rate, 230 microinches, rms. Fig. *b*: 26 ipm feed rate, 140 microinches rms; magnification, ×20.)

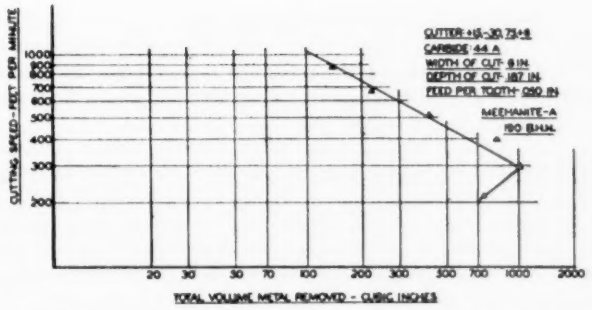


FIG. 12 CUTTING SPEED VERSUS TOTAL VOLUME OF METAL REMOVED TO DULL TOOTH WITH AXIAL RAKE OF +15 DEG, RADIAL RAKE OF —30 DEG, AND CORNER ANGLE OF 75 DEG

quently, higher production, but as is evident from the curve, this can be gained only at the expense of cutter life.

COST OF MILLING AND RATE OF PRODUCTION

From the foregoing discussion it is evident that the selection of speed and feed in milling must take into consideration a number of factors such as tool life, surface quality, production rate, breakout of trailing edge of work, etc., any one of which may be of paramount importance in a particular case. In the final analysis, the best combination must be determined by economic considerations; in other words, by the best balance between production rate and cost per piece. Hence it is necessary first to study in detail all of the elements entering into the cost of production.

In the paper[3] previously mentioned, the factors that determine milling cost were combined into the following equation

$$C = \underbrace{\left[\left(M_{LO}\right)\left(T_m + \frac{T_o}{N_L} + \frac{T_r}{N_S}\right)\right]}_{\text{Milling cost}} + \underbrace{\left[C_u\right]}_{\substack{\text{Initial}\\ \text{cost of}\\ \text{cutter}}} + \underbrace{\left[\left(G_{LO}\right)\left(\frac{T_S}{N_S} + \frac{T_B}{N_B}\right) + C_a + W\right]}_{\text{Cutter preparation cost}}$$

where

C = total cost to mill one piece, dollars
M_{LO} = labor + overhead on milling machine, \$/min
G_{LO} = labor + overhead on cutter grinder, \$/min
B_{LO} = labor + overhead on brazing unit (assumed = G_{LO}), \$/min
T_m = total time to mill one piece, min = feeding time + rapid traverse time + loading and unloading time
T_o = original set-up time on milling machine, min
N_L = total number of pieces in lot
T_r = time to change and reset cutter, min
T_s = time to resharpen cutter, min
N_s = number of pieces milled per cutter sharpening
T_B = time to rebraze teeth (or reset blades), min
N_B = number pieces milled per brazing (or resetting)
C_u = original cutter cost per workpiece
C_a = carbide (or blade) cost per workpiece
W = wheel (diamond or abrasive) cost per sharpening

From this equation the production rate in pieces milled per 60-min hr (P) can be derived

$$P = \frac{60}{T_m + \frac{T_o}{N_L} + \frac{T_r}{N_s}}$$

The cost equation also indicates that the two major factors which determine the cost of milling are the actual milling cost (or metal-removal cost), and the cutter preparation cost. The original cutter cost per piece milled is generally negligible, except for short jobs that require special cutters.

In order to illustrate the application of a cost analysis to speed and feed selection in practical cases, specific examples will be presented to show the effect of such factors as work material, cutting speed, feed per tooth, number of teeth in the cutter, loading and unloading time, number of pieces in the lot, and the length of cut. The following assumptions will be common to all of the examples:

Operation: Face mill cast-iron block
Cut dimensions: 6 in. wide, $^3/_{16}$ in. deep, 20 in. long (except where noted)
Cutter: 10 in. diam, +15 deg axial rake, —30 deg radial rake, 75 deg corner angle, +6 deg true rake, 12 teeth (except where noted)
Feed per tooth: 0.050 in. (except where noted)
Approach to work: 10 in.
Overtravel of cutter past work: 10 in.
Number of pieces in lot: 10,000 (except where noted)
Time to load and unload: 1 min (except where noted)

Labor cost on milling machine	\$1.00 per hr
Overhead on milling machine	\$4.00 per hr
Labor cost on cutter grinder	\$1.00 per hr
Overhead on cutter grinder	\$1.25 per hr

Then M_{LO} = \$.0832 per min
G_{LO} = \$.0374 per min

Rapid traverse rate = 300 ipm

T_o = 60 min
T_r = 10 min
T_s = 20 min per tooth
T_B = 5 min per tooth
$N_B = 4\,N_s$

$$C_u = \frac{\text{Original cutter cost}}{\text{No. of pieces milled with cutter}} = \frac{\$200}{50{,}000} = \$0.004$$

$$C_a = \frac{\$2.00 \times \text{No. teeth}}{3\,N_B}$$

$$W = \frac{\$0.20 \times \text{No. teeth}}{N_s} \text{ (for diamond grinding wheel)}$$

The time to mill one piece T_m will then be

$$T_m = \frac{10 + l}{f} + \frac{10 + l + 20}{r} + T_L$$

where

l = length of cut, in.
f = feed rate, ipm
r = rapid traverse rate, ipm
T_L = time to load and unload, min.

The number of pieces milled before the cutter has to be resharpened, N_s, will be

$$N_s = \frac{\text{No. teeth} \times L}{\text{Cubic inches removed per piece}}$$

where

L = tool life, cu in. removed to dull one tooth, obtained from cutting-speed versus tool-life curves (such as Fig. 12)

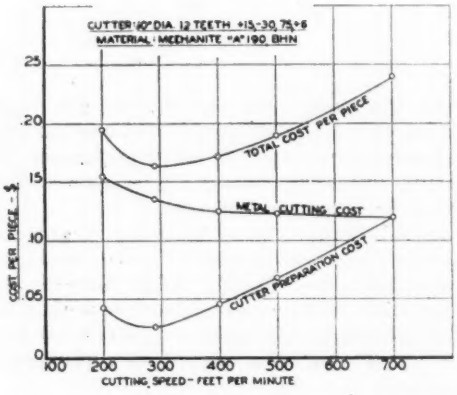


FIG. 13 ANALYSIS OF TOTAL MILLING COST IN TERMS OF ITS PRINCIPAL COMPONENTS
(Dimensions of cut: 1/16 in. deep, 6 in. wide, 20 in. long.)

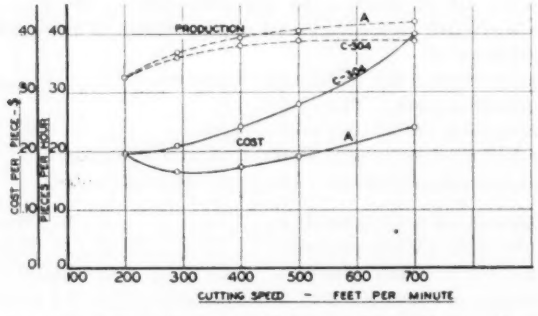


FIG. 14 PRODUCTION RATE AND COST PER PIECE VERSUS CUTTING SPEED
(Dimensions of cut: 1/16 in. deep, 6 in. wide, 20 in. long.)

The manner in which the cutting cost components vary with cutting speed, in milling Meehanite A, is shown in Fig. 13. The cutter preparation cost is a minimum at 290 fpm, because at this speed the tool life was a maximum (see Fig. 12). The metal-cutting cost drops rapidly as the speed is increased from 200 to 400 fpm, but at higher speeds the milling cost remains practically constant because the increase in feed rate is offset by the time lost in changing and resetting cutters which results from the decreased tool life. The total cost per piece is the sum of the cutter preparation cost and the metal-cutting cost. This total cost is likewise seen to be a minimum at 290 fpm.

But the cost per piece may not be the most important factor. Under certain conditions, the production rate may be equally important as the cost per piece, and in some cases may be even more important. The production rate required on a machine may be determined by the capital investment and by the inconvenience or delay in obtaining additional equipment. For example, it may be desirable to sacrifice tool life by operating at higher cutting speeds in order to obtain a definite production rate with a given number of milling machines.

The production rate, measured in number of pieces milled per 60-min hr, and the cost per piece, vary with cutting speed as shown in Fig. 14. The production rate for both of the materials tested (Meehanite A and Meehanite C-304) rises rapidly as the speed is increased from 200 to 400 fpm, but at the higher speeds these increases are less pronounced owing to the increase in time lost when changing cutters. The total cost per piece for Meehanite C-304 is practically constant between 200 and 300 fpm, but at the higher speeds the cost rises rapidly. The differences in cost and production between the two grades of Meehanite are due to the differences in their machinability characteristics. From Fig. 14 the speed which gives the best combination of cost and production can be readily determined. In milling Meehanite A it is obvious that 300 or 400 fpm would be a more economical speed than 200 fpm.

Quantitative comparisons may also be made. Thus in milling Meehanite C-304, the cost at 300 fpm would be 1.07 times as high as at 200 fpm, whereas the production rate at 300 fpm would be 1.11 times as high. Thus at 300 fpm, for a 7 per cent increase in cost, one could obtain a production increase of 11 per cent. In a like manner, the economy of operation at other cutting speeds can be compared.

In the case just discussed, the feed per tooth was held constant at 0.050 in. A thorough analysis of cost and production, however, must take into consideration a wide range of feeds per tooth as well as cutting speeds.

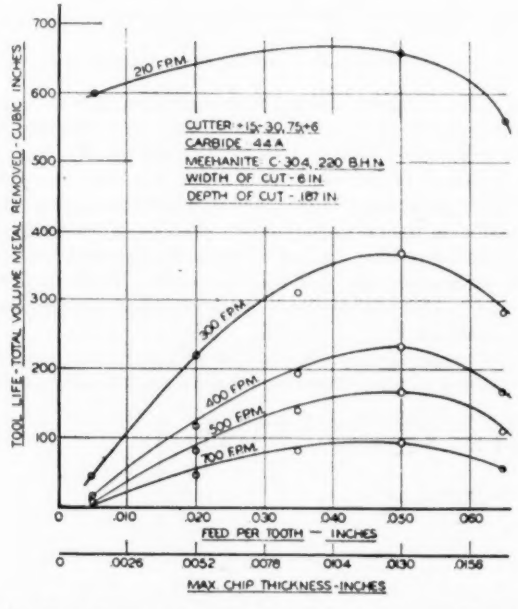


FIG. 15 TOOL LIFE, IN TERMS OF TOTAL VOLUME OF METAL REMOVED VERSUS FEED PER TOOTH, AT CONSTANT CUTTING SPEED

In Fig. 18 of the paper by Field and Bullock[3] (reproduced here as Fig. 15), the interrelation of feed per tooth and cutting speed, with tool life, is shown for the 75-deg corner angle cutter when milling Meehanite C-304. Here the tool life (expressed in cubic inches of metal removed per tooth) is plotted against feed per tooth at constant cutting speeds. Note that here the maximum tool life occurs at 0.050 in. feed per tooth, regardless of the cutting speed. In Fig. 16 the cost and production rate have been plotted against feed per tooth, at constant cutting speeds, using the tool-life data from Fig. 15. Inspection of Fig. 16 shows that the minimum cost likewise occurs at 0.050 in. feed per tooth for all cutting speeds.

Many interesting facts are revealed by a study of the curves in Fig. 16. For instance, it will be noted that for cutting speeds of 200 to 400 fpm, the cost curves are relatively flat with feeds per tooth between 0.040 in. and 0.060 in., but rise rapidly with feeds per tooth below 0.040 in. For cutting speeds above 400 fpm, the cost curves show a sharp minimum at about 0.050 in. feed per tooth. In contrast, all the production-rate curves rise rapidly with feeds per tooth up to 0.040 in., while above 0.040 in. only those for cutting speeds of 400 fpm and under continue to rise appreciably. At 500 fpm the production-rate curve is rela-

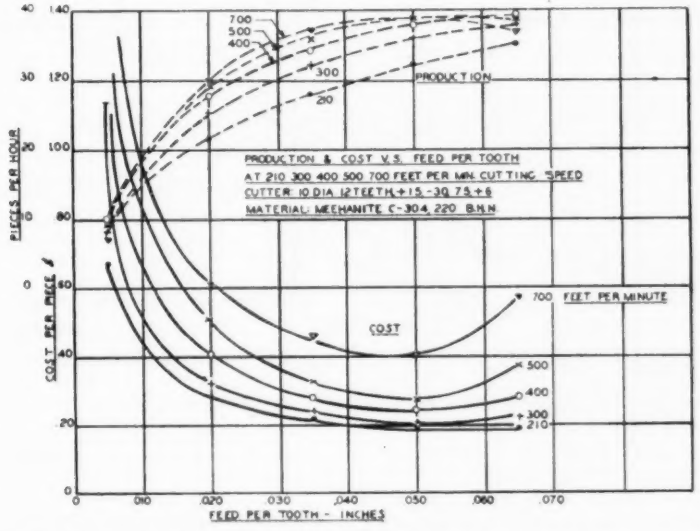


FIG. 16 PIECES PER HOUR AND COST PER PIECE VERSUS FEED PER TOOTH AT CONSTANT CUTTING SPEEDS
(Dimensions of cut: 1/16 in. deep, 6 in. wide, 20 in. long.)

tively flat above 0.040 in. feed per tooth, while at 700 fpm, the curve actually peaks at a feed per tooth of 0.050 in. In this neighborhood the vertical interval between the production-rate curves decreases as the speed is increased, while the interval between the cost curves rapidly increases.

From the curves in Fig. 16 it is therefore apparent that for this particular example of cutter and work, the most desirable combination, from the standpoint of both cost and production, is with a cutting speed of about 300 fpm, and a feed per tooth of about 0.050 in. to 0.055 in. If the cutting speed were increased from 300 to 400 fpm, the cost per piece would be increased 10 per cent, while the production rate would increase only 5 per cent. On the other hand, if the cutting speed were reduced from 300 to 200 fpm, the cost would be decreased only 5 per cent, while the production rate would decline 10 per cent.

With a cutter of 9⅝ in. mean diam, (as in Fig. 2), a 300-fpm cutting speed would correspond to a rotation of 120 rpm. With 12 teeth in the cutter and a feed per tooth of 0.055 in., the feed rate would then be 120 × 12 × 0.055, or 80 ipm. Under these conditions, the total volume of cast iron, Meehanite C-304, which could be removed before the cutter would need resharpening (using the data from Fig. 15), would be about 4200 cu in. or approximately 1200 lb.

If a cutting speed of 400 fpm were used, the feed rate would be 107 ipm, but the total volume of metal removed before sharpening would be reduced to 2640 cu in. Under these conditions, using the data from the curves in Fig. 16, it can be shown that the production rate would be increased 5.4 per cent while the cost per piece would be increased 22 per cent.

From the tool-life curve in Fig. 12, it is interesting to note that if Meehanite A had been used instead of Meehanite C-304, the volume of metal removed before sharpening, at a cutting speed of 300 fpm, would be 12,000 cu in., or approximately 3100 lb.

OTHER FACTORS INFLUENCING PRODUCTION RATE AND MILLING COST

There are still other important factors than quality specifications and tool life, however, that influence production rate and cost of milling.

Number of Teeth in Cutter. In Fig. 17 is shown the effect of the number of teeth in the cutter when using an optimum combination of cutting speed and feed per tooth. Here it will be

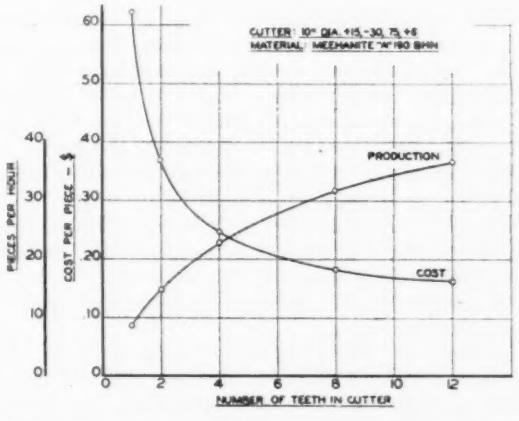


FIG. 17 PIECES PER HOUR AND COST PER PIECE VERSUS NUMBER OF TEETH IN CUTTER
(Dimensions of cut: 1/16 in. deep, 6 in. wide, 20 in. long.)

seen that there is a rapid drop in cost and a rapid rise in production rate as the number of teeth is increased from 1 to 4 in this 10-in-diam cutter. As the number of teeth is further increased, both the cost and the production curves flatten out because the feeding time eventually becomes small in comparison with other fixed portions of the cycle time, such as the rapid traversing time, and the loading and unloading time.

Loading Time. The effect of loading and unloading time on cost and production is shown in Fig. 18, for two conditions: (*a*) 280 fpm cutting speed and 65 ipm feed rate; and (*b*) 500 fpm cutting speed, and 105 ipm feed. From this chart it will be seen that the cost at 500 fpm is a constant amount higher than at 280 fpm, regardless of the loading time. Furthermore, the cost per piece is a linear function of the loading time. The production-rate curves are flat at a high loading time because the feeding time here is short compared to the time to load and unload. However, when the loading time is decreased below one min, the production rates increase sharply. It will also be noted that no appreciable increase in production will be obtained by selecting the high speed and feed, unless the loading time is decreased. For example, at 0.1 min loading time, 102 pieces per hr could be milled at 500 fpm, compared to 80 pieces per hr at

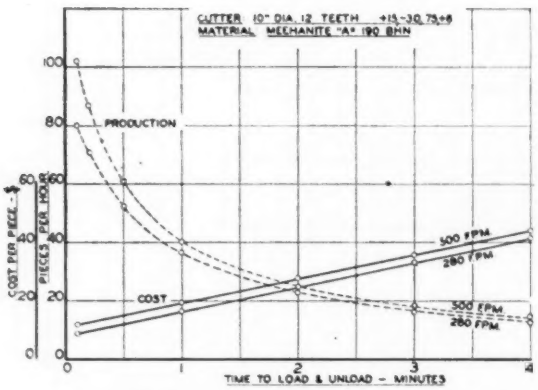


FIG. 18 PIECES PER HOUR AND COST PER PIECE VERSUS TIME TO LOAD AND UNLOAD
(Dimensions of cut: 3/16 in. deep, 6 in. wide, 20 in. long.)

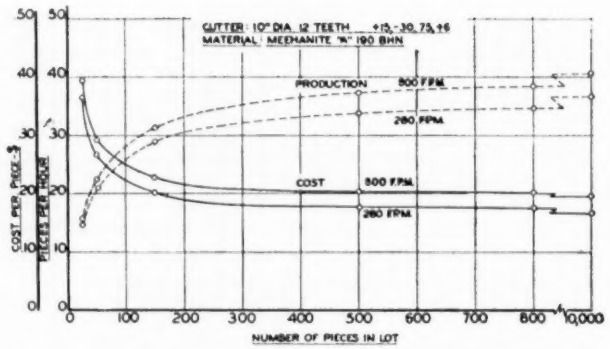


FIG. 19 PIECES PER HOUR AND COST PER PIECE VERSUS NUMBER OF PIECES IN LOT
(Dimensions of cut: 3/16 in. deep, 6 in. wide, 20 in. long.)

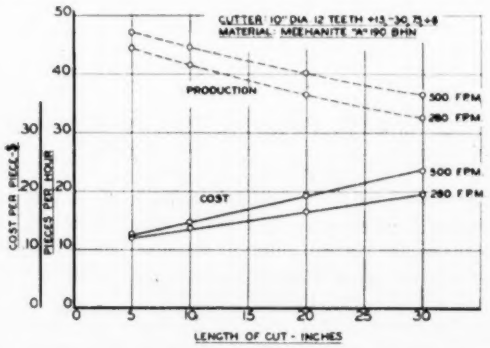


FIG. 20 PIECES PER HOUR AND COST PER PIECE VERSUS LENGTH OF CUT
(Dimensions of cut: 3/16 in. deep, 6 in. wide.)

280 fpm. This is an increase of about 27 per cent. In contrast, for a 2-min loading time, 22.5 pieces per hr could be milled with the high speed and feed, compared to 21 pieces per hr with the low speed and feed; an increase of only 7 per cent.

Number of Pieces in Lot. The effect of the number of pieces in the lot being milled is shown in Fig. 19. If the number of pieces in the lot is small, the original setup time may seriously decrease the production rate and may add appreciably to the cost of milling. In the example chosen, it is seen that the cost and production curves change rapidly if there are fewer than 200 pieces in the lot. However, for larger lots the changes in the curves are very small. It is furthermore interesting to note the small difference between 800- and 10,000-piece lots. There is a constant difference in cost per piece between the 500- and 280-fpm curve. The difference in production rates between the two cutting speeds is small for very small lots. However, this difference increases and eventually becomes practically constant above a 300-piece lot.

Length of Cut. The effect of the length of cut on cost and production is shown in Fig. 20. The cost was about the same for both cutting speeds for a 5-in. length of cut. As the length of cut increased, the cost per piece to mill at the higher cutting speed increased over that of the lower cutting speed. However, the production rate at 500 fpm was substantially higher than at 280 fpm for lengths of cuts of 5 to 30 in.

MILLING OF STEEL

Turning now to the milling of steel, we may cite as an example an analysis made of an actual production milling job performed in the authors' plant. The workpiece was a steel forging (S.A.E. 4340, 415 Bhn) used as a "drag link" on the landing gear of the B-29 Superfortress. Two major milling operations were performed on this forging, namely, milling the inside and outside surfaces of the yoke on each end. The inside of the yoke was milled, with the setup shown in Fig. 21, on a Cincinnati horizontal Hydrotel using two staggered-tooth slotting cutters, 14 in. diam, having 8 teeth, tipped with a steel-cutting grade of carbide. The teeth were ground with an axial rake of —20 deg, a radial rake of —20 deg, and 1/4 in. radius. Each cutter took a cut 5/16 in. deep and 3 3/4 in. wide. The work was fed into the cutter at a rate sufficient to provide a feed per tooth of 0.008 in. The return feed was made at the same rate so as to reduce the dimensional error due to springing of the workpiece, and to avoid marring the work, as a finish under 50 microinches (rms) had to be obtained.

Three cutting speeds were chosen, 235, 290, and 370 fpm, respectively. From Fig. 22 it is seen that minimum cost and maximum production were obtained at 290 fpm. Designating the cost and production rates at this optimum speed 100 per cent, it is seen from the curves that, at a cutting speed of 235 fpm, the cost increased to 104 per cent while the production dropped to 94 per cent, whereas at 370 fpm, the production remained at 100 per cent while the cost rose to 107 per cent. Obviously, a cutting speed in the neighborhood of 300 fpm was the best for this particular operation.

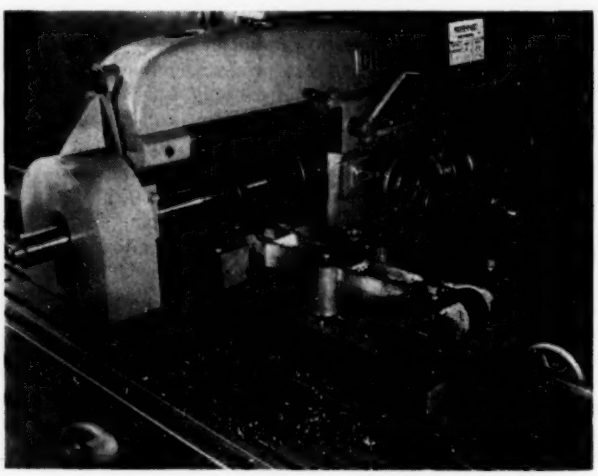


FIG. 21 SETUP FOR MILLING INSIDE OF YOKE ON ALLOY STEEL FORGING
("Drag link" for B-29 Superfortress.)

The second major operation analyzed was the straddle-milling operation on the outsides of the yoke. This operation was performed on a Cincinnati 4–48 duplex Hydromatic miller, with the setup shown in Fig. 23, using a pair of right- and left-hand, 6-in-diam 6-tooth shell-end mills. The cutters had an axial rake of —20 deg, a radial rake of —20 deg, and a corner angle of 30 deg. These cutters also took a cut $^{5}/_{16}$ in. deep and $3^{3}/_{4}$ in. wide. Again, in order to obtain the specified surface finish and accuracy, the cutters were fed fully across each yoke surface. As shown in Fig. 24, the minimum cost per piece and maximum production rate occurred at 285 fpm. Designating this condition as 100 per cent, it is seen that at 210 fpm the cost remained at 100 per cent, while the production dropped to 88 per cent. At 380 fpm, however, the cost jumped to 181 per cent while the production rate dropped to 88 per cent. It is therefore evident that a cutting speed of about 300 fpm was the optimum for this operation.

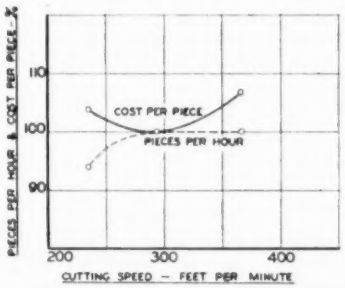


FIG. 22 PRODUCTION RATE AND COST PER PIECE VERSUS CUTTING SPEED FOR MILLING INSIDE OF YOKE ON DRAG LINK

Cutters: 14 in. diam, 8 teeth, —20 deg axial rake, —20 deg radial rake, $^{1}/_{4}$ in. radius. Material: S.A.E. 4340, 415 Bhn. Depth of cut, $^{5}/_{16}$ in.; width of cut, $3^{3}/_{4}$ in.)

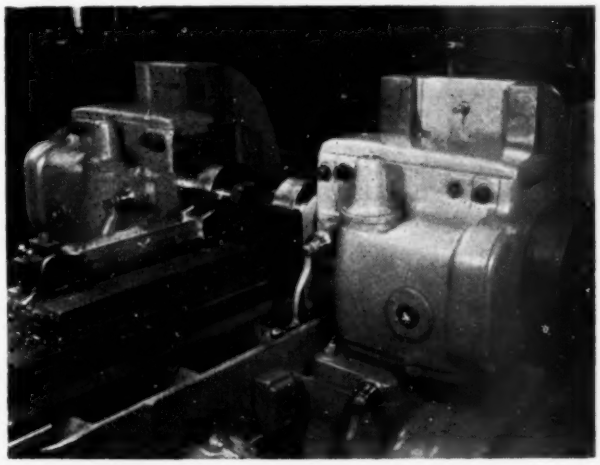


FIG. 23 SETUP FOR MILLING OUTSIDE OF YOKE ON DRAG LINK

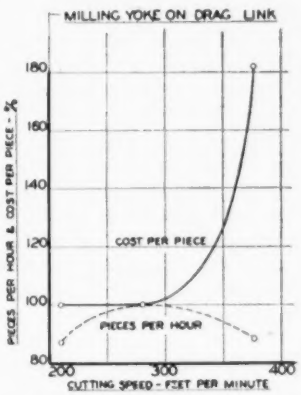


FIG. 24 PRODUCTION RATE AND COST PER PIECE VERSUS CUTTING SPEED FOR MILLING OUTSIDE OF YOKE ON DRAG LINK

(Cutters: 6 in. diam., 6 teeth, —20 deg axial and radial rake, 30 deg. corner angle. Material: S.A.E. 4340, 415 Bhn. Depth of cut, $^{5}/_{16}$-in.; width of cut, $3^{3}/_{4}$ in.)

CONCLUSIONS

The following conclusions can be drawn from the results of the work done thus far:

1 It is not possible to extrapolate tool-life curves into the low-speed range from the results of tests made at cutting speeds over 500 fpm, for the following reasons:

(*a*) From the results of tests made thus far it appears that the cutting-speed versus tool-life curve may often contain a maximum tool-life point toward the lower end of the speed range. This point seems to exist at a lower value for the harder grades of cast iron.

(*b*) In certain cases the curve of cutting speed versus tool life is not a straight line in the lower speed range when drawn on log-log paper.

2 Practical tests of multitooth cutters with the combination of very large corner angle (70 to 80 deg), large negative radial rake (—30 to —45 deg), and large positive axial rake (+15 to +20 deg), have shown that this combination has unusually long life in terms of volume of metal removed before grinding. It also permits the use of very high feed rates and consequent high production without clogging of chips, and yet meets normal quality specifications of flatness, surface finish, and breakout.

3 Curves showing the relationship between cutting speed, feed, and tool life are essential for an intelligent selection of speed and feed. However, selection of speed and feed for practical milling operations cannot be made directly from these tool-life curves, but must take into consideration also the effect of tool life on both cost and production. Proper balance between these two factors can be made only on the basis of a complete cost analysis.

4 Selection of speed and feed must also be made on the basis of meeting quality specifications, such as flatness, surface finish, and breakout.

5 Cost and rate of production are also affected by number of teeth in the cutter, loading time, length of cut, and number of pieces in the lot. A complete analysis of a milling operation should take into consideration the relationship between these factors and cutting speed and feed.

ACKNOWLEDGMENT

The authors wish to express their appreciation to Dr. M. E. Merchant and Mr. Norman Zlatin of the research department of the Cincinnati Milling Machine Co., for their aid in the preparation of this paper, and to Mr. Walter Deer of the engineering service department, who helped in conducting the shop tests.

(Owing to travel emergency conditions existing when this paper was presented, discussion will be accepted until May 10, 1946)

Analysis of Initial Contact of Milling Cutter and Work in Relation to Tool Life

By M. KRONENBERG,[1] CINCINNATI, OHIO

Sintered-carbide tools, made of the hardest metal man has ever produced, have played a predominant role in speeding up war production. While appreciable experience has been acquired in connection with the turning of artillery shells and other implements of war, the application of sintered-carbide tools is often more difficult in milling than in turning operations because face-milling cutters, end mills, straddle mills, side mills, etc. are subjected to several hundred impacts per minute, which may destroy the tools prematurely due to their brittleness. Control of impact is therefore vital, a problem not encountered with high-speed steel tools.

It is the purpose of this paper to present methods for determining readily the impact conditions for any shape of the cutting edge as a function of positive and negative rake angles, corner angle, cutter diameter, position of the cutter relative to the workpiece, feed per tooth, and depth of cut. Furthermore, tests are discussed indicating a variation in the wear of sintered-carbide tools with a variation of impact conditions obtained by altering the relative position of cutter and work.

Introduction

WHILE carbide-tipped tools with negative rake angles have been successfully employed for a number of years in intermittent turning operations, this technique is a relatively recent development in the case of milling operations. The reason for this may well lie in the more complex nature of initial contact of milling cutter and work compared with that of a turning tool and work.

In the simple case of machining a slotted flange in a plunge-cut operation, the location of the initial contact can be easily controlled. As shown in Fig. 1, a negative back rake is the only requirement for shifting the initial contact from the sharp point "S" of the tool to a point farther back, where the tool is stronger.

Turning a shaft with a keyway, using a longitudinal feed, is a more difficult case in that three tool angles affect the location of the initial contact when the tool is "on center," namely, back rake, side rake, and side-cutting-edge angle.

In the case of milling operations, a fourth quantity, which is not a property of the tool itself, must be taken into consideration; it depends on the position of the milling cutter relative to the work. This fourth quantity, later referred to as the "angle of engagement," plays a significant part in the location and magnitude of impact.

Three questions present themselves for the analysis of the impact problem. They can conveniently be used for subdividing the subject of this paper as follows:

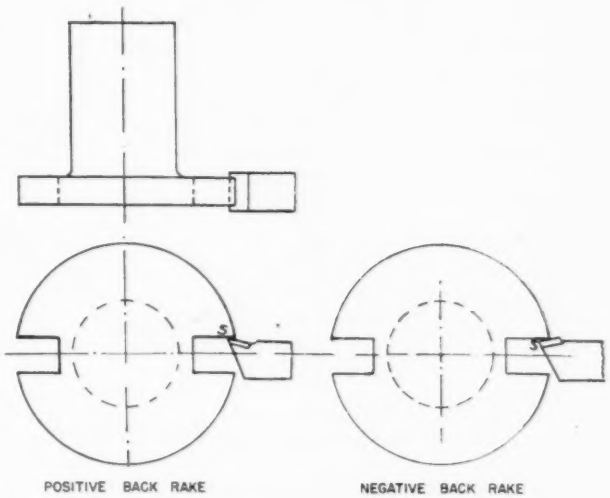


FIG. 1 INITIAL CONTACT PRODUCED BY POSITIVE AND NEGATIVE BACK RAKE, WHEN TURNING A SLOTTED FLANGE

1 Where does the impact of tooth and work occur? That is, what point on the tool face hits the work first? (Location of impact.)

2 How great is the impact? (Magnitude of impact.)

3 How is tool wear affected by location and magnitude of impact?

1—LOCATION OF IMPACT

Model, Demonstrating Location of Contact

A face-milling cutter is shown in Fig. 2 at an instant shortly before the tooth engages the side wall of the work, termed "plane of engagement." This plane is always assumed parallel to the cutter axis and extending in the direction of feed motion. It is evident from the close-up in the upper corner of Fig. 2 that the material removed by a tooth with a straight cutting edge is indicated by a parallelogram *S-T-U-V*. Its height depends on the depth of cut, while the width is determined by the feed per tooth represented by a dotted line on the top of the work. This parallelogram *S-T-U-V* develops gradually as the tooth enters the work, and the question arises, what spot on the contour of the parallelogram is generated first. This spot will obviously be the point of initial contact.

It will be seen from Fig. 2 that the tooth, before contacting the work, passes through the removed portion of the plane of engagement. This happens when the cutter axis is on the "workside" of the plane of engagement, as shown in Fig. 2.

In the analysis of initial contact, it is necessary to consider only the region of cutter and work indicated in the close-up, Fig. 2. This same region is represented in Fig. 3 as a large-scale model, seen in the direction of the arrow of cutter rotation, Fig. 2.

In Fig. 3 the "tool face" is a glass plate shaped to the contour of a tooth, intersecting the "plane of engagement" in line *L-M*.

---

[1] The Cincinnati Milling Machine Company.

Contributed by the Research Committee on Metal Cutting Data and Bibliography, and on Cutting Fluids, and the Production Engineering Division and presented at the Fall Meeting of the Cincinnati Section, Cincinnati, Ohio, Oct. 2–3, 1945, of THE AMERICAN SOCIETY OF MECHANICAL ENGINEERS.

NOTE: Statements and opinions advanced in papers are to be understood as individual expressions of their authors and not those of the Society.

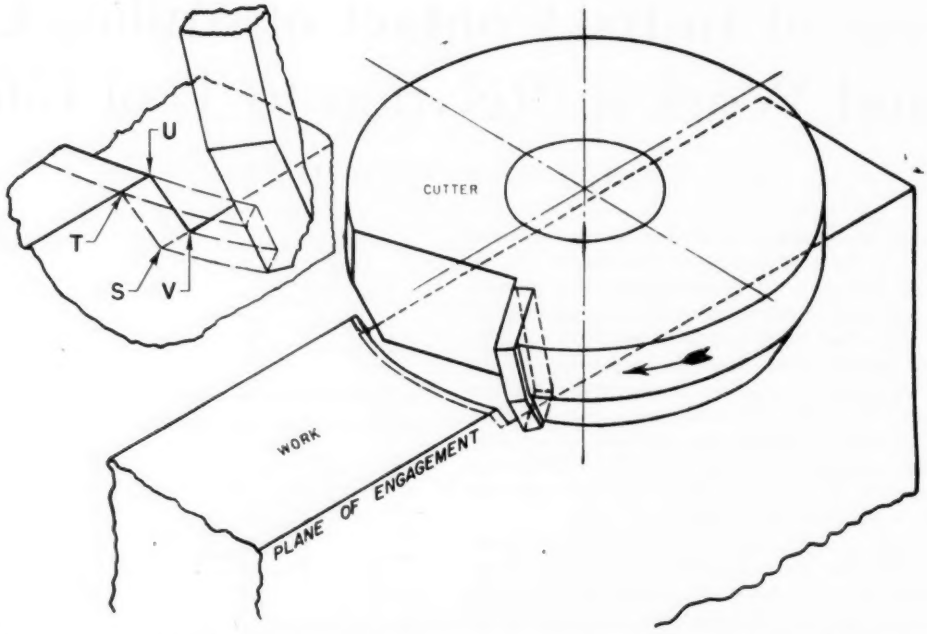


FIG. 2 DIAGRAMMATIC VIEW OF CUTTER AND WORK, ILLUSTRATING AN INSTANT SHORTLY BEFORE INITIAL CONTACT

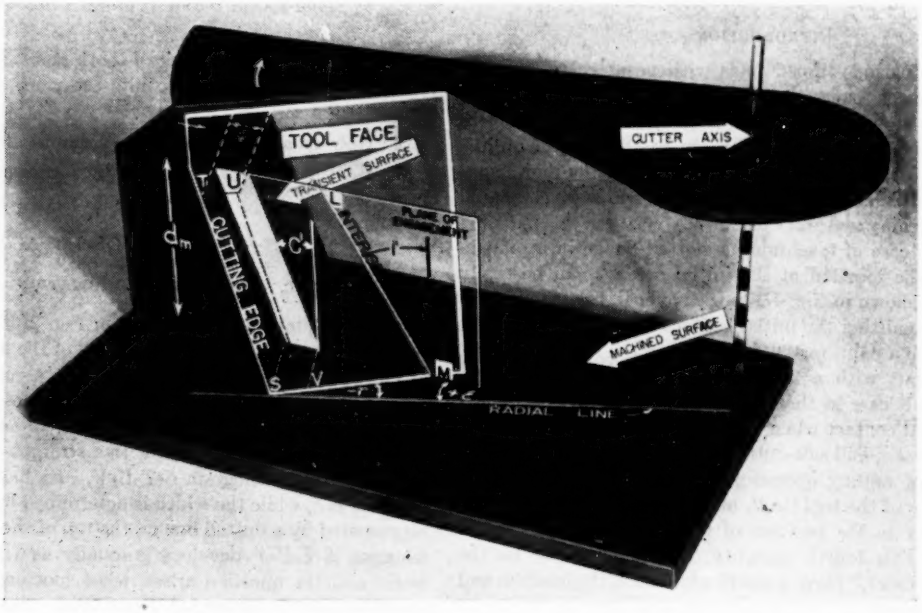


FIG. 3 MODEL OF CUTTER AND WORK ILLUSTRATING INTERSECTION LINE OF TOOL FACE AND PLANE OF ENGAGEMENT

The axial rake and the radial rake are both negative and the cutting edge is a straight line in this model.

The direction of cutter rotation is indicated by an arrow pointing into the workpiece.

The "cutter axis" is connected with the tool face by a top piece symbolizing the face of the cutter body. The cutter axis is actually more distant from the tool face than shown in the model.

On the workpiece, dimension d_m is the depth of cut, while dimension f_t represents the feed per tooth.

The chip cross-sectional area is indicated by a white parallelogram on the workpiece. The corresponding points on the tool face are marked S, T, U, and V, in clockwise order.

The distance traveled by the tooth from the instant shown, to the instant of contact, is very short and it may therefore be assumed that the tool moves in a straight line during this very short interval of time, instead of traveling in a circular path. In other words, the tool face is assumed to advance parallel to itself in the direction of the white dotted lines which connect the points, *S*, *T*, *U*, *V*, on the tool face with the white parallelogram. The white lines are continued on the top of the work because the cutter movement is also considered straight for a short distance within the workpiece.

Point *S* is the sharp point of the tool and its weakest spot. Initial contact there is undesirable.

Point *T* is the top point of the active cutting edge and is located at a height above the machined surface equal to the depth of cut (d_m).

Point *U* indicates a point on the tool face, at the same height as point *T*, but remote from the cutting edge by approximately the feed per tooth.

Point *V* is a point on the face edge, located at a distance from point *S* approximately equal to the feed per tooth.

It is evident from Fig. 3 that in the case of this model, point *U* on the tool face will contact the work first, because this point is nearest to the white parallelogram. This can be judged by comparing the length of the four dotted white lines connecting points, *S*, *T*, *U*, and V with the work. Point *U* has the shortest distance. This type of contact is called "*U*-contact."

If the tool face would be inclined at a positive axial rake, point *V* would have the shortest distance on the model and contact first (*V* contact).

It shall now be assumed that the tool face in Fig. 3 is advancing parallel to itself, in the direction of the white dotted lines toward the workpiece. Point *U* on the tool face will then travel toward the upper right corner of the white parallelogram; simultaneously point *L* of the intersection line will likewise move toward the upper right corner on the workpiece. At the instant when point *U* contacts the white parallelogram at its upper right corner, point *L* of the intersection line must have arrived at that same point also.

If the tool face would be inclined at a positive axial rake and the angle *i'* would be to the right of the vertical line in the plane of engagement, it would be points *V* and *M* which would arrive at the same instant but at the lower right corner of the white parallelogram.

Consequently, the spot on the tool face which contacts the work first is indicated by the point of the intersection line LM, which first contacts the white parallelogram.

This is an important finding, because it furnishes not only the basis for the derivation of mathematical formulas for contact conditions in the case of straight cutting edges but also principles for a graphical solution of the more involved problems connected with nonstraight cutting edges and with the magnitude of impact.

Mathematical Conditions for Location of Initial Contact

Mathematical formulas are required for preparing diagrams and for other graphical methods which can directly be employed by production and tool engineers in their daily work.

The following nomenclature will be used in connection with the derivation of formulas:

a = axial rake
A' = distance of cutter axis from plane of engagement (see Fig. 4)
c = corner angle of tool
c' = slope of transient surface produced by corner angle c ($\tan c' = \tan c/\cos \epsilon$)
c_a = chamfer angle of tool
d_m = depth of cut
D = cutter diameter
ϵ = angle of engagement
f_t = feed per tooth
i = index angle
i' = intersection angle of tool face and plane of engagement ($\tan i' = \tan i/\cos \epsilon$)
I = impact factor (rate of increase of chip cross-sectional area) sq in. per sec
L_d = distance traveled by index line in direction of depth of cut during penetration time
L_f = distance traveled by index line in the direction of feed during penetration time
r = radial rake
T_p = penetration time, i.e., time elapsing between instant of initial contact and instant when both cutting edge and face edge of tool have engaged the work
T_e = exit time, i.e., time elapsing between instant when first point of tool leaves work and instant when both cutting edge and face edge are disengaged

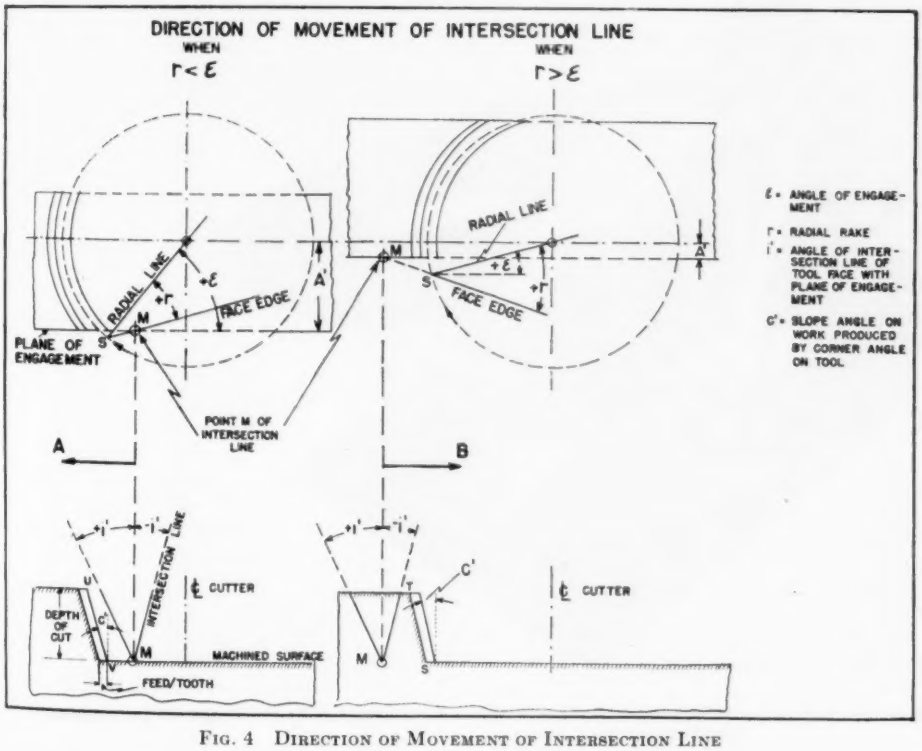


FIG. 4 DIRECTION OF MOVEMENT OF INTERSECTION LINE

Referring to Fig. 3, two important angles, c' and i', will be seen in the plane of engagement.

Angle c' is the slope of the "transient surface" measured in the plane of engagement. This angle has been produced by the preceding tooth and depends therefore on the shape of the cutting edge and on the angle of engagement, as will become evident later.

Angle i' is an angle formed by line LM (which is the intersection line of tool face and plane of engagement) and a line parallel to the cutter axis. Angle i' is called "intersection angle."

The model, Fig. 3, refers only to the case where the intersection line is outwardly inclined with respect to the cutter axis and where the cutter axis is on the workside of the plane of engagement.

For a more general consideration, reference is made to Fig. 4. It will be seen from the lower sketches that the intersection angle i' can be positive or negative with respect to the vertical line parallel to the cutter axis, that is, it can be outwardly or inwardly inclined. Furthermore, the radial rake, formed by the face edge and a radial line, is shown in Fig. 4, marked r. In addition, the angle formed by the plane of engagement and the radial line is indicated; it is the angle of engagement (ϵ).

For determination of the direction of movement of the intersection line, it is sufficient to consider only its lower point M which is also a point of the face edge of the tool. In the case of the left-hand sketch in Fig. 4, point M moves toward the left as the cutter continues to rotate. Hence the intersection line will always move "away" from the cutter axis, due to cutter rotation, when $r < \epsilon$. Consequently, in cases where $r < \epsilon$, initial contact can occur only at the right-hand contour of the chip cross-sectional area, that is, in the case of a straight cutting edge, either at point U, or along line U-V or at point V, depending on the relationship of the two angles c' and i'.

Changing the setup (right-hand sketch in Fig. 4), by moving the workpiece into a different position with respect to the cutter axis, will change the relationship between the angles r and ϵ.

Point M of the intersection line is now located on the other side and will move "toward" the cutter axis, as the cutter continues to rotate. Consequently, in cases where $r > \epsilon$, initial contact can occur only at the left-hand contour of the chip cross-sectional area, that is, in the case of a straight cutting edge, either at point S, or T, or along line ST.

The following mathematical relationships for initial contact of straight cutting edges can therefore be derived from inspection of Fig. 4

$$S = \text{contact occurs when } r > \epsilon \text{ and } i' > c' \quad [1a]$$

$$S\text{-}T \text{ (line)} = \text{contact occurs when } r > \epsilon \text{ and } i' = c' \quad [1b]$$

$$T = \text{contact occurs when } r > \epsilon \text{ and } i' < c' \quad [1c]$$

$$U = \text{contact occurs when } r < \epsilon \text{ and } i' > c' \quad [1d]$$

$$U\text{-}V \text{ (line)} = \text{contact occurs when } r < \epsilon \text{ and } i' = c' \quad [1e]$$

$$V = \text{contact occurs when } r < \epsilon \text{ and } i' < c' \quad [1f]$$

There are three more types of initial contact possible in the case of straight cutting edges, namely, when $r = \epsilon$. In these special cases, the intersection line and therefore point M is at infinity because the face edge enters the work parallel to the plane of engagement. The mathematical conditions for these cases will be discussed later.

In order to express the contact conditions as functions of axial rake, radial rake, angle of engagement, it is now necessary to find the relationship between these three angles and the intersection angle i'.

Referring to Fig. 5: Dropping a perpendicular line from point L of the intersection line L-M, produces a vertical triangle L-N-M

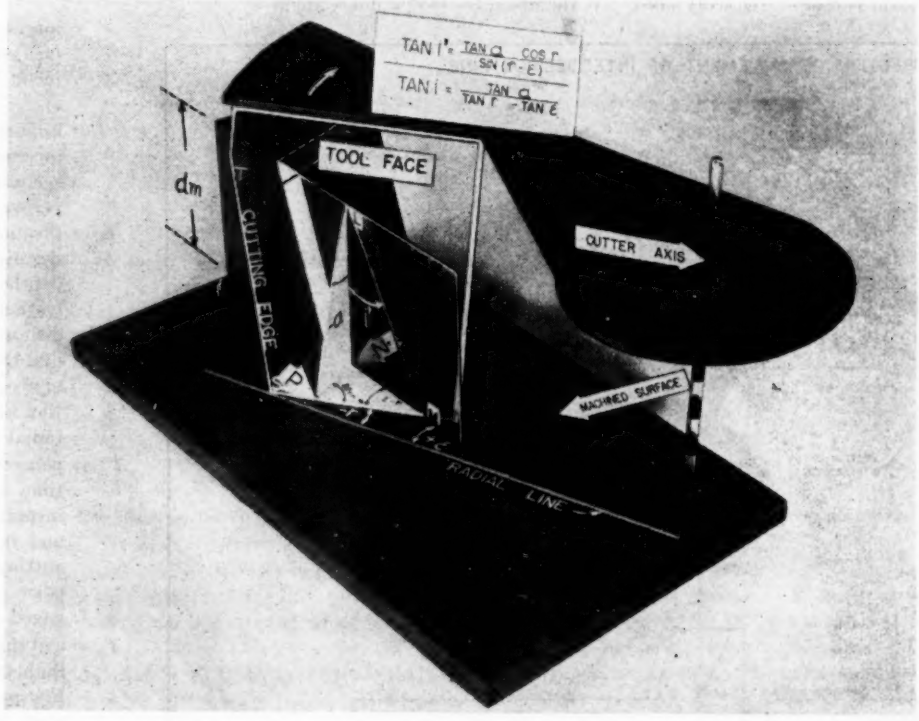


FIG. 5 MODEL OF CUTTER AND WORK ILLUSTRATING RELATIONSHIP BETWEEN AXIAL RAKE, RADIAL RAKE, ANGLE OF ENGAGEMENT, AND INTERSECTION ANGLE

TABLE 1 MATHEMATICAL CONDITIONS FOR THE NINE TYPES OF INITIAL CONTACT FOR STRAIGHT CUTTING EDGES

	TYPE OF CONTACT	Relationship: radial rake(r) & angle of engagement (ε)	Relationship: corner angle(c) and index angle (i)	Relationship corner angle(c) axial rake(a) radial rake (r) and angle of engagement (ε)
1	S	$r > \epsilon$	$c < i$	$\tan c < \frac{\tan a}{\tan r - \tan \epsilon}$
2	T	"	$c > i$	$\tan c > \frac{\tan a}{\tan r - \tan \epsilon}$
3	U	$r < \epsilon$	$c < i$	$\tan c < \frac{\tan a}{\tan r - \tan \epsilon}$
4	V	"	$c > i$	$\tan c > \frac{\tan a}{\tan r - \tan \epsilon}$
5	ST	$r > \epsilon$	$c = i$	$\tan c = \frac{\tan a}{\tan r - \tan \epsilon}$
6	UV	$r < \epsilon$	$c = i$	$\tan c = \frac{\tan a}{\tan r - \tan \epsilon}$
7	VS	$r = \epsilon$	$i = 90°$	$a = +$
8	UT	"	"	$a = -$
9	FACE	"	NO LINE INTERSECTION	$a = 0$

in the plane of engagement. This triangle L-N-M contains angle i'. The base line N-M equals

$$d_m \cdot \tan i'$$

The axial rake is measured, according to definition, in a plane located in the direction of cutter rotation, that is, in a plane perpendicular to the radial line. Such a plane is represented in Fig. 5 by the white vertical triangle L-N-P, containing the axial rake ($-a$) which is shown negative. The base line N-P equals

$$d_m \cdot (-\tan a)$$

The two base lines N-M and N-P, together with portion P-M of the face edge, form the horizontal, white triangle P-N-M, with the angles

$$(90 + r)$$

and

$$(\epsilon - r)$$

Applying the sine law to the horizontal triangle results in the formula

$$\tan i' = \frac{\tan a \cdot \cos r}{\sin (r - \epsilon)} \quad \ldots\ldots\ldots\ldots\ldots [2]$$

Equation [2], however, is inconvenient for use in a diagram, because the radial rake r appears twice.

A simplification can be obtained by multiplying both sides by cos ϵ. This transformation gives

$$\tan i = \frac{\tan a}{\tan r - \tan \epsilon} \quad \ldots\ldots\ldots\ldots\ldots [3]$$

It will be noticed that Equation [3] refers to an angle i instead of angle i'. This is due to the multiplication of Equation [2] by cos ϵ. Equation [3] represents therefore a different angle, called "index angle" (i).

The relationship between the intersection angle (i') and the index angle (i) follows from

$$\tan i = \tan i' \cos \epsilon \quad \ldots\ldots\ldots\ldots\ldots [4]$$

Index angle i is a projection of intersection angle i', on a vertical plane which can be erected in the radial line. This plane, called reference plane, forms the angle ϵ with the plane of engagement, but is not shown in the model.

In order to maintain the mathematical relationship between slope angle c' and intersection angle i' when determining the location of initial contact (see formulas [1a] to [1f], inclusive), it is necessary to multiply the slope angle c' also by cos ϵ as was done with angle i'. The slope angle c' is thus substituted by the corner angle c (or bevel angle) as ground to the tool itself, which is measured in the reference plane. The corner angle c is mathematically a projection of the slope angle c' on the reference plane. The relationship between slope angle c' and corner angle c is given by

$$\tan c = \tan c' \cdot \cos \epsilon \quad \ldots\ldots\ldots\ldots\ldots [5]$$

The multiplication of Equation [2] by cos ϵ does not only simplify the formula, but allows using the corner angle c of the tool instead of the slope angle c' on the work.

The following general equation is obtained for initial contact in the case of straight cutting edges by substituting Equations [3] and [5] into formulas [1a] to [1f]

$$\tan c \begin{matrix} > \\ = \\ < \end{matrix} \frac{\tan a}{\tan r - \tan \epsilon} \quad \ldots\ldots\ldots\ldots\ldots [6]$$

The individual formulas for the nine possible contacts in case of straight cutting edges are summarized in Table 1. The last three cases, where $r = \epsilon$, follow if Equation [6] is solved for tan a

$$\tan a \begin{matrix} > \\ = \\ < \end{matrix} \tan c \, (\tan r - \tan \epsilon) \quad \ldots\ldots\ldots\ldots\ldots [6a]$$

The right side becomes zero if $r = \epsilon$, indicating that these three contact conditions are determined by the fact as to whether the axial rake "a" is positive, zero, or negative.

Cutter-Engagement Diagram

For practical use in engineering offices a "cutter-engagement diagram," Fig. 6, has been prepared, based on the foregoing mathematical analysis. It refers primarily to cases where the cutting edge is a straight line and where only a determination of the location of initial contact is desired.

A more general method is described later on in this paper which includes the determination of the progress of engagement and of the magnitude of impact, in addition to the location of impact.

Four fields will be seen in Fig. 6, marked in counterclockwise order; S-contact, T-contact, U-contact, and V-contact. Three smaller rectangles flanked by these four fields refer to three types of line contacts as indicated on the diagram. The two remaining types of contact, S-T line-contact and U-V line-contact are determined by the border lines between the S-field and T-field, and the U-field and V-field, respectively.

The type of contact can easily be determined by tracing along horizontal and vertical straight lines. This is indicated by a dot and dash line marked "example."

The example refers to a case where, at a distance of 2 in., a cutter with a diameter of 12 in. is located on the workside, which is the usual condition with face mills, end mills, etc. The radial rake and the axial rake are assumed 10 deg negative. Following

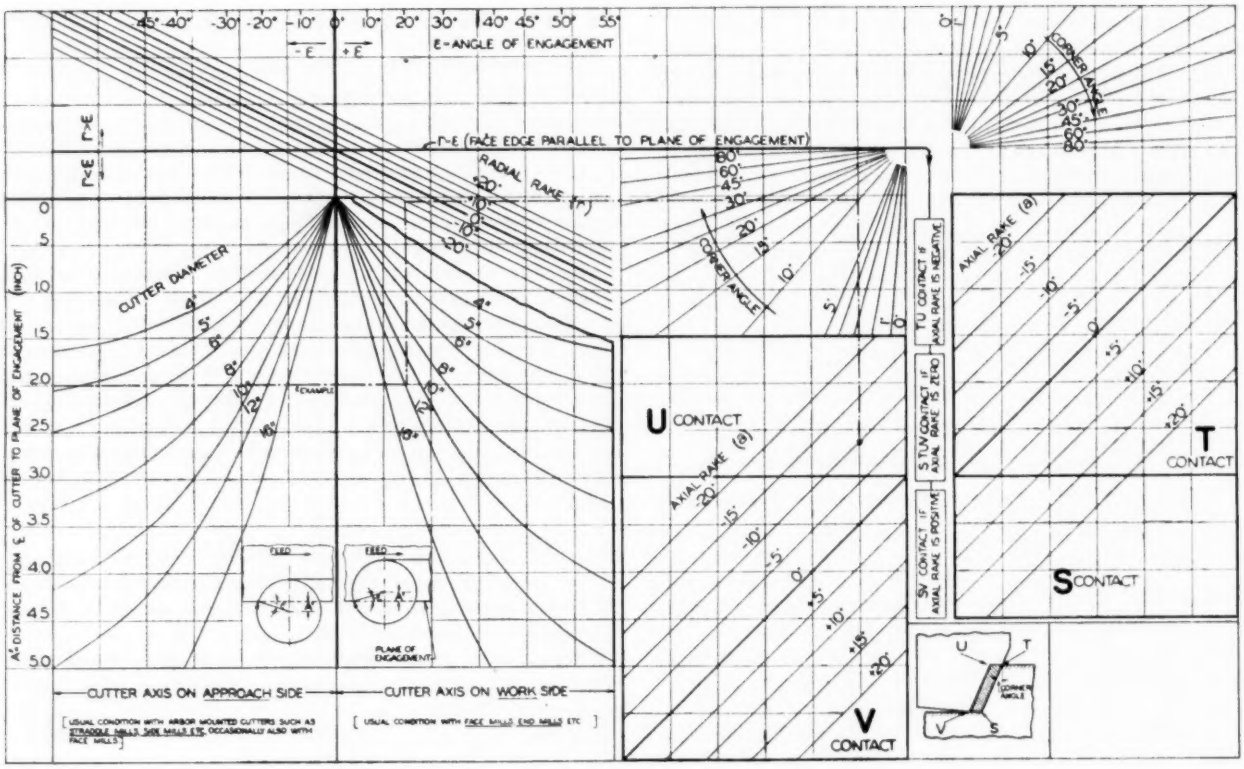


FIG. 6 CUTTER-ENGAGEMENT DIAGRAM

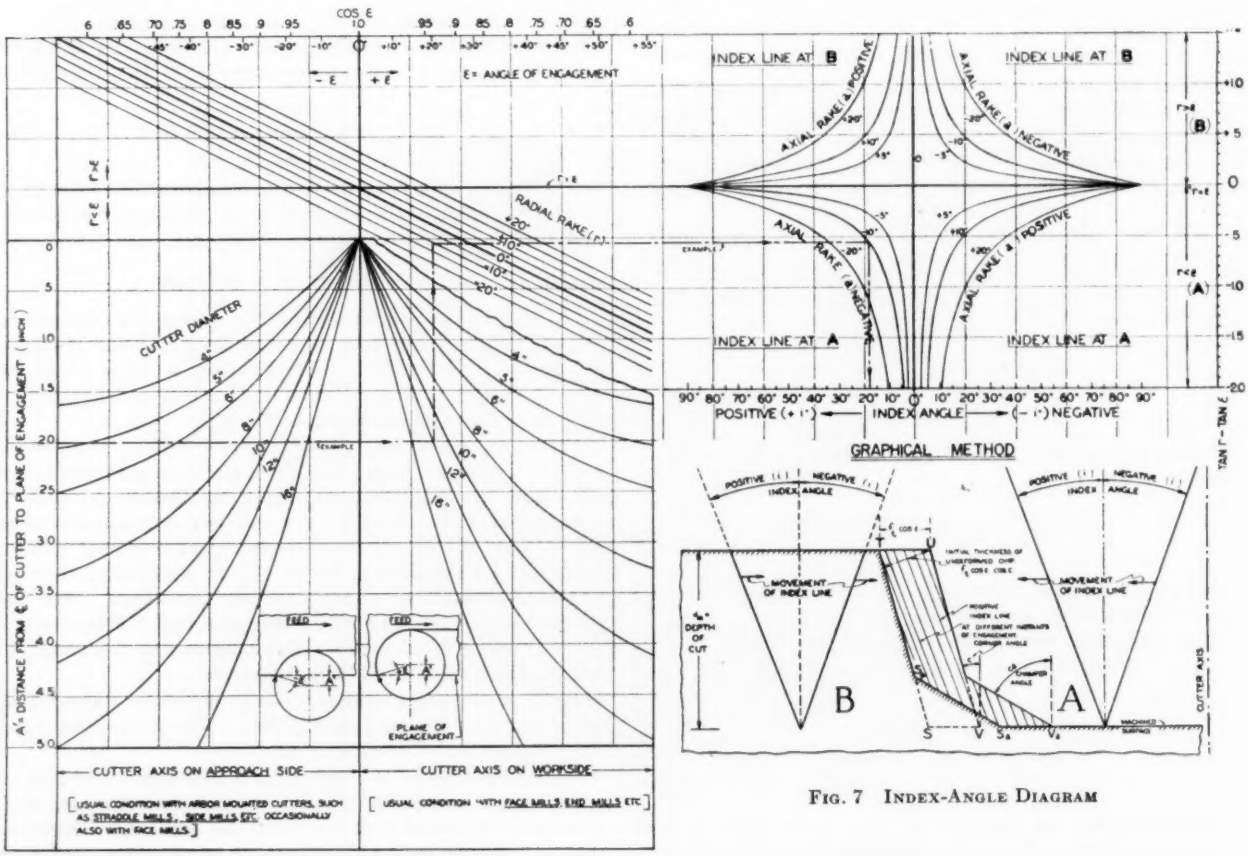


FIG. 7 INDEX-ANGLE DIAGRAM

the dot-and-dash line leads to the U-field. Hence U-contact will ensue from this combination of rake angles, corner angle, cutter distance A', and cutter diameter.

The angle of engagement can be read at the top of the cutter-engagement diagram ($\epsilon = 20$ deg); it is however, not necessary to read this angle when using the diagram.

Graphical Solution of Contact Problems for any Shape of Cutting Edge

Complex formulas for the contact conditions result if the cutting edge is chamfered or rounded. However, a graphical method which gives, also, a mental picture of the engagement of cutter and work has been developed for solving such cases on the drawing board. The graphical method covers a broad field in that it includes the progress of engagement and disengagement, and also the magnitude of impact in addition to solving problems of initial contact for any shape of the cutting edge. Exit conditions existing when the cutter leaves the work can likewise be solved with the graphical method.

It has already been stated, in connection with Fig. 3, that the spot on the tool which contacts the work first is indicated by the point where the intersection line first contacts the white parallelogram.

Thus in order to determine graphically the location of initial contact, it is only necessary to draw the chip cross-sectional area (white parallelogram) to scale and to move a line at angle i' toward it. Where this line touches the chip cross-sectional area first, initial contact occurs.

It is, however, more convenient to move a line at angle i (index line) instead of the intersection line at angle i', because the corner angle c can then be used when drawing the chip cross-sectional area instead of the slope angle c'.

Furthermore, referring to Equation [3], it will be seen that the index angle i is independent of the corner angle c and therefore independent of the contour of the cutting edge.

Hence initial contact can be determined graphically by moving a straight line at index angle i toward a chip cross-sectional area of any shape, not only a parallelogram.

The index angle i, which is the compound angle of axial rake, radial rake, and angle of engagement, can either be calculated from Equation [3] or be determined without use of mathematics by means of the "index-angle diagram," Fig. 7. The left-hand portion of this diagram is identical with the left-hand portion of the "cutter-engagement diagram," Fig. 6, while the right-hand part of Fig. 7 is different, having curves for the axial rake, instead of the contact fields. The example in Fig. 7 corresponds to that on the cutter-engagement diagram. Tracing along the dash-dotted example line, however, leads, in Fig. 7, to an index angle of +18 deg and to the instruction that the index line must be placed at A, meaning that it moves away from the cutter axis (because $r < \epsilon$). Compare arrow "A" in Fig. 4.

The graphical solution (see Fig. 8) includes the following:

1 Construct a figure proportional to the initial chip cross section, indicated by the cross-hatched area, where d_m is proportional to the depth of cut, distances TU, SV, S_aV_a proportional to the feed per tooth · cos ϵ and where c = corner angle, c_a = chamfer angle.

2 Draw index line at index angle i at A (or B) of cross-hatched area, as determined from diagram. [A is indicated if $r < \epsilon$, and B if $r > \epsilon$.]

3 Move index line toward cross-hatched area. (If $r = \epsilon$ the index line is moved vertically; upward when the axial rake is positive, or downward when the axial rake is negative. No index line exists for face contact, i.e., when $r = \epsilon$ and the axial rake is zero.)

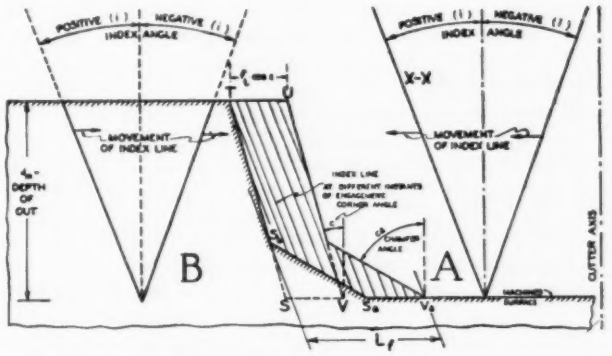


Fig. 8 Graphical Method for Determining Initial Contact of Cutter and Work, and Also the Progress of Their Engagement for Any Shape of the Cutting Edge

4 *Initial contact of cutter and work is indicated by the point or line where the moving index line touches the contour of the cross-hatched area first.*

In the given example when moving an index line x-x at +18 deg the initial contact occurs at point V_a.

5 Progress of engagement: The graphical method, however, permits not only determination of initial contact, but also the progress of engagement. Continuing the movement of the index line, x-x it, will be seen that

2nd point to engage is S_a
3rd point to engage is U
4th point to engage is T
5th point to engage is S_b

A closer inspection, by slowly moving the index line across the cross-hatched area, reveals even more details about the progress of engagement, for example, the fact that the engagement of point U follows very closely the engagement of point S_a. It will also be seen that a chip develops at first by deforming a triangle with the base V_aS_a, while later on a second chip develops from point U. Both chips unite at the instant when the vertex of the obtuse angle (i.e., the point opposite S_b) engages.

If the cutting edge is straight, the chip cross-sectional area is represented by parallelogram S-T-U-V in Fig. 8. Initial contact occurs in the case of $i = +18$ deg at point U instead of at V_a as was the case in the foregoing example for a chamfered cutting edge.

In the case of this example, chamfering of the cutting edge changes the initial contact from U to V_a. Chamfering, however, does not always have this effect. If the conditions for radial rake, axial rake, and angle of engagement are such as to give a negative angle i, initial contact of a tool having a straight cutting edge would occur at V, not at U, and the change due to chamfering would then be only a shifting of the initial contact from V to V_a.

Exit conditions when the cutter leaves the work can likewise be determined by the graphical method. Only one modification is necessary. Instead of using the distance of the cutter axis from the plane of engagement, the distance of the cutter axis from the exit plane must be used, when determining the index angle i in diagram Fig. 7. The terms "cutter axis on approach side" and "cutter axis on workside" are then to be used with reference to the exit plane.

2 MAGNITUDE OF IMPACT

The second problem, namely, the question, "How great is the impact?" is important because it may well be that the magnitude

of impact is a vital factor in cutter life. The magnitude of impact can be determined by further expanding the graphical method, used previously for determining the location and progress of engagement.

From the graphical method, Fig. 8, it will be realized that a chip does not exist at the instant of contact; that is, at the instant when the index line touches the contour of the cross-hatched area. However, as the index line travels across the cross-hatched area, the chip develops gradually, reaching its full size when the index line has moved all the way across the cross-hatched area. At that instant, all points of the tool face that take part in the metal removal have engaged the work.

For instance, in the example where $i = +18$ deg, no chip exists when the index line touches point V_a, but the full chip has been generated when the index line has arrived at point S_b of the cross-hatched area.

Conclusion: During the period of time in which the index line travels across the chip cross-sectional area, the chip has developed from zero to full size. This time interval is called "penetration time."

The shorter the penetration time, i.e., the faster the chip develops, the larger the impact.

The rate of increase of chip cross-sectional area can therefore be used as an "impact factor."

$$\text{Impact factor} = \frac{\text{Chip cross-sectional area}}{\text{Penetration time}} \quad \ldots\ldots [7]$$

In order to find the impact factor, it is necessary to determine only the penetration time and to divide it into the chip cross-sectional area. The impact factor has the dimension of square inch per sec.

Since "time" is the ratio of "distance traveled" to "velocity," it is possible to determine the penetration time T_p by dividing the distance L_f, which the index line has traveled across the cross-hatched area, by the velocity of this travel v_f.

As shown in Fig. 8, distance L_f can be measured directly from the graph between the contact position and end position of the index line when the graph is drawn to scale.

It remains to find the velocity of travel of the index line.

The velocity of travel v_f can be determined from the model shown in Fig. 9. In the horizontal triangle *N-P-M*, dimension *P-N* lies in the direction of cutter rotation and can therefore be taken as the "cutting speed vector." Dimension *M-N* lies in the direction of travel of the intersection line *L-M*, and represents therefore the "velocity vector" of the intersection line.

From the geometry of the horizontal triangle *N-P-M*

$$v'_f = \frac{\tan i'}{-\tan a} v_c \quad \ldots\ldots [8]$$

The same conversion as before is necessary in order to find the velocity of the index line instead of the intersection line. The result is

$$v_f = \frac{-v_c}{\tan r - \tan \epsilon} \quad \ldots\ldots [9]$$

It will be seen that the travel velocity v_f of the index line is a function of the cutting speed v_c, the radial rake, and the angle of engagement.

The minus sign in Equations [8] and [9] indicates the direction of travel, i.e., v_f is counted positive when the index line moves away from the cutter axis.

The penetration time in seconds is therefore

$$T_p = \frac{5L_f}{v_f} = \pm \frac{5\,L_f\,(\tan r - \tan \epsilon)}{v_c} \text{ sec} \quad \ldots\ldots [10]$$

where the factor 5 is due to conversion from feet per minute to inches per second.

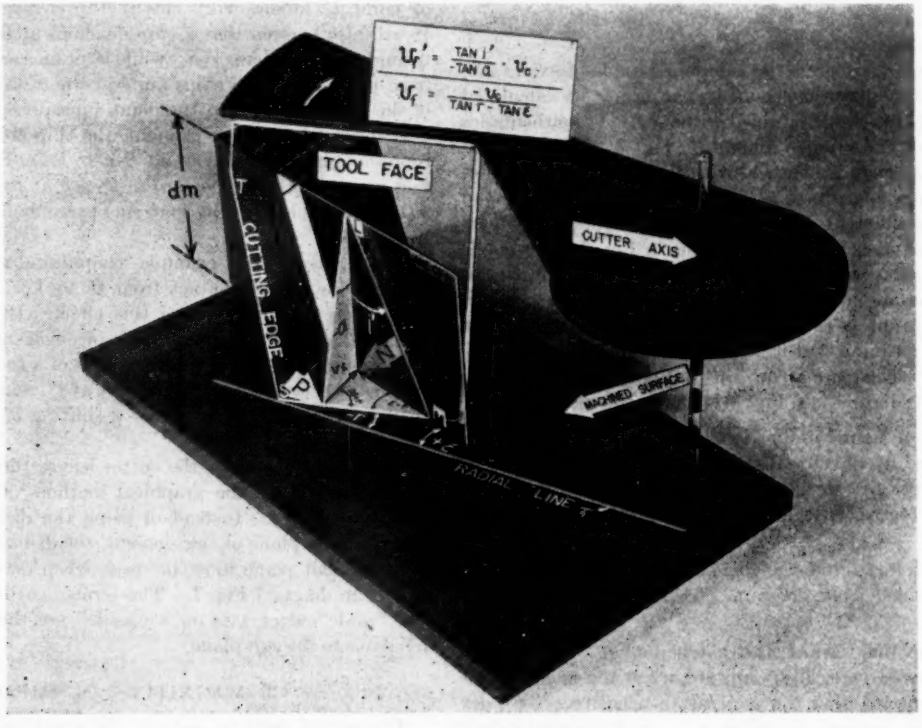


FIG. 9 MODEL OF CUTTER AND WORK ILLUSTRATING RELATIONSHIP BETWEEN CUTTING SPEED AND TRAVEL VELOCITY OF INTERSECTION LINE

When dimension L_f is very large, it is more convenient to use dimension L_d, Fig. 10, and the velocity (v_d) of the apparent travel in this direction.

Since this velocity, v_d is perpendicular to velocity v_f, their relationship is expressed by

$$v_d = \frac{v_f}{\tan i} = \frac{v_f\,(\tan r - \tan \epsilon)}{\tan a} \quad \ldots\ldots\ldots\ldots [11]$$

Upon substitution of Equation [9], the following formula results for the penetration time

$$T_p = \pm \frac{5L_d \cdot \tan a}{v_c} \quad \ldots [12]$$

When comparing the magnitude of impact for various tool-angle combinations, it is often *not* necessary to determine penetration time and impact factor from Equations [10], [12], and [7], but it is sufficient to compare only the dimensions L_f (or L_d),

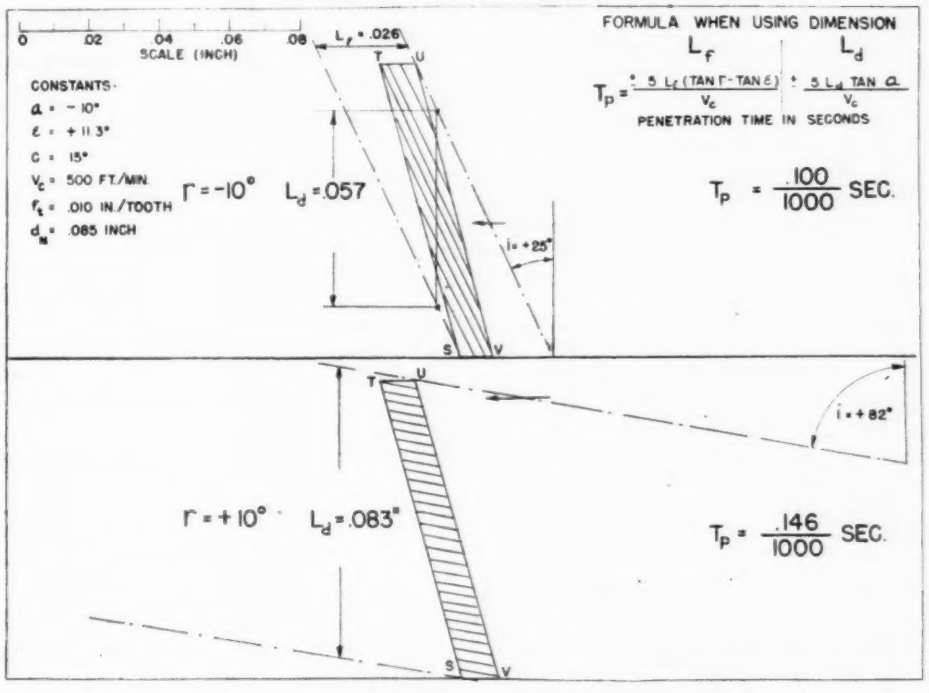


FIG. 10 DETERMINATION OF PENETRATION TIME AND MAGNITUDE OF IMPACT

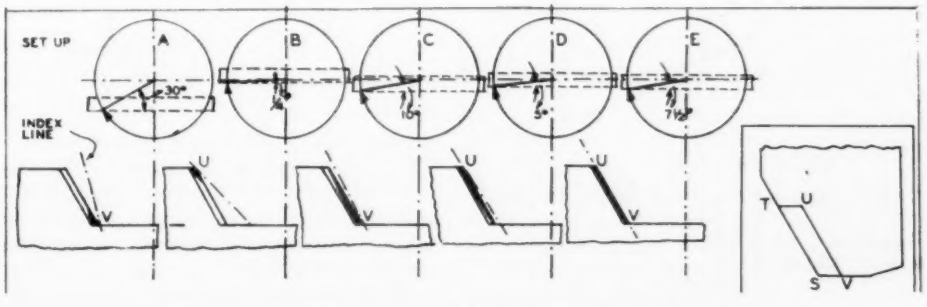


FIG. 11 SETUP OF CUTTER AND WORK USED IN TOOL-WEAR TESTS

Setup	Distance of cutter axis from plane of engagement, in.	Angle of engagement, deg	Location of impact	Magnitude of impact (impact factor) sq in. per sec
A	2.000	30	V	3.4
B	0.020	1/4	U	12.3
C	0.700	10	V	19.5
D	0.360	5	U	24.5
E	0.520	7 1/2	UV	44.5

Constants:

Axial and radial rake, deg	10 negative
Corner angle, deg	30
Feed per tooth, in.	0.009
Depth of cut, in.	1/8
Cutting speed, fpm	490

obtained graphically as the travel distance of the index line across the chip cross-sectional area from contact position to end position.

The following rules apply:

(*a*) The longer distance L_f, the less the impact, provided that the axial rake is the only variable involved in a comparison of impact.

(*b*) The longer distance L_d, the less the impact, provided that the radial rake or the angle of engagement is the variable involved in the comparison.

(*c*) The longer either distance L_f or L_d, the less the impact, provided that the corner angle c is the only variable involved in the comparison of impact.

The two examples shown in Fig. 10 indicate that the impact will be smaller in the lower case, because L_d is here longer than in the upper case. The L_d comparison is used because the radial rake is the variable in the examples. The ratio of impact is inversely proportional to the distance L_d, i.e., the impact is 46 per cent greater in the upper case than in the lower one.

3 HOW IS TOOL-WEAR AFFECTED BY IMPACT?

Tool-life tests have been carried out in order to determine the relationship between impact and tool wear.

A single-tooth cutter was employed for each run, changing the tooth after 13,300 impacts. Tests were also made with 20,000 impacts, and 26,600 impacts.

The location and magnitude of impact were varied by changing the distance of the cutter axis from the plane of engagement, that is, by changing the angle of engagement (ϵ). It was necessary only to adjust the knee of a horizontal milling machine up or down for each setup. Five different setups were tested as indicated in Fig. 11.

It will be noticed that the variation in the angle of engagement (ϵ) was small; this was done in order to keep the initial chip thickness and the exit conditions of the cutter as constant as possible.

The width of the workpiece was only $^3/_4$ in. in order to reduce tool wear due to cutting, in comparison with the wear due to impact.

The average depth of the crater on the tool face, measured after the same number of impacts, was taken as the basis for comparison of tool wear. The results are indicated in Figs. 12 to 16, inclusive.

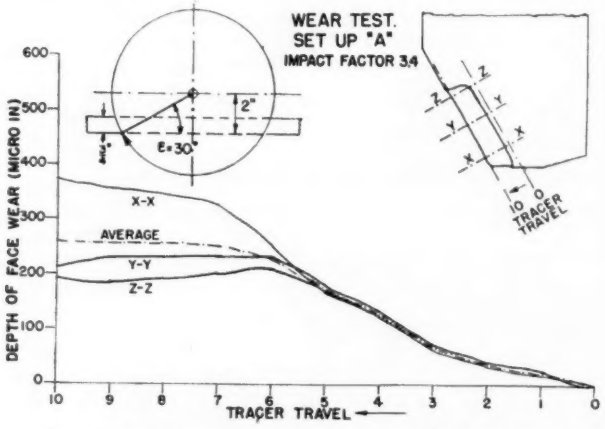


FIG. 12 WEAR TEST, SETUP A; SMALLEST IMPACT FACTOR

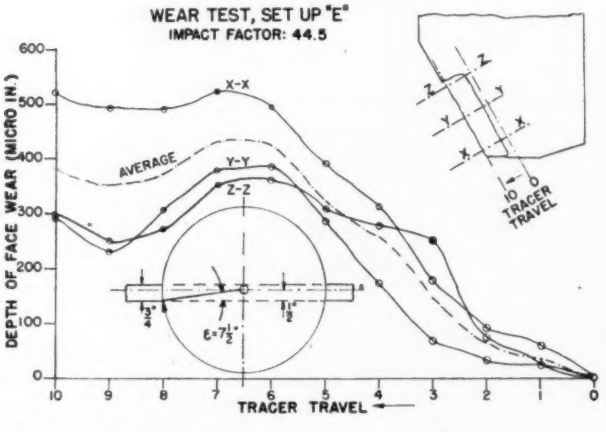


FIG. 13 WEAR TEST, SETUP E; LARGEST IMPACT FACTOR

Fig. 12 shows the results of the wear test for setup A where the distance from cutter axis to plane of engagement was 2 in., corresponding to an angle of engagement of 30 deg.

The wear was measured at ten points in each of the three planes marked *X-X*, *Y-Y*, and *Z-Z*, perpendicular to the cutting edge. The wear at each point was measured repeatedly.

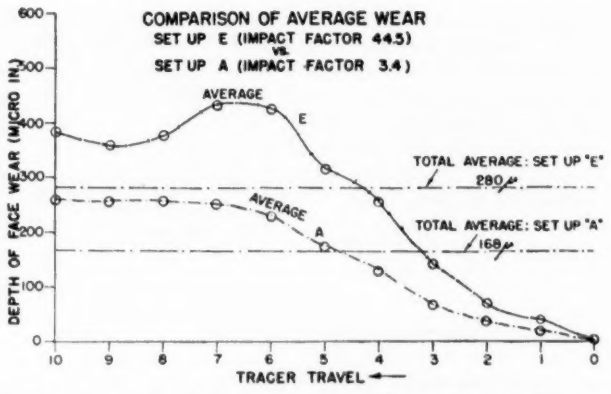


FIG. 14 COMPARISON OF AVERAGE WEAR; SETUP E VERSUS SETUP A

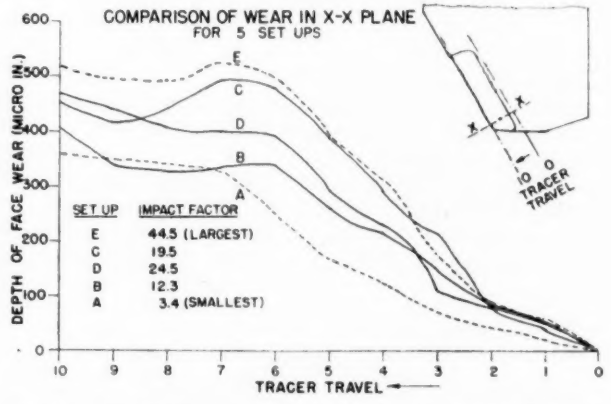


FIG. 15 COMPARISON OF WEAR IN *X-X* PLANE FOR FIVE SETUPS

It will be seen that the wear in the *X-X* plane was the greatest, with a maximum at tracer travel point 10 (that is, on the cutting edge). Tracer point 0 indicates the surface on the tool face not touched by the chip.

The dash-dotted line indicates the average of the wear in the three planes *X-X*, *Y-Y*, and *Z-Z*.

Setup A is the case where the impact factor is the smallest of the five setups tested.

Fig. 13 refers to the wear in the case of the largest impact factor (setup E), again measured in three planes perpendicular to the cutting edge. The distance of the cutter axis from the plane of engagement was $^1/_2$ in., the angle ϵ was $7^1/_2$ deg.

The averaged value of the three curves is again indicated by a curve marked "average."

Setup E and setup A are compared in Fig. 14, where the average curves of these two setups only are plotted. It will be seen that the wear in the case of the larger impact (setup E) was always greater than the wear of the smallest impact (setup A). Totaling the wear indicated by each one of the average curves results in a figure called "total average." This figure represents the over-all wear for each setup and is the result of about 200 values.

In the case of setup A, the total average was 168 microinches but as much as 280 microinches in the case of setup E. This appreciable difference of nearly 70 per cent is caused by the slight difference in the relative position of cutter axis to workpiece, and its resultant change in location and magnitude of impact.

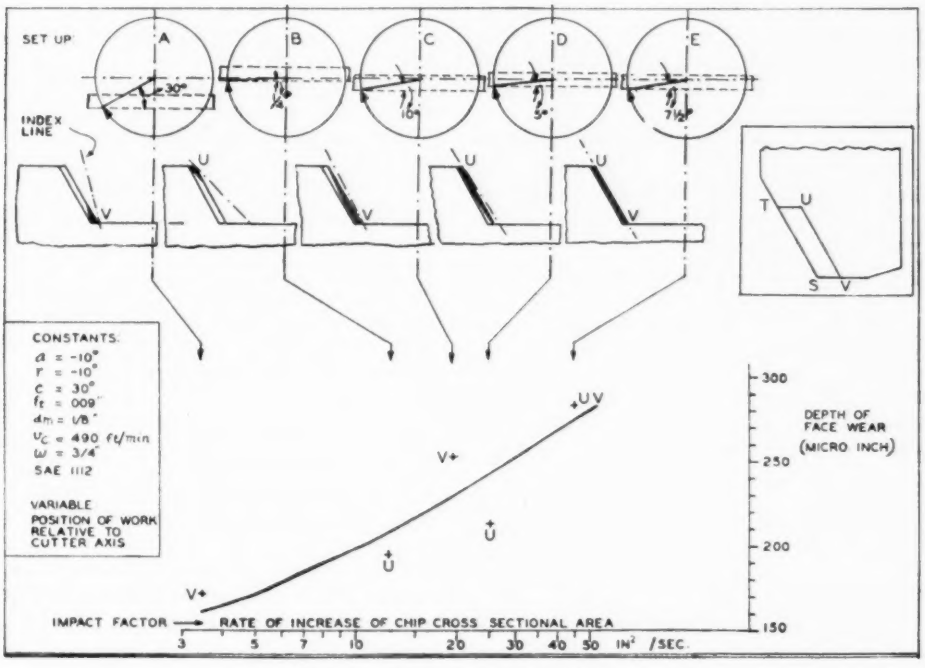


FIG. 16 SUMMARY OF WEAR TESTS

Diagram, Fig. 15, has been prepared in order to compare the wear for all five setups. Wear values in the X-X plane have been selected as an example, but the same trend holds also for the other planes.

It will be seen that the wear curves follow each other in approximately the same order as the impact factors.

Reading from the bottom up, the smallest wear (curve A) occurred in the case of the smallest impact; the second curve (curve B), referring to a larger impact factor, indicates also greater wear, and the greatest wear is found in the case of the largest impact factor.

Only curves C and D are reversed, because D has a smaller wear but a higher impact factor than curve C.

An explanation for this reversal is offered in Fig. 16 which is a summary of the wear tests. The impact factor is plotted logarithmically on the x-axis; the depth of the face wear on the y-axis, which is arithmetical.

Each of the five points is the result of approximately 200 values and represents the total average of the wear for the respective setup, indicated diagrammatically at the top. A definite trend is indicated by the curve, namely, the finding that tool-face wear increases with increasing impact factor, that is, with the rate of increase of chip cross-sectional area. It will furthermore be noticed that the points indicating the wear in case of U-contact are below the trend curve, while those for V-contact are above the curve.

It may well be the case that, within limits, a large impact applied at point U causes less wear than a small impact at point V. This may explain the reversal of the C and D curves in Fig. 15 where the D curve represents the case of a large impact applied at a favorable point of the tool (U-contact), while the C curve refers to a small impact applied at the less favorable point V. This would also indicate that equal impacts will cause less wear when applied at U than at V.

In so far as our tests indicate up to now, it is concluded that a small impact at point U is the most desirable condition, but a large impact at this same point (U) is worse than a small impact at V.

It appears that both the location and the magnitude of impact should be taken into consideration for determining favorable tool-life conditions. Their combined effect is a major factor in tool wear.

There are naturally other factors affecting tool wear; if these other factors cannot be kept constant when varying the location and magnitude of impact, they may change the trend indicated by the curve. The curve may run more horizontally or rise more rapidly. This will be the subject of further research.

CONCLUSIONS

With the aid of the graphical method, the following conclusions can readily be drawn from exploring contact conditions of various combinations of axial rake, radial rake, cutter diameter, distance of cutter from work, and for various shapes of the cutting edge:

1 For face mills and end mills, usually located on the work-side of the plane of engagement:

(*a*) The most frequent type is V-contact, that is, at a point on the face edge, remote from the sharp point of the tool by a distance approximately equal to the feed per tooth.

(*b*) U-contact can occur only when the axial rake is negative; the radial rake, however, may be either positive or negative, but must be smaller than the angle of engagement. This latter condition ($r < \epsilon$) is usually satisfied with face mills and end mills, except when the cutter axis is nearer to the plane of engagement than about 20 per cent of the cutter diameter.

(*c*) The larger the corner angle, the less likely is U-contact.

(*d*) Chamfering of a cutting edge renders it more difficult to obtain U-contact.

(*e*) Changing the corner angle c does not always affect initial contact. There is no effect if the axial rake is positive. There may be, however, an effect if the axial rake is negative. (If c is small, initial contact will be at U, if c is large, initial contact will be at V.)

2 For arbor-mounted cutters, such as straddle mills, side mills (and occasionally also for face mills, when only a portion of the width of the workpiece is machined):

(*a*) The most frequent type is *T*-contact, that is, contact at the top point of the cutting edge.

(*b*) The undesirable type of *S*-contact, at the weakest spot of the tool, can be eliminated by grinding a negative axial rake to the tooth.

(*c*) A negative radial rake alone does not necessarily eliminate the undesirable type of *S*-contact.

(*d*) Chamfering of a straight cutting edge having *T*-contact will not change this type of contact and is therefore ineffective as far as contact conditions are concerned.

(*e*) Chamfering of a straight cutting edge, however, having *S*-contact, will eliminate such contact by shifting the location of the contact point either to S_a (along the face edge) or to S_b (out of the plane of the machined surface), depending on the size of the chamfer angle.

(*f*) Changing the corner angle affects contact conditions of arbor-mounted cutters differently from those of face mills and end mills. In the case of arbor-mounted cutters, a change in the corner angle does not affect initial contact, when the axial rake is negative. However, if the axial rake is positive, it may be either *T*-contact or *S*-contact, depending on the relationship of index angle and corner angle.

3 *For all types of milling cutters: Tool angles on milling cutters such as face mills, end mills, straddle mills, side mills alone do not determine any type of initial contact. It is always necessary to consider also the angle of engagement.*

An existing cutter with given rake and corner angles may have different types of initial contact, depending on the position of the workpiece relative to the cutter axis, and on the cutter diameter. Tool life may therefore vary with the setup of cutter and work.

4 Exit conditions:

(*a*) The point of initial contact is not necessarily identical with the point that leaves the work first.

(*b*) The wider the workpiece, the less likely is the identity of the point of initial contact with the point that leaves the work first.

(*c*) Most frequently, the top point *T* of the cutting edge emerges first (*T*-exit).

(*d*) When the top point of the cutting edge contacts the work first (*T*-contact) it also leaves first (*T*-exit).

(*e*) In the case of a positive axial rake: *V*-contact may be followed by either *S*-exit or *T*-exit; *S*-contact may be followed by *T*-exit, depending on the width of the work and the combination of the other tool angles.

(*f*) In the case of a negative axial rake: *V*-contact may be followed by either *U*-exit or *T*-exit; *U*-contact may be followed by *T*-exit, depending on the width of the work and the combination of the other tool angles.

5 Tool wear:

(*a*) The combined effect of location and magnitude of impact is a major factor in the wear of sintered-carbide tools.

(*b*) A small impact at *U* seems to be the most desirable condition, but a large impact at this point is worse than a small impact at *V*.

(*c*) The most desirable condition can be obtained by careful co-ordination of axial rake, radial rake, corner angle, chamfer angle, and angle of engagement.

ACKNOWLEDGMENT

The author wishes to express his appreciation to Mr. Hans Ernst, research director, and to Dr. M. E. Merchant, physicist, for their helpful advice. The able assistance of Mr. Norman Zlatin, research engineer, and Mr. Robert Adams, who conducted the tool-wear tests, is also acknowledged. Mr. Emil Suhr, laboratory assistant, and Miss Jane Alexander assisted in the preparation of the models.

(Owing to travel emergency conditions existing when this paper was presented, discussion will be accepted until May 10, 1946)

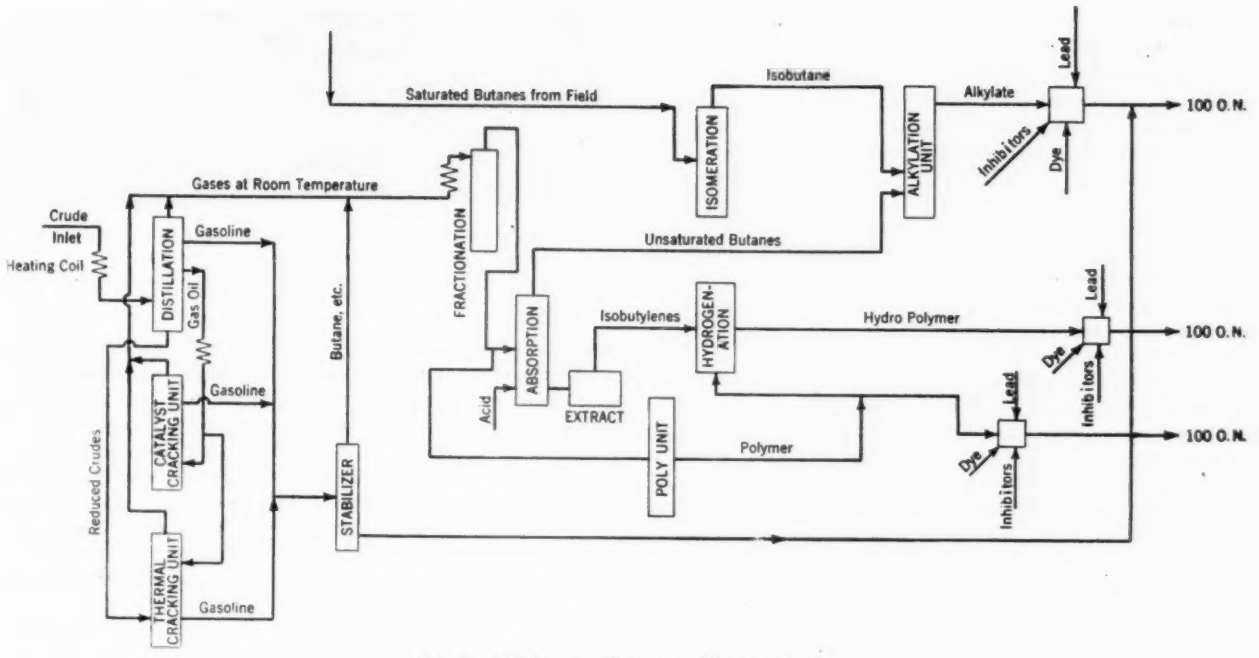


FIG. 1 100-OCTANE GASOLINE MANUFACTURE

Resistance of Nickel-Containing Alloys to Corrosives Encountered in the Petroleum Refineries

BY B. B. MORTON,[1] NEW YORK, N. Y.

Production of bulk gasoline in a modern petroleum refinery is accompanied by corrosion during topping and cracking from sulphur and from weak hydrochloric acid which is formed from salts in the crude. Organic acids such as naphthenics are also often present and are quite corrosive. Solutions of refinery corrosion problems are considered in this paper.

THE modern petroleum refinery under the stress of producing war essentials, such as high-octane gasoline, rubber, etc., has become a most complex organization.

Fig. 1, which is a rather simplified flow sheet of the processes employed in making 100-octane gasoline, hints at the complexities involved. A view of the towers, tanks, lines, and equipment involved would be more impressive but possibly less instructive.

As a homely comparison a refinery may be likened to a kitchen in which many cooks are turning out a large volume of good soup (standard gasoline). Other cooks, specialists, are busy making a sauce to be added in small parts to the soup to make it superlatively good. This sauce is the additives, made by polymerization, alkylation, hydrogenation, etc. These additives bring up the octane number of the bulk gasoline produced. The final step is the addition of lead compound, the supersauce.

The production of the bulk gasoline is accompanied by corrosion, during topping and cracking, from sulphur and from weak hydrochloric acid which is formed from salts in the crude. Organic acids, as naphthenics, also are often present and are quite corrosive. These acids are apparently becoming more of a corrosive factor during distillation as a result of the crudes used at the present time.

The corrosion problems associated with the formation of the additives are much more pronounced and are more varied than those associated with topping and cracking. This can be understood by considering some of the reagents involved in the manufacture of the additives:

Acids: Hydrochloric, sulphuric, hydrofluoric, phosphoric, etc.
Bases: Sodium hydroxide, potassium hydroxide, ammonia, etc.
Salts: Aluminum chloride, boron chloride, etc.

CORROSION IN REFINERIES

The author has found it convenient to consider refinery corrosion as possessing two different identities, the dividing line being

[1] Development Engineer, Development and Research Division, The International Nickel Company, Inc. Mem. A.S.M.E.

Contributed by the Petroleum Committee of the Process Industries Division and presented at the Annual Meeting, New York, N. Y., Nov. 26–29, 1945, of THE AMERICAN SOCIETY OF MECHANICAL ENGINEERS.

NOTE: Statements and opinions advanced in papers are to be understood as individual expressions of their authors and not those of the Society.

the temperature level at which water is no longer present; an arbitrary figure of 500 F has been taken. Above this temperature "dry" corrosion is considered to take place due to the action of sulphur and also some organic acids; below this temperature "wet" or electrolytic corrosion is assumed to take place.

The nature of electrolytic corrosion has been described in detail in the literature. It is pointed out that a metal tends to go into solution at an anode while hydrogen or another metal plates out at the cathode. It is generally recognized that the areas of the electrodes, the presence of depolarizing agents, and also the relation of the electrodes in a galvanic series, all affect the rates of corrosion. The gradual changes in composition of the film at the face of the electrodes can greatly affect the rate, direction, and nature of the corrosion.

It has been widely pointed out, though not well heeded, that the current passing is the important factor in corrosion by electrolysis rather than the potential between electrodes.

The electrolytic conception of corrosion has provided a working insight into much corrosion. It has also furnished an ingenious but often erroneous explanation of some corrosion. It has awakened a dread of the presence of dissimilar metals, sometimes unwarranted.

A galvanic series of some metals in salt water is provided in Table 1 (1).[2] This series will prove of interest in combating refinery corrosion[3] in condensers, run-down lines, separators, etc. It has been found that galvanic corrosion is greatly suppressed in the absence of oxygen, and this should be considered in evaluating galvanic corrosion in refineries. As light on this subject, Fig. 2 is provided. It will be noted that the nickel plate on the steel sucker rod has failed to produce as serious undercutting as might be expected from the coupling of these two metals. The rod was exposed to the corrosive brine of an Arkansas well. The metal removed is the result of contact with the tubing. The absence of oxygen is assumed to account for the absence of marked galvanic corrosion.

TABLE 1 GALVANIC SERIES OF METALS AND ALLOYS

Corroded End (anodic, or least noble)
Magnesium
Magnesium alloys
Zinc
Galvanized steel or galvanized wrought iron
Aluminum 52SH
Aluminum 4S
Aluminum 3S
Aluminum 2S
Aluminum 53S-T
Alclad
Cadmium
Aluminum A17S-T
Aluminum 17S-T
Aluminum 24S-T
Mild steel
Wrought iron
Cast iron
Ni-Resist[a]
13% chromium stainless steel type 410 (active)
50-50 lead-tin solder
18-8 stainless steel type 304 (active)
18-8-3 stainless steel type 316 (active)
Lead
Tin
Muntz metal
Manganese bronze
Naval brass
Nickel (active)
Inconel (active)
Yellow brass
Admiralty brass
Aluminum bronze
Red brass
Copper
Silicon bronze
Ambrac
70-30 copper nickel
Comp. G-bronze
Comp. M-bronze
Nickel (passive)
Inconel (passive)
Monel
18-8 stainless steel type 304 (passive)
18-8-3 stainless steel type 316 (passive)
Protected End (cathodic, or most noble)

[a] Reg. U. S. Pat. Off.

[2] Numbers in parentheses refer to the Bibliography at the end of the paper.



FIG. 2 STUDY OF NICKEL-PLATED STEEL SUCKER ROD FROM CORROSIVE WELL; OXYGEN ABSENT; ×8
(Note absence of undercutting where plate has worn through in contact with the tubing.)

That highly vigorous attack can be produced under conditions favorable to galvanic attack is shown in Table 2. The data of this table were derived by coupling metals with a carbon-containing material which is used to line vessels against acid attack or to form packing or equipment in vessels. The necessity of insulating to prevent forming a couple of metal with this carbon-containing material can be readily seen. The difficulties of insulating effectively will be great in many cases.

TABLE 2 PRELIMINARY STUDY OF A CARBONACEOUS ELECTRODE COUPLED WITH SOME ALLOYS

Areas	Carbonaceous electrode	1.07 dm²
	Coupled metals	0.25 dm²
Electrolyte		65 per cent sulphuric acid
Temperature		193 C (379 F)
Aeration		None

Couple	Time, hr	Corrosion rates of alloys — M.d.d.	In. per year
Carbon and Hastelloy B[a]	4	59626	9.0+
Carbon and Hastelloy D[a]	16	1266	0.23
Carbon and Monel[b]	4	40413	6.5+

[a] Normally quite resistant to these conditions.
[b] Normally fairly resistant to these conditions.

It must not be assumed that galvanic corrosion is an unmitigated evil. This form of corrosion can be usefully employed and is widely used though often without recognition of the fact. Galvanizing is a nice example of the use of galvanic effects. The iron is protected by the sacrifice of zinc. In general, to use galvanic protection a metal "less noble" than the one to be protected must be coupled with the metal whose life it is desired to prolong. No parsimoniousness can be tolerated in the use of the less noble metal. It must be considered definitely expendable and must be present in suitable mass and area to invite and to sustain attack over the desired period.

The destruction of the less noble metal need not be complete. Some Monel (2/3 nickel, 1/3 copper) bolts from a condenser, Fig. 3, provide a good example of protection without destruction of the less noble metal. The cast iron in contact with the bolts built up a graphitic layer which protected itself while offering protection to the Monel. The vast area of the cast-iron pipes also tended to offset the attack directed to the pipe by the bolts. The use of greater area of the less noble metal is a common means of

[3] It must be recognized that in a different medium the placement of the metals might differ slightly.

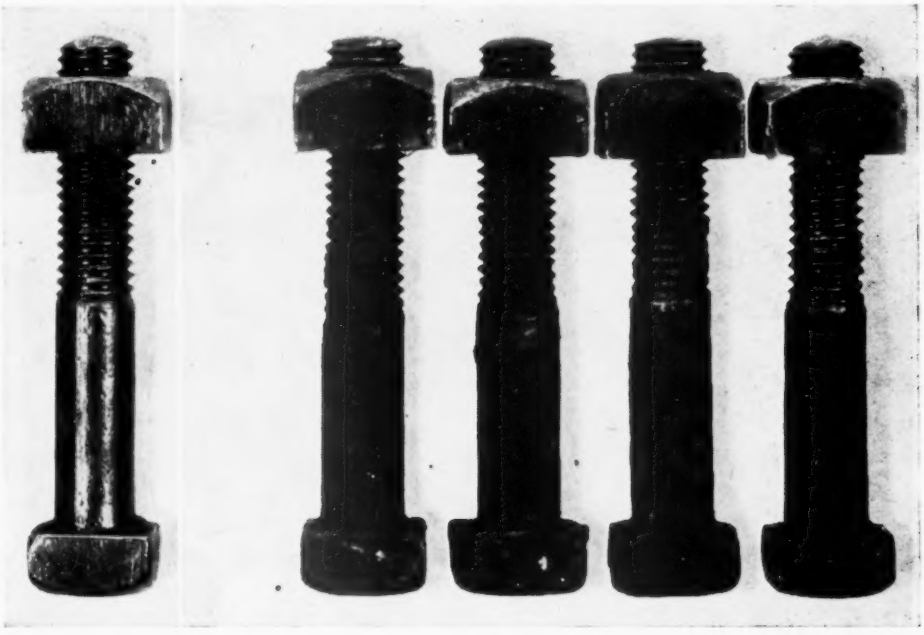


FIG. 3 MONEL BOLTS EXPOSED 22 YEARS IN A CONDENSER BOX TO CONTAMINATED SALT WATER OF THE KILL VAN KULL

utilizing galvanic corrosion to protect a part, as a weld or a rivet head, without unduly injuring the less noble material.

GENERAL SOLUTION TO REFINERY CORROSION

A general solution to the two distinct types of corrosion occurring in a petroleum refinery appears as follows:

(*a*) *Elevated Temperature* (*Above 500 F*). Chromium is the metallic element most useful to resist the action of sulphur. The necessary concentration of chromium in the metal appears to depend upon the temperatures used and the concentration of the sulphur compounds; also the nature of these compounds. Metals showing resistance to sulphur which are in wide use are listed in descending order as follows: 18 per cent chromium, 8 per cent nickel; 11 to 14 per cent chrome steels; 4 to 6 per cent chrome steels.

The variety of mechanical properties of these alloys as well as their corrosion resistance dictate the particular choice.

Where naphthenic acids are a source of corrosion at temperatures above 500 F, the following alloys are employed:

Inconel[4] (approximately 80 per cent Ni, 13 per cent Cr)
Type 316 (approximately 18 per cent Cr, 14 per cent Ni, 2–3 per cent Moly)

In some investigations reported, (2) it has been pointed out that 18-8 is more vigorously attacked by naphthenic acid under conditions of elevated temperature than is carbon steel. Both metals were vigorously attacked. Alloy 18-14-3, however, appears quite resistant. Inconel appears to be highly resistant, possibly since nickel itself is, and the 13 per cent chromium present gives protection against sulphur attack which might take place on nickel above 500 F.

Type 316 stainless steel 18-14-3 is finding increasingly wider uses in refineries as they turn toward the manufacture of chemicals from petroleum products. Its resistance to many organic acids is outstanding. It is considered less subject to "weld decay" than is regular 18-8.

The practical application of material to resist corrosion at elevated temperature consists in using tubing of 4–6 per cent chrome or of 18 per cent chromium, 8 per cent nickel alloy, lining equipment with 18-8 or 11 to 15 per cent chromium stainless. Where strip or other welding is used, 18-8, or better, 25 per cent chrome, 20 per cent nickel rod is used.

In some equipment as in certain bubble towers, a wide temperature gradient exists along the axis, say, from 700 to 370 F. In this case a stainless steel is indicated for the temperature region above 500 F, and Monel for the cooler top region Fig. 4. Some very large towers have 18-8 lining, trays, and caps in the high-temperature region and Monel lining, caps, and trays in the top.

Some exchangers exposed to attack from naphthenic acid at temperatures of 700 to 850 F are tubed and equipped with Inconel (approximately 80 per cent nickel 13 per cent chrome).

(*b*) *Low-Temperature Corrosion* (*Below 500 F*). Corrosion occurring within the temperature region below 500 F is considered to be electrolytic in character. It is assumed that liquid water is present to form an electrolyte. The solution to the corrosion of this type is more difficult than in the case of corrosion at elevated temperature, owing to the complex nature of the attacking agents. No single element is effective against corrosion at low temperature as is chromium at elevated temperature against sulphur.

The most satisfactory means for studying corrosion of any type appears to be to install specimens of metals under operating conditions and to observe results. This is particularly true for electrolytic corrosion. Insulating between samples is necessary for this temperature region where water can exist, and this complicates testing. The test spool, Fig. 5 (3), has been developed and improved over a period of years by the author's company. Thousands of specimens have been exposed in various industries, and an impressive mass of data have been accumulated.

From a study of the data it appears that no general rule can be applied to the selection of a material for use in a refinery in order to combat electrolytic corrosion. The selection is best done by studying the exposed samples. Such a study is helpful in picking the most economical material, as the samples will indicate the relative life and the tendency toward pitting. Often the short life of refinery equipment, due to becoming obsolete, dic-

[4] Registered trade-mark name; The International Nickel Company, Inc.

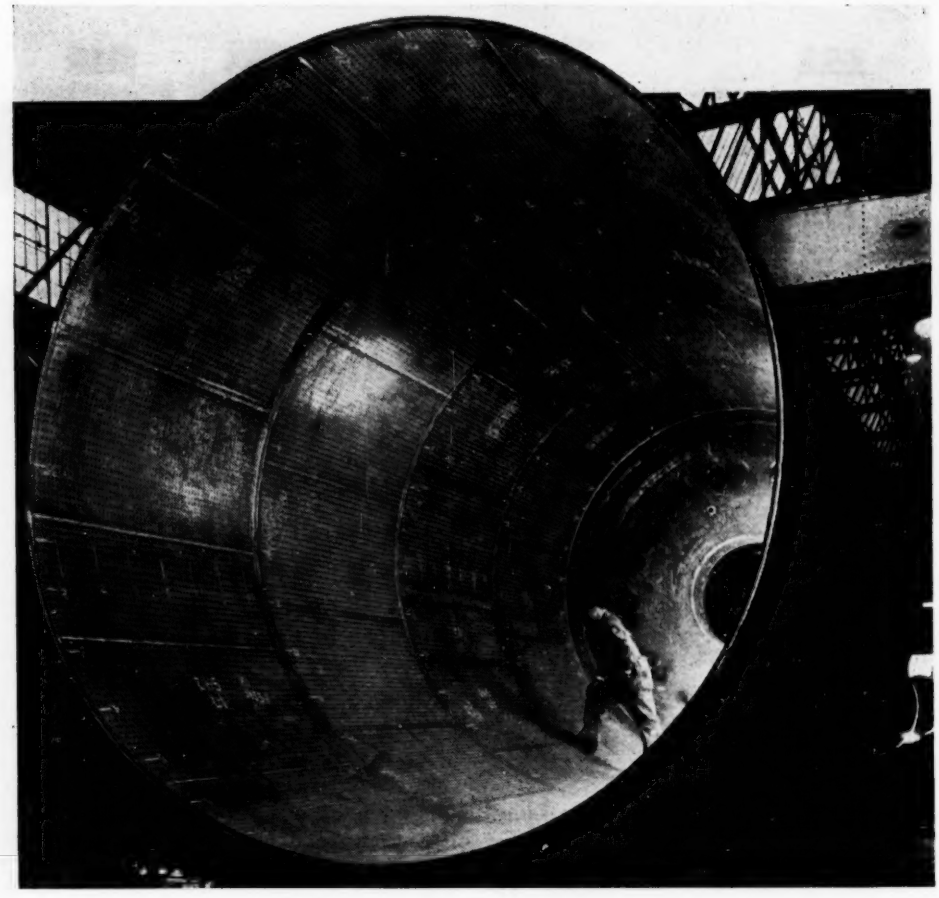


FIG. 4 SECTION OF LARGE FRACTIONATING TOWER THE TOP PART OF WHICH IS "SMITHLINED" WITH MONEL SHEET TO WITHSTAND CORROSION BY DILUTE HCL. THE BOTTOM LINING IS OF 18-8 TO RESIST SULPHUR

(Monel tower linings are confined to top sections where temperatures do not exceed 500 F.)

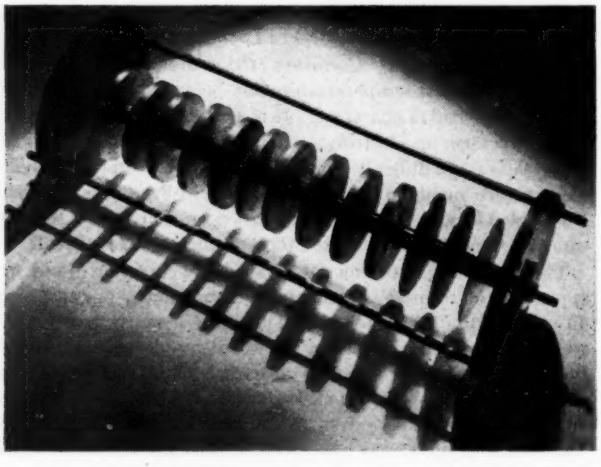


FIG. 5 SPOOL-TYPE SPECIMEN HOLDER USED IN TESTING CORROSION OF METALS

tates a less expensive material than would be selected if indefinite life is desired.

The use of nonferrous alloys to combat electrolytic corrosion is widespread, as will be evident in the consideration of material used in parts of refinery equipment exposed to corrosives.

CONDENSING EQUIPMENT

Condensing equipment suffers much from electrolytic corrosion. As the tendency is increased to improve the efficiency of this equipment the need for better and more corrosion-resistant materials is felt, that is, as the submerged coil of cast-iron pipe is abandoned for shell-and-tube or submerged-tube segments, the need for better material is noted.

Condenser shells are formed either of Monel-clad steel or are protected locally by liners of this alloy, Fig. 6. Where Admiralty tubing is suffering dezincification, the trend before the war was to use 70-30 copper-nickel tubes. Other nickel-containing tubing to thwart dezincification is hinted at as postwar materials.

The 70-30 copper-nickel tube offers greater resistance to impingement attack than does Admiralty tubing.

ISOMERIZATION EQUIPMENT

The introduction of HCL gas as an atmosphere in an isomerization operation has greatly intensified refinery corrosion problems.

Hastelloy B, an alloy of approximately 60 per cent nickel, 32 per cent molybdenum, is apparently one of the most resistant of commercial alloys to the corrosive conditions evoked by the use of the HCL atmosphere in the isomerization operation. Some data, Table 3, obtained by exposure of samples in an operating unit serve to place Hastelloy B in comparison with some other materials. The position of nickel is also indicated. It has been

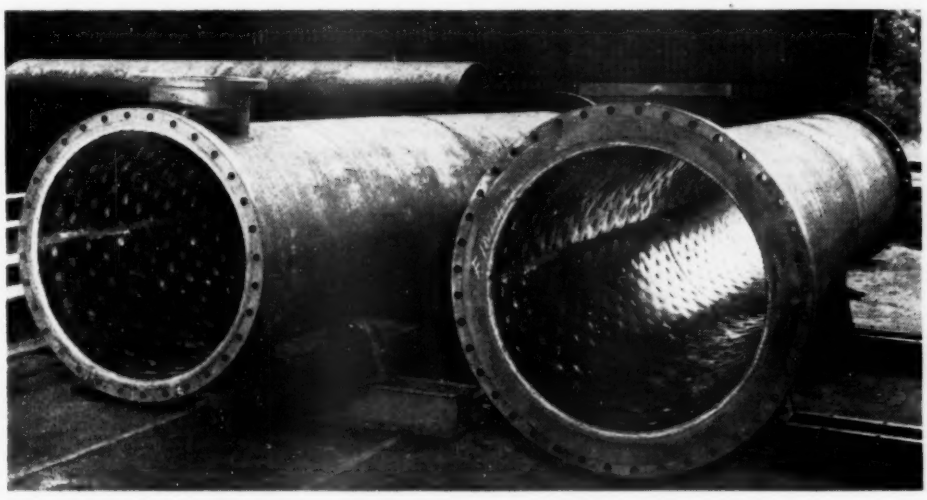


FIG. 6 MONEL-CLAD HEAT-EXCHANGER SHELLS

noted in service that nickel is somewhat erratic in its resistance. The cause is not known for the variation noted.

The study of materials for use in isomerization units is proceeding apace. The widespread use of nickel would indicate that certain refinery units understand and can control its rate of corrosion. The success may depend on the efficiency of the dehydrating equipment. High efficiency of these drying units will permit use of the cheaper materials of construction.

ALKYLATION UNITS

Alkylation is carried out with the use of hydrofluoric and sulphuric acids as catalysts.

Monel has emerged as possibly the most useful of the commercial materials for parts of units using HF acid for the catalyst. It is now used as liners for vessels; as rings and packing; as valves and fittings, etc. There may be a tendency to use Monel lining with carbon packing. The corrosion engineer so inclined to this use is referred to Table 2 and is warned.

"S"-Monel, a high-silicon alloy (4 per cent Si) (see Table 5) has such excellent resistance to seizing and galling that its use as the plug and other parts of valves was considered for use in HF alkylation units. The vigorousness with which hydrofluoric acid attacks silica caused some concern that the silicon of S-Monel might be attacked. Laboratory results indicate that S-Monel is not attacked with especial vigor by HF, and use is made of this alloy as a plug material.

A welding rod to permit an overlay of S-Monel has been developed by the author's company. Since the rod must of necessity have a silicon content greater than that of S-Monel to compensate losses during the overlaying, the rod was tested in HF acid with results noted in Table 4. The rate of attack on the rod material itself is tolerable, and since the overlay will have the composition of S-Monel, which is apparently adequately resistant, the rod will probably fill a need for a corrosion- and a galling-resistant surface for valve parts.

Sulphuric acid presents many corrosion problems in refineries, especially when it is used as the catalyst in an alkylation unit or as a solvent. This is due to variations in concentrations and temperature. Table 5 lists some materials used in handling sulphuric acid in petroleum refineries.

When the problem involves concentrating acid, Hastelloy D has proved useful and it is used for the elements to introduce heat into the acid.

Pump and valve parts are made from the alloys listed in Table 5, and from similar alloys.

The behavior of sulphuric acid is so influenced by the presence or absence of oxidizing reagents, by the presence of chlorine or other halogens, also by the presence of salts that can form hydrochloric acid, that general recommendations rarely can be made.

TABLE 3 STUDY OF ALLOYS IN ISOMERIZATION UNITS

Corrosive.....Hydrochloric gas and acid
Process.....Isomerization of Butane
Duration.....1050 Hr
Temperature.....240 F avg

	Spool No. 1 (tar)		Spool No. 2 (vapor)	
	Corrosion rate, in. per year (avg)	Pitting during test, in. surface (max)	Corrosion rate, in. per year (avg)	Pitting during test, in. surface (max)
Monel	0.026	.....	0.024	0.004
Nickel	0.009	.....	0.012	0.010
Inconel	0.010	.....	0.012	0.002
18-8 Stainless	....	0.002[a]	.....	0.008
Type 304	0.094	0.002[b]	0.050	0.010
18-8 Mo Stainless	....	.....	.....	0.006
Type 316	0.111	.....	0.048	0.004
Hastelloy B	0.000	.....	0.000	.....
Silver	0.047	Perforated	0.065+	Entirely corroded away
Copper	0.13+	Entirely corroded away	0.043	0.003
85-5-5-5 Bronze	0.145	.....	0.058	.....
Ni-Resist	0.052	.....	0.051	.....
Mild steel	0.162	0.005[c]	0.081	0.002
Cast iron	0.085	.....	0.082	.....

[a] 1/2 of specimen corroded away.
[b] 1/3 of specimen corroded away.
[c] 1/4 of specimen corroded away.

TABLE 4 MONEL VERSUS HYDROFLUORIC; COMPARISON OF SILICON-CONTAINING "H" AND "S" MONEL WITH REGULAR MONEL[a]

Duration of tests, air-free..... 6 Days
Duration of tests, air-saturated..... 1 Day (24 hr)
Velocity.....42 to 73 fpm

	Average corrosion rate, in. penetration per year			
	At 86 F		At 176 F	
	Air-free	Air-saturated	Air-free	Air-saturated
	Hydrofluoric acid 25 per cent (by weight)			
Monel sheet	0.0002	0.037	0.0024	0.011
Cast Monel	0.0006	0.019	0.0013	0.020
H-Monel	0.0004	0.019	0.0004	0.022
S-Monel	0.0002	0.009	0.0002	0.021
	Hydrofluoric acid 50 per cent (by weight)			
Monel sheet	0.0001	0.008	0.0006	0.039
Cast Monel	0.0005	0.006	0.0022	0.037
H-Monel	0.0002	0.007	0.0009	0.044
S-Monel	0.0004	0.003	0.0020	0.046
S-Monel welding rod, 6.6 per cent silicon				0.018
S-Monel welding rod, 5.2 per cent silicon				0.013

Note accelerating effect of oxygen. In refinery service this factor rarely appears.

[a] Laboratory tests in 25 per cent and 50 per cent hydrofluoric acid at 86 F, and 176 F. Specimens were suspended in liquid hydrofluoric-acid solutions in a closed nickel autoclave equipped with nickel reflux condenser. Tests in air-free solutions made by bubbling nitrogen continuously through the acid, and air-saturated tests made by bubbling air continuously through.

TABLE 5 REPRESENTATIVE LIST AND APPROXIMATE COMPOSITIONS OF SOME NICKEL-CONTAINING ALLOYS USED IN CONNECTION WITH SULPHURIC ACID

Material	Nickel, per cent	Copper, per cent	Iron, per cent	Chromium, per cent	Molybdenum, per cent	Aluminum, per cent	Silicon, per cent	Manganese, per cent	Tungsten, per cent	Carbon per cent
Nickel	99.4[a]	0.1	0.15	...	..	..	0.05	0.2	...	0.1
Monel	67.	30.	1.4	...	..	..	0.1	1.	...	0.15
H-Monel[b]	65.	29.5	1.5	...	..	..	3.	0.9	...	0.1
S-Monel[b]	63.	30.	2.	...	..	..	4.	0.9	...	0.1
K-Monel	66.	29.	0.9	...	..	2.75	0.25	0.4	...	0.15
Inconel	79.5	0.2	6.5	13.	..	..	0.25	0.25	...	0.08
Hastelloy A	53.	..	22.	...	22.	..	1.	2.	...	..
Hastelloy B	60.	..	6.	...	32.	..	1.	1.	...	..
Hastelloy C[b]	51.	..	6.	17.	19.	..	1.	1.	5.	..
Hastelloy D[b]	85.	3.	...	...	..	1.	10.	1.	...	..
Illium G[b]	60.	4.	6.	21.	6.	..	1.	1.	1.	..
Illium R	60.	3.	8.	21.	5.	..	1.	1.	1.	..
LaBour[b]	53.	5.0	8.0	23.	4.0	..	4.0	0.5	2.0	..
Duramet T	22.	1.0	Bal.	19.	3.5	..	...	...	...	0.07
Worthite	24.	1.7	Bal.	20.	3.0	..	3.3	0.6	...	0.07

[a] Including cobalt.
[b] Only as castings.
NOTE: Specific use can be determined by making tests or by seeking suggestions from suppliers.

The action of the presence of copper from copper-alloy fittings in the destruction of otherwise resistant alloys has been reported (2).

The most resistant metallic materials to a wide variety of concentrations of sulphuric acid and to temperature variations and impurities in the acids to come to the author's attention are the high-silicon cast irons, such as "Duriron" and "Corrosiron." The brittleness of these materials somewhat limits their usefulness but when considered in design they are used for many pieces of equipment.

Caustic Regenerators

Caustic is used both to neutralize acid and as a solvent for organic compounds. As an example of the latter consider mercaptan scrubbing and recovery.

Monel appears to be one of the most useful materials with which to line caustic regenerators, and for caps and trays. The tubes of the reboiler are often of Monel which appears quite satisfactory. The service of the tubes is severe since boiling and high attending velocity often injure protective films. An alloy of 70-30 copper nickel appears unsatisfactory for this service of tubes in reboilers in units recovering mercaptans from caustic. The vigorous attack of sulphur upon the copper-rich alloy and subsequent injury of film may account for the failures of 70-30 so far reported.

Before undertaking to line an existing tower that has been in a caustic regenerating unit with Monel, it is well to consider that sulphur on the steel wall may cause embrittlement of plug or other welds. The sulphur and adhering caustic must be entirely removed. Discussion of the proposed lining with the Technical Service group of the author's company might be advisable since observations to date could be presented.

Ni-Resist cast iron, a nickel or nickel-copper cast iron which is austenitic in structure, i.e., nonmagnetic, is useful for pumps and valve parts of equipment handling caustic.

Nickel-clad steel appears to be the favorite material of construction in units employing caustic and an organic compound to act as a solvent for mercaptans.

Solvents

Many solvents find application in petroleum refineries. In fact the use of selective solvents has revolutionized the art of refining.

Many of the solvents are corrosive toward steel. Others not originally corrosive become so after use and contamination.

For such solvents as phenol, furfural, and chlorinated compounds, Monel or 18-8 stainless will be found quite satisfactory. The 18-8 is the proper material to use at temperatures above 500 F. Monel is considered more satisfactory for use with chlorinated solvents at the temperature at which these solvents are used.

Solvents are often used at subzero temperatures of —50 F, —75 F, and —150 F. At these low temperatures corrosion ceases to be a problem but the impact value of many nonheat-treated steels suffers deterioration. Normalized nickel-containing steels retain a large part of the room-temperature impact value at low temperatures when properly made for this service. Nickel steels of $2^1/_2$ per cent are used at temperatures down to —75 F. Nickel steels of $3^1/_2$ per cent, properly deoxidized and aluminum-treated, should provide suitable material for vessels to operate at —150 F. The carbon of the steel should be low, preferably below 0.10 per cent. For uses at lower temperatures one should consider the austenitic stainless steels or Monel.

In the foregoing, plates and large parts capable only of being normalized are considered. Nearly all alloy steels that can be fully hardened by quenching and drawing will give good impact value at very low temperatures.

Hydrogen Attack

Hydrogenation is an important tool in petroleum refineries. Under conditions of temperature and high partial pressure of hydrogen, attack takes place upon steel and other materials in that there is a tendency toward decarburization and mechanical disintegration.

Sulphur attack also is a factor in much of the hydrogenation of petroleum.

The alloy, 18 per cent chrome, 8 per cent nickel, is highly resistant to hydrogen attack. It suffers some temporary loss in mechanical properties due to mechanical presence of hydrogen in the metal. The hydrogen can be removed by heating, and the properties restored.

For other steels the presence of carbide-forming elements as chromium, tungsten, molybdenum, and others are required to prevent decarburization. In general, the more complex the carbide the more resistant is the metal to decarburization under hydrogenation conditions. Unless 12 per cent or more of chromium is present sulphur attack must be expected.

BIBLIOGRAPHY

1 "Some Observations of the Potentials of Metals and Alloys in Sea Water," by F. L. LaQue and G. L. Cox, Proceedings of the A.S.T.M., vol. 40, 1940.

2 "Corrosion of Petroleum Refineries," by B. B. Morton, *Petroleum Engineer*, May, 1944; reprints available, International Nickel Company, 67 Wall St., New York, N. Y.

3 "Corrosion Testing Methods," Bulletin T-10, The International Nickel Company, 67 Wall St., New York, N. Y.

Creep of Neoprene in Shear Under Static Conditions

By W. N. KEEN,[1] WILMINGTON, DEL.

This paper presents some of the mechanical properties, particularly the creep characteristics, of neoprene and natural-rubber vulcanizates. Included along with the creep data are the mechanical properties obtained in both compression and shear on the vulcanizates used in this study.

IN an earlier paper Yerzley (1)[2] showed how changing the base composition by the use of different types of softeners and reinforcing fillers influenced the physical properties, particularly the creep characteristics, of neoprene vulcanizates.

This paper shows how the creep in shear of neoprene vulcanizates in the hardness range of 40 to 60 durometer (Shore Type A) is influenced by the following:

1 Degree of vulcanization.
2 Preconditioning in shear at elevated temperatures.
3 Changes in composition.

The long-time static creep-tests discussed herein show that as the degree or state of vulcanization of neoprene compositions is increased, the rate of creep and the set of these vulcanizates are decreased without appreciably altering other important mechanical properties.

Preconditioning at elevated temperatures reduces both the rate and the magnitude of creep to a greater extent for the neoprene vulcanizates than for the natural-rubber vulcanizate tested.

The greatest improvement in creep characteristics has resulted from changes in the composition of the vulcanizates.

Both the composition and the degree of vulcanization must be studied in order to obtain the most desirable combination of properties for a given application. Such a study should be broad enough to cover independent evaluation of the important mechanical properties involved.

Method of Testing Samples

The tests described in this paper were conducted at a controlled temperature of 82 F ± 2 F under a load of 17.75 psi. The sandwich or specimen designed for evaluating vulcanizates in shear on the Yerzley oscillograph (2) was used in this work. Fig. 1 shows the static-creep test stand with specimens under test. The rectangular rubber members of the specimen are each 0.5 × 0.5 × 0.882 in. The schematic sketch, Fig. 2, gives the details of the loading bar showing its knife-edge construction and the connecting linkage between the test specimen and the loading bar. The linkage is readily adjustable so that the bar may be leveled as creep takes place in the specimen. Creep in inches was measured by a dial gage (0.001) equipped with a special jig.

In order to present the data for the several compositions on a comparable basis, they are expressed in terms of relative creep, as defined by Yerzley (1). Relative creep may be expressed mathematically as follows:

$$\text{Relative creep} = \frac{\text{Total deformation} - \text{initial deformation}^*}{\text{Initial deformation}^*}$$

In other words, the relative creep at 5 min is zero in all cases.

* Deformation obtained 5 min after loading.

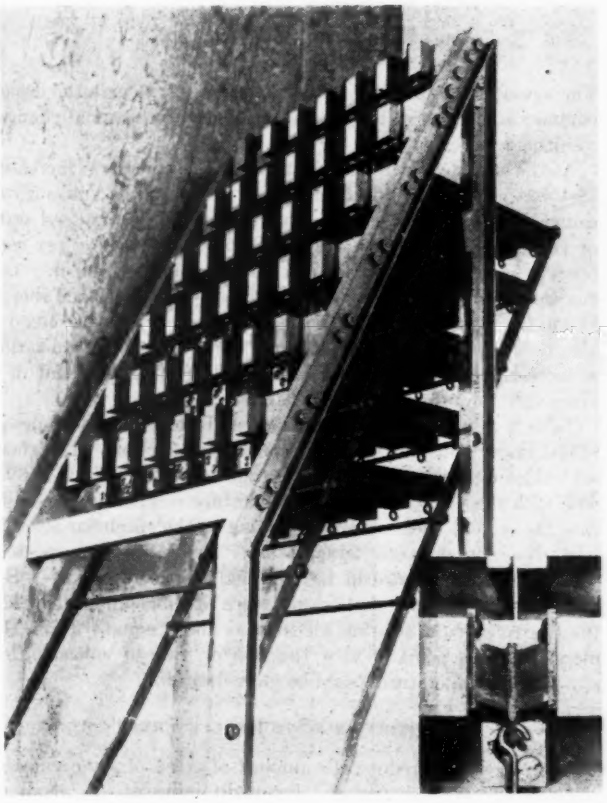


FIG. 1 STATIC-CREEP TEST STAND AND DETAIL OF SPECIMEN

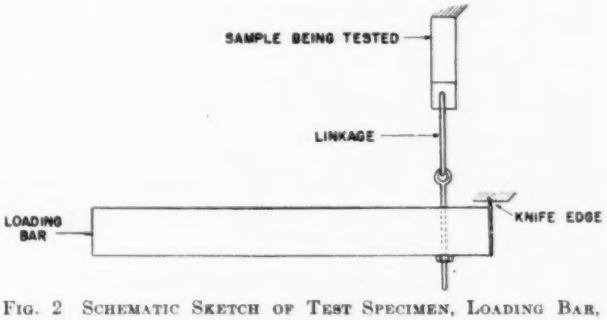


FIG. 2 SCHEMATIC SKETCH OF TEST SPECIMEN, LOADING BAR, AND LINKAGE

[1] Rubber Chemicals Division, Organic Chemicals Department, E. I. du Pont de Nemours & Company. Jun. A.S.M.E.

[2] Numbers in parentheses refer to the Bibliography at the end of the paper.

Contributed by the Rubber and Plastics Division and presented at the Annual Meeting, New York, N. Y., Nov. 26–29, 1945, of THE AMERICAN SOCIETY OF MECHANICAL ENGINEERS.

NOTE: Statements and opinions advanced in papers are to be understood as individual expressions of their authors and not those of the Society.

TABLE 1 MECHANICAL PROPERTIES OF COMPOSITIONS

Specimen	A.S.T.M. grade no.	Cure min/deg F	Hardness, Shore A	Compression characteristics: Per cent set, A.S.T.M. methods A	B	Resilience at 20 per cent deformation, per cent	Frequency, cycles per min	Static modulus, psi: At 0 per cent	At 20 per cent deformation	Load at 20 per cent deformation psi	Effective dynamic modulus, psi
S-1	SC-425	30/287	44	21	39	87	225	485	650	107	792
S-2	SC-525	60/287	46	13	25	88	227	490	690	117	797
S-3	SC-525	30/307	47	12	24	88	227	470	685	115	857
S-3D	SC-525	30/307	...	...	...	...	...	...	...	...	...
S-4	SC-425	80/307	41	11	18	83	234	435	645	105	847
S-6	SC-420	80/307	43	12	19	64	273	345	390	71	884
S-7	RN-530	15/287	46	11	24	90	193	500	810	130	835
S-7D	RN-530	15/287	...	...	...	...	...	...	...	...	...
S-8	SC-614	40/307	59	10	32	75	...	...	795	160	...
S-9	SC-612	65/307	59	10	18	58	...	...	770	160	...
S-10	SC-614	45/307	59	4	9	77	237	710	870	200	1070

The actual creep in inches is included in order to give the design engineer some idea of the magnitude of the dimensional changes resulting from creep.

As the state or degree of vulcanization of neoprene is increased (S-1 versus S-2), the rate of creep and the set of the vulcanizates decrease. The decrease in the rate of creep with increased state of vulcanization is shown graphically in Fig. 3, where per cent relative creep is plotted against time on log-log paper. The change in rate of creep or slope values B are given in Table 1. It will be noted in Fig. 3 that the magnitude of relative creep is also reduced for this composition as the degree of vulcanization is increased. The numerical values for creep at the end of 3 years and 9 months are given in Table 1.

Table 1 also gives the compression and shear set values determined under constant load and constant deflection. The shear set values were determined in accordance with A.S.T.M. D-395-40T with respect to time and temperature. These values indicate the actual shear strain remaining in the specimen after 30 min recovery at room temperature. As would be expected, there is little difference in the physical properties between S-2 and S-3 since the time and temperature relationship is such that the degree of vulcanization for them is about equal. From the manufacturer's point of view the shorter time of vulcanization at a higher temperature would be more desirable.

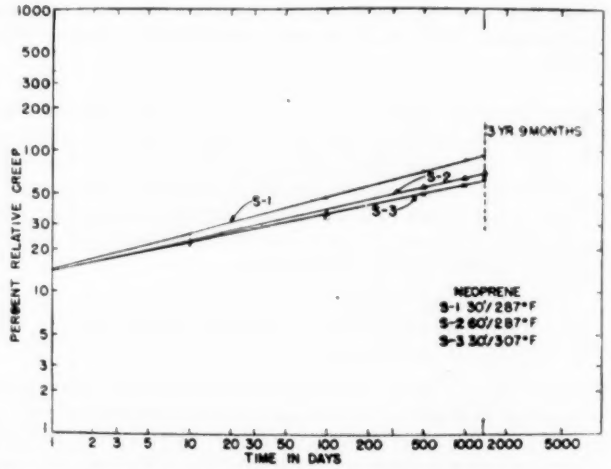


FIG. 3 INFLUENCE OF DEGREE OF VULCANIZATION ON STATIC CREEP IN SHEAR OF VULCANIZATES OF SAME NEOPRENE COMPOSITION

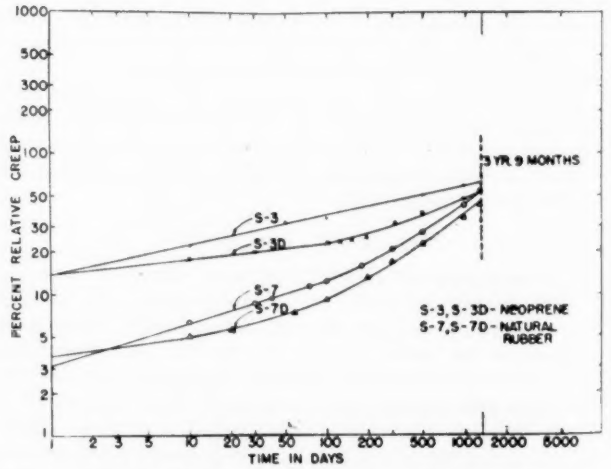


FIG. 4 INFLUENCE OF PRECONDITIONING, IN SHEAR, ON CREEP IN SHEAR OF NEOPRENE VULCANIZATE, COMPARED TO NATURAL-RUBBER VULCANIZATE

PRECONDITIONING TO REDUCE CREEP

Another way to reduce the amount of creep of some vulcanizates is by preconditioning. Preconditioning of the neoprene (S-3D) and the natural-rubber (S-7D) specimens consisted of straining them 30 per cent in shear and heating in this condition for 24 hr at 158 F. After the heating period, the specimens were removed from the jig and permitted to rest for one week at 82 F before being mounted on the static-creep test stand. Fig. 4 shows how this preconditioning in shear reduces the rate of creep for a limited time for both neoprene and natural-rubber vulcanizates. These curves indicate that neoprene is more receptive to preconditioning as a means of reducing creep than is natural rubber. Deviations from a straight-line function similar to those exhibited by curves S-3D, S-7, and S-7D have been reported by other investigators (3).

EFFECT OF CHANGING COMPOSITION

Fig. 5 presents some idea of how the relative creep may be varied by changing the composition. If this group of curves is considered from the standpoint of slope or rate of change of relative creep, they are all superior to the natural-rubber control except specimens S-4 and S-10. Specimens S-6, S-8, and S-9, would undoubtedly be of greatest interest to the design engineer because of their low rate of creep, as indicated by their slopes of less than 0.20. It will be noted, however, that while all of the curves except S-4 and S-10 have a lower slope than the natural rubber (S-7); all of them except S-10 have a higher per cent relative creep after 1 day. This higher initial creep can readily be taken care of by the engineer in his design of a spring or mounting.

In view of the fact that the relative creep - time curves are linear when plotted on logarithmic co-ordinates, they may be expressed by the equation

$$\text{Relative creep} = At^B$$

where A = Y intercept at 1 day
B = slope of curve
t = time in days

TABLE 1 (*Continued*)

Specimen	Shear characteristics: Per cent set constant load, 17.75 psi	Per cent set constant deflection, 20 per cent	Resilience at 20 per cent deformation, per cent	Frequency, cycles per min	Static modulus, psi: At 0 per cent deformation	Static modulus, psi: At 20 per cent deformation	Load at 20 per cent deformation, psi	Effective dynamic modulus, psi	Static-creep characteristics in shear: Under load of 17.75 psi: Initial deformation, in.	Initial shear, per cent	Per cent relative creep, 3 yr 9 mo	Creep in inches, 3 yr 9 mo	Y intercept A	Slope B
S-1	5.0	3.5	85	167	100	106	20	204	0.0930	18.6	92.3	0.0858	0.158	0.244
S-2	4.2	2.8	86	169	120	107	22	210	0.0858	17.2	69.4	0.0595	0.140	0.222
S-3	4.0	2.7	87	176	115	105	22	227	0.0883	17.7	63.0	0.0556	0.142	0.205
S-3D	...	...	...	...	...	...	...	...	0.0843	16.9	53.6	0.0452	0.140	0.121[a]
S-4	4.6	3.6	83	159	102	95	20	180	0.0935	18.7	42.0	0.0393	0.050	0.295
S-6	6.3	3.8	66	174	91	73	17	224	0.1530	30.6	65.0	0.0995	0.217	0.155
S-7	4.5	4.0	90	161	121	125	25	231	0.0707	14.1	54.2	0.0383	0.031	0.285[a]
S-7D	...	...	...	...	...	...	...	...	0.0717	14.3	46.0	0.0330	...	...
S-8	...	...	80	202	150	145	30	363	0.0591	11.8	104.0	0.0615	0.296	0.174
S-9	...	...	63	193	135	130	28	314	0.0649	12.9	50.6	0.0328	0.194	0.129
S-10	1.8	2.4	81	187	197	173	38	365	0.0465	9.3	22.0	0.0102	0.026	0.294

[a] Slope of straight-line portion of curve.

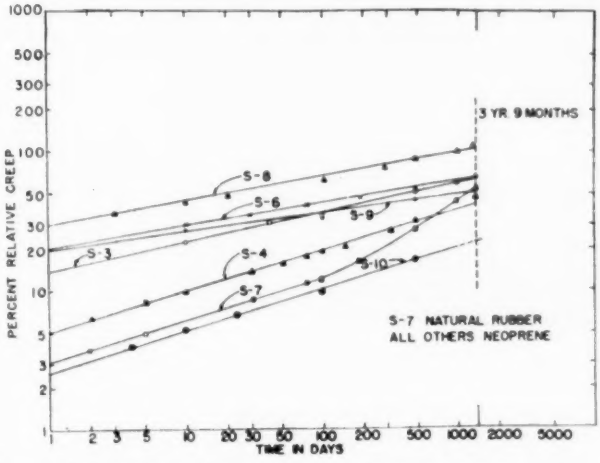


FIG. 5 INFLUENCE OF COMPOSITION ON CREEP IN SHEAR OF NEOPRENE VULCANIZATES

Table 1 gives the values for A and B for all of the curves except S-7D which has a variable slope.

As has been shown, the A.S.T.M. set, and the creep characteristics of neoprene are improved as the state of vulcanization is increased. Likewise some of the other mechanical properties in both compression and shear are increased as the state of vulcanization progresses (see Table 1). The compression characteristics were determined on cylinders 0.75 in. diam and 0.5 in. high, molded from the same composition used in making the shear specimens.

In view of the popular belief that high resilience is indicative of low creep, it is interesting to note that neoprene specimens S-6, S-8, and S-9, which have the lowest rate of creep of the compounds investigated, also have the lowest resilience. This is further evidence to confirm Yerzley's (1) statement that there is no simple correlation between creep rate and resilience.

CHANGE IN PROPERTIES WITH AGE AND TEMPERATURE

Since engineers are always interested in knowing how age affects the material with which they are working, the following data were obtained. The static creep test in shear after 3 years was terminated on specimens of S-1, S-4, S-7, and S-10, and the set in shear remaining 24 hr after removing the load was recorded. The change in the mechanical properties of these four specimens and in the specimens of the same four vulcanizates which had been stored at 82 F in an unstressed condition for 3 years were obtained by means of the Yerzley oscillograph. Data given in Table 2 show that natural aging for 3 years has caused a slight stiffening of the neoprene vulcanizates which is reflected by the increase in resilience, frequency, and moduli. There is little difference between samples aged in a stressed condition and those aged in an unstressed condition.

Knowledge of how the mechanical characteristics of a vulcanizate are affected by changes in temperature is for most applications essential to the design engineer. Riesing (4) has shown the effect of temperature on some of the physical properties of neoprene vulcanizates. He presented data showing the functional stability of neoprene at different temperatures by installing neoprene motor mountings, muffler support, and spring-shackle bushings in a car and conducting tests at ambient temperatures of —40 F and +140 F.

Both Forman (5) and Liska (6) have reported that some neoprene vulcanizates show delayed stiffening on long exposure to moderately low temperatures (32 F). This stiffening is the result of crystallization of the elastomer. From a practical consideration crystallization is not as serious as it sounds because the vulcanizate returns to its original state when the ambient temperature is increased or when there is mechanical work done on the vulcanizate. Recent technological advancements in the

TABLE 2 EFFECT OF NATURAL AGING ON MECHANICAL PROPERTIES

Specimen	A.S.T.M. grade no.	Cure: Min/deg F	Resilience at 20 per cent deformation, per cent	Frequency, cycles per min	Static modulus, psi: At 0 per cent deformation	Static modulus, psi: At 20 per cent deformation	Load at 20 per cent deformation, psi	Effective dynamic modulus, psi	Creep, in.	Shear strain, per cent	Per cent relative creep	Per cent shear set (24-hr recovery)
Original shear characteristics												
S-1	SC-425	30/287	85	167	100	106	20	204				
S-4	SC-425	80/307	83	159	102	95	20	180				
S-7	RN-530	15/287	90	161	121	125	25	231				
S-10	SC-614	45/307	81	187	197	173	38	365				
Shear characteristics after a 3-year static-creep test (under a load in shear of 17.75 psi at 82 F)												
S-1			90	175	115	118	24	225	0.0675	34.7	81.3	18.4
S-4			85	174	128	118	24	224	0.0366	28.6	39.2	13.5
S-7			90	161	133	130	26	232	0.0315	24.0	43.3	9.5
S-10			83	194	220	195	41	396	0.0092	14.5	19.9	6.0
Shear characteristics after 3 years of aging in an unstressed condition at 82 F												
S-1			91	170	125	110	24	212				
S-4			82	183	115	118	22	246				
S-7			91	163	130	135	27	236				
S-10	No specimen available											

processing of neoprene have led to a practical way of preventing crystallization (7).

Although static-creep tests give valuable information, an obvious disadvantage is the fact that they are time-consuming, and technical advancement often results in a composition becoming obsolete before the testing is completed. This emphasizes the desirability for a more rapid method of testing the creep characteristics of elastomeric materials. Considerable experimentation was carried out in the du Pont rubber laboratory during the past year for the purpose of developing a satisfactory dynamic-creep test. Apparatus has been built and is in operation.

Acknowledgment

The author takes pleasure in acknowledging the important contributions of N. L. Catton and A. M. Neal of the Rubber Chemicals Division of the du Pont Company to the progress of this work. He is also indebted to M. A. Gass, who made most of the measurements.

BIBLIOGRAPHY

1 "Creep of Neoprene in Shear," by F. L. Yerzley, *Mechanical Engineering*, vol. 63, 1941, pp. 343–345.

2 "A Mechanical Oscillograph for Routine Tests of Rubber and Rubber-Like Materials," by F. L. Yerzley, Proceedings of the A.S.T.M., vol. 39, 1939, pp. 1180–1188.

3 "The Creep of Natural and Synthetic Rubber Compounds in Shear," by S. H. Hahn and I. Gazdik, *India Rubber World*, vol. 103, 1941, p. 51.

4 "Synthetic-Rubber Mechanical Parts in Present and Postwar Vehicles," by E. F. Riesing, presented at S.A.E. Meeting, Detroit, Mich., Jan. 8, 1945.

5 "Effect of Elastomer Crystallization on Tests for Freeze Resistance," by D. B. Forman, *Industrial and Engineering Chemistry*, vol. 36, 1944, p. 738.

6 "Effect of Low Temperatures on Young's Modulus of Elastomers," by J. W. Liska, *Industrial and Engineering Chemistry*, vol. 36, 1944, p. 40.

7 "Freeze Resistance of Neoprene GR-M," du Pont Rubber Chemicals Division Technical Report BL-196, May 5, 1945.



FIG. 1 "PLASPREG" BLOCK SERVES FOR LAMINATING PURPOSES

Physical Properties of Resin-Impregnated Plaster

BY JOHN DELMONTE,[1] LOS ANGELES, CALIF.

While development work on impregnated plaster bodies has been in progress for many years, it was not until 1945 that the process was finally commercialized with low-viscosity furane resins, and extensive applications undertaken in the tooling field, and in general improvements of plaster-of-Paris patterns and forms. The impregnation of plaster of Paris with liquid thermosetting resins and the subsequent conversion of the product with heat, result in the formation of a material which has been called "Plaspreg." In this paper the methods of producing this material, its physical properties, and applications are discussed.

THE impregnation of plaster of Paris with liquid thermosetting resins and the subsequent conversion of the product with heat results in the formation of an entirely new material of construction. The resinified plaster body still retains the crystalline structural network formed on the hydration of $2CaSO_4.H_2O$, although considerably augmented through infusion with synthetic resins. In appearance and feel the impregnated plaster body resembles a cast plastic material more than it does the ordinary plaster-of-Paris bodies, though the improvements which are possible extend much further than the appearance, as all properties are greatly enhanced.

While development work on impregnated plaster bodies has been in progress for many years, it was not until 1945 that the process finally became commercialized with low-viscosity furane resins, and extensive applications undertaken in the tooling field and in general improvements of plaster-of-Paris patterns and forms. While the range of usefulness of resin-impregnated plaster (Plaspreg) forms will be analyzed more completely later in this paper, it will suffice for the moment to point out that among the applications are master models built of plaster of Paris (weighing several hundred pounds) which have been rendered much harder and more permanent through proper impregnation of furane resin; dies for hydropress operation in forming sheet metal; Keller pattern and duplicating dies; core boxes for the foundry; forms for laminating polyester resins; contoured shapes for shaping acrylic plastics; and general improvement in properties of dozens of plaster-of-Paris patterns of industrial and decorative value.

METHOD OF APPLICATION

The application of low-viscosity furane resins to the hardening

[1] Consulting Engineer, Furane Plastics and Chemicals Company, Los Angeles, Calif., and Technical Director, Plastics Industries Technical Institute. Mem. A.S.M.E.

Contributed by the Rubber and Plastics Division and presented at the Annual Meeting, New York, N. Y., Nov. 26–29, 1945, of THE AMERICAN SOCIETY OF MECHANICAL ENGINEERS.

NOTE: Statements and opinions advanced in papers are to be understood as individual expressions of their authors and not those of the Society.

of plaster-of-Paris bodies is a relatively simple procedure. Plaster of Paris or "hydrocal" forms are prepared in exactly their usual manner, i.e., added to water in certain optimum proportions and then stirred and poured. Depending upon the grade of plaster, the forms set in approximately 15 to 20 min, reproducing with the utmost fidelity the finest details of the mold. The sections can be splash castings 1/4 in. thick or sections measuring several feet in thickness. The hydration process is an exothermic reaction and some heat is developed although temperatures seldom exceed 50 C. After the plaster has firmly set, it may be removed from the mold. There is a considerable amount of free water present which should be evaporated for best results. This can be accomplished by forced drying or leaving in the open for several days. Up to this point the process is standard practice in so far as the plaster industry is concerned. The next step is the application of low-viscosity furane resin which is applied by dipping, brushing, or spraying. The rate of resin diffusion is very rapid, and after thorough impregnation parts are generally cured at temperatures of 140 to 160 F. The final impregnated body is the entirely new structural material which has proved so useful.

The application of organic plastics to plaster-of-Paris bodies is not entirely a new idea, as coatings have been sprayed on the material for many years, largely to seal its surface or to apply some decorative finish. The writer first began experimenting with the impregnation of plaster some 5 years ago and has successfully applied many types of thermosetting urea, melamine, phenolic, and polyester resins and thermoplastic resins. Some of the background leading to the development of furane-resin-impregnated plaster was described in a recent paper before the S.P.I. (1).[2]

The final procedure selected for preparing Plaspreg involved a low-viscosity furane resin whose viscosity could be readily adjusted to meet various application conditions, not by methods of diluting with solvents such as water, alcohol, or acetone, but through proper polymerization conditions. Thus a complete liquid resin capable of conversion to an infusible, insoluble body was developed exclusively for plaster-of-Paris treatment.

A typical application of furane-resin impregnation to plaster-of-Paris bodies is shown in Fig. 1 illustrating a die for laminating purposes. A polyester resin has been laminated about the impregnated form and cured at 250 F. The technique of plaster impregnation was suggested by the author in 1943 (2). Further work upon hydrocal was cited in a more recent publication (3). A further example of furane-resin impregnation is shown in Fig. 2. The many fine details made possible by this impregnation and curing process are emphasized.

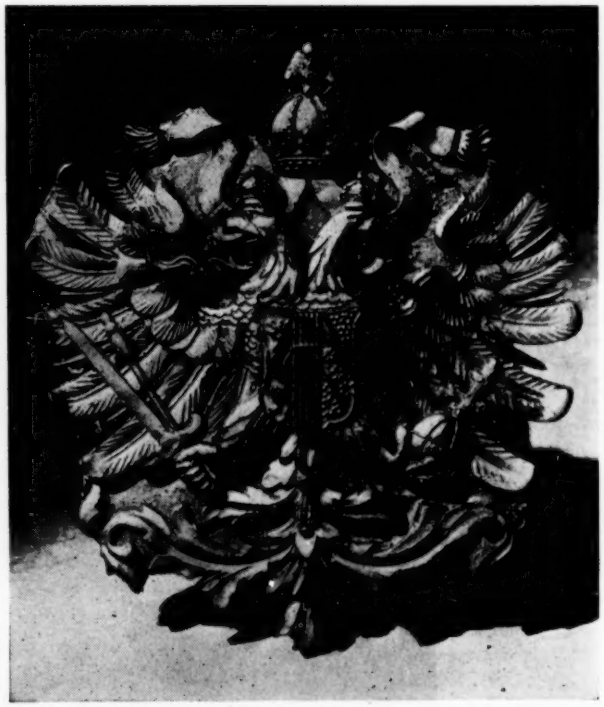


FIG. 2 COMPLICATED DESIGN DETAILS, MAINTAINED IN RESIN-IMPREGNATED PLASTER

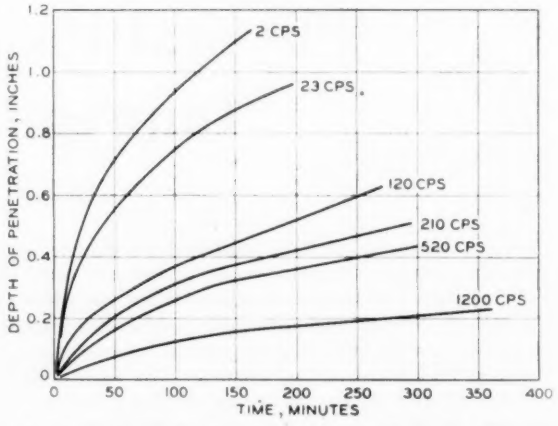


FIG. 3 AMOUNT OF PENETRATION VERSUS TIME FOR DIFFERENT VISCOSITIES OF THE SAME FURANE RESIN

VARIABLES WHICH INFLUENCE RATE AND EASE OF IMPREGNATION

Throughout all of the work which has been accomplished in the impregnation of plaster of Paris, it has become apparent that best results are obtained through infusion with low-viscosity resins into dry plaster-of-Paris bodies. There are several variables which will influence the rate and ease of impregnation. These are as follows: (*a*) Inherent resin viscosity in the absence of solvent; (*b*) relative porosity of the plaster structure, determined largely by the initial solids-to-water ratio; (*c*) temperature of the plaster-of-Paris body; (*d*) presence of impurities upon the surface. Inasmuch as the correct development of the physical properties of resin-impregnated plaster depends upon these variables, they will be discussed briefly.

(*a*) *Resin Viscosity.* The resin viscosity has a definite influence upon the rate of penetration into the plaster. The higher the viscosity, the higher is the molecular weight and the slower the rate of penetration. The mobility of the resin and its ability to wet surfaces are functions of resin viscosity and, due to the capillary nature of the diffusion process into plaster bodies, resin viscosity is most important. This fact is graphically illustrated in Fig. 3 where the amount of penetration is plotted against time for different viscosities of the same furane resin. The much slower penetration rate of the higher-viscosity resins should be noted. Variations in viscosity were achieved by polymerizing the resin to various degrees, otherwise the material is chemically the same. Another interesting observation which can be made is that the rate of penetration approaches a constant value after a period of time.

While the test method adopted precluded measurements of penetrations much beyond 1 1/4 in., it will be noted that complete cessation of penetration did not occur. A relatively simple technique was devised in which the plaster of Paris was poured into a

[2] Numbers in parentheses refer to the Bibliography at the end of the paper.

glass vial and then given an opportunity of thorough drying at low temperatures. Because of the slight expansion in setting, a tight fit was insured against the side of the glass vial. The penetration could be observed at the side of the glass vial and measurements made at frequent intervals. These checked completely with any observation upon samples cut open after different intervals of immersion in the resin.

From the data accumulated it was possible to express the rate of penetration by the following equation:

$$r = r_0 \left(1 - e^{\frac{-kt}{u}}\right)$$

where

r is rate of penetration at any time
r_0 is final steady-state penetration rate
k constant, depending upon physical factors, such as porosity
t time
u viscosity

Thinning the resin with low-viscosity solvents does not produce increased rates of penetration of anything except the solvent, primarily because the plaster-of-Paris body will act as a filtering medium and separate the higher molecular-weight components from their carrier. This means that a thick resin, such as a phenolic casting resin, may presumably be thinned to a low enough viscosity for good penetration. However, during application only the solvent will penetrate, with the high-viscosity phenolic resin remaining near the surface. Other variable factors such as method of application of the resin impregnant, will influence the penetration of the resin. Brushing on the resin and keeping it in motion will aid penetration.

(*b*) *Porosity of Plaster.* The porosity of the plaster has a definite bearing on the amount of resin which can be absorbed. It is seldom possible to produce a workable mix of plaster and water with less than 60 lb of water per 100 lb of plaster. Of the water used, however, only 18.5 lb are required to set the plaster chemically and the balance of 42.5 lb represents free water. This water is evaporated or forced out by oven-drying, leaving voids to be filled by the resin impregnant. While the author has employed a number of water-soluble resins for diffusion into plaster, and in this manner obtained a good penetration followed by subsequent hardening, the total amount of resin pickup is obviously less than when a 100 per cent resin impregnant is employed for application to a plaster in which the free water has been removed.

In Fig. 4 the relationship between the water and plaster ratio and the maximum theoretical pickup is illustrated (calculated on the basis of a 1.18 specific-gravity resin). The resin pickup is based on the total removal of free water after the cast has been made. In addition, the decrease in compressive strength of the plaster is illustrated, indicating that when large amounts of water are employed, the percentage of voids is greater and the effect upon the strength more pronounced. The values for compressive strength of the non-resin-treated plaster are obtained upon dry plaster which is appreciably stronger than wet plaster. At the same time, the compressive strength of resinified plaster is also illustrated. The reinforcing effect of the furane-resin impregnant is quite apparent, as even low-density lightweight plasters are considerably improved. The same improvement is also noted if, during the process of drying or during use, some of the water of crystallization is removed. Resin impregnation overcomes weakness or loss of strength in plaster.

To demonstrate the increased rates of resin impregnation for more porous plasters, a group of test specimens was prepared from 100/60 (solid-to-water ratio) to a rate of 100/100. When these had been thoroughly dried of free water, resin-impregnation tests

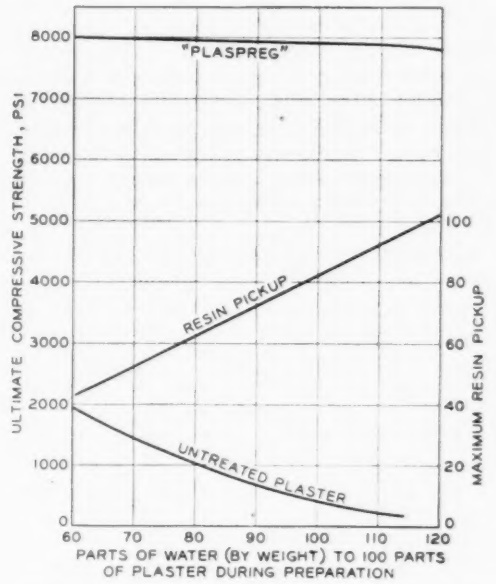


FIG. 4 RELATIONSHIP BETWEEN WATER AND PLASTER RATIO AND MAXIMUM THEORETICAL PICKUP OF FURANE RESIN

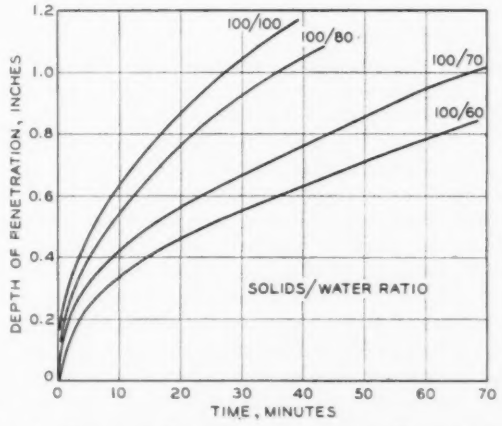


FIG. 5 EFFECT OF POROSITY OF PLASTER ON PENETRATION

were conducted and depth of penetration versus time observed. Averages of several test results are reported in Fig. 5 for a furane resin of initial viscosity of 2 to 3 centipoises. Viscosity measurements were conducted at 25 C, with a "Zahn" viscosimeter cup purchased from the General Electric Company. The increased rates of penetration for more porous plasters are readily indicated upon this curve sheet.

The porosity may also be checked by the water absorbed and in some processes, such as pottery manufacture, this is an important procedure. Aside from this application, low water absorption is an asset. In resinified plaster, where voids are substantially filled with furane resin, water absorption is very low; less than 2 per cent A.S.T.M. water absorption in 24 hr when properly prepared. Herein lies the utility of furane-resin-impregnated plaster tools and articles from a weathering standpoint; they are substantially more satisfactory than untreated plasters. Within a few minutes' immersion, most plasters of the 100/plaster/60 H_2O composition will have a water absorption of 25 per cent. Parts will deteriorate rapidly, while nonporous resinified plaster is infinitely more satisfactory.

(*c*) *Temperature of Plaster.* While not of major consequence

the temperature of the plaster at time of impregnation will influence the rate of penetration of the resin. By raising the temperature of the plaster it is possible at the time of resin application to obtain quicker penetration. From a practical point of view, as forms are removed from the drying oven they can be immediately treated with the resin impregnant without waiting for them to cool. In Fig. 6 is compared the rate of penetration of a 1 to 2-centipoise-viscosity furane resin at room temperature of 75–80 F, 135–140 F, and 180–185 F, respectively. The faster

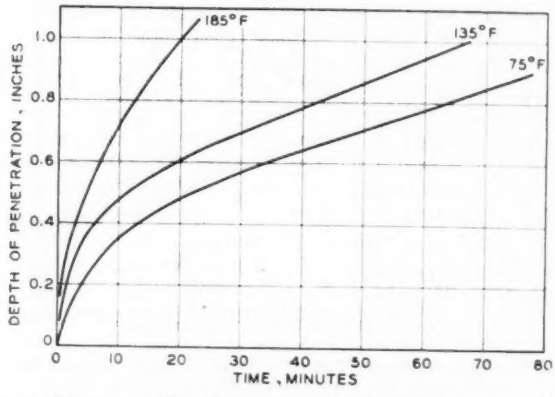


FIG. 6 EFFECT OF TEMPERATURE ON PENETRATION INTO 100/60 PLASTER

rate at 185 F is immediately observed. After a period of time the higher temperature has a retarding action inasmuch as the resin impregnant begins to cure or polymerize, resulting in a decrease in the rate. The plaster used in this experiment and others, unless otherwise indicated, is 100 solids to 60 parts of water.

(*d*) *Impurities on Surface.* There are several types of surface impurities which may influence the rate of penetration of the resin into the plaster. This becomes of practical importance when, for example, treating large surfaces and uniform appearance is necessary. One of the more common surface imperfections may arise from too liberal use of a parting agent in preparing plaster-of-Paris molds and patterns. Stearic acid is largely used for this purpose, as well as various soaps. These materials, if present, would restrict penetration of resin into the surface. However, if removed by light sanding or finishing operations upon the plaster surface, uniform pickup of resin is assured. In applying furane resin to develop resinified plasters, these surface irregularities can be readily observed, and a few spots where an excess amount of lubricant is present may be easily detected. A light touch with very fine sandpaper eliminates this problem.

Another type of surface imperfection finds origin in the mixing of the plaster. This imperfection is known to the plaster trade as a "hard spot." It occurs, generally, on large smooth surfaces, particularly near sharp corners or edges where rapid drying occurs. The hard spots are due simply to portions of plaster not too thoroughly mixed with the balance of the batch. If this is the case, such that a higher solids-to-water ratio is present, the plaster will tend to be harder, and porosity a little less. Once again, however, light sanding over this region will make the pickup of resin more uniform.

AMOUNT OF RESIN REQUIRED

While best physical properties are obtained upon fully impregnated forms, it is also feasible to consider surface penetrations of $^1/_4$ to $^1/_2$ in. without necessarily going through several inches of plaster. For many contour blocks and tools this procedure has been followed for reasons of economy, and a good hard surface obtained without full treatment of the plaster. The amount applied may be controlled to some extent by the number of times the surface is gone over with a brush that has been saturated with liquid furane resin. Absorption of resin into the surface may be likened to the absorption of ink into a piece of blotting paper. Penetration takes place instantaneously upon the initial application, though at a slower rate after 10 or 15 min.

While vacuum and pressure vessels have been employed to obtain even faster and more thorough penetrations, the entire procedure is conducted at atmospheric pressure and temperature. When thin, low-viscosity resins are employed, the amount of build-up on the surface is negligible. However, when high-viscosity impregnating resins are employed, there is some build-up on the surface which must be wiped off before the part is cured. For greatest accuracy of dimensions this is quite important. Likewise, obscuring of surface details is avoided, and the plaster-of-Paris part is unaffected in detail though materially improved in substance.

For quick estimates of the amount of resin required to impregnate completely a plaster-of-Paris body, the article is weighed and approximately 40 per cent of its weight is prepared in impregnating resin. The actual amount required depends, however, on how thorough a penetration is desired, how well the plaster has been dried, and the other variable factors previously described.

CURING IMPREGNATED PLASTER

After the plaster has been properly impregnated, it is cured to develop optimum physical properties, which are consistently a 300 to 400 per cent improvement over the straight plaster-of-Paris structure. The curing procedure does not invite any special complications, simply requiring placing the form in an oven and slowly raising the temperature to about 145–150 F. The rate at which temperature is raised or the rate at which it is lowered must be conducted, of course, with concern for thermal expansion and shrinkage characteristics, in order to avoid the development of internal stresses at any position such as may mark the meeting of a thick or thin section of material.

While a very slight initial shrinkage may be observed, of the order of 0.05 per cent, the aftershrinkage of resinified plaster is negligible, and dimensions are held with utmost accuracy. This is a fortunate circumstance when considering the problems brought on by cast liquid resins, and the excessive shrinkages they have incurred, even with a judicious selection of fillers. Even after prolonged heating at 185 to 190 F, the dimensions are unchanged in resinified plaster.

At the same time these tests were made, the thermal-expansion coefficient was determined at 0.000022. This value approximates the expansion coefficient of aluminum alloys. This property has been utilized to advantage in providing for localized reinforcement of resinified plasters at positions of high stress concentration. The insertion of aluminum-alloy strips or corners, folded from sheet metal, gives the end product greater toughness where it is most needed. At first, this reinforcement may be viewed as an obvious procedure. However, the fact remains that cast plastics tooling has not been reinforced with metal strips because the plastics are too unstable and their aftershrinkage characteristics would create conditions for internal stresses and ultimate cracks in the casting. The complete absence of aftershrinkage in resinified plaster and the coincidence of identical thermal-expansion coefficients make a sound combination with aluminum alloy.

In Fig. 7 are curves showing the attainment of cure conditions at different temperatures. There are two stages to the cure: One in which the impregnating resin takes a set and turns to a dark color and the other in which the strength is progressively increased. The criterion proving most useful for this work is the

value of compressive strength, measured upon 1-in. cubes at frequent intervals during cure time. Impact-strength measurements run parallel to these. This set of results is also quite significant and explains in part why resinified plasters are much harder and more chip-resistant than unimpregnated materials. Of course, the values of impact strength indicated will not prevent the part from breaking, although there are various design principles which can be followed to give improved results. These design

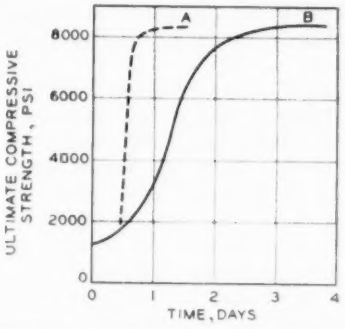


FIG. 7 ATTAINMENT OF CURE CONDITIONS AT DIFFERENT TEMPERATURES

(*A*—Initial cure at 135 F; followed by 180–190 F. *B*—Cure at 130–140 F. Resin XP, impregnated plaster.)

principles place emphasis upon generously rounded corners and ample sections of materials to withstand load conditions. Impregnated plaster is not flexible, as the modulus of elasticity is quite high and hence when loaded, as in the application to a hydropress forming operation, the base should be perfectly flat and preferably mounted upon a true surface without any "bowing" before load is applied.

Additions of various fillers to the plaster composition to achieve even higher impact strength, will be discussed later in this paper. Comparative physical properties with various methods of reinforcement will also be outlined.

TEMPERATURE STABILITY

One of the most important gains registered in furane-resin-impregnated plasters over unimpregnated plaster is improvement

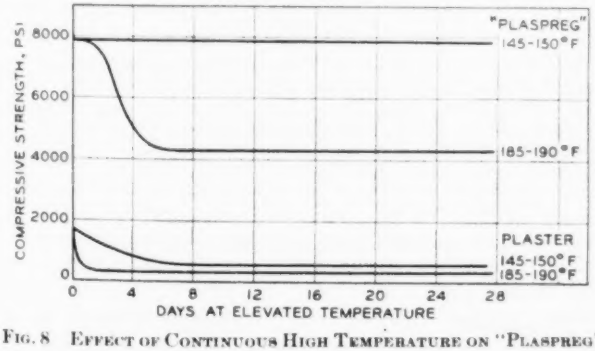


FIG. 8 EFFECT OF CONTINUOUS HIGH TEMPERATURE ON "PLASPREG"

in temperature stability. This has already been indicated in part by pointing out that the material has a negligible aftershrinkage. The study, however, goes deeper than that and in two respects resinified plaster is far superior to ordinary plaster:

1 Maximum continuous operating temperature which it will withstand without suffering any permanent change in physical properties is in the neighborhood of 180 F. This value is appreciably more than straight plaster, the temperature limit of which is about 120 F, because above this it loses water of crystallization and strength. Likewise, the liquid casting resins have temperature limits of about 140 F or thereabouts, because at higher degrees they shrink too excessively.

2 The maximum temperature at which resin-impregnated plaster can operate continuously and still be stronger than the initial plaster, is about 250 F. Above 180 F the strength may fall off slowly to a certain level and then stop, although it will be stronger than the original plaster of Paris. This has been quite important to foundry work where plaster forms and core boxes have not been considered because of the rapidity with which they lose strength when raised in temperature.

The permanency of the physical properties of resin-impregnated plaster is indicated by the retention of its strength over a long period of time. Impregnated bodies prepared a few years ago test as strong as when they were first cured. To accelerate the aging of resinified plaster, a constant-temperature oven at 185–190 F is employed and compressive strength is observed after various intervals of time. Typical results are shown in Fig. 8. For purposes of comparison, straight plaster has also been tested. The loss in strength of plaster is due to loss of strength on removal of water of crystallization at high temperature. Retention of strength after exposure to high temperatures is indicative not only of the permanency of the materials, but also of operating temperature limits. As is the experience with most thermosetting plastics, short exposures to high temperatures in excess of continuously operating temperature limits will not be damaging.

Limiting factors in the temperature resistance of resinified plaster are (*a*) the loss of water of crystallization, and (*b*) the temperature limits of the furane-resin polymer, which lie about 250–300 F. Further improvements in temperature stability can be realized by substituting an inert filler such as powdered silica for part of the plaster of Paris. This can be accomplished without weakening the total cured structure.

CHEMICAL RESISTANCE

The chemical resistance of furane-resin-impregnated plaster is much more satisfactory than is that of untreated plaster. Water-absorption tests at room temperature are shown graphically over a long period of time in Fig. 9. Not only is water absorption greatly reduced because of the presence of furane resins to fill the voids, but furane-resin solids (100 per cent) show an A.S.T.M. water absorption of less than 0.05 per cent in 24 hr. In Fig. 9 sanded surfaces are compared with polished surfaces. For maximum weather protection, resinified-plaster toolings are polished or rubbed by hand with a wax suitable for finishing purposes. This will enable parts to be stored in the open, whereas in the past plaster has fallen apart or was seriously weakened by such exposures.

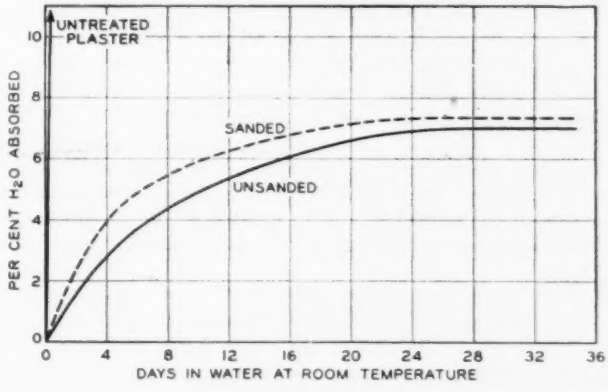


FIG. 9 WATER ABSORPTION OF FURANE-RESIN-IMPREGNATED PLASTER

Strong acids and alkalies affect resinified plaster only slightly, whereas they cause untreated plaster to decompose. As evidence of their good chemical resistance, various resinified plaster parts have been electroplated after first applying a thin high-polymer film, followed by stannous chloride and then a silvering solution.

For general chemical and temperature resistance, the parts shown in Fig. 1 illustrate the utility of resinified plasters as tooling for low-pressure laminating. The service life of plaster parts is increased quite appreciably owing to the much higher strength. In addition, forms are rendered quite impervious to various polyester resins which must be cured at temperatures as high as 300 F. In the illustration shown, XRS-16631 served as the laminating resin for glass cloth which was cured under vacuum pressure. A vinyl-resin lacquer provides a good release agent for the parts in question.

In another important laminating problem for complicated ducts for aircraft, a removable core of plaster was necessary for each operation, requiring breakage to take the piece out. The plaster cores did not possess sufficient strength to stand up under the laminating operation, although the problem was solved by subsequent treatment with furane resins. By impregnation they acquired sufficient strength to withstand the pressure of the laminating operation. A number of air ducts for fighter airplanes was produced in this manner.

Physical Properties of Resinified Plasters

The discussion so far has centered upon furane-resin-impregnated plaster of Paris. Results are even more noteworthy when various fibrous reinforcements are included in the plaster. Long fibers such as hemp or sisal fiber have been known to strengthen plaster patterns and tooling. They likewise add considerably to the strength of the resin-impregnated plasters. Glass flock, in particular, is effective in forming a strong and tough body which can take much mechanical abuse, and its introduction into plaster before impregnation is an important step.

In Table 1 some of the physical properties of furane-resin-impregnated plaster are noted.

TABLE 1 PHYSICAL PROPERTIES OF RESINIFIED PLASTERS

Material Property:	Unimpregnated plaster	Resinified plaster no filler
Specific gravity	1.15 (dry)	1.65
Compressive strength, psi	1500–1800	7500–8000
Flexural strength, psi	400–500	2500–3500
Impact strength, Charpy unnotched, ft-lb per in.	0.15–0.25	0.8–1
Water absorption, per cent in 24 hr.	35	2

All of the physical tests followed the applicable A.S.T.M. standards with the exception of compressive-strength tests which employed 1-in. cubes instead of $^1/_2$-in. cubes. The unimpregnated plaster and resinified plaster contained 100 parts of solids and 60 of water at the time of preparation. Materials were dried at room temperature for 3 or 4 days and then overnight at 140 F, to remove all traces of free water. They were impregnated with low-viscosity resins and cured about 48 hours at 150 F.

In conclusion, it appears desirable to sum up some of the advantages and disadvantages of resinified plaster. It represents the application of a new thermosetting resin, the 100 per cent furane resin, into the plastics picture and the development of a new and important outlet for plastics in the ceramics industry. A new, low-cost tooling material with negligible shrinkage has made its appearance.

The advantages of resinified plaster are as follows:

Low Cost. Resinified plaster is prepared from a low-cost base material, plaster of Paris, which costs about 1 cent per lb. When fully impregnated, the cost of the treated plaster is appreciably less than that of a thermosetting cast-phenolic resin.

Ease of Fabrication. From the standpoint of ease of fabrication and workability, plaster has few equals. In the resin-impregnation process, plaster of Paris or hydrocal tools, forms, or patterns are prepared in their usual manner and set at room temperature. A very stable structure is prepared with simple tools. Upon resinifying and hardening, this form is rendered permanent.

Physical, Chemical, and Thermal Properties. These properties have been vastly improved over the straight plaster, placing fully resin-impregnated plaster in the same class as liquid-cast resins, with the important advantage of zero aftershrinkage.

Applications. No form is too small or section too big to be handled by this process. Resin penetrations up to several inches have been accomplished at room temperature and atmospheric pressure. Wherever plaster is used resin impregnation may be applied to convert these articles to permanent, stronger materials of construction.

The disadvantages of resinified plaster are as follows:

Drying. For best results the plaster forms should be thoroughly dried out. This necessitates an additional step in preparing plaster and lengthens the time lapse before the tool can be used.

Breaking. While all properties are improved some 300–400 per cent, furane-resin-impregnated forms can still be broken, and one should not expect the treatment to convert plaster into a rubberlike, unbreakable material.

BIBLIOGRAPHY

1 "Impregnation of Plaster of Paris With Synthetic Resins," by John Delmonte, S.P.I., Los Angeles, Calif., August 28, 1945.

2 "New Developments in Furane Resins," by John Delmonte, *Modern Plastics*, vol. 21, February, 1944, pp. 102–104.

3 "Furfural Resins as Low Viscosity Impregnants," by John Delmonte, *Plastics*, vol. 2, March, 1945, p. 112.

The Control of Fouling Organisms in Fresh- and Salt-Water Circuits

By JOHN G. DOBSON,[1] SHORT HILLS, N. J.

The difficulties encountered by industrial water users due to fouling organisms are discussed. To control such fouling, a knowledge of the organism's life cycle and reactions to stimulus is necessary. Typical mollusks, Bryozoa, sponges, barnacles, and tunicates are considered. Their control can be effected by heat, change of salinity, change of oxygen content, increased velocity, acids, antifouling paints, screening and poisoning with a number of different poisons. It is concluded that chlorination is the most effective and economical of these methods justifying itself in most plants by improved heat transfer alone. Factors to be considered in designing water systems that may foul are also outlined.

INTRODUCTION

Examples of Problems

THE growth of marine macroorganisms, both plant and animal, has been a continuing source of difficulty to power stations, oil refineries, and other users of industrial water. Although much has been written concerning accumulation of microorganisms of the capsulated and slime-forming types on heat-exchanger surfaces with attendant reduction of heat-transfer efficiency (1, 2, 3),[2] little has been published on the growth and control of the macroorganism in closed water circuits. This paper deals with those fouling organisms visible to the naked eye which cause industrial difficulties.

One of the more important, although perhaps the least obvious of the difficulties resulting from fouling by the larger aquatic organisms, is the reduction in the carrying capacity of a pipe line by reduction of the Hazen and Williams coefficient and also by actual reduction of the pipe-line diameter. In addition to some fresh-water grasses and mats of fresh-water algae in the sunlit portions of the water conduits, the most common organisms responsible for this blocking of fresh water lines are the Bryozoa, notably *Pectinatella magnifica*, and the sponges. In salt-water or brackish-water lines, the various hydroids and Bryozoa, as well as Mollusca and Tunicates, are responsible for such reduction.

Sponges, both of the calcareous and of the siliceous or fiber types have been responsible for occasional fouling of pipe lines. In one southwestern city the Hazen and Williams coefficient has dropped from 145 to 94.5 on a 60-in. iron pipe line due to sponge accumulations. Occasionally large cast-iron pipe lines have become almost completely blocked with various Mollusca, notably *Mytilus edulis* and *Pecten latiauratus* in salt-water circuits and various *Dreisseniidae* in fresh-water circuits. As much as 266 tons of shells have been removed yearly from the circulating tunnels of one New England power station. Another station has an accumulation of dead shells 3 ft to 6 ft deep in a tunnel with a 6 × 11-ft cross section and 400 ft long. Figs. 1 to 4 inclusive, illustrate conditions in a tunnel on October 1, 1945. The tunnel walls and floors had been made broom clean by scraping 4 months before. Where salt water is used in fire service, these same organisms have not only reduced carrying capacity of the line, but shells loosened by sudden rush of water due to fire demands have blocked valves, hydrants or other irregularities, and have completely shut off water supplies with disastrous results.

Similar difficulties have been encountered where salt water is used for displacement of gasoline or fuel oil from underground storage.

Sea-going vessels in harbor waters of temperate climate and most tropical waters have had fire and flushing lines clog with marine growths.

Growths, particularly of shelled organisms, continue to enlarge until their exposed area becomes so great that they are torn from their moorings on the pipe line and are swept into screens, tube sheets, or pumps. In one Gulf Coast refinery, Bryozoa so blocked the tube sheet of divided water-box condensers that the pressure from circulating-water pumps burst through the dividing wall and forced whole sections of the refinery "off stream."

When the lines or tunnels serving shell-and-tube or surface condensers become fouled with these organisms, additional difficulties are encountered. After the organisms break off or die, the shells float up with the circulating water. Many seaboard stations and some stations using river and lake water have had to shut down entire turbogenerator units two or three times a day to permit removal of shells that are blanketing the tube sheets. Some shells in these cases are sure to enter the tubes and cause high impingement velocities with attendant erosion and reduction in tube life (4).

The presence of macroorganisms, as well as that of microorganisms on the surface of metals, cause differential cells and attendant corrosion (5), particularly of steel materials. Attacks on nonmetallic structural materials also occur (6).

Mechanics of Fouling

The exact mechanics of fouling have been studied to only a limited extent. Most of the work has been done on smooth metal or glass plates simulating conditions on a ship's bottom. The first organisms to attach to a newly immersed plate are the unicellular capsulated bacteria, Fig. 5. Whether these organisms attach first merely because of their rapidity of growth, or whether they form a necessary footing for other larger organisms is not clear.

Some "conditioning" of a surface has been thought necessary before fouling begins, even in the case of natural rock (7). This "conditioning" apparently consists of a roughening of the surface and possibly the elimination of the material being leached from the surface.

After that period of "conditioning," first one and later other organisms may become predominant (8). Eventually stable conditions result (9).

History of Control

Early recorded experimental work (10) covering control of

[1] Industrial Division, Wallace & Tiernan. Jun. A.S.M.E.

[2] Numbers in parentheses refer to the Bibliography at the end of the paper.

Contributed by the Power Division and presented at the Annual Meeting, New York, N. Y., Nov. 26–29, 1945, of The American Society of Mechanical Engineers.

Note: Statements and opinions advanced in papers are to be understood as individual expressions of their authors and not those of the Society.



FIG. 1 CIRCULATING-WATER-INTAKE BAR RACK
(The rack had been completely cleaned of all growth 2 months before this view was taken.)



FIG. 2 CEILING OF CONCRETE TUNNEL
(The luxuriant growth of *Tubularia crocea* is 7 in. long and some of it has already dropped off and decomposed on the tunnel floor in the 4 months since the last cleaning.)

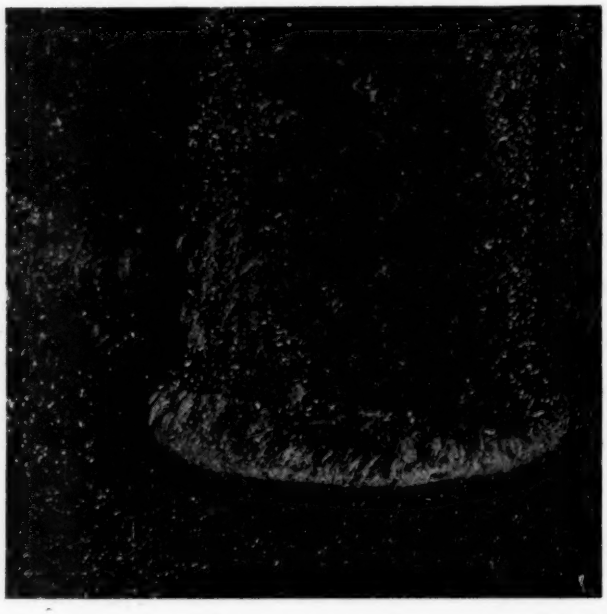


FIG. 3 PUMP-SUCTION BELL IN SAME TUNNEL AS FIG. 2, WITH LARGE GROWTH OF MYTILUS
(These mussels are already large enough to blanket tube sheets if they break off in mats or to lodge in a tube if they break off as individuals.)

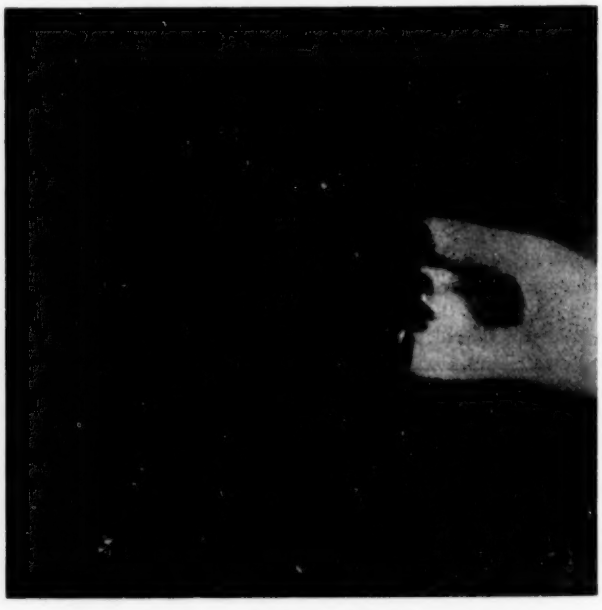


FIG. 4 CLOSE-UP OF THE SAME PUMP BELL AS FIG. 3
(The area at the right has had the mat of mussels torn off to show depth of growth. The hand merely indicates dimension.)

fouling organisms in closed water circuits was begun when the consulting-engineering firm of Kennedy and Donkin was commissioned early in 1919, by the Electricity Committee of the Edinburgh Town Council to make recommendations regarding the control of marine growths in the circulating tunnel of the Portobello Generation Station, which was then in process of design.

The investigators studied various control methods which had been previously attempted. One private firm at the Leith Docks had attempted to control mussels by annual flushings with high concentrations of sulphuric acid. This control was partly successful but severe corrosion resulted. Others had attempted annual or semiannual cleanings of inlet pipes by use of tight-fitting balls and other cleaning implements being dragged through tunnels; but several pipe lines were severely damaged. At Portsmouth an electrically insulated pipe line had been freed to some extent of mussels by using electrical discharges between the pipe and a central electrode.

Screening to prevent the entrance of small organisms, the use of various antifouling paints, and the use of various mechanical

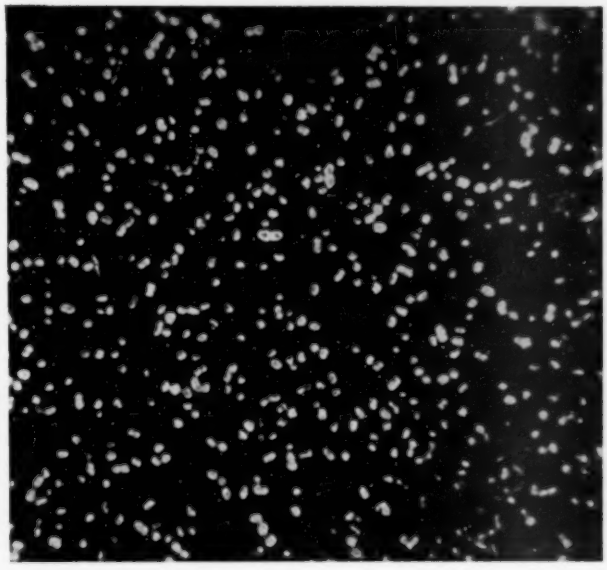


FIG. 5 SMALL GRAM NEGATIVE ENCAPSULATED COCCOBACILLI TYPICAL OF SLIMING MICROORGANISMS IN SALT WATER; ×930

cleaning methods, were considered and rejected as impractical. Chemical means were then attempted.

It was found that sulphuric acid in concentrations of 1 part in 10,000 was unsuccessful; that the larger mussels, after immersion in fresh water even for as long as 120 hr, were unaffected.

Experiments were then tried with heated water. Mussels were removed from sea water at 69 F and placed in salt-water tanks which were gradually heated. Selective killing occurred above 100 F during immersion periods of 25 to 50 min. All mussels failed to revive when returned to normal sea water, after immersion at 106 F for 22 to 63 min.

Based on these experiments, it was recommended in 1921 that the Westbank Station of Portobello be built so as to permit the reversal of flow in the condenser cooling waters, and that that reversal be carried forward at about 4-week intervals. It was also recommended that during this reversal period, the circulating water flow be throttled so as to increase the water temperature on the exit of the condenser to at least 110 F.

Various other attempts were made in the succeeding decade to obtain satisfactory chemical methods of control. These were summarized by the British Electrical and Allied Industries Research Association (11) in 1929. Apparently based on abstracts, the author reported successful control of marine growths by use of chlorine. The major paper upon which the author relied (12) had merely suggested that since chlorination would kill slime-forming and other microorganisms, and since these organisms were the food for mussels, chlorination might control *Mytilus edulis*. No experimental work had been done and since we now know that *Mytilus edulis* does not require living organisms for food, the hypothesis was unsatisfactory.

A German professor (13) has been widely quoted as reporting successful control of the fresh-water mussel *Dreisseniidae polymorpha* in the flumes of a powerhouse on the Glambacksee near Berlin. His report in 1921 indicated that the larvae of this organism died in the laboratory under chlorine dosage but apparently no unchlorinated control was used. No plant-scale work had been carried out. Some confirming laboratory work was done in Germany in 1929 (14). Similar discussions of the use of chlorine were later published (15, 16).

The first work in this field in the United States was started under the direction of W. J. O'Connell. In 1924 experimental work on intermittent treatment of condenser cooling water for the control of slime-forming microorganisms in cooling-water systems had begun in co-operation with Commonwealth Edison Company of Chicago, and the first plant-scale experiments of such intermittent treatment were tried at the Kearny Power Station of the Public Service Electric and Gas Company of New Jersey. The extension of this work to the control of marine growths was started in 1929, at the Northport Station of Long Island Lighting Company with the co-operation of L. H. Curley. The work there and at Corpus Christi indicated that it was possible, by intermittent chlorination, to eliminate completely the growths of the grasses and higher algae, and to reduce effectively the growth of bivalve forms. However, at that time eliminations of the order of 99 per cent were not attempted.

TYPICAL ORGANISMS

The life history, method of reproduction, food, responses to various unfavorable environments, and living habits of fouling organisms must be thoroughly understood before any intelligent plan can be suggested for their control. It is impossible to cover the wealth of material that is available about all the fouling organisms, but representative types can be discussed. However, before commercial installations are started, details regarding the organisms responsible for the particular fouling should be known.

Luckily for the engineer interested in controlling such growths, very few of the approximately 822,000 invertebrate animals which have so far been described by the biologists, cause fouling difficulties.

THE MOLLUSCA

Of the fouling organisms, the members of the phylum *Mollusca*, which includes the snails and other single-shelled *Gastropoda;* and the clams, oysters, mussels, and other bivalve or two-shelled *Lamellibranchiata* are the most troublesome. *Mytilus edulis*, or the edible or black mussel, is probably the most common fouling mollusk throughout the world. This organism has been responsible for most of the fouling difficulties in the British Isles and along the North Atlantic coast of the United States. The closely related *Mytilus californianus* has been responsible for



FIG. 6 HYDROIDS GROWING IN LOW-VELOCITY AREA OF A TUNNEL (Young mussels appear at right; dead mussel shells in upper left-hand corner.)

much of the fouling difficulties which have occurred along the western coast of the United States.

The black mussel (17) is familiar to all who have frequented any rocky coast of the northeastern United States. The shell is wedge-shaped, pointed in front and round behind; black or dark brown outside with indistinct circumferential growth rings around the shell. The interior of the shell is pearly with violet margins. Shells vary in length to a maximum of about 4 in. Its life history is typical of many other of the fouling invertebrates (18). Other *Mytilus* have nearly identical life cycles. The sexes are separate, but one individual may be male one year and female the next. The eggs and sperm from near-by individuals are discharged almost simultaneously and the eggs are fertilized in the open water. The sperm has only limited range of locomotion (19). An average female discharges from 5,000,000 to 12,000,000 eggs although a female $3^1/_2$ in. long may release as many as 25,000,000 eggs. Cell division begins immediately after fertilization and is completed within 20 min. The first cilia begin developing at the end of 4 hr (based on 68 F sea-water temperature), and at the end of 5 hr the embryo is completely free-swimming.

Development continues and at the end of 24 hr the organism is a very active swimmer; and by the end of 40 hr the complete digestive tract and the glands for forming the shell are becoming evident. At the end of 44 hr the organism has attached to some stable hard material such as rock, concrete, glass, rubber, or similar solid support, and has begun to develop the first single shell. At the end of 69 hr the elementary single shell or prodissoconch has completely enclosed the fleshy portions. The organism is still capable of rapid swimming and is able to crawl on solid surfaces, vertical walls, and the tops of horizontal tunnels. Some time later the true bivalve shell or dissoconch develops. Contrary to popular belief, the organism, which is now attached by long clear threads, known as byssus threads, (20) is still capable of motion, and if conditions of poor feeding, inadequate oxygen supply, or mechanical or chemical irritation develop, the organism will break the byssus threads from their point of attachment and crawl by a "foot" which projects out of the shell near the hinge. Such "walking" is similar to the locomotion of the familiar terrestrial snail. The mussel can also move by secreting new byssus threads and breaking off older ones.

The greatest growth rate occurs when the organism is completely submerged at all times, although under natural conditions predatory fauna may reduce the number of organisms below the low-water line (21).

Under normal conditions the adult *Mytilus edulis* will leave the shell open about 15 to 20 deg, the cilia on the mantle will vibrate rapidly and water containing food will be forced through the digestive tract. This flow of water amounts to about 10–20 gal per day in a specimen 2 in. long (22, 23) and seems to be constant, provided the organism is not irritated. This water circulation is called "drinking." The rate of digestion, on the other hand, seems to vary with metabolism demands. The shell remains open about three quarters of the total time in a temperature range of 31 to 77 F (24) without any variation with temperature.

As the water is circulated through the digestive tract any suspended solid matter adheres to the mucus surfaces. Digestive juices then digest such material as is usable for food, and this is assimilated. The balance is excreted as fecal pellets. By this process, mussels are capable of clearing cloudy and turbid water.

The exact nature of the food requirements is still little known. It was originally believed that living microorganisms mostly diatoms and algae, Fig. 7, were required, and they undoubtedly make up a large part of the natural food (25, 26). Robinson (12) based his theory of killing of mussels on this postulate. However, more recent work has indicated that while organic matter is

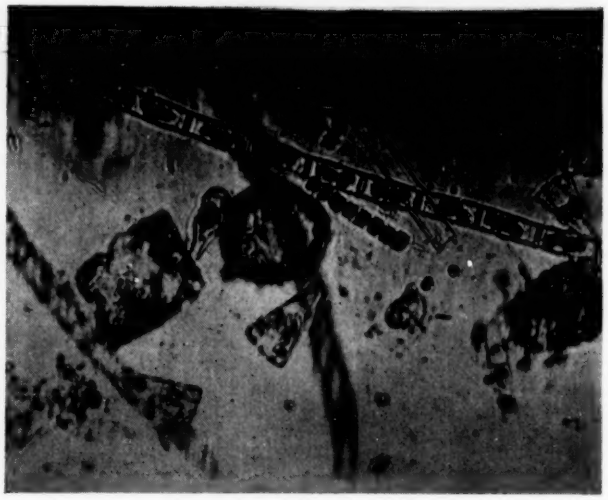


FIG. 7 ALGAE AND DIATOMS WHICH FORM BASIC NATURAL FOOD OF MUSSELS; ×460

necessary as food, decaying animal and vegetable material is as efficient as living organisms (27, 28, 29). It is known that domestic-sewage pollution, provided continuous anaerobic conditions are not set up, encourages growth.

Each species has its own preference as to conditions of light. The author has repeatedly placed *Mytilus edulis* and *Modiolus modiolus* in equal quantities in adjoining and connected cells, one light and the other dark. Marked migration of *Mytilus edulis* toward the dark and *Modiolus* toward the light is always noticed. *Mytilus* grows three times as fast in total darkness as in sunlight (30), although a weak light may be still more favorable. Optimum growth occurs at 50 to 68 F, and is seriously inhibited by heating for even a few minutes a day (31).

If any unfavorable conditions develop or anything disturbs the organism, the shell will close within a fraction of a second and only after an extended period will the mussel open the shell slightly and "drink" very cautiously. This ability to close its shell tightly makes all adult *Lamellibranchiata* very difficult to control. All mussels have a cushion pad which forces the shell open as soon as the adductor muscle is out or relaxed. Therefore a gaping shell can be considered as a sign of damage to the organism.

Pecten (scallops) (32) are not usually responsible for fouling, but *Pectens latiauratus*, which attaches with byssus thread reduced an 18-in-diam cast-iron line serving a South Carolina power plant to 6 in. in about 12 months.

The various fresh-water mussels have a life history similar to *Mytilus edulis*. However, important differences exist. Instead of releasing single-celled eggs, the adult female permits the eggs to be fertilized while still within the mantle, and free-swimming "glochidia" about 0.014 in. diam are released (33). A parasitic period on host fish is necessary before metamorphosis into shelled forms can take place. *Dreisseniidae* is limited in range to fresh or brackish water of less than 1 per cent salt content (34).

Dreisseniidae is similar in appearance to *Mytilus edulis* but lacks the pearly shell interior. The organism is common in Germany, having been responsible for actually shutting down a power station on the Glambacksee with a 12-in-thick growth on tunnel walls (13). The American oyster (*Ostrea virginica*) is a common Mollusca responsible for severe fouling of power inlets on our South Atlantic and Gulf coasts, where it is easily recognized by its rough shell and white interior. Its life history, together with that of its European cousin (*Ostrea edulis*) has been carefully

studied because of its importance in the culture of oysters for food. Its life history is similar to the edible mussel (35). However, its spats are apparently considerably more delicate. The period of pelagic or larvae life varies from 13 to 17 days (36), depending upon temperature. The spat prefers a dark place to settle, and metamorphosis can be delayed by failure to find a suitable resting place (37). Spawning can be stimulated out of season by raising the water temperatures from 82 to 86 F (38). It can be induced by the presence of eggs or sperm in the water, not only of its own specie but those of other mollusks, or by various chemicals (39). The season of normal spawning varies with location, being from April to June in some eastern United States waters and from July to August in others (40). In Denmark it occurs from late May to mid July, while in Holland spawning occurs in September.

The daily rate of growth varies with age of the organism and water temperature, but does not vary with the actual size of the organism (41).

The Sponges

The sponges (*Porifera*) are the simplest of the fouling macroorganisms. A "sponge," as normally seen with the naked eye, is a colony of individuals with the large number of "pores" on the outer surface. Through these pores, water containing food material is circulated by flagella, and as it passes through the cloacal cavity, exposed cells absorb food material and transmit it to near-by cells. No truly "specialized" organs exist.

Reproduction is by three separate and distinct methods, i.e., by budding, by the formation of gemmules, and by sexual methods.

Budding takes place within the organisms and results in a single "sponge" increasing in size or even dividing, but does not permit the formation of new groups at a distance from the previous place of attachment.

The formation of gemmules is similar to a formation of "spores" in microorganisms. A living cell migrates to the center of the colony and is covered with a capsule secreted by the adjoining cells. When unfavorable conditions of temperature (in fresh water lakes) or dryness (in tropical lakes) occur, these dormant forms resist those unfavorable conditions and upon the return of conditions conducive to development, burst the capsule and begin development of a new sponge.

Sexual reproduction is in the main responsible for the development of new colonies. "Some sponges are hermaphroditic, others are unisexual. No special sexual organs are present, the ova and sperm developing from ... the inner cells .... The ... egg develops into a ciliated two-layered larva which swims actively about in the water, which finally attaches itself and, after metamorphosis, develops into the adult animal" (42).

It is during the larva stage that the sponge is most vulnerable to attack by poisons. They are relatively sensitive to changes in pH (43).

The Bryozoa

The Bryozoa, or Polyzoa as they are called in England, are minute colonial animals that are often confused with seaweed and sponges both by the layman and the early naturalists. There are about 3000 marine species and 35 fresh-water species. Upon first examination, they may appear as red or white encrusting patches, as groups of dead sticklike organisms, brown or purple in color, projecting from a rock or as branched sticks with plumed ends (*Plumatella*). The familiar jelly balls in fresh-water lakes (*Pectinatella*) are also Bryozoa.

Each colony or "zoarium" increases in size by budding. Sexual reproduction also takes place; the eggs and sperm being released into an inner cavity and developing to a larva stage there. The larva are released either through special openings or by the death and disintegration of the parent. Other specie (notably the fresh water *Plylactoloemata*) are capable of forming "statoblasts" to resist unfavorable conditions similar to those developed by sponges.

Statoblasts of *Pectinatella magnifica* can endure much drying but not absolute desiccation. They are not harmed by brief exposure to temperatures as low as 31 F and as high as 130 F; while the adult form or "polypids" survive only in a range of 50 to 104 F (44). The statoblasts of fresh-water Bryozoa usually germinate at 62 to 66 F. These statoblasts not only provide a means of surviving unfavorable conditions, but also provide a ready form for transportation by wind and birds.

Grave (45) has reported on the development of *Bugula flabellata*, one of the common Bryozoa on the New England coast. The breeding season at Woods Hole, Mass., extends from June 10 to November 15. The young are expelled from the colony as swimming embryos. After a free-swimming period of 4 to 6 hr, the larva attaches, profound metamorphosis takes place involving the loss of some larva organs, and the colony begins development. At the end of a week the colony has increased by budding to 8 or 10 individuals, at the end of 2 weeks to 100 individuals, and by the end of a month the colony is half grown and has reached sexual maturity. Colonies $1^1/_2$ to $1^3/_4$ in. diam are able to hibernate successfully and resume growth in early May. Even more rapid growth occurs in South Atlantic and Gulf Coast waters where the time from first infection to serious difficulty in industrial water circuits may be only a matter of weeks. Colonies of *Bugula neritina* grow as long as 4 in. at Beaufort, N. C. (46). Many fresh-water Bryozoa flourish in dark as well as light, and cause serious fouling in water mains (47).

The Barnacles

The barnacles are probably the best known of the fouling organisms, since they have been responsible for most of the serious fouling of ships' bottoms. Because of their hard shell with several parts and because they seemed to "drink" like the mollusks, they were so classified by the early zoologist. J. V. Thompson in 1830 was the first to show definitely that they were Crustacea, closely related to the crayfish, lobster, and soft-shelled crab. Darwin (48) in 1850, made an extensive study of the group (49).

Moore (50) on the Isle of Man and Grave at Woods Hole, Mass. (51), among others, have made extensive studies of the barnacles. They are mostly hermaphroditic but in a few cases are unisexual. Some species have a male form which is very tiny and lives parasitically within the shell of the female.

The eggs (52) are held within the mantle cavity and the larvae are released as free-swimming forms after hatching. The "nauplei" changes form slightly with each moult into forms known as "meta-nauplei," and then metamorphoses into an entirely different type of organism known as the cypris larvae or the "cyprid." This later stage lasts from 7 days for *B. amphitri* to two weeks for *B. balanoides*. During this stage the cyprid swims with a sudden backward motion of the appendages. The barnacles then settle down on a suitable place of attachment and begin to undergo a second metamorphosis and form a shell. Actually the organisms will make several attempts to find a suitable place to attach and if the one selected is not satisfactory the barnacles will break away even after they have become partially attached. After finally reaching a suitable place, some small motion in an area of about $^1/_2$ in. is still possible (53).

"In immature barnacles tissue growth continues throughout the year but is most rapid in the spring and autumn. In mature barnacles there is a sharp drop in growth rate during the summer

and a slight one during winter associated with the development of the larva." In exposed places, below mean-tide level, the *Chthamalus* reach sexual maturity in the first year and die in their third year. In less exposed places, the organisms reach sexual maturity in their second year and die in their fifth year (54).

The spat will choose its resting place partly on the basis of light intensity, apparently making a choice of optimum light, shying away from too bright and too dark places. The organism apparently can only distinguish light from dark areas. Light has also some control on growth (55, 56), and the adult organisms will close their shells when a shadow passes over them (57).

Barnacles also react to changes in potassium (58), alcohol (59), carbon dioxide (60), calcium (61), salt-water dilution (62), strong electrolytes, urea, glucose, and glycerol (63).

The Tunicates

The highest organisms responsible for fouling in industrial plants are the tunicates. They represent a "subphylum" of the phylum *Chordata* to which also belong the vertebrates including fish, mammals, and man. They derive the name from their thick, hard, cellulose coating and are one of the few animals capable of synthesizing cellulose.

Of these, one of the most common is *Molgula manhattensis*. It consists of a brown sac with two distinct openings at the end of noticeable tubes. While the individual organisms are only about 1 in. in diameter, they form large colonies which break off in mats from tunnel walls and often blanket tube sheets. It is also not uncommon, for example in the Kill Van Kull off Staten Island, for these mats to be broken off by wave action and block inlet screens and sometimes even bar racks. Related specimens with nearly clear tunics have been clogging powerhouse screens in Stamford, Conn., harbor. They are commonly called "squirt balls" because of the habit of ejecting water from their body cavity sometime after they have been lifted from water.

The life history of the *Molgula manhattensis* has been carefully studied by Berrell (64). Eggs of about 0.006 in. diam are released in the water and fertilized there. The time taken from fertilization to hatching varies with temperature, being approximately 120 hr at 46 F, and 40 hr at 62 F. The hatched egg yields a "polliwog" which is free-swimming with an active tail. The tunicates have a heart, elementary circulatory system, digestive tract, liver, a nerve cord, and a gangula which is an early form of the brain. After a period of 160 to 450 hr, which period depends on CO_2 content of water, salinity, pH, and temperature, the "polliwog" attaches to rock, inlet tunnel or tube sheet, or other structure, with three sticky tentacles and begins a retrogressive metamorphosis. Powers of locomotion are lost, the existing digestive tract disappears, and a new one begins to form on the remaining portion of the animal.

Even this high animal can reproduce by "budding" and thus form extended colonies. In order to attain maximum efficiency in control of tunicates, control methods must be timed to attack the organism during the early active larvae stage or during early metamorphosis, before the larvae alimentary canal, through which both food and oxygen are absorbed, is eliminated from use.

Al arge number of standard zoological texts, as well as specialized books and articles, give further details on the life history of the fouling and related organisms. Pratt (42) is a good representative general text for identification of invertebrates; while Ward and Whipple (65) give more detailed treatment covering the fresh-water organism.

A good recent review of the reactions of invertebrates to stimuli has been published by Warden, Jenkins, and Warner (66).

CONTROL METHODS

Numerous methods have been suggested for preventing the settling of larval forms and the killing of adult forms of fouling organisms. Among them are the following:

1 Heating the water.
2 Increasing or decreasing salinity of the water.
3 Creating anaerobic conditions in the water.
4 Increasing water velocity in tunnels.
5 Poisoning with acids.
6 Antifouling paints.
7 Screening the tunnel entrance.
8 Poisoning with miscellaneous poisons.
9 Poisoning with chlorine.

Any theory of killing or method of control is only as valuable as it can be proved in actual practice at plant scale. Heat, increased velocity, surface treatment, acid, and chlorine are the only methods that have been put into practice on a large scale.

In selecting a particular method of operation, it is well to bear in mind the factors to be considered. While there will be differences of opinion as to the relative importance of these various factors, most designers will wish to consider them all.

1 The method should not materially increase the operating cost of the plant. Too often in evaluating the various methods involved, designers are likely to decide against one particular method, because of a direct cost of operation and decide upon another that disproportionately increases pumpage costs or lowers the general efficiency of the plant.

2 The method should have lowest possible first cost consistent with low operating cost. Particular care should be taken in evaluating cost of special equipment for control of marine growths compared with increased cost of general plant equipment to make possible other methods of control.

3 The method should assure that no organism can grow to a size that will be detrimental to plant equipment, and a method should be available for recovering control of the growth if, for any reason, the treatment method must be interrupted.

4 The method should permit operation of the plant at full capacity without interruption.

Control by Heat

The earliest method of control used on plant scale was heating circulating water. One power station throttled the circulating-water flow until the desired heat balance was obtained. The amount of heating required is dependent upon the normal average temperature and normal range of temperatures of the water in which the organism has grown.

Without reporting initial temperature of the water from which the organisms were removed, Henderson (67) found that by raising water temperature gradually and removing specimens to cooler water for recovery, the lethal temperatures for various mollusks were *Leda tenuisulcata*, 88.7 F; *Cardium boreulis*, Conrad, 88.9 F; *Modiolaria discors*, Beck, 89.4; *Saxicava rugosa*, Lamaich, 91.0 F; *Crenella glandula*, Atoms, 91.0 F; *Cardium pinnulatum*, Conrad, 91.8 F; *Astarte undata*, Gould, 92.4 F; *Pandora trilineata*, Say, 92.4 F; *Modiolaria nigra*, Loven, 94.2 F; *Yoldia sapotilla*, Simpson, 94.7 F; *Zirpoea crispate*, Gray, 92.4 F; *Mactra solidissoma*, Chemnitz, 98.6 F; *Mya arenaria*, Linne, 105 F; *Mytilus edulis*, Linne, 105.4 F; *Nacoma fusca*, Atoms, 108.2 F; *Venus mercenaria*, Linne, 113.3 F; and *Ostrea virginica*, Lister, 119.3 F.

It is interesting to note that *Tubularia* in water above 68 or 70 F, remains dormant, although it is able to recover when held for 3 days at 65 F (46, 68). In Scotland successful control of

Mytilus edulis on plant scale has been obtained by heating the circulating water to 120 F.

The cost of operating such a system can be extremely high. Assuming that a power station with initial steam conditions of 400 psi and 500 F, and capacity of 25,000 kw is fully loaded, and assuming that the circulating-water temperature must be raised from 65 to 120 F, the fuel cost alone due to the corresponding loss in vacuum for a 2-hr period will amount to approximately 40 tons or, computed at $2 a ton, $80. The load capacity of the plant is, of course, at the same time reduced.

In addition, increasing the temperature of the condenser may cause leaking ferrules and other leaks due to uneven expansion of tubes and tube sheets. Any operator who has experienced a failure of condenser water supply will appreciate this problem.

The cost of the initial installation of such a heating system for a steam power plant will also be higher than other methods of marine-growth control. This can be readily appreciated when it is realized that the entire circulating-water system, and particularly the pumps must be designed for reverse flow. For plants not having waste heat available, the cost of such heating would be prohibitive.

Control by Changes of Salinity

Fresh water has been used as a means of eliminating marine growth from fouled surfaces since ancient times. Early mariners ran their vessels up fresh-water streams to loosen the ship's fouling load.

Most marine organisms are adversely affected by reductions of salinity, but the absolute value that will support life varies with the species, the salinity of environment from which they are removed (69), and the rate at which the change in salinity occurs. Because of the number of variables, it is difficult to correlate various experimental results. Sudden reductions to 30 per cent of normal salinity have been found to be fatal to *Mytilus* (70). *Ostrea virginana* will not fatten below 20 per cent salinity (71). The critical salinity for maintaining life and for growth varies from individual to individual within a given specie (72).

Most fresh-water invertebrates die in salt concentrations above 5 grams per liter NaCl (73) but *Physa heterostropha* have been known to live actively in 25 per cent sea water if the concentration is slowly increased to that figure (74). Contrary to the average tendency, the oyster drill grows to a larger size in brackish water than in salt water (75). Increase or decrease of salinity from that of normal sea water acts as an anesthetic, causes loss of sense of balance in the motile organisms and paralysis of the motor systems (76, 77).

Practical applications of this method for control of growths in industrial-plant water circuits are difficult, unless brackish streams varying in salinity with rainfall are readily available. Unfortunately even for plants with such streams available the problem is not fully solved for all the fouling organisms are not as sensitive as those just mentioned, and some will thrive under conditions of widely varying salinity.

Plants on such brackish streams are faced with another problem which is acute along the St. Johns and Hillsboro Rivers in Florida. Spring rains almost invariably change these streams from brackish to fresh water. The mussels and barnacles which have set in the circulating-water tunnels are killed, and the shells and debris of the dead organisms float up and clog pipe lines and blanket tube sheets. No operator having tube sheets badly clogged with shells will say that natural variation of salinity is a cure for his marine-growth problems!

Control by Creating Anaerobic Conditions in Water

The reduction of oxygen content of the water below certain critical levels will eliminate many organisms. The exact value of dissolved oxygen which will support life varies with species. All fish and most of the invertebrates require free dissolved oxygen. At least one of the contributing causes of death of oysters in water heavily polluted with paper-mill waste has been the reduction of oxygen content (78, 79).

However, no practical means are available to remove oxygen from industrial-water circuits. The gross pollution which has been so common in some of our tidal streams has effectively done this in certain areas; but the disagreeable odors and prevention of recreational use of the streams are too high a price to pay for elimination of fouling organisms (80, 81). As pollution of streams is reduced with improved waste treatment, these anaerobic conditions will be eliminated. This trend will probably be greatly accelerated in the near future, both by governmental pressure to eliminate such public health hazards and by the realization by industry that many valuable products may be recovered by proper treatment of their industrial wastes. Even in streams having completely anaerobic conditions certain mollusks are still able to survive. *Mya arenaria* (82), *Saxidomus gigantea* (83), and various others (84) have been shown to be capable of acting as facultative anaerobes. By this is meant that they are capable of obtaining energy by the breakdown of organic matter without use of oxygen.

It has not yet been conclusively demonstrated whether the Mollusca can continuously live under these circumstances, or whether they must be subjected at regular intervals or at stated times in their metamorphosis to aerobic conditions.

Sewage pollution will also encourage certain seaweed growth such as sea lettuce (*Ulva latissima*) (85), which also often blocks screens and tube sheets.

Control by Increasing Velocity

Where high velocities in the line can be obtained without unduly increasing the cost of pumping, such increased velocities may be used for the control of aquatic growths. The author has observed that *surface* velocities in excess of 1 fps minimize the set of mussel and barnacle larvae on smooth metal surfaces. However, very much higher *average* velocities must be attained to arrive at surface velocities of 1 fps on rough surfaces; such as, cast-iron pipe and concrete tunnel walls. *Mytilus*, which have already formed bivalve shells have been successfully removed by increasing the water velocity in cast-iron pipes to $13^1/_2$ fps for a period of 1 hr each week. However, such a means of eliminating marine growths is practical only where catch basins or strainers can be economically installed to eliminate the debris before it reaches critical equipment; such as condensers and pumps. The idea of high-velocity flushing is definitely practical for application in small plants. However, in large installations, particularly where large circulating- and cooling-water flows are required, the cost of pumps to attain these velocities, and the cost of power to operate them at the higher friction losses make the method economically impractical.

Control With Acids

The shifting of pH of the water was one of the earliest methods of control of fouling organisms attempted. Plant-scale experiments were carried out with partial success as early as 1915. Extensive studies of the effect of lowered pH on various mollusks were later carried out by Prytherch (86, 87) who was searching for an easier method of opening oysters to expedite commercial shucking. The natural pH of sea water and its buffer capacity varies slightly from place to place in the open sea (88) and varies considerably where industrial pollution is present. Fig. 8 is a typical curve of a buffer capacity of sea water, as measured by glass-electrode titration of samples taken in the open sea off the New Jersey coast.

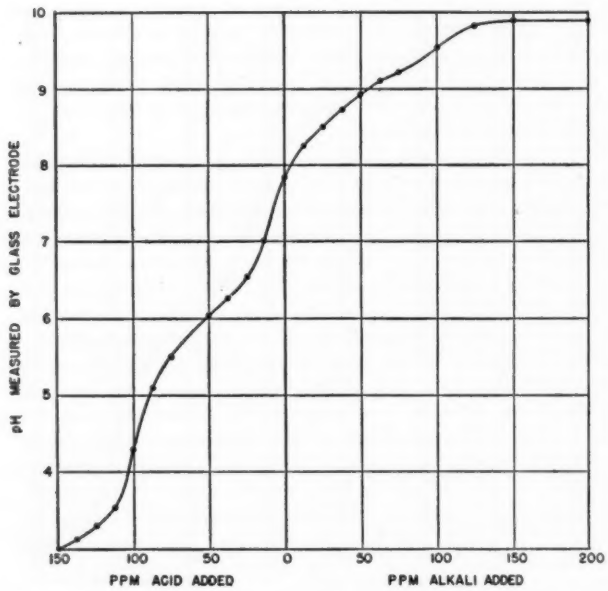


FIG. 8 BUFFER CAPACITY OF SEA WATER MEASURED AS pH BY GLASS ELECTRODE WITH SULPHURIC ACID AND SODIUM HYDROXIDE
(The curves remain flat at pH 9.9 until all calcium carbonate has been precipitated.)

It has been found that maintenance of pH between 2 and 5 depending upon the organism, and for periods varying from 1 to 3 hours will anesthetize the average *Lamellibranchia* and cause the shell to open sufficiently wide to permit insertion of a knife. Considerably longer periods are required actually to kill the organism. Corrosion, at these pH values, particularly of brass condenser tubes, is serious. As will be noted from the curve, 150 ppm acid is required to obtain a pH of 3. Translated to plant scale on a 25,000-kw electric generation station, it would require 5625 lb of 60-deg Bé sulphuric acid for a 3-hr period. Computed at current prices of $1.25 per cwt, that would amount to $70 per day of treatment. Corresponding increase in cost would, of course, occur in larger plants. Lower concentrations are useless. Ritchie (10) found that 10 ppm of sulphuric acid in water had no effect on mussels after submergence for 240 hr.

CONTROL WITH ANTIFOULING PAINTS AND SURFACES

A large amount of carefully detailed experimental work and large-scale tests have been carried out by the United States and British navies and by various laboratories and paint manufacturers in an attempt to discover antifouling paints and surfaces for ships' bottoms. Literally thousands of patents have been issued covering various surface treatments to prevent the accumulation of fouling organisms. Paints containing as wide a variety of materials as mercurials, arsenicals, silicates, lead, copper, zinc, strychnine, cyanides, phenols, creosote, resins, asphalt, hair, guano, asafetida, and cow dung have been suggested (89). A smooth surface, while it will discourage fouling, will not prevent it, for even a smooth plate-glass panel will foul. Some authors (90) have suggested that paints can be compounded so as to slough off at high rates and take the load of fouling organisms with it. However, the required rates are high enough to make the method impractical.

Copper and copper-bearing paints have been found to be the most efficient antifouling materials, and recent exhaustive tests (91) have indicated that the antifouling properties of copper-bearing paints are directly related to the leaching rate of the metallic copper. Means of making laboratory determinations of leaching rates which correlate with fouling determinations have been devised (91).

Antifouling paints, which necessarily leach out material and become porous, should never be used to prevent corrosion. Protective primers of known corrosion-preventative ability should always be used under antifouling finishes.

All antifouling finishes eventually lose their efficiency; most of them after a single season. In long cast-iron pipe lines and on cement tunnel surfaces, the surfaces are too rough to make the use of paint economical. This is particularly true in plants where dewatering once a season for the renewal of the painted surface would be extremely expensive, as well as creating a hardship due to the required plant shutdown. On ships' bottoms and other metal surfaces which must be painted at regular intervals to prevent corrosion, it is the best method of preventing fouling yet devised.

CONTROL BY SCREENING

Water inlets of all power stations and other large users of industrial water are screened. However, to have a screen fine enough to catch the larvae forms of the fouling organisms, which are less than $^1/_{100}$ in. at early stages of development, is totally impractical. Any screen which would catch such organisms would quickly clog with microbiological accumulations, and unless made of corrosion-resistant material, would soon become permanently blocked with corrosion products.

POISONING WITH ACTIVE POISONS

Various active poisons have been suggested as controls for marine growths. Cyanide has been suggested but has been rejected because of extreme danger to human life.

Some plants have used coal oil, gas-oil drip, kerosene, creosote, and similar oily products for control. Sections of the circulating-water tunnels between high and low tide become coated with these materials and become unsatisfactory places of attachment for fouling organisms. Some control is thereby obtained but no control is effected below the low-water line. Any method using a poison which is not dissipated, or consumed by mixing with other sea water, is dangerous in that it is likely to kill near-by oyster and clam beds and to cause public-health hazards at near-by beaches. Release of such poisons could well become the subject for damage suits and injunctive relief by the owners of proprietary oyster beds near the industrial plant using such poisons. Also, in almost all cases the cost of these poisons at the required dosage are prohibitive.

Other chemicals are useful in the control of particular organisms. For instance, quicklime spread over oyster beds at the rate of 400 lb per acre will kill starfish without affecting the oysters. This material burns the soft flesh of the starfish and causes lesions that fail to heal (92).

A patent (93) has been issued covering the use of cyanide in conjunction with chlorine for freeing a ship's bottom of fouling organisms.

CONTROL BY CHLORINATION

Chlorine is the most economical and widely used means of controlling fouling organisms in both salt- and fresh-water circulating systems. It has proved successful in many plants throughout the world. A few plants have experimented with chlorine and have failed to achieve control. These failures have occurred because of lack of appreciation of the need of proper residuals (i.e., active chlorine left in the water), proper treatment periods, proper variations of treatment with breeding periods, and proper control and distribution of chlorine in the circulating water.

Early experiments using chlorine have already been detailed.

Power stations scattered along the Atlantic coast from Massachusetts around the tip of Florida and as far along the Gulf coast as Corpus Christi have chlorinated successfully. The organisms thus controlled have covered a wide range of species.

Cursory details of English experience (94) and the installation at the United States Naval Air Station at Quonset Point, R. I. (95), have already been published.

It has been reported that successful control of *Mytilus edulis* has also been obtained with chlorine at the Corporation Power Station at Belfast and Dublin, Ireland, and Brighton and Southampton, England.

Early attempts using chlorine were based on continuous chlorination. Later short intermittent treatments were found unsuccessful. We have now found that properly spaced intermittent-treatment schedules are more economical than continuous treatment and are completely satisfactory. It will be remembered that all fouling organisms have a spat or larvae stage during their sexual reproduction and that infections in new areas can begin only by the ingress of such larvae. Therefore if the larvae can be killed at regular intervals, before they have completed metamorphosis, no new fouling will occur. In this the design engineer is fortunate, for most organisms during metamorphosis have a higher metabolism than at any other time in their lives and therefore are more vulnerable to poisoning.

It is obvious that if chlorination is carried out periodically so as to kill all the larvae in the tunnel, and is then repeated before any new larvae that enter the tunnel after treatment stops have had time for complete metamorphosis, complete control will be established. Such a statement is, however, an oversimplification of the problem. It is always possible, and will occasionally occur, that some larvae will arrive in the tunnel in an advanced stage of development and will complete metamorphosis almost immediately. When it is realized that a normal fouled shore line may contain a thousand million barnacles per mile and that these will release a million million larvae, or that a single *Mytilus edulis* may release as high as 25,000,000 eggs, it will be realized that only a very small percentage of the larvae need escape to cause serious difficulty.

A distinction should be drawn between complete prevention of fouling and substantial reduction or control of fouling. In all cases where fouling must be completely prevented, continuous chlorination during the fouling season must be used. However, where control only is required, intermittent chlorination may be used more economically.

In those cases where intermittent preventative treatment is to be used the lines should be purged by continuous treatment for short periods at regular intervals. Glass flanges should be inserted in pipe lines or test blocks should be inserted into tunnels and observations made at weekly intervals. As soon as the residual fouling that is not being prevented by the intermittent treatment, reaches the point where the organisms threaten to cause plant operating difficulty, then a corrective treatment should be instituted. This treatment will consist of chlorination at higher residuals and for longer periods than the preventative treatment. The reason for this longer period is obvious, since all of the *Lamellibranchia* are capable of closing and remaining closed for long periods. Chlorination periods must be extended until the organisms are forced to open their shells to obtain food or oxygen.

Observations by the author on experimental troughs set up at the inlet slip of the power station of the New York, New Haven, and Hartford Railroad at Cos Cob, Conn., through the courtesy of Mr. Sidney Withington, Mr. E. F. French, and Mr. John Coolidge, will illustrate the method of killing adult organisms. A large group of shelled *Mytilus edulis* of varying size was removed from the piers near the site of the experiment and placed in untreated wooden troughs with fresh sea water continuously circulated through the troughs. Time was allowed for the organisms to become acclimatized and no treatment was begun until all specimens were fully attached by byssus threads. Chlorination was then begun in different troughs at levels sufficient to yield 2.5, 5, and 10 ppm chlorine residuals.

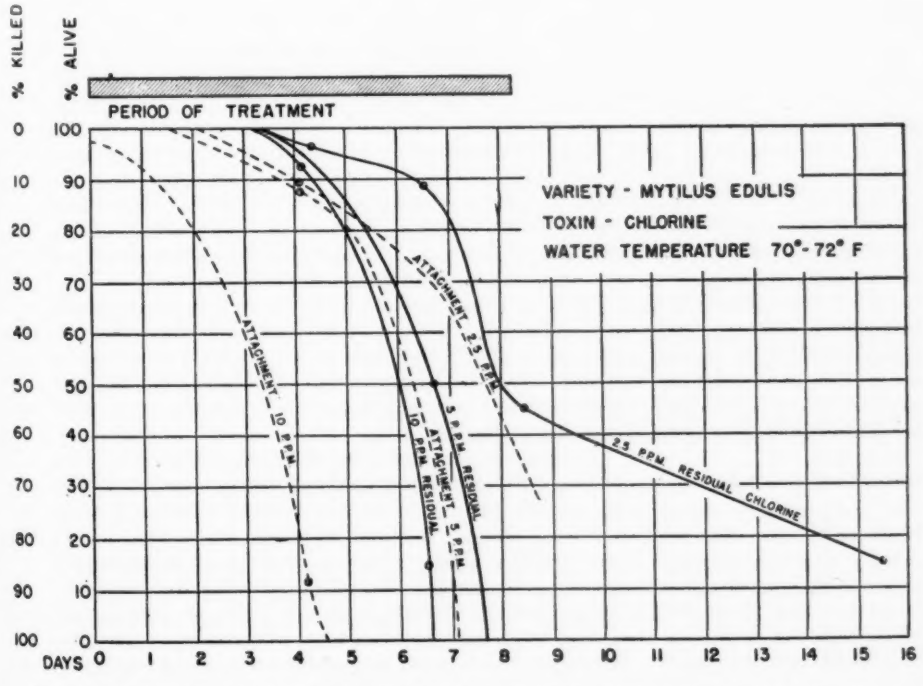


FIG. 9 TIME REQUIRED TO FORCE MUSSELS TO DETACH AND TO KILL MUSSELS IN VARIOUS CONCENTRATIONS OF CHLORINE

Fig. 9 illustrates the rate of detachment and rate of killing of these adult organisms. It will be noted that the mussels break their byssus threads and attempt to migrate to more favorable environments before chlorination actually kills them. Killing, in this case, is defined as reaching a state such that when the organism is removed to clear fresh sea water it does not recover and in a few hours or days it has opened its shell and actual decomposition has begun.

Most larvae, as contrasted with adult forms of fouling organisms, are killed by chlorine residuals of 0.5 ppm applied continuously. This has been confirmed by experiments at various places along the Atlantic Coast from Massachusetts to Florida. However, on one plant scale operation in Virginia 0.5 to 0.6 ppm chlorine residuals maintained continuously failed to control mussels and barnacles.

In another case, an electric plant in New England chlorinated

during one season at 0.5 ppm chlorine residuals on schedules of 20 min each, six times per day, and obtained complete slime control on condenser tubes, but showed no noticeable reduction in their annual accumulation of 600 cu ft of mussel and barnacle shells. The following season the same plant chlorinated at residuals of 0.7 ppm on a schedule of two 1-hr periods per day. The accumulation that year was 25 cu ft. Further reduction could have been effected.

In June, 1944, the plant of the Montaup Electric Company in Somerset, Mass., removed 20 tons of growth from its tunnels. This was considered a normal annual accumulation. Chlorination was started in January, 1945, and examination in June, 1945, showed less than $^1/_2$ ton of fouling-organism accumulation. Observation indicated that most of this had accumulated prior to the beginning of treatment. Because of physical variations among different plants with regard to water-circulating tunnels and the piping arrangements, as well as predominating fouling organisms, these experimental results and previous plant experiences should be used as a basis of design in other plants only with extreme caution.

Care should also be taken in instituting plant scale operations. For instance, in the beginning of treatment of a circulating-water system that has been in use for some time, a large quantity of organisms, usually sufficient to block tube sheets, and often sufficient to cause serious damage to circulating-water pumps, will be released if curative treatment is immediately applied. To prevent this, chlorine residuals should be held at low levels and chlorination should be short at the beginning, gradually lengthening as less and less fouling organisms remain in the tunnel.

In the preventative treatment, extreme care must be taken that the regularity of intermittent schedule be uninterrupted. The author inspected one tunnel that had been under treatment. Because of failure to obtain chlorine in the required time, the plant had been without treatment for 4 days. No continuous curative treatment was attempted to fill in the deficit. Three months later a full $1^1/_2$ in. thickness of *Pecten* of nearly uniform size had developed. During the 2 years following when no interruption in treatment occurred, no fouling was found.

The chlorination of salt water carried in steel lines has certain distinct difficulties. If continuous treatment is used, the slime film which ordinarily would inhibit salt-water attack on the line is completely removed and corrosion is aggravated. Cases have been observed in which $^1/_4$-in-thick scales have developed on steel lines within a few months. However, if corrosion-resistant alloy or cast-iron lines are used so that the natural aggressive action of salt water is minimized, chlorination will prevent bacteriological corrosion (96, 97, 98) and thus materially increase metal life. Where the water is naturally aggressive and the use of steel lines is indicated, intermittent chlorination, which will permit the reformation of protective slime films during idle periods, will minimize salt-water corrosion and yet maintain macroorganism control and also heat-transfer efficiency. Where the water is not naturally aggressive, such as is normally the case in fresh-water lines, continuous chlorination at properly controlled residuals will reduce rather than increase corrosion rates.

The means of applying chlorine to large circulating-water flows should be carefully considered. Chlorine is only slightly soluble in fresh water and is still less soluble in salt water. For this reason special apparatus for obtaining completely dissolved chlorine in water solution must be provided. In order to obtain marine-growth control in large tunnels and pipe lines, the chlorine solution must be evenly distributed through the circulating-water flow. Unless wide experience is available as to the type of flow that will be found in screen wells and suction chambers, it is likely that a point of application and means of diffusion will be selected which will completely free one area of serious growth and permit uncontrolled growth in other areas. It also should be remembered that while chlorine in the low concentrations required for the killing of these organisms is not corrosive to normal materials of construction, it is highly corrosive in higher concentration and particularly if released as a gas. Therefore, if adequate mixing and dilution are not provided local areas of high concentration may severely corrode pump bells, impellers, and casings.

The chlorination of circulating water will have no adverse effect on oyster or clam beds lying off shore nor on near-by bathing beaches. This can be readily appreciated when it is realized that the "chlorine demand" of normal sea water is such that the mixing of chlorinated water with an equal volume of sea water will eliminate or materially reduce the residual chlorine so as to be no longer toxic to oyster beds. The residuals carried approximate those used in swimming pools, and therefore if pH is maintained as it will be by the natural buffer capacity of sea water, beneficial rather than harmful effects would occur from swimming directly in the discharge water.

Throughout this discussion the term "chlorine residual" has been used to indicate a free chlorine residual or active HOCl as contrasted to a bound or chloramine residual, where the chlorine is bound by reaction with ammonia or amino compounds. Recent work (99, 100, 101) has indicated the wide difference between the killing power of chlorine and chloramine residuals. Chloramine residuals have distinct use for specific purposes since they are more stable in the presence of organic matter. They are therefore highly useful for the sterilization of swimming-pool water, and stock and pulp systems in paper mills. However, where ammonia content is not high, and this is true in most applications where marine fouling by macroorganisms is a problem, the use of free chlorine is recommended. Unfortunately, even if no ammonia is added, chloramine residuals often still occur because of the high ammonia and amino-nitrogen content of water which has been subjected to organic pollution. In those cases a question arises as to whether it is more economical to use "Break Point" chlorination and remove the ammonia, or to take the longer killing periods and higher required residuals of the chloramine. The determination as to whether a particular water with a particular chlorine dosage and contact period is yielding a chlorine or chloramine residual can easily be determined by the Laux-Nickel test (102, 103) or by titration with arsenite (104).

Chlorination should be carried out only at the higher residuals necessary to kill macroorganisms in their larvae form during those periods when the larvae are in the water. Naturally, most industries will desire to chlorinate at lower residuals during the remainder of the year to prevent formation of microorganic slime and thereby maintain heat-transfer efficiency (105).

The cost of marine fouling control with chlorine can usually be economically justified. A 25,000-kw station will usually be able to achieve control for about $3.50 per day during the fouling season. More than this amount will be saved due to improved vacuum as well as reduction in cleaning cost and outage resulting from marine fouling.

The time of year during which fouling will occur and rate of fouling will be dependent upon the fouling organism responsible for the difficulty, upon the water temperature, and upon the particular season. Seasonal variations are in turn dependent upon whether a large or small group of adult organisms succeeded in establishing themselves in the near-by waters during the previous reproductive periods, and whether these organisms survive to the next breeding time. Conditions of tide, particularly as it affects water temperature, will also influence fouling periods and rates. These factors are too numerous and varied to permit accurate forecasting. To obtain this type of informa-

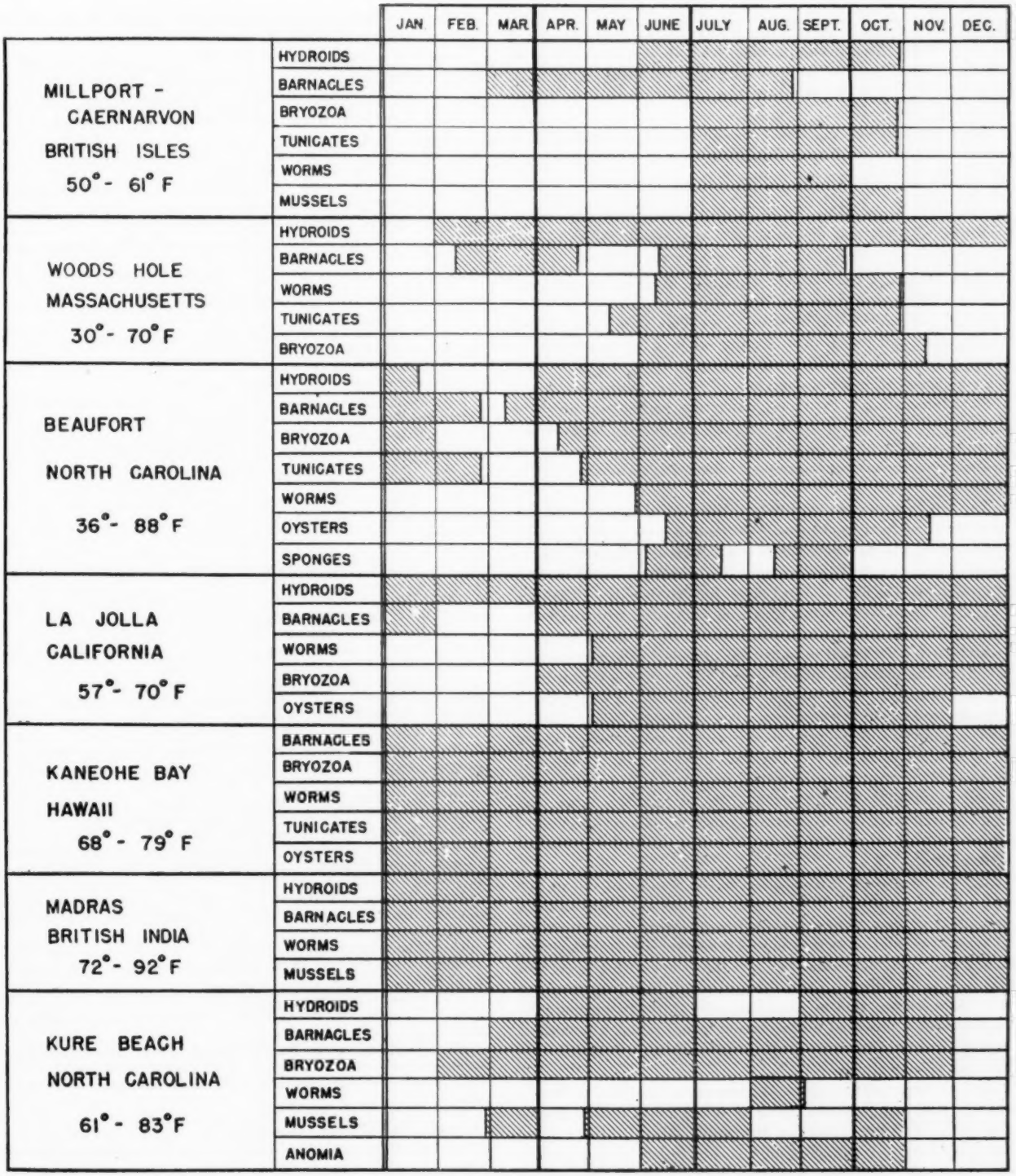


FIG. 10 FOULING PERIODS IN VARIOUS HARBORS

tion, the William F. Clapp Laboratories of Duxbury, Mass., and the Woods Hole Oceanographic Institution of Woods' Hole, Mass., have maintained for a number of years test blocks and panels at a large group of stations on the Atlantic and Gulf Coasts and elsewhere. These specimens are returned to the laboratories at regular intervals and examined to determine both settling rates and growth rates for the particular station and time. From these examinations much valuable information has been amassed.

The technique of setting such panels in order to obtain reproducible results over a long period is beyond the scope of this paper. Color and material of the panel depth and angle of submergence, type of support, and location of the tested area with respect to contaminating influxes and tidal rips are a few of

the factors to be considered. While results obtained from such test blocks cannot be used to forecast particular conditions at a station unless those tests are taken from the circulating flow of that particular station, some of the published results may be of interest (46). Fig. 10 indicates the fouling periods at widely scattered points.

In shipping or storing specimens for later examination, they may best be preserved by draining surplus water from them and placing in sealed bottles containing 98 per cent alcohol.

Designing for Fouling Conditions

In the design of new plants using fresh or tidal water likely to foul, two questions must be answered: (*a*) What will be the extent and nature of the fouling organism? (*b*) What design steps must be taken to overcome them?

Often forecasts of fouling conditions have been made, based on studies of test panels or of fouling on logs, piers, rocks, and structures near the site of a proposed plant, or on studies of fouling conditions at an adjoining plant.

Such forecasting is extremely dangerous and should never be relied upon. Industrial water supplies taken from large bodies of water usually afford ideal conditions for invertebrate growth in their screen chambers, pump-suction wells, supply pipes, and flumes.

The sessile organisms naturally dependent upon water motion to carry their food to them will thrive and grow at rates unprecedented on the previous shore line. This is naturally due to water velocities usually in the range of $^1/_{10}$ to 2 fps. Differentials of growth rates as high as 3 to 1 have, for instance, been recorded for barnacles in wave-swept waters as compared with barnacles living in comparatively still tidal water. Still faster rates of growth have been noted in industrial tunnels. Where the water taken by the industrial plant is used for cooling an additional factor which cannot be forecast is introduced. The enormous heat output in cooling water from a large power station or refinery is often sufficient to shift the over-all temperature of the body of water as much as 15 deg F. This shift in water temperature may be enough to encourage year-round growth and reproduction of an organism that has previously been dormant a large part of the year, or may permit overwintering and luxurious growth of some organism which has been previously subject to seasonal extermination.

A good example of this occurred in the Southwest during the war. A new plant was to be erected on tidal water and take its cooling-water flow from a brackish stream only a few hundred feet from the inlet of an existing oil refinery. Design engineers, basing their judgment upon the fact that the existing plant had experienced no difficulty, and upon a belief, based upon rather limited experience, that no organism could thrive in varying salt-content water, provided no protection from fouling. Luxuriant Bryozoa growth shut down the plant before a single year of operation had been completed.

For another example, there are two power stations in Rhode Island whose cooling-water inlets are a city block apart. Negligible differences exist between the plants in so far as salinity, water temperature, sewage pollution, and other normal factors are concerned. The plant upstream from the sea has had severe fouling with *Mytilus edulis;* the one nearer the sea has had none. The difference probably exists in variations in river bottoms. Some plants have experienced severe fouling recently after a period of comparative freedom, probably due to changes in industrial and domestic pollution in their water source.

It should be realized that even though conditions are known to be unfavorable to the fouling organisms that exist near the proposed plant site, these same conditions of salinity, temperature, and pollution may encourage luxurious growth of some other organism, not now native, when changed water flow and temperature due to the new operations occur.

It is only sound engineering to design as though fouling will occur. Satisfactory design will require that all portions of the system be accessible for inspection and manual cleaning; and preferably be capable of being readily dewatered; but such manual cleaning should be considered only as an emergency measure. From the standpoint of efficiency, of continuity of operation, and of cost of cleaning, control methods as previously discussed are more satisfactory than manual cleaning. Designing with such control methods in mind from the very inception of plans will often substantially reduce corrective construction and operating costs.

BIBLIOGRAPHY

1 "Chlorination of Condenser Cooling Water," by R. B. Martin, Trans. A.S.M.E., vol. 60, 1938, pp. 475–483.

2 "Chlorination of Cooling Water," by N. C. Estes, *Refiner and Natural Gasoline Manufacturer*, vol. 17, 1938.

3 "Chlorination of Industrial Waters," by F. J. Matthews, *Power and Water Works Engineering*, vol. 32, 1937, pp. 19–21.

4 "Keep Your Condenser Tubes in Service," by F. G. Smith, *Southern Power and Industry*, vol. 60, 1942, pp. 136–138.

5 "Overgrowth and Corrosion in Condenser Tubes of Electro-Station," *Mikrobiologiya*, vol. 10, 1941, pp. 890–895.

6 "Effect of Biological Processes on the Destruction of Structural Materials," by L. W. Haase, *Korrosion und Metallschutz unter Einbeziehung des Allgemeinen Werkstoffschutzes*, vol. 16, 1940, pp. 155–160.

7 "The Colonization of a New Rocky Shore at Plymouth," by H. B. Moore, *Journal of Animal Ecology*, vol. 8, 1939, pp. 29–38.

8 "The Sequence of Events in the Fouling of Submerged Surfaces," by C. E. ZoBell, Official Digest, Federation of Paint and Varnish Production Clubs, no. 178, 1938, pp. 379–385.

9 "Cut Throat Competition in the Sea," by W. E. Allen, *Scientific Monthly*, vol. 48, 1939, pp. 111–119.

10 "Reports on the Prevention of the Growth of Mussels in Submarine Shafts and Tunnels at Westbank Electric Station, Portobello," by James Ritchie; M'Lagan and Cummins, Edinburgh, 1927.

11 "The Prevention of Trouble Due to Aquatic Growths in Condenser Systems With Special Reference to the Destruction of Mussels," by D. V. Onslow, British Electrical and Allied Industries Research Association, Publication H/T 15, 1929.

12 "Chemical Treatment of Condensing Water," by L. L. Robinson, *Electrical Times*, vol. 61, June 22, 1922, p. 607.

13 "Beitrage zur praktischen Biologie des Wandermuschel Dreissensia polmorpha und ihrer Bekampfung in Wasserwerken," *Deutsche Wasserwirteschrift*, vol. 18, 1923, no. 7, pp. 107–108; no. 8, pp. 119–120; no. 9, pp. 125–126.

14 "Chlorine in Water and Its Action on Fish and Other Water Animals," by G. Ebeline and T. H. Schrader, *Wasser und Abwasser*, vol. 27, 1929, p. 95.

15 "The Prevention of Trouble Due to Aquatic Growths in Condenser Systems," by D. V. Onslow, *World Power*, vol. 13, 1930, pp. 379–381.

16 "Slime and Mussel Control in Surface Condensers and Circulating Tunnels," by S. T. Powell, *Combustion*, vol. 4, 1933, pp. 7–13.

17 "Mytilus," by K. M. White, vol. XXXI, Liverpool Marine Biological Committee Memoirs on Typical British Marine and Fresh Water Plants and Animals, University Press of Liverpool, England, 1937.

18 "Biology and Economic Value of Sea Mussel, *Mytilus Edulis*," by I. A. Field, Bulletin of the Bureau of Fisheries, vol. XXXVIII, Document 922, United States Government Printing Office, 1921–1922, pp. 127–259.

19 "The Longevity and Swimming Ability of Spermatozoa," by B. H. Grave and R. C. Downing, Proceedings of the Indiana Academy of Science, vol. 37, 1928, p. 308.

20 "The First Physiological Observation on the Secretion of Byssus," by L. Pigorini, *Archives italiennes de biologie*, vol. 72, 1923, pp. 133–141.

21 "The Ecological Study of the Sea Mussel," by A. E. Warren, *Journal of the Biological Board of Canada*, vol. 2, 1936, pp. 89–94.

22 "The Rate of Water Propulsion by California Mussel," by D. L. Fox, H. V. Sverdrup, and J. P. Cunningham, *The Biological Bulletin*, vol. 72, 1927, pp. 417–438.

23 "Report on Mussel Purification," by R. W. Dodgson, Min-

istry of Agriculture and Fisheries, Fishery Investigations, Series II, vol. 10, no. 1, H. M. Stationery Office, London, 1928, pp. 1–498.

24 "Shell Movements of the Edible Mussel, Mytilus Edulis (L) in Relation to Temperature," by V. L. Loosanoff, *Ecology*, vol. 23, 1942, pp. 231–234.

25 "Bacteria as Food for Certain Marine Invertebrates," by C. B. ZoBell and C. B. Feltham, *Journal of Marine Research*, vol. 1, 1938, pp. 312–327.

26 "The Rearing of Oyster Larva on an Algae Diet," by J. R. Bruce, Margery Knight, and M. W. Parke, *Journal* of the Marine Biological Association of the United Kingdom, vol. 24, 1940, pp. 337–374.

27 "The Food and Feeding of Fresh Water Mussels," by W. R. Allen, *Biological Bulletin*, vol. 27, 1914, p. 127.

28 "Digestive Processes in Marine Invertebrates and Fish," by C. M. Yonge, *Journal du Conseil permanent international pour l'exploration de la mer*, vol. 6, 1931, p. 175.

29 "The Importance of Dissolved Substances in the Nutrition of Water Animals," by August Krogh, *Zeit. vergleich Physiology*, vol. 12, 1930, pp. 668–681.

30 "Effect of Light on the Growth of Mytilus," by A. G. Huntsman, Trans. of the Royal Society of Canada, sec. V, vol. 15, 1921, pp. 23–28.

31 "Growth of Sea Mussels," by H. S. Coulthard, *Contributions to Canadian Biology and Fisheries*, vol. 1, 1929, pp. 126–136.

32 "Pecten," by W. J. Dakin, Liverpool Marine Biological Committee, Memoirs of Typical British Marine Plants and Animals, vol. XVII, University of Liverpool Press, England, 1908.

33 "Studies on the Life Cycles of Two Species of Fresh Water Mussels Belonging to the Genus Anodonta," by M. E. Tucker, Biological Bulletin of the Marine Biological Laboratory, vol. 54, 1928, pp. 117–127.

34 "The Harmfulness of Dreissensia Polymorpha to Water Plants," by F. Roch, *Gesundheits-Ingenieur*, vol. 48, 1925, pp. 97–99.

35 "Oyster Biology and Oyster Culture," by J. H. Orton, Edward Arnold and Company, 1937.

36 "Investigation of Spawning and Settling of Oysters in Barnegat Bay, New Jersey," by T. C. Nelson, Report of the Department of Biology, New Jersey Agriculture Experiment Station, 1927, pp. 77–83.

37 "Some Observations and Experiments on the Settling Behavior of Larvae of Ostrea Edulis," by H. A. Cole and E. W. K. Jones, *Journal du Conseil permanente international pour l'exploration de la mer*, vol. 14, 1939, pp. 86–105.

38 "Spawning Reactions of Three Species of Oysters," by P. S. Galtsoff, *Journal* of the Washington Academy of Science, vol. 22, 1932, pp. 65–69.

39 "Physiology of reproduction of Ostrea Virginica. III—Stimulation of Spawning in the Male Oyster," by P. S. Galtsoff, *The Biological Bulletin*, vol. 78, 1940, pp. 117–135.

40 "Investigation of the Physical Conditions Controlling Spawning of Oysters and the Occurrence, Distribution, and Setting of Oyster Larvae in Milford Harbor, Conn.," by H. F. Prytherch, Bulletin of the United States Bureau of Fisheries, vol. 44, Document 1054, 1928, pp. 428–539.

41 "The Daily Rate of Growth of Oysters During the Summer," by B. Havinga, *Journal du Conseil permanente international pour l'exploration de la Mer*, vol. 3, 1928, pp. 231–245.

42 "A Manual of the Common Invertebrate Animals Exclusive of the Insects," by H. S. Pratt, P. Blakiston Sons and Co., Inc., Philadelphia, Pa., 1935.

43 "Environmental Selection of the Fresh Water Sponges of Michigan," by M. C. Old, Trans. American Microscopical Society, vol. 51, 1932, pp. 129–136.

44 "Notes on the Statoblasts and Polypides of Pectinatella Magnifica," by C. M. Brooks, Proceedings of the Academy of Natural Science of Philadelphia, Pa., vol. 81, 1929, pp. 427–441.

45 "The Natural History of Bugula Flabellata at Woods Hole, Massachusetts," by B. H. Grave, *Journal of Morphology and Physiology*, vol. 49, 1930, pp. 355–384.

46 "Sessile Marine Invertebrate of Beaufort, North Carolina," by K. D. McDougall, *Ecological Monographs*, vol. 13, 1943, pp. 321–371.

47 "The Ecology of the Fresh Water Polyzoa in East Anglia," by H. E. Hurrell, *Journal* of the Royal Microscopic Society of London, vol. 47, 1927, pp. 135–142.

48 "A Monograph of the Subclass Cirripedia," by Charles Darwin, 1851.

49 "Sessile Barnacles," H. A. Pilsbry, Bulletin of the United States National Museum, vol. 93, 1916.

50 "The Biology of Balanus Balanoides," by H. B. Moore, *Journal* of the Marine Biological Association, vol. 19, 1934, pp. 851–858; vol. 20, 1935, pp. 263–277; pp. 279–307.

51 "Rate of Growth, Age at Sexual Maturity and Duration of Life in Sessile Organisms at Woods Hole, Massachusetts," by B. H. Grave *The Biological Bulletin*, vol. 65, 1933, pp. 375–386.

52 "Le Spermatozoide de la Balane Balanus Perforatus Burg," by P. P. Grasse and Odette Tuzet, *Comptes Rendus des seances de la Société de Biologie et de ses Filiales et Associées*, vol. 99, 1928, pp. 1543–1545.

53 "Reaction of the Cyprid Larvae of Barnacles at Time of Attachment," by J. P. Visscher, *The Biological Bulletin*, vol. 54, 1928, p. 327.

54 "The Biology of Chthamalus Stellatus," by H. B. Moore and J. A. Kitching, *Journal* of the Marine Biological Association of the United Kingdom, vol. 23, 1939, pp. 521–541.

55 "Light as a Controlling Factor in the Growth of Balanus Balanoides," by A. B. Klugh and C. L. Newcombe, *Canadian Journal of Research*, Sec. D, vol. 13, 1935, pp. 39–44.

56 "The Influence of Surface Angle and of Light on the Attachment of Barnacles and Other Sedentary Organisms," by C. M. Pomerat and E. R. Reiner, *The Biological Bulletin*, vol. 82, 1942, pp. 14–25.

57 "Observations et Experiences sur le Peuplement des Cotes Recheuses par les Cirripedes," by Harry Hatton and E. Fischer-Piette, Bulletin de l'institute Oceanographique (Monaco) no. 592, 1932, pp. 1–15.

58 "Chemical Action of the Rhythm and Duration of Retraction of the Cirripedia of Balanus Perforatus," by Vera Waldes, *Zeit. für Vergleichende Physiologie*, vol. 26, 1938, pp. 347–361.

59 "Chemical Stimulation by Alcohols in the Barnacles, the Frog and Planaria," by W. H. Cole and J. B. Allison, *The Journal of General Physiology*, vol. 14, 1930, pp. 71–86.

60 "The Physiology of Marine Organisms," by H. F. Roaf, *Journal of Physiology* (U.S.S.R.), vol. 43, p. 449.

61 "Surface Permeability of Marine Invertebrates as the Cause of the Toxicity of Seawater of Abnormal Composition," by Albrecht Bethe, *Archiv für die gesamte Physiologie des Menschen und der Tiere* (Pflugers), vol. 221, 1928, pp. 344–362.

62 "The Relation between Temperature and the Pedal Rhythm of Balanus," by W. H. Cole, *The Journal of General Physiology*, vol. 12, 1929, pp. 599–608.

63 "Response of the Barnacles to Some Strong Electrolytes, to Urea, Glucose and Glycerol," by W. H. Cole and J. B. Allison, *Physiological Zoology*, vol. 10, 1937, pp. 405–411.

64 "Studies in Tunicate Development, Part I, General Physiology of Development of Simple Ascidians," by N. J. Berrell, Philosophical Transactions of the Royal Society of London, Section B, vol. 218, no. 415, 1929, pp. 37–78.

65 "Fresh Water Biology," by H. B. Ward and G. C. Whipple, John Wiley and Sons, Inc., New York, N. Y., 1918.

66 "Comparative Psychology; a Comprehensive Treatise, vol. II, Plants and Invertebrates," by C. J. Warden, T. N. Jenkins, and L. N. Warner, Ronald Press Co., New York, N. Y., 1940.

67 "Lethal Temperatures of Lamellibranchiata," by J. T. Henderson, Contributions to Canadian Biology and Fisheries, vol. 4, 1929, pp. 399–411.

68 "The Role of Temperature in Hydranth Formation in Tubularia," by H. A. Moore, *The Biological Bulletin*, vol. 76, 1939, pp. 104–107.

69 "The Accommodation of Some Marine Invertebrates to Reduced Osmotic Pressure," by F. L. Topping and J. L. Fuller, *The Biological Bulletin*, vol. 82, 1942, pp. 372–384.

70 "Physiological Effects of a Hypotonic Environment II Shock Effect and Accommodation in Cilia Following Sudden Salinity Changes," by G. P. Wells, I. C. Ledingham, and Mary Gregory, *Journal of Experimental Biology*, vol. 17, 1940, pp. 378–385.

71 "Influence of Temperature and Salinity on the Condition of Oysters," by J. C. Medcof and A. W. H. Needler, *Journal* of the Fisheries Research Board of Canada, vol. 5, 1941, pp. 253–257.

72 "Influence of Rapid Variation of Salinity on the Oxygen Consumption of Mytilus Edulis," by H. Bouxin, *Bulletin de l'institute Oceanographique* (Monaco), no. 569, 1935, pp. 1–11.

73 "Action of NaCl on Aquatic Mollusks," by H. Rajat-Vichy, *Comptes Rendus des seances de la Société de Biologie et des ses Filiales et Associées*, vol. 80, 1917, pp. 172.

74 "The Resistance of Fresh Water Snail Physa Heterostropha to Sea Water," by H. G. Richards, Biological Bulletin of the Marine Biological Laboratories, vol. 57, 1929, no. 5, pp. 292–299.

75 "Salinity and Size of Urosalphix Cinerea," by H. Federight *American Naturalist*, vol. 64, 1930, p. 183.

76 "Study of the Action of an Anisotonic Solution on a Marine Mollusk," by Cencettina Scordia, *Bollettino della societa italiana di biologia serimental*, vol. 1, 1926, pp. 745–749.

77 "Ability of Marine Invertebrates to Live in Diluted Sea

Water," by A. S. Pearse, Biological Bulletin of the Marine Biological Laboratory, vol. 54, 1928, pp. 405–408.

78 "Effect of Pulp Mill Pollution on Oysters," by A. E. Hookins, P. L. Galtsoff, and H. C. McMillin, United States Department of Commerce Bureau of Fisheries Bulletin, vol. 6, 1931, pp. 1–186.

79 "Cause of the Decline of the Oyster Industry of the York River, Virginia, and the Effect of Pulp Mill Pollution on Oysters, by P. S. Galtsoff, W. A. Chipman, Jr., A. D. Hasler, and J. B. Engle, United States Bureau of Fisheries, Investigation Report, no. 37, 1938, pp. 1–42.

80 "Industrial Waste and Fish Life," by M. M. Ellis, *Water Works and Sewage*, vol. 95, 1945, pp. 171–174.

81 "Effect of Sewage Pollution on Aquatic Life," by P. G. Barnickol, *Journal* of the Missouri Water and Sewerage Conference, vol. 15, 1944, pp. 57–63.

82 "The Respiratory Processes of Mya Arenaria and Other Marine Animals," by J. B. Collip, *The Journal of Biological Chemistry*, vol. 49, 1921, pp. 297-310.

83 'Anaerobic Respiration in Pelecypod," by C. Berkeley, *The Journal of Biological Chemistry*, vol. 46, 1921, pp. 579–98.

84 "The Crystalline Style as a Possible Factor in Anaerobic Respiration of Certain Marine Molluscs," by C. Berkeley, *The Journal of Experimental Zoology*, vol. 37, 1923, pp. 477–488.

85 "Ulva Latissima and Its Relation to the Pollution of Sea Water by Sewage," by E. A. Letts and John Hawthorne, Chemical News, vol. 82, pp. 164–165.

86 "New Method of Opening Oysters and Improving Their Condition for Market," by V. Koehring and H. F. Prytherch, United States Department of Commerce, Bureau of Fisheries, Investigational Report no. 15, Government Printing Office, 1932.

87 "Method of Opening Bivalves," by H. F. Prytherch and Vera Keohring, United States Patent 2,041,727, dated May 26, 1936.

88 "Wher das Kohlensauresystem in Meerwasser," by K. Buch, H. W. Harvey, H. Wattenberg, and S. Grippenberg, Conseil permanente International pour l'exploration de la Mer., Rapp et Proc.-verb, vol. 79, 1932.

89 "Primary Film Formation by Bacteria and Fouling," by C. E. ZoBell, *Collectors News*, vol. 14, 1939, pp. 2–3.

90 "The Biological Approach to the Preparation of Antifouling Paints," by C. E. ZoBell, National Paint, Varnish and Lacquer Association, Circular 588, 1939, pp. 149–163.

91 "Evaluation of Antifouling Paints by Leaching Rate Determinations," by B. H. Ketchum, J. D. Ferry, A. C. Redfield, and A. E. Burns, Jr., *Industrial and Engineering Chemistry*, vol. 37, 1945, pp. 456–460.

92 "Use of Lime in Controlling Starfish," by V. L. Loosanoff and J. B. Engle, United States Fish and Wild Life Service Reports, vol. 2, 1942, pp. 1–29.

93 "Method and Apparatus for Freeing the Bottoms of Vessels From Barnacles and the Like," by J. W. Van Meter, United States Patent 1,430,773, October 3, 1922.

94 "Condenser Fouling Prevented by Chlorine," by W. E. Warner, *Power Plant Engineering*, 1930, pp. 1129–1130.

95 "Power and Steam for the Naval Air Station at Quonset Point, Rhode Island," by A. W. Kramer, *Power Plant Engineering*, vol. 49, June, 1945, pp. 70–79.

96 "Role of Bacteria in the Corrosion of Iron and Steel," by A. H. Thomas, Proceedings of the Second Annual Water Conference Engineers Society of Western Pennsylvania, November 3–4, 1941.

97 "Corrosion of Water Pipes in a Steel Mill," by C. L. Clark and W. J. Nungester, Proceedings of the American Society for Metals, vol. 31, 1943, pp. 304–320.

98 "Characteristics of Microbiological Deposits in Cooling Water Circuits," by W. J. O'Connell, Jr., American Petroleum Institute, Proceedings of the Eleventh Midyear Meeting, Tulsa, Oklahoma; sec. 3, Refining, 1941, pp. 66–83.

99 "Electro-Chemical Properties of Chlorinated Water," by F. C. Schmelkes, E. S. Horning, and G. A. Campbell, *Journal* of the American Water Works Association, vol. 31, 1939, p. 1524.

100 "Progress Report on Studies of Water Chlorination," by H. W. Streeter, *Journal* of the American Water Works Association, vol. 35, 1943, p. 421.

101 "Influence of pH and Temperature on the Survival of Coliform and Enteric Pathogens When Exposed to Free Chlorine," by C. T. Butterfield, Elsie Wattie, and C. W. Chambers, Public Health Reports, vol. 58, 1943, p. 1837.

102 "A modification of the Flash Color Test to Control Breakpoint Chlorination," by P. C. Laux and J. B. Nickel, *Journal* of the American Water Works Association, vol. 34, 1942, p. 1785.

103 "Colorimetric Determination of Chlorine Residuals up to 10 ppm With Ortho-tolidine," by N. S. Chamberlin and J. R. Glass, *Journal* of the American Water Works Association, vol. 35, 1943, pp. 1065 and 1205.

104 "Determination of Active Chlorine," by F. J. Hallinan, *Water Works and Sewage*, vol. 90, 1943, p. 413.

105 "Chlorinated Condenser Water Averts Cleaning, Saves Fuel," by R. L. Gillespie and L. P. Sudrab, *Electrical World*, vol. 19, 1943, p. 36.

106 "Growth of Sedentary Marine Organisms on Experimental Blocks and Plates for Nine Successive Years," by W. R. Coe and W. E. Allen, Bulletin of the Scripps Institute of Oceanography, Technical Series, vol. 4, pp. 101–136.

Discussion

S. P. EWING.[3] This paper is an excellent condensation of the extensive and scattered information on fouling organisms as related to circulatory salt-water systems, and the Bibliography will be helpful to those who wish to learn more about this interesting subject. The paper is another example of the economic and engineering value of pure science. Certainly the engineer cannot expect to deal effectively with the fouling problem unless he uses the knowledge of the marine biologist.

There is little that the writer can add to the subject of the paper. But it might be worth while to mention a few other instances where the engineer must deal with fouling organisms, and show how in each case the problem is an economic or engineering problem where the marine biologist could contribute to the solution.

The salt-water piping system on ships is similar to the shore cooling system. The fouling problem is in some respects more important because the piping is designed for relatively high velocities, the pipes are relatively small so that comparatively little fouling may greatly reduce the capacity. On combat ships, failure of the piping at a critical time might result in loss of the ship. Hence it is not sufficient to be able to remove the fouling at intervals. The piping and also the hull must be kept free of fouling at all times because nearly perfect performance at all times is essential. It is impossible to design and operate the ship's piping so that the water velocity exceeds the minimum required to prevent fouling. Nor is it possible to close completely parts of the system at regular intervals, and thus kill small attached organisms by suffocation. The use of chlorine or other poisonous chemicals is objectionable on combat ships because of space limitations and the added hazard of these materials in case of battle damage.

The possibilities thus seem to be limited to the use of (1) copper alloys which will prevent fouling, (2) antifouling paints on the interior of the pipes, and (3) chlorine generated electrolytically from sea water. One might think that with a large power plant available, it would be a simple matter to produce enough chlorine from the electrolytic decomposition of sea water to prevent fouling in salt-water pipes. The work that has been done by the Bureau of Ships and the experience on ships indicates that the best solution is to use copper-nickel pipes, which corrode enough to prevent fouling for at least 1 year and then use antifouling paint or abrade the interior of the pipe so as to restore its antifouling characteristics. With steel pipes, the best solution is the use of antifouling paint.

Another well-known instance where marine organisms interfere with the activities of man is the damage to wooden structures caused by marine borers. Here the best defense is to treat the wood so that these organisms are discouraged from boring in it, or to cover it with a material which the borers cannot penetrate. The method used since ancient times to prevent attack on wooden

[3] Bureau of Ships, Navy Department.

NOTE: The opinions expressed in this discussion are not to be construed as those of the Navy Department or the Naval Service at large.

vessels has been to cover the underwater hull with sheet copper. This method was used extensively on early steel and iron vessels. An elaborate and expensive system of wooden sheathing was used between the copper and steel to control the galvanic couple and thus prevent rapid corrosion of the steel.

There are numerous types of structures where fouling in itself is not particularly objectionable. For example, fouling on a wooden pier does not interfere with the proper functioning of the pier, so long as the organisms do not penetrate the wood and weaken it. Fouling on steel piers, lock gates, buoys, submarine nets, and submerged pipe lines is not particularly objectionable so long as the organisms do not penetrate the organic protective coating and cause corrosion of the steel. On lock gates, buoys, and submarine nets, the added weight may affect buoyancy because the shells are heavier than the water. However, the effect on buoyancy is only about 1/4 of the total weight in air of the fouling growth.

It is well known that when certain barnacles grow on relatively soft bituminous materials and some paints, the shell of the barnacle gradually penetrates the organic material so that after the barnacle reaches its full growth its shell is in intimate contact with the steel over nearly the entire area of its base. Serious corrosion of the metal often occurs in this area, especially if the electrical conditions are favorable for corrosion. This situation has occurred on lock gates and submerged pipe lines. Other unidentified marine organisms are reported to attack asphalt coatings in a somewhat similar manner.

There are several possible ways to prevent damage to the coated metal. An antifouling paint might be applied over the bituminous coating, but this will be effective for only a limited time, since most antifouling paints lose their effectiveness in less than one year. Tests may show that a sufficiently hard coating will prevent penetration. This is certainly the case with barnacles. A sufficient amount of hard mineral filler in the bitumen may be an effective means for discouraging other types of boring or digging animals. If the attack of the marine organisms on the coating is rather slow, and only a few holes are made in a relatively long period, the use of cathodic protection to prevent corrosion at the holes in the coating may be the most economical solution. Each case will have to be studied in order to arrive at the most effective and economical solution; and the solution will probably require identification of the culprit, and a knowledge of its life history.

L. W. Hutchins.[4] This paper fills a gap in the literature of fouling problems. The engineer is presented with an introduction to some of the complex biology involved in the fouling of water circuits, and, indeed, of any fouling. On the other hand, the biologist is offered an excellent review of the practical problems from the engineer's standpoint. The number of new observations recorded and the extensive review of the practical literature, which generally does not come to the attention of biologists, are particularly worthy of praise.

The author has pointed out very well the extent to which the solution of engineering problems must depend on competent biological knowledge. His remarks on the inadequacies of fouling control by screening, on the possible variations of control by heat, and in particular, the variable dosages of chlorine which must be adjusted both to the types of organisms present and the stages of their life histories are good cases in point.

It happens not infrequently that biologists are not able to give the best possible consulting advice about fouling problems simply from ignorance of the practical aspects of the situation. This situation can be alleviated by papers such as this which present both sides of the picture.

[4] Woods Hole Oceanographic Institution, Woods Hole, Mass.

Cases have come to the writer's attention in which plants and designers have refused to allow dissemination of the factual information about the fouling problems they have encountered, in the rather naïve belief that the occurrence of fouling in their setup was a reflection on the abilities of the operator or designer. That view is quite incorrect.

The only sound procedure, as the author points out, is to design with the expectation—a practical certainty—that fouling will occur, and to make suitable provisions accordingly for inspections, cleanouts, and, if desired, attempted control. The failure of any intended control system, moreover, does not necessarily reflect on the engineer, but as often as not, on the inadequacies of the biological knowledge concerning his problem.

Improvement in this general subject can be obtained only by a thorough understanding of both points of view so that the biologist can know the lines which his investigations should follow, and the engineer can have a true picture of the information available for application in designing and operating control measures.

The need for more exact biological knowledge has become increasingly clear along two lines. In so far as the economical use of control measures must involve their quantitative relation to the incidence of fouling, it is obviously desirable to know as fully as possible the fouling expectancy and the effects of factors modifying it. The particular fouling population which will develop in a highly localized site appears to depend on the natural populations to which that site is accessible. In harbors and other such locations generally of interest to industry this question of accessibility appears to be highly complicated. The set of local currents may profoundly alter the probable accessibility as judged by simple geography. Pollution, which may be either somewhat beneficial or detrimental to the growth of individual species, depending upon its nature and extent, is another factor believed to be of very great importance in such areas. Far too little is known, however, about the effects of individual contaminants to permit predicting localized harbor fouling conditions with any assurance. There is a need for further facts about all such factors modifying the incidence of fouling.

The second line along which further exploration is indicated is that of the knowledge of toxicity and factors which may be utilized in control of fouling. The investigations of possible toxics other than chlorine and heavy metals can hardly be said to have been prosecuted with any vigor. Knowledge is inadequate even as to possibilities, particularly in the line of organic toxics. Similarly, with reference to chlorination, it would seem worth while to investigate much more thoroughly than has been done the problem of control by intermittent treatment. Even with the intermittent applications now in use, the cost appears sufficiently high so that possible savings would more than justify considerable research aimed at the reduction in chlorine usage. This is a problem in which the biologist must go first, studying the effects of various concentrations and of various time dosages on a wide variety of organisms and attempting thereby to develop generalizations which can be put into practice by the engineer.

The writer feels that the greatest importance of the paper is as an aid to the further profitable co-operation between professional biologists and engineers.

F. L. LaQue.[5] On the basis of some of our investigations in related fields, the writer is able to confirm some of the author's conclusions:

1 We have found that when sufficient chlorine is used to prevent the development of slime films, as well as fouling organisms,

[5] In Charge Corrosion Engineering Section, Development and Research Division, The International Nickel Company, Inc., New York, N. Y.

corrosion of steel pipe lines by sea water moving at high velocity is increased, presumably through the loss of the protective effect of slime films and accumulations of macroorganisms. At the same time, there has been some evidence that small amounts of chlorine in sea water retard rather than accelerate corrosion of some nonferrous alloys, such as Admiralty brass and 70:30 cupro-nickel, perhaps through some reinforcement of protective films. Likewise, the prevention of fouling and perhaps, also, a slight increase in the oxidizing capacity of sea water due to the presence of a small amount of chlorine, have been found to exert a beneficial effect on the performance of stainless steels.

2 Our observations generally confirm those of the author with respect to the influence of water velocity on the fouling of smooth surfaces. We have found that macroorganisms are not likely to become attached at steady flow rates much above about 3 fps, but once attached during periods of lower velocity flow, they may be able to retain a foothold and grow in contact with water moving at much higher velocities, e.g., 10 fps.

3 Examinations of many specimens of steel covered with fouling organisms after exposure to sea water have failed to indicate any significant effect of the organisms in accelerating corrosion through differential cell action as suggested by the author. However, with highly alloyed steels, such as stainless steels and other passive alloys, local attack believed to be due to differential cell action under fouling organisms is common.

Since the possible effects of chlorination on corrosion of equipment are of natural concern to those contemplating the use of chlorine to prevent fouling, it is hoped that more extensive investigations of this phase of the subject, and particularly with respect to intermittent chlorination, will be made and that the results will be made available.

S. T. Powell.[6] The author has given an excellent history of methods undertaken for the control of biological microorganisms responsible for fouling condensers and similar equipment. In addition to this valuable record, he has presented a very clear and concise discussion of the specific types of organisms which have been responsible for such difficulties and has submitted a constructive review of miscellaneous corrective treatments and their application. The paper also includes one of the most complete bibliographies which has been published, and this material alone is an invaluable contribution to this subject.

That portion of the paper dealing with "control by chlorination" is a concise statement of the value and limitation of this type of treatment and should correct many misconceptions as to the application of chlorination.

In general, the paper is a worth-while contribution to the literature and represents an authoritative reference work with a high degree of reliability.

Lester Randall.[7] The writer in support of the facts given in the paper is able to provide some results obtained at the power station of The Connecticut Power Company, Stamford, Conn.

The Stamford station has grown from the early days of the industry so that when an additional unit of 25,000 kw capacity was installed in 1940–1941, a complete new intake system for this unit was necessary. The circulating pumps are propeller type, located in the screen house on the waterfront. The intake tunnels are two 36-in. cast-iron pipe lines from the pumps to the condenser, one line to each side of the divided water box. The combined length of the two lines is 262 ft.

Circulating pumps for the old portion of the plant are of the submerged slow-speed centrifugal type, located in another screen house also on the water front. The intake tunnel for the old plant is also 36-in. cast-iron pipe but laid out as a loop, like a hairpin, with the two ends connected through valves to a header located near the pumps. Take-offs to the condensers are on one leg of the hairpin so that in effect there is a cooling-water header supplying the old condensers, this header being fed from both ends. Division valves make it possible to inspect sections of this line while other sections are still operating. The whole length of this loop, including leads to condensers, is 680 ft, but only 570 ft are in active use, the remaining section being connected to units not regularly operated, and because of a closed division valve very little water circulates through it.

The new unit was put in service during October, 1941. Intermittent chlorine treatment was started in January, 1942, for this unit and in April for the old part of the station. Prior to this time no method of controlling intake fouling had been used. Heavy growths occurred in the pipes and had to be scraped out at least twice a year. The fouling included all sorts of marine animals but mussels predominated.

The new plant has operated as a base-load unit, being shut down over a week end every 6 to 8 weeks for inspections and maintenance. The old plant seldom operates over a week end and when shut down no chlorine is fed, although a small amount of water is kept circulating through the lines.

Circulating water is taken from the harbor, an arm of Long Island Sound. Normal water velocities during the summer in the several pipes are 5 fps for the new plant; 6 fps for a 325-ft section of the old intake piping; and 7.5 fps for another 240 ft.

Until July 20, 1942, the program for chlorination was three 20-min periods per 24 hr, at which time the treatment was increased to four 20-min periods. The following year, 1943, the program was changed to two periods of 60 min each 24 hr. This was started May 12, 1943, and has been in effect most of the time since.

Residuals have been carried at 0.5 ppm, except during July, August, and September, when it has been kept slightly higher, from 0.55 to 0.65 and occasionally, for short periods, to 0.7 ppm. Samples for residual determination are taken from the condenser outlet in the new plant and condenser inlet in the old plant.

Results have been gratifying. Considering the old plant only, the 1942 program of three and four 20-min chlorinating periods per 24 hr reduced the total amount of material to be removed manually by 50 per cent. The two 60-min periods per 24 hr has reduced it by more than 95 per cent when compared with conditions before chlorine treatment.

Results for the new plant are even more interesting. From October, 1941, to August 12, 1945, nearly 4 years, a total of 10.5 cu ft of material, all mussels, has been removed from the 262 ft of 36-in. pipe and 8-in. suction lines to the cooling-water booster pumps. One half of this total was taken out the first year, 1942, when using the 20-min chlorinating period. Probably an important reason for the small amount this first year was the smooth condition of the pipe surfaces, which had been given a shop coat of bitumastic paint.

Prior to chlorine treatment, it was regular operating practice during parts of the year to drain half a condenser at night and pick out the mussels and shells that were wedged in the ends of tubes. Sometimes it was necessary to do it during the noon hour. This operation has been completely eliminated. Rubber plugs are blown through all condenser tubes every 4 weeks to remove such shells as do lodge in the tubes and might cause failures.

The cost of chlorination for the combined plant is 15 tons of chlorine per year; generation for the same time is up to 300,000,000 kwhr.

Considerable time has been given to studying mussels. The beginning and duration of the spawning season and the rate of

[6] Chemical Engineer, Baltimore, Md. Mem. A.S.M.E.

[7] The Connecticut Power Company, Stamford, Conn.

growth are important considerations. Four years of observation has pretty well determined that with the present chlorine treatment, mussels will not begin to appear in the pipes until July 1. It has also been determined that if the pipes are cleaned after October 15, they will remain free of any growth except a scattering of barnacles, for the following 8 months. For removing such mussels as do get started two cleanings are made, the first about August 20, the second about October 20. Using this schedule, mussels that may get started are removed before they get large enough to crowd each other loose from the pipe surface and be carried along by the current.

These results apply to Stamford station. Other stations must determine the treatment best suited for their particular conditions. Some of the factors to consider are nature of tunnel surfaces; velocity of water; size of tunnels; continuity of service and chlorine treatment; nature of fouling organisms.

The author suggests installation of glass inspection plates or hanging test pieces in tunnels. The writer considers that method unreliable, especially for salt-water plants.

In the old plant, during the summer of 1945, a solid blanket of mussels covering 8 ft of 36-in. pipe became established in a section between a condenser take-off and a closed division valve. Also a good-sized patch started in the 24-in. connection at one side of one of the old condensers. Why these patches start in an otherwise clean pipe is difficult to explain. In the new plant, water for the turbine coolers (hydrogen and lubricating oil) is taken through 8-in. suction lines to two 750-gpm booster pumps, one on each main intake pipe. One pump is operated at a time for 1-week intervals. Each summer, mussels completely blanket the insides of these suction lines. Also, in the new plant mussels completely filled the crease in the reinforced rubber expansion joints just below the water boxes.

So far only intake pipes have been mentioned. The pump and screen wells do collect growths on the walls. This is due to a design that does not give good mixing of chlorine with the water in the wells. Chlorine feed pipes are placed just in front of the pump suction, between the pump and the screen, so the chlorine passes directly to the pump and into the pipes.

Chlorine has eliminated all non-shell-bearing animals, slimes, etc., and nearly all mussels from the circulating-water piping. However, barnacles do not seem to be affected, in fact it would seem they like the clean surfaces. In the old-plant intake lines they will nearly cover the surface by midsummer. They are hard to scrape off but because they are so securely fastened to the pipe walls and are so small, they are not a hazard in operation of the plant.

W. D. Bissell.[8] At the time the chlorination system was installed at Montaup Electric Company one of the condensers had been completely retubed the previous year and another condenser was completely retubed at the time the treatment was started.

The selection of sampling points for observation and control was carefully considered and these were located at the discharge elbow of the circulating pumps, each condenser discharge elbow, half the distance along the pump discharge tunnel where house service pumps are located, and also at the combined discharge of all condensers.

As the tunnel system was known to have considerable growth, extreme care was used when treatment was first started in February, 1945, in order to observe the sluffing-off of this growth. A thirty-minute cycle per day was used for about two weeks maintaining a residual of 0.3 ppm at the condenser outlet. The cycle was then changed to fifteen minutes of treatment three times daily and the residual was increased to 0.5 ppm, where it has been maintained since. No difficulty was experienced from accumulated growth dropping off during the initial cleaning period.

It was interesting to observe, during the difficulty which was experienced maintaining chlorine residual during the first month of treatment, that the discharges of the pumps would vary in chlorine residual from day to day. This variation leveled off later so that each pump discharge would indicate the same residual.

It is believed that this variation was due to the uneven deposits in the pump suction and the gradual cleaning of them resulted in the leveling off of residual at all pumps.

The greatest demand of chlorine was along the distance from the river intake screens to the pump discharges which was three or four times greater than through the condensers from the inlet to the outlet. Due to having sampling points at these important locations close observation could easily be obtained. The results were accurately logged which was of great assistance in maintaining machine control and residual control.

When the water temperature reached about 45 deg in the spring of the year the chlorine demand increased very rapidly until 50 deg was reached. From that time to 75 deg, chlorine demand was observed to be quite normal. During the period of warm water operation at temperatures of from 68 deg to 80 deg, an interesting changeable condition would occur in the foam on the surface of the condenser discharge water. This would be very dark brown for a few days at a time and would then change to a light yellow and the chlorine demand would change rapidly.

The control of chlorination was obtained by results as indicated on the condenser tubes, sheets, inlet and discharge water boxes, at regular frequent inspections. When chlorination was first started the growth of so-called moss and marine growth was about $^3/_8$ in. thick on the internal surfaces of the water boxes with some adhering to the tube sheets. After several weeks of treatment this could be easily removed by rubbing with the hand. In about three months this growth was completely removed and the surfaces could be coated with red lead.

Previous to chlorination the condensers were rather foul-smelling and it was extremely difficult for men to make repairs or to stay in them any length of time. Extended periods of working in a condenser would make a man ill. Since chlorination has been used the condensers have not been odorous to any extent, and are not objectionable for men to remain inside for extended periods to make any necessary repairs.

The purpose of using chlorination was to remove slime deposits on the heating surfaces chiefly. Mussels in the intake tunnel were of considerable nuisance and also would collect in various station salt-water lines and valves which caused considerable trouble in the past.

Chlorination has completely removed the slime and reduced the mussel growth so that it is negligible. The station water lines have been free from any growth or deposits and it has not been necessary to clean cooler surfaces, etc. Previous to chlorination such conditions as described in Figs. 2, 3, and 6 were usually found when the tunnel was dewatered.

The use of chlorination has been quite satisfactory in keeping the condensers and the condenser water system clean and we feel that good results have been obtained. However, some points have been raised such as the following:

1 In keeping condenser tubes free from slime and any organic growth by the use of chlorination, will this permit corrosive action caused from oxygen or any corrosive gases in the circulating water to attack the condenser tubes, which may shorten their life?

2 (*a*) Does the type of bacteria change at different seasons of the year? (*b*) Do they change at different temperatures? (*c*)

[8] Engineer, Somerset, Station Montaup Electric Company, Fall River, Mass.

Is it usual to have chlorine demands change rapidly from causes such as mentioned above?

3 In the process of first applying chlorination will chlorine demands change rapidly in initial cleaning periods?

4 Do river-bed deposits change gradually from year to year, thereby affecting the type of growth and gases in the water which may result in changes in the chlorine demand?

5 (*a*) Is it considered advisable to discontinue chlorination during the winter period when temperatures are at 33 deg or thereabouts? (*b*) Should the chlorine cycle be reduced in frequency? (*c*) Should the chlorination residual also be reduced?

6 If marine growth and fouling organisms vary from season to season at various temperatures, is not the best means of control obtained from observation of results which can actually be a guide for correct residuals, thereby obtaining positive control?

7 Since variable conditions of the tide are observed to have an effect on the chlorine residual, can this be explained?

Author's Closure

The author wishes to express his appreciation to the various discussors for their thoughtful and well-prepared contributions. The discussions papers by W. D. Bissell and L. E. Randall are interesting in that they present the viewpoint of the problems as seen by the operating man.

Mr. Bissell has pointed out a familiar observation that the chlorine demand, as indicated by the difference between chlorine dosage in the screen well and chlorine residual in the tailpipe, is made up of two parts: (1) The demand of the water itself during the time of contact permitted, and (2) the demand or absorption of chlorine by the surface accumulations on the tunnels and heat-exchanger tubes. Naturally, when large accumulations exist in a concrete tunnel, considerable chlorine will be absorbed by this organic matter until such time as it has been completely oxidized, and in most cases, has completely sloughed off. Mr. Bissell has raised certain specific questions which the writer will attempt to answer. The question as to whether the chlorination of condenser tubes and the resultant bright tube condition will permit the aggressive action of salt water, of dissolved gases, and of other corrosive fluids to increase the corrosion rate of these tubes over the corrosion rate existing in slime-covered tubes is a subject which will still bear considerable investigation. Mr. LaQue, in his discussion of this paper, seems to feel that such accelerated corrosion does not exist, and that, in fact, the elimination of the slime film and macroorganism fouling will retard the corrosion of nonferrous metals. Further research should be carried out in this field; but suffice to say, from a practical viewpoint, corrosion rates of installed tubes have never been demonstrated to have been increased by chlorination. A few cases are on record where the tube corrosion rate increased simultaneously with the use of chlorine for elimination of slime accumulations, but in all cases where the chlorine was abandoned for a period, the increased corrosion rate continued unabated.

The type of bacteria and other slime-forming organisms responsible for heat-exchanger sliming do not vary in terms of the season. However, the type of organism present at any time is dependent upon water temperature, upon food supply, and upon other factors such as oxygen content in the water. Since these factors, in turn, have seasonal variations, it is possible that specific flora will be more regularly found at certain seasons of the year. Certain microorganisms multiply very rapidly at specific temperatures, but are in practically static conditions in all but a very narrow range of temperature. Certain others are tolerant to much wider temperature conditions, and will thrive throughout the temperature range of normal circulating-water conditions. Mr. Bissell has outlined in his own discussion a very clear demonstration of the high chlorine demand of fouled surfaces during the initial clean-up period of a circulating water system. His experience is quite typical of the conditions in a normal circulating-water tunnel.

The variations of river bottom do not have a particular effect upon the growth of microorganisms in circulating water. In most cases these organisms exist free-floating in the water, and unless the river bottom is contributing changes of water conditions, such as oxygen depletion or hydrogen sulphide production, the condition of the river bottom will not seriously affect the growth of microorganisms on heat-exchanger surfaces. However, the macroorganisms, such as mussels, have only a limited field of locomotion between the point of fertilization of the egg and final point of attachment of the larva animal. For this reason, an invasion of mud over a rocky bottom, which quite frequently occurs in tidal water, may well eliminate the breeding grounds and ultimately the source of infection for macroorganisms for a given tunnel.

The question as to what changes of treatment should be made as water temperatures approach freezing is one that can be answered only after a study of the particular problem. It should be remembered, however, that temperature at which the organism is breeding is not the temperature of the water, but rather the surface temperature of heat-exchanger metal, and for this reason, even at 32 deg water temperature there may be lively growth of the microorganism. As a practical matter, chlorination should be continued at residuals sufficiently high, properly spaced, and of sufficient duration to kill the flora attached to the flume, condenser, or other surfaces.

The answer to Mr. Bissell's sixth question is again a matter of practical application of biological facts. If a station could afford to have continuous studies by an experienced biologist to determine when the spat form of each organism is present in the water, then residuals and dosage periods could easily be varied in accordance with season and water-temperature conditions, so as to yield maximum economies of chlorine use. But the average plant finds it much easier to feed chlorine at residuals sufficiently high to kill the spat form of the macroorganisms during the entire period when water temperature is sufficiently high, or seasonal advance is sufficiently completed to warrant a belief that some of the fouling organisms may be breeding.

Variations of chlorine demand with tidal conditions is quite common. The common condition of a polluted stream moving into a relatively clear estuary will yield high chlorine demands during periods of ebb-tide, due to the preponderance of river water and low chlorine demands while the tide is in flood due to the preponderance of sea water. In any particular harbor the question of what mixing will occur at various tides can become extremely complex.

Mr. Randall's report is an excerpt from the data which he has accumulated during the past six years. These experiments are the most carefully controlled and fully observed plant-scale demonstrations of the control of fouling organisms by chlorination known to the writer. I hope that Mr. Randall will publish his very carefully detailed data in the near future. His experiences have indicated some of the pitfalls which may well trap the unwary operator attempting chlorination for the elimination of fouling organisms. No plant which is circulating any salt water should permit that salt water to circulate for a period of more than twelve hours without treatment. Mr. Randall's difficulty with his dead-ends in the old station is typical of the problems which will occur if this precaution is not taken. In the placing of test panels or plate-glass windows in circulating-water tunnels, the place chosen for test must be representative of conditions throughout the entire station, and if any doubt exists as to whether the place chosen is representative, spot checks throughout the system should be made. The control of barnacles re-

quires slightly higher residuals than those required for the killing of other fouling organisms, and therefore unless barnacles are giving trouble it is uneconomical to chlorinate at these higher residuals.

In the cleaning up of fouled tunnels either when starting to control fouling in existing tunnel, or in the cleaning of a tunnel which has been under treatment and which has been permitted to foul to a limited extent by "preventative treatment" recommended in the original paper, there is always a question of the economy as to whether chlorination or manual cleaning should be used. In all cases where plant shutdown and dewatering is readily possible and access to the tunnel can be made without undue expense, it would seem advisable to choose manual cleaning. Under other circumstances chlorination might easily be the answer.

Dr. Ewing's discussion of problems related to the fouling of circulating-water systems has been very valuable in rounding out the view of the subject. The writer has had some contact with the design work involved in the production of chlorine cells for use on board fighting ships. Certainly considerably more improvement of those cells, and improvement of the antifouling materials for lining the ships' pipes is in order. Such development can best be carried on by the co-operation of all interested parties.

Dr. Hutchins' discussion of this problem from the viewpoint of the biologist will warrant careful study by the designing engineer. His warnings of the unpredictability of fouling in tidal waters should be a warning to all designers faced with this problem. His plea for effective co-operation between the professional biologist and the engineer will, I hope, encourage further publications by operating men and designers who have experienced difficulty in this field.

Mr. LaQue's authoritative discussion on corrosion is much appreciated. It is the writer's hope that further work along these lines will be undertaken within the near future.

All the discussors have been kind enough to point to the gravity of the problem of fouling organisms to circulating-water systems, and the writer trusts that these discussions will lead to a fuller appreciation of the problem and careful consideration by the designers in the planning of future circulating-water tunnels.

Discussion

In 1945, when there was a ban on national meetings, some papers originally scheduled for these meetings were presented before local groups. In the case of these papers the Committee on Publications suspended its rule, which requires simultaneous publication of paper and discussion, and accepted discussion based on the published paper.

Irreversibility in the Theoretical Regenerative Steam Cycle[1]

G. M. Dusinberre.[2] To future workers on this subject the writer recommends the analysis based on 1 lb throttle steam as used by the author. This seems more straightforward than to base on 1 lb through steam.

The author's Fig. 5 is a concise way of presenting the data on this cycle. But if a need really exists for data on the properties of this cycle, the writer feels that neither heat-rate tables nor the entropy-increase diagram is adequate, for two reasons: (1) Reheat cannot be handled except in a roundabout manner, as the author points out. (2) This ideal cycle is based on net work, that is, turbine work less feed-pump work. The practical use of the data would probably be in the study of high pressures where pump work is relatively large. Since there is no necessary relation between turbine and pump efficiencies, the application of any sort of efficiency factor to the ideal heat rate at least makes the fourth significant figure look a little foolish.

The writer concludes that the most useful form in which the data could be presented is (*a*) to use the divided cycle proposed by Markson,[3] and (*b*) to tabulate or plot the turbine work, pump work, and through steam, for 1 lb throttle steam: The corresponding heat items are readily obtained from the steam tables.

If the pump work is required, the author's integration is not directly useful as we need values of $(1 - w)$ for $\int (1 - w)v_f dp$. To get these, the writer has found that $\int \frac{T_f}{H - h_f} ds_f$ is more convenient than the function used by Selvey and Knowlton,[4] as the curvature is less.

When data are in graphical form, such as an indicator card, the logical method of integration is to use a planimeter, and not to pick off points for numerical integration. But when the data are in numerical form, as in the present case, it is equally more logical to use some method of numerical integration rather than to introduce the extra step of plotting a curve.

H. G. Elrod, Jr.[5] A completely accurate alternative to the author's Equation [6] can be obtained readily in the following manner.

Consider a regenerative cycle *ABCXZfA* in the author's Fig. 1. When 1 lb of throttle steam is circulated in this cycle, $(1 - w)(s_x - s_f)$ units of entropy are rejected by the system, and $(s_c - s_a)$ entropy units are received. The net entropy increase of both the system and its surroundings is given by

$$\Delta S = (1 - w)(s_x - s_f) - (s_c - s_a) \quad [1]$$

The variation of ΔS with exhaust conditions is found by differentiating Equation [1] of this discussion

$$d(\Delta S) = -(1 - w)ds_f - (s_x - s_f)dw \quad [2]$$

Using the author's Equation [3] (corrected to include a minus sign), we obtain

$$d(\Delta S) = -(1 - w)\left[1 - \frac{T_f(s_x - s_f)}{H_x - h_f}\right] ds_f \quad [3]$$

Substituting the value of $(1 - w)$ from Equation [1] into Equation [3] of this discussion, we find

$$\frac{d(\Delta S)}{s_c - s_a + \Delta S} = d\ln(s_c - s_a + \Delta S) = -\left[\frac{1}{s_x - s_f} - \frac{T_f}{H_x - h_f}\right] ds_f \quad [4]$$

The left-hand side of Equation [4] is directly integrable. The right-hand side may be evaluated in the manner illustrated by the author.

A comparison of Equation [4] with the author's Equation [6] shows that the author's approximation amounts to the assumption that $\ln(1 + x) = x$. Using Equation [4], we obtain for the example cited by the author

$$\ln\left(1 + \frac{\Delta S}{s_c - s_a}\right) = 0.0288 \quad [5]$$

or

$$\Delta S = 0.5425 \times 0.02922 = 0.01585 \quad [6]$$

The corresponding heat rate is 6000, which more closely agrees with the accurate value of 6001.2 computed by Shapiro.[6]

Ernest L. Robinson.[7] When the writer first became interested in this subject, there were great gains to be made in station performance. In 1923 he published curves for the efficiency of the extraction cycle which extended up to 1000 psi and 700 F, pressures and temperatures far beyond anything in use at that time.[8] The extraction cycle is now commonplace with steam conditions far above those. The gains looked forward to 20 years ago have been more than realized, and modern discussions are largely confined to the technique of calculation.

The writer has always believed that the best technique of calculation is to formulate the difference from some precisely known relationship and then to calculate that difference with care.

---

[1] By R. E. Hansen, published in the October, 1945, issue of Trans A.S.M.E., vol. 67, pp. 557–560.

[2] Department of Mechanical Engineering, Virginia Polytechnic Institute, Blacksburg, Va.; now on duty at U. S. Naval Academy, Annapolis, Md. Mem. A.S.M.E.

[3] Discussion by A. A. Markson of "Theoretical Regenerative-Steam-Cycle Heat Rates," by A. M. Selvey and P. H. Knowlton, Trans. A.S.M.E., vol. 66, 1944, pp. 504–505.

[4] Selvey and Knowlton, reference (3) of the paper.[1]

[5] Department of Marine Engineering, U. S. Naval Academy, Annapolis, Md. Jun. A.S.M.E.

[6] Discussion by A. H. Shapiro, of "Theoretical Regenerative-Steam-Cycle Heat Rates," Trans. A.S.M.E., vol. 66, 1944, p. 508.

[7] Turbine Engineering Department, General Electric Company, Schenectady, N. Y. Mem. A.S.M.E.

[8] "The Margins of Possible Improvement in the Central Station Steam Plant," by Ernest L. Robinson, Trans. A.S.M.E., vol. 45, 1923, p. 644.

Mr. Hansen has selected the Carnot cycle for his precisely known relationship and has proceeded to formulate the departure of the extraction cycle from perfect reversibility when superheated steam is bled.

This is an excellent method to pursue, as it enables attention to be focused on the magnitude of the departure itself, and thus the errors of calculation become errors of the second order of smallness.

The author takes advantage of this to introduce as an approximation the assumption that the weight flow throughout the cycle is in inverse proportion to the entropy difference between steam and feedwater. The close check with the Selvey and Knowlton tabular values justifies the assumption.

However, since the author uses graphic integration anyway, it does not seem to the writer as if it would complicate his calculation if the correct expression for weight flow were used. When the writer first set down this expression, he used w to represent the weight flow of extracted steam per pound to the condenser. Thus the weight flow in the turbine per pound to the condenser is

$$1 + w = e^{\left[\int_{h_G}^{h} \frac{dh}{H-h}\right]}$$

In evaluating the integral for high pressures it would be desirable, as Selvey and Knowlton pointed out, to allow for the feed-pump work.

Thus

$$1 + w = e^{\left[\int_{h_G}^{h} \frac{1 - \frac{vdp}{Jdh}}{H-h}\, dh\right]}$$

The author uses w to represent the weight flow of extracted steam per pound to the throttle. Thus, using his notation, the weight flow in the turbine per pound at the throttle is

$$1 - w = \frac{1}{e^{\left[\int_{S}^{S_A} \frac{Tds}{H-h}\right]}}$$

In conclusion the writer would like once more to call attention to the advantage of weight-flow curves in extraction-cycle analysis. Especially with reference to a fixed exhaust pressure, such as 1 in. Hg, they may be drawn on the Mollier chart as characteristic lines per pound to the condenser for any stage efficiency. With the weight flow throughout the cycle known, performance is easily computed from cycle input and output. This technique is particularly useful for actual efficiencies other than 100 per cent.[9]

ASCHER H. SHAPIRO.[10] The relation between Equations [2], [5], and [7] of this paper, and the first and second laws of thermodynamics is most obscure, due, it is felt, to the only too common practice of not clearly defining the system under consideration. What mass of material, for example, does the dS of Equation [2] refer to? Analysis indicates that it is the increase in entropy in an infinitesimal heater per unit of throttle flow. Referring to Fig. 1 of this discussion, we get for the increase in entropy flux of an infinitesimal open heater.

$$dS_{\text{heater}} = (1 - w + dw)s_f - s_x dw - (s_f - ds_f)(1 - w)$$

After simplification and combination with the "heat balance," Equation [3] of the author's paper, this becomes

$$dS_{\text{heater}} = [H_x - h_f - T_f(s_x - s_f)]\,\frac{dw}{T_f} \quad \ldots\ldots [7]$$

which is identical with Equation [2] of the text. Note that in deriving this equation it is unnecessary to allude to fictitious "lost-work" effects.

Thermodynamically, the chief criticism of the writer is that the

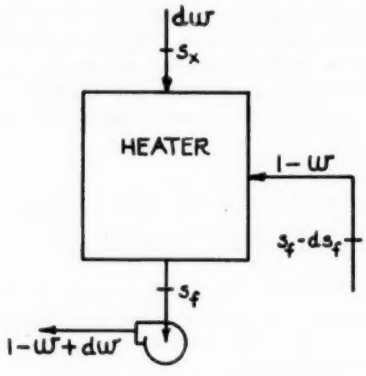


FIG. 1 FLOW DIAGRAM FOR INFINITESIMAL HEATER

author identifies the value of $\Sigma dS_{\text{heater}}$ found from Equation [2] with the ΔS of Equation [7] of the paper. The writer sees no connection between this reasoning and the laws of thermodynamics.

The actual definition of the ΔS of Equation [7] of the paper resides in Equation [7] itself. For the heat rate of the cycle we may write

$$\text{Heat rate} = \frac{3412.75(H_C - h_A)}{H_C - h_A - (1 - w)_{\text{cond.}}\,(H_D - H_G)} \quad \ldots\ldots [8]$$

where the flow rate to the condenser (based on unit flow rate to the throttle) is found through integration of Equation [3] of the author's paper, to wit

$$(1 - w)_{\text{cond.}} = e^{-\int_{\text{cond}}^{\text{throttle}} \frac{T_f ds_f}{H_x - h_f}} \quad \ldots\ldots [9]$$

If Equations [8] and [9], herewith, are compared with Equation [7] of the author's paper, the exact definition of ΔS is found to be

$$\Delta S_{\text{exact}} = (s_C - s_A)\left[\frac{(s_C - s_G)/(s_C - s_A)}{e^{\int_{\text{cond}}^{\text{throttle}} T_f ds_f/(H_x - h_f)}} - 1\right] \quad \ldots\ldots [10]$$

Equation [6], giving the author's formula for ΔS, becomes, after a slight rearrangement

$$\Delta S_{\text{Hansen}} = (s_C - s_A)\left[\log_e \frac{s_C - s_G}{s_C - s_A} - \int_{\text{cond}}^{\text{throttle}} \frac{T_f ds_f}{H_x - h_f}\right] \quad \ldots\ldots [11]$$

A comparison of Equation [10] with Equation [11] of this discussion shows that the author's formula for ΔS is correct only when

$$\log_e \frac{s_C - s_G}{s_C - s_A} = \int_{\text{cond}}^{\text{throttle}} \frac{T_f ds_f}{H_x - h_f} \quad \ldots\ldots [12]$$

or, in other words, only when ΔS is identically zero.

Equation [12] is not a thermodynamic identity, and can at best be satisfied only approximately. It appears that for the cases given in the author's Table 2, the agreement is fairly good.

[9] "Notes on the Comparison of Steam Turbine Efficiencies," by Ernest L. Robinson, *General Electric Review*, vol. 29, 1926, pp. 503–510.

[10] Assistant Professor of Mechanical Engineering, Massachusetts Institute of Technology, Cambridge, Mass. Jun. A.S.M.E.

Taking, for example, the steam conditions of Table 1, we get

$$\log_e \frac{s_C - s_G}{s_C - s_A} = 1.006; \quad \int_{\text{cond}}^{\text{throttle}} \frac{T_f ds_f}{H_x - h_f} = 0.977^*$$

Since the author's method apparently rests on the fortuitous fact that Equation [12] is approximately satisfied when steam is the working fluid, an important consideration concerns the maximum error which might be incurred through its use. For example, is one likely to encounter considerably greater errors than the largest error in Table 2, viz., 7 Btu per kwhr?

As regards the author's claim that his method requires less labor of computation than that of Selvey and Knowlton, attention is called to the writer's discussion of the Selvey and Knowlton paper. In that discussion it was shown that Selvey and Knowlton's procedure could be improved slightly as regards the thermodynamic analysis itself, and improved in considerable measure as regards computation technique. The method employed in that discussion was essentially equivalent to integrating Equation [9] of the present discussion with the aid of Simpson's rule and then substituting in Equation [8] of the present discussion to solve for the heat rate. With steam conditions of 3200 psia, 1200 F, 1 in. Hg, it was found that with only four calculations similar to those of Table 2 in the present paper, heat rates could be calculated with an accuracy of about 1 or 2 Btu per kwhr. With eight such calculations, the accuracy of the method is of the order of 0.1 or 0.2 Btu per kwhr.

H. Le H. Smith.[11] The author's three-dimensional consideration of temperature-entropy-quantity of steam is of special interest. Some of the general treatment raises questions of rigor, where fluid quantities are spoken of when fluid rates of flow are seemingly meant.

In dealing with adiabatic expansion and the resulting theoretical cycles, the treatment does not come to grips with reality. The author says, "Usually engineers are reluctant to utilize the concept of entropy except when it remains constant,....." Can these things be?

The problem of the heat-cycle loss when superheated steam is bled for feedwater heating is an important problem, but surely its importance in a realistic sense is in application to real turbines, expanding nonadiabatically.

Toward the end of the paper explicit statements are made concerning the procedures by which the method could be modified to transfer it from the status of dealing with an unrealistic hypothetical turbine to that of dealing with a real turbine.

It would be an enlightening contribution if the author would make this transfer in a supplementary paper.

Author's Closure

The suggestion by Lieutenant Elrod eliminates the approximation to which objection is made in two of the discussions, without adding appreciably to the work involved. However, the error introduced by the approximation is negligible at any temperature likely to be employed in practice for some time to come, as may be shown by solving Equation [5] of the discussion for ΔS, letting A equal the area found graphically or otherwise.

$$\Delta S = (S_C - S_A)(e^A - 1) \quad [13]$$

The exponential may then be expanded into an infinite series, by means of Maclaurin's theorem.

$$e^A = 1 + A + \frac{A^2}{2!} + \frac{A^3}{3!} + \ldots + \frac{A^n}{n!} \quad [14]$$

The approximation employed in the paper amounts to rejecting all terms beyond the second. If the value of A so found is of the order of 0.03, as in the example worked out in Table 1, the error introduced through letting $(e^A - 1)$ equal A, amounts to 0.00045, which would affect the heat rate by approximately 2 Btu per kwhr. If the value of A is 0.0014, as in the third line of Table 2, the error amounts to 0.000001, which would affect the heat rate by less than 0.01 Btu per kwhr. There is thus no justification for assuming that the discrepancies shown in Table 2 are due to this "approximation." The author has solved Equation [9], using Simpson's rule with eight intervals, and obtained a heat rate at 400 psia 700 F throttle conditions of 8228.3 Btu per kwhr. This indicates that a major part of the discrepancy referred to may be attributable to inaccuracy in the Selvey and Knowlton value of 8222.

Solution either of Equation [6] of the text or of Equation [13] just given is facilitated by the use of Simpson's rule. The following have been computed from data given in Table 1, by plotting the figures in column 10 and reading values at desired intervals.

No. of intervals	A	ΔS	Heat rate, Btu/kwhr
2	0.0284	0.0156	5999
3	0.0288	0.01585	6000.4
4	0.0288	0.01585	6000.4
8	0.0290	0.01595	6001.2

Three intervals[12] are sufficient to obtain an accuracy within one Btu per kwhr, compared with eight necessary if Equation [9] is used. At throttle temperatures below 1000 F, probably two intervals would prove ample. A still rougher approximation would be

$$A = \frac{S_A - S_G}{3}\left[\frac{1}{S_C - S_A} - \frac{T_A}{H_C - h_A}\right] \quad [15]$$

The derivation in the paper is predicated on one pound of throttle steam. The time interval involved does not enter the discussion, hence it is unnecessary to employ terms indicating flow rate.

The manner in which reheat may be handled, merely by addition of the ΔS for each expansion, seems to the author exceedingly simple. Commander Dusinberre's observations regarding turbine and pump work are apt. However, it does not appear that theoretical pump work can be of much value, inasmuch as actual feed-pump work usually bears little relation to the theoretical.

It has been pointed out that much remains to be done before a rapid method of estimating real plant heat rates with high accuracy can be made available. The intention in the present paper has not been to indicate exactly how this may be done. It has rather been to clarify the concept of regeneration in the superheat region as an irreversible process, as implied by the title chosen, with the particular purpose of showing how quantitative results may be obtained.

One further step may be taken in the direction of actuality by making an analysis similar to Lieutenant Elrod's, but considering S_X to be variable, and letting feed-pump efficiency be m (assuming motor-driving the feed pump to have 100 per cent efficiency). This leads to the following

$$\Delta S = (S_C - S_A)(e^{(a + b + c)} - 1) \quad [16]$$

* The value 0.977 is taken from the writer's discussion of the Selvey and Knowlton paper, author's reference (3).

[11] Supervisor, Power Department, B.M.T. Division, Board of Transportation, City of New York. Mem. A.S.M.E.

[12] Statement of Simpson's rule given in most handbooks applies only for an even number of intervals; with three intervals, y being the value in Table 1, column 10

$$\text{Area} = \frac{S_A - S_G}{8}(y_0 + 3y_1 + 3y_2 + y_3)$$

in which

$$a = -\int\left[\frac{1}{S_x - S_f} - \frac{T_f}{H_x - h_f}\right] dS_f \quad [17]$$

$$b = \int \frac{dS_x}{S_x - S_f} \quad [18]$$

$$c = -\frac{1-m}{m}\int \frac{v_f dp}{Hx - h_f} \quad [19]$$

All integrals are of course between limits of throttle and condenser pressure. (Statement in paper that "ΔS value because of irreversibility in turbine expansion can be read from the expansion curve" is obviously incorrect, as such a value would not take into account the reduced quantity of steam reaching condenser.) Of the three components of the exponent, only b would be comparable in magnitude with the exponent to be evaluated if Equation [9] is employed, being of the order of half of the latter. Using Simpson's rule, not more, and probably fewer, than eight intervals would be required. If the steam flow is wanted, it can be found from the following

$$(1 - w) = \left[\frac{T_G\,(S_C - S_A)}{H_D - h_G}\right] e^{(a+b+c)} \quad [20]$$

The inference may be drawn that other factors could be devised to be added to the exponent in Equations [16] and [20], to cover other departures from complete reversibility.

Development of the Lysholm-Smith Torque Converter[1]

AUTHOR'S CLOSURE

The author regrets that owing to wartime conditions, he has not been able to close the paper before.

Mr. Eksergian agrees with the author that the flow of a multistage reaction converter increases with reduced speed. The influence of this increased flow on the input torque is, however, not correctly interpreted by Mr. Eksergian. By using his theory, the input would increase on both sides on the optimum point, which is not substantiated by the test results. For the converter in question, the last turbine stage acts like a guide to the pump impeller giving a counterrotating vortex. The higher the secondary speed is, the less the circulation of this vortex will be, causing an increased unloading of the impeller. It has also been confirmed by tests made by the author that if a stationary guide is arranged before the pump impeller, the input torque will be substantially constant near the optimum point but, due to the increased flow decreases somewhat at stalling and racing. The dimensions of the various parts of the converter may be obtained from Fig. 1, which is drawn to a scale of 1:6.7.

Mr. Wislicenus comes to the conclusion that by using the equation given below Fig. 2, the actual pressure drop will be twice as great as derived from Equation [1]. This is not correct, as Equation [1] applies both to guide and rotating blades, thus making up for the missing factor of 2. The author regrets that this was not stated in his paper.

The author agrees that it is very difficult to separate losses in a hydraulic converter. The approximate method used when computing Table 1 was to estimate leakage, rotation, and mechanical losses according to usual formulas and try to balance the remaining losses in a reasonable way to correspond to the total losses obtained by the tests.

The carry-over losses are the losses in the open space between turbine and pump, or vice versa.

The author's Equation [2] was taken over from a similar equation used for calculating losses of the Ljungström double-rotation steam turbine. As shown in Fig. 4, this factor is by no means constant, but varies considerably over the range of inlet angles.

The rate of flow indicated in Fig. 2 is valid for constant input horsepower—that is to say, a constant value of $Q\Sigma\,\Delta h$. The values have been computed from test data for a great number of primary and secondary speeds by means of a Pitot tube fitted after the guide blade C in Fig. 1. This characteristic has to be accepted as correct on account of these tests, but it is also possible to confirm the test results by the cut-and-try method described below Fig. 2 in the paper.

A. LYSHOLM.[2]

[1] By A. Lysholm, published with discussion in the July, 1944, issue of the Transactions of the A.S.M.E. Because of wartime conditions the author was unable to submit a closure.

[2] Consulting Engineer, Stockholm, Sweden.

Experimental Study of the Flow of Coal in Chutes at Riverside Generating Station[1]

R. F. LEGGET.[2] This lucid account of an exhaustive experimental study into a complex operating problem has proved of unusual interest to the writer since he was working on an allied problem at the University of Toronto, apparently simultaneously with the authors of the paper. His findings, which to some extent supplement those of the authors, will be presented at a future date.

The writer's investigation was concerned with the clogging of bituminous coal in the large reinforced-concrete bunkers of the new steam-generating plant of the Polymer Corporation at Sarnia, Ontario. A model of a bunker was used, one-twelfth full size, but made of wood and not of such a convenient material as pyralin. The grading of the coal used did not correspond with that shown in Fig. 1 of the present paper; however, the coal used for experiments was modified as the authors suggested.

In all the experiments conducted at Toronto, no "scale effect" was noted, and the writer is therefore puzzled by the authors' statement with regard to this matter, especially since it is difficult to see what should cause a difference between the behavior of coal in model and prototype. Possibly the authors will discuss this matter further in their closure.

The comment given on the use of "wetting agents" confirms the writer's experience; he cannot but think, however, that in some way these remarkable chemical products may one day assist in the solution of problems involving the movement of coal.

In view of the differing character of the units being studied, it is the authors' interesting discussion of the physical properties of the coal which provides the closest link between the two investigations. Although the approaches to the study of the properties of coal were somewhat different, the moisture content is paramount in both. Accordingly, it would be helpful if the authors would state how their moisture contents are expressed, i.e., as percentages of the dry or of the wet weights of coal.

[1] By E. E. Wolf and H. L. von Hohenleiten, published in the October, 1945, issue of Trans. A.S.M.E., vol. 67, pp. 585–599.

[2] Associate Professor of Civil Engineering, University of Toronto, Toronto, Ontario, Canada.

Failure of Ductile Metals in Tension[1]

By G. SACHS[2] and J. D. LUBAHN,[3] CLEVELAND, OHIO

The extensive fabrication of aluminum-alloy sheet in the aircraft industries has revealed the lack of fundamental knowledge regarding the phenomena which explain the performance of metals under various stress and strain states. Previous investigations appear to have neglected entirely both the effects of the part geometry and the fact that the strength of the metal and limit of forming are frequently determined by a process of instability, or "necking," rather than by the process of fracturing. In this paper a theory of necking is developed in order to predict the forming limits for various stress or strain states based upon an analysis of the true stress-strain curve in pure tension. A criterion for necking is advanced, based upon the maximum-load (or pressure) conception of instability, and is applied to different geometrical shapes formed at room temperature. Future publications will present, in support of the criterion advanced, experimental analyses of the forming of different geometrical shapes under various loading conditions and stress and strain states.

Nomenclature

The following nomenclature is used in the paper:

A = cross-sectional area

e = ordinary principal strain = $\frac{L - L_0}{L_0}$

F = tensile load

F_{max}/A = stress at maximum load point

L = length of longitudinal element

p = internal pressure in tube, sphere, or circular bulge

R = radius of curvature to inside surface of thin-walled tube, sphere, or circular bulge

s = principal stress

h = thickness of element, or wall thickness of a tube or sphere

V = volume of element

w = width of element

ϵ = natural strain or logarithmic strain = $\ln (1 + e)$

0 = subscript denoting conditions before straining

1 = subscript denoting direction of principal stress or strain of greatest algebraic value

2 = subscript denoting direction of principal stress or strain of intermediate algebraic value

3 = subscript denoting direction of principal stress or strain of least algebraic value

Introduction

THE general term "forming limit" may cover a variety of fundamentally different metal characteristics. It generally defines the maximum strain, or rather the magnitude and state of strain, which may be achieved with a certain type of equipment. This forming limit may be determined by the "cohesive" strength or "ductility" of the metal, which is often considered to be the only forming limit. However, a process may be limited by the strength of the equipment rather than by the ductility of the metal. In many commercial processes, particularly those of the compression type, the maximum strain is limited only in this manner.

Another rather peculiar type of forming limit results from a condition of loading which causes a local breakdown of the metal. A generally known and much discussed group of phenomena of this type is called "buckling." The buckling of a slender structural member limits its strength in a manner quite comparable to a brittle failure. Besides those phenomena of buckling discussed in textbooks on elasticity, there is also a variety of types of plastic buckling known which limit the forming under certain stress states, such as the wrinkling of deep-drawn cups and the folding of sunk or necked tubing.

The general characteristics of buckling may be defined as a load condition where an increase in strain occurs without an increase or with a decrease in load. Such an instability, therefore, should occur always when the load F goes through a maximum, or when the differential of the load becomes zero

$$F = \text{maximum} \qquad dF = 0$$

This condition determining the forming limit in buckling also applies to another group of instability phenomena, the best known representative of which is the local "necking" of a part strained in tension. When the load passes through a maximum, and the strain increases by a small amount at some location, this location becomes less strong in comparison with the remainder of the part. Then all further strain will occur here while it will discontinue at other locations, thus resulting in a "neck." The necking of a regular tensile-test specimen has attracted considerable interest, and numerous publications deal with stress-strain conditions conducive to necking (1–7).[4]

The condition of necking for pure tension can be written as follows:

$$dF = d(As) = 0$$

$$\frac{ds}{s} + \frac{dA}{A} = 0$$

where s is the true stress corresponding to a cross-sectional area A. This rather lucid formulation of the necking condition relates the instability to the fact that the rate of increase in tensile load by the increase of stress (due to strain-hardening) is no longer able to compensate for the decrease in tensile load be-

---

[1] This paper is one of a series of reports on the research program on hot-forming of aluminum alloys conducted at Case School of Applied Science under contract with the Office of Production Research and Development of the War Production Board. This research, which was supervised by the War Metallurgy Committee under the "restricted" project NRC-547, is the basis of this paper which has been released for publication by the OPRD.

[2] Professor of Physical Metallurgy, Department of Metallurgical Engineering, Case School of Applied Science. Mem. A.S.M.E.

[3] Department of Metallurgical Engineering, Case School of Applied Science.

Contributed by the Metals Engineering Division and presented at the Annual Meeting, New York, N. Y., Nov. 26–29, 1945, of The American Society of Mechanical Engineers.

Note: Statements and opinions advanced in papers are to be understood as individual expressions of their authors and not those of the Society.

[4] Numbers in parentheses refer to the Bibliography at the end of the paper.

cause of decreasing cross-sectional area. The necking condition in this form has been applied to processes other than uniaxial tension, such as a sheet subjected to biaxial tension (13), a rotating disk, and a tube subjected to internal pressure (8, 9, 11).

In order to develop an instability condition that is applicable to the wide variety of commercial conditions of loading and geometry, the original maximum-load conception must be extended. Already it can be concluded from previous analyses that the instability of a flat sheet and of a tube subjected to the same stress state occur at different strains. Therefore the conception is advanced in this paper that instability occurs, or "necking" begins, if, with increasing strain, one of the external loads passes through a maximum. So far only the tensile load has been considered ($dF = 0$). However, the primary source of stress in parts subjected to internal pressure is this pressure p and consequently instability should then occur when

$$p = \text{maximum} \qquad dp = 0$$

The purpose of this and subsequent papers will be as follows:

1 To develop the conception that under various load and geometrical conditions the forming limit for a homogeneous metal may be determined by instability, and to associate this "necking" with a maximum in either the tensile load or the internal pressure, as discussed previously.

2 To develop a theory of instability which may be applied to the stress-strain curve as experimentally derived for the load conditions and geometrical conditions actually present.

3 To extend this criterion of instability to predict the forming limit for any stress state and condition of geometry considered, using only the stress-strain curve in pure tension.

In the present analysis equations have been developed which apply to actual relations between the stresses and strains that exist during a particular type of test on a particular material. These relations, which are necessary in order to predict the necking strain, may be determined experimentally in a simple manner for certain conditions of geometry and loading, such as a tube subjected simultaneously to internal pressure and longitudinal tension. In this case the stresses and strains are calculated readily from the measured load, the pressure, and the dimensional changes, such as the changes in length and diameter of a tube. However, in other instances of geometry, such as a circular hydraulically formed bulge, a tedious experimental analysis and possibly also a theoretical analysis is necessary to establish the stress-strain relations that are required for the application of the derived necking condition.

Experimentation generally supplies the three principal stresses and the three principal strains for each point of the test, thus defining completely the stress and strain states, respectively. To apply the graphical construction, particular stresses and strains, or functions of these, must be selected to yield a suitable stress-strain relation. It would be desirable that various stress states could be represented by a single, or "universal," stress-strain curve, by plotting a suitable function of the three principal stresses versus a suitable function of the three principal strains. There are several possibilities, and the question as to which is the most suitable is still a matter of considerable argument. In most problems of plasticity the simplest possible condition has been found to yield sufficiently accurate results.

The following analysis applies only to biaxial-tension stress states, defined by the fact that the algebraically smallest principal stress s_3 is zero. In this case the larger of the two tensile stresses s_1, may be plotted versus the numerically largest of the three natural principal strains, as the simplest possible conception that yields a nearly universal stress-strain relation.[5]

Other stress and strain functions yield stress-strain curves for various stress states which agree more closely, but also which require more elaborate calculations. It should be noted that two of the stress states which are considered particularly in this paper, namely, pure tension and balanced biaxial tension, yield identical stress-strain curves, according to any of the recognized theories. The stress state which may be particularly affected regarding the accuracy of the solution by any such assumption would be the condition of plane strain which is intermediate between pure tension and biaxial tension.

The present approach to the problem has the particular advantage that the resulting differential equations allow the direct determination of the necking point on the experimental or equivalent stress-strain curve, using a simple geometrical construction. Also, the equations derived in this paper are basic, and may be extended to include any desired universal stress-strain relation. Finally, the stress may be approximated algebraically as a function of the strain, to permit an algebraic rather than a graphical solution. However, considering the rather large amount of work which such an algebraic analysis requires, it appears that the graphical method of solution is more flexible, is more lucid, and offers less possibility of error; consequently, this will be used in the analyses in subsequent publications.

Regarding the effect of the part geometry on the instability strain for balanced biaxial tension, it will be shown that the results are rather different for the three types of curvature, or changes in curvature, represented by (*a*) a flat sheet, (*b*) a sphere under internal pressure, or tubing under longitudinal tension and internal pressure, and (*c*) a circular hydraulic bulge formed by pressure from flat sheet. Previous experimentation confirms the results of some phases of the theoretical analysis, and additional evidence will be submitted in subsequent publications.

Necking of a Tensile Test Specimen

The well-known necking of a ductile tensile test specimen has been recognized by Considére (1) and Ludwik (2), as a phenomenon of instability. It is associated with a maximum in the load-strain diagram. As long as the load F increases, the specimen stretches approximately uniformly over its length,[6] while a decreasing load indicates necking.

(*a*) If s_1 is the true principal stress, i.e., the load F divided by the actual cross section A of the metal, the beginning of necking is given by the condition (see Sachs, 7)

$$F = s_1 A = \text{maximum}$$

$$dF = 0 = A\,ds_1 + s_1\,dA$$

$$\frac{ds_1}{dA} = -\frac{s_1}{A} \qquad [1]$$

As illustrated in Fig. 1, the point of necking, or maximum load point, is a point in the s_1 versus A diagram, such that the tangent at this point intersects the ordinate at $A = 0$ at a height

[5] This is a special case (for biaxial tension) of the conception that all stress states yield identical stress-strain curves if the maximum shear stress $\left(\frac{s_1 - s_3}{2}\right)$ is plotted versus the maximum (absolute) natural strain.

[6] The "uniform" strain is considered as the presumably constant value of strain encountered at room temperature outside necked areas along the length of a sufficiently long tensile specimen. This value represents the greatest strain the metal will exhibit without necking under ideal conditions.

$\frac{2F_{max}}{A}$, giving a slope value of $-\frac{s_1}{A}$ (see footnote[7]).

This solution becomes particularly simple if the s_1 versus A diagram is a straight line in the vicinity of the maximum load point, as shown by Koerber (4), and pointed out previously by Moellendorff and Czochralski (3); see also Koerber and Rohland (6).

(*b*) The strain may also be expressed by the stretch e_1 of a certain length, $L = L_0 (1 + e_1)$, determined by the constancy of volume V

$$V = L_0 A_0 = LA = L_0 (1 + e_1) A$$

$$1 + e_1 = \frac{A_0}{A}$$

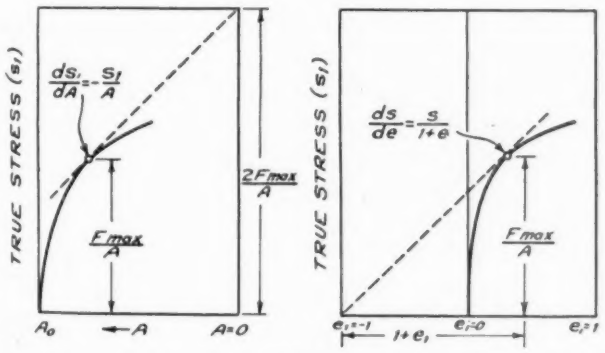
where the subscript zero denotes conditions before straining. The condition of necking then becomes

$$F = A_0 \left(\frac{s_1}{1 + e_1} \right) = \text{maximum}$$

$$dF = A_0 \left[\frac{ds_1}{1 + e_1} - \frac{s_1 de_1}{(1 + e_1)^2} \right] = 0$$

$$\frac{ds_1}{de_1} = \frac{s_1}{1 + e_1} \quad \ldots\ldots\ldots\ldots\ldots\ldots [1a]$$

In the s_1 versus e_1 diagram, Fig. 2, the maximum load point is



FIGS. 1 AND 2 CONSTRUCTION OF THEORETICAL NECKING CONDITION IN PURE TENSION FOR s VERSUS A AND s VERSUS e CURVES

determined by the condition that its tangent shall intersect the abscissa at a value $e_1 = -1$, yielding a slope equal to $s_1/(1 + e_1)$, see Considére (1), Nielsen (5), and Gensamer (13).

(*c*) By a third method which will be used generally throughout this paper, the strain can be expressed as the natural strain

$$d\epsilon_1 = \frac{de_1}{1 + e_1}$$

The necking condition then can be written (see Equation [1*a*])

$$\frac{ds_1}{d\epsilon_1} = s_1 \quad \ldots\ldots\ldots\ldots\ldots\ldots [1b]$$

As illustrated in Fig. 3, the maximum load point may be determined by the condition that its tangent intersects the abscissa of the s_1 versus ϵ_1 diagram at the value $-(1 - \epsilon_1)$, yielding the slope $s_1/1$.

[7] In the graphical solution for a particular metal, using experimental data, it is more accurate actually to plot the slope (ds_1/dA) and the ratio (s_1/A) against A and note their intersection (see also Fig. 9), rather than use the type of construction indicated in the various figures.

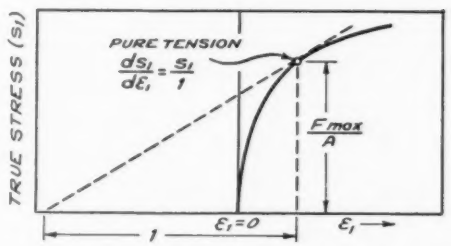


FIG. 3 CONSTRUCTION OF THEORETICAL NECKING CONDITION IN PURE TENSION FOR s VERSUS ϵ CURVE

NECKING OF FLAT SHEET UNDER BIAXIAL TENSION

When a flat sheet is subjected to biaxial tension, the normal stress s_3 is zero, and the maximum shear-stress condition indicates that the largest principal stress s_1 (2 times the largest shear stress) is always the decisive stress.

Under these conditions, the stress-strain curve becomes very similar to that for uniaxial tension if this decisive stress is plotted against the decisive strain, i.e., the numerically largest principal strain. Considering the intermediate natural strain ϵ_2, two general cases of biaxiality arise. When ϵ_2 is less than zero, ϵ_1 remains the decisive strain; when ϵ_2 is positive (but smaller than ϵ_1, according to definition), ϵ_2 becomes the decisive strain.

(*a*) The general condition of instability (necking) for a flat sheet will now be postulated to be the occurrence of a maximum in the force applied in the direction of the maximum tension s_1, this resulting in the same equation as for uniaxial tension Equation [1]

$$F = s_1 A = \text{maximum}$$

$$dF = 0 = s_1 dA + A ds_1$$

$$\frac{ds_1}{s_1} = -\frac{dA}{A} \quad \ldots\ldots\ldots\ldots\ldots\ldots [2]$$

Using the constant-volume condition

$$\left.\begin{aligned} A &= A_0 (1 + e_2)(1 + e_3) \\ dA &= A_0 (1 + e_3) de_2 + A_0 (1 + e_2) de_3 \\ \frac{dA}{A} &= \frac{de_2}{1 + e_2} + \frac{de_3}{1 + e_3} = d\epsilon_2 + d\epsilon_3 \end{aligned}\right\} \quad \ldots\ldots [3]$$

The general instability condition, Equation [2], becomes

$$\frac{ds_1}{s_1} = -d\epsilon_2 - d\epsilon_3 \quad \ldots\ldots\ldots\ldots\ldots [3a]$$

$$\frac{ds_1}{s_1} = d\epsilon_1 \quad \ldots\ldots\ldots\ldots\ldots\ldots [3b]$$

(*b*) Strain ϵ_1 remains decisive for any biaxiality where $0 > \epsilon_2 > -\frac{\epsilon_1}{2}$, the limiting conditions being uniaxial tension $(\epsilon_2 = -\epsilon_1/2)$ and plane strain $(\epsilon_2 = 0)$. For this whole range of biaxiality, therefore, the same condition Equation [3*b*], applies as that for uniaxial tension

$$\frac{ds_1}{s_1} = d\epsilon_1$$

For the case of plane strain, Baranski (10) has observed previously that the natural necking strain is practically the same as for pure tension.

(*c*) For biaxialities where $\epsilon_1 > \epsilon_2 > 0$, ϵ_2 becomes the decisive

strain, the limiting conditions being plane strain ($\epsilon_2 = 0$) and balanced biaxiality ($\epsilon_1 = \epsilon_2 = -\epsilon_3/2$).

Introducing the quantity n, defined by

$$\epsilon_2 = -n\epsilon_3 \quad [4]$$

where $^1/_2 > n > 0$ (for ϵ_3 being decisive), the basic Equation [3a] becomes

$$\frac{ds_1}{s_1} = -d\epsilon_3(1 - n) \quad [3c]$$

This equation can also be solved graphically.

(*d*) In the special case of balanced biaxial tension, $\epsilon_2 = -\epsilon_3/2$, $n = {}^1/_2$, and the instability condition assumes the following form

$$\frac{ds_1}{s_1} = -\frac{1}{2}d\epsilon_3 \quad [5]$$

or

$$\frac{ds_1}{d\epsilon_3} = -\frac{s_1}{2} \quad [5a]$$

As shown by Gensamer (13), the graphical solution of this equation can be obtained by the same method as employed in Fig. 3 and illustrated in Fig. 4.

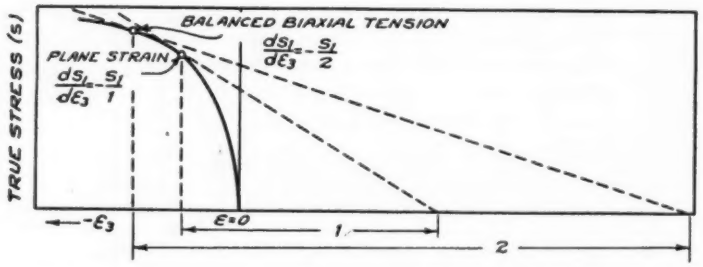


FIG. 4 CONSTRUCTION OF THEORETICAL NECKING CONDITION IN BIAXIAL TENSION FOR s VERSUS ϵ CURVE

(*e*) In the limiting case of plane strain, $\epsilon_2 = 0$, $\epsilon_3 = -\epsilon_2$, $n = 0$, the two solutions, Equations [3b] and [3c], yield identical results (see Figs. 3 and 4)

$$\frac{ds_1}{s_1} = -d\epsilon_2 = d\epsilon_1$$

It can be seen that for identical stress-strain curves, as noted previously, ϵ_3 at the maximum load point of balanced biaxial tension is much larger than ϵ_1 at the maximum load point of uniaxial tension, Fig. 3. Thus the uniform stretch in balanced biaxial tension, $\epsilon_1 = -\epsilon_3/2$, must be greater than one half the uniform stretch in pure tension, and may be either larger or smaller than the uniform stretch in pure tension, depending upon the strain-hardening characteristics of the metal.

INSTABILITY OF THIN-WALLED TUBES SUBJECTED TO INTERNAL PRESSURE

The condition for the necking of a thin-walled tube subjected to internal pressure has not been thoroughly understood up to the present time. Some attempts by Laszlo (8, 9) and Siebel and Kopf (11) indicate that such a tube will neck at considerably smaller strains than a tensile test specimen of the same material.

It appears that the uniform strain of a tube subjected primarily to an internal pressure p, is determined by the condition that this pressure reaches a maximum. For a thin-walled tube having an initial inside diameter $2R_0$ and an initial wall thickness h_0, this pressure is given by the well-known equation

$$p = s_1\frac{h}{R} = s_1\frac{h_0(1 + e_3)}{R_0(1 + e_1)} \quad [6]$$

where e_1 and e_3 are the circumferential and normal strains, respectively.

This condition should apply for any condition of biaxiality where the circumferential stress is the decisive stress (and possibly also for conditions where the longitudinal stress is the decisive stress).

Regarding the decisive strain, again two conditions arise, where $0 > \epsilon_2 > -\frac{\epsilon_1}{2}$, and where $\epsilon_1 > \epsilon_2 > 0$.

(*a*) The general condition of instability, Equation [6], can now be written as follows

$$dP = 0 = \frac{h_0}{R_0}\left[ds_1\frac{1 + e_3}{1 + e_1} + s_1\frac{de_3}{1 + e_1} - s_1\frac{de_1(1 + e_3)}{(1 + e_1)^2}\right]$$

This yields the final equation

$$\frac{ds_1}{s_1} + \frac{de_3}{1 + e_3} - \frac{de_1}{1 + e_1} = 0 \quad [6a]$$

or

$$\frac{ds_1}{s_1} + de_3 - de_1 = 0 \quad [6b]$$

(*b*) For pure (uniaxial) circumferential tension, ϵ_1 is the decisive strain, and $\epsilon_3 = \epsilon_2 = -\frac{\epsilon_1}{2}$. Consequently, the instability condition, Equation [6b], assumes the following form

$$\frac{ds_1}{s_1} = \frac{3}{2}d\epsilon_1$$

or

$$\frac{ds_1}{d\epsilon_1} = \frac{s_1}{2/3} \quad [7]$$

This latter form can again be solved graphically by the method of trial and error, Fig. 5. A comparison with the condition for pure tension for which the same stress-strain curve exists, Equation [1b], shows clearly that the tube would become unstable at a smaller circumferential strain than the (longitudinal) necking strain of a tensile test bar. This difference is due to the change in curvature, rather than to differences in the stress state.

(*c*) If $0 > \epsilon_2 > -\frac{\epsilon_1}{2}$, the decisive strain remains ϵ_1. Introducing the relation

$$\epsilon_2 = -n\epsilon_1;\ \epsilon_3 = -\epsilon_1 - \epsilon_2 = (+n - 1)\epsilon_1 \quad [8]$$

where $1/2 > n > 0$, the general condition of instability can be written as follows

$$\frac{ds_1}{s_1} = d\epsilon_1(2 - n) \quad [6c]$$

(*d*) For plane strain, $\epsilon_2 = 0$, $n = 0$, and the instability condition then becomes

$$\frac{ds_1}{d\epsilon_1} = \frac{s_1}{1/2} \quad [9]$$

The graphical solution for this case of biaxiality is also illustrated in Fig. 5. The circumferential strain at which the tube would become unstable, under such conditions, would be still smaller than that for a tube subjected to pure circumferential pressure.

(*e*) If $\epsilon_1 > \epsilon_2 > 0$, the decisive strain becomes ϵ_3. Using the relation of Equations [8]

$$\epsilon_1 = \frac{\epsilon_3}{n-1} \quad \ldots\ldots\ldots\ldots\ldots [8a]$$

where $0 > n > -1$, the general condition of instability can be written as follows (see Equation [6*c*])

$$\frac{ds_1}{s_1} = d\epsilon_3 \left(\frac{2-n}{n-1}\right) \quad \ldots\ldots\ldots [6d]$$

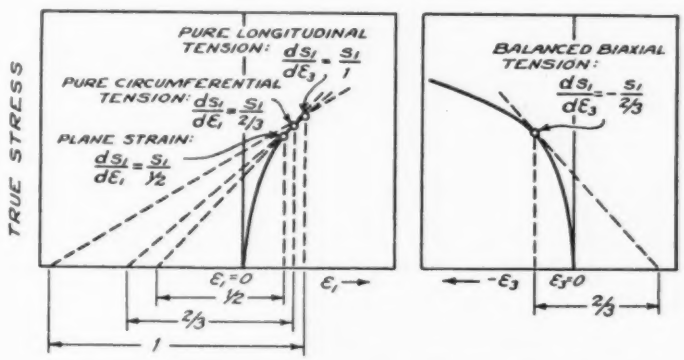


FIG. 5 CONSTRUCTION OF THEORETICAL NECKING CONDITION IN TUBING UNDER VARIOUS STRESS STATES

(*f*) For balanced biaxial tension, $\epsilon_1 = \epsilon_2 = -\frac{\epsilon_3}{2}$, $n = -1$ and the instability condition yields the equation

$$\frac{ds_1}{d\epsilon_3} = -\frac{s_1}{2/3} \quad \ldots\ldots\ldots\ldots\ldots [10]$$

The same graphical solution now applies as for pure circumferential tension, Fig. 5, the decisive strain, however, being ϵ_3. The circumferential strain, in the case of balanced biaxial tension, however, would be only one half of that for uniaxial circumferential tension, because of $\epsilon_1 = -\frac{\epsilon_3}{2}$. As noted previously, in balanced biaxial tension, approximately the same curve is obtained by plotting s_1 versus ϵ_3 as that obtained in uniaxial tension by plotting s_1 versus ϵ_1. Furthermore, Equations [10] and [7] apply, respectively, to these two curves in the same manner, yielding as the solutions identical values of necking strain (ϵ_3 and ϵ_1, respectively). In the case of balanced biaxial tension, however, the uniform stretch ϵ_1, which is only one half of the normal instability strain ϵ_3 is therefore also only one half of the uniform stretch in uniaxial circumferential tension.

INSTABILITY OF THIN-WALLED SPHERE SUBJECTED TO INTERNAL PRESSURE

The same approach as used for a tube should be valid when applied to a sphere subjected to an internal pressure, p. The pressure for a sphere having an initial diameter $2R_0$ and an initial wall thickness t_0, is given by the well-known equation

$$p = 2s_1 \frac{h}{R} = 2s_1 \frac{h_0}{R_0} \frac{1+e_3}{1+e_1}$$

where $s_1 = s_2$ is the tensile stress and $e_1 = e_2$ the tangential strain (in the surface of the sphere), and e_3 is the normal (and decisive) strain.

The instability condition then becomes

$$dp = 0 = 2\frac{h_0}{R_0}\left[ds_1 \frac{1+e_3}{1+e_1} + s_1\left(\frac{de_3}{1+e_1} - \frac{de_1\,(1+e_3)}{(1+e_1)^2}\right)\right]$$

or

$$\frac{ds_1}{s_1} + \frac{de_3}{1+e_3} - \frac{de_1}{1+e_1} = 0$$

or

$$\frac{ds_1}{s_1} + de_3 - de_1 = 0 \quad \ldots\ldots\ldots\ldots [11]$$

And using the relation $\epsilon_1 = -\frac{\epsilon_3}{2}$, the same equation results as for tubing under balanced biaxial tension, Equation [10], the graphical solution of which is illustrated in Fig. 5.

INSTABILITY OF CIRCULAR HYDRAULICALLY FORMED BULGE

The criterion for necking presented here is limited to uniform stress and strain states over the region in question. This requires that for any section of the specimen both the thickness and radius be uniform at any instant during the test, and that there be no variation of metal properties throughout the specimen.

During the bulging of a thin circular disk clamped at its periphery, neither the thickness nor the radius is uniform over the entire bulge. However, experimentation has shown that at and around the pole there is a rather large area which is close to spherical and where the magnitudes of the stresses and strains are nearly constant. Consequently, an analysis similar to that used for other geometrical shapes should be applicable. The validity of this conception has been verified by experiments which will be presented in a later publication.

Fundamentally, the same condition should determine the strength of a ductile disk, subjected to hydraulic pressure, as that which determines the strength of a sphere subjected to internal pressure, namely, that when the pressure p, reaches a maximum, instability should occur, provided that the metal is sufficiently ductile to "neck" before fracturing. This pressure p is given, as in the case of the sphere, by the equation

$$p = 2s_1 \frac{h}{R} = 2s_1 \frac{h_0(1+e_3)}{R}$$

where $s_1 = s_2$ is the tension at the pole of the bulge, at which location the highest strains are exhibited, and $e_1 = e_2$ and e_3 are the tangential strains and normal strain, respectively, Fig. 6. The necking condition in terms of the strain e_3 then becomes

$$dp = 0 = 2h_0\left(ds_1 \frac{1+e_3}{R} + s_1 \frac{de_3}{R} - s_1 dR \frac{1+e_3}{R^2}\right)$$

or

$$\frac{ds_1}{s_1} = \frac{dR}{R} - \frac{de_3}{1+e_3}$$

This equation can be written in the logarithmic form[8]

$$d(\ln s_1) = d(\ln R) - de_3$$

or

$$\frac{d\,(\ln s_1)}{de_3} = \frac{d\,(\ln R)}{de_3} - 1 \quad \ldots\ldots\ldots\ldots [12]$$

[8] $\ln = \log_e$

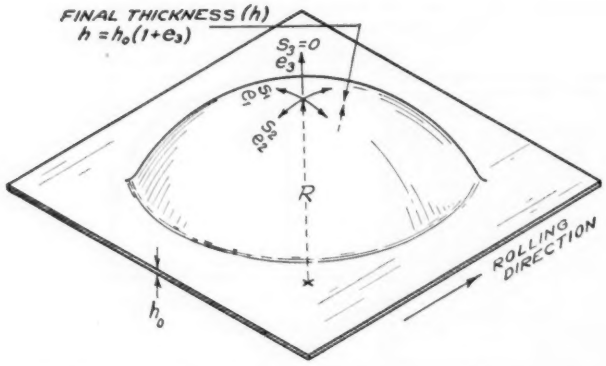


FIG. 6 STRESS AND STRAIN STATE AND GEOMETRICAL CONDITIONS IN A CIRCULAR BULGE

This equation differs from that of a sphere because the radius of curvature in this case is an unknown function of the strain. No theory of bulging is yet available which would yield the curvature during bulging if the other quantity were known. Therefore, a graphical solution, based upon experimentally determined values of stress, strain, and curvature, is necessary. The stress-strain curve, s_1 versus ϵ_3, and the radius-strain curve, R versus ϵ_3, are necessary in order to determine the two functions

$$\frac{d\ (\ln s_1)}{d\epsilon_3} \text{ and } \frac{d\ (\ln R)}{d\epsilon_3}$$

The radius is determined experimentally from contour measurements. The normal strain ϵ_3 is calculated from the measured tangential strains $e_1 = e_2$ according to the equation

$$\epsilon_3 = \ln\left[\frac{1}{(1 + e_1)^2}\right]$$

The stress is determined from the experimentally measured quantities, radius, pressure, and tangential strain, related by the following equation

$$s_1 = \frac{pR\ (1 + e_1)^2}{2t_0}$$

These values can be employed in the graphical solution of Equation [12]. Thus, as shown in Figs. 7(*a*) and 7(*b*), ln R and ln s_1 are plotted as functions of ϵ_3, (ϵ_3 being negative). The values of

$$\frac{d\ (\ln R)}{d\epsilon_3} - 1 \quad \text{and} \quad \frac{d\ (\ln s_1)}{d\epsilon_3}$$

are determined from these curves and plotted as functions of ϵ_3, Fig. 7(*c*). The ϵ_3 value at the intersection then determines the strains at the necking point, according to

$$\epsilon_1 = \epsilon_2 = -\frac{\epsilon_3}{2}$$

This strain value is considerably higher than that for the sphere and usually also higher than that for plane biaxial stress, because of the decrease in radius R, with increase in strain.

ACKNOWLEDGMENT

The authors are indebted to Mr. G. Espey and Mr. W. F. Brown, Jr., of the Department of Metallurgical Engineering, Case School of Applied Science, for their valuable assistance and criticism of the original manuscript.

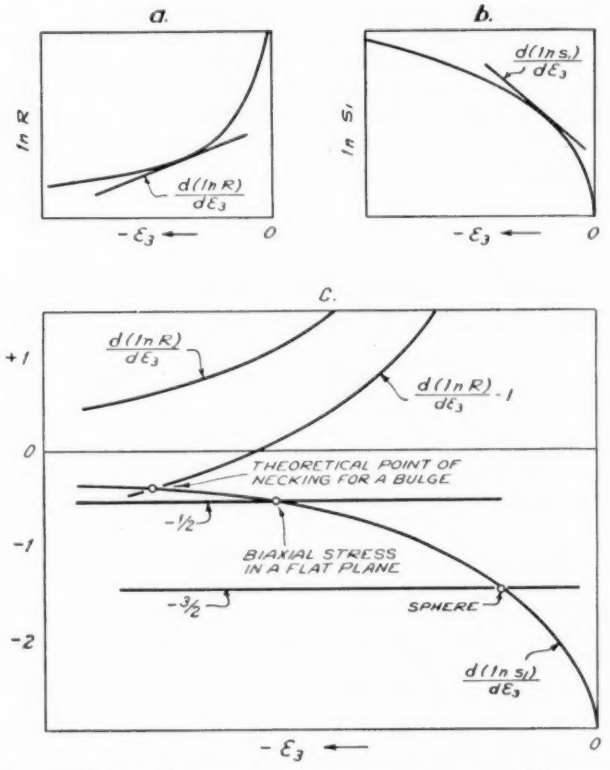


FIG. 7 STEPS IN GRAPHICAL SOLUTION OF EQUATION FOR NECKING OF A CIRCULAR BULGE [11], AND COMPARISON OF THE INSTABILITY STRAIN WITH THAT FOR A SPHERE AND FOR A FLAT PLANE SUBJECTED TO BALANCED BIAXIAL TENSION

BIBLIOGRAPHY

1 "The Application of Iron and Steel for Constructions," by M. Considére, Vienna, Austria, 1888.

2 "Elements of Technological Mechanics," by P. Ludwik, Berlin, Germany, 1909.

3 "Technological Conclusions From the Crystallography of Metals," by W. v. Moellendorff and J. Czochralski, *Zeitschrift des Vereines deutscher Ingenieure*, vol. 57, 1913, pp. 931–935.

4 "Strain-Hardening and Tensile Strength," by F. Koerber, Mitteilungen Kaiser-Wilhelm Institut Eisenforsch, Duesseldorf, vol. 3, 1922, pp. 1–15; *Stahl und Eisen*, vol. 42, 1922, pp. 365–370.

5 "The Determination of the Tensile Strength of a Ductile Metal From a Compression Test," by F. Nielsen, *Stahl und Eisen*, vol. 42, 1922, p. 1687.

6 "The Influence of Alloying Additions and Temperature Changes on the Strain-Hardening of Metals," by F. Koerber and W. Rohland, Mitteilungen Kaiser-Wilhelm Institut Eisenforsch, Duesseldorf, vol. 5, 1924, pp. 55–68.

7 "An Analysis of the Tensile Test," by G. Sachs, Werkstoffausschuss, *Verein Deutscher Eisenhuettenleute*, Report No. 52, 1925.

8 "Rotation of Bodies Having Rotational Symmetry in the Range of Permanent Strains," by F. Laszlo, *Zeitschrift für Mathematik und Mechanik*, vol. 5, 1925, pp. 279–293.

9 "Overstraining by Rotation and Internal Pressure," by F. Laszlo, *Maschinenbau*, vol. 5, 1926, pp. 210–213.

10 "Tensile Tests Under Plane Plastic Strain," by G. Baranski, *Zeitschrift für Metallkunde*, vol. 26, 1934, pp. 173–180.

11 "Tests on the Strength Properties Under Internal Pressure," by E. Siebel and E. Kopf, *Zeitschrift für Metallkunde*, vol. 26, 1934, pp. 169–172.

12 "The Design and Manufacture of Bursting Discs," by G. F. Lake and N. P. Inglis, *Engineering*, July 14, 1939, pp. 58–60; and July 31, 1939, pp. 88–89.

13 "Flow and Fracture of Sheet Under Combined Tensile Stresses," by M. Gensamer, Modern Industrial Press, Sept., 1942, pp. 36–38 and 43.

The Necking of Tensile-Test Specimens[1]

By J. D. LUBAHN,[2] CLEVELAND, OHIO

The conventional tensile test is the basis of acceptance tests, and its results are extensively used to evaluate the structural metals regarding their relative performance in forming and their strength in service. However, it appears that the significance of the phenomena encountered in a tensile test are little understood, in spite of a large number of investigations. In this paper, the strains encountered in long rectangular tensile-test bars of the aluminum alloys 24S-O and 24S-T have been investigated in detail. The theoretical conceptions previously advanced,[3] regarding the necking of tensile-test bars, have been confirmed experimentally.

THE present theory of necking correlates the occurrence of a maximum in the external load with a change in the strain condition from a uniform strain state to a nonuniform strain state, i.e., local necking. The simplest example of uniform stress and strain conditions throughout the metal should be that encountered in a regular tensile-test bar which is subjected presumably to "pure tension" before necking occurs.

The validity of the necking condition for test bars strained in "pure tension" has been the subject of numerous investigations listed in a previous paper.[3] Recently, however, the existence of a really uniform strain in a tensile test bar has been considered as doubtful. It must be emphasized that commercial metals are not entirely uniform, and therefore their strains in pure tension will be nonuniform to an extent depending upon the variations in metal properties. Frequently, also, test bars and sections that are stretched commercially lack uniformity of cross section along their length and these variations likewise cause the strains to be nonuniform even before instability, or "necking," occurs.[4]

In addition to the foregoing considerations, the stress state of a standard tensile-test specimen at failure is rather complex as a result of two factors: (*a*) The transverse tension near the ends of the gage length, because of enlarged "heads" of the specimen; and (*b*) the transverse tension in the neck itself, which is in effect a notch of large radius of curvature. In a relatively short gage length, such as that of a standard tensile-test specimen, it has been observed that the regions where lateral contraction is restrained, corresponding to the two regions of lateral tension just described, may overlap. This makes it impossible to determine by strain analysis of a standard (American) tensile-test specimen any such strain as the uniform elongation, or the strain under conditions of uniaxial tension at which local necking begins.

Tensile-Test Procedure

In order to study the phenomenon of necking under conditions which avoid the difficulties mentioned, a few tensile tests were made on aluminum-alloy strips 20 in. long, of bare 24S-O and bare 24S-T sheet, Figs. 1 and 2. The strips were reduced in the center portion from a sheared width of $1^1/_2$ in. to a width of 1 in., in order to form a 13-in. gage length of constant width with edges free from nicks and cold work. The edges were prepared by milling to a depth at least equal to the thickness, followed by polishing on a belt sander. The longitudinal direction[5] of the sheet was selected as the direction of testing, in order to obtain the most nearly constant thickness and the most nearly uniform metal properties along the length of the specimen.

The specimens were subjected to tension loads that continuously increased at a very small rate. During tests, measurements of width and thickness were made at 24 stations spaced $^1/_2$ in. apart. By a process of interpolation, the measurements, and thus also the strains, were computed for the same point of time at all the stations. Thus in Figs. 1 and 2, each curve represents the strain distribution at one particular instant during the test. Such a representation illustrates the gradual change in shape of the strain-distribution curve as the test proceeds.

It is apparent from Figs. 1 and 2 that the strains are nearly constant with position along the length of the specimen up to a strain of approximately 8 per cent. With further increasing strain, small nonuniformities appear which are not local necks in the sense of an instability effect, because they do not represent points where the strain continues to increase in the absence of strain at other points. There is a certain maximum strain, however, which has been denoted as the necking strain, above which the strains continued to increase in only one localized region, called the "neck," Figs. 1 and 2. It can be seen that this necking strain was approximately 18.5 per cent for the investigated 0.040-in. 24S-O bare specimen, and 17.5 per cent for the 0.125-in. 24S-T bare specimen. Apparently, for 24S-T bare, the strain at a load of 8980 lb was the maximum-load strain, Fig. 2, since the strain after fracture differed only by the amount of elastic recovery that is to be expected for this alloy.

The curves of (true) stress versus reduction of cross-sectional area for the two materials were obtained by plotting (for one particular station) the cross-sectional areas corresponding to the various strain curves in Figs. 1 and 2 versus the corresponding stresses. The same stress-strain curve was obtained for various stations, thus indicating the correctness of the interpolation process for obtaining the strain-distribution curves. For the purpose of this investigation, the stress-strain curves were extended only to the largest strain encountered outside the region of fracture, to avoid introducing the effects of transverse tension in the neck. The curves so obtained were found satisfactory for the following analysis, in that they exceeded by a few per cent the theoretical point of necking.

---

[1] This paper is one of a series of reports on the research program on hot-forming of aluminum alloys conducted at Case School of Applied Science under contract with the Office of Production Research and Development of the War Production Board. This research, which was supervised by the War Metallurgy Committee under the "restricted" Project NRC-547, is the basis of this paper, which has been released for publication by the OPRD. The project was directed by G. Sachs, Case School of Applied Science.

[2] Department of Metallurgical Engineering, Case School of Applied Science.

[3] "Failure of Ductile Metals in Tension," by G. Sachs and J. D. Lubahn, published on pages 271–276 of this issue of the Transactions.

[4] The results of recent tests show that these variations are large, even under the most accurate conditions of material selection and machining. Variations in strain along the length of the specimen may be correlated directly with variations in initial cross section.

Contributed by the Metals Engineering Division and presented at the Annual Meeting, New York, N. Y., Nov. 26–29, 1945, of The American Society of Mechanical Engineers.

Note: Statements and opinions advaced in papers are to be understood as individual expressions of their authors and not those of the Society.

[5] Tests on transverse specimens were abandoned because of excessive variations in thickness across the width of the rolled sheet.

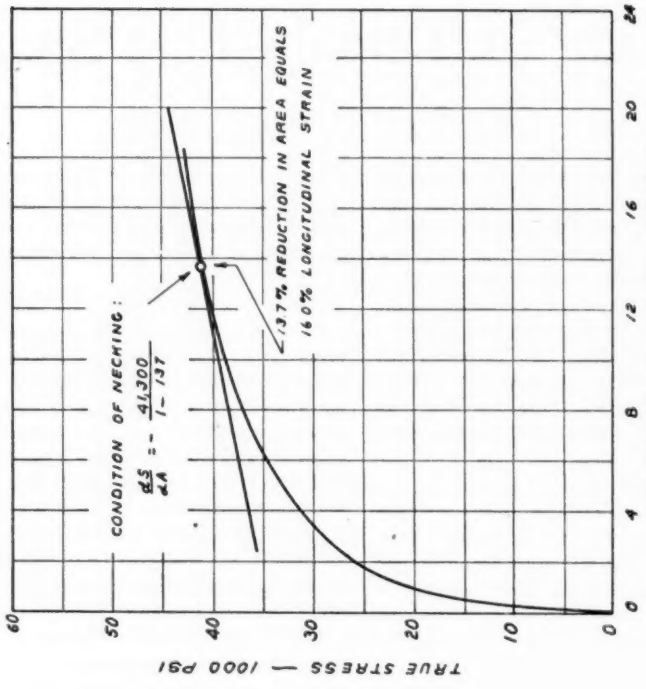


FIG. 3 STRESS-STRAIN CURVE FOR 0.040-IN. BARE 24S-O SHEET, SHOWING THEORETICAL CONDITION FOR NECKING

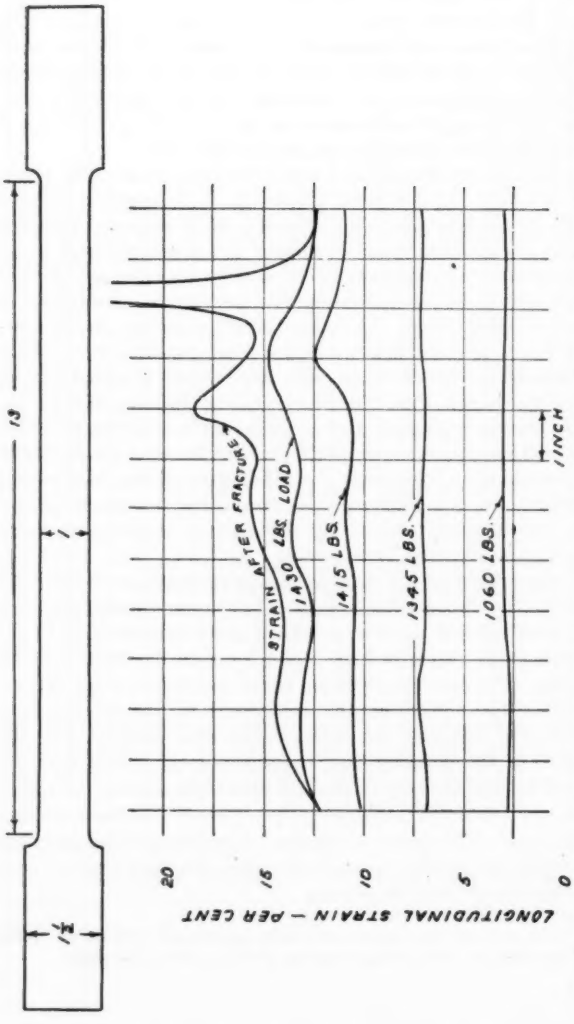


FIG. 1 PROGRESSIVE CHANGES IN DISTRIBUTION OF LONGITUDINAL STRAINS IN STRIP TENSILE SPECIMEN CUT LONGITUDINALLY FROM 0.040-IN. BARE 24S-O SHEET

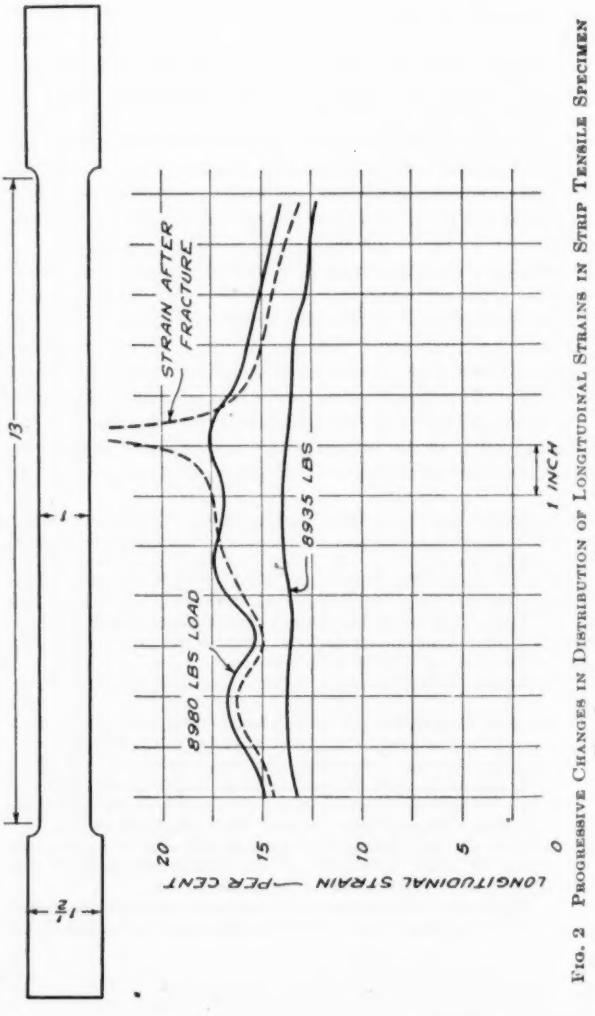


FIG. 2 PROGRESSIVE CHANGES IN DISTRIBUTION OF LONGITUDINAL STRAINS IN STRIP TENSILE SPECIMEN CUT LONGITUDINALLY FROM 0.125-IN. BARE 24S-T SHEET

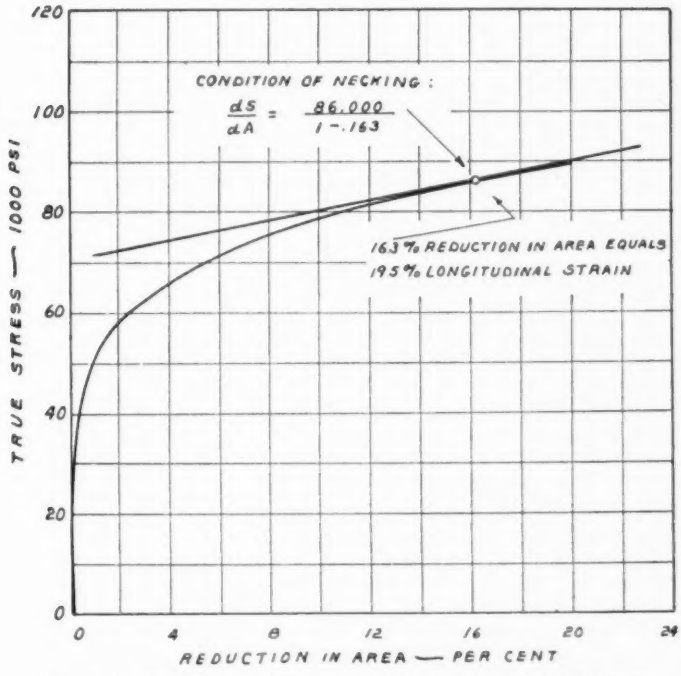


FIG. 4 STRESS-STRAIN CURVE FOR 0.125-IN. BARE 24S-T SHEET, SHOWING THEORETICAL CONDITION FOR NECKING

ANALYSIS OF RESULTS

The stress versus reduction (of area) curves thus obtained are shown in Figs. 3 and 4, together with the construction lines for determining the strain at necking, according to the theory developed previously.[3] The values of longitudinal strains obtained from the necking theory for 24S-O bare, and 24S-T bare, are 16 and 19.5 per cent, respectively. These values are in good agreement[4] with the corresponding experimentally determined uniform strains of 18.5 and 17.5 per cent, respectively, Figs. 1 and 2.

The accuracy with which the strain at necking can be determined from a stress-reduction curve, such as that in Fig. 4, depends primarily upon the accuracy with which the slope of the stress-area curve is measured. In order to illustrate the probable extent of the scattering of the slope measurements, the necking condition has been solved, in Fig. 5, by intersecting the two functions s_1/A and $-ds_1/dA$. The curve shows that typical errors of slope measurements may result in errors in the strain at necking of approximately plus or minus 1 per cent.

[4] A larger number of subsequent tests show that the necking strain determined theoretically from the stress-strain curve is 1 or 2 per cent above that observed in the strain-distribution curve, and this phenomenon has not been explained as yet. It should be observed, however, that this difference is smaller than the rather large experimental errors associated with instability phenomena.

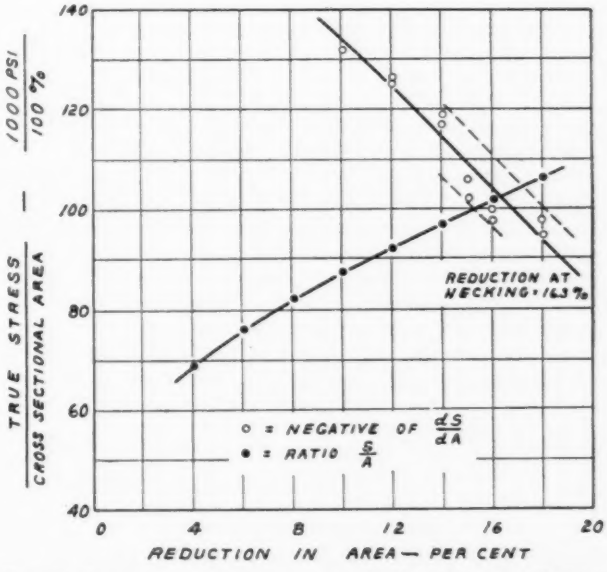


FIG. 5 CONDITION FOR NECKING OF 0.125-IN. BARE 24S-T SHEET, SHOWING EQUALITY OF ds/dA AND s/A, AND INDICATING POSSIBLE ERRORS RESULTING FROM INACCURATE SLOPE MEASUREMENTS

Instability of Thin-Walled Tubes Subjected to Internal Pressure[1]

By G. ESPEY,[2] CLEVELAND, OHIO

A preceding paper advances the criterion that the maximum-load or pressure conception of instability is applicable to geometrical shapes other than the tensile test. This paper presents experimental analysis to support the theoretical conception advanced for the necking of tubing subjected to pure longitudinal tension, to balanced biaxial tension, and to plane strain with the major strain being circumferential. It also shows that the stress-strain curve in uniaxial tension can be used to predict the necking strain for tubing under various stress states.

LOAD conditions other than pure tension which can be readily investigated are those encountered in tubing which is simultaneously subjected to a major circumferential tension and a minor longitudinal tension.[3]

The following analysis should reveal the validity of the conception advanced[4] that a tube subjected to the stress state mentioned, if it does not fracture in a brittle manner, fails by instability when the internal pressure reaches a maximum. This failure should be of much the same type as that of a tensile specimen which fails by local instability or "necking" when the tensile load passes through a maximum.[5]

Some results have been published recently by Davis,[6] which present a series of tests suitable for a comparison of the theoretical instability strains with experimentally derived forming limits for various stress states. Cylindrical copper tubes 1.45 in. OD, 1.25 in. ID, and having an 8-in. length were machined from solid rod. These were subjected to various ratios of longitudinal and circumferential tension which were kept approximately constant in any one test but which were in different proportions for different tests. Both stresses were progressively increased during a test by increasing the internal pressure and the longitudinal tension. The strains were carefully measured during these tests, and for an investigation of the instability condition the final dimensions of the fractured specimens were also secured later for the purposes of this analysis (lot B of reference 6). Of the tubes tested under combined tensions, the stress and strain conditions of balanced biaxial tension $\left(\frac{s_2}{s_1} = 1, \frac{\epsilon_2}{\epsilon_1} = 1\right)$ and plane strain $\left(\frac{s_2}{s_1} = 1/2, \epsilon_2 = 0\right)$ were available for the analysis.

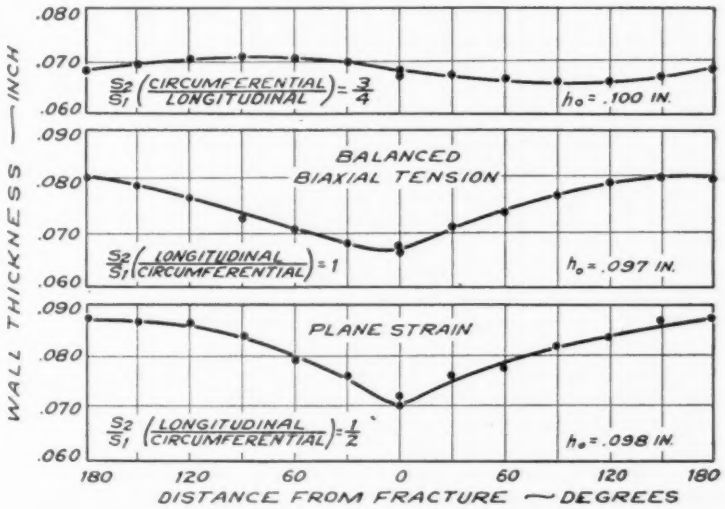


FIG. 1 DISTRIBUTION OF WALL THICKNESS WITH CIRCUMFERENCE AT THE CENTER OF TUBES TESTED UNDER VARIOUS STRESS RATIOS AND HAVING LONGITUDINAL FRACTURES

CORRELATING TEST RESULTS

To correlate the necking performance of tubes under uniaxial tension with those under biaxial tension, a tube tested in pure tension was also investigated. The individual (true) stress-strain curves obtained in the various tests were used as the basis for the determination of theoretical stress and strain conditions of instability under plane strain and balanced biaxial tension.

As might be expected, the tubes which had been subjected primarily to internal pressure failed by splitting longitudinally. The fracture appeared to be rather brittle; furthermore, the occurrence of a longitudinal fracture in the specimen tested with a ratio of circumferential stress to longitudinal stress of 3:4 indicated that the ductility in the circumferential direction was considerably less than in the longitudinal direction and possibly low enough to cause brittle fracture. Measurements of the distribution of thickness h, around the circumference at the longi-

---

[1] This paper is one of a series of reports on the research program on hot-forming of aluminum alloys conducted at Case School of Applied Science under contract with the Office of Production Research and Development of the War Production Board. This research, which was supervised by The War Metallurgy Committee under the "restricted" Project NRC-547, is the basis of this paper which has been released for publication by the OPRD. The project was directed by G. Sachs, Case School of Applied Science.

[2] Department of Metallurgical Engineering, Case School of Applied Science.

[3] As yet, the condition or combination of conditions determining instability for tubing under a major longitudinal tension and a minor circumferential tension is not clearly understood. However, the limiting conditions of pure longitudinal tension and balanced biaxial tension are known and discussed. The results of tests in the region between these two limits are later reported in Fig. 9.

[4] "Failure of Ductile Metals in Tension," by G. Sachs and J. D. Lubahn, published on pages 271–276, of this issue of the Transactions.

[5] "The Necking of Tensile-Test Specimens," by J. D. Lubahn, published on pages 277–279, of this issue of the Transactions.

[6] "Increase of Stress With Permanent Strain and Stress-Strain Relations in the Plastic State for Copper Under Combined Stresses," by E. A. Davis, Trans. A.S.M.E., vol. 65, 1943. p. A-187.

Contributed by the Metals Engineering Division and presented at the Annual Meeting, New York, N. Y., Nov. 26–29, 1945, of THE AMERICAN SOCIETY OF MECHANICAL ENGINEERS.

NOTE: Statements and opinions advanced in papers are to be understood as individual expressions of their authors and not those of the Society.

tudinal center of fracture for this tube showed no definite evidence of local necking, Fig. 1. This therefore indicates that if any instability took place it occurred at a strain very near the limit of ductility.

The instability condition can be applied only if the ductility of the metal is sufficiently high to exceed that required by the necking condition. Measurements of the thickness distribution for tubes tested under balanced biaxial stress ($s_1/s_2 = 1$) and in plane strain ($s_2/s_1 = 1/2$), Fig. 1, reveal the presence of necks. The presumably uniform normal strain under both of these load conditions was considerably less than the normal strain at the fracture, which was approximately the same for all three tubes that failed longitudinally.

Thus it appears that the two tubes representing balanced biaxial tension and plane strain were suitable for a comparison of the theoretical with the experimental instability conditions.

First, however, the validity of the instability condition for the tube tested in pure longitudinal tension was confirmed. The load reached a maximum, Fig. 2, and from measurements of the thickness (radial strain, ϵ_3) and diameter (circumferential strain, ϵ_2) of the fractured specimen, a neck was found to extend over approximately 1 in. on each side of the failure. The remainder of the tube was strained rather uniformly, by a value of natural longitudinal strain, $\epsilon_1 = -2\epsilon_2 = 0.39$. This is practically the same value as that obtained by graphical solution, Fig. 3.

The pressure versus strain curves obtained for the tubes subjected to internal pressure show the decrease in slope which generally precedes a maximum, Figs. 5 and 7. However, no decrease in load was observed because of the explosive failure which occurs. Such failure is expected when the forces become unbalanced, i.e., when instability starts.

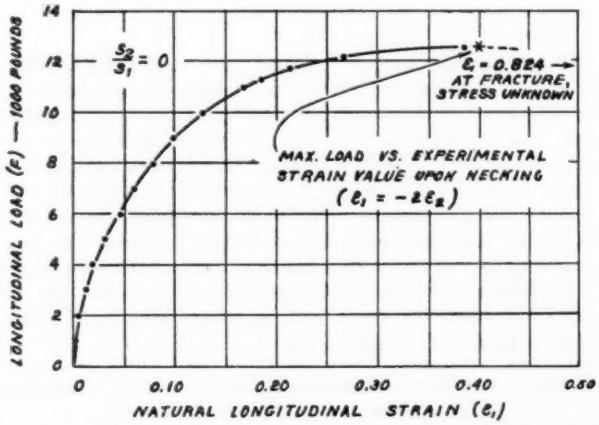


FIG. 2 LOAD-STRAIN CURVE FOR COPPER TUBING IN PURE TENSION

For the two combined tension tests made under balanced biaxial tension and plane strain, the thickness measurements taken around the circumference of the tubes at the longitudinal center of the fracture also showed no pronounced distinction between uniform and local straining, as the thickness gradually decreased toward the fractures, Fig. 1. This type of nonuniformity of strain which may be caused to some extent by slight variations in wall thickness of the original specimens, makes it difficult to determine definitely the circumferential strain at the moment of instability.

However, in the case of perfectly balanced biaxial tension, the uniform strain can be derived indirectly from the condition that before instability occurs the circumferential strain will equal the longitudinal strain; and since the fracture occurs in the longitudinal direction, the longitudinal strain should discontinue as soon

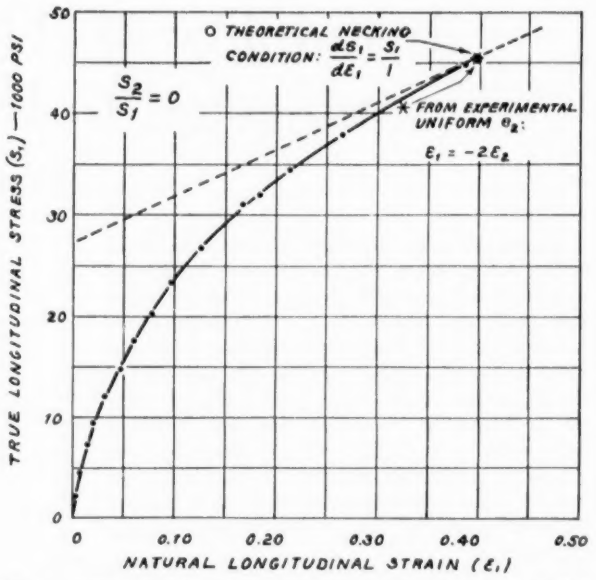


FIG. 3 TRUE STRESS-STRAIN CURVE FOR COPPER TUBING IN PURE TENSION WITH A COMPARISON OF THEORETICAL AND EXPERIMENTAL POINTS OF INSTABILITY

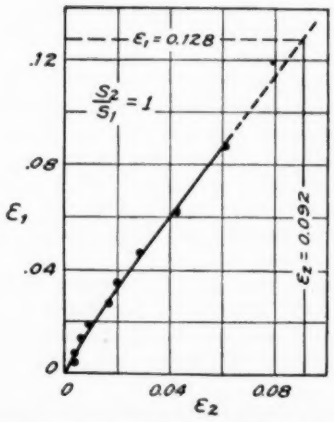


FIG. 4 EXTRAPOLATION OF ϵ_1 VERSUS ϵ_2 TO OBTAIN THE VALUE OF ϵ_1 UPON NECKING FROM THE CORRESPONDING VALUE OF ϵ_2
(Balanced biaxial tension test.)

as instability is initiated. Therefore the uniform strain in the longitudinal direction should be the same as the circumferential strain present at the start of instability. However, for the case considered, the circumferential stress (s_1) was approximately 13 per cent higher than the longitudinal stress when instability started; consequently there was a corresponding difference between the longitudinal and circumferential strains, Fig. 4. A value of circumferential strain equal to 0.128 at the point of instability was obtained by extrapolation of the curve in Fig. 4 to the measured value of uniform longitudinal strain of 0.092. The corresponding value of normal strain is

$$\epsilon_3 = -\epsilon_1 - \epsilon_2 = -0.092 - 0.128 = -0.22$$

The strain values obtained by graphical solution of the necking condition, Fig. 6, were $\epsilon_1 = 0.13$ and $\epsilon_3 = 0.25$. They are again in good agreement with the experimental values.

In the case of plane strain, Fig. 7, the lack of any change in length ($\epsilon_2 = 0$) of the specimen makes it impossible to use this strain as a criterion of the point of instability; and the lack of a

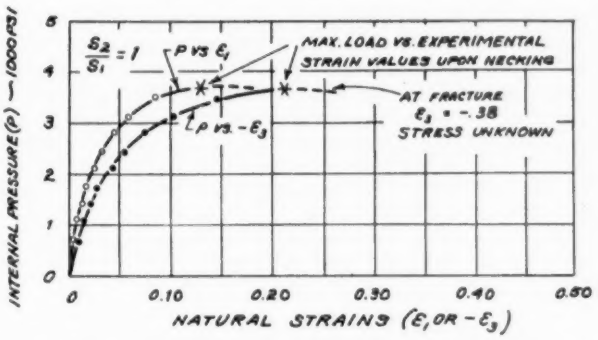


FIG. 5 PRESSURE-STRAIN CURVES FOR COPPER TUBING IN BALANCED BIAXIAL TENSION

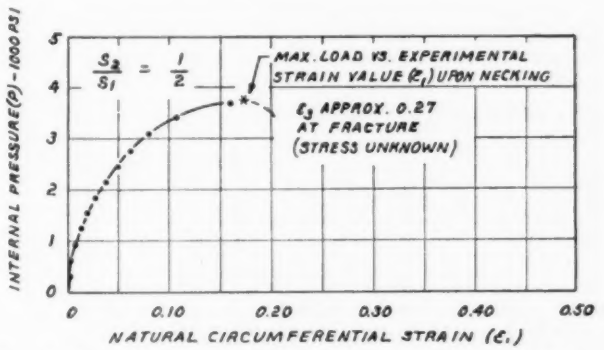


FIG. 7 PRESSURE-STRAIN CURVE FOR COPPER TUBING IN PLANE STRAIN

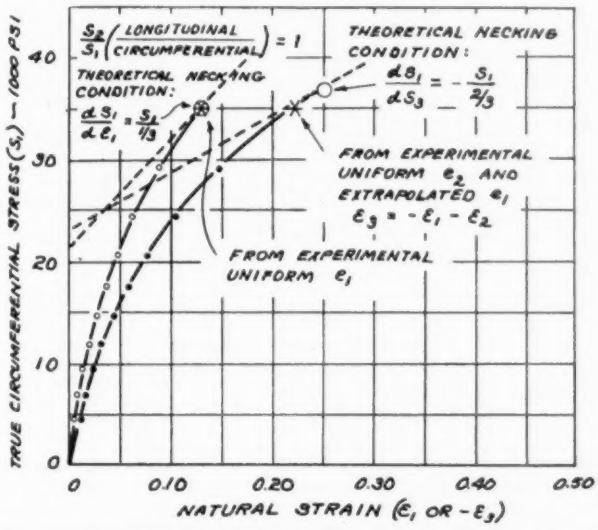


FIG. 6 TRUE STRESS-STRAIN CURVES FOR COPPER IN BALANCED BIAXIAL TENSION WITH A COMPARISON OF THEORETICAL AND EXPERIMENTAL POINTS OF INSTABILITY

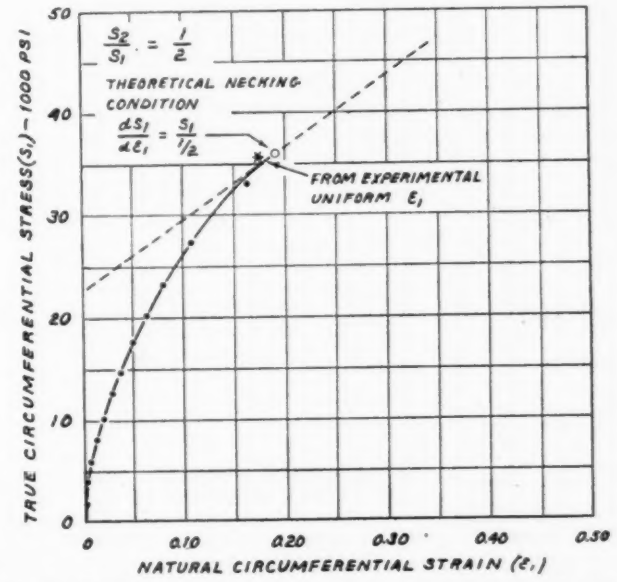


FIG. 8 TRUE STRESS-STRAIN CURVE FOR COPPER TUBING UNDER CONDITIONS OF PLANE STRAIN, I.E., LONGITUDINAL STRAIN = 0, WITH A COMPARISON OF THEORETICAL AND EXPERIMENTAL POINTS OF INSTABILITY

region of uniform thickness about the circumference after fracture, Fig. 1, eliminates a second possible method of determining the uniform strain. However, the measured average circumferential strain may be used as the experimental strain at instability, although it is somewhat inaccurate because of the small effect on the average value of the larger strain at the neck. Measurement of the outside diameter after fracture at points $^1/_2$ in. beyond the ends of the fracture yielded a mean value of 1.699 in. This value may be corrected by the corresponding thickness (0.081 in.), obtained by extrapolation of the outside-diameter versus thickness curve, to yield a value of uniform natural circumferential strain of $\epsilon_1 = 0.175$.

As in the case of pure tension, the accuracy of the "theoretical necking strains" for the tubes investigated depends upon the accuracy of the slope measurements. Also, there is likely to be some additional error because of the scarcity of experimental points in the vicinity of the region of necking, with the corresponding uncertainty in the shape, and thus the slope of the curve.

The graphical solution of the instability condition for plane strain yields a strain value $\epsilon_1 = -\epsilon_3 = 0.19$ (approximately) which is again in good agreement with the experimental value $\epsilon_1 = 0.175$, Fig. 8.

Thus the analysis of tubes subjected to internal pressure confirms the conception that a maximum in the internal-pressure curve of a sufficiently ductile metal is associated with a localized strain region or "neck" in the circumferential direction, and a lack of any further strain in other parts of the specimen.

The investigation of the various load conditions also reveals that in accordance with the theoretical analysis, a thin-walled tube subjected either to "pure" internal pressure (plane strain) or to balanced biaxial tension will fail by instability at a considerably smaller circumferential strain than the longitudinal strain which occurs on necking of a tensile test specimen made from the same metal, Figs. 3, 6, and 8. A tube subjected to pure internal pressure will become unstable at only approximately one half of the circumferential strain as a tube subjected to pure longitudinal tension. It can be shown that the conventional strength is a function of these strains; and the bursting strength of tubes, therefore, should be considerably lower than the tensile strength, the difference depending upon the strain-hardening characteristics of the metal and the degree of biaxiality.

In Fig 9 the three principal strains at the point of instability are represented for the tubes tested by Davis,[8] as obtained both experimentally and by theoretical analysis. The experimentation also covered four tubes not analyzed, which were subjected to a major longitudinal and to a minor circumferential tension. As previously discussed, the experimental evidence indicates

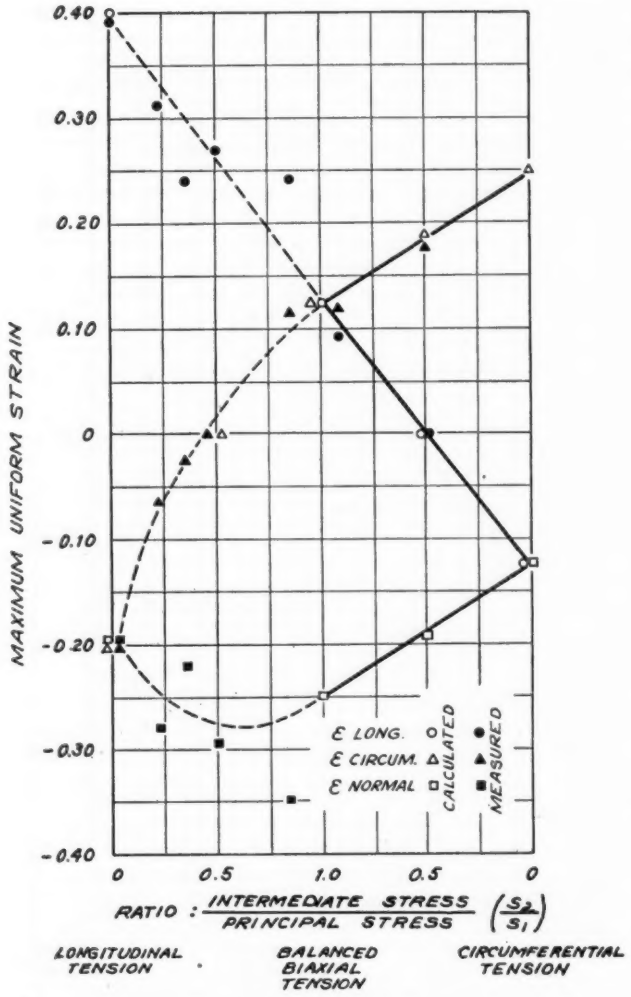


FIG. 9 MAXIMUM UNIFORM STRAINS FOR VARIOUS STRESS RATIOS EXISTING IN TUBING WHEN NECKING STARTS

that the longitudinal strain at which a circumferential neck occurs should decrease as the internal pressure superimposed on the longitudinal tension increases, Fig. 9. The condition that the longitudinal load reaches a maximum, obviously does not account for the observed changes in longitudinal necking strain with increasing internal pressure, until balanced biaxial tension is

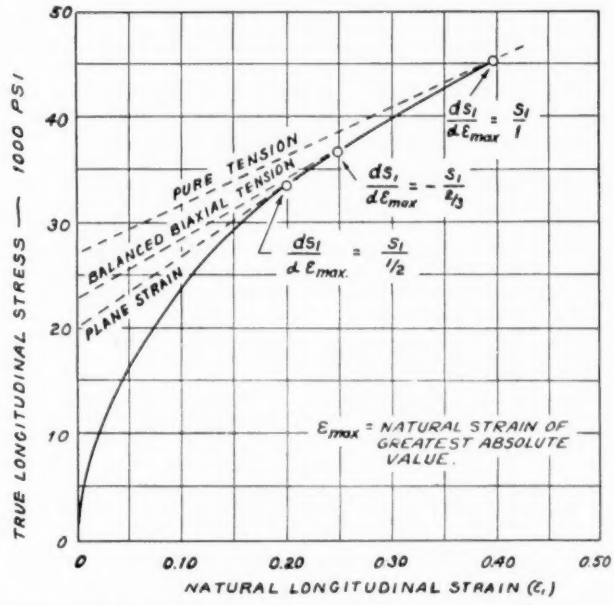


FIG. 11 NECKING CONDITION FOR TUBING UNDER VARIOUS STRESS STATES AS THEORETICALLY DETERMINED, I.E., GRAPHICALLY, FROM TRUE STRESS-STRAIN CURVE IN PURE TENSION

reached. The effect of the internal pressure in this range has not been accurately investigated as yet.

PREDICTION OF INSTABILITY STRAINS FROM STRESS-STRAIN CURVE IN PURE TENSION

The instability condition has been developed in such a manner[4] that it may be used to predict the forming limits by necking from

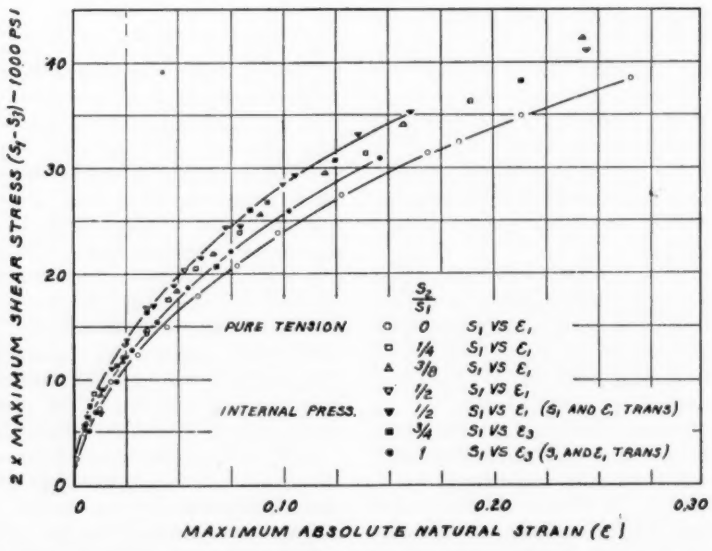


FIG. 10 CURVES OF MAXIMUM SHEAR STRESS VERSUS MAXIMUM ABSOLUTE STRAIN FOR COPPER TUBING TESTED UNDER VARIOUS STRESS STATES

the true stress-strain curve in pure tension for various conditions of geometry and stress ratios.

The data on copper tubing offer the opportunity to investigate the possibility of predicting the instability strain in this manner since the relation between the stresses and strains are known for this condition of geometry. As was previously mentioned, such application involves the assumption that true stress-strain curves for various stress states will be similar (particularly regarding slope), if the maximum shear stress is plotted against the largest absolute strain. While this maximum shear-stress criteria for flow may lead to considerable error in stress value, it can be shown that no considerable error in predicted strains will result.

In this paper only cases of uniaxial ($s_2 = s_3 = 0$) or biaxial tension ($s_3 = 0$) are considered and therefore the curves for various stress states should be similar if the largest stress s_1 is plotted against ϵ_{max}.

Fig. 10 shows such a plot for copper tubing in various stress states from $s_2/s_1 = 0$ to $s_2/s_1 = 1$. While these curves are not identical, it must be remembered that the slope of the curves is of greater importance than the ordinate value in determining the necking condition and that for a given abscissa value, the slopes for the various curves are nearly identical.

The instability theory has been applied to the true stress-strain curve in pure tension to predict the necking strain for copper tubes in plane strain and balanced biaxial tension, as shown in Fig. 11. Table 1 shows these values together with those obtained by the instability theory from the stress-strain curve for the particular stress state considered and also for the actually measured forming limit. These strain values obtained from the stress-strain curve in uniaxial tension are in good agreement with those derived experimentally.

TABLE 1 STRAIN VALUES FROM STRESS-STRAIN CURVES AND MEASURED NECKING STRAIN

Stress ratio in tubing	Necking strain from stress-strain curve corresponding to stress state	Necking strain from stress-strain curve in pure tension	Measured necking strain
$\frac{s_2}{s_1} = 0$	$\epsilon_1 = 0.40$	$\epsilon_1 = 0.40$	$\epsilon_1 = 0.39$
$\frac{s_2}{s_1} = 1$	$\epsilon_1 = 0.13$	$\epsilon_1 = 0.125$	$\epsilon_1 = 0.11$ $(= -\epsilon_2/2)$*
$\frac{s_2}{s_1} = 1/2$	$\epsilon_1 = 0.19$	$\epsilon_1 = 0.20$	$\epsilon_1 = 0.175$

* Corrected to apply to the stress ratio of $s_2/s_1 = 1$.

ACKNOWLEDGMENT

The author is indebted to Dr. A. Nadai and Dr. E. A. Davis, Westinghouse Research Laboratory, East Pittsburgh, Pa., for permission to measure the special dimensions of the test specimens after failure, and for the original data on pressure, load, and strain values.

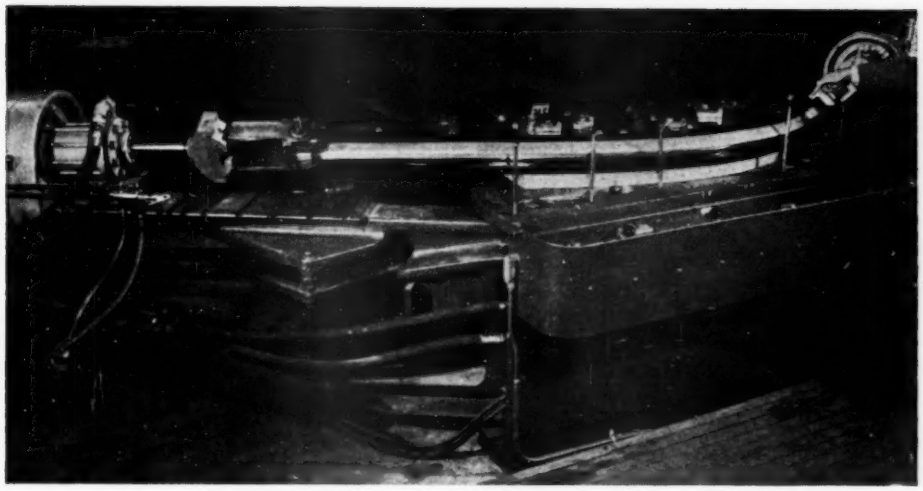


FIG. 1 TYPICAL CONTOUR-FORMING MACHINE IN WHICH TENSION IS COMBINED WITH BENDING

Distortion Due to Contour-Forming of Extrusions and Preformed Sheet-Metal Sections

BY WILLIAM SCHROEDER,[1] BURBANK, CALIF.

The effect of springback on the radius of curvature due to contour-forming of extrusions or preformed sheet-metal sections is analyzed. A number of the commonly used methods of forming are considered. Equations for computing values for change in radius are derived and sample calculations are compared.

NOMENCLATURE

The following nomenclature is used in the paper:

a = area
b = width
c = distance from innermost fiber to neutral axis of bending
d = depth of section
e = strain
e_1 and e_2 = strains due to forming; outer and inner fibers, respectively
ϵ_1 and ϵ_2 = components of elastic strain due to springback that cause a change in radius; outer and inner fibers, respectively
ϵ_x and ϵ_y = components of springback strain at point (x, y) due to elastic bending about the X- and Y-axes, respectively
F = force
I_x and I_y = moments of inertia about the X- and Y-axes, respectively
I_{xy} = product of inertia about the X- and Y-axes
$K = \frac{r}{s_0 R_p}$
m = first moment of area
M = moment of force
q_x and q_y = parameters
r = modulus of strain-hardening or slope of true stress-strain curve
R_p = radius of part
R_d = radius of die
R' = transverse radius of curvature due to springback distortion
s = true stress
s_0 = yield strength of material or s_i whichever is greater, see Fig. 5
x and y = co-ordinates with reference to X- and Y-axes
$\bar{x}$ = distance from vertical reference in section to centroid of area
$\bar{y}$ = distance from inner fiber to centroid of area
y_a = distance from inner fiber to axis, parallel to neutral axis, which divides area of section equally

INTRODUCTION

Several methods for computing springback in contour-forming have appeared in the technical literature.[2, 3] These, however, apply only to one type of forming, namely, simple bending, and are trial-and-error methods which are very laborious. Many of the present methods of contour-forming have not previously been analyzed.

The springback resulting from contour-forming extrusions and preformed sheet-metal sections may conveniently be classed as

[1] Research Engineer, Lockheed Aircraft Corporation. Mem. A.S.M.E.

Contributed by the Metals Engineering Division and presented at the Aviation War Conference, Los Angeles, Calif., June 11–14, 1945, of THE AMERICAN SOCIETY OF MECHANICAL ENGINEERS.

NOTE: Statements and opinions advanced in papers are to be understood as individual expressions of their authors and not those of the Society.

[2] "Data on Springback of Metals," by R. E. Oestreich, *Aero Digest*, vol. 45, 1944, pp. 77–81 and 138.

[3] "Determining Springback," by R. G. Sturm and B. J. Fletcher, *Product Engineering*, vol. 12, 1941, pp. 526–528 and 590–594.

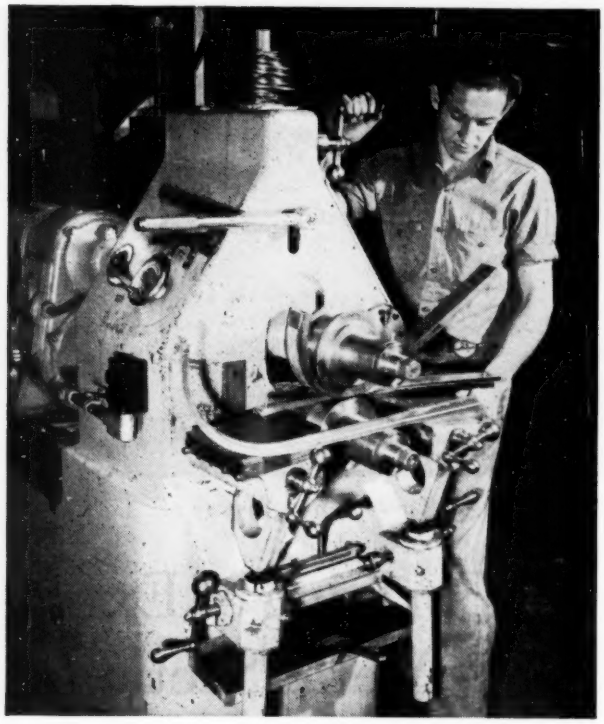


FIG. 2 TYPICAL CONTOUR-FORMING MACHINE OPERATING ON PRINCIPLE OF SIMPLE BENDING
(The part is bent by the rolls to the contour of the curved steel bar.)

consisting of a change in the over-all length or a change in radius of curvature of the part. A change in length of a part is generally of little significance because parts are normally trimmed to the desired lengths after forming; however, a change in curvature usually produces a significant error in contour that must be corrected. For this reason, changes in radius due to springback will be treated as important and changes in length as incidental.

In the hand-forming methods of forming stringer sections, the effect of springback may be corrected in the process of forming. When contour-forming machines[4] of various kinds, requiring dies or form blocks, are used, it becomes desirable to be able to predict the change in curvature due to springback in order to reduce the developmental costs of the dies.

The amount of radius change depends upon the forming method employed. Simple bending methods produce relatively large changes in radius while contour-stretching methods produce much less.[5] Many parts can be formed with these contour-stretching machines without excessive springback; nevertheless, under certain conditions springback allowance in the dies must still be made.

SPRINGBACK DUE TO CONTOUR-FORMING

The phenomenon of springback may be explained in terms of the stress-strain relationship for a bar loaded in tension and compression, as shown in Fig. 3. If the loading is interrupted at some point as at a and the load removed, the stress and strain decrease on the line a to c. The elastic recovery or decrease in strain is from b to c. In a similar manner, unloading the bar from point a'

[4] "Methods of Forming Aluminum Alloy Extrusions and Preformed Sheet Metal Sections," by William Schroeder, *Automotive and Aviation Industries*, vol. 90, 1944, pp. 28–31 and 100.

[5] "Elastic Theory in Sheet-Metal Forming Problems," by F. R. Shanley, *Journal of Aeronautical Sciences*, vol. 9, 1942, pp. 313–333.

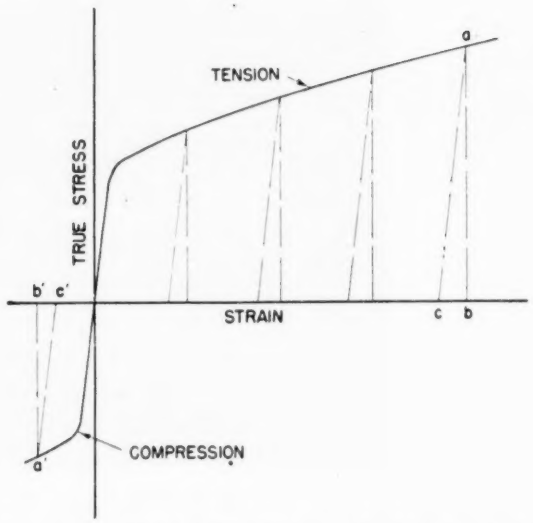


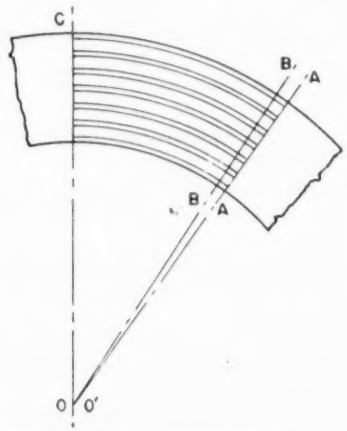
FIG. 3 STRESS-STRAIN CURVE AND SPRINGBACK IN TENSION AND COMPRESSION

in compression changes the strain from b' to c'. The amount of plastic recovery is indicated for a number of values of strain in order to show the approximate manner of variation with strain.

It has already been mentioned that springback from contour-forming depends upon the method and technique of forming. The amount and nature of springback furthermore depend upon the shape of the section. For the purpose of discussion, a number of typical cases will be discussed.

METHOD I—FORMING TO APPROXIMATE CONTOUR, HEAT-TREATING, AND STRETCHING TO FINAL CONTOUR

One method which may be expected to give a negligible amount of change in radius due to springback is to form the part approximately to contour by any of the contour-forming methods, follow with a solution heat-treatment or anneal, and stretch the part between 1 to 3 per cent over a block or die. This produces approximately the result illustrated in Fig. 4.



BY METHOD I POINT O AND O' COINCIDE.

FIG. 4 EFFECT OF SPRINGBACK BY FORMING METHOD I

Owing to the heat-treatment following the forming, all fibers have the same temper at the time of stretching. Furthermore, all fibers are subjected approximately to the same stretching stress and strain since the part is already formed nearly to contour prior

to stretching. The elastic recovery is therefore proportional to the curved length of the fiber. Hence the fibers terminating on the plane *A-A*, while under stretching load, spring back to the position in plane *B-B*. If the line *B-B* is extended to intersect with line *C-O*, it is found that the new center of curvature *O'*, coincides with the center of curvature *O*, before springback. Hence the radius of curvature remains unchanged even though the curved length has decreased.

This result applies equally to all sizes and shapes of cross sections. There is, furthermore, no tendency for the part to distort out of the plane of bending or become twisted.

Inconsistencies in this and all the following methods may result from nonhomogeneity of strength distribution over the cross section of the part. Such nonhomogeneity is sometimes associated with a nonhomogeneous grain structure.

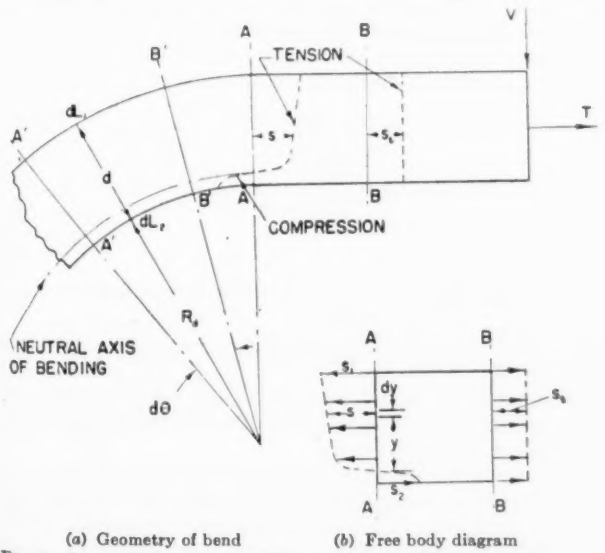
Method II—Forming to Approximate Contour and Stretching to Final Contour

When parts are formed to approximately the correct contour and subsequently stretched without intermediate heat-treatment, a result somewhat different from Method I is obtained. The material becomes strain-hardened nonuniformly in the forming operation, the strain-hardening being greatest in the outer and inner radius fibers and decreasing toward the middle. Springback from stretching a part with such nonuniform strain-hardening will generally produce slight distortion. The amount and type of distortion will depend on the shape of the cross section and the method of contouring. The part will also distort from the plane of bending if the cross section or distribution of strain-hardening is not symmetrical about an axis parallel to the plane of bending. (The plane of bending corresponds to the *Y*-axis n the figures of this paper.)

Since a wide variety of conditions for this method can exist, each leading to a different result, no attempt to solve any specific case has been made.

Method III Simultaneous Wrap and Stretch-Forming With Constant Force

One rather common method of contour-forming consists of bending and stretching progressively. By this method the part is usually first loaded in tension to a stress corresponding to a very small permanent set. The part is then wrapped around the die. This wrapping action is basically one of bending. It differs from pure bending by the fact that the bending is done under the influence of the tensile force, Fig. 5. Simple bending may be considered as a special case in which the force $T = 0$.



(*a*) Geometry of bend (*b*) Free body diagram

Fig. 5 Contour-Forming an Extrusion, or Preformed Section, With Constant Tensile Force

Neutral Axis of Bending With Tensile Force. As a step in analyzing the effect of springback on the radius, the neutral axis of bending will be considered first.

From the geometry of the bend, Fig. 5, it may be seen that

$$d\theta = \frac{dL_1}{R_d + d} = \frac{dL_2}{R_d} \quad \ldots\ldots [1]$$

By definition

$$\frac{dL_1}{dL_0} = 1 + e_1 \quad \ldots\ldots [2]$$

and

$$\frac{dL_2}{dL_0} = 1 + e_2 \quad \ldots\ldots [3]$$

where dL_0 = unstrained length of dL_1 and dL_2.

Therefore

$$\frac{1 + e_1}{R_d + d} = \frac{1 + e_2}{R_d} \quad \ldots\ldots [4]$$

or

$$\frac{d}{R_d} = \frac{e_1 - e_2}{1 + e_2} \quad \ldots\ldots [5]$$

Stretching of the straight portion of the part may result from the original application of the tensile force; however, the main forming action takes place in the region adjoining section *A-A*, Fig. 5. The stress conditions are approximately as in Figs. 5(*b*) and 6. The outside fibers elongate and increase in strength according to the stress-strain behavior of the material. In order for the material between sections *A-A* and *B-B* to be in equilibrium, it is necessary that the net force represented by the area under the stress-distribution curves for sections *A-A* and *B-B* be equal. This condition is expressed by

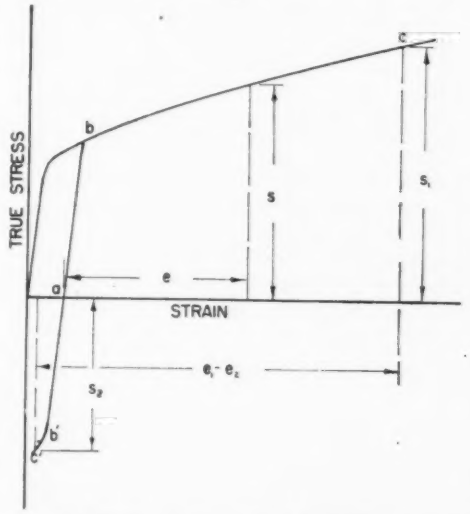


Fig. 6 Stress-Strain Relation for Contour-Forming With Constant Tensile Force

$$-\int bs\,dy + as_i = 0 \quad \ldots\ldots [6]$$

It is assumed that the strain imposed by bending is proportional to the distance from the neutral axis. In this case, the neutral axis of bending is defined as the fiber in the section that has zero stress.

The solution of Equation [6] depends on the relation between s and y, which in turn depends upon the stress-strain diagram. An exact solution is difficult to obtain; however, a useful solution may be obtained by assuming that the stress-strain diagram a-b-c, Fig. 6, may be expressed by

$$s = s_0 + re \quad [7]$$

and a-b'-c' by

$$s = -s_0 + re \quad [7a]$$

In this expression

$$e \simeq \frac{y}{R_d} \quad [8]$$

where y is measured from the neutral axis of bending.

For all cases except $s_i = 0$ (pure bending), it may be assumed that $s_0 = s_i$. For $s_i = 0$, s_0 equals approximately the yield strength of the material.

Substituting Equations [7], [7a], and [8] into [6] gives

$$-\int_0^{d-c} bs_0 dy + \int_{-c}^{0} bs_0 dy - \int_{-c}^{d-c} \frac{b}{R_d} ry\,dy + as_0 = 0 \quad [9]$$

or

$$-s_0(a_a - a_b) - \frac{r}{R_d} a(\bar{y} - c) + as_0 = 0 \quad [9a]$$

where

$$a_a = \int_0^{d-c} b\,dy = \text{area above neutral axis}$$

and

$$a_b = \int_{-c}^{0} b\,dy = \text{area below neutral axis}$$

Equation [9a] will be evaluated for cross sections composed of rectangular components as in Fig. 7. It may be demonstrated that $(a_a - a_b)$ is equal to twice the shaded area between y_a and c, where y_a is the distance from the inner fibers to an axis, parallel to the neutral axis, that divides the cross-sectional area into two equal parts. Several special cases have been evaluated as follows:

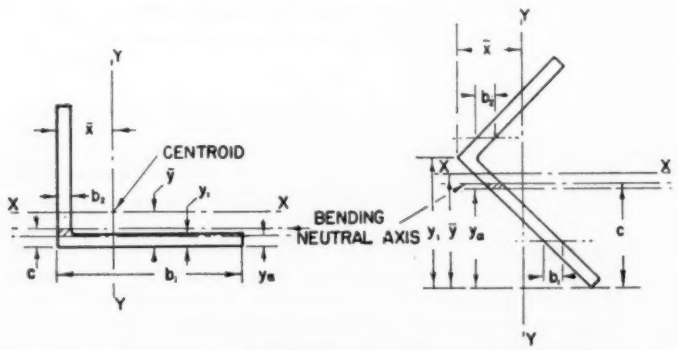


FIG. 7 DIMENSIONS REQUIRED FOR COMPUTING SPRINGBACK DUE TO CONTOUR-FORMING

Case (a): When $y_a \gtrless y_1$, Fig. 7. For this case, Equation [9a] becomes

$$-2s_0b_1(y_a - c) - \frac{r}{R_d} a(\bar{y} - c) + as_0 = 0 \quad [10]$$

and

$$c = \frac{2b_1y_a + Ka\bar{y} - a}{2b_1 + Ka} \quad [11]$$

where

$$K = \frac{r}{s_0R_d}$$

Case (b): $y_a > y_1 > c$, Fig. 7. Substituting into Equation [4a]

$$-2s_0b_2(y_a - y_1) - 2s_0b_1(y_1 - c) - \frac{ra}{R_d}(\bar{y} - c) + as_0 = 0 \quad [12]$$

and

$$c = \frac{2b_2(y_a - y_1) + 2b_1y_1 + Ka\bar{y}}{2b_1 + Ka} \quad [13]$$

Neutral Axis in Simple Bending:

(a) For simple bending the value of c lies between y_a and $\bar{y}$; and $T = 0$. When $c \gtrless y_1$ and $y_a < y_1$

$$c = \frac{2b_1y_a + Ka\bar{y}}{2b_1 + Ka} \quad [14]$$

(b) For $y_a < y_1$ and $c > y_1$

$$c = \frac{2b_1(y_a - y_1) + 2b_2y_1 + Ka\bar{y}}{2b_2 + Ka} \quad [15]$$

(c) For $c > y_1$ and $y_a \lesssim y_1$

$$c = \frac{2b_2y_a + Ka\bar{y}}{2b_2 + Ka} \quad [15a]$$

DETERMINATION OF PART RADIUS AFTER SPRINGBACK

The springback in contour-forming with a constant tensile force may be analyzed by considering the moments required for bending and the change in moments due to springback. The bending moment depends upon the shape of the section and the plastic properties of the material, while the moment due to springback depends upon the elastic properties of the section. The following equilibrium conditions must be satisfied

$$\Sigma M_x = 0 \quad [16]$$

$$\Sigma M_y = 0 \quad [17]$$

$$\Sigma F_n = 0 \quad [18]$$

where

M_x and M_y = moments about the X- and Y-axes, respectively

F_n = force normal to X-Y plane

In this case, the X- and Y-axes are taken through the centroid of the section with the Y-axis in the plane of bending.

Since springback is a purely elastic phenomenon, the principle of superposition may be applied and the changes in stress and strain may be resolved into components as due to bending about each of the two axes and a uniform change in strain normal to the X-Y plane. The uniform

strain component produces no distortion, as previously explained, and can therefore be neglected in the following discussion. The other elastic components are related as follows

$$\epsilon = \epsilon_x + \epsilon_y \quad [19]$$

Since Equation [18] yields information only on the uniform component of strain, it may be omitted from further discussion.

Based on Fig. 5, the moments due to bending are expressed by

$$M_{1x} = \int_s syda \quad [20]$$

and

$$M_{1y} = \int_s sxda \quad [21]$$

where $\int_s$ means a surface integral over the cross-sectional area and da refers to an area element with dimensions dy and dx. The changes in moment due to springback are

$$M_{2x} = \int_s E\epsilon yda \quad [22]$$

and

$$M_{2y} = \int_s E\epsilon xda \quad [23]$$

Substituting into Equations [16] and [17]

$$\int_s syda + \int_s E\epsilon yda \quad [24]$$

and

$$\int_s sxda + \int_s E\epsilon xda \quad [25]$$

The solution of Equations [24] and [25] depends mainly upon the stress-strain curve between points c' and c, Fig. 6. An approximate but useful result is again obtained by assuming

$$s = s_0 + re \text{ and } s = -s_0 + re$$

The elastic bending strain ϵ may furthermore be assumed to be composed of ϵ_x and ϵ_y, where ϵ_x is due to bending about the X-axis, and ϵ_y due to bending about the Y-axis. Assuming that planes before forming remain planes after forming

$$\epsilon_x = \frac{\epsilon_{x1} - \epsilon_{x2}}{d} y = q_x y \quad [26]$$

and

$$\epsilon_y = \frac{\epsilon_{y1} - \epsilon_{y2}}{d} x = q_y x \quad [27]$$

For the condition after springback, Equation [5] becomes

$$\frac{d}{R_p} = \frac{(e_1 - \epsilon_{x1}) - (e_2 - \epsilon_{x2})}{1 + e_2 + \epsilon_{x2}} \quad [28]$$

and

$$\frac{d}{R_p} \simeq \frac{d}{R_d} + \frac{\epsilon_{x1} - \epsilon_{x2}}{1 + e_2} = \frac{d}{R_d} + \frac{q_x d}{1 + e_2} \quad [29]$$

This may be rearranged to give

$$R_p = \frac{R_d}{1 + \dfrac{q_x R_d}{1 + e_2}} \quad [30]$$

The distortion arising from springback tending to bend the extrusion from the plane of bending may be expressed in terms of

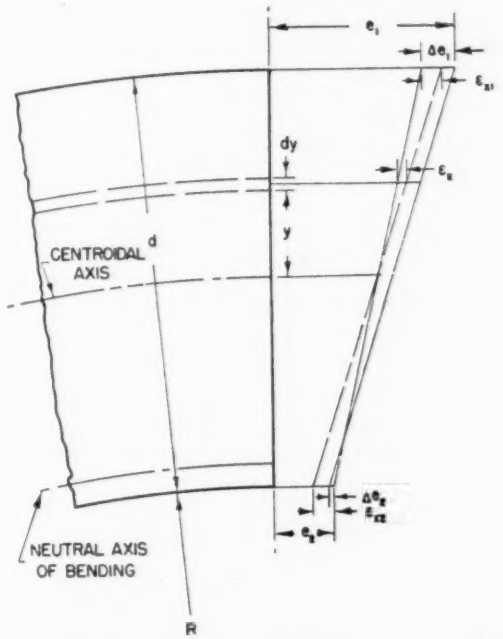


FIG. 8 STRAIN RELATIONS IN CENTROIDAL PLANE ABOUT X-AXIS DUE TO FORMING AND SPRINGBACK

q_y. The transverse radius of curvature R' is obtained by substituting ϵ_{y1} and ϵ_{y2} for e_1 and e_2, respectively, in Equation [5]; thus

$$\frac{d}{R'} = \frac{\epsilon_{y1} - \epsilon_{y2}}{1 + \epsilon_{y2}} \simeq \epsilon_{y1} - \epsilon_{y2} \quad [31]$$

Combining Equations [31] with [26]

$$R' = \frac{1}{q_y} \quad [32]$$

Values for q_x and q_y may be obtained by solving Equations [24] and [25]. After substituting for s and ϵ, Equation [24] becomes

$$s_0 \int_{c-\bar{y}}^{d-\bar{y}} yda - s_0 \int_{-\bar{y}}^{c-\bar{y}} yda + \frac{r}{R_d} \int_s y^2 da + E \int_s (q_x y + q_y x) yda = 0 \quad [33]$$

and

$$s_0(m_{x1} - m_{x2}) + \frac{r}{R_d} I_x + \frac{r}{R_d} a(c - \bar{y})^2 + Eq_x I_x + Eq_y I_{xy} = 0 \quad [34]$$

where

m_{x1} = first moment of area above the neutral axis of bending taken about the X-axis

m_{x2} = first moment of area below the neutral axis of bending taken about the X-axis

Similarly Equation [25] becomes

$$s_0(m_{y1} - m_{y2}) + \frac{r}{R_d} I_{xy} + Eq_x I_{xy} + Eq_y I_y = 0 \quad [35]$$

where

m_{y1} = first moment of area above the neutral axis of bending taken about the Y-axis

m_{y2} = first moment of area below the neutral axis of bending taken about the Y-axis

It may furthermore be demonstrated that in Equations [34] and [35]

$$m_{x1} = -m_{x2} \text{ and } m_{y1} = -m_{y2}$$

In computing springback for the conditions of forming with a constant tensile load, specific values are substituted into Equations [34] and [35] to solve for the values of q_x and q_y. The values of q_x and q_y are then substituted into Equations [30] and [32] for R_p and R'.

Forming Method IV—Simultaneous Wrap and Stretch Forming With Increasing Tensile Force

When the extrusion is contoured and stretched with an increasing tensile force the whole section is subjected to tensile stress and the neutral axis, as defined, does not exist. Since the X- and Y-axes are centroidal axes and under the present condition the area above the neutral axis is the whole area a, and the area below the neutral axis is zero, it follows that

$$m_{x1} = m_{x2} = m_{y1} = m_{y2} = 0$$

From Equations [34] and [35]

$$q_y = 0 \text{ and } q_x = -\frac{r}{ER_d}$$

Substituting these values into Equations [30] and [32]

$$R_p = \frac{R_d}{1 + \frac{r}{E(1 + e_2)}} \quad \ldots\ldots [36]$$

and

$$R' = \infty \text{ (no transverse curvature)} \quad \ldots\ldots [37]$$

Discussion of Forming Methods

Comparison of Springback. The relative amounts of radius change resulting from the foregoing forming methods are computed for one specific condition and compared in Table 1. It may be seen that the radius change is negligible for Method I and is progressively greater for Methods IV, III with tensile pull, and Method III without tensile pull (pure bending). The results for Method II are difficult to predict but are expected to range between the results for Methods I and IV. Of the methods discussed, I and IV will produce little tendency to distort the part from the plane of bending even though the section is not symmetrical about the Y-axis.

TABLE 1 COMPARISON OF COMPUTED RESULTS FOR FORMING A 3/4-IN. × 1-IN. BY 0.070-IN. EXTRUSION WITH 3/4-IN. LEG IN PLANE OF BENDING

(Material: 24S-T aluminum alloy; and R_d = 20 in.)

Method of forming	Part radius in plane of bending R_p, in.	Resulting transverse radius of curvature R', in.
I	20	∞ (no distortion)
II (values not computed but range is estimated)	20–20.55	6000—∞
III (*a*) s_t = 53.000 psi	20.94	6000 (slight)
III (*b*) s_t = 0 (simple bending)	22.6	71 (appreciable)
IV	20.55	∞ (no distortion)

In any of the methods that involve stretching it is important that the jaws for gripping are so designed that they will develop the necessary gripping force without weakening or twisting the section to be formed. Another serious difficulty of contour-forming by stretching is due to friction between the part being formed and the die. This friction makes it difficult and sometimes impossible to stretch the part throughout the length in contact with the die when using Methods I and II. This factor may also interfere with the proper execution of Method IV. The use of a good lubricant and vibrating the die are beneficial for reducing friction between part and die.

Experience may show that friction between the part and die may make it impractical or impossible to attain the conditions assumed in Method IV, and that minimum amounts of springback in practice will correspond more nearly to those for Method III using a constant tensile force.

Accuracy of Results

There has been little opportunity to compare computed with measured values for change in radius due to springback. Where checks have been possible the results have agreed within the limits of accuracy of the measurements. Due to the simplifying assumptions that were made some slight disagreement between computed and measured values may be expected; however, experience has indicated that the error from this cause is considerably less than the variation that may be expected from non-homogeneity and variation in physical properties of material used in forming.

(Owing to travel emergency conditions existing when this paper was presented, discussion will be accepted until June 17, 1946)

Design Considerations for Welded Machinery Parts

By G. L. SNYDER,[1] COATESVILLE, PA.

Only some basic considerations for the designer in developing weldments are brought out in this paper, because of the wide scope of the subject. Separately, these basic considerations may seem elementary and self-evident, but when considered collectively in developing a weldment, their complexity becomes apparent. At least twelve different types of components can be utilized by a designer in his weldment and each of these components can be used in several ways. So, the designer must be familiar with limitations in processing weldments and with the scope and limitation of equipment and methods used in their production. These are the factors discussed here. However, this discussion is limited to dynamically loaded welded machinery parts.

HOT-rolled steel plate, a basic element, probably is the most universal component used in welded machinery parts. Undoubtedly, the freedom offered by the many sizing and shaping possibilities of hot-rolled steel plate has much to do with its widespread use as weldment components. Basically flexible raw material from the stand-point of dimensions, hot-rolled plate is obtainable in variable sizes to 195 in. wide or to 25 in. thick.

Flat Components

Shearing usually is the most economical method of sizing or shaping a plate to rectangular or circular dimensions. But when a plate is to be sheared to size, the designer should keep in mind the existence of shear droop which is the abrupt break in flatness that occurs around the sheared edge, because localized stresses imposed by the shearing pressure exceed the elastic limit of the material. Since this effect is confined to the area adjacent to the edge, it can be practically disregarded when the component is subjected to subsequent trimming or when it is in light gages, 3/8 in. and under.

Flame-cutting undoubtedly is the most common method of shaping and sizing weldment components, particularly when the number of duplicate weldments required is small. Probably a big reason for this is the fact that many components of weldments necessarily are irregular in shape.

Since regular configuration generally is cheaper, the designer should think in such terms where possible. However, he need not be concerned if an edge is sheared or flame-cut so long as he designs the part so that the supplier is free to use either method or both on a particular component.

Fig. 1 shows an example of component produced entirely by flame-cutting. Fig. 2 is a plate part produced by a combination of shearing and flame-cutting.

Of course, in addition to shaping and sizing, the cutting torch also makes welding chamfers, or kerfs, on the edges of a component which provide the "grooves" for welds, other than plain fillets, when assembled with adjoining components.

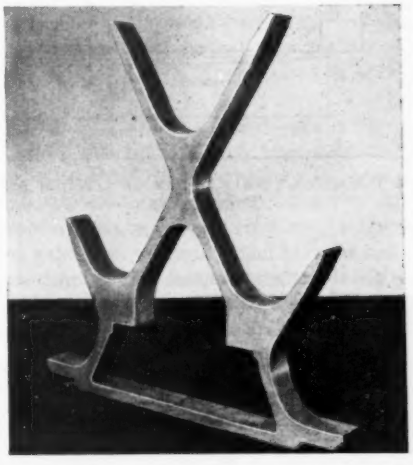


Fig. 1 Component Flame-Cut to Shape from Hot-Rolled Plate

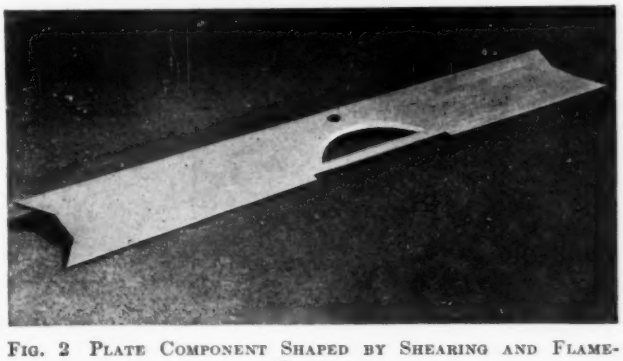


Fig. 2 Plate Component Shaped by Shearing and Flame-Cutting

Tolerance on components, disregarding the method used in producing them, merits careful consideration by the designer of weldments for an accumulation of tolerances can cause costly difficulty in fabrication, as is shown in Fig. 3. This illustration pictures a highly improbable coincidence of tolerance accumulation. Nevertheless it could occur within the limits of necessary commercial tolerances on flatness and straightness. Tolerances are important considerations on flatness and straightness, particularly if the fabricator's facilities for performing such operations cannot be operated as cheaply as those of the supplier of components.

Often it is advantageous to size components on machine tools, if only for the reason that much closer tolerances are obtainable. For a complicated assembly with much welding on it, prefabrication machining is indicated. Also, at times, machining of components will help achieve close tolerance on a complete weldment. The more generous the tolerances on components, the more prevalent the gaps in fitting. Gaps require the deposition of a

---

[1] Chief Engineer, Lukenweld, Inc., Division of Lukens Steel Company.

Contributed by the Production Engineering Division and presented at the Annual Meeting, New York, N. Y., Nov. 26–29, 1945, of The American Society of Mechanical Engineers.

Note: Statements and opinions advanced in papers are to be understood as individual expressions of their authors and not those of the Society.

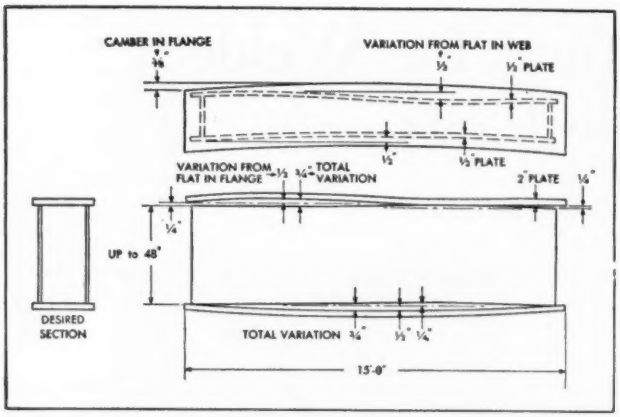


FIG. 3 BOX BEAM SHOWING RESULTS OF CAMBER AND FLATNESS TOLERANCES

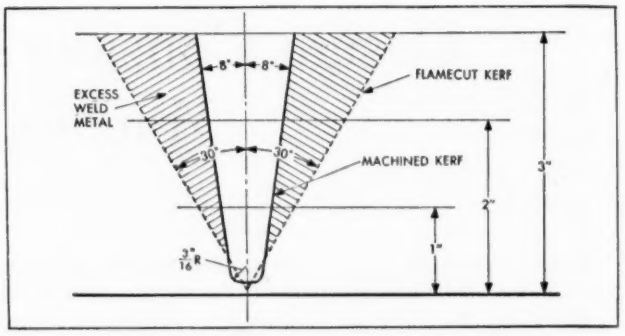


FIG. 6 COMPARISON BETWEEN "U" AND "V" WELDING KERFS

greater amount of weld metal, thereby increasing costs and destroying the metal-to-metal contact which resists tendencies to shrink or warp.

The main structural parts of the weldment shown in Fig. 4 are

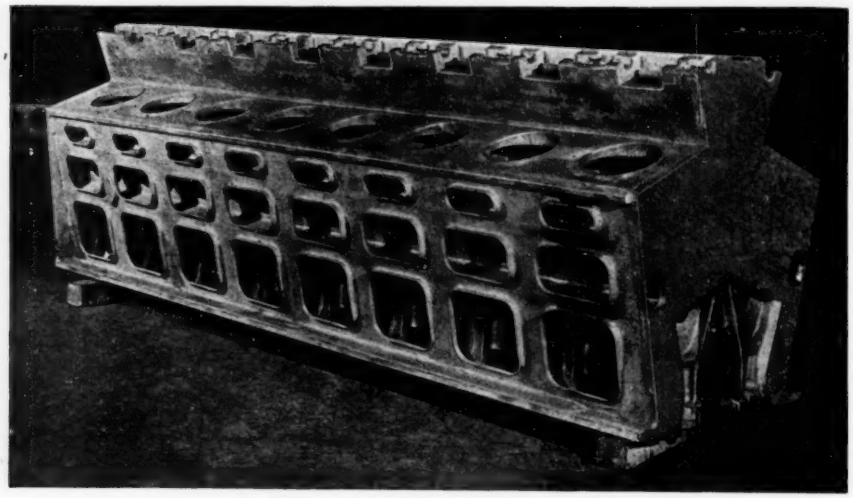


FIG. 4 16-CYLINDER, V-TYPE, WELDED DIESEL-ENGINE FRAME

premachined. Since this item is one of mass production, individual peculiarities in each weldment caused by the nonuniform accumulation of component tolerances could not be allowed.

Sometimes design considerations dictate prefabrication machining as in the case of the joint between the heavy web and flange shown at the left in Fig. 5. This might be a detail of construction on the bed of a large hydraulic or mechanical press. The loading in the region of the compression flange of those machines is such that the joint detail, shown at the right in Fig. 5, would be necessary if the edge of the web were not machined. When machined, the metal-to-metal bearing, to withstand concentrated compression loads, is achieved. Fillet welds as indicated in this illustration are adequate then for withstanding the horizontal shear components in this region of the beam. The edging of such webs to a relatively close tolerance is a simple operation on a plate planer.

Another reason for prefabrication machining is the provision of economical welding kerfs in combination with good joint fit-up, particularly in welding thick plates. A kerf must be sufficiently wide to clear the tip of the welding electrode to permit the depositing of weld metal at the root of the weld; for as the plate thickness increases, it is apparent that the amount of metal wasted in the angularity of V-shape flame-cut kerfs in contrast to the U-shaped ones, as shown in Fig. 6, becomes an important factor.

Prefabrication machining is necessary, too, in instances of conflicting tolerances, in the fitting of circular components within each other. Studies of minimum tolerances reveal that gaps between pieces so fitted are inevitable but machine fits reduce such

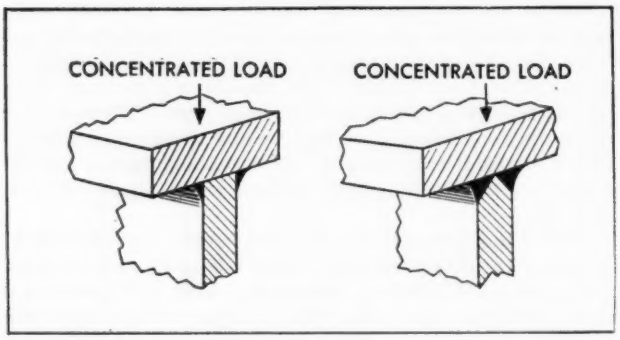


FIG. 5 JOINT BETWEEN HEAVY FLANGE AND WEB, SHOWING MACHINED EDGE AT LEFT AND FULL WELD AT RIGHT

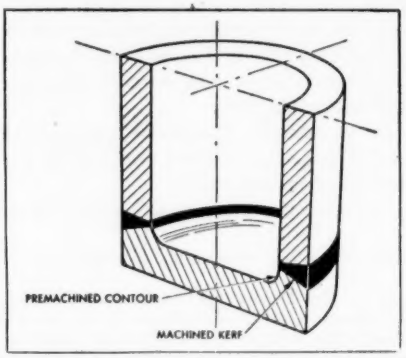


FIG. 7 BOTTOM OF HYDRAULIC CYLINDER, TYPICAL OF THOSE USED IN HEAVY HYDRAULIC PRESSES

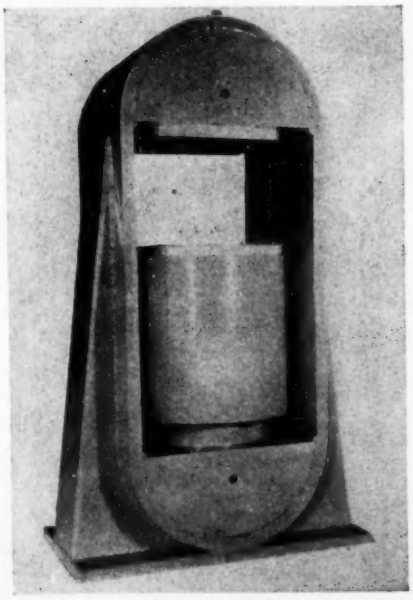


FIG. 8 CYLINDER ON HYDRAULIC PRESS



FIG. 9 BLANKED, AND BLANKED AND PUNCHED COMPONENTS MADE OF 1/4-IN-THICK STEEL PLATE

which is simply shearing, using knives of special shapes, can be justified, usually, only when quantities required warrant the expense of dies. Fig. 9 shows typical blanked or blanked and punched pieces.

A simple example of blanking or punching is the shearing of a rectangular plate. By blanking the piece only one operation is required in comparison to four operations for each piece which would be necessary in shearing. Hence a comparison of blanking and shearing costs can be made merely by multiplying the cost of the added three shearing operations by the number of pieces required and comparing this with the cost of tooling. Naturally, the estimate will be approximate since the relative cost per hour of the machines used might affect the comparison. Another important benefit gained by blanking is the comparatively close tolerance that can be achieved.

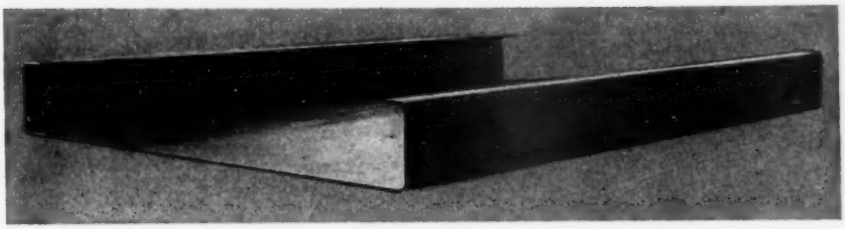


FIG. 10 HORIZONTAL ANGULAR BENDS PROVIDED BY PRESS-BENDING

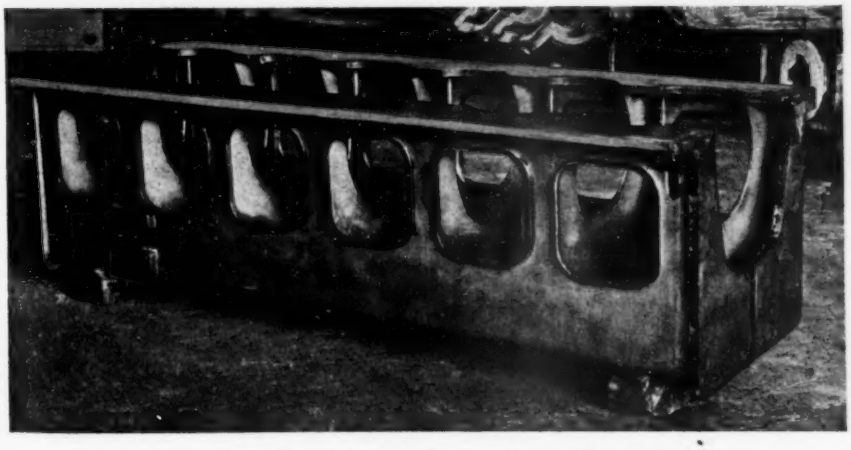


FIG. 11 WELDMENT SHOWING UTILIZATION OF FLUED OPENING

gaps to a negligible point. Prefabrication machining is necessary at times, also, for providing proper contours in highly stressed weldments, or in those subject to fatigue. Fig. 7 shows such an instance in the bottom plate of a hydraulic cylinder premachined to provide proper curved contour at the corners. This sketch also illustrates an application of machined kerfs on thick plates. Fig. 8 shows the cylinder of a hydraulic press designed on such principles.

Another method used frequently for shaping plate components is "blanking" or "punching" on a power press. This operation

"FORMED" COMPONENTS

Thus far we have considered only flat pieces in the preparation of components but we must give thought also to "formed" type components which are required frequently in weldments. Several methods are in general use for forming components for weldments. One of these is press-bending to make horizontal angular bends as are shown in Fig. 10.

Definite reasons for forming operations such as bending or fluing have been evolved. One is lower cost, for angular bends eliminate one or more welded joints. The cost of bending seldom equals that of the alternative assembly and welding. Careful examination of the design proportions of metal sections might show the economy of using the same metal thickness of web and flange to utilize the advantage of a bent section. A bent com-

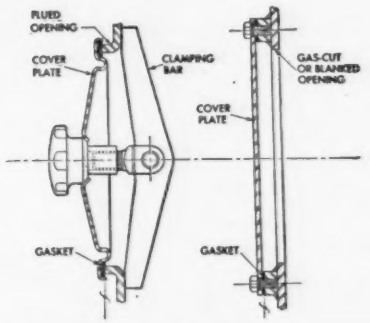


FIG. 12 THE FORMED SEAT COVER AT THE LEFT IS DESIGNED TO BE FASTENED BY AN INNER CLAMP

(Assembly, welding and consequent warpage, and the cost of drilled and tapped holes are eliminated as in the case of the cover at the right.)



FIG. 13 MELTING POTS USING FLANGED PRODUCTS AS COMPONENTS

ponent naturally is more rigid than a flat one. This can be important in the control of shrinkage and warpage.

Another method often of value in component production is the specialized forming operation known as fluing. Flued openings such as shown in Fig. 11, when machined, provide formed seats for covers. Generally, such a cover is designed to be fastened by an inner clamp as shown at the left in Fig. 12. Treatment permitted by the flued opening eliminates assembly, welding, and consequent warpage, and the cost of many drilled and tapped holes as shown at the right in Fig. 12. In addition, weight reduction is achieved.

Another function of flued openings in weldments is to provide stiffening lips which are executed normally by welding a band around the opening where required by design considerations.

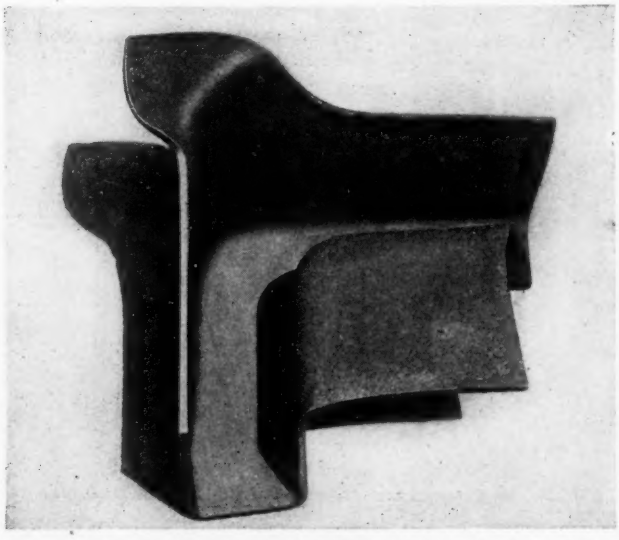


FIG. 14 CORNER STAMPING FOR WATER-COOLED FURNACE DOOR

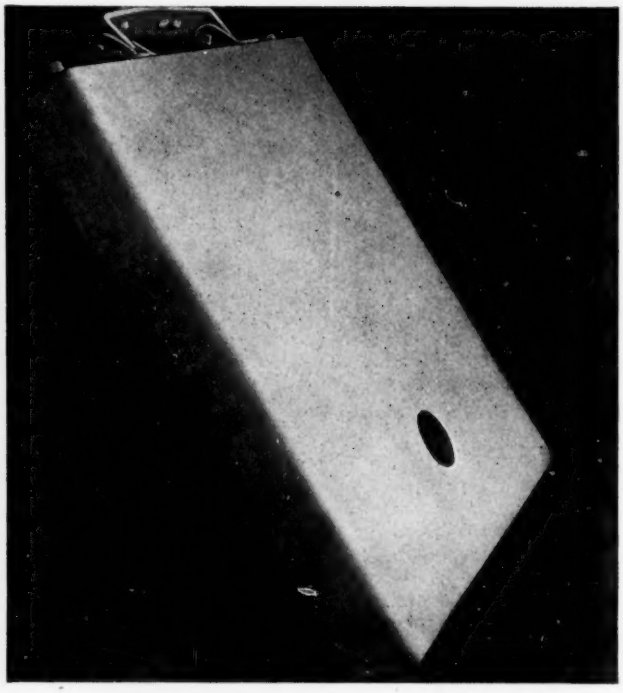


FIG. 15 FURNACE DOOR USING CORNER STAMPINGS SHOWN IN FIG. 14

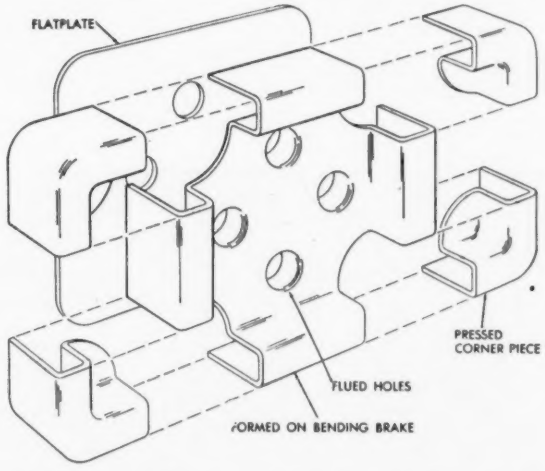


FIG. 16 EXPLODED VIEW OF WATER-COOLED FURNACE DOOR SHOWING CONSTRUCTION

Since dies are necessary, flued openings are unwarranted economically unless the quantity of openings justifies their use. When flued openings are being considered the designer should consult the supplier for it is possible that dies exist which can be adapted.

Products of the flanging or spinning machines often are utilized to advantage in weldments, as their applications in the melting pots in Fig. 13 show. The bottom corners of the pot in the lower illustration are composed of a flanged head split in half, with one half serving for each corner.

The use of flanged products as components may provide component rigidity, possibly simpler welding conditions, or a reduction in welding. Flanging also provides curved contours which may be desired for proper functioning or for appearance.

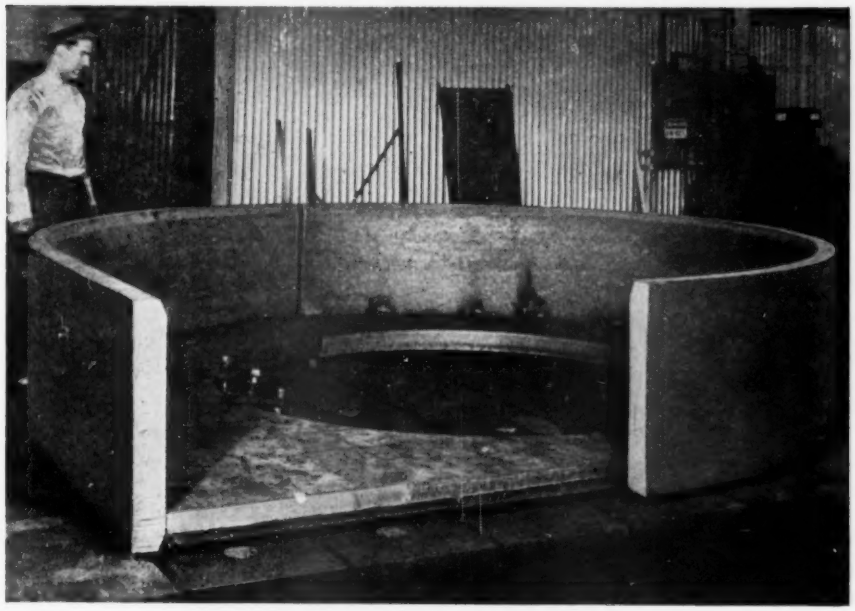


FIG. 17 PLATES 4 IN. THICK FORMED ON BENDING ROLL

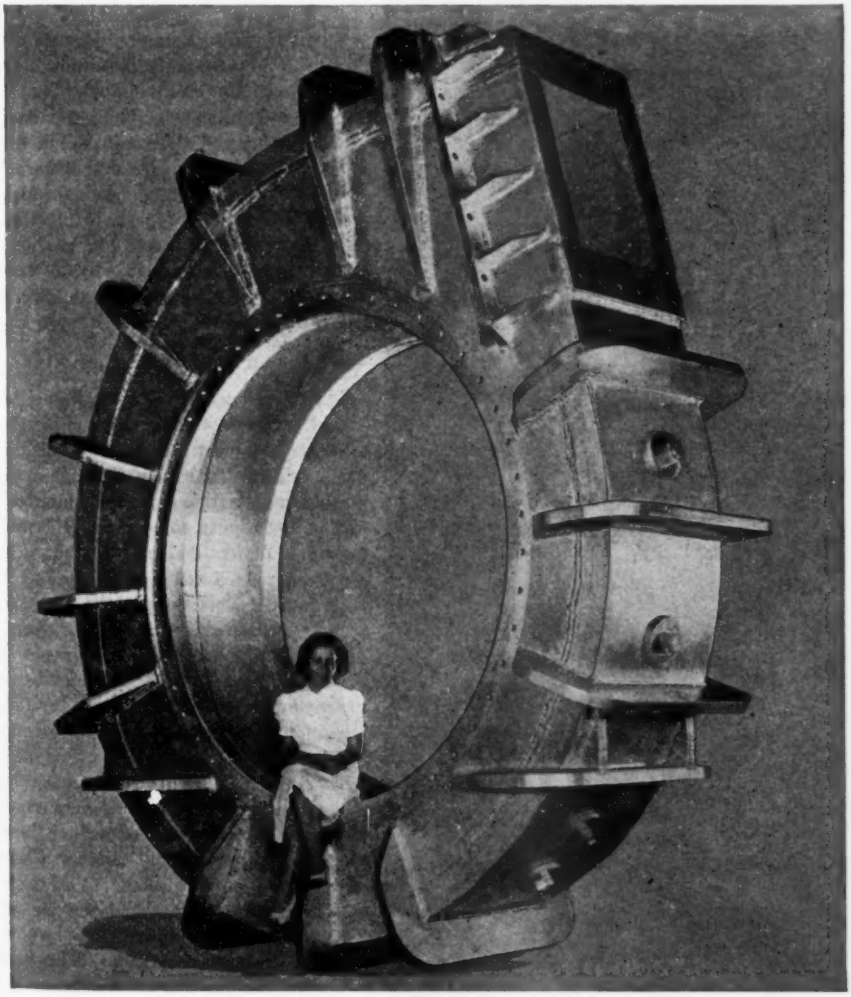


FIG. 18 PUMP CASING UTILIZING COMPONENTS SHOWN IN FIG. 17

STAMPING AND PRESSING

When quantities justify, formed components produced in special shapes by forming dies on power presses may be used advantageously. Fig. 14 shows a small stamping and Fig. 15 shows the weldment in which four of these stampings form the corners of the piece. Forming, required on the remaining components, is done on a press brake. Fig. 16 shows the relation of the various components in this weldment.

A useful method of shaping cylindrical contours is provided by bending rolls. A component formed in such a manner is shown in Fig. 17. This component is seen readily in the finished weldment shown in Fig. 18.

SHAPES FORMED ON ROLLING MILL

At times, shapes formed on a rolling mill may be used justifiably in weldments. Their value as components results from two factors: A reduction in cost because of elimination of welding and initial rigidity which can tend to simplify fabrication problems of shrinkage and warpage. In considering the use of structural rolled shapes, the tolerances possible in such rolling-mill products should be studied carefully for they may affect adversely the design requirements.

Steel castings are used extensively as components in weldments where economy in producing complicated shape requirements or special contours at given points in a particular assembly are involved. When castings are to be used in weldments their physi-

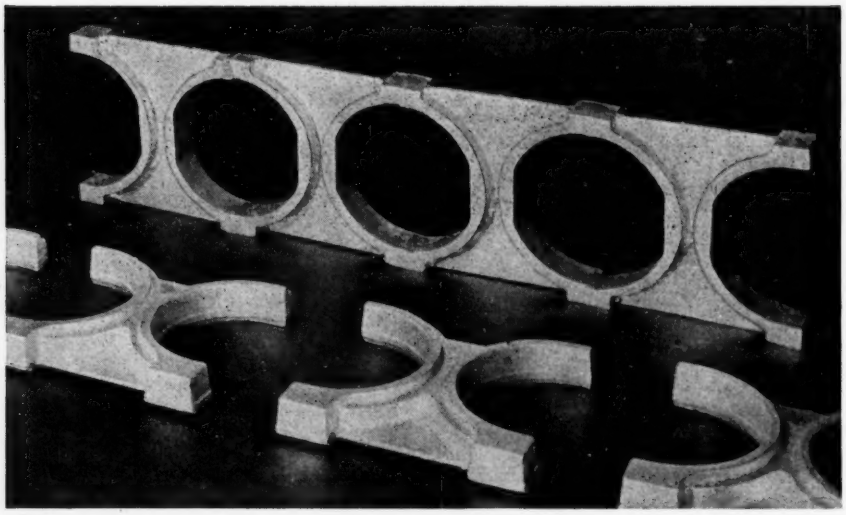


FIG. 19 TYPICAL USE OF DROP FORGINGS AND FLASH-WELDING TO PROVIDE COMPONENTS OF IRREGULAR SHAPE AND DIFFICULT PROPORTIONS

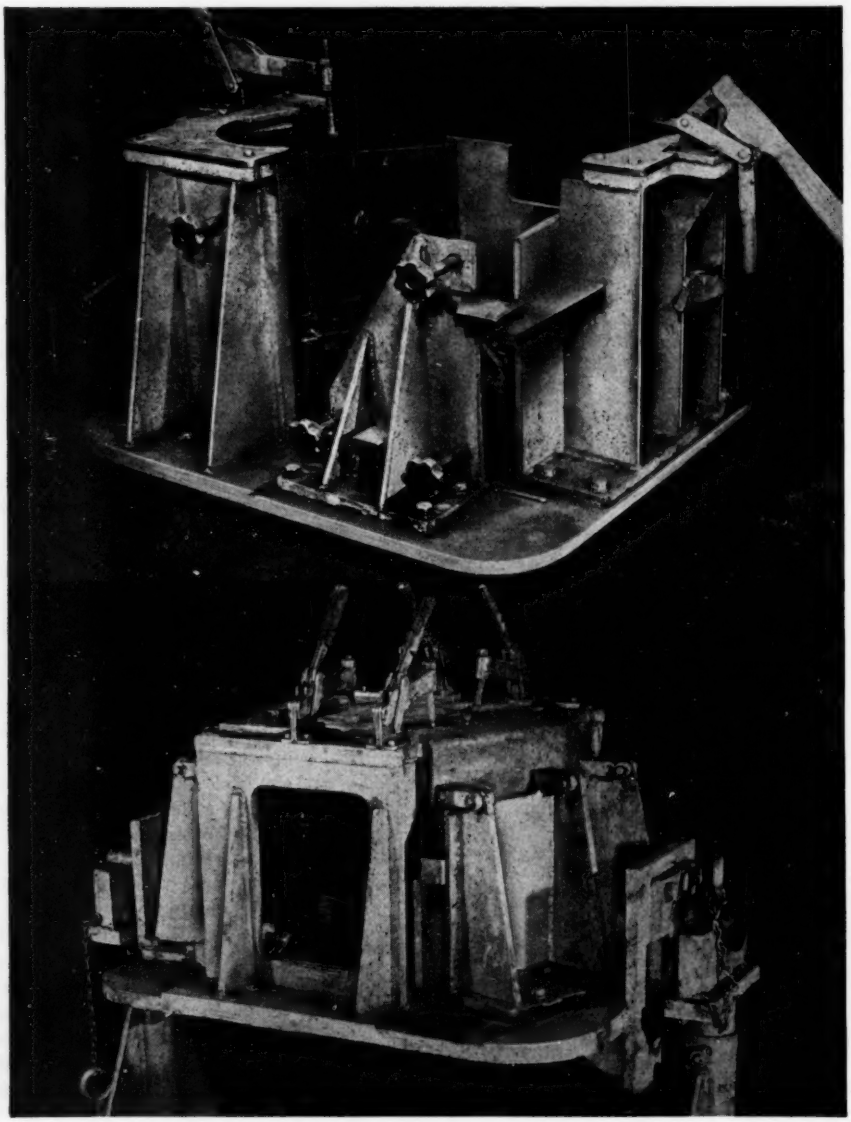


FIG. 20 TWO SPECIALLY DESIGNED FIXTURES FOR TOOLING WELDMENTS IN QUANTITY PRODUCTION

cal and chemical properties should be specified carefully. Also, where size permits, it is desirable to have castings of electric-furnace steel which seems to possess greater cleanliness. This is important in obtaining good welds with minimum difficulty.

Drop forgings also may be used when their size and quantity justify the investment in dies. This product has good homogeneous properties, and when properly controlled, its tolerances are close. Fig. 19 shows such application where several drop forgings have been joined by flash-welding.

FABRICATION OF WELDMENTS

Having considered the production and application of components, the subject of fabrication from the designer's viewpoint in developing a weldment is the next consideration. The first aspect covers the type and extent of available equipment in a weldery which will produce the pieces designed. This is important since the more flexible and extensive the equipment, the more freedom there is in design. In addition, when quantities are involved, advantage may be gained in designing the job to suit particular facilities of a weldery. Usually it is well to consult with the engineering staff of the weldery most likely to be involved regarding these matters, particularly if repetitive items are contemplated.

Production methods concerning the fabrication of weldments may be considered from two aspects. The first involves the extent of what might be termed "universal" equipment, such as positioning facilities, automatic welding units, inspection methods,

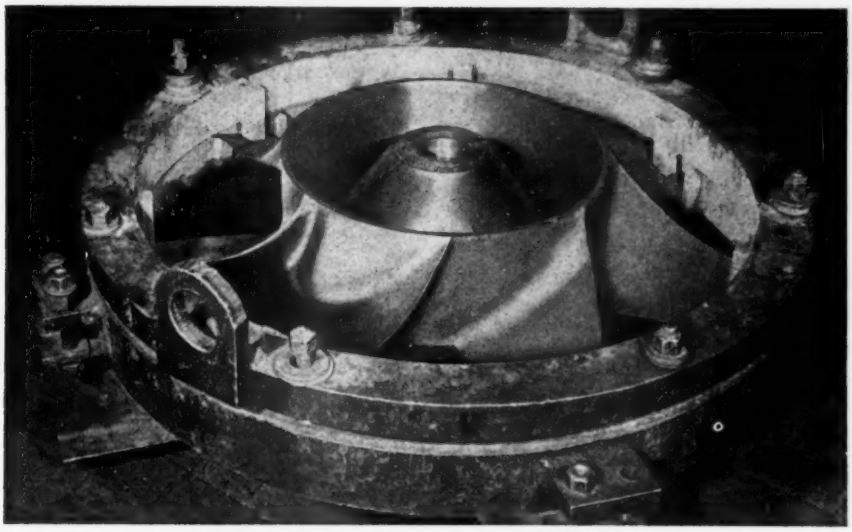


FIG. 21 HIGH-SPEED FAN, AND JIG IN WHICH IT IS WELDED

and stress-relieving facilities. Many types and sizes of positioning equipment are in use in welderies today. The other aspect involves special jigs or fixtures or other types of tooling that might be justified or imperative. Usually, if the product is to any degree repetitive in quantity, the possibilities in special tooling should be considered.

Also to be considered by the designer to promote economy and quality is the possibility of breaking up the weldment into subassemblies in sizes to suit production equipment. If the final size of the part as designed exceeds the limits of available equipment, possibly it can be redesigned so that a minimum of handling of the piece in its final size is necessary. Often the use of automatic welding equipment with its finite scope and features merits a thought in designing the weldment, especially in considering the advantage such equipment offers for cost reduction.

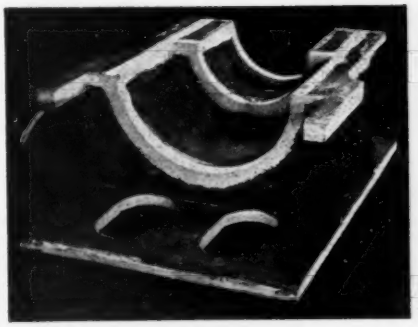


FIG. 22 SUBASSEMBLED COMPONENT OF A WELDMENT
(Welding is completed before further assembly is done.)

With special tooling, the designer should keep in mind that he is dealing still with rough component parts despite measures that might have been taken to minimize tolerances. Weldshop tooling naturally is more restricted than that usually available in machine shops. Tools, such as jigs or fixtures, should be designed with the necessity of flexibility in mind. Fig. 20 shows two special fixtures which are typical.

Special tooling also might be mandatory in order to hold components in proper relation to each other during the welding operation. Fig. 21 shows a special fixture with the weldment in place.

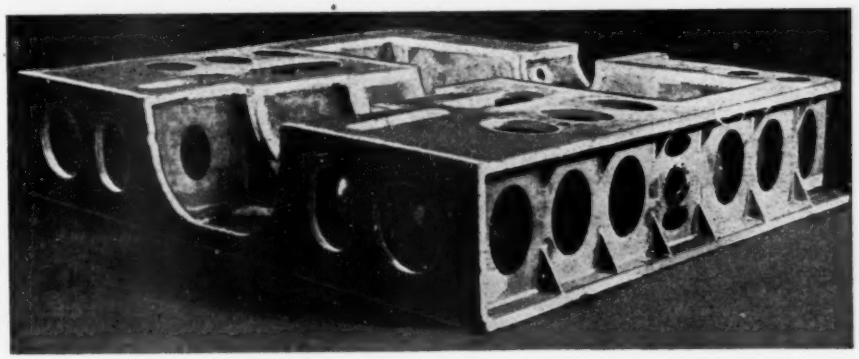


FIG. 23 LOWER SECTION OF WELDED GEAR-REDUCTION HOUSING

Although subassemblies frequently are important to the designer of weldments, design limitations often prohibit their use. Obviously, the more work done on small pieces, the easier and quicker will be the completion of the final assembly.

A completely welded subassembly is shown in Fig. 22. The final weldment is pictured in Fig. 23. Here, design controls the method of fabrication, for the lower flange member could be made in one piece. In that case at least a portion of the subassembly welding would have been required on the larger and more cumbersome piece.

Subassemblies of components should be made so that particular portions in certain instances can be sized before they become part of the final weldment. This practice helps insure that the final weldment is close to required dimensions. Where tolerances have accumulated, straightening or trimming might be involved. The effect of the welding on the completed subassembly from the standpoint of warpage or shrinkage has been eliminated as a factor on the finished weldment.

Sometimes in very complicated structures involving considerable welding, various subassemblies are stress-relieved be-

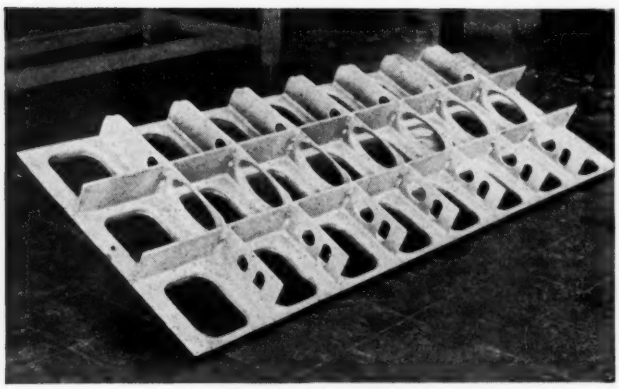


FIG. 24 WELDED SUBASSEMBLY WITH ALL WELDING READILY ACCESSIBLE

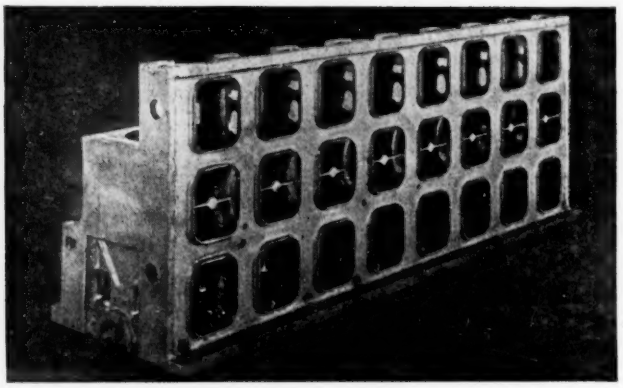


FIG. 25 WELDMENT OF WHICH SUBASSEMBLY SHOWN IN FIG. 24 IS A PART

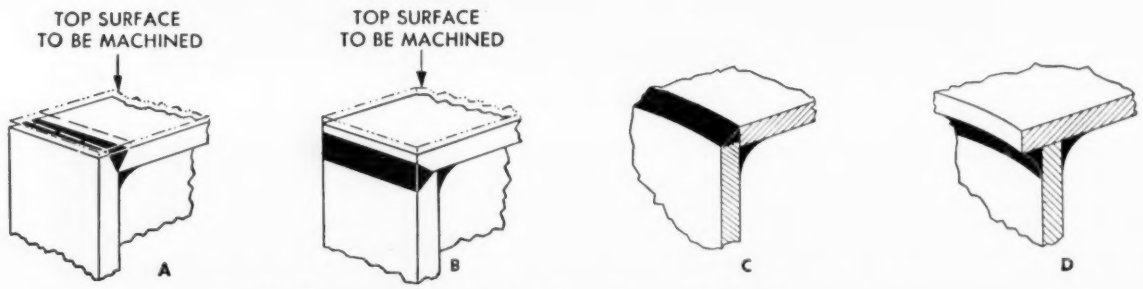


FIG. 26 TYPES OF WELDED JOINTS WHICH DESERVE DESIGN CONSIDERATION

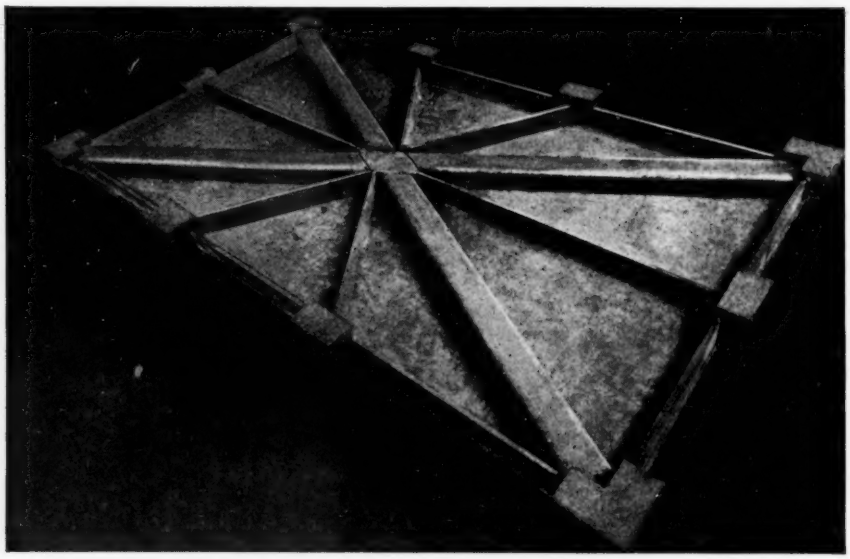


FIG. 27 STIFFENER ARRANGEMENT ON UNDERSIDE OF MACHINE BED

fore being assembled into the whole structure to reduce the accumulation of residual stresses. Subassemblies also facilitate inspection of welds. At times, where x-ray inspection is specified, subassembly welding is necessary, for if the welding were not completed and x-rayed in the subassembly, the interference of adjacent components in the completed assembly might make it impossible to x-ray or repair such welds. At times, subassemblies are welded completely when they include compartments subjected to pressure or oil-retention tests.

Tests are made and necessary repairs completed on the subassembly piece. Clearly, such practice is more economical than to attempt such work on the final piece, if only from the standpoint of the relative bulk to be handled in testing and repairing.

An important reason for careful consideration of subassembly possibilities in design is the provision of maximum access for the greatest possible amount of the welding to be done, for the more accessible the welding, the less it will cost. Also, quality is more readily achieved if the welding operator can work under open or accessible conditions. Fig. 24 shows a subassembly on which all welding to be done is before the operator. Fig. 25 shows the

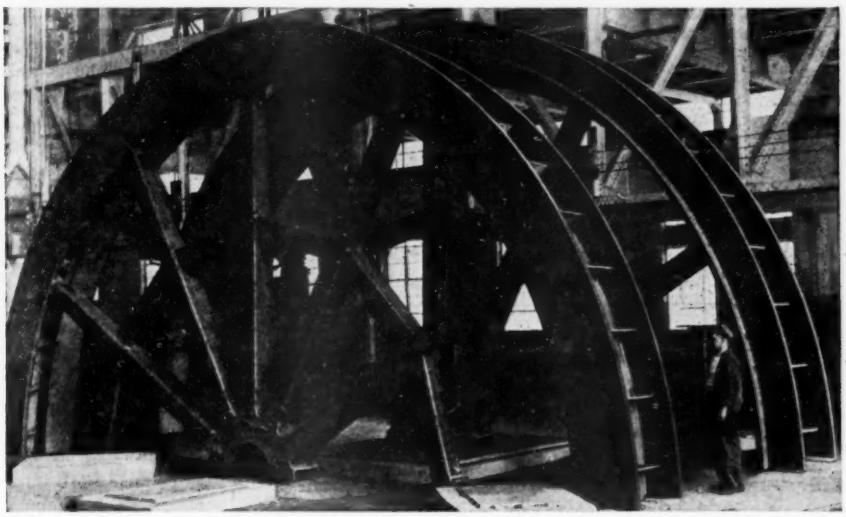


FIG. 28 TWO HALVES OF LARGE WELDED MACHINE PART WHICH ARE ASSEMBLED AND WELDED INTO ONE PIECE AFTER SHIPMENT

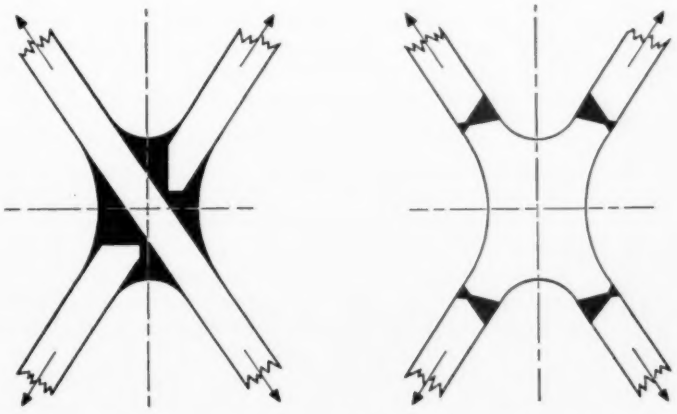


FIG. 30 TYPES OF INTERSECTION WITHOUT AND WITH TRANSITION PIECE

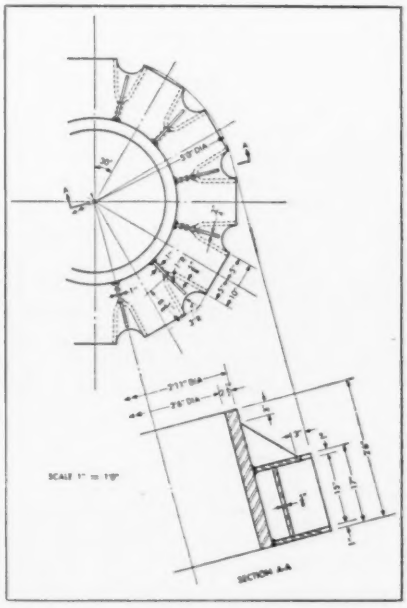


FIG. 29 DETAIL OF CONSTRUCTION OF CENTER HUB ON PIECE SHOWN IN FIG. 28

completed weldment with the subassembly in place. Obviously, welding has been simplified since the joining welds between subassembly and main assemblies are completed by working through the access openings shown. If the welding had not been completed in the subassembly it would have had to be performed through such openings. This would have necessitated the use of a mirror by the welder with resulting slow and consequently expensive welding.

At times it is advantageous to design so that progressive subassembly is possible. Thus one portion of the weldment is completed before it is assembled and welded to other components as a step in the final assembly of the completed weldment.

When maximum access is provided by subassembly practice or other design control, inspection can be more conclusive. Fig. 23 illustrates design for accessibility with elliptically shaped openings, permitting access to the inner side of the joints to be welded. Here desirable structural qualities of a box member are not sacrificed for access but care has been taken in shaping the openings so that abrupt discontinuities in the contour of the members are avoided.

Welded joints of maximum quality and predictability from the standpoint of either external contour or internal soundness are almost impossible to execute with the manual arc if the joint is not reasonably accessible from both sides. However, at certain points where stresses are of secondary nature and fatigue-loading is not present in structures, the joints do not require work on both sides.

In addition to the type of welded joints used, their position in the weldment deserves careful design consideration for several important reasons besides positioning them for maximum access. Where machined surfaces occur in the design, care in placing joints can effect economy, as comparative illustrations given in Fig. 26 show. Clearly, if the joint is placed as in Fig. 26 (A), a portion of the deposited weld metal will be removed in machining operations. Depositing weld metal is expensive and removing it is wasteful. The joint placed in Fig. 26 (B) shows how the amount of necessary weld metal has been reduced. The joint shown need have only the cross-sectional area of that shown in Fig. 26 (A) after it is machined. Economy may be possible by positioning a joint as shown in Fig. 26 (C) which eliminates the kerf and its cost, or Fig. 26 (D) which also simplifies fitting, in contrast to the same joint detailed in Fig. 26 (A).

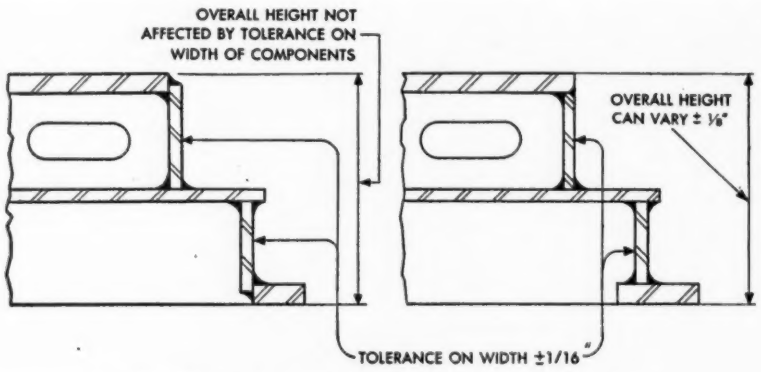


FIG. 31 EFFECTS OF CONTROLLING CUMULATIVE TOLERANCES

At times spoked or diagonal members are indicated by design considerations and their intersection usually presents a type of joint difficult to fit and costly to weld if proper external contours are to be maintained. An example is shown in Fig. 27. Here the diagonal pattern of the box stiffeners on the underside of this machinery bed is highly desirable from the standpoint of maximum rigidity. However, their central intersection presents a problem of the nature just described. By the utilization of a flame-cut central member, square joints at the intersection have been obtained; hence, fitting and welding are simplified.

Fig. 28 shows a simple treatment of an intersection of spokes. The central member in this is a subassembly so designed that the spokes do not converge on each other with obviously poor fitting and welding conditions resulting. An illustrative sketch showing the construction of this central hub is given in Fig. 29.

At intersections of members subject to high stress levels, fatigue, impact, or a combination of these, careful design treatment is imperative. Contrasting designs of such an intersection are shown in Fig. 30, where the left illustration shows the intersection as welded without benefit of a transition member. Clearly, in order to provide curved contours, an inordinate amount of weld metal would be necessary. In addition, it is practically impossible to execute such a welded joint so that full predictable strength will result. If necessary, x-ray inspection is practically impossible. Fitting conditions are poor and the excessive amount of weld metal adds to warpage and shrinkage problems. Desirable features of a similar joint as executed in the right illustration are self-evident.

The designer should remember the generality that in a weldment the fewer separate and different components required, the cheaper and better the design will be.

At times, particularly with secondary members such as ribs or stiffeners, slight changes will permit uniformity in size of different components. Such consideration might make quantity production by blanking economically possible. Another somewhat minor consideration is the difficulty caused the assembler or fitter in trying to identify parts that appear almost the same.

The designer should keep in mind, also, the possible utilization of hot-rolled-bar stock, for often such material can be used by making a slight change in dimension of a given cross section to conform to standards.

All components, regardless of the method of producing them, are subject to dimensional tolerances. The designer must keep this in mind for economy and good fit-up so that he can control the ill effects of cumulative tolerances. Fig. 31 gives a simple illustration of a typical weldment in which the designer has kept cumulative tolerances in mind. The drawing at the left shows a partial cross section, while the drawing at the right shows a similar cross section in which the point has been ignored.

Shrinkage and warpage problems which exist in the production of weldments will continue to be a factor so long as drastic heat gradients occur during welding. A degree of experience is needed to be able to predict such effects and to control and counteract them. It is impossible to discuss this factor here in detail. The designer should, however, sense the general aspects of such phenomena so that he does not develop designs that may be impossible to produce within necessary tolerances.

Warpage will occur to a great or little degree depending on the relative size of given welds and their distances from the neutral axis of the assembly. This is due simply to the relative ability of a member to resist shrinkage stress imposed at different points in its cross section with respect to the neutral axis of that cross section.

Welding results in shrinkage both longitudinally and at right angles to the weld metal. The extent varies for sizes as well as types of welds. When the number of different sizes and types of welds occurring in an average weldment, and their length and position with respect to each other are considered, it can be realized that control of warpage is to a large degree a matter of practical experience. Sequence of welding also should be carefully controlled as a counteracting measure. At times special fixtures are used to restrain warpage during welding.

CONDITIONING AND INSPECTION METHODS

Following completion of welding, it is an established practice to condition the weldment by removing spatter, grinding edges or surfaces where specified because of design requirements, and gritblasting when size permits.

Spatter is removed for appearance and to insure that it will not drop off progressively when the weldment is in service. Spatter can be detrimental mechanically if, for instance, it were left in a lubricating-oil compartment.

Weldments are gritblasted to remove mill scale from plate surfaces and to facilitate visual inspection of welds. Undercuts usually are more difficult to detect before the weld is gritblasted. Welds are inspected visually for proper size, surface cracks or other surface defects. X ray is used to inspect welds for internal defects. Various specifications such as those of the A.S.M.E. and the U. S. Navy provide inspection standards for the acceptance or rejection of welds by means of x-ray photographs.

Hydrostatic testing often is required by design specification. Oiltight compartments should be checked and tested before the part leaves the weldery. Finally, the weldment should be laid out for a final inspection at the weldery to verify that it is dimensionally correct within specified tolerances.

Any weldment to be machined, subsequently, to any appreciable degree should be stress-relieved if the machined surface or other parts of the weldment are to hold their relationship within service life. Any weldment subjected to severe stresses or to fatigue or impact, also should be stress-relieved. Especially is this advisable since locked-up stresses, the magnitude or direction of which cannot be predicted, can be of a high order following welding. If normal service loading imposes design stresses having the same direction at a given point as that of a residual or locked-up weld stress, structural distress or failure can result.

Many weldments are in use that have not been stress-relieved. Hence definite predictions cannot be made that difficulty will result for a given type of weldment in the unstress-relieved state. Stress-relief therefore may be regarded somewhat like insurance having a low premium rate because the per pound cost of stress-relieving is usually only a fraction of a cent.

Specifications for Weldments

A weldment should be specified clearly and concisely so that no misunderstanding results, and to insure from the equitable standpoint, that each potential vendor is quoting on the same conditions. It is important, for instance, that the weldery know if the weldment must be produced under a code requirement.

Over-all tolerance requirements on various dimensions of the weldment should be considered carefully. The designer might be inclined to make everything tight to "be on the safe side." But this can be a costly practice compared to that of evaluating requirements intelligently. Often, a relatively close tolerance, under given conditions of size, shape, and amount of welding, at some point in a weldment can be costly to achieve. Proper study might show that the tolerance can be loosened without affecting the service performance of the weldment. In this instance it is common practice to consult with the weldery to achieve, mutually, the best conditions.

This check list of specifications and drawing information will give the weldery proper and clear directions:

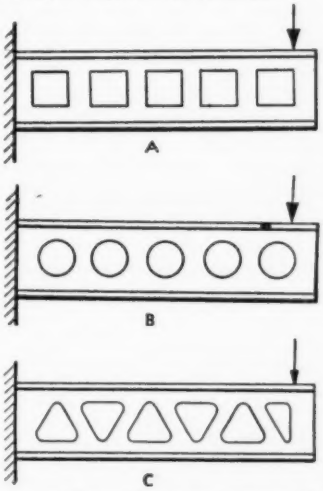


Fig. 32 Cantilever Beam Showing Three Designs in Web Openings

Steel specification?
Inspection agency, if any?
Weld sizes and to what standard?
General tolerances or any special tolerances?
Gritblast?
Grind? If so, where?
Stress relieve?
Paint? If so, what type and how many coats?
X-ray requirements? To what code?
Test—hydrostatic? If so, at what pressure?
Test—oiltightness?

Many types of weldments or components for weldments can be designed effectively into welded machinery parts. Categorically, machinery parts, as distinguished from other types of structural members, can be defined as parts required to resist or support moving forces; parts subjected to dynamic loading.

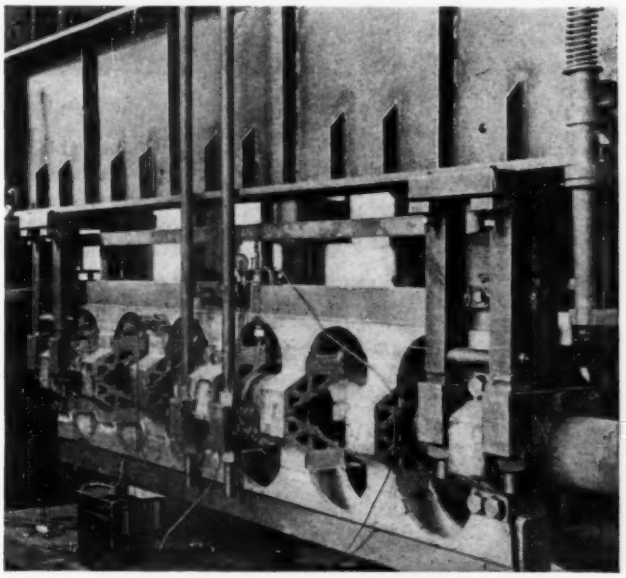


Fig. 34 Analysis on Model of Welded Engine Bed (Stresses under lateral load can be read from the strain gages visible in the illustration.)

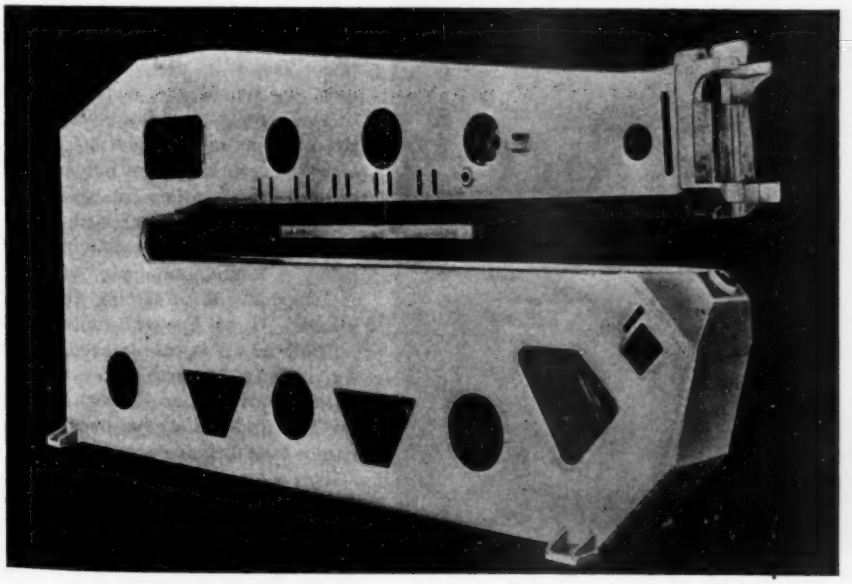


Fig. 33 Circle Shear Frame

Dynamic loading or applied forces in motion can involve additional factors or criteria, i.e., fatigue and impact, to be considered in the design of the part and the proper selection of its material. These two factors, alone or in combination, often can affect materially, or control the shape, material, and manner of fabrication of a mechanical structural member.

If fatigue and impact are of major consideration, those properties of the material determining its resistance to such loading should be known. As we know, such properties generally are referred to as the endurance limit with respect to fatigue, and impact resistance in relation to impact. This latter property sometimes is related to temperature.

External contours of a part subjected

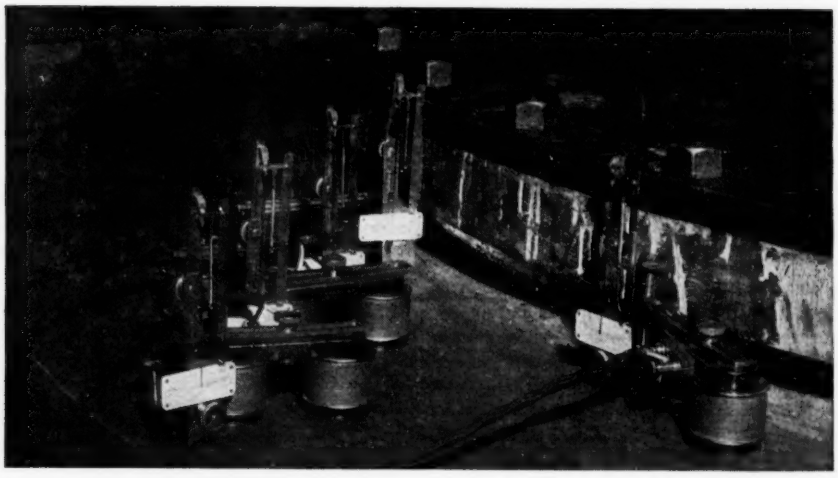


FIG. 35 TEST SETUP TO DETERMINE ACTUAL STRESSES UNDER LOAD ON PIECE SUBJECTED TO INTERNAL HYDROSTATIC PRESSURE

to dynamic loading, particularly when fatigue is probable, are an important consideration especially when the member is subjected to primary loads. They are extremely important at the points of changes in contour in a structure of irregular shape.

Contours influence the effectiveness of a load-carrying member from a general standpoint. Proper contour denotes efficient disposition of material which is fundamental in control of weight. As an example, the component shown in Fig. 32 (A) is less rigid for a given over-all weight than that shown in Fig. 32 (B). Disposing metal as shown in Fig. 32 (C) is more effective from this standpoint. An example of such design thought in an existing welded structure is shown in Fig. 33.

Internal contours, those bounding openings in a structure, are worthy of careful consideration in the design of machine parts, especially since mechanical structures usually require openings of varying sizes and shapes for such reasons as fabricating or operating accessibility, or for mechanical clearance.

Often the effectiveness of proper, flowing contour, particularly its value in rigidity, is mathematically indeterminate. Where maximum rigidity or strength for least weight is important, model analysis is possible. Fig. 34 shows the setup for such an analysis of a welded machine part. Actual stresses in a product also can be determined by the use of instruments such as strain gages shown in Fig. 35.

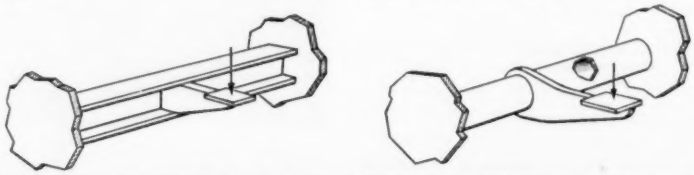


FIG. 36 ABSTRACT EXAMPLE OF TWO METHODS OF RESISTING TORSIONAL FORCE

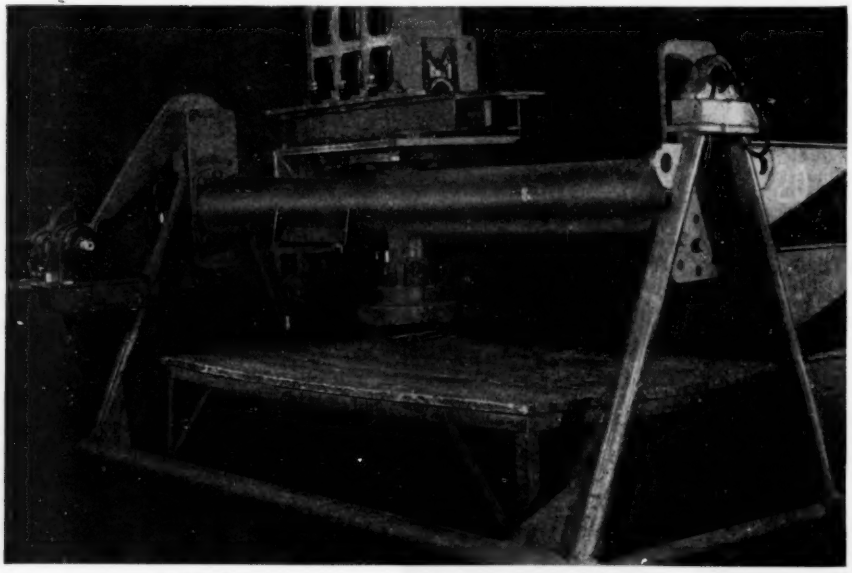


FIG. 37 APPLICATION OF WELDED TUBULAR STRUCTURE
(Main beam of this welding positioner is tubular in cross section. It is subjected to combined bending and torsional stresses.)

WEIGHT CONTROL

Frequently, minimum weight is a major factor in designing structural members of machines, and the weight of a mechanical part can be controlled by one or more considerations. Sufficient strength is the first fundamental. Several considerations can be involved in designing for the strength factor. One is a properly adjusted factor of safety. A minimum factor of safety is important in designing for least weight. If it is known definitely that no internal voids can or need exist in a given cross section subject to primary dynamic stress, one element making up the factor of safety has disappeared, or at least is under control.

This control can be exercised in production of weldments if design permits. It is axiomatic that in designing for least weight the shape should be as regular and flowing as possible, as the previous discussion of contours reveals.

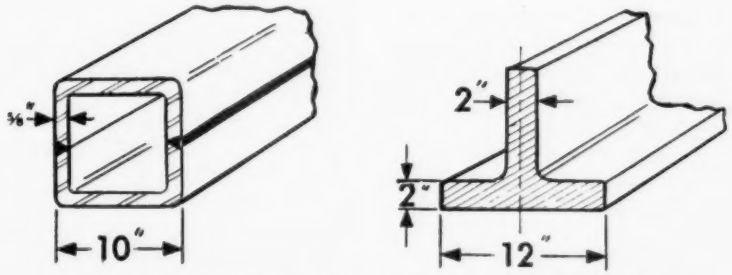


FIG. 38 DESIGN DETAIL OF SPOKES IN A WELDED MACHINE PART

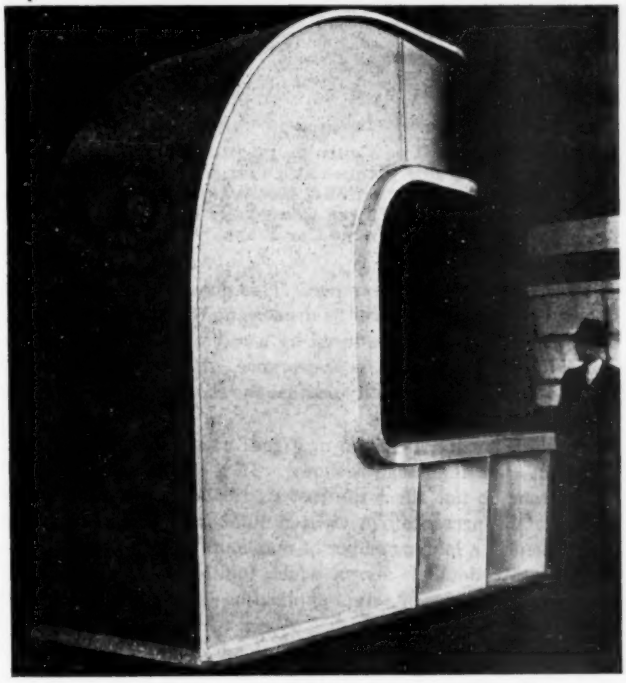


FIG. 39 WELDED FRAME FOR C-TYPE, OR OPEN-SIDE, HYDRAULIC PRESS

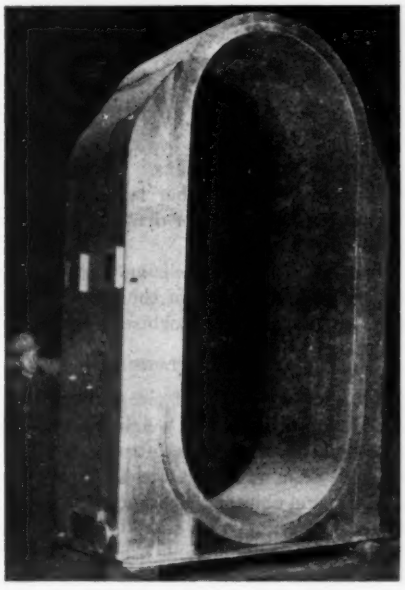


FIG. 40 WELDED-STEEL CONTINUOUS BAND HYDRAULIC-PRESS FRAME

Another consideration in the strength factor is the exactness of knowledge of the magnitude, direction, and location of the dynamic forces with respect to each other and their reactions involved in the machine. In designing machine parts, particularly for least weight, it is important that these be predicted as closely as possible.

After this has been done, the material resisting or supporting such forces or reaction can be disposed in a weldment to best advantage consistent with mechanical clearance requirements balanced against the necessity for least weight.

As an instance, Fig. 36 shows an abstract example of two methods of resisting a torsional force. There is no questioning the effective disposition of metal in a tubular design. Nor is there any questioning that the effective disposition of metal insures least weight. Fig. 37 shows an example of this concept in an existing machine part.

Another example of effective metal disposition is shown in the spokes of an enormous machine part, the cross section of which appears at the left in Fig. 38. The illustration at the right shows the spoke as it was designed initially because of casting limitations.

RIGIDITY A VITAL FACTOR

The dominant factor in the design of structural parts for machines sometimes is rigidity, or stiffness, rather than strength as in the instances just discussed. The primary function of the spokes in Fig. 38 is maintenance of alignment between machined parts in the structure to the greatest possible degree. Rigidity or minimum deformation dominates in the design of the C-type, or open-side press frame shown in Fig. 39. This weldment is composed exclusively of hot-rolled plate with metal thickness at any point dictated solely by design requirements.

A welded design that embraces directional control of rigidity is shown in Fig. 40. Purely vertical deformation or elongation is a secondary consideration in the function of this machine. A somewhat normal design for the structural parts of such a press is composed of top beam or platen, lower beam or bed, and side housings; all separate pieces integrated by two or four vertical tie rods secured by nuts at both ends.

In such a design, it can be seen readily that in addition to vertical, straight-line elongation, the upper and lower beams will tend to deflect as beams in a manner detrimental to the alignment of tools and work in the press. That such detrimental tendency is practically eliminated is shown in this design where the single structural member resists the working forces imposed on it in direct uniform tension.

The stabilization of thin and unsupported expanses of metal is a new element which requires watchfulness in the design of weldments for machinery, since the basic properties of the component materials are more predictable and process limitations on the thinness of metal sections are nonexistent. These thin and un-

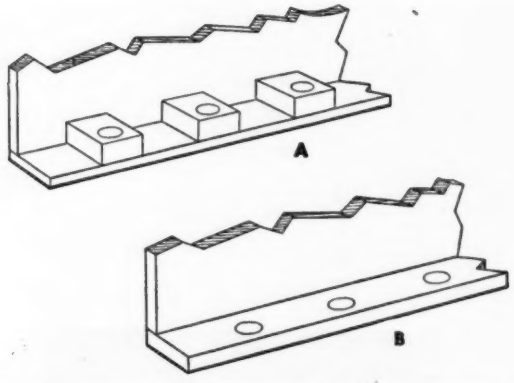


FIG. 41 COMPARATIVE TREATMENTS OF BOLTING FLANGES IN A WELDED PART

supported expanses of metal may be detrimental to the operation of the machine for several reasons. One is the possibility of "drumming" or vibration, another is fundamental instability, and the third is the possibility of dents or distortion in normal handling of the structure.

Many possible methods of stabilizing expanses of cross section exist. Usually the imagination of the designer is fertile in the solution of the problem, if it is recognized.

SIZE LIMITATION

Generally, the fewer number of pieces required to make up a machine structure, the less it will weigh and cost, and the stiffer it will be in contrast to a one-piece structure. The only limitations on the size of a weldment are those imposed by stress-relieving facilities and shipping clearance.

Another type of freedom that should be kept in mind by the designer of weldments is the possible use of higher-strength weldable alloys in highly stressed portions of the structure. The secondary components or elements of the piece can be of cheaper, plain carbon steels. Weldable alloys, of course, add nothing in rigidity or stiffness since the modulus of elasticity remains practically the same.

Factors of primary importance in the economic balance or competitive comparison of a welded-steel design must be evaluated clearly. The fundamental reason for assuming that a weldment is the proper medium must be unmistakably defined. This reason may include natural adaptability, and predictability, minimum weight, and initial cost. Having established this, it must be realized that the weldment undoubtedly will not resemble a casting in appearance. This does not imply that the welded machinery part will be displeasing to the eye. It means simply that anything produced by a radically different process logically will be different in appearance. If it is not, the design should be reviewed critically because the chances are that it is not economical as a weldment.

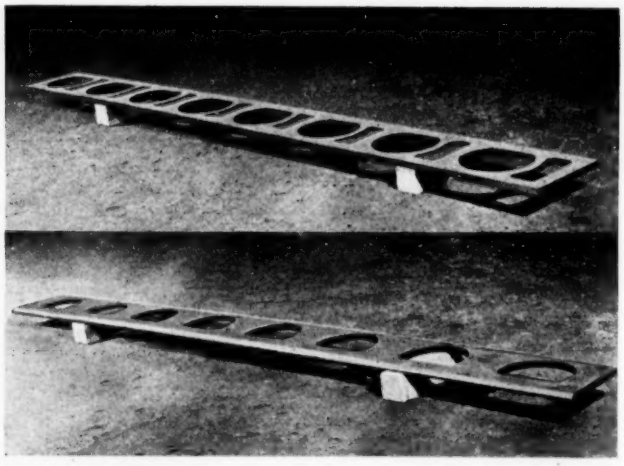


FIG. 42 IN THESE TWO COMPONENTS, THE UPPER ONE WAS DESIGNED FOR MINIMUM WEIGHT BY CUTTING OUT AREAS OF FULL THICKNESS BETWEEN FUNCTIONAL HOLES AND FILLING THEM WITH THINNER PLATE. THE LOWER COMPONENT IS COMPOSED OF ONE FLAME-CUT PLATE

A simple instance is shown in Fig. 41 where at A, the common detail of a bolting flange is shown. In a casting many changes in contour do not affect the cost particularly. In a weldment such details necessitate a greater number of components and consequently a larger number of manhours to join them. At B an alternate detail is shown which fulfills the same function. These are examples of actual applications in use in thousands of weldments.

On the other hand, if weight reduction is of critical importance, the over-all economic balance might dictate the added complication in the weldment. A natural question here is, "why not cast it?" The answer has been found to be that if weight reduction is the primary criterion for given requirements of space and over-all size, a weldment can be designed which will weigh less than a casting and not affect the strength or rigidity.

Another comparison between two components of a weldment that perform the same function is shown in Fig. 42. The upper

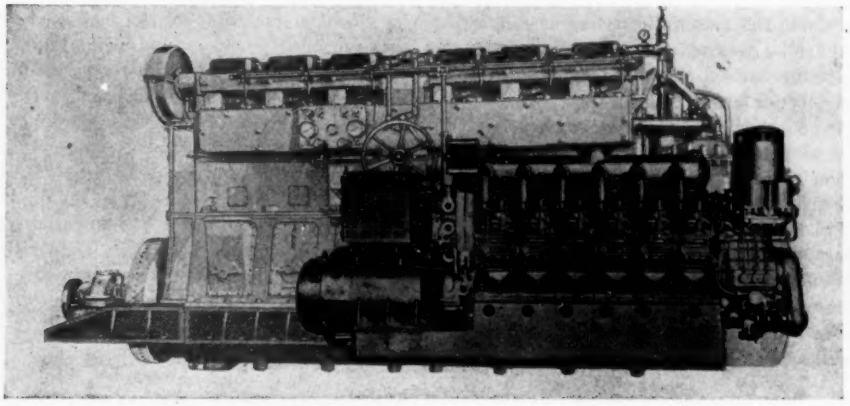


FIG. 43 COMPARATIVE ILLUSTRATION SHOWING A DIRECT-DRIVE 4-CYCLE DIESEL ENGINE OF 1926 WITH AN ELECTRIC-DRIVE 2-CYCLE DIESEL ENGINE OF TODAY

detail is more costly but lighter in weight than that shown in the lower half. If quantities of duplicate parts are involved, other methods of achieving minimum weight at lowest cost also are possible.

In making a decision on the value of weldments as structural members in a machine, the broad measures of their desirability should be known and considered. Logically, a weldment should not be used simply because a desire exists to design in this medium. By the same token a casting or forging should not be used if a weldment presents greater advantages.

In this discussion weight control or reduction may seem to have been emphasized. This is due simply to the progressive recognition of the fact, particularly in relatively large pieces weighing 200 lb or more, that weldments have been applied admirably where weight is important. Undoubtedly, the inherent features making this possible are predictability and the fact that the process practically imposes no limit on the thinness of sections. The weight factor can be important in machine design for many reasons. Fundamentally, it is the minimizing of inertia forces in moving parts of machinery. Another is the pyramiding of the effects of weight or mass in mechanisms subject to high velocity, as the modern railroad passenger car.

Conclusion

In conclusion, the result of the practical application of the many factors discussed probably can be best illustrated by a particular instance of weight and space efficiency in the use of weldments. A comparison, in Fig. 43, of a direct-drive four-cycle Diesel engine of 1926 with an electric-drive two-cycle Diesel engine of today shows that the modern smaller engine represents a reduction of 67.39 per cent in cubic feet occupied per brake horsepower, and also a reduction of 58.40 per cent in weight per brake horsepower. The development of welded-steel-type construction has materially helped in reducing weight. At the same time, the lighter engine of today is 50 per cent more efficient than the heavier engine of 20 years ago.

Stress-Rupture Characteristics of Various Steels in Steam at 1200 F[1]

By J. T. AGNEW,[2] G. A. HAWKINS,[3] and H. L. SOLBERG[4]

Small tensile specimens made from low-carbon, carbon-moly, 2¼ Cr- 1 Mo, 5 Cr-Mo-Si, 9 Cr-Mo-Si, 12 Cr, 18 Cr-8 Ni, 25 Cr-20 Ni, and 5 Cr-Mo-Ti steels were placed in a steam reaction chamber at 1200 F and stressed in tension for periods of time ranging from 10 hr to 7700 hr. Data were taken on time to rupture, elongation, reduction in area, depth of scale layer, effect of type of flow, and type and angle of fracture. A photomicrographic study was made of the ruptured specimens. The straight-line relationship between stress and time to rupture on log-log co-ordinates postulated by White, Clark, and Wilson for tests in air also holds for tests in steam.

As the conditions of temperature and pressure to which alloy steels are exposed in modern steam power plants and other industrial apparatus become more severe, the need for experimental data concerning the behavior of these alloys under such conditions becomes more acute. This paper describes an investigation in which small steel specimens were placed in tension in an atmosphere of steam at 1200 F until rupture occurred. The stress-rupture data for various alloy steels in contact with high-temperature steam are needed for the design of various types of high-temperature steam-generating equipment.

TABLE 1 CHEMICAL ANALYSIS AND HEAT-TREATMENT FOR STEELS USED IN THE TESTS

Type of steel	Type number	Chemical Analysis C	Mn	P	S	Si	Mo	Cr	Ni	Ti	Heat-treatment
Low carbon	1	0.16	0.47	0.084	0.023	0.20					1650 F Air cooled - roll. temp. strain tempered from 650C
Carbon-moly	2	0.20	0.53	0.01	0.016	0.24	0.50				An. 1550 F
2.25 Cr-1 moly	3	0.16	0.39	−0.03	0.03	0.33	0.90	2.24			An. 1550 F Nor. 1750 F
5 Cr-Mo-Si	4	0.10	0.38	−0.03	0.03	1.55	0.51	4.83			T. 1500 F 6 Hr O.Q. 950 C
9 Cr-Mo-Si	5	0.12	0.44	−0.03	0.03	0.67	0.95	9.5			Air cooled-625-635C
12 Cr	6	0.11	0.41	0.014	0.013	0.286		12.66	0.385		Nor. 1700 F
25–20	7	0.11	0.58	−0.03	0.03	0.75		23.6	20.65		W.Q. 2000 F
18–8	8	0.06	0.50	−0.03	0.03	0.61		17.75	9.25		An. 1650 F
5 Cr-Mo-Ti	9	0.10	0.44	−0.03	0.03	0.38	0.50	4.98		0.51	

Description of Apparatus

Small steel specimens were placed in tension inside four horizontal steel reaction chambers, each of which consisted of a 10-ft length of extra-heavy 2-in. steel pipe. These reaction chambers were uniformly heated externally to the test temperature by means of resistance heaters. The steam entering the reaction tubes was presuperheated to test temperature by means of gas-fired superheaters and, after leaving the reaction chambers, was conducted to water-cooled copper-tube condensers. In each reaction chamber, several specimens were connected end to end by universal joints and were loaded in tension by means of rods which passed through packing glands at either end of the reaction tubes. One end of each tension rod passed through a calibrated spring which, when compressed, caused the specimens to be placed in tension. Chromel-alumel thermocouples were used to measure the temperature at several positions along each reaction tube. The temperatures were evaluated by means of a Leeds & Northrup portable potentiometer.

The chemical analysis and heat-treatments of the various steels used in these tests are reported in Table 1. The numbers used to designate a specimen, for example, 913, have the following significance: The first number is the type of steel, as given in Table 1, the second number is the test number, and the third (or third and fourth) number is the specimen number. Therefore, 913, would be the third sample of 5 Cr-Mo-Ti steel used in test No. 1.

Test specimens similar to the one shown in Fig. 1 were machined from round stock of 1 in. diam. The dimensions of the straight central section of the test specimens were in the same proportions as the standard tensile specimen which is 2¼ in. long and 0.505 in. diam. The straight central section of each specimen was machined to a tolerance of ±0.01 in. in length, and the diameter of the test section was held to ±0.001 in. For the specimen with the smallest test section, 0.138 in. diam and 0.61 in. long, this could result in an error of ±400 psi in the calculated stress, and for the specimen with the largest test section,

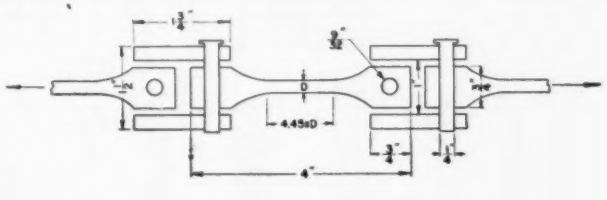


Fig. 1 Schematic Drawing of Test Specimen and Couplings

[1] Based on a doctoral thesis, Purdue University, Lafayette, Ind., 1944, by one of the authors.[2]

[2] Assistant Professor of Mechanical Engineering, Purdue University.

[3] Professor of Thermodynamics, Purdue University. Mem. A.S.M.E.

[4] Head, School of Mechanical and Aeronautical Engineering, Purdue University. Mem. A.S.M.E.

Contributed by the Power Division and presented at the Critical Pressure Steam Boiler Session of the Annual Meeting, New York, N. Y., Nov. 26–29, 1945, of The American Society of Mechanical Engineers.

Note: Statements and opinions advanced in papers are to be understood as individual expressions of their authors and not those of the Society.

0.366 in. diam and 1.63 in. long, an error of ±30 psi in the calculated stress would be possible. Holes 9/32 in. diam were drilled in the large ends of the specimens, as shown in Fig. 1, for the purpose of allowing several specimens to be coupled together. Eight specimens were coupled together and placed in each tube by means of collars and pins shown in Fig. 1. The collars consisted of 1 3/4-in. lengths of 1 1/2-in-OD × 1-in-ID 18 Cr-8 Ni stainless-steel tubing. Stainless-steel pins 1/4 in. diam were passed through the holes in the collars and specimens to hold the specimen train together. The pinholes in each collar and specimen were placed 90 deg apart around the circumference in order that each collar might act as a universal joint. The end collars of the specimen train were drilled and tapped with a standard 1/4-in. pipe thread. Tension rods were screwed into the end collars and extended to the outer steel framework. The outer ends of the tension rods passed through holes in parallel I-beams which formed the end pieces of a rectangular frame around the reaction chambers. A collar, thrust bearing, and nut were placed on the end of the extension rod nearest the superheater to transfer the tension load to the I-beam frame. The tension rod at the other end of the specimen train passed through a calibrated coil spring which was compressed against the I-beam frame by means of a collar, thrust bearing, and adjusting nut on the tension rod. The springs were compressed to exert a constant force of 500 lb on the train of specimens.

By using specimens whose test sections were of various diameters, any desired value of stress could be obtained. The diameters and stresses used for the various specimens are indicated in Tables 2 and 3. The compression of the calibrated loading springs was checked continuously by means of gage bars, and the springs were held to the correct length with an accuracy of ± 0.005 in. so that the absolute force exerted by the springs was 500 lb ± 4 lb. For a specimen 0.2 in. diam this would mean a stress of 15,900 ±100 psi. A stop was provided to restrict the movement of the broken assembly to not more than 1/2 in. Approximately 45 min were required to remove a ruptured specimen and replace it with a new one. The temperature at one end of the tube dropped to approximately 1150 F during this operation but returned to 1200 F within 1 hr after a new specimen was inserted.

Test Program

It was decided to conduct a short preliminary test on several specimens of the same steel to investigate the effect of type of steam flow and pressure upon the corrosion rate. Eight specimens of 5 Cr-Mo-Ti steel, designated as series 9 in the tests, were machined so that, with a load of 500 lb, four of the specimens would be under a stress of 6900 psi, and the other four under a stress of 6200 psi. One specimen corresponding to each stress was placed in each reaction chamber so that each chamber contained two specimens. The temperature, pressure, and steam-flow conditions were maintained as indicated in Table 2. The results of the test are also given in Table 2.

Specimens 916, 917, and 918, under a stress of 6200 psi, were not ruptured during the test. While waiting for specimens 911, 912, 913, 914, and 915 to break, additional specimens of three different types of steel were inserted into the reaction tubes to gather what additional stress-rupture data could be obtained. The results obtained from these additional specimens are included in Table 2. Since the results from this preliminary test were not conclusive, it was decided to maintain different flow and pressure conditions in the four reaction chambers during the remainder of the test program with several samples of each steel being exposed to the various conditions.

On the basis of the data of the relation of stress to time to rupture in steam, as determined from the preliminary test, the second or regular test was started with eight specimens in each reaction tube. The results of this test are given in Table 3. Flow rates were adjusted to maintain laminar flow with a Reynolds number of 1100 in the reaction chambers containing steam at 5 psig, and turbulent flow with a Reynolds number of 5500 in the reaction chambers in which steam was used at 75 and 100 psig, as indicated in Table 3. Each time a specimen ruptured it was replaced by a new specimen. A complete history of each specimen including temperature, type of steam flow, stress, time to rupture, type and angle of fracture, elongation in area, etc., is given in Table 3. The stress-rupture results are plotted in Fig. 2, with stress as the ordinate and time to rupture as the abscissa on log-log co-ordinates.

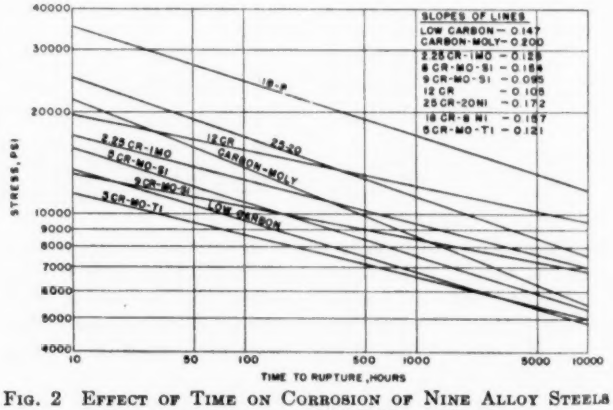


Fig. 2 Effect of Time on Corrosion of Nine Alloy Steels Exposed to Steam at 1200 F Under Stress

TABLE 2 RESULTS OF PRELIMINARY STRESS-RUPTURE TESTS

(Temperature: 1200 F ± 10 F)

Test No. 1
Test chamber *W* — Re = 1100, P = 130 psig
Test chamber *S* — Re = 5500, P = 130 psig
Test chamber *N* — Re = 5500, P = 75 psig
Test chamber *E* — Re = 1500, P = 5 psig

Spec. no.	Test chamber	Time for rupture, hr	Stress, psi	Elongation, ± 2 per cent	Reduction in area, ± 3 per cent	Depth of scale layer, in.	Type and angle of fracture D—Ductile B—Brittle
911	W	318	6900	88	77	0.0044	D — 45°
912	S	833	6900	79	63	0.0066	D — 45°
913	N	869	6900	104	71	0.0072	D — 45°
914	E	1010	6900	90	71	0.0105	D — 60°
915	W	545	6200	71	74	0.0049	D — 45°
916	S		Not broken				
917	N		Not broken				
918	E		Not broken				
711	W	159	14300	32	38	<0.0003	B — 90°
511	W	113	10800	89	81	0.0007	D — 80°
512	W	256	9600	68	82	0.0013	D — 85°
811	W	1305	16000	8	19	<0.0003	B — 90°

The elongation of the ruptured specimens is reported in Tables 2 and 3 as a percentage of the original length of the specimen and was determined by measuring with a pair of dividers the length of a straight section of each test specimen between two punch marks before insertion into the reaction chamber and repeating the measurement on the ruptured specimen with the two sections of the broken specimen placed as close together as possible in the positions they occupied prior to rupture.

The reduction-in-area data presented in Tables 2 and 3 are reported as the ratio of the difference between the original

TABLE 3 RESULTS OF STRESS-RUPTURE TEST NO. 2

(Temperature: 1200 F ± 10 F)

TEST NO. 2

SPECIMEN NUMBER	TIME FOR RUPTURE, HOURS	STRESS, PSI	ELONGATION, ±2%	REDUCTION IN AREA ±3%	DEPTH OF SCALE LAYER, INCHES	STEAM PRESSURE, PSIG	TYPE OF FLOW EXPOSED TO L-LAMINAR T-TURBULENT	TEMPERATURE	VISUAL DETERMINATION OF TYPE AND ANGLE OF FRACTURE D-DUCTILE I-INTERMEDIATE B-BRITTLE	INITIAL LENGTH OF TEST SECTION, INCHES	INITIAL DIAMETER OF TEST SECTION, INCHES
121	3588	5770	19	29	SCALE SHATTERED	75	T		B-45°	1.48	0.333
122	4671	4740	12	50		100	T		B-90°	1.63	0.366
126	10	12500	26	61	0.0047	5	L		D-45°	1.00	0.225
127M*	57	9500	37	66	0.0075	5	L		D-45°	1.15	0.259
128M	75	8200	24	59	0.0101	5	L		D-45°	1.24	0.279
129M	1261	7000	20	42	0.0367	100	T		B-80°	1.34	0.301
1210	27	16000	30	54	0.0045	5	L		I-90°	0.88	0.199
1211	857	6800	21	41	0.0288	5	L		B-45°	1.36	0.306
221	63	15200	32	46	0.0080	5	L		B-90°	0.91	0.204
222	151	12600	36	42	0.0124	5	L		B-60°	1.00	0.224
223	696	10700	20	29	0.0182	100	T		B-85°	1.08	0.243
224	253	9550	36	46	0.0218	5	L		B-70°	1.15	0.259
225	760	8400	20	47	0.0322	5	L		B-45°	1.23	0.276
226	3047	7800	13	35	0.0596	75	T		B-80°	1.27	0.285
227	1301	7400	23	41	0.0398	5	L		B-60°	1.30	0.292
228	7587	6900	16	47		75	T		B-80°	1.34	0.302
229		5900								1.47	0.329
2210	144	16000	20	40	0.0101	75	T		I-90°	0.88	0.199
2212M	312	9100	29	37	0.0208	5	L		B-90°	1.18	0.265
321	226	11300	62	89	0.0164	5	L		D-45°	1.05	0.236
322	1114	10400	45	80	SCALE SHATTERED	100	T		D-80°	1.10	0.247
323	2884	9200	21	70		5	T		D-45°	1.17	0.263
324		8600								1.21	0.271
325	1908	8400	41	89	SCALE SHATTERED	5	L		D-90°	1.23	0.276
326	1519	8400	61	88	SCALE SHATTERED	100	T		D-90°	1.23	0.276
327		7750								1.28	0.287
328	46	14400	49	89	0.0075	5	L		D-90°	0.94	0.210
329	50	13000	71	91	0.0079	5	L		D-60°	0.98	0.220
421	154	9550	117	91	0.0016	75	T		D-85°	1.15	0.259
422	209	8500	113	84	0.0058	5	L		D-60°	1.22	0.273
423	1237	7750	67	78	0.0069	100	T		D-45°	1.28	0.287
424	1709	7300	68	71	0.0088	75	T		D-45°	1.32	0.295
425	2522	6700	56	66		100	T		D-45°	1.37	0.308
426		6450								1.40	0.314
427		6400								1.41	0.316
428	4007	6100	60	56		100	T		I-45°	1.44	0.323
429	3613	5450	52	55		5	L		I-90°	1.52	0.341
4210	142	11000	158	89	0.0029	100	T		D-70°	1.07	0.240
4211	1166	7600	61	75		75	T		D-60°	1.29	0.289
4212M	1340	6900	82	65	0.0075	75	T		D-45°	1.35	0.303
521	56	12000	114	86	0.0006	5	L		D-90°	1.02	0.230
522	83	11000	85	84	0.0007	5	L		D-90°	1.07	0.240
523	287	9100	107	86	0.0013	5	L		D-80°	1.18	0.264
524	258	8600	155	84	0.0016	5	L		D-85°	1.21	0.272
525	1734	8300	95	81	0.0019	75	T		D-85°	1.23	0.277
526	1970	8300	84	78	0.0023	75	T		D-70°	1.23	0.277
527		7650								1.29	0.289
528	616	9100	87	83	0.0018	100	T		D-90°	1.18	0.265
529	946	8800	78	83	0.0016	100	T		D-90°	1.20	0.270
5210M	498	8100	94	82	0.0013	5	L		D-85°	1.25	0.280
621	164	15100	30	27	0.0007	5	L		B-90° CUP	0.91	0.205
622	624	13700	38	48	0.0008	100	T		B-90°	0.96	0.215
623	942	12300	43	54	0.0009	100	T		B-85°	1.01	0.226
624	260	11800	51	68	0.0009	5	L		I-80°	1.03	0.231
625	538	11000	53	71	0.0012	5	L		I-80°	1.07	0.240
626	2284	10700	68	81		75	T		D-90°	1.09	0.244
627	2792	10400	71	78		75	T		D-90°	1.10	0.247
628	2517	10000	59	79	0.0017	75	T		D-85°	1.12	0.252
629M	15	17750	58	92	0.0002	5	L		D-90°	0.85	0.190
6210	339	16100	30	46	0.0011	100	T		I-70°	0.88	0.198
6211	899	13000	20	53		100	T		I-80°	0.98	0.220
6212M	569	11700	57	88	0.0012	75	T		D-85°	1.03	0.232
721	937	12500	58	36	> 0.0001	75	T		B-90°	1.00	0.224
722	1552	9950	75	49	> 0.0001	100	T		B-90°	1.13	0.253
723	3810	8400	70	42		5	L		B-90°	1.23	0.276
724	107	17000	49	31	> 0.0001	5	L		B-90° CUP	0.86	0.193
725	177	15300	40	41	> 0.0001	5	L		B-80°	0.90	0.203
726	977	11000	64	44	> 0.0001	75	T		B-90°	1.07	0.240
821	263	19000	36	33	> 0.0003	5	L		B-85°	0.81	0.183
822	7720	14000	15	11		75	T		B-85°	0.95	0.213
823M	151	22600	28	31	> 0.0003	5	L		B-90°	0.75	0.168
824	15	33400	23	25	> 0.0003	5	L		B-90° CUP	0.61	0.138
825	45	27600	51	38	0.0008	5	L		B-90°	0.68	0.152
826	1145	17000	43	31	0.0013	75	T		B-80°	0.86	0.193
921	182	9400	83	71	0.0038	100	T		D-45°	1.26	0.260
922	291	7000	81	66	0.0088	5	L		D-45°	1.34	0.301
923	2606	6300	77	61	0.0102	75	T		I-45°	1.42	0.318
924	3109	5950	52	49		75	T		B-45°	1.46	0.328
925	55	9700	61	70	0.0049	5	L		D-45°	1.14	0.256
926	288	8000	55	59	0.0084	5	L		I-?	1.25	0.281
927	1100	7000	45	49		100	T		I-45°	1.34	0.301

ALL TEMPERATURES 1200F ± 10F

*THE LETTER "M" REFERS TO A SPECIMEN WHOSE TEST SECTION WAS MACHINED FROM A PREVIOUSLY TESTED UNBROKEN SPECIMEN (SEE DISCUSSION OF RESULTS)

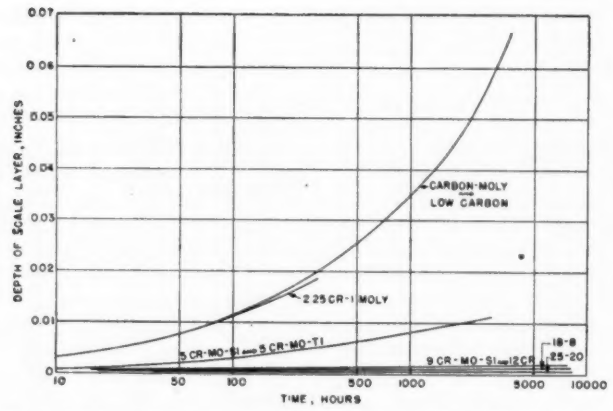


FIG. 3 STRESS-RUPTURE CHARACTERISTICS OF NINE ALLOY STEELS IN STEAM AT 1200 F

and final areas to the original area in per cent and are based on a measurement of the original diameter of the specimen by a micrometer and a measurement of the final diameter, not including the scale layer, by a pair of dividers.

Due to the size and shape of the specimens it was not possible to determine the loss of metal due to corrosion by electrolytic stripping as was used in previous corrosion studies (1, 2, 3, 4, 5)[5] at Purdue University. Some of the specimens were exposed to the steam for a short time interval, thereby producing a thin layer of oxide which could not be removed by the electrolytic stripping method. For the small specimens used in these stress tests a satisfactory method of determining the penetration of the scale layer was developed. A small section of the scale-covered ruptured specimen approximately 1/4 in. long was cut off by means of a cut-off wheel. This section was molded in bakelite and polished. By means of a precision microscope it was possible to measure the thickness of the scale layer quite accurately. The results of the corrosion measurements are given in Tables 2 and 3, and in Fig. 3.

DISCUSSION OF RESULTS

The slopes of the stress versus time-to-rupture lines for the various alloys, as plotted in Fig. 3, are as follows: Low carbon, 0.147; carbon-moly, 0.200; 2 1/4 Cr-1 Mo, 0.128; 5 Cr-Mo-Si, 0.154; 9 Cr-Mo-Si, 0.095; 12 Cr, 0.105; 25 Cr-20 Ni, 0.172; 18 Cr-8 Ni, 0.157; and 5 Cr-Mo-Ti, 0.121. The significance of these various slopes is that a steel with a large slope would not be expected to have a high rupture stress for long time intervals such as 100,000 hr. Table 4 presents the stress required to rupture each of the steels for time intervals of 10, 1000, and 10,000 hr.

Of the nine steels tested, carbon moly is sixth in order at 10,000 hr, whereas it was third at 10 hr. 9 Cr-Mo-Si was eighth at 10 hr, is fifth at 10,000 hr and would be third at 100,000 hr if the straight-line relationship continued to hold.

In general, the stress required for rupture in a given time in an atmosphere of steam at 1200 F is higher than the stress required for rupture in the same time in air at 1200 F, the air values being taken from the data of the Timken investigators (6, 7, 8). The nine alloys which were included in this investigation are listed in Table 5, in the order of decreasing magnitude of the differences between the stress in steam and the stress in air required for rupture in 10,000 hr. The magnitude of the ratio of stress in steam to stress in air is indicated following each alloy.

[5] Numbers in parentheses refer to the Bibliography at the end of the paper.

TABLE 4 STRESS REQUIRED TO CAUSE RUPTURE OF VARIOUS ALLOY STEELS AT 1200 F

	In 10 hr		In 1000 hr		In 10,000 hr[a]	
(1)	18 Cr-8Ni	35000	18 Cr-8 Ni	16800	18 Cr-8 Ni	11600
(2)	25 Cr-20Ni	25000	12 Cr	12000	12 Cr	9400
(3)	Carbon-moly	21500	25 Cr-20 Ni	11200	25 Cr-20 Ni	7550
(4)	12 Cr	19500	2 1/4 Cr-1 Mo	9400	2 1/4 Cr-1 Mo	7000
(5)	2 1/4 Cr-1Mo	17000	Carbon-moly	8600	9 Cr-Mo-Si	6800
(6)	5 Cr-Mo-Si	15500	9 Cr-Mo-Si	8500	Carbon-moly	5450
(7)	Low carbon	13500	5 Cr-Mo-Si	7600	5 Cr-Mo-Si	5300
(8)	9 Cr-Mo-Si	13200	Low carbon	6900	5 Cr-Mo-Ti	5000
(9)	5 Cr-Mo-Ti	11500	5 Cr-Mo-Ti	6700	Low carbon	4900

[a] Extrapolated.

TABLE 5 DIFFERENCES BETWEEN STRESS IN STEAM AND STRESS IN AIR REQUIRED FOR RUPTURE IN 10,000 HR OF VARIOUS ALLOYS

	Type of steel	Ratio of stresses in steam to air
1	Low carbon	3.6
2	12 Cr	3.2
3	Carbon moly	1.8
4	25 Cr-20 Ni	1.4
5	5 Cr-Mo-Si	1.2
6	18 Cr-8 Ni	1.2
7	2.25 Cr-1Mo	1.2
8	9 Cr-Mo-Si	1.1
9	5 Cr-Mo-Ti	0.98

The results of the attempt to determine the effect of turbulent or streamline flow upon the stress-rupture results were inconclusive and no definite conclusions could be drawn concerning this effect.

The results of the measurement of the thickness of the scale layers are given in Tables 2 and 3, and in Fig. 3. As in previous tests at Purdue University (1, 2, 3, 4, 5), the chromium content of the alloy is the critical factor in the determination of the depth of corrosion. The alloys can be divided into four general groups relative to the type and extent of corrosion. The two alloys, low carbon and carbon-moly, show serious corrosion, having a thick, porous but tightly adhering layer of scale. Alloys 2 1/4 Cr-1Moly, 5 Cr-Mo-Si, and 5 Cr-Mo-Ti show appreciable corrosion and have a brittle flaky layer of scale. Alloys 9 Cr-Mo-Si and 12 Cr exhibit a slight amount of corrosion, while the corrosion of alloys 18 Cr-8 Ni and 25 Cr-20 Ni is very slight. It is to be noted that the corrosion results of the stress-rupture tests cannot be directly compared to the corrosion results obtained previously at Purdue University (1, 2, 3, 4, 5), since in the previous tests the results were reported as penetration in inches as computed from measured loss of metal, whereas in the stress-rupture tests the results are reported as depth of scale layer on the ruptured specimen. An examination of the data reveals no correlation between type of steam flow and depth of scale layer.

A comparison of the types and characteristics of the fractures of the various alloys is of considerable interest in that it gives some indication of the type of fracture that can be expected in service. A discussion of the fracture of each alloy will be given. A metallographic study was made of the original microstructure and the microstructure of two fractured specimens of the longest and shortest fracture time and the following comments are a result of these studies:

(*a*) Low-Carbon Steel (Alloy No. 1). Of the eight specimens tested, three had ductile fractures, four had brittle fractures, and one had an intermediate fracture. However, the values of ductility as measured by elongation were consistently low (from 12 to 37 per cent) with the ductile fractures giving the greater elongation. By an intermediate fracture is meant a fracture with just a slight amount of necking at the break as compared to no perceptible necking for a brittle fracture and considerable necking for a ductile fracture. This method of classification holds for all nine alloys. The three low-carbon specimens with the ductile fractures, 126, 127M, and 128M, and the one with the intermediate fracture, 1210, had the largest elongation and reduction of area at rupture. The short-time ductile fracture of specimen

126 was characterized by stretching of the grains while the long-time brittle intergranular fracture of specimen 121 was characterized by the remaining equi-axed grains pulling apart at the grain boundaries. In both the long- and short-time specimens a dark intergranular material appeared which was probably an oxidation product together with voids resulting from parting of the grains. Spheroidization of the carbides present in the original sample occurred in both the long- and short-time specimens of this alloy with considerable agglomeration of the spheroids present in the long-time specimen.

No clearly defined graphite was detected in the structure of the specimens.

(*b*) Carbon-Moly (Alloy No. 2). All of the carbon-moly specimens had the brittle type of fracture except specimen 2210 which showed a slight amount of necking and was classified as having an intermediate fracture. All of the specimens had low values of ductility as measured by elongation (13 to 36 per cent). As in the case of the low-carbon alloy, the only appreciable change in the microstructure was general spheroidization of the carbide structure. Very little agglomeration was present in the microstructure of the short-time specimen, 221, the original normalized structure still being somewhat in evidence. Considerable agglomeration of the carbides was present in the long-time specimen, 226. Parting of the grains had occurred in both specimens 221 and 226, but to a greater extent in the short-time specimen 221. This parting resulted in intergranular fracture for both the long- and short-time intervals and also resulted in the presence of dark areas between the grains, probably consisting both of oxidation product and voids.

No clearly defined graphite was observed in the microstructure of the carbon-moly specimens.

(*c*) 2¼ Cr-1 Mo (Alloy No. 3). In contrast to the carbon-moly steel, all of the specimens of 2¼ Cr-1 Mo steel had the ductile type of fracture as evidenced by the higher values of ductility as measured by elongation (21 to 71 per cent). Without exception, all of the specimens necked considerably at the break, resulting in high values for reduction in area. Another peculiarity of this alloy was the very brittle flaky type of scale which curled away from the parent metal as the corrosion progressed, thus continuously leaving fresh metal exposed to the steam. Due to the excessive necking at the break, the metal there should have been very highly strained. The microstructure of the short-time specimen 328 showed considerable elongation of the grains. The microstructure of the fractured specimens showed coalescence of the carbides which were present in the original steel before testing. The degree of coalescence was considerably higher in the long-time specimen 325 than in the short-time specimen 328. The specimens showed more than normal inclusions which, however, did not appear to be graphite when examined unetched. Since there was evidence of some inclusions in the original microstructure of this steel, it is not believed that the inclusions present in the microstructure of the fractured specimens is due to any appreciable extent to oxidation and stress. This steel is to be contrasted to the low-carbon and carbon-moly steels which did show parting of the grains and a resultant dark constituent at the grain boundaries.

(*d*) 5 Cr-Mo-Si (Alloy No. 4). This alloy was characterized by a very ductile fracture resulting in high values for elongation and reduction in area, the values of elongation ranging from 52 to 158 per cent. The surface of the scale was lined with deep cracks but the scale itself adhered very tightly to the parent metal. The comments made concerning the microstructure of 2¼ Cr-1 Mo steel (Alloy No. 3) in paragraph (*c*) apply equally well to the microstructure of Alloy No. 4, that is, the amount of inclusions did not increase over those present in the unstressed steel, no clearly defined graphite was detected, and coalescence of the carbides originally at the grain boundaries occurred.

(*e*) 9 Cr-Mo-Si (Alloy No. 5). This alloy was also characterized by high values of elongation (from 68 to 155 per cent) and reduction in area which indicated a ductile fracture. The fracture specimens were covered with a smooth tightly adhering layer of scale which was lined with a fine network of cracks. Photomicrographs of the microstructure of this alloy indicated that the only significant change was an increasing degree of agglomeration of the carbide spheroids with time under the test conditions. In the long-time specimen, 526, a preferred orientation and stretching of the spheroids and other elements of the microstructure could be detected.

(*f*) 12 Cr (Alloy No. 6). The fractures for this alloy varied considerably. Of the twelve specimens tested there were three with brittle fractures, five with ductile fractures and four with intermediate fractures. The ductility as measured by elongation was fairly low, ranging from 20 to 71 per cent. The scale formed on fractured specimens of this alloy resembled very closely that formed on specimens of Alloy No. 5 (9 Cr-Mo-Si). There was practically no change in the microstructure of specimens of this alloy except for enough agglomeration of the carbide spheroids to make them appear to have a uniform and random distribution, whereas in the original structure the outline of the austenitic grains was indicated by the chain of spheroids.

(*g*) 25 Cr-20 Ni (Alloy No. 7) and 18 Cr-8 Ni (Alloy No. 8). Both of these alloys were characterized by very brittle fractures for both the long- and short-time intervals, resulting in low values for reduction in area and elongation. The values for elongation for the fractured specimens of 18 Cr-8 Ni ranged from 8 to 51 per cent while those for 25 Cr-20 Ni were a little higher, ranging from 32 to 75 per cent. Specimens of these alloys were covered with a thin film of scale which visually appeared to be thicker on the stressed test section than on the relatively unstressed part of the specimen. The only noticeable change in the microstructure of the 25 Cr-20 Ni specimens was the growth and coalescence of the carbides and of the peculiar black phase which has been reported by other investigators (9). The exact identity of this black phase is not yet known. The short-time specimen, 824, of 18 Cr-8 Ni which was very highly stressed (33,400 psi), resulting in a very short time to rupture (15 hr), suffered a decided change in grain size; the grain size for the ruptured specimen being much smaller than that of the original structure. Considerable carbide precipitation at the grain boundaries and inside the grains appears to have taken place. Also, the black phase which is known to appear in 25 Cr - 20 Ni steel as just described appears to be present in the microstructure of the long-time specimen, 826, of the 18 Cr - 8 Ni alloy. It is doubtful that this black phase is graphite since chromium is known to be a very effective inhibitor of graphitization and the carbon content of this steel is only 0.06 per cent.

(*h*) 5 Cr-Mo-Ti (Alloy No. 9). This alloy tended to be somewhat erratic in its behavior. Referring to Tables 2 and 3 it can be seen that of the twelve specimens tested, eight had ductile fractures, three had intermediate fractures, and one had a brittle fracture. However, it should be noticed that the one brittle fracture was the longest time specimen, 924, whose time to rupture was 3109 hr and whose value of elongation was 52 per cent. The values for elongation (45 to 104 per cent) and reduction in area tended to be somewhat lower than those for Alloy No. 4 (5 Cr-Mo-Si), an alloy differing only in the content of Si and Ti. The scale formation was identical to that of Alloy No. 4, the specimens having a fairly thick layer of scale heavily lined with deep cracks. The only appreciable change in microstructure was spheroidization of the carbides which were originally present at the grain boundaries.

Referring again to the data in Tables 2 and 3 concerning the measurements of reduction in area and elongation, it would appear that the relative ductility of the nine alloys as measured by these two methods is not the same. For example, Alloy No. 3 (2¼ Cr-1 Mo) has relatively low ductility as measured by per cent elongation, but as measured by per cent reduction in area, as a group it has the highest ductility. The authors are of the opinion that per cent elongation is the safest indication of ductility because it is a measure of ductility over a longer period of time. Again taking Alloy No. 3 as an example, the high values of reduction in area are due simply to the fact that the specimens necked down considerably before actual rupture, which probably took place during the last few minutes of the life of the specimen.

The carbon steels tested, i.e., low-carbon (Alloy No. 1) and carbon-moly (Alloy No. 2), corroded excessively so that the reduction-in-area values could be attributed both to mechanical shrinkage due to the stress and loss of metal due to corrosion.

It can be seen in examining Tables 2 and 3 that for all of the alloys tested the values of elongation tend to be less when the brittle-type fracture occurs. A good example is Alloy No. 6 (12 Cr) in which the five specimens with the highest values of elongation all had ductile fractures while the specimens with intermediate and brittle fractures all had lower values of elongation. For the other alloy which had all types of fracture, Alloy No. 9 (5 Cr-Mo-Ti), the only specimen with a brittle fracture had the second lowest value of ductility as measured by elongation.

For all of the nine alloys taken as a whole no satisfactory correlation between time to rupture and either elongation or reduction in area could be obtained.

An examination of the microstructure of all the alloys revealed no clearly defined graphite in any case. An extensive study was made of the three alloys most likely to be susceptible to graphitization, low-carbon, carbon-moly and 2¼ Cr-1 Mo, by the research department of The Detroit Edison Company (13). They reported that while each of the steels responded "abnormal" to the McQuaid-Ehn test, no clearly defined graphite was found in any of the samples examined.

Conclusion

1 The straight-line relationship between stress and time to rupture on log-log co-ordinates, postulated by White, Clark, and Wilson, for tests in air (9) also holds for tests in steam.

2 The break in the stress-rupture line encountered in air tests by other investigators (9, 10) was not found in the present tests in steam.

3 The tests indicate that for the small specimens of the nine alloys tested the stress required for rupture in steam in 10,000 hr or longer is higher than the stress required in air at 1200 F.

4 The type and characteristics of the scale formed on the stress-rupture specimens affects the position of the stress-rupture line on log-log co-ordinates.

5 The slope of the stress-rupture line is important since an alloy whose stress-rupture line on log-log co-ordinates has a low value of slope might not appear to be desirable at short rupture times, but for long rupture times might be better than other alloys which were superior at short rupture times.

6 Ductility values, as measured by per cent elongation, are more reliable values for ductility over a long period of time than are ductility values as measured by reduction in area. Also reduction-in-area values are more affected by the amount of corrosion.

7 For the two austenitic alloys tested, the fractures were the brittle type, even for short time intervals.

8 In general, the ductility, as measured by elongation for all of the alloys tested tends to decrease as the time to rupture increases.

9 Longer times and lower stresses are favorable for the production of brittle fractures.

10 The tests confirm the conclusion based on air tests (11), that elongation for a given steel is always less when the brittle fracture occurs.

11 As in unstressed tests, the chromium content of the alloy is the critical factor in determining the amount of corrosion taking place. The corrosion decreases as the chromium content increases.

Acknowledgments

The authors wish to express their appreciation to the following for their co-operation in the preparation and the analysis of the microstructures of the fractured specimens: Dr. C. L. Clark of the Timken Roller Bearing Company, Canton, Ohio; Dr. H. K. Ihrig of the Globe Steel Tubes Company, Milwaukee, Wis.; Mr. C. H. Fellows and Mr. I. A. Rohrig of The Detroit Edison Company, Detroit, Mich.; Mr. J. P. Magos, Mr. N. A. Ziegler, Mr. J. J. Kanter, and Mr. W. L. Meinhart of Crane Company, Chicago, Ill.; and Mr. R. J. Raudebaugh, Assistant Professor of Metallurgical Engineering, Rochester University, Rochester, N. Y.

BIBLIOGRAPHY

1 "Investigation of the Oxidation of Metals by High-Temperature Steam," by A. A. Potter, H. L. Solberg, and G. A. Hawkins, Trans. A.S.M.E., vol. 59, 1937, pp. 725–732.

2 "Corrosion of Unstressed Steel Specimens and Various Alloys by High-Temperature Steam," by H. L. Solberg, G. A. Hawkins, and A. A. Potter, Trans. A.S.M.E., vol. 64, 1942, pp. 303–316.

3 "Corrosion of Unstressed Specimens of Alloy Steels by Steam at Temperatures Up to 1800 F," by G. A. Hawkins, H. L. Solberg, J. T. Agnew, and A. A. Potter, Trans. A.S.M.E., vol. 65, 1943, pp. 301–308.

4 "The Corrosion of Alloy Steels by High-Temperature Steam," by G. A. Hawkins, J. T. Agnew, and H. L. Solberg, Trans. A.S.M.E., vol. 66, 1944, pp. 291–295.

5 "The Corrosion of Stressed Alloy-Steel Bars by High-Temperature Steam," by H. L. Solberg, A. A. Potter, G. A. Hawkins, and J. T. Agnew, Trans. A.S.M.E., vol. 65, 1943, pp. 47–52.

6 Digest of Steels for High-Temperature Service, Fourth edition, The Timken Roller Bearing Company, Canton, Ohio.

7 Résumé of High Temperature Investigations Conducted During 1940–1941, The Timken Roller Bearing Company, Canton, Ohio.

8 Résumé of High Temperature Investigations Conducted During 1941–1942, The Timken Roller Bearing Company, Canton, Ohio.

9 Résumé of High Temperature Investigations Conducted During 1943–1944, The Timken Roller Bearing Company, Canton, Ohio.

10 "The Fracture of Carbon Steels at Elevated Temperatures," by A. E. White, C. L. Clark, and R. L. Wilson, Trans. American Society for Metals, vol. 25, Sept., 1937, pp. 863–888.

11 "The Rupture Strength of Steels at Elevated Temperatures," by A. E. White, C. L. Clark, and R. L. Wilson, Trans. American Society for Metals, vol. 26, March, 1938, pp. 52–80.

12 "Fracture of Steels at Elevated Temperatures after Prolonged Loading," by R. H. Thielemann and E. R. Parker, Trans. A.I.M.E., vol. 135, 1939, pp. 559–582.

13 Determination of the Normality and Extent of Graphitization of Three Different Steels After Stress-Rupture Test in 1200 F Steam. Research Department Report 9063, I. A. Rohrig, Oct. 24, 1945.

Discussion

Arthur McCutchan.[6] The steam-corrosion work at Purdue has been followed with great interest. The stress rupture characteristics of various steels in steam should be of particular value to designers of high-temperature equipment. The choice of 1200 F as the test temperature doubtless was made on the basis of accelerating the scaling effect. Since the field of usefulness

[6] Engineer, Engineering Division, The Detroit Edison Company, Detroit, Mich. Jun. A.S.M.E.

of the low-carbon and carbon-moly steels will, in general, be below 1000 F, and the $2^1/_4$ per cent chrome-moly steel below 1100 F it is of importance to recognize that in some cases the higher temperature of test may give a false indication of the relative value of these materials for high-temperature service.

Through the co-operation of Professor Solberg, a number of the ruptured specimens of low-carbon, carbon-moly and $2^1/_4$ per cent chromium, 1 per cent molybdenum steels were examined for graphite by I. A. Rohrig of The Detroit Edison research department. Despite the fact that all were found to be "abnormal" in their response to the McQuaid-Ehn test, no graphite was reported. Since, in abnormal low-carbon and carbon-moly steels, graphite is readily produced by heating for 1000 hours or less at 1000 to 1100 F, failure to produce graphite in heating periods of 4000 to 7000 hours at 1200 F might be considered unusual. It has been hazarded that the AC_1 temperature of these materials might be lowered sufficiently in the presence of stress so that 1200 F is above the temperature at which graphite tends to precipitate.

Because of the possible precipitation of graphite, particularly at welded joints, the long-time load-carrying ability at, say, 1000 F of the low-carbon and carbon-moly steels is much less than that of the $2^1/_4$ per cent chromium, 1 per cent molybdenum steel. It would seem therefore that the stress rupture data which are given in this paper should be considered as directly applicable only at 1200 F.

On the basis of a rupture time of about 1200 to 1500 hours it is of interest to note the relatively high stress supported by the low-carbon steel in 1200 F steam. The stresses supported by the several materials were as follows:

STRESS CAUSING RUPTURE IN 1200 TO 1500 HOURS IN 1200 F STEAM

	Specimen	Stress, psi
Low carbon steel	129 M	7000
Carbon molybdenum	227	7400
$2^1/_2$ per cent chromium, 1 per cent molybdenum	326	8400

The authors' conclusions regarding the tendency to intergranular fractures are particularly noteworthy. The point that longer times and lower stresses are favorable for the production of brittle intergranular fractures of many creep-resistant steels is not always appreciated. The ductile type of fracture of the $2^1/_4$ per cent chromium — 1 per cent molybdenum steel would seem to be a count in its favor.

Authors' Closure

The authors wish to thank Mr. McCutchan for his interesting discussion. It is true that the temperature of 1200 F is severe for low-carbon, carbon-moly, and $2^1/_4$ Cr-1 moly steels, but it is felt that the data will be applicable in the future when steam temperatures in power plants and other industrial apparatus become higher.

Also it should be pointed out that the effects of specimen size and type and characteristics of the scale formed in a steam atmosphere are two variables which are yet to be thoroughly investigated.

Effect of Molding Pressure and Resin on Results of Short-Time Tests and Fatigue Tests of Compreg

By W. N. FINDLEY,[1] W. J. WORLEY,[2] and C. D. KACALIEFF[3]

Tests were performed on six samples of compressed-impregnated plywood, including static tension tests, static compression tests, static torsion tests, and rotating-beam type of fatigue tests. The results provide data on the effect of different molding pressures and different resins on the "static" strength properties, stiffness, and fatigue strength of "compreg."

THE tests reported in this paper were undertaken in order to provide information on the effect of different molding pressures and different resins on the "static" strength properties, stiffness, and fatigue strength of compressed-impregnated plywood (compreg).

The following tests were performed on six different samples (described later) at a temperature of 77 F and a relative humidity of 50 per cent: Static tension tests, static compression tests, static torsion tests, and rotating-beam-type fatigue tests. All specimens were cut with their long axis parallel to the grain of the wood used in making the compreg. Values of ultimate strength, yield strength, and modulus of elasticity were obtained from all of the static tests. The fatigue tests were carried out as far as 10,000,000 cycles.

Several investigators have reported the static properties (1–9)[4] of compreg and some other investigators have studied fatigue characteristics (10, 11) of this type of material.

Material Used for Tests

Six compreg panels were prepared especially for this series of tests by the United States Forest Products Laboratory, Madison, Wis. The panels were made from rotary-cut sap yellow-birch wood of 1/16-in. plies. All veneers were from the same shipment and met the grain requirements of Army Air Forces Specification 15065. Prior to laminating, the 1/16-in. birch veneers were cylinder-treated for 6 hr in the case of the water-soluble resin and 16 hr in the case of the alcohol-soluble resin at 75 psi and dried for 18 hr at 130 F. All plies were glued on one face with Bakelite XC7381 resin, using 6.7 g of dry glue per sq ft of glue line; all panels were pressed at the indicated pressure (see Table 1) under conditions such that the center of each panel was held at 305 to 310 F for 15 min. All panels were cooled to 150 F in the press before releasing the pressure. The data in Table 1 were prepared by the Forest Products Laboratory. As shown in the table, three different resins, *A*, *B*, and *C* were used, and two panels were made with each resin. One panel for each resin was molded at 1500 psi; the other panel for each resin was molded at 600 psi.

TABLE 1 FOREST PRODUCTS LABORATORY DATA

Panel number	204	205	206	207	208	209
Type of resin[a]	*A*	*A*	*B*	*B*	*C*	*C*
Resin content,[b] per cent	28.5	28.0	31.5	32.0	28.0	28.5
Number of plies	17	15	17	15	17	15
Bonding pressure, psi	1500	600	1500	600	1500	600
Specific gravity	1.36	1.22	1.36	1.24	1.37	1.24
Shear parallel to laminations,[c] psi	4840	3640	4450	4230	4340	3620
Izod,[d] ft-lb per in. notch	10.0	8.3	7.8	6.1	9.4	6.6
Water absorption,[e] per cent	3.0	7.0	1.7	5.0	2.0	6.7
Swelling,[f] per cent	14.2	13.9	9.7	9.9	11.5	12.2
Residual swelling,[g] per cent	2.90	2.97	1.87	2.22	2.28	2.00

[a] Resin *A* Bakelite BV 10678 (alcohol-soluble) by Bakelite Corporation, Bloomfield, N. J.
Resin *B* Bakelite BV 15100 (water-soluble) by Bakelite Corporation, Bloomfield, N. J.
Resin *C* Compregnite (water-soluble) by Casein Company of America, Bainbridge, N. Y.

[b] Resin content on basis of dry weight of untreated wood.

[c] Shear tests made by Forest Products Laboratory block-shear method in plane of laminations.

[d] Izod values calculated from notched-toughness values, using empirical conversion factor obtained from Izod and notched-toughness tests on matched specimens.

[e] Measurements made according to Army Air Forces specifications No. 15065 on 3 in. × 1 in. × 3/4-in. specimens (1 in. in fiber direction), immersed in water for 24 hr.

[f] Specimens were cut the full thickness of the panel and 1/8 in. long in the direction of the grain. The specimens were immersed in water for 48 hr at room temperature and were measured in the direction of the thickness of the original panel before and after immersion.

[g] Thickness of specimens used for swelling tests after subsequent air-drying and oven-drying, expressed as a percentage of the thickness of a matched specimen subjected to the same drying cycle but not to the water immersion. The "thickness" measured was in the direction of the thickness of the original sheet.

The test panels were made from large sheets of veneer from which six matched panels were laminated with the grain of all plies parallel. The six panels were matched with two crosswise of the grain and three lengthwise of the grain.

Additional data shown in Table 1 include the percentage resin content, the code number for the resin, number of plies used in the panel, the specific gravity, the shear strength parallel to the laminations, the impact strength (expressed as an equivalent Izod test), percentage water absorption, percentage swelling, and percentage recovery after wetting.

Preparation of Specimens

A drawing of the "static" specimens used in this investigation is shown in Fig. 1, and the fatigue specimen is shown in Fig. 2. All specimens were cut from the panel with their long axis parallel to the grain of the wood. All specimens were machined on a lathe and were finished by polishing with grade 2/0 emery paper. Some of the tension specimens were machined with a straight cylindrical portion and used for stress-strain data; other of these specimens were machined with a reduced section or neck at the center of the gage length and were used to determine the ultimate strength of the compreg in tension.

The compression specimens were turned on a lathe to the two lengths shown in Fig. 1(*c*). The 2-in. specimen was used as shown in Fig. 6, to obtain stress-strain relationships. The short specimen was used to obtain ultimate-strength values only. The torsion specimens were also made by turning on a lathe.

[1] Assistant Professor of Theoretical and Applied Mechanics, College of Engineering, University of Illinois, Urbana, Ill. Jun. A.S.M.E.

[2] Instructor in Theoretical and Applied Mechanics, College of Engineering, University of Illinois. Jun. A.S.M.E.

[3] Research Assistant in Theoretical and Applied Mechanics, College of Engineering, University of Illinois.

[4] Numbers in parentheses refer to the Bibliography at the end of the paper.

Contributed by the Rubber and Plastics Division and presented at the Annual Meeting, New York, N. Y., Nov. 26–29, 1945, of The American Society of Mechanical Engineers.

Note: Statements and opinions advanced in papers are to be understood as individual expressions of their authors and not those of the Society.

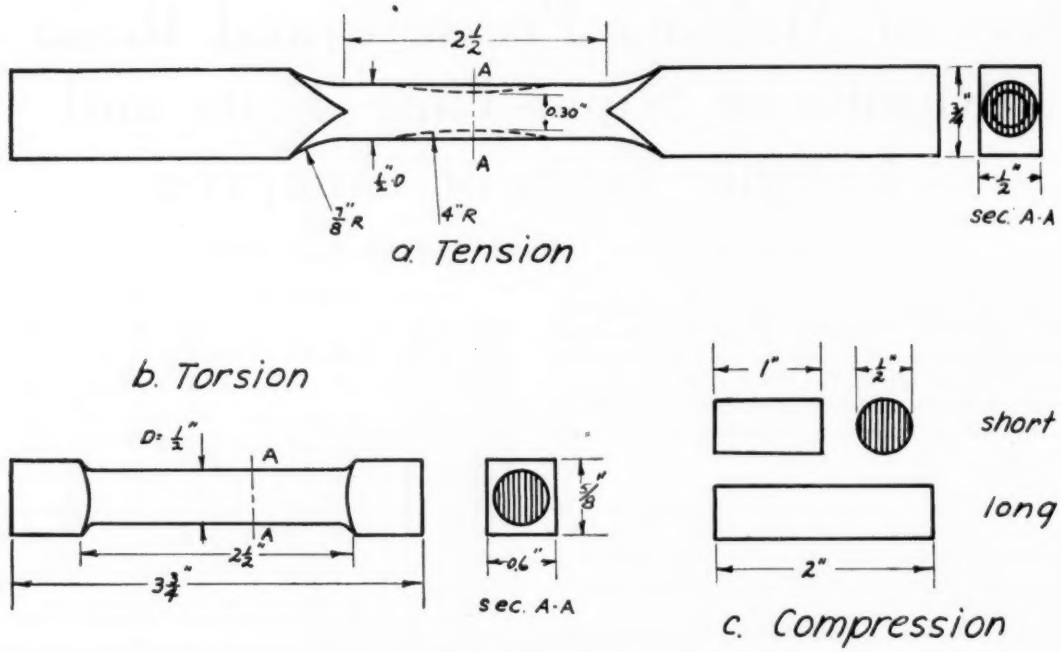


FIG. 1 STATIC SPECIMENS USED IN TEST

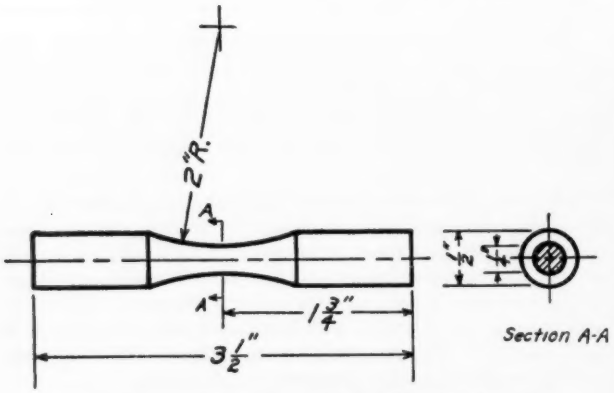


FIG. 2 ROTATING-CANTILEVER-BEAM FATIGUE SPECIMEN

The machining of all specimens was done in a laboratory maintained at constant temperature and constant relative humidity. After the specimens were completed, they were allowed to remain in this room, which was maintained at a constant temperature of 77 ± 1 deg F and constant relative humidity of 50 ± 2 per cent, for at least 2 weeks before the tests were started.

TENSION TESTS

Short-time tension tests were performed on specimens as shown in Fig. 1(*a*). These specimens were tested in tension on an Olsen 10,000-lb four-screw machine, of the beam-weighing type, equipped with a separate variable-speed drive. The specimens were held in Templin wedge grips *A*, Fig. 3, mounted in such a way as to provide an axial load on the specimen. Strain of the specimen was measured by means of a Moore-Hayes 2-in-gage-length extensometer *B*, Fig. 3. This instrument provided a multiplication such that one division on the dial indicated a strain of 0.0001 in. per in. in the specimen. In order that these specimens need not support the weight of the extensometer and to prevent damage to the instrument if the specimen should fracture while the extensometer was attached, the extensometer

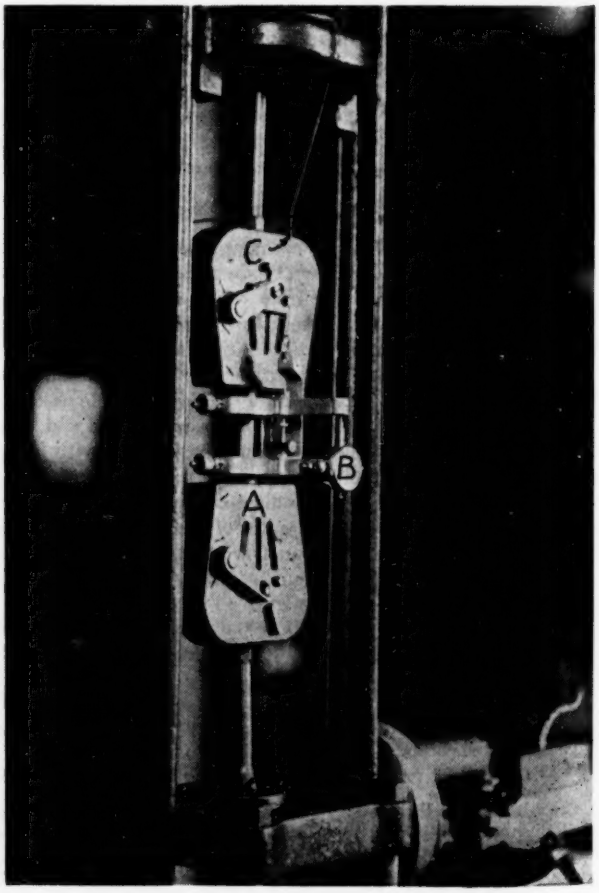


FIG. 3 TENSION APPARATUS

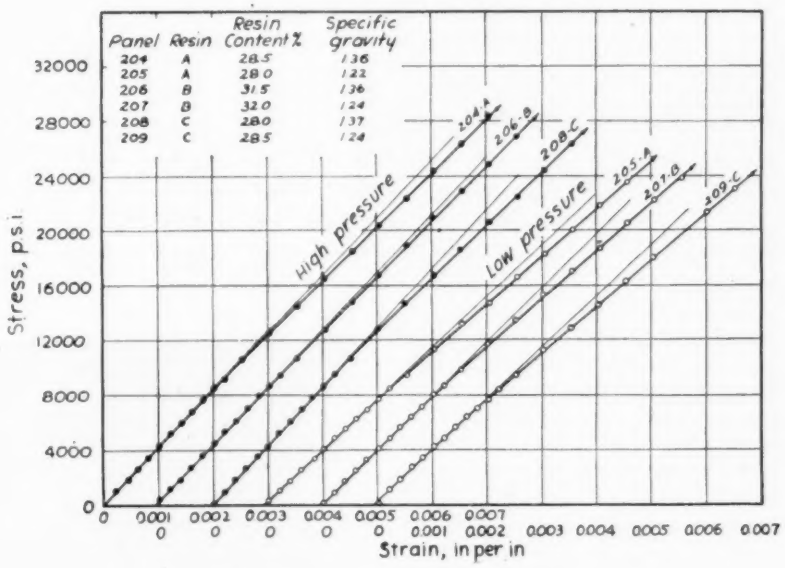


FIG. 4 TENSION TESTS OF COMPREG

was supported by means of the light coil spring C, shown in Fig. 3.

Two sets of tension tests were run; one set in which the stress-strain characteristics were determined, and the other set in which only the ultimate strength was obtained. In the former group the gage section of the specimen was straight and readings of load, deformation, and time were simultaneously obtained "on the run" throughout the test. In the latter case only the load at fracture was recorded. For this purpose the specimens were necked down by turning on a lathe to a 4 in. radius. This was accomplished by rotating the compound of the lathe. These specimens were reduced from $^1/_2$ in. diam at the end of the test section to $^9/_{10}$ in. diam at the center. This reduction was found necessary in order to cause the specimen to fail at the center of the test section rather than in the shoulder of the specimen. Straight specimens failed at the shoulder as a result of the stress concentration.

A preliminary test was made to determine the testing speed required to produce a rate of tensile strain of about 0.0016 in. per in. per min. All succeeding tests were run at or near this rate of strain. This rate was selected in order to permit correlation between the results of these tests and tests performed by the authors on other material (12). This rate of strain corresponds roughly to the rate of strain produced by testing machines operated at a head speed of 0.05 in. per min. However, it should be noted that different machines, and even different materials tested in the same machine at the same rate of crosshead motion will not in general produce the same rate of strain in the specimen. This is due to different relative stiffnesses of the machine, specimen, and auxiliary gripping apparatus.

The rate of strain was made uniform in these tests rather than the rate of increase of stress as used by some investigators, because the same rate of strain can be used without difficulty in testing materials which differ widely in modulus of elasticity, whereas if such materials are tested at the same rate of stressing, the required testing-machine speeds become excessive for materials of low modulus, and the rate of strain becomes too high to follow with ordinary equipment.

Both the tension and the compression tests were performed outside of the air-conditioned laboratory. The temperature of the testing room was about 75 F, and the relative humidity was variable. In order to minimize the effect of differences in temperature and relative humidity, the specimens were placed in an insulated box while being transferred from the conditioned storeroom to the laboratory, and the tests were conducted within 5 to 10 min after the specimen was removed from the insulated box. During the test, readings of load, deformation, and time were recorded up to a point within a few per cent of the load at which failure was expected. The extensometer was removed before failure.

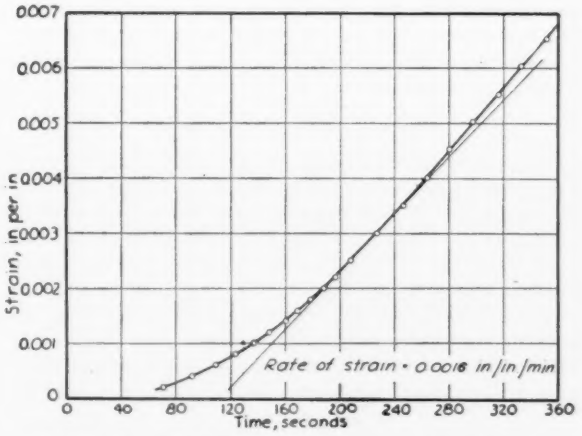


FIG. 5 STRAIN-TIME CURVE OF COMPREG IN TENSION

From these data the stress and strain were computed. Then diagrams of stress versus strain, Fig. 4, and strain versus time, Fig. 5, were plotted. The modulus of elasticity was determined in each case from the slope of the initial part of the stress-strain curve. The yield strength[5] at 0.05 and 0.2 per cent offset could not be determined owing to the fact that the straight specimens failed at the shoulder before the stress in the gage section became high enough to produce an offset of 0.05 per cent.

The rate of strain was determined from a time-strain curve (see Fig. 5), by measuring the slope of this curve in the region just below the value of strain above which the stress was no longer

[5] See "Standard Definitions of Terms Relating to Methods of Testing," A.S.T.M. Standards, part 3 (E6-36), 1942, p. 849.

TABLE 2 TENSION TESTS*

Stress-strain tests (constant cross section specimens)						
Panel number	204	205	206	207	208	209
Type of resin	*A*	*A*	*B*	*B*	*C*	*C*
Molding pressure, psi	1500	600	1500	600	1500	600
No. of specimens tested	2	2	2	2	2	2
Modulus of elasticity, psi × 10^{-6}	4.10–4.13	3.70–3.74	4.20–4.20	3.90–3.94	4.12–4.34	3.86–3.90
Average	4.12	3.72	4.20	3.92	4.23	3.88
Approximate rate of strain, in. per in. per min	0.0017	0.0013	0.0017	0.0015	0.0015	0.0014
Ultimate-strength tests (reduced cross section at center of specimen)						
No. of specimens tested	3	3	3	2	3	2
Ultimate strength, psi	56500–51700	44500–42800	55600–53600	44400–42600	53000–50000	49000–46800
Average	53700	43600	54600	43500	51300	47900

proportional to strain. The tangent line used is shown in Fig. 5.

Results of the tension tests are shown in Table 2. The average modulus of elasticity in tension was found to vary from 3,720,000 to 4,230,000 psi, depending on the resin and molding pressure used; and the average ultimate strength was found to vary from 43,500 to 54,600 psi, depending on the resin and molding pressure. The data in Table 2 show that both the ultimate strength and modulus of elasticity are higher for compreg molded under 1500 psi pressure than for compreg molded at 600 psi. This is true for each of the three resins investigated. The increase in ultimate strength, resulting from increasing the molding pressure from 600 to 1500 psi, was 23.2 per cent when resin *A* was used, 25.5 per cent when resin *B* was used, and 7.1 per cent when resin *C* was used. The corresponding increase in tensile modulus of elasticity was 10.7 per cent with resin *A*, 7.2 per cent with resin *B*, and 90 per cent with resin *C*.

Short-Time Compression Tests

Compression specimens were tested in the same machine as the tension specimens and under the same temperature and humidity conditions. In order to minimize the effect of possible eccentric loading the specimens were tested by using a compression tool *A*, shown in Fig. 6. A compressometer *B*, of 1 to 1 ratio having a 0.0001-in. "Last Word" dial and 1-in. gage length was used to determine the strain. As in the case of the tension tests, the instrument was supported on a light coil spring.

Two different shapes of specimen, Fig. 1, were required, one to determine stress-strain relations and the other the compressive strengths. The 2-in. specimen $\left(\frac{l}{r} = 16\right)$* was used with the 1 in-gage-length compressometer to determine the compressive strength of the material.

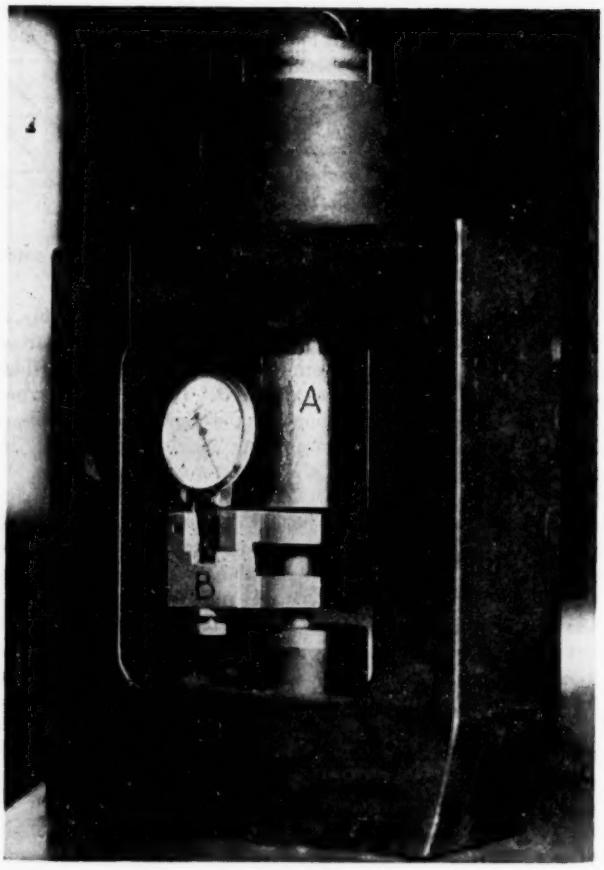


FIG. 6 COMPRESSION APPARATUS

* $\frac{l}{r}$ is the ratio of the length of the specimen to the radius of gyration of the cross section of the specimen.

TABLE 3 COMPRESSION TESTS

Stress-strain tests (2-in. specimens)						
Panel number	204	205	206	207	208	209
Type of resin	*A*	*A*	*B*	*B*	*C*	*C*
Molding pressure, psi	1500	600	1500	600	1500	600
Number of specimens tested	2	2	3	3	3	2
Modulus of elasticity, psi × 10^{-6}	4.00–4.42	3.64–3.94	4.16–4.18	3.92–4.20	4.30–4.38	3.90–3.98
Average	4.21	3.81	4.17	4.07	4.33	3.94
Yield strength at 0.2 per cent offset psi	20900–20400	18500–19300	21400–22500	20400–21600	21500–21800	19500–20200
Average	20700	19000	21900	21000	21600	19900
Yield strength at 0.05 per cent offset psi	18900–19500	16400–18100	19800–20300	19000–20200	20000–20100	18200–19000
Average	19200	17500	20000	19400	20100	18600
Approximate rate of strain, in. per in. per min	0.0014	0.0015	0.0015	0.0014	0.0015	0.0015
Compressive-strength tests (1-in. specimens)						
Number of specimens tested	3	4	4	4	4	4
Ultimate strength, psi	24100–24200	22400–22800	26600–27000	25000–25300	23800–25600	22600–23000
Average	24200	22700	26800	25200	24500	22800

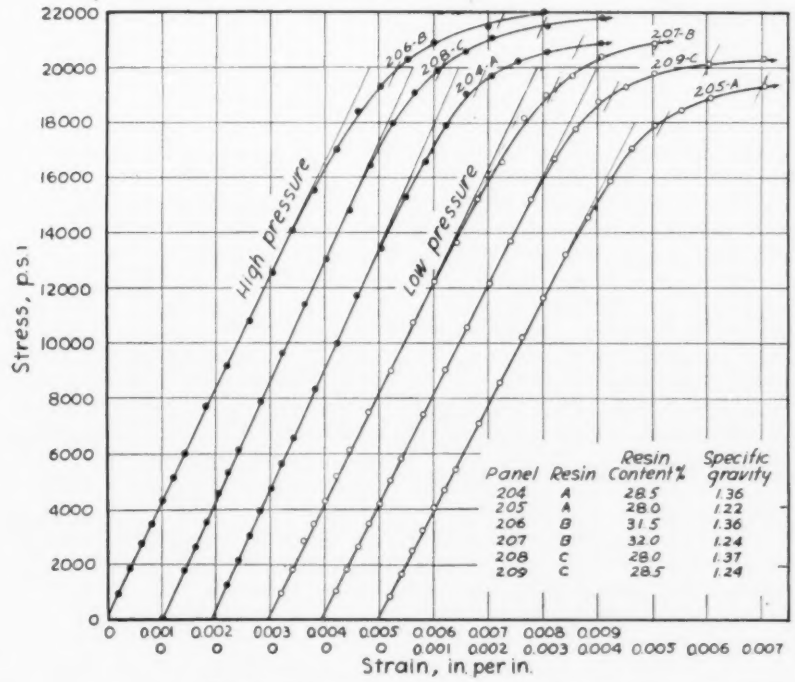


FIG. 7 COMPRESSION TESTS OF COMPREG

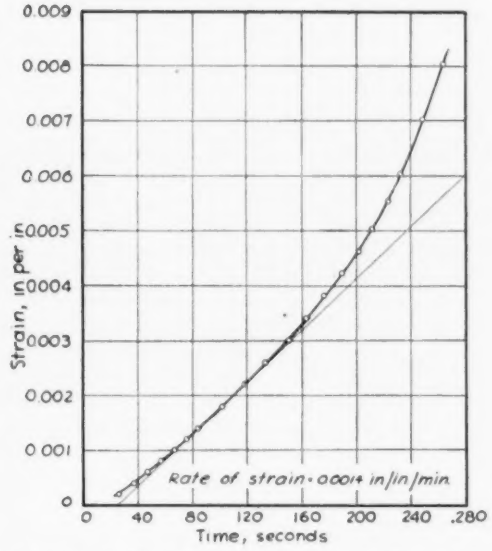


FIG. 8 STRAIN-TIME CURVE OF COMPREG IN COMPRESSION

During the compression tests of the 2-in. specimens, readings of load, deformation, and time were recorded. From these data the stress and strain were computed, and stress-strain and strain-time curves were plotted. Fig. 7 shows the stress-strain curves for the compression tests, and Fig. 8 shows a sample strain-time curve from a compression test. The modulus of elasticity, yield strength at 0.05 and 0.2 per cent offset, and the rate of strain were determined from these curves. The rate of strain in the 1-in. specimen was determined by comparing the loading rate with the loading rate in a 2-in. specimen. The loading rate was obtained by plotting a load-versus-time curve.

Results of the compression tests are shown in Table 3. The average modulus of elasticity in compression was found to vary from 3,810,000 to 4,330,000 psi, depending on the resin and

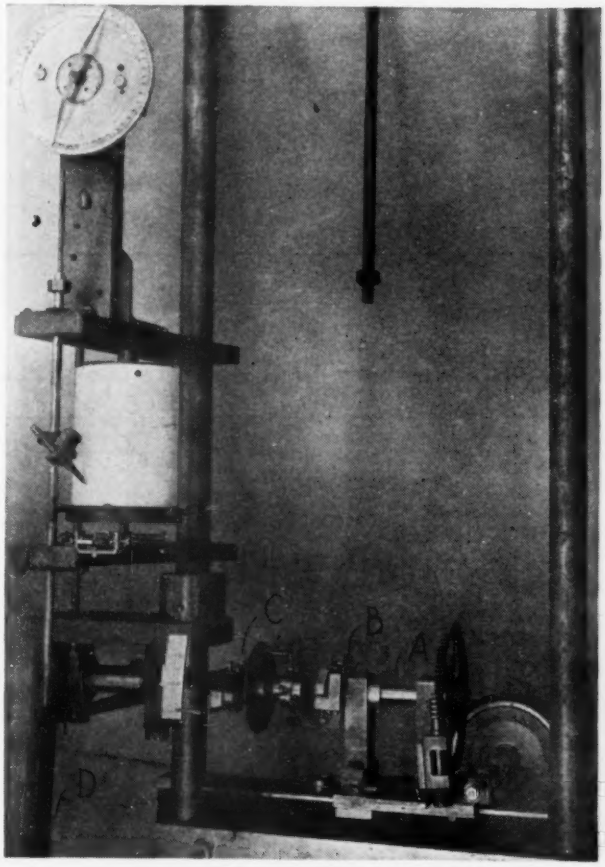


FIG. 9 TORSION APPARATUS

molding pressure used, and the average ultimate strength in compression was found to vary from 22,700 to 26,800 psi, depending on the resin and molding pressure. The data in Table 3 show that the modulus of elasticity, ultimate strength, and yield strengths in compression are about 5 per cent higher for compreg molded under 1500 psi pressure than for compreg molded at 600 psi. This is approximately true for each of the resins investigated.

The increase in modulus of elasticity in compression resulting from increasing the molding pressure from 600 to 1500 psi was 10.5 per cent when resin *A* was used, 2.5 per cent when resin *B* was used, and 9.9 per cent with resin *C*. The corresponding increase in ultimate strength was 6.6 per cent with resin *A*, 6.3 per cent with resin *B*, and 7.5 per cent with resin *C*. The increase in yield strength at 0.2 per cent offset was 8.9 per cent with resin *A*, 4.3 per cent with resin *B*, and 8.5 per cent with resin *C*. Corresponding values for the yield strength at 0.05 per cent offset are 9.7, 3.1, and 8.1 per cent, respectively.

Short-Time Torsion Tests. The special torsion-testing machine used for these tests is shown in Fig. 9. The machine was constructed as an attachment for a low-capacity tension-testing machine. The pendulum-weighing system of the tension-testing machine was used as the torque-measuring device for the torsion machine. This was accomplished by attaching to the tension machine a twisting head, *A*, Fig. 9, driven by a double worm drive. A special chuck *B* was attached to the shaft of this twisting head and another chuck *C* to the axis of the pendulum *D*. These chucks were designed to apply a torque to the specimen with slight danger of inducing bending. This action was further assisted by mounting the specimen on centers and applying the torque as a couple by means of adjustable screws.

The gage used for measuring the shearing strain is shown in Fig. 10. It was designed to accommodate materials whose ultimate shearing strain was relatively small and also materials which might twist 2 or 3 revolutions in a length of 2 in. The instrument consisted of two rings *A*, Fig. 10, which were slipped over the specimen and fastened to it by three adjusting screws in each ring. A gage length of 2 in. was obtained by use of a removable spacer *B*. To one of the rings was fastened a circular scale *C*, for measuring large angles of twist. Two 10-in. arms *D* fastened to the same ring carried scales on the ends, which were used to measure small shearing strain. Adjustable pointers *E*, were attached to the other ring in such a way as to indicate the readings on their respective scales.

Laminated materials, such as the compreg described herein, are anisotropic, that is, their properties are not the same in all directions. In the tension and compression specimens the maximum normal stress was parallel to the grain direction throughout the test specimen. However, in a torsion specimen with axis parallel to the lamination, both the tension and shearing stresses had different directions (relative to the direction of the wood grain and the plane of laminations) at different points around the circumference of the specimen. Thus the equations of stress and strain for torsion of an isotropic member cannot be expected to indicate accurately the stress or strain in this anisotropic material. Nevertheless, the following equations developed for isotropic materials were used here to give nominal values of shearing stress and strain as a basis for comparison: The equation for shearing stress in a circular member of an isotropic material subjected to torsion is $\tau = \frac{Tc}{J}$, and the corresponding equation for shearing strain is $\gamma = \frac{c\theta}{l}$.

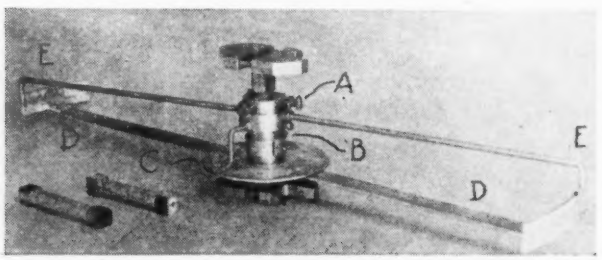


FIG. 10 DETRUSION GAGE

In the case of a laminated material, the torsion test may serve as an indication of the relative shearing strength of the bond between laminations, that is, in a wood-laminated material failure is likely to take place by shearing parallel with the grain.

Short-time torsion tests were performed on specimens, Fig. 1(*b*), cut from the sheet with their longitudinal axes parallel to the grain.

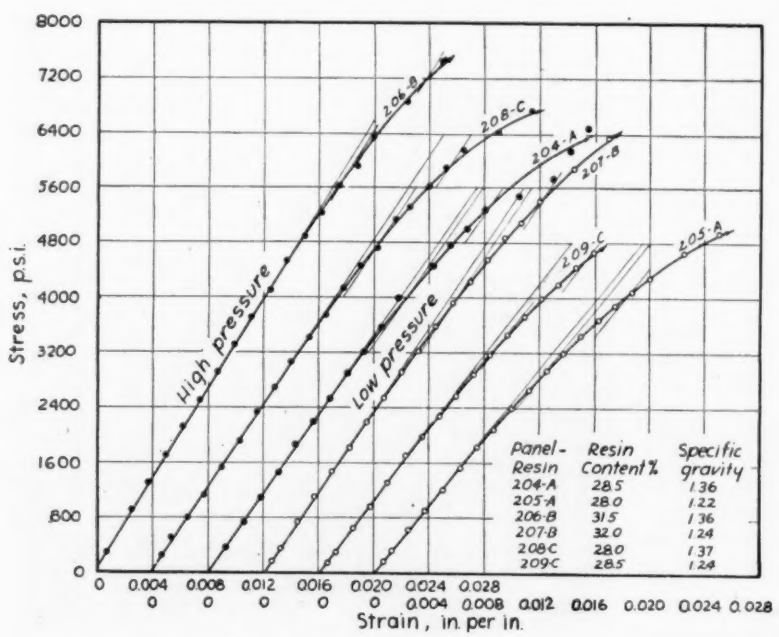


FIG. 11 TORSION TESTS OF COMPREG

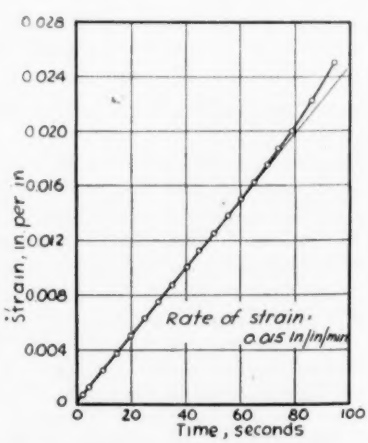


FIG. 12 STRAIN-TIME CURVE OF COMPREG IN TORSION

TABLE 4 TORSION TESTS

Panel number	204	205	206	207	208	209
Type of resin	*A*	*A*	*B*	*B*	*C*	*C*
Molding pressure, psi	1500	600	1500	600	1500	600
No. of specimens tested	2	3	3	3	2	2
Shearing modulus of elasticity, psi $\times 10^{-6}$	0.286–0.292	0.246–0.249	0.326–0.347	0.295–0.302	0.303–0.308	0.238–0.263
Average	0.289	0.248	0.337	0.298	0.306	0.251
Shearing yield strength at 0.2 per cent offset, psi	4740–5460	4040–4420	7230–8000	5610–5820	5840–5920	4540–5150
Average	5100	4180	7720	5700	5880	4850
Shearing yield strength at 0.05 per cent offset, psi	3180–3980	2760–3340	5840–6700	3960–4400	4460–4580	3420–4290
Average	3580	2960	6340	4120	4520	3860
Modulus of rupture in torsion, psi	6720	4940–5110	9630–9960	6740–7120	8400	4670–5680
Average	6720[a]	5060	9800[b]	6980	8400[a]	5180
Approximate rate of strain, in. per in. per min	0.015	0.016	0.014	0.015	0.015	0.016

[a] One specimen.
[b] Two specimens.

During the torsion test simultaneous readings of torque, angle of twist, and time were recorded. The nominal shearing stress at the surface of the cylindrical specimen and the nominal shearing strain were computed from the relationships just given.

Curves of shearing stress versus shearing strain, Fig. 11, and time versus shearing strain, Fig. 12, were then plotted. The shearing modulus of elasticity G and rate of shearing strain were determined from these curves as in the case of the tension tests. It may be observed that the strain-time curve for torsion is practically a straight line, as compared with the curved strain-time diagrams for tension and compression. This is due largely to the greater stiffness of the machine compared to that of the specimen in the case of the torsion tests.

The results of the torsion tests are given in Table 4. The average shearing modulus of elasticity G, as determined from a torsion test, was found to vary from 248,000 to 337,000 psi, depending on the resin and molding pressure used, and the average modulus of rupture varied from 5060 to 9800 psi, depending on the resin and molding pressure. The data in Table 4 show that the shearing modulus of elasticity, modulus of rupture, and yield strengths were higher for compreg molded under 1500 psi pressure than for compreg molded at 600 psi. This was true for each of the three resins. The increase in modulus of rupture was particularly marked. The increase in shearing modulus of elasticity resulting from increasing the molding pressure from 600 to 1500 psi was 16.5 per cent with resin *A*, 13.1 per cent with resin *B*, and 21.9 per cent with resin *C*. The corresponding increases in modulus of rupture were 32.8 per cent for resin *A*, 40.4 per cent for resin *B*, and 62.1 per cent for resin *C*. The yield strengths at 0.2 per cent offset were increased 22.0, 35.4, and 21.2 per cent for resins *A*, *B*, and *C*, respectively; and the yield strengths at 0.05 per cent offset were increased 21.0, 53.9, and 17.1 per cent for resins *A*, *B*, and *C*, respectively.

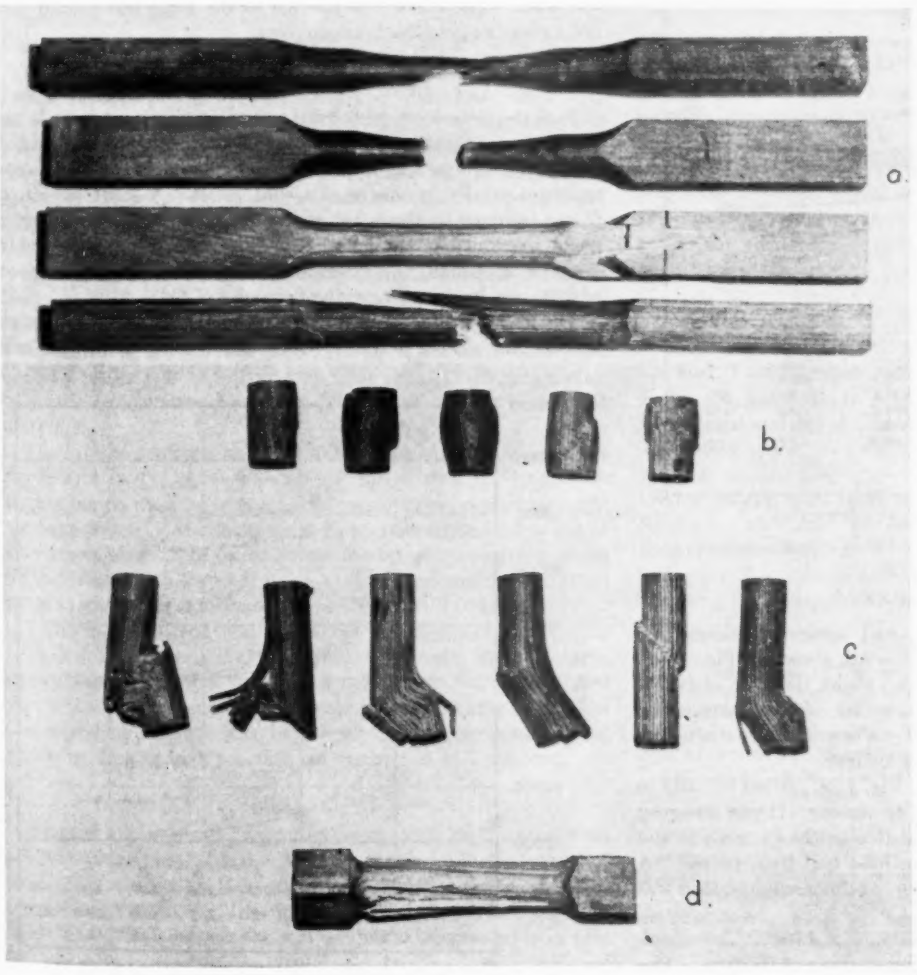


FIG. 13 FRACTURED SPECIMENS
(*a*, Tension; *b*, short compression; *c*, long compression; *d*, torsion.)

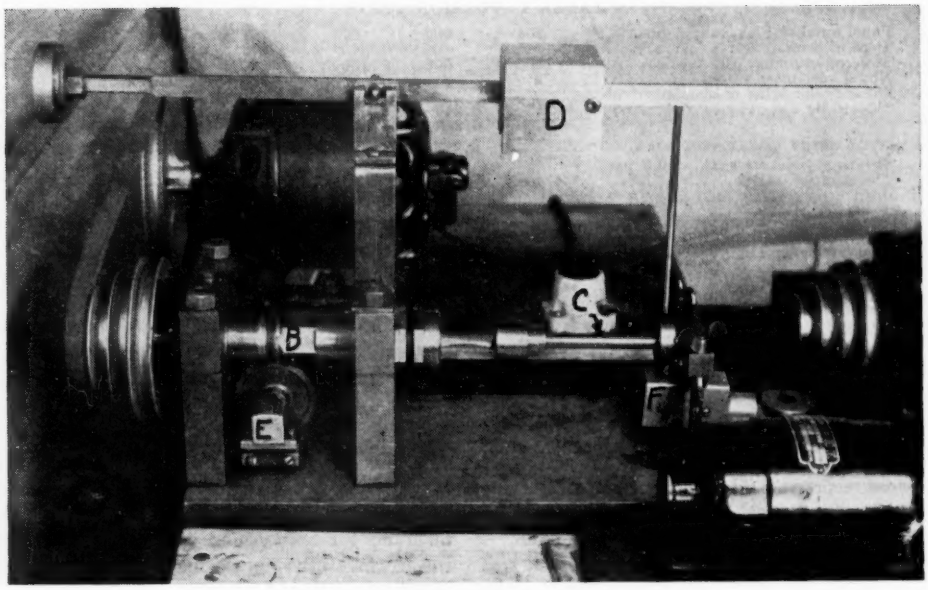


FIG. 14 ROTATING-CANTILEVER-BEAM FATIGUE MACHINE

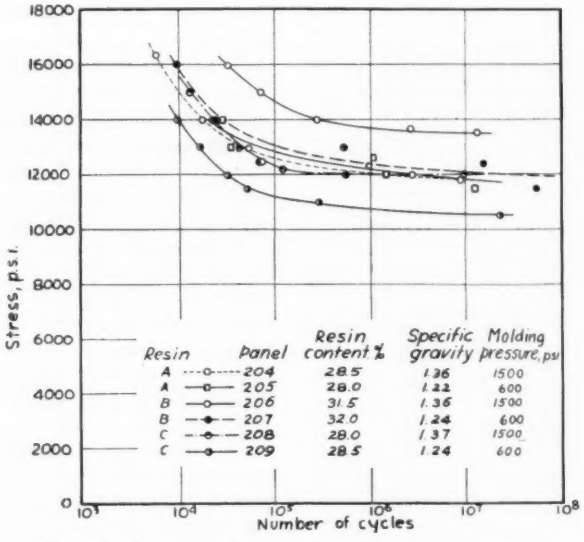


FIG. 15 ROTATING-BEAM FATIGUE TESTS OF COMPREG

MODE OF FAILURE

Fractured tension, compression, and torsion specimens are shown in Fig. 13. Tension specimens are shown in Fig. 13(*a*). One of the straight tension specimens shows the type of failure which frequently occurred at the shoulder. Short compression specimens are shown in Fig. 13(*b*). These failures started as shear failures at 45 deg to the axis of loading.

The long compression specimens, Fig. 13(*c*), failed initially in much the same manner as the short specimens. It was observed that the shear failures which are visible in the illustration did not occur until after the maximum load had been passed. A slight bulging was observed, however, as the maximum load was approached.

A failed torsion specimen is shown in Fig. 13(*d*). This specimen has been severely twisted to show the type of fracture. The initial fracture in each torsion specimen was a slight longitudinal crack resulting from the shearing stress parallel to the axis of the specimen. The crack was parallel to the grain but usually did not follow the glue line between plies.

FATIGUE TESTS

Fatigue tests were performed on a rotating-cantilever-beam type fatigue machine shown in Fig. 14. This machine consisted of a motor-driven spindle *B* to which the specimen *A* was attached coaxially by means of a split collet. A shaft extension *C* was fastened to the other end of the specimen by means of a collet machined integral with the shaft. The entire assembly (spindle, specimen, and extension shaft) was rotated at a speed of 6200 rpm by a motor driving through a V-belt.

The specimen was bent downward by a load applied through a small ball bearing to the end of the extension shaft. This load

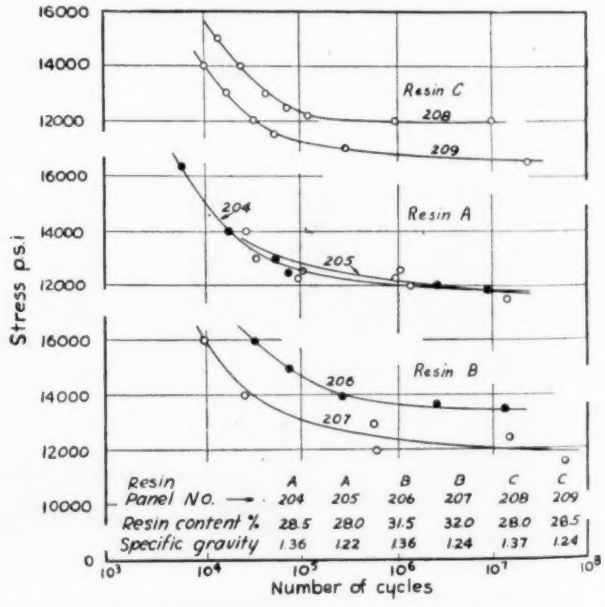


FIG. 16 ROTATING-BEAM FATIGUE TESTS OF COMPREG

TABLE 5 SUMMARY

Number	Item	Resin *A*		Resin *B*		Resin *C*	
1	Panel number	204	205	206	207	208	209
2	Molding pressure, psi	1500	600	1500	600	1500	600
3	Specific gravity	1.36	1.22	1.36	1.24	1.37	1.24
4	Tension modulus, psi $\times 10^{-6}$	4.12	3.72	4.20	3.92	4.23	3.88
5	Tension strength, psi	53700	43600	54600	43500	51300	47900
6	Compression modulus, psi $\times 10^{-6}$	4.21	3.81	4.17	4.07	4.33	3.94
7	Compression strength, psi	24200	22700	26800	25200	24500	22800
8	Compression yield strength at 0.2 per cent offset psi	20700	19000	21900	21000	21600	19900
9	Torsion (shearing) modulus, psi $\times 10^{-6}$	0.289	0.248	0.337	0.298	0.306	0.251
10	Modulus of rupture (torsion), psi	6720	5060	9800	6980	8400	5180
11	Shearing (torsion) yield strength at 0.2 per cent offset, psi	5100	4180	7720	5700	5880	4850
12	Shear strength parallel to laminations, psi	4840	3640	4450	4230	4340	3620
13	Impact, ft-lb per in. of notch	10.0	8.3	7.8	6.1	9.4	6.6
14	Fatigue strength at 10^7 cycles, psi	11800	11800	13400	12000	12000	10600
15	Water absorption, per cent	3.0	7.0	1.7	5.0	2.0	6.7
16	Swelling, per cent	14.2	13.9	9.7	9.9	11.5	12.2
17	Recovery, per cent	2.90	2.97	1.87	2.22	2.28	2.00

was produced by a beam-and-poise mechanism *D*. The stress σ at the minimum section of the specimen was computed from the equation $\sigma = \frac{Mc}{I}$ in which M was obtained from the load applied by the poise with suitable correction for the moment produced by the extension shaft.

In order to determine the number of cycles to cause failure a counter *E* was attached to record the number of cycles and a microswitch *F* was used to stop the machine when a crack had started in the specimen.

The data obtained from the fatigue tests of the six compreg panels is shown in Fig. 15, plotted as $\sigma - N$ diagrams. The tests were carried out to at least 10,000,000 cycles. It was observed that the fatigue-test results were nearly the same for four out of the six panels. The panel made with resin *B* and molded at the high pressure had the best fatigue characteristics, while the panel made with resin *C* and molded at low pressure had the poorest fatigue characteristics.

Fig. 16 shows the fatigue curves grouped in pairs according to the resin used. This diagram shows that the fatigue curves for resin *A* are almost identical. The different molding pressures made no difference. In the case of resins *B* and *C*, however, the ordinate (stress) of the fatigue curve was about 12 per cent higher when the panels were molded at 1500 psi than when molded at 600 psi.

The fatigue strength at 10,000,000 cycles is tabulated as item number 14 in Table 5. The term "fatigue strength"[7] refers to the maximum amplitude of an alternating stress cycle which will not cause fracture of the material for a given number of cycles of alternating stress. In other words, the fatigue strength is given by the ordinate to the $\sigma - N$ curve at the given number of cycles. In this report, the number of cycles used was 10,000,000.

The fatigue strength at 10,000,000 cycles was 11,800 psi with resin *A* for both molding pressures; with resin *B*, the fatigue strength was 12,000 psi, for the low molding pressure and 13,400 psi for the high pressure, an increase of 11.7 per cent; with resin *C* the fatigue strength was 10,600 psi for the low pressure and 12,000 psi for the high pressure, an increase of 13.2 per cent.

Comparison of Results

Average values of all properties determined for the six panels are summarized in Table 5. A study of this table discloses that panel 206, molded at 1500 psi with resin *B*, showed the best properties in 9 out of 14 items tabulated (numbered 3 through 16). The 17th item, recovery, was difficult to evaluate in this manner and will not be included in the comparison. This panel (number 206) was next to the highest in tensile modulus, compression modulus, and shear strength parallel to the laminations, but was fourth from the highest in impact strength, and of course had a higher specific gravity than the materials molded at low pressure. Panel 204 had the highest impact strength and shear parallel to the laminations; and panel 208 had the highest tension and compression moduli.

When the properties of the three panels molded at low pressure were compared, it was found that panel 207 molded with resin *B* had the best properties in 11 out of 14 items. It had a specific gravity slightly higher than panel 205, a tensile strength inferior to that of panel 209, and had the lowest impact strength of the group.

No account was taken of the specific gravity in comparing the properties of the six panels so that the low-pressure panel of resin *B* may be as good or better (depending on the property and application) than the high-pressure panel with resin *B*, for applications where weight is a prime factor.

[7] See A.S.T.M. designation D671-42T, A.S.T.M. Standards part III, 1942, p. 1251.

Acknowledgment

As previously noted, this project was carried out as a part of the work of the Engineering Experiment Station of the University of Illinois, Dean M. L. Enger, Director, in the Department of Theoretical and Applied Mechanics of which F. B. Seely is head. The authors are indebted to F. B. Seely for assistance in the preparation of this manuscript.

The authors wish to express their appreciation to the Forest Products Laboratory for preparing the samples and supplying the information quoted.

A part of tests reported herein were conducted as a senior thesis by C. D. Kacalieff.

BIBLIOGRAPHY

1 "Superpressed Plywood," by R. K. Bernhard, T. D. Perry, and E. G. Stern, *Mechanical Engineering*, vol. 62, March, 1940, pp. 189–195.

2 "The Compression of Wood," by R. M. Seborg and A. J. Stamm, Forest Products Laboratory, mimeograph R1258.

3 "Resin-Treated, Laminated, Compressed Wood," by A. J. Stamm and R. M. Seborg, Forest Products Laboratory, mimeograph R1268.

4 "Forest Products Laboratory Resin-Treated, Laminated, Compressed Wood (Compreg)," by A. J. Stamm and R. M. Seborg, Forest Products Laboratory, Mimeograph R1381.

5 "Effect of Resin Treatment and Compression Upon the Properties of Wood," by R. M. Seborg and A. J. Stamm, Forest Products Laboratory, Mimeograph R1323.

6 "Bearing Strength of Plastic Materials," by R. T. Schwartz and E. Drugger, Jr., Army Air Forces Technical Report, No. 4998, August, 1943.

7 "Variation of Tensile Strength and Elongation of Plastic Materials With Temperature," by R. T. Schwartz, Army Air Forces Technical Report No. 5062, December, 1943.

8 "Resin Impregnation of Wood," by R. Casselman, *Modern Plastics*, vol. 21, Nov., 1943, pp. 124–126 and 168.

9 "Effect of Prolonged Heating on Some Physical Properties of Compreg," by D. Baker and J. E. Gurvitch, *Modern Plastics*, vol. 22, Sept., 1944, pp. 142, 176, and 178.

10 "Mechanical Properties of Plastic Materials at Normal and Subnormal Temperatures," by T. T. Oberg and R. T. Schwartz, Air Corps Technical Report No. 4648, June, 1941.

11 "Fatigue Tests on Compressed and Impregnated Laminated Wood," by A. G. H. Dietz and H. Grinsfelder, A.S.T.M. Bulletin No. 129, August, 1944, pp. 31–34.

12 "Short-Time Static Tests and Creep Tests of a Paper Laminated Plastic," by W. N. Findley and W. J. Worley, Proceedings of the A.S.T.M., vol. 44, 1944, pp. 949–966.

Discussion

A. G. H. Dietz.[8] The authors have carried out an excellent series of tests and have obtained information which extends our knowledge of the behavior of compreg.

In an attempt to correlate their results with those reported by the writer and his collaborator in a previous joint paper,[9] the results summarized in Table 5 of the paper have been reduced to a common base by dividing the values obtained in tests 4 to 14, inclusive, by the specific gravities of the individual panels. Furthermore, taking panels 206 and 207 as points of reference, because they have the highest resin contents and also, generally speaking, have the highest values, ratios of values for panels 206 and 207 to those of 204 and 208, and 205 and 209, respectively, have been drawn. The results are summarized in Table 6 of this discussion.

It is, of course, not safe to generalize from these results, but certain factors are worthy of note because they may be indicative of trends:

1 When reduced to a common base (specific gravity reduced to 1.00) most of the values become more nearly equal, but considerable differences still exist. In panel-pairs 204–205 and 206–207, the higher density material has higher tensile strength, but the reverse is true of 208–209. In every pair, however, the lower density material has the higher compressive strength. Furthermore, in every pair the lower density material has higher moduli of elasticity in both tension and compression, although the differences are generally slight.

2 Shear characteristics and impact strength, unlike the general trend in tension and compression, appear to be benefited by higher densities. With one exception, every test, e.g., torsion (shearing) modulus, torsion modulus of rupture, shearing yield strength, shear strength parallel to laminations, impact, the higher density material is superior to the lower. The one exception is in 206–207, shear strength parallel to laminations.

3 In fatigue, the results are apparently not so clear. In pairs 206–207 and 208–209, the higher density material is slightly superior, in 204–205 the reverse is decidedly indicated.

It is interesting to compare panels 206 and 207, which have the highest resin contents, with the other panels made at the same pressures. In the high-density panels, the resin ratios for 206/204 and 206/208 are 1.10 and 1.13, respectively. For the low-density panels, the ratios for 207/205 and 207/209 are 1.14 and 1.12, respectively. With these in mind, the following factors may be worthy of note:

1 Although the ratios of most of the tensile and compressive values of panels 206 and 207, as compared with the other panels, are greater than unity, none of them is as great as the ratios of the resin contents. Increasing the resin content does not appear to increase these values proportionately. As might be expected from the characteristics of wood and resin, compressive strength is most nearly proportional, tensile strength less so.

2 With the exception of shear strength parallel to laminations, all the ratios of shear values, e.g., torsion (shearing) modulus, torsion modulus of rupture, shearing yield strength, are proportionately higher than the ratios of resin content. Increasing resin content appears to aid these properties. Shear parallel to laminations is proportionately lower in the high-density panels but the reverse in low density.

3 Impact values follow previous experience; the higher the resin content, the lower the impact strength.

4 Fatigue values are inconclusive, high-density panels give results favorable to higher resin content, low-density panels the reverse.

In the paper previously referred to,[9] fatigue results were compared with static moduli of rupture (bending). In the present paper no moduli of rupture are given, but if it is assumed, as a rough approximation, that moduli of rupture lie halfway between the tensile and compressive strengths, the fatigue values are approximately 30 to 35 per cent of the moduli of rupture. This is in approximate agreement with the results previously reported.[9]

Henry Grinsfelder.[10] The matching of panels is not entirely clear to the writer. Will the authors explain this matter more fully?

Do the values obtained with resin B represent definite proof that this is the best of the three resins tested, or is the improvement obtained by virtue of the higher resin content?

While the properties tested and the values obtained show the merit of compreg as it is prepared initially, is there any knowledge of how much of its strength is retained after outdoor exposure for one year?

[8] Associate Professor of Structural Engineering and Materials, Department of Building Engineering and Construction, Massachusetts Institute of Technology, Cambridge, Mass.

[9] Reference 11 of authors' Bibliography.

[10] The Resinous Products & Chemical Company, Philadelphia, Pa.

TABLE 6 AUTHORS' TABLE 5 REDUCED TO COMMON BASE[a]

No.	Item	204	205	206	207	208	209	Panel ratios 206/204	206/208	207/205	207/209
	Panel number	204	205	206	207	208	209				
1	Resin content, per cent	28.5	28.0	31.5	32.0	28.0	28.5	1.10	1.13	1.14	1.12
2	Molding pressure, psi	1500	600	1500	600	1500	600				
3	Specific gravity	1.00	1.00	1.00	1.00	1.00	1.00	1.00	0.99	1.02	1.00
4	Tension modulus, psi 10^{-6}	3.04	3.05	3.09	3.16	3.09	3.13	1.02	0.99	1.05	1.01
5	Tension strength, psi	39500	35800	40100	35100	37500	38600	1.02	1.06	1.00	0.91
6	Compression modulus, psi 10^{-6}	3.10	3.12	3.06	3.28	3.16	3.18	0.99	0.97	1.07	1.03
7	Compression strength, psi	17800	18600	19700	20300	17900	18400	1.11	1.09	1.11	1.10
8	Compression yield strength at 0.2 per cent offset, psi	15200	15600	16100	16900	15800	16000	1.06	1.01	1.10	1.05
9	Torsion (shearing) modulus, psi 10^{-6}	0.212	0.203	0.248	0.240	0.224	0.202	1.17	1.20	1.10	1.19
10	Modulus of rupture (torsion), psi	4940	4150	7200	5630	6130	4180	1.45	1.17	1.38	1.35
11	Shearing (torsion) yield strength at 0.2 per cent offset, psi	3750	3430	5680	4600	4300	3900	1.51	1.31	1.36	1.17
12	Shear strength parallel to laminations, psi	3650	2980	3270	3410	3170	2920	0.92	1.03	1.16	1.17
13	Impact, ft-lb per in. of notch	7.4	6.8	5.7	4.9	6.9	5.3	0.78	0.83	0.74	0.92
14	Fatigue strength at 10^7 cycles, psi	8700	9700	9900	9700	8800	8600	1.14	1.12	1.02	1.03

[a] Specific gravity reduced to unity.

A. J. STAMM.[11] While the tests on compreg are obviously not extensive enough to afford a close quantitative evaluation of the effect of molding pressure and resin content on static and dynamic strength, the fact that the veneer was carefully matched in making up the samples affords a means of securing fairly accurate comparative values for the three resins and two pressures used. The data, however, should not be construed as necessarily representing average values for compreg made with these particular resins, such as would result from more extensive sampling.

The Forest Products Laboratory has, in the past, advocated the use of a water-soluble phenolic resin in preference to an alcohol resin for making compreg, largely because of the greater dimensional stability and lack of recovery. The alcohol-soluble resin used in the panels described in the paper, however, gave much less water absorption, swelling, and recovery than the alcohol-soluble resins in use in making compreg at the beginning of the war. The explanation is that this alcohol-soluble resin has been modified to make it more like the water-soluble resins with a low degree of condensation and high fiber-penetrating power, and still retain its advantage in giving higher impact strength. The advantages claimed in various Forest Products Laboratory reports for water-soluble resins, although still existing, are no longer as important.

It is felt that all three of the resins used in making the panels for which test data are given in this report are suitable for making high-quality compreg.

AUTHORS' CLOSURE

The authors wish to express their thanks to the discussers for their valuable contributions to this paper. Mr. Dietz has made some very interesting comparisons, but there is one point on which the authors are in disagreement with him. He has implied that dividing the various mechanical properties by the specific gravity reduces them to a common base for all panels.

This seems misleading. The results as reported by the authors were on a common base with regard to actual strength, stiffness, etc., and as indicated in the paper the relative merits of the panels might be different for different applications when weight is considered.

Mr. Dietz has implied that the strength of structural members of equal weight made of materials of different specific gravity can be compared by dividing the appropriate mechanical property by the specific gravity and comparing the resulting quantity. This is true for only certain specific cases, such as: tension members of the same length, short compression blocks of the same length, beams of the same length and depth, and long columns of the same length and depth of section which fail by buckling in the plane of the depth dimension.

However, this is not true for many other cases. The ultimate load-carrying capacity of beams of equal weight having the same length and the same width but made of materials having different specific gravity may be compared by dividing the flexural modulus of rupture for each material by the *square* of its specific gravity and comparing the resulting quantities.

Similarly the ultimate torque-carrying capacity of circular shafts of equal weight and length may be compared by dividing the torsional modulus of rupture of each of the materials by its (specific gravity)$^{1/2}$ and comparing the resulting quantities.

Also the ultimate load-carrying capacity of long columns of equal weight and of the same length and *width* of section which fail by buckling in the plane of the depth dimension may be compared by dividing the effective elastic modulus for bending of each of the materials by the *cube* of its specific gravity.

The stiffness of structural members can be compared in a similar manner. The stiffness of bars of equal length subjected to axial loads of either tension or compression (where no buckling is involved) can be compared by dividing the appropriate elastic modulus of each material by its specific gravity; and the stiffness of circular shafts of equal length in torsion can be compared by dividing the shearing modulus of elasticity of each material by the *square* of its specific gravity.

These relationships can be derived from the equations for load or stiffness and the given restricting conditions such as the same weight for both structural members and the same length for both structural members.

Inasmuch as the panels for these tests were prepared by A. J. Stamm, who has been directly connected with the development of compreg, the authors have referred the questions raised by Mr. Grinsfelder to Mr. Stamm. His reply is as follows:

"The panels were matched as follows: Eighteen sheets of $^1/_{16}$ by 28 by 54 in. rotary cut yellow-birch sapwood veneer conforming to AAF Specification 15065 were stacked and cut into 8 piles of plies approximately 14 in. wide and 13$^1/_2$ in. long. The stacks of plies were numbered 204 to 211; 204, 206, 208 and 210 being matched consecutively in the fiber direction, and 204 and 205, 206 and 207, 208 and 209, and 210 and 211 being matched in the tangential direction of the tree. Stacks 210 and 211 were retained by the Forest Products Laboratory for future reference. Stacks 204 and 205 were treated with resin A, 206 and 207 with resin B, and 208 and 209 with resin C. The even-numbered stacks were assembled at 1500 psi and the odd numbers at 600 psi. As matching in the fiber direction of the wood is better than side matching, the matching for the resin type variable was better than for the pressure variable.

"The data presented in this paper are insufficient to draw conclusions regarding the small variations in properties. The only differences which we believe are real on the basis of other data obtained by the Forest Products Laboratory are the water absorption, swelling, and recovery, and the compressive strength and impact strength (Izod). Water-soluble resins of the type illustrated by resin B, we believe, penetrate the cell-wall structure more completely than the alcohol-soluble resins as represented by resin A.

"This greater penetration results in somewhat better moisture stability and makes the cell wall more rigid, resulting in an increase in compressive strength but a decrease in impact strength. Tensile strength, modulus of rupture in bending, and shear strength appear to be affected little by the type of resin used. Little significance can be placed on differences in these values.

"All three of these compregs have excellent properties. From the user's standpoint there is little to choose between them. Resin A, however, is exceptional among alcohol-soluble resins in giving high dimensional stability. More advanced alcohol-soluble resins will give inferior dimensional stability properties."

[11] Chief, Division of Derived Products, U. S. Forest Products Laboratory, U. S. Department of Agriculture, Madison, Wis.

Glue-Line Stresses in Laminated Wood

By A. G. H. DIETZ,[1] HENRY GRINSFELDER,[2] and ERIC REISSNER[3]

With intensified use of timber beams, consisting of laminations of relatively thin boards and planks glued together, the problem of glue lines coming apart under changing conditions of moisture content in the timber has become of considerable importance. From an examination of glued timbers undergoing changes in moisture content, it appears that delamination, when it occurs, most frequently does so when the moisture content is being reduced; during such a dehydrating phase not only does shrinking take place but also checking of the wood. Results of experimentation and field trials indicate that thin laminations are better than thick ones for gluing, and wood species with low moduli are better than species with high moduli. Adhesives must be employed which have high shearing strength and high tensile strength perpendicular to the glue line if laminated beams are to be dependable in service.

Introduction

WITHIN recent years, timber beams, consisting of laminations of relatively thin boards and plank glued together to form large curved or straight members, have found rapidly increasing use. It has been customary to employ cold-water-mixed room-temperature-setting adhesives in the fabrication of such timbers. Experience indicates that under conditions of changing moisture content in the timber, glue lines sometimes come apart.

It has been known for some time that thick wood members are more difficult to glue than thin. Plywood has been successfully bonded over a period of years with resin adhesives, but serious difficulty has often been encountered when the thickness of one or more plies has exceeded about $^1/_4$ in. It is also known that plywood made of $^1/_8$-in. veneer is more apt to delaminate during outdoor exposure than is plywood made of $^1/_{16}$-in. veneer. In edge-glued lumber difficulties have been caused by sunken joints. Troubles have arisen in gluing plywood surfaces to lumber cores. More recently, considerable interest has been aroused by the problem of laminating oak for exposure to such severe conditions as are found around ships' keels.

The difficulty has not been one of obtaining a good initial bond but rather one of preventing delamination after relatively short periods of exposure to service conditions. In the laboratory, joints which initially fail in the wood at values above 2800 psi, when tested in compression-shear blocks, are frequently delaminated by immersing in water for 7 days and drying to 8 per cent moisture content. The glues used are those usually considered to be waterproof or water-resistant.

Many theories, i.e., acids of the wood, tannins in the wood, high hydrogen-ion content of the wood in salt water, each or all weakening the adhesive bond, have been advanced to explain this phenomenon. However, no real proof has been produced supporting these theories, and from an analysis of the available facts, it would appear that certain fundamentals concerning wood and gluing need re-examination.

When wood increases in moisture content it expands. If wood is glued and then permitted to increase or to decrease in moisture content, either the wood expands and takes the adhesive with it, the adhesive restrains the wood and prevents expansion, or delamination occurs and the wood leaves the adhesive. However, when wood shrinks due to loss of moisture, wood failure in the form of splits, or "checking," may occur in place of glue failure or delamination. In laminated wood, unlike plywood, noticeable expansion and contraction take place as the moisture content of the laminations changes. Good glue joints, therefore, depend upon the ability of an adhesive to follow or to restrain the wood during the changes in dimensions caused by changes in moisture content.

Glue-Line Stresses Caused by Moisture Changes

In order to obtain an indication of the nature of the stresses set up in the glue lines of laminated timbers as the moisture content changes, two cases have been investigated mathematically. In both, the beam consists of two parallel-grain laminations of equal thickness, Fig. 1(*a*). They represent the

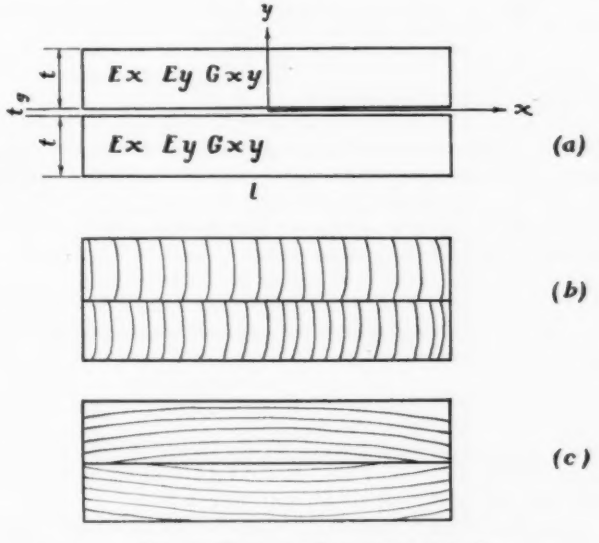


Fig. 1 Types of Laminated Beams

(*a*, Cross section through two-layer laminated beam of material having Young's moduli E_x and E_y in x- and y-directions; shear modulus G_{xy}, and dimensions shown. *b*, Two-layer beam of edge-grain wood. *c*, Two-layer beam of flat-grain wood.)

probable extreme cases; one in which high shear stresses are set up in the glue line without any normal stress perpendicular; the other in which high normal stresses perpendicular to the glue line occur but no shear stresses. For most beams consisting of several laminations, the usual condition would be intermediate between these extremes.

The mathematical analysis, omitted here for the sake of brevity, leads to conclusions which follow:

[1] Associate Professor of Building Engineering and Materials, Massachusetts Institute of Technology, Cambridge, Mass.

[2] Laboratory Head, Resinous Products and Chemical Company, Philadelphia, Pa.

[3] Associate Professor of Mathematics, Massachusetts Institute of Technology. Jun. A.S.M.E.

Contributed by the Wood Industries Division and presented at the Annual Meeting, New York, N. Y., November 26–29, 1945, of The American Society of Mechanical Engineers.

Note: Statements and opinions advanced in papers are to be understood as individual expressions of their authors and not those of the Society.

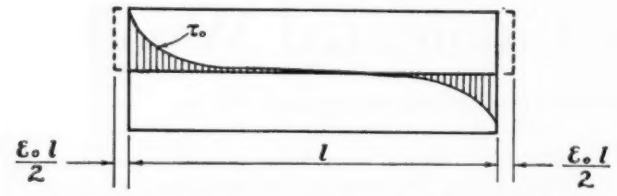


FIG. 2 CASE 1—CROSS SECTION THROUGH TWO-LAYER BEAM WITH ONE LAMINATION TENDING TO EXPAND OR CONTRACT UNIFORMLY BECAUSE OF UNIFORM CHANGE IN MOISTURE CONTENT
(Other lamination unchanged in moisture content. Shear stresses have sharp maxima at edges of beam.)

Case 1. Two laminations of equal thickness, one of which undergoes uniform moisture change tending to increase or decrease its width whereas the other remains unchanged, as illustrated in Fig. 2.

No normal stresses perpendicular to the glue line are set up. "Rolling" shear stresses do occur as one lamination tends to expand or contract past the other. These stresses are largely concentrated at the ends of the glue line, decaying toward zero over a distance approximately equal to the thickness t of the lamination. Their maximum intensity is, approximately

$$\tau_{0max} = 0.7\epsilon_0\sqrt{E_x G_{xy}} \quad [1]$$

$$\epsilon_0 = \alpha(M_2 - M_1) \text{ (see Fig. 2)}$$

where α = hygroscopic coefficient of expansion
M_1 = initial moisture content
M_2 = final moisture content
E_x = Young's modulus of laminations in x-direction (parallel to glue line)
E_y = Young's modulus of laminations in y-direction (perpendicular to glue line)
G_{xy} = Shear modulus in xy-plane

Case 2. Two laminations of equal thickness, in which the moisture content changes in a parabolic manner, as shown in Fig. 3. Moisture change is symmetrical about the glue line, and no shear stresses are set up in the glue line. Normal stresses σ_0 occur perpendicular to the glue line, with maximum intensities at the ends, as shown in Fig. 3. For isotropic materials their maximum intensity is given by

$$\sigma_{0max} = 0.45\epsilon_0 E_x \quad [2a]$$

A modification of this formula for anisotropic materials, such as wood, is

$$\sigma_{0max} = 0.45\epsilon_0\sqrt{E_x\sqrt{2E_y G_{xy}}} \quad [2b]$$

where the symbols have the same significance as in Equation [1], except that ϵ_0 is now the difference in hygroscopic strain between the outermost fibers and the fibers at the glue line.

Equations [1] and [2a] have been obtained by minimum energy methods. A stress distribution was assumed of known shape in the direction across the thickness of the laminations while the variation of the stresses in the direction of the glue line was determined entirely by the energy method. A further approximation was made by saying that the state of stress was plane. It is believed that the values of the maximum stresses will be changed slightly only if plane strain is assumed instead of plane stress but this should still be confirmed by calculation. With regard to Equation [2b] it should be said that this is a plausible generalization of Equation [2a] for the isotropic material. Equation [2b] has, however, not been obtained by solving directly the problem for the anisotropic material. It is hoped that the theoretical work leading to the foregoing results may be continued so as to cover the points mentioned, as well as to obtain results which go beyond those given here.

Numerical Examples. In order to obtain numerical values of stress for the foregoing expressions, it is necessary to find values of shear modulus and Young's moduli across the grain, and of expansion across the grain caused by changes in moisture content.

In Table 1 are given some measured and some estimated values of shear modulus and Young's moduli for various species of wood. Shear modulus is in the radial-tangential plane (cross section of the wood); Young's moduli are in the radial and tangential directions of the cross section.[4] In Table 1 are also given estimated average values of the hygroscopic coefficient of expansion α_r and α_t in the radial and tangential directions. These are based largely upon values of shrinkage from fiber-saturation point to oven-dry condition.[5] The hygroscopic coefficients α are therefore the expansion per unit width of material for each per cent increase in moisture content.

Case 1. Example. Suppose, for example, that at the time of gluing the lumber is at 12 per cent moisture content (M_1) and that subsequently one lamination of the glued-up beam rises to the fiber-saturation point (M_2) or 28 per cent. The total expansion per unit width then occurs over a range of 16 per cent, and

$$\epsilon_0 = 16\alpha_r$$

for edge-grain material, (Fig. 1*b*).

$$\epsilon_0 = 16\alpha_t$$

for flat-grain material, (Fig. 1*c*).

For the various species of Table 1, the values of maximum shear-stress intensity, as calculated by Equation [1], are then approximately as given in Table 2 under the heading Case 1.

These values must be considered approximate, because the various constants, especially the moduli, are known only approximately and show wide variation. Nevertheless, it becomes clear that heavy shear-stress concentrations may be set up at the outside edges of glue lines when only the outer lamination under-

[4] "Report on Materials of Construction Used in Aircraft," by C. F. Jenkin, Aeronautical Research Committee (British), 1920; (also, from data of Forest Products Laboratory.)

[5] Wood Handbook, U. S. Department of Agriculture, Forest Products Laboratory. (Slightly revised June, 1940.)

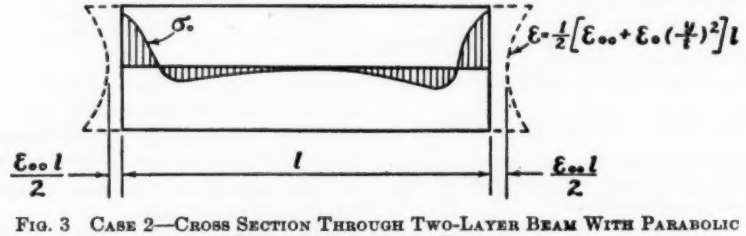


FIG. 3 CASE 2—CROSS SECTION THROUGH TWO-LAYER BEAM WITH PARABOLIC CHANGE IN MOISTURE CONTENT
(Normal stresses perpendicular to glue line have sharp maxima at edges of beam.)

TABLE 1 HYGROSCOPIC AND ELASTIC CHARACTERISTICS OF SELECTED SPECIES

Species	Hygroscopic coefficients		Elastic constants		
			Young's moduli		Shear modulus
	Radial α_r	Tangential α_t	Radial E_r, psi	Tangential E_t, psi	G_{rt}, psi
Ash	0.00179	0.00272	238000	140000	36000
Douglas fir	0.00178	0.00278	155800	113200	7100
Mahogany	0.00170[a]	0.00270[a]	140000	70000	22000
Oak	0.00189	0.00321	175000[a]	91000[a]	35000[a]
Spruce	0.00154	0.00274	130000	70000	4600
Walnut	0.00185	0.00253	172000	92000	34000

[a] Estimated.

goes marked change in moisture content while the others remain unchanged. This "rolling" shear stress would be sufficient to rupture either the wood or the glue line for a short distance inward, and failure would be progessively inward until the ratio of thickness of lamination to width of unruptured glue line became large enough to cause a diminution of shearing-stress intensity. It is worthy of note that stresses set up by edge-grained laminations are generally less than those set up by flat-grained laminations.

This is, of course, an extreme case, and one not apt to occur very often in practice. The usual conditions are more nearly approximated by Case 2, which will be examined next.

Case 2, Example. In this example parabolic distribution is assumed for the change in moisture content across the total depth of a two-layer beam, Fig. 3. It was shown that under these conditions there would be no shear in the glue line, but that normal stresses perpendicular to the glue line would be induced as given by Equation [2*a*] for isotropic materials and by Equation [2*b*] for anisotropic materials such as wood.

Assuming, for the sake of comparison with case 1, a 16 per cent change in moisture conditions; that is

$$\epsilon_0 = 16\alpha_t$$

or

$$\epsilon_0 = 16\alpha_r$$

the normal stresses perpendicular to the glue line for the various species of Table 1, are as given in Table 2 under the heading Case 2. As was true of case 1, flat-grain laminations induce higher stresses than do edge-grain laminations, but the difference is considerably greater than was true of Case 1.

It is to be noted that the normal stresses given in Table 2 are maximum compression when the moisture content is increasing, and maximum tension when the moisture content is decreasing.

Here again we have a case in which extreme conditions are postulated. The beam is only two layers thick and both layers are undergoing extreme moisture changes, tending to cause both of them to bow in opposite directions. It must be kept in mind, also, that all the constants are subject to wide variation and that the data supporting all of them are meager. It is entirely probable that some of them change markedly with moisture content. If so, the computed stresses will be altered.

To summarize, depending upon the distribution of moisture during a change in the moisture content of a laminated beam and depending upon whether the change is an increase or a decrease, the extreme conditions are as follows:

1 No normal stress in the glue line, but shear occurring with a sharp maximum at the ends of the glue line. "Rolling" shear stresses as high as 2100 psi or more are indicated under severe conditions.

2 No shearing stresses in the glue line, but normal stresses occurring with a sharp maximum, either compression or tension, at the ends of the glue line. Theoretical stresses as high as 3240 psi are indicated.

In a laminated beam consisting of a number of pieces, the outer laminations would undergo the most marked moisture changes,

TABLE 2 SHEAR AND NORMAL STRESS INTENSITIES IN GLUE LINES

Species	Case 1 τ_{max} —Shear stresses, psi—		Case 2 σ_{max} —Normal stresses, psi—	
	Edge-grain laminations	Flat-grain laminations	Edge-grain laminations	Flat-grain laminations
Ash	1850	2160	1740	3020
Douglas fir	660	880	940	1580
Mahogany	1060	1150	910	1720
Oak	1660	2020	1360	3240
Spruce	420	550	550	1130
Walnut	1590	1590	1330	2130

and the inner laminations would change moisture content along their exposed edges. Under these conditions both shear and direct stress perpendicular to the glue lines would occur, each perhaps one half as large as indicated in Cases 1 and 2. In any event, stresses would probably be concentrated at the ends of the glue lines, tending to cause delamination there.

Conclusions

From an examination of glued timbers undergoing changes in moisture content, it has appeared that delamination, when it occurs, most frequently does so when the moisture content is being reduced. In other words, the dehydrating phase of a moisture-change cycle is the more severe. Not only does glue-line delamination occur more frequently during shrinkage but so also does checking of the wood.

Extensive experimentation and field trials lead to the conclusion that thin laminations are better than thick for gluing, and that wood species with low moduli are better than species with high moduli. Increased strength of the wood when dry abetted by loss of plasticizing water in the glue line apparently are cumulative and a severe test for a glue.

Consideration of the factors causing glue-line delamination should enable timber laminators to produce better, more durable stock. Lower bonding temperatures or shorter high-temperature schedules may be used if the glue-line stresses are reduced, so that in many instances the extra cost of thinner laminations or a thicker beam of a weaker species may be offset by increased production and durability performance. In any event, adhesives must be employed which have both high shearing strength and high tensile strength perpendicular to the glue line both when dry and when wet if laminated beams are to be dependable in service.

Discussion

F. J. Hanrahan.[6] The authors are to be commended for their exploratory mathematical studies on intensity and distribution of glue-line stresses caused by moisture-content changes in wood; also for suggesting a method of reducing these stresses by interlaying thin veneer in each glue line.

There are some features of the paper on which additional data, explanation or discussion would be desirable.

In case 1, it is stated, "These stresses are largely concentrated at the ends of the glue line, decaying toward zero over a distance

[6] Structural Engineer, National Lumber Manufacturers Association, Washington, D. C. Mem. A.S.M.E.

approximately equal to the thickness t, of the lamination." Is this statement based upon internal stress-strain studies or is it an assumption as to distribution of intensity of stress? Does this statement mean that the shear stresses set up at the glue line are independent of the face width (beyond a width equal to twice the thickness of lamination) of the lumber laminations glued together?

The formula for maximum intensity of stress (authors' Equation [1]), appears to contain no thickness-of-lamination factor. Does this mean that the intensity of the shear stresses set up at the glue line due to moisture change is independent of the thickness of the laminations glued together?

Without further explanation it is difficult to reconcile the foregoing quoted statement with the following statement under Case 1: ". . . failure would be progressively inward until the ratio of thickness of lamination to width of unruptured glue line became large enough to cause a diminution of shearing-stress intensity."

Also it would be of interest if the authors could suggest an explanation of why the use of a thin interlayer of low-density low-moduli veneer between laminations of dense strong woods reduces or prevents delamination. Could it be that the thin relatively weak wood flows plastically, tending to permit some relative lateral movement of the denser layers? Or is the movement believed to be purely elastic?

In such a complicated investigation one should not expect complete answers from early investigations but additional light on the subject, if available, would be helpful.

VERNE KETCHUM[7] AND O. H. SCHRADER.[8] Fearing the possibility that the opening paragraph of this paper may leave the impression that delamination of glue lines in laminated wood construction is a common occurrence in service, it is suggested that explanation be included that fabricators do not class such types of glue as waterproof or intended for exterior use, except where adequately protected from the elements.

It would also be desirable to explain the reasons for increased difficulty in gluing with thick laminations. At least three factors enter into this relationship: (1) The problem of accurate surfacing; (2) the effect of dimensional changes that take place after surfacing, both of which are emphasized with an increased thickness; and (3) the difficulty of obtaining intimate contact between laminations as pressure is applied.

Both white oak and Douglas fir have been successfully laminated in quantity for ship parts at the two pilot plants, established by the WPB during the war, and numerous laminated boat parts have successful records of years of service under the severest kind of service conditions. In fact, not a single failure by delamination has occurred in these boat parts, and delamination need not be a problem if adhesives now on the market are used under the conditions for which they are fitted.

The authors leave the impression that the cold-water-mixed room-temperature-setting adhesives, such as casein or urea-resin types, should resist delamination after exposure to exterior conditions. Late tests by the Forest Products Laboratory show that under such service conditions only phenol, melamine, or resorcinol-type glues, employed with careful observance of the required curing conditions, will withstand extreme service conditions. It would be well to indicate that "waterproof" and "water-resistant" are not synonymous terms, as the plywood manufacturers have spent a great deal of money in recent years in attempting to make this plain to the buying public, and to engineers and designers who may employ plywood under a wide range of service conditions.

The formulas and calculations seem valid in so far as the constants employed are valid. However, there are also several other factors which might have a bearing upon the mechanics of the problem:

1 It is known that wood possesses certain "plastic-flow" or "yield" characteristics, although at present no accurate determinations of these factors have been reported in literature. This property of wood is now the subject of extended study at the Forest Products Laboratory. The plastic-flow characteristics of wood are materially affected by changes in moisture content and may be responsible for the observed fact that delamination or wood failure along a glue line is far more evident during the drying or shrinking phase than in the swelling phase of laminated timbers.

2 The assumption is made that a glue line in laminated wood is a continuous sheet or film and is capable of transmitting stresses as a continuous member. Actual observations of glue lines, made after delamination tests or shear tests, disclose that the continuous-sheet theory is not entirely substantiated, but it is found that the glue line is frequently broken and separated into strips which often coincide with the distribution of springwood and summerwood on the face of the lamination.

In summarizing, the authors' conclusions 1 and 2 should both be modified by the consideration of the plastic-flow characteristic which will tend to reduce the computed stresses.

Again, under conclusions, the phrase, "consideration of the factors causing glue-line delamination," is so used that it infers that timber fabricators are not concerned with these factors. This is not the case, as witness the many sound efforts made to improve commercial gluing techniques, the interest in specifications that is being manifested, and the research on this subject that has been carried out in recent years. The fabricator is ready and willing to adopt any practice that will improve the quality without undue increase in cost. The use of low-strength interlayers of thin veneer would seem to increase cost and decrease shear and bending strength.

It would be desirable to distinguish between "delamination," and "wood failure at the glue line," as the former may result from improper laminating practices or improper use of adhesives, while the latter would indicate that it results from severe exposure and may be corrected by providing surface protection of paint, boxing or other type water-resisting coverings.

It is important to bear in mind that laminating is a new industry which is laboring under severe handicaps in the development of machinery and methods adaptable to volume production. It is desirable to make every effort to encourage good practices, provided they are not prohibitive from the cost standpoint, as it is certain that the industry will strongly oppose methods which increase the cost differentials that are now encountered in a competitive market.

T. D. PERRY.[9] This paper reveals a problem in the use of laminated timber that is fundamental, i.e., the internal stresses that may occur within the timber and independent of any superimposed load. However, it is quite unlikely that two adjacent layers will at any time have a net differential of as much as 16 per cent moisture content, since exterior moisture diffuses inward at a diminishing ratio, and even the imperfect barrier of a glue line will not retard such diffusion to any substantial extent. Do the authors agree with this statement?

Another point to consider is the width of the glue joint across the grain of the lumber. It is conceivable that unit stresses would not be troublesome over a 1-in. width, but they might be very serious over a 12-in. width. It is probably a fair assumption that the percentage of shrinking or swelling over a 16 per cent

[7] Chief Engineer, Timber Structures, Inc., Portland, Ore.
[8] Chief Wood Technologist, Timber Structures, Inc.

[9] Development Engineer, Resinous Products & Chemical Co., Inc., Philadelphia, Pa. Mem. A.S.M.E.

moisture-content range might be as much as 2 per cent, which would not be appreciable for pieces 2 or 3 in. wide, but on a 12-in. width it would amount to $^1/_4$ in. It is doubtful whether any adhesive would maintain a strong joint between two pieces of 4/4-in. lumber, one of which was endeavoring to increase its width by $^1/_4$ in., and was restrained only by the strength of the glue line. If the widths were greater or the percentage higher, the magnitude of this stress would be much more serious. Have the authors any comment to make on this?

It has been a rough and ready rule among plywood manufacturers that test pieces, made with a suitable resin adhesive, of an all-veneer construction with $^1/_{16}$-in. veneer layers, can be put through prolonged wet-dry cycles without delamination. When $^1/_8$-in. layers are used, the case becomes marginal and delamination may occur. If, however, $^3/_{16}$-in. or $^1/_4$-in. layers are glued together, delamination is reasonably certain to take place. This has been explained by the theory that the total expansive power of a $^1/_8$-in. layer is about double that of a $^1/_{16}$-in. layer, and in other ranges varies approximately as the thickness. My observation, without scientific analysis, seems to confirm this theory. Therefore, would the thickness of the adjacent layers invalidate or modify any of the assumptions or conclusions made in the paper?

G. M. Rapp.[10] The paper is stimulative and timely; because, within the writer's knowledge, it is the first time that methods of the mathematical physicist and of the structural engineer have been applied to the long-observed phenomena of delaminating surfaces; and furthermore, because the application of laminating and modern gluing techniques, which have been so notably advanced during the war, gives promise of even greater acceleration and much wider use in the immediate future. With the "rediscovery" of wood as one of our foremost structural materials, it is necessary that we advance our knowledge of its behavior under varying conditions of moisture and temperature, quantitatively, rather than to treat these, as heretofore, as anomalies to be allowed for but not accounted for. The authors are to be congratulated for pointing out a specific problem relating to a very important limitation of wood, i.e., its dimensional instability under moisture change in glued assemblies.

The writer has long been interested in the intrinsic causes underlying the delamination of adhered surfaces. Although the authors have confined themselves to wood, the question really is a far more general one to which mathematical analyses can bring much in the way of a clearer understanding of the adverse actions involved and the remedies possible. Not only wood but most organic materials are susceptible to dimensional change with moisture content, with the inevitable result that stresses are produced in heterogeneous assemblies and even in the homogeneous materials themselves when they are subjected to moist environments. It is the writer's opinion that somewhat the same action as postulated by the authors in a simplified example of a laminate, obtains also in paint coatings on wood, ceramic glazes on clay tile, plaster on walls, in fact, in any combination where materials, which are unlike in their moisture-expansion properties, are adhered to each other. He agrees wholeheartedly with the conclusion that the cause of many observed delaminations is induced stresses. For example, the "popping" of an expanding plaster on a wall, the lifting or peeling of paint, the crazing of the glaze on tiles and of portland-cement-mortar overlays. An extreme illustration, and one intriguing to the analytically minded, is the crackling of glass produced by certain glues; a phenomenon put to practical use by the glass technologists.

Furthermore, like the authors, the writer has attempted to evaluate some of these problems as the stress analyst would investigate a bridge or other structure. After all, with a quantitative knowledge of the moisture change and other elastic properties of the materials involved, the only difficulties in obtaining a solution are those of defining correctly the equilibria conditions, establishing reasonable assumptions for simplification, and solving the mathematical equations. Analogous problems exist and have been solved in such cases, for example, as determining the stress performance of bimetallic elements (from unequal thermal-expansion coefficients) and in the calculating of the shear stresses induced in fillet-welded joints in steel members or, again, in theorizing as to the distribution of bond stresses along a concrete reinforcement bar. In all these cases, as in the authors' case, the general pattern of the stress distribution along the joint follows the exponential (e^x) law, which follows naturally from the fact that the changes in stress along the bond line are proportional in some way to the stress itself. Thus it would be expected, as the authors show, that maximum stresses would occur at the ends of the glue line and dissipate themselves rapidly as the neutral point is approached.

It is impossible to comment authoritatively upon the authors' formulas since their mathematical derivations have been omitted from the paper. It is regrettable that this was done inasmuch as the reasonableness and true significance of the conclusions depend so completely upon the mathematical processes. However, the final equations given appear to be rational though apparently simplified by the insertion of certain limits which, although they serve the purpose of a solution for the specific problem, do not permit of generalization. Obviously, the authors have made assumptions in their analysis which do not appear in the paper. Presumably one of these was that there is no slip in the glue line itself. Such an assumption would complicate the mathematics but might be a valuable addition to the theory in view of the greater attention being given to thermoplastic adhesives and to the use of "cushioning" interlays.

The writer objects to the terminology "hygroscopic coefficient of expansion." He would suggest the expression "coefficient of moisture expansion," which applies regardless of whether absorption or adsorption processes are involved, and whether the environment is air with a high water-vapor content or merely liquid water.

In his own attempts to solve similar problems mathematically, the writer has usually ended up with expressions which include the thickness of the laminate. The necessary summation of the distortions from the tensile, compressive, and shear stresses induced in both cases illustrated is dependent upon this thickness factor. The authors have contented themselves with stating that observation has shown adverse results with thicker veneers.

Also, one's attention is drawn to the statement under Case 1, "no normal stresses perpendicular to the glue line are set up." In considering infinitesmal elements directly beneath and above the glue line and the combination of the shear and direct stresses acting upon these elements, the conclusion is inevitable that there must exist a resultant or principal stress which is not parallel to the glue line. These principal stresses, which also exist in beams, have therefore components normal to the glue line, which predicate the presence of tensile or compressive forces, dependent upon the relative magnitude and direction of the shear and direct stresses. Tensile stresses, if they truly exist, may be significant in accounting for delamination. In fact some theorists go so far as to hypothesize tension as a prerequisite for every material failure.

The authors properly point out the greater susceptibility of flat-grain as compared with edge-grain veneers to delamination and checking. This is accounted for by the relatively greater dimensional change tangentially in most woods. The writer

[10] Assistant Director, John B. Pierce Foundation, New Haven, Conn.

has just seen a somewhat dramatic corroboration of this in certain tests in his laboratory involving the moisture changes in edge-grain and flat-grain laminated oak. It is a fact of practical significance worthy of note by fabricators.

The authors are to be commended for the realistic approach which they take in Case 2, wherein they assume a parabolic distribution of moisture content throughout the depth of their sample beam. Because all wood structures absorb and desorb moisture from the outside inward, this has special significance. It might well be pointed out, however, that the induced stresses will be dependent upon the rate at which such moisture gradients are generated within the wood or, in other words, on the time element. This factor, which is well known to everyone experienced in the kiln-drying of wood, offers a possible means of control against delamination in laminating practice, i.e., controlled curing.

In closing, the writer wishes to appeal to the authors to submit their mathematical analyses either in an appendix to this paper or in a future presentation. It is the only foundation upon which the true significance of their results can be appraised.

C. B. Norris[11] and A. C. Knauss.[12] It is difficult to comment on this paper without the inclusion of the mathematical analysis which leads to the results obtained. The mathematical analysis is exceedingly difficult and has not previously been accomplished. Probably some simplifying approximations have been made and the results therefore may be misleading.

It has been found that wood flows plastically at stresses well below the published proportional-limit stresses. This plastic flow will materially modify results obtained by use of the mathematical theory of elasticity. It does not seem that sufficient is known about the plastic behavior of wood to make the solution of the problem possible.

We believe that some of the assumptions and conclusions drawn are not generally applicable to nor borne out in experience with laminated-timber construction, although they may be applicable in certain specific instances.

C. D. Dosker.[13] The authors' suggestions are in line with the writer's observations of the behavior of laminated timbers when exposed to variable moisture conditions. It is true that delamination tends to take place along the exterior edges of the glue lines. It is true, also, that the first evidence of delamination frequently occurs with the first substantial change in moisture content, but does not continue to increase in depth with subsequent moisture changes. The authors' analysis suggests an interesting and seemingly logical explanation of this phenomenon.

One question which occurs to the writer concerns the distribution of stress assumed in Case 2, as illustrated in Fig. 3. No "rolling shear" stress is assumed and this assumption is undoubtedly correct if it is assumed further that there has been no change of moisture content in the fibers immediately adjacent to the glue line. If a moisture change develops adjacent to the glue line, however, and if the glue exerts a restraining influence, it would seem that some shear stress would be present on both edges of the glue line. In the absence of a moisture change adjacent to the glue line, all stress would be normal to the glue line as indicated by the authors.

It is not apparent, however, why this stress should be zero at the center part of the glue line, as is indicated in Fig. 3. On the contrary, it would seem that in the case illustrated, the maximum tension stress should occur at the center point. This, however, would not in any way tend to invalidate the conclusions derived by the authors.

[11] Forest Products Laboratory, U. S. Department of Agriculture, Madison, Wis. Mem. A.S.M.E.

[12] Forest Products Laboratory, U. S. Department of Agriculture, Madison, Wis.

[13] President, Gamble Brothers, Louisville, Ky.

Authors' Closure

The comments made in the foregoing discussions serve the very useful purpose of emphasizing certain aspects of the investigation and of indicating again its limits.

Only two cases, capable of a reasonably close mathematical solution, were selected. These two cases, furthermore, represent two extreme conditions, one in which only shear stresses are induced at the glue line, and one in which only stresses normal to the glue line are induced. Both of these lead to high stress values. In an actual instance, the true condition would probably be intermediate between these extremes.

The discussion re-emphasizes that a 16 per cent change in moisture content is an extreme case. This case was used in computing the values given in the tables, and would represent material changing from fiber-saturation point (green wood) to air-dry. Such a condition would seldom occur.

Basic to all this discussion, of course, is the uncertainty respecting the constants employed. These are known only approximately, are subject to wide variation, and presumably vary considerably with changes in moisture content. Furthermore, as re-emphasized several times in the discussion, wood is probably subject to plastic flow and therefore the constants are subject to considerable modification .

These factors not withstanding, the principal point brought out by the analysis is that both shear and tension perpendicular to the glue line may be induced by changes in moisture content, the stresses may be high, and the maximum intensity is likely to occur at the ends of the glue lines. It follows, of course, that the same stresses exist in the wood directly adjacent to the glue, and the high-quality glues presently employed in the laminating industry have shown themselves capable of withstanding any stresses which wood itself will withstand. Fabricators of laminated timber, who understand and appreciate these various factors, select their adhesives for the conditions under which they are to be employed, and also understand the necessity of taking into account the moisture content of the wood at the time of fabrication as well as in service. The analysis presented in this paper to a large extent substantiates analytically what has been found in a general way to be true by experience, as pointed out in several of the discussions.

As to the question of the nature of the mathematical analysis employed we should like to quote the following paragraph of the paper which had been inserted after the discussors had seen the paper but before the authors had seen the discussions.

"Equations [1] and [2*a*] have been obtained by minimum energy methods. A stress distribution was assumed of known shape in the direction across the thickness of the laminations while the variation of the stresses in the direction of the glue line was determined entirely by the energy method. A further approximation was made by saying that the state of stress was plane. It is believed that the values of the maximum stresses will be changed slightly only if plane strain is assumed instead of plane stress but this should still be confirmed by calculation. With regard to Equation [2*b*] it should be said that this is a plausible generalization of Equation [2*a*] for the isotropic material. Equation [2*b*] has however not been obtained by solving directly the problem for the anisotropic material. It is hoped that the theoretical work leading to the above results may be continued so as to cover the points mentioned as well as to obtain results which go beyond those given here."

The authors are fully conscious of the fact that they have only made a beginning and that much more remains to be done before

the problem of this paper can be considered to be fully solved. They are confident, however, that within the limitations stated the mathematical results will be confirmed by future work.

Early experiments with the use of thin interlayers had led to the belief that stress relief might be obtained thereby. However, continued exposure to alternate wet and dry cycles proved this belief to be in error. It did appear that the interlayers relieved to an appreciable extent the shear stresses, but did not relieve the normal stresses induced during the drying cycle. Statements regarding the use of thin veneer interlayers were omitted at the oral presentation, but unfortunately were in the earlier copies offered to the discussors. These statements are also absent from the final paper.

Considering the question presented regarding the classification of glues into waterproof and water resistant grades, the paper attempts to indicate that glues may be completely waterproof but not able to withstand the normal or shearing stresses imposed during changing moisture content of a laminated beam. Proper selection of the glue must necessarily be dependent on the wood specie as well as the beam size, lamina size, and service conditions to be expected. It would appear that a glue for spruce need not be anywhere near as strong as a glue for oak. Conditions for use of the glue also must enter into consideration, so that the possibility of using a lower temperature of cure, or a less expensive glue with the less stress inducing joints may be worthy of consideration by the timber fabricators.

Tests of Oil-Film Journal Bearings for Railroad Cars

By S. J. NEEDS,[1] PHILADELPHIA, PA.

This paper presents results of a special series of tests made with fitted and broached railway-car journal bearings as part of the program of the Journal Bearing Development Committee of the Association of American Railroads. Three recently developed bearings, each containing less bronze than the old standard A.A.R. bearing, were tested. Comparative tests were run with bath, pad, and waste-pack lubrication. Quantitative effects of fitted and broached bearing surfaces and method of lubrication on operating temperature, frictional power loss, and the all-important minimum film thickness are given. An attempt has been made to separate the friction of the bearing from that of the pad or waste-pack lubricator. Total frictional power losses of the box are given in terms of drawbar pull.

Introduction

IN December, 1941, the Association of American Railroads organized a journal-bearing development committee[2] for the purpose of studying and redesigning the railway-car journal bearing. The main object of this committee was conservation of nonferrous metals. According to recent figures (1)[3] there are about 250,000 tons of nonferrous metals in the journal bearings of railroad rolling stock in this country. Any possible reduction in weight of these bearings, consistent with safety, would mean important tonnages of copper, lead, and tin available for other war purposes. Since there are some 2,000,000 cars in service, and the rate of bearing renewal is about two bearings per car per year, any possible saving would soon become apparent.

The first steps taken by the A.A.R. Journal Bearing Development Committee were to redesign the standard journal bearing and to invite bearing manufacturers and other interested parties having ideas on how strategic metals could be saved, to submit bearings for test. These tests were conducted in the laboratory of the Railway Service and Supply Corporation in Indianapolis under the direction of a full-time resident committee. Bearings successfully passing the laboratory tests were further tested in actual service.

Two obvious methods of reducing the amount of strategic metal in a bearing are to reduce its dimensions, or to replace the metal by some material more plentiful. Since there appears to be no satisfactory substitute for babbitt, reduction in quantity is the only open course. It has been found possible, however, to lighten the bronze back considerably, also to replace a large percentage of the bearing bronze with ferrous metals.

The old standard $5^1/_2 \times 10$ bearing weighed about $25^1/_2$ lb. The bronze back weighed $20^1/_2$ lb, and the $^1/_4$ in. thickness of babbitt lining averaged about 5 lb. In redesigning this bearing the committee reduced the weight of the back by about $2^1/_2$ lb and took the same weight from the lining. Thus 12 per cent of the bronze and 50 per cent of the babbitt were saved. These changes in design not only save 5 lb of metal but have resulted in mechanical improvements by eliminating several sources of trouble in the old bearing. One feature of this improved bearing is the depressed back, patented by E. S. Pearce (2), which applies the load near the ends of the bearing instead of at random, thus permitting the bearing to bend axially and conform to the flexure of the loaded journal. The back is now machined, which increases contact area and thus improves heat transfer to the wedge. Another improvement is broaching or boring the babbitt bearing surface to a uniform diameter which provides a smooth machined surface for the journal instead of the rough cast surface permissible in the old design. The improved bearing, known as the A.A.R. Emergency, D23-5/29/42, is shown in Fig. 1.

A design submitted by the author's company removes another $3^1/_2$ lb from the bronze back of the $5^1/_2 \times 10$ bearing by using ribs instead of solid construction. In this design the load is applied to the back on four properly located bosses. Due to the greater flexibility of the back and the predetermined points of load application, the bearing can flex circumferentially as well as axially. This results in increased bearing area and greater film thickness, which reduces unit load and rate of wear. Thus the $20^1/_2$-lb back of the old A.A.R. bearing has been lightened some 6 lb, or about 30 per cent, with improved bearing characteristics and performance. This bearing is shown in Fig. 2.

A bearing which goes considerably further in conservation of bronze has been submitted by the Railway Service and Supply Corporation. This design, called the "V" bearing (3), abandons the one-piece idea and employs a relatively thin bronze shell fitted into a malleable-iron back. In the $5^1/_2 \times 10$ size this composite bearing requires only 5.7 lb of bronze, as compared with 14.4 lb in the flexible-back bearing, 17.7 lb in the A.A.R. improved bearing, and 20.5 lb in the old A.A.R. bearing. The malleable-iron back weighs somewhat less than $9^1/_2$ lb. This bearing is shown in Fig. 3.

Many other bearings were submitted to the committee for test. The three mentioned are typical examples of practical substitute bearings. They performed well in service and were selected for a special series of tests herein described, to determine their operating characteristics. A full report of the committee's work is beyond the scope of this paper.

---

[1] Service Manager, Kingsbury Machine Works, Inc. Mem. A.S.M.E.

[2] Membership of this committee includes Chairman W. I. Cantley, Mechanical Engineer, Association of American Railroads; C. B. Bryant, Assistant to Vice-President, Research and Tests, Southern Railway System; J. W. Hergenhan, Assistant Engineer, New York Central System; J. R. Jackson, Engineer of Tests, M. P. Lines; L. B. Jones, Engineer of Tests, Pennsylvania Railroad; J. Mattise, General Air Brake Inspector, C.&N.W. Railway; S. J. Needs, Kingsbury Machine Works, Inc., A.S.M.E. Representative; V. C. Barth, C.&N.W. Railway, R. V. Brinkworth, New York Central System, and J. M. Wingert, Pennsylvania Railroad, members of resident committee.

[3] Numbers in parentheses refer to the Bibliography at the end of the paper.

Contributed jointly by the Research Committee on Lubrication and the Railroad Division and presented at the Annual Meeting, New York, N. Y., Nov. 26–29, 1945, of THE AMERICAN SOCIETY OF MECHANICAL ENGINEERS.

NOTE: Statements and opinions advanced in papers are to be understood as individual expressions of their authors and not those of the Society.

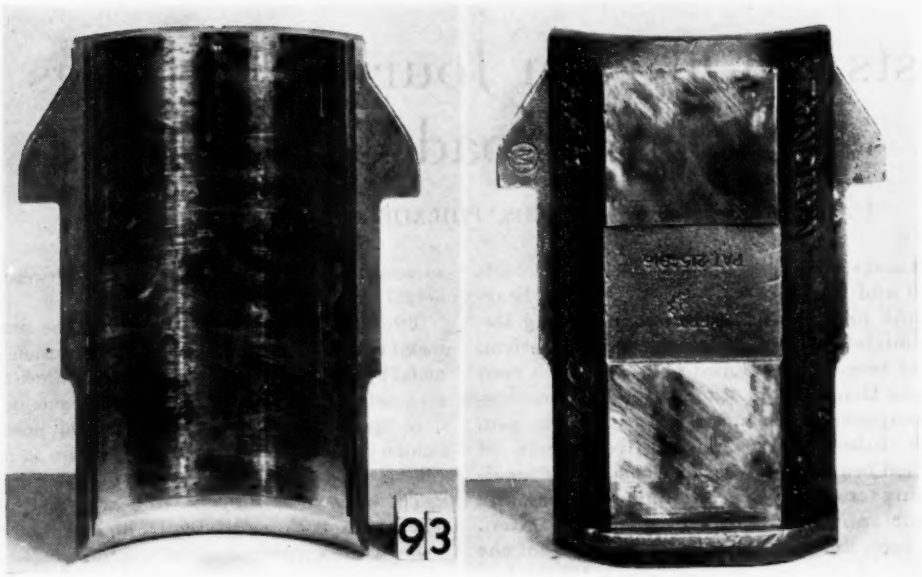


FIG. 1 A.A.R. EMERGENCY BEARING 93 (D23-5/29/42)
(Fitted to test journal under load.)

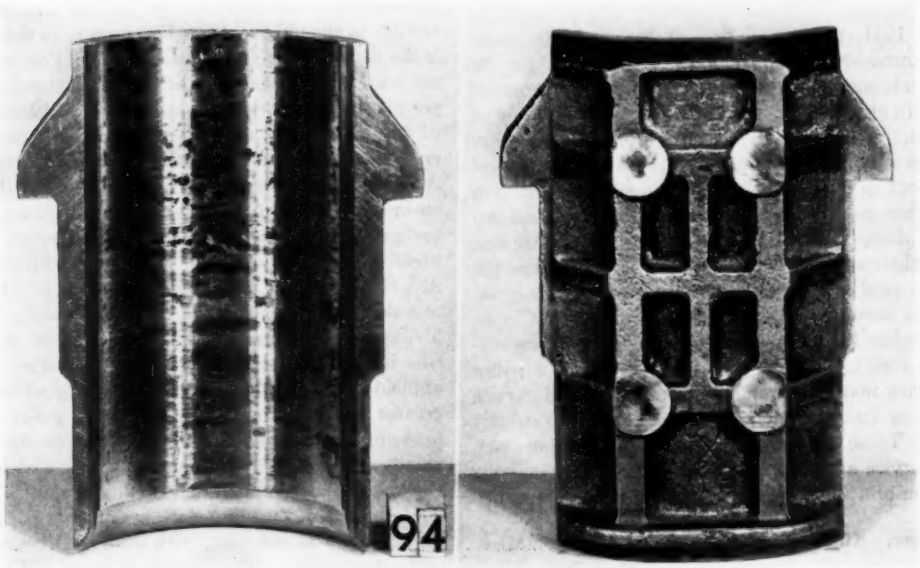


FIG. 2 KINGSBURY FLEXIBLE-BACK BEARING 94
(Fitted to test journal under load.)

FEW IMPROVEMENTS IN HISTORY OF RAILWAY-CAR BEARINGS

Despite the importance of the railway-car bearing and the great number replaced annually, little effort has been made to improve its performance. The basic design of the bearing in use today dates back to the early days of the American railroads. Lack of progress has been due to several factors, perhaps most important of which is the fact that the bearing behaves very well in service without requiring too much attention. Considering the vast number of bearings in operation, actual failures are few and far between. The only machined surface required on the prewar bearing was the bore to which the babbitt lining was applied. In many cases the bearing surface and back were used as cast. For example, the lining of the $5^1/_2 \times 10$ bearing was rough-cast to $5^9/_{16}$ in. diam. Corresponding journal diameter could vary from $5^1/_2$ in. when new to 5 in. before the axle was condemned. The $5^9/_{16}$-in-diam rough-cast babbitt bearing surface was applied to the journal with permissible diametral running clearance from $^1/_{16}$ in. to $^9/_{16}$ in. After establishing load-carrying area by wear, the bearing would run for an average of 4 years under loads often exceeding 1000 psi of actual bearing area, lubricated by oily waste usually contaminated by appreciable quantities of dirt, grit, and water. The journal was finished by roller-burnishing, a process hardly conducive to a geometrically perfect surface. In the general case part of the contamination in the lubricant embedded itself in the babbitt and aided by sidesway, the bearing became an effective lap which improved the journal

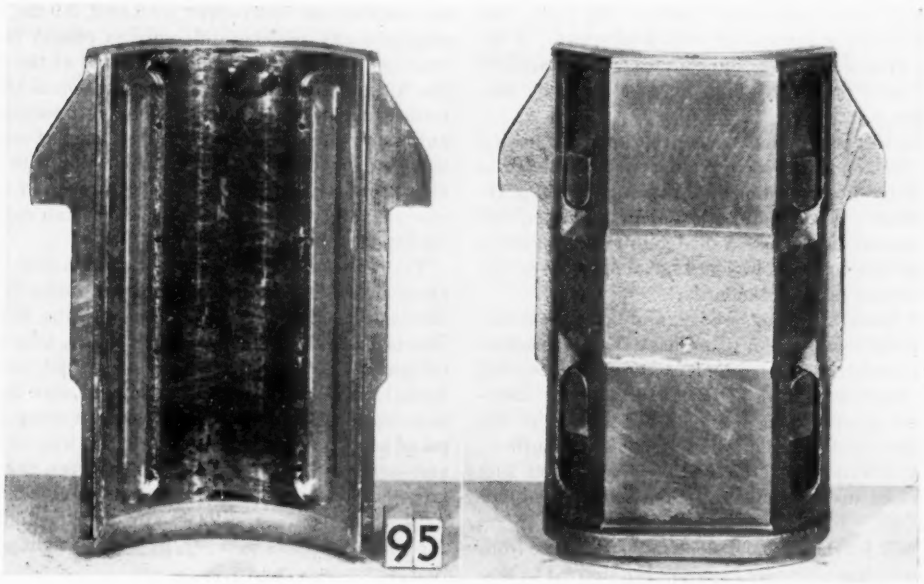


FIG. 3 RAILWAY SERVICE & SUPPLY CORPORATION "V" BEARING 95
(Fitted to test journal under load.)

surface. As bearing area increased with wear, film thickness and load capacity increased and the bearing became safer. After the initial wearing-in period the rate of wear dropped to 0.001 to 0.002 in. per 1000 miles. At the end of its average life of 4 years the bearing was removed for one of many reasons but seldom because of crown wear, since only three in every hundred bearings removed are worn out in the crown.

Considering the geometrical perfection of oil film designed into bearings for modern high-speed machinery, the behavior of the crudely constructed railway journal bearing is most impressive. Occasionally there might be an epidemic of hotboxes but year in and out the general performance has been satisfactory. Hence aside from economic considerations, there appeared to be no urgent necessity for changes.

Regardless of its record, however, the railway-car journal bearing is susceptible of improvement. One reason for improvement is the fact that in 1943 there were about 135,000 "set-outs" due to bearing trouble in freight cars, with resultant loss of time, service, and revenue. It is obvious that the frictional drag of the waste-pack consumes power which could be used in hauling useful load. It is also clear that a better fit between journal and bearing would result in less load per unit of bearing area, increased oil-film thickness, and greater load capacity.

Minimum film thickness is the criterion of bearing safety. In operation a properly fitted bath-lubricated bearing is completely separated from its journal by an oil film of appreciable thickness, except at the moments of starting and stopping. Thus wear is reduced and bearing safety increased. These considerations are not new. Fitted journal bearings are common on European railway cars and replacement of waste pack by bath lubrication has been made successfully abroad (4). The problem has also received some attention here.

To evaluate the possibilities in this direction the committee undertook comparative tests of fitted and broached bearings lubricated by bath, pad, and waste pack. The object of this paper is to describe these particular tests and to draw some general conclusions therefrom.

THE TESTING MACHINE

The machine used for the journal-bearing tests is shown in Fig. 4 and is fully described elsewhere (5). Essential elements of this machine consists of a horizontal axle supported by two roller bearings with a $5^1/_2 \times 10$-in. test journal overhung as in the conventional railway car. The axle is connected through a flexible coupling to a 25-hp d-c motor which draws its power from the city lines through a motor generator set. The machine is able to start under full test load and maintain constant rpm

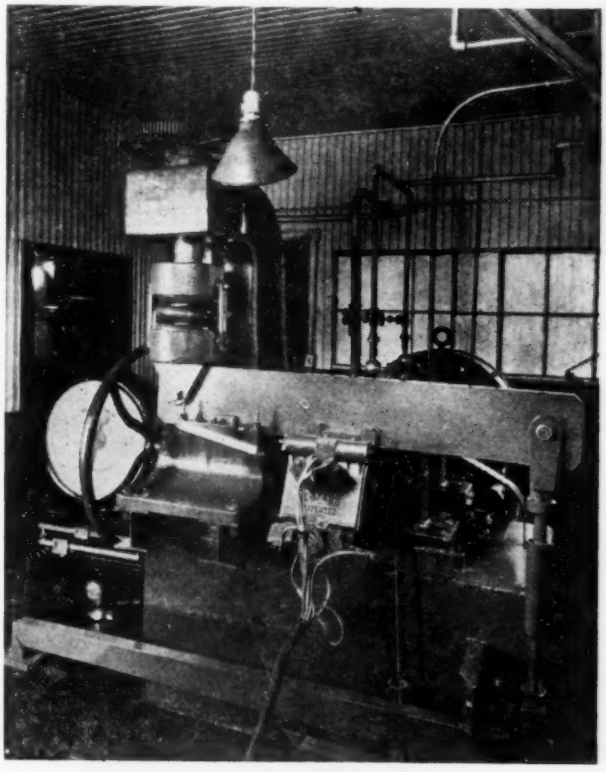


FIG. 4 JOURNAL-BEARING TESTING MACHINE

corresponding to any speed from zero to above 100 mph. An automatic recorder makes a continuous record of speed. A recording wattmeter gives continuous indication of power applied to the motor and more precise readings may be made by ammeter and voltmeter.

The bearing under test is mounted in a conventional box loaded by a beam across the top much as in regular service. Load is applied to the beam by direct-reading scales through an amplifying lever arrangement. During all tests herein described the load was held constant at 16,375 lb. A dust guard was applied to the inside end of the box to control oil leakage. All parts of the box assembly conform to A.A.R. standards.

Temperatures of journal, bearing, wedge, and box were measured by thermocouples located in a plane near the longitudinal center line of the assembly. Journal temperature was measured in a central hole in the journal drilled from the outer end. Bearing temperature was measured in a similar hole drilled in the center of the bronze back parallel with the bearing surface. Wedge temperatures were measured on each side, and box temperatures were measured at several points around the inner side.

Diameter of the test journal was 5.4385 in. A departure from usual railroad practice was made by grinding the journal to size instead of finishing by roller-burnishing. The journal was not reground for these particular tests. An entirely satisfactory surface was obtained with no measurable decrease in diameter by light honing with a fine hard stone.

Bearings, Lubrication, and Oil

Bearings included in this study are shown in Figs. 1, 2, 3, and 5. Bearing 93 is the A.A.R. emergency design D23-5/29/42, manufactured by the National Bearing Metals Corporation. Bearing 94 is the flexible-back design manufactured by the Pennsylvania Railroad from a drawing furnished by the author's company. Bearing 95 is the "V" design of the Railway Service and Supply Corporation, and Bearing 92 is the A.A.R. emergency design manufactured by Magnus Metals Corporation and known as the "Magnus Special."

Analyses of the backs show the metals are closely alike. Average contents are 73.6 copper, 19.8 lead, 5.9 tin, and 0.5 zinc. To eliminate any possible difference in results due to the linings, bearings 93, 94, and 95 were babbitted at the St. Louis plant of the National Bearing Metals Corporation at the same time with metal from the same pot. This babbitt contained 87.1 lead, 8.1 antimony, 4.7 tin, 0.1 arsenic, and a trace of copper. Bearing 92 was lined, by Magnus Metals Corporation, with a metal composed almost entirely of lead. Its contents were 97.6 lead, 1.7 tin, 0.4 calcium, and 0.2 magnesium. The alkali earth was added to harden the lead.

The four bearings were bored or broached to the journal diameter and fitted by hand-scraping under full test load, thus eliminating effects of journal and bearing flexure due to load. Bearings 92, 93, and 94 were each $5^3/_8$ in. long in the direction of motion. This is equivalent to an angular length of 113.2 deg. Actual bearing area was 45.7 sq in. and since the total load in all tests was 16,375 lb, the three bearings carried a unit load of 358 psi of actual bearing area. Bearing 95 was compound-broached, and its fitted length was $2^5/_8$ in. between the two longitudinal grooves. This is equivalent to an angular length of 55.4 deg. Actual bearing area was 22.3 sq in., and the unit load was 735 psi. All bearing surfaces were $8^1/_2$ in. wide at right angles to the direction of motion.

When fitting the bearing surfaces it was noted that the alkali-earth-hardened metal was appreciably harder than the babbitt. This is also shown in the illustrations of the fitted bearing surfaces. Fig. 5 shows the hardened lead lining spotted much as if the metal were tin-base babbitt. Figs. 1, 2, and 3, however, show the spotted areas extending over practically the entire surfaces. This intimate contact was brought about by wear and plastic flow of the high spots under load. The scraper removed most of the metal, and short circumferential back and forth movements of the dry journal under load produced sufficient wear and flow to fit the bearing to the journal. Scratches in the journal, however slight, were imprinted on the bearing surfaces. In fact this metal was so soft that gentle rubbing with clean cheesecloth would produce scratches. Its Brinell hardness was 17.8, as compared with 23.8 for the alkali-earth-hardened lead. Brinell hardness of tin-base babbitt (85–10–5), is about 23.9.

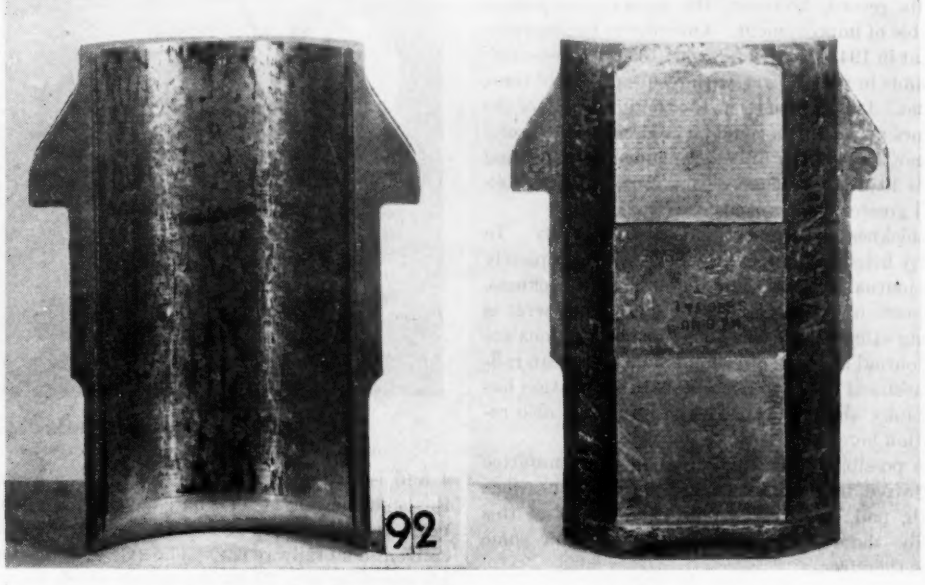


Fig. 5 A.A.R. Emergency Bearing 92; "Magnus Special"
Lined with alkali-earth-hardened lead.)

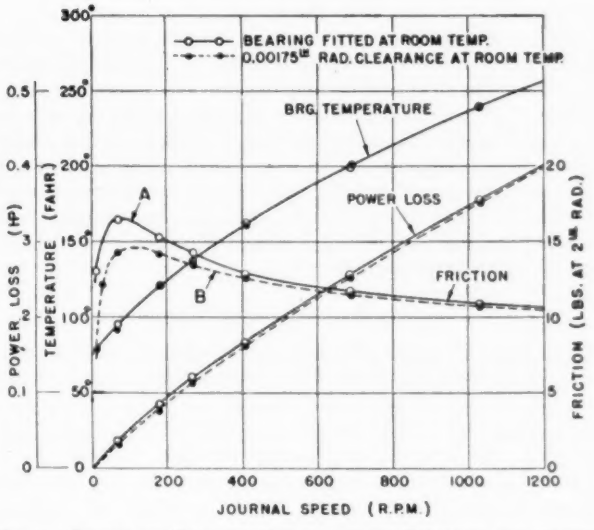


FIG. 6 EFFECT OF BEARING CLEARANCE ON FRICTION AND POWER LOSS

(120-deg centrally loaded bearing; 4 in. diam × 4 in. wide. Load 16,760 lb = 1200 psi of projected bearing area. Atreco XB oil, viscosity $14.4(10)^{-6}$ lb sec per sq in. at 100 F.)

When bronze bearings are fitted to a steel shaft at a given temperature they remain fitted only at that temperature. Bearings 92, 93, 94, and 95 were fitted at about 75 F. Since operating temperatures were well above room, the bearings automatically provided their own running clearance by differential expansion of bronze bearing and steel journal. The importance of this clearance is shown in Fig. 6 which refers to a bath-lubricated 120-deg bronze bearing 4 in. diam × 4 in. long, carrying a load of 1200 psi of projected bearing area. Curve *A* shows variation of friction with speed when the bearing is running with a shaft fitted at room temperature. Curve *B* shows friction variation when running with a shaft 0.0035 in. smaller in diameter than the shaft to which the bearing was fitted. At higher speeds the temperature rise provides running clearance for the fitted bearing, and the increased clearance with the smaller shaft is not particularly effective in reducing friction. At lower speeds, however, the temperature is not high enough to cause much difference in expansion of bearing and journal and these surfaces remain at substantially equal radii. Under such conditions the friction of the fitted bearing is appreciably greater than that of the clearance bearing. At 10 rpm, friction with the fitted bearing is about 70 per cent greater than with the clearance bearing.

In addition to fitting the bearing surfaces, attention was given to the backs and wedge to avoid possible torsion of the bearings when loaded. Some time was also spent fitting the insert of bearing 95 to its malleable-iron back.

In all tests with bath lubrication the oil level was set at $^3/_4$ in. above the bottom of the journal at the start of each run. Oil circulation, thermal expansion, and leakage altered this level during the test but the quantity of oil in the box was kept substantially constant by replacing the small amount lost with fresh oil.

The journal lubrication pad used in the tests was developed by the Railway Service and Supply Corporation. It is described elsewhere (6) and has been successfully used in railroad service. Oil level with the pad was set at $^5/_8$ in. below the bottom of the journal at the start of each test.

The waste pack used for lubrication in these tests weighed 8 lb. It consisted of $3^1/_4$ lb of oil for each pound of new oven-dried cotton waste.

Oil used in the tests was neutral reclaimed car oil. Viscosity was 348 S.S.U. at 100 F, 154 sec at 130 F, and 53.8 sec at 210 F. Specific gravity was 0.9123 at 60 F and 0.8877 at 130 F. Oil from the same barrel was used throughout the study.

TEST OF BEARING WITH ALKALI-EARTH-HARDENED LEAD LINING

Bearing 92, with the alkali-earth-hardened lead lining, was first run bath-lubricated at 40 mph, which is equivalent to 374 rpm of a 36-in-diam wheel. Bearing temperature became constant at 176 F and the test was discontinued at the end of 6 hr. Upon inspection the bearing surface was found practically unchanged. Fitted spots in the central bearing area seemed to have lost some of their polish but were still quite distinct. Several tiny holes were found in the bearing surface near the lug end from which oil seeped as the bearing cooled. If all oil is removed from the bearing surface seepage will continue even at this writing, more than a year after the bearing was tested.

An 8-hr run was made at 40 mph the following day. Final bearing temperature was 196 F. There was no change in appearance of the bearing surface but a longitudinal seam had opened about $1^3/_4$ in. from the entering edge, running parallel with the bearing axis to within about 1 in. from each end. This seam corresponded to the edge of the large babbitt groove which in this design is cast in the back. No doubt the disturbed metal around the edges of this seam had interfered with action of the oil film and accounted for the higher operating temperature.

A run was made next day at 80 mph (747 rpm). The power-input curve was very uneven, and several times the normal motor input of 3.5 kw increased momentarily to more than 7 kw. After about 3 hr of such operation the bearing temperature reached 300 F and then began to decrease. At 6 hr the temperature had dropped to 275 F, and the machine was unloaded and stopped. Upon removal the bearing area was found badly

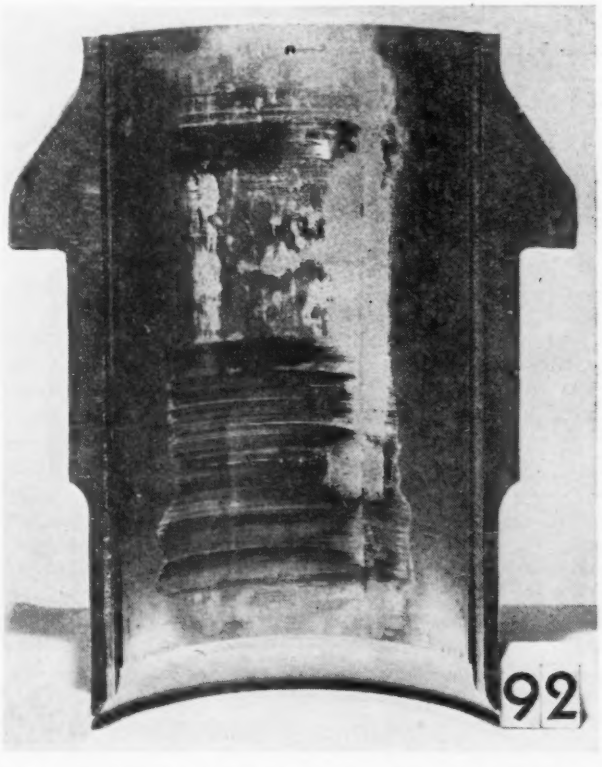


FIG. 7 CORROSION AND WIPING OF ALKALI-EARTH-HARDENED LEAD BEARING METAL

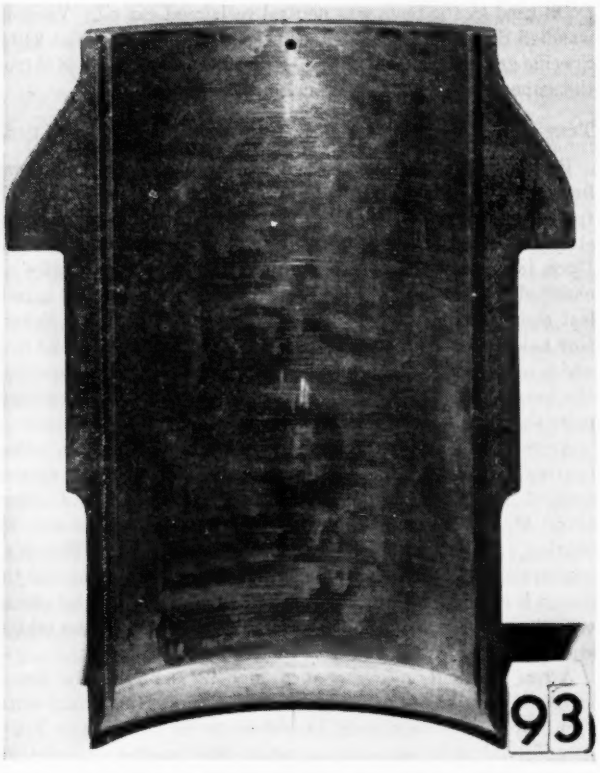


FIG. 8 FITTED A.A.R. EMERGENCY BEARING 93 AFTER TESTS
Note that scraped pattern is still visible after bearing has "traveled" 3680 miles, indicating complete separation of bearing and journal.)

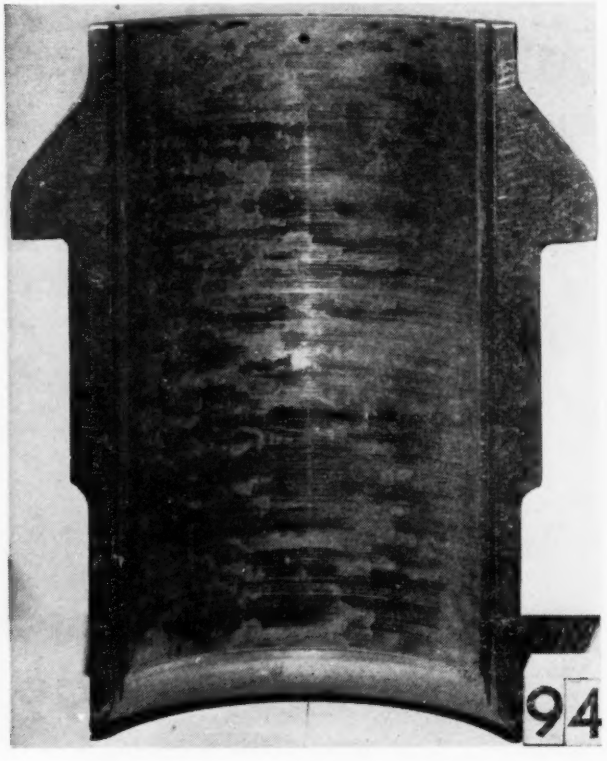


FIG. 9 FITTED KINGSBURY FLEXIBLE-BACK BEARING 94 AFTER TESTS
(Note that scraped pattern is still visible after bearing has "traveled" 3680 miles, indicating complete separation of bearing and journal.)

corroded and in some spots the corrosion had caused wiping, as shown in Fig. 7. Cause of corrosion remains to be determined but the only obvious difference between this run which resulted in failure due to corrosion, and the previous runs in which no corrosion occurred, was an increase in bearing temperature due to increased speed. Corrosion of high-lead alkali-earth-hardened linings had been observed in earlier tests of broached waste-packed bearings. This lining was included in the present study to discover whether or not the phenomenon would reappear when bearing and journal were more widely separated by the thicker oil film of the fitted bearing.

TESTS OF BABBITT-LINED BEARINGS

(*a*) *Fitted Bearings.* Procedure in all tests with babbitt-lined bearings followed the same routine. All bearings were run bath-lubricated before continuing with pad and waste pack. Fresh oil was used with each change in method of lubrication of each bearing. An 8-hr run was made with each bearing at each speed. Machine and bearing were permitted to cool overnight. Approximately one half the test period was required to warm the parts and reach stabilization temperature at which rates of heat generation and dissipation became equal. From then on there was little, if any, temperature change. No special cooling was provided for the box, hence operating temperatures were appreciably higher than would obtain in service where the box is air-cooled as the car moves along. The machine was started and stopped with the load removed to avoid possibility of surface abrasion in the absence of an oil film.

The fitted bearings are shown after the tests in Figs. 8, 9, and 10. Each bearing had "traveled" 3680 miles and except for circumferential scratches, due to insoluble particles passing

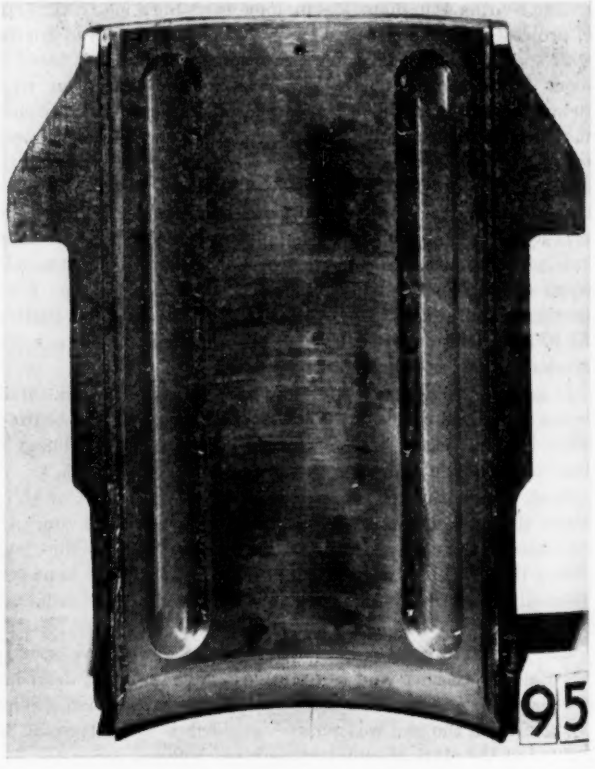


FIG. 10 FITTED RAILWAY SERVICE AND SUPPLY CORPORATION "V" BEARING 95 AFTER TESTS
(Note that scraped pattern is still visible after bearing has "traveled" 3680 miles. Scratches are somewhat more pronounced than in bearings 93 and 94 due to thinner oil film.)

TABLE 1 RAILROAD-CAR $5^1/_2 \times 10$ JOURNAL BEARINGS; BEARINGS FITTED UNDER LOAD[a]

SPEED	40 M.P.H. (373.6 R.P.M.)									80 M.P.H. (747.2 R.P.M.)									100 M.P.H. (934 R.P.M.)								
BEARING	93			94			95			93			94			95			93			94			95		
LUBRICATION	BATH	PAD	WASTE	BATH	PAD	WASTE	BATH	PAD	WASTE	BATH	PAD	WASTE	BATH	PAD	WASTE	BATH	PAD	WASTE	BATH	PAD	WASTE	BATH	PAD	WASTE	BATH	PAD	WASTE
JOURNAL TEMP.	168	195	225	164	200	232	176	207	240	234	261	307	230	270	322	223	279	330	270			275			255		
BEARING TEMP.	166	192	221	164	199	231	174	201	231	232	256	301	229	267	320	219	267	316	266			274			251		
BOX TEMP.	151	142	138	144	141	131	154	147	135	200	171	168	198	173	163	191	189	165	226			231			218		
ROLLER BRG. TEMP.	130	133	137	130	132	135	134	132	138	158	158	164	159	156	168	155	167	165	174			175			172		
ROOM TEMP.	90	90	93	90	90	92	94	90	91	95	88	91	92	88	95	89	95	90	96			96			98		
JOURNAL TEMP. RISE	78	105	132	74	110	140	82	117	149	139	173	216	138	182	227	134	184	240	174			179			157		
BEARING TEMP. RISE	76	102	128	74	109	139	80	111	140	137	168	210	137	179	225	130	172	226	170			178			153		
BOX TEMP. RISE	61	52	45	54	51	39	60	57	44	105	83	77	106	85	68	102	94	75	130			135			120		
MOTOR INPUT (WATTS)	1849	1886	1909	1817	1857	1966	1870	1852	1964	3090	3024	3090	3117	2990	3106	3139	2976	3231	3984			4040			3871		
MIN. OIL FILM (IN) ①	60	46	35	61	42	32	31	23	20	45	40	33	47	37	30	29	21	18	35			31			23		

① MULTIPLY BY $(10)^{-5}$ TEMP. AND TEMP. RISE IN DEG. F.

[a] Load 16,375 lb; journal diameter 5.4385 in. Stabilized running condiditions, 8-hr test runs.

TABLE 2 RAILROAD-CAR $5^1/_2 \times 10$ JOURNAL BEARINGS; BEARINGS BROACHED TO $5^{17}/_{32}$ IN. DIAMETER; DIAMETRAL CLEARANCE 0.093 IN.[a]

SPEED	40 M.P.H. (373.6 R.P.M.)									80 M.P.H. (747.2 R.P.M.)									100 M.P.H. (934 R.P.M.)								
BEARING	93-A			94-A			95-A			93-A			94-A			95-A			93-A			94-A			95-A		
LUBRICATION	BATH	PAD	WASTE	BATH	PAD	WASTE	BATH	PAD	WASTE	BATH	PAD	WASTE	BATH	PAD	WASTE	BATH	PAD	WASTE	BATH	PAD	WASTE	BATH	PAD	WASTE	BATH	PAD	WASTE
JOURNAL TEMP.	172	199	218	167	195	230	170	209	225	213	257	297	207	262	304	215	275	322	241			229			235		
BEARING TEMP.	170	194	213	167	194	230	168	201	216	211	250	288	207	260	302	212	263	307	240			229			232		
BOX TEMP.	148	138	138	142	126	125	144	138	131	176	158	165	172	158	155	178	176	167	198			187			197		
ROLLER BRG. TEMP.	137	140	140	136	131	135	137	134	137	159	155	163	155	160	165	162	161	165	171			165			172		
ROOM TEMP.	100	106	98	98	90	90	100	91	93	94	95	94	98	91	95	103	96	95	99			95			102		
JOURNAL TEMP. RISE	72	93	120	69	105	140	70	118	132	119	162	203	109	171	209	112	179	227	142			134			133		
BEARING TEMP. RISE	70	88	115	69	104	140	68	110	123	117	155	194	109	169	207	109	167	212	141			134			130		
BOX TEMP. RISE	48	32	40	44	35	35	44	47	38	82	63	71	74	67	60	75	80	70	99			92			95		
MOTOR INPUT (WATTS)	1811	1721	1829	1747	1752	1910	1790	1879	1836	3016	2889	2970	2902	2908	2995	2916	2970	3044	3736			3634			3569		
MIN. OIL FILM (IN) ①	16	13	11	20	16	12	14	11	10	16	13	11	20	15	12	14	10	8	15			20			14		

① MULTIPLY BY $(10)^{-5}$ TEMP. AND TEMP. RISE IN DEG. F.

[a] Load 16,375 lb; journal diameter 5.4385 in. Stabilized running conditions, 8-hr test runs.

through the oil films, there is little change in appearance of the surfaces. Original scraped patterns are clearly visible indicating complete separation of bearing and journal during the tests. Scratches on the left or trailing side of bearing 95 seem somewhat more marked than in the other bearings. This would be expected since the film thickness of bearing 95 was less because of its shorter bearing arc. Results of the tests are given in Table 1.

(*b*) *Broached Bearings.* Upon completion of the fitted-bearing tests the bearings were broached to $5^{17}/_{32}$ in. diam. To identify the broached bearings the letter A was added to the bearing number. The same shaft was used as in the previous tests, hence the diametral running clearance of the broached bearings was almost exactly $^3/_{32}$ in. The oil used was from the same source as in the previous tests. The bearings were first run bath-lubricated at 40, 80, and 100 mph, followed by pad- and waste-pack-lubricated runs at 40 and 80 mph. Test results are given in Table 2.

Figs. 11, 12, and 13 show the bearings after the tests. Due to load concentration, a worn or crown area was found in the center of each bearing. The greater the difference between journal and bearing diameters, the shorter the arc of contact and the heavier the load concentration. When difference between journal and bearing diameters is appreciable, application of load causes local deformation of the bearing surfaces, possibly accompanied by plastic flow of the relatively soft bearing metal. Thus the line contact of cylindrical bearing surfaces of different radii is increased to contact over an appreciable area. If the bearing surfaces are smooth and sufficient area is in contact, rotation of the journal introduces an oil film which separates bearing and journal and permits running without wear. If sufficient area is not in contact, wear will continue until the contact area is large enough to permit formation of a load-carrying film. Figs. 11, 12, and 13 show these effects. Under load but not running, intimate contact of the bearing surfaces occurred over an area somewhat less than is shown worn in the illustrations. Running under load, a greater area than that worn was effective in carrying the load. The circumferential scratches covering the worn areas were made by insoluble particles passing through the films. In general, the outline of the worn area is more distinct on the left than on the right. Journal rotation was from right to left and the oil film was thinner on the left or trailing side.

Other things being equal, length of crown area in direction of motion depends on the stiffness of the back and the method of loading the bearing. With an absolutely rigid back, bearing area could be developed only by elasticity, wear, or flow of bearing surfaces. In these tests the bearings showed no signs of plastic flow

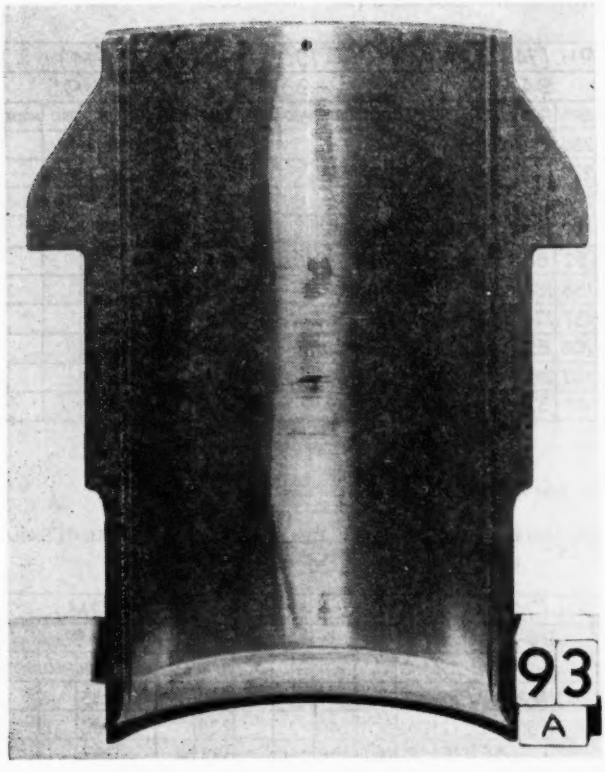


FIG. 11 BROACHED A.A.R. EMERGENCY BEARING 93-A AFTER TESTS

when examined after the runs. The mean crown length of bearing 93-A was found to be 21 deg by planimeter measurements of tracings of worn area. Due to controlled points of loading which permit flexure in the circumferential direction, the mean crown length of bearing 94-A is $27^1/_2$ deg. Mean crown length of bearing 95-A is $17^1/_2$ deg due, no doubt, to the rigidity of its malleable-iron back. Some area on either side of the worn crown probably is effective in supporting load-carrying film. In the absence of definite information it is assumed that this area is of the order of 20 per cent of the worn crown area. Hence, for calculation, useful length of oil film has arbitrarily been taken as 25 deg for bearing 93-A, 32 deg for bearing 94-A, and 21 deg for bearing 95-A. On this basis the same total load of 16,375 lb gives unit loadings of 1625, 1270, and 1930 psi, respectively.

The foregoing runs were repeated after rebroaching the bearings $^3/_{32}$ in. larger than a new shaft diameter of 5.406 in. In addition to the usual tests, runs were made, pad- and waste-pack-lubricated, at 100 mph. The rebroached bearings are designated by the letter B. Due to rebroaching, babbitt thickness was reduced to about $^3/_{32}$ in. and a porous spot appeared in the lining of bearing 93-B. Results were somewhat erratic with this bearing and are not included with the results of the other bearing tests given in Table 3. Comparison of Tables 2 and 3 shows operating temperatures of the A and B bearings in good agreement.

Average results for the three fitted bearings and the five broached bearings are given in Table 4. Calculated bearing losses refer to the test bearing only. Calculation of these frictional power losses is necessary since this information cannot be found directly from the testing machine. For example, consider the fitted bearing running bath-lubricated at 40 mph. Under stable temperature conditions average power input to the motor is 1845 w, from Table 4. Curves are available giving power losses at various speeds and roller-bearing temperatures when the

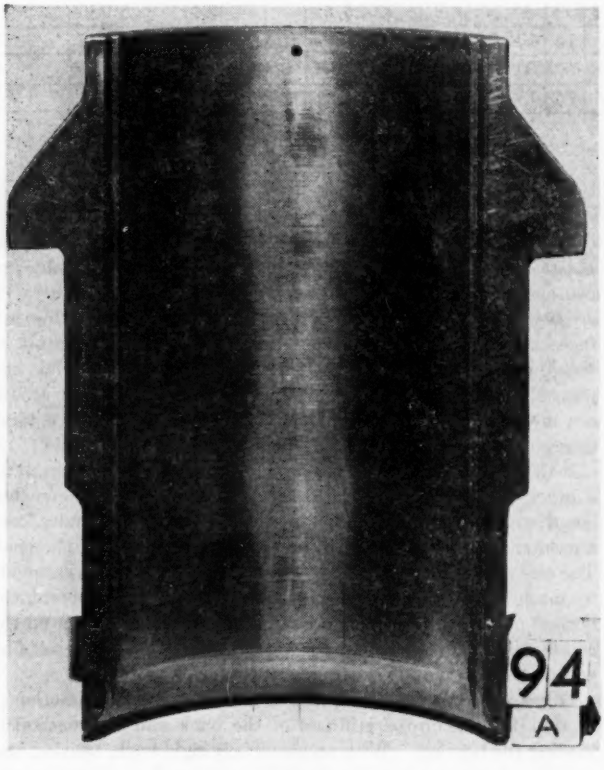


FIG. 12 BROACHED KINGSBURY FLEXIBLE-BACK BEARING 94-A AFTER TESTS

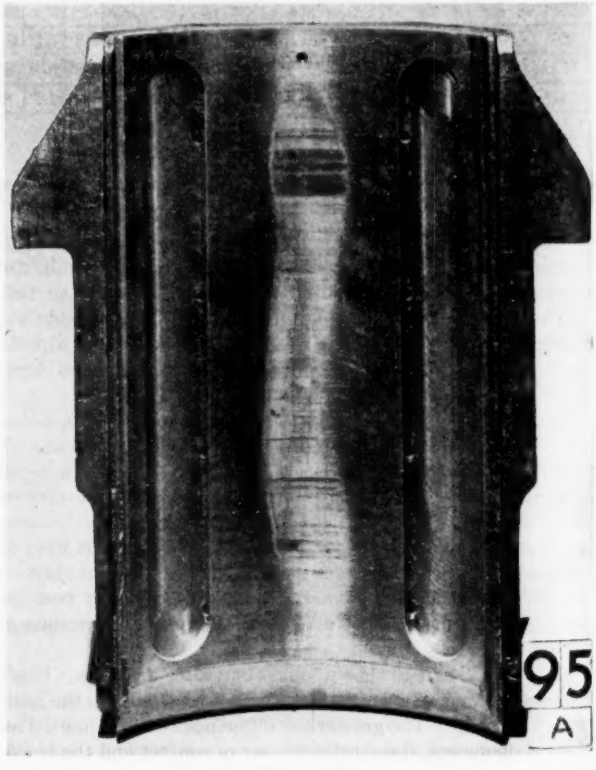


FIG. 13 BROACHED RAILWAY SERVICE & SUPPLY CORPORATION "V" BEARING 95-A AFTER TESTS

TABLE 3 RAILROAD-CAR 5½ × 10 JOURNAL BEARINGS; BEARINGS BROACHED TO 5.498 IN. DIAMETER; DIAMETRAL CLEARANCE 0.092 IN.*

SPEED	40 M.P.H. (373.6 R.P.M.)						80 M.P.H. (747.2 R.P.M.)						100 M.P.H. (934 R.P.M.)					
BEARING	94-B			95-B			94-B			95-B			94-B			95-B		
LUBRICATION	BATH	PAD	WASTE	BATH	PAD	WASTE	BATH	PAD	WASTE	BATH	PAD	WASTE	BATH	PAD	WASTE	BATH	PAD	WASTE
JOURNAL TEMP.	166	199	230	169	205	227	206	264	326	208	302	305	218	289	353	223	351	396
BEARING TEMP.	165	197	228	165	195	216	206	261	323	205	285	289	218	284	349	220	331	375
BOX TEMP.	139	134	128	144	130	126	171	147	159	172	165	152	179	158	163	181	185	177
ROLLER BRG. TEMP.	134	140	138	134	135	137	164	165	165	160	158	168	170	172	170	171	173	173
ROOM TEMP.	89	98	93	93	90	88	93	94	97	93	92	89	95	97	88	94	97	88
JOURNAL TEMP. RISE	77	101	137	76	115	139	113	170	229	115	210	216	123	192	265	129	254	308
BEARING TEMP. RISE	76	99	135	72	105	128	113	167	226	112	193	200	123	187	261	126	234	287
BOX TEMP. RISE	50	36	35	51	40	38	78	53	62	79	73	63	84	61	75	87	88	89
MOTOR INPUT (WATTS)	1869	1857	1860	1821	1822	1907	2855	2806	2976	2910	3040	3008	3299	3295	3649	3426	3634	3816
MIN. OIL FILM (IN) ①	18.0	13.7	11.1	15.5	12.0	10.3	19.7	14.0	10.4	15.8	10.0	9.7	20.2	13.9	10.7	16.0	9.1	8.1

① MULTIPLY BY $(10)^{-5}$ TEMP. AND TEMP. RISE IN DEG. F.

* Load 16,375 lb; journal diameter 5.406 in. Stabilized running conditions, 8-hr test runs.

TABLE 4 AVERAGE OF TEST RESULTS FROM TABLES 1, 2, AND 3; 5½ × 10 RAILROAD-CAR JOURNAL BEARINGS; FITTED AND BROACHED BEARINGS, BATH, PAD, AND WASTE-PACK LUBRICATED

	FITTED BEARINGS							BROACHED BEARINGS								
SPEED	40 M.P.H.			80 M.P.H.			100 M.P.H.	40 M.P.H.			80 M.P.H.			100 M.P.H.		
LUBRICATION	BATH	PAD	WASTE	BATH	PAD	WASTE	BATH	BATH	PAD	WASTE	BATH	PAD	WASTE	BATH	PAD	WASTE
JOURNAL TEMP.	169	201	232	229	270	320	267	169	201	226	210	272	311	229	320	375
BEARING TEMP.	168	197	228	227	263	312	264	167	196	220	208	264	302	228	308	362
BOX TEMP.	150	143	135	196	178	165	225	143	133	130	174	161	160	188	172	170
ROLLER BRG. TEMP.	131	132	136	157	160	166	174	136	136	137	160	160	165	170	173	172
ROOM TEMP.	91	90	92	92	90	92	97	96	95	92	96	94	94	97	97	88
JOURNAL TEMP. RISE	78	111	140	137	180	228	170	73	106	134	114	178	217	132	223	287
BEARING TEMP. RISE	77	107	136	135	173	220	167	71	101	128	112	170	208	131	211	274
BOX TEMP. RISE	59	53	43	104	88	73	128	47	38	38	78	67	66	91	75	82
OIL FILM VISCOSITY ①	2.02	1.24	0.814	0.823	0.546	0.344	0.540	2.07	1.26	0.90	1.06	0.54	0.37	0.81	0.35	0.24
MOTOR INPUT (WATTS)	1845	1865	1946	3115	2997	3142	3965	1808	1806	1868	2920	2923	2998	3533	3465	3733
					*										*	
CALC. BRG. LOSS (HP)	0.242	0.189	0.173	0.441	0.332	0.274	0.548	0.190	0.149	0.125	0.387	0.277	0.230	0.485	0.324	0.266
LUBRICATOR LOSS (HP)		0.080	0.204			0.203			0.038	0.145		0.114	0.261		0.070	0.487
TOTAL BOX LOSS (HP)	0.242	0.269	0.377	0.441		0.477	0.548	0.190	0.187	0.270	0.387	0.391	0.491	0.485	0.394	0.753

① UNITS LB. SEC. PER SQ. IN.-MULTIPLY BY $(10)^{-6}$ TEMP. AND TEMP. RISE IN DEG. F.

* AVERAGE MOTOR INPUT PROBABLY LOW.

machine is unloaded and no test bearing is in the box. According to these curves, 1238 w are required to run the machine when unloaded. With no test-bearing load the roller bearings carry only the weight of the shaft, hence the 607 w difference between power input with and without test-bearing load represents friction of the test bearing and dust guard, and added friction due to the test load on roller bearings and motor. By calculation, test-bearing friction was 0.242 hp or 181 w. This leaves 426-w loss due to dust-guard friction and load on roller bearings and motor. Since the total of these unknown losses is some 2¼ times the power loss of the test bearing, it is obvious that there is no hope of arriving at test-bearing power losses directly from motor input.

It is possible, however, to estimate power losses due to pad and waste pack by assuming that at a given load, speed, and roller-bearing temperature, the machine losses will remain constant. With this assumption any difference in power input in the tests with bath, pad, and waste-pack lubrication can be attributed to variation of friction in the box. From Table 4 the power input for the fitted bearing running bath-lubricated at 40 mph is 1845 w. Calculated power loss is 0.242 hp at the bearing temperature of 168 F. The same bearing, running pad-lubricated at the same speed, requires a power input of 1865 w. In the latter case calculated power loss for the bearing alone is 0.189 hp at the operating temperature of 197 F. Difference in box loss between pad and bath lubrication is 1865 — 1845 = 20 w or 0.027 hp. Therefore total box loss is 0.242 + 0.027 = 0.269 hp, and since the power loss of the bearing alone is 0.189 hp, the difference, or 0.080 hp, represents the power loss due to the pad. In like manner power loss in the waste-packed box at 40 mph is 0.173 hp for the bearing and 0.204 hp for the waste pack at the test temperature of 228 F.

Applying this reasoning to the pad-lubricated fitted bearing at 80 mph, it is found that the total power loss for bearing and pad is 0.049 hp less than the calculated loss for the bearing alone. Apparently, observed value of motor input is low. This is not the case, however, with the broached bearings, and since power

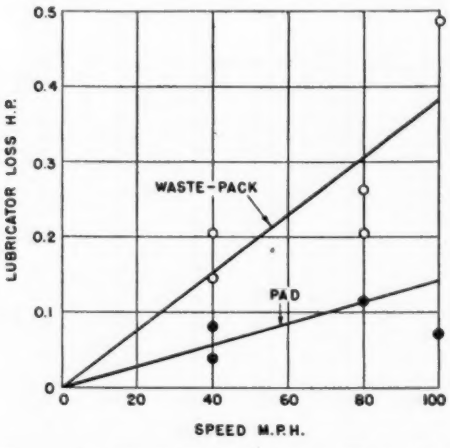


FIG. 14 FRICTIONAL POWER LOSS OF PAD AND WASTE-PACK 5½ × 10 BEARINGS
(Load 16,375 lb.)

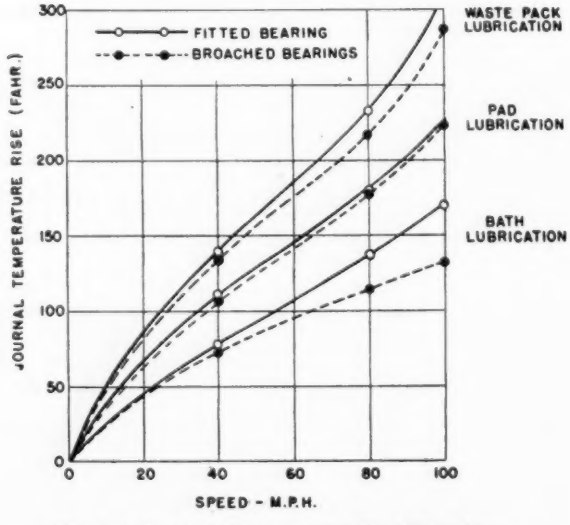


FIG. 15 JOURNAL TEMPERATURE RISE WITH SPEED
(5½ × 10 bearings; load 16,375 lb; average room temperature 93 F.)

losses of the lubricators do not depend on the bearings, the same pad loss would be expected with fitted and broached bearings. To arrive at pad and waste-pack power losses from the test results, lubricator losses in Table 4 are plotted in Fig. 14. Maximum departure of observed points from the curves represents errors in average motor input of about 2 per cent. Since box losses are a relatively small part of motor input, small errors in power measurement are greatly magnified when computing total box loss.

DISCUSSION OF RESULTS

Variation of journal temperature rise with speed is shown in Fig. 15, where the solid lines refer to the fitted bearings and broken lines to the broached bearings. Journal temperature rise in all cases is somewhat less with broached than with fitted bearings. Since friction losses of pad and waste pack are independent of the bearing, lower operating temperatures indicate that the broached bearing operates with less friction than the fitted bearing. Calculation also shows this to be true. Against this slight advantage in friction, however, the broached bearing has the serious disadvantages of considerably less oil-film thickness and higher unit loading due to its shorter angular length. Because of its thinner film the reserve load capacity of the broached bearing is much less than that of the fitted bearing. Greater film thickness and reserve load capacity are the real advantages of the fitted bearing.

Maintenance of sufficient oil-film thickness is the deciding factor in successful bearing operation. When due to overload, overheating, or low speed, the oil film becomes thinner than the heights of the irregularities on the bearing surfaces, these high spots are no longer completely separated and metallic wear occurs. Wear may also be caused by particles in the oil too large to pass freely through the film. All wear is accompanied by temperature increase, and if heat is generated more rapidly than it can be dissipated the bearing eventually overheats and fails. If, however, an oil film thick enough to separate the bearing surfaces completely can be maintained under all conditions, metallic wear will be eliminated and the bearing cannot fail. Factors tending to thick films are high viscosity, high speed, and low unit loading.

In the absence of metallic contact, rate of heat generation depends on rate of oil-film shear. With a given load, rate of shear increases with speed, and heat thus generated reduces film viscosity. Operating temperatures will rise until the gradient between oil film and box is sufficient to dissipate the heat as rapidly as it is generated. This stable temperature may be so high that the increase in film thickness due to speed is more than offset by the decrease in thickness from reduced viscosity; and in that case, film thickness decreases with increasing speed. In these tests this decrease was more marked with the fitted than with the broached bearings, as shown by the curves of calculated oil-film thickness in Fig. 16. In service, higher speeds are accompanied by induced air currents which cool the box, thus maintaining lower operating temperatures and thicker oil films.

Effect of speed and method of lubrication on frictional power loss are shown in Fig. 17, in which average curves are plotted for fitted and broached bearings, bath, pad, and waste-pack lubricated. Power losses in the box are made up of bearing and lubricator frictions. Dust-guard friction and losses due to oil churning are comparatively small and are neglected. In each graph the lower curve represents bearing friction calculated for the conditions of the test. With bath lubrication the only source of power loss in the box is the bearing itself, hence there is but one curve in the graphs for bath lubrication. With pad and waste-pack lubrication, however, friction losses due to the lubricators are added to the bearing friction. These additional losses are represented by the shaded areas in Fig. 17, superimposed on the curves for bearing friction. The upper curves then represent bearing and lubricator friction or the total friction of the box. With each of the three types of lubrication, mean power loss in the box averages 16 per cent greater with the fitted than with the broached bearing. This agrees with the lower-operating-temperature curves for the broached bearings shown in Fig. 15.

From comparison of the shaded areas in Fig. 17, and from the curves in Fig. 14, it is interesting to note that the friction of the waste pack is 2.7 times the friction of the pad. Comparison of shaded and unshaded areas shows the waste-pack friction to be 115 per cent of the bearing friction. Similarly, friction loss due to the pad is 37 per cent of the bearing friction. From this it appears that for all practical purposes the friction of the waste pack is about the same as the friction of the bearing, and the friction of the pad is approximately ⅓ that of the waste pack.

In addition to the friction of pad and waste pack, the heat-insulating properties of these lubricators add considerably to the higher operating temperatures. This is clearly shown in Fig. 18, which gives average results for the three fitted bearings at 80 mph. In each test curves were plotted from temperature readings around the longitudinal center line of the box after equi-

librium temperature had been reached. Mean temperature, found from each curve by planimeter, is listed in the tables as box temperature. Temperatures at the top of the box are little influenced by method of lubrication. Temperatures at sides and bottom, however, are greatly affected by the heat-transmission characteristics of the lubricator. When the bearing is bath-lubricated, agitation by the rotating journal facilitates transfer of heat from journal to box where it is dissipated to the atmosphere. In this case the oil is acting as a coolant as well as a lubricant.

With pad lubrication there is some oil cooling of the journal but the bath is considerably less agitated due to the presence of the pad, and heat transfer between journal and box is less efficient than with the bath. Rubbing of the pad on the journal adds to the heat generated by the bearing and this, together with poorer heat-transfer characteristics from journal to box, accounts for the higher operating temperature. Because of the higher operating temperature, however, oil viscosity has dropped to the point where the sum of bearing and pad frictions is about the same as the friction of the bath-lubricated bearing. Since total friction is the same, the higher operating temperature of the pad-lubricated bearing must be due entirely to the heat-insulating characteristics of the pad.

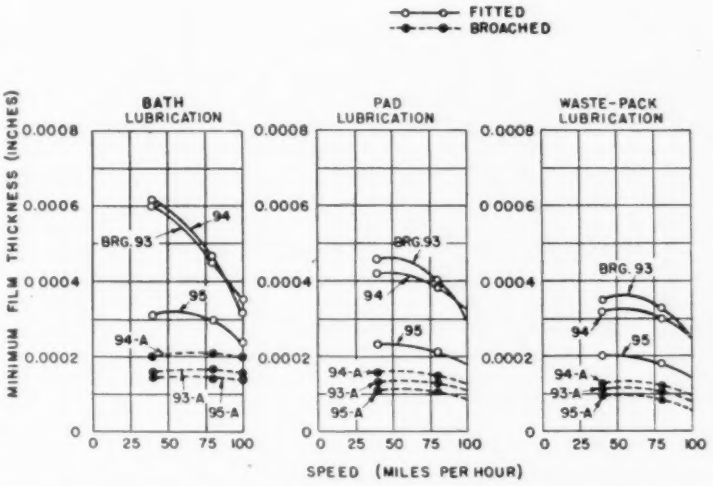


FIG. 16 VARIATION OF CALCULATED MINIMUM OIL-FILM THICKNESS WITH SPEED
($5^1/_2 \times 10$ bearings; load 16,375 lb.)

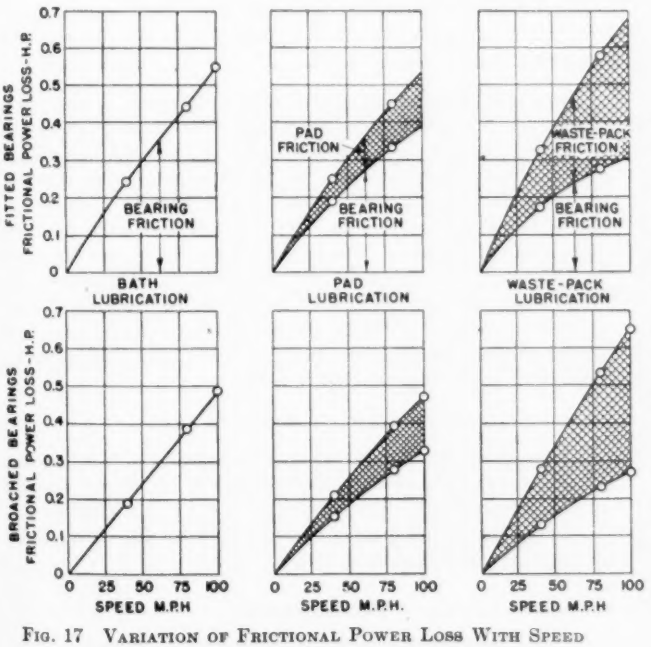


FIG. 17 VARIATION OF FRICTIONAL POWER LOSS WITH SPEED
($5^1/_2 \times 10$ bearings; load 16,375 lb.)

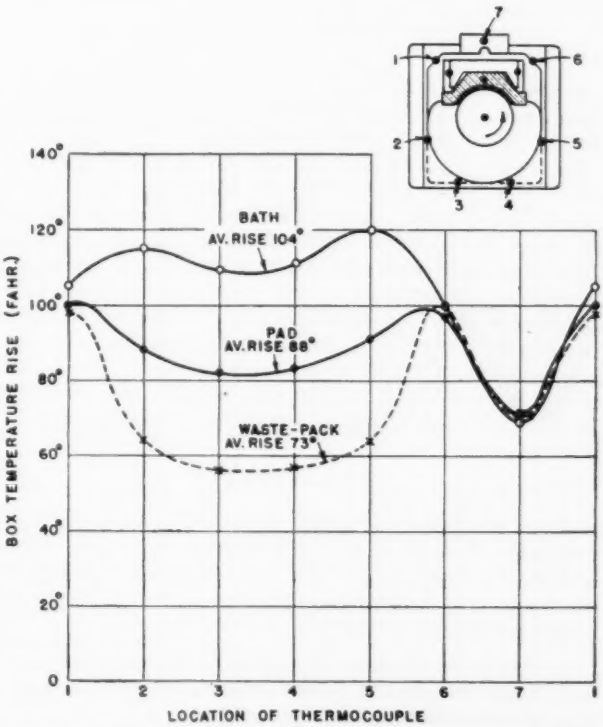


FIG. 18 TEMPERATURE VARIATION AROUND LONGITUDINAL CENTER OF BOX WITH BATH, PAD, AND WASTE-PACK LUBRICATION
($5^1/_2 \times 10$ fitted bearings at 80 mph; load 16,375 lb; average room temperature 91 F.)

The situation becomes more pronounced with the waste pack. In this case there is little, if any, cooling effect of the oil. Friction between waste and journal is relatively high, and the pack acts as an effective heat insulator between journal and box, as shown by the lower box temperature rise. As temperature increases, rate of oil viscosity drop with temperature decreases and decrease in bearing friction becomes less rapid. The sum of waste-pack and bearing frictions becomes greater than with bath or pad lubrication, and temperature gradient between journal and box increases in order to dissipate the additional heat. Higher operating temperatures are undesirable, even when accompanied by reduced bearing friction, since film thickness and bearing safety are less at higher temperatures.

Variation of box temperature rise with journal temperature rise is shown in Fig. 19, for the three methods of lubrication. With perfect heat transmission between journal and box the temperatures would be the same at these points. This condition is represented by the dot and dash line *A*, the slope of which is unity. Slopes of the other curves show clearly the relative heat-insulating effects of the three methods of lubrication. From Fig.

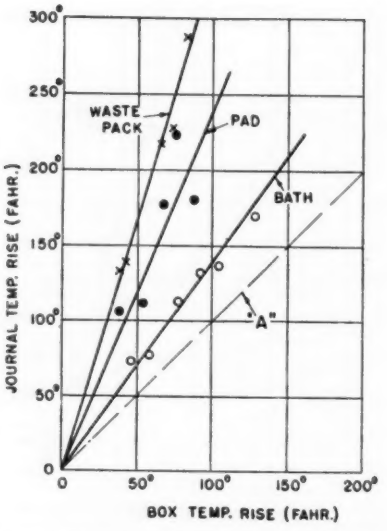


FIG. 19 TEMPERATURE GRADIENTS BETWEEN JOURNAL AND BOX
(5½ × 10 bearings; load 16,375 lb; average room temperature 93 F.)

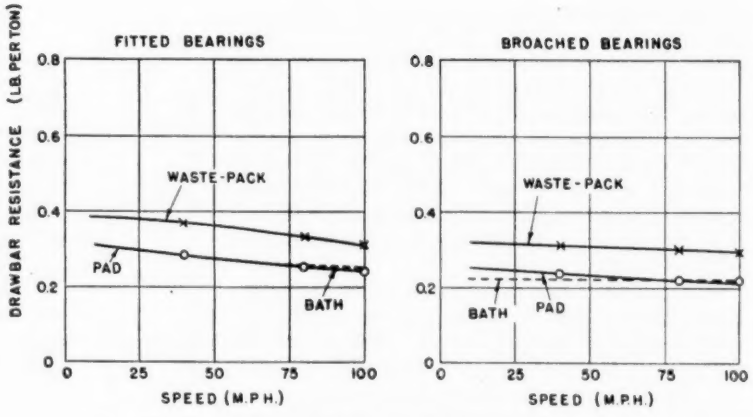


FIG. 20 VARIATION OF DRAWBAR RESISTANCE WITH SPEED
(5½ × 10 bearings; load 16,375 lb.)

19 average temperature rise of the box is 72 per cent of the temperature rise of the journal with bath lubrication, 42 per cent with pad, and 30 per cent with waste pack. The importance of this relationship in maintaining cool bearings is obvious.

Friction losses given in Fig. 17 are readily converted into drawbar resistance. Variation of drawbar resistance with speed is given in Fig. 20 for the fitted and broached bearings, bath, pad, and waste-pack lubricated. Resistance is expressed in pounds per ton carried by the bearing and, as usual, speed is given in miles per hour. A 36-in-diam wheel is assumed. Since frictional power losses with bath and pad lubrication are closely alike, drawbar resistance is also nearly the same. Due to higher power losses with the waste-packed bearings, average drawbar resistance is about ⅓ greater than with the other two methods of lubrication.

CONCLUSIONS

Fitted and broached bearings have been tested at 40, 80, and 100 mph. Data at 20 and 60 mph would have been useful in plotting the curves and for confirming results at the other speeds. On the basis of our present information, however, the following conclusions appear warranted:

1 Pad and waste pack are capable of supplying sufficient oil to maintain complete fluid-film lubrication at speeds at least as high as 100 mph.

2 The railway-car bearing is capable of carrying its maximum load without failure at temperatures at least as high as 375 F.

3 Operating temperatures and frictional power losses are somewhat less with the broached than with the fitted bearing. These advantages are offset by the fact that under similar operating conditions the oil-film thickness of the broached bearing averages only ⅓ that of the fitted bearing. Hence the broached bearing has less reserve load capacity and safety.

4 In a waste-pack-lubricated box, friction of the waste pack is approximately the same as the friction of the bearing.

5 Friction of the pad used in these tests is about ⅓ that of the waste pack.

6 Total friction with bath and pad lubrication are nearly the same, due to the higher operating temperature caused by the pad.

7 Total friction with waste-pack lubrication is higher than with bath or pad despite the higher operating temperatures due to the friction and blanketing effect of the waste pack.

8 Because of its lower operating temperature the bath-lubricated bearing has greater oil-film thickness, hence greater reserve load capacity and safety. This is particularly important at high speeds.

9 Frictional power loss and drawbar resistance of the waste-pack-lubricated bearing are approximately ⅓ greater than with bath or pad lubrication.

10 Method of lubrication has a profound effect on the heat-dissipation characteristics of the box and the temperature gradient between journal and box.

From the foregoing discussion and conclusions it is clear that the crown, or useful load-carrying area of the bearing, should be as large as possible since it results in reduced unit load, increased film thickness, and less wear. It would be interesting to check these conclusions in actual service on a car or tender making considerable mileage per month. The same type bearing could be applied to all journals. One half should be fitted and the other half broached. Wheels, axles, and trucks should be in good condition so that the test would not be terminated by bearing end wear or broken collars. Periodic inspections and careful measurements of wear should give some interesting and impressive information on bearing reliability and life.

ACKNOWLEDGMENT

The author greatly appreciates the assistance of the Resident Committee and the splendid co-operation of Mr. Pearce and his staff. Acknowledgment is especially due L. G. Taylor and J. Roller for the careful manner in which they conducted the series of test runs reported in this paper.

BIBLIOGRAPHY

1 "Secondary Copper for Bearings, War Work, and Alloy Steel," by the Advisory Committee of the National Academy of Sciences to the War Production Board, *Metal Progress*, vol. 42, Aug., 1942, p. 223.

2 U. S. Patent No. 2,154,916.

3 "Composite Railroad Bearing Conserves Copper," by E. S. Pearce, *Metal Progress*, vol. 42, Sept., 1942, p. 368.

4 "Film Lubrication Applied to Railway Axle Bearings," by J. Foster Petree, Proceedings of the General Discussion on Lubrication and Lubricants, The Institution of Mechanical Engineers, vol. 1, 1937, pp. 234–240.

5 "Locomotive and Car Journal Lubrication," by E. S. Pearce, Trans. A.S.M.E., vol. 58, 1936, pp. 37–45.

6 "Report of Committee on Lubrication of Cars and Locomotives," Association of American Railroads, Operation and Maintenance Department, Mechanical Division. Circular No. DV-1006, May 19, 1941, pp. 3–4.

Discussion

P. G. EXLINE.[4] The writer is particularly interested in this paper because of some work of a similar nature carried out at the laboratories of the Gulf Research & Development Company during 1942. A standard A.A.R., 5 × 9 journal and bearing was used for a series of tests to compare the performance of a bearing having a normal diametral clearance of $^1/_{16}$ in. with that of a bearing having 0.005 in. clearance. The load, 30,000 lb, was above normal, while the speed range was equivalent to $2^1/_2$ to 30 mph on a 36-in. wheel.

Measurements were not made of the coefficient of friction, but the bearing temperatures indicated a qualitative agreement with the data reported by the author.

It was noted that after a period of operation at 30 mph, the standard-clearance bearing would often show signs of distress when the speed was reduced to $2^1/_2$ to 5 mph. This did not occur with the 0.005-in-clearance bearings, indicating a higher factor of safety. The standard-clearance bearing also took a longer time to accommodate itself to a reversal of the direction of rotation even though it had been well run-in in the forward direction. In this respect, the low-clearance bearing behaved as one which had been well run-in for both directions of rotation.

The test journal was mounted substantially the same as the Pearce machine, in that it was supported by a spherical roller bearing at the wheel seat. This bearing was cooled by adjusting the temperature of the stream of oil pumped through it. It was found that changes in the temperature of this bearing could influence the temperature of the test bearing. It seems evident that the wheels of a railroad car can act as cooling fins and dissipate an important fraction of the heat developed in the oil film.

The author's results and those of the writer suggest that a properly designed railroad bearing with bath or oil-ring lubrication and having adequate protection against oil loss and tampering would provide trouble-free performance with less maintenance than the present bearings.

M. D. HERSEY.[5] This report not only tells how the problem of conservation of bronze and babbitt was solved, but offers in connection therewith a large amount of carefully checked information on the design and performance of railroad-car bearings. Of special interest is the use made of the theory of lubrication to calculate the "all-important" minimum oil-film thickness, and also the friction loss, with the aid of actual temperature measurements.

Might it not add to the permanent value of this record if the author would refer to the formulas or curves used for these calculations? The necessary procedure is not entirely obvious to the writer, and doubtless many other students of lubrication would appreciate an outline of the steps in a completely worked example.

J. R. JACKSON.[6] It was the writer's privilege to be associated with the author during the test program treated in this paper. The data made available through this research constitute a distinct contribution to the knowledge of railroad-car journal-bearing design and lubrication. Furthermore they indicate the direction for the betterment of the journal-box assembly of the future by utilizing more completely the advantages which an oil-lubricated solid-type bearing has over the present conventional waste-pack journal box.

It is perhaps difficult to understand why the present conventional design of railway-car journal-box assembly has been retained down through the years, and why advantage has not been taken of advances in the art of bearing lubrication to replace the waste-pack originally used and continued without essential change on the American railroads for a hundred years. The answer is simplicity and reliability together with long-established standards and practices of operating cars in interchange service, and the relatively large number of units in use.

It probably should be stated that the simple expedient of removing the waste pack and filling the bottom of the journal box with oil, as was done during the laboratory tests, would not work out in service because the oil could not be retained in the box. Bath or flood lubrication would necessitate a redesign of the conventional box to insure oil retention. This question of oil retention in the conventional journal box is also pertinent, in lesser degree, to some forms of pads or wick-type lubricators which have had limited service trials on railway equipment in this country. Completely redesigned journal-box assemblies, employing flood lubrication and other refinements, including provision for oil retention, have been developed and used in considerable numbers on some roads on equipment operated in on-line service. These have not found sufficient favor to be considered for adoption as standard in interchange freight service.

The increasing use of roller bearings for passenger equipment and their development for freight equipment will no doubt result in a reconsideration of the design, service, and economics of railway-car journal bearings in the immediate future. It is felt that this paper is a distinct contribution to the literature on this subject, and that a similar line of investigation of the roller bearing for railway equipment should be carried out.

L. B. JONES.[7] In studying this report it should be borne in mind that the comparison between broached and fitted bearings was made with broached bearings which were just "starting out," so to speak. In other words, in actual service the broached bearing will continue to enlarge its contact area until it approaches the condition of the fitted bearing, with resultant improvement in oil-film condition.

While the tests were run mainly to determine oil-film conditions, it will be of interest to railroad men to note that the A.A.R. standard journal lining gave a good account of itself, and nothing developed in the test to indicate the necessity for a change in its composition.

The two principal indictments of the time-honored waste pack, pointed out by Mr. Pearce in his comments on this paper, are again high-lighted in this report. The actual friction of the waste pack is equal to, or greater than, the bearing friction; and it also acts as a thermal insulator to discourage radiation of heat from the journal.

The drawbar resistance in pounds per ton due to the friction load on the journal, as indicated in Fig. 20 of the paper, shows that the journal friction is a relatively small part of the total resistance of loaded freight cars on level track, as determined by dynamometer tests. It therefore appears that improvements in journal-box performance will pay their largest dividends in hot-box insurance rather than in decreasing the rolling resistance of the train.

F. K. MITCHELL.[8] The author prefaces his remarks on the his-

[4] Section Engineer, Gulf Research & Development Company, Pittsburgh, Pa. Mem. A.S.M.E.

[5] Research Associate in Mechanical Engineering, Massachusetts Institute of Technology, Cambridge, Mass. Fellow A.S.M.E.

[6] Engineer of Tests, Missouri Pacific Lines, St. Louis, Mo. Mem. A.S.M.E.

[7] Engineer of Tests, The Pennsylvania Railroad, Altoona, Pa. Mem. A.S.M.E.

[8] Assistant General Superintendent of Motive Power and Rolling Stock, New York Central System. Mem. A.S.M.E.

tory of the improvements on railway-car bearings by the statement, "Despite the importance of the railway-car bearing and the great number replaced annually, little effort has been made to improve its performance." If he intended to say by that remark that the bearing itself had undergone very little improvement prior to the war period, his statement is unquestionably true, but the insinuation that little effort has been made to improve the performance of the bearing cannot be substantiated. Over the years, journal boxes, dust guards, wedges, and other related parts used in the assembly, of which the journal bearing is a part, have been subjected to a great deal of experimentation, and many important facts have been learned thereby, and certain very productive changes worked out and put into practice.

It is essentially true that the most extensive changes in the bearing itself have come about since the beginning of the war, and are children of necessity. These changes involved not only the bearing but also the lining and were promulgated through the necessity of minimizing the amount of critical materials required to produce a bearing of a certain size. As to the lining, the efforts in this respect have been confined generally to reducing its thickness and to producing a lining made of substitute material, both in order to save babbitt. It is generally conceded that the reduction in the thickness of the lining accomplished the required end. Substitute lining described by the author as a metal composed almost entirely of lead, alkali-earth-hardened, has not been entirely satisfactory, which fact cannot be discounted. On the other hand, the results so far obtained in the use of such a lining certainly do not warrant the complete discarding of the idea of its use. On the contrary, it is evident from the experience to date that further experimentation and development of such a lining offer worth-while possibilities.

The second series of major changes in the bearing itself, made to reduce the amount of critical material in the bearing back, has been enlightening, and also seems to be producing the desired results. There are still some features in connection with the various redesigned backs which have been offered for this purpose that need further study. These studies will no doubt be undertaken by the committee, of which the author is a member, in due time. Further comment in this regard will be made later.

It is unfortunate that the laboratory test equipment which was used to make the study under discussion does not duplicate in a practical manner the actual service conditions to which bearings are, in fact, subjected. It will be noted that the bearings were subjected to a constant uniform load of 16,375 lb. In actual service the load, of course, varies. Furthermore, in actual service the bearing is subjected to severe vertical and longitudinal shocks which the test equipment as used was unable to duplicate. This, it is felt, in itself materially affects the practicability of the information developed. It is pointed out by the author, under "Discussion of Results," "maintenance of sufficient oil-film thickness is the deciding factor in successful bearing operation." Therefore it would appear quite evident that the maintaining of such an oil film under the conditions imposed by the test apparatus is an entirely different problem from that which is found in actual service where, even under normal conditions, the bearing is constantly being disturbed by vertical shocks originating from uneven rail joints, etc., and longitudinal shocks arising from brake applications, slack action, etc.

While discussing the matter from the point of view of oil film, it should also be understood that with the laboratory test equipment used in these experiments, the journal being the driving instead of the driven element, the greater bearing clearance occurs on the rising side of the journal, whereas in actual practice the journal is driven by the bearing and the greater clearance is on the opposite side of the bearing. Hence under laboratory conditions the oil film produced by any method of lubrication, and under any bearing conditions, would be more favorable than under circumstances of actual usage where the clearance is the minimum on the rising side of the journal.

These facts in themselves make questionable the acceptability of some of the results obtained in this series of tests. They certainly do so to the point of discrediting the definite conclusion that "pad and waste pack are capable of supplying sufficient oil to maintain complete fluid-film lubrication at speeds at least as high as 100 mph, and that "the railway-car bearing is capable of carrying its maximum load without failure at temperatures at least as high as 375 F." Here it might also be noted that because many failures of bearings result from causes other than heat generated, the design of the back is an important factor, and unless it is shown that the back, however physically composed, is not only so designed as to distribute uniformly the load over the bearing area, but also is of such strength as to prevent breakage, then it cannot be concluded that the railway-car bearings tested were capable of carrying their maximum load without failure; this regardless of temperature. It is quite obvious that no failures from causes other than heating would be expected when the tests were conducted with the laboratory equipment which was used in these experiments, and the answer to this question was not obtained for any of the bearings under test.

It might also be said in passing that in the observation regarding heat transfer from the bearing to the related parts of the bearing-and-box assembly two confusing statements are incorporated in the report. The first is that the depressed-back (E. S. Pearce patent) bearing applies the load near the ends of the bearing instead of at random. Actually, this bearing applies the load over all but the one third of the area in the center. The application of the load near the extreme ends of the bearing has long since been proved to be mechanically incorrect. It is further stated that the back of the so-called "depressed-back bearing" is now machined. It will be found on check of the records that only a few railroads actually machine the back of the so-called "depressed-back bearing" for bearings used in passenger service, and that generally no roads are machining the depressed-back bearing used in freight service.

As to the transfer of heat, because of the greater contact area and therefore the improved heat transfer to the wedge, it will be interesting to note that bearings 93 and 95 have the large back area referred to, whereas bearing 94 has only four small bearing areas, nowhere comparable to that offered by bearings 93 and 95, yet the tests show that bearing 94 produced journal-temperature, bearing-temperature, and box-temperature rises at various speeds which generally lay between that of bearings 93 and 95. No explanation for this fact either in the case of the fitted bearing or the broached bearing is offered.

Regarding the question of whether or not the broached and unfitted bearing is more satisfactory than the broached and fitted bearing: The author concludes, and the data developed indicate, that better results can be expected from a fitted bearing. While this is interesting, and no doubt true, it has no practical value for the reason that the expense and delay involved in fitting the bearing, particularly to freight cars, would in no wise be offset by the results obtained.

The data developed and conclusions reached in connection with the relative values of bath, pad, and waste lubricating systems would indicate that the committee has concluded from the results obtained that waste-packed lubrication is less satisfactory than pad lubrication and bath lubrication. This is no doubt true if it were not for the practical side of the problem. Certainly bath lubrication is a far cry from being practical at present. Pad lubrication is more or less in its infancy and offers considerable possibilities, yet, at the moment, the writer knows of no practical means of avoiding excessive loss of lubricant in the present freight-

car box assembly where either bath or pad lubrication is used. Here again a factor arises which the test equipment used by the committee does not bring out. The entire matter does emphasize the necessity for further experimentation and development along the desirable lines indicated by the tests.

As to the effect on drawbar resistance, neither the data having to do with the friction of the broached or unbroached bearing nor pad nor waste-packed boxes are of much practical value.

It is worthy of note that speeds for use in connection with these experiments (40, 80, and 100 mph) were selected. While 40 mph represents pretty closely the present freight-train movement, the immediate future no doubt will mean speeds for freight-train movement between the figures of 40 and 80, throughout which range the report is silent as to what might be expected. The author comments on this fact in his conclusions. It is regrettable that data were not also secured for speeds of 50, 60, and 70 mph.

While as previously indicated, the data submitted in this report are interesting, although in a great many respects somewhat impractical, it is respectfully suggested that either test equipment which will more closely simulate actual operational conditions should be designed and used for such a series of experiments, or final conclusions should be based on actual experience in the field.

E. S. Pearce.[9] On certain phases of railroad journal operation this paper sets out most clearly two points of general and practical interest:

1 The very low power loss chargeable to the conventional journal-box assembly.

Power loss in journal friction as a factor in total train resistance is a particularly timely subject, as the railroads are contemplating operation at higher maximum and higher average speeds. The values given by the author cast considerable doubt on the advisability of substitution of roller bearings for solid bearings as a matter of sound economics.

2 The separation of the power loss between bearing and lubricating medium.

To those confronted with the everyday problems of journal operation, the significance of packing friction losses relative to those of the bearing alone will be of considerable practical interest.

Analyzing the author's paper in the light of the two major disclosures, obviously, much of constructive value to the railroads in the operation of a conventional journal-box assembly would result from a further exploration of this subject through a lower range of speeds and temperatures in combination with various methods of lubrication, lubricants, and bearing construction now available.

The accepted formula for calculating freight-car resistance on straight level track is[10]

$$R = 1.3 + \frac{29}{w} + 0.045V + \frac{0.0005AV^2}{wn} \quad \ldots\ldots [1]$$

Fig. 21 of this discussion has been superimposed upon the author's Fig. 20 demonstrating what a small portion of total resistance can be charged to journal friction at the load and speeds used in the paper.

The values given by the author for power losses are roughly one tenth of that given by the first two terms of Equation [1] of this discussion.

Journal operating temperatures in this paper are at a level much higher than the generally accepted limit for safe performance in service. This is due in large part to operation in the still air of the laboratory. Pearce[11] shows the magnitude of this difference at lower speeds than covered in this paper.

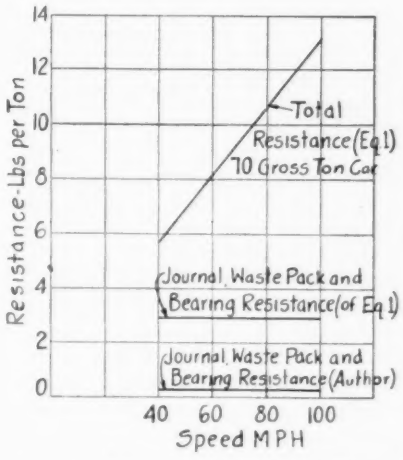


Fig. 21 Relation of Journal Resistance to Total Resistance of a Freight Car

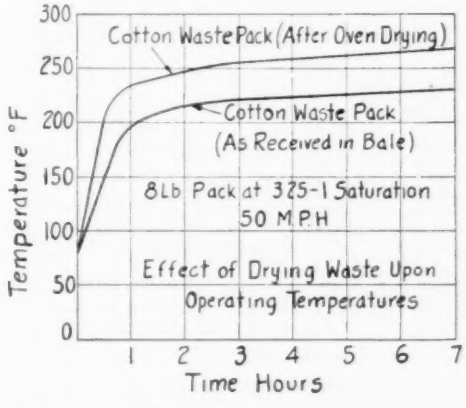


Fig. 22 Effect of Drying Waste Upon Operating Temperatures

Another contributing factor to the high temperature obtained with the waste pack was the use of "oven-dried" waste as so designated by the author. In investigations of this kind, in the interest of accurate duplication of results, oven-drying of waste is done to offset the variation in moisture content and the effect on temperature which would otherwise exist between various samples of waste. In preparing the waste for test purposes it is dried at a temperature of 220 F. The effect of this drying upon operating temperatures is shown in Fig. 22 of this discussion.

The contribution of the lubricating medium to the total power loss of the bearing assembly has never been fully appreciated. The placing of a waste pack in a journal box is very similar to the installation of an opposed bearing, as there is an upward pressure of the waste pack against the lower half of the journal. Fig. 23 shows how this contributes to the elevation of the running temperature as the amount of packing at the same oil-waste ratio, is varied in the same journal box.

To verify the power losses of the lubricating medium, as shown in Fig. 14 of the paper, a study was made of the reduction in power input to the driving motor by the momentary lowering of the lubricating medium from contact with the lower half of the

[9] President, Railway Service and Supply Corporation, Indianapolis, Ind. Mem. A.S.M.E.

[10] "The Steam Locomotive," by R. P. Johnson, Simmons-Boardman Publishing Corporation, New York, N. Y., 1944, p. 184.

[11] "Temperature Distribution and Sources in the Conventional Railway Journal Box," by E. S. Pearce, Trans. A.S.M.E., vol. 62, 1940, pp. 633–638.

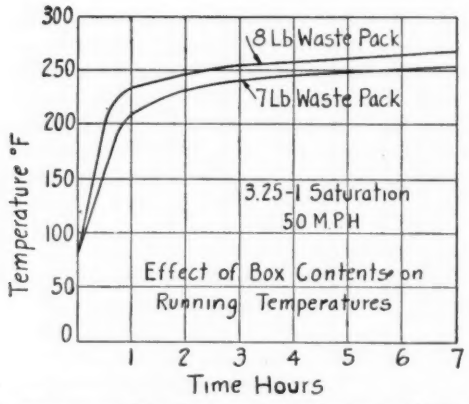


FIG. 23 EFFECT OF BOX CONTENTS ON RUNNING TEMPERATURES

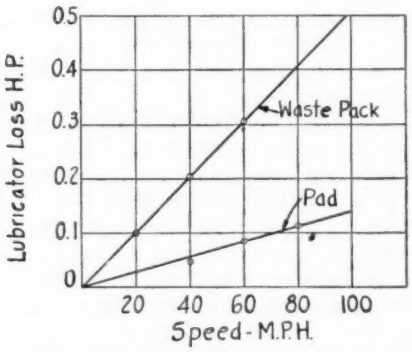


FIG. 24 FRICTIONAL POWER LOSS OF PAD AND WASTE PACK, AS DETERMINED BY MOMENTARILY DROPPING LUBRICATOR FROM CONTACT WITH JOURNAL

journal. This was accomplished by the use of the bearing described by Pearce[12] as bearing No. 18, this bearing being capable of operation for sustained periods on the stored oil. This time interval was quite adequate to take the necessary instrument readings. The box used was split on its horizontal center line and mounted on a jack so that it could be quickly lowered and again raised. Results are shown in Fig. 24 of this discussion, and comparison with the author's Fig. 14 indicates that the calculated loss of the lubricating medium is in good general agreement with the experimental findings.

R. J. SHOEMAKER.[13] In connection with the results obtained with pad lubrication reported in this paper, we may state that one of the major trunk-line railroads of this country has been using pad lubrication (Magnus type) very successfully for a number of years past in connection with oil lubrication of driving-box brasses of main passenger and freight power, also on main-line passenger cars, locomotive tender, and locomotive truck and trailer brasses.

By the use of pad lubrication, considerable economy of operation has been accomplished as shown by reduction in the number of hotboxes, increased service life of bearings, and corelated parts, reduction in friction, etc., as compared with results obtained with conventional lubrication formerly used.

With regard to the economy of materials accomplished in the tests of new types of bearings reported in the paper, the author states, "Since there appears to be no satisfactory substitute for babbitt, reduction in quantity is the only open course." The author further states that in redesigning the prewar type of journal bearing, the babbitt metal was reduced 50 per cent in weight, or in other words, reducing the lining metal from $^1/_4$ to $^1/_8$-in. thickness, as was done in the A.A.R. emergency-type bearing used in the early years of the war. However, in view of the unsatisfactory performance in service of this $^1/_8$-in. lining, the babbitt metal was later restored to its original $^1/_4$-in. thickness, as now used by the railroads in the present type of A.A.R. emergency journal bearing.

[12] "Locomotive and Car Journal Lubrication," by E. S. Pearce, Trans. A.S.M.E., vol. 58, 1936, pp. 37–45.

[13] Magnus Metal Corporation, Chicago, Ill.

TABLE 5 DEGREES BRINELL HARDNESS OF VARIOUS BEARING METALS

(500 kg load)

Deg F	Satco	Tin-base babbitt	A.A.R. babbitt	Antimonial lead
70	23.8	22.2	17.8	15.0
212	17.2	12.9	9.5	6.2
300	12.0	7.6	4.2	*
400	7.7	*	*	*

* Indicates metal too soft to measure hardness using 500-kg load.

TABLE 6 COMPRESSIVE STRENGTH OF VARIOUS BEARING METALS

(Pounds per square inch; 25 per cent deformation)

Deg F	Satco	Tin-base babbitt	A.A.R. babbitt	Antimonial lead
70	16300	17200	15600	13000
212	10200	7500	6100	5000
300	7000	4000	2700	1100
400	3700	2000	1200	*

* Metal too soft to determine compressive strength due to excessive deformation.

With regard to a satisfactory substitute for babbitt metal, we may mention that our company developed and put on the market a number of years ago an alkali-earth-hardened lining metal for bearings known as "Satco" metal, which is having widespread and successful use as a substitute for lead- and tin-base babbitts, block tin, etc., in various types of railway and other bearings.

This metal is a lead-base alloy containing from 95 to 98 per cent lead with the balance calcium, tin, and other hardeners. It contains no antimony or copper. During the late war great economies were effected by the use of Satco bearing metal in vital materials such as tin, copper, antimony, etc.

Satco metal has a melting point approximately 150 F higher than that of babbitt metals with a correspondingly greater hardness at elevated temperatures. Tables 5 and 6 of this discussion show comparative physical properties of Satco metal, A.A.R. babbitt, tin-base babbitt and antimonial lead at normal and elevated temperatures.

Because of its greater heat resistance Satco-lined bearings perform satisfactorily at temperatures which cause failure by melting in babbitt-lined bearings, consequently the alloy is more resistant to "waste grabs" which are a frequent cause of failure in railway bearings.

In addition to the various types of railway-car and locomotive bearings, Satco metal is also used as a lining in main and connecting-rod bearings and motor-support bearings of Diesel engines. The successful performance of the alloy in this service has been reported by L. M. Tichvinsky.[14]

The author further reports that the lining metal in the "magnus special" bearing tested by the committee showed indications of corrosion during the 80-mph schedule. In this connection we wish to state from our experience with Satco-lined bearings, that corrosion is the exception rather than the rule. In the railway field particularly, corrosion of Satco linings is of rare occurrence.

Under certain conditions, however, particularly with lubricating oils which are compounded with free fatty acids, all types of lining metals regardless of their composition will corrode to some extent.

[14] "Diesel-Engine Bearings," by L. M. Tichvinsky, *Mechanical Engineering*, vol. 67, 1945, pp. 297–308.

Author's Closure

The discussion has brought to light some additional experimental work on the subject. It is hoped that Mr. Exline plans to publish the results of the railway-car journal bearing studies conducted in the laboratories of the Gulf Research and Development Company.

Data on lubricator power losses furnished by Mr. Pearce are most interesting inasmuch as they check the results given in the paper by an entirely independent method. With waste-pack lubrication, Fig. 24 shows the losses somewhat greater than the author's Fig. 14. Losses with the pad are in close agreement. Mr. Pearce's direct method of obtaining his data is probably somewhat more accurate than the author's indirect approach. The results, however, are in good agreement as has been pointed out, and may be said to verify some of the conclusions reached in the paper. Mr. Jones's comment that journal friction is a relatively small part of the total car resistance is well illustrated in Fig. 21.

Detailed procedure in the calculation of bearing oil-film thickness and friction, referred to by Mr. Hersey, was purposely omitted to reduce the length of the text. Basic data for these calculations will be found in previously published papers by Kingsbury[15] and Needs.[16]

The test results bring out the very interesting fact that despite the relatively large clearances of the railway journal bearing, clearances far beyond those permitted in other machinery, the bearing friction is slightly less than with the more normal clearances obtained by running the fitted bearings at operating temperatures. In other words, it appears that the friction of the bearing itself is about as low as can be expected and improvement can be hoped for only through method of lubrication. In this respect, statements by Mr. Jackson and Mr. Shoemaker that some of the railroads of this country have been using flood and pad lubrication for a number of years are significant.

A comparison of the test results given in the paper with similar data on roller bearings for railroad equipment as suggested by Mr. Jackson would be very interesting indeed and it is hoped that the Committee will be able to release such information in the not too distant future.

Mr. Shoemaker's data on variation of bearing-lining hardness with temperature are particularly interesting. From the fact that bearing 95-B carried a load of 1930 psi at 375 F with "A.A.R. babbitt" there appears to be ample babbitt hardness safety factor when operating at the usual loads and temperatures encountered in service.

That part of the discussion which is critical stresses the fact that a bearing under test in the laboratory is not meeting actual service conditions, and for this reason the test results are not of practical nature. When planning the tests the difference between laboratory and service conditions was realized. For example, it was not expected that the machine in which the tests were run would give any information on the ability of the bearing to withstand collar cracking forces. Such information is readily obtained by placing the bearing in service. The main objects of the laboratory tests were to investigate bearing friction and method of lubrication under steady comparable conditions and to compare these characteristics with those of the fitted bearing on the assumption that the fitted bearing was the best obtainable for the service. Since all successful bearings in actual service operate by virtue of their oil films, comparisons under comparable conditions of various methods of feeding these oil films are entirely valid, hence practical, regardless of whether the data are accumulated in the laboratory or on the railroad. In order to make the tests comparable they had to be run under steady conditions and since there are very few stretches of track where a train can run 80 or 100 mph for eight consecutive hours, the difficulty of obtaining our data from service is apparent. In some respects the conditions of the laboratory tests were more severe than the bearing would meet in service. Proof of this is the fact that every bearing surviving the laboratory test gave a good account of itself in service.

One or two other points raised by Mr. Mitchell can be answered more specifically. It is quite true that in a railroad car the two opposite bearings push the axle and wheels along. The horizontal component of the load which provides this force is essentially small as compared with the vertical component due to the weight of the car and its load. However small the horizontal load may be it does cause the bearing center line to lead the journal center. This, however, has no effect whatever on formation of the oil film. Only the converging portion of the oil film can possibly generate positive load-carrying pressures. In the testing machine the load-carrying area is in the center of the bearing as shown in Figs. 11, 12, and 13. Because the bearing must carry the axle and wheels along in actual service the load-carrying bearing area will be shifted from the center a very slight distance opposite the direction of rotation. Under comparable operating conditions the films will be exactly the same otherwise.

Regarding heat transfer from bearing to wedge, the test results seem to indicate that the smaller contact area of bearing 94 is not a matter of concern. As Mr. Mitchell has pointed out, the operating temperatures of bearing 94 are much the same as the temperatures of the other two bearings under the same operating conditions. This would be expected inasmuch as friction is approximately the same with each of the three bearings. It will be noted from the tables, however, that the temperatures of bearings 93 and 95 are generally several degrees lower than the journal. With bearing 94 this difference is only a degree or so, the smaller difference being due to less contact area between bearing and wedge.

[15] "Optimum Conditions in Journal Bearings," by A. Kingsbury, Trans. A.S.M.E., vol. 54, 1932, paper RP-54-7, pp. 123–148.

[16] "Effects of Side Leakage in 120-Degree Centrally Supported Journal Bearings," by S. J. Needs, Trans. A.S.M.E., vol. 56, 1934, paper APM-56-16, pp. 721–732.

Dimethyl-Silicone-Polymer Fluids and Their Performance Characteristics in Unilaterally Loaded Journal Bearings[1]

By J. E. BROPHY,[2] R. O. MILITZ,[3] AND W. A. ZISMAN[4]

This investigation concerns the practicability of using the dimethyl silicone polymer fluids as lubricants in unilaterally loaded journal-bearing machines. A specially designed bearing machine was used having forced-feed lubrication up to pressures of 26 psi. It was operated at a speed of 1725 rpm, and the oil-sump temperatures varied from 115 to 130 F, while the bearing temperatures varied from 150 to 240 F. Plain or chrome-plated high-carbon-steel shafts were used in conjunction with bearings of copper-lead, bronze, tin-base babbitt, cast iron, commercial brass, aluminum (17S), copper and Alfin metal. Cast-iron or steel bearings used in conjunction with steel journals were entirely unsatisfactory when lubricated with the silicone fluid. All of the nonferrous bearings performed satisfactorily with the silicone fluid. It was found that an organic silicon-containing film was formed during the long, slow, break-in process. The need for such a long break-in could be eliminated by the application of a technique of pretreating or lacquering the bearings with silicone oil before assembling the test machine. The method of pretreatment is described briefly. It was also discovered that such pretreated bearings were able to carry much higher than normal loads when operated in contact with petroleum lubricating oil.

Introduction

THIS is part of a larger investigation made by the Naval Research Laboratory during the war at the request of the Bureau of Ships. It concerns the physical and chemical properties of the silicone polymer fluids (or polyorganosiloxanes) and their application to, and development for, naval lubrication problems. As the dimethyl silicone polymer fluids have the smallest temperature coefficients of viscosity of any of the available silicones (or of any other known pure liquids in the viscosity range of lubricants), and as they are especially stable to oxidative decomposition, they have been the most thoroughly studied, and they alone are discussed here.

The dimethyl silicone fluids are included among the various new silicones developed and manufactured by both the Dow Corning Corporation and the General Electric Company and are now commercially available from each supplier under his own trade name.[5,6] At the start of this investigation only one manufacturer was in commercial production and able to supply large enough quantities of the desired fluid; hence all the data given here relate to several large batches of a well-reproduced fluid made by the Dow Corning Corporation.

Comparisons with the latest available and comparable grades of dimethyl silicone polymer fluids manufactured by both producers showed them to behave identically as lubricants. The fluid used here was specially stripped of volatiles, making it noninflammable to incendiary fire. It was identified by the producer as Dow Corning fluid, series 500, batch 369–62–69, and its viscosity-temperature characteristics are summarized as follows:

Temperature, deg F	Kinematic viscosity, centipoises
210	29.8
130	55.6
100	73.5
0	275.0
—20	390.0
—40	600.0

Prior to the investigation of this laboratory all of the lubrication tests reported by the producers and by the numerous other laboratories having access to these fluids had led to the conclusion that the silicones were poor lubricants. However, these fluids were considered so promising in other respects and the need for low- and high-temperature lubricants and noninflammable hydraulic fluids was so great that it was deemed unsound to drop them from consideration on the basis of the usual quick tests for load-carrying capacity.

After some search, a simple technique was found suitable for observing quickly some of the lubricating peculiarities of silicones. This is described in another paper.[7] Using this technique to separate the promising metal combinations from those obviously having no promise, it was found that whereas a number of nonferrous metals were suitable for bearings, steel or cast iron were uniquely unpromising. It was therefore decided to study these extreme types of metal combinations in both a bearing machine and a hydraulic pump system. The results obtained in hydraulic systems are described elsewhere,[7] while the first results obtained in bearing machines are reported here.

Since the theoretically best understood and most common type of lubrication occurs in the unilaterally loaded journal-bearing machine, it was considered to be the appropriate machine for studying load-carrying capacity (or seizure load) as affected by the fluid, the break-in procedure, and the bearing composition. By going from light loads with full hydrodynamic conditions

---

[1] The opinions or assertions contained in this paper are the authors' and are not to be construed as official or reflecting the views of the Navy Department.

[2] Associate Mechanical Engineer, Lubrication Section, Naval Research Laboratory, Washington, D. C. Mem. A.S.M.E.

[3] Lieutenant, U.S.N.R., Lubrication Section, Naval Research Laboratory, Washington, D.C.

[4] Head Lubrication Section, Naval Research Laboratory, Washington, D. C. Mem. A.S.M.E.

Contributed by the Special Research Committee on Lubrication and presented at the Annual Meeting, New York, N. Y., Nov. 26–29, 1945, of THE AMERICAN SOCIETY OF MECHANICAL ENGINEERS.

NOTE: Statements and opinions advanced in papers are to be understood as individual expressions of their authors and not those of the Society.

[5] "The Silicones—A New Plastics Family," *Plastics*, vol. 2, January, 1945, pp. 112–115.

[6] "The Organo-Silicon Polymers," by E. G. Rochow, *Chemical and Engineering News*, vol. 23, 1945, p. 612.

[7] "Dimethyl-Silicone-Polymer Fluids and Their Performance Characteristics in Hydraulic Systems," by V. G. Fitzsimmons, D. L. Pickett, R. O. Militz, and W. A. Zisman, published on pages 361–369, of this issue of the Transactions.

prevailing, to heavy loads with intermittent metallic contact, it was believed that important peculiarities of the fluid could be noted. It was necessary to design a special bearing machine for this work.

Owing to the originally limited availability and high cost of the silicone fluid, this machine was of small capacity. Nevertheless it was desirable to be able to employ commercially available insert bearings and to secure adequate freedom from shaft deflections and bellmouthing of bearings, which meant that good bearing alignment and accurate boring and finishing of bearings were essential. Several models were built, the final one used for this investigation being shown in Figs. 1 to 4, inclusive.

Due to the poor lubricating value of the silicones in steel-on-steel or steel-on-cast-iron sliding loaded surfaces, the forced-feed oil system of the machine had to be operated with a low-pressure low-flow-rate gear pump designed to avoid such loading. The machine used was equipped with a specially designed gear pump having bronze bearings. Later models of the machine were equipped with Pesco 1P-349N aviation gear pumps run at low speeds.

Experimental Equipment and Methods

Fig. 1 shows the bearing machine completely assembled with weights on the pan of the loading arm. Fig. 2 is a partial test assembly of the bearing machine revealing the placement of the bearings, journal, and thermocouple. Fig. 3 is an assembled view of the support bearings, test bearing, journal, and flinger. Fig. 4 is a view of the component parts of the test assembly shown in Fig. 3.

The small motor A beneath the drain pan, Fig. 1, drives a special vertical, bronze, gear pump B. The pump is immersed in its own reservoir C to minimize the volume of fluid needed. The high-pressure feed line extends from the side of the pump to the aircraft-type Skinner filter D. One copper tube from the filter feeds the support bearings. This tube and its end connection to the support block are shown in Figs. 2, 3, and 4. Another copper tube from the filter goes to a needle valve and thence to a rotameter-type flowmeter E. The fluid pressure is measured at the outlet of the flowmeter. A coiled copper tube connects the flowmeter with the test-bearing holder F. The load on the bearing is applied through the long beam G and a secondary lever system that is connected to the test-bearing holder.

The method of supplying the lubricant to the bearings is shown in Figs. 3 and 4. The flare fitting on the block H is connected to both support bearings by drilled holes. The small hole at the top of the test bearing J shown in Fig. 4, is the supply orifice for the lubricant. The test holder is drilled to connect the flare fitting and the bearing. A spring-loaded thermocouple is screwed into the bottom of the test-bearing holder at point K and contacts the outer surface of the test bearing.

Plain bearings with one hole drilled top center (opposite loaded area) were used. The bore was 0.687 in. and the length of the bearing was $^1/_2$ in. The bearing clearance (bore diameter minus journal diameter) was held to 0.0010 in. ± 0.0001 in. A special boring technique, developed and made available to this laboratory by Russell Dayton of the Battelle Memorial Institute, was used to assure true cylindrical holes in the test bearing and support bearings. The journals were of chromium-plated high-carbon steel with the exception of that used in run N, in which case it was copper-plated steel. The bearings were pressed into the test-bearing holder and the support block. If rough-boring was necessary, it was accomplished before pressing the bearings into the holder and block. Finish-boring was accomplished in the lathe in a special fixture using the boring technique mentioned previously. This fixture was built to isolate the eccentricities of the lathe spindle from the work and

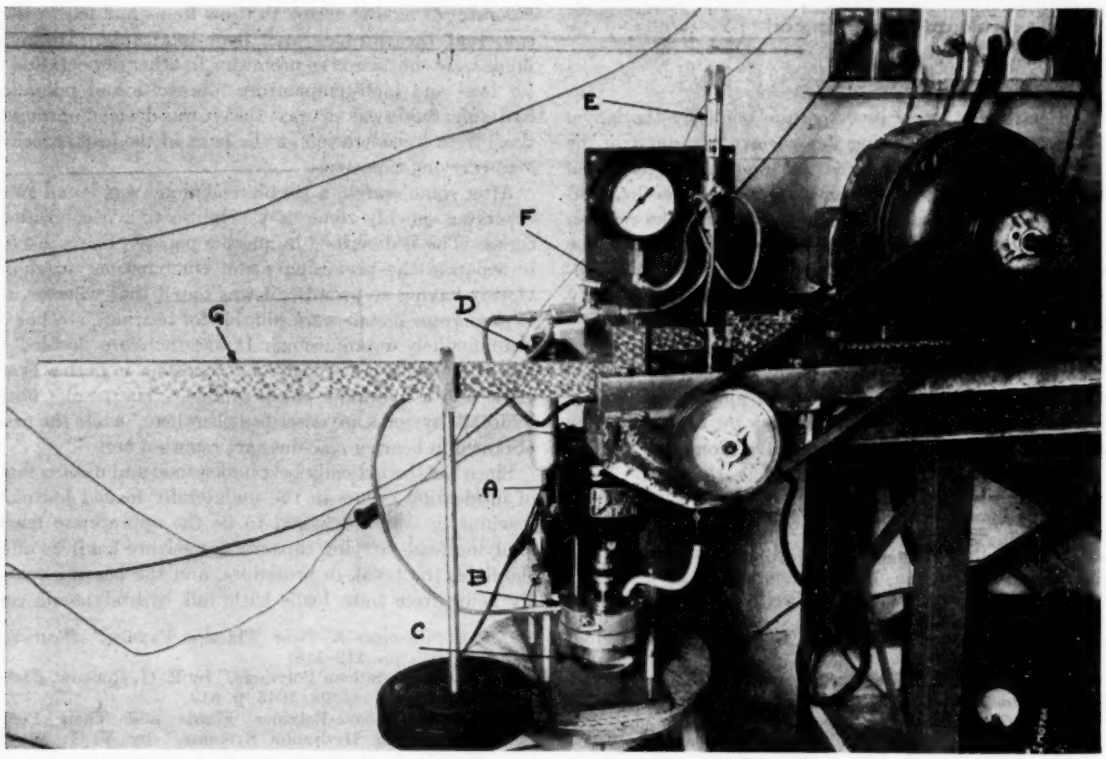


Fig. 1 Bearing-Test Machine, Assembled for Test Run

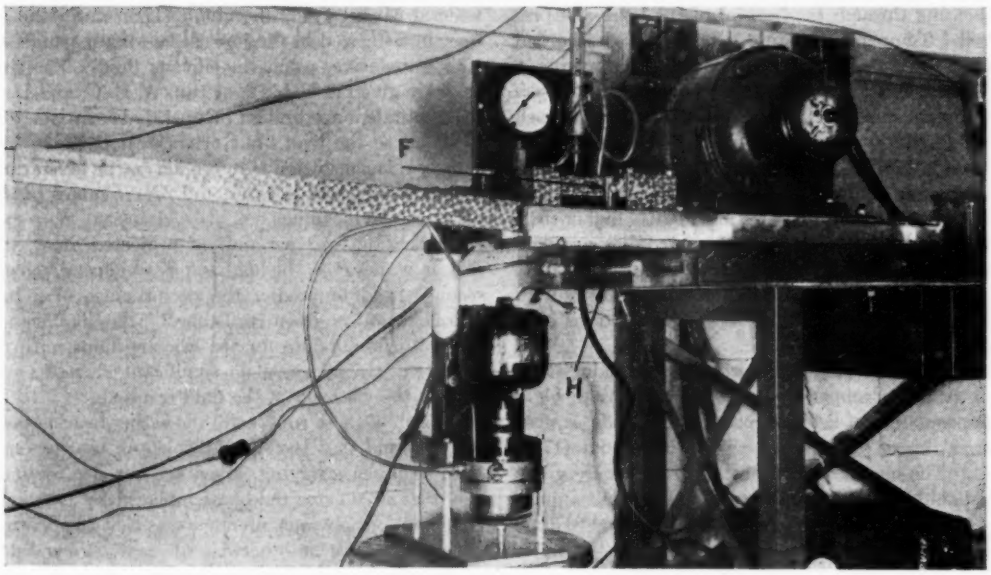


FIG. 2 BEARING-TEST MACHINE WITH OIL PAN AND DRIVE PULLEY REMOVED

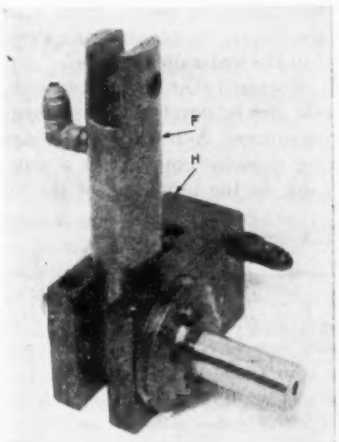


FIG. 3 ASSEMBLY OF SUPPORT AND TEST BEARINGS

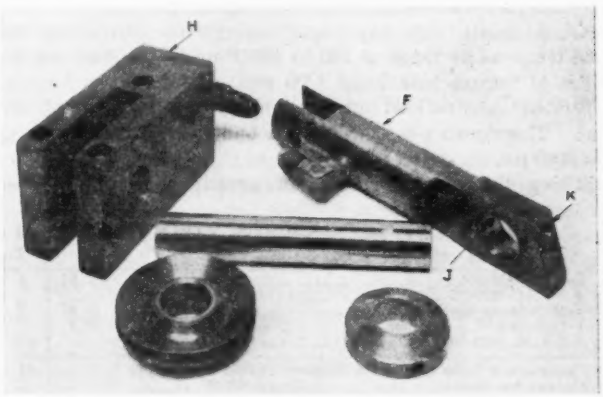


FIG. 4 COMPONENT PARTS OF A BEARING TEST

to insure reproducible finishings in the bearing. All parts in the test setup, including the bearings, were washed either in unleaded gasoline or in benzene and blown dry with clean air. All bearing surfaces were wet with the silicone fluid prior to assembly in the machine.

Due to the low surface tension of the silicone fluid, approximately 20 dynes per cm, it was difficult to prevent leakage of the fluid from the system. In the first bearing machine developed for this work it was found that the standard labyrinth-type seal, used so much in modern equipment, was entirely unsatisfactory. Flinger rings were found to work if properly shaped. As for the standard synthetic-rubber seal rings, it was found necessary to change the composition of the rubber to a silicone plasticized Hycar compound, described in the accompanying paper on hydraulics.[7]

The gear pump was operated to deliver the silicone fluid to the test bearing at a pressure of approximately 26 psi. No attempt was made to maintain the same ambient temperature or bearing temperature throughout the various runs. Bearing temperatures ranged from 152 to 240 F, while temperatures of the oil in the sump ranged from 118 to 129 F. The journal speed throughout was 1725 rpm. The load in all the tests was limited to a maximum of approximately 6000 psi. This limit was imposed by the design of the machine, since higher loads would cause excessive shaft deflection and bellmouthing of the bearings.

After some experimentation, several procedures were adopted for breaking in the bearings. A slow break-in consisted of an initial overnight run of 16 hr at 500 psi, and thereafter an increase in the load of 100 psi per hr. This load was continued until failure occurred, or the load limit of the machine was reached (6000 psi). If no seizure occurred the load was cycled between 500 and 6000 psi. One run of 157 hr duration was made. Once broken in, the bearings were run 8 hr per day at 6000 psi after a 15-min warm-up run at 500 psi. The 157-hr run was stopped because of a failure in the power supply to the oil-pump motor. A fast break-in had only 2 hr initial operation at 500 psi, and the load was increased 500 psi every 15 min. A very fast break-in has been used in which the bearing was operated at 500 psi for 2 hr and then loaded to 3000 psi and increased to 6000 psi 15 min after that. The bearing was then cycled between 500 and 6000 psi.

The temperature of the test bearing was taken at the outer

surface of the bearing through the bottom of the holder as previously described. Temperatures were measured and recorded continuously on a Leeds & Northrup potentiometer having a range of 0 to 350 F, and a time of full-scale travel of 27 sec. With this type of instrument it is impossible to follow flash temperatures or temperatures at final seizure, but general operating temperatures were recorded very well. The temperature of the bearing rose slightly after each increase in load, but fell in a few minutes to an equilibrium temperature slightly higher than that for the previous load. This temperature-recording arrangement has proved satisfactory for observing incipient seizure. However, in the runs described in this paper, no difficulties with incipient seizure were found in the silicone-lubricated runs over the load range used.

The bearing metals used included cast iron, babbitt, a high lead and a high-tin bronze, copper-lead alloys containing high, medium, and low amounts of lead, copper-nickel silicide, copper (hard), commercial brass (half-hard temper), aluminum (17S), and Alfin metal. The chemical analyses and sources are given in Table 1. It should be understood that these materials are not the only ones of promise but simply all those investigated to date.

Some Load-Carrying Characteristics of Chemically Untreated Bearings

The first bearing machine built was tried with bearings of cast iron, 80-10-10 bronze, and Delco bushing (copper-lead), and steel-backed babbitt. The nonferrous bearings were satisfactory over the temperature range of 140 to 180 F up to the load-carrying limit of the machine (only 2200 psi). The cast-iron bearings operated under no load but failed promptly at loads of only 250 psi. Therefore a new machine was built permitting loading up to 6000 psi.

Using the break-in procedure already described, copper, Federal Mogul F-16, aluminum (17S), and Alfin alloy bearings were investigated in the journal-bearing machine shown in Figs. 1 to 4, inclusive, using the silicone fluid. The summarized results are given in Table 2, as runs A, B, C, and D. In all cases these metals, once broken in, operated as satisfactory bearings at loads up to the load limit of the test machine (6000 psi). Of course, this conclusion is restricted to the given range of bearing temperatures, oil-flow rates, and ZN/P values (Z, N, and P having the usual meanings, i.e., Z = viscosity; N = rpm of journal; P = bearing load per unit of projected area). The quantity PV (in which P = the load and V = journal velocity in feet per second) used to predict the performance of a bearing with a petroleum oil is given in Table 2. No significance can yet be given to these values for the silicone fluids until more data are collected. In all cases no significant change (±1 per cent or less) in the viscosity of the fluid resulted.

In each of these runs, as in the earlier bearing tests mentioned, it was found that the slowly broken-in bearings not only developed high load-carrying capacities, but also retained them when the original silicone fluid was replaced by new and unused silicone oil. An obvious inference was that the bearing surface had been chemically or otherwise altered. A careful inspection of each bearing surface following the slow break-in procedure revealed that each loaded surface was coated with a thin transparent film or lacquer roughly 0.0001 in. thick and varying from water-white to pale yellow in color. Such a lacquer had also been found on the bronze bushings of the Pesco high-pressure gear pumps used in the hydraulic pump.[7]

It is now well recognized that bearings carefully run-in on petroleum lubricants slowly develop a dark lacquer coating on the loaded-bearing surface. As it was considered possible that the high load-carrying capacity obtained in a slow break-in with silicone oil was due to the formation of the observed film or

TABLE 1 ANALYSES OF BEARING METALS USED

Bearing metal	Cu	Pb	Sn	Zn	Sb	Fe	Ni	Al	C	Si	Mg	S	P	Mn
Delco bushing[a]	88.92	3.79	4.01	3.28	0.01	0.01	..	...	..	..	...	...	..	..
A.S.T.M.-B62-36	...	...	...	...	..	..	...	..	..	..	...	...	..	..
F-16 (copper-lead)[b]	74.63	19.04	5.47	0.6	0.1	0.5	..	...	..	..	...	...	..	..
F-1 (bronze)[b]	86.95	0.1	9.5	2.5	0.1	0.1	0.05	0.05	..	..	...	...	..	..
A.S.T.M. B60-36	...	...	...	...	..	..	..	...	..	..	...	...	..	..
Commercial brass (half-hard temper)	60.2	2.69	...	37.0	..	0.05	..	0.1	..	..	...	...	..	..
Copper bar (hard)	99.9	...	...	...	..	..	..	...	..	..	...	...	0.9	..
Aluminum (17S)	4.0	...	...	...	..	..	..	95.0	..	..	0.5	...	..	0.2
Alfin metal[c]	0.05	...	6.32	...	..	0.89	..	93.0	..	0.07	...	...	..	..
Copper-nickel-silicide[d]	96.0	...	...	...	...	...	2.19	...	..	0.8	...	...	..	..
Babbitt	3.77	0.07	89.2	...	7.64	0.01	..	...	..	..	...	0.088	0.40	..
Cast iron	..	..	..	..	..	...	..	...	3.36	1.2	...	...	..	0.48
Bronze	79.9	10.0	10.0	0.02	0.01	..	..	...	..	..	...	...	..	..

[a] Manufactured by Delco Appliance Division, General Motors Corporation (Pc. No. 5029150).
[b] Manufactured by Federal-Mogul Corporation.
[c] Manufactured by Al-Fin Corporation, Jamaica Long Island, N. Y. (obtained through courtesy of N.A.C.A.).
[d] Manufactured by P. R. Mallory & Company, Inc. (known as Mallory No. 53).

TABLE 2 RESULTS OF JOURNAL-BEARING TESTS WITH SILICONE FLUID

Run no.	Bearing material[a]	Bearing load,[b] psi	Bearing temp.,[c] deg F	Oil-sump temp., deg F Initial	Final	$\frac{ZN}{P}$	PV	Treated bearings	Type of break-in
A	F-16	6000	165	118	122	11.5	31400	No	Slow
B	Aluminum (17S)	5300[d,e]	145	120	127	15.5	27200	No	Slow
C	Alfin	5700[d,e]	163	127	127	12.1	29700	No	Slow
D	Copper	6000[d]	163	122	122	11.5	31400	No	Slow
E	Delco	6000	152	118	127	12.7	31400	Yes	Fast
F	Delco	500[d]	...	...	...	..	2590	No	Fast
G	Delco	6000	240	120	122	6.8	31400	Yes	Fast
H	Delco	6000	146	122	125	13.4	31400	Yes	Fast
J	Delco	6000	190	120	125	9.3	31400	Yes	Fast
K	Delco	6000	137	118	125	14.5	31400	Yes	Fast
L	Commercial brass	6000	196	116	120	9.0	31400	Yes	Fast
M	F-1	6000	152	115	122	12.7	31400	Yes	Fast
N	Cold rolled steel[g]	5500[d]	135	116	118	16.6	25500	Yes	Fast
V	Cast iron	2000[d]	115	120	120	53.6	10800	Yes	Fast
W	Cast iron	2500[d,f]	126	116	118	37.8	13500	Yes	Fast

[a] All shafts except where noted were chrome-plated high-carbon steel.
[b] Load limit of test machine was approximately 6000 psi.
[c] Highest steady-state temperature prior to seizure.
[d] Bearing seized at this load.
[e] Run terminated due to accidental failure of power to oil-supply pump.
[f] Incipient seizure at 1521 psi.
[g] Copper-plated high-carbon-steel shaft, support bearings—Delco.

lacquer, it was decided to try to produce artificially such films on bearings and investigate the resulting change in the break-in and load-carrying characteristics of the bearings lubricated with silicone fluids.

Silicone Lacquers and their Use in Silicone-Fluid-Lubricated Systems

Previous research of this laboratory on the oxidation stability of the dimethyl silicone polymer fluids had shown them to be very stable at temperatures up to approximately 300 F. At higher temperatures some formaldehyde and formic acid were evolved, and eventually the oil thickened until it set to form a water-white transparent gel. The rate of oxidation and of viscosity increase was considered negligible for most purposes at temperatures of 300 F, but at higher temperatures they became increasingly more serious. In the temperature range of 300 to 500 F and in the presence of the common metals, Cu, Fe, Al, bronze and babbitt, the rate of oxidation was decreased somewhat. However, pure lead and pure tin were found to be catalysts for accelerating the oxidation and gelation of the oil. From this work and other related research of this laboratory it was concluded that the films on the bearings, as described previously, were silicon-containing organic lacquers or thin films formed during contact of the metal with the products of the silicone-oil oxidation reaction.

The test bearing metals and also the supporting bearings were immersed in beakers of the silicone oil and were heated in the open air for long periods of time at 300 F or higher. The desired lacquers eventually formed, the time required varying with the temperature and metal. Numerous variations of this method of forming lacquers on the bearings have been tried and developed. The method used in preparing the bearings throughout the test discussed in this report involved the use of temperatures of 300 F for as long as 100 hr, or 500 F for only 24 hr. Longer times of exposure were necessary for steel than for nonferrous metals.

With the exception of run F, all of the runs E to N, inclusive, in Table 2 were made with lacquer-coated bearings previously prepared by the chemical method described. After the lacquer treatment the bearings were allowed to cool, were washed with benzene, and were then assembled in the test machine. Following this, the test fluid was added and the bearing test was run according to the loading schedule indicated in Table 3. It will be noted from Table 2 that all these treated bearings carried the maximum load of the machine (6000 psi), while the break-in time was reduced to only 2 hr. Also no significant changes (±1 per cent or less) in the viscosity of the fluid resulted.

In run F an untreated Delco bearing was used, and it was initially loaded up to and held at 500 psi. After 1¼ hr operation at that load seizure occurred. This is to be contrasted with the five equally or more rapidly loaded runs, E, G, H, J, and K, on the same bearing metals up to maximum loads of 6000 psi. The low load seizure in run F indicates the need for a slow break-in to obtain load-carrying capacities in excess of 1000 psi. It can now be concluded that a silicone film or lacquer formation on the bearings is necessary for the operation at high unit loads of silicone-fluid-lubricated journal bearings.

In runs L and M on commercial brass and F-1 (high tin-bronze) bearings, respectively, each was chemically treated by the method described, and each could be rapidly and successfully loaded to the maximum load-carrying capacity of the machine. In run N a copper-plated high-carbon-steel journal, rotated in a previously lacquered, cold-rolled steel, test bearing, operated successfully under rapid loading until seizure occurred at 5500 psi. This is to be compared with the very low loads (250 psi) at which seizure occurred with steel-on-cast-iron silicone-lubricated bearings as described in the earlier tests.

Runs V and W were made using lacquer-treated bearings of cast iron and journals of chromium-plated high-carbon steel. Seizures occurred at loads of approximately 2000 and 2500 psi. In another paper,[7] it is shown that Pesco high-pressure gear pumps, fitted with cast-iron bushings, failed in a few minutes at a hydraulic pressure of 600 psi. Therefore, although the silicone-lacquer treatment did not increase the load-carrying capacity of cast-iron bearings to values as high as it did the nonferrous bearings studied, a considerable and perhaps valuable increase did result. This increase in ability to carry loads is especially significant when one considers the very rapid loading schedule followed (see Table 3).

Silicone-Lacquered Bearings and Their Use With Petroleum Oils

The advantages found in silicone-fluid systems in treating bearings with silicone lacquer suggested the investigation of the value of using such treated bearings in petroleum-oil-lubricated systems. In runs P, Q, R, S, and T (see Tables 4 and 5), Navy Symbol 1080 petroleum oil was used for the bearing tests. This is a high V. I. nonadditive aviation-engine lubricant, and the batch used had the following viscosity-temperature characteristics:

15.5 centipoises at 210 F
74.5 centipoises at 130 F
360.0 centipoises at 77 F
2700.0 centipoises at 32 F

The viscosity is identical with that of the silicone fluid used at 148 F, which is not far from a mean of the bearing temperatures encountered.

Before beginning runs P and Q, the bearings were lacquered with a silicone oil by the chemical methods already described. Runs R, S, and T were made without any preliminary chemical treatment of the bearings. It was found that the lacquered

TABLE 3 TREATMENT AND LOADING SCHEDULE AND FOR JOURNAL-BEARING TESTS WITH SILICONE FLUID

Run no.	Bearing material	Lacquer treatment	Loading schedule	
A	F-16	None	500 psi for 15½ hr	100 psi increments in load 1 hr after each equilibrium temperature was reached
B	Aluminum	None	500 psi for 17 hr	Same loading as in A
C	Alfin	None	Same as in A	
D	Copper	None	500 psi for 19 hr	Same loading as in A
E	Delco	Bearings cooked in silicone oil 150 hr at 300 F	500 psi for 2 hr	250 psi increments in load every 15 min
F	Delco	None	500 psi load	Bearing seized after 1¼ hr
G	Delco	Bearings cooked in silicone oil 24 hr at 430 F	500 psi for 2¼ hr	500 psi load increments every 15 min
H	Delco	Bearing cooked in silicone oil 24 hr at 380 F	500 psi for 2 hr	3000 psi load increments every 15 min
J	Delco	Bearing cooked in silicone oil 24 hr at 380 F	Same as run H	
K	Delco	Bearings cooked in silicone oil 44 hr at 300 F	500 psi for 2 hr	6065 psi added immediately after break-in
L	Commercial brass	Cooked in silicone oil 89 hr at 300 F	500 psi for 2 hr	Load increase same as run G
M	F-1	Cooked in silicone oil 108 hr at 300 F	500 psi for 2½ hr	Load increase same as in run G
N	Cold-rolled steel	Shaft and bearing cooked in silicone oil Bearings—137 hr at 300 F Shaft—168 hr at 300 F	Same as in run E	
V	Cast iron	Shaft and bearings cooked in silicone oil Bearings—178 hr at 300 F Shaft—167 hr at 300 F	500 psi for 2¾ hr	Same load increase as in run G
W	Cast iron	Bearings cooked in silicone oil 8.5 hr at 500 F	Same as in run G	

TABLE 4 RESULTS OF JOURNAL-BEARING TESTS USING NAVY SYMBOL 1080 PETROLEUM OIL

Run no.	Bearing material[a]	Bearing load, psi	Bearing[b] temp, deg F	Oil-sump temp, deg F Initial	Final	ZN/P	PV	Treated bearing	Type of break-in
P	Commercial brass	5800[c]	158	110	112	10.0	31000	Yes	Fast
Q	Delco	4300[c]	147	101	102	18.3	22900	Yes	Fast
R	Delco	2100[c]	126	127	129	58.8	11300	No	Slow
S	Delco	2600[c]	143	141	124	30.6	13900	No	Fast
T	Delco	2300[c]	136	136	136	40.7	12600	No	Fast

[a] All shafts were chrome-plated high-carbon steel.
[b] Highest steady-state temperature prior to seizure.
[c] Seizure load.

TABLE 5 TREATMENT AND LOADING SCHEDULE FOR JOURNAL-BEARING TESTS WITH N.S. 1080 PETROLEUM OIL

Run no.	Bearing material	Lacquer treatment		Loading schedule
P	Commercial brass	Bearing cooked in silicone fluid 96 hr at 300 C	72 psi for 2 hr	250 psi load increments every 15 min
Q	Delco	Bearing cooked in silicone fluid 118 hr at 300 F	500 psi for 2 hr	Load increase same as in run P
R	Delco	None	72 psi for 16 hr	Load increments of 250 psi 1 hr after each equilibrium temperature was reached
S	Delco	None	72 psi for 4 hr	Load increased 250 psi every 30 min
T	Delco	None	72 psi for 2½ hr	Load increased as in run S

bearings did not seize during a fast break-in until loads were used of 5800 psi with brass and 4300 psi with Delco bearings, respectively. In contrast, the unlacquered Delco bearings seized at from 2100 to 2600 psi, depending upon the loading schedule followed during the break-in. Therefore, with a petroleum-oil-lubricated system, the silicone-lacquer bearing treatment was found to increase considerably the permissible rate of break-in and the seizure load.

Discussion of Experiments

Due to the care used in boring, aligning, and finishing the bearings and journal, reasonably good reproducibility was obtained, and seizure loads did not vary more than approximately 10 per cent from the mean. In this work high enough values of ZN/P were selected to remain usually in the region of hydrodynamic lubrication. It is of immediate interest to learn how much above 6000 psi are the seizure loads for the various nonferrous metals studied. Inasmuch as increases in seizure loads with lacquer formation of from 100 to 200 per cent were found, there is no doubt of the reality of the improvement obtained with lacquering.

Considerable variations were found in the maximum bearing temperatures before seizure. However, this is not unexpected because of the wide range of loading schedules followed during the break-in operations. These temperature variations are not considered as important in silicone-fluid as in petroleum-fluid-lubricated systems, due to both the smaller temperature coefficient of viscosity and the greater oxidation stability of the silicone fluid. As in the hydraulic work,[7] no significant viscosity changes occurred during the bearing runs not accounted for by initial loss of volatiles. This eliminates shear instability of the fluid as a cause of the peculiar lubricating properties of steel-on-steel or cast-iron bearings.

Conclusions

A number of the common bearing metals have been found very promising for use in unilaterally loaded journal bearings, lubricated with the silicone fluid. Among them are copper-lead, bronze, commercial brass, babbitt, copper, aluminum (17S), and Alfin alloy. These were especially effective with chromium-plated high-carbon-steel journals. Cold-rolled steel bearings operated with copper-plated high-carbon-steel journal bearings also showed promise. These nonferrous bearings have been successfully operated at the load limit of the bearing machine used (6000 psi), with load increments of as much as 5500 psi applied during cycling tests.

For the maximum load-carrying capacity the bearings should have either a long gradual break-in or be suitably treated with a silicone lacquer prior to operation. The long, slow break-in process formed a silicon-containing organic film on the bearing. It was found that such film-coated bearings had load-carrying capacities comparable to those of artificially silicone-lacquered bearings.

Bearing systems of steel on steel and steel on cast iron were not satisfactory for operation with silicone fluids. However, a very slow break-in process or a preliminary treatment of the bearings with silicone lacquer enabled them to stand loads of up to approximately 2000 psi. Suitable bearing-lacquer coatings have been formed by completely immersing the bearings in dimethyl silicone polymer fluid (viscosity at room temperature of 50 to 100 centipoises or more may be used) and maintaining them at a temperature of from 300 to 500 F in the presence of air. The time of exposure varied with the metal, being longest for steel and least for copper. Exposures of from 100 hr were needed at 300 F and 24 hr at 500 F.

Acknowledgments

The skillful mechanical and experimental work of John Larson MM 2/c and the able machine work of William Kostowicz MM 2/c were of considerable aid in this work. Their interest and suggestions are much appreciated. Analyses of the test oils before and after the bearing runs were made through the courtesy of Carl Hechmer, Lieutenant, U.S.N.R., and Eleanor Bried, Sp (X) 2/c. Chemical analyses of the bearings listed in Table 1 were made through the co-operation of the Analytical Section of the Metallurgy Division.

Dimethyl-Silicone-Polymer Fluids and Their Performance Characteristics in Hydraulic Systems

By V. G. FITZSIMMONS,[1] D. L. PICKETT,[2] R. O. MILITZ,[3] AND W. A. ZISMAN[4]

This investigation concerns research on the polymethyl siloxanes or dimethyl-silicone polymers, and their uses as lubricants and hydraulic fluids. It is shown that these new fluids give excellent results when operated in a standard aircraft-type Pesco gear pump. It was found that the silicones when used in a gear pump fitted with cast-iron bushings caused serious wear and disintegration of the bushings at pump pressures of only 600 psi. It is concluded that the loaded surfaces of steel sliding on cast iron or on steel are not adequately lubricated by the silicone fluid, whereas steel sliding on bronze is effectively lubricated. A simple manually operated slider-and-plate test method was discovered capable of permitting the discrimination between good, bad, and indifferent bearing combinations for use with silicone fluids. Results with 156 combinations of metals are summarized. There is also given a means of relating these observations to the practical problem of selecting suitable metals for use in lubricating the sliding parts of machinery with silicones. The results are related to observations on the choice of suitable metals for gear pumps, piston pumps, and journal bearings. It is shown that the same conclusions relative to steel sliding on steel or on bronze are reached from tests with the Vickers piston pump.

Introduction

EARLY in the war the Naval Research Laboratory was requested by the Bureau of Ordnance to investigate the possibility of using the new silicone-polymer fluids (or polyorganosiloxanes) as recoil and damping fluids. When difficulties due to the inflammability of present aircraft hydraulic fluids became apparent, the Bureau of Aeronautics also became interested in the development of these fluids for use in aircraft hydraulic systems. A description of some of the properties of these fluids by the two producers will be found in the literature.[5,6]

Many of the physical and chemical properties of interest in the evaluation of hydraulic fluids were investigated by this laboratory prior to commencing tests in hydraulic equipment. It was concluded that of the various silicone-polymer fluids, the dimethyl silicones were the most desirable because they had the smallest temperature coefficients of viscosity of any pure fluids known, and also had unusual stability to oxidation. The resistance of the dimethyl-silicone fluids to various fire hazards was studied, and it was concluded that they were adequately resistant to the fire hazards of interest in this investigation. Laboratory tests and M-1 incendiary-bullet firing tests on properly stripped silicones verified that, under such fire hazards, these fluids would not ignite nor would the liquid spray propagate a flame front. This made it of interest to study the operation in hydraulic equipment of a carefully stripped silicone fluid.

Both manufacturers of the silicones were requested to prepare one sample each of the fluid having a viscosity at 210 F of approximately 25 to 30 centistokes. The viscosity-temperature characteristics obtained in each case were within the following narrow ranges:

Temperature, deg F	Viscosity, centistokes
210	26–30
130	52–56
100	68–74
0	259–275
—20	385–390
—40	600–610

The two fluids submitted were used throughout this investigation and no important differences in behavior were found. Other less viscous fluids can be obtained having the advantage of being much less viscous at lower temperatures. Thus a silicone fluid has since been obtained having the advantages that, while the viscosity at 210 F is 18 centistokes at 0 F it is 160 centistokes, and at —40 F it is only 360 centistokes. Such a single hydraulic fluid can at once satisfy all present military requirements in so far as viscosity, volatility, and pour point are concerned. The high viscosity at 100 F of the fluid used here was considered desirable at the commencement of this investigation because the tendency of the silicones to leak out of the hydraulic system and the inflammability were decreased by using the highest possible viscosity consistent with approximating both the low-temperature ordnance and aircraft hydraulic specifications, O.S. 2943 and AN-VV-O-366b.

Experimental Equipment

At the commencement of this investigation the available supply of silicone fluids was very limited and hence the laboratory hydraulic tests were made in systems operated with the small-size high-pressure pumps used in aircraft. These were the 1P-349-N Pesco gear pump and the Vickers model No. PF-2713-10, constant-delivery aircraft piston pump.

The Pesco pump has nitrided gears running in high-lead bronze bushings. The bushings are pressure-loaded against the sides of the gears. Any wear resulting from a test is therefore noticed on the face of the gears and the sliding surface between the thrust face of the bushings and the side of the gears.

The Vickers pump is a 7-piston constant-delivery pump. Several points are observed for wear, one being the hardened-steel

[1] Assistant Technologist, Lubrication Section, Chemistry Division, Naval Research Laboratory.

[2] Associate Technologist, Lubrication Section, Chemistry Division, Naval Research Laboratory.

[3] Lieutenant, U.S.N.R., Lubrication Section, Chemistry Division, Naval Research Laboratory.

[4] Head, Lubrication Section, Chemistry Division, Naval Research Laboratory. Mem. A.S.M.E.

[5] "The Silicones—A New Plastics Family," *Plastics*, January, 1945.

[6] "The Organo-Silicon Polymers," by E. G. Rochow, *Chemical and Engineering News*, vol. 23, 1945, p. 612.

Contributed by the Special Research Committee on Lubrication and presented at the Annual Meeting, New York, N. Y., Nov. 26–29, 1945, of The American Society of Mechanical Engineers.

Note: Statements and opinions advanced in papers are to be understood as individual expressions of their authors and not those of the Navy Department or of this Society.

universal link on which are pivoted, on steel pins, four hardened-steel knuckles. Through two steel retainers this assembly serves to connect the drive shaft to the bronze cylinder block. As a result of the angle (10 deg) between the drive shaft and cylinder block, each revolution of the shaft causes the knuckles to rotate 10 deg around the steel pins of the universal link. Bronze bearings at either end of the universal link are lubricated by the fluid pumped being forced through a small hole in the link. The action of the piston in the cylinder block and the sliding of the cylinder block on the valve plate are also observed. Five ball bearings, one thrust loaded, two radial loaded, and two with a combination load, serve to make this pump very desirable as almost every type of wear is represented.

The hydraulic system used is shown in Fig. 1. The reservoir *A* was designed to produce a long liquid path within the sump from inlet to outlet in order to facilitate deaeration of the fluid. Two sizes of sumps were used, depending upon the amount of the test fluid available. When the smaller was used the total capacity of the hydraulic system was 1.25 gal, while with the larger sump it was 3 gal. Thermometer *T* was used for reservoir temperature measurements. The line *C* was $^{5}/_{8}$ in. OD 0.035-in-wall copper tubing. Line *D* was a standard flexible high-pressure rubber hose with $^{13}/_{32}$-in. ID conforming to the specification AN-863-8-21. All other tubing was $^{1}/_{2}$-in. OD and 0.035-in. wall copper. Standard 24S-T aluminum alloy or equivalent AN-type flare fittings were used throughout. The driving motor used, *M*, was a General Electric type K, frame 225, 220/440-volts, 3-phase, rated at 5 hp at 3600 rpm. Pressure was controlled by a Vickers No. C-167-E relief valve *H*. The gage *I* was used on the high-pressure side of the valve. This was a Lonergan gage with a range up to 3000 psi. Gage *J* was used to measure the pressure drop across the relief valve, and gage *K* measured the pressure drop across the filter *L*. This filter was either a Purolator aircraft-line type, using a paper element impregnated with what is reported to be a phenol-formaldehyde resin, or a Skinner aircraft-instrument-type filter, using a paper-disk element enclosed in a cloth sheath. The hydraulic fluid was cooled in flowing through cooler M_1, which consisted of 20 ft of $^{3}/_{8}$-in. copper tubing inserted in 20 ft of $^{3}/_{4}$-in. copper tubing and then coiled in a helix. The test fluid passed through the space between the inner and outer tubes, and

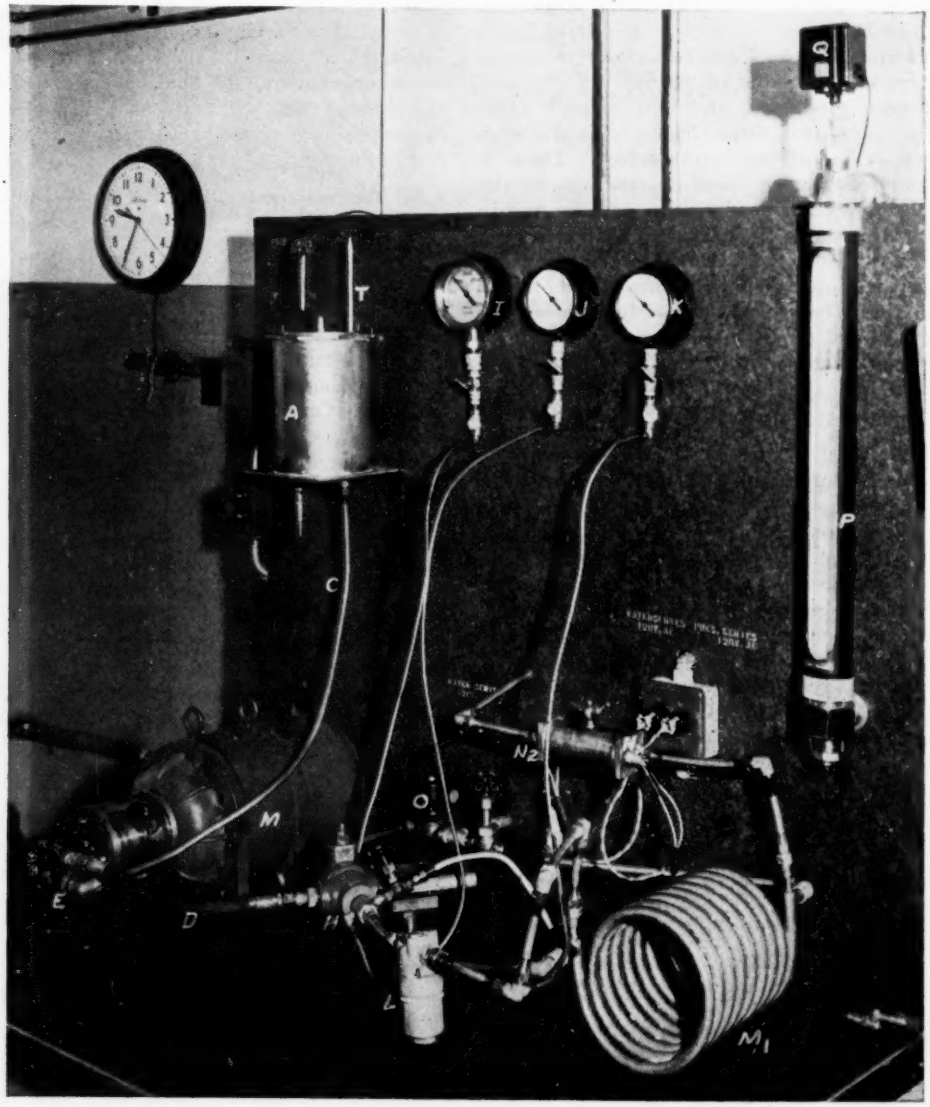


FIG. 1 HYDRAULIC TEST SETUP USED

a flow of cooling water passed through the inner $^3/_8$-in. tube. Where necessary the helix was immersed in a cooling bath.

The device N_1 was a Fenwal thermoswitch which was connected with the motor control, the purpose being to shut off the driving motor if the temperature of the hydraulic fluid exceeded the desired test temperature. This device was in the nature of a safety shutoff in case of water failure to the cooler. The device N_2 was also a Fenwal thermoswitch which controlled the sump oil temperature through a solenoid O in the water-supply line to the cooler. The test fluid then passed through P, a Fisher and Porter rotameter Stabl-vis type 12 P7, capable of measuring flow rates from 0 to 5 gpm. On top of the rotameter a Minneapolis-Honeywell Pressuretrol Q was installed. This was a safety device to switch off the power to the drive motor if for any reason the pump failed to deliver fluid. It was caused to operate by the slight pressure in the line from the rotameter to the reservoir which was generally in the neighborhood of 1 or 2 psi. When this pressure was not present the switch moved to the "off" position, thereby breaking the circuit to the drive motor. The fluid left the rotameter through a line which entered the side of the reservoir near the top and then directed the flow against the wall of the container. This caused the test fluid to take a circular path to the pump inlet, thereby allowing any entrapped air bubbles the greatest possible time to escape to the surface of the fluid. The liquid velocity was not sufficient to cause the fluid to vortex in the reservoir.

Operating Technique

Before each test the entire hydraulic system was dismantled and cleaned with suitable solvents. Repeated washing with unleaded gasoline was sufficient to clean the system if previously operated with the silicone fluid. Where polymer-thickened petroleum hydraulic fluids had been used previously, it was necessary to wash all parts in unleaded gasoline to remove the petroleum fluid and to follow that with successive washings with methyl cellosolve and acetone. The cleaning procedure was completed with drying the system with a forced draft of clean air. In using these fluids precautions were necessary owing to the pronounced ability of the dimethyl silicones to creep over surfaces and to leak through mechanical joints. All tubing flares had to be made as nearly perfect and tight as possible, and it was found valuable to use wherever practicable a pipe-thread sealing compound. An available material which was found satisfactory was "Tite-seal," a product of the Radiator Specialty Company of Charlotte, N. C.

Before each run and before a gear pump was placed on the test stand, it was fitted with a new set of bushings and gears. Both the gears and the bushings were thoroughly washed in benzene, dried, and weighed to the nearest tenth of a milligram on an analytical balance. As the pump was assembled, all moving parts and all O-ring seals were wetted with the fluid to be tested. When the system was assembled and secured, it was charged by filling the reservoir and turning the pump slowly until the entire system was filled. The drive motor was then started and the fluid circulated with no restriction offered by the Vickers relief valve until it could be ascertained that the system was operating satisfactorily. The Vickers relief valve was then adjusted to the desired pressure and as the fluid began to heat up, the adjustments on the thermoswitches were made.

Most of the runs were made for 100 hr of continuous operation or until a failure caused discontinuance. Samples of the hydraulic fluid were taken at the end of each run and the viscosity, neutralization number, and precipitation number were measured, the latter two measurements being made only when the reference petroleum fluids were used. The gears and bushings were removed from the pump, washed, and weighed at the end of each run to determine the amount of wear occurring during the test period. The rest of the system was examined for any unusual manifestations such as corrosion, solvent effects, and deposits.

Piston-pump performance was characterized by observations of the flow rate at the beginning and end of each run, appearance of metallic particles in the test fluid or the filter, and condition of the working parts, as evidenced by weight losses, appearance, and fits. Due to the size and mass of the working components as well as to the presence of many crevices impossible to clean perfectly, measurements of weight losses were not considered satisfactory for observing wear.

A new filter core was used for each run and in some cases where a Skinner filter was used, a cloth bag covered the core. After each run the filters were examined for deposits. In some of the runs thermocouple readings were taken to determine temperatures after the fluid had passed through the pump and again after passing through the relief valve. These thermocouple installations were temporary in that the temperature was found to rise 10 deg F passing through the valve. The results were consistent for a number of runs, thus making such observations superfluous and hence they were not made routine observations. The approximate number of cycles which the fluid made per run was calculated by multiplying the time of the run by the flow in gallons per minute and then dividing by the system capacity. The flowmeter readings were not corrected for density or viscosity of the fluid. These readings were all made at running temperature for the purpose of determining losses in volumetric efficiency of the pumps at a determined pump speed. These readings were approximately 4 per cent higher than the actual flow rates.

The reference petroleum hydraulic fluids tested had the following viscosity-temperature characteristics:

Temperature, deg F	Viscosity, centistokes	
	AN-VV-O-366b	O.S. 2943
210	5.16	10.0
130	10.1	...
100	14.1	29.1
0	90.3	223.5
—25	...	556.3
—40	406.4	...

Packings for Systems Operated With Dimethyl-Silicone-Polymer Fluids

If the dimethyl-silicone-polymer fluids are to be used in hydraulic systems, it may be necessary to change the composition of the packings. It was found essential to change the composition of the O-ring seals which are so commonly used especially in aircraft. Whatever the ingredients used as plasticizers for the synthetic rubber of the O-ring seals, these plasticizers gradually were extracted by the silicone fluids, and as a result the rings shrank and became brittle. This shrinkage was of such magnitude as to cause serious leakage from the pumps and other hydraulic components using such rings. As might be expected, the solubility of the plasticizers was increased with time and temperature. It was found that serious leakage occurred after 24 hr of pump operation at 180 F sump temperature. However, it was found possible to run the pump for 500 hr continuously at 140 F without serious leakage, but after that run had been completed the seals had become so brittle that they shattered when an attempt was made to remove them. Even in systems operating at lower temperatures than 140 F, there may be trouble with present O-ring packings after long exposures occurring in peacetime practice or in long storage. There was evidence that the solubility effect was present even at room temperature.

A solution to the problem of the shrinkage of O-ring seals was found. The same solution will probably care for difficulties with

many other types of hydraulic packings. It seems that the most commonly used plasticizers of synthetic rubber are all soluble to some extent in dimethyl-silicone fluids. Therefore the High Polymer Section of this laboratory compounded a new packing with a small amount of the silicone hydraulic fluid under test. The rubber used was basically a Hycar compound having a durometer reading of 60 and a tensile strength of 2000 psi, an elongation of 325 per cent, and a freezing point of —60 F. A small percentage of graphite was also included in the manufacture of this material to reduce the friction of these seals on moving parts. It was found that O-rings made from this stock gave completely satisfactory performance in pumps using silicone fluids for 100 hr continuous running at from 180 to 200 F, the highest temperatures employed in this investigation. It was found later that suitable gaskets necessary for journal-bearing experiments[7] could be made from the same material.

Behavior of Silicone Fluids in Gear Pumps

The results obtained on the reference petroleum oils and on the silicone fluid are given in Tables 1 and 2. The sometimes variable finish and hardness of the gears and bushings furnished by the manufacturers of the pumps caused irregular weight measurements during the break-in of new gears as can be seen when comparing the gear weight losses on all runs, especially runs P-20 and

TABLE 1 GEAR-PUMP RUNS ON ORDNANCE AND AERONAUTICAL HYDRAULIC PETROLEUM OILS

	AN-VV-O-366b		O.S. 2943 (PRL 1081)	
	P-60	P-63	P-29	P-31
Time in hrs.	100	100	100	100
Sump temp. °F	180	180	140	140
PSI high	1500	1500	1500	1500
PSI low	38-40	37-45	65-40	65-45
Flow GPM:				
Start	3.08	2.97	3.03	3.01
Finish	3.04	2.92	3.04	3.04
Cycles approx.	18,000	16,000	18,180	18,120
Wt. loss grams:				
Drive gear	.0439	.0535	.0115	.0075
Driven gear	.0372	.0592	.0178	.0052
Max. one bushing	.1782	.0102	.0574	.0044
Total bushings	.4452	.0204	.1873	.0079
Visc. cs.:				
Start	13.37	13.37	28.39	29.10
Finish	7.884	8.485	12.70	14.45
Filter type	Purolator Line type	Purolator Line type	Purolator Line type	Purolator Line type
Appearance of oil after run	--	--	Normal, clear	Normal, clear
Gears & bushings	New	Broken in 100 hrs.	New	New

TABLE 2 GEAR-PUMP RUNS ON DIMETHYL-SILICONE-POLYMER FLUID

	Run No.								
	P-11	P-13	P-18	P-19	P-20	P-21	P-22	P-23	P-25
Time in hours	48	50	41	100	100	100	100	100	500
Sump temp. °F	180	180	180	180	180	180	200	200	140
PSI high	1500	1500	1500	1000	1500	1500	1500	1500	1500
PSI low	135	110	150	150	175	140-155	160	165-195	210-300
Flow GPM:									
Start	3.24	3.25	3.35	3.24	3.34	3.35	3.24	3.36	3.51
Finish	3.27	3.35	3.24	3.24	3.34	3.34	3.12	3.35	3.43
Cycles approx.	9,360	9,750	8,118	19,440	20,040	20,040	19,080	20100	105,000
Wt. loss grams:									
Drive gear	.0066	--	.0117	.0034	.0048	.0006	.0092	.0044	.0030
Driven gear	.0045	--	.0072	.0000	.0020	.0011	.0041	.0000	.0028
Max. one bushing	.0034	--	.0068	.0081	.0010	.0010	.0086	*.0004	.0168
Total bushings	.0042	--	.0133	.0171	.0024	.0020	.0137	*.0010	.0208
Visc. cs.:									
Start	--	69.35	69.27	69.27	69.27	71.11	69.27	71.11	71.11
Finish	--	68.51	68.23	68.58	69.23	72.05	70.39	72.34	70.16
Filter type	Skinner no bag	Purolator line type	Skinner with bag	Skinner with bag	Skinner no bag*	Skinner with bag	Skinner no bag**	Skinner with bag	Skinner no bag
Appearance of oil after run	Cloudy gel	Light amber, clear	Hazy	Hazy	Hazy	Clear, light amber	Hazy amber	Clear amber	Clear deep yellow
Gears & bushings	New	New	New	New	From P-19	From P-19&P-20	New	New	New

* After 40 hours.
** After 60 hours.

P-21 of Table 2. It can be noticed from runs P-19, P-20, and P-21 that when the same set of gears was re-used the weight losses became less, thus indicating that at least part of the weight loss was not due to the fluid alone but rather to mechanical variables. These three runs are the only ones in which gears were re-used, and so it can be concluded that the weight losses in the other runs represent the highest wear rates to be expected in the history of a given pump operated on clean oil.

It was noticed that when using the petroleum "ordnance hydraulic fluid" O.S. 2943, the weight losses were much greater than when the silicone fluid was used. Values of approximately 0.015 g per gear per 100 hr, using the new gears and bushings with petroleum fluid, should be compared with values of often much less than 0.009 g using the silicone fluid. It was also found that higher rates of bushing wear occurred when petroleum was used than with silicone.

It is believed the cause of the low wear rates on the silicone-lubricated pressure faces of the bronze bushings was the formation of a protective resin consisting of cross-linked polymers developed by oxidation of the fluid. Early research on the oxidation of silicones had shown that gels and eventually cross-linked polysiloxane resins resulted. Similar deposits were obtained by this laboratory when strips of polished metal were immersed in the silicone fluid during the oxidation tests.

Although it was found difficult to detect the presence of gel in the silicone fluid because of the small difference in the refractive indexes of gel and fluid, careful examination under a microscope definitely revealed the presence of particles of gel in the fluid

[7] "Dimethyl-Silicone-Polymer Fluids and Their Performance Characteristics in Unilaterally Loaded Journal Bearings," by J. E. Brophy, R. O. Militz, and W. A. Zisman, published on pages 355-360 of this issue of the Transactions.

which had been run for 100 hr. In every run some soft black gel was found on the filter element. In the 500-hr run, P-25, there was enough gel formed in the fluid so that it could be scraped from the filter walls with a spatula, permitting the recovery of 10 ml. Apparently the only reason for the fluid casting out the gel under normal conditions was that the gel would attach itself to minute particles of more dense material in the fluid and would thereby become heavy enough to be thrown out at points where flow direction changed abruptly such as happened in the filter.

Some attempts were made to concentrate the gel formed by the use of a centrifuge but this method proved unsatisfactory. As a result of the formation of gel in the silicone fluid, it was found that a definite build-up of back pressure occurred on the Skinner filters fitted with bags, accompanied by a gradual clogging of the pores by slime. The rate of clogging, however, was not sufficient to cause trouble in normal operation. Using either the purolator filter or the Skinner filter without a bag, serious clogging of the filter occurred after 500 hr of continuous operation at 140 F and 1500 psi operating pressure.

It will be noticed in Table 2 that there was no significant viscosity change (less than 2 per cent) in the silicone fluid after having been pumped at a pressure of 1500 psi continuously for as long as 500 hr (or 105,000 cycles). For comparison, the petroleum fluid O.S. 2943 decreased in viscosity to less than 50 per cent of its original value after 18,000 cycles.

A set of cast-iron bushings (3.3 per cent carbon content) was made to fit the Pesco 1P-349-N pump to replace the usual bronze bushings. Results with O.S. 1113 petroleum hydraulic oil as well as the silicone fluid are given in Table 3. When operated on

TABLE 3 GEAR-PUMP RUNS USING CAST-IRON BUSHINGS

	Hydraulic fluid			
	Silicone		OS-1113 petroleum oil (commercial)	
Run No.:	P-14	P-14A	P-14B	P-14C
Time in hours	0.25	0.33	2.0	1.0
Sump temp. °F	180	180	180	180
PSI high	600 (failed)	600 (failed)	800 (satisfactory	800 (satisfactory
PSI low	110	110	110	110
Flow GPM:				
Start	3.80	--	3.60	3.60
Finish	2.20	--	3.60	3.60
Cycles approx.	75	--	--	--
Filter type	Purolator line type	Purolator line type	Purolator line type	Purolator line type
Appearance of oil after run	Black with iron particles	Black with iron particles	Clear	Clear
Gears and bushings	New	New	New	New

silicone fluid, the pump ran normally at 200 psi for 15 min. Therefore the pressure was increased gradually. At 600 psi the pump began to fail rapidly and the fluid became black with such finely dispersed particles of iron that they were not retained by the filter, while the volumetric efficiency of the pump fell approximately 33 per cent in 5 min, leading to the discontinuance of the entire run. A microscopic examination revealed that much gel had formed in the silicone fluid. Several more runs were made using new cast-iron bushings and pump failures were obtained. The roughened appearance of a set of the cast-iron bushings following such a disastrous run is evident in Fig. 2.

Finally, similar runs were made using the Navy Ordnance petroleum hydraulic fluid O.S. 1113. It was found that the pump operated well at a pressure of 800 psi. When examined after 2 hr of operation, there was only a slightly galled spot on the bushings as evidence of wear.

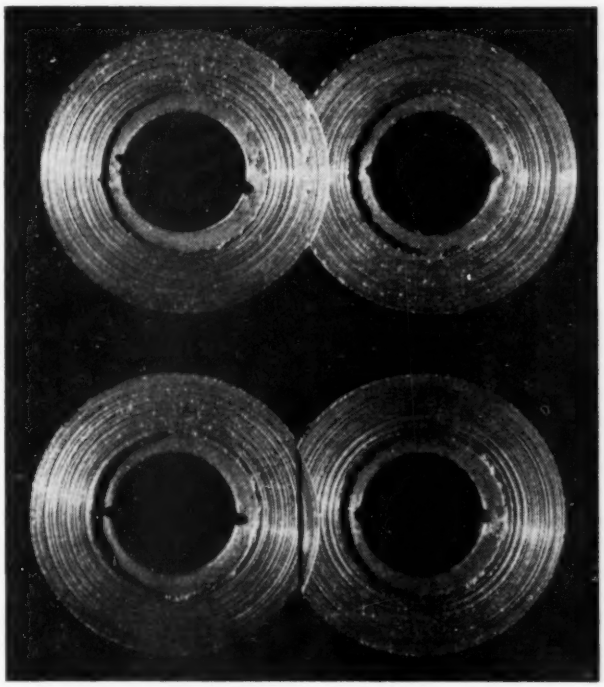


FIG. 2 CAST-IRON BUSHINGS AFTER 0.25 HR IN SILICONE

SELECTION OF BEARING METALS FOR USE WITH SILICONE LUBRICANTS

The contrast in the high rate of wear of silicone-lubricated surfaces of steel rubbing on cast iron, and the negligible rate of wear of steel on bronze in the gear-pump runs described, suggested the possibility that other combinations of rubbing metal surfaces might exist which were also well lubricated by this fluid. It was evident that an undesirably large amount of shop and time-consuming testing machine work would be needed if the large number of metal combinations of interest were tried as pump bushings or test bearings.

In endeavoring to duplicate the serious rate of wear and eventual seizure at low pressures of steel sliding on polished cast iron or on polished steel, a simple technique was found valuable in the rapid sorting out of the good, bad, and indifferent metal combinations lubricated with the silicone fluid. This "slider-and-plate" method consisted in sliding manually a flat cylindrical and polished metal slider having a diameter of 1 in. upon a lubricant-covered, flat, polished metal plate $1^1/_2$ in. wide and 6 in. long while exerting a downward pressure on the slider. The edge of the cylinder was rounded off to make the cylinder operate as a sled and so invite formation of an oil wedge between slider and plate.

In the middle portion of each long back-and-forth stroke of the slider a condition of thick-film lubrication prevailed unless the unit load had become high enough to cause metal-to-metal contact. The maximum load obtainable by exerting pressure manually was approximately 20 psi with the 1-in. slider. Loads of around 40 psi could be obtained using sliders of smaller diameter, although the need for preventing rocking did not permit the use of sliders much smaller than $^5/_8$ in. diam.

The existence of serious wear was determined by the sense of touch, by an inspection of the sliding metal surfaces, by observations of the fluid for deterioration, and especially for the presence of abraded metal. This method may not be equally useful, however, in examining fluids of entirely different chemical compositions.

A series of these simple tests was made, using thirteen different sliders and twelve different plates. The metals used included bronze (80-10-10), brass (commercial), copper, aluminum, magnesium, tin, babbitt (lead-base), cold-rolled steel, stainless steel, and steel plated with nickel, chromium, cadmium, zinc, and silver. This permitted observing 156 combinations of bearing metals. For comparison, a sample of naval specification petroleum oil NS-1047 was used. This high V.I. nonadditive oil had viscosities of 6.3 centistokes at 210 F, 41 centistokes at 100 F, and 2300 centistokes at 0 F.

It was chosen because at the test temperature (68 F), it had the same viscosity as the silicone fluid used. The plated metal surfaces were buffed to a high polish before use in these tests. The other metals were polished, using successively finer grades of emery paper and ending with 4/0 grade paper. All surfaces were previously cleaned with hot c.p. toluene. Although the degree of surface polish somewhat affected the results of this test in so far as doubtful cases were concerned, it was found that the differentiation between the relatively good and bad cases was not changed.

The results of an attempt to classify the observations using the slider-and-plate tests are presented in Tables 4, 5, and 6. In each table the qualitative results are indicated for the silicone oil and for the comparison oil. From the relative performance of all the combinations of lubricated metals tried, three groups were made. The good metal combinations are listed in Table 4. None of these exhibited any adverse characteristics. The bad combinations are listed in Table 5. The doubtful ones, listed in Table 6, had some bad features, such as relatively high friction or the presence of a metallic sludge in the oil after rubbing, but these characteristics were not considered pronounced enough to classify them as definitely bad.

TABLE 4 GOOD SILICONE-LUBRICATED METAL COMBINATIONS AND CORRESPONDING RATINGS USING PETROLEUM OIL N.S. 1047

Slider	Plate	Corresponding petroleum test result
Brass	Brass	Good
	Nickel	Good
	Cadmium	Good
	Tin	Good
	Zinc	Good
	Aluminum	Doubtful
	Chromium	Good
Bronze	Babbitt	Good
	Nickel	Good
	Copper	Good
	Chromium	Good
	Cadmium	Good
	Zinc	Good
	Aluminum	Good
	Silver	Good
Babbitt	Brass	Good
	Silver	Good
	Nickel	Good
	Chromium	Good
	Cadmium	Doubtful
	Zinc	Good
Nickel	Tin	Good
	Silver	Good
	Chromium	Good
	Aluminum	Good
Zinc	Brass	Good
	Tin	Doubtful
	Nickel	Good
	Cadmium	Good
	Zinc	Good
	Aluminum	Good
Magnesium	Tin	Doubtful
	Nickel	Doubtful
	Chromium	Doubtful
	Cadmium	Doubtful
Aluminum	Brass	Bad
	Copper	Bad
	Magnesium	Bad
	Nickel	Good
	Chromium	Good
	Zinc	Good
Cadmium	Brass	Good
	Copper	Good
	Babbitt	Good
	Tin	Good
	Stainless Steel	Good
	Silver	Good
	Nickel	Good
	Chromium	Good
	Cadmium	Good
	Zinc	Good
	Aluminum	Good
Silver	Brass	Good
	Copper	Doubtful
	Babbitt	Good
	Tin	Doubtful
	Stainless Steel	Good
	Nickel	Good
	Chromium	Good
	Zinc	Good
	Aluminum	Good
Tin	Copper	Good
	Babbitt	Good
	Tin	Doubtful
	Stainless Steel	Good
	Nickel	Good
	Chromium	Good
	Aluminum	Doubtful
Cold rolled Steel	Nickel	Doubtful
	Cadmium	Doubtful
Copper	Aluminum	Good
	Brass	Good
	Copper	Good
	Babbitt	Good
	Magnesium	Good
	Tin	Good
	Silver	Good
	Nickel	Good
	Chromium	Good
	Cadmium	Doubtful
	Zinc	Good

In contradiction to the original conclusion of earlier investigators that silicone fluids were not good lubricants, the results of this study revealed 81 bearing-metal combinations with which they may be found to be useful lubricants. The original reports were based upon the failure of silicone fluids to lubricate steel on steel where petroleum oils behaved very well. It is of interest to point out here that there are cases where the N.S. 1047 petroleum oil behaved poorly, while the silicone fluid produced good lubrication. From Table 4 may be cited such cases as aluminum on brass; copper on magnesium; magnesium on tin, nickel, chromium and cadmium; and cold-rolled steel on nickel and cadmium.

In contrast, the following metal combinations were lubricated well by N.S. 1047 but were not well lubricated with the silicone fluid: Steel, aluminum, copper, and nickel sliding on steel; nickel on brass and on nickel; tin on cadmium, and many others given in Tables 5 and 6.

It is apparent that each particular oil fails to lubricate certain definite metal combinations and that specificity of lubrication is a phenomenon not limited to silicone fluids alone. For example, the difference in the load-carrying capacity between N.S. 1047 oil and white mineral oil or a pure hydrocarbon like dodecylbenzene could be discerned, but in no case was there the serious scratching and seizure encountered with the silicone fluid.

TABLE 5 BAD SILICONE-LUBRICATED METAL COMBINATIONS AND CORRESPONDING RATINGS USING PETROLEUM OIL N.S. 1047

Slider	Plate	Corresponding petroleum test result
Brass	Magnesium	Bad
	Silver	Bad
Tin	Silver	Good
Magnesium	Brass	Doubtful
	Copper	Doubtful
	Babbitt	Doubtful
	Magnesium	Doubtful
	Aluminum	Doubtful
Cold rolled Steel	Aluminum	Good
	Stainless Steel	Good
Copper	Stainless Steel	Good
Aluminum	Tin	Bad
	Silver	Doubtful
	Stainless Steel	Good
Babbitt	Aluminum	Doubtful
Nickel	Copper	Good
	Babbitt	Good
	Cadmium	Good
	Zinc	Good
	Stainless	Good
Chromium	Tin	Doubtful
	Silver	Bad
	Nickel	Bad
	Chromium	Bad
	Cadmium	Bad
	Zinc	Bad
	Babbitt	Bad
	Copper	Bad
	Magnesium	Bad
	Brass	Bad
	Aluminum	Bad
	Stainless Steel	Bad

TABLE 6 DOUBTFUL SILICONE-LUBRICATED METAL COMBINATIONS AND CORRESPONDING RATINGS USING PETROLEUM OIL N.S. 1047

Slider	Plate	Corresponding petroleum test results
Brass	Babbitt	Good
	Copper	Doubtful
	Stainless steel	Doubtful
Babbitt	Magnesium	Good
	Tin	Good
	Stainless steel	Good
	Babbitt	Doubtful
	Copper	Doubtful
Nickel	Brass	Good
	Magnesium	Doubtful
	Nickel	Good
Zinc	Copper	Doubtful
	Babbitt	Doubtful
	Magnesium	Doubtful
	Stainless steel	Doubtful
	Silver	Good
	Chromium	Doubtful
Cadmium	Magnesium	Doubtful
Aluminum	Cadmium	Bad
	Aluminum	Doubtful
	Babbitt	Bad
Bronze	Tin	Good
	Brass	Good
	Magnesium	Good
	Stainless steel	Good
Silver	Magnesium	Doubtful
	Silver	Good
	Cadmium	Doubtful
Tin	Brass	Doubtful
	Magnesium	Doubtful
	Cadmium	Good
	Zinc	Good
Magnesium	Stainless steel	Doubtful
	Silver	Doubtful
	Zinc	Doubtful
Cold rolled steel	Brass	Doubtful
	Copper	Doubtful
	Babbitt	Doubtful
	Magnesium	Doubtful
	Tin	Doubtful
	Silver	Doubtful
	Chromium	Doubtful
	Zinc	Doubtful

In the case of steel on steel, the N.S. 1047 lubricated specimens were given the maximum manual loading (40 psi with a $^5/_8$-in. slider) and still no tendency toward seizure was noticed. Similar plates when lubricated with silicone oils and placed under loads of only 5 psi could be felt to scratch as though an abrasive were present. Slightly higher loads caused deep scratches or even sudden seizures, and with loads of 30 to 40 psi, movement of the slider almost instantly became an impossibility due to the seizure. In spite of such pronounced differences as this, in individual cases with most of the combinations of metals, the silicone fluid and the N.S. 1047 behaved alike. Thus in Table 4, of every five cases where silicones were found to be good, four were also good with the petroleum oil. From Tables 5 and 6, of every five cases in which silicones were found to be bad or doubtful, petroleum was found to give bad or doubtful results in three.

A qualitative relation can be established between the predictions from these simple tests and the results of tests with other more complex machines such as the journal-bearing machine.[7] In the case of the unilaterally loaded journal-bearing machine, the flat plate of these experiments corresponds to the shaft, and the slider corresponds to the bearing. Thus the slider (like the bearing) will accumulate thermal effects and reaction products which, depending upon the oil, may help or hinder lubrication. In contrast, each element of surface area of the plate (like the journal) will bear the load only periodically, allowing better distribution of the heat and chemical products generated. By similar considerations it is believed that these results can be interpreted for many applications to machinery and mechanisms of a more complex nature.

In trying to relate these slider-and-plate observations to some of the performance characteristics to be expected of more complex machines, another factor must be taken into account. The sliding test does not permit ascertaining the effect of break-in. For example, it has been found in the journal-bearing machine that a steel shaft rotating in a bronze bearing does very well if, and only if, a proper break-in procedure is followed.

In the Pesco pump runs it was found that bronze bushings rubbing against the face of steel gears worked well but developed lacquer coatings. This particular combination of metals belongs to the doubtful class in Table 6 because a slight sludge was noticed. Under careful break-in conditions in a pump or journal bearing,[7] this initial wear is avoided, a protective lacquer is formed, and subsequently the bearing is able to stand higher loads than with petroleum oil under similar conditions. Similar observations apply to the case of a brass slider upon steel, and may apply to other combinations. In agreement with this conclusion, when the slider and plates were coated with silicone lacquer by the method described in the companion paper, reference[7] no difficulties were encountered with seizures or scratching in the slider test.

Behavior of Silicone Fluids in Piston Pumps

Prior to observing the performance of the silicone fluid in the Vickers piston pumps, a 300-hr test run at 1500 psi and 180 F sump temperature was made on the petroleum oil AN-VV-O-366b, to provide reference data. Observations and a thorough inspection were made after 100, 200, and 300 hr of continuous operation, and the results are given in Table 7. The wear rates with this petroleum fluid were negligible. The general pump condition remained excellent throughout the test, while the oil remained clear, although an appreciable darkening in color was observed. The viscosity steadily decreased as usual due to shear breakdown of the polymer thickener. The viscosity decrease in the first 5000 cycles was approximately 24 per cent, and as usual the rate of viscosity breakdown rapidly became less after the first 5000 cycles.

TABLE 7 PISTON-PUMP RUNS ON PETROLEUM OIL AN-VV-O 366b

(Sump temperature 180 F)

	Start	After 100 hrs.	After 200 hrs.	After 300 hrs.
Test pressure (psi)	1500	1500	1500	1500
Pressure drop across relief valve (psi)	1450	1450	1450	1450
Flow rate GMM	2.94	2.68	2.85	2.84
Approx. number of cycles	0	5360.	11390.	16450.
Visc. cs. at 100°F	14.27	10.73	9.637	9.58
Percent visc. change	0	24.8	32.4	32.9
Filter type used	Skinner	Skinner	Skinner	Skinner
Appearance of oil	Clear red	Clear red	Clear red	Clear red

TABLE 8 PISTON-PUMP RUNS ON SILICONE FLUID

	Run F1 (Steel knuckles)	Run VP1 (Steel knuckles).	Run VP2 (Bronze knuckles)
Time in hours	65	80	650
Sump temp. °F	140	100	180
PSI high	1500	1500	1500
PSI low	190	75	64
Flow GPM:			
Start	3.18	2.7	3.4
Finish	0	0	2.99
Cycles approximately	1908	4500	38900
Visc. cs. at 100°F			
Start:	71.11	71.11	71.11
Finish:	73.22	71.28	73.67
Percent change	+ 0.3	nil	+ 0.36
Filter type	Skinner	Purolator aircraft	Purolator aircraft
Appearance after run	Cloudy gray	Cloudy gray	Clear, light amber
Initial Condition of Pump	100 Hrs. on 366E	New	New

The same pump was thoroughly cleaned with solvents and operated on the silicone fluid. After 65 hr of continuous operation at 1500 psi and 140 F sump temperature, the pump failed through seizure. In another trial, using a new pump and a new batch of silicone fluid, it failed through fracture of the universal link after 80 hr of continuous operation at the same pressure and at 100 F sump temperature. In each trial the oil became dark with dispersed particles of steel before failure occurred. The surfaces of the steel pins and knuckles were so worn where they rubbed each other that their diameters changed by apporximately one half of the original values, see Fig. 3. Enough gel and finely divided metal was created to accumulate in the filters and increase the pressure drop across the filter by 87 psi. Pump failure was directly due to the excessive wear in these members, allowing the piston connecting rods to strike the sides of the cylinders, either causing seizure or breaking of the universal link.

The pump failures in these tests had in each instance been caused by the rapid wearing of the steel universal link and steel knuckle. This was not surprising in view of the results of the slider-and-plate experiments previously described. From that study a number of much more suitable metal combinations than steel on steel suggested themselves for materials to be used in making the link and knuckles. As few would have been available soon enough, 80-10-10 bronze was used instead of the steel knuckles.

Accordingly, a set of four such knuckles was made and installed in a new Vickers pump and tested for 50 hr of continuous operation at 180 F sump temperature and 1500 psi. At the end of this time the system was completely taken down and inspected. No appreciable wear being apparent, the test was con-

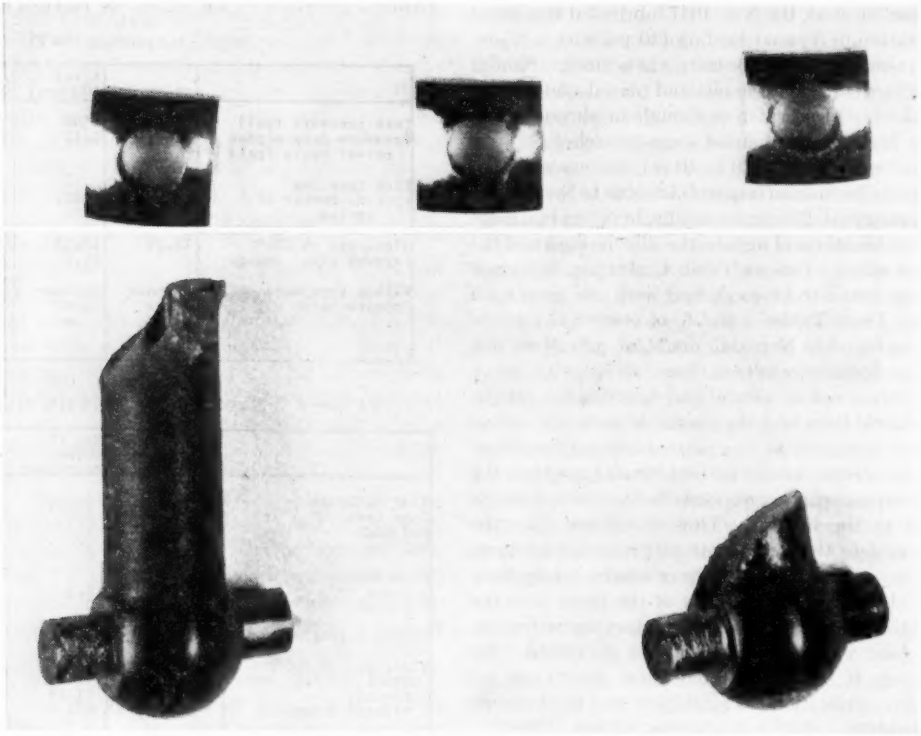


FIG. 3 UNIVERSAL LINK AND STEEL KNUCKLES AFTER 80 HR OPERATION IN SILICONE FLUID; RUN VPL

tinued for a total of 650 hr of operation, after which it was completely disassembled and inspected. The components of the pump were examined carefully. The universal link pins and knuckles were not unduly worn and the general condition of the pump was considered excellent. The silicone fluid remained clear for the entire test and no significant change was observed in the viscosity. No gel was evident in the fluid and the filter showed freedom from clogging or accumulated slime. However, some gel was found collected around the universal link bearings as it was in all the silicone tests. As the results of the Vickers pump design, these points were exposed to a very small flow of the fluid and any gel accumulated there would have little chance of circulating through the hydraulic system and collecting in the filter.

Hence the use of steel pins and bronze knuckles improved the lubrication characteristics so much as to permit the silicone fluid to be a practicable hydraulic fluid in this type of pump. However, it has not been established here that steel pins and bronze knuckles are the best possible choice of materials. Other combinations of metals deserve consideration by those interested in the necessary changes of design required in pumps to be used with these new fluids.

CONCLUSIONS

These experiments make evident the need for discrimination in the use in lubrication and hydraulics of the dimethyl-silicone-polymer fluids. Until a cure is found for the very limited load-carrying capacity of the fluid where both loaded sliding surfaces are ferrous, the application of the fluid to many types of equipment now in use will be limited or impractical. Where one or both of such loaded sliding surfaces are nonferrous or can be replaced by suitable nonferrous metals, much equipment can be adapted to the use of these new fluids. In many cases such changes may require considerable and even undesirable redesign.

The difficulties encountered due to the creeping and leaking tendencies of the silicone fluid will be annoying in some equipment, and the only cure found to date has been in the use of fewer, tighter, and more carefully made mechanical joints. A satisfactory pipe-thread sealant has been found and others probably exist. Its use in tight mechanical joints may be necessary where vibration is severe. The silicone fluids cannot be used where seals are made by metal-to-metal contact without using high sealing pressure or a pipe compound, an example of this difficulty being certain types of aircraft selector valves which require the achievement of a leakproof seal by the use of a steel poppet valve against a steel seat.

The excellent behavior of the silicone fluid in the gear or piston p mps when the proper metal is used for bushings or links and knuckles demonstrates the promise of these new fluids for applications as hydraulic and lubricating fluids. As their peculiarities become better understood, their unusually valuable viscometric, freezing point, and chemical-stability properties will make their adoption increasingly inviting.[6] Therefore, despite the need for redesign, packing changes, tight joints, etc., an increasingly wider use of these remarkable fluids can be expected. The use of the silicone fluid in the composition of the rubber packings instead of the usual plasticizer has shown how readily suitable packings can be prepared.

The protective and durable lacquer formed on the bronze bushings of the gear pump is quite like that found in slowly broken-in journal bearings described elsewhere,[7] and no doubt they are identical in origin and nature. There was no special difficulty with gel formation, for it was significant only after long periods of continuous operation at high sump temperatures. Even then that difficulty appeared adequately cared for by a filter-cartridge change every several hundred hours of continuous operation at high pressure. As the temperature of operation of the pumps rises above 200 F, no doubt the rate of gel formation

will become greater and will necessitate more frequent changes of the filter cartridge.

The results of the simple slider-and-plate tests, although merely qualitative, appear useful. The observed peculiarities of the silicone fluid in lubricating gear and piston pumps, as well as journal bearings,[7] are all in agreement with the predictions made by judicious use of the results of the slider tests, and in fact were used to guide part of the work here described and in the paper on journal bearings.[7] Except for a relatively few combinations, most of the slider-and-plate pairs tried and rated "good" with silicone were also rated "good" with the petroleum oil, and a similar parallelism holds with the combinations rated "bad." Also, many of the metal combinations rated "good" or "bad" for petroleum oil are identical with those experience has shown are useful in bearing systems lubricated with petroleum oils.

The low wear rates found in the gears of the Pesco pumps and the freedom from wear where found in the ball-bearing race of the Vickers pump are considered highly significant with respect to the relation of the behavior of the silicone fluids in rolling and in sliding friction. In both examples of rolling friction encountered here, steel rolled on steel, the unit loads were high, and yet little wear occurred. In contrast, at comparatively very low unit loads in the sliding friction of steel on steel, the failure to lubricate was remarkable. It is well known that sliding friction is less desirable in so far as wear rates are concerned than is rolling friction, but such a contrast as found here requires special explanation. It is suggested that this difference in case of the silicone fluid is due to the fact that, although it has ample chemical stability and adhesiveness to handle high unit loads directed normally to the moving surfaces, it fails under weak loads where sliding occurs as a result of the creation of local hot spots on ferrous and a few other poor-conducting hard metals, causing oxidative breakdown leading to gelling, lacquering, and even local cementing or welding.

Acknowledgments

It is a pleasure to acknowledge the co-operative efforts of other members of the Lubrication Section, especially Charles M. Murphy, Jr., and Eleanor Bried, Sp(X) 2/c, in making available the necessary viscometric data; Lieut. (jg) G. M. Hain for the careful and useful microscopic examinations; William Kostowicz, MM 2/c, for his skillful machine work; and, in particular, Ensign Harrison Shull, for his experimental and analytical assistance in connection with the slider-and-plate experiments. To Dr. Peter King and Ferdinand Thurman, Sp(X) 3/c of the High Polymer Section, we are indebted for their originality and efforts in the development of the indispensable silicone-oil-resistant packings employed throughout this and related investigations.

Rotary-Pump Theory

By W. E. WILSON,[1] WINNETKA, ILL.

A theory describing the performance of rotary positive-displacement pumps and fluid motors in terms of torque and delivery is presented. From the equations for these two quantities, expressions for power input and power output are developed. The concept of torque efficiency as a complement to the concept of volumetric efficiency is introduced. Equations are developed for the volumetric, torque, and over-all efficiencies. Three operating ranges are identified by outstanding characteristics of the performance in each case. Performance charts in dimensionless form are presented and analyzed. Tests on a conventional gear pump operated as a fluid motor yield data which substantiate the theory in one operating range. Additional tests on a cam-type pump give data confirming the predictions of the theory concerning the performance when pumping oils of high viscosity. Alterations of the physical dimensions of the unit are discussed in terms of effect on the performance characteristics. The possibility of the design of units with optimum dimensions is indicated.

General Theory

THE equations which will be developed apply to a rotary positive-displacement unit, acting either as a pump or as a motor. The unit consists of a rotary element, a stationary housing, inlet and outlet passages, and a shaft connected to the rotary element. The definite volume of fluid which is trapped between the rotary element and the housing is positively forced through the unit. Viscous bearing and gear friction as well as other mechanical effects will tend to resist motion of the rotor. These affect the shaft torque by an amount which will be referred to as "torque loss." Flow through the clearances and seals will cause an actual discharge differing from the ideal discharge. These secondary flows are referred to collectively as "slip." A loss in delivery of a pump, not properly designated as slip, is described. This loss is encountered when pumping liquids containing entrained gases, or liquids which vaporize readily.

Three distinct ranges of performance are recognized and defined as follows:

Range 1. All flow of the fluid in the unit in the turbulent range, giving a fluid torque resistance proportional to the square of the angular speed, and slip proportional to the square root of the pressure difference. Slip is independent of the viscosity in this case and torque loss is nearly constant.

Range 2. Laminar flow of the fluid throughout the unit, giving a viscous torque resistance proportional to the first power of the angular speed and first power of the viscosity, and a slip proportional to the first power of the pressure difference and inversely proportional to the viscosity.

Range 3. Laminar flow of the fluid throughout the unit. Slip is negligible due to high viscosity at low speeds. Slip increases as the speed increases due to local heating of the fluid, which in turn is caused by energy dissipated in the shearing action on the viscous liquid. This results in viscous torque loss less than that which would arise from fluid of the original viscosity. Delivery is also reduced by expansion of entrained gases or vapor in the low-pressure region at the pump intake.

In Fig. 1 are shown the characteristics of performance just outlined, in graphical form, in terms of torque and delivery as functions of speed of rotation of rotor shaft at constant pressure differential and constant viscosity at pump intake.

In the development of the theory it is assumed that the rotor shaft is rigid, clearances within the unit remain constant, and the coefficient of friction between unlubricated surfaces is a constant.

Ideal Torque and Delivery

In Fig. 2 is shown a section through a typical rotary pump. Using this sketch for reference, the equations for torque and delivery in general form may be written as follows:

As the rotor of either a pump or a fluid motor rotates, the motion is resisted by a viscous drag which originates in the narrow passages between rotor and housing. In addition there will be resisting torques such as those which originate in the shaft seals which will be nearly constant in magnitude. There are also torques resisting the motion which are proportional to the pressure differential which exists. These torques may originate in the seals if the sealing forces are proportional to the pressure differential, or in the bearings where the resistance is proportional to the bearing load, which in turn depends upon the pressure differential. In the case of the pump the pressure differential causes a torque opposing the motion, and in the case of the fluid motor in the direction of the motion. This torque will be called

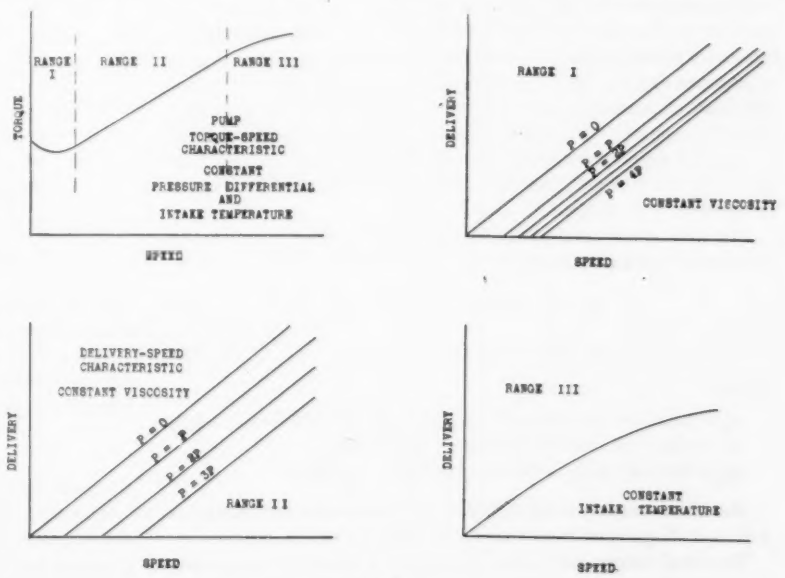


Fig. 1

---

[1] Consulting Engineer, Winnetka, Ill. Mem. A.S.M.E.

Contributed by the Hydraulic Division and presented at the Annual Meeting, New York, N. Y., Nov. 26–29, 1945, of The American Society of Mechanical Engineers.

Note: Statements and opinions advanced in papers are to be understood as individual expressions of their authors and not those of the Society.

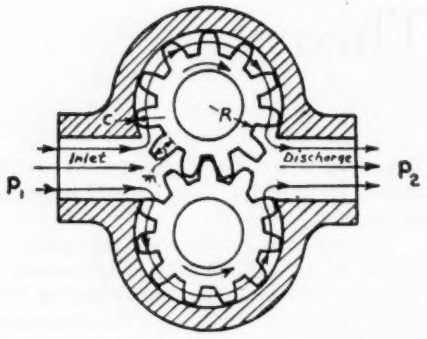


FIG. 2

the ideal torque since it is the torque which would be required to drive the pump or would be developed by the motor if the fluid were frictionless and there were no mechanical friction causing resisting torques.

The torque T required to drive a pump or developed by a fluid motor may be expressed in terms of the torques just discussed as follows

$$\text{Pump:} \quad T = T_i + T_v + T_f + T_c \ldots\ldots [1a]$$

$$\text{Motor:} \quad T = T_i - T_v - T_f - T_c \ldots\ldots [1b]$$

where

T_i is ideal torque due to pressure differential and physical dimensions of unit only
T_v is resisting torque due to viscous shearing of fluid
T_f is resisting torque, due to mechanical friction, which is directly proportional to pressure differential
T_c is resisting torque due to mechanical friction which is constant

The delivery of a pump or fluid motor consists of the fluid which is trapped due to the geometrical features of the unit and bodily transported from the inlet to outlet, less that fluid which is returned from the discharge to the intake by the geometrical features of the unit, less that fluid which flows from discharge to intake by reason of the pressure differential (slip) and, in the case of pumped liquids, less the volume of entrained gases or vapor which are expanded at the intake and compressed at the discharge side of the pump. The ideal delivery is that full quantity which is trapped and transported from intake to discharge less that quantity which is returned from discharge to intake by virtue of the geometry of the unit.

The delivery of the pump or fluid motor may therefore be expressed in general terms as follows

$$\text{Pump:} \quad Q = Q_i - Q_s - Q_L \ldots\ldots [2a]$$

$$\text{Motor:} \quad Q = Q_i + Q_s \ldots\ldots [2b]$$

where

Q_i is ideal delivery of unit due to its geometrical features only
Q_s is slip flow caused by pressure differential
Q_L is delivery loss due to entrained gas or vapor

The ideal torque and ideal delivery of a unit with zero clearance will be distinguished from those of a unit with clearances.

The ideal torque and ideal delivery of a unit with zero clearances may be expressed very simply by considering that the pressure differential acts upon a rotating surface of area A, which by its motion displaces the fluid in a positive manner.

The ideal torque T_i' due to the pressure differential may be expressed in terms of a force $(p_1 - p_2)\,A$, which acts at the distance r from the axis of rotation thus

$$T_i' = (p_1 - p_2)\,Ar \ldots\ldots [3]$$

where

p_1 is pressure at intake
p_2 is pressure at discharge
A is projected area of moving surface on radial plane
r is distance from center of pressure to axis of rotation

Similarly, the ideal delivery Q_i' may be expressed as the volume $Ar\omega$ swept out per unit time by the translation of the area A through the distance $r\omega$ thus

$$Q_i' = Ar\omega \ldots\ldots [4]$$

where

ω is angular speed of rotation of rotor shaft
A is area previously defined
r is distance from axis of rotation to centroid of area A

It is apparent that the quantity Ar is identical in the two expressions given, when the pressure is constant over the area A. Situations in which the pressure is not constant over the area A will not be considered for the present.

Between the peripheral boundary of the area A and the housing lies a small clearance space through which slip flow occurs. The area of this opening in a radial plane must be considered in some manner in calculating ideal delivery and torque. Definitions to provide for this consideration will be given. Expressions for rate of flow and fluid-resisting torque will be developed on the basis of the assumption that the flow in these small passages is approximated sufficiently closely by the flow between infinite parallel flat plates.

We have defined the ideal delivery as the delivery which would represent the full geometrical delivery of the unit. It is apparent that the fluid which adheres to the moving boundary of the area A in a unit with clearances will result in the transport of fluid through the clearance space. The expression for ideal delivery, Q_i, may then be written

$$Q_i = Ar\omega + ar'\omega$$

or

$$Q_i = \alpha\omega \ldots\ldots [5]$$

where

ar' is volume of fluid carried along by translation of periphery of area A through unit angular distance
α is equal to $(Ar + ar')$

The quantity α is simply the ideal displacement of the pump or fluid motor per unit rotation of the rotor shaft. This quantity may be most easily determined experimentally by finding the delivery when the pressure differential across the unit is zero. Under these circumstances there can be no slip flow.

One may proceed in a similar manner to write an expression for the ideal torque T_i of a unit with clearance, and for sake of brevity we shall write immediately the expression

$$T_i = (p_1 - p_2)\alpha \ldots\ldots [6]$$

where all terms have been defined previously.

The use of the quantity α in the expression for torque as well as delivery may be justified quite rigorously for the case of the ideal pump or fluid motor in a rather simple manner. The mechanical power input to the pump or output of the motor is simply the

product of the torque and angular speed, and the hydraulic power output of the pump or input to the motor is the product of delivery and pressure differential. In an ideal unit the input and output must necessarily be equal. For the case of the ideal unit one may then write

$$T\omega = Q\,\Delta p$$

which in the nomenclature used previously is

$$(p_1 - p_2)\alpha\omega = \alpha\omega(p_1 - p_2)$$

This is obviously an identity as it should be if the quantity α may properly be used in this case. The justification for the use of α in the general case is beyond the scope of the present treatment; however, the case of laminar flow will be considered in detail since the mathematical development is relatively simple.

Slip and Torque Loss

Consider now the flow through a clearance space of the dimensions shown in Fig. 3(*a*). The lower plate moves at the speed $U = r\omega$, where r is the distance from the plate to the axis of rotation. The flow ΔQ_1 through the opening is due to both pressure drop and shear transport of the fluid and is assumed to be in the laminar range.

Referring to Fig. 3(*b*), we consider an element of the fluid at the distance y from the fixed plate, and of the dimensions dx, dy, b. The forces acting on this element are the pressure forces $(p + dp)\,b\,dy$ acting to the right and $p\,b\,dy$ to the left, the shear forces $\tau\,b\,dx$ acting to the left and $(\tau + d\tau)\,b\,dx$ to the right. Assuming steady flow, the acceleration of the element is zero, hence the equation of equilibrium is

$$[(p + dp) - p\,]\,b\,dy + [(\tau + d\tau) - \tau]\,b dx = 0$$

which reduces to

$$\frac{dp}{dx} = -\frac{d\tau}{dy}$$

Since the flow is between parallel plates the pressure gradient dp/dx will be constant. We may therefore integrate the equation just given and obtain

$$\tau = -\frac{dp}{dx}\,y + \tau_0$$

Newton's viscosity law may now be introduced to relate the shear stress to the velocity gradient

$$\tau = \mu\,\frac{du}{dy}$$

Substitution of this expression for τ yields the differential equation

$$\mu\,\frac{du}{dy} = \tau_0 - \frac{dp}{dx}\,y$$

This may be integrated to yield

$$\mu u = \tau_0 y - \frac{dp}{dx}\,\frac{y^2}{2} + C_1$$

The boundary conditions are

$$\text{at } y = 0, \quad u = 0$$

$$\text{at } y = c, \quad u = r\omega$$

It follows therefore that

$$c_1 = 0$$

and

$$\tau_0 = \frac{\mu r\omega}{c} + \frac{dp}{dx}\,\frac{c}{2}$$

The velocity u at any distance y from the fixed plate is then

$$u = \frac{r\omega y}{c} + \frac{1}{\mu}\,\frac{dp}{dx}\left[\frac{yc}{2} - \frac{y^2}{2}\right]$$

The total quantity of fluid flowing ΔQ_1 is given by

$$\Delta Q_1 = \int_0^c u \cdot b \cdot dy$$

or

$$\Delta Q_1 = \int_0^c \left\{\frac{r\omega y}{c} + \frac{1}{\mu}\,\frac{dp}{dx}\left[\frac{yc}{2} - \frac{y^2}{2}\right]\right\} b dy$$

and after integration

$$\Delta Q_1 = \left[\frac{r\omega c}{2} + \frac{dp}{dx}\,\frac{c^3}{12\mu}\right] b$$

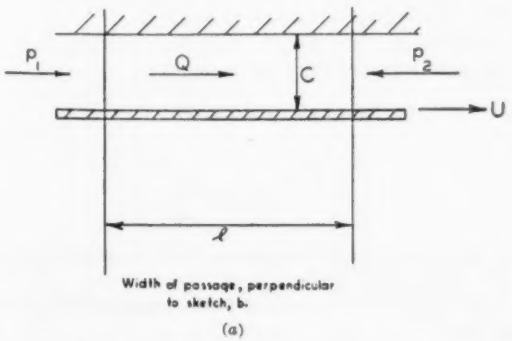
and upon substituting for dp/dx as follows

$$\frac{dp}{dx} = \frac{p_1 - p_2}{l}$$

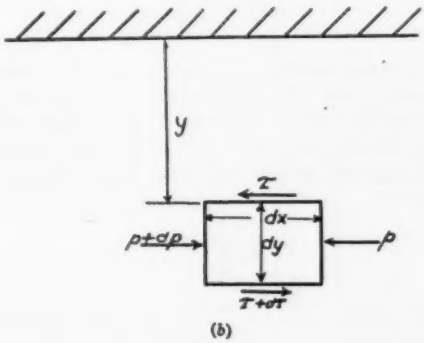
we have finally

$$\Delta Q_1 = \left[\frac{r\omega c}{2} + \frac{(p_1 - p_2)c^3}{12\mu l}\right] b \qquad \text{.....[7]}$$

The unit force τ due to viscous friction which retards the moving plate is given by the value of the shear stress at $y = c$



(*a*)



(*b*)

Fig. 3

$$\tau = -\frac{(p_1 - p_2)}{l}\frac{c}{2} + \frac{\mu r\omega}{c}$$

Since the total force F on the moving plate is

$$F = \tau lb$$

there results a torque ΔT_1 acting on the rotary element of the unit

$$\Delta T_1 = -\left[\frac{(p_1 - p_2)}{l}\frac{c}{2} - \frac{\mu r\omega}{c}\right] lbr \quad [8]$$

There may be several passages through which the fluid will leak, hence it is necessary to consider the total effect on both torque and delivery. The fact that the torque ΔT_1 and flow ΔQ_1 are linear functions of the pressure difference and angular speed of the shaft permits the equations for net delivery and net torque to be written in the following form

$$Q = Q_i' + \Sigma Q_1$$

$$T = T_i' - \Sigma T_1$$

which upon substitution for ΣQ_1 and ΣT_1 yield

$$Q = Ar\omega + \Sigma\left[\frac{r\omega c}{2} + \frac{(p_1 - p_2)c^3}{12\mu l}\right] b$$

$$T = (p_1 - p_2)Ar + \Sigma\left[\frac{(p_1 - p_2)}{l}\frac{c}{2} - \frac{\mu r\omega}{c}\right] lbr$$

These may be rewritten in the forms

$$Q = \omega\left[Ar + \Sigma\frac{rcb}{2}\right] + \Sigma\frac{(p_1 - p_2)c^3 b}{12\mu l} \quad [9]$$

$$T = (p_1 - p_2)\left(Ar + \Sigma\frac{crb}{2}\right) - \Sigma\frac{\mu\omega lbr^2}{c} \quad [10]$$

It is apparent that the quantity

$$\left[Ar + \Sigma\frac{rcb}{2}\right]$$

is the factor ω, and $\Sigma\frac{rcb}{2}$ is the quantity ar' previously defined.

Also in accordance with previous definitions, the delivery loss due to pressure differential is the slip. It follows therefore that the slip ΔQ_s for a single passage is given by

$$\Delta Q_s = \frac{(p_1 - p_2)c^3 b}{12}$$

and the torque loss ΔT_L by

$$\Delta T_L = \frac{\mu\omega lbr^2}{c}$$

Now since in any specific unit (pump or motor) the clearance c, length of path l, width of passage b, and radius to the passage r are different for the various elements of the passages surrounding the rotating element, the expressions for the total torque loss T_L, and total slip Q_s must be written in a more general form. This is done as follows

$$Q_s = \frac{\beta p}{\mu} \quad [11]$$

$$T_L = k\mu\omega \quad [12]$$

where

$$p = p_1 - p_2$$

It is readily shown that both k and β have the dimensions length to the third power and may be expressed thus

$$\beta = \Sigma\frac{c^3 b}{12l}$$

$$k = \Sigma\frac{lbr^2}{c}$$

In order to simplify the equations and without materially decreasing their significance, the torque loss T_L will be considered to include that loss in torque which is due to entrance and exit losses since in the case of laminar flow, these will be nearly proportional to the product of viscosity and angular speed.

Detailed equations for torque, delivery, power input, power output and efficiencies will now be developed for the three performance ranges defined previously.

Torque and Delivery Range 1

In this range of performance the slip is proportional to the square root of the pressure differential and practically independent of the viscosity. The torque losses are principally mechanical in nature, although the fluid resistance will vary with the square of the speed of rotation and will be practically independent of the viscosity of the fluid. The expressions for torque and delivery may now be written, taking into consideration the nature of the slip and resisting torques, thus

Pump: $$T = \epsilon p\alpha + k\rho\omega^2 R^2 + T_e \quad [13]$$

$$Q = \alpha\omega - \frac{\beta}{R}\sqrt{\frac{p}{\rho}} - Q_L \quad [14]$$

Motor: $$T = \epsilon p\alpha - k\rho\omega^2 R^2 - T_e \quad [15]$$

$$Q = \alpha\omega + \frac{\beta}{R}\sqrt{\frac{p}{\rho}} \quad [16]$$

where

T is torque input or output, ft-lb
p is pressure difference, psf
T_e is torque due to mechanical friction independent of pressure, ft-lb
α is ideal displacement, cu ft per radian
k is a coefficient with dimensions, cu ft
μ is viscosity of fluid, slugs per ft-sec
ω is angular speed of shaft, radian per sec
Q is delivery, cfs
β is a coefficient with dimensions, cu ft
ρ is density of fluid, slugs per cu ft
Q_L is loss in delivery in cu ft per sec due to vaporization of liquid, or liberation of entrained gas at intake
R is a characteristic radius of the unit, ft
ϵ is given by the following expression using positive sign for pump and negative sign for motor:

$$\epsilon p\alpha = p\alpha \pm T$$

or

$$\epsilon = 1 \pm \frac{T_f}{\alpha p}$$

T_f is mechanical friction torque which is proportional to pressure differential

Now since T_f is proportional to the pressure differential p, one may write

$$T_f = mp$$

and it follows that

$$\epsilon = 1 \pm \frac{m}{\alpha}$$

which is a constant for any one pump or motor.

Torque and Delivery Ranges 2 and 3

In a similar manner expressions for torque and delivery for both pump and motor in performance ranges 2 and 3 may now be written, using the nomenclature employed previously, as follows

$$\text{Pump:} \quad T = \epsilon p\alpha + k\mu\omega + T_c \qquad [17]$$

$$Q = \alpha\omega - \frac{\beta p}{\mu} - Q_L \qquad [18]$$

$$\text{Motor:} \quad T = \epsilon p\alpha - k\mu\omega - T_c \qquad [19]$$

$$Q = \alpha\omega + \frac{\beta p}{\mu} \qquad [20]$$

The distinction between range 2 and range 3 comes in the variation of the viscosity with speed in range 3, and the difference in order of magnitude of the last two terms in the equation for pump delivery. In range 2 the torque shows a straight-line variation with speed, due to the constancy of the viscosity. Also in range 2 the delivery loss Q_L is negligible. In range 3 the torque does not change as rapidly with speed as would be indicated by a constant value of the viscosity, and the slip is either negligible compared with Q_L or shows an increase with the speed corresponding to the decrease in viscosity which is characteristic of this situation.

Power

Equations for power output and power input may be written on the basis of the fundamental expressions

$$\text{Pump:} \quad \begin{aligned} &\text{Power output} = P_0 = Qp \\ &\text{Power input} \ = P_i = T\omega \end{aligned}$$

$$\text{Motor:} \quad \begin{aligned} &\text{Power output} = P_0 = T\omega \\ &\text{Power input} \ = P_i = Qp \end{aligned}$$

Substitution of the previously given expressions for torque and delivery yields the following equations

Range 1

$$\text{Pump:} \quad P_0 = p\alpha\omega\left[1 - \frac{\beta\sqrt{p/\rho}}{R\alpha\omega} - \frac{Q_L}{\alpha\omega}\right] \qquad [21]$$

$$P_i = p\alpha\omega\left[\epsilon + \frac{k\omega^2R^2\rho}{p\alpha} + \frac{T_c}{p\alpha}\right] \qquad [22]$$

$$\text{Motor:} \quad P_0 = p\alpha\omega\left[\epsilon - \frac{k\omega^2R^2\rho}{p\alpha} - \frac{T_c}{p\alpha}\right] \qquad [23]$$

$$P_i = p\alpha\omega\left[1 + \frac{\beta\sqrt{p/\rho}}{\alpha\omega R}\right] \qquad [24]$$

Ranges 2 and 3

$$\text{Pump:} \quad P_0 = p\alpha\omega\left[1 - \frac{\beta p}{\mu\alpha\omega} - \frac{Q_L}{\alpha\omega}\right] \qquad [25]$$

$$P_i = p\alpha\omega\left[\epsilon + \frac{k\mu\omega}{p\alpha} + \frac{T_c}{p\alpha}\right] \qquad [26]$$

$$\text{Motor:} \quad P_0 = p\alpha\omega\left[\epsilon - \frac{k\mu\omega}{p\alpha} - \frac{T_c}{p\alpha}\right] \qquad [27]$$

$$P_i = p\alpha\omega\left[1 + \frac{\beta p}{\mu\alpha\omega}\right] \qquad [28]$$

Efficiency

In the case of a motor, the ratio of the actual torque to the theoretical torque may be termed the torque efficiency E_T; and the ratio of the theoretical delivery to the actual delivery may be termed the volumetric efficiency E_v. The reciprocals of these quantities are the corresponding efficiencies for the pump. These may be written as follows

Range 1

$$\text{Pump:} \quad E_T = \frac{p\alpha}{T} = \frac{1}{\epsilon + \frac{k}{\alpha}\frac{\omega^2R^2\rho}{p} + \frac{T_c}{p\alpha}} \qquad [29]$$

$$E_v = \frac{Q}{\alpha\omega} = 1 - \frac{\beta}{\alpha}\frac{\sqrt{p/\rho}}{\omega R} - \frac{Q_L}{\alpha w} \qquad [30]$$

$$\text{Motor:} \quad E_T = \frac{T}{p\alpha} = \epsilon - \frac{k}{\alpha}\frac{\omega^2R^2\rho}{p} - \frac{T_c}{p\alpha} \qquad [31]$$

$$E_v = \frac{\alpha\omega}{Q} = \frac{1}{1 + \frac{\beta}{\alpha}\frac{\sqrt{p/\rho}}{\omega R}} \qquad [32]$$

Ranges 2 and 3

$$\text{Pump:} \quad E_T = \frac{p\alpha}{T} = \frac{1}{\epsilon + \frac{k}{\alpha}\frac{\mu\omega}{p} + \frac{T_c}{p\alpha}} \qquad [33]$$

$$E_v = \frac{Q}{\alpha\omega} = 1 - \frac{\beta}{\alpha}\frac{p}{\mu\omega} - \frac{Q_L}{\alpha w} \qquad [34]$$

$$\text{Motor:} \quad E_T = \frac{T}{p\alpha} = \epsilon - \frac{k}{\alpha}\frac{\mu\omega}{p} - \frac{T_c}{p\alpha} \qquad [35]$$

$$E_v = \frac{\alpha\omega}{Q} = \frac{1}{1 + \frac{\beta}{\alpha}\frac{p}{\mu\omega}} \qquad [36]$$

It is convenient to make the following simplification in nomenclature

Let

$$\phi_1 = \frac{\rho\omega^2R^2}{p}$$

in range 1, and

$$\phi = \frac{\mu\omega}{p}$$

in ranges 2 and 3.

The over-all efficiency E is now defined as the power output of the unit divided by the power input; thus

$$E = \frac{P_0}{P_i}$$

The expressions for this over-all efficiency may be written as follows, provided we substitute in each case the appropriate term ϕ or ϕ_1 for the parameters cited previously

RANGE 1

$$\text{Pump:}\quad E = \frac{1 - \dfrac{\beta}{\alpha\sqrt{\phi_1}}}{\epsilon + \dfrac{k\phi_1}{\alpha} + \dfrac{T_e}{p\alpha}} \qquad [37]$$

$$\text{Motor:}\quad E = \frac{\epsilon - \dfrac{k\phi_1}{\alpha} - \dfrac{T_e}{p\alpha}}{1 + \dfrac{\beta}{\alpha\sqrt{\phi_1}}} \qquad [38]$$

RANGES 2 AND 3

$$\text{Pump:}\quad E = \frac{1 - \dfrac{\beta}{\alpha\phi} - \dfrac{Q_L}{\alpha\omega}}{\epsilon + \dfrac{k\phi}{\alpha} + \dfrac{T_e}{p\alpha}} \qquad [39]$$

$$\text{Motor:}\quad E = \frac{\epsilon - \dfrac{k\phi}{\alpha} - \dfrac{T_e}{p\alpha}}{1 + \dfrac{\beta}{\alpha\phi}} \qquad [40]$$

It is pertinent to note that significant simplification of the equations for range 2 may be effected by noting the relative order of magnitude of the terms involved in the various equations just given. When operating in this range at fairly high pressures, e.g., over 300 psi, the term $\frac{T_e}{p\alpha}$ is frequently found to be negligible in comparison with $k\phi/\alpha$ and ϵ. Also by definition, the term $Q_L/(\alpha\omega)$ is small in this range compared with $\beta/(\alpha\phi)$. The simplified equations in range 2 then reduce to

$$\text{Pump:}\quad E_v = 1 - \frac{\beta}{\alpha\phi} \qquad [41]$$

$$E_T = \frac{1}{\epsilon + \dfrac{k\phi}{\alpha}} \qquad [42]$$

$$E = \frac{1 - \dfrac{\beta}{\alpha\phi}}{\epsilon + \dfrac{k\phi}{\alpha}} \qquad [43]$$

$$\text{Motor:}\quad E_v = \frac{1}{1 + \dfrac{\beta}{\alpha\phi}} \qquad [44]$$

$$E_T = \epsilon - \frac{k}{\alpha}\phi \qquad [45]$$

$$E = \frac{\epsilon - \dfrac{k\phi}{\alpha}}{1 + \dfrac{\beta}{\alpha\phi}} \qquad [46]$$

It is immediately apparent that under these circumstances the performance of the pump or fluid motor may be expressed in terms of dimensionless ratios descriptive of the geometry of the unit, namely, k/α and β/α; and the dimensionless parameter expressed as $\phi = \frac{\mu\omega}{p}$, which describes the conditions of operation.

Consideration of the equation for over-all efficiency E in this case leads to the immediate conclusion that there is a particular value of ϕ which corresponds to the maximum efficiency of the unit. The value of ϕ which corresponds to the maximum efficiency may readily be obtained by maximizing the equations for over-all efficiency, considering ϕ as the only variable. The resulting values of ϕ are given by

$$\text{Pump:}\quad \phi_m = \frac{\beta}{\alpha}\left[1 + \sqrt{1 + \frac{\epsilon\alpha^2}{\beta k}}\right] \qquad [47]$$

$$\text{Motor:}\quad \phi_m = \frac{\beta}{\alpha}\left[-1 + \sqrt{1 + \frac{\epsilon\alpha^2}{\beta k}}\right] \qquad [48]$$

where ϕ_m is the value of ϕ corresponding to E_{max}.

The corresponding values of E_{max} are

$$\text{Pump:}\quad E_m = \frac{1}{\epsilon_1\left[1 + 2\theta + 2\sqrt{\theta(1+\theta)}\right]} \qquad [49]$$

$$\text{Motor:}\quad E_m = \epsilon_2\left[1 + 2\theta - 2\sqrt{\theta(1+\theta)}\right] \qquad [50]$$

where

$$\theta = \frac{k\beta}{\epsilon\alpha^2}$$

These expressions for efficiency are shown graphically in Fig. 4

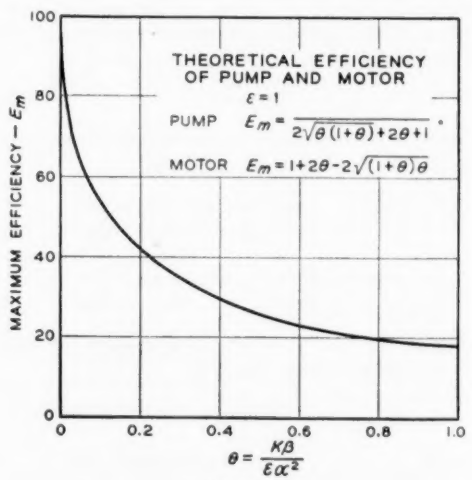


FIG. 4

for the case of $\epsilon_1 = \epsilon_2 = 1$. It is readily shown that motor and pump efficiencies are identical in this case. It is immediately apparent that the maximum efficiency is a function of θ and ϵ only, and that these in turn are determined by the geometry of the unit only.

Since the concept of torque efficiency is somewhat unfamiliar, it is well to point out the relationship which exists between the volumetric efficiency E_v, the torque efficiency E_T, and the over-all efficiency E. By definition the following expressions may be written for a pump

$$E_v = \frac{Q}{Q_i}$$

$$E_T = \frac{T_i}{T}$$

$$E = \frac{Qp}{T\omega}$$

The product of E_v and E_T may then be obtained thus

$$E_v E_T = \frac{QT_i}{Q_i T}$$

Substituting the following quantities for ideal torque and ideal delivery

$$T_i = p\alpha \qquad Q_i = \alpha\omega$$

we obtain

$$E_v E_T = \frac{Qp}{T\omega}$$

from which it may be concluded that the product of the volumetric efficiency and the torque efficiency is equal to the over-all efficiency. A check of the equations given previously for the various cases reveals that they are in agreement with this general conclusion, and a similar demonstration may be made for the case of a motor.

Local Heating of Liquid

It has been pointed out that the reduction in viscosity by the heating developed in the shearing action on the fluid in the narrow passage between rotor and housing is a most important feature of the performance in range 3 (44).[2] An equation describing the important characteristics of this phenomenon will be derived.

The narrow passage, shown schematically in Fig. 3(*a*), will be used as the basis of this development. The work done on the fluid which flows through the passage is equal to the product of the force exerted by the moving plate on the fluid and the speed at which the plate moves. It will be assumed that this energy which is supplied to the fluid is dissipated entirely in raising the temperature of the fluid. The following expressions for work done and heat absorbed may be written

$$\text{Work done on fluid} = \left[\mu\frac{r\omega}{c} + \frac{(p_1 - p_2)c}{2}\right] r\omega bl$$

$$\text{Heat absorbed by fluid} = c_s Q w \Delta T$$

where

c_s is heat required to raise temperature of 1 lb of liquid 1 deg F
w is weight of 1 cu ft of liquid
ΔT is rise of temperature in deg F of liquid in distance l
μ is coefficient of viscosity of liquid in slugs per ft-sec
Q is rate of flow of liquid through narrow opening relative to moving plate, cfs

All other terms have been defined previously or are defined in Fig. 3(*a*).

Equating these rates of energy supply and absorption, assuming no heat loss to the surroundings, introducing the mechanical equivalent of heat J and the value of Q from Equation [7], we have

$$Jc_s\left[\frac{r\omega c}{2} + \frac{(p_1 - p_2)c^3}{12\mu l}\right] bw\Delta T = \left[\frac{\mu r\omega}{c} + \frac{(p_1 - p_2)c}{2l}\right] r\omega bl$$

Suitable algebraic manipulations lead to the following expression for the temperature rise

$$\Delta T = \frac{\mu l r\omega}{c_s c^2 wJ}\left[2 + \frac{1}{\frac{1}{4} + \frac{3r\omega\mu l}{2c^2(p_1 - p_2)}}\right] \quad \ldots\ldots [51]$$

It is readily determined that the expression contained within the brackets must have a value between 2 and 6. For purposes of simplification it is assumed that a constant value of 4 for the quantity within the bracket will yield results sufficiently reliable for practical use.

While it is necessary to calculate the temperature rise in the slip passage, it is further required that the change in viscosity be determined. For purposes of calculation the viscosity μ of the liquid is approximated by the expression

$$\mu = \mu_0 e^{-\gamma T} \quad \ldots\ldots [52]$$

where

μ_0 is viscosity at $T = 0$
γ is a constant for any particular liquid
e is base of natural logarithms

Considering now the change dT in the temperature along a length dx of the passage, we may rewrite Equation [51] upon using the value 4 for the bracket thus

$$\frac{dT}{\mu_0 e^{-\gamma T}} = \frac{4r\omega}{c_s w c^2 J}\, dx$$

This may be integrated to yield

$$\mu = \frac{B\mu_1}{\mu_1 x + B} \quad \ldots\ldots [53]$$

where

$$B = \frac{c_s w c^2 J}{4\gamma r\omega}$$

and x is the distance along the passage to the point at which the viscosity is μ. The quantity μ_1 is the viscosity at entrance to the pump or motor.

The average value of the viscosity in the passage is of particular significance. Denoting this average value by μ_{avg}, it may be calculated as follows

Define

$$\mu_{avg} = \frac{\int_0^l \mu dx}{l}$$

then

$$\mu_{avg} = \frac{1}{l}\int_0^l \frac{B\mu_1}{\mu_1 x + B}\cdot dx$$

Integration and simplification yield

$$\mu_{avg} = \frac{B}{l}\log_e\left[\frac{\mu_1 l}{B} + 1\right] \quad \ldots\ldots [54]$$

This may be put into a more significant form by dividing both sides of the equation by μ_1 the initial viscosity of the liquid

$$\frac{\mu_{avg}}{\mu_1} = \frac{B}{\mu_1 l}\log_e\left[\frac{\mu_1 l}{B} + 1\right]$$

which may be rewritten in the following form

$$\frac{\mu_{avg}}{\mu_1} = \frac{c_s w c^2 J}{4\gamma r\omega l\mu_1}\log_e\left[\frac{4\gamma r\omega l\mu_1}{c_s w c^2 J} + 1\right] \quad \ldots\ldots [55]$$

The variation of μ_{avg} with angular speed ω with constant pressure differential is particularly significant. When the angular

[2] Numbers in parentheses refer to the Bibliography at the end of the paper.

speed is zero the ratio $\frac{\mu_{avg}}{\mu_1}$ reduces to the form 0/0 which may be shown mathematically to have the value 1, as would be expected from purely physical considerations. As the angular speed increases the ratio $\frac{\mu_{avg}}{\mu_1}$ approaches zero. The viscous torque may be expressed in terms of the reduced viscosity μ_{avg}

$$T_v = k\mu_{avg}\omega$$

and upon substituting the expression for μ_{avg}

$$T_v = \frac{kc_s wc^2 J}{4\gamma rl} \log_e \left[\frac{4\gamma rl\omega\mu_1}{c_s wc^2 J} + 1\right] \quad [56]$$

which shows a continually increasing value of the torque T_v as the speed increases. However, T_v will, under these circumstances, always be less than $k\mu_1\omega$, the torque which would be encountered if the viscosity remained at its initial value μ_1.

A detailed analysis of the problem of the effect of the reduction in pressure in the neighborhood of a pump inlet on delivery has been given by Pigott (42, 44), for the case of volatile low-viscosity liquids. The effect of viscous resistance in reducing inlet side pressures and thereby causing loss in delivery due to the expansion of entrained air, may be analyzed in the elementary manner to be discussed.

Viscosity and Entrained Gases

When pumping extremely viscous liquids the resistance to flow causes excessive reductions in pressure in the intake passages. Entrained gas will expand in low-pressure regions in the neighborhood of the inlet and fill to a greater or lesser extent the volume intended for the transport of liquid from the intake to the discharge of the pump. When this gas reaches the discharge side of the pump its volume is reduced due to the high pressure encountered (39, 42, 44, 45).

The volume of entrained gas per unit volume of liquid is V_g, at the inlet pressure p_1, and this volume increases to V_g', due to the reduction in pressure as the liquid enters the trapping space in the pump. Then the expanded gas and sufficient oil to fill the displacement volume of the pump are transported to the high-pressure side of the pump where the volume of the gas is reduced to V_g''. If the flow in the intake passages and adjacent to the rotor is considered to be as indicated in Fig. 5, and the flow is treated as

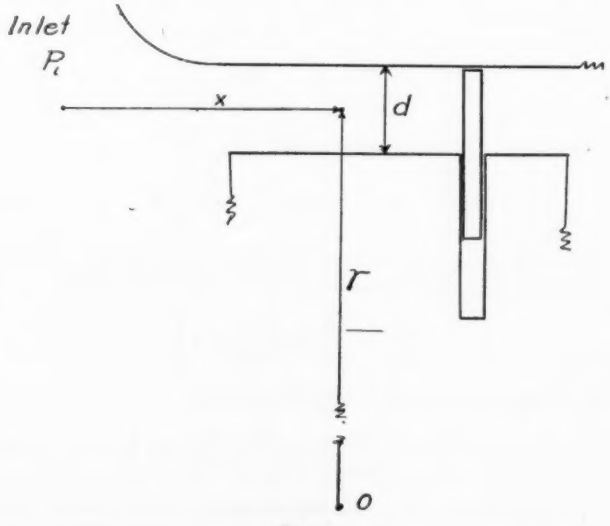


Fig. 5

laminar flow between parallel flat plates, one may state that to fill the space behind the advancing vane a quantity of liquid $bdr\omega$ must be drawn into the space per unit time. Now making use of Equation [7] which describes the flow between parallel flat plates, and setting the rate of flow equal to $bdr\omega$ we have

$$bdr\omega = \left[\frac{r\omega d}{2} + \frac{(p_1 - p)d^3}{12\mu x}\right] b$$

This may be solved for the pressure p and yields

$$p = p_1 - 6\mu\omega \frac{rx}{d^2} \quad [57]$$

where

p is pressure at any point within inlet passage, psf
x is distance in feet from intake to point at which p is measured
r is radial distance in feet to point at which p is measured
d is radial distance in feet from rotor to housing

Equation [57] may be put in dimensionless form

$$\frac{p}{p_1} = 1 - \frac{6rx}{d^2}\frac{\mu\omega}{p_1} \quad [58]$$

The loss in delivery will be caused by the expansion of the entrained gas of volume V_g. Assuming this expansion takes place isothermally, we have

$$\frac{V_g}{V_g'} = \frac{p}{p_1}$$

where

V_g is volume of entrained gas at intake pressure p_1 per unit volume of liquid
V_g' is expanded volume of entrained air at pressure p per unit volume of liquid

As the liquid and gas progress to the region of high pressure a reduction in volume of the gas to V_g'' is accomplished. Assuming isothermal compression, we may write

$$\frac{V_g''}{V_g} = \frac{p_1}{p_2}$$

where p_2 is the pressure at the discharge of the pump. The loss in volume V_L per unit volume of liquid due to expansion of the gas is simply the difference between V_g' and V_g''. Expressing this as an equation, we have

$$V_L = V_g' - V_g'' = \frac{V_g p_1}{p} - \frac{V_g p_1}{p_2}$$

and upon substituting for p_1/p there results

$$V_L = V_g\left[\frac{1}{1 - \frac{6rx}{d^2}\frac{\mu\omega}{p_1}} - \frac{p_1}{p_2}\right] \quad [59]$$

The quantity V_L represents, therefore, the proportion of the displacement which is lost at a point located x feet from the inlet due to expansion of entrained gas. The quantity V_g is simply the ratio of the volume of entrained gas to the volume of liquid at intake pressure.

It will be noted that the loss in displacement V_L is associated with the distance x. In order to obtain the total loss in displacement it is necessary to sum up the losses V_L, at each point x, over the entire region involved.

Although this equation is based on gross oversimplifications it indicates the nature of the variables which describe the phe-

nomenon, and it is evident that greater refinements will lead to expressions containing the same parameters $\frac{\mu\omega}{p_1}$ and $\frac{p_1}{p_2}$ and differing only in algebraic form. Summation of the losses in displacement will again change only the form of the expression and not the quantities involved. Use will be made of this observation in analyzing experimental data.

Experimental Data for Hydraulic Motor

Data obtained in the test of a conventional gear pump operating as a hydraulic motor are presented in dimensionless form in Figs. 6, 7, 8, and 9. The tests were performed on a pump with a theoretical displacement of 0.283 gal per 100 revolutions. Oils with viscosities ranging from 200 SSU to 6000 SSU were used. Pressures ranged from 180 psi to 600 psi. The speed, torque output, capacity, temperature of oil and pressure differences were observed and the viscosity of the oil determined at various temperatures.

In Fig. 6 the torque efficiency is shown as a function of the dimensionless parameter $\frac{\mu\omega}{p}$. In Fig. 7 the reciprocal of the volumetric efficiency is shown as a function of the dimensionless parameter $\frac{\mu\omega}{p}$. In Fig. 8 the reciprocal of the volumetric efficiency is again shown as a function of $\frac{\mu\omega}{p}$, but the abscissa is in this case $\left(\frac{\mu\omega}{p}\right)^{-1}$. In Fig. 9 the over-all efficiency is shown as a function of $\frac{\mu\omega}{p}$. The quantities β and k are evaluated, assuming the quantity T_f to be negligible, from the data shown in Figs. 6, 7, 8, and 9. The solid line in Fig. 9 is computed on the basis of these values.

In Figs. 11 and 12 are shown the plottings of experimental data on the performance of a cam-type rotary pump operating in range 3. The plotting in Fig. 11 of torque input as a function of speed is with constant pressure differential and approximately constant viscosity at intake. In Fig. 12 is shown a plotting of loss in delivery as a function of the parameter $\frac{\mu\omega}{p_1}$, where ω is the speed of rotation of the shaft, for the same pump operating with a wide range of intake pressures and viscosity.

Evaluation of Theory and Data

The data may be considered to provide a striking confirmation of the predictions of the theory concerning the performance characteristics of a conventional gear pump operating as a motor in performance range 2 and of the effect of high viscosity on a pump operating in range 3. The dimensionless plotting of the torque efficiency as a function of the parameter $\frac{\mu\omega}{p}$, shown in Fig. 6, is characterized by a close grouping of the points about a straight line as predicted by theory. The deviation of a small number of points representing runs at the lowest pressure used, namely, 180 psi, indicating as they do a considerable magnitude of the factor $T_e/(p\alpha)$, might well provide material for an interesting study of the pump mechanism. The volumetric efficiency plotted in reciprocal form in Fig. 8, shows an excellent approach to the straight line predicted by the theory. In Fig. 9 points representing data on the over-all efficiency show excellent agreement with the curve calculated from the values of β, k, and ϵ, which were evaluated by means of the previous plottings.

As predicted by Equation [48], the maximum efficiency occurs very close to $\frac{\mu\omega}{p} = 69 \times 10^{-7}$. The peak efficiency with a few exceptions lies in the range 58 to 67 per cent compared with the

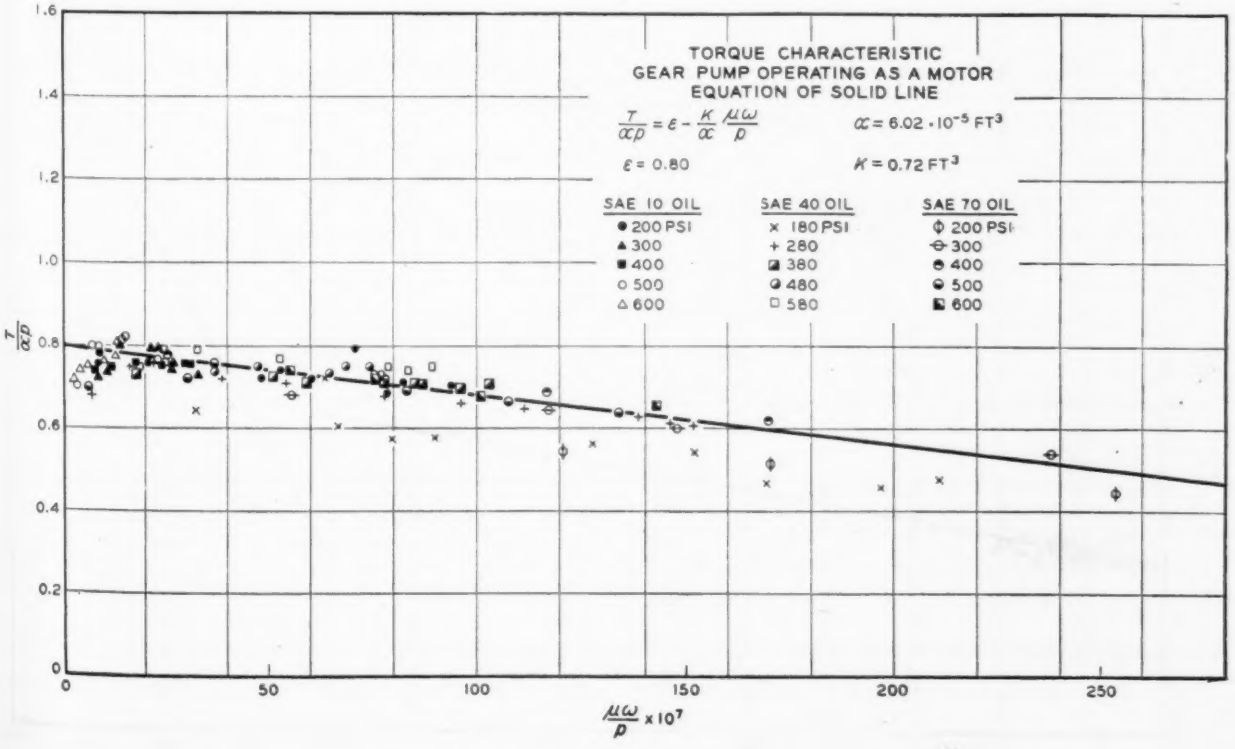


Fig. 6

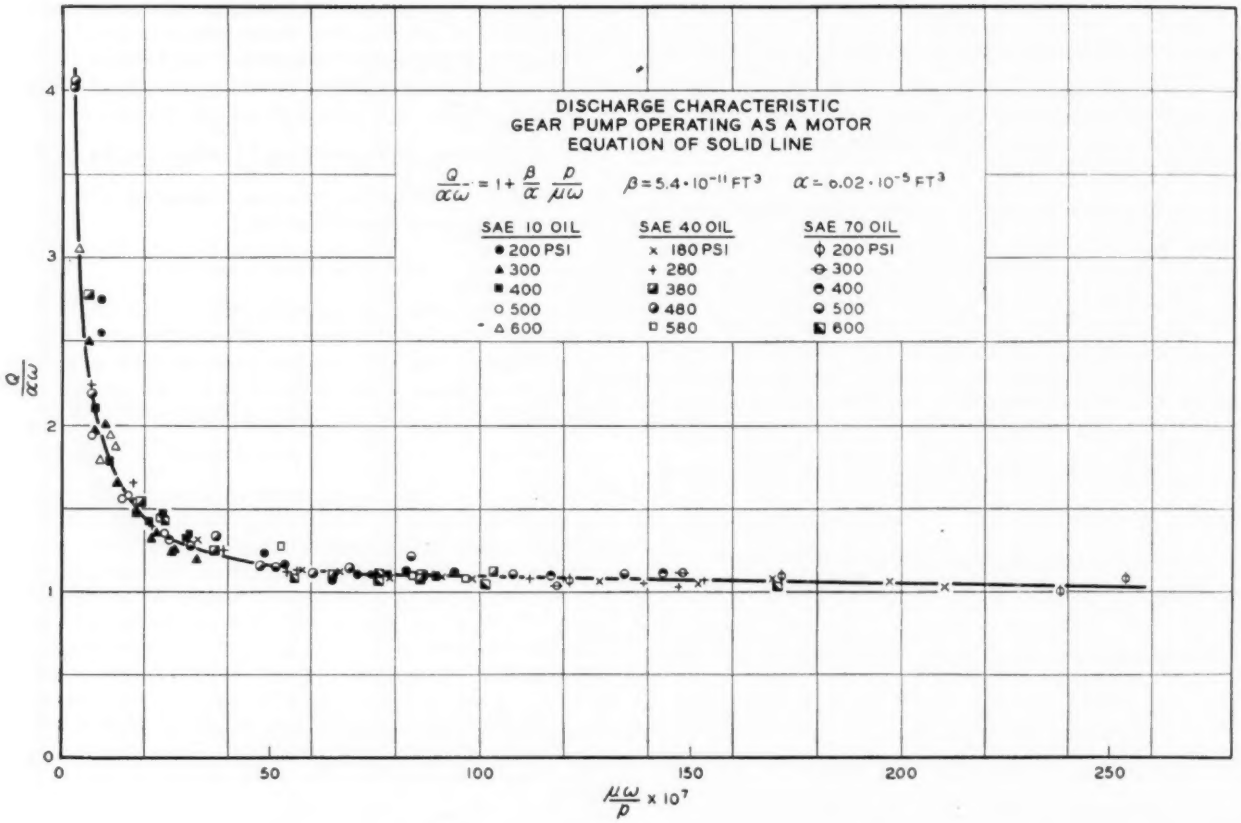

DISCHARGE CHARACTERISTIC
GEAR PUMP OPERATING AS A MOTOR
EQUATION OF SOLID LINE
$\frac{Q}{\alpha\omega} = 1 + \frac{\beta}{\alpha}\frac{p}{\mu\omega}$ $\beta = 5.4 \cdot 10^{-11}$ FT^3 $\alpha = 6.02 \cdot 10^{-5}$ FT^3
SAE 10 OIL
● 200 PSI
▲ 300
■ 400
○ 500
△ 600
SAE 40 OIL
× 180 PSI
+ 280
◪ 380
◍ 480
□ 580
SAE 70 OIL
Φ 200 PSI
⊖ 300
◓ 400
⊜ 500
◥ 600
$\frac{Q}{\alpha\omega}$
$\frac{\mu\omega}{p} \times 10^7$
0
1
2
3
4
50
100
150
200
250

FIG. 7

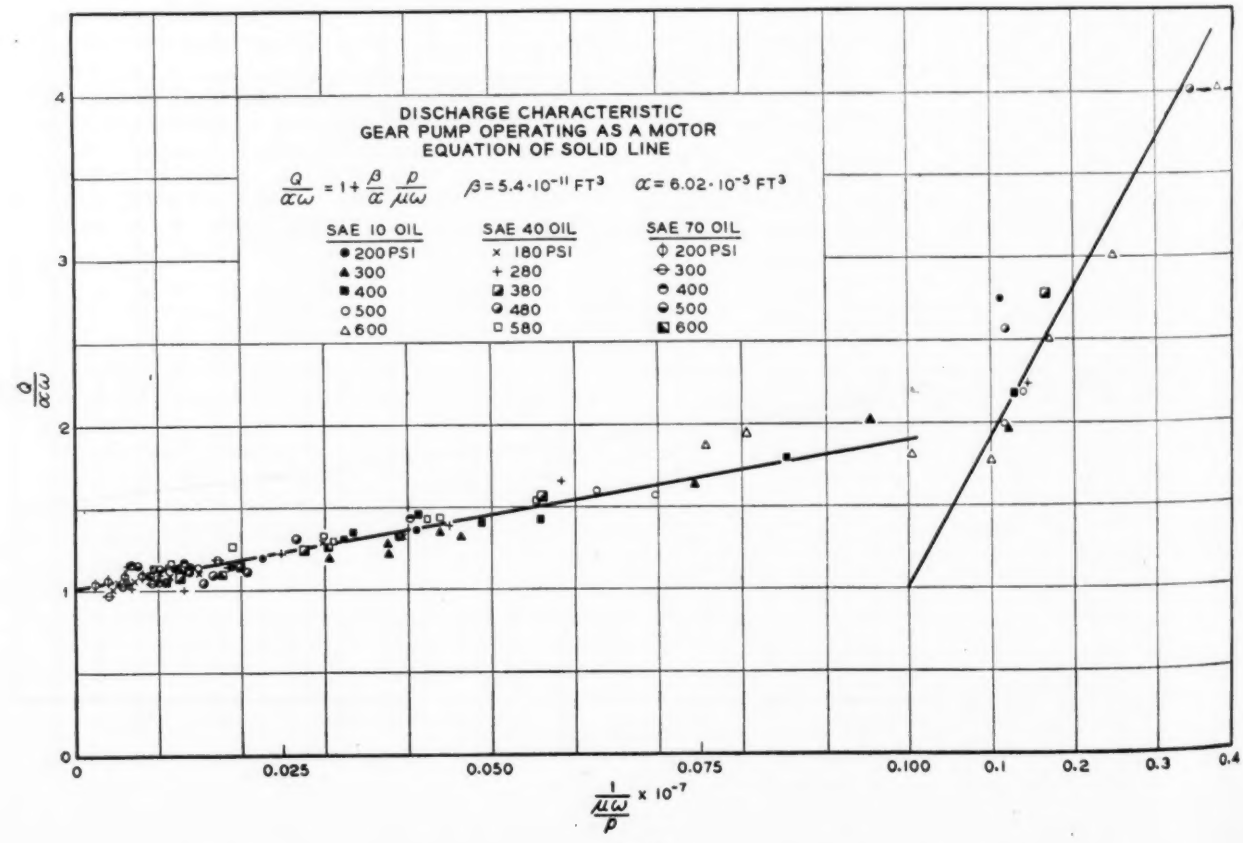

DISCHARGE CHARACTERISTIC
GEAR PUMP OPERATING AS A MOTOR
EQUATION OF SOLID LINE
$\frac{Q}{\alpha\omega} = 1 + \frac{\beta}{\alpha}\frac{p}{\mu\omega}$ $\beta = 5.4 \cdot 10^{-11}$ FT^3 $\alpha = 6.02 \cdot 10^{-5}$ FT^3
SAE 10 OIL
● 200 PSI
▲ 300
■ 400
○ 500
△ 600
SAE 40 OIL
× 180 PSI
+ 280
◪ 380
◍ 480
□ 580
SAE 70 OIL
Φ 200 PSI
⊖ 300
◓ 400
⊜ 500
◥ 600
$\frac{Q}{\alpha\omega}$
$\frac{1}{\frac{\mu\omega}{p}} \times 10^{-7}$
0
1
2
3
4
0.025
0.050
0.075
0.100
0.1
0.2
0.3
0.4

FIG. 8

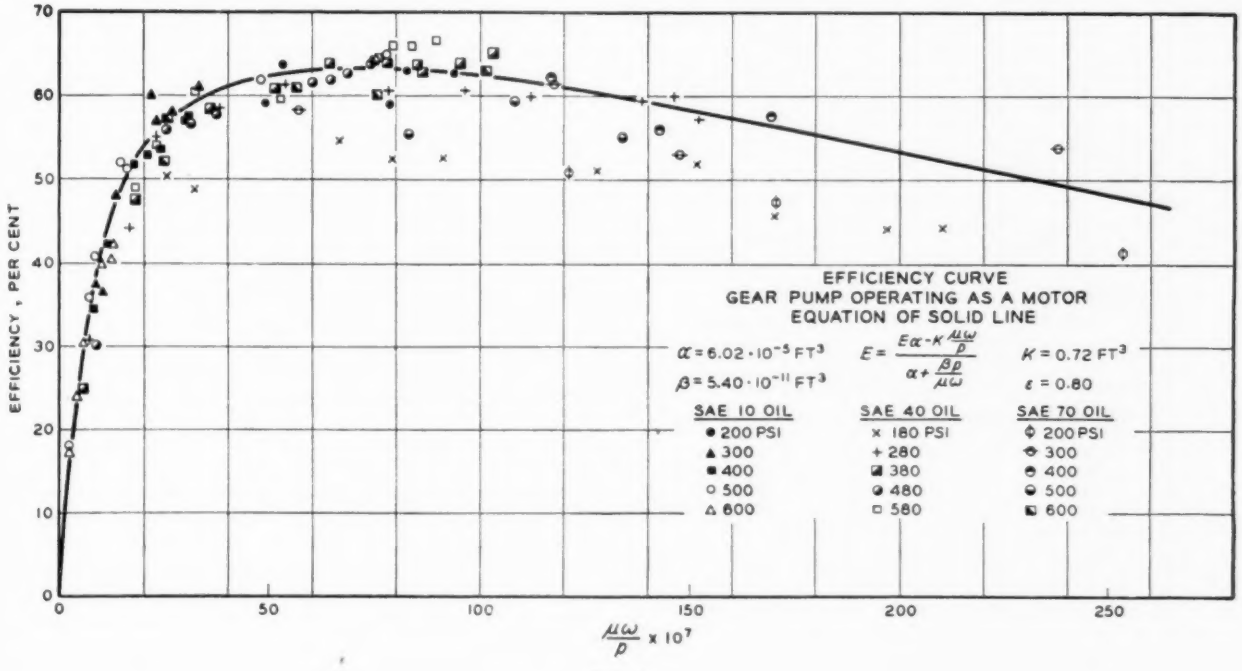


FIG. 9

theoretical maximum of 63.4 per cent, computed by means of Equation [50].

The use of the dimensionless performance curves in evaluating a particular design may now be studied in some detail. In Fig. 10 are illustrated the particular features of these plottings which make them extremely powerful tools in analyzing performance and planning improvements. For simplicity and ease of comparison with the experimental data, the case of a hydraulic motor is considered.

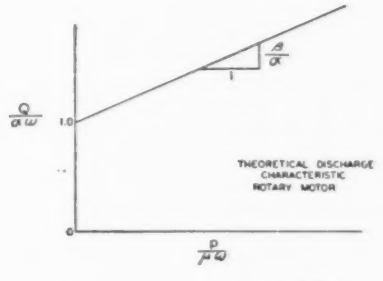
In Fig. 10(*a*) is shown a graphical representation of the discharge characteristics of the unit on the basis of Equation [36] which may be inverted for this purpose

$$\frac{Q}{\alpha\omega} = 1 + \frac{\beta}{\alpha}\frac{p}{\mu\omega}$$

This plots as a straight line on rectangular co-ordinate paper, with $\frac{Q}{\alpha\omega}$ as ordinate and $\frac{p}{\mu\omega}$ as abscissa. The intercept on the vertical axis at $\frac{p}{\mu\omega} = 0$ is necessarily unity, since $\frac{p}{\mu\omega} = 0$ corresponds to either zero pressure difference, infinite speed, or infinite viscosity, each of which obviously necessitates zero slip or $\frac{Q}{\alpha\omega} = 1$. The slope of the curve is $\frac{\beta}{\alpha}$, a physical characteristic of the unit which is a dimensionless ratio. This ratio would be given, if all slip passages corresponded to the idealized case in Fig. 3(*a*), by the quantity

$$\frac{\beta}{\alpha} = \Sigma\,\frac{c^3 b}{12lcrb} = \Sigma\,\frac{c^2}{12lr}$$

where r is the distance from the moving plate to the axis of rotation. In the case of an actual unit this factor $\frac{\beta}{\alpha}$ will depend, as indicated, upon the clearances, lengths of flow paths, and distances to the axis of rotation, for all the passages through which leaks take place.



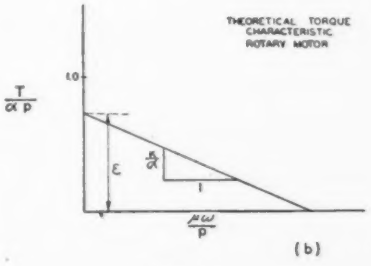


FIG. 10

Similarly in the plotting of torque efficiency $\frac{T}{p\alpha}$ versus $\frac{\mu\omega}{p}$ a straight line is expected, since the simplified expression obtained from Equation [35] for torque efficiency is

$$\frac{T}{\alpha p} = \epsilon - \frac{k}{\alpha}\frac{\mu\omega}{p}$$

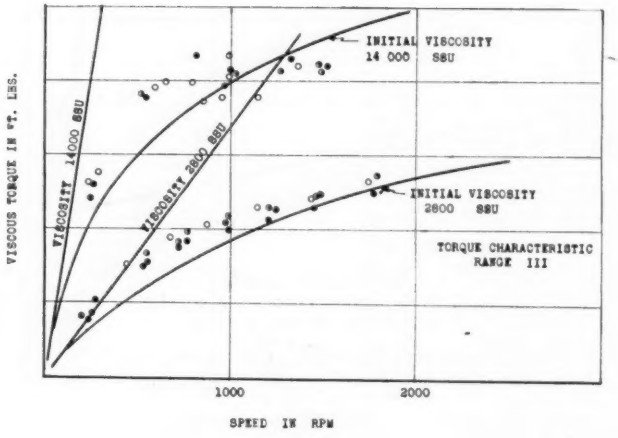


FIG. 11

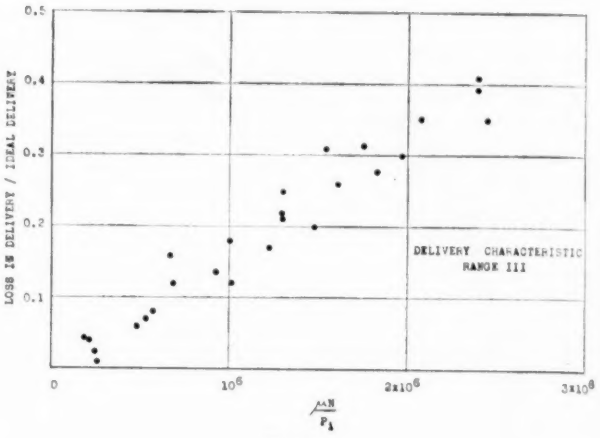


FIG. 12

Deviations of the actual performance from that indicated by the theory will occur if the clearances or alignment of the parts of the unit change, or if the nature of the flow in the unit is different from that assumed, e.g., turbulent rather than laminar. Such changes in clearances and alignment may be caused by pressure increase or decrease or by centrifugal effects due to speed changes.

If in a test the viscosity and pressure difference are held constant at certain values during successive series of runs, one would expect the data to plot as series of points forming straight lines on both types of plottings, shown in Fig. 10. Deviations from the theoretical form of the plots may be of the nature to be indicated and have the significance stated.

If the plotted data give points forming straight lines but the slopes vary from series to series this variation in slope must be caused by changes in the geometrical features of the unit by the pressure, since the viscosity was held constant.

If the curves are not straight lines the reason may be either that the flow is not in the assumed regime, e.g., it is assumed laminar but actually proves to be turbulent, or the geometrical features of the unit change with speed due to centrifugal effects.

If the plottings are parallel straight lines but the intercepts vary from series to series, the cause must be sought in changes in geometry due to pressure resulting in a change in mechanical friction.

The significance of the parameter $\frac{\mu\omega}{p}$ is of note. Since the maximum efficiency occurs at a specific value of the parameter $\frac{\mu\omega}{p}$, it is obvious that this maximum may be attained with various combinations of μ, ω, and p. For example, use of an oil of great viscosity will result in maximum efficiency at very low speed for a given pressure difference. The corresponding speed at a high pressure difference will be proportionately greater. Use of an oil of low viscosity will result in maximum efficiency at higher speeds for the same pressure difference.

A general characteristic of hydraulic units operating with laminar flow is apparent from Equations [49] and [50] in that efficiency of the unit operated as a pump will always be the same as the efficiency of the unit operated as a motor, if $\epsilon = 1$. The difference in efficiency in the two cases will never be very great unless the mechanical friction is greatly different in the two cases.

Specific details of the experimental data will be analyzed, keeping in mind the general principles previously set forth.

The plotting of the data in Fig. 6 makes possible a determination of the coefficient k since $\left(-\frac{k}{\alpha}\right)$ is the slope of the straight line which is taken as a fair representation of the trend of the data. Deviations from the straight line may be due to at least two specific causes, as follows:

1 Local heating of the oil due to energy dissipation causes a local viscosity far different from that measured at the discharge of the unit, thus placing operation in range 3 rather than in range 2 as assumed.

2 Variations in orientation and clearances of the elements of the unit and their lubrication during the runs cause changes in both the mechanical friction and the viscous resistance.

The value of ϵ is given by the value of E_T at $\frac{\mu\omega}{p} = 0$. The plotting of Fig. 7 shows an asymptotic approach of $\frac{Q}{\alpha\omega}$ to the value unity as $\frac{\mu\omega}{p}$ increases as would be expected from the theory. Fig. 8 gives the necessary information to evaluate β since the slope of the solid line is $\frac{\beta}{\alpha}$.

The interpretation of the factor ϵ is important since it represents a major element in the design of hydraulic units. The value of ϵ appears to be essentially a constant for much of the data and its nature as a factor, analogous to a coefficient of kinetic friction describing mechanical friction, appears to be confirmed since the coefficient of kinetic friction is practically independent of speed, pressure, and viscosity. Certain deviations from the expected are evident in the data, especially for runs at 180 psi, which might be interpreted as a change in ϵ but may better be explained on the basis of the neglected term of Equation [35]. The experimentally determined value of 0.80 for ϵ indicates a 20 per cent loss through mechanical friction in this particular pump. A considerable improvement in performance might be effected by a suitable change in design.

It is also pertinent to point out that Equation [50] indicates an efficiency, which might well be termed the hydraulic efficiency, of better than 78 per cent, if $\epsilon = 1$, for all values of θ less than approximately 0.02. It is clear from a consideration of the elements of the pump geometry that a value of θ in excess of 0.02 is a practical impossibility in even a poorly conceived design. The value of θ for the pump studied was approximately 0.013, which corresponds to an efficiency of approximately 79 per cent.

A study of the equations developed reveals the effect of changes in the physical dimensions of the unit which might be made to alter the performance characteristics by changing either clearance or displacement or both.

It is apparent that an increase in clearance results in

1 Decrease in k.
2 Increase in β.

An increase in α results in

1 Increase in torque.
2 Increase in capacity.

However, it is pertinent to point out that a detailed analysis of the performance of a rotary pump as influenced by its geometrical features reveals that for any given value of rotor length and rotor diameter there is an optimum value for the clearance for best performance in range 2. It may be shown also that the performance, solely from a hydraulic standpoint, improves as the ratio of rotor length to rotor diameter is increased. There is of course an obvious limitation on this increase imposed by shaft deflection.

The data for pump performance in range 3 reveals a number of interesting features. The plotting of torque as a function of speed shows the characteristic decrease in slope of the curve as the speed increases. The solid lines indicating the torque which would be expected for the given intake viscosity, if there were no local heating, were obtained from experiments at lower viscosities. The solid curved line for the case of initial viscosity of 2800 SSU was calculated to pass through one of the experimentally determined points thus evaluating the constant $\frac{B}{l}$ of Equation [54] for the pump. The curved solid line for the initial viscosity of 14,000 SSU was then calculated using the same constant. It is apparent that the agreement with the experimental data is as good as could be expected considering the approximate nature of the theory and the oversimplification involved in it.

The relationship between loss in delivery and the parameter $\frac{\mu\omega}{p_1}$ is particularly interesting when it is realized that the plotted points represent a wide variation in viscosity, speed, and intake pressure. The effect of discharge pressure has been neglected in the plotting, hence one may expect that the scattering of points may well be due to some extent to this neglected factor.

A detailed analysis of pump-intake geometry should lead to useful equations predicting the effect on performance in so far as lost delivery with high viscosity is concerned.

Conclusions

On the basis of the experimental data the following conclusions may be derived:

1 Predictions of the theory are borne out.
2 Experimental data may be presented in a compact dimensionless form.
3 Losses in efficiency may be traced readily and the causes determined.
4 Hydraulic and mechanical factors in performance are shown in proper perspective and may be analyzed separately.
5 Performance of units with fluids giving flows in the turbulent range may be expected to be subject to effective study by means of this theory and method of analysis of data.

Acknowledgments

The author wishes to acknowledge the assistance of the Pittsburgh Equitable Meter Company and Mr. W. A. Kates of Chicago in sponsoring the experimental work which forms the basis of this paper.

BIBLIOGRAPHY

1 "An Investigation of a Rotary Pump," by F. V. Bistrom and W. W. White, Trans. A.S.M.E., vol. 51, 1929, paper HYD-51-12.
2 "Rotary Feed Pump With Combined Steam and Electric Drive," *Engineering*, vol. 129, May 23, 1930, p. 683.
3 "Gear-Pump Tests," by A. Castagna, *Aerotecnica*, vol. 10, 1930, pp. 613–628.
4 "New Gear Pump," *Engineer*, vol. 152, Sept. 4, 1931, p. 252.
5 "Rotary Fuel-Oil Pressure Pump," *Engineering*, vol. 131, Nov. 20, 1931, p. 391.
6 "Small Rotary and Plunger Pumps," *Engineering*, vol. 132, Dec. 4, 1931, pp. 698–699.
7 "Rotary Pump for High Vacua," *Engineer*, vol. 151, Feb. 6, 1931, p. 168.
8 "'Moriscot' Petrol Pump," *Engineering*, vol. 131, Feb. 27, 1931, p. 313.
9 "U. S. Army Air Corps Switches From Gear to Vane Type of Fuel Pump," by F. W. Heckert, *Automotive Industries*, vol. 64, 1931, pp. 512–515.
10 "Small Gear Pump," *Engineer*, vol. 153, Feb. 12, 1932, p. 193.
11 "Gear Pumps," *Industrial Pumping Practice* (Supp. to *Mechanical World*), June 9, 1933, pp. 14–15.
12 "Steam-Jacketed Rotary Fuel-Oil Pump," *Engineer*, vol. 155, April 7, 1933, p. 357.
13 "Quelques Nouveantes en Matiere de Pompes et de Compresseurs," by A. Lambrette, *La Pratique des Industries Mechaniques*, vol. 15, 1933, pp. 307–312.
14 "Rotary Displacement Pumps," by C. S. Darling, *Industrial Pumping Practice*, June 9, 1933, pp. 11–13.
15 "Unusual Design Characterizes New Rotary Pump," *Power*, vol. 77, Oct., 1933, p. 512.
16 "Birotor Fixed-Vane Rotary Pump," *Engineering*, vol. 138, Dec. 7, 1934, p. 618.
17 "New Type of Rotary Pump," *Engineer*, vol. 158, Sept. 21, 1934, p. 284.
18 "Rotary Pumps," by W. E. Bakewell, *Power*, vol. 78, Nov., 1934, pp. 602–603.
19 "Producing High Vacuum With Rotary Pumps," by L. H. Bailey, *Chemical & Metallurgical Engineering*, vol. 41, July, 1934, pp. 358–359.
20 "Nothing to Halt Development of Rotary Pump for Fields Occupied by Reciprocating Units," by R. J. S. Pigott, *Oil and Gas Journal*, vol. 32, May 10, 1934, pp. 122–124, 126, and 129.
21 "Birotor Pump," *Metropolitan-Vickers Gas*, vol. 15, 1935, pp. 212–216.
22 "Variable-Discharge Rotary Displacement Pump," *Engineering*, vol. 140, Nov. 8, 1935, p. 498.
23 "Cox Rotary Displacement Pump," *Mechanical Engineering*, vol. 58, 1936, pp. 252–253.
24 "Northey Rotary Pump," *Mechanical Engineering*, vol. 58, 1936, p. 316.
25 "Rotary Pump With Restrained Vanes," *Engineering*, vol. 141, June 26, 1936, p. 708.
26 "Constant-Delivery Rotary Pump," *Engineer*, vol. 164, Dec. 17, 1937, pp. 690–691.
27 "Positive-Displacement Rotary Pump," *Engineering*, vol. 146, Sept. 2, 1938, p. 274.
28 "Rotary Pumps; Their Application and Operation," by K. B. Humphrey, *Mill & Factory*, vol. 24, Feb., 1939, pp. 70–76, and 173.
29 "Theory of Westco Type Rotary Pump," by A. Miyadzu, Society of Mechanical Engineers, Japan, Trans., vol. 5, 1939, pp. 109–115.
30 "Pumps," by F. A. Kristal and F. A. Annett, McGraw-Hill Book Co., Inc., New York, N. Y., 1940.
31 "Cavitation Characteristics of Centrifugal Pumps Described by Similarity Considerations," by G. F. Wislicenus, R. M. Watson, and I. J. Karassik, discussion, Trans. A.S.M.E., vol. 62, 1940, pp. 155–166.
32 "Theory of Gear Pumps," by A. Meldahl, *Brown Boveri Review*, vol. 26, 1939, pp. 259–261.
33 "Trapping of Fluid Between Teeth of Involute Gear Pump," by Y. Takahashi, Society of Mechanical Engineers, Japan, Trans., vol. 6, 1940, pp. 111–6–10.
34 "Theory of Westcot-Type Rotary Pump," by O. Myagi and A. Miyadzu, Tohoku Imperial University Reports, vol. 13, 1939, pp. 264–288.
35 "Application of Rotary Pumps to Molasses," by A. Shaw, J. G. Real, and V. A. Pardo, *Institute of Sugar Journal*, vol. 43, 1941, pp. 176–178.
36 "Gear Rotary Pumps—Selecting Right One for Your Job," by W. A. McGrath, *Power*, vol. 85, Aug. 1941, pp. 70–71.
37 "Investigations on Influence of Air Content on Cavitation and Corrosion," by I. Vuskovic, *Escher-Wyss News*, vol. 13, 1940, pp. 83–90.
38 "Vane Type Rotary Pumps," by B. P. Hetler. *Industry & Power*, vol. 43, Nov., 1942, pp. 70–71 and 110.

39 "Correlation of Ground and Altitude Performance of Oil Systems, Oil Pumps, and Their Operation at High Altitude," by John Dolza, paper at S.A.E. Meeting, June 8, 1942.

40 "Helpful Hints That Insure Good Rotary-Pump Performance," by D. F. Schaub, *Power*, March, 1943, pp. 99–101.

41 "Rotary Pumps," by R. J. Sweeney, *Journal of the American Society of Naval Engineers*, vol. 55, Feb., 1943, pp. 1–24.

42 "Oil Aeration," by R. J. S. Pigott. Presented at S.A.E. National Fuels and Lubricants Meeting, Tulsa, Okla., Nov. 4, 1943.

43 "High- and Low-Pressure Airplane Hydraulics in Europe," by Jean Mercier, Trans. A.S.M.E., vol. 66, 1944, pp. 599–604.

44 "Some Characteristics of Rotary Pumps in Aviation Service," by R. J. S. Pigott, Trans. A.S.M.E., vol. 66, 1944, pp. 615–623.

45 "Lubrication Ceiling," by P. H. Schweitzer, *Aeronautical Engineering Review*, vol. 3, November, 1944, pp. 37, 39, 41, and 43.

46 "An Instrument for Indicating the Amount of Gas in Gas-Liquid Mixtures," by B. R. Walsh and G. S. Peterson, Trans. A.S.M.E., vol. 67, 1945, pp. 399–404.

Air-Gas Ratio Control Applied to Nonatmospheric-Pressure Furnaces

By H. C. McRAE,[1] CLEVELAND, OHIO

For reasons of economy and efficiency, in the burning of fuel gases in industrial furnaces it is essential to maintain the air-gas ratio at approximately the correct point for perfect combustion. Furthermore it is important to control the ratio of air flow to gas flow because of the effect of burned gases or atmosphere upon material being heat-treated. The author discusses in detail the various control processes available, the equipment developed for the purpose, and analyzes the several control circuits, basing the work on the laws of low-pressure gas flow or noncompressible flow.

Introduction

IN the process of burning fuel gases in the combustion chamber of an industrial furnace, usually the approximate amount of air required for perfect combustion is introduced along with the gas in some form or another. For the purpose of fuel economy alone, at elevated temperatures, the air-gas ratio must be held close to the proper amount. Aside from this reason, it is important to control the ratio of air flow to gas flow because of the effect of the burned gases or atmosphere upon the material being heat-treated. Sometimes the reaction produced by a small amount of excess air is desirable, while in other applications a deficiency of air may produce the desired result. Of course the air may be introduced as primary air, that is, air which is mixed with the gas before reaching the combustion chamber, or as secondary air which mixes with the gas as it is burning. "Free" air from the atmosphere is often used for a source of secondary air. In this case the air enters directly through ports in the furnace wall because of furnace draft, or this air may be induced by the momentum of the mixture of primary air and gas through a burner port which is discharging into an opening in the furnace wall. The quantity of free secondary air is difficult to control because it is so easily affected by small changes in furnace pressure and therefore that application is excluded from this discussion.

For manual or automatic control of temperature a variable heat input is required. In batch-type furnaces a high heat input is used to heat up a cold furnace or to heat up a cold load. As the desired temperature is reached the heat input is decreased until it just balances the losses of heat through the furnace wall and out of the flue. In continuous furnaces a variable heat input is used to maintain a variable loading at a constant temperature. Variable heat flow means variable gas- and air-flow rates. Maintenance of the correct air-gas ratio with variable demand of heat flow and with variable furnace-pressure conditions, then, is the subject under discussion.

The amount of air required for perfect combustion of natural gases is approximately 10 parts to 1 of gas and for manufactured gases is about 5 parts to 1 of gas. These two gases are the ones most commonly used, although there are others which require more air and some which require less air. Air is therefore considered to be the principal fluid because of its greater quantity. This means that the energy required for the mixing process and delivery of the mixture to the furnace can best be obtained from the air stream rather than from the gas stream. Another reason for considering the air to be the principal fluid is that it may be conveniently compressed to a pound (per square inch) pressure or so by the use of the proper blower while gas is frequently furnished at only a few ounces (per square inch) pressure. Occasionally, high-pressure gas of several pounds pressure is available, in which case the energy from the gas stream may be used to induce free primary air from the atmosphere, but here again as in the use of free secondary air, the air-gas ratio is upset easily by changes in furnace pressure. The use of free air is therefore not considered here. The following discussion assumes that air may be furnished at a pressure of $^1/_4$ to 2 psi, whether it be primary or secondary air.

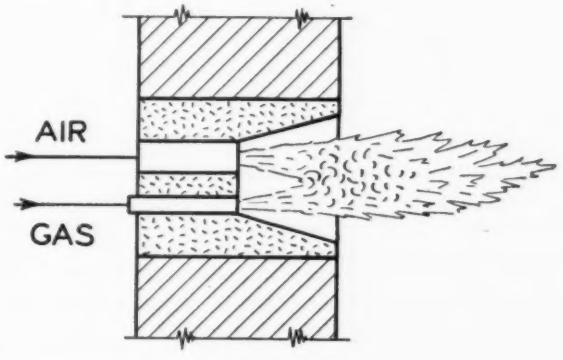


FIG. 1

The gas pressure available will be considered as three distinct cases, low, medium, or high pressure, and may affect the type of control to be used for air-gas ratio control. The low-pressure gas will be reduced to zero pressure or approximately so. Medium-pressure gas will be higher than this, but not as high as the air pressure furnished. High-pressure gas is available at as high a pressure as the air pressure or higher.

The air-and-gas-mixing apparatus or, simply, "mixer" is the unit where the gas and air are brought together and where the mixing process has begun but may not necessarily be completed. In the use of secondary air the mixer is installed in the furnace wall and is usually called the burner, although for purposes of discussion here it shall be considered a mixer. A primary-air mixer discharges the mixture of air and gas to a piping manifold where it is delivered to a single burner or a multiplicity of burners. In either case, there are recognized three distinct classes of mixers. This classification is based upon the effect of the air flow on the gas flow, that is, whether the air tends to help or hinder the flow of gas. This effect may be measured by discharging the mixer into the atmosphere and turning off the gas supply. The resulting pressure obtained at the gas entrance, which is produced by the air flow, is the key to the classification. If the pressure so

[1] Research Engineer, The North American Manufacturing Company.

Contributed by the Process Industries Division and presented at the Annual Meeting, New York, N. Y., November 26–29, 1945, of THE AMERICAN SOCIETY OF MECHANICAL ENGINEERS.

NOTE: Statements and opinions advanced in papers are to be understood as individual expressions of their authors and not those of the Society.

obtained is zero or very nearly so, as in Fig. 1, this type is defined as a neutral mixer. On the other hand, if a back pressure is obtained on the gas connection this is called a back-pressure mixer as in Fig. 2. Fig. 3 is an ejector-type mixer which produces suction on the gas and tends to help the flow of gas. When either back pressure or suction is produced, these values are, in general, proportional to the air-pressure supply to the mixer and, indeed, must be so in order to function as a part of the air-gas-ratio control.

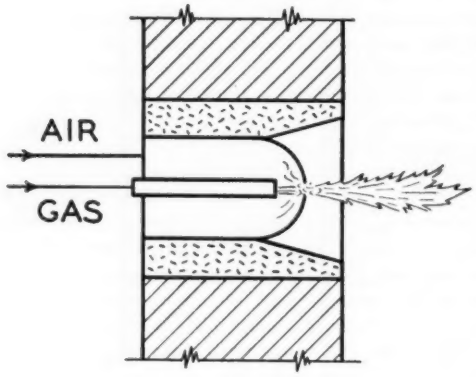


FIG. 2

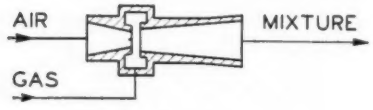


FIG. 3

If, instead of discharging the mixer into atmospheric pressure, it is discharged into a region of back pressure caused by the resistance to flow of a burner or caused by the combustion process itself, the back-pressure effect of a mixer will be increased, or the suction produced by an ejector mixer will be decreased. As long as the back-pressure effect which is downstream from the mixer is constant, it has no detrimental result on the air-gas ratio control, but if this back-pressure effect should become variable, then special allowances must be made in the ratio-control circuit in order to maintain air-gas ratio consistency. In fact, it will be shown how the difference between a constant and a variable back-pressure effect calls for a fundamental difference in the type of air-gas ratio control to be used.

In keeping with the two types of back-pressure effect from the downstream of the mixer, there correspond two classes of furnace-pressure conditions. The first class, a standard-pressure furnace, is defined as one which either has an atmospheric pressure or a back pressure which is in proportion to the mixture pressure being delivered to the furnace by one burner or a group of burners all under the same throttling control. The use of large flue areas and little or no stack effect will maintain zero pressure in the combustion chamber. If a stack is used, an automatic damper control may be installed to maintain zero pressure. Again, in the absence of stack effect, but with limited flue openings, a back pressure is created in the combustion chamber due to the combustion process; however, as long as there is only one throttling control, this back pressure will be in proportion to this throttling-control pressure. With the use of more than one throttling-control on one furnace there is a tendency for interference of one control upon another.

The other type of furnace-pressure condition is called a special pressure furnace and is defined as one which is not standard. This type of pressure is usually variable but may be constant at any value other than zero. The class of special pressures may be produced by the use of a stack, fan, or an extraneous throttling-control system discharging into the combustion chamber of the control group under discussion. Of course the two classes of furnace pressures are relative, not absolute, depending upon the amount of deviation of air-gas ratio that is allowed. In other words, a standard-pressure type of control may be used on an application with a small variation in pressure as long as the corresponding change in air-gas ratio is permissible.

ANALYSIS

At this point it is advisable to review the fundamental gas-flow laws before attempting to analyze the various control circuits. These laws of low-pressure gas flow or noncompressible flow are not exact but are close enough for commercial application. The following terms will be used in the analysis:

Q = volume rate of flow
P = gage pressure
S = specific gravity
R = resistance to flow
A = general bleed constant
K = mixer constant
B, C, D, F, G, H, L, M = general constants

Subscripts:

u refers to upstream
d refers to downstream
1 refers to air stream
2 refers to fuel-gas stream
3 refers to air-gas mixture stream
4 refers to combustion chamber
v refers to bleed valve
o refers to bleed orifice

Any consistent set of units may be used.

The first law of gas flow states that the volume rate of flow of gas (or weight rate of flow if the gas is considered incompressible) is proportional to the square root of the pressure drop or pressure differential across any resistance to flow, such as an orifice plate, Venturi, valve, pipe fitting, etc. This is a common law applied in the metering of gas flow. It is also applied in controlling air-gas ratio. A set of differential pressures indicating air flow and another set of differential pressures indicating gas flow are made to oppose each other through various arrangements of diaphragms.[2] Thus a balance of differential pressures is maintained, which results in a constant air-gas ratio. While it is easily understood how control of the air-gas ratio is obtained using differential pressures, it is much more difficult to understand the control of air-gas ratio by single impulse pressures when used in connection with the various types of mixers and furnace-pressure conditions as heretofore described. If the downstream of an orifice plate is discharged to a known pressure region such as the atmosphere, the upstream pressure tap will indicate flow by itself, since the downstream pressure is known without measurement. In this case the upstream pressure tap becomes the single impulse pressure, by means of which the air-gas ratio must be controlled.

The other gas-flow law is that the volume rate of flow is inversely proportional to the square root of the specific gravity of the gas. Combining the two gas laws

$$Q \sim \sqrt{\frac{P_u - P_d}{S}}$$

[2] "Multiple-Diaphragm Pressure Regulators and Their Application," by H. C. McRae, *Instruments*, vol. 17, September, 1944, pp. 529–531.

It is convenient to express the constant of proportionality as $\sqrt{1/R}$, since the laws have the square-root form and the resistance concept to flow is similar to that used in the electrical, magnetic, thermal, and stress fields. Then, the general law of low-pressure gas flow is

$$Q = \sqrt{\frac{P_v - P_d}{RS}}$$

Any set of units may be used, the resistance unit being defined from the other units. From analogy to the electrical field, resistances may be combined[3] in series and in parallel. Likewise, both of Kirchhoff's laws of electrical networks may be used for gas-flow circuits; namely, (1) the algebraic sum of the gas flows in all the pipes that meet at a point is zero and (2) the total change of pressure around any closed circuit is zero. The resistance form of gas flow and Kirchhoff's first law will be used in the following analysis to prove that the various control circuits do maintain a constant air-gas ratio for variable flow rates. Of course in practice the various control circuits were derived from the analysis.

Although there are several types of control circuits for air-gas ratio control, using single impulse pressures, all of them are derived from the basic form shown in Fig. 4, which is called the

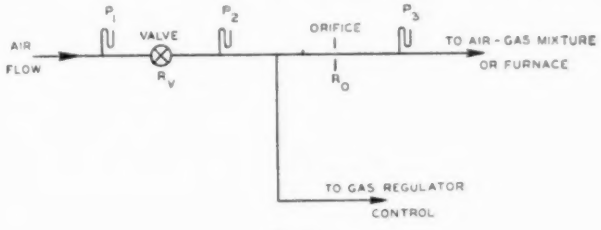


FIG. 4

"general bleed." It must be understood that the bleed mechanism or any of its derivatives is only a small branch of $^1/_4$-in. or $^3/_8$-in. pipe size, going from the main air pipe and usually some point of lesser pressure such as the air-gas mixture pipe, the combustion chamber, or the atmosphere, to the gas-pressure regulator control. Before the complete control circuits can be analyzed it is necessary to develop the following mathematical expressions for the general bleed and other bleed systems.

In Fig. 4 the pipe line going to the gas-regulator control is dead-ended; that is, there is no steady flow of air in this line. Therefore the flow rate through the valve must be equal to the flow rate through the small orifice

$$\sqrt{\frac{P_1 - P_2}{R_v S_1}} = \sqrt{\frac{P_2 - P_3}{R_0 S_1}}$$

Solving this equation

$$P_2 = \left(\frac{R_0}{R_v + R_0}\right) P_1 + \left(\frac{R_v}{R_v + R_0}\right) P_3$$

Let

$$\frac{R_0}{R_v + R_0} = A$$

and, therefore

$$\frac{R_v}{R_v + R_0} = 1 - A$$

[3] "Low Pressure Gas Flow Analyzing by a Resistance Theory," by H. C. McRae, *Industrial Gas*, vol. 19, March, 1941, pp. 17–20.

Rewriting the value of the gas controlling pressure

$$P_2 = AP_1 + (1 - A)P_3 \quad \ldots\ldots [1]$$

where $0 \leq A \leq 1$

Equation [1] is the mathematical expression for the general bleed, stating that P_2 is always a fixed ratio difference between P_1 and P_3, regardless of the rate of flow or how P_1 and P_3 may vary during the control cycle. Since the bleed valve is set once and for all at the beginning of an installation to conform to the particular requirements of the application, R_v and therefore A are constant in the control cycle.

The various types of control are derived from Equation [1] by fixing definite values for A and P_3. For the conditions

$$P_2 = AP_1 + (1 - A)P_3 \quad \ldots\ldots [2]$$

$$0 < A < 1 \quad \text{and} \quad P_3 \neq 0$$

a double connection is required to control the gas (both to P_1 and P_3) and hence the name, "double bleed." If

$$A = 0 \quad \text{and} \quad P_3 \neq 0$$

$$P_2 = P_3 \quad \ldots\ldots [3]$$

For this case the bleed valve is closed or $R_v = \infty$. In practice the bleed valve and orifice are not used, since it is necessary to use only a single pipe to connect the air-gas mixture pressure, P_3, to the gas-regulator pressure, P_2. This class of control is called the "reduced cross connection."

The gas-control pressure may also be connected to the combustion chamber, in which case

$$P_2 = P_4 \quad \ldots\ldots [4]$$

This type of control is called "cross connection to furnace." In fact, if the mixer is mounted directly on the furnace and the air is used as secondary air, the mixture pressure, P_3, becomes the furnace pressure, P_4. In other words, this case is derived from the previous case.

Again, for the condition

$$P_2 = AP_1, P_3 = 0, 0 < A < 1 \quad \ldots\ldots [5]$$

the bleed orifice is discharged directly into the atmosphere. This case is called "single bleed" or abbreviated to simply "bleed."

In addition, if $A = 0$ and $P_3 = 0$

$$P_2 = 0 \quad \ldots\ldots [6]$$

This "zero gas" is the most commonly used type of control; the gas-control regulator need only be vented to the atmosphere and no pipe interconnections between the air and gas are necessary.

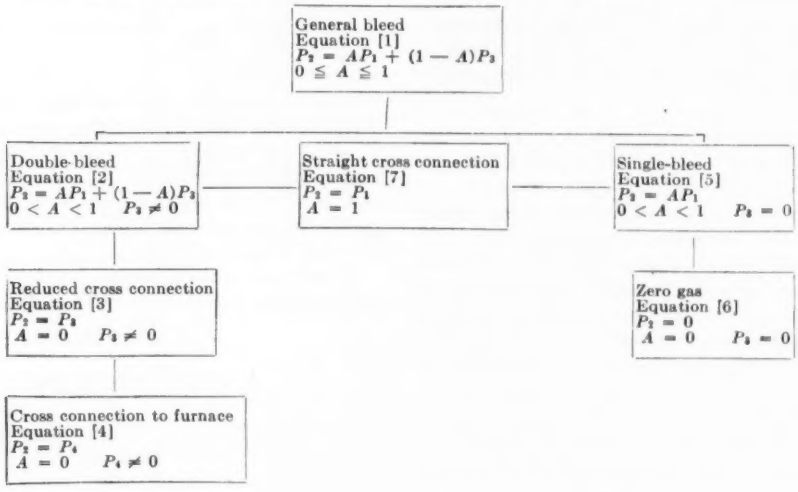
The last type of control is derived either from the single or the double bleed, since P_3 may or may not be zero, because $A = 1$

$$P_2 = P_1 \quad \ldots\ldots [7]$$

This is called "straight cross connection." For this case the bleed valve is open wide with no resistance; $R_v = 0$. Again, in practice, this is equivalent to a single pipe connection between the air pressure and the gas-control pressure.

The foregoing control classifications give all the necessary combinations in air-gas ratio control by single impulse pressures to cope with the various types of mixers, gas pressures available, and furnace-pressure conditions. There are a few other miscellaneous control types, such as connection of the gas-control pressure to the air and to a gas-pressure point just upstream from the mixer, but these controls only duplicate, in need, what has already been derived. Table 1 is constructed for convenience to summarize the various controls and show their relationship. It will

TABLE 1 SUMMARY OF VARIOUS CONTROLS AND RELATIONSHIP



be shown later how the branch on the right side is used for standard-pressure furnaces, while the left branch is used for special pressure furnaces.

Fig. 5 shows the general arrangement of the air and gas piping with the exception of the bleed control itself. As previously mentioned, the mixer and the burner may be only one unit instead of two separate units as shown. It is important to notice the function of the gas-pressure-regulator control. This device is sometimes called a "zero governor" or "atmospheric regulator." It is nothing more than a diaphragm-operated pressure regulator[4] which controls the gas-discharge pressure to be equal to the impulse pressure imposed from the bleed control, providing of course that the gas-supply pressure is high enough. The control valve is adjusted according to heat-input demand. Thus the air pressure, P_1, and air-flow rate are being adjusted continuously, while likewise the gas-flow rate must remain in step with the air flow through the application of the proper bleed control and the gas regulator.

[4] "Simple Pressure Regulators—Principal Types and Their Characteristics," by H. C. McRae, *Instruments*, vol. 15, February, 1942, pp. 44–45 and 59.

Fig. 6 shows the diagrammatic layout of the circuit in Fig. 5; R_1 represents the resistance to flow of air in the mixer and R_2 is the resistance to gas flow in the mixer, including a gas valve for air-gas ratio adjustment. Term R_3 is the resistance of the burner. The expression, $K_2\ (P_1 - P_3)$, is the suction or back-pressure effect of the air on the gas flow as discussed under the subject of mixer classification. The corresponding effect of the gas on the air flow is $K_1(P_2 - P_3)$. The value of K_2 determines the mixer classification: For $K_2 = 0$, a neutral mixer; for $K_2 < 0$, a back-pressure mixer; and for $K_2 > 0$, the mixer is the ejector type.

The air flow through the resistance, R_1, is

$$Q_1 = \sqrt{\frac{P_1 + K_1(P_2 - P_3) - P_3}{R_1 S_1}}$$

The gas flow rate is

$$Q_2 = \sqrt{\frac{P_2 + K_2(P_1 - P_3) - P_3}{R_2 S_2}}$$

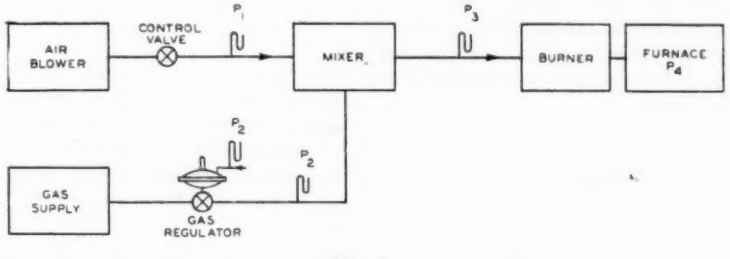


FIG. 5

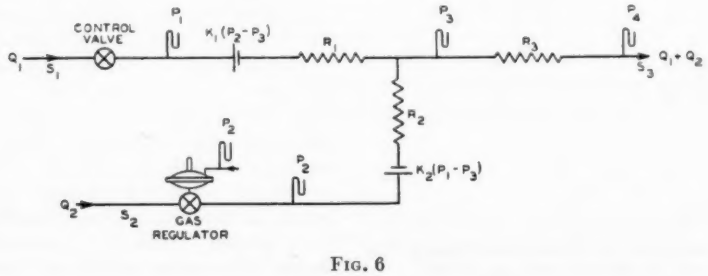


FIG. 6

For the experimental determination of K_2, the gas flow is cut off. Then $Q_2 = 0$ and

$$P_2 + K_2(P_1 - P_3) - P_3 = 0$$

$$K_2 = -\frac{P_2 - P_3}{P_1 - P_3} \text{ (no gas flowing)}$$

In a similar manner, with the air cut off

$$K_1 = -\frac{P_1 - P_3}{P_2 - P_3} \text{ (no air flowing)}$$

In the case that the mixer and the burner become one unit, combustion may affect the K values. For this case the K values will have to be determined under actual combustion and by metering the air- and gas-flow rates; however, P_3 is replaced by P_4.

From the foregoing air- and gas-flow rates the air-gas ratio is

$$\frac{Q_1}{Q_2} = \sqrt{\left(\frac{R_2S_2}{R_1S_1}\right)\left[\frac{P_1 + K_1(P_2 - P_3) - P_3}{P_2 + K_2(P_1 - P_3) - P_3}\right]} \quad \ldots\ldots [8]$$

Since R_1, R_2, S_1, S_2, K_1, and K_2 are constants, it is only necessary to eliminate the pressure terms, which vary in the control cycle, to prove that the air-gas ratio is constant.

Taking a simple case to illustrate the method of proving air-gas-ratio constant, consider a neutral-type mixer discharging into a zero-pressure furnace. In this case, $K_1 = K_2 = P_3 = 0$. Equation [8] becomes

$$\frac{Q_1}{Q_2} = \sqrt{\left(\frac{R_2S_2}{R_1S_1}\right)\left(\frac{P_1}{P_2}\right)}$$

Let $P_2 = AP_1$ be the control chosen, which is a single bleed or straight cross-connection for $A = 1$. After substituting this value for P_2

$$\frac{Q_1}{Q_2} = \sqrt{\left(\frac{R_2S_2}{R_1S_1}\right)\left(\frac{1}{A}\right)} \text{ const}$$

Consider a standard-pressure furnace for which $P_4 = 0$ or in the case that P_4 is proportional to P_2, the furnace resistance to flow may be included in the burner resistance and the flue gases are discharged from the furnace to the atmosphere or zero pressure anyway. In other words, for standard-pressure furnaces the downstream resistance from the mixer is constant. Then, for this case: $P_4 = 0$ and R_1, R_2, R_3, S_1, S_2, S_3 are constant. The control chosen is $P_2 = AP_1$ which is the single-bleed, straight cross connection for $A = 1$, or zero gas for $A = 0$. The pressure, P_3, must be proved to be proportional to P_1, before Equation [8] may be used. Equating the sum of the air and gas flow to be equal to the mixture flow

$$\sqrt{\frac{P_1 + K_1(P_2 - P_3) - P_3}{R_1S_1}} + \sqrt{\frac{P_2 + K_2(P_1 - P_3) - P_3}{R_2S_2}} = \sqrt{\frac{P_3 - P_4}{R_3S_3}}$$

Using the values just given for P_2 and P_4

$$\sqrt{\frac{P_1 - P_3 + AK_1P_1 - K_1P_3}{R_1S_1}} + \sqrt{\frac{AP_1 - P_3 + K_2P_1 - K_2P_3}{R_2S_2}} = \sqrt{\frac{P_3}{R_3S_3}}$$

This equation may be written in more simple form by the use of general constants, since the actual value of P_3 is not needed

$$\sqrt{FP_1 + GP_3} + \sqrt{BP_1 + DP_3} = \sqrt{HP_3}$$

After squaring this equation twice and combining the proper terms in order to eliminate the radicals

$$[(F + B)P_1 + (G + D - H)P_3]^2 = 4[BFP_1^2 + (DF + BG)P_1P_3 + DGP_3^2]$$

Again, simplifying by using general constants

$$P_3^2 + LP_1P_3 + MP_1^2 = 0$$

or

$$P_3 = \frac{-LP_1 \pm \sqrt{L^2P_1^2 - 4MP_1^2}}{2} = \left[-\frac{L}{2} \pm \frac{\sqrt{L^2 - 4M}}{2}\right]P_1$$

and finally

$$P_3 = CP_1$$

Now Equation [8] becomes

$$\frac{Q_1}{Q_2} = \sqrt{\left(\frac{R_2S_2}{R_1S_1}\right)\left[\frac{1 + AK_1 - CK_1 - C}{A + K_2 - CK_2 - C}\right]}$$

which is constant and independent of the control pressure P_1.

Since it is proved that zero gas produces constant air-gas ratio for standard-pressure furnaces or zero-pressure furnaces, this case may be easily extended to prove that cross connection to furnace holds constant air-gas ratio for special pressure furnaces. These two cases become equivalent when all the pressures in the latter case are referred to P_4, the furnace pressure, as a base instead of the atmosphere or gage pressure. In other words, since $P_2 = P_4$, P_2 will always be zero if referred to its value exceeding P_4. Likewise, P_1 and P_3 take on new values that differ from their old gage values by the same amount that P_4 differs from zero gage pressure.

Now consider the general case of special-pressure furnaces. Both P_4 and R_3 become variable for this case, although R_3, the burner resistance, is not usually varied purposely but may vary slightly with temperature change. P_3 is no longer proportional to P_1 and therefore the single-bleed will not hold constant air-gas ratio. Choose

$$P_2 = AP_1 + (1 - A)P_3$$

the double bleed control, the reduced cross connection for $A = 0$, or the straight cross connection for $A = 1$. Equation [8] becomes

TABLE 2 TYPE OF CONTROL FOR GIVEN APPLICATION

Mixer classification	Gas pressure available	Standard pressure furnaces	Special pressure furnaces
Ejector type	Low	Zero gas	Cross connection to furnace
	Medium	Zero gas	Cross connection to furnace
		Single bleed	Reduced cross connection
			Double bleed
	High	Zero gas	Straight cross connection
		Straight cross connection	
Neutral or back-pressure type	Low	No method available	No method available
	Medium	Single bleed	Double bleed
	High	Straight cross connection	Straight cross connection

$$\frac{Q_1}{Q_2} = \sqrt{\left(\frac{R_2S_2}{R_1S_1}\right)\left[\frac{(P_1 - P_3) + K_1(AP_1 + P_3 - AP_3 - P_3)}{AP_1 + P_3 - AP_3 - P_3 + K_2(P_1 - P_3)}\right]}$$

$$= \sqrt{\left(\frac{R_2S_2}{R_1S_1}\right)\left[\frac{(P_1 - P_3) + AK_1(P_1 - P_3)}{A(P_1 - P_3) + K_2(P_1 - P_3)}\right]}$$

$$= \sqrt{\left(\frac{R_2S_2}{R_1S_1}\right)\left[\frac{1 + AK_1}{A + K_2}\right]} \text{ const}$$

Table 2 shows the type of control to use on any given application. The use of the single bleed and the double bleed have been avoided when possible, although these types of control sometimes have to be used to obtain a sufficient quantity of gas. The reason for avoiding these controls is because of the necessity of adjusting the bleed valve properly to get just the sufficient amount of gas pressure without exceeding the gas-supply pressure minus the pressure drop through the gas regulator. All of the other controls require only a single pipe connection to the gas regulator without any adjustments. The zero gas system is the most popular, because in this case no connection need be made to the gas regulator, and there is always a sufficient supply pressure for this control.

Figs. 7 to 11, inclusive, show the complete circuit for some of the most frequent applications.

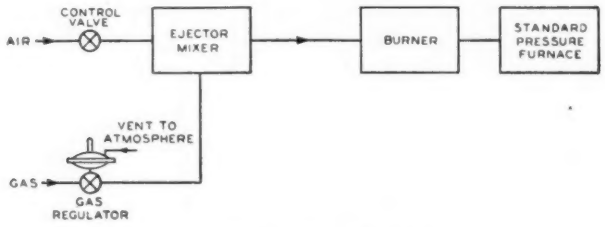


FIG. 7 ZERO GAS

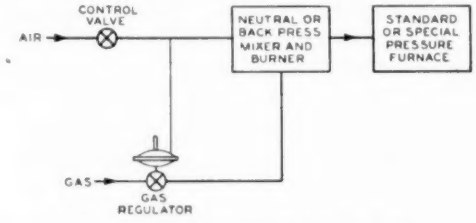


FIG. 9 STRAIGHT CROSS CONNECTION

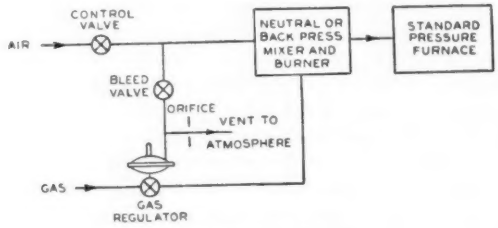


FIG. 8 SINGLE BLEED

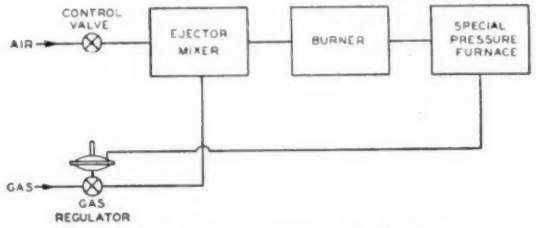


FIG. 10 CROSS CONNECTION TO FURNACE

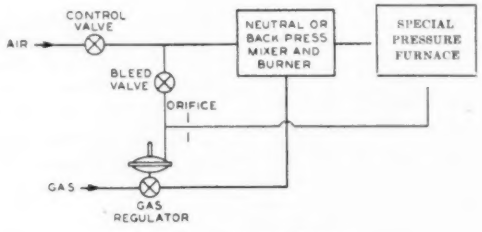


FIG. 11 DOUBLE BLEED

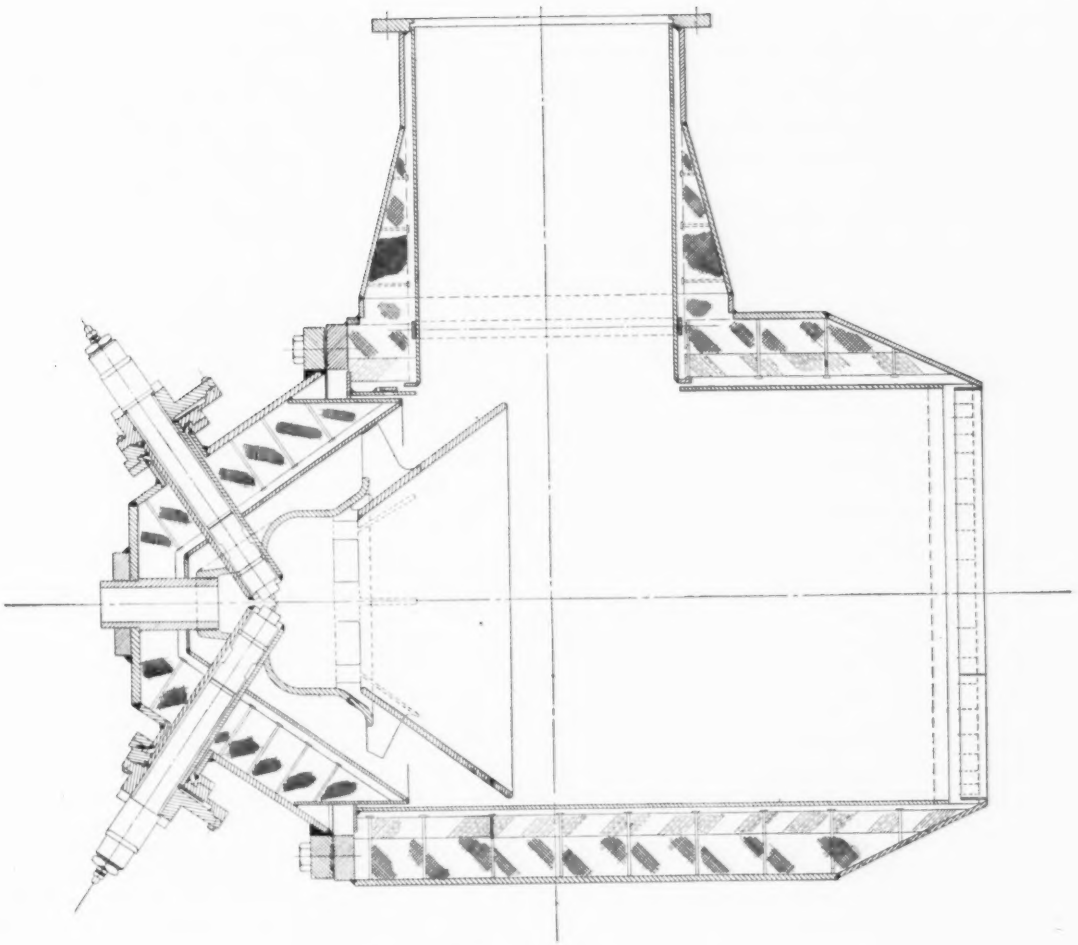


FIG. 1 ELBOW COMBUSTION CHAMBER

The Elbow Combustion Chamber

BY M. A. MAYERS[1] AND W. W. CARTER,[2] JEANNETTE, PA.

A description is given of the "elbow" combustion chamber, developed for use in the gas-turbine power plant designed and built for the United States Navy by the Elliott Company. This type provides extremely high heat-release rates which is an essential characteristic for gas-turbine applications. The fuel-oil-burning system which utilizes standard Diesel fuel-injection equipment has been developed to a high point of efficiency, and may be varied over a range from full load to 1/10 full load without material change in quality of atomization. The paper discusses in detail the air-flow characteristics, fuel supply, ignition and control devices, and analyzes the combustion-chamber performance-test data.

THE "elbow" combustion chamber was developed for use in the gas-turbine power plant designed and built for the U. S. Navy by the Elliott Company during the period 1942–1944. It has turned out to be exceptionally adapted to gas-turbine use in that it permits heat-release rates of 2.5×10^6 Btu per cu ft per hr, with air supplied at 95 psia, and 650 F, when it requires a pressure drop of only 16 in. water column; it permits a "turndown" to $1/20$ of full load; and is extremely insensitive to fuel-air ratio. As shown in Fig. 1, it consists of a right-angle elbow in a duct, of which the upstream arm is smaller in diameter than the downstream one. The upstream end of the large arm which forms the combustion chamber proper, is closed by a head which carries an "ignition cone," the fuel-oil burners, an igniter burner, and the "flame-rod" or contact member of the flame-sensitive controller. The chamber contains no inner shell separating combustion air from tempering air, and all the air in the gas-turbine circuit is supplied to the chamber without the

[1] Formerly Development Engineer, Elliott Company. Mem. A.S.M.E.

[2] Engineering Research and Development Department, Elliott Company. Jun. A.S.M.E.

Contributed by the Oil and Gas Power Division and presented at the Annual Meeting, New York, N. Y., November 26–29, 1945, of THE AMERICAN SOCIETY OF MECHANICAL ENGINEERS.

NOTE: Statements and opinions advanced in papers are to be understood as individual expressions of their authors and not those of the Society.

necessity for separate control of combustion air. Fuel is supplied to the chamber through standard Diesel fuel-injection equipment, producing a pulsating fuel flow which on a single burner may be varied over the range from full load down to $^1/_{10}$ full load without material change in the quality of the atomization. The rate of fuel flow is controlled by adjusting the position of the control rod of the Diesel injection pump.

Gas-Turbine Combustion-Chamber Requirements

The Elliott gas turbine was designed from the basic premise that such an engine, to be a successful prime mover, must have an efficiency comparable with those of others with which it would compete. To accomplish this aim, it was necessary to provide heating of the working medium in two stages, one before the first stage of expansion and a reheat after this; and to reduce the parasitic losses associated with the combustion chambers to a minimum. The thermodynamic advantages to be gained by reheating have been treated elsewhere (1)[3] and need not be repeated; the process does, however, entail the necessity of supplying heat to a flue gas, resulting from the combustion in the initial, or high-pressure combustion chamber, which may contain 2.7 per cent carbon dioxide, 2.6 per cent water vapor, and whose oxygen concentration may be reduced to about 16.5 per cent.

It may not at first be apparent why the pressure drop in the combustion chambers, as well as in the ducts and heat exchangers, must be so severely limited. The loss in gross turbine work is proportional to the ratio of the pressure drop to the absolute pressure at which it occurs and thus does not appear to be serious. Only a portion of the gross turbine work appears as useful output, this fraction being represented by the work ratio, α (1). The proportional loss of net turbine output due to parasitic losses is inversely proportional to α and may be therefore from 2.5 to 4 times as great as the loss in gross turbine work.

Since this machine was designed for naval ship propulsion, it was necessary for it to operate over a wide range of loads. The cubic relation between speed and power in ship propulsion, coupled with the fact that the gas turbine is governed directly by the rate of heat input, demands a high degree of flexibility in the fuel-burning system. Fig. 2 shows how the fuel-burning rate, and the power output depend upon the propeller-shaft speed. For maneuvering at speeds down to 45 per cent of full-power speed the high-pressure chamber must operate stably over a range of burning rates of 10 to 1; while for the design conditions of speeds down to $^1/_3$ of full the turndown must approach 20:1. Conventional marine practice of changing the tips or spray plates of fuel burners is not acceptable for this application, since burner removal from chambers operating under pressures greatly exceeding atmospheric could hardly be made rapid enough.

Associated with the need for wide-range characteristics of the fuel-burning equipment is the necessity that it be insensitive to over-all excess air. It is evident from Fig. 2 that the air-to-fuel ratio covers an extreme range from 600:1 in the low-pressure chamber to about 120:1 in the high-pressure chamber. In addition, variations in operating conditions such as weather, draft of vessel, etc., might impose variations about the curve of air-to-fuel ratio, at any value of speed, of 10–25 per cent. Previous chambers (2) had used separate control of combustion air to meet this type of difficulty. In the present instance this solution was unsuitable because air was supplied to the chambers at such high temperatures that valves or dampers could hardly be expected to operate reliably, and because of the stringency of pressure-drop restrictions.

It is desirable that the combustion chambers for gas-turbine plants permit very high heat-release rates; in fact, the possibility

[3] Numbers in parentheses refer to the Bibliography at the end of the paper.

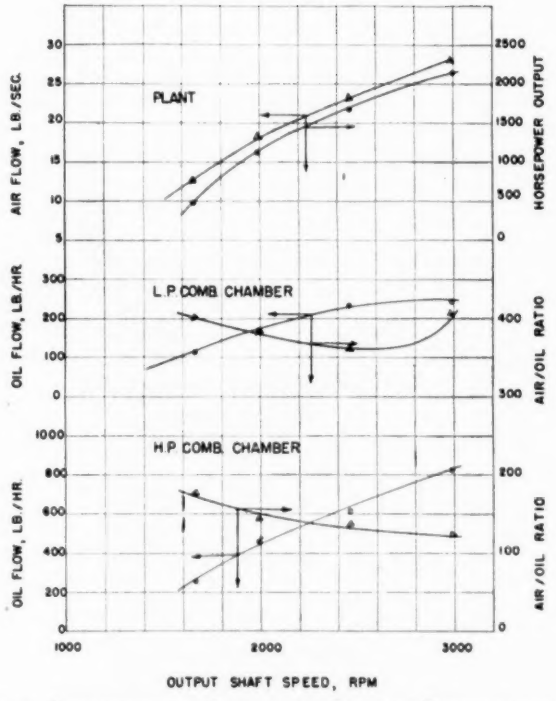


Fig. 2 Dependence of Combustion-Chamber Performance on Output Shaft Speed

that this may be secured is one of the main attractions of the internal-combustion gas turbine. It was, moreover, believed to be essential that these combustion chambers operate with a perfectly clean discharge, as the effect of soot, smoke, or gaseous products of incomplete combustion on the turbines and heat-transfer surfaces could not be predicted. The requirement of clean discharge also made it undesirable to leave exposed surfaces of nonmetallic refractories in the combustion chamber, since spalling or dusting of such material would foul the gas stream. Of course, safety, reliability, and convenience in operation, as well as ease and accessibility for necessary repairs are also desirable characteristics.

Characteristics of Elbow-Type Combustion Chamber

Air Flow. The air, on entering the main combustion chamber through the side inlet, follows the flow pattern characteristic of flow through an elbow in a pipe line (3), producing a double-vortex system. The two vortexes lie on either side of the center line of the inlet duct and have opposite senses of rotation. When the chamber is in operation the centers of these vortices appear as two bright spots to an observer looking upstream from the outlet of the chamber.

The strength of the vortex system is enhanced by making the diameter of the inlet duct less than that of the main chamber. While exact limits of this ratio have not yet been established, it has been found by model tests that the vortexes become less stable and show more tendency to break down into a single vortex having relatively undisturbed laminar flow, when the ratio of the diameters becomes greater than 0.6. The same kind of breakdown is produced by eccentricity of the inlet, or departure of the inlet center line from an extension of a radius of the combustion chamber proper.

A portion of the air entering the chamber is trapped behind the edge of the ignition cone which projects across the inlet air stream. Some of this air flows into the cylindrical part of the ignition cone through the slots shown in Fig. 1, producing a ring

vortex which has been shown to stabilize the ignition of fuel sprays (4), by some such mechanism as the following: Air from the slots in the ignition cone, on meeting the back wall of the ignition cone, turns radially outward, causing the formation of a vortex ring whose sense of rotation is such that the flow through the center of the ring is upstream. This causes the ring to take up a fixed position in relation to the back wall into and out of which air passes without affecting the stability of the vortex system as a whole (5). Thus the vortex ring is similar to a smoke ring, except that it is fixed in position and is continuously replenished. The entering air which has swept over the fuel spray injected into the chamber, carries with it a portion of finely atomized oil and oil vapor which serves as fuel for a continuously regenerated pilot flame established in the vortex ring.

The pilot flame formed by the vortex ring probably serves as a source of heat and of "active centers" to initiate the combustion of the main oil spray with the remainder of the air flowing through the ignition cone. Under conditions of very low oil-air ratio this small amount of air may be sufficient to burn the oil completely within the ignition cone, itself; but at higher loads, this protected region serves only as a space within which the whole mass of fuel may be vaporized and ignited. It should be noted that no rotation about the axis of the chamber is imparted to the flow through this cone. In every instance in which such rotation was produced, drops of burning oil were thrown against the walls of the cone, which eventually produced coke deposits.

The mass of ignited fuel issuing from the ignition cone appears to flow into the centers of the two vortexes formed by the main air flow, in which their combustion is completed. Observation of the bright spots formed by the double-vortex system shows that their size depends on the load, or rate of burning oil. At medium loads, large enough so combustion is not complete within the ignition cone, the spots are quite small and are clearly separated. As the load increases they increase in size until the two spots nearly touch. One might imagine that the flow out of the cone is directed into the centers of the vortices and that the burning fluid diffuses radially out from these centers to an extent determined by the amount of air required to complete its combustion. It has been suggested (6) that the reduction in static pressure at the center of a vortex (7) may be the agency which produces such a directed flow.

That some mechanism, such as that just suggested, governs the operation of the chamber can scarcely be doubted. At no time has there been evidence of incomplete combustion such as would result from the quenching of the burning by too great an amount of excess air, even though the chambers have been operated at air-to-oil ratios as great as 600:1. Moreover, the temperature of the flame, estimated from visual observation of its color, must be of the order of 3000 F, a value associated with combustion with only a small excess of air. Another observation, which helps to show that only the portion of the air that penetrates nearly to the center of the vortexes takes part in the combustion of the fuel, is that the air in the outer filaments of the vortex flow, which sweeps the walls of the combustion chambers, remains cool in the sections of the chamber in which rapid combustion occurs and serves to cool the metallic walls. This portion of the air rises in temperature some distance downstream and is eventually mixed by the residual vortex motion with the combustion air proper.

This characteristic of the elbow combustion chamber makes it almost unique among high-duty chambers; other types, which depend upon partial admission of air into the combustion space vented through liner walls, thereby make the liner wall behave like a ported gas burner except that in this case flames of air in a fuel-rich atmosphere are set up. The proximity of these flames to the chamber wall leads, of course, to overheating of the liner. In the elbow chamber no such overheating or warping of the chamber liner has ever been observed; tests, described below, indicate that no point on the inner shell rises more than 300 deg F above the outlet gas temperature even though it is exposed to direct radiation from a dense flame.

Fuel Supply. Fuel is supplied to these combustion chambers by means of commercial types of Diesel injection equipment. Number 2 Diesel oil is pumped through wound cartridge filters made by Commercial Filter Corporation under the trade name "Fulflo," to the inlet of 8-cylinder pumps made by the American Bosch Corporation. The discharges of all eight cylinders of each pump are led through $^1/_8$-in. $\times$ $^1/_4$-in. hydraulic tubing to a high-pressure manifold in which the lines are brought together. From here they pass through $^1/_4$-in. $\times$ $^1/_2$-in. hydraulic tubing, to a single water-cooled fuel injector, of a standard design produced by Aircraft and Diesel Equipment Corporation. Thus each pump, header, and injector combination forms a single burner unit.

The injection pumps have cylinder bores of 10 mm and actual plunger strokes of 10 mm. The plungers are cam-actuated so as to have essentially constant velocity over the effective or delivery part of the stroke, which can be varied by changing the point at which a relief port is uncovered by the plunger. Thus fuel is delivered at a constant rate during a short variable time interval. The volume of fuel per injection is directly proportional to the length of the time interval during which injection of fuel occurs and is controlled by the position of a pushrod which simultaneously fixes the effective stroke of each plunger. Since the maximum duration of injection from each pump cylinder is 26 deg of camshaft rotation, while the interval between the start of each succeeding injection is 45 deg, it is evident that the discharges do not overlap. The pumps are driven at a constant speed of 1200 rpm, producing a frequency of injection through each burner of 9600 per min, or 160 per sec. Thus the time interval between the start of each injection is 6 milliseconds, which is short enough to assure stable flame, without pulsations, when the fuel is discharged into the ignition cone previously described.

The Adeco injector mentioned previously, contains a spring-loaded differential-area valve which opens when the fuel-oil line pressure reaches 3300 psi. This valve insures clean sharp dis-

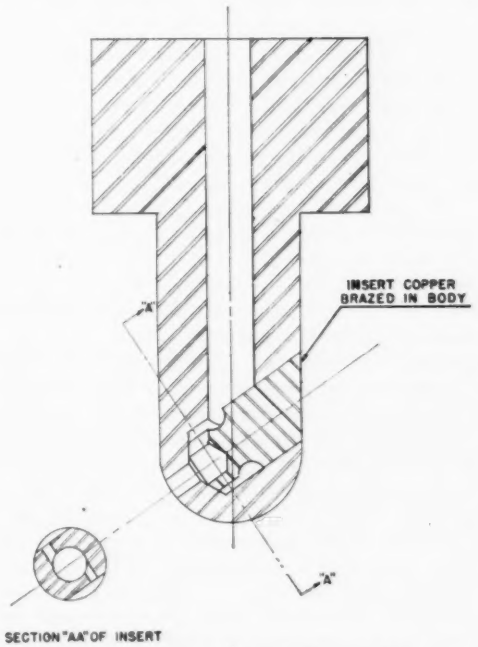


FIG. 3 DIESEL INJECTOR-NOZZLE TIP

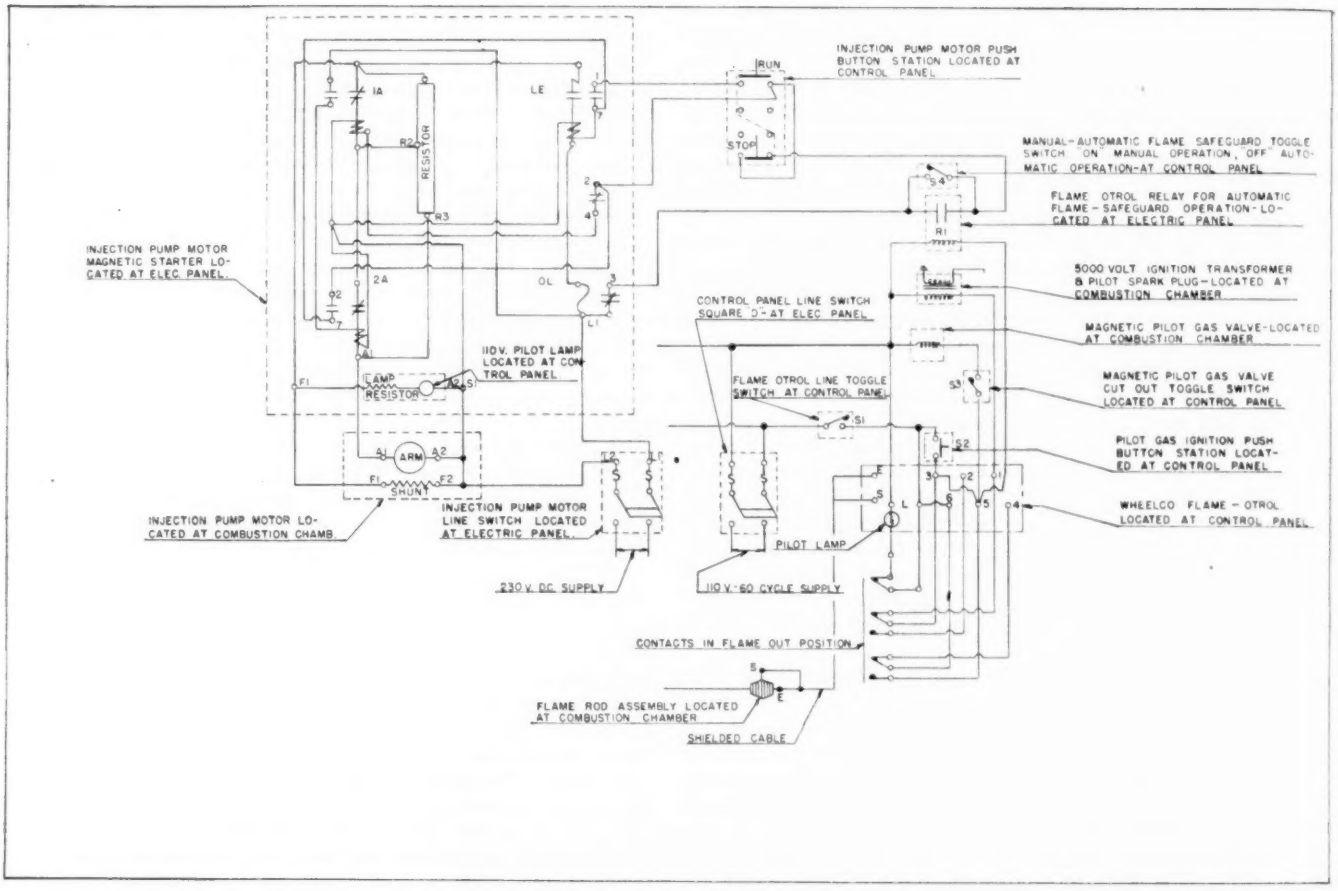


FIG. 4 FLAME-CONTROL CIRCUIT

charges and prevents "dribbling" between pulses. The injector is equipped with nozzle tips whose construction is shown in Fig. 3. By this means the advantages of the fine atomization and uniform distribution produced by a whirling cone spray, used conventionally in large mechanical-atomizing oil-burner nozzles, were secured for the spray from a Diesel injector. The discharge orifice is set at an angle to the axis of the tip to permit inserting two injectors in the same ignition cone with their tips not more than 1 in. apart, and having them discharge axially down through the same cone. The tips are installed in the injector by means of a jig which insures the correctness of their orientation, while the injectors are held in the chamber by a fixture built into the burner support. Since fuel is delivered to the injector at a constant instantaneous rate during the injection interval, the atomizing energy is constant from maximum to minimum capacity and good atomization is obtained over the full range.

Ignition and Control Devices. The head of the chamber also carries a spark-ignited gas-fired igniter burner, and the support for the "Flame-rod" or sensing element of the controller, made by Wheelco Instrument Company, which insures that fuel will not be supplied to the chamber in the absence of a source of ignition. This device uses the electrical conductivity of the flame to balance a bridge circuit, allowing a relay to close. This relay may be connected, as shown in Fig. 4, to hold open a valve for gas supply or to close contactors supplying power to the injection pumps. If the conductivity of the circuit including the Flame-rod is either above or below that of the flame the relay opens, cutting off power from these operations, and lighting a signal lamp. The Flame-o-trol, or measuring and control element of this device, which is mounted on the main operating panel board of the gas-turbine unit, is by-passed at starting by depressing a push button which simultaneously opens the gas-supply valve to the igniter burner and applies a sparking voltage to the electrodes of the igniter.

The igniter burners are supplied with a propane-and-air mixture formed in a Venturi mixer; propane is supplied from commercial tanks. Air to the mixer, and cooling air to the Flame-rod holders is supplied by the high-pressure compressor of the gas-turbine set. A small portion of the discharge of this compressor is drawn off from the main discharge duct ahead of the regenerator, passed through a small aftercooler, and is supplied to these auxiliaries. The air- and gas-piping diagram of these devices is shown in Fig. 5.

Sight glasses are mounted on the combustion chambers at convenient points to permit observation of the flame. Those installed in these chambers do not, unfortunately, permit removal of the glass while the chamber is under pressure, but the sight glasses designed for the future will. To date, no glass has ever broken in service.

Materials and Construction. The inner shell of the chamber, which acts merely as a shield to prevent abrasion of the internal insulation by the gas stream and takes no pressure load, is of 25 per cent Cr, 20 per cent Ni, type No. 310 steel. The inner shell is supported centrally in the chamber by means of two "spoked" supports which permit radial expansion of the shell without altering the center-line position. The shells are fixed axially near the air-inlet position and are free to expand in both directions from this point. Flexible seals to prevent pieces of insu-

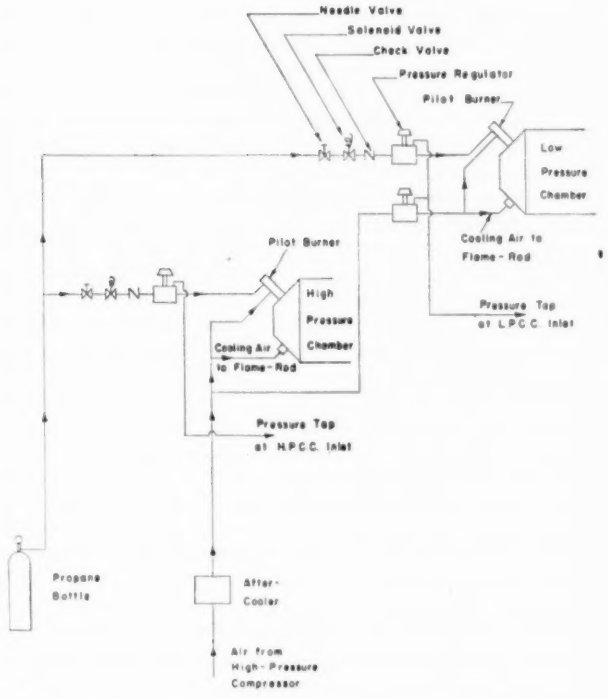


FIG. 5 AIR AND GAS PIPING TO IGNITERS AND FLAME RODS

lation getting into the gas stream are installed at either end of the inner shell.

The ignition cone is cast of chrome iron containing a minimum of 28 per cent Cr. The burner holders are of No. 302 stainless steel. Except for the insulation, which occupies the space between the inner and outer shells, these are the only parts exposed to extreme temperatures.

The internal insulation consists of two layers; the inside, which is exposed to the highest temperature, being of a lightweight brick $1^1/_2$ in. thick. The outer layer is a slag-wool block, wired and cemented to the outer shell. In the high-pressure chamber it was desired to minimize the thermal expansion of the structural member of the combustion chamber, so the block insulation is 2 in. thick and the outer pressure-retaining shell is of mild steel. In the low-pressure chamber some thermal expansion was desired, intermediate between the amount that would be caused by exposure of the shell to gas temperature and that of a "cold" shell. One inch of block insulation was therefore placed inside the shell and $1^1/_2$ in. outside, and the outer shell was made of 18 Cr, 8 Ni, type No. 302 stainless steel.

The heads for both chambers have outer shells of mild steel, inner shells of type No. 310 and are insulated between the shells. They are bolted to the combustion chamber proper by studs tapped into the combustion-chamber flange. The joint is sealed by a double-ring copper-wire gasket. Since the head of the chamber carries all the internal elements, these are immediately accessible for repair or replacement on its removal.

COMBUSTION-CHAMBER PERFORMANCE

An extensive series of tests was made on an experimental combustion chamber, a duplicate in its principal dimensions to the high-pressure combustion chamber. The chamber could be supplied at a maximum pressure of 8 psig, with 5600 cfm of air which could be heated to temperatures up to 1000 F, by burning natural gas in it in a special furnace. The maximum weight flow of air was only about one fifth of that in the gas-turbine set, and only one burner-injection pump unit was installed. It was anticipated, however, that these tests would permit determining if the performance of the combustion chambers would limit the plant operation, as a wider range of air-oil ratios could be tested than would be used in the plant, and shorter burning times could be obtained, since larger volume flows and higher velocities could be produced by lowering the pressure. It was expected that the fourfold increase in pressure in the prototype would permit increasing the heat-release rate by more than the factor of 3 between that of the prototype and that reached in the tests.

These tests were aimed at the determination of the operating efficiency of the combustion chamber. For a system in which the flue-gas discharge temperature is far above the air inlet temperature, it is not immediately obvious how the thermal efficiency should be defined. One possibility is to compare the higher heating value of the fuel with the difference between the enthalpy of all of the products of combustion and that of the air and fuel supplied. The first term in this difference is subject to some error because of uncertainty in the actual amount of moisture in the flue gas, but the results calculated in this manner have been presented in Table 1, under the column heading "Efficiency by Heat-Balance Method." Another method of expressing the efficiency, derivable from the same heat-balance equation, results in a comparison of the change in enthalpy of the air supplied to the chamber with a quantity defined by chemists (8) as the "heating value at the temperature" of the combustion-chamber discharge. The combustion-chamber efficiency thus defined may be expressed

$$\eta = \frac{A}{F}\frac{i_2 - i_1}{H_2} \qquad [1]$$

TABLE 1 TEST RESULTS FROM EXPERIMENTAL COMBUSTION CHAMBER

Run Number	Inlet Temp. (°F)	Outlet Temp. (°F.)	Inlet Pres. (Psia.)	Air Rate (#/Sec.)	Oil Rate (#/Hr.)	Heat Input in Million Btu./Hr.	Air/Oil Ratio	Static Pres. (Psi.)	Eff.-Bu. Ships Method	Eff.-Ht. Bal.
29	498	1050	20.1	6.04	180.5	3.55	120.4	0.63	96.0	97.6
30	497	1258	20.3	6.00	245.0	4.81	88.2	0.71	99.3	99.9
31	130	860	20.0	5.97	217.5	4.28	98.7	0.62	97.1	99.2
32	130	890	18.8	5.95	226.5	4.45	94.6	0.64	99.6	99.2
33	498	1049	19.7	6.12	185.5	3.65	118.8	0.70	94.8	96.0
34	499	1063	19.7	6.14	191.5	3.76	115.3	0.66	94.3	94.7
35	497	1250	19.8	5.99	250.5	4.92	86.1	0.73	95.8	95.6
36a	117	259	16.8	6.19	51.0	1.00	437.2	0.42	83.2	85.6
36b	103	288	15.2	4.00	43.5	.86	331.2	0.21	81.0	80.9
37	1003	1254	20.7	6.18	100.5	1.97	221.4	0.61	86.0	87.3
38	505	1035	19.6	6.13	174.5	3.43	126.5	0.66	96.9	96.3
39	498	1039	19.6	6.15	175.5	3.50	126.2	0.66	98.7	98.3
40	116	290	16.6	5.91	58.5	1.15	363.9	0.42	83.4	----
41	122	1035	18.5	5.64	262.5	5.16	76.9	0.68	97.9	----
42	475	996	18.9	5.85	166.5	3.27	126.5	0.69	93.2	----
43	121	393	17.0	5.92	80.5	1.58	264.7	0.53	95.2	----
44	487	1041	19.1	5.86	178.5	3.51	118.2	0.75	93.0	----
45	465	989	18.9	5.87	167.5	3.29	126.2	0.72	94.3	95.4
46	480	995	19.1	5.92	166.5	3.27	128.0	0.77	94.2	95.9
47	134	1365	18.8	5.23	330.5	6.50	57.0	0.75	101.1	102.7

where η is combustion-chamber efficiency

$\frac{A}{F}$ is air-fuel ratio at which chamber is operated

i_2, i_1 are enthalpies of air at discharge and inlet conditions, respectively

H_2 is heating value of fuel at temperature of combustion-chamber discharge and is defined by

$$H_2 = H_0 - [w_c(i_{C_2} - i_{C_0}) + w_H(i_{H_2} - i_{H_0}) - w_0(i_{0_2} - i_{0_0})] \ldots [2]$$

where H_0 is heating value of fuel determined under standard conditions

w_C, w_H, w_0 are weights of carbon dioxide, water, and oxygen entering the reaction per unit weight of fuel

i_{C_2}, i_{C_0}, etc., are enthalpies of constituents indicated by letter subscripts at the condition of discharge from the chamber and standard condition, respectively.

This efficiency is entered in Table 1, under the column heading "Efficiency by Bureau of Ships Method" (9), and is plotted in Fig. 6.

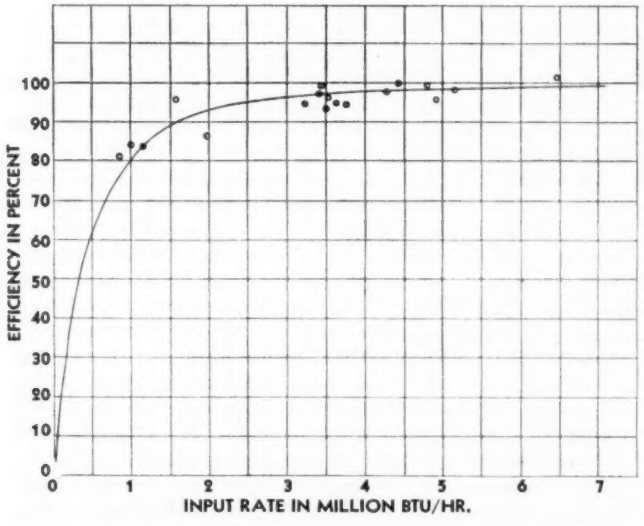


FIG. 6 COMBUSTION-CHAMBER EFFICIENCIES AT VARIOUS LOADS

Instrumentation. Both methods of determining efficiency require accurate measurement of the temperature of the discharge from the combustion chamber. Two methods of measuring this temperature were used. One was similar to that used by King (10) in determining a reference temperature for the calibration of shielded thermocouples, while the other, which also permitted estimating the degree of stratification in the discharge temperature, was based on the average of the indications of three shielded thermocouples (11) placed in the combustion-chamber discharge. The average of the three thermocouples was always higher than the indication of the single reference couple, which could be accounted for by heat loss between the two temperature-measuring stations. Because stratification in the outlet duct cast some doubt on the validity of the average, and since there was a possibility that the temperatures of the shielded couples were influenced by catalytic combustion on the metallic surfaces of the shields, the reference couple was always used for efficiency estimates.

The pressure measurements used for estimation of the pressure drop across the chamber were the subject of rather intensive study. This characteristic of the chamber was of special importance, but was very small in magnitude so that great care was needed in its measurement. The static-pressure measurements in both the inlet and outlet ducts were checked, during cold-air runs, against the indications of a Fecheimer tube (12) to assure freedom from errors due to impact pressures.

Gas samples were drawn from both inlet and outlet ducts and were analyzed on an Ellison three-chamber gas analyzer of the Orsat type. This instrument could not be expected to indicate small concentrations of the products of incomplete combustion, which might, however, have a relatively large effect on the chamber efficiency. In order to permit the diagnosis of losses from this source, a combustible-gas analyzer, having a full-scale range equivalent to 1 per cent of carbon monoxide, was kindly lent us by the Mine Safety Appliances Company, Pittsburgh, Pa., and a series of tests (runs Nos. 40–44 inclusive) were run, covering the range of air-oil ratios, in which gas samples from the regular taps were conducted to the analyzer. As shown in Table 2, the maximum indication of combustible gas during the run was about 0.02 per cent, equivalent to about 0.6 per cent heat loss to incomplete combustion. For the first 10 to 15 min of operation of the chamber after lighting off, a decreasing indication, starting at a peak of about 0.06 per cent equivalent carbon monoxide, was observed. As this analyzer, by producing catalytic combustion of combustible components of the gas stream on the surface of the platinum wire whose temperature affects the balance of a resistance bridge, indicates the presence of all products of incomplete combustion, these tests were considered conclusive proof that the fuel was completely burned out at the discharge of the chamber.

TABLE 2 GAS ANALYSES FROM TESTS ON EXPERIMENTAL COMBUSTION CHAMBER

Run Number	Combustible Gas Content of Outlet Gas by MSA Analyzer	Gas Analysis by Orsat Gas Analyzer					
		Inlet Gas			Outlet Gas		
		CO_2	O_2	CO	CO_2	O_2	CO
29	-	0.8	19.2	0.0	2.8	16.5	0.0
30	-	0.8	19.2	0.2	3.4	15.8	0.0
31	-	0.0	20.9	0.0	2.0	17.8	0.0
32	-	0.1	20.2	0.0	2.2	17.6	0.0
33	-	0.8	19.3	0.0	2.4	17.2	0.0
34	-	0.8	19.4	0.0	2.6	16.8	0.0
35	-	0.8	19.4	0.0	3.2	15.8	0.0
36A	-	0.0	20.9	0.0	0.5	20.4	0.0
36B	-	0.0	20.9	0.0	0.5	20.5	0.0
37	-	2.3	16.3	0.0	3.2	15.4	0.0
38	-	0.8	19.3	0.0	2.3	17.1	0.0
39	-	0.7	19.5	0.1	2.3	17.2	0.0
40	0.02	-	-	-	-	-	-
41	0.	-	-	-	-	-	-
42	0.	-	-	-	-	-	-
43	0.	-	-	-	-	-	-
44	0.01	-	-	-	-	-	-
45	-	0.5	19.8	0.0	2.4	17.2	0.0
46	-	0.5	19.5	0.0	2.4	17.0	0.0
47	-	-	-	-	4.1	14.9	0.0

Test Results. The detailed results of the combustion-chamber tests are presented in Tables 1 and 2, while the efficiency measurements are summarized in Fig. 6. Above fuel-supply rates of 2.5×10^6 Btu per hr, the combustion-chamber efficiency remains above 99 per cent, up to the maximum load carried in these tests, 6.5×10^6 Btu per hr. The limitation on the maximum load was imposed, not by oil-supply capacity or combustion conditions, but by the necessity of limiting the temperature of the discharge, which was vented to the atmosphere through mild-steel ducts.

This maximum represents about 35 per cent of the full-load heat input of the high-pressure chamber in the gas-turbine set. Tests on the chambers installed in the gas-turbine set, in which rates up to the design full-load condition have been carried, indicate no decrease in combustion efficiency as the load is further increased. Of course, these tests are not of as high precision as those on the experimental combustion chamber because of the impracticability of accurate measurement of air flow, and the lack of checks on temperature measurements. A significant result is that neither the stability of operation, nor the combustion efficiency is affected by the presence of products of combustion in

the inlet air, or by the reduction of the oxygen content of the inlet air to 16.3 per cent on the dry basis, corresponding to about 15.6 per cent before condensation of moisture.

As the combustion rate is decreased the efficiency of the chamber appears to fall off to about 81 per cent at a heat-liberation rate of 0.7×10^4 Btu per hr, the lowest stable combustion rate that could be maintained. At the lowest rate the radiation from the outside shell of the chamber accounts for approximately 5 per cent of the heat supplied by fuel, while incomplete combustion accounts for only 1 per cent or so more. The remainder of the apparent loss, amounting to about 14 per cent of the heat in the fuel at the lowest rate, is unaccounted for and must be ascribed to inaccuracies in the measurements.

Preliminary tests had shown that the pressure loss of the air passing through the chamber amounted to approximately one velocity head of the fluid at the entrance to the chamber. These tests were made in a chamber lacking the transition and elbow at the discharge of both the experimental chamber and those in the gas-turbine plant and were not of a high order of precision. The tests reported in Table 1 confirmed this result, however; they also permitted the formulation of a relatively precise expression for the loss in pressure. Study of the data by the methods of correlation analysis (13) showed that the pressure drop was dependent upon the velocity head of the gas leaving the combustion chamber, as well as that at the entrance. Since the quantity of fluid is essentially the same at entrance and exit, these velocity heads are simply related through the ratio of the absolute temperatures at the two sections, designated here as β. Using this convention, the results of these tests may be expressed

$$p = (0.360\beta - 0.077)h_1 \quad \ldots\ldots\ldots\ldots\ldots [3]$$

where

p is static pressure drop in any convenient units

h_1 is velocity head at combustion-chamber inlet in same units

$\beta = \dfrac{T_2}{T_1}$ is ratio of absolute temperature of air leaving to that entering the chamber

This expression represents the data of Table 1 to within about 9 per cent and was used to predict the performance of the chambers for the gas-turbine plant.

Stratification of the gas stream with respect to temperature has been the most troublesome characteristic of the combustion chamber. The difference in temperature across the gas stream may amount to 50 per cent or more of the average temperature rise. Temperature traverses have shown that the hot spot is always displaced from the center line toward the inlet of the chamber. It is curious that the chamber may operate consistently with low stratification at one speed of the turbine and just as consistently with high stratification just a few hundred revolutions higher or lower. Further investigation of this characteristic is being made.

The highest metal temperatures occurring in the chamber are those of the ignition cone. Temperatures of the inner shell were also measured during the early runs on the experimental chamber, but the couples at these positions were broken, before the tests reported here were run, by the axial movement of the inner shell relative to the outer shell accompanying heating up and cooling down. They remained in place long enough, however, to show that the shell at no point exceeded the temperature of the ignition cone. Immediately in front of the cone, at the inlet side, the shell temperature usually approached the maximum cone temperature. The variation of the average ignition-cone temperature with the load on the chamber is quite regular, as shown in Fig. 7. The results shown here may be generalized by the conclusion that at no point in the chamber does the metal temperature exceed the chamber discharge temperature by more than 300 deg F, under any condition of operation.

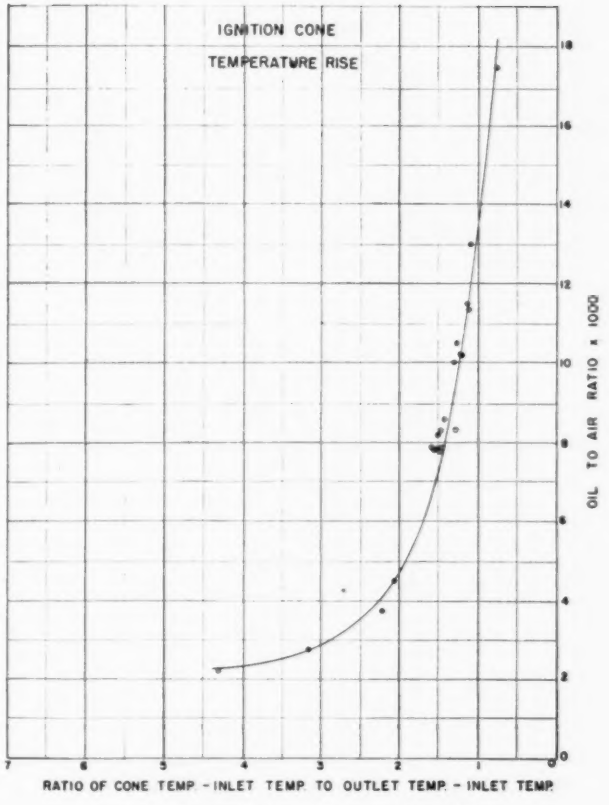


FIG. 7 IGNITION-CONE TEMPERATURE RISE

NOTES ON THE DEVELOPMENT

Work on this project started late in 1942, with an attempt to design a combustion chamber that would fit the space requirements of the proposed plant layout. Several designs following more or less conventional practice were completed and chambers of mild steel were built for testing in an outdoor test stand.

In these conventional chambers combustion air was separated from tempering air by a metal shell (2) since it was thought that the large amount of excess air would quench the burning of the fuel. The largest part of the air passed around this shell while combustion air was admitted to the burner end of the shell through a variety of registers, most of which were equipped with adjustable vanes, as in boiler practice. A "spinless" register was also built, in which the primary air was admitted between two coaxial cones, which produced much more stable ignition in a smaller volume of the chamber than did any of the others. It was also found that such stable ignition was essential, with either continuous or intermittent injection of the fuel, to reduction of the flame length. This register was the elementary form of the ignition cone now in use.

Of the chambers proper, those having circumferential slots which admitted air axially along the walls of the inner shell were found to produce very long flames, while those having round holes producing radial jets gave short flames but required relatively larger pressure drop. The "elbow" form of chamber was produced fortuitously by the removal of all inner shells in an attempt to reduce pressure drop.

ACKNOWLEDGMENTS

The authors wish to acknowledge the assistance and encouragement supplied throughout this development by Commodore R. V. Kleinschmidt and his staff in the Research Section of the Bureau of Ships; and to thank the Chief of the Bureau of Ships for permission to publish this material. We wish also to thank Mr. R. B. Smith, vice-president Engineering, and the rest of the management of the Elliott Company for their support of this work; and to express our gratitude to William Schoenfelt, formerly a member of the Engineering Research and Development Department of the company, and especially to George Schertzinger, for their devoted work on this problem.

BIBLIOGRAPHY

1 "The Gas Turbine as a Possible Marine Prime Mover," by C. R. Soderberg and R. B. Smith, Trans. Society of Naval Architects and Marine Engineers, vol. 51, 1943, pp. 115–130; discussion pp. 131–155.

2 "Combustion Chambers," U. S. Patent 2,268,464 to Claude Seippel (assigned to Aktien Gesellschaft, Brown Boveri & Company), Dec. 30, 1941; also U. S. Patent 2,249,489 to W. G. Noack (assigned to Aktien Gesellschaft, Brown Boveri & Company), July 15, 1941; cf. also "Firing High-Pressure Furnaces," by E. G. Peterson, Trans. A.S.M.E., vol. 66, 1944, pp. 433–438.

3 "Fluid Mechanics for Hydraulic Engineers," by Hunter Rouse, McGraw-Hill Book Company, Inc., New York, N. Y., first edition, 1938, p. 269, fig. 139 (a).

4 Verbal communication by R. V. Kleinschmidt, Capt. U.S.N.R., May, 1943.

5 "Hydrodynamics," by Horace Lamb, fourth edition, Cambridge University Press, 1916, p. 234.

6 Verbal communication by K. E. Wenk, Socony Vacuum Oil Company, Inc., July, 1945.

7 "Introduction to Theoretical Physics," by Leigh Page, D. Van Nostrand Company, Inc., New York, N. Y., second edition, 1935, p. 237, fig. 81.

8 "Thermodynamics and the Free Energy of Chemical Substances," by G. N. Lewis and M. Randall, first edition, McGraw-Hill Book Company, Inc., New York, N. Y., 1923, pp. 101–105.

9 "A Thermodynamic Investigation of Gas Turbine Cycles," by R. V. Kleinschmidt, U. S. Bureau of Ships Research Memorandum No. 1–42, 1942; cf. "Gas Turbine Combustion Chamber—Concept of Efficiency," by A. L. London, U. S. Bureau of Ships Research Memorandum.

10 "The Measurement of High Temperatures in High-Velocity Gas Streams," by W. J. King, Trans. A.S.M.E., vol. 65, 1943, pp. 421–428.

11 "Investigations of High-Temperature Measurements," by H. W. Emmons. Reports nos. 4 and 5 of work undertaken for the Elliott Company, 1943.

12 "The Measurement of Static Pressure," by C. J. Fechheimer Trans. A.S.M.E., vol. 48, 1926, pp. 965–972.

13 "Statistical Methods for Research Workers," by R. A. Fisher sixth edition, Oliver & Boyd, London, England.

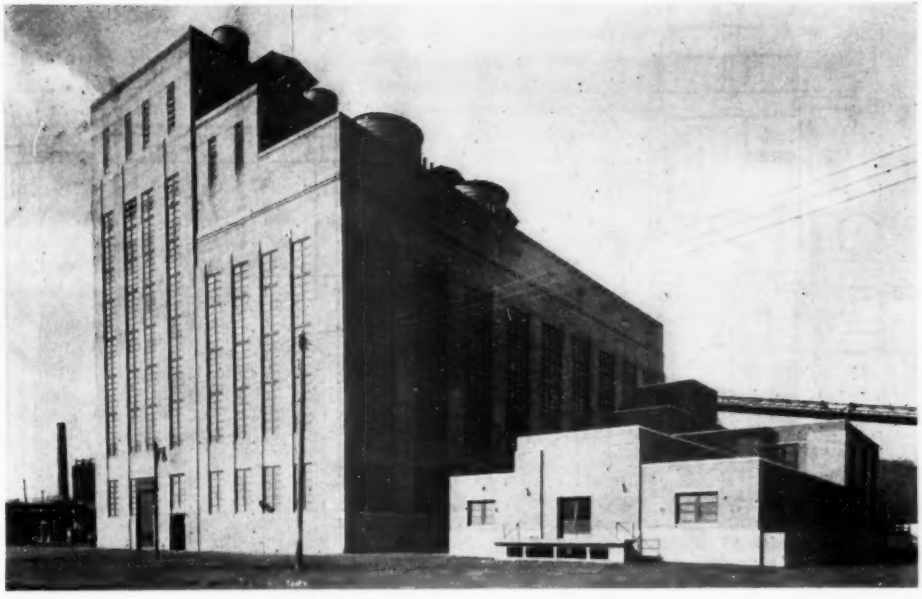


FIG. 1 GENERAL VIEW OF POWER PLANT

A Comparison of Operation of Forced- and Natural-Circulation Boilers

BY G. F. ROSS[1] AND LEONARD WILKINS,[2] KOBUTA, PA.

Steam-generating facilities at the Koppers Company, Incorporated, Butadiene Division, Butadiene-Styrene Chemical Plant, at Kobuta, Pa., include two types of units; natural-circulation boilers and the first forced-circulation boiler to be installed in the United States for industrial-plant processes. Since plant operation began in the summer of 1943, this installation has afforded boiler operators an opportunity to compare the operating characteristics of the two types. This paper describes briefly the design and operating features of these steam generators, together with some of the difficulties encountered and how they were overcome.

THE installation of a controlled forced-circulation boiler unit adjacent to three natural-circulation boiler units of identical rating at the Koppers Company, Incorporated, Butadiene Division, Butadiene-Styrene Chemical Plant[3] has afforded boiler operators an opportunity to compare the operating characteristics of these two types of steam-generating units. Boiler designers and operators are naturally interested in the first application in this country of a forced-circulation boiler unit to supply steam for industrial-plant processes. The steam-generating facilities at Kobuta were built at a time when the steel demand for other urgent war needs was at its peak; the Government directed that a forced-circulation boiler unit should be installed. Plant operations began in June, 1943, with one natural-circulation boiler; in August, 1943, the forced-circulation unit was placed in service.

It will be the endeavor of this paper to describe briefly the design features and compare the major operating differences between the two types of steam-generating units and to outline a few of the operational difficulties that accompany boiler generators of this type. Problems attendant to starting up the units for the first time are intentionally omitted, as boiler designers and operators are well aware that initial operating difficulties rarely recur after the difficulty is once remedied. All boilers installed at this plant met the manufacturers' expected-performance specifications and this paper will deal only with problems arising after acceptance.

It is well to point out that operating personnel was obtained several months prior to operations, in order that start-up of the boiler units could proceed without delay. Operators observed the complete erection of each boiler unit with its auxiliaries, and supervisors conducted short classes with operators to familiarize them with the operating characteristics of each boiler. The wisdom of such a procedure was illustrated by the ability of the operators to start up each unit as it was completed and maintain it on the line as a reliable steam source for plant process. The start-up of the forced-circulation unit was no more of an event than that of the natural-circulation units, as operators had become accustomed to its unconventional design.

---

[1] Assistant Superintendent of Utilities, Koppers Company, Inc., Butadiene Division.

[2] Maintenance Engineer, Koppers Company, Inc., Butadiene Division.

[3] This plant is operated by Koppers Co., Inc., Butadiene Division, an agent for the Reconstruction Finance Corporation, Office of Rubber Reserve, Washington, D. C.

Contributed by the Power Division and presented at the Annual Meeting, New York, N. Y., Nov. 26–29, 1945, of THE AMERICAN SOCIETY OF MECHANICAL ENGINEERS.

NOTE: Statements and opinions advanced in papers are to be understood as individual expressions of authors and not of the Society.

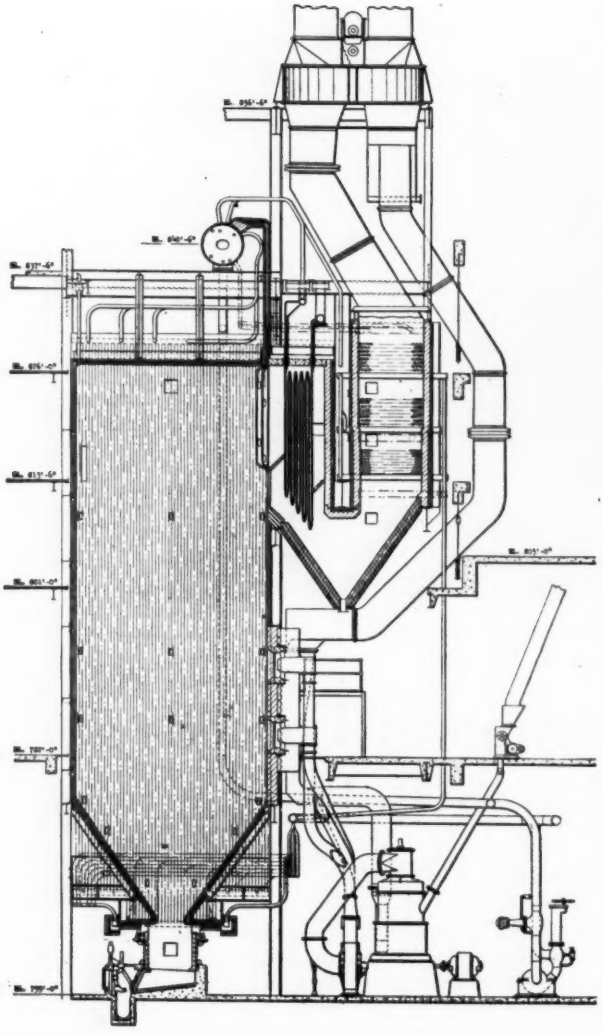


FIG. 2 CROSS-SECTIONAL VIEW, FORCED-CIRCULATION BOILER

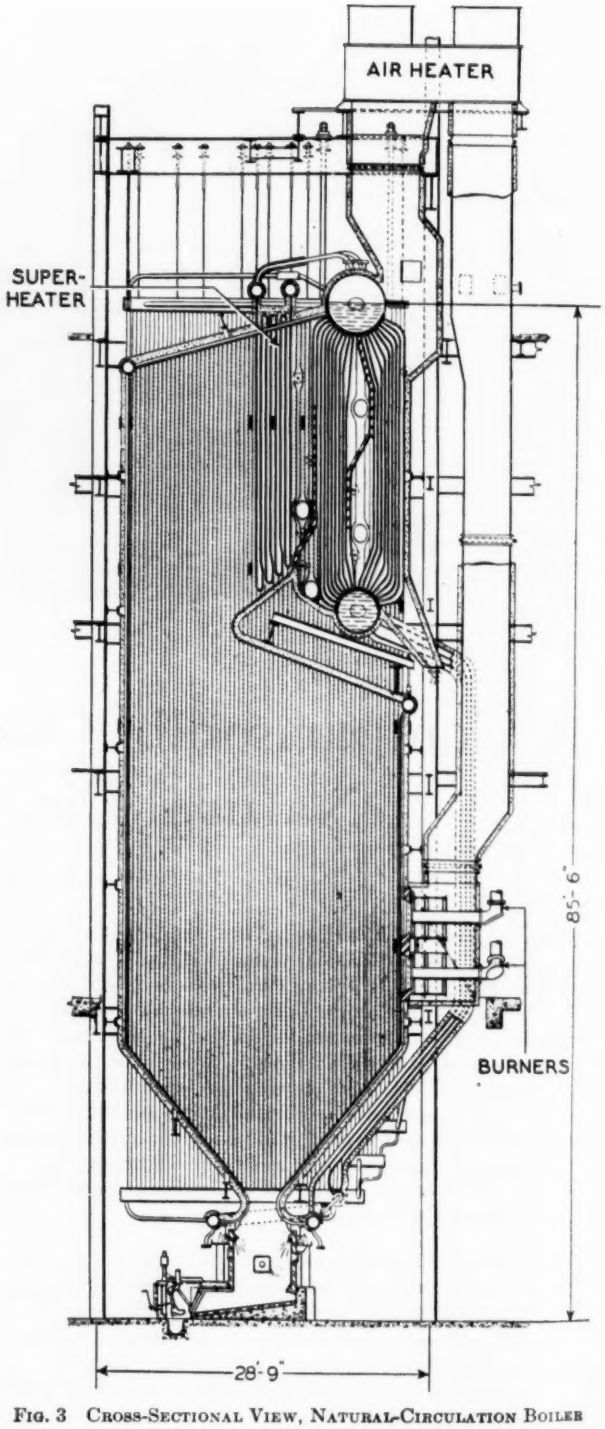


FIG. 3 CROSS-SECTIONAL VIEW, NATURAL-CIRCULATION BOILER

It is beyond the scope of this paper to present in detail the design data of these boiler units. Aside from a secondary interest in these data, boiler operators are primarily interested in the operating characteristics, availability, water control, and maintenance of their steam-generating units. A description of the physical layout of the steam plant is included to better acquaint the reader with its size, design features, and operating conditions. It must be remembered that war regulations prohibited extensive refinements in this steam plant, and these limitations were met remarkably well.

The time limit of construction and operating date prohibited exhaustive studies in layout and operating equipment. That the plant has produced steam consistent with high demand attests to the ability of the designers and operators to meet the wartime limitations. Most boiler operators will agree that boiler auxiliaries present more operating difficulties than the actual furnace, and it is well to note that in this case the boiler auxiliaries are not as a whole duplicated in each of the types of boilers. No attempt will be made to compare these auxiliaries, but the inclusion of the operation of the forced-circulation pumps is made, since it is considered an integral part of the forced-circulation boiler unit.

It is not the intention here to present data to influence the selection of any particular type of boiler unit. Boiler operators pride themselves on being able to fire any type of steam-generating equipment and to secure from it the maximum possible efficiency and reliability. After two years of experience with each of these types of boilers, it is possible to make a comparison of their operation and to present to those interested a summary of our experience at Kobuta.

DESCRIPTION OF PLANT AND BOILER AUXILIARIES

The original steam plant consists of four 350,000-lb per hr

boilers, designed for superheater-outlet conditions of 725 psi pressure and 750 F temperature. The first is a Combustion Engineering Company single-drum controlled forced-circulation boiler, Fig. 2, and the other three are Babcock & Wilcox Company two-drum, radiant-type, natural-circulation units, Fig. 3. Operating experience indicated that the capacity of three boilers was not sufficient to supply all the steam demanded by the chemical-process units with one boiler off the line for inspection and maintenance. Accordingly, a fifth boiler of 180,000 lb per hr capacity at 450 psi pressure without superheat was installed. This latest addition is a Combustion Engineering Company four-drum natural-circulation unit. Total steam-generating capacity available from the five boilers is 1,580,000 lb per hr. The four high-pressure units are housed in a reinforced-concrete boilerhouse, approximately 130 ft high, while the low-pressure unit is installed in a separate annex at the south end of the original concrete boiler room. No further reference will be made to the smaller natural-circulation unit and its auxiliaries.

Draft equipment for each of the high-pressure units is identical, consisting of one induced- and one forced-draft fan per boiler, with turbine drives. An important factor in selecting boiler capacity was the limitation of draft equipment to single fans per boiler so as to require a minimum number of reduction-geared-turbine drives, an extremely critical item during the construction period. Fly-ash collection equipment is within the induced-fan housings, thus minimizing the use of steel. Each boiler is equipped with a Ljungström air preheater. A combination of two coal-and-gas, and two coal-and-oil burners fire the forced-circulation boiler. Natural-circulation-boiler furnaces are equipped with six combination coal-and-oil, and two separate gas burners. All furnaces are dry-bottom, with intermittent ash-sluicing facilities, and continuous ash sprays. The forced-circulation unit is equipped with two Raymond bowl mills, with integral exhausters, and the natural-circulation units are fired with two Hardinge-type ball mills, with remote exhausters located on the operating floor. Suitable feed pumps are installed in the pump bay on the ground-floor elevation. These consist of five units, i.e., three turbine-driven, one motor-driven, and one combination turbine-and-motor dual-drive unit.

Steam at 700 psi and 750 F goes to a 35,000-kw turbogenerator which exhausts at 165 psi back pressure for chemical-plant-process requirements. Total plant electrical load approximates 14,000 kw, the excess electrical energy going into the local utility system. Exhaust steam leaves the turbine discharge and passes into two 24-in. lines at 165 psi and 460 F, which maintains slight superheat to the farthest end of the process-plant distribution lines. Part of this steam is reduced to 75 psi for process, as needed. In order to furnish 165-psi steam with a turbine or utility tie-line outage, desuperheating and pressure-reducing stations are installed between the boiler headers and exhaust lines. Any sudden interruption to exhaust-steam supply operates these stations through master controllers. Desuperheating water is supplied from the condensate system through special pumps installed at the feed-pump bay.

Main high-pressure boiler-plant piping is so arranged that boilers may be isolated into two separate generating systems, each

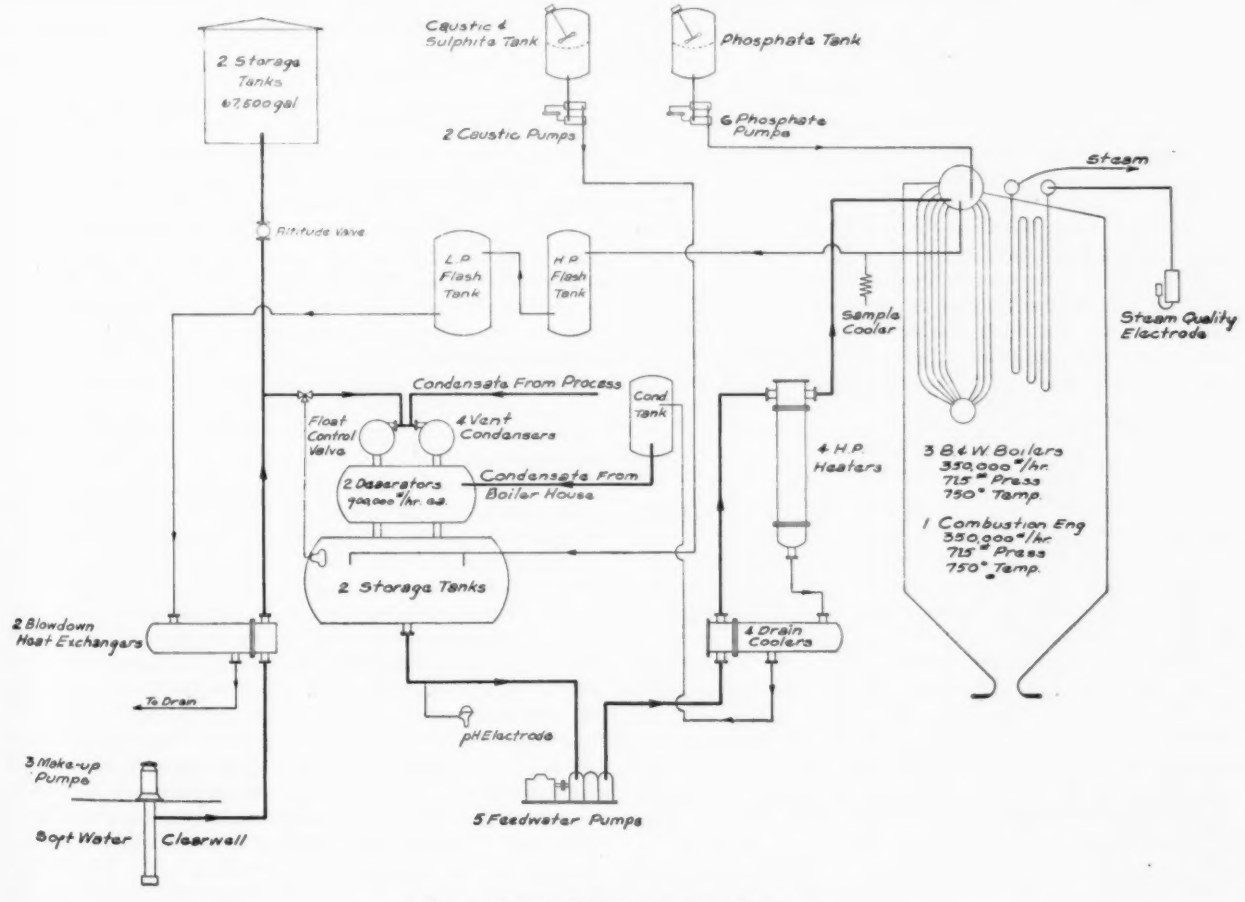


FIG. 4 BOILER-FEEDWATER FLOW DIAGRAM

containing its own feedwater, steam-generating, and blowdown facilities. The forced-circulation main steam lead and one of the natural-circulation units are tied to a common header with the remaining two high-pressure units discharging into a similar header. The turbogenerator is fitted with double inlet valves, one from each main boiler header.

The blowdown system consists of two separate series of high- and low-pressure flash tanks, from which 165-psi and 10-psi steam is supplied to the high-pressure heaters and to the deaerators, the effluent being sewered through the blowdown heat exchangers. It has been noted that during peak loads and high rate of blowdown, approximately 50 per cent of the 165-psi steam requirements for the high-pressure heaters is met by the high-pressure flash steam. The feedwater flow is illustrated in Fig. 4.

Coal comes to the plant by rail, truck, or barge. Belt conveyers transport it from unloading points to storage or directly into the crushers where it is sized to $^3/_4$ in. or less, before entering the bunker house. A feeder tripper distributes coal into eight 250-ton hoppers from which it drops by gravity, through automatic scales to mill feeders and pulverizers at each boiler. Furnace volumes permit carrying full boiler load on coal alone, consuming 1500 to 1700 tons per 24 hr for the four large boilers. All-electric combustion control is duplicated on all boiler units, regulating air and coal feed according to steam demands. Hand preadjustment of the control mechanism assures sufficient combustion air for oil and gas.

Feedwater-pump- and draft-fan-turbine exhaust goes to two deaerating feedwater heaters that handle both return condensate and raw make-up. A reducing valve from the main-turbine exhaust supplies any deficiency. The high-pressure closed heaters receive steam directly from the main-turbine exhaust, supplemented by flash from the blowdown system.

Water-Treating Facilities

Treating-plant equipment and basins are located adjacent to the powerhouse in a separate building and connected to the station by a pipe tunnel. Ohio River water is fed into three Spaulding precipitators in the water-treating plant through a 20-in. line. The raw-water flowmeter controls the rate of chemical input. Lime, soda-ash, and copperas solutions are fed by individual pumps into the inlet flume of the precipitators. At the maximum rate of flow through the precipitators, the detention time is 90 min. The water, having been clarified and partially softened in its passage through the precipitators, flows by gravity to six Anthrafilt filters. The filtering capacity is 3900 gpm and

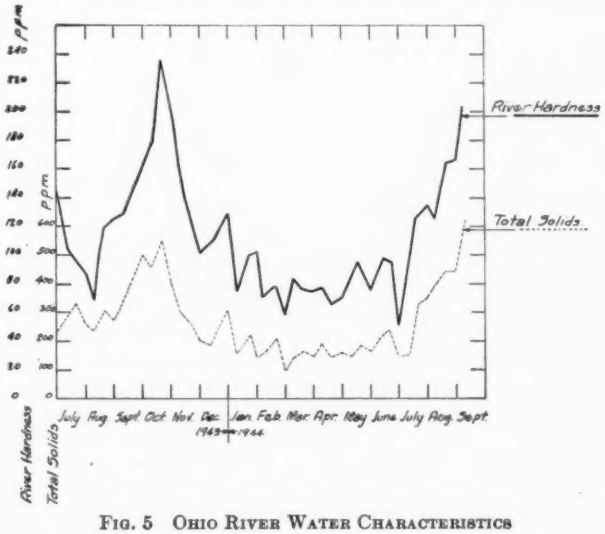


Fig. 5 Ohio River Water Characteristics

the flow of water through the filters is regulated by rate-of-flow controllers. In leaving the filters, the water is discharged into an acid-mixing chamber before passing into a filter clearwell, and a pH value of 8.3 is maintained to prevent deterioration of the zeolite in the final softeners.

After the water is clarified, partially softened, filtered, and acidified to the correct pH, it is pumped to six gravity-flow zeolite softeners. The design of the equipment was based on a hardness of 55 ppm from the filter clearwell. With this capacity setting, each unit is capable of softening about 770,000 gal of water in each regeneration. The zeolite operates in the sodium cycle with rock salt for preparation of the solution. The treating process is capable of delivering the required boiler make-up water to the boilerhouse with a residual hardness rarely exceeding 2 ppm even during periods of peak hardness of the raw water.

Make-up water is pumped from the soft clearwell to two deaerators located in the boiler plant. Each deaerator is designed to operate at a pressure of 10 psi with a guarantee to remove the oxygen from 900,000 lb of feedwater per hr. To protect the equipment from corrosion attack, sodium sulphite is fed into the deaerator storage tank. Caustic soda is also added at this point to maintain a safe pH value in the feedwater, as it passes through the feed pumps and high-pressure heaters. Caustic-soda feed is also used to maintain the specified alkalinity range in the boiler water. Sodium-metaphosphate solution is fed directly into the upper drums of the four boilers to satisfy demands of residual hardness of the boiler feedwater and acts as a sludge-forming accelerator. Each boiler is equipped with a boiler-water-sample cooling coil located at the upper drum, and two Straub condensers with conductivity cells and recorders are provided to obtain a continuous check on the quality of steam leaving the boiler drum.

Controlled Forced-Circulation Unit

The sectional view of the forced-circulation unit shows no lower or mud drum. Forced circulation eliminates the need for the lower drum with its interconnecting generating surface necessary to set up circulation between the lower and upper drums. Boiler feedwater enters the single drum after passing through the economizer which is located in the upper section of the convection zone, immediately below the air preheater. The feedwater is introduced into the drum through a submerged pipe which extends the entire length of the drum, discharging the water through perforations. Two 10-in. downcomer pipes, located about 6 ft from each end of the drum, carry the water down to the circulating pumps. These downcomer openings are protected by wire screens as mechanical protection for the circulation-pump impellers and are also fitted with downtake spiders to eliminate vortex formation.

The circulating pumps are 10 × 10 Allis-Chalmers horizontal single-stage type, Fig. 6, rated at 4500 gpm, 151 ft head, 517 F, and suction pressure of 800 psi. They have an end suction and a side discharge and are driven by horizontal steam turbines through a Fast "spacer" coupling. Ball-thrust bearings absorb all the thrust load of the pump. Through close co-operation between the representatives of the boiler and pump manufacturers, the pumps are so designed to maintain a constant and unfailing flow of water through the boiler and to operate continuously and without interruption, in order to protect the boiler tubes. To facilitate removal of the rotating element, there has been incorporated in the design of the pump a casing cover, or end head, through which all the internal parts of the pump can be removed. A close-clearance bushing directly behind the pump impeller is used with "bleed-in" and "bleed-off" connections to reduce the temperature and pressure on the stuffing box. The bleed-in connection permits a water flow of 20 gpm at 240 F and 900 psi from the boiler feed pump discharge main to enter the inner end

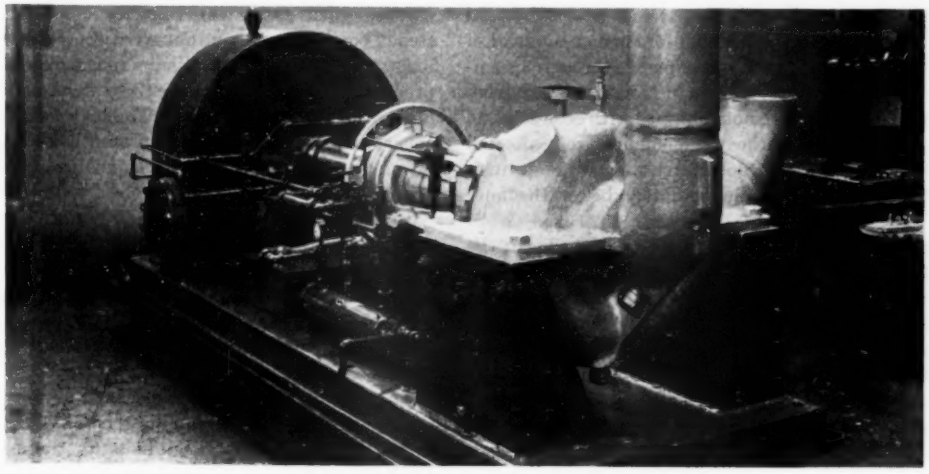


FIG. 6 FORCED-CIRCULATION-BOILER PUMP
(Rated at 4500 gpm, 151-ft head, 1500 rpm, 517 deg F; suction pressure 800 psi.)

of the reducing bushing. This flow of water at a pressure higher than pressure in the pump maintains a water flow at 240 F out of the bushing into the pump, instead of the hot boiler water in the pump flowing back toward the packing. About 2 gpm of 240 F water flows into the pump, and the remaining 18 gpm is bled off through the bleed-off connection. By this arrangement it is possible to pack against a low pressure and low temperature, rather than against the normal boiler pressure and temperature. Further reference is made to this feature later in the text.

The circulating pumps located on the ground floor withdraw water from the drum and discharge into a loop which supplies water to wall-distributing headers. Two of these headers supply the burner and rear-wall tubes, two supply the central section of the side walls, four others supply the outside sections of the side walls, and the remaining one supplies water to the secondary generating section.

Flow of water from the headers to the wall and secondary-generator tubes is controlled by a series of combination orifice strainers, consisting of a nipple approximately 6 in. long perforated by $^{3}/_{16}$-in. holes and drilled with a control orifice. The arrangement is such as to permit removal of the orifice strainers from the headers for inspection and cleaning. One orifice strainer serves a tube nozzle which is trifurcated for the three wall tubes which arise from it. A total of 276 strainer orifices are provided to supply 183 tubes on each of the burner and rear walls, 198 tubes on each of the side walls, and 32 tubes in each section of the secondary generator located immediately below the economizer. Front- and rear-wall tubes lead directly into the top of the drum above water level, while the side-wall and secondary-generator elements collect into headers and pass into the drum through 4-in. risers entering the drum above the water level.

The 54-in-drum internals are so arranged that the water-steam mixture is first directed downward by a deflector baffle at the tube entrances. The flow is then reversed in direction permitting the water to separate from the steam. This reversal permits the steam part of the mixture to continue directly to the screen driers, while the remainder of the mixture bubbles through a submerged screen below the water level. Steam at relatively low velocity passes through three sets of screen driers for the complete removal of any entrapped moisture. In leaving the drum, the steam passes around deflector plates located directly under the tubes leading to the superheater.

The superheater element hangs directly in the gas stream at the entrance to the convection section and is protected by a slag screen of staggered front-wall tubes, three rows deep. Combustion gases pass out of the furnace through the front-wall screen, across the superheater bank, through the convection bank containing two sections of generating tubes, and through the economizer. The last banks are supported on water-cooled beams which are part of the secondary-generator circuit. Soot is removed below the superheater, and by the dust collector in the induced-draft-fan housing.

It will be noted that in the forced-circulation unit there is no need for generating tubes to be suspended in the gas passes and baffles for routing gas flow are not required. The forced-circulation unit thus approaches a favorable design of gas passes and tube arrangement to overcome any fly-ash erosion difficulties.

Boiler dimensions of the forced-circulation unit are given in Table 1.

TABLE 1 FORCED-CIRCULATION-UNIT DATA

Furnace volume, cu ft gross	25,400
Boiler heating surface, sq ft	4,510
Waterwall surface, sq ft	8,470
Superheater surface, sq ft	4,430
Economizer surface, sq ft	9,830
Air preheater surface, sq ft	38,900
Operating water volume, lb	36,643
Steam drum	54″ diam × 28′–9½″ long
Upper wall tubes	1¼″ OD × 0.120″ wall thickness
Lower wall tubes	1¼″ OD × 0.150″ wall thickness

NATURAL-CIRCULATION UNITS

As noted by the sectional side view, Fig. 3, the natural-circulation boilers have two drums with pendant superheater. Feedwater enters the upper drum through a perforated pipe below the water level and passes down to the mud drum through interconnecting generating and heating tubes. Water is then distributed to the waterwalls through eight headers located at the bottom of the furnace. Two of these supply front and rear walls, two supply the center and rear section of the side walls, and the other four supply the front sections of the side walls. Rear- and front-wall tubes terminate directly in the steam drum entering below water level. The side-wall tubes terminate in headers at the top of the furnace and continue to the drum by risers entering the drum above water level, but inside the internal baffle compartment.

The 60-in-drum internals cause the water and steam mixture in the wall and generator tubes to enter a baffled compartment from which the mixture passes tangentially into 44 cyclone steam separators. As a result of the whirling action of the cyclones, the

water is directed downward while the steam passes upward through the corrugated scrubber elements for further removal of moisture. In leaving the drum the steam passes through a twin-type steam scrubber where the last trace of moisture is removed. The natural-circulation boilers are not equipped with economizers. The convection bank and superheater elements are protected from direct radiation by a water-cooled arch extending approximately halfway into the furnace, immediately below the mud drum.

Attention is called to the baffle arrangement as shown in the sectional view, Fig. 3. The baffle between the first and second pass is of tile construction. The upper section of the baffle separating the second and last pass was originally as shown in Fig. 3 and is also of tile construction, the sloping portion being of the poured type, and the lower section again of tile construction. In recent months two generating-tube failures have occurred on two of these natural-circulation units due to fly-ash erosion of the tube metal. In the first case, leakage of dust-laden gas through the baffle, separating the second and last pass, seriously eroded the generating tubes directly behind this baffle, a short distance below the top drum. In the other case, concentration of fly ash sweeping down the slope of this same baffle eroded tubes in the row just ahead of this baffle at a point just below the baffle slope. Baffle changes have been completed on all three of the natural-circulation units by making the entire baffle vertical from the drum downward. This arrangement should overcome both difficulties as well as afford convenient access to the furnace for inspection of the baffle for leakage. Soot is removed at the second pass of the convection bank at mud-drum level, as well as by collection in the induced-draft fan similar to the forced-circulation unit.

Boiler dimensions of the natural-circulation units are given in Table 2.

TABLE 2 NATURAL-CIRCULATION-UNIT DATA

Boiler heating surface, sq ft	20,640
Waterwall surface, sq ft	6,367
Superheater surface, sq ft	4,030
Total steam-generating surface, sq ft	31,007
Air-heater surface, sq ft	38,600
Volume of combustion space, cu ft	29,900
Operating water volume, lb	150,680
Front-wall tubes	3¼″ OD × 0.203″ wall thickness
Steaming drum	60″ diam. × 30′ long
Mud drum	42″ diam. × 29′ long
Rear-wall tubes	2½″ OD × 0.170″ wall thickness
Side-wall tubes	2½″ OD × 0.170″ wall thickness
Roof tubes	4″ OD × 0.213″ wall thickness
Generating tubes	2½″ OD × 0.148″ wall thickness

Operating Conditions

During the latter part of 1943, the entire year of 1944, and the first quarter of 1945, the directed rate of chemical production demanded a peak steam load of 1,300,000 lb per hr, with an installed capacity of 1,400,000 lb per hr at that time. It was the responsibility of the boiler operators to maintain maximum steam generation under extreme varying conditions. Boiler outages were purposely kept to an absolute minimum by maintenance forces on a 24-hr schedule to keep the boiler units in operating service. Initial planning called for scheduled outages of boiler units each 6 months, but revisions were made on first inspections and subsequent tube failures to remove the forced-circulation boiler from the line each 60 days for inspection, and the natural-circulation units each 180 days. This schedule was adhered to during the entire period of peak steam demands.

The complexity of the butadiene-styrene chemical process, with its large number of stills, compressors, and heat exchangers, imposed on the boilers the requirement of maintaining correct pressure and temperature at all times. The chemical process is extremely sensitive to variations in steam conditions and slight steam upsets curtail chemical production. During boiler difficulties, when generating capacity could not maintain proper steam conditions, operators were reluctant to drop steam delivery to process because subsequent readjustment to normal production rate would require 24 to 48 hr, in addition to entailing large losses of raw materials. The boilers were called upon to recover from adverse conditions promptly and in most cases, boiler operators were able to maintain a continuity of steam flow to the process units.

In contrast to the operation and performance of a boiler under central-power-station conditions where make-up water rarely exceeds 2 per cent, and where even this amount is supplied by evaporation, boiler make-up here at Kobuta has been of the order of 60 to 70 per cent due to process-steam requirements. These steam requirements necessitate discarding two thirds of the steam condensate in process wastes.

Ohio River water, which is the raw-water source, contains principally sulphate salts and is generally slightly acid in nature, with a pH of 6.5. Total hardness for the major portion of the year ranges between 70 and 90 ppm expressed as calcium carbonate.

In Table 3 the analysis given for Ohio River water may be considered as being the average.

TABLE 3 TYPICAL ANALYSIS OF OHIO RIVER WATER

	Ppm
Bicarbonate (HCO_3)	7
Sulphate (SO_4)	96
Chloride (Cl)	15
Silica (SiO_2)	5
Iron (Fe)	4
Calcium (Ca)	23
Magnesium (Mg)	5
Sodium (calc.) (Na)	23
Suspended solids	17
Total dissolved solids	195
Soap hardness as $CaCO_3$	78

Composition of the water is subject to wide variations in hardness and dissolved solids, as shown in Fig. 4. During the 2 years that the plant has been in operation, control of water conditioning and continuity of operation have been maintained under conditions where hardness of the water has fluctuated from a low of 60 ppm during the winter and early spring seasons, to a high exceeding 250 ppm during periods of low river flow. Similarly, dissolved solids fluctuated from a low of 100 ppm to a high exceeding 600 ppm. Obviously with boiler make-up exceeding 60 per cent, and with solids concentrating in the boilers in a very short time during periods of peak dissolved solids, conditions exist which tax a conventional natural-circulation boiler to the limit and impose on the operation of a forced-circulation unit the additional measures necessary to prevent an accumulation of suspended matter at its control orifice strainers great enough to cause tube failures. Blowdown equipment is adjusted to maintain a dissolved-solids content of 2000 ppm in the boiler water.

On the basis of the average analysis of raw water in which dissolved solids were 178 ppm a blowdown of 10 per cent was expected. As most of the heat-recovery equipment was designed to handle this quantity, the blowdown facilities were vastly overloaded when it became necessary to blow down 30 per cent of the feedwater in order to maintain the desirable boiler-water conditions when the dissolved solids in the raw water exceeded 600 ppm. After installing larger blowdown valves and pipes, and with the continuous-blowdown equipment operating at maximum, it is still necessary to supplement this with continuous blowing of the mud drums. With the installation of the fifth boiler, blowdown-equipment arrangements can be made to modify the blowdown lines in such a manner as to recover the heat normally lost in the use of the mud-drum blows.

Residue oil and gas furnished from the process units is delivered to the boilerhouse for burning in combination with the

coal obtained from the local bituminous mines. Normally, moisture content of the coal does not exceed 4 per cent, but there have been periods during transportation difficulties, when 10 to 15 per cent moisture coal has been delivered to the pulverized-fuel equipment; such periods occurring when steaming capacity was at a premium. While the ability to satisfy steam demand under these moisture conditions is a function of the fuel-burning and handling auxiliaries, boiler operators were called upon to adjust boiler ratings continuously to maintain proper pressure and loading. These periods made it possible to observe the individual boiler response to the demands for steam to process. That no particular difference between the boiler units was found might be surprising to those who believe that the forced-circulation unit responds and recovers load in less time than the natural-circulation units of the same capacity. With the units equipped with different types of mills, any indication of such conditions might be attributed to the mill performance rather than to that of the boiler.

Local strip-mined coal, ranging in quantities of 25 to 50 per cent of the total fuel, has been fired in all boilers. Two generating-tube failures and severe erosion of generating tubes in the natural-circulation boilers have led several consultants to consider these conditions to be the result of the high silica content of the ash of this strip-mined coal.

Operating Characteristics

The forced-circulation boiler, with $1^1/_4$-in-OD wall tubes and only one drum, has considerably less water in it than the natural-circulation unit has, with two or more drums and larger-diameter wall and generating tubes. The forced-circulation boiler holds approximately 37,000 lb of water at steaming level, compared to the natural-circulation boiler which holds 155,000 lb, or nearly $4^1/_4$ times as much. This causes a greater sensitivity in the forced-circulation boiler to changes in feedwater conditions or changes in controls.

With the natural-circulation boiler operated at 350,000 lb of steam per hr for a period of 2 hr with the blowdown completely shut off and with 400 ppm dissolved solids in the feedwater, an increase of 1800 ppm in the solids concentration of the boiler water would result. This added to the normal 2000 ppm carried would mean a total concentration of the boiler water of 3800 ppm. Actual operating data indicate that these boilers can be operated at 400,000 lb per hr with 4000 ppm dissolved solids. Should the continuous blowdown be completely shut off on these natural-circulation boilers, no serious results would be experienced before the boiler operators could remedy the condition.

In the case of the forced-circulation unit under the same conditions, the concentrating effect of evaporation would result in a total dissolved solids content of 9600 ppm. At a steam rate of 350,000 lb per hr, solids carry-over would probably begin with a concentration of 5000 ppm and would doubtless be experienced if the blowdown were stopped for only $^1/_2$ hr.

To be reasonably free from upsets of the nature described, analyses of the boiler waters are made every 2 hr, total solids being checked by the conductivity method. In so far as the natural-circulation boiler is concerned, this 2-hr frequency is adequate to detect any major change in conditions before the results become serious. Such is not the case in the forced-circulation unit. Carry-over has been experienced on several occasions with the forced-circulation unit as a result of rapid increase in solids concentration, the carry-over being detected by means of the steam-temperature recorder.

Arrangements are being made to install a conductivity recorder on all the boilers, recording total solids in the continuous blowdown. Especially in the case of the forced-circulation boiler, where the quantity of water at steaming level is relatively small and where the percentage make-up is relatively high, a conductivity apparatus recording total solids should be installed as standard equipment with the boiler.

Natural-circulation units depend on differences in specific gravity to set up circulation; and as a result, circulation rates vary with changes in rating or changes in heat input. In the forced-circulation boiler the rate of circulation is fixed and controlled by means of centrifugal pumps which take the water from the main drum and discharge it to distribution headers where it enters the tubes through control orifices. These orifices are so sized that a reasonable pressure drop is experienced across them and good control of distribution is the result.

It is natural to expect that a centrifugal pump installed in the boiler-water circuit would be regarded as an outstanding weak point in the entire system. In actual practice, this has not proved to be the case at Kobuta. To date there has been no instance of circulation failure due to the pumps. The forced-circulation unit is equipped with two pumps, one operating at rated speed and load, the other idling at approximately 400 rpm. The original installation required manual operation to place the idling pump in service should the loaded pump fail. This arrangement made it mandatory to station an operator at the pumps at all times. Physical layout has placed the pumps remote from the boiler feed pump bay, and in the future, boiler-installation designers might consider locating a forced-circulation boiler in such a manner that the circulation pumps can be attended by the normal boiler feed pump operator or water attendant. The usual interlocks for tripping the coal-pulverizing mills when the pump differential reaches the low limit were provided, but this feature was removed shortly after the unit went into service, because of the feeling that the pump attendant was sufficient protection.

The stationing of the pump attendant was regarded as a stopgap measure for emergency protection of the boiler, and at present quick-opening steam valves have been installed to bring the idling pump to full speed and rating automatically. The control for these valves is taken directly from a differential-pressure controller. On occasions when upsets resulted in low steam pressure to the pumps, and pump differential reached the low safe limit, the idling pump was automatically put in service in a very satisfactory manner. It is now believed that with this feature added, and based on the performance of the pumps to date, the reliability of the circulation system is assured.

Efficiency and performance tests have indicated no outstand-

TABLE 4 PERFORMANCE DATA OF FORCED-CIRCULATION AND NATURAL-CIRCULATION STEAM GENERATORS

	Forced-circulation unit	Natural-circulation unit
Steam output, lb per hr	352500	345000
Temperature of air for combustion, deg F	90	106.3
Temperature of feedwater to boiler, deg F	472	364
Exit gas—CO_2 content, per cent	14.9	15.2
Heat content of coal (as fired), Btu per lb	13695	13095
Steam pressure, psi	720	722
Air pressure at burners, in. water	1.92	2.8
Draft in furnace, in. water	0.139	0.22
Draft at boiler outlet, in. water	1.9	2.98
Draft at economizer outlet, in. water	4.31	.....
Draft at air-heater outlet, in. water	6.81	10.65
Steam temperature, deg F	726	690
Temperature of air leaving air heater, deg F	574	554
Temperature of gases leaving boiler, deg F	1038	658
Temperature of gases leaving economizer, deg F	697	.....
Temperature of gases leaving air heater, deg F	379	376
Temperature of feedwater entering economizer, deg F	350	.....
Combustion space per lb of coal per hr, cu ft	0.78	0.92
Heat absorbed by water in economizer, Btu per lb	133	.....
Heat absorbed by water and steam in boiler, Btu per lb	742.3	864
Refuse, per cent of fuel (as fired), per cent	11.82	15
Rate of heat absorption per lb of fuel, KB	11.54	10.95
Rate of heat absorption per sq ft of steam-generating-unit surface per hour, KB	13.75	11.47
Efficiency of steam-generating unit, per cent	84.3	84.0
Average draft loss, in. water	6.67	10.43
Average air-pressure loss, in. water	5.93	9.65
Steam purity, ppm	0.6	0.7

ing differences in the two types of boiler units. Table 4 gives comparative test data taken from each of the boilers. These data are presented for general information and do not indicate performance under stable conditions. The forced-circulation and the natural-circulation units have been and are consistently operated at 85 per cent efficiency. Steam requirements for normal operation of the pumps of the forced-circulation unit amount to 10,000 lb per hr, or 3 per cent of the boiler capacity. This power requirement imposes an additional loss of over-all steam output, resulting in a lower inherent over-all efficiency of the forced-circulation type of boiler unit.

With the high make-up previously mentioned, and with the boilers being of necessity maintained on the line for considerable periods, it has been observed that the natural-circulation units form considerable sludge in the vicinity of the downcomer tubes at the top drum. In the forced-circulation unit, this sludge with additional scale particles collects on the orifice strainers tending to plug the control orifices. On two occasions this plugging of orifice strainers has resulted in tube starvation and failure. It has been particularly observed that at no time have scale particles been encountered on the natural-circulation units receiving the same feedwater and treatment. The exact location of the origin of these scale particles has not yet been determined, but they appear to form in the region of the distributing headers ahead of the orifice strainers. Chemical composition of these scale particles is identical with that of the soft sludge which is formed in the natural-circulation boilers.

Removal of the sludge is accomplished in the natural-circulation boiler by the conventional tube turbining of the downcomers with final removal at the mud drum. Build-up of this sludge indicates that a scheduled outage once each 6 months is sufficient for its removal with little danger of serious difficulty for longer periods. In the forced-circulation unit, sludge and scale removal is accomplished by removing and cleaning all the orifice strainers. Past operating data indicate that sludge and scale particles in the forced-circulation unit require a boiler outage each 60 days for inspection, thus reducing its availability, as compared to the natural-circulation boilers.

During internal inspections of the circulating pumps for the forced-circulation unit, it has been revealed that at times considerable build-up of scale takes place on the pump impellers with indications of scale breaking off and entering the orifice headers. As previously described, the circulating pumps have an arrangement of bleed-in and bleed-out connections which permit a small amount of boiler feedwater to enter the pump. Water consultants agree that under pH conditions existent in the feedwater, a reaction between the soluble phosphate present in the boiler water and the hardness present in the incoming feedwater results in a precipitation of calcium phosphate which forms a scale rather than the normal soft sludge precipitated in conditioned boiler water. It has been deemed advisable to maintain this "in" leakage to the pump at a minimum, and differential-pressure regulating valves have been installed to maintain a constant differential pressure automatically in the bleed-in line to the pump over the circulating pump discharge pressure. Prior to this installation, manual adjustments were made with probable erratic results.

In an effort to improve the availability of the forced-circulation unit, and to minimize the work required for sludge and scale-particle removal, two external strainer drums have been installed in each of the pump discharge lines as near as possible to the orifice headers. These strainers have openings of exactly the same size as those in the header orifice strainers, and each strainer has a free area more than twice that of the total for all the orifice strainers. These strainers were installed at a time when it was believed the scale particles were being formed between the steam drum and the distribution headers, including the pump impellers. It was hoped these strainers would thus effectively remove all of the scale particles and cause scheduled boiler outages only to clean the external strainers. Results observed on two occasions, since installation, reveal conditions in general to be no better than prior to their installation. It is apparent that scale is formed on the distribution headers ahead of the orifice strainers, a region of non-heat-absorbing surface, a condition which is contrary to that found in the conventional boilers. No definite conclusion concerning scale formation at this location has been advanced, although suspicion has been pointed to velocities, to mechanical agitation due to the pumps, and to minimum chemical-reaction time in the drum.

The apparent failure to remove the scale particles by mechanical means in the forced-circulation unit and the desirability of preventing sludge accumulation in both types of boilers has led all concerned to an attitude that the problem is one of chemical treatment and elimination of the formation of the sludge and scale rather than removal of scale particles after they have formed. A modified chemical treatment is now being used to overcome this condition and so far the results appear favorable.

The forced-circulation type of boiler has proved to be much more stable than the natural-circulation boilers from the standpoint of water level with varying operating conditions. The fact that the forced-circulation boiler is equipped with an economizer which furnishes the feedwater to the drum at 480 F, as compared with 340 F feedwater entering the natural-circulation drum, is given as one factor for such stability. Another factor is that the rate of circulation is relatively constant for forced circulation at either maximum or minimum rating. This pumping rate is 5100 gpm, or 1,900,000 lb per hr which gives a ratio of circulated water to steam of $5^1/_2$ to 1 at rated load.

In a natural-circulation boiler the rate of water circulation increases with rating, probably resulting in considerable turbulence in the steam drum at higher load conditions. With a slight lowering in drum pressure due to suddenly increased steam demand, the volume of steam bubbles in the generating tubes will increase sufficiently to cause a rise in water level in the drum, since the generating tubes enter the drum below water level. Such a rise, often called "swell," tends to upset feedwater regulation. This condition can only occur in the natural-circulation type of boiler unit. Consequently, the forced-circulation boiler-water level will be upset to a lesser degree by rapid and large load changes regardless of feedwater control than with the natural-circulation boiler. However, the natural-circulation units have, on a number of occasions, experienced load changes from 200,000 to 400,000 lb per hr without seriously upsetting water level and with no sign of carry-over. The ability of the operators and of the feedwater control to handle these conditions indicates that natural-circulation units can take rapid load swings without serious water-level upsets.

The expectation that the forced-circulation boiler with its closely spaced $1^1/_4$-in. tubes would present a nearly solid water-cooled metal surface to the furnace and that slag would not so readily adhere to this surface, has not been realized. Wall soot blowers were installed slightly above burner level to aid in removing this slag deposit. It appears that the greater number of spaces between the tubes for a given width of wall in the forced-circulation unit offers a larger number of points for slag to adhere, thus making it possible for the slag to bridge over more readily in this type of boiler than in the natural-circulation unit with larger wall tubes and greater spacing. With coals of the quality now burned, with an ash-fusion temperature between 2300 F and 2400 F, wall blowers or lancing will not be required for the natural-circulation units.

Tube ruptures at different times on both types of units afforded

the opportunity for boiler operators to compare urgency of removing the boiler from service. With chemical operating units unable to reduce steam demand safely at a moment's notice, the forced-circulation boiler, in one case, was kept on the line at full rating in excess of 3 hr, despite a complete wall-tube rupture. This type of boiler, with its relatively smaller-diameter tubes and small control orifice in the water inlet, in addition to the fact that the generating tubes terminate above the water level in the drum, can suffer a complete tube rupture without the necessity of immediate removal from the line. This is an extremely vital factor in chemical processes where shutdowns must be made in an orderly and safe manner. In the two instances when rupture occurred in a wall tube or generating tube on the natural-circulation units, it was necessary to take the boiler off the line immediately, resulting in pressure upsets to chemical process. A natural-circulation boiler, upon loss of any tube, immediately becomes inoperable.

Conclusion

In summarizing and outlining the characteristics found in these two types of boiler units at the Koppers plant, it is not the intent to suggest advantages or disadvantages of any particular type of unit. That the forced- and natural-circulation principles are radically different would of necessity present different operating characteristics.

The forced-circulation unit has demonstrated particular operating assets as follows:

1 The ability to suffer loss of a tube and continue to operate until other apparatus is brought on the line to take its place, or until load can be sufficiently reduced so that boiler capacity is not required.

2 Water-level stability under conditions of rapid and large load changes.

The natural-circulation units have particular operating assets as follows:

1 Greater availability in comparison with forced-circulation type.

2 Less sensitivity to changes in feedwater conditions, rendering it more suitable for high make-up with high solids in the feedwater.

3 Lower susceptibility to scale formation under equivalent feedwater conditions.

The operating record of both of these types of steam generators reveals their ability to supply process-steam requirements under many adverse conditions. Chemical production of butadiene and styrene has been maintained at high rates throughout the operating period to date, and over-all operation should compare favorably with that of any other steam plant of its size and operating conditions.

Discussion

J. M. Harvey.[4] The character of the water in the Ohio River and its tributaries is such that many problems must be met which do not exist where water of more stable quality, such as water from the Great Lakes, is utilized for boiler-feed purposes. Acid mine drainage and extensive use of these streams for disposal of industrial waste and sewage from the heavily populated surroundings make for extreme variation in the character of the river water.

Characteristic is the trend from a bicarbonate condition, with low dissolved solids and increased suspended material during the heavy run-off in the spring and early summer to a highly acid condition, with high dissolved solids and low suspended material during the low flow in late Summer and Fall. Localized pollution and the presence of river pools may further influence the character of the river water at a particular plant intake.

Generally, the periodic variations in dissolved solids will follow a somewhat fixed pattern with minimum and maximum concentrations reaching about the same value each year, and with the average concentration varying not more than a few ppm over a period of several years. However, combination of conditions may produce considerable deviation from the normal pattern as shown by Fig. 5 in the paper, charting variations during a period when industrial activity was at an unprecedented high.

The wide flexibility of the water-conditioning facilities installed at Kobuta made it possible to cope with the variations imposed and maintain boiler-water conditions within closely defined limits. Even so, characteristics of the river water exert their influence and have been productive of adherent sludge deposits in the boilers. Specific measures were adopted several months ago which we believe, and which are proved in part, will solve this problem.

In January, 1945, silicate treatment was introduced to one of the natural-circulation boilers. At this time the routine water-testing program was expanded to include determination of the silica concentration in the boiler water and saturated steam. These tests soon established the fact that there was no significant difference between the silica present in the steam generated by the boiler receiving silica treatment and the boilers not receiving this treatment.

Since all the natural-circulation boilers had been mechanically cleaned just prior to the introduction of silicate treatment, inspection of these boilers in June, 1945, after a 6-months' run, afforded the opportunity to compare the appearance of the internal surfaces of the boilers. The boiler subjected to silicate treatment was decidedly cleaner than the other natural-circulation boilers.

On the basis of these observed conditions, silicate treatment was extended to all the natural-circulation boilers as well as the forced-circulation boiler. Inspection of the forced-circulation boiler in October, 1945, after a run of approximately 60 days on silicate treatment, revealed accumulation of scale particles in the orifice headers to about the same extent as noted during previous inspections. However, finely divided sludge, which had been found intermingled with the scale particles on previous occasions, was almost entirely absent. The scale particles are identical in chemical composition to the finely divided sludge formerly found along with the scale particles. This is indicative possibly that the scale particles originate at some point in the circulating system where the finely divided sludge adhered and attained more coherent and compact form under conditions existing at that point. Thus we believe there is some possibility that the scale particles will be eliminated with continued operation on the silicate treatment.

In connection with the silicate treatment, it is also worthy of mention that inspection of the 35,000-kw back-pressure turbogenerator in October, 1945, showed the complete absence of any deposits. This inspection was made after approximately 2 years of operation, and silicate treatment was in effect during the last 9 months of operation.

H. J. Klotz.[5] The authors of this paper are to be commended for the unprejudiced presentation of the comparison of the operating characteristics of forced- and natural-circulation boilers of the same capacity installed side by side in an industrial plant and performing under identical conditions as regards load and

[4] Engineering Service, Hall Laboratories, Inc. Pittsburgh, Pa.

[5] Chief Power Engineer, Stone & Webster Engineering Corporation, Boston, Mass. Mem. A.S.M.E.

feedwater. The writer's connection, as consultant to the Office of Rubber Reserve, with the operation of the Koppers plant, has afforded an opportunity to observe that the plant-operating organization has been equally unprejudiced in its handling of the boilers. There has been not the slightest tendency to favor either type of boiler, but a conscientious effort has always been evident to meet any special requirements imposed by the two types of boilers. The fairness of their comparison has thus been assured.

It is, of course, too much to expect that a comparison in one plant only could form the basis to permit final and definite conclusions as to whether one or the other type of boiler should be installed. The principal offsetting features would appear to be the ability of the forced-circulation unit to continue in operation following the loss of a tube, an important item in many processes, compared with the greater availability of the natural-circulation boilers. Corrective measures adopted at the Koppers plant will probably obviate the importance of this comparison as it is believed the causes of the tube ruptures in the natural-circulation boilers have been greatly minimized, and the lower availability of the forced-circulation boiler should eventually be overcome by further progress in chemical treatment of the feedwater plus possible additional mechanical features to prevent sludge accumulation on the orifice strainers.

The extremely variable nature of the make-up water at this plant makes the latter an important consideration and one which, until it is overcome, points to the desirability of the natural-circulation boiler for comparable water conditions.

It is important to note that the pumps required for circulating water with the forced-circulation boiler have imposed no operating problem.

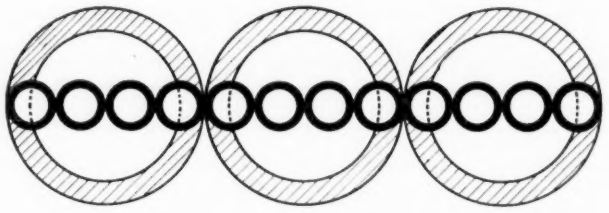
Experience at the Koppers plant indicates that the practicability of the forced-circulation boilers for industrial plants has been sufficiently proved to warrant additional installations, and that any plant considering the choice between the two types would be safe in basing its decision on the relative investments and space requirements after assuring itself that any possible feedwater limitations would be satisfactorily met.

W. S. Patterson.[6] The authors have refrained from comparing differences in design in the two boiler types unless these differences have, up to the present time, resulted in operating assets in favor of one type or the other. However, since forced circulation, applied to large steam generators, is new in this country, it will be of interest to point out some of the reasons for the difference which will be noted from a study of the paper, and some of the potential assets.

Small-diameter tubes are used in forced-circulation boilers because a high flow resistance and velocity in the tubes are desirable, and because a high fluid velocity in the tubes can be realized with a minimum quantity of circulating water handled by the pumps. Small-diameter tubes can have very thin walls, resulting in low hot face skin temperatures and low temperature stress in the tube metal even with very high rates of heat absorption. There is also a saving in weight of tube metal and weight of water in the tubes; but the advantages of small tube diameter are most apparent in high-pressure boilers as will be seen from Fig. 7 of this discussion.

Although bifurcated tubes have been used in natural-circulation-boiler furnaces, this is the first application of trifurcated furnace tubes. Such an arrangement decreases the number of header connections, orifices, and access openings. Before this boiler was placed in operation Pitot tubes were installed in each tube of several of the trifurcated furnace elements to check relative water distribution. The results are presented in Table 5 of this discussion.

[6] Assistant Manager, Forced Circulation Boilers, Combustion Engineering Co., Inc., New York, N. Y. Mem. A.S.M.E.



	4 in.	1 in.
Tube Diameter		
Wall thickness	.48 in.	.15 in.
Velocity ratio	1	4.7
Tube weight ratio	1	.335
Water weight ratio	1	.213
Temp. gradient ratio	**1**	**.326**

Fig. 7 Furnace-Wall-Tube Comparison for Tangent Spacing; Small-Diameter Versus Large Diameter

(Velocity ratio is based upon same circulation ratio for both arrangements.)

TABLE 5 DISTRIBUTION OF FLOW IN TRIFURCATED FURNACE CIRCUITS

Date of tests	Dec. 12 to 21, 1943
No. of tests on each circuit	6
Boiler output	250,000 to 300,000 lb per hr
Boiler pressure	730 to 740 psig

	Front furnace wall								
Trifurcate no.	1			13			22		
Tube no.	1[a]	2	3	37	38	39	64	65	66
Flow through tube, per cent	33.6	34.8	31.6	35.0	34.8	30.2	31.8	37.8	30.4

	Rear furnace wall			Side furnace wall		
Trifurcate no.	6-1			1		
Tube no.	181	182	183[a]	1[a]	2	3
Flow through tube, per cent	27.4	35.8	36.8	26.8	37.8	35.4

[a] Denotes tube in corner of furnace.

The convection boiler, called the "secondary generator," also employs $1^1/_4$-in-OD tubes, but they are fitted with $1^3/_4$-in-high fins and disposed horizontally in a bank below the economizer. These tubes are bifurcated at the end adjacent to the control orifice so that each orifice serves two circuits which are intermeshed, with forged return bends and long-radius bends alternating through the length of each circuit. The tubes are arranged in staggered relationship with $2^1/_2$-in. horizontal and $3^1/_2$-in. vertical spacing, and because of their small diameter and transverse flow of the gases, a very high heat-transfer rate is obtained without the use of baffles and without resorting to a high gas velocity. The surface installed per cubic foot of space in the secondary generator is about twice that of a conventional boiler and each element is independently removable through a large door at one end.

The "water-cooled beams" mentioned in the paper, support the secondary generator and both economizer sections. They are shown at three elevations in Fig. 2 of the paper, and consist of two parallel sets of three headers each, with series flow through each set. The tubes supplying the outer end of the uppermost headers are shown coming off the main distributing header. The water passes through the uppermost headers, thence by external connections to the inner end of the lowest headers, through the latter to the outer end, and thence through external connections to the single secondary-generator inlet header containing the control orifices. The two intermeshed circuits of each secondary-generator element terminate in separate discharge headers which support the lower economizer section. From these headers the steam-water mixture is discharged to the boiler drum.

Since the steam drum is not required to support a bank of steam-generating tubes, it is located entirely outside the setting as shown in Fig. 2 of the paper, which is sometimes possible but

rarely convenient in designing a natural-circulation boiler. In the case of thick drum shells exposed to hot gases, drum protection must be provided, which introduces a maintenance item for the operator; also, where a boiler baffle abuts the drum shell, a positive and tight seal must be maintained to prevent fly-ash erosion of the drum due to baffle leakage. These problems are absent when the drum is outside the setting and therefore represent potential operating assets. It will also be noted that all the drum-tube connections in Fig. 2 of the paper are in one quadrant of the shell, thus reducing to a minimum the amount of thick shell plate required.

The authors point out an operating disadvantage of a high-capacity boiler containing a very small quantity of water, when the rate of blowdown is high due to high make-up of water having high total solids. However, the low weight of water is also associated with low weight of tube metal and this combination results in a lower fuel requirement to place a forced-circulation boiler in service and less heat loss on cooling down. This would be a distinct asset in the case of a boiler subject to week-end shutdowns in many industrial plants. In combination with forced circulation, it also permits entry to the furnace for maintenance within 8 hr of the time the boiler is taken off the line, even in the case of a large high-pressure unit with a wet-bottom furnace. Also, with the increasing popularity of acid cleaning of boilers it is an operating asset to require only one quarter of the amount of acid, flushing water, and neutralizing solution, to say nothing of the time saved in filling, draining, etc.; and 2 min operation of the pumps at hourly or half-hourly intervals will completely mix the solvent, re-establishing a uniform concentration and uniform temperature, both of which are important.

Fig. 2 of the paper shows that each pump is equipped with a shutoff valve at suction and discharge. It was originally intended that only one pump would be in operation and the other held as a spare with suction and discharge valves closed. With the method of operation used at this plant the spare pump idles at 400 rpm and with all suction and discharge valves open. The check valve located at each pump discharge has a bypass which permits operating the spare pump in this manner but limits recirculation through the idle pump. The shutoff valves have never been used during operation because the availability of both pumps has been 100 per cent.

The authors give a figure of 10,000 lb per hr steam consumption for circulating-pump drives but the heat extracted in the turbine is only about 200 Btu per lb or 2,000,000 Btu per hr. The fuel equivalent of this is about 0.50 per cent of the fuel fired at maximum rated capacity and part of this energy is returned to the boiler water in passing through the pump.

The occurrence of scale chips in the orifice headers has not been uniform in all headers, and this was originally explained by the fact that the first supply tubes coming off the main distributing header go to the front or burner wall; the next group at each end go to the side-wall headers and the center group go to the rear-wall header. When the sludge and/or scale chips have been present in serious quantities, the front-wall header has generally contained the most and the rear-wall header the least. In fact, the strainers were not removed from the rear wall during one entire year of operation, and beginning in April, 1944, and ending July, 1944, there was one operating period of 30 days, followed by another of 60 days, during which no significant deposits occurred in any of the orifice headers.

The differential-pressure regulating valves on the bleed-in lines to the pumps were recommended by both the pump and the boiler manufacturer during the design stages but were not installed until the spring of 1945.

The authors mention "minimum chemical-reaction time in the drum," as a possible reason for scale in the orifice headers of the forced-circulation boiler. However, it has been noted that a ring of sludge forms even in the perforations of the submerged feed pipe, which is an indication of very quick reaction.

The furnace-wall soot blowers on the forced-circulation boiler were furnished by the boiler manufacturer in 1943 in lieu of removing superheater elements, because during early operation the steam temperature exceeded the guarantee and it was found that removing ash from a band of the furnace walls just above the burners would give 50 deg F steam-temperature control.

One reason for keeping the steam temperature down on the forced-circulation boiler has been because the natural-circulation boilers do not deliver steam at the predicted temperature (see authors' Table 4), and this results in different steam temperatures in the two turbine leads, which is objectionable. Predicted performance of the forced-circulation boiler was deliberately based upon moderately dirty furnace conditions. At maximum load the contract average gas temperature leaving the furnace was 2110 F. A test in January, 1945, at maximum load using an 18-point traverse with a high-velocity shielded platinum thermocouple at three elevations at the superheater entrance gave the following averages:

Upper 1870 F; middle 2015 F; lower 2025 F; during the test the CO_2 entering superheater was 16.3 per cent, the average steam temperature 760 F; the furnace-wall blowers had not yet been placed in service and the walls were moderately dirty. In reference to the authors' conclusion on availability, it might be added that the boiler manufacturer definitely recommended that the forced-circulation boiler be taken out of service every 60 days for inspection, because this boiler was a new development and frequent inspections would avoid the possibility of any major damage to the unit, as well as decrease the possibility of a forced outage. Nevertheless, the availability of the forced-circulation boiler averaged close to 95 per cent from December 1, 1943, to April 1, 1945, and it would be of interest to learn how much greater availability was realized on each of the natural-circulation boilers to justify the conclusion drawn.

S. T. Powell,[7] H. E. Bacon,[8] and L. G. von Lossberg.[9] Personal inspections of these boilers and studies of the feedwater treatment by the writers confirm the authors' observations. In particular, chemical and x-ray analyses of deposits removed from the forced-circulation boiler at the last inspection, representing the conditions during the feeding of sodium silicate to control magnesium in the sludge, show that the desired precipitate, magnesium silicate, is now being produced. However, our recent inspection indicates that troublesome deposits are still occurring in the orifice strainers.

Our experience with water conditioning for the forced-circulation type of unit has also shown that feedwater of high quality is required to prevent deposits in the control-orifice strainers. Also, the relatively small volume of water contained in this type of boiler limits the concentration of constituents that may be tolerated in the feedwater.

The favorable comparison with regard to the operating characteristics of the forced- and natural-circulation boilers for the production of process steam is noted with interest.

It is our opinion that the operators of the plant are to be complimented upon maintaining continuous operation of the steam-generating facilities and related equipment under the rigorous conditions imposed throughout the 2-year war-production period.

[7] Consulting Chemical Engineer, Baltimore, Md. Mem. A.S.M.E.
[8] Engineering Assistant to Sheppard T. Powell, Consulting Chemical Engineer, Baltimore, Md. Mem. A.S.M.E.
[9] Engineering Assistant to Sheppard T. Powell.

W. F. RYAN.[10] The authors are to be congratulated on the impartiality with which they have presented the facts in regard to these two types of steam-generating equipment. If they have any preference it cannot even be inferred from their paper, and the reader is left to draw his own conclusions. This form of presentation is as commendable as it is unusual in engineering literature.

Steam consumed by the circulating pumps means little unless translated into energy; the latter is obviously a charge against the efficiency of the forced-circulation unit. No discussion is offered of the greater space and building costs required for a natural-circulation design. At Kobuta, it appears that the building design was determined by the space required for the larger boiler and hence no appreciable savings accrued from the installation of a single forced-circulation unit. These savings might have been considerable, however, had the building been designed for four forced-circulation units.

It is unfortunate that Figs. 2 and 3 of the paper, showing cross sections of the two boilers, are not shown to the same scale. The tabulations, however, show that the natural-circulation boiler has 4500 cu ft greater furnace volume. For four boilers, this amounts to 18,000 cu ft which might have been saved had the building been designed for the forced-circulation type of boiler only. Weights are not given, but from the data on heating surface, tube sizes, and water volumes, it is clear that the weight of the natural-circulation boiler, filled with water for test, is more than twice the weight of the forced-circulation unit. As shown in the tables, the operating weight of water in the natural-circulation boiler is more than 4 times that in the other type. These factors materially affect the cost of building steel and foundations and should ultimately have an appreciable effect on the cost of equipment as well.

These are the reasons, of course, that manufacturers and operators are willing to spend time and money on such developments of the art. What we all want are better boilers at less cost than we now have. It is apparent from this paper that forced circulation is a constructive step in this direction.

AUTHORS' CLOSURE

The silicate treatment as mentioned in Mr. Harvey's discussion definitely showed promising results as to the elimination of sludge in the natural circulation boilers. Duplicate treatment in the forced-circulation boiler has not produced hoped for results and all inspections of this boiler unit since the treatment was initiated revealed scale at the orifice strainers in amounts equal or greater than on previous inspections. Sludge accumulations were, however, somewhat reduced. Operations at this boiler plant are now such that continued observation of this method of feedwater treatment is not possible as the forced circulation boiler has been out of service since early in November due to low steam demand to process. The elimination of the troublesome scale at the orifice strainers remains as an important factor in securing greater availability of the forced circulation unit, and the authors believe that feedwater consultants will overcome this difficulty by introduction of other suggested treatments, should the silicate not produce the desired results. The divergence in results of this duplicate treatment of the feedwater for both types of boilers further demonstrates that the natural circulation boilers are less susceptible to scale formation under equivalent feedwater conditions than the forced circulation unit.

Mr. Patterson's discussion of certain design features and potential operating assets of the forced circulation boiler enhances the value of the paper for design engineers and operators of boiler plants. The authors, as operators, are naturally inclined to overlook design features unless they materially affect the boiler operation or are modified to improve the operation. The references to savings in weight, "secondary generator," "water-cooled beams," and drum location will no doubt be of great interest to all readers, and the authors concur in his discussion on certain minor advantages gained by low weight of water and lower requirements for acid cleaning. The further explanations of Mr. Patterson in regard to pump operation, soot blowers, and steam consumption of the pumps contributes much to enlighten the reader on points which the authors unintentionally might have slighted.

The conclusion that the natural circulation boiler has greater availability has been demonstrated by the operating records of the two types of units. While operating at near peak demands, the outage schedule required that each natural circulation boiler be taken off the line every six months with the outage time limited to three days. The outage schedule of the forced circulation unit required an outage each two months with outage time limited also to three days. The amount of maintenance work required on both types was relatively equal. Thus it can be seen that on a percentage of availability basis the natural circulation boilers would reach 98.36 per cent or 6 days outage per operating year while the forced circulation boiler would reach 95.08 per cent or 18 days outage per operating year. While the percentage availability difference does not seem too great, it is significant that the scheduled outage time required by the forced circulation unit amounts to three times that of the natural circulation boilers.

The authors appreciate the discussions of all these engineers and the favorable comments contained in these discussions. That the Kobuta Plant has had such an outstanding operating and performance record is partially due to the suggestions and recommendations of these outstanding men of the steam-generation field.

It is well to point out that since preparation of this paper all the 3 in. tubes between the pump discharge header and the orifice headers were mechanically turbined. The amount of scale removed during this operation has led us to believe that these tubes are the source of scale particles, and their scheduled turbining at times of boiler outages would do much to increase the operating time between outages of the forced circulation boiler.

It will be noted that the operating assets of the forced circulation unit are inherent for this type of boiler unit, while those of the natural circulation boiler are not limited by its type. It would thus seem that further developments to overcome any deficiency of operating assets for forced circulation will enable us to attain better boilers at less cost as asked by Mr. Ryan.

[10] Assistant Chief Mechanical Engineer, Stone & Webster Engineering Corporation, Boston, Mass. Fellow A.S.M.E.

Operating History and Performance of 2000-Psi Forced-Circulation Boiler at Somerset Station of Montaup Electric Company

By G. U. PARKS,[1] W. S. PATTERSON,[2] and W. F. RYAN[3]

In this paper the operating experiences with the high-pressure forced-circulation boiler at Somerset station of the Montaup Electric Company are given in considerable detail. Special test and research activities on the installation are reported in this and companion papers. The conclusion is reached that the selection of a bare-tube, slagging-bottom, radiant, forced-circulation boiler for this high-pressure application has been verified by its operating record.

THE forced-circulation boiler at Somerset Station was installed during 1940–1942, as part of the topping installation. Initial pressure and temperature were dictated by the necessity of obtaining 25,000 kw by topping a 375-psi 750 F plant. The size and shape of the boiler were determined by the floor space and headroom available in a vacant space in the existing boiler room which had been allocated in 1925 to a future boiler of 120,000 lb per hr capacity.

The subject boiler has a guaranteed maximum output of 650,000 lb per hr at 960 F at the superheater outlet. Drum safety valves are set to blow at 2000 psi, but average drum pressure over an extended period of time has not exceeded 1925 psi. Pressure at the superheater outlet averages approximately 1850 psi, which gives name-plate pressure at the topping-turbine throttle. The reheater takes exhaust steam from the topping turbine at 400 psi 603 F, and exhausts to the station's low-pressure header at 380 psi 765 F. The boiler and related equipment have been described in detail in references (1)[4] and (2).

Normally the station burns West Virginia semibituminous coal or bunker "C" fuel oil, and the boiler was therefore designed to use either fuel or any combination of the two. Since the station's pulverized-coal system is of the storage-bin type, and it is necessary to supply this new slagging-bottom furnace and the older dry-bottom furnaces from the same supply, the furnace and combustion equipment were so designed that coals with ash-softening temperatures between 2200 F and 2600 F could be used satisfactorily.

It is the purpose of this paper to discuss the operation problems encountered and their solution and present the results of research and tests on circulation, tube temperatures, and performance.

Although all equipment manufacturers have been very co-operative, wartime conditions have made it impossible to effect some changes when they were desired. It is hoped that the complete topping installation can be discussed at some later date when changes and modifications in equipment in no way related to the boiler have been completed.

After 3 months' preliminary operation, delivering steam through the by-pass line, the boiler was placed in commercial operation with the turbine on October 26, 1942, and has been taken out of service 54 times from that date to the present time, November 1, 1945.

The longest outages, which are identified by numbers in Fig. 1, were chargeable to equipment as listed below the chart. Table 1 supplements this list and shows that there were in the first three years of commercial operation, 8 forced outages and 46 scheduled outages, about half of which were directly chargeable to research and tests. Most of the outages charged to research merely consisted of taking the unit off the line for a few hours for checking dissolved and suspended solids in the boiler water. The scheduled outages charged to other equipment were sometimes also used for scheduled boiler maintenance if time permitted. On the other hand, the forced outage in 1944, charged to slag in the superheater, was caused by malfunctioning of the air-flow recorder and operation with low excess air.

Fig. 1 also shows average output calculated from steam-flow-integrator readings for the duration of each operating period, without correction for pressure or steam temperature. The meter is calibrated for 1825 psi and 960 F.

Although the boiler has been operated in excess of 650,000 lb per hr with both coal and oil firing, output during the past two years was normally limited to approximately 585,000 lb per hr, and the average monthly load is under 500,000 lb per hr. This has been for the following reasons, rather than desire or necessity due to boiler limitations:

(*a*) The necessity for keeping spinning reserve on the system at other points.

(*b*) The large amounts of hydro-generated power which tie lines make available during evening and night hours.

(*c*) The rebuilding of the 10-in. pressure-reducing and desuperheating station which leaves only the 4-in. station with 200,000 lb per hr capacity in case of turbine failure.

(*d*) Vibration and shaft whip in the topping turbine under certain load conditions.

(*e*) Inability of the low-pressure plant to absorb more than 500,000 lb per hr when either low-pressure unit is not on the line.

Since October, 1942, it has been impossible for the station to receive coal from the normal suppliers in the Pocahontas No. 3 seam or the Sewall seam. Based on monthly composite samples, the heat content of coal as received has varied from 13,000 Btu per lb to 14,000 Btu per lb, moisture from 4 to 8 per cent, ash from 6 to 13 per cent, and grindability from 70 to 100 per cent on the Hardgrove scale. Ash-softening temperature has varied between 2100 and 2800 F. A substantial part of the coal burned has been from either West Virginia or Pennsylvania strip operations.

[1] General Manager, Montaup Electric Company, Fall River, Mass. Mem. A.S.M.E.

[2] Assistant Manager, Forced-Circulation Boilers, Combustion Engineering Company, Inc., New York, N. Y. Mem. A.S.M.E.

[3] Engineering Manager, Stone & Webster Engineering Corporation, Boston, Mass. Fellow A.S.M.E.

[4] Numbers in parentheses refer to the Bibliography at the end of the paper.

Contributed by the Power, Industrial Instruments and Regulators Divisions, and the Joint Research Committee on Boiler Feedwater Studies, and presented at the Annual Meeting, New York, N. Y., November 26–29, 1945, of The American Society of Mechanical Engineers.

Note: Statements and opinions advanced in papers are to be understood as individual expressions of authors and not of the Society.

TABLE 1 OUTAGE TABULATION

Reason for Outage	Annual Period Nov. 1 to Nov. 1			3-Yr Period
A - Forced Outages	1942-43	1943-44	1944-45	1942-45
Furnace Tube Failure	2	1	1	4
Reheater Tube Failure	0	0	2	2
Slag in Superheater	1	1	0	2
Total Forced Outages	3	2	3	8
B-Scheduled Outages				
Research and Tests	7	15	1	23
Piping External to Boiler	2	2	2	6
Low Pressure Station Repairs	0	2	1	3
Pressure Reducing Station	1	0	1	2
Miscellaneous Boiler Items	1	1	0	2
Safety Valves	0	0	2	2
High Pressure Turbine	0	1	1	2
Acid Cleaning Boiler	1	0	0	1
Soot Blowers	1	0	0	1
Reheater Repairs	0	0	1	1
Boiler Vent Valve	0	0	1	1
Electrical Trouble	1	0	0	1
Drum Internal Changes	0	1	0	1
Total Scheduled Outages	14	22	10	46
Total Outages	17	24	13	54

Due to overworked mills, the amount of pulverized coal through a 200-mesh screen has rarely been as high as 80 per cent, and averages 70 per cent, with 3 to 4 per cent retained on 60 mesh.

The normal operating crew has been the boiler operator, stationed at the control panel, and his assistant who keeps the log sheet and also operates blowdown, soot blowers, and attends to changing and cleaning oil burners. They are assisted part of the time by an oiler on the feeder and fan floor, who also works on the fans and feeders of five low-pressure boilers, and by a pump tender who operates the high-pressure heaters and drip pumps, as well as the circulating pumps. When coal from normal suppliers is available, the latter also acts as ashman. Feedwater chemistry is directly controlled by the station's own laboratory on a single-shift basis. The high-pressure-turbine operator acts as chemist on the other two shifts.

The arrangement of the boiler unit as originally installed with changes and modifications from 1942 to 1945, inclusive, indicated in notes, is shown in Fig. 2. Following is a summarized description of operating experiences with the boiler unit including a discussion of changes made and the reasons for them.

Operating History and Changes

Evaporating Surface. A furnace-tube failure occurred within the first 2 months of preliminary operation. It was in the front wall a short distance below the roof and in the second tube from the right side wall. A short section of tube was welded in for repair. Microscopic examination of the failed section indicated overheating but the reason for overheating was not immediately determined.

A second tube failure occurred in January, 1943, in the furnace roof in the same tube that had failed previously. This failure was occasioned by pitting on the inside surface of the tube, one of the pits having extended entirely through the tube. A large amount of solid deposit found on the inside surface of the tube was considered to be a contributing factor to the corrosion. Repair was made by welding-in a replacement section, and an attempt was made to locate any source of free oxygen which might have contributed to this failure. Consultants were also engaged to study the conditions which caused the deposition of foreign matter on the inside tube surface.

The third tube failure occurred in February, 1943, while this investigation was in progress. This failure was in the left side wall, third tube from the rear wall. Microscopic examination of the failed portion indicated overheating and the cause was thought to be plugging of one of the orifice strainers.

Each time the boiler was drained substantial amounts of foreign matter were found in the orifice headers, particularly near

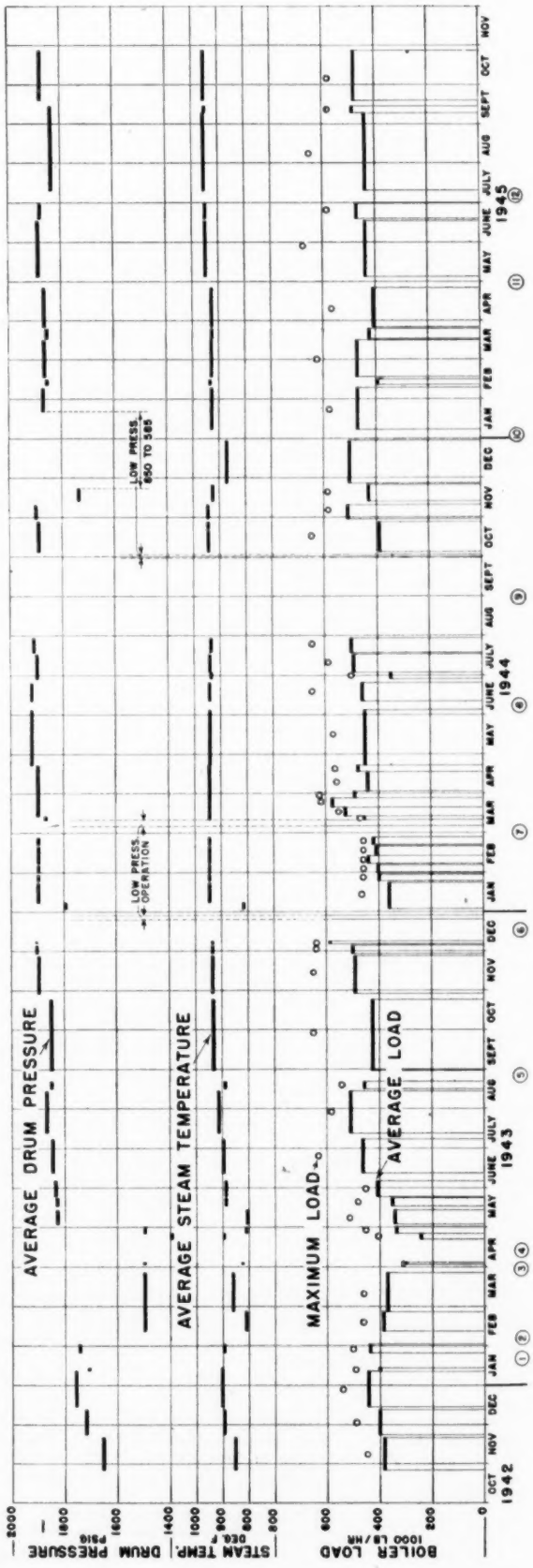


FIG. 1 LOAD, TEMPERATURE, PRESSURE, AND OUTAGE CHART

The numbered outages were charged as follows:

1 Furnace tube failure
2 Furnace tube failure
3 Research
4 Acid-cleaning boiler
5 Miscellaneous boiler changes
6 Furnace tube failure and acid-cleaning
7 Miscellaneous boiler changes
8 Drum internal changes
9 High-pressure-turbine overhaul
10 Pressure-reducing station
11 Reheater repairs
12 High-pressure turbine

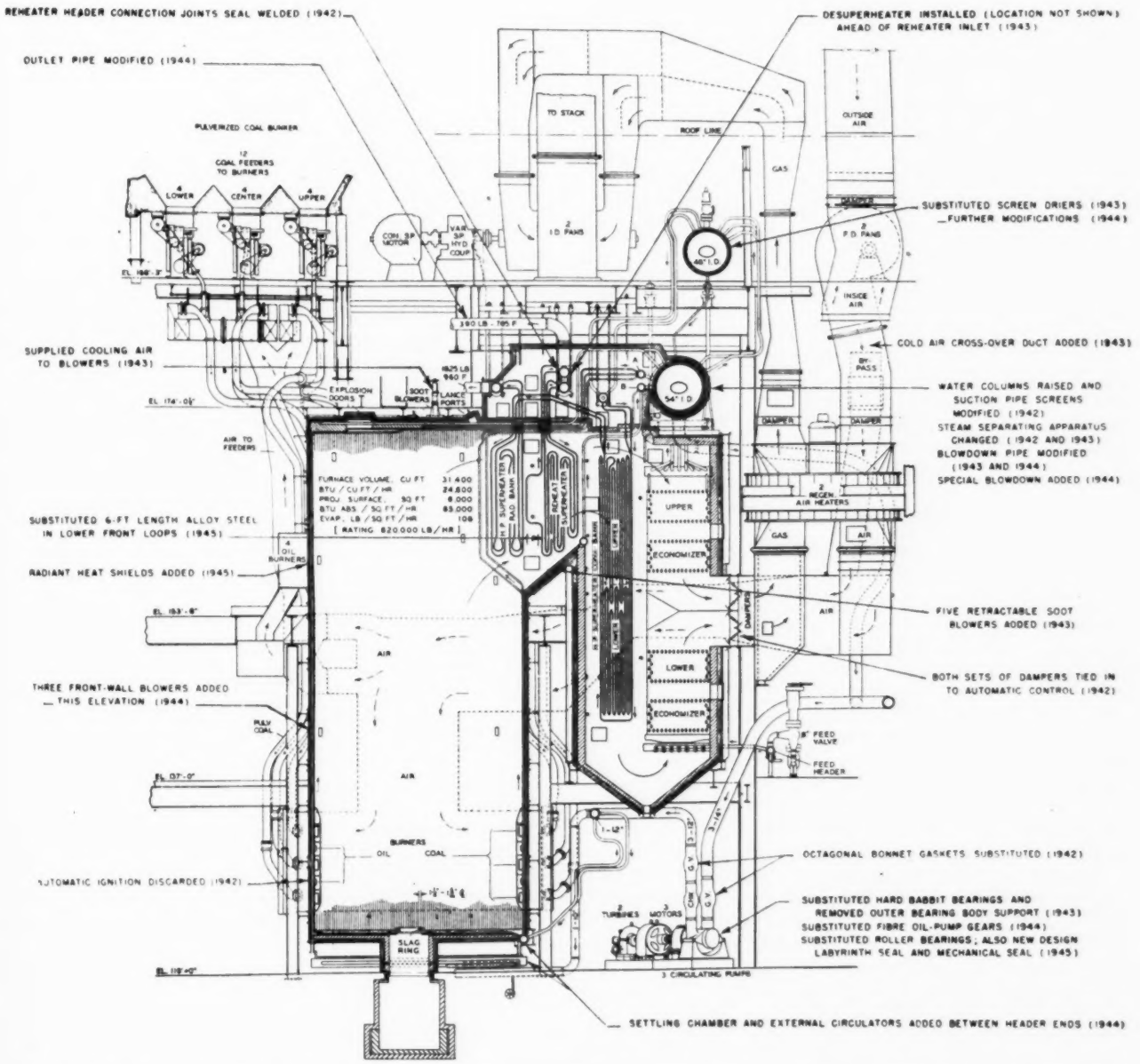


FIG. 2 ARRANGEMENT OF BOILER UNIT AS ORIGINALLY INSTALLED WITH CHANGES FROM 1942 TO 1945, INCLUSIVE, INDICATED BY MARGINAL NOTATIONS

the ends. Prior to the second tube failure, a sample of header washings was found to contain 66 per cent iron shot, 17 per cent mill scale, and miscellaneous oddments such as steel shavings, turnings, chips, and weld splatter. A sample collected at the time of the second failure contained 30 per cent weld splatter, 20 per cent mill scale, and 13 per cent iron shot, plus oddments.

The 54-in. boiler drum had been shotblasted in the shop after the junction headers had been attached and, although the headers had been blown out with compressed air, it was impossible to do an adequate job, since the header ends were closed at the time. The boiler had been carefully washed out and boiled out, with the orifices and strainers removed, prior to operation. Headers were washed at every available opportunity but the recurrence of foreign particles and substantial amounts of mill scale persisted for some time in the lower headers. There was also evidence of chemical hide-out whenever the boiler was taken off the line.

In order to clean tube surfaces thoroughly and remove mill scale, the boiler was washed with inhibited hydrochloric acid in April, 1943. All orifices were removed and the circulating pumps were not operated during the washing and it was therefore impossible to maintain uniform temperatures. In spite of this, tests showed that substantial amounts of mill scale and foreign material had been removed. Prior to this time feedwater was normally treated with standard sodium chemicals (phosphate, hydroxide, and sulphite). After the acid cleaning the potassium treatment developed by Dr. R. E. Hall was introduced (3, 4).

In December, 1943, after 7 months' operation with potassium treatment, including silica feed, the fourth tube failure occurred. This was the third failure in the same tube (second tube from the left side wall), and was in the section of the tube which passed across the roof of the furnace. The inside surface of several other tubes examined at the same time was coated with thick

sludge and scale, but the actual failure was considered to be caused by a plugged orifice strainer. The evidence of such plugging was missing, due, no doubt, to the disturbance created in the header when the tube failed; but repeated failures only in tubes served by orifices close to the dead end of the headers indicated the most probable cause to be sludge accumulations at the header ends.

Study of orifice-header pressures showed that there was sufficient pressure difference between the rear and the side headers so that if a small circulator were installed between each end of the rear header and the rear end of each side-wall header, there would be sufficient flow between the interconnected headers to preclude any sludge accumulation near the orifice strainers which serve the tubes in which failures had occurred. Circulators of $1^1/_4$ in. were installed between the rear header and the side headers, each provided with a small baffled settling chamber with sampling connections and blowdown valves and upper closure plugs to permit measuring the depth of sludge in the chambers. After establishing the fact that they collected a considerable quantity of sludge, they were connected into the existing drain lines, and are blown down once a week as part of the operating routine. Since the headers have been interconnected, very little sludge accumulation within them has been evident and very few of the strainer openings are found closed. In fact the strainers have not been removed in nearly 2 years except a few for inspection purposes.

At the time of the fourth failure representative tubes were sampled. There were substantial sludge deposits on all of them and acmite scale on most. Therefore, before the boiler was returned to service it was again acid-cleaned, using inhibited hydrochloric acid, supplemented by a fluoride. In order to insure a thorough acid cleaning at recommended temperatures, one circulating pump was operated 1 min during each half hour of the cleaning period, and thermocouples installed for the purpose showed that recommended temperatures were being maintained. Immediately after the cleaning and washing period the circulating pump was dismantled and the impeller removed for examination. There was no evidence of any attack by the acid.

Since this fourth failure the potassium treatment of feedwater without silica has been used. Tube samples taken in February, 1944, August, 1944, and September, 1945, from several parts of the walls showed very little sludge accumulation, and what did exist was not adherent but easily brushed away. There was evidence of very little, if any, corrosion or pitting of wall surfaces.

Periodically throughout the 3-year operating period of this boiler the external surfaces of representative furnace tubes have been checked for external corrosion. Although an adherent "enamel" coating of fused slag has been found, similar to that which has been credited with causing corrosion in other furnaces, actual corrosion has been negligible or nonexistent up to October 26, 1945.

On October 26, 1945, about 22 months after the last internal cleaning of the boiler, three small leaks occurred in the rear furnace wall, one located less than 1 ft above the floor and two about 20 ft above the floor in a different tube. The tubes which had failed were found to be heavily coated with sludge and, on the fire side, iron-oxide scale had formed between the sludge and the tube wall, indicating that the sludge had caused overheating of the tubes. An adjacent tube near the floor in the rear wall was in similar condition on the inside but a tube almost directly opposite, near the floor of the front wall, although heavily coated with sludge, had most of the deposit on the casing side where it could not cause overheating. This latter tube was perfectly clean at an elevation 17 ft above the floor, and a tube in the right side wall 15 ft above the floor was also nearly as clean as the same tube had been a month earlier.

There is evidence to indicate that a recent disturbance has caused this trouble because on this last outage there was appreciable external tube corrosion on some of the rear-wall tubes in the region of the lowest leak. Due to failure of the water seal below the slag hole and malfunctioning of the flue-gas oxygen recorder a deficiency of air near the walls and consequent abnormally high gas temperatures probably occurred.

Before the boiler was again placed in service it was acid-cleaned, using one circulating pump a few minutes of each hour to maintain uniform solvent temperature throughout the unit. Two tubes were sampled after the cleaning to make sure of a thorough job.

Superheater: High Pressure. There have been no failures, changes, or maintenance in either the convection bank or radiant bank.

It had been originally expected to obtain automatic superheat control by having the controller operate only the by-pass dampers located at the outlet of the upper economizer. However, it was found that manual operation of the main-passage dampers at the outlet of the lower economizer was necessary to obtain quick response. The controls were therefore modified so that both sets of dampers are automatically operated, that is, as the by-pass dampers open the other dampers close a proportionate amount.

Superheater: Reheat. The steam reheater which operates at 400 psi was provided with bolted ball-and-socket joints where the elements are attached to the headers. On account of numerous leaks during the first 2 months and the difficulty of access to the joints for refacing, it was decided to seal-weld all these joints.

Operation at high rates of output indicated that reheated-steam temperatures would be too high at maximum load for continuous operation with carbon-steel reheater elements. It was decided not to reduce the heating surface but rather to correct the difficulty by installation of a manually controlled steam-atomizing spray-type desuperheater. This was installed between the high-pressure turbine and the reheater in July, 1943, and has given satisfactory control.

It will be noted from the side-elevation view of the boiler that the lower portion of the front loop of the reheater is not effectively screened from the radiant heat of the furnace, particularly if the rear-wall screen tubes are kept clear of ash accumulation. Soon after a soot-blower overhaul in August, 1944, reheater-tube failures in this front loop began to occur. These were quickly repaired on each occasion by welding-in a new piece of carbon-steel tubing, but at the end of April, 1945, the lower end of the front loop, including the lower bend, of all 58 elements, was replaced with chrome-molybdenum-titanium alloy tube sections about 6 ft long. This is the same material as used in the front section of the superheater for 960 F steam temperature and since the reheated-steam temperature is only 765 F, no further trouble from this cause is anticipated. All other parts of the reheater are quite effectively shaded from radiant heat.

Economizer. There have been no failures or changes in the economizer. There has also been no maintenance except to seal up a few air leaks at the economizer doors and in the suspended arch where the hanger rods pass through the roof.

Steam Drums and Drum Internals. Because of the forced-circulation feature it was possible to operate the pumps with cold water and observe the flow of water into and out of the drum with the manholes open. Before placing the boiler in operation the flow of water toward the two suction pipes at the ends of the drum was photographed, and it was observed that a vortex was created over each suction-pipe nozzle, and that air was drawn into the suction pipes when the water level was low. The design of suction-pipe screens was changed and a coverplate was incorporated to eliminate the undesirable turbulence.

In reference (1) Fig. 13, it will be noted that the feedwater from

the economizer outlet discharges into the drum through tubes entering the bottom of the shell and that a deflecting baffle was installed directly above the outlet of these tubes. It was found that this resulted in low shell temperatures between this region and the suction-pipe nozzles. This baffle was removed in December, 1942, in order that the feedwater, which is at a temperature 100 deg F below that of the boiler water, can mix with the latter more quickly and thus eliminate this undesirable condition.

The original steam-separating means consisted of a combination of "hydraulic baffle" and metallic baffles in the wet drum and a combination of baffles and rod-type drier in the dry drum. During the first few months of operation the boiler was sensitive to carry-over when the water level approached the center line of the drum and, because the feedwater regulators were not functioning properly, the capacity was limited to 400,000 lb per hr, although higher capacity could have been carried with better water-level regulation. Minor modifications were tried but showed little promise of correcting the trouble so an entire new set of wet-drum internals of the "reversing-hood" type was substituted in October, 1942 (see Fig. 13 of reference 1 of Bibliography).

The blowdown line in the boiler drum as originally installed was found to be unsatisfactory after the reversing-hood type of internals had been installed because considerable feedwater was entering the blowdown piping. To correct this condition, six open-ended collecting pipes were extended upward above the water level so that concentrated boiler water from the hoods would discharge directly into the collecting pipes.

Although the reversing-hood steam separators in the wet drum resulted in satisfactory steam purity at loads up to 500,000, it became obvious in June, 1943, that further improvements would be necessary to meet the guarantee of 0.50 ppm solids in steam. Furthermore, the gaskets of the drum internals had deteriorated during the acid wash of the boiler in April, 1943, so that in August, 1943, the wet-drum internals were regasketed with copper-covered asbestos and screen driers were substituted for the rod driers in the dry drum.

Early in 1944 special laboratory evaporating apparatus, which permitted the determination of solids in steam by evaporating a 4-liter sample every 24 hr, was used to check the solids in steam. It was found that at maximum guaranteed output the guaranteed 0.50 ppm was being exceeded. Part of the difficulty was believed due to the fact that the steam-discharge tubes from the dry drum are not uniformly spaced along the drum but are arranged in three groups. A new set of low-velocity screens was substituted and a perforated baffle plate was installed ahead of each group of steam-discharge tubes to produce uniform velocity through the screens.

The steam line supplying the high-pressure soot blowers was originally connected to a nozzle near the center of the dry drum. The steam was taken out of the drum from the space between the screen driers and the steam-discharge tubes, and it was found that when the soot blowers were operated there was an increase in moisture in the steam in the saturated header of the superheater. To improve this condition the soot-blower steam nozzle was extended to take steam from the drum before it passes through the final drying screens. Gasketed joints in the wet drum were seal-welded at this time.

Excellent steam quality is now obtained from this unit and the results are included elsewhere in this paper.

Although there are generally only 10 to 20 lb of sludge in the wet drum after several months of operation, it has been noted that when the fires are extinguished preparatory to taking the boiler out of service, the blowdown water sample always becomes very turbid. The theory was advanced that the most quiescent zone in the wet drum during the steaming period is on the bottom of the shell between the 18 feedwater discharge nozzles which project into the drum about 2 in. This would then be a logical place for sludge to accumulate; but when the feedwater flow rate is reduced on shutting down the boiler the flow of water toward the suction pipes might wash this deposit away. Accordingly, in February, 1944, a special blowdown pipe was placed on the bottom of the drum and connected externally, through valves, to the continuous blowdown pipe. A study was made of the increase in turbidity of the blowdown sample on opening these valves and it is now part of operating routine to operate this special blowdown once a week.

In a boiler of this type it is possible to check the circulating ratio quite accurately by determining the solids concentration in the water at the circulating pumps and in the concentrated water leaving the steam-generating circuits, provided a representative sample of the latter can be collected. Fig. 3 shows a novel means

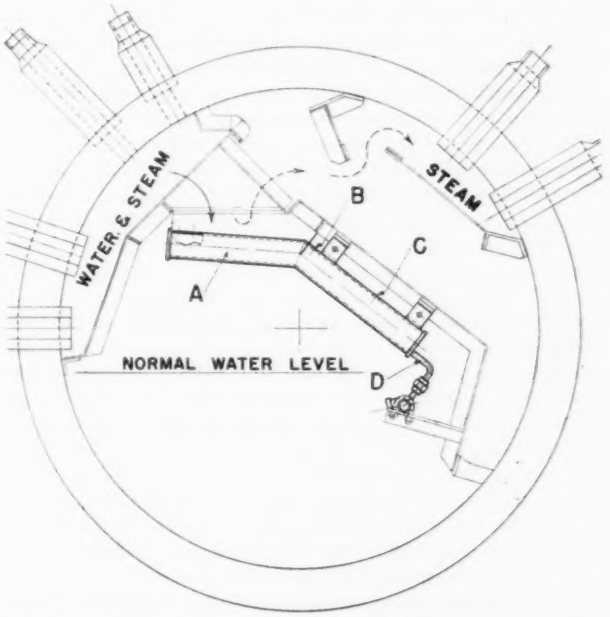


FIG. 3 ARRANGEMENT OF CONTINUOUS BLOWDOWN COLLECTORS

of collecting this sample from the concentrated water discharged into the drum above the water level. Six such blowdown collectors are uniformly spaced across the drum. The horizontal portions *A* are located directly under the slots of the reversing hoods which discharge water and steam into the drum. The upper surface of pipe *A* is perforated and designed to collect water at a rate several times greater than the maximum rate of blowdown. Any steam which enters pipes *A* is vented through an opening at *B* and the excess water is discharged through an opening at *C*. By proportioning the latter opening properly, a high collecting rate can be maintained in pipe *A* without filling the pipe, and the collecting rate is also independent of the rate of blowdown from the lower end of the collector at *D*. These blowdown collectors have been very satisfactory and result in minimum blowdown rate since they collect only the concentrated water which is discharged from the steam-generating tubes.

Air Heaters. The air heaters have given excellent service and there has been practically no maintenance. The steam soot blowers have never been used nor have the heaters been washed. They have been air-lanced on three or four occasions during scheduled outages but the necessity for this has never been urgent. In accordance with manufacturers' recommendations, compressed-air blowers were recently installed to bring the installation up to date.

Soot Blowers. Fig. 2 shows the location of the low-pressure soot-blower elements and also the position of the high-pressure retractable blowers located in the roof. These latter blowers had a sleeve around the blowing nozzle providing an annular passage to permit room air to be drawn in by furnace draft for cooling the blowers. After about a year of operation it was found that the portion of the sleeve projecting into the furnace was burned off and that the blowing elements were also badly damaged. In October, 1943, air under pressure was piped to these blowers to provide additional cooling.

When the boiler was operated at 550,000 lb per hr or higher, continuous output, it was found that an accumulation of ash occurred in the crotch and on the slope below the reheater. There was a tendency for this accumulation to grow quite rapidly and extend up the sloping screen tubes to the superheater. Five retractable mass-type blowers were installed on the slope in August, 1943.

In 1944 the coal was poorer than normal and quite variable. Slag was sometimes difficult to remove from the furnace walls. The soot blowers in the superheater-reheater zone were badly damaged and practically useless and it was found that the steam pressure at the high-pressure blowers was considerably below the recommended operating pressure. Since the coal situation might get worse before it got better, it was decided to review completely the soot-blower situation with the manufacturer and take steps to improve the situation during the August, 1944, annual outage.

During overhaul, additional bearings were provided for several of the low-pressure elements, particularly in the superheater-reheater zone. Replacement elements with larger nozzles were installed between reheater and front superheater and the wall boxes which were out of alignment were relocated. Operating mechanism of all blowers was overhauled and some changes made to facilitate operation. Two of the roof blowers were moved down to the side walls to replace wall blowers at the elevation of, and just in front of, the bottom of the slope below the reheater to assist the slope blowers which were not very effective near the side walls. The two side blowers thus replaced, plus one blower "stolen" from the upper front wall above the auxiliary burners, were located in the front wall at the elevation of the first row of observation doors above the burners.

During the process of overhauling all the retractable blowers it was found that part of the damage and malfunctioning was due to lack of lubrication. A lubrication schedule was set up and central lubricating stations were installed so that several blowing elements could be lubricated from each station. With the exception of the slope blowers there was very little soot-blower maintenance during the following year and at the end of that time all of the blowers except those in the slope were still in good condition. The cleaning effectiveness of the blowers as a whole has also been very good since this August, 1944, overhaul. Part of this improvement can be attributed to the higher steam pressure available at the high-pressure blowers after repairing the pressure-reducing valve through which this steam passes.

At the present time the nozzles of the slope blowers do not retract far enough to protect the blowing heads and there is considerable maintenance. Also, in spite of frequent lubrication, some of these blowers have become inoperative due to the action of heat on the lubricant. Correction of these difficulties is still being followed by the soot-blower manufacturer, but in fairness to him it should be pointed out that space limitations had made it necessary to install blowers with only 5-in. travel. The blowers must advance far enough so as not to cut the tubes in the slope and at the same time retract far enough to be out of the heat, and the blowing head is about 2 in. long with three large nozzles covering about 100 deg of blowing arc.

Circulating Pumps. Except for two leaks at the circulating-pump heads, the circulating pumps performed satisfactorily during the first 3 months of preliminary operation but toward the end of October, 1942, trouble developed in the labyrinth of one of the pumps. As described in reference (1) the labyrinth provides a means of sealing the pump against leakage of hot boiler water at nearly saturation temperature by introducing lower-temperature feedwater at a higher pressure at one end of the labyrinth passage. The labyrinth is a close-clearance passage between moving and stationary parts and as the sealing water flows toward the leak-off point adjacent to the packing gland the pressure breaks down to about 150 psi. An increase in leak-off pressure could be caused by increased flow through leak-off piping and is an indication of increased sealing-water quantity due to excessive wear in the labyrinth. This is how the first labyrinth trouble was detected. When the pump was opened up, the labyrinth surfaces were found to be badly worn, but new parts were installed without any changes except to realign the pump.

The *A* pump which had a labyrinth failure in October, 1942, had another similar failure in November, 1942, and toward the end of December, 1942, the labyrinth in the *B* pump failed. New sleeve bearings were installed in the *A* and *B* pumps during January, 1943, and the bearings of all three pumps were changed to hard babbitt in February, 1943.

During the overhaul for bearing replacement on the *C* pump, it was discovered that the pump could not be rotated until the support under the coupling end of the bearing body was removed, and in March, 1943, the supports were also removed from under the coupling end of the bearing body on both *A* and *B* pumps. Indicators were used to record the amount of vertical and horizontal movement of each bearing body when the support was removed. It was found that these supports had been exerting a strain on the bearing body which probably was resulting in misalignment of the shaft in the labyrinth. It was later found that temperature changes within the pump and/or piping would produce a few thousandths of an inch movement of the floating end of the bearing body and that the upper and lower parts of the bearing-body bracket were not at the same temperature. Insulation was added to the lower part of the bracket to correct this latter condition.

Also in March, 1943, the *A* pump labyrinth failed for the third time but the trouble was found to be corrosion or erosion of the casing in the labyrinth section. This was repaired by applying stainless steel and remachining. The other two pumps were overhauled during April and May, 1943, and there were no further failures in the labyrinths. However, there were several failures of *B* and *C* oil-pump spur gears later in the year; fiber gears were substituted and gave much longer life than the bronze gears.

Bearing troubles were encountered not only with the circulating-pump motors but on other pump motors in the station. The trouble in the case of the circulating pumps was diagnosed as being due to expansion of the pump shaft toward the motor a sufficient amount to put a thrust on the motor bearings. This movement had not been allowed for in the design of the motors. After the replacement of several sets of motor bearings, the pump manufacturer corrected the trouble by the installation of limit stops in the flexible couplings located between motor and pump.

Although there was no trouble or maintenance on the circulating pumps since the spring of 1943, except oil-pump drive gears, the amount of water used to seal these pumps greatly exceeded the manufacturer's predictions. The pipe carrying this water to the pumps from boiler feed pump discharge was therefore much overloaded, thus making it necessary to carry a pressure at the feed pumps about 200 psi above boiler pressure in order to have sufficient sealing-water pressure at the pumps. In order to be able to operate with closer clearances in the labyrinth, to reduce the sealing-water requirements, the pump manufacturer decided to rebuild the bearing body and to substitute roller bearings in

place of the babbitted sleeve bearings. The design of the labyrinth was also changed to accommodate a mechanical seal between the sealing-water injection point and the impeller chamber. This seal reduced the leak-in of seal water to the pump practically to zero. Further reduction in sealing-water requirements was accomplished by the close clearances in the labyrinth passages so that the over-all result was to reduce the injection water, leak-off and leak-in, to amounts far below the original predictions, and the high-pressure leak-off was eliminated completely. One of these pumps was rebuilt about February 1, 1945, and there has been no perceptible increase in sealing-water requirements. This pump was dismantled after 2 months' operation and the boundary surfaces of the labyrinth passage were in excellent condition. The second pump has just been changed over and the third pump will have also been rebuilt by the time this paper is presented.

Water-Level Indicators. Four water-level devices were installed on this boiler, consisting of a recorder and an Eye-Hye gage on the operating panel, a double-window Bi-Color gage with 21-in. visibility and mirrors on one end of the drum, and a double-window Micasight gage with 18-in. visibility on the other end of the drum. The indirect-type gages have been very satisfactory but they do not give a true indication when the pressure is below the design value, due to change in water density.

The center of both water-level gages was originally located 10 in. below the drum center line. This meant that in one gage the water level was still visible when there was only $6^1/_2$ in. of water in the drum, which would expose the modified suction-pipe cover plate, and result in steam entering these pipes. The water columns were both raised so that the normal water level and center of gage are now 5 in. below the center of the drum.

Illumination of the double-window Micasight gage was not sufficiently bright to permit the water level to be observed from the operating floor. The manufacturer decided that it would be a physical impossibility to line up the double-window gage for good visibility because there was only one spot on the operating floor from which the gage could be seen and part of the window was obstructed by a steel beam. A single-window gage of 12-in. visibility was substituted in August, 1943, but after a short period of operation the image of the water level became too faint to be seen from the operating floor. In October, 1945, the gage manufacturer installed a new improved illuminator and mirrors to reflect the water-level image to a convenient point near the operating floor. Visibility of the image with new mica windows was very clear but decreased rapidly. It remains to be determined how often the mica will have to be renewed to maintain satisfactory visibility.

The Bi-Color gage has required frequent maintenance. It has been necessary to have a spare gage available for replacement due to the frequency of failures. One of the gages was modified by the manufacturer in February, 1944, but the modified gage was no improvement. The other gage was modified in a different manner in September, 1945, but failed after 8 days in service. One of the gages was recently assembled in an improvised manner and at the time of writing, has been in service 5 weeks which is the best record so far. However, visibility of the water line at the end of that time is only fair due to dirty mica.

Burners. The automatic ignition system used light oil, mechanically atomized and electrically ignited. From a control station it was possible to start up the oil pump, insert the ignition torches and ignite the oil. The principal trouble encountered was with the mechanism used to insert and retract the oil burners. The automatic features were discarded in favor of torches of steam-atomizing type using heavy oil and which are moved into position by hand.

The pulverized-coal burners are located in the four corners and fire tangentially. No changes have been made except to incline the lowest row slightly downward to improve slag fluidity on the floor.

There are four auxiliary oil burners in the upper front wall which are required to maintain maximum steam temperature at reduced load when the unit is operating with a clean furnace and 100 per cent oil fuel. These burners are not required to supplement coal-firing nor are they necessary with intermittent coal and oil firing. They have never been used and were found to be damaged due to radiant heat from the furnace after a year of disuse. The vanes and other metal parts were burned or distorted. They were repaired and removable Fahrite protecting plates inserted to shield them from the furnace heat.

Miscellaneous: Valves, Piping, Ducts. During the period of preliminary operation, with frequent starting and shutting down, considerable trouble was encountered due to leaks in the bonnet joints of the large gate valves in the suction and dicharge lines of the circulating pumps. These flanged bonnets were originally installed with ring gaskets of oval section. Leakage troubles were corrected by changing to gaskets of octagonal section.

Two outages were charged to safety valves because two shutdowns were scheduled to lap-in the seats of leaky valves.

There are two forced-draft fans and two air heaters with a common preheated-air duct below the air heaters. Although dampers were provided at the inlet to each fan and air heater and, in the cold-air by-passes, these dampers did not prevent the preheated air from leaking through to the idle fan, when only one fan was in operation, and burning the paint on the fan. A crossover duct was installed in 1943, between the cold-air outlet ducts of the two fans to correct this condition.

A program involving several changes in the exhaust-steam piping between the high-pressure turbine and the low-pressure station header is in progress at this station for the purpose of reducing the pressure drop between those points. The first change was to modify the outlet connection of the reheater, in August, 1944, when it was realized that a reduction in pressure drop of several pounds per square inch could be obtained. The reheater originally had a single outlet near the center of the outlet header, and two additional 6-in. outlet pipes were added.

Another piping modification was to install a by-pass line around the high-pressure feedwater heaters permitting both heaters to be out of service without having to shut down the high-pressure boiler. The by-passline also increases flexibility of operation by facilitating an increase in the quantity of low-pressure steam from the high-pressure boiler without increasing the output of high-pressure steam. Under certain load conditions this would obviate the necessity of placing another low-pressure boiler in service or in any event decrease the urgency.

Research and Tests

Special Provisions. Before the boiler was placed in operation more than 100 thermocouples were installed at various points throughout the unit for the purpose of checking operating metal temperatures on furnace-wall tubes, superheater, reheater, economizer, steam drum (lower), feedwater connections to drum and circulating-water connections to pumps. Nearly one half of these were installed on the hot face of the furnace-wall tubes at an elevation about 3 ft above the furnace floor. Pressure taps and Pitot tubes were also installed at various points in the circulating system, as illustrated in Fig. 4. Actually, the Pitot-tube locations were further from the elbow than this sketch indicates.

During the course of subsequent special studies, after the boiler had been placed in operation, additional thermocouples were added to lower drum, circulating pumps, reheater, and on the furnace tubes at different elevations, bringing the total number of thermocouples installed up to about 275.

Steam-sampling connections were initially provided on super-

heater inlet and dry drum, but for special studies additional sampling connections were made at dry drum, reheater outlet, high-pressure-turbine inlet, and high-pressure-turbine outlet.

A special calorimeter was installed to check for the presence of steam in the suction pipes to the pumps and its operation is described in reference (5).

The method of installing the thermocouples and the technique of using Pitot tubes has been described in references (6) and (7).

Circulation. One of the first research studies was to check the total circulation and distribution of circulation to the four separate groups of parallel circuits comprising the four furnace walls. In each wall one circuit had been chosen for installation of a pressure tap on the downstream side of the orifice. The pressure difference between header and the downstream tap beyond the orifice could then be used to determine the rate of flow through the orifice, using calibration data reported in reference (8) Fig. 39, which were determined for the orifice assembly shown in Fig. 38, this being an exact replica of the arrangement used in the Montaup boiler. All the orifices serving the circuits of a given wall are the same size; and, since the pressure drop across the orifices is large compared to the drop across the parallel heated circuits, very little error is introduced by using the flow through one orifice to calculate the flow for the entire wall. Furthermore, all heated tubes of a given wall are nearly the same length and all have approximately the same exposure to heat. By measuring the pressure drop across four furnace-wall orifices, it was therefore possible to determine the total circulation of the unit since there is no other steam-generation surface or no other stray circuits except a connection to the economizer inlet; this is used to circulate boiler water through the economizer when the unit is being brought up to pressure preparatory to placing in operation.

The Pitot tubes in the two suction pipes to the circulating pumps provided another means of determining the total circulation, except that this would not include the sealing water which

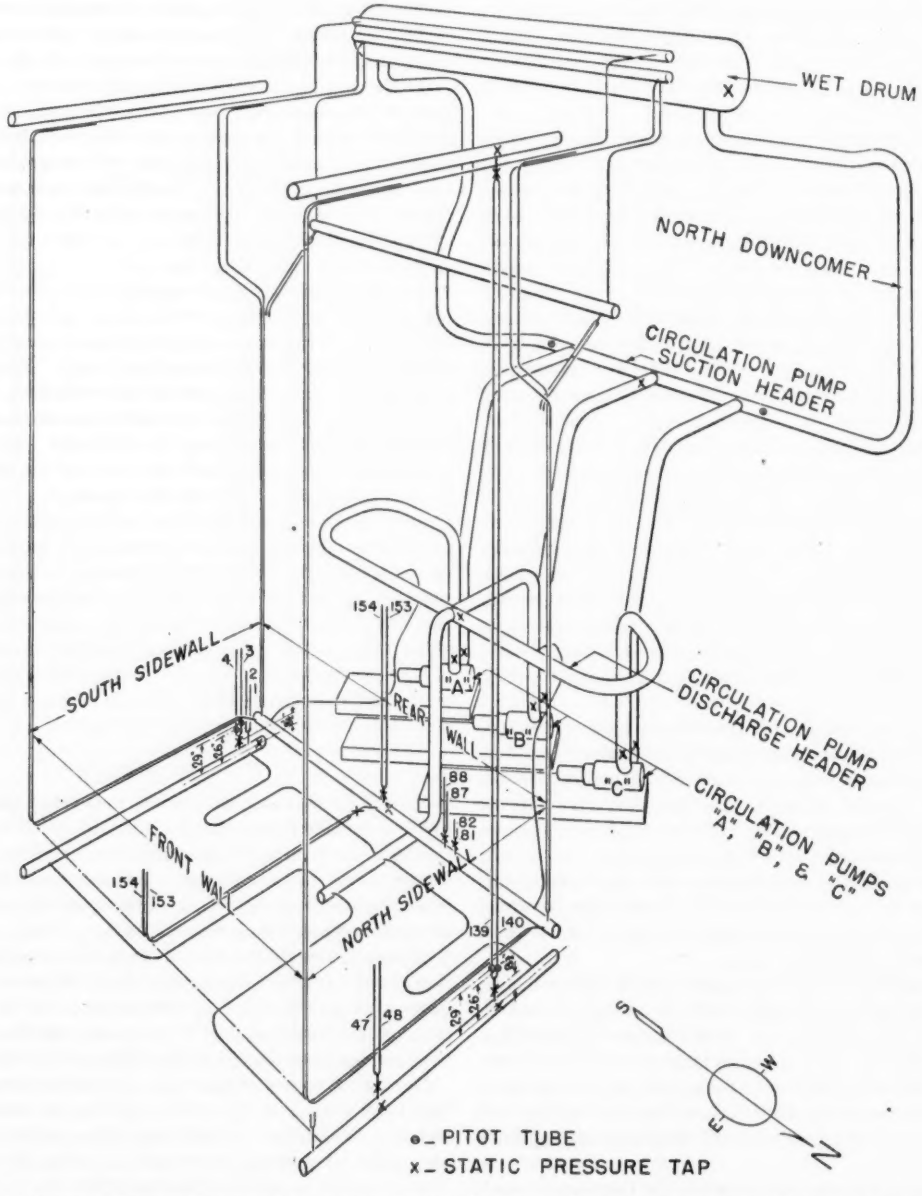


FIG. 4 ISOMETRIC SKETCH SHOWING LOCATION OF SPECIAL PRESSURE CONNECTIONS USED IN TESTS ON CIRCULATION

leaks into the pump. This leak-in can be checked by determining the difference between rate of feedwater flow and steam flow and of course making an allowance for blowdown. This was done on certain tests during 1944, but the flow data were taken during 1942 and 1943, and no correction for leak-in was made because the quantity was of the order of 0.50 to 1 per cent of the water being handled by the pumps, and the accuracy of the flow data did not warrant this refinement since it is not claimed to be correct within 1 per cent.

Measurement of the pump head provided a third means of checking the pump capacity because a pump characteristic curve had been determined by shop test. Unfortunately, however, these tests were conducted up to a capacity of only 5000 gpm and the curve had to be extrapolated for comparison with some of the field data.

A fourth method of checking the total circulation was by determining the difference in solids concentration in the water at pump discharge and leaving the evaporating circuits. The following equation shows the relationship of the variables involved

$$W/S = C_1/(C_1 - C_e)$$

where W = weight of water entering furnace circuits
S = weight of steam generated in furnace circuits
C_e = concentration of solids in water entering, ppm
C_1 = concentration of solids in water leaving, ppm

Since the feedwater is introduced at the bottom of the drum and does not mix with the steam in the drum, it is not heated to saturation before entering the suction pipe. There is, of course, some condensation of steam in both drums, and this would tend to make the weight of steam generated in the furnace circuits greater than the weight of steam metered at the superheater outlet. Consequently, the determination of W by using the weight of metered steam for S would give a value of W which would be lower than the true value.

When this method was first used the difference in concentration of chloride, sulphate, and total solids were all determined for comparison of the results but the time required for analysis of the water samples was too great to permit frequent checking. The results reported herein are based on analysis for chlorides only. The chloride concentration at the pumps was generally between 200 and 260 ppm, and it was considered possible with this concentration to determine the chloride by titration without involving an error of more than about 2 ppm.

Fig. 5 shows a plot of the total flow of water through the orifice headers, based on measured orifice pressure drop using a mercury manometer. The data were collected at different operating pressures and rates of output, but the total flow appears to be independent of these variables over a wide range. There is, however, a marked increase in circulation when the boiler is not steaming and when the water temperature is low.

Fig. 6 is a similar plot of flow data based on pressure differential measured by a mercury manometer across the Pitot tubes in the suction pipes. There is a greater spread in the data probably due to the effect of variable leak-in of sealing water, and the effect of the economizer circulating line which was open during the period when most of the downtake flow data were taken. However, this plot substantiates the previous statement that the total flow is quite independent of load and pressure. Figs. 5 and 6 illustrate the fact that the flow with one pump is about 70 per cent as great as with two pumps. Three pumps were not operated during the period when these data were taken, except at atmospheric pressure with cold water (100 to 125 F) under which conditions three pumps produced only 15 per cent more flow than two pumps.

Fig. 7 is a plot of measured flow rate in the suction pipes and

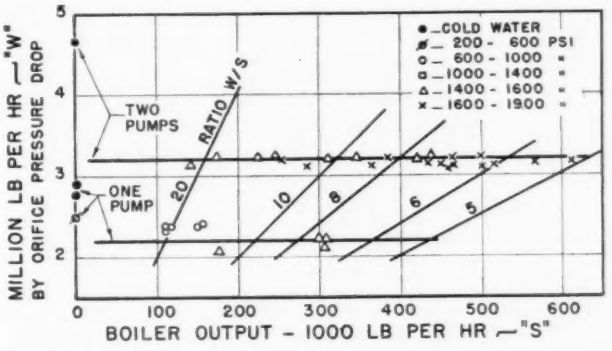


FIG. 5 TOTAL CIRCULATION TO LOWER FURNACE-WALL HEADERS BASED UPON PRESSURE-DROP MEASUREMENTS ACROSS ORIFICES

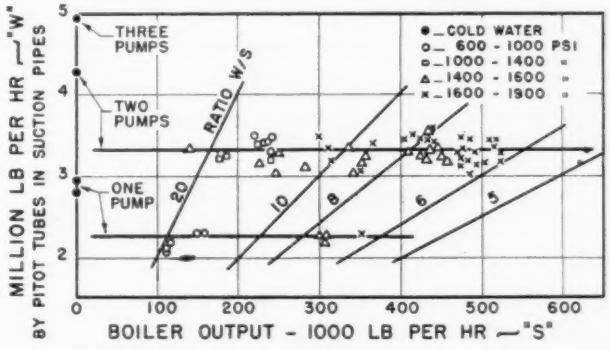


FIG. 6 TOTAL CIRCULATION ENTERING PUMPS BASED UPON PRESSURE DROP MEASUREMENTS TAKEN ON PITOT TUBES IN SUCTION PIPES

measured pressure difference between pump outlet and pump inlet, uncorrected for acceleration across the pump, superimposed on characteristic pump curves. The pressure difference was determined by dual connections to a 12-in. Crosby test gage having 5-lb graduations which may have introduced considerable error in the pressure data. This may explain why some of the data do not fit the characteristic curves too well, but a small error in the flow rate may also be partly responsible. Also, the pump-head curves are plotted for 1750 rpm, and the pumps are motor-driven and operate at considerably less than full load amperage, particularly when the water density is low, so the actual pump speed may have at times approached 1790 rpm. The pump speed was not determined but the extent to which this variation would displace the head curve is indicated on the chart. The system resistance lines drawn through the test data can be considered as only approximate since the data for one pump operation are meager and subject to large error in the pressure reading.

Fig. 8 is a plot of total water flow calculated from chemical concentration at pump discharge and leaving evaporating circuits, the latter based on water samples from the continuous-blowdown collectors shown in Fig. 3. The data are plotted for two-pump and three-pump operation and two chemists worked independently on these results which explains why two different kinds of points are plotted for each series of tests. No allowance was made for steam condensed in the drum, which explains why total circulation by this method is lower than the results of the two other methods.

It has been shown that the total circulating-water flow calculated from the pressure drop across four orifices checks very well with the total flow calculated from Pitot-tube measurements in the suction pipes. The distribution of circulating water to the

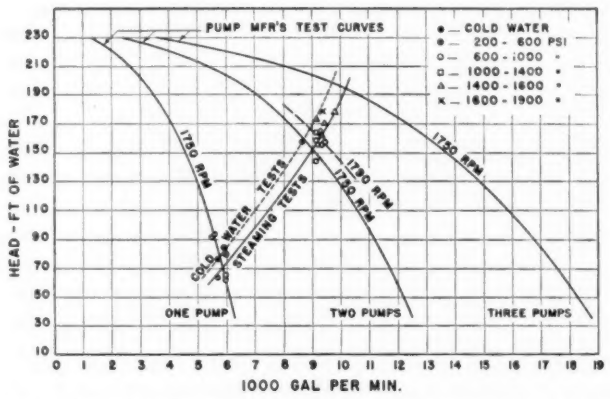


FIG. 7 CIRCULATING-PUMP CHARACTERISTICS, COMPARED TO MEASURED PUMP HEAD PLOTTED AGAINST SUCTION-PIPE FLOW RATE

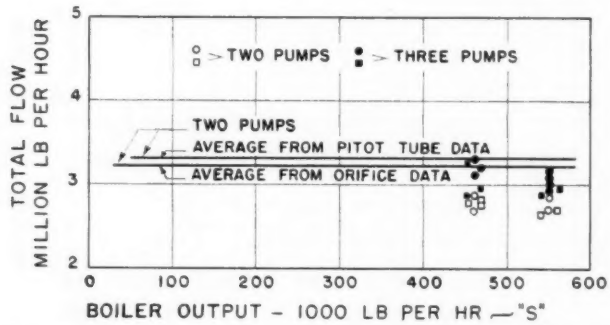


FIG. 8 TOTAL CIRCULATION CALCULATED BY CHEMICAL METHOD COMPARED TO AVERAGES BY OTHER METHODS

walls can therefore be quite accurately determined from the same orifice pressure-drop measurements and the results of several tests are given in Table 2. When this unit was designed the orifices were selected so as to control the water flow to each wall in proportion to the calculated distribution of heat to the walls. The table shows how closely this distribution and control are being realized with only two orifice sizes, namely, 0.34 and 0.40 in., and also illustrates that the distribution is practically the same for any load or pressure.

The distribution of water to the two suction pipes was found to be practically 50–50 when the two outside pumps or the center pump was operating. It was sometimes nearly equal when the center and one of the outside pumps were used but on other occasions the distribution was 45–55.

Fig. 4 shows that pressure drop could be measured across two orifices in the right side wall. Equal pressure drops were often noted but the maximum difference in flow rate on any test was 1.5 per cent.

A study was also made of water distribution to the two legs of bifurcated circuits in the right-hand and left-hand walls. These circuits are indicated in Fig. 4. In each circuit the orifice pressure drop was measured to determine water flow to the circuit and average velocity in the two tubes, assuming equal distribution. A calibrated Pitot tube was installed in each leg to check the distribution of flow. The average velocity based on Pitot-tube differential was lower than the velocity calculated from the measured orifice flow but the distribution was nearly equal as indicated by Table 3.

A calorimeter similar to that described in reference (5) was used to check for the presence of steam in the suction pipes. These tests involved not only the measurement of water temperature in the pipes but a check on the heat exchange in cooling this water

TABLE 2 COMPARISON OF MEASURED DISTRIBUTION OF CIRCULATING WATER WITH CALCULATED DISTRIBUTION OF HEAT TO STEAM-GENERATING SURFACES

Test Date	Operating Pressure	Boiler Output	Distribution of Circulating Water		
			Front	Rear	Sides
6-20-43	1825	285,000	37.2%	30.5%	32.3%
6-16-43	1840	450,000	37.3	30.1	32.1
6-19-43	1850	515,000	37.6	30.2	32.2
6-21-43	1875	565,000	37.7	30.5	31.3
6-24-43	1880	610,000	37.7	30.5	31.8
* 6-5-43	380	0	37.4	28.9	33.7
6-5-43	1840	252,000	37.4	29.9	32.7
6-5-43	1850	385,000	37.3	29.9	32.8
6-4-43	1850	465,000	37.3	30.1	32.6
4-22-43	1500	175,000	37.7	29.7	32.6
4-23-43	1500	245,000	37.6	29.5	32.9
4-23-43	1500	340,000	37.4	30.0	32.6
4-23-43	1500	420,000	37.3	30.1	32.6
7-20-42	850	110,000	35.6	30.0	34.4
7-22-42	900	156,000	34.3	30.1	35.6
* 8-31-42	0	0	37.0	29.0	34.0
* 8-31-42	0	0	38.4	30.1	31.5
8-31-42	0	0	37.0	28.6	34.4
			Calculated Distribution of Heat		
			37.4%	29.5%	33%

*One pump used for these tests; all other tests based on two pump operation.

TABLE 3 DISTRIBUTION OF FLOW IN BIFURCATED CIRCUITS

Date, 1943		6-16	6-18	6-20	6-21	6-24
Boiler output, 1000 lb/hr		450	515	285	565	610
Boiler pressure, psig		1840	1845	1825	1875	1880
Right-hand Furnace Wall -	Circuit No. 70 Tubes No. 139 and 140					
Flow Thru Tube 139 - %		49.8	50.0	49.1	49.0	48.1
" " " 140 - %		50.2	50.0	50.9	51.0	51.9
Left-hand Furnace Wall -	Circuit No. 2 Tubes No. 3 and 4					
Flow Thru Tube No. 3 - %		50.5	50.2	51.7	51.0	51.0
" " " 4 - %		49.5	49.8	48.3	49.0	49.0

about 200 F in the calorimeter. This gives a check on the presence of entrained steam and none could be detected by this method.

Other tests were conducted to check the water temperature at several points in the suction pipes between the drum and the pumps, by the use of iron-constantan thermocouples peened into the metal of the pipes under the insulation. A precision potentiometer, using an ice cold junction, was used and the data of Table 4 are typical of the results obtained with two-pump operation. The difference between saturation temperature in the drum and the measured temperatures was 6 to 9 F which is about one half the calculated difference assuming no condensation of steam to heat the feedwater in the drum. Therefore these tests indicate that the rate of steam condensation in the drum was 10 to 15 per cent of the rate of steam flow leaving the unit and this correction, if applied to the Fig. 8 data, would bring the results of the chemical method in very close agreement with the total flow determined by Pitot tube and orifice pressure drop.

Furnace-Tube Temperatures. The measurement of the fire-side skin temperature of furnace-wall tubes is of considerable interest to boiler manufacturers and users. Thermocouples if carefully installed will give reliable readings over a period of several months and some have been in service more than 2 years. The skin temperature can be used to give an approximate evaluation of the rate of heat absorption at different levels in the furnace and to study the rate of slag or ash accumulation, as well as the effect of slag removal by blowers or by lowering the rate of steam generation. Several papers discussing the effect of slag and ash on heat absorption are to be found in a recent publication (9), and some of the results of the studies at Montaup are included in these papers.[5] Another reference (10) discusses the effect of metal thick-

[5] Reference (9), Fig. 9, p. 13; (see Fig. 14 of this paper).

TABLE 4 CIRCULATING-WATER TEMPERATURE MEASUREMENTS

Date, 1943		July 6	July 13	July 14	July 15
Boiler output, 1000 lb/hr		550	530	550	550
Boiler pressure, psig		1875	1870	1875	1875
Feed temperature to drum	F	510	520	500	525
Saturated Steam Temp.	F	628	628	628	628
Temp. N. Pipe below upper elbow,	F	--	621	619	621
Temp. at suction header,	F	622	622	619	--
Temp. at "A" pump inlet,	F	621	622	619	621
Temp. at "B" pump "	F	621	--	--	--
Avg.(to nearest deg.)	F	621	622	619	621
Difference from saturation	F	-7	-6	-9	-7

ness, heat absorption, and internal-surface factors on the tube-metal temperature.

The data obtained at Montaup and already published show that even in a bare-tube furnace and in the zone of highest flame temperature with pulverized-fuel firing, the hot face metal temperature with normal slag covering was only about 50 deg F above saturation temperature. The tubes are $1^1/_4$ in. OD 0.165 in. minimum wall thickness, but the average wall thickness is probably more nearly 0.180. It may therefore be readily calculated from the charts and equations of reference (10) that the heat absorption at the point of temperature measurement was only about 50,000 Btu per hr per sq ft, allowing for reasonable drop at the evaporating film. These data also show the effect of deliberately removing the slag and ash coating from a portion of the wall, thus exposing a small surface to the full radiation of the flame at a temperature approaching 3000 F. Under these conditions the skin temperature rose to a maximum value 172 deg F above saturation (786 F — 614 F saturation temperature), and the corresponding heat-absorption rate would be about 150,000 Btu per hr per sq ft, allowing for temperature gradient between inside surface and the evaporating water. These values represent the extreme rate of heat absorption to which these bare tube walls could be subjected because if a larger area in the zone of high temperature were clean the radiating temperature and the average heat-absorption rate would both be lower.

In June and July, 1943, a study was conducted to learn the effect of circulation rate on the polished interior surface of several tube specimens installed in several furnace-wall circuits. In each of three circuits having different-size orifices a pressure tap was available on the downstream side of the orifice so that the water-flow rate in each could be determined by measuring the orifice pressure drop. The results of the flow measurements appear in Table 5, section A.

There were three thermocouples at the 30 ft elevation on side-wall tubes Nos. 3 and 5, and at the 24 ft elevation in the rear wall there were three couples on tube No. 87 and two on tube No. 81. When tube-temperature measurements on the side-wall tubes are compared to those on the rear-wall tubes, it should be considered that the side-wall tubes are very close to a corner of the furnace. The couples on tubes Nos. 81 and 87 were quite close to a furnace wall blower, and the temperature readings reflected the effect of blower operation. At the end of 2 weeks continuous operation, with coal-firing, and with the boiler operating at maximum guaranteed output, tube-temperature data were collected; some of the readings are included in Table 5, section B.

All these thermocouples were read daily at less than hourly intervals for a month. It was noted that tube No. 81 was more sensitive to wall blowing than No. 87 but never did the temperature of either tube exceed 720 F even immediately after operating the blowers. On some occasions after soot-blowing, the temperature spread for the five couples was less than 10 deg F. From these observations it was concluded that variation in circulation from 57 to 230 per cent of normal had no effect on the tube temperatures.

TABLE 5 EFFECT OF VARIABLE ORIFICE SIZE ON CIRCULATION AND TUBE TEMPERATURE AS SHOWN BY (A) FLOW DATA AND (B) TEMPERATURE DATA

A - Flow Data - June 14 & 15, 1943 - 1845 psi - 465,000 lb/hr output

Wall Location	Left	Left	Rear	Rear
Circuit Tube No.	3 & 4	5 & 6	87 & 88	81 & 82
Orifice diameter, in.	0.50	0.34	0.34	0.25
Water Flow, lb/hr	12,000	*5,150	6,400	3,625
Inlet Tube Velocity, ft/sec.	9.1	3.9	4.82	2.73

B - Temperature Data - June 22, 1943 - 1880 psi - 650,000 lb/hr output

Tube No.	3	5	87	81
Elevation above floor, ft	30	30	24	24
No. of couples	3	3	3	2
Max. Temp., F	663	657	690	702
Min. Temp., F	639	644	652	644

* There was no downstream orifice pressure tap on this circuit but the water-flow figure given was obtained on the same size orifice in the opposite side wall.

In October, 1944, the boiler was placed in operation with oil-firing after an outage. Under these conditions the furnace walls were clean and remained clean while tube temperatures were taken. Oil was fired tangentially through burners interposed between the coal burners, and it would therefore be expected that tube temperatures in the lower part of the furnace would be much higher than with coal-firing. Fig. 9 illustrates the results of these tests and shows the variation in tube temperature at different elevations above the furnace floor when the boiler output was varied from 260,000 to 560,000 lb per hr. At each elevation noted two thermocouples were installed 1 in. apart, one as a check against the other, because previous experience had indicated that a couple sometimes becomes shorted against the cover plate, thus giving a high and erroneous reading. At the time these studies were made a panel of eight tubes in the right-hand side wall was being used for another special study of the effect of the orifice size on internal tube conditions, but tubes No. 133 and 139 were the only two tubes of the group which had couples installed at the 5-ft and 11-ft elevations. Tube No. 133 is one of a pair served by a normal-sized 0.34 in. orifice in the trunk of the bifurcate; tube No. 139 was one of a pair having no orifice below the bifurcate but having an individual orifice of 0.25 in. in each tube above the bifurcate. The calculated water-flow rate to each of these tubes is the same. The location of this group of tubes is one where maximum flame temperature would most likely occur but it will be noted that the maximum tube temperature measured was 720 F.

The object of the special study started in 1944, and just mentioned as involving a group of eight tubes in the right side wall, was to confirm over a 1-year operating period, with routine boiler-water control, the general conclusions resulting from the shorter study of tube temperature and interior-surface condition of the rear-wall and left side-wall tubes. The four bifurcated elements chosen were side by side in a zone of high heat absorption and actually straddled a wall-blower element located about 34 ft above the furnace floor. Test specimens of new tubing were installed in all eight tubes, extending from approximately 18 to 25 ft above the floor, and two thermocouples were installed on each tube at each of the following elevations: 18 ft, 24 ft, and 26 ft. One bifurcated circuit had a normal orifice, one an oversize, one an undersize, and one element had individual orifices in each leg which were installed at two butt-welded tube joints in the form of a diaphragm-backing-ring with the orifice hole drilled through the center of the diaphragm. During the first month the boiler was coal-fired at design pressure and daytime load generally be-

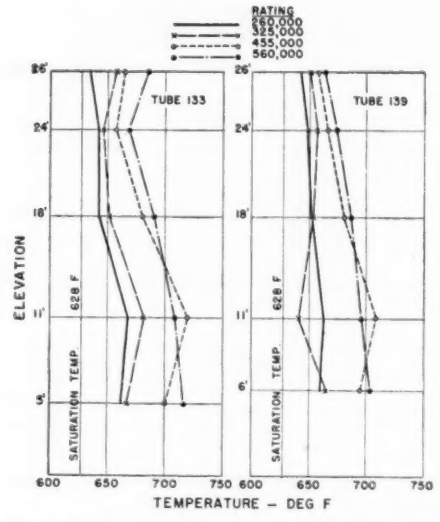


FIG. 9 PLOT SHOWING EFFECT OF RATING AND ELEVATION IN FURNACE ON TUBE TEMPERATURES WITH OIL-FIRING

tween 550,000 and 610,000 lb per hr, followed by 4 days' operation with 100 per cent oil at 550,000 lb per output. Table 6 presents the range of readings at each elevation on each of the eight tubes during these two periods of operation.

It will be noted that tube No. 139 had abnormally high temperatures at the 18-ft elevation, although they were normal at the two higher elevations. The boiler was taken off the line July 16 for a scheduled outage, and a blister was found on tube No. 139 at about 10 ft above the floor. A short piece was welded in and the boiler placed in operation the following day, but temperatures were still somewhat higher than normal at this one elevation. Subsequently, a probe was run up into these two individual orifices to make sure they were clear and after that the boiler was operated for over a year with normal temperatures. In October, 1945, these individual orifices were removed and it was discovered that the probable cause of the blister was welding scale which had formed on and near the orifice during welding and which had subsequently flaked off and restricted the flow. In further discussion of the temperatures in Table 6, the figures given for tubes Nos. 139 and 140 will not be considered.

Table 6, section A, shows a wide variation in temperature due to the effect of ash building up and falling or being blown off the tubes. At the lower elevations the metal was practically at saturation temperature when covered with ash and never exceeded 705 F under normal operating conditions. At the highest elevation which was still about 8 ft below the nearest wall blower the minimum and maximum temperatures were higher due to more effective cleaning and lower rate of accumulation after cleaning. Table 6, section B, shows that with oil-firing the spread in temperature at all couples was much less than with coal, due to more uniform ash conditions at the absorbing surface. This part of the table also shows that with oil-firing the tubes are hotter at the lower elevations as would be expected with a cleaner furnace. In no case is there any significant difference in temperature that can be attributed to orifice size.

Steam Purity. Because of the several changes and modifications which were necessary before satisfactory steam purity was obtained, considerable data were collected on this subject. During the early part of this work samples were taken from the "dry" drum to determine the effectiveness of the separating apparatus in the "wet" drum and from the inlet header of the superheater to determine the final result. However, it was found that

TABLE 6 FURNACE-TUBE TEMPERATURES AT DIFFERENT ELEVATIONS ON TUBES HAVING DIFFERENT SIZE ORIFICES WITH (A) COAL-FIRING AND (B) OIL-FIRING

A – Coal Firing – 4 Weeks at 550,000 to 610,000 lb/hr Load

June 12 – July 12, 1944

Orifice Size		.34		.30		.50		.25	.25
Circuit Tube No.		133	134	135	136	137	138	139	140
Elev. 18'	Max.	705	705	665	680	675	690	790	700
	Min.	630	630	630	630	630	630	630	630
Elev. 24'	Max.	705	695	685	695	680	680	690	685
	Min.	630	630	630	635	635	635	635	645
Elev. 26'	Max.	725	---	710	720	---	---	695	720
	Min.	645	---	650	650	---	---	645	655

B – Oil Firing – 4 Days at 550,000 lb/hr Load

July 12 – July 16, 1944

Tube No.		133	134	135	136	137	138	139	140
Elev. 18'	Max.	690	715	700	710	720	710	785	695
	Min.	680	670	665	665	670	670	710	655
Elev. 24'	Max.	690	685	680	680	675	695	690	690
	Min.	655	660	660	650	640	655	650	650
Elev. 26'	Max.	690	—	670	685	—	—	680	690
	Min.	665	—	655	660	—	—	655	660

under certain conditions the steam conductivity was lower (indicating better purity) entering the final drying screens than leaving the screens, as determined by the superheater inlet-header sample. Switching the conductivity cells at the two sampling points did not change the results. Some time later it was discovered that if steam conductivity data were collected during a period when saturated steam was being taken from the dry drum for operation of the soot blowers, the conductivity of the superheater inlet-header sample fluctuated rapidly, and the average was much higher than when the soot blowers were not being used. This led to the installation of a sampling nozzle in the superheated-steam line near the high-pressure-turbine inlet, and it was found that this sample had a lower conductivity and did not fluctuate or increase very much during soot-blowing periods.

When the final changes were made to the dry-drum internals, a long sampling nozzle was installed at the outlet of the final drying screens between the screens and the several off-take tubes leading to the superheater. Furthermore, the off-take nozzle for supplying soot-blower steam was extended through the screens, as mentioned elsewhere in this paper. A sampling connection was made in the side of a horizontal run of this small soot-blower steam pipe (dictated by convenience), and subsequent checks on steam purity entering the final drying screens were made only during periods of soot blowing.

It was found that the source of make-up water and the season of the year had a very marked effect on steam conductivity leaving the high-pressure boiler. For example, there was a period during the spring of 1944, when it became necessary to use one of the low-pressure boilers as an evaporator for the make-up water. Raw water was evaporated in the boiler and condensed in the low-pressure units and it was found that the conductivity almost immediately increased about 1 mmho all through the station at points where it was being measured, such as at condenser hot wells, feed line and high-pressure-boiler steam outlet. This increase was found to be due to an increase in ammonia. There is also a seasonal variation in ammonia caused by the make-up water from the evaporators, even though the make-up is only about 2 per cent. For example, the uncorrected conductivity of steam in August, 1945, was about 3.5 times greater than the corrected value but less than 1.5 times greater in the month of May, 1945. The corrected value is currently obtained by passing the condensed sample of steam through a degassifier; earlier values of the gas correction were obtained either by checking for ammonia and carbon dioxide in the sample or by comparing the uncorrected conductivity with the results of gravimetric measurement of the total solids.

Fig. 10 shows the relation between total solids, determined by evaporation, and the conductivity of undegassed samples of condensed steam. The generally accepted conversion factor by which conductivity of a degassed-water sample is multiplied to obtain ppm of dissolved solids, is 0.60. Fig. 10 shows that when the evaporators were used for make-up the factor was about 0.40 in the cold-weather months, and 0.20 or less in the warm-weather months; but when the low-pressure boilers were used to evaporate the make-up, the factor was only about 0.20, even in the cold-weather months.

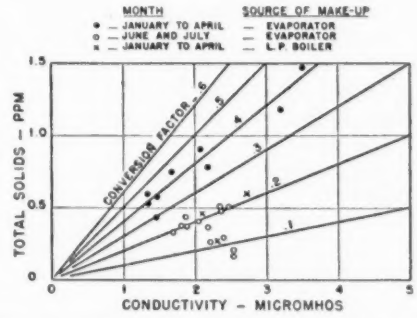


FIG. 10 RELATION BETWEEN CONDUCTIVITY AND TOTAL SOLIDS DETERMINED BY EVAPORATION

All the condensed-steam samples which were evaporated for total-solids determination after the final changes were made in the drum internals were obtained at boiler loads between 550,000 and 650,000 lb per hr. For each of these determinations a 3-liter sample was evaporated to dryness in the special steam-sample evaporator which is described in another paper of this series (11), and the results are given in Table 7.

The conductivity of undegassed-steam samples taken from the dry drum ahead of the final drying screens was found to be 4.23 mmho and 4.56 mmho at boiler loads of 620,000 and 650,000 lb per hr, respectively. Other samples, evaporated during the same week, indicated that the conversion factor was 0.20 or less, so the corresponding total solids in the dry drum would be 0.85 and 0.91 ppm, respectively. This would indicate that without the dry drum the purity would be equal to or better than the minimum guarantee of 1 ppm which has now been recommended by the American Boiler Manufacturers Association and Affiliated Industries (A.B.M.A. and A.I.). The guarantee on this unit was 0.50 ppm, and the screens in the dry drum removed enough moisture to bring the final results below the guarantee as will be seen from the results given in Table 7.

TABLE 7 STEAM-PURITY DETERMINATIONS BY EVAPORATION

June 13 to July 20, 1944

Boiler Output lb/hr	Number of Determinations	Boiler Water Avg.* T.S.ppm	Steam Sample Avg.* T.S.ppm
550,000	3	593	0.34
572,000	3	1107	0.34
610,000	7	598	0.37
650,000	1	1137	0.37

* T.S. is total solids determined by evaporation.

Effect of Circulation Rate on Internal Surface of Tubes. In June, 1943, the boiler was placed in operation with one oversize and one undersize orifice. The location of the circuits, orifice size, and relative circulation rates are given in Table 5, section A. Table 5, section B, lists the number and location of thermocouples which were installed in 2-ft-long sections of new tubing having polished inside surfaces. These sections were installed to determine whether corrosion would occur on polished surfaces with the new potassium treatment, including the feeding of silica, and whether rate of circulation had any effect. A polished section was also installed in the adjacent rear-wall circuit near the discharge end, in the zone above the furnace roof where the tube would not be exposed to heat.

At the end of 1 month of operation at 470,000 lb per hr average load and 630,000 lb per hr maximum load, one half of the polished sections were removed from the two rear-wall tubes. A superficial examination revealed no difference between the two tubes; each was lightly and uniformly coated on the inside with a film of gray sludge, and under the coating of each the metal had been slightly attacked on the fire side but less so on the side toward the casing.

At the end of another month of operation at an average load of 510,000 lb per hr, the remaining half of the original polished sections were removed from the rear-wall tubes. Again a superficial examination revealed no difference between the two sections but there were a few small pits on each. The polished sections from the side wall were not removed for examination at this time since the study of the rear-wall tubes had shown no difference in appearance even with relative circulation rates of nearly 2 to 1. The results of a more elaborate examination of the foregoing and other polished sections removed at later dates are discussed in another paper of this series (12).

In June, 1944, when it had become apparent that the omission of silica from the water treatment had resulted in improved conditions, another special study was commenced involving four circuits in the right side wall as previously mentioned and described (see Table 6). After a year of operation tube sections were removed from these circuits in September, 1945. Again, superficial examination of the tubes indicated that the rate of circulation, within the range of 200 to 75 per cent of normal, had little effect on the appearance of the surface. Regardless of rate of circulation, all the tubes had a light coating of black sludge of less thickness than had been found the year previous; the side toward the fire was much cleaner than the side toward the casing; metal under the film was very smooth on both fire side and casing side except for numerous small pinpoint pits which occurred more frequently on the unheated side than on the heated side.

Table 8 shows the marked difference in weight of deposit for the fire side compared to the casing side; in each case the tubes were split along the vertical axis separating the fire side and the casing side, and all the sludge deposit from a 5-in. length was removed and weighed. It will also be noted that the tube which had the highest rate of circulation also had the largest deposit of sludge.

TABLE 8 COMPARISON OF WEIGHT OF SLUDGE SCRAPINGS FROM TUBES WITH UNDERSIZE, OVERSIZE, AND NORMAL ORIFICES

Orifice Designation		Oversize	Normal	Undersize
Orifice Diameter - in.		0.50	0.34	0.30
Tube Number		138	134	136
		Weight of Sludge - Milligrams		
Fire Side		162.1	96.0	97.5
Casing Side		244.1	179.0	146.7
	Total	406.2	275.0	244.2

The results of a carefulexamination of the surfaces of other specimens from the same tubes are discussed in another paper of this series (12).

PERFORMANCE

Circulating Pumps. The boiler is normally operated with two

pumps running and the third pump idle with suction and discharge valves closed. Normally, at least one dual-drive pump is always in service and after 3 years of operation a power failure did occur and trip out both pump motors; the turbine drive on one pump took over the load and maintained full speed on one pump. Test data plotted in Figs. 5 and 6 show that two pumps handle about 3,200,000 lb per hr and since the operating water content of the boiler is about 30,000 lb (exclusive of economizer), this represents a recirculation rate of more than 100 times per hr. The ratio of water to steam for any rate of output can also be readily determined from either Fig. 5 or Fig. 6. It will be noted that at maximum load of 650,000 lb per hr, this ratio is about 5 with two-pump operation, and the same ratio would be maintained with one pump up to a load of about 450,000 lb per hr. At 650,000 lb per hr load with one pump the water-to-steam ratio would be nearly 3 to 1, a condition which should not cause any trouble during an emergency period since it has been proved in experiments with circuits that operation at one half normal circulation over a period of 2 months produced no ill effect. It has, however, been the practice not to exceed 400,000 lb per hr output with one pump, particularly if the other two pumps were not in condition to operate. There were short periods early in 1943 when only one pump was in operating condition, but Table 1 shows that no outage of the boiler was ever caused by the circulating pumps.

The circulating-pump specifications rate each pump at 3500 gpm 50 psi head (184 ft) when handling water at 630 F and operating at 1750 rpm, but shop tests by the manufacturer indicated the total head to be 192 ft at the capacity mentioned. Owing to conservative pressure-drop calculations for the circulating system, the actual resistance for a given flow rate is lower than anticipated, and consequently, the pumps operate at higher than design capacity. Fig. 7 would indicate that when two pumps are operating, each is handling about 4600 gpm rather than 3500 gpm and that with single-pump operation the capacity is nearly 6000 gpm.

With two-pump operation each pump uses an average of 37 amp at 2300 v which is equivalent to about 3,500,000 Btu per hr in fuel fired, or a gross input to the two motors equal to less than 0.5 per cent of the fuel fired at maximum load. The hydraulic horsepower under the same conditions would be 240 for two pumps, which represents input of energy to the water at the rate of about 600,000 Btu per hr, so the net consumption of the pump drivers would be equivalent to 0.35 per cent of the heat in the fuel fired at maximum output.

Heat Absorption and Distribution. No attempt was made to check the actual distribution of heat to the various furnace walls but it can be calculated from average heat-absorption rate and exposed surface with due allowance for surface effectiveness. Table 2 shows that measured distribution of water to the various furnace walls is almost identical to calculated distribution of heat.

Distribution of heat to various other parts of the unit such as superheater, reheater, economizer, and air heater, is readily checked by measuring temperature rise or drop of one or both fluids and calculating or measuring the quantity of the fluids. Total heat absorption of each part of the unit was very close to manufacturer's predictions, except in the case of the reheater which was too conservatively designed. The method of correcting the reheated-steam temperature has been discussed elsewhere in this paper.

Figs. 11 and 12 show the results of informal tests in October and November, 1943, with both coal and oil firing, compared to predicted performance for coal-firing represented by the curves. The steam-temperature controller was set to maintain 950 to 960 F, according to the Micromax recorder, and the reheat temperature was also being regulated according to recorder, but at the end of the tests the recorder was checked and found to be reading 15 deg F too high. The corrected temperatures are plotted and therefore fall below the predicted values. However, for the tests above 450,000 lb per hr output higher steam temperature could readily have been obtained, because during these tests the by-pass dampers were being used to reduce the temperature of high-pressure steam, and the reheated-steam temperature was being reduced by desuperheating.

In comparing the results of the oil-firing and coal-firing tests it should be noted that oil was used only for the duration of the tests and coal was used during about 16 hours of each day. Therefore the furnace walls and other heating surfaces were not as clean as would be the case with prolonged used of oil.

Although the average gas temperature leaving the two heaters was close to contract predictions, the air temperature during these tests was higher than predicted. The three factors responsible for this were: (*a*) lower ratio of air to gas (*b*) higher gas-inlet temperature, (*c*) higher air-inlet temperature; but because of conservative selection of air-heater surface, the air-heater heat absorption was close to predictions. Air leaks into the economizer were responsible for the low ratio of air to gas, and these have been stopped, thus reducing both air-outlet and gas-outlet temperatures.

Superheat Control. Steam temperature from the high-pressure superheater is automatically controlled and the equipment used is described in another paper of this series (13). Automatic regulation of both sets of dampers at the economizer outlet results in very close regulation. Starting with the conditions which exist immediately after operating the furnace wall blowers, the by-pass damper is fully closed or slightly open depending upon the rate of output. As the furnace accumulates ash and the gas temperature increases, the by-pass dampers automatically open and maintain the steam temperature within ±5 F of the desired limit. At the end of an 8-hr operating period the by-pass dampers will be 50 to 80 per cent open, depending upon the output rate and the nature of the coal. Then, as the wall blowers are operated, the by-pass dampers operate automatically to compensate for the effect of removing the ash from the walls and maintain the same close regulation of steam temperature during the cleaning period. Tests were conducted to determine the full effect of operating the by-pass dampers from closed to 75 per cent open. As mentioned elsewhere the lower economizer dampers close as the by-pass dampers open, but a stop on the regulator cylinder prevents the former from closing fully, because full closing has never been necessary to obtain the desired control. Fig. 13 shows the results of these tests and illustrates how the heat absorption of the combined economizers increases as the by-pass dampers open, thus compensating for the decreased superheater absorption and resulting in very little increase of final gas temperature. Oil-firing was used in order to maintain uniform conditions of furnace cleanliness during the tests.

Capacity and Flexibility. The maximum peak capacity of the boiler has never been determined. The maximum demand has been 670,000 lb per hr but the feeders, burners, fans, and circulating pumps are adequate for higher output.

At reduced pressure there is no decrease in circulation, and the volumetric percentage of steam in the mixture leaving the generating tubes will increase so the average velocity in the tubes is greater. The unit is therefore very flexible as regards operation at variable pressure, and the upper limit of capacity would be governed by considerations of steam purity and steam temperature rather than circulation. These upper limits were not determined. During special tests on the high-pressure turbine, wide swings in pressure, output, and steam temperature were accomplished very rapidly and with an excellent degree of control.

The boiler has a very stable water level even under extreme op-

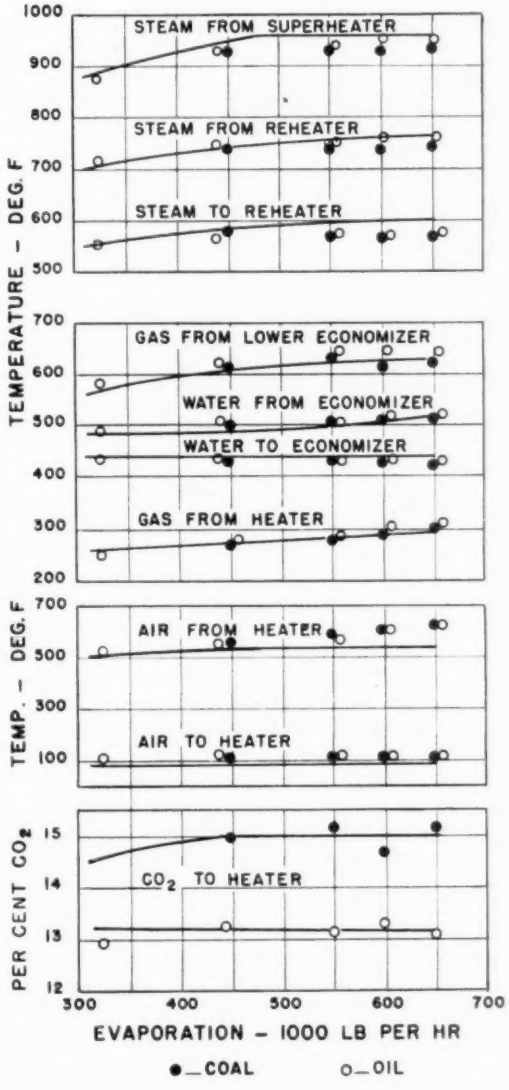


FIG. 11 RESULTS OF TESTS WITH COAL- AND OIL-FIRING COMPARED TO PREDICTED PERFORMANCE

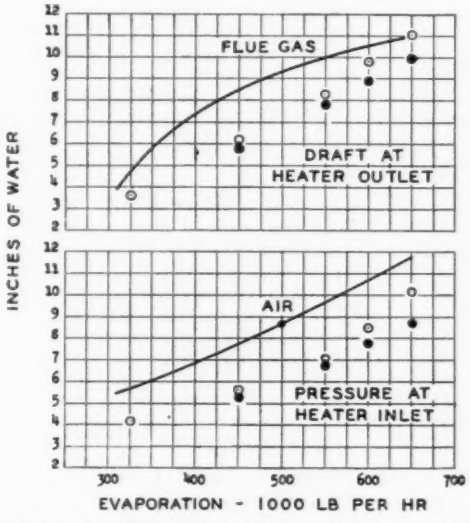


FIG. 12 RESULTS OF TESTS WITH COAL- AND OIL-FIRING COMPARED TO PREDICTED PERFORMANCE

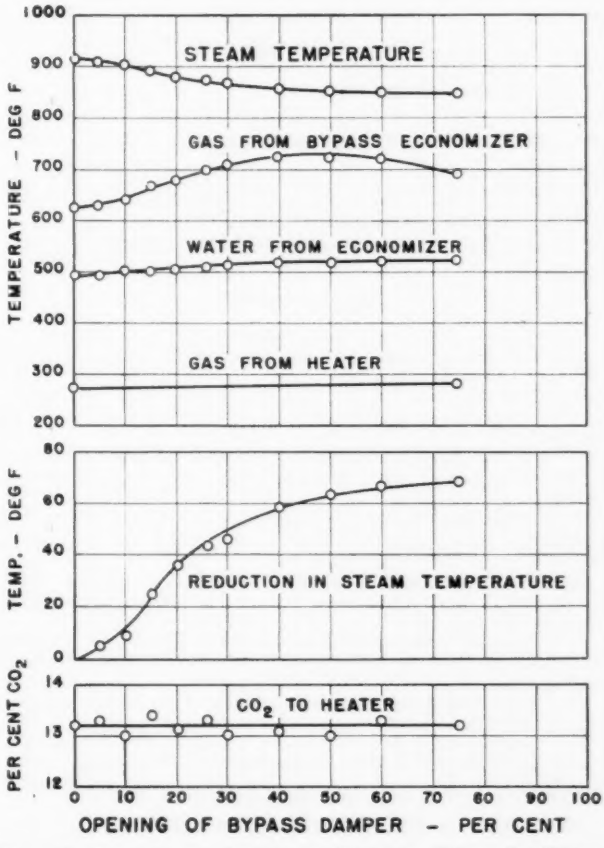


FIG. 13 RESULTS OF SUPERHEAT-CONTROL TEST, OIL-FIRING, 560,000 LB PER HR OUTPUT, 1900 PSI DRUM PRESSURE

erating conditions of sudden load increase or decrease. In fact, sudden emergency load changes have occurred without any perceptible change in water level. Also, on the occasion of furnace-tube failures, it has not been difficult to maintain water level while reducing load and pressure in an orderly manner.

Efficiency. Coal and ash samples were not collected during the informal tests conducted in 1943, so complete heat-balance figures are not available.

The contract over-all efficiency with coal-firing at 650,000 lb per hr output was 89.3 per cent, based on coal of 14,200 Btu per lb, with 2.8 per cent moisture as fired; and based on 15 per cent CO_2 in gases at the economizer outlet, with 290 F gas temperature leaving the air heater, 80 F entering-air temperature, and with 0.6 per cent allowance for unburned combustible.

During the reported tests at 650,000 lb per hr output, the CO_2 at the economizer outlet averaged 15.2 per cent, the air entering the heaters was 110 F, and gas leaving the heaters 306 F. Tests to determine heat loss due to combustible in fly ash were conducted at a later date when the maximum load demand on the boiler averaged 572,000 lb per hr, the CO_2 entering the convection superheater section was 16 per cent, and the average heat loss in the fly-ash combustible for two tests was 0.47 per cent. The results of two other tests with 15 per cent CO_2, at the same output, averaged 0.34 per cent heat loss in the fly-ash combustible.

CONCLUSION

The authors have revealed all the experiences with this high-

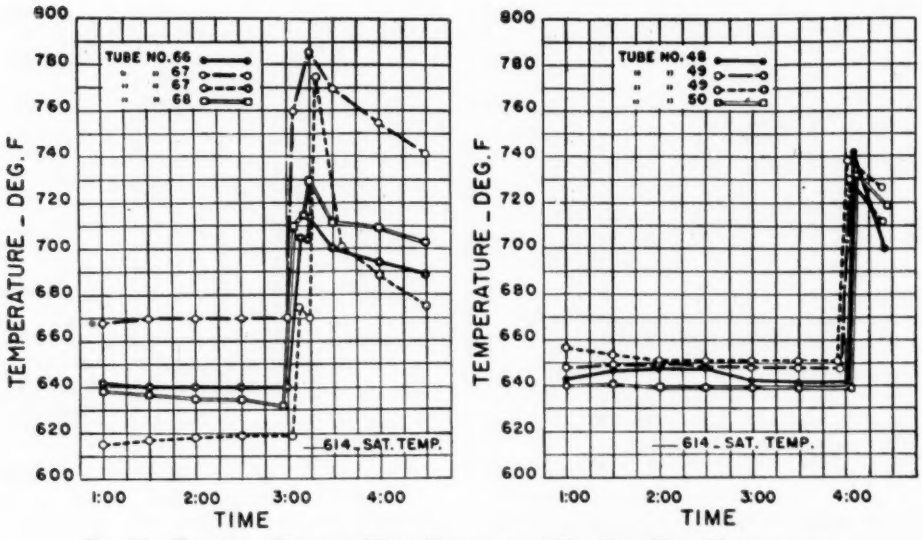


FIG. 14 EFFECT OF FURNACE WALL CLEANING ON HOT FACE TUBE TEMPERATURE

pressure boiler in considerable detail so that others may benefit from a knowledge of what has been going on at this station during the last 3 years. The special test and research activities reported in this and its companion papers (11, 12, 13) represent only a part of the total number of special studies conducted. Many of these were associated more with operation problems of the station as a whole than with problems peculiar to the forced-circulation boiler. The judgment of those responsible for selecting a bare-tube, slagging-bottom, radiant, forced-circulation boiler for this high-pressure application has been verified by the operating record of this boiler.

BIBLIOGRAPHY

1 "1825-Lb-Pressure Topping Unit With Special Reference to Forced-Circulation Boiler," by F. S. Clark, F. H. Rosencrants, and W. H. Armacost, Trans. A.S.M.E., vol. 65, 1943, pp. 461–474.

2 "First American Utility Plant Uses Forced-Feed Circulation," by F. S. Clark, *Electrical World*, vol. 116, August 23, 1941, pp. 52–54, and 66.

3 "A New Approach to the Problem of Conditioning Water for Steam Generation," by R. E. Hall, Trans. A.S.M.E., vol. 66, 1944, pp. 457–474.

4 "Experience With Sodium and Potassium Chemicals for Boiler-Water Conditioning at Montaup Electric," by G. U. Parks, Trans. A.S.M.E., vol. 67, 1945, pp. 335–338.

5 "Qualitative Determination of Steam-Water Mixtures," by T. Ravese and C. G. R. Humphreys, *Combustion*, vol. 16, January, 1945, pp. 37–39.

6 "Thermocouples for Furnace Tube Surface Temperature Measurements," by C. G. R. Humphreys, *Combustion*, vol. 16, December, 1944, pp. 53–55.

7 "Measurements of Boiler Circulation by Means of Pitot Tubes," by T. Ravese, *Combustion*, vol. 16, October, 1944, pp. 43–45.

8 "Studies of Heat Transmission Through Boiler Tubing at Pressures From 500 to 3300 Pounds," by W. F. Davidson, P. H. Hardie, C. G. R. Humphreys, A. A. Markson, A. R. Mumford, and T. Ravese, Trans. A.S.M.E., vol. 65, 1943, pp. 553–579.

9 "Furnace Performance Factors," A.S.M.E. Pamphlet published May, 1944. Consisting of papers presented at the 1943 Annual Meeting of the American Society of Mechanical Engineers.

10 "Factors Affecting Metal Temperature of Furnace and Boiler Tubes," by W. S. Patterson, *Combustion*, vol. 12, 1940, pp. 24–29.

11 "Special Studies of the Feedwater-Steam System," by W. D. Bissell, B. J. Cross, and H. E. White, published on pages 429–442 of this issue of Transactions..

12 "Results of Potassium Treatment," by W. W. Cerna and A. K. Scott, published on pages 443–451 of this issue of Transactions.

13 "Experience With Instruments and Control Equipment for 2000-Psi Boiler at Somerset Station of Montaup Electric Company," by W. D. Bissell and E. B. Powell, published on pages 453–466 of this issue of Transactions.

Discussion

LEWIS J. DAWSON.[6] It may be in order at this time to restate the suction conditions under which the circulating pumps operate in order that the importance of the labyrinth design can be understood. The water handled by the impeller is at full boiler pressure of about 1900 psi and at the corresponding saturation temperature of 630 F. The pressure, temperature, and incipient flashing preclude the possibility of using a conventional stuffing box in which the packing is subjected to suction conditions. The injection and bleed-off arrangement is required to give safe stuffing-box conditions and normal packing life. The labyrinth must be of a reasonable length and of close clearance to reduce injection water requirements. These two factors make it important that labyrinth alignment be maintained.

After it became apparent that misalignment was causing the labyrinth failures, the support under the coupling end of the bearing body was removed which allowed the pump to move freely with the piping so that no internal misalignment could occur. Measurements were taken of the movement of the free end under various operating and stand-by conditions. These measurements revealed that pipe movement was the major factor, with uneven bracket temperature of secondary importance. Variations in these measurements, both vertical and horizontal, could be obtained by warming and starting one of the remaining two pumps, showing that temperature changes in the common piping affected alignment of the unit being measured. Equalization of bearing-bracket temperature did not restore alignment.

The units are equipped with spacer-type gear couplings, so that the resultant 0.030 to 0.040 in. misalignment between pump and driver can be tolerated. In connection with the couplings, the author has mentioned the limit stops which were installed to prevent motor bearing failure. It is a sad commentary on motor design that all large motors must be protected in this manner because of inadequate thrust-bearing capacity.

Failures of oil-pump spiral drive gears were found due to wear in the oil-pump shaft bearings. This resulted in improper alignment and tooth contact between gear members. The new-design bearing housing has incorporated a ball-bearing oil-pump shaft support.

---

[6] Field Engineer, Cameron Engineering Service, Ingersoll-Rand Company, Phillipsburg, N. J. Jun. A.S.M.E.

With reference to Fig. 7 of the paper, it is probable that the actual operating speed is close to 1790 rpm under the reduced horsepower loading. The majority of the steaming test points fall reasonably close to the revised head-capacity curve. We note that the field points having greatest deviation are all from high-temperature water readings. Checking the point of greatest deviation, calculating the water horsepower and comparing it to brake horsepower input, we arrive at a pump efficiency 21 per cent greater than the manufacturer's shop test curve value at the corresponding capacity. This would lead us to believe that the Pitot tube calibration is off at high water temperatures and corresponding low densities.

Authors' Closure

The same data which Mr. Dawson used in arriving at his statement that pipe movement was the major cause of pump misalignment can be interpreted differently when all the operating procedures occurring at the time of measurement are also taken into consideration.

Fig. 4 shows the position of the suction pipes to each pump, and the suction header which is common to all three pumps. The horizontal movement of these three pipes was measured at an elevation 20 ft above the pumps during the process of raising pressure on the boiler and it was found that there was no movement of the center pipe while the movement of each outside pipe was about $^1/_4$ in., but in opposite directions, as would be expected due to expansion of the suction header. This being the case, one would expect the movement of the coupling end of the bearing to be in opposite directions on *A* and *C* pumps, and no movement on *B* pump, if due to pipe strain. Instead this end of the bearing body moved downward on all three pumps, from a cold to hot condition, and the cause of the pump misalignment therefore is a controversial subject. The fact remains that the trouble was corrected by merely allowing the coupling end of the bearing to float freely and by taking steps to equalize upper and lower bearing bracket temperatures.

The authors desire to comment further on the tube failures which occurred on October 26, 1945. The amount of sludge found in the drum after this failure was greater than had previously accumulated during any operating period of equal duration, and this sludge was nearly 70 per cent copper. Sludge deposits from the generating tubes were also higher in copper content than previously noted. This would indicate that prior to this failure unusual feedwater contamination in the form of corrosion products, including copper, had been prevalent.

The failures located 20 ft above the floor were diagnosed as having been caused by sludge deposits and subsequent overheating sufficient to cause weakened metal and intergranular rupture. The failure close to the furnace floor may also have been started by sludge accumulation which increased the outside surface temperature a sufficient amount to accelerate external tube corrosion. Concurrently corrosion was causing a thinning of the metal from the inside and laying down a deposit of the corrosion product, iron oxide, to further insulate the inside of the tube. When the tube became thin enough a small bulge occurred which quickly overheated locally until rupture occured.

After acid washing the boiler, thermocouples were installed at four elevations between 8 in. and 24 ft above the floor on the tube which had failed close to the furnace floor. During the past five months these couples have been read twice daily and some of them connected to a recorder for a continuous record. The metal temperature 8 in. above the molten slag on the floor varies between saturation temperature (about 630 F) and 765 F but there has been no gradual increase as would be expected if sludge were again accumulating on the inside surface. The maximum temperature at higher elevations has been 10 to 20 deg F lower. The furnace tubes were checked for external corrosion about January 1, 1946, and there was no evidence of any further attack on any of the walls.

Special Studies of the Feedwater-Steam System of the 2000-Psi Boiler at Somerset Station of Montaup Electric Company

By W. D. BISSELL [1] B. J. CROSS [2] AND H. E. WHITE [3]

In conjunction with other studies on the high-pressure forced-circulation boiler at the Somerset Station of the Montaup Electric Company during the past 3 years, tests to determine, particularly, the extent of dissolution of iron throughout the system, and the formation of high-iron sludges were made. A summary of the findings of this investigation are given in this paper.

DURING the course of a complete investigation of the high-pressure forced-circulation boiler at the Somerset Station of the Montaup Electric Company covering the past 3 years, a special study was made on the feedwater and steam system particularly with regard to the dissolution of iron throughout the system, and the formation of high-iron sludges within the boiler. This paper gives a summary of the findings of these studies.

The period covered by this work was from January, 1944, to October, 1945. The boiler was thoroughly cleaned by acid treatment late in December, 1943. The boiler water has been continually on potassium-salt treatment since May, 1943.

Over the past few years the occurrence of iron oxide in boilers has become a matter of interest, if not concern, to operators of high-pressure boilers, as the presence of this substance must always indicate corrosion in some part of the system. Usually the amount of iron oxide is small by comparison with the large area of steel surfaces involved, and the indicated loss of metal, if uniformly distributed, is not large enough to be a cause of great concern. If, however, there are small areas of concentrated attack, the amount of iron oxide found may well indicate serious corrosion leading to failures.

Even in the case of uniform corrosion of iron which in itself may not be a serious matter, the accumulation of the solid products might lead to failures in the boiler by insulation effect on surfaces receiving heat and also by obstructing passages and thereby interfering with circulation of water.

Sludge deposits found in the high-pressure boiler at the Somerset Station were of particular concern because tube failures that had occurred were attributed to these deposits either on the surfaces of the tubes or on the strainers protecting the orifices in the tube circuits.

The examination of samples of tubes cut from furnace walls at periodic examinations disclosed a thin film of deposit on the entire inner surface of the tube. On the evaporative surfaces the deposit was usually baked on in a semiscalelike form. On the inactive surfaces it occurred as a slime which dried out to a dust. Both types of deposits could be removed with a stiff brush. Slime deposits of sludge also were found in the inlet headers, on orifice strainers and on other surfaces not exposed to external heat. Scalelike flakes of caked sludge have been found lodged in the holes in the strainers. Some of these flakes had a curvature indicating that they had formed in headers or downtake piping. Deposits found in the drum were more granular than those found in the tubes and probably represent the heavier components of the sludge.

The composition of the sludge varied somewhat with location but all deposits had a high proportion of black iron oxide. Typical analyses of sludges are given in Table 1.

TABLE 1 TYPICAL ANALYSES OF SLUDGES

SAMPLE NUMBER	1	2	3	4	5	6
IRON AS Fe_2O_3 - PER CENT	53.3	47.0	78.3	27	63	42
PHOSPHATE AS P_2O_5 - PER CENT	18.5	3.3	6.0	20-25	6-8	12-15
SILICA AS SiO_2 - PER CENT	.6	TRACE	.5	.5	1	TRACE
CALCIUM AS CaO - PER CENT	12.3	4.1	6.5	20.0	10	15-20
MAGNESIUM AS MgO - PER CENT	10.3	1.6	5	12-15	4-8	8-10
COPPER AS Cu - PER CENT	-	41.3	4.2	-	7	2

1. SUSPENDED SLUDGE AT BLOW DOWN.
2. DRIFT DEPOSIT IN WET DRUM.
3. DEPOSITS ON STRAINERS.
4. DEPOSIT ON DOWNCOMER SCREENS
5. DEPOSITS IN REAR HEADER COLLECTING CHAMBER.
6. SLUDGE FROM REAR HEADERS.

The high proportion of iron oxide in these sludges naturally led to some concern as, if it were formed entirely within the boiler, it might indicate severe local corrosion or pitting that would result ultimately in failure.

The accumulation of sludge, regardless of its composition, in the boiler might result in stoppages of furnace circuits or overheating of metal by insulation of heat-absorbing surfaces. Corrosion may occur as a result of the concentration of boiler-water salts under deposits of sludge on heating surfaces. It is known that adherent scales may form under such deposits on steam-generating surfaces as a result of the concentration of the components in the sludge "sponge" and the higher metal temperature resulting from the insulation of the metal.

The high-pressure boiler at this station delivers steam at 1850 psig and 950 F to the high-pressure turbine. This turbine exhausts through a reheater to the low-pressure system. The water supplied to the boilers is condensate with make-up supplied by evaporators. The principal outside sources of contamination were condenser leakage and evaporator carry-over.

A simplified diagram of the feedwater system is shown in Fig. 1. The condensate from the hot-well pumps passes successively through the oil cooler, 15th-stage heater, deaerating heater, 10th-stage heater, low-pressure feed pumps, exhaust heater, extraction heater, high-pressure feed pumps, high-pressure heaters, and to the economizer. The drips from the various heaters are re-

[1] Somerset Station, Montaup Electric Company, Fall River, Mass.
[2] Combustion Engineering Company, Inc., New York, N. Y. Mem. A.S.M.E.
[3] Stone & Webster Engineering Corporation, Boston, Mass. Mem. A.S.M.E.

Contributed by the Power, Industrial Instruments and Regulators Divisions, and the Joint Research Committee on Boiler Feedwater Studies, and presented at the Annual Meeting, New York, N. Y., Nov. 26–29, 1945, of THE AMERICAN SOCIETY OF MECHANICAL ENGINEERS.

NOTE: Statements and opinions advanced in papers are to be understood as individual expressions of authors and not of the Society.

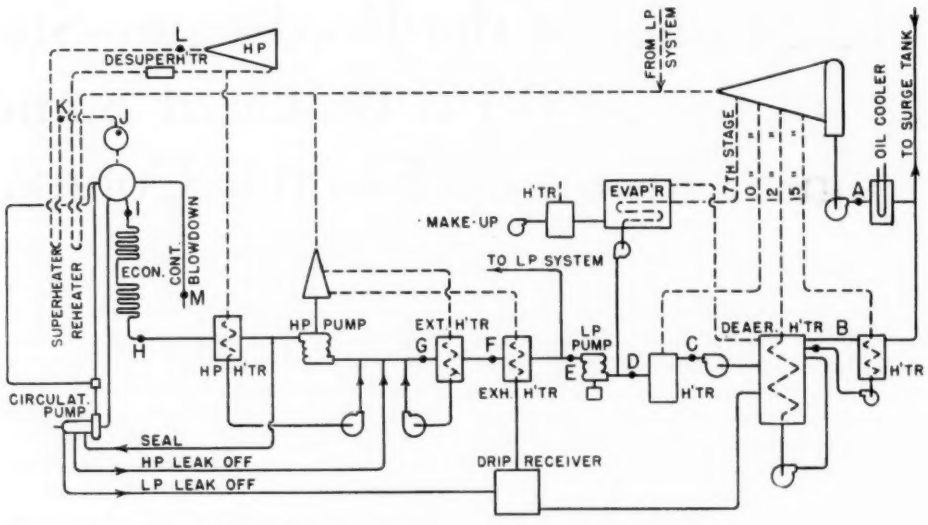


FIG. 1 SIMPLIFIED DIAGRAM OF FEEDWATER SYSTEM

turned to the main stream as indicated. The gland water for the circulating pumps is taken before the high-pressure heaters. The high-pressure leak-off is returned to the feed-pump suction and the low-pressure leak-off to the deaerating heater. Sampling points are indicated in this diagram and are also listed in Table 2. The fluid temperature and pressure and the type of cooling coil used are given in this Table.

TABLE 2 LOCATION AND DATA OF SAMPLING POINTS

	TEMPERATURE °F	PRESSURE LB/SQ IN	COOLING COIL
POINT A - HOT WELL PUMP	80–100	40	NONE
B - 15TH STAGE HEATER	160	40	ST. STEEL
C - DEAERATOR OUTLET	215	80	COPPER
D - 10TH STAGE HEATER	240	80	"
E - LOW PRESSURE PUMP	250	500	"
F - EXHAUST HEATER	290	500	"
G - EXTRACTION HEATER	340	500	"
H - ECONOMIZER INLET	450	2150	"
I - ECONOMIZER OUTLET	520	2150	"
J - STEAM DRY DRUM	630	1950	MONEL
K - STEAM SATURATED HEADER	630	1930	"
L - SUPERHEATED STEAM	950	1850	"
M - BOILER BLOW DOWN	630	1950	"

This diagram represents the condition at the time most of the work reported was done. Minor changes have since been made.

SCOPE OF INVESTIGATION

The feedwater study may be divided into several phases both on the basis of the nature of the work done and on the time periods. Because of wartime restrictions of both manpower and equipment, all of the work could not be carried on simultaneously. Each phase of the investigation is listed in the following tabulation and is discussed in order:

Period 1.

(*a*) The continuous measurement of hydrogen in feedwater and steam and oxygen in feedwater.

(*b*) The measurement of total solids in feedwater, steam and blowdown.

(*c*) The measurement of suspended solids in boiler water at shutdowns of the boiler.

(*d*) The study of gases in steam, particularly as affected by small variation in boiler-water conditions and the normal irregularities in the functioning of auxiliary equipment.

Period 2. The exploration of the feedwater system for dissolved hydrogen, dissolved iron and changes in alkalinity (pH).

Period 3.

Miscellaneous studies as follows:

(*a*) Copper in feedwater.
(*b*) Bead column and ion exchanger column tests.
(*c*) Tube-temperature measurement.
(*d*) Corrosion detector.

The work under Period 1 was done during January, February, and March, 1944.

Period 1 (*a*). Recording hydrogen meters were set up to give a continuous record of the dissolved hydrogen in feedwater and in the steam delivered by the boiler. As hydrogen is one of the products of the reaction of water with iron, the amount of hydrogen evolved may be taken as a measure of the rate of corrosion. As irregularities in the performance of the deaerating heater were suspected, a dissolved-oxygen meter was also installed to sample the feedwater to the boiler. With the exception of short outages for adjustments and maintenance, these instruments have been in continuous operation since January, 1944. Originally they were installed close to the point of sampling but later moved, when stainless-steel tubing became available, to a more convenient location for observation by the boiler operators.

The hydrogen record for the 3-month period, January, February, and March is plotted in Fig. 2. Steam flow and boiler pressures are also shown on this chart. It may be seen that while the hydrogen content of the feedwater is substantially constant, the hydrogen in steam showed relatively high values in the early part of January, with a gradual reduction in these values until they leveled out at $1^1/_2$ to 1 part per billion over the feedwater values. While the high hydrogen values during the first week of the month may be partly accounted for by the lower rating, it is believed that they are in greater part due to residual hydrogen in the system following the acid wash.

The feedwater sample was usually taken from the economizer inlet. It was, however, occasionally taken at the economizer outlet. The values for hydrogen at the economizer outlet fell between those of the inlet and the steam leaving the boiler.

The significant feature of these hydrogen curves is the fact that they show that a large part of the hydrogen in the steam enters the boiler with the feedwater. Also there is an indication from the few readings taken that there is an increase in hydrogen across the economizer.

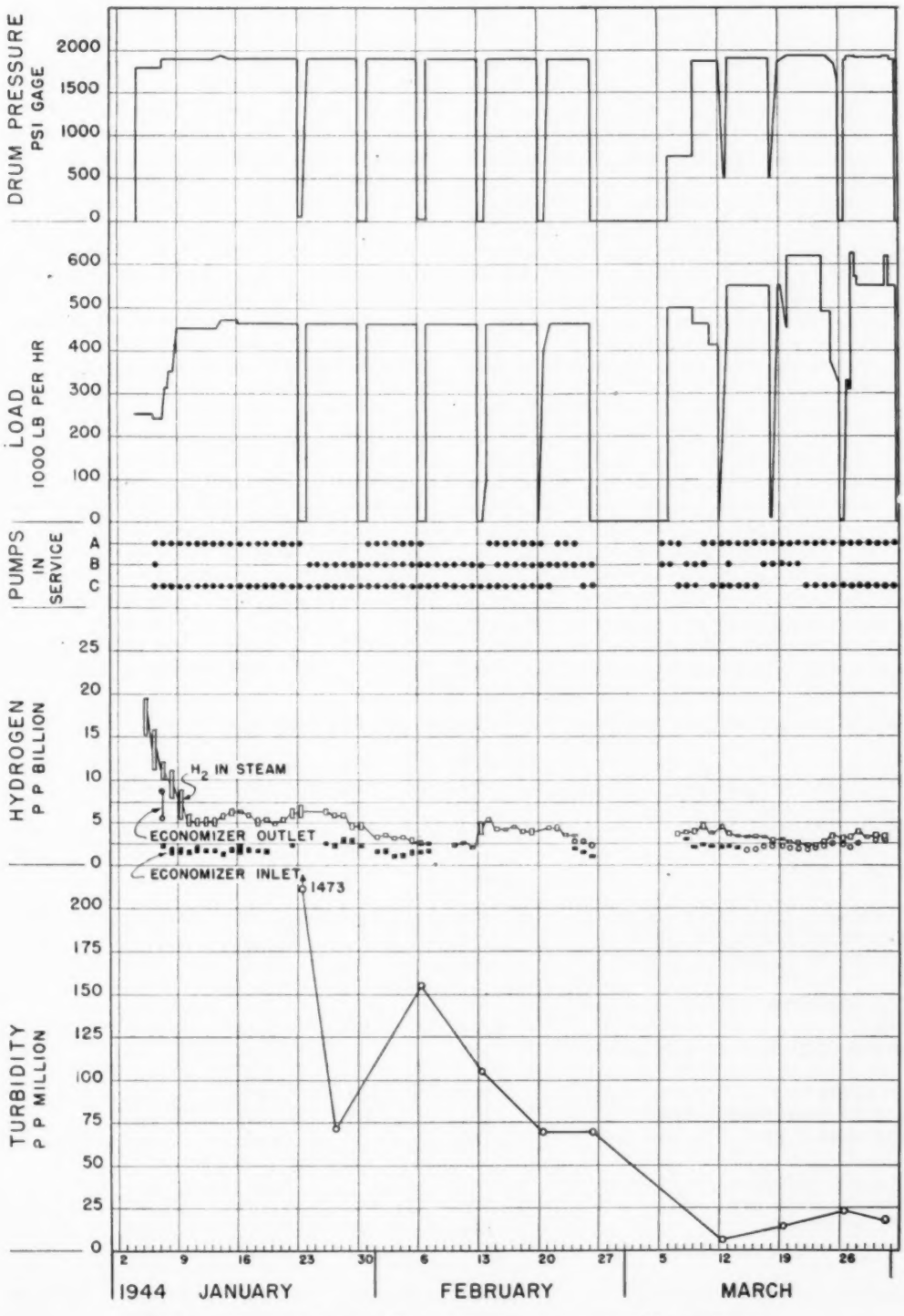


FIG. 2 HYDROGEN CONTENT RECORD OF FEEDWATER FOR 3-MONTH PERIOD

A consideration of the probable reaction of iron with water presents the possibility that hydrogen may be evolved in the economizer and boiler without any reaction involving the metal of the boiler. It has been proposed that in the lower-temperature areas the reaction may be

$$Fe + 2H_2O \rightarrow Fe(OH)_2 + H_2$$

At the higher temperature of the boiler and economizer the ferrous hydroxide may react to form magnetic oxide

$$3Fe(OH)_2 \rightarrow Fe_3O_4 + 2H_2O + H_2$$

If, however, all of the hydrogen formed in the boiler came from this second reaction, the relative amounts of H_2 in feedwater and

steam would be 3 to 4. Actually it is nearer to 2 than 3, which indicates some reaction with the boiler metal.

During the 3-month period represented by this chart there were sporadic occurrences of small amounts of dissolved oxygen in the feedwater to the high-pressure unit. Changes in the deaerating system, made in the spring of 1944, resulted in consistently good removal of air and since that time the feedwater has been substantially oxygen-free.

Period 1 (b): Total Solids in Feedwater, Steam, and Blowdown. The first approach to the sludge problem was a study of the amounts of total solids delivered to the boiler in the feedwater and leaving the boiler with the steam produced and the blowdown removed. Samples of feedwater, steam and blowdown were collected in hourly increments over an 8-hr period. These samples were evaporated to dryness and the residues weighed. The standard-size samples were 3 liters for the feedwater, 3 to 4 liters for the steam, and $^1/_2$ liter for the blowdown. All samples were evaporated without boiling in closed containers ventilated with filtered air.

The results of a number of determinations are given in Table 3, with the calculations leading to the total amounts of solids delivered to the boiler and removed from the boiler for a 24-hr period. Feedwater and steam flows were taken from station meters. The boiler blowdown was passed through cooling coils and weighed. Because of the dilution of the feedwater with condensate from the high-pressure and the extraction heater after the point of sampling, it was necessary to correct the total solids in feedwater by analysis for this dilution. Also, because some of the steam produced is diverted through the high-pressure heater and returned to the boiler as feedwater, the measured steam flow must be reduced by that amount.

It will be noted that there is in each case a positive unaccounted-for balance which presumably remains in the boiler.

In a number of tests the iron content of the total-solids residues was determined. The calculations for iron were carried out in the same manner as for the total solids and a figure for iron remaining in the boiler was obtained. These results also are given in Table 1. As with total solids, there is a positive unaccounted-for amount of iron.

Period 1 (c): Suspended Solids in Boiler Water. A measure of the relative amount of sludge formed and remaining in the boiler was afforded by the determination of turbidity of the boiler water that occurs when the boiler is taken out of service. It had long been noted that on shutting down the boiler the water becomes turbid and that the maximum concentration of suspended solids occurred at the pressure interval of 600 to 400 lb pressure; this being at the time the fires were extinguished. Advantage is taken of this period to remove much of the accumulated sludge by blowing down. During January, February, and March, 1944, each week was a test period during which modifications in operating procedure were tried. After each week the boiler was taken out of service and the turbidity measured while the boiler was being blown down.

A graphic log of a typical shutdown is shown in Fig. 3. The various observations and measurements are plotted against time.

The rate of reduction in load and pressure is shown in the lowermost graphs with notation of various operations. The

TABLE 3 RESULTS OF TESTS TO DETERMINE TOTAL SOLIDS IN FEEDWATER, STEAM, AND BLOWDOWN

DATE - 1944		1/26	2/1	2/8	2/16	2/22	3/14
STEAM FLOW (METER) 1000 LB/HR		461	461	464	461	465	554
HP HTR DRIPS (EST) 1000 LB/HR		80	80	80	80	80	90
STEAM TO LP SYSTEM 1000 LB/HR		381	381	384	384	385	464
TOTAL SOLIDS IN STEAM - PPM		.76	.275	.47	.60	.40	.77
IRON IN STEAM - PPM		.026	-	.017	-	.029	.055
F.W. FLOW (STEAM + B.D.) 1000 LB/HR		461,500	461,487	464,475	461,596	465,590	554,594
T.S. IN FEED WATER (EXTR.HTR.) PPM		1.76	1.77	1.26	1.73	2.03	1.93
IRON IN FEED WATER (EXTR.HTR.) PPM		.146	-	.038	-	.06	.065
TOTAL SOLIDS CORRECTED (DILUTION BY H.P. DRIPS)		1.59	1.50	1.12	1.53	1.75	1.74
IRON CORRECTED (DILUTION BY H.P.DRIPS)		.123	-	.034	-	.055	.063
BLOW DOWN - LB/HR		500	487	475	596	590	594
TOTAL SOLIDS IN BLOW DOWN - PPM		454	458	591	668	600	690
IRON IN BLOW DOWN - PPM		.160	-	.05	-	.032	.076
FLOW - 1,000,000 LB/DAY							
FEED WATER AT EXTR. HTR.		11.075	11.076	11.147	11.150	11.175	13.310
STEAM TO L.P. SYSTEM		9.144	9.144	9.216	9.216	9.144	11.147
BLOW DOWN		.0112	.0117	.0114	.0143	.0142	.0143
SOLIDS - LB/DAY -	IN FEED WATER	17.609	16.614	12.485	17.059	19.556	22.159
	IN STEAM	6.949	2.515	4.331	5.500	3.696	8.583
	IN BLOW DOWN	5.448	5.349	6.737	9.552	8.520	9.867
UNACCOUNTED TOTAL SOLIDS		5.212	7.874	1.317	2.007	7.340	4.709
IRON - LB/DAY -	IN FEED WATER	1.362		.379		.625	.839
	IN STEAM	.238		.157		.268	.613
	IN BLOW DOWN	.003		.0006		.0004	.001
UNACCOUNTED - IRON		1.121		.221		.357	.225

boiler had been in operation approximately 1 week using the *B* and *C* circulating pumps.

The dissolved hydrogen in feedwater and steam are plotted only up to the time that reduction in pressure occurs. The readings beyond that time had no significance as the flow of sample was too much reduced. The slight rise in hydrogen as the steam flow is reduced is characteristic of most of the shutdowns and may be due to the increased concentration of hydrogen with reduced flow of steam.

The reduction in concentration of chloride and sulphate is the result of increased rate of blowdown and is a measure of the dilution of boiler water with the increase in feedwater rate.

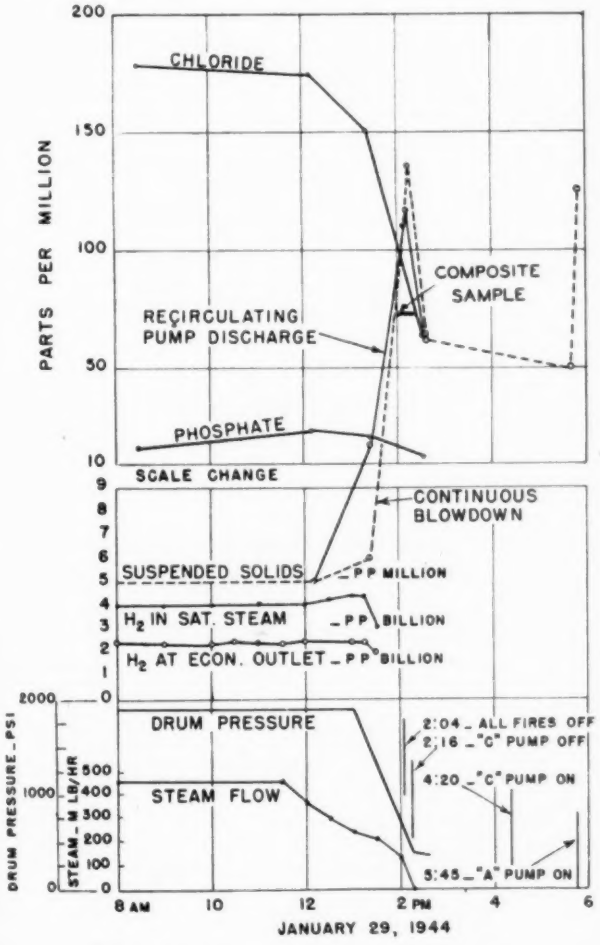


FIG. 3 LOG OF A TYPICAL BOILER SHUTDOWN

The phosphate does not show a corresponding reduction in concentration, indicating a slight "hideout" of that chemical. When corrected for dilution, a recovery of about 1 lb of phosphate as PO_4 is indicated. There is also a slight increase in the silica content of the water.

There are two graphs for boiler-water turbidity, one based on samples taken at the boiler blowdown, the other on samples taken at the discharge of the circulating pumps. While there is good agreement in the two sets of samples, the latter are regarded as the more accurate as the sampling lines were much shorter. The turbidity rose sharply to a maximum value of 135 ppm at the time the fire was extinguished, then decreased to 50 ppm by 5:40 pm. At that time the *A* circulating pump which had been out of service for a week was started. The increase in turbidity from 50 to 125 ppm was caused by the sludge that had settled out on the valves at the pump. As the water content of the boiler under nonsteaming conditions is about 50,000 lb, this increase in turbidity corresponds to $3^1/_2$ lb of sludge.

The composite sample taken over a 20-min period at the time indicated in the graph was assumed to represent the maximum sludge brought into suspension. The peak turbidity was of short duration and the sludge was probably not thoroughly distributed in the mass of the boiler water.

The shutdown procedure, as indicated on this chart, was established for the shutdown of January 29 and was followed as closely as possible on all subsequent tests.

The results of the turbidity measurements for January, February, and March, 1944, have been plotted in the lower graphs of Fig. 2 using, with the exception of January 22, the results of the composite samples. On the January 22 shutdown no composite sample was taken and the point indicated off scale was that of the maximum turbidity sample.

As may be noted, there is a decrease with time in the amount of sludge stirred up at shutdown periods. The high turbidity of the January 22 samples, which represented a full-pressure operating period of about 2 weeks, may be attributed at least in part to the effect of the acid wash. The gradual reduction in sludge over the 3-month period was principally the result of a closer control of condenser leakage and evaporator carry-over. Subsequent to this period of operation, sludge-collecting chambers were installed between the ends of the rear-waterwall inlet header and the side-wall inlet headers and also a sludge blowdown pipe was installed at the bottom of the main boiler drum. These were blown down once a week and the accumulated sludge thus removed during operation.

Period 1 (d): Gases in Steam. The study under this item was in greater part unrelated to the work covered in this report. A portion of the program, however, was a measurement of the gases in feedwater and steam and the results afforded an independent check on the hydrogen, indicated by the recorders. Samples of water and steam were passed through a special degasifier and the gases removed were accumulated until the quantity was sufficient for analysis by a modified Orsat apparatus. The results of these determinations indicated hydrogen values of the same order as those shown by the recording instruments. The readings of the dissolved-oxygen recorder were also checked using a modification of the Winkler test.

Period 2: Hydrogen, Iron, and pH. The work covered by this period was carried on during the interval, October, 1944, to April, 1945, after two additional hydrogen recorders had been acquired. The two original recorders had been set up permanently to sample the feedwater entering the economizer, and the steam leaving the desuperheater. One of the new recorders was set up at the hotwell-pump discharge, and the second one was arranged so that it could be moved to various locations along the line of feedwater flow.

The pH of the water was measured at the sampling points and samples were taken for the determination of iron. The pH was measured by an electrometric meter using a flow cell located at the point of sampling. It was found to be essential in the measurement of pH of water of high purity that the samples be not exposed to the air. Large errors may result from absorption and possibly the release of gases. Water samples of 1 liter were taken in hourly increments for the iron determination. A laboratory sample of 500 ml was evaporated to dryness in a dust-free atmosphere, then taken up with 1 ml of hydrochloric acid and diluted to 50 ml. The iron was determined by a colorimetric method using a photoelectric colorimeter.

In the determination of these very small quantities of iron

extreme care was necessary to avoid contamination of the samples. For this reason the samples were not filtered as this operation would involve a hazard of contamination through exposure to the air. Although the samples were all crystal-clear, occasionally one would show an inordinately high iron content, and it was suspected that an unnoticed particle of sludge had been included. In such cases the result was discarded.

The results of a number of tests are shown in the graphs in Fig. 4. Various conditions of load and pressure are represented. The values for dissolved hydrogen, pH, and iron are plotted for the various sampling points. The plotted points represent the average of daily samples taken over a 6- to 8-day period. It was not possible to take samples from all points during any one test period and usually 6 points were selected for each test. The selection was varied for different tests so that samples at all points were obtained during the course of the study.

For the study of hydrogen the plan was to have one meter stationed at the hot well and to advance the second one successively to stations along the line of flow. The hot-well sample consistently showed zero hydrogen throughout the study. No hydrogen was found at the deaerator outlet or the 10th-stage-heater outlet. Sporadic readings of low values were obtained at the discharge of the low-pressure boiler feed pump. From this point on there was a gradual increase in the quantity of dissolved hydrogen along the path of flow to the maximum values shown for the superheated steam. This study shows that all of the hydrogen which appears in the boiler feedwater originates in the feedwater system. The hydrogen in the steam is removed

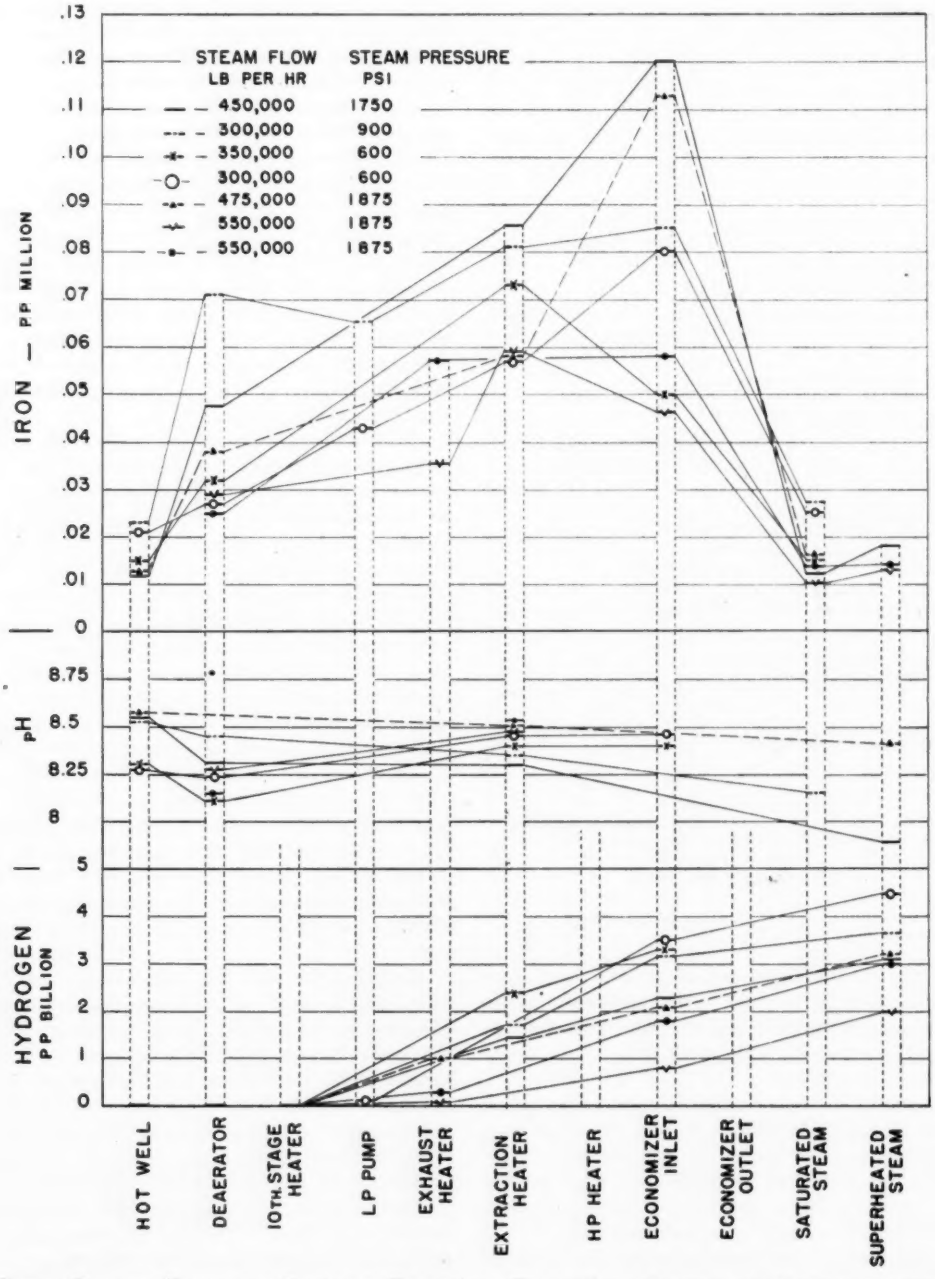


FIG. 4 CURVES SHOWING VALUES FOR DISSOLVED HYDROGEN, pH, AND IRON PLOTTED FOR VARIOUS SAMPLING POINTS

TABLE 4 RESULTS OF TESTS TO DETERMINE AMOUNT OF COPPER IN FEEDWATER

COPPER - PARTS PER MILLION

SAMPLE	TEST NO. 3 9/19	9/20	9/22	9/24	9/27	AVERAGE TEST 3	AVERAGE TEST 2	AVERAGE TEST 1	TEST 1-2-3
15TH STAGE HEATER DRIPS	.007	.005	.004	.004	.007	.005	.009	.007	.007
HOT WELL	.009	.022	.007	.006	.009	.011	.009	.012	.011
DEAERATOR OUTLET *	.012	.006	.007	.007	-	.008	.011	.012	.011
DEAERATOR OUTLET **	.013	.008	.009	.009	.017	.011	.011	.014	.012
SATURATED STEAM	.008	.007	.006	.006	.013	.008	.009	.012	.010

AMMONIA NITROGEN - PARTS PER MILLION

15TH STAGE HEATER DRIPS	.10	.10	.15	.10	.08	.11	-	-	.11
HOT WELL	.15	.15	.20	.20	.18	.18	-	-	.18
DEAERATOR OUTLET	.12	.15	.15	.18	.18	.16	-	-	.16
STEAM	-	.18	.20	.25	.25	.22	-	-	.22

* COPPER COOLING COIL
** STAINLESS STEEL COOLING COIL

in the condenser and none is recirculated to the feedwater.

The pH value of the samples varied over a relatively narrow range during this series of tests. The pH values at the hot well were between 8.3 and 8.6. There was a reduction in the deaerator due to removal of gases, apparently NH_3. The rise in pH at the extraction heater is ascribed to the effect of the treatment chemicals that are introduced ahead of that point, although it may be due in part to vapor from the evaporators which is introduced into the deaerator.

The values for the iron content of the water at the various sampling points are given in the upper group of points. The points of each test are connected by lines to form curves only the better to identify the several points of the test. While there is wide divergence in values, particularly at the economizer inlet, the points of each test form the same general pattern. No relation is evident between the iron content of the water and changes in pressure and boiler load. It may be concluded only that iron and dissolved hydrogen increase together. If we may be permitted to use the average of the rather scattered points for iron values at the economizer inlet, it may be pointed out that this average value corresponds closely to the amount of hydrogen in the superheated steam. From the equations given earlier, of the probable reactions for the dissolution of iron, one part per billion of hydrogen is the equivalent of 0.021 ppm of iron. The average hydrogen of the steam is 3.3 ppb corresponding to 0.069 ppm of iron. The average of the economizer feedwater is 0.079 ppm iron. There is as close an agreement as could be expected.

The miscellaneous projects listed under Period 3 represent work done at various times during the course of the investigation.

Period 3 (a): Copper in Feedwater. The measurement of copper in the feedwater was made because of the presence of that element in all deposits found in the boiler. As the condensers were suspected of being the principal source of contamination from copper, the study was limited to this equipment. Samples of condensed steam from the 15th-stage-heater drips were taken as representative of steam delivered to the condenser and a sample was taken at the discharge of the hot-well pumps for comparison. Samples were also taken of water leaving the deaerator and saturated steam leaving the boiler.

The analysis was made on 500-ml samples evaporated to dryness in the same manner as for iron. The determination of copper was by a colorimetric method. As there was a question of possible contamination of the samples by the use of copper cooling coils, a comparison was made between copper and monel coils and between copper and stainless-steel coils. There was no indication of contamination from the copper coils and in fact the very small differences in copper content of the samples from the three coils favored the copper coils. The sample reported is that taken with the stainless-steel coil.

The results of the series of tests are given in Table 4. Daily results for a 5-day period are given with the average for this period and the average for two similar periods. While the amounts of copper reported are quite small, there is a consistent increase across the condenser. The indication of copper in the condensed-steam sample is rather surprising. These samples were condensed in a monel coil, and there is a possibility of contamination from that source. The comparative tests of monel and steel coils at the deaerator outlet where the sample was cooled only in the coil cannot be taken as assurance that there is no contamination under condensing conditions.

It should be noted that there are other possible sources of copper contamination than the condenser that were not investigated. These are the 10th stage heater and low-pressure pumps having bronze impellers. There are also steam-air heaters in the coal-preparation house, the drips from which are returned to the feedwater system.

Period 3 (b): Bead and Ion-Exchange Columns. The plating out of iron-rich deposits on conductivity cells, glass tubing, and rubber tubing through which samples of feedwater and steam were drawn has been observed in a number of plants.

At the Somerset Station attention was first called to this phenomenon by the necessity of cleaning the conductivity cells and their glass containers at least once a week. It was first assumed that the deposit was a result of oxidation of a ferrous salt and the deposition of the more insoluble ferric compound. The cell and thermometer were inserted in the container through a rubber stopper, not necessarily an airtight seal. It was, however, noted that the glass and rubber connections between the cooling coil and the cell, where there was little possibility of air leakage, were also coated with a similar deposit.

This deposit was easily removed by washing with dilute hydrochloric acid. Usually a slight to strong odor of hydrogen sulphide was noted when the cell on the steam sample was washed.

In order further to study this plating-out effect, bead columns were made up consisting of $\frac{1}{2}$-in-ID pyrex tubing packed with $\frac{1}{8}$-in. soda-glass beads. These were set up at sampling points so that a sample could be drawn through them slowly and at a measured rate. The sample stream was arranged to flow across the top of the column into a spill tube, and the sample to the column was drawn from this stream. There was thus no syphon effect and the pressure at the connections was always above atmospheric. The rate of flow was adjusted to 1 liter per hr, and the tests were continued until 25 liters were drawn through the column. The effluent was measured in 10-liter graduated bottles.

A synthetic-resin ion-exchange column, operating on the hydrogen cycle, was prepared and tested together with the bead column. It had substantially the same dimensions as the bead column and took a sample from the same stream and at the same rate of flow. The purpose of the test was to determine the possibility of the quantitative removal of small amounts of dissolved salts and their recovery in the column wash in more concentrated solution. If successful, this method could be used instead of the usual one involving the evaporation of large samples, except, of course, where the determination of silica is involved. The exchange medium used was an analytical grade of a commercial product.

Daily samples were taken of the influent and analyzed for iron. Electrical conductivity and pH were measured for both influent and effluent. At the end of the sampling period the deposit in the bead column was dissolved with dilute hydrochloric acid, and the total solids as chlorides weighed. Iron and copper were determined in the residue. The ion exchange column was regenerated with dilute hydrochloric acid followed by a rinse with distilled water, and the extracted solids were recovered. Total solids as chlorides, iron, and copper were determined.

The results of two tests, one on a sample from the deaerating heater and the other on a sample from the extraction heater are given in Table 5. The ion exchange column is designated by the letter A and the bead column by B. The columns were in operation for 8 hr daily for a period of 3 days. Based upon the inlet and outlet samples, the recovery of iron on test 1 was 100 per cent for the A and 50 per cent for the B column. The actual recovery by extraction of the columns was 63 per cent for A and 25 per cent for B. It was found that the extraction of the ion-exchange bed was incomplete, and in the second test the acid strength was increased with resulting better recovery.

The recovery of iron for test 2 on the basis of inlet and outlet samples was 69 per cent for the A column and 39 per cent for the B column, compared with 99 per cent and 39 per cent, respectively, by extraction. The values by extraction are believed to be more nearly correct as at the higher concentration a greater accuracy of analysis is possible.

It will be noted that both conductivity and pH are reduced by the bead column which might indicate that the iron removed is in the form of ferrous hydroxide. The changes in conductivity and pH across the ion exchange column are what would be expected. When the positive ions are retained in the ion exchange process an equivalent amount of acid is produced.

The principle involved in the plating-out effect exemplified in the bead column is not known but is believed to be a surface-adsorption effect. Iron appearing in the deposit is in the form of ferric oxide; hydrated ferric oxide and magnetite. Silica also is present, its source probably being the soft glass beads. It is probable that the silica in the deposit is incidental and is not involved in any reaction with the iron. The iron deposits occur in pyrex tubing, rubber tubing, and on the inner surfaces of the various cooling coils. The entire feedwater system is undoubtedly lined with this deposit and probably much of the iron de-

TABLE 5 RESULTS OF TESTS TO DETERMINE TOTAL SOLIDS AS CHLORIDES, IRON, AND COPPER USING BEAD AND ION EXCHANGE COLUMNS AT DEAERATING HEATER AND AT EXTRACTION HEATER

TEST NUMBER	1						2					
SAMPLE	DEAERATOR OUTLET						EXTRACTION HEATER OUTLET					
SAMPLE VOLUME	25 LITERS						25 LITERS					
WATER TO COLUMNS	1		2		3		1		2		3	
IRON - PPM	.014		.012		.050		.069		.058		.056	
CONDUCTIVITY - MMHO	3.0		6.5		3.05		4.35		5.05		2.65	
PH	8.55		8.60		8.59		8.36		8.48		8.34	
	COLUMN						COLUMN					
	A			B			A			B		
WATER FROM COLUMNS												
IRON - PPM	0	0	0	.007	.006	.026	.011	.032	.013	.041	.043	.026
CONDUCTIVITY - MHO	8.0	15.5	6.3	3.5	7.25	2.95	9.84	9.85	3.70	4.0	4.7	2.35
PH	7.0	4.65	6.0	8.5	8.4	8.2	4.75	4.77	5.05	7.76	8.20	8.09
COLUMN EXTRACTION	MG	PPM		MG	PPM		MG	PPM		MG	PPM	
TOTAL SOLIDS	63.6	2.52		21.0	.84		68.0	3.72		3.50	.140	
IRON	.396	.0158		.159	.006		1.153	.060		.600	.024	
COPPER	.945	.0378		.635	.025		.530	.021		.325	.013	
RECOVERY OF IRON												
1 BASED ON INLET AND OUTLET	100 %			50 %			69 %			39.5 %		
2 BASED ON INLET AND RECOVERY	63 %			25 %			99.2 %			39.4 %		

posits noted in the boiler tubes may be accounted for by this property of plating-out on all surfaces.

The concentration of salt cations by means of the ion-exchange column did not work out well, principally because it was difficult to make a complete extraction of the retained material, and particularly the iron. While the residue remaining in the bed after regeneration was very small, even when the conventional wash was used, it represented a relatively large percentage of the total. This objection could be met by using a larger sample so that the unextracted portion would be negligible. The actual capacity of the bed was in only very small fraction realized by the 25-liter sample used. It is believed that this method of concentration of sample has promise and should be further explored.

Period 3 (c): Tube-Temperature Measurement. Tube-temperature measurements have been reported in another paper of this group. One purpose of these measurements was to determine whether or not there was any progressive increase in tube temperature that might be ascribed to internal deposits. Daily readings of temperatures of a group of tubes in the north wall gave no indication of appreciable internal deposits. The thermocouples were located at elevations of 5 to 25 ft above the hearth. A recent inspection following a tube failure at a 1-ft level, however, disclosed sludge deposits that would have been indicated by a couple at that elevation.

Period 3 (d): Corrosion Detector. In an attempt to obtain a quantitative check on the rate of solution of iron in the feedwater, a corrosion detector was installed in one branch of the boiler feed line leading to the economizer. This corrosion detector consisted of a short rod of carbon steel machined flat on two sides. It was mounted so that it could be removed without disturbing any of its original surface. This detector was recently examined after an exposure of 1 year. After being carefully cleaned in an ammonium-citrate solution, it was found to have lost 0.25 g of its original weight of 14 g. This loss if evenly distributed corresponds to 0.0001 in. penetration. There was, however, one small pit of about 0.005 in. depth. The surface was darkened and coated with a powdery film of what appeared to be an iron oxide. This corrosion detector was returned to its position in the feed line and will be again examined after a period of exposure.

The rate of metal loss, as indicated by the direct determination of iron content of the water and also by the measurement of the evolved hydrogen, is not large. Translated into inches penetration per year over the areas of the preboiler equipment and of the boiler itself, it would not be an impressive figure and would not lead to any great apprehension as to the imminent failure of any part of the equipment. There would, however, be cause for concern if the loss of metal were restricted to local areas such as has been noted in boiler feed pumps. While the hydrogen evolution appears to indicate a greater activity in the high-temperature end of the feedwater system, there is no evidence to indicate that localized attack occurs. It is, however, doubtful that loss of metal from erosion, such as may occur in feed pumps, is accompanied by the evolution of hydrogen.

The rate of loss of metal from the steam-side surface of the condenser tubes, as indicated by the measurements of dissolved copper, is extremely low. The loss on the cooling-water side is probably much greater, and also localized attack is known to occur. Failure of condenser tubes is more likely to occur as a result of attack on the outside, that is, the cooling-water side of the condenser.

One disquieting thing about the dissolution of iron and copper in the feedwater system is that the mechanism of the corrosion is not well understood, nor have preventative conditions been well established. It is generally agreed that dissolved ammonia is the principal factor in the corrosion of copper, and methods for the removal of this substance have been proposed. It is indicated that the dissolution of iron can be reduced by the control of pH. However, the permissible range of pH in the feedwater is limited by boiler-water conditions particularly when the rate of boiler-water blowdown is low.

The principal concern over the presence of iron and copper compounds in the boiler feedwater is caused by the propensity of these substances to form adherent sludges on the boiler surfaces. The iron is transformed probably completely to magnetic oxide and the copper is in large part at least reduced to the metallic state.

Slime deposits of sludge are found on all internal surfaces of the boiler and are often heavier on the unheated areas than on active steam-generating surfaces. It is indicated that this deposit is laid down mechanically, that is, there is no general chemical attack under sludge deposits. Small pits of pinpoint dimensions have been noted but are believed to be only incidental and not generally related to the deposits. While the sludge-collecting pots at the waterwall headers and a special sludge blowdown in the drum permit the removal during operation of accumulated sludge, they have not completely eliminated the hazard. The chief danger of the sludge deposit lies in its insulating effect on active steaming surfaces where it may build up to a thickness that results in overheating of the tube metal.

Basically the sludge problem in boilers results from the introduction into the boiler with the feedwater of solids or salts that form solids, at a higher rate than the rate of removal. Inevitably this must lead to trouble.

There are two obvious lines of attack on this problem: (*a*) to prevent or minimize the production of the metallic ions which are the principal components of the sludge in the feedwater system, and (*b*) to provide for a better continuous removal of sludge with the blowdown from the boiler.

The chances of complete solution of the problem by either or both of these efforts are not particularly promising and it is probable that a periodic cleaning of boilers will be necessary.

Apparatus and Methods

The hydrogen analyzer and recorder used in the investigation was a commercially available instrument utilizing the difference in thermal conductivity of gases. The analyzer consists of a Wheatstone bridge, two legs of which are formed by identical platinum-wire spirals. These spirals are electrically heated, a constant potential being applied. One of these spirals is surrounded by saturated air and the other by air that has bubbled through the sample which flows to the analyzer at a measured rate. Hydrogen of the sample is present in the latter air in proportion to its concentration in the sample. Because of the higher thermal conductivity of the air containing hydrogen, the temperature of the second spiral and hence its electrical resistance is reduced and the bridge is thrown out of balance. The balance is then restored automatically by a potentiometer which records the off-balance as hydrogen. At the usual low concentrations of hydrogen in feedwater the unit is parts per billion.

The principle of the dissolved-oxygen recorder is similar to that of the hydrogen recorder. Pure hydrogen which is generated electrolytically surrounds the reference spiral and hydrogen which scrubs the sample and has the equilibrium content of oxygen surrounds the analyzer spiral.

These instruments are extremely sensitive. Two parts of hydrogen in 10 billion parts of sample will give a scale deflection. It is necessary to check the zero of these instruments daily and it is desirable also to make frequent checks of the scale. This is done by introducing hydrogen to the sample at a measured rate. The hydrogen is made electrolytically and the rate of introduction of hydrogen is measured by current used.

While the meters are simple in principle, considerable attendance is required in order to assure their continuous accuracy.

The steam-sample evaporator is shown in Fig. 5. It consists essentially of a 5-liter flask having a tubulature extending downward with the open end in the evaporating dish in which the sample is being evaporated. The end of this tube is ground to a standard taper to which a platinum thimble is fitted. This thimble is weighed with the dish. As the water level in the dish recedes, the open end of the tube is uncovered allowing air to enter the flask and more water to flow into the dish. In starting the evaporator, the stopper is inserted at the end of the delivery tube and the measured sample, 3 to 4 liters, is poured in at the top opening. The cap with the manometer is then replaced and suction is applied to obtain an indication of about 1 in. on the manometer, and the stopcocks *A* and *B* are closed. The weighed dish is then placed in position on the heater assembly which is held on a ring stand below and to one side of the evaporator bell. The stopper is then removed and the heater and dish assembly quickly placed in the operating position. To do this without spilling the sample requires practice, and it is recommended that the operation be rehearsed with the flask empty until the necessary skill is acquired. The stopcock *B* is open during the evaporation.

The sample is evaporated without boiling, most of the heat being applied over the surface of the liquid. When the sample container is empty, the mercury switch closes and actuates a relay which shuts off the current to the heaters and closes the valve through which the air is admitted. There is enough residual heat in the heater and bell to complete the evaporation. At the end of the evaporation the flask is rinsed with a jet of distilled water and the washings added to the dish and evaporated. The rate of evaporation is about 200 ml per hr.

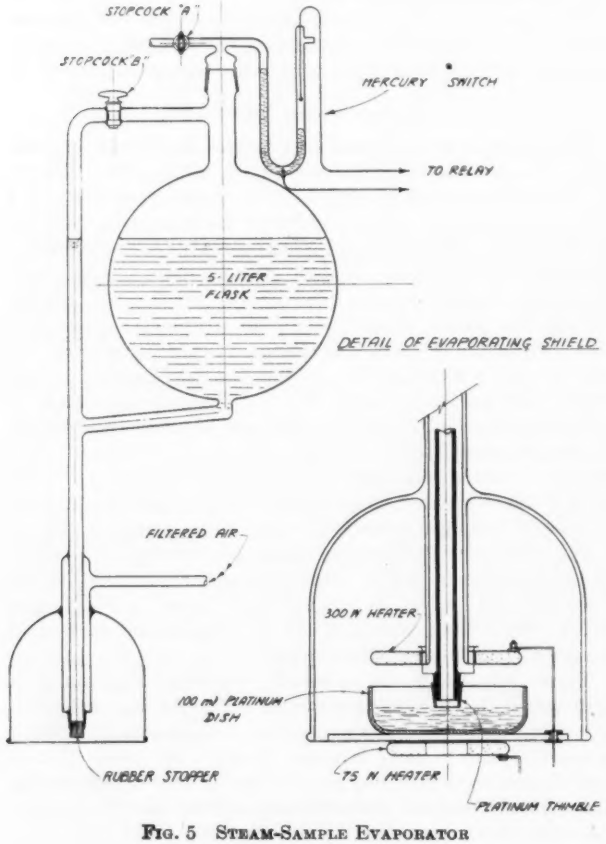


FIG. 5 STEAM-SAMPLE EVAPORATOR

The sample concentrator for the determination of iron is shown in Fig. 6. It consists merely of a 1-liter Erlenmeyer flask covered with a vented hood through which filtered air is blown. A 500-ml sample is evaporated to dryness without boiling in about 4 hr. The residue is then taken up in 1 ml of concentrated acid and diluted to 50 ml for analysis.

Most of the analyses were made by a colorimetric method using thiocyanate. Measurement of color was by means of a photoelectric colorimeter. A second method using orthophenanthrolene was tried and although it proved more sensitive, it also required concentration of the sample and the simpler thiocyanate method was preferred.

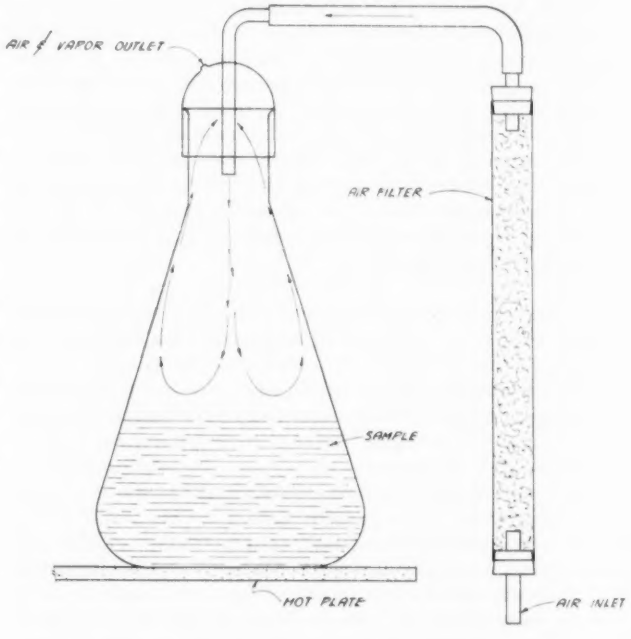


FIG. 6 SAMPLE CONCENTRATOR FOR DETERMINATION OF IRON

Extreme care is necessary to prevent contamination of the samples. It was found that if a sample was stored even for a day an appreciable amount of iron was lost because of the plating-out effect on the walls of the flask. To reduce the error due to the plating-out tendency, a small measured amount of acid and an organic reducing agent were placed in the flask in which the sample was collected, and the storage time was reduced to a minimum. Any iron present in reagents was corrected by means of blank samples.

Samples for copper determinations were prepared in the same apparatus used in the iron analysis. A colorimetric method using sodium diethyl-dithio carbamate in alkaline solution was used. This method was generally very satisfactory. In a very few instances an interfering turbidity resulted and it was necessary to extract the color with an organic solvent.

The bead-column and the ion-exchange-column arrangements are shown in Fig. 7. The columns were set up at the point of sampling. The sample flow was arranged so that a constant head was provided and also so that all connections were under pressure and no air would be drawn into the columns. The rate of sample flow was 1 liter per hr, and the effluent was collected in calibrated bottles so that the total flow could be measured.

At the end of a sampling period the assembly was taken to the laboratory where the extracts were removed by acid treatment and the columns prepared for another run. A 10 per cent

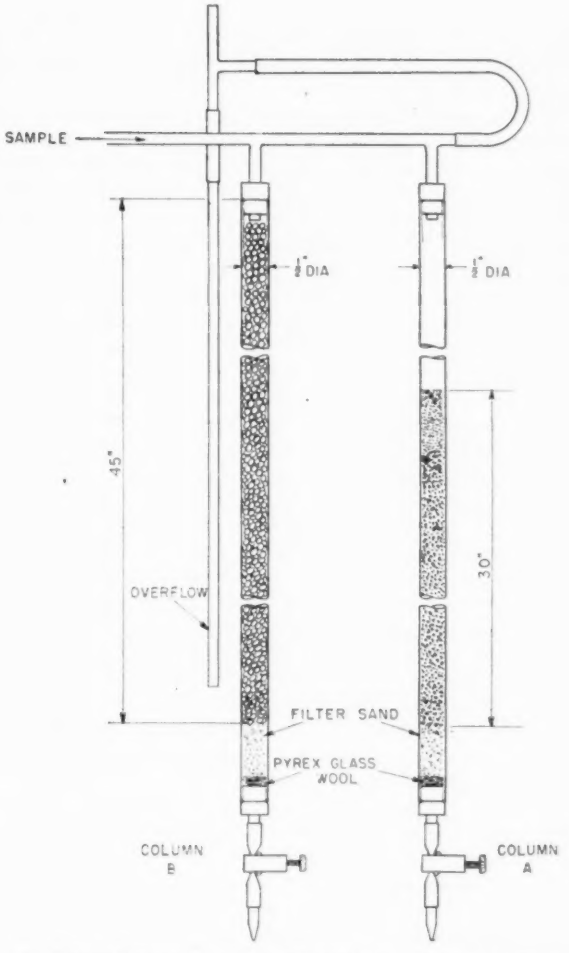


FIG. 7 BEAD COLUMN AND ION EXCHANGE COLUMN ARRANGEMENTS

hydrochloric acid, 300 ml in amount, was used in regeneration of the ion exchange column, followed by a 300-ml water wash. Distilled water that had previously been passed through the bed was used for the wash water.

The 600-ml recovery sample was reduced to 500 ml for convenience and analyses were made on aliquot portions. Colorimetric methods previously described were used for the iron and copper determinations.

Discussion

R. C. COREY.[4] The excellent experimental data presented by the authors serve, among other things, to place one important phase of corrosion in high-temperature steam cycles on a factual basis, and those concerned with iron-oxide sludges now have available something more substantial than opinion or, as is frequently the case, " . . . . ill-begotten equations supported by bad data;" as it is stated by Lewis and Randall.[5] The experimental work conducted by the authors to establish the source of iron oxide in boilers and the probable mechanism of its formation, by means of hydrogen and dissolved-iron surveys of the steam and water cycles, is unique to the extent that no published data from similar work are to be found elsewhere. In some respects, which will be mentioned later, their results confirm certain conclusions of laboratory and theoretical studies of the fundamental reactions between iron and pure water. To this end there is support of the contention that there are yet many more questions than there are answers to the problem of corrosion by pure water at elevated temperatures.

It is a curious fact that although one may find in corrosion literature data on the rate of corrosion of iron and steel in contact with almost every conceivable inorganic or organic material, under widely different conditions of independent variables, there are no published data on the rate of corrosion of iron and steel in pure water. A possible reason for this may lie in the fact that in pure water the rate of corrosion is insignificant compared to that in acids, bases, and certain salt solutions. It is obvious, however, from the results of the present paper and the current problem of feed-pump corrosion which appears to be related in some way to pure condensate, that there is a definite need for an investigation of the rate of corrosion of iron and steel in pure water up to around 600 F, and under various conditions of flow and pH.

Evaporated feedwater make-up and highly efficient steam-washing and deaerating equipment result in feedwater of extreme purity, and as so clearly expressed recently,[6] "It dissolves to some extent anything that it comes in contact with on its way from the condenser to the boiler. This dissolving action starts in the last stages of the turbine where the first condensation occurs." It may be asked what is meant by "pure" water. Qualitatively it may be defined as water which contains no dissolved gases and which produces no residue on evaporation. A quantitative definition for pure steam condensate might be based upon its electrical conductivity when there are no ions present other than hydrogen and hydroxyl ions resulting from the ionization of the water.

On the other hand, it is possible that the conductivity of pure water may not change after contact with an iron vessel, due to the formation of Fe_2O_3 or FeOOH which are insoluble. In such a case the buffer index might be a useful criterion for purity, this being defined as the differential ratio dB/d(pH), in which d(pH) is the increment of pH when an increment of base dB, in terms of gram equivalents of hydroxyl ion, is added. An increment of hydrogen ion would be equivalent to —dB. Thus pure condensate would have a buffer index of 0.1429, and if iron oxide were added this value would increase due to the fact that the oxide would react with added hydrogen ion.

The authors have shown clearly that in the subject plant most of the hydrogen and dissolved iron result from corrosion of external piping and heat-exchange equipment, a very small amount being due to corrosion within the boiler. They postulate that the ferrous hydroxide formed in the primary corrosion reaction decomposes to Fe_3O_4 and more hydrogen. There is experimental and theoretical work to support this. Schikorr[7] found that when iron turnings were placed in contact with pure water, pressures of 18 atm and higher of hydrogen developed, and Fe_3O_4 was formed. In later experiments he demonstrated that ferrous hydroxide spontaneously decomposed to hydrogen and Fe_3O_4 at a rate inversely proportional to the pH.[8] Investigation of the

[4] Research and Development Department, Combustion Engineering Company, Inc., New York, N. Y.

[5] "Thermodynamics," by G. N. Lewis and M. Randall, McGraw-Hill Book Company, Inc., New York, N. Y., 1923.

[6] "Properties of Pure Boiler Feedwater," *Combustion*, Feb., 1945, p. 45.

[7] "On the System Iron-Water," by G. Schikorr, *Zeit. für Elektrochemie*, vol. 35, 1929, p. 62.

[8] "Ferrous Hydroxide and a Ferromagnetic Ferric Hydroxide," by G. Schikorr, *Zeit. für Anorganische und allgemeine Chemie*, vol. 212, 1933, p. 33.

reactions at room temperature between iron and pure water[9] demonstrated that Fe_3O_4, hydrogen, and about 0.2 ppm of dissolved ferrous iron were the final products, and the pH rose to 8.3. The dissolved iron was considered to be an intermediate stage in a chain of reactions,

$$Fe \rightarrow Fe^{++} \rightarrow Fe(OH)_2 \rightarrow Fe_3O_4$$

No attempt was made, however, to correlate the dissolved-iron concentration and pH because of (*a*) lack of information on the state of the dissolved iron, that is, whether it was colloidal or poorly ionized; (*b*) disagreement in the literature as to the solubility and the solubility product of $Fe(OH)_2$; and (*c*) inability to determine which of the foregoing reactions controlled the rate to the right. Thermodynamic calculations have shown[10] that iron reacts with oxygen-free water to form Fe_3O_4 more readily than $Fe(OH)_2$, although it is conceded possible that the latter may be an intermediate phase. Thus it is a necessary conclusion that $Fe(OH)_2$ will decompose to Fe_3O_4 and hydrogen.

All of these facts find confirmation in the results obtained by the authors if it is kept in mind that it is very unlikely that equilibrium between iron and condensate ever is attained in the short time of contact between the hot well and the boiler. Thus the relative amounts of Fe^{++}, $Fe(OH)_2$, Fe_3O_4, and H_2 may be expected to vary considerably from equilibrium values.

One question concerning these investigations with iron and pure water is whether the iron determinations represent only dissolved iron or varying mixtures of dissolved iron and an extremely finely divided form of magnetite.

In one of the afore-mentioned investigations,[9] there were indications that despite careful filtering a small amount of iron oxide, possibly of colloidal dimensions, occasionally contaminated the samples. This is merely a question of academic interest, related to the fundamental corrosion reaction, and therefore does not affect the results and conclusions of the authors.

It may be asked, why, if the rate of corrosion of iron and steel by pure water at elevated temperatures is insignificant when uniformly distributed throughout the system, it receives the attention it does in the present paper. The authors have very clearly resolved the problem in two parts: (1) There was the question whether the iron oxide originated in the boiler as the result of attack of steaming surfaces; and (2) the possibility that excessive deposits of iron oxide on steaming surfaces would lead to overheating due to a decrease in the over-all coefficient of heat transfer. In so far as the subject plant was concerned, it was demonstrated that the greater part of the iron oxide was carried into the boiler from external sources. This confirms the consensus of a number of operators. Regarding the ultimate effect of deposits of iron oxide on steaming surfaces, there is, in addition to the insulating effect, the possibility that boiler-water salts may concentrate in and beneath the oxide, and if sufficient free caustic is present localized, rapid attack may occur.[11]

Another factor that may be considered is the possibility that metallic copper, invariably associated with iron oxide in boilers, deposited on a baked-on sludge of iron oxide may set up an electrolytic cell, the tube metal being anodic, the copper cathodic, and the iron oxide between, serving as a porous matrix for salt-saturated liquid. This, of course, is hypothetical and until data are available on the emf between copper (or copper oxide) and iron, and on time-potential curves, which indicate whether anodic or cathodic polarization is controlling the rate of corrosion, this theory offers possibilities.

Thus as suggested by the authors, iron-oxide deposits in high-pressure boilers cannot be ignored, and if it has been established that excessive quantities of iron oxide are being carried into a boiler from outside sources, then steps should be taken to minimize corrosion in external equipment even though the rate is not sufficient to cause significant attack in such equipment itself. Theoretically attack can be minimized either by raising the pH of the feedwater or by applying a protective coating to the ferrous materials with which the feedwater comes in contact. Assuming, however, that there were no practical difficulties to the first of these steps, the fact remains that we do not know the optimum pH at which the feedwater should be maintained to minimize corrosion under operating conditions, because no investigation has been made of the rate of corrosion of steel under these conditions at various values of pH.

The data on hydrogen and iron throughout the system are extremely interesting. Regarding the increase in hydrogen across the economizer, not shown in Fig. 4 of the paper, it would be of interest to know what values were obtained at the economizer outlet and also the iron determinations, if available. If the iron and hydrogen did not increase together then it might be inferred that the increase in the hydrogen was the result of decomposition of ferrous hydroxide rather than corrosion in the economizer.

If the authors have made any conductivity determinations at the various sampling points, they would be a valuable supplement to the other data and may help to explain some questions of fundamental importance.

It was noted that the concentration of hydrogen in the steam did not vary with the load. This confirms experiments conducted by the American Gas & Electric Service Company at Logan, where the concentration was found to be constant at about 3 ppb between a steam output of 400,000 and 850,000 lb per hr.[12] The average concentration at Montaup was 3.3 ppb.

Regarding the results for dissolved iron, it is interesting to note that the iron in the steam was approximately the same as found in the hot well. It would be of interest if the authors described the method they adopted for determining the iron, that is, whether it was a modified thiocyanate, orthophenanthroline, or similar scheme.

At the present time little can be said about the manner of formation of metallic copper in the boiler or its effect with regard to corrosion. It has been stated[13] that the corrosion of copper or copper alloys by ammonia is negligible in the absence of oxygen. Relatively, this may be so but it appears that in oxygen-free condensate sufficient solubility, in the presence of less than 0.1 ppm NH_3, occurs to produce large amounts of copper in boilers. Dissolved carbon dioxide, either as free CO_2 or bicarbonate ion, also is a factor in the corrosion of copper.

The corrosion detector, installed in one branch of the boiler feed line leading to the economizer, offers excellent possibilities for determining, under actual operating conditions, the rate of corrosion of low-carbon steel. It is suggested, however, that it is not advisable to re-use the specimen for a subsequent test, more acceptable results being obtainable if new specimens are used for each test. Also, if possible, it would be desirable to install an identical specimen in a location where the temperature and pH of the liquid are the same but of different velocity.

---

[9] "The pH, Dissolved Iron Concentration and Solid Product Resulting From the Reaction Between Iron and Pure Water at Room Temperature," by R. C. Corey and T. J. Finnegan, Proceedings of the A.S.T.M., vol. 39, 1939, pp. 1142–1260.

[10] "Thermodynamic Considerations in the Corrosion of Metals," by J. C. Warner, Trans. Electro Chemical Society, vol. 83, 1943, pp. 319–333.

[11] "Co-Ordination of Water Conditioning With Operating Problems," by R. E. Hall and C. E. Kauman, *Power Plant Engineering*, vol. 45, September, 1941, pp. 61–64, and October, 1941, pp. 59–61.

[12] Publication No. H-11, Edison Electric Institute, 1940.

[13] "The Reaction of Copper and Oxygen-Saturated Ammonium Hydroxide," by R. W. Lane and H. J. McDonald, *Journal of Corrosion*, Aug., 1945, pp. 1–8.

The experiments with bead columns to study the effectiveness of various materials in removing small amounts of solids from water are of considerable interest, particularly with regard to the comparative efficiency of the glass and the synthetic resin.

The authors suggest that silica is not involved in the action between the glass beads and iron-bearing water. The writer submits that in experiments with pure water and iron in pyrex vessels there seemed definitely to be reaction of dissolved iron with the glass. The pH of the water rose to 9.0–9.5 and a flaky anisotropic material formed which microchemical tests showed to contain iron and silicon; possibly being a hydrated iron silicate.

In conclusion, it is believed that this investigation has emphasized the need for more fundamental work on the reactions of iron with pure water. A program for such an investigation might be as follows:

1 Determination of the rate of corrosion of iron and steel in water as a function of pH, velocity, and temperature, up to 600 F.

2 Study of the time-potential curves for iron under the same conditions as item 1.

3 Preparation of pure ferrous hydroxide and determination of the following:

(*a*) Its solubility and pH in pure water.

(*b*) Rate of decomposition to Fe_3O_4 and H_2 as a function of temperature and pH.

The results of such an investigation should, among other things, determine the minimum pH of feedwater required to effect maximum protection of steel surfaces, at various temperatures related to operation.

E. R. Mueller.[14] Of interest primarily to chemists rather than engineers is the reference given in the subject paper to the use of an ion-exchange material as a tool in the analysis of feedwater or steam samples. The application discussed is a clear-cut example of the manner in which the analytical grade Amberlite resins can be used as analytical tools. The investigators are taking advantage of the unique properties of these resinous exchangers, in this case, the cation exchanger, one such property being the complete adsorption of heavy metal ions such as iron, copper, etc.

It has been stated in the paper that dilute hydrochloric acid was first employed with incomplete recovery of the full metal content from the exchanger. Although the concentration was not indicated in the paper, this was pointed out to be 5 per cent. By the use of 10 per cent acid, the higher concentration referred to in the paper, better results were obtained. It is suggested that in both cases more complete recovery of the metal ions from the exchanger could have been accomplished by the recycling of a relatively small but adequate portion of either concentration of acid. This technique would have the added advantage of keeping the eluting solution at the smallest possible volume, thereby reducing the time required later for evaporation.

Since the resinous exchanger is entirely organic in composition, it is suggested that the analytical technique might be improved upon by wet-ashing the entire sample of exchanger upon which the metal ions have been adsorbed. This would eliminate the elution step altogether, thereby insuring the analyst against an error in the results brought about by incomplete elution of the metal ions.

In general, the particular problem represents an unusual application of the properties of ion-exchange resins.

[14] The Resinous Products & Chemical Company, Philadelphia, Pa.

W. F. Ryan.[15] A becoming but regrettable modesty has restrained the authors of this paper from acclaiming the outstanding achievement of their part of the investigations at Montaup. The statement "recording hydrogen meters were set up" is a masterpiece of condensation. The "setting up" of these meters required many weeks of painstaking engineering, involving a degree of scientific knowledge, technical skill, patience and determination more readily associated with the instrumentation of the atomic-bomb project than of a steam boiler. Perhaps Mr. White can be persuaded at a later date to publish in detail this story of measuring hydrogen in fractions of a part per billion under the pressure and temperature conditions prevailing in this station, and securing accurate and continuous records, in spite of the difficulty in maintaining reasonable equilibrium between the fluids being analyzed and the metals which contained them.

The hydrogen-meter installation was expensive not only in money but in engineering manpower, and there were many discouraging periods during which the patience of operators and contractor's representatives was sorely tried, and many of us would cheerfully have thrown the project overboard. Fortunately, however, the work was carried to successful completion, and the importance of the results well repaid the time and effort expended.

The boiler, presumably in common with all boilers working at elevated temperatures, is subject to continuous, but infinitesimal, widely distributed, and therefore substantially harmless, oxidation. It may also be subject, at irregular and unpredictable intervals, to intensified localized oxidation. When the meter shows a sudden or abnormal evolution of hydrogen in the boiler it is a clear indication that such oxidation is taking place; the meter is raising a danger signal as significant as low water in a gage glass and calls for equally prompt and vigorous action.

We are feeding all of the high-pressure boilers in the country with water contaminated by oxides. The deleterious effects may not be serious in some instances but it is not of record that it ever did a boiler any good. We are now groping in the dark to combat, in the boiler, a contaminant which should never have been allowed to enter it, and there have been widespread difficulties with boiler feed pumps and high-pressure heaters that are all a part of the general problem. Mastery of the hydrogen-meter technique offers an opportunity at least to locate the source or sources of the trouble. It is hoped that some utility or combination of utilities may sense the importance of this possibility and undertake to measure hydrogen evolution throughout a high-temperature cycle from the superheater outlet to the condenser and back again through the feed heaters, feed pumps, economizer, boiler, and superheater. When this work is undertaken, the project will be greatly facilitated by the solution at Montaup of the many and difficult technical problems involved.

T. J. Finnegan.[16] The record of hydrogen throughout the cycle given in this paper by Bissell, Cross, and White adds confirmation to the opinion held by many persons that much of the loose black-oxide sludge in the boiler is of external origin. They do not accept the theory voiced by some extremists that none of the black oxide is formed in the boiler, except perhaps where overheating occurs. They support their opinion by the implied acceptance of the two equations which would explain the formation of hydrogen by decomposition of $Fe(OH)_2$ rather than by direct attack of the metal. In other words, they admit the possibility that the fundamental corrosion reaction

[15] Assistant Engineering Manager, Stone & Webster Engineering Corporation, Boston, Mass. Fellow A.S.M.E.

[16] Chemical Engineer, Buffalo, Niagara Electric Corporation, Buffalo, N. Y. Mem. A.S.M.E.

$$3Fe + 4H_2O = Fe_3O_4 + 4H_2$$

might occur in two steps, the velocity of which is strongly influenced by temperature.

While it is almost certain that the fundamental reaction is a chain one, it has yet to be established that the separate steps of the chain can occur at a delayed rate. For example, it is easily shown that when iron is placed in oxygen-free water at room temperature the products are loose Fe_3O_4 and hydrogen. Whether or not a large amount of $Fe(OH)_2$ may be mixed with the Fe_3O_4 and have potentiality for decomposing at higher temperatures is an interesting question.

Theoretical speculations of this sort as well as those referring to the reaction of copper given in the comment on the limitations of the hydrogen recorder in the paper by Bissell and Powell[17] make one admire the attempts which are made to give a rational explanation to the observed phenomenon, but they also emphasize the need for more fundamental work on the pure chemistry of the water-metal systems. We are continually being confronted with the results of chemical reactions, the nature of which we do not understand because they have not been thoroughly studied, especially over extended ranges of temperature.

An investigation made some years ago showed that the products of the reaction of iron with oxygen-free water at room temperature are hydrogen and Fe_3O_4.[18] The oxide did not form a protective coating but settled as a loose powder on the bottom of the reaction vessel. This investigation was made in a power-company laboratory which was not equipped for carrying out the obvious extension of the work, and it would be interesting if some research organization would repeat the experiments and continue them into higher-temperature regions, with particular attention to the matter of protective coatings, the existence of $Fe(OH)_2$, and to any factors which tend to limit the reaction.

Authors' Closure

The authors appreciate Mr. Corey's very carefully prepared discussion. His observations on the possible reactions that may take place in the feedwater system emphasize the need for further work on that subject. While no quantitative data were obtained, there is evidence that iron in the feedwater at the Somerset Station occurs both in colloidal and dissolved states. The iron is reported as total iron as the samples were evaporated to dryness and the residues were taken up with acid. In some samples where the iron content was high enough to be determined without concentration of the sample, lower values for iron were obtained on the sample before evaporation than on an evaporated sample. When the sample was acidified and heated increasing values for iron were obtained with increasing time of digestion.

[17] "Experience With Instruments and Control Equipment for 2000-Psi Boiler at Somerset Station of Montaup Electric Company," by W. D. Bissell and E. B. Powell, published on pages 453–466 of this issue of the Transactions.

[18] "pH, Dissolved Iron Concentration and Solid Product Resulting From Reaction Between Iron and Pure Water at Room Temperature," by R. C. Corey and T. J. Finnegan, Proceedings of the A.S.T.M., vol. 39, 1939, p. 1242.

There is also evidence that much of the iron is in the ferrous state. For example, in bead column tests a heavier deposit is obtained when the sample is aerated. The deposit is also of a deeper red color.

Mr. Corey suggests that there may have been a reaction between the glass of the beads and the iron in the water. Our conclusion that the silica was only incidental was based on the fact that the same type of deposit occurred in rubber-tube connections and also in the copper tubes of the cooling coils. This, of course, does not preclude the possibility that an iron-silica reaction does take place—the source of the silica being other than the glass.

While the hydrogen content of the steam is reasonably constant in the record shown in Fig. 2, the variation in rating is not large. There is, however, a definite trend of increase in hydrogen concentration with decrease in load. This may be noted in the hydrogen curves of Fig. 4 and also in Fig. 3. The change in the hydrogen values is not large and is sometimes masked by other unexplained variations.

As reported in the paper the corrosion indicator was removed for weighing at the end of one year and was at once restored to service in the pipe line. A duplicate corrosion indicator of carbon steel was machined, however, and was installed in October, 1945, in place of the original one, just as Mr. Corey has proposed.

His suggestion is that an additional corrosion indicator be installed where it would be exposed to identical conditions except for velocity would yield informative data. Because of daily and seasonal variations in boiler load, however, the present indicator is exposed to appreciable changes in velocity, and under existing conditions it appears impracticable to select a second location where the feedwater velocity would remain in approximately constant ratio to that at the existing corrosion indicator.

The valuable suggestions of Mr. Mueller are appreciated. The advantages of the ion exchange method of sample concentration are many and the results so far are encouraging. The alternate method of evaporation is laborious and time-consuming and it requires a very careful technique for its successful application.

The authors are gratified by Mr. Ryan's very kind discussion and appreciate his comments on the broader significance of the investigation.

The authors must agree with Mr. Finnegan that in what little experimental work has been done on the reactions of water and iron, there is little or no evidence of ferrous hydroxide in the corrosion products. The experiments, however, have been conducted under conditions such that chemical equilibrium was established. It is doubtful that such equilibrium could be attained in the feedwater system at the Somerset Station.

Recent analyses of bead-column deposits indicate that 50 to 70 per cent of the iron is in the ferrous state. The work is being continued and the feedwater system will be explored for the ferrous ferric ratio. There is no question but that the final product is Fe_3O_4. Under nonequilibrium conditions the ratio of ferrous to ferric iron should depend upon the relative reaction rates of the formation and decomposition of ferrous hydroxide.

Water Conditioning for the 2000-Psi Boiler at the Somerset Station of Montaup Electric Company

By W. W. CERNA[1] and R. K. SCOTT[1]

Considerable interest has been aroused in the chemical treatment used for the high-pressure boiler at the Somerset Station of the Montaup Electric Company. The theoretical aspects of the present treatment, which has been in use since January 1, 1944, are given in a paper by Hall.[2] Details of the results obtained with the different types of treatment used on this boiler have been given in a paper by Parks.[3] It is largely the purpose of this paper to present the reasons for the various methods of chemical treatment which have been used, and for the changes made, which have resulted in stabilization of the boiler-water conditioning since January 1, 1944.

Period of Sodium Treatment

WHEN the high-pressure boiler of the Somerset Station first went into operation in the summer of 1942, a fairly standard treatment, using sodium chemicals, was used with the following control limits:

Alkalinity as sodium hydroxide, NaOH, ppm	50–60
Sodium phosphate, Na_3PO_4, ppm	50–70
Total solids, ppm (max)	1000

Some months later it was also decided to feed and maintain a positive reserve of sodium sulphite in the boiler water. During the period this treatment was used several tube failures occurred, as discussed in a previous paper of this series by Parks, Patterson, and Ryan.[4] Internal boiler conditions were also found unsatisfactory as described in the reference paper by Parks.[3] Evidence of the "hide-out" of sodium sulphate and sodium phosphate was also found which indicated that some of the boiler water was being concentrated very much beyond the limits of the normal over-all boiler water.

For example, using the published data of Schroeder, Berk, and Gabriel[5] for the solubility equilibria of sodium sulphate and sodium phosphate at boiler temperatures, a boiler water at 595 F, containing 350 ppm of sodium sulphate (Na_2SO_4) and 70 ppm of trisodium phosphate (Na_3PO_4) representative of that in the Montaup boiler at the time, would have to concentrate about 185 times before the first deposition of these substances would commence. Neglecting the effect of the sodium hydroxide on the solubility equilibria, which would actually be in the direction of increasing the number of concentrations, no deposition of sodium sulphate or sodium phosphate from the boiler water would be possible until the concentration of sodium hydroxide had likewise increased 185 times. If the initial concentration were 60 ppm of sodium hydroxide, the water just about to lay down solid sodium sulphate and sodium phosphate at the evaporative surface would necessarily contain 11,000 ppm of sodium hydroxide or a 1.1 per cent solution of NaOH. Thus it is apparent that in establishing the water conditioning for such high-pressure boilers, it is necessary to think in terms of the concentrated films, and not merely of the over-all boiler-water analysis, such as represented by the analysis of a representative sample taken from the boiler.

In so far as the over-all boiler water was concerned we had protective conditions. But the change which could occur on concentrating the boiler water from 60 ppm NaOH to 11,000 ppm NaOH is well illustrated by the curve in Fig. 1, originally developed by Partridge and Hall[6] from the experimental data of Berl and van Taack.[7] With 60 ppm caustic soda, the concentration is in the region of the most protective-to-iron zone. At 11,000 ppm NaOH (275 epm), the rate of attack found by Berl and van Taack on steel powder at 590 F was as great as in an acid solution containing about 25 ppm, HCl (0.7 epm).

The 11,000-ppm caustic-soda solution may seem fancifully high and difficult to attain. Actually, this is not the case. Dissolved substances lower the vapor pressure of a solution at any definite temperature. Correspondingly, under an externally applied temperature increase, the concentration of dissolved solids in a film of boiler water must necessarily increase to maintain constant pressure. As the terms Δt and Δts will be used frequently in this paper, a graphic representation of the meaning of the terms is given in Fig. 2 which consists simply of the vapor pressure-temperature curves of water and a saturated solution of potassium chloride. The Δt is the difference between the temperature of the concentrating film at the heat-transfer surface and the boiling temperature of pure water at the same pressure. The Δts is the Δt which corresponds to the existence of a saturated solution. If Δt is increased beyond this point, a solo solution will evaporate to dryness. Thus from Fig. 2, the film temperature can exceed the over-all boiler-water temperature at 1950 psia by about 140 deg F before potassium chloride will go to dryness in solo solution. At lower film temperature or Δt

---

[1] Hall Laboratories, Inc., Pittsburgh, Pa.

[2] "A New Approach to the Problem of Conditioning Water for Steam Generation," by R. E. Hall, Trans. A.S.M.E., vol. 66, 1944, pp. 457–488.

[3] "Experience With Sodium and Potassium Chemicals for Boiler-Water Conditioning at Montaup Electric," by G. U. Parks, Trans. A.S.M.E., vol. 67, 1945, pp. 335–338.

[4] "Operating History and Performance of 2000-Psi Forced-Circulation Boiler at Somerset Station of Montaup Electric Company," by G. U. Parks, W. S. Patterson, and W. F. Ryan, published on pp. 411–427 of this issue of the Transactions.

[5] "Solubility Equilibria of Sodium Sulphate at Temperatures From 150–350°C. III Effect of Sodium Hydroxide and Sodium Phosphate," by W. C. Schroeder, A. A. Berk, and Alton Gabriel, *Journal of the American Chemical Society*, vol. 59, 1937, pp. 1783–1790.

Contributed by the Power, Industrial Instruments and Regulators Divisions, and the Joint Research Committee on Boiler Feedwater Studies and presented at the Annual Meeting, New York, N. Y., Nov. 26–29, 1945, of The American Society of Mechanical Engineers.

Note: Statements and opinions advanced in papers are to be understood as individual expressions of their authors and not those of the Society.

[6] "Attack on Steel in High-Capacity Boilers as a Result of Over-Heating Due to Steam Blanketing," by E. P. Partridge and R. E. Hall, Trans. A.S.M.E., vol. 61, 1939, pp. 597–622.

[7] "The Action of Caustic and Salts on Steel at High Pressures," by E. Berl and F. van Taack, *Forschungsarbeiten auf dem Gebiete des Ingenieurwesens*, V.D.I. Verlag, Berlin, Germany, No. 330, 1930.

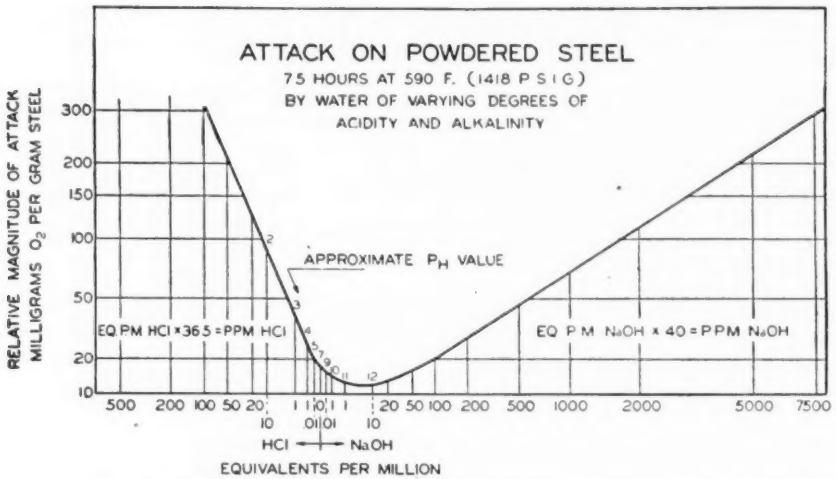


FIG. 1 RELATIVE ATTACK OF STEEL AT 590 F BY HYDROCHLORIC ACID AND SODIUM HYDROXIDE
(From laboratory data of Berl and van Taack.)

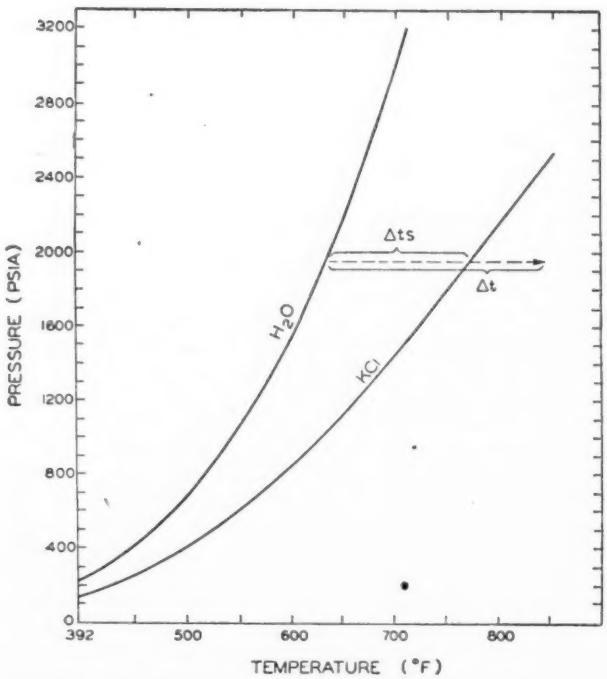


FIG. 2 PRESSURE-TEMPERATURE RELATIONSHIPS

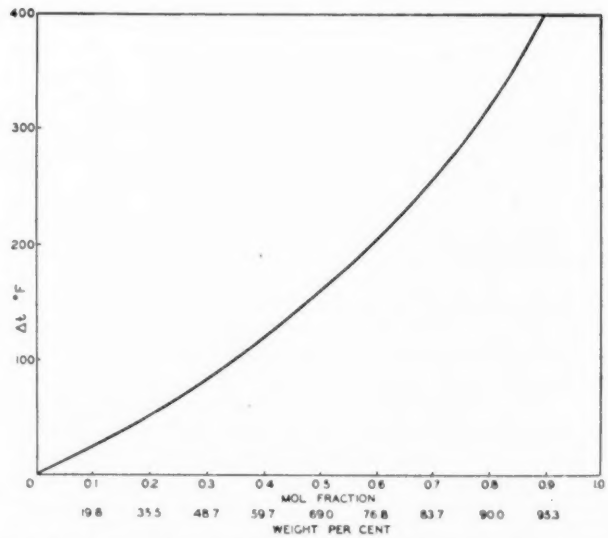


FIG. 3 CAUSTIC-SODA RELATION OF CONCENTRATION IN SOLO SOLUTION TO Δt

differential, the film boiler water will simply concentrate to keep its vapor pressure the same as that of the over-all boiler water. If the film temperature or Δt exceeds 140 F the water will evaporate from the solution leaving a dry residue of potassium chloride.

Fig. 3 shows the caustic-soda concentrations produced in solo solution by various Δt values. How much Δt would be required to produce the 11,000 ppm NaOH concentration? The answer is only a little more than 1 deg F. With a Δt of 5 deg F the film concentration would be about 45,000 ppm (1125 epm) NaOH, with corrosive action (from Fig. 1) at relatively the same rate as an acid solution of about 300 ppm (8 epm) HCl.

That such small or even larger increases in film temperatures can result in a high-pressure boiler is hardly to be denied. Fortunately, for the most part such concentrated films are not continuous, but when they are, failure soon results. However, even with relatively good circulation such small increases in film temperature, or Δt, and concentrated solutions if soluble solids are present, can occur for at least short periods of time. Examples of such periods would be occasions when the slag falls off of a section of waterwall, exposing the tubes to higher temperature than the surrounding area which is insulated by the slag covering, or in certain tube sections immediately following soot blowing.

Obviously, in view of such factors, it becomes the duty of the water-conditioning engineer to think in terms not only of protective conditions for the over-all normal concentration of boiler water, but also in terms of maintaining the concentrating film as protective as possible.

Fortunately, by the time the need for improving boiler-water conditions at Montaup became apparent, considerable of the work developed in the paper by Hall[3] had already been made available. Therefore the boiler was cleaned of existing deposits by means of inhibited acid (Dowell) and a different treatment instituted.

Preliminary Potassium-Treating Period

The studies developed by Hall[2] indicated that while sodium silicate would "hide-out" and be scale-forming, the same was not true for potassium silicate as long as the silica-to-alkali ratio, in equivalents, was maintained at 1.6 or less, so that the highly soluble potassium metasilicate or disilicate would exist, even though considerable concentration due to film-boiling might occur. This made the maintenance of some silica in the boiler water, if it could be kept in the soluble form, desirable as a means of decreasing the amount of sodium-hydroxide concentration which could develop in a concentrating film. Furthermore, considerable magnesium phosphate had been found in various boiler deposits during the period of sodium treatment, and the maintenance of some silica in the boiler water would be advantageous for precipitating the magnesium as magnesium silicate, which has been proved to be the most desirable form of magnesium sludge in boiler water, with minimum tendency for the formation of adherent deposits. To obtain the advantage of these developments the boiler-water-conditioning control, started after the acid cleaning in April, 1943, was established as follows:

pH value	10.2–10.7
Phosphate (PO_4), ppm	30–50
Sulphite (SO_3), ppm	2–5
Silica (SiO_2), ppm	7–10
K to Na ratio, equivalents (min)	2:1
SiO_2 to alkalinity ratio, equivalents (max)	1.2:1

Inasmuch as the plant uses tidewater for cooling purposes, so that even small amounts of condenser leakage introduced considerable sodium in the boiler water, it was necessary to feed potassium chloride, in addition to the potassium phosphate, sulphite, and silicate, to maintain the desired potassium to sodium ratio.

A number of tests which were conducted after the boiler was returned to service with the use of potassium chemicals showed quite promising results. One of the most interesting features was the virtual elimination of sulphate and phosphate hide-out. The results of typical hide-out tests during the periods of sodium and potassium treatment, respectively, are shown in Fig. 4. The upper curves show the chloride concentrations as the load on the boiler was decreased. The lack of hide-out with potassium-treated boiler water contrasts sharply with the large amount of hide-out indicated by the sodium sulphate and sodium phosphate, obtained during the period of sodium treatment.

Several boiler inspections after relatively short runs, following the use of potassium chemicals, also showed promising results inasmuch as the boiler internals proved to be quite clean. Therefore the boiler was operated at full design pressure and the maximum load desired by the plant, generally between 550,000 and 600,000 lb of steam per hour.

A series of special tests were also made during this period which produced a number of interesting results. For example, it was found that in this boiler high-silica concentrations were unstable, and it was therefore inadvisable to try maintaining more than 10 ppm of silica in solution in the boiler water.

The work of Hitchens and Purssell[3] indicated that very little decomposition or auto-oxidation of sodium sulphite occurred up to a steam pressure of 1775 psi. However, in the Montaup boiler, considerable decomposition of sodium sulphite had been indicated whenever efforts were made to maintain more than a few ppm thereof in the boiler water. In this respect the potassium sulphite proved similar, and therefore the decision was made to maintain only a few ppm of sulphite in the boiler water, to serve primarily as an indicator of whether or not dissolved oxygen was entering the boiler with the feedwater.

[3] "The Behaviour of Sodium Sulphite in High-Pressure Steam Boilers," by R. M. Hitchens and J. W. Purssell, Jr., Trans. A.S.M.E., vol. 60, 1938, pp. 469–473.

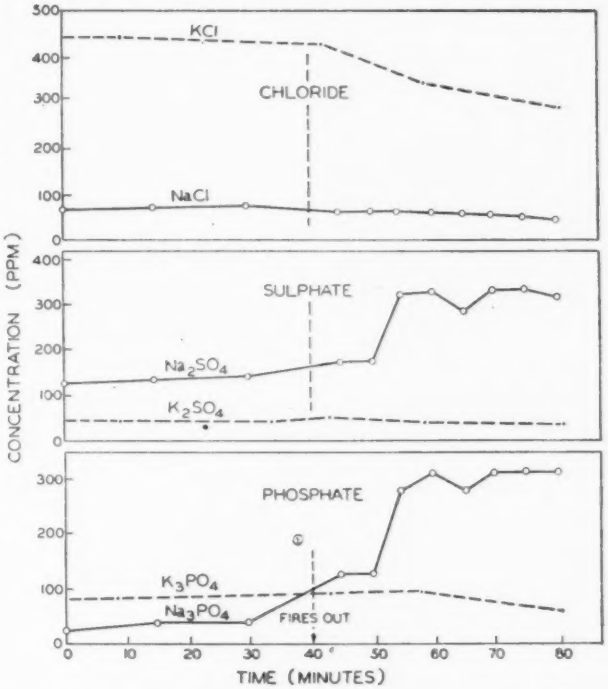


Fig. 4 Presence and Absence of Hide-Out With Na and K Salts

In December, 1943, No. 2 roof tube failed, apparently due to sludge accumulation in the rear-wall header around the strainer supplying the orifice which fed this particular tube. A number of tube sections were cut out at this time and considerable iron-oxide formation was found on the tubes, particularly on the fire side. Pickling some of the tube sections also disclosed a thin yellow ribbon of acmite, sodium iron silicate scale, on the fire side of a number of the tubes. Details of this are given in the reference paper by Parks[2] and need not be repeated here. It is perhaps noteworthy that during the period of potassium and silicate treatment the boiler had been operating at full design pressure and had generated considerably more steam with but one tube failure than it had during the period of sodium treatment during which three tube failures had occurred.

The boiler was again acid-washed by Dowell, using inhibited hydrochloric acid with some bifluoride added in order to remove the silicate scale as well as the iron-oxide formation. In order to eliminate further sludge accumulations at the ends of the rear header, arrangements were also made to interconnect each end of the rear-wall header with the adjacent side-wall header.

Potassium Treatment in Use Since January 1, 1944

In putting the boiler back on the line, it was decided to discontinue the feed of silica because of the slight but definite acmite formation which had been produced on the fire sides of a number of the tubes. It was also deemed advisable to continue with potassium boiler-water treatment because of the lack of hide-out when potassium chemicals were used in the boiler-water conditioning. Furthermore, a number of other plants which had substituted potassium chemicals in place of sodium chemicals for high-pressure-boiler water conditioning, had also found considerably less phosphate sludge in the boilers following this change

even though silica feed had not been used. This factor was also an influence in the decision to continue with potassium treatment.

Our laboratory has been doing considerable work with various solo solutions and mixtures of various salts in high-temperature bombs to determine the vapor pressures of the solutions at various temperatures and pressures. The results of a series of such tests are plotted in Fig. 5, from the data of Kaufman,

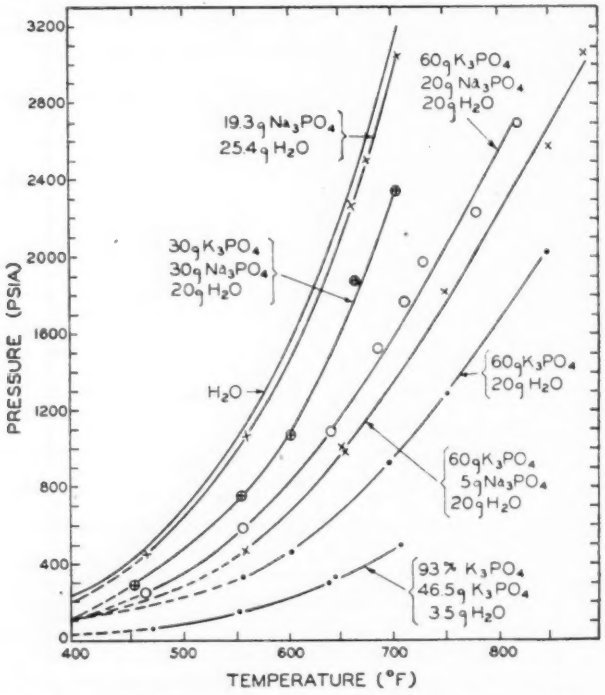


FIG. 5 VAPOR PRESSURE OF SODIUM PHOSPHATE, POTASSIUM PHOSPHATE, AND MIXED PHOSPHATE SOLUTIONS

Marcy, and Trautman.[9] These curves show why hide-out is readily obtained with sodium phosphate and not with potassium phosphate. For example, the Δt for sodium phosphate is only approximately 5 to 9 deg F for the entire temperature range from 400 to 3200 psia. Thus a film temperature of only 5 to 9 deg F above that of the main body of boiler water would be necessary to produce Δts, or a saturated solution. If the film temperature exceeds this, the solution will go to dryness, or, in this case, result in hide-out of sodium phosphate. With solo solutions of potassium phosphate, a Δt of several hundred degrees would be required before saturation and hide-out could occur. Mixtures of sodium and potassium phosphates show intermediate behavior, with an increasing Δts as the ratio of potassium to sodium is increased.

Fig. 6 shows the vapor pressures for a number of solo solutions compared to those of water at various temperatures. It will be noted from Fig. 6 that many of the sodium salts such as sodium phosphate, sodium sulphate, and sodium silicate have very low Δts values, or would go to dryness at a film boiler temperature of 10 deg or less in excess of the temperature of the saturated steam. A considerably larger Δts value is indicated for sodium chloride and even greater values are obtained for potassium chloride. As mentioned in connection with Fig. 5, the Δts of potassium phosphate is so large that it would seem almost impossible to obtain a film temperature sufficiently high to precipitate potassium phosphate out of solution unless actual overheating of a tube occurs to a considerable degree. With either sodium or potassium hydroxides, concentration of the solution occurs without going to dryness. In other words, in a boiler, or in a water-hydroxide system, Δts is practically nonexistent for sodium or potassium hydroxides.

As pointed out in connection with Fig. 1, concentration of hydroxide, such as obtained by only a few degrees elevation in temperature due to film boiling, can produce conditions decidedly corrosive to boiler metal. Therefore in thinking in terms of the concentrated solution which can develop, it is desirable to introduce other salts of sufficient Δts to remain in solution in case of film boiling, and thereby reduce the concentration of caustic which can result. In order to accomplish this, the joint means were used of decreasing the range of alkali to be maintained in the boiler water and increasing the potassium chloride concentration. The effectiveness of this was checked in the laboratory by means of accelerated tests. Bombs were charged with 250 g of solids (anhydrous) and 30 g of water. The temperature within the bomb was raised to approximately 1022 F in a period of 3 hr, after which the heating was discontinued and the closed bomb allowed to cool to room temperature. The residual pressure due to the hydrogen generated during this test was measured after cooling. The results obtained for mixtures of potassium chloride and potassium hydroxide, potassium phosphate and potassium hydroxide, and mixtures of both potassium chloride and potassium phosphate with potassium hydroxide are plotted in Fig. 7. It will be noted from this figure that the amount of hydrogen formed, which is a direct indication of the amount of attack on iron, dropped very rapidly as the molar ratio decreases below 0.2 for mols KOH over the total mols of chemicals present. Thus for benefit to be obtained from this source it is indicated that the chloride concentration, in equivalents, should be at least 5 times that of the hydroxide concentration, and for added safety in this respect a ratio of 10 to 1 chloride to alkalinity was

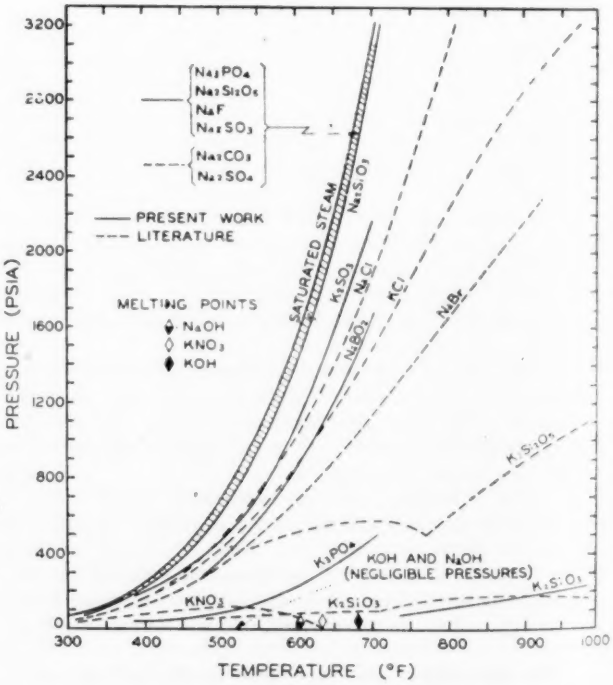


FIG. 6 VAPOR PRESSURE OF SATURATED SOLO SOLUTIONS

[9] "The Behaviour of Highly Concentrated Boiler Water," by C. E. Kaufman, V. M. Marcy, and W. H. Trautman, Proceedings of the Sixth Annual Water Conference, Engineers Society of Western Pennsylvania, October, 1945.

established as a minimum for the chemical control of the Montaup boiler water.

The detailed control limits which were established and have been maintained since January 1, 1944, are as follows:

pH value	9.8–10.4
Phenolphthalein alkalinity (ml, N/30 acid required for 100-ml sample)	0.5–1.6
Phosphate (PO_4), ppm	8–20
Chloride:hydroxide ratio, epm	Minimum = 10:1
Potassium:sodium ratio, epm	Minimum = 3:1
Total solids, ppm	Maximum = 1000

Actually, the control has worked out so that the chloride to hydroxide ratio, in equivalents, is seldom below 50:1. Thus in a film-boiling solution with Δt of 5 deg F, instead of obtaining a caustic concentration of 4.5 per cent, this concentration will be only about 0.09 per cent (900 ppm or 22.5 epm), or still within

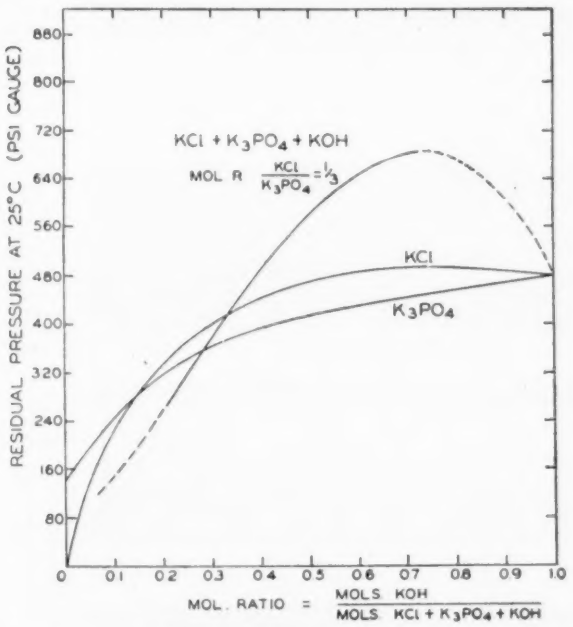


FIG. 7 RESIDUAL HYDROGEN PRESSURE DEVELOPED BY ACTION OF KCl-K_3PO_4-KOH MIXTURES

the protective range of minimum attack by hydroxide on steel at high-pressure-boiler temperatures, as indicated by the data of Berl and van Taack plotted in Fig. 1.

HIGH-PRESSURE-BOILER FEEDWATER

The nature of the boiler feedwater is also a factor which cannot be ignored, especially in the operation of high-pressure boilers.

The boiler feedwater at Montaup is obtained from the turbine condensers plus a small amount of evaporated make-up water. Control to maintain good feedwater conditions is normally maintained at the plant, as proved by some 15 years' operation of the 400-psi boilers without difficulty in the preboiler equipment. However, with the advent of the early difficulties encountered in the operation of the high-pressure boiler, steps were taken further to improve the quality of the feedwater wherever possible. Operation of the two deaerators was adjusted so that they would always be under positive pressure to assure good elimination of dissolved oxygen. The turbine condensers were also retubed in 1944, to assure minimum contamination by the tidewater used for condenser cooling.

These steps have resulted in feedwater which generally shows zero values for dissolved oxygen. Carbon dioxide in the system is also very low, due to the feedwater to the evaporators being a sulphate rather than a carbonate water. Tests made on the steam indicate that the carbon-dioxide content is of the order of 0.01 ppm. Measurement by means of a Leeds & Northrup pH meter on flowing cooled samples, right at the sampling points after the deaerators, generally shows pH values of about 8.5.

Condenser leakage is immediately indicated on the condensate-conductivity recorders, and if this becomes at all high, the condenser is taken out of service as soon as possible and the leaking tubes located and plugged. As a result of this control the turbine condensate used for feedwater has averaged less than 5 micromhos per cm conductivity, since the summer of 1944.

EXAMINATION OF BOILER-TUBE SECTIONS

The removal of tube sections for examination rather than merely examination and analysis of such deposits as are found in the wet-steam drum, has greatly facilitated the determination of internal conditions of the Montaup boiler. We have thus been able to study the distribution of constituents of the deposit between the fire and cold sides of the tubes, as well as between the surface of the deposit and the area next to the metal. Examples of this variation are the presence of acmite ($Na_2O.Fe_2O_3.4SiO_2$) on the fire side of some tubes in a thin layer next to the metal. In some instances this layer was so thin that it would never have been detected had the tube section not been pickled. The bulk of the deposits was iron oxide and contained little or no acmite. Another example is the presence of a considerably higher percentage of phosphate sludge on the cold side of some tubes rather than on the fire side. A third example of variation is found in the appearance of the internal surfaces of some tubes. Many of these specimens examined showed smooth continuous films of magnetic iron oxide, while others exhibited considerable roughness and thicker surface deposit. Pickling of the specimens showed that those tubes which exhibited a rough surface very frequently showed evidence of metal attack.

The first set of specimens examined by us was removed from the boiler on January 13, 1943, at the time of failure in the No. 2 roof tube. The general condition of these tubes has already been reported in the paper by Parks.[3] Also in this paper were presented for comparison photographs of tubes examined after the boiler had been on potassium-silicate treatment. In both of these sets of tubes a hard dense deposit, consisting chiefly of magnetic iron oxide, was found on the fire side of the specimens examined. This was, at least in the specimens removed after potassium-silicate treatment, found to overlie a very thin film of acmite ($Na_2O.Fe_2O_3.4SiO_2$). The specimens removed after sodium treatment were not pickled to determine if a layer of acmite adjacent to the metal was present. The cold side of the tubes, while showing a relatively rough surface, did not exhibit the hard, dense iron oxide found on the fire side in either of these sets of specimens. The material on the cold side of the tube was soft and powdery, as was the surface layer on the fire side which covered the hard, dense material.

Appreciable roughening of the metal surface of a number of the tubes was evident. This roughening was believed due in part, at least, to small tears produced in the tubes during cold-drawing. A specimen of this sort of tubing, carefully polished to remove the tears before installation, did not show as much attack on the metal surface although this tube section was not in operation as long as the unpolished tube. It is not known whether acid-cleaning of the boiler contributed to this roughening.

The first set of specimens removed after the discontinuance of silica feed still showed some patches of the dense iron oxide, which patches were coated with metallic copper. Since these specimens had been in the boiler during silica feed and the acid-cleaning which was done following the silica treatment, it seems quite

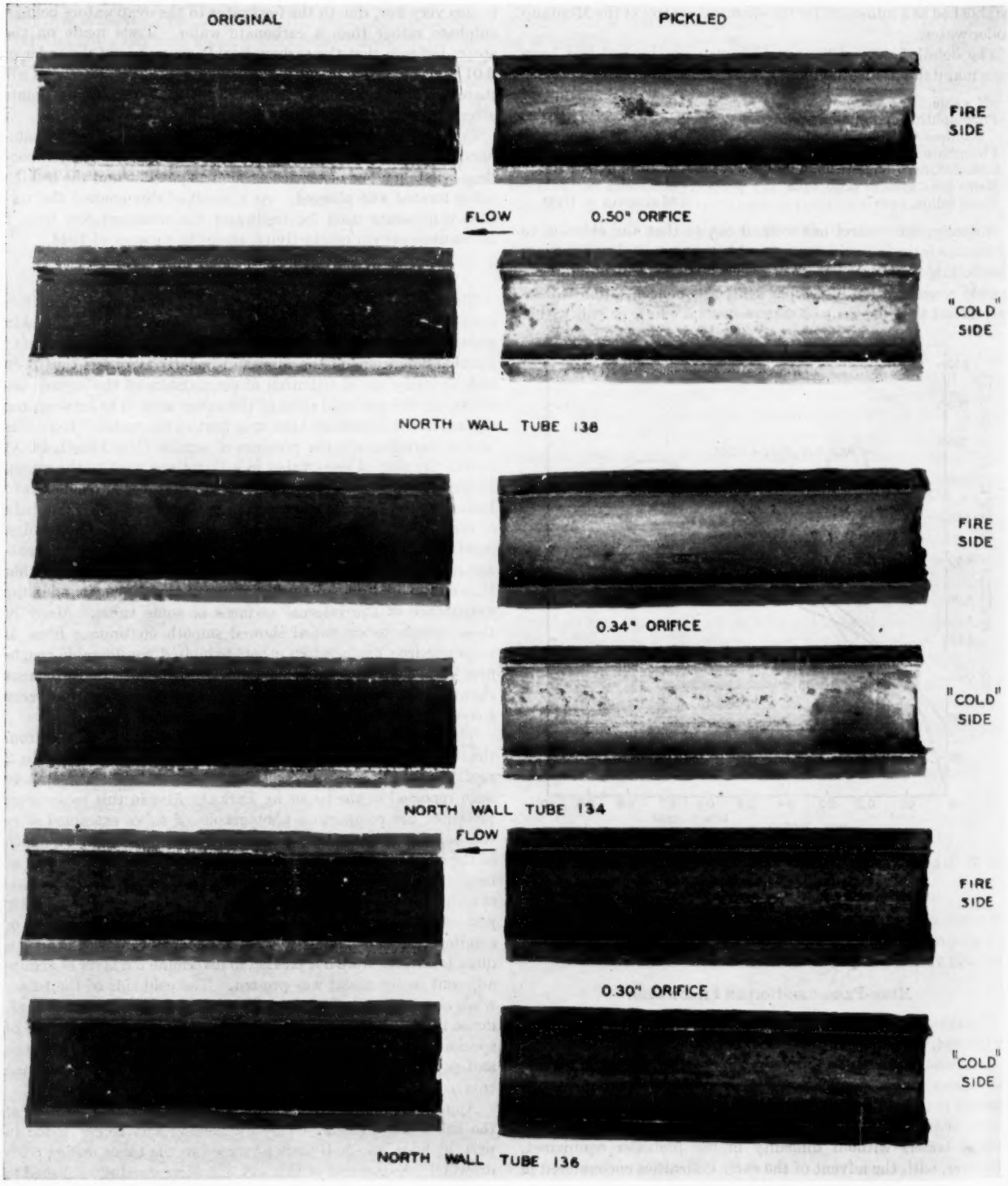


FIG. 8 APPEARANCE OF BOILER TUBES FROM BIFURCATED SECTIONS AFTER 14 MONTHS OF OPERATION WITH PRESENT POTASSIUM TREATMENT

(Each tube is one of a pair of bifurcated tubes fed by a single orifice. Tube No. 138 is fed from a 0.50-in-diam orifice; tube No. 134 is fed from a 0.34-in-diam, or normal size orifice; tube No. 136 is fed from a 0.30-in-diam orifice.)

possible that the deposition of copper and even part of the pitting might have occurred during the acid-cleaning. Tube sections removed up to September, 1945, showed that none of the tubes which have been installed since the December, 1943, acid-cleaning contained any significant amount of this hard dense iron oxide. One or two localized patches of scale had developed, but this is believed due to restricted circulation from welding slag in the particular tube orifice, as will be explained later.

Since the surfaces of the tubes originally installed in the boiler were found quite rough, particularly on the fire side, it was decided, in order really to evaluate the present method of treatment, to examine only specimens which have been installed since the December, 1943, acid-cleaning. Special orifices were installed in the strainers feeding six of the north-wall tubes. A fairly large section of these tubes, plus an adjacent pair, fed by the normal orifice, was replaced in June, 1944, with new tubing and we were therefore able to determine the general effect of treatment and also the effect of the special orifices on the same set of samples.

The specimens from this section examined during the latter part of 1944, contained considerably more calcium and magnesium phosphate than had previously been seen on the tubes since the institution of potassium treatment, although there was no evidence of marked attack on the tubes such as had been experienced with the tubes examined previously. It was found that much of the sludge and iron oxide could be removed from the boiler by operating for a 24-hr period at 400 psi and high blowdown. Until the October, 1945, failure of two rear-wall tubes, this treatment of the boiler indicated that accumulation of deposit was insignificant.

Prior to the use of tubes installed in 1944, for examination, it was almost impossible to tell from the condition of the metal surface or from the amount of sludge accumulation just what the extent of attack really was. This was because the amount of metal loss and consequent roughening of the surface seemed to be a function of the number of tears occurring in the metal surface during cold-drawing, as well as operating conditions. The accumulation of iron oxide and also the precipitation of phosphate sludge appeared to be proportional to the amount of roughening of the metal surface. Of particular interest along this line was the fact that the phosphate sludge tended to pile up on the downstream side of a high spot in the iron-oxide surface, especially behind a tubercle on the cold side of the tube. We are at a loss to explain why there should be more phosphate on the cold side, unless the increased turbulence on the fire side of the tube prevented it from settling out. The phenomenon has, however, been observed too frequently to be pure coincidence.

Fig. 8 shows portions of tubes removed from the north wall after approximately 15 months of the present potassium treatment. Tube No. 134 is one of a pair of tubes being fed through a normal 0.34-in. orifice. It will be noted that the surface of the

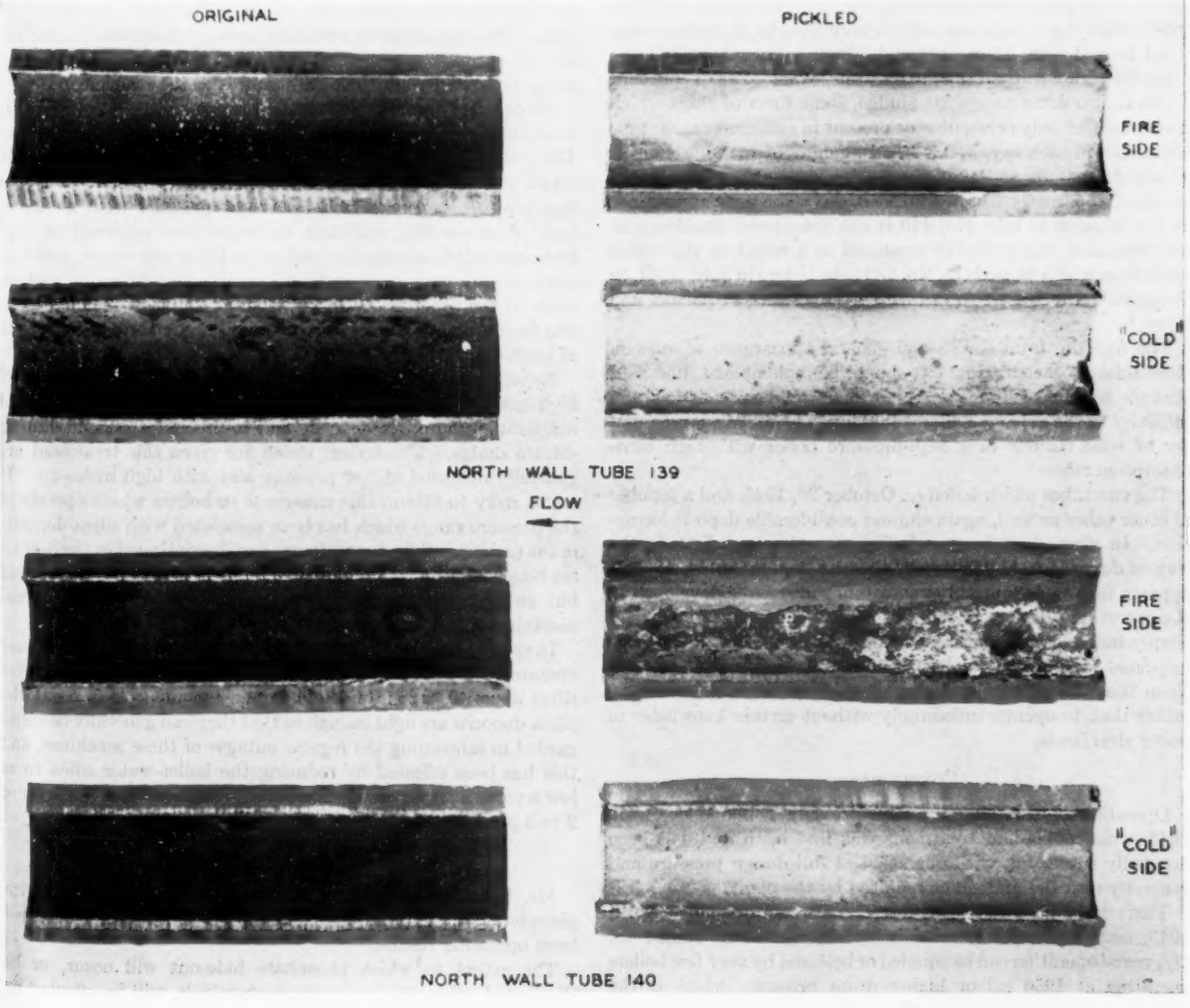


FIG. 9 APPEARANCE OF BOILER TUBES FED BY SINGLE, SEPARATE, 0.25-IN-DIAM ORIFICES AFTER 14 MONTHS OF OPERATION WITH PRESENT POTASSIUM TREATMENT

oxide film is fairly smooth and that there is no evidence of significant attack on the metal in the pickled specimen, either on the fire or cold side. Tube No. 138 is one of a pair of tubes being fed by a special 0.50-in. orifice and is similar in appearance to No. 134 tube with the normal orifice. Tube No. 136 is one of a pair of tubes being fed by a reduced-sized orifice, 0.30 in. In the original specimen from this tube the definite roughening of the surface of the deposit can be noted on both the fire and cold sides. In the pickled specimen there is a little more roughening of the surface on the fire side, Fig. 9.

Tubes Nos. 139 and 140, Fig. 9, normally a pair fed by a single 0.34-in. orifice, are fed by two separate 0.25-in. orifices. These two separate small orifices would transmit about the same total water flow as through a single 0.34-in. standard orifice. It will be noted that there is no more attack evident on the pickled specimens of tube No. 139 than in the normal tubes. The flaking off of deposits on the cold side of tube No. 139 is believed to be due purely to mechanical causes during shipment of the tube, since light tapping of the tube in the laboratory removed more of the deposit. The particular section of tube No. 140 shown was photographed because of the apparent difference in the nature of the deposit. This is the only hard patch on any of this set of tubes, and does not extend over the remainder of the specimens from this tube. The main constituent of this very thin, hard, scalelike material is still iron oxide, although there is considerably more hematite (Fe_2O_3) than magnetic iron oxide (Fe_3O_4) present. There is also some phosphate sludge, some form of silica which was not sufficiently crystalline or present in sufficient amount for identification by x ray, and a small amount of metallic copper. Traces of sodium and potassium salts were also found in the deposits, apparently trapped in the scale. The poor appearance of the fire side of tube No. 140 is not considered significant as this condition was probably produced as a result of the orifice restriction which caused the No. 139 tube failure in July, 1944, as discussed in the first paper of this series by Parks, Patterson, and Ryan.[4]

The freedom from sludge and general appearance of most of these tubes is encouraging. It should be remembered, however, that the amount of sludge or scale which would cause little if any difficulty in the average boiler would likely result in a large number of tube failures in a high-pressure boiler with high heat-absorption rates.

The two tubes which failed on October 26, 1945, and a number of other tubes as well, again showed considerable deposit formation. In view of the long period of operation with little in the way of deposits from January 1, 1944, to September 14, 1945, it appears that some unusual circumstance may have developed in the operation prior to October 26. On the other hand, this may simply indicate that inasmuch as only the tubes cut out can be inspected for internal conditions, it would be advisable to acid-clean the unit at regular intervals such as annual shutdowns, rather than to operate indefinitely without certain knowledge of boiler cleanliness.

Conclusions

Operation of the Montaup high-pressure boiler since April, 1943, when potassium treatment was first instituted, has been decidedly successful, with operation at full design pressure and generally near design load as required by the plant.

There have been only two forced boiler outages since April, 1943, associated with internal boiler deposit. This record for $2^1/_2$ years' operation can be equaled or bettered by very few boilers operating at 1950 psi or higher drum pressure, which is the operating pressure of the Montaup unit.

In arriving at the boiler-water control for high-pressure boilers, not only the over-all boiler-water conditions must be considered, but attention must also be focused on the type of water which will develop when abnormally high concentrations occur, such as follow with but a few degrees film-temperature increase above the over-all boiler water and saturated-steam temperatures.

It is felt that the advantages of potassium equilibrium in the boiler water have been definite contributing factors to the operating record of this boiler, similarly to a number of other boilers operating at pressures of 600 psi or above, where definite improvements in internal boiler conditions or maintenance of turbine capacities, or both, have resulted.

Discussion

T. J. Finnegan.[10] This paper describes the application of potassium treatment to the Somerset Station and presents curves which show that under that treatment hide-out did not occur, while under sodium treatment it was present. This is in agreement with our experience with three high-pressure natural-circulation boilers which operate at 1265 psia and 900 F at the turbine inlet and deliver 900,000 lb of steam per hr. In our experience, however, it has been found that hide-out of phosphate is absent only when the PO_4 content of the boiler water is kept at a low figure and consequently we do not allow it to exceed 10 ppm. There is probably a relation between boiler design and the amount of hide-out which will occur, and this must be considered along with the purely chemical features of the problem.

We can also support the statement regarding the decomposition of sulphite in the boiler water and can demonstrate that the condition which permits it to occur may be very delicately established and difficult to define. In one of two 900,000-lb per hr high-pressure boilers, which had been operated with about 15 ppm of excess SO_3, sufficient decomposition occurred so that hydrogen sulphide could be smelled easily in the steam, and copper sulphide deposits were found on the high-pressure heaters, while in the other boiler no evidence of sulphite decomposition was found. Both boilers were operated under similar conditions of loading.

Reports have been received of good results in the treatment of high magnesium boiler water with silicates in order to avoid magnesium-phosphate deposits and to precipitate magnesium as silicate sludge. The boilers which are given this treatment are generally operated at low pressure and with high make-up. It seems risky to extend this treatment to boilers which operate in the pressure range which has been associated with silica deposits in the turbine. Silicate treatment was discontinued in the Somerset boiler because a small amount of silica scale had been found but an equally important consideration would be the internal condition of the turbine.

In spite of the fact that the three high-pressure units mentioned operate with less than 1 per cent make-up, at one time severe silica deposits had been found in the turbine. At present the silica deposits are light enough so that they can generally be disregarded in scheduling the regular outages of these machines, and this has been effected by reducing the boiler-water silica to as low a value as it is possible to obtain; it is usually of the order of 2 to 3 ppm of silica.

Authors' Closure

Mr. Finnegan's comments in regard to actions observed with phosphate and sulphite contribute to the information obtained from operating results.

The extent to which phosphate hide-out will occur, or be eliminated, when using potassium chemicals, will be affected by

[10] Chemical Engineer, Buffalo, Niagara Electric Corporation, Buffalo, N. Y. Mem. A.S.M.E.

the ratio of potassium to sodium present, and the Δt as illustrated by Figs. 2 and 5 of the reference paper.

The use of silica, properly controlled, has been of decided benefit in reducing the amount of adherent sludge in many boilers. Successful experiences in this respect include boilers operating at as high as 750-psi drum pressure, with no increase in the turbine deposition. The precipitation of residual magnesium entering the boiler as the silicate, instead of the hydroxide or phosphate, produces the most favorable conditions for the prevention of adherent sludges.

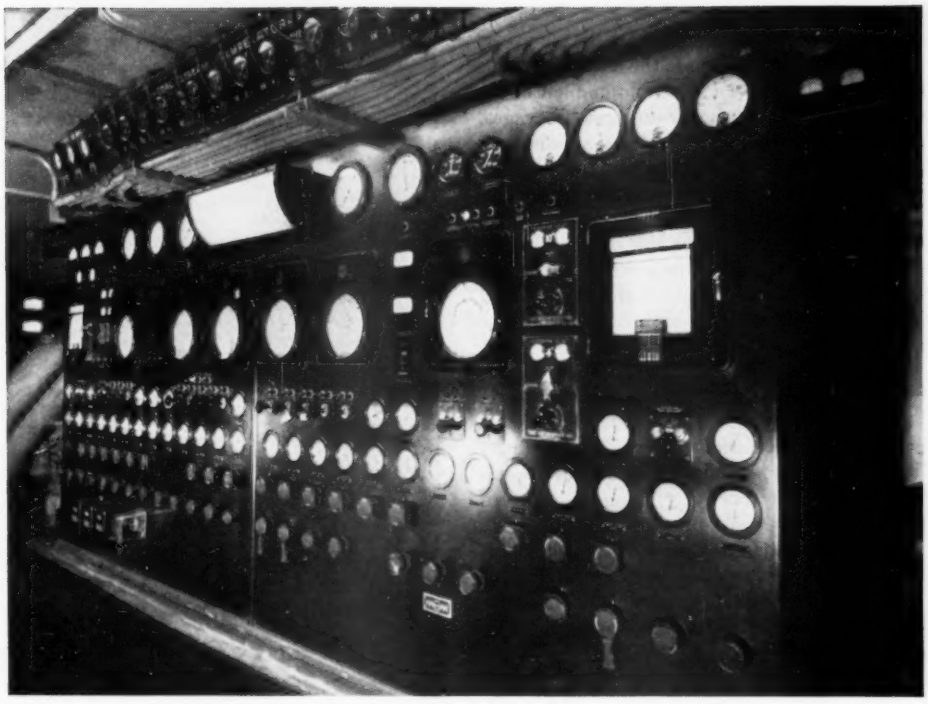


FIG. 1 MAIN CONTROL BOARD 2000-PSI BOILER 6; GR. 137

Experience With Instruments and Control Equipment for 2000-Psi Boiler at Somerset Station of Montaup Electric Company

BY W. D. BISSELL[1] AND E. B. POWELL[2]

This paper presents comprehensive descriptions and operating experiences with the instruments and control equipment as applied to the high-pressure high-capacity boiler of the Somerset Station. Details are given not only of the completely automatic operating and control equipment but also of the indicating and recording instruments which enable the operators to follow constantly the operating conditions of the boiler and thus permit immediate manual adjustment when the need is indicated.

THE 2000-psi boiler at Somerset Station is numbered 6 from location and sequence of installation in the station and, for brevity, will be referred to as boiler 6 in this discussion. The instruments and automatic regulating devices which serve for operation control on the boiler are conveniently considered in three groups. In group (1) is classed equipment serving primarily for stabilization of output and efficiency of combustion; in group (2), equipment for maintenance of water conditions. For ready identification of equipment associated with the distinguishing characteristic of the boiler, a third grouping is employed for permanent instruments and controls installed to meet the special needs of forced circulation.

[1] Somerset Station, Montaup Electric Company, Fall River, Mass.
[2] Stone & Webster Engineering Corporation, Boston, Mass. Mem. A.S.M.E.

Contributed by the Power, Industrial Instruments and Regulators Divisions, and the Joint Research Committee on Boiler Feedwater Studies and presented at the Annual Meeting, New York, N. Y., Nov. 26–29, 1945, of THE AMERICAN SOCIETY OF MECHANICAL ENGINEERS.

NOTE: Statements and opinions advanced in papers are to be understood as individual expressions of their authors and not those of the Society.

CONTROL OF BOILER OPERATION AND COMBUSTION EFFICIENCY

The functions served by the instruments and control equipment of group (1), as classified in the preceding paragraph, are essentially those to be met in the operation of any modern boiler of equal capacity, i.e., pressure gages for steam, water, and air; flowmeters for steam, water, and fuel oil; feeder speed indicators for pulverized coal; instruments for evaluation of combustion efficiency; boiler-drum water-level recorder and drum water-level indicators; combustion and steam-pressure control; steam-temperature control; feedwater-pressure and flow-control devices. Interest in experience with this equipment is found chiefly in the instances where pioneering has been involved. Other equipment will be sketched merely for perspective.

Main Control Board. The main control board, mounting in-

struments and controls primarily of group (1), is shown in Fig. 1. The operating signal lights for the boiler circulating pumps at the extreme left near the top of the board are the only equipment of this figure not classed as of group (1). At right and left of the board are independently mounted primary-air pressure gages. Above the board are fuel-oil pressure gages and coal-stream temperature indicators. On the board proper the top row includes coal-feeder tachometers at the extreme left, and fan-motor ammeters at the extreme right, multipoint draft gages in the middle, with water- and steam-pressure gages. The row of recording instruments includes recorders for temperature of steam and boiler feedwater at the extreme left, and temperature of flue gases and air for combustion at the extreme right, with boiler-feedwater flow and pressure, and steam pressure, boiler-drum water level, main steam flow - air flow, reheater steam flow, fuel-oil pressure, and flue-gas oxygen in sequence in intermediate positions. At left and right of the feedwater flow recorder are mounted, respectively, controls for feedwater regulation and one of the drum water-level indicators. Similarly, at the sides of the flue-gas oxygen recorder are mounted, respectively, induced-draft-fan motor-exciter voltmeter and the steam-pressure reducing-valve controls. The lower half of the board is devoted almost exclusively to combustion and steam-pressure control, providing for manual control of the combustion system as a whole or for selective use of manual or automatic control as desired on the different elements of the system.

The flue gas-oxygen recorder is one of the highly informative instruments of the board. However, this instrument had barely passed the experimental development stage when purchased. As to be expected with novel equipment, a number of difficulties have been encountered from those frailties which it seems experience alone can fully bring to light. Experience has also proved the value of the instrument as a guide in control of combustion, giving more definite and precise indication of furnace conditions than the steam flow - air flow recorder which it serves to supplement. The flue-gas oxygen recorder is now to be extensively rebuilt.

Mounted on a hinged panel at the left of the recorder row are indicating pyrometers for main superheated-steam and reheated-steam temperatures. Mounted on a separate panel on the opposite side of the aisle, facing the main control board and not shown in the figure, is a group of instruments serving primarily to place control of the temperature of 375 psi superheated steam, delivered to the turbine throttle, in the hands of the high-pressure-boiler operator. This temperature control is effected by regulation of water supply to the desuperheater preceding the steam reheater normally, to the by-pass desuperheaters when the latter are in operation. The equipment of the panel includes two temperature indicators and recorders, one for each of the low-pressure-turbine throttles, an indicator for temperature of steam from the reheater, and water controls for the 4-in. by-pass desuperheater. Control valves for the desuperheating station ahead of the reheater, while not operated from the panel, are readily accessible at the rear of the boiler at the same grade. Controls for the 10-in. by-pass pressure-reducing and desuperheating station and for pressure reduction ahead of the 4-in. desuperheater are on the main board.

Variations in superheated-steam temperature on the low-pressure system are caused usually by variations in loading of low-pressure boilers which take up all load swings within the limits of their operating capacity. The throttle steam temperature on the low-pressure turbines must be held within close limits. Obviously, maintenance of mere constancy of reheated-steam temperature would not meet the requirements. Accordingly, manual adjustments are made in desuperheating the low-pressure steam prior to reheating, or in automatically controlled

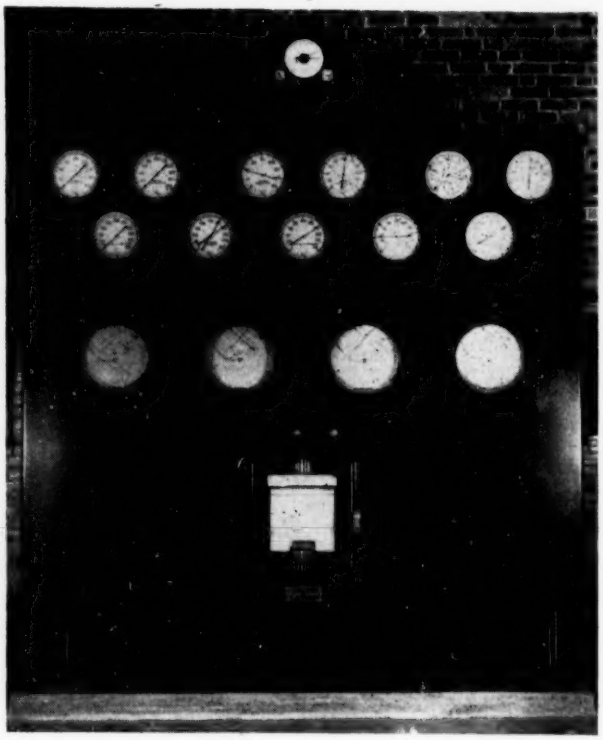


FIG. 2 BOILER-FEED-PUMP INSTRUMENT PANEL; GR.137

temperature of pressure-reduced steam, or in both, as required to give substantially constant temperature at the low-pressure-turbine throttles. The indicating pyrometers on reheated steam and the temperature indicators and recorders on steam at the throttles of the two low-pressure turbines give the operator clearly readable and closely concurrent values at these points at all times.

Adjacent to the low-pressure-system steam-temperature control panel is a 12-point potentiometer indicator for checking recorders and for reading instantaneous temperatures. With multipoint recorders, several minutes may elapse between temperature measurements for a particular point. The indicators bridge the gap and give values instantly or continuously as desired.

Boiler-Feed-Pump Instruments. Fig. 2 shows the boiler-feed-pump instrument panel on the main operating floor, Gr. 137, on which are mounted a recorder for steam flow to turbine-driven feed pumps and for high-pressure-boiler feedwater flow and pressure, and a recording pyrometer for feedwater temperature at several stages of heating, as well as indicating gages for individual pump suction and discharge pressures, pump-turbine-drive exhaust and extraction pressures, and pressure differential between boiler drum and main feedwater header. Additional feedwater-system pressures and temperatures are indicated on the gages of the feedwater-heater instrument panel shown in Fig. 3. On this panel are also mounted controls for motor-operated feed-line valves at the high-pressure heaters and alarms for water levels in the shells of closed-type heaters. This panel is located on the ground floor, Gr. 118.

Regulation of Boiler-Feedwater Flow and Feed-Line Pressure. The feedwater flow recorder on the main board records the total of the separate flows in the two feedwater lines to the boiler economizer. The feedwater-regulator controls mounted adjacent to this recorder provide for adjustment of water-level position in the drum, for changes from automatic control from the corresponding drum-end thermostat to manual control, and

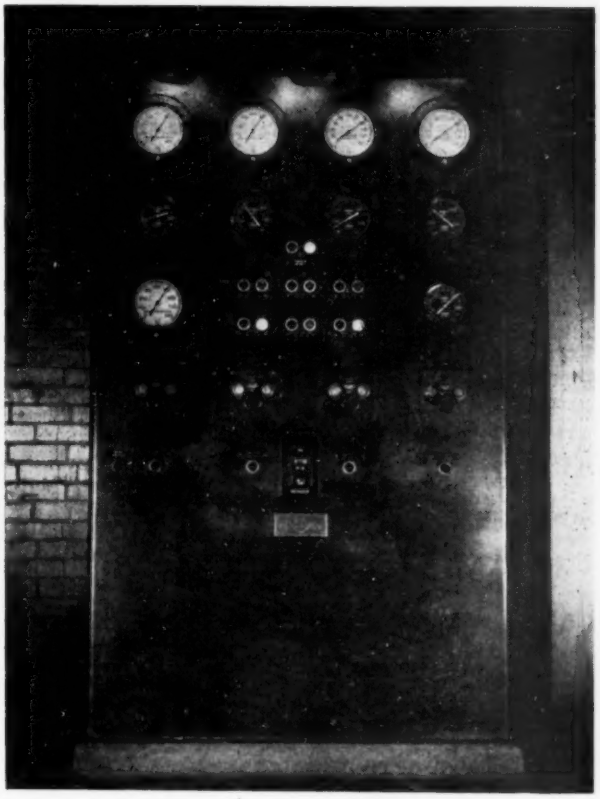


FIG. 3 FEEDWATER-HEATER INSTRUMENT PANEL; GR. 118

vice versa on either or both feed-line flow regulators, and for the manual control of feed-line flow through either or both regulators. Valve position indicators immediately above the controls show at all times the degree of opening of each regulator. Separate line flow indicators, which are of value in equalizing regulator operation, are mounted adjacent to the respective individual metering orifices. The master controller, which functions to maintain the required head differential on the feedwater regulating valves and a definite pressure excess in the feedwater line for sealing the glands of the boiler circulating pumps, is mounted at the rear of the boiler and, as its adjustments are of relative permanence, is not arranged for control from the main board.

Transmission of the primary impulses from the drum end thermostats to the receiving diaphragms on the feedwater regulators, and from the feed-line excess-pressure master controller to the receiving diaphragms for adjusting the speed settings of the boiler feed pump turbine governors, has been accomplished eminently satisfactorily with compressed air. For the actual motivating fluid on the feedwater-regulator pistons, water was found during preliminary operation to give a smoother and more precise control and, accordingly, was adopted. On failure of the motivating water supply, the feed-regulating valve is automatically locked in position. Shifts back and forth between automatic and manual controls are effected easily and smoothly and, since the change in motivating fluid on the water-flow-regulator pistons, the functioning of the system has creditably met all demands, positively controlling the water level in the drum over the full capacity range of feed-line flow down to the condition of complete feedwater supply through circulating-pump gland leakage. Maintenance, aside from wear on the feed-pump low-load flow-recirculating valves, has called for little more than routine of inspection, cleaning, and lubrication of parts.

The feed-line pressure-control system provides not merely for high-pressure feed-pump speed adjustment but also for automatic spilling of the high-pressure feed-pump-drive turbine exhaust to the 15-psig exhaust system, and to atmosphere if required in the emergency of failure of one of the normally two such pumps in operation.[3] As there has been no high-pressure boiler-feed pump service failure, this last provision has not been called into operation.

The automatic control of recirculation of feedwater, required at low loads on the high-pressure boiler-feed pumps,[3] is also one of the functions of the high-pressure boiler-feed regulating system. The recirculating valve is operated by air impulse from the feed-pump-governor speed-setting control. As commented above, wear on the valve parts from the 2150-psi to 500-psi pressure reduction taken in the valve has been about the only source of significant replacement called for in maintenance of the high-pressure-feed regulating system. It is now believed that the life of these parts can be increased by change in design.

Combustion Control. Combustion control is of course initiated by change in steam pressure, with auxiliary adjustments from the accompanying steam flow and gas flow. The measurements of steam pressure and steam flow are usually direct and accomplished with adequate precision without regard to boiler design. On the other hand, for the modern boiler with heating surface almost exclusively of the radiant type, especially where the superheater is under gas by-pass control as in boiler 6, inherent sources of draft loss appropriate for the measurement of combustion-gas flow or combustion air flow become not so obvious. Control equipment and certain instruments used for giving a running check on control efficiency are dependent upon the precision of this measurement. The problem of providing the essentials for this measurement adequately and economically may well receive the careful attention of both boiler manufacturer and plant designer.

Before going into the experiences in measurement of combustion-gas flow on boiler 6, it should be pointed out that superheated-steam temperature is controlled by diverting through the upper economizer a part of the combustion gas flow which would otherwise make full travel of the convection bank of the superheater. The diversion of gas flow is accomplished by adjustment of main and by-pass dampers at the gas outlet of the economizer, shown diagrammatically in Fig. 4. Steam temperature is held very closely, swings in temperature rarely exceeding 5 F even during operation of soot blowers.

As first arranged, air flow for combustion was evaluated by summation of straight-line functions of gas pressure drops across the two parts of the economizer, utilizing connections at points about as indicated by *C* and *D* and *E* and *F* in Fig. 4. For recording steam flow - air flow relations, the combustion-gas flow initially was to be based upon the differential across the steam reheater between points indicated by *A* and *B*, also in Fig. 4. It early became evident, however, that the normal gas resistance of the reheater was not great enough to give consistent measurement of gas flow, and connections were made to provide for summation of straight-line functions of economizer-draft drops, paralleling the corresponding arrangements for combustion control. For metering purposes, however, an effort was made to compensate for variations in gas density by making the two pressure connections on the flue at the same level and extending the trailing pressure lead to the outlet of the economizer within the gas stream.

Attempts toward close co-ordination in combustion control en-

[3] "1825-Lb-Pressure Topping Unit With Special Reference to Forced-Circulation Boiler," by F. S. Clark, F. H. Rosencrants, and W. H. Armacost, Trans. A.S.M.E., vol. 65, 1943, pp. 461–477.

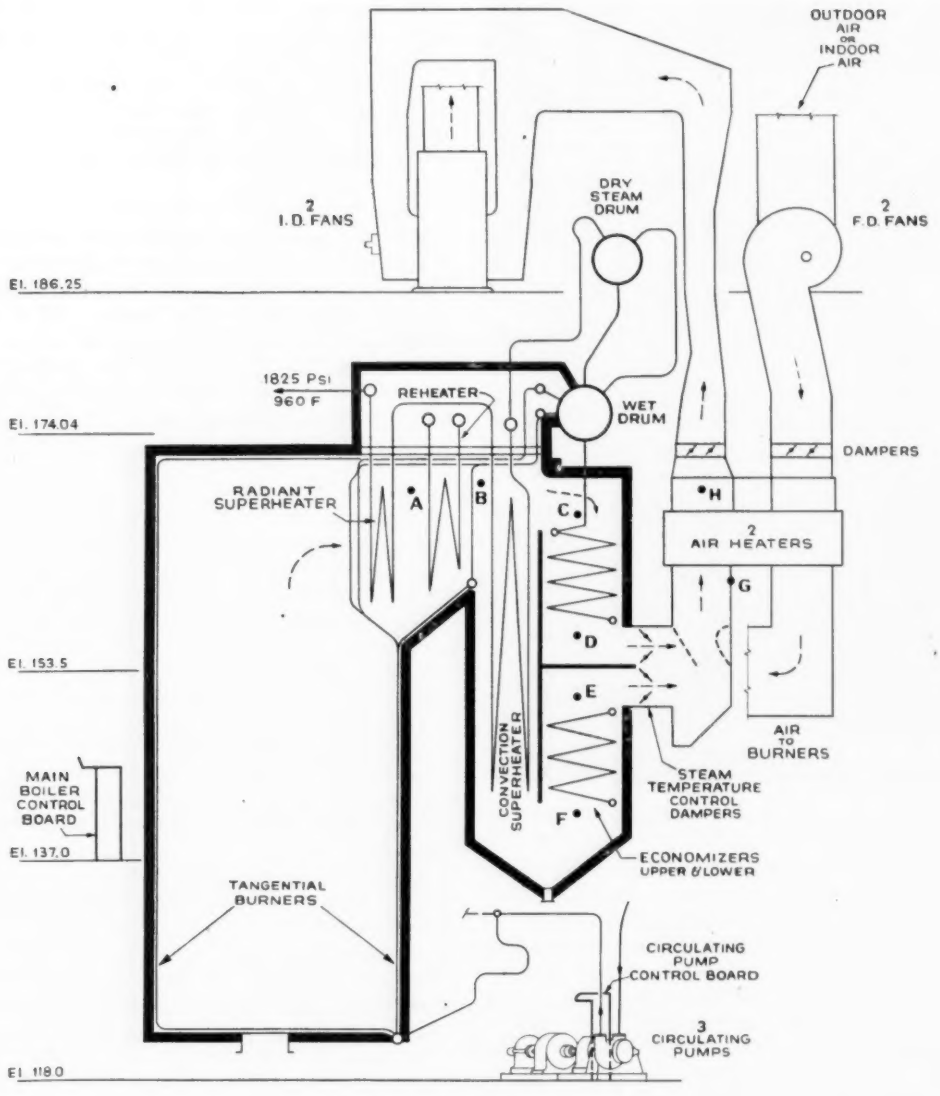


FIG. 4 DIAGRAMMATIC SECTION BOILER 6

countered the situation that pressures measured at the downstream connections in the economizer casings were seriously influenced by flow disturbances varying with the positions of main and by-pass dampers. In addition, during the first few months of operation, apparently the economizer gas-pressure differentials were affected by accumulating deposits on economizer surfaces and by flow disturbances from slag and ash accumulations in the superheater and reheater ahead of the economizer. These factors gave an annoying lack of consistency in gas-pressure differential in relation to actual rate of gas flow. After exhaustive efforts to improve performance, it was decided to abandon use of the steam-generating equipment proper as a source of gas-pressure differential and install restricting baffles to form an orifice in the short length of flue between the economizer-outlet dampers and the air heater, as indicated in Fig. 4. Observations with this arrangement, however, demonstrated that the pressure loss, as measured across the restricting baffles, was also influenced by the position of the dampers.

Air heaters of the rotating type are generally regarded as too unstable in draft characteristics for evaluating rates of gas flow, their variations in leakage and in resistance of path being thought too great to permit use of a device of that kind in the control of combustion and the metering of gas flow. However, use of the air-heater pressure differentials was adopted as a last resort. Connections for metering gas flow and the gas-flow factor in combustion control were shifted to G and H, Fig. 4. The results have been very promising. The arrangement has now been in operation more than 6 months, and combustion control and air-flow measurement have been found to respond satisfactorily not only to normal fluctuations but in meeting severe sudden changes in load.

Protective devices associated with the combustion control are arranged to give instant stoppage of fuel, coal or oil, on loss of primary air, on excessive back pressure in the furnace, or on failure of both induced-draft fans and, under this last condition, forced-draft and primary-air fans will be tripped out. The use of controlled circulation requires also that all fuel be instantly cut off on failure of circulation, which in this case is effected by the pressure differential across the circulating pumps on dropping to 20 psi.

Although not news to many associated with power-plant opera-

tion, it still cannot be too strongly stressed that successful operation of automatic controls is inescapably dependent upon their conscientious routine inspection and maintenance and, where compressed air is the control-impulse fluid as on boiler 6, absolute cleanliness and dryness of air and reliability of air supply are of vital importance. Control service compressors are provided in duplicate, each of capacity for full requirements, with the station compressed-air system as emergency reserve, each brought in automatically on predetermined fall in control-line pressure.

Control of Boiler Circulation

The control and instrument equipment of group (3), having to do primarily with control of the boiler circulation, are of the general type of group (1). Aside from the signal lights and emergency cutoff for fuel supply mentioned in discussing the equipment of group (1), and certain gages mounted directly on the circulating pumps, the present control equipment of group (3) is identified on the boiler-circulating-pump panel, Fig. 5, which is

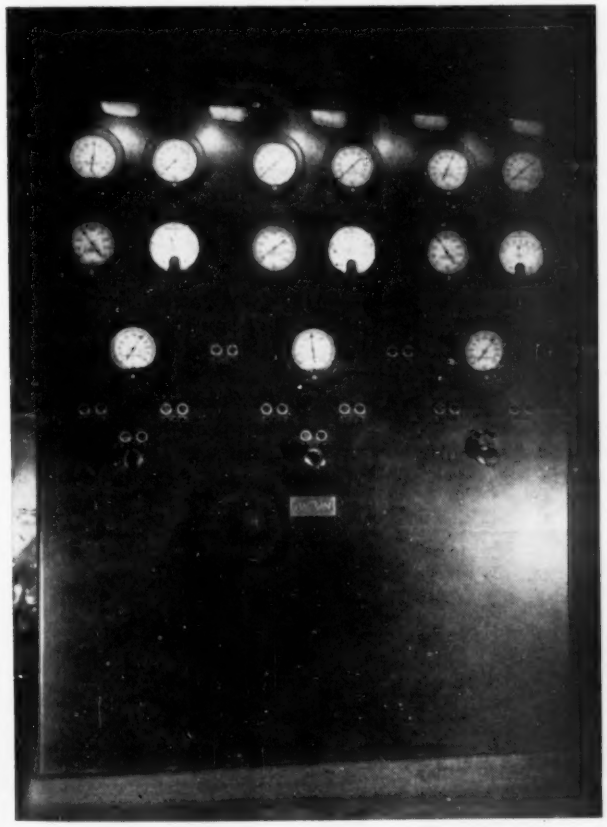


Fig. 5 Circulating-Pump Panel; Gr. 118

set up immediately beside the pumps as indicated in Fig. 4. There are three pumps, one motor-driven and two with combined motor-and-turbine drives. The gages of the two upper rows on the panel are arranged in three groups, showing for each pump labyrinth-seal injection and leak-off pressures and pump-drive-motor amperes.

Rise in labyrinth leak-off pressure, indicating an increase in sealing-water requirements, has served to give warning of wear in the labyrinth gland. The three gages of the next row below are for pump suction and discharge header pressures and steam pressure available at the pump-drive-turbine throttles. Operating signal lights for the two turbines are mounted in intermediate positions in this row. Below are, first a row of signal lights to indicate the position of the individual pump suction and discharge valves, whether open or closed and, below these, the motor-circuit-breaker controls and their open and closed position signal lights. For convenience of the pump operator for close observation while the boiler is being brought up to pressure or taken off pressure, injection pressure gages are mounted close to the injection control valves at the individual pumps.

In addition to the control facilities at present in use, three differential-pressure recorders have been provided and are now mounted in place, but not yet connected, on a separate panel near the main operating board of boiler 6 on Gr. 137. These recorders will give, for each of the three pumps, continuous record of pressure differentials between suction and discharge and between discharge and labyrinth-gland-seal injection. As pointed out in a paper by Parks, Patterson, and Ryan,[4] in the original sealing arrangement the breakdown from the operating pressure of the circulating pump to the final leak-off pressure of approximately 125 psi was effected by labyrinth exclusively. Water flow for sealing purposes and required boiler-feed line pressure, however, proved considerably higher than anticipated. With this condition corrected, the purpose of the new recorders is both to give continuous record of circulating-pump over-all performance and to permit taking full advantage of the gland-seal improvement in lowered feed-line pressure and feed-pump power consumption.

Control of Water Conditioning

As is to be inferred from the other papers of this series, experience with the instruments of group (2) has been of major interest at the station. Preliminary operation of the high-pressure unit early demonstrated that the simple routine of daily tests which had served for the older 375-psi plant was far from meeting the needs of close control of water conditions for boiler 6. More observations and more frequent observations were necessary to avoid too long continuance of contamination or too wide discrepancy between coincident chemical requirements and actual chemical concentrations. Specific factors determined as commonly contributing to upsets of water conditions and found calling for more prompt detection have included condenser leakage; evaporator carry-over; chemical-feed variations; change in continuous-blowdown recirculation; change in continuous blowdown to waste; contamination of stored condensate; subatmospheric pressure in deaerators; carry-over by steam from low-pressure boilers.

Hazards associated with condenser leakage in a seaboard plant hardly need comment. Evaporator carry-over at Somerset Station presented a greater than usual problem because the make-up feed is drawn from a surface supply subject to seasonal organic contamination of a sort which markedly affects the boiling properties of the water. The severe foaming which, prior to the installation of supplemental washing scrubbers on the evaporator vapor lines in the summer of 1944, was liable to occur at unexpectedly low evaporator concentration, was also very liable to pass undetected by any usual spot-sampling routine. The other factors mentioned have recognizable counterparts in most power stations. Factors less usual and less liable to occasional occurrence have also come to attention. All have important potentialities in any high-pressure-boiler plant.

Inspection following the overheating of a furnace-roof tube on January 13, 1943, had shown incipient pitting on tube interior surfaces with corrosion products constituting the major part of the

[4] "Operating History and Performance of 2000-Psi Forced-Circulation Boiler at Somerset Station of Montaup Electric Company," by G. U. Parks, W. S. Patterson, and W. F. Ryan, published on pages 411–427 of this issue of the Transactions.

deposited material within the tubes. It appeared that temperature rise in the metal from the insulating effect of a solid deposit on the interior surface of the tube might be promoting corrosion and so adding to the build-up of solid material with accelerating effects. Recording instruments to reveal and identify corrosive and other unfavorable conditions as they occurred seemed of pressing importance.

Hydrogen evolution at the steel surface was believed to give a reliable index of the rate of metal loss in the absence of free oxygen in the system. Consequently, among the first of the new instruments selected was a two-point hydrogen single-point oxygen recorder, its commercial development and possibilities having been brought to the attention of one of the authors by Sheppard T. Powell. Also, for the utmost promptness in detection and identification of departures from scheduled conditions, so as to minimize the continuance and effects of water variables, recorders were provided to cover continuously the highly informative test values of high-pressure feedwater and boiler-water pH and conductivity, and high-pressure steam and evaporator vapor conductivity. It was further recognized that instruments of this class should be under practically constant surveillance of operators who would themselves take any indicated corrective measures or would be in a position promptly to give proper instructions to others. In setting up the permanent installation, the hydrogen-and-oxygen recorder, the high-pressure feedwater and boiler-water continuous-blowdown pH recorder, the high-pressure feedwater and superheated-steam conductivity recorder, and the high-pressure boiler-water continuous-blowdown conductivity recorder were mounted on the high-pressure turbine-room main operating control board shown in Fig. 6, and the evaporator vapor-conductivity recorder was installed in the low-pressure station pump and evaporator room.

The high-pressure-turbine operator makes an hourly log of chemical-pump operation and continuous-blowdown valve settings; also, of recorded high-pressure feedwater oxygen and hydrogen concentrations, conductivity, and pH; boiler-water conductivity; and superheated-steam hydrogen concentration and conductivity. In logging these values entry is made of the temperature of the samples to the different recorders. Because of the importance of stability of water conditions in boiler 6, the operator makes hourly tests of the high-pressure continuous-blowdown water for alkalinity, phosphate concentration, and pH value as running checks on the recorders. With the close observation of water conditions so maintained in such comprehensive scope, even a slight change is quickly detected and usually its source rather promptly identified so that, in general, correction can be made before any serious effects have resulted. Nevertheless, much more in this direction can still be done. Meanwhile the broadened and heightened interest of the turbine operators, and their conscientious follow-up of irregularities observed in water conditions, are worthy of note and of emulation.

The more complete daily analysis of high-pressure-boiler water and boiler feedwater is made once daily by the plant laboratory and the results of these analyses are used as the over-all check on the hourly tests for basic control of water conditioning. The extremely low values to which contamination from hardness-producing salts is held in the condensate of this tidewater station make it practicable to recirculate boiler blowdown water to assist in stabilizing feedwater alkalinity and deliver the normal dosage of all water-conditioning chemicals continuously at the outlet of the deaerators to be carried through all high-temperature heat-exchange equipment to the boiler. A high-pressure chemical pump is available for delivery of chemicals directly to the boiler drum as special conditions may require.

Notwithstanding the generally small values of feedwater contamination, the recording instruments give very practical demonstration of the importance of continuity and uniformity in chemical feed. With intermittent delivery of chemicals, if there is serious condenser leakage or evaporator priming during an interval between periods of chemical introduction, there are prompt reflections in phosphate concentration and pH value, followed by increase in hydrogen evolution shown by the sample streams of both steam and feedwater. It is an almost invariable observation that serious upset in water conditions causes response in at least some discernible degree in the three feedwater test recorders. On this account, if one instrument shows an unusual in-

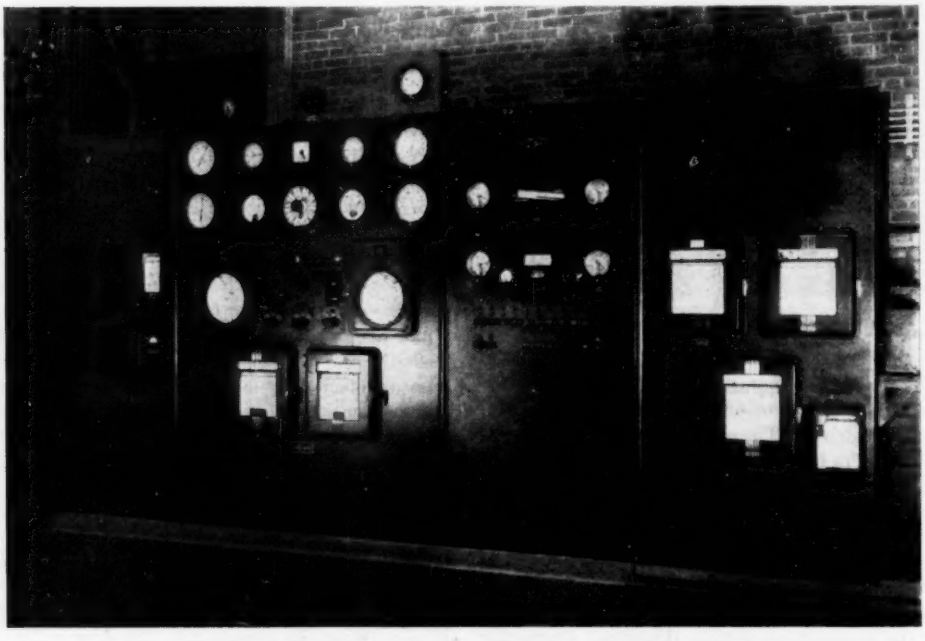


FIG. 6 MAIN CONTROL BOARD HIGH-PRESSURE TURBINE; GR. 137

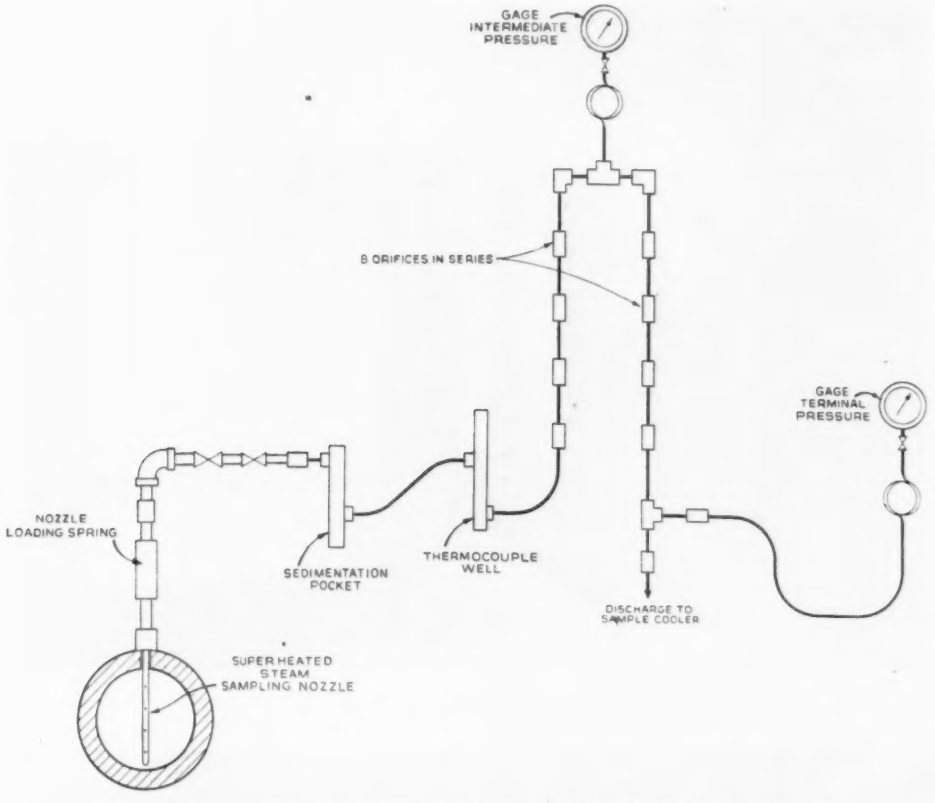


FIG. 7 DIAGRAM OF HIGH-PRESSURE SUPERHEATED-STEAM-SAMPLING CONNECTION

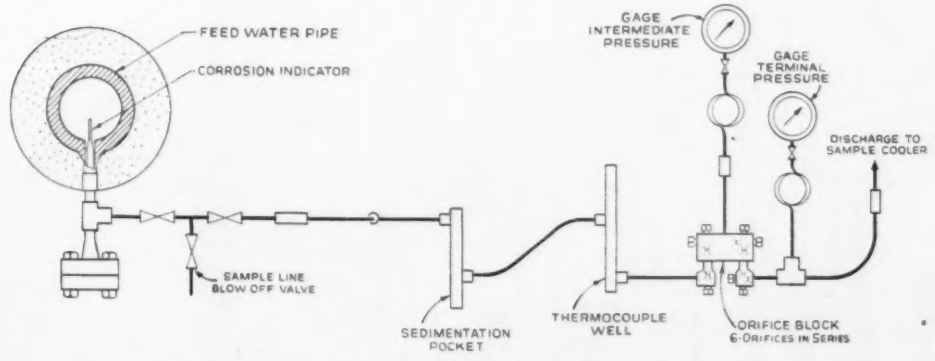


FIG. 8 DIAGRAM OF BOILER-FEEDWATER-SAMPLING CONNECTION

dication without response of any sort in the records of the others, the condition and accuracy of that instrument are investigated.

Initial sampling connections and piping to the analyzing blocks of the hydrogen and oxygen recorder were temporary in anticipation of exploratory studies to be conducted. With the aid of degassing and sampling apparatus made available in March, 1944, through the courtesy of the American Gas and Electric Service Corporation and Beech Bottom Power Company, several weeks were spent in calibration of the hydrogen equipment and the potential accuracy and dependability of the analyzer and recorder demonstrated. After considerable preliminary investigation of sources of hydrogen liberation in the high-pressure system, permanent connections for sampling were established, and the installation was completed early in 1945. The oxygen-analyzing block of the recorder was connected to the high-pressure feedwater line immediately ahead of the boiler 6 economizer. One of the hydrogen-analyzing blocks receives its sample from the same point. The second hydrogen-analyzing-block connection was made to the high-pressure superheated-steam lead of the 1800-psi 950 F topping turbine.

Steam- and Water-Sampling Arrangements. General arrangements of the high-pressure steam- and feedwater-sampling connections are shown in Figs. 7 and 8. Fig. 9 is from a photograph of the feedwater-sampling connection immediately ahead of the economizer. The steam-sampling nozzle is stabilized stainless steel, and to avoid complexities associated with welding to the carbon-molybdenum steel of the adjacent outer fittings, this nozzle is held to seated position by a special alloy spring. The initial pressure of the steam sample is broken down through a series of eight orifices to about 100 psig. The sample is then led through stainless steel to cooling coils in which it is condensed and the temperature brought to approximately 120 F or some-

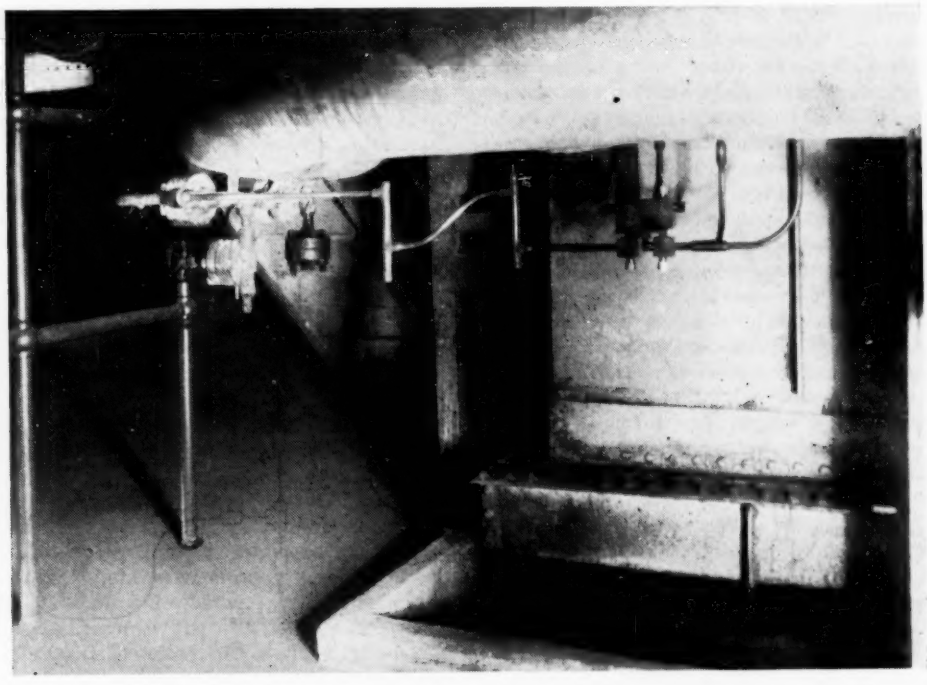


FIG. 9 VIEW OF BOILER-FEEDWATER-SAMPLING CONNECTION

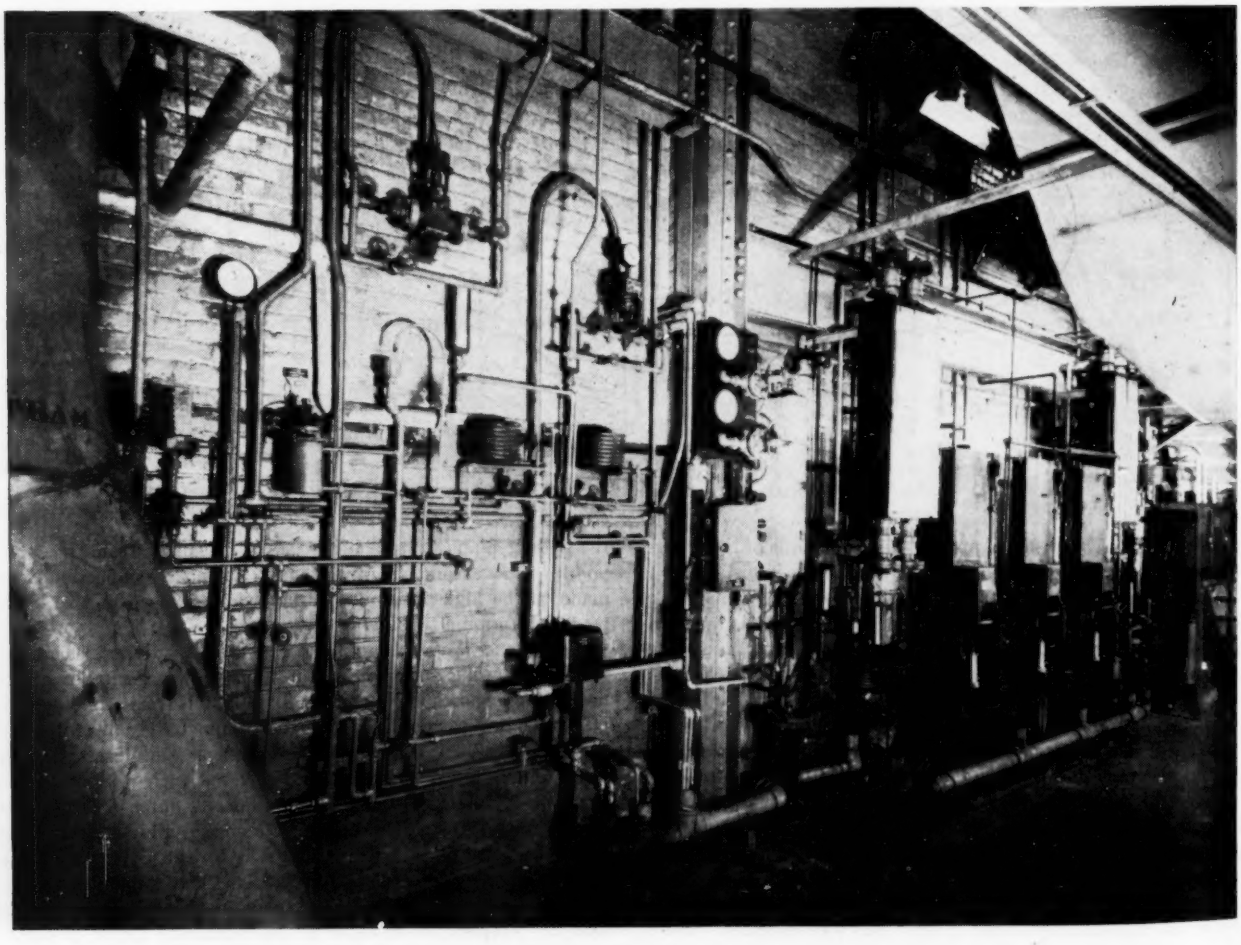


FIG. 10 HYDROGEN-ANALYZING BLOCKS, pH, AND CONDUCTIVITY CELLS AND ACCESSORIES

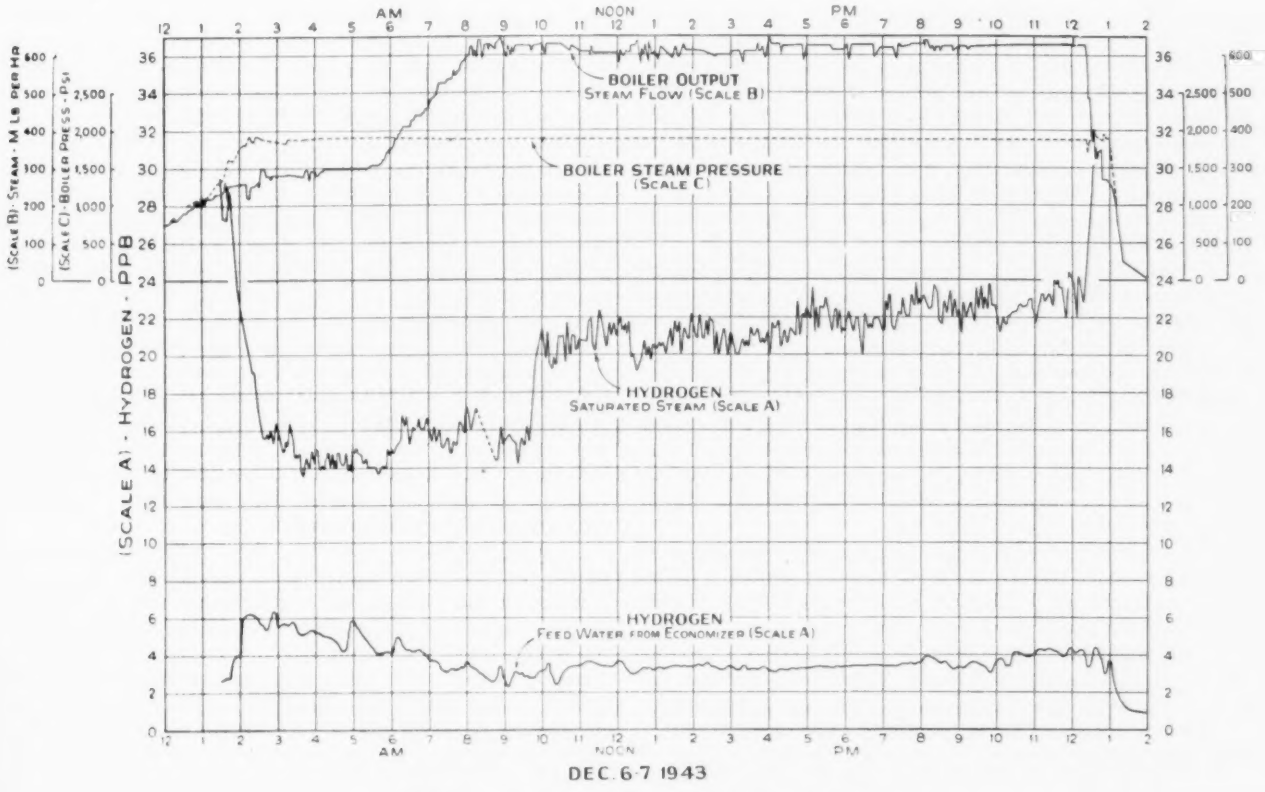


FIG. 11 GRAPHIC LOG: DECEMBER 6 and 7, 1943

what higher for the hydrogen-analyzing block, and for degassing when a precise measure of steam conductivity is desired.

A part of the condensed sample is cooled further, to about 100 F, for purposes of the routine conductivity record. The high-pressure feedwater sample passes first over the corrosion-indicating specimen mentioned in a current paper by Bissell, Cross, and White,[5] then flows through a six-orifice stainless-steel pressure-reducing block in which the pressure is brought down to somewhat under 300 psig. The feedwater sample is also cooled to 120 F or somewhat higher, for the oxygen and hydrogen analyzing blocks, and parts are cooled further to 90 F, approximately, for conductivity and pH measurement. As in the case of the condensed sample of high-pressure steam, the tubing used to convey the feedwater sample is of stainless steel. Intermediate and terminal pressure connections are provided for the series of orifices on each sampling line.

Although used initially for checking the flow capacities of the orifices, the gages are part of the permanent installation to give warning of change in flow characteristics from accumulation of iron oxide in the orifices or from wear. The iron oxide present in the feedwater and steam, which is an important topic of another paper of this series,[5] deposits in the orifices of the feedwater-sampling system, but apparently has had no effect on steam sampling. It has so far rather frequently proved necessary to clean the orifices of the feedwater system when returning the boiler to service after an outage. Similarly, at the end of approximately 1 year, the steam-sample flow rate through the orifice series was unchanged and the water-sample flow rate had been increased by roughly 40 per cent. The sample cooling coils and analyzing elements for the group (2) recorders mounted on the high-pressure-turbine operating board are shown in Fig. 10.

Records of Operation. Under current normal operating conditions, oxygen concentration recorded is "zero," expressed in parts per million (ppm), and the approximately full-load concentrations of hydrogen are close to 2 parts per billion (ppb) in the feedwater at the boiler 6 economizer entrance and below 3 ppb in the superheated steam as delivered to the high-pressure turbine. Other full-load characteristics recorded by the instruments of group (2) are conductivity of steam about 1.5 micromhos as sampled, varying with the seasons, and 0.6–0.7 micromho degassed; conductivity of chemically treated feedwater about 5 micromhos; conductivity of boiler water about 1000 micromhos; pH value of feedwater 8.3; and pH value of boiler water 10.3.

To illustrate the potential value of instruments of this general class it has seemed advantageous to select records of important departure from the characteristic performance. Figs. 11, 12, 13, and 14 have been prepared with this in view.

The hydrogen-and-oxygen recorder had been placed in operation November 7, 1943. The manufacturer's field calibration was undertaken within the next 10 days. On placing the instrument in service, the points of sampling at that time being at the economizer outlet and the dry drum of boiler 6, recorded hydrogen concentrations in the saturated steam seemed high, 10 ppb to 18 ppb at times, and showing progressive increase.

On November 27, 1943, the boiler was taken out of service for low-pressure blowdown, and on December 5, 1943, for complete change of water and cleaning of the main drum. Eleven pounds of solids, approximately 45 per cent magnetic oxide of iron from the analysis, were removed from the drum and the boiler was

[5] "Special Studies of the Feedwater-Steam System of the 2000-Psi Boiler at Somerset Station of Montaup Electric Company," by W. D. Bissell, B. J. Cross, and H. E. White, published on pages 429–442 of this issue of the Transactions.

returned to service, attaining full rated pressure and an output of 620,000 lb per hr shortly after 8 a.m. on Monday, December 6.

Values shown in Fig. 11 for hydrogen in feedwater and steam are probably not very significant prior to 12:30 or 1:00 a.m. when the boiler pressure had passed above 1000 psi. Full designed pressure was attained shortly after 2:00 a.m. The progressive fall in hydrogen concentration of the saturated steam shown prior to about 3:30 a.m. is probably due to dilution accompanying the increasing rate of steam generation which at 3:30 was approximately 375,000 lb per hr.

There had been a period of leakage in one of the condensers between midnight and 1:00 a.m. and this was probably, at least in part, responsible for the relatively high evolution of hydrogen in the feed system during the early morning hours. Feedwater make-up at the time was being drawn from the distilled-water storage tank and may have been not entirely free from solids contamination. It will be noted that instead of a fall in hydrogen concentration of the steam which is a usual accompaniment of an increase in rate of steam generation, the increase in boiler loading between 5:30 a.m. and 8:30 a.m. brought a small rise in hydrogen concentration of the steam.

Without much further change in loading, this was followed at 9:30 a.m. by rapid increase in rate of hydrogen evolution in the boiler by about 6 ppb, attaining a concentration in the saturated steam of 20–22 ppb at 10:00 a.m. With this substantially full-rated-load operation continuing the balance of the day, there was gradual progressive increase in rate of hydrogen evolution in the system until at 12:25 a.m., December 7, with the hydrogen concentration in the steam having reached 24 ppb, one of the roof tubes ruptured and the boiler was thereupon promptly taken off the line. The increases in hydrogen evolution in the feedwater system, raising the hydrogen concentration of the feedwater to 4 ppb at 8:00 to 8:20 p.m., and to a maximum of 4.4 ppb after 10:00 p.m., may have been due to leakage of one of the condensers. Records are not complete for the period.

In the light of subsequent experience it is of course perfectly obvious that on at least part of the boiler surface, temperatures had been excessive throughout the full period of operation prior to December 7, during which the hydrogen-and-oxygen recorder had been in service but at the time there was still much doubt regarding the interpretation to be placed upon the indications of the instrument.

As stated in the first paper of the series,[4] there have been two subsequent failures from overheating of furnace tubes in boiler 6. At the time of the first of these failures, discovered on taking the boiler off the line on July 16, 1944, the analyzing block for hydrogen concentration in steam had been out of order for several days, so depriving the operators of the possibility of a warning indication. The circumstances of the second failure October 26, 1945, are discussed later in the present paper under "Value and Limitations of Hydrogen Recorder."

Fig. 12 was prepared primarily to show by means of 6-hr averages immediate and cumulative effects of continued tube leakage in a service water heater. It will be noted, however, that the records show other features of interest. The steam condensed in the service heater was returned at intervals to the boiler-feed system by a trap. The water being heated was from the same surface supply from which water for the boiler-feed make-up evaporators is taken and is very low in dissolved inorganic solids but carries small and somewhat varying proportions of

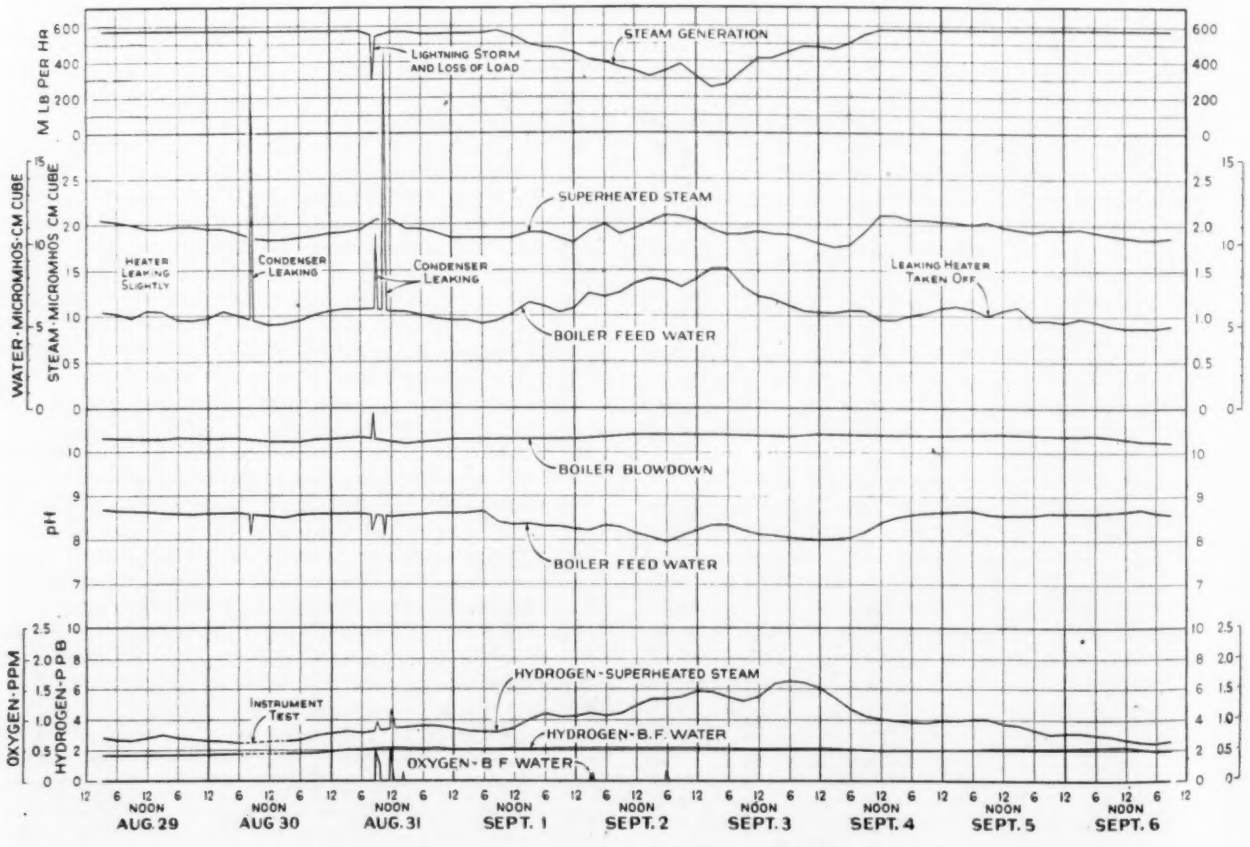


FIG. 12 GRAPHIC LOG: AUGUST 29 TO SEPTEMBER 6, 1945, INCLUSIVE

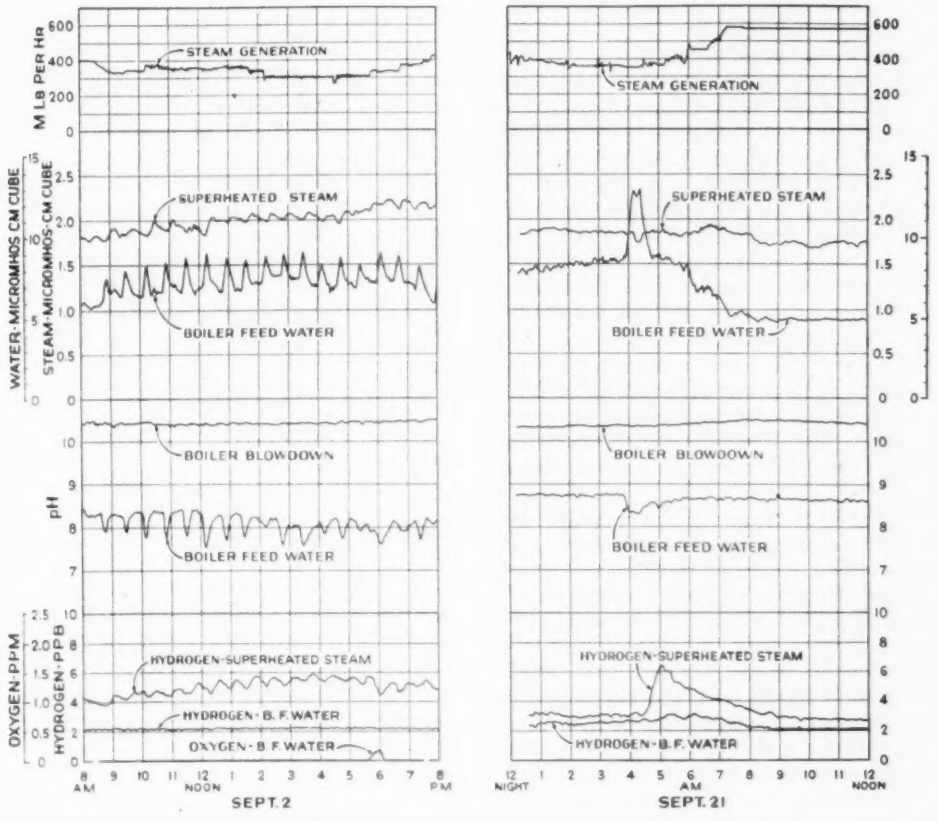


FIG. 13 GRAPHIC LOGS: SEPTEMBER 2 and SEPTEMBER 21, 1945

carbon dioxide and ammonia. Instantaneous effects of the operation of the trap during the height of the heater leakage are shown in some detail in Fig. 13.

Apparently the service-heater leakage on August 29, 1945, was comparatively slight and the irregularities in feedwater characteristics were not immediately sufficient to attract the attention of the operators. However, after the swings in feedwater conductivity became noticeable, it was some time before the source of contamination could be identified, on the evening of September 3, and then it was not found feasible to take the heater out of service for repair until September 5.

The rise in average feedwater conductivity over the period of September 1 to September 3, inclusive, is probably all to be accounted for as a reflection of the week-end and Labor Day holiday sag in load. The sag in feedwater pH average over the same period is believed similarly accountable as due to decrease and absence of low-pressure-boiler blow-down recirculation.

On the other hand, it seems that the high-pressure superheated-steam hydrogen concentration may be reflecting the effects of feedwater contamination to some extent and, on September 2 and 3, was also influenced by the low feedwater pH occurring on those days. As to be inferred from Fig. 13, the gas content of the raw water entering the system through the leaking heater causes increase in the conductivity of the superheated steam. The main cause of the higher-than-usual average conductivity of the steam was probably a high proportion of make-up coupled with seasonal increase in gas content of the raw make-up water.

On August 30 and on August 31 the effects of the service-heater tube leakage were augmented by main-condenser-tube leakage. Shortly after 8:00 a.m. on August 30 leakage of one of the surface condensers caused a brief rise in high-pressure-boiler feedwater conductivity from about 5 micromhos to 22 micromhos. The leakage was rather promptly corrected. The effect on pH value of feedwater was recorded by coincident drop from pH 8.6 to pH 8.1. Any effect on the rate of hydrogen evolution in either boiler-feed system or high-pressure boiler was masked by the test on the instrument begun shortly thereafter.

At about 8:20 a.m. on August 31 a severe lightning storm took out transmission lines which caused an abrupt drop in boiler load equivalent to about 275,000 lb steam generation per hr. The resulting temperature stresses in the condensers caused tube-joint leakage which was reflected in rise of feedwater conductivity from 5–6 micromhos to over 10 micromhos, drop in feedwater pH value from pH 8.6 to pH 8.2, and rise in hydrogen concentration in the superheated steam from 2.7 ppb to 3.5 ppb, the last mentioned being doubtless in part a simple reflection of loss of load. At the same time apparently the abrupt temperature change in the boiler-furnace tubes was sufficient to cause some release of "hide-out" alkalinity, as reflected by the abrupt rise in pH value of boiler water from around pH 10.35 to pH 10.9.

The initial stoppage of the condenser leakage was only temporary, and further leakage was registered about 10:30 a.m. which caused an abrupt and very brief increase in feedwater conductivity from about 6 micromhos to 20.5 micromhos with accompanying drop in pH value of boiler feedwater from pH 8.6 to pH 8.15 and somewhat marked increase in rate of hydrogen evolution in the high-pressure boiler, raising the concentration in the superheated steam from about 3 ppb to 4.4 ppb. The loss of load and leakage of condensers were both accompanied by oxygen contamination of the boiler feedwater. Whether this was due to unbalance of steam supply to the deaerators at the time is uncertain. There was further appearance of dissolved oxygen in

the feedwater on September 2 which is mentioned in the following discussion of Fig. 13.

Eight hours of chart records for Sunday loading on September 2 have been plotted at the left in Fig. 13 to show more clearly the response of the high-pressure-boiler feedwater steam system to the leakage in the service heater. As to be expected, the effects of the discharge of the heater drain trap are most acutely reflected in the conductivity and pH value of the boiler feedwater. The intermittent contamination, probably chiefly from the gaseous content, also appears in the conductivity of the superheated steam. The rate of hydrogen evolution in the boiler-feedwater system seems not to have been influenced, continuing practically constant at around 2.2 ppb as measured at the entrance to the boiler 6 economizer. The effect on hydrogen evolution in the boiler is, however, only slightly less noticeable than that on boiler-feedwater conductivity and pH value. It will be noted that in their general trend, the values for conductivity of superheated steam and boiler feedwater, the pH value of boiler feedwater, and the hydrogen evolution in the boiler are all responsive to the rate of steam generation.

The appearance of dissolved oxygen in the boiler feedwater beginning about 5:40 p.m. and reaching a value of about 0.2 ppm at 6:00 p.m., may have been due either to unbalance of steam supply to the deaerators resulting from the accompanying increase in boiler load or to admission of air-contaminated water in preparing one of the boiler feed pumps for return to service, actually put on the line about 6:50 p.m.

The graphs at the right in Fig. 13, for 12 hours of the morning of September 21, are intended primarily to show the recording of an instance of severe condenser leakage occurring shortly before 4 a.m., and so further illustrating the sensitivity of the feedwater line and boiler system to corrosive and otherwise adversely reactive constituents in the feedwater. The trends of the several values also reflect effects of change in rate of steam generation. Boiler 6 was carrying the entire station load up to 7:15 a.m.

The relatively high conductivity shown by the boiler feedwater prior to the development of the condenser leakage was probably the result of continuing the chemical-feed delivery at the average rate which had been adjusted for the higher load conditions of the previous day. The condenser leakage brought a rather abrupt rise in feedwater conductivity from about 8.5 micromhos to 12.5 micromhos and was effectively checked about one-half hour later, as will be noted from the rapid fall in feedwater conductivity to a value governed essentially by the rate of feedwater flow.

The conductivity of the superheated steam responded in a brief fall of about 0.1 micromhos, suggesting either a fixation of a part of the ammonia or carbon dioxide by dissolved solids of the contaminating harbor water or stabilizing effects of the chloride content of the harbor water. The pH value of the boiler feedwater dropped substantially simultaneously with the increase in conductivity. The recovery of pH value was more gradual. The trend of the dissolved-hydrogen values recorded for the boiler feedwater would suggest a somewhat delayed response. The response in rate of hydrogen evolution in the boiler, however, was quite marked and prolonged, the increase in concentration in the superheated steam being approximately 3.4 ppb, requiring a full 4 hours for recovery.

An item, possibly of interest in connection with the detection of condenser leakage, was met in the early investigation of potential sources of contamination which would affect the operation of boiler 6 when it was found that salt in considerable quantity could be added at the condenser hot well without effect upon the recorded condensate conductivity although appropriately increasing the feedwater conductivity. The hot-well conductivity cells drew their sample from the top of the condensate line ahead

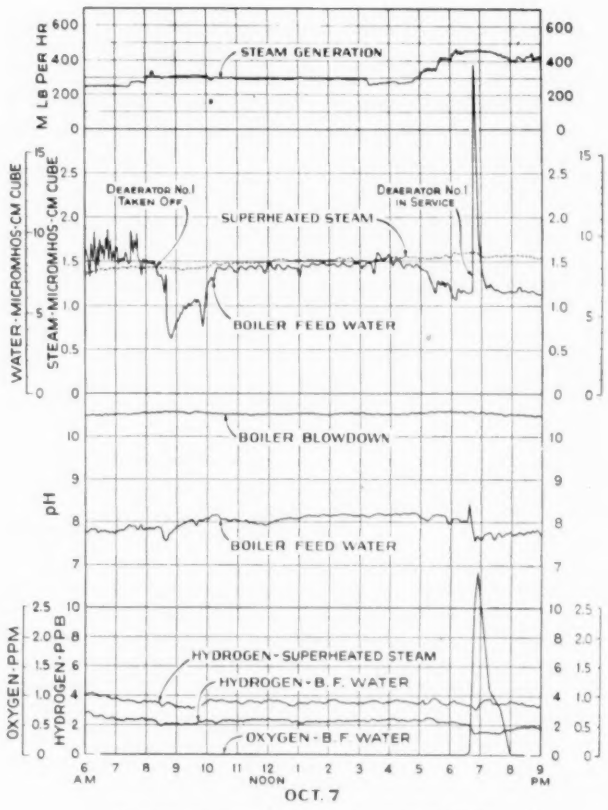


FIG. 14 GRAPHIC LOG: OCTOBER 7, 1945

of the hot-well pump. Dispersion in the condensate line evidently was not sufficiently rapid.

Fig. 14 shows recorded effects associated with taking one of the station deaerators out of service, and its return, on Sunday, October 7, 1945. The graphs give a 15-hr record. It seems probable that with the light loading of the early morning, there were sufficient differences in deaerator pressures to cause fluctuations in chemical-feed distribution between the two deaerators, resulting in the fluctuations in feedwater conductivity and pH noticeable between 6:00 a.m. and 8:00 a.m. Around 8:30 a.m. steps were taken to cut deaerator No. 1 out of service. The chemical feed to that deaerator was not immediately shut off. With the falling pressure in the first deaerator, chemical feed to the other deaerator was automatically discontinued.

The absence of chemical feed caused immediate drop in conductivity of feedwater from about 8.0 to 3.5 micromhos, accompanied by a drop in pH value of feedwater of about 0.3. On returning the deaerator to service shortly after 6:30 p.m., the abrupt delivery to the feed line of the chemical solution earlier accumulated in the deaerator brought a brief increase in feedwater conductivity from a value of approximately 6 micromhos to somewhat over 20 micromhos, with an accompanying increase in feedwater pH value from about pH 7.8 to pH 8.25. The water first delivered to the feed system from the deaerator returned to service also contained sufficient dissolved oxygen to cause the high-pressure-boiler feedwater to register concentration in excess of 3 ppm, and dissolved oxygen in considerable concentration was not entirely out of the high-pressure-boiler-feed system until more than 1 hour later.

Apparently a part of the oxygen in the feed system was consumed in reaction with the hydrogen evolved in that system. The rate of hydrogen evolution in the boiler shows increase as

an effect of the sudden introduction of the chemical charge but the hydrogen in the feedwater fell appreciably. A corresponding effect on the hydrogen concentration in the boiler feedwater, but of lesser magnitude, is noticeable when the deaerator was taken out of service, although the recorded rise in dissolved-oxygen content at that time was exceedingly brief and reached a maximum of only about 2 ppm. It would seem likely that in this latter instance the effect on rate of hydrogen evolution recorded for the feedwater system was due more to the marked decrease in feedwater conductivity without great loss in pH value than to reaction of evolved hydrogen with oxygen.

Value and Limitations of Hydrogen Recorder. It had of course been recognized that hydrogen evolved in the feedwater system or boiler might combine to some extent with oxygen where found dissolved in the water in contact with the metal surface. A contingency overlooked was that an oxide of copper might function in the system as a source of oxygen. The practical importance of chemical action of that sort was brought strongly to attention by the October 26, 1945, furnace-tube failures taking place without marked increase in recorded rate of hydrogen evolution in the boiler.

One of the low-pressure-turbine stage heaters, temporarily operated as an evaporator condenser with feedwater entering at 215–218 F and condensing vapor of about 16 psig pressure, corresponding to about 250 F, had been returned to this vapor-condensing service October 10, in the midst of the season of maximum organic contamination of the evaporator water supply and immediately following installation of 468 new tubes of Admiralty alloy. Apparently the copper carried into the feedwater system in oxidized form from the corrosion of the new Admiralty alloy tubes was sufficient to cause practically complete disposal of the hydrogen evolved from the overheating of the boiler tubes. Although the boiler had been in operation less than 6 weeks following an inspection when the drum had been cleaned, considerably in excess of the quantity of metallic sludge to be expected from 6 months of operation was found to have accumulated in this brief period, and the sludge was approximately two-thirds copper, which is one and one-half times the maximum proportion of that metal previously found.

A factor which will be recognized as commonly responsible for hydrogen concentrations out of step with temperature or other corrosive influences normally to be associated with concurrent operation is the abnormally high chemical activity of the metal surface following an acid-cleaning of the boiler. The rate of hydrogen evolution which occurs during the first few weeks of operation of an acid-cleaned boiler may be so high as to mask any increase in rate of hydrogen evolution which might result in the boiler from other than extreme contamination or actual overheating.

Notwithstanding such interfering factors as mentioned, hydrogen evolution in a boiler gives the best known indication of corrosion or solution of the boiler metal and the measurement of the rate of this evolution affords the only feasible basis for judging the extent of corrosion taking place while the boiler is in operation. Means for minimizing the effects of interfering factors are being studied.

Conclusions

It will be obvious from the experience in operation of boiler 6 that on modern steam-generating equipment, instruments appropriate to the requirements, especially recording instruments, can be not merely informative but of tremendous instructive value and sources of heightened interest in operating personnel. The importance and the potentialities of such instruments doubtless increase with the degree of operating efficiency which it is desired to maintain, and for a base-load unit of the capacity and type of boiler 6, become essential. To fulfill their potentialities, in fact to avoid real hazard from their presence, the instruments must be rugged by the station environment standard rather than by that of the laboratory and must be followed with definitely scheduled routine inspection, calibration, and maintenance of frequency and thoroughness that will assure precision of indication within acceptable limits at all times.

Comment on the importance of control-equipment maintenance is given earlier in the paper, and should not need repetition. High standard of upkeep in instruments is hardly less vital and, from the point of view of subsequent analysis of operating events, dependable instrument charts can contribute invaluably to the continuity of informative records.

Acknowledgments

The authors desire to record their appreciation of valuable suggestions on the text of the paper made by Mr. G. U. Parks, and of his permission for use of the station data, and of the assistance of Mr. H. E. White in arrangement of these data. They would also record their appreciation of the very constructive criticism of the text by Mr. W. S. Patterson.

The authors take this occasion to express appreciation of the very generous co-operation afforded them by Mr. Philip Sporn, and Mr. W. L. Webb of the American Gas and Electric Service Corporation, and Mr. J. R. McDermet of the Elliott Corporation, which aided greatly the studies conducted in preliminary exploration of hydrogen evolution in the high-pressure system at Somerset Station. Appreciation is also expressed of the very exceptional patience shown by Mr. G. U. Parks and his operating organization and their co-operation in adapting their plant operation to the needs of this investigation.

Discussion

W. W. Cerna.[6] The authors have gone to considerable pains to present complete descriptions and operating experiences of useful instrumentation and control equipment applied to the operation of a high-pressure high-capacity boiler. These descriptions and operating experiences cover not only completely automatically operating and control equipment, but also indicating and recording equipment to enable the operators to have constant knowledge of conditions, and thus provide for ready manual adjustments when the need is indicated.

The authors refer to the log of operations maintained and hourly simple control tests conducted by the high-pressure-turbine operator, in connection with chemical feed, blowdown, etc., for the No. 6 boiler. It has been of particular interest and satisfaction to note that a few minutes spent each hour on these readings and control, plus the daily complete check and establishment of the expected chemical-feed requirements for the next 24 hours by the chemical laboratory, have resulted in boiler-water conditions of unusual uniformity. This is of particular significance when one considers the fact that the Somerset Station is a tidewater plant, using salt water for condenser cooling. The significance of "close control" of boiler-water conditions at this plant will be particularly apparent by referring to the control ranges of various chemicals and salts maintained in the No. 6 boiler water, as given in another paper of this Montaup series by Scott and the writer.[7]

In discussing both the value and limitation of the hydrogen recorder, the authors also point out that copper oxide in the water

[6] Hall Laboratories, Inc., Pittsburgh, Pa.

[7] "Water Conditioning for the 2000-Psi Boiler at the Somerset Station of Montaup Electric Company," by W. W. Cerna and R. K. Scott, published on pages 443–451 of this issue of the Transactions.

system might serve as a means of combining with hydrogen to prevent the indication of hydrogen formation. That this mechanism can and does occur has been confirmed by some laboratory work carried out by Messrs. Kaufman and Trautman of our research department. The tests were conducted in laboratory bombs. One test, using a synthetic but highly concentrated boiler water with considerable alkali present to insure the formation of hydrogen at the test temperature, showed, as expected, considerable hydrogen formation. In another test synthetic boiler water of the same composition was used to which some solid copper oxide was added. The test conditions were repeated, with the result that very little free hydrogen was found and considerable of the copper oxide had been reduced to metallic copper.

Under similar boiler conditions copper salts or compounds would be effective in preventing hydrogen indication and recording by the recording instrument, as illustrated by the following reactions:

$$CuO + H_2 \rightarrow Cu + H_2O$$

$$Cu_2Cl_2 + H_2 + 2KOH \rightarrow 2Cu + 2KCl + 2H_2O$$

R. R. Donaldson.[8] Automatic combustion control, which started out as a convenient accessory for holding constant steam pressure, today has virtually the status of an integral part of the boiler plant. It is depended upon to perform the twin functions of regulating the operation of the boiler so as to satisfy the load demands in a desired manner and of automatically maintaining optimum controlled fuel-air ratios.

In accomplishing the latter function, that of production of proper fuel-air ratios, the ability to measure fuel input and air input is paramount in the present state of the art. It is fair to state that for the present, the production of desired fuel-air ratios by flow proportioning of fuel Btu and air represents the most advanced engineering solution. While someday we may reasonably expect to have gas-analyzing apparatus which is rapid and dependable enough to be used for automatic control of combustion, we have not yet reached that point.

The authors found that it was necessary to do considerable experimental work on their boiler before a satisfactory location for measurement of products of combustion or air flow could be obtained. Their final use of the Ljungström preheater drop gave them a satisfactory solution for this installation.

The difficulties encountered in measurement of air flow for boiler control are not unique with Montaup. There are many installations where perfection of results is limited chiefly by ability to measure air flow satisfactorily.

Admittedly, the problem of metering the products of combustion or the air supply to a large steam-generating unit is far more difficult than the ordinary metering of fluid flows. If, however, in the inception of every new steam-generating installation, the purchaser and the manufacturer of the equipment would spotlight this feature of the boiler design, there is no doubt that better operating installations from the standpoint of maintained furnace efficiencies would result.

The present paper will serve as a stimulus and spearhead to a concerted program for investigating and improving the metering characteristics of modern steam-generating equipment.

[8] Hagan Corporation, Pittsburgh, Pa. Mem. A.S.M.E.

Authors' Closure

Mr. Cerna has contributed valuably in presenting results from bomb tests conducted by Hall Laboratories, Incorporated, in studying the possibilities of reduction of copper oxide in high-pressure boiler water by hydrogen evolved from the boiler metal. Through the courtesy of the Laboratories we learn that similar tests more recently conducted in continuing their investigation have demonstrated that, by increasing the proportion of copper oxide added to the bomb solution, actual evolution of hydrogen may be practically prevented and that the same general effects are observed to occur in the bomb at the temperature with which we are concerned whether or not alkali other than from the boiler metal is present.

Mr. Finnegan's pressing emphasis[9] on the need for more fundamental work on the pure chemistry of the water-metal systems, especially throughout the high-temperature range, is very gratifying. Lack of fundamental information on the reactions of both iron and copper in the range of temperature and other environmental conditions met in the feedwater-boiler water-steam circuits of the high-pressure unit has been a serious handicap throughout the operation of boiler 6 to date.

Mr. Donaldson underscores very aptly the present necessity for dependable, instantaneous, mechanical evaluation of combustion air-flow from the standpoint of the control-equipment designer and manufacturer. The authors concur fully that provisions for evaluation for air-flow rate should be made one of the elementary considerations in design of the modern fuel-burning steam-generating unit.

The improvement work on the flue-gas oxygen-recording equipment and on the boiler-feed-pump flow recirculating valves, mentioned in the paper as to be undertaken, is going ahead promisingly but has not in either case progressed sufficiently to warrant further comment now. The installation of the boiler-circulating-pump pressure differential recorder also is not yet complete. In regard to the last-mentioned equipment however, such brief preliminary observations as have been made have brought to attention valuable data on pressure conditions during periods of boiler start-up and shutdown which would not otherwise have been noted and present impressions are that the information made available by the graphic record will prove even more useful than initially contemplated.

[9] "Special Studies of the Feedwater-Steam System of the 2000-Psi Boiler at Somerset Station of Montaup Electric Company," by W. D. Bissell, B. J. Cross, and H. E. White. See discussion by T. J. Finnegan, pages 441 and 442 of this issue of Transactions.

The Supply of Air to Coal-Fired Steam Locomotives

By R. A. SHERMAN,[1] W. H. BROWNE,[2] and R. B. ENGDAHL[2]

As part of the program of research for Bituminous Coal Research, Inc., means by which the performance of coal-fired steam locomotives can be improved are being investigated. Because of the importance of the method and of the rate of supply of air in any combustion process, an analysis has been made of the factors that govern the supply of air to the locomotive by its unique method of discharge of the exhaust steam to the stack through the front-end nozzle. The analysis shows that for any given front-end arrangement and locomotive, there is a definite upper limit of output of the locomotive at which the weight of air supplied will equal that required for the fuel burned. A similar but lower limit applies on the basis of fuel fired. Below these limits the percentage of excess air will increase with decreasing output of the locomotive; above the limits there will be a deficiency of air. The position of the limits is determined by the performance characteristics of the engine, of the boiler, and of the front-end arrangement. A program of research is outlined which is aimed to supply information (*a*) on the design of front ends for maximum combustion efficiency through proper excess air and minimum carry-over of cinders, and for maximum power output through reduction in back pressure on the cylinders, and (*b*) on the merits of overfire air in improving combustion efficiency through reduction in carry-over of cinders.

THE method of supplying air to steam locomotives is unique. Whereas the stationary boiler plant has a high stack or, more commonly, fans to provide the pressure difference necessary to force the air through the fuel bed and the combustion gases over the heat-absorbing surfaces of the boiler, the steam locomotive has only a short stack that barely projects above the boiler shell. The pressure difference, usually called draft, is provided by discharging the steam exhausted from the cylinders through a nozzle at the base of the stack.

Furthermore, whereas the stationary boiler is equipped with dampers or other means by which the rate of air supply can be closely adjusted to the requirements of the load or of the fuel, the locomotive has, practically without exception, no independent control of the air supply. As the output of the engine increases, the amount of steam admitted to and exhausted from the engine increases, and the rate of supply of air for combustion of the fuel increases.

This simple method of supplying the air also serves to a considerable degree to decrease the objectionable noise of the exhaust steam. It was for this purpose that Trevithick and Stephenson, to whom first use of the method is variously credited, originally turned the exhaust steam into the stack. However, although the steam must be exhausted from the engines, the movement of air in this way is, obviously, not without expenditure of energy. The increase in back pressure on the cylinders, necessitated by the restriction of the nozzle, materially decreases the horsepower output of the locomotive.

This paper analyzes the available data on the performance of the air-supply system of locomotives to determine its relation to the efficiency of combustion and to that of the engine at various power outputs. The particular purpose is to determine what information on the problem of air supply is lacking that might be obtained by research, that the performance of coal-fired locomotives may be improved.

Previous Work

Few parts of the locomotive lend themselves to such ease of trials of changes as the exhaust nozzle and its arrangement with relation to the stack. Hence much cut-and-try work has gone on and has been reported in the literature. The International Railway Fuel Association and its successor, the Railway Fuel and Traveling Engineers Association, have long had a Standing Committee on Front Ends, Grates and Ash Pans, and the committee has, with few exceptions, had an annual report. No attempt will be made here to review completely these many reports.

One of the most thorough discussions of exhaust arrangements is that of Chapelon (1)[3] in his book on the steam locomotive, but this has not been generally available in this country. MacFarland (2) presented a discussion principally directed to a demonstration of the power loss through high back pressures because of restricted nozzles and made a plea for induced-draft fans. Jackson (3) recently gave a review of the problem of drafting locomotives with a discussion of the attempts at variable-exhaust nozzles.

Young (4) has presented a complete analysis of the early work on the drafting problem as an introduction to the report of his exhaustive experimental investigation of the performance of various types of nozzles. His work was done on a one-fourth-scale model of a locomotive.

Fry (25) has recently shown that the performance of the front end affects the efficiency of combustion and sets the maximum output of the locomotive.

Methods for Evaluation of Exhaust Arrangements

Despite the long use of the steam nozzle to move air and gases in the locomotive and its extended use in other applications as the boiler-feedwater injector, the steam-jet ejector for air-conditioning systems, and the steam jet for blowing air in overfire-air applications, the action of the nozzle is not wholly understood. The ability of the jet to entrain and to move air is apparently a function not only of the kinetic energy of the steam, but is also related to the exposed surface of the steam. Because of the importance of the latter factor the steam is often divided into multiple streams as in the pepperbox nozzle, or the surface is in-

[1] Supervisor, Fuels Division, Battelle Memorial Institute, Columbus, Ohio. Mem. A.S.M.E.

[2] Research Engineer, Fuels Division, Battelle Memorial Institute. Jun. A.S.M.E.

Contributed by the Fuels and Railroad Divisions and presented at the Annual Meeting, New York, N. Y., Nov. 26–29, 1945, of The American Society of Mechanical Engineers.

Note: Statements and opinions advanced in papers are to be understood as individual expressions of their authors and not those of the Society.

[3] Numbers in parentheses refer to the Bibliography at the end of the paper.

creased by a star-shaped section, or by bridges. It is interesting to note, however, that Young (4) found, as a result of his tests, a difference from the worst to the best no greater than 12 per cent in the performance of various nozzles as expressed by the ratio of the weight of air moved to the weight of steam exhausted through the nozzle.

Because of the obvious necessity of high differences of pressure, or draft to move the gases through the restricted area of the long fire tubes of the locomotive boiler, and also the obvious undesirability of high back pressures on the engine cylinders, the number of inches of water draft in the front end per pound of back pressure has long been used as the criterion of the performance of front-end arrangements. Although this may apply for a given locomotive of fixed resistance to flow, an attempt to apply such a criterion to locomotives of different design and size is obviously in error. It is as incorrect as it would be to rate the capacity of fans by the static pressure that they develop, or to express the capacity of boilers by the pressure at which they operate.

Young (4, 5) clearly recognized that the value of a front-end arrangement should be measured by its ability to move air; this could not be measured by draft alone. In a discussion (6) of the paper by Jackson, he has made a good statement of the problem as follows:

"The actual problem of front-end design is to produce an arrangement which will pull an optimum weight of air through the fire for each pound of steam generated and discharged, maintaining at the same time, three mechanical conditions: 1 Minimum back pressure, 2 clearing the smokebox, and 3 lifting the smoke above the train. The greatest difficulties lie in the mutual incompatibility of these mechanical requirements."

Factors Affecting the Performance of Front Ends

Engdahl and Holton (7) in an investigation of steam-air jets for supplying overfire air have shown that with air tubes whose area is large relative to the area of the steam nozzle, ratios of the order of 200 to 500, as much as 15 to 20 lb of air could be moved per lb of steam used. They found, as others have shown, that the entrainment ratio increases as the steam pressure decreases and as the ratio of the area of the air tube to that of the steam nozzle increases. As they were interested in the jets as blowers to move air at high velocities against small differences in pressure, they did not investigate the effect of resistance to flow, but this should, obviously, affect the performance of jets. The temperature of the gases moved should also be important.

Effect of Steam Pressure at Nozzle. As the output of a locomotive increases, the weight of steam used and exhausted from the cylinders through the nozzle increases. The back pressure at the nozzle increases approximately as the square of the weight of steam discharged. Hence the range of back pressures at the nozzle is large.

Fig. 1 shows the variation of the entrainment ratio, the ratio of weight of gases to weight of steam, with back pressure for a typical locomotive. As expected, the air-steam ratio decreases with increase in back pressure. The ratio is much lower than those quoted from the work of Engdahl and Holton (7) on overfire-air jets because, as will be shown later, of the difference in area ratios of stack to nozzle, and because of the resistance to the flow of gases.

Effect of Ratio of Areas of Stack and Nozzle. As previously noted, almost every steam locomotive has been the subject of experiments on the exhaust nozzle and front-end arrangements and thus has had the ratio of the area of the stack to the nozzle changed. In these experiments, however, facilities have not been available to measure the air flow as well as the steam flow.

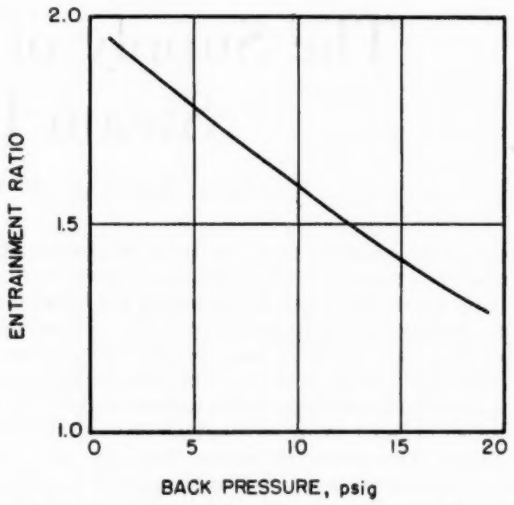


Fig. 1 Relation of Entrainment Ratio to Back Pressure on Nozzle for Typical Locomotive
(Ratio, area of stack to nozzle, 6.2. Resistance ratio, 4.5×10^{-6}.)

For data on the effect of this variable the work of Young (4) is used.

Fig. 2 shows the relation derived from Young's data of the entrainment ratio to the ratio of areas of stack and nozzle. As his data were obtained on a quarter-scale model, the original data have been corrected by the factors that he derived from principles of similarity. The pressures and dimensions are multiplied by 4, the reciprocal of the scale of the model, and weights of air and steam by $4^{5/2}$ or 32.

The curves show the increase of the entrainment ratio as the ratio of the area of stack to that of the nozzle increases. Curves for two steam pressures, 8 and 32 psig, are included. Again, the reduction of the entrainment ratio with increase in pressure is shown.

Effect of Resistance Against Which Gas Is Moved. A third factor which governs the performance of a locomotive front end is the resistance against which the gases must be moved. The resistance is determined by the path of the gases in the front end, the area and length of the tubes and flues of the boiler, the area of the throat back of the arch, the thickness of the fuel bed, the area of the air openings in the grate, and of the air openings into the ashpan.

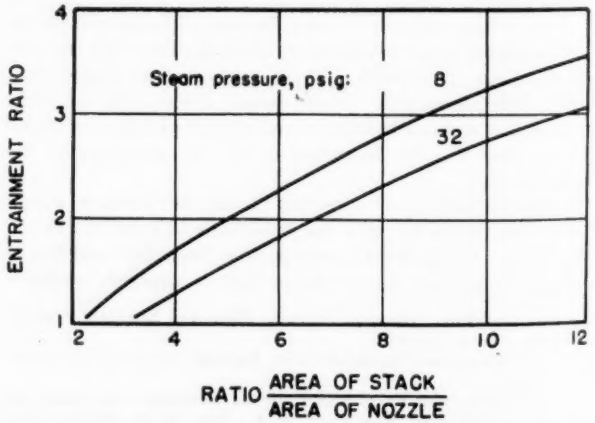


Fig. 2 Relation of Entrainment Ratio to Ratio of Area of Stack to Nozzle
(Resistance ratio, 2.8 to 3.0×10^{-6}. Data from Young (4) corrected for size ratio.)

The data in Fig. 2, as were most of the data presented by Young (4, 5), were taken with a fixed resistance made up of that of the locomotive model and an orifice of fixed area. The resistance was so chosen by Young as to simulate that of a full-scale locomotive.

Fig. 3 presents data obtained by Young in a series of tests in which the area of the orifice in the system was changed to vary the resistance. The solid portion of the curves covers the range of data given by Young; the dashed portion was drawn from data taken at Battelle on a $^1/_{16}$-scale model. Each curve represents one constant steam pressure on the nozzle.

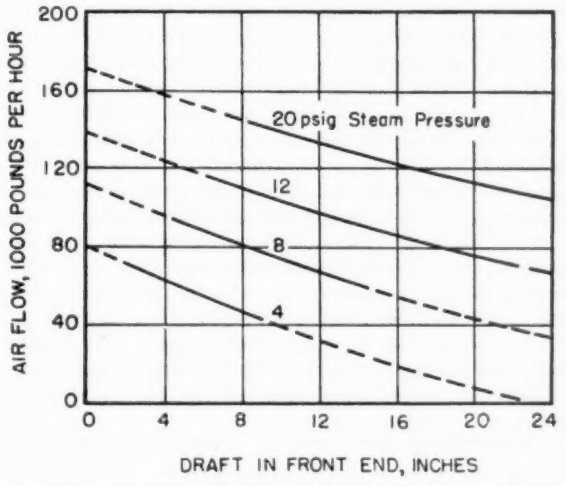


FIG. 3 RELATION OF AIR FLOW TO DRAFT IN FRONT END AND TO STEAM PRESSURE
(Ratio of area of stack to nozzle, 11.1. Data from Young (4) corrected for size ratio.)

The curves in Fig. 3 show the way in which the rate of air flow decreases as the resistance, as indicated by the draft, increases. This figure demonstrates clearly the inadequacy of the draft as a criterion of the performance of front ends. By increase of resistance the draft obtained with a given nozzle and steam pressure can be increased, but the air supplied, which is the true measure of the performance, decreases.

Concept of Resistance to Gas Flow. In consideration of the flow of electricity, we have a concept of three definite measures; current, voltage, and resistance, and the familiar relation that

$$\text{Current} = \frac{\text{Voltage drop}}{\text{Resistance}}$$

In the flow of fluids we have, corresponding to current, the volume or weight of the fluid, and to voltage, the pressure drop, but no term for resistance is in common use. As a result the pressure against which the pump, fan, or ejector moves the fluid is often used as a measure of the resistance. In locomotives the pressure is less than atmospheric and is termed draft.

Unfortunately, also, the term draft is often confusedly used not only as a measure of pressure drop and resistance, but also of rate of flow of gas as well; that is, a high draft is often assumed to be synonymous with a high rate of flow of gas. As just shown in Fig. 3, this is far from necessarily true.

The general relation of the rate of flow of gases to the pressure difference in turbulent flow is

$$Wa = K\sqrt{d}$$

where

Wa = rate of flow in pounds per hour

K = a constant coefficient involving a number of physical factors in the system of flow

d = pressure difference or draft in inches of water

Legein (8) introduced the conception of a factor of temperament, T, in his studies of locomotive drafting, and Chapelon (1) and Young (5) have also used it, but otherwise it has not been used in this country. The temperament is equivalent to the constant coefficient K in the foregoing equation. Thus we have

$$Wa = T\sqrt{d}$$

$$T = \frac{Wa}{\sqrt{d}}$$

Compared with the flow of electricity, the temperament T corresponds to the conductivity.

The reciprocal of the conductivity can, however, be as conveniently used, and we have

$$Wa = \frac{\sqrt{d}}{R}$$

$$R = \frac{\sqrt{d}}{Wa}$$

This expression considers both the pressure difference or draft and the rate of flow of gas and thus permits proper comparison of different locomotives or parts of the gas-flow system of a given locomotive.

Fig. 4 presents Young's data used for Fig. 3 in which the ratios of weights of air and steam are plotted against the resistances to flow. The curves show a sharp decrease in the entrainment ratio with an increase in the resistance. The curves emphasize again the impossibility of accurate comparison of the performance of front ends of locomotives without consideration of the resistance of the gas-flow system.

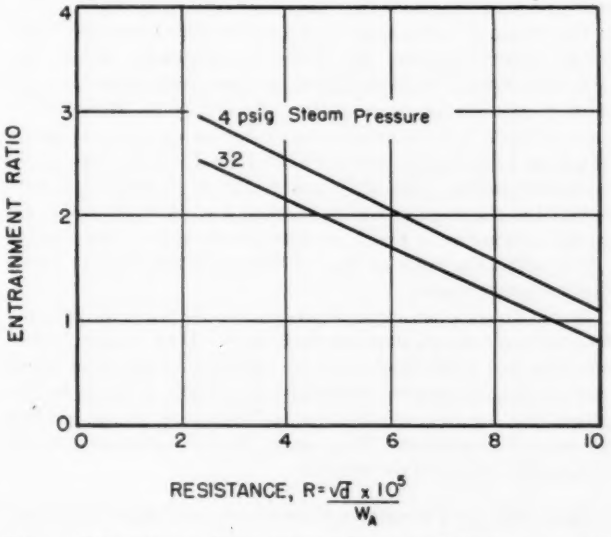


FIG. 4 RELATION OF ENTRAINMENT RATIO TO RESISTANCE TO AIR FLOW
(Ratio of area of stack to area of nozzle, 11.1. Data from Young (4) corrected for size ratio.)

Effect of Temperature of Gas. The data of Young that have been used are for the movement of air at atmospheric temperatures, for which most of his tests were run. He did, however, investigate the effect of temperature, and Fig. 5 shows the relation that he found. The reduction in the entrainment ratio was as

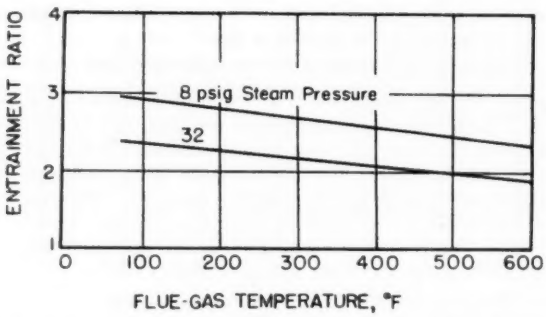


FIG. 5 RELATION OF ENTRAINMENT RATIO TO FLUE-GAS TEMPERATURE

(Ratio of area of stack to area of nozzle, 8.5; resistance ratio, 2.8 to 3.0 × 10^{-6}. Data from Young (4) corrected for size ratio.)

great as 25 per cent for gas at 600 F as compared to gas at room temperature.

The percentage reduction in entrainment ratio by increase in the flue-gas temperature increased as the rate of flow of gases increased. Hence it may be concluded that the effect of temperature in full-scale locomotives would probably be greater than found by Young. His model did not include a boiler, although it did have flues, and thus the temperature gradient in the gases was obviously lower than in a locomotive.

Summary of Factors Affecting Front-End Performance. The data that have been presented show that all four factors, steam pressure, ratio of area of stack to nozzle, resistance of the gas-flow system, and the flue-gas temperature are of major importance in determining the performance of the locomotive front end. Other factors, as the distance between the nozzle and base of stack, and length and taper of stack, also affect the performance but are of less importance. The data also show that it should be possible to predict the performance of a front end and to eliminate the cut-and-try methods that have been so largely used.

That Young's data are applicable to full-scale locomotives may not be apparent at once. Fig. 1 showed entrainment ratios of the order of 1.25 to 2, while the figures prepared from the model tests showed entrainment ratios of the order of 2 to 3. However, we note in Fig. 2 that the entrainment ratio for a steam pressure of 32 psig and a stack- to nozzle-area ratio of 6.2, which is that of the locomotive in Fig. 1, is slightly less than 2. If we apply that point to Fig. 4 at the resistance ratio of about 3 × 10^{-6}, the resistance for the locomotive of Fig. 1, an entrainment ratio of the order of 1.5, or within the range of Fig. 1 will result, even without correction for temperature.

Hence Young's data provide an excellent basis for the development of basic design data for front ends. They require supplementary and confirming tests on full-scale locomotives where care is taken to obtain accurately the weight of gases moved. More data are also required on the resistance of the gas-flow system in locomotives. This, again, requires accurate information on the weight of gas moved.

RELATION OF FRONT-END PERFORMANCE TO AIR-FUEL RATIO

Now that we have established the general effect of the several pertinent factors on the amount of gas moved by the front end, let us examine how it satisfies the air requirements of a locomotive at various power outputs.

Fig. 6 presents six plots that develop the relation for a typical locomotive between the requirements and the supply of air. Plot (A) shows the relation between the hourly steam output of the boiler and the locomotive output in drawbar horsepower. This is a straight-line relation because the cylinder efficiency and the mechanical efficiency were practically constant over the range of outputs.

Plot (B) shows the relation between the heat-liberation requirements expressed in pounds of coal per hour and the steam output. This is essentially a straight line as the efficiency of heat absorption is practically constant. Note that this is the heat liberated from the coal burned and not the coal fired. As is well known and as will be discussed later, there is a large loss of heating value of the coal fired at high rates because of the solid combustible matter that passes out of the firebox unburned. Combustible matter that does not burn does not use air and is thus not here considered.

Plot (C) shows the relation of the weight of air required per hour to the coal burned. As a definite weight of air is required per pound of coal, this relation, too, is obviously a straight line. Plot (D) shows the relation between the entrainment ratio, weight of air per pound of steam, and the output of steam. Because the back pressure on the cylinders increases as the rate of steam output increases, and because the entrainment ratio decreases with increase of pressure, we have the relation shown.

Plot (E) shows the relation of the air requirements and the air supplied to the drawbar-horsepower output of the locomotive. Combining relations shown in plots (A), (B), and (C) gives us the curve of air required, which is a straight line. Combining (A), (B), and (D) gives us the curve of air supplied. The nozzle in this particular locomotive gave such entrainment ratios that the rate of air supply first increased at a faster rate than the rate of

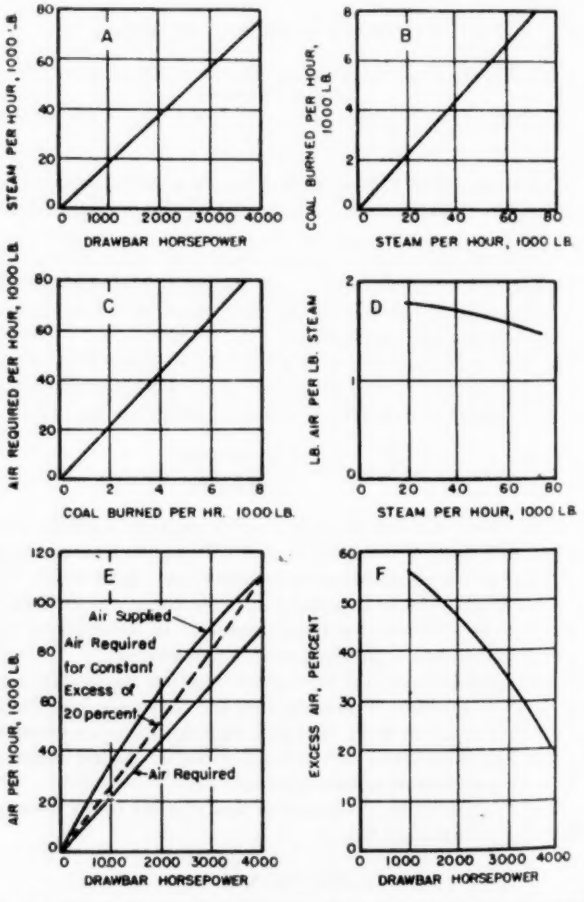


FIG. 6 DEVELOPMENT OF RELATION BETWEEN AIR REQUIREMENTS OF LOCOMOTIVE AT DIFFERENT RATES OF POWER OUTPUT AND AIR SUPPLIED BY FRONT END

air requirements but, because of the decrease of the entrainment rate with increase in back pressure, the rate of increase dropped off at high power outputs.

Combustion of any fuel requires a certain amount of excess air, either to avoid losses in unburned gaseous combustible matter, or to avoid excessively high temperatures. This excess, for good efficiency in heat transfer, should be at a minimum. Whether the excess should be constant over the range of rates of operation, or whether it should increase or decrease with the rate cannot be definitely and generally answered; it depends upon the design of the combustion device.

However, it can be stated with assurance that the amount of air supplied should never be less than required. If it were, although by firing more fuel, the output of the boiler and engine would continue to increase, the unburned combustible losses would become excessive, and the over-all efficiency would be low.

Plot (F) in Fig. 6 shows the relation of the excess air as calculated from the curves of air required and air supplied in plot (E). It can be seen that the percentage excess was rapidly decreasing; if the locomotive had been carried to higher outputs there would have been an actual deficiency of air.

If the front end of the locomotive had been so designed as to follow exactly the air requirements at low outputs the drooping characteristics of the air-supplied curve would have resulted in a deficiency of air at a much lower power output.

The dashed curve in plot (E) shows the correct characteristic for a constant excess of 20 per cent for this locomotive.

Calculations of Conditions for Equilibrium of Requirements and Supply of Air. The relations established by curves as in Fig. 6 can also be worked out by simple mathematical relations. The following expressions give the relations between the weights of air supplied and required:

$$\left[\frac{\textit{Locomotive}}{\textit{Performance}}\right]\left[\frac{\textit{Boiler}}{\textit{Performance}}\right]$$

$$\frac{\text{Lb air req'd}}{\text{Dhp}} = \frac{\text{Lb steam}}{\text{Dhp}} \times \frac{\text{Lb coal}}{\text{Lb steam}} \times \frac{\text{Lb air req'd}}{\text{Lb coal}} \quad \ldots [1]$$

$$\left[\frac{\textit{Locomotive}}{\textit{Performance}}\right]\left[\frac{\textit{Nozzle}}{\textit{Performance}}\right]$$

$$\frac{\text{Lb air supplied}}{\text{Dhp}} = \frac{\text{Lb steam}}{\text{Dhp}} \times \frac{\text{Lb air entrained}}{\text{Lb steam}} \quad \ldots [2]$$

But in Equation [1]

$$\frac{\text{Lb coal}}{\text{Lb steam}} = \frac{\dfrac{\text{Btu}}{\text{Lb steam}}}{\dfrac{\text{Btu absorbed}}{\text{Btu liberated}} \times \dfrac{\text{Btu}}{\text{Lb coal}}}$$

$$= \frac{\text{Btu}}{\text{Lb steam}} \times \frac{\text{Btu liberated}}{\text{Btu absorbed}} \times \frac{\text{Lb coal}}{\text{Btu}} \quad \ldots [3]$$

and

$$\frac{\text{Lb air req'd}}{\text{Lb coal}} = \frac{\text{Lb air req'd}}{\text{Btu}} \times \frac{\text{Btu}}{\text{Lb coal}}$$

It is well established, although not so widely recognized as it should be, that the weight of air required per Btu is practically constant for solid, liquid, and most gaseous fuels. The value is 7.56 lb of air per 10,000 Btu or 7.56×10^{-4} per Btu. Hence we have

$$\frac{\text{Lb air req'd}}{\text{Lb coal}} = 7.56 \times 10^{-4} \times \frac{\text{Btu}}{\text{Lb coal}} \quad \ldots [4]$$

Substituting values in Equations [3] and [4] in [1],

$$\frac{\text{Lb air req'd}}{\text{Dhp}} = \frac{\text{Lb steam}}{\text{Dhp}} \times \frac{\text{Btu}}{\text{Lb steam}} \times \frac{\text{Btu liberated}}{\text{Btu absorbed}} \times \frac{\text{Lb coal}}{\text{Btu}} \times 7.56 \times 10^{-4} \times \frac{\text{Btu}}{\text{Lb coal}}$$

which becomes

$$\frac{\text{Lb air req'd}}{\text{Dhp}} = \frac{\text{Lb steam}}{\text{Dhp}} \times \frac{\text{Btu}}{\text{Lb steam}} \times \frac{\text{Btu liberated}}{\text{Btu absorbed}} \times 7.56 \times 10^{-4} \quad \ldots [5]$$

The factor of calorific value of the coal cancels out and the weight of air per drawbar horsepower is dependent only on the efficiency of the locomotive in the use of steam, the enthalpy of the steam, and the absorption efficiency of the boiler, and is independent of the calorific value of the coal.

This proves that if the not infrequent statement that a locomotive was correctly drafted for one coal, but not for another, is correct, it is not so because of differing air requirements based upon calorific value. It may, however, have a basis in the fact that one coal may require a higher excess of air, either to avoid losses in unburned gaseous combustible, or to avoid clinkering and slagging difficulties because of the fusion characteristics of its ash.

Returning to Equations [2] and [5] for the air supplied and required, it can be seen that in equating them the factor of locomotive performance is eliminated and we have

$$\frac{\text{Lb air entrained}}{\text{Lb steam}} = \frac{\text{Btu}}{\text{Lb steam}} \times \frac{\text{Btu liberated}}{\text{Btu absorbed}} \times 7.56 \times 10^{-4} \quad \ldots [6]$$

Using Equation [6], we can calculate the entrainment ratio we must have under given conditions. For example, if the Btu per pound of steam, its enthalpy, is 1300, and if the boiler absorption efficiency is 80 per cent

$$\frac{\text{Lb air entrained}}{\text{Lb steam}} = 1300 \times \frac{100}{80} \times 7.56 \times 10^{-4}$$

$$= 1.23$$

The entrainment ratio of the front end must be 1.23 if the theoretical air requirements of the coal burned are to be met. If an excess of 20 per cent is required, the entrainment ratio must be $1.20 \times 1.23 = 1.48$.

Thus as has also been shown by Fry (25) the calculation of the required entrainment ratio for the front end reduces to an extremely simple basis. If we knew accurately the values of the several variables that fix the entrainment ratio, the design of a front end could be reduced to an exact engineering operation.

Relation of Excess Air to Power Output. Relations similar to those in Fig. 6 have been worked out for several locomotives from data from testing plant tests of the Pennsylvania Railroad and the University of Illinois. They all show similar relations to those presented and it is needless to burden this report with them.

The percentage excess air can, of course, be calculated from the composition of the flue gases and it is usually a standard item in the report of a locomotive test. The excess air calculated from the flue-gas composition gives, it must be recalled, the excess on the basis of the fuel burned and not on the basis of the fuel fired. Hence the values obtained are comparable with those presented in Fig. 6.

Fig. 7 presents the relation of the percentage excess air to the output for four locomotives: a Mikado 2-8-2 tested at the Uni-

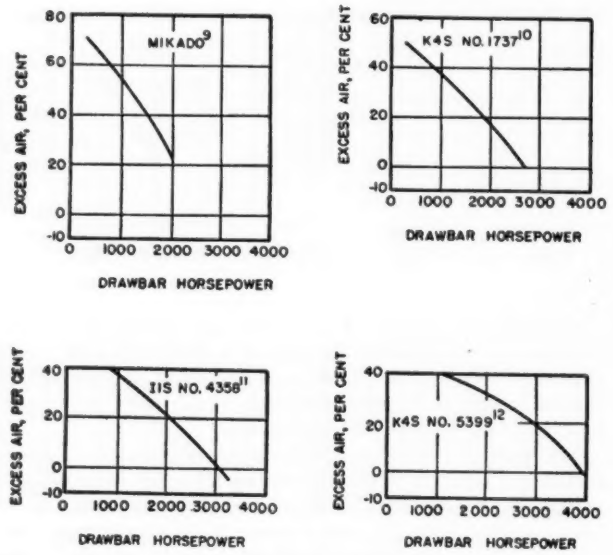


FIG. 7 RELATION OF EXCESS AIR TO POWER OUTPUT FOR FOUR LOCOMOTIVES

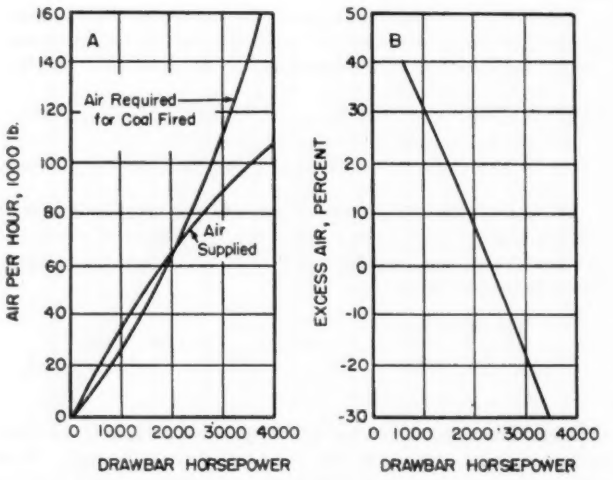


FIG. 8 RELATION OF WEIGHT OF AIR REQUIRED AND SUPPLIED, AND OF PERCENTAGE EXCESS AIR TO POWER OUTPUT OF LOCOMOTIVE ON BASIS OF COAL FIRED

versity of Illinois (9); a K-4-S No. 1737 (10); an I-1-S No. 4358 (11); and a K-4-S No. 5399 (12); all tested at the Altoona testing plant of the Pennsylvania Railroad.

The four curves have the same characteristic shape. Two of them reached zero excess air, and one showed an actual deficiency, at the maximum output at which they were tested.

Relation of Air Supplied by Front End to Air Required for Coal Fired. The calculations and considerations up to this point have been on the basis of the coal burned or heat liberated. It is more customary, however, in locomotive practice, to consider the over-all performance on the basis of the coal fired to the grate.

Fig. 8 shows on this basis the relation of the air required and supplied for the same locomotive used as an example in Fig. 6. The method of development was the same as for the former figure, but only the curves for the air required, and the air supplied, and the curve of percentage excess air are shown in plots (A) and (B), respectively.

Above an output of 2200 drawbar horsepower (dhp), the amount of air supplied by the front end was less than that required for the coal fired, and the deficiency amounted to 30 per cent at an output of 3500 dhp. On the basis of the heat liberated from the coal burned, plot (F) in Fig. 6 showed that there was still an excess of 28 per cent at that power output.

Fig. 8 shows that at an output of 3500 dhp the air required for the coal fired was 142,000 lb per hr. At this output, as shown in Fig. 6, the steam generated and exhausted through the nozzle was 65,000 lb per hr. For the front end to have supplied the air required, each pound of steam would have had to have entrained 2.18 lb of air. Actually, the entrainment ratio at this output was 1.50.

The data on locomotive performance which have been examined in this study have shown no front ends that had entrainment ratios of over 2 at high outputs, although conceivably, one might be designed for such performance.

If, however, the front end did supply enough air for the coal fired at an output of 3200 dhp and if, as it must, the performance curve was the same as shown in Fig. 8, plot (A), then it is obvious that the percentage excess air at all lower outputs would have been very great.

General Law of Front-End Performance. From the foregoing considerations one can draw the following generalization or law on the performance of front ends relative to their function of moving the air and combustion gases:

For any given front-end arrangement and locomotive there is a definite upper limit of output of the locomotive at which the weight of air supplied will equal that required for the fuel burned. A similar but lower limit applies on the basis of fuel fired. Below these limits the percentage of excess air will increase with decreasing output of the locomotive; above the limits there will be a deficiency of air. The position of the limits is determined by the performance characteristics of the engine, of the boiler, and of the front-end arrangements.

To use terms common in locomotive practice, this law means that if a locomotive is correctly drafted at a given output it will be overdrafted at all lower outputs and underdrafted at higher outputs. It does not follow, necessarily, that all locomotives are correctly drafted at the maximum output at which they are designed to operate. They may be either underdrafted or overdrafted at that point, but it follows that the trend will be toward overdrafting at lower rates and underdrafting at higher rates. The possibility of manual or automatic controls to maintain a constant excess of air will be discussed later.

RELATION OF PERFORMANCE OF FRONT END TO LOSS OF HEAT IN CINDERS

Fig. 9 shows the relation of the percentage heat loss in cinders, together with that of the excess air, on the basis of the coal fired as in plot (B) Fig. 8, to the power output of a locomotive. The rather rapid rise of the loss in cinders at the power outputs in which the air supplied drops below the air required would seem to indicate that the cause of the rise in cinder loss might be the deficiency of air.

This can best be analyzed, perhaps, by comparison of the cinder loss in locomotives where the rate of air supply is a variable, dependent upon the rate of steam generation, and in stationary boilers where the rate of air supply is a variable, independent of the rate of steaming or rate of firing, and is controlled by dampers or fans.

Fig. 10 shows a comparison of the relation of the cinder loss to the rate of firing in pounds of coal per square foot for a locomotive fired by a stoker, and for a stationary boiler fired by underfeed stokers. Data on a stationary boiler fired by spreader stokers would have been preferred, but they were not found. The locomotive data are from the tests by Collins (13) of a J-1-b; the

stationary-boiler data are those given by Driscoll and Sperr (14).

Two facts stand out in these data, as follows: (*a*) At low rates of firing of the locomotive when there is an ample excess of air, the cinder loss is higher than for the stationary boiler; (*b*) at a rate of approximately 75 lb of coal per sq ft per hr, the loss of cinders from the stationary boiler equals that of the locomotive and the direction of the curve is steeply upward.

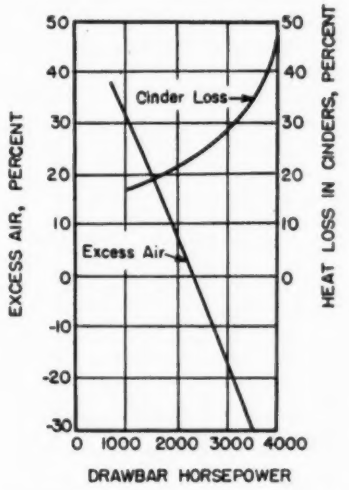


Fig. 9 Relation of Excess Air on Basis of Coal Fired and Cinder Loss to Power Output of Locomotive

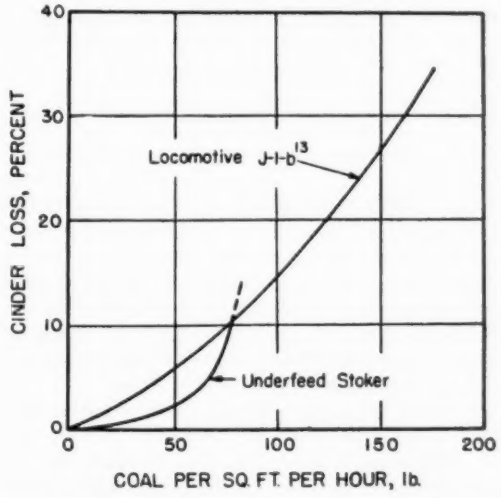


Fig. 10 Comparison of Relation of Cinder Loss to Rate of Firing in Locomotives and Stationary Boilers Fired With Underfeed Stokers

As there was no question of deficiency of air supply in the stationary boiler, the conclusion to be drawn is that the deficiency in air supply, on the basis of the coal fired, is not the major cause of the high cinder loss at high rates of firing in the locomotive. Rather, the high cinder loss is the result of the high carrying power of the gases for solids at the high velocity with which they move through the combustion chamber at high rates of operation. Coal is both carried out of the bed and is swept out of the stream of coal being fired before it reaches the fuel bed.

The probability is that the loss might be somewhat lower if an excess of air were present because the rate of burning in suspension is affected by the amount of oxygen present in the gas. But because the time is so short only the smaller particles would have an opportunity to burn.

Effect of Back Pressure on Power Output

As mentioned in the introduction of the paper, the back pressure on the cylinders which is required to discharge the steam through the nozzle, both increases the amount of steam required for a given output and reduces the maximum power developed. This has always been well recognized, and MacFarland (2) presented extensive data on the back-pressure power loss as calculated from indicator diagrams. Hence but one example will be required to demonstrate the magnitude of the loss of power.

Fig. 11 shows the relation of the horsepower loss by back pressure for locomotive No. 4358 of Class I-1-S (11) to the output. The back-pressure horsepower was calculated as the difference

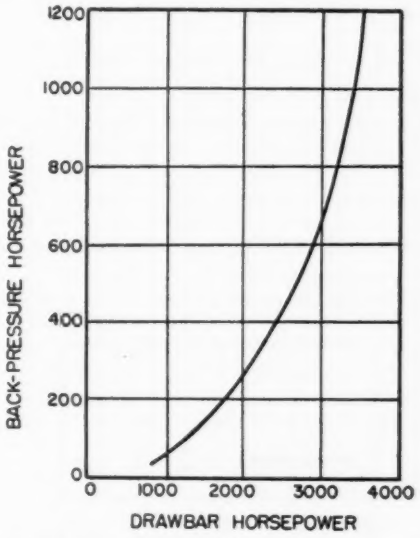


Fig. 11 Horsepower Loss by Back Pressure on Locomotive I-1-S, No. 4358 (Reference 11)

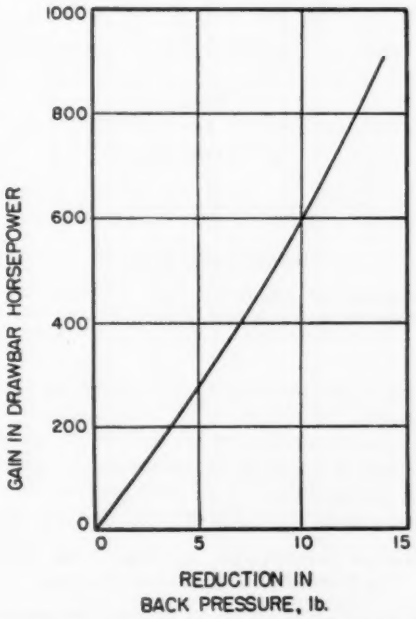


Fig. 12 Gain in Power Output of Locomotive I-1-S, No. 4358, by Reduction in Back Pressure From 14 Psig

in the horsepower actually developed and that which would have been developed if the steam had been expanded to one tenth of the gage back pressure. Although this degree of reduction in pressure was arbitrarily selected, it is satisfactory to illustrate the order of the power loss.

The loss in power increases rapidly with the increase in the net power output and amounts to about 1200 hp or one third of the net maximum output of the locomotive. The desirability of reduction of this loss is obvious.

Fig. 12 presents one further demonstration of the gain in power output by decrease in back pressure. This shows, for the same locomotive as Fig. 11, the gain in output for the same steam consumption by reduction in the back pressure at an output of 2930 dhp, and a back pressure of 14 psig. The gain is slightly more than directly proportional to the reduction in pressure, but for this locomotive each 1-lb reduction means a gain of approximately 60 dhp.

Efficiency of Front End

Fig. 13 shows the power required to supply the air and move the combustion gases through the boiler for the same locomotive used in the example, Fig. 11. The air horsepower was calculated in the usual manner from the rate of flow of the gases, with correction for temperature, and the pressure against which the gases were moved.

Also shown in Fig. 13 is the ratio of the power required to move the gases to the power lost by the back pressure. Above an output of 1000 dhp the ratio is about constant at $^1/_{10}$, that is,

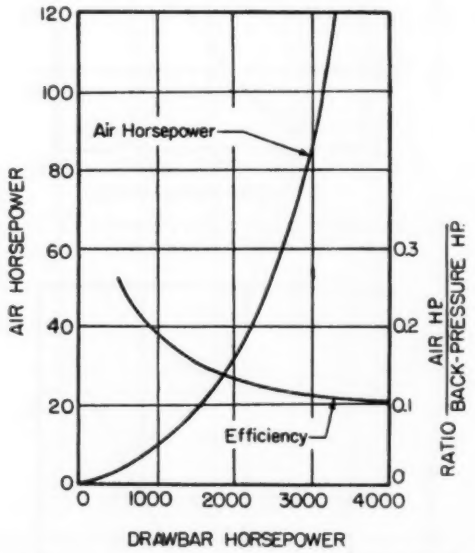


Fig. 13 Relation of Air Horsepower Required to Move Air and Gases and of Ratio of Air Horsepower to Back-Pressure Horsepower to Output of Locomotive

the efficiency of the front end, by this method of calculation, is 10 to 20 per cent.

Young (4) has shown that on the basis of the kinetic energies in the gases and in the steam at the nozzle, the efficiency of the front end is of the order of 5 per cent, but it is considered that the foregoing calculation is of greater significance.

Possibilities of Improvement in Design and Performance of Locomotive Air-Supply Systems

The lines along which efforts to improve the combustion efficiency and over-all performance of the coal-fired locomotive should proceed become clear from the analysis that has been presented. They are as follows: (*a*) To control the drafting appliance that the percentage excess of air for the coal burned will be essentially constant at all rates of operation; and (*b*) to move the air and combustion gases with the minimum back pressure on the cylinders.

With these objectives in mind we shall review the various methods of improvement that have been tried in the past. These include the following: (*a*) Change in area or shape of the nozzle; (*b*) change in area of stack; (*c*) change in resistance to air flow; (*d*) manually and automatically variable nozzles; and (*e*) induced- and forced-draft fans.

Change in Area and Shape of Nozzle. Probably the most common method of changing the locomotive to improve its "drafting" is to change the diameter of the nozzle or to change to one of

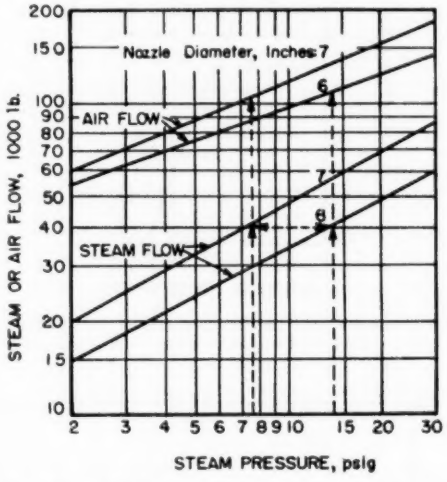


Fig. 14 Relation of Steam Pressure at Nozzle to Rate of Flow of Air and Steam
(Data from Young, reference 4, corrected for size ratio.)

special shape. If the engine does not "steam" properly the usual step is to insert a small nozzle. If it seems wasteful of fuel or emits excessive cinders, a larger nozzle is put in.

Fig. 14 presents curves from Young's work (4) which permit an analysis of what happens when the size of the nozzle is changed. The relations between the steam pressure on the nozzle and the rate of steam and of air flow are plotted on logarithmic paper on which they assume straight lines.

Let us assume first that the locomotive has a 7-in-diam nozzle and is found not to steam properly. A 6-in. nozzle is installed. The dashed lines indicate, as an example, that when the pressure at the nozzle was 7.6 psi, the rate of flow of steam was 40,000 lb per hr, and the rate of flow of air was 105,000 lb per hr. If the flow of steam remains the same, the back pressure with the 6-in. nozzle will be 14 psi; the air flow will be 109,000 lb per hr. The increase is only 4 per cent and is caused, it is to be noted, not because of the increased steam pressure, as we have seen that this decreases the entrainment ratio; instead, it is because of the increase in the ratio of area of stack to nozzle because of decrease in the area of the latter.

Actually, to maintain the same power output from the locomotive with the smaller nozzle would necessitate an increase in steam flow because of the increased loss in power by increase in back pressure. The cutoff would have to be increased, the rate of flow of steam and the back pressure would increase, and the flow of air would increase. A greater net output will be obtained from the engine but at a lower engine efficiency.

Conversely, it can be seen that if a change was made from a 6-

in. to a 7-in. nozzle, the cutoff could be decreased to obtain the same output and the steam flow and air flow would decrease more than shown by the dashed lines.

The size of the nozzle must be of course that which will give the design output of the locomotive, but data should be made available which would make unnecessary a trial-and-error method to establish the correct size. As for special designs and shapes, some have merit, but Young's findings have already been recalled; namely, that among all that he tried the best was only 12 per cent better than the poorest.

Although the size of the nozzle may be varied, we have seen that the laws of flow are such that the percentage excess air supplied will decrease with increase in rate of output of the locomotive, and a fixed nozzle cannot change this fundamental relation.

Change of Area of Stack. The dimensions of the stack of a locomotive once built are not susceptible of simple change and less experimenting has been done with the stack.

For maximum performance of any given combination of stack and nozzle, the distance from the nozzle to the top of the stack must be such that the steam will fill or "seal" the stack. Because the height of the stack is limited by the clearances of the right of way, there is a limit to the stack diameter that can be used.

Furthermore, as the stack diameter is increased, the velocity of discharge of the gases is decreased and trailing smoke that obscures vision may result. European locomotives have often used "wings" to lift the gases above the train. They have also been used to some extent in this country.

Change of Resistance to Air Flow. The analysis in the earlier part of the paper showed that the resistance against which the air and gases are moved is one of the principal factors that determine the entrainment ratio of an exhaust nozzle. The expression for resistance

$$R = \frac{\sqrt{d}}{Wa}$$

was suggested.

Table 1 gives some of the data on five locomotives, the average over-all resistance calculated from the draft in the front end, the resistance of the tubes from the pressure drop across them, and the ratio of the two resistances.

Resistance values from individual tests of each locomotive showed no general trend with locomotive output but were, with few exceptions, nearly constant at the average value shown. When it is seen that the resistance of the tubes is 67 to 75 per cent as large as the total resistance, it is not surprising that the over-all resistance should not change with a change in the thickness of the fuel bed or other variables in the course of tests at various rates of output.

Table 2 gives the pressure drop across various parts of the air- and gas-flow system of a locomotive, the resistance of each section, and the ratio of each to the over-all resistance.

The last column of Table 2 gives the ratio of the resistance of each of the several parts of the system to the over-all resistance. It must be remembered that the sum of the resistances is not equal to the total resistance; instead, the total resistance equals the square root of the sum of the squares of the resistances of the separate parts..

Resistance of Diaphragm and Tubes. The two largest single resistances in the system are those of the diaphragm and tubes. They are, respectively, 59 and 51 per cent of the over-all resistance or together

$$\frac{100\sqrt{2.3^2 + 2.0^2}}{3.9} = 78 \text{ per cent of the total}$$

Hence it would seem that here lies the greatest opportunity for reduction in the resistance and thus the improvement in the performance of the exhaust system.

The function of the diaphragm is to break up and extinguish cinders that they may be discharged freely and harmlessly from the stack. Many variations, such as so-called cyclone front ends, have been tried. A review of all suggested designs and an experimental program on new designs would now be in order.

The resistance of the tubes is high because of the high velocity with which the gases are passed through them. This high velocity results in excellent heat transfer but, as previously pointed out, at the expense of a loss of efficiency of the engine because of the high back pressure.

The over-all efficiency of the locomotive in its use of the heat liberated from the coal is the product of the efficiency of the engine and that of the boiler. As the efficiency of the engine decreases and that of the boiler increases, as the area of the tubes is decreased or their length is increased, there is a value for area and length at which the over-all efficiency is at an optimum.

An analysis to establish whether the values now used in locomotive design are the optimum should be made. If not, experimental research to establish the optimum should be carried out.

Resistance of the Arch. The resistance to the flow of gases backward to the throat of the arch and then by a hairpin turn forward is an important part of the resistance, but the gain in combustion efficiency by this turbulence and in absorption efficiency by the surface of the tubes is large and cannot be sacrificed. It is possible, however, that in the locomotive used as an example, and others, the throat is too small and should be increased.

Resistance of Fuel Bed and Grate. What part of the resistance of the fuel bed and grate is caused by the fuel bed and what by the grate separately is not known. They must be considered together. The total is the smallest of the four resistances so far considered. Even if the resistance could be removed entirely, the flow through the system would not be greatly increased.

For example, the over-all pressure drop would be reduced from

TABLE 1 AVERAGE RESISTANCE TO FLOW OF GAS FOR FIVE LOCOMOTIVES

Locomotive	Max dhp	Grate air openings, per cent	Areas, sq in.		Ratio, (Area of stack) / (Area of nozzle)	Resistance		Ratio, R(tubes) / R(total)
			Nozzle	Stack		Total	Tubes	
I-1-S 4358(11)	3334	32	35.9	314	8.8	5.0	3.7	0.74
H-8-8B 387(15)	1588	27	30.9	227	7.3	5.7	4.3	0.75
Mikado 1742 (9)	1833	37	28.3	265	9.4	4.5	3.1	0.69
K-4-8 1737(10)	2876	28	38.2	214	5.6	5.2	3.5	0.67
K-4-8 5399(12)	3934	15	51.2	310	6.1	4.0	2.7	0.68

TABLE 2 DRAFT, PRESSURE DROPS, AND RESISTANCE TO GAS FLOW IN LOCOMOTIVE[a]

Position	Draft, in. water	Pressure drop, in. water	R, $\frac{\sqrt{d}}{Wa} \times 10^8$	Ratio to over-all resistance
Front end	20.1	...	3.9	1.00
Across diaphragm	..	6.9	2.3	0.59
Back of diaphragm	13.2	...	...	...
Across tubes	..	5.3	2.0	0.51
At flue sheet	7.9	...	...	...
Across arch	..	4.2	1.8	0.46
Firebox	3.7	...	...	...
Across fuel bed	..	3.0	1.5	0.38
Ashpan	0.7	...	...	...
To atmosphere	..	0.7	0.7	0.18

[a] Drawbar horsepower = 3839. Air flow = 114,600 lb per hr.

20.1 to 17.1 in. and the resistance would be as 20.1 to 17.1 or as 4.5 to 4.1. The rate of flow for a given draft varies inversely as the resistances. Hence for the same draft in the front end the rate of flow without the resistance of the fuel bed and grates would be $\frac{4.5}{4.1} = 110$ or 10 per cent greater.

This shows that the effect of reductions in the percentage air openings in the grates, which is often now as low as 7 to 10 per cent compared to 40 to 50 in earlier locomotives, is not that of so increasing the resistance that the ratio of air to fuel is decreased. Instead, the advantage of reduced air openings is that they improve the distribution of the air over the grate and prevent the passage of a large amount of air through a hole that may occur in the fuel bed.

Resistance of Ashpan. The resistance offered to the flow of air by the inlets to the ashpan is much the smallest of the several resistances, but the fact that there should be any resistance, as evidenced by a draft in the ashpan, has often been questioned by engineers.

Even if it were removed, the change in the over-all resistance would be small, of the order of

$$\frac{\sqrt{20.1 - 0.7}}{\sqrt{20.1}} = \frac{4.4}{4.5} = 0.98$$

that is, a 2 per cent decrease. This is small but a reduction would undoubtedly be desirable. The seemingly prevalent rule that the area of the inlets to the ashpan should be 15 per cent of the area of the grate may well be questioned.

Manually and Automatically Controlled Front Ends. Many suggestions have been made of variable nozzles, some controlled manually from the cab and some automatically. The history of the manually controlled nozzles has been that they were difficult to maintain in working order at the temperatures of the front end or that they were closed to their minimum at all times. Their acceptance in this country has not been great.

Lewis Nozzle. Of the several automatically controlled nozzles, the Lewis, described by Jackson (3), attained some use. It was a slot-type nozzle in which two vanes were mounted on shafts which were geared together and connected to a weighted loading arm damped by a dashpot. The vanes "pumped" at low engine speeds as the back pressure varied, but at high speeds they rode at balance, opening further as the pressure increased. The desired functioning was never clearly described in terms of rate of air flow at various outputs. One statement was made that a constant draft was obtained. This is obviously impossible and undesirable as the draft must increase as the rate of output increases.

The action must have been that by opening with increased pressure, the back pressure was held down but because the ratio of area of stack to nozzle was decreased, the rate of air supply was less than it would have been with a fixed nozzle. The reverse has been shown to be the desirable action.

Bertram Automatic Drafting. A device for automatic control of the draft on a locomotive is covered by two patents (16, 17) to Bertram, and some results have been described. It consists of several spring-opposed (18) valves in a line leading from the exhaust pipe to the atmosphere. The valves start to open at a pressure of 5 to 6 lb, and by by-passing part of the steam from the exhaust nozzle the back pressure is reduced. Also, it must reduce the amount of air moved by a nozzle of the same size; whereas we have seen that the need is for a greater amount of air at high rates and a reduction at low rates.

If a smaller nozzle than normal for a nonautomatic nozzle were used and the spring-loaded valves opened early to by-pass a part of the steam at low rates, some measure of the desired action might be attained, but neither the patents nor descriptive literature clarify the exact action. The article states that 59 locomotives of the Lehigh Valley were equipped with the device from 1938 to 1941, but it is understood that all have now been removed.

The Clemac Front End. Another automatically controlled front end has been recently developed by W. H. Clegg, general superintendent, Motive Power and Car Equipment, and R. R. McIntosh, mechanical engineer, Grand Trunk Western Railroad. Only a short discussion has been published (19), but Messrs. Clegg and McIntosh have kindly made all details available to the authors. The development is also well described in two patents (20, 21).

The essential features are as follows:

1 Back-pressure relief valves of the weighted poppet type to govern back pressure on the cylinders by exhaust of steam to the atmosphere.

2 A draft-relief valve that opens to admit air to the front end and thus limits the draft. The draft at which the valve opens increases as the output of the locomotive increases because the valve is loaded by the pressure of the steam at the nozzle through a piston on the upper end of the stem of the valve.

3 A cinder ejector which consists of a pipe that extends from the point of maximum draft inside the skirt of the stack to the bottom of the front end.

4 The elimination of the diaphragm, table plate, draft sheet, and netting from the front end.

The action of the back-pressure relief valve is not essentially different from that of the Bertram, and the same objections apply.

The draft-relief valve may have merit in that it should be possible to maintain the air-fuel ratio constant or to vary it as desired over the range of outputs.

The elimination of the diaphragm, table plate, draft sheet, and netting should decrease the over-all resistance to the flow of gases, permit a larger nozzle, and thus reduce the back pressure on the cylinders. Why these supposedly essential features can be eliminated by the inclusion of the back-pressure and draft-relief valves is not clear. However, the two locomotives equipped with the device have been approved from the standpoint of danger of forest fires for operation in Michigan by the Conservation Department, and in Canada for operation on the associated lines of the Canadian National Railways.

Admittedly, there is much that is not known about the factors that control the pickup and carry-over of cinders. If the carry-over varies as some power, greater than 1, of the rate of flow of gases, the carry-over will undoubtedly be high at the instant the exhaust valve on the engine cylinder opens, when the rate of discharge of steam is at a maximum. Thus it is conceivable that the carry-over would be considerably less for the same total flow if the rate of flow of gases were continuously at the average value than if the rate varies widely, as it must with the intermittent exhaust of steam at widely varying pressure.

Correct Principles of Automatic Control of Air Supply. The automatic devices described appear to have been designed in the belief that a locomotive is overdrafted at high rates and underdrafted at low rates, whereas we have seen that the reverse is true. The correct principle is to install a nozzle of the correct size to give the required output of the locomotive and the desired excess air at that output and to open the nozzle, to by-pass steam, or to relieve the front-end draft at lower outputs to maintain a constant excess of air.

If this were manually controlled an indicator in the cab would be required as a guide to the proper setting. A dual gage, one pointer indicating flow of steam by pressure drop across a nozzle, the other indicating flow of gas by pressure drop across the tubes

with such adjustment of the linkages that when the pointers were together the rate of air supply was correct, would be suitable. This is the principle of the Bailey boiler meter, widely used on stationary boilers and adaptable to automatic control. The difficulties of application to locomotives with widely varying pressures, particularly at low speeds, are apparent.

Induced- and Forced-Draft Fans. The possibility of the application of either forced- or induced-draft fans to the locomotive has occurred to many. MacFarland (2) as the result of his studies of the power losses because of back pressure, designed an induced-draft fan operated by high-pressure steam. The design was applied to one switcher and three road locomotives of the Atcheson, Topeka and Santa Fe Railroad from 1912 to 1914. From 1920 to 1927 Dr. W. F. M. Goss experimented with a turbine-driven induced-draft fan using exhaust steam.

Jackson (3) reports that both of these failed because of the impossibility of maintenance of the blades against the erosion by slag particles and cinders.

The Committee on Front Ends, Grates, and Ash Pans of the International Railway Fuel Association (22) has described a forced-draft installation on a locomotive of the Texas and Pacific, burning both Texas lignite and bituminous coal. Although the first results were promising, no further application seems to have been made. The fan was operated by a turbine, presumably on exhaust steam, although this was not definitely stated. The exhaust of the turbine passed through a nozzle to the stack. Both the nozzle and stack were considerably enlarged as compared to normal practice.

The difficulties of forced draft are obvious. The firebox will be under pressure greater than atmospheric, and the firing door cannot be opened unless the fan is shut off.

Overfire Air. The use of overfire-air jets to decrease the loss by unburned combustible gases and to decrease the smoke has long been practiced and is now coming into greater favor because of the work of Bituminous Coal Research, Inc. (7, 23, 24). This work has given the correct principles of design of steam and fan-driven jets and has shown how the noise which so often prevented their use, can largely be eliminated by a simple silencer. More than 600 locomotives on 24 railroads have now been equipped with jets based on the BCR design.

If 10 or 20 per cent of overfire air is desirable, the question arises whether the supply of 30 to 50 per cent of the air would not be more desirable.

The introduction of the air over the fire would do little to relieve the work on the front-end nozzle and thus reduce the back pressure because the gases would still have to be moved around the arch, through the tubes, and around the diaphragm. We have seen that these constitute the bulk of the resistance of the system.

Whether the use of large proportions of overfire air would reduce the large losses in cinder at high rates depends upon the amount of this carry-over that comes from the fuel bed and the amount that is carried from the coal thrown from the stoker and thus never reaches the bed. Only experimental research will determine the value of overfire air, but as the possible gains are great, a thorough research is warranted.

Conclusions and Recommendations for a Program of Research

This analysis of the problem of the supply of air to coal-fired locomotives by means of the "front-end" system of exhausting the steam from the cylinders into the stack through a fixed nozzle shows the following:

1 That the design of the front end definitely establishes at all rates the efficiency of combustion of the coal, as measured by the excess of air, and the efficiency of the cylinders except for some modification possible by the engineer by position of the throttle and cutoff.

2 That the front end does not increase the rate of supply of air proportionately to the rate of output of the locomotive but leads to a decreasing excess or even a deficiency of air at high rates.

3 That the loss of heat in cinders carried out of the combustion chamber at high rates is not necessarily the result of the deficiency of air supply by the front end.

4 That the high back pressures on the cylinders at high rates lead to large losses of power output.

5 That one of the principal reasons why high back pressures are required is the high resistance offered to gas flow by the diaphragm and the tubes.

6 That most attempts at manually or automatically controlled front ends have been based on the assumption that locomotives are overdrafted at high rates of output and underdrafted at low rates, whereas the reverse is true.

A program of research to improve the performance of the coal-fired steam locomotive by improvement of the air-supply system should include the following:

1 A program of tests on a full-scale locomotive to fix definitely the value of the factors, ratio of area of stack to nozzle, steam pressure, temperature of the gas, and resistance to gas flow that determine the entrainment ratio of a nozzle.

This information can be obtained on standing tests using throttled desuperheated steam. Of particular importance is that the weight of gases moved be accurately measured. This is preferably obtained by movement of the gases with a fan and measurement by means of a nozzle or a Pitot tube.

With this information and with knowledge of the resistance to gas flow and of the consumption of steam of a given locomotive, the proper size of nozzle for a given performance could be established by calculation, and cut-and-try methods of adjustment of the front end would be eliminated.

2 Review of design of front ends and experimental research to develop a design with the minimum resistance to the flow of gas consistent with proper self-cleaning characteristics.

3 Review of the problem of heat transfer in the boiler tubes to fix the area and length to make the over-all efficiency of the locomotive an optimum.

4 Conduct a thorough program of experimental research to determine the value of overfire air in elimination of smoke, reduction of losses in gaseous combustible, and of losses in cinders.

BIBLIOGRAPHY

1 "La Locomotive à Vapeur," by A. Chapelon, Bailliere, Paris, France, 1937.

2 "Locomotive Drafting and Its Relation to Fuel Consumption," by H. B. MacFarland, Proceedings of the Fourth Annual Convention, International Railway Fuel Association, 1912, pp. 143–227.

3 "The Drafting of Steam Locomotives," by J. R. Jackson, Trans. A.S.M.E., vol. 60, 1938, pp. 573–582.

4 "A Study of the Locomotive Front End, Including Tests of a Front-End Model," by E. G. Young, Bulletin No. 256, Engineering Experiment Station, University of Illinois, Urbana, Ill., 1933.

5 "A Supplementary Study of the Locomotive Front End by Means of Tests on a Front-End Model," by E. G. Young, Bulletin No. 274, Engineering Experiment Station, University of Illinois, 1935.

6 Discussion of Paper by J. R. Jackson, by E. G. Young, Trans. A.S.M.E., vol. 61, 1939, pp. 453–454.

7 "Overfire Air Jets," by R. B. Engdahl and W. C. Holton, Trans. A.S.M.E., vol. 65, 1943, pp. 741, 754.

8 "The Exhaust of Locomotives," by F. Legein, Bulletin of the International Railway Congress, vol. 2, 1920, pp. 319–359.

9 "Tests of a Mikado-Type Locomotive Equipped with Nicholson Thermic Syphons," by E. C. Schmidt, E. G. Young, and H. J. Schrader, Bulletin No. 220, Engineering Experiment Station, University of Illinois, 1930.

10 "Tests of a Class K-4-S Locomotive," Bulletin No. 29, Pennsylvania Railroad Company, Locomotive Testing Plant, 1915.
11 "Tests of a Class I-1-S Freight Locomotive," Bulletin No. 32, Pennsylvania Railroad System Locomotive Testing Plant, 1924.
12 "Test of Locomotive No. 5399," Pennsylvania Railroad Testing Plant.
13 "Report on Tests Made by the New York Central Railroad at Selkirk," by W. F. Collins, Proceedings of the Railway Fuel and Traveling Engineers Association, 1940, pp. 157–185.
14 "Ten Years of Stoker Development at Hudson Avenue," by J. M. Driscoll and W. H. Sperr, Trans. A.S.M.E., vol. 57, 1935, pp. 49–58.
15 "Tests of a Modified Class H-8-SB Locomotive," Bulletin No. 10, Pennsylvania Railroad Company, Locomotive Testing Plant, 1914.
16 "Draft Control," by B. C. Bertram, U.S. Patent No. 2,222,501, November 19, 1940.
17 "Draft Control," by B. C. Bertram, U.S. Patent No. 2,222,502, November 19, 1940.
18 "Locomotive Operation Improved by Automatic Draft Control," by F. S. Williams, *Railway Age*, vol. 111, 1941, pp. 338–341.
19 "Discussion of Report of Committee on Front Ends, Grates, Arches, and Ash Pans," by W. H. Clegg, Proceedings of the Railway Fuel and Traveling Engineers Association, 1943, p. 81.
20 "Apparatus for Controlling Draft," by R. R. McIntosh, U. S. Patent No. 2,377,895, June 12, 1945.
21 "Method and Apparatus for Draft Control," by R. R. McIntosh, U. S. Patent No. 2,379,916, July 10, 1945.
22 "Controlled Draft in Locomotives," Report of the Locomotive Economy Devices Committee, Proceedings of the International Railway Fuel Association, 1927, pp. 247–251; also "The Use of Forced Draft on Texas and Pacific Locomotive No. 524," Report of Committee on Front Ends, Grates, and Ash Pans, Proceedings of the International Railway Fuel Association, 1928, pp. 402–414.
23 "Design Data for Overfire Jets," by R. B. Engdahl, *Combustion*, vol. 16, March, 1944, pp. 47–51.
24 "Application of Overfire Jets," by R. B. Engdahl, Technical Report No. 7, Bituminous Coal Research, Inc., May, 1944.
25 "Steam Production and Air in the Locomotive Boiler," by L. H. Fry, Proceedings of the Railway Fuel and Traveling Engineers Association, 1944, pp. 162–171.

Discussion

E. D. Benton.[4] While investigations and testing of various combinations and arrangement of front-end parts have been carried on for many years, no one, heretofore, has clearly set forth the principles so that the ability of the front end to move air could be rationalized. Had this been done previously many of the misconceptions of its inherent characteristics would have been known, and much time and effort saved in attempts to design and patent ideas which were doomed to disappointment. The apparently simple fact that steam-air entrainment ratios decrease with either an increase in steam flow at the nozzle or increase in draft, and therefore at maximum output there is no surplus steam exhausted, has not been appreciated except by a few people. This has resulted in many attempts to improve the front end by the application of principles which, in effect, did just the reverse.

The development of a simple formula for calculating entrainment ratios, based upon the fact that both the air rate per Btu in the coal and boiler-absorption efficiency are essentially constant thus leaving only one variable, that of total heat or enthalpy of the steam, is particularly valuable. It, of course, assumes that all of the steam generated is exhausted through the nozzle or absorbed by the boiler feedwater. However, a sizable percentage of the steam generated by the boiler does not pass through the exhaust nozzle, such as the heat lost from continuous boiler blowdown, the steam-air pump, cab and headlight generator, stoker engine and jets, train heating, etc. Obviously, a factor representing this should be included in Equation [6].

The paper, by inference, brings out an interesting but seldom appreciated point, that exhaust pressures must be higher for modern high-pressure high-superheat engines than for older or saturated-steam engines. Assume two engines with the best possible front-end arrangement, but one engine producing steam having an enthalpy of 1200 Btu per lb, and the other engines with steam conditions giving 1395 Btu per lb. Then the engine with the greater enthalpy must entrain $\frac{1395 - 1200}{1200} \times 100$ or 16 per cent more air per lb of steam exhausted. If Young, in his investigations at the University of Illinois, was able to measure a difference of only 12 per cent between the best and the worst front-end nozzle-stack arrangement, it becomes apparent that the engine having the highest enthalpy must have a well-designed front end, and particular attention must be given the resistance offered to the flow of gases from the ashpan to the front end. It would appear that Young's statement, "the mutual incompatability of the mechanical requirements of the front end," has another difficulty, i.e., that of enthalpy.

The concept of resistance and resistance ratios as presented in the paper should prove helpful to anyone experiencing drafting difficulties, particularly when attempting to compare front-end proportions between engines having substantial differences in enthalpy of the steam generated. That grate and fuel-bed resistance is only about 15 per cent of the total will surprise many stationary-power-plant men who usually consider the fuel bed as the major resistance to the flow of air. It is for this reason that engines appear to steam equally well with a fuel and ash bed free of clinkers of 14 in. in thickness as with one only 6 in. thick.

If the steam turbine is to enjoy the success it justly deserves, considerable attention must be given the optimum "resistance train" in order to lower back pressure and improve water rates, since an increase in enthalpy of the steam is handicapped by an increase in exhaust pressure.

J. R. Jackson.[5] In the main, the writer follows the analysis and subscribes to the points advanced by the authors, particularly that "draft," as expressed in pressure differential, is not the proper basis for the study of the flow of heat through the locomotive boiler, and that the composition, weight, and temperature of the gases moved, at various locations in progression through the boiler, should be determined for different rates of power development. It is agreed with that in this respect there is a lack of information and a field for investigation which should yield a better understanding of the factors in the burning of solid fuels on grates throughout the normal range of power development of a steam locomotive boiler and possibly lead to an extension of the economic range over that heretofore obtainable.

However, there are two points made by the authors which the writer finds it difficult to subscribe to:

1 The evaluation of the resistances to flow through the boiler, particularly to the relatively small value attributed to the fuel bed.

2 The statement of "the correct principles of automatic control of air supply."

As to the first point, fire-bed resistance; the front-end plates and spark-arrester appliances, the tubes and flues, the arch, the grates, and the ashpan openings are the fixed resistances; the fire bed is the variable resistance and consequently the only means the locomotive fireman has to regulate and control air supply. While fire-bed resistance as the authors show, is of a relatively small magnitude as compared with the fixed resistances, it is a most important factor in the control of steam generation for any given rate of power development in any existing coal-

[4] Fuel Engineer, Louisville and Nashville Railroad Company, Louisville, Ky. Mem. A.S.M.E.

[5] Engineer of Tests, Missouri Pacific Railroad, St. Louis, Mo. Mem. A.S.M.E.

fired steam locomotive. The difference between a good fireman and a poor one is essentially the manner in which he regulates fire-bed resistance to control air supply.

As to point 2, i.e., automatic control of air supply. If by "correct size to give the required output of the locomotive" the authors mean maximum output, a nozzle of relatively large area is essential if the cylinder back-pressure horsepower loss is to be kept at the desired minimum for those conditions. However, in practice, with the relatively large nozzle desired for maximum output, it is too large for the lower rates of power development and the locomotive will "steam hard" or "fail for steam" as the rate of flow of exhaust steam through the nozzle is decreased by throttle or cutoff control. The universal remedy followed to improve steaming at the lighter loads under the conditions as just set forth is to reduce the nozzle area. This is directly the opposite procedure to the authors' statement of the correct principles of automatic control of the air supply and wherein the writer finds it difficult to agree. The case of a relatively large-nozzled locomotive in effect approaches the authors' concept for the automatic control of air supply, and yet it does not work out in practice.

It has been realized for many years that the back-pressure horsepower loss in the reciprocating steam locomotive is relatively high at the higher rates of power development. The writer has had considerable experience in attempts to bring about improvement in this direction and still believes that this angle requires further study and experimentation in any program of research looking to the improvement of the conventional reciprocating steam locomotive.

The control of air flow through the grates or above the fire in a coal-fired steam locomotive, throughout the relatively wide range of power development, is not a simple problem but it is believed that the approach, as suggested by the authors in this paper, should yield long-needed supplementary information and gives promise of realizing some worth-while improvements in the efficiency of the steam locomotive within the relatively narrow thermal-efficiency limitations attainable in this type of motive power.

In conclusion, the writer is thoroughly in sympathy with the authors' recommendations for a program of research employing a full-sized locomotive and hopes that it will be carried out along the general line as set forth in this paper.

R. R. McIntosh[6] and W. H. Clegg.[7] We note in the section, "Relation of Air Supplied by Front End to Air Required for Coal Fired," the authors refer to a locomotive developing 3500 dhp, at which output there was a deficiency of 30 per cent in excess air required for the coal fired, while actually for the coal burned, there was still an excess of 28 per cent at that power output. This fact seems to offer the most lucrative field for research in correcting the factors leading to such a tremendous loss in unburned fuel.

It is also noted in "Relation of Performance of Front End to Loss of Heat in Cinders," that the authors conclude that the high cinder loss is the result of the high carrying power of the gases for solids at the high velocity with which they move through the combustion chamber at high rates of operation, and that coal is both carried out of the bed and swept out of the stream of coal being fired before it reaches the fuel bed.

It is apparent that these undesirable conditions exist at high rates of output where they are influenced by the higher back pressure developed, which rapidly increases the ratio of the loss of back-pressure horsepower to the drawbar-horsepower output, as illustrated in Fig. 11. The small percentage of increase of air flow obtained by large increases in back pressure is obtained only at a very high price and is entirely out of proportion. It is therefore reasonable to assume that much may be accomplished in this direction where both high values of back pressure and air flow are automatically controlled, especially where such permits the locomotive to develop its boiler and tractive-effort capacity by reducing materially the ratio of back pressure-horsepower loss to drawbar-horsepower output and maintaining a more satisfactory range of entrainment ratio in the movement of gases.

We heartily concur in the authors' conclusions and recommendations for a program of research which should embrace a careful study of past and present designs of air-flow control, and the effect of unburned fuel loss by the control of back pressure, especially in view of the high ratio of back pressure - horsepower loss to drawbar-horsepower output. It is obvious from the authors' conclusions that they regard high back pressure as a very important factor which should be minimized by reduction of resistance to air flow, and we believe this to be well within the bounds of possibility with automatic control.

Authors' Closure

Mr. Benton has correctly pointed out that an increase in enthalpy of steam, by increase in pressure or in superheat, or both, results in an increase in the required entrainment ratio of the front end. His conclusion that this means that an engine having higher enthalpy must have a well-designed front end is also sound as there is little purpose in increasing the energy in the steam at the high level if one must decrease the size of the nozzle and thus throw the energy away in increased back pressure.

Mr. Jackson questions the conclusion that the resistance of the fuel bed plays a small part in control of the flow of air through the system. His belief that the fireman can control the amount of air by the thickness of the bed is natural and it is true that if the pressure drop through the fuel bed is increased, the supply of air will decrease, but it is not true that it will decrease greatly for normally expected changes in resistance.

If we take, for an example, the conditions shown in Table 2, when the pressure drop across the entire system was 20.1 inches of water and that across the fuel bed was 3 inches, and assume that the drop across the bed is doubled, then the increase in resistance will be

$$\frac{\sqrt{23.1}}{\sqrt{20.1}} = 1.07$$

or seven per cent. That is, the air flow would be decreased by seven per cent, certainly not a large amount, for a doubling of the pressure drop across the fuel bed. The authors will certainly agree with Mr. Jackson that the difference between a good fireman and a poor one is the manner in which he maintains the uniformity of his fuel bed. For example, if the fireman fires too much coal and greatly increases the thickness of the bed, the result may be heavy smoke and loss due to carbon monoxide and unburned volatiles, not because the increased thickness of bed reduced the amount of air appreciably but because it changed the air-coal ratio by too much coal.

Conversely, a decreased rate of firing will lead to a thin fuel bed, low CO_2, and falling steam pressure, not because the air has increased a great deal but because the coal has decreased.

Mr. Jackson questions whether the authors mean maximum output in the statement, "correct size to give the required output

[6] Chief Draftsman, Grand Trunk Western Railroad Company, Battle Creek, Mich.

[7] General Supt. of Motive Power and Car Equipment, Grand Trunk Western Railroad Company, Battle Creek, Mich. Mem. A.S.M.E.

of the locomotive". The answer is that they mean the maximum output desired for the given locomotive, although this is usually the maximum that can be obtained. The authors recognize that as the size of the nozzle is decreased to give a higher entrainment ratio and more air, the cylinder output decreases because of the increased back pressure and the efficiency of the engine will decrease. Hence there should be an optimum size of nozzle for maximum output, but often a higher output can be obtained even at lower efficiency and this sacrifice is made.

The authors confess to lack of practical locomotive experience, but fail to see why, if a given nozzle gives satisfactory operation at high outputs, there should be "hard steaming" at lower outputs. The mathematical relations, fully confirmed by test data, show that the entrainment ratio of a nozzle increases as the flow of steam and thus the back pressure decreases. The "hard steaming" cannot be for lack of air. Could it be from too great an excess?

Messrs. McIntosh and Clegg appear to be in full accord with the conclusions of the paper and suggest that it is possible to obtain automatic control to avoid back pressures. The authors agree as to desirability, but point out again that the method of by-passing steam is wrong in principle because, when more air is needed, it can definitely not be obtained by not passing part of the steam through the nozzle.

Analysis of Special Electronic-Tube Tests

By J. H. CAMPBELL[1] and C. G. DONSBACH,[2] SCHENECTADY, N. Y.

The complexity of manufacturing electronic tubes is such that professional groups normally associated with design and laboratory activities are called upon to work in the factory. These groups contribute considerably to the control of material assembly, test, and the outgoing quality of the product. In this industry many variables exist and because none of the tube parts can be tested electrically until the tube is completed, a system of "statistical quality control" is in order. This paper illustrates improvements which may be accomplished through special tests on tubes in the course of production, followed by statistical analysis of the results.

THE complexity of the manufacture of many articles has been greatly increased in the past few years due to at least one or more of the following conditions:

1 The large number of new devices.

2 The relatively short period of time allowed for development.

3 The large quantities on order.

4 The precise quality and limitations imposed by critical wartime requirements.

There are probably few manufacturing processes more complex than the manufacture of electronic tubes. In order to cope with the situation many professional groups, normally associated with design and laboratory activities, must be called upon to work in the factory. The regular complement of production engineers in an electronic-tube factory must have the assistance of chemical and metallurgical engineers as well as glass technologists. This technical help in manufacturing contributes considerably to the control of material assembly, test, and the outgoing quality of the product.

Another important tool which is gaining in popularity and use in most industries is statistical quality control. In the electronic-tube industry the need for control of the many variables is especially acute since none of the parts can be tested for electrical characteristics until the tube is completely made. These variables start from the material composition of the parts and continue through all processing stations to the final test for electrical characteristics. When properly applied to manufacturing, statistical analysis becomes a library of information to help engineers, foremen, and operators make the right decision at the right time.

This paper is intended to illustrate what can be accomplished through the use of special tests in the production of electronic tubes, with particular emphasis on the need for statistical analysis of the results.

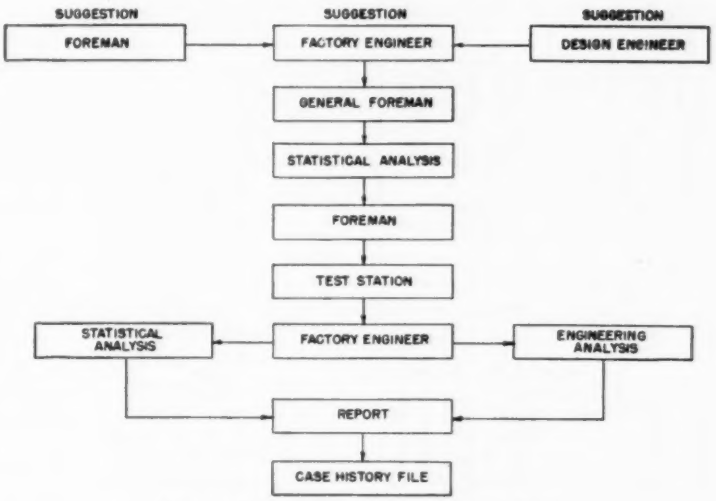


FIG. 1 START AND FINISH OF SPECIAL TEST

"SPECIAL TESTS" FOR ELECTRONIC TUBES

In order to avoid confusion in the term "special test," which will be referred to quite often, the following explanation is given:

The making of electronic tubes like many other manufacturing processes is accomplished by means of standard instructions. These instructions are the best known method of producing a particular tube type at the time the tube is considered developed and ready for manufacture. A special test usually has one variable which is not within the standard instructions. The engineer or person who suggests the test believes the one variable introduced in the manufacture of the tube will improve the quality and/or reduce manufacturing losses. If the test accomplishes either or both of the improvements, the corresponding change is made in the standard instructions.

It is therefore obvious that the special test is one of the most important tools for the factory to improve the quality of its product or reduce the losses in manufacture.

In order to utilize the test method to its fullest extent, complete co-ordination of all the groups in the factory must be obtained. Fig. 1 shows how this is accomplished. In general, the three groups who initiate a test are the engineers in the factory, the foremen, and the design engineers. The factory engineer's office serves as a clearing house for all technical information and the engineer accepts or rejects a special test based on the value of the information he expects may be gained by conducting it.

When a test is approved from a technical viewpoint, the general foreman is consulted regarding the priority the test should have in the production schedule. The written test form is then studied by the statistician to determine whether the method to be used will properly isolate the one variable being tested. The foreman then receives complete instructions and the tubes are assembled and tested. It then becomes the joint responsibility of the engineer and the statistician to analyze the data to determine whether the results are significant enough to require a change in standard instructions. A case history is then kept for future reference. The data are arranged by tube type and subject and made available to all who may have occasion to use them. When

[1] Factory Engineer, General Electric Company, Schenectady Tube Works.

[2] General Electric Company, Schenectady Tube Works.

Presented at the Spring Meeting of the Metropolitan Section, New York, N. Y., May 8, 1945, of THE AMERICAN SOCIETY OF MECHANICAL ENGINEERS.

NOTE: Statements and opinions advanced in papers are to be understood as individual expressions of their authors and not those of the Society.

this file is properly kept it serves to avoid duplication of effort as well as to provide information on past experience to help solve difficult problems in the future.

Production Flow Chart

To give an idea as to the number of variables encountered in the making of a tube, a typical flow chart of production is shown

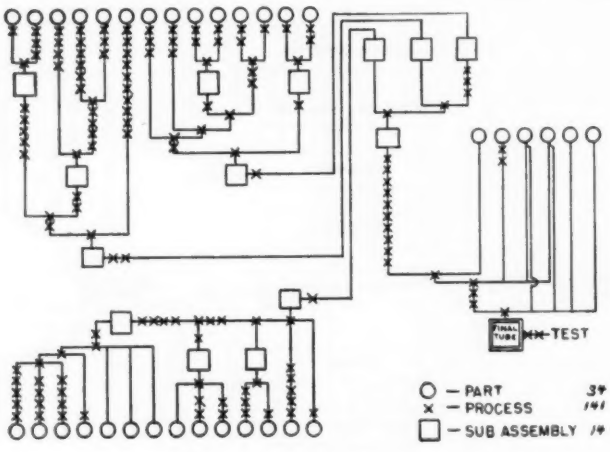


Fig. 2 Flow Chart Showing Possible Variables

in Fig. 2. It will be noted that this chart contains 34 parts, 141 manufacturing processes, and 14 subassemblies. In the manufacturing processes we have not included on the chart any subprocesses such as cleaning schedules of parts, exhaust schedules, etc. Likewise, Fig. 2 does not indicate the number of different machines, or operators, or test sets that may be in use at any one time. For ease of illustration these additional variables were omitted from the flow chart. It is important to note that practically any number of these variables or combinations of them may affect one or more of the electrical characteristics of the tube. The decision as to the total possible number of variables which can be encountered will be left to the reader's imagination.

Control over these variables is maintained statistically in many ways, a few of which may be listed as follows:

(*a*) Control over incoming material by sampling procedures.

(*b*) Control over processing stations by per cent defective, and variables control charts based upon 100 per cent and/or sampling inspection.

(*c*) Control at the test station by means of per cent defective, and variables control charts based upon 100 per cent and/or sampling tests. This may mean control over previous processing procedures since the results at test are, in many cases, directly or indirectly related to processing.

(*d*) Control by means of special tests.

In the remainder of the paper we will point out the method employed in analyzing special tests and some of the results obtained by the use of this system in an electronic-tube plant.

Procedures Followed in Special Tests

Fig. 3 is a flow chart which will give the general basis for the instigation, analysis, and disposition of such tests. An explanation of this chart follows:

The various reasons for running a test may arise from four general sources: 1 It may be the suggestion of a production worker, a foreman, or an engineer to change a certain processing procedure in the hope of improving the quality of the tube. 2 If a rise occurs in the per cent of defective tubes, it is the engineer's responsibility to isolate and correct the cause. This is often done by means of a special test where the suspected cause is the only variable. These troubles may in some cases be outstanding, as when the tubes suddenly become defective, or when per cent defective and/or variables control charts indicate trouble. 3 Another cause for which a special test may be run is to determine whether any differences exist among processing procedures such as among operators or machines. This source also uses special tests to compare test sets. 4 A special test may result from a necessity of control over certain incoming materials such as base metals, filaments, grids, etc., or from necessity of material control over certain processing materials, such as, emission-coating mixes, etc.

In general, regardless of the reason for conducting a special test, the procedure is to manufacture a small sample of tubes under prescribed conditions. Because of the large number of variables encountered it is absolutely necessary to send a control test along with the special test so that conclusions can be studied

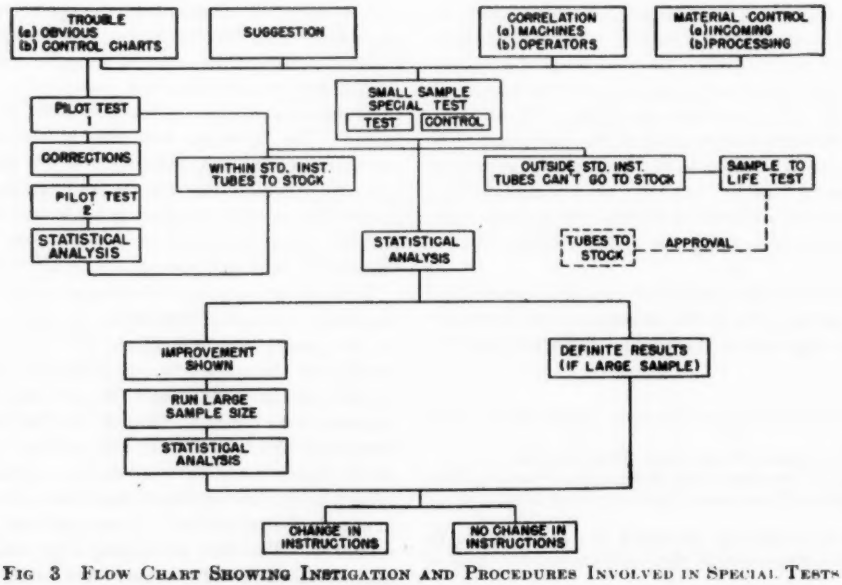


Fig 3 Flow Chart Showing Instigation and Procedures Involved in Special Tests

properly. This is the means used for reducing experimental error by holding constant all factors except the one under investigation. It means that the control test must be processed by exactly the same machines and same conditions (except for the one variable being tested) as the special test. Unless this is done, the results of the special test are not indicative.

These special tests may be further classified into two catagories, i.e., those in which the procedures are within standing instructions, and those which are outside standing instructions. In the case of the former the tubes may go directly to stock, but where the test is for tubes made under procedures which are outside standing instructions, the tubes cannot be stocked until the quality is determined by means of a life test or equivalent on a reasonable sample of the lot. If the tubes pass the additional prescribed test they may then go to stock.

As soon as the tubes are tested the results of the special test are compared with those of the control test. It is in this comparison that the use of the statistical analysis is applied. Fig. 4 shows the various statistical tests applied to determine whether the special-test results are different from normal production (control test). A brief explanation of each of these tests will be given, but for the basic theory the reader is referred to the Bibliography of this paper.

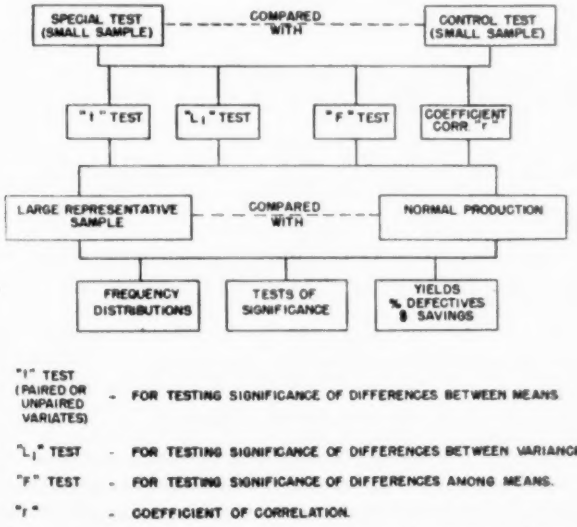


FIG. 4 FLOW CHART SHOWING METHODS OF STATISTICAL ANALYSIS

STATISTICAL COMPARISON OF TEST RESULTS

In the statistical comparison of test results the usual procedure is to figure the mean and standard deviation of the individual electrical characteristics for both the special and control tests, and then be sure that a controlled process exists. The question which then arises is, "Are these means and variations statistically different between the special and the control tests?"[2] In order to determine this, various statistical tests of significance are applied. One of these is the t test. This determines on the basis of the sample size whether the "averages" are significantly different from each other. The t test may be subdivided into two categories, i.e., that of paired, and that of unpaired variates. In all cases where control tests are run along with special tests, it is possible only to use the t test for unpaired variates. In other cases where partial special tests are run without control tests, such as in checking test equipment, the t test for paired variates is used. This is illustrated in Example 4.

The L_1 test is used to determine the significance of differences in "variance" between the special and control tests. The methods of computing the values of the t and L_1 are shown in examples 1 and 4, and the significance is determined from tables prepared for the purpose.[3]

Where there are more than two means and/or variances to be compared, the F test is generally used. Example 3 is an illustration of the use of this F test. Where correlation studies are indicated, the coefficient of correlation and line of regression are computed.

If the results of the special tests show fairly significant differences or are borderline cases, it is usually the procedure to send through a larger representative sample; perhaps a day's production or more. The control for this test is actually normal production before and after the large sample is run. In running this larger test care is taken to see that all parts and processes are randomized as is normal production. If three machines and three operators normally work on one of the tube processes, then this test is run so that the tubes are randomized among these machines and operators as they are in normal production.

After the tubes are tested for electrical characteristics, the results are statistically compared to normal production. The method of best presenting the results of this comparison has been found to be by cumulative frequency distributions, sometimes plotted on probability paper. This not only gives the shape of each distribution but enables one to estimate the average and standard deviation as well as per cent defective. This type of comparison is illustrated in examples 1 and 2. Where it is thought necessary, statistical tests of significance are also applied to these large sample sizes. However, in most cases a study of the curves together with the small-sample analysis are sufficient to determine whether or not to change normal production over to the new procedure.

PILOT TESTS

As mentioned previously, there are instances where special tests are run in about the same manner as normal production. The cause for running this test (which is called a "pilot test") is to determine if the yield of percentage of good tubes can be increased. The principle used is first to observe every process in the production of the tube. During this observation period referred to as pilot test 1, no corrections are made but are merely noted. The results of the yield of this are tabulated with all possible discrepancies. Then pilot test 2 is run with all corrections applied. The corrections are decided upon by engineers who consult with foremen and test observers.

Fig. 5 shows the yield of a certain tube (not yet out of the developmental stage) plotted over a period of time. Note the yield of pilot test 1 and then note the upward trend resulting as corrections were applied. Pilot test 2 showed almost a 71 per cent increase in yield over pilot test 1. The yield on this tube has continued along the yield obtained by pilot test 2.

The examples given in the appendix are taken from case histories of recent special tests. They have been selected as representative cases of actual production and are believed to be self-explanatory. The number of these tests being run and the results obtained from them can be illustrated by the following figures for April, 1945:

Number of tests started	50
Number finished	34
Number of those completed showing improvements	16

The program, as explained in this paper, is being followed actively at the present time. It is helping to produce the highest-quality product. In the postwar period the ultimate consumer will derive benefits in the form of increasingly good quality.

[3] Tables are available in various texts on the subject. (Refer to Bibliography following.)

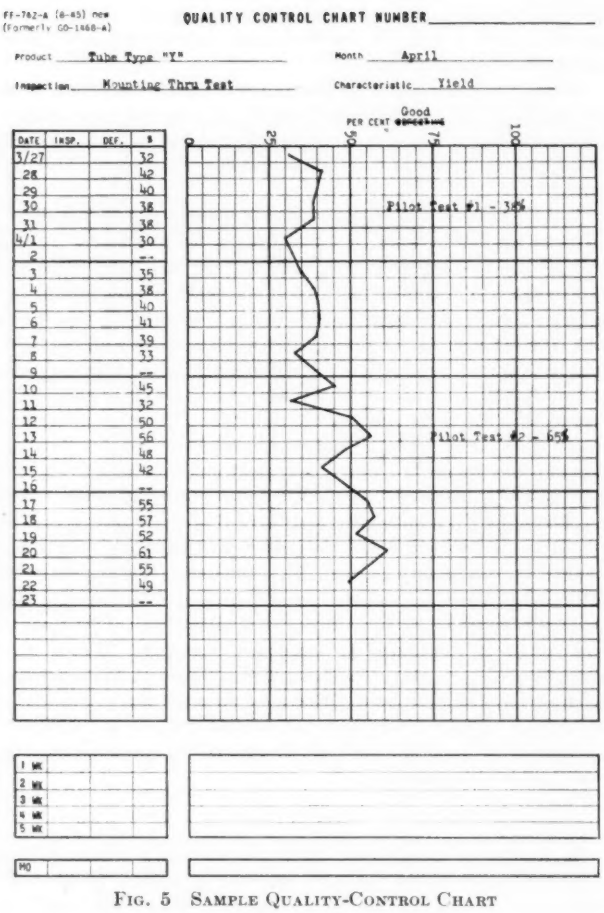


FIG. 5 SAMPLE QUALITY-CONTROL CHART

BIBLIOGRAPHY

1 American Standards Association Publication Z1.1, Z1.2, and Z1.3, 1941–1942.

2 "Laboratory Handbook of Statistical Methods," by T. H. Brown, McGraw-Hill Book Company, Inc., New York, N. Y., 1931.

3 "The Design of Experiments," by R. A. Fisher, Oliver and Boyd, Ltd., London, England, 1942.

4 "Statistical Methods for Research Workers," by R. A. Fisher, G. E. Stechert and Company, New York, N. Y., 1944.

5 "Industrial Statistics," by H. A. Freeman, John Wiley & Sons, Inc., New York, N. Y., 1942.

6 "An Engineer's Manual of Statistical Methods," by Leslie E. Simon, John Wiley & Sons, Inc., New York, N. Y., 1941.

7 "Economic Control of Quality of Manufactured Product," by W. A. Shewhart, D. Van Nostrand Company, Inc., New York, N. Y., 1931.

Appendix

EXAMPLE 1 SPECIAL TEST RUN AS RESULT OF SUGGESTION TO IMPROVE QUALITY

On one tube type the electrical characteristic "grid current" was the cause for a fairly large percentage of loss. The engineer decided that a change in the method of assembly would narrow the tube-to-tube variation and eliminate a considerable number of electrical defects.

After considering the daily production schedule and the number of possible variables present, it was decided to send through a special test of 50 tubes together with a control test of 50 tubes. For the control test, every part used came from the same lot of material and all processing operations were made by the same operators and on the same machines, under the same conditions as the special test, except for the one variable being tested.

The following results were tabulated for the grid characteristic:

	Test	Control
Sample size (n)	50	50
Average ($\bar{X}$), ma	37.4	42.0
Standard deviation (σ), ma	4.2	7.1

Were these results statistically different? The statistical t test was applied to determine the significance of the difference between the averages, and the L_1 test was applied to determine whether this difference in averages was due to inequality in variances.

For the t test, applying the formula

$$t = \frac{d}{\sqrt{\frac{\Sigma(X_t - X_t)^2 + \Sigma(X_c - X_c)^2}{n_t + n_c - 2}\left(\frac{1}{n_t} + \frac{1}{n_c}\right)}}$$

we have

$$t = \frac{4.6}{\sqrt{\frac{890 + 2518}{50+50-2}\left(\frac{1}{50} + \frac{1}{50}\right)}} = 3.9$$

which for 98 deg of freedom is significant.[4]

Applying the formula for the L_1 test

$$L_1 = \frac{s_t^2 s_c^2}{s_a^2 s_a^2}$$

where

$$s_a^2 = {}^1/_2(s_t^2 + s_c^2)$$

we have

$$L_1 = \frac{(17.8)(50.4)}{(34.1)(34.1)} = 0.78$$

$$+ \; s = {}^1/_2(17.8 + 50.4)$$

The value of L_1 for sample sizes of 50 is 0.9612, beyond which lie 5 per cent of all values of L_1. The value 0.78+ is far below this and indicates that the variances of the two assumed normal populations from which these samples were drawn differ significantly.

Because of the results in the special test of 50 tubes, it was decided to obtain a larger representative sample by running at least a day's production with the new assembly technique. In doing this the day's production was run with all shifts, all machines, and other variables that would be encountered in normal production. The distribution curves plotted on probability paper, Fig. 6, will give approximately the whole comparison as follows:

	Test	Normal production
n	309	500
$\bar{X}$	36.8	44.1
σ	4.5	8.0
Per cent defective	1.0	14.0

The actual yield (per cent good from starting 100 assemblies) showed an increase from 74 to 83. This increase in yield represents a monthly saving of $2500 to $3000, based upon the current production schedules.

[4] Degrees of freedom represent the number of independent values in the comparison.

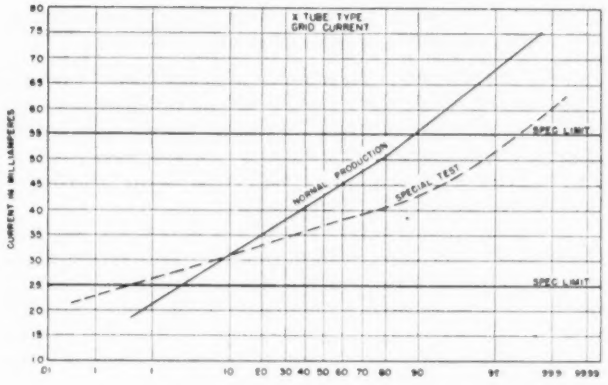


FIG. 6 X-TUBE TYPE GRID CURRENT

The following nomenclature is used in this section:

d = difference between means
X_t = individual value of each special-test reading
X_c = individual value of each control-test reading
$\bar{X}_t$ = average of special-test readings
$\bar{X}_c$ = average of control-test readings
n_t = sample size of special test
n_c = sample size of control test
s_t^2 = variance of special test
s_c^2 = variance of control test
σ = standard deviation

EXAMPLE 2 SPECIAL TEST RUN TO REDUCE HIGH PER CENT DEFECTIVE AS SHOWN BY STATISTICAL CHARTS

On a very critical tube type the per cent defective chart, Fig. 7, indicated a large loss at test due to a plate-voltage characteristic. This characteristic is primarily determined by the relative spacing of certain elements of the tube, which had previously been done by mechanical means. The engineer decided an improvement could be obtained by spacing the tube electrically with a capacitance bridge. This equipment was built for the test and arranged so that a predetermined reading of capacitance could be obtained while the tube was being assembled (the correlation of capacitance and spacing is shown in Fig. 8).

In using this fixture a small lot of tubes was made and the analyzed results indicated so much improvement that a special test was run on 420 tubes. These tubes were made on a completely randomized basis so that a correct comparison could be made with normal production.

Cumulative frequency distributions were plotted and are shown in Fig. 9. The results in the form of per cent defective are tabulated below:

	Normal production	Special test
Plate voltage	15.0	0.5
Capacitance	10.0	0.8
Gassy	3.7	1.4
Shorts	6.6	1.7

The reduction in gassy and shorted tubes was due to the more uniform spacing.

Statistical tests confirmed the differences in plate voltage and capacitance to be significant.

The device was put into use and the control chart in Fig. 7 shows the results in improvement in losses and quality. The over-all yield on this tube increased 49 per cent due to this factor, and the dollar savings amounted to over $7500 per 1000 tubes to stock.

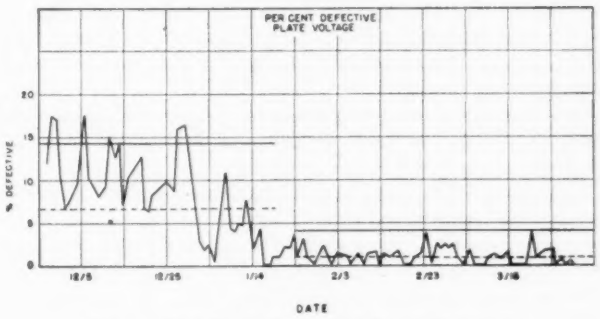


FIG. 7 PER CENT DEFECTIVE PLATE VOLTAGE

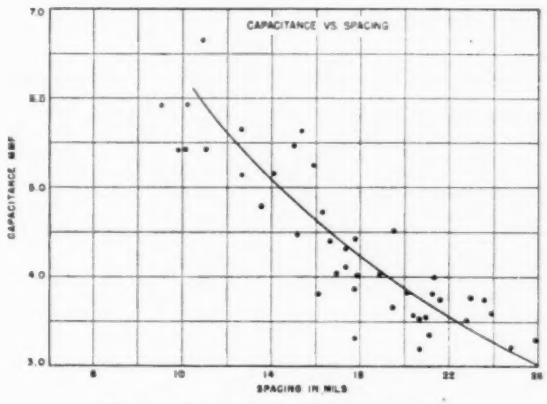


FIG. 8 CAPACITANCE VERSUS SPACING

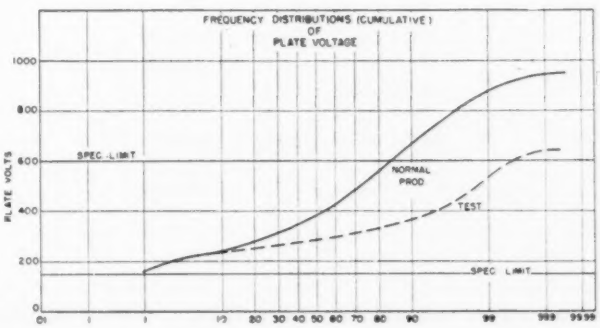


FIG. 9 FREQUENCY DISTRIBUTIONS, CUMULATIVE, OF PLATE VOLTAGE

EXAMPLE 3 COMPARISON OF EXHAUST SCHEDULES THROUGH USE OF L_1 AND F TESTS

Considerable difficulty was encountered in obtaining proper emission on a particular tube type. One of the possible variables which could affect this was the schedule by which the tubes were exhausted.

The engineer ran a special test using four different exhaust schedules. The following results were tabulated:

Exhaust schedule	A	B	C	D
n	16	24	28	19
$\bar{X}$	28	20.2	27	21

From the averages given in the table, schedules B and D look much better than schedules A and C. However, do the averages of these schedules differ significantly among themselves, or do they most likely come from the same homogenous population?

In order to determine this the F test was applied (after applying the L_1 test which showed that the variances of the assumed normal populations from which these samples were drawn were not significantly different).

In the F test we simply segregate the total variances into the variances among schedule means, and the variances within schedule means. We compute the ratio and compare it to the known distribution of F ratio for random samples. In other words, "we compute the ratio of an estimate associated with a suspected 'cause' to the estimate which best defines the error of the experiment. If the probability is small, say, less than 0.05, that this ratio could have occurred by chance in sampling from normal populations of identical means and variances, the hypothesis that such were the populations is rejected."

The following shows the computation of F for the comparison of exhaust schedules:

Source of variation	Sum of squares	Degrees of freedom	Mean square
Among schedules..	$\Sigma(\bar{X}_c - \bar{X})^2$	$K - 1$	$\sigma_1^2 = \dfrac{\Sigma(\bar{X}_c - \bar{X})^2}{K - 1}$
	873.7	3	291.2
Within schedules...	$\Sigma(X - \bar{X}_c)^2$	$n - K$	$\sigma_2^2 = \dfrac{\Sigma(X - \bar{X}_c)^2}{n - K}$
	9631.0	83	116.0
Total.....	$\Sigma(X - \bar{X})^2$	$n - 1$	
	10504.7	86	

where

$$\Sigma(\bar{X} - \bar{X})^2 = \Sigma\bar{X}_c^2 - \frac{(\Sigma X)^2}{n}$$

$$51080.55 - 50206.9 = 873.7$$

$$\Sigma(X - \bar{X}_c)^2 = \Sigma X^2 - \Sigma\bar{X}_c^2$$

$$60711.50 - 51080.55 = 9631.0$$

$$\Sigma(X - \bar{X})^2 = \Sigma X^2 - \frac{(\Sigma X)^2}{n}$$

$$60711.50 - 50206.9 = 10504.7$$

$$\text{where } \Sigma\bar{X}_c^2 = \frac{(\Sigma X_1)^2}{n_1} + \frac{(\Sigma X_2)^2}{n_2} + \frac{(\Sigma X_3)^2}{n_3} + \frac{(\Sigma X_4)^2}{n_4}$$

$$F = \frac{291.2}{116.0} = 2.501$$

The table of values of F for 3 and 83 deg of freedom produces the ratio of 2.72. Since the value of 2.501 is less than this, we must take it as an indication that the exhaust schedules all come from the same homogenous population and therefore they had no significant effect on the electrical characteristic.

The meaning of terms is as follows:

X = individual value of electrical characteristic
n = sample size
K = number of samples

Example 4 Showing Control Over Test Equipment by Means of Correlation Between Test Sets

One of the methods of maintaining adequate control over test equipment is to check factory sets with standard laboratory sets for all electrical characteristics. Although this does not strictly adhere to the full procedure of running complete special tests in order to make these correlations, the actual testing procedure is considered in the category of a special test.

The usual method is to take a small sample of tubes, test them on the one set, and then test them on the standard set (using the same operator). The results are then analyzed for statistical significance between averages by means of the t test for paired variates. The following is a good example of what can be done with statistical tests of significance in such correlations on a certain tube type:

Electrical characteristic	Factory average	Laboratory average	Difference	Statistical significance
A	183.9	177.6	6.3	Significant
B	4.44	4.35	0.09	Significant
C	4.70	4.62	0.08	Significant
D	0.255	0.268	0.013	Not significant
E	4.28	4.31	0.03	Significant
F	2.11	2.00	0.11	Significant
G	0.322	0.307	0.015	Not significant
H	0.311	0.317	0.006	Not significant
I	0.573	0.423	0.114	Significant
J	0.533	0.428	0.105	Significant
K	21.1	21.5	0.4	Significant

Although many of these differences show statistical significance, only three of them were "practically" significant. The factory sets were recalibrated until these differences were not significant.

The t test of significance is illustrated for the "A" characteristic as follows:

$$t = \frac{\bar{d}}{\sigma/\sqrt{n}}$$

where

$$\sigma^2 = \frac{\Sigma d^2 - \dfrac{(\Sigma d)^2}{n}}{n - 1}$$

where

$\bar{d}$ = difference between means
n = sample size
Σd^2 = sum of individual differences squared
$(\Sigma d)^2$ = square of sum of individual differences

$$t = \frac{6.3}{\sigma/\sqrt{21}} = 3.45$$

$$\sigma^2 = \frac{2237 - \dfrac{(133)^2}{21}}{20}$$

$$\sigma = 8.35$$

The Effect of Heat Loss on the Performance of Exchangers With Interconnected Walls

By P. R. TRUMPLER,[1] NEW YORK, N. Y.

Equations are derived for the calculation of exchangers in which the passage walls are bonded to each other, providing substantially uniform wall temperature over any cross section normal to the flow. Results are presented for both countercurrent and cocurrent exchangers and an example illustrating the solution is given.

Nomenclature

The following nomenclature is used in the paper:

- h_s = thermal conductance, based on surface A_s, between metal wall and the surroundings at temperature θ_s, Btu hr^{-1} ft^{-2} deg F^{-1}
- A_s = reference surface for h_s, sq ft per ft of exchanger length
- Q_s = heat flow from metal wall to surroundings, positive for heat flow to surroundings, Btu hr^{-1}
- W = fluid-flow rate, lb hr^{-1}
- c = specific heat at constant pressure, Btu lb^{-1} deg F^{-1}
- h = fluid film conductance, Btu hr^{-1} ft^{-2} deg F^{-1}
- A = surface washed by fluid, sq ft per ft of exchanger length
- θ_s = temperature of surroundings, deg F
- θ = temperature of warm fluid, deg F
- T = temperature of cold fluid, deg F
- η = temperature of metal wall, deg F
- z = length co-ordinate, parallel to fluid-flow directions, positive in direction of flow of cold fluid, ft
- L = exchanger length, ft

Subscripts T and θ refer to the fluids having those temperatures
Subscript 0 refers to value at $z = 0$
Subscript 1 refers to value at $z = L$

Introduction

Under certain conditions heat transfer between an exchanger and its surroundings can have an important effect upon the performance of the exchanger. Even a small heat leak may appreciably alter the temperature difference between the two fluids as calculated for adiabatic performance. Heat-loss effects are often appreciable where a small temperature difference between the fluids is required by the necessity for high thermal efficiency in the process, or where the exchanger operates at a temperature far from the ambient. Examples are found in plants for the separation of gases by deep refrigeration, and at the other end of the temperature scale, in the gas-turbine recuperator.

For the case of a double-pipe exchanger the effect of heat loss has been investigated by Nesselmann.[2] The recent development of extended-surface exchangers, particularly for deep-refrigeration processes, has brought practical importance to another case, namely, exchangers of the general type shown in Fig. 1. For purposes of the present analysis this type is characterized by passages bonded together in such a manner that the wall-temperature variation over any cross section normal to the flow is small compared to the temperature difference between the wall and the surroundings.

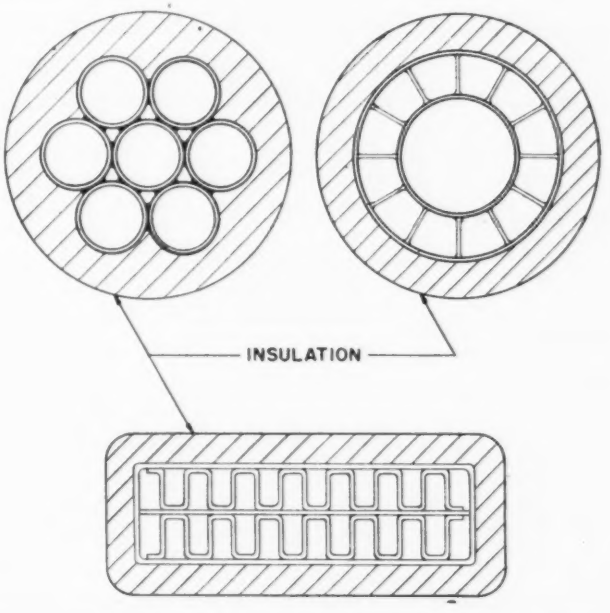


Fig. 1 Typical Heat Exchangers With Interconnected Walls

It will be seen that the results are applicable to exchangers in which the passages are not bonded together, provided the temperature difference between the various walls at a cross section is small. This is generally true of double-pipe or shell-and-tube exchangers in which either (1) the film coefficient of the shell fluid is very much higher than that of the tube fluid or (2) if the two fluids are exchanging heat at a small temperature difference.

Under what conditions should the effect of heat loss be investigated? The equations appear to yield no simple criterion. If, however, a rough estimate of the heat loss shows that the mean temperature difference based on terminal values is appreciably changed, a check for the effect of heat loss should be made.

The performance equations derived in the following section are limited only by the usual assumptions, which require that conductances and specific heats remain constant for the length of the exchanger, and that heat conduction in the metal or the insulation along the length of the exchanger is not important. The effect of heat conduction through fins, wall, bonding material, and fouling films may be taken into account by correcting the individual film coefficients.

Countercurrent Flow

The three basic equations are:

[1] Development Engineer, M. W. Kellogg Company. Jun. A.S.M.E.

[2] "The Influence of Heat Loss From Double-Tube Heat Exchangers," by K. Nesselmann, *Zeitschrift für die Gesamte Kälte-Industrie*, vol. 35, 1928, pp. 62–67.

Contributed by the Heat Transfer Division and presented at the Annual Meeting, New York, N. Y., Nov. 26–29, 1945, of The American Society of Mechanical Engineers.

Note: Statements and opinions advanced in papers are to be understood as individual expressions of their authors and not those of the Society.

$$W_\theta c_\theta d\theta = W_T c_T dT + h_s(\eta - \theta_s)A_s dz \quad [1]$$

$$W_T c_T dT = h_T A_T(\eta - T)dz \quad [2]$$

$$W_\theta c_\theta d\theta = h_\theta A_\theta(\theta - \eta)dz \quad [3]$$

Eliminating η from Equations [2] and [3]

$$\frac{W_T c_T dT}{h_T A_T dz} + \frac{W_\theta c_\theta d\theta}{h_\theta A_\theta dz} = \theta - T \quad [4]$$

Eliminating η and z by Equations [3] and [4], Equation [1] becomes

$$\frac{W_\theta c_\theta}{W_T c_T}\left[1 + \frac{h_s A_s}{h_\theta A_\theta}\left(1 - \frac{\theta - \theta_s}{\theta - T}\right)\right]d\theta = \left[1 + \frac{h_s A_s}{h_T A_T}\left(\frac{\theta - \theta_s}{\theta - T}\right)\right]dT \quad [5]$$

The variables may be separated if we make the transformation

$$x \equiv \frac{\theta - \theta_s}{\theta - T} \qquad y \equiv \theta - T \quad [6]$$

$$xy = \theta - \theta_s$$

$$xdy + ydx = d\theta \qquad dT = (x - 1)dy + ydx \quad [7]$$

Substituting also

$$D \equiv \frac{W_\theta c_\theta}{W_T c_T} \quad [8]$$

Equation [5] becomes

$$\frac{dy}{y} = \frac{1 - D - D\frac{h_s A_s}{h_\theta A_\theta} + \left(\frac{h_s A_s}{h_T A_T} + D\frac{h_s A_s}{h_\theta A_\theta}\right)x}{1 + \left(D + D\frac{h_s A_s}{h_\theta A_\theta} + \frac{h_s A_s}{h_T A_T} - 1\right)x - \left(\frac{h_s A_s}{h_T A_T} + D\frac{h_s A_s}{h_\theta A_\theta}\right)x^2}dx \quad [9]$$

Using Equation [9] to eliminate y from Equation [4] we determine x as a function of z

$$\int_{x_0}^{x} \frac{dx}{1 + (a + D - 1)x - ax^2} = \int_0^z \frac{dz}{K} \quad [10]$$

where

$$a \equiv \frac{W_\theta c_\theta}{W_T c_T}\frac{h_s A_s}{h_\theta A_\theta} + \frac{h_s A_s}{h_T A_T}$$

$$K \equiv W_\theta c_\theta\left[\frac{1}{h_\theta A_\theta} + \frac{1}{h_T A_T}\left(1 + \frac{h_s A_s}{h_\theta A_\theta}\right)\right] \quad [11]$$

Integration yields

$$x = \frac{1}{2\left(\frac{D}{h_\theta A_\theta} + \frac{1}{h_T A_T}\right)}\left\{\frac{1}{h_T A_T} + \frac{D}{h_\theta A_\theta} + \frac{1}{h_s A_s}\left(D - 1 + r\frac{R_0 e^{(r/k)z} + 1}{R_0 e^{(r/k)z} - 1}\right)\right\} \quad [12]$$

where

$$r \equiv \sqrt{(D - 1 + a)^2 + 4a}$$

$$R_0 \equiv \frac{-2ax_0 + (a + D - 1) - r}{-2ax_0 + (a + D - 1) + r} \quad [13]$$

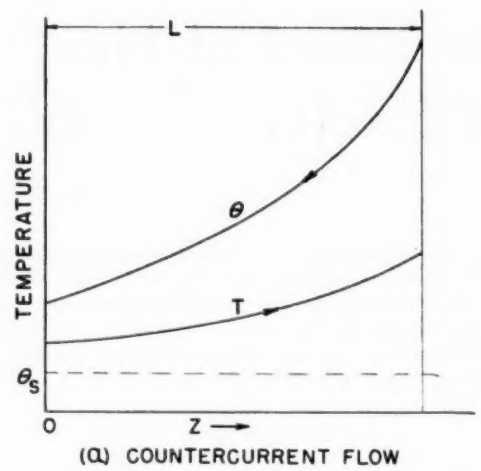


FIG. 2

Integrating Equation [9] and eliminating x by Equation [12] we obtain y as a function of z

$$\frac{y}{y_0} = me^{p_z} + ne^{q_z} \quad [14]$$

where

$$m \equiv \frac{1}{2r}\left\{r - D + 1 - h_s A_s(1 - 2x_0)\left(\frac{D}{h_\theta A_\theta} + \frac{1}{h_T A_T}\right)\right\}$$

$$n \equiv \frac{1}{2r}\left\{r + D - 1 + h_s A_s(1 - 2x_0)\left(\frac{D}{h_\theta A_\theta} + \frac{1}{h_T A_T}\right)\right\}$$

$$p \equiv \frac{U_\theta A_\theta}{2W_\theta c_\theta}\left\{r - D + 1 - h_s A_s\left(\frac{D}{h_\theta A_\theta} - \frac{1}{h_T A_T}\right)\right\}$$

$$q \equiv \frac{U_\theta A_\theta}{2W_\theta c_\theta}\left\{-r - D + 1 - h_s A_s\left(\frac{D}{h_\theta A_\theta} - \frac{1}{h_T A_T}\right)\right\}$$

$$\frac{1}{U_\theta A_\theta} \equiv \frac{1}{h_\theta A_\theta} + \frac{1}{h_T A_T}\left(1 + \frac{h_s A_s}{h_\theta A_\theta}\right)$$

$$r \equiv \sqrt{(D - 1 + a)^2 + 4a}$$

$$a \equiv h_s A_s\left(\frac{D}{h_\theta A_\theta} + \frac{1}{h_T A_T}\right)$$

$$D \equiv \frac{W_\theta c_\theta}{W_T c_T}$$

Equations [12] and [14] completely define the exchanger performance. Two special cases will be noted.

$$\underline{h_s A_s = 0}$$

Then

$$a = 0 \qquad r = D - 1 \qquad n = 1$$

$$m = 0 \qquad p = 0$$

$$q = \frac{U_\theta A_\theta}{W_\theta c_\theta}\left(1 - \frac{W_\theta c_\theta}{W_T c_T}\right)$$

and

$$y = y_0 exp\left[\frac{U_\theta A_\theta}{W_\theta c_\theta}\left(1 - \frac{W_\theta c_\theta}{W_T c_T}\right)z\right] \quad [15]$$

which is the equation of the adiabatic exchanger.

$h_s A_s \to \infty$ with other film coefficients finite

$$a \to \infty \qquad r \to \infty$$

$$\frac{r}{h_s A_s} = \frac{D}{h_\theta A_\theta} + \frac{1}{h_T A_T}$$

and Equation [14] becomes

$$y = (\theta_0 - \theta_s)exp\left(\frac{h_\theta A_\theta}{W_\theta c_\theta} z\right) - (T_0 - \theta_s)exp\left(-\frac{h_T A_T}{W_T c_T} z\right) \ldots [16]$$

Exchanger Length. The calculation of exchanger length is of prime importance to the heat-transfer engineer. The length may be determined by the following procedure:

From Equation [4]

$$\frac{W_T c_T}{h_T A_T}\int_0^1 dT + \frac{W_\theta c_\theta}{h_\theta A_\theta}\int_0^1 d\theta = \int_0^L (\theta - T)dz \ldots [17]$$

or

$$\frac{W_T c_T}{h_T A_T}(T_1 - T_0) + \frac{W_\theta c_\theta}{h_\theta A_\theta}(\theta_1 - \theta_0) = \int_0^L (\theta - T)dz \ldots [18]$$

Also

$$\int_0^L (\theta - T)dz = \int_0^L y dz = y_0 \frac{m}{p}(e^{pL} - 1) + y_0 \frac{n}{q}(e^{qL} - 1) \ldots [19]$$

Three of the terminal temperatures must be given in the statement of the problem. There are four possible combinations of the three temperatures, and the solution for each case will be given.

Case 1. Given θ_0, θ_1, and T_0:

From Equation [14]

$$\theta_1 - T_1 = y_0 m e^{pL} + y_0 n e^{qL} \ldots [20]$$

Substituting Equations [19] and [20] into Equation [18]

$$\frac{W_T c_T}{h_T A_T}\left(\frac{\theta_1 - T_0}{\theta_0 - T_0}\right) + \frac{W_\theta c_\theta}{h_\theta A_\theta}\left(\frac{\theta_1 - \theta_0}{\theta_0 - T_0}\right) + \frac{m}{p} + \frac{n}{q} = m\left(\frac{1}{p} + \frac{W_T c_T}{h_T A_T}\right)e^{pL} + n\left(\frac{1}{q} + \frac{W_T c_T}{h_T A_T}\right)e^{qL} \ldots [21]$$

Equation [21] fixes the value of L.

Case 2. Given θ_0, T_1, and T_0:

Substituting θ_1 from Equation [20], the solution is

$$\frac{W_T c_T}{h_T A_T}\left(\frac{T_1 - T_0}{\theta_0 - T_0}\right) + \frac{W_\theta c_\theta}{h_\theta A_\theta}\left(\frac{T_1 - \theta_0}{\theta_0 - T_0}\right) + \frac{m}{p} + \frac{n}{q} = m\left(\frac{1}{p} - \frac{W_\theta c_\theta}{h_\theta A_\theta}\right)e^{pL} + n\left(\frac{1}{q} - \frac{W_\theta c_\theta}{h_\theta A_\theta}\right)e^{qL} \ldots [22]$$

Case 3. Given θ_0, θ_1, and T_1:

The solution may be readily obtained by changing the direction of the z-axis and interchanging subscripts 0 and 1 of the terminal temperatures. Note that this requires changing x_0 to x_1 in the equations defining m and n. The solution is

$$\frac{W_T c_T}{h_T A_T}\left(\frac{\theta_0 - T_1}{\theta_1 - T_1}\right) + \frac{W_\theta c_\theta}{h_\theta A_\theta}\left(\frac{\theta_0 - \theta_1}{\theta_1 - T_1}\right) + \frac{m}{p} + \frac{n}{q} = m\left(+\frac{1}{p} + \frac{W_T c_T}{h_T A_T}\right)e^{-pL} + n\left(+\frac{1}{q} + \frac{W_T c_T}{h_T A_T}\right)e^{-qL} \ldots [23]$$

Case 4. Given θ_1, T_1, and T_0:

The solution is found as in Case 3

$$\frac{W_T c_T}{h_T A_T}\left(\frac{T_0 - T_1}{\theta_1 - T_1}\right) + \frac{W_\theta c_\theta}{h_\theta A_\theta}\left(\frac{T_0 - \theta_1}{\theta_1 - T_1}\right) + \frac{m}{p} + \frac{n}{q} = m\left(+\frac{1}{p} - \frac{W_\theta c_\theta}{h_\theta A_\theta}\right)e^{-pL} + n\left(+\frac{1}{q} - \frac{W_\theta c_\theta}{h_\theta A_\theta}\right)e^{-qL} \ldots [24]$$

Calculation of Heat Loss:

Case 1. Given θ_0, θ_1, and T_0, or θ_0, T_1, and T_0:

T_1 or θ_1 may be calculated from y_1 where

$$y_1 = y_0 m e^{pL} + y_0 n e^{qL}$$

Knowing the terminal temperatures, the heat loss may be calculated

Case 2. Given θ_0, T_1, θ_1, or T_0, T_1, θ_1

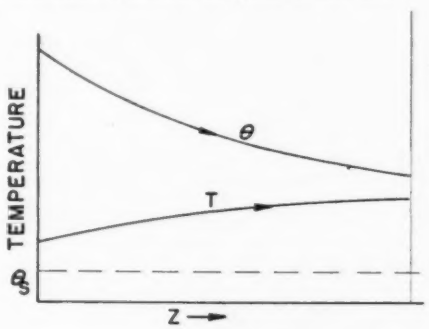
T_0 or θ_0 may be calculated from

$$\frac{\theta_0 - T_0}{\theta_1 - T_1} = m e^{-pL} + n e^{-qL} \ldots [25]$$

Note that x_0 must be changed to x_1 in the equations defining m and n.

Parallel Flow

The three basic equations for parallel flow are



(b) PARALLEL FLOW

Fig. 3

$$-W_\theta c_\theta d\theta = W_T c_T dT + h_s(\eta - \theta_s)A_s dz \ldots [26]$$

$$W_T c_T dT = h_T A_T(\eta - T)dz \ldots [27]$$

$$-W_\theta c_\theta d\theta = h_\theta A_\theta(\theta - \eta)dz \ldots [28]$$

By a treatment similar to that for countercurrent flow the solution is found to be

$$x = \frac{1}{2\left(\frac{1}{h_T A_T} - \frac{D}{h_\theta A_\theta}\right)}\left\{\frac{1}{h_T A_T} - \frac{D}{h_\theta A_\theta} - \frac{1}{h_s A_s}\left(D + 1 + r_c \frac{R_{c0}e^{(r_c/k)z} + 1}{R_{c0}e^{(r_c/k)z} - 1}\right)\right\} \ldots [29]$$

where

$$r_c \equiv \sqrt{(D + 1 - a_c)^2 + 4a_c}$$

$$R_{c0} = \frac{2a_c x_0 + (D + 1 - a_c) - r_c}{2a_c x_0 + (D + 1 - a_c) + r_c}$$

$$a_c \equiv h_s A_s\left(\frac{1}{h_T A_T} - \frac{D}{h_\theta A_\theta}\right)$$

and

$$\frac{y}{y_0} = m_c e^{p_c z} + n_c e^{q_c z} \quad \ldots\ldots\ldots\ldots\ldots [30]$$

where

$$m_c \equiv \frac{1}{2r_c}\left\{r_c - D - 1 - h_s A_s(1-2x_0)\left(\frac{D}{h_\theta A_\theta} - \frac{1}{h_T A_T}\right)\right\}$$

$$n_c \equiv \frac{1}{2r_c}\left\{r_c + D + 1 + h_s A_s(1-2x_0)\left(\frac{D}{h_\theta A_\theta} - \frac{1}{h_T A_T}\right)\right\}$$

$$p_c \equiv \frac{U_\theta A_\theta}{2W_{\theta c_\theta}}\left\{r_c - D - 1 - h_s A_s\left(\frac{D}{h_\theta A_\theta} + \frac{1}{h_T A_T}\right)\right\}$$

$$q_c \equiv \frac{U_\theta A_\theta}{2W_{\theta c_\theta}}\left\{-r_c - D - 1 - h_s A_s\left(\frac{D}{h_\theta A_\theta} + \frac{1}{h_T A_T}\right)\right\}$$

If $h_s A_s = 0$

$$y = y_0 \exp\left[-\frac{U_\theta A_\theta}{W_{\theta c_\theta}}\left(1 + \frac{W_{\theta c_\theta}}{W_T c_T}\right) z\right] \quad \ldots\ldots [31]$$

If $h_s A_s \to \infty$

$$y = (\theta_0 - \theta_s)\exp\left(-\frac{h_\theta A_\theta}{W_{\theta c_\theta}} z\right) - (T_0 - \theta_s)\exp\left(-\frac{h_T A_T}{W_T c_T} z\right) [32]$$

Exchanger Length. The equation corresponding to Equation [18] is

$$\frac{W_T c_T}{h_T A_T}(T_1 - T_0) - \frac{W_{\theta c_\theta}}{h_\theta A_\theta}(\theta_1 - \theta_0) = \int_0^L (\theta - T)dz \quad [33]$$

$$\int_0^L (\theta - T)dz = \int_0^L y dz = y_0 \frac{m_c}{p_c}(e^{p_c L} - 1) + y_0 \frac{n_c}{q_c}(e^{q_c L} - 1) \quad \ldots\ldots [34]$$

Case 1. Given θ_0, θ_1, T_0:

$$\frac{W_T c_T}{h_T A_T}\left(\frac{\theta_1 - T_0}{\theta_0 - T_0}\right) - \frac{W_{\theta c_\theta}}{h_\theta A_\theta}\left(\frac{\theta_1 - \theta_0}{\theta_0 - T_0}\right) + \frac{m_c}{p_c} + \frac{n_c}{q_c} = m_c\left(\frac{1}{p_c} + \frac{W_T c_T}{h_T A_T}\right)e^{p_c L} + n_c\left(\frac{1}{q_c} + \frac{W_T c_T}{h_T A_T}\right)e^{q_c L} \quad \ldots\ldots [35]$$

Case 2. Given θ_0, T_1, T_0:

$$\frac{W_T c_T}{h_T A_T}\left(\frac{T_1 - T_0}{\theta_0 - T_0}\right) - \frac{W_{\theta c_\theta}}{h_\theta A_\theta}\left(\frac{T_1 - \theta_0}{\theta_0 - T_0}\right) + \frac{m_c}{p_c} + \frac{n_c}{q_c} = m_c\left(\frac{1}{p_c} + \frac{W_{\theta c_\theta}}{h_\theta A_\theta}\right)e^{p_c L} + n_c\left(\frac{1}{q_c} + \frac{W_{\theta c_\theta}}{h_\theta A_\theta}\right)e^{q_c L} \quad \ldots\ldots [36]$$

Case 3. Given θ_0, θ_1, T_1:

$$\frac{W_T c_T}{h_T A_T}\left(\frac{\theta_0 - T_1}{\theta_1 - T_1}\right) - \frac{W_{\theta c_\theta}}{h_\theta A_\theta}\left(\frac{\theta_0 - \theta_1}{\theta_1 - T_1}\right) + \frac{m_c}{p_c} + \frac{n_c}{q_c} = m_c\left(+\frac{1}{p_c} + \frac{W_T c_T}{h_T A_T}\right)e^{-p_c L} + n_c\left(+\frac{1}{q_c} + \frac{W_T c_T}{h_T A_T}\right)e^{-q_c L} \quad [37]$$

Note that x_0 becomes x_1 in m_c and n_c.

Case 4. Given θ_1, T_1, T_0:

$$\frac{W_T c_T}{h_T A_T}\left(\frac{T_0 - T_1}{\theta_1 - T_1}\right) - \frac{W_{\theta c_\theta}}{h_\theta A_\theta}\left(\frac{T_0 - \theta_1}{\theta_1 - T_1}\right) + \frac{m_c}{p_c} + \frac{n_c}{q_c} = m_c\left(+\frac{1}{p_c} + \frac{W_{\theta c_\theta}}{h_\theta A_\theta}\right)e^{-p_c L} + n_c\left(+\frac{1}{q_c} + \frac{W_{\theta c_\theta}}{h_\theta A_\theta}\right)e^{-q_c L} \quad [38]$$

Note that x_0 becomes x_1 in m_c and n_c.

Example

An exchanger of the type shown in Fig. 1 is employed to exchange heat between two air streams. Stream θ with a flow of 10,000 lb per hr is to be cooled from 1000 F to 350 F by 9500-lb per hr air entering at 300 F. Each air stream has a surface of 50 sq ft per ft of exchanger length and a corrected film coefficient of 20. The exchanger is lightly insulated, and the outside conductance, based upon a surface of 5 sq ft per ft of exchanger length, may be considered uniform at 1 Btu per hr per sq ft per deg F. Consider the specific heat of the air for each stream as constant and equal to 0.25 Btu per lb. Surroundings are at 100 F. Calculate the outlet temperature of the cold stream and the required exchanger length.

Solution. (Countercurrent exchanger)

$$D = \frac{10{,}000}{9500} = 1.053$$

$$h_s A_s = 5 \qquad x_0 = \frac{\theta_0 - \theta_s}{\theta_0 - T_0} = \frac{350 - 100}{350 - 300} = 5$$

$$h_\theta A_\theta = 1000$$

$$h_T A_T = 1000$$

$$a = 5\left(\frac{1.053}{1000} + \frac{1}{1000}\right) = 0.010265$$

$$r = \sqrt{(0.053 + 0.010265)^2 + 0.04106} = 0.212$$

$$m = \frac{1}{0.424}\left\{0.212 - 0.053 - 5(1-10)(0.002053)\right\} = 0.593$$

$$n = \frac{1}{0.424}\left\{0.212 + 0.053 + 5(1-10)(0.002053)\right\} = 0.407$$

$$U_\theta A_\theta = \frac{1}{\frac{1}{1000} + \frac{1}{1000}\left(1 + \frac{5}{1000}\right)} = 498$$

$$p = \frac{498}{2 \times 10{,}000 \times 0.25}\left\{0.212 - 0.053 - 5\left(\frac{1.053}{1000} - \frac{1}{1000}\right)\right\} = 0.01583$$

$$q = \frac{498}{20{,}000 \times 0.25}\left\{-0.212 - 0.053 - 5\left(\frac{1.053}{1000} - \frac{1}{1000}\right)\right\} = -0.0264$$

$\theta_0 = 350$ $\quad \theta_1 = 1000$ $\quad T_0 = 300$

$$\frac{\theta_1 - T_0}{\theta_0 - T_0} = \frac{1000 - 300}{350 - 300} = 14 \qquad \frac{\theta_1 - \theta_0}{\theta_0 - T_0} = \frac{1000 - 350}{350 - 300} = 13$$

Using Equation [21]

$$\left(\frac{9500 \times 0.25}{1000} \times 14\right) + \left(\frac{10{,}000 \times 0.25}{1000} \times 13\right) + \frac{0.593}{0.01583} + \frac{0.407}{-0.0264} = 0.593\left(\frac{1}{0.01583} + \frac{9500 \times 0.25}{1000}\right)\exp(0.01583L) + 0.407\left(-\frac{1}{0.0264} + \frac{9500 \times 0.25}{1000}\right)\exp(-0.0264L)$$

Simplifying

$$2.26 = \exp(0.01583L) - 0.372\exp(-0.0264L)$$

By trial and error

$$\underline{L = 54 \text{ ft}}$$

Cold Gas Outlet:

$$\frac{y_1}{y_0} = 0.593\ exp(0.01583 \times 54) + 0.407\ exp(-0.0264 \times 54)$$

$$= 1.491$$

$$\frac{1000 - T_1}{350 - 300} = 1.491$$

$$\underline{T_1 = 925 \text{ F}}$$

For Adiabatic Exchanger:

$$10{,}000 \times 650 = 9500(T_1 - 300)$$

$$\underline{T_1 = 984 \text{ F}}$$

Mean temperature difference = L.M. of 50 and 16 = 30 deg F

$U = 10$

$$\text{Exchanger length} = \frac{2500 \times 650}{30 \times 10 \times 50} = 108 \text{ ft}$$

TABLE 1 COMPARISON OF EXACT AND ADIABATIC VALUES

	Exact	Adiabatic
Outlet temperature, cold gas, deg F	925	984
Temperature difference, hot end, deg F	75	16
Exchanger length required, ft	54	108

ACKNOWLEDGMENT

The writer wishes to express his appreciation to the M. W. Kellogg Company for permission to publish this paper.

Discussion

R. S. LEIGH.[1] In reviewing this paper, mathematics and discussion of the author's derivation are to be omitted, since the writer agrees with this method as being one of several equally accurate methods available for use, although a much simpler method will now be given.

For the better understanding of the problem two sets of curves have been drawn, Figs. 4 and 5 of this discussion, based on varying lengths and varying degrees of insulation, with all other factors as in the paper. Case 1 is set up as a completely insulated exchanger where the loss through the insulation is taken as zero. Case 2 is a moderately insulated exchanger with the over-all coefficient from either the gas side or the air side to the outside equal to 0.214 Btu hr^{-1} ft^{-2} deg F^{-1}. This corresponds to 2 in. of 85 per cent magnesia. Case 3 is the lightly insulated exchanger as used in the example by the author, where the over-all coefficient equals 0.952 Btu hr^{-1} ft^{-2} deg $F.^{-1}$

After calculating the exchanger, taking lengths of 27, 54, 81, and 108 ft, we find that the losses through the insulation and out the stack result in the curves shown in Fig. 3. In any heat-transfer apparatus or part of a heat cycle, the item of interest is the over-all efficiency. In this case, it may be seen that for a lightly insulated (case 3) exchanger, there is a maximum efficiency at about 65 ft of length. To equal the efficiency of a 54-ft-long (case 3) exchanger, the moderately insulated exchanger (case 2) would be only 37 ft long and the (case 1) perfectly insulated exchanger would be 35 ft long. Naturally, the lightly insulated exchanger would have the lower gas temperature leaving, but this would be due to losses, not to greater efficiency.

Fig. 5 illustrates the various gas and air temperatures obtainable with varying amounts of insulation and varying exchanger lengths. Of interest is the fact that the log-mean-temperature difference is fixed for any length, regardless of the amount of insulation. The quantity of heat actually transferred from the gas to the air divided by the over-all coefficient, 10 Btu hr^{-1} ft^{-2}

[1] Project Engineer, Development Department, Chase Brass & Copper Company, Waterbury, Conn.

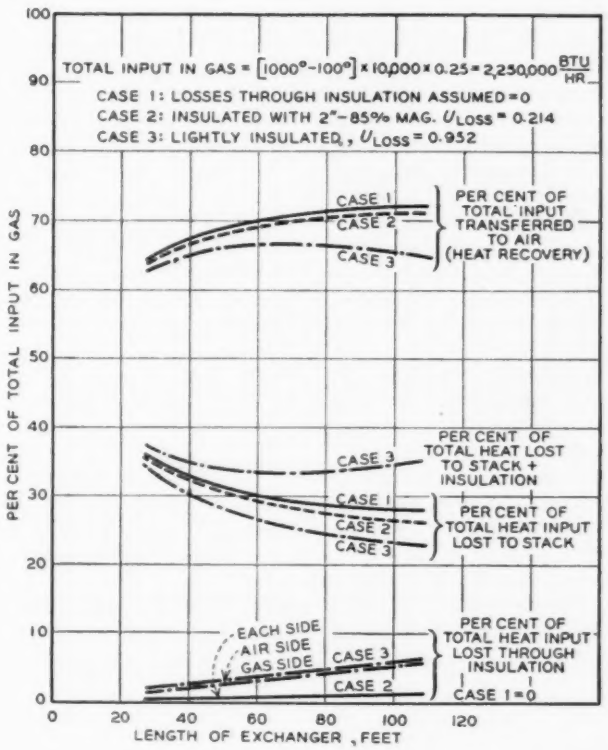


FIG. 4 HEAT BALANCE

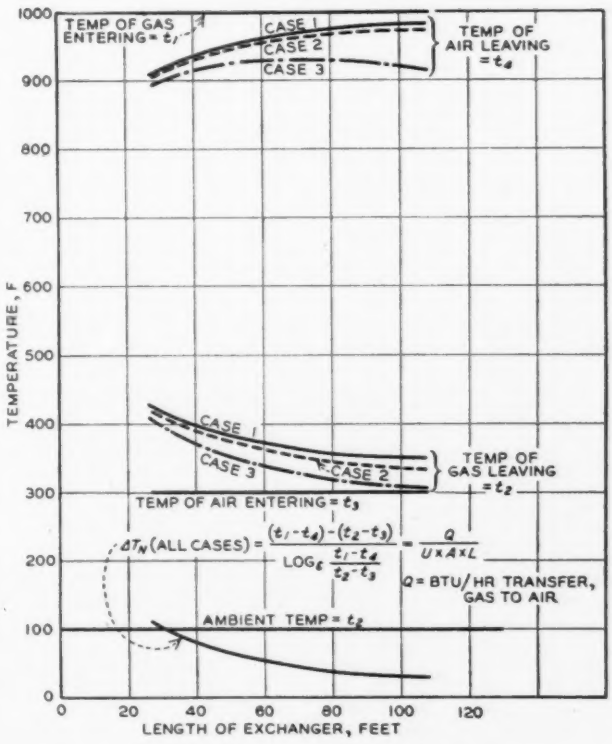


FIG. 5 GAS AND AIR TEMPERATURES

deg F^{-1} times the area per foot of length times the length in feet equals the log-mean-temperature difference and is also constant for any given length. A solution based on this should give a simpler derivation than that in the paper. The amount of heat removed from the gas is simply this given amount plus the losses on the gas side. The amount of heat leaving the exchanger in the air is equal to this given amount minus the losses on the air side.

The solution in which the insulation is neglected (case 1) is simple to calculate. From this calculation the number of Btu per hour actually transferred may be determined, as well as the log-mean-temperature difference for any given length. To this quantity of heat add the gas-side losses and divide by pounds of gas per hour times the specific heat, to obtain the gas temperature drop. Then subtract the air-side losses from the given quantity of heat transferred and divide by pounds of air per hour times the specific heat, to obtain the air temperature rise.

Of interest is the slight difference between a moderately insulated (2 in. of 85 per cent magnesia) exchanger, case 2, and a completely insulated exchanger, case 1, indicating that the results obtained in the paper were exceptional only because the losses were allowed to be excessive.

The effect of the friction should be included in any problem such as this, since the friction on either the gas or air side tends to increase the leaving temperature slightly. This gain would tend to offset the loss through the insulation.

The use of standard symbols and nomenclature should be encouraged and every effort bent to this end.

Author's Closure

The author is not aware of any other methods to solve the heat-loss problem, other than a tedious step-by-step integration. Unfortunately, no references are given in the discussion. The author cannot agree with Mr. Leigh that his method offers a solution to the problem. It should be obvious that the logarithmic mean cannot be used as the mean temperature difference in a nonadiabatic exchanger.

Contrary to Mr. Leigh's statement, the effect of frictional work on a fluid in a heat exchanger usually has negligible significance on the fluid temperature. This is true because the change in temperature with change in pressure, under adiabatic conditions (Joule-Thomson coefficient), is very small except for a gas near the critical region. For a perfect gas the Joule-Thomson coefficient is zero. If one wishes to take the effect into account the result is almost always a cooling, not a heating, of the fluid.

The author regrets that, through ignorance, standard symbols were not used in the paper.

Temperature Uniformity in Heating-Up Processes

By M. P. HEISLER,[1] NEW YORK, N. Y.

The treatment of temperature-uniformity problems by the method first introduced by Paschkis is extended and enlarged. It is shown that uniformity calculations can be reduced to the solution of a simple trigonometric relation which can be readily solved and analyzed. Standard Gurney-Lurie charts for cylinders and spheres are given in a more complete form than is available at present. A chart is included for determining temperature history in plates subjected to two-dimensional heat flow. Finite cylinders are discussed and three-dimensional heat-flow problems are briefly considered.

Introduction

A temperature-uniformity problem results when a body is to be heated to a given surface and a given center temperature. Such a problem cannot be directly solved by means of the standard heating charts because the furnace temperature and the heating time required to produce the specified uniformity are not known. The possibility of applying the simple heating and cooling charts of Groeber, Hottel, Schack, Newman, and others to temperature-uniformity calculations was first recognized by Paschkis.[2] He prepared a set of curves from the Groeber charts and thereby introduced a fundamentally new parameter, which he called the "temperature-uniformity factor." This temperature-uniformity factor, which he defined as (surface temperature — center temperature)/(surface temperature — temperature of surroundings), was obtained by eliminating the furnace temperature from the standard dimensionless temperature ratio Y, used in all of the charts mentioned. By eliminating the furnace temperature Paschkis was able to derive a new set of curves from which, given only the final surface and center temperatures to which the workpiece was to be heated, the unknown furnace temperature and heating time could be found, provided that the following conditions prevailed:

1 Workpiece was of a simple shape; plate, cylinder, or sphere.

2 A suddenly impressed and thereafter constant furnace temperature was used.

3 Workpiece had constant thermal properties, i.e., properties were temperature-invariant.

4 There was constant boundary resistance throughout the heat period.

5 Uniform surface temperatures existed, e.g., on opposite sides of a slab or plate.

Unfortunately, these conditions are never met in practice, although in particular cases they may be approached. In general, the use of constant average thermal properties in place of the true temperature-varying properties results in relatively slight error. The assumption of simple shape introduces an error proportional to the degree to which the actual shape approximates the assumed one, but it is difficult to measure the exact degree of approximation. The influence of boundary resistance is even more difficult to gage, because boundary resistance is, among other things, a function of the temperature difference existing between furnace and surface of stock and therefore is subject to wide variations during the heating cycle.

In fuel-fired furnaces, constant furnace temperatures are virtually nonexistent. If the charge and furnace are heated-up together, the cold walls and charge will lower the initial furnace temperature. Even after the walls and charge are heated up there will still be temperature fluctuations caused by the temperature control. It may be argued that these latter temperature fluctuations are never very large, yet if they are compared with the temperature differences encountered in the stock at the end of the heating period it will be seen that they may have considerable influence on the temperature uniformity. Similar arguments can be made for cases where the cold charge is suddenly introduced into the hot furnace.

Finally, uniform surface temperatures seldom prevail, whether the charge be heated from one or from all sides. Skids, hearth, contact with neighboring stock, corners, edges—all tend to produce unequal temperature distributions on the surface. Nevertheless, for the sake of obtaining some numerical values average conditions are generally assumed. Very often, even though only approximate, analytical methods yield valuable results.

Of these factors the relative boundary resistance m is of particular importance because the accuracy of the analytical solution depends largely upon how accurately m is known. It has become standard practice to use an average surface heat-transfer coefficient in calculating the relative boundary resistance, the proper choice of the average value leaning heavily upon practical experience. In many instances the engineer has little to use as a guide and the boundary resistance used in his calculations may then largely be the result of concentrated wishful thinking.

In general, surface heat transfer occurs mainly by radiation from some constant furnace temperature to a lower varying surface temperature. It is suggested here, as an initial step in placing the determination of a suitable average boundary resistance on a rational basis, that an average surface temperature be used in calculating the surface heat-transfer coefficient. For example, consider a slab, initially at 70 F, heated in a 2000 F furnace. If it can be assumed that heat transfer takes place largely by radiation, then the conditions illustrated in Table 1 exist. In the table, column 1 shows various surface temperatures of the slab; column 2 shows h values for black-body radiation from 2000 F to the given surface temperature; column 3 shows h

TABLE 1 HEATING-UP DATA FOR SLAB IN 2000 F FURNACE

Surface temperature, deg F	h Btu/(sq ft)(hr)(deg F)	$h/102$	Temperature (deg F)/2000
0	31.2	0.306	0
200	35.0	0.344	0.1
400	38.8	0.390	0.2
600	43.3	0.425	0.3
800	49.0	0.481	0.4
1000	54.8	0.537	0.5
1200	62.0	0.608	0.6
1400	70.0	0.686	0.7
1600	80.0	0.785	0.8
1800	90.0	0.883	0.9
2000	102.0	1.0	1.0

[1] Heat Transfer Research Laboratory, Columbia University.

[2] "Electrische Industrieofen für Weiterverarbeitung," by V. Paschkis, Julius Springer, Berlin, Germany, 1932.

Contributed by the Heat Transfer Division and presented at the Annual Meeting, New York, N. Y., November 26–29, 1945, of The American Society of Mechanical Engineers.

Note: Statements and opinions advanced in papers are to be understood as individual expressions of their authors and not those of the Society.

expressed as a fraction of its value at 2000 F; and column 4 the surface temperature expressed as a fraction of the final value of 2000 F. It can be seen that h is directly proportional to the surface temperature over a large part of the temperature scale, the proportionality becoming better as the temperature increases. This latter fact is particularly important because the surface will be at high temperatures for a considerably longer time than it will be at low temperatures. It is evident, then, that a time average of the surface temperature will be nearly proportional to a time average of the boundary resistance m. A relatively simple method for determining the time-average surface temperature will be given later.

In most instances the workpiece is heated to a center temperature that will be as near to the final surface temperature as an economical heating time will permit. In problems of this type two m values must be used. One based upon the time-average surface temperature, to find the heating time; and the other based upon final surface temperature, to find the temperature at the center. To make this clear consider two identical slabs, one at the temperature of the surroundings, the other at a uniform temperature of 1000 F. The slabs are put into a 2200 F furnace at the same instant and are kept there until the surfaces reach a temperature of 2180 F. It is evident that when the surfaces of the slabs reach 2180 F (at different times, of course) their respective center temperatures will, for all practical purposes, be very nearly identical. However, if the center temperatures are calculated in the customary manner from heating and cooling charts, they will not appear to be the same because the average boundary conductances will be based in one case upon initial radiation from 2200 to 1000 F, and in the other case on initial radiation from 2200 F to the temperature of the surroundings. What actually happens is the following:

As the final surface temperature is approached there is little change in the boundary resistance because of little change in surface temperature. As a result, the center temperature which originally lagged considerably behind the fast-changing surface temperature, has time to catch up to the now slowly changing surface temperature and assumes values determined, not by the time-average surface temperature, but by the actual surface temperature at the end of the heating cycle. It is evident then that in any heating to a high degree of uniformity the center temperature should be determined from the boundary conductance at the end of the heating cycle. This can then be adjusted to take care of the slight lag which will still exist between center temperature and surface conductance.

A temperature-uniformity problem therefore resolves itself into determining average and end boundary conditions. The first will yield the heating time, the second the furnace temperature. The determination of the latter is the simpler and will be considered first.

Nomenclature

m = relative boundary resistance, (conductivity)/(surface heat-transfer coefficient) (half thickness)
m_x = relative boundary resistance for two-dimensional heat flow, based upon half thickness in direction of x-axis
m_y = relative boundary resistance for two-dimensional heat flow, based upon half thickness in direction of y-axis
t' = furnace temperature or temperature of hot ambient
t = surface temperature
t° = center temperature
t_b = uniform base temperature of solid
t_a = time-average surface temperature
t_x = temperature in solid at distance x from center
t^* = edge temperature of long rectangular rod
X = dimensionless time (diffusivity)(time)/(half thickness squared)
X_0 = value of dimensionless time when surface has reached final temperature
X_x = dimensionless time for two-dimensional heat flow, based upon half thickness along x-axis
Y_x = dimensionless temperature ratio at distance x from center of solid (furnace temperature—temperature at point x)/(furnace temperature — base temperature)
Y = dimensionless temperature ratio at surface of solid (furnace temperature—temperature of surface)/(furnace temperature—base temperature)
Y° = dimensionless temperature ratio at center of solid, (furnace temperature—center temperature)/(furnace temperature—base temperature)
Y_a = dimensionless temperature ratio for finding average surface temperature (furnace temperature—average surface temperature)/(furnace temperature—base temperature)

One-Dimensional Heat Flow

It was pointed out that in furnace calculations it is customary to make use of dimensionless parameters, m, X, and Y. Many charts by Newman, Hottel, Bachmann, Gurney-Lurie, etc., have been plotted which give the temperature history of simple shapes like semi-infinite plates, infinite cylinders, and spheres. All of these charts, with the exception of Bachmann's, are plotted as functions of m, X, and Y.

Some modifications must be made in these standard charts before they can be used for temperature-uniformity calculations, because neither the furnace temperature nor the heating time is known. However, once the surface and center temperatures of the workpiece are specified and the relative boundary-resistance factor m is determined, the furnace temperature and the heating time are fixed. To see that this is true consider the following equation, which applies to the heating-up of semi-infinite plates

$$Y_x = \frac{t' - t_x}{t' - t_b} = \sum_{k=1}^{\infty} \frac{2(\sin w_k)(\cos w_k x) \exp(-w_k^2 X)}{w_k + (\sin w_k)(\cos w_k)} \quad [1]$$

where w_k is defined by the characteristic number equation $mw = \cot w$, and

t_x is temperature, varying with distance x and dimensionless time X
t' is temperature of hot ambient—furnace temperature
Y_x is relative temperature at position x and time X
t_b is initial temperature of slab

Now, it is a fact that in the expansion all terms after the first can be neglected for X in the neighborhood of 0.2, since for values of X larger than 0.2, these terms rapidly vanish. To illustrate the extreme rapidity of convergence, consider the first two roots of $mw = \cot w$ when m is equal to 1. The first root is $w = \cot w = 0.8603$; the second root is $w = \cot(w + \pi) = 3.4256$. Suppose X is equal to 1. Then, for the first root $\exp(-w^2X)$ becomes 0.477, and for the second root 0.0000076. Thus if only the exponential factor is considered, it is obvious that the second term in the expansion becomes insignificant; the trigonometric factor serves to reduce the numerical value even more. Since the values of X encountered in temperature-uniformity calculations are generally very much greater than 0.2, Equation [1] can be reduced to

$$Y_x = \frac{2(\sin w)(\cos wx) \exp(-w^2X)}{w + (\sin w)(\cos w)} \quad [2]$$

where the first root of $mw = \cot w$ determines w. In the derivation of Equation [1] it was assumed that the origin was at the mid-plane of the slab. Therefore at the surface $x = 1$ and at the center $x = 0$, and

$$\text{(surface)}\quad Y = \frac{t' - t}{t' - t_b} = \frac{2(\sin w)(\cos w)\exp(-w^2X)}{w + (\sin w)(\cos w)} \quad \ldots\ldots [3]$$

$$\text{(center)}\quad Y^\circ = \frac{t' - t^\circ}{t' - t_b} = \frac{2(\sin w)\exp(-w^2X)}{w + (\sin w)(\cos w)} \quad \ldots\ldots [4]$$

where t is the surface temperature and t° the center temperature of the slab. Dividing Y by Y° gives

$$Y/Y^\circ = \cos w = (t' - t)/(t' - t^\circ) \quad \ldots\ldots [5]$$

Equation [5] is plotted in Fig. 1 as a function of m; and since m, t, and t° are known, the unknown furnace temperature t' can be found. To find t', enter Fig. 1 with the known m as abscissa, go vertically to the curve for the plate and thence horizontally and read the ordinate. The ratio $(t' - t)/(t' - t^\circ)$ will hereafter be called the relative-temperature-uniformity ratio, since it is a measure of the relative temperature uniformity existing between stock and furnace at the end of the heat period.

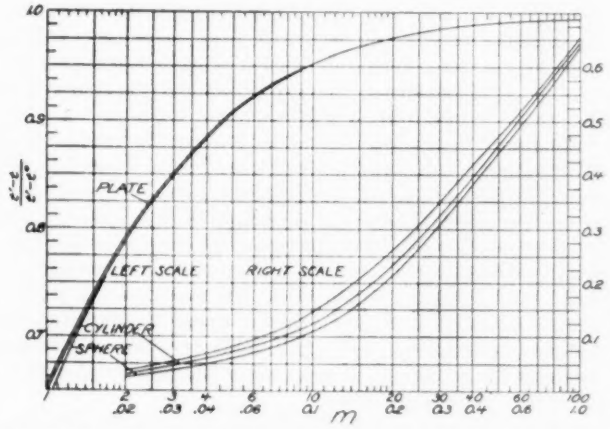


FIG. 1 CHART FOR DETERMINING RELATIVE TEMPERATURE-UNIFORMITY RATIO

Equation [5] shows that the furnace temperature is a function only of the relative boundary-resistance factor m and the given surface and center temperatures. If it were possible to have an infinite heat-transmission coefficient h, m would become zero, cos w would also become zero, and the surface temperature would equal the furnace temperature. For any given surface and center temperatures m is a direct measure of the required furnace temperature. If m is large, which, other things being equal, is tantamount to having poor surface heat transmission, cos w approaches 1. This means that a high furnace temperature is necessary to produce the desired uniformity. Conversely, if m is small the furnace temperature approaches the surface temperature as a minimum. The equation clearly shows that lower furnace temperature and better temperature uniformity within a given time are obtained by increasing surface heat transmission from flame to stock.

By comparison with the Gurney-Lurie-type charts it can be seen that small m's also imply low heating times. The relation of furnace temperature and heating time to boundary resistance is shown in Fig. 2. The curves were obtained from Fig. 1 and illustrate how heating times and furnace temperatures increase with boundary resistance. The curves shown hold for a slab

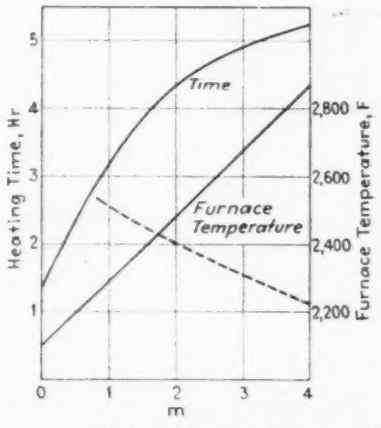


FIG. 2 VARIATION OF HEATING TIME AND FURNACE TEMPERATURE WITH RELATIVE BOUNDARY RESISTANCE

heated to a surface temperature of 2100 F and a center temperature of 2000 F. The dimensions and thermal properties of the slab are not given because the curves are intended to show trends only. For the sake of illustration no distinction was made between average and end boundary conditions.

In the introduction it was pointed out that the relative boundary resistance m is a function of the furnace temperature. Since the furnace temperature is not known, the relative boundary resistance cannot be directly determined, and inversely, since the boundary resistance is not known the furnace temperature and heating time cannot be calculated. One of the necessary calculations in furnace design is a plot showing the relation of the surface heat-transmission coefficient to furnace temperature. This chart must be calculated from the various flame characteristics, such as thickness of flame, composition of the hot gases, amount of dissociation, luminosity of the flame, emissivity and temperature of the surface, and the like. From this chart the surface heat-transmission coefficient can readily be converted into the relative boundary resistance m. Since the furnace temperature increases with increasing h, it will decrease with decreasing m. Suppose that the broken line in Fig. 2 is this calculated temperature versus end m relation for the given flame properties. Then the intersection of the broken temperature line with the solid temperature line (determined from Fig. 1) gives the value of m and the furnace temperature that will, approximately, produce the desired temperature uniformity.

The heating time is determined from the same heat-transmission curve from which the furnace temperature was determined, but in this case an average m is used. To illustrate, suppose such a heat-transmission chart is available and that the time-average surface temperature over the heat period is known. With this average surface temperature the average surface heat-transfer coefficient can be read directly and therefore the average m is determined. With this m, the heating time can be found from the standard heating-cooling charts. The average surface temperature is found as follows:

$$Y_{avg} = \int_0^{X_0} \frac{Y\,dX}{X_0}$$

where X_0 is the value of the dimensionless time when the final surface temperature is reached. Therefore

$$Y_{avg} = \int_0^{X_0} \sum_{k=1}^{\infty} \frac{2(\sin w_k)(\cos w_k)\exp(-w_k^2X)dX}{X_0(w_k + \sin w_k \cdot \cos w_k)}$$

$$= \sum_{k=1}^{\infty} \frac{2(\sin w_k)(\cos w_k)[1 - \exp(-w_k^2 X_0)]}{w_k^2 X_0 (w_k + \sin w_k \cdot \cos w_k)}$$

Since X_0 is greater than 0.2 this can be simplified to

$$Y_{avg} = \frac{Y[\exp(w^2 X_0) - 1]}{w^2 X_0} = \frac{t' - t_a}{t' - t_b}$$

where t_a is the average surface temperature during the interval of exposure. Eliminating Y, this can be written

$$\frac{t' - t_a}{t' - t} = Y_a = \frac{\exp(w^2 X_0) - 1}{w^2 X_0} \quad \ldots\ldots\ldots\ldots [6]$$

Values of w^2 can be read from Fig. 3 and values of Y_a from Fig. 4. The use of the charts will become clear from the following example: A 6-in. steel slab of diffusivity 0.5 sq ft per hr, conductivity 25 Btu/(ft)(hr)(deg F) is to be heated to a surface temperature of 1970 F in a furnace at 2070 F. The temperature of the surroundings is 70 F. Heat transfer is assumed, for simplicity, to take place by radiation only, although it should be noted that the method will apply to any heat transfer for which a curve can be drawn. What is the average surface temperature over the interval? What will be the temperature at the center at the end of the heat period?

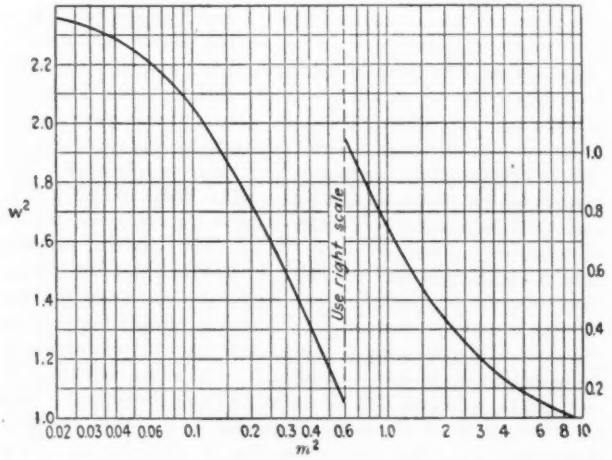


FIG. 3 CHART FOR DETERMINING SQUARE OF CHARACTERISTIC NUMBER w

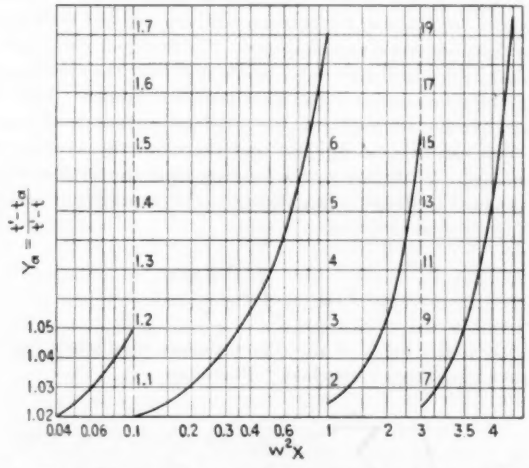


FIG. 4 TEMPERATURE RATIO FOR DETERMINING AVERAGE SURFACE TEMPERATURE OF SLAB

The temperature-time curve of the surface is reasonably parabolic. Therefore assume an initial average surface temperature of (2/3)(1970) = 1315 F. From radiation charts,[3] for radiation between two infinite parallel plane surfaces, one at 2070 F and the other at 1315 F, the surface heat-transmission coefficient h is found to be 70 Btu/(sq ft)(hr)(deg F). Therefore m = (25)/(70)(3/12) = 1.43. From standard cooling charts,[3] for m = 1.43 and Y = (2070 — 1970)/(2070 — 70) = 0.05, X_0 is found to be 4.9. From Fig. 3, when m is equal to 1.43, w^2 is 0.565. Therefore $w^2 X_0 = 4.9 \times 0.565 = 2.77$. From Fig. 4, $Y_a = 5.45 = (2070 - t_a)/(2070 - 1970)$. Solving this, t_a is found to be 1525 F.

The procedure is now repeated with the new t_a. For t_a = 1525, h is 80 Btu/(sq ft)(hr)(deg F). Solving for m, we find it to be 1.25. From this X_0 = 4.35 is obtained and also w^2 = 0.628. From Fig. 4, for $w^2 X_0 = 0.628 \times 4.35 = 2.73$, Y_a is read as 0.53. Solving, it is found that the average surface temperature is 1540 F. This is sufficiently close to the previous value and further refinement is unnecessary.

To find the center temperature proceed as follows: For radiation between 2070 and 1970 F, McAdams[3] gives an h of 110 Btu/(sq ft)(hr)(deg F). From this m is 0.91 and from Fig. 1 $(t' - t)/(t' - t_0)$ is 0.629. Solving for t_0 gives t_0 = 1875 F.

The difference between average and end-boundary-resistance ratios is pronounced, and it is evident that quite different center temperatures will be obtained with both m values. Strictly speaking, neither temperature will be exact, but that obtained from the final boundary conditions will certainly be more correct than that obtained from average boundary conditions.

The foregoing analysis was carried through for a semi-infinite plate. Equations similar to Equation [5] are derived in the Appendix for infinite cylinders and for spheres. It is sufficient here to remark that the curves shown in Fig. 1 for cylinders and spheres can be used in the manner described for the semi-infinite plate. Average surface-temperature equations can be easily derived. One restriction is placed on all these curves; they apply only for values of X equal to or greater than 0.2. However, this does not detract from their applicability because, as is shown, values of X encountered in temperature-uniformity calculations are always far greater than 0.2.

Figs. 5 and 6 are included here because no standard heating-cooling charts of the Hottel type are available for cylinders and spheres, and temperature-uniformity calculations frequently require the use of curves which give small temperature ratios accurately. Only the center temperatures are given. To find the surface temperatures, multiply the ordinate from Fig. 5 or 6 with the corresponding ordinate from Fig. 1. Figs. 5 and 6 give $Y^\circ = (t' - t^\circ)/(t' - t_b)$, and Fig. 1 gives $(t' - t)/(t' - t^\circ)$. The product gives $(t' - t)/(t' - t_b)$, from which the surface temperature can be found. A more complete discussion is given in the Appendix and the relation is extended to include all in-between points.

It should be emphasized that the relative temperature-uniformity ratio and the uniformity factor are not single-valued parameters and do not in themselves determine a unique solution of the problem. To see that this is true consider the uniformity factors 1 — (1900/2000) and 1 — (3800/4000). The factors are numerically equal and give the same heating times, based upon the Paschkis charts,[2] but they will not result in the same furnace temperatures. Similarly, a given relative temperature-uniformity ratio has an infinite number of dimensionless time ratios X. The system is uniquely determined only by the parameters Y, m, and X. The relative temperature-uniformity ratio and the uniformity factor are auxiliary parameters which show certain

[3] "Heat Transmission," by W. H. McAdams, second edition, McGraw-Hill Book Company, Inc., New York, N. Y., 1942.

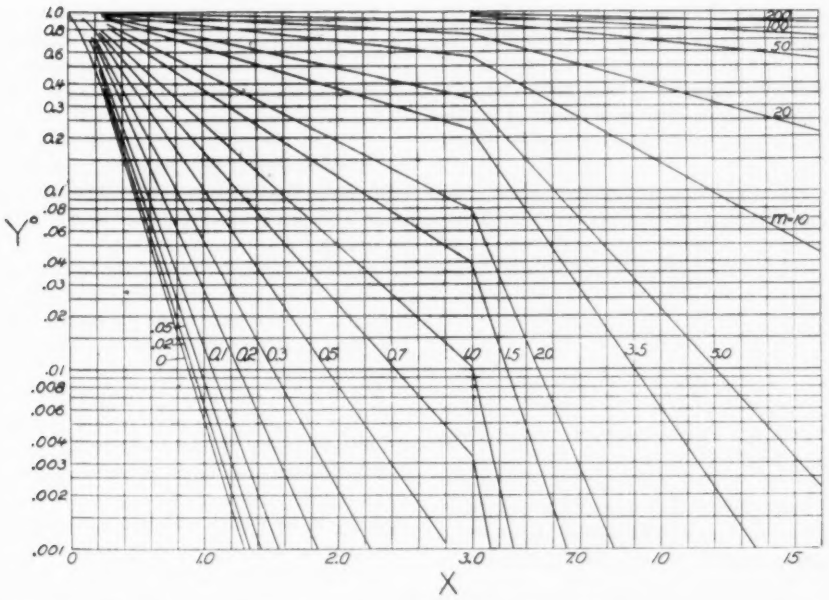


FIG. 5 CHART FOR DETERMINING TEMPERATURE HISTORY AT THE AXES OF CYLINDRICAL BODIES

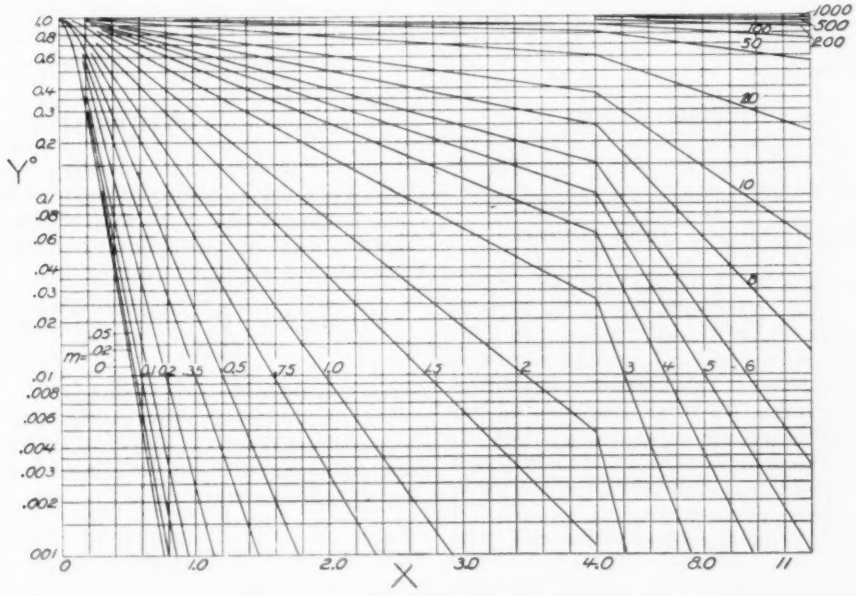


FIG. 6 CHART FOR DETERMINING TEMPERATURE HISTORY AT CENTER OF SPHERICAL BODIES

relations that exist among the different variables; the former ties in the furnace temperature and the latter the heating time with boundary resistance and surface and center temperatures. Each depends upon the other; if taken together they eliminate the necessity for using the standard cooling charts, but they cannot be combined into a single chart.

Summary. In the preceding paragraphs simple equations have been presented which enable uniformity calculations to be made readily. It is pointed out that the simplicity of the relations derived makes it a comparatively easy task to determine the mutually dependent furnace temperature and relative boundary resistance. Temperature-time-space curves are given to supplement and add to those available at present.

TWO-DIMENSIONAL HEAT FLOW

The definition of temperature uniformity is based upon maximum surface and minimum mid-plane temperatures. In two-dimensional heat flow maximum surface temperatures occur at the edge. In the heating of a plate infinite in one direction only, for example, a long rod, or a short plate insulated on two opposite faces, if the origin of a rectangular system of co-ordinates is thought of as placed at the geometric center of the plate, Fig. 7, it is shown in the Appendix that edge, center, and furnace temperatures are related by

$$(t' - t^s)/(t' - t^\circ) = (\cos w)_x(\cos w)_y \ldots\ldots\ldots [7]$$

where as before t' and t° are furnace and center temperatures,

respectively; t^* is the edge temperature; $\cos(w)_x$ and $(\cos w)_y$ are found from Fig. 1 by calculating the relative boundary resistances m_x and m_y for heat flow in the x- and y-directions, respectively, just as is done for one-dimensional heat flow. Since t^* and t° are given by the specifications and m is assumed for the present to be known, the furnace temperature t' can be found.

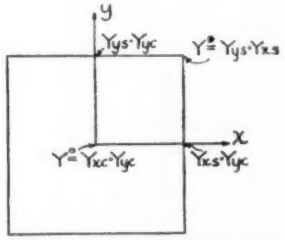


FIG. 7 Y-FACTOR RELATIONS FOR TWO-DIMENSIONAL HEAT FLOW IN PLATE

A chart similar to Fig. 1 can be plotted, but in place of a single curve there will be a family of curves with either m_x or m_y as abscissa and m_y or m_x as parameter. In general m_x will not be equal to m_y.

If the sides of the body are of equal length, $(\cos w)_x$ will equal $(\cos w)_y$ and $(t' - t^*)/(t' - t^\circ)$ will equal $(\cos w_x)^2 = (\cos w_y)^2$, since the two will be numerically equal. In this case the solution can be obtained from Fig. 1 and the standard heating-cooling charts. For example, let $m_x = m_y = 1$, and let the surface temperature be 2100 F and the center temperature be 2000 F. From Fig. 1 and Equation [2]

$$(t' - t^*)/(t' - t^\circ) = (0.654)^2 = 0.428$$

Therefore $t' = 2172$ F. From Equation [18] of the Appendix the temperature ratio at the center is

$$\sqrt{(2172 - 2000)/(2172)} = \sqrt{0.0781} = 0.2795$$

From the cooling curves for $m = 1$, X is found to be 1.88.

When the sides are not of equal length, the cooling charts for one-dimensional heat flow cannot be used. As yet only a few two-dimensional charts have been prepared (an unpublished work by Rohsenow and his co-workers at Yale University, under direction of Professor Wohlenberg). To cover completely all conditions requires an inpracticably large number of such graphs. In the second section of the Appendix it is shown that the system, in so far as temperature-uniformity problems are concerned, can be completely defined by the six parameters m_x, m_y, x/y, X_x, $1 - t^\circ/t'$, and $1 - t^*/t'$. X_x is the dimensionless time ratio, with thickness squared being the square of the length of the smallest side; x/y, a shape factor, is the ratio of the lengths of the sides. The other parameters have already been described. To cover completely all practical combinations of these variables would require (for 15 values of m_y and 5 of x/y) 75 charts of conventional form for each of the two temperature ratios, or 150 charts in all. Such a presentation is obviously out of the question. If an intersection chart is substituted, however, it is possible, by imposing a few restrictions which will be considered later, to cover in a single chart most of the cases met in practical applications. A chart of this type, applying to plates only, is shown in Fig 8.

The chart is somewhat more difficult to use than the simple cooling charts, but some sacrifice in simplicity must be made in order to obtain generality. For temperature-uniformity calculations m_x, m_y, x/y, and Y° will be known (Y° having been found from Fig. 1) and the unknown will be the relative heating time X_x. To find X_x:

1 With the given m_y as abscissa go to the first quadrant and locate the intersection of the vertical from m_y with the curve of constant m_x. From the point of intersection proceed horizontally to the second quadrant and locate the point of intersection with Y°.

2 With the given x/y as abscissa enter the fourth quadrant, go horizontally to m_y; from m_y proceed perpendicularly to m_x and thence horizontally to X. The intersection of this horizontal with a perpendicular from the value of Y° located in the first step determines X.

As an example, the case of the square bar, solved previously by using the one-dimensional cooling chart, is shown (dotted line in Fig. 8). In this case enter the fourth quadrant at $x/y = 1$ and the first quadrant at $m_x = 1$. The intersection in the third quadrant gives $X_x = 1.88$.

Fig. 8 is not restricted to temperature-uniformity calculations, but can be applied to heating and cooling problems in general. However, in any problem neither X_x nor X_y should be less than 0.2 for values of m equal to zero. For larger m values, X less than 0.2 may be used, a simple criterion being to refer to the Gurney-Lurie charts and find for what value of X the lines of constant m have not begun to curve.

In the terminology of this paper X_y will always be less than X_x, because $X_y = X_x(x/y)^2$. Therefore for small values of x/y, X_y should always be calculated to find out if it is within the imposed limit. In general, though, small values of x/y will mean that heat flow in the y-direction is of negligible influence; therefore these cases can be treated as one-dimensional problems, using the standard charts. Fig. 8 can be applied to nearly all problems that cannot be treated one-dimensionally.

Appendix

Infinite Cylinders. Bodies having circular symmetry can be treated in a manner similar to that used for plates. The equation, in dimensionless form, for the heating-up of an infinite cylinder, or a short cylinder insulated at both ends, can be written

$$Y(x,X) = \sum_{k=1}^{\infty} \frac{2J_1(u_k)J_0(u_k x)\exp(-u_k^2 X)}{J_0^2(u_k) + J_1^2(u_k)} \cdot \frac{1}{u_k} \quad \ldots [8]$$

where u_k is defined by $J_0(u) = muJ_1(u)$.

It is true also for cylinders that the values of X encountered in temperature-uniformity calculations are such that in the expansion all terms after the first become negligible. Therefore Equation [8] can be reduced to

(surface) $$Y = \frac{2J_1(u)J_0(u)\exp(-u^2X)}{J_0^2(u) + J_1^2(u)} \cdot \frac{1}{u} \quad \ldots [9]$$

(center) $$Y^\circ = \frac{2J_1(u)\exp(-u^2X)}{J_0^2(u) + J_1^2(u)} \cdot \frac{1}{u} \quad \ldots [10]$$

Proceeding as before

$$Y/Y^\circ = J_0(u) = (t' - t)/(t' - t^\circ) \quad \ldots [11]$$

Equation [11] is plotted in Fig. 1 (see curve for cylinder). The furnace temperature is found in the same manner as was prescribed for the plate. The heating-up time can be found from the cooling chart for the cylinder, Fig. 5. Charts other than the Gurney-Lurie type are not suited for temperature-uniformity calculations because they do not have accurate readability in the small temperature ratios. Charts are given only for center temperatures because, as was pointed out previously, temperatures for the surface can be found from the relation $Y^\circ(Y/Y^\circ) =$

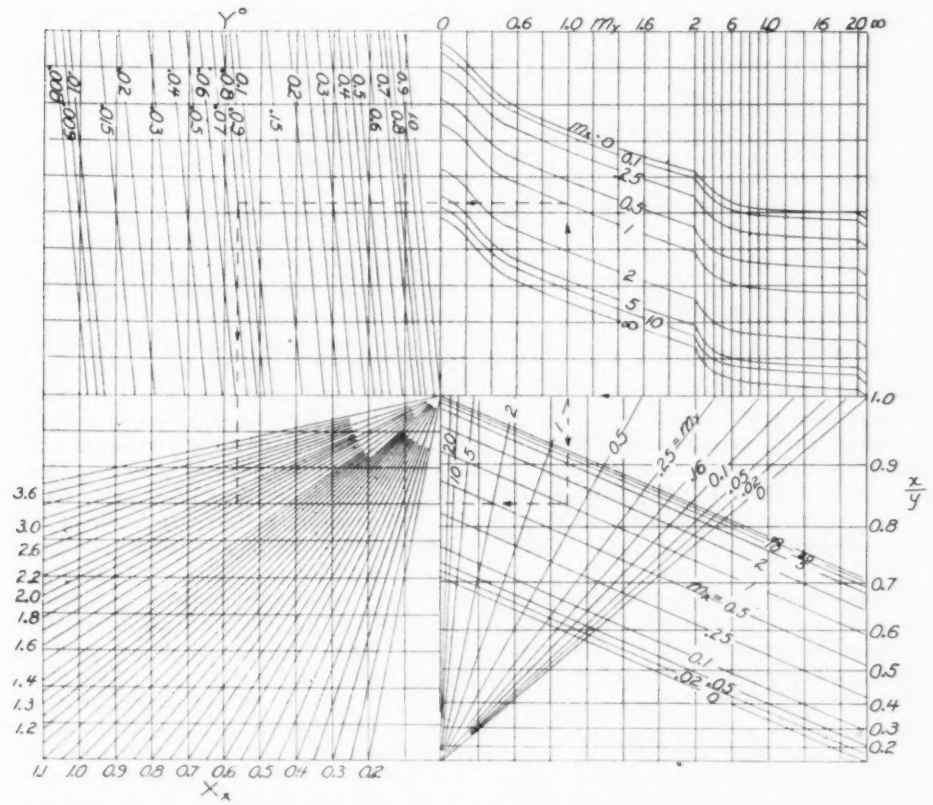


FIG. 8 CHART FOR DETERMINING TEMPERATURE HISTORY AT MID-PLANE OF PLATE SUBJECTED TO TWO-DIMENSIONAL HEAT FLOW

Y. This relation is exact for all values of Figs. 5 and 6 in which the temperature curves are straight lines and this covers practically the entire range of the charts. Little is lost by not being able to use this relation in the small remaining portion of the charts because Gurney-Lurie type charts are not suited for temperature ratios at small values of X; these can be found best by charts derived from short-time expansion formulas.

Spheres. The equation for the sphere is

$$Y(x,X) = \sum_{k=1}^{\infty} 2\frac{(\sin v_k - v_k \cos v_k)\exp(-v_k^2 X)}{v_k - (\sin v_k)(\cos v_k)} \cdot \frac{\sin(v_k x)}{v_k x} \quad [12]$$

and the corresponding characteristic number equation is $mv = (m-1)\tan v$. Again, in temperature-uniformity calculations, all terms after the first can be neglected and the equation reduced to

$$\text{(surface)} \quad Y = 2\frac{(\sin v - v\cos v)\exp(-v^2X)}{v - (\sin v)(\cos v)} \cdot \frac{\sin v}{v} \quad [13]$$

$$\text{(center)} \quad Y^\circ = 2\frac{(\sin v - v\cos v)\exp(-v^2X)}{v - (\sin v)(\cos v)} \quad [14]$$

From the equations for the surface and center

$$Y/Y^\circ = (\sin v)/v \quad [15]$$

Summary. In the preceding paragraphs it has been shown that by eliminating the dimensionless time from the heat equations for plates, spheres, and cylinders, simple equations result which relate surface, center, and furnace temperatures to boundary resistance. From these elemental relations dimensionless temperature ratios can be formed which make it possible to use standard heating-cooling curves to find the time required to obtain the desired temperature uniformity. In addition, the simple temperature and boundary-resistance relations make it comparatively easy to determine the unknown boundary resistance.

Temperature-time-space curves for cylinders and spheres are given to supplement those available at present. These curves are given for center temperatures only, but can be readily extended to surface temperatures by the use of Fig. 1, and to all in-between points by forming the products $Y^\circ \cos(wx)$, $Y^\circ J_0(ux)$, and $Y^\circ(\sin vx)/v$ for plates, cylinders, and spheres, respectively. In all instances these relations are restricted to values of X equal to or greater than 0.2.

TWO-DIMENSIONAL HEAT FLOW

Supplementing the nomenclature previously given, the following additions will be used:

Y° relative temperature for center $= (1 - t^\circ/t')_x, (1 - t^\circ/t')_y$

Y^* relative temperature for edge of a finite plate $= (1 - t/t')_x, (1 - t/t')_y$

Y_y, Y_x relative temperatures at surfaces perpendicular to x- and y-axes, respectively, when body is considered as a semi-infinite solid $= (1 - t/t')_x, (1 - t/t')_y$

Y_{yc}, Y_{xc} relative temperatures at mid-planes perpendicular to x- and y-axes, respectively, when body is considered as a semi-infinite solid $= (1 - t^\circ/t')_x, (1 - t^\circ/t')_y$

x distance from vertical mid-plane to surface

y distance from horizontal mid-plane to surface

d diffusivity

θ time (not dimensionless)

t_b assumed to be zero

Finite Plate. In two-dimensional heat flow essentially the same methods are applied as in one-dimensional heat flow. The heat-flow equation must now satisfy the differential equation

$$\frac{\partial t}{\partial \theta} = d\left(\frac{\partial^2 t}{\partial x^2} + \frac{\partial^2 t}{\partial y^2}\right) \quad [16]$$

where x and y are rectangular co-ordinates indicating the direction of heat flow, and d is the diffusivity. Newman[4] showed that if Y_x was the solution of

$$\partial t/\partial \theta = d(\partial^2 t/\partial x^2)$$

and its boundary conditions, and Y_y was the solution of

$$\partial t/\partial \theta = d(\partial^2 t/\partial y^2)$$

and its boundary conditions, then $Y_x Y_y$ was a solution of Equation [16]. McLachlan,[5] following the method of Newman, showed that in the heating of solids the partial differential equation is satisfied by a solution of the form $1 - Y_x Y_y$, where Y_x is the expansion part of Equation [1] and Y_y is the expansion part of the same equation with y introduced in place of x. The corresponding heating-up temperatures are $H_x = 1 - Y_x$ and $H_y = 1 - Y_y$.

In two-dimensional heat flow the maximum temperatures will occur at the edges of the body and the minimum temperature at the center. The desired temperature uniformity will be given in terms of the edge and center temperatures t^* and t°, respectively, and the following relations (see Fig. 7) then hold

$$\text{(edge)} \qquad Y^* = 1 - t^*/t' = Y_{y_s} Y_{x_s} = 1 - H^*$$

$$\text{(center)} \qquad Y^\circ = 1 - t^\circ/t' = Y_{y_c} Y_{x_c} = 1 - H^\circ$$

To simplify the form of the equations let

$$a_x = 2(\sin w)/(w + \sin w \cos w)$$

$$b_x = \cos(wx)$$

$$c_x = \exp(-w^2 X_x)$$

for heat flow in the direction of the x-axis. For heat flow in the direction of the y-axis, use the same notation but replace the subscript x by y. Then

$$\text{(edge)} \qquad Y^* = (abc)_{x_s}(abc)_{y_s} \quad [17]$$

$$\text{(center)} \qquad Y^\circ = (ac)_{y_c}(ac)_{x_c} \quad [18]$$

Dividing Equation [17] by Equation [18] gives

$$(t' - t^*)/(t' - t^\circ) = (\cos w)_x(\cos w)_y \quad [19]$$

Solution of this equation yields the furnace temperature. The heating time requires a solution of

$$Y^\circ = 1 - t^\circ/t' = (2 \sin w)_x (2 \sin w)_y \{\exp -X_x[w_x^2 + (w_y x/y)^2]\}/(w + \sin w \cdot \cos w)_x \cdot (w + \sin w \cdot \cos w)_y$$

This equation is plotted in Fig. 8. Only center temperatures are plotted. The surface temperatures can be found from Y°, Fig. 1, and the following relations, Fig. 7:

$$\text{(vertical mid-plane)} \qquad Y_{y_s} Y_{x_c} = Y^\circ(\cos w)_y \quad [20]$$

$$\text{(edge)} \qquad Y_{y_s} Y_{x_s} = Y^\circ(\cos w)_x(\cos w)_y \quad [21]$$

$$\text{(horizontal mid-plane)} \qquad Y_{x_s} Y_{y_c} = Y^\circ(\cos w)_x \quad [22]$$

Finite Cylinders. The handling of finite cylinders is the same as for finite plates. If the axis of the cylinder is taken in the direction of the x-axis, it follows, from the similarity between the heat-flow equations for bodies having circular symmetry and those for plates, that

$$(t' - t^*)/(t' - t^\circ) = J_0(u)(\cos w)_x$$

Values of $(\cos w)_x$ and $J_0(u)$ can be obtained from Fig. 1; from their product the furnace temperature can be calculated. As in the case of two-dimensional heat flow in slabs, the solution of the heating time is dependent upon the preparation of the requisite temperature-time-space charts. A chart similar to Fig. 8 can be prepared, or perhaps other methods of plotting, more convenient in form, may be evolved. Equations for determining temperatures at points other than at the edge and center, for example, equations similar to Equations [20], [21], and [22] can be readily derived, the only restriction being that neither dimensionless time ratio be less than 0.2.

The treatment of three-dimensional heat-flow problems follows directly from the methods given for one- and two-dimensional heat flow.

In two- and three-dimensional heat flow an additional complication enters in determining the average boundary resistance, because of the variation of surface temperature from edge to center of the face. Not only will a time average of surface temperature have to be determined, but also a space average, since the faces do not have uniform temperature distribution, and therefore do not have uniform boundary resistances.

Comment. In the preceding discussion only homogeneous solids have been considered. In the case of laminated solids in which the thermal conductivity may be different along the various axes, the value of thermal diffusivity may be correspondingly adjusted for the different directions, and the calculation carried out as usual. If the surface heat-transmission coefficient is different at the various faces, these different values of h may be used, the only limitation being that of maintaining symmetry: the values of m must be the same for any pair of parallel faces.

ACKNOWLEDGMENT

This paper is largely an extension of the work on temperature uniformity originally initiated by Dr. Victor Paschkis, head of the Heat and Mass Flow Analyzer Laboratory at Columbia University. The author is indebted to him for having brought the subject to his attention.

Discussion

F. S. BLOOM.[6] To the engineer who is familiar with practical furnace design and operation, the paper would appear to offer some difficulty, because of the necessary assumptions which the author was forced to make in obtaining a practical solution.

However, he has developed from his mathematical analysis certain facts which agree with test observations of heating furnaces. Some of these statements are worth while emphasizing. For instance, the author states, "As the final surface temperature is approached, there is little change in the boundary resistance, because of little change in surface temperature. As a result, the center temperature, which originally lagged considerably behind the fast-changing surface temperature, has time to catch up to the now slowly changing surface temperature."

---

[4] "Heating and Cooling Rectangular and Cylindrical Solids," by A. B. Newman, *Industrial and Engineering Chemistry*, vol. 28, 1936, pp. 545–548.

[5] "Complex Variable and Operational Calculus," by N. W. McLachlan, Cambridge University Press, 1939; also The Macmillan Company, New York, N. Y., 1942.

[6] Bloom Engineering Company, Pittsburgh, Pa.

By this statement he approaches the conclusions of Williams and Allen, who have previously stated that center temperatures, or temperatures under the surface of the material, follow the pattern of the surface temperature, and ultimately increase or decrease at the same rate as the surface temperature. From this we can conclude that a temperature history or curve of center temperature will follow, at some later time, the temperature history of the surface. In other words, if we plot surface-temperature history for a piece being heated, we can approximate the history of the center temperature.

If we go further in this analysis, we approach the conclusion that temperature uniformity "center to surface" must be considered with time.

The center temperature knows nothing about what happens to surface temperature at any specific time, although it is similarly affected after some delay. This delay or time lag is a factor dependent upon material size, but is constant regardless of speed of heating, that is, a 6-in. square can be heated in 20 min or 6 hr, but still the time for center temperature to equal surface temperature is the same. The magnitude of temperature difference is very large with fast heating, but after the proper equal time interval, temperature uniformity is the same. We do not produce temperature uniformity by slow heating.

The author's work as expressed in this paper stresses temperature uniformity. The writer does not think he intended to convey this impression. Let us face this problem. We heat a slab to a surface temperature of 2300 F, center temperature 2250 F. It is taken from the furnace and lies on the mill table for 15 sec. The surface cools down while the center continues to increase. We end up in the mill with a mixture of temperatures which cannot be equalized. So why demand or think of perfect uniformity.

Temperature-uniformity data are lacking. What we need is a complete study of temperature differences "surface to center" as related to specific industrial-mill operation. The author's method of calculation could be used for such a study. As is quite general, we get the "cart before the horse." Similarly, we get ourselves involved in calculations which get nowhere except to scare engineers into being cautious where it is not necessary. Let us find out the temperature uniformity demanded by the process.

The author also states, as his conclusion of the calculations, that a lower furnace temperature and better temperature uniformity can be obtained by higher heat transmission. He means luminous flames, thick flame blanket, and greater wall area, which in turn means ample roof height. This factor has been seen time and again on many billet-heating furnaces where a heavy luminous flame produces a better scale condition and a better working piece in the mill operation.

He touches gently on temperature control with which the writer fully agrees. There is no use soaking steel if the surface temperature is changing up and down. A 50-deg F temperature difference is easy to produce with such conditions. Good temperature control on heating furnaces is a necessity for uniform temperature distribution. It should be operated by measuring surface temperature, and in this manner a complicated heating-furnace operation can be reduced to the normal temperature-control problem.

The author has presented an outstanding theoretical paper. It is too complicated for the writer fully to comprehend. He must be pretty close to the right answer, because his conclusions seem accurate. It is suggested that he study mill and furnace conditions and then calculate from surface temperature and mill data the permissible out-of-balance temperatures which mill operations can stand.

VICTOR PASCHKIS.[7] The author is to be congratulated for a valuable piece of research. He refers to some previous work of the writer.[2] It may be interesting to compare the two methods of determining the temperature uniformity as follows:

In order to obtain a desired uniformity expressed either by the "temperature-uniformity factor" or by the "relative temperature-uniformity ratio," a definite furnace temperature and a definite heating time must be applied. Both should be expressed in dimensionless units. The determination from the temperature-uniformity factor or the relative uniformity ratio compare as follows:

	Heisler	Paschkis
Unknown	Determines the unknown from	
X	Gurney-Lurie charts	$\frac{t - t_0}{t - t_b} = f(m, x)$
t'	$\frac{t' - t}{t' - t_0} = f(m)$	Gurney-Lurie charts

The writer does not see a particular advantage of the new method above the known one and wonders what advantages can be claimed for it.

The most important part of the paper, as far as one-dimensional problems are concerned, is that dealing with the dual relationship between surface temperature, furnace temperature, and m value.

The recommendation that the heating time should be calculated with the time average m lacks proof, and it would be interesting to obtain definite proof. Incidentally, the step-by-step method described for finding t_a could be conveniently replaced by a procedure similar to that used in Fig. 2 of the paper.

It seems regrettable that the paper does not contain curves for cylinders and spheres, similar to those presented in Figs. 3 and 4, for slabs; also that the curves for the relative temperature-uniformity ratios for rectangular bodies are not developed. Only if curves are available can it be hoped that functions such as those presented in this paper will be widely used in industry. It is hoped that the author will develop such curves and present them at a later time. The author seems to exclude from consideration convection-type furnaces which today certainly gain in importance.

W. TRINKS.[8] While the author presents an excellent mathematical study, it is, however, too involved and obscure for the average engineer and will, for that reason, not be appreciated. Many an engineer will spend a couple of hours on it and will then lay it aside. With a few changes the usefulness of the paper could be vastly increased.

A sketch of the temperature distribution in a solid with notation of the temperature differences which are sought would be of great value.

In the "Introduction," condition No. 6 should be added; namely, that at the beginning of the heating process the work blank has uniform temperature throughout.

What is meant by the "time average" of boundary resistance m? This question is asked in view of the author's statement that boundary resistance is to be constant. It may be advisable to define boundary resistance and to give the units. Several definitions of boundary resistance are current.

The writer is at a loss to understand how the heat-transfer coefficient h is obtained when both the surface temperature and the flame temperature are alike. Can there be any heat transfer in that case?

The author does not say how Equations [1] and [8] were obtained. It is surmised that J_0 and J_1 are Bessel's functions. If so, that fact should be stated.

[7] Head, Heat and Mass Flow Laboratory, Columbia University, New York, N. Y.

[8] Consulting Engineer, Pittsburgh, Pa. Mem. A.S.M.E.

In modern heating practice, we do not bring the surface of the work blank up to furnace temperature and soak it a long time. We do something else. We heat the work blank quickly to a surface temperature which is above the desired final temperature and then soak it in a somewhat cooler furnace section, where the surface temperature drops and the center temperature rises. It would be wonderful if the author could solve, with Bessel's functions, the final temperature distribution which we obtain with that heating method.

Author's Closure

In the text the author has mentioned that Roshenow and coworkers' charts for two-dimensional heat flow have not yet been published. These charts have since appeared in the February, 1946, issue of the transactions of the A.S.M.E.

Both Mr. Bloom and Mr. Trinks stressed the desirability of solving problems involving step temperature functions. Mr. Bloom mentioned the case of a hot slab cooling on a mill table, and Mr. Trinks that of a slab heated quickly to a surface temperature which is above the final desired temperature and then soaking in a somewhat cooler section of the furnace. Many problems of a similar nature arise in metal heating. For example, in some types of heating operations, after the charge is brought to a given surface temperature, the furnace is turned off, and both charge and furnace are allowed to cool together. Another case occurs in surface hardening by high-frequency induction heating followed by internal quenching. Numerous others could be cited. Though the thermal operations involved are entirely unrelated physically, yet all of them are decidedly similar when considered in a mathematical sense. For instance the problem mentioned by Mr. Trinks is mathematically identical to the problem of surface hardening by high-frequency induction heating followed by an internal quench. Both of these can be readily solved by means of existing temperature charts, such as those shown in Figs. 6 and 7. In general all the problems mentioned simply involve relaxing from an initial known temperature distribution. The author is at present preparing a paper on the general solution of problems of this type.

Mr. Bloom points out that center temperatures can be approximated when surface temperatures are known, because of the constant time lag between equal surface and center temperatures. The magnitude of the time lag for any given surface-center temperature can be found from

$$t = \frac{-L^2 \log_e (\cos w)}{d\, w^2}$$

where

t = time lag in hours.
d = diffusivity in sq ft per hr
L = half thickness of slab in feet
w = first root of $m\, w = \cot w$

Values of w^2 are plotted in Fig. 3 and cos w in Fig. 1. Obviously, the time lag varies directly as the square of the thickness and inversely as the diffusivity. Because of the factor w, it also depends on the boundary resistance, decreasing as the boundary resistance increases.

Regarding the "time-average" of boundary resistance, mentioned by both Mr. Trinks and Mr. Paschkis: It is true that in the mathematical problem boundary resistance is considered to be constant. However, in actual heating-up processes boundary resistance varies throughout the heating cycle. Therefore, in applying mathematical formulas to actual thermal problems, it is necessary to estimate in some way or other the average value of the boundary resistance over the heating period, substitute this average value into the formulas, and solve as though the boundary resistance were constant. This average boundary resistance can be based on various thermal concepts. The author has suggested basing it on a time-average surface temperature. Even though, as Mr. Paschkis points out, this method lacks proof, it is nevertheless based on what appears to the author to be much more reasonable assumptions than those which are usually made. In fact, to the author's knowledge, it is the only method advanced so far which is not based on hit or miss guessing.

In regard to Mr. Paschkis' query as to the advantages of the present method of solving temperature-uniformity problems over that previously used: The two methods are in fact complementary. In the previous method heating times and in the present furnace temperatures can be found directly without resorting to Gurney-Lurie type charts. The present method covers a wider range of variables and requires just one simple chart, Fig. 1, in place of the three—each with a family of curves—which are required in the method of Paschkis.

Mr. Trinks is at a loss to understand how the heat-transfer coefficient h can be obtained when both the surface temperature and the flame temperature are alike. By definition, for blackbody radiation

$$h = 0.173 \frac{[(T_a/100)^4 - (T_s/100)^4]}{T_a - T_s}$$

where

T_a = flame temperature in degrees Rankine (F + 460)
T_s = surface temperature in degrees Rankine
h = Btu per sq ft, hr, F

After factoring $T_a - T_s$ from the numerator, this reduces to

$$h = \frac{0.173}{(100)^4} (T_a^2 + T_s^2)\, (T_a + T_s)$$

and when T_s is equal to T_a

$$h = \frac{(0.173)\ (4)\ (T_a)^3}{(100)^4}$$

Although h is finite, there can be no net exchange of heat because no temperature difference exists.

Dynamic Behavior and Design of Servomechanisms[1]

By G. S. BROWN[2] and A. C. HALL,[3] CAMBRIDGE, MASS.

This paper aims to set forth the criteria that are important in the design of certain servomechanisms and to show how certain analytical procedures can be applied to almost any problem to define quantitatively the properties that the control should have in order to make the servomechanism perform in the manner desired. The nomenclature used is essentially that proposed by Draper (1).[4] It is used in the treatment of the problem of synthesizing a controller for a servomechanism whose controlled member is to be rotated and can be defined in terms of inertia plus viscous and coulomb friction, plus a load torque. The broad objective of the designer is assumed to be that of designing a controller which will keep the dynamic error in controlled angular position of the controlled member a minimum under certain operating conditions. The transient and steady-state error for certain forms of motion, the criteria for stability, the effects of viscous friction, coulomb friction and load torques on the desired performance, and other related matters are treated. Several nondimensional charts and tables are included in the paper and show quantitatively the performance of any particular servomechanism with a controlled member of the kind treated, when the system has the various forms of control.

1 Introduction

SERVOMECHANISMS (2) or, more generally, closed-cycle automatic-control systems have become during the past decade exceedingly important elements in, for example, manufacturing, the process industries (3, 4), the steering (5) and operation of ships and aircraft, and many important scientific devices (6). As the applications have been increased in number, the demands imposed on the reliability, precision, and speed of operation of the mechanisms have also been increased. Fortunately, many of these demands have been satisfied because of developments in the various branches of engineering and physics that have taken place simultaneously with the growth of automatic control, but at the same time the complexity of the mechanisms has often been increased. The result of all this has been that the design of servomechanisms or automatic-control systems has now become almost a science, so that for the skillful and straightforward design of a high-caliber system one requires, (*a*) a clear appreciation of the fundamental principles involved in the correct functioning of an automatic-control system, and (*b*) an accurate knowledge of the properties of the mechanisms of which it is composed.

The purpose of this paper is to set forth in fairly simple terms the criteria that are important in the design of servomechanisms and to show how certain simple analytical procedures can be applied to almost any system to define the properties that the control should have in order to make the mechanism perform in the manner demanded.

2 Factors That Characterize a Servomechanism

A servomechanism is a power-amplifying automatic-control system characterized by the presence of a control element that is actuated by some function of the "difference" between the response desired of the system and its actual response. In other words, the system is error-sensitive, and the control is some function of the "error" in the behavior or state of the system. Usually a continuous change in the actuating quantity or the input signal is to be followed by a continuous action of the controller. The input signals usually come from low-power sources and may be random with time, but are preferably continuous. Systems of this kind are closed-cycle continuous-control systems, and it is this closed-cycle property that identifies them as servomechanisms. Their component elements generally tend to be complex, and because of the dependence of the operation of their control upon the result of the control operation, their design must conform to certain basic principles.

Because of widespread application of servomechanisms the actuating and controlled quantities are found in diverse forms. In the servomechanisms used for the automatic steering of ships or aircraft the actuating quantity or input signal is given by a low-power device sensitive to the course setting on a magnetic or gyro compass, and the output or controlled quantity is the direction in which the ship is headed. In servomechanisms used for the control of an automatic die-cutting machine, for example, the cutting head might be required to follow automatically a pattern laid out on a master pattern, or the contour of an existing member, as in replica production. An application such as this would probably result in maintaining the angular position of a shaft operating at a high-power level automatically in synchronism (or in step) with the angular position of a shaft as established by a low-power mechanism. The input signal might be the angular position of a cam-operated shaft, and the controlled quantity or output might be the angular position of the lead screw carrying the cutting head. In practice the angular positions of the two shafts are compared by one of several means common in the art, a measuring device detects the error in the position of the output and establishes a control signal, a controller is actuated by this control signal and operates either directly on the shaft of the high-power member or through some accessory device to bring the output shaft into the desired position.

Confusion occasionally exists among those working in automatic control, concerning the designation of a servomechanism

---

[1] The first portion of this paper was prepared during the summer of 1940, for the Subcommittee on Machine Design, Machine-Shop Practice Division of the A.S.M.E. At the request of the N.D.R.C. it was withdrawn from open publication and privately printed for restricted release. Sections 1 through 9 are substantially as originally written. Sections 10 through 12 have been added for this printing. Sections 13 through 19 have been adapted from an M.I.T. doctorate thesis by A. C. Hall and published for restricted distribution by the Technology Press.

[2] Director, Servomechanisms Laboratory, Massachusetts Institute of Technology.

[3] Assistant Professor, Electrical Engineering, Massachusetts Institute of Technology.

[4] Numbers in parentheses refer to the Bibliography at the end of the paper.

Contributed by the Instruments and Regulators Division and presented at the Annual Meeting, New York, N. Y., Nov. 26–29, 1945, of The American Society of Mechanical Engineers.

Note: Statements and opinions advanced in papers are to be understood as individual expressions of their authors and not those of the Society.

and a servo. In this paper the entire array of apparatus beginning with the input member and going through to the high-power output member and including all measuring and control equipment is called a servomechanism. In particular, the torque, force, or power-producing member that is actuated by the control to restore the equilibrium condition is called a servo, or servomotor.

3 Basic Design Problem

Since a servomechanism should perform in a manner that meets a certain specification, the design of the system should be carried out only after an analysis that yields performance data for each component mechanism, in a form readily subject to quantitative interpretation for design purposes, has been concluded. The component elements can be described in terms of certain quantities, and the analysis should be carried out in a manner that shows the relations that must exist among these quantities in order to provide (*a*) a system that is stable and (*b*) a system whose transient and steady-state operating errors are within the specified limits.

This work is aided by subdividing the system into its essential component mechanisms, for example, the input member, the error-measuring element, the controller, the controlled member, and the output member. With all systems, good judgment is necessary in carrying out this subdivision, and in the more complicated systems a rather detailed subdivision may be desirable (see section 10). A block diagram representative of the manner of interconnection of these component mechanisms is, as a rule, readily drawn. After the analysis has been completed the performance of the mechanisms assigned to the various boxes in the block diagram can be defined, and their design and construction eventually carried out. If the performance specifications are reasonable the designer is limited only by cost, space or weight restrictions, availability of devices having the desired rating and characteristics, and so forth. In other words, the designer's problem is basically that of reducing certain requirements to practice.

To illustrate the procedure for the analysis of a simple mechanism, consider the block diagram shown in Fig. 1. Here the

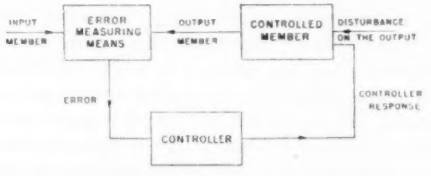


Fig. 1 Block Diagram for a Servomechanism

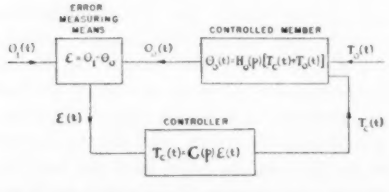


Fig. 2 Block Diagram for a Servomechanism Showing Symbolic Representation of Elements

entire system is represented by five elements: namely, the input member, the error-measuring device, the controller, the controlled member, and the output member. Each component element may comprise much apparatus but this is unimportant for the present. For a generalized treatment let the system be defined in terms of the symbols shown in Fig. 2, where

$\theta_i(t)$ = input disturbance as a function of time
$\theta_0(t)$ = response of output as a function of time
$\epsilon(t)$ = error between desired and actual response as a function of time
$T_c(t)$ = response of controller as a function of time
$T_0(t)$ = any disturbance applied to output as a function of time

Also let these symbols be related in the following manner

$$\epsilon(t) = \theta_i(t) - \theta_0(t) \quad [1]$$

$$T_c(t) = C(p)[\epsilon(t)] \quad [2]$$

$$\theta_0(t) = H_0(p)[T_c(t) + T_0(t)] \quad [3]$$

In Equation [2] $C(p)$ is a differential operator in the form of a polynomial in p, where p represents d/dt. It operates on the time expression for the error and thereby gives the time expression for the controller response. It is called the "controller operator" and is to be determined from the analysis. $H_0(p)$ of Equation [3] is also an operator called the "output member operator." It is characterized by the physical properties of the device or process to be controlled.

Since, in general, the control is intended to keep the error zero, the extent to which the objectives of the control have been achieved is best indicated by deriving the expression for the error in terms of the operators $C(p)$ and $H_0(p)$, the input signal $\theta_i(t)$, and the output disturbance $T_0(t)$. From Equations [1], [2], and [3]

$$\epsilon(t) = \frac{1}{1 + C(p)H_0(p)}\,[\theta_i(t) - H_0(p)T_0(t)] \quad [4]$$

$$\theta_0(t) = \frac{C(p)H_0(p)\theta_i(t) + H_0(p)T_0(t)}{1 + C(p)H_0(p)} \quad [4a]$$

wherein $C(p)$ is frequently the only design variable. Equation [4] is the basic equation for a closed-cycle control system such as that shown in Fig. 2, and the expression $[1 + C(p)\,H_0(p)]^{-1}$, being an over-all system operator or characteristic equation, summarizes the system behavior. This use of an over-all system operator $[1 + C(p)H_0(p)]^{-1}$ to summarize the theory of design of a closed-cycle system of automatic control originated, to the authors' knowledge, with John Taplin in 1937, while he was a special student in electrical engineering at the Massachusetts Institute of Technology. Taplin no doubt recognized the similarity between the closed-cycle control problem and the feedback-amplifier problem as presented by Black (7) and Nyquist (8).

The applications of automatic control are numerous and varied and it is impossible to say that θ, T, or ϵ always represents any particular quantity. Reference to a few of the applications cited in the literature will show that θ, T, or ϵ may be an angular displacement, a flow, a voltage, a torque, a light flux or any of the physical quantities commonly encountered. However, since interest in an analysis is usually stimulated by speaking in terms of some physical application, the control of an automatic replica-cutting machine is considered as an example. It is assumed that $\theta_i(t)$ is an angular displacement indicated by a delicate cam-operated mechanism which displaces a low-power input shaft in accordance with the motion $\theta_0(t)$ desired of a high-power output shaft. The error $\epsilon(t)$ is assumed to be a voltage made proportional to error angle by any of the commonly used methods. The controller response $T_c(t)$ is assumed as a torque applied to the controlled member. The controlled member is a lead screw carrying a cutting head. Thus the controller, in effect, serves also as the prime mover or servomotor for the lead-screw drive. Fig. 3 shows a schematic arrangement of the essentials of this system.

The output member operator $H_0(p)$ can now be formulated. The cutting-head lead-screw drive of a typical milling machine

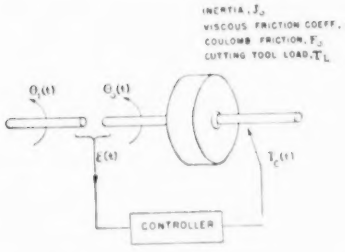


FIG. 3 SCHEMATIC DIAGRAM OF SERVOMECHANISM USED FOR ILLUSTRATIVE EXAMPLE

would comprise shafts, screws, gears, and tool holder and could be defined in terms of an inertia J_0, and a viscous-friction coefficient f_0. The output member would be subjected to a coulomb friction torque and a load torque, which jointly can be represented as $-T_0(t)$. On the assumption that the parameters are constant or the system is linear for small ranges of operation, the differential equation of motion for the output member when considered as a single unit is

$$J_0 \frac{d^2\theta_0}{dt^2} + f_0 \frac{d\theta_0}{dt} = T_c(t) - T_0(t) \quad [5]$$

It is expedient now to express $\frac{d\theta_0}{dt}$ by $p\theta_0$ and $\frac{d^2\theta_0}{dt^2}$ by $p^2\theta_0$, and to write Equation [5] as

$$(J_0p^2 + f_0p)\theta_0(t) = [T_c(t) - T_0(t)] \quad [5a]$$

where the expression in parenthesis preceding $\theta_0(t)$ is an operator, which operates on $\theta_0(t)$ as indicated. When solved for $\theta_0(t)$, Equation [5a] gives

$$\theta_0(t) = \frac{1}{J_0p^2 + f_0p}[T_c(t) - T_0(t)] \quad [6]$$

which, by analogy with Equation [3], gives the output member operator as

$$H_0(p) = \frac{1}{J_0p^2 + f_0p} \quad [7]$$

The substitution of $H_0(p)$ from Equation [7] into Equation [4] gives, after some reduction

$$\epsilon(t) = \frac{1}{J_0p^2 + f_0p + C(p)}[(J_0p^2 + f_0p)\theta_i(t) + T_0(t)] \quad [8]$$

Alternatively, if the input disturbance is a velocity

$$\omega_i(t) = \frac{d\theta_i(t)}{dt} = p\theta_i(t)$$

the error equation becomes

$$\epsilon(t) = \frac{1}{J_0p^2 + f_0p + C(p)}[(J_0p + f_0)\omega_i(t) + T_0(t)] \quad [9]$$

Expressions typified by Equations [8] and [9] are extremely useful in the design or analysis of control systems since they express the error in terms of the parameters of the system, the input disturbance, the disturbing or load torques on the controlled member, and the controller operator $C(p)$. When any mechanism is to be converted to automatic control, the problem for the designer is the synthesis of the simplest and most practical controller that will have the operator $C(p)$ required to meet the specified operating conditions. The next sections present a generalized treatment of the problem of deriving a form of the operator $C(p)$ required by the various conditions of servomechanism operation commonly encountered in practice.

4 SIMPLE FORM OF CONTROLLER OPERATOR

In any particular application it would be desirable to know the expected form of the input disturbance and to choose the controller operator $C(p)$ on the basis of a certain specified performance under the expected operating conditions. In general, however, the input disturbance is random, so that its description in an analytical form which is of much use in the analysis is usually impractical. It is common practice therefore to evaluate the performance afforded by possible designs on the basis of the nature of the transient and steady-state responses of the respective systems to certain test disturbances.

The well-known transient response of a system defined by Equation [8] or [9] is

$$\epsilon(t) = A + Be^{r_1t} + Ce^{r_2t} + \text{etc.} \quad [10]$$

A direct guide to the simplest form of controller operator that will give a workable system is afforded by a characteristic demanded of the exponents r_1 and r_2 of Equation [10]. For instance, r_1 and r_2 are the roots of the operator $J_1p^2 + f_0p + C(p)$ which may conveniently be a polynomial. Clearly the simplest form of $C(p)$ that will make this operator a polynomial is

$$C(p) = k \quad [11]$$

and for the corresponding simple controller, Equation [2] reduces to

$$T_c(t) = k\epsilon(t) \quad [12]$$

Also, for the system to be stable r_1 and r_2 must have negative real parts, and if they are complex the magnitudes of their imaginary parts must fall within a certain range because of operating restrictions. Hence the magnitude of k is obviously restricted.

A further restriction on k can be deduced from the steady-state operating error given by the quantity A of Equation [10], which can be written down by inspection from Equation [8] or [9]. For a constant input angle θ_i, or a constant input velocity ω_i, and constant load torque, the steady-state error is given by putting the operator p zero everywhere in Equations [8] and [9]. If then $C(p)$ is defined by Equation [11], the steady-state errors become, respectively

$$\epsilon_{ss} = \frac{T_0}{k} \quad [13]$$

for θ_i and T_0 constant; and

$$\epsilon_{ss} = \frac{f_0\omega_i + T_0}{k} \quad [14]$$

for ω_i and T_0 constant.

A controller having an operator as just defined applies torque to the controlled member in proportion to the indicated error. Since this definition makes no allowance for response lag in the controller, which here is assumed to include the servomotor, a perfect element is assumed. Actually, of course, response lags exist in all controller servomotors encountered in practice though frequently the lag is negligible in comparison with the periods of response of the system as a whole. Section 10 discusses the problem of treating the controller synthesis when the servomotor has response lags. Servomechanisms employing controllers characterized by Equation [11] are found frequently in practice. They are called simple-error controller servomechanisms and, as a rule, are confined to the class that involves prime movers rated less than a few watts for reasons that later are made clear.

The problem now to be handled is that of selecting the best value of k. Unfortunately, the selection involves a compromise because from Equations [13] and [14] high precision of operation requires that k be large and f_0 and T_0 small, whereas the stability restriction implied in Equation [10] imposes a limit on the largeness of k or the smallness of f_0, because the entire damping is here supplied by viscous friction in the output. Obviously the restrictions on the magnitude of T_0 are practical operating ones. The answers to these questions are best obtained from an examination of the transient response of the system, which is the subject of the next section.

5 Transient Response of Error-Controlled Servomechanism

The transient response of a servomechanism following the sudden application of a constant disturbance to the input member gives data that are useful (*a*) for appraising the quality of the performance of the system as a whole and (*b*) for proportioning f_0 and k to meet certain performance specifications. The response to this suddenly applied input disturbance completely characterizes the system.

The transient solutions are herein given as dimensionless expressions in a form convenient for engineering use, using the procedure and notation introduced by Draper (1). Coulomb friction and applied torque are neglected during the preliminary analyses since it is unnecessary to include them in order to evaluate the quality of the transient performance. Furthermore, their effects can be readily determined and taken into account by applying the principle of linear superposition of causes to give the total effects.

For identification purposes a servomechanism comprising a simple-error controller defined by Equation [12] is classified herein as type 1. For this controller, and with coulomb friction and load torque neglected, Equation [9] has the following form

$$\epsilon(t) = \frac{1}{J_0 p^2 + f_0 p + k_1}(J_0 p + f_0)\omega_i(t) \quad [15]$$

where the subscript 1 in Equation [15] and the following indicates that the parameters are for the system with a type 1 controller.

It is convenient now to define certain new symbols ζ_1 and ω_{n1} by the relations (1)

$$\zeta_1 = \frac{f_0}{2\sqrt{J_0 k_1}} \quad [16]$$

$$\omega_{n1} = \sqrt{\frac{k_1}{J_0}} \quad [17]$$

and to rewrite Equation [15] in terms of these symbols thus

$$\epsilon(t) = \frac{1}{p^2 + 2\zeta_1\omega_{n1} p + \omega_{n1}} (p + 2\zeta_1\omega_{n1})\omega_i(t) \quad [18]$$

In Equation [18] ζ_1 is the damping ratio, that is, the ratio of the actual damping to the damping which would cause aperiodic response of the system. It is a dimensionless parameter and of course equals unity for critical damping; ω_{n1} is the undamped natural frequency of the system.

The response of the system defined by Equation [18] is oscillatory, aperiodic, or overdamped depending upon whether the roots of the denominator of Equation [18] when equated to zero, are conjugate complex, equal reals, or unequal reals, that is, whether ζ_1 is less than unity, unity, or greater than unity. The general form of the expression for the roots is

$$r_1, r_2 = -\zeta_1\omega_{n1} \pm j\omega_{n1}\sqrt{1 - \zeta_1^2} \quad [19]$$

$$= -\frac{1}{\tau_1} \pm j\omega_1 \quad [20]$$

where τ_1 is the characteristic time and ω_1 is the actual angular frequency.

The complete solution of Equation [18] for the case when a velocity ω_i is suddenly applied to the input member with the system at rest and ω_i is afterward maintained constant, and when the roots r_1, r_2 are conjugate complex, is

$$\epsilon(t) = \frac{2\zeta_1\omega_i}{\omega_{n1}}\left[1 - e^{-\frac{t}{\tau_1}}\left(\cos\frac{\sqrt{1-\zeta_1^2}}{\zeta_1}\frac{t}{\tau_1} + \frac{2\zeta_1^2 - 1}{2\zeta_1\sqrt{1-\zeta_1^2}}\sin\frac{\sqrt{1-\zeta_1^2}}{\zeta_1}\frac{t}{\tau_1}\right)\right] \quad [21]$$

Equation [21] thus gives the transient response and can be written in a nondimensional form convenient for plotting as

$$\frac{\epsilon(t)}{\epsilon_{ss}} = 1 - \frac{1}{2\zeta_1\sqrt{1-\zeta_1^2}} e^{-\zeta_1\omega_{n1}t}\sin\left(\sqrt{1-\zeta_1^2}\,\omega_{n1}t + \phi\right) \quad [22]$$

where

$$\epsilon_{ss} = \frac{2\zeta_1}{\omega_{n1}}\omega_i \quad [23]$$

and

$$\phi = \tan^{-1}\frac{2\zeta_1\sqrt{1-\zeta_1^2}}{2\zeta_1^2 - 1} \quad [24]$$

For the critically damped case Equation [22] reduces to

$$\frac{\epsilon(t)}{\epsilon_{ss}} = 1 - e^{-\omega_{n1}t}\left(1 + \frac{\omega_{n1}t}{2}\right) \quad [25]$$

where

$$\epsilon_{ss} = \frac{2\omega_i}{\omega_{n1}} \quad [26]$$

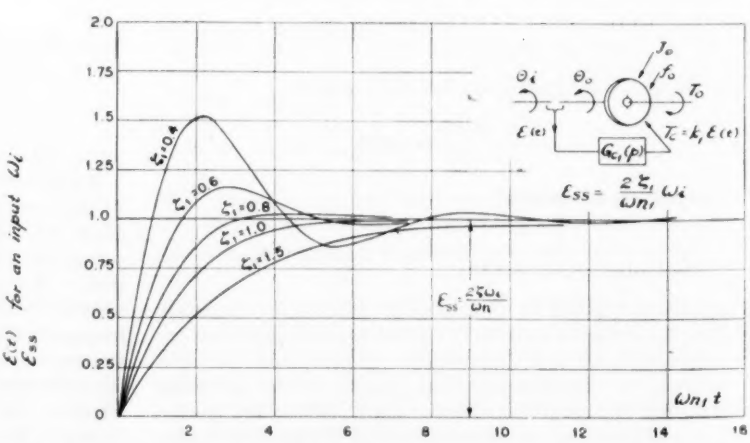


Fig. 4 Dimensionless Transient Error Curves for a Servomechanism With Type 1 Controller When Subjected to Suddenly Applied Input Velocity ω_i

The nature of the transient response is well illustrated by the family of curves in Fig. 4 which shows the dimensionless ratio $\frac{\epsilon(t)}{\epsilon_{ss}}$ as a function of the dimensionless quantity $\omega_{n1}t$ for various values of ζ_1. Load torque and coulomb torque are assumed to be zero. If the viscous-damping coefficient f_0 is assumed to be the only variable in the system, ω_{n1} is constant. Hence when the family of curves is examined with respect to the dimensionless abscissa scale $\omega_{n1}t$, the relative positions of the curves on the plot indicate the relative times of duration of the transient for the particular values chosen for ζ_1.

An inspection of Fig. 4 shows at once: (*a*) that for a type 1 servomechanism with constant ω_{n1} the actual time required for the system to reach substantially its steady-state error is practically independent of ζ_1 when $0.6 < \zeta_1 < 1.0$, whereas the time required for the system to attain any substantial part of its final steady-state error decreases as ζ_1 decreases; (*b*) that the overshoot or tendency to oscillate increases as ζ_1 is decreased; and (*c*) that the steady-following error is proportional to the ratio ζ_1/ω_{n1}. It follows therefore that any design of a type 1 controller is inherently a compromise unless certain specific performance requirements predominate, such for example as a given steady-state error at a given maximum velocity of operation of a given controlled member.

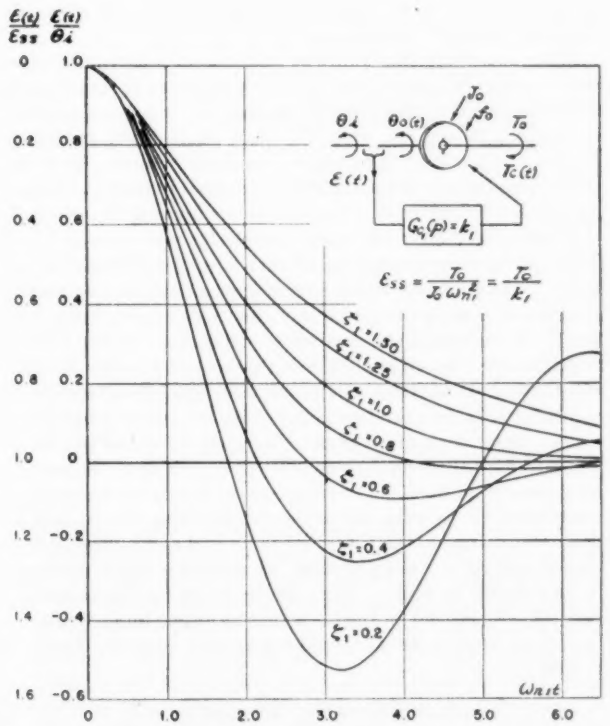


FIG. 5 DIMENSIONLESS TRANSIENT ERROR CURVES OF A SERVOMECHANISM WITH A TYPE 1 CONTROLLER WHEN SUBJECTED TO A SUDDENLY APPLIED INPUT ANGLE θ_i OR A SUDDENLY APPLIED LOAD TORQUE T_0

Fig. 5 shows the dimensionless solutions of Equation [8] for the angle and torque disturbances considered separately. Notice that a single family of curves satisfies both solutions if the ordinate scale for $\epsilon(t)/\theta_i$ for an angle disturbance is inverted to give the ordinate scale $\frac{\epsilon(t)}{\epsilon_{ss}}$ for the torque disturbance.

6 ILLUSTRATIVE EXAMPLE

The effectiveness with which the foregoing data may be used to direct the path of a typical design, and also the fundamental objection usually leveled at mechanisms with a type 1 controller, are readily demonstrated by the following example:

Suppose a given output member is to be automatically controlled in angular velocity and position and that the controller is to be capable of driving this member at 120 rpm with a steady-state following error, due only to viscous friction, of not greater than π radians. Assume that the moment of inertia of the controlled member plus its connected servomotor is 1 slug ft^2. Assume also that the system is to be critically damped. Determine the control constant k_1, and the viscous friction coefficient f_0.

From Equation [23]

$$\omega_{n1} = \frac{2\zeta_1\omega_1}{\epsilon_{ss}} = \frac{2 \times 4\pi}{\pi} = 8 \text{ radians per sec} \quad [27]$$

From Equation [17]

$$k_1 = \omega_{n1}^2 J_0 = 64 \text{ lb-ft per radian} \quad [28]$$

From Equation [16]

$$f_0 = 2\zeta_1\sqrt{J_0 k_1} = 16 \text{ lb-ft sec per radian} \quad [29]$$

From the curves in Fig. 4 the system reaches the steady-state velocity in a dimensionless time $\omega_{n1}t$ of approximately 5.5, or an actual time t of $5.5/8$ = approximately 0.7 sec.

The design constants and the time of duration of the transient are now known quantitatively. However, when it is realized that the power dissipated in viscous friction at maximum speed is $f_0\omega_1^2$, which in practical units is

$$\frac{16 \times (4\pi)^2}{550} \text{ or } 4.57 \text{ hp} \quad [30]$$

the objection to a type 1 mechanism is realized. It is clearly apparent that the designer faces a difficult task when he comes to devise means to dissipate this power in viscous friction and to devise a controller that will be essentially instantaneous and linear in operation and develop torques as great as 200 lb-ft. Furthermore, the entire viscous power serves only to damp the system, and serves no real productive purpose.

Smaller damping losses are achieved by resorting to underdamped operation, accepting a larger error, or decreasing inertia. For the same steady-state error and inertia, but with ζ_1 reduced to 0.6, the new constants are

$$\left.\begin{aligned} \omega_{n1} &= 4.8 \text{ radians per sec} \\ k_1 &= 23 \text{ lb-ft per radian} \\ f_0 &= 5.75 \text{ lb-ft sec per radian} \end{aligned}\right\} \quad [31]$$

The task of the designer has now been eased in proportion to ζ_1^2, and the power dissipated in damping reduced to 1.65 hp. The transient now exists for a dimensionless time $\omega_{n1}t$ of approximately 5, so that $t = 5/4.8$, or about 1 sec, compared with 0.7 sec formerly. The power lost in damping is still appreciable, however, and is the reason why viscous-damped servomechanisms are rarely built for power ratings greater than a few hundred watts.

7 CONTROLLERS IN ABSENCE OF OUTPUT DAMPING

The basic-error equation will now be examined to see whether the controller characteristic can be modified to permit the elimination of output damping power loss. Assume first that substantially all the viscous damping in the output member is eliminated by appropriate modifications to the design. The damping term then disappears from the denominator of Equation [9], the damp

ing ratio ζ_1 becomes substantially zero, the system tends to permit sustained oscillations and hence is impracticable. If by appropriate redesign of the controller, however, a new controller operator $C(p)$ can be obtained which has a term proportional to the time derivative of the error as well as to the error, a damping term is re-established in the denominator. The controller operator then has the form

$$C(p) = k + lp \quad [32]$$

and for the system to be stable it is necessary only that the magnitude of the coefficient l be such that the roots of the expression

$$J_0{}^2 + C(p) = 0 \quad [33]$$

have negative real parts.

This method of arriving at a desirable controller characteristic, while perhaps somewhat heuristic, is actually a very useful one because once the need for improvement in servomechanism performance is realized, the possibilities for achieving it by the design of a controller having the appropriate operator $C(p)$ become obvious after relatively little thought.

The use of control coefficients proportional to the derivative of the error is not new. The features which make this so-called derivative control desirable were pointed out by Minorsky (5) as early as 1922, and used by him in experiments on the automatic steering of ships prior to 1930. Later treatments are given by Hazen (6), and Mitereff (23). For purposes of identification a controller whose operator involves only the error and its derivatives is herein classified as type 2. To increase the scope of the analysis both first- and second-derivative control are assumed and the controller operator is written as

$$C_2(p) = k_2 \pm l_2 p \pm m_2 p^2 \quad [34]$$

In this expression k_2, l_2, and m_2 are positive real numbers, the subscripts 2 signify control coefficients for a type 2 controller, and the algebraic signs signify the possibility of designing the controller to apply components of torque in a positive or a negative direction for a given error or time rate of change of error. Obviously, there is no choice regarding the algebraic sign before k_2.

The substitution of the expression for $C_2(p)$ in Equation [9] gives, when coulomb friction and load torque are neglected

$$\epsilon(t) = \frac{(J_0 p + f_0)\omega_i(t)}{(J_0 \pm m_2)p^2 + (f_0 \pm l_2)p + k_2} \quad [35]$$

$$= \frac{(J_0 p + f_0)\omega_i(t)}{J_2 p^2 + f_2 p + k_2} \quad [36]$$

where

$$J_2 = J_0 \pm m_2 \quad \text{and} \quad f_2 = f_0 \pm l_2 \quad [37]$$

When Equation [36] is written in terms of nondimensional parameters, the expression is

$$\epsilon(t) = \frac{\sigma_2 p + 2\alpha_2\zeta_2\omega_{n2}}{p^2 + 2\zeta_2\omega_{n2}p + \omega_{n2}{}^2}\,\omega_i(t) \quad [38]$$

where

$$\left.\begin{aligned} \sigma_2 &= \frac{J_0}{J_2}, \qquad \zeta_2 = \frac{f_2}{2\sqrt{J_2 k_2}} \\ \alpha_2 &= \frac{f_0}{f_2}, \qquad \omega_{n2} = \sqrt{\frac{k_2}{J_2}} \end{aligned}\right\} \quad [39]$$

The general form of the roots of the denominator of Equation [38] are

$$r_1, r_2 = -\zeta_2\omega_{n2} \pm j\omega_{n2}\sqrt{1-\zeta_2{}^2} = \frac{1}{\tau_2} \pm j\omega_2 \quad [40]$$

The solution of Equation [38] in dimensionless form for the case of a velocity ω_i suddenly applied to the input member with the system at rest, with ω_i afterward maintained constant, and with ζ_2 less than unity is

$$\frac{\epsilon(t)}{\epsilon_{ss}} = \left[1 - e^{-\frac{t}{\tau_2}}\left(\cos\frac{\sqrt{1-\zeta_2{}^2}}{\zeta_2}\frac{t}{\tau_2} + \frac{2\alpha_2\zeta_2{}^2 - 1}{2\alpha_2\zeta_2\sqrt{1-\zeta_2{}^2}}\sin\frac{\sqrt{1-\zeta_2{}^2}}{\zeta_2}\frac{t}{\tau_2}\right)\right] \quad [41]$$

With critical damping the solution is

$$\frac{\epsilon(t)}{\epsilon_{ss}} = 1 - e^{-\frac{t}{\tau_2}}\left(1 + \frac{t}{\tau_2}\right) + \frac{1}{2\alpha_2}\frac{t}{\tau_2}e^{-\frac{t}{\tau_2}} \quad [42]$$

where in each instance

$$\epsilon_{ss} = \frac{2\alpha_2\zeta_2}{\omega_{n2}}\omega_i \quad [43]$$

Equations [41] and [42] therefore indicate the transient response of a servomechanism with a type 2 controller when subjected to a velocity disturbance.

When obtaining the transient response of a servomechanism with a controller which has derivative response, it should be remembered that $p^2\theta_i$ is an infinite impulse at $t = 0$ when a velocity ω_i is suddenly applied, and that both $p\theta_i$ and $p^2\theta_i$ are infinite impulses at $t = 0$ when an angle is suddenly applied. If the law of control given by Equation [34] is assumed to hold at all times, and these particular test disturbances are applied, the controller is required to deliver an infinite torque for zero time at $t = 0$. This, of course, is a requirement that no physical controller can fulfill. Thus a word of warning is appropriate here concerning the matter of using the methods of Heaviside's operational calculus (2, 9) to obtain the solution of expressions of the form of Equation [38] for an applied step function of velocity or angle. Operational calculus methods as ordinarily applied will assume the controller to be ideal and to comply with the law of control at all times. Solutions performed using the methods of LaPlace (9, 22) will introduce the boundary conditions applicable to the particular system conditions. The results given herein for the transient response of servos using derivative control recognize (*a*) that the maximum torque of the controller is limited and (*b*) that a finite torque applied to a mass member for zero time causes no change in its velocity or angle. The solution given by Equations [40] and [41] are derived on the basis that at a time immediately following the application of a suddenly applied velocity, that is, at $t = 0^+$

$$\left.\begin{aligned} &\epsilon,\ \theta_i, \text{ and } \theta_0 = \text{zero};\ p\epsilon = p\theta_i = \omega_i \\ &p\theta_0 = \text{zero};\ p^2\theta_i = \text{zero} \\ &p^2\epsilon = -p^2\theta_0 \end{aligned}\right\} \quad [44]$$

An examination of Equations [36], [41], and [42] indicates certain points regarding the algebraic sign which should be used with the coefficients l_2 and m_2 of Equation [34] to give the best system performance. For example, since the coefficient f_2 in Equation [36] must be positive to insure stability, and since the principal argument for derivative control is to allow output damping to be negligible, only the use of the positive algebraic sign with the coefficient l_2 has practical significance.

For design purposes quantitative data concerning the effects of varying the magnitude of first-derivative response in the controller are highly desirable. If it is assumed, in the interests of simplicity, that the entire damping is supplied by l_2, (the so-called derivative damping) α_2 is zero and the steady-state error as given by Equation [43] is zero. Equations [41] and [42] for the transient response can then be written in a form convenient for the study of the effects of varying l_2 as

$$\frac{\epsilon(t)\omega_{n2}}{\omega_i} = \frac{1}{\sqrt{1-\zeta_2^2}} e^{-\zeta_2\omega_{n2}t} \sin \sqrt{1-\zeta_2^2}\omega_{n2}t \Bigg|_{\alpha_2=0} \quad \ldots [41a]$$

for the oscillatory case, and as

$$\frac{\epsilon(t)\omega_{n2}}{\omega_i} = \omega_{n2}t\, e^{-\omega_{n2}t} \Bigg|_{\alpha_2=0} \quad \ldots\ldots\ldots\ldots [42a]$$

for the critically damped case.

The nature of the transient response of the system now obtained is well illustrated by the family of curves in Fig. 6 which shows the plot of $\frac{\epsilon(t)\omega_{n2}}{\omega_i}$ as a function of the dimensionless quantity $\omega_{n2}t$ for various values of ζ_2. To the extent that angle is considered dimensionless the curves in Fig. 6 are dimensionless. Load

The task of making available a controller that will establish the component of first-derivative response with a high degree of fidelity is frequently somewhat difficult. When it comes to making available a controller that will establish a component of second-derivative response the task becomes one of another order of difficulty. Even the problem of providing a component of response that merely resembles second derivative is frequently difficult. It is highly desirable therefore that a designer have available quantitative data to aid him in balancing the cost of producing a certain amount of second-derivative response against the improvement in the performance of the system which the use of this amount affords.

This matter concerns the question of both the algebraic sign and the magnitude of m_2 which should be used in any particular system. On a heuristic basis it might be argued that the introduction of second-derivative control is in effect the introduction of inertia. Negative inertia as afforded by the use of the negative sign with m_2 might therefore appear to be preferable in order to decrease the magnitude of the apparent inertia of the system. On the basis of this argument a coefficient m_2 equal in magnitude to J_0 and used with the negative algebraic sign might appear to provide the optimum adjustment. It should be clear, however, that values of m_2 greater than J_0 used in conjunction with the

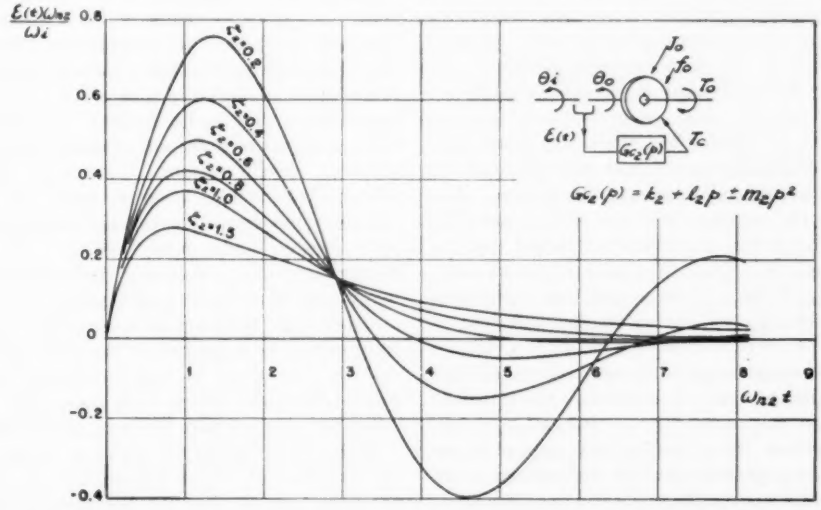


FIG. 6 TRANSIENT ERROR CURVES FOR A SERVOMECHANISM WITH A TYPE 2 CONTROLLER WITH $\alpha_2 = 0$ AND WITH σ_3 CONSTANT, WHEN SUBJECTED TO A SUDDENLY APPLIED INPUT VELOCITY ω_i

torque and coulomb friction are assumed zero in addition to output damping being zero. Since the abscissa variable ω_{n2} is not affected by changes in l_2 this family of curves indicates directly the true relative times of duration of the transient for the values of ζ_2 assumed. The curves also show some rather interesting conditions. For example, the error is substantially independent of ζ_2 when $\omega_{n2}t$ is approximately 3. Also any benefits which might result from attempting to decrease the time of the duration of the transient by decreasing ζ_2 are offset to some extent by an increase in the peak magnitude of the transient error. Specifically, a decrease in ζ_2 from unity to 0.8 decreases the time of the duration of the transient by about 30 per cent, but increases the peak error during the transient by about 13 per cent. Since a decrease in ζ_2 tends to decrease the controller design difficulties and costs, there appears therefore to be genuine merit in the use of a type 2 controller adjusted to give values of ζ_2 such that $0.6 < \zeta_2 < 1.0$, unless a system that oscillates even to only a slight extent is barred because of circumstances peculiar to the particular application.

negative algebraic sign give negative values of J_0, make the system unstable, and hence are barred. Unfortunately, this argument is inadequate for appraising quantitatively the benefits of specific amounts of second-derivative response.

The work involved in preparing quantitative data for this problem can be simplified without much loss generality of the results by again assuming output damping to be zero, thereby making α_2 and the steady-state error zero. If both l_2 and k_2 are held constant as $\pm m_2$ is varied, it follows readily from Equations [39] that ζ_2 and ω_{n2} are proportional to $\sqrt{\sigma_3}$, and hence dependent upon $\pm m_2$. Since the scales of ordinate and abscissa in Fig. 6 involve ω_{n2}, Equations [41a] and [42a] are not in a particularly convenient form for studying the effects of varying amounts of second-derivative control. It is possible, however, to express the error in a form which does not involve ω_{n2} by using a new characteristic time τ_2' defined as

$$\tau_2' = \frac{f_0 \pm l_2}{k_2} = \frac{2\zeta_2}{\omega_{n2}}$$

giving

$$\tau_2' = 2\zeta_2^2\tau_2 \quad [45]$$

In terms of this new characteristic time a dimensionless form of the error equation convenient for studying the effect of varying $\pm m_2$ is

$$\frac{\epsilon(t)}{\omega_i\tau_2'} = \frac{1}{2\zeta_2\sqrt{1-\zeta_2^2}}\, e^{-\frac{2\zeta_2 t}{\tau_2'}} \sin 2\zeta_2\sqrt{1-\zeta_2^2}\,\frac{t}{\tau_2'} \quad [41b]$$

for the oscillatory case and

$$\frac{\epsilon(t)}{\omega_i\tau_2'} = \frac{t}{\tau_2'}\, e^{-\frac{2t}{\tau_2'}} \quad [42b]$$

for the critically damped case.

Fig. 7 gives a plot of a family of curves of the dimensionless quantity $\frac{\epsilon(t)}{\omega_i\tau_2'}$ as a function of the dimensionless time $\frac{t}{\tau_2'}$ for various values of ζ_2. Load torque and coulomb friction are assumed zero in addition to output damping being assumed zero. Neither the ordinate nor the abscissa variables are here functions of $\pm m_2$. Therefore the family of curves indicates directly the true relative times of duration of the transient and the true relative magnitudes of the peak transient error for the assumed values of ζ_2. It must be remembered, however, that variations in the magnitude or the algebraic sign used with the component of second-derivative response of the controller vary ζ_2, since ζ_2 is proportional to $\sqrt{\sigma_2}$. Changes in controller design which affect the second-derivative response are nevertheless readily transferred into quantitative data giving the changes in the performance of the system. The procedure is to compare the response indicated by the curve for the damping ratio in effect before the design is changed, say, ζ_{2a}, and the curve for a ζ_2 equal to $\zeta_{2a}\sqrt{\sigma_2}$. For example, assume that a particular design has $\zeta_{2a} = 0.5$. Then assume that a proposed design modification will change $\pm m_2$ by an amount sufficient to increase σ_2 by a factor of 4. The system then has $\zeta_2 = \sqrt{4}\zeta_{2a} = 1.0$, and the effect of the design change on the relative magnitudes of peak transient error and the times of duration of the transient is shown quantitatively by the curves for $\zeta_2 = 0.5$ and $\zeta_2 = 1.0$, respectively. At first glance these results may appear to be strange for they show that a system originally underdamped and having a rather large peak error can be made to have a substantially smaller peak error, be less oscillatory, and be substantially faster in response by increasing σ_2.

The data in Figs. 6 and 7 serve (*a*) to confirm the heuristic conclusion that the negative algebraic sign should be used with m_2; (*b*) to show that the magnitude of m_2 must be substantial if a substantial decrease in the time of the duration of the transient be brought about; and (*c*), that operation with less than critical damping justifies consideration. It should be remembered, however, that it is probably undesirable to approach too close to the condition in which $\sigma_2 > 10$, that is, $m_2 = 0.9\ J_0$, because of the likelihood that the system will become unstable if accidentally J_2 becomes negative.

The optimum damping ratio for use in any application depends, of course, on the magnitude of the transient departure from the steady-state error that is permissible. Since there is likely to be both viscous and coulomb friction in the output member, the steady-state error is actually finite. A net damping ratio such that $0.6 < \zeta_2 < 0.8$ is then generally satisfactory from the standpoint of small overshoot and preferable from the standpoint of speed of response, because the error is brought within the steady-state operating band about as rapidly as is practicable.

On the basis of the foregoing arguments and the data in Figs. 6 and 7 there should be no doubt about the economic value of introducing a component of first-derivative response into the controller, since by doing so the cost and difficulty of adding damping to the output member are eliminated, the unusually large power rating required of the servomotor, and the ridiculously low over-all efficiency of such a system are obviated. The data herein given permit the designer to evaluate quantitatively the relative merits of first- and second-derivative response when designing a specific system. Considering the practical difficulties that are encountered when the task of designing a controller to yield a second-derivative response with high fidelity is undertaken, there are, no doubt, many instances where the returns hardly justify the costs. Obviously circumstances alter cases, and in many important control applications it is entirely proper to pay a rather large premium to decrease the time of duration of the transient or the magnitude of the peak transient error by a factor of even 2 or less. At such times only a moderate amount of control response, which even then only approximates second-derivative control, may prove to be extremely valuable.

Transient solutions for angle or torque disturbances applied to a system with a type 2 controller are readily obtained by the procedure given. For the boundary conditions at the instant immediately following the application of torque or angle, that is, at $t = 0^+$ such that

$$\epsilon = \theta_i;\ \theta_0 = \text{zero};\ p\epsilon = p\theta_i = p\theta_0 = \text{zero}$$

$$p^2\epsilon = -p^2\theta_0 \text{ and } p^2\theta_i = \text{zero}$$

the time solutions are identical for those obtained for a system with a type 1 controller with the exception that ζ_2 and ω_{n2} replace ζ_1 and ω_{n1}, respectively. The curves in Fig. 5 therefore apply to a type 2 controller if ζ_2 and ω_{n2} are used instead of ζ_1 and ω_{n1}.

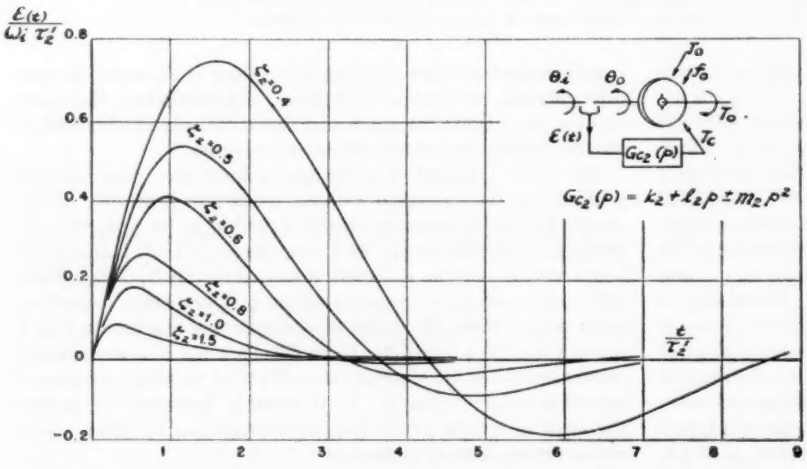


FIG. 7 DIMENSIONLESS TRANSIENT ERROR CURVES FOR A SERVOMECHANISM WITH A TYPE 2 CONTROLLER WITH $\alpha_2 = 0$ AND WITH l_2 CONSTANT, WHEN SUBJECTED TO A SUDDENLY APPLIED INPUT VELOCITY ω_i

8 CONTROLLERS TO COUNTERACT COULOMB OR LOAD TORQUES

In control applications where the output member is principally inertia, an acceptable steady-state error is frequently obtained by decreasing the viscous and coulomb frictions in the output member to a practical minimum and introducing derivative control to establish transient stability. At such times type 2

control is adequate. However, in applications such as precision machine-tool control, calculating machine servomechanisms, and so forth, exceedingly precise performance is often demanded even when the output member is required to operate against a substantial disturbing or load torque T_L, in addition to coulomb friction. At such times it is really difficult to obtain highly precise performance.

Although only mechanical systems have been discussed thus far, it should be remembered that where the mechanisms involve electrically operated elements or hydraulic elements, resistance in the electric circuits or fluid circuits is just as effective in causing steady-state error as mechanical viscous friction. Similarly, the induced voltage of an electromagnetic machine, or the operating fluid pressure of a hydraulic system, and similar phenomena, usually cause effects analogous to those of an output load torque. Also, magnetic hysteresis in the magnetic circuits of electromagnetic machines, and dielectric hysteresis in the dielectric of capacitive elements, are analogous to coulomb fricton and equally undesirable. Thus there is inherently a definite limit to the degree of precision with which almost any servomechanism having type 1 or type 2 controller can operate.

If means to combat these difficulties are to be devised they can come about only as a result of a modification to the controller, since the controller characteristic is really the only design variable. Accordingly the basic-error equation will again be examined, but this time with a view to devising for the controller operator $C(p)$ an expression that will insure not only a stable and rapid system, but one which will counteract the effects of coulomb or load torques.

For the system under consideration the error equation is, by analogy with Equation [9]

$$\epsilon(t) = \frac{(J_0p + f_0)\omega_i(t) + F(\omega) + T_L(t)}{J_0p^2 + f_0p + C(p)} \quad \ldots\ldots [46]$$

where the symbol F signifies coulomb friction torque which is a function of the velocity of the output shaft. Since the direction of this torque reverses as the direction of rotation reverses, Equation [46] is nonlinear and is difficult to handle mathematically. If, however, it is assumed that coulomb friction can be represented as a constant torque which appears only after t = zero, the analysis becomes relatively straightforward and the results are still sufficiently general to be useful. On this basis the error equation can be written for a velocity input as

$$\epsilon(t) = \frac{(J_0p + f_0)\omega_i(t) + F + T_L}{J_0p^2 + f_0p + C(p)} \quad \ldots\ldots [47]$$

For optimum performance it is desirable that the controller counteract the results of F and T_L during the period of transient operation as well as during the steady state. The transient-error behavior is indicated to a considerable extent by the nature of the roots of the denominator of Equation [47]. The steady-state error for a constant disturbance, however, is given directly by the foregoing error equation if p is put equal to zero after the equation is converted to the ratio of two polynomials. Therefore from the mathematical viewpoint at least, the steady-state error would be made zero if the controller were modified so that the law of control would have the effect of multiplying F and T_L by p in Equation [47]. Then when this is done an attempt might be made to adjust the magnitudes of the resulting function $C(p)$ to give the desired transient performance. Thus both objectives would be achieved.

The process of synthesizing a controller operator $C(p)$ which would achieve these objectives can logically start by multiplying the numerator and denominator of Equation [47] by p. The error equation then has the form

$$\epsilon(t) = \frac{p(J_0p + f_0)\omega_i(t) + p(F + T_L)}{p[J_0p^2 + f_0p + C(p)]} \quad \ldots\ldots [48]$$

The steady-state error is now zero, provided the denominator is a polynomial containing a constant term. The restrictions that may be imposed on the operator $C(p)$ to achieve satisfactory transient response are that the roots of the polynomial

$$\left.\begin{aligned} p[J_0p^2 + f_0p + C(p)] &= 0 \\ \text{or} \qquad J_0p^3 + f_0p^2 + pC(p) &= 0 \end{aligned}\right\} \quad \ldots\ldots [49]$$

have substantial negative real parts and, if complex, have magnitudes of the imaginary parts that provide reasonable periods for the oscillation of the system. Since one of the criteria to be satisfied in order for the roots to have negative real parts is that the polynomial have all the coefficients of the same algebraic sign, the simplest form for the function $pC(p)$ is

$$pC(p) = ap + b \quad \ldots\ldots [50]$$

where a and b are positive real quantities.

The result of this analysis has been to show that in order to counteract constant output torques a controller is required whose response is proportional to the error plus the time integral of the error. Actually, it has been known for some time that this response is of value in control problems of the type herein discussed, since it was demonstrated by Minorsky (5) as early as 1922 and treated by Mitereff (23) in 1935.

To those already familiar with automatic-control theory, moreover, it may appear that the foregoing analysis amounts to much ado about nothing This really is not so, however, for while to some persons it may have been obvious after a little thought that the inclusion of an integral term in the controller response would achieve the results desired in the simple example cited, it is not always so easy to reach reliable conclusions in more complicated control problems. On the other hand, the procedure here presented whereby the form of controller characteristic is deduced (*a*) by first examining the error equation with a view to seeing what properties it must have to yield the solution desired and (*b*) by manipulating it mathematically to give it these properties, is quite powerful and widely applicable in control problems. It readily yields data that are directly interpretable in terms of the design of a suitable controller.

In the analysis which follows the integral-plus-proportional controller is referred to as type 3. For the purposes of generality, and also in the interests of improved transient response of a servomechanism with this type of controller, the general form of the operator for type 3 control is taken as

$$C_3(p) = k_3 \pm l_3p \pm m_3p^2 + \frac{n_3}{p} \quad \ldots\ldots [51]$$

where k_3, l_3, m_3, and n_3 are all positive real quantities and, except for l_3 and m_3, they can be associated only with the positive algebraic sign because of stability criteria.

The substitution of $C_3(p)$ from Equation [51] in Equation [48] gives for the error of a servomechanism with a type 3 controller

$$\epsilon(t) = \frac{(J_0p^2 + f_0p)\omega_i(t) + p(F + T_L)}{J_3p^3 + f_3p^2 + k_3p + n_3} \quad \ldots\ldots [52]$$

where

$$J_3 = J_0 \pm m_3 \quad \text{and} \quad f_3 = f_0 \pm l_3 \quad \ldots\ldots [53]$$

9 Transient Solution of Servomechanisms With Type 3 Controller

Equation [52] does not readily yield a solution adaptable to simple graphical presentation from the design standpoint, because

of the large number of design variables and the complexity resulting from the third-order denominator. As Equation [52] stands, however, it shows that the steady-state error is zero for either a constant input angle, a constant input velocity, or a constant disturbing torque on the controlled member. However, if the input undergoes a constant acceleration, $p\omega_i$, the steady-state error is

$$\epsilon_{ss} = \frac{f_0}{n_3}(p\omega_i) \quad \ldots\ldots [54]$$

The question of an ideal versus a nonideal controller arises when a solution of Equation [52] is attempted for a step-function disturbance of angle or velocity. It is seen by inspection of Equation [52] written in the form of a step function of angle, that the operational solution at $t = 0$ for the equation as it stands is

$$\epsilon(0) = \frac{J_0}{J_3}\theta_i$$

This result can be obtained by taking the limit of the error equation as p tends to infinity. For this value of $\epsilon(0)$ to occur the output member would have to undergo a finite displacement in zero time. No physical controller can accomplish this with an output member that comprises mass because the mass cannot be moved in zero time by only a finite torque. This argument is given only briefly for simplicity. If the differential equation of Equation [52] is solved by classical methods subject to physically realizable boundary conditions at $t = 0$, and especially that $\epsilon(0) = \theta_i(t)$ at $t = 0$, the solution will be correct. Alternatively, if methods of formulating the equation such as those of LaPlace (9) are followed, the term J_3 appears in the numerator of the error equation, and not J_0. For these reasons the liberty is taken here of writing the error equation in corrected operational form for a velocity disturbance as

$$\epsilon(t) = \frac{(J_3p^3 + f_0p)\omega_i + p(F + L)}{J_3p^3 + f_3p^2 + k_3p + n_3} \quad \ldots\ldots [55]$$

and for an angle disturbance as

$$\epsilon(t) = \frac{(J_3p^3 + f_3p^2)\theta_i + p(F + L)}{J_3p^3 + f_3p^2 + k_3p + n_3} \quad \ldots\ldots [56]$$

It is desirable to attain some simplification of Equations [55] and [56] before attempting a solution. Simplification occurs, partially at least, by writing the equation in a dimensionless form. Two forms have been found useful. One follows from a method originally indicated by Weiss (10). The other follows by recognizing that the factors of a cubic equation can be written as a quadratic times a real root. Both forms are helpful in design studies. Weiss has prepared useful charts (10) giving the roots of the cubic in forms that aid many design problems. Liu (11) and Evans (12) have prepared charts in the form that is of special significance when the cubic is written as a quadratic factor and a real root. These charts have been found somewhat more useful than those of Weiss, because they permit the solution to be written in terms of damping ratios and undamped natural frequencies, with the result that the data already given in dimensionless form for type 1 and type 2 servos can be made immediately applicable semiquantitatively simply by matching characteristics of the oscillatory components for ζ and ω_n.

The dimensionless form that follows from the work of Weiss writes the denominator of the type 3 servo

$$p^3 + \frac{f_3}{J_3}p^2 + \frac{k_3}{J_3}p + \frac{n_3}{J_3} = 0 \quad \ldots\ldots [57]$$

in the form

$$p^3 + 2\zeta_c\omega_n p^2 + \omega_n{}^2 p + S\omega_n{}^3 = 0 \quad \ldots\ldots [58]$$

where the terms ζ_c, ω_n, and S are merely defined by applying the approach used for nondimensionalizing the quadratic, and in the case of ζ_c and ω_n do not represent a damping ratio or undamped natural period. By definition

$$\left.\begin{aligned} S &= 2\zeta_3\gamma_3 = \frac{n_3}{k_3}\sqrt{\frac{J_3}{k_3}} \\ \zeta_c &= \frac{f_3}{2\sqrt{J_3k_3}}, \quad \omega_n = \sqrt{\frac{k_3}{J_3}} \end{aligned}\right\} \quad \ldots\ldots [59]$$

where γ_3 comes from a stability ratio $\frac{J_3n_3}{f_3k_3}$ using Rouths' stability criteria.

The alternate form, as used by Liu and Evans, writes the denominator as

$$(p + \xi\omega_{nq})(p^2 + 2\zeta_q\omega_{nq}p + \omega_{nq}{}^2) = 0 \quad \ldots\ldots [60]$$

where ζ_q and ω_{nq} now represent specifically the damping ratio and undamped natural period of the quadratic factor or oscillatory component.

The relations between S, ζ_c, ω_n and ξ, ζ_q, and ω_{nq} are

$$(2\zeta_q + \xi)\omega_{nq} = 2\zeta_c\omega_n = \frac{f_3}{J_3} \quad \ldots\ldots [61a]$$

$$(2\zeta_q\xi + 1)\omega_{nq}{}^2 = \omega_n{}^2 = \frac{k_3}{J_3}; \text{ and } \xi\omega_{nq}{}^3 = S\omega_n{}^3 = \frac{n_3}{J_3} \quad \ldots\ldots [61c]$$

An interesting application of the merits of these so-called dimensionless forms of equations results from a study of the following problem: Assume that integral response is to be introduced into a controller which initially has a ratio of output damping to total damping $\alpha_3 = 0.2$ and a damping ratio ζ_2 which is also $\zeta_0 = 0.8$. Assume that it is desired to investigate the form of the transient response to a suddenly applied velocity or angle as integral response is introduced into the controller in amounts represented by $S = 0$, 0.2, 0.4. Since the servo without integral control has already been studied in terms of curves using $\omega_n t$ as the dimensionless time, see Figs. 4, 5, and 6, the same form of dimensionless time can again be used to advantage.

Table 1 shows the dimensionless solution for the error equation of the form

$$\epsilon(t) = \frac{[p^2 + \omega_{nq}\alpha_3(2\zeta_q + \xi)p]\omega_i}{(p + \xi\omega_{nq})(p^2 + 2\zeta_q\omega_{nq}p + w_{nq}{}^2)} \quad \ldots\ldots [55a]$$

$$\epsilon(t) = \frac{[p^2 + \omega_{nq}(2\zeta_q + \xi)p^2]\theta_i}{(p + \xi\omega_{nq})(p^2 + 2\zeta_q\omega_{nq}p + \omega_{nq}{}^2)} \quad \ldots\ldots [56a]$$

where load torques are neglected.

Figs. 8 and 9 show the solution of $\frac{\epsilon(t)\omega_n}{\omega_i}$ and $\frac{\epsilon(t)}{\theta_i}$ as a function of $\omega_n t$.

The numerical solutions were obtained using the cubic chart prepared by Liu (11). Values of ζ_c and S are known and are the values used to enter the chart for determining the values of ζ_q, ξ. Finally ω_{nq} is computed from S and ξ using the relation

$$\omega_{nq} = \left(\frac{S}{\xi}\right)^{1/3}$$

One observation predominates from an inspection of Figs. 8 and 9, namely, that a system which initially is well damped and

TABLE 1 RESPONSE OF A SERVOMECHANISM WITH A TYPE 3 CONTROLLER

For a suddenly applied input velocity disturbance ω_1

$$\epsilon(t) = \frac{(J_3p^2 + f_0p)\,\omega_1}{J_3p^3 + f_3p^2 + k_3p + n_3}$$

$$\epsilon(t) = \frac{\left[p^2 + a_3(2\zeta_q + \xi)\,\omega_{nq}\right]\omega_1}{(p + \xi\omega_{nq})\,(p^2 + 2\zeta_q\omega_{nq}p + \omega_{nq}^2)}$$

$$\frac{\epsilon(t)\omega_n}{\omega_1} = k_1\epsilon^{-\xi\omega_{nq}t} + k_2\epsilon^{-\zeta_q\omega_{nq}t}\cos\left(\omega_{nq}\sqrt{1-\zeta_q^2}\,t + \theta\right)$$

$$k_1 = \frac{\sqrt[3]{\xi}\left[(2\zeta_q + \xi)\,a_3 - \xi\right]}{\sqrt[3]{S}\left[\xi^2 - 2\zeta_q\xi + 1\right]}$$

$$k_2 = \frac{\sqrt[3]{\xi}\sqrt{a_3^2\,(2\zeta_q + \xi)^2 - 2a_3\zeta_q\,(2\zeta_q + \xi) + 1}}{\sqrt[3]{S}\sqrt{(1-\zeta_q^2)\,(\xi^2 - 2\zeta_q\xi + 1)}}$$

$$\theta = \tan^{-1}\frac{\zeta_q - a_3\,(2\zeta_q + \xi)}{\sqrt{1-\zeta_q^2}} - \tan^{-1}\frac{\sqrt{1-\zeta_q^2}}{\xi^2 - \zeta_q}$$

For a suddenly applied input angular disturbance θ_1

$$\epsilon(t) = \frac{(J_3p^3 + f_3p^2)\,\theta_1}{J_3p^3 + f_3p^2 + k_3p + n_3}$$

$$\epsilon(t) = \frac{\left[p^3 + (2\zeta_q + \xi)\,\omega_{nq}p^2\right]\theta_1}{(p + \xi\omega_{nq})\,(p^2 + 2\zeta_q\omega_{nq}p + \omega_{nq}^2)}$$

$$\frac{\epsilon(t)}{\theta_1} = k_1\epsilon^{-\xi\omega_{nq}t} + k_2\epsilon^{-\zeta_q\omega_{nq}}\cos\left(\omega_{nq}\sqrt{1-\zeta_q^2}\,t + \theta\right)$$

$$k_1 = \frac{-2\zeta_q\xi}{(\xi^2 - 2\zeta_q\xi + 1)}$$

$$k_2 = \frac{\sqrt{(1+\xi\zeta_q)^2 + (\xi\sqrt{1-\zeta_q^2})^2}}{\sqrt{1-\zeta_q^2}\sqrt{\xi^2 - 2\xi\zeta_q + 1}}$$

$$\theta = \tan^{-1}\frac{1 + \zeta_q\xi}{\xi\sqrt{1-\zeta_q^2}} - \tan^{-1}\frac{\sqrt{1-\zeta_q^2}}{\xi - \zeta_q}$$

$$J_3 = J_o \pm m_3 \qquad G_c(p) = k_3 \pm \ell_3 p \pm m_3p^2 \pm \frac{n_3}{p}$$

$$f_3 = f_o \pm \ell_3$$

$$\sigma_3 = \frac{J_o}{J_3}$$

$$a_3 = \frac{f_o}{f_3}$$

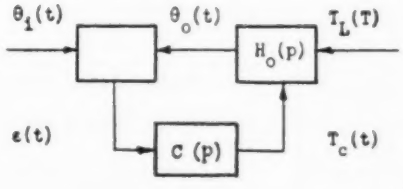
$$\zeta_3 = \frac{f_3}{2\sqrt{k_3J_3}}$$

$$2\zeta_3\,\omega_n = (2\zeta_q + \xi)\,\omega_{nq}$$

$$\omega_n^2 = (2\zeta_q\xi + 1)\,\omega_{nq}^2$$

$$S\omega_n^3 = \xi\omega_{nq}^3$$

$$\omega_{n3} = \sqrt{\frac{k_3}{J_3}}$$



fast becomes more oscillatory and faster as integral control is increased. To procure a reduction in the degree of oscillation, it is apparent immediately that ζ_q must be increased because this parameter controls the oscillatory component. A valuable feature of the dimensionless study using curves such as those prepared by Liu is now recognized because the curves of either Weiss or Liu quickly show the manner in which ζ_c or S must be varied to give the desired ζ_q. Although these parameters are dimensionless, their transformation into real parameters is simple so that actually the curves directly give quantitative data. It is interesting to note that there is always a value of ζ_c beyond which little improvement in ζ_q is obtained, thus necessitating a review of the whole design problem.

10 Systems Involving Energy Storage Elements in Controller or Output

In the preceding analysis the controller has been assumed to be an element that correctly obeys the law of control as given for $C(p)$. While this condition is approximated in many systems, certain inherent properties of physical elements cause the introduction of other considerations into the analysis. For example, the output stages of controllers, which involve power amplification or the servomotor driving the output member, will frequently include (*a*) inductance if it is electromagnetic, (*b*) elastance of oil lines or inertia of valves or pistons if it is hydraulic, (*c*) elastance of air lines if pneumatic. Thus energy storage and energy dissipation occur throughout the system with attendant so-called "response delays." The over-all controller response $T_c(t)$ is then not in phase with the signal that actually initiates the action of the servomotor elements, as is implied by Equation [12].

When the response of any element is fast compared with the system response, its response may be considered instantaneous because the energy storage can usually be neglected. When its response becomes comparable with the speed of system response it is necessary to modify the operator for the controller to introduce the effects of these energy storage elements into the analysis. To do this let a new operator $D(p)$ be used to describe the over-all performance of the controller-servomotor combination, where $D(p) = C(p)\,A(p)$ and in which $C(p)$ characterizes only the portion of the controller that receives the error signal $\epsilon(t)$ and operates on it to yield the proportional, derivative, or integral components of control, and $A(p)$ takes account of the energy storage or "response delay" in the controller output or the servomotor. Equation [2] now becomes $T_c(t) = C(p)\,A(p)\,\epsilon(t)$ and the over-all system operator from Equation [4*a*] becomes

$$1 + C(p)\,A(p)\,H_o(p)$$

As an illustration, consider that the controller comprises a

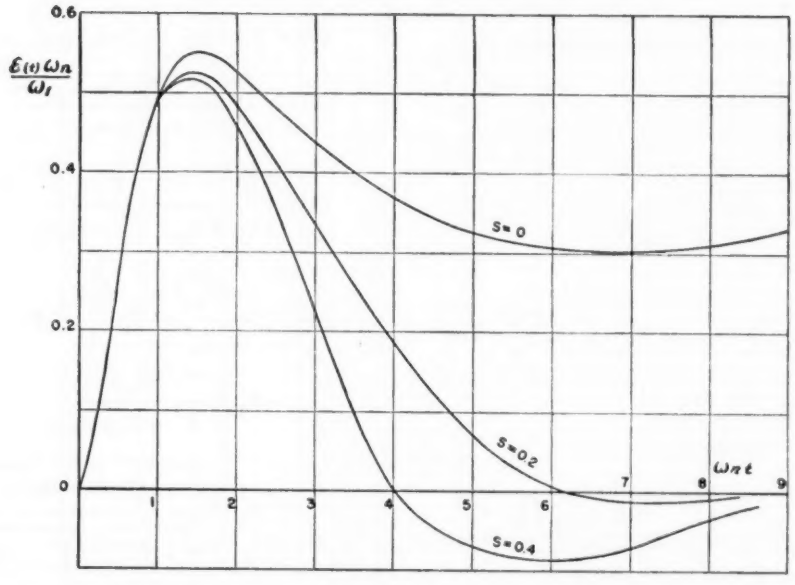


FIG. 8 TRANSIENT ERROR CURVES FOR A VELOCITY DISTURBANCE SHOWING EFFECT OF INTRODUCING INTEGRAL CONTROL INTO A TYPE 2 SERVOMECHANISM FOR WHICH INITIALLY $\zeta_2 = 0.8$ AND $\alpha_2 = 0.2$
(Amount of integral control is given by $S = 0$, 0.2, and 0.4.)

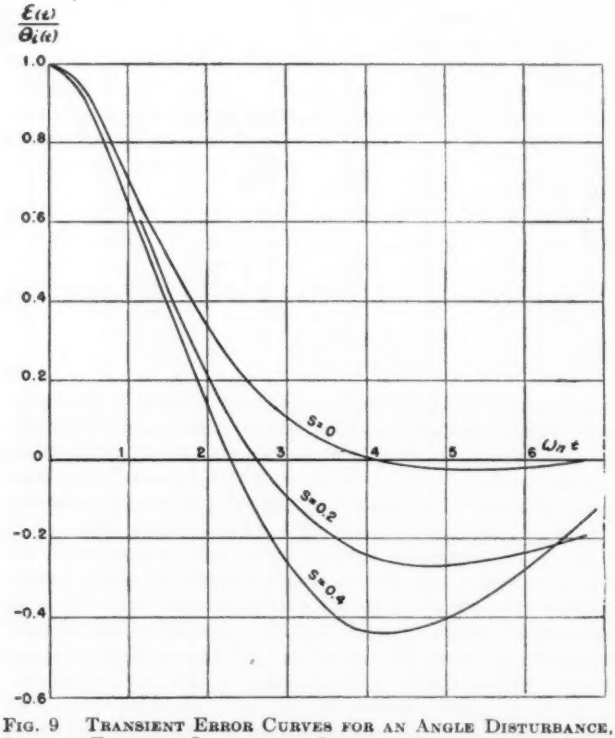


FIG. 9 TRANSIENT ERROR CURVES FOR AN ANGLE DISTURBANCE, SHOWING EFFECT OF INTRODUCING INTEGRAL CONTROL INTO A TYPE 2 SERVOMECHANISM FOR WHICH INITIALLY $\zeta_2 = 0.8$ AND $\alpha_2 = 0.4$
(Amount of integral control is given by $S = 0$, 0.2, and 0.4.)

vacuum-tube amplifier that energizes the field of a generator supplying an electric servomotor. The operator $C(p)$ characterizes the vacuum-tube amplifier field circuit of the generator. If it is assumed that the build-up field flux in the generator is substantially in phase with the grid signal on the amplifier, the principal response lag will be in armature current. The build-up of servomotor torque will lag the generator-field flux because of inductance L_a and resistance R_a of the two armatures. The operator $A(p)$ characterizing the servomotor would then have the form

$$A(p) = \frac{K}{L_a p + R_a}$$

Thus for the system considered in Fig. 3, Equation [9] would take the form

$$\epsilon(t) = \frac{L_a p + R_a}{K(J_0 p^2 + f_0 p)(L_a p + R_a) + C(p)} [(J_0 p + f_0)\omega_i(t) + T_0(t)]$$

A typical block diagram for a system involving several ele-

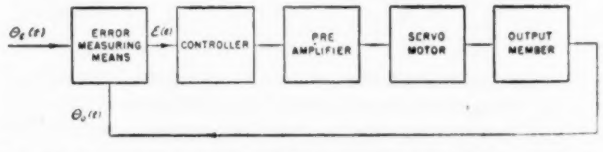


FIG. 10 BLOCK DIAGRAM FOR SERVOMECHANISM COMPRISING SEVERAL ENERGY STORAGE ELEMENTS IN CASCADE

ments, each with response lag, is shown in Fig. 10. The over all system operator for such a system is

$$1 + \begin{bmatrix}\text{Controller}\\ \text{Operator}\end{bmatrix}\begin{bmatrix}\text{Preamplifier}\\ \text{Operator}\end{bmatrix}\begin{bmatrix}\text{Servomotor}\\ \text{Operator}\end{bmatrix}\begin{bmatrix}\text{Output}\\ \text{member}\\ \text{Operator}\end{bmatrix}$$

which leads to a characteristic equation involving high powers of p for which the labor in getting transient solutions may be considerable. The matter is discussed in section 13.

11—SYSTEMS WITH OUTPUT FEEDBACK

In many servomechanisms the error signal given by the error-measuring means is of such a form that it cannot even be easily differentiated once to give good control signals for stabilizing purposes, as previously discussed for a type 2 system, let alone be differentiated twice. In some cases the particular embodiment that the servomechanism takes makes it undesirable to employ

derivative networks. Frequently the error is of such form that good techniques for giving its time rate of change do not exist.

Methods of control that will yield the desired stability or dynamic performance without error differentiation therefore become necessary. The method most commonly used is to feedback (14) to the input a signal that is some function of the response of the servo output, or a response just ahead of the output. Fig. 11 shows the block diagram for a typical system involving

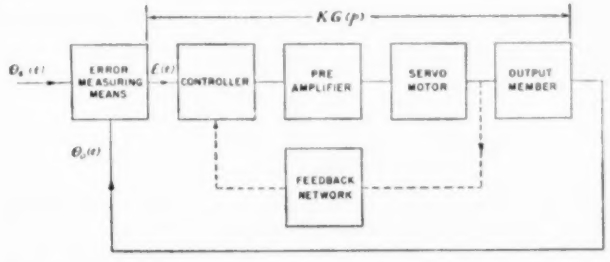


FIG. 11 BLOCK DIAGRAM FOR SERVOMECHANISM COMPRISING SEVERAL ENERGY STORAGE ELEMENTS IN CASCADE AND FEEDBACK WITHIN CLOSED LOOP

feedback. The particular functional relationship between the output and the feedback signals is established by an arrangement of elements inserted specifically for the purpose, and for which a feedback operator is known or can be deduced. No standard rule can be given for the form of the operator used for the feedback (14) since the choice of derivative, integrative, or even the number of feedback elements becomes a function of the specific application for which the servomechanism is intended.

As a general rule the introduction of feedback networks adds energy-storage elements into the system and increases the powers of p in the characteristic equation. By the application of the operator relations for the resulting network the over-all system operator becomes for Fig. 11

$$1+\begin{bmatrix}\text{Controller}\\ \text{Operator}\end{bmatrix}\begin{bmatrix}\text{Preamplifier}\\ \text{Operator}\end{bmatrix}\begin{bmatrix}\text{Servomotor}\\ \text{Operator}\end{bmatrix}\begin{bmatrix}\text{Output}\\ \text{Operator}\end{bmatrix}$$
$$1-\begin{bmatrix}\text{Controller}\\ \text{Operator}\end{bmatrix}\begin{bmatrix}\text{Preamplifier}\\ \text{Operator}\end{bmatrix}\begin{bmatrix}\text{Servomotor}\\ \text{Operator}\end{bmatrix}\begin{bmatrix}\text{Feedback}\\ \text{Operator}\end{bmatrix}$$

12 TRANSIENT ANALYSIS OF SYSTEMS INVOLVING HIGH-ORDER CHARACTERISTIC EQUATIONS

In the systems of the types discussed in sections 10 and 11 the characteristic equations invariably involve high powers of p. The transient analysis then becomes complicated because of (a) the difficulty of determining the parameters of all elements such as inertia, elastance, inductance, damping, amplification, torque gradient, and so forth, for each element in the system and (b) the labor of getting the roots and the time solutions to problems involving characteristic equation of high orders. While the analysis may be classified as tedious, the synthesis of controllers and feedback elements by the transient methods is difficult because the coefficients of the powers of p in the characteristic equation are a heterogeneous arrangement of many of the parameters of the elements of the system. Thus even when the work of obtaining the transient solution has been completed it is difficult to identify any particular element in the system that must be changed to cause any preselected modification in system behavior.

A qualitative knowledge of the transient behavior that is useful for many purposes may, however, be obtained by recognizing that the characteristic equation can be factored into the product of quadratic factors as follows

$$p^n + bp^{n-1} + cp^{n-2} + \ldots = (p^2 + 2\zeta_a\omega_{na}p + \omega_{na}^2)(p^2 + 2\zeta_b\omega_{nb}p + \omega_{nb}^2)\ldots(p + a)$$

Each quadratic factor contributes to a mode of oscillation in the solution having damping ratios ζ_a, ζ_b, ζ_c and undamped natural frequency ω_{na}, ω_{nb}, ω_{nc}, and so forth. Then by the principle of linear superposition the servomechanism response is the sum of the responses attributed to the specific modes a, b, c, etc. Thus for each component of error response the duration of the transient is given qualitatively by reference to the types of solutions given in the body of the paper for simple quadratics, and the relative magnitudes of the transients can often be approximated from the observation that the higher the magnitude of the root the smaller the coefficient of the time solution involving that root. It should be remembered that the parameters of the several elements in a system are not always known to high degrees of accuracy, and that approximate or graphical methods (11, 12, 19, 20, 22) that give the roots to the characteristic equations[5] to a few significant figures are justifiable and timesaving.

Because of the difficulties mentioned the transient method of analysis of complicated systems becomes most valuable as an aid to the visualization of the performance of a system rather than an aid in its design. If a designer has carried out the analysis of the dynamic performance based upon transient studies he can correlate the information with the actual performance if he gives any physical system a transient disturbance by any one of several means readily available to him and then observes or measures the response.

The next section of the paper treats a method of analysis that is particularly useful in the design of complicated systems. This method is sometimes termed the transfer-loci method and is based upon the frequency-response characteristic of the servomechanism.

13 FREQUENCY RESPONSE OF A SERVOMECHANISM

The difficulties of analyzing or synthesizing a complex servomechanism or automatic-control system by the transient method of analysis early became apparent to several investigators and a search was made for a more powerful and less cumbersome method of analysis. During this search it was natural to examine the methods employed in electrical analysis since complex electrical circuits had been analyzed and synthesized effectively for many years. Circuit analysis has been effectively carried out for some time through the study of its frequency-response characteristics. It appeared that the same general approach might prove effective in servomechanism design. Nyquist had developed a powerful means of determining the stability of feedback amplifiers through a study of its frequency-response characteristics and the similarity between feedback amplifiers and servomechanisms had been recognized. In 1942 Harris (21) pointed out that genuine improvements in design technique might result from applying the frequency-response method of analysis to servomechanism design, and in 1943 Hall (13) presented a thorough treatment of servomechanism analysis and synthesis by frequency-response methods. As a result of these investigations the frequency-response approach to servomechanism analysis has been developed into a powerful tool. Most of the remainder of the present paper is adapted from the paper by Hall (13).

The term "frequency-response characteristic," when applied to a mechanism, refers to the relationship between the input and the output of that mechanism when the input is a sinusoidal function of time. In servomechanism terminology, if $\theta_i(t)$ is the input and $\theta_0(t)$ is the output of a servomechanism (see Fig. 2) then if

[5] For a summary of graphical and analytical methods of obtaining the roots to characteristic equations, see Appendix C of the book by Ed S. Smith (22).

$$\theta_i(t) = A \sin \omega t \quad [57]$$

and A is small it will always be true that

$$\theta_0(t) = B \sin (\omega t + \phi) \quad [58]$$

In these equations A is known as the amplitude of the input, B is known as the amplitude of the output, ω is the angular frequency of motion of $\theta_i(t)$ and $\theta_0(t)$ (equal to $2\pi f$ where f is in cycles per second), and ϕ is the relative phase angle between $\theta_i(t)$ and $\theta_0(t)$.

The amplitude ratio B/A, and the phase angle ϕ, when determined as functions of angular frequency ω, comprise the frequency-response characteristic of the servomechanism.

As just shown, the relationship between $\theta_0(t)$ and $\theta_i(t)$, when $\theta_i(t)$ is a sinusoidal function of time, is specified by a magnitude (B/A) and an angle (ϕ). These two quantities can be considered as the defining properties of a vector whose amplitude is (B/A) and whose phase is ϕ. Thus it is frequently stated that a vector relationship exists between $\theta_i(t)$ and $\theta_0(t)$, when $\theta_i(t)$ varies sinusoidally with time. This vector relationship is represented symbolically by $\frac{\theta_0}{\theta_i}(j\omega)$ in which $j(=\sqrt{-1})$, itself, is generally thought of as a vector and emphasizes the vector properties of the ratio. The vector ratio, $\frac{\theta_0}{\theta_i}(j\omega)$ is characterized by an amplitude

$$\left|\frac{\theta_0}{\theta_i}(j\omega)\right|, \text{ and a phase, arc } \left[\frac{\theta_0}{\theta_i}(j\omega)\right]$$

The preceding development is briefly summarized as follows: If in a servomechanism

$$\theta_i(t) = A \sin \omega t \quad [57]$$

then

$$\theta_0(t) = B \sin (\omega t + \phi) \quad [58]$$

By definition the frequency response is denoted by $\frac{\theta_0}{\theta_i}(j\omega)$. The amplitude response is given by

$$\left|\frac{\theta_0}{\theta_i}(j\omega)\right| = \frac{B}{A} \quad [59]$$

and the phase response is represented by

$$\text{arc}\left[\frac{\theta_0}{\theta_i}(j\omega)\right] = \phi \quad [60]$$

The amplitude and phase response curves of a typical servomechanism are illustrated in Fig. 12.

The curves in Fig. 12 may be obtained (*a*) by calculation, if the constants of an actual or proposed design are available, or (*b*) by measurement, if the servomechanism itself is available. The frequency-response characteristic is measured by moving the input sinusoidally at a fixed amplitude but at various frequencies. At each frequency the amplitude of the output and its phase relation to the input motion is measured. The ratio of the amplitudes, plotted for each frequency, yields the first of the curves in Fig. 12. The phase difference between the input and output plotted for various frequencies gives the second of the curves in Fig. 12. The curves in Fig. 12 are readily calculated if the constants of the system and the differential equation relating the output to the input are known. The calculation is effected by replacing the operator p by the frequency operator $j\omega$ (where $j = \sqrt{-1}$) and applying conventional vector arithmetic.

The frequency response of a servomechanism may be closely correlated with its transient response. Important natural frequencies in the transient response are indicated by peaks in the amplitude-response curve. The magnitudes of the peaks of the amplitude response are measures of the relative damping of the natural frequencies of the transient response. The frequency band over which the amplitude response has a substantially constant magnitude is a measure of the speed of response to transients, since a high natural frequency (and therefore a high speed of response) is linked with a high resonant frequency in the amplitude response. When, as just indicated, the frequency-response characteristic is correlated with the transient-response characteristic, the former becomes a powerful means of analysis. The correlation between the sinusoidal and transient characteristics is illustrated by comparing the transient and frequency response of a simple servomechanism, representable by a second-order differential equation. Such a servomechanism comprises a servomotor with a moment of inertia and damping and whose output torque is proportional to the error.

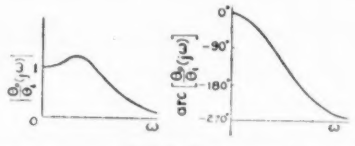


FIG. 12 AMPLITUDE- AND PHASE-RESPONSE CURVES OF A TYPICAL SERVOMECHANISM

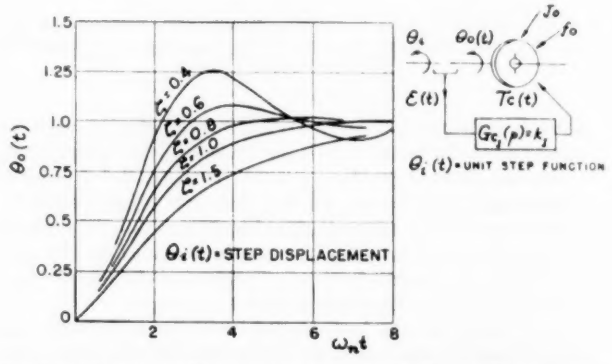


FIG. 13 TRANSIENT RESPONSES OF A SECOND-ORDER SERVOMECHANISM

If the input $\theta_i(t)$ is a step displacement and the output $\theta_0(t)$ is determined for various values of the damping ratio, the set of transient responses illustrated in Fig. 13 results. If $\theta_i(t)$ is made a sinusoidal function

$$\theta_i(t) = A \sin \omega t$$

and the amplitude response of the output $\theta_0(t)$ is determined, the set of curves in Figs. 14 and 15 is obtained. Comparison of the transient and frequency responses reveals a number of points of correspondence: (*a*) The frequency at which the transient response oscillates (the natural frequency) is approximately the same as the frequency at which the amplitude response has a peak (the resonant frequency); (*b*) as the damping ratio is reduced the transient response becomes more oscillatory, and the peak in the amplitude response is magnified; (*c*) when the damping ratio is made larger than unity the transient response becomes sluggish and the amplitude response falls off rapidly without a peak.

It is frequently convenient to combine the information contained in the amplitude-response curve and in the phase-response curve of a system by a single graph. This can be accomplished by remembering that the amplitude ratio and the phase angle are

quantities defining a vector which relates the output and input. As the frequency of the input is varied this vector varies in phase and magnitude and the amplitude- and phase-response curves present the information on the manner in which these two properties of the vector change with frequency. The same information can be provided in an alternative way by plotting on polar co-ordinate paper the path followed by the tip of the vector as the frequency varies over the band of interest. If various points of the curve are labeled with the frequency to which they correspond one curve will supply the information contained in

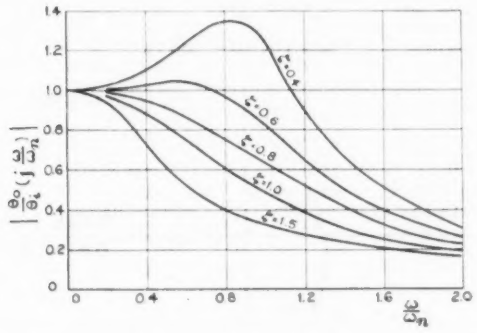


FIG. 14 AMPLITUDE-RESPONSE CURVES OF SECOND-ORDER SERVOMECHANISM

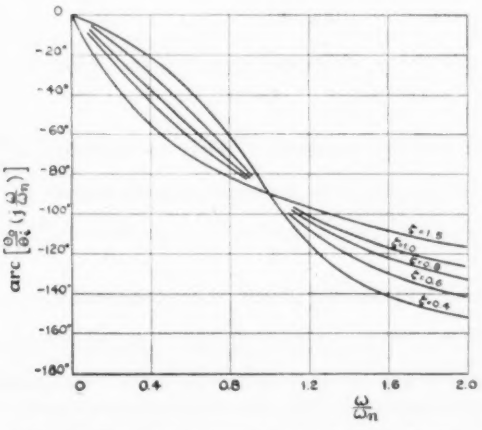


FIG. 15 PHASE-RESPONSE CURVES OF SECOND-ORDER SYSTEM

two curves when the amplitude and phase response are plotted separately. This graphical presentation is known as the locus of the frequency-response characteristic. It is illustrated in Fig. 16 which was drawn for the same second-order system to which the curves in Figs. 14 and 15 apply. The principal advantage of presenting information in this fashion lies in the means it provides for visualizing the frequency response and in the fact that it emphasizes the very important relationship that always exists between the amplitude and phase responses of a system.

14 SERVOMECHANISM TRANSFER FUNCTION

It is clear from the block diagram in Fig. 11 that a single function completely defines the performance of a servomechanism in which the feedback link contains no frequency-dependent elements. The defining function is the relationship between the servo output θ_0 and the error ϵ. If this relation is known in operational; sinusoidal, or time-response forms, the performance of the system is completely defined for all conditions that may be imposed upon it. This function, relating the servomechanism output to its error, has been termed the "transfer function" of the

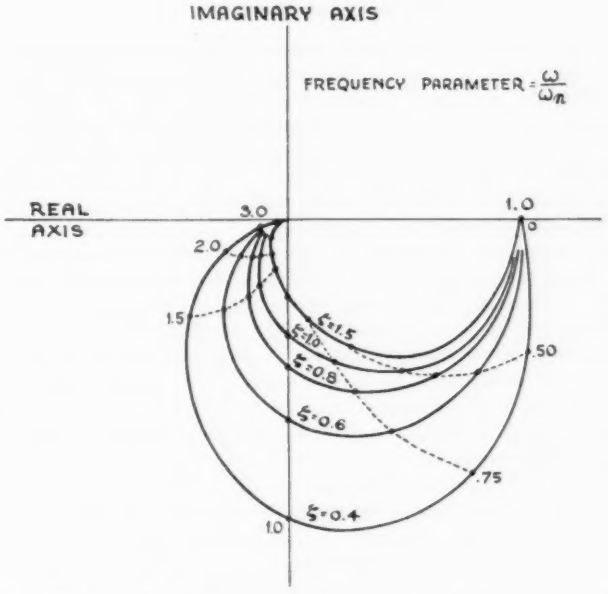


FIG. 16 LOCUS OF FREQUENCY-RESPONSE CHARACTERISTIC OF SECOND-ORDER SYSTEM

servomechanism. When the sinusoidal or frequency-response form of the transfer function is studied it becomes a powerful analysis and synthesis tool. The transfer function may be derived from a known frequency-response characteristic of the servosystem, it may be measured directly, or if system constants are known, it may be calculated directly.

In terms of the nomenclature previously established in this paper the operational form of the transfer function is written $\frac{\theta_0}{\epsilon}(p)$. The sinusoidal form of the transfer function is obtained by replacing the operator p by $j\omega$, giving $\frac{\theta_0}{\epsilon}(j\omega)$. This function is a vector quantity with an amplitude and a phase characteristic just as the ratio $\frac{\theta_0}{\theta_i}(j\omega)$ is a vector quantity.

The transfer function of a servo system is always the product of two parts, one that is invariant with frequency and a second that is frequency-dependent. The fact that these two components exist is emphasized by writing the transfer function in the following form

$$\frac{\theta_0}{\epsilon}(j\omega) = KG(j\omega) \quad [61]$$

The term K represents that part of the transfer function which is invariant with frequency. This portion is known as the gain or the sensitivity factor and is a function of amplifier gain, gear ratios, etc. The second part of the transfer function is denoted by $G(j\omega)$ and represents the portion of the transfer function which changes with frequency.

The frequency response of the servomechanism is connected with the transfer function by the following vector equation

$$\frac{\theta_0}{\theta_i}(j\omega) = \frac{KG(j\omega)}{1 + KG(j\omega)} \quad [62]$$

The transfer function of a system is calculated by straightforward circuit-analysis techniques, or by determining the differential equation relating the output to the error and replacing $\frac{d}{dt}$ by $j\omega$.

15 The Transfer-Function Locus

The transfer function can be studied by means of its frequency characteristics just as other functions have been so studied. The amplitude- and phase-response curves of the transfer function can be drawn and these curves completely define the characteristics of the transfer function of the servomechanism and therefore completely define the system itself. Just as the phase- and amplitude-response curves were combined into a single polar plot with frequency as a parameter, so can the frequency- and phase-response curves of the transfer function be combined. This parametric polar plot of the transfer function has been called the "transfer-function locus," or simply the transfer locus of the servomechanism. The transfer locus completely defines the characteristics of the servo system. A study of its nature provides an effective method for the synthesis of servomechanisms intended for particular applications and a useful general guide to the adjustment of servomechanism parameters in order to secure optimum performance.

The reason for the effectiveness of employing the transfer function $KG(j\omega)$ as a means of analysis is explained as follows:

If it is desired to analyze the response of a servo and design compensation circuits for improving its performance, the function $\frac{\theta_0}{\theta_i}(j\omega)$ is awkward to work with directly. The reason for this arises from the complex nature of the relation between $\frac{\theta_0}{\theta_i}(j\omega)$ and the system parameters. On the other hand, it has been shown that the performance of the servo is completely determined once the transfer function $KG(j\omega)$ is known. A much simpler relation generally exists between the system parameters and the transfer function so that it is comparatively easy to synthesize a controller once the required form of the transfer function is known. The system design is applied to choosing, altering, and improving the servomotor or servo controller, the characteristics of which directly affect the transfer function $KG(j\omega)$.

Design criteria expressed in terms of restrictions upon the transfer function are therefore most easily translated into physical design. However, the final decision as to the quality of the performance of a particular servo is made from a knowledge of the character of its output function, and it is necessary therefore to translate restrictions upon the output and function into restrictions upon the transfer function. The situation is summarized as follows:

It is necessary to know the phase and magnitude of $\frac{\theta_0}{\theta_i}(j\omega)$ in order to decide if the servo is satisfactory. In synthesizing a servo it is easier to work with the transfer function $KG(j\omega)$. By correlating the transfer-function characteristics with the properties of the system frequency response, an effective design procedure can be developed. The correlation of these two functions is most easily effected graphically, as described in the following:

If a parametric frequency plot of the transfer function $KG(j\omega)$ is available, the magnitude and phase of the function $\frac{\theta_0}{\theta_i}(j\omega)$ may be found by graphical calculation. The function $\frac{\theta_0}{\theta_i}(j\omega)$ has been related to the transfer function by Equation [62].

A plot of a typical transfer function $KG(j\omega)$ is illustrated in Fig. 17. Suppose it is desired to calculate $\frac{\theta_0}{\theta_i}(j\omega_c)$ for a particular frequency ω_c, with only the transfer locus available. The transfer function at ω_c, $KG(j\omega_c)$, is represented by the vector $\overline{oc}$ while the vector $\overline{ac}$ represents the term $[1 + KG(j\omega_c)]$, since the point a is located at $(-1 + j0)$. Therefore the magnitude of $\frac{\theta_0}{\theta_i}(j\omega_c)$ is given by

$$\left|\frac{\theta_0}{\theta_i}(j\omega_c)\right| = \frac{|KG(j\omega_c)|}{|1 + KG(j\omega_c)|} = \frac{|\overline{oc}|}{|\overline{ac}|} \quad [63]$$

while the phase of $\frac{\theta_0}{\theta_i}(j\omega)$ is given by

$$\text{arc}\left[\frac{\theta_0}{\theta_i}(j\omega_c)\right] = \text{arc } (oca) \quad [64]$$

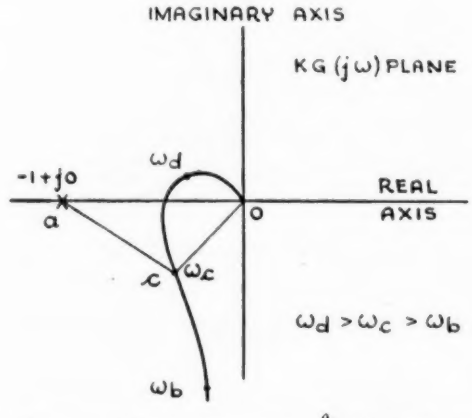


Fig. 17 Graphical Determination of $\frac{\theta_0}{\theta_i}(j\omega)$ From Transfer Locus

The angle, arc (oca), is negative. Thus the magnitude of $\frac{\theta_0}{\theta_i}(j\omega_c)$ is equal to the ratio of the magnitudes of the vectors $\overline{oc}$ and $\overline{ac}$ and the phase of $\frac{\theta_0}{\theta_i}(j\omega_c)$ is equal to the angle between these two vectors.

Equations [62] and [63] permit ready visualization or calculation of the magnitude and phase of $\frac{\theta_0}{\theta_i}(j\omega)$. At small frequencies such as ω_b (see Fig. 17), both vectors $\overline{oc}$ and $\overline{ac}$ are large and approximately equal, and their ratio is approximately unity. The angle between the two vectors, the phase of $\frac{\theta_0}{\theta_i}(j\omega)$, is small at this frequency. As the frequency increases the angle between the two vectors increases and their lengths become smaller so that differences in their lengths cause the ratio $\frac{\overline{oc}}{\overline{ac}}$ to depart from unity. Whether the ratio $\frac{\overline{oc}}{\overline{ac}}$ (the magnitude of $\frac{\theta_0}{\theta_i}[j\omega]$) increases or decreases as the frequency increases depends upon the shape of the curve relative to the origin and the point $(-1 + j0)$. A continuation of this reasoning for the remainder of the frequency range permits the general shape of the phase and magnitude of the servo output to be completely determined. If desirable, the phase and magnitude curves can be determined from the transfer locus with accuracy and ease by using a protractor and divider and measuring the angles and lengths directly from the graph.

Correlation between other servomechanism characteristics and the shape and form of the transfer locus are described in the following sections.

16 Absolute Stability Criterion

The primary requirement that almost every servomechanism

must satisfy is that of stability. Although a servo system must be more than barely stable to be satisfactory, a stability criterion of one type or another is generally the first test applied to proposed servomechanism design. Several criteria exist; however, the one described here was developed primarily for application to feedback amplifiers. It is at once apparent to those familiar with feedback-amplifier theory that the transfer locus of a servomechanism is analogous to the Nyquist diagram of a feedback amplifier. The term Nyquist diagram has been given to this type of plot for a feedback amplifier because of a very useful criterion developed by Nyquist (8) for determining the stability of a feedback amplifier. This criterion may be applied equally well to the transfer locus in order to determine from its shape and position whether or not the servomechanism for which it is drawn is stable. To apply the Nyquist stability criterion to servomechanisms, the following procedure is employed: (*a*) The transfer locus [$KG(j\omega)$ plotted in polar form] is drawn for all frequencies from zero to infinity; (*b*) the conjugate of the transfer locus is drawn. The conjugate of a curve is the mirror image of the original curve about the real axis; (*c*) if the curves so formed enclose the point $(-1 + j0)$, the system is unstable. If the curves do not enclose this point, the system is stable. The application of this criterion is illustrated in Fig. 18.

The foregoing criterion applies to curves of closed form; that is, it applies to transfer loci of such character that the loci and their conjugates join at zero and at infinite frequency. Actually the transfer loci of most servomechanisms are of the open form and some extension is required in order to apply the stability criteria to these forms of transfer loci. The open form of the transfer locus can be changed into the closed form by connecting the curve and its conjugate at the zero-frequency point by means of a circle of infinite radius. The connection should always be made in such a way that no phase discontinuity occurs along the path of the curve.

This is illustrated in Fig. 19 in which are plotted the transfer loci of two common types of servomechanisms, both of which are stable.

17 Transfer Loci for Various Types of Steady-State Performance

The performance of a servomechanism under steady-state conditions is always of great importance. If the servomechanism is primarily a positional device it is desirable that the servomechanism take up various positions without requiring an error to maintain it in that position. Similarly it is frequently necessary for the servomechanism to follow an input of constant velocity, that is, one in which $\theta_i(t) = kt$. In this case it is desirable for the servomechanism to follow various velocities as required without the necessity of a system error to maintain that velocity. Servomechanisms that satisfy the first condition frequently are termed zero-displacement-error servomechanisms and servos that meet the second condition similarly are called zero-velocity-error

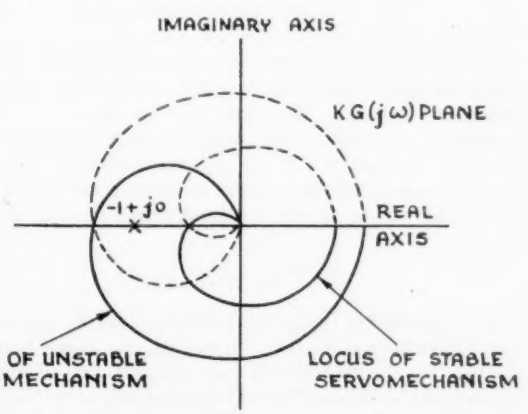


Fig. 18 Application of Nyquist Stability Criterion to Servomechanisms With Positional Error

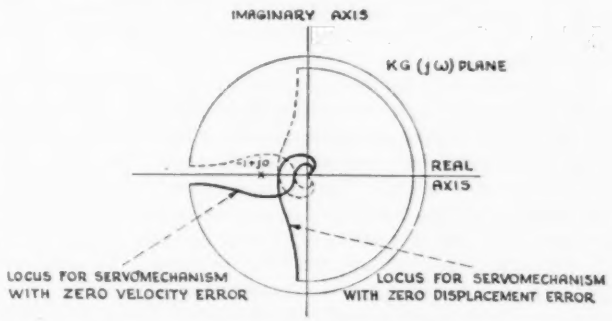


Fig. 19 Extension of Nyquist Stability Criterion to Zero-Displacement-Error and Zero-Velocity-Error Servomechanisms

servomechanisms. It can be readily shown that if the transfer locus of a servomechanism approaches infinity along the negative imaginary axis, the servo will have zero-displacement error. Similarly if the transfer locus of a servomechanism approaches infinity along the negative real axis that servo will have zero-velocity error. The zero-velocity-error servo will, of course, have zero-displacement error also. In Fig. 19 is illustrated the transfer loci of a zero-velocity-error system and of a zero-displacement-error system.

This concept can be extended to servo systems that will follow a constant input acceleration without steady-state error, and so forth.

18 Determination of the Gain Factor (K)

The particular servo parameter most easily adjusted is, perhaps, the gain factor K, which is the frequency invariant portion of the transfer function, $KG(j\omega)$. If the servocontroller is an electronic amplifier, the gain may be fixed, in general, by adjusting a voltage divider controlling the gain of the amplifier. The gain factor of systems incorporating controllers other than electronic amplifiers may be less easily adjusted, but the procedure in most cases is still relatively simple. Since the gain is easily adjusted and since its setting is so important in determining the characteristics of a servomechanism, it is important to develop a technique of gain adjustment that yields optimum results in servo performance.

The effects of increasing the gain or sensitivity of the servomechanism are (*a*) the velocity error of the system is reduced if the servomechanism is of the zero-displacement-error type; (*b*) errors caused by restraining torques on the servo output are reduced; (*c*) errors caused by mechanical misalignment in the servomotor or controller are reduced; (*d*) the imaginary components of the complex roots of the system (the natural frequency or frequencies of the system) are increased in most cases; (*e*) the magnitudes of the real roots of the system are increased in most cases; and (*f*) the real parts of the complex roots of the system (the damping constants) in general are decreased. The first three of these effects reduce the system steady-state error; the next two increase the speed of response of the system, and the last reduces the speed of response of the system in that the time required for a transient oscillation to damp out is increased. A general rule that can be deduced from the factors given is that

the servomechanism sensitivity should be as high as is compatible with proper servo stability.

Any physical closed-cycle system can be made unstable if the sensitivity is sufficiently increased. This is evident from the transfer locus of a physical servomechanism since such a locus always crosses the real axis and therefore as the sensitivity or gain factor K is increased, the locus will enclose the $(-1 + jO)$ point at some finite sensitivity and the servo will become unstable. The gain factor should always be adjusted to avoid instability.

Most applications, however, require not only that the servo be stable but that its degree of stability be satisfactory. The degree of stability determines the damping of the oscillatory components of the servo transient response and in general the gain factor should be so selected that these response components are well damped. When the oscillatory components are insufficiently damped the transient response requires an excessive time to reach its final value and exhibits excessive overshoot. In addition, the amplitude response possesses excessively high peaks. The effect on the transient response is illustrated in Fig. 13 which shows that as the damping ratio is decreased the oscillatory nature of the system is more pronounced. The effect on the amplitude response is indicated in Fig. 14 which shows that as the damping ratio is decreased the magnitude of the peak in the response is augmented.

When a servomechanism is designed on the transient basis the degree of stability is controlled by requiring the effective damping ratio to be of the order of 0.5. When a servomechanism is designed on the frequency-response basis it has been found that an equally satisfactory criterion is to limit the magnitude of peaks in the amplitude response to approximately $1^1/_3$. Neither requirement is based upon exact mathematical criteria; both have been found to give good results in almost every application.

The determination of the gain factor K, that will limit the maximum value of the amplitude response to a prescribed value and thus provide adequate damping in the system, is easily carried out graphically through the use of the transfer locus of the system. If the ratio $\left|\frac{\theta_0}{\theta_i}(j\omega)\right|$ is denoted as M for a particular frequency, curves of constant M can be drawn in the $KG(j\omega)$ plane. These curves turn out to be circles whose centers and radii are easily determined. A set of these circles is illustrated in Fig. 20 together with the transfer locus of a typical servomechanism. The significance of these curves lies in the fact that wherever the transfer locus crosses one of these circles it indicates that at the frequency for which the intersection occurs the value of $\left|\frac{\theta_0}{\theta_i}(j\omega)\right|$ is equal to the M corresponding to the intersected circle. Thus in Fig. 20 $\left|\frac{\theta_0}{\theta_i}(j\omega)\right|$ for the system whose transfer locus is denoted by $K - 1$ will have a value of 1.1 at 1 cycle per sec, 1.5 at 2 cycles per sec, 0.75 at 3 cycles per sec, etc. A value of M can generally be found so that the circle corresponding to this M value is tangent to the transfer locus at some point. A point of tangency indicates that the function $\left|\frac{\theta_0}{\theta_i}(j\omega)\right|$ has a maximum or a minimum at that point. Thus in Fig. 20 the transfer locus drawn for $K = 1$ is tangent to the $M = 1.5$ circle, indicating that the output function has a maximum of 1.5 at 2 cycles per sec.

Also drawn in Fig. 20 are the transfer loci for the same servomechanism with different values of gain factors. It is evident that the maximum value of the output function increases as the gain factor is increased. The proper degree of stability is determined by so choosing the gain factor that the transfer locus corresponding to this gain factor is tangent to the circle drawn for the predetermined maximum value of M.

19 Basic-Design Procedure

Since the transfer-function approach is perhaps most useful in the design and synthesis of servomechanisms, the principal steps in the design procedure employing the frequency-response approach are summarized as follows:

(*a*) Determine the transfer function $KG(j\omega)$ for the first approximation to the complete servomechanism. This requires the determination of the amplitude and phase characteristics of $KG(j\omega)$.

(*b*) Plot this transfer function in the form of a transfer locus using the specific values determined from (*a*).

(*c*) Decide on the degree of stability required in terms of the M ratio discussed in section 18 and determine the gain factor that will produce tangency between the transfer locus and the circle drawn for the maximum permissible value of M. The gain factor can then be used to determine actual sensitivities in the servosystem. Determine the frequency at which the maximum value of $\left|\frac{\theta_0}{\theta_i}(j\omega)\right|$ occurs.

(*d*) From a knowledge of the permissible sensitivity, the frequency at which the function $\left|\frac{\theta_0}{\theta_i}(j\omega)\right|$ is maximum, and the zero-frequency behavior of the transfer locus, answers can be obtained to the following questions:

1 Is the servomechanism of the type (zero-displacement-error servo, zero-velocity-error servo) suitable for the particular application?

2 Can the gain factor be adjusted to secure adequate damping?

3 Is the sensitivity permitted by adequate damping sufficiently high to minimize the effect of nonlinear factors such as sticky valves, dry friction on the output member, etc., and linear factors such as velocity and acceleration error, etc.?

4 Is the natural or resonant frequency sufficiently high to provide the speed of response required by the application?

(*e*) If the answer to any of the foregoing questions is negative remedial action must be taken. Readjustment of certain of the parameters or minor changes in design may be sufficient. Otherwise major design changes must be made or corrective devices incorporated in the system. These corrective devices can be designed: (*a*) To improve the transient response; (*b*) increase the sensitivity permitted by adequate stability; or (*c*) change the basic type (zero-displacement error, zero-velocity error) of the servo. If the corrective element is introduced as an element cascaded with the controller in such a way that no mutual reaction with other elements occurs, the new transfer function is the product of the old transfer function and the transfer function of the corrective element. The new transfer locus can be formed graphically by multiplying amplitudes and adding phases for a particular frequency. If the corrective element is inserted in the system in a different manner straightforward circuit-analysis techniques can be applied to the determination of the transfer function.

20 Summary

Two approaches to the mathematical analysis of servomechanisms have been pointed out in this paper. It has been demonstrated that, in general, a broad understanding of servomechanisms could be obtained by an understanding of both approaches, and in particular, that valuable performance and design data could be obtained. It has been shown that the transient approach

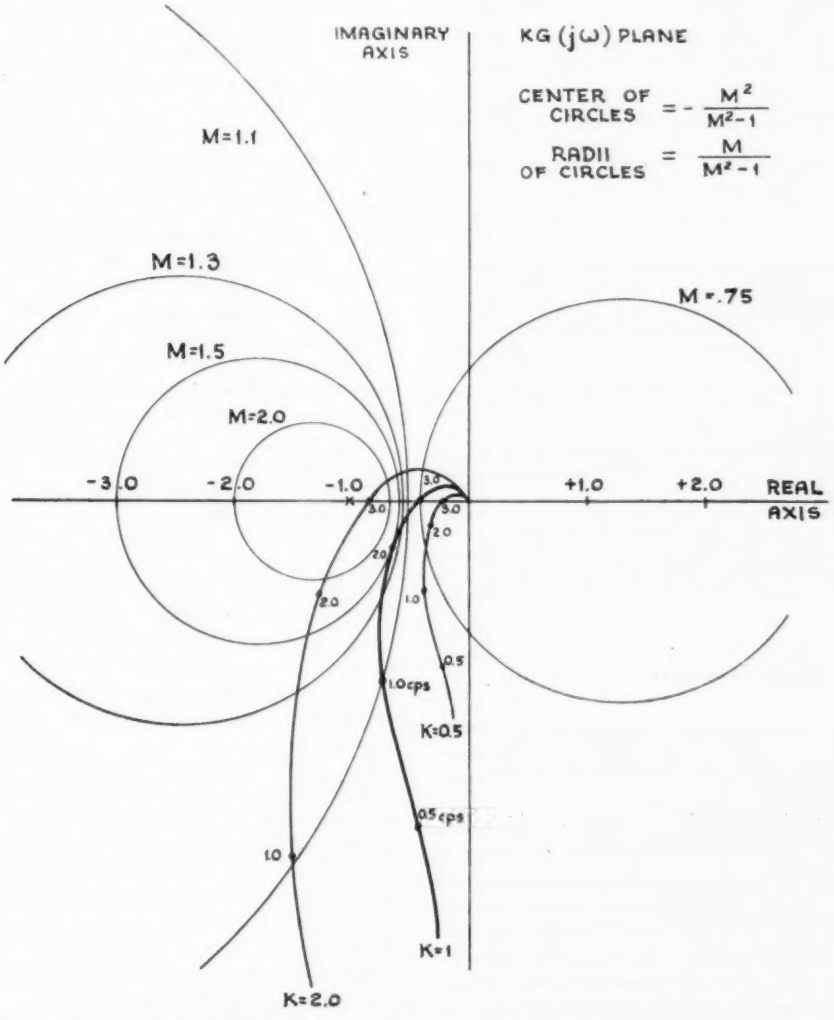


FIG. 20 GRAPHICAL DETERMINATION OF GAIN FACTOR OF TRANSFER LOCUS

is particularly valuable when the exact response to known inputs is required, and in the analysis of simpler servo systems. It has been further shown that the frequency-response approach is indispensable when the analysis and synthesis of complex servo systems is required.

ACKNOWLEDGMENT

The authors gratefully acknowledge the co-operation and assistance of their colleagues at the Massachusetts Institute of Technology. Particular thanks are due to Mr. H. T. Marcy and Mr. G. J. Schwartz for their many valuable suggestions, and to Mr. D. P. Campbell for his contributions to the transient-analysis approach.

BIBLIOGRAPHY

1 "Design Factors Controlling the Dynamic Performance of Instruments," by C. S. Draper and G. P. Bentley, Trans. A.S.M.E., vol. 62, 1940, pp. 421–432.

"General Principles of Instrument Analysis," by C. S. Draper and G. V. Schliestett, *Instruments*, vol. 12, 1939, pp. 137–142.

2 "Theory of Servomechanisms," by H. L. Hazen, *Journal of The Franklin Institute*, vol. 218, 1934, pp. 279–331.

"Design and Test of a High-Performance Servomechanism," by H. L. Hazen, *Journal of The Franklin Institute*, vol. 218, 1934, pp. 543–580.

3 "Automatic Control in the Presence of Process Lags," by C. E. Mason and G. A. Philbrick, Trans. A.S.M.E., vol. 62, 1940, pp. 295–308.

4 "Quantitative Analysis of Single-Capacity Processes," by A. F. Spitzglass, Trans. A.S.M.E., vol. 60, 1938, pp. 665–674, and vol. 62, 1940, pp. 51–62.

5 "Directional Stability of Automatically Steered Bodies," by N. Minorsky, *Journal of the American Society of Naval Engineers*, vol. 34, 1922, pp. 280–309.

"Automatic Steering Tests," by N. Minorsky, *Journal of the American Society of Naval Engineers*, vol. 42, 1930, pp. 285–310.

6 "An Automatic Curve Follower," by H. L. Hazen, J. J. Jaeger, and G. S. Brown, *Review of Scientific Instruments*, vol. 7, 1936, pp. 353–357.

7 "Stabilized Feedback Amplifiers," by H. S. Black, *Bell System Technical Journal*, vol. 13, 1934, pp. 1–18.

8 "Regeneration Theory," by H. Nyquist, *Bell System Technical Journal*, vol. 11, 1932, pp. 126–147.

9 "Transients in Linear Systems," by M. F. Gardner and J. L. Barnes, John Wiley & Sons, Inc., New York, N. Y., 1942.

10 "Constant Speed Control Theory," by H. K. Weiss, *Journal of the Aeronautical Sciences*, vol. 6, no. 4, February, 1939, pp. 147–152.

11 "Servomechanisms: Charts for Verifying Their Stability and for Finding the Roots of Their Third and Fourth Degree Characteristic Equations," by Y. J. Liu; privately printed by Massachusetts Institute of Technology, Department of Electrical Engineering, 1941.

12 "Solution of the Cubic Equation and the Cubic Charts," by L. W. Evans; privately printed by Massachusetts Institute of Technology, Department of Electrical Engineering, 1943.

13 "The Analysis and Synthesis of Linear Servomechanisms," by

A. C. Hall. A publication of the Technology Press, Massachusetts Institute of Technology, May, 1943.

14 "Considerations in Servomechanism Design," by S. W. Herwald, A.I.E.E. Transactions section, vol. 63, December, 1944, pp. 871–876.

15 "Network Analysis and Feedback Amplifier Design," by H. W. Bode, D. Van Nostrand Company, Inc., New York, N. Y., 1945.

16 "Theory of Servomechanisms," by L. A. MacColl, D. Van Nostrand Company, Inc., New York, N. Y., 1945.

17 "Contributions to the Theory of Automatic Controllers and Followers," by D. G. Prinz, *Journal of Scientific Instruments*, vol. 21, no. 4, 1944, pp. 53–63.

18 "Theory of Automatic Control Systems," by D. P. Campbell, *Industrial Aviation*, September, 1945, pp. 62–64 and 94–95.

19 "Method of Successive Approximations of Evaluating the Real and Complex Roots of Cubic and Higher Order Equations," by Shih-Nge Lin, *Journal of Mathematics and Physics*, vol. 20, August, 1941, pp. 231–242.

20 "Comparison of Methods for Evaluating the Complex Roots of Quartic Equations," by H. S. Sharp, *Journal of Mathematics and Physics*, vol. 20, August, 1941, pp. 243–258.

21 "The Analysis and Design of Servomechanisms," by H. Harris, printed, 1942, under the auspices of the Fire Control Committee (Sec. D-2) of N.D.R.C., O.S.R.D. No. 454.

22 "Automatic Control Engineering," by Ed Sinclair Smith, McGraw-Hill Book Company, Inc., New York, N. Y., 1944.

23 "Principles Underlying the Rational Solution of Automatic Control Problems," by S. D. Mitereff, Trans. A.S.M.E., vol. 57, 1935, pp. 159–163, FSP 57–9; discussion and closure, January, 1936, pp. 55–65.

Discussion

C. CONCORDIA.[6] The writer is greatly interested in the steady-state method of analysis of control systems described in this paper and would like to comment on what he considers its scope in relation to other aspects of the control problem.

If one starts from scratch and constructs a control system for a particular job, one's first task is to make sure that the system is stable. For this purpose it seems best to find regions of stable operation in terms of those parameters which are within our control by the application of Routh's stability criteria to the characteristic determinant of the system. Such a study gives information over a great range of system parameters very quickly, without the necessity of studying any one system in detail.

Following such a study, one becomes concerned with the response of the system. The most direct method might appear to be to compute directly the transient response to the various disturbances which are of interest. However, for the reasons discussed by the authors, this sort of calculation does not tell immediately what to do in order to improve performance. Thus it is convenient to devise on a semiempirical basis criteria of probable transient performance in terms of steady-state performance and to make steady-state studies of the system as they have described.

However, even after this is done, one may still wish to make sure that performance will be satisfactory by a direct study of the transient performance. This is especially true in those cases where the system may be subjected to a variety of different kinds of disturbances. An example of this is an airplane-engine turbosupercharger regulator, which may be subjected to disturbances of the pressure-boost setting, the engine-speed setting, or the throttle setting. It will be apparent to those familiar with control-system performance that the optimum stabilizer design for one type of disturbance will not be the same as that for the others, so that the over-all optimum must be a matter of engineering judgment rather than of mathematical criteria.

For the purpose of making such studies of transient performance we have found it convenient to use the differential analyzer. Of course, once a problem is set up on the differential analyzer it is a simple matter to change parameters and run off the resulting transient-response curve, and in fact in many cases this has been so attractive that we have shortcircuited completely the intermediate steady-state analysis method.

A further reason for this is that in many cases, as the refinement of design proceeds, one becomes primarily interested in studying more and more the effects of those nonlinear elements such as friction, backlash, saturation, etc., that are left out of the linear analysis which has been described. A further related factor is that a linear analysis becomes more nearly valid as the control means become better. In many cases very limited control means may be available, and these may be essentially off-on or some other kind of contact control. In these cases it is almost necessary to determine the transient response directly if a good idea of the quality of actual performance is to be had.

L. A. MACCOLL.[7] It is shown in the paper that the function $KG\ (i\omega)$ plays a dominant role in the theory of the particular servomechanism which is under consideration. Perhaps it will be well to point out explicitly that this function, suitably generalized, is fundamental in the theory of any single-loop servomechanism, and to indicate how the generalized function can be determined experimentally.

Let us consider a general single-loop servomechanism, in which we have a "forward circuit," consisting of certain components $C_1, C_2, \ldots, C_l$ connected in tandem, and a "feedback circuit," consisting of certain components $C_{l+1}, C_{l+2}, \ldots, C_{l+m}$ connected in tandem.

The typical component C_n is characterized by a complex-valued function $Y_n\ (i\omega)$, having the following significance: In the steady state, in which all of the signals in the system are varying sinusoidally with time with the radian frequency ω, the absolute value of $Y_n\ (i\omega)$ is the ratio of the amplitude of the signal at the output of C_n to the amplitude of the signal at the input of C_n, and the angle of $Y_n\ (i\omega)$ is the phase difference between these two signals.

Now it is easily shown, by reasoning like that employed in the paper, that the function

$$Y(i\omega) = Y_1(i\omega)Y_2(i\omega)\ldots Y_l(i\omega)\ Y_{l+1}(i\omega)Y_{l+2}(i\omega)\ldots Y_{l+m}(i\omega)$$

plays the role in the theory of the present system that the function $KG\ (i\omega)$ plays in the theory of the system discussed in the paper.

Let us consider the physical significance of $Y\ (i\omega)$. Suppose that we open the feedback loop between any two consecutive components, say the components C_n and C_{n+1}, adding the proper terminations, if necessary, so that the impedance relations within the system will not be disturbed. Then let us impose a known sinusoidal signal at the input of C_{n+1}, and let us measure the amplitude and phase of the resulting signal at the output of C_n. It is readily seen that the ratio of the amplitude of the signal at the output of C_n to the amplitude of the signal at the input of C_{n+1} is the absolute value of $Y\ (i\omega)$, and that the phase difference of the two signals is the angle of $Y\ (i\omega)$. On this account $Y\ (i\omega)$ is commonly called the "loop transmission ratio of the servomechanism."

We note that where we open the feedback loop, whether between C_1 and C_2, or between C_2 and C_3, or elsewhere, is indifferent in principle. However, as far as experimental technique is concerned, it may not be practically indifferent. In many cases the physical nature of the signals changes from point to point in a servomechanism. At one point the signal may be the angular position of a shaft, at another point it may be an electromotive force, and at a third point it may be the pressure of a fluid. In

[6] Engineer, General Electric Company, Schenectady, N. Y. Mem. A.S.M.E.

[7] Bell Telephone Laboratories, Inc., Murray Hill, N. J.

such a case it may well be that we can perform the measurements just described more accurately and conveniently at one point in the loop than at another. We should, of course, select the point at which we open the loop, and perform the measurements accordingly.

Referring to the significance and use of the Nyquist diagram: Suppose that we have a servomechanism with a Nyquist diagram which encloses the critical point $(-1, 0)$, so that the system is unstable, or which, while it does not actually enclose the critical point, passes near to that point, so that the system is barely stable. In either case, we have to modify the system in some way, in order to make its performance satisfactory.

One rather obvious thing we may do is simply to vary the value of some one constant parameter, seeking a particular value which gives a satisfactory performance. This procedure, which is discussed at length in the paper, may be entirely satisfactory in many cases. However, it is evident that this procedure is quite restricted, and it is to be expected that we can often achieve more satisfactory results in other ways. Here the Nyquist diagram performs a great service; for it reveals a great variety of means for obtaining a satisfactory system, many of which are not suggested at all by the older methods.

In so far as satisfactory stability of a servomechanism is concerned, all that is necessary is that the curve of the Nyquist diagram shall neither enclose the critical point $(-1, 0)$ nor pass too near to that point. In order to achieve a curve which is satisfactory in this sense, we can confine ourselves to varying element values, if that is sufficient, or we can insert additional frequency-selective elements in the system, so as to alter the very form of the curve in a drastic manner. The possibilities of the latter sort are particularly valuable when we are dealing with complicated systems subject to stringent requirements.

Ed S. Smith.[8] The authors deserve the thanks of mechanical engineers for the release of this material as soon as the wartime restrictions lifted. It is high time for this M.I.T. group of electrical engineers to claim due credit for its excellent work and real contributions to the war effort. The writer is glad to acknowledge here his professional and personal indebtedness to Bush, Hazen, Gardner, Draper, Brown, Harris, Hall, Campbell, Kochenberger, Taplin, Philbrick, and Ahrendt, to name a representative number of its more active contributors to the art. At the same time, it must be remembered that the pioneering in servomechanisms has been shared by another group of electrical engineers at the Bell Telephone Laboratories: Nyquist, Bode, Black, Ferrell, Dietzold, MacColl, and Barnes whose work with Gardner at M.I.T. is but one tie of many between these two groups.

As a mechanical engineer, the writer's primary interest is to see how these electrical-engineering techniques may be best made available to other engineers, for use in control generally. For this "transmission problem" it is good that such an experienced and co-operative teacher as Brown heads the A.I.E.E. activity in this field. For the sake of continuity, it is hoped by the writer, as the current chairman of the A.S.M.E. Instruments and Regulators Division, that such activity will be most intimately tied in with the work of this division which sponsored this paper. This division in the past has followed control theory as exemplified by papers by Ivanoff, Minorsky, and division members including Fairchild, Grebe, Mason, Sperry, and the present writer to mention a token few. The following comments are purely individual:

It might offhand seem that servomechanisms should form ideal examples of control for mechanical engineers since the familiar elements are the inertia of a mass, the damping of a dashpot, and the proportional effect of a spring. However, from the standpoint of the process-control engineer, these happen to overstress inertial and oscillatory effects. Also mechanical analogs are a bit more farfetched than the hydraulic which has the advantage of more closely corresponding with the electrical systems in which these electrical engineers really think.

Ideally, each actual system should be directly followed in setting up the mathematical formulation which would then be used in a pure form in obtaining results. But this procedure would deprive the creative engineer of the stimulus derived from working in the medium of his experience. Since so much of the literature will be on electrical-engineering techniques, it appears that each active control engineer should become adept in their use.

The experts in the servomechanism and control fields are unfortunately not exceptions to the rule that the experts in an art always ball up the terminology and notation until they can be followed only by a like expert. To a control engineer, if a regulated temperature is too high, the error would be positive and taken as $(T_{\text{actual}} - T_{\text{set}})$. To a "servomechanist," it would seem that the temperature setting T_i was not being followed by the actual temperature T_0 and that the error would be $(T_i - T_0)$. For another example; probably the most important factor in control is the variable "load" which often affects a most inconvenient part of the plant with effects echoing around and around the system, whereas too often the servomechanist either entirely neglects the load change or shrugs it off as mere "hash" or "noise," a mere random impulse without the dignity of identity.

Again, the "controlleer" is charged with habitually over-simplifying analyses, using an occasional integral or appropriate derivative in visualizing the ills and cures of regulated systems reference (16), whereas the servomechanist seems to tend to stick to the more readily available means for obtaining a typical $(1 + Tp)$ term without, in so far as the present writer can see now that the veil of wartime secrecy has been pierced, creating any essentially new form of regulator. At least the controlleer can directly express a ratio of effect to its cause and the lag without becoming involved in the width of a hypothetical frequency-transmission band and in such an acoustical abstraction as "decibels per octave."[9] The point appears to be that the tools of the different arts have different advantages to those who are familiar with their use.

Finally, on this point, the controlleer's need is for an approach which will enable him most flexibly to solve a wide variety of control problems, whereas to the servomechanist, the temptation appears to be irresistibly strong to go overboard on overspecialized treatments, e.g., the nondimensional approach, for the sake of greater efficiency in his special field at the expense of widest utility, with the result that anyone not working steadily in that field will usually save considerable time and be more certain of the correctness of his results if he starts from scratch and sticks to the closest relation between the physical phenomena and the mathematics.

A noteworthy exception to this is that grand tool, the Nyquist method of testing stability. This is essentially so simple that it is difficult for even experts to confuse although they bring in the "conjugate complex," and the idea of "negative frequencies." It may be well here to restate the Nyquist criterion following Harris' rule: A regulated system is unstable only if, 1 the sensitivity (effect/cause) exceeds unity at a lag of 180 deg, and 2, the lag there increases with increasing frequency at the least value of sensitivity which is greater than unity. Of course in

[8] Eclipse-Pioneer Division, Bendix Aviation Corporation, Teterboro, N. J. Mem. A.S.M.E.

[9] "The Servo Problem as a Transmission Problem," by E. B. Ferrell, Proceedings of the Institute of Radio Engineers, vol. 33, November, 1945, pp. 763–766.

any actual system the sensitivity finally must decrease to zero with increasing frequency.

It may lend confidence in this method to note that this was independently approached from purely practical considerations. The writer in 1936 remarked[10] that the time lags in a regulated system were best observed by taking effects in the same direction as their causes, which amounts to dropping the 180 deg for the control relation, as is now conventional. Ivanoff in 1938 (U. S. patent 2,268,285) showed familiarity with the requirement that the lag be 180 deg for steady hunting. And Fairchild in 1940 (Temperature Symposium) noted that the further requirement for steady hunting was that the over-all sensitivity be unity. (Incidentally, as Le Corbeiller noted, to tend to sustain oscillations reliably at substantially a definite amplitude, there must be such a nonlinearity that, upon a decrease of amplitude, the over-all sensitivity or "gain" increases. All other material in this discussion is limited to linear systems.)

In evaluating the advances claimed in the paper: Apparently Harris (21) advanced the Nyquist technique mainly by using the grids of the paper's Fig. 20 to show the sensitivity, with maximum and minimum values of (θ_0/θ_i) where the circles are tangent to the Nyquist loci of the vectors. The advance of Hall (13) is mainly in the systematic correlation of the circuits and networks with their control relationships; and Taplin's pioneering use of $(1 + gh)$ in the denominator, while limited to very simple systems such as elementary servomechanisms without multiple feedback loops, still had wide implications and represents a logical operational advance. The foregoing is an offhand effort to bring the work of these contemporaries into better focus.

It is unquestionably valuable to "block up" a system for the purpose of setting up the equations as a standard procedure, and to use a-c network techniques in obtaining the over-all sensitivity, gain, or transfer ratio, expressed by the appropriate $gh\ldots$ relations. This is useful both as a test for stability and as an indication of the transient performance of the system under such standard forcing functions as the impulse, step, ramp, etc., by the use of the frequency-analysis techniques, notably the Fourier, as recently advocated by Harris. In other words, the formal transient analysis may be entirely replaced by the frequency approach.

Since the paper refers to several publications of the authors' group, it may be a service to engineers attempting to use such publications to note the following: In reference (1), Draper and Bentley, in Figs. 3 and 6, 1.58 should be 1.74. In reference (10), Weiss, the cubic chart III*a* is incorrect in part, a correction having appeared only in a classified paper by one of the authors; and in reference (11), Liu, an approximation-producing assumption appears to be unstated therein which affects the accuracy of this approach in certain ranges which are still useful in control. It is hoped that any like points which later turn up in present and future papers in this field will be scrupulously cleared by publication.

Nothing of the foregoing discussion is to be construed as minimizing the value of the papers by this group. Instead, the writer has noted that the "servomechanism approach" is also of value[11] in control generally, paradoxically including self-operating regulators. The writer is happy to express his indebtedness to members of this group and their works.

It is the main purpose of the writer, as an occasional worker on control, objectively to direct the attention of other mechanical engineers to useful control tools wherever found.

[10] "Automatic Regulators, Their Theory and Application," by Ed S. Smith, Jr., Trans. A.S.M.E., vol. 58, 1936, pp. 291–303.

[11] "Stabilizing a Suction-Relief Valve," by Ed S. Smith, Trans. A.S.M.E., vol. 67, 1945, p. 87.

Authors' Closure

The authors appreciate the comments made by Messrs. Concordia, MacColl, and Smith, particularly for their efforts to supplement the work given in the paper.

Mr. Concordia's comments on the usefulness of a Differential Analyzer to aid in the design are very pertinent though such devices are not widely available. However, as the work on similators or transient analyzers[12] for dynamical systems progresses and more of them become available their use may get widespread adoption. The one difficulty still remaining will be that of determining the parameters of the elements of the system or the various functional relationships that define the system elements. Then, of course, when these data are known a great deal can be done by steady-state sinusoidal analyses by persons not having the use of a Differential Analyzer. By skillful direction of experimental techniques during the determination of much of the basic data on the components, the work of applying the steady-state methods of analysis is considerably reduced.

Dr. MacColl's comments are very pertinent, particularly when one realizes the wide range of physical quantities encountered in any single control system and the relative ease with which certain quantities can be measured in practice and the relative status of the art of measurement of other quantities. For example, at one end of the scale one observes the simplicity and accuracy with which time-varying electrical quantities can be measured compared with the difficulties at the other end of the scale involved in measuring time-varying quantities such as acceleration, pressure, strain, fluid flow and the like.

Dr. MacColl's comments on the need to change the shape of the locus on the Nyquist diagram are appreciated for they give added emphasis to the point which, while included in the treatment under section 19 of the paper, was probably not stressed as much as it might have been.

Mr. Ed Smith's summary of the control analysis and synthesis picture as it exists today is a very timely one. Wartime emphasis on extending analytical techniques in this field were very intense. The old oft-stated gap that used to exist between the various engineering professions is rapidly narrowing as the analytical techniques of the communications engineer are explained to the mechanical engineer, and the "systems" concept is applied more and more vigorously to control problems. The integration within the professions is being stimulated by discussions between professional groups who, until a few years ago, had few common problems. Nowadays one finds a great deal of mathematics, electronics, circuit theory, electrical machinery theory, hydraulic machinery theory being interwoven into a co-ordinated systems design with corresponding benefit to that branch of the art being developed by each group. But this interweaving or integrating is occurring with harmony and a degree of co-operation between engineers of widely different background, in a very interesting way.

[12] "Electrical Analogy Methods Applied to Servomechanism Problems," by G. D. McCann, S. W. Herwald, and H. S. Kirschbaum, Trans. A.I.E.E., vol. 65, February, 1946, pp. 91–96.

Conversion of Measurements of Power Output of Diesel Engines to Standard Atmospheric Conditions[1]

By MARTIN A. ELLIOTT,[2] BRUCETON, PA.

This report presents and analyzes data obtained on the effect of ambient or atmospheric conditions on the power output of three normally aspirated commercial four-stroke-cycle Diesel engines. Different ambient conditions were simulated by maintaining the desired pressure in each of two surge tanks, one connected to the intake and one connected to the exhaust of the engine. The simulated absolute pressures ranged from 20 to 30 in. of mercury. Most of the tests were made at the prevailing atmospheric temperature but a series of tests with one engine was made at an intake temperature of approximately 230 F. Analysis of the results showed that an algebraic relation could be obtained between so-called "derived indicated efficiency" and fuel:air ratio. This relation is independent of ambient conditions and is used in the development of rational procedures for correcting measurements of power output made at existing test atmospheric conditions to any arbitrarily selected standard ambient condition. Using certain of the basic relations developed, an expression was derived for computing the brake horsepower of an engine at any ambient density and rate of fuel consumption. Computed values were within 0.7 hp of values determined experimentally. The report also reviews previous work in the field and indicates the need for further work to obtain the complete solution of the problem desired by the A.S.M.E. Special Research Committee on Internal-Combustion Engines.

Introduction

IN making performance tests of Diesel engines, differences in the density and moisture content of the ambient atmosphere are inevitable at different test locations and at different times in the same location. Since the power output of a Diesel engine operated at a given speed and throttle setting is affected by changes in the density of the intake air, it is desirable to develop methods for correcting the power output of an engine determined at existing ambient conditions to power output at some arbitrarily chosen standard ambient condition.

Members of this Society, who were instrumental in organizing the Special Research Committee on Internal-Combustion Engines, recognized the need for fundamental information on methods for expressing the power output of Diesel engines at standard ambient conditions, and a program of research (4)[3] was prepared outlining the work required to develop the necessary information. In formulating this program an analysis was made of performance data on Diesel engines obtained incidentally by the Bureau of Mines in studies of the effect of barometric pressure on the composition of the exhaust gases produced by Diesel engines. The tests were limited in scope in so far as engine performance is concerned since the main objective of the Bureau of Mines investigation was to determine the hazards of operating Diesel engines underground in places where the barometric pressure might be low. In spite of this, analysis of the data furnished considerable information on possible methods for correcting the power output of Diesel engines to standard ambient conditions and on the probable magnitude of the correction factors. The committee thought that it might be desirable to publish this information in a progress report discussing the general problem, analyzing the data available, and indicating the additional information required to obtain a complete solution. Accordingly the following report has been prepared:

The paper presents methods for converting measurements of power output determined at existing ambient conditions to power output at some arbitrarily selected standard ambient condition. This general procedure is commonly referred to in technical literature as correcting power output to standard ambient conditions and the multiplying factors for doing this are referred to as correction factors. This terminology is used in this paper but it is pointed out that the tests reported here were not broad enough in scope to permit the development of correction factors applicable to all engines. Because of this the somewhat more general term conversion has been used in the title to describe basic procedures developed.

Review of Previous Work

Tests on the effect of atmospheric conditions on the power output of Diesel engines are reported in the literature, but none of the previous investigations has provided a generally applicable method for correcting measurements of the power output of Diesel engines to standard ambient conditions.

The results of tests to determine the effect of humidity, temperature, and pressure on the power output of a four-cylinder, four-stroke-cycle Diesel engine were reported by Everett (5). From these tests it was concluded that, at a given speed and throttle setting, humidity did not affect power output significantly, and that both temperature and pressure affected power output but the fundamental variable was density.

Everett's work (5) and later work of Doolittle (2) furnish experimental evidence on the very minor effect of humidity when excess air is present.

The results obtained by Everett (5) on the effect of pressure on power output may not represent the effect under normal operating conditions because in his tests the pressures at the intake and

[1] Progress Report No. 1, for the A.S.M.E. Special Research Committee on Internal-Combustion Engines. Published by permission of the Director, Bureau of Mines, United States Department of the Interior, Washington, D. C.

[2] Supervising Engineer, Internal-Combustion Engine Research Section, Explosives Division, Experimental Mine and Explosives Testing Station.

Contributed by the Special Research Committee on Internal-Combustion Engines and presented under the auspices of the Oil and Gas Power Division at the Annual Meeting, New York, N. Y., Nov. 26–29, 1945, of The American Society of Mechanical Engineers.

Note: Statements and opinions advanced in papers are to be understood as individual expressions of their authors and not those of the Society.

[3] Numbers in parentheses refer to the Bibliography at the end of the paper.

TABLE 1 DESCRIPTION OF ENGINES TESTED

Engine Type	A Four-stroke-cycle, normally aspirated	B Four-stroke-cycle, normally aspirated	C Four-stroke-cycle, normally aspirated
Number of cylinders	4	4	6
Cylinder bore, in.	4 1/4	4	4 7/8
Piston stroke, in.	5 1/2	4 1/2	6
Piston displacement, cu in.	312.1	• 226.2	672
Maximum rated speed, rpm	1400	2600	1800
Maximum rated bhp with all accessories except fan	44	70	150
Fuel pump	Individual pump for each cylinder; fuel delivery controlled by pump-plunger bypass	Individual pump for each cylinder; fuel delivery controlled by pump-plunger bypass	Single-plunger, low-pressure metering and distributing type
Type of injection valve	Single hole orifice, flat-faced valve seat	Circumferential orifice (pintle nozzle); conical valve seat	Cam-actuated plunger-type injector for each cylinder. Six spray holes in each injector
Operating pressure of injection valve discharging into air at atmospheric pressure, psi	1500	1650	...
Combustion system	Cylindrical precombustion chamber with cone-shaped ends	Spherical turbulence or air-swirl chamber	Directed spray; small air-cell in piston head
Cooling system	Positive circulation, thermostatically controlled	Positive circulation, thermostatically controlled	Positive circulation, thermostatically controlled

final exhaust were not equal. For example, the pressure at the intake ranged from 10 to 16 psia, but the pressure at the final exhaust was always atmospheric (28.79–29.15 in. of mercury). Differences between the pressure at the intake and final exhaust may cause flow into or out of the cylinder during the period of valve overlap, depending upon the relation between the two pressures. This condition is abnormal, and it is desirable therefore to maintain equal pressures at the intake and final exhaust in studies of the effect of ambient conditions on the power output of Diesel engines.

Results reported by Taylor (11) and some of the results reported by Doolittle (2) also were obtained by operating engines at reduced intake pressures and atmospheric exhaust pressure and therefore may not represent normal operation at reduced ambient pressures. Data given by Taylor (11) and Doolittle (2) on the effect of temperature apply only to the engine tested and no attempt was made to generalize the results quantitatively although qualitative generalizations were made by Taylor (11).

Dennison (1) proposed a method for comparing the performance of different Diesel engines, but this method was intended to facilitate comparison of competitive designs and is not adaptable to the development of correction factors for power output.

Moore and Collins (8) have published the results of extensive tests on the effect of atmospheric conditions on the performance of a single-cylinder Diesel engine. These tests included determination of the effect of temperature at constant pressure; the effect of pressure at constant temperature; and the effect of changing both temperature and pressure simultaneously. All of these tests were made with the pressure at the intake equal to the pressure at the final exhaust. In addition, tests were made with intake pressure greater than and less than the pressure at the final exhaust. Moore and Collins contributed considerable information but many of their tests were made at fuel : air ratios far on the rich side, a condition of little practical interest. Furthermore, their analysis of the results was not carried sufficiently far to develop the fundamental theory on the effect of atmospheric conditions on power output of Diesel engines.

In preparation for an investigation by the Bureau of Mines on the effect of atmospheric conditions on the exhaust gases produced by Diesel engines, a study was made of the published results mentioned. This study disclosed that correlation of indicated thermal efficiency with fuel : air ratio had not been examined in analyzing the results of performance tests made at different ambient conditions. Such a correlation is of interest because thermodynamic considerations show that these factors are related in the theoretical fuel : air cycle (6, 10). Furthermore, it might be expected that this fundamental relationship would be unaffected by changes in ambient conditions at least over a relatively wide range of conditions. That this was true was indicated by an analysis (3) of the data of Moore and Collins (8). Once this had been established it was possible to suggest a rational basis (3) for developing methods of correcting the power output of a Diesel engine to standard ambient conditions.

Scope of Present Report

This report includes a discussion of the results of performance tests made at different simulated ambient conditions on three different commercial, four-stroke-cycle, normally aspirated Diesel engines. Methods for analyzing the data are presented and methods for correcting power output to standard ambient conditions are developed and applied to the results of actual tests. These methods are modifications or extensions of the fundamental theory presented in a previous paper (3) by the author.

APPARATUS AND PROCEDURE

Engines Tested. The principal features of the three engines tested are summarized in Table 1. Engines B and C were directly coupled to the dynamometer. Engine A was coupled to the dynamometer through a clutch. An auxiliary cooling system was used and all engines were tested without radiator or fan. The cooling-water circulating pump was driven by the engine in all tests.

Fuel. The chemical and physical properties of the fuels used are given in Table 2. Fuel F was used in tests of engine A at 600,

TABLE 2 CHEMICAL AND PHYSICAL PROPERTIES OF FUELS

Designation of fuel	F	G
Flash point (P.M.C.C.), F.	157	150
Water and sediment	Trace	Trace
Viscosity, S.U. at 100 F, sec.	34	33
centipoises at 100 F.	1.93	1.74
Carbon residue on 10% bottoms, per cent by weight	0.010	0.016
Specific gravity 60/60 F.	0.8295	0.8314
Pour point (upper), F.	—2	—20
Cetane number	Not less than 50	Not less than 50
Sulphur, per cent by weight	0.1	0.2
Hydrogen, per cent by weight	13.4	13.4
Carbon, per cent by weight	86.1	86.2
Oxygen, per cent by weight	0.4	0.3
Nitrogen, per cent by weight	0.0	0.0
Heating value, (upper), Btu per lb	19590	19560

1000, and 1400 rpm; fuel G in tests of engine B; and fuel F in tests of engine C.

Dynamometers. Tests of engines A and C were made using a water-cooled induction-type dynamometer rated at 200 hp from 1200 to 4000 rpm. A direct-current dynamometer rated at 45 hp from 1200 to 2500 rpm was used in tests of engine B. This latter dynamometer was used in determining friction horsepower in motoring tests of all three engines.

Equipment for Simulating Operation at Different Ambient Conditions

Operation at different ambient conditions was simulated by maintaining the desired pressure in each of two surge tanks. One of these tanks was connected to the intake of the engine and one to the exhaust (see Fig. 1). The intake surge tank was 17.5 in. diam and 84 in. in length. The exhaust surge tank was 22 in. diam and 60 in. in length.

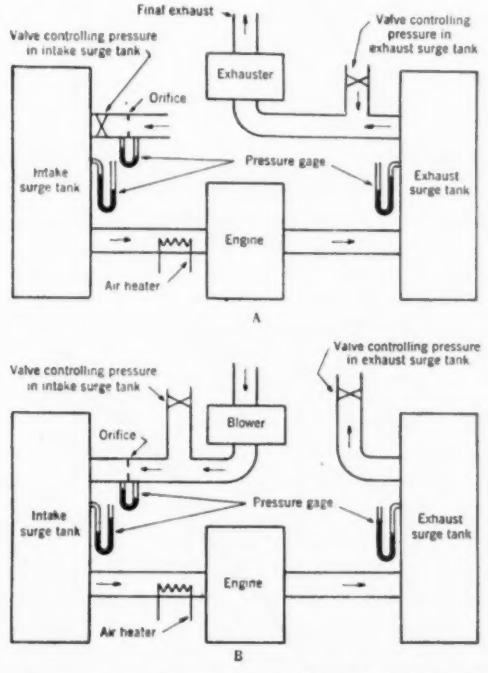


Fig. 1 Diagrammatic Sketch of Arrangements for Tests at (*A*) Ambient Pressures Less Than Prevailing Barometric Pressure and (*B*) Ambient Pressures Greater Than Prevailing Barometric Pressure

In tests at low ambient pressures (20 and 25 in. of mercury abs), the desired pressure in the intake tank was obtained by throttling a valve on the upstream side of the tank. The pressure in the exhaust surge tank was maintained the same as that in the intake surge tank by a Roots-Connersville exhauster driven in some tests by a gasoline engine and in others by an electric motor (see Fig. 1*A*).

In tests at a simulated ambient pressure of 30 in. of mercury abs, which was greater than the prevailing barometric pressure, the Roots-Connersville exhauster was used to compress air to the intake surge tank. The pressure in the exhaust surge tank was maintained at 30 in. of mercury abs by throttling a valve on the downstream side of the tank (see Fig. 1*B*).

In some tests arrangements were made for heating the intake air by manually controlled strip heaters installed in an insulated pipe 6 in. diam just upstream from the intake manifold (see Fig. 1).

Test Procedure

The desired pressures in the intake and exhaust surge tank were obtained as just outlined when the engine was operating at the speed and load selected. Final adjustments were then made in speed, load, and pressure in intake and exhaust surge tanks. The engine was then operated until equilibrium was attained and the test data recorded.

Fuel consumption was determined by an automatic fuel-weighing device which operated an electric clock and revolution counter.

Air was measured by noting the differential pressure across a thin-plate orifice upstream from the intake surge tank. The orifice and connections were installed in accordance with the published recommendations of the A.S.M.E. Special Research Committee on Fluid Meters.

In most tests with each engine the composition of the exhaust gases was determined by analysis in a Haldane apparatus. From this analysis and from the analysis of the fuel it was possible to compute the fuel:air ratio. The values obtained agreed very closely (generally within ±2 or 3 per cent) with values computed from direct measurements of fuel and air consumption.

It was not possible to motor engines connected to the induction-type dynamometer. Therefore friction-horsepower determinations were made with the engines motored by the direct-current dynamometer. In these tests the engine was warmed up

TABLE 3 RESULTS OF TESTS OF ENGINE B AT 1000 RPM NORMAL TEMPERATURES AND DIFFERENT SIMULATED AMBIENT PRESSURES

Test no.	Brake[1,2] hp.	Corrected brake hp[3]	Fuel consumption, lb per hr[2]	Fuel: air ratio, lb per lb	Volumetric efficiency, percent	Temperature at intake, F	Density at intake, lb per cu ft
Nominal absolute pressure at intake and exhaust, 30 in. of mercury[4]							
47	0.3	0.3	2.05	0.0079	90	78	0.0728
51	0.9	0.9	2.28	0.0094	87	92	0.0708
48	2.5	2.5	2.58	0.0103	88	80	0.0725
56	2.6	2.6	2.74	0.0108	87	76	0.0738
49	5.0	5.1	3.30	0.0133	88	81	0.0721
57	5.1	5.1	3.42	0.0135	88	80	0.0735
52	7.5	7.6	4.13	0.0168	87	85	0.0718
58	10.0	10.1	4.92	0.0197	87	82	0.0733
53	12.5	12.7	5.67	0.0232	87	86	0.0715
50	12.5	12.8	5.66	0.0237	84	83	0.0720
59	15.0	15.3	6.50	0.0261	87	83	0.0730
60	17.5	17.7	7.34	0.0294	87	84	0.0733
54	20.0	20.4	8.27	0.0343	86	89	0.0711
61	22.5	22.9	9.22	0.0378	86	86	0.0726
62	25.0	25.7	10.41	0.0429	85	88	0.0725
55	27.5	28.6	11.68	0.0498	84	91	0.0709
63	27.5	28.1	11.50	0.0480	84	90	0.0722
Nominal absolute pressure at intake and exhaust, 25 in. of mercury[5]							
97	0.2	0.3	1.98	0.0096	90	100	0.0588
75	0.3	0.4	2.03	0.0100	88	102	0.0587
76	5.1	5.4	3.38	0.0167	88	102	0.0587
77	10.1	10.7	5.00	0.0248	87	102	0.0589
78	15.0	16.1	6.76	0.0341	86	103	0.0587
111	15.2	16.1	6.67	0.0319	87	80	0.0612
112	17.6	18.8	7.71	0.0371	86	82	0.0611
79	20.1	22.0	8.80	0.0456	84	102	0.0587
113	22.6	24.7	10.14	0.0496	85	84	0.0610
114	23.8	26.4	11.18	0.0559	84	84	0.0608
80	25.2	29.3	12.43	0.0656	82	103	0.0586
Nominal absolute pressure at intake and exhaust, 20 in. of mercury[6]							
87	0.4	0.6	2.06	0.0118	84	100	0.0469
100	0.4	0.6	2.10	0.0131	87	100	0.0469
104	0.3	0.5	2.13	0.0133	88	100	0.0466
83	5.0	5.4	3.30	0.0151	86	101	0.0471
89	10.2	11.5	5.11	0.0328	84	101	0.0470
101	12.6	14.4	6.12	0.0396	83	100	0.0475
90	15.1	17.7	7.19	0.0467	83	101	0.0472
115	15.2	17.5	7.18	0.0434	86	73	0.0491
116	17.3	20.6	8.44	0.0520	84	81	0.0484
117	18.3	22.1	9.03	0.0570	83	82	0.0484
119	18.8	23.4	9.88	0.0625	83	86	0.0480
118	19.2	25.0	11.06	0.0706	83	82	0.0484
91	19.6	27.7	12.45	0.0840	80	100	0.0471

[1] At test intake conditions.
[2] Corrected to nominal speed of 1000 rpm.
[3] Corrected to intake conditions of 29.92 in. of mercury absolute pressure, temperature 60 F, density of 0.0765 lb per cu ft. Equation [23] used.
[4] Actual range of pressure 29.5—30.1 in. of mercury.
[5] Actual range of pressure 24.9—25.1 in. of mercury.
[6] Actual range of pressure 19.9—20.3 in. of mercury.

until the equilibrium lubricating-oil temperature was attained and motoring friction determined at this condition.

Test Results

The results of a typical series of tests on one of the engines are given in Table 3. To eliminate minor effects of deviations of actual speed from the nominal speed, the data on speed, fuel consumption, and horsepower are corrected to the nominal speed by assuming horsepower and fuel consumption to be directly proportional to speed. The correction is minor as the average speed was generally within ±5 rpm of the nominal speed and never exceeded ±15 rpm.

DISCUSSION OF RESULTS

Basis for Comparing Results. The effect of ambient conditions on the power output of a Diesel engine can be determined by maintaining constant all engine operating conditions and all ambient conditions except the one whose effect is being studied. This means that comparisons of the results of tests in which a particular ambient condition is varied must be made at the same speed and throttle setting. In the Diesel engine the position of the throttle or throttle setting fixes the quantity of fuel injected at a given engine speed. If both speed and throttle setting are maintained constant, it is obvious that the quantity of fuel supplied, or in other words the fuel consumption, will be constant and will not be affected by ambient conditions. Therefore comparison of power outputs obtained at different ambient conditions must be made at the same rate of fuel consumption. This comparison can be made most conveniently by plotting brake horsepower against fuel consumption for each ambient condition studied.

Effect of Ambient Conditions on Brake Horsepower

The effect of ambient pressure on the brake horsepower of engines A, B, and C is shown in Figs. 2, 3, 4, and 5. The effect of ambient temperature (at ambient pressures of 30 and 20 in. of mercury abs) on the brake horsepower of engine B is shown in Fig. 6.

These results are presented to give a general idea of the magnitude of the effect of ambient conditions on brake horsepower and to show how the effect varies throughout the operating range of the engine tested. The following generalization may be made:

Reductions in ambient pressure or increases in ambient temperature cause significant reductions in brake horsepower at high rates of fuel consumption (higher loads). Ambient pressure or temperature does not affect brake horsepower significantly at low rates of fuel consumption (light loads).

The foregoing discussion is on the basis of the effect of the independent variables, pressure and temperature. It will be shown subsequently that density is the fundamental variable, and from the foregoing it is evident that reductions in ambient density cause reductions in brake horsepower at the higher loads but that ambient density does not affect brake horsepower significantly at light loads.

If data similar to those presented in Figs. 2 to 6, inclusive, were available for an engine it would be possible to determine correction factors graphically. However, it is desirable to develop other methods that might be more convenient and more generally applicable. In the succeeding sections the data are analyzed further to develop more rational procedures for determining correction factors for power output.

Relation Between Indicated Efficiency and Fuel : Air Ratio

The theoretical or maximum possible thermal efficiency of a given internal-combustion engine can be computed from the thermodynamic properties of the working fluid. Since these properties are related to fuel : air ratio it is evident that thermal efficiency must also be related to fuel : air ratio.

The relation between computed maximum thermal efficiency and fuel : air ratio for a limited-pressure fuel : air cycle and for an assumed compression ratio of 13.9 to 1 is shown in Fig. 7. The details of this computation have been reported previously (3) but it should be mentioned here that the limited-pressure cycle was chosen because it represents a rational criterion for comparing actual cycles of high-speed Diesel engines. The limited pressure at a given fuel : air ratio was obtained from data published by

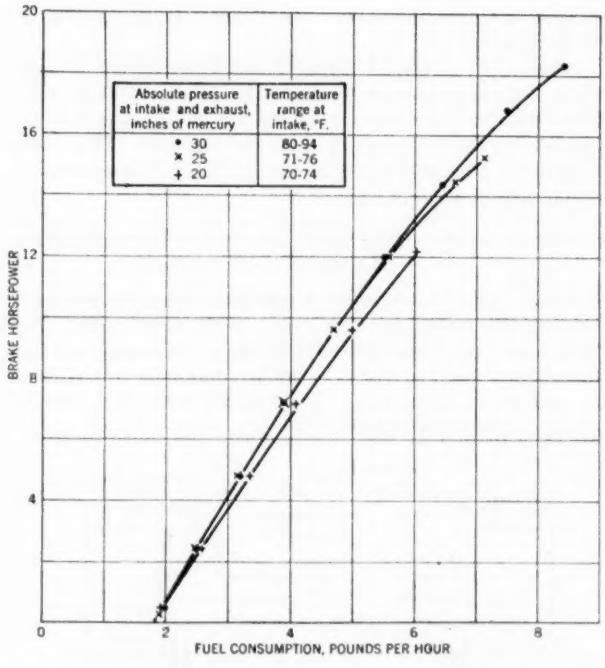


Fig. 2 Effect of Ambient Pressure on Brake Horsepower of Engine A at 600 Rpm

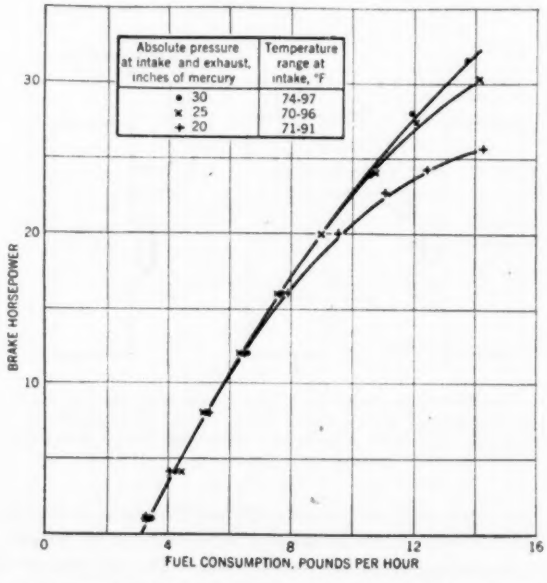


Fig. 3 Effect of Ambient Pressure on Brake Horsepower of Engine A at 1000 Rpm

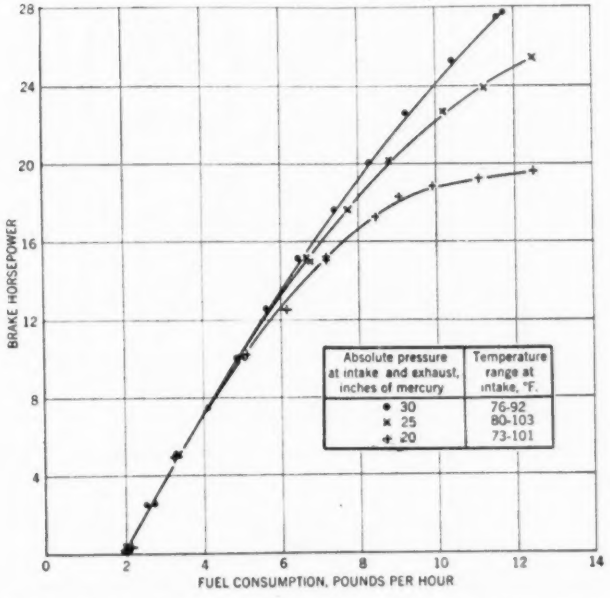


FIG. 4 EFFECT OF AMBIENT PRESSURE ON BRAKE HORSEPOWER OF ENGINE B AT 1000 RPM

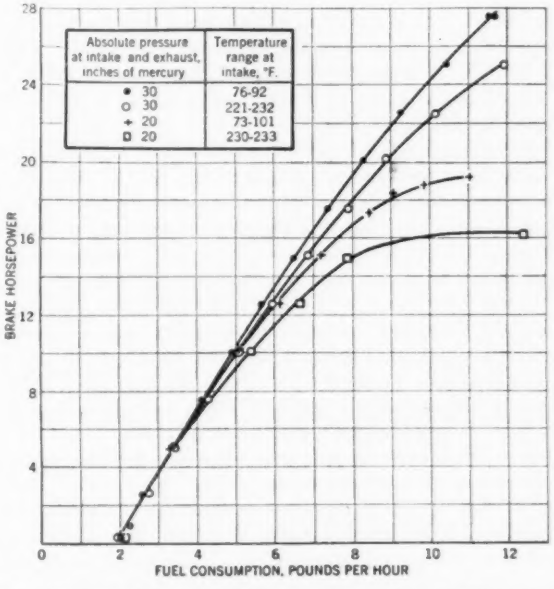


FIG. 6 EFFECT OF AMBIENT TEMPERATURE ON BRAKE HORSEPOWER OF ENGINE B AT 1000 RPM

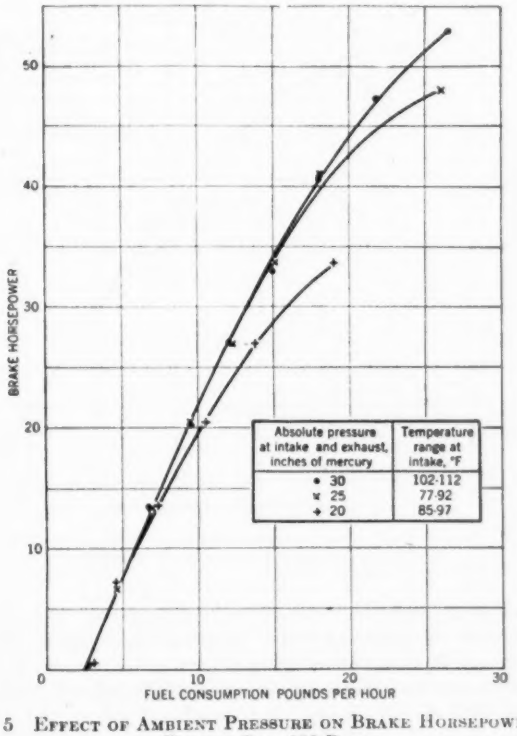


FIG. 5 EFFECT OF AMBIENT PRESSURE ON BRAKE HORSEPOWER OF ENGINE C AT 600 RPM

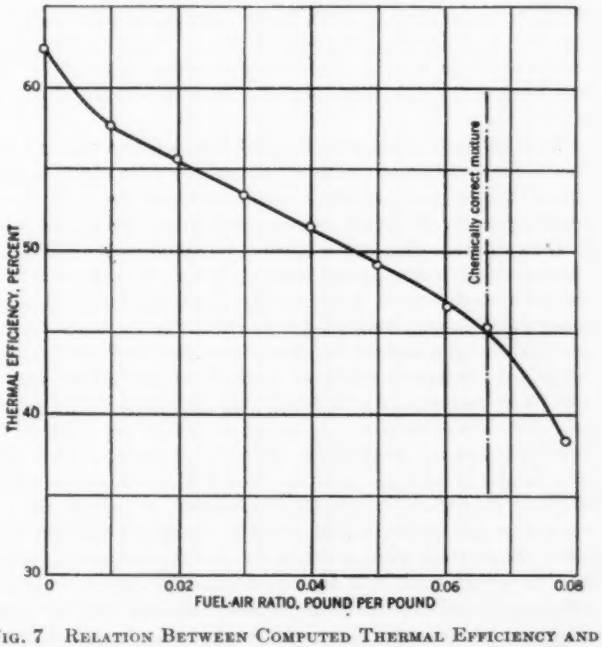


FIG. 7 RELATION BETWEEN COMPUTED THERMAL EFFICIENCY AND FUEL : AIR RATIO FOR A LIMITED PRESSURE FUEL-AIR CYCLE WITH OCTANE FUEL AND AN ASSUMED COMPRESSION RATIO OF 13.9

Rothrock and Waldron (9) who made tests on an engine having a compression ratio of 13.9 : 1.

Fig. 7 shows that at fuel : air ratios, within the normal operating range of a Diesel engine, the relation between computed thermal efficiency and fuel:air ratio is linear. Since this relation is fundamental it might be expected that it would be independent of ambient conditions. It is of interest therefore to examine the relation between indicated efficiency and fuel : air ratio for the actual test results obtained at different ambient conditions.

RELATION BETWEEN FUEL : AIR RATIO AND INDICATED EFFICIENCY DETERMINED FROM BRAKE HORSEPOWER AND MOTORING FRICTION

Facilities for determining indicated horsepower directly were not available in the Bureau of Mines tests. Accordingly, as an approximation, indicated horsepower was assumed to be equal to brake horsepower plus friction horsepower determined in motoring tests. It is recognized that indicated horsepower determined in this manner may be in error because of the well-known limitations (10) in determining friction horsepower in motoring tests. It should be mentioned, however, that errors in determining fric-

tion horsepower become less significant at the higher power outputs because if these errors are not too great they represent only a relatively small fraction of the indicated horsepower. For this reason trends at higher power outputs (higher fuel : air ratios) can be considered as being relatively unaffected by errors in determining friction horsepower.

For convenience, indicated efficiency will be expressed as indicated horsepower-hours per pound of fuel (ihp ÷ lb of fuel per hr). This factor does not have the same numerical value as indicated efficiency, but it is directly proportional to indicated efficiency when the heating value of the fuel is substantially constant as it was in the tests reported herein. For brevity, this factor will be referred to as "indicated efficiency" in this report. Obviously, indicated horsepower-hours per pound of fuel can be converted to indicated thermal-efficiency ratio by multiplying by the factor 2545 ÷ (heating value of fuel, Btu per lb). This conversion would of course be essential in analyzing results obtained with fuels having widely different heating values.

The relation between indicated efficiency determined as outlined and fuel : air ratio is shown in Figs. 8, 9, 10, 11, and 12. Figs. 11 and 12 which represent, respectively, results of test of engine B at 1000 rpm and engine C at 600 rpm, show that the relation is linear and independent of ambient conditions at fuel : air ratios greater than approximately 0.02 lb per lb. Figs. 8, 9, and 10 which represent, respectively, the results of tests of engine A at 600, 1000, and 1400 rpm, show that for all practical purposes the relation is independent of ambient conditions and could be approximated by a linear function at fuel : air ratios greater than approximately 0.025 lb per lb. However, at fuel : air ratios less than this the results of tests of engine A indicate that the relation is not independent of ambient conditions and is not linear.

Since theoretical considerations strongly suggest that the relation between indicated efficiency and fuel : air ratio should be unaffected by changes in ambient conditions, it is necessary to seek an explanation for deviations of test results from this presumption.

If combustion efficiency is affected by ambient conditions, it is obvious that indicated efficiency will not be independent of ambient conditions as predicted by thermodynamic considerations which assume complete combustion. In the tests reported here precise gas-analysis methods were used and carbon monoxide and aldehydes, which are products of incomplete combustion, were determined with considerable precision. The method used for carbon monoxide is sensitive to 0.01 per cent carbon monoxide and the method for aldehydes is sensitive to 5 ppm. The results of such gas analyses showed that the concentration of these products of incomplete combustion at a given fuel : air ratio were not affected significantly by changes in ambient pressure. Since there was no detectable increase in smoke production, it would seem that the apparent reductions in indicated efficiency at the low ambient pressures and low fuel : air ratios could not be accounted for on the basis of reductions in combustion efficiency.

Combustion knock was observed at the lower ambient pressures. Ignition delay probably is greater under such conditions because of the lower partial pressure of oxygen. The apparent effect of ambient conditions on indicated efficiency might have been due to the increased tendency to knock. However, if this were the case it would seem that a significant effect would have been observed at the higher fuel:air ratios where combustion knock was most severe. Since the indicated efficiency was apparently affected significantly by ambient pressure only at the lower fuel:air ratios, it is possible that combustion knock may not have been a factor. This cannot be stated definitely without further refinements in testing methods.

Indicated horsepower is only approximated when it is determined from measurements of brake horsepower and friction horsepower in motoring tests. As mentioned previously any inaccuracy in determining friction horsepower will be a larger proportion of the indicated horsepower at light loads (low fuel : air ratios) than at higher loads. It is possible therefore that the apparent effect of ambient pressure on indicated efficiency at the lower fuel:air ratios may have been only the result of unavoidable inaccuracies in determining friction horsepower.

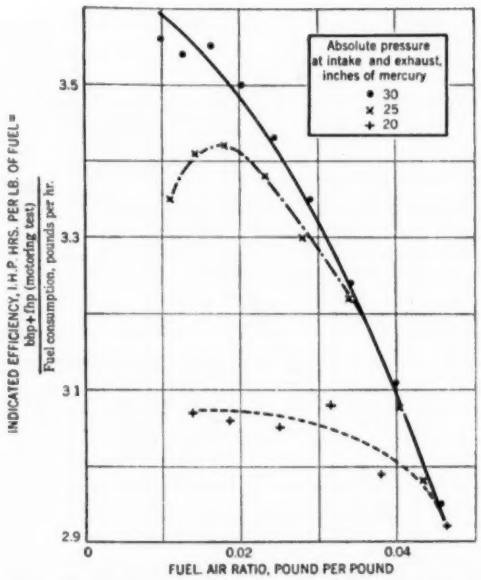


FIG. 8 RELATION BETWEEN INDICATED EFFICIENCY AND FUEL : AIR RATIO IN TESTS OF ENGINE A AT 600 RPM

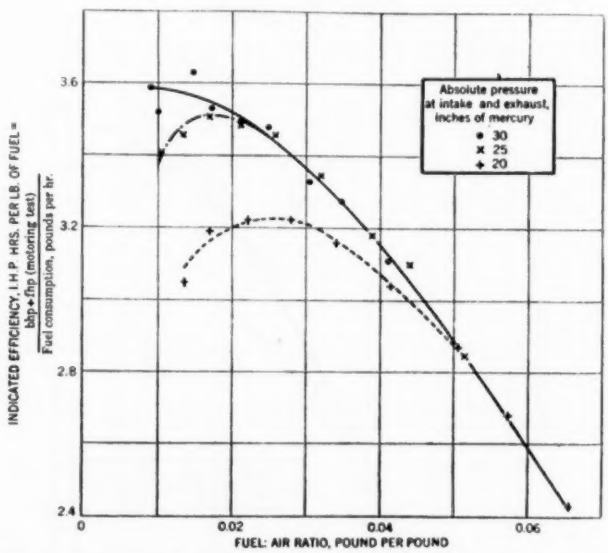


FIG. 9 RELATION BETWEEN INDICATED EFFICIENCY AND FUEL : AIR RATIO IN TESTS OF ENGINE A AT 1000 RPM

It seems desirable therefore to seek a method for approximating indicated horsepower and ultimately indicated efficiency that does not involve determination of friction horsepower in a motoring test. Such a method is described in the following section.

DERIVED INDICATED EFFICIENCY

As mentioned previously, theoretical considerations point to a relation between indicated efficiency and fuel : air ratio that is

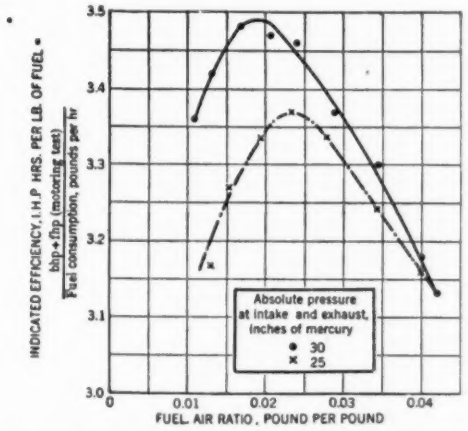


FIG. 10 RELATION BETWEEN INDICATED EFFICIENCY AND FUEL : AIR RATIO IN TESTS OF ENGINE A AT 1400 RPM

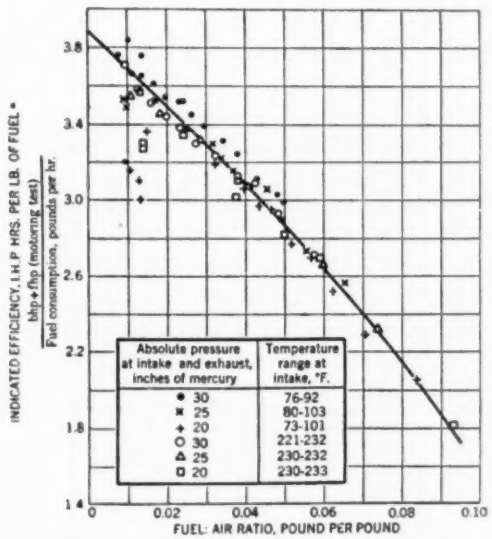


FIG. 11 RELATION BETWEEN INDICATED EFFICIENCY AND FUEL : AIR RATIO IN TESTS OF ENGINE B AT 1000 RPM

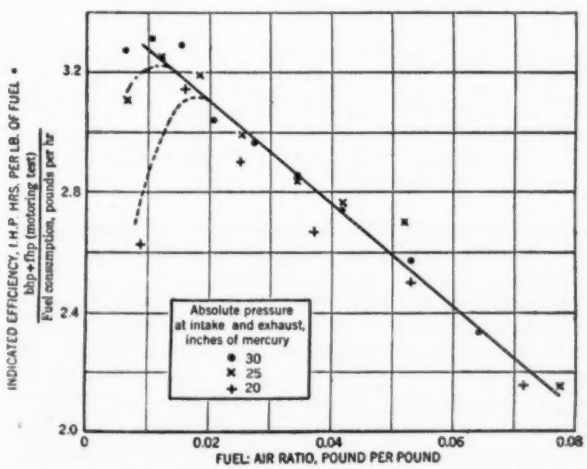


FIG. 12 RELATION BETWEEN INDICATED EFFICIENCY AND FUEL : AIR RATIO IN TESTS OF ENGINE C AT 600 RPM

independent of ambient conditions. The test results analyzed, as outlined, show that for all practical purposes this is true at the higher fuel : air ratios and that the relation is linear under these conditions. Let us assume therefore that linear relation exists in the actual engine and let the indicated efficiency determined from this relation be designated as "derived indicated efficiency." The assumed linear relation can be expressed by the following equation

$$e = e_0 - af \quad \ldots\ldots [1]$$

in which

e = derived indicated efficiency, expressed as ihp-hr per lb of fuel
f = fuel : air ratio, lb per lb
e_0 = intercept on y-axis (constant for a given engine and given engine speed)
a = slope (constant for a given engine and given engine speed)

Using the following nomenclature:

b = brake horsepower
c = derived friction horsepower (assumed constant for a given engine and given engine speed)
i = derived indicated horsepower
F = fuel consumption, lb per hr
v = volumetric efficiency (expressed as a ratio)
ρ = density of ambient atmosphere, lb per cu ft
Q = volume displaced by pistons on intake stroke, cu ft per hr

Then $$i = eF \quad \ldots\ldots [2]$$

Substituting in Equation [2] the value of e from Equation [1], we obtain

$$i = (e_0 - af)F \quad \ldots\ldots [3]$$

Since $$i = b + c \quad \ldots\ldots [4]$$

then from Equations [3] and [4]

$$b + c = (e_0 - af)F \quad \ldots\ldots [5]$$

If a series of tests is made at constant speed, at selected loads from no load to full load, and at a given set of ambient conditions, the value of b, F, and f will be obtained at each test condition. If we select from the data one set of values b_1, F_1, and f_1 then from Equation [5]

$$b_1 + c = (e_0 - af_1)F_1 \quad \ldots\ldots [6]$$

Subtracting Equation [6] from [5] and assuming that c is constant at a given speed and is independent of load

$$b - b_1 = e_0(F - F_1) - a(fF - f_1F_1) \quad \ldots\ldots [7]$$

Dividing Equation [7] by $(F - F_1)$ we obtain

$$\frac{b - b_1}{F - F_1} = e_0 - a\,\frac{fF - f_1F_1}{F - F_1} \quad \ldots\ldots [8]$$

Remembering that b, F, and f can be any set of values in a series of tests at constant speed but at different loads and that b_1, F_1, and f_1 are one particular set of values chosen arbitrarily, then Equation [8] shows that if $\frac{b - b_1}{F - F_1}$ is plotted against $\frac{fF - f_1F_1}{F - F_1}$, a straight line should result and it will be possible to evaluate the constants e_0 and a. It is apparent therefore that Equation [8] offers a method for determining the relation between derived indicated efficiency and fuel : air ratio by measuring only brake horsepower, fuel : air ratio, and fuel consumption in a series of tests at constant speed but at different loads.

To determine the applicability of the foregoing method of

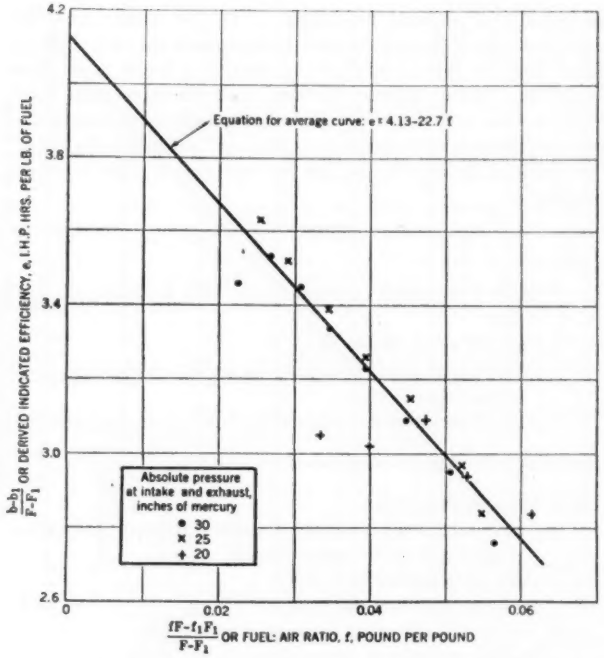


FIG. 13 RELATION BETWEEN DERIVED INDICATED EFFICIENCY AND FUEL : AIR RATIO FOR ENGINE A AT 600 RPM

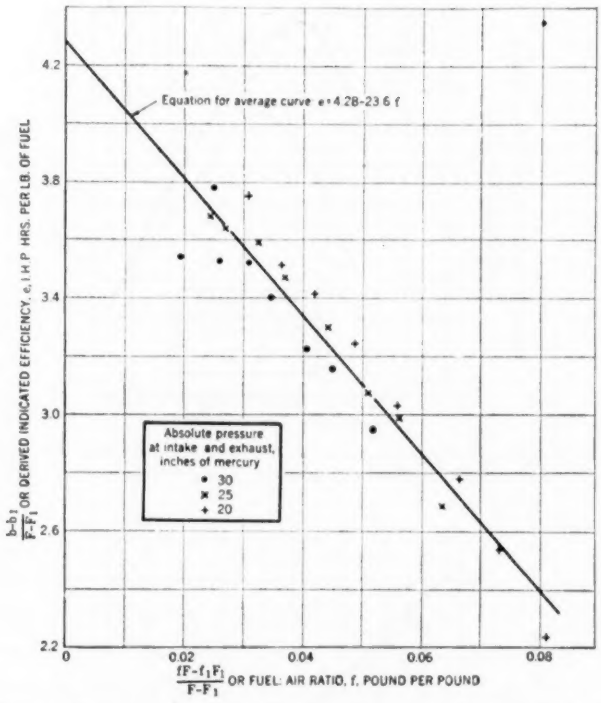


FIG. 14 RELATION BETWEEN DERIVED INDICATED EFFICIENCY AND FUEL : AIR RATIO FOR ENGINE A AT 1000 RPM

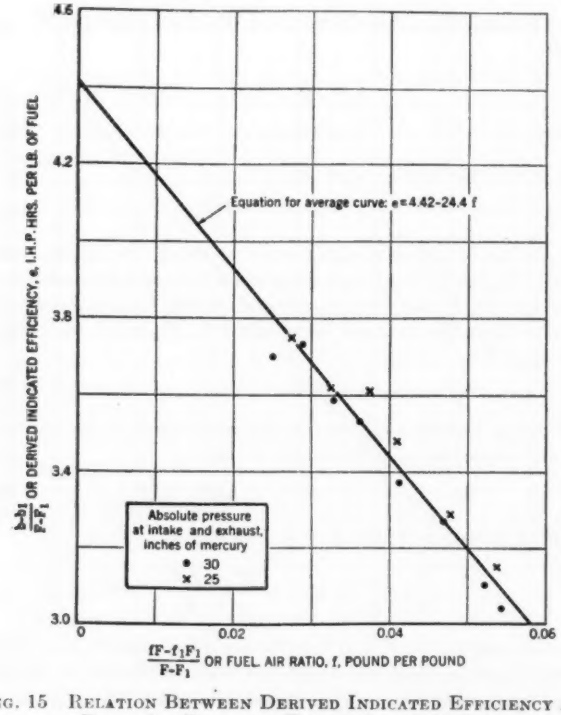


FIG. 15 RELATION BETWEEN DERIVED INDICATED EFFICIENCY AND FUEL : AIR RATIO FOR ENGINE A AT 1400 RPM

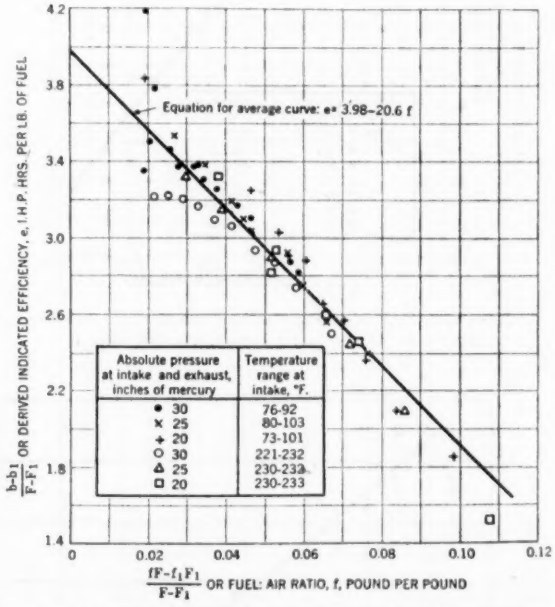


FIG. 16 RELATION BETWEEN DERIVED INDICATED EFFICIENCY AND FUEL : AIR RATIO FOR ENGINE B AT 1000 RPM

analysis, the values of $\frac{b-b_1}{F-F_1}$ and $\frac{fF-f_1F_1}{F-F_1}$ were computed from the test results and are plotted in Figs. 13, 14, 15, 16, and 17. In making the computation, the test at minimum load for each constant ambient condition was arbitrarily chosen for determination of the value of b_1, F_1, and f_1.

Figs. 13, 14, and 15, respectively, represent test results obtained with engine A at 600, 1000, and 1400 rpm. It will be observed that at a given speed the results obtained at all ambient conditions can be represented with good precision by a linear relation. The same conclusion is indicated by Fig. 16 which represents data obtained in tests with engine B at 1000 rpm, and by Fig. 17 which represents data obtained in tests with engine C at 600 rpm. The average deviation from the average curve is approximately 0.08 ihp-hr per lb of fuel. Thus the average curve represents derived indicated efficiency with an average relative error that

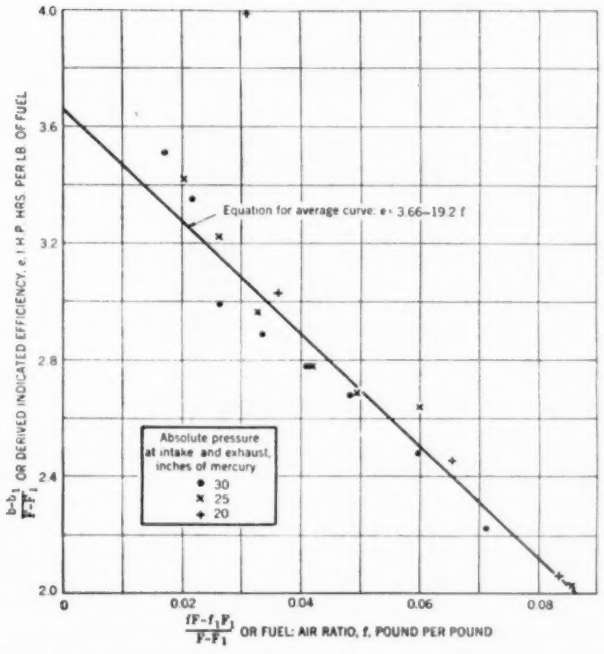


FIG. 17 RELATION BETWEEN DERIVED INDICATED EFFICIENCY AND FUEL : AIR RATIO FOR ENGINE C AT 600 RPM

ranges from approximately 2 to 3 per cent. It will be observed that individual points are dispersed at the lowest values of $\frac{fF - f_1F_1}{F - F_1}$ (see Fig. 16). This occurs because the different $b - b_1$ cannot be determined precisely when this difference is low. For example, an absolute error of 0.2 hp represents a relative error of 10 per cent when $b - b_1$ is of the order of 2 hp.

The values of the parameters e_0 and a were determined by the method of averages (7) and are given in Table 4. In determining the average points the data for each engine speed were divided into two groups above and below an arbitrarily selected value of $\frac{fF - f_1F_1}{F - F_1}$. The values selected were in the middle of the range of this term and were as follows: 0.04 for tests of engine A; 0.05 for tests of engine B; and 0.045 for tests of engine C. Table 4 also shows values of $\frac{e_0}{a}$ as these are required in a subsequent section of the report.

TABLE 4 VALUES OF e_0 AND a IN RELATION $e = e_0 - af$

Engine	Engine speed, rpm	e_0	a	$\frac{e_0}{a}$
A	600	4.13	22.7	0.182
A	1000	4.28	23.6	0.181
A	1400	4.42	24.4	0.181
B	1000	3.98	20.6	0.194
C	600	3.66	19.2	0.191

It will be observed that the values of e_0 and a appear to be affected by engine speed and type of engine. Therefore each set of values applies only to a particular engine and a particular engine speed. However, from the limited data available it appears that $\frac{e_0}{a}$ is approximately the same for the three engines tested and may not be affected by engine speed. If this is true for a number of engines, it would be possible to develop one set of correction factors applicable to all engines.

In connection with the apparent constancy of $\frac{e_0}{a}$, it is of interest to note that $\frac{e_0}{2a}$ is the fuel : air ratio at which both derived indicated horsepower and brake horsepower pass through a maximum. This can be shown by substituting for F its value $fQv\rho$ in Equation [3] or [5]; taking the derivative of i or b with respect to f; equating the derivative to zero and solving for f. Since the fuel : air ratio at which maximum horsepower is obtained is a function chiefly of the thermodynamic properties of the working fluid, it is not surprising that $\frac{e_0}{a}$ which is twice this ratio should be approximately the same for different engines. It should be pointed out that Equation [1] only approximates derived indicated efficiency at fuel : air ratios on the rich side and therefore $\frac{e_0}{2a}$ probably is not the exact fuel : air ratio that results in maximum power. Nevertheless $\frac{e_0}{2a}$ is an approximation of this particular fuel : air ratio and therefore it is not unreasonable to expect that it has the same general property of being determined principally by thermodynamic considerations and of being more or less independent of engine design.

From the foregoing it is apparent that we have a relation that is independent of ambient conditions and that can therefore be used in the development of rational procedures for correcting power output to standard ambient conditions. It is not claimed that the value of e obtained from Equation [1] is the true indicated efficiency, and for that reason it has been called derived indicated efficiency. Although the value of e is somewhat empirical, nevertheless we can operate algebraically with Equation [1] since it represents actual test data with reasonable precision.

The evaluation of the parameters e_0 and a permits evaluation of the parameter c in Equation [5]. It will be remembered that c is designated as "derived friction horsepower." Solving Equation [5] for c we obtain

$$c = (e_0 - af)F - b \quad \ldots\ldots\ldots\ldots\ldots\ldots [9]$$

Since the values of b, F, and f are known for any test condition it is possible to determine c.

The values of c obtained using the values of e_0 and a for the engine and engine speed in question (see Table 4) are given in Table 5. Values of $\frac{c}{Q}$ are also given as they are required in a subsequent section of the report.

It will be observed that the average values of derived friction horsepower given in Table 5 are always greater than the friction horsepower determined in motoring tests (except for engine B at 30 inches absolute pressure and normal temperature). In general, the value of c tends to decrease as the ambient pressure is reduced. This same tendency was observed in the friction horsepower determined in motoring tests. The maximum and minimum values of c for each series of tests are given in Table 5 and indicate that at a given engine speed c is "constant" within reasonable limits. The computed values of c did not appear to be related to fuel : air ratio.

METHODS OF CORRECTING POWER-OUTPUT DETERMINATIONS TO STANDARD AMBIENT CONDITIONS

Derivation of Relations. Starting with Equation [1] which is independent of ambient conditions, we can derive expressions for converting measurements of power output to standard ambient conditions. Several expressions can be derived depending upon which parameters are retained. One such expression is derived in this section and two other forms of the correction equation are given.

If the subscript s denotes standard ambient conditions and the

TABLE 5 VALUES OF DERIVED FRICTION HORSEPOWER, c

Engine	Engine speed, rpm	Absolute pressure at intake and exhaust, in. of mercury	Temperature range at intake, F	Values of c			Friction horsepower from motoring test	$\frac{c}{Q}$
				Maximum	Minimum	Average		
A	600	30	80–94	7.8	7.1	7.3	6.6	0.00224
A	600	25	71–76	7.2	6.8	6.9	6.0	0.00212
A	600	20	70–74	7.1	6.4	6.8	5.3	0.00209
A	1000	30	74–97	14.0	12.6	13.2	11.2	0.00247
A	1000	25	70–96	13.1	11.6	12.0	10.0	0.00223
A	1000	20	71–91	13.3	11.5	11.9	9.1	0.00220
A	1400	30	90–105	20.6	19.5	19.8	15.4	0.00261
A	1400	25	76–80	18.9	18.4	18.7	14.2	0.00246
B	1000	30	76–92	7.7	6.9	7.3	7.4	0.00186
B	1000	25	80–103	7.8	6.7	7.3	6.8	0.00186
B	1000	20	73–101	7.8	6.6	7.1	6.1	0.00181
B	1000	30	221–232	8.3	7.3	7.7	7.2	0.00196
B	1000	25	230–232	7.5	7.2	7.3[a]	6.8	0.00186
B	1000	20	230–233	7.2	6.4	6.8[a]	6.2	0.00173
C	600	30	102–112	10.9	9.2	10.2[a]	8.7	0.00146
C	600	25	77–92	10.1	7.5	9.3[a]	8.2	0.00132
C	600	20	85–97	10.6	8.8	9.8[a]	7.7	0.00140

[a] Values of c in tests at fuel : air ratios greater than the chemically correct value not included in average.

subscript t denotes ambient conditions at the time of a test, then from Equation [3]

$$i_s = (e_0 - af_s)F_s \quad [10]$$

and

$$i_t = (e_0 - af_t)F_t \quad [11]$$

In converting power output to standard ambient conditions the rate of fuel consumption must be the same at the standard condition as at the test condition; therefore

$$F_s = F_t \quad [12]$$

and equating the values of F_s and F_t determined from Equations [10] and [11], we obtain

$$\frac{i_s}{e_0 - af_s} = \frac{i_t}{e_0 - af_t} \quad [13]$$

or

$$\frac{i_s}{i_t} = \frac{e_0 - af_s}{e_0 - af_t} \quad [14]$$

Subtracting 1 from both sides of Equation [14], we obtain upon simplification

$$\frac{i_s}{i_t} = 1 + \frac{1 - \frac{f_s}{f_t}}{\frac{e_0}{af_t} - 1} \quad [15]$$

Since

$$f = \frac{F}{Qv\rho} \quad [16]$$

then when $F_s = F_t$ we obtain

$$\frac{f_s}{f_t} = \frac{v_t\rho_t}{v_s\rho_s} \quad [17]$$

Substituting for $\frac{f_s}{f_t}$ in Equation [15] its value from Equation [17], we obtain

$$\frac{i_s}{i_t} = 1 + \frac{1 - \frac{v_t\rho_t}{v_s\rho_s}}{\frac{e_0}{af_t} - 1} \quad [18]$$

Without introducing a significant error it can be assumed that $v_t \doteq v_s$. The basis for this assumption is discussed in a subsequent section of this report. With this approximation Equation [18] becomes

$$\frac{i_s}{i_t} \doteq 1 + \frac{1 - \frac{\rho_t}{\rho_s}}{\frac{e_0}{af_t} - 1} = R \quad [19]$$

Equation [19] gives a relation for correcting indicated horsepower to standard ambient conditions. However, in practice the principal interest is in the correction of measurements of brake horsepower to standard ambient conditions. This may be done by substituting for i_s and i_t the values obtained from Equation [4] which gives

$$\frac{b_s + c_s}{b_t + c_t} = R \quad [20]$$

Equation [20] is not in a convenient form unless the value of c_s is known but from Equation [20] we may obtain the relation

$$\frac{b_s}{b_t} = R + \frac{c_tR - c_s}{b_t} \quad [21]$$

The value of c is not affected to a great degree by changes in ambient conditions. Therefore, as a close approximation we can assume $c_s \doteq c_t$ and we obtain

$$\frac{b_s}{b_t} \doteq R + \frac{c_t}{b_t}(R - 1) \quad [22]$$

Substituting in Equation [22] the value of R from Equation [19] and rearranging we obtain

$$\frac{b_s}{b_t} \doteq 1 + \frac{\left(1 - \frac{\rho_t}{\rho_s}\right)\left(\frac{c_t}{b_t} + 1\right)}{\frac{e_0}{af_t} - 1} \quad [23]$$

When e_0 and a are known Equation [23] can be used to correct to standard ambient conditions measurements of power output made at any ambient condition. It is necessary to know the fuel : air ratio at the test condition and the value of c_t. This latter factor can be computed from Equation [9] or it can be determined in a motoring test. A relatively large error in c_t has comparatively little effect on the value of the ratio $\frac{b_s}{b_t}$.

By retaining different parameters in the correction equation other forms may be obtained. The following form contains the parameters a and c

BRAKE HORSEPOWER CORRECTED TO AMBIENT CONDITIONS OF 29.92" OF MERCURY AND 60° F.

$$\frac{b_s}{b_t} = 1 - \frac{c_s - c_t}{b_t} - \frac{aF_t^2}{Qb_t}\left(\frac{1}{v_s\rho_s} - \frac{1}{v_t\rho_t}\right) \quad [24]$$

With the simplifying assumption made previously, Equation [24] becomes

$$\frac{b_s}{b_t} \doteq 1 - \frac{aF_t^2}{Qv_t b_t}\left(\frac{1}{\rho_s} - \frac{1}{\rho_t}\right) \doteq 1 - \frac{af_tF_t}{b_t}\left(\frac{\rho_t}{\rho_s} - 1\right) \quad [25]$$

Another form containing the parameters e_0 and c is as follows

$$\frac{b_s}{b_t} = \frac{e_0F_t}{b_t}\left(1 - \frac{v_t\rho_t}{v_s\rho_s}\right) + \left(1 + \frac{c_t}{b_t}\right)\frac{v_t\rho_t}{v_s\rho_s} - \frac{c_s}{b_t} \quad [26]$$

With the simplifying assumptions made previously, Equation [26] becomes

$$\frac{b_s}{b_t} \doteq \frac{e_0F_t - c_t}{b_t}\left(1 - \frac{\rho_t}{\rho_s}\right) + \frac{\rho_t}{\rho_s} \quad [27]$$

Correction of Test Results to Standard Ambient Conditions

The test results have been corrected to standard ambient conditions of 29.92 in. of mercury and 60 F[4] by using Equation [23]. This equation has been selected for illustrative purposes, although either Equation [25] or [27] could be used. Figs. 18, 19, 20, and 21 show brake horsepower at standard ambient conditions (corrected brake horsepower) in relation to fuel consumption. It will be observed from these figures that a single curve represents the relation between corrected brake horsepower and fuel consumption regardless of the ambient conditions of the tests. In general the average deviations from the average curve are of the order of 0.5 hp or less. Part of this deviation is caused by normal experimental errors; part is caused by deviations of actual results from the average relation between derived indicated efficiency and fuel : air ratio; and part is caused by the simplifying assumptions made in deriving Equation [23]. The largest deviations of corrected brake horsepower from the average curve occurred in two tests of engine B at the highest rate of fuel consumption and at an ambient pressure of 20 in. of mercury (see Fig. 20). In these two tests the fuel:air ratios (0.0706 and 0.0840 lb per lb, respectively) were greater than the chemically correct value of 0.068. At these high fuel : air ratios combustion is incomplete and the derived indicated efficiency is not linear with fuel : air ratio (see Fig. 7). Therefore actual test results are not represented precisely by the average curve.

From the foregoing it is apparent that Equation [23] yields reasonably precise results when used to convert brake horsepower at test ambient conditions to brake horsepower at standard ambient conditions. The same order of precision of corrected brake horsepower may be obtained by using either Equation [25] or Equation [27]. It appears therefore that the principles outlined here may be useful in developing rational methods for correcting brake-horsepower determinations to standard ambient conditions. However, before such methods can be developed for universal application it will be necessary to obtain information on many more engines and to study the performance of each engine more intensively than was possible in the Bureau of Mines investigation. As mentioned previously, this investigation was concerned principally with the effect of ambient conditions on exhaust-gas composition, and performance data were obtained only incidentally.

The principal reason for choosing Equation [23] for illustrative purposes is that it can be put into a form convenient for graphical representation, which enables us to obtain a general idea of the magnitude of correction factors for power output of Diesel engines over a wide range of conditions. The value of $1 + \frac{c_t}{b_t}$ can be expressed in terms of fuel : air ratio and known parameters by utilizing Equations [5] and [16], which gives

$$1 + \frac{c_t}{b_t} = \frac{1}{1 - \frac{c_t}{(e_0 - af_t)Qv_t\rho_t f_t}} \quad [28]$$

[4] This represents a commonly used engineering standard condition. The A.S.M.E. Test Code for Internal Combustion Engines, September, 1943, refers gas volumes to a standard condition of 29.92 in. of mercury and 68 F. The maximum difference between horsepower corrected to either condition is less than 0.9 per cent.

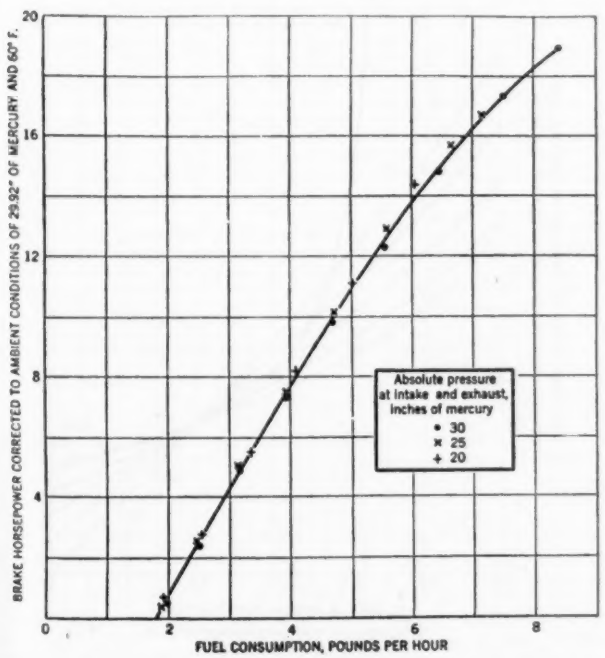


Fig. 18 Relation Between Corrected Brake Horsepower and Fuel Consumption for Engine A at 600 Rpm

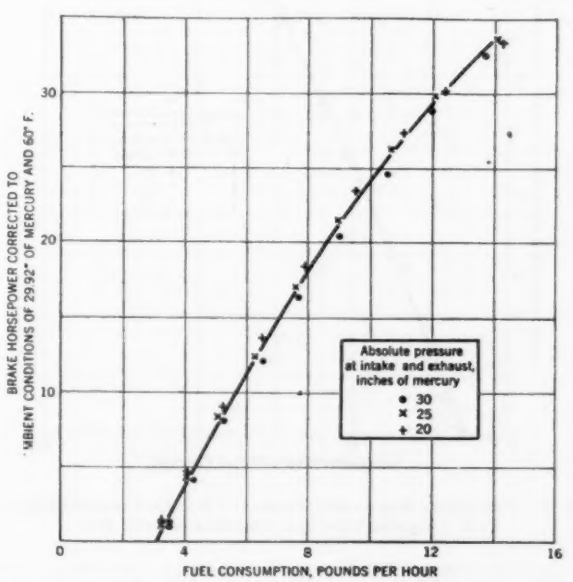


Fig. 19 Relation Between Corrected Brake Horsepower and Fuel Consumption for Engine A at 1000 Rpm

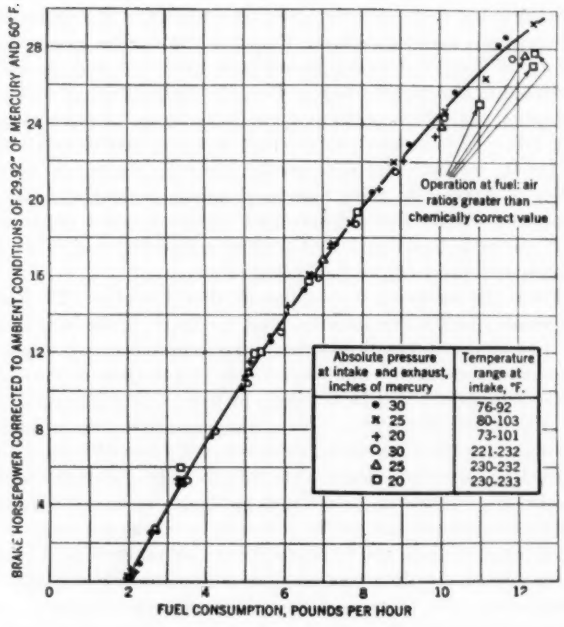


FIG. 20 RELATION BETWEEN CORRECTED BRAKE HORSEPOWER AND FUEL CONSUMPTION FOR ENGINE B AT 1000 RPM

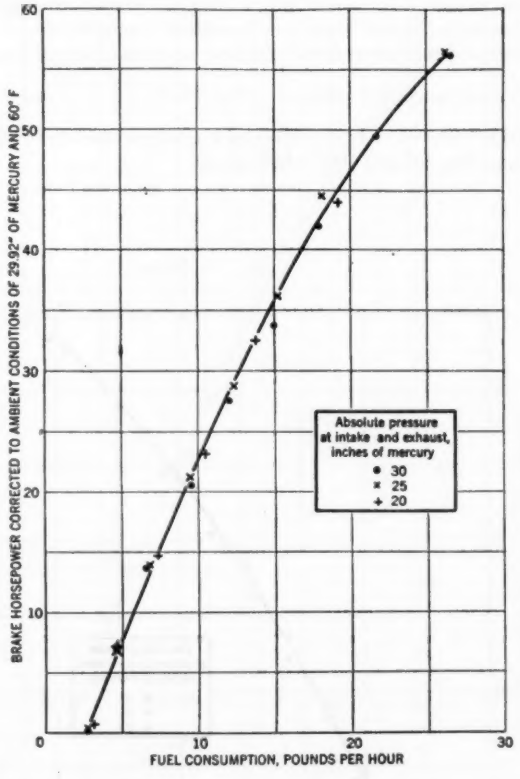


FIG. 21 RELATION BETWEEN CORRECTED BRAKE HORSEPOWER AND FUEL CONSUMPTION FOR ENGINE C AT 600 RPM

Substituting in Equation [23] the value of $1 + \frac{c_t}{b_t}$ from Equation [28], we obtain upon simplification

$$\frac{b_s}{b_t} \doteq 1 + \frac{1 - \frac{\rho_t}{\rho_s}}{\frac{e_0}{af_t} - \frac{c_t}{Qaf_t^2 v_t \rho_t} - 1} \quad \ldots\ldots\ldots\ldots [29]$$

Equation [29] shows that $\frac{b_s}{b_t}$ can be expressed in terms of $\frac{\rho_t}{\rho_s}$ and f_t when the values of e_0, a, c_t, Q, and v_t are known. If we use the data for engine B and assume $e_0 = 3.98$, $a = 20.6$; $c_t = 7.2$; $Q = 3930$; and $v_t = 0.85$ (range of values of v_t for all test conditions at normal temperatures was 0.88 to 0.82) we obtain

$$\frac{b_s}{b_t} = 1 + \frac{1 - \frac{\rho_t}{\rho_s}}{\frac{0.194}{f_t} - \frac{0.000105}{f_t^2 \rho_t} - 1} \quad \ldots\ldots\ldots [30]$$

Equation [30] is shown graphically in Fig. 22 for an assumed ρ_s of 0.0765 lb per cu ft (corresponding to an absolute pressure of 29.92 in. of mercury and a temperature of 60 F). From this figure we may obtain an excellent idea of the approximate magnitude of the correction factor for brake horsepower throughout a wide range of possible operating conditions. It is emphasized that Fig. 22 applies only to one engine and one engine speed, and until further information is developed each engine and engine speed should be considered as an individual case in preparing charts similar to Fig. 22. However, from the data available it appears that correction factors for any engine and engine speed will be within a few per cent of the factors shown in Fig. 22, except at low fuel : air ratios. The reason for this is that the values of $\frac{e_0}{a}$ and a do not vary greatly with type of engine and engine speed. Furthermore the value of $\frac{c_t}{Q}$ is not affected greatly by engine speed within the range studied because both c_t and Q are a function

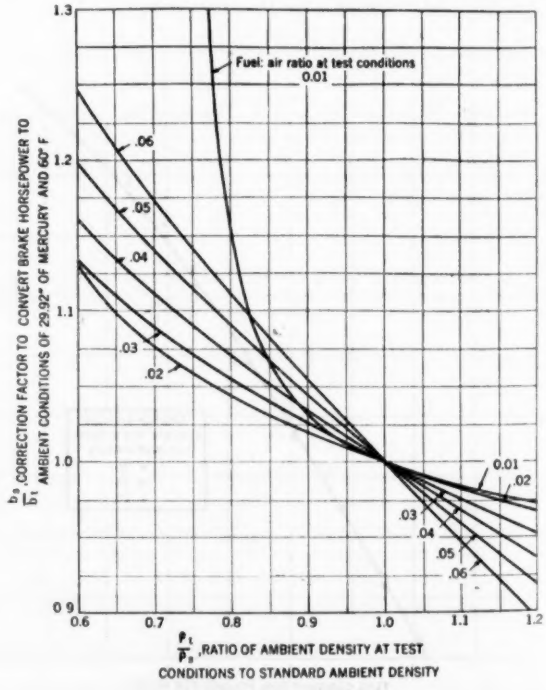


FIG. 22 RELATION BETWEEN $\frac{b_s}{b_t}$, $\frac{\rho_s}{\rho_t}$, AND f_t FOR ENGINE B AT 1000 RPM (For assumed standard ambient conditions of 29.92 in. of mercury and 60 F.)

of engine speed. The value of $\frac{c_t}{Q}$ is affected by type of engine; however, a study of Equation [29] shows that comparatively large variations in $\frac{c_t}{Q}$ have relatively little effect on $\frac{b_s}{b_t}$ at the higher fuel : air ratios.

The most desirable form of the correction equation can be determined only when additional data are available. If further tests show that $\frac{c_0}{a}$ is approximately constant for a number of engines then it may be possible to use Equation [23] with an average value of $\frac{c_0}{a}$ for all engines except when extreme precision is required. The value of a may not vary widely from engine to engine, in which case Equation [25] might be more desirable.

The conditions under which correction factors may have a significant effect on measurements of power output of Diesel engines will depend principally upon the precision of the measurement of power output, on the ratio of the ambient density during the test to the standard ambient density, and on the fuel:air ratio at which the engine is operated during the test. In this connection it is interesting to note that the A.S.M.E. Test Code for Internal-Combustion Engines, September, 1943, permits a maximum deviation from specified operating conditions of ±3 per cent of the absolute barometric pressure specified and of ±5 per cent of the equivalent absolute temperature specified. Correction factors for power output are not required within these limits. With these permissible deviations it would be possible for ambient density to deviate ±8 per cent from the specified value. From Equation [30] it is evident that this deviation in ambient density would cause a deviation in specified brake horsepower of ±3.5 per cent in the case of engine B operated at a fuel:air ratio of 0.05 lb per lb. It appears, therefore, that in some instances consideration might be given to the application of correction factors for power output even though the test ambient conditions are within the permissible limits specified by the A.S.M.E. Test Code.

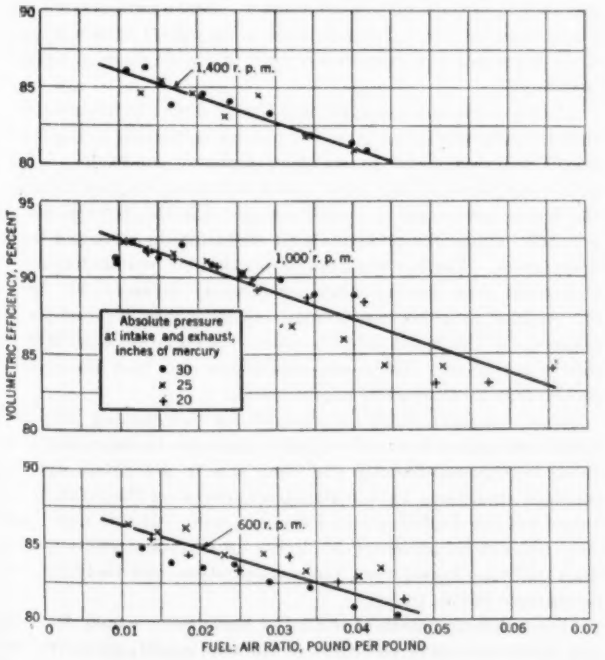


Fig. 23 Relation Between Volumetric Efficiency and Fuel: Air Ratio in Tests of Engine A

Effect of Ambient Conditions on Volumetric Efficiency

In deriving Equation [23], one of the simplifying assumptions was that volumetric efficiency was not affected significantly by changes in ambient conditions. It is of interest therefore to present the evidence supporting this assumption.

Figs. 23, 24, and 25 show the relation between volumetric efficiency and fuel:air ratio. It will be observed that volumetric efficiency decreases slightly as fuel : air ratio increases. The relation is apparently independent of ambient pressure within the range studied, as the deviations of volumetric efficiencies at different ambient pressures are generally within the limits of experimental error (approximately 2 to 3 per cent).

Fig. 24 shows a significant increase in volumetric efficiency as the temperature is increased. This apparent effect is a result of the method of heating the air and probably would not be observed if other more suitable arrangements were provided for heating the intake air. In the tests at elevated temperatures the intake air was heated electrically just before it entered the intake manifold. This method was used to avoid insulation of the intake surge tank. The addition of heat to the intake air results in an expansion in volume and therefore the work done during this expansion, which occurs at substantially constant pressure, must be considered. Under the test conditions a relatively large mass of intake air was on the upstream side of the air heater and a relatively small mass was on the downstream side. It would appear therefore that most of the work resulting from expansion during

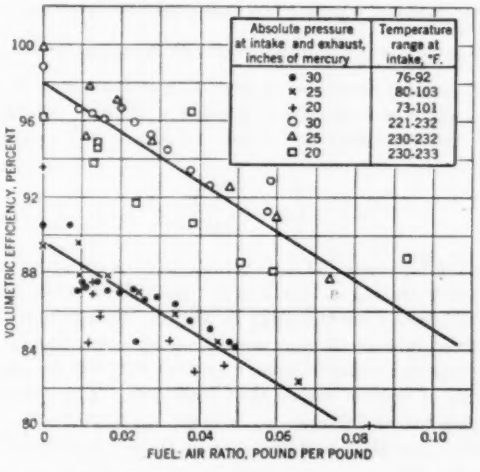


Fig. 24 Relation Between Volumetric Efficiency and Fuel: Air Ratio in Tests of Engine B at 1000 Rpm

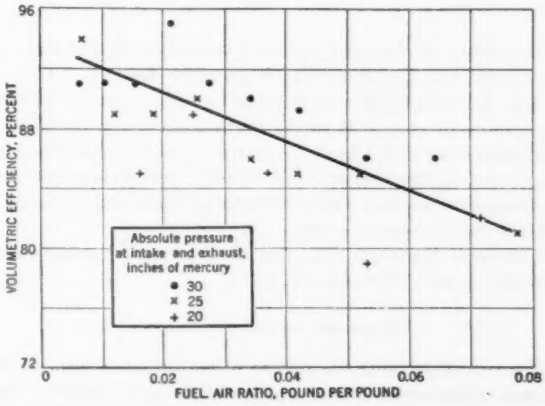


Fig. 25 Relation Between Volumetric Efficiency and Fuel: Air Ratio in Tests of Engine C at 600 Rpm

heating would be done on the relatively low mass of air downstream from the heater. It might be expected therefore that volumetric efficiency would be improved. It is believed that the foregoing explanation of the apparent effect of temperature is correct but additional experimental evidence will be required before it can be stated definitely that ambient temperature has no significant effect on volumetric efficiency.

In a Diesel engine operated at constant speed, changes in ambient conditions result in changes in fuel : air ratio if the throttle setting (rate of fuel consumption) is maintained constant. Accordingly, volumetric efficiency will be affected slightly by ambient conditions. If it is assumed that the ratio of ambient density during the tests to standard ambient density is as low as 0.6 the volumetric efficiencies under the two conditions do not differ by more than 3 per cent in any of the engines tested. If this difference were taken into consideration in Equation [23] the correction factor would be approximately 1 per cent greater at the high rates of fuel consumption.

If it is desired, volumetric efficiency can be related to fuel : air ratio by an equation of the following form

$$v = v_0 - df \quad [31]$$

in which v_0 and d are constant for a given engine and engine speed. This equation could then be used to determine the ratio of $\frac{v_s}{v_i}$. However, for the ordinary range of ambient conditions encountered it is doubtful whether this refinement is necessary.

Predicting Engine Performance by Algebraic Relations

The equations developed in preceding sections may be used to predict engine performance at any given ambient condition and rate of fuel consumption. From Equations [5] and [16] we obtain

$$b = \left(e_0 - \frac{aF}{Qv\rho}\right) F - c \quad [32]$$

In applying Equation [32] an average value of v may be assumed without introducing a significant error. If desired, v can be eliminated from Equation [32] by the use of Equation [31] but the resulting relation is much more inconvenient to handle.

For purposes of illustration, Equation [32] will be applied to the results of tests of engine B at 1000 rpm. The values of the parameters are as follows: $e_0 = 3.98$; $a = 20.6$; $Q = 3930$; $v = 0.85$ (range 0.82 to 0.88); $c = 7.2$; and Equation [32] becomes

$$b = 3.98\,F - 0.00640\,\frac{F^2}{\rho} - 7.2 \quad [33]$$

A comparison of observed values of brake horsepower and values calculated from Equation [33] is given in Table 6. This comparison shows that the equation can be used to predict the brake horsepower of engine B in its normal operating range with a maximum error of 0.7 hp. The error is greater when the engine is operated on the rich side (see Table 6, test 91) because under these conditions a linear relation between indicated efficiency and fuel : air ratio no longer holds.

If desired, Equation [33] can be represented graphically to show the relation between b, F, and ρ.

Summary and Conclusions

This report presents the results of performance tests on three different commercial Diesel engines at different ambient conditions. Operation at different ambient conditions was simulated by controlling conditions in surge tanks connected to the intake and exhaust of the engines. The tests were limited in scope because the principal interest in the investigation was the effect of ambient conditions on composition of the exhaust gases produced by the engine.

TABLE 6 COMPARISON OF BRAKE HORSEPOWER OF ENGINE B, CALCULATED FROM EQUATION [33], WITH OBSERVED BRAKE HORSEPOWER

Nominal ambient pressure, in. Hg, abs								
30			25			20		
Test no.	Calc. bhp	Obs. bhp	Test no.	Calc. bhp	Obs. bhp	Test no.	Calc. bhp	Obs. bhp
47	0.4	0.3	97	0.2	0.2	87	0.4	0.4
57	5.3	5.1	76	5.0	5.1	88	4.4	5.0
58	10.2	10.1	77	9.9	10.1	89	9.6	10.2
59	14.9	15.0	78	14.7	15.0	90	14.4	15.1
54	19.5	20.0	79	19.4	20.1	119	19.2	18.8
63	26.9	27.5	80	25.5	25.2	91	21.5	19.6

The performance data were analyzed, and a method was developed for deriving a relation between so-called derived indicated efficiency and fuel:air ratio that is independent of ambient conditions. The existence of such a relation would be predicted from theoretical thermodynamic considerations. The report presents a method for deriving the relation between indicated efficiency and fuel:air ratio from determination of brake horsepower, fuel consumption and fuel:air ratio at different loads throughout the operating range at a given engine speed.

The relation between derived indicated efficiency and fuel:air ratio is used as the basis for developing rational procedures for correcting to standard ambient conditions brake-horsepower determinations made at ambient conditions prevailing during the tests. The methods developed were applied to the results of tests at different ambient conditions and it was shown that the corrected brake horsepower at a given rate of fuel consumption was independent of the ambient conditions during the tests. Thus the methods developed appear to be suitable for determination of correction factors at least for the three engines on which data were obtained.

The relation between derived indicated efficiency and fuel:air ratio may also be used as the basis for algebraic expressions which permit determination of the brake horsepower of an engine at any rate of fuel consumption and at any ambient density when all the parameters in the equation are known. Brake horsepowers computed from the derived equation are in very good agreement with brake horsepowers determined in tests at a wide range of ambient conditions.

The data and analysis presented in this report have shown that rational procedures can be developed for correcting brake-horsepower determinations to standard ambient conditions. However, only three engines were tested and these engines were not studied as intensively as would be required in the development of generally applicable procedures for determining corrected brake horsepower. Further work may show that the parameters in the correction equation are not significantly different for different engines, in which case a single equation may be used for all engines. If this is not true, the correction equation will differ for different engines. There are indications also that these parameters may be affected by engine speed.

In an extensive study of methods for determining corrected brake horsepower it would be highly desirable to determine indicated horsepower directly and from this to determine whether ambient conditions have a significant effect on the relation between indicated efficiency and fuel:air ratio. If this were done it would not be necessary to derive an empirical relation from data on brake horsepower, fuel consumption, and fuel : air ratio as outlined in this paper.

Direct determination of indicated horsepower would also permit determination of the effect of ambient conditions on friction horsepower and of the effect of engine load on friction horsepower. If this fundamental information were available, more precise

methods could be developed for determining corrected brake horsepower.

Surge tanks connected to the intake and exhaust were used in the present investigation because of their simplicity and availability. However, in an extended investigation it probably would be advisable to test engines in a chamber in which the desired ambient conditions are maintained.

Acknowledgments

The author gratefully acknowledges the encouragement and support given to work on Diesel engines by A. C. Fieldner, chief, Fuels and Explosives Branch, and Wilbert J. Huff, consulting explosives chemist, Explosives Division, Bureau of Mines.

Particular acknowledgment is due to A. P. Rowles, principal engineering aide, Explosives Division, who obtained all test data, and to C. J. Ney, explosives testing station assistant, Explosives Division, and G. H. Hindman, assistant physical science aide, Explosives Division, who assisted in the test work.

The author is also grateful for the encouragement given by members of the A.S.M.E. Special Research Committee on Internal-Combustion Engines and particularly for the interest shown by Lee Schneitter, chairman.

BIBLIOGRAPHY

1 "A Rational Basis for Comparing Diesel Engine Performances," by E. S. Dennison, Trans. S.A.E., 1935, pp. 210–214.

2 "Effect of Variations in Atmospheric Conditions on Diesel Engine Performance," by J. S. Doolittle, Trans. A.S.M.E., vol. 63, 1941, pp. 91–95.

3 "A Rational Basis for Correlating Data on Compression-Ignition Engine Performance Obtained at Different Intake and Exhaust Conditions," by M. A. Elliott, *S.A.E. Journal*, vol. 40, 1941, pp. 532–543.

4 "Proposed Program of Research to Determine Correction-Factors for Converting Measurements of Power Output of Diesel Engines to Standard Atmospheric Conditions," by M. A. Elliott; unpublished report prepared for A.S.M.E. Special Research Committee on Internal-Combustion Engines, September 8, 1944.

5 "Reducing the Performance of a Solid-Injection Diesel Engine to Standard Conditions," by H. A. Everett, *Diesel Power*, vol. 11, 1933, pp. 541–545.

6 "A Thermodynamic Analysis of Internal-Combustion Engine Cycles," by G. A. Goodenough and J. B. Baker, University of Illinois Engineering Experiment Station, Bulletin No. 160, 1927.

7 "Graphical and Mechanical Computation. Part II—Experimental Data," by Joseph Lipka, John Wiley & Sons, Inc., New York, N. Y., 1921.

8 "Compression-Ignition Engine Performance at Altitudes and at Various Air Pressures and Temperatures," by C. S. Moore and J. H. Collins, Jr., N.A.C.A. Technical Note 619, 1937.

9 "Effects of Air-Fuel Ratio on Fuel Spray and Flame Formation in a Compression-Ignition Engine," by A. M. Rothrock and C. O. Waldron, N.A.C.A. Technical Report No. 545, 1936.

10 "The Internal Combustion Engine," by C. F. Taylor and E. S. Taylor, International Textbook Company, Scranton, Pa., 1938.

11 "Correcting Diesel Performance to Standard Atmospheric Conditions," by C. F. Taylor, Trans. S.A.E., 1937, pp. 263–272.

Water Injection in a Spark-Ignition Engine

By W. P. GREEN[1] and C. A. SHREEVE, JR.[1]

The present war witnessed a revival of interest in the use of water as a coolant and detonation suppressor inside the engine cylinder. Aircraft engines when operated with water injection have been boosted in output above normal sea-level capacity and have functioned satisfactorily. This paper gives a review of past tests on the use of water as a coolant and detonation suppressor in gasoline engines. It presents new data regarding the use of water in very high compression ratio engines to promote increased part-load efficiencies with low octane fuels.

THE introduction of water into the mixture, entering the cylinder of a spark-ignition engine, was tried as early as 1866, and was common on carbureted engines burning kerosene a few decades ago. Its action was not fully understood but its purpose was to prevent detonation and to promote smooth combustion. In 1935 Ford L. Prescott reported tests on supercharged aircraft engines in which as much as 2.83 lb of water were added per lb of fuel. No loss in thermal efficiency and an increase in power output were noted. M. S. Kuhring has reported tests in which water was injected into the mixture at the supercharger, with results similar to those obtained by Prescott. Kuhring noted cooling effects on the spark plugs, cylinder heads, and valves when the water was injected.

Colwell, Cummings, and Anderson have presented results of recent work on the injection of water, and water-alcohol into the mixture of truck engines. Data are given to show no increase in wear or other harmful effects on engine life as a result of using water in the combustion chamber.

Steinitz has pointed out that the use of water with its attendant equipment complicates the engine and increases weight. Also there is the possibility of the water freezing unless mixed with an antifreeze solution.

Past research has established the following facts in regard to use of water injection as a detonation suppressor:

1 There is no loss of thermal efficiency with low rates of water injection.

2 Cooling of the engine is not so important a problem at high outputs.

3 Supercharged engines will give higher outputs due to cooling of the mixture by the injected water. The higher manifold pressures increase maximum cylinder pressures and engine output. Detonation is suppressed by the water.

4 Space and weight requirements for carrying the water may be excessive unless condensing equipment is used to secure water from the exhaust gases.

5 There is danger of the water freezing unless mixed with an antifreeze solution.

Purpose of Present Tests

In the light of previously published information the authors felt that tests conducted over a wide range of compression ratios and rates of water injection would accomplish the following:

1 Add valuable data as to quantity of water needed to prevent detonation at a number of load conditions and compression ratios.

2 Determine whether worthwhile gains could be made by operating an overcompressed engine without water at low loads, with detonation suppressed in the high load range by water injection.

3 Indicate effect of injected water on such items as exhaust temperature and heat loss to cooling water.

Test Equipment. A single-cylinder water-cooled N.A.C.A. Universal test engine, located in the mechanical-engineering laboratories of the University of Maryland, was used for all tests, Fig. 1. This engine has a 5-in. bore and 7-in. stroke. Its

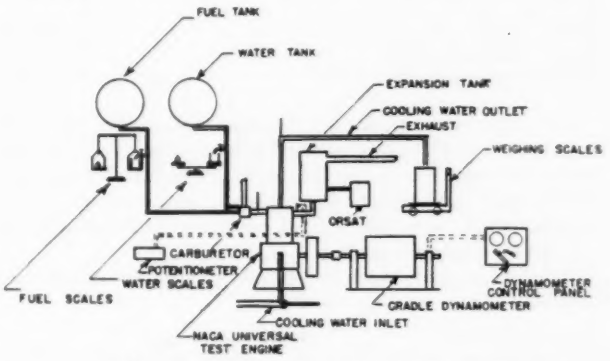


FIG. 1 SCHEMATIC LAYOUT OF TEST EQUIPMENT

compression ratio may be continuously varied from 4 to 1 to as high as 14 to 1. The engine is equipped with a valve-in-head combustion chamber, with two intake and two exhaust valves. A magneto ignition system was used with a single spark plug located at the top of the combustion chamber. Engine output and friction horsepower were measured with a Sprague-type electric dynamometer.

Water was fed from a $^1/_2$-gal beaker, mounted on a weighing scale, to a small jet located in the carburetor venturi. Flow of water was controlled manually.

A standard fuel-weighing set-up was used to measure fuel-consumption rates. Mixture temperatures were measured with a thermometer inserted in the intake manifold 10 in. from the intake-valve port. Mixtures were checked during each test with an Orsat apparatus. Samples of exhaust gas analyzed were taken from an expansion tank located 4 ft from the engine-exhaust-valve port. Exhaust-gas temperatures were measured by an unshielded thermocouple located in the engine exhaust and read by a potentiometer. Exhaust temperatures were corrected for radiation and recovery losses as suggested by King (1)[2] and Hottel (2).

Cooling water from laboratory mains entered a recirculating system actuated by a pump on the engine. Its temperature was measured at the inlet to the recirculating system. After passing through the engine cylinder and head to a thermometer well at the outlet, the water was caught in a tank and weighed. An RCA piezoelectric indicator was used to take cards and to check detonation visually.

[1] Associate Professor of Mechanical Engineering, University of Maryland, College Park, Md. Mem. A.S.M.E.

Contributed by the Oil and Gas Power Division and presented at the Fall Meeting, Cincinnati, Ohio, October 2–3, 1945, of THE AMERICAN SOCIETY OF MECHANICAL ENGINEERS.

NOTE: Statements and opinions advanced in papers are to be understood as individual expressions of their authors and not those of the Society.

[2] Numbers in parentheses refer to the Bibliography at the end of the paper.

Test Procedure. It was decided to operate the engine on one type of fuel at four different throttle openings, thus varying the output between 30 per cent load and full load. At each throttle position tests were run at a number of compression ratios. The first run at each throttle opening was made at a low enough compression ratio so that no detonation occurred under normal operating conditions. No water was injected on this run. Succeeding runs were made at higher compression ratios with just enough water being injected to suppress detonation. Detonation was detected by ear and by the oscillograph on some tests.

Table 1 shows items which were maintained constant on all runs.

TABLE 1 ITEMS WHICH WERE CONSTANT DURING TEST RUNS

Fuel used	gasoline
Octane no. of fuel	68
Revolutions per minute	1000
Spark advance, deg Btdc	25
Air-fuel ratio (approx)	14:1
Cooling-water temperature in cylinder head and cylinder wall, deg F	180 ± 5
Oil temperature, deg F	125 ± 5
Oil pressure, psi	42
Exhaust pressure	atmospheric
Inlet air, deg F	60 ± 5
Mixture temperature, deg F	65 ± 3
Barometer reading, in. Hg	30 ± 0.10

The engine was operated for approximately $2^1/_2$ hrs, until readings indicated that all operating conditions were constant. Several test runs of 15 minutes were conducted at each compression ratio. Whenever the compression ratio was changed at least 30 minutes were allowed for conditions to stabilize before new test readings were taken.

Primary test data taken in addition to readings of standard conditions were as follows:

Compression ratio	Dynamometer load
Duration of run	Cooling-water temperature at inlet
Pounds of fuel consumed	Cooling-water temperature at outlet
Pounds of injection water	Pounds of cooling water
Average rpm	Exhaust temperature

Orsat analysis

Results. Results computed from the data are plotted in Figs. 2, 3, 4, 5, and 6. Each figure shows the engine performance at one throttle opening for various compression ratios and throttle openings.

It is apparent from a study of these figures that as the load is increased, water injection must start at lower compression ratios in order to prevent detonation. If, however, effective compression ratios are considered, it is necessary to start water injection at compression ratios between 4.2 and 5.1 to 1 for all tests on this engine.

Indicated horsepower, brake horsepower, and thermal efficiency show marked gains with increase in compression ratio, especially in the case of throttle opening No. 1. At compression ratios larger than 11:1 there is no appreciable gain in efficiency and power due to the action of the injected water.

Exhaust temperatures and heat to cooling water decrease rapidly with increased compression ratios and water rates.

Fig. 6 shows a typical mechanical-efficiency curve for this engine. It was found that the variations in throttle opening and compression ratio had little effect on this curve. All points fell within ± 2 per cent of the curve.

Quantities and Effects of Injection Water

Fig. 7 shows a family of curves indicating the pounds of water required per pound of fuel to prevent detonation for various horsepower and compression ratios on this engine. It will be noted that higher outputs and compression ratios required higher rates of water injection. In connection with these curves, it should be noted that in the high-load and compression-ratio ranges the engine did not detonate although it ran roughly and occasionally misfired. It is possible that misfiring could have been prevented by use of other types of spark plugs, although this was not investigated.

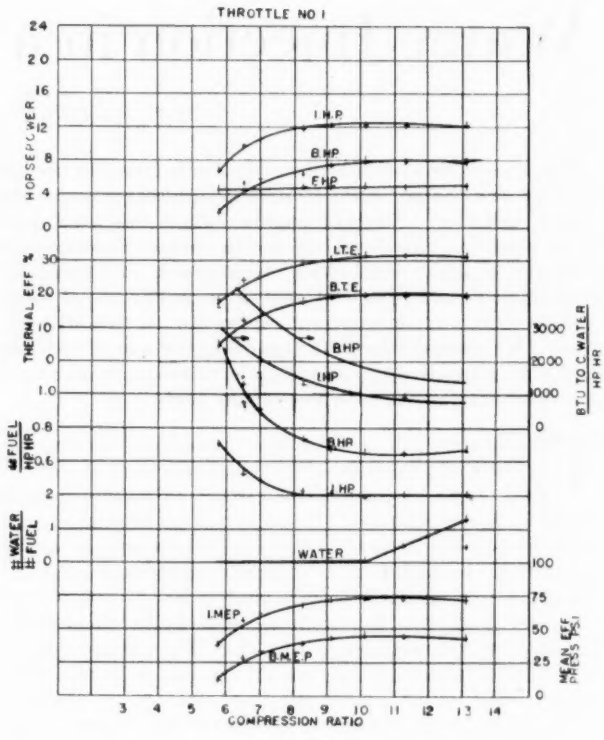


FIG. 2

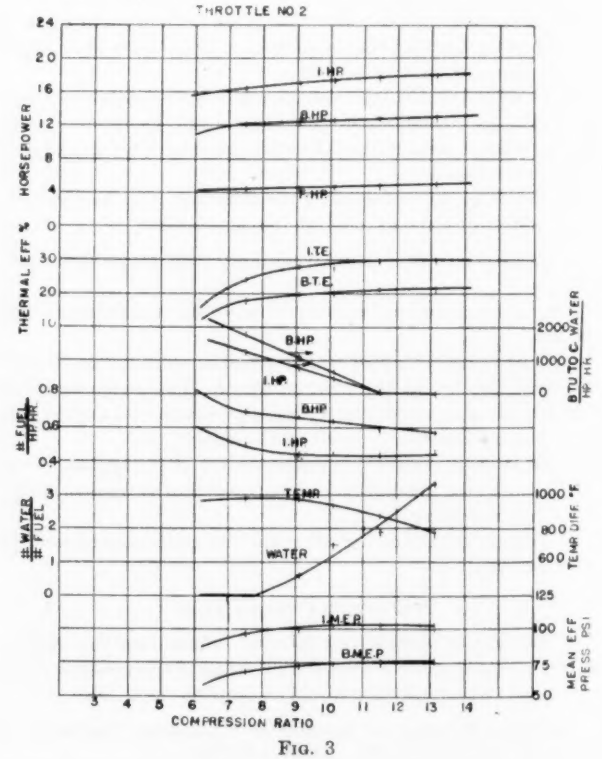


FIG. 3

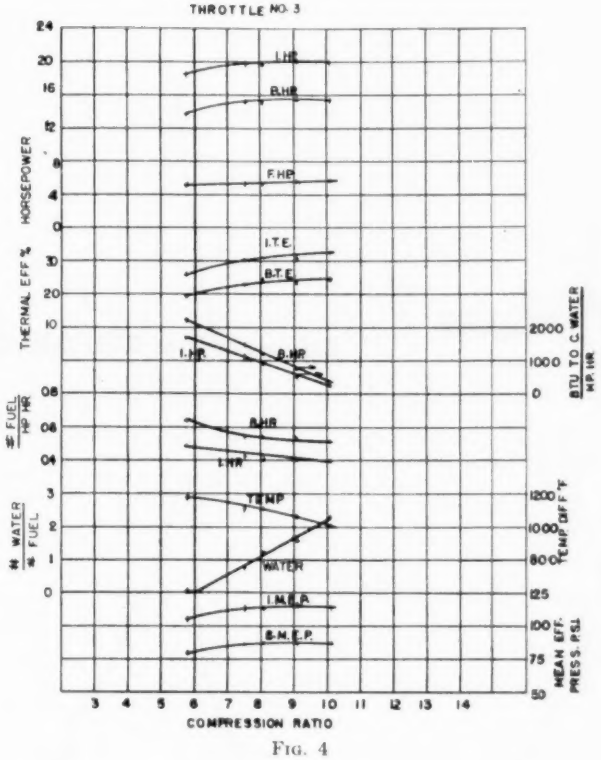


FIG. 4

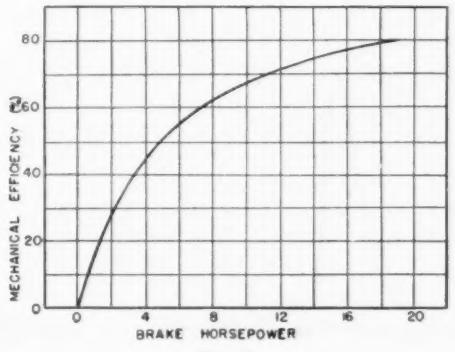


FIG. 6

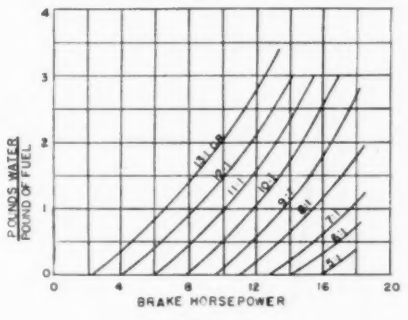


FIG. 7

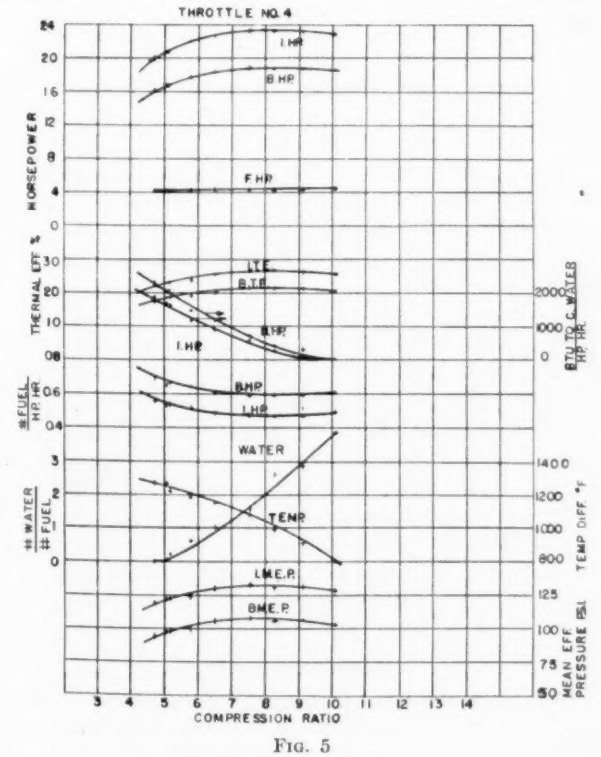


FIG. 5

Fig. 8 shows a set of typical pressure-time-indicator cards for this engine at full throttle and with various compression ratios, using a slightly different gasoline from that of the preceding tests.

At the 4.8:1 compression ratio it was not necessary to add water to prevent detonation. At 5.2:1 compression ratio slight detonation was evidenced by the sharp peak at the top of the card. This was remedied on the next card by the addition of just enough water to prevent detonation. It will be noted that the first effect of the water was to lower the maximum pressure.

As the compression ratio was increased it was necessary to increase the water-injection rates to prevent detonation. It will be noted that the effect of high rates of water injection was to decrease the slope of the expansion line to a marked degree.

The 9:1 compression-ratio card has an excess of water and definitely shows the effect of the water vapor on the expansion line.

Fig. 9 shows the effect of the addition of water on the cooling loss (Btu/bhphr). This curve indicates that the heat loss to cooling water is largely dependent on the water-injection rate. It also shows that for higher rates of water injection the cooling problem is reduced to a point where it is possible that no external cooling other than that done by radiation and the lubricating oil will be required.

Fig. 10 shows the effect of brake horsepower and compression ratio on brake specific fuel consumption. Water was added where necessary to prevent detonation in the amounts indicated in Fig. 7. At the lower brake horsepowers there is a marked difference between the specific fuel consumption at the various compression ratios, while at the higher outputs the water required to suppress detonation lessens the gains due to higher compression ratios.

Fig. 11 shows a comparison between the fuel required for the various compression ratios in per cent of fuel required for 6:1 compression ratio. At the lower loads the 11:1 compression ratio will save about 50 per cent of the fuel required at the 6:1 compression ratio. As the load increases the fuel economy due to the higher compression ratio decreases until at full load the amount of injected water may actually make the higher ratio slightly less economical.

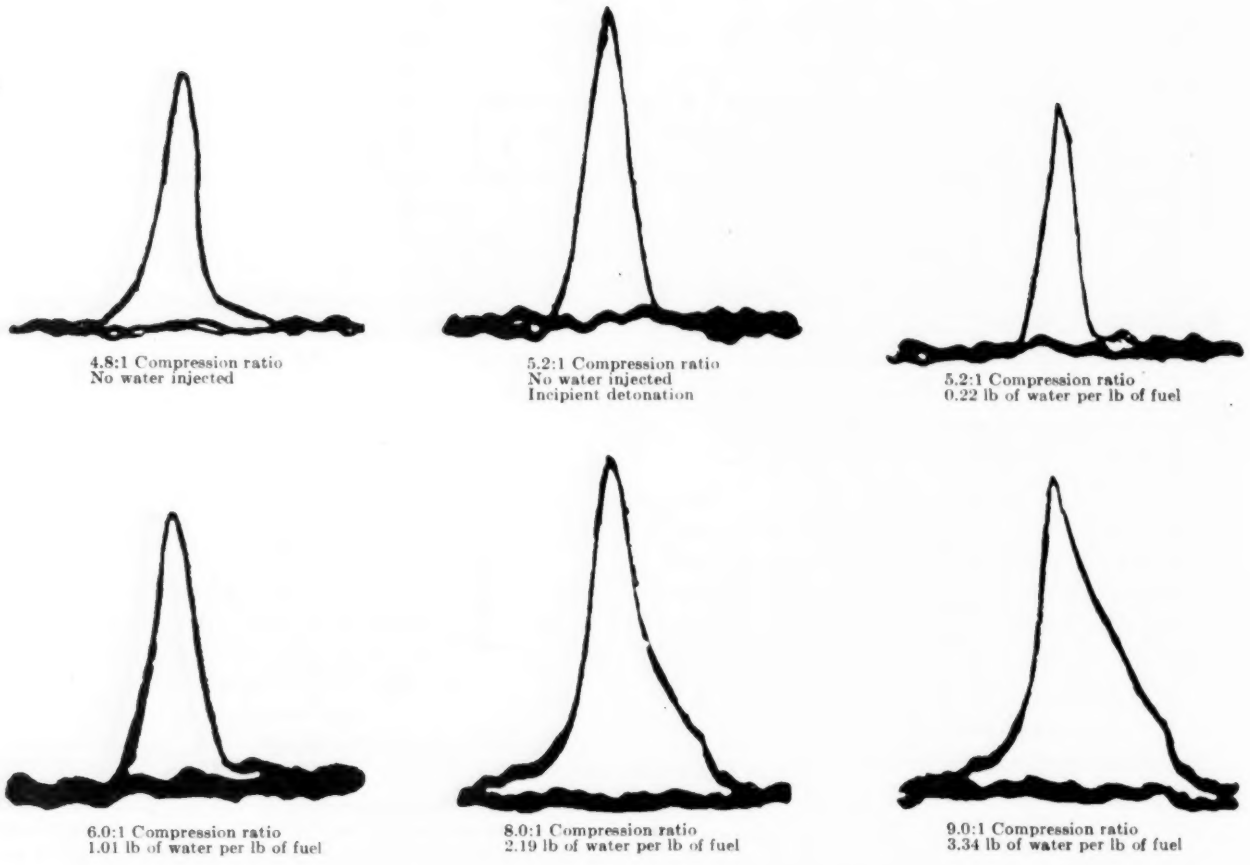


FIG. 8 INDICATOR CARDS OF N.A.C.A. 5-IN. × 7-IN. ENGINE, 1000 RPM, TESTED AT THE MECHANICAL ENGINEERING LABORATORY, UNIVERSITY OF MARYLAND

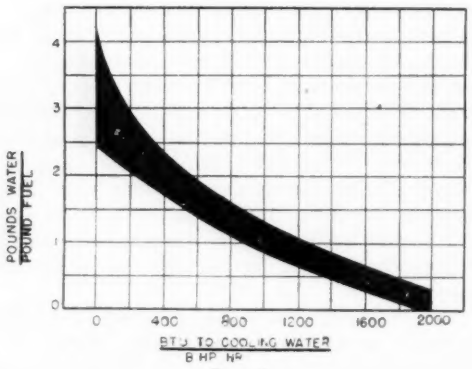


FIG. 9

CONCLUSIONS

The injection of water into the engine cylinder decreases the maximum pressure and tends to decrease the slope of the expansion line with little or no change in thermal efficiency.

Savings shown by the curves in Fig. 11 indicate the desirability of the use of water injection in engines that will operate the greater portion of the time in the low-load range, with only occasional use at full power.

Exhaust temperatures are reduced by water injection although a portion (or all) of the normal heat transferred to the cooling water now appears in the exhaust.

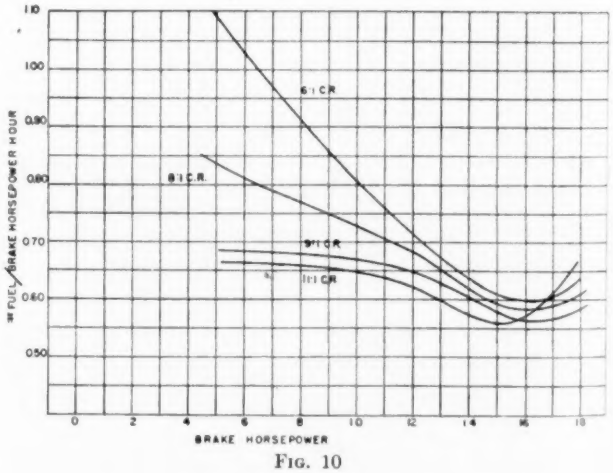


FIG. 10

ACKNOWLEDGMENT

The authors wish to acknowledge the assistance of A. E. Seigel and N. C. Eckhardt, senior mechanical engineering students, in setting up equipment and running preliminary tests.

BIBLIOGRAPHY

1 "Measurement of High Temperatures in High-Velocity Gas Streams," by W. J. King, Trans. A.S.M.E., vol. 65, 1943, pp. 421–431.

2 "Temperature Measurements in High-Velocity Air Streams," by H. C. Hottel and A. Kalitinsky, Trans. A.S.M.E., vol. 67, 1945, p. A-25.

3 "Distillate as a Tractor Fuel," by E. L. Barger and J. L. Gale, *Agricultural Engineering*, vol. 10, Feb., 1938, pp. 67–76.

4 "L'action chimique dans les moteurs a injection d'eau et emploi d'autres fluid auxiliares," by Clerget, *Technique Automobile and Aerienne*, vol. 25, 1934, pp. 45–49.

5 "Alcohol-Water Injection," by A. T. Colwell, R. E. Cummings, and D. E. Anderson, *S.A.E. Journal* (Transactions Section), vol. 53, 1945, pp. 358–372.

6 "Water and Water-Alcohol Injection in a Supercharged Jaguar Aircraft Engine," by M. S. Kuhring, *Canadian Journal of Research*, vol. 16, sect. A, August, 1938, pp. 149–176.

7 "Military Aircraft Engines of the Future," by F. L. Prescott, *Automotive Industries*, vol. 73, 1935, pp. 758–760.

8 "Water Injection," by E. W. Steinitz, *Automobile Engineer*, vol. 34, 1944, pp. 372–374.

9 "Description of the N.A.C.A. Universal Test Engine and Some Test Results," by Marsden Ware, N.A.C.A. Technical Report No. 250, 1927.

10 "A New Method of Cooling Gas Engines," by Bertram Hopkinson. Proceedings of the Institution of Mechanical Engineers, July, 1913, pp. 679–695 and 696–715.

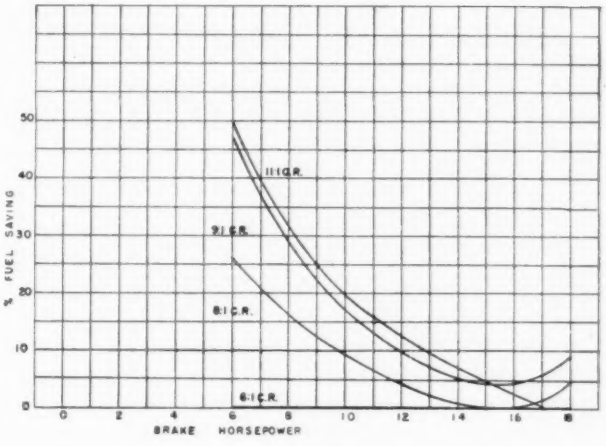


FIG. 11

(Owing to travel emergency conditions existing when this paper was presented, discussion will be accepted until August 16, 1946)

Relation Between the Impact and Flexural Tests for Molded Plastics

By L. E. WELCH[1,2] and H. M. QUACKENBOS, JR.[1]

A theoretical treatment of the phenomena of impact is presented which indicates that rupture under dynamic stress-strain conditions results from the same basic considerations as those governing static or flexural failure. This thesis is proved experimentally by reducing the problem to one of stress rather than the usual method of energy evaluation. When this is done with the aid of newly developed high-speed electronic techniques, it is conclusively demonstrated that impact loading is merely a special case of static loading whereby the stress-strain conditions are identical except for a slight elevation in strength under dynamic conditions. It is shown that the existing methods of impact-strength evaluation such as the standard Izod and Charpy tests lead to erroneous results since the machines in use are apparently of too light a construction, and the technique is oversimplified. It is suggested that the static flexural-test technique when properly carried out to evaluate the energy required for fracture and the notch sensitivity, is sufficient to predict the service characteristics of essentially brittle materials under conditions of both static and impact loading.

Nomenclature

The following nomenclature is used in the paper:

A, B = constants in Equation [16]
b = width of specimen
E = modulus of elasticity of specimen
g = gravitational acceleration
h = depth of specimen (taken outside notched area where bar was notched)
I = moment of cross section of specimen
K, K_M, K_S = spring constant of system, machine and specimen, respectively
l = distance from plane of loading to center of gage for cantilever
L = span of specimen, or length in Equation [4]
M = mass of impacting element
P = force exerted in either static or dynamic loading
t = time after impact
t_1 = total time duration of nonfracture impact
u = mass per unit length of specimen
U = strain energy in specimen under flexural or impact loading
U_0 = kinetic energy of falling (impacting) element
U_S, U_M = energy stored in specimen spring and machine spring, respectively
w = frequency of natural vibration of specimen
v_0 = velocity of impacting element at moment of impact
ϵ = maximum strain in specimen
σ = maximum stress in specimen
y = deflection of specimen in bending test
y_M, y_S = deflection of machine spring and specimen spring, respectively, at any time during impact
y_M', y'_S = maximum values of y_M and y_S during impact

Introduction

Three tests have been generally accepted for evaluating the mechanical properties of rigid plastics. These are the tests for tensile, flexural, and impact properties. Of these the Izod and Charpy impact tests on a notched bar are the most valuable because they differentiate between materials that show similar tensile and flexural results. For example, with the phenolic-resin molding materials with which this paper is largely concerned, the flexural strength usually falls in the range 7000 to 15,000 psi, while the tensile strength displays a smaller variation. The type of filler (wood flour, fabric, mineral, etc.) is more responsible than the type of resin for these changes. The Izod impact strength, however, may vary from 0.15 ft-lb per notched specimen for the wood flour filled to 2.5 ft-lb and higher for the fabric filled. Moreover, the impact evaluation is usually a fair forecast of the toughness of a molded object, especially where internal corners exist. But there are many instances where the agreement between impact tests and practical experience breaks down completely, and so an examination of the Charpy and Izod tests for rigid plastics was undertaken.

A brief description of the flexural and impact tests can well precede a review of the literature. In the standard flexural test a molded specimen, $5 \times 1/2 \times 1/2$ in., is loaded on a 4-in. span. The load-deflection curve is often linear to failure and if ductility is exhibited, it is small. The usual modulus of elasticity (hereinafter referred to as simply modulus) for phenolic molding materials ranges from $1\text{–}4 \times 10^6$ psi. The Charpy and Izod machines are similar to those used for testing metals, except that they are of much lighter construction to accommodate the relatively brittle plastic materials. The standard Izod machine weighs approximately 120 lb. In each test the standard specimen is $1/2 \times 1/2$ in. with a milled notch 0.100 in. deep, and with a radius of 0.010 in. at the bottom. The Izod specimen is a cantilever $1 1/4$ in. long struck 0.866 in. above the point of clamping. The Charpy specimen is supported on a 4-in. span and is struck on the side opposite the centrally disposed notch.

The impact strength, that is, the energy loss of the pendulum, is usually considered to be composed of three main parts:

1 Actual strain energy to break the specimen.
2 Machine losses; vibration and damping in the base of the machine.
3 Energy lost by the pendulum in projecting the broken end (Izod) or ends (Charpy) of the specimen.

Item 3 has been the subject of several recent papers (1, 2, 3, 4, 5).[3] The "end effect" was eliminated either by lowering the

[1] Research and Development Laboratories, Bakelite Corporation, Bloomfield, N. J.
[2] East Orange, N. J.

Contributed by the Rubber and Plastics Division and presented at a meeting of the Metropolitan Section, New York, N. Y., February 7, 1946, of The American Society of Mechanical Engineers.

Note: Statements and opinions advanced in papers are to be understood as individual expressions of their authors and not those of the Society.

[3] Numbers in parentheses refer to the Bibliography at the end of the paper.

pendulum in the orthodox tests until it possessed just enough energy to fracture the specimen, or by using a drop-weight machine in which the specimen is struck blows of increasing severity until fracture is caused. The energy associated with the end effect varies considerably with the filler. It is a small or negligible proportion of the measured impact strength with the tougher materials having a filler of fiber. With the more brittle wood-flour type the proportion may be 60 per cent and as high as 85 per cent with a high-density lead-filled composition. Consequently, quite a different comparison between the common molding materials is given when the end effect is eliminated.

With the energy of projection disposed of, the residual impact energy is then the sum of items 1 and 2, that is, the strain energy plus the machine losses. Most opinions place the machine losses as nearly zero (2, 3, 6). This leaves the residual impact energy as strain energy, and one could reasonably expect it to agree with the energy in a flexural test. Recent tension impact tests of metals (7, 8) have demonstrated that the same stress-strain behavior often occurs in both dynamic and static loading. Early work (9) on wood in long-span flexure shows the same agreement. A paper by Hazen (10) points out that the static flexural energy is a better criterion of service toughness than the standard Izod impact value. Yet the residual impact energy is about 25 per cent higher than the corresponding flexural energy in the Charpy test and is 3 or 4 times as high in the Izod test. The Izod flexural energy for the cantilever of 0.866 in. was calculated in the orthodox way, from the ratio of the spans, as 0.866/4 in. times the energy at a flexural span of 4 in., with a 32 per cent increase to allow for shear.

These discrepancies between the static and dynamic energies suggest the following possibilities: (*a*) The stress-strain relations under impact loading are different from those under static loading; (*b*) machine losses are appreciable.

To resolve these questions the stress-strain diagram in impact has been determined in the Izod and Charpy machines and compared with that for static loading at the same spans. The strain energy in impact absorbed by the specimen can be calculated from the relation between stress and strain. The difference between this energy and that applied by the pendulum, with the end effect eliminated, is taken as machine losses. As machine losses were appreciable, their variation with span was established in a drop-weight type of impact machine.

As to the stress-strain diagram in impact, the strain was measured with a resistance-wire strain gage cemented to the specimen. The voltage change across the gage on straining was amplified and passed to an oscillograph where the displacement of the oscillograph spot then became a measure of the strain. The measurement of dynamic strain in this fashion is an established technique in a number of laboratories (8, 11, 12). The determination of dynamic stress requires a delicate method (8) that could be avoided here because most of the materials used possess a linear stress-strain relation to failure. The dynamic modulus was calculated from the frequency of natural vibration and assumed equal to the modulus present under impact loading. The dynamic stress was derived as the product of this modulus and the measured strain.

Experimental Procedure

Experiments covered the range of common, phenolic molding materials having a variety of fillers and included work on cast iron and steel. All bars had a rectangular cross section. The molding materials were either molded as individual specimens or cut from molded plates 8 in. × 10 in. The laminated specimens were cut from plates. The cut surfaces were smoothed by grinding. The cast iron was cast as a single plate, 12 × 12 × $^3/_8$ in., and bars were cut therefrom 6 × $^3/_8$ × $^3/_8$ in. and finished by grinding. The single steel specimen used was 6 × $^1/_2$ × $^1/_2$ in. from cold-rolled stock. Some of the plastic specimens having a section $^1/_2$ × $^1/_2$ in. contained standard notches, 0.100 in. deep, 0.010 in. radius, milled in the center of one face. Table 1 summarizes the materials.

TABLE 1 LIST OF MATERIALS USED

Material	Description
BM-021	Phenolic resin + wood flour
BM-120	Phenolic resin + wood flour
BM-262	Phenolic resin + mica
BM-1914	Phenolic resin + kraft paper
BM-3510	Phenolic resin + fabric
BM-6260	Phenolic resin + wood flour + cotton floc
XM-9131	Pure phenolic resin — no filler
BM-13080	Phenolic resin + wood flour + cotton floc
BM-16468	Phenolic resin + fabric
Steel	
Cast iron	

The plastic specimens were conditioned 2 days at 50 C and were kept until tested in the laboratory maintained at 25 C, 50 per cent relative humidity.

The following tests were performed: To remove directional effects the same face (e.g., a top molded or cast face) was always in tension.

1 Flexural test on a span of 4 in., according to A.S.T.M. D790–44T: Load-deflection curves were recorded with a Templin stress-strain recorder which magnified the deflection 40 times. Spans other than 4 in. were used occasionally. The measured deflection includes deformation of the machine parts and indentation into the specimen of the edges for loading and supporting. A load-deflection curve was run at zero span (supporting edges together) to give a correction to the measured deflection. For the common thermosetting materials in the form of a bar of $^1/_2$ × $^1/_2$ in. cross section this correction is about 5 per cent at a span of 4 in.

With deflection corrected, modulus for an unnotched bar was calculated from the slope of the load-deflection curve according to

$$E = \frac{PL^3}{4ybh^3}\left[1 + \frac{3h^2}{L^2}\right] \quad [1]$$

and flexural energy from the area under the load-deflection curve.

Modulus was also measured by loading an unnotched bar having a strain gage cemented to the tension face of the specimen. The gage (Baldwin Southwark type SR-4, A-5, length $^1/_2$ in.) was connected to an SR-4 strain meter in the usual way. The center of the gage was vertically below the loading column. The observed strain for a given load must be multiplied by $L/(L - {}^1/_4)$ to give the maximum strain in the plane of loading. Load was converted to stress by

$$\sigma = 1.5\,\frac{PL}{bh^2} \quad [2]$$

and modulus calculated from the slope of the curve of stress versus maximum strain.

2 Static cantilever test: Modulus was determined with resistance-wire strain gages for a span of 0.866 in. If the center of the gage was distance l from the plane of loading, the stress by which the observed strain was divided to give the modulus was calculated from

$$\sigma = \frac{6Pl}{bh^2} \quad [3]$$

A notch, when present, was located on the tension side with its "vee" in the plane formed by the faces of the gripping members and a "modulus" was calculated as if the notch were absent.

3 Dynamic modulus: The frequency of natural vibration

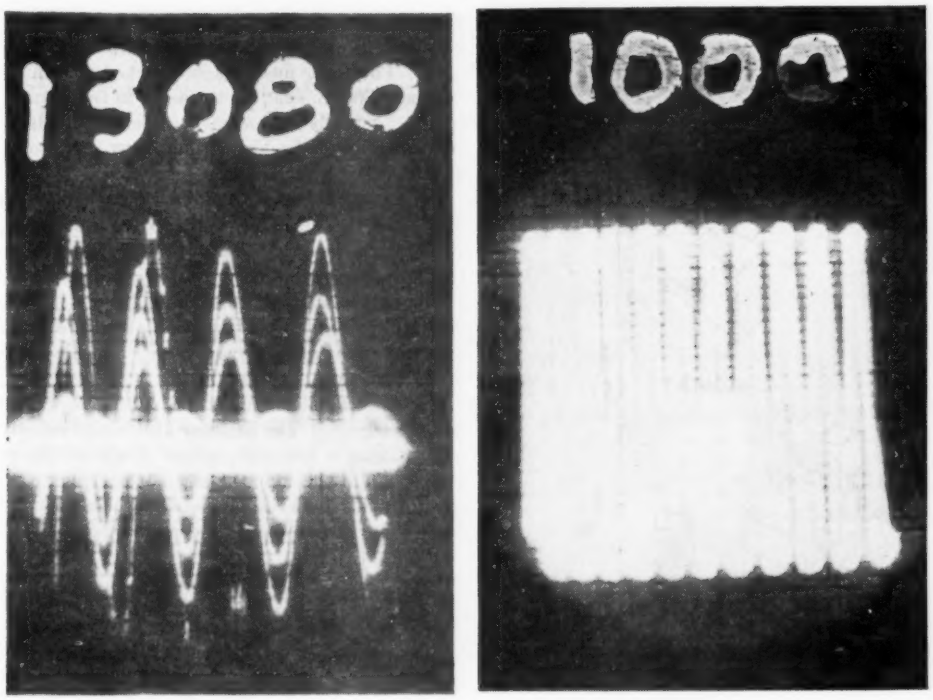


FIG. 1 FREQUENCY OF NATURAL VIBRATION FOR BM-13080, 1/2 × 1/4 IN. AND 1000 CYCLES PER SEC CALIBRATION

was determined mainly for bars having a cross section 1/2 × 1/4 in. An SR-4 A-5 gage was cemented to the central area of the specimen. The gage was connected into the dynamic-strain circuit described in the Appendix. With the oscillograph spot spread into a line, the vibrations of the bar when held lightly at one end and struck at the other cause a wave to appear on the screen of the oscillograph, Fig. 1. This wave is photographed and compared with a wave of 1000 cycles per sec induced by an oscillator. From the natural frequency w, modulus E is (13)

$$w = \frac{22.4}{L^2}\sqrt{\frac{EI}{u}} \quad \ldots\ldots\ldots\ldots\ldots\ldots\ldots\ldots [4]$$

4 Measurement of applied impact energy: The Izod and Charpy machines were fitted with movable spring releases to allow the pendulum to be dropped from any desired height. The heights used were such that the impact velocity varied between 2 and 11.4 fps. The specimen was either given a light blow, insufficient to break, or a blow such that the swing-through after fracture was small. The energy applied to the specimen in either case is calculated as in the Appendix. The Izod machine is a standard type manufactured according to the specifications of the Bell Telephone Laboratories. The Charpy instrument was of lighter weight and was made in the bakelite machine shop.

In the drop-weight tester, Fig. 2, a grooved weight released magnetically slides down vertical stainless-steel wires. The base is a steel plate set in a concrete block, 18 × 12 × 4 in. The energy is the product of the height and the weight with an allowance for friction established in a calibration with an electrical timer. The energy of fracture was determined by an increment method. The height was raised 10 per cent each time from an initial height adjusted so that 2 to 4 blows were needed for fracture.

5 Measurement of impact strain and time: The distribution of strain was established with A-8 gages which were good

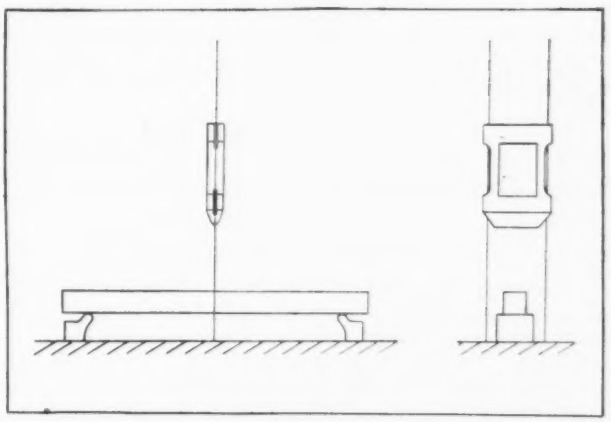


FIG. 2 THE DROP-WEIGHT IMPACT MACHINE, SHOWING WEIGHT SLIDING DOWN WIRES

indicators of essentially point conditions by virtue of their extremely small gage length of 1/8 in. The A-8 gage was also used to detect any compression of the bar against the pendulum and against the supports. Fig. 3 illustrates the disposition of the gages for these experiments.

Once the strain was found to be distributed linearly, subsequent experiments were carried out with A-5 gages which are 1/2 in. long. The maximum strain was calculated from the observed strain at a certain position assuming linear distribution.

With most experiments in which the bar was struck lightly the oscillograph beam of electrons was narrowed to a spot and its displacement was observed by eye as a mean of several blows. Photographs confirmed the precision of this visual method. When photographs were taken the circuit was modified so that the spot was traveling across the face of the oscillograph at a constant rate. The impact then appears as a loop with strain in

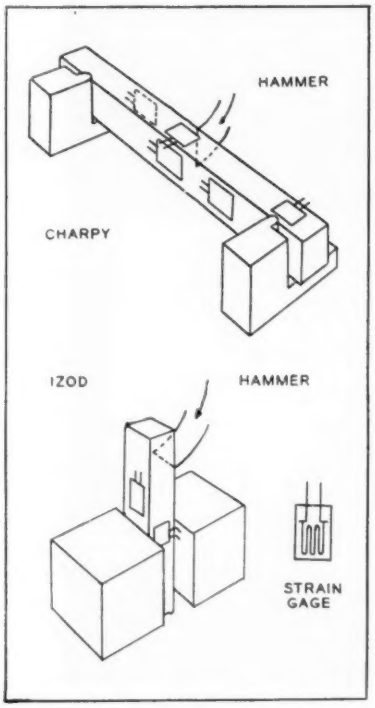


FIG. 3 DISPOSITION OF STRAIN GAGES ON CHARPY AND IZOD SPECIMENS

vertical units and time in horizontal units. The calibration of the vertical and horizontal units is described in the Appendix. Where the bar was broken photographs were taken with a Contax.

In any one set of tests all bars of one material were from the same batch but different batches were frequently used for different tests. This explains slight variations in modulus from test to test.

DISCUSSION OF RESULTS

In analyzing the response of a bar to impact loading it is natural to compare with conditions under static loading. The criteria of comparison are modulus and distribution of strain.

Dynamic Modulus. The dynamic modulus is in most instances the same as the flexural modulus, Table 2. Later when calculations were made of impact strain energy in the specimen, the modulus used was the flexural modulus, except for BM-3510, BM-16468, and BM-1914, where the flexural moduli were increased 20 per cent, 10 per cent, and 10 per cent, respectively. Two simplifications are implied when calculations on this basis are made for specimens of various dimensions in the Charpy and Izod tests and for notched bars in the latter. These are as follows:

TABLE 2 DYNAMIC AND STATIC MODULI; 4 IN. SPAN

Material	Flexural modulus psi × 10^{-6}	Dynamic modulus psi × 10^{-6}
BM-120	1.25	1.20
BM-262[a]	4.66	4.55
BM-1914	1.53	1.69
BM-3510	1.47	1.80
BM-6260	1.13	1.14
XM-9131	0.98	1.04
BM-13080	1.15	1.15
BM-16468	1.33	1.46
Steel	29.5	(29.5)
Cast iron	10.5	(10.5)

[a] Specimen, 1/2 × 1/2 in. All others 1/2 × 1/4 in.
NOTE: Dynamic modulus assumed equal to static modulus for steel and cast iron.

(*a*) While nearly all the results of Table 2 are for bars having a section 1/2 × 1/4 in., they are assumed to hold for all dimensions.

(*b*) The static modulus for notched and unnotched cantilever beams (0.866-in. span) is the same as the flexural modulus (4-in. span). Actually the former (notched) tends to be a few per cent lower, and the latter (unnotched) the same degree higher, as established by strain gages.

Deformation Under Static and Dynamic Loading. Fig. 4 illustrates the variation with distance of the dynamic surface strain for a beam tested in the Charpy machine. In general this strain increases from zero at the supports to a maximum at the center, the point of striking, just as it would under similar flexural loading. This was true for several values of the span length and several specimens of different dimensions struck blows insufficient to cause fracture.

There were anomalous effects but these were small enough to be ignored: (*a*) The hammer knife-edge indents into the specimen causing a low compression strain at the point of impact, Fig. 4; (*b*) at the supports and at the striker a local compression wave travels between the surface being hit and the opposite face; (*c*) at the supports the bending strain is not quite zero.

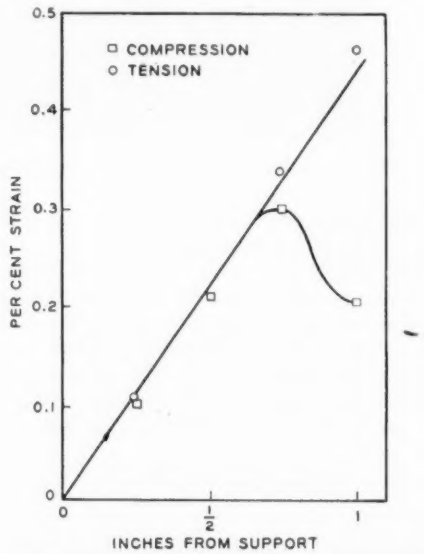


FIG. 4 IMPACT STRAIN VERSUS DISTANCE FROM SUPPORT IN CHARPY MACHINE
(BM-021, Span = 2 in., b = 0.5 in., h = 0.5 in.)

Similar anomalies were observed in the unnotched Izod specimen, but otherwise the surface strain increased in linear fashion from the plane of striking to the plane of clamping.

Taken in conjunction with the agreement between the static and the dynamic modulus these findings permit the conclusion that strain, stress, and load build up from zero in the same way in both tests.

Energy Absorbed by the Impact Specimen. In these circumstances the impact strain energy can be computed from the measured impact strain by exactly the same equations that hold for static loading. The strain energy absorbed by a rectangular beam in reaching a maximum strain in flexure ϵ, at the surface, in the plane of loading is given by

$$U = \frac{1}{216} bhLE\epsilon^2 \left(1 + 3\frac{h^2}{L^2}\right) \quad [5]$$

This is a standard textbook formula (14). The factor in parentheses allows for shear energy and is predicated on a value of

TABLE 3 ENERGY ABSORPTION IN CHARPY MACHINE FOR UNNOTCHED BARS STRUCK WITH BLOW INSUFFICIENT TO FRACTURE

Material	b in.	h in.	Span in.	Dynamic modulus, E, psi $\times 10^{-6}$	Measured absorption, per cent	Calculated absorption,[a] per cent
BM-021	0.50	0.50	2 1/16	1.25	36	36
BM-262	0.50	0.50	2 1/16	4.55	16	13
			4 1/8		81	52
BM-3510	0.50	0.50	2 1/16	1.90	34	27
			4 1/8		72	73
Cast iron	0.375	0.375	2 1/16	10.5	43	16
			4 1/4		91	58
BM-120, BM-1914, BM-3510, BM-6260, XM-9131, BM-13080, BM-16468	0.50	0.25	4 1/4	See Table 2	102 (mean)	96–97

[a] Calculated absorption based on BM-021 as explained in text.
NOTE: Energy applied varied from 0.1 to 0.22 ft-lb; corresponding velocities of impact being 2 and 3 fps. All bars unnotched.

0.3 for Poisson's ratio, which is true for most plastics (15). The formula for a cantilever is similar (14)

$$U = \frac{1}{216} bhLE\epsilon^2\left(1 + \frac{h^2}{L^2}\right) \quad [6]$$

where ϵ is now the strain at the grip.

A sample calculation for the Izod machine will illustrate the method. Material BM-021, $b = 0.50$ in., $h = 0.50$ in., no notch. Observed strain for gage with center 19/64 in. from grip = 3000 microinches per in. Maximum strain at grip = $3000 \times 0.866/(0.866 - 19/64) = 4560$ microinches per in.; $E = 1.25 \times 10^6$ psi. Hence energy absorbed by specimen U, from Equation [6] with $L = 0.866$ in. is 0.034 ft-lb. Energy applied by hammer = 0.131 ft-lb. Per cent measured absorption by specimen = $0.034/0.131 \times 100 = 26$ per cent. Measured absorptions for the Charpy machine are arrived at in the same way by means of Equation [5].

Measured absorptions calculated by these methods are listed in Tables 3 and 4 for the two impact machines. The significance of calculated absorption will be discussed later.

When the specimen does not break there are, of course, no end effects, and these have been eliminated from the applied energy when it does break. It is seen that generally not all the applied energy is absorbed by the specimen, the remainder presumably being lost to the machine. According to the figures presented, the per cent absorption varies from material to material in both machines and is especially erratic for specimens broken in the Izod test. Further, in the Izod test there is a considerable variation in energy absorbed from one specimen to another, sometimes as high as ±18 per cent. This in spite of the fact that the percentage absorption for one specimen struck lightly varies only ±6 per cent. Changes in clamping pressure seemed responsible to only a small extent.

In view of these findings, the energy lost by the pendulum, corrected for the end effect, has no absolute or comparative significance in either of the impact tests. The energy absorbed gives the correct answer, but even this is unsatisfactory in the Izod test because of its variability. A new test to replace the Izod test is suggested later in this paper.

There are certain disagreements in Table 4, as yet unexplained, between the energy absorption at fracture and that under a light blow. This is so when the filler is fabric, kraft, or floc.

Theory of Energy Absorption. It has been established that the energy absorbed by a specimen is only a part of that applied by the impact hammer. A reasonable assumption is that the remainder is lost by absorption in the impact machine. The system comprising the machine and specimen may then be compared to two elastic springs and the energy absorption should follow a certain pattern. An ideal system is illustrated in Fig. 5

TABLE 4 ENERGY ABSORPTION IN IZOD MACHINE

Material	b	h	Modulus, E psi $\times 10^{-6}$	Measured energy absorption, per cent	Calculated energy absorption,[a] per cent
BLOW INSUFFICIENT TO BREAK[b]					
Unnotched					
BM-021	0.50	0.50	1.25	26	26[a]
BM-13080	0.50	0.50	1.07	23	29
BM-3510	0.50	0.50	1.90	26	19
BM-262	0.50	0.50	4.7	21	9
Steel	0.50	0.50	29.5	12	1.5
Cast iron	0.375	0.375	10.5	36	11
BM-3510, BM-13080, BM-6260	0.49	0.25	Table 2	33–36	62–72
Notched					
BM-1914	0.5	0.5	1.69	21	21
BM-3510	0.5	0.5	1.90	25	19
BM-13080	0.5	0.5	1.15	25	29
BLOW TO BREAK[c]					
Unnotched					
BM-021	0.50	0.50	1.25	25	26
BM-262	0.50	0.50	4.7	17	9
BM-1914	0.50	0.50	1.69	24	21
BM-13080	0.50	0.50	1.07	24	29
BM-3510	0.50	0.50	1.90	12[d]	19
Notched					
BM-021	0.50	0.50	1.25	22	26
BM-1914	0.50	0.50	1.69	12	21
BM-13080	0.50	0.50	1.07	14	29

[a] Calculated absorption based on BM-021 as explained in text.
[b] Applied energy varied from 0.098 to 0.39 ft-lb, and velocity of impact from 2.5 to 5 fps.
[c] Velocity of impact varied from 7 to 11.3 fps, except that it was 3 to 4 fps from BM-262.
[d] This is the only material broken in Table 4 that exhibits any ductility near fracture. A gage outside the region, near the clamp, of high strain will not reflect this slight ductility so that the energy absorption is low.

in which a falling weight (the pendulum) drops onto a pan attached to the springs representing the machine and the specimen. An analysis can be made on the following assumptions: (*a*) No damping in any components; (*b*) no loss of energy from the system, e.g., through the machine spring to the rigid foundation to which it is attached; (*c*) both springs weightless and elastic; (*d*) displacement of the springs during impact is small compared with the height of fall of the weight.

At any time during impact the force P, exerted by the falling weight is the same for each spring, and with spring deflections y_M and y_S and spring constants K_M and K_S is given as

$$P = K_M y_M = K_S y_S = K(y_M + y_S) \quad [7]$$

where K = spring constant for total system.

When the strain in the specimen reaches a maximum all the energy U_0, of the pendulum is given up to the springs, i.e.

$$U_0 = U_S + U_M = {}^1/_2 K_M y_M'^2 + {}^1/_2 K_S y_S'^2 = {}^1/_2 K (y_M' + y_S')^2 \quad [8]$$

where the primes denote maximum deflections. This is true for nonfracture, and for fracture where end effects are eliminated. Therefore from Equations [8] and [7]

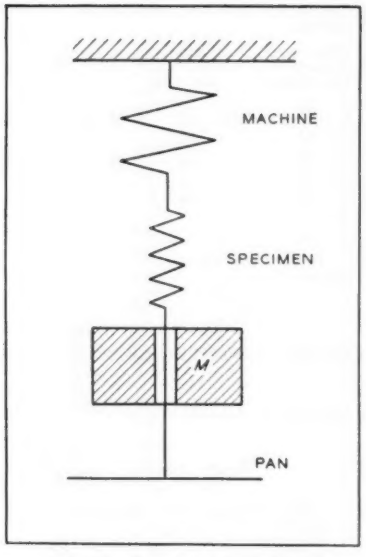


FIG. 5 IDEAL IMPACT SYSTEM

$$\frac{U_S}{U_0} = \frac{K_S y_S'^2}{K\,[y'_M + y'_S]^2} = \frac{K_S}{K} \cdot \frac{K^2}{K_S^2} = \frac{K}{K_S} \quad \ldots\ldots [9]$$

Now from Equation [7] also

$$K = \frac{K_S K_M}{K_M + K_S}$$

and on substitution in Equation [9]

$$\frac{U_S}{U_0} = \frac{K_M}{K_M + K_S} \quad \ldots\ldots [10]$$

Note that U_S/U_0 is the ratio of the energy absorbed by the specimen to that applied by the hammer.

By definition, the spring constant of the specimen K_S is equal to P/y_S and for the beam (Charpy) type of specimen the ratio is given by Equation [1]

$$y_S = \frac{PL^3}{4Ebh^3}\left(1 + \frac{3h^2}{L^2}\right) \quad \ldots\ldots [1]$$

or

$$K_S = \frac{P}{y_S} = \frac{4Ebh^3}{L^3\left(1 + 3\,\frac{h^2}{L^2}\right)} \quad \ldots\ldots [11]$$

The formula for K_S for the Izod specimen is similar so that

$$K_S = \frac{Ebh^3}{4L^3\left(1 + \frac{h^2}{L^2}\right)} \quad \ldots\ldots [12]$$

Now let these equations be applied in practice. For the Charpy machine $U_S/U_0 = 0.36$ for BM-021 when $L = 2^1/_{16}$ in., $b = 0.50$ in., $h = 0.50$ in., $E = 1.25 \times 10^6$. Hence K_S for BM-021 in this instance is 3.01×10^4 lb per in.; K_M can then be calculated from Equation [11] as 1.69×10^4 lb per in.

With these facts it is possible to predict the absorption that will be exhibited by any other bar of any dimensions and modulus and at any span. The procedure is to calculate K_S from Equation [11] and then compute the absorption U_S/U_0, from the relationship.

$$\frac{U_S}{U_0} = \frac{1.69 \times 10^4}{1.69 \times 10^4 + K_S}$$

Table 3 illustrates a fair agreement between calculated and measured absorptions. The correlation is poorest with the materials of higher modulus, BM-262 and cast iron.

With the Izod machine $U_S/U_0 = 0.26$ for BM-021 unnotched having $b = 0.50$ in., $h = 0.50$ in., $E = 1.25 \times 10^6$ psi, $L = 0.866$ in. K_S calculated from Equation [12] is 2.26×10^4 lb per in., so that K_M from Equation [10] is 0.80×10^4 lb per in. The energy absorption can be predicted in a manner already outlined for the Charpy machine. There is generally a wider difference between the actual and the predicted values than in the Charpy machine, especially when the specimen constant K_S, is high (BM-262, steel and cast iron) or low ($^1/_2 \times {}^1/_4$-in. materials).

The analogy of the system to two springs emphasizes that the low energy absorption is not some mysterious attribute of impact testing but arises simply because the machine constant K_M, is too small. Low energy absorption can equally well be observed in a flexural test but the usual testing machine is massive enough to make energy absorption practically 100 per cent.

The results for steel and cast iron are good only for small impact loadings in the elastic range, and the figures are no criterion of tests carried to ductile yielding or to failure. From the spring analogy one might conclude that in the ductile region the energy absorption would be nearly 100 per cent because there the specimen constant K_S, is low in keeping with the effective "modulus" in the ductile range.

Impact Energy Versus Span in a Drop-Weight Machine. From Equation [10] the energy of the falling weight U_0 is

$$U_0 = U_S\left(1 + \frac{K_S}{K_M}\right) \quad \ldots\ldots [10]$$

When U_0 is just sufficient to break the specimen at a given strain ϵ, the energy U_S, taken by the specimen, is

$$U_S = \frac{1}{216}\,bhLE\,\epsilon^2\left(1 + 3\,\frac{h^2}{L^2}\right) \quad \ldots\ldots [5]$$

and as

$$K_S = \frac{4Ebh^3}{L^3\left(1 + 3\,\frac{h^2}{L^2}\right)} \quad \ldots\ldots [11]$$

$$U_0 = \frac{1}{216}\,bhLE\,\epsilon^2\left(1 + 3\,\frac{h^2}{L^2}\right)\left[1 + \frac{4Ebh^3}{L^3K_M\left(1 + 3\,\frac{h^2}{L^2}\right)}\right] \quad \ldots\ldots [13]$$

If the breaking strain ϵ, is considered constant it is easy to demonstrate that a plot of U_0 versus span L goes through a minimum either by plotting values or differentiating a simplified expression with $h^2/L^2 = 0$. In the latter instance the span-depth ratio at the minimum L/h is

$$\frac{L}{h} = \sqrt[3]{\frac{Eb}{K_M}} \quad \ldots\ldots [14]$$

The effect of the depth of specimen h on the location of the minimum is elegantly illustrated by Fig. 6. For span-depth ratios higher than the minimum value the energy absorption soon reaches 100 per cent, as required by Equations [10] and [11], and the dynamic curve becomes a straight line. The absorption for the static curve is, of course, always close to 100 per cent.

In its linear region the dynamic curve lies well above the static,

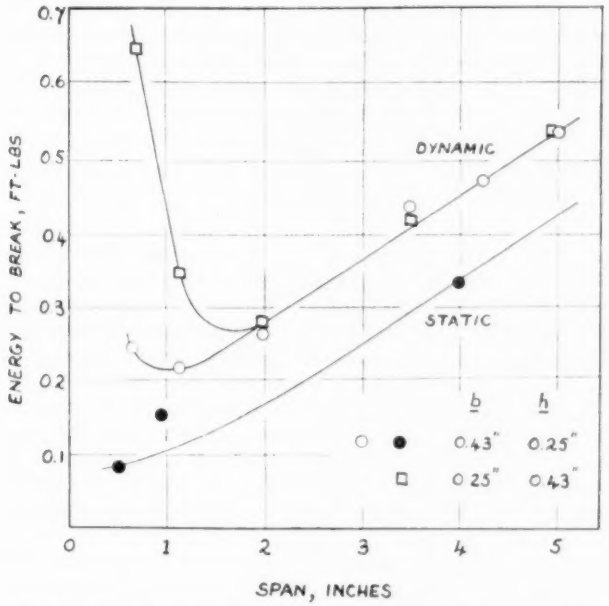


FIG. 6 EFFECT OF SPAN ON ENERGY TO BREAK FOR BM-13080
(Dynamic test in drop-weight machine; static test in Amsler 60,000-lb testing machine.)

suggesting that the breaking stress is considerably elevated in impact loading. Measurement of dynamic strain in the drop-weight machine did not confirm this suggestion. In fact dynamic and static breaking stresses were equal and the energy absorption reached not 100 per cent but only a steady 70 per cent. Presumably the loss is in damping in the rather "dead" concrete base.

The existence of damping losses distorts this analogy of the impact system to two elastic springs but probably not too seriously if such losses remain constant with span.

Further Conclusions From Spring Analogy. The connection between displacement y, and time t, for the two springs is described by

$$M\frac{d^2y}{dt^2} + Ky = 0 \quad \ldots\ldots\ldots\ldots\ldots\ldots [15]$$

the solution of which is

$$y = A \sin \sqrt{\frac{K}{M}}\cdot t + B \cos \sqrt{\frac{K}{M}}\cdot t \quad \ldots\ldots\ldots [16]$$

Time of impact t_1, from the moment the pendulum strikes the specimen until the moment at which it leaves the specimen on the rebound for a blow insufficient to fracture is, from Equation [16]

$$t_1 = \pi\sqrt{\frac{M}{K}} \quad \ldots\ldots\ldots\ldots\ldots\ldots [17]$$

This time, as required by Equation [17] and established by experiment, is independent of the velocity and energy of impact provided that the specimen does not fracture. When the Izod hammer weighs 1 lb and $K_S = 2.26 \times 10^4$ lb per in. (BM-021, $b = 0.5$ in., $h = 0.5$ in., $E = 1.25 \times 10^6$ psi) and K_M (Izod) $= 0.80 \times 10^4$ lb per in.

$K = K_S K_M/(K_S + K_M)$ (from Equation [7]) $= 0.59 \times 10^4$ lb per in.

Hence $t_1 = 2.1$ millisec.

Strain-time photographs establish a mean for t_1 of 1.7 millisec for BM-021 and similar materials like BM-1914 and BM-13080. Fig. 7 shows sample photographs. The strain-time curves are often of a faintly saw-tooth outline, showing that the hammer momentarily loses contact with the specimen, which then starts to return to the initial undeformed position until the hammer overtakes it again. The slight oscillations dying away, in Fig. 7,

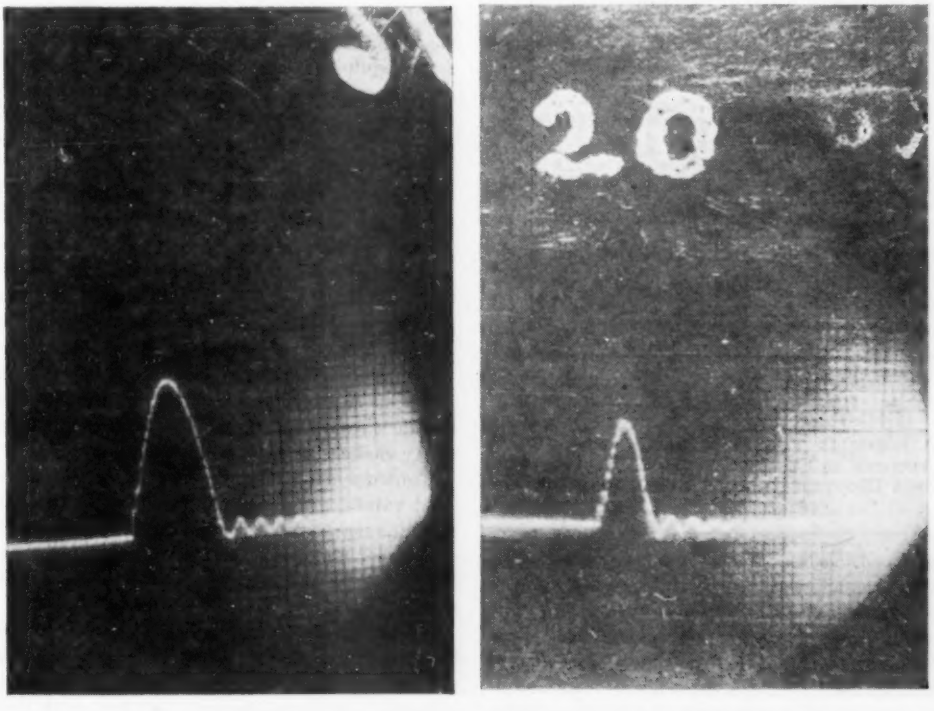


FIG. 7 STRAIN-TIME RELATIONS FOR NONFRACTURE IMPACT IN IZOD MACHINE
(BM-13080, left, 1/2 × 1/2 in. notched, and cast iron, right, 3/8 × 3/8 in. unnotched.)

arise because after the hammer has rebounded the specimen continues to vibrate feebly at its natural frequency.

When impact is violent enough to cause fracture the time of impact evidently must fall as the velocity of the striker is raised more and more. This is confirmed by photographs which resemble Fig. 7 except that the trace breaks off when the peak is reached.

When the limiting conditions: $t = 0$, $y = 0$, $dy/dx = v_0$ are applied to Equation [16] to evaluate the constants, it becomes

$$y = v_0 \sqrt{\frac{M}{K}} \sin \sqrt{\frac{K}{M}} \cdot t \quad \ldots\ldots\ldots\ldots [18]$$

The maximum value of y is when

$$\sin \sqrt{K/M}\, t = 1 \text{ or } \sqrt{K/M}\, t = \pi/2$$

then

$$y = v_0 \sqrt{\frac{M}{K}} \quad \ldots\ldots\ldots\ldots\ldots [19]$$

The force P_0 at this point is given by

$$P_0 = Ky = v_0 \sqrt{MK} = v_0 M \frac{\pi}{t_1} \quad \ldots\ldots\ldots [20]$$

where t_1 is the time of total nonfracture impact. Fig. 8 demonstrates that P_0 is linear in $1/t_1$; P_0 was calculated from readings of strain by the orthodox formula.

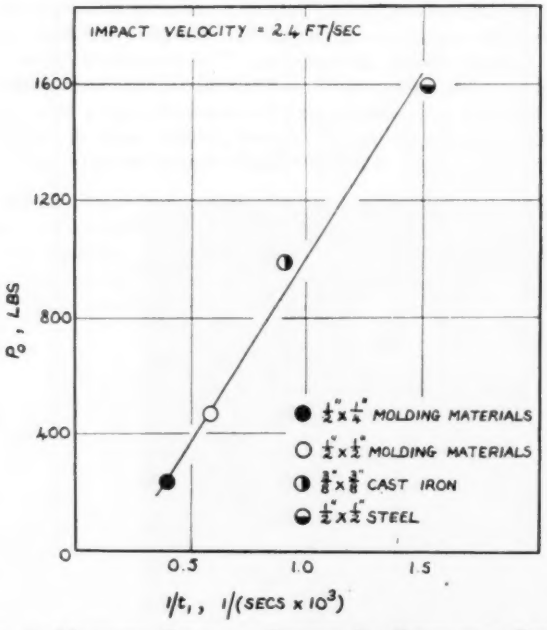


FIG. 8 MAXIMUM FORCE IN POUNDS P_0, DEVELOPED DURING IMPACT AGAINST SPECIMEN AS FUNCTION OF TOTAL TIME OF NONFRACTURE IMPACT FOR CONSTANT HAMMER ENERGY IN IZOD MACHINE

Limitations to Spring Analogy. The comparison of the impact system to two springs has allowed a successful interpretation of the experimental results in the following respects: (*a*) The effect of span, modulus, and dimensions on the per cent energy absorption in the Charpy machine; (*b*) the time of impact and its relation to maximum force; (*c*) the existence of a minimum in the curve of impact energy versus span in the drop-weight machine.

Deficiencies in the theory have appeared in the differences between results and predictions for the materials of higher modulus in both machines and for all materials in the Izod tester.

It is possible that these defects are connected with the assumption that the energy applied by the striker, divided between the specimen and the machine, is completely recovered on rebound, that is, that

$$U_0 = U_S + U_M$$

Actually this is never so with the Izod machine. The energy recovered, judged by the rebound of the pendulum, is as low as 45 per cent for a steel specimen. The energy not accounted for is probably lost by damping in the machine and its foundations. The magnitude of damping losses has already been discussed for the drop-weight machine.

The machine losses probably depend largely upon the machine itself and not too much on its attachment to a foundation, provided that the attachment is fairly rigid. It is possible that the nature of the foundation may have a marked effect on damping losses so that the Izod value indicated by the machine may depend upon its location.

Dynamic Breaking Strain. A specimen deforms into exactly the same shape as demonstrated by the distribution of strain, whether the loading is gradual or dynamic. Further, there is a close agreement between the dynamic and static moduli. So much has been proved.

In regard to breaking strain, sufficient results are not available for a final judgment. For velocities of impact up to 11 fps, it is tentatively concluded that the dynamic and static breaking strains do not differ by more than 10 per cent for the common phenolic molding materials. If this conclusion is firmly established it will follow that impact loading in the orthodox machines is, when properly analyzed, practically no different from flexural loading. This possible consequence opens up attractive vistas of simplification. The energy absorbed by the specimen in impact is incomparably more significant than the orthodox Izod and Charpy values. However, there are the objections that the end effect is not easily eliminated and the use of electronic strain equipment is undesirable for general testing. The simple alternative is to use the area under the flexural curve as the real impact energy. The flexural bar may be notched or unnotched according to the geometry of the molded object to which the results are to be applied.

The use of flexural energy brings out a very important point which has been concealed by the false results of the Izod test. Most common molding materials possess nearly the same linear load-deflection curve in flexure with nearly equal values of modulus of elasticity and of flexural strength. The unnotched impact strength is then almost constant. When there is a notch the impact strength is decided by the notch sensitivity, which is a measure of the ability of a material to withstand the weakening effect of stress concentration. Here the materials begin to show a wide range of real impact strength simply because notch sensitivity varies so much with the filler used (16).

Consequently, the "high-impact" materials, which have high Izod values, are of special value only when the molded object contains sharp notches or their equivalents; and their superiority over other molding materials almost vanishes when notches are eliminated by careful design and when they are not formed during service.

From considerations of notch sensitivity, the standard notched-bar impact tests, faulty as they are, have a much greater power of differentiating between molding materials than the orthodox tensile and flexural tests for which the specimen is not notched.

The effect of not only a notch but of modulus of elasticity, flexural strength, and ductility on resistance to impact is brought out clearly by the use of flexural energy.

Conclusions

The following conclusions are based on molded thermosetting plastics and certain thermoplastics:

Stress-Strain Diagram. The static and dynamic stress-strain diagrams are essentially identical, differing primarily only in the magnitude of breaking stress.

Strength. The dynamic breaking stress or strength is slightly elevated over the static flexural strength by approximately 10 per cent, resulting from the very high rate of loading. This is in agreement with previous data on the rate-of-loading effect as determined by other investigators.

Modulus of Elasticity. No perceptible variation in the modulus of elasticity is encountered under dynamic stressing compared with static loading.

Energy Distribution. In the static flexural test the energy absorption by the specimen is virtually 100 per cent. In the standard impact tests the energy absorption by the specimen varies from 10 to 50 per cent of the indicated energy loss of the pendulum. The remainder of the energy is lost in the machine and in kinetic energy of the broken parts of the specimen.

Notch Sensitivity. The ability of the standard notched-bar impact tests to differentiate between materials of like tensile- and flexural-strength properties is primarily due to the large variation in notch sensitivity in these materials.

Static Flexural Test. Static-flexural-test techniques employed to evaluate the energy of fracture and notch sensitivity for molded thermosetting plastics are concluded to be sufficient for predicting the service characteristics of such materials under both static and impact loading.

Theory. The theoretical concepts developed are not restricted to the testing of plastics but may be applied to the testing of metals and all other materials of construction.

Appendix

Izod and Charpy Energies at Low Swings. When the pendulum is released from a lower point than that for which the machine is calibrated, the energy is deduced from the scale reading (position to which pointer is carried by pendulum) for a free swing without any specimen in the vise. For example, for a 2-ft-lb machine having a velocity of impact of 11.3 fps:

Free swing, usual position, pointer carried = 0.060 ft-lb
Above repeated, pointer carried from 0.060 = 0.032
Therefore windage correction, full swing = 0.032
Windage correction, half-swing = 0.016
From lowered position, free swing, pointer carried = 1.381
For this reading after a specimen broke, correction to be subtracted is 0.036, according to calibration by manufacturer.

It can be shown, then, that energy at impact for free swing of 1.381 is

$$1.984 - 1.381 + 0.036 = 0.639 \text{ ft-lb}$$

$$\text{Velocity}^2 \text{ at impact} = \frac{0.639}{1.984} \times 11.3^2$$

or

Velocity = 6.4 fps

If specimen breaks when struck from lowered position and swing-through after fracture is to 1.945, then impact strength, i.e.

Energy loss of pendulum = 1.945 — correction for 1.945
— (1.381 — 0.036)
= 0.577 ft-lb

Dynamic-Strain Circuit. The entire strain circuit is illustrated in Fig. 9. Normally the measuring strain gage G is switched in, and the calibrating circuit is out. When the specimen is subjected to an impact strain the condenser allows only the voltage change to pass to the amplifier and to the oscillograph. With the strains measured, varying from 0.1 to 1 per cent, the extra amplifier A, is needed to supplement that already embodied in the oscillograph (Dumont, Model 208). The amplifier A is essentially identical to that of the second and third stages of the Y-axis amplifier of Model 208. Its chief virtue is the possession of a constant amplitude gain over a wide frequency range (60 to 10,000 cycles per sec).

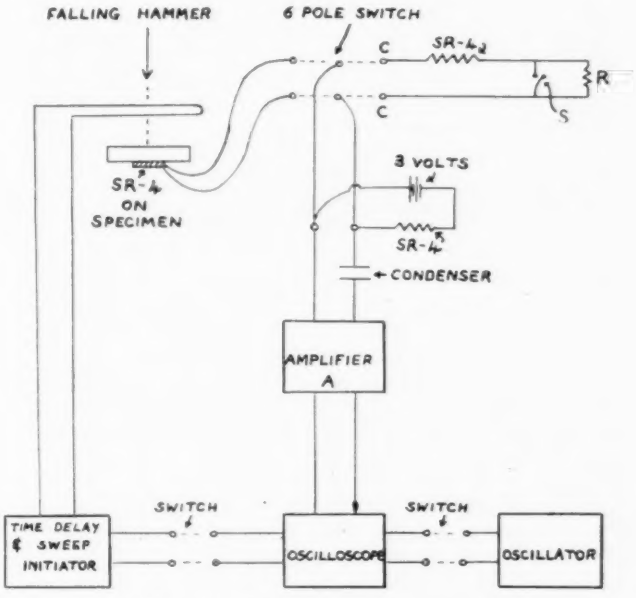


Fig. 9 Dynamic-Strain Circuit

When dynamic strain only is to be measured, the basic circuit, alone, comprising gages, amplifier, and oscillograph, is used. The oscillograph beam is narrowed to a spot, and the displacement on impact is estimated by eye. The screen is calibrated frequently by switching out the measuring gage and bringing in the calibrating circuit. When the microswitch S (normally closed), is opened by hand, an additional small resistance R is suddenly introduced and displaces the spot of the oscillograph. The value of this resistance R in terms of strain is determined as the difference in two readings when the calibrating circuit is attached to an SR-4 strain meter with the microswitch held steady closed and steady open.

Two additional circuits are added when strain-time relations are to be established, i.e., the oscillator circuit and the time-delay and sweep-initiating circuit. The latter device operates in the following fashion:

Initially the spot is off the screen. During its fall the hammer breaks a circuit which, after an adjusted time delay, causes the spot to sweep across the screen at a known rate. The sweep is in the center of the screen when the hammer striking the specimen superimposes a vertical strain displacement on the horizontal travel. The result is a record of the type shown in Fig. 7. The single horizontal sweep across the screen is secured by means of a

multivibrator circuit. With proper measures the velocity of sweep across the screen can be made constant throughout the travel. The time-delay device is a modified multivibrator in which one of the plate-grid connections is purely resistive. The tube containing this plate becomes nonconducting when the circuit receives a pulse on being broken by the falling hammer. Conduction through this tube to the sweep initiator is not re-established until there is a leak of charge from the grid to ground. The rate of leak can be varied by changing the capacity of the capacitive grid-plate connection.

After the strain-time relations are determined the oscillator circuit is brought in to determine the sweep rate. A sinusoidal vibration of 1000 cycles per sec is superimposed on the sweep across the screen so that a photograph gives a calibration of the horizontal axis in terms of time. The oscillator is of the resistance-capacity tuned feedback type.

When natural frequencies of vibration were being measured the external sweep initiator was eliminated and replaced by the built-in sweep circuit of the Dumont oscilloscope. This allowed a record of the type shown in Fig. 1 when the specimen was struck, and a calibration of the X-axis in terms of time when the oscillator was brought in.

Acknowledgment

Several of our colleagues in the Bakelite Corporation assisted and encouraged this work. Dr. C. E. Staff, Assistant Superintendent of Research at Bloomfield, and Mr. V. E. Meharg, Superintendent of the Development Laboratories at Bound Brook, were responsible for securing conditions favorable to its completion and publication. Mr. Walter Miller and Mr. Lloyd Wartman, Research Engineers at Bloomfield, loaned the equipment which they had designed for dynamic-strain measurements. Mr. W. A. Zinzow, Chief Physicist at Bloomfield, made available his staff, Mrs. J. Cairns and Mrs. R. Van Nest, for carrying out many of the experiments and calculations.

BIBLIOGRAPHY

1 "The Falling Weight Impact Test for Ebonite," by H. F. Church and H. A. Daynes, Trans. Institution of the Rubber Industry, vol. 13, 1937, pp. 96–108.

2 "New Methods for Mechanical Testing of Plastics," by L. H. Callendar, *British Plastics*, vol. 13, 1942, pp. 445–458, 506–519.

3 "Impact Testing of Plastics—I: Energy Considerations," by D. Telfair and H. K. Nason, Proceedings of the A.S.T.M., vol. 43, 1943, pp. 1211—1225.

4 "Preliminary Studies on a Drop Ball Impact Machine," by G. Lubin and R. R. Winans, A.S.T.M. Bulletin, May, 1944, pp. 13–18.

5 "Ball Impact Tester for Plastics," by C. R. Stock, A.S.T.M. Bulletin, October, 1944, pp. 21–26.

6 "Impact Testing of Insulating Materials," by W. W. Werring, Proceedings of the A.S.T.M., vol. 26, part 2, 1926, pp. 634–650.

7 "Stress-Strain Relations Under Tension Impact Loading, by D. S. Clark and G. Dätwyler, Proceedings of the A.S.T.M., vol. 38, part 2, 1938, pp. 98–106.

8 "Measurement of Dynamic Stress and Strain in Tensile Test Specimens," by R. O. Fehr and E. R. Parker, *Experimental Stress Analysis*, vol. 1, no. 1, 1943, pp. 76–82.

9 "Impact Tests of Wood," by T. R. C. Wilson, Proceedings of the A.S.T.M., vol. 22, part 2, 1922, pp. 55–70.

10 "Toughness of Molding Materials," by T. Hazen, *Modern Plastics*, vol. 21, October, 1943, pp. 103–106 and 144.

11 "Measurement of Stresses in Steam Hammer Piston Rods," by J. M. Lessels and G. S. Chernak, *Experimental Stress Analysis*, vol. 2, no. 1, 1944, pp. 34–40.

12 "Transverse Impact Transients," by C. O. Dohrenwend, D. C. Drucker, and P. Moore, *Experimental Stress Analysis*, vol. 1, no. 2, 1943, pp. 1–10.

13 "Mechanical Vibrations," by J. P. Den Hartog, second edition, McGraw-Hill Book Company, Inc., New York, N. Y., 1940, p. 186.

14 "Strength of Materials," by S. Timoshenko, part 1, second edition, D. Van Nostrand Company, Inc., New York, N. Y., 1940, p. 174.

15 "Method for Estimating the Shear Modulus of Elasticity," by L. E. Welch, *Product Engineering*, vol. 15, 1944, pp. 215–216.

16 "Plastics in Structural Design," by V. E. Meharg and L. E. Welch, *Modern Plastics*, vol. 22, September, 1944, pp. 117–119 and 182.

Data From Activity-Recording Instruments Applied to Textile Machinery

By C. S. PARSONS,[1] NEW BEDFORD, MASS.

The author advocates the adoption of activity recorders in the analysis of production machinery operations widely throughout the textile industry, as a means of achieving improved performance and lowered costs. After describing the several types of equipment and their applications to the study of textile-machine operations, the paper explains the procedure followed in analyzing the data recorded.

Use of Machinery-Activity Recorders

THE textile industry in general has not recognized the advantages of obtaining graphically data regarding machinery operations. There are four explanations for this as follows:

1 Low costs of labor and machinery compared with other industries.

2 In general, many productive units per machine operator.

3 Much engineering has been done by consultants, and the installation of this equipment for limited observations is expensive.

4 Nature of the machine does not readily lend itself to adapting the instruments.

With increased manufacturing costs, the use of machine-activity recorders becomes of much greater importance than formerly.

Wages have risen to new peaks and reduced costs must be realized through the more efficient use of manpower. Prices for machinery are also higher today, due not only to the increased cost of building the equipment but also because of the higher speeds, resulting in the necessity for better machining and closer tolerances.

The description which follows will show methods for analysis of machinery operations that will assist in reducing production costs.

Examples of Application

The use of recorders in studying weaving will serve as an illustration for this discussion. However, for mills that are not primarily interested in weaving, three of many other possible applications will be mentioned:

1 For cloth-finishing processes, the analysis of operation time will serve as a record of machinery utilization, as well as uniformity of cycle times for control of quality.

2 Another example of an indirect installation is that of the standard makes of regain controls, Fig. 1, which record the moisture remaining in the yarn after drying. When the sizing machine is stopped the instrument registers zero. As a result, data are available for the frequency of machine stops, time lost by the machine at the beginning of the work day, cleaning, or other reasons. In this operation the machine investment and wages for labor are comparatively high and the machinery efficiency is low due to fixed setup times.

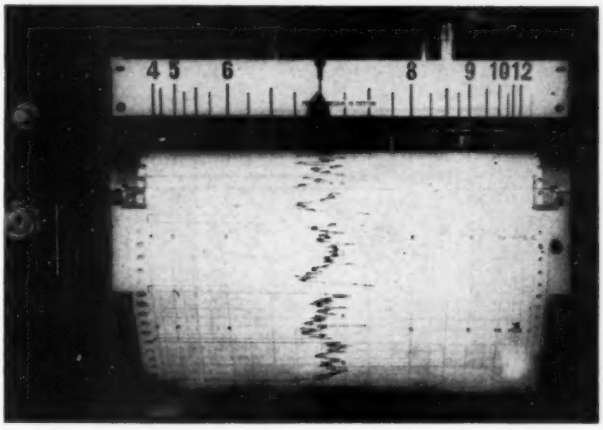


Fig. 1 Type of Regain Controller

3 Roving frames serve as an interesting example since many mills are installing new long-draft machinery to reduce the number of operations. The greatest causes of lost efficiency are end breakage, doffing, and creeling. In conjunction with conventional time studies, graphic recorders assist in the analysis of roving-frame operations for frequency of occurrence and time spent by the operator on the machine, as well as the time that the frame is not receiving the attention of the operator. This last down time includes the time when more than one of the tender's frames are stopped simultaneously.

Description of Recorders

Recording wattmeters, Fig. 2, may be used for obtaining data on one or more machines according to the electrical drive. However, their use is somewhat limited due to variable conditions in a group of machines and interpretation of average data.

Before considering the advantages of the use of instruments for loom studies, a brief description will be given of the design of recorders that are intended for machine activity only.

There are two common types of recorders and their selection will depend on the following factors:

(*a*) Permanency of the installation of the machine or instrument.
(*b*) Flexibility for use on other machines.
(*c*) Accuracy with which charts can be read.
(*d*) Ease in comparison of records from various machines to be studied.
(*e*) Availability of charts during study.
(*f*) Original cost of recorders per machine to be studied.
(*g*) Installation cost of instruments.
(*h*) Maintenance costs of charts.

For simplicity, the two types for looms will be identified as mechanical and electrical.

The mechanical type is clamped or bolted to the loom and any mechanical motion that will move or swing the pendulum located within the device will also move the stylus and make a record on the chart. In use, the recorder case is closed so that

[1] Superintendent, Hathaway Manufacturing Company. Mem. A.S.M.E.

Contributed by the Textile Division and presented at the Annual Meeting, New York, N. Y., Nov. 26–29, 1945, of The American Society of Mechanical Engineers.

Note: Statements and opinions advanced in papers are to be understood as individual expressions of their authors and not those of the Society.

the stylus marks the chart only during the time when the pendulum is put in motion by the working activity of the machinery to which the recorder has been attached. The circular charts used on this device are 4 in. or 6 in. diam and are designed for 1, 3, or 7-day operation.

The electrical type (Fig. 3 for example) is manufactured by at least two different companies. It is beyond the present purposes to make comparisons of the differences in design. The following description will be limited, therefore, to one maker's design, Fig. 4. This particular instrument is built for blocks of twenty machines and records their production on a continuous running chart with the records of each machine spaced about 1/4 in. apart. The electrical type may have a mechanical clock mechanism, but the operation of the machine is transmitted to the recorder by means of an electrical switch connected to the shipper mechanism or photronic equipment.

When the productive machine is in operation an electromagnet raises the pen about 0.1 in. above the base line. When the machine is stopped, the electric current stops and the pen returns to its normal position. The chart is fed through the machine so that previously printed horizontal lines spaced 0.1 in. apart normally designate 1 or 2 min according to the type selected.

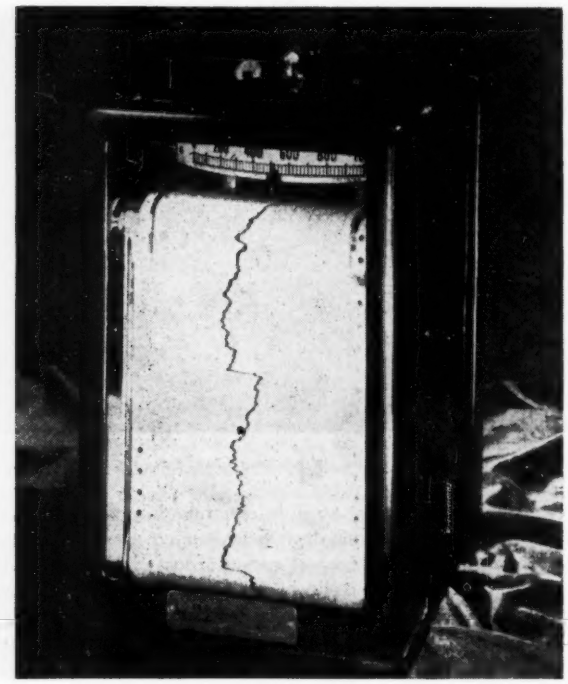


FIG. 2 MODEL A.W. SWITCHBOARD GRAPHIC INSTRUMENT

APPLICATION TO A LOOM

On a loom with an electrical stop motion the current is shut off when the loom stops. This switch is then used for operating the

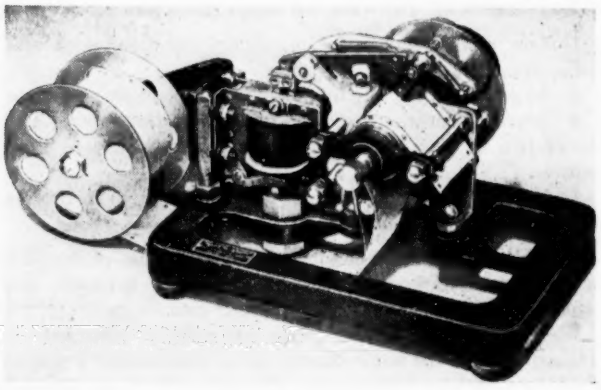


FIG. 3 ONE TYPE OF ELECTRICAL RECORDER

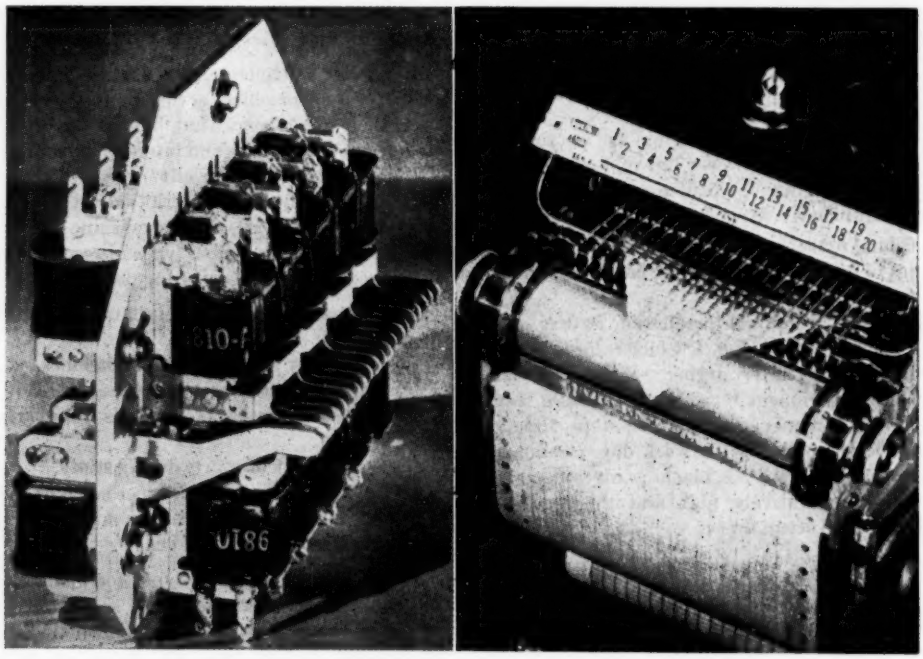


FIG. 4 TWENTY-PEN MACHINE-ACTIVITY RECORDER

(All of the electromagnets of a twenty-pen operation recorder are mounted on a single plate, but each is removable as a unit. Tilting the scale plate automatically lifts all twenty pens of the operation recorder to allow easy threading of the chart.)

pen of the recorder for indicating the stoppage for all causes. However, it is possible to cut into the wiring of the electrical stop motion and indicate on another pen the warp stoppage. A device could be arranged so that the filling-detector mechanism would actuate a third pen. Thus on one third the number of looms as might be otherwise studied, an analysis could be made of total stoppage, filling and warp stoppage, and by deduction, all other causes. The records would then conform with current practice of observing three major classifications of loom stoppage.

Explanation of Chart

One of the first impressions obtained in observing a chart such as Fig. 5, is the great variation from loom to loom even on the same cloth construction. This is readily apparent to those who are not acquainted with time-study analysis. The activity of the looms is more effectively shown by graphs than by figures, as is true of graphic presentation of such data.

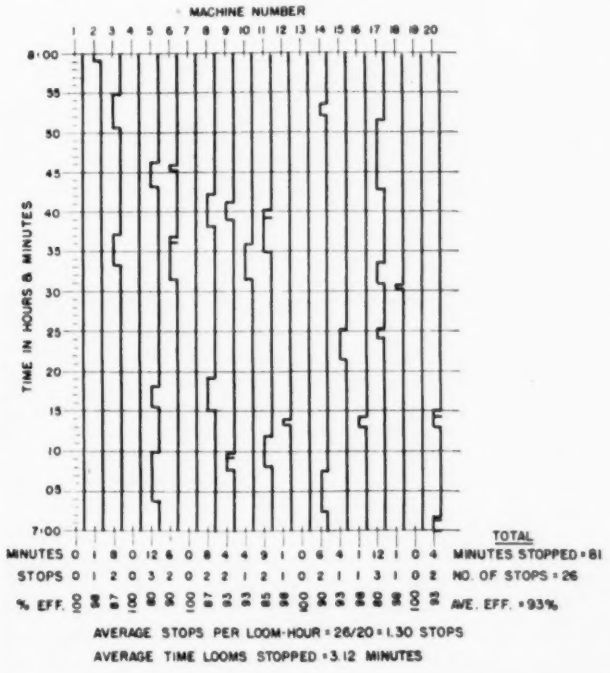


Fig. 5 Chart Made From Data Obtained With Electrical Recorder

Some engineers record operations in the sequence of their occurrence, which requires considerable clerical work in the summation of the data to follow the activity of any one particular machine. In contrast, some time-study observers record their findings directly according to the machine, irrespective of actual sequence. As a result, in a 4-hr study, considerable trouble may occur in a brief period, for example, in $\frac{1}{2}$ hr, and for the remaining seven eighths or $3\frac{1}{2}$ hr of the test the performance might be normal. Such instances are clearly seen by the use of graphic recorders.

Further examination of Fig. 5 shows that the machine numbers are across the line on the top of the page. One hour has been taken to illustrate this chart. There are 60 horizontal lines with 12 heavy lines representing 5-min intervals, as shown on the extreme left-hand margin. It will be seen that loom No. 3 was stopped for 4 min from 7:33 to 7:37.

Beneath the chart are the total stops for each loom for the hour and the total number of minutes stopped.

The efficiency of each loom can be readily calculated from the minutes of lost production.

By adding across each minute line, as shown in the right-hand column, data may be obtained on the number of looms stopped during each minute.

This twenty-pen machine-activity recorder, Fig. 4, makes graphic records of the production of twenty machines at one time. By suitable electrical connections to the starting or knockoff mechanism of the machine it is possible to determine the following:

1 Number of stops.
2 Duration of stops.
3 Frequency of stops for any period.
4 The number of machines stopped at any given period.
5 The amount of down time for that period.

This machine will give a graphical record of the quantitative analysis of the production and, if customary time studies are made in conjunction with it, there should be an accurate analysis which could not be obtained by other means. It is recognized that a complete analysis of any problem should contain quantitative and qualitative studies. For the work in textile mills the cause of machine stoppage is of secondary importance if the frequency can be accurately obtained, since if there is not a large amount of machine stoppage, the causes are not of great importance. Frequently it may be necessary to make a special analysis of the production of the machinery in order to determine the cause of machinery being stopped. This device will not give an accurate unit time that the operator spends in starting the machine in all cases, inasmuch as the machine will be stopped automatically in most cases and as a result, the down time of the machine will include:

(*a*) Time spent by the operator arriving at the machine.
(*b*) Time spent by the operator working to get the machine in operation.
(*c*) Actually starting the machine.

In most cases, such as weaving, the last two factors are very closely related and for most practical purposes can be combined.

Weekly Variations Per Machine

In order to determine the operation of one style a chart has been made from data obtained with the electrical recorder. In Fig. 6 is shown the analysis of the stops per loom-hour from ten looms operating 81 hr in 1 week. Loom No. 11 had an average of 3.04 stops per loom per hr, and an efficiency of 77.1 per cent. Loom No. 17 showed much less stoppage and operated at 90 per cent efficiency.

The test was operated for only 5 hr on the first shift Monday, 8 hr on the second shift that day. On Tuesday the results of 7 and 8-hr shifts are shown. It is interesting to observe that loom No. 12 operated at more nearly normal efficiency and although it ran poorly Thursday morning, it ran well the last of the week.

Variations Per Machine

Fig. 7 shows a probability curve of the variation in stops per hour. From this graph it is apparent that 21 per cent of the stops per loom per hour will be the average for the total test. Likewise, $7\frac{1}{2}$ per cent will vary approximately 30 per cent below or above the average and 10 per cent of the stoppage will be approximately 25 per cent higher or lower than average.

Similar data were obtained and analyzed for an entirely different cloth construction. In this case 32 per cent of the stoppages were average instead of 21 per cent. Approximately 8 per cent of the recorded stoppages varied 30 per cent above or below the mean.

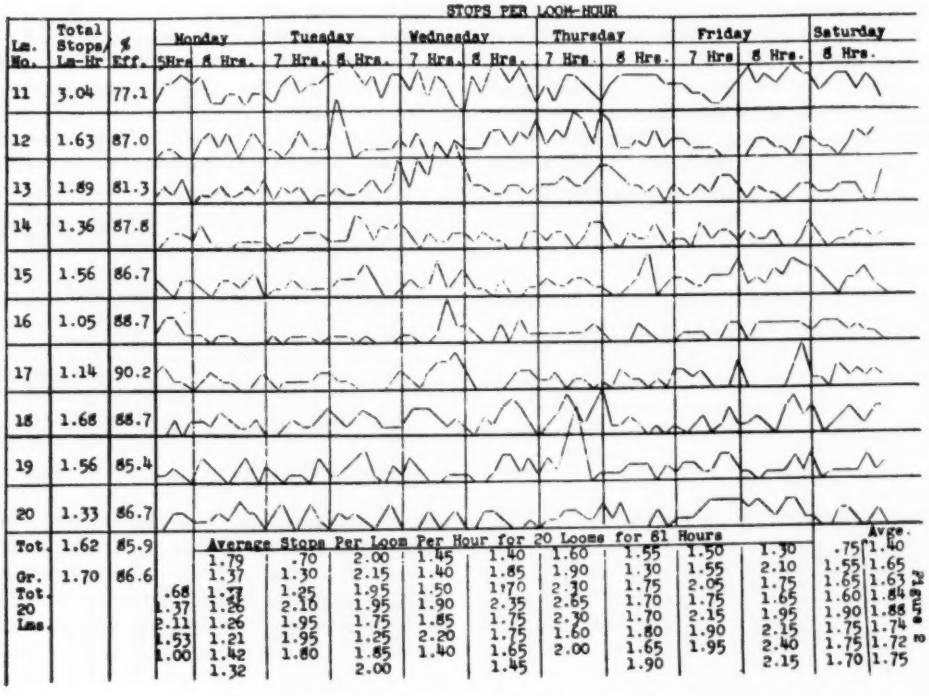


FIG. 6 STOPS PER LOOM PER HOUR FOR EACH DAY

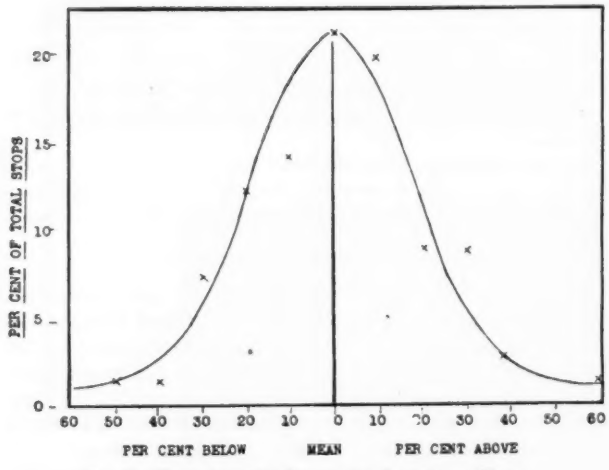


FIG. 7 VARIATION IN STOPS PER LOOM PER HOUR
(Average 20 looms; continuous testing for 81 hr.)

These data are of interest in selecting a representative test when conventional time studies are made.

STOPS PER HOUR VERSUS UNIT TIMES

Fig. 8 shows the relationship between stops per loom-hour and weaving efficiency from a 50-hr study of twenty looms. Unfortunately, this relationship is not always recognized and the values do not closely correspond since (1) the elemental time values will vary according to the nature of the stop, and (2) the weaver is not always immediately available to start the loom.

STOPS PER WEAVER AND PRODUCTION EFFICIENCY

If the recording instruments are to be used for weavers' work assignment, it will be interesting to examine Fig. 9, an analysis of stops per weaver per hour. In the upper half of this chart is

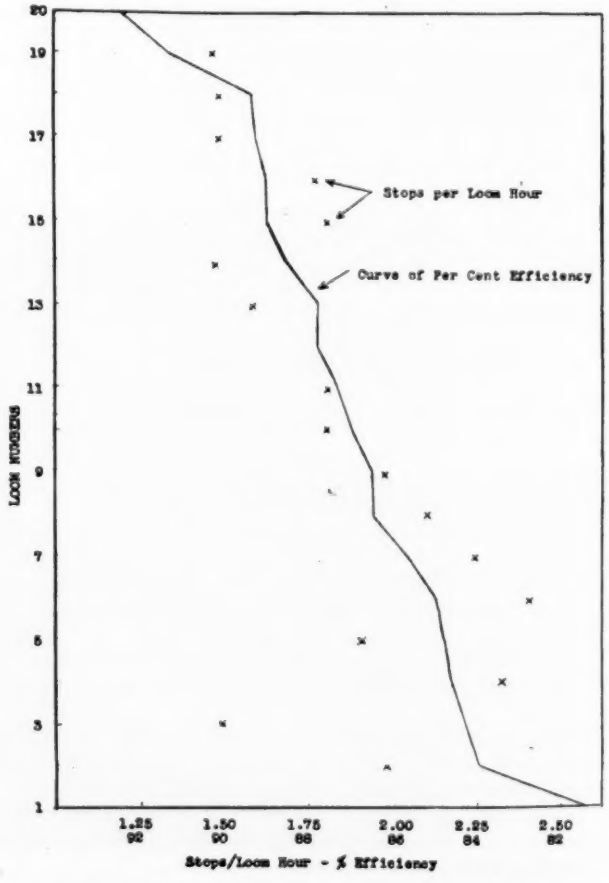


FIG. 8 GRAPH SHOWING RELATION OF PER CENT EFFICIENCY TO STOPS PER LOOM PER HR

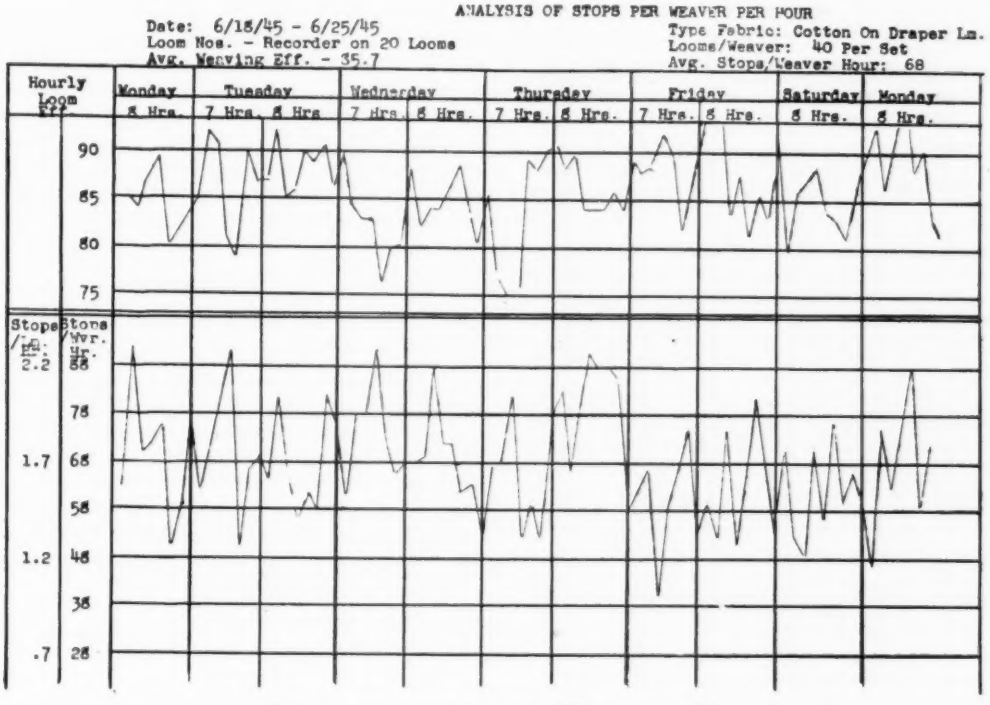


FIG. 9 ANALYSIS OF STOPS PER WEAVER PER HR

the hourly fluctuation in weaving efficiency of twenty looms for two shifts operating one week.

In the lower half of this figure is the variation in stops per loom-hour. The best shift performance was on the first shift Friday. No third shift was in operation and yet the looms ran well the first hour in spite of their being stopped. It is apparent that a test for only a few hours on one day probably would not give representative data.

MACHINE INTERFERENCE

Published material on time studies contains very little regarding the problems resulting from multiple machine jobs. As was previously mentioned, the number of looms stopped at one time is a limiting factor of machine efficiency. An automatic loom has stop motions which operate when a yarn breaks or certain mechanical parts are not in correct adjustment. When all looms are in operation the weavers' duties are limited to inspection and a few minor tasks. Therefore the measurement of the amount of time when a varying number of looms are stopped is of great importance. To obtain these data by personal observation is difficult when a large number of looms is tended by one weaver. However, the electrical recorder makes an ideal record which not only makes the data easily obtainable but also shows graphically when abnormally poor conditions occur.

INTERFERENCE TIME

Interference time, as previously mentioned, occurs when more than one machine is stopped and the operator is able to work on only one machine at a time. For example, assume an operator is assigned four machines; at certain periods all machines may be running; then one stops, and he works on that machine. Then a second machine may stop before the other machine has been put back in operation and interference time occurs. The amount of lost time for this reason will depend on the following:

1 The machine setup time.
2 Number of machines per operator.
3 Average time to start one machine.
4 Frequency with which the machine stops.
5 The number of other employees that may assist in the operation of the same machines and the amount of their time.

In order to measure interference time, formulas have been set up by several engineers, but as yet there is none that has been generally accepted. This is unquestionably due to the difficulty in obtaining the data for proving the formulas. The present purpose is to show that with the use of activity recorders the desired information can be readily obtained, and that unless sufficient data are accumulated, erroneous deductions may result. In order to appreciate the importance of interference time it should be mentioned that in a recent weavers' arbitration an allowance in earnings of $7^1/_2$ per cent was claimed.

EXAMPLE OF INTERFERENCE

An actual example of loom-stoppage tests to illustrate the importance of the problem is given in Fig. 10. Conventional time studies were made simultaneously with the activity recorder during 4-hr periods. Two of these tests were chosen showing the effect of the weaver on the production. In the case of weaver A, 88 per cent efficiency was obtained, and weaver B, working on the same job on the second shift, obtained 95 per cent efficiency. Each of the first four curves represents one hour's work of weaver A.

These graphical records analyze the number of looms stopped at $^1/_2$-min intervals. In the top curve, for instance, it is seen that at the start of the test all looms were running; $^1/_2$ min later one was stopped; and at the end of 1 min three were stopped. Four looms had stopped in the first $1^1/_2$ min of the test. At the end of 5 min all looms were again in operation. After 35 min all looms were running for approximately 5 min.

It is apparent that the four lower curves representing weaver B show much better weaving efficiency, since there is less area enclosed by the curves above the base line.

The summary of these tests is shown in Fig. 11. These illustrate that when weaver A ran the looms for 26.5 per cent of the

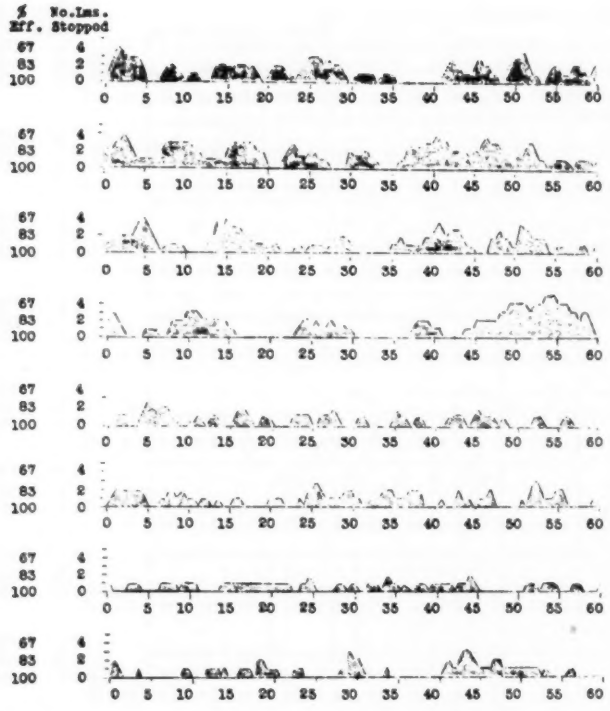


FIG. 10 ANALYSIS OF LOOMS STOPPED AND WEAVING EFFICIENCIES (Results of eight 1-hr tests. Observations made at ½-min intervals.)

480 observations, no loom was stopped, and 28.3 per cent of this time one loom was stopped. In contrast, weaver B with the higher efficiency, had all looms in operation 48.1 per cent of the time, and only one loom stopped 40 per cent of the time.

It is believed that these data can be used as a basis for determining certain qualifications of the weaver, such as skill, effort, etc.

It should be emphasized that the number of looms stopped at one time does not necessarily indicate the running qualities of the job, but how the job was operated. The data below Fig. 11 are significant, namely, 7 per cent less production, 40 per cent greater unit time, resulting in much greater time lost and the looms not in operation. The interference time in the first case is 5.2 per cent and 1.2 per cent as shown for weaver B.

The number of looms that should be assigned to a weaver is governed by the frequency of loom stoppage and time spent working on such duties. In addition there must be adequate allowances for patroling the job, miscellaneous tasks, and personal time. The patrol and inspection time frequently established is 20 per cent of the total weaver's time. Modern quality-control methods establish statistical procedures for analyzing the frequency of inspection. Today less inspection is required in many instances than was formerly practiced. It therefore becomes of greater importance to demonstrate that other work is not required of the weaver. The methods just described will prove that there is not an excessive number of looms stopped requiring work by the weaver.

Conventional time studies show the amount of time the operator is not occupied performing his regular weaving duties to keep his machines in operation. When it is found that additional work can be performed, the total available time may be divided by the number of such time-study readings to obtain an average unit time available for other work. This elemental time used in conjunction with data regarding the average number of machines stopped at one time, may be of assistance in establishing the correct work assignment.

The data obtained from this recording device accumulate so quickly that the need for modern statistical analysis of test data soon becomes apparent. By means of such analysis standard deviation of data can be obtained. In addition, the adequacy of test observations can be calculated. This will unquestionably result in establishing new standards for the length of time that observations are necessary. Frequently, substantial savings in the cost of time-study observations will result.

CONCLUSIONS

It is apparent that the following information is readily available from the charts:

1 Frequency of stoppage per hour or any other desired period.

2 Duration of time for each stoppage.

3 Machine efficiency of any recorded unit or machines for any time period of the test.

4 Comparison of performance of similar machines.

5 Comparison of the performance with similar products.

6 A number of machines in one operator's job can be recorded at one time on one sheet.

7 Variation in operations:

(*a*) per shift.

(*b*) comparison of shifts.

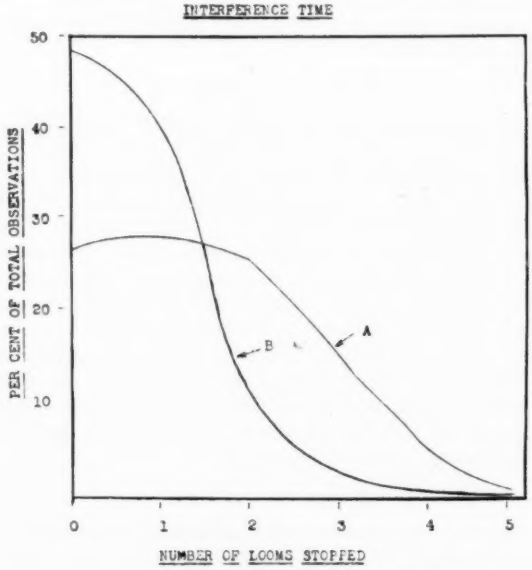
(*c*) comparison of performance on different days or even greater periods.

8 Starting and stopping time of shift.

9 Instantaneous records for immediate investigation.

10 After installation, continuous records at minimum expense.

Other data were accumulated for further analysis which frequently are not easily obtainable, such as the following:



	WEAVER A	WEAVER B
Weaving Efficiency	88	95
Stops per Producing Loom Hour	2.4	2.1
Average Time per Stop in Minutes	.90	.70
Per Cent of 4 Hours Weaver Spent on Stops	54%	29%
Interference Time (Waiting for Weaver)	5.2%	1.2%
Average Number of Looms Stopped When Weaver was Available	1.1	.34

FIG. 11 INTERFERENCE TIME

1 Weekly variations per machine.
2 Variations for similar machines.
3 Stops per operator and production efficiency.
4 Machine interference.

Adoption of activity recorders in the analysis of production machinery operations will result in improved performance, which will automatically reduce costs. The data obtained from these instruments will serve for work-load assignments based on adequate evidence of frequencies of occurrence.

Discussion

N. M. MITCHELL.[2] The paper obviously has as its objective the pointing out of benefits which may be obtained through intelligent use of recording instruments.

The author discusses his activities in connection with the use of the Esterline-Angus unit which has proved so useful to him in his own mill-engineering work. He obviously recognizes that the data which can be collected by means of this equipment can be misleading and actually dangerous if used either after insufficient testing to cover truly representative periods, or without due consideration of the practical elements, such as types of operatives, types of fabrics, conditions of machinery, and surrounding conditions.

The crying need in the textile industry today from an engineering standpoint is the determination of the true value of interferences of all types in direct-labor operating activities. The type of instruments described by the author comes more nearly to providing a means for the correct determination of interference than any equipment which has been presented for consideration to date. The fact that the type of equipment referred to is costly and somewhat cumbersome should not deter engineers from purchasing and using it, because its improvement and ultimate meeting of the real need for the industry can come only through reasonably wide distribution and use by engineers in the various mills.

There is definite need that the engineering profession recognize the fact that publication of information collected in a casual manner can be of far more damage to a mill than would be the case if the subject were to be loft untouched. The use of recording instruments in connection with work-load studies or machine studies will unquestionably expand and become general throughout the field, providing its early use is not abused, or the information reported as a result of its use is not based upon incomplete or short-period testing.

This paper, covering as it does the use of recording instruments, furnishes a great deal of valuable background information. It is interesting to note the state of operational affairs from the standpoint of loom stoppage, recorded in the chart Fig. 5. This indicates that the loom stoppages at given intervals throughout the study ranged from zero to four. It would be extremely difficult to establish this fact without this type of recording instrument. Analysis of this information can serve as a means of evaluating interference and its influence on a weaver or operative of any type of multiple-machine operations. Without accurate means of measuring consecutive and respective stoppages in machinery in multiple-load activities, it would be extremely difficult to evaluate interference and properly analyze the situation.

The writer believes there is great need to devote intensive study to work-load interference in order to prevent the subject becoming one of mystery and possible misuse in respect to establishing work loads and piece rates in the textile industry. There is a possibility that the subject may have a harmful psychological influence on mill operatives unless it is treated intelligently and resolved into matter-of-fact common-sense usage by mill management.

The use of recording instruments will unquestionably bring about the revelation of substandard mechanical conditions which otherwise might pass unnoticed if these conditions had to depend only on observations of work-load students, without the use of a means for multiple coverage of a job.

Present-day labor-management conditions make it necessary to establish accurate true facts relative to all phases of machine operations as well as that for the human being. The writer is of the strong opinion that the equipment described in the paper and used along the lines obviously applied in the collection of the information which was submitted, is very much worth while and its use should be encouraged if possible in all mills.

A. PALMER.[3] Many mills are faced with problems relating to work assignment that can be solved only by scientific methods. In many cases time studies and loom-stoppage studies are satisfactory. In others they are not, either because they are resented by the employees or because they do not give the kind of information that is needed.

We have been asked by mills recently how loom-stoppage data can be obtained without taking time studies. Our reply has been to refer them to this paper.

As the author points out, the time-study data that many of us have been taking show the average performance of a set of looms. Unless we analyze the data very carefully, we have no knowledge of the performance of each individual loom. The recording instruments used by the author give him not only the average picture, but also a clear one of the performance of each individual machine.

Is it possible to use these recording instruments to show the causes for loom stoppage? If these instruments can be connected to differentiate warp breaks, filling breaks, and miscellaneous stoppages from each other, some very desirable information can be obtained.

One problem that, in so far as the writer knows, no one has been able to solve satisfactorily is the question of loom interference. Years ago Mr. McElroy and various others tried to set up work-assignment formulas that took this element into consideration. They did exceptionally well with the information that they had at their disposal, but they will probably agree, at least in some measure, with the writer's feeling that there still is work to be done in this connection by someone who is familiar with higher mathematics, particularly with the theory of probability.

In this connection it seems to me that from the records taken by instruments such as the one the author has been using, much essential basic data could be obtained. Put into the proper hands, these figures should enable someone who knows how to supply the necessary mathematical theory to develop a formula that would be useful, at least in the case covered by the particular records that were used.

Much work of this nature has been done by Dr. Thornton C. Fry of the Bell Telephone Laboratories. He has supplied some of the mathematical procedures developed for the use of the telephone companies to the problem of assigning work loads in industry. To the layman his computations appear to be very complicated, not only because of the fundamental mathematical processes, but also because of the large number of variables that he includes.

In our opinion, Dr. Fry could help the textile industry if that industry supplied him with data similar to that which has been accumulated by the author. It is believed also that if the textile industry indicated to Dr. Fry that a simplified process was re-

[2] President, Barnes Textile Associates, Inc., Boston, Mass. Mem. A.S.M.E.

[3] Vice-President, Crompton & Knowles Loom Works. Worcester, Mass.

quired, he might be able to give us a sufficiently complete answer. If we know the average length of time during which looms stop; if we know the frequency of the occurrences and any other data that are pertinent to the loom-stoppage question, isn't it enough to determine what the best number of machines per operative is to keep the operator fully occupied but not overburdened, and to give the maximum production per loom?

If the writer understands Dr. Fry's work, he has included many considerations such as the weavers' wages, overhead expenses, and items of that nature, all of which are necessary but which seem to complicate the problem at the outset. If we can find out, on the basis of the loom-stoppage data, the number of looms that an operator should run to give the maximum production per loom, then the cost items automatically take care of themselves. It is therefore the writer's suggestion that as soon as the author, Mr. McElroy, and others who are doing this work, have sufficient data, they consult Dr. Fry to see what he can do with them.

A. N. SHELDON.[4] The advantages accruing from the information provided by the use of activity-recording instruments seems quite obvious from the paper. The utility of its general adoption would appear to justify the cost if the data derived therefrom become the basis of a careful and continuing analysis; the records are accurate, impersonal, visual, and permanent, for guidance of both management and operatives.

There is one deduction that appears possible from the data in Fig. 5, and that is that for this particular example there were too many looms per weaver; out of 20 looms there were only 5, (looms 1, 4, 7, 13, and 19) that operated continuously throughout the hour covered by the record, and the remaining 15 looms stopped 26 times and were unproductive for a total of 81 min. Consequently the efficiency of these 15 looms was only 90 per cent; the stops per loom per hour were 1.7, and the average duration of each stop was 5.4 min. Expressed in another way, out of these 20 looms, 1.30 looms were stopped for the entire hour. For a group of 1000 looms this is equivalent to 65 looms continuously idle, if the record for 1 hr is typical of all other hours. Since the capital invested in a single loom might be $1500 (including the cost of loom, building, air conditioning, power and light wiring, heating, etc.) there would be approximately over $100,000 of invested capital totally and always unproductive.

Fig. 5 also shows that there were only 12 min in the hour, or 20 per cent of the time, when all 20 looms were running simultaneously, which together with the average duration of stoppage of 5.4 min per loom, is strong circumstantial evidence that the weaver's job for this particular situation was too extended, with consequent loss in production from the looms and unproductive effort by the weaver.

Whether or not the foregoing conclusion is correct, the activity recorder presents a reliable device for investigating its validity, and as indicated by the chart in Fig. 5, there is nothing gained by increasing the looms per weaver beyond the point where loss of production, arising from "interference time" becomes the dominant factor. Incidentally, it does not seem consistent to penalize the loom-operative efficiency with interference time just because the weaver is not present to run it.

---

[4] F. P. Sheldon and Son, Engineers, Architects, Appraisers, Providence, R. I. Mem. A.S.M.E.

Discussion

In 1945, when there was a ban on national meetings, some papers originally scheduled for these meetings were presented before local groups. In the case of these papers the Committee on publications suspended its rule, which requires simultaneous publication of paper and discussion, and accepted discussion based on the published paper.

Heat Transfer in the Locomotive Boiler[1]

F. P. Huston.[2] The author presents in this paper a procedure for determining the output of any given quality of steam from conventional locomotive boilers for given rates of heat release and gas production.

The first part of the computation deals with the transfer of heat through radiation to the firebox and combustion surfaces. The second part deals with the transfer by convection through the walls of the tubes, flues, and superheater pipes. The author shows that the results of the computations are in reasonably close agreement with test data.

The variations between the maximum evaporation estimated by present methods and the maximum obtained on test, as reported by the late C. A. Brandt,[3] on ten locomotives range from 47 per cent more evaporation obtained on test over the estimated maximum to 14 per cent less. This wide spread is apparently due to the rule-of-thumb methods now in use, as exemplified by the 55-lb rule, dating back to 1912, as the result of the "Coatesville tests," or Baldwin's 80-lb rule. Either of these figures will apply at some low to moderate firing rate, but many locomotives are used today at near the maximum steaming capacity where the evaporation from the firebox surfaces may approach a rate of 125 lb of water per sq ft per hr.

The author, in presenting the formulas derived from the generally accepted fourth-power equation for the transfer by radiation in the firebox and the double logarithmic equation for transfer by convection in the flues, provides a means to compute the expected performance of the present-day conventional boiler to greater accuracy and enables a better proportioning to be made between the firebox and the flue areas. His contribution should prove of great value in studying the influences of changes which obviously must be made in the combustion of the fuel and features of design to enable steam-locomotive boilers to meet the requirements imposed by the modern trend toward higher steam pressures, greater demands, higher superheat temperatures, and better fuel economy.

H. S. Vincent.[4] In the opinion of the writer the author's Fig. 5 would be more useful had it been constructed to show the temperature of the combustion gases at the rear flue sheet instead of a mythical equilibrium temperature. With such data the heat absorbed through the walls of the firebox would be given by the expression

$$H_a - H_t = h_f \quad [1]$$

where

H_a = available heat of combustion
H_t = heat in gases at rear tube sheet
h_f = heat absorbed through walls of firebox.

The use of the author's Equation [1] for radiation from combustion gases cannot be defended, as has been shown conclusively by Schack (1),[5] Hottel (2), and other investigators. Equation [1] of the paper can apply only to radiation from solid fuel where the total radiations are normal to the cold surface. To give correct results the equation must include a factor allowing for the average angle through which the radiating surface "sees" the absorbing surface. Hottel (3) has given data for evaluating such a factor in cubical furnaces as well as in other types of heat exchangers. In so far as the writer is aware nothing of this character has been worked out for the locomotive furnace.

About 10 years ago the writer published a series of articles (4) on the general subject of heat transfer in the locomotive boiler with the particular purpose of determining the proportion of available heat taken up by its various components, viz., firebox, tubes, and superheater. The data there given were derived from 62 laboratory tests of nine different types of locomotive boilers. The method used in determining heat transfer through the walls of the firebox is given by the writer's Equation [1]. The principal chance of error in using this method is from excess air introduced through the fire door or above the fire. With automatic-stoker-firing, this contingency does not often arise.

It will be observed from the author's Fig. 3, especially in the series C, that there is excessive fluctuation in the measured temperature of the gases in the firebox in relation to the rate of firing. The reason for this abnormal variation in recorded temperature is that only one temperature determination is made for each complete test whereas for the temperature in the smokebox, as well as for all other data, frequent determinations are made. In any calculation based upon the firebox temperature it is evident that the results will be more logical and accurate if a mean of the observed firebox temperatures is taken rather than those actually recorded. This was the method pursued by the writer in the articles referred to.

The author has given as criteria his Table 4 and Fig. 5, for estimating the heat transfer through the firebox walls for any given locomotive. Using these data, the writer has prepared Table 1 of this discussion, for the locomotive series C, for which the author includes four tests. The writer's Table 1 includes eleven tests of this locomotive, only two of which coincide with tests cited by the author.

The data for columns 4 and 5 of Table 1 are taken from the articles cited and are based upon the Fry (5) method of calculating these quantities. Column 6 gives the equilibrium temperatures, as established from the author's Fig. 5, although they do not agree with those shown in his Table 3, column 4. Column 7 of Table 1 is the so-called "radiation factor," taken from the author's Table 4, at the appropriate temperature. Column 8 of Table 1 gives the heat absorbed through the firebox walls in per

[1] By Lawford H. Fry, published in the February, 1946, issue of Trans. A.S.M.E., vol. 68, pp. 107–113.

[2] In Charge of Railroad Development, Development and Research Division, The International Nickel Company, Inc., New York, N. Y. Mem. A.S.M.E.

[3] "The Locomotive Boiler," by C. A. Brandt, Trans. A.S.M.E., vol. 62, 1940, pp. 379–419.

[4] Consulting Engineer, East Harwich, Mass. Mem. A.S.M.E.

[5] Numbers in parentheses refer to the Bibliography at the end of this discussion.

TABLE 1 EXPERIMENTAL DATA AND COMPUTED VALUES FOR PERCENTAGE OF AVAILABLE HEAT TRANSMITTED THROUGH THE FIREBOX WALLS OF LOCOMOTIVE BOILER SERIES C

Series	Test no.	Firing rate lb dcf per sfg per hr	Heat available for absorption btu per sq ft of firebox hs	Mixed gas lb per hr per sq ft of firebox hs	Equilibrium temperature, author's Fig. 5	Radiation factor, author's Table 4	Heat absorbed through firebox walls in per cent of heat available for absorption		Difference in columns 8 and 9, per cent
							Author's method	Writer's method	
1	2	3	4	5	6	7	8	9	10
C	532	67.3	119200	157.5	1810	41600	34.9	48.3	13.4
	539	80.5	136500	185.1	1850	44700	32.7	43.9	11.2
	511	94.4	167200	210.5	1970	54900	32.9	45.8	12.9
	520	105.4	180100	213.0	2040	61700	34.2	46.8	12.6
	521	108.8	178600	212.5	2040	61700	34.5	45.9	11.4
	530	112.8	194200	241.5	2040	61700	31.7	42.6	10.9
	519	122.0	202000	247.1	2060	63700	31.5	42.3	10.8
	526	128.1	204100	230.0	2130	71200	34.8	46.0	11.2
	531	146.9	224000	272.5	2115	69550	31.1	38.8	7.7
	527	174.6	267000	325.0	2160	74600	27.9	35.8	7.9
	523	231.2	336500	386.0	2300	92000	27.3	30.1	2.8

NOTE: Dcf = dry coal fired; sfg = square feet of grate area; hs = heating surface.

cent of the heat available for absorption, using the author's method of calculation. Column 9 gives data similar to those of column 8, but calculated in accordance with the writer's Equation [1]. Column 10 shows the difference in percentage between columns 8 and 9. This varies from about 3 to 13 per cent and indicates to the writer that firebox absorption, as determined by the author's formulations, is too low by this amount.

In the present state of the art it seems inadvisable to attempt to show the exact method by which the available heat reaches the firebox walls. This determination must await the patient work of investigators who are equipped to take all of the complex elements of the problem into consideration. A very great need today is for many more laboratory tests of the locomotive with the results made available to all who can use them. It seems most fitting that such tests should be made under the auspices of the Federal Government and could well be conducted by the Bureau of Standards. It can be said without contradiction that our present knowledge of the thermodynamics of the steam locomotive is largely due to the generosity of the Pennsylvania Railroad in making available records of tests conducted at their plant in Altoona.

BIBLIOGRAPHY

1 "The Influence of Radiation in Coal-Fired Furnaces, Etc.," by W. J. Wohlenberg and E. L. Lindseth, Trans. A.S.M.E., vol. 48, 1926, Appendix 5, p. 922.

2 "The Radiation of Furnace Gases," by H. C. Hottel and R. B. Egbert, Trans. A.S.M.E., vol. 63, 1941, p. 297.

"Radiant Heat Transmission From Water Vapor," by H. C. Hottel and R. B. Egbert, Trans. A.I.C.E., vol. 38, 1942, p. 531.

3 "Heat Transmission," by W. H. McAdams, first edition, McGraw-Hill Book Publishing Company, Inc., New York, N. Y., 1933, p. 50.

4 "Heat Transmission in Locomotive Boilers," by H. S. Vincent, *Railway Mechanical Engineer*, vol. 109, May, 1935, p. 180.

5 "A Study of the Locomotive Boiler," by L. H. Fry, Simmons-Boardman Publishing Corporation, New York, N. Y., 1924.

C. J. SURDY.[6] In more recent years the so-called "80 lb rule" has been quite generally used by locomotive builders in calculating the evaporative values of the boiler direct-heating surfaces. The presence of these new and higher values has been mentioned by both Johnson and Brandt but Mr. Fry in his paper has clearly and pointedly attributed this to high rates of combustion. Table 3 (columns 3 and 6) of the paper offers abundant proof of the existence of a 55 lb-125 lb evaporative range per sq ft of direct heating surface, depending upon combustion rates.

The present work may be viewed as an extension of the author's treatise "A Study of the Locomotive Boiler" (Simmons-Boardman Publishing Corporation, New York, N. Y., 1924) in which tables 5, 9, 10, 11, 12, 13, and 14 show exhaustive test results forming the original premise of the conclusions set forth there and expanded in the present paper. In this earlier treatise the steam produced at the various rates of combustion is equated in terms of the total heating surface of the locomotive firebox. However, it is clear from this study and the present paper that a definite relationship exists between rate of combustion and evaporation per square foot of heating surface.

To locomotive design engineers this paper presents an authoritative exposition of the factors which make the modern high-capacity steam locomotive possible. The author should be complimented for this further contribution to his studies of the locomotive boiler.

[6] Assistant to President, The Standard Stoker Company, Inc. Mem. A.S.M.E.

AUTHOR'S CLOSURE

The author appreciates the comments made by Messrs. Surdy and Huston.

Mr. Vincent's discussion contains several points of interest. The author welcomes comparison between the present paper and Mr. Vincent's extensive and valuable study of heat transfer in locomotive boilers (4) published in 1935 which deserves to be better known. Mr. Vincent took the results obtained in nine series of locomotive tests and by noting the rate of heat release in the firebox, the weight of the gases of combustion, and the temperature at which they left the firebox, he computed the rate at which heat was taken up in the firebox. From this the total heat taken up by the boiler could be separated with considerable precision into its three components, heat absorbed in firebox, heat absorbed in flues and tubes, and heat absorbed in superheater. In his discussion of the present paper, Mr. Vincent points out that his values for heat taken up in the firebox are higher than those given in the paper. This is true and further consideration of the problem leads to the conclusion that a modification should be made of the statement in the paper that "radiation at the equilibrium temperature corresponds to the heat actually taken up by the firebox." Some correction should be made for the fact that the equilibrium temperature is higher than the temperature at which the gases leave the firebox. Mr. Vincent's figures, which confirm some of the author's earlier figures (5), show that the heat actually taken up by the firebox is larger than that computed as radiated by Equation [1] of the paper by about 12 per cent at low rates and by about 5 per cent at high rates of operation.

It might be possible to arrange a corrective formula to give better correlation between rate of heat transfer in the firebox and the radiation at the equilibrium temperature. It is however not highly important to determine the exact rate of heat transfer in the smokebox. Radiation at the equilibrium temperature gives a reasonably good qualitative picture of the distribution of heat absorption between the firebox and the flue bundle, and for the present attention is directed to the fact that the method as a whole gives a remarkably exact procedure for estimating the over-all output of locomotive boiler. Mr. Vincent in a private

communication says that he has made a number of checks of the method and has found no case in which it deviates from the measured results by more than one per cent.

Rather than strive for too high a degree of idealistic perfection, the author prefers, as stated in the preamble of the paper, to work with an admittedly empiric method that produces useful practical results.

NOTE: Computed equilibrium temperature for Test 527 Series C should be 2120 not 2320.

Rate of Temperature Change in Short-Length Round Timbers[1]

MAX JAKOB.[2] In the paper under discussion one finds sentences like the following: "Each curve....was prepared by plotting the temperatures for each heating period for the logs of different diameters." These logs are not logarithms, but real logs. Unfit for mathematical treatment as they may seem to be, the paper subjects them to such treatment. It contains and illustrates the solution of the differential equation for simultaneous axial and radial thermal conduction in short cylindrical pieces of timber which are suddenly heated and then kept at constant temperature all over the surface.

Strange enough, almost the same solution as needed and used here in conditioning timber logs was previously needed and derived for a similar practical purpose, namely, glass cooling, by Williamson and Adams.[3] The author's solution also includes the case of different thermal conductivities in axial and radial directions as occurs in timbers; this, however, causes only a slight change in the main equation.

The paper contains a great number of useful graphs, representing the temperature distribution in logs, 4 and 8 ft long, of different diameters for different time intervals. These graphs can easily be converted to be used under different conditions.

Two items in this very valuable paper are to be regretted: The author does not use the letter symbols for heat flow as recommended by the American Standards Association.[4] The American Standards symbol for thermal diffusivity, for instance, is α. The author, however, uses h^2 and q^2 for the diffusivities in the radial and axial direction, respectively, which is particularly undesirable because the American Standards employ h for surface coefficient of heat transfer and q for heat-flow rate. For time the author uses T which the Standards reserve for temperature on absolute scale as generally adopted.

The other objection is that the author, though knowing very well that diffusivity is a property of the substance in which conduction occurs, proceeds as though it were different for heating the timber in steam or water. His statement, "The diffusivity values determined from experimental tests may be considered as values which apply for the heating medium used," is likely to confuse readers who are not quite familiar with the concept of "diffusivity." It is significant that the author speaks of a "diffusivity factor for radial heating" instead of, "diffusivity factor for radial direction." What he actually has in mind is that the surface coefficient which we call h, is generally greater for condensing steam than for water in contact with the surface, and that increasing h accelerates the propagation of temperature in a solid as does an increase of the diffusivity α. The effect of an increase of h may therefore be approximated by raising the value of α. Then, however, one should call this an "apparent" or "equivalent" diffusivity and express it by a different symbol, for instance, α_e. Both lines in the author's Fig. 1 obviously represent equivalent rather than true diffusivities, since the author neglects the temperature difference between the heating medium and the surface of the timber samples.

[1] By J. D. MacLean, published in the January, 1946, issue of Trans. A.S.M.E., vol. 68, pp. 1–16.

[2] Consultant in Heat Research, Armour Research Foundation, and Research Professor of Mechanical Engineering, Illinois Institute of Technology, Chicago, Ill. Nonresident Research Professor of Heat Transfer, Purdue University. Mem. A.S.M.E.

[3] "Temperature Distribution in Solids During Heating or Cooling," by E. D. Williamson and L. H. Adams, *Physical Review*, vol. 14, 1919, pp. 99–114.

[4] American Standard Letter Symbols for Heat and Thermodynamics Including Heat Flow," A.S.A., Z10.4–1943, published by A.S.M.E.

Temperature-Time Distribution in Rectangular Bars[1]

G. M. DUSINBERRE.[2] The authors suggest the use of their curves in the calculation of cooling rates during quenching of steel. There are two difficulties here, as follows:

The first lies in the way the results are plotted, log of the temperature-change ratio against a function involving time directly. This is a widely used convention. It has the advantage, in plotting, that the lower end of each curve approaches a straight line. However, this region will ordinarily be of little interest. The authors wisely give a better chart in the same space by omitting values of T_x less than 0.02, which values are shown on many similar charts.

Consider the cooling of steel from 1600 F to 100 F. The most important changes occur around 1300 F, or $T_x = 0.8$. The logarithmic plotting constricts this part of the chart. Therefore a uniform scale of T_x would be an improvement. A further improvement would be to use $\sqrt{a\theta/w}$ as abscissa to expand the time scale in the region of practical importance.

The second difficulty lies in the use of constant values of the thermal properties (k, c_p, and h) and neglect of the latent heat of phase change. These simplifications are unavoidable under the conventional mathematical treatment, although not under a numerical treatment.

Take an experimental temperature-time curve for a steel slab or billet. There is a definite "flat" in the critical range not shown on curves such as the authors'. If, by choice of mean values of the properties, we attempt to fit a theoretical curve to this, we will find that it must be in error, perhaps 10 to 15 per cent in position at some point and even more in regard to slope. This makes any question of two- or three-figure "accuracy" rather academic.

The fact is that calculus is not adequate for this problem. If we have to get solutions by calculation rather than experiment, then the writer feels that we should use the less esthetic but more accurate finite-step methods.

AUTHORS' CLOSURE

The authors appreciate Commander Dusinberre's amplifying statements regarding the mathematical method of solution. The log plot for T_x function has become a generally adopted method of plotting this type of data. The authors realize that it is sometimes desirable to plot the results in a different way from the one they chose; hence they have included the tabular results shown in Tables 1 through 5, which may be used in plotting the curves in any desired manner.

This method of solution involving the solution of the partial

[1] By W. M. Rohsenow, M. A. Aronstein, and A. C. Frank, published in the February, 1946, issue of Trans. A.S.M.E., vol. 68, pp. 135–141.

[2] Department of Mechanical Engineering, Virginia Polytechnic Institute, Blacksburg, Va. Mem. A.S.M.E.

differential equation is limited to cases in which the thermal properties (k, Cp, and h) are essentially constant and in which there are no phase changes and no latent heat. This method may be applied to the steel slab mentioned by Commander Dusinberre provided the temperature range does not include the critical point.

Measurements of Temperatures in Metal Cutting[1]

K. J. Trigger.[2] The authors present interesting results of average chip temperatures versus cutting speed, Fig. 2 of their paper. The reasoning for the observed constancy of chip temperature at the higher range of speeds appears logical. The results do, however, emphasize the desirability of determining the temperature at the tool-chip interface, or contacting surface, since, as pointed out, this is where tool failure has its inception.

The most direct approach to the tool-chip interface temperature is probably by means of the tool-work thermocouple, which is, in reality, composed of many thermocouples in parallel so that the emf measured is the average emf of all the points of contact (thermocouples) of the tool and chip. A temperature so determined represents therefore the average temperature at the tool-chip interface, and in this discussion is referred to as the cutting temperature. The writer has been investigating cutting temperatures utilizing the tool-work thermocouple principle and using a steel-cutting grade of cemented carbide as the tool and annealed NE8640 as the workpiece.

Since the authors used carbide tools on steel it would seem that the results of the cutting-temperature tests should apply quite directly, and sample curves are submitted to supplement the authors' statements concerning the temperature of the tool.

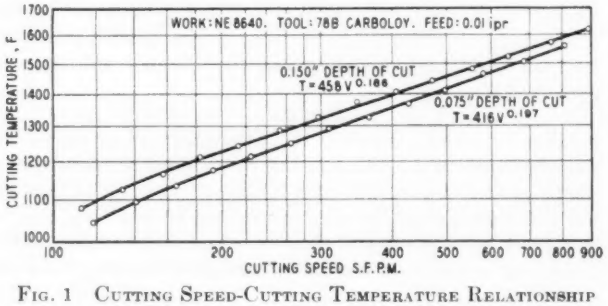


Fig. 1 Cutting Speed-Cutting Temperature Relationship

Fig. 1 of this discussion shows the effect of cutting speed upon cutting temperature for two depths of cut at constant feed. Many similar curves have been obtained, all of the same general shape.

It is generally observed that the curves droop at low speeds and/or light cuts. Examination of the chip under such conditions reveals some scuffing or roughness on the separating surface coincident with the presence of a significant built-up edge on the tool. The effect of the built-up edge would be to remove some of the thermocouples from the separating surface, and thus lower the indicated (average) emf. Supporting this belief is the fact that when the chip shows no scuffing the points lie on the straight-line portion of the curve. Such conditions have been observed in many tests to date.

Within the range of conditions herein reported, the writer believes that cutting temperature is essentially a power function of cutting speed, and is expressed by the relationship $T = CV^n$, where C is a constant and n the exponent. This contention receives support from the older and more common relationship for tool life and cutting speed, i.e., $VT^n = C$, where V = cutting speed, sfpm; T = tool life, min; C = const; and n = exponent.

Various investigators, including the authors, report constant cutting force if cutting speed is the only variable. If, then, the tool life is shortened exponentially with increased cutting speed, it is presumably due to increased temperature at the tool surface in a similar sort of relationship, that is, exponential.

Authors' Closure

Professor Trigger's comments on the paper, "Measurements of Temperatures in Metal Cutting," are very much appreciated. Professor Trigger's method of measuring the cutting temperatures between the chip and tool by using a tool-work thermocouple appears to be a logical procedure to determine the maximum temperatures developed in metal cutting. In fact, Professors Gilbert and Boston first presented a paper before the A.S.M.E. in December, 1934, entitled, "Relation Between Cutting Force Temperature and Tool Life in Cutting Steel With Single-Point Tools." The time of this presentation coincided with the depression and the paper was never published. Another paper entitled, "Cutting Temperatures Developed by Single-Point Turning Tools," was presented to the American Society for Metals[3] by Professors Gilbert and Boston. Both of these papers showed that the cutting temperature as a function of cutting speed was practically a straight line for any shape of tool, except for speeds below approximately 25 fpm, where the curve was concave downward but above the normal line. Professor Trigger's definition that the thermocouple is composed of many thermocouples in parallel is in agreement with the authors' opinion. In fact, the concave portion of the temperature-cutting speed curve for the lower speeds is presumably due to this particular principle, in that at lower speeds the built-up edge becomes larger, and actually introduces a considerable amount of worked metal between the newly formed chip and the tool face. This is one of the objections of the tool-work thermocouple. Apparently Professor Trigger's work as shown in Fig. 1 was carried out at speeds where the built-up edge did not exist or was small in size. His lowest speeds were about 120 fpm, with tool temperatures above 1000 F.

An objection to the tool-work thermocouple is the difficulty of calibration. The authors have found that the electrical properties of all tool bits are not identical, and that the calibration must be carried out between a piece of the work being cut and that particular cutting tool doing the cutting. It is also necessary to make a new calibration for each material cut. It would be interesting to know Professor Trigger's procedure in calibrating his tool-work thermocouple.

The two-tool thermocouple in which two dissimilar tool materials form the cutting edge, eliminated the need of calibrating against the material cut. The greatest trouble was in regrinding the tool, and also the sintered carbide wore faster than the other tool material at cutting speeds below 100 fpm. This two-tool thermocouple had the advantage of being able to cut any material, the emf developed between the two tools being a direct function of the temperature at the cutting edge and independent of the material cut. This permitted the use of this two-tool thermocouple to compare cutting temperatures under standard sizes of cuts when turning steel, cast iron, nonferrous metals, etc.

Later a double tool-work thermocouple was developed in which

[1] By A. O. Schmidt, O. W. Boston, and W. W. Gilbert, Trans. A.S.M.E., vol. 68, 1946, pp. 47–49.

[2] Professor of Mechanical Engineering, College of Engineering, Department of Mechanical Engineering, University of Illinois, Urbana, Ill. Mem. A.S.M.E.

[3] Trans. American Society of Metals, vol. 33, no. 3, September, 1935, pp. 703–726.

one tool of high-speed steel, and a second tool of cast nonferrous alloy, identical in shape, were used when cutting a bar at the same speed, feed, and depth of cut. The reading on the potentiometer was independent of the material being cut, the tool grinding was simplified, and the accuracy of reading was improved.

All of these types of thermocouples gave practically straight-line relationships between the cutting speed and temperature. In this respect the authors' work does not agree with Professor Trigger's, due perhaps to the fact that our temperatures are normally below 1000 F, whereas Professor Trigger's are normally above. It would therefore appear that further work on this subject to establish the relationship between the temperature and the tool life as a functior of cutting speed would be well worth while.

Summary Report on the Joint E.E.I.-A.E.I.C. Investigation of Graphitization of Piping

By S. L. HOYT,[1] R. D. WILLIAMS,[2] AND A. M. HALL[3]

Following the failure in January, 1943, of a welded joint in a high-pressure steam line at the Springdale Station of the West Penn Power Company, among the several investigations undertaken, a research program was initiated at Battelle Memorial Institute to study the fundamental causes of graphitization and the restoration of graphitized joints. The present paper is a summary of the findings to date on graphitization and includes not only work of the Institute but elsewhere. It gives the present status of significant points which have emerged in relation to manufacture and fabrication.

Introduction

THE failure in January, 1943 (1)[4] of a welded joint in a high-pressure steam line at the Springdale Station of the West Penn Power Company made the whole power industry, as well as the metallurgical world, acutely aware, for the first time, that graphite could form in steel piping operating at steam temperatures, and that its presence in certain instances could so weaken the piping as to produce a service hazard.

Among the several investigations immediately begun by various interested groups was a research program at Battelle Memorial Institute under the auspices of a Joint Subcommittee on Graphitization, initiated by the Edison Electric Institute and the Association of Edison Illuminating Companies. The program was set up to study the fundamental causes of graphitization and the restoration of graphitized joints. For new pipe, it was desired to know one or more kinds of steel which would be resistant to graphitization.

In particular, interest centered about the segregated type of graphite found in the Springdale pipe. This occurred as a continuous film across the entire cross section of the pipe, at or near that zone of a welded joint which had been heated to the Ac_1 point of the steel during welding, i.e., the low-temperature edge of the weld-heat-affected zone. Instead of being plane, this film of graphite was scalloped in conformity with the heat-affected zone and in a cross section through weld and stock, showed a characteristic "eyebrow" formation. Graphite nodules might have formed elsewhere in the pipe, but with their random distribution they were thought to be relatively harmless. The segregated streaks, however, tended to form a weak and brittle plane across the entire pipe and it was imperative that their formation be prevented.

This paper is a summary of the findings to date on graphitization investigations, both at Battelle and elsewhere. These include reports by approximately 40 operating companies on the condition of their steam lines[5] and by additional investigators, principally staff members of the power companies and of suppliers who had individual points under study.

In general, no attempt is made in this paper to distinguish between the sources of the data discussed, although this has been done in the Battelle progress reports to the Joint Subcommittee.

It is intended in this summary report to give the status to date on points that have emerged as being of greatest significance in manufacture and fabrication. Fortunately, it is possible to give reasonably good answers to some of the more important questions, but it should be recognized that the exploration of a new field is likely to raise additional questions, the existence of which had not been anticipated. That is true in the present instance and is principally responsible for the tentative position which must be taken on some of the points.

Influence of Deoxidation and Alloying Elements

Aluminum Deoxidation. Among the plain-carbon steels the high-aluminum-deoxidized types (i.e., 1.5–2 lb Al per ton) were found to be relatively susceptible to graphitization at the higher steam temperatures. Plain-carbon steels, low-aluminum-deoxidized (i.e., 0.5 lb Al per ton, or less) or straight silicon-deoxidized, appear resistant to graphitization at present steam temperatures. These findings are confirmed by both plant and laboratory investigations (2). Bead-welded high-aluminum-deoxidized plain-carbon steel showed graphitization after only 500 hr at test temperatures of 925 F and 1025 F. At the same test temperatures a low-aluminum-deoxidized plain-carbon steel contained no more than possible traces of graphite after 7700 hr.

Residual aluminum in the steel, or some factor which runs parallel with it, seems to promote graphitization very strongly. In this connection there is some evidence, though it is inconclusive, to suggest that it is residual aluminum as metallic aluminum, rather than as Al_2O_3, which is effective. This point will be again considered when the relationship between graphitization and microstructure is discussed.

Molybdenum. The presence of about 0.5 per cent molybdenum in the carbon-molybdenum steel retards graphitization to some extent. However, molybdenum was originally added to improve creep strength, and its retardation of graphitization is a secondary effect, far outweighed by the action of aluminum deoxidation as an accelerator. Thus while low-aluminum-killed or straight silicon-killed carbon-molybdenum steel was found to be very resistant to graphitization, high-aluminum-killed carbon-molybdenum steel graphitized to an appreciable extent, though not as readily as high-aluminum-killed plain-carbon steel. The graphitization of carbon-molybdenum steel and the effect of aluminum deoxidation may be seen by comparing Fig. 1 with Fig. 2.

---

[1] Technical Adviser, Battelle Memorial Institute, Columbus, Ohio.

[2] Welding Engineer, Battelle Memorial Institute.

[3] Research Engineer, Battelle Memorial Institute.

[4] Numbers in parentheses refer to the Bibliography at the end of the paper.

Contributed by the Joint A.S.T.M.-A.S.M.E. Research Committee on Effect of Temperature on the Properties of Metals and presented at the Annual Meeting, New York, N. Y., Nov. 26–29, 1945, of THE AMERICAN SOCIETY OF MECHANICAL ENGINEERS.

NOTE: Statements and opinions advanced in papers are to be understood as individual expressions of their authors and not those of the Society.

[5] Of the forty stations reporting, seven had cases of severe graphitization (chain-eyebrow-type or heavily segregated nodules), two had cases of moderately severe graphitization (segregated nodules), four had cases of moderate graphitization (random nodules), three had cases of slight graphitization (a few random nodules), and 23 had found no graphite.

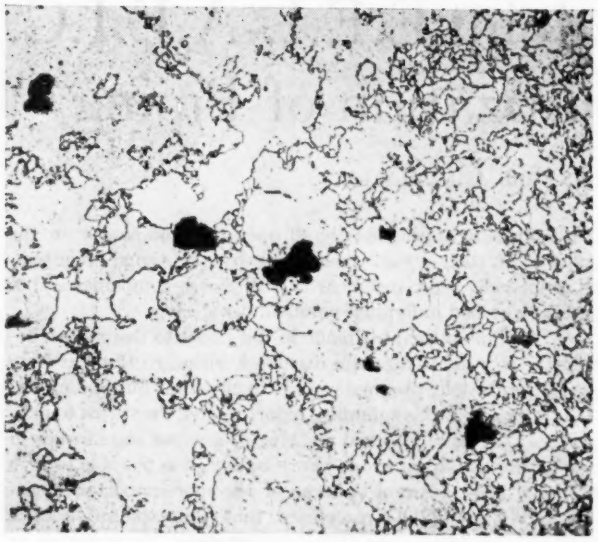


FIG. 1 HIGH-ALUMINUM-KILLED CARBON-MOLYBDENUM STEEL BEAD-WELDED AND TREATED 9700 HR AT 1025 F
(Random graphitization. Nital etch; ×250.)

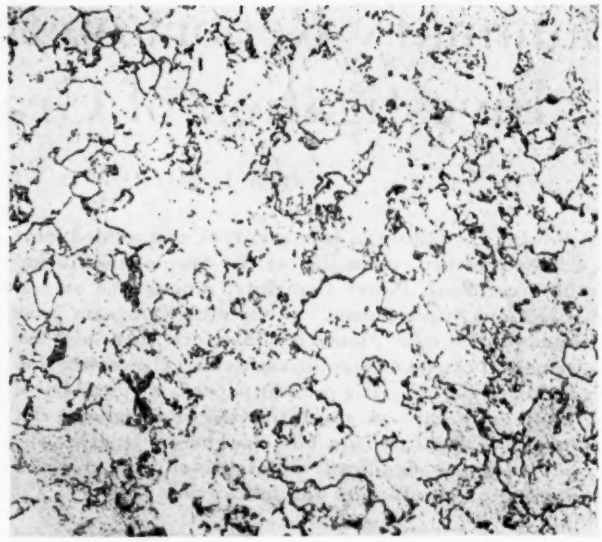


FIG. 2 LOW-ALUMINUM-KILLED CARBON-MOLYBDENUM STEEL BEAD-WELDED AND TREATED 9700 HR AT 1025 F
(No graphitization. Nital etch; ×250.)

Chromium. Examination of the chromium-molybdenum steels has developed a feature of the microscopic identification of graphite that deserves mention. Chromium is added, in this case, to produce a carbide of such stability that it will be immune to any tendency to form graphite at operating temperatures. There is considerable evidence to support this belief, and one expects the microscopic examination of heated test samples to show nothing of the nature of graphite. Actually, one observes very small particles, even in samples containing 1 per cent of chromium or more, and he is inclined to report "traces of graphite." One of these small particles is shown in Fig. 3. The occurrence of graphite is highly doubtful and the situation calls for positive identification of these particles, if not in the present samples in which the task would be relatively difficult, then in samples which have been heated long enough for them to grow into a more convenient size. Unfortunately, at this time it has not been possible to carry out the work necessary to complete the identification—they might be chromium oxide or some other unsuspected reaction or precipitation product.

With this in mind it is noted that chromium-molybdenum steels, even one containing as little as 0.25 per cent chromium and made with high-aluminum deoxidation, did not appear to graphitize in a laboratory test. After heating at 925 F and 1025 F for 5000 hr, careful metallographic examination showed so little graphite, if any, that it could not be identified with certainty. Under the same conditions, control specimens, similar in composition except that no chromium was added, graphitized after 2500 hr. Figs. 4 and 5 indicate these differences. Thus the stabilizing or retarding capacity of chromium is much greater than that of molybdenum, and is apparently sufficient to offset the accelerating tendency of aluminum.

Nickel. It has been reported that nickel in amounts up to 3.43 per cent does not increase the tendency of low-carbon molydenum steel toward graphitization in the temperature range of 950 F to 1050 F and may quite possibly decrease it.

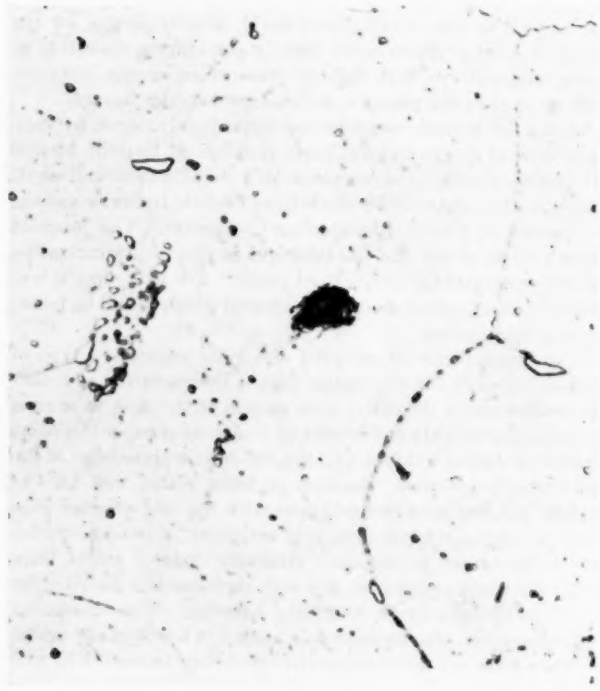


FIG. 3 SMALL DARK PARTICLE IN LOW-ALUMINUM-KILLED CHROMIUM-MOLYBDENUM STEEL, 0.5 PER CENT CR, 0.5 PER CENT MO, TREATED 2500 HR AT 1025 F; ×2000

EFFECT OF PRIOR HEAT-TREATMENT AND STRUCTURE

Welding. The striking peculiarity in the graphitization problem confronting the power industry is the fact that when segregated graphite forms in pipe during service it usually occurs in a narrow zone in the pipe immediately adjacent to a weld. It is evident that the location of this zone and the degree of graphite segregation in it are largely determined by the thermal gradients imposed on the pipe during welding. Microscopic examination shows that this zone of graphite segregation is the narrow band through the wall of the pipe near the weld and following the weld contour, which has been heated approximately to the Ac_1 point of the steel by the welding operation. The influence of welding heat is shown in Figs. 6 and 7 for a high-aluminum-killed plain-carbon steel.

Welding is not the only factor operating to produce segregated

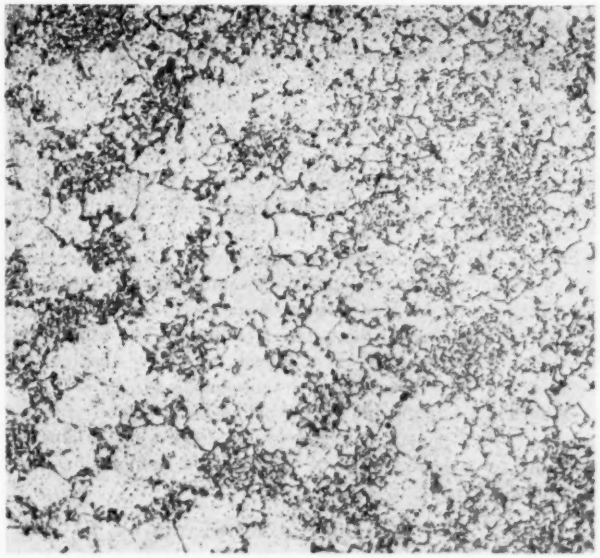


FIG. 4 HIGH-ALUMINUM-KILLED CHROMIUM-MOLYBDENUM STEEL, 0.50 PER CENT CR, BEAD-WELDED AND TREATE › 5000 HR at 1025 F
(No graphite. Nital etch; ×250.)

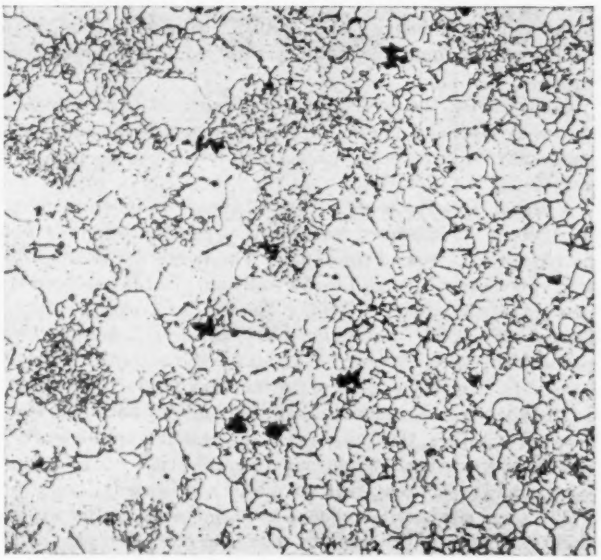


FIG. 5 HIGH-ALUMINUM-KILLED CARBON-MOLYBDENUM STEEL, 0.0 PER CENT CR CONTROL, BEAD-WELDED AND TREATED 5000 HR AT 1025 F
(Graphitization tending to segregate at Ac_1 isotherm. Nital etch; ×250.)

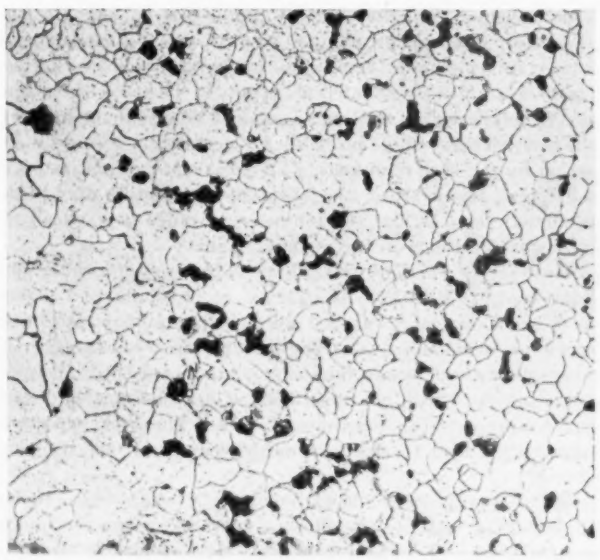


FIG. 6 HIGH-ALUMINUM-KILLED PLAIN-CARBON STEEL, BEAD-WELDED AND TREATED 7700 HR AT 1025 F
(Graphitization in zone just above Ac_1 isotherm. Nital etch; ×250.)

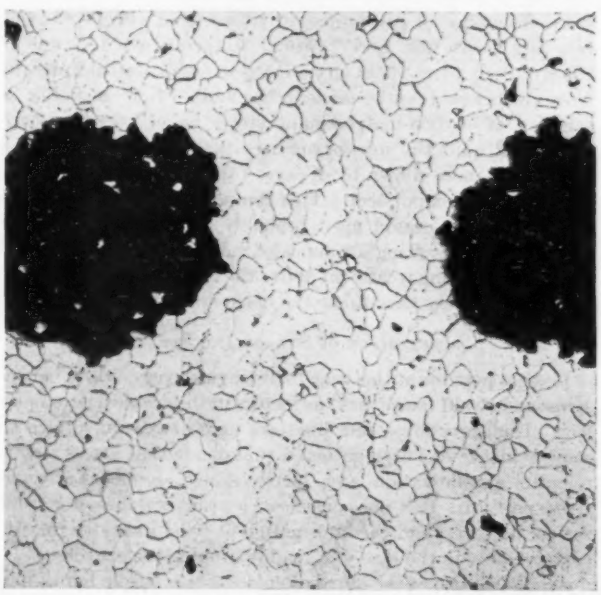


FIG. 7 HIGH-ALUMINUM-KILLED PLAIN-CARBON STEEL, BEAD-WELDED AND TREATED 7700 HR AT 1025 F
(Graphitization in stock unaffected by welding heat. Nital etch; ×250.)

graphite; we must not overlook the simple fact that the steel must be inherently graphitizable. Thus the thermal treatment accompanying welding is a necessary but not a sufficient condition for the production of a brittle zone of segregated graphite.

Carbide Particle Size. There is evidence to indicate that it is the structure of the carbides in the zone heated to the Ac_1 point which induces the graphite segregation. In particular, the observations suggest that a spheroidized or coarse-carbide structure, such as may obtain at the Ac_1 isotherm after welding, is especially susceptible to graphitization. Fine carbides appear to be more resistant to graphitization. This was brought out in a test of a high-aluminum-killed plain-carbon steel which was heated 1350 hr at 1025 F. Specimens water-quenched from 2000 F or 1600 F, or normalized at 1650 F, (all containing fine carbides) showed no graphite, while specimens annealed at 1400 F, or spheroidized 65 hr at 1250 F, had graphitized, forming random graphite nodules. Furthermore, welded carbon-molybdenum steel pipe, normalized at 1650 F, was also resistant to graphitization, presumably because the susceptible structure near the weld was replaced by a relatively fine and resistant structure. It is to be assumed that longer heating would ultimately produce random graphite, a point that is more adequately treated under the kinetics of graphitization.

Normality. The accumulated evidence seems to confirm the hypothesis that a steel which is structurally completely "normal" in the McQuaid-Ehn test is highly resistant, though not necessarily absolutely immune, to graphitization (2). In this light the action of aluminum as an accelerator of graphitization may be its known capacity for promoting spheroidization of car-

bides and for inducing "abnormality" in steel. Thus the influence of aluminum may actually arise from its effect on structure.

Contrariwise, the persistence of well-defined lamellar pearlite shown by Kerr and Eberle for long-continued heating of normal steels may be directly associated with freedom from graphitization (2).

Postweld Heat-Treatment. Postweld heat-treatments at 1200 F or 1300 F have shown a little less graphitization as compared to the as-welded condition. The reason for this small effect is not clear, though for molybdenum steel it has been suggested that the effect of 1300 F is due to the formation of molybdenum carbide (3). A striking effect, however, is produced by a postweld stress relief carried out slightly above the Ac_1 temperature of the steel which re-forms the structure produced by welding. In tests of a high-aluminum-deoxidized plain-carbon steel, stress-relieved at 1370 F, the formation of segregated graphite was completely prevented, although random graphitization was not prevented, and in fact may even have been accelerated.

The same steel, stress-relieved at 1290 F or less, after welding, developed segregated graphite near the Ac_1 isotherm. These tests were carried out at 925 F and 1025 F for time intervals up to 7700 hr.

It may be pointed out here that some instances of resorption of segregated graphite have been observed in test samples.

Creep Strength. One of the points immediately considered upon discovery of the apparently beneficial effects of stress-relieving above the lower critical temperature (Ac_1) was the effect of such a treatment on the creep strength of steel so treated. Creep tests could not be made in the limited time available, but samples of carbon-molybdenum steels were "stress-relieved" at 1425 F, and the microstructures thus produced were compared with those shown by Weaver (4), in his study of creep in carbon-molybdenum steel. This comparison suggested that the creep properties would most probably correspond to Weaver's specimens representing an annealed initial condition. As such, the stress-relieving treatment above the lower critical point would not be excessively harmful to the creep strength.

Influence of Stress and Strain

It is not possible at this time to distinguish very clearly between stress and strain (cold work) as factors in the graphitization problem. High-pressure steam lines are under stress in service and some evidence has been gathered to indicate that stress may accelerate graphitization and in so doing, produce a typical stress pattern. It is not considered a primary cause of graphitization, however, and the information at hand indicates that it is effective only in the case of a readily graphitizable steel.

As an example of the effect of cold work, a tensile bar of high-aluminum-deoxidized plain-carbon steel was pulled to fracture at room temperature and heated 1350 hr at 1025 F. Random graphitization was found in the bar, increasing in severity toward the fracture. A similar test in a low-aluminum-killed plain-carbon steel produced no graphite whatever. Straining by bending at room temperature slightly increased graphitization in a high-aluminum-killed plain-carbon steel, while compressive straining at 1025 F considerably increased the amount of graphitization. No relationship was found between the strain lines (Lüders' lines) produced in a steel specimen by tensile deformation and the location of graphite nodules.

The information so far accumulated points toward stress, and particularly that developed at steam-line operating temperatures, as a probable accelerator of graphitization which should not be overlooked.

Effect of Joint Preparation

Among the original questions raised by the power industry regarding the susceptibility of carbon-molybdenum steel pipe to graphitization, three dealt with the possible effect of joint preparation as a cause of graphitization. Specifically these were: (*a*) Is grease applied to the pipe end during fabrication a possible source of graphite? (*b*) Does gas-cutting of pipe ends preparatory to welding cause graphite to form? and (*c*) Does cold-working, such as produced by too coarse a tool feed in machine-beveling of pipe ends, cause graphite to form?

Tests indicate that none of these three factors is likely to contribute to the graphitization of steam lines. However, the evidence is not absolutely conclusive, particularly in regard to the effect of grease. Hence it appears advisable to adhere to the practice of cleaning all joints free from grease and other foreign matter prior to welding. It is known, of course, that perfectly clean steel graphitizes if it is of the susceptible type.

As for flame-cutting and heavy tool feeds, it is believed, in view of the depth of penetration of weld metal below the original surface of a joint, that neither of these surface preparations would cause the formation of graphite.

Kinetics of Graphitization

On the basis of preliminary work that has been done an attempt has been made to apply the principles of chemical kinetics to the problem of graphitization.

The approach consists in treating the graphitization process as a slow chemical reaction and determining its course with time at constant temperature, as given by the fraction of carbon transformed from the initial condition (carbide) to the final condition (graphite), for different intervals of time. The plot of the fraction of total carbon transformed, against time at temperature, is the reaction curve of the process. By correlating a series of reaction curves, each representing the progress of graphitization at a different temperature, the effect of temperature may be determined; at least for the temperature range over which the mechanism of the process remains the same.

Fig. 8 shows reaction curves obtained from data for the graphitization at 925 F, 1025 F, and 1125 F, of "reconditioned"[6] specimens of the original Springdale pipe, a high-aluminum-deoxidized carbon-molybdenum steel. The fraction of carbon transformed to graphite was determined by metallographic methods and plotted semilogarithmically against time. The solid portion of each curve represents the experimental data. The broken portions have been added to show the probable form of the complete curves.

For the purpose of illustration only it was decided to use these data to indicate the effect of temperature on the rate of graphitization. For this the half-life time at each of the three test temperatures was read directly from the reaction curves as the time required to convert one half the total carbon in the steel to graphite. These half-life times for 925 F, 1025 F, and 1125 F, plotted semilogarithmically against the reciprocal of the absolute temperature, yielded the approximately straight-line relationship shown in Fig. 9.

Reports on the progress of graphitization usually make use of some simple description of amounts, particle size, and distribution, with photomicrographs of typical areas. That is not adequate for quantitative treatment; and for the present work it was necessary to determine the amount of graphite in each sample. This was done by polishing several microsections of each sample and then estimating the average area covered by graphite. This figure in per cent gives the per cent by volume. Upon converting the volume per cent to weight per cent, it was necessary to apply a correction factor which was experimentally determined by a comparison of a limited number of microscopic determinations with direct chemical analyses for free carbon.

Some refinements in technique are still desirable but the data

[6] Air-cooled from 2200 F and normalized at 1650 F.

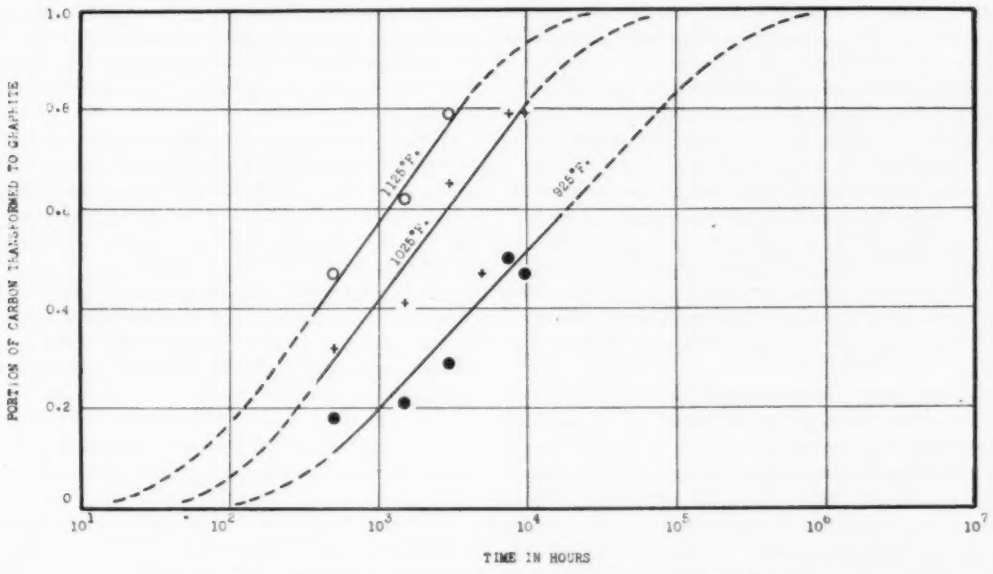


FIG. 8 REACTION CURVES FOR GRAPHITIZATION OF SPRINGDALE PIPE

presented are doubtless adequate for illustrating the principles. At this time no great accuracy can be claimed for the individual determinations. However, the data are good enough at least to suggest that the graphitization process, when it occurs, follows a definite law. Furthermore this law, whatever it may be, appears to be reasonably uniform in behavior over the range of temperature involved in the test program. Should this initial finding be corroborated by additional and more precise determinations, this is a conclusion of major significance since it gives legitimate grounds for predicting, from the findings at higher and accelerating test temperatures, what will happen at lower temperatures, or down to approximately 925 F. There is some reason to believe that at some temperature below 925 F, which would probably be different for different steels, some sort of change in the process sets in, such as one or more of the conditions for graphitization dropping out, and hence that a temperature range of immunity is entered. That temperature, if adequately determined and defined, would then become the maximum safe operating temperature for the steel in question.

While this preliminary study was conducted for the primary purpose of checking the soundness of the use of accelerating test temperatures, in other words, checking the experimental approach to the problem, it suggests, and possibly justifies, certain speculations on the type of data or observations which are needed to give an adequate understanding of the process. That should be the ultimate goal of an experimental program which seeks the control of graphitization. Since this is speculation, the discussion will be brief.

There is some thought that graphitization is a nucleation and growth process. The characteristics of such a process are: (*a*) An incubation period of nucleation over which it appears that nothing happens; (*b*) a period of relatively rapid change with corresponding depletion in the reacting substance; and (*c*) a final slow change to the end point. The graphitization data indicate that the reaction starts relatively fast and proceeds at a decelerating rate. (The curves in Fig. 8 do not show this on account of the logarithmic scale, but it becomes clear when time is plotted on a linear scale.) At least the data are consistent with the idea that nuclei are already present in the steel used for this test, though in other graphitizable steels that might not be so and the difference should show up in the reaction curves. Of course if the second type of steel were tested for too short a time one might erroneously conclude that it was immune.

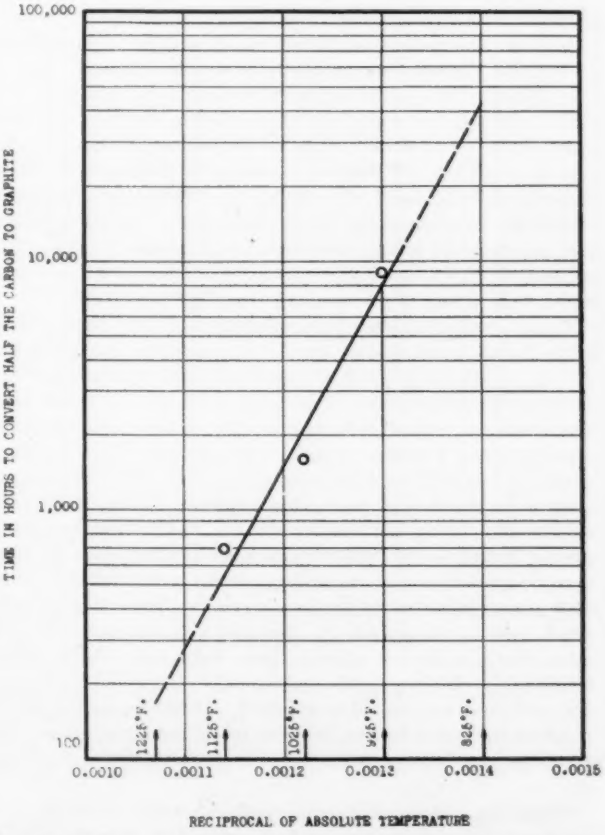


FIG. 9 EFFECT OF TEMPERATURE ON RATE OF GRAPHITIZATION PROCESS

The idea of graphite nuclei being present in some steels is not without support since Mr. Bolton of the Lunkenheimer Company has shown by chemical analysis that the Springdale steel before service contains about 0.04 per cent free carbon. Other steels

which are either immune or relatively resistant, ran about 0.01 per cent. These amounts are too small to be seen under the microscope.

An experimental verification of these points is greatly to be desired. While they may appear to be of greater theoretical than practical interest, that would probably be a shortsighted viewpoint. Laboratory tests of 10,000 hr duration are relatively long, yet an accelerated test at 1125 F, which steps up the rate thirteenfold would require over 30,000 hr to produce the effect of normal operating life at 925 F. In other words, we are required by the force of circumstances to pass judgments which are based on relatively short acquaintance with the steels in question. Obviously, the more complete our understanding of graphitization, the better able we will be to appraise steels and structures in short-time tests.

Another line of speculation which may not be without interest relates to the effect of structure, particularly the striking segregation of graphite along the Ac_1 isotherms. From thermodynamics it is known that the slope of the straight line in Fig. 9 is proportional to the energy change involved in the mechanism which controls the rate of the reaction. Calculation gives a heat value (32,900 cal per mol) which is consistent with the assumption that the controlling factor is diffusion, presumably the diffusion of carbon atoms through the ferrite matrix from the carbide source to the graphite nodules. This immediately raises the question of what carbide particles serve as sources.

In most processes of nucleation and growth it is not difficult to identify the reacting material, or source. For the case of graphitization, the malleabilization of white cast iron comes to mind, with nodules of graphite surrounded by uniform, impoverished zones. The present type of graphitization departs from this ideal picture, at least in numerous instances, in that the graphite nodules may be surrounded by carbide-containing areas. Obviously, those areas did not provide carbon for the graphite; the carbon must have come from more distant points. This seems to be just a simple statement of the facts, and if correct it shows that not all of the carbon is equally "available."

There is some evidence on availability. In the Battelle program it was found that a steel that was either quenched and drawn, or normalized, did not graphitize under test conditions which produced graphite in the same steel when it was annealed. The obvious structural difference is a fine carbide in the first two conditions and a coarse carbide in the latter. The concept of availability is sufficiently intriguing to induce one to attempt to apply it to the case of segregated graphite. Upon heating the steel to Ac_1 during welding the carbide has an opportunity to coarsen and this would probably be aided by aluminum deoxidation. If graphite nuclei are already present, graphitization would start almost immediately by drawing carbon from those carbides which were able to provide it. Even so, the process is slow and, particularly at service temperatures, some time would elapse before much visible graphite had formed. If nuclei had to form first, still more time would be required. In either case the graphite which formed at the Ac_1 isotherm preferentially would serve as a "sump" and drain carbon from coarsened carbides in the vicinity.

While this picture may be adequate for some of the cases of graphitization, a review of the findings to date indicates that it by no means covers all cases. Smith and Brambir (5) found, for example, in experiments with an end-quenched bar of graphitizable steel that the quenched end produced graphite on being heated subsequently. That seems to contradict the work at Battelle on a quenched and drawn sample, but more likely it is probably just telling a different story.

Without going into all the details, this seems to be the status of our knowledge of the graphitization process. By this we mean that from the standpoint of understanding the process, the data which have been accumulated do not fall into one simple pattern, They suggest, rather, that there are varying and multiple conditions which must be satisfied for the initiation and progress of graphitization.

Work on the kinetics of graphitization suggests that it should be valuable for distinguishing between the cases of free graphite initially present in the steel and of the spontaneous generation of nuclei. The latter condition would require a longer period for the growth of finite particles, and in the incubation period would be difficult to distinguish from the case of a nongraphitizable steel. (The determination of free graphite might make this possible.) Furthermore, it now appears that absence of graphitization at a given time interval may be due either to (*a*) absence of nuclei in an otherwise graphitizable steel, (*b*) absence of available carbon in an otherwise graphitizable steel, or (*c*) stable carbide. Conditions (*a*) and (*b*) could conceivably become modified with additional time and produce late graphitization. Condition (*c*) is the case desired for good practice, for both fabrication and service.

The ultimate use of the kinetic approach would be to make it possible to make reasonable predictions of behavior in service from accelerated test data gathered in the laboratory.

Summary

Considerable information has been gathered on the effects of several of the variables operating in the graphitization of high-pressure steam lines. Some data have been accumulated on the influence of deoxidation and the composition of the steel, on the effects of welding heat and other preservice heat-treatments, and on the influence of microstructure and cold deformation. While the results are largely qualitative, they throw some light on the mechanism of graphitization and give a basis, the only one at present, for prescribing the steel to be used and for setting safe operating temperatures.

In summarizing, it is thought that the following can be said on the points that appear now to be most important in this problem:

Deoxidation. The deoxidation practice used in making steels which are presumably of the graphitizable type is of great importance. In particular, the use of $1^1/_2$ to 2 lb of aluminum per ton is known to have a pronounced effect. This applies to both carbon and carbon-molybdenum steels of the type used for steam lines. This effect of aluminum has been found by controlled tests to be more pronounced than is the stabilizing effect of 0.5 per cent molybdenum. Steels which have been tested with not over 0.5 lb per ton and straight silicon-killed steels are relatively immune. These steels are characterized by showing a highly normal case structure in the McQuaid-Ehn test while the same steels deoxidized with the larger amount of aluminum showed the abnormal structure. While there is still some small doubt as to the absolute immunity of these normal steels, they should be regarded as highly resistant and capable of operating under more severe conditions without graphitizing than the same steels of the abnormal type. (No. = 0.001 ± per cent; Ab. = 0.020 + per cent Al).

Composition. Since carbon is the element which produces the graphite, it would seem advisable to keep it on the "low side," although no quantitative determinations have been made of the effects of different carbon contents. Chemical analysis reports a small amount of free carbon in these steels as manufactured. The indications to date are that the nongraphitizing steels contain not over 0.01 per cent free carbon and the graphitizing steels about 0.04 per cent. This lead is so important that it should be followed up. This might be done by determining free carbons on new lots of both wrought and cast steels for information purposes.

Manganese and silicon are both known to affect graphitization in general. In the present case these elements have been held at fairly constant levels and to date no specific effects of these elements have been uncovered.

Molybdenum is known to form a (metallic) carbide and has been shown to exert a stabilizing effect on pipe steels. Molybdenum also has a characteristic effect on the structure of steel and may have a secondary effect of this type. Just what this effect might be has not been worked out as yet, certainly not quantitatively.

It has been reported that heating the molybdenum steels at about 1300 F has a pronounced beneficial effect on graphitization. It was suggested that this is due to the conversion of iron carbide to the more stable molybdenum carbide, but apparently it is not known that this molybdenum carbide would remain stable at the lower operating temperatures or that the immunization is permanent.

Chromium also forms a highly stable carbide and is now thought to be the best element to add to carbon or carbon-molybdenum steels to keep them from graphitizing in service. In contrast to molybdenum, the addition of as little as 0.25 per cent chromium has at least checked graphite in high-aluminum-killed steel. While tests of chromium-containing steels have not as yet given definite or final answers, particularly on the amount of chromium which would be needed, the tests do indicate that chromium prevents or vastly retards graphitization. In this connection, however, it should be mentioned that tests of steels containing as much as 1 per cent chromium, or more, have shown "traces" of some new substance. Since one is looking for graphite in these samples, he is inclined to refer to this material as graphite since it occurs as very tiny dark specks. On the other hand, this material has not been identified, a determination which would not be without difficulties.

Welding. While random graphitization can occur in pipe steels without causing undue alarm, the heat effects of welding establish a highly critical zone where the stock has been heated to about the Ac_1 temperature. This is the major cause of segregated graphite.

While the usual stress-relieving temperatures of 1200 to 1300 F retard graphitization, it seems to be necessary to eradicate the structure of the heat-affected zone to have any important effect on the elimination of segregated graphite. Such a stress-relieving would be carried out just above the critical temperature for a long enough time to accomplish this. This treatment should be regarded as a good "corrective measure" for use with a known or suspected graphitizable steel, but by no means as a substitute for a stable steel.

Inasmuch as welding sets up the structural conditions which invite graphite segregation, welding techniques should be looked for to ameliorate this condition. The use of a high heat input and preheat which widen the heat-affected zone should be beneficial and should improve the effectivenss of stress-relieving above Ac_1.

Prior Structure. Prior structure of the part as welded does not appear to have a dominating effect on graphitization. While the point has been kept in mind by investigators, it does not appear to warrant very much attention. Even so it might have a secondary effect on the susceptible structure which is set up by welding. With this factor, as with various other factors of graphitization, an analysis of its precise effects is far less important than finding a steel which is immune to graphitization and not sensitive to deoxidation, welding, structure, etc. In particular, it is not thought that the structure set up by hot-upsetting, hot-forming, etc., is of primary importance in the graphitization problem.

Cold Work. The manufacture of pipe and castings for steam lines does not involve cold work except scarfing and similar operations. On this account the effects of cold work do not enter into the problem in a practical way, but laboratory tests have shown that cold deformation of graphitizable steels accelerates the process. On this account it might be used in a testing program to distinguish between graphitizable and nongraphitizable steels.

Service Temperatures. In view of the present interest in higher steam temperatures it is advisable to point out that the various investigational programs have all related to service temperatures not above the 925 F to 950 F mean-operating-temperature range. Steam temperatures of the order of 1000 F and above would very likely call for a different type of steel.

Suggestions for Power Industry. (*a*) For new steam-line installations it is suggested that a "normal" (low-aluminum-, or silicon-killed) carbon-molybdenum steel with initial graphite content of not more than 0.01 per cent, or a chromium-molybdenum steel containing 0.50 to 1 per cent chromium and 0.50 per cent molybdenum be used. Also, since postweld stress-relieving is general practice, it appears advisable to stress-relieve these steels above their Ac_1 temperature after welding. Future work may show this to be unnecessary.

(*b*) Though joints exhibiting some graphitization in service can generally be "healed" by normalizing at 1650–1700 F, they should be checked periodically.

(*c*) When a joint is severely graphitized, the only safe procedure is to cut it out and reweld, or replace it with a spool of new pipe. In fact, where severe graphitization is encountered in a large number of joints throughout the installation, it is safest to replace all the pipe with a type resistant to graphitization.

Acknowledgments

The authors wish to express their appreciation of the advice and assistance given by the members of the Joint E.E.I.-A.E.I.C. Subcommittee on Graphitization of Piping, Messrs. Alex D. Bailey, Sabin Crocker, L. E. Hankison, and T. E. Purcell; and to thank Messrs. C. E. Sims, Francis Boulger, and J. R. Heising for their valuable contributions to this paper; and Miss Jean Kernahan for metallographic assistance.

Furthermore, the authors wish to acknowledge the data from other research investigations and operating company reports made available to the Joint Subcommittee from which they have drawn freely.

BIBLIOGRAPHY

1 "Symposium on the Graphitization of Steel Piping," presented at the A.S.M.E. Annual Meeting, New York, N. Y., December, 1944; pamphlet on "Graphitization of Steel Piping," included in Trans. A.S.M.E., vol. 67, 1945; also, Edison Electric Institute Bulletin, vol. 11, No. 10, October, 1943, p. 307.

2 "Graphitization of Low-Carbon and Low-Carbon-Molybdenum Steels," by H. J. Kerr and F. Eberle, A.S.M.E. pamphlet on "Graphitization of Steel Piping," included in Trans. A.S.M.E., vol. 67, 1945.

3 "A Possible Means of Avoiding Local Graphitisation of Steels in Service at Elevated Temperatures," by G. V. Smith and R. F. Miller, A.S.M.E. pamphlet on "Graphitization of Steel Pipng," included in Trans. A.S.M.E., vol. 66, 1944.

4 "The Effect of Carbide Spheroidization Upon the Creep Strength of Carbon-Molybdenum Steel," by S. H. Weaver, Proceedings of the A.S.T.M., vol. 41, 1941, p. 608.

5 "Graphitization of Welded and of End-Quenched Carbon and Molybdenum Steels," by G. V. Smith and S. H. Brambir, A.S.M.E. pamphlet, "Graphitization of Steel Piping," included in Trans. A.S.M.E., vol. 67, 1945.

Discussion

Arthur McCutchan.[7] This paper is an excellent summary of

[7] Engineer, Engineering Division, The Detroit Edison Company, Detroit, Mich. Mem. A.S.M.E.

the findings both at Battelle and elsewhere. The tentative position taken in answering some of the important questions is justified by incompleteness of the findings and the different conclusions possible from the data at hand.

From a comparison of microstructures the authors have concluded that a postweld heat-treatment just above the lower critical temperature will not be excessively harmful to the creep strength. It is hoped that subsequent creep tests will support this conclusion. Examination of weld-probe samples from both high- and low-aluminum-deoxidized carbon-molybdenum welded joints after a few years' service at 900 F shows that a definitely spheroidized structure has resulted. It would seem important therefore to have creep tests and stress-rupture tests made on this spheroidized material for comparison with service creep measurements.

Efforts to reproduce the "strain-line" type of preferential graphitization apparently were not successful. The importance of understanding the cause of this type of graphitization is so great that further efforts should be made to reproduce this phenomenon under laboratory conditions.

While the structure produced by hot-upsetting may not, as stated by the authors, be of primary importance in the graphitization problem, it is the writer's opinion that the segregated type of graphite found adjacent to the welds and in the strain lines at Springdale is in some manner related to hot-upsetting.

I. A. Rohrig.[8] The data embodied in this report represent a vast amount of work and constitute a fundamental contribution that can be utilized in the selection and specification of new high-temperature-steam pipe material.

In association with graphitization, the effect on the physical strength of infected joints that are in service is of the greatest importance. In an endeavor to evaluate the effect of graphitization, two 10-in-diam welded joints in medium-carbon steel A.S.T.M. A-106 Grade B pipe that had been in service at 825 F for 59,000 and 64,000 hr, respectively, were investigated by the writer's company. Each weld joined a corrugated filler at the downstream side and a pipe bend at the upstream side. The graphitization that had occurred at these joints was judged to be "moderate" in amount and is shown in Fig. 10 of this discussion. Tensile tests made on samples taken from the joints indicate that the graphitization had no adverse effect on the tensile strength. Notched-bar tests made on samples cut from the two joints showed, however, a reduction in shock resistance in three of the four graphitized areas tested.

The results from these tests are given in Table 1 of this discussion. Samples from the same joints were laboratory-heated at temperatures that were varied between 850 and 950 F for a period of 6000 hr to develop further graphitization. Typical graphitization found in these samples after laboratory-heating is shown in Fig. 11. Since only small samples were used, notched-bar tests were not made after laboratory-heating, but bend tests made on strips cut from these laboratory-heated samples resulted in a distinct crack at one side of one weld as shown in Fig. 12. These samples were taken from welds in vertical piping, and it is interesting to note that the most severe graphitization at each weld occurred at the lower or downstream side of the weld.

The results obtained for these joints after laboratory-test-heating of samples removed from service show that although only moderate graphitization had developed as a result of 60,000 hr of service, a critical type of graphitization might possibly develop in these joints as a result of somewhat longer service.

The results presented by the authors regarding stress-relieving

[8] Research Department, The Detroit Edison Company, Detroit, Mich.

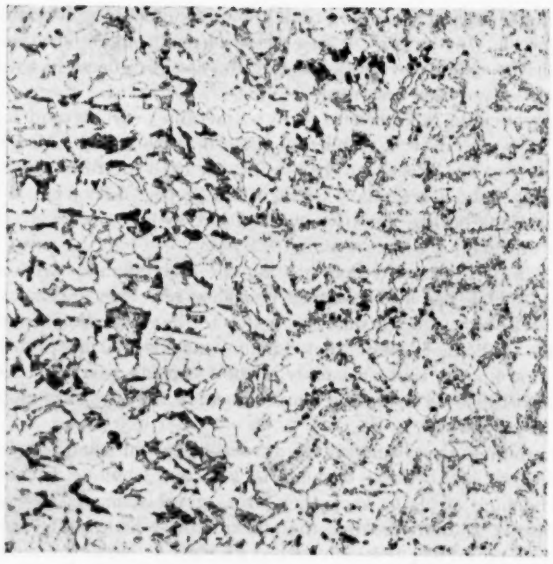


Fig. 10 Moderate Graphitization in Heat-Affected Area of Weld in Medium-Carbon Steel Pipe After 59,000 Hr of Service at 825 F; ×100

TABLE 1 NOTCHED-BAR DATA FOR WELDED JOINTS IN MEDIUM-CARBON STEEL AFTER HIGH-TEMPERATURE SERVICE

	Charpy V-notch toughness, ft-lb			
	Pipe metal unaffected by welding		Heat-affected area containing graphite	
Joint No. 1				
After 59,000 hr of service at 825 F:				
Corrugated filler	41		34	
	41		22	
	44	42	35	30.3
Pipe bend	72		78.5	
	72.5		86	
	76	73.5	102	88.8
Joint No. 2				
After 64,000 hr of service at 825 F:				
Corrugated filler	59		46	
	43		35	
	46	49.3	55	45.6
Pipe bend	103.5		81	
	65		77	
	69.5	79.3	57	71.6

treatments above the lower critical temperature are of particular interest since heat-treatment within or above the critical-temperature range after welding offers a means of overcoming dangerous graphitization. A graphitization test is under way at the writer's company, using welded samples of three different heats of A.S.T.M. A-206 low-aluminum carbon-molybdenum pipe material in the normalized, and also in the hot-rolled and drawn condition. Some of the samples received a treatment of 2 hr at 1400 F, following welding. The graphitization test is being conducted using laboratory-test-heating and temperatures varying between 950 and 1150 F. The results obtained after 1500 and also after 2500 hr of test are given in Table 2 herewith. In one of the heats under test, namely, heat 10,600, the 1400 F stress-relieving treatment appears to be effective in preventing graphitization, whereas in heats 3099 and 6347 graphite was found in the samples that received the 1400 F treatment. Further study is to be made of the time-temperature relationship of various heat-treatments in that temperature range.

Each of the three heats was judged to be "normal" in the McQuaid-Ehn test. Heat 6347 had the most clearly defined normal structure and was classed "Type 1," while the other two

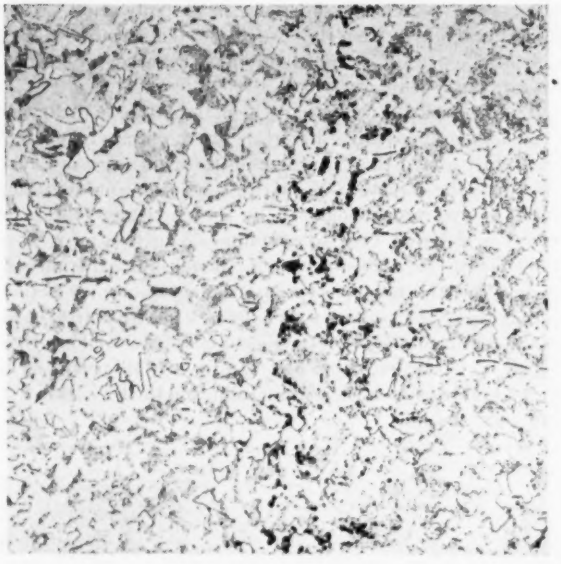


FIG. 11 GRAPHITIZATION AFTER 59,000 HR OF SERVICE FOLLOWED BY 6000 HR OF LABORATORY-TEST-HEATING: ×100

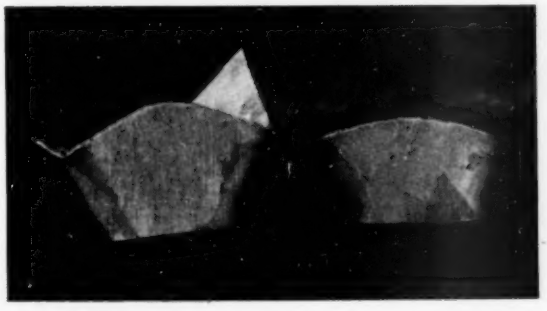


FIG. 12 BEND SPECIMENS OF WELDED SAMPLES THAT WERE LABORATORY-HEATED AFTER REMOVAL FROM SERVICE

TABLE 2 GRAPHITIZATION TEST OF LOW-ALUMINUM CARBON-MOLYBDENUM PIPE MATERIAL

(Test temperature varied between 950 and 1150 F)

	Hot-rolled and drawn			Normalized 1725 F		
	As welded	S-R 1200 F	S-R 1400 F	As welded	S-R 1200 F	S-R 1400 F
Heat 3099						
1500 hr...	None	None	Little	None	None	Little
2500 hr...	Little	Little	Increased	Little	Little	Increased
Heat 6347						
1500 hr...	None	None	None	None	None	None
2500 hr...	None	None	Trace	None	None	Trace
Heat 10,600						
1500 hr...	Little	Little	None	Little	None	None
2500 hr...	Increased	Increased	None	None	None	None

heats were classed as "Type 2." At the end of 2500 hr of test the least amount of graphite was found in the samples of the steel classed as having Type 1 normality.

With respect to the influence of strain in promoting graphitization, as given in the paper, the results obtained from an examination of stress-rupture samples may be of interest. Stress-rupture samples of low-carbon carbon-molybdenum, and chromium-molybdenum steel that had been tested at Purdue University in 1200 F steam, were examined for graphitization by the writer. These samples have been discussed in detail in a paper by J. T. Agnew, G. A. Hawkins, and H. L. Solberg.[9] The samples were obtained through the courtesy of Professor Solberg and were examined for the presence of possible graphitization and for determination of their response to the McQuaid-Ehn test.

Six specimens of each of the three types of steel were examined. Although each of the three steels was highly "abnormal," which indicated that graphitization might have been expected in the carbon and carbon-molybdenum samples, no clearly defined graphite was found in any of the samples. While this result is different from that reported in the paper by Dr. Hoyt, it should be remembered that the samples obtained from Professor Solberg, and here referred to, were tested at 1200 F instead of at 1025 F. The range of stresses under which the samples were tested as well as the hours of test are shown in Table 3 of this discussion. The absence of graphitization in the carbon and carbon-molybdenum samples, even though abnormal, may have been due to lowering of the Ac_1 temperature for the steels as a result of stress at the relatively high temperature of test. Because of its alloy content it is unlikely that graphitization would occur in the chromium-molybdenum samples.

In other work a probable indication of graphitization as influenced by stress was found in a failed low-carbon superheater tube. Creep failure had occurred as a longitudinal crack at the front of the tube due to overheating. It was interesting to note

[9] "Stress-Rupture Characteristics of Various Steels in Steam at 1200 F," by J. T. Agnew, G. A. Hawkins, and H. L. Solberg, Trans. A.S.M.E., vol. 68, 1946, pp. 309–315.

TABLE 3 STRESS-RUPTURE TEST IN 1200 F STEAM

	Type of steel	Stress during test, psi[a]	Duration of test, hr[a]	Result
1	Low carbon[b]	4740	4620	No graphite
2	Low carbon[b]	5770	3588	No graphite
3	Low carbon[b]	6800	857	No graphite
4	Low carbon[b]	7000	1261	No graphite
5	Low carbon[b]	12500	10	No graphite
6	Low carbon[b]	16000	27	No graphite
7	Carbon-0.50 Mo[b]	6900	7590	No graphite
8	Carbon-0.50 Mo[b]	7400	1300	No graphite
9	Carbon-0.50 Mo[b]	7800	3047	No graphite
10	Carbon-0.50 Mo[b]	9100	312	No graphite
11	Carbon-0.50 Mo[b]	10700	696	No graphite
12	Carbon-0.50 Mo[b]	16000	144	No graphite
13	2-1/4 Cr-1 Mo[b]	8400	1519	No graphite
14	2-1/4 Cr-1 Mo[b]	8400	1908	No graphite
15	2-1/4 Cr-1 Mo[b]	9200	2885	No graphite
16	2-1/4 Cr-1 Mo[b]	10400	1114	No graphite
17	2-1/4 Cr-1 Mo[b]	11300	226	No graphite
18	2-1/4 Cr-1 Mo[b]	14400	46	No graphite

[a] Purdue University data.
[b] "Abnormal" in the McQuaid-Ehn test.

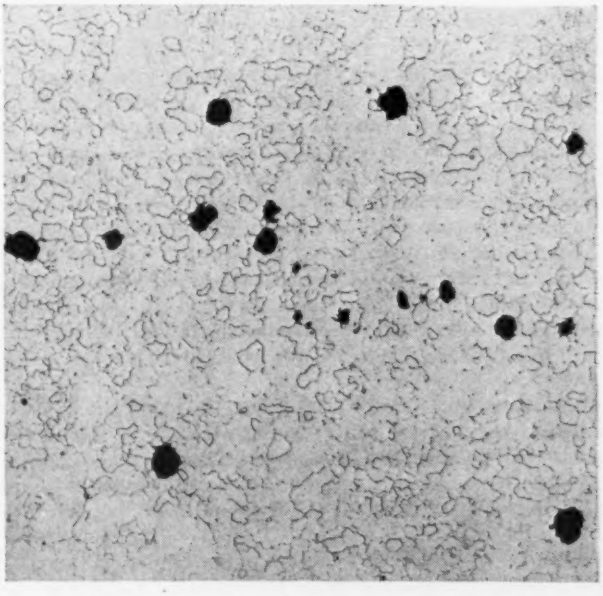


FIG. 13 GRAPHITE IN A LOW-CARBON STEEL, 1 3/4-IN-OD SUPERHEATER TUBE; ×100

that graphitization had occurred parallel to the failure and at a short distance at either side of the failure where it appeared to be localized as a result of probable critical stressing of the tube wall. Graphitization found in the tube is shown in Fig. 13 of this discussion. This is believed to be one of the few instances reported of the occurrence of graphitization in tubing smaller than 4 in. diam.

Authors' Closure

The authors appreciate Mr. McCutchan's thoughtful analysis of the present status of the graphitization situation. The determination of the creep strength of pipe steel in various structural conditions does not come within the scope of the investigation of graphitization, but they concur in Mr. McCutchan's comments. As for possible effects of hot-upsetting, we have examined many samples which compared structures produced by heating the steel to 1650 and 2200 F, respectively, and have observed no significant difference in graphitization. Therefore it seems unlikely that the structure from hot-upsetting is significant though, of course, there may be other effects of that operation which are.

The discussion of Mr. Rohrig is an important contribution and is greatly appreciated. Referring to the stress-relieving treatment just above the critical temperature, that was devised to eliminate the structure of the heat-affected zone and hence to remove what was thought to be the particular reason for the highly segregated type of graphite. The treatment at about 1400 F appears to be successful, though our experiments have shown that the random type of graphitization may actually be accelerated. Of course, it is only a corrective treatment and would not be needed with the right kind of steel. The other data which are contributed by Mr. Rohrig are all pertinent to the broad problem and are a welcome addition to the E.E.I.-A.E.I.C. program.



FIG. 1 4-KEEL TEST-BLOCK CASTING SHOWING GATE AND RISER

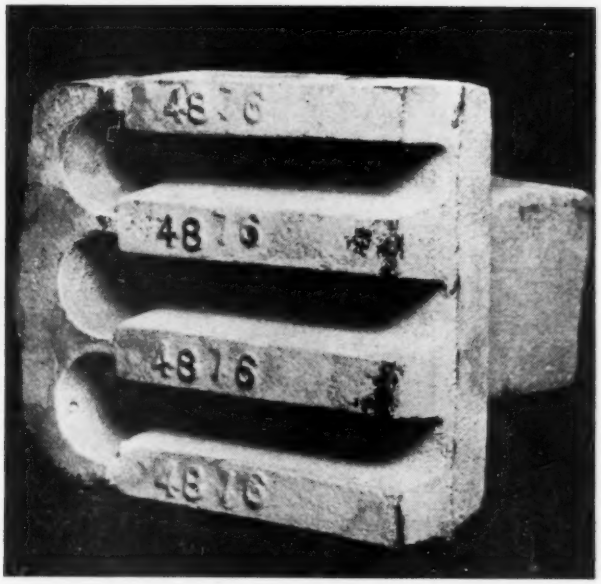


FIG. 2 4-KEEL TEST-BLOCK CASTING, DRAG SIDE, SHOWING COUPONS MEASURING APPROXIMATELY 1 × 1 × 6 IN.

Studies on Susceptibility of Casting Steels to Graphitization

BY J. J. KANTER,[1] CHICAGO, ILL.

This is a progress report for project No. 29 of the Joint A.S.T.M.-A.S.M.E. Committee on Effect of Temperature on the Properties of Metals. One of the activities undertaken by project No. 29 has been the study of certain aspects of the graphitization problem applying to the carbon-molybdenum casting steels used in welded piping structures. The steels so involved are of the types covered in A.S.T.M. Specifications A217 covering Pressure Alloy Castings Suitable for Fusion Welding such as valves, flanges, fittings, and other pressure-containing parts for high-temperature services. This investigation was undertaken in co-operation with the Manufacturers Standardization Society (M.S.S.) of the Valve and Fitting Industry, through a committee representing the constituent manufacturers engaged in the founding and manufacture of steel valves, flanges, and fittings.[2]

A program of tests was adopted by a group of manufacturers[2] from the valve and fitting industry for comparing the graphitization susceptibilities and general high-temperature stability of weldable grades of alloy cast steel using test castings in the form of a 4-keel block. This block, used by all of the investigators, is cast in green sand with the keels in the drag position, each fed from an end and through a risered mass above the keels as illustrated in Figs. 1 and 2. Fig. 1 shows the orientation of the casting as it is made, while Fig. 2 is a view of the four keels and the manner in which they are fed is more apparent.

The keels were removed from the blocks by sawing after heat-treatment, consisting of normalizing and drawing. The sawed surfaces of these keels were then machined flat. Upon the machined surface was deposited a single bead weld as illustrated in Fig. 3. The procedure in laying on the bead was essentially that established at Battelle Memorial Institute for the studies sponsored jointly by E.E.I.-A.E.I.C. The steel test coupon is placed in water at 60 to 65 F, at a level $^1/_4$-in. below the face machined for depositing, using end slugs for starting and finishing the bead. Using a $^5/_{32}$-in-diam type 7010 (C-Mo 0.50) electrode and a travel of approximately 6 ipm, the bead is deposited with direct-current negative polarity, at 25 to 30 volts and 125 to 135 amp.

After deposition of beads, the test specimens were given a stress-relieving heat-treatment at 1200 F. A cross section of a bead so deposited is illustrated in Fig. 4, showing the structure gradient between heat-affected zone and parent metal thus provided for study of susceptibility to segregated graphitization upon aging.

Drawing upon the experience at Battelle Memorial Institute in the E.E.I.-A.E.I.C. studies, aging treatments on the weld-bead cast-steel specimens have been made at 1025 F to attain an accelerated indication of graphitization susceptibility. Cur-

[1] Materials Research Engineer, Crane Company. Mem. A.S.M.E.

[2] The various manufacturers contributing steel test castings and investigational services include the following: Chapman Valve Manufacturing Company, Crane Company, Edward Valve and Manufacturing Company, Inc., Lunkenheimer Company, Powell Company, Reading-Pratt & Cady Division, Walworth Company.

Contributed by the A.S.T.M.-A.S.M.E. Research Committee on Effect of Temperature on the Properties of Metals and presented at the Annual Meeting, New York, N. Y., November 26–29, 1945, of THE AMERICAN SOCIETY OF MECHANICAL ENGINEERS.

NOTE: Statements and opinions advanced in papers are to be understood as individual expressions of their authors and not those of the Society.

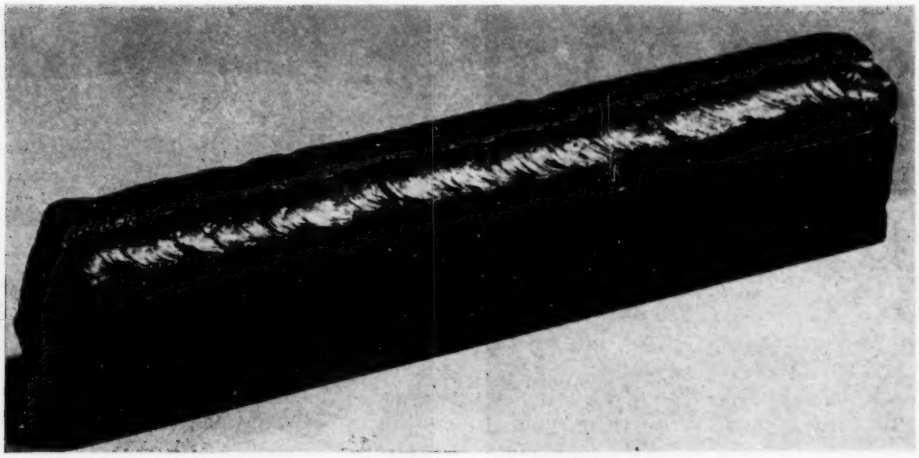


FIG. 3 WELD-BEAD SPECIMEN FOR GRAPHITIZATION TEST

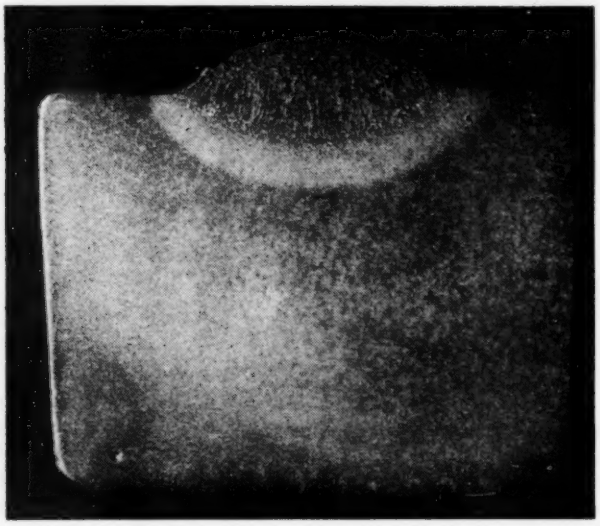


FIG. 4 ETCHED SECTION FROM SPECIMEN SHOWN IN FIG. 3 AT 3 DIAM

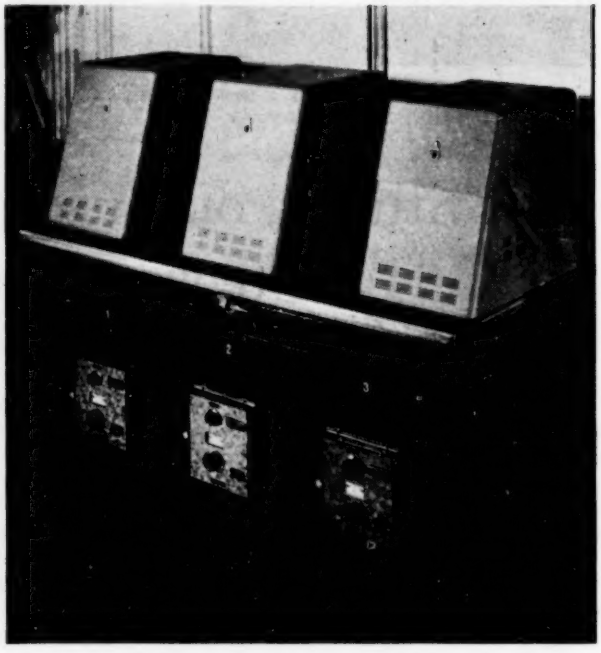


FIG. 5 ONE OF FOUR INSTALLATIONS OF FURNACES IN USE FOR AGING WELD-BEAD SPECIMENS SHOWN IN FIG. 3

rently, a number of studies in these series of tests are available for aging periods up to about 6000 hr and the specimens are continuing to age in furnaces at four of the co-operating laboratories. One of the furnace installations being so used exclusively for graphitization agings at 1025 F is shown in Fig. 5.

The original plan of the M.S.S. group was to survey the difference in graphitization susceptibility and stability of high-temperature properties in the carbon-molybdenum cast steels as made by various electric melting processes, namely, acid arc, basic arc, induction. Test heats by these processes were separately made using two types of deoxidation practice, including silicon addition, and silicon addition plus 2 lb aluminum per ton.

Almost unanimously, the co-operators reported difficulty and inability to obtain test-block castings free of "pinholes" using the straight silicon addition and it did not appear practicable from the standpoint of steel-pressure-vessel founding to consider such a practice. It was therefore decided to add another series of test materials using silicon addition plus $\frac{1}{2}$ lb aluminum per ton, which produced reasonably satisfactory test-block castings. Through this additional series of test castings it was expected that a variety of residual metallic aluminum contents would be obtained among the various heats, which would afford a basis for correlation with graphitization susceptibility.

Each co-operator furnished another set of test blocks by one or more of the electric melting processes containing 0.5 per cent of chromium in addition to the 0.5 per cent of molybdenum. These chromium-bearing castings were all made using the silicon plus 2 lb per ton aluminum-killing practice.

RESULTS OF STUDIES

The results of the studies from the cast-steel test bars upon observation after agings up to 6000 hr seem to bear out the already well-known contention that aluminum additions to carbon-molybdenum steels make for graphitization susceptibility as will be apparent from the comparison of photomicrographs, Fig. 6. A companion McQuaid-Ehn carburized structure is shown on this chart for each of the aged structures. It becomes further apparent that these tend to substantiate the Kerr-Eberle con-

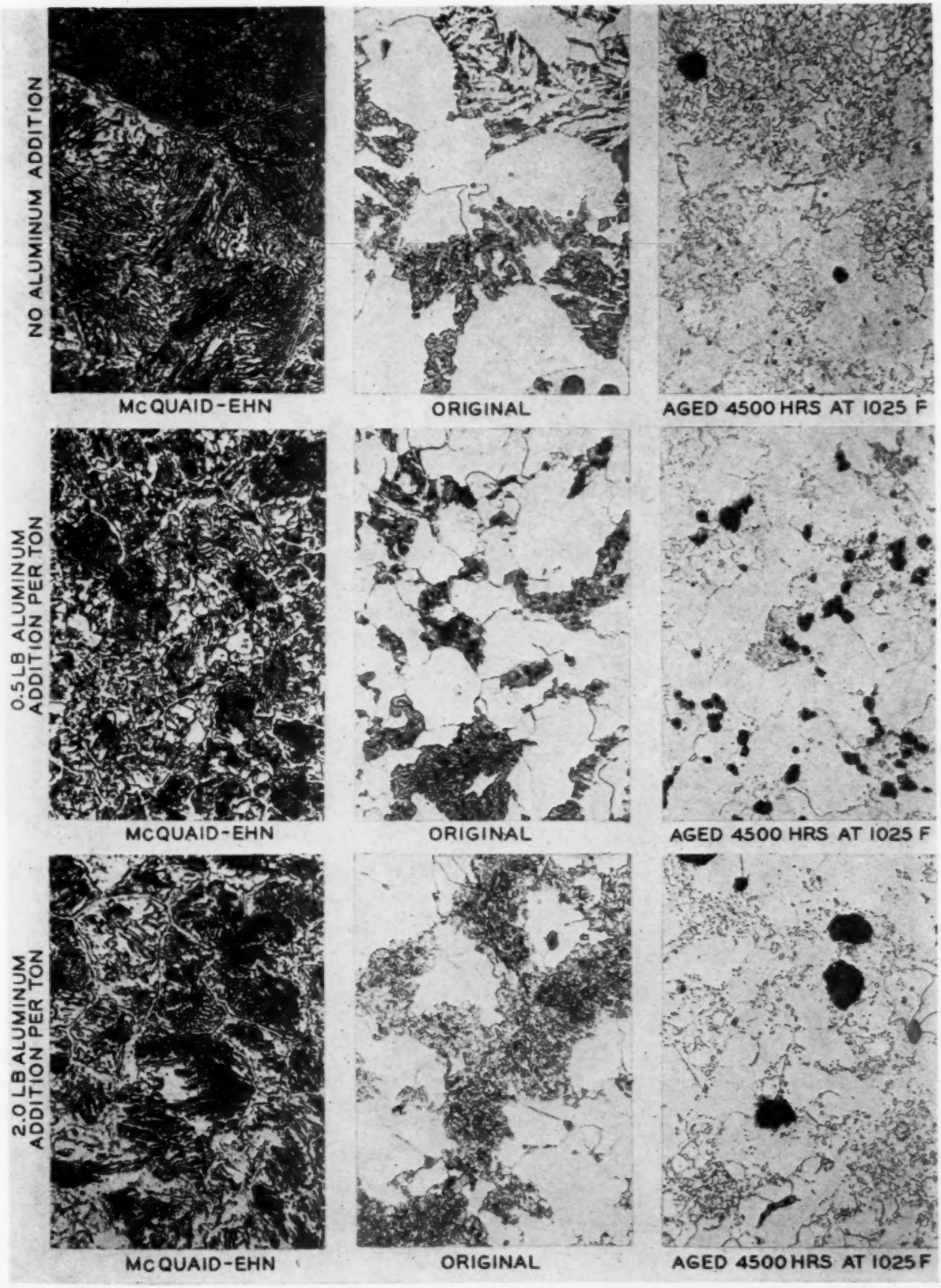


FIG. 6 COMPARISONS OF TYPICAL McQUAID-EHN CARBURIZED STRUCTURES FOR CARBON-MOLYBDENUM CAST STEELS WITH STRUCTURES AT HEAT-AFFECTED ZONE AT 500 DIAM

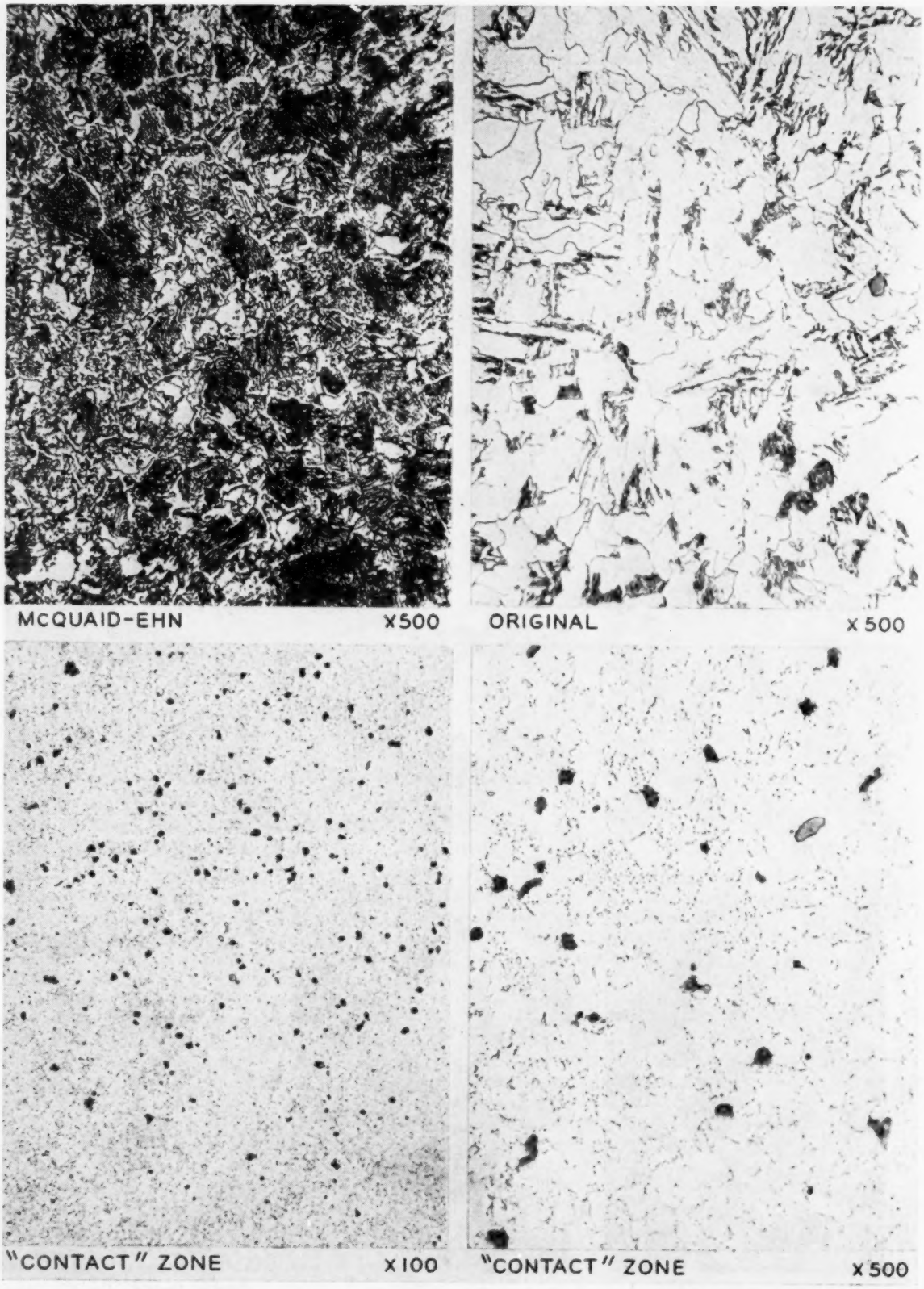


FIG. 7 GRAPHITE DEVELOPED AT HEAT-AFFECTED ZONE OF CARBON-MOLYBDENUM CAST STEEL WITH 2 LB OF ALUMINUM ADDITION PER TON, NORMALIZED AFTER WELDING, AGED 4500 HR AT 1025 F

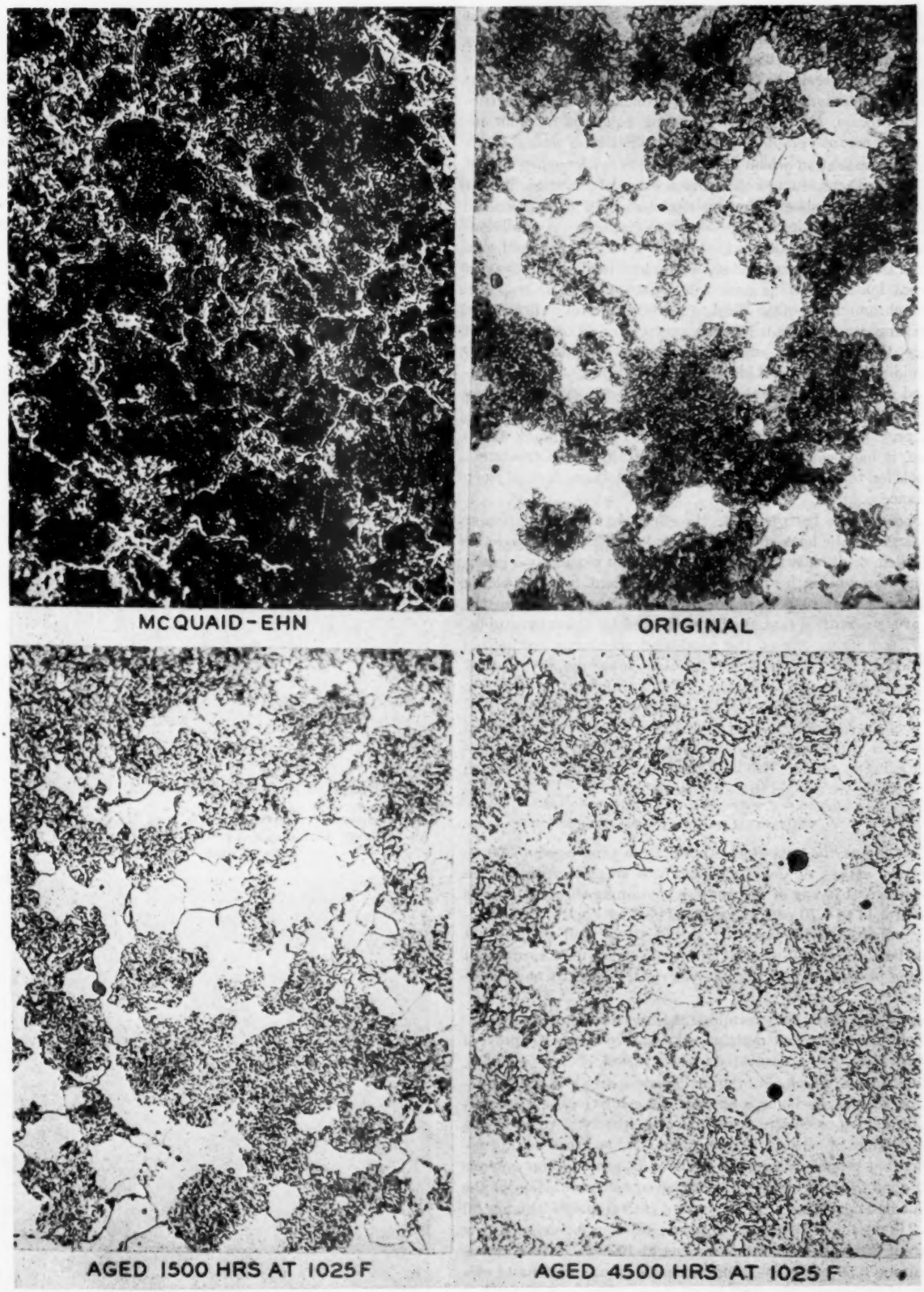


FIG. 8 TYPICAL STRUCTURES AT 500 DIAM OF CHROMIUM-BEARING CARBON-MOLYBDENUM CAST STEEL WITH 2 LB OF ALUMINUM ADDITION PER TON, AT HEAT-AFFECTED ZONE BEFORE AND AFTER AGING AT 1025 F

tention that "abnormal" structure by this criterion is an index of graphitization susceptibility in aluminum-treated carbon-molybdenum steels. This rule, however, does not necessarily apply to the steels having chromium additions. Study of microstructures indicates that the particular kind of electric-furnace process, all other factors being equal, is a minor influence as regards graphitization susceptibility.

One generalization which seems to apply with regard to the tests under discussion as well as much other observation, is that the inception of spheroidization agglomeration or coalescence of the carbide precedes its breakdown to graphite. A number of examples have been observed where in a single microfield, one spheroidized-carbide area will show graphite nodules, whereas an adjacent lamellar-carbide area will show no signs of graphite. Where chromium or other alloying ingredients prove effective in preventing graphitization under a certain condition of thermal history, the inhibition seems to be associated with resistance to spheroidization of the carbide. The susceptibility of aluminum-treated steel to graphitization seems to be associated with an accelerated tendency toward spheroidization.

In previous reports by the Joint A.S.T.M.-A.S.M.E. Committee, it has been apparent that strong aluminum treatment of steels led to easy spheroidization and consequent lack of creep resistance.

Proposals have been made to the effect that graphitization at the margin of the heat-affected zone or "contact zone" might be forestalled, or at least reduced to an impotent nature by a grain-refining normalizing heat-treatment subsequent to the welding operation. That such a treatment may not be effective in the case of a susceptible cast steel is evidenced by the micrographs, Fig. 7, comparing one of the weld-bead specimens normalized after deposition. It is seen that "contact zone" graphite has not been inhibited in this specimen. The transformation resulting from welding in the heat-affected zone seems to have some persistent effect, although it does appear that the zone of segregated graphite is somewhat broader, diffuses, and perhaps requires longer aging to detect. Studies upon more specimens normalized after welding are needed to clarify the effect.

Chromium in Cast Steels

In so far as the cast-steel studies have progressed (3000 to 5000 hr of aging), no definite evidence of graphitization has become apparent in any of the samples containing chromium in the range of 0.43 to 0.70 per cent as witnessed by Fig. 8, where relatively spheroidization-resistant carbides are well defined. It should be noted that the lowest chromium content is 0.43 and that the time periods involved are as yet relatively short and inconclusive.

It may eventually be determined that resistance to spheroidization is a necessary and perhaps sufficient condition to prevent graphitization over an expected service period.

Specimens of a number of the cast steels upon which the graphitization studies are being made are aging for the eventual purpose of making creep-strength studies on structures representing various stages of carbide deterioration. It has become quite apparent that graphitization has occurred in some of the coupons being aged for creep tests after advanced spheroidization of the carbide had developed. In the case of carbon-molybdenum steel with 2 lb per ton of aluminum addition, well-developed graphite is apparent after about 4000 hr of aging at 1025 F. The coupons containing 0.50 per cent chromium have shown no definite evidence of graphite after 5000 hr of aging. The committee has decided to continue the aging of all coupons for creep tests up to at least 10,000 hr before considering the starting of creep-rate determinations upon any of them.

Discussion

I. A. Rohrig.[3] This report shows that under suitable conditions graphitization may readily occur in cast as well as in wrought carbon-molybdenum steels. The observation of an apparent "persistent effect" resulting in segregated graphite in the heat-affected area of a weld even after normalizing is of particular significance because normalizing has appeared to be the most effective postwelding treatment for preventing segregated graphite. With respect to the normalizing of welds, the results of laboratory graphitization tests conducted on normalized welded samples by The Detroit Edison Company may be of interest.

A sample of high-aluminum carbon-molybdenum pipe mate-

[3] Research Department, The Detroit Edison Company, Detroit, Mich.

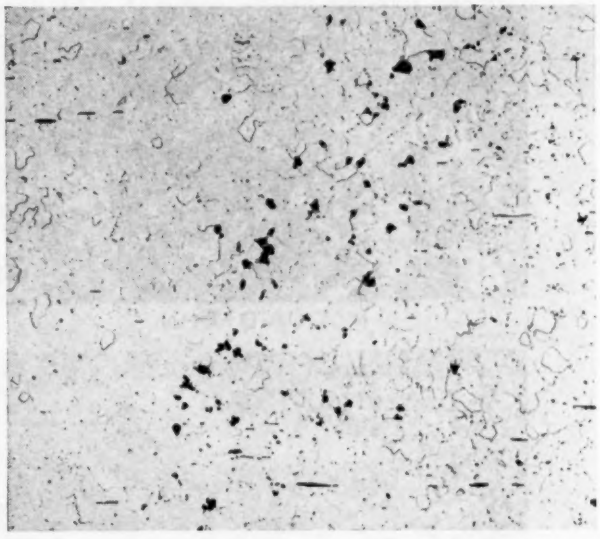


Fig. 9 Segregated Graphite in the Heat-Affected Area of "As-Welded" Carbon-Molybdenum Sample After 10,300 Hr of Laboratory Test Heating

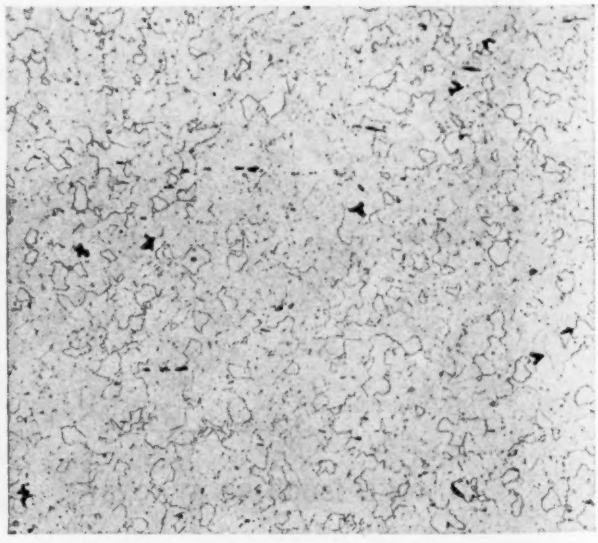


Fig. 10 Random Graphite in Former Heat-Affected Area of a Normalized Weld in Carbon-Molybdenum Sample That Was Laboratory-Heated for 10,300 Hr After Normalizing

rial was welded to low-aluminum material and then normalized by heating for 1 hr at 1725 F, followed by air-cooling. To promote graphitization, "as-welded" as well as "normalized" samples were heated at temperatures varied between 1000 and 1060 F for 3300 hr, and then at temperatures varied between 900 and 1150 F for an additional 7000 hr. After a total time of 10,300 hr of test heating, the as-welded samples showed a distinct segregation of nodular graphite in the heat-affected area whereas the normalized samples showed only random graphitization. Segregated graphite in the heat-affected area of as-welded high-aluminum material is shown in Fig. 9 of this discussion. Random graphitization at the former heat-affected area of the sample that was normalized after welding is shown in Fig. 10. Similar results were found in the low-aluminum material with the exception that considerably less graphite was present.

These results indicated that the normalizing treatment of 1 hr at 1725 F had been fully effective in removing the nucleation effect resulting from the heat of welding. Kerr and Eberle[4] have also reported on the apparent beneficial effect of normalizing after welding as a means of preventing the formation of segregated graphite. The results obtained from test prompt the suggestion therefore that the normalizing treatment used by the author, and which is not stated in the paper, may not have been fully effective in reconstituting and homogenizing the structure of the heat-affected area in his sample.

The author's suggestion that resistance to spheroidization may be a necessary and perhaps sufficient condition to prevent graphitization is probably based upon the hypothesis that spheroidization is the first stage of graphitization. Referring again to the work of Kerr and Eberle,[4] it is noted that they have reported on a number of cases in which steels that had spheroidized were found to be resistant to graphitization. Although spheroidization and graphitization may be parallel phenomena in steel at high temperature, it does not necessarily follow that spheroidization is the first stage of graphitization. In this association it might be pointed out that although the photomicrographs presented in Fig. 6 of the paper, are for the apparent purpose of showing the graphitization susceptibility of the aluminum-treated sample in contrast with the graphitization resistance of the sample having no aluminum addition, the two samples appear to be about equally spheroidized.

[4] Graphitization of Low-Carbon and Low Carbon-Molybdenum Steels" by H. J. Kerr and F. Eberle, A.S.M.E. pamphlet "Graphitization of Steel Piping," included in Trans. A.S.M.E., vol. 67, 1945.

Author's Closure

Mr. Rohrig's evidence that a sample of high-aluminum carbon-molybdenum pipe material, welded and normalized at 1725 F showed only random graphitization, is in interesting contrast to that on the carbon-molybdenum cast steels studied in the Project No. 29 investigation. Of seven different heats of carbon-molybdenum steel with 2 lb of aluminum addition per ton and normalized at 1650 F for one hour after welding by the various contributors of the specimens, all specimens showed a development of graphite after 5,000 hours of aging at 1025 F, of which the "contact" zone photomicrographs of Fig. 7 are typical. Since the presentation of the report in question, these aging tests have progressed far enough to show that upon 10,000 hours, the average degree of contact zone graphitization for the seven heats of steel normalized after welding is about the average degree which was obtained for a group of six similar heats of steel stress-relieved only after welding upon 4000 hours of aging. This degree of deterioration represents about one third of the carbon transformed to graphite. While normalizing has served to retard the development of graphite at the contact zone, it by no means promises to be a satisfactory measure of control for the carbon-molybdenum cast steels.

Mr. Rohrig questions the observation that spheroidization of carbide is a prelude to graphitization and supports his objection by pointing out that certain samples reported upon showed spheroidization but no graphitization. However, since the report was presented, examinations after 10,000 hours of aging at 1025 F have revealed further spheroidization and graphitization in a number of samples where it had not been found after 5000 hours, including those containing one half of one per cent of chromium, thus indicating that the development of graphite in sequence to spheroidization may be an eventual effect to be always considered relative to aging time, temperature stress, and the composition of the steel.

Comparative Graphitization of Some Low-Carbon Steels With and Without Molybdenum and Chromium

By G. V. SMITH,[1] S. H. BRAMBIR,[1] AND W. G. BENZ[1]

Study of several experimental heats of steel containing 0.5 per cent molybdenum and up to 1.20 per cent chromium showed that in steels containing 0.5 per cent or more of chromium, no graphitization occurred in 3000 hr at 1025 F; but this finding requires confirmation by study of additional heats, particularly of commercial manufacture. Additional studies relating to the effect of deoxidation practice, particularly in plain carbon steels, and of the effect of posttreatment of welds on graphitization are described.

Introduction and Summary

IN continuation of investigations (1, 2, 3)[2] begun shortly after the now well-publicized pipe failure at the Springdale Generating Station of the West Penn Power Company (4), we have studied the occurrence of graphitization in the following samples:

1 Unwelded samples of 10 heats of 0.1–0.2 per cent carbon steel made and deoxidized differently.

2 A series of experimental heats of chromium-molybdenum steels to ascertain the effectiveness of chromium in preventing graphitization.

3 Molybdenum steel treated to simulate the structures occurring in the heat-affected region of a weld.

4 Molybdenum steel (0.5 per cent), which had been heated at 1300 F after welding, as a means of preventing localized graphitization in the heat-affected region.

The results are as follows:

1 In normalized samples from ten heats of 0.1–0.2 per cent carbon steel of different manufacturing and deoxidation practice exposed for 2000–3000 hr at 1025 F, graphite formed in only four steels. These four had been deoxidized with 2 lb or more of aluminum per ton of steel and were fine-grained and moderately abnormal in the carburizing test. Steels with 1 lb or less of aluminum per ton did not graphitize, even though in some cases slightly or moderately abnormal.

2 The results indicate that in a 0.5 per cent molybdenum steel at least 0.5 per cent chromium is necessary to prevent graphitization, but do not prove that this would always suffice. Experimental heats containing 0.5 per cent or more of chromium did not graphitize under the conditions of our experiments, no matter how they were deoxidized or treated before or after welding. This inference should be checked by additional tests on commercial heats, however, since, although a 0.25 per cent chromium—0.5 per cent molybdenum steel, deoxidized with more than 1 lb of aluminum, graphitized locally under certain conditions, a similar steel without chromium did not. Graphite did not form in the 0.25 per cent chromium—0.5 per cent molybdenum steel when the welded sample had been heated to 1300 F for 4 hr prior to exposure at 1025 F.

3 Simulation of the temperature-time cycles which occur during welding indicated that the maximum amount of graphite appears in that zone of the weld-heat-affected region which reached a temperature in the vicinity of 1400 F. This temperature is only an approximation and is interrelated with the time at temperature and cooling rate. Further confirmation was obtained of the efficacy of a 1300 F treatment, prior to simulated service, in preventing graphitization.

4 In a sample of pipe from the Schuylkill Generating Station normalized from 1650 F, graphitization was entirely suppressed by a treatment of 4 hr at 1300 F after welding and prior to simulated service. On the other hand, similar tests on samples which had not been normalized showed some graphite; exposure for 8 and 12 hr, instead of 4, at 1300 F still further reduced the amount of graphite to the point where it could hardly warrant concern.

I Graphitization of Ten Carbon Steels (0.1–0.2 Per Cent Carbon), Made and Deoxidized Differently, at 1025 F

Because of indications that manufacturing and deoxidation practices affect the tendency to formation of graphite in steels, we exposed samples of ten commercial carbon steels which happened to be available, in a furnace at 1025 F for a period of (*a*) 1000 hr, (*b*) 2000 hr, and (*c*) in the case of Nos. 1, 2, and 3, 3000 hr. The samples were examined metallographically for the presence of graphite, with results given in Table 1, along with the composition and mode of deoxidation of each steel. Each steel had initially been normalized from 1650 F; the samples were 3 in. long and $^3/_4$ to 1 in. thick. We also carburized[3] a sample of each steel and determined the resulting grain size and structure "normality" because of the recent claim that degree of "abnormality" is an indicator of tendency to graphitize.

Graphite was detected in only four of these ten steels, namely, in Nos. 7, 8, 9, and 10, as illustrated in Fig. 1. These four comprise all which had been deoxidized with 2 lb or more of aluminum, had residual aluminum in excess of 0.025 per cent, and were fine-grained; on the other hand, the six which did not graphitize had been deoxidized with not more than 1 lb of aluminum, had less than 0.007 per cent residual aluminum, and were coarse-grained. The four which graphitized were moderately abnormal, but so were some of those (Nos. 4 and 5) which did not; thus these limited data indicate that although carbon steels which graphitize are abnormal, the converse is not necessarily true. Consequently, the normality cannot be regarded as a reliable indicator of tendency to graphitize. More-

[1] Research Laboratory, United States Steel Corporation, Kearny, N. J.

[2] Numbers in parentheses refer to the Bibliography at the end of the paper.

Contributed by the Joint A.S.T.M.-A.S.M.E. Research Committee on Effect of Temperatures on the Properties of Metals and presented at the Annual Meeting, New York, N. Y., Nov. 26–29, 1945, of The American Society of Mechanical Engineers.

Note: Statements and opinions advanced in papers are to be understood as individual expressions of their authors and not those of the Society.

[3] By holding 8 hr at 1700 F in a commercial carburizing compound (Houghton's Pearlite No. 50) and furnace-cooling at a rate which averaged 4 deg F per minute in the range 1700 to 1000 F.

TABLE 1 CHEMICAL ANALYSIS, DEOXIDATION PRACTICE, CARBURIZED GRAIN SIZE AND STRUCTURE NORMALITY, AND GRAPHITIZATION SUSCEPTIBILITY OF TEN HEATS OF CARBON STEEL

Grade	No.	Main deoxidizers added,[a] in lb per ton		Chemical analysis[b] C	Mn	P	Si	Al	After carburizing test A.S.T.M. grain size	Structure normality	Graphitization at 1025 F[c] 1000 hr	2000 hr	3000 hr
Open-hearth, 0.15 carbon	1	FeSi	1Al	0.13	0.45	0.011	0.19	0.007	2–4	Slightly abnormal	No	No	No
Open-hearth, 0.15 carbon	2	FeSi	1/2Al 4FeCTi	0.14	0.47	0.008	0.21	0.004	1–4	Slightly abnormal	No	No	No
Open-hearth, 0.15 carbon	3	FeSi	6FeCTi	0.14	0.46	0.009	0.19	0.005	3–4	Slightly abnormal	No	No	No
Capped open-hearth	4		1/4Al	0.07	0.45	0.006	0.01	...	1–4	Moderately abnormal	No	No	..
Capped bessemer	5			0.08	0.38	0.079	0.01	...	2–3	Moderately abnormal	No	No	..
Grade B, Si-killed	6	FeSi		0.27	0.52	0.016	0.22	0.006	2–4	Normal	No	No	..
Grade B, Si-Al-killed	7	FeSi	2Al	0.24	0.86	0.013	0.23	0.033	7–8	Moderately abnormal	Slight amount	Slight amount	..
Grade XB, bessemer	8	FeSi	4Al	0.14	0.54	0.074	0.19	0.025	7–8	Moderately abnormal	Yes	Yes	..
Grade XB, bessemer	9	FeSi	3Al	0.13	0.48	0.087	0.21	0.047	7–8	Moderately abnormal	Yes	Yes	..
Grade XB, bessemer, Al-killed	10		4Al	0.18	0.51	0.077	0.03	0.066	8	Moderately abnormal	Yes	Yes	..

[a] Other than FeMn which was added in all steels.
[b] Sulphur was less than 0.04 in all steels.
[c] No—none detected.

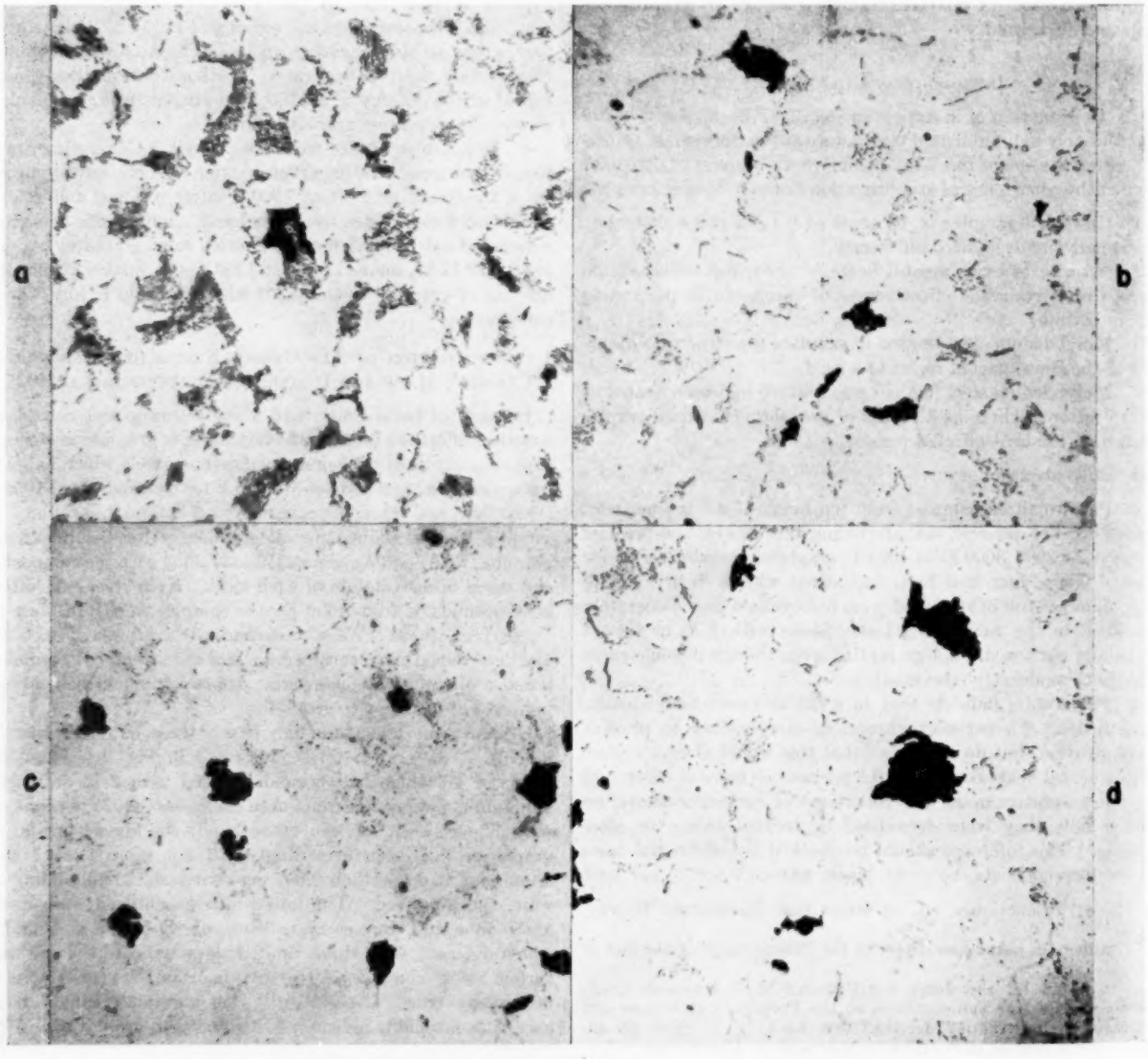


FIG. 1 TYPE AND AMOUNT OF GRAPHITE IN NORMALIZED CARBON STEELS
(*a*, No. 7; *b*, No. 8; *c*, No. 9; *d*, No. 10 of Table 1, after 1000 hr at 1025 F. Picral etch; ×500.)

over, according to these observations, the amount of residual aluminum, even though the accuracy of the analytical procedure is uncertain, appears to be a better indicator of tendency to graphitize than is the abnormality of the carburizing test.

The amount of graphite was greatest in steel 9, and progressively less in Nos. 8, 10, and 7, as determined by counting the number of nodules in the following manner: In an area at the center of the $^3/_4$-in. × 1-in. polished but unetched surface, the number of nodules in 50 fields 1 mm apart was determined after both 1000 and 2000 hr at 1025 F. To test whether a sufficient number of observations had been made to obtain a true picture, a second set of 50 observations was made, midway between the original ones. The results are given in Table 2.

TABLE 2 NUMBER OF GRAPHITE NODULES IN STEEL SAMPLES

Steel no.	Hours at 1025 F	Number of nodules in First 50 fields	Second 50 fields	Total 100 fields
7	1000	2	2	4
	2000	4	9	13
8	1000	77	88	165
	2000	123	114	237
	1000	191	202	393
	2000	272	257	529
10	1000	16	22	38
	2000	31	28	59

Taking into account both this number and the size of the nodules in Fig. 1, it is evident that the amount of graphite is greatest in steel 9 and progressively less in steels 8, 10, and 7. It was hoped that the counts would also provide an indication of whether the number of graphite nuclei is limited or increases with time. The data appear, on first thought, to show an increase; but when it is considered that nodules already present continue to grow, and that the chance of intersecting a nodule (by the plane of polish) increases with its size, it is realized that the evidence is insufficient to permit any decision on the matter.[4] It can be said, however, that if new nodules form, their rate of appearance between 1000 and 2000 hr at 1025 F is not great.

[4] If the nodules were uniform in size (which they probably are not), the number counted should increase in proportion to the increase in radius, and since this number did not even double (except for steel 7), it would be necessary to make precise measurements of nodule size and size distribution.



FIG. 2 LONGITUDINAL CROSS SECTION OF WELD SAMPLE EMPLOYED IN SECOND SECTION OF PAPER
(Weld deposited for $^1/_2$, 1, 2, 4, or 8 sec. Nital-picral etch; ×1.)

The amount of graphite in the several steels could not be correlated with chemical composition nor with initial microstructure.

II EFFECTIVENESS OF CHROMIUM IN PREVENTING GRAPHITIZATION OF 0.5 PER CENT MOLYBDENUM STEEL

Among the suggestions for preventing graphitization in 0.5 per cent molybdenum steel is that of adding chromium, which is one of a group of elements that, when present in sufficient proportion, combine with carbon in steel to form so-called alloy carbides. Molybdenum, also one of this group, is reputed (5) to possess stronger affinity for carbon and presumably forms a more stable carbide than does chromium; consequently, if carbide stability is a factor, there is no a priori reason for thinking that chromium addition will be more effective than equivalent increase in molybdenum.

Materials and Procedure. In an effort to ascertain whether chromium is effective in preventing graphitization and, if so, the minimum amount necessary, we investigated a number of heats with 0.5 per cent molybdenum and up to 1.20 per cent chromium, deoxidized with $^1/_4$ or $1^1/_4$ lb of aluminum per ton or with ferrosilicon-zirconium, as listed in Table 3. These were 20-lb induction-furnace heats, forged to $^1/_2$-in. × 1-in. bars, which were cut into 3-in. lengths. Two specimens of each were heated at 1450, 1650, or 2200 F for $^1/_2$ hr and air-cooled. After rough-grinding to remove scale, five weld deposits were made on each sample, as illustrated in Fig. 2, using molybdenum-steel weld rod ($^3/_{16}$-in. Murex C-Mo 50); the rod was held for $^1/_2$, 1, 2, 4, or 8 sec at different locations, the sample being cooled to room temperature before each deposit. In this manner, it was hoped that the effect of steepness of the temperature gradient through the heat-affected region during welding could be determined, since an earlier study (3) showed susceptibility to graphitization to be greater the steeper this gradient. One of each pair of specimens was then heated 4 hr at 1300 F to determine the effectiveness of this posttreatment in preventing localized graphitization (1, 3). All samples were then heated for 3000 hr at 1025 F in a muffle furnace, after which they were sectioned longitudinally through the weld deposits, and examined microscopically for graphite.

We also carburized a sample of each steel

TABLE 3 CHEMICAL ANALYSIS, DEOXIDATION PRACTICE, AND CARBURIZED GRAIN SIZE AND STRUCTURE NORMALITY OF CHROMIUM-MOLYBDENUM SERIES OF STEELS

Ident.	C	Mn	Si	Cr	Mo	Zr	Al	Al_2O_3	Deoxidation, lb Al per ton	After carburizing—test at 1700 F: A.S.T.M. grain size	Structure normality
A	0.14	0.45	0.17	..	0.52	..	0.007	0.008	$^1/_4$	4–6	Moderately abnormal
B	0.15	0.46	0.16	..	0.52	..	0.032	0.019	$1^1/_4$	8–9	Quite abnormal
C	0.16	0.52	0.18	0.27	0.54	..	0.010	0.015	$^1/_4$	2	Slightly abnormal
D	0.15	0.54	0.24	0.27	0.53	..	0.055	0.025	$1^1/_4$	8	Moderately abnormal
E	0.14	0.61	0.25	0.60	0.54	..	0.012	0.022	$^1/_4$	7–8	Slightly abnormal
F	0.13	0.61	0.23	0.60	0.53	..	0.073	0.030	$1^1/_4$	7–8	Slightly abnormal
G	0.14	0.58	0.22	1.17	0.52	..	0.013	0.014	$^1/_4$	7–8	Slightly abnormal
H	0.14	0.57	0.23	1.17	0.54	..	0.031	0.018	$1^1/_4$	7–8	Slightly abnormal
I	0.15	0.66	0.26	0.03	0.48	0.05	..	..	Fe-Si-Zr	6–7	Normal
J	0.16	0.55	0.20	0.12	0.54	0.05	..	..	Fe-Si-Zr	5–6	Slightly abnormal
K	0.17	0.57	0.21	0.58	0.54	0.04	..	..	Fe-Si-Zr	6–7	Slightly abnormal
L	0.15	0.41	0.16	1.19	0.53	0.03	..	..	Fe-Si-Zr	4–6	Slightly abnormal

NOTE: Sulphur and phosphorus were less than 0.035 or 0.01 per cent, respectively, in steels I, J, K, and L and were not determined in the remainder.

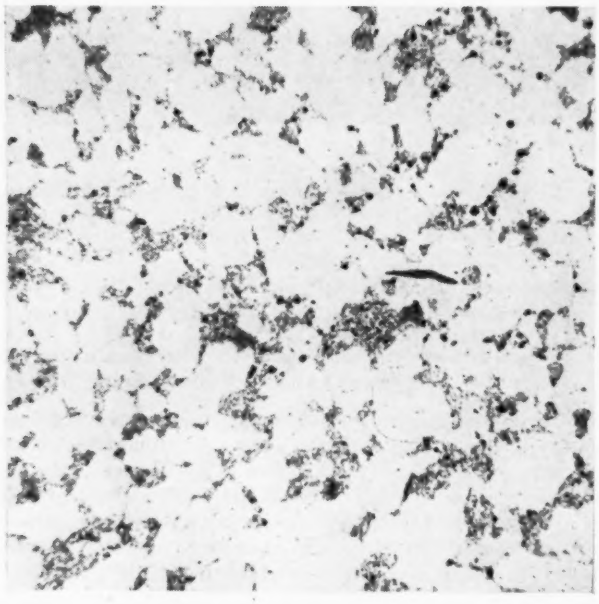


FIG. 3 GRAPHITE IN HEAT-AFFECTED ZONE OF WELD IN STEEL D, 1/2 MO-1/4 CR, AFTER 3000 HR AT 1025 F
(Picral etch: ×500.)

and determined the resulting grain size and normality, with results given in Table 3.

Results and Discussion. Only two samples definitely graphitized; these were both of steel D, 0.25 per cent chromium–0.5 molybdenum, deoxidized with 1 1/4 lb of aluminum per ton. In the samples of this steel normalized from 1450 or from 1650 F before welding, graphite formed in the heat-affected region of all welds, the amount being not appreciably different among the welds, contrary to our earlier finding (3). The graphite nodules were quite small, Fig. 3, and only a very few were found in unaffected base metal. No graphite was observed in the companion samples heated 4 hr at 1300 F after welding and prior to exposure at 1025 F, in further confirmation of the efficacy of this proposed preventive treatment (1, 3), nor was any found in samples previously normalized from 2200 F, confirming a tendency, reported earlier (3), toward increased resistance to graphitization of structures resulting from normalizing at high temperature.

None of the others showed any graphite in any condition of prior or posttreatment, with the possible exception of B, normalized at 1650 F before welding and not heated at 1300 F after welding. In this there were several widely scattered nodules which appeared to be graphite, but because they were so small and so few, we cannot be certain. That this steel did not graphitize more extensively, in one or more original conditions, was unexpected, since it was thought that the molybdenum steel would be more prone than the chromium-molybdenum to form graphite.

This possible inconsistency in behavior emphasizes again the danger of basing claims on observations on a small number of heats; the results do indicate, however, that more than 0.25 per cent chromium must be present in order to inhibit localized graphitization.

All these steels were to some extent "abnormal" in the carburizing test except I, the plain 0.5 per cent molybdenum steel deoxidized with ferro-silicon-zirconium. Because of lack of graphitized steels in this series it is not possible to correlate "abnormality" with tendency to graphitization. However, the normality ratings are of some interest in themselves, showing, for example, that it is difficult to produce a strictly normal steel; that 0.5 per cent molybdenum steel is "normal" when deoxidized with ferro-silicon-zirconium confirms an earlier finding (7).

III SIMULATION OF STRUCTURES OF HEAT-AFFECTED REGION WHICH GRAPHITIZE

It has been shown that the zone of localized graphitization in welded molybdenum steels is that which during welding reached a temperature slightly above the lower critical, A_1 (1340 F). To learn more about this phenomenon, samples of a molybdenum steel, susceptible to graphitization, were heated for short times in the range 1350–1450 F, and gradiently cooled, thin samples being used to insure rapid temperature change.

From a sample of Springdale Station[5] pipe, air-cooled as a 3/4-in. section after 1/2 hr at 1650 F, a number of samples approximately 1/16 × 1/4 × 1 in. were prepared. Using a coke-covered, deoxidized lead bath held at constant temperature within the range 1350–1450 F, and tongs heated to the bath temperature, one end of a sample was grasped in the tongs, and the whole immersed in the lead bath for 1/2 min; its free end was then immersed to a depth of 1/4 in., in water at room temperature and held until reasonably cool. A duplicate set of samples was treated at each of the temperatures 1350, 1375, 1400, 1425, and 1450 F. Each set was then sealed, in vacuo, in a silica bomb to prevent subsequent oxidation and decarburization, and one of these was heated at 1300 F for 4 1/2 hr; both were held for 1000 hr at 1025 F, and each sample was then examined metallographically upon a longitudinal section for graphite.

The samples were held for only 1/2 min in the lead bath, because we thought this might simulate welding conditions. In such a short time at only slightly above the lower critical temperature, there is time for only partial transformation of ferrite and carbide to austenite, and the small regions, necessarily rich in carbon, of this latter constituent presumably set the stage for localized graphitization (1). The specimens were gradiently quenched to provide a progression of cooling velocities, one of which should correspond to the fairly fast rate of the heat-affected region of a weld.

After 1000 hr at 1025 F, graphite was observed in each of the five samples which had not received the 1300 F treatment, but not in any of the companion five which had been so treated. The photomicrographs in Fig. 4, taken approximately 1/4 in. from the quenched end, show a comparison of the five samples. The 1300 F sample showed no graphite in the quenched zone, Fig. 4(*a*), but there were a few small nodules in the tong-held end. At 1375 F there was some graphite near the quenched end, Fig. 4(*b*), but practically none in the opposite end. The quenched zone of the 1400 F specimen, Fig. 4(*c*), showed the maximum amount of any sample, and the tong-held end showed an intermediate amount. At 1425 F the amount in the quenched zone had decreased sharply, Fig. 4(*d*), and there was an appreciable amount in the tong-held end. At 1450 F there were very few nodules at either end, Fig. 4(*e*).

Thus these experiments indicate that graphite forms most readily in that portion of the heat-affected region which, during welding, was at a temperature in the neighborhood of 1400 F. This is only an approximation since our holding time of 1/2 min may not exactly simulate welding conditions; the temperature in any event is not critical. The experiments also indicate that cooling rate is significant. That no graphite occurred in any sample postheated at 1300 F provides further confirmation (3) of the utility of this treatment.[6]

IV POSTTREATMENT AT 1300 F AS A PREVENTIVE OF LOCALIZED GRAPHITIZATION

Sometime ago we suggested (1) that localized graphitization

[5] Of West Penn Power Company, where the problem first arose (4).
[6] See also the second and fourth sections of this paper.

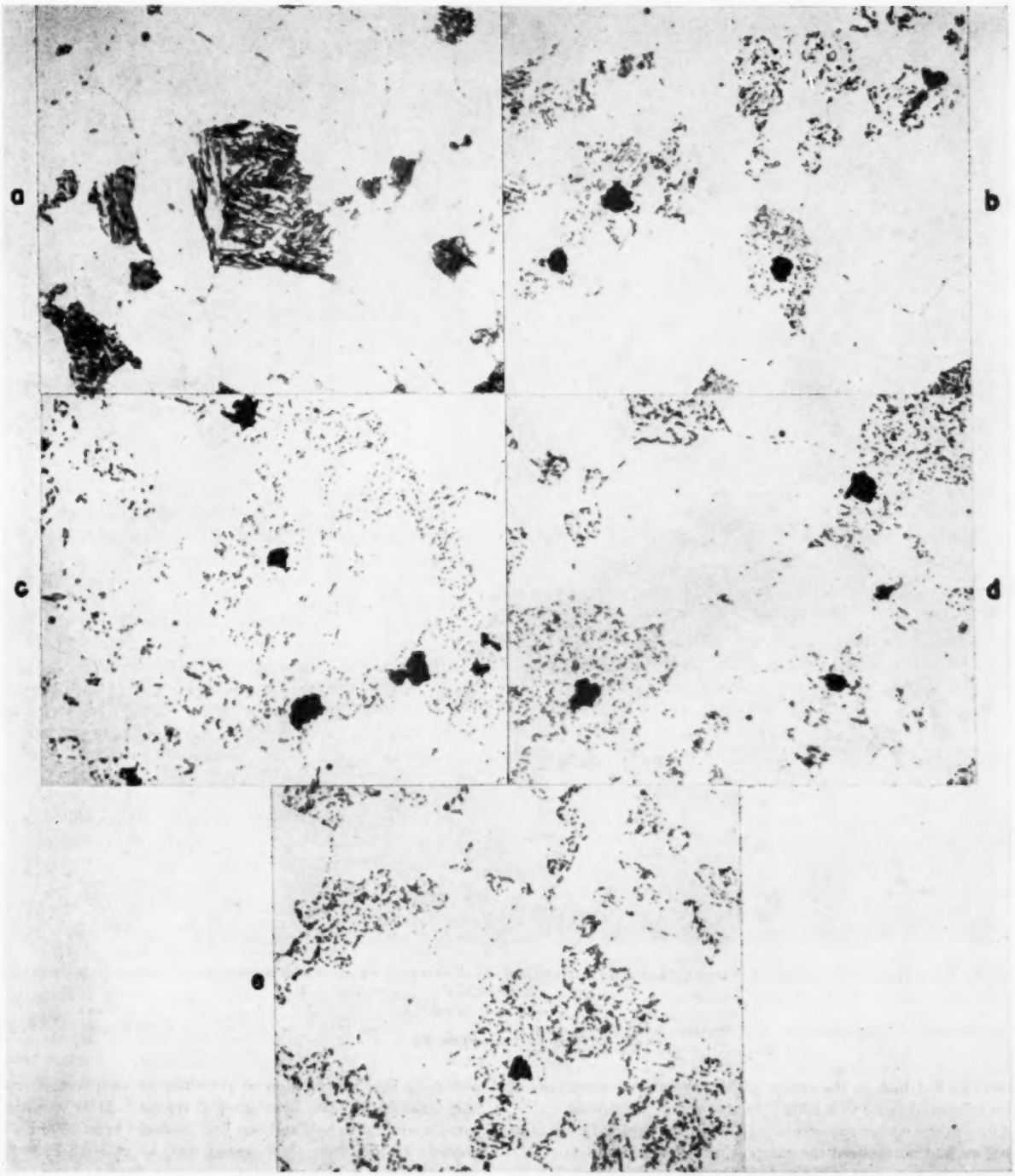


FIG. 4 REPRESENTATIVE REGION NEAR QUENCHED END OF THIN SAMPLES OF 1/2 PER CENT MOLYBDENUM STEEL
(Heated to *a*, 1350 F; *b*, 1375 F; *c*, 1400 F; *d*, 1425 F; and *e*, 1450 F, for 1/2 min and gradiently quenched, then heated at 1025 F for 1000 hr. Picral etch; ×1000.)

might be avoided by heating to 1300 F after welding and prior to service, and recently obtained experimental corroboration (3) of the efficacy of this treatment on samples of Springdale Station pipe.[8]

Shortly after our results were published, H. Weisberg of Public Service Electric and Gas Company, reported privately that he had been unable to prevent graphite formation by using this suggested treatment although its amount had been reduced; he then kindly supplied us with a sample of his steel, which was used in the following experiments.

The samples were reported to be from a 0.5 per cent molybdenum-steel pipe manufactured by National Tube Company, Heat No. 6532, in 1937 to A.S.T.M. specification A158-36, Grade P-1, was deoxidized with 1.8 lb of aluminum per ton, and was furnished for the Philadelphia Electric Company's Schuylkill Station as annealed between 1350 and 1400 F. It had not been

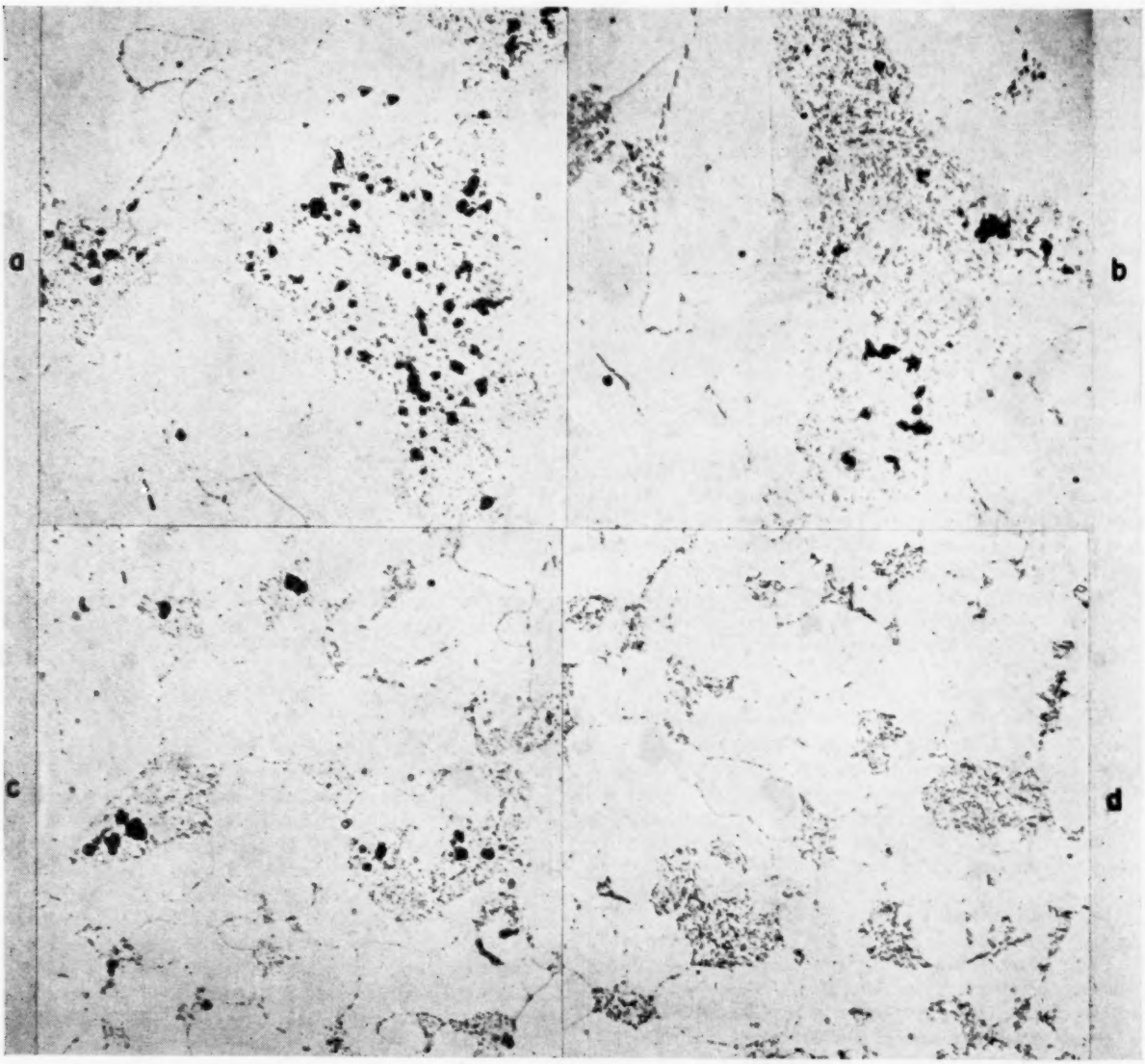


FIG. 5 GRAPHITIZATION IN HEAT-AFFECTED REGION OF 1/2 PER CENT MOLYBDENUM STEEL FROM SCHUYLKILL STATION PIPE AFTER 1000 HR AT 1025 F

(Picral etch: ×500.)

(*a*, As-received, not posttreated; *b*, as received, posttreated 4 hr at 1300 F; *c*, normalized 1650 F, not posttreated; *d*, normalized 1650 F, posttreated 4 hr at 1300 F.)

in service but had, in the course of Mr. Weisberg's experiments, been subjected twice to a 1200 F "stress-relief" treatment.

Since in our earlier experiments (3) with the Springdale Station pipe, we had normalized the samples prior to test, and since Mr. Weisberg had conducted his tests in the as-received condition, we decided to test in both conditions. Accordingly, two specimens approximately $1 \times 2^1/_4 \times 3^3/_8$ in. were prepared, one as received, the other normalized 1/2 hr at 1650 F. Upon each of these a "narrow" and a "wide" weld bead, illustrated in Fig. 6, were laid down according to the following conditions:

Preheat	None	
Electrode	Murex C-Mo 50	
Weld type	Bead weld deposited in flat position	
	Narrow	Wide
Current, amp	200	285
Arc voltage, volts	28	30
Speed, ipm	9	3
Heat input, Btu per in.	37	171

The purpose in having both a narrow and a wide weld bead was to obtain further information on the effect of steepness of temperature gradient in the heat-affected region. After welding, each sample was cut in half and one half heated 4 hr at 1300 F and air-cooled; all four were then heated 1000 hr at 1025 F, sectioned, and examined microscopically.

Figs. 5(*a*), (*b*), (*c*), and (*d*), representing the structure of the low-temperature zone of the heat-affected region of the narrow weld bead of each sample, illustrate the results. In the as-received sample, not heated at 1300 F after welding, much graphite had formed, Fig. 5(*a*), but the companion section heated at 1300 F after welding showed considerably less, though there was some, Fig. 5(*b*), corroborating Mr. Weisberg's finding. The sample normalized before welding also showed considerably less graphite, Fig. 5(*c*), and the companion section heated at 1300 F after welding showed none at all, confirming our earlier observations on the normalized Springdale Station pipe. In those which had graphitized the amount was greater in the heat-affected region of the narrow than of the wide weld bead. Graphite was not observed in the unaffected base metal of any sample.

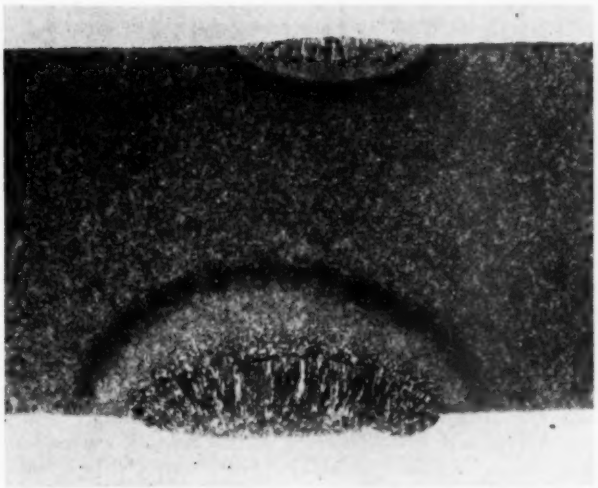


FIG. 6 TRANSVERSE CROSS SECTION OF WELD SAMPLE EMPLOYED IN SECTION IV
(Nital-picral etch: ×2.)

We do not know why graphite formed in the as-received but not in the normalized sample heated at 1300 F after welding. As apparent in Fig. 5, the as-received material was coarse-grained, indicative of a comparatively high temperature during its last supracritical treatment; this, however, probably would contribute to greater rather than to less resistance.[7] One suspicious factor is the 1350–1400 F annealed condition in which presumably the steel was furnished, this being the range (see preceding section) in which the stage is set for graphitization in the heat-affected region of a weld. With this beginning, the two stress-relief treatments at 1200 F which the material had undergone, may have so stabilized the graphite nuclei that they were not dissolved by subsequent heating for 4 hr at 1300 F,[8] i.e., treatment at 1200 F may have initiated the formation of graphite, but was too short to result in visible nodules. Some credence is given to this hypothesis by the results of the following experiment:

Upon another as-received sample a weld bead was laid under conditions identical with those just described for the narrow bead (since this produced more graphite). The sample was then cut in half, and one half heated for 8 hr, the other for 12 hr at 1300 F; both were then exposed for 3000 hr at 1025 F and examined microscopically. Both samples contained graphite in the heat-affected region, but in such small amount that it was difficult to find; Fig. 7 illustrates the largest amount. The amount appeared to be about the same in both samples,[9] and none was observed in the unaffected base metal of either. Thus longer heating at 1300 F resulted in considerably less graphite, presumably because the graphite nuclei had been dissolved or had reverted to carbide.

[7] See reference (3) and also the second section of this paper.

[8] In an earlier paper (2), we showed that graphite in a similar steel could be caused to revert to carbide by heating at 1300 F.

[9] On afterthought, it is realized that the choice of 12 hours was poor; 16 or 24 hours would have been better.

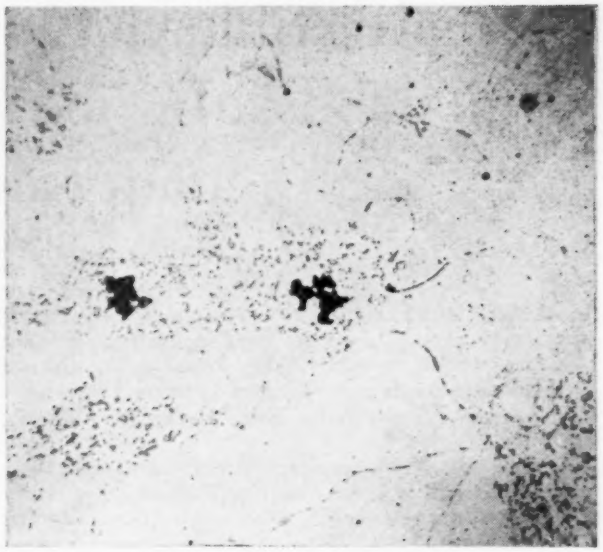


FIG. 7 MOST SEVERE GRAPHITIZATION IN HEAT-AFFECTED ZONE OF SCHUYLKILL STATION PIPE WELDED IN "AS-RECEIVED" CONDITION AND THEN POSTTREATED 8 HR AT 1300 F AND HELD AT 1025 F FOR 3000 HR
(Picral etch: ×500.)

ACKNOWLEDGMENTS

Dr. R. F. Miller of Carnegie-Illinois Steel Corporation and Mr. E. C. Wright of National Tube Company furnished the steels studied except for item 4, which was supplied by Mr. H. Weisberg of the Public Service Electric and Gas Company, and for a sample of the Springdale pipe supplied by Mr. R. W. Emerson of Pittsburgh Piping and Equipment Company.

BIBLIOGRAPHY

1 "A Possible Means of Avoiding Local Graphitization of Steels in Service at Elevated Temperatures," by G. V. Smith and R. F. Miller, "Graphitization of Steel Piping," included in Trans. A.S.M.E., vol. 66, 1944.

2 "Precipitation and Reversion of Graphite in Low-Carbon Low-Alloy Steel in the Temperature Range 900–1300 F," by G. V. Smith, R. F. Miller, and C. O. Tarr, Trans. A.I.M.E., vol. 158, 1944, p. 387.

3 "Graphitization of Welded and of End-Quenched Carbon and Molybdenum Steels," by G. V. Smith and S. H. Brambir, *Welding Journal*, Research Supplement, vol. 24, 1945, p. 153, included in Trans. A.S.M.E., vol. 67, 1945.

4 "Graphitization of Steel Piping," pamphlets included in Trans. A.S.M.E., vol. 66, 1944, and vol. 67, 1945.

5 "Functions of the Alloying Elements in Steel," by E. C. Bain, A.S.M., Cleveland, Ohio, 1939.

6 "Graphitization of Low-Carbon and Low-Carbon-Molybdenum Steels," by H. J. Kerr and F. Eberle, *Welding Journal*, Research Supplement, vol. 24, 1945, p. 86-s. Included in Trans. A.S.M.E., vol. 67, 1945.

7 "Structural Changes in Carbon and Molybdenum Steels During Prolonged Heating at 900 to 1100 F, as Affected by Deoxidation Practice," by G. V. Smith, R. F. Miller, and C. O. Tarr, American Society for Testing Material, preprint 19a, 1945.

Further Observation of Graphitization in Aluminum-Killed Carbon-Molybdenum-Steel Steam Piping

By R. W. EMERSON[1] and MATHEW MORROW[2]

Among graphitization of steel pipe studies being carried on, the present one deals with what the authors have termed "slip-plane" graphitization, which describes a condition of graphite segregation along slip planes where local "yielding" or localized plastic deformation had previously occurred. Such graphitization has been found to vary widely from the outside to inside of a pipe and from quadrant to quadrant around the pipe periphery. It has been determined that "nodular" graphite segregation whether of the "isotherm" or slip-plane type is as effective as "chain" graphite in reducing the ductility of low-carbon or low-carbon-molybdenum steel.

Introduction

THE graphitization of steel containing less than 1 per cent carbon and particularly less than 0.2 per cent carbon, at subcritical temperatures although reported in the literature (1)[3] was, prior to 1943, of little more than academic interest.

The complete circumferential failure of a carbon-molybdenum-steel steam pipe in January, 1943, which was attributed to subcritical graphitization, and the subsequent discovery of the same phenomenon in pipe lines in many other high-temperature steam power plants during the past 3 years has, however, resulted in the establishment of numerous intensive research programs which have been sponsored by both private industry and joint investigating committees. The results of these various investigations have been viewed by both the consumer and the producer with increasingly keen interest.

A report of the failure mentioned was given, together with three other papers dealing with graphitization, before this Society in December, 1943 (2, 3, 4, 5). The many investigations which have been carried out during the past 3 years have shown that graphite tends to segregate along the extremity of the heat-affected zones of welded joints, provided the steel is one in which the carbide is potentially unstable.

In February, 1945, however, routine sampling of several joints at the Springdale Power Station, at which station the original failure occurred, revealed a condition of graphite segregation which was not only of a serious nature, but one which was totally different from anything previously encountered. Whereas the terms "isotherm" and "eyebrows" were used to describe graphite segregation encountered adjacent to welded joints, due both to the location and macroscopic appearance of the graphite, the authors have chosen in this case the term "slip-plane" graphitization, to describe a condition of graphite segregation which appears to have unquestionably occurred along slip planes where local "yielding" or localized plastic deformation had previously occurred.

Although the discovery of slip-plane graphitization adds further to the general field of knowledge about graphitization, it also points to the over-all complexity of this general problem with which we are dealing.

Location of Slip-Plane Graphitization

In sharp contrast to "isothermal" graphitization adjacent to welded joints, slip-plane graphitization varies markedly from ID to OD and from quadrant to quadrant on the pipe periphery. For this reason the location of the graphitized area with respect to the boiler lead in which the difficulty was found, as well as its location with respect to the original failure, is given in Fig. 1. Twelve inches of pipe, including the upset pipe end of No. 4 boiler lead, was removed at the time of the failure in January, 1943. This was replaced by a spool of pipe from one of the three heats of pipe originally used in this installation in 1937. This pipe, however, had never been in service and was used without

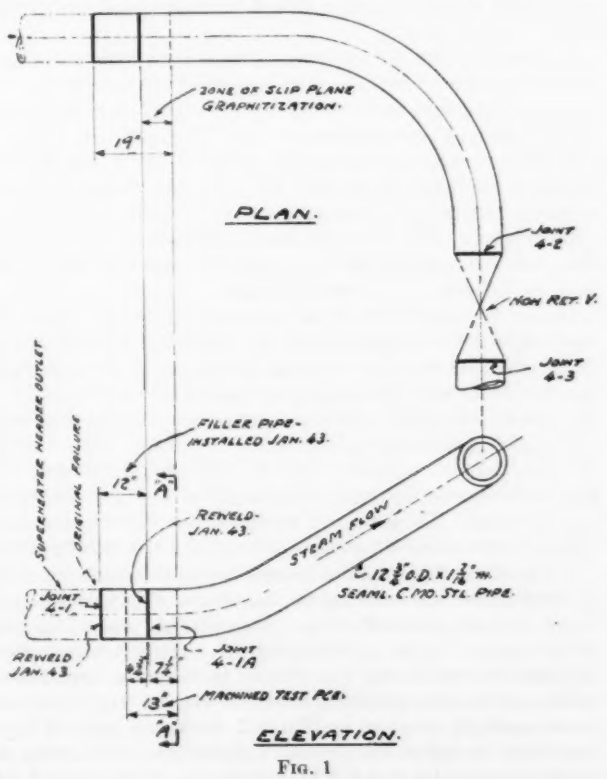


FIG. 1

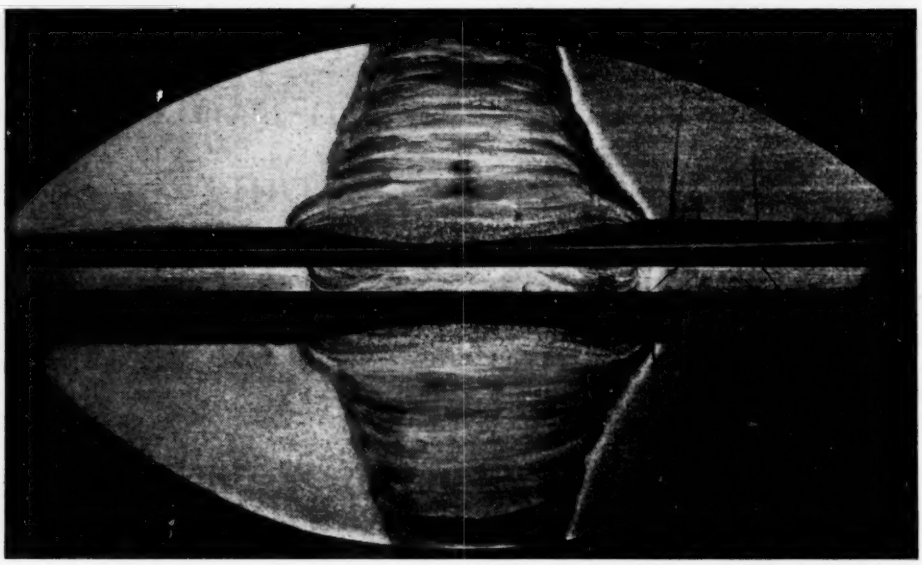
[1] Metallurgist, Pittsburgh Piping and Equipment Company, Pittsburgh, Pa.

[2] Assistant Metallurgist, Pittsburgh Piping and Equipment Company.

[3] Numbers in parentheses refer to the Bibliography at the end of the paper.

Contributed by the Joint A.S.T.M.-A.S.M.E. Research Committee on Effect of Temperature on the Properties of Metals and presented at the Annual Meeting, New York, N. Y., Nov. 26–29, 1945, of THE AMERICAN SOCIETY OF MECHANICAL ENGINEERS.

NOTE: Statements and opinions advanced in papers are to be understood as individual expressions of their authors and not those of the Society.



12 × In. Spool Weld Original Pipe

FIG. 2a PANORAMIC VIEW OF GRAPHITIZATION AS FOUND IN "WELD PROBER" SPECIMEN FROM JOINT NO. 4-1A, 12-IN. SCH. 160 PIPE-TO-PIPE WELD; ×1

(Graphitization runs from OD to ID and on 45-deg angle with respect to longitudinal direction of pipe. Plastic deformation along planes of maximum shear stress is believed to be responsible for nucleation of graphite.)

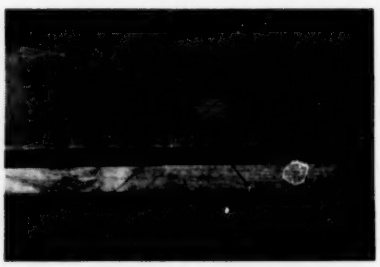


FIG. 2b CIRCUMFERENTIAL CRACKS AT OD WHICH RUN AT A 45-DEG ANGLE TO DIRECTION OF PIPE ROLLING

upsetting. Joints 4-1 and 4-1A as shown in Fig. 1, were welded, using a 400 F preheat and a 1200 F stress-relieving heat-treatment.

In January, 1944 (1 year later), $1^1/_2$-in-diam trepanned plugs were removed from both the inlet and outlet sides of joints 4-1A and the inlet (pipe) side of joint 4-2. Microscopic examination revealed incipient graphitization of the 12-in. spool as well as a mild reinfection (graphitization) of both the outlet side of joint 4-1A and the inlet side of joint 4-2. Segregated graphite of a serious nature, however, was not present in the plugs examined.

In February, 1945 (2 years later), "weld-prober" specimens were removed from the same two joints at approximately 45 deg from the location of the trepanned plugs.

During the preparation of the specimen from joint 4-1A it was observed that two cracks were present in the old pipe which had all the characteristics of previously encountered graphite segregation but which were in no way associated with the extremity of the heat-affected zone. Further examination revealed that these cracks, although extending from the OD toward the ID to a depth of $^5/_8$ in., did not run transverse to the direction of rolling on the pipe circumference but rather at an angle of 45 deg to the direction of rolling. The pattern of the cracks, as shown in Fig. 2, is typical of that which is produced in material which fails by shear.

Inasmuch as this condition existed across the entire width of the weld-prober specimen and not knowing to what extent it continued into the pipe or whether or not additional planes of graphite were present in the pipe remaining in service, it was deemed advisable to replace the entire bend between the superheater header and nonreturn valve as shown in Fig. 1. This pipe bend was accordingly removed on March 2, 1945, and replaced by a 1 per cent chromium 0.5 per cent molybdenum steel having an analysis comparable to A.S.T.M. Specification A 213 Grade T-12.

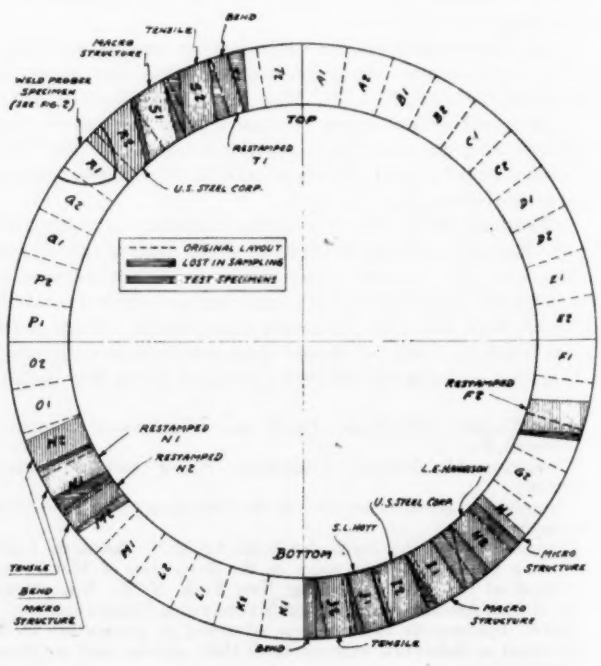


FIG. 3

Results of Macroscopic Investigation

In an effort to determine the extent of the grossly segregated slip-plane graphitization which was found in the weld-prober specimen from joint 4-1A, a 13-in. section from the bend was removed, comprising the joint mentioned, 4.75 in. of the 12-in-long spool which was installed at the time of failure, and 7.25 in. of the old pipe which had been in service since 1937, and which extended to a distance of 19 in. from the original failure.

Having previously found that heavily segregated graphite could be made visible to the unaided eye by either rough-grinding or machining, the surface of the 13-in. length of pipe was "turned" in a lathe to obtain a clean machined surface on both the OD and ID (2, 12).

After machining, the pipe section was stenciled in accordance with Fig. 3, and subsequently quarter-sectioned longitudinally. Before removing any test pieces, however, both the inside and outside pipe surface of each quarter-section was photographed. Figs. 4 to 7, inclusive, show the severity of slip-plane graphitization as revealed by surface-machining only. It is to be emphasized that no special machining, grinding, polishing, or etching techniques are required to locate heavily segregated graphite such as shown in Figs. 4 to 7, inclusive.

Several distinct lines of heavily segregated graphite, running at both a plus and minus 45-deg angle, can be seen in the upper right-hand corner in Fig. 4. (Section F-1 to J-2, inclusive, see Fig. 3.) A multitudinous number of fine lines of segregated graphite are also present in the upper center of Fig. 4. A good example of "isotherm" graphitization (graphite segregation at the extremity of a weld-heat-affected zone) is shown by the semicircular pattern in the upper left of this figure. This condition was produced by the fillet-welding of a 1-in-sq bar to the pipe, apparently for mechanical reasons during the original erection of this piping. This in effect is the result of a "weld-bead" test similar to that devised and used by Battelle Memorial Institute, and others in 1943, as a simple test for determining the susceptibility of steel to graphitization. The bead test shown in this illustration, however, was given an aging treatment of 935 to 950 F for approximately 65,000 hr (actual operating conditions), as contrasted with the artificial accelerated aging tests of 2000 to 8000 hr or longer at 1000 to 1050 F. Also present in Fig. 4 are several lines of graphite adjacent and running into weld joint 4-1A.

Lines of heavily segregated graphite running at both plus and minus 45-deg angles as well as a multitudinous number of the finer lines of graphite were found in section K1 to 02 inclusive (see Fig. 3). This is shown in Fig. 5. In addition to the foregoing, many other small speckled patches of localized graphite segregation of unknown origin are present in this figure. It is to be pointed out that lines of heavily segregated graphite are not present in the location of the trepanned plug (upper left, Fig. 5) which was removed in January, 1944. This plug was removed from the side of the pipe at the location 02-P1 shown in Fig. 3. Metallographic evidence, however, indicated that not only was heavily segregated slip-plane graphitization present at the time this plug was removed in 1944, but that this condition actually existed at the time the 12-in. spool was welded into the line in January, 1943. When sampling pipe for evidences of slip-plane graphitization therefore it cannot be overemphasized that the mere fact that such a condition is not detected in a test specimen does not mean that such a condition is nonexistent in the general vicinity of such a test specimen.

The location of the weld-prober specimen, the macrographs of which are shown in Fig. 2, is shown in Fig. 6 (section P1 to T2, inclusive), and it may be seen that it was coincidental that the location was so chosen that the heavily segregated slip-plane graphitization was intersected by the specimen removed. Had the specimen been removed anywhere between section A1 and E2 this condition would have gone undetected, and this pipe might possibly still be in service. The longest length of slip-plane graphitization, shown in Fig. 6, was found to be 4.5 in.

The inside pipe surface was machined to determine if the condition described could be located on the inside pipe surface or if the graphite segregation found on the outside of the pipe had actually penetrated the entire pipe wall. The condition found on the inside pipe surface, although confined to sections F1 to M2, is believed to be even a more striking example of a graphitization pattern, the orientation of which is unquestionably the direct result of stress.

Having observed the macroscopic appearance of both the inside and outside pipe surface, Figs. 8, 9, and 10 illustrate the graphite pattern found through the pipe wall at sections I1 and S1. A roughly ground and unetched view of section I1 is shown in Fig. 8 at normal magnification.

The same section as shown in Fig. 8 is shown in Fig. 9, after polishing and deep-etching in hot 50 per cent hydrochloric acid. This illustration which takes in a larger area than Fig. 8, is shown at two magnifications.

Since many of the lines of graphite segregation appear to emanate from the weld, it first appears that these lines formed as a result of and after joint 4-1A was completed (January, 1943). On the contrary, however, close examination of this figure reveals that these lines have been partially eradicated along the heat-affected zone of the weld. Microscopic observations further substantiate that re-solution of the graphite took place in the heat-affected zone as a result of the localized high temperature during the rewelding of this joint. This fact was subsequently substantiated by G. V. Smith and S. H. Brambir, U. S. Steel Corporation Research Laboratory (14). Furthermore, had the lines of graphite shown in Fig. 9 been initiated at the time of or subsequent to the welding of joint 4-1A, the condition of stress which initiated the graphite pattern in the old pipe would have been transmitted through the weld into the 12-in. spool and it would therefore be expected that similar lines of graphite segregation would be present in the 12-in. spool which was installed at the time joint 4-1A was made, and which was of similar chemistry and deoxidation as the original pipe.

Still another reason for believing that this condition was initiated prior to and present in 1943 is that the average graphite-nodule size of the grossly segregated slip-plane graphitization closely approaches the size of random graphite located in the many specimens of the originally installed material previously examined microscopically. Although growth of isotherm graphite nodules have been followed in several welded joints exhibiting incipient graphitization in 1943, there have been no cases where the rate of nodule growth over a 2-year period would approach that found in this case (assuming this condition to have developed after the original failure).

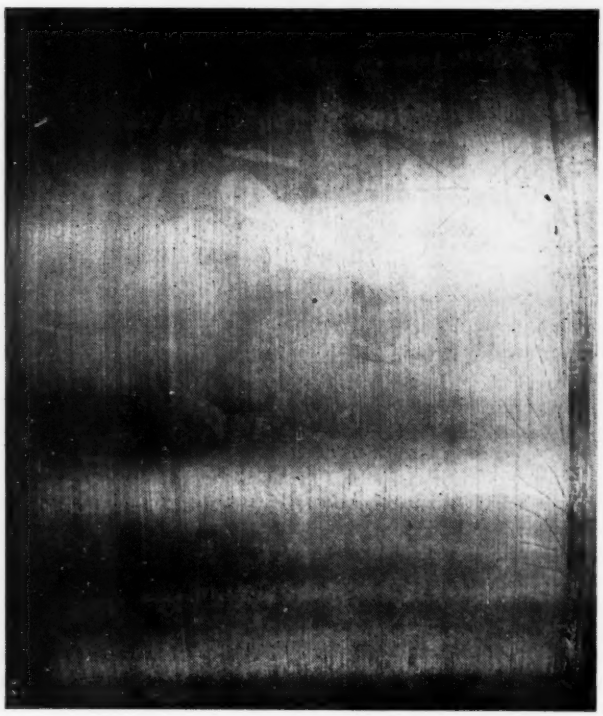
The depth and direction of the graphite segregation through the pipe wall at section S1 is shown in Fig. 10.

Physical Properties

Several bend and tensile tests were made on pipe sections, the locations of which are shown in Fig. 3. The results obtained are shown in Figs. 11 and 12 and in Table 1. These tests were made principally to confirm the authors' belief that gross segregation of "nodular" graphite whether of the isotherm or slip-plane type is as effective as "chain" graphite in reducing the ductility of low-carbon or low-carbon-molybdenum steel.

The bend test shown in Fig. 11 was removed from section T1 (see Fig. 3). From the location of the fissures it may be noted that this specimen was cut from the upper portion of the quadrant shown in Fig. 6. Although the graphite segregation in this case has no direct relation to the heat-affected zone of a weld, it is to

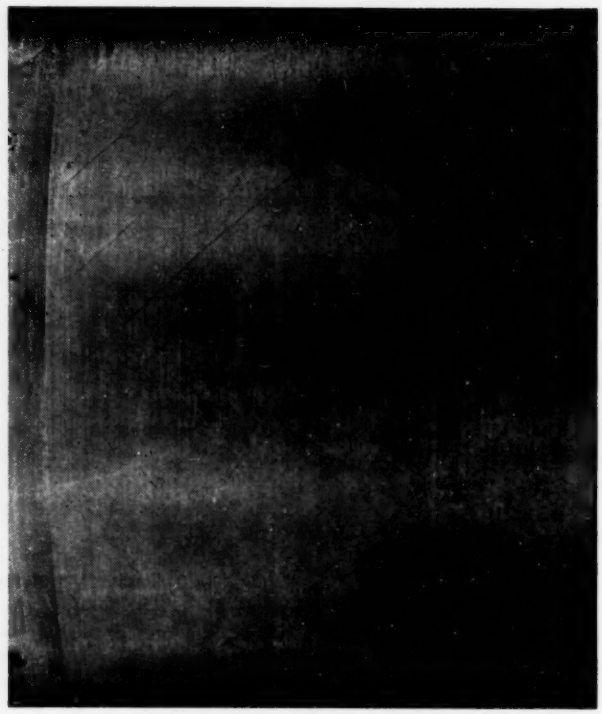
F1



J2

FIG. 4 GRAPHITE PATTERN ON MACHINED OUTSIDE PIPE SURFACE OF SECTION F1 TO J2; ×0.8

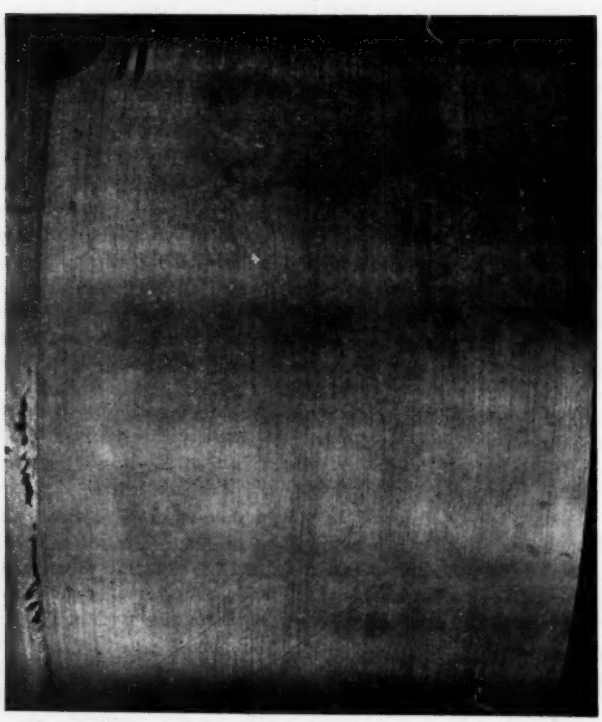
T2



P1

FIG. 6 GRAPHITE PATTERN ON MACHINED OUTSIDE PIPE SURFACE OF SECTION P1 TO T2; ×0.8

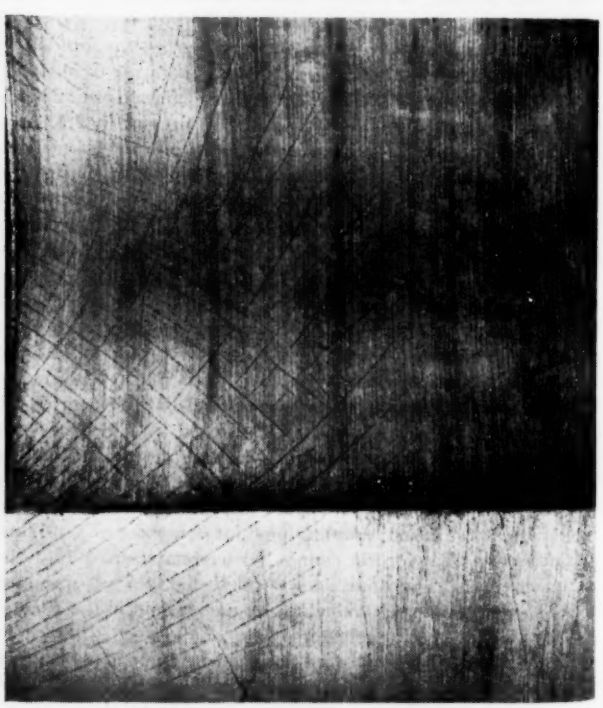
O2



K1

FIG. 5 GRAPHITE PATTERN ON MACHINED OUTSIDE PIPE SURFACE OF SECTION K1 TO O2; ×0.8

F1



N1

FIG. 7 GRAPHITE PATTERN ON MACHINED INSIDE SURFACE OF SECTION F1 TO N1; ×0.8



FIG. 8 UNETCHED MACROGRAPH OF SECTION I1 SHOWING LINES OF SEGREGATED NODULAR GRAPHITE RUNNING FROM ID TOWARD OD OF PIPE; ×1

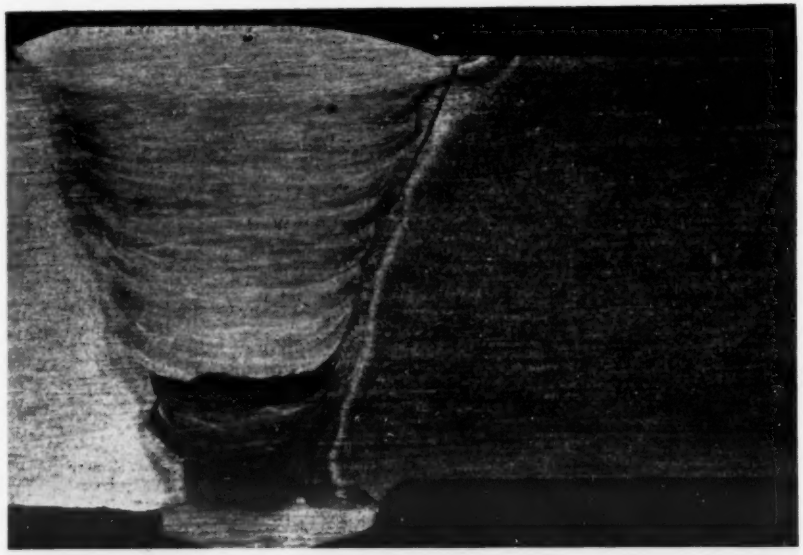


FIG. 10 MACROSECTION S1, SHOWING SLIP-PLANE GRAPHITIZATION; ×1½
(Etchant, hot 50 per cent hydrochloric acid.)

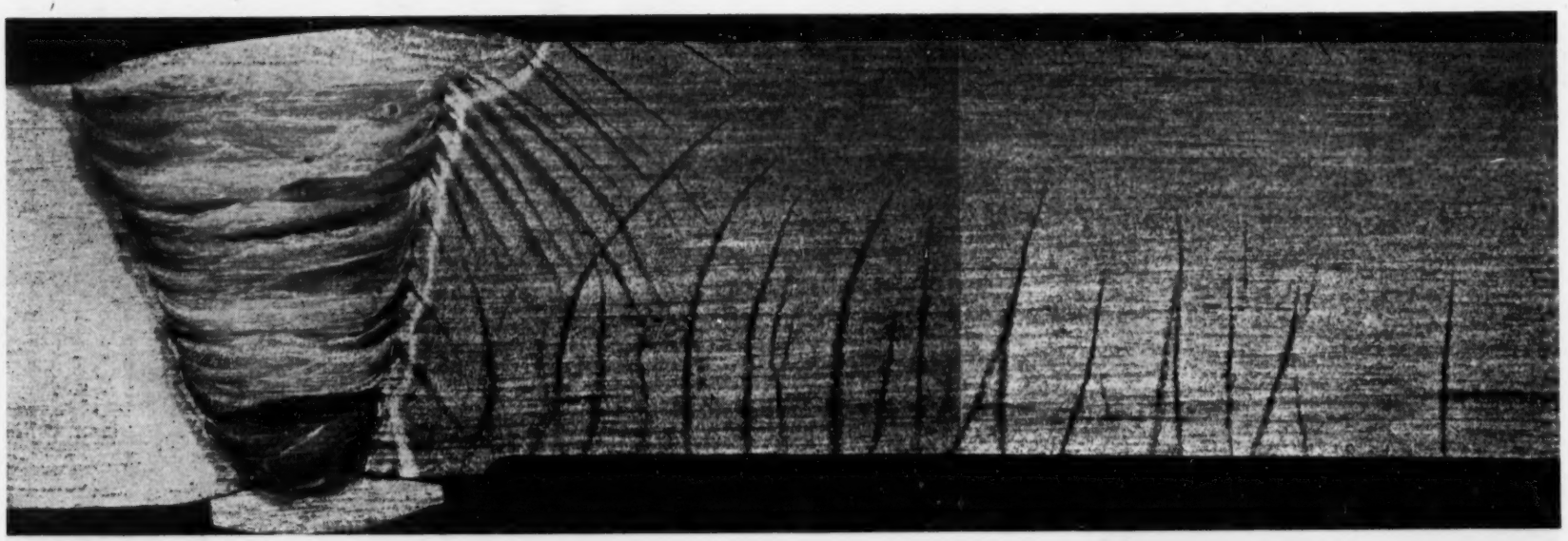


FIG. 9 TWELVE-INCH SPOOL, REWELDED JOINT NO. 4-1A AND ORIGINAL PIPE 12 IN. TO 16 IN. FROM ORIGINAL FAILURE; ×1.8
(Location II, see Fig. 3. Note large graphite stringers emanating from ID and intersecting those emanating from OD adjacent to weld. Etchant, hot 50 per cent hydrochloric acid.)

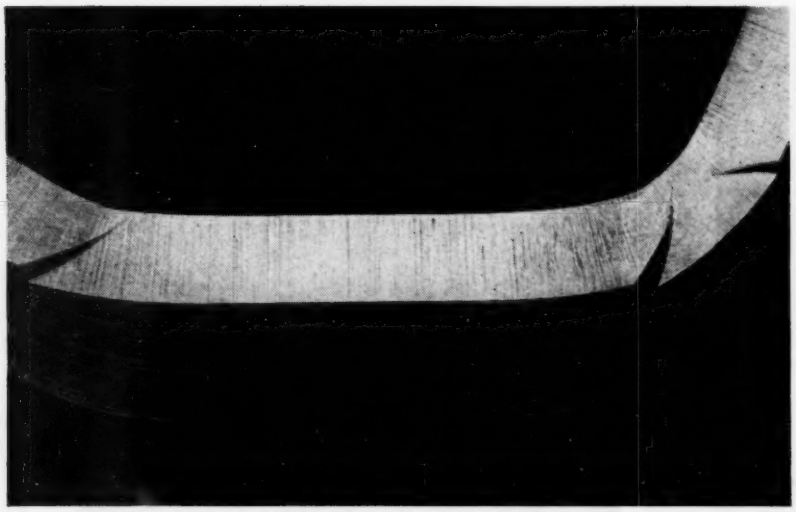


FIG. 11 BEND TEST ON SECTION T1, SHOWING FISSURING ALONG GRAPHITIZED SLIP PLANES; ×1

TABLE 1
Tensile Tests Removed From Graphitized Pipe

Section	Tensile strength, psi
J2	59130
N2	58860
S2	46050

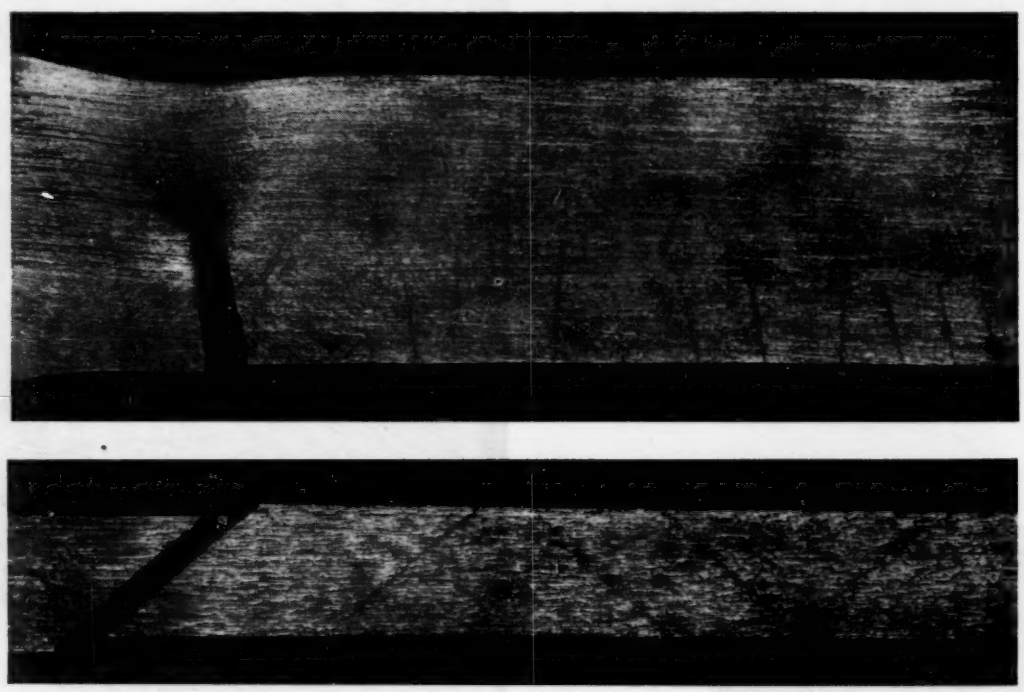


FIG. 12 SIDE AND EDGE VIEWS OF TENSILE BAR, MACHINED FROM SECTION J2; ×1½
(Note that failure occurred along one of the planes of graphite segregation.)

be carefully noted that its ultimate effect on the ductility of the pipe is similar to that which has been found to occur at the "contact" zone of a welded joint.

Both the side and edge view of a partially pulled tensile bar removed from section J2 is shown in Fig. 12. Planes of graphite may be observed to be "running" at both plus and minus 45 deg on the edge of the machined specimen. The edge view shown was adjacent to the inside pipe surface before removal of the specimen from the pipe. Numerous planes of graphite may be seen to extend from the ID toward the OD in the side view of this specimen. Failure occurred abruptly along one of the graphite planes at a stress of 59,130 psi, followed immediately by a necking-down of the ductile portion of the specimen.

MICROSCOPIC EXAMINATION

Although macroscopically, slip-plane graphitization as shown in Figs. 4 to 12, inclusive, appears as a continuous crack, microscopically it appears as discontinuous large gray nodules. The relative size and spacing of these nodules determine the resultant ductility of the material.

One of the planes of segregated graphite which was intersected by weld 4-1A in January, 1943, is shown at a magnification of 100 in Fig. 13. It may be seen that the nodules which were outside of the heat-affected zone of the weld remained unchanged, whereas those just within the heat-affected zone were partially put into solution. Those nodules which were in the immediate vicinity of the line of fusion may be seen to be completely dis-



FIG. 13 INTERSECTION OF SLIP-PLANE GRAPHITIZATION WITH LINE OF FUSION OF WELDED JOINT 4-1A; ×100

solved by the heat from welding. The sudden solution of the graphite in the austenite, followed by the rapid rejection of the carbon (graphite) as a carbide phase, resulted in the formation of

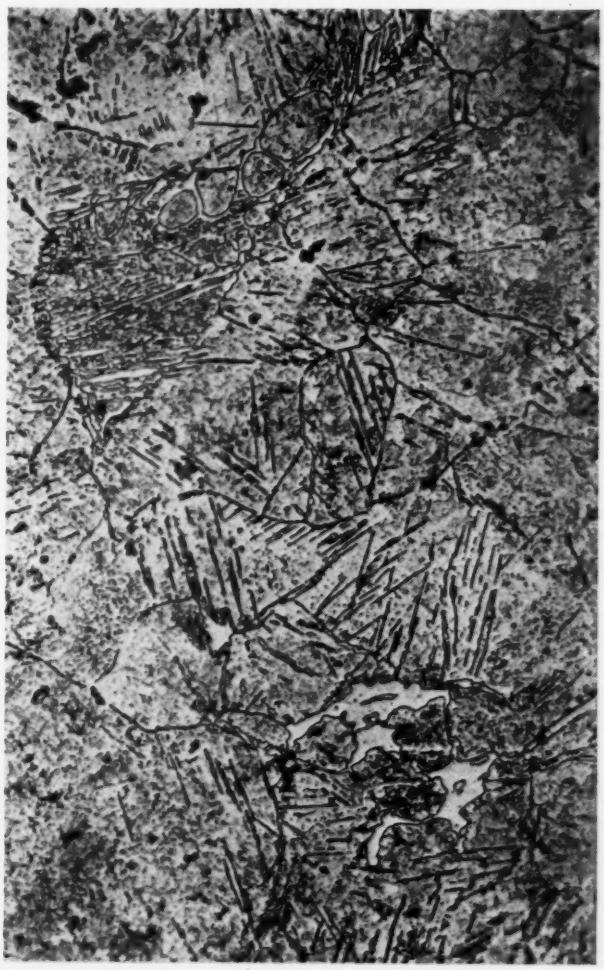


FIG. 14 PARTIAL VIEW OF FIG. 13, AT HIGHER MAGNIFICATION, SHOWING STRUCTURAL DETAIL OF AREA IN WHICH GRAPHITE WAS REDISSOLVED AND REPRECIPITATED AS A CARBIDE PHASE DURING WELDING; ×600

a localized band of steel of hypereutectoid composition. The carbide present in the darkened area in Fig. 13, which is probably in the range of 1 to 2 per cent carbon, can be seen in Fig. 14 to have partially regraphitized in the 2-year period following its inception.

The fact that the graphite was put into solution by the heat from the rewelding of joint 4-1A in 1943, is believed to be adequate proof that the graphite was present some time prior to the welding of this joint.

Further proof of this fact is offered in Figs. 15 to 17, inclusive. Slip-plane graphitization at a remote distance from the weld is shown at a magnification of 100 in Fig. 15. The size and detail of these segregated graphite nodules are shown in Fig. 16 at a magnification of 600.

In following the rate of growth of graphite adjacent to welded joints under both actual operating conditions and in accelerated aging tests made in laboratory furnaces, the authors have never encountered a rate of growth of graphite over a 2-year period in low-carbon-molybdenum steel which would even approximate that shown in Figs. 15 and 16.

This is believed to be substantiated by the published work of Kerr and Eberle (3, 6); Smith, Miller, and Brambir (4, 11); Weisberg (5, 12); Hoyt and Williams (7); Van Duzer, McCutchan,

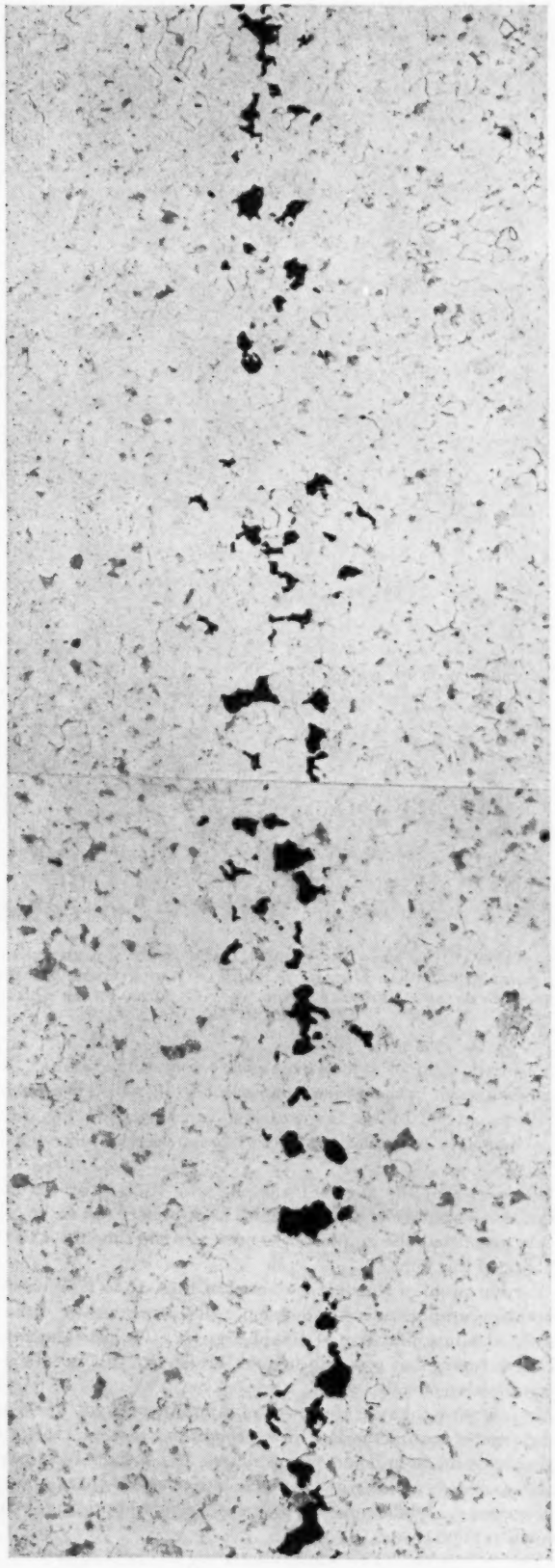


FIG 15 GROSS SEGREGATION OF NODULAR SLIP-PLANE GRAPHITIZATION; ×100



FIG. 16 SIZE AND DETAIL OF GRAPHITE NODULES SHOWN IN FIG. 15; ×600

and Rohrig (8, 9); as well as certain unpublished work on this subject by other investigators. In contrast to Figs. 15 and 16, however, the rate of growth of graphite over a 2-year period in the contact zone adjacent to joint 4-2 is shown at a magnification of 600 in Fig. 17. This joint was also rewelded in January, 1943, and it is known that graphite did not exist adjacent to this joint at the time it was rewelded.

Since such a vast difference in nodule size exists between Figs. 16 and 17, it is concluded by the authors that the slip-plane graphitization was initiated prior to 1943, and that the many graphite planes which appear to emanate from the weld are coincidental.

DISCUSSION AND PROBABLE CAUSE OF SLIP-PLANE GRAPHITIZATION

Owing to the over-all complexity of the graphitization problem as it is known to exist, an attempt has been made to correlate the existing facts with other published information. In so doing

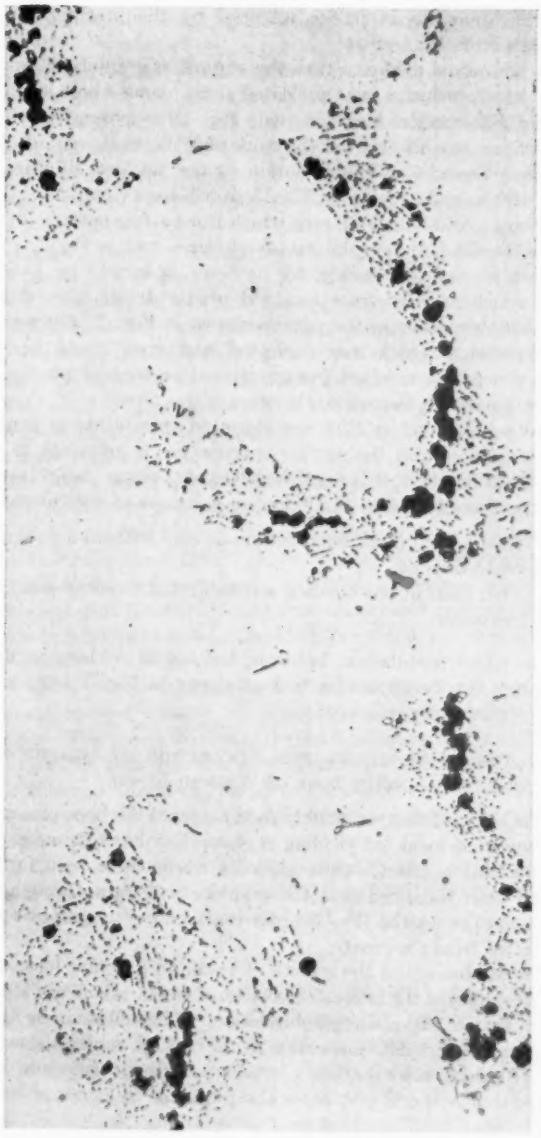


FIG. 17 GROWTH OF GRAPHITE IN REGRAPHITIZED JOINT NO. 4-2 AFTER 2 YEARS OF SERVICE; ×600

certain postulations could not be avoided in this discussion.

The iron - iron carbide system, although extremely useful and of real importance to the ferrous metallurgist, has been recognized for many years as a metastable system; the iron-carbon system being the truly stable one. Hoyt and Williams recently stated, "In spite of the apparent stability of iron carbide in the common carbon steels, in which it is the active strengthening and hardening constituent, it has a definite, although usually slight tendency, to change to the more stable form of graphite" (7).

A logical theory regarding the precipitation of carbon (graphite) in steam piping subjected to fluctuating temperatures was presented before this Society in 1944 by F. B. Foley (13). His theory was based upon the slope of the solubility curve of the alpha phase of the iron - iron carbide diagram together with the composition of the alpha phase (ferrite) with respect to aluminum or silicon or both.

It has been shown by Fink and Smith that in precipitation-hardening alloys of the duralumin type, precipitation of the $CuAl_2$ upon aging will always occur preferentially along slip planes resulting from any plastic deformation, before general precipitation occurs (15).

In this respect, it is to be pointed out that the solubility curve for the aluminum-rich solid solution in the aluminum-copper system is qualitatively the same as the solubility curve of the alpha phase in the iron - iron carbide system.

Luders' lines, or "stretcher strains" have been stated by Winlock and Leiter "to occur as a result of the uneven and non-uniform flow of metal at the yield point, caused by the sudden transition of different grains or groups of grain from the elastic to the plastic state." They further state, "Luders' lines occur in the range of deformation corresponding to an elongation of 1.5 to 10 per cent" (16).

On the basis of the foregoing it is believed that slip-plane graphitization is initiated by localized yielding or plastic deformation along slip planes with the formation of Luders' lines or stretcher strains. In the case under discussion major slippage occurred along planes of maximum shear stress. In Fig. 1 it is to be noted that the slip-plane graphitization is located along the pipe length just outside of the 30-deg bend. It is postulated that although this bend was made hot, a sufficient load was applied in making the bend to produce a critical strain (1.5 to 10 per cent elongation) in the cold pipe just outside of the hot-bent region. This bend was subsequently furnace-stress-relieved at 1150 to 1200 F before installation. This temperature was apparently too low to remove the effects of previous strain, in fact it is suggested that the stress-relieving temperature may have initiated actual submicroscopic graphitization along the planes which received localized plastic deformation by virtue of the increased solubility of carbon in alpha iron at the stress-relieving temperature, followed by graphite precipitation upon cooling in accordance with the theory advanced by F. B. Foley.

Just why graphite, or for that matter any precipitating phase should precipitate preferentially along planes which have been plastically deformed is not too clear, although it is suggested by Smith and Brambir that it is due to a greater ease of nucleation of the precipitating phase in the plastically deformed regions (14).

After nucleation of graphite once occurs, its continual growth along either slip planes or isotherms appears quite logical. It is believed, however, that temperature fluctuations in a steam line will result in graphite precipitation only at those locations where a graphite nucleus or a strong graphite nucleating effect is present. It is believed that temperature fluctuations will otherwise result only in the solution and reprecipitation of iron carbide. During this time, however, diffusion of the carbide from the carbide-rich areas toward the ferrite areas, which are low in carbon owing to the slow but continual precipitation of graphite at the graphite nuclei, is taking place.

As the graphite nodules grow in size the surrounding ferrite becomes depleted of carbon. The ferrite around the graphite nodules can therefore only precipitate graphite upon each cooling cycle as fast as the carbon in the alpha iron (ferrite) can diffuse from the carbide-rich areas to the ferrite surrounding the graphite.

Based upon the foregoing assumptions, the rate of graphite precipitation for a given set of temperature conditions would appear to depend upon the number of graphite nuclei present and the rate of diffusion of carbon in alpha iron. This is in general agreement with the postulation made by Smith and Miller who stated, "Conceivably, then, graphite in a limited region could bring about, in time, the substantial depletion of carbide within an entire specimen."

Contrary to the belief or implied belief by many that graphite forms directly from the carbide (Fe_3C) phase due to the higher carbon content of this phase as compared to the alpha phase (ferrite), it is believed by the authors that the mechanism by which graphite precipitation occurs is through the gradual solu-

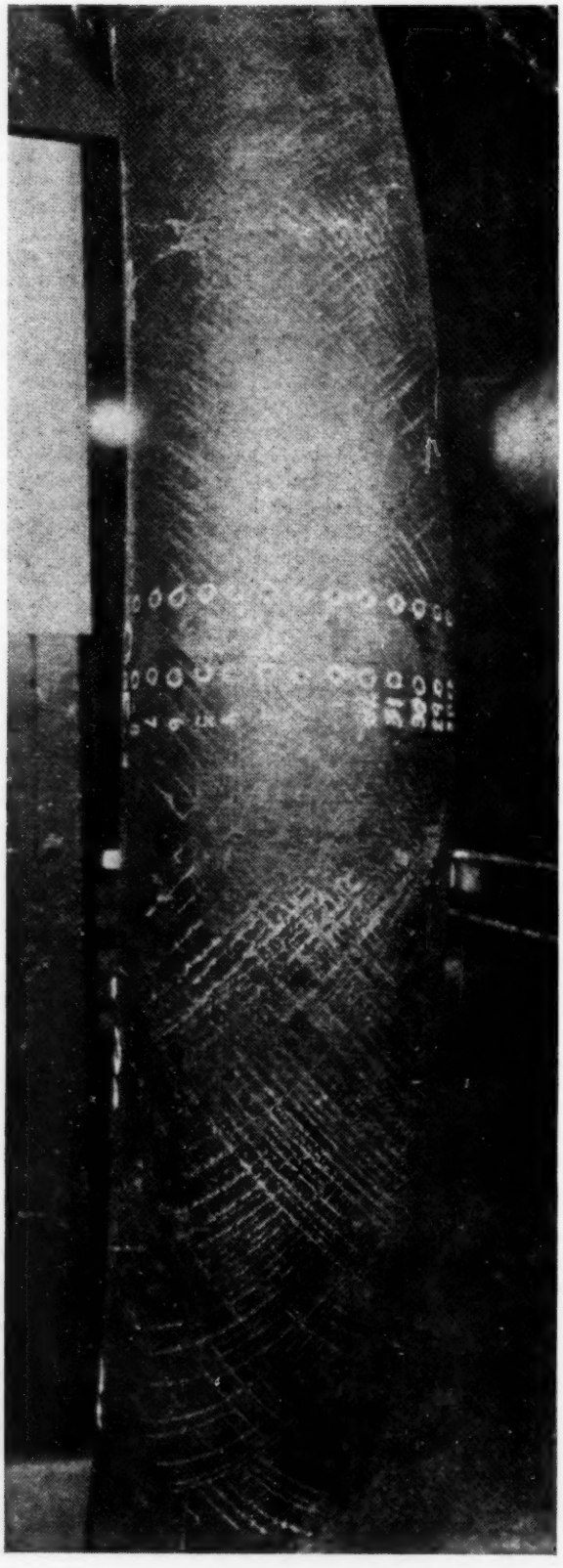


FIG. 18 LUDERS' LINES ON BACK OF 8-IN. PIPE AFTER COLD-BENDING

tion of cementite in ferrite followed by the precipitation of graphite from the ferrite.

As additional evidence that the slip-plane graphite shown in Figs. 4 to 7, inclusive, was nucleated along planes where localized plastic deformation had occurred, Fig. 18 is presented. This illustration was taken from the work of William Hovgaard (17), and was brought to the attention of the authors by Messrs. McCutchan and Crocker, of The Detroit Edison Company. Fig. 18 shows a cold-bent 8-in. pipe which has a stress pattern identical to the slip-plane graphitization pattern shown in Fig. 7. The pattern on the pipe in Fig. 18, however, is formed by Luders' lines which resulted from localized plastic deformation during cold-bending, whereas the pattern shown in Fig. 7 is slip-plane graphitization which was nucleated and grew along Luders' lines which also resulted from a critical amount of plastic deformation during the original bending of this pipe.

Assuming therefore that a material is susceptible to general graphitization, and the service temperature is adequate to obtain graphitization, it is suggested that slip-plane graphitization may be encountered in the following locations of critical strain:

1 Entire bend if the bend was made cold without subsequent full heat-treatment.

2 Cold ends of hot bends if not subjected to subsequent full heat-treatment.

The latter postulation, however, has not as yet been verified, although two bends similar to that shown in Fig. 1 have since been removed for examination.

NEW THEORY SUGGESTED FOR NUCLEATION OF GRAPHITE AT CONTACT ZONE OF WELDED JOINTS

It is believed that reasonably good evidence has been presented to show that localized yielding or plastic flow has a strong graphite nucleating effect. Once graphite nuclei have been formed it has been theorized that the graphite will grow through the solution of cementite (Fe_3C) in ferrite, followed by graphite precipitation from the ferrite.

The mechanism of the growth of isotherm graphite formed at the extremity of the heat-affected zone of welds, is believed identical to that of slip-plane graphitization. The condition or agent which causes graphite nucleation at the contact zone adjacent to welded joints, however, has not been too clear. It is now suggested that isotherm graphite is also nucleated by stress, although of a somewhat different nature.

Whereas, slip-plane graphitization is believed to be nucleated by plastic flow from an externally applied load, isotherm graphitization is believed to be nucleated by self-compensated stresses known as "tessellated stresses."

The work of Dr. F. Laszlo on tessellated stress was brought to the attention of the authors by C. H. Davy[4] (18, 19, 20, 21, 22).

Although Dr. Laszlo approaches the subject of tessellated stress mathematically, the following extract which qualitatively defines the subject, is taken from his work: "Anisotropy of the single crystals of most materials and the difference between the bulk physical properties of the components of compound solids readily cause internal self-compensated stress systems to develop around such centers as crystals or components of the compound structure, respectively. These self-compensated stress systems are called tessellated stresses."

One of the first conclusions drawn, after the examination of the pipe failure at the Springdale Power Station, was that the failure occurred at the Widmanstätten grain boundaries at a distance from the weld where the temperature from the welding was

[4] Chief Research Engineer, Babcock & Wilcox, Ltd.

just sufficient to cause grain-boundary transformation.[5] It was also this location where grain-boundary graphite of the "chain" type was located and which was the basic reason for failure.

Just outside of the heat-affected zone the metal structure consists of iron carbide or complex iron-molybdenum carbide, embedded in a matrix of alpha iron (ferrite) whereas, just within the heat-affected zone a portion of the alpha iron goes through a phase change to gamma iron, simultaneously absorbing the carbide phase or as much of it as time will permit under the short heating cycle during welding. Rapid cooling of the heat-affected zone may result in the formation of minute amounts of martensite. There is present in the transition zone (zone of isothermal-graphite formation), therefore, alpha iron which has a body-centered cubic lattice, iron carbide or complex iron-molybdenum carbide which has a complex lattice structure, austenite which has a face-centered cubic lattice, and martensite if formed, which goes through a transition structure of body-centered tetragonal and finally to a body-centered cubic lattice.

Along the transition zone adjacent to a weld, therefore, numerous crystal structures, all of which have their own physical constants and which are surrounded by each other, exist at one time or another during the welding cycle. It is common knowledge that a considerable volume change occurs when alpha iron transforms to gamma iron (austenite) and that upon rapid cooling such as occurs in welding the metal does not go back to its exact original dimensions.

It seems quite reasonable to believe therefore that a system of self-compensated stress is developed around crystals or grains at the transition zone between the heat-affected and unaffected parent metal adjacent to a weld, owing to the different physical constants and directional properties of the several different crystal structures which exist at this location during the welding operation.

It is therefore postulated that graphite is nucleated in the contact zone adjacent to a welded joint by self-compensated stresses known as tessellated stresses.

Summary

1 The term slip-plane graphitization has been chosen to describe a condition of graphite segregation which appears unquestionably to have occurred along slip planes where local yielding or localized plastic deformation had previously occurred.

2 Slip-plane graphitization, unlike isotherm graphitization which has been found to be reasonably uniform through the pipe wall and around the pipe circumference, varies markedly from OD to ID and from quadrant to quadrant around the pipe periphery.

3 Slip plane like isotherm graphitization (if severe) is readily visible to the unaided eye after machining or rough-grinding.

4 Gross segregation of "nodular" graphite, whether of the isotherm or slip-plane type, is as effective as chain graphite in reducing the ductility of low-carbon or low-carbon-molybdenum steel.

5 Substantial evidence has been presented to show that plastic deformation is an excellent nucleating agent for graphite of the slip-plane type.

6 The mechanism of graphite growth of either the isotherm or slip-plane type is believed to occur through the solution of the carbide phase in ferrite, followed by the precipitation of graphite from the ferrite.

7 Having presented evidence to show that slip-plane graphitization is nucleated by stress, the postulation is made that isotherm graphite is also nucleated by stress. In this case, however, a self-compensated stress system is believed to be set up, resulting from the difference in directional properties and physical constants of the several different crystal structures which exist in the transition zone adjacent to a welded joint at the time of welding. Self-compensated stresses of this nature are known as tessellated stresses.

[5] This is known as the lower critical temperature (Ac_1) which is approximately 1350 F for carbon-molybdenum steel.

Acknowledgments

The authors wish to extend their appreciation to Mr. L. E. Hankison, West Penn Power Company, and Mr. G. Sinding Larsen, vice-president, Pittsburgh Piping & Equipment Company, for their co-operation, helpful suggestions, and inspiring influence during the investigation and preparation of this manuscript.

The authors are further indebted to the West Penn Power Company for its permission to publish the results of this investigation.

BIBLIOGRAPHY

1 "Graphite in Low-Carbon Steel," by A. B. Kinzel and R. W. Moore, Trans. A.I.M.E., vol. 116, 1935, pp. 318–329.

2 "Carbide Instability of Carbon-Molybdenum Steel Piping," by R. W. Emerson, "Graphitization of Steel Piping," included in Trans. A.S.M.E., vol. 66, 1944.

3 "Graphitization Caused by Testing Conditions on Carbon-Molybdenum Tubular Creep-Test Specimens," by H. J. Kerr and F. Eberle, "Graphitization of Steel Piping," included in Trans. A.S.M.E., vol. 66, 1944.

4 "A Possible Means of Avoiding Local Graphitization of Steel in Service at Elevated Temperatures," by G. V. Smith and R. F. Miller, A.S.M.E. pamphlet, "Graphitization of Steel Piping," 1944.

5 "Report on High-Temperature Pipe Weld Investigation," by Herman Weisberg, "Graphitization of Steel Piping," included in Trans. A.S.M.E., vol. 66, 1944.

6 "Graphitization of Low-Carbon and Low-Carbon-Molybdenum Steels," by H. J. Kerr and F. Eberle, "Graphitization of Steel Piping," included in Trans., A.S.M.E., vol. 67, 1945.

7 "Progress Report on Graphitization of Steam Lines," by S. L. Hoyt and R. D. Williams, A.S.M.E. pamphlet, "Graphitization of Steel Piping," 1945.

8 "Investigation of Graphitization at Detroit," by R. M. Van Duzer, Jr., I. A. Rohrig, and Arthur McCutchan, "Graphitization of Steel Piping," included in Trans. A.S.M.E., vol. 67, 1945.

9 "A Study of Austenitic Welding for Control of Graphitization in Steel," by I. A. Rohrig, "Graphitization of Steel Piping," included in Trans. A.S.M.E., vol. 67, 1945.

10 "Graphitization of Carbon-Molybdenum Steel in High-Temperature Steam Piping," by George A. Timmons, "Graphitization of Steel Piping," included in Trans. A.S.M.E., vol. 67, 1945.

11 "Graphitization of Welded and of End-Quenched Carbon and Molybdenum Steels," by G. V. Smith and S. H. Brambir, "Graphitization of Steel Piping," included in Trans. A.S.M.E., vol. 67, 1945.

12 Discussion of Kerr-Eberle paper (6), by H. Weisberg.

13 Discussion of Kerr-Eberle paper (6), by F. B. Foley.

14 "U.S. Steel Corporation Memorandum No. 622 (private communication), June, 1945.

15 "Age Hardening of Aluminum Alloys—I," by W. L. Fink and D. W. Smith, Technical Publication No. 706, A.I.M.E., February, 1936.

16 "Some Factors Affecting the Plastic Deformation of Sheet and Strip Steel and Their Relation to the Deep-Drawing Properties," by Joseph Winlock and Ralph W. E. Leiter, Trans. A.S.M., vol. 25, 1937, pp. 163–165.

17 "Bending of Curved Pipes," by William Hovgaard, Proceedings of the Third International Congress for Applied Mechanics, Stockholm, Sweden, vol. 2, 1930, pp. 331–341.

18 "Tessellated Stresses—I," by Dr. F. Laszlo, *Journal of the Iron and Steel Institute*, vol. 148, 1943, pp. 173P–199P.

19 "Tessellated Stresses—II," by Dr. F. Laszlo, *Journal of the Iron and Steel Institute*, vol. 148, 1943, pp. 137P–159P.

20 "Tesselated Stresses—III," by Dr. F. Laszlo, *Journal of the Iron and Steel Institute*, preprint, vol. 150, August, 1944, pp. 183P–209P.

21 "Tessellated Stresses—IV," by Dr. F. Laszlo, *Journal of the Iron and Steel Institute*, preprint November, 1945; advance paper.

22 "Graphitization of Steel Influenced by Tessellated Stresses," *Journal of the Iron and Steel Institute*, vol. 148, 1943, p. 201.

Graphitization in Some Cast Steels

By A. J. SMITH,[1] J. B. URBAN,[1] AND J. W. BOLTON[1]

Field service and controlled laboratory experiments have demonstrated that it is not possible to insure against graphitization of carbon-molybdenum steel through any of the controlled procedures of melting and deoxidation practice or heat-treatment. It is probable that freedom from graphitization is to be sought through the use of alloy additions which confer greater stability to the carbide. A hypothesis has been put forth concerning the mode of graphitization based upon the observed graphitization behavior of both plain-carbon and carbon-moly steels. Use has been made of this hypothesis to explain the resistance to graphitization of the nickel-chrome-moly steels. The experimental evidence would appear to indicate that the hypothesis is substantially correct.

GRAPHITIZATION characteristics of steels for steam service at elevated temperatures have been a subject of study by many workers since the original failure of a welded carbon-molybdenum steel pipe at the Springdale Station of the West Penn Power Company in January, 1943. Subsequent to that failure graphitization has been found in various classes of wrought and cast products, particularly in weld-affected zones, in the examination of piping systems made by the different power companies.

Happily, the Springdale failure was not disastrous, and to our knowledge none of the other piping systems examined has shown equally extensive graphitization. Nevertheless, it is highly desirable to ascertain means whereby deterioration due to graphitization can be avoided. At the same time it is necessary to preserve in graphitization-resistant material high mechanical properties such as creep strength, soundness, good weldability, and overall economy.

For increasing efficiency in power-plant operation increase in operating temperature is among the promising approaches. Increase to the present 900-950 F has been a development of the past decade. Even now plans are under way for 1000 F operating temperature, and the end of the upswing does not seem in sight. With longer experience acquired as to serviceability of materials at these temperatures, undesirable characteristics have been revealed which hitherto have been unsuspected. From this experience some materials have been shown to be unsuitable for the service. Carbon steel which serves admirably at lower temperatures shows marked loss in mechanical properties at 800 F and is not recommended. Carbon-molybdenum steel which has excellent mechanical properties at 900 to 950 F now is revealed to possess unfortunate graphitization characteristics, limiting its useful application to perhaps 850 F as top operating temperature where welding is a consideration.

In developing and prescribing steels for these higher temperatures, close attention must be paid toward avoiding failures that by chance might occur. All the factors that could contribute to deterioration and failure must be thoroughly investigated. This point is emphasized by occurence of the Springdale failure.

[1] The Lunkenheimer Company, Cincinnati, Ohio.

Contributed by the Joint A.S.T.M.-A.S.M.E. Research Committee on Effect of Temperature on the Properties of Metals and presented at the Annual Meeting, New York, N. Y., Nov. 26–29, 1945, of THE AMERICAN SOCIETY OF MECHANICAL ENGINEERS.

NOTE: Statements and opinions advanced in papers are to be understood as individual expressions of their authors and not those of the Society.

The Springdale failure was unexpected. Prior to the failure but one instance of graphitization of low-carbon steel had been reported in the literature (1).[2] Use of molybdenum in steels in high-temperature service led graphitization to be an unsuspected probability since molybdenum is normally considered a relatively strong carbide former and as such likely to promote carbide persistence. There have been arguments for many years on the logic of a double iron-carbon constitutional diagram. Weight of the evidence indicates, however, that iron and graphite are the equilibrium forms, iron carbide or cementite being at best metastable. Since a vast amount of work was required for assuring suitable strength at temperature, possibility of graphitization and other types of structural degradation were neglected.

THE GRAPHITIZATION PROBLEM

The problem of graphitization is complex. It would be quite impossible to study the problem in all of its various phases simultaneously, and it becomes necessary to isolate the various factors and study them individually before any attempt may be made at a comprehensive answer. The problem may be broken down into several subheads, among which are the following:

1 Effects of steel-making practice.
2 Effects of alloying and other elements.
3 Effects of heat-treatment.
4 Effects of fabricating practice.
5 Effects of service operating conditions.
6 Mode of graphitization.
7 Repair of graphitized structures now in service.

Most of the product of the authors' company is in the form of castings. Hence its work in general has been restricted to castings. Certain phases of the foregoing outline have not been touched upon in this work and will be brought up only incidentally. In view of the extensive investigation being carried on by the joint E.E.I.–A.E.I.C. Subcommittee on Graphitization of Piping, no work has been done on possible methods of repair of graphitized structures.

Effect of steel-casting-making practice has been studied here in respect to deoxidation practice.

Fabricating practice, i.e., rolling, upsetting, welding, etc., has not been described in the present report although some work is described on graphitization of structures simulating weld structures.

In the work of the authors' company, some 1300 specimens have been prepared and examined under various conditions of alloy, heat-treatment, and aging-treatment. In this report only those samples will be commented on which were productive of positive evidence in these studies. The others represent duplicate tests for verification of original findings, tests on samples from other heats for the same purpose, cycling tests, etc. The samples chosen for illustration thus should be considered as representing generic classes of structures. The evidence presented for them has been fully corroborated.

GRAPHITIZATION IN STEEL CASTINGS

After the Springdale failure many piping systems were examined by the various power companies chiefly by removal of bolt samples from the welded joints. An early discovery of graphiti-

[2] Numbers in parentheses refer to the Bibliography at the end of the paper.

zation in a valve casting led to replacement of the valve in the line so that complete and more leisurely examination could be made. The valve was used as a boiler stop valve at nominal operating temperature of 900 F and was in service a period of 44,137 hr, 1909 of which were 950 F or above, 4½ at 1000 F.

The casting had been made in 1936 by the older melting practice of "catching the heat coming down" with partial aluminum deoxidation in the ladle, the remainder in the stream on pouring the mold. Total aluminum added was 1.86 lb per ton.

Analyses were made at several locations. Analyses of inlet and outlet ends were as given in Table 1.

TABLE 1 ANALYSES OF INLET AND OUTLET ENDS OF PIPE

	Inlet, per cent	Outlet, per cent
Total carbon	0.31	0.31
Graphitic carbon	0.12	0.04
Silicon	0.40	0.41
Manganese	0.77	0.76
Phosphorus	0.020	0.021
Nickel	0.11	0.05
Copper	0.05	0.04
Molybdenum	0.42	0.44
Chromium	None	0.01
Aluminum (as Al_2O_3) per cent Al	0.012	0.010
Free aluminum per cent Al	0.017	0.018
Total aluminum per cent Al	0.029	0.028



FIG. 1 GRAPHITE IN WELD-AFFECTED ZONE OF CASTING GRAPHITIZED IN SERVICE; ×500

It will be seen that there is no significant difference except in graphite content between the two ends of the valve. Marked visible graphitization had taken place at the inlet end, none could be discovered microscopically in examining several segments of the outlet end. The original cast structure throughout was fine pearlite-ferrite. Graphite in the weld-affected zone was nodular and associated with the carbide areas as shown in Fig. 1.

The wrought-pipe structure was coarse Widmanstäten-ferrite, graphite being similar in amount, type, and distribution to the casting. Just as graphite was not found in the outlet end of the casting neither was it found in the pipe welded thereto. Welding conditions, in so far as they can be judged at this time and presumably as closely as they can be held commercially, were identical.

Service conditions are suspect, yet graphitization was fully reversed in a stop valve from another boiler just adjacent with both high-pressure lines leading to the same manifold. In this other case graphitization was found in the outlet but not in the inlet of both pipe and casting. Truly remarkable circumstances but illustrative of the point that graphitization is in some cases a "hair-trigger" proposition.

Mechanical properties of the graphitized inlet end were investigated, with the finding that there was little impairment of tensile strength and appreciable impairment of elongation and impact. Actual properties were as follows:

Yield strength, psi	57000
Tensile strength, psi	72000
Reduction of area, per cent	54
Elongation, per cent	11.2
Charpy (check tests) ft-lb	7, 9, 6

The tensile bar was made with axis normal to the weld interface, yet the break occurred in the weld metal, not in the graphitized zone. Vee notches in the Charpy bars were placed at the line of graphitization. (Impact value for the base metal of the casting was 18 ft-lb.)

In bend tests made with the bend at the graphitized zone, samples withstood a bend of 90 deg without cracking.

These values show that graphitization has by no means approached the point where it can be considered dangerous, even though it is undesirable. A metal with 6-9 Charpy is hardly "brittle."

GRAPHITIZATION OF WELDED STRUCTURES

Inasmuch as the Springdale failure was associated with a weld-affected structure, it became incumbent on investigators to include in their agenda of research, studies of this phase of the graphitization problem. Previous extensive studies on welding by the authors' company and others indicated that for an investigation of this type there are too many variables involved for proper assignment of causes of acceleration of graphitization. While normal control of welding insures a commercially desirable result in most cases, absence of exact thermal and composition control leads more to speculation than to scientific fact in considering graphitization rates.

It was evident from our examination and that of others of the Springdale failure that graphitization was most acute in metal which had been raised to the neighborhood of the lower critical temperature. In any work this, then, is a zone of interest. To simulate such structure under closely controlled conditions of temperature, yet free from such influences as composition, gas, slag, etc., present in welds, standard bars (⅞ in. round × 6 in. long) were heated at one end in a bath at 1600 F, the other end at 600 F, and after holding at temperature 1 hr the bars were quenched. Hardness surveys were then made to determine the critical zones, whereupon the bars were placed in aging furnaces at 975 F, 1025 F, and 1100 F. Graphitization was found to be most rapid at 1100 F, very slow at 975 F, hence 975 F was discontinued as an aging temperature.

In steels prone to graphitization, graphite appeared first in the critical zone, subsequently appearing in the zone quenched from a higher temperature, and later in the zone quenched from a lower temperature. From this it would appear that welding, *per se*, is not responsible for the severe graphitization in the weld-affected zone, but that this condition is induced by heating the material to perhaps just above the critical followed by rapid cooling. To verify this point several samples were heated to various temperatures

TABLE 2 COMPOSITIONS AND MECHANICAL TEST PROPERTIES OF STEEL SAMPLES

Heat	A	B-S	B-A	C-S	C-A	D	E-S	E-A	F
Carbon, per cent	0.30	0.28	0.28	0.21	0.20	0.27	0.26	0.23	0.25
Silicon, per cent	0.42	0.38	0.42	0.42	0.53	0.40	0.27	0.36	0.43
Manganese, per cent	0.65	0.70	0.70	0.75	0.74	0.64	0.61	0.59	0.70
Phosphorus, per cent	0.037	0.034	0.031	0.036	0.034	0.027	0.024	0.020	0.025
Sulphur, per cent	0.044	0.034	0.033	0.033	0.034	0.026	0.026	0.029	0.020
Molybdenum, per cent	...	...	...	0.57	0.56	0.51	0.90	0.40	0.36
Nickel, per cent	...	...	...	...	...	...	0.81	0.93	0.99
Chromium, per cent	...	...	...	...	...	...	0.39	0.53	0.63
Aluminum (total), per cent	0.070	0.008	0.053	0.007	0.058	0.085	0.0030	0.024	0.063
Al_2O_3, per cent	0.023	...	0.019	...	0.018	0.026	...	0.015	0.026
Al in Al_2O_3, per cent	0.012	...	0.010	...	0.010	0.014	...	0.0079	0.014
Yield point, psi	48900	38100	44800	53200	53100	56400	75000	57000	71400
Tensile strength, psi	75800	69000	78100	79400	79000	81200	100700	88300	94400
Elongation, per cent	26.9	32.6	27.2	27.8	29.5	84.4	18.8	24.1	21.0
Reduction in area, per cent	36.7	60.1	49.2	61.0	57.8	46.0	44.9	45.1	41.6



FIG. 2 GRAPHITIZATION IN CARBON-MOLY STEEL AFTER 500 HR AT 1100 F IN SAMPLE, QUENCHED FROM 1390 F; ×1000

within this critical range. Graphitization was found to occur most rapidly in samples heated to 1390 F and water-quenched, appearing extensively as early as 500 hr at 1100 F. Time of heating these samples at 1390 F was 3 hr. Graphitization as it appears is shown in Fig. 2.

Welding and its effects on graphitization in piping systems are not to be set aside briefly. However, simple one-bead welds, or restriction to a single set of welding conditions are likely to lead to unsound conclusions. Precise time-temperature conditions (at given locations) and other variables are neither known nor controllable in usual welding techniques. This means that welding studies, to be safely useful, must include many variations in welding practices, hence must be voluminous in respect to experimental manipulations. Extensive investigation is under way to study its full bearing on the problem, the results of which it is hoped will be presented at an early date.

If heating to a zone in the neighborhood of 1390 F (for carbon-molybdenum steels) is critical for promotion of graphitization, as is indicated by the foregoing experiments, and the time at this temperature is not too significant, as the experiments also suggest, then any method of differential heating (welding or other) will produce a zone critical for graphitization. This would call for viewing with caution any method designed to offset the effects of welded structures such as have been proposed, for example, austenitic welding, postnormalizing, etc. Such procedures might serve merely to move the zone to a different location without certain amelioration.

EFFECTS OF DEOXIDATION PRACTICE AND HEAT-TREATMENT ON GRAPHITIZATION TENDENCIES

Certain studies were carried out to ascertain some of the effects of silicon and silicon-aluminum deoxidation and of various structures and treatments on the graphitization tendency of carbon (A.S.T.M. A-216-WC-B), carbon-molybdenum (A.S.T.M. A-217-WC-1), and nickel-chrome-moly (A.S.T.M. A 217-WC-4) steels.

Steels were made up according to regular commercial practice, i.e., $2^1/_2$-ton charges in acid electric furnace. Practice includes ore addition and boil, followed by recarburization and furnace deoxidation by ferrosilicon, ferromanganese, and silicomanganese. Before pouring, tests of such metal lie quietly due to the "silicon deoxidation." ("Silicon-deoxidized" samples were taken at this period.)

When the steel is poured into a large ladle, aluminum is plunged in, 2.4 lb per ton being used. Samples taken therefrom are referred to as "silicon-aluminum-deoxidized."

All samples received a normalize after 5 hr at 1650 F, and were drawn for 5 hr at 1200 F, before subsequent experimentation.

Compositions and room-temperature mechanical test properties of the steels referred to are given in Table 2.

Carbon Steel— WC-B (Heat A). Samples, silicon-aluminum-deoxidized, were heated 3 hr at 1550 F, and quenched into molten tin at 1300 F, at which temperature they were held for 30 sec, 2 min, 20 min, 2 hr, and 5 hr, followed by water-quenching. A complete range of structures was developed, from martensite to lamellar pearlite. Substantial amounts of proeutectoid ferrite were evident in all samples. A comparison sample quenched directly into water from 1550 F, yielded a martensitic structure with small amounts of proeutectoid ferrite appearing only in the boundaries of the original dendrites.

Aging 2000 hr at 1100 F produced full spheroidization, of about the same particle size, and graphitization, to about the same degree, in all samples.

Carbon Steel—Heat B. This metal was divided into silicon-deoxidized and silicon-aluminum-deoxidized portions. A series of isothermal quenching treatments was performed on samples of both coarse and fine austenitic grain size. Coarsening temperature was 1900 F, followed by furnace-cooling to 1550 F, and quenching. Refining was carried out by heating to 1550 F, followed by direct quenching. Quenching was carried out in a controlled tin bath.

Temperatures employed were those used in earlier work on car-

bon-molybdenum steel (4) and which gave the structures for carbon moly shown in Table 3.

TABLE 3 CARBON-MOLYBDENUM STEEL STRUCTURES, HEAT B

	Structure (carbon moly)	Transformation temperature, deg F
I	Coarse pearlitic	1200
II	Coarse mixed pearlitic-acicular	1000
III	Coarse acicular	800
IV	Coarse martensitic	500
V	Fine pearlitic	1200
VI	Fine mixed pearlitic-acicular	1000
VII	Fine acicular	800
VIII	Fine martensitic	500

The acicular structure of the carbon-moly steels is not a member of the plain-carbon-steel series, hence was not developed in this experiment. Also it was not possible to develop a martensitic structure at 500 F in this carbon steel. However, since we are more concerned with comparative temperature levels in processing these materials than in the actual structures, it was thought desirable to retain the quenching-bath temperatures used earlier and on which fairly complete data were available.

TABLE 4 CARBON-STEEL STRUCTURES

	Structure (carbon steel)	Transformation temperature, deg F
I	Coarse pearlitic	1200
II	Coarse mixed pearlitic-bainitic	1000
III	Coarse upper bainitic	800
IV	Coarse lower bainitic	500
V	Fine pearlitic	1200
VI	Fine mixed pearlitic-bainitic	1000
VII	Fine upper bainitic	800
VIII	Fine lower bainitic	500

In the carbon steels Table 4 gives the structures approached. The structures shown in Figs. 3 to 6 respectively, are of the coarse series, and it may be seen that they do not correspond in all respects to the type description. This is because of the difficulty of securing a homogeneous austenite in cast materials. Because of these inhomogeneities there was marked separation of proeutectoid ferrite similar to that developed in conventional heat-treatment of castings. This alters the effective carbon concentration in the carbide areas and affects the time of reaction at a given temperature.

All of the silicon-aluminum-deoxidized samples graphitized within 1000 hr at 1100 F. Graphitization was most general in the type VIII sample (fine lower bainite). Size of graphite particles was about the same in all samples.

Of the silicon-deoxidized samples the following graphitized at 1100 F within the time indicated:

I	Coarse pearlitic	2000 hr
II	Fine pearlitic	6000 hr
VII	Fine upper bainitic	4000 hr

The following were resistant for the duration of the test, 6000 hr:

II	Coarse mixed pearlitic bainitic
III	Coarse upper bainitic
IV	Coarse lower bainitic
VI	Fine mixed pearlitic-bainitic
VIII	Fine lower bainitic

The foregoing suggests that fine and uniform distribution of carbide may lessen initial graphitization tendency. Since such distribution indicates less steep carbon-concentration gradients, such influence might be expected, at least in initiation of the reaction. However, once action is started, a more general nucleation might well cause more general graphitization.

In case of this carbon steel, silicon-aluminum deoxidation favors graphitization, but the absence of aluminum does not always prevent it.

The two deoxidation practices influence hardenability, silicon deoxidation tending toward coarser grain and deeper hardening. Since bainitic structure in silicon deoxidized graphitized, the effects of differences in hardenability characteristics (as influenc-



FIG. 3 COARSE PEARLITIC CARBON STEEL; ×500



FIG. 4 COARSE MIXED PEARLITIC BAINITIC CARBON STEEL; ×500

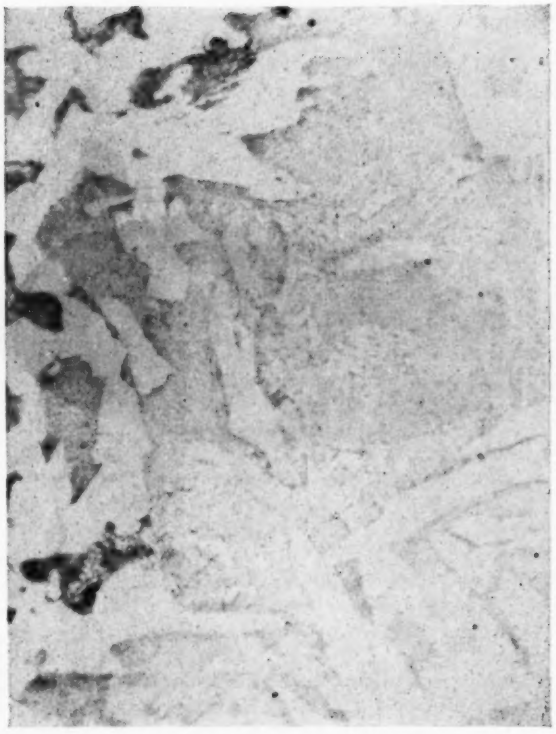


FIG. 5 COARSE UPPER BAINITIC CARBON STEEL; ×500

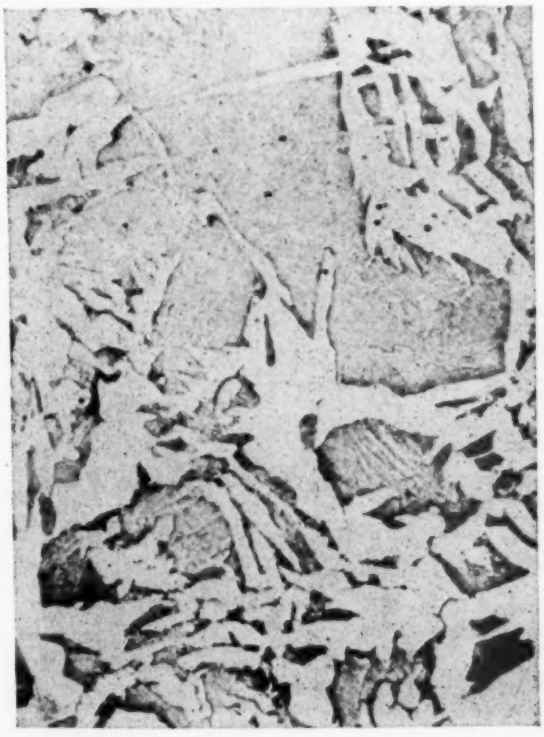


FIG. 6 COARSE LOWER BAINITIC CARBON STEEL; ×500

ing graphitization) may be somewhat discounted. However, a number of these points require more extensive study before firm generalities can be safely made. Subject to this qualification, the experimental work on carbon steel (WC-B) suggests the following:

(*a*) Silicon kill retards graphitization tendency, but does not safely prevent it.

(*b*) Carbon-concentration gradients appear to promote the earlier formation of graphite.

(*c*) Greater carbon homogeneity may promote more general graphitization, once the reaction is initiated.

(*d*) Coarser austenitic grain and deeper hardening characteristics tend toward greater resistance, but may not assure it. (This might well be independent of agencies promoting such structure.)

Conventional normalize and anneal, under production conditions permitted graphitization in both silicon and silicon-aluminum-deoxidized conditions. Silicon-aluminum deoxidized graphitized in less than 4000 hr; silicon deoxidized in 6000 hr.

Principal structures aged at 1100 F were aged in duplicate at 1025 F. Of the silicon-aluminum deoxidized all had graphitized at 1000 hr, with the exception of the mixed pearlitic-bainitic, again showing the resistance of this structure to graphitization. Otherwise little difference was to be noted from 1100 F aging.

Carbon Moly (WC-1) Steel (Heat C). This material was divided into silicon-deoxidized and silicon-aluminum-deoxidized portions. Samples were put into the following structural conditions, and graphitization time as it appeared in the silicon-aluminum deoxidized samples which developed graphite within 6000 hr is as given in Table 5.

TABLE 5 CARBON-MOLYBDENUM STRUCTURES; HEAT C

Structure (carbon moly)	Graphitization
Coarse pearlitic	2000 hr
Coarse-pearlitic-acicular	None
Coarse acicular	2000 hr
Coarse martensitic	None
Fine pearlitic	6000 hr
Fine pearlitic-acicular	None
Fine acicular	None
Fine martensitic	None

In these structures there was considerable separation of proeutectoid ferrite leaving the carbides as islands in a ferritic ground mass. This appears to be the common pattern developed in carbon-moly steels. In looking for graphitization such structures are suspect. On the other hand, the structure description describes the state of aggregation of the carbide to much better degree than was found for the carbon steels.

No graphitization was found in the corresponding silicon-deoxidized samples, within 6000 hr.

The grain size for the silicon-deoxidized portion was 2-3 with normal McQuaid-Ehn as shown in Fig. 7.

In heat D, silicon-aluminum, killed, similar samples all graphitized within 6000 hr or less. Grain size and normality were similar for both silicon-aluminum-killed heats, i.e., 6-7 and markedly abnormal McQuaid-Ehn, Fig. 8.

Production heat-treatment of normalize from 1650 F yielded graphitization within 2000 hr in the silicon-aluminum-deoxidized, none within 6000 hr in the silicon-deoxidized. However, graphitization was found in 6000 hr in a silicon-deoxidized sample held 5 hr at 1650 F, and furnace-cooled as shown in Fig. 9. The sample illustrated is the only one that has been developed experimentally in our work showing an approach to chain graphite. All others have been nodular. The correspondingly treated silicon-aluminum-deoxidized sample showed nodular graphite.

The results on carbon moly (WC-1) indicate that silicon deoxidation resulting in coarse-grain normal McQuaid-Ehn structures retards graphitization, but does not always prevent it, as was established also in case of carbon (WC-B) steel. It is apparent that as compared with carbon steel the molybdenum content of WC-1 increases carbide persistence.

In another experiment on a silicon-aluminum-deoxidized sample, heat C was held 5 hr at 1650 F and furnace-cooled, then

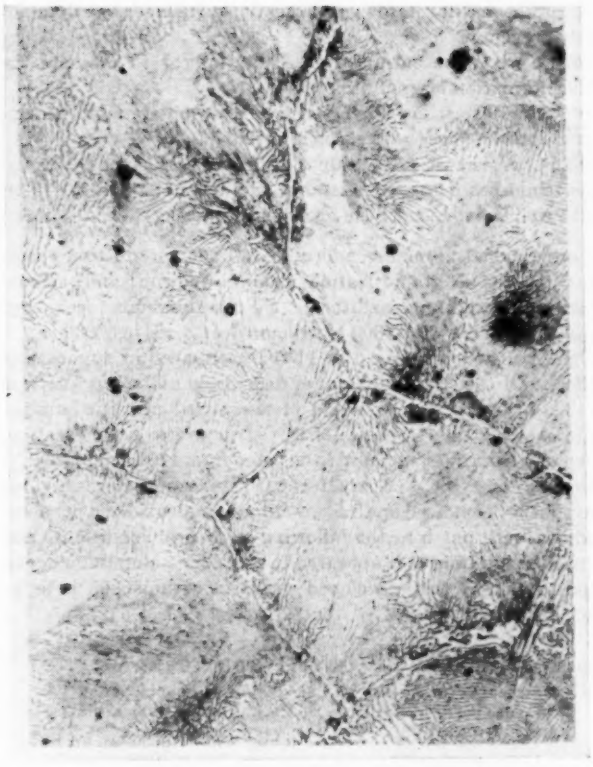


FIG. 7 McQUAID-EHN CASE HEAT C SILICON DEOXIDIZED; ×500



FIG. 8 McQUAID-EHN CASE HEAT C SILICON-ALUMINUM DEOXIDIZED; ×500



FIG. 9 GRAPHITIZATION IN SILICON-DEOXIDIZED, HEAT C; ×500

drawn for 10 hr at 1300 F; graphitization being produced within 4000 hr at exposure to both 1025 and 1100 F.

This treatment was employed to determine the effectiveness of high-temperature annealing in order to stabilize the carbides in somewhat different form as suggested by Smith and Miller (5).

Consideration of these and other studies, and of the published literature and field data, indicates that carbide persistence is influenced by many variables; some whose general influence seems clear, others which must be better known and evaluated before conclusions can be drawn.

Since strength at temperature is fully as important as structural stability, creep tests were run at 950 F on samples from heat D, heated for prolonged periods at the suggested stabilizing temperature, i.e., 110 hr at 1320 F, after normalizing from heating at

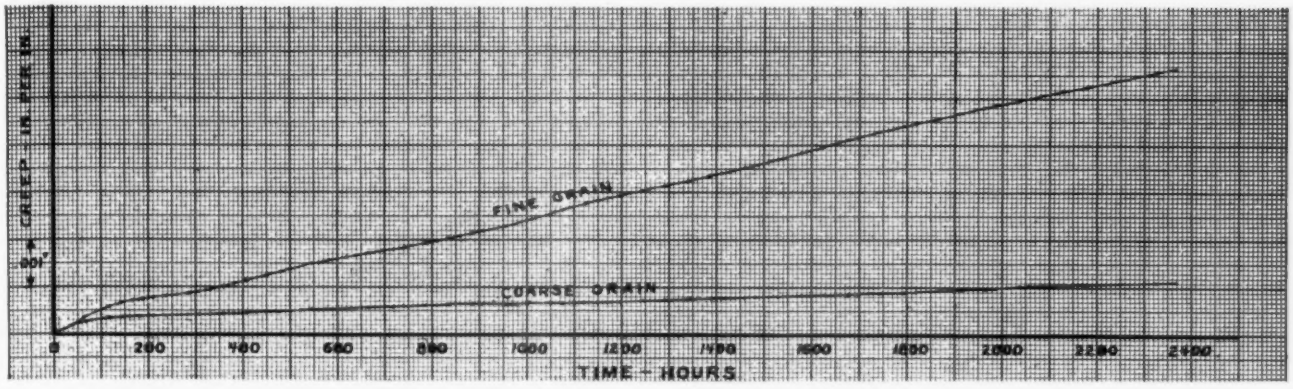


FIG. 10 CREEP CURVES FOR CAST CMO STEEL

1550 F in one case and from heating at 2200 F, followed by furnace-cooling to 1550 F in another to yield both fine- and coarse-grained structures in a highly spheroidized condition. The resulting creep curves are shown in Fig. 10. Tests were carried out for a period of 2400 hr under loads of 12,000 psi. In both cases graphitization was found after test. The test temperature of 950 F was the lowest at which graphitization has been produced in this laboratory. At least in this steel, treatment at 1320 F has not insured against graphitization. Structures of the samples before and after test are shown in Figs. 11 to 14, inclusive.[3]

Nickel-Chrome Moly (WC-4) Steel. Samples of silicon-deoxidized and silicon-aluminum-deoxidized metal, heat E, were prepared. Each series was placed in the eight structural conditions listed for carbon moly (WC-1) given previously. After exposures to a maximum of 6000 hr at 1100 F, no graphization appeared in any sample.

In another series of experiments on a silicon-aluminum-deoxidized heat, heat F, with samples placed in the same structural condition, no graphite was found after 7976 hr at 1100 F. Duplicate experiments at 1025 F also failed to reveal any evidence of graphite development.

As in the carbon-moly steels, creep tests on nickel-chrome-moly steel were carried out with identical prior heat-treatment including commercial normalize and draw conditions. No graphitization was found in the bars after test. Structures before and after testing were as shown in Figs. 15 to 18, inclusive.

It will be noted that a number of the structural and deoxidation conditions in which WC-4 was placed correspond to those in which

[3] "Coarsened" means coarsened austenitic grain size. This treatment results in greater carbon homogeneity. Thus the resulting transformation product aggregations (Figs. 11 to 14, inclusive) give appearance of finer "grain" in the coarsened sample photomicrographs. There is no anomaly. The reader is cautioned not to confuse "pearlitic" grain-size appearance with austenitic grain which is not shown.

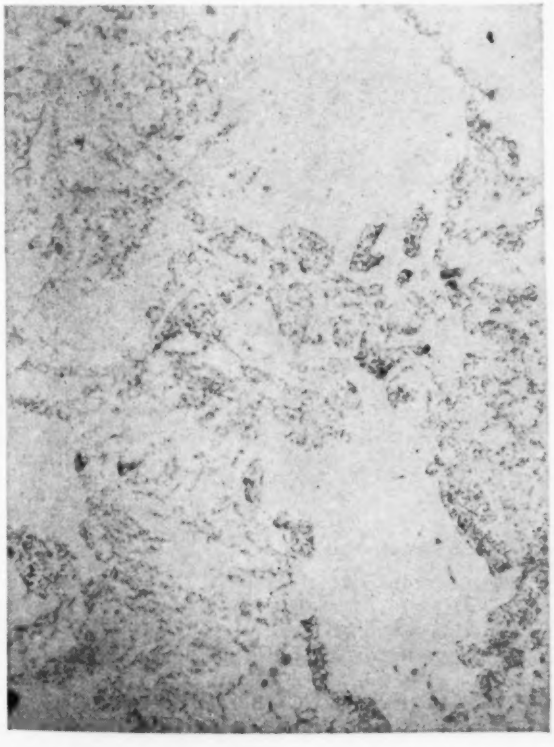


FIG. 11 COARSENED WC-1 BEFORE CREEP; ×500



FIG. 12 REFINED WC-1 BEFORE CREEP; ×500



FIG. 13 COARSENED WC-1 AFTER CREEP; ×500



FIG. 14 REFINED WC-1 AFTER CREEP; ×500

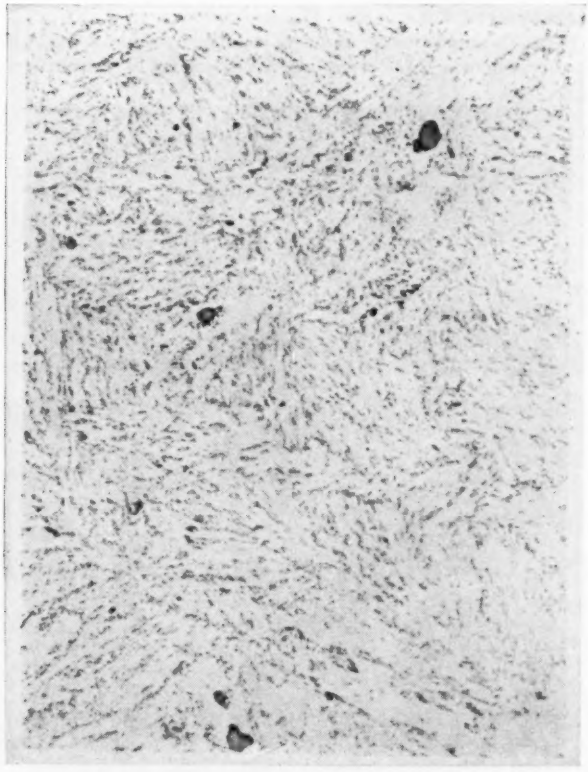


FIG. 15 COARSENED WC-4 BEFORE CREEP; ×500

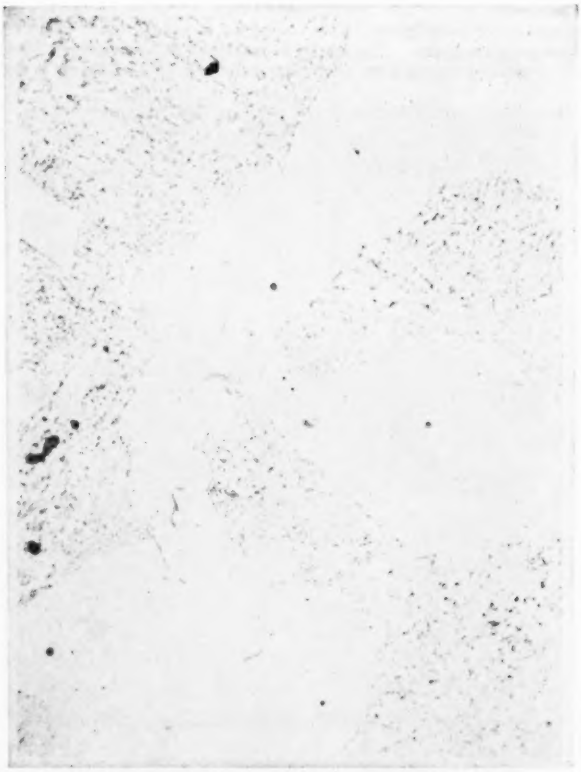


FIG. 16 REFINED WC-4 BEFORE CREEP; ×500

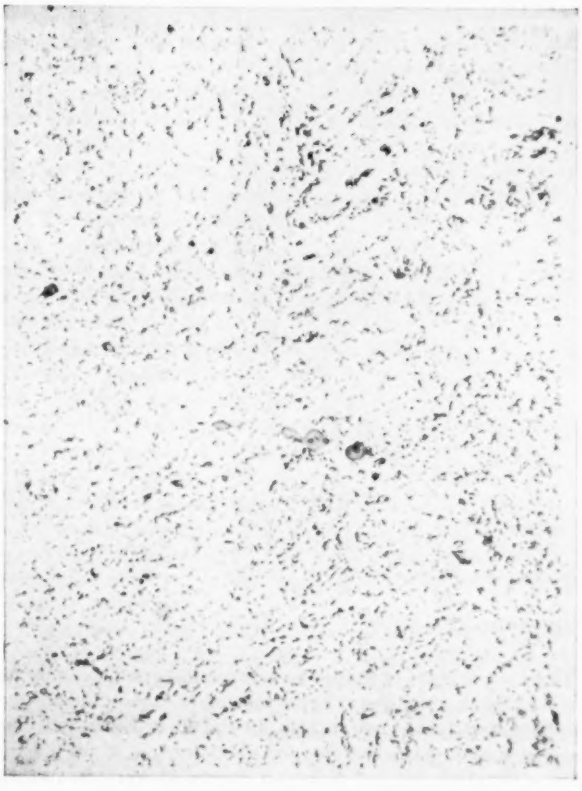


FIG. 17 COARSENED WC-4 AFTER CREEP; ×500



FIG. 18 REFINED WC-4 AFTER CREEP; ×500

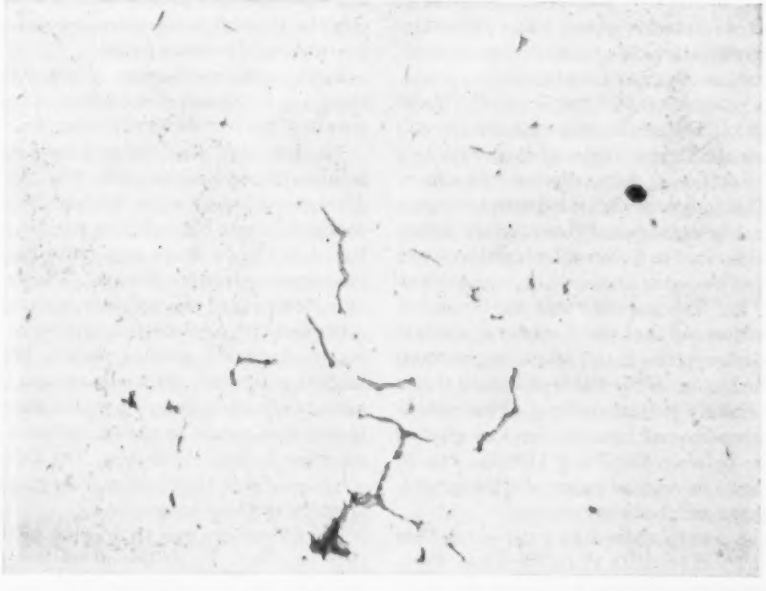


FIG. 19 PIPE REMOVED FROM SERVICE AND GIVEN CYCLING TREATMENT; ×500

rapid graphitization was found in carbon-moly (WC-1) steel. Work on WC-4 was confirmed by study of several heats. (Differential quench samples also showed no graphitization.)

MODE OF GRAPHITIZATION

Emerson (6) has distinguished between two types of graphite formation, "nodular" and "chain." Our study suggests the desirability of including a third type, "flake," a formation shown in Fig. 19. Graphite formations and groupings in reality are in three dimensions, not two, as they appear in a photomicrograph. This must be borne in mind in any attempt to evaluate apparent orientations in respect to their evolution and effects.

Emerson (6) has illustrated the chain formation in such a way as to leave little doubt as to its distribution and possible conse-

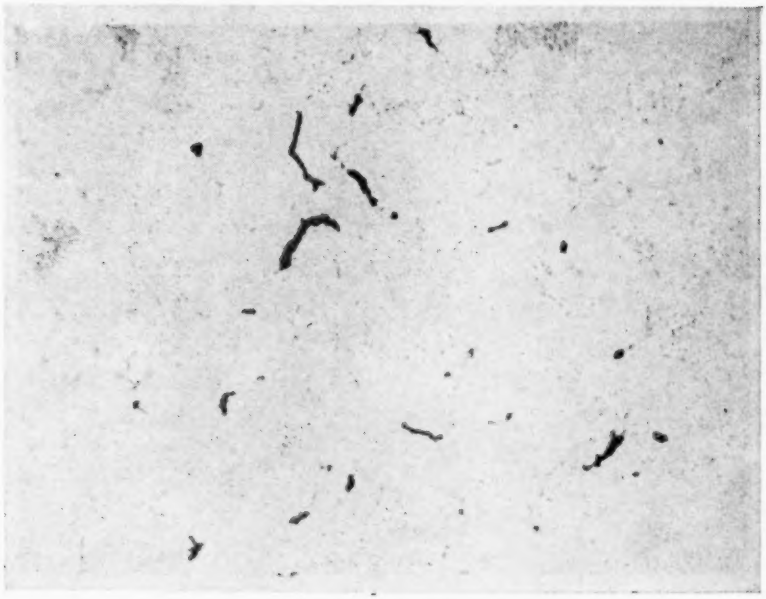


FIG. 20 CASTING AS REMOVED FROM SERVICE; ×500

quence. A flake may be but a progressive development of a chain although our studies suggest otherwise.

For the purpose of identifying graphite, polarized light has been very useful. Graphite crystallizes in the hexagonal system and shows extreme pleochroism and birefringence in polished section (7). Using a first-order red compensator plate, the change from red to green with stage rotation is striking and distinctive. This and other characteristics of graphite have been observed before in this laboratory in the course of its studies on cast iron. Hence the tool fits very nicely into investigations of graphitization in steel.

The color change at extinction for a particular crystal depends, among other factors, on its orientation with respect to the plane of polarization of the light. Differently oriented anisotropic crystals will show extinction at different angles of stage rotation. Nodular graphite shows a mottling of red and green with a first-order red compensator. This indicates that it is formed of many small crystallites of various orientations. However, in many of the graphite formations described as flake, uniform extinction of the whole flake was shown at the same angle. This was evident in the flakes shown in Fig. 19. This suggests that the formation is of uniform crystal orientation and is of the character of a single crystal, bearing close similarity to the flakes found in cast iron. The massive portion attached to one of the flakes of Fig. 19 shows the mottled effect and is definitely polycrystalline. This sample was from a segment of pipe removed from service and given a cycling treatment for 800 hr between 950 F and 1100 F. Fig. 20 is from a sample taken from a casting as removed from service. It also shows the single crystal or flake behavior.

Were these flakes built up from a chain it is improbable that there would be crystallographic uniformity along the whole chain. The Widmanstätten relationship which exists between matching planes of precipitate and matrix can be met in several different ways with respect to the plane of polish, so there is no requirement that all graphite particles separating from a single ferrite grain should have the same orientation with respect to the plane of polish even though the growth mechanisms are identical. Thus a plate of graphite built up from a series of particles originally in chain form would be expected to be broken up crystallographically into a number of segments which would be clearly revealed by examination in polarized light.

There is one point of similarity between flake and chain formation which seems significant in attempting to explain the mode of graphitization. As shown in Figs. 19 and 20, in Emerson's illustrations of chain formation (6), and also in certain of the illustrations of Weisberg (8) and Kerr and Eberle (9), graphite in these instances is located in the ferrite grain boundaries. Nodular graphite usually is associated with the carbide areas. While chain and flake graphite may be attached to carbide areas, perhaps at other locations than the plane of polish, the formations extend out into regions of primary ferrite.

The general mechanism of graphite formation involves two steps, i.e, formation of a nucleus or initial graphite particle, and growth of the particle by diffusion of carbon to it.

The first step necessitates a local concentration of carbon together with some nuclear influence. The nuclear influence may be developed in many ways, submicroscopic impurities or other discontinuities probably playing a major role. A grosser sort is illustrated in Fig. 14 where a graphite flake is seen radiating from a manganese-sulphide inclusion. The second step requires diffusion of carbon toward the first formed particles from carbides or from other graphite particles less capable of sustained growth. As the region about the growing particle becomes depleted in carbon, migration through the ferrite occurs. Ferrite dissolves a certain amount of carbon (varying with temperature) and local depletion in one area results in carbon diffusion from another, thus maintaining a statistical balance. The diffusion distance is extreme in some cases as in the chain or flake graphite lying at some distance from the carbide "reservoirs."

Thus there are two approaches in the problem of preventing deterioration: Promotion of relative carbide stability; and the lessening of the possibility of diffusion of carbon through ferrite.[4]

Other factors being equal, tendency toward graphitization in the iron-carbon series increases with increasing carbon content. Hypereutectic cast irons (with primary cementite) graphitize in the freezing range with the formation of kish or free graphite in the partly liquid metal. The gray irons graphitize rapidly in the

[4] "Stability," as used in this paper implies resistance to breakdown over a normally expected service life. It is not possible to say that any carbide is stable in the true equilibrium sense. However, the term is descriptive when used in its practical sense.

interval between the eutectic and eutectoid temperatures. This graphitization may continue even below the eutectoid under slow-cooling conditions or in the presence of sufficient silicon.

In the case of malleable iron, the composition is so chosen that there is no graphitic carbon as cast. Subsequent treatment is such that the cementite is graphitized both above and below the eutectoid-transformation range. The mechanism of carbon diffusion through the ferrite toward graphite particles is perhaps most vividly shown by the formation of "bull's eyes," graphite particles surrounded with ferrite in a general pearlitic matrix.

Graphitic steel is a product of commerce. Austin's work (10) shows how readily high-carbon steel can be graphitized in quite a short time.

In normal carbide areas the concentration of carbon is high, well above that of the average for the whole sample. As more and more proeutectoid ferrite is present in a given analysis, it is readily seen that the carbon concentration in the carbide areas becomes much greater, ultimately approaching the eutectoid composition. With such concentration gradients a graphitizable steel will usually graphitize most readily regardless of state of aggregation of carbide. Thus steels with large areas of free ferrite are more suspect for serious graphitization than steels of a more homogeneous character even though the more homogeneous steels may ultimately graphitize.

The problem of stabilizing the carbide and preventing diffusion in ferrite is complex but its solution is necessary for insuring against service failures due to graphitization. All of the carbide formers have a solubility in ferrite and under proper circumstances may dissolve even when carbon is present, e.g., in the presence of a stronger carbide former. In a straight molybdenum steel the molybdenum undoubtedly is associated in large measure with the carbide. Hence with little distortion of the ferrite lattice, the interstitially dissolved carbon is able to diffuse at will. The binding forces of the molybdenum are evidently satisfied fully as well in an iron-molybdenum carbide as in a straight molybdenum carbide with the result that carbon can be given up by the molybdenum to be subsequently precipitated as graphite by the ferrite without too greatly altering the state of free energy of the system.

Although good creep properties have been shown for carbon-free iron-molybdenum alloys (11) in the normal steels, molybdenum is depended upon for conferring strength at elevated temperatures in the formation and distribution of a stable and resistant carbide. Yet it is known that certain amounts are dissolved in the ferrite. In a higher-carbon steel, 0.70 carbon, Bowman, Parke, and Herzig (12) have shown the amount in the ferrite to be of fairly low order, possibly less than 20 per cent of the total. Partition data on steels such as described in this report, are not available. It may be reasoned, however, that the partition coefficient would be changed with composition and with lower carbons more molybdenum would dissolve in the ferrite. Carbon-molybdenum steel castings for ET service contain some 30 to 50 per cent more carbon than carbon-moly piping, and hypothetically, the partitionment of molybdenum in ferrite in the piping would be greater than in the castings. Yet the piping materials graphitized perhaps more readily than the castings, at least such appears to be the case from the service record. This suggests that increasing molybdenum dissolved in ferrite would not bring about assurance of freedom from graphitization.

Creep properties at elevated temperatures are markedly altered by carbide pattern and distribution. Hence it would appear that the superior creep properties of molybdenum-bearing steels are dependent in large part upon the molybdenum or iron-molybdenum carbide and are not to be sought in steels alloyed with stronger carbide formers in which the molybdenum would be forced to much greater extent into the ferrite, leaving the new alloying element, such as vanadium or titanium, to form the principal carbides. Such steels have not been shown to possess superior elevated-temperature properties in the absence of molybdenum and improve molybdenum steels to but minor extent. Thus such carbides cannot be looked on as a source of strength at such temperatures.

To protect against graphitization by use of alloys it appears that greater success might be achieved by use of weaker carbide formers than molybdenum or by noncarbide formers, which would dissolve in the ferrite and force more molybdenum into the carbide. By distortion of the iron lattice with dissolved elements, diffusion is interfered with and at the same time the ferrite is strengthened. The molybdenum being forced further into the carbide should confer additional elevated temperature strength to the carbide. Copper, cobalt, and nickel do not form carbides and might be found to perform this particular function. Chromium would show similar behavior since, although a carbide former, it is weaker in this respect than molybdenum. It is probable that combinations of these would be of more effect than when used singly, in accordance with general knowledge of the behavior of alloying elements.

The foregoing reasoning is hypothetical. Partition data are not as yet available by which the hypothesis can be fully evaluated. However, behavior of steels of the type of WC-4, nickel-chrome-moly lends substantiation to its correctness. This steel could not be graphitized under any set of conditions in the laboratory and has not graphitized in service.

Furthermore, it has creep properties superior to carbon-moly steel as is indicated by the various creep studies. Creep tests with various comparable structures confirm this. (They are not a part of this report since they in themselves have little bearing on the graphitization problem.) The nickel may play an important part in this stabilization or it may be looked upon more as a safety measure since, not being a carbide former, it opposes ferrite solution of the other elements but would not in itself be partitioned. The finding by Smith, Miller, and Tarr (13) that a molybdenum steel containing 0.17 chromium was readily graphitizable and by Hoyt (14) that a 0.50 chromium steel could be graphitized leads to some question whether steels containing this chromium alone (as has been proposed) would provide complete assurance against graphitization. It remains for subsequent work to demonstrate conclusively whether or not such additions can be relied on for this purpose, over a wide range of manufacturing, fabrication, and operating conditions.

Discussion of Results of Studies

While the Springdale failure was disconcerting, possibilities of graphitization probably should not have been unexpected. In the high-carbon steels the problem had been studied rather extensively, especially by Austin and co-workers. A failure in straight low-carbon steel also had been observed under quite similar circumstances.

In detection of early stages of graphitization the most useful tool is the microscope. To observe graphite in a polished section a special technique is involved for its retention in the section, the graphite being readily removed in the the normal polishing operation. Undoubtedly, were graphite present it would have been preserved with inclusion polishing. However, inclusions almost invariably are studied before extended heat-treatment rather than after. This probably accounts for graphite not being detected even in creep samples until its presence was suspected.

The major question that arises is whether or not any carbide is stable under all conditions of temperature and pressure. It is entirely possible that none is, ultimately; yet certain carbides may prove sufficiently persistent to endure for the expected service life of the parts without undue deterioration.

It is not known what conditions are required for carbide stability. Molybdenum is normally considered a strong carbide former yet failure took place in a molybdenum-bearing steel. Chromium is less strong as a carbide former than molybdenum yet a nickel-chrome-moly steel proved quite resistant to graphitization experimentally and evidence from field service supports the laboratory findings. Results of others suggest that sufficient percentages of chromium likewise might be proved effective. The hypothesis has been advanced in the present paper that ferrite plays an active part at least in chain or flake graphitization. It must play a part in nodular graphitization also. If this hypothesis is correct, then an explanation of the stability of the nickel-chrome-moly steel may be found in the fact that the nickel is dissolved in the ferrite, and, with a stronger carbide former, molybdenum, being present than the chromium, the chromium likewise is largely dissolved in the ferrite, resulting in the conferring of stability to the ferrite against carbon rejection in the form of graphite.

It is believed that if a steel initially is seriously unstable from its composition, no amount of "doctoring" will insure sufficient stability for prolonged service. Thus production of a straight carbon-moly steel of coarse grain size and normal McQuaid-Ehn structure is not sufficient to prevent graphitization over normal service periods although the graphitization rate may be very considerably slower or its initiation require more unfavorable fabricating and operating conditions. A desirable initial structure likewise may retard but will not insure against graphitization. This has been shown not only for different distribution of constituents but also for their constitution, as, contrary to the suggestion of some workers, steels annealed at temperatures which would promote formation of a presumably more stable molybdenum carbide subsequently graphitized at lower temperatures.

It appears also that little is to be safely hoped for by modification of weld practice short of normalizing the whole assembly before installation since any type of localized heating will result in some zone being heated into the temperature range critical for graphitization.

Thus far, critical field graphitization has been found adjacent to welds. In many instances, however, noncritical graphitization has been found elsewhere in piping and castings. In no case that has come to the authors' attention has graphitization proceeded as far as at Springdale. Thus it is perhaps fortuitous that critical graphitization has not been found in regions not associated with welds. The recent finding at Springdale of graphite precipitated on slip planes well removed from a weld leads to suspicion that finding of such critical graphitization may be made in the not too remote future.

The use of alloys for stabilization appears to offer the most promising hope against such a condition. As indicated, it may be as fully necessary to stabilize the ferrite as to stabilize the carbide. Both laboratory and field experience appear to indicate that a steel conforming to A.S.T.M. A-217-WC-4 is an approach in this direction.

Summary

From many samples studied both from field service and controlled laboratory experiment it has not been shown possible to insure against graphitization of carbon-molybdenum steel through any of the controlled procedures of melting and deoxidation practice or heat-treatment. The evidence would appear to indicate that freedom from graphitization is to be sought through the use of alloy additions which confer greater stability to the carbide. Cases cited in the literature of graphitization of low-alloy chrome-molybdenum steel at conventional service temperatures lead to little assurance of freedom from graphitization over the normal service life by the use of such low chromium additions to the moly steels alone. Critical percentage ranges, if existent, should be revealed by co-operative work being undertaken by various agencies. Extensive experimental data lead to such assurance for the nickel-chrome-moly steels within the present specification range of A.S.T.M. A-217-WC-4. Experiments with carbon-moly steel have been duplicated for the most part with nickel-chrome-moly steel with special reference to those conditions which are critical for carbon-moly steel, silicon-aluminum kill resulting in a highly abnormal steel structure. In no case has graphitization been found in the nickel-chrome-moly steel.

A hypothesis has been put forth concerning the mode of graphitization based on the observed graphitization behavior of both plain-carbon and carbon-moly steels. Use has been made of this hypothesis to explain the resistance to graphitization of the nickel-chrome-moly steels. The experimental evidence would appear to indicate that the hypothesis is substantially correct.

BIBLIOGRAPHY

1 "Graphite in Low-Carbon Steel," by A. B. Kinzel and R. W. Moore, Trans. A.I.M.E., vol. 116, 1935, p. 318.

2 "The Effect of Normalizing on the Properties of Welds in Carbon-Molybdenum Steel Pipe," by I. A. Rohrig, D. H. Corey, and Sabin Crocker, *Welding Journal*, vol. 22, 1943, pp. 5215–5275.

3 "A Study of Austenitic Welding for Control of Graphitization in Steel," by I. A. Rohrig, pamphlet "Graphitization of Steel Piping," included in Trans. A.S.M.E., vol. 67, 1945.

4 "Structure and Creep Characteristics of Cast Carbon Molybdenum Steel at 950°F," by H. E. Montgomery and John Urban, A.S.T.M. Bulletin 125, 1943, p. 13.

5 "A Possible Means of Avoiding Local Graphitization of Steels in Service at Elevated Temperatures," by G. V. Smith and R. F. Miller, pamphlet "Graphitization of Steel Piping," included in Trans. A.S.M.E., vol. 66, 1944.

6 "Carbide Instability of Carbon Molybdenum Steel Piping," by R. W. Emerson, pamphlet "Graphitization of Steel Piping," included in Trans. A.S.M.E., vol. 66, 1944.

7 "Dana's System of Mineralogy," by C. Palache, H. Berman, and C. Frondel, seventh edition, John Wiley & Sons, Inc., New York, N. Y., 1944, p. 152.

8 "Report on High-Temperature Pipe Weld Investigation," by Herman Weisberg, pamphlet "Graphitization of Steel Piping," included in Trans. A.S.M.E., vol. 66, 1944.

9 "Graphitization of Low Carbon and Carbon Molybdenum Steels," by H. J. Kerr and F. Eberle, pamphlet "Graphitization of Steel Piping," included in Trans. A.S.M.E., vol. 67, 1945.

10 "Factors Controlling Graphitization of Carbon Steels at Sub-Critical Temperatures," by C. R. Austin and M. C. Fetzer, Trans. A.S.M., vol. 35, 1945, p. 485, including bibliography.

11 "Graphitization of Carbon-Molybdenum Steel in High-Temperature Steam Piping," by G. A. Timmons, pamphlet "Graphitization of Steel Piping," included in Trans. A.S.M.E., vol. 67, 1945.

12 "The Alpha Iron Lattice Parameter as Affected by Molybdenum and an Introduction to the Problem of the Partition of Molybdenum in Steel," by F. E. Bowman, R. M. Parke, and A. J. Herzig, Trans. A.S.M., vol. 31, 1943, p. 487.

13 "Structural Changes in Carbon and Carbon-Molybdenum Steels During Prolonged Heating at 900–1100 F as Affected by Deoxidation Practice," by G. V. Smith, R. F. Miller, and C. O. Tarr, A.S.T.M. Preprint 19a, 1945.

14 "Fundamental Investigation of Graphitization of Piping," Progress Report No. 4 Joint E.E.I.-A.E.I.C. Subcommittee on Graphitization of Piping, Edison Electric Institute Bulletin, vol. 13, 1945, p. 209.

Discussion

F. Eberle.[5] One of the most important facts developed in this paper is the experimental evidence of the fundamental instability and, incidentally, also of the relatively great stability of straight silicon-killed McQuaid-Ehn coarse-grained and normal carbon-molybdenum steels. At 975 F, which may be considered as an upper temperature limit for the use of this steel in steam-

[5] Research Metallurgical Engineer, The Babcock & Wilcox Company, Barberton, Ohio.

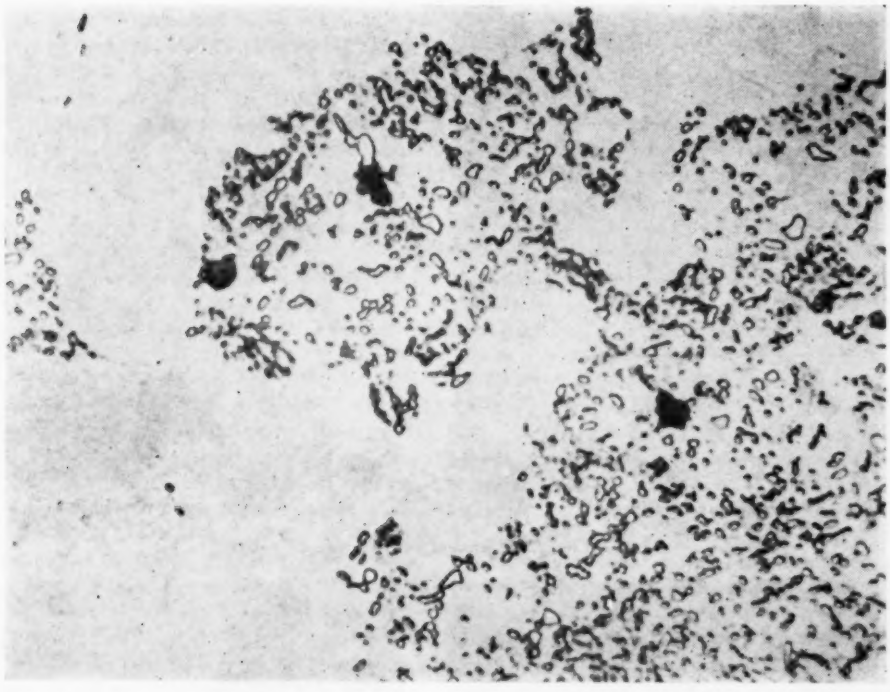


FIG. 21 LOW-TEMPERATURE END OF WELD-AFFECTED ZONE IN CREEP-TEST SPECIMEN CASE 3; ×2000

plant operation, the authors found the rate of graphitization to be very slow and therefore they conducted most of their experiments at 1100 F. Even at this extreme and impractical temperature only one out of the described ten test samples of straight silicon-killed carbon-molybdenum steel produced graphite within 6000 hr. The sample which did graphitize had been in the 1650 F-furnace-cooled condition in which the steel is most susceptible to graphitization.

As a further illustration of the fundamental instability and the relatively great stability of McQuaid-Ehn normal carbon-molybdenum steel, we present the following results of tests and examinations conducted in the laboratory of the writer's company:

Case 1. A creep-rupture specimen containing a 1200 F, stress-relieved, standard, multiple-pass arc weld in the center of the gage length was found free of graphite after 11,400 hr at 950 F under 20,000 psi which is $2^1/_2$ times the allowable working stress. The steel was silicon-aluminum-deoxidized (0.75 lb. of aluminum per ton) and was McQuaid-Ehn normal- and medium-grained (grain size No. 6). Prior to the welding the steel had been normalized at 1650 F.

Case 2. A creep-test specimen made of 1650 F normalized unwelded silicon-aluminum-killed carbon-molybdenum steel (0.5 lb. of aluminum per ton) also was found free of graphite after 8380 hr at 950 F under 10,000 psi which is $1^1/_4$ times the permissible working stress. This steel, too, was McQuaid-Ehn normal- and medium-grained (grain size No. 4-5 with some No. 6).

Case 3. A creep-test specimen made of the same material as previously described (case 2), but containing a standard multiple-pass arc weld, stress-relieved at 1200 F, in the center of the gage length, was found to contain a very few tiny graphite nodules in the low-temperature end of the weld-affected metal after 8380 hr at 950 F under 10,000 psi which again is $1^1/_4$ times the allowable working stress. These graphite nodules were so small that they could be recognized only at very high magnification and then identification was not absolutely assured (see Fig. 21 of this discussion).

Case 4. Another creep-test specimen, again made of the same material as used for the last described two samples, but containing repeatedly arc-welded and unstress-relieved shoulder pads at the ends of the gage length, was found totally free of graphite after 7002 hr at 950F under 10,000 psi which is $1^1/_4$ times the permissible working stress.

Case 5. A creep-test specimen made of straight silicon-killed McQuaid-Ehn normal- and coarse-grained carbon-molybdenum steel (grain size Nos. 2-4) in the 1650 F annealed (slow-furnace-cooled) condition and containing a standard multiple-pass arc weld, stress-relieved at 1200 F, in the center of the gage length, was found free of graphite after 5800 hr at 1000 F under 10,000 psi which is twice the working stress permitted by the Boiler Code.

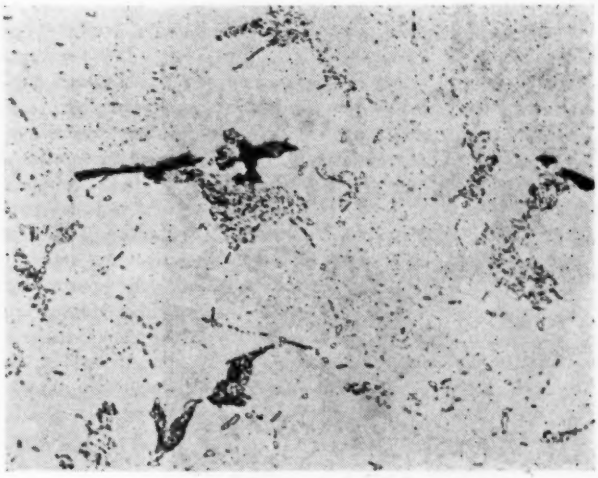
Case 6. An identical creep-test specimen as just described, but with an unstress-relieved weld in the center of the gage length, was found to contain scattered medium-sized graphite nodules in both the weld-affected and weld-unaffected metal after 13,420 hr at 1000 F under 10,000 psi, which again is twice the allowable working stress, Fig. 22 (*a* and *b*).

Case 7. Another creep-test specimen of the same annealed straight silicon-killed carbon-molybdenum steel as previously described (cases 5 and 6) and again containing a 1200 F stress-relieved standard multiple-pass arc weld in the center of the gage length, also displayed scattered medium-sized graphite nodules in both the weld-affected and weld-unaffected metal after 13,440 hr at 1000 F under 10,000 psi. Number and size of the graphite nodules were not markedly different from those in the unstress-relieved weld specimen of case 6, Fig. 23 (*a* and *b*).

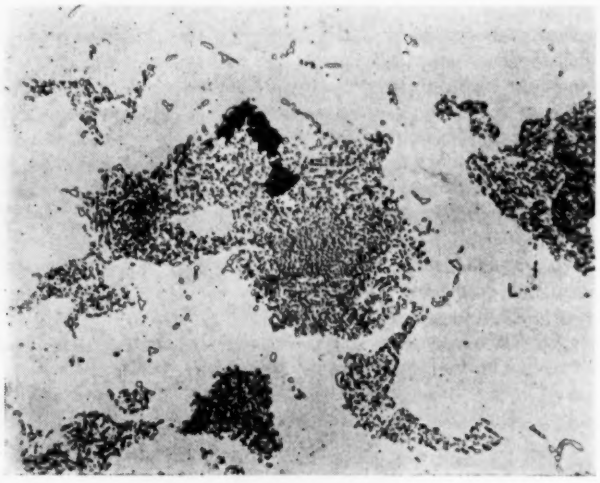
Case 8. An unwelded section of a refinery tube of straight silicon-killed McQuaid-Ehn normal and coarse-grained carbon-molybdenum steel was found free of graphite after 39,420 hr service at 1050 F under 2140 psi. The steel of this tube contained also 0.61 per cent nickel.

Case 9. Another straight silicon-killed carbon-molybdenum steel refinery tube, containing 0.45 per cent nickel, likewise was found free of graphite after 30,660 hr of service at 1050 F to 1070 F under 2080 psi.

Case 10. A third, straight silicon-killed, carbon-molybdenum

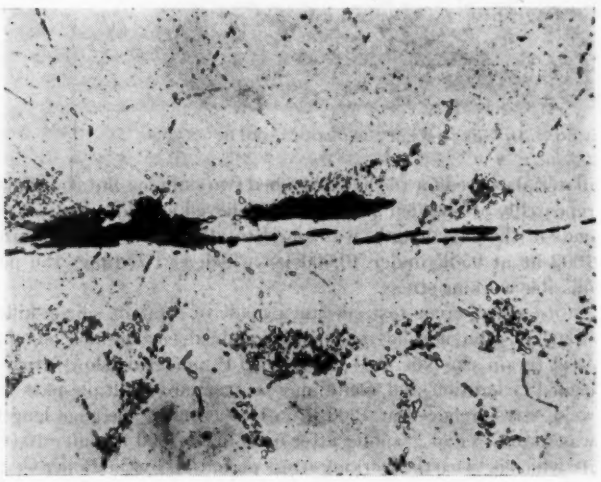


(*a*) Low-temperature end of weld-affected zone; ×500

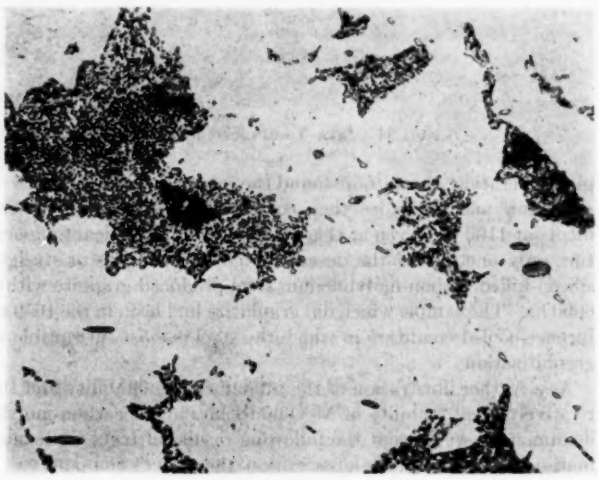


(*b*) Weld-unaffected metal; ×500

FIG. 22 CREEP-TEST SPECIMEN CASE 6.



(*a*) Low-temperature end of weld-affected zone; ×500



(*b*) Weld-unaffected metal; ×500

FIG. 23 CREEP-TEST SPECIMEN CASE 7

steel refinery tube with 0.48 per cent nickel also was found free of graphite after 30,660 hr of service at temperatures of 1080 to 1100 F under 1860 psi.

These examples permit some interesting deductions. A study of cases 1 and 3 shows that susceptibility to graphitization is not a direct function of the amount of aluminum added in deoxidization practice and that two steels may possess similar McQuaid-Ehn case characteristics and yet display a marked difference in susceptibility to graphitization.

A comparison of cases 2 and 3 demonstrates that weld-affected metal in the stress-relieved condition is decidedly more susceptible to graphitization than normalized and stress-relieved metal.

Cases 5 to 7 show that straight silicon-killed McQuaid-Ehn coarse-grained and normal carbon-molybdenum steel is fundamentally unstable and will graphitize under extreme conditions.

The absence of graphite in the three nickel-containing refinery tubes raises the question whether the resistance to graphitization of these tubes is due to the nickel in the steel. The authors have expressed the opinion that nickel, dissolved in the ferrite, may prevent graphitization by interfering with the carbon diffusion due to distortion of the ferrite lattice and by forcing more molyb-

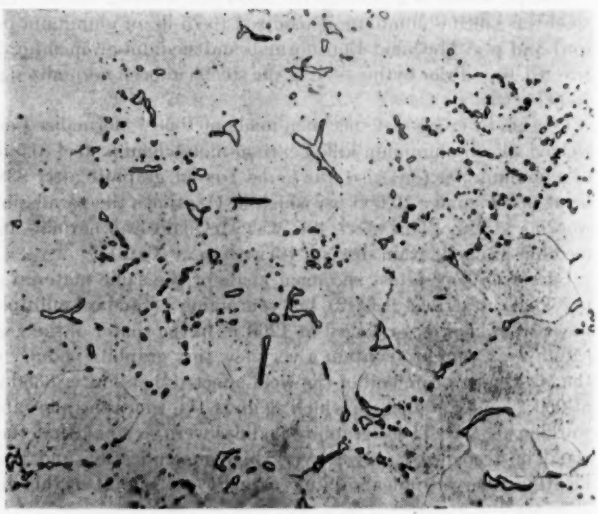


FIG. 24 MICROSTRUCTURE OF REFINERY-TUBE, CASE 9; ×500

denum into the carbide. The microstructure of the three refinery tubes, an example of which is depicted in Fig. 24 of this discussion, shows a high degree of carbide diffusion, spheroidization, and coalescence. One can readily imagine that a low rate of carbon diffusion may retard the beginning of graphite formation and the growth of the graphite cells formed, but in the case of a steel which has undergone fargoing carbide diffusion and coalescence, the rate of carbon diffusion does not seem to have been a factor in preventing graphitization. It also appears to us to be doubtful that nickel conferred stability to the ferrite against carbon rejection in the form of graphite by mechanically strengthening the ferrite, i.e., by increasing the work to be done by the volume expansion resulting from the carbide dissociation, since another element, silicon, which is a much more powerful ferrite strengthener than nickel, is known to promote carbide dissociation. However, the possibility that nickel dissolved in the ferrite forces more molybdenum into the carbide, as suggested by the authors, remains.

One may also wonder if the addition of an element which dissolves in the ferrite, such as nickel, does not modify the electrostatic balance in the ferrite lattice in a manner which is less favorable to carbon rejection in the form of graphite. It all goes to show that there is much to be learned yet before a full understanding of the phenomenon of graphitization is attained. The authors have presented some significant facts and have indicated a new approach to the solution of this difficult problem for which they deserve appreciation and thanks.

L. H. Carr.[6] In the Edward laboratories, we have been making extensive graphitization tests for the past year and a half. We have obtained a certain amount of test data which does not differ in its essential details from most of that which has been presented already. The tests show up many of the same anomalies which have already been pointed out. They seem to show that we all know a number of factors which definitely have to do with a tendency toward graphitization, but that we do not know for sure of an economical solution which can be applied to steelmakers the country over which will guarantee the absence of graphite for service times of 5 to 25 years.

For example, we have found such conflicting data as the following: Samples of cast carbon-molybdenum steel from one foundry source deoxidized with 2 lb of aluminum per ton will develop graphite in every test. Samples of the same material again deoxidized with 2 lb of aluminum per ton from another foundry source have never developed graphite in any of our tests. On the other hand, the foundry source whose material graphitizes with high aluminum addition, has made a number of test bar heats of either no aluminum or $^1/_2$ lb per ton. None of these specimens has graphitized in our tests, but other investigators have found graphite developing in steels of low aluminum additions. We have tested a good many heats of steel graphitized when stress-relieved at 1200 F after welding, and none of them showed graphite when stress-relieved at 1300 F after welding. Again, however, other investigators have reported this as not being a foolproof preventive. We have tested a number of heats of cast carbon-molybdenum steel containing from 0.40 to 0.60 per cent chromium for test periods as long as 10,000 hr at 1025 F. Again none of these specimens has shown graphite, although we have heard from other investigators that they have found graphite in some steels containing chromium.

Again, we might call attention to a number of pipe investigations wherein graphite has been found distributed in a number of random locations away from any apparent welding or heating. It would seem therefore that perhaps graphitization is a little bit like creep in that at high temperatures we will always have some, and that the engineering and metallurgical problem is to minimize this tendency toward graphitization, rather than to try to erase it 100 per cent in all cases.

In view of the fact that different steelmakers, using nominally the same practice, produce carbon-molybdenum steels of widely differing graphitization tendencies, it would seem that too much weight could not be given to the results of any one graphitization investigator. Furthermore, it is felt that too many suggested solutions to the whole problem have been discarded because of just one or two graphite spots widely distributed in a sample. Since no simple cure-all for the matter has been developed, it would seem that the best way to give engineers the information they need today would be to summarize all available test information in some sort of a statistical score sheet. This might show, for example, that of several thousand specimens of high-aluminum carbon-molybdenum steel 30 per cent would show graphitization at the end of a certain testing time. It might show in the case of several thousand other low-aluminum carbon-molybdenum steels that 3 or 4 per cent would show graphitization under similar time and temperatures. Again, it might show that of specimens stress-relieved at 1300 F, a certain per cent would show graphitization. Several hundred specimens of chromium containing carbon-molybdenum steels might show that only one or two had developed any graphite. It would also be desirable to work out some simple method of classifying the degree of graphitization. A simple statement of "Yes, it is present," or "No, it is not," leads to the condemnation of many test samples which are structurally quite sound, but which show one or two isolated graphite spots. Samples in which two out of three fields of view show no graphite in the critical area should perhaps receive a separate classification.

It is believed that a large amount of data of this sort is now available in laboratories throughout the country, which will represent the widest possible range of steel manufacture. A table of this sort should enable engineers to select materials for today's problems on a much more rational basis than merely listening to the opinions of any one or two investigators.

Authors' Closure

The authors are indebted to Mr. Eberle and Mr. Carr for their discussions and interest. The cases cited by Mr. Eberle are significant in illustrating the profound influence of minor variations of treatment on graphitizing tendency. In our own work we have found that in certain samples which were presumed to be homogeneous, since they were cut out of larger parts which had been treated as a whole, a particular region would display a marked shower of graphite particles while the remainder of the sample would be devoid of visible graphite (on the same polished section). This made for great tedium in the microscopic examination for the failure to find graphite at the first examination gave no assurance graphite was not present and in significant quantity. Particular conditions of divorcement of ferrite and carbide were suspect, as brought out in the paper and if graphite was not found in the first instance, the sample was ground down and repolished through successive layers until there was reasonable assurance that graphite either was or was not present.

This critical examination was required by the nature of the Springdale failure and by the findings on the graphitized valve body described in the paper. The graphite found on a particular section may not be significant in revealing the degradation of the whole member. This was brought out by Blumberg in the general discussion of graphitization at the December, 1943, meeting of the A.S.M.E.

The foregoing comments will partially serve in reply also to Mr. Carr. The compilation and statistical analysis of graphitiza-

[6] Director Research, Edward Valves, Inc., East Chicago, Ill. Mem. A.S.M.E.

tion data suggested by Mr. Carr would possess a certain interest but would afford small satisfaction to the design engineer. To lay out a power plant with the knowledge that 30 per cent or even 3 per cent of the steels involved would graphitize within the normal service life, perhaps seriously, would not be very comforting. It is quite true that we shall always have a little creep at these high temperatures but creep is something that can be measured and predicted and loading values are selected so that total creep over service expectancy is kept small in amount. However, the action through which controlled creep takes place does not lead to marked degradation of the physical properties. Graphitization involves degradation and may in some instances lead to serious failure. We therefore believe that erasing of graphitization 100 per cent *is* the metallurgical problem and to fail to strive for that end is not sound.

Question has been raised regarding usage of 1100 F as a graphitization test temperature. The results presented at this session of the Joint E.E.I.-A.E.I.C. Investigation supports our position in this. Although we made no detailed attempt to measure graphitization quantitatively, qualitatively it appeared from our results that time was the principal factor affected by using higher temperatures. Furthermore, 1100 F is a directly significant temperature when it is considered that in some newer installations operating swings will closely approach it.

We affirm our position that for increasing the relative stability the judicious use of alloys offers the safest approach. Also, the mechanisms are such that simple concepts, for example that thermodynamic stability of carbides is the only factor, may be not only misleading, but also dangerous. In support of our findings on WC-4 steel other investigators working within the chemistry of this specification have found samples with weld metal deposited thereon resistant to graphitization in the weld-affected zone over periods up to 10,000 hours at 1100 F. If the chart on graphitization rates prepared for the Summary Report of the Joint E.E.I.-A.E.I.C. may be presumed correct this would be the equivalent of 100,000 hours at 925 F.

Influence of Heat-Treatment Upon the Susceptibility to Graphitization of High-Aluminum-Deoxidized Carbon-Molybdenum Steel

By F. EBERLE,[1] BARBERTON, OHIO

Susceptibility to graphitization of carbon-molybdenum steels may be influenced by heat-treatment of the material prior to installation. Tests are reported in this paper on high-aluminum-deoxidized pipe with welded upset ends, the upsetting being carried out at 2000 F without subsequent heat-treatment. Graphitization in certain zones of the pipe were in evidence. Subsequently the influence of prior heat-treatment or weld heat effects upon susceptibility to graphitization was explored. The procedure and results attained are recorded in this paper.

Introduction

A STUDY of the behavior of carbon-molybdenum steels in long-time service at steam-plant operating temperatures led to the observation that susceptibility to graphitization may be influenced by the heat-treatment of the material prior to installation. For example, in high-aluminum-deoxidized pipe with welded upset ends, the upsetting being carried out at 2000 F without subsequent heat-treatment, the following conditions might be encountered:

(*a*) High-temperature end of weld-affected upset material: not graphitized.

(*b*) Low-temperature (1300–1400 F) zone of weld-affected upset material: graphitized.

(*c*) Weld-unaffected upset part of pipe: not graphitized.

(*d*) Transition zone from the upset to the unupset part of the pipe which had been heated to and cooled from a temperature of 1300–1400 F: graphitized.

(*e*) Heat-unaffected unupset body of the pipe: graphitized or not graphitized, depending on the heat-treating temperature and rate of cooling prior to installation.

This influence of prior heat-treatment or weld heat effects upon susceptibility to graphitization was subsequently explored with a series of experiments designed to examine the following factors:

1 Rapid cooling from very high temperatures as sometimes encountered in upset pipe ends and in the high-temperature zone of weld-affected metal.

2 Slow cooling from very high temperatures, sometimes found in pipes and heavy castings.

3 Rapid cooling from temperatures above but in the vicinity of the A_3 point of the steel as employed in standard normalizing treatment.

4 Slow-cooling from temperatures above but in the vicinity of the A_3 point of the steel as met in "normalized" heavy castings.

5 Rapid and slow cooling from temperatures just above the A_1 point of the steel after heat-treatments (1) to (4) as may occur in the low-temperature zone of weld-affected metal ("contact zone").

6 Quenching of normalized material from temperatures just above and just below the A_1 point of the steel as may be encountered in the contact zone between weld-affected and weld-unaffected metal.

7 Annealing at 1200 F and 1300 F, respectively, as employed for stress-relieving.

No attempt was made in these experiments to reproduce exact fabrication conditions, i.e., the rate of cooling in the normalized samples was sometimes faster, the quenching of the quenched samples more drastic, and the cooling of the annealed samples slower than in fabricated material. This was done purposely in order to establish fundamental trends and, if possible, to shed more light on the mechanism of graphitization.

Experimental Procedures

For some of the tests only unwelded specimens were used, consisting of $^3/_4$-in. cubes machined from the heat-treated material so as to eliminate oxidized and decarburized surface metal. In general, the heat-treating was done in a salt or lead bath. Some tests with unwelded material were run in duplicate, one set of specimens remaining in the heat-treated and machined condition, while identical specimens of a second set were 50 per cent cold-compressed in a tensile machine prior to the soaking in the lead bath at 1000 F. This severe cold deformation had been found generally to promote or accelerate graphitization and helped to induce the formation of graphite in some conditions of heat-treatment where it would otherwise not occur, at least not within the chosen duration of the tests.

A second set of experiments was conducted with special spot welds consisting of 1-in-diam × $^1/_8$-in-thick disks which were prepared by placing them between the water-cooled electrode tips of a spot-welding machine and applying sufficient current to fuse the core of the disks from cold to fusion within $^1/_{15}$ sec, $^2/_{15}$ sec, and $^1/_5$ sec, respectively, the disks then cooling to room temperature within 1 sec. These tests were intended to give information on the effect of extremely rapid cooling under conditions of welding.

A third series of tests was carried out with regular multiple-pass arc welds prepared by joining two plates which had been water-, air-, or slow furnace-cooled from 2200 F and 1650 F, respectively, prior to the welding, water-cooled plate being welded to water-cooled plate, and air-cooled plate to air-cooled plate, etc. Each

---

[1] Research Metallurgical Engineer, The Babcock & Wilcox Company.

Contributed by the Joint A.S.T.M.-A.S.M.E. Research Committee on the Effect of Temperature on the Properties of Metals and presented at the Annual Meeting, New York, N. Y., Nov. 26–29, 1945, of The American Society of Mechanical Engineers.

Note: Statements and opinions advanced in papers are to be understood as individual expressions of their authors and not those of the Society.

of these test welds was then cut into three sections, one section remaining in the as-welded condition, a second section being standard stress-relieved at 1200 F and the third section annealed at 1300 F for 20 hr. These tests were intended to furnish information on the effect of various heat-treatments under actual fabricating conditions.

All graphitization tests were conducted in a charcoal-covered lead bath held at 1000 F.

Materials

Two types of carbon-molybdenum steel were employed: Two high-aluminum deoxidized steels of great susceptibility to graphitization (steels A and B) and a high-aluminum-deoxidized steel of low susceptibility to graphitization (steel C). The deoxidation practice, McQuaid-Ehn case characteristics, and chemistry of these steels are given in Tables 1 to 6 which also contain summaries of the test results.

TABLE 1 TEST SERIES A—TESTS WITH UNWELDED SPECIMENS IN VARIOUS CONDITIONS OF HEAT-TREATMENT

(Specimens 3/4-in. cubes machined from heat-treated material)

Steel "A": Si-Al Killed (1.8 lb. Al/Ton), McQuaid-Ehn Grain Size 7 (Abnorm.)
.19C, .48Mn, .16Si, .018P, .024S, .52Mo, .039 Al, .009 Al_2O_3

Specimen	Heat Treatment	Results of 3000 hr Tests At 1000F	Illustration
B1	1 hr 2200F/Air	No Graphite	
B2	1 hr 2200F/Air +50% Cold Reduction	No Graphite	
B3	1 hr 2200F/Air +1 hr 1400F/Fce (1°/hr)	Very Few Scattered Very Small Nodules	
B4	1 hr 2200F/Air +1 hr 1400F/Fce (1°/hr) +50% Cold Reduction	Scattered Small Nodules	Fig. 1
E1	1 hr 1650F/Air	No Graphite	
E2	1 hr 1650F/Air +50% Cold Reduction	Scattered Small Nodules	Fig. 2
E3	1 hr 1650F/Air +1 hr 1400F/Fce (1°/hr)	No Graphite	
E4	1 hr 1650F/Air +1 hr 1400F/Fce (1°/hr) +50% Cold Reduction	Few Scattered Small Nodules	
E5	1 hr 1650F/Air +1 hr 1400F/Air	Very Few Scattered Very Small Nodules	
E6	1 hr 1650F/Air +1 hr 1400F/Air +50% Cold Reduction	Few Scattered Small Nodules	
E7	1 hr 1650F/Air +1 hr 1400F/Water	Few Scattered Very Small Nodules	
E8	1 hr 1650F/Air +1 hr 1400F/Water +50% Cold Reduction	Scattered Very Small Nodules	
C1	1 hr 2200F/Fce (50°/hr)	Scattered Large Nodules	Fig. 3
C2	1 hr 2200F/Fce (50°/hr) +50% Cold Reduction	Increased Number Of Scattered Large Nodules	
C3	1 hr 2200F/Fce (50°/hr) +1 hr 1400F/Fce (1°/hr)	Very Few Scattered Small Nodules	
C4	1 hr 2200F/Fce (50°/hr) +1 hr 1400F/Fce (1°/hr) +50% Cold Reduction	Grain Boundary Chain Graphite And Scattered Medium Sized Nodules	Fig. 4
F1	1 hr 1650F/Fce (50°/hr)	Segregated Graphite At Surface Only	
F2	1 hr 1650F/Fce (50°/hr) +50% Cold Reduction	Scattered Small Nodules	
F3	1 hr 1650F/Fce (50°/hr) +1 hr 1400F/Fce (1°/hr)	Few Scattered Small Nodules	
F4	1 hr 1650F/Fce (50°/hr) +1 hr 1400F/Fce (1°/hr) +50% Cold Reduction	Scattered Small Nodules	Fig. 5
F5	1 hr 1650F/Fce (50°/hr) +1 hr 1400F/Air	Very Few Scattered Small Nodules	
F6	1 hr 1650F/Fce (50°/hr) +1 hr 1400F/Air +50% Cold Reduction	Scattered Small Nodules	
F7	1 hr 1650F/Fce (50°/hr) +1 hr 1400F/Water	Few Scattered Small Nodules	
F8	1 hr 1650F/Fce (50°/hr) +1 hr 1400F/Water +25% Cold Reduction	Scattered Small Nodules	Fig. 6

TABLE 2 TEST SERIES B—TESTS WITH UNWELDED SPECIMENS IN VARIOUS CONDITIONS OF HEAT-TREATMENT

(Specimens 3/4-in. cubes machined from heat-treated material)

Steel "B": Si-Al Killed (1.8 lb. Al/Ton), McQuaid-Ehn Grain Size 6-7 (Abnorm.)
.11C, .45Mn, .14Si, .012P, .026S, .53Mo, .036 Al, .006 Al_2O_3

Specimen	Heat Treatment	Results Of 3000 hr Tests At 1000F
SR1	4 hr 2200F/Fce (50°/hr)	No Graphite
SR2	4 hr 2200F/Fce +4 hr 1200F/Fce	Localized Nodules At Surface Only
SR3	4 hr 2200F/Fce +4 hr 1300F/Fce	Some Scattered Medium Nodules At Surface Only
SR4	4 hr 2200F/Fce +50% Cold Reduction	Numerous Small To Medium Nodules
SR5	4 hr 2200F/Fce +50% Cold Red. +4 hr 1200F/Fce	Numerous Small To Medium and Some Large Nodules
SR6	4 hr 2200F/Fce +50% Cold Red. +4 hr 1300F/Fce	Medium Amount Of Small To Medium And Some Large Nodules
SR7	4 hr 2200F/Water	No Graphite
SR8	4 hr 2200F/Water +4 hr 1200F/Fce	No Graphite
SR9	4 hr 2200F/Water +4 hr 1300F/Fce	No Graphite
SR10	4 hr 2200F/Water +50% Cold Reduction	No Graphite
SR11	4 hr 2200F/Water +50% Cold Red. +4 hr 1200F	No Graphite
SR12	4 hr 2200F/Water +50% Cold Red. +4 hr 1300F	No Graphite

TABLE 3 TEST SERIES C—TESTS WITH UNWELDED SPECIMENS IN VARIOUS CONDITIONS OF HEAT-TREATMENT

(Specimens 3/4-in. cubes machined from heat-treated material)

Steel "A": Si-Al Killed (1.8 lb. Al/Ton), McQuaid-Ehn Grain Size 7 (Abnorm.)
.19C, .48Mn, 16Si, .018P, .024S, .52Mo, .039 Al, .009 Al_2O_3

Specimen	Heat Treatment	Results Of 1500 hr Tests At 1000F
G1	1 hr 2200F/Air + 1 hr 1300F/Fce	No Graphite
G2	1 hr 2200F/Air + 1 hr 1300F/Fce + 50% Cold Reduction	Small Nodules At Surface Only
G3	1 hr 1650F/Air + 1 hr 1300F/Fce	No Graphite
G4	1 hr 1650F/Air + 1 hr 1300F/Fce + 50% Cold Reduction	Few Small Nodules At Surface Only
G5	1 hr 1650F/Air + 20 hr 1300F/Fce	No Graphite
G6	1 hr 1650F/Air + 20 hr 1300F/Fce + 50% Cold Reduction	Few Small Nodules At Surface Only
H1	1 hr 2200F/Fce (50°/hr) + 1 hr 1300F/Fce	Some Small To Medium Nodules At Surface Only
H2	1 hr 2200F/Fce (50°/hr) + 1 hr 1300F/Fce + 50% Cold Red.	Numerous Small Nodules
H3	1 hr 1650F/Fce (50°/hr) + 1 hr 1300F/Fce	Some Small Nodules At Surface Only
H4	1 hr 1650F/Fce (50°/hr) + 1 hr 1300F/Fce + 50% Cold Red.	Few Small Nodules
H5	1 hr 1650F/Fce (50°/hr) + 20 hr 1300F/Fce	Some Small Nodules At Surface Only
H6	1 hr 1650F/Fce (50°/hr) + 20 hr 1300F/Fce + 50% Cold Red.	Some Small Nodules At Surface Only

TABLE 4 TEST SERIES D—TESTS WITH UNWELDED SPECIMENS QUENCHED FROM TEMPERATURES JUST ABOVE AND JUST BELOW THE A_1 POINT OF THE STEEL

(1/8 × 1/4 × 1/4 in. specimens, normalized at 1650 F)

Steel "B": Si-Al Killed (1.8 lb. Al/Ton), McQuaid-Ehn Grain Size 6-7 (Abnorm.)
.11C, .45Mn, .14Si, .012P, .026S, .53Mo, .036 Al, .006 Al_2O_3

Specimen	Heat Treatment	Results of 10000 hr Tests At 1000F
K1	½ hr 1400F/Ice-Brine	Uniformly Scattered Graphite
K2	½ hr 1350F/Ice-Brine	Less Uniform And Less Graphite Than In K1
K3	½ hr 1300F/Ice-Brine	As In K2
K4	½ hr 1250F/Ice-Brine	As In K2

TABLE 5 TEST SERIES E—TESTS WITH DISKS CONTAINING SPOT-WELD-FUSED CORES

(Specimens 1 in. diam × 1/8 in. thick, machined from material normalized at 1700 F and heated between the water-cooled electrode tips of a spot-welding machine)

Steel "B": Si-Al Killed (1.8 lb. Al/Ton), McQuaid-Ehn Grain Size 6-7 (Abnormal)
.11C, .45Mn, .14Si, .012P, .026S, .036 Al, .006 Al_2O_3

Specimen	Heating Time To Fusion	Cooling Time To Room Temp	Fused Core	Results of 10000 hr Tests At 1000F Contact Z. Weld-Aff./Weld-Unaff. M.	Weld-Unaff. Metal
L1	1/15 sec.	1 sec.	No Graphite	Few Scattered Nodules	Few Scattered Nodules
L2	2/15 sec.	1 sec.	No Graphite	Few Scattered Nodules	Few Scattered Nodules
L3	1/5 sec.	1 sec.	No Graphite	Few Scattered Nodules	Few Scattered Nodules

TABLE 6 TEST SERIES F—TESTS WITH STANDARD MULTIPLE-PASS ARC WELDS

(Specimens 5 × 5 × 1-in. plate sections in various conditions of heat-treatment, welded together and post-weld-treated as indicated)

Steel "C": Si-Al Killed (1.5 lb. Al/Ton), McQuaid-Ehn Grain Size 5-7 (Slight To Medium Degree of Abnormality)
.18C, .83Mn, .23Si, .016P, .023S, .49Mo, .041 Al, .029 Al_2O_3

Specimen	Heat Treatment Of Plate Pair	Postweld Treatment	Results Of 6000 hr Tests At 1000F: 2200F Treated Material, Weld-Unaff. M.	2200F Treated Material, Heat-Aff. Z. (Contact Z.)	1650F Treated Material, Weld-Unaff. M.	1650F Treated Material, Heat-Aff. Z. (Contact Z.)
M1	2200F/Water—1650F/Water	None	No Graphite	No Graphite	No Graphite	No Graphite
M2	2200F/Water—1650F/Water	1 hr 1200F	No Graphite	No Graphite	No Graphite	No Graphite
M3	2200F/Water—1650F/Water	20 hr 1300F	No Graphite	No Graphite	No Graphite	No Graphite
M4	2200F/Air—1650F/Air	None	No Graphite	No Graphite	Some Nodules In Some Cold Worked Surface Zones	No Graphite
M5	2200F/Air—1650F/Air	1 hr 1200F	No Graphite	No Graphite	Some Nodules In Some Cold Worked Surface Zones	No Graphite
M6	2200F/Air—1650F/Air	20 hr 1300F	No Graphite	No Graphite	No Graphite	No Graphite
M7	2200F/Fce*—1650F/Fce*	None	A Few Isolated Nodules	Some Widely Scattered Medium Nod.	Some Nodules In Cold Worked Surface Zones Only	Some Scatt. Small To Med. Nodules
M8	2200F/Fce*—1650F/Fce*	1 hr 1200F	A few Widely Scatt. Nodules	Some Scatt. Medium Nod.	Some Large Nod In Surface Zones Only	No Graphite
M9	2200F/Fce*—1650F/Fce*	20 hr 1300F	No Graphite	No Graphite	No Graphite	No Graphite

* Cooled 50° per hour

Test Results

Evaluation of the test results led to the following conclusions:

1 Carbon-molybdenum steels deoxidized with the same nominal amount of aluminum, possessing practically identical chemistry and displaying practically identical abnormal McQuaid-Ehn case characteristics may show differences in susceptibility to or rate of graphitization.

2 Annealing at very high temperatures followed by rapid cooling seems to inhibit or retard graphitization at the contemplated temperatures. This was found to be true also for specimens which had been 50 per cent cold-reduced by compression prior to the subcritical annealing at 1000 F.

3 Annealing at temperatures above, but near the A_3 point of the steel followed by rapid cooling appears to be much less effective in retarding graphitization than rapid cooling from very high temperatures. When severely cold-deformed, such material may form graphite within 1500 to 3000 hours at 1000 F.

4 Annealing at very high temperatures followed by slow cooling seems to promote or accelerate graphitization. In this condition relatively large scattered graphite nodules are formed within 1500 hours at 1000 F.

5 Annealing at temperatures above, but near the A_3 point followed by slow cooling renders the steel less susceptible to graphitization than slow cooling from very high temperatures, but more susceptible than air cooling from temperatures above but near the A_3 point.

6 Reheating steel which had been rapidly cooled from very high temperatures and thereby made insensitive to graphitization, to temperatures just above the A_1 point renders it again susceptible, irrespective of the subsequent rate of cooling.

7 Heating to just above the A_1 point (1400 F) followed by water-quenching renders the steel more susceptible to graphitization than slow furnace-cooling from the same temperature. On the other hand, slow-cooling from just above the A_1 point favors graphitization more than air-cooling. In this connection it should be remembered that quenching from very high temperatures inhibited the formation of graphite more effectively than any other heat-treatment. The high susceptibility to graphitization resulting from quenching from just above the A_1 point therefore deserves particular attention.

8 Steel which previously had been heated to very high temperatures appears to be rendered slightly more susceptible to graphitization when subsequently reheated to just above the A_1 point than steel which previously had been heated to temperatures above but in the vicinity of the A_3 point.

9 Material which had been slow furnace-cooled from temperatures above the A_3 point appears to be slightly more susceptible to graphitization when subsequently reheated to temperatures just above the A_1 point than previously fast-cooled material. Steel slowly cooled from very high temperatures, reheated to above the A_1 point and then severely strained, shows a tendency to form continuous grain-boundary chain graphite.

10 Quenching from temperatures just above the A_1 point seems to favor graphitization more than quenching from temperatures just below the A_1 point.

11 Annealing at 1200 F as used in conventional stress-relieving appears to have little effect upon the formation of graphite unless accompanied by a reduction or elimination of stresses. Under like conditions, annealing at 1300 F for the same length of time seems to reduce the number of graphite nodules, but does not seem to prevent their formation.

12 Long-time annealing at 1300 F considerably retards the formation of graphite and also tends to reduce the number of nodules formed.

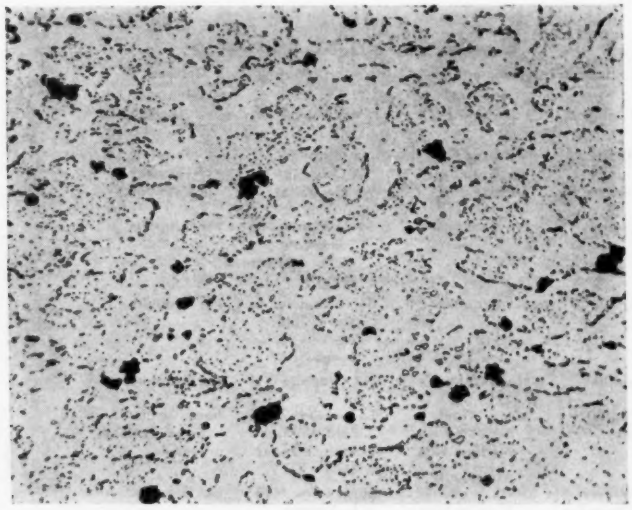


Fig. 1 Specimen B4 After 3000 Hr at 1000 F; ×500
(Steel A, 1 hr 2200 F/Air plus 1 hr 1400 F/Fce (1 deg per hr) plus 50 per cent cold reduction.)



Fig. 2 Specimen E2 After 3000 Hr at 1000 F; ×500
(Steel A, 1 hr 1650 F/Air plus 50 per cent cold reduction.)



Fig. 3 Specimen C1 After 3000 Hr at 1000 F; ×500
(Steel A, 1 hr 2200 F/Fce (50 deg per hr).)

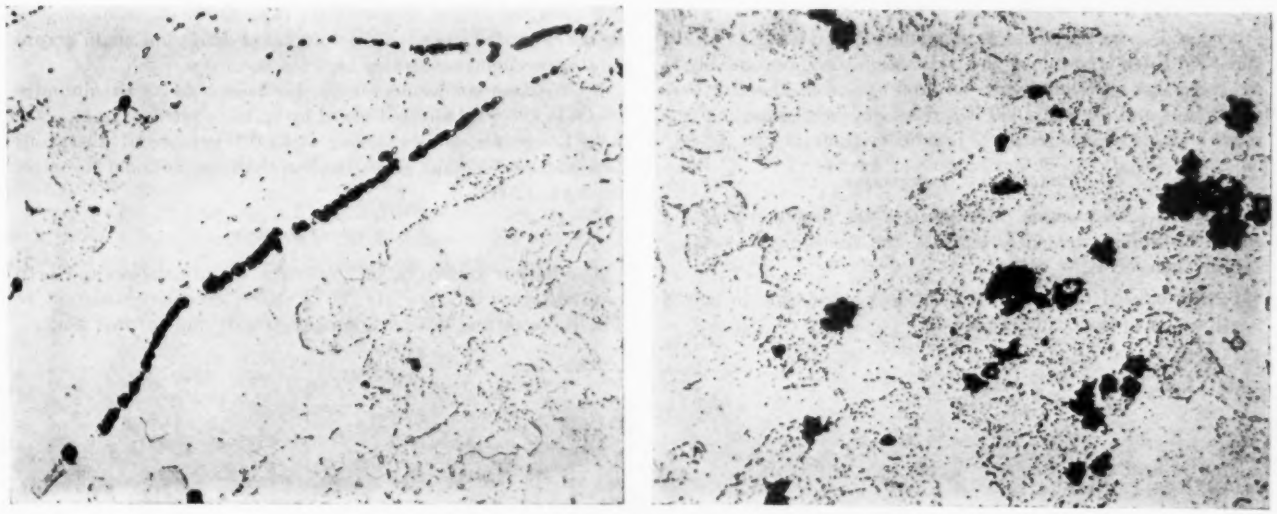


FIG. 4 SPECIMEN C4 AFTER 3000 HR AT 1000 F; ×500
(Steel A, 1 hr 2200 F/Fce (50 deg per hr) plus 1 hr 1400 F /Fce (1 deg per hr) plus 50 per cent cold reduction.)

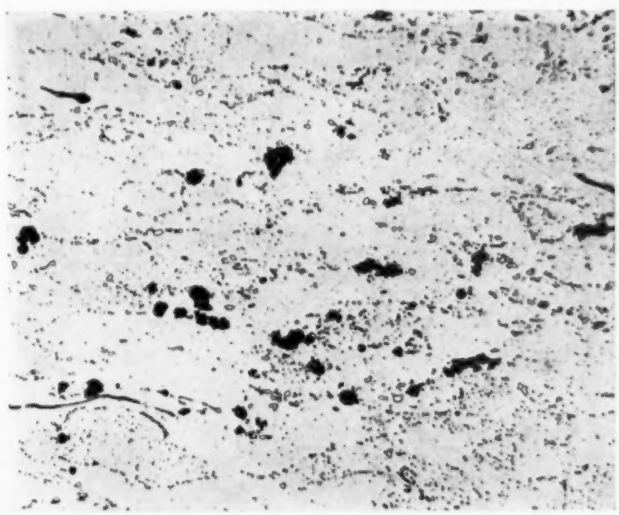


FIG. 5 SPECIMEN F4 AFTER 3000 HR AT 1000 F; ×500
(Steel A, 1 hr 1650 F/Fce (50 deg per hr) plus 1 hr 1400 F/Fce (1 deg per hr) plus 50 per cent cold reduction.)

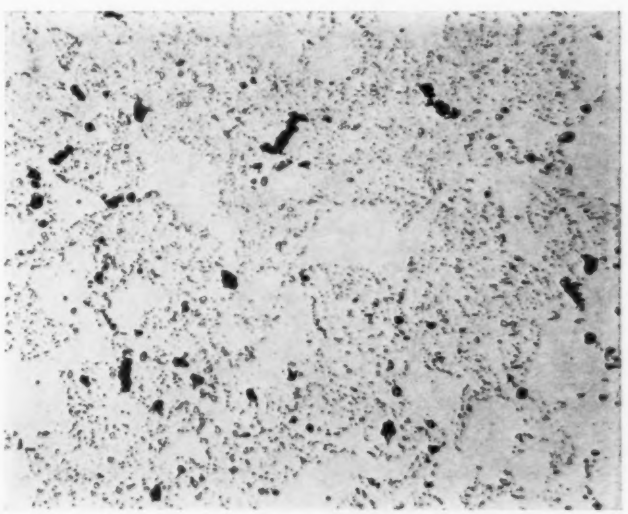


FIG. 6 SPECIMEN F8 AFTER 3000 HR AT 1000 F; ×500
(Steel A, 1 hr 1650 F/Fce (50 deg per hr) plus 1 hr 1400 F/water plus 25 per cent cold reduction.)

GENERAL DEDUCTIONS

The pattern of susceptibility to graphitization obtained with the various heat-treatments preceding the isothermal graphitization tests at 1000 F clearly indicates the involvement of a submicroscopic precipitation phenomenon as suggested by Austin and Fetzer.[2] There seems to be a substance, elements or compounds, which upon precipitation in a certain state promote carbide instability. The solution temperature of this substance seems to be rather high and its precipitation from solution relatively sluggish. Air-cooling from temperatures above 2000 F appears to suffice to retain these elements or compounds in solution even in the extremely sensitive high-aluminum-deoxidized steels and in this condition the steel will not graphitize within 10,000 hr at 1000 F, as demonstrated by the behavior of the spot-weld-fused samples. Heating the steel to intermediate temperatures above but in the vicinity of the A_1 point apparently does not create complete solution, and diffusion of the submicroscopic phase and abnormal steel air-cooled from such temperatures will therefore graphitize under favorable conditions, as for instance, when severely cold deformed. Slow cooling from very high and from intermediate temperatures precipitates the phase and renders the steel susceptible to graphitization. Complete solution and diffusion of the phase as obtained at very high temperatures seems to result in a more effective state of precipitation than incomplete solution and diffusion as obtained at intermediate temperatures.

If steel which had been rapidly cooled from high temperatures is subsequently reheated to temperatures just above the A_1 point, the dissolved phase will at least partly precipitate and render the steel again susceptible to graphitization. It is suspected that the allotropic transformation at the A_1 point, particularly when combined with straining, aids the precipitation of the submicroscopic phase. The preferential occurrence of graphite in the low-temperature zone of weld-affected metal may be similarly explained. Short-time annealing at 1200 F and 1300 F apparently

[2] "Factors Controlling Graphitization of Carbon Steels at Subcritical Temperatures," by C. R. Austin and M. C. Fetzer. Trans. A.S.M., vol. 39, 1945, pp. 485–535.

fails to bring about effective precipitation of the phase. On the other hand, once the phase is precipitated, annealing at 1200 F and 1300 F tends to render the phase ineffective, presumably by coalescence or agglomeration. At 1200 F, this effect seems to be very slight and even at 1300 F a relatively long annealing time is required to produce results of practical significance.

Practical Conclusions

Applying the foregoing deductions to the practical aspect of graphitization in welded structures, the following conclusions suggest themselves:

1 Normalized material is slightly less susceptible to graphitization than annealed material.

2 Normalizing at temperatures close to the A_3 point offers a better safeguard against the formation of dangerous chain graphite than normalizing at very high temperatures.

3 Welding conditions should be chosen so as to minimize strain in the weld-affected metal by suitable preheating.

4 Long-time stress relieving at 1300 F is more advantageous as a safeguard against graphitization than conventional stress-relieving at 1200 F.

Acknowledgment

The author gratefully acknowledges the inspiration and help received from the late Mr. H. J. Kerr, executive assistant of The Babcock and Wilcox Company, in carrying out this work.

General Discussion of Graphitization Papers

S. H. Weaver.[1] The General Electric graphite furnace heats bars with a lengthwise weld bead to 900 F at one end and 1300 F at the other end. All bars were notched at the 1100 F location for examination after 3000 hr. The 6200-hr study has been partially completed.

Fig. 1 of this note, for items 1 to 7, Table 1, gives the graphitic growth by chemical analysis in 3000 hr for different temperatures upon 0.15 per cent carbon steel with different deoxidization. The 1200 to 1300 F points were omitted because of decarburization of the steel. The furnace was then changed to dry nitrogen atmosphere.

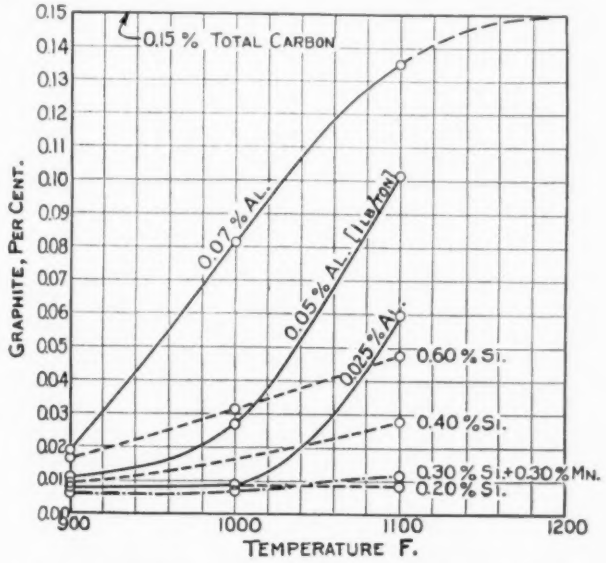


Fig. 1 Growth of Graphite at 3000 Hr in 0.15 Per Cent Carbon Steel

In the alloy series in Table 2 of this note, items 8 to 16 have no microscopic graphite after 6200 hr at 1100 F.

Table 3 lists nine conditions of pipe to A158-36P1 with 2 lb per ton of aluminum where at 1100 F in 3000 and 6200 hr all contained small nodular graphite except the 2300 F upset-end sample.

The four items of pipe in Table 4 to A206-42T with 1 lb per ton of aluminum, and the four items in Table 5, with 0.4 lb per ton of aluminum have shown no graphite at 1100 F. No examination has been made at other temperatures.

There are 19 other bars in the furnace including samples of 1 per cent Mo; 1 per cent Mo, 0.2 per cent V; 0.5 per cent Cr, 0.5 per cent Mo, in each case with varying practices as regards heat-treatment and deoxidization practice. No graphite has been observed after the first 1700 hr. A longer soak will be required before any conclusion can be drawn from these latter test bars.

[1] Turbine-Generator Engineering Division (retired), General Electric Company, Schenectady, N. Y.

TABLE 1 INDUCTION FURNACE HEATS, DIFFERENT DEOXIDIZATION

Heat Treatment: 1700 F—2 hr air cool
1200 F—2 hr furnace cool

Item	C	Al	Si	Mn
1	0.15	0.025	..	..
2	0.15	0.050	..	..
3	0.15	0.075	..	..
4	0.15	..	0.20	..
5	0.15	..	0.40	..
6	0.15	..	0.60	..
7	0.15	..	0.30	0.30

Note: Graphite nodules in 3000 hr. See Fig. 8 for graphite chemical analysis with temperature.

TABLE 2 INDUCTION FURNACE HEATS, EFFECT OF ALLOYS

Heat Treatment: 1700 F—2 hr air cool
1200 F—2 hr furnace cool

Item	C	Si	Mn	Mo	Cr
8	0.15	0.30	0.70	..	..
9	0.15	0.30	1.30	..	..
10	0.15	0.30	0.30	0.50	..
11	0.15	0.30	0.70	0.50	..
12	0.15	0.30	0.90	0.50	..
13	0.15	0.30	..	0.50	0.30
14	0.15	0.30	..	0.50	0.70
15	0.15	0.30	..	0.50	0.90
16	0.15	0.30	..	0.50	1.30

Note: No graphite in 6200 hr at 1100 F but fully spheroidized.

TABLE 3 PIPE SPECIFICATION A.S.T.M., A158-36P1

(2 lb al per ton)

1	"As received;" 1200 F- 2 hr, furnace cool
2	"As received;" 1300 F- 2 hr, furnace cool
3	Upset, 2300 F- 1 hr, furnace cool
4	1600 F- 2 hr, water quench, 1200 F- 1 hr, furnace cool
5	1700 F- 2 hr, air cool, 1200 F- 2 hr, furnace cool
6	1700 F- 2 hr, air cool, 1100 F- 2 hr, furnace cool
7	1700 F- 2 hr, air cool, 1000 F- 2 hr, furnace cool
8	1700 F- 2 hr, air cool, no draw
9	575 F weld cycle, 1200 F- 2 hr, furnace cool

Note: Except upset item all had small nodules of graphite at 3000 and 6200 hr at 1100 F.

TABLE 4 PIPE SPECIFICATION A.S.T.M., A206-42T

(1 lb al per ton)

1	"As received;" 1200 F- 2 hr, furnace cool
2	"As received;" 1300 F- 6 hr, furnace cool
3	Upset, 2300 F- 1 hr, air cool
4	575 F weld cycle, 1200 F draw

Note: No graphite at 1100 F in 3000 or 6200 hr.

TABLE 5 PIPE SPECIFICATION A.S.T.M., A206-42T

(0.4 lb al per ton)

1	"As received;" 1200 F- 2 hr, furnace cool
2	"As received;" 1300 F- 6 hr, furnace cool
3	Upset, 2300 F- 1 hr, air cool
4	575 F weld cycle, 1200 F draw

Note: No graphite at 1100 F in 3000 or 6200 hr.

Some Stress-Corrosion Studies on Austenitic Cast Irons

By J. B. URBAN,[1] J. W. BOLTON,[1] AND A. J. SMITH[1]

Experimentation is the most adequate approach to stress-corrosion problems and should involve various mechanical loadings of a material under corrosive conditions. When corrosive conditions are held constant in respect to concentration and temperature, useful threshold stresses if existent can be ascertained and suitable safety factors adopted. The procedure for studying austenitic cast irons on this basis is discussed, the investigation indicating that at very high stresses, such irons are subject to stress corrosion in strong hot caustic. However, threshold stresses have been found to be relatively high, markedly exceeding stresses contemplated in design and application. Thus the desirable properties of such material can be utilized to good advantage, with margin to assure adequate safety in this corrosive medium.

PROBLEMS of stress corrosion have concerned engineers for many years. "Season-cracking" in brasses and embrittlement of ductile boiler-plate steel in presence of alkaline media are familiar examples. A material may possess apparently adequate strength and adequate corrosion resistance, as ascertained by separate conventional tests. Yet some materials are known to fail prematurely when exposed to certain combinations of these factors.

It is known that triaxiality of stresses may bring about acceleration of failure, or failure at lower loading than would be expected from conventional formulas for mono- and biaxial loading. Somewhat similarly, "corrosive stress" may be considered as an additional stress imposed upon a normally loaded system, giving the effect of higher stress order than contemplated by formulas. The safest approach to stress-corrosion problems is experimentation on various mechanical loadings under corrosive conditions. When corrosive conditions are held constant in respect to concentration and temperature, useful threshold stresses if existent can be ascertained and suitable safety factors adopted.

Since stress corrosion is initiated as a surface effect, it is essential that surface stress intensities (as imposed by loading) be determined accurately, so that the result of imposition of a corrosive condition can be evaluated. The resistance-wire (SR-4) type strain gage has proved quite useful in this respect.

Strong hot caustic (sodium hydroxide) is a powerful corrosive toward many metals, and produces embrittlement in some. Suitable grades of gray cast iron have fairly good resistance toward the corrosive effect and also are relatively free from stress-corrosion deterioration. Some of the high-nickel austenitic cast irons have excellent corrosion resistance toward strong caustics, even at elevated temperatures. This suggests their consideration[2] where contamination of caustic must be held to a minimum and where maximum life under such corrosive conditions is desired.

The present investigation indicates that at very high stresses the austenitic cast irons are subject to stress corrosion in strong hot caustic. However, threshold stresses have been found to be relatively high, markedly exceeding stresses contemplated in design and application. Thus the desirable properties of such material can be utilized to good advantage, with margin to assure adequate safety in this corrosive medium.

Experimental Procedures

Compositions of the materials examined are given in Table 1. Samples of austenitic-type cast iron were immersed in 50 per cent caustic solutions and boiled, using reflux condenser, for periods up to 6 months. These were broken in impact test. The test results were equal to those of companion samples not exposed to caustic. This showed that caustic embrittlement does not result when stress is absent.

TABLE 1 COMPOSITION OF MATERIALS

	Austenitic cast iron A, per cent	Austenitic cast iron B, per cent	Austenitic cast iron C, per cent	Austenitic cast iron D, per cent	No. 25 cast iron, per cent
Carbon	2.44	2.10	2.66	2.75	3.25
Graphite	1.98	2.01	...	...	...
Silicon	1.84	1.77	1.88	1.97	2.75
Manganese	0.90	0.74	0.92	0.98	0.58
Phosphorus	0.050	0.049	0.14	0.13	0.33
Sulphur	0.020	0.015	0.028	0.025	0.055
Nickel	19.82	20.61	19.86	19.09	...
Chromium	1.60	None	1.65	1.75	...
Molybdenum	0.74	0.90	0.63	0.62	...
Copper	4.10	0.06	4.55	4.33	...

Other samples were loaded under standard creep-test conditions.[3] These tests showed that the materials involved withstand stresses to 15,000 psi at 350 F, without measurable flow or "creep." After removal from the creep test and breaking, no differences in strength and ductility from companion unstressed samples were observed. These and other tests indicate that even at relatively high stresses the material is not adversely affected by mechanical loadings, even at temperatures appreciably above 350 F. The question then is whether the combined actions of stress and exposure to the corrosive medium produce effects not indicated by these factors operating independently.

The corrosive medium and condition chosen was 50 per cent by weight commercial sodium hydroxide (aqueous solution) at 280 F.

Three methods of stress application utilized were as follows:

[1] Metallurgical Department, The Lunkenheimer Company, Cincinnati, Ohio.

Contributed by the Metals Engineering Division and presented at the Fall Meeting, Cincinnati, Ohio, October 2–3, 1945, of The American Society of Mechanical Engineers.

Note: Statements and opinions advanced in papers are to be understood as individual expressions of their authors, and not those of the Society.

[2] Austenitic cast irons also are resistant to many other corrosive agents, both alkaline and acid, wherein long experience has shown that stress corrosion is not a factor.

[3] "Recommended Practice for Conducting Long-Time High-Temperature Tension Tests of Metallic Materials," A.S.T.M. Standards, 1941, E22-41.

(*a*) tensile loading, (*b*) cantilever loading, and (*c*) beam loading.

All specimens were cast in green sand and tested in the unmachined condition. (This simulates the surface conditions of cast product as commonly used.)

Tensile Loading Method

The arrangement of equipment is shown in Fig. 1. The test specimen was mounted between high-nickel-alloy pulling bars supported at the top with a ball-and-socket joint and a dead load applied to the bottom. The bottom bar passed through the base

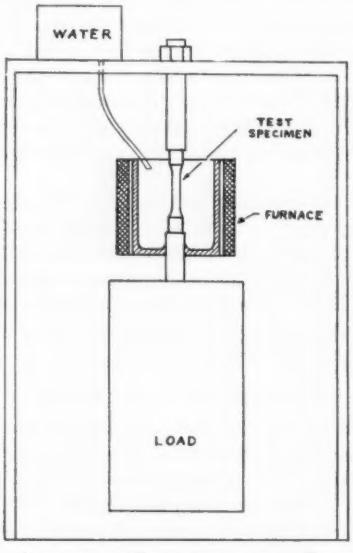


Fig. 1 Stress-Corrosion Test Setup for Tensile Loading

of a high-nickel-alloy container with a watertight seal, the container being filled with solution of commercial sodium hydroxide. A heating element around the container maintained the desired temperature of 280 F, through a potentiometer controller and thermocouple. (This temperature is very near the boiling point.) Water lost through evaporation was replaced continuously through a simple gravity-feed mechanism holding the solution concentration relatively constant. The average stress intensity over the affected area was established by the sum of the weights of container and contents, lower pulling bar, and applied weights.

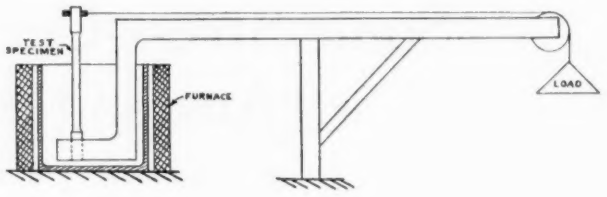
Simple- and Cantilever-Beam Loading Methods

These systems are shown in Figs. 2 and 3. The ends of the test specimens were attached to the load through a wire passing over a ball-bearing-mounted pulley of low frictional resistance. By means of this arrangement stresses on the specimens were independant of flexural changes in the supports, within reasonable limits of flexure of specimens.

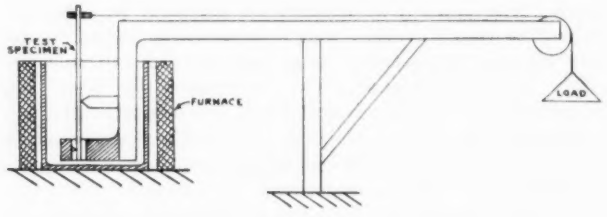
Tests were carried out both on round specimens 0.5 in. diam, and specimens of rectangular cross section measuring 1 × 0.4 in. Specimens were $8^1/_2$ in. in length in the cantilever test; in the simple-beam tests the outer knife-edges were $9^1/_2$ in. apart, the center knife-edge $3^1/_2$ in. from the lower fixed edge.

In conventional engineering practice stress intensities (as rupture moduli) usually are calculated by the beam formulas. These formulas are based upon the assumptions of elasticity and equivalent stress-strain moduli in both tension and compression. Cast irons do not comply with these assumptions. As shown by the authors' company[4] and others, the stress-strain curve of cast

[4] "Some Notes on Mechanism of Deformations in Grey Iron," by J. W. Bolton, Proceedingsof the A.S.T.M., vol. 32, part 2, 1932, p. 477.



CANTILEVER BEAM TYPE LOADING



SIMPLE BEAM TYPE LOADING

Fig. 2 Stress-Corrosion Test Setup for Beam-Type Loading

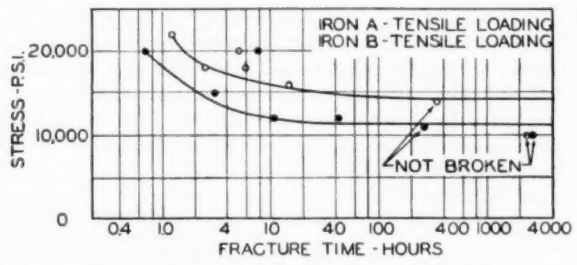


Fig. 3 Stress-Corrosion Rate for Austenitic Cast Irons; Tensile Loading

TABLE 2 SUMMARY OF TENSILE TESTS

Tensile stress, psi	Time for fracture, hr: Austenitic cast iron A	Austenitic cast iron B	No. 25 cast iron
25000	...	...	284[a]
22000	...	1.25	...
20000	0.7 and 7.7	5.2	...
18000	...	2.5 and 6	...
16000	...	15	...
15000	3.1	350[a]	...
12000	11 and 43	...	...
11000	270[a]	...	...
10000	2600[a]	2600[a]	2600[a]

[a] Not broken.

irons combines both elastic and plastic components. Also, properties are not equivalent in tension and compression. Thus the neutral stress axis does not coincide with the geometric axis.

Since stress-corrosion phenomena are (at least at their incidence) influenced by surface conditions, accurate measurement of fiber stress is necessary for evaluation. Strain-resistance (SR-4) gages are quite useful for this purpose. SR-4 gages and instrumentation have been described in detail in recent literature. Many applications have been to elastic materials. In such applications the measured strain is interpreted in terms of stress by introduction of Young's modulus.

Since the materials studied are but quasi-elastic, a modified procedure was required. Relationship of strain to stress not being constant, strain readings must be compared to a separately determined stress-strain curve to ascertain the corresponding stress intensities. The details of procedure and the various calibrations are described in the Appendix. The SR-4 strain-measurements'

accuracy compared very favorably with measurements by other extensometric devices and results were readily reproducible. The facility with which these gages can be applied to locations and shapes where strains are not measurable by other devices extends the field of testing engineering. SR-4 gages can be used not only on simple test shapes but also on products and other complicated shapes subjected to stress and strain.

Test Results

Tensile Tests. These are summarized in Table 2 and are shown graphically in Fig. 3. The gray cast iron sustained a tensile load of 25,000 psi for 284 hr and 10,000 psi for 2600 hr without breaking. The solution discolored and the bars showed evidence of surface corrosion but there was no evidence of corrosion being accelerated by the stress, or suggestion that embrittlement was effected.

Austenitic iron failed in a comparatively short time under a load of 20,000 psi, 0.7 hr on one bar, 7.7 hr on another, both from the same heat. Decrease of stress to 12,000 psi increased the time to fracture by almost 3 times. At a stress of 10,000 psi load was sustained for 2600 hr without fracture. The curves indicate that there is a limiting stress below which failure will not occur in caustic solutions. (This is confirmed by long-time service experience with the condition and material.) Above the limiting stress very slight increases in stress profoundly shorten the time to failure. This indicates the desirability of suitable choice of design stress, and measurements under operational conditions to reveal it.

The tensile strength of iron A, cast as a 0.5-in-diam specimen was 38,500 psi. The specimen removed unbroken after 270 hr in hot caustic under a stress of 11,000 psi was subsequently broken at room temperature and showed a tensile strength of 37,900 psi. A piece of the test specimen which failed after 43 hr at 12,000 psi was broken at room temperature, giving a tensile strength of 38,600 psi. It would appear that the caustic is effective only in lowering the time to fracture under stress when material is under the corrosive and temperature influence.

Beam Loadings. Results obtained from beam loadings of specimens are recorded in Table 3, and plotted in Fig. 4. The upper curves show the tensile fiber stress as calculated from the beam formula, the lower from conversion of actual strain measurements according to the method described in the Appendix. The marked error occasioned by use of the beam formula is evident.

These results are in good agreement with those found for tensile loading, the limiting or threshold stress being about 10,000 psi.

Conclusion

These studies show that for the corrosive and temperature considered there is a limiting stress below which the effects of stress corrosion on austenitic irons are either negligible or nonexistent. This stress is relatively high in respect to contemplated stresses for cast-iron products. Thus the good corrosion resistance of these metals in hot caustic can be advantageously utilized as sound engineering practice. This confirms field experience.

As shown by these studies (and described in the Appendix), the SR-4 resistance-strain-gage method is a valuable tool for the metallurgist and test engineer in their evaluation of quasi-elastic materials.

TABLE 3 RESULTS OF BEAM-LOADING SPECIMENS

Calculated stress from beam formula, psi	Stress from stress-strain curve, psi	Fracture time, hr: Austenitic cast iron C, simple beam	Austenitic cast iron C, cantilever beam	Austenitic cast iron D, cantilever beam
49200	26300	...	...	0.1
46800	26000	...	0.5	...
41400	24200	...	1.8	...
39600	23700	...	...	0.7
31100	20800	...	...	1.2
25800	18400	...	12.4	...
24900	18000	...	...	5.0
23200	17000	8.1	...	...
22600	16700	...	...	7.1
22000	16400	...	236	...
20400	15400	...	...	15.5
19650	14800	243[a]	...	...
18200	13900	...	...	152
16370	12600	...	...	468

[a] Not broken.

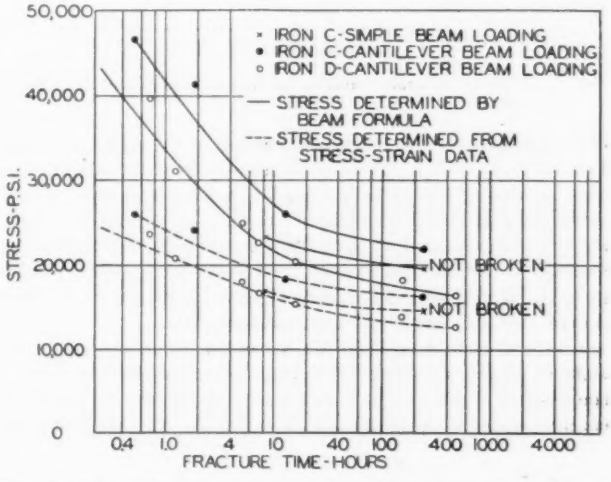


Fig. 4 Stress-Corrosion Rate for Austenitic Cast Irons; Transverse Loading

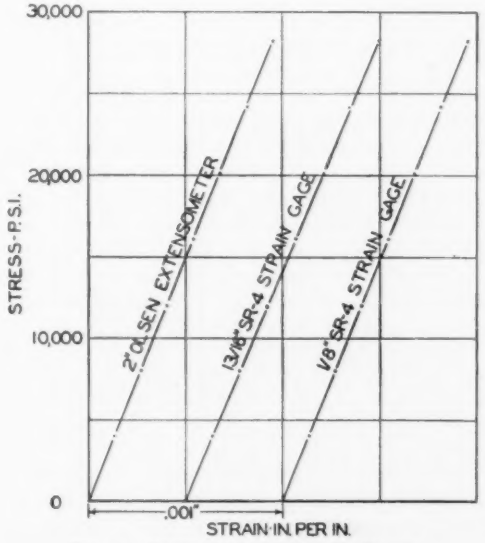


Fig. 5 Comparison of Strain Gages

(Gages mounted on steel tensile-test specimen. Readings were taken simultaneously on all gages.)

Appendix

The foregoing paper indicates the necessity of correct stress evaluation in studies of stress-corrosion effect.

Stresses due to tensile loading are determined readily and directly. Those due to various transverse loadings are not so easily determined. This is especially so in case of quasi-elastic materials, such as cast irons, where the premises of beam formulas do not apply, and strain measurements by conventional extensometric devices are not readily made.

SR-4 resistance-type strain gages were used to determine the

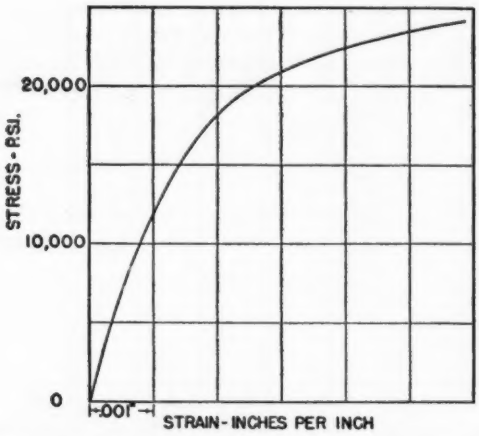


FIG. 6 TENSILE STRESS-STRAIN CURVE FOR AUSTENITIC CAST IRON

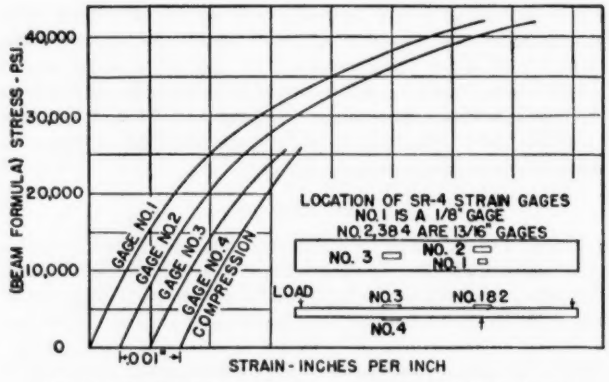


FIG. 7 STRESS-STRAIN CURVE ON AUSTENITIC CAST IRON
(Simple beam loading.)

strain readings for the transverse loading of the stress-corrosion tests. To check the accuracy and sensitivity of the SR-4 strain gages a steel tensile-test specimen was made long enough to accommodate an Olsen extensometer (2 in. gage length), a $^{13}/_{16}$-in. SR-4 strain gage, and a $^{1}/_{8}$-in. SR-4 strain gage. Simultaneous readings of strains and applied load were taken. The results given in Fig. 5 show good agreement, especially when it is borne in mind that different gage lengths are involved.

A typical tensile stress-strain curve for austenitic cast iron is shown in Fig. 6. Four SR-4 strain gages were mounted on a specimen as shown in Fig. 7, and the specimen was subjected to simple loading in the setup shown in Fig. 2. The applied loads were converted to stress as indicated by the beam formula and plotted against the corresponding strain as shown in Fig. 7. The apparent moduli by beam-formula fiber stress versus strain are considerably higher than those obtained from tensile stress-strain data especially at higher stresses. This emphasizes the fact that stresses determined from beam formulas deviate considerably from the true stresses. The stress-strain data shown in Fig. 7 were obtained on as-cast specimens not subjected to previous stressing. Cast irons are quasi-elastic materials. Therefore stressing will result in plastic deformation and alter the stress-strain characteristics of the material. When strain determinations on a quasi-elastic material are converted to stress, it is imperative that the stress-strain data used in the conversion be obtained on material of similar prior stress history.

Modern Methods in the Heat-Treatment of Steel

By E. R. MERTZ,[1] BURBANK, CALIF.

The construction of time-temperature-transformation curves (S-curves) and their use in developing the interrupted-quench processes for steels are treated in this paper. Of these processes, martempering, austempering, and cyclic annealing are explained in detail. Martempering results in greatly reduced stresses in quenched parts, as compared to the conventional quench and temper method of hardening steel, and hence much less cracking and distortion is apparent. Austempering, an isothermal process producing bainite, develops surprisingly high impact properties in the region of 250,000 psi or 50 Rockwell C. Cyclic annealing is an elevated-temperature isothermal annealing process to produce a predetermined degree of softness, and saves much valuable time in the annealing of the higher alloy steels. The use of hardenability curves in establishing size limitations for particular heats of steel and in selecting accurate tempering temperatures is demonstrated.

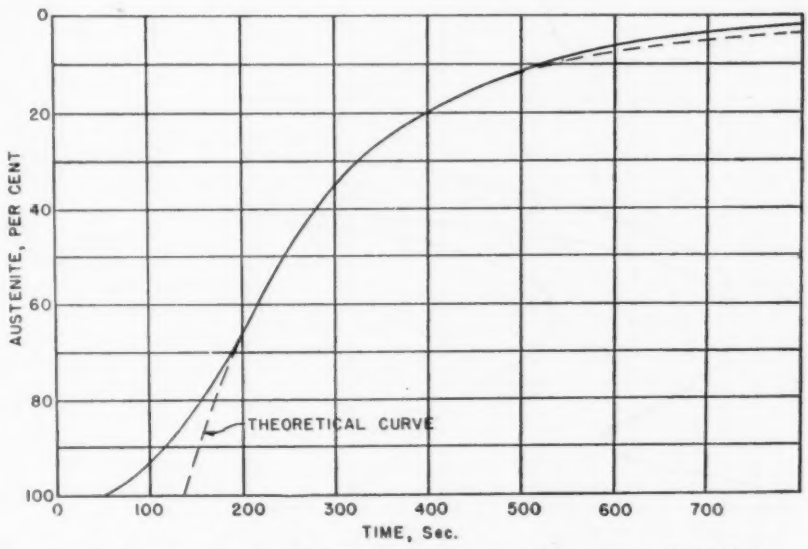


FIG. 1 REACTION RATE OF AUSTENITE COMPARED TO THEORETICAL FIRST-ORDER REACTION CURVE

INTRODUCTION

MOST of the processes involved in the heat-treatment of steel depend upon the decomposition of austenite into one or more of its transformation products, and the physical properties produced depend upon the nature of the product or products formed. Austenite is a solid solution of carbon in iron which is stable (for most steels) only at elevated temperatures, and when it is cooled below a certain critical temperature the normal solubility of carbon in iron is reduced to a negligible amount. As a result, a reaction occurs which involves a change in the crystallographic structure of the iron, and in most cases the formation of iron carbide and/or other carbides. Bain and Davenport (1)[2] demonstrated that the product formed from the decomposition of austenite was dependent upon the temperature at which the reaction occurred rather than the speed at which the austenite was cooled.

AUSTENITE DECOMPOSITION; S-CURVES

Fig. 1 illustrates how closely the isothermal transformation of austenite follows a first-order chemical reaction in which the rate of reaction at any instant is proportional to the amount of reacting material remaining. However, there are several notable deviations from a true first-order reaction. Such a reaction begins immediately at a maximum rate and continues at a constantly diminishing rate. Theoretically, it never reaches completion.

Austenite apparently goes through an incubation period before decomposition starts, does not reach its maximum rate until the reaction has progressed an appreciable amount, and does reach completion in a finite time.

Bain and Davenport (1) studied isothermal transformation rates of austenite at various subcritical temperatures and plotted curves of temperature versus time for beginning and end of transformation. The result was the now familiar "S-curve."

Fig. 2 illustrates (2) how these curves were constructed. The progress of transformation at a chosen temperature was followed by quenching numerous thin samples from an austenitizing temperature into a molten metal bath maintained at the chosen temperature. Periodically, specimens were drastically quenched from the constant-temperature bath so that any untransformed austenite would be converted to martensite, the product formed from austenite at low temperatures. Microscopic examination of such specimens properly etched revealed the dark-etching pearlite or bainite in contrast to the lighter-etching martensite.

Thus accurate data on the beginning and virtual end of transformation of austenite to pearlite or bainite were established, but the data on austenite to martensite transformation remained in doubt. Inasmuch as the formation of martensite apparently involves only a space-lattice change, it does not require time for diffusion. Hence many metallurgists were of the opinion that time was not a function of the process, and temperature was the controlling factor.

---

[1] Associate Professor in General Engineering, University of Southern California, Los Angeles, Calif. Formerly Research Engineer, Lockheed Aircraft Corporation.

[2] Numbers in parentheses refer to the Bibliography at the end of the paper.

Contributed by the Metals Engineering Division and presented at the Aviation War Conference, Los Angeles, Calif., June 11–14, 1945, of THE AMERICAN SOCIETY OF MECHANICAL ENGINEERS.

NOTE: Statements and opinions advanced in papers are to be understood as individual expressions of their authors and not those of the Society.

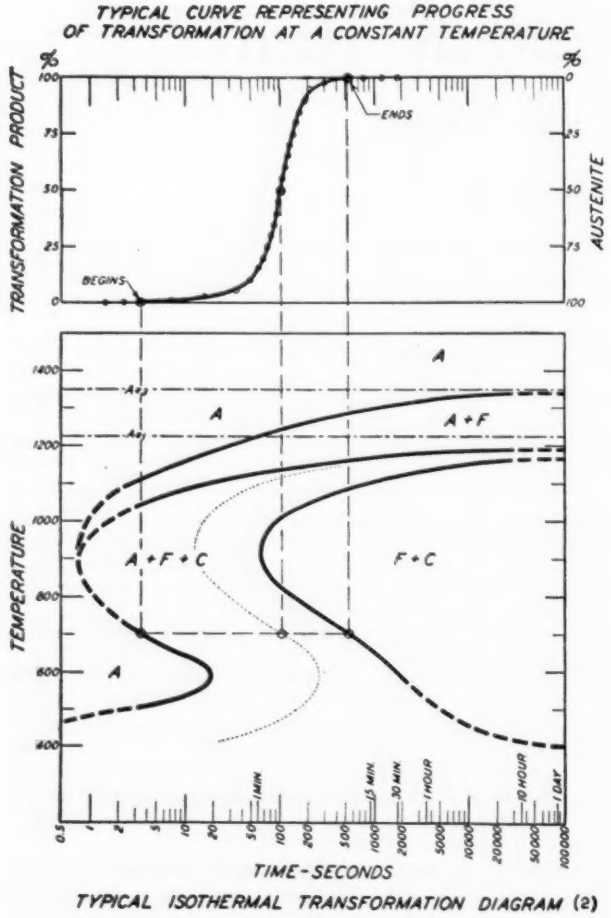


FIG. 2

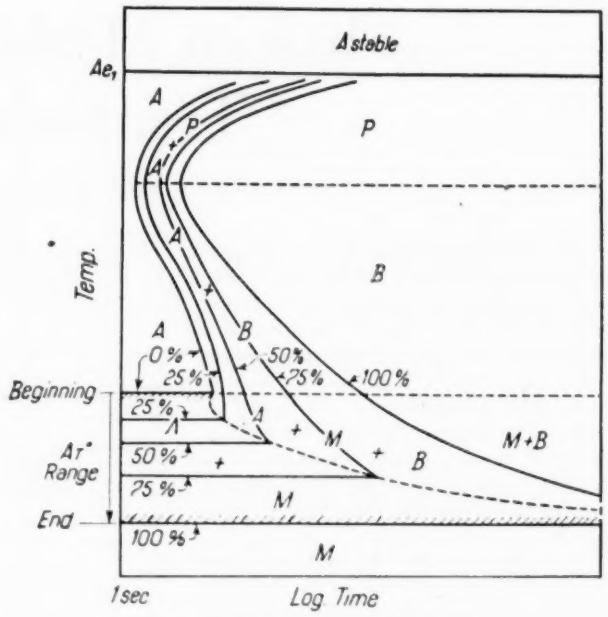


FIG. 3 MODIFIED S-CURVE DIAGRAM

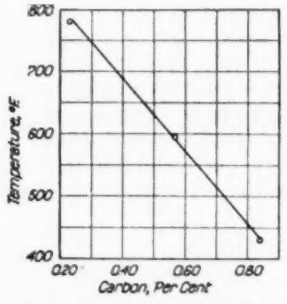


FIG. 4 EFFECT OF CARBON ON THE M_s OF PLAIN-CARBON STEEL

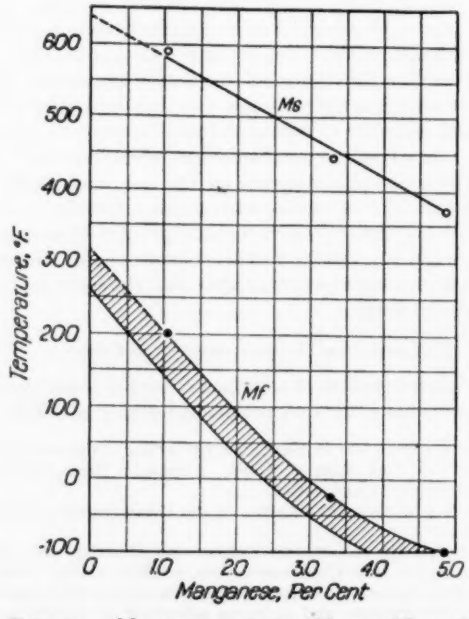


FIG. 5 EFFECT OF MANGANESE ON THE M_s AND M_f OF 0.50 PER CENT CARBON STEEL

MARTENSITE FORMATION; M_s AND M_f POINTS

In a recent investigation Greninger and Troiano (3) were able to follow the progress of austenite to martensite formation by tempering for a short time at a higher temperature the specimens quenched into a low-temperature isothermal bath. The tempering treatment caused any martensite formed to etch darker than freshly quenched martensite, and microscopic examination revealed it in sharp contrast to that formed by quenching after the tempering treatment. The lighter-etching martensite formed by quenching after tempering, represented the untransformed austenite from the original isothermal quench. The results of this investigation established that martensite formation was essentially dependent upon temperature alone. At a given temperature a certain percentage of martensite was formed almost instantaneously and no more was formed unless the temperature was lowered. A constant-temperature product began to appear after a considerable time lag, which amounted to days or weeks at room temperature. This latter product was no doubt a result of diffusion, and was bainitic in structure.

Fig. 3 represents a modified S-curve, or time-temperature-transformation (TTT) curve constructed by Cohen (3), in which the "timeless" nature of martensite formation is incorporated. The dotted line represents the beginning of formation of the isothermal product, which Cohen includes with bainite.

The temperature indicating the beginning of formation of martensite has been designated M_s, and that representing the end, M_f. Fig. 4 is a curve constructed by Greninger (4) showing that the M_s point decreases linearly with increasing carbon content.

Alloys have a similar effect on both the M_s and M_f point, as indicated in Fig. 5 by Payson and Savage (5). They have submitted the following formula for calculating the M_s point, provided, of course, that the austenitizing temperature used is one at which all carbides will be completely in solution in the austenite.

$$M_s \text{ in deg F} = 930 - 570\,C - 60\,Mn - 50\,Cr - 30\,Ni - 20\,Si - 20\,Mo - 20\,W$$

In many steels of high-carbon and high-alloy content the M_f point is well below room temperature, and considerable amounts of austenite are retained by conventional heat-treating procedures. The distortion of accurate gages after long storage may be explained by the eventual transformation of such retained austenite to the isothermal product formed at the storage temperature. Subzero treatment of such steels often transforms much of the retained austenite to martensite, giving a more uniform product, and in many cases a much harder one.

Interrupted-Quench Processes

Complete hardening of a steel part requires the formation of essentially 100 per cent martensite, necessitating a cooling rate at the center fast enough to miss the "nose" of the S-curve where much softer products are formed. Fig. 6 illustrates (6) the conventional quenching process. With rapid quenching the temperature gradient is sufficient to allow the surface of the steel to be almost wholly martensitic while the center is still wholly austenitic. Thus when the center does transform, the expansion due to the austenite-martensite transformation produces tensile stresses in the rigid outer layer of martensite which are often sufficient to produce cracking or at least severe distortion. Such conditions may be minimized by quenching into an isothermal bath above the M_s point and holding at temperature long enough to equalize the temperature throughout the cross section. Air-cooling from this temperature will produce complete hardening, and the thermal gradient will be small enough to allow martensite formation to take place more uniformly from surface to center, minimizing residual stresses. This process is called "martempering," and is illustrated in Fig. 7 (6). The quenching is followed by the usual tempering treatment to produce desired properties.

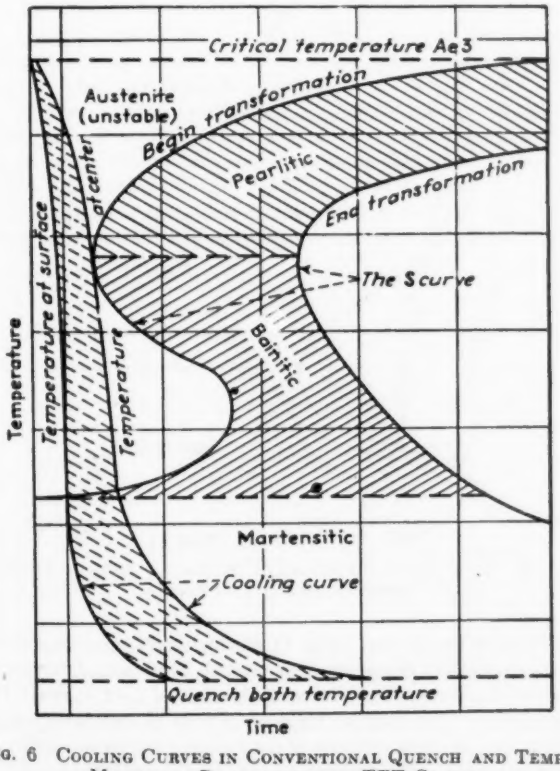


Fig. 6 Cooling Curves in Conventional Quench and Temper Method in Relation to the TTT Curve

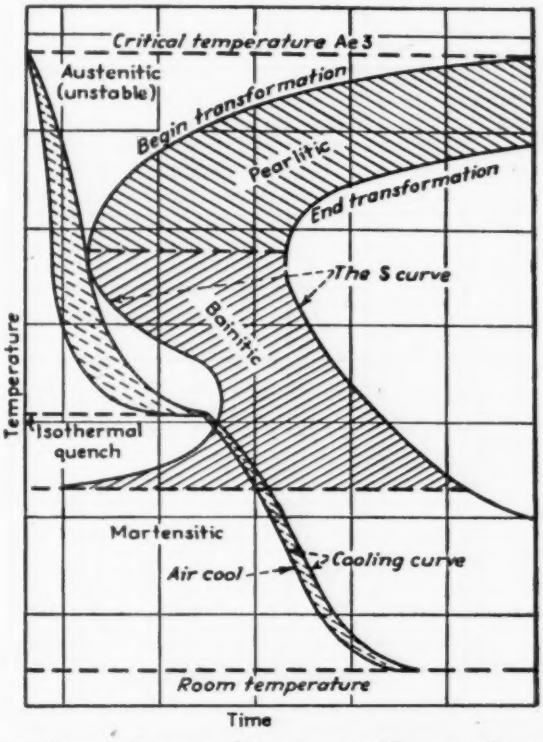


Fig. 7 Cooling Curves in Martempering Method in Relation to the TTT Curve

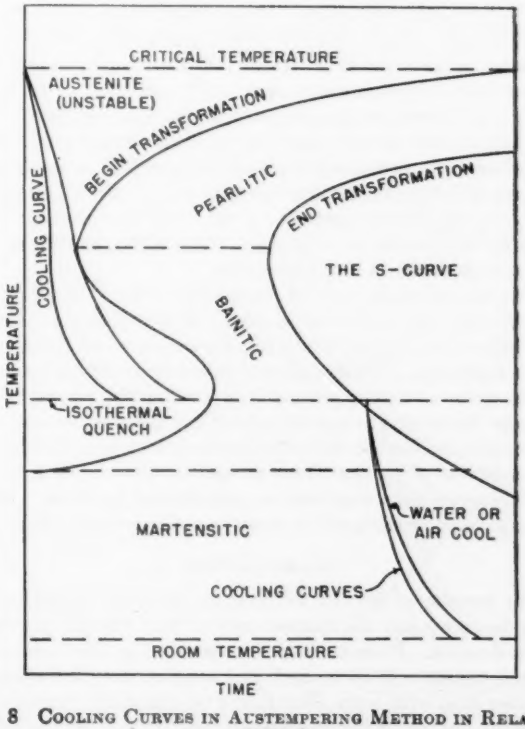


Fig. 8 Cooling Curves in Austempering Method in Relation to the TTT Curve

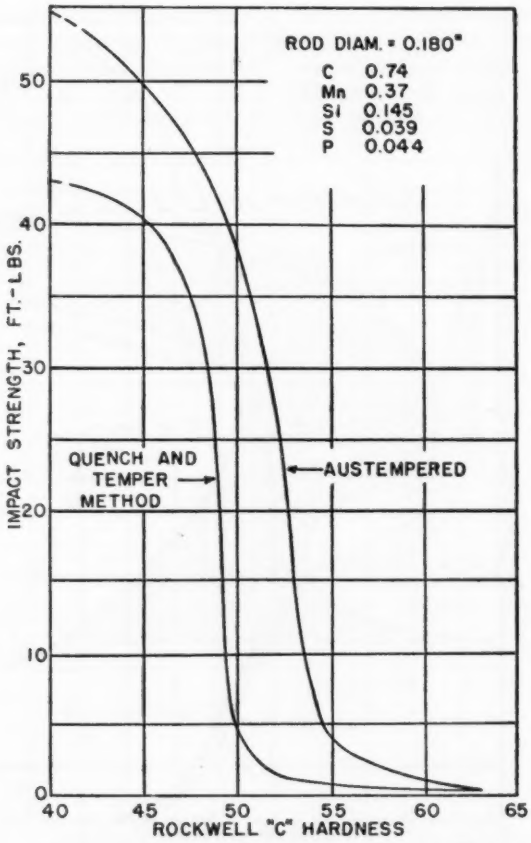


FIG. 9 COMPARISON OF IMPACT STRENGTHS AT VARIOUS HARDNESSES OF AUSTEMPERED AND QUENCHED-AND-TEMPERED STEELS

Fig. 8 illustrates (6) a method of heat-treatment which eliminates the need for tempering. The process, known as "austempering," consists of quenching the steel into a bath held at a temperature where bainite is formed and allowing the austenite to transform isothermally to bainite. The selection of bath temperature determines the hardness of the final product. Steels treated in this manner show considerable improvement in impact resistance, especially in the vicinity of 50 Rockwell C hardness or 250,000 psi, as illustrated in Fig. 9 (7). This process has been applied successfully in the heat-treatment of certain springs, knives, chisels, and other parts where toughness combined with hardness is of importance.

The annealing of steels by furnace-cooling to produce a soft, machinable structure is often a very slow process, especially in the higher-alloy grades which require very slow cooling to avoid some hardening. Much valuable time may be saved by the use of the cyclic annealing process illustrated in Fig. 10 (6). An air furnace operating at constant subcritical temperature may often be substituted for the isothermal quench with little loss of time. The selection of isothermal temperature is dictated by a compromise between time consumption and desired hardness. Higher temperatures produce softer structures, but require longer time.

HARDENABILITY

The severity of quench required for complete hardening of a steel depends upon the reaction rate of that steel at the "nose" of the S-curve. If the cooling curve crosses the nose some pearlite and bainite will be formed, and a softer structure obtained. Another steel with more alloy might be completely hardened by the same quench, indicating that its reaction rate at the nose of

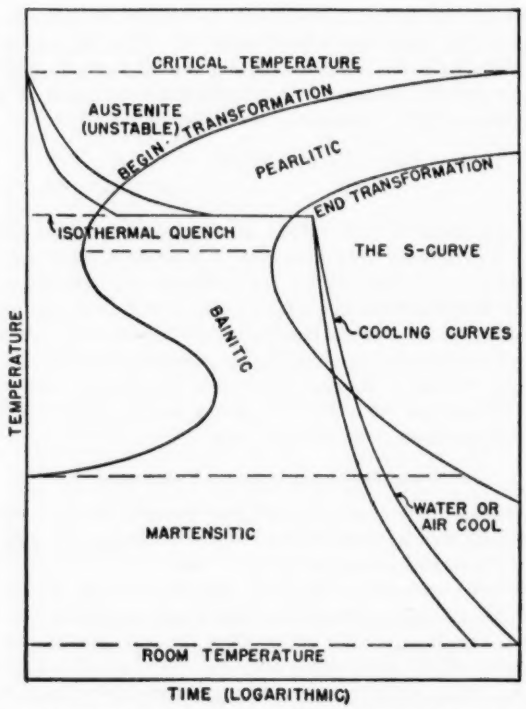


FIG. 10 COOLING CURVES IN CYCLIC ANNEALING METHOD IN RELATION TO THE TTT CURVE

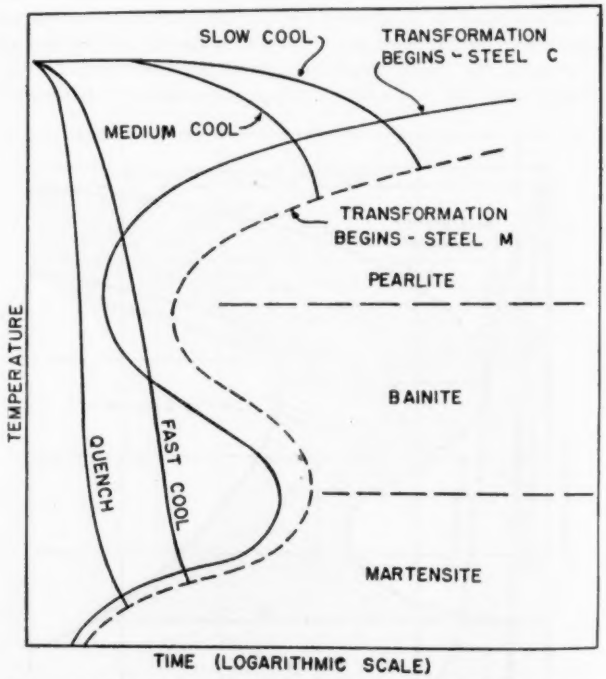
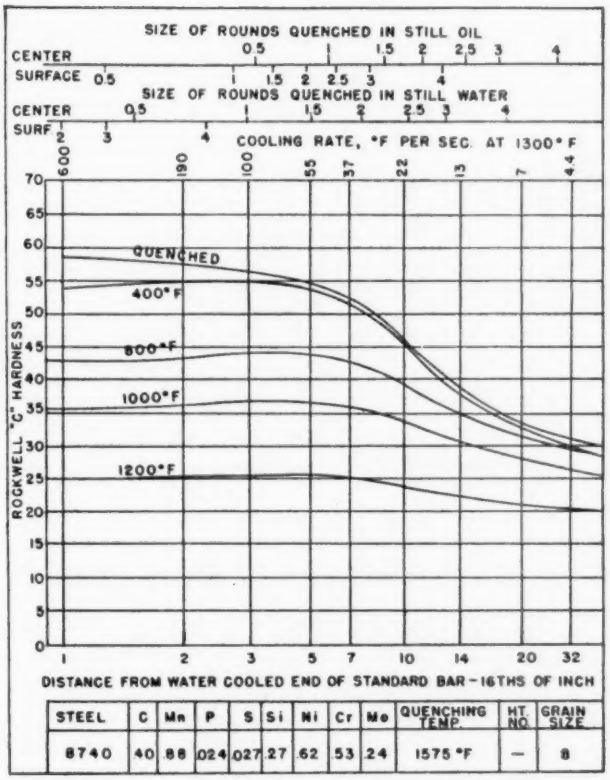


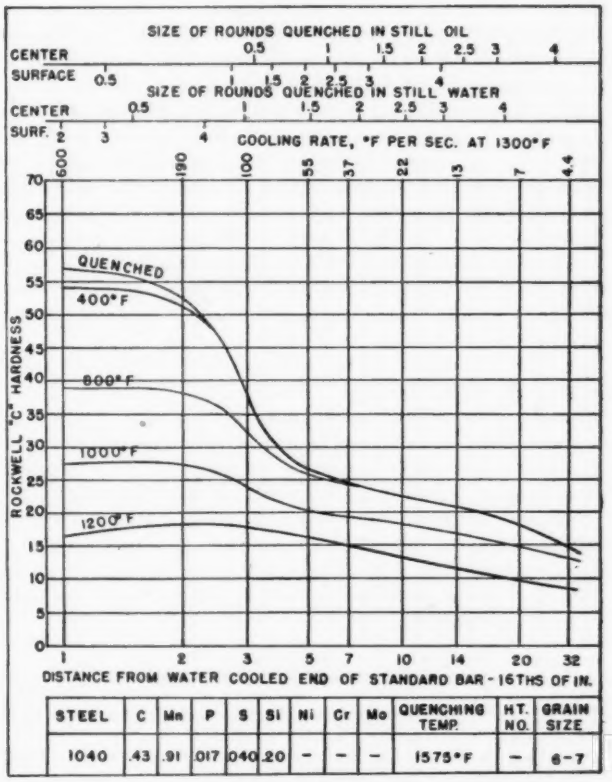
FIG. 11 COMPARISON OF COOLING RATES TO OBTAIN DESIRED STRUCTURES FOR TWO STEELS

the S-curve was slower. Fig. 11 illustrates (7) this comparison. The fast cool completely hardens steel M, but incompletely hardens steel C, inasmuch as it crosses the nose of the S-curve. The construction of an S-curve for a given heat of steel is very time-consuming, so other methods of determining the hardenability of steels are used. Most popular is the end-quench hardenability



STEEL	C	Mn	P	S	Si	Ni	Cr	Mo	QUENCHING TEMP.	HT. NO.	GRAIN SIZE
8740	40	88	024	027	27	62	53	24	1575 °F	—	8

FIG. 12 STANDARD END-QUENCH HARDENABILITY CURVES FOR AN NE-8740 STEEL



STEEL	C	Mn	P	S	Si	Ni	Cr	Mo	QUENCHING TEMP.	HT. NO.	GRAIN SIZE
1040	.43	.91	.017	.040	.20	—	—	—	1575°F	—	6-7

FIG. 13 STANDARD END-QUENCH HARDENABILITY CURVES FOR AN S.A.E. 1040 STEEL

test devised by Walter E. Jominy. This test makes use of the fact that a heated steel bar, quenched only on the end by a jet of cold water, will have a very rapid cooling rate at the point of impingement of the water jet, and a continually decreasing cooling rate at increasing distances from the quenched end. Inasmuch as such cooling rates have been established, a longitudinal hardness traverse of an end-quenched bar will determine what cooling rates are necessary to produce specific hardnesses in the steel from which the bar was made. By correlation of these cooling rates with known cooling rates in fully quenched bars, the hardnesses in such bars may be predicted.

Figs. 12 and 13 show end-quench hardenability curves for two steels. These are supplemented by curves for the same steels tempered at various temperatures.

CORRELATION OF HARDENABILITY DATA TO CROSS-SECTIONAL HARDNESS DATA

Figs. 14 and 15 are correlation charts to be used in conjunction with hardenability curves to convert rapidly end-quench hardness values to cross-sectional hardness values. These charts were constructed by plotting established cooling rates (8) as abscissas against section size as ordinates. Cooling rates are necessarily

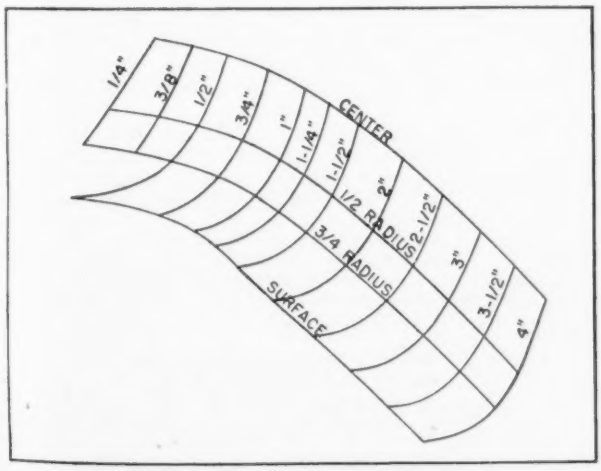


FIG. 14 CORRELATION CHART; END QUENCH TO SECTION HARDNESS; OIL QUENCH

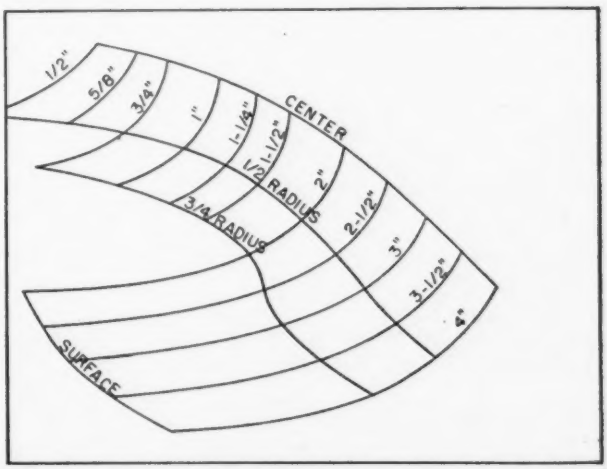


FIG. 15 CORRELATION CHART; END QUENCH TO SECTION HARDNESS; WATER QUENCH

on the same scale as those which appear in Figs. 12 and 13. Construction lines are deleted to avoid confusion. For use, the correlation charts are constructed on transparent paper or copied on photographic film. The use of the water-quench correlation chart is illustrated in Fig. 16. The chart is superimposed on Fig. 13 so that the vertical index line at the left falls on the left border line of Fig. 13. By sliding the chart up or down (keeping the vertical lines indexed) hardness values are read at the intersection of the hardenability curve and the selected bar size and section-location curves. In Fig. 16 point A indicates that the center of a 1-in. round of this heat of S.A.E. 1040 steel would have a hardness of approximately 38 Rockwell C when quenched in water. To find the anticipated hardness halfway between the surface and the center, the correlation chart is moved up until the junction of the half-radius and 1-in. curves intersects the hardenability curve. Here a hardness of 48 Rockwell C is obtained. The oil-quench correlation chart is used in a similar manner.

These correlation charts permit the rapid translation of hardenability data to cross-sectional hardness data for various tempering temperatures as well as the as-quenched values by using tempering curves like those appearing in Figs. 12 and 13. They also permit the rapid determination of hardness depth for incompletely hardened parts and the establishment of limiting size of a given steel for a particular quench when a minimum acceptable hardness has been decided upon.

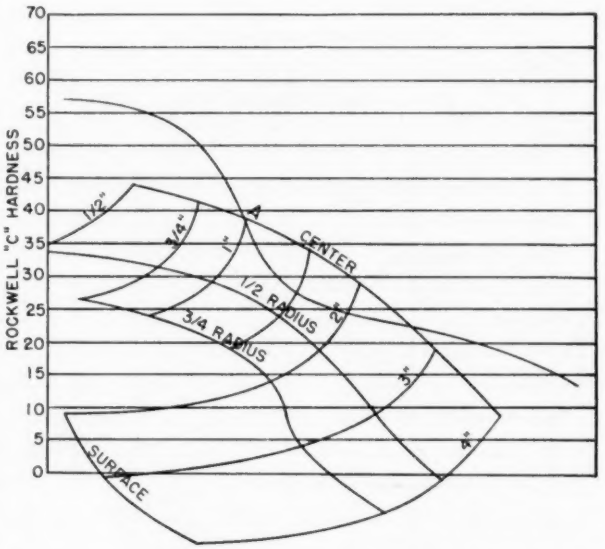


FIG. 16 USE OF WATER-QUENCH CORRELATION CHART ON END-QUENCH HARDENABILITY CURVE FOR AN S.A.E. 1040 STEEL

BIBLIOGRAPHY

1 "The Transformation of Austenite at Constant Subcritical Temperatures," by E. S. Davenport and E. C. Bain, Trans. A.I.M.E., vol. 90, 1930, p. 117–154.

2 Atlas of Isothermal Transformation Diagrams, United States Steel Corporation, Pittsburgh, Pa., 1943.

3 "Kinetics of the Austenite to Martensite Transformation in Steel," by A. B. Greninger and A. R. Troiano, Trans. A.S.M., vol. 28, 1940, p. 537–574; discussion by Marcus Cohen.

4 "The Martensite Thermal Arrest in Iron Carbon Alloys and Plain Carbon Steels," by A. B. Greninger, Trans. A.S.M., vol. 30, 1942, p. 1–26.

5 "Martensite Reactions in Alloy Steels," by P. Payson and C. H. Savage, Trans. A.S.M., vol. 33, 1944, p. 261–280.

6 "Salt Bath Quenching Processes," by H. J. Babcock, *Metals and Alloys*, vol. 20, October, 1944, p. 964–972.

7 "The Industrial Application of Austempering," by E. E. Legge, *Metals and Alloys*, vol. 10, August, 1939, p. 228–242.

8 S.A.E. Handbook, 1944, p. 321.

Elevated-Temperature Stretch-Flanging of Some Aluminum Alloys

By E. G. THOMSEN,[1] D. M. CUNNINGHAM,[2] and J. E. DORN[3]

Many aircraft parts consisting of a flat web and a concave flange are produced by rubber-die-forming on a hydropress. The forming action consists of bending the flange around the die radius and stretching the outer fiber of the flange from its original length to that which is achieved when it contacts the die. Several types of failures and defects are encountered, the most important being a radially directed fracture initiated at the outer fiber of the flange. When this fracture occurs without necking, the maximum per cent stretch that may be produced approximates the per cent local ductility in the tension test. If, however, fracture is preceded by necking, the permissible per cent stretch is intermediate between the uniform and local per cent strain in tension. Increasing the forming temperature permits greater per cent stretches for some of the more-ductile alloys.

Introduction

MANY aircraft parts consist of a flat web with a concave flange. Such parts are usually produced by rubber-die-forming on a hydropress at atmospheric temperature. Although many aircraft materials exhibit ample deformation to permit successful forming of concave flanges, other materials, particularly those in the aged condition, have such limited deformability that satisfactory flanges cannot be produced. The Western Aircraft War Production Council recommended that the War Metallurgy Committee investigate the mechanics of concave flanging and the possibilities of improving this operation by forming at elevated temperatures. This report is based on investigations conducted by Project NRC-548 for the Office of Production Research and Development of the War Production Board.

The rubber-die hydropress-forming of concave flanges has been described in several papers.[4,5,6] A blank of radius R_b, as illustrated in Fig. 1, is placed on a die block having a contour radius R_c somewhat greater than R_b. As the rubber contained in the head of the press is impressed against the die, the blank is bent around the die radius along the die contour line until the formed flange touches the die. Since the extreme fiber of the flange is stretched from a radius R_b to the larger radius it assumes when contact is achieved, the operation is commonly called stretch-flanging.

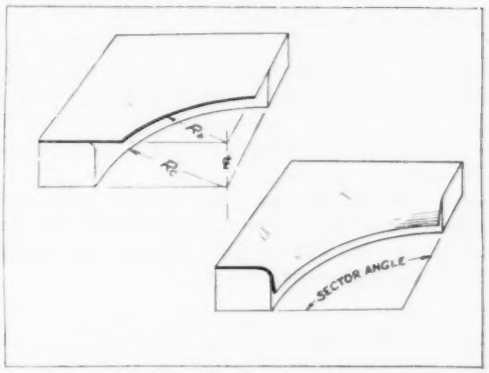


Fig. 1 Blank and Flanged Part of Die

Experimental Procedure

Scope of Investigation. Tests were planned to determine the stretch-flanging limits of a number of aluminum-alloy sheet materials at forming temperatures of 70 F, 300 F, 400 F, and 450 F. The maximum temperature of 450 F was selected because of rapid deterioration of the rubber pad at higher temperatures and possible detrimental changes in physical properties of some of the precipitation-hardened alloys. The general survey of the effect of temperature on the stretch-flange formability was carried out on a 4-in-contour-diam die with blanks having 360-deg flange sectors. Spot tests were made on other variables, such as other contour diameters, sheet thicknesses and sector lengths, in order to observe the major trends introduced by these variables.

Materials. The standard aluminum sheet materials that were investigated included 3S-O, 52S-O, 24S-O, 61S-O, 75S-O, 24S-T, 24S-T86, 61S-T, R301-T, and 75S-T covering thicknesses from 0.020 in. to 0.081 in.

Equipment. The hydropress consisted of a modified 200-ton aircraft-type press. The platen was 15 in. wide and 28 in. long arranged with electric-resistance heaters and automatic temperature control.

The normal platen pressure was 1050 psi, but pressures as high as 7000 psi were obtained with special platens and rubber heads. The mild-steel die blocks had contour diameters of 3, 4, 6, and 8 in.; $^3/_{16}$-in. bend radii were provided on all dies in order to eliminate bend failures.

Specimens. The specimens were sheared from sheet stock with die-locating holes and blank pilot center hole jig-drilled. The desired blank-hole diameter was machined with a fly cutter to an accuracy of 0.010 in. of the nominal blank-hole diameter. All blank holes were polished with 2/0 Behr Manning polishing paper after machining, in order to provide uniformly controlled edge conditions.

Experimental Technique. The specimen blanks were preheated to the forming temperature for 10 min in an air furnace and rapidly transferred to the die block. A light layer of asbestos powder was screened over the blank in order to prolong the useful

[1] Assistant Professor of Mechanical Engineering, University of California, Berkeley, Calif.

[2] Lecturer in Mechanical Engineering, University of California.

[3] Associate Professor of Physical Metallurgy, University of California.

[4] "Forming Methods—Forming by Single Action Hydraulic Press," International Textbook Company, Bureau of Aeronautics, Navy Department, Washington, D. C., 1943.

[5] "Elastic Theory as a Tool in Sheet Metal Forming Problems," by F. R. Shanley, *Journal of the Aeronautical Sciences*, vol. 9, 1942, pp. 313–333.

[6] "Design Factors for Aircraft Sheet-Metal Forming," by W. Schroeder, *The Modern Industrial Press*, October, 1943.

Presented at the National Meeting of the Aviation Division, Los Angeles, Calif., June 3–6, 1946, of The American Society of Mechanical Engineers.

Note: Statements and opinions advanced in papers are to be understood as individual expressions of their authors and not those of the Society.

life of the rubber pad. The press head was then moved against the platen to a predetermined pressure which permitted complete forming of the blank. A series of blanks were thus formed with blank-hole diameters varying in steps of 0.10 in. (flange widths varying in 0.05-in. steps). The critical blank diameter was evaluated as the minimum diameter that was successfully formed. Frequently in the region of the critical diameter a specimen would fracture, whereas a duplicate specimen would form successfully. In this case the critical value of blank diameter was taken as the larger and more conservative value.

In order to obtain forming temperatures in the blank approaching those of the die it was necessary to hold the blank under light pressure for 1 min between rubber pad and heated die before forming the stretch flange. All temperatures reported herein are those of the heated die but represent the blank temperature to within 10 deg F.

Geometry of Stretch Flanges. The simplest type of stretch flange consists of a 360-deg sector produced on a block having a 90-deg die angle. For this type flange the per cent stretch of the outer fiber of the flange is simply

$$\text{Per cent } S = \frac{(R_e - R_b)}{R_b} \times 100 \quad \ldots\ldots [1]$$

As smaller values of R_b are employed the per cent stretch of the outer fiber of the flange increases. Finally a critical value is reached resulting in fracture of the flange. The maximum permissible stretch is given by

$$\text{Per cent } S_{max} = \left(\frac{R_e}{R_{b\,min}} - 1\right) \times 100 \quad \ldots\ldots [2]$$

and the corresponding true strain is

$$\phi_{max} = \ln \frac{(R_e)}{R_{b\,min}} \quad \ldots\ldots [3]$$

If the sector angle is less than 360 deg, another geometrical factor enters the analysis. The induced circumferential tensile stresses causing stretching vanish at the sector edges and the per cent stretch that is obtained becomes less than the value calculated from Equation [1]. The actual stretch is therefore less than the theoretical stretch, and consequently flanges of greater heights may be produced without encountering failures.

For small sector angles, the arc length of the flange approaches the corresponding chord length. Since the energy that is required to form a straight flange is less than that required for a curved flange of the same contour length, flanges of small sector angle frequently form straight flanges along the chord.

In order to produce a part having a flange at 90 deg to the web, the part must be slightly overformed so that the desired angle is obtained after springback. The per cent stretch for dies having angles that differ from 90 deg is derived in Appendix 1.

Experimental Results

Types of Fracture. The forming of stretch flanges is limited by several forming defects and failures which are shown in Fig. 2, and are briefly described as follows:

(*a*) *Stretch Rupture.* Stretch rupture, illustrated in Fig. 2(A), is the most common type of forming failure. This type of fracture was encountered in most of the 360-deg flanges that were tested. Two types of fracture were observed. The annealed alloys at all temperatures and some of the precipitation-hardened alloys at 450 F exhibited local necking preceding fracture; some of the precipitation-hardened alloys fractured without necking at the lower temperatures.

(*b*) *Bulging Rupture.* The second type of rupture which limits the formability is shown in Fig. 2(B), and was named a bulging rupture. This type of rupture was obtained when small blank-hole diameters were employed. Instead of forming a flange the blank bulged in a manner similar to that obtained in the absence of a central hole. Fracture occurred along the die-contour radius before the outer fiber reached its limiting ductility. This type of fracture was not obtained when the hole diameter was increased to the critical value for stretch rupture.

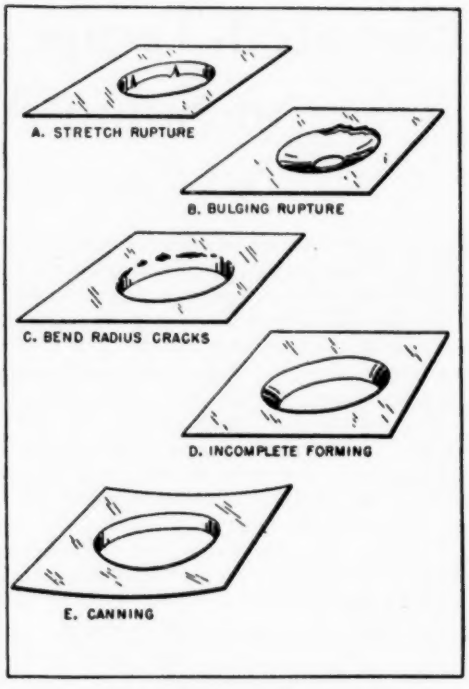


Fig. 2 Forming Defects

(*c*) *Bend Cracks.* If the die bend radius is too small the strains of the fiber on the top surface of the blank may exceed the permissible strain before the outer fiber of the flange reaches its critical stretch value, resulting in fracture of the upper surface of the blank along the die bend radius. This type of fracture is shown in Fig. 2(C). In the present investigation the die bend radii were maintained sufficiently large to prevent the formation of bend cracks.

(*d*) *Incomplete Forming.* In forming stretch flanges the blank is bent as well as stretched. Consequently the pressure required for forming stretch flanges is greater than that required for straight flanges. If the pressure is not great enough an incompletely formed flange results, as shown in Fig. 2(D). The pressures for the present investigation were maintained sufficiently large to insure contact of the outer fiber of the blank and the die.

(*e*) *Canning.* Canning, as shown in Fig. 2(E), results from springback after forming. No attempt was made to evaluate completely the springback after forming, but it was observed that the springback for stretch flanges is slightly less than that for straight bends for the same conditions of forming temperature, sheet thickness, and bend radius.

Maximum Per Cent Stretch. The effect of temperature on the maximum per cent stretch that may be achieved in a number of aluminum alloys is shown in Fig. 3. It is evident from these curves that increased stretch-flange formability is achieved at temperatures above 300 F for all alloys investigated. Each alloy, however, exhibits its own peculiar maximum per cent stretch-temperature curve.

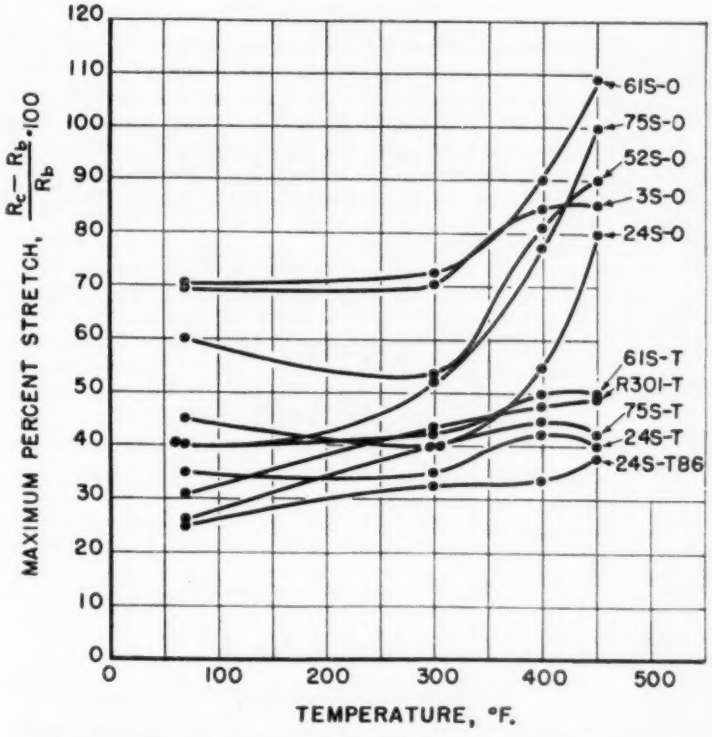


FIG. 3 EFFECT OF TEMPERATURE ON MAXIMUM PER CENT STRETCH

A few tests were made to evaluate the effect of contour radius on the maximum per cent stretch. Materials which necked during flanging yielded decreasing per cent stretch with increasing contour radii.

The effect of thickness was studied for 24S-O and 61S-T formed at atmospheric temperature on a 6-in-contour-diam die. Slightly greater per cent stretch was observed as the thickness was increased from 0.020 to 0.081 in., but results were too varied to warrant a more definite statement.

The effect of the angle of sector of the blank on the maximum per cent stretch is given in Fig. 4 for atmospheric and 450 F forming temperatures. The plain open and solid circles refer to maximum per cent stretch limited by stretch fracture, whereas the crossed symbols refer to maximum per cent stretch limited by fracture at the edge of the segmented blanks near the die bend radius. For the two alloys investigated the maximum per cent stretch with atmospheric-temperature forming rises moderately with decreasing sector angle to a maximum at approximately 90 deg. Blanks with sector angles of 30 deg could not be fractured at all forming temperatures. At 450 F alloy 24S-O could not be fractured with sector angles of 90 deg or less.

Discussion of Results. A major objective of investigations on the formability of metals is the development of a useful philosophy that will permit the prediction of forming limits from a few simple, easily obtainable test data. Most metal-forming processes, however, are so complex that this objective has not been completely achieved; stretch flanging is not an exception. The results of this investigation, however, show that the forming limit for stretch flanges can be approximated in a few simple cases.

The fracture causing a stretch-rupture failure during forming starts at the outer fiber of the flange. Although, in some alloys, local plastic action precedes fracture in this critical region, in other alloys fracture occurs without evidence of necking. Many alloys that neck when tested in simple tension do not neck when stretch-flanged.

An estimate of the maximum per cent stretch is possible for alloys that do not neck when stretch-flanged. Since the outer fiber of the flange is known by grid analyses to be essentially stressed by simple circumferential tension, it is logical to assume that stretch rupture is initiated when the circumferential tension stress equals the true fracture stress in tension. This assumption implies that the maximum true strain for stretch-flange forming should approximate the true local strain in tension defined by

$$\phi_{max} = \ln \frac{A_0}{A_f}$$

where

A_0 = original cross-section area
A_f = cross-section area at fracture

A comparison of the maximum true stretch with tension data,[7] obtained from standard A.S.T.M. specimens, shown in Fig. 5, illustrates the agreement that may be expected. Materials 24S-T86 at all temperatures, R301-T and 75S-T up to 300 F, and 24S-T up to 400 F exhibited stretch ruptures without evidence of necking. For these conditions the maximum true stretch approximated the true local strain in tension. In all other cases necking preceded fracture, and the maximum true stretch that could be achieved was intermediate between the true uniform and the true local strains in tension. Thus the maximum true stretch that can be achieved in the absence of necking approaches the true local strain at fracture in tension.

No satisfactory analysis is available for predicting the stretch-flange-forming limits of materials under conditions where necking is obtained; the maximum true stretch is significantly greater than the true uniform strain in tension. Since necking is known to begin when the resistance to the forming load passes a maximum value, it is logical to suspect that necking in stretch-flanging requires a complete analysis of the stress and strain distribution in the entire flange. Thus changes in contour diameter may affect

[7] "Tensile Properties Affecting the Formability of Aluminum-Alloy Sheet at Elevated Temperatures," by A. E. Flanigan, L. F. Tedsen, and J. E. Dorn. To be published in the *Journal of the Aeronautical Sciences.*

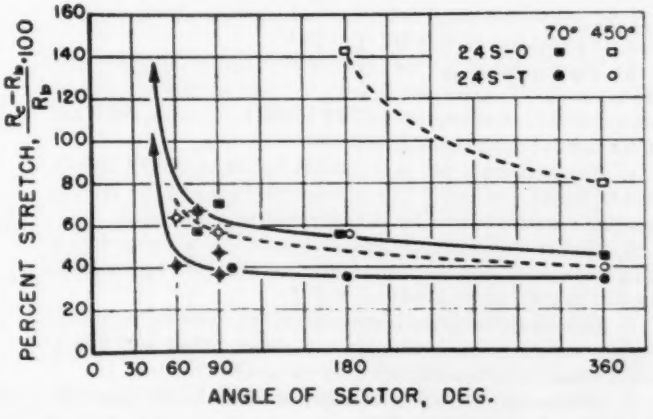
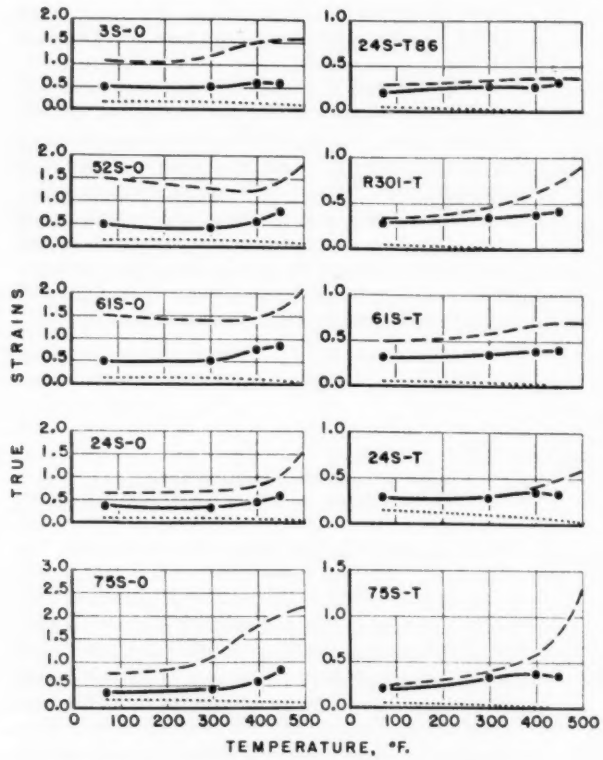


FIG. 4 EFFECT OF ANGLE OF SECTOR ON MAXIMUM PER CENT STRETCH



— — — $\ln(A_o/A)$ = True strain at fracture in the tensile test.

..... $\ln(l_u/l_o)$ = True maximum uniform strain in the tensile test.

——— $\ln(R_c/R_b)$ = Maximum stretch in stretch flanging.

FIG. 5 COMPARISON OF STRETCH-FLANGING DATA WITH TENSILE DATA

the per cent stretch. The complex distribution of stresses in the flange are not yet known and therefore complete knowledge of stretch-forming limits will have to await the development of this involved analysis.

SUMMARY AND CONCLUSIONS

1 Forming of 360-deg-sector stretch flanges in a number of aluminum alloys is limited by stretch rupture, radius-bend cracks, or available press pressure.

2 Materials 24S-T, 24S-T86 and 75S-T fractured without evidence of necking when formed at 70 F to 300 F; for all remaining materials and temperatures investigated, fracture was preceded by necking except R301-T at 70 F.

3 The maximum per cent stretch obtained with 24S-T, 24S-T86, and 75S-T agrees closely with the local ductility in tension when formed at temperatures of 70 F to 300 F; between 300 F and 450 F some necking preceded fracture.

4 The maximum per cent stretch for 3S-O, 52S-O, 24S-O, 61S-O, 75S-O, and 61S-T falls between the local and the uniform per cent strain in tension for all temperatures investigated.

5 Higher stretch-flange-formability may be achieved with a 3-in. than with an 8-in-contour-diam die at a forming temperature of 70 F for alloys 24S-O and 61S-T.

6 Increasing thickness from 0.020 in. to 0.064 in. results in higher stretch-flange-formability for alloys 24S-O and 24S-T when formed on a 6-in-contour-diam die and 70 F.

7 Sectors may be formed to a greater flange height than 360-deg flanges for 24S-O and 24S-T.

8 Springback of stretch flanges is slightly less than for straight bends for the same die radius and sheet thickness.

ACKNOWLEDGMENT

The authors wish to acknowledge the support of the Office of Production Research and Development of the War Production Board on this investigation. They are particularly indebted to the Western Aircraft War Production Council for suggestions and assistance in planning this investigation. The authors also wish to thank Messrs. T. Robinson, V. Gudmendsen, and Miss Barbara Roney, for their assistance on the experimental phases of the investigation.

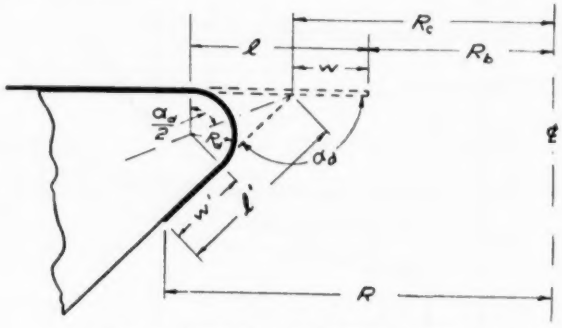


FIG. 6 GEOMETRY OF STRETCH FLANGE

Appendix 1

PER CENT STRETCH FOR 360-DEG FLANGES

Assuming that the changes in thickness and length are minor, an approximate calculation of the effect of the die angle on the stretch is readily obtainable from Fig. 6.

Let

$$l' = w' + R_d \tan \frac{\alpha_d}{2}$$

$$w' = l - \alpha_d R_d$$

$$l' = l - \alpha_d R_d + R_d \tan \frac{\alpha_d}{2}$$

$$l = w + R_d \tan \frac{\alpha_d}{2}$$

$$l = R_c - R_b + R_d \tan \frac{\alpha_d}{2}$$

$$l' = R_c - R_b + R_d \tan \frac{\alpha_d}{2} - \alpha_d R_d + R_d \tan \frac{\alpha_d}{2}$$

$$R = R_c - l' \cos \alpha_d = R_c - \left[R_c - R_b + R_d \left(2 \tan \frac{\alpha_d}{2} - \alpha_d \right) \right] \cos \alpha_d$$

$$\text{Per cent } S = \left(\frac{R - R_b}{R_b} \right) \cdot 100 = \left[\left(\frac{R_c}{R_b} - 1 \right) (1 - \cos \alpha_d) - \frac{R_d}{R_b} \left(2 \tan \frac{\alpha_d}{2} - \alpha_d \right) \cos \alpha_d \right] \cdot 100$$

Accordingly, the true strains of the outer flange fiber are

$$\phi = \ln \frac{R}{R_b} = \ln \left[\frac{R_c}{R_b} - \left\{ \frac{R_c}{R_b} - 1 + \frac{R_d}{R_b} \left(2 \tan \frac{\alpha_d}{2} - \alpha_d \right) \right\} \cos \alpha_d \right]$$

Actually, the length l' is somewhat smaller than assumed in the foregoing analysis owing to simultaneous thinning of material and shortening of the flange during stretching. Usually this factor may be neglected, as it is generally a small correction term.

Folding in Tube-Sinking

By GEORGE SACHS[1] and W. M. BALDWIN, JR.[2]

An experimental study of the folding tendency of tubes during the process of sinking was made. It was determined that tubes with a fold-free point, having a wall thickness of less than 1 per cent of the diameter, can be sunk without folding. However, if it is attempted to sink tubes with points containing folds beyond a certain critical reduction, the fold contained in the point will be perpetuated throughout the length of the tube. This critical reduction increases almost linearly with the ratio of thickness to diameter of the tube, and is little affected by the die angle, the metal, and its temper. The length of the fold during its formative period is found to increase with increasing reduction, with decreasing relative thickness, and to be relatively unaffected by die angle. The stress required to sink a tube with folds was found to increase only slowly beyond the limiting stress for sinking such a tube without folding to the smallest possible diameter.

Nomenclature

THE following nomenclature is used in the paper:

A = cross-sectional area of tube
D = mean diameter of tube
L = gage length of tube
P = force required to sink tube
s_1 = average longitudinal tension in sinking
t = wall thickness of tube

NOTE: o as a superscript refers to original dimensions. Primed symbols refer to final dimensions.

Introduction

Certain metal-forming operations are performed in such a manner that the metal is not completely constricted in its flow by the forming tools, with the result that the metal may escape the desired or intended shaping by buckling or folding. Of these operations, the following are industrially important:

"Sinking," where a tube is drawn through a die without support on its internal surface. Circumferential or hoop stresses may cause the tube to fold along its length if the wall of the tube is thin, Fig. 1 (*a*).

"Necking," "tapering," and "nosing," where a tube is pushed through a die without internal support. In this case the tube may fold along its length, Fig. 1 (*b*), but may also develop transverse folds under the action of longitudinal stresses, Fig. 1 (*c*).

"Stripping," where a shell or cup is removed from a draw punch. The cup is supported on its internal surface by the punch but not on its exterior surface. The longitudinal compressive stresses may therefore develop transverse folds, Fig. 1 (*d*).

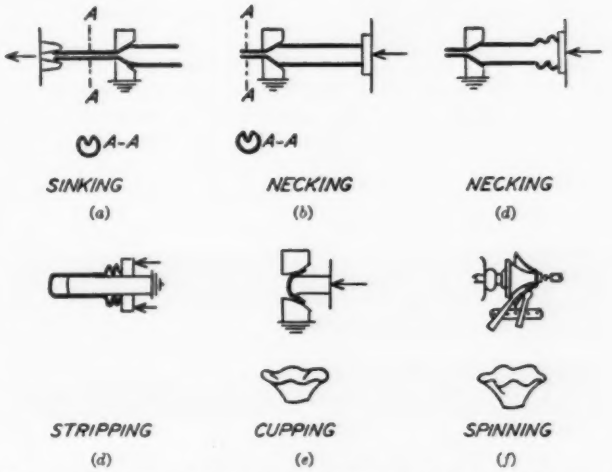


FIG. 1 VARIOUS INDUSTRIALLY IMPORTANT PLASTIC-FORMING OPERATIONS IN WHICH FOLDING CAN OCCUR

"Cupping," or "deep drawing," where a blank is pushed by a punch through a die, forming a cup or shell. The sheet cannot always be supported sufficiently by holddown pads to prevent radial wrinkles or creases caused by compressive hoop stresses, Fig. 1 (*e*).

"Spinning," where a sheet is rotated in a lathe while forming tools work the sheet onto a forming block to produce a cup. Circumferential stresses again can develop radial wrinkles, Fig. 1 (*f*).

These folds and wrinkles appear to be specific cases of the general class of buckling failures and as such are characterized by two features: (*a*) they occur in "slender" articles, i.e., in thin metal, and (*b*) they are caused by compressive stresses lying in the plane of the sheet or the wall of the tube and acting in a direction normal to that in which the fold occurs.

The only one of the phenomena described which has been made the subject of theoretical considerations is the wrinkling of a deep-drawn cup (1).[3] However, this analysis has been applied principally in predicting the number of waves into which the flange would buckle rather than to the limiting conditions under which the cupping operations could be successfully conducted.

In the present work the factors involved in the folding or collapsing of tubes being sunk will be studied experimentally. The variables studied will be the alloy, its temper, the wall thickness of the tube, and the die contour.

Materials and Procedure

For the experimental investigation tubes of four different materials were used: (*a*) hard phosphorus-deoxidized copper (Rockwell 30-T, 59–66); (*b*) soft phosphorus-deoxidized copper (annealed 1 hr at 1000 F in a forced-convection furnace); (*c*) soft tube brass (66.5 per cent copper, 0.5 per cent lead, balance zinc, annealed 1 hr at 1000 F); and (*d*) soft aluminum (2S, annealed 15 min at 600 F).

The tubes were drawn commercially to different diameters ranging from 0.580 to 1.375 in., and possessed a wall thickness

[1] Professor of Physical Metallurgy, Case School of Applied Science, Cleveland, Ohio. Mem. A.S.M.E.

[2] Metallurgical Engineer, Chase Brass and Copper Company, Inc., Midwestern Division, Euclid, Ohio.

Contributed by the Metals Engineering Division and presented at the Spring Meeting, Chattanooga, Tenn., April 1–3, 1946, of THE AMERICAN SOCIETY OF MECHANICAL ENGINEERS.

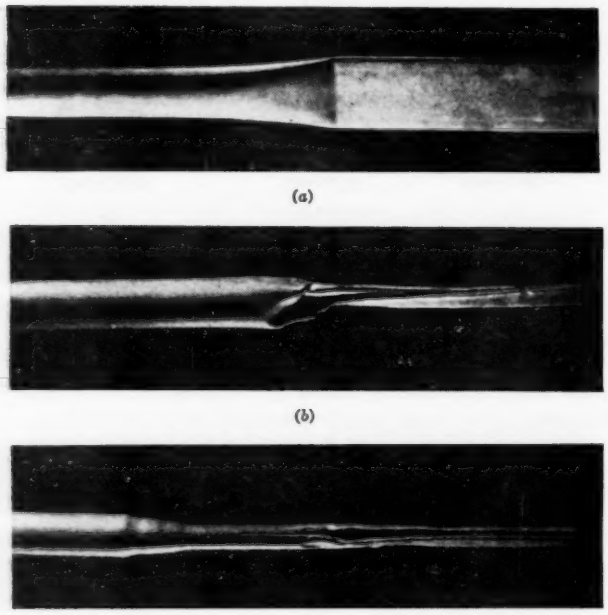
NOTE: Statements and opinions advanced in papers are to be understood as individual expressions of their authors and not those of the Society.

[3] Numbers in parentheses refer to the Bibliography at the end of the paper.

varying between 0.009 to 0.050 in. In the case of the hard copper, the reduction in cross-sectional area after the last anneal (but before sinking) was approximately 50 per cent.

Tube specimens, approximately 40 in. long, were drawn through three different sets of conical steel dies, possessing half die angles of 7, 14, and 27 deg, respectively, to an outside diameter ranging from 0.375 to 1.300 in. The polish on the 7-deg die was inferior to that of the 14- and 27-deg dies.

Two types of points were put on the tubes, i.e., a folded point and a fold-free point. The first type of point was obtained by first flattening the tube, and then folding the flattened section under as shown in Fig. 2 (*a* and *b*). The fold-free point was obtained by sinking a tube progressively with a folded point in sufficiently small steps for a short length of the tube to eliminate the fold, Fig. 2 (*c*).



(*a*)

(*b*)

(*c*)

FIG. 2 PROCEDURE OF POINTING TUBE

(*a*, Flattened tube end. *b*, Flattened section folded under. *c*, Tube drawn in a series of small reductions which eliminates folds and produces "fold-free" point.)

The sinking was performed on either an Olsen 60,000-lb, or a Baldwin Southwark 100,000-lb tensile-testing machine, at a speed of approximately 0.5 fpm. For this purpose a special die holder was attached above the upper jaw of the testing machine and the point of the tube was gripped and pulled with the regular lower jaw. A commercial soap-base lubricant with a high free-fat content (Nopco No. 6) was employed.

The load required to sink the tube was generally found to remain constant within ±5 per cent over the entire length of each tube.

Micrometer measurements were made on both the initial and the drawn tube in order to compute the sinking stress s_1, and the reduction in mean diameter, D. The sinking stress was calculated from the formula

$$s_1 = \frac{P}{A'} = \frac{P}{\pi t' D'}$$

The significant strain for the strain-hardening of the metal in tube-sinking is the reduction in mean diameter for those cases where the wall thickness increases during the operation. This was the case for all tubes investigated since in no instance did the ratio of the wall thickness to mean diameter exceed 0.05, at which value, according to Baldwin and Howald (2), the wall thickness increases for reductions in outside diameter as high as 50 per cent.

This reduction in mean diameter R was computed by means of the equation

$$R = 1 - \frac{D'}{D}$$

The relative thickness of a tube is defined in the present work as the ratio of the wall thickness of the tube to the mean diameter of the tube, t^0/D^0.

If no restriction were put on the angle at which the tube entered the die, the tube would assume a cant, especially with the heavier drafts, when a fold was being perpetuated, Fig. 3. In general, the cant was toward the fold when the tube was sunk through wide-angle dies, whereas the tube assumed a cant away from the fold in the case of the narrow-angle die, although there were a few exceptions to this general rule. Experiments conducted with a restricting cage to force the tube into an axial position, however, showed that this factor had a negligible effect on the critical reductions that could be made.

THEORY OF FOLDING

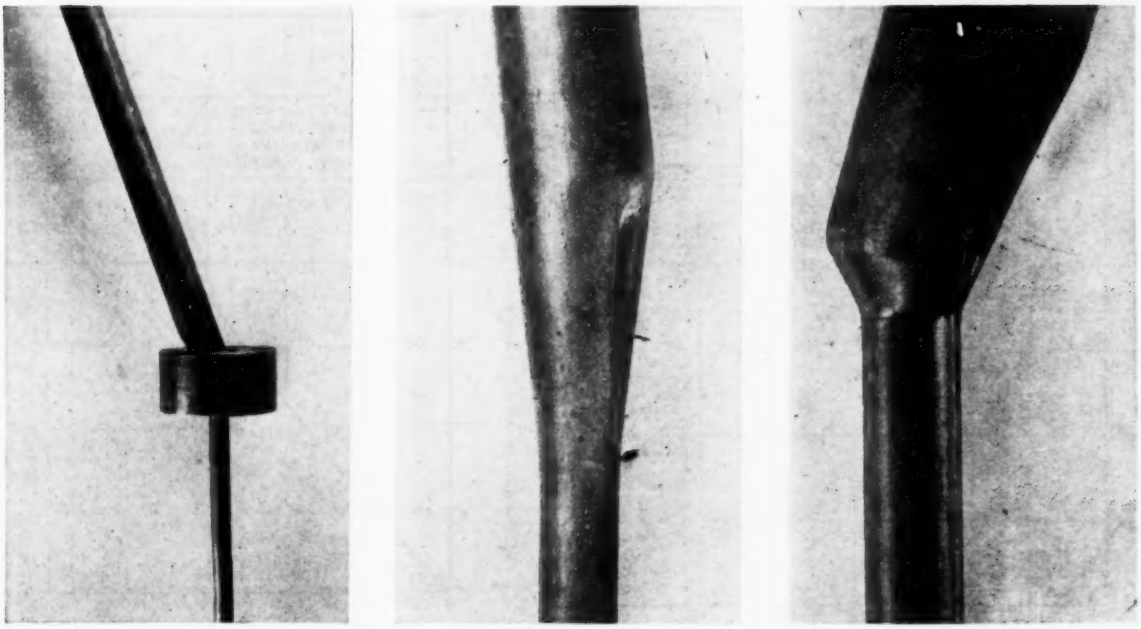
The folding during tube-sinking and the closely related process of necking (primarily observed in cartridge cases) are, according to all external appearances, phenomena of plastic buckling, Figs. 12 to 14, inclusive. The stress responsible for folding is clearly the compressive hoop stress. This hoop stress varies for a fold-free tube along the length of the tube portion in the die, being determined for a given material primarily by the reduction from the original to the considered cross section.

If certain unknown conditions, regarding the magnitude and distribution of the hoop stresses required to draw a fold-free tube, exist the tube wall would be expected to collapse. It was therefore believed at the beginning of this investigation, that folding during tube-sinking might be closely related to the collapsing of a tube under external pressure. In any buckling process one of the decisive factors is the metal thickness; and the expected effect of wall thickness was also found to occur in folding, as discussed later. In the case of collapsing, increasing length of the portion exposed to pressure reduces the unit collapsing pressure (3, 4, 5, 6). The conclusion to be drawn from this fact, that a sunk tube drawn with an acute die (i.e., a long contact length) should collapse after a smaller reduction than a tube drawn through a large-angle die, has not been verified by the following experimentation.

In addition, it was found that no folds could be obtained within the limits of the investigated dimensions without the presence of a preformed fold. Therefore the phenomenon of folding probably is not related to a true buckling process, but comprises a new problem of plastic flow. The results of this investigation may help to reveal the nature of this problem, which, of course, must be recognized before any theoretical analysis can be attempted.

EXPERIMENTAL RESULTS

Sinking of Tubes With a Fold-Free Point. As already mentioned, it was not found possible to collapse any tube with a fold-free point. The circular contour appears to be highly resistant to buckling, even in tubes with the thinnest wall and subjected to the highest possible reduction. An extreme example was soft-copper tube with $D^0 = 1$ in. and $t^0 = 0.009$ in. (i.e., a ratio $t^0/D^0 = 0.009$) and a reduction in mean diameter of approximately 50 per cent.



(a) (b) (c)

FIG. 3 TUBES SHOWING A CANT WHEN SUNK WITH FOLDS
(a, Tube in a 27-deg die. b, Tube removed from 7-deg die showing cant away from fold. c, Tube removed from 27-deg die, showing cant toward fold.)

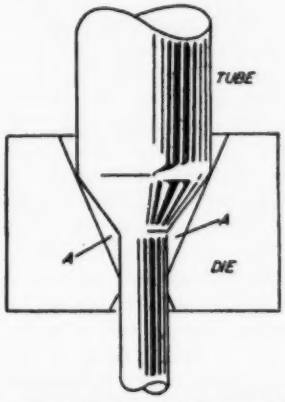


FIG. 4 ENTRAPMENT OF LUBRICANT BETWEEN TUBE AND DIE
(If the tube was prepared with a fold-free point whose angle was greater than that of the die, the lubricant could be entrapped in the cavities *A-A*. Being incompressible, it would force folds into the tube being sunk.)

Such fold-free tubes, however, are obtained only if the tubing is free from dents, and seams. In addition, it was observed that any lubricant entrapped between the die and tube surface caused folding, as illustrated schematically in Fig. 4.

The same facts were found also to exert a considerable influence in the necking of cartridge cases. A high percentage of rejections encountered in regular production was eliminated in one instance by avoiding any denting on handling the mouth of annealed cases, and in another case by designing the die contour such that no lubricant was entrapped in successive tapering operations.

Conditions for the Development of Folds in Sunk Tubing. Either one of two cases occurred when drawing a tube with a folded point: When subjected to small reductions in diameter, the resulting tube was fold-free, while beyond a certain reduction it folded along its entire length. Close to this limiting reduction the fold was eliminated only after the tube was drawn for a considerable length, occasionally as much as 12 in.

In the case of a tube which contained folds when sunk, the reduction in mean diameter possesses no physical significance. In order to evaluate the data, however, it is necessary to know what reduction could have been attained if folding had not occurred.

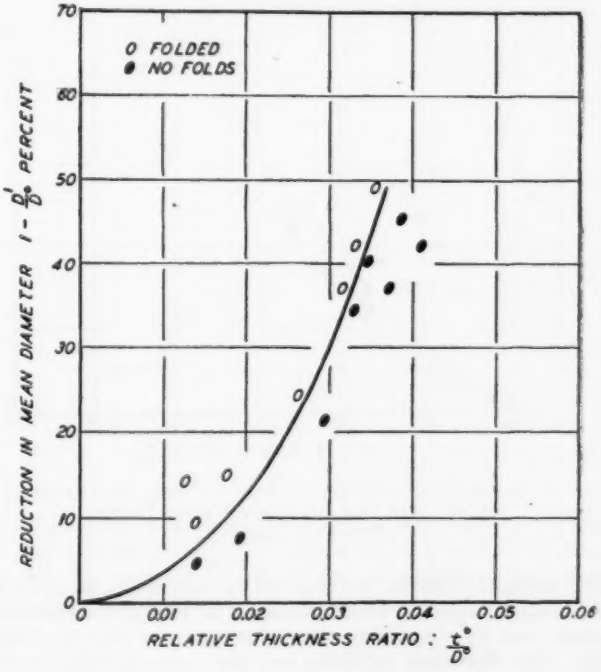


FIG. 5 TYPICAL SET OF DATA ON FOLDING
(For soft copper sunk through a polished steel die having a half-angle of 14 deg.)

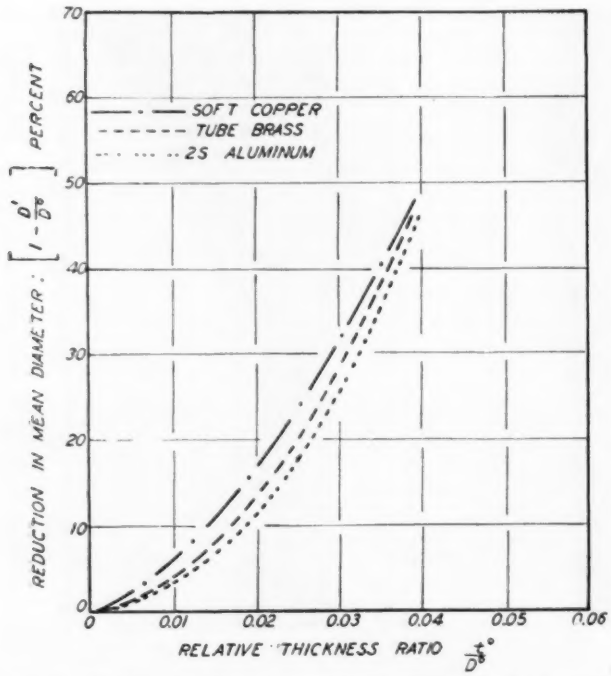


FIG. 6 LIMITING REDUCTION TO WHICH TUBES OF DIFFERENT METAL MAY BE SUNK USING FOLDED POINTS
(Data for 7-deg dies.)

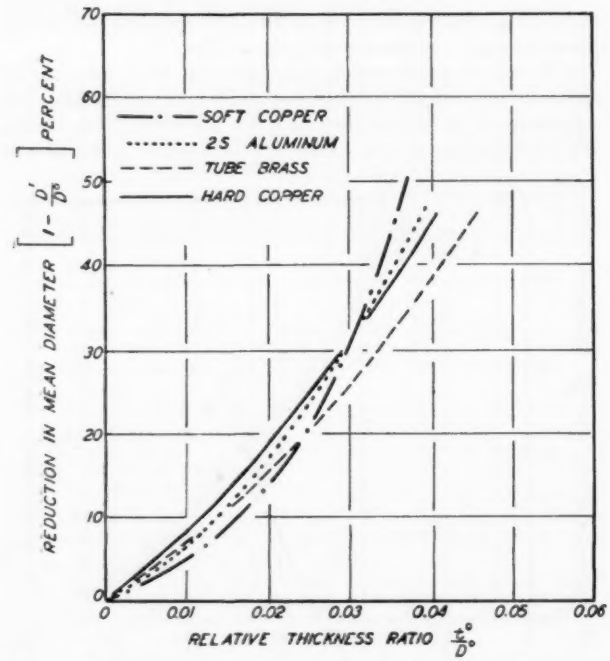


FIG. 7 LIMITING REDUCTION TO WHICH TUBES OF DIFFERENT METALS MAY BE SUNK USING FOLDED POINTS
(Data for 14-deg dies.)

This intended reduction was obtained by interrupting the sinking process, which produced folds; preparing the tube with a fold-free point; and then resuming the sinking process without folding. The (intended) reduction was then taken as that of the fold-free tube.

A typical set of experimental data is represented in Fig. 5. It assembles the results obtained on tubes of varying wall thick-

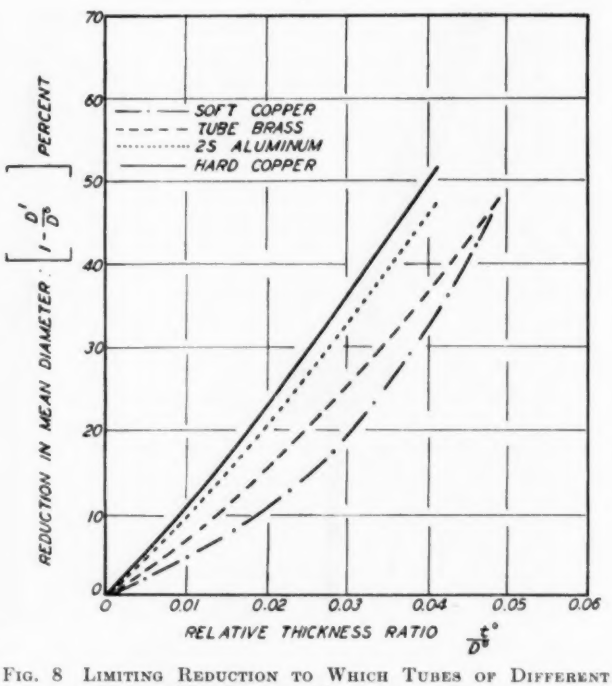


FIG. 8 LIMITING REDUCTION TO WHICH TUBES OF DIFFERENT METALS MAY BE SUNK USING FOLDED POINTS
(Data for 25-deg dies.)

ness of a particular alloy and drawn through a particular die. A solid line has been drawn separating the conditions where a fold was perpetuated in the sinking process from those conditions where folds are eliminated. This graph illustrates the degree of accuracy in determining the dividing line between folded and fold-free tubing. In general, the position of this line appears to be accurate within approximately ±3 per cent reduction.

In Figs. 6 to 8, inclusive, all the experimentally determined boundary lines are shown for the three different dies, the various curves in each graph belonging to the different alloys. These graphs illustrate that the reduction in mean diameter, up to which a tube can be sunk fold-free depends primarily upon the relative thickness of the tube. In general, it increases slightly faster than proportional to the reduction, for all conditions investigated. Any one of the investigated alloys could be sunk with any one die to the commercial reduction limit of approximately 50 per cent, if the wall thickness is larger than 5 per cent of the outside diameter. On the contrary, no tube investigated possessing a wall thickness of approximately 1 per cent of its diameter could be drawn fold-free (with a folded point) by more than approximately 10 per cent reduction.

This relation was found to be comparatively independent of either the alloy, according to Figs. 6 to 8, inclusive, or the die angle, according to Figs. 9 to 11, inclusive. A possible effect of the alloy, exceeding the accuracy limits of experimentation, was observed only for the wide-angle 27-deg die. Contrary to expectations for a buckling phenomenon, hard copper could be sunk fold-free to higher reductions than soft copper.

Also, regarding any effect of die angle, it could have been expected that a large-angle die, because of its length of contact, would permit larger reductions than an acute die. Numerous investigations on the collapse of tubes when subjected to external pressure reveal a profound effect of specimen length on collapse pressures (3, 4, 5, 6). It would normally be expected that this effect would apply to tube-sinking if the fold development was a phenomenon of buckling.

Observations on Fold Development. This anomalous behavior

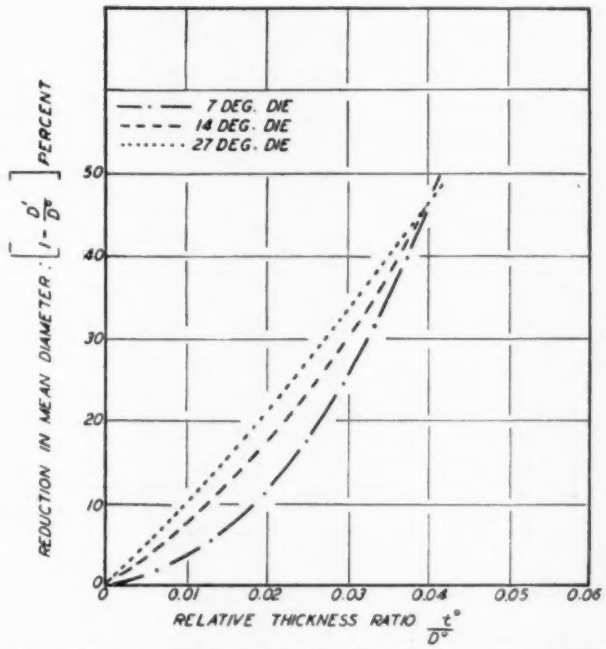


FIG. 9 LIMITING REDUCTION TO WHICH SOFT 2S ALUMINUM MAY BE SUNK USING FOLDED POINTS

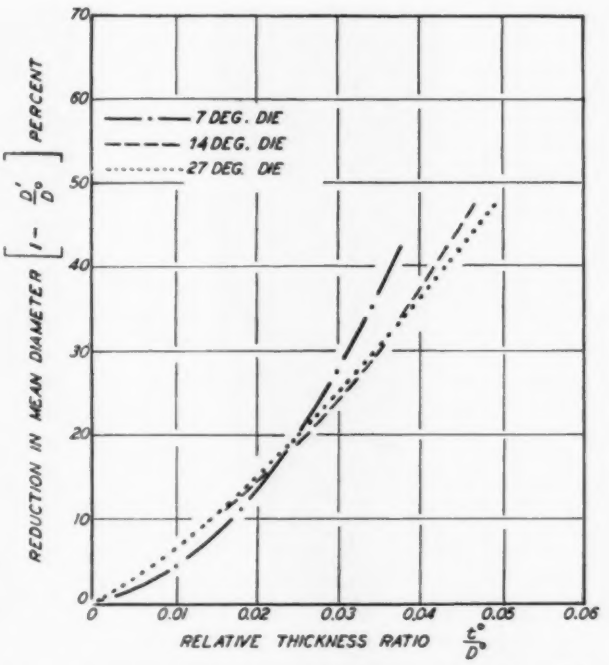


FIG. 10 LIMITING REDUCTIONS TO WHICH SOFT TUBE BRASS MAY BE SUNK USING FOLDED POINTS

is more readily understood, however, if the geometry of the fold is studied. The manner in which the fold is perpetuated along the length of the tube is illustrated in Figs. 12 to 14, inclusive. The point of inception of the fold is shallow, but as the metal proceeds through the die, the fold deepens generally, first becoming broader and then narrower. When the metal leaves the die the edges of the fold are brought together. This cycle occurs for all reductions, heavy or light. The length of the fold depends primarily upon two factors, i.e., the intended reduction Fig. 12, and the relative thickness, Fig. 13. It is, however, practically independent of the die angle, other factors being constant, Fig. 14. Consequently, the point of inception of the fold may be either inside or outside of the die. It appears interesting that the die contour, and consequently the length along which the forces act, which cause the reduction in diameter, has practically no effect on the fold development.

The length of the fold was measured for a number of soft copper tubes drawn through the 27-deg die, Fig. 15. The critical reductions for the various relative thickness ratios have been also entered in Fig. 15, as arrows. It is seen that the length of fold at the critical point is roughly equal to the diameter of the initial outside diameter.

In fold-free sinking the reduction in diameter causes the length of the tube to increase, while the thickness remains practically constant, as mentioned previously. If the formation of a fold were merely a matter of the tube wall being folded into a lobe as the tube was drawn through the die, little change in the cross-sectional area of the original tube would be anticipated. The reduction in diameter would then cause primarily a bending in the area containing the fold, while the remaining portion of the cross section would be only slightly curved. Such a process would result in no change in length of the tube. Some measurements, however, reveal that during the sinking of a folded tube the cross-sectional area is definitely reduced and that, consequently, the entire cross section is subjected to plastic flow.

To determine any increase in length, 2-in. intervals were scribed along the length of tubes. The tubes were sunk with folds, and the segments were then measured. From the assumption that the volume of the metal remains constant during plastic deformation, the ratio of the initial length to the final length of a tube section yields the reduction in cross-sectional area affected by the process

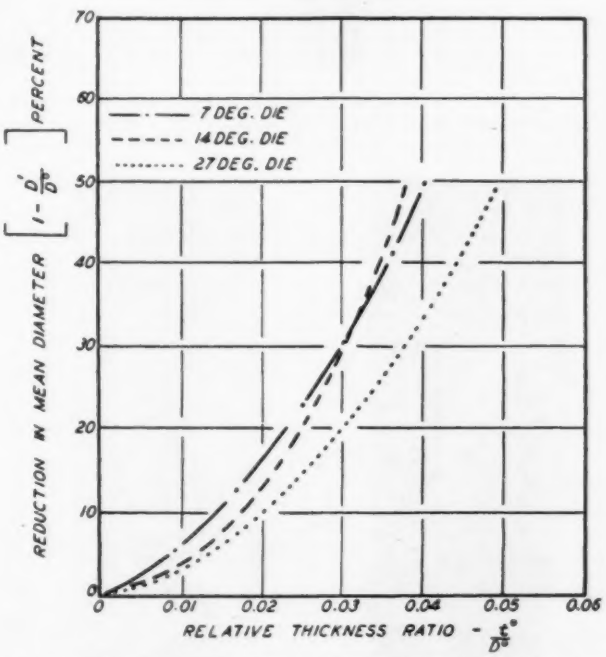


FIG. 11 LIMITING REDUCTIONS TO WHICH SOFT COPPER MAY BE SUNK USING FOLDED POINTS

$$R' = 1 - \frac{L^\circ}{L'}$$

In Fig. 16 the reduction in area determined in this manner is plotted as a function of the intended reduction (in mean diame-

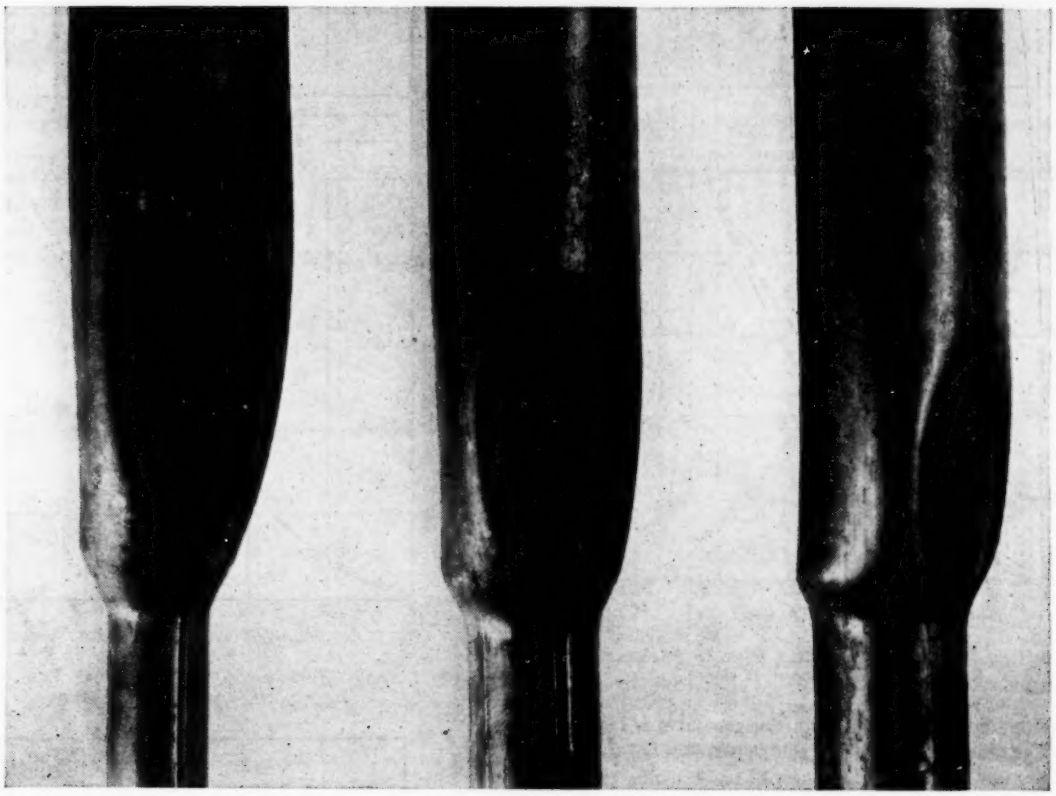


FIG. 12 LENGTH OF FOLD DURING FORMATIVE PERIOD AS A FUNCTION OF INTENDED REDUCTION IN MEAN DIAMETER
(All tubes were 1 in. × 0.020 in. soft copper [$t^o/D^o = 0.021$] sunk through 27-deg dies. Left to right: sunk to 0.500 in. diam, sunk to 0.650 in. diam, sunk to 0.750 in. diam, respectively. Slightly larger than natural size.)

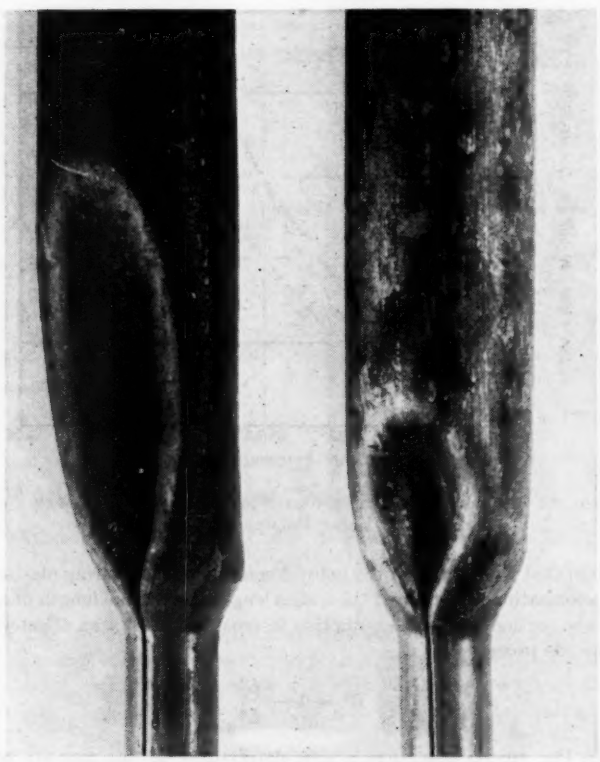


FIG. 13 LENGTH OF FOLD DURING FORMATIVE PERIOD AS A FUNCTION OF RELATIVE THICKNESS
(Left-hand tube is a 1-in. × 0.020-in. soft copper tube [$t^o/D^o - 0.021$] sunk to 0.500 in., showing relatively long fold. Right-hand tube is a 1-in. × 0.038-in. soft copper tube [$t^o/D^o - 0.040$] sunk to 0.500 in. showing relatively short fold. Both tubes sunk through a 27-deg die. Slightly larger than natural size.)

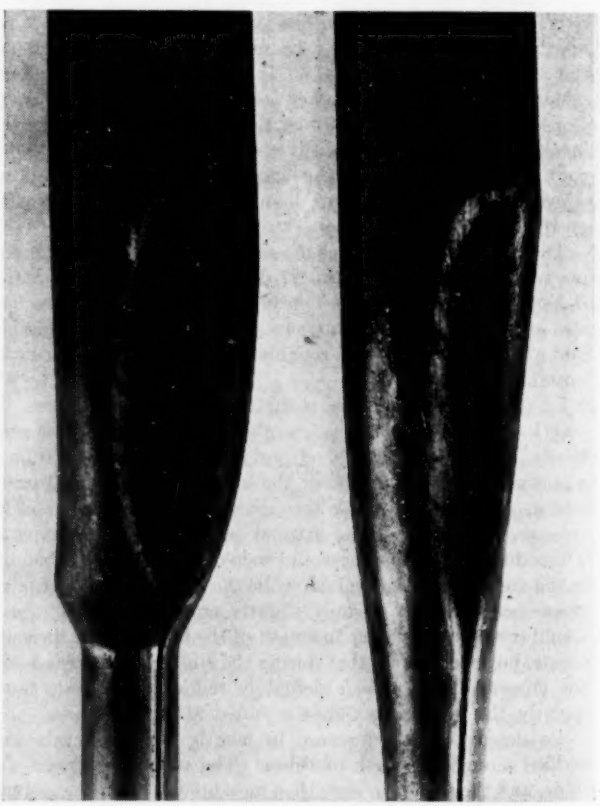


FIG. 14 LENGTH OF FOLD DURING FORMATIVE PERIOD AS A FUNCTION OF DIE ANGLE
(Both tubes were 1 in. × 0.020 in. soft copper [$t^o/D^o - 0.021$], sunk to 0.500 in. diam. Left-hand tube sunk through 27-deg die. Right-hand tube sunk through a 7-deg die. Slightly larger than natural size.)

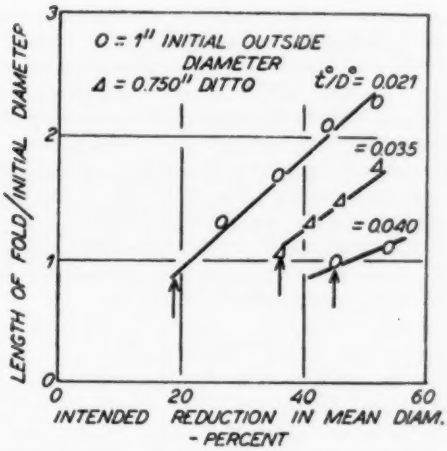


FIG. 15 GRAPH SHOWING LENGTH OF FOLD AS A FUNCTION OF INTENDED REDUCTION AND RELATIVE THICKNESS RATIO
(Data are for soft copper through 27-deg die. Critical reductions are indicated by arrows.)

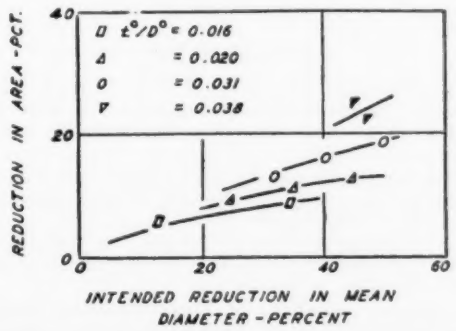


FIG. 16 REDUCTION IN CROSS-SECTIONAL AREA OF TUBES SUNK WITH FOLDS
(Data are for soft tube brass sunk through a 14-deg die.)

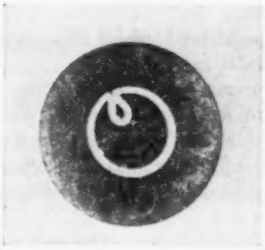


FIG. 17 CROSS SECTION OF TUBE SUNK WITH FOLD
(Tube wall is variable in thickness, being thickest at point diametrically opposite the fold.)

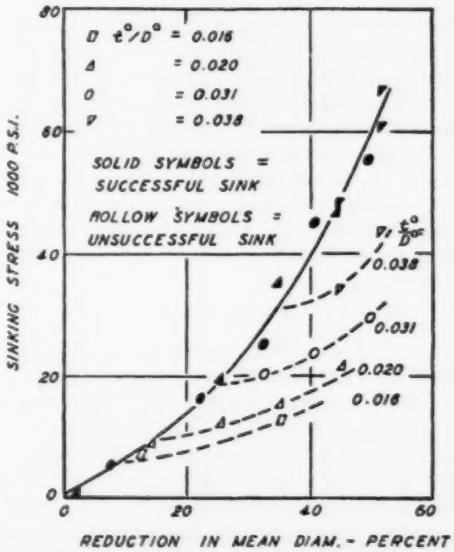


FIG. 18 STRESSES REQUIRED TO SINK TUBE WITH FOLDS
(Data are for soft tube brass sunk through a 14-deg die.)

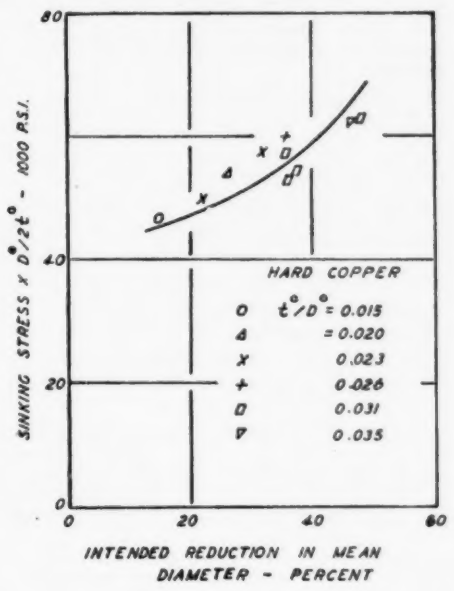


FIG. 19 STRESS REQUIRED TO SINK TUBE WITH FOLDS DIVIDED BY RELATIVE THICKNESS RATIO
(a, Data for hard copper and 14-deg die. b, Data for soft tube brass and 14-deg die.)

ter). It is apparent that an increase in both the intended reduction and the relative thickness ratio of the tube leads to an increase in the actual reduction in area.

Thickness measurements revealed that 1.0 thickness changes occur before the folded tube enters the die. Within the die, however, the wall thickness increases. As shown in Fig. 17 this deformation is not uniform around the circumference as the wall thickens to the greatest extent at a point diametrically opposite to the fold.

Stresses to Sink Folded Tubes. The unit stress s_1, required to pull the folded tube through the die is determined by the equation

$$s'_1 = \frac{P}{A'} = \frac{P}{A^\circ}\frac{L'}{L^\circ}$$

In Fig. 18 the stresses required to sink (with folds) brass tubes of various initial relative thickness ratios, through a 14-deg die, are plotted as a function of the intended reduction. It is to be noted that the curves so obtained intersect the curve for sinking without folds, reported previously (7), at the critical reduction, for the relative thickness ratio in question.

The curves for various relative thickness ratios can be further reduced to a single master curve if the values for the individual stresses are divided by the relative thickness ratio. This has been carried out in Figs. 19 and 20 for tube brass and hard copper, respectively.

Conclusions

The results of this investigation cannot be reconciled with the conventional theory of buckling or collapsing. The factors which determine the perpetuation or elimination, respectively, of a fold in tube-sinking are different from those which determine definite buckling phenomena such as the collapsing of a tube.

The only factor which is conducive to both collapsing and fold formation is a small thickness-to-diameter ratio. Other factors, however, such as the length along which pressure is applied and the elastic and plastic metal properties which are important in collapsing, have only a minor influence on folding.

The predominant effect of the reduction in diameter cannot be satisfactorily explained. However, it has been observed that a fold is enlarged only if the circumferential force is smaller for this process than for fold-free sinking, assuming that the differences in the respective sinking forces also indicate proportional differences in the circumferential forces, other conditions being equal. This would also explain the observation that if the sinking forces for folded tubes equal those for fold-free tubes, the tendency to fold disappears. In other words, a fold will be perpetuated only if the resistance against bending into the fold is smaller than the resistance against a uniform compression of the diameter. No theoretical approach to this phenomenon has been developed as yet.

It has been also observed that it is much more difficult to obtain a fold on sinking a circular cross section than on sinking a section with a preformed fold. This result may be compared with the buckling forces required to deform permanently bars under concentric and eccentric loading, respectively.

Acknowledgment

Acknowledgment is made to Prof. K. H. Donaldson, head of the Metallurgical Engineering Department of Case School of Applied Science, and to Dr. H. P. Croft, director of technical control and research, Midwestern Division, Chase Brass and Copper Company, Inc., for their encouragement and help. The authors are also indebted to B. H. Higgins, Linderme Tube Company, Cleveland, Ohio, who kindly supplied the aluminum tube used in this research.

BIBLIOGRAPHY

1 "Plastic Folding of the Walls of Hollow Cylinders and Some Other Folding Phenomena in Bowls and Sheets," by J. W. Geckeler, *Zeitschrift für angewandte Mathematik und Mechanik*, vol. 8, 1928, pp. 341–342.

2 "Dimensional Changes Encountered in Tube Sinking," by W. M. Baldwin, Jr., and T. S. Howald, Trans. American Society of Metals, vol. 33, 1944, pp. 88–102.

3 "The Resistance of Tubes to Collapse," by A. P. Carman and M. L. Carr, University of Illinois, Engineering Experimental Station, Bulletin No. 5, 1906.

4 "Collapse or Instability of Thin Cylindrical Shells Under External Pressure," by D. F. Windenburg and C. Trilling, Trans. A.S.M.E., vol. 56, 1934, pp. 819–825.

5 "The Collapse of Short Thin Tubes by External Pressure," by G. Cook, *Philosophical Magazine*, vol. 28, 1914, pp. 51–56.

6 "The Critical External Pressure for Tubes," by R. von Mises, *Zeitschrift des Vereines deutscher Ingenieure*, vol. 58, 1914, pp. 750–755.

7 "Stress Analysis of Tube-Sinking," by G. Sachs and W. M. Baldwin, Jr., published on pages 655–662, of this issue of the Transactions.

Stress Analysis of Tube-Sinking

By GEORGE SACHS,[1] and W. M. BALDWIN, JR.[2]

A theoretical stress analysis was made of the tube-sinking operation, equations being set up to yield the sinking stress as a function of the reduction in mean diameter. The equations were confirmed by experimentation on annealed and full hard copper and on annealed tube brass for conical dies of various tapers. The coefficients of friction existing during tube-sinking have been determined and are found to be of the same magnitude as those determined previously for wire drawing.

Nomenclature

The following nomenclature is used in the paper:

A = cross-sectional area of tube
B = parameter = $\dfrac{\tan \alpha + f}{\tan \alpha}$
D = mean diameter of tube
f = friction coefficient
k = flow stress (or yield strength in tension)
k_0 = $1.1\,k$
P = force required to sink tube
s_1 = algebraically largest principal stress, assumed to be average longitudinal tension in sinking
s_2 = intermediate principal stress, assumed to be die pressure
s_3 = algebraically smallest principal stress, assumed to be average hoop stress
t = wall thickness of tube
x = longitudinal co-ordinate
α = angle between die wall and tube axis = half die angle of conical die

Note: o as a superscript refers to original dimensions. Primed symbols refer to final dimensions.

Introduction

The analysis of the stresses occurring in a number of forming processes, in which the metal is continuously subjected to deformation, follows in each case a similar pattern. The processes to which such an analysis has been applied so far, wire-drawing (1, 2),[3] strip-rolling (3, 4, 5, 6, 7), and tube-drawing with a moving mandrel (8) have one feature in common, namely, that the mean stresses acting on each cross section can be derived from the equilibrium of the longitudinal forces.

An analysis of tube-sinking has not been attempted previously. In a paper dealing with the stress and strain relations in tube-sinking, it was assumed that the stresses in this process are identical with those occurring in wire-drawing (9).

The following discussion presents a theoretical and experimental analysis of the tube-sinking process. In order to develop a differential equation for the stresses occurring in the process, it was found necessary to consider not only the equilibrium of the longitudinal but also that of the transverse forces. This results from the fact that in contrast with the processes just mentioned the largest and smallest principal stresses in tube-sinking do not occur in a longitudinal plane but in a circumferential plane.

In the experimental analysis, the high tendency of the tube being sunk to develop folds was eliminated by a special pointing procedure. This yielded a fold-free point, which permitted sinking operations with tubes with the smallest available wall thickness to maximum reductions without folding, and thus to measure the sinking forces over a wide range of conditions. The problem of folding will be considered in a subsequent publication.

Materials and Procedure

For the experimental investigation, tubes of three different materials were used: (*a*) hard phosphorus-deoxidized copper (Rockwell 30-T, 59–66); (*b*) soft phosphorus-deoxidized copper (annealed 1 hr at 1000 F in a forced-convection furnace); and (*c*) soft tube brass (66.5 per cent copper, 0.5 per cent lead, balance zinc, annealed 1 hr at 1000 F). The tubes were drawn commercially to different diameters, ranging from 0.580 to 1.375 in., and possessed a wall thickness of 0.015 to 0.050 in. In the case of the hard copper, the reduction in cross-sectional area after the last anneal (but before sinking) was approximately 50 per cent.

Tube specimens, approximately 40 in. long, were drawn through three different steel dies, possessing half die angles of 7, 14, and 27 deg, respectively, to an outside diameter of 0.50 in. The polish on the 7-deg die was inferior to that of the 14- and 27-deg dies.

The sinking was performed on either an Olsen 60,000-lb, or a Baldwin Southwark 100,000-lb tensile-testing machine, at a speed of approximately $^1/_2$ fpm. For this purpose, a special die holder was attached above the upper jaw of the testing machine, and the point of the tube was gripped and pulled with the regular lower jaw. A commercial soap-base lubricant with a high free-fat content (Nopco No. 6) was employed.

The load required to sink the tube was generally found to remain constant within ±5 per cent over the entire length of each tube.

Micrometer measurements were made on both the initial and the drawn tube in order to compute the sinking stress s_1', and the reduction in mean diameter. The sinking stress was calculated from the formula

$$s_1' = \frac{P}{A'} = \frac{P}{\pi t' D'}$$

The significant strain for the strain-hardening of the metal in tube-sinking is the reduction in mean diameter for those cases where the wall thickness increases during the operation. This was the case for all tubes investigated, since in no instance did the ratio of the wall thickness to mean diameter exceed 0.05, at which value, according to Baldwin and Howald (10), the wall thickness increases for reductions in outside diameter as high as 50 per cent.

The reduction in mean diameter R was computed by means of the equation

$$R = 1 - \frac{D'}{D^o}$$

---

[1] Professor of Physical Metallurgy, Case School of Applied Science, Cleveland, Ohio. Mem. A.S.M.E.

[2] Metallurgical Engineer, Chase Brass and Copper Company, Inc., Midwestern Division, Euclid, Ohio.

[3] Numbers in parentheses refer to the Bibliography at the end of the paper.

Contributed by the Metals Engineering Division and presented at the Spring Meeting, Chattanooga, Tenn., April 1–3, 1946, of The American Society of Mechanical Engineers.

Note: Statements and opinions advanced in papers are to be understood as individual expressions of their authors and not those of the Society.

Stress-strain curves by means of tensile tests were determined for the various metals before and after sinking in the conventional manner. The reduction in area is the significant strain in the tensile test, being equivalent to the reduction in mean diameter in tube-sinking. The significant strain of a sunk tube subjected to a tensile test is therefore the sum of the two strains referred to in the initial cross-sectional area.

Theoretical Analysis

The method of analysis used here assumes (*a*) that a pressure normal to the working tool-metal interface operates on the interface of tube and die, and that, neglecting the presence of the shear stress, this pressure is one of the principal stresses; (*b*) that because of friction, a shear stress operates at the interface; (*c*) that transverse sections are free of shear stresses; (*d*) that the normal stress acting on the transverse sections is uniformly distributed over the cross section and that it is another principal stress; (*e*) that the wall thickness of the tube is small in comparison to the tube diameter; and (*f*) that the wall thickness of the tube remains constant through the process. This last assumption is not strictly valid but has been found to be true within ±5 per cent (9, 10).

With these assumptions, two equations can be derived from Fig. 1, using the equilibrium of the forces in the longitudinal and radial directions. Summation of the longitudinal forces supplies one equation

$$\cos\alpha[(s_1 + ds_1)(A + dA) - s_1A] + p\sin\alpha\frac{dx}{\cos\alpha}\pi D + fp\cos\alpha\frac{dx}{\cos\alpha}\pi D = \cos\alpha\, d(s_1A) + pdx\pi D(\tan\alpha + f) = 0 \quad [1]$$

Using the geometrical relations, Fig. 1

$$D = 2x\tan\alpha \qquad dD = -2dx\tan\alpha \quad [2]$$

$$A = \pi tD \qquad dA = \pi t dD = 2\pi t\, dx\tan\alpha \quad [3]$$

transforms Equation [1] to

$$\pi t d(s_1D)\cos\alpha\,\pi DdD\,p\frac{\tan\alpha + f}{2\tan\alpha} = \pi t d(s_1D)\cos\alpha\,{}^1/_2\,\pi DdD\,pB = 0 \quad [4]$$

where

$$B = \frac{\tan\alpha + f}{\tan\alpha} \quad [5]$$

Summation of the radial components of forces yields

$$p2B\frac{D}{2\cos\alpha}\frac{dx}{\cos\alpha} + 2s_3Bt\frac{dx}{\cos\alpha} = 0$$

or

$$p = -s_3\frac{2t\cos\alpha}{D} \quad [6]$$

Substituting Equation [6] into Equation [4] results in the general differential equation of tube-sinking

$$d(s_1D) = Bs_3dD \quad [7]$$

Equation [7] is of the same form as that derived for rolling (3, 4, 5, 6, 7), wire-drawing (1, 2), or tube-drawing (8), the only difference being that the parameter B takes on different values for the various forming operations.

To relate the quantities s_1 and s_3 in Equation [7], some condition of plasticity must be invoked. The most accurate available is the strain-energy condition

$$(s_1 - s_2)^2 + (s_2 - s_3)^2 + (s_1 - s_3)^2 = 2k^2 \quad [8]$$

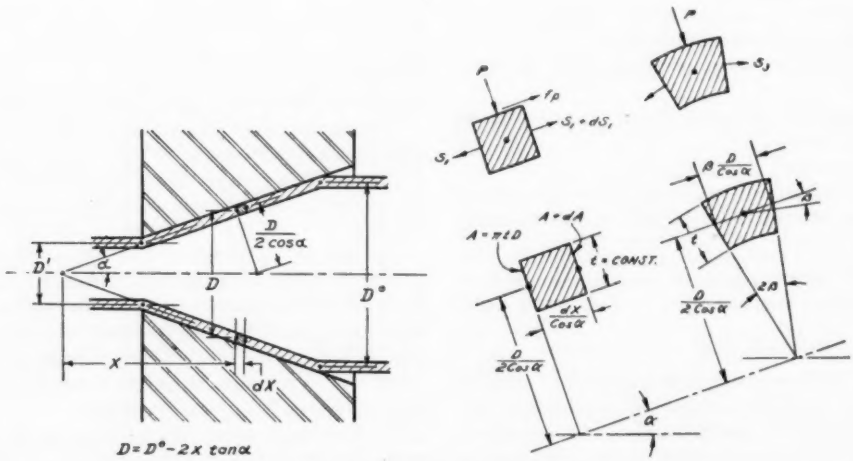


Fig. 1 Stresses in Tube-Sinking

where the quantities s_1, s_2, and s_3, are the three principal stresses in algebraically decreasing order of magnitude and k is the flow stress or yield strength of the metal as determined in simple tension or compression. However, the use of this condition involves considerable calculations. Under most general conditions Equation [8] sets certain limits on the values that $s_1 - s_3$ can assume, namely

$$k \leqq (s_1 - s_3) \leqq 1.15\,k \quad [8a]$$

For the present case a constant average value may be taken as sufficiently accurate to represent the condition of plasticity throughout the sinking process, namely

$$s_1 - s_3 = 1.1\,k = k_0 \quad [8b]$$

Substitution of Equation [8*b*] in Equation [7] and making the variable D dimensionless by multiplying the equation with D^0 finally yields the linear differential equation

$$\frac{ds_1}{d(D/D^o)} + (1 - B)\frac{s_1}{D/D^o} = -B\frac{k_0}{D/D^o}$$

If the parameter B, is considered constant throughout the sinking process (i.e., if the die angle and coefficient of friction are constant) this equation may be integrated as follows

$$s_1 = -B\left(\frac{D}{D^o}\right)^{B-1}\int_1^{\circ} k_0\frac{d(D/D^o)}{(D/L^o)^B} + s_1^o\left(\frac{D}{D^o}\right)^{B-1} \quad \ldots\ldots[9]$$

where s_1^o is the stress for zero reduction, $D = L^o$.

The parameter B passes to unity as the coefficient of friction goes to zero. If the metal is further assumed to possess no strain-hardening (i.e., k_0 is constant) then Equation [9] becomes, neglecting s_1^o

$$s_1 = k_0 \log_e \frac{D^o}{D} \quad \ldots\ldots[9a]$$

This equation is commonly associated with ideal (i.e., frictionless) conditions, and has been deduced, for example, for wire-drawing, not only by using a method analogous to the present one (1, 2), but also by using stress-analysis methods based on the balance of the work consumed (11).

Another special case of the general Equation [9] is that in which friction exists but no work-hardening occurs. In this case k_0 is independent of D; and Equation [9] may be integrated to yield the following equation

$$s_1 = \frac{Bk_0}{B-1}\left[1 - \left(\frac{D}{D^o}\right)^{B-1}\right] + s_1^o\left(\frac{D}{D^o}\right)^{B-1} \quad \ldots\ldots[9b]$$

This equation yields the longitudinal stress at any position D, for a given D^o, and consequently also the sinking stress, $s_1 = s_1'$, at the exit, $D = D'$

$$s_1' = \frac{Bk_0}{B-1}\left[1 - \left(\frac{D'}{D^o}\right)^{B-1}\right] + s_1^o\left(\frac{D'}{D^o}\right)^{B-1} \quad \ldots\ldots[10]$$

Experimental Results

Hard Copper. The comparison of experimental data with the theory may be first made for hard copper. This material was selected for the investigation primarily because it represents a practical example of the conditions assumed to develop Equation [9*b*], namely, a material which does not strain-harden during the sinking process. In Fig. 2 the yield strength k, of the hard copper is shown as a function of the (mean) diameter change, after sinking through the 14-deg (half-angle) die. It will be noticed that an average value of $k = 60{,}000$ psi would describe the yield strength over the entire range of reduction, within ±3 per cent. A family of curves for the sinking stress s_1, obtained by substituting the value $k_0 = 1.1\,k = 66{,}000$ psi, and a series of values for the parameter B, in Equation [9*b*] are also represented in Fig. 2.

The value of the integration constant C was determined experimentally by sinking a tube with the negligibly small reduction of 0.25 per cent, approximately; the measured value of 3000 psi agrees well with that extrapolated from the experimental sinking stresses for larger reductions.[4]

[4] Abundant experimental evidence may be found in the literature where a wire-drawing stress extrapolates to a definite positive stress value for zero reduction, see Thompson (12), Lueg and Pomp (13), Davis and Dokos (2). In discussing this positive value, Thompson describes it as "the extra pull required merely to overcome the frictional resistance in the die." Poeschl (14) and Davis and Dokos (2) attribute this positive value to a small transitional region of elasticity. Poeschl has attempted a mathematical analysis for this elastic region. In the present paper such positive values for soft copper or tube brass were found to be negligible whereas for hard copper they were found to be considerably higher, thus tending to confirm Poeschl's theory.

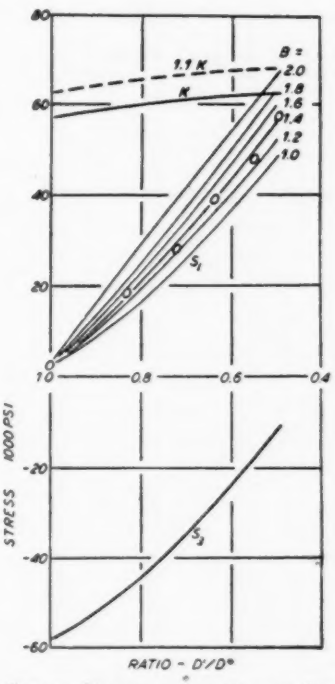


Fig. 2 Stress-Strain Diagram and Sinking-Stress Data for Hard Copper

(Experimental sinking-stress data for a 14-deg die half-angle have been entered as circular symbols.)

The experimental data agree rather closely with the theoretical curve for which the parameter B has a value of 1.4, approximately.

The hoop stress, $s_2 = s_1 - k_0$ Equation [8*b*] is also shown in Fig. 2, for a value of $B = 1.4$. The curve for the hoop stress represents its distribution over any length of contact, as its value is determined only by the local reduction of the considered cross section, irrespective of the total reduction of any particular draw.

Annealed Copper and Brass. For any soft material such as annealed copper and brass, the yield strength is primarily a function of the reduction. The stress-strain curves for these two metals derived from tensile tests are shown in Figs. 3 and 4.

The theoretical sinking stress can be obtained by graphical integration of Equation [9]. In Figs. 5 and 6, families of curves for the sinking stress, for a series of values for the parameter B, are given for soft copper and brass, respectively.

In comparing these theoretically derived curves with experimental data, it should be borne in mind that the stress-strain curve for a tube which had been sunk differs from that derived from a soft tube, as illustrated for one example in Fig. 7. This factor can be taken into account by a method employed by Sachs (15) for wire-drawing. From a comparison of the stress-strain curves in tension with those of sunk tubes as given in Fig. 7, a chart giving the effective reduction as a function of the actual reduction can be constructed.[5] Such a chart is shown in Fig. 8 for tubes sunk through the three different die angles included in this research. It will be noted that for large reductions the ideal and effective reductions become approximately equal. It is for this reason that this correction was not required for hard copper.

Figs. 9 to 13, inclusive, show the theoretical sinking stresses

[5] The difference between effective and actual reduction is attributed to the presence of shear stresses and shear strains. These have been demonstrated by means of grids on the cross section of wire, in both soft and hard copper, by Taylor and Quinney (16), and by Siebel (17).

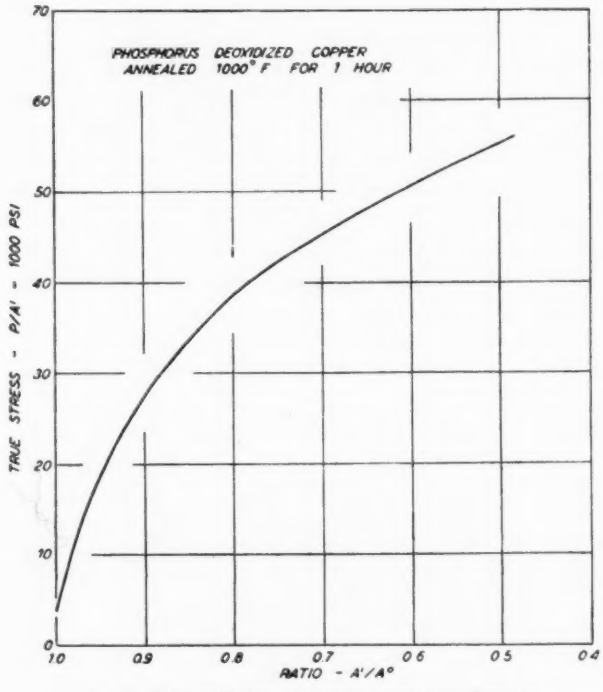


FIG. 3 STRESS-STRAIN DIAGRAM FOR SOFT COPPER

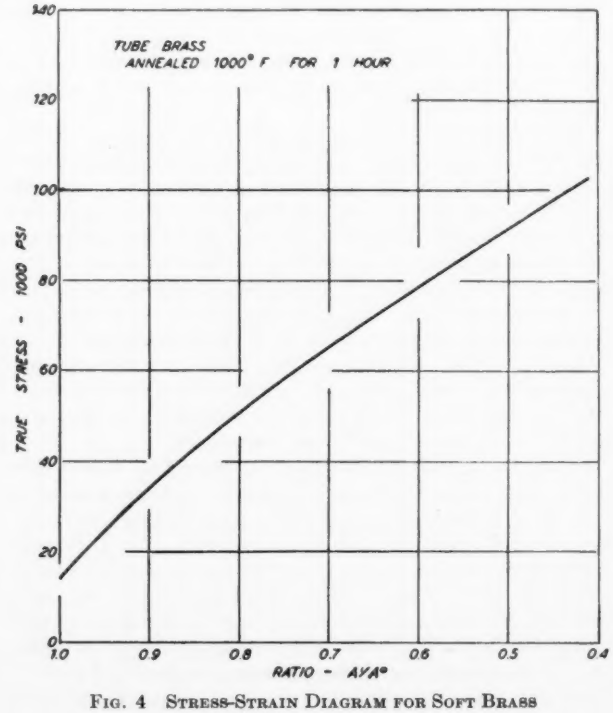


FIG. 4 STRESS-STRAIN DIAGRAM FOR SOFT BRASS

transformed by means of Fig. 8 from functions of the actual reductions, Figs. 5 and 6, into functions of the effective reductions. Each graph now applies only for a given alloy and a given die angle; and the range of parameter values B, represented in each graph covers the range of experimental scattering.

The experimental sinking stresses are shown in Figs. 9 to 13, inclusive, as open circles. It will be noticed that the scatter is greatest in the case of the 7-deg die and progressively lessens in

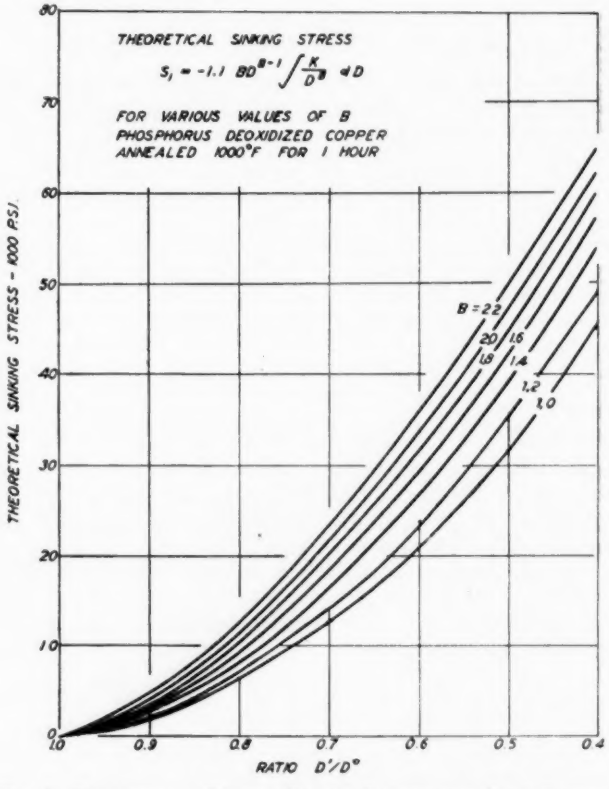


FIG. 5 THEORETICAL SINKING-STRESS CURVES FOR SOFT COPPER FOR VARIOUS VALUES OF PARAMETER B

the case of the 14- and 27-deg die. These observations indicate that some variation in friction was encountered in the experiments.

In general, however, there is a fair agreement between the experimental value and a theoretical curve for a particular value of the parameter, B.

Coefficients of Friction. From the parameter B, and the die angle α, the frictional coefficient $f = \tan \rho$, can be readily determined by means of Equation [5]

$$\frac{\tan \alpha + f}{\tan \alpha} = B$$

In Fig 14 the parameter B is plotted as a function of the coefficient of friction, $\tan \rho$, for the three die angles, $\alpha = 7$, 14, and 27 deg employed in this investigation.

In Table 1 the parameters B are tabulated for the various metals and die angles investigated. The corresponding values of the coefficient of friction, f, are also included in Table 1.

TABLE 1 PARAMETERS, DIE ANGLES, AND COEFFICIENTS OF FRICTION OF METALS INVESTIGATED

Material	Die angle, deg	Parameter, B	Coefficient of friction, f
Hard copper	14	1.4	0.10
Soft copper	14	1.4	0.10
	27	1.3	0.15
Tube brass	7	2.6	0.20
	14	1.5	0.13
	27	1.3	0.15

These coefficients of friction are for both the 14- and 27-deg die of the same order of magnitude as those obtained by other investigators for wire-drawing (1, 2). However, for the 7-deg die, which was not as finely polished as the 14- or 27-deg die, the friction was found to be approximately twice as great.

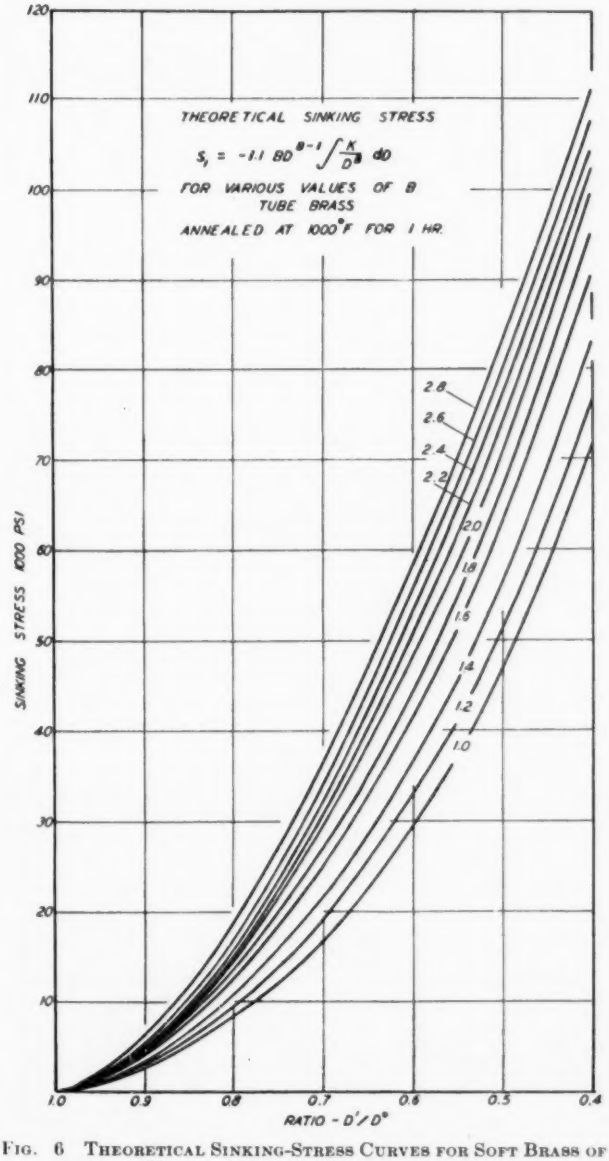


FIG. 6 THEORETICAL SINKING-STRESS CURVES FOR SOFT BRASS OF VARIOUS VALUES OF PARAMETER B

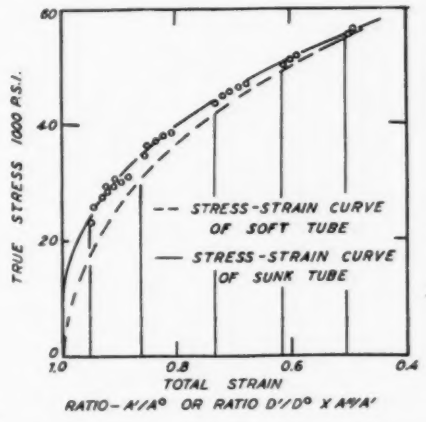


FIG. 7 COMPARISON OF STRESS-STRAIN CURVE OBTAINED FROM SOFT COPPER AND FROM COPPER SUNK THROUGH 14-DEG DIE

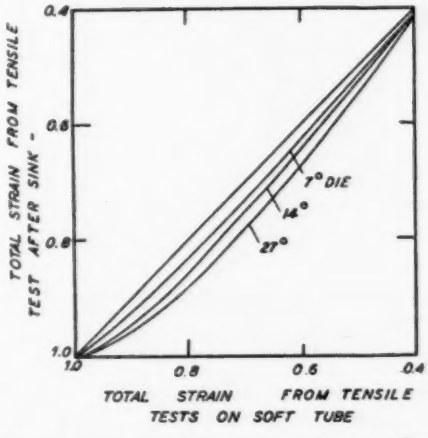


FIG. 8 CHART CORRELATING REDUCTION IN AREA FOR GIVEN STRESS ON STRESS-STRAIN DIAGRAMS OF SOFT TUBES AND SUNK TUBES

CONCLUSIONS

Any theory of a metal-forming process involves a number of simplifying assumptions in order to obtain sufficiently simple equations to allow numerical or graphical evaluation. Some discrepancies between theory and experimentation may therefore be expected. The analysis of tube-sinking presented here contains some minor refinements as compared with previous analyses of related processes in that no mathematical approximations are used other than that employed for the condition of plasticity. The experimentation indicates that this has yielded the gratifying result that the sinking stresses (i.e., the draw forces and the power consumption, excluding the losses in the equipment) can be calculated satisfactorily to within ± 2000 psi for soft copper drawn with a 27-deg die, and to within ± 9000 psi for soft tube brass drawn with a 7-deg die. This range of agreement is comparable to that reported in studies on wire-drawing, tube-drawing, etc.

It must be emphasized, however, that such an agreement cannot be claimed for either the distributions of the stresses or the strains over the cross section in drawing processes. So far, no theoretical analysis is available which promises to yield accurate results regarding the stress and strain distributions. This knowledge would be very desirable as the stress distribution is important in respect to various commercial problems, particularly those involving residual stresses.

Appendix

COMPARISON OF TUBE-SINKING WITH WIRE-DRAWING; EFFECTS OF TUBE THICKNESS

The experimental data on tube-sinking were obtained with thin-walled tubes, their ratio of wall thickness to diameter (relative thickness) being between $t_0/D^o = 0.01$ to 0.05. Tubes having a larger relative thickness were not investigated.

However, some indication regarding the effect of relative thickness can be obtained by comparing the stresses required to draw, respectively, thin-walled tube with those required to draw wire (or rod), other conditions (metal, dies, lubricant) being identical.

The wire represents the limiting condition of a tube, the relative wall thickness being $t_0/D^o = 0.5$. The wire-draw stress is given, according to Sachs (1) by the equation

$$s_1'' = \frac{B_1 k}{B_1 - 1}\left[1 - \left(\frac{D'}{D^o}\right)^{2(B_1-1)}\right] \quad \ldots\ldots\ldots [11]$$

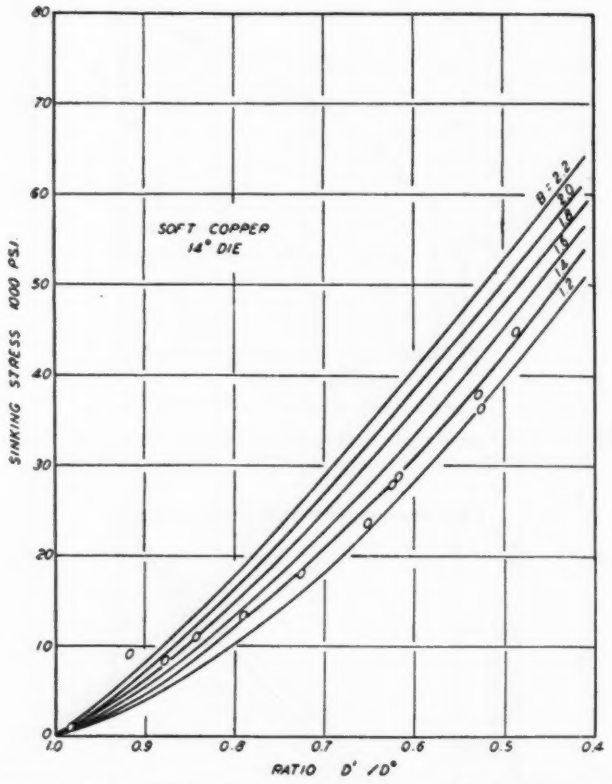


FIG. 9 THEORETICAL SINKING-STRESS CURVES CORRECTED FOR DIFFERENCES IN STRESS-STRAIN DIAGRAMS SHOWN IN FIG. 7
(Curves are for soft copper sunk through a 14-deg die. Experimental data are represented as circles.)

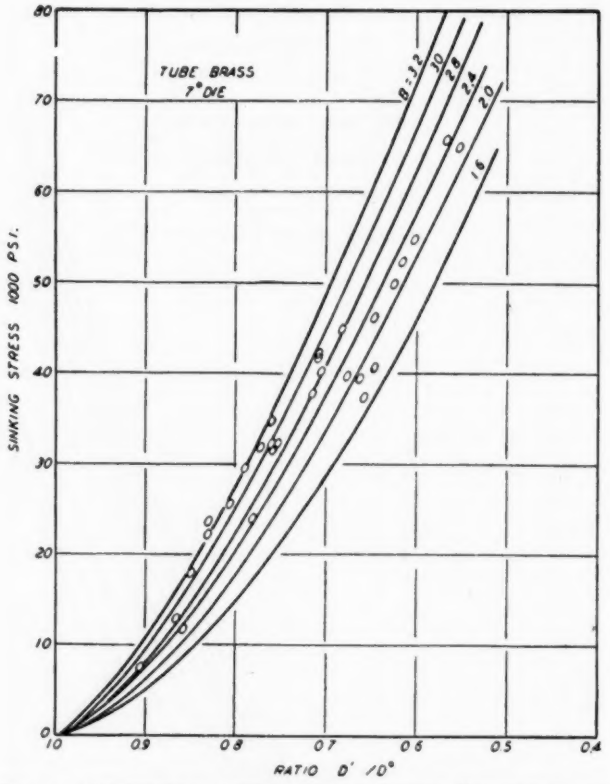


FIG. 11 THEORETICAL SINKING-STRESS CURVES CORRECTED FOR DIFFERENCES IN STRESS-STRAIN DIAGRAMS SHOWN IN FIG. 7
(Curves are for soft tube brass sunk through a 7-deg die. Experimental data are represented as circles.)

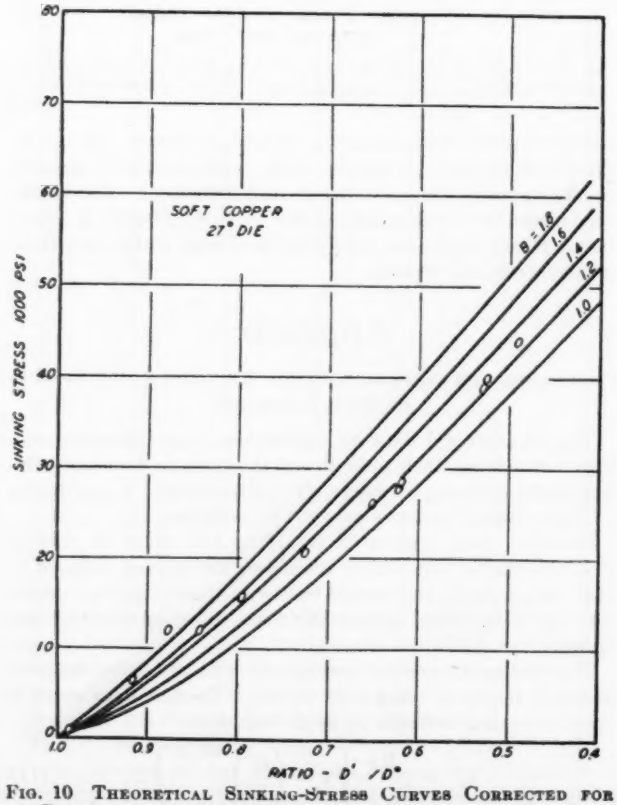


FIG. 10 THEORETICAL SINKING-STRESS CURVES CORRECTED FOR DIFFERENCES IN STRESS-STRAIN DIAGRAMS SHOWN IN FIG. 7
(Curves are for soft copper sunk through a 27-deg die. Experimental data are represented as circles.)

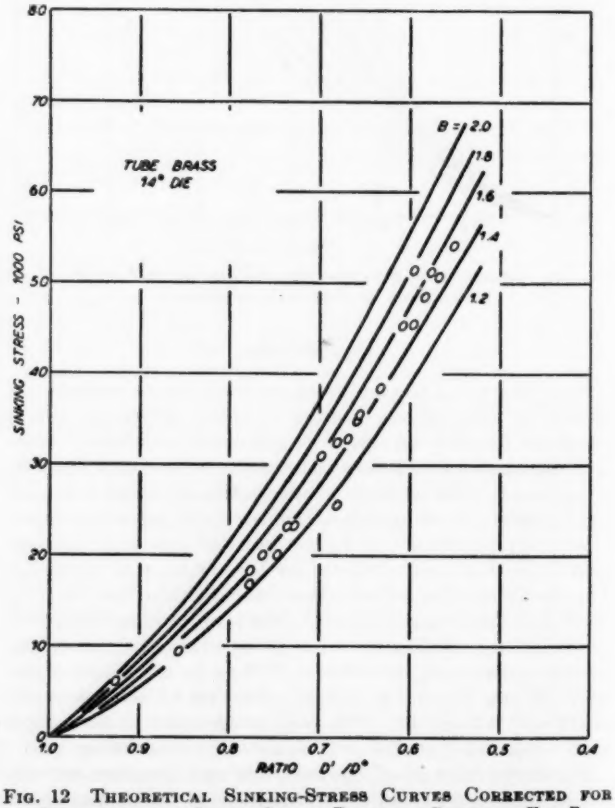


FIG. 12 THEORETICAL SINKING-STRESS CURVES CORRECTED FOR DIFFERENCES IN STRESS-STRAIN DIAGRAMS SHOWN IN FIG. 7
(Curves are soft tube brass sunk through a 14-deg die. Experimental data are represented as circles.)

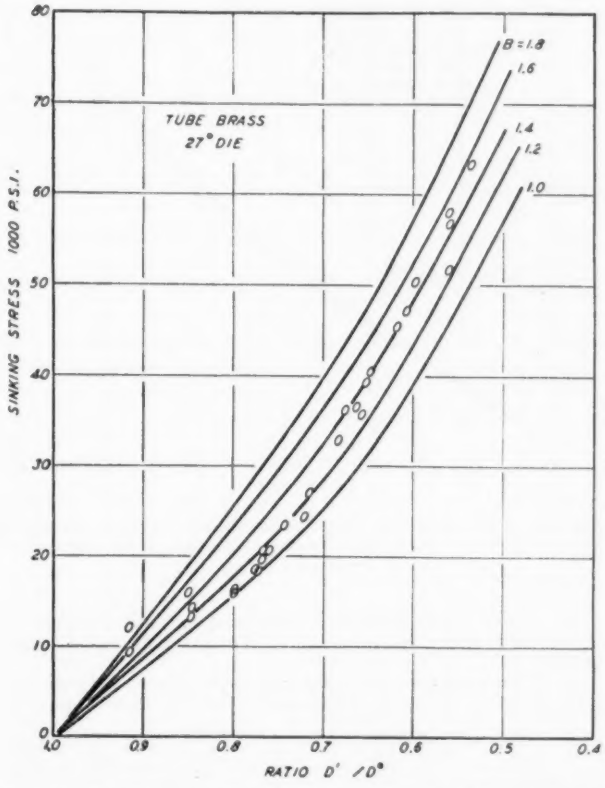


FIG. 13 THEORETICAL SINKING-STRESS CURVES CORRECTED FOR DIFFERENCES IN STRESS-STRAIN DIAGRAMS SHOWN IN FIG. 7
(Curves are for soft tube brass sunk through a 27-deg die. Experimental data are represented as circles.)

Neglecting the back pull s_1°, the sinking stress given by Equation [10] becomes

$$s_1' = \frac{Bk_0}{B-1}\left[1-\left(\frac{D'}{D^\circ}\right)^{B-1}\right] \quad \ldots\ldots\ldots [10a]$$

The parameters, B_1 and B, in Equations [11] and [10a] are identical (see Equation [5])

$$B_1 = B = \frac{\tan\alpha + f}{\tan\alpha}$$

Considering that the cross-sectional area in wire-drawing is

$$A_1 = \pi D^2$$

consequently

$$\frac{A_1'}{A_1^\circ} = \left(\frac{D'}{D^\circ}\right)^2 \quad \ldots\ldots\ldots\ldots\ldots [12]$$

On the other hand, the cross-sectional area in tube-sinking is

$$A = \pi t D$$

consequently

$$\frac{A'}{A^\circ} = \frac{D'}{D^\circ} \quad \ldots\ldots\ldots\ldots\ldots [13]$$

Introducing Equations [12] and [13] into Equations [11] and [10a], respectively, yield the following

For wire-drawing

$$s_1^\circ = \frac{Bk}{B-1}\left[1-\left(\frac{A_1'}{A_1^\circ}\right)^{B-1}\right] \quad \ldots\ldots\ldots [11a]$$

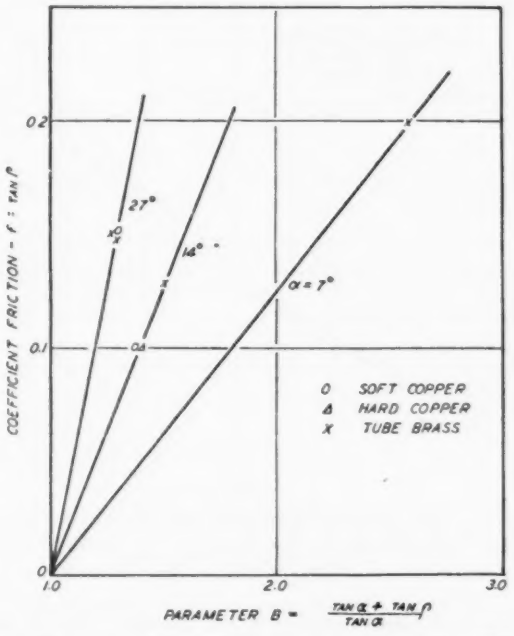


FIG. 14 PARAMETER B AS A FUNCTION OF COEFFICIENT OF FRICTION AND DIE ANGLE

and for tube sinking

$$s_1' = \frac{Bk_0}{B-1}\left[1-\left(\frac{A'}{A_1}\right)^{B-1}\right] \quad \ldots\ldots\ldots [12a]$$

Thus for a given ratio of cross sections at the entrance and exit, the ratio of the draw stresses for wire-drawing and tube-sinking should be

$$\frac{s_1^\circ}{s_1'} = \frac{k}{k_0} = \frac{k}{1.1\,k} = 0.91$$

So far, the comparison of the two processes has not considered the effects of the shear stresses at the interface between die and metal, which increase the yield strength over that of a homogeneously deformed metal, as discussed previously. If these effects are larger in tube-sinking than in wire-drawing, the ratio k/k_0 would be larger than 0.9, and vice-versa.

To test these conceptions, two series of tests with a 14-deg and a 27-deg (half-angle) die, respectively, were carried out on annealed copper. The processing of both the copper tubes and the copper wire was such that identical stress-strain curves were obtained, represented in Fig. 3. All test conditions were also the same, as described previously for tube-sinking.

The results of the experimentation are shown in Figs. 15 and 16. For the smaller die angle, 14-deg, the ratio of the draw stresses for wire-drawing and tube-sinking respectively, is possibly slightly larger than 0.9. For the larger die angle this ratio is rather close to unity. Considering that the effects of shear increase with increasing die angle, the following conclusions can be drawn from these tests: (*a*) The draw stresses in tube-sinking and wire-drawing, respectively, correspond approximately to the fundamental difference in the flow stress derived from the difference in their stress states; (*b*) the shear stresses occurring under commercial processing conditions affect the metal flow in wire-drawing to a (slightly) greater extent than in sinking a thin-walled tube.

BIBLIOGRAPHY

1 "Contribution to the Theory of the Drawing Process," by G. Sachs, *Zeitschrift für angewandte Mathematik und Mechanik*, vol. 7, 1927, pp. 235–236.

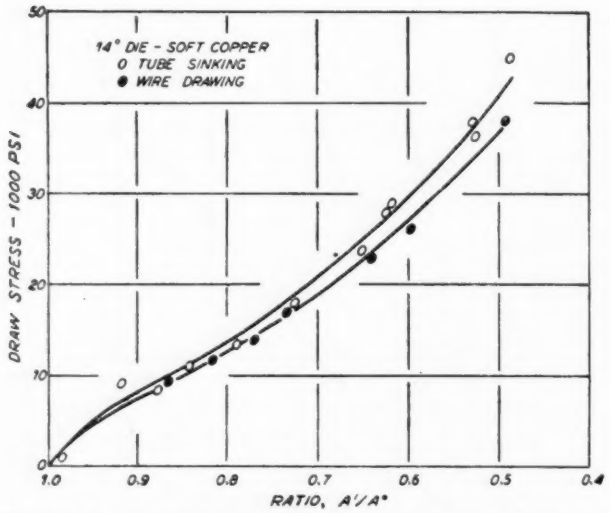


FIG. 15 COMPARISON OF DRAW STRESSES FOR SINKING ANNEALED COPPER TUBE AND DRAWING ANNEALED COPPER WIRE THROUGH A 0.50-IN-DIAM 14-DEG DIE

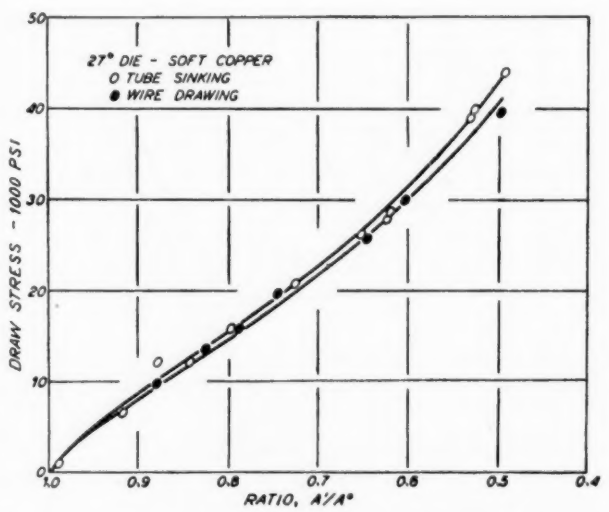


FIG. 16 COMPARISON OF DRAW STRESSES FOR SINKING ANNEALED COPPER TUBE AND DRAWING ANNEALED COPPER WIRE THROUGH A 0.50-IN-DIAM 27-DEG DIE

2 "Theory of Wire Drawing," by E. A. Davis and S. J. Dokos, *Journal of Applied Mechanics*, Trans. A.S.M.E., vol. 55, 1933, p. A-193.

3 "Forces and Flow of Material During Plastic Deformation," by E. Siebel, *Stahl und Eisen*, vol. 35, 1925, pp. 1563–1566.

4 "Contribution to the Theory of the Rolling Process," by T. von Kármán, *Zeitschrift für angewandte Mathematik und Mechanik*, vol. 5, 1925, pp. 139–141.

5 "Experimentation on the Determination of Normal Stresses During the Process of Rolling," by K. Huber, *Zeitschrift für angewandte Mathematik und Mechanik*, vol. 8, 1929, p. 454.

6 "The Influence of External Friction and Tension on the Pressure of the Metal on the Rolls in Rolling," by A. I. Tselikov, *Metallurg*, 1939, pp. 61–76.

7 "The Calculation of Roll Pressure in Hot and Cold Flat Rolling," by E. Orowan, Proceedings of The Institution of Mechanical Engineers, vol. 150, 1943, pp. 140–167.

8 "Drawing Thin-Walled Tubing With a Moving Mandrel Through a Stationary Die," by G. Sachs, J. D. Lubahn, and D. P. Tracy, *Journal of Applied Mechanics*, Trans. A.S.M.E., vol. 66, 1944, p. A-199.

9 "Stresses and Metal Flow in Drawing Tubing," by E. Siebel and E. Weber, *Stahl und Eisen*, vol. 55, 1935, pp. 331–334; *Mitteilungen aus dem Kaiser-Wilhelm-Institut für Eisenforschung*, Duesseldorf, vol. 16, 1934, pp. 217–224.

10 "Dimensional Changes Encountered in Tube Sinking," by W. M. Baldwin, Jr., and T. S. Howald, Trans. A.S.M., vol. 33, 1944, pp. 88–102.

11 "Regarding the Mechanical Phenomenon in the Die Opening," by E. Siebel, *Zeitschrift für Technische Physik*, vol. 7, 1926, pp. 335–337.

12 "The Drawing of Non-Ferrous Wires," by E. L. Francis and F. C. Thompson, *Journal of the Institute of Metals*, vol. 46, 1931, pp. 313–351.

13 "The Effect of Back Tension in Drawing of Steel Wire," by W. Lueg and A. Pomp, *Stahl und Eisen*, vol. 63, 1943, pp. 229–236.

14 Calculation of the Drawing Forces and Stress States in Wire Drawing," by Th. Poeschl, *Metallwirtschaft*, vol. 22, 1943, pp. 428–434.

15 "Experiments on the Properties of Drawn Wire and the Power Consumption in Wire Drawing" ("Spanlose Formung der Metalle"), G. Sachs and others, *Mitteilungen der deutsche Materialprüfungsanstalten*, Sonder Heft no. 16, J. Springer, Berlin, 1931, pp. 38–67.

16 "The Distortion of Wires on Passing Through a Draw Plate," by G. I. Taylor and H. Quinney, *Journal of the Institute of Metals*, London, vol. 49, 1932, pp. 187–202.

17 "Deformation Relationships in Wire Drawing," by E. Siebel, *Mitteilungen aus dem Kaiser-Wilhelm-Institut für Eisenforschung*, Düsseldorf, vol. 16, 1934, pp. 213–216.

The Design of Mechanical Auxiliaries for TVA Hydroelectric Plants

By H. J. PETERSEN,[1] KNOXVILLE, TENN.

Sixteen hydroelectric power plants have been designed by the Tennessee Valley Authority during the past ten years. Changes and improvements have been incorporated in each successive design, as a result of experience gained in operation of each plant. This applies particularly to mechanical auxiliaries involved. It is this phase of the design which is treated in the present paper, specific reasons being given for adoption of the particular auxiliaries discussed.

DURING the past decade the Tennessee Valley Authority has designed sixteen hydroelectric power plants which include almost every type of plant except those using Pelton wheels. These plants were all designed by essentially the same organization, which resulted in a succession of improved designs as experiences gained in the earlier plants were incorporated in the designs of the later plants. This is especially true in the case of the mechanical auxiliaries since considerable latitude is permitted in the design of these systems. Consequently, it has been possible to standardize on a good many features of these auxiliaries which have proved themselves in service.

This paper will discuss the design of the various mechanical auxiliaries for hydroelectric power plants as developed by the Authority, outlining the reasons establishing the designs adopted. It is expected that these designs will be superseded by later and better designs as operating experiences and improved techniques dictate. It is not intended that this paper shall represent a comprehensive treatise on hydroelectric power-plant piping and auxiliaries, as these subjects are well handled in numerous textbooks and manuals; however, the scope of this discussion makes it desirable to complement the specific references to TVA design with a review of certain related principles which the author considers good general piping practice.

In general, the term "mechanical auxiliaries" includes those systems usually consisting of one or more machines connected by piping to the main prime movers to aid them in their proper functioning, or other systems distributed throughout the powerhouse for services such as water, air, drainage, and so forth. Because they occupy relatively small spaces and usually are located in out-of-the-way places in the powerhouse, these systems sometimes do not receive their full share of attention and may be slighted in the design. In almost all cases they are vital to successful and economical operation, and thought given to their design in the preliminary stages will pay dividends in the long run in the trouble-free operation of the plant.

However, the amount of time and effort spent in the design of these features should be justified by the results required. Elaborate calculations and long and complicated empirical and theoretical formulas should be resorted to only when the results prescribed make their use unavoidable. Only a novice will carry out a computation to two or three decimals when a lesser number of significant figures will suffice. An experienced designer is aware of this and has available a number of charts, tables, and curves, from which he is able to pick certain approximate values which facilitate his design. Also, a practical designer will always maintain a close liaison with the department that will operate the plant in order to ascertain its likes and dislikes in the matter of machinery and equipment. Many times that department, because of its operating experiences, can make worth-while contributions to the design.

General Considerations

Before reviewing the design of the individual systems, several features common to all systems and on which generalizations may be made will be discussed.

Piping. The fundamental requirement for any piping system is that it shall be functionally correct. All valves and items of equipment should be in proper relation to each other, so that the system operates in the most efficient manner possible.

The best way to obtain this result is by making a valve-operation diagram. Fig. 1 is such a diagram for a governor and lubricating-oil system at one of the Authority's plants. It will be noted that this diagram outlines the entire system, including all valves, equipment, and machinery. From this it is an easy matter to check the over-all design of the system from a functional standpoint. This diagram, made in sketch form before any drawings are begun, serves as a guide to the draftsman in making the detailed drawings. When made into a final drawing, it has the further purpose of aiding the field erection forces in the installation of the piping, and finally it enables the operators to visualize the system as a unit which promotes more efficient operation. Each valve on each system is marked with an aluminum tag describing its function (see Fig. 2). Tags A, B, and C are attached to the valve handwheels underneath the nut, while tag D is attached to the valve-bonnet bolt, to the valve stem, or to the operating chain. Each valve is numbered according to a standard system, and an experienced operator can tell the relative location of a valve in the piping system by its number. The symbols shown on this drawing for the various kinds of valves and items of equipment are standard for the diagrams for all plants.

During the preliminary stages of the design of the powerhouse, adequate consideration should be given to the physical location of the pipe lines. It is absolutely essential that all the various systems be considered as a group in order to lay out the space requirements properly. Close co-ordination between the piping designer, the architect, and the concrete designer is essential at this stage of the design in order to insure proper space for pipe galleries, tunnels, and riser shafts.

Fig. 3 shows a gallery containing a number of piping systems. It will be noted that the gallery is of ample size, that all the pipes are racked along the wall parallel to the building lines, and that they provide adequate headroom. As a contrast, one of the earlier designs showing the piping around the top of a shaft is illustrated in Fig. 4. Note the pipe at angles to building walls, the inaccessibility of valves, some valves upside down, and the general appearance of having been designed one system at a time instead of as a group. The improvement in the oil piping shown

---

[1] Head Mechanical Engineer, Tennessee Valley Authority. Mem. A.S.M.E.

Contributed by the Hydraulic Division and presented at the Spring Meeting, Chattanooga, Tenn., April 1–3, 1946, of The American Society of Mechanical Engineers.

Note: Statements and opinions advanced in papers are to be understood as individual expressions of authors and not of the Society.

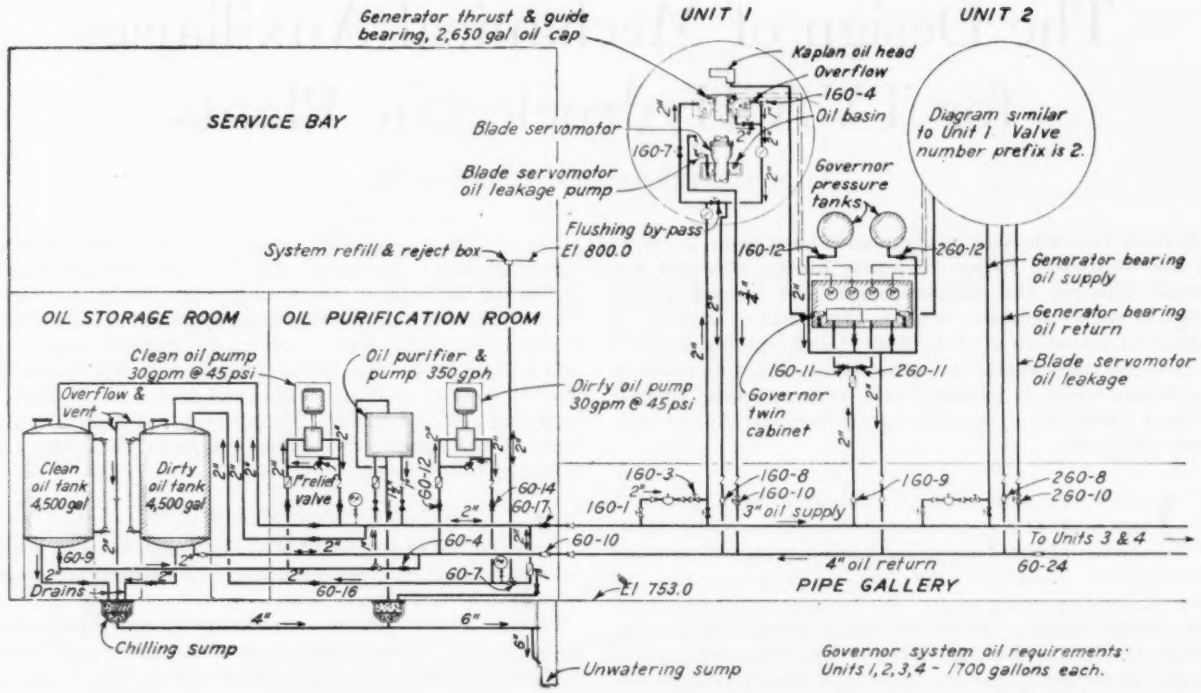


FIG. 1 VALVE-OPERATION DIAGRAM; GOVERNOR AND LUBRICATING-OIL SYSTEM; FORT LOUDOUN PROJECT
(Units 3 and 4 and some valve numbers omitted for condensation and clarity.)

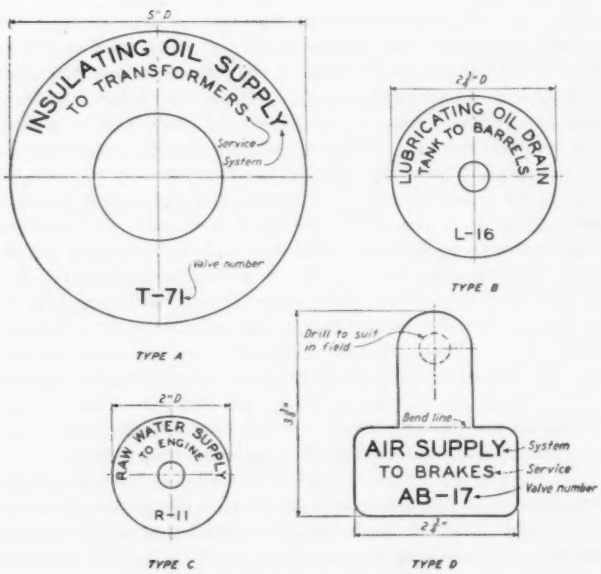


FIG. 2 VALVE MARKER TAG

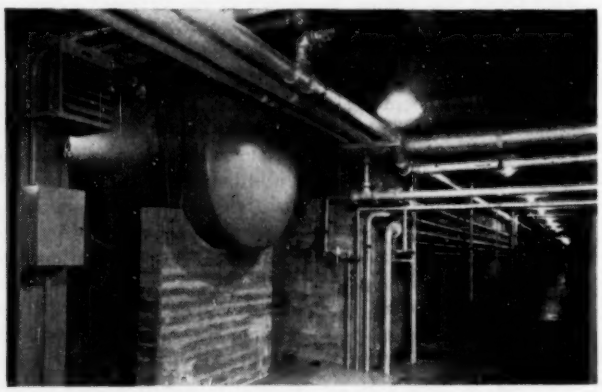


FIG. 3. PIPING IN GALLERY

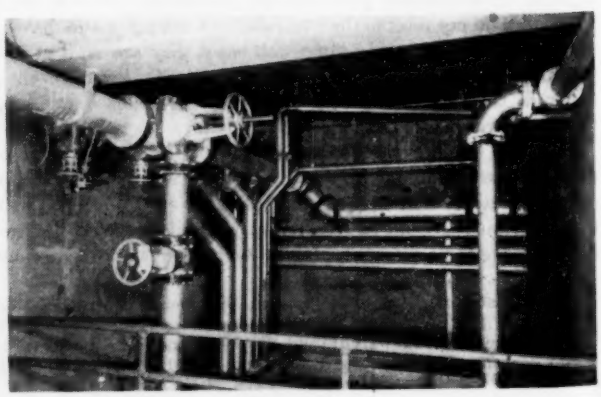


FIG. 4 PIPING AT TOP OF SHAFT

in Fig. 6, over that shown in Fig. 5, is evident. Fig. 5 has large radii bends combined with welding fittings, pipes crossing each other at angles, pipe in more than one plane, and a multiplicity of valves and piping.

By locating the equipment closer to the walls and by using three-way cocks, as shown in Fig. 6 for a similar system in a later powerhouse, it was possible to eliminate many valves and some of the piping. The use of welding fittings throughout and the uniform spacing of the headers result in a piping design which places the accent on simplicity and good appearance as well as

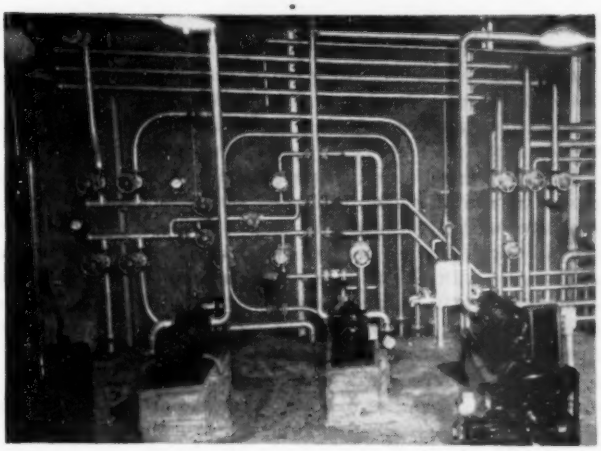


FIG. 5 PIPING IN OIL-PURIFICATION ROOM IN ONE OF EARLIER PLANTS

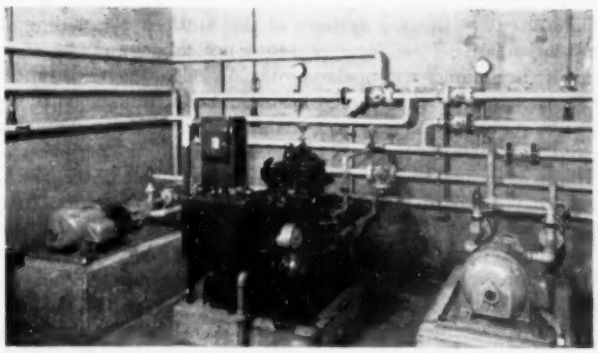


FIG. 6 PIPING IN OIL-PURIFICATION ROOM IN LATER PLANT

functionalism. The choice of the operator between these two designs is obvious.

The greatest part of the steel pipe used by the Authority for hydroelectric plants is purchased under A.S.T.M. Specification A 120, standard weight (ASA-B36.10). For certain pipe assemblies where considerable bending or coiling of the pipe is necessary, the pipe is specified as A.S.T.M.-A53, Grade A. Wrought-iron pipe is purchased under A.S.T.M. Specification A72. All cast-iron pipe is bell and spigot centrifugally cast, with class depending upon the pressure. Cast-iron pipe for pressure lines is purchased cement-lined, as it may be had at little or no increase in price, and experience has proved that it is much more resistant to tuberculation. Cast-iron pipe is purchased in 16- or 18-ft lengths, depending upon the supplier. Shorter lengths are seldom used because of the added calking expense.

In some of the larger-size mains, it has proved advantageous to use spiral-welded pipe. This is especially true in drainage lines embedded in concrete where the cost of steel or cast-iron pipe would not be justified. Steel pipe is purchased in random lengths with ends threaded and coupled, or beveled for welding, as the case may be. We find that it is cheaper to weld pipes 4 in. and larger than to use screwed flanges. It also saves time and expense to have complicated welding pipe assemblies shop-welded into subassemblies which are then welded together in the field.

The Authority makes single-line detailed construction drawings for piping systems using pipe 2 in. and smaller and for large-scale yard piping of all sizes. They can be made much faster and, except in some congested areas, they give a satisfactory physical picture. Any congested areas are developed either with standard double-line drawings or by isometric projection. Duplication of views, notations, dimensions, and mark numbers are avoided as they add to the design expense and increase the chances for error.

Where lines lead directly to headwater or tail water, heavier construction is used up to the first valve to guard against possible breakage. A special connection is used where embedded lines emerge from the concrete in the various galleries. In smaller lines a screwed coupling is placed flush with the face of the concrete wall; this permits ready replacement in case of breakage in the line. In larger steel lines a standard cast-iron sleeve is placed flush with the concrete wall, and the exposed pipe is calked therein. Cast-iron lines emerging from concrete are placed with the end of a bell flush with the face of the wall.

Pipes passing through walls and floors are sleeved, with sleeves in floors extending 1 in. above the floor to permit floor washing without water spilling to the room below. Black steel pipe is used for sleeves, except where rust action would prove objectionable, in which case galvanized sleeves are used. Piping systems are provided with drains at the low points to facilitate repairs and to drain water lines which are subject to freezing. A good designer always provides a closure piece in a piping system between two pieces of equipment where there are intervening flanged fittings or valves, instead of designing the system fitting to fitting. This is necessary because fittings and valves seldom are furnished to exact dimensions, and the closure piece takes up the inaccuracies in dimensions. Pipe lines are arranged to provide adequate access to machinery for inspection and repair, and to permit the removal of equipment without the necessity of dismantling large sections of piping. Fig. 6 is a good example of this.

It is of prime importance in the design of a piping system to provide for the maximum ultimate requirements. This is especially true in trunk lines for water-supply mains and plumbing waste lines. Our experience has been that as a project develops, more and more demand is placed upon these two systems. A liberal estimate of ultimate requirements is the best insurance against insufficient capacity in the future.

Next in importance to functionalism in a piping system is that the design shall be economical. This factor involves the proper selection of the material, type, and size of the various pipe, valves, and equipment. It is compounded from a great many elements, some of the more important of which are (1) expected life versus cost, (2) higher pumping costs because of reduced sizes versus smaller initial investment, and (3) increased operating conveniences and reduced maintenance expense versus the added cost for obtaining these features. If these three points are carefully evaluated in the design of each system, it is fairly certain that an economical design will result.

From past experience and from technical data on the subject, the expected life of a pipe or valve may be closely estimated. Obviously, the longer life is more desirable, but it is necessary for the designer to balance the extra years of service against the added cost necessary to obtain it.

The size of each pipe line, once the maximum flow is established, is almost entirely a function of the pressure drop due to friction in the line. It is necessary to investigate each line for head loss, using the friction characteristics for the fluid carried. Sizes of equipment connections should never be construed as indicative of proper pipe size. In most cases the size of pipe mains for water systems is dictated by the flow necessary for fire protection. In evaluating pumping costs and pipe sizes, it must be remembered that station power is cheap in a hydro plant. On the other hand, most of the added cost of a larger-size pipe is the material itself, since the labor of installing each-size line is practically the same. It is advisable not to have too many different

sizes and kinds of pipe in a plant since this requires a larger stock of replacement parts for valves and specialties.

The amount of money that should be spent for operating conveniences and reduced maintenance is largely determined by experience and judgment. A good many operating conveniences may be had without extra cost if the systems are properly designed. Valves should be located so that their purpose is apparent at a glance, and they should be accessible, especially those required in an emergency, using chain wheels where necessary. There should be sufficient unions in screwed lines to facilitate disassembly. All waste and drain lines, especially those buried in concrete, should have cleanouts at strategic points. The practice of burying plumbing or other piping in walls should be avoided; it is much better to provide access corridors behind the fixtures for service and maintenance.

Valves. The function of a valve in a piping system is either to regulate the flow of the fluid in the line or to sectionalize a piece of equipment or part of the system. Globe valves are used for the first function and gate valves for the second. Since most of the valves in hydro plants require only infrequent operation and are seldom used for throttling service, gate valves are used in the majority of cases. Globe valves are used on by-passes around special valves and regulators with a gate valve on either side of the equipment by-passed.

The Authority prefers a rising-stem valve to a nonrising-stem valve because the position of the stem indicates the position of the disk and because the stem threads are not in contact with the fluid. The O.S.&Y. type of rising-stem valve has the further advantage that the stem threads are outside the valve when open, making it possible to examine and lubricate them with the valve in service. The additional headroom which is required for the rising-stem valve over a nonrising-stem valve is of small importance.

Globe valves usually are purchased with plug-type disks because that type of disk gives excellent throttling service, has great resistance to wear, and is easily repaired. The so-called composition disk has not proved as satisfactory for throttling and wears out quickly. Gate valves 2 in. and larger usually are purchased with double disks, and smaller than 2 in. with wedge disks. A double-disk valve gives a tighter shutoff and is more easily repaired in the field. Sometimes a larger-size wedge-disk valve is used when it is impossible to install the valve with the stem up. In this position the disk of the double-disk valve is liable to jam. Gate valves smaller than 2 in. are purchased with wedge disks because, in our opinion, the various parts in a double-disk valve in those sizes are too small.

Valves 2 in. and smaller, both gate and globe, usually are purchased all brass because the extra cost involved is nominal. Larger valves are purchased iron body, bronze-mounted. The use of cleanouts in valve bodies has not been found necessary, nor has it been necessary to specify air-tested valves. Pressures encountered in hydroelectric plants seldom call for by-passes around valves, although at times it has been necessary to provide gearing for the larger-size valves. This, of course, is a function of the pressure on the valve and is investigated for each condition. Larger valves which require fast operation, or are remotely controlled, are fitted with motor operators.

Check valves are used on the discharge of pumps and at all other places where it is imperative to prevent backflow of the fluid. Swing-check valves are preferred, but in some cases lift-check valves are used, especially for upward flow. A balanced-disk or spring-loaded check valve is used to prevent slamming and excessive surges in the higher-head lines.

Bolts and Gaskets. Flange bolts are purchased under A.S.T.M. Specification A 107, with regular unfinished square heads and heavy unfinished hexagon nuts. In rare cases where the bolts are inaccessible and subject to excessive corrosion, such as for fastening inlet gratings to the upstream face of a dam, stainless-steel bolts are used. The thinnest possible gasket consistent with the roughness of the flange, is used, with no gaskets over $^1/_{16}$ in. Ring gaskets are used in preference to full-face gaskets as they make a tighter joint.

Hangers, Supports, and Expansion Joints. In a well-designed piping system the weight of the pipe and its contents are always supported so that no stresses are transmitted to any of the valves or machinery. The stresses introduced in equipment in this manner, coupled with vibration, may eventually break the casting of a pump or valve. Standard commercial hangers are used where possible, as they are cheaper than designing special hangers for individual applications.

While the temperatures encountered in hydro-plant piping systems do not give rise to many expansion problems, the long lengths of the lines in a multiunit plant do call for some expansion design. The Authority uses pipe bends and offsets, where possible, in preference to guided slip joints with packing boxes. Sometimes, where vibration is coupled with expansion in a pipe line, a corrugated type of joint is used.

Painting. All piping systems of the Authority, including all insulation, are painted for appearance, protection, and identification, in accordance with a standard color code. Each system has its own color, and this standard is maintained throughout all the plants. The whole system is first painted with an aluminum paint, and identification is obtained by painting the periphery of flanges or by painting an occasional screwed elbow or tee, as the case may be, with the color of that particular system. If the length of line between these identification points is long, a narrow band is painted around the pipe at intervals. Arrows are sometimes painted on pipe lines where the direction of flow is not evident at a glance.

Control Valves. Control valves are used by the Authority in hydro plants for pressure regulating, temperature regulating, pressure relief, and maintaining liquid level. Pressure-regulating valves are used for reducing the water pressure to generator air and oil coolers, turbine oil coolers and runner seals, air-conditioning equipment, air-compressor jackets and aftercoolers, and general plant services. Where the pressure drop is low direct-operated spring-loaded diaphragm valves are installed, while pilot-operated valves are used for high-pressure drop. The pilot-operated valves are of the hydraulic or pneumatic type. The pneumatic type has proved more satisfactory for use on raw river water, as trouble has been experienced with the hydraulic type owing to fouling of the pilot valves, necessitating the installation of strainers in the pilot lines. We have found that filters installed in the air lines ahead of pneumatic valves are a good investment. Small valves and valves used for dead-end service are single-seated, while large valves are double-seated. A pressure gage is always installed on either side of a reducing station.

The sizing of pressure-regulating valves for hydro plants presents a problem because of varying headwater elevations. Since the valves must pass the required amount of water under any head condition, a valve large enough under low headwater may be too large under maximum headwater levels. Likewise a regulating valve on plant service sometimes must also be used for fire protection. This means that water requirements must be estimated very closely, and valves must be selected which have characteristics best suited for their particular service.

Two types of temperature-regulating valves are used, i.e., solenoid and motor-operated from a thermostatic element. Solenoid valves are used on air-compressor jackets and similar services to control cooling water so as to prevent flow and condensation when the service is intermittent. Motor-operated valves, actuated from thermostatic elements, are used on air-

conditioning equipment and to control the cooling water to generator air coolers in remotely controlled plants.

Both spring-loaded hydraulic relief valves and diaphragm back-pressure valves have been used after pressure-regulating valves. Spring-loaded hydraulic relief valves are used in the small sizes and where the comparatively wide relief range is not objectionable. Diaphragm back-pressure valves have proved more satisfactory for large sizes and where close control is required. Relief valves are sized to pass the total amount of water which the pressure-regulating valve will pass under highest head conditions.

Level controls are used in open tanks and station drainage sumps, and for depressing tail water in the draft tube when units are motored. The types used are: the ordinary balanced float valve to maintain a constant level in an open tank from a pressure main, float-operated mercury switches and cam-type float switches to start and stop pumps, and diaphragm valves actuated by float-operated pilots and compressed air to depress tail water in the draft tube when units are motored for condenser operation.

Motors. All machinery in the hydro plants of the Authority is driven by electric motors because of the availability of a reliable power supply and because of the dependability of the modern motor and its simplicity of control.

Motors driving station auxiliaries are general-purpose, N.E.M.A. standard, with class A insulation. Motors driving constant-speed equipment, such as pumps, compressors, and ventilating fans, are squirrel-cage induction type with normal torque and starting current; those for variable speed and torque, such as cranes and hoists, are wound-rotor slip-ring type. Integral-horsepower-size motors are rated 440 volts, 3 phase, 60 cycles. No auxiliaries require motors large enough to make voltages above 440 economical. Fractional-horsepower sizes are 110 or 220 volt single phase. A few auxiliaries, such as emergency turbine guide-bearing, lubricating-oil pumps, and important valves, are provided with 250-volt d-c motors operated from the station service batteries.

Motors in locations where windings might become damaged by water or oil are provided with moistureproof insulation and splashproof or dripproof frames; others have open frames. In very damp locations it has been found necessary to apply strip-type heaters or to circulate a small amount of current through the motor coils to avoid sweating while the motors are shut down.

Controls are centralized on auxiliary-power switchboards for groups of related equipment. Each motor circuit contains a manually operated disconnecting switch, a set of fuses as protection against short circuit, and a magnetic contactor for full-voltage starting and thermal overload protection. Push-button stations for manual control generally are located at or near the motors. Motors under automatic control also have a push button which provides manual control for inspection. Power supply is sufficiently duplicated to assure continuous operation of auxiliaries during usual maintenance and under any reasonable fault conditions.

Individual Systems

Compressed Air. Compressed air is used in the hydro plants of the Authority for operating pneumatic tools, for generator brakes, for pneumatically operated regulating valves, for depressing tail water below the runners for synchronous-condenser operation in those plants where tail water level is normally above the runner, and in one plant (Kentucky) for preventing the formation of ice on the spillway gates.

Pneumatic tools operate most efficiently using air at 80 to 100 psi, and since the other uses for compressed air require pressures of less than this, 100 psi has been adopted as a standard pressure for the compressors. One stationary 105-cfm compressor has been found to have sufficient capacity for all normal plant needs in all plants except Kentucky. This is supplemented by a portable machine of approximately 100-cfm capacity at each plant which is used when major repair work requires additional air capacity.

The Authority has standardized on a horizontal, crosshead type, double-acting, water-cooled, 325-rpm, V-belt-driven, single-stage compressor for the stationary machine. Its low rotative speed and low bearing loads, together with its all-round rugged construction, make it a most dependable machine, capable of giving continuous service over a period of many years with very little maintenance. Dual control is used with these compressors. This control can be set to operate the compressor continuously when there is a steady demand for air, or it can be set to start and stop the compressor automatically when the demand for air is intermittent. The latter control is the one normally used, with the motor being operated by a pressure switch on the receiving tank. All compressors unload to atmosphere to prevent starting the motors under load.

The portable compressor is an air-cooled, single-acting, 2-stage, motor-driven machine complete with intercooler, air receiver, wheeled truck, and all standard accessories. The motor is controlled by a magnetic starter and push-button station mounted on the machine. The compressor is motor-driven because electrical outlets are provided throughout each plant area which make it possible to use the compressor either in isolated locations, such as up on the roadway crossing the dam, or in the powerhouse to supplement the stationary machine.

A water-cooled aftercooler is always used after single-stage compression to remove the excess moisture in the air before it condenses in the distribution system. An "air through the tubes" type of aftercooler with moisture receiver at one end is installed in the discharge piping. The small amount of moisture and oil from the compressor cylinder carried over to the distribution line is removed by traps. These traps are placed at low points in the line for gravity drainage.

An air receiver is placed in the discharge line after the aftercooler to damp the pulsations of the reciprocating compressor and to provide storage of compressed air when the peak demand is greater than the capacity of the compressor. Since the air cools in a receiver, its dew point is lowered and additional condensation takes place, which is removed by a blowoff or a trap. Because air is compressible, the damage resulting from a ruptured receiver is likely to be severe; consequently, the Authority always specifies that the tank shall be fabricated in accordance with the A.S.M.E. Code for Unfired Pressure Vessels.

Certain features of design are observed in the layout of the compressed-air system; some of these are essential and others are desirable. The air intake is connected to outside air whenever possible and fitted with a filter. When this is not feasible, the compressor is located in the lower levels of the substructure where the air is relatively cool and clean. A valve is never placed in the discharge line between compressor and receiver without an intervening safety valve. All air-hose connections are made at the tops of headers to prevent picking up moisture. Cooling water is discharged through an open funnel so that it may be tested for temperature by feeling. The Authority uses black steel uninsulated pipe for air lines. Internal corrosion from condensate has not evidenced itself up to the present time.

The use of air for depressing tail water below the runner[2] and for protection against ice at spillway gates[3] has been fully de-

[2] "Hydraulic Turbine Practice of the TVA," by H. J. Petersen and J. F. Roberts, *Mechanical Engineering*, vol. 65, 1943, pp. 237–244.

[3] "Kentucky Dam Project of TVA, Part II," by C. L. Norris and R. M. Gardner, *Power Plant Engineering*, vol. 49, March, 1945, pp. 79–81.

scribed in other articles and will be omitted from this paper.

Governor and Lubricating Oil. The Authority uses the same oil for the governor pressure system and for the lubrication of the generator thrust bearing. Some difference of opinion between the governor and generator manufacturers has arisen lately over the viscosity of this oil. The generator manufacturers prefer an oil with a viscosity in excess of 300 S.S.U. at 100 F, while the governor manufacturers prefer this viscosity to be around 250 S.S.U. at 100 F. In order to avoid the necessity of two separate oil systems, oil with a viscosity of 300 S.S.U. at 100 F will be purchased in the future.

We have found that purifying oil by centrifugal force is satisfactory and economical, and we have standardized on that type of machine. A self-contained and enclosed stationary 350-gph unit, complete with centrifuge, motor, pump, electric heaters, temperature control, and all standard accessories, is purchased for each plant. In the early stages of the Tennessee Valley Authority program consideration was given to the use of a portable machine which could be transported to individual plants as required. A central purifying depot, where oil from all plants could be shipped for processing, was also considered. These were both ruled out because of operating inconveniences involved and because the cost of a purifying system is a very small percentage of the total cost of each plant.

Two tanks are provided for each project, one for clean oil and one for dirty oil. Each tank has sufficient storage for the oil in one unit thrust bearing, plus the oil in one governor system, plus a few hundred gallons of extra capacity. When space permits, these tanks are located in the powerhouse adjacent to the oil-purification room. In plants where no space is available the tanks are buried in the fill outside the powerhouse wall. Tanks placed in this manner are designed with an extra $^1/_{16}$ in. of metal to allow for corrosion. In either case the storage tanks are always located so that they may be filled by gravity from the ground level and still provide a positive head on the pumps.

One clean-oil pump and one dirty-oil pump are furnished for each powerhouse. The pumps are standard positive-displacement type with built-in relief valves and are rated 30 gpm when pumping oil at 50 F. A complete piping system is installed at each plant between the units and the purification facilities. The Authority uses black steel, scale-free uninsulated pipe for these oil lines. Experience has proved that it is difficult to prevent leaks in piping using screwed malleable fittings, especially when the oil is hot, as around the centrifuge. Consequently welded joints are used throughout, except at valves and unions, with forged-steel socket welding fittings used for sizes 2 in. and smaller. Oil-resistant gaskets are used when it is necessary to use flanges. No matter how well a pipe line is cleaned, there will always be scale and welding particles carried along in the oil, especially when starting the system. For this reason a filter is installed in the line leading to each unit and a standard Y-type strainer with $^1/_{32}$-in. perforations is used on each pump suction. These filters have 0.005-in. openings through metal slots and are equipped with built-in knife-blade cleaners.

Insulating Oil. Because of its different characteristics from lubricating oil, a separate oil-purification system is installed in each plant for the insulating oil used in the transformers, circuit breakers, and other oil-filled electrical equipment. The same type of machine is used as just described, but because of the larger volumes handled, its capacity is increased to 600 gph. A filter press which raises the purifying capacity to 900 gph is added to this machine to remove the colloidal carbon from the oil.

One clean- and one dirty-oil pump are installed in each plant. They are of the same type as the pumps for the lubricating-oil system, with the capacities increased to 100 gpm each. At some plants it is possible to return the dirty oil from the switchyard to the storage and purification rooms by gravity, and no dirty-oil pump is supplied. One clean-oil tank, one dirty-breaker-oil tank, and two dirty-transformer-oil tanks are provided at each plant. In this way the breaker oil and transformer oil are never mixed after they once have been used. Each of the circuit-breaker-oil tanks (clean and dirty) has storage capacity for one breaker, and the two dirty-oil transformer tanks have a total storage capacity for one transformer.

The same comments apply for the piping as for lubricating oil, except that black wrought iron is used for underground lines in the switchyard. The supply and return lines in the switchyard are not permanently connected to the transformers and breakers; instead, a valve is located in each line near the equipment and a flexible hose is used when filling or draining is necessary. This hose has a specially treated synthetic-rubber lining and is equipped with a flexible ball-joint fitting to facilitate attachment to the service valve. Because the oil is changed at infrequent intervals we find this arrangement entirely satisfactory.

Runner-Hub Oil. In the main river plants which have Kaplan turbines the runner hub is filled with a heavy oil for lubricating the internal blade-operating mechanism. This oil has a viscosity of approximately 1700 S.S.U. at 100 F. Whenever the runner is dismantled for inspection or repair, it is necessary to remove this oil, and since there are approximately 1500 gal of oil in each hub, the Authority salvages it for re-use.

A black steel pipe header is installed in the access gallery located below the units in each plant. Branch headers lead from this line to the draft-tube access doors of each unit, and connection to the hub is made with a flexible hose. An 8-gpm motor-driven screw-type portable pump and two portable storage tanks are provided for transporting and storing the oil during the dismantling of the unit. Because of the infrequency of this operation, the storage tanks and the pump were made portable so that they may be transferred from plant to plant as required. Two storage tanks were supplied to reduce the volume of each tank to facilitate handling.

Raw Water. Raw water is used in the Authority's plants for cooling water for the main generators, for the air compressors, and for the air-conditioning equipment, and in some plants for fire protection, for lubricating the turbine guide bearing, and for supplying make-up for the treated-water system.

In the low-head plants water is taken from the scroll case of each unit and pumped through a multiple basket strainer having $^3/_{16}$-in. openings to a header leading to the station system. One pump is located at each unit to insure a positive cooling-water supply, and a stand-by pump is installed in the service bay of each plant. This latter pump is connected to the forebay by a separate intake and can supply any unit with cooling water in an emergency. All the pumps are connected into a header running the length of the powerhouse so that the chances of any one unit being without cooling water are remote.

The pumps are horizontally split-case, double-suction, single-stage, volute-type centrifugal units. Specifications include enclosed bronze impeller with wearing rings, bronze shaft sleeves through the stuffing box, water-seal piping, and deep stuffing boxes. Experience has proved that this type of pump will give years of service with little maintenance except occasional repacking or lubrication of the bearings. A booster pump is installed in each plant service system using raw water where the forebay pressure is insufficient for a gravity supply. Sometimes the operating requirements of two or more of these systems make it possible to supply them with water from one pump. Quantities involved are usually low, and single-stage single-suction pumps are used. The Authority has found the close-coupled type of pump very satisfactory for this service.

In the high-head plants a separate intake from each unit pen-

stock is connected to a central manifold from which the individual systems are supplied, with pressure-reducing valves installed as required. An air-cushion chamber is installed on the manifold to absorb the water hammer caused by the operation of the system. When the raw-water system supplies the make-up for the treated-water system, intakes at different levels are provided in the dam to enable the operator to take advantage of the varying water temperatures, turbidities, and chemical contents of the lake water at different levels.

The Authority uses black steel pipe for exposed raw-water piping, except that galvanized steel is sometimes used in the smaller sizes. Welded joints are used, except that flanged joints are used around equipment and valves. Gaskets are $^1/_{16}$-in. red rubber. Raw-water lines buried in the ground are cast iron, bell and spigot, in accordance with standard waterworks practice. Black wrought-iron pipe is used for buried lines in sizes $1^1/_2$ in. and smaller, for sprinkler and general yard service.

Lines are insulated in locations where sweating of the cold pipe would prove objectionable. Standard commercial insulating felt molded in 3-ft lengths and covered with 8-oz canvas jacket is used for straight runs of pipe. Fittings and irregular surfaces are covered with a layer of hair felt sealed with a waterproof-tape wrapping and a coating of asphaltic sealing compound. Insulation of 1 in. thickness has been found sufficient to prevent sweating for the water temperatures and air humidities encountered in the low-head hydro plants, but $1^1/_2$ in. of insulation is necessary in the high-head plants because of the colder water. Regranulated cork has been used in some instances to prevent sweating, but unless it is applied very carefully and built up to a thickness of $^1/_4$ in. or more, it is not as satisfactory as hair felt. This is especially true in the high-head plants where water temperatures sometimes go as low as 36 F. Raw-water lines subject to freezing temperatures are insulated with built-up hair felt. The required thickness is a function of the temperatures encountered and the amount of water passing through the line and is investigated for each condition.

Treated Water. Treated water is used in the various hydro plants for all sanitary services, and in some plants for fire protection. Whenever possible the Authority obtains its treated water from a near-by community, even if this involves laying a mile or two of transmission main. We have found it to be more economical to purchase water in this manner than to install a treating system in the plant, requiring the services of an operator. However, it has been necessary to install water-treating systems in most of the projects because of their isolated locations.

At some projects the plant operators live close at hand and use water from the system. This increases the required capacity to the point where a conventional rapid sand gravity filter plant, with mixing chamber, coagulation basin, dry-chemical feeders, and chlorinator is justified. The water treated in this area is such that alum and soda ash or lime are the reagents used. At some of the projects the demand is 10 gpm or less, and pressure filter plants are installed. Originally, pot feeders actuated by differential flow across the orifices were installed for chemical feeding in the pressure filter plants, but our experience with them has not been satisfactory, and they have been replaced with solution-feeder pumps. Pot feeders are difficult to keep regulated, especially when the temperature of the water supply varies considerably as it does with intermittent use.

System pressure is obtained by using elevated storage tanks which usually are transferred from the construction activities at the project. At some of the high-head plants, where such a tank was not available and where raw water for fire protection could be obtained from pond storage, a pneumatic tank was installed for the treated-water system pressure. However, the controls for these tanks require a great deal of attention to keep them in proper working order, and an elevated storage tank is much preferred for this service.

The foregoing comments for pumps, piping, and insulation of the raw-water system apply to the treated-water system also except that in the latter case more galvanized-steel pipe is used.

Fire Protection. Raw water is used for fire protection in all plants where the minimum lake level provides sufficient pressure. The Authority has adopted 40 psi at the hose nozzle as the minimum pressure for this service, but a pressure of 60 to 70 psi is preferred and is used when obtainable. In plants where this pressure is not obtained, fire protection is obtained from the treated-water system or by means of a booster pump.

Fire-hose racks containing 50 ft of $1^1/_2$-in. unlined linen hose with cast-brass nozzles are located throughout each powerhouse at strategic points for inside fire protection. Standard 4-in. A.W.W.A. fire hydrants, fitted with two $2^1/_2$-in. nozzles, are located throughout the plant area and switchyard. A fire-hose cart equipped with a reel and three 50-ft lengths of $2^1/_2$-in. double-jacketed, flat-cured, cotton, rubber-lined hose with rocker-lug couplings is provided for switchyard fire protection. This is supplemented by a wheeled cart containing two 100-lb cylinders of CO_2. National standard fire-hose threads are used for the $2^1/_2$-in. hose and standard-iron-pipe threads for the $1^1/_2$-in. hose. Standard underwriters' play pipes are provided for outdoor fires, except that for electrical fires a nozzle is used which atomizes the water spray to the point where it will not conduct electricity.

Considerations were given to installing built-in fire-protection systems, using either water or CO_2, in the switchyards. These were ruled out because the remote possibility of these fires would not justify the cost of the installation. Sometimes transformers are installed very close to the powerhouse, as on the draft-tube deck. In such cases a fire might cause considerable damage, and built-in water systems, using fog nozzles, are installed. These systems are set off either manually by remote control, automatically by thermostats, or by the tripping of the transformer differential relay which is actuated by a short circuit in the transformer.

Carbon Dioxide. In addition to water fire protection, a complete CO_2 system is provided for each plant. This system protects the main generators, the oil-purification room, and the oil-storage rooms. The CO_2 system is designed in accordance with the standards of the National Board of Fire Underwriters for class A systems, which calls for total flooding of enclosed spaces.

A central supply of 50-lb storage cylinders sufficient to provide the gas concentration for one generator called for by the standards mentioned, is connected to all the generators by a complete piping system. This system is energized either manually by remote control or automatically by thermostats located in each generator. A separate system of cylinders and piping is provided for the oil-purification and storage rooms. It is controlled either manually or by thermostats in the room being protected. When this system trips off, all doors and openings automatically close to confine the gas, and pumps, ventilating fans, and other moving equipment shut down. The gas-discharge nozzles in an oil-purification room for one plant may be seen in Fig. 6. Portable containers of carbon dioxide in the 4- and 15-lb sizes are located at various points throughout the powerhouse to supplement the built-in systems.

Drainage and Unwatering. Roof, deck, and floor drainage in each plant is discharged either to the forebay or the tailrace whenever possible; however, it is necessary to carry some of the drainage to the station sump during periods of high tail-water levels. Galvanized steel pipe usually is used for roof drains, and black steel pipe for deck and floor drains. Screwed cast-iron drainage fittings which have recessed shoulders are used for all

systems. Expansion of roof-drain riser pipes is taken care of just under the roof either by fitting offsets in the pipes or by patented slip joints made for that purpose. Lines are uninsulated, except that deck drains are insulated against sweating when they run above false ceilings in the office areas.

Lead and special-alloy cast-iron lines were originally installed for battery-room drains as a protection against acid. This has been changed to standard steel pipe because the weak concentration of the acid solution does not justify the extra cost of special pipe.

The station sump in each plant is unwatered by two 300-gpm, float-controlled, deep-well-type, vertical-shaft turbine pumps operating in echelon. This type of pump keeps the motor above the wet conditions of an open sump. Very little sand or abrasive matter is present in the water, so enclosed or semienclosed impellers are specified. The pumps are bronze-mounted and oil-lubricated automatically by a solenoid valve energized with the motor circuit.

At times it is necessary to unwater the draft tube of a unit for inspection. Each unit draft tube is connected to the station sump with a large-size cast-iron line containing a sectionalizing valve. The first project of the Authority had the outlet in the bottom of the draft tube, but this soon filled up with sediment and later projects have this outlet about 15 in. from the bottom of the draft-tube floor. Most plants have two deep-well-type vertical unwatering pumps which range in capacity from 2500 to 5000 gpm, according to the volume of the draft tube. They are manually operated and can augment the station sump pumps in an emergency. In those plants where sufficient head is available, unwatering is done by eductors. Since this pressure water comes from the unit penstocks and since it is possible for the penstocks to be empty, the station drainage eductor is supplemented by one motor-driven sump pump. No supplementary pump is installed for draft-tube unwatering as unwatering operations may be scheduled for the times when a penstock is full of water.

Piezometers. The Authority installs piezometers in the various water passages at each plant to check the hydraulic performance of the units, penstocks, and spillways and to operate flowmeters. These lines are $^3/_4$-in. type K, extra-heavy, hard-copper tubing with solder-joint streamline fittings. Lines are installed carefully to avoid pockets and have a minimum pitch of 1 in. in 10 ft from the connection at the water passage to the terminal board.

Plumbing. In general, the design of the plumbing systems in the hydro plants of the Authority follows the "Recommended Minimum Requirements for Plumbing" established by the Subcommittee on Plumbing of the U. S. Department of Commerce.

Water closets and urinals are provided with flush valves, with those on the urinals being foot-operated. All lavatories are equipped with mixing faucets. Hot water is supplied by thermostatic-controlled tanks with immersion-type elements. These tanks vary in size from 10 to 120 gal. Where the hot-water lines are of considerable length, a small circulating pump is installed; however, in some instances it has been found more economical to purchase more than one heater, thus eliminating long runs of piping. A mixing valve is used in the showers to prevent the possibility of scalding. Drinking water is furnished by self-contained electric coolers located throughout each plant. Wall fountains supplied with chilled water from the remote connections on the water coolers are also used. Acid-resisting, enameled, cast-iron sinks have replaced stoneware sinks which were used in the battery rooms of some of the earlier hydro plants.

Type K, extra-heavy, hard-copper tubing with solder-joint fittings is used for all sanitary-water service because its small additional cost is justified by its longer life and its ease of installation. Air chambers 18 in. long are installed as close to the fixtures as possible to absorb the surges caused by quick-closing faucets or valves. Water pressures are maintained at approximately 50 psi, with no pressures exceeding 85 psi at a fixture. Excessive pressure results in leakage, water hammer, and high maintenance costs. Valves are provided at each fixture to permit repairs without shutting off a whole group of fixtures. Vacuum breakers are installed on all fixtures that are directly connected to the water supply to prevent polluted water from being siphoned into the water lines. Although ordinarily the pressure in the water lines prevents the entrance of polluted water, sometimes a partial vacuum occurs which causes siphoning unless vacuum breakers are installed. Floor drains in the toilet rooms have been eliminated in the later plants because they are so infrequently used that water evaporates in the traps and sewer gas enters the room.

All exposed soil and waste lines are standard-weight, galvanized, wrought-iron pipe with black, screwed, cast-iron drainage fittings. Extra-heavy cast-iron soil pipe and fittings are used for embedded lines. Galvanized wrought-iron pipe with black malleable-iron fittings is used for vent lines; where possible, the vents are all connected to the main vent stack to reduce the number of pipes projecting above the roof. A septic tank is installed in each plant with effluent discharged to tail water.

Hot-water piping is insulated with standard molded 3-ft sections of 6-ply preshrunk corrugated asbestos paper, 1 in. thick, and covered with 8-oz canvas pasted on. Fittings in hot-water lines are covered with insulating cement.

Heating, Ventilating, and Air Conditioning. Since the powerhouses are relatively large, with limited occupancy, and the materials of construction are such as to absorb large quantities of heat, the power requirements for general heating to comfort conditions are greater than can be justified. Consequently, only those areas where attendance is required are heated to 72 F, while the rest of the spaces are heated only as required for the relief of dampness or excessive chill.

All heating is by electric-resistance heaters. Except for the air-conditioned areas, heaters, in general, are thermostat-controlled, fan-type, 440-volt, three-phase units, with auxiliary on-off-auto manual switches. In some of the smaller areas 220-volt, single-phase, thermostat-controlled heaters are used. They are either gravity convection heaters recessed in the walls or suspended fan units as space or architectural considerations may require. In addition to these permanent heaters, outlets are provided throughout each powerhouse to which portable electric heaters may be connected as desired. In some of the powerhouses air used for ventilating electrical equipment is recirculated, thus utilizing the heat dissipated. In one plant this reclaimed heat amounted to more than 100 kw.

Ventilation is provided in the several areas of each plant according to the need for human comfort, for the dissipation of heat from electrical equipment and solar radiation on roofs, walls, and decks, and for the relief of dampness. In a number of plants where the arrangement and design of the electrical equipment require, parts of the electrical apparatus, including the main generator leads, are ventilated to prevent damage from overheating. Ventilation is provided in the tunnels and lower galleries for the relief of excessively damp and stagnant conditions.

The scheme of ventilation is a problem which must be solved in each individual plant. The usual practice of the Authority is to introduce air into the generator room and lower parts of the service bay and to exhaust this air through the other spaces to be ventilated by separate fans. In a few plants the fresh air is introduced by gravity, but in most powerhouses a number of supply fans are employed. The arrangement of each powerhouse usually is such that most of the more important spaces adjoin the generator room or are connected to it by open passages. These spaces are grouped together according to location and similarity of ventilating requirements into a number of groups, and each group is

served by a separate exhaust system. In the semienclosed type of hydro plant, where the intake deck is just above the generators, the excess heat from the generators and from solar radiation on the deck above escapes through louvers in the generator hatch covers over the machines. These louvers may be closed in winter, if desired, to conserve heat.

For convenience of maintenance and for economy of space, all the fans in the powerhouse are grouped usually into two separate fan stations. Fig. 7 shows an exhaust-fan station for one plant. It may be seen from this view that both direct-connected and

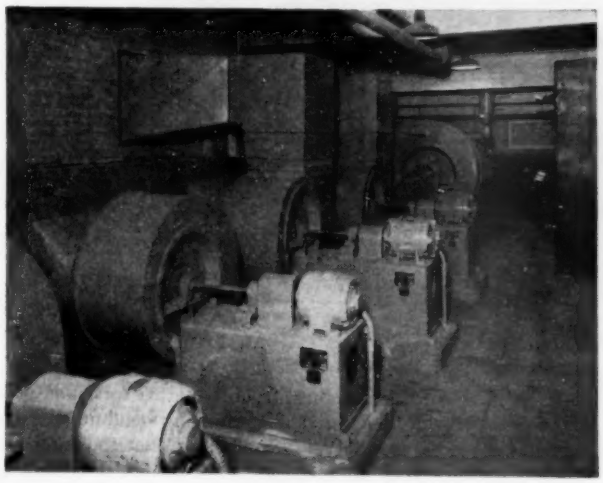


FIG. 7 EXHAUST-FAN ROOM

belt-driven fans are used. When the discharge pressure is fairly constant, fans with forward-curved blades at low rotative speeds are sometimes used. However, most of the fans used by the Authority have backward-curved blades because of their high efficiencies over a wide range of performance and because of the nonoverloading characteristic of that type of blade. It is also better suited to high speeds and hence more adaptable to direct connection. Inlet dampers are used where close control of the discharge pressure or of the delivery of a fan is desired. These dampers are operated by either a pneumatic or an electric motor actuated by the discharge pressure. Resilient bases, usually rubber-mounted, are used under fans when it is necessary to eliminate vibration or reduce noise.

Air conditioning is provided in certain spaces of each powerhouse for the protection of delicate electrical equipment and for human comfort. Because of variations in the heating and cooling requirements of the different parts of the powerhouse, the air-conditioning spaces usually are divided into three systems. One system serves the control room and its related spaces, another system serves the office areas, while the third system serves the public spaces, including the lobby and entrance vestibules. Other spaces, such as the telephone-equipment room, the laboratory, the assembly room, and the first-aid station, are served by one or more of the three systems. The control-room-system areas are grouped together because with their limited outside exposures and heavy heat losses from electrical equipment, they may require cooling at times when the other spaces require heating. The office system areas are served together because of similarity of exposure and thermal load, and the spaces served by the public spaces system are grouped together because of their proximity.

The individual air-conditioning systems may be used for ventilating, heating, and humidifying, or cooling and dehumidifying as required. Electric blast heaters are used for heating, and their operation is thermostatically regulated with auxiliary manual control. Humidification is provided by discharge of live steam generated by an electric immersion heater in an open pan in the plenum of each system. Cooling is by finned-type surface coolers, using chilled water in the coils. In the high-head plants where storage water is available at 55 F or less, lake water is used; in the other plants water is chilled by mechanical refrigeration.

Each of the air-conditioning systems can be placed on the heating, cooling, or ventilating cycles as desired and the control and operation of each is independent, that is, one system may be operating on the heating cycle while the other systems are on the cooling or ventilating cycles. Each system is complete with fan, electric blast heaters, humidifier, cooling coils, and filters, together with the manual, thermostatic, and other automatic control and safety devices necessary for its operation. Fans for air conditioning have two-speed motors or adjustable variable-speed motors, with the low speed used for the heating cycle and the high speed used for the cooling cycle.

The air filters are of the dry-filter type with filtering medium of paper, felted cotton, or felted glass fiber. Cell-type construction is used, and spare cells and filter media are provided at each plant.

In those plants having mechanical refrigeration, one water-chilling system serves all air-conditioning systems. The water-cooling equipment consists of one or more single-acting, multicylinder refrigerant compressors, a shell-and-tube-type water cooler, and a shell-and-tube-type condenser, all piped together and assembled as a unit. Welded joints are preferred for the steel refrigerant piping to minimize leakage, but tongue-and-groove-type flanged joints are used for connections to the compressor and refrigerant specialties. Piping smaller than 1 in. is usually extra-heavy copper tubing with sweated joints. The refrigerant is freon-12 which is nontoxic, noninflammable, and nonexplosive. Lake water, usually supplied by gravity, is used for condensing.

The air-conditioning system in each plant is automatic and in order to prevent excessive starting and stopping of the compressor a separate storage tank of chilled water is provided. Water is circulated from this tank by a small pump which responds to demands for cooling water. The chilled-water piping is insulated with cork, glass fiber, or mineral cork, ice-water thickness, and covered with a sealing tape and compound. Supply ducts are insulated with 1-in. boards of the same material and sealed with an airtight coating. Return-air ducts are not insulated. Fans, tanks, and plenums are insulated as required in the same manner as the ducts.

Machine-Shop Equipment. Each plant has a permanent machine shop, usually located just off the erection space on the generator floor. The size of the machine shops and the amount of equipment in them vary in the various plants according to the proximity of outside repair service. However, even in the isolated plants which have the maximum complement of machine tools, it is not intended that they be able to make all major repairs which may be necessary.

Experience has shown that the following list of machine tools is sufficient to take care of all the normal repair work in any plant:

1—8-in. engine lathe
1—9-in. bench lathe
1—24-in. shaper
1—30-in. upright drill
1—10-in. sensitive drill
1—9 × 9-in. power hack saw
1—12-in. grinder
1—portable pipe-threading machine, ½ in. to 2 in.
1—tool-post grinder

The larger machine tools are specified for medium-duty general-purpose precision work. In addition to these machines, each

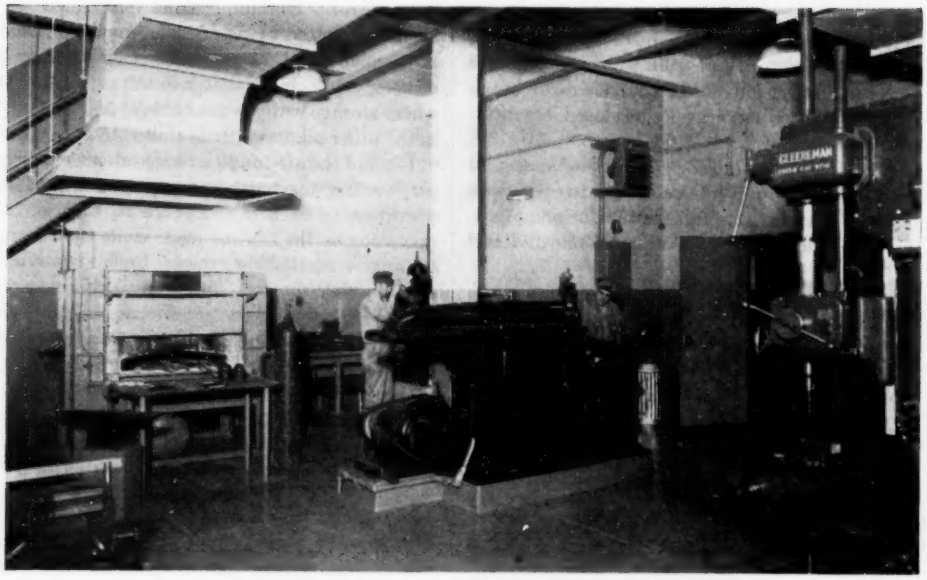


FIG. 8 TYPICAL MACHINE SHOP

plant is provided with a portable forge, blacksmith accessories, and a full complement of small tools. Fig. 8 shows a typical machine shop. The forge in this view has been superseded in later plants by a portable forge.

ACKNOWLEDGMENT

The author acknowledges valued assistance from members of the mechanical-engineering staff in preparing data for parts of this paper and for constructive criticism of the paper as a whole.

Discussion

SABIN CROCKER.[4] The paper is principally devoted to describing the several piping systems required in hydroelectric plants and gives an excellent analysis of the basic considerations for good design of such systems. In general, the writer subscribes to and endorses the author's views on simplicity and neatness of arrangement with a view to improving appearance and at the same time making the purpose of the connections and valving readily apparent. Those interested in furthering a better understanding of the requisites of good design are indebted to the author for having taken the trouble to discuss the fundamental principles of piping layouts in a published paper where the information will be available to young engineers interested in improving their piping technique.

There is only one point noticed by the writer which seems to warrant further explanation. This relates to the following observation:

"In some of the larger-size mains, it has proved advantageous to use spiral-welded pipe. This is especially true in drainage lines embedded in concrete where the cost of steel or cast-iron pipe would not be justified."

The writer would like to inquire whether the foregoing statement should be construed to mean that the author considers it desirable to cast concrete solidly around drain pipes or other pipes conveying fluids. This question is prompted by the fact that cracking or settlement of concrete is apt to fracture any pipe solidly embedded therein, thus permitting the contents to escape or seep away to the general detriment of the piping system and plant. As a protection against trouble of this sort it is usual practice to provide a continuous protecting conduit of larger diameter around a pipe buried in concrete so that the outer conduit can fracture from any moderate settlement without damage to the pipe itself. The writer would like to inquire whether the author recommends dispensing with such outer conduit for drain lines and if so, under what conditions he considers this advisable.

J. B. CUTLER.[5] The author's paper is very interesting and should be of value to hydroelectric-power engineers as it gives a general description of the type and arrangement of mechanical auxiliaries that the TVA engineers consider to be the most satisfactory after many years of operating experience in many plants.

It may be of some interest to mention a few of the mechanical features in our Safe Harbor Hydroelectric Station, which was first placed in operation in 1931, that are different or operate on a somewhat different basis from the TVA equipment referred to in the paper.

Piping and Color Code. The piping systems at Safe Harbor are identified by a color code. The greater portions of these lines, where visible, are painted solidly in the selected code color, and it is our opinion that with this arrangement, quick identification of a service line in an emergency is possible. An exception to this rule is made only for a small portion of some of these lines where, for architectural reasons, another color may be desirable.

All of the valves are identified by tags in a manner similar to that used by TVA, but at Safe Harbor only the valve code number is indicated. The service is readily identified by the solid code color of the pipe line, and the code numbers indicate the main power unit which is served by that line and the position of the valve therein. Odd numbers indicate the supply, and even numbers the return lines. A typical identification number for a valve in the raw-water system, serving power unit No. 3 and being the fifth valve in sequence in the supply line, would be 3-RW-5.

Control Valves. At Safe Harbor, when it is desired to operate a unit as a synchronous condenser, the elevation of water in the draft tube is automatically depressed by the admission of compressed air through the head cover of the turbine. An adjustable

[4] Consulting Engineer, Detroit, Mich. Mem. A.S.M.E.

[5] Mechanical Engineer, Pennsylvania Water & Power Company, Baltimore, Md. Mem. A.S.M.E.

type of reducing valve is used to maintain a constant pressure below the head cover, and although it is necessary to reset this valve for changes in the tail-water elevation greater than 8 or 10 ft, such changes are very infrequent. This system has operated satisfactorily since the units were first installed and no trouble has been encountered. Inspections are made, however, every 3 or 4 years, and as the result of some of these inspections it has been found desirable to overhaul the valve mechanisms.

The float-operating systems used by TVA would have the advantage of maintaining a constant level of water in the draft tubes regardless of the variations in tail-water elevations. It would be interesting to learn from the author whether any mechanical difficulties have ever been experienced in the operation of these floats.

Governor and Lubricating Oil. Similar to the arrangement used in the TVA plants, one grade of oil is used at Safe Harbor for both the governor and the unit guide and thrust bearings, and this oil is handled by one pipe, purifying and storage system. This arrangement has proved to be entirely satisfactory and the same quality of oil has been used since the date of initial operation of this plant. The viscosity of the oil at Safe Harbor is approximately 250 SSU at 100 F, which is somewhat lower than the viscosity value of the oil used in the TVA systems. The oil at Safe Harbor is purified about once a year using a centrifugal type of purifying unit for this operation. It would be interesting to learn how frequently it has been found desirable to purify the oil now being used for TVA.

Runner-Hub Oil. The oil used in the runner hubs of the Safe Harbor turbines has a viscosity of approximately 1600 SSU at 100 F. At 40 F the viscosity is very much higher or somewhere around 19,000. This grade of oil has proved to be satisfactory for this service both during the summer and winter seasons.

The author states that the oil used for this same purpose in the TVA stations has a viscosity of only about 1700 at 100 F, which, it will be noted, is a very much thinner grade than the oil selected for Safe Harbor. In view of this very wide difference in viscosity characteristics any further information the author may submit in regard to TVA operating experience with their oil should be interesting.

Author's Closure

Mr. Crocker's comment relative to the embedment of pipe in concrete is pertinent. The proper procedure under such circumstances should be determined by consultation between the piping designer and the concrete designer. The concrete designer has no wish to design a structure which will crack or settle, as the resulting damage to the dam or powerhouse holds as much or more risk as the damage which may be caused by a cracked pipe. The TVA has made every effort to design concrete structures with a minimum of cracking, and actual experience in the embedding of pipe solidly in this concrete has proved completely successful. However, if the concrete designer decides that unusual settlements may be expected, or if he must put in special contraction joints to care for possible cracking, then the piping designer must be aware of these facts in order that he may design his piping with such special protection as is necessary. It should be pointed out that if the embedded pipe has any bends in it, it would be very difficult and expensive to provide a continuous conduit of larger diameter around the pipe as Mr. Crocker suggests.

Mr. Cutler's comments on this paper are very interesting as the writer formerly was associated with him and helped develop some of the features he mentions about the Safe Harbor hydroelectric station.

The author believes the TVA method of painting piping systems is an improvement over the Safe Harbor method. The Authority's system, which paints all the various pipes with one color (aluminum) with identifying colors at fittings and flanges, provides a more pleasing appearance. This is obtained without sacrificing quick identification in case of emergency, because all valves are painted with the identifying color, and it is the valve, not the pipe, which controls an emergency.

Regarding the identifying valve tags, anything which aids the operator in establishing the function of a valve is to be desired. The naming of a system on the tag performs that function and adds very little to the cost of the tag. The Authority uses the same system of numbering valves on supply and drain lines as Safe Harbor.

We have found the float-operated valve very satisfactory for controlling the water level below the runner when it is operating as a synchronous condenser. It is preferred over the pressure-operated control in that it is much more sensitive and does not need to be reset. No operating difficulties have been experienced with the float-operated valve.

Under normal operating conditions the oil in the governor and lubricating-oil systems is purified once a year, at the time of the annual inspection.

The oil used in the rubber hub has a viscosity of 1700 at 100 F. The 40 F figure as given in the preprint was an error which slipped through all the checkings of this article.

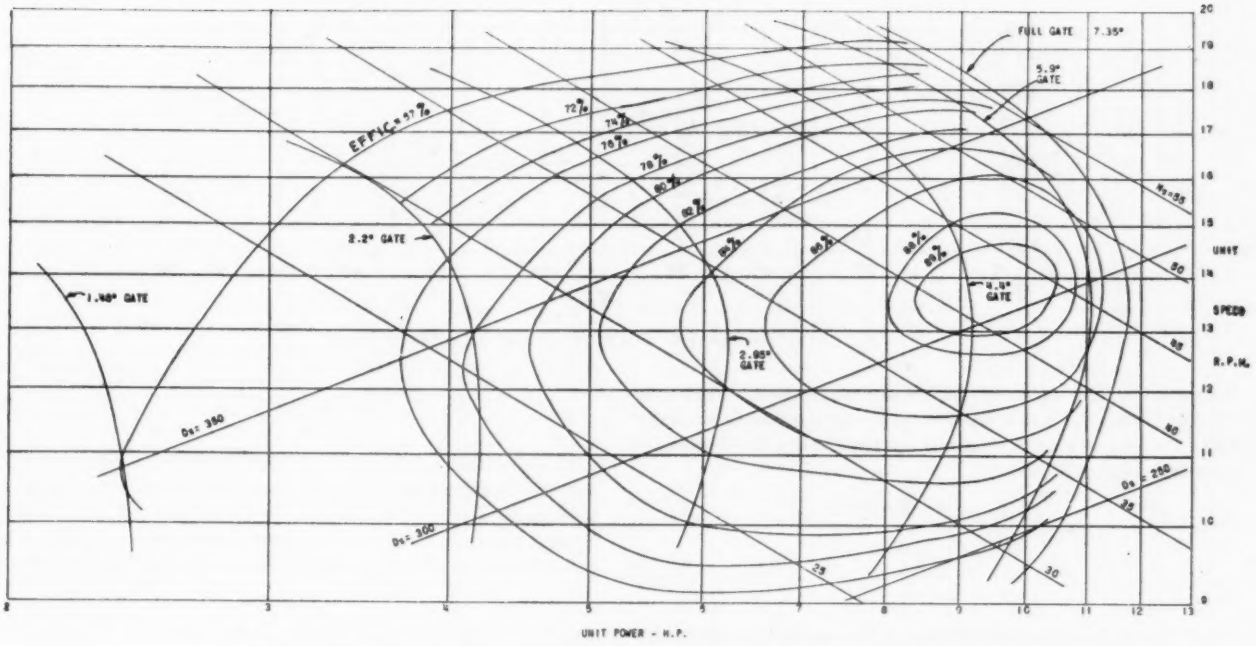


FIG. 1 PERFORMANCE DIAGRAM OF 100-IN-DISCHARGE-DIAM FRANCIS TURBINE
(Efficiencies from model test, not stepped up.)

A Better Method of Representing and Studying Water-Turbine Performance

BY R. A. SUTHERLAND,[1] NEW YORK, N. Y.

The author indicates that the contour form of turbine-efficiency diagram has advantages in giving a clearer picture of performance than the usual efficiency curves. An example illustrates that several different variables can be shown on such diagrams. Formulas are derived for finding the discharge diameters of runners and are illustrated by examples. A simple method of determining the mutual influence of turbine speed and water hammer during transient conditions is illustrated by an example. Finally, the operating stability of a water turbine supplying an independent load is brought forward for discussion.

INTRODUCTION

WATER-turbine performance is usually represented by "performance curves" consisting of a series of power-efficiency curves for different heads; the efficiencies shown may be either "expected" or "guaranteed," and the curves of course apply only to a selected size and speed of runner of a selected type. Such curves are made by "picking off" from test curves which give unit power and efficiency of a given size of runner at various gate openings in terms of "unit speed" or sometimes of "peripheral coefficient." Such curves have been reproduced elsewhere[2] and need not be repeated here.

The performance curves contain the minimum amount of information required by a purchaser and for many purposes are entirely adequate.

Another type of performance curve is in the form of an efficiency contour diagram, examples of which appear in several texts.[3]

The author has found that the contour type of diagram is well adapted for the following purposes:

1 The synthesis of available data on turbine performance.
2 Comparison of different runners.
3 Guide to operation.
4 Study of turbine behavior under transient conditions.

TYPICAL EFFICIENCY DIAGRAM

Fig. 1 represents an efficiency-contour performance diagram for the Norris and Hiwassee turbine model, the data being plotted from the published test diagrams.[2] The size assumed in Fig. 1 is 100 in. discharge diam, to facilitate ready conversion for other sizes. In addition to efficiency, gate openings, and specific speed,

[1] Hydraulic Engineer, Ebasco Services, Inc. Mem. A.S.M.E.

Contributed by the Hydraulic Division and presented at the Spring Meeting, Chattanooga, Tenn., April 1–3, 1946, of THE AMERICAN SOCIETY OF MECHANICAL ENGINEERS.

NOTE: Statements and opinions advanced in papers are to be understood as individual expressions of their authors and not those of the Society.

[2] "Francis-Turbine Installations of the Norris and Hiwassee Projects," by G. R. Rich and J. F. Roberts, Trans. A.S.M.E., vol. 64, 1942, p. 26.

[3] For example, "Water Power Engineering," third edition, by H. K. Barrows, McGraw-Hill Book Company, Inc., New York, N. Y., 1943, p. 239.

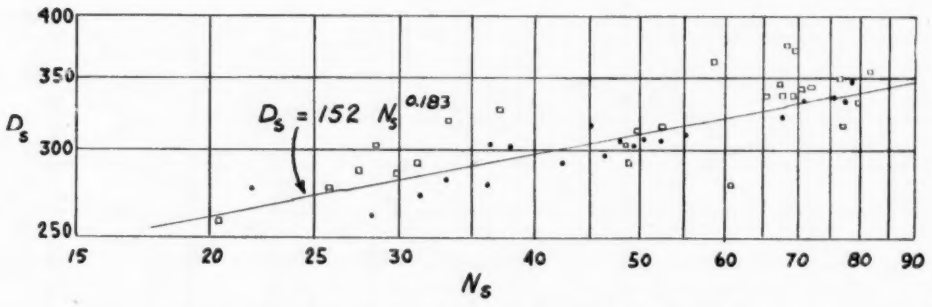


FIG. 2 FRANCIS RUNNERS; DIAMETER NUMBER IN TERMS OF N_s

the diagram also includes some lines representing "diameter number," which is a new concept as far as the author is aware. The expression for D_s is obtained by eliminating head from the basic homologous equations

$$\mathrm{Hp} = A\ D^2\ H^{3/2} \quad [1]$$

$$N = B\ \frac{H^{1/2}}{D} \quad [2]$$

where A and B are constants, just as the well-known expression for specific speed is obtained by eliminating D from these equations. By eliminating H from Equations [1] and [2], we obtain

$$D = \left(\frac{B}{A}\right)^{1/4} \frac{\mathrm{Hp}^{1/4}}{N^{1/4}} = D_s\ \frac{\mathrm{Hp}^{1/4}}{N^{1/4}} \quad [3]$$

In the present paper discharge diameters (in inches) are used throughout and values of the diameter number D_s are similarly applicable to discharge diameters (in inches). The symbol D_s has been represented by analogy with the universally used symbol for specific speed, but the author has avoided the use of the word "specific diameter," since D_s is not dimensionally a length, any more than N_s is dimensionally a speed.

The diagram shown in Fig. 1 can readily be converted by the principles of homology to apply to any selected size of runner of the same model type. The values of the efficiency should be stepped up to give an appropriate peak value, as determined by experience or by the use of the Moody formula applied to the original model. The 100-in-discharge-diam runner represented in Fig. 1 would be suitable for use at a normal head of 170 ft, and at a speed of 180 rpm. The unit speed would be 13.8 rpm, and the full-gate unit power at normal head would be 11.8 hp. Allowing a 5 per cent margin in power, the rated horsepower of such a turbine would be 25,000 hp. The D_s value at rated power would be

$$100 \times \frac{180^{1/4}}{25{,}000^{1/4}} = 298$$

SYNTHESIS OF DATA

By tabulating data from a number of turbine tests, expressions can be obtained for various factors in terms of N_s. In the limitations of space only D_s will be considered here. Fig. 2 shows values of D_s for Francis turbines in terms of N_s, each being for rated horsepower, which in the case of models has been assumed 5 per cent less than the full-gate power at rated best speed. The graph can be represented by the equation

$$D_s = 152\ N_s^{0.183} \quad [4]$$

Combining Equations [3] and [4] gives the following expression for discharge diameter

$$D = 152\ N_s^{0.183}\ \frac{\mathrm{Hp}^{1/4}}{N^{1/4}} \quad [5][4]$$

This equation is believed to be more logical as a means of finding the discharge diameter of a Francis runner than others involving head, for the reason that the rated head can always be altered a few feet, while a synchronous speed must be used. The equation can, however, be expressed in these alternative forms

$$D = \frac{152}{N_s^{0.417}} \times \frac{\mathrm{Hp}^{1/2}}{H^{1/4}} \quad [6]$$

$$D = 152\ N_s^{0.583}\ \frac{H^{1/2}}{N} \quad [7]$$

Table 1 shows a comparison of diameters obtained by Equation [5] with actual diameters of a number of turbines, and the results of other methods as noted are given for comparison.

If the specific speed of a Francis turbine be assumed to equal $\frac{632}{H^{1/2}}$, Equation [5] can be simplified (at the cost of some approximation) to the following form

$$D = \frac{1088\ \mathrm{Hp}^{0.139}}{N^{0.722}} \quad [8]$$

Equations [6] and [7] could, of course, be similarly simplified. Equation [8] is represented in Fig. 3.

If a further simplifying assumption is made, namely, that rated load efficiency is 88 per cent, then Equation [8] reduces to the form

$$D = \frac{3.127}{H^{0.0413}}\ Q^{1/2} \quad [9]$$

Values of the coefficient of $Q^{1/2}$ vary only from 2.51 at 600-ft head to 2.81 at 40-ft head, so that Equation [9] leads to a simple "rule of thumb" for finding approximate discharge diameter of a turbine required to use a given amount of water. A simple rule of this type is often useful in preliminary investigation.

For the sake of completeness, equations for the diameters of fixed-blade-propeller and Kaplan runners will be given without description of the supporting data.

For fixed-blade-propeller runners

$$D = 79\ N_s^{0.35}\ \frac{\mathrm{Hp}^{1/4}}{N^{1/4}} \quad [10]$$

For Kaplan runners

$$D = 445\ \frac{\mathrm{Hp}^{1/4}}{N^{1/4}} \quad [11]$$

[4] This equation can be readily solved on a log-log slide rule without resort to tables or charts.

TABLE 1 DISCHARGE DIAMETER OF FRANCIS TURBINE

No.	Name	Head in feet	HP	Speed RPM	Spec. Speed N_s	Disch. dia D_2 inches	Diameter No. D_s	Discharge Diameter, Inches By Eqn. 5	By Creager & Justin	By Kent
	(1)	(2)	(3)	(4)	(5)	(6)	(7)	(8)	(9)	(10)
1	Stevens Creek	27	3 125	75.	68.1	141	376	123.5	131.5	123
2	Amoskeog	46	7 500	112.5	81.5	126	359	119.	130	117
3	Mitchell	70	24 000	180	76.5	166	350	159.5	172.5	157
4	Upper Falls	64	14 250	105.8	69.8	153.5	372	137	145.5	136
5	Sherman Island	66	10 000	150	79.8	104	333	106	115	104.5
6	Muscle Shoals	95	30 000	100	58.4	179.5	362	158.5	160	168
7	Sturgeon Pool	105	6 300	277	65.2	66.7	338	64.5	67.5	64
8	Bridgewater	115	13 200	171.5	52.3	96	315	95	97	96.5
9	Rock Island	142	22 000	164	49.6	108	311	107.5	107.5	108.5
10	Shawinigan	145	49 000	138.3	60.9	126	279	146.5	151	145.5
11	Kern River Canyon	240	12 000	257	29.8	67	286	66	59.5	66.5
12	Queenston	305	63 500	187.5	37.0	129	328	116.5	109	118
13	Kerckhoff	315	15 000	360	33.2	64	320	57.5	53.5	59
14	Davis Bridge	350	20 000	360	31.0	62	293	60.5	53.5	59
15	Pit River No. 1	421.5	45 000	257	28.5	93	304	85.5	77	86.5
16	San Francisquito	515	22 000	428	25.8	56	277	53.5	47	53.5
17	Oak Grove	849	36 200	514	20.4	50	259	51	43.5	49.5
18	Norris	180	81 600	112.5	48.8	165	292	174.5	174	177
19	Bartlett	112	26 700	150	67.2	132	347	125	132.5	124
20	Wilson	92	40 400	100	70.5	179.5	342	174.5	186	173
21	Conowingo	89	54 000	81.8	69.5	213	339	208	221.5	206
22	Boulder	475	115 000	180	27.5	132	289	127.5	112.5	128
23	Hiwassee	190	80 000	120	48.1	165	305	167	166.5	169.5
24	Dnieprostroy	123	100 000	88.2	68.0	230	338	224	238	222
25	Beauharnois	80	53 000	75	72.0	228	345	219.5	234.5	217.5
26	Holtwood	62	20 000	94.7	77.0	149.5	316	159	172	157
27	Waterville	840	57 000	400	21.1	65.4	---	65	---	---
28	Diablo	327	90 700	171.5	37.2	127.5	---	131.5	---	---
29	Fifteen Mile Falls	180	54 200	138.5	48.9	143.5	---	142.5	---	---
30	Shipshaw	208	85 000	128.5	47.3	160	162	162	---	---
31	Chute a Caron	150	65 000	120	58.3	165	---	166	---	---
32	Bellows Falls	57	17 500	85.7	72.4	173	---	163	---	---
33	Parker	80	40 000	94.7	79.0	187	---	184	---	---
34	White Rapids	28	4 200	100	101.0	128	---	118.5	---	---

NOTE: Items 1 to 17 incl. from "Water Power Engineering" by Barrows, McGraw-Hill, NY, 1943, pages 424-7, omitting plants earlier than 1920.
Items 18 to 21 incl. from "Preliminary Selection of Hydraulic Turbines," W.L. Voorduin, T.V.A. 1941, p. 13, Fig. 2
Items 22 to 26 incl. Ditto p. 12, Fig. 1
Items 27 to 34 incl. Supplied by S. Morgan Smith Coy
Items in Col. 9 from "Hydro-electrical Handbook," Creager & Justin, Wiley, N.Y., 1927, p. 604, Fig. 395. An enlarged diagram was used.
Items in Col. 10 from "Mechanical Engineer's Handbook-Power," Kent, Wiley, N.Y., 1936, p.2-46, Fig. 12. An enlarged diagram was used.

Results obtained by these formulas are given in Tables 2 and 3, respectively, the former of which includes also the results of other methods.

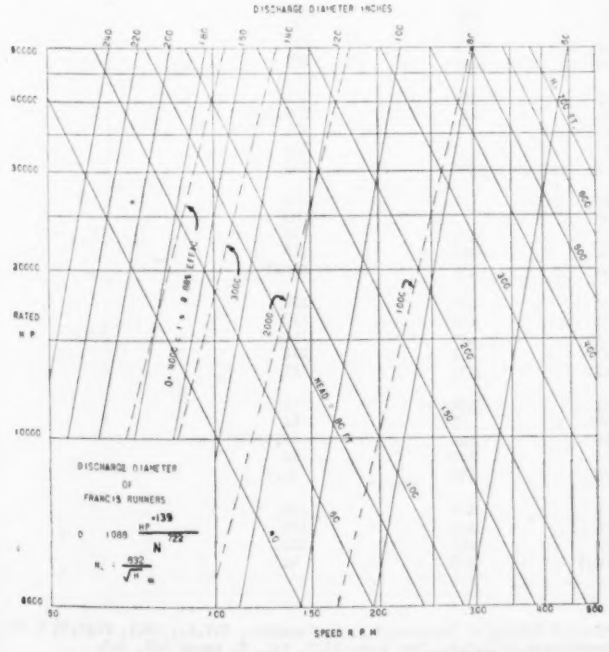


FIG. 3 DISCHARGE DIAMETER OF FRANCIS RUNNERS

The important bearing of sigma value on the best speed of propeller and Kaplan runners militates against obtaining accurate values of diameter for such runners by a formula which does not allow for the effect of the setting.

Equations such as [5], [10], and [11] are useful in the preliminary stages of powerhouse design.

COMPARISON OF DIFFERENT RUNNERS

If diagrams similar to Fig. 1 are available for different runners of approximately the same specific speed, the runners can be compared by superposition of the diagrams. The logarithmic scale enables the "spread" of any efficiency contour (such as 85 per cent or 90 per cent) to be compared as a measure of the percentage of full load over which a given efficiency will be reached or surpassed.

The contour diagram can be used equally as well as the more usual test diagram for "picking off" performance curves of two or more possible runners for given conditions. It can also be used to pick off directly the performance of a turbine at constant output under varying heads, a requirement which may apply to a plant which is used for peaking by being operated a limited number of hours per day at full generator capacity. The last-named pickoff is made by the use of an appropriate D_s line, since these lines represent constant output once the size and speed of the unit have been fixed. It is known that some runners have a better sustained output at low heads than others, and this is at once shown on the contour diagram by the full-gate line continuing to slope upward to the right, instead of bending back to the left. Such a runner might be advantageous in cases of peaking

TABLE 2 DIAMETER OF FIXED-BLADE-PROPELLER RUNNERS

No.	Name	Head in feet	HP	Speed RPM	Spec. Speed N_s	Disch Dia. D_2 Inches	Diameter No D_s	Discharge Diameter, Inches By Equation 10	By Creager & Justin	By Kent	By Voorduin
	(1)	(2)	(3)	(4)	(5)	(6)	(7)	(8)	(9)	(10)	(11)
1	London	22.4	6 600	90	150	177	454	178	181	173.5	148
2	Crisp Co. Ga	27.8	5 500	100	116	148	418	148	---	152	79.5
3	Holyoke No. 8	27.8	5 500	128	149	118	381	141	141	135	131
4	Drummondville	30	6 000	138.5	152	133	450	135	137	132	---
5	Beebe Island	32.4	5 500	150	144	118	426	124.5	126.5	122	109
6	Slave Falls	34.3	13 800	94.7	134	187	432	190.5	196	190.5	141.5
7	Lewiston	35	7 000	138.5	136	141	463	134	137	133	---
8	Louisville	37.8	13 800	100	125	180	430	179.5	186	183	134
9	Proser	39.5	4 200	200	130	98	443	96	97	95	76
10	Wheeler	46.7	46 000	81.8	144	264	433	274	279	269	314.5
11	Chat Falls	52.5	27 600	125	145	195	457	192	194	187	254
12	Island Falls	56	14 000	163.6	126	139	439	136	139	137	---
13	Great Falls	56	28 000	138.5	151	189.	471	184	186	179	---
14	Cize Bolozon	57.4	11 400	187	126	121	431	121	123.5	121	---
15	La Gabelle	65.2	36 500	120	124	195	422	197.5	202	200	216
16	Seven Sisters	67	38 200	138.5	141	195	456	191	194	187.5	254
17	Flat Rock	7.5	503	80	144	118	471	113	114	110	---
18	Dixon	8	790	80	167	130	476	130	---	125	---
19	Matte	11.4	305	200	168	63	481	62.5	---	60	---
20	Troy	13.2	2 200	80	151	154	459	154	156.5	150.5	---
21	Wyman	15.5	2 460	107	174	126	437	138	---	134	---
22	Rheinfelden	17.1	2 220	107	144	131	463	127.5	129	124	---
23	Lilla Edet	21.4	11 430	62.5	145	236	436	243.5	248	238.5	---
24	Kachlet	25.2	7 350	75	114	177	398	184	---	191	---
25	Canadian	30.1	3 450	180	151	103	467	101	105	101	---
26	Forshuvud	34	10 050	94	119	167	404	174	---	180.5	---
27	Louisville	37	13 300	100	126	179	424	182	185.5	182	---
28	Manitoba	56.2	27 600	138.5	150	189	471	183.5	186.5	178.5	---
29	La Gabelle	60.2	29 600	120	124	188	425	189	194.5	200	---

NOTE: Items 1 to 16 inclusive from "Preliminary Selection of Hydraulic Turbines," W.L.Voorduin, T.V.A. 1941, pages 42, 43. Nos. 4, 7, 12, 13, 14 are at rated head. Others in this group are at "critical head" as defined by Voorduin.
Items 17 to 29 inclusive from "Hydraulic Structures," A. Schoklitsch, A.S.M.E., New York, 1937, Vol 2, pages 946-7.
Items in Col. 9: See note on Col. 9, Table I. Items in Col. 10: See note on Col. 10, Table I.
Items in Col. 11: From source noted in second note on Table I, p. 43, Fig. 23.

TABLE 3 DIAMETER OF KAPLAN TURBINE RUNNERS

No.	Name	Head	HP	Speed RPM	Spec. Speed N_s	Disch. Dia. D_2 (inches)	Diameter Number D_s	Disch. diameter, inches by Equation 11
	(1)	(2)	(3)	(4)	(5)	(6)	(7)	(8)
1	Klingmau	26.9	20,000	75	173	254	466	242
2	Laholm	28	16,000	83.3	165	216	442	217
3	McIndoes	29	5,100	150	159	120	439	124.5
4	Lanforsen	30.4	13,000	94	152	188	433	193
5	Guntersville	42	38,000	69.2	126	265	419	288
6	Dogern	33	33,000	75	168	276	458	268
7	Chickamauga	35.5	37,300	75	168	264	428	274
8	Aborrforsen	35.8	16,000	107	155	180	428	187
9	Swir	36.1	37,500	75	164	292	472	275
10	Ryburg	37.7	42,000	75	165	269	426	281
11	Pickwick	39.6	43,000	75	156	292	460	282
12	Jonage	42.6	6,000	214	152	101	443	100.5
13	Bonneville Units 1 & 2	60	60,000	75		280		301
14	Bonneville Units 3 to 10	65	74,000	75		280		314
15	Munkfors	50.5	15,000	167	151	147	464	141
16	Safe Harbor 25	55	42,000	100		220		236
17	" " 60	55	42,000	109.1		220		223
18	Cize Bolozon	53.5	10,000	187	130	118	431	122
19	Mixnits	64.5	12,000	214	129	121	463	116
20	Semo Antschali	65.7	17,000	167	116	146	450	144.5
21	Santee Cooper	70	40,000	120	118	192	408	210
22	Groenvollfoss	75.5	18,400	214	130	133	466	127
23	Wettingen	76.3	10,700	214	98	114	445	114
24	Hojum	102	62,000	136.3	105	197	414	212
25	Shannon	106	33,000	167	89	161	434	165
26	Stromberg	13.8	480	250	226	61	488	56
27	Lanforsen	13.8	590	214	214	67	468	64
28	Kanyakeski	17.1	790	214	172.5	67	442	67.5
29	Siebenbrun	17.8	960	250	212	75	520	64
30	Tolfforsen	21.3	690	300	171	55	456	53.5
31	Lilla Edet	21.3	13,800	62.5	159	228	405	250
32	Gratewein	26.3	3,450	167	164.5	106	449	105
33	Mori	27.8	5,520	150	174.5	128	460	124
34	Hogforsen	33.3	4,030	214	170	94.5	449	94

Note: Items 1 to 12, 15 and 18 to 25, from "Preliminary Selection of Hydraulic Turbines," W. L. Voorduin, T.V.A., 1941, Figs.31 & 34.
Items 26 to 34 incl. from "Hydraulic Structures," A. Schocklitsch, A.S.M.E., New York, 1937, Vol. 2, pages 948, 949.
Items 13, 14, 16 and 17, by S. Morgan Smith Coy.

plants subject to occasional low head, in that a better firm power position could be demonstrated.

In the study of surge-tank stability, the rate of change of efficiency with head (power remaining constant) is one of the factors used.[5] This rate of change may be found directly from the contour curve by use of an appropriate D_s line.

Guide to Operation

Fig. 4 illustrates a typical contour diagram for a Kaplan turbine 132 in. in diam operating at 180 rpm.[6] In addition to efficiency curves, the diagram includes curves for gate opening and blade angle, and the D_s lines have been shown to represent horsepower. It is also readily possible on a large-scale diagram to show discharges and cavitation limits, but they are not included in Fig. 4, to avoid confusion. A diagram of this type is useful as a guide to operating in any desired manner, viz , to obtain highest efficiency, or to maintain a uniform discharge in the river, under varying operating heads.

Study of Turbine Behavior Under Transient Conditions

In so far as the author knows, previous studies of transient conditions in turbines have always been based upon some approximation as regards turbine discharge, and sometimes on a number of approximations. The contour diagram makes it readily possible to study correctly what happens in such cases. To illustrate the procedure, the turbine represented in Fig. 1 is taken.

Steady-load conditions are as follows:

Head, ft	170
Horsepower	25000
Speed, rpm	180
Gate, in	6.2
Efficiency, per cent	89.3
WR^2, psf	8×10^6

The effect of gate closure in 4 sec is studied in the following cases:

Case 1. Pressure rise neglected. This case is not attainable in practice, but might simulate conditions if a large surge tank were installed immediately upstream of the turbine.

Case 2. Turbine supplied by a penstock such that the effective characteristics of the water conduit are as follows:

Length, ft	300
Diameter, ft	13
Velocity of propagation, fps	3000

The unit is tripped off the line by relay operation.

Case 3. Similar to Case 2, but the load is reduced by load-limit control, the unit remaining on the line. (It may be noted in passing that according to previous methods the discharge history for this condition would be the same as in Case 2.)

In each case the effect of generator windage has been ignored for the sake of simplicity. It can readily be taken into account by adding another column to Table 4.

Fig. 5 shows the efficiency contours on a network of "unit speed" and "unit power" lines, and the gate lines shown are in accordance with the gate-time curve shown at the left in Fig. 6. The several data given have been selected for simplicity, but illustrate the procedure equally well as though an actual installation were considered. The complexity of the conditions that can be studied are limited only by the patience of the computer.

Pressure changes are determined by the graphical method, which has been described in many published articles.[7] Speed changes are determined by the formula

$$N_2^2 - N_1^2 = \frac{3{,}238{,}000 \times \text{Hp sec during interval}}{WR^2}$$

[5] See "Hydraulic Stability," by A. W. F. McQueen, *The Engineering Journal*, vol. 16, 1933, p. 13.

[6] This diagram has actually been falsified from a turbine test and is thus illustrative only.

[7] One of the most recent being "Water-Hammer Problems in Connection With the Design of Hydroelectric Plants," by E. B. Strowger, Trans. A.S.M.E., vol. 67, 1945, p. 377.

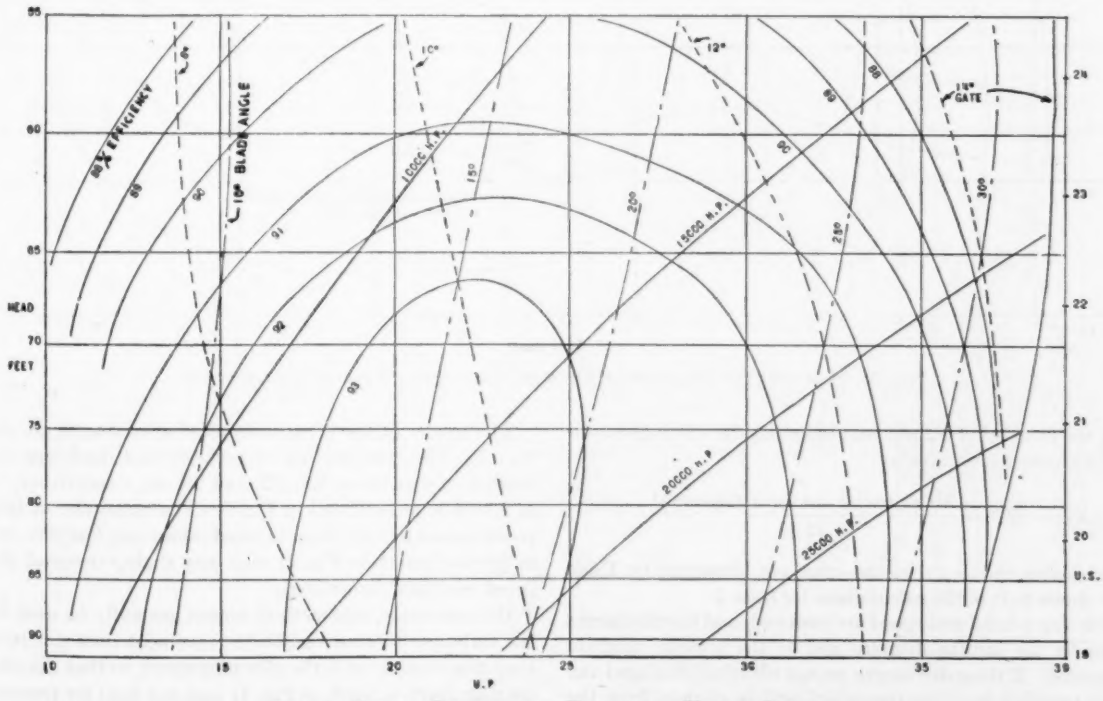


Fig. 4 Typical Performance Diagram of Kaplan Runner

TABLE 4 PART OF COMPUTATION OF CASE 2

Time	Gate	Trial Head	Trial Speed	Unit Speed	Unit Power	H.P.	Ave. excess H.P.	$N_2^2 - N_1^2$	N_2^2	N_2	Effic. %	Discharge required for H.P. pressure		Remarks
(1)	(2)	(3)	(4)	(5)	(6)	(7)	(8)	(9)	(10)	(11)	(12)	(13)	(14)	(15)
0.00	6.2"	170	180	13.8	11.28	25,000			32,400	180	89.3	1450	1450	
0.20	6.0	175	186	14.06	11.13	25,780	25,390	2052	34,452	185.5	90.0	1439	1442	Speed wrong
		176	185.6	13.98	11.14	26,000	25,500	2062	34,462	185.6	90.0	1445	1442	O.K.
0.40	5.8	182	190.8	14.13	10.92	26,820	26,410	2138	36,600	191.3	90.7	1431	1416	Speed wrong Q wrong
		179	191.2	14.28	10.9	26,160	26,050	2108	36,570	191.2	90.6	1417	1420	O.K.
0.60	5.55	182	196.2	14.53	10.62	26,100	26,100	2110	38,680	196.6	91.1	1384	1390	Speed wrong
		183	196.6	14.53	10.62	26,300	26,200	2120	38,690	196.6	91.1	1390	1389	O.K.
0.80	5.25	186	202.0	14.80	10.26	26,020	26,160	2116	40,806	202.0	91.4	1348	1348	O.K.

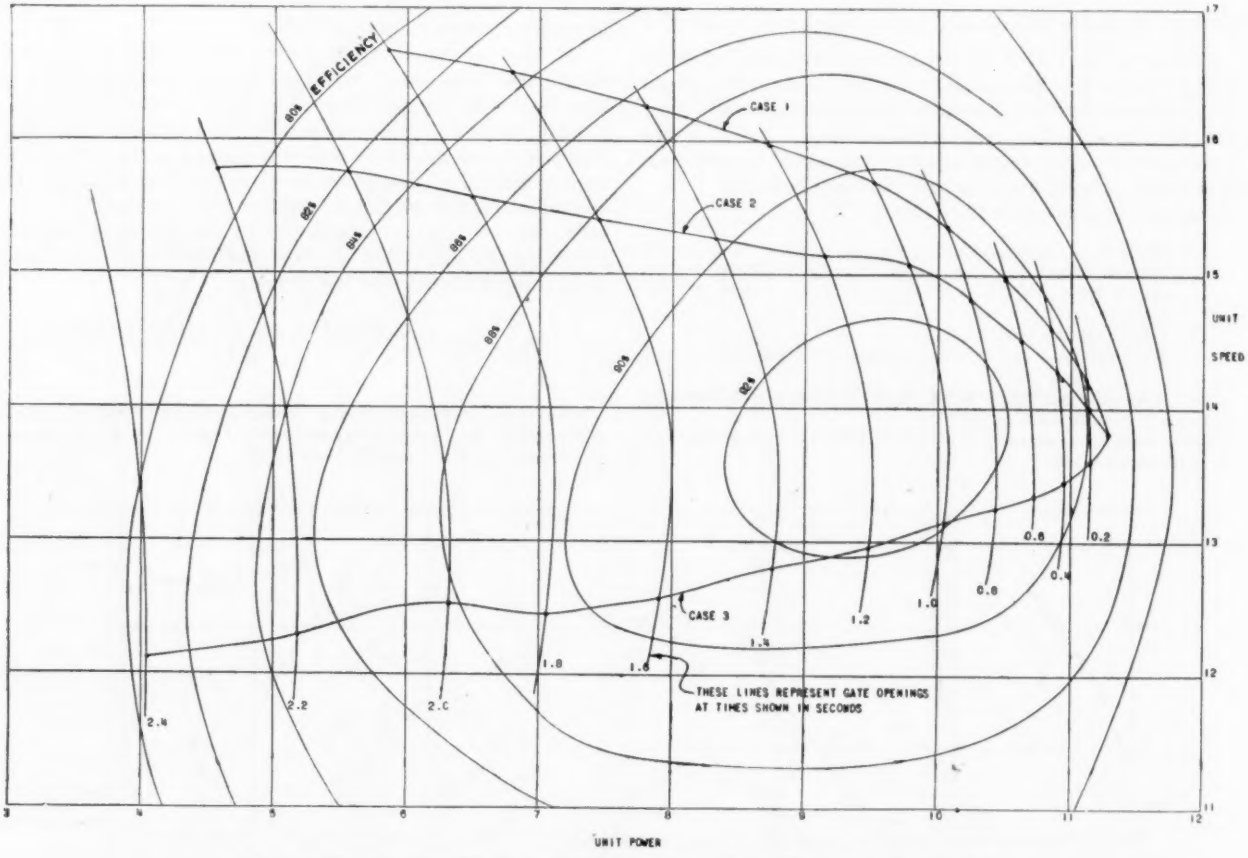


FIG. 5 PERFORMANCE DIAGRAM OF FRANCIS RUNNER FOR TRANSIENT CONDITIONS

Using the interval of 0.2 sec, and inserting the value given for WR^2, this expression reduces to

$$N_2^2 - N_1^2 = \frac{\text{Mean excess hp during interval}}{12.36}$$

The procedure used is a trial-and-error one, illustrated by Table 4, which shows part of the calculations for Case 2.

At each step a head and speed are assumed, and the discharges called for by the turbine diagram and by the pressure diagram are computed. If these discharges are not identical, the head and speed are modified in a direction which will be obvious from the first trial until substantial or exact agreement is obtained.

The results of the three cases cited as examples are shown in Fig. 7. The computation of pressure and discharge has been carried only as far as 1.8, 2.2, and 2.4 sec, respectively, for cases 1, 2, and 3, as indicated in Fig. 5. The remainder of the horsepower curves beyond the computed values can, however, be drawn in (shown broken in Fig. 7) with only slight error and the total speed rise thus determined.

Unfortunately, this method cannot generally be used for Kaplan turbines, because the blade movement does not in general keep time exactly with the gate movement, so that the efficiency-contour diagram (such as Fig. 4) does not hold for transient conditions.

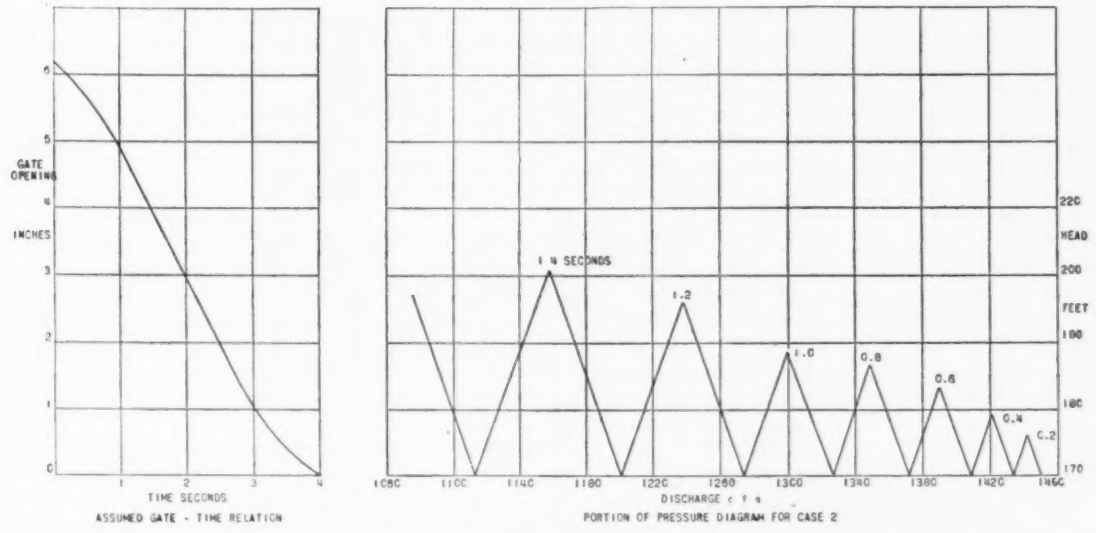


FIG. 6 GATE RELATION AND TYPICAL PRESSURE DIAGRAM FOR FRANCIS TURBINE GATE CLOSURE

This method of studying transient conditions is obviously more refined than is generally necessary, but has been of inestimable value in studying one important and unusual installation, in which not only were numerous closure operations studied, but also governing stability of the unit when supplying independent loads. The computed behavior was closely checked by prototype tests.

GOVERNING STABILITY

Operating stability of a hydroelectric plant generally requires the provision of an amount of WR^2 in the generator considerably in excess of that normally built in by the generator manufacturer. The leading generator makers have tables which show the "normal WR^2" for various sizes and speeds, and Fig. 8 has been prepared by the author to show the resulting regulation constant C. This diagram is useful as a preliminary guide to the amount of excess WR^2 required to give a desired value of C. The regulation of a hydroelectric unit connected to a system has been ably treated by numerous writers. In the exceptional case of a unit supplying an independent load, the stability may require study.

The moving water column contained in the penstock and draft tube represents a considerable amount of kinetic energy, which must be reduced or increased when the turbine gates close or open, respectively, as a result of any governor action, however slight. In the case of gate closure, part of the kinetic energy in the column is in effect transferred to the unit, which is already burdened with the excess energy which gave rise to the speed and gate change.

In the case of the gate-opening movement, the unit needs a quick supply of energy, which the water column is unable to furnish, being burdened with the necessity of increasing its own energy. Thus the water column always acts for an appreciable time in opposition to the governor, and it is easily seen that instability may occur if the water-column kinetic energy becomes too large in proportion to that of the unit.

The author has been able to observe only one case of this kind in practice, in which a unit was supplying a rheostat load and operated stably at small outputs, but became violently unstable as the output was increased. The ratio of the kinetic energy of

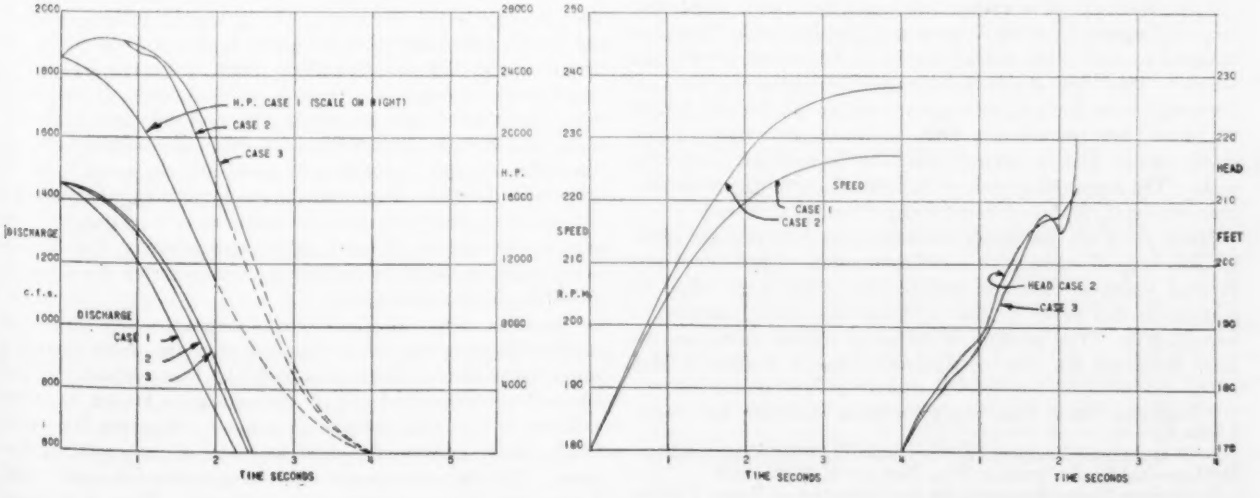


FIG. 7 DISCHARGE, HORSEPOWER, SPEED, AND HEAD DURING GATE CLOSURE UNDER DIFFERENT CONDITIONS

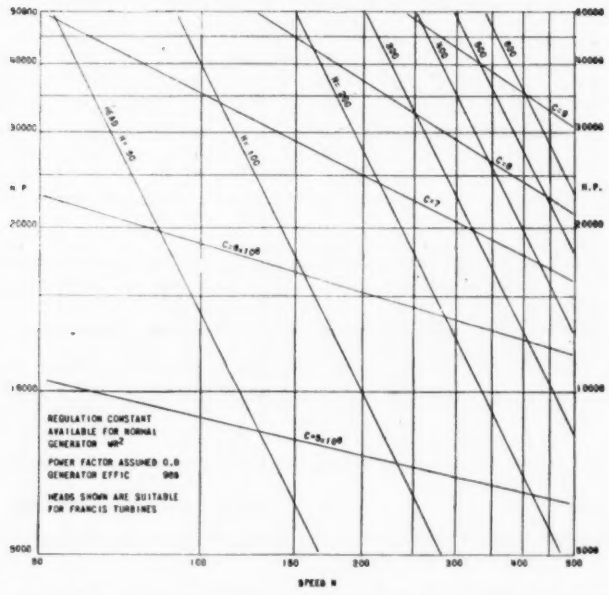


FIG. 8 REGULATION CONSTANT AVAILABLE FOR NORMAL WR^2 OF GENERATORS

the water column to that of the unit, when instability occurred, was about 0.2. This ratio is obviously not the only factor involved, but is believed to be an important one, and the author suspects, from a study of other plants, that not a few units which now operate very sweetly on the line would be unstable if supplying a rheostat load.

The problem is analogous to but more complicated than the stability of surge tanks; and the author wishes at this time to bring the phenomenon into the open for discussion.

ACKNOWLEDGMENT

The author's thanks are due to Mr. L. F. Harza, who greatly stimulated his interest in turbine performance, and to Mr. George A. Jessop, for suggestions and data.

Discussion

L. F. HARZA.[8] The author has urged the use of a valuable form of diagram in which to present hydraulic-turbine test data designed to display the characteristics of the turbine vividly and clearly. This form of turbine characteristic curves was used extensively in the first and subsequent editions of a text by Daniel W. Mead,[9] first published in 1908, on which the writer collaborated, except with a natural instead of logarithmic horizontal scale. The logarithmic scale adds little, if anything, to the diagram except the N_s lines become straight instead of curved.

Many years ago the writer developed standard platting paper for this type of curve with a sufficient range of horizontal and vertical scales so that any turbine then being built could be platted on this paper.[10] The N_s lines were curved because of natural scale. The position of the set of turbine curves on the sheet indicated the type of turbine. Thus a turbine of high unit speed and unit power would be platted, in the author's form of diagram, in the upper right-hand portion of the sheet, and a high head and therefore low-speed turbine in the lower left-hand portion of the sheet.

The author has added one new feature, namely, his D_s curve, whose usefulness the writer is not as yet prepared to evaluate without more experience in using it. The author refers to N_s and D_s characteristics, the former generally known as "specific speed," as not actually dimensional constants. In this the writer differs; N_s is the speed of a 1-hp turbine under 1 ft head, the turbine being of design homologous to the large turbine. Likewise D_s would appear to be the diameter of a homologous turbine which would run at 1 rpm and develop 1 hp. There would appear to be less value, however, in the mental conception of the meaning of this constant as compared with N_s.

The use of the relation curve, Fig. 2 of the paper, between N_s and D_s is not clear except as to the preliminary studies in laying out a hydroelectric station. It cannot be more than a general indication as to the diameter at the outlet of a turbine of an assumed N_s, sufficiently close for a first layout or assumption. It will be noted that the points from which this curve is projected are scattered widely. For example, at $N_s = 30$ the D_s may vary from about 260 to 300 because of the great difference in dimensions and turbine characteristics of different manufacturers, or the different types of turbines of essentially the same N_s of the same manufacture. For other than the first preliminary studies it is always necessary to use the dimensions of the individual type and size of turbine offered by the manufacturer. The D_s constant might be useful for preliminary studies before this more detailed information is available.

The author offers his Fig. 4 type of diagram as one suitable as a guide for operation, but in the opinion of the writer there is a much better form of diagram available for that purpose.[11] After the turbine is installed and its characteristics known by extrapolation or field test, there is no value in continuing the use of "unit speed" and "unit power" as scales of the operating diagram. The curve mentioned uses the operating head and actual horsepower of the prototype as co-ordinates. Thus at a glance

[8] President, Harza Engineering Company, Chicago, Ill. Mem. A.S.M.E.

[9] "Water Power Engineering," by Daniel W. Mead, second edition, McGraw-Hill Book Company, Inc., New York, N. Y., 1915.

[10] "Further Means Suggested for Interpretation of Water-Turbine Test Data," by L. F. Harza, *Engineering News Record*, vol. 72, October 30, 1915, pp. 542–544.

[11] Ibid., Fig. 5, p. 544.

the operator can pick off the best horsepower at which to run the unit at each head. This should be carried one step further using gross head horizontally and kilowatts vertically, because these are the figures which the operator reads and which he can use without any conversion such as deduction for hydraulic losses to obtain net head, or converting horsepower to kilowatts.

The author presents some applications of his curves to the study of transient phenomena and governing stability which are well worth careful study and application.

Manufacturers generally do not put their test data into the "efficiency-contour" form of curves, or at least if they do, the customer never sees them. The information displayed to the engineer by this form of platting is so far superior to that of the usual form of characteristic curves submitted by a manufacturer, that the extra work of platting is well justified on the part of the purchaser's engineer.

J. D. McLaughlin.[12] The method given for studying the behavior of hydraulic turbine - generator units under transient conditions makes it possible as the author has outlined, to estimate with reasonable accuracy the power, discharge, speed, or head versus time relationships for unusual or unconventional hydroelectric installations.

The behavior under transient conditions of the hydroelectric unit installed at the Fort Peck Project during the war emergency required special analytical consideration in the manner outlined due to the fact that it was installed without the surge tank contemplated in the original design. Prediction of the behavior of the unit under anticipated operating conditions made possible the forecasting of operating regulations and the installation of special accessory features as means of adapting the unit to prevent excessive pressure surges in the penstock. The pressure-surge limitation was met by restricting the wicket-gate closure time to a minimum of approximately 42 sec. Overspeed of the unit, resulting from heavy load rejection at the line circuit breaker, was controlled within reasonable limits by automatic transfer of the generator output to a water rheostat which was preset to dissipate approximately 75 per cent of the load rejected.

The writer, being familiar with the installation, initial tests, and test conditions referred to under "Governing Stability," desires to elaborate upon the causes of instability of the Fort Peck unit when supplying a rheostat load, for the conditions that applied during the tests witnessed by the author. Observations upon which these comments are based were made during the operation of the unit without surge tanks over a period of approximately 3 years, during which time several series of tests were run to obtain specific data for use in designing a continuous-rating water rheostat. Throughout this period the behavior of the unit was one important consideration.

The resistivity of the river water, used in all rheostat tests, is relatively low, being approximately 600 ohms per cu cm. This factor had the effect of making a water rheostat located in the powerhouse tailrace extremely sensitive to fluctuations of the water surface.

The temporary, and what proved upon analysis to be unsatisfactory location of the water rheostat in the powerhouse tailrace during the initial test period undoubtedly intensified and perhaps initiated the instability noted in the operation of the unit supplying an independent load provided by the water rheostat. When operating in this manner, the load on the generator is determined by the depth of the electrode immersion. Surges and surface waves in the tailrace, whether due to the discharge from the adjoining tunnels or from the powerhouse draft tube, changed the depth of electrode immersion, and thus varied the generator load, by changing the water elevation of the tailrace.

An increase in tail-water elevation of 6 in. would produce an increase of approximately 22 per cent in a generator load of 20,000 kw, and would decrease, by the above increment, the head available to the unit. The former would increase the demand for kinetic energy from the water column, while the latter would decrease the energy available in the water column. Conversely, a decrease in tail-water elevation of 6 in. would decrease the load on the generator by approximately 28 per cent and would increase the energy available in the water column. In either case the governor would respond with a gate movement tending to restore the speed to normal, and in both cases would tend to "overadjust" the gate. Since the surging is periodic, it is believed that should the period achieve the proper magnitude with respect to the speed of the governor, serious operating conditions would result from this cause.

C. B. Spellman.[13] This paper arrives at certain new formulas for approximating the discharge diameters of various types of reaction-turbine runners. It appears to the writer that the application of these formulas for diameter is somewhat awkward, because they involve functions other than the basic engineering conditions and on this account the diameter number or the discharge diameter for a given project cannot be determined until one has first determined the specific speed or the speed in rpm. Also, it is suggested that a somewhat more definite idea of the runner size would be obtained if it were expressed as "throat diameter" rather than discharge diameter. The throat diameter seems more definitely fixed by considerations of flow and head, whereas the discharge diameter of a runner having a given throat diameter may vary depending upon the peculiarities of individual runner design. The ratio of discharge diameter to throat diameter might vary from as much as 1.20 down to even less than unity for very low-specific-speed runners.

For purposes of quick approximation of the throat diameter for a given set of basic conditions, the formula

$$\text{Diameter of throat} = \sqrt{\frac{68 \times \text{Horsepower}}{\text{Head}}}$$

has been developed. It will be noted that this formula involves only the two fundamental variables of horsepower and head.

We are indebted to R. B. Willi of the I. P. Morris Department for a very useful formula, involving only these same basic variables, for determining approximately the operating speed of vertical-shaft Francis or Kaplan turbines. This formula is

$$\text{Rpm} = \frac{C \times H^{5/4}}{\sqrt{\text{hp}}}$$

where C is equal to 632 for Francis turbines and 950 for Kaplan turbines.

As a check on the accuracy of these formulas, the writer has tabulated a comparison of the approximate diameter and speed with the actual values, for many of the I. P. Morris installations of both the Francis and Kaplan type (Tables 5 and 6 of this discussion). The tabulation indicates that the error in the formula for throat diameter averages less than 1 per cent and for speed less than 4 per cent. It must be admitted that in some few cases errors of the order of 20 to 25 per cent are encountered, but this occurs only when, for some reason, the specific speed selected for the design was at variance with the permissible value indicated by the "experience curve" of N_s versus head. When more accurate

[12] Engineer (Electrical), Hydroelectric Branch, Engineering Division, U. S. Engineer Office, Fort Peck, Mont.

[13] Assistant Supervising Engineer, I. P. Morris Department, Baldwin Locomotive Works, Philadelphia, Pa. Mem. A.S.M.E.

TABLE 5 I. P. MORRIS FRANCIS TURBINES; SIZE AND SPEED

Plant	Head	Hp	Rpm	$\frac{632H^{3/4}}{\sqrt{hp}}$	Rpm, per cent error	D_{th}	$\frac{\sqrt{68\ hp}}{H}$	D_{th}, per cent error
Berlin, N. H.	83	20500	128.6	121.9	−5.2	126.0	129.7	+2.9
Sauzal	387	33600	300.0	303.5	+1.0	76.0	76.9	+1.1
Ixtapantongo	1028	39000	600.0	582.0	−3.0	48.6	50.75	+4.3
Boulder Dam	510	115000	180.0	201.2	+11.8	130.0	123.8	−4.9
Apalachia	360	53000	225.0	228.0	+1.1	103.0	100.1	−2.6
Yuba Narrows	235	13500	300.0	326.0	+8.8	66.0	62.5	−5.2
Marshall Ford	120	27000	144.0	140.0	−2.7	128.5	124.0	−3.6
Columbus	112	18000	150.0	162.5	+8.2	108.0	104.5	−3.1
New Kanawha	157	35000	150.0	150.0	0.0	125.0	123.0	−1.5
Hardy Dam	99	14800	163.6	163.6	0.0	103.5	101.0	−2.5
Carpenter	89	39500	94.7	97.8	+3.1	173.0	174.0	+0.4
Cobble Mountain	420	19200	450.0	426.0	−5.3	54.0	55.7	+3.2
Cobble Mountain	420	8550	600.0	638.0	+6.1	36.0	37.2	+3.4
Morony	82.5	31000	81.8	98.5	+20.5	173.0	160.0	+7.6
Lower Tallassee	88	36000	100.0	96.1	−4.9	165.2	166.8	+0.9
Colton	270	15700	360.0	338.0	−6.2	62.5	63.0	+0.8
Cadyville	156	4300	450.0	426.0	−5.4	40.0	43.3	+8.2
Upper Tallassee	55	25000	80.0	81.6	+2.0	175.0	176.0	+0.5
Lake Chelan	377	34000	300.0	295.0	−1.6	75.5	78.2	+3.6
Conowingo	89	54000	81.8	78.9	−3.6	194.0	203.0	+4.6
Chapala	233	8000	360.0	424.0	+17.6	51.5	48.3	−4.1
Norwood	70	31100	90.0	86.5	−3.9	170.5	174.0	+2.0
Cherokee Bluff	145	45000	120.0	124.7	+3.9	147.0	145.3	−1.1
Cheat Haven	81.5	18000	133.3	127.1	−4.6	121.0	122.8	+1.3
Rumford Falls	97	10000	200.0	195.5	−2.2	85.0	83.6	−1.4
Cutler	124	21500	150.0	159.7	+6.3	111.0	108.6	−2.1
Exchequer Dam	300	24500	257.0	292.0	+13.5	73.6	74.5	+1.2
Wallenpaupack	330	28500	300.0	292.0	−2.6	73.6	76.6	+4.1
Soft Maple	121.5	10500	225.0	227.5	+1.0	78.6	76.5	−2.6
Lighthouse Hill	62	5250	150.0	192.8	+28.5	83.5	76.0	−9.0
Dix River	220	9850	300.0	369.0	+23.0	58.8	55.1	−6.1
St. Croix	48	4550	150.0	172.8	+15.1	82.0	80.2	−2.2
Amoskeag	46	7500	112.5	130.0	+15.2	110.0	91.1	−17.1
Holtwood	62	20000	94.7	99.0	+4.4	149.5	148.2	−0.9
				Avg	+3.7			Avg −0.56

TABLE 6 I. P. MORRIS KAPLAN TURBINES; SIZE AND SPEED

Plant	Head	Hp	Rpm	$\frac{950\ H^{3/4}}{\sqrt{hp}}$	Rpm, per cent error	D_{th}	$\frac{\sqrt{68\ hp}}{H}$	D_{th}, per cent error
Fort Loudoun	65	50000	105.8	97.5	−7.6	222.0	229.0	+3.0
Watts Bar	52	42000	94.7	90.1	−4.8	234.0	234.5	+0.2
Safe Harbor	55	42500	100.0	93.9	−6.1	220.5	229.5	+4.0
High Point	70	10000	225.0	229.0	+1.8	101.0	98.5	−2.5
Chickamauga	36	36000	75.0	74.1	−1.3	264.0	261.0	−1.2
Buzzard's Roost	60	7400	240.0	241.0	+0.6	92.0	91.5	−0.5
Mattaceunk	39	5900	171.4	195.1	+13.9	109.5	101.5	−7.3
				Avg	−0.5			Avg −0.61

data are required, manufacturers' recommendations, of course, should be obtained.

The principal application which I. P. Morris has found for the contour type of diagram has been in the Kaplan field, where it greatly facilitates the preparation of expected-performance curves for proposed prototype turbines. Without the contour diagram the preparation of such curves is very laborious, as the basic test data comprise a series of tests for various fixed-blade positions. Thus a performance curve has to be derived for each blade position, and the envelope of these individual performance curves drawn to indicate the performance obtainable with automatic adjustability of the runner blades. The reason for this is that each different blade position, in effect, makes a different runner is so far as performance is concerned. This, of course, does not hold true in the Francis field where the blades are immovable. Hence the Francis performance curve is readily obtainable from a single set of model test readings. For this reason there has not been the same incentive to use contour diagrams for the Francis models as there has been for the Kaplan models.

E. B. Strowger.[14] In discussing turbine behavior under transient conditions, the author makes use of the contour form of turbine-efficiency diagram for showing the performance relations in terms of power, speed, and gate opening. On these diagrams the speed is shown in terms of unit speed and the power in terms of unit power rather than in terms of rpm and power output of the unit under normal head conditions. The writer prefers to show the transient performance in terms of the normal head performance rather than reduce the data to 1 ft head. In this connection he wishes to call attention to the joint paper he wrote with S. L. Kerr in 1926, on this subject,[15] where the step-by-step or arithmetic integration method was first applied to the problem and the solution was first made by a rational method rather than by rough approximation. He also wishes to call attention to a discussion of Arnold Pfau's paper which was published in 1930.[16] The author's method is the same as that shown in these publications except that he has substituted the contour diagram for the runner ϕ curves, and the graphical method of water-hammer determination for the arithmetic-integration method. These substitutions do not change the basic character of the method of computation.

Case 3, cited by the author, assumes that during load rejection the unit remains on the line. Consequently, with the unit connected to a large system, the speed of the unit will remain sensibly constant. However, because the head is increased, due to water hammer, the unit speed decreases as shown by the curve, marked Case 3 in the author's Fig. 5. The author states that according to previous methods the discharge history for this condition would be the same as in Case 2. The writer believes that the method shown in the references cited would give a discharge history which would not be the same as the author's Case No. 2 but would agree with the author's results for Case 3.

It should be pointed out perhaps that the time-horsepower curves for Cases 1 and 2, as shown in the author's Fig. 7, should be modified in the dotted portions to show that the power output becomes negative near the end of the governor stroke due to the overspeed, forcing the governor to close the gates below the speed-no-load point.

[14] Hydraulic Engineer, Buffalo Niagara Electric Corporation, Buffalo, N. Y. Mem. A.S.M.E.

[15] "Speed Changes of Hydraulic Turbines for Sudden Changes of Load," by E. B. Strowger and S. L. Kerr, Trans. A.S.M.E., 1926.

[16] "Mechanics of Hydraulic Turbine Pressure Regulation," by Arnold Pfau, Trans. A.S.M.E., vol. 52, 1930; discussion, HYD-52-4.

Author's Closure

Mr. Harza questions the value of logarithmic plotting of turbine test data. The main advantage, in the author's experience, is the ease of transferring from one size of unit to another. In such case the curves need not be replotted but only the scales need be shifted. Disadvantages are that the portion of the diagram near full gate has the smallest divisions and that the diagram cannot well be extended down to small gate openings. Mr. Harza's definition of "specific speed" is frequently used but nevertheless is believed to be inaccurate, for the insertion of dimensional values will show that it is not a speed. One at least of the makers recognizes this by using the more correct term "characteristic speed number." Similarly the author's term D_s could be called the characteristic diameter number. Its value, as Mr. Harza indicates, lies in giving a first approximation to the size of runner to meet given conditions, just as the N_s parameter is used in finding a suitable speed, and it is believed that the author's Tables 1, 2, and 3 indicate that it serves this purpose. The author's formulas were developed in self-defense against the insistent demand of the structural men for dimensions, in the early planning of hydroelectric projects. One of the engineers of a large public body has devoted a whole book to this and allied questions (Table 1, second footnote). It is true as Mr. Harza points out, that there is quite a spread in the experience values of D_s, but it is believed that this is due largely to the turbine makers' use of developed models for heads or speeds for which they are not ideally suited. It is the author's belief, which unfortunately may never be proved or disproved, that if all turbines were specially designed for optimum operation at their rated head and speed, the spread would be very small.

Mr. McLaughlin's discussion of the Fort Peck installation is of particular interest to the author, who took part in the tests made prior to regular operation. It is hoped that Mr. McLaughlin can be prevailed upon to publish the results of the later tests which he indicates have been made, for this wartime installation was of unusual interest from an hydraulic point of view and reflects considerable initiative and courage on the part of the U. S. Engineer Department. The author is unable to agree with Mr. McLaughlin's suggestion that "the location of the water rheostat in the tailrace perhaps initiated the instability noted." He will, however, agree that it complicated the phenomenon. In a certain report[17] are shown oscillograms obtained during operation both with a tank rheostat (Plate 14, Test D-1) and with the tailrace rheostat (Plate 16, Test H-1) and each shows the same characteristic instability, the period being of the order of 14 seconds. Actually the rate of pressure rise in the case of the tank rheostat appears to be appreciably sharper than in the case of the tailrace rheostat. Instability of this type is comparatively little known in the United States, due to interconnection of plants, but appears to be more familiar to European engineers, and in fact has been ably discussed by Daniel Gaden in a recent text.[18]

Mr. Spellman's contribution is distinctly useful and practical and his formulas have the advantage of being easily remembered. His suggestion that "a more definite idea of the runner size would be obtained if it were expressed as throat diameter rather than as discharge diameter" is no doubt valid, and for a maker's engineer the throat diameter is no doubt the more fundamental dimension. The author's use of his formulas was mainly for the limited purpose of determining in the first place the dimensions of draft tubes, etc., as a means of fixing approximate powerhouse dimensions. This he did by means of various empirical relationships referred to discharge diameter and specific speed. The same purpose could be served if such data were available in terms of throat diameter, which could then be obtained by Mr. Spellman's formulas. The author is interested to note that Mr. Spellman's company values the facility of the contour type of diagram, in the case of Kaplan turbines. It is a fact that the contour diagram is not only capable of containing a surprising amount of information in one diagram without confusion, but is very revealing as to the suitability of a runner for a given head and speed and for this reason has been given the apt name, by Mr. Harza, of the "goldfish bowl" diagram.

Mr. Strowger's eminence in his field makes his contribution especially appreciated by the author, who is glad to state that he regards the first paper cited by Mr. Strowger[15] as the original "gospel" on the subject. Mr. Strowger believes that the methods shown in the references cited by him would give results which would agree with the author's Case 2 and Case 3. Mr. Strowger's Fig. 5 (loc. cit.) gives the gate-time relationship and one turbine efficiency curve, which is presumably taken at the rated head and speed, and therefore at a constant unit speed. It is not apparent to the author that efficiencies taken at a constant unit speed could correctly be applied to the behavior of a turbine whose actual unit speed, on account of the pressure and speed changes, is varying throughout the phenomenon, although no doubt the error involved might be negligible for many purposes. The second reference cited by Mr. Strowger[16] contains a very excellent exposition of his procedure of determining the change in head and speed during the phenomenon of a change in load. It takes into account both the changes in head and speed during the transient as shown by his Tables 2, 3, and 4. Two complete sets of computations are required, the second applying trial and error principles to the first.

The author's procedure seems to be more direct in that each point in the computation is arrived at by trial and error to satisfy simultaneously two sets of conditions, viz., the water-hammer conditions and the turbine characteristics. The accuracy is limited only by the correctness of the physical data and the patience of the computer. The author feels considerable confidence in this method for it was successfully used to predict pressures in the Fort Peck installation under various conditions, and was found to give quite appreciable differences in pressure with the same gate closure, depending on the amount of water rheostat load thrown on the generator during the gate-closing operation. In general, the pressure rise increased as the rheostat load used decreased, although this would not necessarily hold true for other operating heads.

Referring to the author's Fig. 5, if the operating head were different, the starting point of Cases 1, 2, and 3 would likewise be different from that shown, and the lines marked Case 1, Case 2, etc., would cut across the efficiency contours in a different manner and other results than those just mentioned might occur. The Fort Peck tests referred to by Mr. McLaughlin required turbine closures with a water conduit about a mile long and no surge tank, and the element of risk involved warranted the most painstaking investigation prior to embarking on such tests. The author's method also successfully predicted hydraulic instability on rheostat load. This was possible because the slow governor time considered rendered the behavior of the unit amenable to computation by reason of the governor compensation effect being negligible. The author believes that an additional advantage of his procedure lies in its giving a graphical picture at each instant, and this is particularly apparent in studying stability, where what might be called the "history line" (like the lines marked Case 1, etc., on the author's Fig. 5) wanders around the diagram somewhat in the form of a lemniscate.

[17] Field Pressure Measurement, Fort Peck Powerhouse Penstock, Technical Memorandum no. 206–1, U. S. Waterways Experiment Station, May 15, 1944.

[18] "Considérations sur le Problème de la Stabilité—Contribution à l'Etude des Régulateurs de Vitesse," Lausanne, Editions La Concorde, 1945.

Mr. Strowger correctly points out that the "tail end" of the author's horsepower curve, Fig. 7, should dip down to a negative value. The excuse for not doing so is that a good runner of the specific speed illustrated would run at speed-no-load with a very small gate (in the case of Fort Peck about 0.04), so that this negative dip would be negligible, and secondly, that makers generally fail to test runners at very small gate openings so that data would ordinarily be unavailable to compute this negative dip, even though it is known to exist. In certain cases, however, it is recognized that this negative power may be of considerable importance, and in any case the existence of the negative portion of the horsepower-time curve would make the speed curve peak earlier, viz., at the instant the horsepower changes from positive to negative.

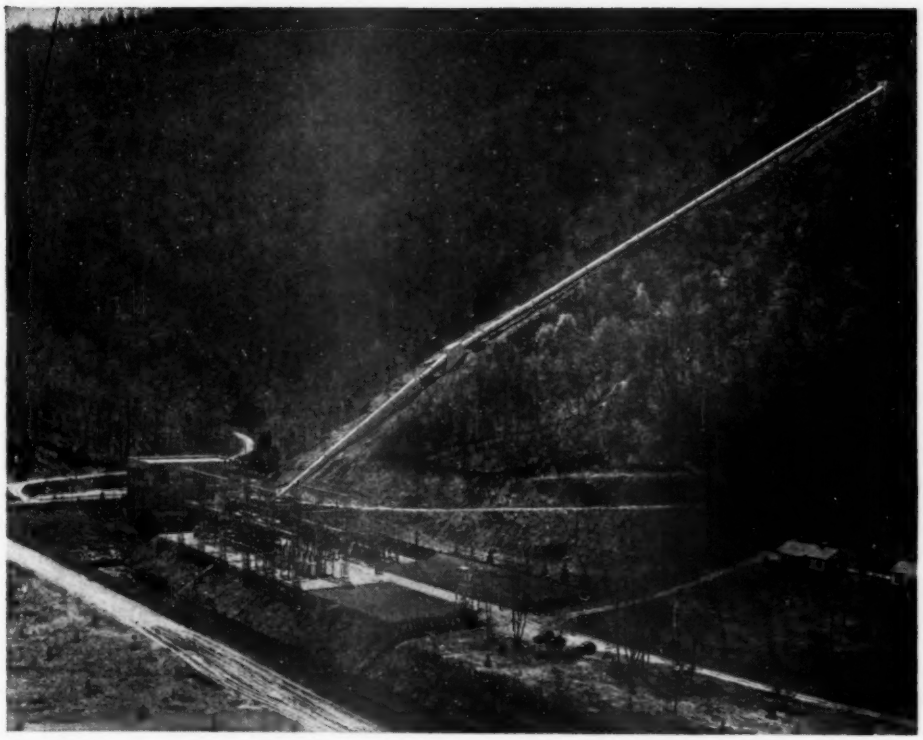


FIG. 1 GENERAL VIEW OF THE NANTAHALA POWERHOUSE

Nantahala Turbine

BY J. P. GROWDON,[1] R. V. TERRY,[2] AND H. H. GNUSE, JR.[3]

The Nantahala plant of the Nantahala Power and Light Company is located near Franklin, N. C., and was designed by the Aluminum Company of America. The 60,000-hp hydraulic turbine operates under 925 ft rated net head at 450 rpm. The static head on the plant of 1008 ft is the highest for any reaction-type turbine installed in the United States. The design and construction of this turbine and butterfly valve are described, followed by results of the field tests. Operation and maintenance work undertaken since the unit was installed are frankly discussed. The field tests showed an efficiency of 93.7 per cent. Considerable stainless steel was used in the original installation and its use has been greatly extended since the unit was placed in operation.

INTRODUCTION

THE Nantahala hydroelectric development is owned and operated by the Nantahala Power and Light Company, a subsidiary of the Aluminum Company of America. It is situated on the Nantahala River in southwestern North Carolina, where the steep slopes permit a high-head development in a relatively short reach of river. It was completed in July, 1942, and has been in successful operation since that date.

The acquisition and design of this development has been carried on by the owner and its parent company since 1911. In this period of 35 years, many different types of development have been proposed and studied. As finally designed and built, the Nantahala hydroelectric development consists of an earth-faced rock-fill dam, 250 ft high, creating a reservoir with 125,000 acre-ft of usable storage. The water from the reservoir is taken to the powerhouse through an unlined pressure tunnel, approximately 5.3 miles long, and a penstock 1391 ft long. A differential surge tank is located 1991 ft from the turbine. The powerhouse, shown in Fig. 1, contains a single hydroelectric unit, consisting of a 60,000-hp reaction turbine, operating under a maximum static head of 1008 ft, directly connected to a 3-phase 60-cycle generator, with the necessary transformers and auxiliary equipment. The power output is fed into a transmission system so that it is not required to operate the unit when for any reason transmission is interrupted.

A great deal of study was given to the problem of selecting a turbine which would combine the following characteristics: Low cost per horsepower; maximum efficiency; satisfactory and reliable operation.

At this head, either an impulse or reaction turbine appeared feasible. For the total capacity at least two impulse turbines would be required, with an expected efficiency of 88 per cent.

[1] Chief Hydraulic Engineer, Aluminum Company of America, Pittsburgh, Pa. Mem. A.S.M.E.

[2] Assistant Chief Engineer, Newport News Shipbuilding & Dry Dock Company, Newport News, Va. Fellow A.S.M.E.

[3] Chief Electrical Engineer, Nantahala Power & Light Co., Franklin, N. C.

Contributed by the Hydraulic Division, and presented at the Spring Meeting, Chattanooga, Tenn., April 1–3, 1946, of THE AMERICAN SOCIETY OF MECHANICAL ENGINEERS.

NOTE: Statements and opinions advanced in papers are to be understood as individual expressions of authors and not of the Society.

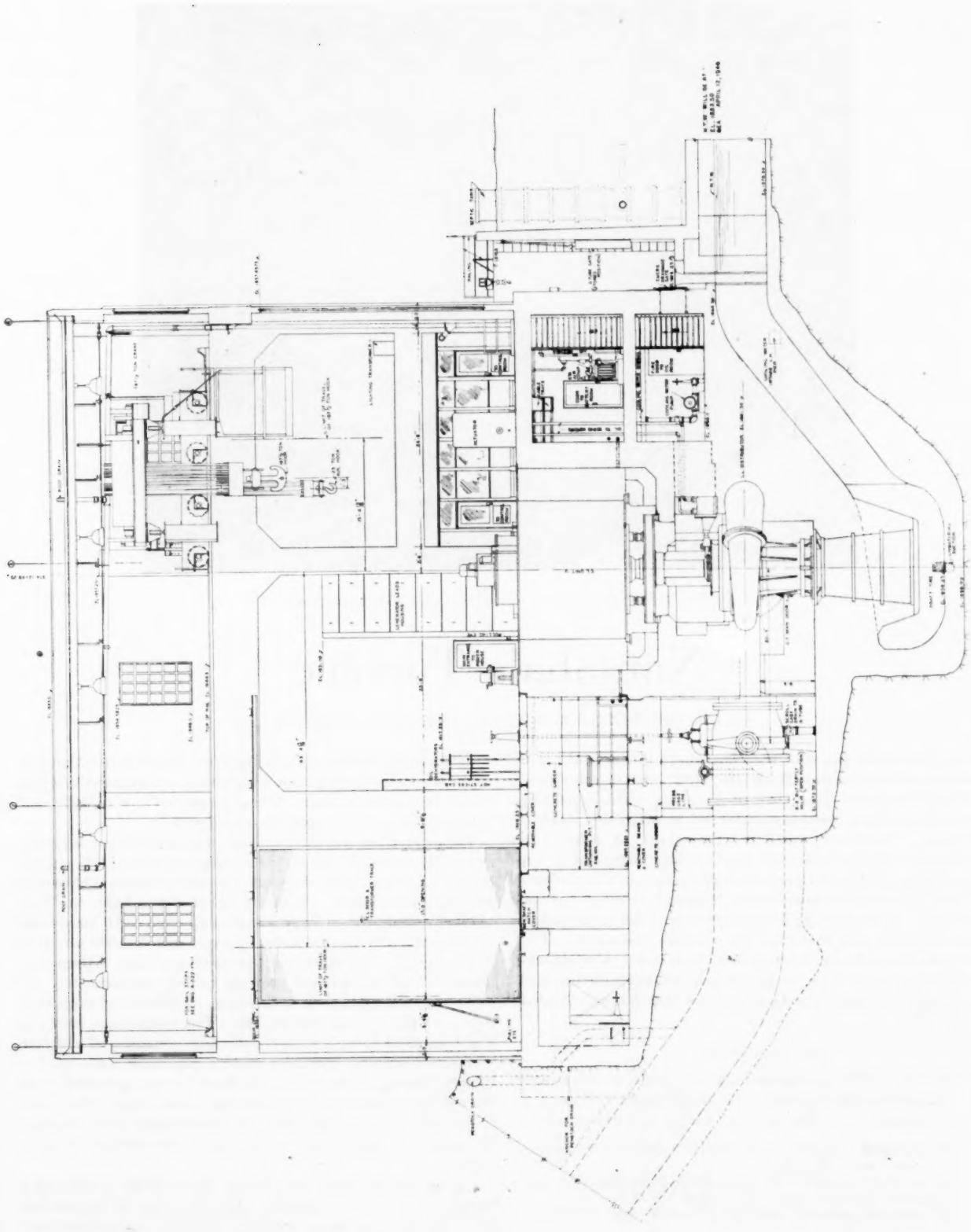


FIG. 2 LONGITUDINAL SECTION THROUGH POWERHOUSE

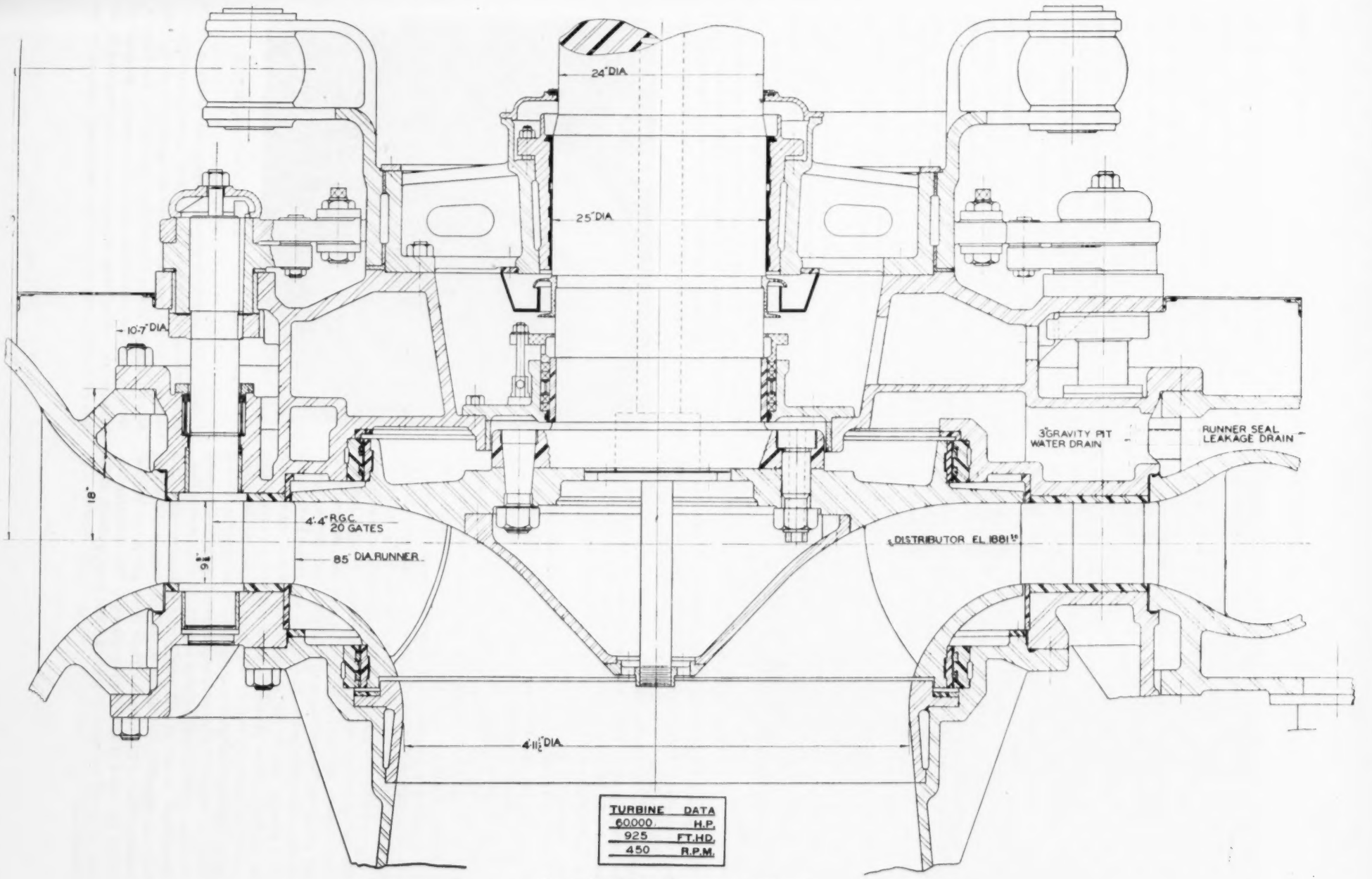


FIG. 3 SECTIONAL VIEW OF THE TURBINE

Since the power requirements did not necessitate operation at low loads, and since the large reservoir provides an opportunity for periodic inspection and repairs, without wasting water, the two units are no more useful than a single unit and would cost considerably more.

A reaction turbine of this capacity, having an efficiency of more than 90 per cent, appeared to be feasible. Due to the permissible lower turbine setting, it would regain a few feet of head which the impulse turbine could not utilize. A single-unit reaction turbine, with its direct-connected generator, would cost considerably less than the two impulse units previously mentioned. It was realized that the head is higher than any other reaction turbine in America, and that reaction turbines under somewhat less head had developed many operating difficulties.

The parent company had had some experience with high-head reaction turbines and believed that as a result of this experience and the increased knowledge of the turbine designers, it would be possible to design and build a reaction turbine which would meet the requirements of the Nantahala hydroelectric development better than any other type and which would be free from serious operating difficulties.

Several turbine manufacturers agreed with this conclusion, and after consideration of all turbine builders' proposals, the contract was awarded to the Newport News Shipbuilding & Dry Dock Company for the design and manufacture of a 60,000-hp (925-ft head), 450-rpm vertical reaction turbine, with all essential auxiliaries, operating under a maximum static head of 1008 ft, and an 8-ft-diam butterfly valve to be located immediately above the scroll case.

Nantahala Turbine

The turbine selected for the Nantahala plant is of the vertical-shaft single-runner Francis type, rated 60,000 hp under a net head of 925 ft, operating at a speed of 450 rpm. This gives a specific speed of 21.6. It is designed for a maximum net head of 1000 ft, the maximum static head on the plant being 1008 ft. This is believed to be the highest-head reaction-type turbine installed in the United States and to be the highest-powered extremely high-head reaction turbine in the world.

The Francis type was selected in preference to an impulse type after giving due consideration to several factors. The efficiency of the reaction-type turbine is several per cent higher (about 4.5 per cent) than that of the impulse type. The speed is considerably higher, resulting in a much smaller and less expensive generator. The unit is sufficiently large so that reasonable clearances could be employed and yet maintain relatively small leakage losses. The disadvantages are that load cannot be changed as rapidly as with an impulse turbine and that there is some element of danger in operating the unit unwatered as a synchronous condenser.

Fig. 2 shows a longitudinal section through the powerhouse. The turbine setting includes a hydraulically operated butterfly valve between the turbine-casing inlet pipe and the penstock, and a cast-steel spiral casing in 3 sections with 20 vanes, one opposite each wicket gate. The vertical part of the draft tube is of the straight conical type, the upper part being of cast steel and the lower part of steel plate. The upper part includes a removable section just below the runner. This permits removing the runner and throat ring from below and gives access for repair or renewal of the seal rings and other work on the turbine without disturbing the crown plate and other parts supported by the crown plate. Downstream of the conical part of the draft tube there is a collecting chamber which discharges diagonally upward and then around a bend to the tailrace. There is one pier in the diagonal portion and bend of the discharge passage. The discharge passage is vented upstream of the bend and near the wall of the powerhouse.

Runner and Seal Rings. Fig. 3 shows a sectional view of the turbine. The runner is of the conventional Francis type of cast steel in one piece, 85 in. nominal diam, with 21 vanes, arranged for a bolted connection to the main shaft. The bolted connection is arranged for easy removal of the runner. There are ten tapered bolts used primarily to take shear and four loose-fitting straight bolts to carry the hydraulic thrust and weight of the runner.

The entrance edges of the vanes are sloped circumferentially and a large radial gap of about 6 in. is left between the runner vanes and wicket gates so as to result in smooth flow from the gates into the runner. This arrangement has proved highly satisfactory and cannot be too greatly emphasized.

The runner carries two straight steel seal rings shrunk on, one on the crown and one on the band. The two rings are of equal diameter to provide good hydraulic balance and at the same time are interchangeable. The rings are placed at as small a diameter as possible so that a small running clearance could be used and the leakage area reduced. A radial clearance of 0.015 in. is employed. The clearances at the periphery of the runner are purposely left large to preserve hydraulic balance. The seal rings are supplied with 80 gpm of clear water through a check valve, piping, and radial holes between the inserts in the stationary seal rings.

Provision is made for checking the seal clearances periodically from above and below the runner, with the turbine shut down. Leakage through the top seal is carried out through the crown plate and a pipe to a point above tail water where the amount of leakage may be observed at any time during operation.

The runner was dynamically balanced and the shaft-connection holes drilled and reamed before shipment to the generator manufacturer. A cast-steel fairwater is bolted to the bottom of the runner. Fig. 4 shows a shop view of the runner and spare runner.

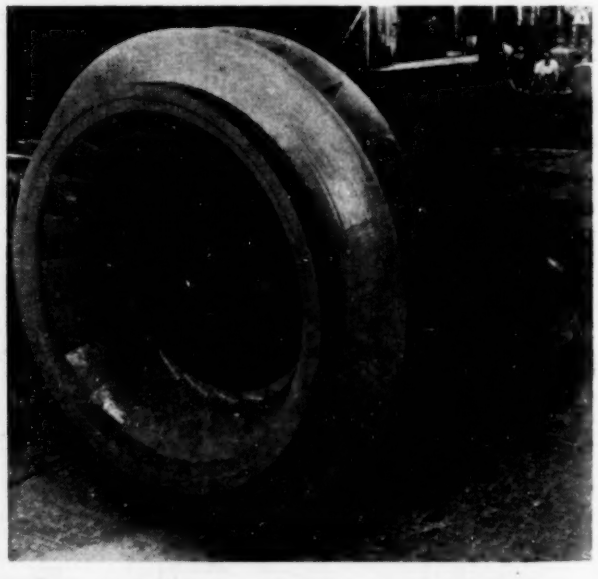


Fig. 4 Shop View of Runner and Spare Runner

Shaft. The usually separate turbine and generator shafts were combined and furnished in one piece by the generator manufacturer. This is practicable since the runner is removed from below. The shaft has a nominal diameter of 24 in. The flange for connection to the runner was drilled and reamed by the generator manufacturer using templates and drilling jigs furnished by the turbine manufacturer who had previously used them in drilling

and reaming the runners. A rather elaborate set of jigs was required owing to the necessity for having the runner, spare runner, and any future replacements interchangeable. The generator builder fitted each runner to the shaft and checked alignments before shipping to the field. The shaft is provided with a stainless-steel sleeve in halves, opposite the turbine stuffing box. A turbine manufacturer's representative supervised the installation of the sleeve and witnessed the shaft and runner alignment.

As usual on large forgings of this kind, a hole was provided in the shaft. This hole was used for certain generator leads and to admit a small amount of venting air to the draft tube through a pipe in the runner cone or fairwater. The hole was also used at first for passing a cable for handling the runner but this was later dispensed with in favor of a jacking arrangement.

Main Bearing and Lubrication. The unit has three bearings, a turbine bearing, a generator-guide bearing below the rotor, and a spherical Kingsbury guide-and-thrust bearing above the rotor. The turbine bearing is of the babbitted oil-lubricated type, 25 in. diam, rather short, being only 16 in. long. The shell is in halves, machine-grooved, tinned, babbitted, bored, and scraped to a clearance of 0.010 in. on diam.

The oil sump is of 74-gal capacity placed in a sector of the crown plate. Oil is supplied to the bearing through a cooler by an a-c motor-driven pump with a d-c motor-driven pump as a stand-by arranged to cut in upon loss of pressure. The pumps, cooler, and gage board are located in an alcove in the turbine pit. The oil supply enters the bearing in an annular groove about one third down from the top, flowing both ways to lubricate the bearing. A reservoir of oil is left at the top of the bearing to act as a supply when changing from a-c to d-c pump or other temporary lack of supply. Excess oil overflows through a pipe to the sump.

Crown and Curb Plates. The crown and curb plates are of cast steel in one piece and of usual construction except that the curb plate is removable from below, after removal of the draft-tube section. This gives access for removal of the wicket gates from below and for maintenance of certain wearing plates and rings under the crown plate.

Wicket Gates and Operating Mechanism. The 20 wicket gates are of forged steel with integral stems. The wearing surfaces at each end of the body of the gates were overlaid by welding with one layer of stainless steel, using a 25 chromium - 20 nickel rod. A total clearance of 0.020 in. was provided.

Each gate has three bearings, one below and two above the body. The lower bearings are greased from below as ample space is available from the passageway around the removable section of the draft tube. Cup leather packing instead of the usual type of square packing is used in the upper gate-stem packing boxes to seal against the high pressures involved. A thrust collar on each gate stem carries the upward thrust against the crown plate.

Each gate lever is made in two sections connected by the usual safety shear pin.

The operating ring and two servomotors, etc., are of usual construction designed for operation with oil at 250 to 300 psi, the displacement of the servomotors being 18.3 gal. In order to suit the design of penstock and surge tank, positive stops were installed on the servomotors to limit the stroke to about 90 per cent, corresponding to a discharge of 635 cfs and about 60,000 hp at 935 ft head.

Governor. The governor is of the Woodward cabinet actuator type with 3-in. pipe connections and rated about 85,000 ft-lb at 250 psi; the governor being designed for a maximum pressure of 300 psi. The minimum time for full gate stroke was specified as 4 sec. However, due to the pipe-line conditions, the closing stroke is limited to 12 sec by $^{17}/_{32}$-in. orifices in the port piping to the servomotors, and the opening stroke to 22 sec by a special small relay valve with limited stroke.

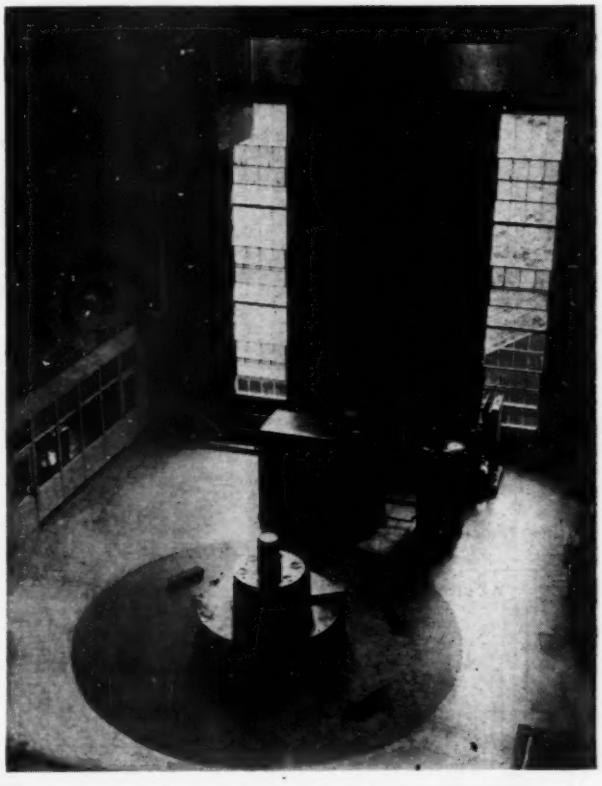


FIG. 5 INTERIOR VIEW OF POWERHOUSE, INCLUDING THE GOVERNOR

The flyballs are driven by a permanent-magnet generator mounted on the generator. Oil pressure is supplied by two 50-gpm motor-driven pumps with echelon control.

The WR square of the generator is about 4 000,000 ft² lb, giving a regulating constant, WR^2N^2 divided by horsepower, of 13,500,000.

Fig. 5 shows an interior view of the powerhouse, including the governor.

Butterfly Valve. Fig. 6 shows a sectional arrangement of the butterfly valve and operating gear. The valve has a nominal diameter of 8 ft at inlet, reducing to 6 ft 6 in. diam at discharge. Its center line was placed about 20 ft upstream from the center line of the turbine so that there would be no question about the valve disk creating a disturbed flow that would affect the efficiency of the turbine. Body and disk are each in one piece made of cast steel. The shaft is of forged steel keyed to the disk. An 8-in. by-pass is provided for filling the turbine casing before opening the valve, although the valve is designed for opening or closing under full static head of 1008 ft. A 3-in. Crispin air-and-vacuum valve permits the air in the casing to escape and automatically closes when the casing is filled with water. It also admits air when the casing is being drained.

Special care was devoted to the design of the seal rings to reduce the leakage to a minimum and to prevent erosion when the valve was left closed for long periods with the penstock under pressure. Body and disk seal rings are both made of stainless steel of different grades to prevent the possibility of galling. The body seal ring was bored after installation in the body. The disk ring is in halves, secured in its groove, but free to float like a piston ring so that it will adjust itself properly when the valve is closed. This arrangement has proved very satisfactory and there has been little increase in leakage during the 4 years since installation. The choice of stainless steel for the seal rings has proved to be wise.

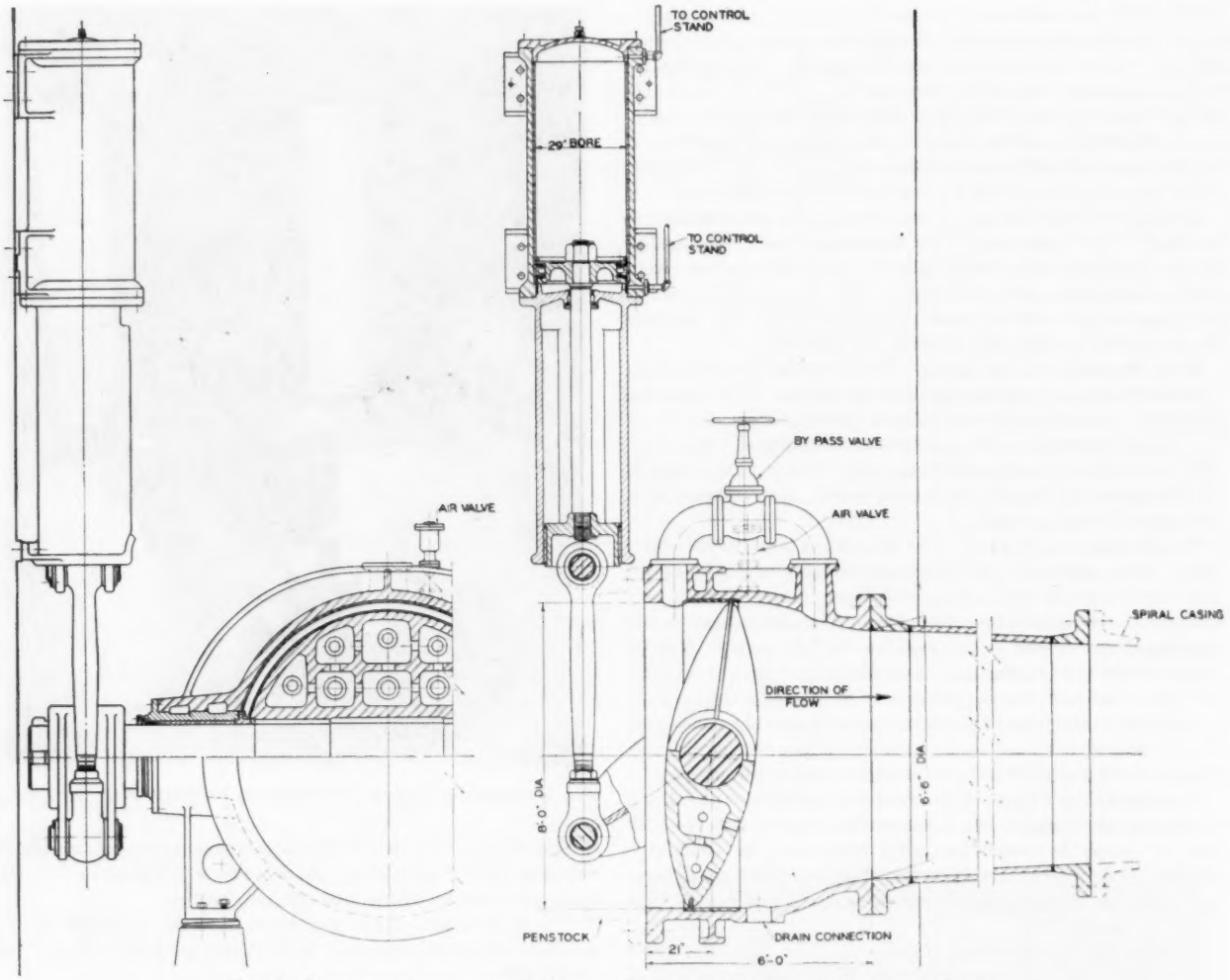


FIG. 6 SECTIONAL ARRANGEMENT VIEW OF BUTTERFLY VALVE AND OPERATING GEAR

The valve is arranged to be opened or closed in about 2 min from a control stand on the powerhouse floor, by means of penstock pressure in a bronze-lined cylinder 29 in. diam by about 5-ft stroke. The opening and closing time are limited by the size of the control piping.

Weights. The total weight of the turbine, not including shaft and spares but including governor equipment, was about 300,000 lb. The weight of the complete butterfly valve was about 150,000 lb.

SHOP ERECTION AND TESTS

The turbine spiral casing, inlet section, and butterfly valve were erected and tested in the shop under a hydrostatic pressure of 700 psi, for 2 hr. Fig. 7 shows these parts assembled with a cast-steel test head bolted to the upstream end of the valve housing. The crown plate and curb plate were in place, and a test ring was fitted between the crown and curb plates opposite where the periphery of the runner would be in the field. The wicket-gate stem holes were temporarily plugged for this test and the butterfly-valve disk was in the open position.

The space between the upstream face of the valve disk and the test head was given a separate test at 700 psi, after closing the disk with a torque of about 80,000 ft-lb. The valve leakage was measured at a pressure of 435 psi, corresponding to full head in the field, and found to be 0.135 cfs. The leakage in the field was much less for then the closing moment was about 10 times as much or 800,000 ft-lb.

A tightness test of 500 psi was placed on the casing and butterfly-valve body in the field before pouring concrete.

TURBINE MODEL AND FIELD TESTS

A homologous model was built with a 22-in-diam runner and tested in the manufacturer's hydraulic laboratory before construction of the turbine was started. The homologous parts consisted of all parts which affected the water passages from the inlet to the butterfly valve to the discharge end of the conical draft tube. The model tests were made under a reduced head of about 30 ft. The best efficiency obtained was 89.5 per cent. These tests were made both with and without the butterfly disk in place. No differences in results could be detected.

A complete field test was made in accordance with the A.S.M.E. Test Code for Hydraulic Prime Movers, the water being measured by the Gibson method. Fig. 8 shows the results of the field test, the maximum efficiency being 93.7 per cent.

Sixty-two thousand hp was obtained at 87.5 per cent gate opening which is the maximum gate opening at which the turbine is operated. Above 85.5 per cent gate opening or 60,000 hp, a cavitation noise starts in the draft tube.

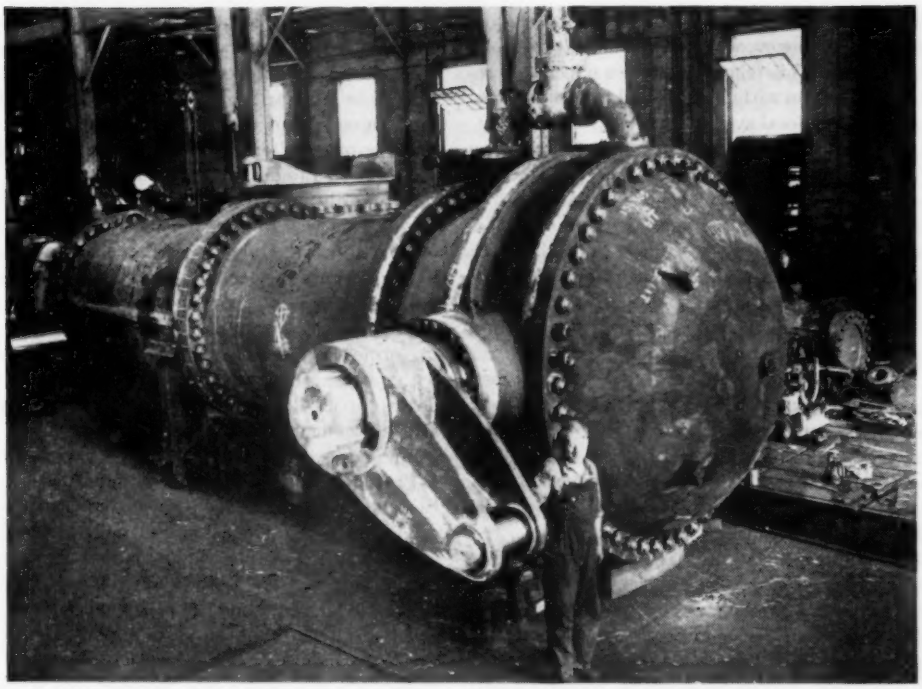


FIG. 7 ASSEMBLY VIEW OF TURBINE-SPIRAL CASING, INLET SECTION, AND BUTTERFLY VALVE AS ERECTED IN THE SHOP FOR TESTING

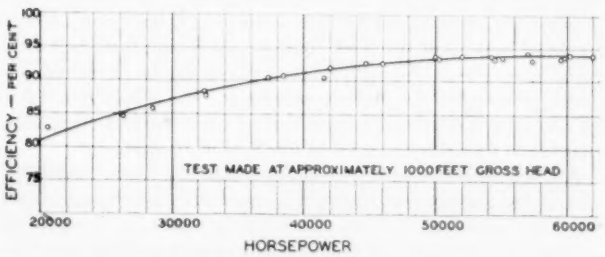


FIG. 8 RESULTS OF FIELD TESTS; MAXIMUM EFFICIENCY 93.7 PER CENT

Other results of field tests are as follows:

Gate opening required to bring unit up to speed, per cent	6.0
Pressure rise for full load off—148 ft or (per cent)	16.0
Speed rise for full load off, per cent	33.0
Power required to motor, runner submerged, kw	1750
Power required to motor, runner unwatered, kw	560
Wicket-gate leakage under full head, cfs	8.2
Oil pressure required to move gates, unwatered, psi	12
Oil pressure required to open gates, full head, psi	175

Gate leakage is sufficient to keep the unit running at 135 rpm before closing the butterfly valve but not sufficient to start unit from rest.

Following is a comparison of guaranteed, model, and field test efficiencies at 925 ft net head:

Per cent load	Efficiencies, per cent		
	Guaranteed	Model test	Field test
100	87.0	89.0	93.7
Best	89.5	89.5	93.7
75	88.5	86.6	93.0
50	84.0	79.0	88.0

Water Velocities. The following tabulation shows the approximate water velocities from the entrance to the butterfly valve to the discharge end of the draft tube, based upon the field test discharge of 610 cfs at rated load and head:

Location	Velocity, fps
Penstock	12.1
Butterfly valve	19.3
Casing entrance	23.5
Casing	29.8
Speed-ring discharge	49.5
Wicket gates	118.0
Entrance to runner, absolute	165.0
Entrance to runner, relative	38.0
Discharge from runner, absolute	37.0
Discharge from runner, relative	115.0
Draft tube, throat	31.2
Draft tube, bottom of cone	10.7
Draft tube, discharge passage	4.3

OPERATION

The turbine was placed in operation July 2, 1942. The field tests were made in August, 1942.

The operation of the Nantahala turbine is not unusual except for several operating limitations that are imposed due to certain design features that resulted from the high head. Some of the original limitations have been mitigated by slight changes in design and by the use of more suitable materials when repairs have been made. The remaining limitations as will be indicated do not impose any serious restrictions on the operation of this unit, in view of the fact that the Nantahala turbine is always operated as part of a large co-ordinated system in which it can normally serve as a base load plant.

The physical location of the powerhouse made a relatively long pipe line necessary between the surge tank and the unit. In order to protect this pipe line against excessive surge pressures it was felt desirable to provide relatively slow governor time. This slow governor timing makes it impossible to use the Nantahala unit for any tie-line load regulation which requires quick changes of load. The slow closing speed also results in an overspeed upon sudden loss of full load of approximately 33 per cent. Since the small load which would normally remain connected to this unit upon the loss of tie line can usually be taken care of by generation at smaller plants, it was considered very desirable to separate the Nantahala unit completely from the remainder of the system upon the sudden loss of load. To accomplish this an overspeed "inertia" relay was interlocked through a watt relay and con-

nected to trip the generator breaker immediately upon the occurrence of a fast rise in frequency, which would indicate loss of a major portion of the load. This relay installation effectively removes the unit from the system within 1/2 sec and prevents excessive overspeeds on the small local system.

The runner of the Nantahala unit is partially submerged by the normal tail water, even when the unit is not in operation. This center line elevation was purposely selected in an effort to minimize cavitation of the runner during normal operation. This results in a positive pressure under the runner for loads up to approximately 57,500 hp at rated head, at which point the velocity head of the water and other disturbances create a negative pressure at the periphery of the draft-tube throat. It was found that when this negative pressure exceeds approximately 14 psi, cavitation noises start in the draft tube. Since the load at which this disturbance occurs varies with the gross head, a table has been prepared showing "maximum gate limit setting versus head," so that the wicket gates will not be opened beyond this critical setting. It has been found that the output varies from approximately 55,500 hp at the minimum head to 65,000 hp at the maximum head before these cavitation noises occur.

The setting of the runner below normal tail water makes it impossible to use the unit as a synchronous condenser without providing special features, such as compressed air to lower the tail water and to provide additional equipment to assure water lubrication to the seal rings during extended periods of operation as a synchronous condenser. After considerable discussion and investigation, this equipment was not considered justified due to the fact that the reactive kva can always be supplied from other units which are located closer to the load center.

A further limitation which was originally imposed on the operation of the machine was a precaution against operating for extended periods below one half rated load due to the excessive wear which would result from operation at light loads. This consideration is no longer as critical as it was originally due to the use of stainless steel in the repair of various of the wearing parts.

Maintenance

It was generally agreed, even before the turbine was installed, that considerable maintenance, particularly of the runner, would be required owing to the high head and high water velocities which exist in this unit. However, some additional problems were experienced which required some redesign as well as some repair.

As originally designed, an oil sump of 74-gal capacity was placed in a sector of the crown plate with the thought that sufficient cooling would be provided by contact of the underside of the oil sump with the water discharged through the turbine. This oil sump provided lubrication through one set of oil pumps to both the generator and turbine guide bearings. It was soon found that there was not sufficient heat transfer through the oil sump to cool the oil adequately, so a heat exchanger was inserted in the oil line between the oil pumps and the bearings.

The first difficulty with this system was experienced due to water spray from the shaft packing gland entering the oil system through the oil-collector pan underneath the turbine guide bearing. This water caused considerable rusting and pitting of the turbine-generator shaft just above the guide bearings, and also a rough rusty appearance on the actual bearing surfaces of the shaft. This condition was corrected by using a rust-inhibiting oil which was very effective in eliminating the rusting, pitting, and sludging which had taken place in the original oil. Admission of water into the system from the packing gland was later effectively eliminated by adding a water deflector to the shaft just above the packing gland, but moisture continued to be present due to condensation on the cool surfaces of the sump walls.

Although the location of the oil sump in the crown plate conserves space in the structural design of the powerhouse, it results in a very unsatisfactory location from a maintenance standpoint. It is practically impossible to clean out completely the sump and to remove all traces of moisture and sediment. In order to remove moisture of condensation effectively, a continuous small blotting-paper filter has been installed in series with the oil line.

It was also found that the one oil-pumping system would not satisfactorily lubricate both the turbine and the generator bearings. This was due to the fact that the generator bearing is located approximately 7 1/2 ft above the turbine bearing, and also to the fact that the generator bearing was supplied through a small orifice, whereas the turbine bearing was supplied through a 3/4-in. pipe. Any small or slight obstruction in the generator piping orifice would merely force the oil into the turbine bearing without resulting in an appreciable rise in pressure to remove the obstruction. This combination system was separated to provide an independent forced oil lubrication system with separate oil sump and heat exchanger for the generator guide bearing.

Provision was made in the original design of the turbine for the runner to be removed by means of a cable through a hole in the generator shaft. The cable and runner could then be handled by means of the main powerhouse crane. However, the upper portion of the hole through the shaft was also used for the generator-field leads which extend from the field poles to the collector rings. Early experience indicated that considerable time and effort would be required to remove and reinstall the generator leads every time the runner was removed. It would also be difficult to keep the runner centered when it was being lifted by the cable due to the close seal-ring clearances. It was therefore decided to remove the runner by means of jack bolts and a special frame so that all of the work could be carried on from below the scroll case where the entire operation could be observed and closely checked by the maintenance force. It has been found that by use of this device, a runner can be removed and completely reinstalled by a six-man crew in five 8-hr work shifts.

Another small detail which developed was the fact that under certain conditions when filling the draft tube and scroll case, a water hammer was created which forced water up through the hole in the shaft and out into the generator rotor, and also into the main thrust-bearing oil sump. Since it was felt that the hole served a useful purpose of admitting air to the draft tube, this problem was corrected by installing a check valve at the lower end of the shaft in such a manner that air would be admitted through the shaft to the draft tube but water would be checked and prevented from rising up the shaft.

After the completion of the original installation it was noticed that the wicket gates would not completely pinch when closed against full water pressure. Upon release of the water pressure from the scroll case, the gates would move to the completely closed position. It was found that due to an unbalanced pressure under the gate stem, amounting to an upward thrust of several tons per gate, the upper flange of the crown plate against which the thrust collars pressed deflected sufficiently to allow the top of the gates to rub the upper wearing plate. This condition was corrected by readjusting the thrust collars on the stems and by installing lugs and additional bolts to minimize the deflection of this flange. Whereas it was originally necessary to close the butterfly valve in order to bring the unit completely to a stop, the unit can now be brought to a stop by merely closing the wicket gates.

The major portion of the maintenance and repair of the unit results from pitting and erosion that are caused by the high water velocities and pressures. Realizing that considerable maintenance would be necessary, frequent inspections were made of the unit after it was placed in service. After about 6 months of operation, the wicket gates and the back side of the nonoverlapping parts of the runner vanes began to show signs of erosion or pitting.

After a year's operation, the wearing plates opposite the top and bottom surfaces of the gates had started to erode, the seal-ring clearances had increased from 0.015 to 0.020 in., and considerable wiredrawing could be observed on the closure contact surfaces of the gates, despite the fact that the butterfly valve was always closed and pressure removed from the scroll case within a few minutes after the wicket gates were closed.

After two seasons of operation the Nantahala unit was dismantled with the intention of making minor adjustments and repairs, such as the welding in the field of small areas of the wicket gates, wearing plates and runner that showed wear from an inspection of the completely assembled machine. However, upon removal of the runner the complete extent of the wear could be observed, and it was evident that a major overhaul would be required. It was decided that the following parts should be renewed or repaired: runner and seal rings, throat ring below runner, wicket gates, curb and crown-plate wearing plates and rings.

The stainless steel originally applied to the ends of the wicket gates and the stainless seals used for the butterfly-valve seals showed no sign whatever of erosion or other damage. Fig. 9 shows a typical wicket gate before being repaired. The curb and crown-plate wearing rings and the seal rings on the runner had originally been made of S.A.E. 1045, a carbon-manganese steel, heat-treated to a Brinell hardness of 200 to 235. It was thought that this material would be suitable for resisting the erosion from the high velocities, but this was not the case. The stationary seal rings were made of cast steel, each with two bronze inserts held in place with calking strips. The bronze inserts eroded faster than the carbon-steel rings on the runner.

The parts to be restored were shipped back to the turbine manufacturer and were treated as follows:

The nonoverlapping back sides of the runner vanes and the inside of the runner band from the vanes to the bottom edge were recessed about $^1/_8$ in., overlaid with 25-20 stainless welding and refinished. The runner wearing rings were replaced with steel rings overlaid with 25-20 stainless-steel welding. It would have been less expensive to use stainless bar material for this purpose but necessary early delivery could not be obtained during the war.

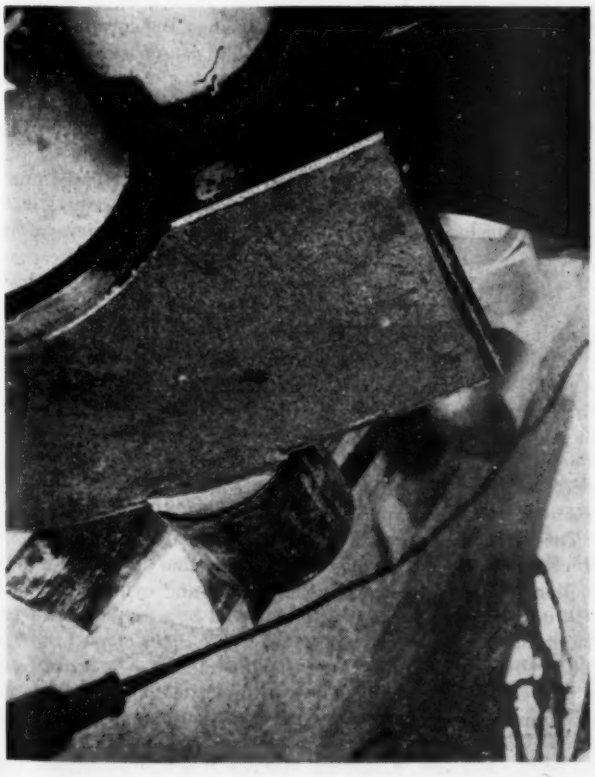


FIG. 9 TYPICAL WICKET GATE BEFORE BEING REPAIRED

The bore of the cast-steel throat ring for a distance of 6 in. from the top was similarly treated with a stainless overlay.

The bronze inserts in the stationary seal rings were replaced with inserts made of a 13 chrome-stainless steel. This gave two different grades of stainless steel working opposite each other so that even if they should accidentally touch in operation, galling would not result.

The entire downstream side and one third of the upstream side of the body of each forged-steel wicket gate were overlaid with 25-20 stainless welding and refinished. The intermediate and lower wicket-gate stem bearings which had pitted somewhat from corrosion were restored with a stainless metal-spray finish, and a collar was shrunk on the lower gate stem adjacent to the gate to help retain grease on the lower bearing surface.

The curb and crown-plate wearing plates and rings opposite the runner periphery were renewed with mild steel overlaid with 25-20 stainless welding. At the same time total clearance at the end of the wicket gates was reduced from 0.020 to 0.015 in.

In order to make the foregoing repairs the unit was taken out of service on March 6, 1944, and by working continuously it was put back into operation on May 2, 1944. No water was lost from the reservoir during the 56 days the unit was down.

As a result of the changes the power output was increased about 5 per cent, 3000 hp, because the runner-discharge openings were increased. The leakage through the runner seals was even less than when the unit was first installed. With the smaller wicket-gate clearance and complete closure of the gates, the unit would stop of its own accord with the gates closed and the butterfly valve left open, whereas previously it would not.

After two additional seasons of operation the runner was again removed for a detailed inspection of the unit. All of the stainless steel which had been properly applied was still in perfect condition. Even the tool and the file marks still showed, indicating that very little if any metal had been removed due to erosion or pitting. The closure contact surfaces of the wicket gates were also in perfect condition. A number of spots were found on which the stainless-steel weld had been almost completely removed when the piece was remachined and those spots were pitting or eroding appreciably. These small areas were chipped out and filled in with 18-8 stainless-steel rod; and subsequent inspection indicates that this work was very effective.

Evidence of the effectiveness of stainless steel was clearly demonstrated by surfaces of the stationary wearing ring which is installed in the crown plate opposite the periphery of the runner. Through an oversight in the repair work, an inside vertical surface of this ring was coated with $^1/_8$-in. stainless-steel overlay but the lower horizontal surface which adjoins the wearing plate was not coated except for the $^1/_8$ in. vertical overlay that extended to this lower horizontal surface. After two seasons of operation the mild steel between the wearing plate and the $^1/_8$-in. stainless-steel overlay was eroded or pitted to a depth of $^1/_{16}$ to $^3/_{32}$ in. This area was repaired in place by chipping out and filling in with stainless-steel welding rod.

After the runner was removed for this inspection it was decided to install the spare runner and to perform additional stainless-steel welding on the original runner to cover areas which were not repaired when the unit was returned to the factory. These areas consist primarily of the top and bottom edges of the periphery of the runner and a portion of the working face of the vanes where the water impinges upon starting. Considerable

erosion occurs on these faces because the runner acts as an impulse rather than a reaction wheel at small gate openings.

It was gratifying to note that even the seal rings did not show any wear. The manufacturer showed good judgment in applying different grades of stainless steel to the stationary and movable seal rings, since it was found that they had actually touched in a few spots without appreciable damage. It was found that the contact between the two surfaces was due to warpage of the inserts, which probably resulted from internal stresses which had not been relieved. This was corrected by grinding the stationary seal-ring inserts to a true circle by means of a field-constructed jig, and by buffing the movable rings. All of the surfaces were trued up and refinished without changing the original clearances appreciably.

The use of stainless steel has greatly reduced the amount of maintenance work which would have been required to keep the unit in a safe and efficient operating condition. By maintaining smooth surfaces it undoubtedly greatly increases the average long-term efficiency of the unit and removes some of the previous limitations that had been imposed to reduce wear on the unit.

Conclusion

During the more than 3 years' operation of this unit, all the difficulties encountered have been corrected. It is believed that the moderate initial cost (as compared with other types), the very high efficiency, and the absence of serious operating difficulties have amply justified the selection of the Francis type for the conditions under which this turbine operates, and that it will have a long life, with only moderate renewals and repairs.

Discussion

G. D. Johnson.[4] The use of Francis instead of impulse turbines under head of 1000 ft and over has again been vindicated by the Nantahala turbine.

Because of the high efficiencies attainable and the economies in first cost due to high-speed equipment with small space requirements for the amount of power developed, there is a natural inclination to use Francis turbines for higher and higher heads. However, because of operating difficulties experienced with previous high-head installations, there are today only a few Francis turbines in the entire world operating under heads approximating 1000 ft. Apparently use of stainless steel and improved welding techniques will now assure satisfactory, reliable operation of units of this type without excessive maintenance.

The writer was privileged to witness a vivid illustration of this modern trend, when in November, 1945, he visited the Lages Plant of the Rio de Janeiro Tramway, Light, and Power Company (The Light) in Brazil. At present this plant contains eight four-jet vertical-shaft impulse turbines and two vertical-shaft Francis turbines, all of European manufacture, operating under a rated head of 310 m (1018 ft). The small space occupied by the 50,000-hp 600-rpm Francis units, as compared with the size of the 9000-hp and 19,000-hp 300-rpm impulse units, was striking. Moreover, the maintenance on the Francis wheels, installed in 1940, and 1942, respectively, and equipped with special alloy-(stainless-) steel runners, has consisted mainly of stainless-steel welding on the gates and is no more than is required on the runners, needles, and nozzles of the impulse wheels. No erosion or cavitation of the runners was apparent after 3 to 5 years of service. This is due, of course, to the use of special material in the castings, but it is apparent that, as in the case of the Nantahala turbine, the liberal use of stainless steel results in units requiring a minimum of maintenance.

[4] Hydraulic Engineer, S. Morgan Smith Co., York, Pa. Mem. A.S.M.E.

The writer congratulates the authors on the courage and skill demonstrated in the conception and design of the Nantahala turbine and on the success which they have achieved in its operation, as well as on the manner in which they have presented the complete story in their excellent paper. Their generous discussion of design considerations and operating experiences will undoubtedly promote further worth-while developments in the application of hydraulic turbines to high-head power generation.

S. J. Needs.[5] The paper was particularly interesting to the writer, who happened to be at Nantahala on several occasions while the machine was being installed. It is also timely in that it discusses a most unusual machine after it has been proved successful in service. Comparison with larger machines makes it difficult to realize that such a small turbine can develop so much power. Its high output is due, of course, to the exceedingly high head and this is one of the features which make the installation so outstanding.

The authors mention the spherical thrust bearing selected for this machine, and since the bearing is also quite unusual and interesting, a few words about it are in order. Instead of the flat thrust and cylindrical upper guide bearing, common in vertical machines of this type, a spherical thrust bearing is used. This bearing is capable of supporting radial as well as vertical loads, hence it eliminates the upper generator guide bearing.

The spherical thrust bearing for the Nantahala unit is shown in Fig. 10 of this discussion. It is located at the top of the machine and it runs in an oil bath with a cooler like most Kingsbury bearings in hydroelectric service. It is 51 in. diam and to date is the largest spherical bearing that has been built. The rubbing surface of the runner A is a zone of a sphere, the center of which is on the shaft axis. Six segmental spherical shoes B are fitted to the runner and pivoted in the usual Kingsbury manner. The bearing angle of the shoes is 39 deg with respect to the shaft center line. Total vertical thrust load is 575,000 lb or about 96,000 lb per shoe. Due to the bearing angle the normal load per shoe is about 123,000 lb and its horizontal component is approximately 78,000 lb. The shaft is held concentrically by the horizontal components of the thrust load acting radially at each shoe. The babbitt surface area of each shoe is 261 sq in. and loading per unit area is 472 psi.

At the normal operating speed of 450 rpm the average minimum film thickness along the trailing edges of the shoes is 0.0026 in. under the loading cited. When a horizontal load comes on the bearing the shaft can move sidewise due to the slight decrease in oil-film thickness at the more heavily loaded shoes. A side load of 10 per cent of the vertical thrust will decrease the minimum film thickness 0.0004 in., or 15 per cent. Twenty per cent side load will decrease the minimum film thickness 0.0006 in. or 24 per cent, and 40 per cent side load will cause the normal minimum film thickness to decrease somewhat less than 0.001 in. or about 36 per cent. Sidewise movement of the shaft is approximately the same as the change in minimum film thickness, from which it follows that the shaft is held very close to a central running position, even under appreciable side loads.

Total frictional power loss at full load and speed due to oil-film shear is 175 hp. This is about the same as the combined frictions of the corresponding flat thrust and cylindrical guide bearings. The frictional heat is removed by a cooling coil consisting of approximately 1000 ft of $1^1/_8$-in-diam copper tubing. Oil is circulated around the cooler by means of a centrifugal pump consisting merely of two opposite holes drilled in the runner at an angle. At 450 rpm the peripheral speed of the

[5] Service Manager, Kingsbury Machine Works, Philadelphia, Pa. Mem. A.S.M.E.

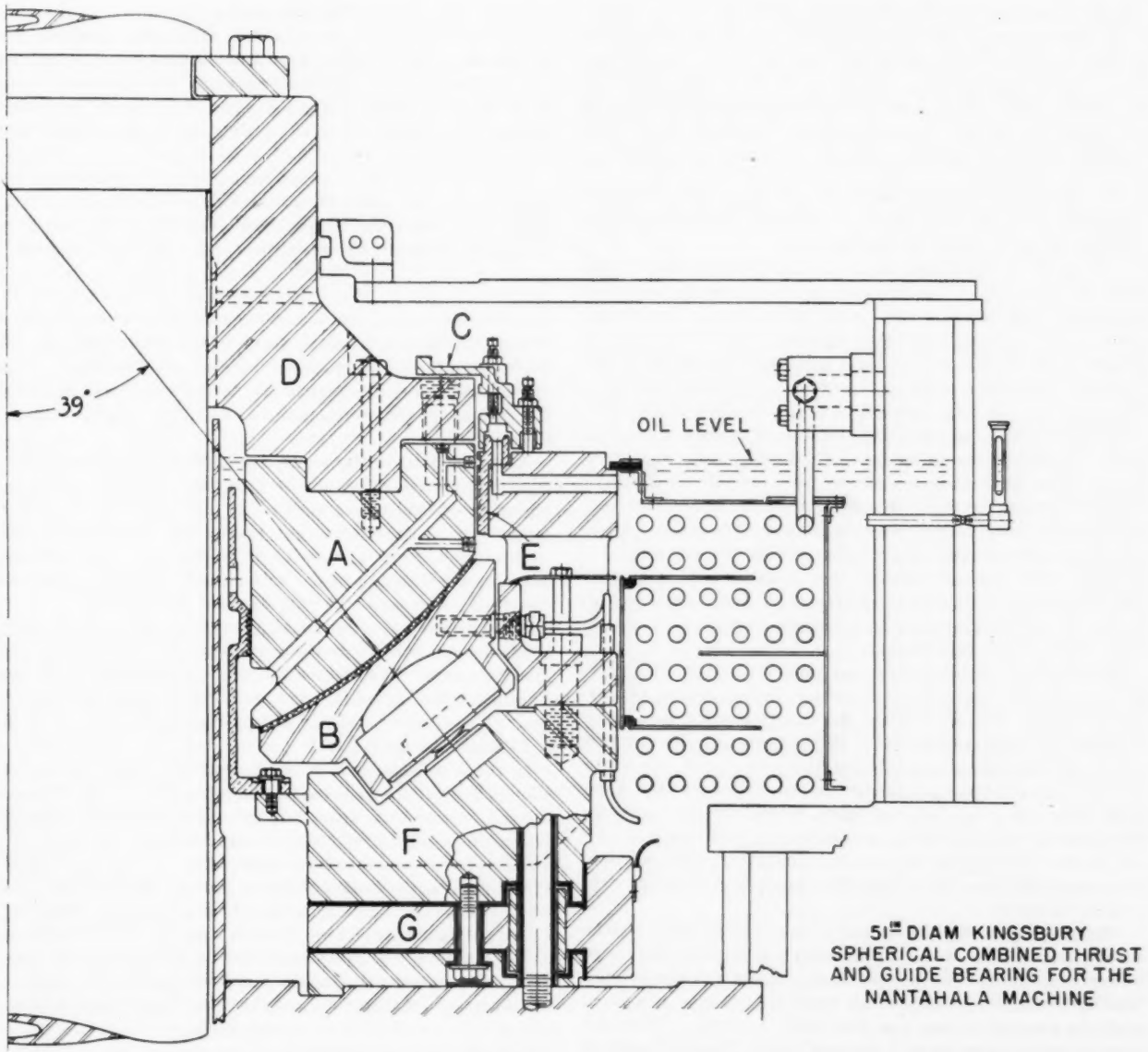


FIG. 10 SPHERICAL COMBINED THRUST AND GUIDE BEARING FOR THE NANTAHALA MACHINE; 51 IN. DIAM

runner is 101 fps or about 69 mph. Static pressure at the discharge ends of the pumping holes is 43 psi and about 35 gpm is circulated around the cooler tubes. This flow is increased by the centrifugal action of the runner surface on the oil in the spaces between the shoes.

Clearance between the air-seal ring *C* and the removable thrust block *D* is so adjusted that oil is maintained in this space, thus sealing the bath against entrance of air. The inner air-seal ring at the runner bore prevents air from entering the oil at that point. Due to these seal rings the top of the bath is clear and practically motionless.

In the unlikely event that the shaft should ever rise, a cylindrical bronze guide bearing *E* is provided. Radial clearance between the outside diameter of the thrust runner and the guide bearing is $^1/_{16}$ in., hence this emergency bearing is practically frictionless in normal operation.

Beneath the solid base ring *F* the bearing is provided with double insulation against shaft currents. A lead from the inter-base *G* makes it possible to test the insulation at any time.

The principal advantages claimed for the spherical thrust bearing are as follows:

1 The shaft is held in a concentric running position as if in a guide bearing of zero clearance.

2 Any inaccuracies of the thrust block and ring key are compensated for by the permissible rolling action of the spherical runner. Movement so induced at right angles to the direction of motion would be of small amplitude and practically unresisted by the fluid oil film. Hence galling between thrust block and shaft and shaft throwout at the turbine bearing due to thrust-block inaccuracies are eliminated.

3 The spherical bearing simplifies design of the thrust bracket by eliminating the cylindrical upper generator guide bearing and the special oil pump and piping usually required for its lubrication.

4 The spherical bearing is so constructed that at zero speed the babbitt faces of the shoes are segments of a true spherical zone and will bear equally against the runner. Thus equal shoe

loading is inherent, no field adjustments of loading are necessary.

5 The vertical center lines of bearing and shaft will intersect at the center of the runner sphere, but it is not essential that these center lines coincide. Hence equal shoe loading will obtain despite shifting of foundations and appreciable departure of the shaft from plumb. To obtain this self-alignment with a flat bearing requires the use of leveling-plate equalizing construction.

J. F. Roberts.[6] This 60,000-hp Francis-type turbine, operating under 925 ft net head, has set a new mark in American practice for high-head reaction-type turbines.

One point which strikes us as particularly important is the marked improvement which stainless steel shows as compared with either cast steel or rolled steel in resisting cavitation and scour erosion due to the high velocities under these relatively high heads. This further confirms data gathered in regard to cavitation of Kaplan and propeller-type wheels. Possibly the Europeans are right in their conclusions that it is well worth while to make the runners and some other vital parts entirely of stainless steel. In this particular case, had the runner, guide vanes, and facing plates been made of stainless steel, possibly all of the repairs required at the end of 2 years of operation might have been avoided. Until recently it has been impossible to secure a stainless-steel runner in this country, but during the war several of the steel foundries have enlarged their stainless-steel casting capacity and several stainless-steel runners are now being manufactured. It will be interesting to see whether or not these outlast their carbon-steel predecessors.

The fact that stainless steel was used in the butterfly valve both as the seal ring on the disk and seat in the housing with excellent results further confirms the data regarding its greater resistance to wear and erosion. While discussing the butterfly valve, the excellent streamlining on the downstream side of the disk so as to maintain practically uniform velocity as the water flows from the valve into the spiral casing deserves mention. The housing contracts rapidly so that there is no decrease in velocity as the water leaves the area surrounding the disk, which in this case probably occupies from 25 to 30 per cent of the effective area in the valve.

The company with which the writer is connected built a 30,000-hp impulse turbine of the double-overhung type for this same power company at about the time the Nantahala turbine was built. The difference in efficiency of an impulse turbine as compared with the reaction turbine was more than expected. While the impulse turbine gave about 1 per cent higher than the expected 88 per cent, or about 89 per cent, it still was over $4\frac{1}{2}$ per cent below the 93.7 per cent obtained on the Nantahala turbine. Mr. Growdon and the other officials of the Nantahala Power Company, in discussing this difference, agree with the writer that if we had had as much experience with high-head reaction turbines at the time of building these plants, both plants, that is, Glenville as well as Nantahala would have been of the high-head reaction type.

The tabulation showing the comparison in efficiency between the 22-in. model and the 85-in. Nantahala turbine deserves consideration, especially the increase of 9 per cent at half load from the model to the full-sized unit in the field. This is also one of the rare cases where the actual field tests showed a greater improvement in the plant than is indicated by the Moody formula, as the Moody formula would show only about 92.5 per cent efficiency as compared with the 93.7 per cent actually obtained.

While the Nantahala turbine is set with the center line of the spiral casing about 4 ft below the average tail water, the fact that serious cavitation noises occurred at loads slightly below rated capacity indicates the desirability of setting this type of turbine even lower in order to decrease such cavitation. Had this turbine been set some 4 or 5 ft lower than it actually was, we feel that the cavitation limit would have been materially improved, that is, larger capacity would be possible without cavitation noises and, undoubtedly, considerably less pitting and erosion would have shown up on the runner.

The authors are to be complimented on the frankness of their discussion in placing this valuable information before the Society. There is no doubt that this paper will be beneficial to many other prospective users of this specialized type of hydraulic equipment.

F. H. Rogers.[7] This paper is of great interest to both the operating companies and the turbine manufacturers as the use of Francis turbines for heads of about 1000 ft is exceptional. The authors are to be congratulated on the frank description of the original difficulties experienced and the corrective methods used. The maximum efficiency obtained of 93.7 per cent is indeed a splendid record.

As pointed out in the paper, the successful use of a Francis-type unit instead of the impulse type results in higher efficiency, higher speed, and lower cost. The difficulties to be guarded against are unstable operation, pitting due to cavitation, and wear of internal parts, caused by the extremely high velocities and abrasive materials in the water, and loss of the original efficiencies due to wear at the runner seals.

An interesting comparison with the Nantahala turbine is the 39,000-hp unit built by the writer's company for the Ixtapantongo Development of the Comision Federal de Electricidad in Mexico. This unit was designed for a net head of 1028 ft at a speed of 600 rpm. The specific speed is 20.3, only slightly less than the value of 21.6 given in the paper.

In the Nantahala unit a radial clearance of about 6 in. was allowed between the wicket gates and entrance to the runner vanes to result in smooth flow from the gates into the runner. For the Ixtapantongo unit the corresponding clearance was about $2\frac{1}{2}$ in. It is our experience that so large clearance is not necessary if wicket gates are so streamlined as to produce smooth flow. This smaller clearance results in decreased size of unit and lower cost.

The authors describe how the heavy upward hydraulic thrust on the bottom of the gate stems caused a deflection of the upper flange of the crown plate, which permitted the top of the gates to rub the upper wearing plate, and this friction prevented sufficient gate closure to stop the turbine completely.

This difficulty was avoided in the Ixtapantongo unit by extending the lower gate stems through stuffing boxes in the lower cover, thus eliminating all upward thrust.

The repairs made after 2 years of operation are of particular interest. It is noted that considerable wear occurred on the runner, throat ring, gates, curb, and crown-plate wearing rings and seal rings, and that these parts were repaired by welding the surfaces with 25-20 stainless-steel rods.

In the case of the Ixtapantongo unit, the same carbon-manganese steel (S.A.E. 1045) was used for the wearing rings and seal rings, and the same bronze inserts in the stationary seal rings. This unit, however, has been in operation only about 18 months, but the power company reported that an inspection made after the first year of operation showed no appreciable pitting or wear of the internal parts.

The authors speak of erosion or mechanical wear rather than pitting and the writer would like to know if this wear was caused by erosive action from sand or other abrasive materials in the water. It is noted that water is carried through an unlined pres-

[6] Manager, Hydraulic Department, Allis Chalmers Manufacturing Company, Milwaukee, Wis. Mem. A.S.M.E.

[7] Manager, Hydraulic Turbine Sales, Baldwin Locomotive Works, Philadelphia, Pa. Mem. A.S.M.E.

sure tunnel, which might result in foreign materials being present in the water.

It has been our practice to use 18-8 stainless steel on the runner vanes, gates, wearing rings- and seal rings to resist pitting rather than the higher chrome-nickel materials. We understand that recent tests made at the Massachusetts Institute of Technology indicated that a 17-7 stainless steel showed greater resistance to pitting than the higher combination of chrome and nickel.

It is quite possible that the 25-20 stainless steel used at Nantahala has a higher Brinell hardness and will stand up better where sand is present under these extremely high velocities. We would like to have the authors' opinions on this matter.

The efficiencies obtained on the field test as compared to the model test are unusual, as at best efficiency the prototype shows 93.7 per cent and the model 89.5 per cent; a gain of 4.2 per cent. The well-known Moody formula[8] would show for the runner sizes and heads stated, a gain of $3^1/_4$ per cent for a coefficient of $n = 0.25$, and a gain of $2^3/_4$ per cent for a coefficient of $n = 0.20$. The gain at part loads of 6 to 9 per cent over the model efficiencies is even more unusual, as such gains are rarely higher than at the maximum efficiency. Our company is of the opinion that the exponent $n = 0.25$ results in too high an efficiency for the prototype and is now using the value $n = 0.20$.

R. E. B. Sharp.[9] An efficiency of 93.7 per cent with a specific speed of 21.6 represents an important advance in hydraulic-turbine performance. Surrounding conditions, justifying large units of the Nantahala characteristics are rare, and unfortunately the conducting of field tests of such units is even rarer.

It is gratifying for those interested that the Aluminum Company has seen fit to test not only the Nantahala unit, but also four of the Shipshaw units as well, three Allis-Chalmers, and one S. Morgan Smith, with water measurements by the Gibson method and all with excellent efficiencies. The Smith unit attained a maximum efficiency of 93.6 per cent and was one of four built by S. Morgan Smith, Canada, Ltd.

The Ixtapantongo unit, which was designed under the writer's direction and built by The Baldwin Locomotive Works for the Comision Federal Electricidad of Mexico, has, regrettably, not been field-tested. This unit is also of the Francis type, with a rating of 39,000 hp under a net head of 1028 feet, with a specific speed at rated power of 21.8. It was put into operation during the summer of 1944, and therefore does not have as long a case history as the Nantahala unit.

In an effort to predict, on the basis of the Nantahala performance, the maximum efficiency which might be attained from a runner of still lower specific speed, the writer, in Table 1 of this discussion, has made a comparison of those estimated losses which vary most greatly with specific speed.

The disk losses include only the external runner surfaces, both of the crown and band. The Unwin formula

$$2.07 \times 10^{-10} \times \text{rpm}^3 \times \text{diam in ft}^5$$

was used. For the surfaces which depart from a disk shape a summation of small divisions was made. The clearance losses were obtained by determining the velocity head at the seals and deducting this from the head acting, using a coefficient of 0.5 through the area and allowing for the reduced head on the seals due to the centrifugal effect between the runner periphery and the seal location. The authors may be able to state the measured Nantahala clearance loss. The draft-tube losses were calculated assuming a draft-tube efficiency in all cases of 80 per cent. The shock losses are on the assumption that one tenth of the radial velocity head entering the runner is lost. All losses were calculated at best efficiency. While the aggregate losses not included in this comparison amount to more than the sums of those included, it is believed that this comparison gives a fair indication of what efficiency might be expected from a Francis turbine of still lower specific speed for possible use with an appreciably greater head than 1000 ft, that is, something over 92 per cent for such conditions would be in order with a runner of about 85 in. diam. An account[10] has been given of a unit of Escher Wyss design which attained from field test an efficiency of 91.4 per cent when developing 16,000 hp under a head of 918 ft, at a specific speed of 15.07. The diameter of this runner was only 70 in.

TABLE 1 COMPARISON OF ESTIMATED PERFORMANCE OF VARIOUS HYDRAULIC-TURBINE RUNNERS

	Shipshaw	Nantahala	Hypothetical unit
Specific speed at best efficiency	44.3	21.6	15
Speed, rpm	128.6	450	450
Head, ft	208.0	925.0	925.0
Horsepower at best efficiency	74000	60000	29000
Diameter of runner, entrance, in.	154	85	85
Diameter of top draft tube, in.	159.75	59.5	46
Radial clearance at seals, in.	0.0625	0.015	0.015
Disk loss, per cent	0.785	1.340	2.780
Clearance loss, per cent	0.578	0.650	1.007
Draft-tube loss, per cent	0.875	0.327	0.214
Shock loss at entrance, per cent	0.426	0.219	0.146
	2.664	2.536	4.147

The introduction of 80 gpm of clear water into the seals is an interesting feature, but the small amount used leads the writer to question the advantage gained thereby as a means of protecting the seal rings from the passage of foreign matter. Possibly the original reason for the introduction of this water was in connection with synchronous-condenser operation.

One of the principal advantages in obtaining well-conducted field tests, to the turbine designer, is the comparison thereof with the model performance, as this is the yardstick for use in future guarantees and designs. The Nantahala field test is unusual in that the step up in efficiency is so great. The Moody formula on the basis of the losses varying inversely with the one-fourth root of the runner diameters would result in a field efficiency of 92.5 per cent. A field efficiency of 93.7 per cent corresponds with an exponent of about $\frac{1}{2.6}$. Possibly one reason for the large increase might be in the relatively large model seal clearance. For this value to be homologous on the model it would be

$$0.015 \times \frac{22}{85} = 0.0039 \text{ in.}$$

which is an impracticably small value.

On the lower portion of Fig. 11 of this discussion is shown the model curve as compared with the field, as plotted from the data in the authors' paper. It is noted that the guarantees at part load are disproportionately higher than the model curve which falls off quite rapidly. Further information in regard to this point would be of interest.

On the upper part of Fig. 11 a comparison is given of the Shipshaw field and model tests of the Smith unit tested. In this

[8] Moody formula:

$$E_p = 100 - (100 - E_m)\left(\frac{D_m}{D_p}\right)^n \times \left(\frac{H_m}{H_p}\right)^{0.01}$$

where

E_p = efficiency of prototype
E_m = efficiency of model
D_p = runner diameter prototype
D_m = runner diameter model
H_p = effective head on prototype
H_m = effective head on model

[9] Consulting Engineer, S. Morgan Smith Company, York, Pa. Mem. A.S.M.E.

[10] "Vemork Reaction Turbine Operates Under 918-Ft Head," Escher Wyss & Company, *Power*, vol. 73, Jan.-June, 1931, p. 630.

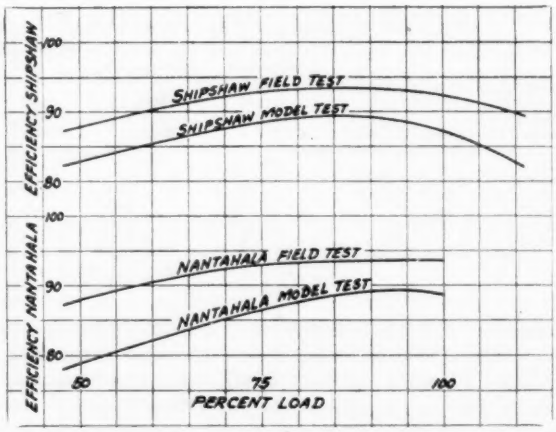


FIG. 11 EFFICIENCY CURVES OF MODEL AND FIELD TESTS OF NANTAHALA AND SHIPSHAW TURBINES

instance the 19.5-in-diam model attained 89.6 per cent efficiency. The Moody formula steps this up to 93.8 per cent field efficiency, which agrees quite closely with the actual value of 93.6 per cent. Both the Shipshaw and Nantahala field tests show satisfactorily high part-load efficiencies, with the Nantahala values somewhat higher if they are both brought to the same percentage of load for maximum efficiency.

The authors make no mention of presence or absence of foreign matter in the water, but it would appear that there is some abrasive matter present, and possibly some degree of acid content. The writer had occasion to examine the seals of Units N5 or N6 at Boulder after about a year of operation under a head above 500 ft, and found the clearances on the average slightly less than when the units were installed, due to the deposit, in some places, of verdigris on the white brass inserts in the stationary rings. The Boulder water was, during this period, exceptionally free from abrasive matter.

The substitution on the Nantahala turbine, of stainless steel on the stationary wearing ring for bronze, while showing gratifying results from the standpoint of maintained low leakage loss, appears questionable to the writer from the standpoint of safety during possible runaway speed. Assuming a runaway speed of 725 rpm, which is believed to be conservative, calculations made indicate an expansion at this speed of about 0.008 in. on the radius, leaving 0.008 in. as the clearance under that condition or a possibility of this being reduced to 0.003 in. if the shaft swings to its extreme position in the bearing. Even though the rotating and stationary seal surfaces are not subject to galling, the presence of two broad surfaces of hard metals under this admittedly abnormal condition might result in violent seizure due to heating after contact. In view of the excellent resistance of stainless steel for these surfaces, as brought out by the authors, labyrinth seals of this metal along the lines used in steam-turbine design might be a good solution from all standpoints.

On the Ixtapantongo unit mentioned the lower gate stems extended through stuffing boxes in the bottom, or curb plate, and were of the same diameter as the upper stems. This was for the purpose of avoiding the heavy upward thrust on the stems, and also of avoiding the loss of grease due to water passing under the lower ends of the stems and forcing the grease upward on the sides of the stems nearest the runner.

The writer wishes to congratulate Mr. Terry on the excellent design and performance of the Nantahala turbine, and all of the authors on the frank manner in which they discuss the difficulties encountered. This attitude is of distinct long-range benefit both to manufacturers and users.

AUTHORS' CLOSURE

The extent and quality of each of the several discussions is greatly appreciated by the authors. These discussions add greatly to the value of the paper.

While the spherical Kingsbury thrust bearing is installed on the generator, it is of course an essential part of the turbine as well. Mr. Needs's description of the design and construction of this bearing is most interesting and timely. So far, the bearing has functioned perfectly and we would definitely favor its use for hydroelectric units.

Mr. Roberts has misinterpreted the statement in the paper with respect to cavitation noises in the draft tube, since these noises only occur at loads above rather than slightly below the rated load for the various heads. The turbine operates regularly at between 45,000 and 46,000 kw under a net head of 951 ft without cavitation noises in the draft tube.

Several of the discussers raised questions relative to the presence of abrasive materials or acid in the water. The tunnel is driven through hard insoluble Arkose rock. It is unlined except near the portals. It was thoroughly cleaned and washed out before being filled. The washing removed most of the rock dust and small gritty particles. Some rock dust remained and was taken out by the water during the first few hours of operation. The water velocity in the unlined section of the tunnel at full load is approximately 4.75 fps, which is insufficient to transport loose material through the tunnel. Practically no rocks or sand have been found in the rock catcher, which is located at the end of the unlined tunnel just before the water enters the steel penstock. Except for the first few hours of operation, we believe that no sand or rock dust has passed through the turbine.

The drainage area is generally heavily wooded, with oak trees predominating. The water from this drainage area is therefore slightly acid. It does not affect the rate of corrosion.

The runner seal-ring clearances for the turbine model were 0.008 in., or relatively twice as large as for the main unit, which partly accounts for the large step up in efficiency, particularly at the lower percentages of output.

While the bulk of the welding with stainless was done with a 25-20 rod, some repair work was done in the field using 18–8 and 17–7 rods. These three grades of stainless rods have apparently stood up equally well in the field. 25–20 was selected because of the manufacturer's experience with the application of this grade. The resulting deposit, is, of course, diluted by the parent metal in any case, dilution varying somewhat with welding technique. The 25–20 rod is quite readily applied, and the resulting weld is somewhat more ductile than the other two.

The 80 gpm of cooling water supply to the runner seal rings was intended for use if the unit was operated as a synchronous condenser and not for the exclusion of any foreign matter. The unit is not, however, used as a synchronous condenser but the operators make a practice of turning on the seal water just before starting the machine. The supply valves are left open as long as the unit is in operation. The actual necessity for this procedure is questionable but it is certainly on the safe side. The seal supply pressure is limited. Consequently, the supply line is provided with a check valve to keep the water from backing up in the line as the turbine wicket gates are opened and the pressure builds up in the seal spaces.

The Ixtapantongo unit described by Mr. Rogers is of considerable interest. Experience with that unit for the first year closely parallels that of the Nantahala Unit. It was only after two years of operation at Nantahala that the extent of the wear with the carbon steel was appreciated. In other words, carbon steel stands up satisfactorily under this head for a limited time but it is the authors' opinion that stainless is needed for long-time trouble-free service.

New Developments in Combination Controls

By J. W. KELLY,[1] BURBANK, CALIF.

This paper deals with combination controls, which present advantages of weight and cost saving which in recent years have been greatly enhanced by the dependability and ruggedness which can be built into them. Small electric motors, developed for aircraft-accessory operation, have permitted the construction of motor-operated valves. Both solenoid- and motor-operated valves now give the aircraft designer a wide choice of control characteristics. New methods and improvements in older types of follow-up systems for hydraulic controls are discussed in the paper.

Introduction

COMPETITION between mechanical, hydraulic, and electrical modes of actuation has, through the last few years in the aircraft industry, produced certain results that would probably not have been obtainable otherwise.

After maximum efficiency with minimum weight had been obtained from each separately, it became obvious that combinations of the mechanical, hydraulic, and electrical systems, utilizing the best of each, would produce results heretofore unobtainable.

Hydronic Units

Realizing this condition, the author's company undertook a program several years ago of developing what we term "hydronic" controls (hydraulic-electrical combinations) and various mechanical-hydraulic combinations.

Solenoid Valves. The first of the hydronic units (the electrical-hydraulic combination) to be developed were the solenoid-operated selector valves. The field of available solenoids was thoroughly covered for possible standard units usable to operate selector valves. Unfortunately, none was found that came within our weight expectations; therefore a series of developmental solenoids were made. The results of tests on these solenoids set up the general type of solenoid to be used for valve actuation. One of the first solenoids put into production is the one shown in Fig. 1, which, with a weight of 21 oz, gives a pull of 60 lb over a stroke of $^1/_8$ in. at 18 volts. This solenoid was designed for intermittent operation and would reach a maximum temperature of 250 F after several hours of continuous operation.

Still not satisfied with the original solenoids, attempts were made to reduce the weight further. Finally a double-coil arrangement was worked out with a primary and secondary coil. When the solenoid is first energized, both coils contribute to the pull. The plunger, upon reaching the end of the stroke, operates a switch as shown in Fig. 2, interrupting the current to the primary coil, allowing the secondary coil to apply a holding pull. Thus an instantaneous high-amperage input operates the valve; and the secondary coil, with low-amperage input, taking advantage of the principle that pull increases inversely to the air gap, holds the valve in the desired position. This type of solenoid gives an exceedingly high pull with a minimum of weight.



Fig. 1 First Solenoid Design; Weight 21 Oz

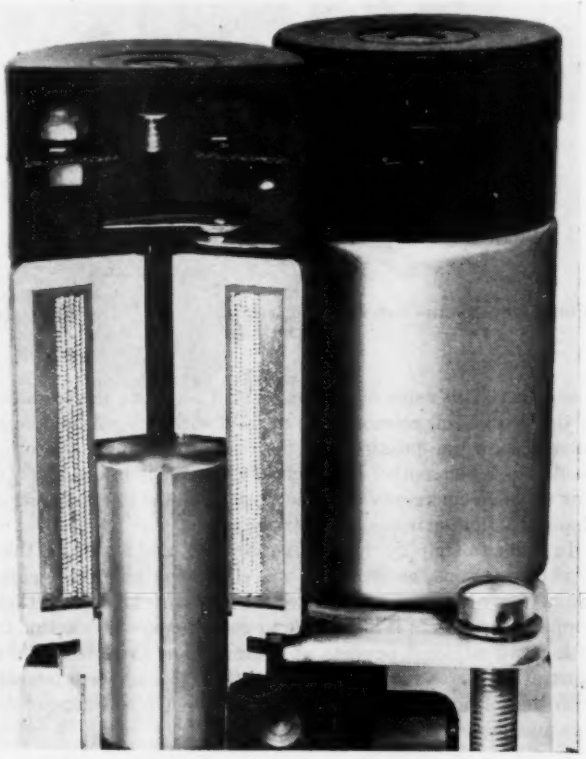


Fig. 2 Improved Solenoid Design; Weight 15 Oz

Having developed a suitable solenoid, a valve had to be designed to utilize the high-pull and short-stroke characteristics of the solenoid. One of the first solenoid valves built by the company used a rocker arm but did not require a neutral position. A 30-lb spring loads the rocker arm in one direction; the solenoid pulls 60 lb, thus 30 lb is available in both directions.

Fig. 3 indicates a valve having a rocker arm operated by dual

---

[1] Chief Engineer, Adel Precision Products Corporation.

Contributed by the Industrial Instruments and Regulators Division and presented at the Aviation War Conference, Los Angeles, Calif., June 11–14, 1945, and at the Annual Meeting, New York, N. Y., November 26–29, 1945, of The American Society of Mechanical Engineers.

Note: Statements and opinions advanced in papers are to be understood as individual expressions of their authors and not those of the Society.

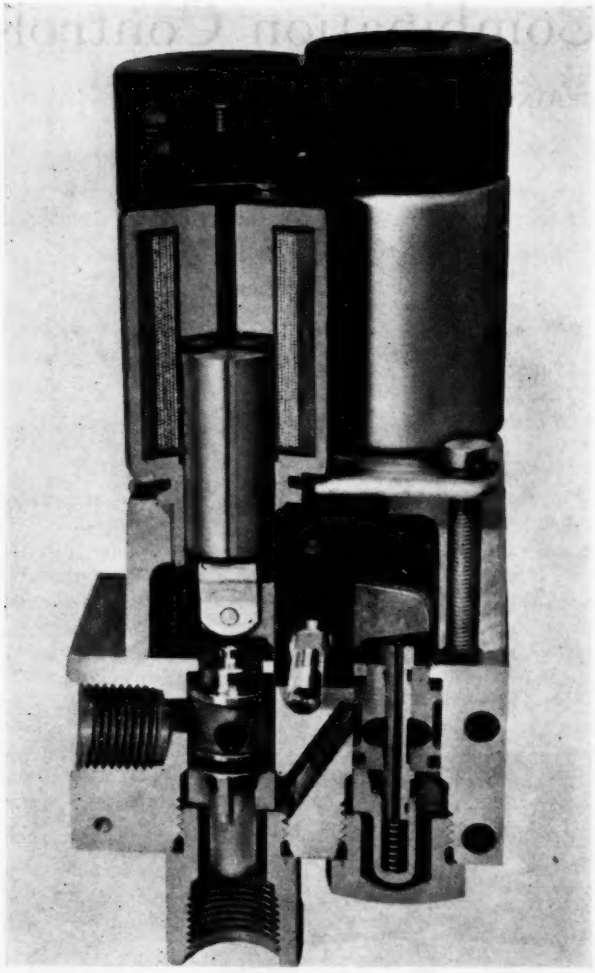


FIG. 3 SOLENOID-OPERATED SELECTOR VALVE, INCORPORATING ROCKER ARM

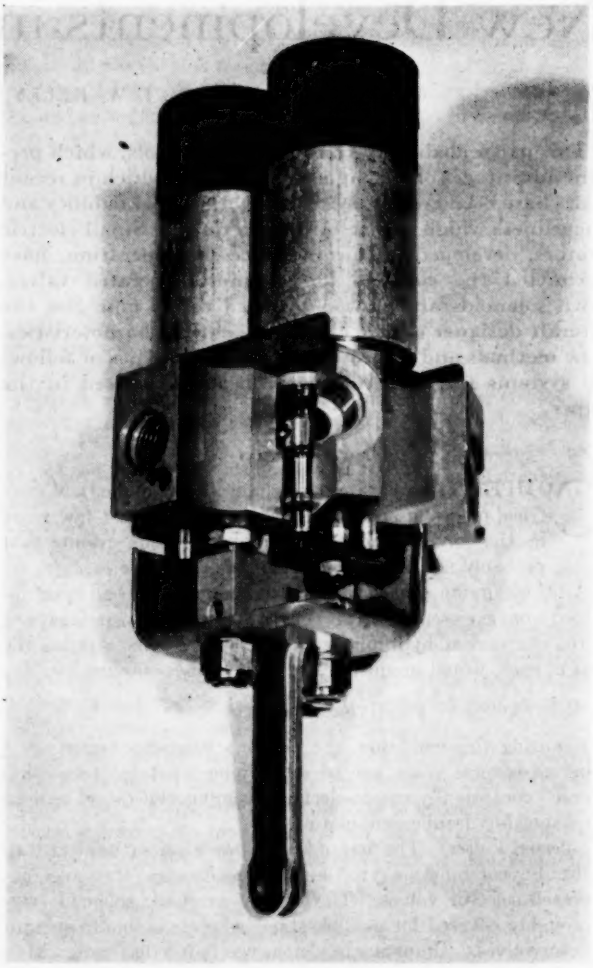


FIG. 4 SOLENOID-OPERATED SELECTOR VALVE; CROSSBAR REPLACES ROCKER ARM

solenoids. This valve requires a neutral position; therefore two of the double-coil solenoids are utilized with one solenoid being energized for one position and the other solenoid for the other position. When neither is energized the valve is in neutral. On this valve an emergency override lever is added to allow for mechanical actuation in case of electrical failure.

In order to simplify design, over-all cost, and weight, a third type of actuation, as in Fig. 4, was developed which eliminated the need for a rocker arm. Because of the pressure and return-poppet arrangement it is possible to get a 4-way-valve action by lifting two adjacent poppets at a time; thus as shown in this illustration, a crossbar is put between these two adjacent poppets with the solenoid pulling on this crossbar. On this type of design manual actuation is easily provided.

Various types of valves for operating pressures of 1500 and in some cases 3000 psi, including the shutoff, 3-way and 4-way, have been designed for solenoid actuation having single solenoids, utilizing spring returns or double solenoids with and without rocker arm.

Electric-Motor-Actuated Valves. The advent of small inexpensive electric motors allows motor-operated valves to become competitive with solenoid-operated valves. Although the cost of the motor-operated valve is slightly higher at present, proper production engineering on either motor or solenoid valves may give either the cost advantage. Over and above cost consideration, performance requirements may dictate the use of either mode of actuation in that both have advantageous characteristics for particular applications.

Solenoid actuation has the advantage over motor actuation in conventional selector valves requiring a neutral position. Limit switches are required to obtain a neutral position in motor-operated valves; whereas, it is a natural function with solenoid-operated valves. Obviously, this advantage is lost to solenoid actuation on valves requiring no neutral position.

Emergency manual override is easier to obtain on the solenoid-operated valves, due to the free movement allowed in a solenoid when the current is not energized. A manual override on a motor valve leads to complications in design. Solenoid valves have the advantage where fast actuation is required, operating in a fraction of a second, whereas the time of motor-operated valves is usually measured in seconds. This applies, however, to direct-connected conventional poppet-design solenoid valves and not to pilot-operated valves which are inclined to be somewhat slow and erratic in operation.

Extremely high starting loads, usually obtained in the larger valves, are handled more effectively by motors which give out high initial torque as against the low initial torque of a solenoid.

A motor-operated valve can be readily designed to stay in

either extreme position without being energized, whereas a solenoid requires continuous energizing to hold its position, unless locking mechanism is provided.

In the weight-comparison graph shown in Fig. 5, solenoid valves are seen to be lighter in the smaller sizes than motor-operated valves, with the lines crossing slightly above the 1/2-in-size valves. Above 1/2-in-line size, the motor-operated valves have definite weight advantages.

Power Package. The power package, a combination of electrical and hydraulic units, has provided the industry with another unit of extreme versatility with weight saving. Several years ago, when the need presented itself for a valve actuator required to hold the valve in extreme positions for a protracted period of time, the device shown in Fig. 6 was developed. An electrical-mechanical actuator, originally contemplated, presented overheating problems when held in a stalled position. By utilizing a small electric-driven gear pump, taking fluid from the return side of the valve, a simple reversible pump-and-cylinder combination was worked out, providing easy actuation of the valve with a minimum of weight. No overheating problems were present due to the built-in leakage in the gear pump and the cylinder.

This device led to the development of a power package for actuation of landing gears and flaps for light aircraft. This unit combines a motor-driven gear pump, submerged in the hydraulic reservoir; the reservoir is surrounded by a glass tube, allowing visual inspection; an integral selector valve allows positioning; by-pass valve avoids any possibility of overflowing the reservoir; and a built-in relief provides adequate thermal protection. This unit weighing 4 3/4 lb, dry, has an output of 1/2 gpm at 300 psi operating pressure.

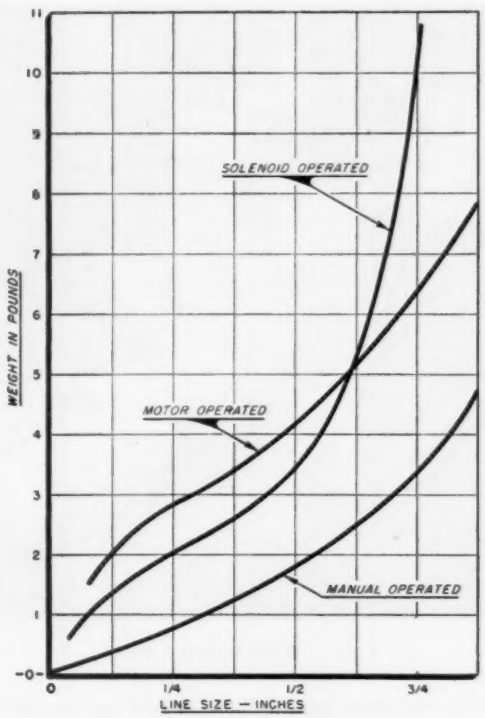


FIG. 5 RELATIVE WEIGHTS
(Manual, solenoid- and motor-operated 4-way selector valves.)

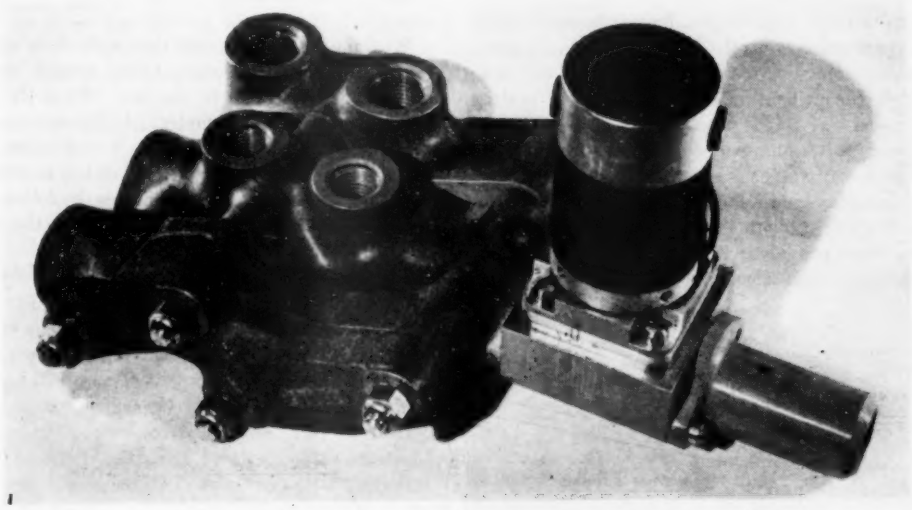


FIG. 6 ELECTRICAL-HYDRAULIC ACTUATOR

Later requirements for a heavier-duty unit dictated a slightly sturdier design as shown in Fig. 7. Designed primarily for emergency power stand-by, it incorporates a motor, pump, reservoir, relief, and pressure and return ports. The glass-reservoir cover is replaced by a casting, with fluid level being easily determined by the use of a dip stick. Provision is made for the adaptation of the Adel Stacking Midget[3] (a manifold-type selector valve), thus a package unit can be obtained incorporating a motor, pump, reservoir, relief valve, auxiliary pressure and return ports, and/or 1, 2, 3 or more selector valves. This unit gives 800-psi output at 0.7 gpm with 1/3 gal capacity for 11 lb weight, dry.

Another problem, somewhat different from the others, led to the development of the pump-and-tank combination which forms the basis of a power package. Difficulties in pumping oil at 35,000 to 40,000 ft altitude led to this particular pump design, which shows no cavitation effects at high altitude under high- or low-temperature conditions. The unit has a pump, motor, reservoir, with a built-in relief; selector valve, and other hydraulic components can be added to produce a power package which gives 6-gpm flow at 1000 psi with a weight of 37 lb. The

[3] "Hydraulic Control Standardization," by J. W. Kelly, *Aero Digest*, vol. 41, Dec., 1942, pp. 211–212, 215–216, 218, 276, and 279.

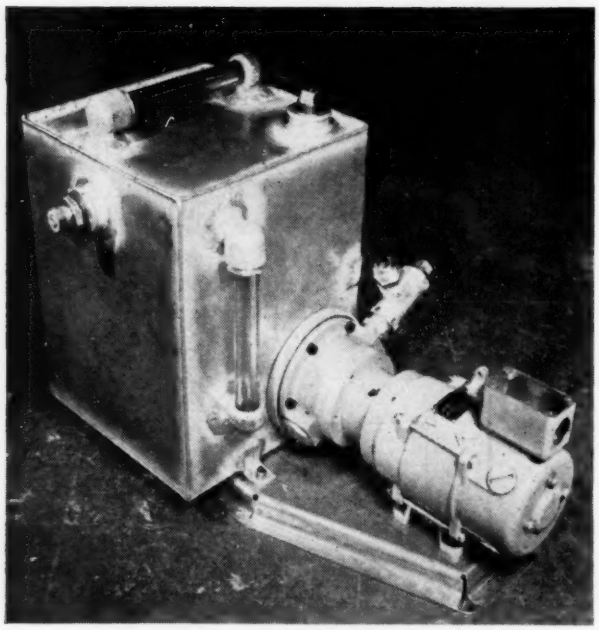


FIG. 7 HIGH-ALTITUDE PUMP

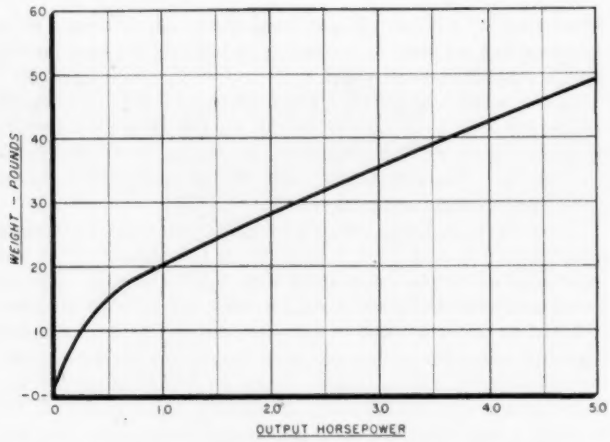


FIG. 8 WEIGHT OF ELECTROHYDRAULIC POWER PACKAGES AT VARIOUS HORSEPOWERS

weights of the power packages are plotted against output hydraulic horsepower in the curve, Fig. 8. It is interesting to note the slope in the horsepower ratings below the 1-hp point.

POWER POSITION CONTROLS

The need for combination controls is definitely brought out in the field of the power position control. Utilizing hydraulic power as the desirable power source, three different types of follow-up systems which allow the utilization of efficient power position control will be discussed.

Mechanical Follow-Up. A simple mechanical follow-up system applied to hydraulic 4-way valves is shown in Fig. 9. We have developed several planetary-gear follow-up systems; but find that this walking-beam system, through sheer simplicity, has much to offer. The walking beam provides a simple follow-up mechanism on a sensitive rocker-arm-type selector valve. Movement of the master or control lever, opens the valve which in turn operates the power cylinder; displacement of the follow-up mechanism shuts off the valve when the cylinder reaches the desired position. Being of a simple and straightforward type, motoring and hunting and other difficulties usually present in power position controls, are absent.

Hydraulic Follow-Up. Another method, shown schematically in Fig. 10, utilizing the "Adel isodraulic" system, has a hydraulic follow-up. It offers many advantages in weight saving, installation, simplicity, and smooth operation. It consists basically of three cylinders in parallel; cylinder 1 forming the master unit, cylinder 2 the valve-operating unit, and cylinder 3 the follow-up unit.

Working on the principle that with three cylinders in parallel, one being held, the second being moved, the third will move an amount equivalent to the first. Thus the follow-up cylinder is held by the power cylinder. As the master cylinder is moved, the second cylinder operates the 4-way valve which in turn applies pressure to the proper side of the power cylinder. Movement of the power cylinder operates the follow-up cylinder which automatically shuts off the valve when the desired position is reached.

Electrical Follow-Up. Utilizing the electric control on hy-

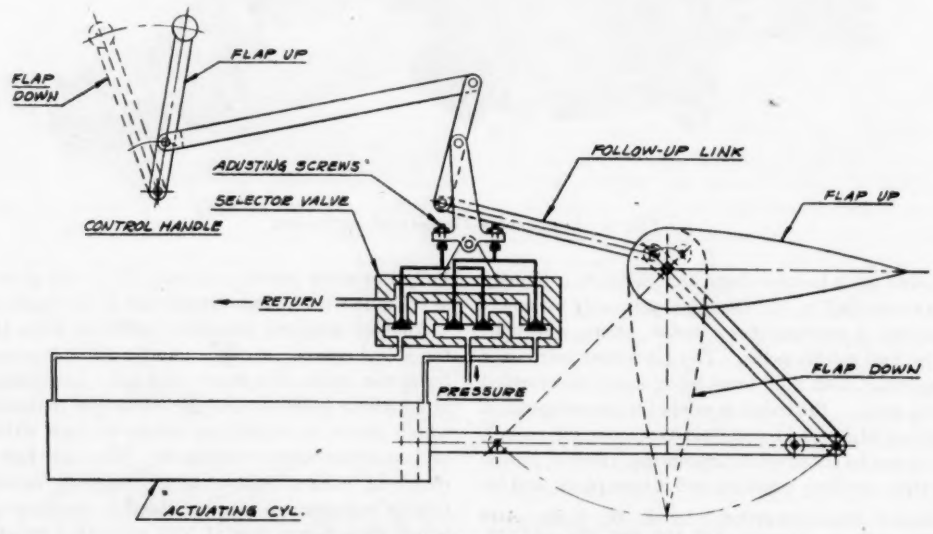


FIG. 9 SCHEMATIC OF MECHANICAL FOLLOW-UP SYSTEM

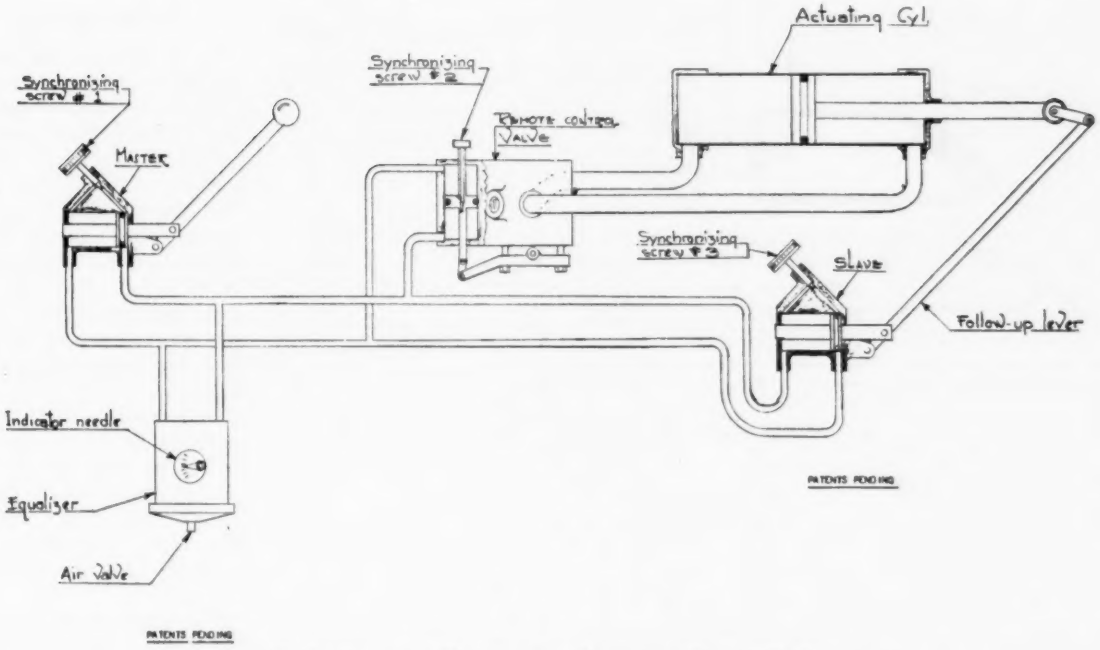


FIG. 10 SCHEMATIC OF HYDRAULIC OR ISODRAULIC FOLLOW-UP SYSTEM

draulic power, through the medium of a solenoid 4-way valve, another type of power-position-control combination is presented. Fig. 12 shows such a hydronic follow-up system. The master potentiometer upsets a bridge relationship with the follow-up potentiometer; thus the relay control box actuates the solenoid valve which in turn allows the cylinder to go to the desired position at which the follow-up potentiometer shuts the valve off.

"Hydronic" system, for long distances, is the lightest of the three, as shown in the graph, Fig. 13. Up to around 50 ft distance, the isodraulic position control enjoys weight advantages; and below 20 ft distance the mechanical system is the lightest.

Other factors, however, invariably enter into the follow-up choice. Actual position indication and system "feel" are naturally obtained in the mechanical and isodraulic; whereas, no feel is obtainable in the hydronic. Long distances are easiest to install with the hydronic, with the isodraulic coming second, and the mechanical third. The isodraulic and mechanical follow-up systems are self-contained and not dependent upon any outside source of power for actuation and followup; whereas, electrical power is required for hydronic operation. Multiple installations are easier to obtain electric-wise, requiring only slight revisions in circuits. For utmost simplicity and comprehension, when servicing in the field, the mechanical would rate first; with isodraulic second; and hydronic third.

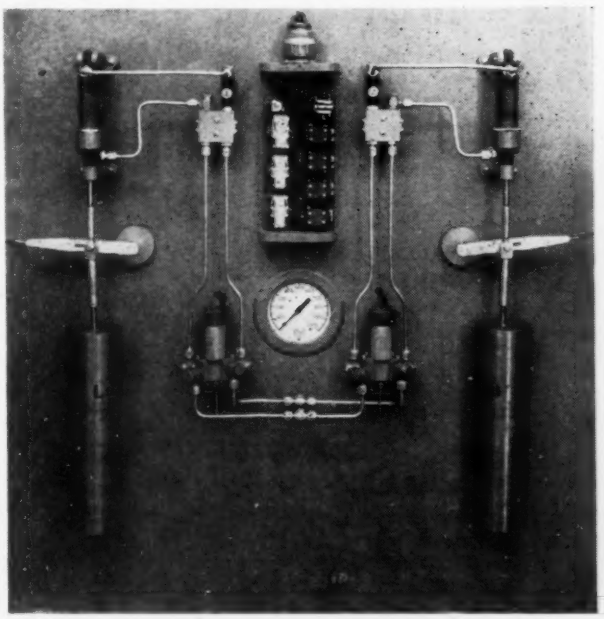


FIG. 11 ELECTRICAL OR HYDRONIC FOLLOW-UP SYSTEM

CONCLUSION

Combination controls have presented many features which have and will be used to weight- and cost-saving advantages in the future as well as in the past. Actual manufacturing experience and operation of solenoid valves over the past several years have given much desirable and worth-while knowledge which allows us to design into these units more dependability and ruggedness than originally conceived.

Utilization of small electric motors, currently being supplied on other aircraft devices, has allowed us to design and build dependable motor-operated valves. Both solenoid- and motor-operated valves appear to be permanently in the picture and give the aircraft designer a wide choice of characteristics from which to choose.

The power package is beginning to come into its own; and as further improvements are made, weight-savings and operational advantages will become more and more apparent.

New methods and advancements of old methods on follow-up systems for hydraulic controls, utilizing basically mechanical, hydraulic, and electrical combinations, give to the industry versatility with smooth hydraulic power.

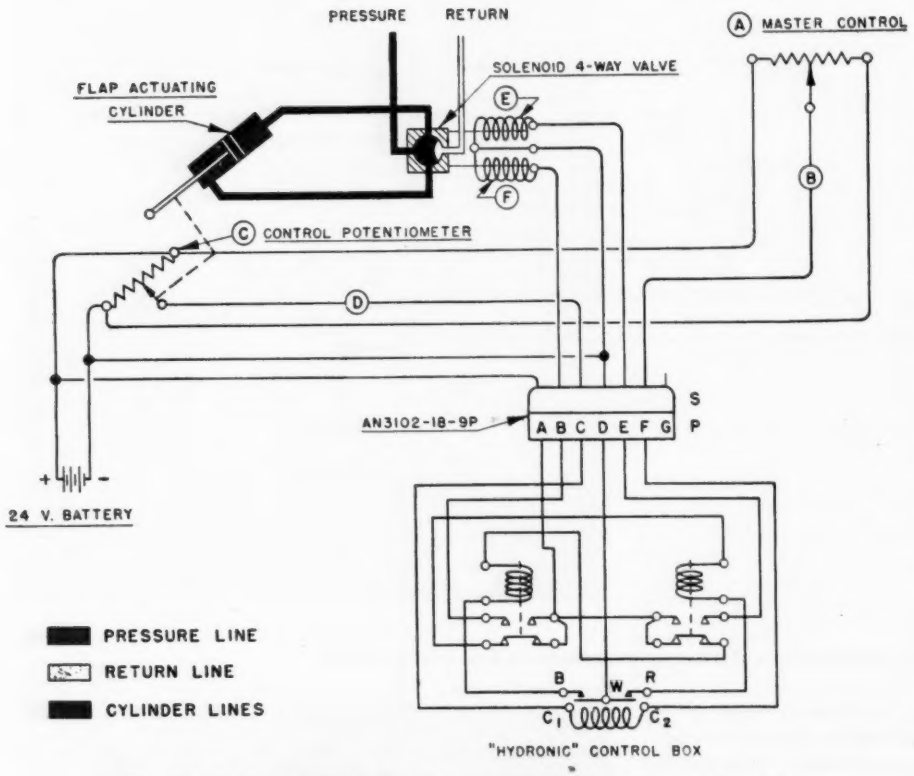


FIG. 12 SCHEMATIC DIAGRAM OF FOLLOW-UP SYSTEM SHOWN IN FIG. 11

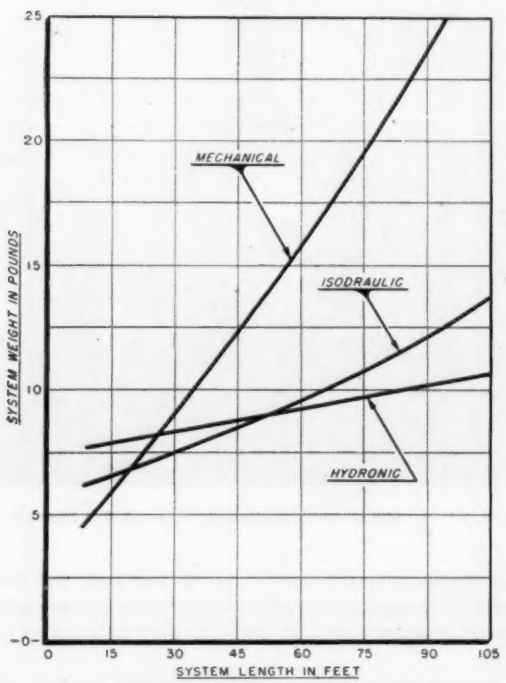


FIG. 13 RELATIVE WEIGHTS OF POWER-POSITION-CONTROL SYSTEMS

Discussion

R. A. GUND.[3] In discussing combination controls for aircraft, the author assumes that hydraulic power is the desirable power. It should be pointed out that for minimum weight the desirable power source may be either hydraulic or electric, depending on the characteristics of the load. Another factor which must be evaluated is the power supply on the aircraft—is it principally hydraulic or electric?

On large airplanes, where the power applications are generally located at some distance from one another, hydraulic lines are more difficult to run than electric wires. In military craft hydraulic lines are much more vulnerable.

The most versatile system would be one employing electric distribution with either electric or hydraulic power applied at the load, depending upon individual requirements. If, for instance, the load requires a starting torque of less than 6 times rated torque, an electric motor should be used to drive the load directly. This will result in minimum weight and maximum efficiency. On the other hand, if a very high torque load must be driven, hydraulic power can be advantageously applied by the use of the combination power package.

As an example, a split series-wound motor driving a screw jack could be directly substituted in place of the solenoid 4-way valve and hydraulic cylinder shown in Fig. 12.

Hydraulic power is most suitable for storing energy, as in power-boost systems and for hydraulic brakes.

Thus we may conclude that for minimum weight and maximum dependability all factors should be considered, and hydraulic power used only if it gives the most desirable results.

AUTHOR'S CLOSURE

In this paper the author has tried to avoid the controversial argument of hydraulic versus electrical modes of control. However, the author's assumption that hydraulic is the more desirable power source is further emphasized by Mr. Gund, and the arguments on the relative weight values of hydraulic and electric systems should be considered along with the many other factors involved before deciding which is the more desirable as a system.

---

[3] General Electric Company, Schenectady, N. Y.

The Effect of Measurement Dead Time in the Control of Certain Processes

By D. P. ECKMAN,[1] PHILADELPHIA, PA.

The purpose of this paper is to report on a series of automatic-control tests which demonstrate the importance of instantaneous controller-mechanism response in self-balancing potentiometer controllers. The automatic-control tests were made with both two-position and proportional-reset control. Other tests, dealing with the importance of measurement dead zone of the controller, are included, noting the relation between dead zone of measurement and dead time of controller response.

Introduction

ONE of the most important factors in automatic control of industrial processes is the manner in which the controller mechanism responds to changes in the measured variable. This measuring lag, as it is often called, forms an extensive part of the input-output controller-response relationship.

Generally, the factors of measurement dead time and dead zone are neglected in process-control analysis, particularly in mathematical analysis where their inclusion results in complications of a high order. Therefore it seems desirable to investigate the effect of these factors in automatic control in order to aid in the application of theoretical or empirical data to control problems.

Potentiometer controller mechanisms which incorporate continuous rather than periodic principles of rebalancing provide an opportunity for comparison test of these types of measuring means. Under simulated control conditions it is possible to analyze the dynamic action of the control system and the effectiveness of continuous measurement.

The measuring lag of a temperature controller is composed of two main parts: the lag of the primary element, and the lag of the controller detecting mechanism. It is this second part of the measuring lag, that due to the detecting mechanism, which we wish to study. For purposes of discussion we may classify the many methods of operation of self-balancing potentiometer controllers under two general types, i.e., periodic action and continuous action. A periodic-action potentiometer (recording type) is generally identified by a periodic mechanical system for detecting the position of a galvanometer pointer. When an unbalance of voltages is produced by a change in measured temperature, the detecting mechanism determines the amount of unbalance and drives a voltage divider or slide wire to balance against the new value of measured voltage. The periodic-action potentiometer is in wide general use for both measurement and control of process variables.

The continuous-action potentiometer (recording type) is generally identified (1)[2] by the use of continuous uninterrupted drive means, usually electronic, for obtaining the balance of measured against standard voltages. The use of continuous action in potentiometer balancing eliminates any lag due to a rebalancing mechanism, and avoids periodicity whereby a small dead time may elapse before changes in controlled temperature can be detected.

Tests With Two-Position Control

In order to determine the effect of dead time in the measuring system, it is desirable to conduct tests of two-position control. By this means all extraneous factors may be eliminated from the tests of automatic control. Processes were selected on the process-analog control board (2) by using various combinations of capacitance, resistance, and dead time.

The reaction curves for the processes to be tested are shown in Figs. 1 and 2. A reaction curve is determined by setting the

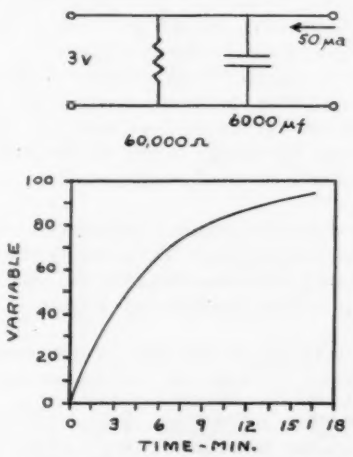


Fig. 1 Diagram and Reaction of Process No. 1

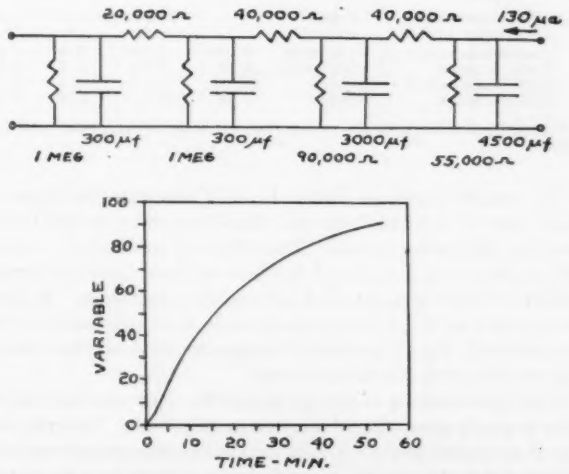


Fig. 2 Diagram and Reaction of Process No. 3

---

[1] Development Engineer, The Brown Instrument Company. Jun. A.S.M.E.

[2] Numbers in parentheses refer to the Bibliography at the end of the paper.

Contributed by the Industrial Instruments and Regulators Division and presented at the Annual Meeting, New York, N. Y., Nov. 26–29, 1945, of The American Society of Mechanical Engineers.

Note: Statements and opinions advanced in papers are to be understood as individual expressions of their authors and not those of the Society.

valve position and allowing the measured variable to balance. A small sudden movement of the valve to a new fixed position will result in gradual increase of the measured variable to a new balanced value. The resulting time rate of change of the measured variable is the reaction curve. All processes indicate that self-regulation is present. Although the reaction curves are shown for only one direction of change, it may be assumed that the negative change produces a similar curve.

Process No. 1, shown in Fig. 1, is essentially a single-capacity process with a time constant of about 6 min, which is the time required to achieve 63 per cent of final value. Process No. 2 is identical in characteristics except that a dead time of 0.1 min was introduced between controller action and resultant valve movement.

Process No. 3, shown in Fig. 2, is a two-capacity process and thus involves slight transfer lag as can be noted by the slower initial rate of change on the reaction curve. Process No. 4 is identical in characteristics except that a dead time of 0.25 min was introduced between controller action and resultant valve movement.

Each process analog was connected, in turn, to the potentiometer controller. Each potentiometer controller, a periodic-action type and a continuous-action type, was fitted with both pneumatic and electric two-position "on-off" control. Pneumatic control was accomplished through a pneumatic diaphragm mechanism. The proportional band (throttling range) of the pneumatic on-off controllers was 0.6 per cent of controller scale. The on-off pneumatic controller is not actually a two-position controller but is a proportional controller with a very narrow band. This controller, however, is commonly termed on-off. Electrical control was arranged so that the control contacts directly actuated the energy supply to the process. The differential gap of both electrical on-off controllers was 0.05 per cent of controller scale.

With all process and controller combinations, a cycle of controlled variable was recorded. The resulting control cycle is described in Table 1 which shows amplitude, and Table 2 which shows period of cycle of the controlled variable.

TABLE 1 AMPLITUDE OF CONTROL CYCLE; PER CENT SCALE

Potentiometer controller with	Type of control	Process no. 1	2	3	4
Continuous action	Pneumatic	0.12	4.2	2.2	5.4
Periodic action	Pneumatic	1.80	4.6	4.2	7.1
Continuous action	Electric	0.25	3.8	2.3	6.1
Periodic action	Electric	1.00	4.2	4.0	6.8

TABLE 2 PERIOD OF CONTROL CYCLE; MINUTES

Potentiometer controller with	Type of control	Process no. 1	2	3	4
Continuous action	Pneumatic	0.10[a]	0.28[a]	2.4	4.5
Periodic action	Pneumatic	0.50	0.80	3.7	5.0
Continuous action	Electric	0.03	0.25	2.4	4.7
Periodic action	Electric	0.27	0.67	3.9	5.0

[a] Actually throttling to the extent that valve never completely opens or closes.

The results shown in Tables 1 and 2 illustrate the improvement caused by eliminating the dead-time delay in the potentiometer measuring means. This effect is particularly noticeable in processes Nos. 1 and 3, where all dead time in the controlled system is concentrated in the measuring means. In processes similar to No. 4 where considerable dead time exists in the process itself, the elimination of measurement dead time results in proportionately less improvement.

Dead time existing in any portion of the controlled system results in nearly proportional increase in amplitude. It is obvious that if automatic control is to maintain an adequate process balance then dead time in the controlled system must be reduced to a minimum.

Applying the results of these tests to applications of automatic control, it is probable that in electrically heated furnaces and baths where the process lags are very small, the elimination of measurement dead time would result in much closer temperature control.

On the other hand, when controlling the temperature of such processes as heat exchangers, where the process lags may be of minutes duration, the elimination of measurement dead time may bring no noticeable improvement.

It is interesting to note that the measuring lag may be computed from the results of controlling process No. 1 with the electrical two-position controller. Here virtually all of the lag aside from the time constant of the process is associated with the potentiometer measuring means. Since in two-position control the period of cycling is about 4 times the total lag (3), then the measuring lag should be the period divided by 4.

Thus the measuring lag calculates to be about 0.0075 min for the continuous-action potentiometer measuring means and about 0.0645 min for the periodic type.

Tests With Proportional-Reset Control

In order to demonstrate the effect of dead zone in the measuring means, a controller may be applied to a process, and the deviation during a recovery from a load change may be expected to show differences depending upon the magnitude of dead zone (4). The dead zone is generally defined as the greatest range of scale values within which changes in value of the controlled variable are not detected.

With self-balancing potentiometers, the width of dead zone is generally related to the construction of its detecting and balancing mechanisms. As one contributing factor, the width of dead zone is inversely proportional to the number of active convolutions of the potentiometer rebalancing slide-wire since the controller pen and controller mechanism are generally positioned to the convolution of the slide-wire nearest the balance point.

The self-balancing continuous-action potentiometer used in the previous tests has 1600 active convolutions on the slide-wire (1). It was desired to test this same potentiometer with 800 and 400 convolutions on the slide-wire, thus multiplying the dead zone by 2 and 4, respectively.

These arrangements were made by altering the mechanical relation between full-scale pen motion and slide-wire contactor travel. An oversize drum on the slide-wire driving shaft reduced the amount of slide-wire contactor motion while maintaining the same pen motion. This change does not alter the responsiveness of the potentiometer balancing motor to a given unbalanced emf, but reduces the amount of slide-wire contactor travel for the same pen travel when a rebalancing action occurs. The electronic voltmeter on the process-analog control board was then readjusted to maintain the same range of 0 to 5 volts for full-scale pen travel.

The net result of these changes is to alter the number of slide-wire convolutions corresponding to a given pen travel while maintaining the same dynamic balancing action and the same scale calibration.

Three processes were selected and are described in Figs. 3, 4, and 5. Process No. 5, described in Fig. 3, is a relatively simple process having a moderate reaction rate and slight transfer lag Process No. 6, described in Fig. 4, possesses a moderate reaction rate and appreciable transfer lag. Process No. 7, described in Fig. 5, has a fast reaction rate and slight transfer lag. In all tests only the dead time inherent in the system was present and no dead time was intentionally added.

Each process analog was connected to the potentiometer controller and optimum adjustments of proportional band and reset rate selected (5). A pneumatic proportional-reset type con-

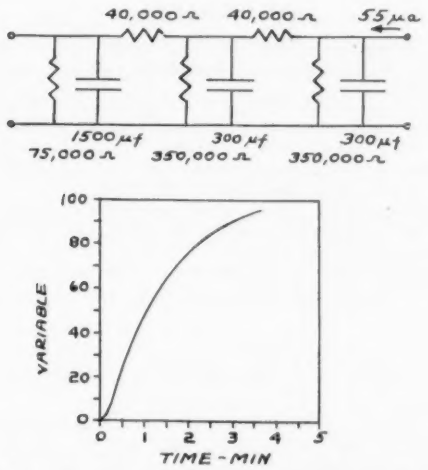


FIG. 3 DIAGRAM AND REACTION OF PROCESS NO. 5

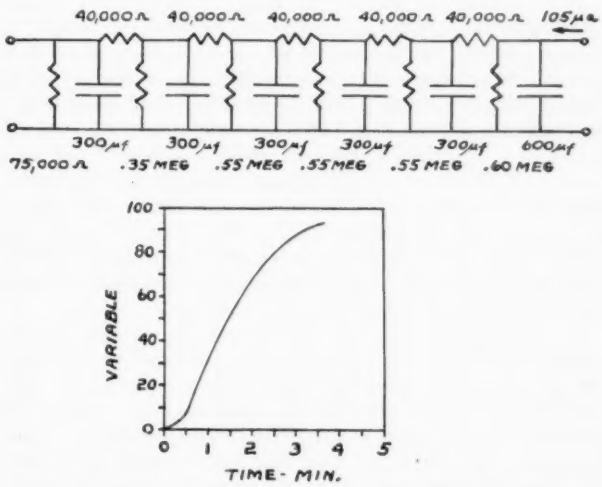


FIG. 4 DIAGRAM AND REACTION OF PROCESS NO. 6

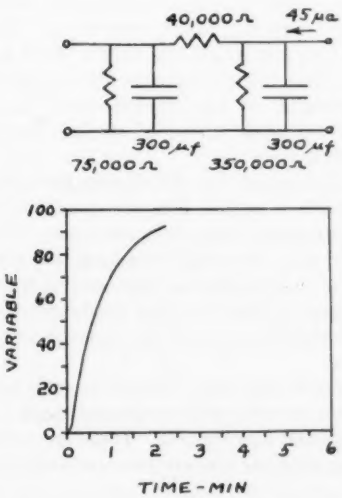


FIG. 5 DIAGRAM AND REACTION OF PROCESS NO. 7

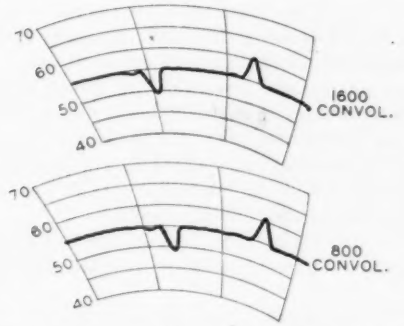


FIG. 6 RECOVERY CURVES FOR PROCESS NO. 5
(45 per cent band, 0.8 per min reset rate. 1 time division equals 4 min.)

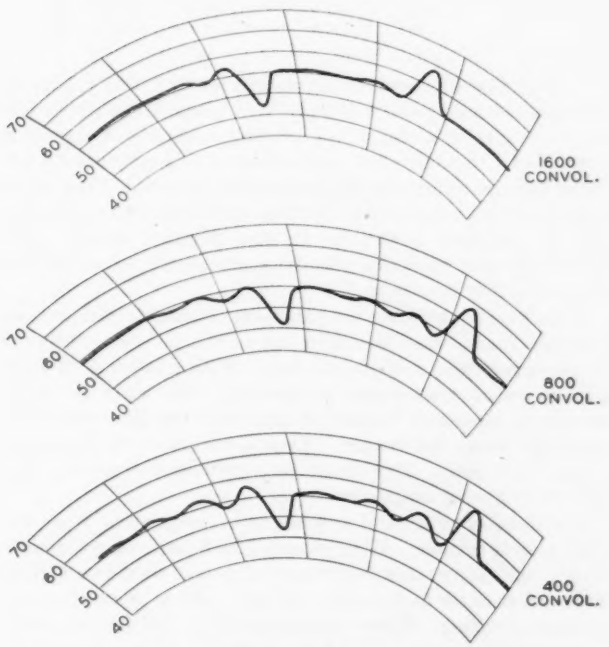


FIG. 7 RECOVERY CURVES FOR PROCESS NO. 6
(60 per cent band, 0.4 per min reset rate. 1 time division equals 4 min.)

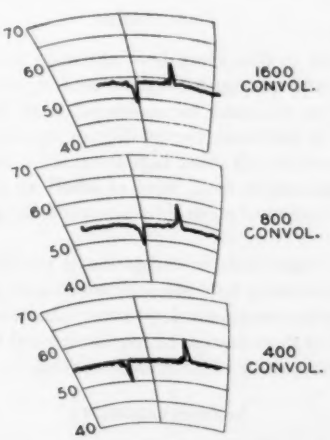


FIG. 8 RECOVERY CURVES FOR PROCESS NO. 7
(25 per cent band, 3 per min reset rate. 1 time division equals 4 min.)

troller was employed for these tests. After the controlled variable had stabilized, a change in supply of energy to the process was made and the controller recovery curve obtained.

The supply change was introduced by adding a bias voltage to the existing voltage supplied to the current-input unit on the process-analog control board. This is, in effect, a change of flow through the control valve caused by a variation in pressure drop and requires that the controller correct for this change. The control valve has 200 effective positions.

The charts showing the recovery curves are reproduced in Figs. 6, 7, and 8. The results of these tests are given in Table 3.

TABLE 3 RESULTS OF TESTS

Process no.	Prop. band, per cent	Reset rate per min	Maximum deviation for supply changes of No. of effective convolutions 1600	800	400
5	45	0.8	11.2	11.7	..
6	60	0.4	16.7	17.7	18.1
7	25	3.0	10.0	10.4	10.6

As shown by the recovery curves in Figs. 6, 7, and 8, both an increase and a decrease in supply were made. The increase in supply results in a rise of the controlled variable before it is corrected by the controller, and a decrease in supply results in a fall of the controlled variable before it is corrected. The maximum deviation was found by adding both the positive deviation and the negative deviation. In this manner various small nonlinearities in valve characteristics, process time-constant, and process lag may be averaged.

The difference between the various maximum deviations from a supply change may be attributed to the different widths of measurement dead zone in each test. With a larger dead zone, a short period must elapse between the time when an actual change in measured variable begins and the time when the controller senses the change. Thus a measurement dead zone creates dead time. This delays the controller corrective action and allows greater deviation.

The stability of control appears to be more cyclic when the dead zone is greater. With process No. 6 particularly, the recovery curve shows that the proportional band should be slightly increased in order to maintain the same ratio of succeeding amplitudes of cycling. There is an appreciably consistent lengthening of period when the dead zone is greater. The apparent decrease in stability of control and the lengthening of period of control points to the conclusion that an additional lag exists when the measuring means of the controller possesses a finite dead zone.

Conclusion

The brief test results given here illustrate the importance of measuring lag and measurement dead zone in automatic control. It is desirable to maintain measurement dead time as small as possible since it increases the quality of control, especially on such processes where all other lags are small. It is desirable to maintain measurement dead zone as small as possible since it increases the quality of control by accomplishing a reduction of dead time.

It is evident that more investigation is required to establish further the relationship between each component part of measuring lag and the measurement dead zone. In most control problems the effect of these factors cannot be ignored because of their influence on the quality of automatic control.

Acknowledgment

The author gratefully acknowledges the suggestions of Mr. T. R. Harrison in the investigation.

Bibliography

1 "A Self-Balancing Potentiometer," by T. R. Harrison, W. P. Wills, and F. W. Side, *Electronic Industries*, vol. 2, May, 1943, pp. 68–69 and 153.

2 "Electrical-Analogy Method for Fundamental Investigations in Automatic Control," by D. P. Eckman and W. H. Wannamaker Trans. A.S.M.E., vol. 67, 1945, pp. 81–86.

3 "Principles of Industrial Process Control," by D. P. Eckman, John Wiley & Sons, Inc., New York, N. Y., 1945.

4 "Theoretical Foundations of the Automatic Regulation of Temperature," by A. Ivanoff, *Journal of the Institute of Fuel*, vol. 7, February, 1934, pp. 117–138.

5 "Optimum Settings for Automatic Controllers," by J. G. Ziegler and N. B. Nichols, Trans. A.S.M.E., vol. 64, 1942, pp. 759–768.

Discussion

W. F. Hickes.[3] The author has shown us the detrimental effect of "dead time" in process control and has presented some evidence on the effects of "dead space" in terms of slide-wire turns. The results are interesting because they confirm the conclusions reached in our own laboratory investigations and field work.

It is difficult in practice to speak of dead time without bringing in dead space and vice versa because the two are so closely related. Let us assume we have a furnace at 1500 F. Let us further assume that with full heat on we have a heating rate of 5 deg F per min. Now if we have an instrument with a 0 to 1600-deg scale range and 1600 slide-wire turns, each turn will represent 1 deg, that is, the instrument will have 1 deg dead space. With a 5 deg per min change of temperature, the instrument should move every $^1/_5$ min and can hardly be much better than a periodic instrument with a dead time of $^1/_5$ min and could be expected to be inferior to a periodic instrument with the usual period of $^1/_6$ to $^1/_{10}$ min. It might be added that the figures quoted represent an actual furnace installation.

In comparing measuring instruments the author has described two types, the so-called continuous and the periodic. Actually there are at least four types. There is the periodic type described by the author, which has dead space due to slide-wire turns and dead time due to its periodic balancing action. There is another type which has dead time but not dead space, since the slide-wire serves only to set the control point, and the control mechanism operates directly from the galvanometer deviation. This type is nonrecording but has been very successful as a controller. There is the "continuous" type, cited by the author, which eliminates dead time by its continuous action but which still has the dead space due to slide-wire turns. There is finally a fourth type which has inherently neither dead space nor dead time, the dead time being eliminated by the same type of continuous balancing as in the previous case, dead space being eliminated by the substitution of stepless balancing for the conventional slide-wire.

The author has stated that the elimination of dead time is of greatest value where process lags are small and may bring no noticeable improvement where lags are large. This is undoubtedly correct although it should be realized that the typical thermal processes of inconsequential lags such as heat-treating furnaces have in general relatively slow maximum rates of temperature change so that dead time may be much less objectionable than dead space.

The really interesting cases would appear to lie in the extension of electronic controls of these general types to problems involving pressure and flow control. There are at present several makers offering units to convert pressure and differential pres-

[3] Foxboro Company, Foxboro, Mass.

sure into electrical values such as resistance which can then be measured on the type of instruments described. Since pressure and flow controls are normally characterized by very small lags and in many cases also by very rapid changes, the value of a truly continuous instrument free from inherent dead space as well a dead time should be apparent.

Author's Closure

The discussion of Mr. Hickes is greatly appreciated since it brings out many of the factors affecting the quality of automatic control when controller dead zone is present. As is stated, in control problems of inconsequential lag measurement, dead time becomes an appreciable factor.

Mr. Hickes's conclusion with regard to dead time due to dead zone is open to controversy because having a slidewire in which one convolution represents an interval of 1 F is not identical to having a dead zone of 1 F. Without going into the many details involved, a high amplifier "sensitivity" produces a condition wherein a rise in thermocouple emf will cause the slidewire contact to move entirely across one convolution to the edge of the adjacent convolution. Thus with gradually changing temperatures it is possible to obtain a relatively greater response with a slidewire balancing device having discreet positions than with a continuously balancing device.

With respect to measurement and controller dead zone, there are four general cases: (*a*) Control systems and process with a relatively fast reaction rate and little lag, (*b*) with relatively slow reaction rate and little lag, (*c*) with relatively fast reaction rate and large or appreciable lag, and (*d*) with relatively slow reaction rate and large or appreciable lag. The effect of dead zone is different in each case.

For example, in process control with fast reaction rate and little lag such as in flow or speed control, the author has observed cases of pseudo stability at narrow proportional bands which, with large, sudden upsets become cyclically unstable, sometimes violently so. This passage from the stable to the unstable region is apparently initiated by a fast change of the controlled variable through the dead zone and there may be little subsequent evidence of a square top wave.

With processes having a slow reaction rate and appreciable lag, the dead zone evidences itself as a consistent, additional lag and the quality of control is proportionately reduced.

Mechanical Oscillators and Their Electrical Synchronization

By S. W. HERWALD,[1] R. W. GEMMELL,[2] and B. J. LAZAN[3]

Mechanical oscillators provide an excellent means for obtaining structural serviceability tests. The adjustable-while-running type is particularly flexible. With it the answers to certain fundamentally difficult problems can be obtained quickly. The electrical system presented provides accurate remote control of frequency and phase angle between forces of two or more mechanical oscillators. In addition, means are incorporated for changing and indicating remotely the amount of unbalance of each oscillator unit. Rototrol units used with electronic and magnetic controls are the basic elements of this precise servomechanism.

HIGHER speeds in modern transportation and machinery, and present-day design trends toward greater efficiency and lighter weight have emphasized the importance of dynamic forces as a factor in design. The urgency of dynamic testing of materials and structures is indicated by a few recent studies (1),[4] which show that very few service failures in machine and structural members can be attributed to static forces alone; over 80 per cent involve dynamic forces.

Practical mechanical testing may be of three types, as follows:

(*a*) Testing carefully prepared specimens under simplified conditions of stress and environment to determine basic material properties.

(*b*) Testing actual shapes, assemblies, or structures under conditions which closely simulate actual service to secure direct design data.

(*c*) Testing in actual service.

Theoretically, if basic material properties and service conditions are known, one should be able to predict the behavior of a structure. Reasonable success has been achieved in such analysis of structures under static loads. However, predicting the behavior of a structure under dynamic loads in this manner is often unreliable because of such difficult variables as stress concentration, natural frequencies, damping, load distribution, etc. Thus past experiences indicate that at present the best procedure is to use specimen testing as a guide to the selection of materials and as an aid during the initial design stages; but to rely on structure testing for refining a design and checking actual serviceability.

Of course, no test of serviceability is as foolproof as actual service. However, to rely exclusively on actual service is usually impractical, time-consuming, and very expensive. Thus the simulated service test is a vital link in modern engineering analysis.

One of the most useful tools in simulated service tests is the mechanical oscillator, a device for producing sinusoidal alternating force or torque of controlled magnitude, direction, and frequency. Generally, it is a portable machine which may be carried to the structure and attached to it for field testing. Oscillators of this type are particularly useful in producing sinusoidal forces of large magnitude at relatively low frequencies. Furthermore, two or more of these oscillators can be connected electrically so that a definite phase relationship of the force outputs can be maintained. This provides the possibility of a more complete test, because a number of definitely related forces can be introduced to the structure simultaneously.

The Mechanical Oscillator

Probably the first mechanical oscillator capable of producing linear sinusoidal force was developed by W. Spath (2) in 1928, for testing railroad bridges. This oscillator utilizes the centrifugal force of eccentrically supported rotating masses as a source of alternating force (see Fig. 1). An eccentric E is attached to each of two shafts S which are motor-driven and geared so as to rotate in opposite directions. When both eccentrics E point vertically downward, position a in Fig. 1(a), the radial centrifugal forces add and the resultant force is vertically downward. After 90 deg of rotation to position b, the two centrifugal forces point in opposite directions and cancel each other. When the eccentrics reach position c they again add to produce a vertically upward force, and at position d they again cancel. In general, the net force is the vector sum of the two radial centrifugal forces, which is a sinusoidal alternating force such as shown in Fig. 1(b).

The same oscillator may be arranged to produce pure torsional vibration about an axis perpendicular to the plane of the paper at b in Fig. 1(c), by driving shafts S in the same direction and rearranging the eccentrics as shown.

The frequency of the alternating force equals the frequency of rotation of the oscillator, and the magnitude of the force equals the total inch-pound unbalance in eccentrics E multiplied by the angular velocity squared. The value of the unbalance can be adjusted by changing either the radial location or the size of eccentric E.

Variations of the Spath unit have been developed using four (3) or six (4) eccentrics, or using a different arrangement for the eccentrics so as to permit greater flexibility in governing the direction of types of possible forces. Oscillators have been built (4) capable of producing alternating forces as high as ± 44,000 lb; others have unbalanced masses with eccentricity as high as 6800 in-lb.

In many types of tests it is imperative that the weight of the oscillator be kept to a minimum. Mechanical oscillators developed to meet this requirement include the scotch yoke and the hypocyclic oscillator (3). However, none has been as successful as the centrifugal-force type from point of view of simplicity of operation, ease of maintenance, and purity of the sinusoidal force. The scotch-yoke oscillator, for example, generally induces rather severe harmonics which make analysis of results difficult.

During the dynamic testing of a structure it is generally necessary to cover a wide range of alternating forces. In the early os-

[1] Special Products Engineering, Westinghouse Electric Corporation, Pittsburgh, Pa. Mem. A.S.M.E.

[2] Manager, Aircraft Sales, Westinghouse Electric Corporation.

[3] Associate Professor and Director of Testing and Metallurgy Laboratories, Syracuse University, Syracuse, N. Y. Formerly Vice-President and Chief Engineer, Sonntag Scientific Corporation, Greenwich, Conn. Mem. A.S.M.E.

[4] Numbers in parentheses refer to the Bibliography at the end of the paper.

Contributed by the Industrial Instruments and Regulators Division and presented at the Annual Meeting, New York, N. Y., Nov. 26–29, 1945, of The American Society of Mechanical Engineers.

Note: Statements and opinions advanced in papers are to be understood as individual expressions of their authors, and not those of the Society.

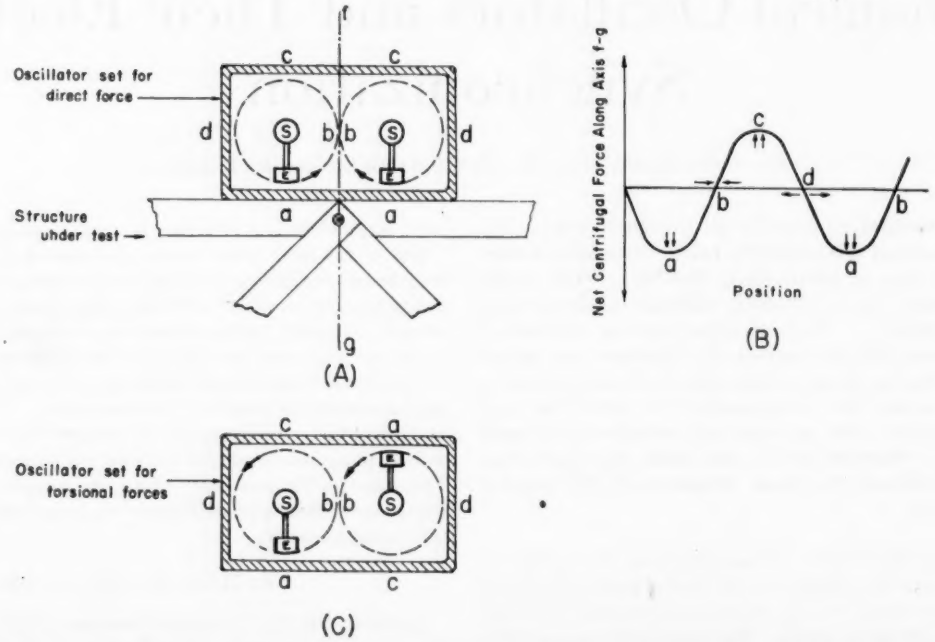


FIG. 1 PRINCIPLE OF OPERATION OF CENTRIFUGAL-FORCE-TYPE OF OSCILLATOR WITH TWO ECCENTRICS

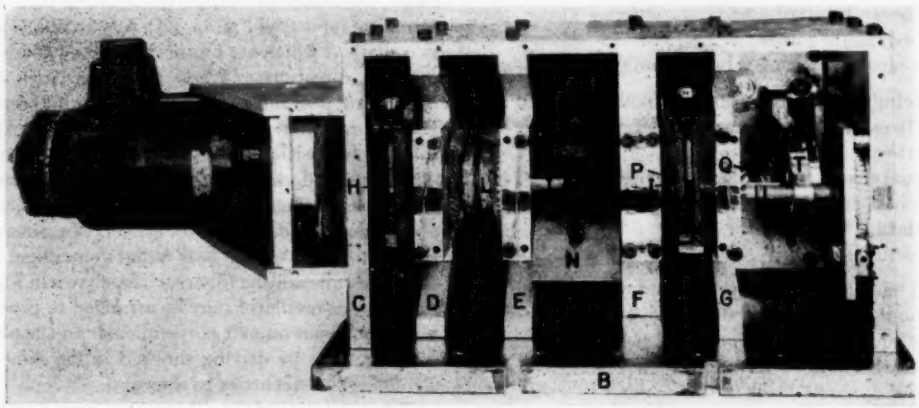


FIG. 2 ADJUSTABLE-WHILE-RUNNING OSCILLATOR OF THE 45-DEG RACK TYPE WITH DRIVE MOTOR AND SYNCHRONIZATION CONTROL EQUIPMENT ATTACHED

cillator every change in unbalance required stopping the unit and manually moving or changing the eccentric. This procedure not only consumed time, but also made certain types of tests very difficult. Recent improvements in centrifugal-force oscillators permit stepless adjustment of unbalance without stopping the unit. This may be accomplished either by adjusting a remotely controlled electric drive or by turning a knob attached to the oscillator.

Three different types of unbalance-changing mechanisms have been used: (*a*) differential gear changer (5); (*b*) helical key changer (6), which is now the most popular adjustable-while-running oscillator in use; and (*c*) 45-deg rack changer. Inasmuch as the special electric synchronization equipment to be described later was developed for the oscillator with the rack changer, this unit will now be described in detail.

The principle of operation may be understood by referring to Fig. 2. The oscillator consists of a base plate *B* to which are mounted pedestals *C*, *D*, *E*, *F*, and *G*. The ball bearings contained within the pedestals support rotating shaft *H* between *C* and *D*, rotating shaft *I* between *E* and *F*, and rotating shaft *J* between *F* and *G*. Shafts *H* and *J* are mechanically connected by a shaft running through the center of *I* so that they rotate together at the same speed and in the same direction. Spiral bevel gears *L* connect shafts *H* and *I* so that they rotate in opposite directions but at the same angular velocity. An eccentrically supported mass is attached to each of the three rotating shafts; eccentric *M* to shaft *H*, eccentric *N* to shaft *I*, and eccentric *O* to shaft *J*. At any given setting of the oscillator, eccentric *N* has an inch-pound unbalance equal to the sum of the unbalance in eccentric *M* and *O*. Furthermore, the inch-pound eccentricities in *M* and *O* are inversely proportional to the distances of *M* and *O* from eccentric *N*. This results in cancellation of moments.

Since eccentric *N* rotates in one direction as eccentrics *M* and *O* rotate at the same velocity in the opposite direction, pure sinusoidal force results (see previous explanation of Spath unit). It is possible to produce sinusoidal vibration in any direction perpendicular to the axis of rotation by unmeshing gears *L* (which enables shaft *I* to turn freely without a corresponding rotation of

shafts H and J), turning shaft I as desired, and remeshing the gears L.

The unbalance of all three eccentrics may be remotely and steplessly varied from zero to the maximum value while the oscillator is either stationary or running. This is accomplished as follows:

Each eccentric consists mainly of a large unbalanced mass and two racks P containing square teeth which make a 45-deg angle with the axis of the rack. These straight racks P slide in rectangular slots cut in the three shafts H, I, and J. Contained within these three tubular shafts are round members Q which have 45-deg square teeth cut on two sides to mesh with the 45-deg teeth on straight racks P. Thus as racks Q are moved axially, the meshing teeth will cause straight racks P to move radially, thereby changing the radial location of the center of gravity of the eccentrics. At zero unbalance, racks Q are so located that the center of gravity of the eccentric assembly consisting of P, etc., is at the center of rotation. To increase the eccentricity, the center of gravity of the eccentric is moved radially outward from the center of rotation.

Ball bearings contained within the shafts H, I, and J hold the racks in rigid axial location, but allow them to have angular freedom so that they can rotate with the parts they locate. This axial location is determined by the position of yoke T which is moved by motor-driven worms and screws U to adjust the radial location of the eccentrics.

This oscillator has a maximum unbalance of 150 in-lb and can produce alternating forces up to ± 1000 lb at speeds as low as approximately 500 rpm. Further refinements incorporated in this unit will be discussed in another section.

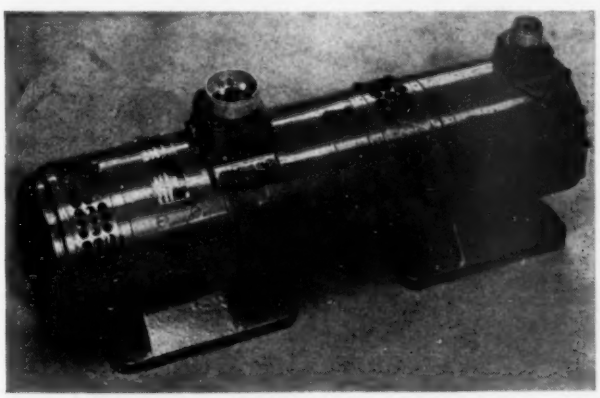


Fig. 3 Aircraft Rototrol of 3000 W

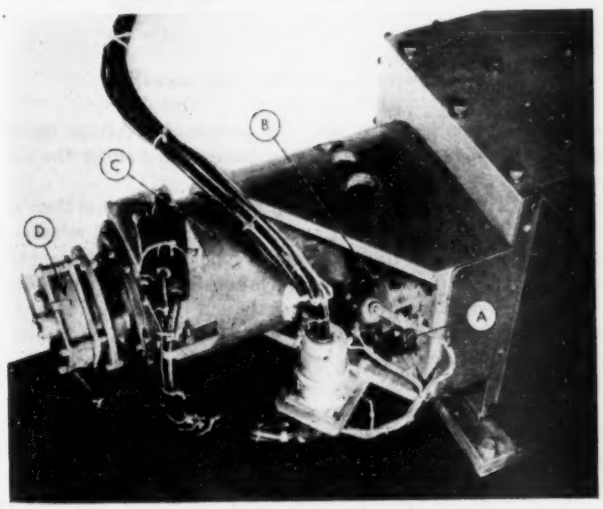


Fig. 4 Drive-Motor End of 45-Deg Rack-Type Oscillator

Electrical Control

The basic electrical equipment used to control accurately the frequency and force-phase relationship of two oscillators of the type shown in Fig. 2 is the Rototrol (7). This machine is illustrated in Fig. 3. When it is used with the proper electronic control, it provides the power required for precise regulation of the oscillator drive motors. The drive motors, shown as C in Fig. 4, rotate the unbalanced masses in the oscillators, producing sinusoidal forces in the manner described in Fig. 1. The motor shown is rated 3 hp at 3600 rpm.

Complete control of both oscillator units is obtained at the control box shown in Fig. 5. From here the speed of the oscillators,

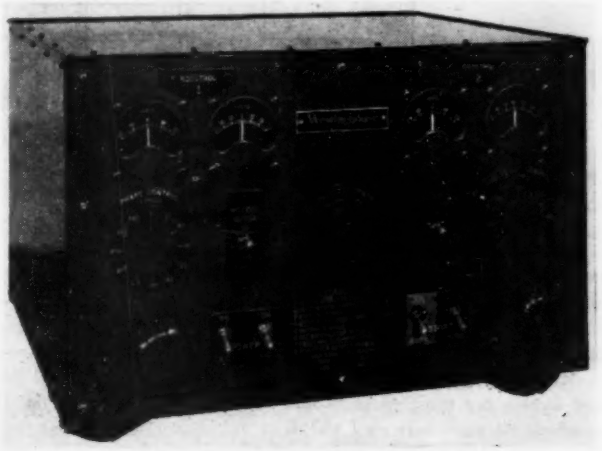


Fig. 5 Front View of Oscillator Control Box

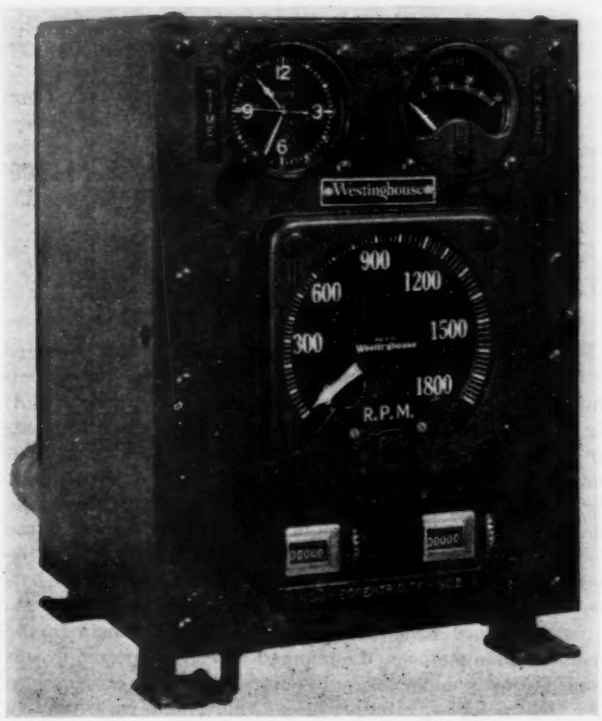


Fig. 6 Front View of Oscillator Indicating Panel

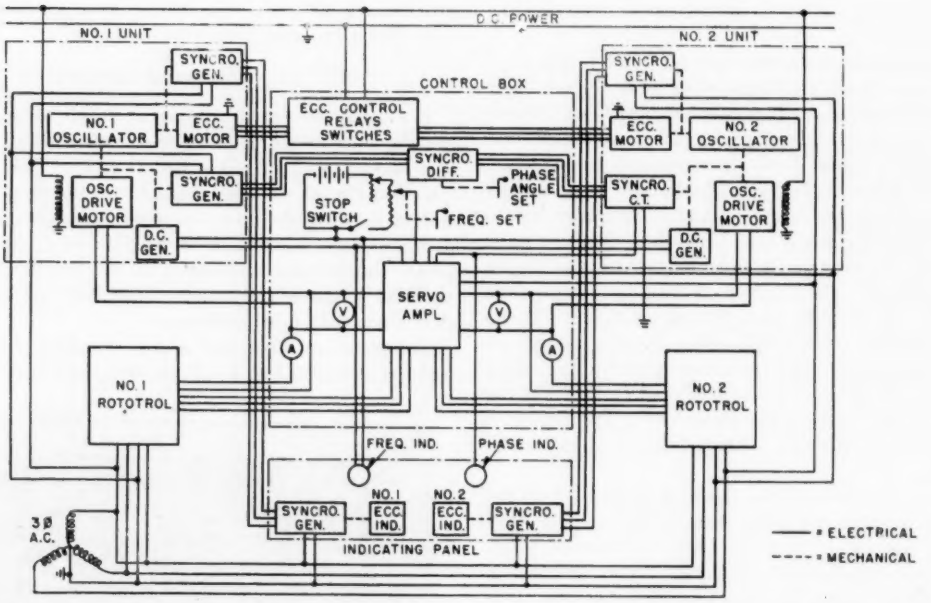


FIG. 7 SCHEMATIC OF FREQUENCY, SYNCHRONIZATION, AND ECCENTRICITY CONTROL OF TWO OSCILLATOR UNITS

the phase angle between their force outputs, and the amount of unbalance in each unit can be varied while the oscillators are running. Here also are the normal and emergency braking switches used to obtain decrement curves and emergency shutdown, respectively. Frequency can be fixed at anywhere from 100 to 1800 cycles per min; phase angle between forces can be fixed anywhere between zero and 360 deg; unbalance can be changed from zero to 150 in-lb on each oscillator independently.

Fig. 6 shows the indicating panel associated with this equipment. It contains the test record and is conveniently arranged for photographing. Thus the time of test, the frequency, the eccentricity in each of the units, and the phase error between the units can all be obtained on one photograph. The phase error mentioned should not be confused with the phase-angle setting on the control panel. Phase error is merely the inaccuracy of the phase angle as set on the control unit. The phase-error meter reads directly in degrees. In operation it showed substantially less than ± 15 deg, even with large eccentricities and with the units 180 deg out of phase.

The schematic diagram of the electrical system used to control the oscillators is given in Fig. 7.

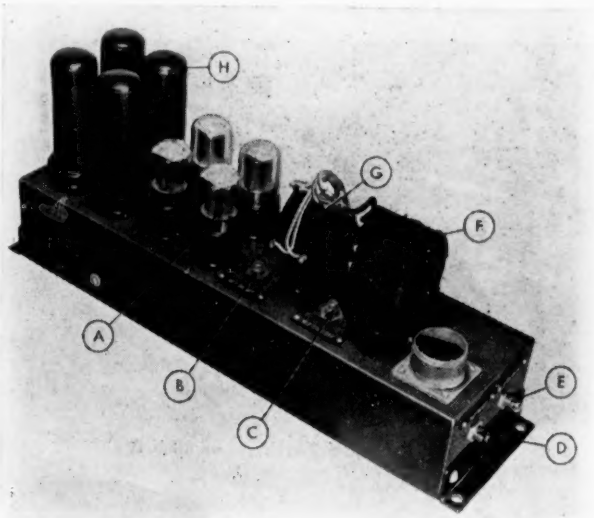


FIG. 8 TWO-CHANNEL SERVOAMPLIFIER

FREQUENCY AND PHASE CONTROL

For the No. 1, or master unit, a desired frequency is maintained within close limits by matching the preset portion of the control-unit battery voltage with that of a d-c tachometer generator *A*, Fig. 4, driven by the No. 1 oscillator motor *C*, Fig. 4. The voltage difference which occurs when the generator voltage does not match the battery potentiometer voltage is fed into the amplifier, Fig. 8. The amplifier output controls the output voltage of the No. 1 Rototrol generator which in turn changes the speed of the No. 1 oscillator drive motor so as to reduce the voltage error between the tachometer generator and the preset portion of the battery voltage. Thus except for a very small voltage difference required to produce enough Rototrol output voltage to maintain the oscillator drive motor at the required speed, the system is self-compensating, tending always to reduce the voltage error. Since a d-c tachometer generator produces a voltage that varies linearly with speed, all one has to do to vary frequency is to adjust the battery potentiometer *B*, Fig. 9. This, of course, causes the drive motor to change speed so that the tachometer voltage again matches the portion of the battery voltage picked off by the potentiometer.

The No. 2 unit operates in a similar manner, except that there is one added feature. In order to maintain a given phase relationship between the Nos. 1 and 2 units, a synchrosystem is used to detect error from the desired phase relationship. This error is detected as an a-c voltage that varies as the sine of the angle of deviation from the desired phase relationship of the Nos. 1 and 2 units. An electrical schematic of this synchrosystem is shown in Fig. 11. The rotor of the synchrogenerator which has salient poles is excited single phase. This sets up the flux field *A* which cuts the stator windings. These stator windings are usually displaced mechanically 120 deg and connected to exactly similar windings of the synchrodifferential. The currents that flow in similar windings such as *a* and *a'* or *b* and *b'* of the generator stator and the differential rotor are identical. Therefore flux field *B* has the

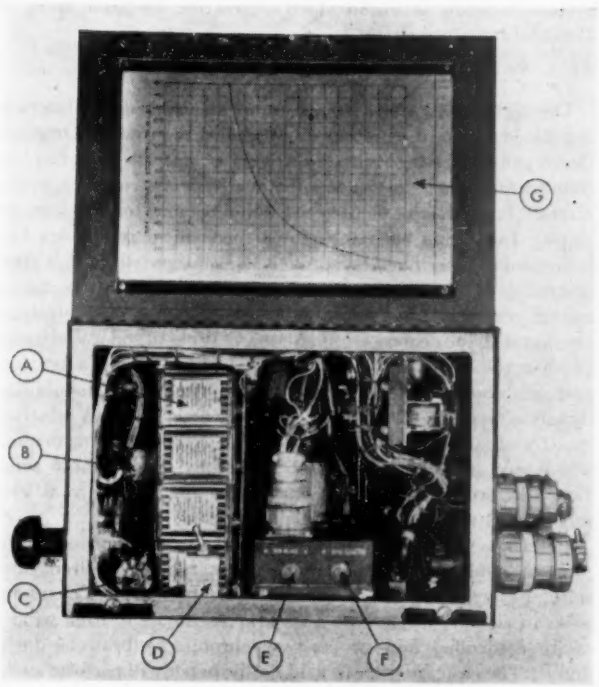


FIG. 9 RIGHT-SIDE VIEW OF OSCILLATOR CONTROL BOX

same position relative to the windings as flux field A and the windings have served as a means of indicating generator-rotor position in the differential. Similarly the combination of the synchrogenerator-rotor and the differential-rotor positions is indicated by the synchrocontrol-transformer flux field C. Thus the apparent position of the generator rotor as indicated to the control transformer by flux field C can be changed by rotating the synchro differential rotor.

The control transformer is similar to the synchrogenerator except that the rotor has a distributed winding to reduce reaction torque. With the synchrocontrol transformer rotor in the position shown in Fig. 11, no error voltage appears across terminals T_1 and T_2 as the rotor is at right angles to the flux field C. As the rotor is rotated the component of flux intercepted is proportional to the sine of the angle of rotation, consequently, the error voltage at T_1 and T_2 also varies as the sine of the angle of control-transformer-rotor rotation. The rotation of either the synchrogenerator or differential rotor produces a voltage at T_1 and T_2 that varies as the sine of the angle of rotation. This occurs because movement of either rotor shifts flux field C relative to the control-transformer rotor.

If the generator and control-transformer rotors are rotated at

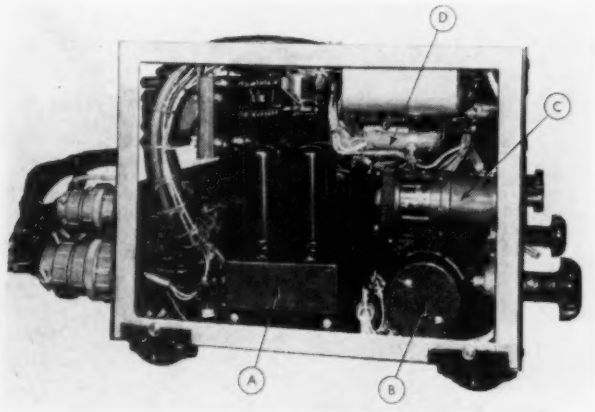


FIG. 10 LEFT-SIDE VIEW OF OSCILLATOR CONTROL BOX

exactly the same speed the voltage at T_1 and T_2 does not vary as the relative position of flux field C and the control-transformer rotor does not change.

As used in this system the synchrogenerator B, Fig 4, is driven by the No. 1 motor and is electrically connected through the synchrodifferential C, Fig. 10, in the control unit to the synchrocontrol transformer which is physically located on the No. 2 unit exactly as in B, Fig. 4. The control transformer is driven by the No. 2 motor. The phase-relationship-error voltage obtained from the synchrosystem, as described, is superimposed on the frequency control in the amplifier channel for the No. 2 unit.

The voltage output of the No. 1 tachometer generator is used to give an indication of the frequency. A voltmeter, see Fig. 6, in the indicating panel, calibrated in cycles per min, is used for that purpose. The control-transformer error voltage, which is a measure of the phase-angle error between the Nos. 1 and 2 units, is indicated by an a-c voltmeter on the indicating panel. This phase-angle error is required so that enough control-transformer error voltage is produced at the No. 2 unit amplifier channel to hold a fixed phase relationship between the Nos. 1 and 2 units.

ECCENTRICITY CONTROL

The eccentricity of an oscillator unit is varied by operating a switch on the control-unit panel. It is a two-way momentary "on" switch, and by using relays and limit switches D and E, Fig. 12, the eccentricity motor B, Fig. 12, is operated in either direction so as either to increase or to decrease the eccentricity.

A synchrogenerator C, Fig. 12, is driven by the eccentricity motor. By electrically connecting this synchrogenerator to a similar one in the indicating-panel unit which drives a counter, an indication of the eccentricity in each of the units is obtained. This, of course, is the standard synchrotie connection. The

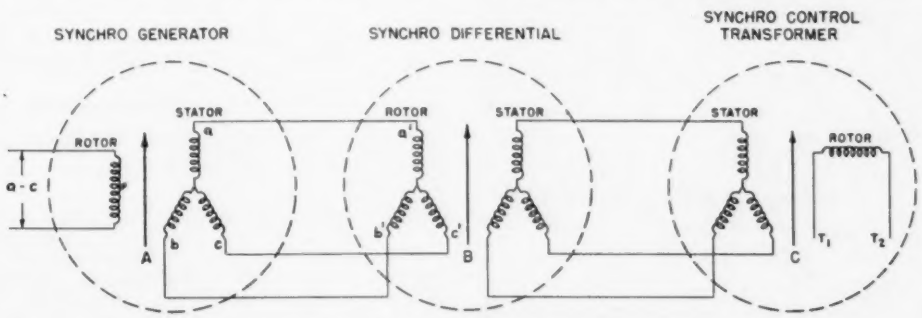


FIG. 11 SYNCHROSYSTEM SCHEMATIC

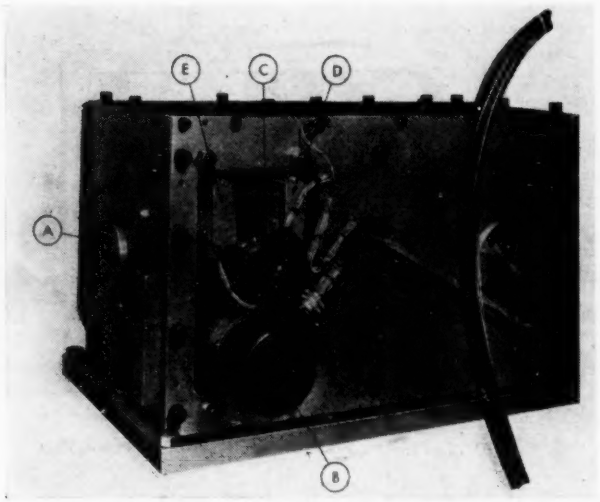


FIG. 12 ECCENTRICITY MOTOR END OF 45-DEG RACK-TYPE OSCILLATOR

amount of unbalance in the unit can be determined mechanically by inserting a calibrated needle gage in bolt hole of *A*, Fig. 12.

AMPLIFIER OPERATION

The amplifier shown in Fig. 8 is used as a means of detecting the low-power-level intelligences offered by the battery, d-c tachometer, and synchro machine circuits, and of converting them almost instantaneously into intelligence at a power level sufficiently high to control a Rototrol generator-control field. A Rototrol is in itself a fine power amplifier. Its power output, which is regulated by the control field, is great enough to run an oscillator drive motor, and yet it is a fast machine electrically, responding quickly to the intelligence the amplifier transmits to its control field.

The Nos. 1 and 2 channels of the amplifier are similar. Each has two stages of push-pull d-c voltage amplification for which a pair of 6SL7's are used, *A* Fig. 8, and one push-pull power-amplification stage in which two 6L6's, *H* Fig. 8, are used. A dynamotor *B*, Fig. 10, supplies direct current for the plates of the 6SL7's, whereas the plate supply for the 6L6's is alternating current. Each pair is supplied by a separate secondary winding of the same transformer. The difference between the two channels of the amplifier is that the synchrocontrol-transformer error voltage is introduced into the No. 2 channel only. This locks the No. 2 oscillator in a definite phase relationship to the No. 1 oscillator. As previously described, this phase relationship can be varied from zero to 360 deg by rotating the differential synchromachine rotor.

As in the case of all servomechanism (8) systems, proper damping means must be used to prevent "hunting." In this oscillator system damping is obtained by derivative feedback from the Rototrol armature circuit.

CONCLUSION

During the past 17 years the use of mechanical oscillators for simulated service testing has enjoyed steady growth. Originally developed for testing railroad bridges, oscillator testing has been found applicable to testing many other types of structures, such as aircraft, land vehicles of all types, buildings and foundations, and ships. In testing such structures mechanical oscillators have been used to determine such properties as fatigue strength, natural frequency of vibration, damping capacity, resonant stress, flutter, riding comfort, and other vibration-response characteristics. Oscillators have also been used for many types of soil investigation (such as the behavior of an airport landing strip under vibration), and as a laboratory tool to study fatigue, stress-relief possibilities, dynamic modulus of elasticity, dynamic creep, etc. A relatively small oscillator is a particularly powerful dynamic testing machine when used to produce resonant vibrations; under these conditions the force exerted on the part under test may be from 10 to more than 100 times the oscillator force (3).

Certain types of dynamic testing require two or more oscillators properly synchronized and controlled to induce a desired vibration. For example, one method of determining flutter characteristics in aircraft wings is to attach an oscillator to each wing to excite controlled and properly synchronized vibrations during flight. The equipment described in this paper will perform such a task. The combination Rototrol and electronic control will maintain precisely the frequency and phase relationship of two or more oscillators. Additional electrical control provides means of adjusting the frequency, phase, and eccentricity of the oscillators while the units are operating.

BIBLIOGRAPHY

1 "Present-Day Knowledge of Fatigue" (Symposium), Report of Research Committee on Fatigue of Metals, Proceedings of the American Society for Testing Materials, vol. 30, part 1, 1930, pp. 260–310.

2 "Dynamische Untersuchungen an technischen Gebilden," by W. Spath, *Zeitschrift des Vereines deutscher Ingenieure*, vol. 73, 1929, pp. 963–965.

3 "Some Mechanical Properties of Plastics and Metals Under Sustained Vibration," by B. J. Lazan, Trans. A.S.M.E., vol. 65, 1943, pp. 87–98.

4 Catalog No. 2280-2000 published in May, 1932, by Losenhausenwerk, Dusseldorf, Germany.

5 "Testing Apparatus," Rudolf K. Bernhard, U. S. Patent No. 2,206,386, July 2, 1940.

6 Bulletin No. 202, Baldwin Southwark Division, Philadelphia, Pa.

7 "Rototrol—A Versatile Electrical Regulator," by W. H. Formhals, *Westinghouse Engineer*, May, 1942, p. 51.

8 "Considerations in Servomechanism Design," by S. W. Herwald, Trans. A.I.E.E., vol. 63, 1944, pp. 871–876.

Precision Tachometer for Use in Wind-Tunnel Testing

By R. K. FAIRLEY[1] and H. L. CLARK[1]

The equipment described is a high-speed high-accuracy tachometer developed primarily to measure rotative speed during the power-testing of airplane models in wind tunnels by measuring the frequency of a tachometer generator. The frequency being measured is automatically compared with that of a tuning fork and indicated on an instrument having a scale length of 86 in.

ONE of the largest laboratory devices we have today is the modern wind tunnel, built to analyze the performance of planes and their component parts. While all tunnels are custom-built, they have one common characteristic, that is, the need for many accurate instruments. In addition to fairly good accuracy, good precision is also required since precision or constancy of indication will reveal trends resulting from model changes.

To build instruments of the accuracy required is sufficiently difficult, but to add to the difficulty, such instruments should be self-reading or recording. As the design of airplanes increases in complexity, the number of instruments which must be read simultaneously is multiplied. To expedite research work, not to mention economics which is sometimes forgotten under the stress of war work, it is highly desirable to obtain such readings at the touch of a button. Automatic recording avoids the errors of an observer, particularly those caused by fatigue. Not only are such errors obviated by self-recording features, but such readings may also be recorded in a calculating machine and much laborious manual calculating work avoided.

Some phases of model testing involve so-called "power on tests." This means that the model plane will be provided with a propeller and a power plant, usually an electric motor or motors. When a test is in progress it is necessary to know accurately the speeds of these electric power plants and the developed torques. Torque is usually measured indirectly, first, by calibrating each motor in a dynamometer and measuring the electrical input at each given speed. The motor is then mounted in a model plane in the wind tunnel, and at the same speed, the same watts, volts, and amperes are applied and the calibrated torque obtained.

During a test run the watts, volts, amperes, and speed are continuously measured and numbers set up in a printing machine. When stable conditions are reached these quantities, together with their associated multipliers, etc., are simultaneously recorded in the printing machine.

It is the purpose of this paper to describe the equipment which measures the speed and actuates the printing machine.

Principle of Operation

Accurate measurements are usually facilitated by comparison with a known value, commonly referred to as a standard. For example, accurate measurements of weight can better be made with a balance, using tested weights, than with a spring scale. The balance uses the comparison principle while the spring scale uses the deflection principle.

A similar principle applied to the measurement of frequency is often used employing an oscilloscope and Lisajou figures. The ratio between the unknown and known frequencies, such as $^2/_4$, $^5/_8$, etc., is deduced from the shape of the pattern. The equipment to be described automatically obtains this ratio using a self-contained known frequency, and indicates the value of the unknown frequency on a special long-scale instrument.

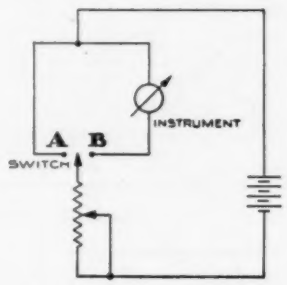


Fig. 1 Basic Circuit, Deflection Principle

A simplified circuit showing the principle of operation is illustrated in Fig. 1. The switch, normally in position A, snaps over to position B at the beginning of the cycle being measured. This is shown at point 1 in Fig. 2(a). After a definite length of time this switch automatically switches back to position A and stays there until the beginning of the next cycle of the frequency being measured (point 2). Current will flow through the instrument while the switch is in position B. The wave shape of this current is shown in Fig. 2(b), in which t_1 shows the definite length of time the switch stands in position B, and t_2 is the time for one cycle of the frequency being measured. The instrument will indicate the average value of the current, shown as i_{av}. When a higher frequency is being measured, as shown in Fig. 2(c), the switch snaps from position A to position B at the beginning of the cycle, stands in position B for the same definite length of time as before, then snaps to position A, and then waits in position A until the beginning of the next cycle. The current flows through the instrument as shown in Fig. 2(d). Since the pulses of current are spaced more closely together, the average current will be higher. This average current is given by

$$i_{av} = i_{max} \frac{t_1}{t_2} \quad \ldots\ldots [1]$$

Since the frequency being measured is

$$f = \frac{1}{t_2} \quad \ldots\ldots [2]$$

the average current is then

$$i_{av} = i_{max}\, t_1 f \quad \ldots\ldots [3]$$

---

[1] General Engineering and Consulting Laboratory, General Electric Company, Schenectady, N. Y.

Contributed by the Industrial Instruments and Regulators Division and presented at the Annual Meeting, New York, N. Y., Nov. 26–29, 1945, of The American Society of Mechanical Engineers.

Note: Statements and opinions advanced in papers are to be understood as individual expressions of their authors and not those of the Society.

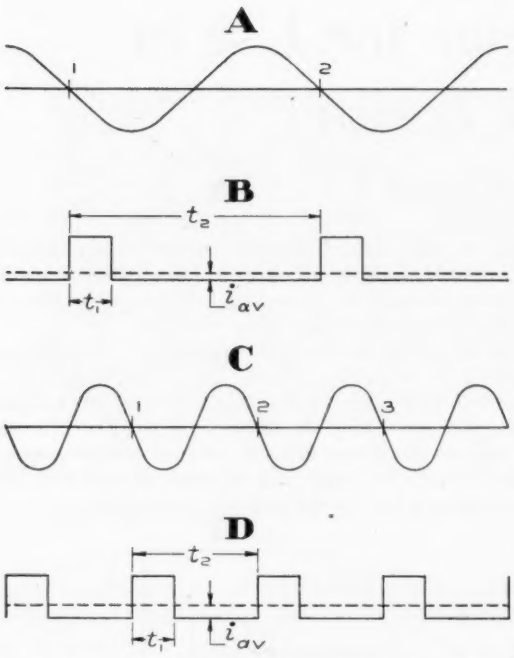


FIG. 2 CURRENT IMPULSES, SHOWING OPERATION OF SWITCH

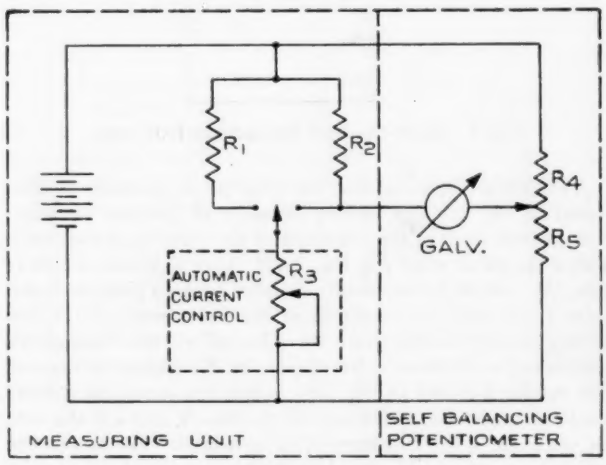


FIG. 3 BASIC CIRCUIT, BALANCE PRINCIPLE

Equation [3] shows that the average current through the instrument is proportional to the frequency being measured.

However, the use of an ordinary indicating instrument to measure the average current makes use of the deflection principle instead of the more accurate comparison principle. Rearrangement of Equation [3] gives

$$\frac{i_{av}}{i_{max}} = t_1 f \quad \ldots\ldots\ldots\ldots\ldots\ldots\ldots\ldots [4]$$

Here we see that the ratio between the average and maximum current is proportional to the frequency being measured since t_1 is a constant.

This ratio may conveniently be measured by using a self-balancing bridge, the basic circuit of which is shown in Fig. 3. The bridge consists of resistors R_2, R_3, and R_4 plus R_5 which is a self-balancing potentiometer. (The resistor R_3, denoted "Automatic Current Control," is required to hold the current through this arm of the bridge strictly proportional to the supply voltage. This is necessary because of the somewhat variable voltage drop across the switching element which is to be described later.) The voltage across R_2 is proportional to i_{av}, while the voltage across R_2 plus R_3 is proportional to i_{max}. When the slider on the potentiometer is adjusted so that no current flows through the galvanometer

$$\frac{i_{av}}{i_{max}} = \frac{R_4}{R_4 + R_5} = t_1 f \quad \ldots\ldots\ldots\ldots\ldots\ldots\ldots\ldots [5]$$

Here we see that the value of the frequency being measured is determined by the ratio of two resistances and the constant t_1 which is the time for one cycle of the tuning fork.

Since changes in the value of the supply voltage produce like changes in i_{av} and i_{max}, the ratio of i_{av}/i_{max} remains unchanged. Variations in the power-supply voltage do not change the value of the frequency indicated.

As shown in Fig. 4, the equipment consists of two essential units, a measuring unit and a self-balancing potentiometer. The measuring unit performs the switching operations which determine the ratio of i_{av}/i_{max} while the self-balancing potentiometer measures this ratio.

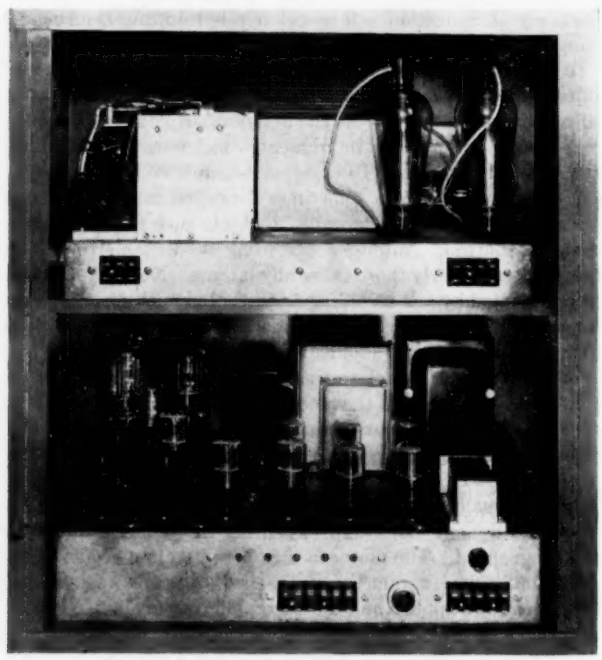


FIG. 4 PRECISION TACHOMETER

MEASURING UNIT

Since the required switching speed is very high, electronic instead of mechanical switches are used. To form an electronic switch two tubes are connected as shown in Fig. 5. Each tube acts as one pole of a single-pole double-throw switch, that is, only one tube conducts current at a given time. For instance, assume tube V_1, in Fig. 5, is carrying current. This current flows through R_1, causing a voltage drop. Through the voltage divider R_5 and R_6, the grid of V_2 is held so far negative with respect to its cathode that no current flows in this tube. There is no voltage drop across R_4 so that through the divider R_2 and R_3, the grid of V_1 is held positive, and V_1 continues to conduct current.

To change the switch from its original position a negative impulse may be applied to the grid of V_1 decreasing the current in V_1,

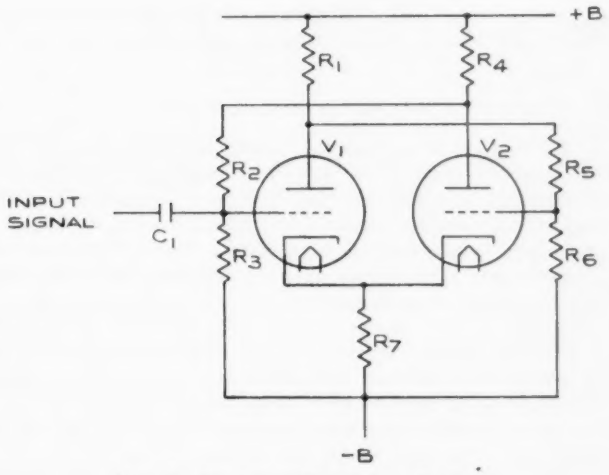


FIG. 5 CIRCUIT OF ELECTRONIC SWITCH

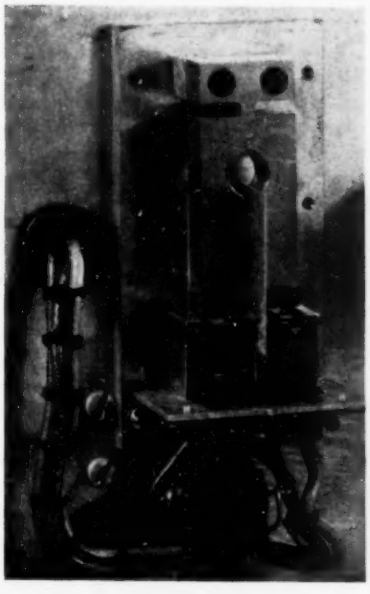


FIG. 6 TUNING FORK

causing its plate voltage to rise. Through the voltage divider the grid of V_2 is driven positive, causing this tube to conduct current. The resulting voltage drop across R_4 will, through the voltage divider, drive the grid of V_1 negative, thus holding off tube V_1 while tube V_2 conducts current. Thus a voltage impulse applied to one of the grids causes a transfer of current to take place similar to that of a single-pole double-throw switch.

Several of these electronic switches are used in combination to obtain the current pulses as shown in Fig. 2.

The timing element of the equipment is a tuning-fork oscillator. A close-up view of the tuning fork is shown in Fig. 6. A small Alnico magnet is mounted on the end of each tine of the tuning fork, and a coil opposite each magnet. Motion of the tuning fork generates a voltage in the coils, one of which is connected to the grid of an amplifier tube. This voltage, after being amplified, is applied to the other coil, thus sustaining the oscillations.

The frequency of the tuning fork, which is approximately 3000 cycles per sec, must in most cases be 3 times the highest frequency to be measured. Such a tuning fork can be made to provide a high degree of accuracy. The principal cause of inaccuracy is the temperature coefficient of the material. A material having a temperature coefficient of 5 parts per million per centigrade degree is used so that an accuracy of the order of 0.05 per cent is easily obtained.

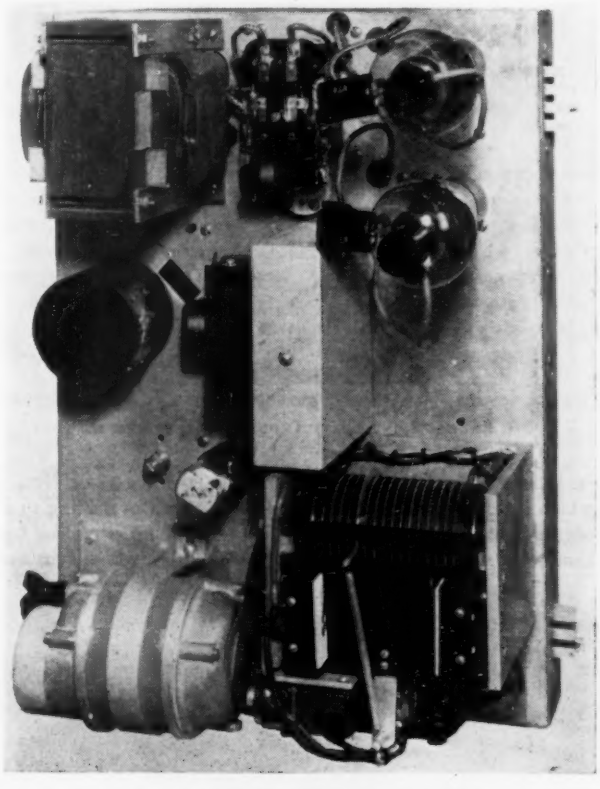


FIG. 7 SELF-BALANCING POTENTIOMETER

SELF-BALANCING POTENTIOMETER

The self-balancing potentiometer shown in Fig. 7 uses as a galvanometer an ordinary microammeter with a mirror instead of a pointer. This galvanometer reflects a beam of light from the light source to two phototubes, dividing it equally between the phototubes when the circuit is balanced. If one phototube receives more light than the other, one of the thyratrons passes current through the motor, which through a gear reduction drives the potentiometer in the direction which will bring the galvanometer to balance. The potentiometer will accurately follow variations of 2 per cent of full scale per second and has a maximum speed of 15 per cent per second. This speed is ample to follow the speed variations encountered in the application described.

The potentiometer consists of 10,000 or more turns of fine resistance wire wrapped around a core of Formex-insulated copper wire, and 14 turns of the whole wrapped around a grooved drum. A split nut carrying the slider rides in a groove so that as the drum rotates the slider follows the resistance wire. A pin on the split nut rides against a cam which is shaped so as to advance or retard the slider to compensate for nonlinearity of the resistance wire. The potentiometer unit is made accurate to 0.1 per cent or better.

Also connected to the gearing is a selsyn transmitter so that the position of the potentiometer can be transmitted to a remote location for operating the recording mechanism for indication or control. The indicating instrument shown in Fig. 8 has two hands, one of which makes 10 revolutions while the second hand indicates the number of revolutions made by the first hand. The



FIG. 8 LONG-SCALE INDICATING INSTRUMENT

scale length for 10 revolutions is 86 in., making each division, which is 0.1 per cent, very nearly $^3/_{32}$ in. so that a reading to the accuracy of the equipment can be made without estimating fractions of a division. The transmitter and receiver selsyns each turn 150 revolutions for full scale so that an error of 5 deg in the selsyn, for example, would cause less than 0.01 per cent error in the indication.

ACCURACY OF INSTRUMENT

The method of calibration is largely responsible for the high degree of accuracy obtainable with this equipment. The known frequency of the tuning fork is connected to the input of the equipment with the circuits so arranged that one half the frequency of the tuning fork is measured. The indicating circuit is then adjusted so that the proper reading is obtained, thus correcting for any variations in the electronic circuit. Since the circuit is essentially independent of tube characteristics, these initial variations are small, and after being corrected as described, are negligible. The factors entering into the accuracy of the measuring unit then are the frequency of the tuning fork and the values of several precision resistors which are accurate to 0.05 per cent or better.

Adding up the several factors, 0.05 per cent for the tuning fork, 0.05 per cent for the resistors, and 0.1 per cent for the self-balancing potentiometer, the over-all accuracy of the device is 0.2 per cent or better.

Electromagnetic Torquemeter

By M. W. HIVELY[1] and D. F. LIVERMORE[1]

The electromagnetic torquemeter is a dynamometer of the transmission type. A calibrated shaft unit is directly connected in the rotating shaft where the torque is to be measured. This paper describes a slip-ring type of torquemeter in which the small torsional deflections in the shaft unit are measured by electromagnetic-gage elements and associated electrical components to give a continuous direct reading of torque with an accuracy of 1 per cent of full-scale torque. By proper mechanical and electrical design, effects of centrifugal forces and changes in brush resistance are held to negligible values. Several torquemeters of this type are now in use. They cover a range of 250 lb-ft at 8000 rpm to 10,000 lb-ft at 400 rpm. The same general torquemeter principle is readily applicable to much higher torque ranges.

Introduction

THERE is a growing demand for torquemeter equipments to measure the torque transmission through a rotating-shaft system. Some typical examples are the torque applied to an aircraft propeller or helicopter rotor, the torque transmission from a prime mover to a compressor load, and the torque transmission through drive shafts and axles in automobiles and trucks. The torquemeter will, of course, not replace the conventional cradled-dynamometer equipments which are often used for similar purposes, but nevertheless it has a very definite field of application of its own.

The torquemeter development has been going on for many years, and the various designs are almost as numerous as the development engineers who have worked in this field. Substantial progress has recently been made.

The electromagnetic torquemeter discussed herein is a transmission dynamometer of the torsion type in which a calibrated shaft unit is inserted as a section of the rotating shaft.

Most torquemeters for rotating shafting make use of the same fundamental physical principle: An elastic member, when subjected to an external torque within the elastic limit of the member, will deflect torsionally an amount proportional to the applied torque, and will return to its original state when the load is removed. The amount of angular twist in a fixed length of shaft is measured by some means. It is in this means of measuring the twist that the several types of torquemeters vary. The General Electric electromagnetic shaft unit, to which most of the discussion to follow is devoted, measures the torsional deflections, over a fixed shaft length, with electromagnetic gages. Changes in torque produce corresponding changes in the air gaps of the gages mounted in the shaft unit. These changes can be measured electrically by use of suitable electrical components which are a part of the torquemeter equipment.

Description of Electromagnetic-Torquemeter Shaft Unit

The electromagnetic torquemeter consists of the shaft unit and electrical components required to translate torsional deflections of the shaft unit into electrical-instrument readings.

The shaft unit is shown in Figs. 1 and 2. It consists of a hardened alloy-steel shaft 20 to 30 in. long which is coupled between the prime mover and the load. A section of this shaft is made with a reduced diameter so that approximately $^1/_8$ deg of torsional displacement is obtained in 2 to 4 in. of shaft length.

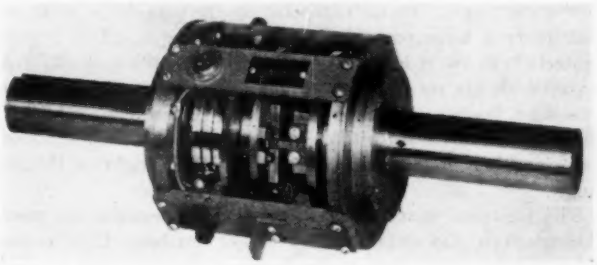


Fig. 1 Electromagnetic-Torquemeter Shaft Unit

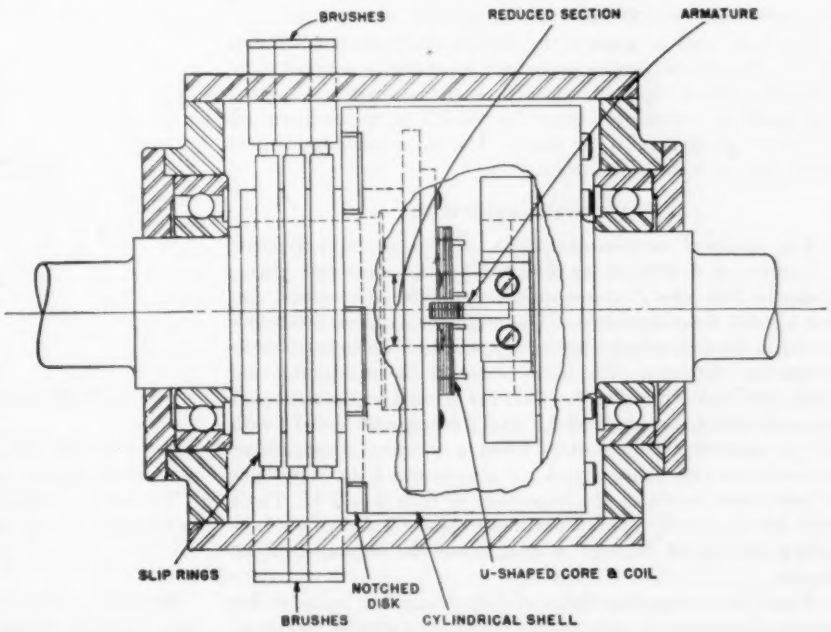


Fig. 2 Shaft-Unit Assembly

[1] General Engineering and Consulting Laboratory, General Electric Company, Schenectady, N. Y.

Contributed by the Instruments and Regulators Division and presented at the Annual Meeting, New York, N. Y., Nov. 26–29, 1945, of The American Society of Mechanical Engineers.

Note: Statements and opinions advanced in papers are to be understood as individual expressions of their authors and not those of the Society.

A bracket fastened rigidly on one end of this section transfers this torsional displacement to the other end of the reduced section where it is measured by securely attached electromagnetic-gage elements, consisting of two U-shaped laminated cores and associated coils with an armature common to both of them. Two such brackets and gaging elements are located diametrically opposite each other with the gaging elements electrically connected together. Pure torque affects each of these elements equally. Torque and shaft-bending affect one element such that it sees a displacement which is a function of the torque, plus a displacement which is a function of bending. The other element sees a displacement which is a function of torque minus the bending effect. The two gage elements electrically average these displacements, and the bending effect in one element is canceled by an opposite effect in the other element.

A cylindrical shell spanning this reduced section of shaft and covering both gage elements is securely fastened to the shaft just beyond one end of the reduced section. A disk is securely attached to the shaft just beyond the other end of this reduced section. Both cylindrical shell and disk are notched and fitted together in such a manner that they do not touch each other until the torque is approximately 250 per cent of the maximum rating of the shaft unit. From that point on the cylindrical shell and disk carry a large part of the overload torque. This feature protects both the reduced section of shaft and the gage elements if overloads are encountered. Such overloads might occur due to sudden loading or excessive torsional oscillations. In Fig. 1 the shaft unit is shown with cover and cylindrical shell removed; however, the notched disk can be seen at the right of the slip rings.

The electrical connections to the gaging elements are made through three slip rings and two sets of brushes. Careful consideration has been given in the design of the shaft unit to minimize the effects due to variation in contact resistance between brushes and slip rings. How this is accomplished is discussed in the section entitled "Design Considerations."

Each slip ring is engaged by two brushes located 180 deg apart. The brush rigging and cover assembly is supported by end plates which are held concentric with the shaft by standard ball bearings, serving to locate the brushes in the proper axial position with respect to the shaft. The cover assembly is held stationary by a suitable anchor.

Electrical Components

The electrical components shown in Figs. 3 and 4 translate the torsional deflections as detected by the shaft-unit gaging elements into electrical-instrument readings. The shaft unit has already been described. The oscillator supplies 2000-cycle power to the torquemeter power unit which contains impedance-comparing elements. The basic circuit of the power unit and shaft unit is shown in Fig. 5. Coil 1 is located on the shaft unit diametrically opposite to coil 3. Coil 2 is adjacent to coil 1 with coil 4 diametrically opposite. When a torsional displacement increases the impedance of coil 1, it also increases the impedance of coil 3 and decreases the impedance of coils 2 and 4. These coils are connected to two capacitors $C1$ and $C2$ and to the indicating instrument through a unique rectifier arrangement as shown.

When the average impedance of coils 1 and 3 is equal to the average impedance of coils 2 and 4, there is no current flowing in the torque indicating instrument. For average impedance of 1 and 3 greater than that of 2 and 4, the current will flow in the opposite direction from that obtained when the average impedance of 1 and 3 is less than that of 2 and 4.

An electrical zero-position adjustment of the torque indicating instrument is obtained by potentiometer R. The voltmeter V is used when setting the transformer-secondary voltage at a predetermined value to give correct sensitivity.

The torque indicating instrument is a direct-current milliammeter with its scale marked in pound-feet of torque.

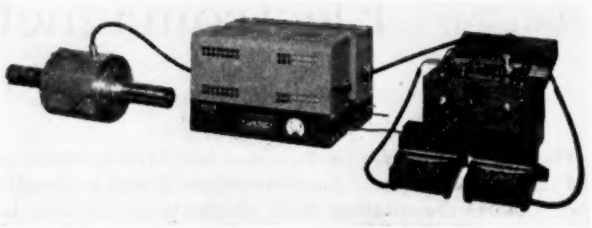


Fig. 3 Electromagnetic-Torquemeter Shaft Unit With Electrical Components

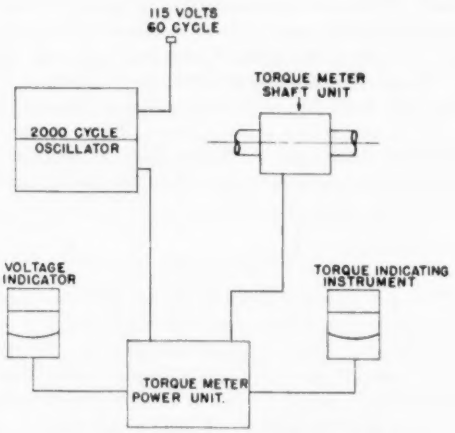


Fig. 4 Interconnection Diagram

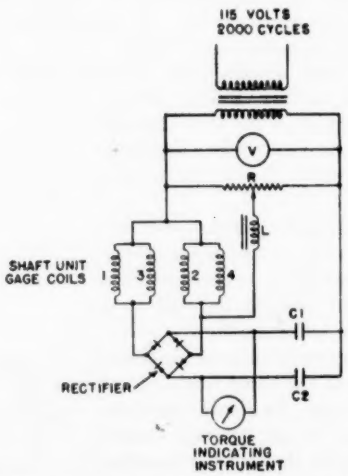


Fig. 5 Schematic Diagram of Torquemeter-Gage Circuit

Design Considerations

Since the electrical connections to the gaging elements are made through brushes and slip rings, the contact resistance between brushes and slip rings constitutes a part of the impedance measured by the electrical components. By making the impedance of a gaging element large in comparison to the effective alternating-current resistance, the brush-contact resistance has a negligible effect on the impedance. For example, consider the vector diagram shown in Fig. 6; R, X, and Z are, respectively,

the effective alternating-current resistance, the reactance and the impedance of the gage element, including brush and lead resistances. Let ΔR be the change in R due to variations in brush-contact resistance. If ΔR is 1 per cent of the total R, Z is changed by 1 per cent for $\theta = 0$, by 0.65 per cent for $\theta = 30$ deg, by 0.25 per cent for $\theta = 60$ deg, and by approximately zero per cent for $\theta = 90$ deg.

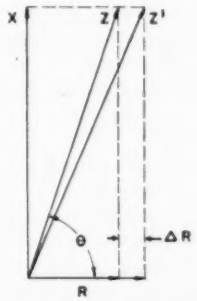


FIG. 6 VECTOR DIAGRAM OF GAGE ELEMENT

A value of θ close to 80 deg is obtained by use of laminated cores and armatures of very good magnetic properties, the use of coils with a large number of turns, and the use of 2000-cycle excitation. At 80 deg a 1 per cent change in total resistance produces only 0.04 per cent change in impedance. The electric circuit used compares impedances independent of phase angles. Since an impedance differential of 40 per cent is obtained at 100 per cent torque, this 0.04 per cent change in impedance due to 1 per cent resistance change will produce only 0.1 per cent change in torque reading. The variation in brush resistance observed under normal operating conditions is from 1 to 2 per cent of the total resistance. This small change in brush-contact resistance is obtained by using silver slip rings and graphite brushes.

Variation in brush resistance was found to increase somewhat with increased slip-ring surface speed. While a sharp line cannot be drawn as to the limiting speed to be tolerated, it has been found desirable to keep the slip-ring peripheral speeds at 80 fps or less.

The action of centrifugal forces on the gage elements is also an important consideration. Gage coils and laminations must be supported rigidly and strongly: (1) to hold the gages in place and (2) to prevent centrifugal forces from displacing the gage elements in a manner which would produce a drift in torquemeter readings as a function of speed. The particular unit shown in Fig. 1 has been run at speeds over 5000 rpm without encountering difficulties from centrifugal effects. A torquemeter of the same general type has successfully been run at 8000 rpm. This was accomplished by a more rigid gage-element supporting structure and by using small slip rings.

OVER-ALL PERFORMANCE

In general, an accuracy of 1 per cent and a repetitive accuracy of 0.5 per cent of full-scale torque can be expected with the electromagnetic torquemeter described in this paper. Tests made using a cradled dynamometer to calibrate the shaft unit at operating speeds show that static calibrations agree so closely with dynamic calibrations that only static calibrations are needed. A typical calibration curve is shown in Fig. 7. The calibration is seen to be very linear except for a slight deviation at full torque. When best accuracy is required, corrections obtained from calibration data should be applied to the torquemeter readings.

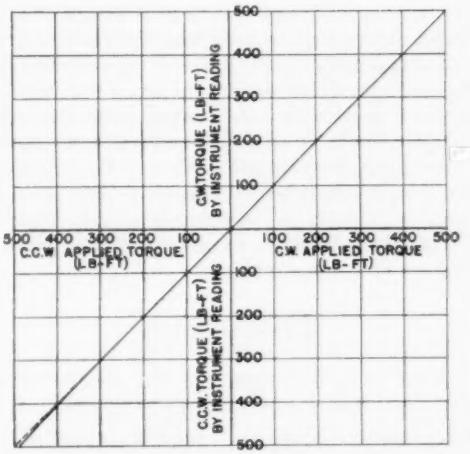


FIG. 7 CALIBRATION CURVE FOR SHAFT UNIT RATED AT 500 LB-FT MAXIMUM TORQUE

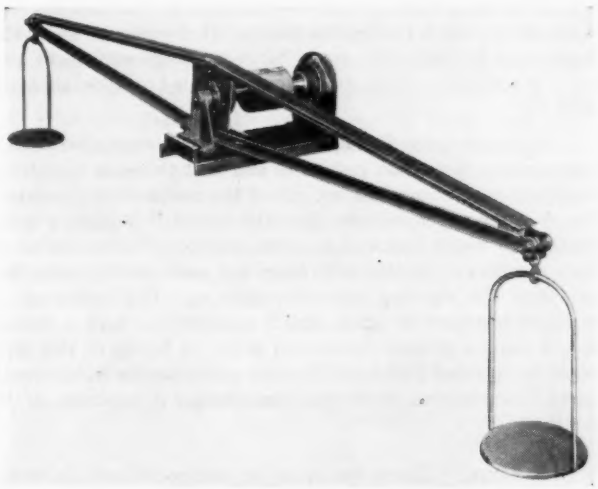


FIG. 8 STATIC CALIBRATING STAND

CALIBRATION

Fig. 8 shows a static calibrating stand with a shaft unit bolted by the attached half-couplings to a fixed plate on one end of the calibrating stand and a pivoted torque arm on the other, through which a known load is applied by adding standard weights to the weight pans hanging from knife-edges at the ends of the arm. The knife-edges provide an accurate loading point, and the ball-bearing central pivot supports the applied weights and provides a nearly frictionless pivot, making it possible to apply an accurately known torque. Thus very accurate calibrations can be obtained.

APPLICATIONS

The operation of electromagnetic torquemeters now in practical use has proved to be very satisfactory. The torque and speed ranges covered by these torquemeters extend from 250 lb-ft at 8000 rpm to 10,000 lb-ft at 400 rpm. These ranges are by no means considered as limits for electromagnetic torquemeters.

Modern trends in the design of rotating equipment are toward lightweight with accompanying high stresses. Therefore it becomes not only desirable but essential, in many cases, to know just what torque is being delivered through a section of shafting.

In addition to the torque instrument reading obtained, the torquemeter output may be used with electronic control equipment for regulating the torque delivered by a rotating shaft.

Someday torquemeters of one type or another will be standard equipment in large aircraft, on ships, and many other places where rotating shafts are used to transmit power. For the present, however, torquemeters will likely find their greatest use in production-test setups where comparative data are needed to standardize a product, or in research and development test installations where they can be used to obtain data useful in improving the design of a product.

Discussion

J. G. Fleming.[2] It is suggested that the following points discussed by the authors might be further clarified:

1 An accuracy of 1 per cent of full scale is cited in the paper. How long can this accuracy be maintained under normal operating conditions without rechecking for calibration and zero stability?

2 What is the speed of response of this instrument?

3 The application of the electromagnetic torquemeter for large-aircraft use is cited in the paper. How compact would the instrument be and what would be its approximate weight and cost for application with aircraft engines rated at approximately 1000 hp?

4 It is stated that the slip-ring contact resistance is very small compared to the circuit resistance and that therefore variations in slip-ring resistance do not affect the instrument operation. Fig. 5 of the paper indicates that the output is fed into a rectifier bridge which operates a galvanometer. The resistance of such rectifiers is usually quite large and undoubtedly much larger than the slip-ring contact resistance. The resistance of rectifiers increases on aging, and it appears that such a change would cause a gradual calibration drift. A bridge of this type could be operated with a null-balance galvanometer which would make the measuring circuit free from changes in resistance in the rectifiers.

N. S. Muir.[3] The writer wishes to confirm the authors' belief that the application of electromagnetic principles to the measurement of torque can provide a very satisfactory method capable of wide application in various mechanical systems. The authors may be interested in learning something about a similar application of the electromagnetic principle in a transmission dynamometer developed at the Royal Aircraft Establishment in England about 13 years ago which aimed at giving an accurate record of the mean torque transmitted by an aircraft engine to a propeller.

The research which preceded the development and construction of this particular torquemeter was initiated by the British Air Ministry early in 1930, aiming at the evolution of a satisfactory transmission dynamometer for the measurement of engine power in flight and in the then proposed 24-ft wind tunnel. From a critical discussion of the available methods as one would employ them in a practical transmission dynamometer, it was decided that the variable-air-gap method would provide a basic arrangement which would be favorable compared with the others, such as piezoelectric crystals, capacity units, resistance-pressure elements, etc.

One of the main features of the electromagnetic system in common with that of a capacity unit is that no direct connection need exist between the two moving members other than the flexible element providing the desired relationship between force and deflection. The line of attack chosen therefore for the research was the construction of a torquemeter in which the angular deflection of a spring element inserted in the drive between an engine and airscrew would be measured by electrical means, using variable air gaps. Thus we had two of the time-honored foundations for the transmission dynamometer design being remolded and combined in the light of modern knowledge of the application of scientific principles and the use of new materials. The basis of the electrical system chosen was attributable to Ford and may be described briefly as one in which the electromotive force (emf) due to change of inductance of a transformer secondary coil, consequent upon a change of air gap in an adjacent iron circuit forming the core, is balanced by an equal and opposite emf generated in a remotely situated receiver having a similar circuit operated by hand.

In the torquemeter being described, the deflection of the spring element was arranged to vary the air gaps in the system specially developed for the purpose, and an electrical balance was obtained by means of a micrometer-screw device on the receiver; the balanced position of the air gaps being read off a scale attached to the screw as in the Ford torsion meter. The null-reading condition of electrical balance is indicated by a moving-coil current-measuring instrument of adequate sensitivity. When forced torsional oscillations are present in the drive, the air gaps vary cyclically about the mean value, and the true mean deflection is still readable in terms of electrical balance of the moving-coil instrument, the mechanism of which is then suitably damped.

In the earlier air-gap instruments of Denny, Ford, and Moullin, the systems were energized from small alternators or by interrupted direct current of relatively low frequency. This latest unit to which reference is made is fed from a special 1500-cycle alternator designed to have a purely sinusoidal voltage output. The high frequency is essential to deal with the presence of torque oscillations in the airscrew drives in aero engines up to about 200 per sec, so that integration of the torque variation may be sufficiently accurate.

The basic design for our first torquemeter was completed in March, 1930, and the apparatus was ready for calibration in May, 1931. Preliminary experience was gained with this first unit, covering some 70 or 80 hr running on the test bench on a Jupiter VII supercharged direct-drive engine and using the Froude brake as the criterion of torque. At constant speeds, accuracy within 0.3 per cent was obtained, while over a range of speeds the greatest error was within 2 per cent. The apparatus was then transferred to an aircraft and successful use in flight was achieved. Special apparatus was provided to obtain an accurate measure of the rotational speed of the engine, since the computation of horsepower depends upon the product of speed and torque.

A second unit was provided primarily for use in the then proposed 24-ft wind tunnel at Farnborough to enable full-scale testing of propellers to be carried out. In this case the spring element took the form of a one-piece wheel in which the rim, spokes, and hub were carved out of a solid disk of about 18 to 20 in. diam and was capable, in conjunction with the electrical system, of giving readings of torque over a wide range from one-quarter to full torque of engines up to about 1000 hp.

It will be appreciated that the null-reading electrical system chosen is not the same as that described in the paper just presented, which uses an electrical system on the lines of that used by Moullin, where the output of an alternator or 2000-cycle oscillator is modulated by the torquemeter coils to give a direct rectified indication of torque. At an early stage of our investigation it was found essential to have an especially accurate apparatus for carrying out static-torque calibrations, and a tackle was

[2] The Bristol Company, Waterbury, Conn.

[3] Chief, Engine Development Section, British Supply and Air Commission, Washington, D. C.

specially designed for the purpose, which permitted the rolling load of a beam system to impose pure torques on the shaft carrying the torquemeter so that positive and negative torques could be smoothly applied according to the direction of motion of the load from the central position of no torque. The apparatus has ball bearings at every moving joint and is extremely delicate in its operation; torques of only 2 or 3 lb-in. being accurately obtained.

Limit stops were provided on the spring element which permitted a range of torque of from 60,000 lb-in. to approximately —12,000 lb-in. and some idea of the accuracy of the spring element in maintaining its zero at no torque is given by the fact that after taking the spring through several cycles of stress on the torque loading elements previously mentioned to remove any slight hysteresis in the material and then determine its zero setting, it returned after subsequent cycles of stress to this zero position within 1/40,000 in. at 9.625 in. radius. This radius refers to the position of a dial-gage reading to 1/10,000 in. which was attached in such a way as to record this circumferential deflection of the spring as it deflected. This dynamometer was used satisfactorily in large 24-ft wind tunnel at Farnborough for the measurement of torque in full-scale propellers.

Many applications of such a system can be made, and a dynamometer of this type lends itself to use either as a transmission coupling or as a static unit mounted in conjunction with aero-engine reduction gears or in any position where the torque to be measured reacts on a stationary member. From the writer's experience with this torquemeter, assurance can be given to the authors that their application is well worth development along the lines which they propose and for the applications which they mention. The writer's opinion, however, is that a null-reading system is much more likely to give enhanced accuracy than the use merely of the output from an unbalanced coil system. One important feature which must not be overlooked is, as previously stated, the accurate calibration of the spring element whether it be a piece of shaft or actual springs. This, in fact, is particularly important where in measurement on ship's propeller shafts a relatively long length of shaft is chosen. The writer agrees with the authors' attention to the slip rings and brushes used in the system. In the British torquemeter which the writer has just described, we have recently redesigned the recording circuit so as to eliminate completely any errors arising from faulty slip-ring contacts.

Author's Closure

Mr. Fleming brings up several points which will be discussed briefly in order.

(1) The electromagnetic torquemeter described should maintain its calibration. However, the zero adjustment may have to be made occasionally and should be checked whenever possible.

(2) The speed of response is limited by the indicating instrument and is approximately two seconds. A magnetic oscillograph may be used in place of the indicating instrument to record rapid torque variations up to several hundred cycles per second.

(3) The electromagnetic torquemeters described in the paper are not suitable for general flight applications on aircraft engines.

(4) The resistance of the rectifier section is approximately 20 ohms which is small in the light of the several hundred ohm gage circuit impedances. The advantages of a null system are recognized and are frequently put to good use. A continuous indicating system has the advantage of convenience over a null system where the balancing must be done manually. Accurate automatic null balancing systems are available.

Taking the Mystery Out of the Kadenacy System of Scavenging Diesel Engines

By P. H. SCHWEITZER,[1] C. W. VAN OVERBEKE,[2] AND L. MANSON[3]

The "Kadenacy effect" of the Diesel-engine exhaust is utilized to create a vacuum in the cylinder for introducing the fresh charge. The result of the application of this system is exemplified in tests in 1939, of a converted Junkers opposed-piston engine in which the power was raised from 11 to 25 hp, or an increase of 130 per cent. This was accomplished solely by changing the characteristics of the inlet and exhaust ports and passages in accordance with the Kadenacy patents. However, the theory expounded by the inventor has been subject to question, as the authors explain, and while the results are entirely matters of record, the phenomenon can be accounted for by conventional thermodynamics based upon simple adiabatic expansion. This fact the authors have demonstrated by experiment. The formulas derived check closely with those of Kadenacy but they are based upon a more rational approach to the problem than Kadenacy's contention that supersonic velocities are involved in the exhaust process.

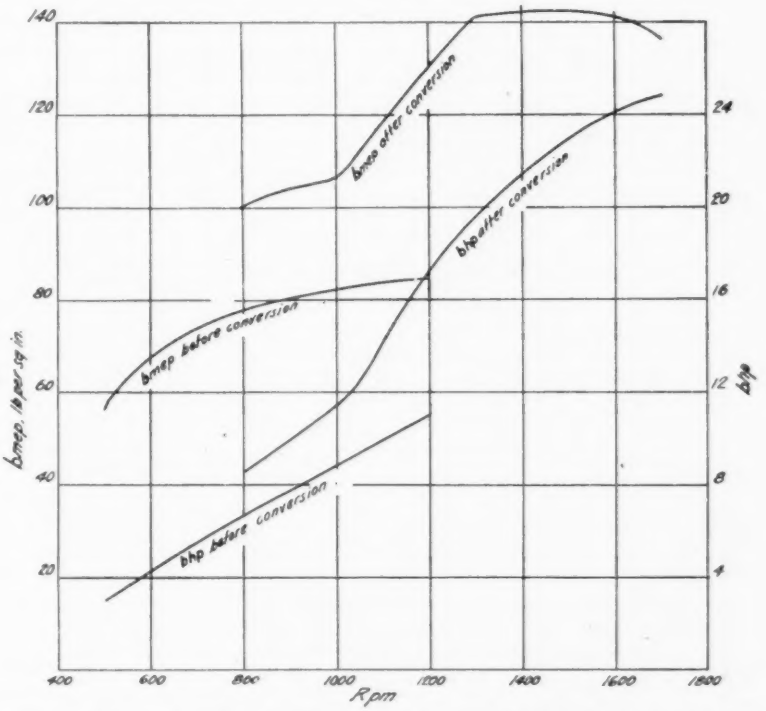


FIG. 1 HORSEPOWER AND BRAKE MEAN EFFECTIVE PRESSURE OF JUNKERS OPPOSED-PISTON ENGINE BEFORE AND AFTER CONVERSION TO KADENACY SYSTEM

DURING the last few years the Kadenacy system of scavenging Diesel engines has attracted some attention in this country and more abroad. That system is best known in the form of a blowerless two-stroke-cycle engine. The "Kadenacy effect" of the exhaust is utilized to create a vacuum in the cylinder for introducing the fresh charge. That by itself would not be remarkable if we were to attribute the effect to a tuned exhaust pipe. The Kadenacy system, however, embraces more than that. In numerous patents (1)[4] an ever-recurring sentence is that "at least a substantial portion of the burnt gases leaves the cylinder at a speed much higher than that obtaining when a flow resulting from an adiabatic expansion only is involved, and in such a short interval of time that it is discharged as a mass, leaving a depression behind it which is utilized in introducing a fresh charge into the cylinder, etc." This has been quoted from U. S. Patent 2,168,528. Kadenacy's other patents include various versions of the same statement and explain that mass means a "coherent mass" (Patent No. 2,123,569), "having properties similar to those of a resilient body" (Patent No. 2,102,559), and that the "ballistic" speeds involved in the evacuation are about 4 times higher than "the speed of adiabatic expansion," leaving behind them "a high depression which may reach a complete vacuum" (Patent No. 2,131,957).

The foregoing notions are so unorthodox that many engineers ignored and even ridiculed them. But it is not wise to ignore test results and Kadenacy has astonishing results to his credit.

The first commercial blowerless Kadenacy engine was built by Petter (2), and the same company is still building Kadenacy-type engines of an improved design (3); however, with a blower attached.

According to tests (4), described in 1939, the conversion of a Junkers opposed-piston engine resulted in a substantial increase of power. Some test results are reproduced in Fig. 1. The maximum power was raised from about 11 to 25 hp, an increase of 130 per cent. This is claimed to have been obtained without any alteration to the combustion chamber or fuel-injection equipment, solely by changing the characteristics of the inlet and exhaust ports and passages, in accordance with the Kadenacy patents. The scavenge pump was rendered inoperative and the inlet ports, which were still controlled by the upper piston, were arranged so that they communicated directly with the atmosphere. With the Kadenacy system fitted to the engine it was possible to run the engine to a much higher speed without any ill effects, it is claimed. The pistons remained in a cooler condition, the maxi-

[1] Professor of Engineering Research, Pennsylvania State College, State College, Pa. Mem. A.S.M.E.

[2] Ex-Cell-O Corporation, Detroit, Mich.

[3] DeLaval Steam Turbine Company, Trenton, N. J.

[4] Numbers in parentheses refer to the Bibliography at the end of the paper.

Contributed by the Oil and Gas Power Division and presented at the Annual Meeting, New York, N. Y., Nov. 26–29, 1945, of THE AMERICAN SOCIETY OF MECHANICAL ENGINEERS.

NOTE: Statements and opinions advanced in papers are to be understood as individual expressions of their authors and not those of the Society.

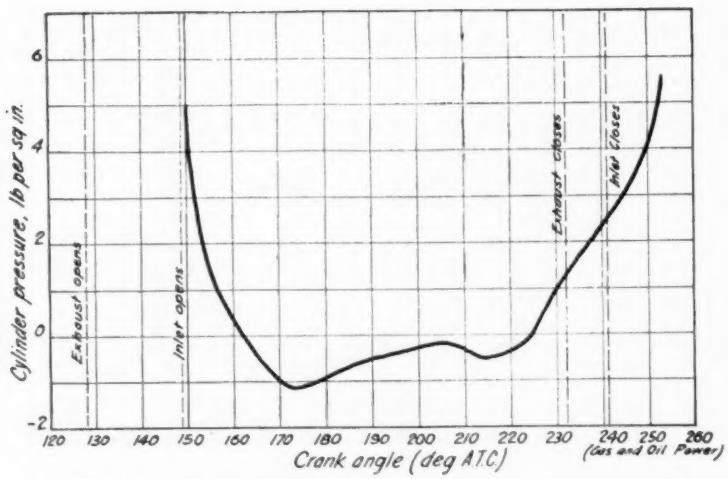


FIG. 2 CYLINDER PRESSURES IN THE JUNKERS-KADENACY OPPOSED-PISTON ENGINE

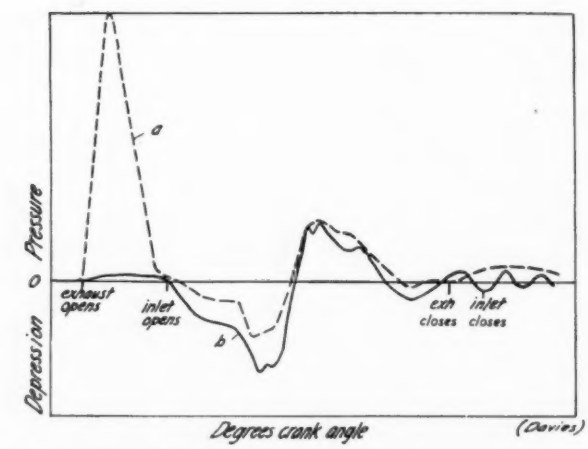


FIG. 3 PRESSURE FLUCTUATIONS IN EXHAUST DUCT—LINE A—AND INLET DUCT—LINE B—OF A JUNKERS-KADENACY ENGINE; 650 RPM

mum pressures were lower and the specific fuel consumption also was lower.

Fig. 2 shows the cylinder pressures in the Kadenacy-Junkers engine operating without scavenging air pump. It is notable that a depression over 1 psi below atmospheric occurred in the cylinder 50 deg after the exhaust ports had opened.

Fig. 3 shows the pressures in the intake and exhaust ducts of the converted Junkers engine from which it is seen that pressure changes are transmitted from the exhaust ducts to the intake ducts without appreciable delay. Tests at 800 rpm with various lengths of exhaust pipes gave Fig. 4 which shows that the Kadenacy effect does not depend upon a particular pipe length, only the time of maximum depression was retarded when the exhaust-pipe length was increased.

We have dwelt on this Kadenacy-Junkers engine because part of the tests reported were made by such an unquestioned authority as Prof. S. J. Davies of London, England.

Conversions of other two-stroke engines of either uniflow or the cross-scavenge type gave similar results, although not quite as spectacular as those shown in Fig. 1. Some engines fitted with the Kadenacy system had blowers and others had none. When a blower was used the scavenge-air pressure was considerably less, and significantly it decreased when the load increased. In the original engine the scavenging pressure increased with the load. The difference is explained by the fact that with the Kadenacy system as the load becomes greater the energy in the exhaust also becomes greater and with it the suction effect in the cylinder, thus reducing the resistance to the delivery of the air from the blower. Converted engines consistently showed appreciable power increase with lower specific fuel consumption and lower exhaust temperatures.

The mechanics of the Kadenacy principle were investigated by Davies (5) with a free-moving piston in a cylinder. He compressed a mixture of air and gasoline vapor with a hand crank and ignited it with a spark plug. The gas pressure sent the piston downward until it uncovered a slot through which the burnt gases discharged into the atmosphere. This sudden discharge caused so great a depression in the cylinder that the free piston rose in the cylinder and came to rest at about two thirds of its upward travel. With photoelectric apparatus, Davies recorded the piston travel and showed that the entire process was completed in a very short time. With a cylinder of 2.4 in. bore and 2.2 in. effective stroke the exhaust process lasted only 3.2 milliseconds and the residual depression was 17 in. Hg abs. Experiments with various lengths of exhaust pipes showed that the resulting depression and the time during which the exhaust slot remained uncovered were largely unaffected by the exhaust pipe. For instance, when the exhaust-pipe length was changed from 7.5 to 53 in., the duration of the exhaust period changed only about 6 per cent. The gas flow in the exhaust pipe was shown by high-speed photography of a lightweight "cursor" in a glass exhaust pipe. This revealed a very rapid back-and-forth movement of the gas column.

While the results obtained with the Kadenacy system are fully discussed in the literature, the constructional details are not disclosed. One or more of the expedients shown in the patent drawings such as tapered exhaust pipes and reflection-wave stoppers might have been employed to obtain the excellent results but apparently no particular importance is attached to them.

In view of these reports, the authors felt a necessity to de-

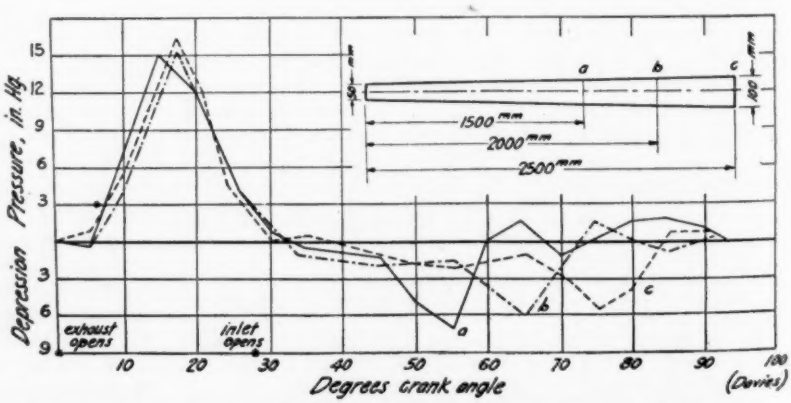


FIG. 4 PRESSURES IN EXHAUST PIPE OF JUNKERS-KADENACY ENGINE WITH VARIOUS LENGTHS OF EXHAUST PIPES; 800 RPM

termine in a conclusive manner whether the so-called Kadenacy effect really exists, aside from the pipe effect the nature of which is fairly well known (6).

Investigation of the Kadenacy Effect

Kadenacy claims that upon opening the exhaust port the gas leaving the cylinder with a very high (supersonic) velocity will evacuate it, leaving a partial or complete void behind, irrespective of whether a pipe is attached to the cylinder or not.

The depression thus created in a cylinder, no matter how short in duration, can be measured and no combustion needs to be involved in the test.

In order to measure the depression following a sudden gas outflow, a special setup was built at The Pennsylvania State College. It consists of a steel cylinder, Fig. 5, closed by a lid locked with a quick-acting latch. This lid is forced open by the initial cylinder pressure when the latch is released. Orifices of different diameters or nozzles were fixed at the lid end of the cylinder. A pickup for determining the lowest pressure reached in the cylinder during the exhaust was fixed at the closed end of the cylinder. This pickup consists of a brass diaphragm of $2^1/_4$ in. diam and 0.025 in. thick, exposed to the cylinder pressure on one side, and to an adjustable depression on the other. The diaphragm opens an electric contact when the pressure in the cylinder drops below the adjusted depression; the contact is inserted in a 6-volt circuit in series with a transformer coil. A neon lamp is placed in series with the secondary winding of the transformer. This gives a flash when the primary circuit opens.

The depressions have been measured for different orifice diameters and different initial tank pressures. The results are shown in Fig. 6 where the maximum depression after the gases have rushed out of the cylinder, are plotted against the cylinder gage pressure before the cylinder was opened. With the 6-in. orifice there was in effect no plate, as the cylinder was wide open. One curve corresponds to the use of a convergent-divergent nozzle with 2-in. throat diameter and $3^1/_8$-in. length. The opening on the pressure side was $4^1/_2$ in. and convergence took place for 2 in. Over the remaining $1^1/_8$ in. the nozzle diverged uniformly at an angle of 15 deg.

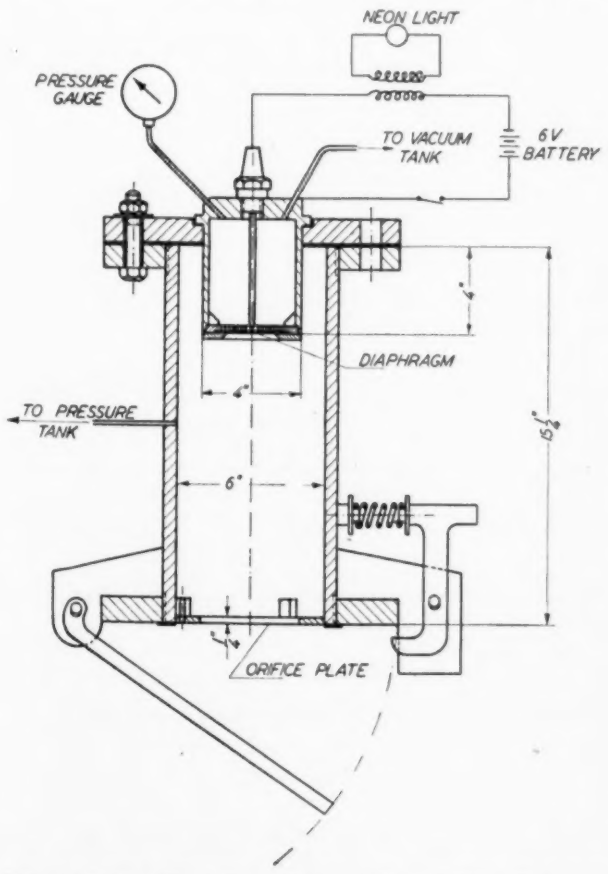


Fig. 5 Vessel With Quick-Opening Lid to Test Kadenacy Effect

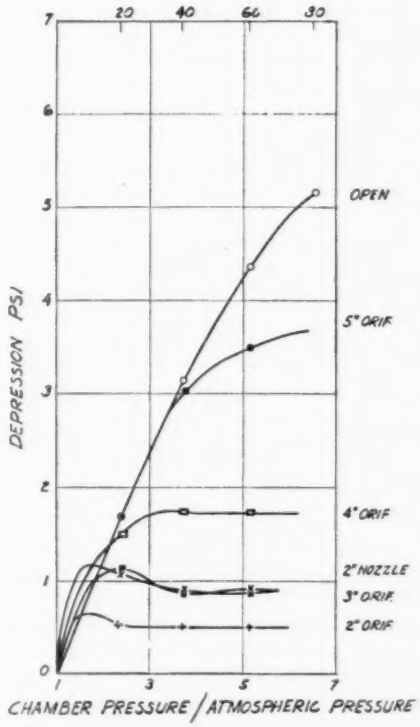


Fig. 6 Kadenacy Effect; Observed Depressions by Sudden Pressure Release, Penn State Experiments

The experiments show that the depression, although far from a complete void, is great enough to account for the results on two-stroke Diesel engines applying Kadenacy's patents.

Theory of the Kadenacy Effect

Various explanations of the Kadenacy effect have been published. Giffen (7) calculated the pressure waves generated by the sudden evacuation of a cylindrical vessel and obtained depressions of the order that we have observed. His calculations even showed that with an orifice appreciably smaller than the cylinder the depression does not increase continuously with the increase of the initial cylinder pressure but it reaches a maximum when the initial cylinder pressure is around 20 psia, and if it exceeds that, the depression begins to decrease. This agrees with our observations with orifices and nozzles of 3 in. diam or smaller.

Geyer (8) proposed a rather simple theory of the Kadenacy effect. He attributes the evacuation of the cylinder to the kinetic energy of the gases still in the cylinder, yet rushing out of the cylinder.

It is not improbable that Geyer got the idea for his theory from Kadenacy himself. For instance, in U. S. Patent No. 2,123,569, Kadenacy is using the analogy of a coil spring to explain what happens in the cylinder. He visualizes a helical spring on a table compressed, with a certain amount of energy

stored in it. If the spring is released gradually by allowing it to expand against a resistance, it will return to its free length. The work done by the spring will then become stored in the resistance. This, he states, corresponds to the release of compressed gases from a container through an orifice which is opened gradually.

On the other hand, if the spring, after having been compressed on the table, is released suddenly by removing the compressing means in a short interval of time, the spring while expanding will leave the table bodily. The energy stored in the spring imparts momentum to the spring. During its flight through the ai after it has left the table, oscillations will occur in the spring but these oscillations will bear no direct relation with the motion of the spring body from the table. This case corresponds to the sudden release of the gas from the cylinder according to Kadenacy.

Geyer goes through a somewhat similar reasoning. The potential energy of the compressed gas is transformed into kinetic energy. The gas will leave the cylinder with a velocity that corresponds to this energy. At the time the pressure inside of the cylinder has dropped to atmospheric, the gas in the cylinder still has some kinetic energy, which will perform work against the atmospheric pressure. This work consists of displacing a certain volume of air against ambient pressure. The equivalent volume of air to replace the volume must come from the cylinder, and so a depression is created by the discharge of that amount of air.

Geyer's simple theory can have no pretension of describing accurately such a complex phenomenon as the sudden evacuation of a cylinder. Yet it not only gives a correct mental picture of the mechanism of the Kadenacy effect but surprisingly it even gives tolerable agreement with observed results. Geyer has applied his calculations to Davies' experiments (8), and we to the Penn State experiments (9), which are shown in Fig. 7.

In Fig. 8 is reproduced a comparison of the observed and calculated depressions when the sudden removal of the lid uncovered the full cylinder opening. With smaller orifices the observed depressions are higher than those calculated.

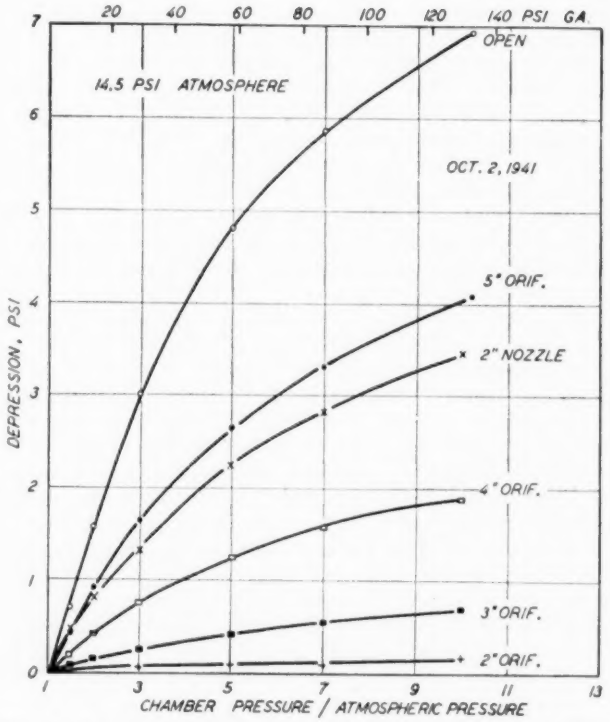


FIG. 7 KADENACY EFFECT; GEYER'S THEORY APPLIED TO PENN STATE EXPERIMENTS

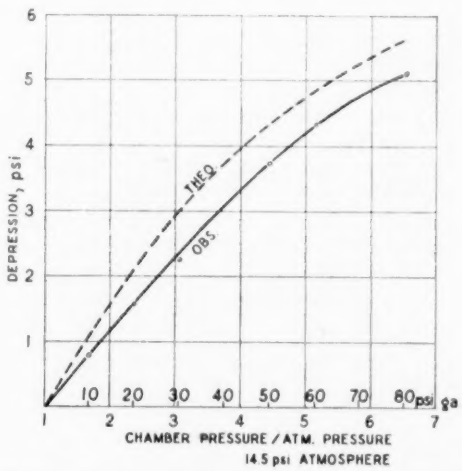


FIG. 8 KADENACY EFFECT; OBSERVED AND CALCULATED DEPRESSIONS; OPEN END

BALLISTIC VELOCITIES

A recurrent statement in most Kadenacy patents is that the burnt gases discharge through the exhaust ports at a speed far in excess of the speed of adiabatic expansion. Patent No. 2,123,569 gives the "speed of adiabatic expansion" as 350 to 450 m per sec, and gives the "ballistic speed" of exhaust due to the "ballistic force" as 1400 to 1800 m per sec, that is about 4 times as high.

The velocity of sound in a diatomic gas of a temperature about equal to that of the exhaust gases is as a matter of fact 350 to 450 m per sec. In a straight or convergent orifice this is also the upper limit of discharge velocity of the gas.

The authors were unable to find out where figures of 1400 to 1800 m per sec had been obtained. But Kadancy uses these figures in porting design and obtains good results. This may be an indirect proof that his figures are correct. Let us examine this evidence.

Since the pressure in the cylinder when the exhaust port opens is about 5 atm, Kadenacy reasons, 4 volumes of exhaust gases have to be discharged to bring the pressure down to atmospheric during the blowdown period. It takes, he states, as much time to discharge 4 cylinder volumes of gas at 1800 m per sec velocity as one volume of gas at $^1/_4 \times 1800 = 450$ m per sec velocity. Therefore he envisages the "hypothetical velocity" of 450 m per sec and designs his exhaust ports in such a manner that the gas column which projects through the exhaust port during the exhaust-lead period with the hypothetical velocity of 450 m per sec, is just equal to 1 cylinder volume. If V denotes this volume in cubic meters, A_m the mean uncovered exhaust-port area during the exhaust lead (blowdown period) in square meters, and L the length of the hypothetical gas column in meters, then

$$V = A_m L \quad \ldots\ldots [1]$$

the hypothetical velocity which is 450 m per sec, is given by

$$V_{hyp} = \frac{L}{t} \quad \ldots\ldots [2]$$

where t is the time of the blowdown period in seconds, and

$$t = \frac{\alpha}{6n} \quad \ldots\ldots [3]$$

Here α is the exhaust lead in degrees and n is the engine speed in revolutions per minute.

From Equations [1], [2], and [3]

$$V = A_m V_{hyp} \frac{\alpha}{6n} \quad \ldots\ldots [4]$$

Putting $V_{hyp} = 450$ and rearranging, we get

$$A_m\alpha = V n \frac{6}{450} = \frac{V n}{75} \quad m^2 \text{ deg} \quad \ldots\ldots [5]$$

This is Kadenacy's reasoning, and the resulting formula is identical with Kadenacy's formula Patent No. 2,144,065

$$\frac{W}{100\,KA} = \frac{a}{360\,N} = t$$

except for the different symbols. From this the proper exhaust lead can be calculated. By converting the metric units used in Kadenacy's Equation [5] to square inches we get

$$A_m\alpha = \frac{(39.4)^2}{(39.4)^3} \frac{Vn}{75} = 0.00034\ Vn \quad \ldots\ldots [6]$$

This is still Kadenacy's formula in a slightly changed form. On the other hand Schweitzer's formula (10) gives

$$A_m\alpha = 0.00033\ V_{disp} n \quad \ldots\ldots [7]$$

Ignoring the difference between V and V_{disp}, Equation [7] differs only 3 per cent from Equation [6].

Equation [6] is a consequence of the Kadenacy theory, but Equation [7] was derived independently of the Kadenacy theory, before we knew of the latter's existence. The Kadenacy theory supposes the existence of "ballistic velocities" which are about 4 times higher than those obtained from adiabatic expansion. Equation [7] was derived by conventional thermodynamics, and the discharge velocities used were substantially the same as sound velocities modified by discharge coefficients obtained by the Nusselt theory. The two theories give practically identical results.

The circumstance that Kadenacy got correct results from incorrect premises casts a doubt on Kadenacy's reasoning.

We believe Kadenacy's reasoning to be fallacious and in the following we try to show the error in it.

Fallacy in Kadenacy Theory

Kadenacy states[5] that instead of applying the true ballistic velocity, 1800 m per sec to 4 cylinder volumes of gases to bring down the pressure from 5 atm to 1 atm, one may use a hypothetical velocity of 1800/4 = 450 m per sec to 1 cylinder volume and get the same results. We believe this to be a mistake. One cylinder volume should be considered and not 4, even if the pressure in the cylinder is 5 atm.

A rough reasoning should suffice to make this clear. Let us consider two cases. In one case the density of the gas does not vary during the discharge. Before, in, and after the exhaust orifice, the density is the same. In this case (which is analogous to the discharge of water) if the cylinder volume V contains gas at 5 atm pressure and that is discharged through an orifice A with 450 m per sec discharge velocity, and $A = V/450$, then at the end of 1 sec all of the gas will be discharged and not $^1/_5$ of it only. It makes no difference whether the pressure in the cylinder was 5, 4, 3, 2, or 1 atm. In every case 450 m per sec discharge velocity is required to evacuate the cylinder in 1 sec. The assumption of a ballistic velocity of 1800 m per sec is unjustified.

[5] U. S. Patent No. 2,123,569, p. 4, lines 33–62.

Let us next consider the change in gas density. The discharge velocity refers to the throat of the orifice, and the specific weight to be considered is the one existing in the throat.

Calculation by conventional thermodynamics shows that the specific weight in the throat is approximately 0.78 kg per cu m in the beginning of the blowdown and drops gradually to approximately 0.4 kg per cu m at the end. Assuming a constant discharge velocity of 450 m per sec and a constant exhaust orifice of A m^2 during the t sec of the blowdown period, we shall discharge

$$450 \frac{0.78 + 0.4}{2} A \text{ kg of air}$$

If, conforming to Kadenacy, we make $A = V/450$, where V is the total cylinder volume, the amount discharged will be

$$D = 0.59\ V \text{ kg}$$

while the amount that has to be discharged to drop the pressure from 5 atm to 1 atm is

$$D_1 = \frac{4}{5} V \gamma_{int} = 0.8\ V\ 0.73 = 0.585\ V \text{ kg}$$

It is seen that D approximately equals D_1, which means the exhaust can be disposed of in the required time period, assuming only sound velocity and no supersonic or ballistic velocity is required.

We conclude that while the value of Kadenacy's hypothetical velocity is sound and should give good results if applied to porting design, it in no way supports the existence of ballistic velocities in excess of sound velocities.

A further confirmation of this conclusion can be found in calculating from Geyer's theory the outflow velocities created by the sudden opening of an air-filled vessel. Fig. 9 shows these velocities, and for comparison, also the calculated sound velocities for various temperatures. For the detailed calculation the reader is

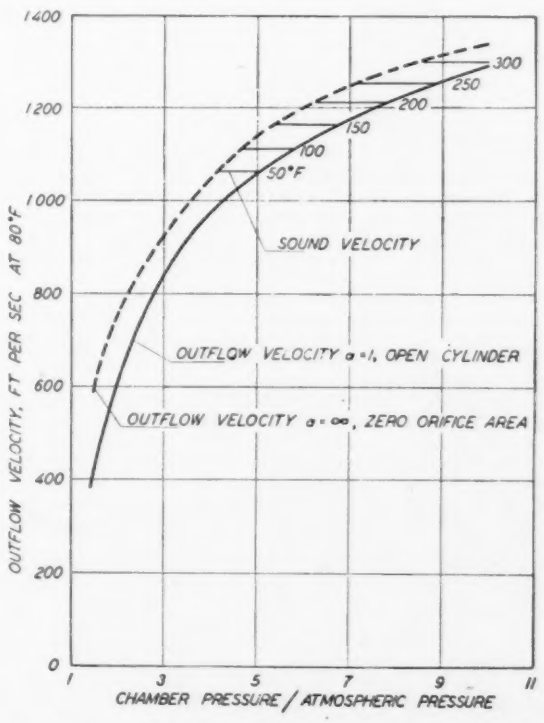


Fig. 9 Outflow Velocities Created by Sudden Opening of Vessel Filled With Air, From Geyer's Theory

referred to (9). An inspection of Fig. 9 reveals that with 5 to 7 atm chamber pressure the outflow velocities do not differ much from the sound velocities.

Conclusions

1 The astonishing performance claimed by Kadenacy engines should not be rejected as incredible as the effect is based upon a demonstrable physical phenomenon; the rarefaction that follows the sudden discharge of compressed gas from a closed vessel.

2 The Kadenacy effect is not due solely to the inertia of the gas column in the exhaust pipe, as 10 in. Hg depression was observed by the authors in a vessel without any exhaust pipe, and reported results show good performance in engines with varying lengths of exhaust pipes.

3 The Kadenacy effect vanishes if the discharge opening becomes relatively small. One inference is that an obstacle of the full exploitation of the Kadenacy effect is that exhaust ports or valves in engines cannot be opened rapidly enough.

4 Geyer's theory seems to give a fair picture of the mechanics of the Kadenacy effect and excellent numerical agreement in case of a large discharge opening.

5 Nothing in our observations supports Kadenacy's contention that velocities in excess of sound velocities are involved in the exhaust process. Conventional thermodynamics based upon simple adiabatic expansion gave formulas practically identical with those recommended by Kadenacy, and Geyer's theory applied to our experiments also successfully indicated discharge velocities of the order of sound velocities and no higher.

BIBLIOGRAPHY

1 Kadenacy U. S. Patents:
2,102,559, 1937
2,110,986, 1938
2,113,480, 1938
2,123,569, 1938
2,131,957, 1938
2,130,721, 1938
2,131,959, 1938
2,134,920, 1938
2,144,065, 1939
2,147,200, 1939
2,167,303, 1939
2,168,528, 1939

2 "Induced Air Scavenge for Two-Stroke Engines," by P. W. Petter, *Engineer*, vol. 158, 1934, p. 157.

3 "Recent Development in Medium-Speed Two-Cycle Oil Engines," by C. B. M. Dale, *British Motor Ship*, vol. 25, January, 1945, no. 300, pp. 346–348.

4 "Improving the Two-Stroke Cycle," *Gas and Oil Power*, vol. 34, Nov., 1939, pp. 294–299.

5 "The Characteristics of Engines of Kadenacy Design," by S. J. Davies, *Engineering*, London, vol. 143, 1937, pp. 685–688.

6 "Improving Engine Performance by Exhaust Pipe Tuning," by P. H. Schweitzer, *Journal of the American Society of Naval Engineers*, vol. 56, 1944, pp. 185–212.

7 "Rapid Discharge of Gas From a Vessel Into the Atmosphere," by E. Giffen, *Engineering*, London, vol. 150, 1940, pp. 134–136, 154–155, and 181–183.

8 "A Theory of the Kadenacy System," by E. W. Geyer, *Engineering*, vol. 151, 1941, pp. 463–464.

9 "The Kadenacy Effect," by P. H. Schweitzer, C. W. Van Overbeke, and L. Manson, *Engineering*, London, September 28, 1945, pp. 241–244.

10 "Porting of Two-Stroke-Cycle Diesel Engines," by P. H. Schweitzer, *Diesel Power and Diesel Transportation*, vol. 20, 1942, p. 818.

Discussion

Paul Diserens.[6] The authors' discussion of the Kadenacy effect is particularly timely in view of the development of two-cycle engines, sponsored by Mr. Kadenacy, on the part of several American manufacturers at this time.

It would appear that the paper is, in effect, a continuation of the extended discussion of the Kadenacy engine which was reported in the British and the Continental technical press during the years 1938 to 1941, inclusive. While the authors make some reference to the numerous articles published at that time, it might be suggested that a bibliography comprising the more important references would constitute a valuable addition to the paper.

The writer finds it of particular interest to compare the apparatus used by the authors in their experiments, with that employed by Prof. S. J. Davies, of Kings College, University of London.[7]

It should be noted that in the Davies apparatus provision is made to insure the greatest possible speed in establishing communication between the pressure vessel and the atmosphere. In the apparatus used by the authors the speed of opening is limited because of the time required to accelerate the communicating valve.

It is evident that the results reported in the paper reflect the influence attributable to the speed of opening and therefore the results might conceivably be quite different if some other speed had been employed. Consequently, conclusion 3, i.e., "The Kadenacy effect vanishes if the discharge opening becomes relatively small." One inference that full advantage cannot be taken of the Kadenacy effect because "exhaust ports or valves cannot be opened rapidly enough," cannot be valid except when the exhaust-valve acceleration at the time of opening is low or at best comparable with that which obtained during the authors' experiments. For this reason it would appear that their results cannot properly be used as the basis for any general theory to explain the phenomena and should not be quoted as confirming such a theory based on pure speculation.

The authors assert that the hypothetical assumed average speed of 450 m per sec is derived from some preconceived theory of operation, and quote from various Kadenacy patent specifications in support of this assumption. This does not conform to my understanding of the Kadenacy patents. From a complete study of all of these it is obvious that the structures covered by the patents rest entirely upon experimental data from which empiric relationships are established. Obviously, variable coefficients must be determined in order to take care of such variable conditions as, for example, speed of opening of the exhaust valve.

An experimental engine, built by the company with which the writer is associated, develops mean effective pressures of more than 100 psi without a blower. Analysis of the exhaust gas, as well as direct measurements indicates that the volume of air passing through an engine exceeds the displacement by 60 per cent.

---

[6] Director of Research and Development, Worthington Pump and Machinery Corporation, Harrison, N. J. Fellow A.S.M.E.

[7] "Sudden Discharge of Air From a Pressure Vessel," by S. J. Davies, *Engineering*, vol. 149, 1940, pp. 17–18.

An Analysis of Intercooled Supercharging

By RALPH H. MILLER,[1] MILWAUKEE, WIS.

In this and in an earlier paper,[2] the author analyzes the internal-combustion engine as a heat engine. He finds that with present-day materials, the output of the internal-combustion engine is limited by the temperatures reached in the internal surfaces and not by lack of air to sustain combustion. A method is developed by which the output capacity of four-cycle engines may be increased by more than 100 per cent without exceeding practical and previously established temperatures of internal surfaces.

IN a previous paper,[2] the author summed up his analysis of intercooled supercharging in a rating graph which is reproduced in Fig. 1, herewith.

Curve *A* in the graph shows that with standard supercharging without air cooling 133 per cent of the mean indicated pressure (mip) is carried at 4 psi pressure with the same cycle mean temperature. This represents a gain of 36 per cent in brake mean effective pressure (bmep). Since that paper was presented a series of tests has been conducted to check the theories presented therein.

Efforts were made to correlate calculated cycle mean temperatures and the surface temperatures of the internal walls, which are obviously what affect the engine parts and not the temperature of the gases.

An engine operating at 600 rpm, and another engine tested at 327 and 360 rpm were used in these tests. Equipment was installed to measure the heat flow to the cooling-water jackets with great accuracy. Means were also installed for controlling the air-intake temperature to the blower or the engine manifold.

The cooling-water mean temperature was kept at 155 F and the rate of circulation maintained constant for all loads and speeds.

The formula for rate of heat transmission

$$dq = U \times dA\ (t_1 - t_0)$$

where

dq = Btu per unit of time
dA = area
$U \times dA$ = over-all conductance of wall per unit of time
t_1 = temperature of internal hot surface
t_0 = temperature of cooling water

permits us to conclude that the internal-wall temperature t_1 is unchanged when, in any given engine, changes are made in manifold pressure or temperature or combustion efficiency, but the load is adjusted so that dq remains constant.

The rate of heat flow to the cooling water (liners and cylinder heads) is plotted in Fig. 2 for the 600-rpm engine. Curve 1 shows the naturally aspirated engine from 58 to 85 bmep. Curve 2 is the engine supercharged with the Buchi system with two exhaust pipes to the turbine. Curve 3 is the same as curve 2 but with intercooling to 90 deg F in the air-inlet manifold.

The naturally aspirated engine is rated at 80 bmep. The heat flow to the cooling water (dq) is 12,000 Btu per min at this load. When the engine is operated supercharged with the Buchi system, a heat flow of 12,000 Btu is reached at a load of 102 bmep. Curve 1 in Fig. 3 shows a supercharging pressure of 6.7 in. Hg (3.3 psi) at 102 bmep.

The theoretical rating curve, Fig. 1, shows that on the basis of equal cycle mean temperature of the gases, a rating of 131 per cent of the naturally aspirated indicated rating should be carried at 3.3 lb supercharging pressure.

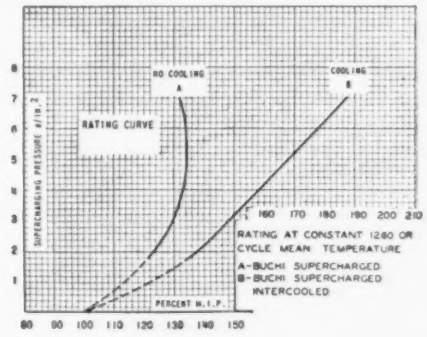


FIG. 1

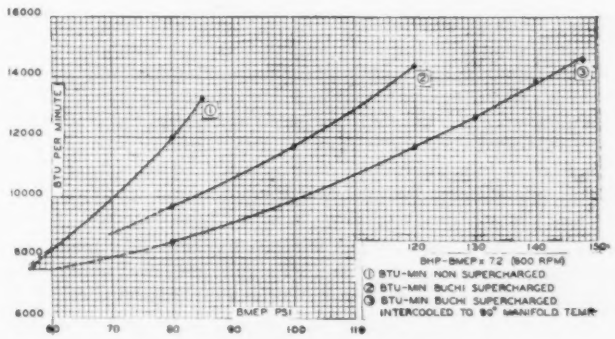


FIG. 2

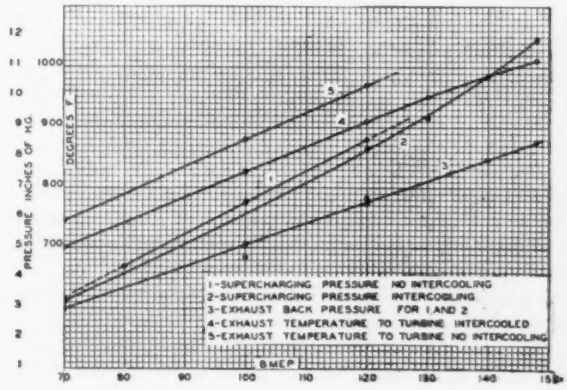


FIG. 3

---

[1] Chief Engineer, Four Cycle Diesel Division, Nordberg Manufacturing Company. Mem. A.S.M.E.

[2] "Rating Supercharged Engines on the Basis of the Mean Temperature of the Cycle," by Ralph Miller, Trans. A.S.M.E., vol. 65, 1943, pp. 685–696.

Contributed by the Oil and Gas Power Division and presented at the Annual Meeting, New York, N. Y., November 26–29, 1945, of THE AMERICAN SOCIETY OF MECHANICAL ENGINEERS.

NOTE: Statements and opinions advanced in papers are to be understood as individual expressions of their authors and not those of the Society.

Assuming a friction mean effective pressure (mep) of 20 psi at 80 bmep and that it increases with the square root of the bmep the mip at 12,000 Btu per min is as follows:

	Mip from Fig. 2	Mip from Fig. 1
Naturally aspirated, $80 + 20 =$	100	100
Buchi supercharged, $102 + \left(20 \times \sqrt{\frac{102}{80}}\right) =$	125	131
Buchi supercharged intercooled, $123 + \left(20 \times \sqrt{\frac{123}{80}}\right) =$	148	158

This shows a difference of $4^1/_2$ per cent in the noncooled and $6^1/_2$ per cent in the intercooled ratings between mip calculated from cycle mean temperatures and actual tests, recording heat flow to cooling water.

This discrepancy is probably caused by increased afterburning and diminishing expansion coefficient with the later cutoff when supercharging. The same cause brings about the nonparallelism of the curves 1 and 2, that is, the combustion efficiency falls off at a faster rate in the nonsupercharged than in the supercharged engine.

In Fig. 4 the rate of heat flow to the cooling water is plotted

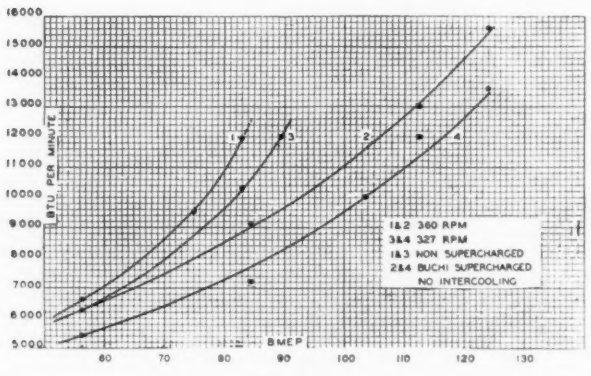


FIG. 4

versus bmep. Curves 1 and 2 show the heat flow nonsupercharged and supercharged at 360 rpm. Curves 3 and 4 are plotted for 327 rpm, nonsupercharged and supercharged.

If a heat-flow rate of 10,000 Btu per min is taken as a maximum for full load the bmep ratings will be as follows:

Engine rpm	327	360
Nonsupercharged oil Diesel, psi	82	77
Buchi supercharged oil Diesel, psi	103	93

The low bmep of this engine when supercharged would seem to be due to insufficient scavenging.

Intercooled Supercharging

At 4 lb supercharging pressure the bmep can be increased between 21 and 26 psi at the same heat flow to the cooling water when the supercharging air in the inlet manifold is cooled to the air temperature at the blower intake.

The graphs in Fig. 5 show manifold temperature versus bmep developed by the high-speed engine at two different rates of heat flow to the cooling water, namely, 10,000 and 12,000 Btu per min. Selecting for an example, the test point at 126 F manifold temperature and 105 bmep with a heat flow of 12,000 Btu per min, a cycle mean temperature of 1262 deg R is calculated as follows:

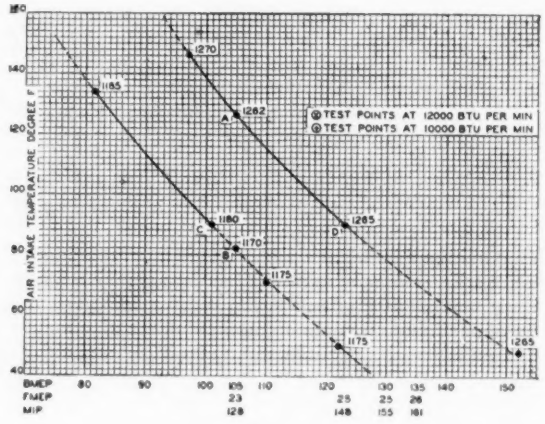


FIG. 5

$$\text{Mip} = 105 + \left(20 + \sqrt{\frac{105}{80}}\right) = 128$$

P_1 = supercharging pressure; nonintercooled line, Fig. 3 = 3.45 psig

Cutoff for 128 mip and 3.45 psi, Fig. 6 = 14.18

Ratio Tm/T_1 for cutoff 14.18, Fig. 7 = 1.92

$T_1 = 126 + 460 + t_{ch}$ = (Equation [9], reference 2) = 657 deg R

$Tm = 1.92 \times 657 = 1262$ deg R

The 10,000-Btu line shows a manifold temperature of 82 deg F at the same load. The initial temperature and the cycle mean temperature at this point are then

$$T_1 = 657 - (126 - 82) = 613 \text{ deg R}$$
$$Tm = 613 \times 1908 = 1170 \text{ deg R}$$

(The supercharging pressure P_1 has dropped from 3.45 to 3.3, Fig. 3, so that the Tm/T_1 ratio changes from 1.92 to 1.908.)

Reducing the manifold temperature from 126 to 82 deg F has reduced the cycle mean temperature from 1262 to 1170 deg R, and the heat flow to the cooling water from 12,000 to 10,000 Btu per min. We then have

$$\frac{12{,}000}{10{,}000} = \left(\frac{1262}{1170}\right)^n$$

where $n = 2.4$.

In other words, when the manifold temperature is reduced the heat flow to the cooling water, and therefore the internal wall temperature, decreases with the power of 2.4 of the cycle mean temperature.

Now, when the load is increased from C to D at 82 deg F manifold temperature to the point where the heat flow to the cooling water is again 12,000 Btu per min, it is seen that heat flow increases with approximately the same power of the cycle mean temperature, as follows:

At point C on the 10,000-Btu line, we have

$T_1 = 90 + 460 + 71.5 = 621.5$ deg R

P_1 = supercharging pressure (from Fig. 3) = 3.1 psig

Mip = 101 + 22.5 = 123.5 psi

Ratio Tm/T_1 (from Fig. 6) = 1.90

Then

$Tm = 621.5 \times 1.9 = 1180$

Point D on the 12,000-Btu line and 90 deg F air temperature reads 123 bmep; then

Mip = 123 + 25 = 148 psi

P_1 (from Fig. 3) = 4.2 psig

$T_1 = 90 + 460 + 70.5 = 620.5$ deg R
Ratio $Tm/T_1 = 2.04$
$Tm = 620.5 \times 2.04 = 1265$

The cycle mean temperature has increased from 1180 to 1265 deg

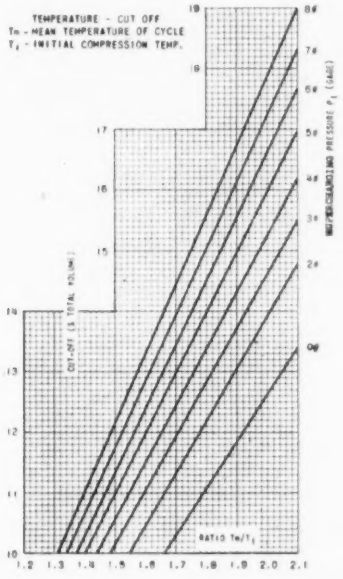


FIG. 6

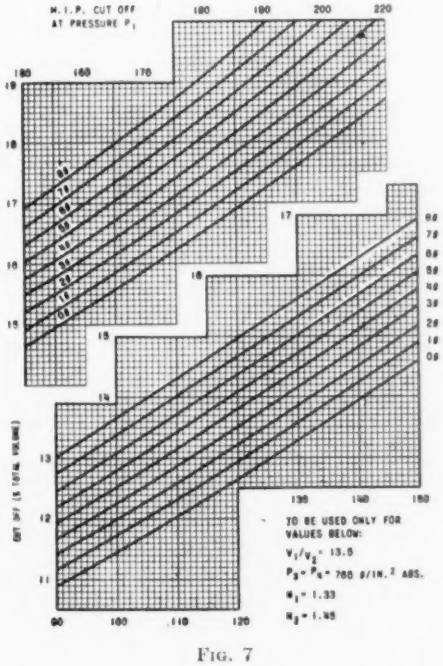


FIG. 7

R, and the heat flow from 10,000 to 12,000 Btu per min, and we have

$$\frac{12{,}000}{10{,}000} = \left(\frac{1265}{1180}\right)^n$$

where $n = 2.6$.

This proves that when the air-intake temperature is changed the load may be adjusted along the line of constant calculated

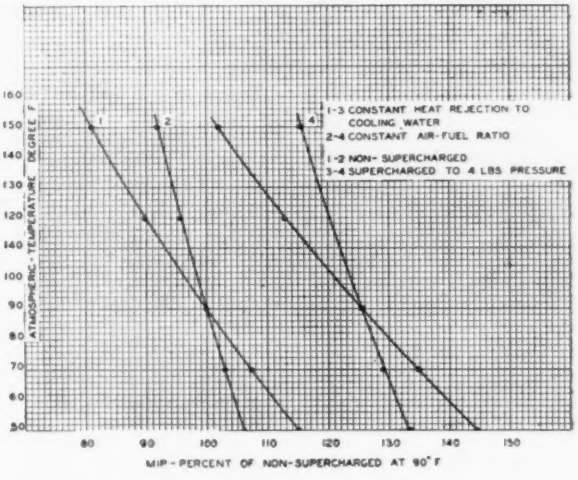


FIG. 8

cycle mean temperature. This loading will maintain the internal temperatures constant as indicated by the rate of heat dissipation to the cooling water.

The constant heat-flow curves in Fig. 5 will show an increase in initial compression pressure with increase in load which is characteristic of turbocharged engines. In Fig. 8 constant cycle temperature lines have been plotted against atmospheric intake temperature and mip for constant manifold pressures; 90 deg F is taken as standard and the point of rating. Curves 1 and 2 are for nonsupercharged and curves 3 and 4 for a supercharged engine. Curves 2 and 4 show the ratings which would be obtained by the conventional method which assumes that the mip is inversely proportional to the absolute temperature, or directly to the air density. This method does not derate sufficiently for temperature increases. Thus if an engine is operating with 115 deg F intake temperature, which is not unusual, it suffers a loss of 8½ per cent in load capacity. Conversely, when the temperature is decreased the load-carrying capacity increases at a rate faster than the air density.

FUEL CONSUMPTION

Table 1 summarizes data from a nonsupercharged, two noncooled, and three intercooled Buchi supercharged tests.

Although the theoretical cycle thermal efficiency is unaffected by the initial compression temperature,[3] these test results show an increase from 34.2 to 35 per cent brake thermal efficiency when cooling the intake air to 90 deg F, at 120 bmep. The fuel consumption is reduced from 0.377 to 0.371 lb per bhp per hr. The heat flow to cooling water drops from 14,500 to 11,700 Btu per min, and the calculated cycle mean temperature from 1365 to 1270 deg R.

When the bmep is increased from 105 to 126 along the 12,300-Btu per min heat-flow line in Fig. 2, the fuel consumption drops to 0.37 lb per bhp per hr, Fig. 9.

The lowest rate of heat flow to the cooling water is 11.15 per cent of the total heat at 147 bmep.

It will be noticed that the excess air is reduced with intercooling. Thus the uncooled engine at 105 bmep shows 27.1, and the cooled engine at 126 bmep 26.4 lb of air per lb of fuel, both at 12,300 Btu heat flow to cooling water.

Where a cooling medium of low temperature is available, such as in cold-storage or ice plants where brine may be used, or in

[3] "Internal Combustion Engine," by D. R. Pye, second edition, Oxford University Press, New York, N. Y., vol. 1, 1937.

TABLE 1 TEST DATA FOR 12-IN. × 14-IN. SIX-CYLINDER ENGINE AT 600 RPM

	Buchi supercharged					
	Noncooled			Intercooled		
Brake mean effective pressure	80	105	120	120	126	147
Mean indicated pressure	100	128	144.5	144.5	151	174
Brake horsepower	576	756	864	864	907	1060
Indicated horsepower	720	921	1040	1040	1087	1253
Fuel consumption per bhp-hr	.386	.375	.377	.371	.3705	.376
Fuel consumption per ihp hr	.309	.313	.313	.308	.308	.317
Total Btu min hhv 19,600	72500	92700	106500	104500	110000	130000
Btu to cooling water	12000	12300	14500	11700	12300	14500
Btu to cooling water per cent of total	16.6	13.3	13.6	11.2	11.2	11.15
Brake thermal efficiency, per cent	33.7	34.7	34.4	35	35	34.5
Supercharging pressure	0	3.45	4.2	4.075	4.38	5.75
Air-intake temperature gage	90	140	147	90	90	90
Initial compression temperature T_1	675	671	677	621	619	617.5
Ratio T_m to T_1	1.895	1.91	2	2.06	2.07	2.19
mip from Figs. 6 and 7	100	127			151	
Total weight of air per minute	101	165	170	184.2	188	200
Weight of air per minute retained in cylinder	101	129.5	134	145	148	158.5
Weight of fuel per minute	3.71	4.76	5.46	5.33	5.6	6.65
Lb of air per lb of fuel	27.2	27.1	24.5	27.2	26.4	23.8
Volume of air, cfm total	1395	2210	2270	2460	2510	2675
Btu removed from air, min				2500	2750	3700
Btu removed per hp per min from air				2.90	3.03	3.5
Btu per cent of total cooling water plus air	16.6	13.3	13.6	13.6	13.6	14.2

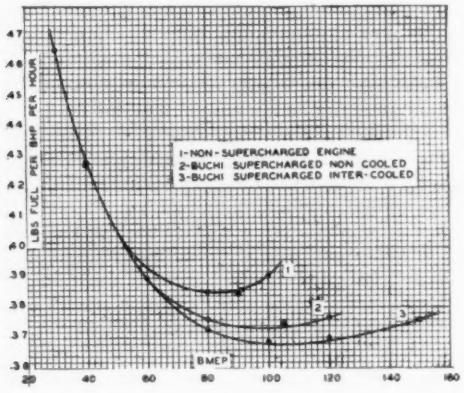


FIG. 9

places where cold well water is available, the air cooling may be carried below 90 deg F to advantage. Fig. 5 shows by extrapolation that with an air-intake temperature of 50 deg F, about 145 bmep is carried with the heat load of 105 bmep on the noncooled Buchi supercharged engine.

In Fig. 10 is plotted the fuel consumption in hhv per hour and per bhp per hour recorded on the intercooled supercharged engine at 327 rpm. The cooling-water heat-flow line for this run is shown on curve 4 in Fig. 4.

The author promoted and directed this development which was started in 1943. The first tests were made in January and February, 1945. The fuel consumption obtained at that time is plotted in curves 3 and 4 in Fig. 10. The engine was operated with air intercooling. At 130 bmep the fuel consumption was 6500 Btu hhv per bhp per hr. This may be the lowest fuel consumption ever recorded on a gas engine.

Without air cooling the consumption will increase about 3 per cent to 6700 Btu. This latter value has recently been confirmed by another enginebuilder who has since taken up the supercharged gas Diesel.

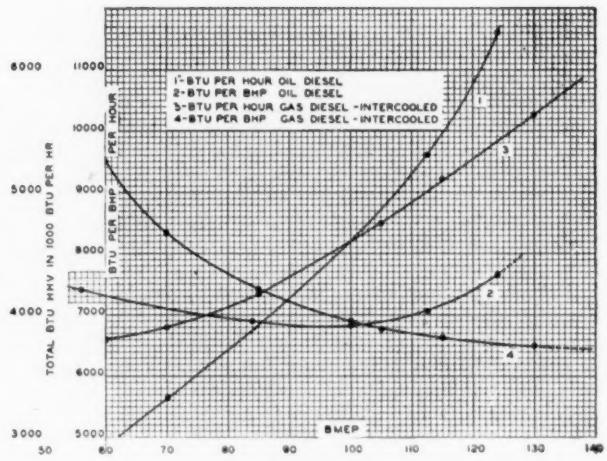


FIG. 10

On the basis of cycle mean temperature, the supercharged gas Diesel will carry a higher mep than the oil Diesel. This is due to better combustion efficiency at high loads.

HIGH-PRESSURE SUPERCHARGING

Points *A*, *B*, and *C*, curves 1 and 2, Fig. 11, are transposed test points on the 12,000-Btu line in Fig. 2. By calculating T_1 for these points, the mean temperature Tm is found, thus permitting other points on the curves to be calculated from Figs. 6 and 7.

If the nonsupercharged engine could be scavenged, the mip would increase from 100 to 109. The curve starting at 109 and 0 supercharging pressure shows the gain obtained by increasing the pressure. The highest load occurs at 5 lb, where the mip is 125. Of this, 9 lb is gained by scavenging and 16 by increasing the supercharging pressure. Above 5 lb gage the load drops off.

By cooling the air in the manifold to 90 deg F or to the intake temperature of the blower, the mip at constant cycle mean temperature will follow curve 2. The 148-mip point is established from the actual heat-flow test curves in Fig. 2. The maximum cylinder pressures are equal at 765 psi for curves 1 and 2 in Fig. 11. The cutoff ratio and compression pressure versus scavenging pressure for rating line 2 is shown on lines 7 and 6. A maximum of 177 mip is reached at 9.5 lb supercharging pressure when the compression pressure equals the maximum cylinder pressure of 765 lb.

Therefore, when maintaining the maximum cylinder pressure of the nonsupercharged engine, the limit of supercharging pres-

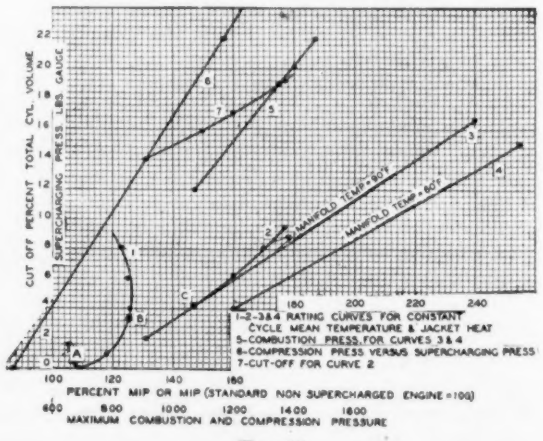


FIG. 11

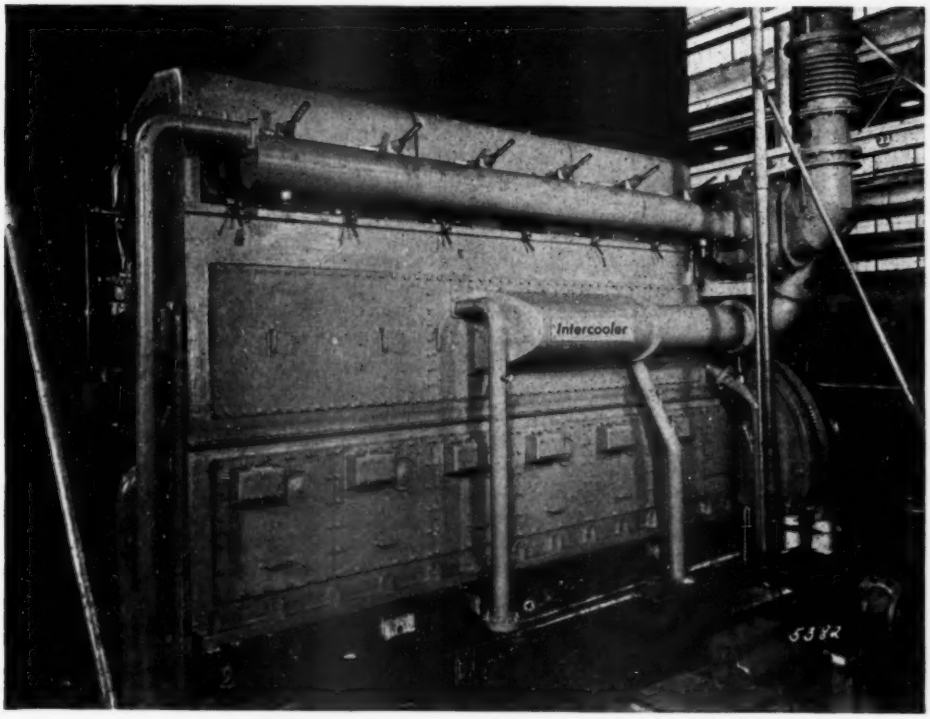


FIG. 12 SUPERCHARGED DIESEL ENGINE WITH INTERCOOLER

sure, with intercooling to blower intake temperature, is reached at about 9.5 lb gage.

Higher supercharging pressures can be used only by permitting the maximum combustion pressure to increase.

The 147-mip point on curve 2 in Fig. 11 has a combustion-to-compression pressure ratio of 1.266. If this ratio is maintained with increasing supercharging pressure and constant air-manifold temperature, we find that with constant cutoff (15.5 per cent) the mip for constant cycle temperature increases directly with the absolute supercharging pressure. The cycle mean temperatures are identical at all loads on curve 3, and the thermal efficiency is constant.[3]

Line 4 in Fig. 11 is plotted for 60 deg F air-intake temperature to indicate the as yet unexplored possibilities of high output of the four-cycle engine. For example, with a supercharging pressure of 22 psig a mip of 318 psi would be carried. The compression pressure would be 1170 psi, and the maximum combustion pressure 1480 psi. The heat flow to the cooling water would be about 5.6 per cent of the total, and the fuel consumption 0.32 lb per bhp per hr; 45.4 per cent of the total heat would go to work and 49 per cent to exhaust and radiation. While these figures will have to be adjusted downward to compensate for increased heat-transfer rate from gas to the walls, due to the increase in gas density, high-pressure supercharging nevertheless holds great promises.

CONCLUSIONS

On the basis of constant internal temperatures, the nonair-cooled Buchi supercharging system permits an increase of 28 to 30 per cent on the brake horsepower of the nonsupercharged engine, or an increase of between 20 and 28 bmep. The cost of equipping an engine with a turbocharger and the Buchi exhaust-pipe system is very nearly in the ratio of this increase so that the final cost per bhp of the supercharged engine is approximately the same as the cost of the standard nonsupercharged engine.

By the simple expedient of adding to the supercharging equipment an air cooler whose dimensions may be 15 in. square × 4 ft long for 2600 cfm, and supplying cooling water at 80 deg F to remove 3 Btu per min per bhp, the engine output is increased to 155 per cent of nonsupercharged rating.

The cost of this cooling equipment will be about $3 to $4 per hp, gained by cooling. The author believes this to be the lowest cost on record for a Diesel-engine horsepower. The extreme simplicity of equipment and ease of operation and maintenance should bring about universal acceptance of intercooling and render the uncooled turbocharged engine obsolete.

Compared with the nonintercooled turbocharged engine, intercooling to 90 deg F reduces the cost per horsepower by about 18½ per cent. The weight and volume of the engine are reduced about 20 per cent for the same horsepower.

Beyond this lies high-pressure intercooled supercharging using multiple-stage turbochargers, which promises in the near future to revolutionize the design of internal-combustion engines. Those engineers who accept the challenge of this discovery and bend their efforts toward the solution of the problems involved in developing this new engine will help to guide the internal-combustion-engine industry toward greater expansion and increased importance in our civilization.

Discussion

G. J. HAISLMAIER.[4] The author analyzes the internal-combustion engine primarily as a heat engine. As such it is important that we maintain a balance of heat, adding it where necessary and removing it where it is undesirable. In the case of the supercharger intercooler, that is, the cooling unit itself, we are interested primarily in the removal of heat and generally

[4] Sales Manager, Contract Products Division, Young Radiator Company, Racine, Wis.

speaking, removing as much as possible. In terms of heat transfer we find the engine jacket water at a temperature level too high to afford a means of cooling the supercharged air. We look therefore to an outside source of water, normally the raw-water supply which is used for cooling the engine jacket water and the oil coolers, or in the case of a marine engine, the sea water, in which case we must be careful to design into the intercooler unit a construction with materials that are resistant to salt-water corrosion.

The intercooling of supercharged air is comparatively new; however, we did accomplish this and in production-lot quantities, starting back in 1939, on the smaller high-speed 4-cycle Diesel engines ranging in the neighborhood of 150 to 200 hp. Later on during the war period we did this for other engines also in the higher-speed Diesels, namely, in the 300-hp range. Fig. 13 of this discussion shows a small cooling unit used with a 300-hp marine supercharged Diesel engine. The core element of this unit is approximately 6 in. square and this will give a relative idea of the over-all size of the cooling unit. This unit is capable of handling anywhere from 300 to 600 cfm of supercharged air and of cooling this down to within about 25 deg of the temperature of the sea water. The unit was designed and manufactured entirely of salt-water-corrosion-resistant materials and, in being furnished for the requirements of the United States Navy, was built in compliance with the applicable specifications of Heat Exchanger Specification 66Cl of the Heat Transfer Section of the United States Navy, Bureau of Ships.

Fig. 14 shows the performance curves for this unit, which basic data have served well in approximating the size of the intercooler units being furnished for some of the larger slower-speed Diesel engines today. It will be noted that all of the characteristics are plotted against engine rpm. The sea-water temperature rise is negligible. The sea-water flow rate is such as dictated by the other parts of the cooling system. The air-pressure drop is within an acceptable range, and it will be noted also that the sea-water pressure drop is almost negligible.

In the meantime some of the engine designers had indicated a preference for an intercooler unit which would be round in shape, and from a design standpoint this seems to be the logical arrangement of heat-transfer surface, because of the over-all shape of the unit, the straight-through air flow, and the ease of installation to the engine. Naturally this round-type intercooler would be more desirable, fitting readily and neatly into the air duct from the supercharger blower to the engine intake manifold, and it is generally conceived by the engine designer as a unit which would be about the same diameter size as the air duct, or at least not much larger. An intercooler of this design has been developed, and is shown in Fig. 12 of the paper. This has been applied to one of the larger supercharged Diesel engines. The cooler itself, Fig. 15 of this discussion, is approximately 22 in. diam with approximately 1100 tubes, $^1/_4$ in. diam, making up the tube nest, the salt water from the engine cooling system flowing through the flanges as shown and the air flowing through the tubes. The unit handles approximately 2000 cfm with a pressure drop of about 8 in. water gage, and cools the air to within about 20 deg F of the water temperature.

As yet this type of unit has not been made available in production-lot quantities and there is some doubt that it will be, at least in its present shape and form. It must be remembered that the raw water, or the salt water in marine applications, passes around the smaller tubes in very narrow and restricted passages inside of this round unit. So far the design of this round-type unit has not been cleanable from the sea-water side. However, that factor is being given further consideration and the round-type intercooler may yet be available for the engine designer in the not too distant future.

As in all engineering considerations, design too is a matter of compromise, and in the design of the supercharger-intercooler unit itself the compromise is that of shape and size with performance in terms of cooling efficiency as well as of maintenance and serviceability in operation. There is also a compromise in the arrangement of the heat-transfer surface, that is, a compromise in over-all height and width against pressure drop in the air stream passing through the cooling unit.

The following is what might be considered an over-all compromise in terms of one of the latest intercooling units now being applied to one of the larger slow-speed Diesel engines. This engine, a six-cylinder model, 16-in. bore, 22-in. stroke, operating at 325 rpm when supercharged, has a rating of 1200 hp as against the 750-hp rating unsupercharged. With supercharger intercooling, it is expected to bring the rating of this engine up to 1500 hp at the same engine speed. The intercooler unit has over-

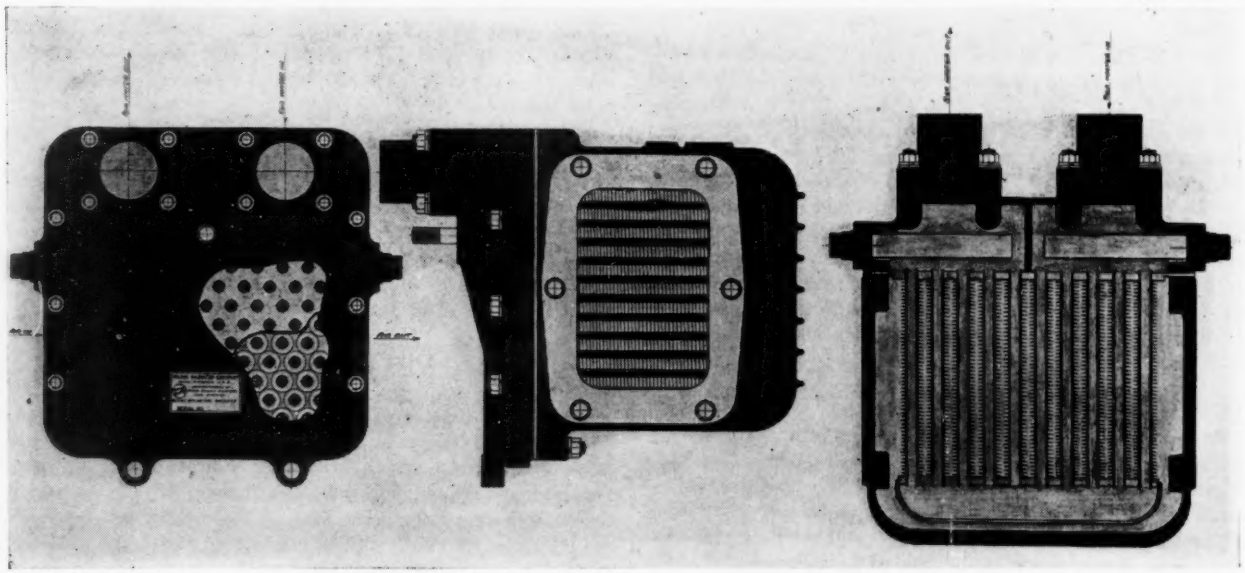


FIG. 13 DETAILS OF SUPERCHARGER INTERCOOLER HEAT EXCHANGER

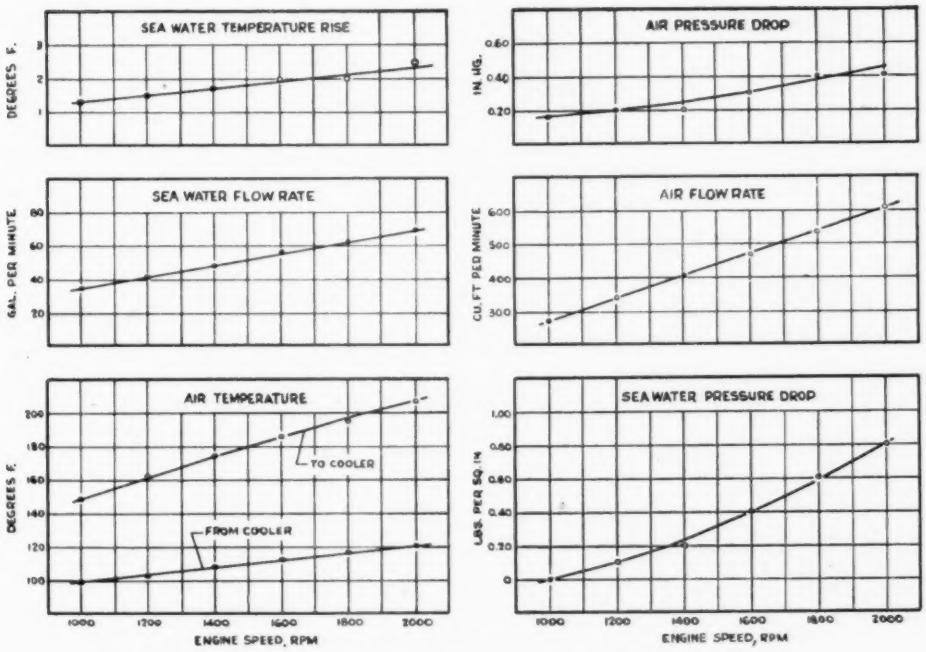


FIG. 14 PERFORMANCE CURVES OF INTERCOOLER HEAT EXCHANGER



FIG. 15 ROUND-TYPE INTERCOOLER UNIT

all dimensions of 53 in. length, 18½ in. height and depth in the direction of air flow of 7⅛ in., although the core element itself to which the supercharged air stream is exposed, measures only 48 in. between the end headers, 16⅛ in. height and 5⅛ in. depth in the direction of air flow.

This unit in over-all volume is somewhat smaller than the intercooler unit to which the author referred in his paper, and it is offered to give cooling performance even a little better than that same unit. More specifically, it is designed to handle an air flow of 3900 cfm with an air-inlet temperature coming from the supercharger at 155 deg F, cooling the supercharged air down to 90 deg F. The cooling-water temperature maximum is 80 deg F, and with lower water temperatures the leaving temperature of the supercharged air coming off the cooling unit will of course be less, that is, approximately 10 to 15 deg above the water temperature.

In this particular case we have figured on a cooling-water flow of from 200 to 250 gpm, which is the same water flow available for the engine jacket-water heat exchangers and the lube-oil heat exchangers. The raw water would flow through the supercharger intercooler before passing through the other heat exchangers as there is only about a 2½ to 3 deg F temperature rise in the cooling water passing through the supercharger intercooler. This unit, incidentally, has approximately 150 tubes, ⅜ in. diam, and in its performance we estimate the pressure drop on the air side will run in the neighborhood of 2½ to 3 in. water gage.

The weight of this intercooler unit is approximately 350 lb. As yet it is not being manufactured in production-lot quantities, but even on the smaller-quantity basis the cost figures today indicate that the $2 per hp figure which the author quotes is not far out of our reach. In fact, depending upon the size of engine and the quantity manufactured at one time, we find current costs on intercooler units of this kind running from $2.50 to about $5 per hp, based upon the increase of horsepower which will be obtained from the intercooling alone. This does not take into account the cost of the application and the additional materials such as the duct work and manifolding which the engine manufacturer will have to consider in his design costs. It is a figure based on the cost of the intercooler itself as an accessory item.

This cost, however, will be less as time goes on, particularly as plans are being made eventually to work out a standard intercooler design which can be made adaptable to more than one engine installation and which conceivably may be manufactured in larger quantities, resulting in ultimately lower costs. It is not unreasonable therefore to look forward to approaching the figure of $2 per hp or possibly even improving upon that figure.

Bavarian Motor Works Altitude-Test Facilities

By E. E. STOECKLY,[1] WEST LYNN, MASS.

Several large-capacity high-altitude low-temperature test chambers for aircraft-engine work were constructed during the war. The present paper describes in some detail the equipment and operation of the first of these at the Bavarian Motor Works.

EARLY in the year 1941 the German Air Ministry authorized the construction of the first large-capacity high-altitude low-temperature aircraft-engine testing laboratory. This decision was predicated on the conviction that the further rapid development of high engine powers at altitudes could most rapidly be accomplished by ground-level testing under actual high-altitude low-temperature high-speed flight conditions. Of paramount importance was the cooling problem of both air- and liquid-cooled conventional engines, and the satisfactory performance and operation under altitude conditions

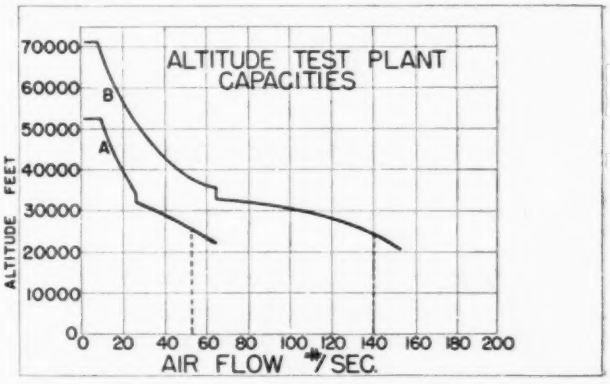


FIG. 1 TEST-PLANT CAPACITIES

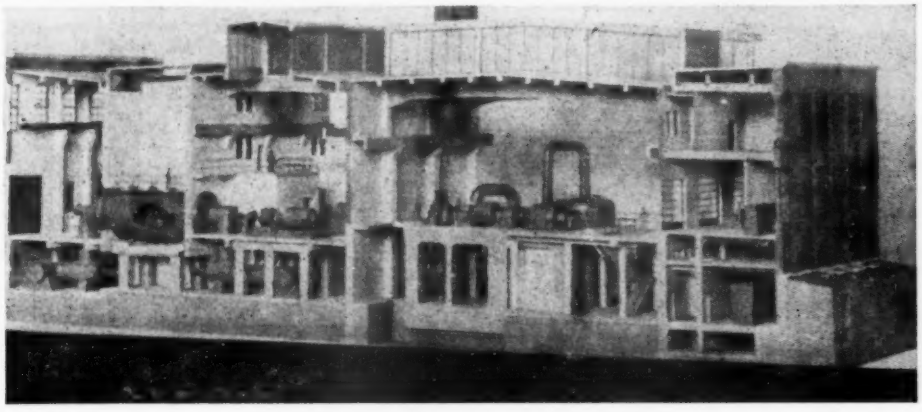


FIG. 2 CROSS SECTION OF TEST PLANT

of their then little-known jet-propulsion engine. Prior to 1941 all laboratory altitude testing consisted of holding only the engine exhaust and carburetor air inlet at altitude conditions. Because of the experience and success that the B.M.W. had with such testing, it was directed to build the first really large altitude-test plant. The plans called for a maximum refrigerated air supply of 53 lb per sec at —80 F, and an evacuation capacity of 53 lb per sec at 26,000 ft altitude, with a maximum operating altitude of 52,500 ft, as given by curve A, Fig. 1.

Shortly after authorizing the first plant, the German Air Ministry, often referred to as R.L.M., authorized the construction of four more such plants, some of which were to be over twice as large as the Bavarian Motor Works (B.M.W.) plant. The new plants were to be for the research establishment of the Luftwaffe, known as E.D.L; German Experimental Establishment for Aviation, know as D.B.L; Daimler Benz and Junkers Motor Works. This policy was to make altitude-testing facilities available to the three leading German reciprocating and gas-turbine aircraft-engine manufacturers, as well as the two leading government research institutions. The two government plants were to have exhausting and refrigerating capacities as shown by curve *B*, Fig. 1. The plants at the three engine manufacturers were to be as given by curve *A*, Fig. 1, with space and foundations provided for eventually increasing the plant capacity to curve *B*, Fig. 1.

Between 1941 and 1943, as the hopes for larger engines rose and fell, doubling the capacity of the B.M.W. plant was authorized and canceled several times. Some 3 years after construction was started, the B.M.W. plant, a cross-section model of which is shown in Fig. 2, went into operation in October, 1944, with a refrigeration and evacuation capacity of 53 lb per sec at 26,000 ft altitude and a maximum working altitude of 52,500 ft. The plant operated successfully from the very beginning and was in continuous service up to the time of occupation by the American forces, except for short outages to repair bomb damage. Be-

[1] Engineer, Aircraft Gas Turbine Division, General Electric Company. Mem. A.S.M.E.

Contributed by the Oil and Gas Power Division and presented at the Annual Meeting, New York, N. Y., Nov. 26–29, 1945, of THE AMERICAN SOCIETY OF MECHANICAL ENGINEERS.

NOTE: Statements and opinions advanced in papers are to be understood as individual expressions of their authors and not those of the Society.

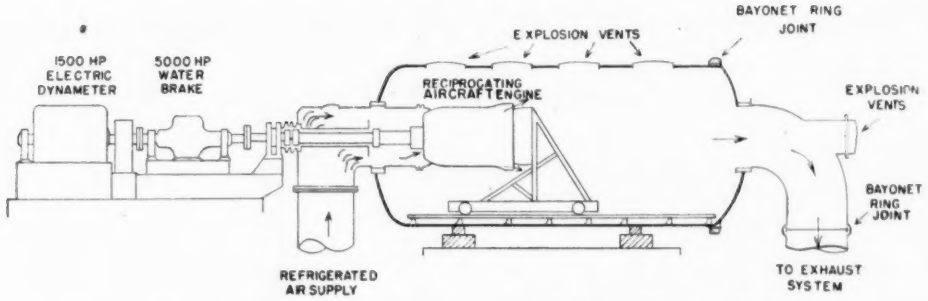


FIG. 3 ALTITUDE TEST CHAMBER FOR RECIPROCATING ENGINES

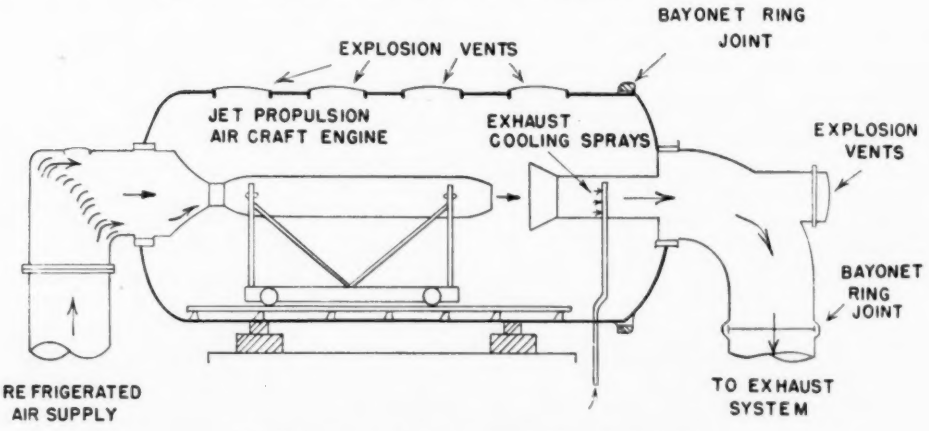


FIG. 4 ALTITUDE TEST CHAMBER FOR JET ENGINES

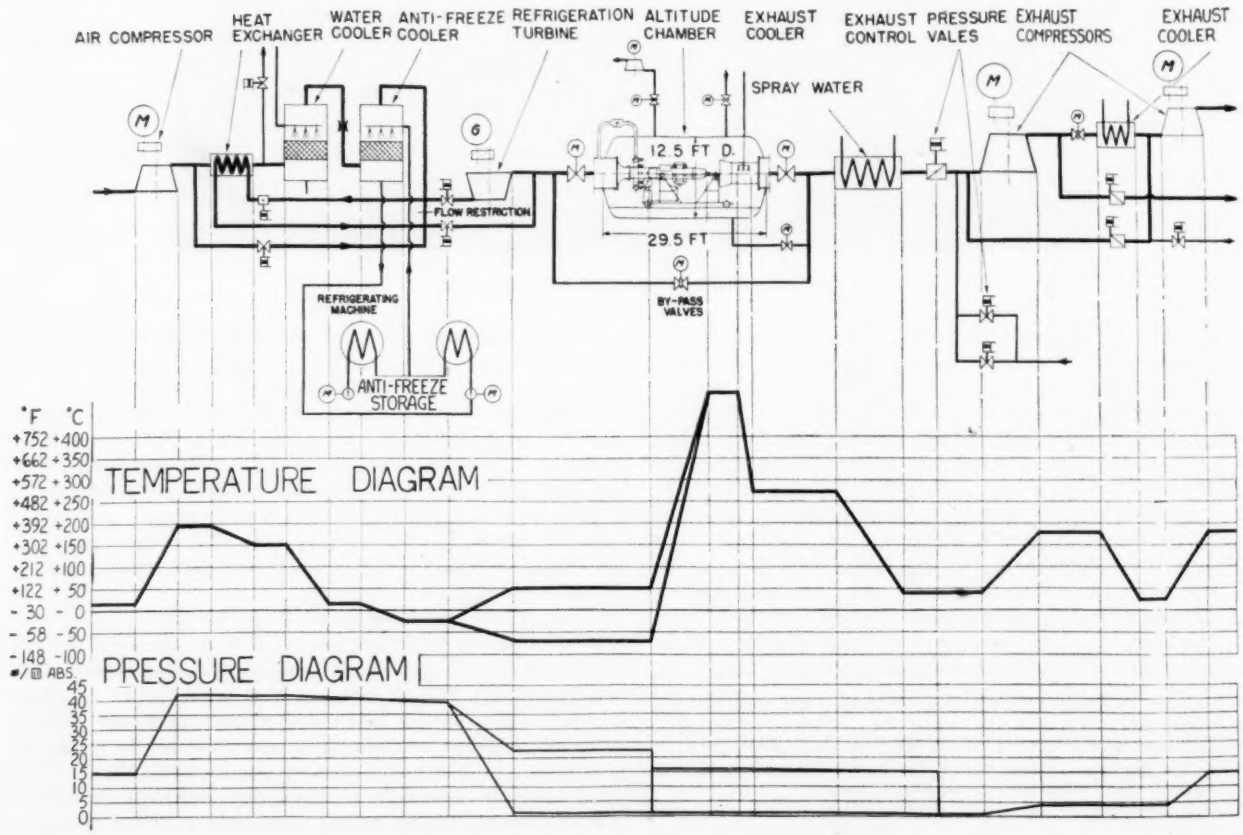


FIG. 5 SCHEMATIC PIPING ARRANGEMENT, B.M.W. PLANT

cause of the critical shortage of electric power in the Munich area, brought about by heavy Allied air bombardment, the plant could be operated only from late evening until early morning. As the construction of the other test plants was lagging behind, the German Air Ministry made the B.M.W. plant available to the other engine manufacturers on a priority basis.

From October, 1944, to April, 1945, several reciprocating engines and approximately 20 Junkers 004 and B.M.W. 003 jet-propulsion engines were completely altitude-tested.

B.M.W. Plant and Equipment

Test Chamber. The altitude test chamber, as shown in Fig. 3, consists essentially of a large cylinder in which the aircraft engine to be tested is mounted on a movable carriage. Refrigerated air under the desired conditions of temperature, altitude, pressure, and velocity is rammed into the front end of the engine. The exhaust system connected to the rear section of the cylinder removes the exhaust gases and cooling air. In the case of air- or liquid-cooled reciprocating engines and propeller-drive aircraft gas turbines, the power output is transmitted by a drive shaft through the inlet-air elbow to a combination water brake and electric dynamometer located on the left-hand side of the test chamber.

Fig. 4 shows the manner in which a jet-propulsion engine is mounted for testing. The air connection to the front end of the engine is through a free-sliding labyrinth joint transmitting no axial forces. With the unit mounted in a frame on rollers, the thrust output of the engine is transmitted by a system of links and bell cranks to a thrust-measuring scale located in the test chamber and read through a turnable periscope from the operating control room.

Fig. 5 is the schematic piping arrangement of the entire test plant with the principal pressures and temperatures at various points. The left-hand side of the figure shows the refrigerated-air-supply system, and the right-hand side shows the exhausting system. Starting on the left-hand side, normal atmospheric air is compressed to approximately 2.6 atm, cooled by direct-contact water sprays to 60 F, followed by cooling to — 10 F, by an anti-freeze solution, and finally cooling to altitude temperature and pressure by expansion through an air-refrigeration turbine. In order to make available a wide latitude of air temperatures and pressures at the test-chamber entrance, the by-pass lines and heat exchanger shown in the line diagram were added. As will

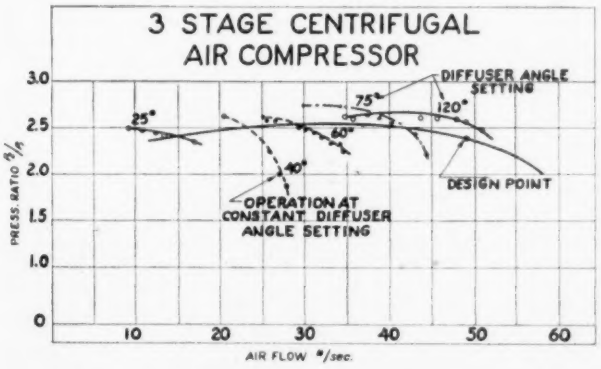


Fig. 6 Characteristics Air-Supply Compressor

be shown later, the purpose of the heat exchanger is to make possible rapid changes in temperature to the altitude test chamber without producing icing conditions.

Air Compressor. The air compressor is a three-stage radial-flow centrifugal unit with automatically controlled variable

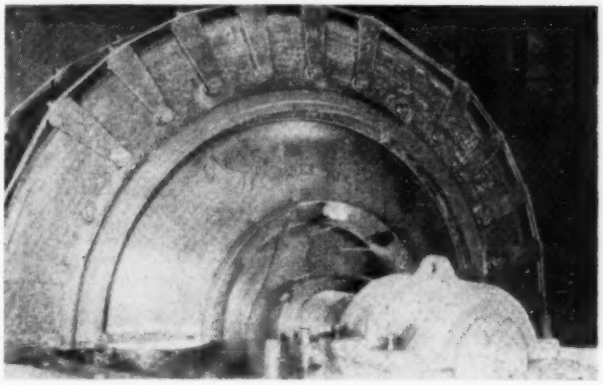


Fig. 7 Variable-Diffuser-Control Air-Supply Compressor

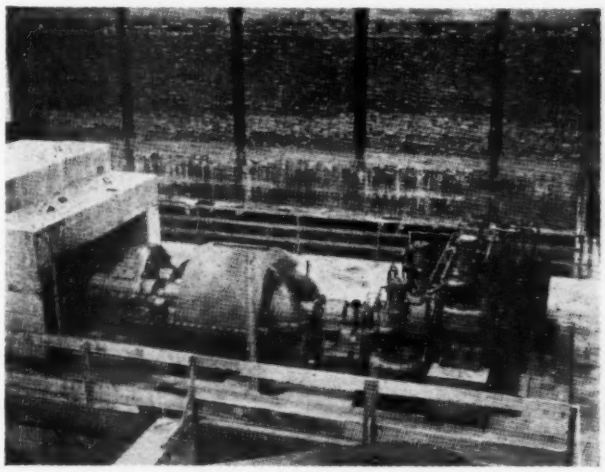


Fig. 8 Air-Supply Compressor and Refrigeration Turbine

diffuser vanes and was built by the Brown Boveri Company. Fig. 6 shows a plot of pressure ratios for various air flows for this compressor. The design point and expected curve are given for various constant values of diffuser angle from 25 to 120 deg. These curves show that the compressor can operate stably between air flows of 10 lb per sec to approximately 55 lb per sec. An automatic control, actuated by air flow, varies the diffuser angle setting for operation along the designed curves. Fig. 7 shows the cable and linkage system used to control the angle of the diffuser vanes.

Fig. 8 is a view of this compressor with the refrigeration turbine that drives it shown on the right-hand side. The difference in power between the turbine and compressor is made up by the 3300-kw motor on the left-hand side, which is connected to the compressor through a step-up gear.

The compressor driving motor was made large enough to carry full load on the compressor without the help of the refrigeration turbine. Operation of the compressor and refrigeration turbine is at a constant speed of 4370 rpm, while the driving motor runs at 990 rpm. The concrete blocks surrounding the motor were placed there during the last few months of the war as a protection against damage due to Allied bombing attacks. Similar concrete protection was placed around all other vulnerable apparatus as protection against bomb damage.

Air-Cooling System. The air leaving the air-supply compressor is cooled by a heat exchanger from 0 to 70 F, depending upon the method of operation. The next stage of cooling is accomplished

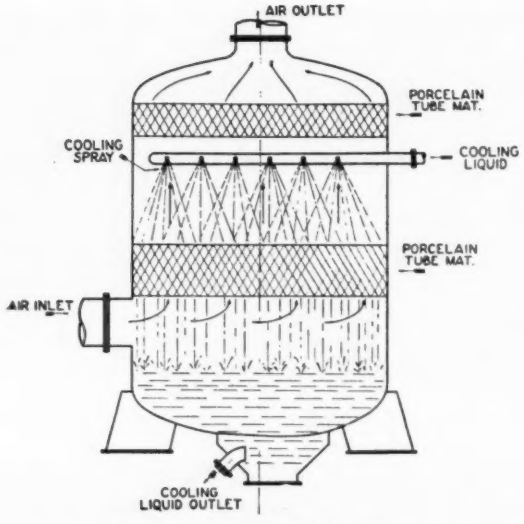


FIG. 9 AIR-COOLING CHAMBER

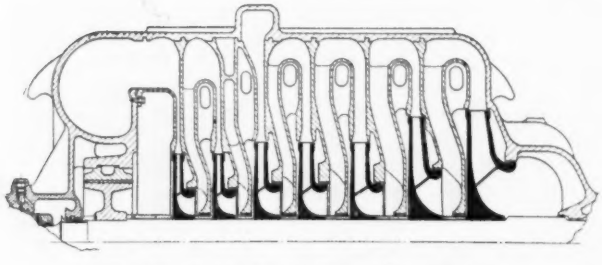


FIG. 10 SEVEN-STAGE FREON COMPRESSOR

in a water-cooling cylinder, a cross section of which is shown in Fig. 9. The air enters at the bottom left-hand side and passes up through a mat of small porcelain tubes each about $^5/_8$ in. long and $^3/_4$ in. OD × $^1/_2$ in. ID. These tubes are piled indiscriminately to form a mat with large surface area and many projecting corners. The total depth of this mat is approximately 36 in. Cooling water that is distributed evenly over this mat by means of sprays flows down through and around the tubes, finally collecting in the bottom of the cooler.

After the air has been cooled by contact with the water flowing over the surfaces of the short porcelain tubes, it goes up through another similar mat of tubes approximately 24 in. thick. In going through this second mat the excess moisture carried in suspension is effectively removed by the many sharp corners and narrow twisting paths up through which the air must go. Air leaving the top of this cooling cylinder is approximately at the compressor-discharge pressure of 2.6 atm and saturated with water vapor at a temperature of 60 F. At this temperature and pressure the air will hold in saturation approximately 50 grains of moisture per lb of air. In summer time this may be less moisture than in the incoming air but more than it is likely to hold in the winter months.

The next stage of cooling is similar in construction and operation except that an antifreeze solution is used instead of water. The outgoing air temperature from the second stage of cooling is about 10 F below zero. At this temperature and 2.6 atm, the saturation moisture content is reduced to 1.5 grains per lb of dry air. To accomplish this cooling the antifreeze solution enters the cooling chamber at —16 F and is removed at —6 F. Due to lowering the air temperature, approximately 1320 lb of moisture is condensed out of the air every hour. This is absorbed in the antifreeze solution from which it is removed by special multiple-effect evaporators. This is done on a continuous basis by sending a small fraction of the liquid leaving the air cooler through the concentrating process before going to the antifreeze cooling system. The antifreeze solution used was obtained under the trade name of Reinhartin and is believed to be of a calcium-chloride base with an inhibitor to reduce corrosion.

Cooling Antifreeze Solution. Cooling of the antifreeze solution is accomplished by an integrally designed refrigeration unit manufactured by Brown Boveri Company and sold under the trade name of "Frigibloc." This unit, consisting of a seven-stage centrifugal freon compressor, shown in Fig. 10, is built integrally with a condenser, evaporator, and all necessary accessories. Ther efrigerant gas used is freon F-11. It is extracted at the end of five stages and after passing through an intercooler is returned to the entrance of the sixth stage. Elaborate oil shaft seals are used to prevent air leakage in and freon leakage out. The compressor is driven by a 400-kw direct-connected motor running at 2950 rpm.

Fig. 11 shows the schematic arrangement of the component parts. The centrifugal compressor is shown at the center top and the evaporator, consisting of a tube heat exchanger with the antifreeze solution circulating inside the tubes, is shown directly below the compressor. The intercooler between the fifth and sixth stages is shown on the left-hand side, while the condenser with its liquid aftercooler is shown on the right-hand side. The schematic system for the shaft seal is shown in the upper left-hand corner, while the purging system is shown in the lower left-hand corner.

Refrigeration Turbine. The —10 F air coming from the antifreeze cooling chamber is expanded to altitude pressure in a refrigeration turbine designed and built by Brown Boveri Company. It is of conventional design having a single stage and eight equal admission-valve arcs. Good mixing between the air being by-passed around the turbine and that going through was obtained by building the by-pass directly into the turbine. The turbine buckets and wheel were made of a special nickel steel to withstand the low temperatures encountered. No insulation was applied to the outside of the turbine as it was felt it would interfere with accessibility and maintenance. This results in some heat absorption by the cold air but does not appear to be serious. The turbine is operated at a constant speed of 4370 rpm and is directly connected to the air-supply compressor as a means of loading. Fig. 12 gives the minimum air temperature that can be obtained at the test chamber after correcting for turbine and pipe-line heat loss. As can be seen from the curve, a minimum test-chamber air-inlet temperature of approximately 50 deg F below standard N.A.C.A. altitude temperatures can be maintained with flows of 20 lb per sec and more up to 40,000 ft altitude.

DANGER OF ICING

In the operation of a turbine-expansion cycle of this type for air-cooling there is always the danger of icing resulting from moisture condensation. As air is expanded to lower pressures, at constant temperature, it will hold greater amounts of moisture in saturation. As the temperature is reduced at constant pressure, the amount of moisture that can be held in saturation is rapidly reduced. Fig. 13 shows the plot of constant-saturation-moisture-content lines on a pressure-temperature field. From these curves it can be seen that with a turbine-inlet moisture content of 1.5 grains per lb of dry air, the moisture content can be kept below saturation along the N.A.C.A. altitude-temperature curve only up to 30,000 ft altitude and again above approximately 65,000 ft altitude. Between these two altitudes at N.A.C.A. temperatures and through broader limits at lower

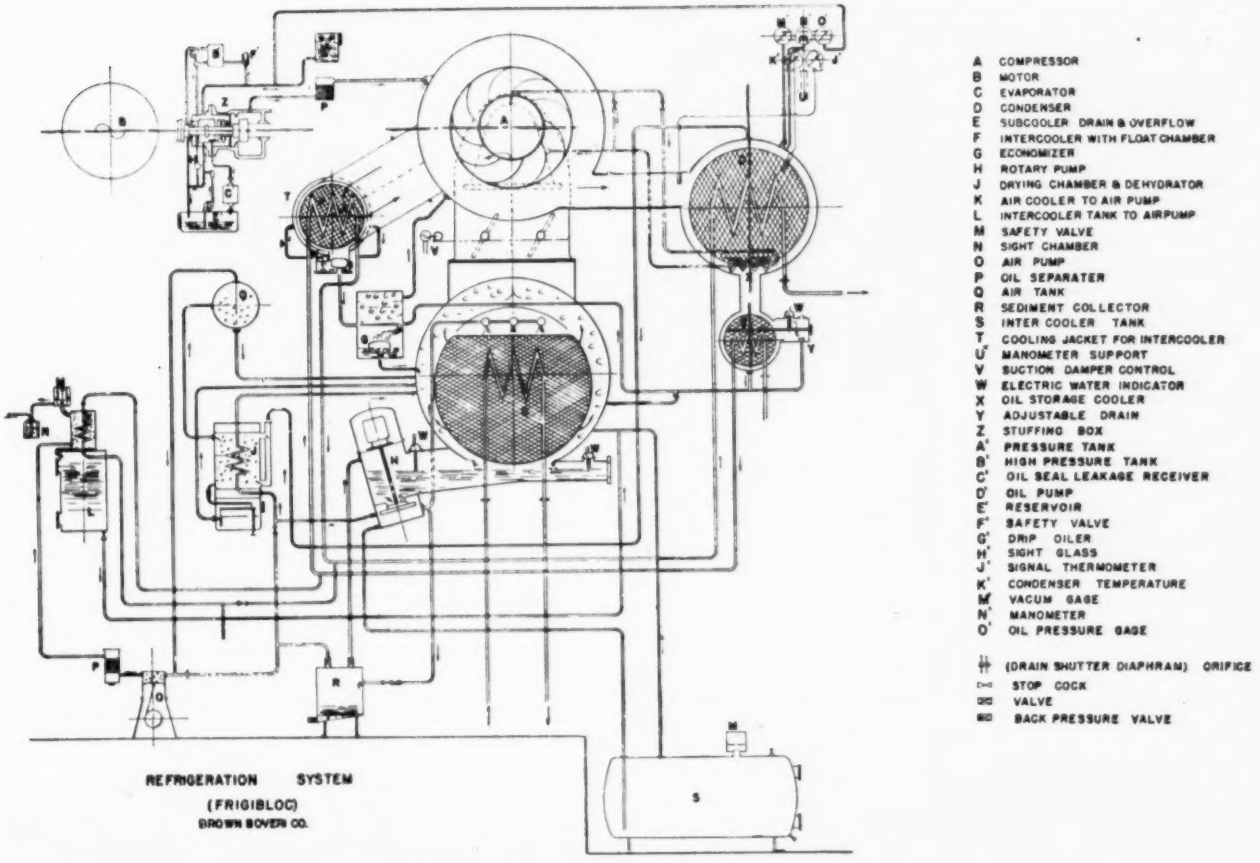


FIG. 11 SCHEMATIC ARRANGEMENT OF FRIGIBLOC REFRIGERATION UNIT

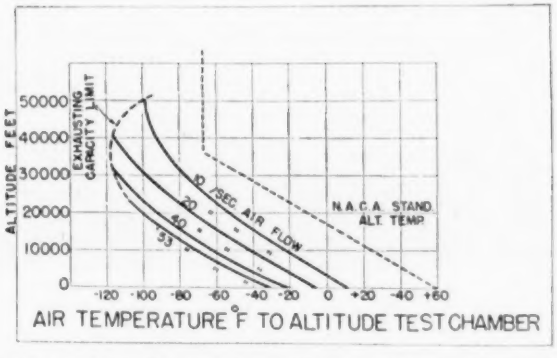


FIG. 12 MINIMUM AIR TEMPERATURE TO ALTITUDE CHAMBER

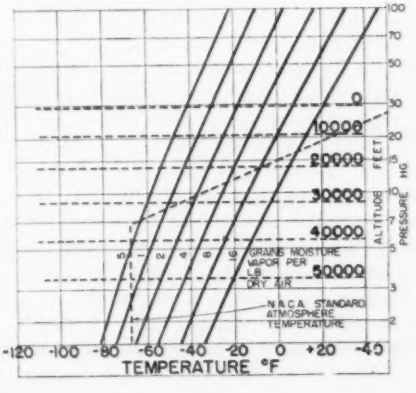


FIG. 13 SATURATION MOISTURE CONTENT AT VARIOUS TEMPERATURES AND ALTITUDES

than N.A.C.A. temperatures, the air has more moisture than it can hold in saturation and the possibility of ice formation exists.

The designers of the B.M.W. test plant were aware that such icing might give trouble and considered in the initial design stages the installation of chemical driers for removing additional moisture from the air. Because of the size and expense of such driers, they decided to try the system without and find out by experience just how serious the icing problem would be. To date they have operated the plant several hundred hours, although not more than 6 hours continuously, in the range in which icing troubles should occur, as indicated in Fig. 13, and report that they have had no sign of trouble.

The author's personal experience with similar altitude-refrigeration equipment in the United States has shown that icing problems increase rapidly as the air-moisture content gets above 3 to 4 grains per lb and decreases rapidly below 3 grains. This evidence indicates that quite likely little icing trouble will be encountered if the moisture content can be held down to 1.5 grains.

If air temperatures higher than those obtained going through the refrigeration turbine are desired, air can be by-passed around the turbine and the air temperature to the test chamber raised to —10 F, with a moisture content of not over 1.5 grains. If still warmer air is desired, the piping is so arranged that the —10 F air from the antifreeze cooling chamber can be returned to

a heat exchanger between the supply air compressor discharge and the first water air cooler. The maximum temperature that can be obtained in this manner is 120 F. By this method air dried to 1.5 grains can be delivered to the test chamber at temperatures ranging from +120 F to —100 F. This is of particular value when obtaining compressor efficiencies by the temperature-rise method, especially with low inlet-air temperatures.

The heat exchanger between the compressor and the water cooler is used to rapidly heat the cold-air lines between the turbine discharge and the test chamber when shifting from a low temperature point to a higher temperature point. The by-pass valve from the air-compressor discharge to the turbine inlet is rarely used because of the moisture and icing problems encountered by moisture-laden warm air striking cold surfaces.

The inlet-air temperature to the altitude cylinder is controlled by changing the ratio of the air by-passed around the refrigeration turbine to the air that goes through the turbine, with the controls set so as to hold a constant total air flow. The inlet-ram conditions to the engine under test is obtained by varying the total air flow to the test chamber by increasing or decreasing both the air by-passed around the turbine and that going through the turbine. The controls are such as to maintain a constant ratio between the two.

Air-Exhaust System

The altitude cell is exhausted by means of two four-stage motor-driven centrifugal exhausters For low altitudes the exhausting units are operated in parallel while for higher altitudes the exhausters are operated in series. The change-over point is the break noted in curve A, Fig. 1. The larger of the two exhausters, shown in Fig. 14, operates at 3200 rpm and is driven by a 4500-kw 990-rpm motor through a step-up gear. The smaller unit operates at 4785 rpm and is driven by a 2700-kw 990-rpm motor through a step-up gear. These exhausters were built as multiple-stage centrifugal units rather than axial flow because of the belief they would have broader stability limits and would be less subject to performance deterioration due to accumulation of dirt.

Fig. 15 gives the pressure-ratio air-flow characteristics of the two exhausters. Fig. 16 is an outside view of the V1104 or smaller of the two exhausters. The two projecting flanges on the top half-casing hold membrane-type explosion vents that blow out in case of an explosion in the exhaust system. The motors driving these exhausters and the air-supply compressors are of the three-phase alternating-current asynchronous type with wound rotors. Starting is accomplished by inserting liquid resistors between the slip-ring connections. As the speed increases the liquid resistance is decreased until it becomes zero for normal operation. It was originally planned to control the exhaust pressure by speed control obtained by varying the rotor resistance. This did not prove to be practical and as a result the exhausters are operated at full speed, and chamber altitude pressure is maintained regardless of flow, within the limits of operation, by an automatic hydraulic system controlling the throttling valve just ahead of the first exhauster. When the system air flow gets below the stable range of the exhauster, air is bled in from atmosphere to the exhauster inlet.

The exhaust system is so valved that the change-over from series to parallel operation can be made by remote control while the units are operating and the test is going on. Smooth change-over is obtained on the three valves that it is necessary to change by making two self-acting, nonreturn check valves, and the third, a motor-operated gate valve. In changing over it is necessary to change only the motor-operated gate valve and the other two valves automatically follow in the proper sequence.

The hot exhaust gases leaving the test-chamber discharge

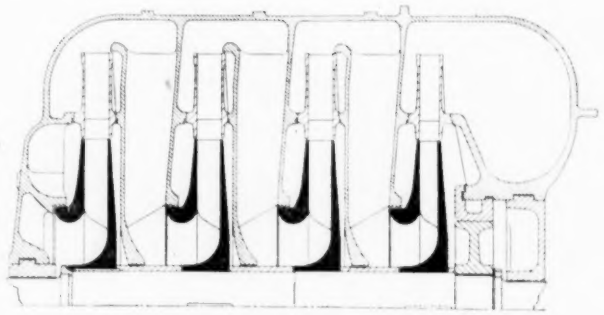


Fig. 14 Four-Stage Centrifugal Exhauster

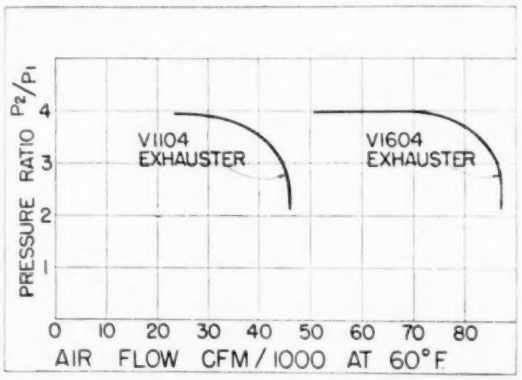


Fig. 15 Characteristics of Exhausters

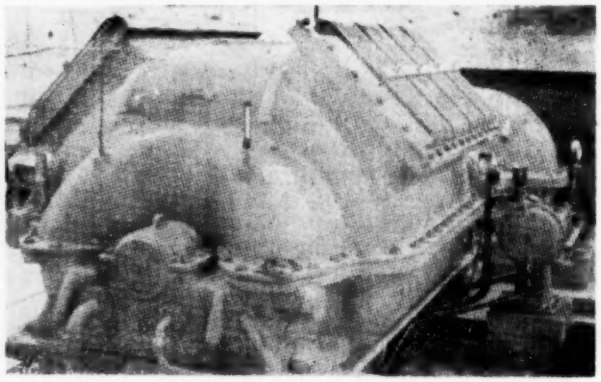


Fig. 16 Four-Stage Centrifugal Exhauster

are reduced to approximately 525 F by automatically operated water sprays. Additional cooling of the exhaust gases to approximately 100 F is accomplished by a surface gas cooler using water as a cooling medium. When the exhausters operate in parallel each discharges to the atmosphere through a brick stack. When the two operate in series an additional surface gas cooler is placed between the two exhausters to reduce the inlet temperature of the second one to approximately 100 F.

Altitude Test Chamber

The altitude test chamber is a cylindrical body about 26 ft long and 12.5 ft diam. To withstand possible explosions, the chamber was tested with an internal pressure of 150 psi. The side walls are 0.8 in. thick and the end domes 1.38 in. thick. Since they had had no previous experience with such chambers, four large membrane explosion reliefs 34½ in. diam were pro-

vided on the top side of the chamber. In order that the escaping gases from these vents would not damage the building, an explosion shaft was built above the chamber. To date no explosions have been experienced. This has been attributed to the large amount of excess air. Starting of the engine has always been on gasoline and some fires on starting have occurred. These have always been quickly extinguished by closing off the cooling-air supply to the chamber and injecting CO^2 gas. Experimental attempts were made to extinguish fires by quickly raising the altitude to 50,000 ft. This procedure failed to put out the gasoline fires. The author has seen similar oil fires in altitude chambers that were quickly put out by raising the altitude to 40,000 ft.

The entire exhaust-pipe system is protected against explosions and overpressure by a large number of explosion valves built especially for this particular job. These valves are spring-closing check valves of very light construction so that any sudden rise in pressure will quickly open them.

Access to the altitude chamber is obtained by removing the entire end dome and exhaust elbow. This operation is made entirely automatic, requiring only the pressing of several buttons, by the ingenious use of two power-operated bayonet-ring joints. Fig. 17, which is an end view of the altitude chamber, shows the large ring bayonet joint. After the two joints are opened a jib crane supporting the discharge elbow and end dome swings the assembly out of the way. In the center can be seen the exhaust nozzle of the jet engine under test together with the supporting test frame on which it is mounted.

All electrical, pressure, temperature, and fuel-supply lines to the test frame are made by quick connectors. This allows the entire engine assembly to be quickly removed or installed. Such a complete change has been made in less than 2 hr. Fig. 18 is a view of the instrument board in the engine control room. In the center can be seen the turnable periscope used for viewing the engine in the protected altitude chamber. Important temperatures and pressures needed for the proper operation of the engine are given by direct-reading instruments directly in front of the operator. Special test temperatures are read on portable-type potentiometers on the left-hand side of the control board, while special pressures are read on mercury manometers on the right-hand side.

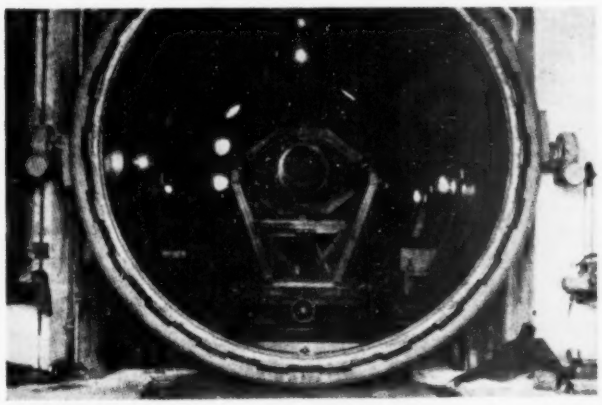


FIG. 17 ALTITUDE TEST CHAMBER

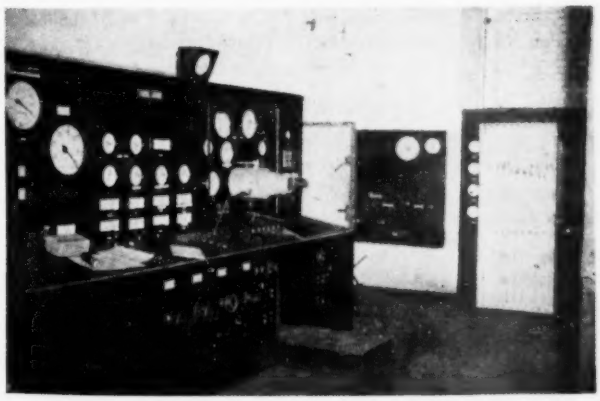


FIG. 18 ENGINE-CONTROL BOARD, ALTITUDE TEST CHAMBER

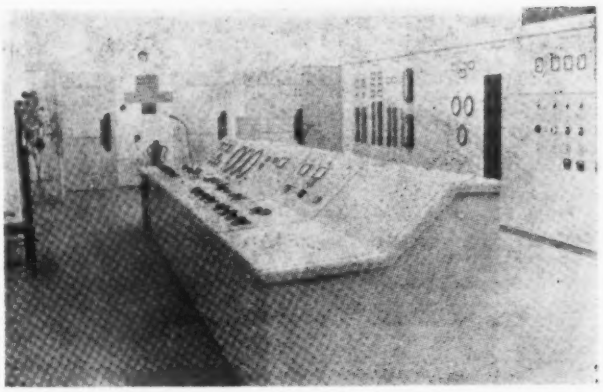


FIG. 19 REFRIGERATION AND EVACUATION CONTROL ROOM

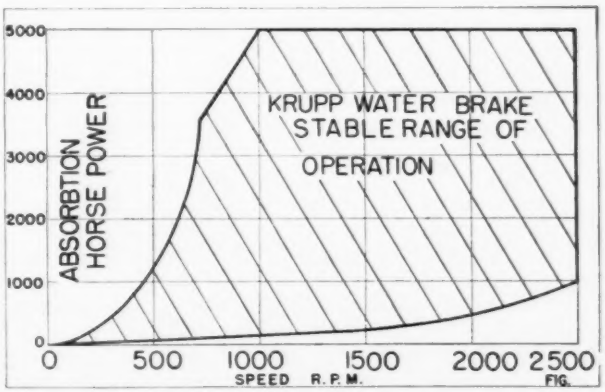


FIG. 20 CHARACTERISTICS OF FROUDE WATER BRAKE

Fuel flow metering equipment is placed in a large tank that is vented to the altitude chamber. Two systems were originally set up to serve as a cross-check. One was a weight-tank system and the other was a volume measurement in which photoelectric cells operated an electric timer. Owing to trouble the photoelectric-cell volume method was discarded and the weigh-tank readings taken without a check method.

Speed measurements were made using a standard aircraft-type tachometer. On jet-propulsion engines, engine speed was held constant and of an exact value by making a matching stroboscopic disk appear stationary. The disk was driven by a small synchronous motor connected to a small synchronous generator on the engine. The flashing light source for the stroboscopic disk was from a special constant-frequency source and did not depend upon power-line frequency.

Fig. 19 is a view of the refrigeration and evacuation control room. From this point the operator controls the altitude pressure in the test chamber, the inlet-air temperature, and the inlet-air velocity or ram pressure. This information is trans-

mitted to the operator from the operator in the engine-control room over a public-address system.

Testing Propeller-Drive Engines

Propeller-drive engines were loaded onto a combination water brake and electric dynamometer. The water brake, whose characteristics are given in Fig. 20, was of the Froude design and had a capacity of 5000 hp over a speed range of 1000 to 2500 rpm. This brake was cradled with and directly connected to a Siemens Schuckert electric dynamometer that was capable of absorbing 1100 kw as a generator and developing 780 kw as a driving motor. The electric load of the dynamometer was loaded into a d-c — a-c motor-generator set that pumped back into the main a-c power lines. The total torque developed by the water brake and electric dynamometer was read on a single electric light beam weigh scale.

In spite of being designed and built under wartime conditions, no effort or expense was spared to make this plant the very best in all respects. That the Germans succeeded in this is testified to in the excellent manner in which the plant operated.

Peanut-Meal Plywood Glue

By R. S. BURNETT[1] AND E. D. PARKER[1]

In this paper the results are given of work done at the Southern Regional Research Laboratory in which specifications were established for peanut meal for use in preparing plywood glue. A satisfactory formula has been developed. Joint tests show that the peanut-meal glue meets the requirements established for casein and casein-type glues. Comparisons of peanut-meal glues with other water-resistant glues are made.

THE FIRST large-scale application of an oilseed meal to the preparation of plywood glues began in 1927 with the use of soybean meal from Manchuria. This development took place in the Pacific Northwest to meet the needs of the Douglas-fir plywood industry for a cheap water-resistant glue. Although soybean-meal glue is more suitable for softwoods than for hardwoods, considerable amounts are used on hardwoods grown in the eastern and southern United States, especially in the manufacture of water-resistant box shooks (1).[2] While the preparation of plywood glue from other oilseed meals such as peanut (2, 3) cottonseed (4), castor-bean (5), and hempseed (6) meals has been investigated, to our knowledge only soybean-meal plywood glue has been used in significant amounts in this country. Of the latter 30,000 tons were consumed in 1942 (7). The present investigation is concerned with the preparation of a plywood glue from peanut meal.

The increase in peanut acreage in the South during the past ten years has made available a supply of protein-rich meal, but the preparation of plywood glue from this meal has been prevented by lack of the necessary technical information. The required information must include the development of a formula for preparing a suitable glue which must not only be capable of making a strong glued joint but must have flow properties that permit the glue mixture to fit effectively into the mechanical processes used to make plywood. Spreading characteristics, "working life," assembly time, etc., are all dependent on good flow properties. It is necessary to know also what influence the processing conditions employed to separate the seed into oil and meal have on the suitability of the meal for use in plywood glue.

As a result of work completed to date at the Southern Laboratory, specifications have been established for a peanut meal suitable for use in preparing plywood glue; a satisfactory glue formula has been developed; and information has been obtained with respect to the behavior of the glue under varying conditions of assembly time, pressure, etc. Comparisons of peanut-meal glues with other water-resistant glues have also been made.

Test Methods

The only way to evaluate a plywood glue is by gluing wood and measuring the strength of the joint obtained. Methods for evaluating plywood glues by the plywood and the block shear tests, developed by the U. S. Forest Products Laboratory, have served as a basis for Federal specifications for water-resistant glues (8, 9). The use and interpretation of data obtained by the application of these methods are discussed in several readily available publications (10, 11, 12). Such methods are subject to many variations which are difficult to control; they are not sufficiently accurate to measure small differences but they provide a means of making relative comparisons of one product with another. What actually is measured by such methods is the strength of the glued joint obtained rather than the strength of the glue. In other words, these methods of evaluation serve as a measure of the success of a gluing operation with a given glue.

The three principal tests required to evaluate a plywood glue are the dry and wet plywood shear test, the block shear test, and the measurement of the viscosity of the glue to determine its working life and setting properties.

The plywood shear test is made on specimens of birch plywood which have been prepared with the glue to be evaluated. The test pieces are subjected to tension in a standard plywood shear-testing machine until the joint fails. The load required to break the test pieces and the amount of wood failure is measured on dry joints and on those which have been soaked in water for 48 hours. This test is especially valuable for measuring the resistance of a glued joint to water. The specifications for casein and casein-type water-resistant glues (8, 9) require dry and wet plywood shear strengths of 340 and 140 pounds per square inch, respectively. There was no wood failure found in any of the wet joints tested except those made with one of the two lots of the casein glue mix containing blood and soybean meal reported in Table 9. In the plywood shear test the grain of the core of the 3-ply test pieces is at right angles to the faces.

In the block shear test the minimum requirement is 2800 lb per sq in. (8, 9). The grain of the two glued hard-maple blocks is parallel and a compression force is applied in the direction of the grain.

According to Federal specifications, "a glue shall be considered to have reached the end of its working life when it reaches a viscosity of 800 poises." For this test an orifice-type viscosimeter is recommended. However, for simplicity and speed of operation, the present investigators prefer to use a MacMichael rotating-cup viscosimeter employing a bob suspended from a torsion wire. When wire No. 26 is used with this instrument a reading of 290 deg is roughly equivalent to the maximum viscosity of 800 poises specified. Since the peanut-meal glues exhibit thixotropy, they must be stirred thoroughly to break down incipient gel formation before reliable viscosity readings can be made.

The gluing schedule followed in all of the plywood shear tests reported herein, unless otherwise indicated, was as follows:

Glue to water, proportion by weight	1 to 3
Temperature of wood and glue	75 to 77 F.
Glue spread	70–75 lb per 1000 sq ft
Closed assembly time	5 to 9 min
Pressure	150 lb per sq in. overnight at 75 to 77 F.
Age of glue mixture when used	1 hr
Moisture content of wood and of test pieces	6 to 7 per cent
Number of tests for each average value reported	15 (3 panels)

[1] Southern Regional Research Laboratory, New Orleans, Louisiana. One of the laboratories of the Bureau of Agricultural and Industrial Chemistry, Agricultural Research Administration, U. S. Department of Agriculture.

[2] Numbers in parentheses refer to the Bibliography at the end of the paper.

Contributed by the Wood Industries Division.

Statements and opinions advanced in papers are to be understood as individual expressions of their authors and not those of the Society.

For the block shear test the gluing schedule was the same as for the plywood shear test with the following exceptions:

Pressure, 200 lb per sq in.
Number of tests for each average value reported, 5–15.

To control the moisture content in the wood and test samples used for the plywood and block shear tests an inexpensive, easily constructed, constant humidity room was built. This was described in a previous publication (13). Test samples held in this room for 72 hours at a relative humidity of 32 per cent reach an equilibrium moisture content of 6 to 7 per cent.

Formula Development

Finely ground oilseed meals are required for the preparation of plywood glues. Because of the 6 to 10 per cent of oil which remains in hydraulic-press meals a flour cannot be prepared by ordinary sifting methods. It is necessary therefore to employ an air separator to obtain a flour of the desired fineness. The peanut flours used in this investigation were ground and sized so that 80 to 90 per cent would pass through a 200-mesh sieve; the sieve tests being run after the oil was removed by means of solvent. The oil remaining in the meal serves to prevent the glue from foaming during the mixing and spreading operations.

A readily available peanut-meal flour, Table 4, meal No. 1, which had been produced under controlled conditions for use as a food was chosen for the preliminary work on the development of a plywood-glue formula. It had a high protein content and was processed to separate the oil and meal at relatively low temperatures. Subsequent work showed this to be a good choice and this flour, or one prepared under similar conditions, was used in the work reported here, unless otherwise indicated.

Casein and soybean-meal glues are usually made up with water and various combinations and amounts of sodium hydroxide, lime, and sodium silicate. As would be expected, preliminary experiments indicated that peanut meal so combined behaved in a manner generally similar to that of soybean meal and casein.

A joint which has a high dry strength can be prepared with peanut meal by the use of sodium hydroxide and water alone. The addition of lime to such a mixture provides an irreversible gel which is necessary for wet strength in the glue bond. The addition of sodium silicate in amounts up to 15 parts per 100 parts of meal greatly improves the spreading qualities of the glue. Best results are therefore obtained when all three alkalies are present in the glue mixture.

Taking into account viscosity characteristics, working life, water requirements, and the wet and dry strengths of the plywood joint obtained, the combination of alkalies which has given the best results with peanut meal is: hydrated lime 15 parts, sodium hydroxide 4 parts, and sodium silicate 15 parts per 100 parts of peanut meal. Some of the data obtained in arriving at this formula are given in Table 1. In the series of tests recorded in the table the amount of sodium silicate and tetrasulphide, discussed later, was held constant. The addition of hydrated lime up to 15 parts per 100 parts of meal was found to increase the wet shear value. The use of less than 10 parts of hydrated lime gave glue mixtures with unstable viscosities, whereas with the addition of 10 and 15 parts of hydrated lime the viscosities were stable at all concentrations of sodium hydroxide shown. Increasing the amount of sodium hydroxide from 2 to 6 parts increased the dry strength somewhat and lowered the wet strength. A good compromise therefore is the formula containing 15 parts of hydrated lime and 4 parts of sodium hydroxide per 100 parts of meal. However, any one of the last six formulas in Table 1 provides good joints and has good viscosity characteristics.

A plywood glue which will produce a joint having a wet strength up to about 80 lb per sq in. can be prepared by the addition of lime, sodium hydroxide, and sodium silicate to the peanut meal. However, to further increase the water resistance of the glue it is necessary to use, in addition to lime, another insolubilizing agent, and the most satisfactory one which has been tried is carbon disulphide (14, 15). Carbon disulphide is recommended for use in soybean glue. It is sold mixed with equal parts of carbon tetrachloride to eliminate hazard of fire and the mixture is called "tetrasulphide." The influence on the plywood shear test of carbon disulphide, in the form of tetrasulphide, is shown in Table 2.

TABLE 1 EFFECT OF SODIUM HYDROXIDE AND LIME ON THE VISCOSITY AND PLYWOOD SHEAR STRENGTH OF PEANUT-MEAL GLUE WITH A 1:3 RATIO OF MEAL TO WATER[a]

Hydrated lime, per 100 g of meal, g	Sodium hydroxide per 100 g of meal, g	Viscosity in MacMichael deg wire No. 26				Plywood shear tests	
		0.5 hr	1 hr	2 hr	4 hr	Dry strength psi; Wood failure %	Wet strength psi
3	2	44	52	48	65	308–10	0
3	4	85	220	300+	...	....	....
3	6	99	172	....	....	....	....
3[b]	6	48	96	234	300+	395–16	80
5	2	37	51	76	191	383–18	128
5	4	70	115	208	....	....	....
5	6	103	187	300+	....	....	....
5[b]	6	48	66	105	154	404–10	122
10	2	50	59	65	88	398–12	138
10	4	48	58	68	74	400–13	134
10	6	78	84	96	88	417–38	136
15	2	44	45	59	63	396–12	151
15	4	56	67	74	76	424–26	139
15	6	81	80	79	63	400–26	121

[a] The amounts of sodium silicate and tetrasulphide were held constant at 15 g and 2 ml, respectively, per 100 grams of meal.
[b] Ratio of meal to water increased to 1:3.25.

TABLE 2 INFLUENCE OF THE CARBON DISULPHIDE IN TETRASULPHIDE[a] ON THE VISCOSITY AND WATER RESISTANCE OF PEANUT-MEAL GLUE

Tetrasulphide per 100 g of meal, ml	Viscosity in MacMichael deg. wire No. 26				Plywood shear tests: Dry strength lb per sq in.; Wood failure, %	Plywood shear tests: Wet strength lb per sq in.
	½ hr	1 hr	2 hr	4 hr		
0	53	45	45	37	432–18	48
1	52	54	57	56	433–13	118
2	51	69	71	73	444–15	140
3	61	97	94	97	412–19	150

[a] Equal parts of carbon disulphide and carbon tetrachloride.

From the standpoint of cost, viscosity stability, and water-resistance the use of 3 parts by weight of tetrasulphide per 100 parts of meal (2 ml per 100 gm) is satisfactory.

The complete formula for peanut-meal glue as compared with two commercial soybean-glue formulas is given in Table 3. This peanut-meal glue formula was used in all the work reported in this article, unless otherwise indicated.

The low water requirement of the peanut-meal glue is important because it permits the addition of less water to the veneer in the gluing operation, with the result that less water need be removed from the plywood in the drying tunnels than is necessary with glues which contain larger amounts of water.

TABLE 3 COMPARISON OF THE FORMULA DEVELOPED FOR PEANUT-MEAL GLUE WITH FORMULAS FOR OTHER WATER-RESISTANT PLYWOOD GLUES

(Quantities shown are parts per 100 parts of meal)

	SRRL peanut-meal glue	Commercial soybean-meal glue	Commercial soybean glue fortified with casein and blood albumin
Sodium hydroxide	4	7	5
Hydrated lime	15	3	12
Sodium silicate:			
Philadelphia quartz N brand or equivalent	15	15	25
Tetrasulphide	3[a]	3	2
Water	300	390	355

[a] Cc per 100 g.

TABLE 4 INFLUENCE OF PROCESSING CONDITIONS USED TO PREPARE THE MEAL ON ITS SUITABILITY FOR USE AS A PLYWOOD GLUE

Meal no.	Conditions used to prepare meal: Cooking time min.	Conditions used to prepare meal: Maximum temp F	Analysis of meal: Protein (N × 6.25) %	Analysis of meal: % of total meal N soluble in 1M NaCl	Analysis of meal: Lipids %	Ratio of meal to water in glue mixture	Viscosity, MacMichael deg, Wire No. 26: ½ hr	1 hr	2 hr	4 hr	Plywood shear tests: Dry strength, psi; Wood failure %	Plywood shear tests: Wet strength psi	Block shear tests strength, psi; Wood failure %	Group
						Commercial hydraulic-press meals								
1	76	215	58.4	81.0	10.5	1:3.0	44	65	90	113	417–15	147	3234–16	I
2	108	240	43.8	44.3	7.0	1:3.46	42	47	51	49	298–12	27	1915–29	II
						1:3.25	64	68	71	66	322–12	55	.....	
3	90	235 to 238	50.2	52.0	7.6	1:3.46	37	38	38	39	366–12	113	2550–17	II
						1:3.25	56	59	64	60	337–16	123	.....	
4	...	....	53.3	38.6	7.2	1:3.46	54	58	58	59	334–10	119	2741–42	II
5	...	....	52.2	60.8	6.7	1:3.46	38	42	52	55	360–12	122	2780–32	II
						1:3.25	51	49	48	43	396–19	51	.....	
						1:3.00	98	103	94	75	365–83	83	.....	
6	80	210	51.0	70.9	8.2	1:3.25	40	50	62	72	342–17	151	.....	I
						1:3.00	53	71	81	...	358–17	194	2780–22	
7	...	....	44.8	63.2	8.8	1:3.46	72	84	97	104	298–13	153	2242–20	II
						1:3.46	63	77	80	...	335–17	134	.....	
8	...	....	52.5	45.5	7.0	1:3.46	58	60	70	...	397–17	136	.....	II
						1:3.46	60	65	75	78	361–15	139	2295–16	
						Commercial expeller meals								
	...	....	57.0	55.3	7.1	1:3.67	41	44	54	56	358–13	42	.....	II
						1:3.34	97	99	97	91	397–11	79	2823–15	
10	...	....	48.2	17.5	10.9	1:3.46	118	126	143	142	319–11	75	.....	II
						Pilot-plant hydraulic-press meals made from 2-year-old nuts[a]								
11	60	219	53.6	75.8	8.4	1:3.25	50	66	76	93	400–14	155	3378–11	I
12	60	240	54.6	69.2	8.5	1:3.25	55	71	80	91	374–23	152	3529–16	I
13	80	262	54.2	37.7	12.8	1:3.25	76	85	106	119	345–14	101	2909–3	II
						Pilot-plant hydraulic-press meals made from fresh nuts[a]								
14	60	220	52.5	72.3	7.0	1:3.25	38	42	49	62	325–14	110	.....	I
						1:3.00	65	81	97	111	398–25	143	2956–19	
						1:3.00	63	80	107	113	374–11	140	.....	
15	60	240	53.7	69.4	8.0	1:3.25	44	48	55	62	340–15	141	.....	I
						1:3.00	54	64	76	86	368–16	147	2829–6	
16	80	262	52.8	40.9	10.8	1:3.25	59	67	72	80	396–19	118	.....	II
						1:3.25	62	65	74	81	389–12	134	3045–22	
17	60	225	51.9	76.0	8.3	1:3.00	53	59	75	76	400–29	155	3308–39	I
						Solvent-extracted meal								
18	Not cooked		57.3	89.5	10.0[b]	1:2.9	45	54	74	85	397–30	148	.....	I

[a] Two lb water added to 50 lb peanut flakes before cooking.
[b] Ten parts peanut oil added to 90 parts solvent-extracted meal in order to prevent the glue from foaming in the spreader.

Choice of Meal

As pointed out, the processing conditions employed to prepare peanut meal have considerable influence on the suitability of the meal for use as a plywood glue. This is shown by the data presented in Table 4.

The solubility of the protein in peanut meal varies with variations in the processing conditions employed to cook and press the rolled meats. This variation referred to as degree of denaturization, can be estimated from the percentage of the total meal nitrogen which is soluble in 1 molar sodium-chloride solution (16). Most commercial hydraulic-press peanut meals appear by this test to be appreciably denatured (low nitrogen solubility) as indicated in Table 4 and in an earlier publication (17). If the meals in Table 4 are divided into those which have a nitrogen solubility in 1M sodium chloride of 69 per cent or better (group I) and those which have a lower solubility (group II) it can be seen that the meals in group I make more satisfactory glues than those in group II. In most cases both dry and wet plywood strengths as well as the block shear strength is low when glues prepared from meals in the low-nitrogen-solubility group are used, the low wet strength being especially marked. The lower test values in group II are probably due, in part, to the necessity for using more water in preparing the glue mixture when the protein in the meal has been appreciably denatured. It is also possible that denaturization inactivates some of the groups in the protein molecule which are capable of reacting with lime and carbon disulphide to increase water resistance.

An examination of the conditions of time and temperature used to prepare commercial meals 1 and 6 (group I) shows that maximum cooking temperatures of 210 to 215 F for 76 to 80 minutes provide conditions for satisfactory oil recovery and at the same time produce a meal which is suitable for use as a plywood glue.

Nevertheless, application of these conditions may not produce a satisfactory meal in all oil mills, and specific directions for preparing meal cannot be given. Each mill will need to determine the best procedure for preparing a meal in which 70 to 80 per cent of the total nitrogen is soluble in 1M sodium chloride. As a further check a plywood-glue test should be made with meals which meet the solubility specification. The complete specifications for meal which has uniformly given good results when used as a plywood glue follow:

Protein (N × 6.25)	50 per cent minimum
Percentage of total meal N soluble in 1M sodium chloride	70 per cent minimum
Sieve test	80 per cent or more through 200 mesh
Oil	6 per cent minimum

The meals listed in Table 4, Nos. 11–17, were prepared in a pilot-plant special-model hydraulic press. Our experience and that of others have shown that meals prepared in a small mill may differ considerably from meals prepared under the same cooking and pressing conditions in a mill of greater capacity. Although a satisfactory meal can be prepared in the pilot plant by heating rolled meats to temperatures as high as 240 F for 60 min (meals Nos. 12 and 15) it would be unsafe to conclude that these conditions would yield the same results in a larger mill.

It is probable that the amount of water present or added to the flaked peanuts and the rate at which the water is driven from the flakes during the cooking operation accounts for the difference in the degree of denaturization of the meal obtained in various mills even though the cooking time and temperature remain the same. Fontaine, Samuels, and Irving (16) have shown the influence of water vapor on the degree of denaturization of the protein in cooked peanuts.

Peanut shells are incompletely removed prior to processing or

are later added to peanut meal which is intended for use as feed, the minimum protein (N × 6.25) requirement being 48 per cent. The presence of shells in meal intended for use as plywood glue, however, acts as a filler and should be avoided. The soybean-plywood-glue manufacturer pays a premium in order to obtain a meal which has a high protein content. The peanut-meal manufacturer should have no difficulty in preparing a meal containing 50 per cent or more protein (N × 6.25) for use in preparing plywood glue.

The first series of pilot-plant meals was prepared from peanuts which were two years old. It was advisable therefore to repeat the tests when a fresh stock of peanuts became available. Results indicate that the age of the seed used has no influence on the gluing characteristics of meal.

Solvent-extracted meal (meal No. 18) can also be used for preparing plywood glue. It is necessary, however, to add oil to the glue made from this type of meal in order to prevent excessive foaming in the spreader.

Influence of Various Factors on the Gluing Characteristics of Peanut-Meal Glue

A satisfactory plywood glue must produce a good joint with the equipment and under the conditions ordinarily encountered in the plywood factory.

The temperature of the glue room and of the water used to prepare plywood glue varies considerably. It was therefore of interest to determine the influence of temperature on the viscosity of peanut-meal glue. The results shown in Table 5 indicate that within the range of 65 to 95 F temperature has little influence on the flow properties of peanut-meal glue.

TABLE 5 EFFECT OF TEMPERATURE ON THE VISCOSITY OF PEANUT-MEAL GLUE

Temperature at which glue was prepared and held, F	Viscosity, MacMichael degrees Wire No. 26			
	1/2 hr	1 hr	2 hr	4 hr
65	50	62	66	76
77	53	59	75	76
85	62	72	86	77
95	59	72	82	71

TABLE 6 EFFECT OF AGE OF THE PEANUT-MEAL GLUE MIXTURE ON PLYWOOD SHEER STRENGTH

Age of glue, hr	Plywood shear tests	
	Dry strength, psi Wood failure, %	Wet strength, psi
1	405–25	132
2	407–14	128
3	392–10	115
4	396–14	104

The influence of the age of the glue mixture on the results obtained with a peanut-meal glue is shown in Table 6. Test panels were prepared with the glue at the end of 1, 2, 3, and 4 hours. The wet strength obtained was somewhat low to begin with and decreased to some extent with age.

In the manufacture of plywood the glued veneer is stacked until a press load is accumulated, an operation usually requiring 10 to 20 minutes. If a glue is too fluid, an excessive amount may be absorbed by the wood during this period or an excessive amount may be squeezed out when the glued veneer is placed under pressure. If the glue is too viscous, absorption of water by the wood may lead to the production of a dry joint, with the result that a thick film of glue and a weak bond are obtained. The influence of the closed assembly time on the strength of the bond obtained with a typical peanut glue is shown in Table 7. The results indicate that an assembly time up to 15 minutes gives a strong bond. This is an acceptable assembly period.

The yellow birch used for plywood tests varies considerably in color, from white through yellow to red, depending on whether the veneer is cut from sapwood or from heartwood. Since the color of the wood to be used in tests is not specified in the literature, it was of interest to compare woods selected for color, and at the same time to determine the influence of pressure on joint strength. The results given in Table 8 indicate that joint strength is not appreciably influenced by variation in veneer color or by variation of pressure within the range ordinarily applied.

TABLE 7 INFLUENCE OF CLOSED ASSEMBLY TIME ON PLYWOOD SHEAR TESTS

Closed assembly time min	Plywood shear tests	
	Dry strength psi; Wood failure, %	Wet strength psi
5	414–24	159
10	397–38	147
15	356–21	142
20	296–22	95

TABLE 8 EFFECT OF PRESSURE ON JOINTS MADE WITH A SINGLE LOT OF PEANUT-MEAL GLUE APPLIED TO RED, YELLOW, AND WHITE "YELLOW BIRCH" VENEER

(In terms of plywood shear strength, psi; Wood failure, %)

Pressure	100 psi		150 psi		200 psi	
	Shear strength psi; Wood failure %					
	Dry psi–%	Wet psi	Dry psi–%	Wet psi	Dry psi %	Wet psi
Red	415–35	131	454–34	139	447–46	142
Yellow	412–22	148	405–44	150	414–32	128
White	402–27	138	391–34	153	398–30	151

Comparison of Peanut-Meal Glue With Other Water-Resistant Glues

A comparison was made of the results obtained with peanut-meal glue and those obtained with other water-resistant glues as shown in Table 9.

It was also of interest to prepare test panels with tupelo and red-gum woods in addition to the usual birch panels since these two southern hardwoods and Douglas fir are used in the greatest amounts for the manufacture of veneers in this country. The relative amounts (thousands of feet, log scale) of these woods consumed in 1937 for the manufacture of veneers was: Douglas fir 306,299, red gum 213,654 and tupelo 170,438 (18).

An examination of Table 9 reveals that peanut-meal glue is equal to soybean-meal glue when tested according to the official birch-plywood test and also when tupelo and red gum are used. Although the results reported in this investigation appear to indicate that the peanut-meal glues tested are slightly superior in most cases to the soybean-meal glues tested, the number of soybean-meal glues examined is too small to justify concluding that there is any significant difference in these two oilseed-meal glues. It is also probable that optimum conditions were not always employed in gluing the three woods with the two glues. The casein glue examined as well as the mixture of casein, blood, and soybean meal are in most instances superior to the oilseed-meal glues.

The satisfactory results obtained by gluing tupelo and red-gum veneers with peanut-meal glue and the proximity of these southern hardwoods to the raw material for preparing peanut-meal-glue presents an opportunity of mutual advantage to southern agriculture and the southern plywood industry.

Influence of Added Blood Albumin and of Hot-Pressing on Peanut-Meal Glue

Blood albumin is sometimes added to soybean-meal glues to increase their water resistance. Glues with or without added blood may be heated in hot presses after the glue joint has been prepared in the usual manner by holding the glued product under pressure for several hours. Therefore preliminary tests which show the effect of hot-pressing at two temperatures and the effect of adding blood to peanut meal, as shown in Table 10, may be of interest.

Hot-pressing of plywood prepared with peanut-meal glue at 180 F has little effect, but raising the temperature to 240 F in-

TABLE 9 COMPARISON OF PEANUT-MEAL GLUE WITH OTHER WATER-RESISTANT GLUES WHEN APPLIED TO VARIOUS WOODS

Description of meal or glue used	Lot no.	Viscosity[a] Change with time in hours ½	1	2	4	Birch Dry strength, psi; Wood failure %	Birch Wet strength, psi; Wood failure %	Tupelo Dry strength, psi; Wood failure %	Tupelo Wet strength, psi; Wood failure %	Red gum Dry strength, psi; Wood failure %	Red gum Wet strength, psi; Wood failure %	Block shear tests strength, psi; Wood failure %
Peanut-meal glue	1	53	80	...	77	364–12	157	327–23	91	382–28	150	.....
	2	..	..	...	...	367–14	147	374–41	138	373–50	110	2857–13
Commercial soybean-meal prepared for use as plywood glue.[b]	1	..	..	...	...	393–26	151	401–7	0	328–9	105	.....
	2	71	72	86	102	396–15	73	268–44	112	352–16	33	2806–6
	3	58	63	71	88	396–30	142	274–43	143	370–10	138	.....
Casein-glue mix ready for use upon addition of water.[b]	1	..	..	...	...	495–30	195	408–25	138	497–77	151	.....
	2	30	42	67	136	523–43	214	357–70	185	403–51	171	3185–32
Casein-glue mix containing blood and soybean meal.[b]	1	48	67	76	...	489–36	259–15	340–21	166–10	356–12	184–13	.....
	2	15	47	148	Gel	409–22	167	251–28	138	341–20	112	3282–40

[a] MacMichael degrees; wire no. 26.
[b] Used as recommended by manufacturer.

TABLE 10 EFFECT ON PLYWOOD SHEAR STRENGTH OF ADDING DRIED BLOOD ALBUMIN TO PEANUT MEAL AND OF HOT-PRESSING

	Peanut-meal glue[b]	Peanut meal, 90 parts;[c] blood albumin, 10 parts	Peanut meal, 80 parts;[c] blood albumin, 20 parts
Ratio of meal to water in glue mix	1:3	1:3.25	1:3.25
Carbon tetrasulphide, ml per 100 g meal	2	1.5	None
Viscosity at ½, 1, 2 and 4 hours (MacMichael degrees, wire no. 26)	59, 68, 77, 77	42, 103, 155,—	180, 180, 188, 170
Plywood shear tests:			
Dry strength psi; wood failure, per cent	396–9	414–10	417–23
Wet strength psi	135	170	166
Shear tests on plywood hot-pressed at 180 F:[a]			
Dry strength psi; wood failure, per cent	395–25	430–19	454–16
Wet strength psi	156	202	224
Shear tests on plywood hot-pressed at 240 F:[a]			
Dry strength psi; wood failure, per cent	464–39	504–25	553–41
Wet strength psi	177	232	260

[a] Plywood dried overnight at 150 lb per sq in. pressure and subsequently hot-pressed at 150 lb per sq in. for 10 min at the temperature shown.
[b] Formula given in Table 3.
[c] Formula given in Table 3 with exceptions noted.

creases both the dry and wet plywood shear strengths. The addition of 10 and 20 per cent of blood albumin to the peanut meal increases the shear strength both before and after hot-pressing for 10 min under 150 lb per sq in. pressure at 180 and 240 F. In each case the panels were held at 150 lb per sq in. pressure overnight before they were hot-pressed.

The presence of blood albumin increased the viscosity of the glue considerably thus making it necessary to increase the amount of water; at the same time it decreased or eliminated the need of tetrasulphide.

Plant-Scale Formula and Details for Preparing the Glue Mixture

The formula recommended for preparing plant-scale batches of peanut-meal glue is as follows: The ingredients are added in the order listed:

Water, 200 lb
Peanut-meal flour, 100 lb
Add flour to water and stir to a smooth paste. Then add
Water, 55 lb
Hydrated lime, 15 lb mixed with 35 lb of water
Caustic soda, 4 lb dissolved in 11.5 lb of water
Tetrasulphide (equal parts carbon disulphide and carbon tetrachloride) (1 qt) 3 lb
Stir for 2 minutes and add silicate of soda (Philadelphia "N" brand or equal), 15 lb. Stir for a few minutes and use.

A spread of about 150 pounds of wet glue per thousand sq ft, 3-ply basis, and a pressure of 150 lb per sq in. is satisfactory for gluing plywood.

The foregoing formula is for application to dry hardwood veneers. It may be necessary to alter the water content of the glue when gluing softwood veneers or wet veneers.

Peanut-meal glue was tried on a plant scale in a commercial plywood factory. The glue performed well throughout the process and gave as good or better joints with poplar and black-gum veneers as did soybean-meal glue which was used under the same conditions on the same lots of veneer.

Summary

Specifications have been developed for peanut meal which is suitable for use in preparing plywood glue.

A glue mixture has been developed which has good flow properties and which is accommodated to ordinary gluing schedules for this type of glue. Joint tests show that the peanut-meal glue meets the requirements established for casein and casein-type glues.

Acknowledgment

The authors wish to express their appreciation to the Raymond Pulverizer Division, Combustion Engineering Company, Inc., Chicago, Ill., for grinding and sizing sufficient peanut meal for plant-scale tests, and to the Mississippi Plywood and Veneer Company, Fernwood, Miss., for making trial runs in their plant.

BIBLIOGRAPHY

1 "Soybean Adhesives," by I. F. Laucks, *The Chemurgic Digest*, vol. 2, 1943, pp. 173–176 and pp. 185–188.
2 U. S. Patent 1,942,109 (1934), I. F. Laucks.
3 U. S. Patent 1,601,506 (1926), G. H. Osgood.
4 U. S. Patent 1,601,507 (1926), G. H. Osgood.
5 First report of the Adhesives Research Committee, p. 41, London, Eng., 1922.
6 "Preliminary Notes on the Use of Sunn Hempseed Proteins as Plywood Adhesives," by D. Narayanamurti, V. Ranganathan, and D. C. Roy. Indian Forest Leaflet No. 52, Forest Research Institute, Dehra Dun, U. P.
7 "He Started a New Industry From Soymeal," *Soybean Digest*, vol. 2, 1942, pp. 6–7.
8 Federal Specification C-G-456, July 8, 1941, Glue; Casein-type, Water-Resistant.
9 Navy Department Specification 52G8c, May 1, 1941, Glue, Casein, Water-Resistant.
10 "The Gluing of Wood," by T. R. Traux, U. S. Department of Agriculture Bulletin No. 1500, June, 1929.

11 "Gluing Wood in Aircraft Manufacture," by T. R. Traux, U. S. Department of Agriculture Technical Bulletin No. 205, Oct., 1930.

12 "Manual for the Inspection of Aircraft Wood and Glue for the U. S. Navy," second edition, 1941.

13 "Controlling Moisture Content in Wood and Glued Test Samples," by R. S. Burnett and A. L. Merrifield, *Mechanical Engineering*, vol. 67, 1944, pp. 475–476.

14 U. S. Patent 1,691,661 (1928), I. F. Laucks and Glenn Davidson.

15 U. S. Patent 1,833,527 (1931), F. F. Lindstaedt.

16 "Properties of Peanut Meal," by T. D. Fontaine, Carolyn Samuels, and G. W. Irving, Jr., *Industrial and Engineering Chemistry*, vol. 36, 1944, pp. 625–627.

17 "Commercial Peanut Meal," by R. S. Burnett and T. D. Fontaine, *Industrial and Engineering Chemistry*, vol. 36, 1944, pp. 284–288.

18 "Statistical Abstract of the United States 1939," p. 718 U. S. Department of Commerce.

Locomotive Fuel From the Coal-Man's Viewpoint

By C. F. HARDY[1]

The sizes of coal for locomotives and the preparation of coal, screening, and segregation are discussed in this paper. It is suggested that from an engineering standpoint coal specifications for locomotives should be standardized because of the changes in equipment and construction, and that extensive tests should be made.

WHEN the credit for winning World War II is apportioned a large share will be given to the coal-burning steam locomotive. With a tremendous task to do, using to a large extent different sizes and types of coal from those that were formerly furnished, the railroads were able to keep the nation's freight and passengers moving. Probably no other major coal user had so much dislocation of normal coal supply as did the railroads. Of necessity a great part of the coal which could be used for by-product, special purposes, or domestic use, was taken out of railroad fuel and replaced in the main by smaller sizes or lower quality. It is doubtful if any other type of fuel-burning equipment than the steam locomotive could have been operated under such adverse circumstances.

Now that the war is over, the possibility of improving sizes, type, and preparation of the coal for locomotive use is again pertinent. There have been tremendous advances in the practices of coal preparation and coal cleaning in recent years. From the simple bar screens of a few decades ago, coal-screening plants can now produce any practical size of coal. Along with this trend of sizing coal has come the study of its impurities and the best methods of removing these. Some coal-producing districts have installed more cleaning plants than others. This trend has been reflected in the type of coal furnished for locomotive use from these producing districts. These questions naturally arise: Why cannot all railroad coal be standardized as to size and preparation? Is it feasible for either the railroad or the coal industry to standardize locomotive coal? Will it help the performance of present or future locomotives?

The economics of the problem are bound up with the well-known interdependence of the railroads and the coal industry. A few details will suffice to show this interdependence. The railroads are the coal industry's best and most consistent customers and have bought during the last decade approximately 21 per cent of the total annual coal production. The railroads, by purchasing sizes which are temporarily not in demand, have permitted many mines to keep in regular production, whereas otherwise they would have to operate sporadically due to the lack of markets for one or more sizes. This effect is also shown by the fact that the monthly stocks of coal which the railroads carry have varied from month to month as much as 40 per cent, plus the fact that they buy widely varying sizes of coal. The other aspect of the interdependence is that the coal industry is responsible for supplying the railroads with 20 per cent of their total gross freight revenue in normal years and more than 80 per cent of the railroads' total annual fuel requirements.

[1] Chief Engineer, Appalachian Coals, Inc., Transportation Building, Cincinnati, Ohio. Mem. A.S.M.E.

Contributed by the Fuels and Railroad Divisions and presented at the Annual Meeting, New York, N. Y., Nov. 26–29, 1945, of THE AMERICAN SOCIETY OF MECHANICAL ENGINEERS.

SIZES OF COAL NOW USED AND RECOMMENDED FOR LOCOMOTIVE FIRING

A complete analysis of sizes of coal used by locomotives entitled "1937 Railway Locomotive Fuel" (1)[2] was prepared by the former Bituminous Coal Division. Two hundred and fifty-two different size designations were shown in this report. A less elaborate compilation was made for 1944 and apparently it agrees fairly well with the 1937 figures. In 1937, 445 railroads used 89,935,580 tons of bituminous coal for locomotive fuel. This tonnage represented 82.6 per cent of all locomotive fuel, including fuel oil, anthracite, and wood. The coal came from all but one of the 23 coal-producing districts set up by the Bituminous Coal Act of 1937. (See map.)

Table 1 shows the amount of on-line, off-line, lake, tidewater, truck, and river, total railroad fuel, and the percentage of the districts' production going to railroad fuel. Of the major producing districts, District No. 7, Southern low-volatile, showed the smallest percentage (1.8 per cent) used for locomotive fuel.

Table 2 gives a breakdown by size groups of the total of all districts and of the six largest railroad-fuel-producing districts. From this table it is seen that run of mine and resultant run of mine of more than 4 in. top size are used to a larger extent than any other size coal both off-line and on-line. Off-line locomotive coal is bought on the open market and in this case the railroad has no specific interest in the coal producer. The railroad is free to specifiy the size it regards best for locomotive performance. In spite of this, there is little difference in the sizes bought off-line and those bought on-line. This total, 52,618,116 tons, is almost $6^1/_2$ times as much tonnage as is in the next-larger-size group. Also, more of it is produced for locomotive fuel than any other size in each district, except District No. 11, Indiana. (See first line of Table 2.)

Table 3 is included to show the comparison of the amount and sizes of locomotive fuel produced by each of the foregoing six districts and also District No. 9, Western Kentucky. The size groups of coals were fairly consistent with the run-of-mine sizes showing the largest increase.

In view of the recommendations in the literature for modified screenings or screenings with part of the fines removed, it is surprising that only about 492,000 tons out of the 6,700,000 tons of screenings were modified. (See second line of Table 2.) Even if the size listed as "nut" (see tenth line of Table 2) which might better be included as modified screenings, were included, it would bring the total up to only about 7,500,000 tons. The widespread use of mine run is substantiated by a series of tests run at the University of Illinois in 1917 which showed that mine-run coal (actually 5-in. resultant) is best suited for locomotive use. This series of tests also showed that 2 × 3-in. nut gave good evaporation at high rates and the lowest cinder loss (2).

Zern (3) and Robinson (4) show agreement fairly well on 5-in. or 6-in. resultant mine run with a limit of 23 per cent of minus 1 in. or $^3/_4$ in. Woodrich (5) advocates that the coal supplied for hand-fired locomotives should be of plus $1^1/_2$ in. or 2 in. when it leaves the mine. He states that the use of these coals would stimulate the coal producers to greater efforts in moving the

[2] Numbers in parentheses refer to the Bibliography at the end of the paper.

TABLE 1 LOCOMOTIVE FUEL BY DISTRICTS, 1937

	District	On line	Off line	Lake, tidewater, truck, river	Total R. R. fuel	Total all coal prod. by district	Per cent to locomotive fuel
1	Central Penn.	5,294,963	4,026,843	28,578	9,350,384	41,106,000	22.7
2	Western Penn.	7,633,309	1,757,774	345,217	9,736,300	72,253,000	13.5
3	Fairmont	3,113,145	4,710,128	495,977	8,319,250	24,010,000	34.6
4	Ohio	4,632,401	2,353,601	1,321,148	8,307,150	25,178,000	33.0
5	Michigan	4,569	35,151	....	39,720	562,000	7.1
6	Panhandle	59,055	16,670	141,815	1,017,540	4,203,000	24.2
7	Southern low-volatile	894,419	31,669	42,654	968,742	54,275,000	1.8
8	Southern high-volatile	7,552,729	5,019,310	633,058	13,205,097	91,874,000	14.4
9	West Kentucky	2,140,591	413,681	....	2,554,272	8,563,000	29.8
10	Illinois	12,027,277	2,899,641	....	14,926,918	51,602,000	28.9
11	Indiana	3,879,186	1,277,341	....	5,156,527	17,765,000	29.0
12	Iowa	638,558	84,320	....	722,878	3,637,000	19.9
13	Alabama	2,716,951	984,341	....	3,701,294	13,459,000	27.5
14	Arkansas, Oklahoma	146,493	3,665	421	150,579	1,967,000	7.7
15	Missouri, Kansas	1,576,170	308,488	200	1,884,858	9,038,000	20.9
16	Colorado	82,818	2,312	166	85,296	2,510,000	3.4
17	Colorado	1,451,611	476,108	....	1,927,719	5,515,000	35.0
18	Arizona, New Mexico	261,436	31,792	....	293,228	884,000	33.2
19	Wyoming	4,144,510	23,446	....	4,167,956	5,918,000	70.4
20	Utah	423,300	344,335	....	767,535	3,810,000	20.1
21	N. and S. Dakota	....	....	....	....	2,298,000	....
22	Montana	1,946,721	171,502	....	2,118,223	2,965,000	71.4
23	Oregon, Washington, and Alaska	509,751	24,365	....	534,116	2,139,000	25.0
	TOTAL	61,929,963	24,996,383	3,009,234	89,935,580	445,531,000	20.2

TABLE 2 SIZES FURNISHED IN 1937, TOTAL ALL DISTRICTS AND SELECTED DISTRICTS, FOR LOCOMOTIVE FUEL

Description of sizes:		All districts	Selected districts 1	2	3	4	8	10	11
Straight ROM and resultant more than 4" top size	On line	36,931,188	4,562,109	5,702,762	2,495,088	2,980,489	2,524,687	6,096,612	743,479
	Off line	15,686,928	2,302,055	1,114,164	3,060,740	1,992,274	3,879,129	1,353,285	457,206
Screenings less than 3" top size, including 492,500 T modified	On line	6,220,594	21,288	253,816	10,542	95,447	3,316,455	1,638,073	85,026
	Off line	510,559	51,190	18,936	16,610	32,079	81,582	56,265	180,655
Chunks, top size 7" to 6" bottom size more than 7/8"	On line	5,751,358	133,323	170,960	398,125	310,883	152,091	1,585,563	1,532,355
	Off line	2,582,213	215,812	273,993	314,257	1,828	174,841	883,593	383,034
Egg, top size 5" to 3" bot. size more than 7/8"	On line	4,658,202	14,927	252,295	12,179	998,392	466,008	2,034,718	605,041
	Off line	2,784,823	320,690	116,757	611,040	218,581	489,214	363,212	163,956
Resultant ROM 3 in. and 4 in.	On line	3,080,414	67,567	334,882	4,613	51,960	627,411	5,242	102,238
	Off line	1,514,664	759,855	33,395	33,620	642	207,013	191	....
Lump, bot. size 3" to 1/4" top less than 8"	On line	2,559,498	291,301	297,319	78,627	167,113	338,048	207,214	494,258
	Off line	1,052,794	246,373	191,622	331,575	72,801	47,197	17,795	83,094
Block, bot. size more than 6 in.	On line	856,078	....	31,150	106,095	8,664	6,644	157,698	196,856
	Off line	79,285	....	....	9,733	4,491	4,481	4,413	1,251
ROM, top size 8 to 10 in.; including crushed and mod.	On line	756,847	....	435,834	4,261	1,810	51,245	45,169	82,294
	Off line	303,531	8,218	....	38,801	30,587	129,289	414	103
Screenings, top size 1 in. or less	On line	603,319	163,702	44,675	3,458	119	21,155	37,033	36,875
	Off line	114,154	17,193	8,029	74,600	....	159	....	....
Nut, top size 2 3/4 in. to 1 in., bot. size more than 28 mesh	On line	512,459	40,746	109,616	157	17,524	48,985	219,955	764
	Off line	367,432	105,457	878	219,152	318	6,405	20,473	8,042
Total		89,935,580	9,350,384	9,736,300	8,319,250	8,307,150	13,205,097	14,926,918	5,156,527

Source: Bituminous Coal Division, "1937 Railway Locomotive and Powerhouse Fuel," Preliminary Analysis, Jan. 16, 1939.

TABLE 3 COMPARISON OF LOCOMOTIVE FUEL BY SIZE GROUPS, YEARS OF 1937[a] AND 1944[b] FOR SELECTED DISTRICTS

Description of sizes	Year	All districts	Selected districts 1	2	3	4	8	9	10	11
Lump coal and double-screened top size over 2 in.	1937	19,374,808	877,083	1,163,598	1,624,531	1,952,807	1,647,493	692,365	5,025,141	3,410,057
	1944	34,623,236	499,046	1,886,401	4,636,788	1,932,403	1,335,446	1,169,257	12,483,640	8,018,754
Double-screened top size not exceeding 2 in.	1937	1,492,155	147,172	33,170	223,317	82,378	117,153	19,300	705,104	57,612
	1944	2,336,088	58,296	176,550	380,497	31,869	479,163	71,201	872,228	154,816
Mine run and minus resultant top size over 2 in.	1937	63,903,181	7,615,848	8,293,585	6,074,051	6,160,233	9,568,849	1,784,920	8,118,499	1,380,243
	1944	87,474,978	8,204,731	9,265,025	9,770,851	9,811,046	13,697,020	5,632,733	10,565,071	1,513,507
Minus resultant and dedusted screenings, top size over 1/4 in. and not exceeding 2 in.	1937	4,632,099	74,165	194,280	140,603	111,613	1,787,688	51,466	1,068,038	265,681
	1944	7,808,968	61,072	759,326	108,235	273,352	2,014,524	151,909	2,380,565	419,387
Minus resultant and dedusted screenings top size not exceeding 1/4 in.	1937	506,453	178,880	51,667	42	119	26,068	6,221	9,065	36,875
	1944	986,355	243,786	62,581	130,076	34,008	105,746	77,331	102,392	1,590
Size not reported	1937	26,884	457,236	.....	256,706	.....	57,846	....	1,071	6,059
	1944	752,965	19,261	63,402	43,213	7,439	79,016	3,600	20,888	77,013
Total	1937	89,935,580	9,350,384	9,736,300	8,319,250	8,307,150	13,205,097	2,554,272	14,926,918	5,156,527
	1944	133,982,590	9,086,192	12,213,285	15,069,660	12,090,117	17,710,915	7,106,031	26,424,784	10,185,067

[a] 1937 Data rearranged in same size groups as 1944 data from "1937 Railway Locomotive Fuel."
[b] 1944 Data from Mineral Market Report, M.M.S. No. 1289.

minus 1 1/2-in. or 2-in. sizes. For stoker-fired locomotives, Woodrich recommends an average of 3-in. top size, with no lumps more than 8 in. maximum, and a bottom size of 3/4 in.

The International Railway Fuel Association, and likewise the Railway Fuel and Traveling Engineers Association, have devoted much time to the subject of coal sizes (6). In 1942 the R.F.T.E.A. committee on coal sizing recommended run of mine with lumps reduced to 4 in. top size as the most economical size for use on hand-fired locomotives. For stoker-fired locomotives not adapted to handle smaller sizes, "properly cleaned coal not to exceed 2 1/2 in. × 0 in." was recommended as the most economical size. For stoker-fired locomotives properly fitted to handle small sizes, 2 in. × 0 in., or coal with a smaller top size, was recommended. It was pointed out that minus 1/4-in. slack was objectionable, particularly in the softer bituminous coals. One-quarter-inch screenings should not exceed 35 to 40 per cent of the total when small sizes are used, according to this committee.

In 1943 the same committee recommended the use of mechanically cleaned coal because it gave the most efficient and economical performance. The principal basis of this recommendation was the experience of a railroad using coal largely from Districts Nos. 10 and 11, Illinois and Indiana.

TABLE 4 STEAM LOCOMOTIVES IN SERVICE OF CLASS 1 RAILROADS
December 31, 1943[c]

	Per cent	Total	Freight	Passenger	Freight or pass.	Switching
Total in service (A) (B)	100	39,498	24,353	6,399	1,738	7,008
No. built before Jan. 1, 1910	24.9	9,814	6,183	1,373	275	1,983
No. built bet. Jan. 1, 1910, and Dec. 31, 1914	23.6	9,330	5,742	1,834	212	1,542
No. built bet. Jan. 1, 1915, and Dec. 31, 1919	18.6	7,341	4,995	792	143	1,411
No. built bet. Jan. 1, 1920, and Dec. 31, 1924	17.2	6,797	4,306	1,225	235	1,031
No. built bet. Jan. 1, 1925, and Dec. 31, 1929	10.1	4,008	1,996	790	404	818
No. built bet. Jan. 1, 1930, and Dec. 31, 1934	2.4	960	485	176	171	128
No. built bet. Jan. 1, 1935, and Dec. 31, 1937	1.2	464	213	94	77	80
No. built bet. Jan. 1, 1938, and Dec. 31, 1942	2.0	777	430	115	221	11
No. installed bet. Jan. 1, 1943, and Dec. 31, 1943		429[d]				
No. installed bet. Jan. 1, 1944, and Dec. 31, 1944		329[d]				

NOTE (A) 15,734 of these locomotives are equipped with stokers.
NOTE (B) As of March 31, 1945, 39,658 locomotives were in service of Class I switching and terminal railroads. 21,710 were listed as freight, 6318 as passenger, and 11,630 as switching.
[c] Compiled by Traffic Department, National Coal Association, from American Association of Railroads, and Interstate Commerce Commission figures.
[d] No breakdown available.

The coal specifications set up by the various railroads are not standardized. Each road has its own specifications for locomotive use and these vary widely as to the sizes considered most suitable. Some roads may have facilities to further prepare the coal before using although the author has no data on this subject.

From the engineering standpoint, standardization of coal specifications for locomotives would seem necessary for the following reasons:

1 New locomotives, embodying fireboxes of different designs and different types of coal-burning equipment, etc., have replaced the older locomotives.

2 The older locomotives have been changed by the addition of stokers, different-type grates, arches, front-end design, etc., so that the former sizes of coal are not satisfactory.

3 Experimental and testing work on locomotives has proved that the size of coal should be changed for greater efficiency and economy.

The age and class of service of locomotives now in use are shown in Table 4. About two thirds of the steam locomotives in service were built before 1919 which would seem to rule out condition No. 1. These tabulations show that approximately 40 per cent of the present locomotives are equipped with stokers, although the relative age of the stoker-fired locomotives is not given.

That a great deal of work has been done on grate designs, arches, and "the combustion train" generally, is shown by the literature. There is no indication that these improvements have necessitated the change in sizes or types of coal, but every indication is that they have resulted in burning the present sizes and types more efficiently. The reduction in consumption of coal per ton-mile shown each year is due partially to these improvements, although increased steam temperatures and pressures, improved bearings, roadbed improvements, and fewer and longer trains have also helped.

The experimental and testing work in locomotives quoted in the literature is all of considerable age, although the types and sizes of locomotives tested are still in service. Undoubtedly other work has been done that has not been reported so that the answer to our third condition is not readily apparent.

The Preparation of Coal

The basic mining and preparation practices which have developed over a period of years in the various coal-producing districts have a vital bearing on the extent to which locomotive coal could be standardized without a serious dislocation of the coal industry's economy. Coal is a natural product and varies in quality, size consist, and chemical make-up, not only according to the mining district, but according to the mine and even from the part of the mine from which it comes. It can be improved or modified to a certain extent by mining methods and after it is mined, but no major changes can be made.

In 1943 there were, in the United States, 6620 mines, each having a production capacity of more than 1000 tons of bituminous coal per year. It is therefore difficult to treat the product of so many mines as one subject. No one mine, seam, or coal-producing district could conceivably furnish all the railroad coal in the country, so that of necessity the same locomotive will have to burn coals from widely separated geographic sources, and with different qualities and burning characteristics. The growing practice of running a locomotive over two or more divisions may result in using coals of widely different sources and characteristics on one trip.

If coal is loaded by hand, face preparation is practiced, that is, rock, bone, slate, and other impurities are not loaded with the coal but are rejected by the miner. This is much easier to do with hand-loaded coal than when the coal is mechanically loaded, inasmuch as a loading machine has no judgment as to what it picks up. The same is largely true of "strip" coal, for in strip-mining there is less chance to inspect the coal.

Once the coal is delivered to the tipple, it can be cleaned in two ways: The first and most universal practice is hand-picking, or removing the visible impurities manually. Sizes as small as 1 in. bottom size can be picked, although it is not generally economical to pick sizes under 3 in. The reduction of impurities by hand-picking depends to a large extent on how the impurities are found in the coal, the number of pickers employed, and their efficiency. In many mines hand-picking does not lower the ash content to a great degree, while in many others, where conditions are favorable, a large reduction in ash content is made. It also tends to waste considerable coal if the pickings are not cleaned by washing afterward (7).

It is difficult to pick run of mine and resultant, and it is the practice in some mines to separate into the various sizes, hand-pick or otherwise clean these, and then recombine them.

The second method, mechanical cleaning of coal, has been steadily increasing in popularity. One method of mechanical cleaning consists simply of "dedusting" or screening out a part of the fines and it is practiced in mines where a large percentage

of impurities are found in the extremely fine coal. The top size of coal removed may be as small as 60 mesh and as large as 1/4 in. Of the 590,177,000 tons of coal produced in the United States in 1943, 145,575,849 tons, or 24 per cent, were mechanically cleaned. Of this total, 85.8 per cent or 124,374,775 tons were cleaned by wet-washing, whereas 21,201,074 tons, or 14.2 per cent, were cleaned by pneumatic methods. Forty-seven per cent of the washed coal was cleaned on jigs and 29.6 per cent was cleaned on launders and upward-current classifiers. Of the total coal cleaned, 30,326,426 tons were mined from strip pits, 125,313,687 tons were mechanically loaded underground, and 67,258,305 tons were hand-loaded underground.

Both the wet-washing and air-cleaning processes depend on the difference between the specific gravities of the coal and the impurity. The specific gravity varies for both the coal and the impurity. The "gravity" of the cleaning medium must be adjusted to remove as much of the impurity as possible without wasting excessive amounts of coal.

Although it is impossible to remove organic sulphur or some of the finely divided pyritic sulphur from coal by washing, it is sometimes possible to reduce other types of sulphur in high-sulphur coals by more than 50 per cent, depending on the efficiency of the washer, the nature of the coal, etc. The ash in high-ash coals may be reduced nearly 50 per cent, depending on the distribution of the ash-producing constituents, friability of the coal, etc. (8).

Air-cleaning of coal is usually confined to the sizes which are too small to be satisfactorily wet-washed because of the increase in moisture content likely to result from washing fines. For example, at a given mine sizes larger than 5 in. may be hand-picked, sizes between 5 in. and 3/8 in. washed, and the 3/8-in. × 0-in. cleaned pneumatically. When all the coal from, for example, 2 in. down is air-cleaned, it is carefully separated into its component sizes before being air-cleaned. For example, if it is desired to clean 2 × 0-in. coal, it is divided into 2 × 1 in., 1 × 3/4 in., 3/4 × 1/2 in., 1/2 × 1/4 in., and so on, and run over separate air-cleaning apparatus. It is difficult to air-clean sizes with wide variations, such as 2 in. × 0 in., in one cleaner.

Mechanical cleaning is necessary and most beneficial to coals containing in the raw state a high percentage of ash and foreign matter and to mechanically loaded coal. Ordinarily when operations in an underground mine are changed from hand loading to mechanical loading, there follows an increase in the percentage of ash in the coal. When a cleaning plant is put in at the same time, the net over-all effect would be to perhaps lower the ash content by one to three per cent over the average encountered in hand-loading methods. The fact that a coal has been washed or air-cleaned is no indication of its quality, as the raw coal from one seam may be superior to the washed or cleaned from another.

The average cost of cleaning is given by Campbell (9) as about 20 to 25 cents a ton. There is an economic limit to the amount of ash and sulphur reduction which may be made by cleaning. Above this, reject losses increase to such a point that it is no longer economically justified to clean it.

Screening Coal

The equipment of mines for screening and preparing coals varies from mine to mine. This depends somewhat on the size of the mine, the amount of coal in reserve or the prospective life of the mine, and on the ultimate use for which the coal is best suited, or those sizes which will return the greatest over-all realization. The problem of screening the coal as it comes to the tipple into those sizes which are most in demand and provide the greatest return for the combination of sizes made is complex and requires both careful study and extensive planning. For example, if the coal from a given mine possesses the peculiar characteristics which make it suitable for domestic stoker coal, it may be profitable to crush some larger sizes to make stoker coal, and not at all profitable to make locomotive fuel.

Mines with no screening facilities of necessity make run-of-mine coal; and mines equipped with bar screens only are able to make two sizes such as 5-in. lump and 5-in. resultant. These mines may be equipped with crushers so that coal can be crushed to a given top size. The bulk of the mines which sell coal for many different uses are equipped with shaker screens and in many cases vibrating screens. A large number of sizes may be made by changing the size of the screens, although the number of sizes which may be made at one time at a given tipple depends on the number of tracks and their usage. The average mine probably makes and loads three or four sizes at a time. The elaborate modern tipples, particularly where mechanical cleaning is employed, may make 12 or more sizes simultaneously, part of which are delivered to bins and may be remixed or blended from the bins before loading. Mines which make only one or two sizes of coal are more likely to be found in the eastern area, that is, in Districts Nos. 1, 2, 3, 4, 6, and 8, than it is in Districts in the Middle West, Nos. 9, 10, and 11.

The practice of furnishing a double-screened washed coal such as 6 in. × 1 in., or similar size, to the railroads, is probably followed to a greater extent in Indiana, District No. 11, (10) (79.3 per cent of locomotive fuel furnished by this district in 1944 was double-screened with a top size of more than 2 in.) than any other producing district. Districts No. 9 (Western Kentucky), No. 10 (Illinois), and No. 4 (Ohio) also furnish considerable coal of this type. It would probably be most difficult for District No. 1 (Eastern Pennsylvania), to furnish sizable amounts of double-screened coals to the railroads due to the relatively soft structure of the coals. District No. 2 (Western Pennsylvania), No. 3 (Northern West Virginia), and No. 8 (Southern high volatile), could furnish a larger amount of double-screened coal and washed coal for locomotive use than is the usual practice. This, however, would only serve to emphasize the difference in quality between these coals and the others which are often used interchangeably on the same locomotive. If these districts were to furnish a double-screened coal, particularly of a smaller top size, it would mean a tremendous investment in screening equipment for many of the mines not now so equipped, and it is doubtful that the resulting small sizes could readily be sold. Many of the smaller mines which now make railroad coal exclusively could not afford to put in screening equipment, because the acreage available to them is limited. Furthermore, if at a normal rate of production a mine will work out within the next four or five years the cost of screening equipment could not be justified.

The remainder of sizes in a commercial mine which customarily produces block or lump, egg, nut, and 2-in., 1 1/2-in., or 1 1/4-in. nut and slack is not seriously disrupted by making run-of-mine or a resultant size such as 5 in. × 0 in. for railroad fuel, as the total production is utilized in the one or two sizes made at this time. If the railroads insisted on a given size, such as 5 in. × 1 in., the mine would undoubtedly have too much of either the large or small sizes at times and would be unable to operate.

Segregation and Degradation

Perhaps the greatest change that can take place between the time coal is mined and used is the segregation of the coal as it is handled. Each time it is dumped or conveyed the larger pieces tend to roll the farthest, as to the outside of the pile, and the smaller pieces tend to stay near the point of dumping. Naturally, as the difference between the top size and the bottom size of the coal increases, segregation also increases under the same conditions of handling. Segregation can be greatly reduced by careful handling, by using nonsegregating chutes and hoppers, by

layer-loading, etc., as well as decreasing the difference between the top and the bottom size.

Segregation is often confused with degradation, and with bad preparation. The user often finds it hard to believe that the fines he discovers in the middle of his coal pile were there when the coal was unloaded, and are not a result of the coal "slacking" or breaking up.

According to Fraser (11) the greatest degradation is in the handling of plus 4-in. lump coal and this amounts to about 4½ per cent. There is very little degradation in the handling of run-of-mine, resultant, or screenings, perhaps due to the cushioning effect of the fine sizes. The same authority shows that the percentage of fines in the mine-run coal as delivered from the hard-structured seams found in Eastern Kentucky and Illinois coals is well within the limit set as desirable by several authorities for locomotive coal. All percentages are under 40 per cent. Subsequent handling, such as filling the fuel bins at coaling stations and coaling the engines would seem to increase the percentage of fines but little.

Briquetting

The briquetting of coal for railroad use in this country has been suggested and extensive tests were run by the U. S. Bureau of Mines in 1908 (12). The first tests were run on No. 3 Pocahontas coal both in the mine-run form and briquetted. As would be expected from the burning characteristics of this coal, the briquettes worked out much better than did the mine run, primarily due to the smaller amounts of fines. Later, briquettes were tried from a wide number of coals and general improvement in burning rates were reported. Apparently then, as now, the higher cost of the briquettes as compared to the cost of raw coal made their use uneconomical. Further research in briquetting methods may in time reduce the processing cost to a more practical figure.

Conclusions

Railroad locomotive fuel is such a large part of the total coal production of the United States that one standard size could not be screened out of the coal as mined without changing the sizes of coal furnished to all other coal users. The mere elimination of all the fines below a certain size would immediately lead to the accumulation of tremendous tonnages of this coal which could not be sold in a normal market.

The present practice of furnishing mechanically cleaned or double-screened coal for locomotive use is confined primarily to those districts where the practice of cleaning has grown over a number of years, due to greater mechanization of the mines, and to some extent to the large amount of impurities in the raw coal. Mechanical cleaning of coal has been developed to a greater extent in some districts and this naturally has resulted in a greater proportion of the locomotive fuel being cleaned. It is true that the trend is in the direction of more careful sizing and cleaning of coal, but it is equally true that all coal mines cannot be changed over immediately to produce a standard size of locomotive fuel. In many cases the raw run-of-mine or resultant sizes from one district will be equal or will be superior to the cleaned or double-screened sizes from another so that there may not be an actual advantage in having the size standardized.

No other type of coal-burning equipment is capable of being operated with such a wide range of size and quality of coals as the coal-fired locomotive. This has helped both the railroads and the coal industry but has also allowed in some cases the buying and furnishing of inferior quality and preparation when better grades were available.

In view of all the factors involved, it would seem that extensive tests should be made, using the different types and sizes of coal in the various sizes and types of present-day and new locomotives so as to determine the best performance under road conditions with as many sizes and qualities of coal as is possible. The published data are so inconclusive that such a procedure would seem prerequisite to making major changes. There is no question that the coal industry is willing to do anything within its power to arrive at the solution of this very important problem of locomotive fuel.

Bibliography

1 "1937 Railway Locomotive and Powerhouse Fuel," Preliminary Analysis, Bituminous Coal Division Report, January 16, 1939.
2 University of Illinois, Bulletin No. 101, 1917.
3 "Railway Fuel," by E. McAuliffe, Simmons-Boardman Publishing Corporation, New York, N. Y., 1927. Quotation from E. N. Zern. p. 20.
4 "Locomotive Fuel," by W. L. Robinson, International Conference on Bituminous Coal, vol. 2, 1928, p. 366.
5 "Railway Fuel," by H. L. Woodrich, et al., International Conference on Bituminous Coal, vol. 2, 1931, p. 116.
6 Railway Fuel and Traveling Engineers' Association, Annual Proceedings, 1942–1943.
7 "Coal Preparation," by D. H. Davis, American Institute of Mining and Metallurgical Engineers, 1943, chapt. 8, p. 247.
8 "Coal Preparation Problems in the Illinois Field," by D. R. Mitchell, American Institute of Mining and Metallurgical Engineers, Technical Publication 362, 1930.
9 "Cleaning Bituminous Coal," by J. R. Campbell, American Institute of Mining and Metallurgical Engineers, Technical Publication 117, 1928.
10 M. A Tuttle, private communication.
11 "Coal Preparation," by T. Fraser and J. S. Johnson, American Institute of Mining and Metallurgical Engineers, 1943, "Screening," chapt. 5, p. 180.
12 U. S. Bureau of Mines, Bulletins Nos. 34 and 37, 1908 and 1911.

Discussion

E. D. Benton.[3] The value of coal as a locomotive fuel is dependent upon several factors, (1) size consist, (2) calorific value, (3) price per ton, (4) per cent of ash, (5) ash-softening temperature.

Which one of the foregoing factors belongs in No. 1 position depends on the limitations of the other four. The fact that a locomotive can burn almost anything that is black is legend. This, in turn, has worked to the disadvantage of the steam engine and in favor of the Diesel. The availability or distance which a locomotive can operate is governed in no small part by the fuel it consumes. If the coal is high in ash there is a definite mileage limit when it must either be taken out of service and another engine substituted or it must suffer lengthy terminal delays while its ashpan and fire are being cleaned. If the fusion characteristics of its ash tend to promote slagging of the tube sheet, the engine is limited in mileage and must be taken out of revenue service, its fire killed and the honeycomb removed. It is often possible to favorably alter slagging difficulties by the use of double-screened coal or limiting the amount of smaller sizes and extreme fines. However, double-screened coal, after passing through storage piles and the resulting multiple-handling, suffers considerably in size consist by the time it reaches the stoker conveyer screw.

Motive power is a tool and its value is measured by the amount of revenue-tons of freight or passenger-car-miles hauled. This sounds like a trite statement, but let us expand it a little further. In the case of coal traffic, the tonnage moved from the mines depends on the ability of the coal mine to produce and sell its product. In normal markets, production capacity is usually in excess of market demands, resulting in mines not producing because of "no bills" on certain sizes. If the railroads are able to step in

[3] Assistant Supervisor, Fuels Division, Battelle Memorial Institute, Columbus, Ohio. Mem. A.S.M.E.

during stress periods and purchase such sizes as to relieve the bottleneck of no bills, then the sizes in demand move to market and the locomotive produces revenue. By and large the railroads take advantage of the steam locomotive's ability to burn a wide variety of coal by purchasing coal sizes not readily marketable. Thus the steam engine as a tool may be evaluated in two ways. There are, of course, limiting circumstances which may alter the ability of any railroad in the purchase of certain sizes.

The number of hand-fired engines and coaling facilities are the principal reasons why mine run or resultant mine run are purchased in such large quantities. Many railroads are unable to separate coals from various producing districts or certain sizes for specific services. Undoubtedly all producing districts would like the top size decreased but appear to be unwilling to do anything about the bottom size. Skimming the cream off the top simply decreases the availability of steam engines, promotes increased maintenance costs due to cinder cutting, tube-sheet slagging, etc., because when the per cent of small-size coal increases, it in turn causes increased carry-over and finally results in an increase in pounds of coal per ton of freight or passenger-car mile. Whenever you increase cost and decrease availability you simply give the Diesel the "green light."

Because of the way railroad fuel must be purchased and the general policy of storing coal during times of slow market demand, individual coals lose their identity in storage piles and its size consist suffers. But if there are not excessive fines due to the top size being sufficiently large when the coal is received for storage, then the coal from storage to the engine tank will contain less fines in spite of the degradation in storage. One thing which is not changed in storage is the amount of impurities in the coal. It would seem to the writer, since ash is the principal "hurdle" which coal must overcome, that rapid attention be given cleaning plants. If coal had no ash there is considerable doubt whether the now competing fuels would be much of a factor. As the per cent of ash increases, more and more difficulty is encountered until, as a practical matter, one of the measures for the distance coal is able to move from the mine is its per cent of ash. If the coal industry could supply the railroads with coal of not over 8 per cent ash it would have a marked influence on increase in availability and decrease in cost of operation. Another thing which the coal industry might well undertake is the active research of an economical method of drying washed coal. Wet coal in cold weather is particularly troublesome and if the removal of surface moisture could be accomplished economically the coal industry would make an outstanding contribution, not only for the railroads but industry in general, and the coal indusdustry in particular.

E. C. Payne.[4] Mr. Hardy has made some good suggestions in his paper and the writer appreciates this opportunity to emphasize those recommendations which will improve the competitive position of the coal-fired steam locomotive.

It has been proposed that extensive tests should be made using different types and sizes of coal for optimum performance on various types of locomotives. In the writer's opinion such a program should be undertaken as soon as possible so that present locomotives will reach the ultimate in efficiency and reliability and the railroads may find it less attractive to consider other types of motive power. If it should develop that prepared sizes are superior to run-of-mine, it would require a gradual change in the distribution of bituminous coal. Mines without screens would be forced to make substantial investments for tipple improvements, but this would certainly be in keeping with the times, in order that a producer meet all types of competition with coals of similar character. Considering the standardization of sizes for locomotive fuel, it is quite probable that top and bottom sizes should be adjusted to compensate for differences in physical and performance characteristics of the coals from different seams and different mines. The test program should establish the proper size for best performance. The old policy of supplying the railroads with run-of-mine and surpluses of any screen size, as a matter of convenience to the producer, undoubtedly has been a contributing factor in the failure to get the best results from the steam locomotive. Even the most expert fireman cannot obtain the best results unless he is furnished a reasonably uniform quality and size with similar burning characteristics for day-to-day operation.

The statistics cited certainly show that the locomotive has been quite versatile in the utilization of practically every size of coal produced by the bituminous industry. This versatility has been accomplished undoubtedly with a substantial sacrifice in efficiency and reliability. The locomotive with all of its limitations of weight, combustion space, and variable performance conditions should not be required to use just any size or grade of coal. It would seem much more feasible to utilize the stationary power plant for wide-range size and quality-coal application instead of using the railroads for balancing the production at the mines. Industrial steam-generating equipment has wider utilization flexibility and there is a definite trend in new power-plant construction toward the use of an even greater range of coal size and quality. Naturally, any change in the distribution of sizes produced by the bituminous industry should be very gradual, but the coal industry should co-operate to the fullest extent in improving the coal-burning steam locomotive.

It would also seem desirable that the coal industry co-operate with the builders of the modern steam-fired locomotives, and the railroads, to give wide publicity to the superior performance results that are being obtained by the modern coal-fired engines. The public should realize that modern coal-fired engines are also pulling modern streamlined trains and that some railroads believe that comfort, reliability, and economy are obtainable with the modern "iron horse." The coal industry must take other active steps to preserve the competitive position of the steam locomotive, analyzing this railroad-fuel business on an over-all economic basis rather than expect any so-called interdependence of the railroads and the coal industry to perpetuate the use of bituminous coal.

Author's Closure

Mr. Benton has brought up a very good point in that railroad fuel loses its individuality after it leaves the mine, so that any change in standards would have to be made system-wide as far as the railroad is concerned, and industry-wide as far as the coal industry is concerned.

I believe that both Mr. Benton and Mr. Payne have made an important point in that all coal preparation should be better, and that more and more coal will have to be cleaned for railroad use. This of course does not get over the hurdle as to the difference in the quality of the coal in the various districts, and the fact that these coals are mixed indiscriminately and used interchangeably many times on the same trip by one locomotive.

Perhaps when and if the suggested series of tests are made, a standard of preparation for each type of coal will be evolved that will somewhat equalize the differences in quality and burning characteristics. Thus the quality of the coal might be standardized to some extent from a performance standpoint although the size actually used would vary widely as to the district and seam involved.

Let us again re-emphasize that the blind changing of standards without such a series of tests would prove nothing but would merely cause a tonnage dislocation without guaranteeing an improvement in performance.

[4] Consulting engineer, Consolidation Coal Company, New York, N. Y. Mem. A.S.M.E.

A Failure-Sequence Indicator for Static Test Specimens

By R. W. POWELL,[1] BURBANK, CALIF.

An instrument is described which has been used to determine the location of initial failure in static tensile-test specimens. Its particular usefulness in aircraft structural development is discussed and technical details of its operation are presented.

IN airframe design there are basically two major problems, the aerodynamic design, and the design of the structure. The structure must be strong enough to withstand the highest expected loading and still be as light as possible. It has been variously estimated that 1 lb of weight-saving in an airplane is worth from 10 to 600 dollars in additional pay-load capacity. Certainly weight is at a premium, and for this reason structural tolerances and factors of safety or ignorance must be small.

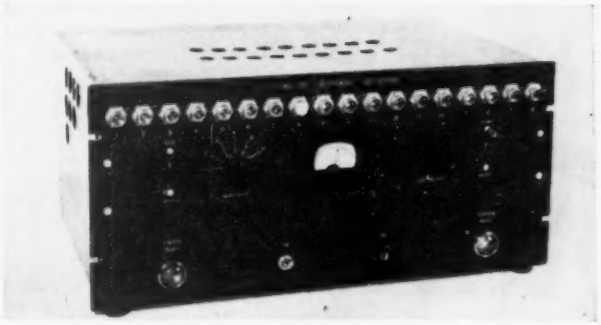
The usual aircraft structure is quite complex so that much of the data for stress analysis must come from empirical tests; and after an analysis has been made it is usually checked by additional tests.

For many years the aircraft industry has used strain gages of various types to obtain much of these data. However, strain gages are useful for measuring relatively small strains over a limited area only, and since the strain distribution in the structure under test is usually the least known factor, it is difficult to be sure that at least one of the strain gages is measuring the highest localized strain. Even if a strain gage is in the proper location and properly oriented, it may not give a good indication for extremely localized strain since a strain gage will average the strain over its active area. Of course, failure, when it occurs, is usually recognizable. However, even after failure, the location of initial failure is not definitely established because an initial failure of a weak section will usually cause progressive failure in adjacent stronger sections due to the resultant redistribution of the applied load.

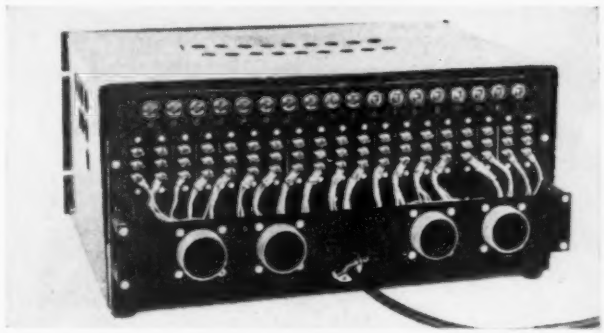
In compression tests the failure is usually in buckling, and in many cases it occurs slowly enough and with enough warning to be easily observed. However, in tension tests in which fracture or actual separation occurs, the failure often gives no warning and can progress, perhaps, at the speed of sound in the material.

For example, in a specimen of 24S-T dural, 3 ft wide, a failure initiated at one side may be complete in as little as 500 microseconds. It is highly desirable to locate the origin of such failures exactly. Ordinary techniques of obtaining data of this nature with the use of high-speed cameras or dynamic strain equipment are not very satisfactory because the interval in which the failure can occur may be from several minutes to several hours, and real difficulties involving film speed and length of film are encountered.

An ideal instrument for this type of measurement should start to record at the instant of initial failure (or slightly before), should be reasonably portable, should be simple to operate and install, and should have no effect on the strength of the structure. The device, Fig. 1, described in this paper incorporates most of these features.



Front View



Rear View

FIG. 1 FAILURE-SEQUENCE INDICATOR

THEORY OF OPERATION OF THE PICKUP

The pickup or activating elements of the instrument are composed of small copper wires which are cemented to the surface of the structure. It has been determined experimentally that such wires, when cemented to aluminum alloy, will fail in tension at almost the same time as the structure, Fig. 2, for example. This is true even if the wire is more ductile than the structure, because at failure the wire is constrained by the cement bond at both sides of the rupture, and consequently the strain in the wire is highly localized.

The wire must be small in diameter so that the cement bond will be strong in comparison to the wire. It must be large enough and of proper material so that its incremental elongation will exceed that of the structure. Number 40 annealed copper wire is suitable for incremental elongations up to about 50 per cent, Fig. 3. In practice No. 40 Formex insulated wires are cemented to the structure with Goodyear MN28C cement and are spaced usually not closer than 4 in.

THEORY OF OPERATION OF THE INSTRUMENT

There are several possible standard methods of recording sequence of failure of the wires but for the most part they are not suitable because of the indeterminate time of failure or because

[1] Research Engineer, Lockheed Aircraft Corporation.

Contributed by the Industrial Instruments and Regulators Division and presented at the Aviation War Conference, Los Angeles, Calif., June 11–14, 1945, of THE AMERICAN SOCIETY OF MECHANICAL ENGINEERS.

NOTE: Statements and opinions advanced in papers are to be understood as individual expressions of their authors and not those of the Society.

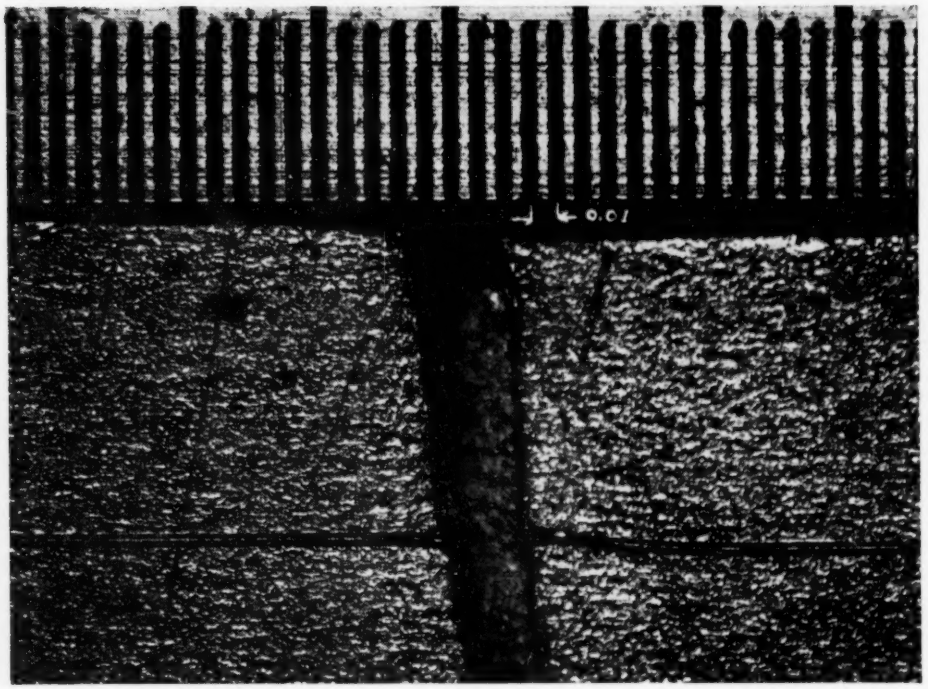


FIG. 2 TYPICAL FAILURE OF FAILURE-SEQUENCE WIRE WHEN CEMENTED TO 24S-T86

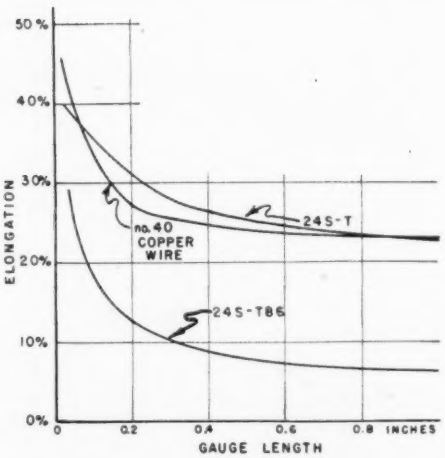


FIG. 3

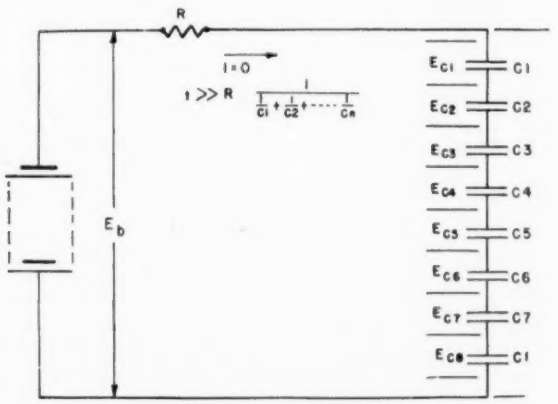


FIG. 4

of the short time involved during failure. The following method, however, has proved practicable:

Consider first several condensers which are connected in series with a battery and resistance, Fig. 4. The sum of the voltages on the condensers is equal to the battery voltage at any time after closure that is considerably greater than the time constant of the circuit. The voltage across each individual condenser is determined by its capacity, leakage, and initial state of charge.

If each condenser is short-circuited by a failure-sequence wire, Fig. 5, the charge on each condenser is zero until the first wire fails, Fig. 6. When this occurs the voltage across the first condenser is

$$E_{c1} = E_b\left(1 - e^{\frac{-t}{RC_1}}\right)$$

At the time of the second wire failure, t_1, it will have a voltage equal to

$$E_{c1} = E_b\left(1 - e^{\frac{-t_1}{RC_1}}\right) = E_1$$

After t_1 the circuit shown in Fig. 6 is modified by the addition of condenser C_2 as shown in Fig. 7. The charging rate of condenser C_1 is changed by the addition of the second condenser. After t_1 the expression for E_{c1} is

$$E_{c1} = E_b\frac{e^{\frac{-t_1}{RC_1}}C_2}{C_1 + C_2}\left[1 - e^{\frac{(t_1-t)(C_1+C_2)}{RC_1C_2}}\right] + E_1$$

At this same time the second condenser will begin to charge so that

$$E_{c2} = E_b\frac{e^{\frac{-t_1}{RC_1}}C_1}{C_1 + C_2}\left[1 - e^{\frac{(t_1-t)(C_1+C_2)}{RC_1C_2}}\right]$$

If the condensers are equal in capacity the expressions will be simplified to

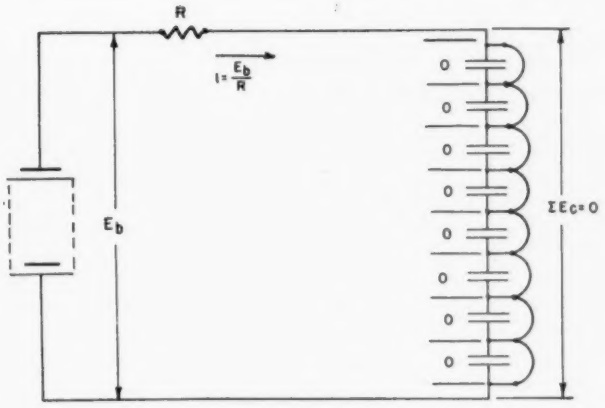


FIG. 5

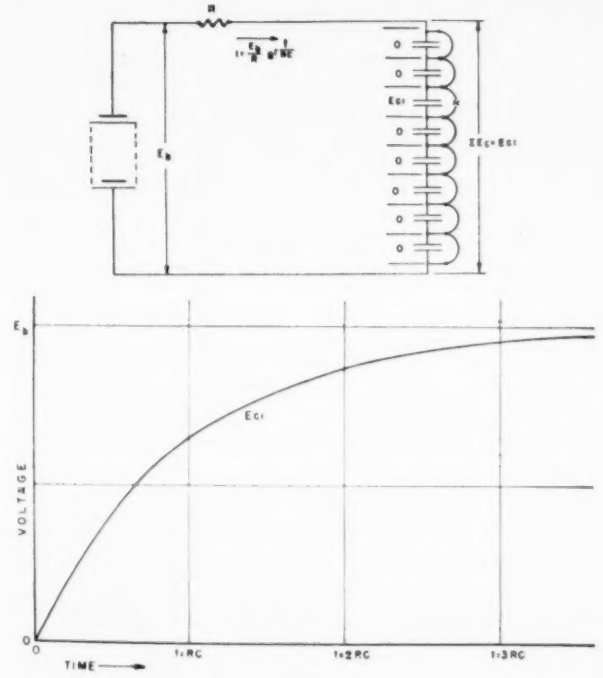


FIG. 6

$$E_{c1} = E_b \frac{e^{\frac{-t_1}{RC}}}{2}\left[1 - e^{\frac{2(t_1-t)}{RC}}\right] + E_1$$

$$E_{c2} = E_b \frac{e^{\frac{-t_1}{RC}}}{2}\left[1 - e^{\frac{2(t_1-t)}{RC}}\right]$$

The voltage on each condenser at t_2 when the third wire breaks is equal to

$$E_{c1} = E_b \frac{e^{\frac{-t_1}{RC}}}{2}\left[1 - e^{\frac{2(t_1-t_2)}{RC}}\right] + E_1 = E_2 + E_1$$

$$E_{c2} = E_2$$

and the equation of charge of each of the three condensers is now equal to

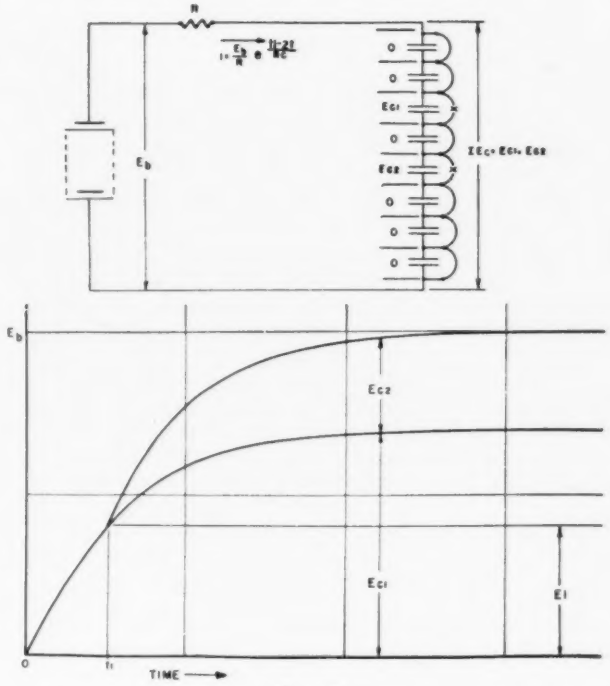


FIG. 7

$$E_{c1} = E_b \frac{e^{\frac{t_1-2t_2}{RC}}}{3}\left[1 - e^{\frac{3(t_2-t)}{RC}}\right] + E_2 + E_1$$

$$E_{c2} = E_b \frac{e^{\frac{t_1-2t_2}{RC}}}{3}\left[1 - e^{\frac{3(t_2-t)}{RC}}\right] + E_2$$

$$E_{c3} = E_b \frac{e^{\frac{t_1-2t_2}{RC}}}{3}\left[1 - e^{\frac{3(t_2-t)}{RC}}\right]$$

and so on (see Fig. 8). It is easy to see that if the condensers are of equal capacity the charge of any one is always greater than that on condensers starting to charge at a later time, and always less than that on condensers that started to charge at an earlier time, Fig. 9. If the leakage is small, the charge on each condenser may be measured after failure by a ballistic galvanometer or a vacuum-tube voltmeter, and the sequence of, and interval between, the failure zones determined.

Unfortunately, it is difficult to keep these leakages small if the condensers remain attached to the specimen and to the battery, Fig. 10. Therefore 10 milliseconds after the failure is complete, all circuits to the condensers are opened automatically so that the slight remaining leakage will merely decrease the charge, leaving the ratios of charge between the several condensers relatively unchanged. The condensers are carefully picked for low dielectric leakage and for uniformity of capacity.

Even with the foregoing precautions the time of recording data manually for a large number of sequence wires could allow excessive leakage. The instrument is therefore provided with an automatic stepping relay that scans the condensers and indicates first failure with a numbered light. Immediately following failure, the scanning relay automatically goes into operation connecting a vacuum-tube voltmeter, which does not discharge the condenser, to each condenser successively. If any condenser has a charge of 80 per cent or more of the applied voltage a relay is actuated, the scanning is stopped, and the corresponding light indicates the location of the first failure.

In case of initial simultaneous wire failures the switch will scan

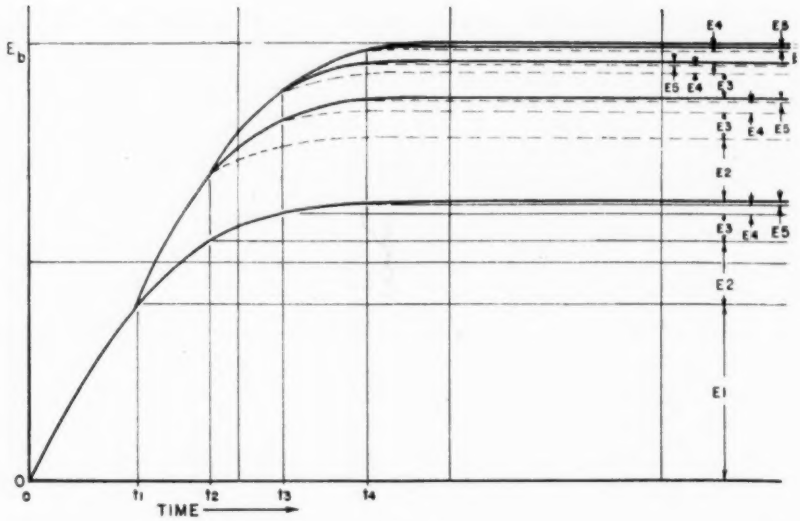


FIG. 8

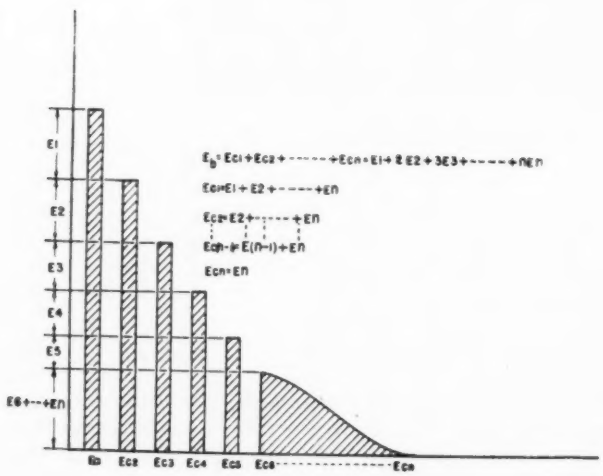


FIG. 9

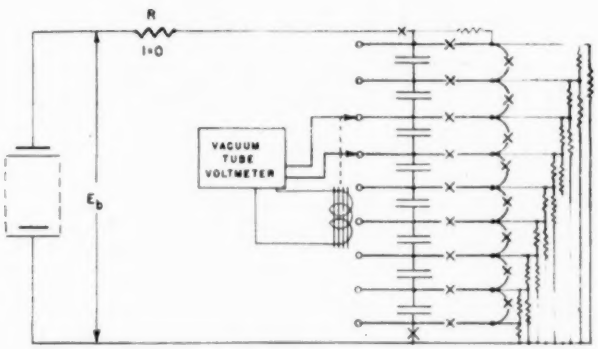


FIG. 10

through once and the operator may increase the voltmeter sensitivity until a stoppage of the scanning relay is effected. The number of the wire is indicated as before by the lights, and the charge on the condenser is indicated by the meter on the front panel. When these data have been recorded the operator may continue the scanning to another stoppage by pressing the "step" switch to restart and adjusting the sensitivity control.

As the instrument is currently used, any number of failure-sequence wires up to 18 may be attached (if necessary, it may be designed for any number of wires). It has an initial time constant of 500 microseconds, which means that a difference in time of failure of 20 microseconds of the first two wires may be detected, or that the second wire to fail may be determined if it occurs as much as 2 millisec after the initial failure. This time range may be changed to other values by changing the size of the resistor or the condensers.

CONCLUSION

The device has been used on static tests of aircraft structures involving 24S-T, 24S-T86, and plexiglas, and in each instance the data obtained were wholly consistent and apparently valid. In several cases structural redesign was based, in part, on the indications obtained by this method, and improved strength and joint efficiency were obtained.

Laminated Edge Attachment for Acrylics

By E. H. SNYDER,[1] BURBANK, CALIF.

As it had been observed that pressure loads encountered on such large acrylic parts as canopies, astrodomes, blisters, noses, windshields, and the like, caused frequent replacements, particularly at attachment points, it was determined that an improved method of attachment must be developed. In this paper is described an improved method of edge attachment for the canopy of the P-80 airplane in which aerodynamic and cockpit pressure loads have imposed higher loads than usual in the acrylic canopy material. In tests, laminated edging integrally attached to acrylic sheeting consistently approached and in certain cases developed the full strength of the cast acrylic sheeting.

Introduction

An examination of a number of service reports on large acrylic parts such as canopies, astrodomes, turrets, blisters, noses, and windshields revealed that replacements were comparatively frequent. Most replacements were necessitated due to crack formations originating at attachment points. The method of edge attachment assumed a role of increased importance with the introduction of high-performing aircraft such as the P-80 airplane. Aerodynamic and cockpit pressure loads encountered in the P-80 imposed still higher loads in the acrylic canopy material.

The present conventional method of attachment requires the drilling of a considerable number of holes along the edges of the canopy. These holes have to be large enough to permit the installation of rubber grommets and steel liners which serve to minimize the possibility of crack formation. A new and improved method of edge attachment was recently developed which consists of bonding integrally a laminate of relatively high strength to the canopy edges. Attachment can then be made directly through the laminated edge strips without the use of grommets and liners.

Until recently the manufacture of such a reinforced edge has not been practical. However, with the development of catalysts which promote rapid polymerization or solidification of the methyl-methacrylate liquid monomer in the presence of ultraviolet light, the bonding of edge strips to the canopy has become feasible.

Preliminary tests showed that this type of attachment was at least twice as strong as the conventional edge attachment. Thus a series of tests was instigated to develop a design and technique which was commercially applicable to regulation canopies. The final objective of this program was to apply the new attachment method to actual airplane parts such as canopies and windows and determine their strengths when tested under conditions encountered in the actual flight of the airplane.

Discussion of Laminating Resin

The acrylic sheeting used in present-day aircraft is made by casting methyl-methacrylate monomer (a water-white liquid) between two glass plates. The addition of a catalyst and the application of closely controlled heat cause the monomer to polymerize or cure into a solid state. Polymerization is accompanied by an exothermic reaction, which, if not properly regulated, would cause the rate of polymerization to progress beyond control and result in the formation of bubbles or perhaps violent boiling of the monomer. This is reviewed in order to point out that polymerization must proceed at a rather slow rate. Several days or a week, depending upon the thickness, are necessary for the curing of the usual cast sheet.

When attention was first directed toward a laminated edging for acrylics, it was conceivable that layers of cloth could be cast integrally around the edges of a cast acrylic sheet. This, however, was beyond the scope of the average aircraft plastics laboratory. It was hoped that a quicker and more practical method could be developed to attach integrally a laminated edging to methyl-methacrylate sheeting.

A light-sensitive catalyst,[2] which caused strips of cloth, impregnated with prepared acrylic monomer to "jell" in 5 to 10 min. and cure into a hard mass in approximately 1 hr of exposure to sunlight, appeared to be the solution to the laminated edge attachment.

Methyl-methacrylate monomer is waterlike in consistency. To make it more suitable for laminating operations, it was thickened or bodied so that it would not run off the laminated or bonded item before the polymerization or solidification reaction was complete. The monomer was bodied or partially polymerized by adding a very small amount (0.2 per cent by weight) of the light-sensitive catalyst and refluxing until the suitable viscosity was attained. Care was exercised in determining the amount of catalyst necessary so that none in excess of the specified amount would be added. Too much catalyst would cause the exothermic reaction which occurs during refluxing to proceed so rapidly that uncontrollable boiling results in complete polymerization. When this bodied resin cooled to room temperature, an additional 3 per cent by weight of the catalyst was added to make it ready for application. In this condition it must be used within a few hours or stored in a refrigerator to prevent complete solidification or polymerization.

Fabrication of Joint Specimens

The test specimens used to determine the strength of the various types of edge attachments were made from $^{5}/_{16}$-in-thick acrylic sheet stock $4^{1}/_{2}$ in. long and 3 in. wide. The thickness and width were thus chosen to approximate 1 sq in. of cross section. The laminates used for the edges of the new type joints consisted of Fiberglas or other fabrics laminated with the same resin that is used for making the actual blown canopy.

Type I—External V-Joint. Some of the first acrylic tension specimens, containing an external "V" on the ends (see Fig. 1) were prepared "wet;" that is, laminae of glass cloth which had just been dipped in the acrylic resin were laid symmetrically on either side of the scarfed ends and the whole assembly sandwiched between cellophane-covered glass plates. After exposure to sunlight for approximately 1 hr, the resin polymerized or cured, and the specimen was then ready for trimming and mounting. It has been found that the time necessary for curing can be substantially reduced by using a good strong source of ultraviolet light instead of natural sunlight.

Since cut Fiberglas cloth tends to fray and become unwoven at the ends, it was practically impossible to keep a few loose glass

[1] Research Engineer, Lockheed Aircraft Corporation.

Presented at the Rubber and Plastics Session of the Aviation Division Meeting, Los Angeles, Calif., June 3–5, 1946, of The American Society of Mechanical Engineers.

Note: Statements and opinions advanced in papers are to be understood as individual expressions of their authors and not those of the Society.

[2] Manufactured by C. C. Sachs, No. Hollywood, Calif.

threads from floating out upon the clear portion of the specimen and being cured in place.

To avoid the problem of these loose Fiberglas threads and also the undesirable handling of the wet laminae in the final preparation of specimens, laminates were cured into flat sheets in the following manner:

Each piece of fabric (about 23 in. square) was dipped into a pan of the prepared resin and laid in place on a 2-ft-sq piece of cellophane-covered tempered glass plate. As each piece was stacked on the glass plate the trapped air bubbles were worked out with a suitable squeegee. When all layers were in place, micarta strips $^1/_2$ in. wide and of proper thickness were nested around all four edges to serve as spacers and also to prevent too much resin from escaping. A second 2-ft-sq piece of cellophane-covered tempered glass plate was then placed over the stack of impregnated fabric and clamped in place with a number of standard C-clamps. After curing, the laminate was machined into strips for bonding to the acrylic-specimen edges. These flat laminated sheets were made in thicknesses equal to one half that of the acrylic component in order to facilitate beveling of the edges of strips which were machined from the flat sheets. Figs. 1 and 2 illustrate how the beveled strips were placed together to form a mating "V." The successful rapid machining of these strips was accomplished by using cutting tools with cemented-carbide tips. The prepared resin was placed on all mating surfaces and the strips cured in place by exposing the assembly to sunlight.

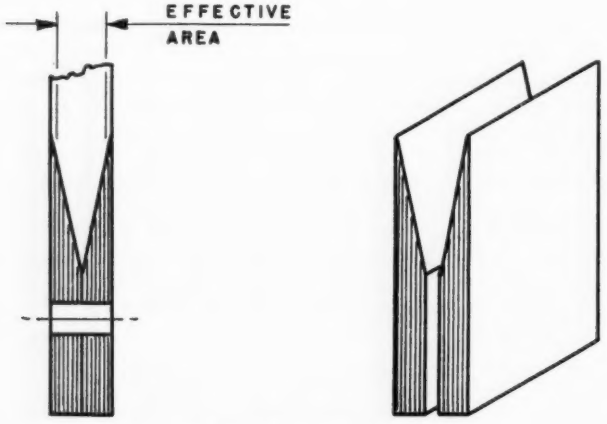


FIG. 1 EXTERNAL V-JOINT

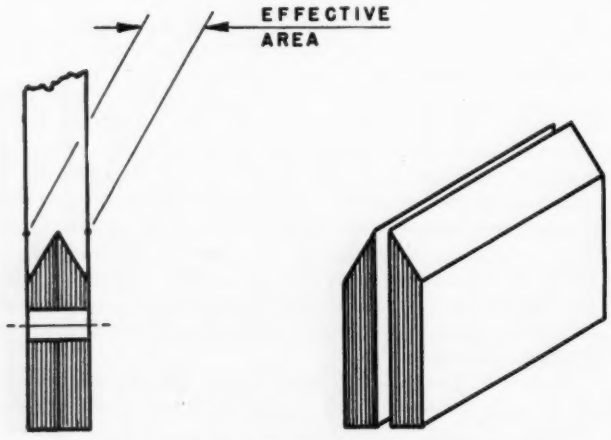


FIG. 2 INTERNAL V-JOINT

Tests made on this type of attachment showed that it had a strength equivalent to that made with individual wet laminae but it, too, had some distinct disadvantages: (1) Due to the shrinkage problem which is difficult to handle and because of the fact that resin cast in this manner has a lower strength than the original acrylic sheet, the scarf of the edge strips had to be of a length which would allow a transition gradual enough to produce an attachment of optimum strength. The length of scarf necessary caused the opaque laminated edge to extend about $^1/_2$ in. above the usual canopy mount, thus decreasing visibility. (2) Any excess resin which was present tended to be forced over the clear adjacent surface. This necessitated laborious polishing to restore the original optical qualities.

Type II—Internal V-Joint. This type of joint was also made by bonding the cured laminated strips to the prepared acrylic edge, but in this case the scarfed edges of the laminate were fitted into an internal "V" in the acrylic edge (see Fig. 2). Tests made on this type of specimen showed that it was stronger than an equivalent external type of joint; and that an internal "V" $^1/_4$ in. deep was as strong as any $^3/_4$ in. external V-joint. In addition, the disadvantages of the external type of joint were eliminated, because it was now possible to keep the opaque edge flush with the canopy mount, and any excess resin present when the edge strips were bonded in place was forced over the opaque laminate instead of the clear adjacent acrylic sheet.

Figs. 1 and 2 illustrate both types of joints and clearly indicate the advantages of the internal type of attachment.

RESULTS OF TESTS

Tension Tests. As a result of stress concentrations, the efficiency of edge attachments in direct tension vary from 30 per cent (for bolted attachments, using rubber grommets and steel liners) to approximately 85 per cent for laminated edge attachments. In terms of average stress at failure, the conventional bolted attachment developed approximately 2500 psi and the laminated edge attachments ranged as high as 6500 psi.

Bearing Tests. Since the specimens containing the laminated Fiberglas edges were failing outside of the actual joint and causing no appreciable elongation of the attachment holes, it was decided that a laminate containing all laminae of Fiberglas was too strong. It was hoped that a laminate of cotton or linen cloth would solve the problem and eliminate the undesirable machining qualities of laminated Fiberglas, but the linen and cotton cloth-filled laminates failed in tension before there was any evidence of bearing failure. A number of laminated bearing specimens were thus fabricated using a combination of cotton cloth and Fiberglas cloth. Elongation of the attaching holes was thereby controlled by substituting cotton cloth for certain Fiberglas laminae.

Fatigue Tests. Test specimens of the conventional rubber grommet-and-liner type and those containing the internal V-type laminated edges were made identical to those used for tension tests. These were tested dynamically at various loadings and frequencies until failure occurred. The fatigue life of the laminated attachment was found to be over 1000 times that of the bolted type.

APPLICATIONS OF THE LAMINATED EDGE ATTACHMENT

(*a*) *Aircraft Canopies.* From the promising results obtained from the small test specimens it was decided to prepare a full-size canopy of the type used on the P-80 airplane with the new type of edge attachment and tested under simulated flight conditions.

The P-80 canopy is of the one-piece "bubble" type, which lends itself to "free-blowing" or vacuum-forming. In this process of forming, a heat-softened acrylic sheet is clamped to a vacuum pot and free-drawn to a controlled depth. The shape of the

vacuum-pot opening gives the general outline required for the canopy edge. After forming is completed the enclosure is finish-trimmed for mounting.

The P-80 production canopy is fabricated from $^{3}/_{8}$-in-thick acrylic sheet. However, the new canopy which was to contain the laminated edging was formed from a $^{5}/_{16}$-in-thick acrylic sheet.

Following is a step-by-step description of the detailed operations required in the preparation of the laminated strips and their subsequent attachment to the canopy edges:

1 Preparation of laminates: As a result of the bearing tests made on various types of laminates, a combination muslin-and-Fiberglas cloth laminate was chosen, which would show an incipient bearing failure in the attaching holes at a load slightly below the average breaking load of the acrylic specimens. This would allow a more uniform distribution of the loads.

The laminated-edge-strip material, which was considered as the optimum for this type of attachment, consisted of two layers of coarse-woven muslin with a layer of ECC-11-148 Fiberglas cloth on each outer surface. These laminates were made in the same manner as previously described, and their nominal thickness was chosen as $^{1}/_{64}$ in. less than $^{1}/_{2}$ of the minimum thickness of the canopy edge, in order to make it possible to produce a completed edge strip with surfaces flush with the canopy surfaces. The laminated panels were cut into strips $1^{1}/_{8}$ in. wide and then beveled on one edge to mate with the canopy edge and also on each end to mate with adjoining strips.

It has been found that the variation in thickness of commercial canopies was as much as 0.100 in. due to manufacturing tolerances; in addition, the thickness variation may further be increased by the canopy drawing or stretching operation. However, by placing a strip of wet uncured resin-impregnated fabric between two cured laminated strips, it was possible to compensate for any variation in thickness normally found.

2 Preparation of canopy edges: The edges of the special blown acrylic canopy were first trimmed shorter than a conventional canopy to allow for the addition of the laminated edge. The edges then were machined to form an internal "V," since the internal V-joint had proved to be superior from the standpoint of strength and ease of fabrication. The internal "V" was machined quite readily by the use of a portable hand router and a special bit.

Transparent contoured fixture strips, which were necessary to hold the laminated edging to the canopy and at the same time permit light to reach the joint to effect curing, were obtained by sawing off the edges of scrap production canopies. These contoured strips were then clamped on either side of the canopy edges so that they extended approximately $1^{1}/_{2}$ in. beyond the machined edges of the canopy. They served their purpose effectively for the forming of the laminated strips and also as transparent fixtures for holding the formed laminated strips in place during the curing cycle.

3 Forming of laminated edge strips: The prepared laminated strips were formed to mate with the ever-changing contour of the canopy edges. Since the resin used to make the laminates was a "thermoplastic" (softens under heat and hardens when cooled), it was only necessary to heat the strips for several minutes in an oven at 300 F and then hold them in place in the grooved canopy edges until they cooled. This was facilitated by the transparent fixtures (edges from scrap canopies) clamped to the prepared canopy edges. The hot pliable laminated strips were forced down onto the machined edges of the canopy and clamped to the overhanging transparent fixture strips until they cooled enough to retain their new contour.

4 Curing of preformed laminates to canopy: The next step in the fabrication of the edge attachment was to sandwich a wet resin-impregnated Fiberglas lamina between two cured formed laminated strips to build up the thickness of these edge strips to equal that of the canopy edge. Excess resin from the wet laminae flowed into any spaces created by the varying edge thickness of the canopy and was thus cast and cured into place around the canopy edges to form a smooth, clear, and continuous transition from the opaque laminated edge to the clear acrylic canopy material.

To simplify tooling, the attaching operation was accomplished in two steps. In the first step the cellophane-covered transparent fixture strips were clamped only to the inside edges of the canopy. The chamfered edges of the inboard cured laminated strips were "doped" with resin, forced into contact with the canopy edges, and clamped in position to the fixture strips for curing. The second curing step was taken after removal of the inboard transparent fixture strips. The wet impregnated Fiberglas lamina was then placed on the previously attached inboard laminated strip. Next, the chamfered edges of the outboard cured laminates were doped with resin and carefully placed in their correct position on top of the wet lamina. The cellophane-covered outboard transparent fixture strips were then placed on top of this assembly and clamped in place to the canopy. As a final operation to assure correct positioning, the outboard cured laminates were forced into intimate contact with the machined edges of the canopy before finally clamping in place to the outboard fixture strips for curing.

The canopy described, having the laminated edging, was subjected to pressurization tests along with production canopies containing the rubber grommet-and-metal liner type of attachment. The laminated-edge-type canopy, blown from $^{5}/_{16}$-in-thick acrylic material, withstood pressurization loads 25 per cent greater than those which produced failure in the $^{3}/_{8}$-in-thick production canopies. This $^{5}/_{16}$-in-thick canopy, containing the laminated edging, was not tested to destruction, but was saved for possible investigation of other variables.

This canopy was actually one of three fabricated with the laminated edging for testing purposes.

The first one, formed from $^{5}/_{16}$-in-thick acrylic sheeting, failed prematurely at a load higher than that withstood by any previous production canopy, when part of the mounting structure failed.

After reinforcement of the mounting structure, the second $^{5}/_{16}$-in-thick canopy was tested as previously described and then saved for possible future investigations.

The last and third canopy was formed from $^{1}/_{4}$-in-thick acrylic sheeting. Considerable speculation awaited the test results of this particular canopy. Unfortunately, however, it was cracked during installation, so further testing was discontinued.

5 Fabrication of canopy from a flat developed pattern: Near the end of the war an ingenious method was developed by a West Coast plastics fabricator[3] for the free-blowing of aircraft canopies from a flat developed pattern. This method consisted of machining a sheet of acrylic to the exact flat developed pattern of the canopy. After heating the flat blank in a specially constructed oven, it was carefully laid on a blowing jig and securely clamped around all edges to effect a perfect seal against air leaks before the blowing operation was started. Positive air pressure was used rather than pulling a vacuum. This enabled the operator to check the part during the blowing process and control the air pressure throughout the operation.

The canopy for North American's P-51 "Mustang" fighter plane was "free-blown" from a flat developed pattern using this method. With North American's permission a P-51 canopy was secured by Lockheed in the flat pattern, and Lockheed's laminated edge attachment was cured to the edges of this pattern.

[3] Stacks Plastics, Culver City, Calif.

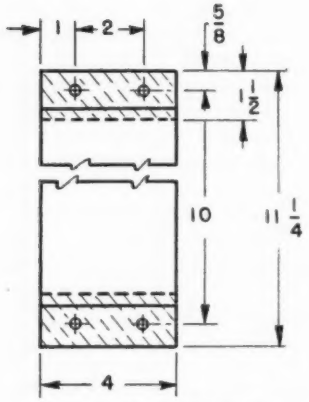


FIG. 3 CREEP SPECIMEN

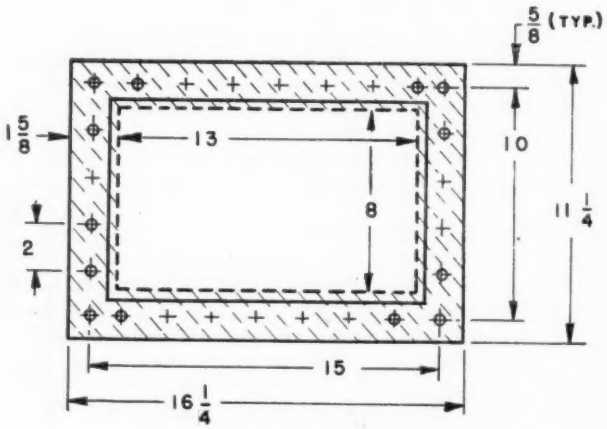


FIG. 4 SHEAR SPECIMEN

Since the curing of the laminated edge strips to a flat sheet obviously entails less difficulty than curing strips of compound curvature to canopy edges of compound curvature, it was desired to determine whether or not the addition of the laminated edging to the flat pattern would alter the forming characteristics of this particular free-blowing method.

No difficulties were encountered in the final operation of blowing this flat developed pattern into a finished canopy with laminated edges.

The hand methods used in fabricating the special laminates and their subsequent attachment to the canopy edges were necessarily laborious. However, when production methods are considered, it is apparent that certain operations could be eliminated or greatly simplified. The method of blowing canopies from a flat developed pattern would further facilitate production if applied to the laminated-edge-type canopy.

(*b*) *Acrylic Panels.* Since joints of 85 per cent efficiency were consistently being produced of laminated strips to acrylic sheeting and developing stresses as high as 6500 psi, the possibility of using stressed acrylic panels was given consideration.

One of the characteristics desired to be known about an acrylic panel, which incorporated a laminated edge attachment, was its behavior when subjected to shear loads both at normal and extreme temperature ranges.

1 Shear tests. The method used in fabricating the shear test specimens was essentially the same as that used for fabricating the canopy laminated edge attachment. Three test specimens were made from $^3/_8$-in-thick acrylic sheeting according to Fig. 4. These panels were mounted in a steel shear frame having pin-connected corners, and the assembly was attached to a rigid floor structure. The shear loads were applied to the panel frame by means of hydraulic jacks and transferred to the plastic panel through the $^1/_4$-in-diameter attaching bolts. Total shear deflections were measured by means of a dial gage. A temperature-controlled enclosure was built around the test panel so that various temperatures could be accurately maintained.

The first panel was loaded at a temperature of 65 F in increments of 50 lb per in. (see Fig. 5). The application, removal, and reversal of shear load was repeated for 1000 cycles at 150 lb per in.; 1000 cycles at 300 lb per in.; and 3000 cycles at 500 lb per in. This repetition of loading showed no change in the shear deflection noted at the beginning of each cycling test. A maximum static load of 850 lb per in. was applied at room temperature without any serious permanent effects.

When the foregoing tests were completed the temperature was lowered to —55 F, and a load of 300 lb per in. was applied and maintained for 2 hr. Upon removal of all load there was no indication of permanent set. The load was then gradually increased to a maximum value of 650 lb per in., whereupon the specimen suddenly shattered.

The second panel was installed and the temperature lowered to —40 F. Loading was applied in small increments, and again when the value of 650 lb per in. was reached, the panel suddenly shattered.

The third and last panel was tested at 130 F. Loading was applied in 50-lb-per-in. increments until a load of 600 lb per in. was attained. Failure occurred approximately 90 sec after application of the 600-lb-per-in. load.

The amount of deflection at various temperatures is compared in Table 1.

2 Tension creep tests. The purpose of these tests was to determine the behavior of an acrylic panel incorporating laminated Fiberglas edges under prolonged tensile loading at various temperatures.

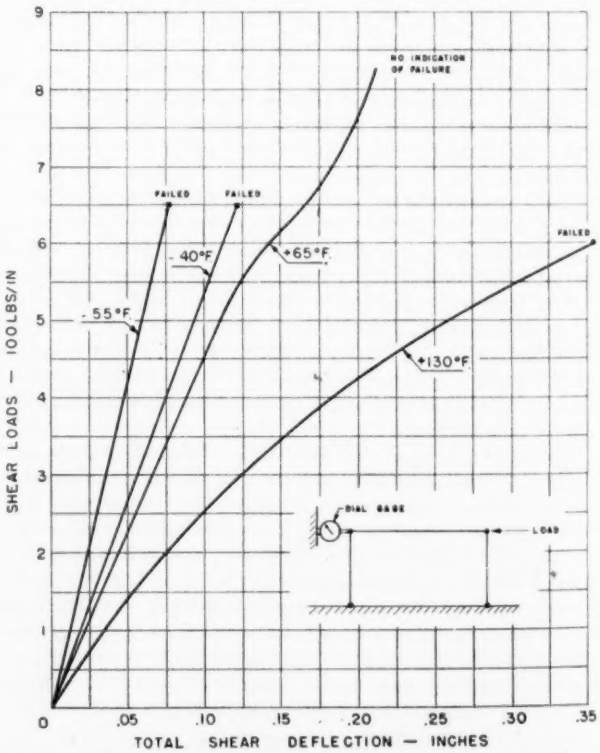


FIG. 5 SHEAR LOAD VERSUS DEFLECTION FOR LAMINATED EDGE-ACRYLIC PANEL

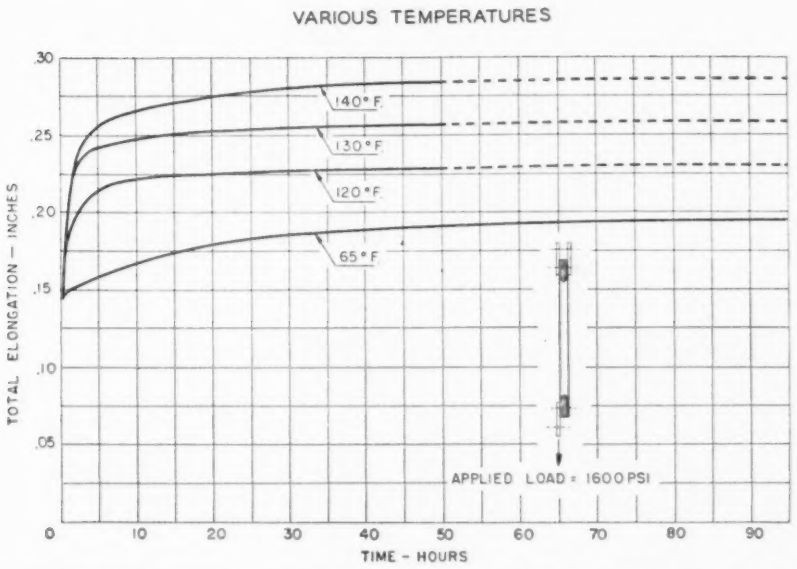


FIG. 6 ACRYLIC CREEP TESTS: ELONGATION VERSUS TIME AT VARIOUS TEMPERATURES

TABLE 1 DEFLECTION OF TEST PANEL AT VARIOUS TEMPERATURES

Temperature, deg F	Shear load, lb per in.	Total deflection, in.
— 40	650	0.120
70	650	0.155
130	600	0.354

Test specimens were made from $^{3}/_{8}$-in-thick sheet stock with the Fiberglas edge attachment at each end, as shown in Fig. 3.

Specimens were suspended in a controlled-temperature enclosure by means of a double-shear-type fitting. At the lower end, arrangement was made for applying 2400 lb (600 lb per in.) through a single shear-type fitting, so that there was an eccentricity of $^{9}/_{32}$ in. between the suspension and the applied load. Two dial gages, calibrated in thousandths of an inch, were installed, one on either side of the specimen, to indicate the total elongation in the 10-in. gage length. Time versus elongation curves for different temperatures are presented in Fig. 6.

The tests indicated that when the load was first applied the rate of creep was high, but that it decreased rapidly over the first several hours.

Creep effect is greatly influenced by temperature, as may be seen by referring to Fig. 6. Considering 10 hr as a reasonable period for "long-duration" loading, it is apparent that under 600-lb-per-in. load and at room temperature, the observed creep constituted only an additional 12 per cent above the elastic (instantaneous) elongation, while at 140 F the deformation would almost double itself. Under this load and at any temperature up to 140 F, 10 hr appears to be sufficient time for a reasonable stabilization of the elongation.

At the conclusion of the tests no permanent elongation of the holes in the Fiberglas-reinforced edge was apparent. It is improbable that any appreciable amount of the observed creep effect occurred in the laminated edges.

SUMMARY

In summarizing, it is pointed out that a laminated edging integrally attached to acrylic sheeting consistently approached and in certain cases developed the full strength of the cast acrylic sheeting.

Where further reduction in load concentrations is necessary at attachment points, various combinations of filler material may be used in the laminated edging to produce controlled bearing failure in the attaching holes.

Rotational Drop-Testing of Airplane Main Landing Gear

By W. H. GAYMAN,[1] BURBANK, CALIF.

The immediate physical objectives of drop-testing are presented, together with a general method for conducting rotational tests that have proper contact velocity and energy relationships coincidental with the absence of undesirable dynamic reactions at the pivot axis. Application of the method to tests of the main landing gear of the Models PV-1 and PV-2 patrol bombers is discussed. Conclusions drawn from dynamic-load measurements emphasize the possibility of attaining excessive loads in the drag-resisting structure when the impact surface is horizontal and the gear is inclined to simulate resultant loading of any particular design condition. It is implied that the practice of dropping the test gear on an inclined platform during translational drop tests may result in unconservative loading unless deliberate compensation is afforded.

Introduction

DROP-TESTING of a newly designed airplane landing gear is commonly included in the structural-test program carried out with a static-test airplane. These tests have as their immediate purpose the demonstration of the degree of compliance with design specifications regarding, fundamentally, the energy-absorption characteristics and related dynamic behavior of the landing gear. While the tests are generally preceded by landing-gear-jig drop-tests, conducted incident to developing or checking the shock-strut design, their specific objectives are the determination of landing-gear functional characteristics with effects of airframe elasticity included, and the checking of the structural integrity of the gear and its supporting members. The latter consideration is in general complementary to other required structural tests.

In the case of an airplane with conventional landing gear, it has been customary to conduct rotational drop-tests independently for both tail gear and main gear. In tests of the former, the airplane is usually permitted to "rotate about the main gear axles" as the tail is raised and dropped. In tests of the main gear, the tail-wheel axle or some other convenient item is utilized as the pivot axis.

The author has failed to discover any literature justifying the basic concept of rotational drop-testing of main landing gear as commonly executed; he presumes that its acceptance has been due to its advantages over translational drop-testing of the entire airplane because of its inherent freedom from additional test variables arising from the following:

1 The problem of assuring simultaneous or at least reproducible contact conditions of main wheels and tail wheel.

2 Interactions of main landing gear and tail landing gear attributable to airplane-pitching accelerations due to different stiffness rates and strokes of the two basic types of landing chassis.

This is not to imply that translational drop tests are conducted infrequently; the advent of tricycle landing gear has given impetus to development of this technique.

However, it is not the purpose of this paper to present a discussion of methods other than rotational drop-testing, or of the philosophy of drop-testing in general. Rather, the intent is to present, from a test engineer's point of view, a discussion of methods that have been under development since the beginning of a program for drop-testing the PV-1 patrol bomber.

1 General Dynamic Considerations

Drop-Test Problems

There appear to be no standard interpretations of drop-test criteria as they reflect on the major aspects of the physical problem. Consequently, the test engineer must formulate his own interpretations from the pertinent general specifications, or perhaps depart from the letter of the specifications in order to rationalize some of the apparent physical incompatibilities. For example, while the drop-test specifications of various agencies are specific enough in defining "drop-height" and "load-factor" requirements for landing gear of various types of aircraft, in general they either leave too much latitude in the test-airplane weight distribution or impose limitations that have no fundamentally rational basis. In the manner of support of the test airplane at its pivot attachment, a specification may impose restrictions, which, if rigidly adhered to, can unwittingly cause local failure of the aft fuselage section in the attempt to obtain tests of the main landing gear, or conversely, failure of the main landing gear or its supporting structure in rotational drop tests of the tail gear.

That instances of such failures exist is a matter of record. In some cases a "too literal" interpretation of the pertinent specification may have been the cause; in other cases lack of precedent, combined with insufficient appreciation of the dynamic aspects of the problem may have been a factor. In any case, however, possible danger to test personnel as well as direct and indirect costs occasioned by such accidents have warranted the direction of efforts to evolve a practical rotational drop-test technique that satisfies all of the basic requirements. Because of the length that would be required to cover specific problems arising in rotational drop-tests of auxiliary gear, the present discussion is necessarily limited to rotational drop-testing of main gear, although the basic dynamical approach is applicable to either.

Rotational drop-testing is simply a convenient means of obtaining landing-gear performance characteristics. Because of the variation of linear acceleration with distance from the center of rotation, this type of test is not intended to constitute a structural test of the entire airplane, but rather is limited to a relatively localized region embracing the test gear.

Test Setup Parameters

In order to impart a maximum of physical meaning to the interpretation of the test results it is important that the test setup

---

[1] Formerly, Research Engineer, Lockheed Aircraft Corporation.

Presented at the Aviation Division Meeting, Los Angeles, Calif., June 3–5, 1946, of THE AMERICAN SOCIETY OF MECHANICAL ENGINEERS.

NOTE: Statements and opinions advanced in papers are to be understood as individual expressions of their authors and not those of the Society.

parameters be consistent with the basic design conditions. Hence for a given test:

(*a*) The magnitude of the static reaction on the test gear should be the same as that established by the design condition. (A value based upon an "equivalent-mass" analysis may be used where applicable.)

(*b*) The wheel contact velocity for a given free-drop height, as measured at the axle (or bottom of the tire), should be the same as that to be obtained in a hypothetical translational drop from the same drop height.

(*c*) The energy to be absorbed by the test gear, resulting from a drop from a given height, as measured at the axle, should be the same as that part of the airplane's total potential energy that would be absorbed by the test gear in a purely translational drop-test from the same drop-height, effects of interactions of main gear and auxiliary gear being discounted.

(*d*) The direction of the impact load on the gear, relative to the shock-strut axis, should be the same as that established by the particular design condition.

Requirement (*c*), as presented here, is really repetitive since ideally the satisfaction of conditions (*a*) and (*b*) automatically fulfills (*c*).

In addition to the attainment of these basic objectives, the test engineer has a few of his own requirements to meet, the foremost, aside from safety for test personnel, being that he avoid structural damage to the test airplane resulting from dynamic loading at the pivot point.

An analytical evaluation of the degree to which all of these criteria may be satisfied may be made by consideration of the dynamics of the compound pendulum.

Consider the case of the rigid pendulum subjected to constrained rotation, Fig. 1. If the pendulum has its motion arrested suddenly by a stop, the nature of the instantaneous loading at the pivot point is dependent upon the following factors:

(*a*) The instantaneous value of the angular velocity.

(*b*) The magnitude of the force exerted by the stop.

(*c*) The direction of the stop force relative to the line containing the center of percussion, the center of gravity, and the center of rotation.

(*d*) The displacement of the line of action of the stop force from the center of percussion of the pendulum.

If the line of action of the stop forces passes through the center of percussion, the tangential component produces no reaction at the pivot axis. However, the radial component adds algebraically to the simultaneous value of centrifugal force.

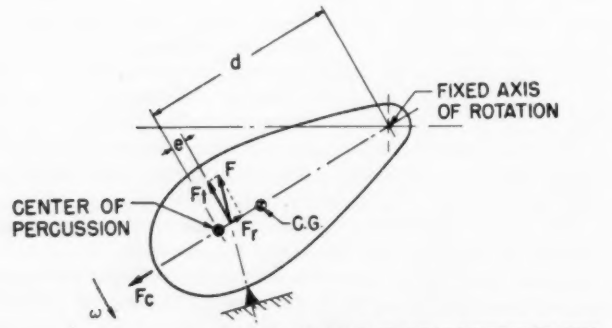


FIG. 1 "FIXED ROTATIONAL" COMPOUND PENDULUM

If, in the case of a semielastic body, the motion is arrested by a sprung stop, the natural frequency of which is very low compared with the natural axial and flexural frequencies of the body, the behavior of the system is quite comparable with that of the inelastic pendulum.

The rigid-body type of analysis applied to a rotational drop-test setup indicates the nature of the problem of avoiding undesirable loading at a fixed pivot point. Consider a case for tests of main landing gear. If the airplane wheels are dropped on a well-greased horizontal surface, it is generally assumed that the landing reactions act vertically. This being granted, it becomes necessary to orient the pitching attitude of the airplane so that requirement (*d*) noted previously is fulfilled, that is, so that the direction of the shock-strut axis relative to the impact load conforms with the design condition.

This factor precludes the probability of avoiding substantial loads at the fixed-pivot axis even if the test airplane's weight is distributed so that the center of percussion is directly over the line of contact of the main-gear wheels. With the airplane in attitudes intended to simulate either "level-landing" or "three-point-landing" conditions, it is not possible to distribute the required mass so that the line containing the center of percussion and the fixed axis of rotation is normal to the landing reactions.

In the case of the Model PV-1, a 26,500-lb normal-gross weight airplane, calculations for drop tests in three-point attitude, with the center of percussion over the main-gear axles and the tail-gear axle a fixed center of rotation, indicate that allowable impact loads on the main gear could produce a tail-gear drag-load component in excess of 24,000 lb. An estimated value of angular velocity at the instant of peak impact load indicates an additional 3000-lb component, due to centrifugal force, giving instantaneously a magnitude of total drag load on the tail gear greater than that of the airplane gross weight.

In order to avoid the imposition of large dynamic loads at the pivot point, it has sometimes been a practice to provide elastic restraint of the pivot by use of shock cord. This technique may well prevent damage to the airplane structure but still may result in violation of requirements (*b*) and (*c*) relative to contact velocity and energy absorption, depending upon the degree of restraint afforded.

The ideal anchorage for the airplane in rotational drop tests is one whereby the axis of rotation may be placed on a horizontal line through the airplane center of gravity (cg).

The "free rotational" compound pendulum represents a system of this type, Fig. 2. If the pivot axis is allowed to move freely in frictionless horizontal guides that offer complete vertical restraint, no horizontal forces can be applied to the body during its free fall, and the center of gravity will drop vertically. During this period the only force existing at the pendulum support is that required to produce angular acceleration of the body about the instantaneous center of rotation, which falls with a vertical velocity the same as that of the center of gravity. Thus the line containing the instantaneous center of percussion (icp) and the instantaneous center of rotation passes horizontally through the center of gravity. If the instantaneous center of percussion is located directly over the stop, the stop force produces no impact at the moving pivot axis.

EQUILIBRIUM EQUATIONS

Several useful and interesting relationships may be obtained from the equilibrium equations of this system during its free-fall period. By referring to Fig. 2 it may be seen that the position, velocity, and acceleration of the center of gravity (cg) relative to the reference axes are described by

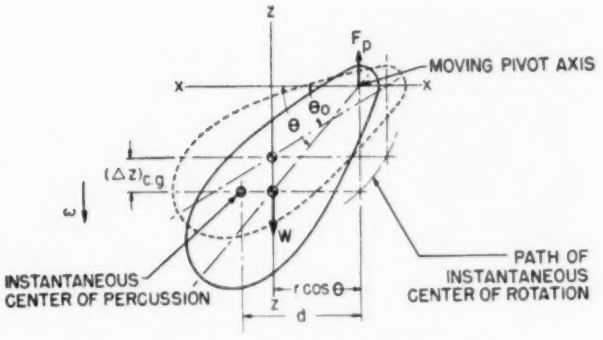


FIG. 2 "FREE ROTATIONAL" COMPOUND PENDULUM

$$(z)_{cg} = r \sin \theta \quad [1a]$$

$$(v_z)_{cg} = r\omega \cos \theta \quad [1b]$$

$$(a_z)_{cg} = r\alpha \cos \theta - r\omega^2 \sin \theta \quad [1c]$$

For translational equilibrium

$$\left(\frac{W}{g}\right)(a_z)_{cg} = W - F_p \quad [2]$$

For rotational equilibrium

$$\left(\frac{W\rho^2}{g}\right)\alpha = F_p r \cos \theta \quad [3]$$

From Equations [1c], [2], and [3],

$$(r^2 \cos^2 \theta + \rho^2)\,\alpha - (r^2 \sin \theta \cos \theta)\omega^2 - gr \cos \theta = 0 \quad [4]$$

Equation [4] may be put in a more convenient form by using $\omega \dfrac{d\omega}{d\theta}$ for α and letting $\omega^2 = 2u$, resulting in

$$\frac{du}{d\theta} - \left(\frac{2r^2 \sin \theta \cos \theta}{r^2 \cos^2 \theta + \rho^2}\right) u = \frac{gr \cos \theta}{r^2 \cos^2 \theta + \rho^2} \quad [5]$$

Solution of this equation yields

$$\omega = \sqrt{\frac{2\,gr\,(\sin \theta - \sin \theta_0)}{r^2 \cos^2 \theta + \rho^2}} \quad [6]$$

where θ_0 is the position angle corresponding to $\omega = 0$.

The term, $r(\sin \theta - \sin \theta_0)$ is simply the change in height of the center of gravity, that is, $(\Delta z)_{cg}$.

By use of the concept of the instantaneous center of rotation the relationship between the drop height of the center of gravity and that of the instantaneous center of percussion is apparent

$$(\Delta z)_{cg} = \left(\frac{r \cos \theta}{d}\right)(\Delta z)_{icp} \quad [7]$$

From basic mechanics $d = \dfrac{k^2}{r}$, where k is the radius of gyration about the axis of rotation, and r is the distance from the center of rotation to the center of gravity.

Here $d = \dfrac{r^2 \cos^2 \theta + \rho^2}{r \cos \theta}$, so that the vertical velocity of the center of percussion in terms of its drop height is

$$(v_z)_{icp} = d\omega = d\sqrt{\frac{2g\,(\Delta z)_{icp}\, r \cos \theta}{(r^2 \cos^2 \theta + \rho^2)\, d}} = \sqrt{2g\,(\Delta z)_{icp}} \quad [8]$$

Since the vertical velocity attained by the instantaneous center of percussion in falling from a given drop height is the same as that attained by a body falling freely from the same height

$$(a_z)_{icp} = g$$

and, from Equation [2] and the counterpart to Equation [7]

$$F_p = W\left[1 - \frac{(a_z)_{cg}}{g}\right] = W\left(1 - \frac{r \cos \theta}{d}\right) \quad [9]$$

If the system is prevented from rotating by an external restraint acting along a vertical line through the instantaneous center of percussion, the static reaction at the pivot axis is

$$R_p = W\left(\frac{d - r \cos \theta}{d}\right) = F_p \text{ for the same values of } \theta$$

FREE ROTATIONAL COMPOUND PENDULUM SYSTEM

The "free rotational" compound pendulum system ideally permits fulfillment of all of the basic rotational drop-test requirements for main gear if it is physically feasible to satisfy the following conditions:

1 The inclination of the shock strut relative to the impact load (assumed acting vertically) may be made to conform with the design condition.

2 With the airplane in the attitude consistent with item 1, a distribution of weight may be made such that, for the entire loaded airplane, (*a*) simultaneous values of $r \cos \theta$ and ρ satisfy a value of d predetermined from a choice of moving-pivot location; and (*b*) simultaneous values of $r \cos \theta$ and W satisfy the requirement for test-gear static reactions.

It is to be noted that the test-airplane gross weight and center-of-gravity position, as such, need not conform with those of the design condition; nor need the disposition of weights in the fuselage be based upon the actual distribution of fixed equipment or useful load. It is, of course, important to avoid local overloading of any part of the structure; the probability of this occurrence may readily be determined by analysis of the weight distribution with regard to anticipated local accelerations.

In practice, deviations from the theoretical performance exist; these may be summarized qualitatively as follows:

(*a*) *Eccentricity and Nonverticality of Impact Load.* Because of the inclination of the shock strut the fore-and-aft position of the axle relative to the airplane varies as the strut is compressed under load. Thus at only one position may the test-airplane instantaneous center of percussion be directly over the axle. The effect is usually very small, however, the maximum eccentricity from this source being of the order of 1 per cent of the value of d. Another contribution to eccentricity may result from change in effective mass. Prior to impact, the airplane may be considered as a relatively rigid body; after impact the semisprung mass of tire, wheel, axle, and piston behaves altogether differently from the rest of the airplane. Here, again, the magnitude of these effects is generally small since the percentage change in "rigid" mass is small.

Potentially of more importance than the horizontal eccentricity of axle relative to the instantaneous center of percussion is the drag-load component resulting from forward or aft motion of the tire on the impact surface. Even with a liberally greased contact surface it is not inconceivable that the direction of resultant load may vary by several degrees from the vertical, depend-

ing upon the coefficient of friction and the moment of inertia of the wheel-and-tire mass. This factor is of little practical consequence in so far as the magnitude of dynamic loading at the pivot axis is concerned; it is more significant that the nature of the effect is generally such as to be additive to the design drag-load component, simulation of which is intended by prior inclination of the shock-strut axis. More will be said about these effects in the discussion of the test results.

(*b*) *Nonrigidity of Airframe.* Potentially, a major reason for differences between the idealized and the actual behavior might appear to lie in the fact that the airplane is not a rigid body. Quantitatively, an analysis of the effects of elasticity is a formidable task (1, 2).[2] Moreover, it would appear to be a misdirection of effort to attempt such an analysis merely for purposes of of drop-testing

Qualitatively, it may be noted that the load-time history of a landing event is usually very long in comparison with the natural period of vibration of any of the significant weight items. Hence pure resonant effects may be discounted. However, both the release shock and the landing shock excite in the airplane components transient oscillations which may have a measurable effect, not merely at the pivot axis, but also on the test-gear dynamic loading. It might be expected that elastic effects would be most noticeable for critical metering pin-and-orifice combinations. Cases are known wherein a particular metering pin, prescribed as a result of landing-gear tests in a translational drop-test rig, was found not to give optimum performance in airplane drop tests. However, it should be noted that differences in overall test techniques, including setup parameters and instrumentation, may well produce differences of comparable magnitude.

2 APPLICATION TO LOCKHEED PV PATROL BOMBER DROP-TESTS

Basic Test Arrangement

The moving tail-pivot test arrangement has been used in drop-tests of the main landing gear of PV patrol bombers. These tests were conducted for both "level-landing" and "three-point landing" conditions to determine energy-absorption and load-factor data throughout a range of drop heights.

As a matter of convenience, the tail-gear axle was chosen as the moving-pivot axis. The tail-gear strut was locked in a fully compressed position by steel straps attached to the torque-knee lugs. The tail wheel, less tire, was set on a steel track laid in the base of a horizontally slotted guide block, which was shimmed up from the floor to the height required to give the specified inclination of shock-strut axes for each landing condition. The installation is shown in Fig. 3.

The weight of the test airplane, consisting primarily of basic structure less outer wing panels, constituted about 20 per cent of the normal gross weight just prior to the start of the test setup. At this time it was desired to add the required mass in such a manner that the proper static reactions were obtained and that the center of percussion of the entire test airplane was placed over the line of contact of both main-gear wheels. From basic weight data the weight, location of the center of gravity, and pitching radius of gyration about the center of gravity were calculated for the empty test airplane. Weight and center-of-gravity location were checked by actual weighing.

As additional weights were placed in the airplane, a running tabulation of the weight-distribution parameters was made until, by successive approximations, the calculations indicated that the desired conditions had been satisfied. For overload conditions weights were added in equal increments both forward and aft of the center of gravity at distances equal to the computed radius of gyration about the center of gravity for the normal-

[2] Numbers in parentheses refer to the Bibliography at the end of the paper.

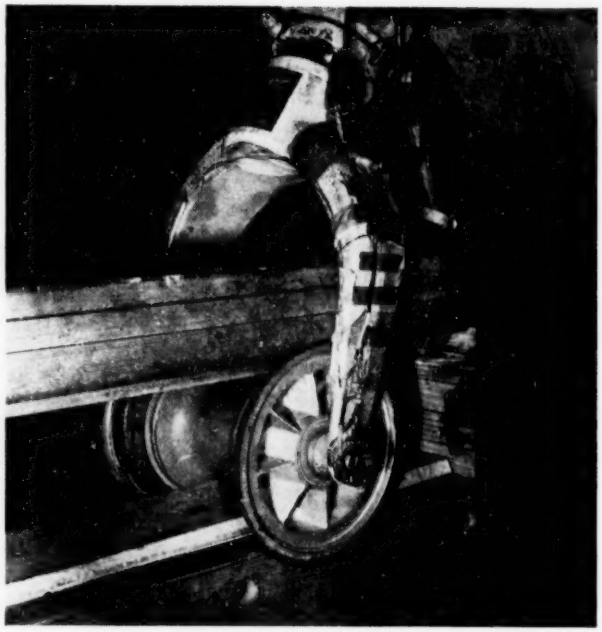


Fig. 3 Tail Wheel Mounted in Horizontal Guide Block During Tests Simulating "Level Landing With Inclined Reactions"

(Thrust line was inclined 18 deg, nose down, and tail gear was swiveled 180 deg to avoid interference between fork and guide block.)

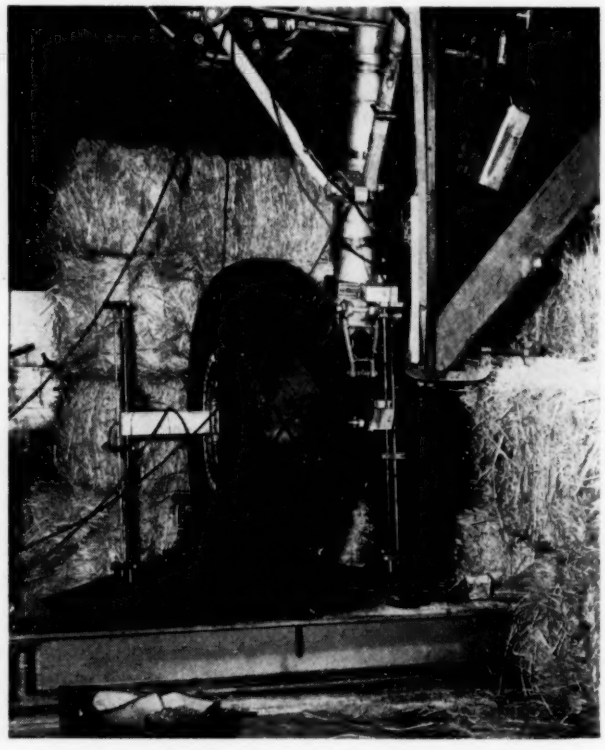


Fig. 4 PV-1 Main Landing Gear Drop-Test Setup

(View shows dynamic "weighing" platform, tire-deflection-measurement slide wires, and strain-gage installation on drag strut. Baled straw was used for protection of personnel and test airplane in event of tire or gear failure.)

gross-weight condition. In this manner the location of the center of percussion was held constant, and the increases in main-gear static reactions were made proportional to the corresponding increases in gross weight of the test airplane.

In the loading of the test airplane no particular effort was made to obtain exact correspondence of fuselage load distribution with the actual airplane weight distribution, although provisions for large items of fixed equipment or useful load greatly influenced the operations. It was considered important, however, to reproduce power-plant weights and centers of gravity locations inasmuch as each engine-mount support structure was closely associated with the landing-gear supporting structure. As a matter of economy the wing outer panels were not installed, having been damaged in previously conducted static tests. However, it is considered that the over-all behavior of the landing gear and wing center section would have been somewhat more representative had it been feasible to effect a normal distribution of wing weight. Moreover, it would undoubtedly have been more rational from the standpoint of wing torsional moments to have reduced "power-plant" dead weight by the ratio of the distance from the instantaneous center of rotation to the instantaneous center of percussion and the distance from the instantaneous center of rotation to the power-plant center of gravity. Yet in all probability such a reduction would have involved overloading the fuselage forebody in the three-point-landing condition because of the necessity of having enough weight forward to locate the instantaneous center of percussion properly.

Drop-Test Instrumentation

Several months prior to the start of the tests it was recognized that a considerable amount of data would need to be taken in as short a period of time as possible because of the pressure of other testing schedules. Accordingly, special instrumentation was devised to permit rapid recording and reduction of the data.

In the PV-1 tests simultaneous and continuous recording was made of the following quantities as a function of time:

1 Load on bottom of tire.
2 Tire deflection.
3 Shock-strut piston travel.
4 Airplane travel from the instant of release.

These measurements were made concurrently on both left-hand and right-hand gear. In addition, the following quantities were recorded on one side only:

5 Landing-gear drag-strut load.
6 Longitudinal deflection of the lower end of the shock-strut outer cylinder relative to the plane of the wing main beam.

In tests of the PV-2 facilities were available for measurements of side-strut and drag-strut axial loads on both sides, as well as tail-pivot loads.

All "load" measurements were made by means of SR-4 strain gages installed on structural members and incorporated in 1000 cycle-per-sec alternating-current bridge circuits, the output voltages of which were amplified, rectified, and impressed on the galvanometer elements in a recording oscillograph. Tire and strut deflections, as well as airplane travel, were recorded in a basically similar manner through the use of specially constructed slide-wire potentiometers. The outer-cylinder deflections were detected by a bending-beam-type of strain-gage pickup.

The measurement of axial loads in tubular struts posed no new problems, since the techniques of dynamic strain measurement and associated calibrations to obtain corresponding loads are fairly well established. However, the determination of dynamic loads on the shock strut required a somewhat different approach, inasmuch as there were no locations on the gear itself where anticipated strains sufficiently large for accurate measurement could be considered as absolutely indicative of load on the member. Accordingly, it was decided to drop the wheels on platforms, each of which was supported by three tubular pedestals to which strain gages were attached. By virtue of identical load-strain sensitivities of the pedestals and of the manner of incorporating the gages in the bridge circuit, the load indication of each platform was made independent of the load center relative to the three supports and also of any local pedestal bending strains that might be developed from horizontal-load components.

A typical oscillogram is shown in Fig. 5. It is to be noted that traces labeled "inboard" and "outboard" deflections of each tire appear. It was found necessary to use two slide-wire potentiometers on each wheel because of cumulative rotation due to bending of wing center section, shock strut, and axle. Thus a means of knowing true deflections at the tire center line was afforded, as well as the magnitude of the rotation. Each oscillogram trace has its own calibration factor in terms of its physical counterpart, the calibration being facilitated by the static conditions prior to release of the airplane and immediately after the airplane came to rest.

Test-Data Interpretation

In the interpretation of the oscillograms it was necessary to correct the platform-load indications for the effects of semisprung mass of wheel and axle, in order to obtain magnitudes of load experienced by the shock-strut outer cylinder and supporting structure. In general, the peak loads on the tire occurred at a time when the shock-strut stroke-time trace indicated very little differential acceleration of sprung and semisprung airplane masses. Accordingly, the peak loads on the outer cylinder were obtainable quite accurately merely by taking the appropriate fraction of the platform-load indication. As a matter of convenience, this same fraction was usually applied to all values of platform load in the process of constructing load-stroke and load-mass travel graphs from the oscillograms. Inasmuch as the semisprung gear weight amounted to only a few per cent of the static platform reaction, the error involved was usually of no practical consequence.

The recording of dynamic loads and deflections on both main gears made possible a determination of over-all energy relationships. By comparing the potential energy of the airplane prior to release with the energy absorbed in both main-strut and tire units up to the time of minimum center-of-gravity height, an estimate of the minimum amount of energy absorbed by the airframe could be made. The term "minimum" is used, since the nominal center-of-gravity travel was used in computations, without regard to the incremental energy accruing from structural deformation.

In the earlier series of tests, analysis of the oscillograms showed that peak drag-strut loads were considerably greater than were anticipated. This condition was true for both three-point-landing and level-landing tests. Two readily apparent reasons for the differences were (*a*) that the peak load on the gear was developed earlier in the stroke than had been the case in previously conducted jig drop tests and (*b*) that the effects of structural deformation had not been included in the preliminary stress analysis. However, even with allowances for these factors, the drag-strut loads appeared to be too large. Qualitatively, the residual discrepancy was attributed to nonverticality of impact load due to inertial or frictional effects.

The PV-2 test instrumentation permitted an indirect evaluation of the degree of main-gear load eccentricity relative to the center of percussion. With the airplane in a "tail-high" attitude intended to simulate "level landing with inclined reactions," the line of action of the hoisting gear very nearly intersected the line

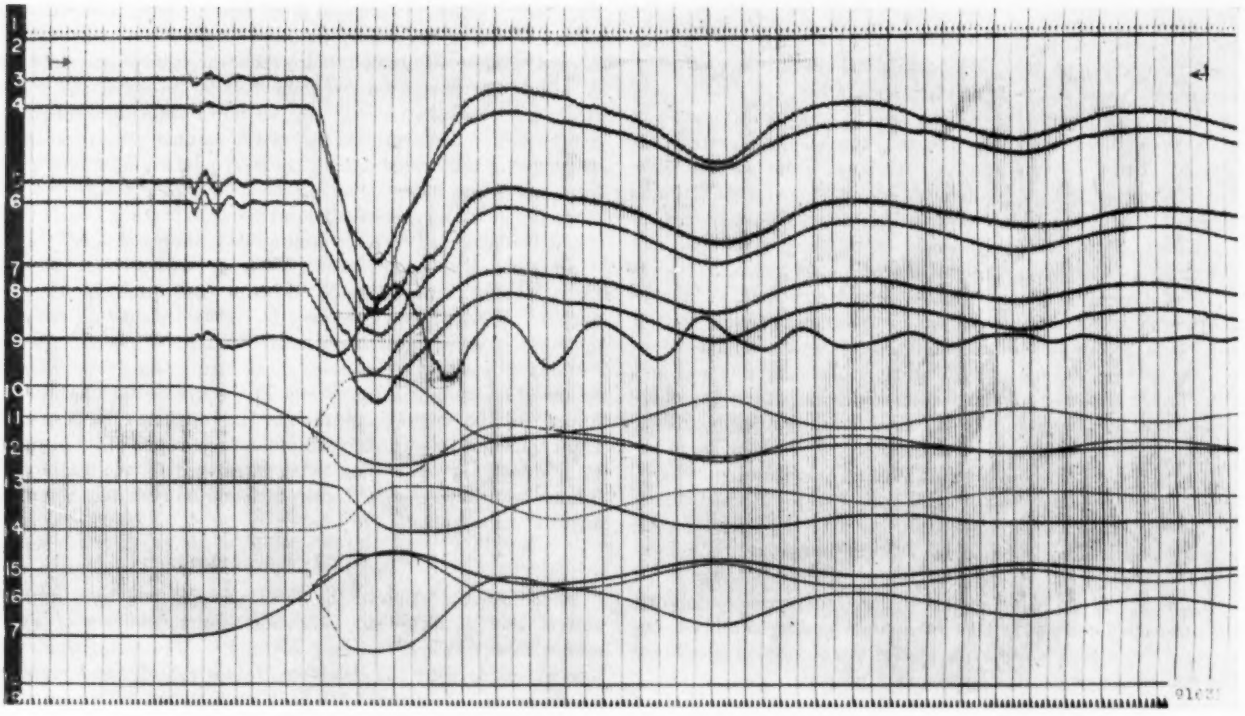


FIG. 5 TYPICAL OSCILLOGRAM, WITH NUMBERED TRACES CORRESPONDING TO PHYSICAL QUANTITIES
(1 and 19, sixty-cycle timing waves; 2 and 18, reference line; 3, left drag-strut load; 4, right drag-strut load; 5, left side-strut load; 6, right side-strut load; 7, left-platform load; 8, right-platform load; 9, tail-gear load; 10, left-wing travel; 11, left tire, outboard deflection; 12, left tire, inboard deflection; 13, left strut stroke; 14, right strut stroke; 15, right tire, inboard deflection; 16, right tire, outboard deflection; 17, right-wing travel.)

of contact of main-landing-gear tires. Hence if the airplane behaved as a rigid body, and if the impact force acted vertically through the center of percussion, no change should have been expected in the tail-gear static reaction other than that occasioned by a slight change in airplane attitude.[3] Actually, a rather significant change in tail-gear reaction occurred, as can be seen by reference to the oscillograph trace in Fig. 5. Statically, prior to release, the bottom track of the horizontal guide applied an upward force on the tail wheel. Shortly after the instant of initial main-gear impact this force diminished to zero, remaining at zero for an instant while the tail wheel traveled freely about 1/16 in. before encountering the restraint of the upper guide. The peak downward load on the tail gear was attained shortly after the peak loads had been reached on the main gear. This behavior was typical for this series of tests, the magnitude of dynamic tail load increasing with main-gear drop height, and the time of maximum occurring at or shortly after maxima on the main gear. The persistence of tail-load oscillations after the main landing event was also characteristic.

An obvious deduction to be made from the tail-pivot loading is that substantial drag forces were developed as the semisprung gear elements moved forward due to compression of the inclined shock struts. Thus the diving moment induced by these drag forces was balanced by a downward dynamic load on the tail pivot. The validity of this conclusion is strengthened by the fact that the recorded peak loads on the landing-gear drag struts are in good agreement with values calculated by means of the instantaneous attitude of the airplane, the measured vertical loads on the gear, and values of drag load required to balance the simultaneous tail-pivot load. The data indicate that at the instant of peak vertical load the unwanted drag load may have been larger than 12 per cent of the vertical load. Thus the direction of impact load relative to the shock-strut axis was considerably more severe than that prescribed by the design condition.

Drop-tests for simulation of "three-point landing with vertical reactions" produced effects in the opposite direction, that is, the aft acceleration of wheel-and-tire masses demanded by the compression of the shock struts led to the development of peak resultant loads acting somewhat forward of vertically upward. Again, the net effects on the gear and its supporting structure were more severe than were intended.

CONCLUSIONS

The author feels that there are two definite conclusions to be drawn from the experiences accumulated both during the drop-test programs discussed herein and during more recently completed rotational-jig drop tests employing the same principles:

1 Drag-load errors arising from wheel inertia or from friction between tires and impact surfaces are not necessarily negligible in any type of drop-testing, whether simulation of the proper drag component is sought either by inclining the shock-strut axis or by inclining the contact surface. It is significant that, in general, the former expedient produces effects in a direction to aggravate loads in the drag-resisting structure, whereas the latter tends to alleviate them, resulting in an unconservative test unless deliberate compensation is afforded. While the control of these factors may be unduly costly, the measurement of their effects on the airplane structure appear to be justified as a standard procedure. The degree of refinement to be attained in instrumentation and in adjustment of test setup parameters is indicated by an over-all view of the problem. Drop-testing to simulate a particular "instantaneous" design condition is one thing; drop-testing to simulate actual critical landing conditions is quite another.

[3] Reference to Equation [9], et seq.

2 The "free-rotational" drop-test method described herein is believed to be an improvement over previously used rotational test methods. Moreover, from the standpoints of safety, accuracy, and ease of airplane control, it appears to offer advantages over translational airplane drop-testing in cases where simulation of dynamic landing loads on the entire airplane structure is not intended.

ACKNOWLEDGMENT

Acknowledgement is due a number of Lockheed engineers for their contributions, especially toward the initial work in 1943. Particular note should be made of the assistance given by G. E. Nichols and W. Bush in the testing and data reduction; of the helpful suggestions made by J. S. Edison, P. C. Mortenson, and R. Contini; of the development of the initial electrical instrumentation by R. E. Rawlins; of the guidance by V. S. Upton under whose direct supervision the work was carried out; and of the basic contributions by W. C. Hurty, whose interest and encouragement made possible the evolution of the new techniques described herein.

BIBLIOGRAPHY

1 "An Analytical Theory of Landing Shock Effects on an Airplane Considered as an Elastic Body," by E. G. Keller, Trans. A.S.M.E., vol. 66, 1944, p. A-219.

2 "Dynamic Loads on Airplane Structures During Landing," by M. A. Biot and R. L. Bisplinghoff, N.A.C.A. Advance Restricted Report 4H10, October, 1944.

3 "Landing Gear Design Considerations," by J. A. Hootman, N.A.C.A. Advance Restricted Report 3D30, April, 1943.

4 "Dynamic Reaction Platforms—Evaluation of," U. S. Navy Department, Bureau of Aeronautics, A.M.L., N.A.M. 2486, Part 1, October, 1945.

Some Suggested Specifications for Thermal Ice-Prevention System for Aircraft

By L. A. RODERT,[1] INDIANAPOLIS, IND.

The general conclusions from research and development of the airplane thermal ice-prevention system are given and additional comments in discussion of present knowledge are made. Details of design are discussed whereby some faults of early applications of the thermal system may be avoided. Specifications for the thermal system are given as an aid to operators and others desiring to provide the most effective protection against the formation of ice on airplanes to be designed for commercial or military use.

Introduction

THE need for closer adherence to scheduled operations becomes increasingly urgent as the military and commercial use of the airplane is extended. Attention therefore is being given to the improvement of equipment and operational methods which will enable the airplane operator to achieve the regularity which is necessary to meet the demands of the public and competition.

The airplane is handicapped during inclement weather by obstructions to visibility and the formation of ice. The maintenance of schedules also is affected at some terminals by congestion of air traffic. While visibility and traffic problems may be solved by signal devices and operating procedures, the ice problem requires an intimate consideration of the airplane.

Research and development activities in many countries have been directed in search of a solution to the ice problem. These activities have, in general, concluded that the problem can be solved by the use of heat. Although it is fortunate that an answer has been found, heat is not entirely a fortunate solution because the internal parts of the airplane are adversely affected and complicated by its application. Engineering skills which can cope with the problems of flight and the internal mechanism therefore have to be directed to the task of applying the thermal system.

The locale, intensity, and distribution of heat and the mechanical, electrical, and aerodynamical details must be considered when the airplane ice-prevention specifications are prepared. The reports of the researchers have been limited in many instances to a discussion of the practicability and thermal requirements of the system, and rightly so, since these were the objectives. During the conduct of the tests, which involved the operation of several airplanes in natural icing conditions, practical design and operational information was also obtained. In the present paper, the practical considerations of design will be considered on a more equal plane with the theoretical objectives of the researches. It is hoped that this treatment of the knowledge will be helpful during the interim between the present and the later date when the manufacturers and operators will have had adequate experience with applied aircraft to establish the needed empiricisms.

[1] Research Engineer, Stewart-Warner Corporation, South Wind Division; Chairman, N.A.C.A. Subcommittee on De-Icing Problems.

Presented at the Aviation Division Meeting, Los Angeles, Calif., June 3–5, 1946, of The American Society of Mechanical Engineers.

Note: Statements and opinions advanced in papers are to be understood as individual expressions of their authors and not those of the Society.

Ice-Prevention Data

After the preliminary exploration in the United States and Germany, from which the practicability of the thermal system of ice prevention was established, many projects were undertaken in order to test the application to various parts of the airplane and to determine the intensity, distribution, and extent to which heating must be applied in order that ice might be alleviated. In this country, the application to all vulnerable parts of the aircraft has been recommended (1, 2, 3, 4, 5, 6, 7);[2] in Canada, the National Research Council has advanced and endorsed the use of heat on the propeller; and in Germany, the thermal system has been applied to lifting surfaces and windshields (8, 9). British researchers, collaborating with and actively participating in the work in this country (due to the difficulties imposed by hostilities over the British Isles), have also approved the thermal system as superior to other methods for all vulnerable parts of the airplane. These results all pertain to aircraft of conventional configuration, size, power loading, and power-plant installation.

Aerodynamic Lifting Surfaces. When heat is delivered to the leading edge 10 per cent region in sufficient quantity to raise the average leading-edge skin temperature 100 deg F above the ambient air temperature, while flying in dry air at 18,000 ft pressure altitude and at 60 per cent rated engine power, adequate heat is provided to prevent or remove ice formations from wings and empennage surfaces. This conclusion has been reached from tests with full-scale aircraft in flight in natural icing conditions. Conclusions based upon the data are considered to be applicable to conventional airfoils of from 4 to 20 ft chord whose pressure distribution is similar to that of the N.A.C.A. 230 airfoil series and whose thickness is from 6 to 18 per cent of the chord. The surfaces of the wings were normally clean but not aerodynamically smooth. The condition of the surfaces was more likely to be hydrophilic than the hydrophobic. The data were established from flights in several aircraft over a period of 5 years' time, over a wide geographical area, in various types of meteorological conditions, and with different observers (1, 2, 3, 5). Encounters with what may be called severe icing conditions have been successfully experienced.

The chordwise heating intensity over the leading edge 10 per cent chord region gave a temperature rise which was uniform within about 15 deg F in one airplane which had satisfactory protection in all conditions.

Ice does not form in the vicinity of the controls or control hinges unless, by peculiar rigging, a part of the control surface is made to protrude beyond the normal boundary layer of air which passes over the wing. Hinges, balances, or other protuberances which may occur from faulty manufacturing techniques will collect ice when the leading edge is heated sufficiently to keep ice off from the stationary part of the airfoil. When ice is allowed to refreeze on the regions rearward from the leading edge by reducing the heat below specified values, the formations have always occurred forward of the control-hinge regions.

Flight in clouds containing unusually large quantities of water at air temperatures below 32 F caused the wing leading edge to be

[2] Numbers in parentheses refer to the Bibliography at the end of the paper.

substantially wetted back to the 5 to 7 per cent chord point on the upper surface. Observations were not made directly on the lower surface, however, the wetted area is thought to be about the same as on the upper side. The area rearward from the 5 to 7 per cent chord region has been observed to be only partially wetted. No ice formed on areas rearward from about the chord point of maximum ordinate on wings of large chord, and, from this observation, it is concluded that no water is in contact with the skin in this region since the temperature of the skin was below the freezing point of water. This conclusion is not thought to be valid for airfoils of 4 ft chord or less.

In flights through cumulo-nimbus clouds of major development, large quantities of water in the form of snow, sleet, and rain, held aloft by strong up-currents have been encountered which caused the deposit of a slushlike formation along the stagnation-pressure region for short periods of time. These formations were as much as 2 in. wide and $^1/_2$ in. thick in some cases of extreme severity.

The delivery of heat to the aerodynamic lifting surfaces has been accomplished by the following means:

1 Exhaust tube within the wing leading edge (1).

2 Circulation of heated air within the leading edge and discharged from the airfoil interior in the vicinity of the trailing edge or control-surface hinge line (5).

3 Circulation of heated air within the leading edge and discharged from the airfoil interior into the boundary air near but to the rear of the transition point on the low-pressure side, high-pressure side, or both (2, 3).

The exhaust tube within the wing was discarded in favor of the air-circulating systems because the latter has been found to be more easily constructed and maintained and to be more readily employed on most airplanes.

Attempts to deliver heat to the wing leading edge by the spanwise flow of heated air along the wing leading edge have not been successful. All successful leading-edge designs have been adaptations of the Junkers leading heat-intercooler design (8) which employs a spanwise plenum, chordwise flow for heat exchange, and either a chordwise or spanwise flow for the outgoing air.

The wing-heating systems have been made without serious deleterious effects on the strength, construction, weight, or maintenance of the aerodynamic surfaces.

Windshield. The vision of the pilot and copilot of airplanes at speeds under 200 mph, indicated, has been maintained during flights in icing conditions by the transmission of about 1000 Btu per sq ft per hr through the outer surface of the windshield glass (2, 4). The prevention of ice on the windshield has also been accomplished on one airplane by the passage of a layer of heated air over the exterior from a slot at the forward edge (5). About 10,000 Btu per sq ft per hr was employed in the externally discharged air-heating system. However, the mechanical design was inferior, and it is believed that less heat would be required in a better arrangement.

Greater amounts of heat than that just indicated have resulted in excessive warmth in the pilot's cabin particularly in airplanes in which the pilot's face is near to the windshield. Heating the windshield to a limited degree increases the resistance of the glass to the impact of bird strikes according to tests conducted by the Civil Aeronautics Authority. Heating the windshield to a temperature above 140 F seriously weakens the glass and has a deleterious optical effect upon the plastic binder of safety glass.

Heat has been transmitted in the necessary quantities by the following:

1 Circulation of heated air between the panels of a double-glazed windshield.

2 Electric power through the use of embedded heating wires in the glass.

3 Circulation of heated air over the exterior surface.

4 Electric power through the use of external heating wires.

5 Electric power through the use of transparent conducting surfaces.

It is very important to remember that vision through the windshield is the important objective in windshield ice prevention.

The solution to this very important part of the ice problem must consider ice prevention on the outside, frost removal on the inside, resistance of the panel to the impact of flying birds, and the other more obvious construction and service requirements. Hope has long been held that a transparent and durable electrical conducting film for the coating of glass could be discovered whereby the windshield panels could be heated with electric power. Such a product has been discovered and developed by the engineers of the Pittsburgh Plate Glass Company. This discovery, which has been given the name of "Nesa," promises to solve the windshield icing problem in an optimum manner for all the factors involved wherever electric power is available in the required quantities.

The improvement of the optical qualities of the doubly glazed windshield has been attempted by the treatment of the glass surfaces for the reduction of the surface reflectivity. Coating the glass surfaces with magnesium fluoride by the evaporative process was not successful in one attempt. The use of the doubly glazed windshield has several disadvantages. Tests have shown the increased reflectivity of the greater number of surfaces to be detrimental to the pilot's vision, particularly at night in the landing maneuver. Water precipitates form on the inner side of the outer glass occasionally on some installations during taxi and take-off runs due to the circulation of high-humidity air past the cold outer panel. The fogging clears soon after the ducts are cleared of the moist air and the temperature of the air rises. The collection of foreign particles on the interior surfaces of the glass necessitates frequent clearing in dusty regions.

Propeller Blades. Ice can be removed or prevented from forming on propeller blades by the provision of heat to the blade leading-edge region or to the entire blade section. The application of the thermal system to the propeller blade has been accomplished by the use of electric power and by passing heated air through the interior of blades having an open passage from root to tip. The minimum quantity of heat required for a propeller blade has not been reliably established; however, sufficient data have been obtained whereby practical and reliable propeller protection can be achieved for blades currently in use. The results indicate that blades for a 12-ft-diam propeller will require from 1000 to 1200 watts of electric power per blade when turning at about 1100 rpm propeller speed and flying at about 180 mph indicated airplane speed (6). Other results indicate that blades of a 15-ft-diam propeller under about the same operating conditions require from 1000 to 1500 watts of electric power per blade (10).

Flight tests in natural and simulated icing conditions by independent researchers have shown that the thermal system for propellers may be operated intermittently with satisfactory protection for the propeller and with a great saving in electric power. When operated intermittently, the power is applied to a propeller for a short time during which the ice is removed and then the heating is interrupted. During the interruption, heating is applied to another propeller on which a small amount of ice has been permitted to form. Intermittent operation is thought to require a slight increase in blade heating in order to minimize the time required for ice removal and reduce the size of ice particles thrown off.

The electric heating of propeller blades has been accomplished by neoprene blade shoes in which an electric resistance of either conducting rubber or wire was constructed. The blade shoes have been about 60 inches long in some successful installations. Some blade shoes have given several hundred hours' service in varied conditions without excessive abrasion while others were severely damaged by one flight in snow and heavy rain.

The shoes were applied to the blade by adhesives. The attachment changed the contour of the blade profiles from 0.050 to 0.065 in. at the leading edge and about 0.010 in. at the 20 per cent chord point. The blade shoes covered about 25 per cent of the blade chord on the camber face and slightly less than 20 per cent on the thrust face on one installation which gave favorable results. The heating intensity of the electrically heated shoes was twice as great over the leading-edge part of the shoe as over the areas immediately to the rear of the leading edge on camber and thrust faces (6).

Power has been successfully supplied to the electrically heated blades by propeller-hub-type alternating-cuttent generators and through slip ring and brushes from an electric power source, such as the regularly installed generator.

Air for use in the air-heated hollow steel propellers was supplied from heat exchangers in one successful demonstration of the system. The energy employed in the propeller air-heated system was excessive and all ice was not prevented in every test, although it should be noted that by baffling the blade interior the heat would have been better employed and better protection would have been provided.

Miscellaneous Parts. Although the results of tests on wings, windshield, and propellers are indicative of how ice may be prevented on other vulnerable parts of the airplane, direct solutions to the miscellaneous problems have not been established. Individually, the collection of ice at points on the airplane other than on the wings, windshield, or propeller may not seriously affect the operation of the craft. Collectively, however, the miscellaneous problems, unless solved in part, may so handicap the airplane that the advantages of the improved protection to the wings, etc., will not reward the operator with the improvement in reliability which would otherwise be achieved.

The formation of ice on exposed frontal parts of the airplane such as the fuselage, engine cowls, and propeller spinner has been observed to be of sufficient size and shape to reduce the performance slightly, create a hazard when the formations become dislodged and fly rearward, and in the case of the cowls create an interference with the propeller blades which might interfere with blade-angle movement in an extreme case.

The formation of ice on radio antenna wires has broken the wires on most airplanes which have been operated in severe icing conditions unless steel cables were used in place of the copper wire which is customarily employed. Ice formations on radio antenna insulators have caused a reduction in the distance over which radio signals could be transmitted.

The formation of ice on the mast to which the static-pressure orifice for the airspeed and altimeter system is mounted causes an error in the meter readings and increases the drag of the airplane. In extreme cases the masts have been broken away from the airplane fuselage.

The formation of ice inside and on the edge of inlets to air ducts will reduce the inlet area and increase the air-pressure losses in the duct. Turning vanes in air scoops will collect ice and cease to be an advantage to the circulation of air. When ice dislodges from the opening and passes into the duct, due to flight into warmer air temperatures, the formations have seriously stopped the flow of air into a duct for a period until the ice has completely melted.

The formation of ice on exposed moving mechanisms has rendered such equipment inoperative. The exposed cable and pulley wheel or similar devices on propeller governors which are mounted on the front face of the engine, and the alternate air-intake door and operating arms for carburetor air intakes are examples of equipment which has been affected by ice formations. Slight accretions have been observed on control-surface hinges and balance weights but not of sufficient size to cause interference since these parts are ordinarily shielded by the forward part of the aerodynamic surface.

Engine Air-Induction System. The established practices of heating the engine air in this country and of heating the parts of the carburetor and induction system walls in the United Kingdom will prevent and remove the formations of ice in the engine air-induction system (7). Most airplane service installations of the air-heating system are unsatisfactory because of high maintenance requirements and the use of unsatisfactory mechanical arrangements for adjusting the carburetor air temperature. The air-temperature rise which is required for the removal or prevention of ice in the induction system is known by most airline and military operators and will not be discussed here.

Equipment

The application of the thermal ice-prevention system has necessitated the invention and development of new and unique mechanisms. The success of the detail design of the system is dependent upon the judicious choice and use of these devices. In the conduct of full-scale research, some experience was gained on some of the mechanical, thermal, and electrical equipment which must be used to implement the thermal system. These data are not a substitute for long service experience but may be helpful in the current phase of the development.

Sources of Heat. Heated air has been provided for wings, empennage, windshield, and propeller by exhaust gas-to-air heat exchangers in service and experimental airplanes, and by combustion heaters in experimental airplanes in this country. In Germany, the heat exchanger, combustion heater, and a mixture of exhaust gas and air have been employed as heat sources. Adequate heat capacity can be achieved with any of these types of heat source although several airplane systems have been designed which failed to meet the design requirements in this regard. Heat exchangers have been employed in service in large numbers which have given no cause for maintenance after thousands of hours flight time. Other heat exchangers have not given satisfactory service and have been replaced. Combustion heaters have been employed in service in sufficient volume and for a long enough time (for cabin-heating purpose) to indicate that this type of source can be made satisfactory. Minor service complaints have been experienced but none has been found which involves unsolvable problems.

Installations of the exhaust-gas exchanger have been made which provide adequate heating under all necessary operating conditions (11). Whereas the use of the combustion heater obviously involves an economic loss due to the use of gasoline for heat, the continuous passage of air and exhaust gas through the heat exchanger also involves a power loss which must be compensated for in increased power of the engines in order to maintain unaltered climb and speed performance (12).

Electric power has been provided by propeller-hub-type alternating-current generators for propeller ice prevention and the airplane's electric system. Service difficulties have been experienced in the use of the hub generators; however, the problems do not appear beyond solution.

Air-Distribution System

The distribution of air from the heat sources to the heated areas has been accomplished with aluminum, aluminum strength

alloys, mild steel, stainless steel, and glass-fabric tubes. The difficulties experienced with the duct systems were as follows:

1 Excessive air-pressure loss due to small size ducts, circuitous paths, internal protuberances, collapsed fabric flexible connectors, sharp corners, and improperly located or shaped guide vanes.

2 Excessive maintenance due to use of soft metals which were easily dented, use of thin metal which fluttered and failed in fatigue, duct connections which made repair of any part very difficult, use of insulation materials which deteriorated under vibration and wear, and control valves which failed elastically or in fatigue due to the use of small metal gages.

3 Off-gassing of pungent volatile materials when hot.

4 Creation of a fire hazard by the absorption of inflammable liquids in duct-insulating materials.

5 Air losses at duct joints and seams.

Controls. An electric control consisting of motor-actuated air valves, overheat turn-off switches, off-on signal lamps, on-off switches and a signal test circuit has been found satisfactory in one experimental system which employed heat exchangers (5). So-called safety devices and alarms failed more frequently than did the equipment against which failure the safety device was to provide.

Instrumentation. The definition of the properties of a thermal ice-prevention system has been accomplished with great difficulty. The use of the very elaborate and expensive measuring equipment and testing methods has not altered this situation (5). The measurement of pressures is handicapped by the turbulent condition usually existing in the duct system. The measurement of pressures is difficult because the instrument usually altered the condition being measured. With care, air flow rates can be measured to within plus or minus 10 per cent. Attempts to invent and develop ice-rate indicators have not resulted in success.

Temperatures can be measured with accuracies as given in Table 1.

TABLE 1 PROBABLE ACCURACY OF TEMPERATURE MEASUREMENT IN FLIGHT

Item	Range, deg F	Accuracy, deg F
Metal structure	0 to 300	±8
Metal structure	300 and above	±20
Ambiant air	−20 to +40	±1[a]
Duct air	0 to 300	±10
Leading-edge skin	0 to 200	±10
Engine exhaust gas	1000 to 1800	±25

[a] With greatest care and with correction for kinetic effect on a wetted thermometer bulb in a moving stream.

The stresses induced in a heated wing have been measured in tests from which apparently reliable results were obtained. The accuracy of this work is stated to be ±400 psi for the stress-change data involved in the heated wing (13).

The measurement of the temperature of the ambient air has been studied with care for the case of the thermometer bulb being located in a moist moving stream (14).

Meteorology

The measurement of the meteorological factors, i.e., water content, droplet size, and air temperature, has been undertaken by several capable engineers and the work continues, but the results thus far have not been encouraging. The best information on water content now available is that measured at mountain top weather bureau stations and that resulting from analytic studies which are based upon fundamental concepts of the physics of the air. Limited flight data substantiate data collected by ground stations and from analytical studies. The data are more satisfactory for stratus-cloud structures than for frontal or vertical developments. The great variations within clouds of vertical development and frontal phenomena make the measurement in these conditions particularly difficult.

The water content and droplet size in stratus clouds have been estimated to approach the values given in Table 2.

TABLE 2 ESTIMATED PHYSICAL DATA ON WATER IN ATMOSPHERE

Air temperature, deg F	Droplet size, μ ($\frac{1}{1000}$ mm)	Water content, g per cu m
0	10	0.50
5	13	0.55
10	16	0.75
15	19	1.15
20	23	1.65
25	26	2.30
30	29	2.85
32	30	3.00

The values given in Table 2 are established by a faired line which has been drawn on a graphical presentation of weather-bureau data (15). The faired curve was drawn so as to give values which in all cases exceeded the data thus far observed and therefore is probably conservative. Our knowledge of the weather is obviously inadequate.

Operational Factors

Flight tests have been made by various observers over the United States from the Pacific Coast to the Great Lakes region, and over Canada from the Lakes to the Atlantic Coast and beyond. No variation in the nature of ice due to geography alone should be expected and none has been observed. Most severe and frequent icing conditions have been observed where a combination of large water content and subfreezing temperatures are encountered. The movement of Pacific air masses over the mountains along the Pacific Coast and the movement of frontal disturbances from the central mid-continent in an easterly and northerly direction cause severe icing conditions. Air mass or local weather does not usually produce dangerous icing conditions except over terminals where traffic is held aloft for long periods at fixed altitudes.

As has been reported by many investigators, formations can occur at air temperatures from 32 F to as low as −40 F or lower. Flight tests have been made in which icing has been encountered up to 18,000 ft pressure altitude. Reports have been recorded from flight operations over the North Atlantic of icing conditions which extend to about 27,000 ft pressure altitude. Icing at altitudes above 20,000 ft is found only in clouds of vertical development and therefore occurs over limited areas or along narrow lines.

Changing the velocity of an airplane will affect the formations of ice in accordance with the kinetic equation (14). Present transport aircraft do not fly sufficiently fast to prevent ice on the wing except at air temperatures near 32 F. The velocity of the outer blade radius sections of the propeller, however, is heated by the kinetic effect to a degree which will prevent the formation of ice under most conditions. In order to take advantage of the velocity effect in the design of propeller ice-prevention equipment, it is necessary to consider the thermal conductivity and other factors involved in the blade-heating problem (16).

The tests in icing conditions have involved sustained flight for over 2 hr in intermittent, moderate, and light icing conditions. Tests in severe conditions have been for short periods only because of the limited size of the regions in which such conditions have been found. Several experiences with severe conditions have been encountered for periods of about 20 min.

The performance of a system cannot be judged by an observation at any one instant because some ice accretions on the surface of an airplane wing which is heated less than that required for complete prevention will accumulate and intermittently be blown away, the bond having been broken by heating which was not adequate for complete prevention.

Operations have been made in icing conditions during engine warm-up, taxi, take-off, climb, cruise, let-down, landing, single engine cruise, and single engine[3] let-down with adequate protection provided. Frost has been removed from the leading-edge regions of the wing and empennage in about 15 min. This operation is usually accomplished in less time than that required for the warming-up of the engines.

The removal of ice from the wings, after accretions have been allowed to form, sometimes is accomplished satisfactorily, other times with some refreezing on the rearward and unheated portions of the wing.

The installation of the thermal system will result in a loss of climb and speed performance at all times when air is passed through a ram-actuated system. The internal and external losses will have almost a negligible effect on the performance of the airplane if care is used in providing the utmost in aerodynamic cleanliness. A poorly designed installation, on the other hand, can cause a loss of as much as 6 mph in speed at 55 per cent power cruise. The use of alcohol blade shoes on propellers has not resulted in a measurable loss in performance, although it is reasonable to believe that a slight loss in propulsive efficiency has been experienced when the design blade section ordinates are changed to the extent necessary in the heater installation. The blade shoes could be expected to have a greater effect on new and well-designed propellers.

The passage of heated air through a propeller and the discharge of air at the propeller tip cause a slight loss in propulsive efficiency. These losses will depend upon the shape, size, and location of the tip outlet, and the nature of the air passage.

Service experience with the heated wing indicates that the construction involved complicates the problems of repair of the leading-edge region. When damaged by hail, rough ground handling, or bird strikes, the replacement of the double-skin regions is particularly difficult. Normal means of corrosion prevention, i.e., alclad and dichromate primers, have retarded corrosion on three experimental airplanes after two years of operation. Metallurgical inspection of structural parts has not revealed any deterioration in the allowable strength, yield strength, elongation, or cyrstalline structure.

Discussion and Specifications

The results of all tests and experience in this country and abroad indicate that the thermal system can be applied to most commercial and military airplanes in a manner which will retain normal operational efficiency and dependability during conditions of icing.

In order for the thermal system to make a contribution in improved dependability, the airplane must be able to operate in icing clouds or freezing rain at any of the various operating conditions. It is not sufficient that the efficiency of ice prevention in the cruising altitude, for instance, be better than present equipment. An improvement in the protection during cruising would improve the safety, but unless the conditions of take-off, taxi, and landing are equally provided for, the operator will not be able to improve greatly his flight regularity.

The engineer therefore must give care in making the thermal ice-prevention installation in order to assure that protection has been provided for all normal altitudes and conditions of flight. A thorough knowledge of applied operations is a necessity in meeting this requirement successfully.

The evolution in design will alter the application of the thermal system, but it will not change the natural truth of ice being melted by heat. The fundamental seems to have been established.

[3] With a twin-engine airplane.

Preliminary to the statement of detail specifications, an expression (or at least understanding) of the general objectives should be formulated. The general specification should define the degree of perfection, and certain specializations which result from the use to which the airplane is to be put, the climate and region in which it will operate, the class of service, and the civil or military codes, compliance to which is mandatory. These general qualifications frequently are stated in part through other sections of the specification for an airplane but not in sufficiently complete detail to define the general requirements of the ice-prevention equipment. A specific statement on perfection is desirable because the results of tests and experience thus far observed show that the costs of perfect protection for an unlimited flight duration in the most severe conditions, and under conditions of a dual emergency (such as engine failure in addition to icing conditions), may penalize the usefulness of the aircraft to an impractical degree. Economically there is a limit to the perfection of ice protection in somewhat the same manner that there is a limit to the load factor or power loading which can be provided in an economically employed vehicle.

In addition to a statement on the degree of protection desired, the following general specifications are recommended:

0:1 The formation of ice on the airplane in any manner or location which shall reduce the operational efficiency, interfere with regularity of service, or reduce the safety of flight shall be prevented.

0:2 The installation of the equipment shall result in the minimum increase in weight and maintenance, and minimum decrease in speed and climb performance.

0:3 The safety, structural capacity, hazards from fire or gaseous poisoning of personnel, and versatility of the airplane shall not be adversely altered in any degree by the installation of the thermal system.

Aerodynamic Lifting Surfaces. Complete protection for the wings, empennage, and control surfaces will preserve the lift, drag, and pressure distribution of the basic airfoil, protect the operation of mechanisms, maintain flow through leading-edge duct inlets, protect the illuminating qualities of lighting equipment mounted thereon, and prevent damage to or interference with other parts of the airplane due to ice on the wing or to ice which has become dislodged from the wing and flies rearward.

The complete prevention of ice requires that the leading edge be maintained at a temperature above 32 F over all regions on which liquid water may reside. An ideal solution in the evaluation of the heat required might consist of determining how much water will strike the leading edge and over what area of an airfoil at the various water contents and droplet sizes given in Table 2. By assuming all or a specified portion of the water evaporated, the remainder to be abraded away by the airstream; by assuming a specified transition from laminar to turbulent flow as affected by the presence of water on the wing; by assuming the surface to be hydrophobic or hydrophilic, or to what degree of each; and by making other simplifying assumptions of aerodynamic nature, the required external heat-transfer coefficient at various chord points may be approximated. These calculations should be done at several air temperatures and therefore at several water-content conditions as given in Table 2 in order to establish the condition of maximum heat requirement and the optimum distribution for all conditions. In order for this method to be completely rigorous, the calculations should also be repeated for several combinations of wing and power loadings. This process does not seem practical because the data of Table 2 are not and have not been purported to be authoritative, nor have other weather data more authoritative been established. The process is of dubious accuracy because nothing is known about the relation of mass

transfer to abrasion losses or the distribution of this relation along the chord of the wing.

A rigorous solution to the external heating requirements on an airfoil will not be possible in the design of the thermal ice-prevention equipment until the weather conditions, i.e., water-content and droplet size variations with air temperature, have been established and recognized by regulating agencies and until the physical and thermal processes on the wing leading-edge exterior are better understood.

The degree of protection given a wing will depend upon the intensity of heating, the extent, and distribution of the heat, the pressure distribution of the airfoil, surface smoothness and wetability, and other factors. The specification should allow freedom in design which will permit the engineer to take advantage of all artifices and fortuitous circumstances. For example, in the propeller-wake region, it may be permissible and desirable to discharge the heated air from the leading-edge system into the boundary layer at about the 15 per cent chord point and thus greatly improve the thermal effectiveness of the system.

The experience gained thus far with the thermal system has shown that airplanes equipped with exhaust-heat exchangers will have been provided with protection for the lifting surfaces if sufficient heat is delivered to the 10 per cent chord leading-edge area to produce 100 deg F skin temperature rise at 18,000 ft altitude, 0 F ambient air, long-range cruise power, and in clean air. In the airplanes with which this experience was gained the heated air was passed through the after region of the wing after it had served its purpose in the leading-edge system. The effect of passing the air through the after section may not be large. It is obvious that some benefit will accrue, however, just as it is obvious that a greater heated chord coverage than 10 per cent will give a more efficient use of the heated air.

Practical limitations of wing leading-edge construction require an internal exchange system similar to the Junker's leading-edge intercooler design and therefore predicate within certain limits the type of distribution of heat which can be achieved with air or gas as the heating medium. While the distribution of heat may not be optimum as transmitted to the outer skin by the Junker's intercooler design, neither is the distribution as obtained particularly wasteful of heat. By tapering the passage of the air gap, a nearly uniform outer-skin temperature can be obtained. The conductivity of the skin will even out peaks or valleys which result from large or small transfers on the inner or outer surface at particular chord points.

A specification for the aerodynamic lifting surfaces such as the following is recommended:

1:1 A thermal system of ice protection shall be provided which shall preserve all of the aerodynamic, mechanical, and control characteristics of the wings, horizontal stabilizer, fin, and all control surfaces.

1:2 The degree of protection shall be equal to or better than that afforded by that quantity of heat which will raise the leading-edge 10 per cent heated region average temperature 100 deg F above static ambient air temperature for the condition of 60 per cent engine rated power at 18,000 ft pressure altitude and maximum load, less fuel required to climb to 18,000 ft pressure altitude.

1:3 All air-duct inlets, outlets, breathers, exposed mechanical devices, and illuminating fixtures on or in the surface shall be provided protection equivalent to that afforded the leading-edge areas as specified in 1:2.

1:4 The intermittent operation of the thermal system as presently designed for the aerodynamic lifting surfaces shall not be allowed except during emergency let-down and landing operations.

Windshield. The practical application of the heated windshield has been extensive and therefore the preparation of specifications for this part of the ice prevention does not involve as many questionable issues as other parts with which service experience is limited. The double-glazed windshield, which is heated by the passage of heated air between the panels, has provided protection but is subject to many faults. Freedom in design is desirable therefore in order that new and better solutions to the problem may be developed in service. The wording of the windshield specification should allow this freedom. Since the air-heated system is the principal method now available, the specification should also seek to stimulate the improvement of this method by manufacturers who desire to continue its use.

The external air film, infrared electric heating, electric conducting transparent film, and embedded resistance-wire electric heating all show promise and may replace the double-glazed arrangements.

Specifications for windshield ice prevention are recommended as follows:

2:1 Means shall be provided through the use of heat whereby the vision of the pilots through the cabin transparencies will not be reduced by the formation of ice, frost, or fog on inside or outside, in any maneuver in flight or on the ground.

2:11 The provision of adequate vision at all times must be achieved without the use of knock-out panels or the opening of windows.

2:2 The heating of the pilot's windshields shall not impair the comfort in the cabin of the airplane or cause irritation to the eyes, nose, or throats of personnel in the pilot's cabin.

2:3 The prevention of ice on the windshield should be accomplished without the resort to water repellents on the outer surface of the glass.

2:4 The operation of the thermal ice-prevention equipment shall not reduce the protection which is afforded by the windshield to the cabin occupants against bird impacts and similar hazards.

2:5 The construction of the heated windshield shall not seriously impede the cleaning of the windshield glass.

2:6 The heating of the windshield shall not cause an optical distortion of the pilot's view.

2:7 The heating of the windshield shall not cause an accelerated deterioration of the plastic binders of safety glass or of elastic or plastic frame seals of the panel in the airplane.

2:8 The protection against ice on the windshield should be equal to or better than that which is afforded when 1000 Btu of heat per sq ft per hr is passed through the outer surface of the transparency at an indicated airspeed of 150 mph.

Propeller Blades. Although the quantity of heat required for the protection of the propeller blades has not been evaluated by analysis, experimental data have been collected whereby adequate specifications can be prepared. As in the case of other equipment previously noted, freedom of design should be permitted because there are several ways in which the thermal system can be employed with apparently equal results. Ice on the blades of a constant-speed propeller reduces the efficiency of the propeller at all blade angles and also reduces the blade angle in accordance with the increase in drag of the blade section. Protection of propellers therefore should be as nearly perfect as possible.

The Army Air Forces Specification No. 29245, November 15, 1945, may well serve as a guide in the detail specifications of the blade-heating equipment. The specifications as follows are also recommended:

3:1 Means shall be provided whereby the propeller blades shall be heated in a manner and to a degree which shall prevent

the loss of propulsive efficiency or excessive propeller unbalance by ice formations or damaging shedding of ice fragments at all operating conditions in the air or on the ground.

3:11 The prevention of ice on a propeller which is feathered shall not be required.

3:2 The protection on the propeller blade should be equal to or better than that which is afforded by the continuous dissipation of 3.2 w per sq in. average over the leading-edge 20 per cent chord region and 75 per cent of the span measured from the hub face, or by the intermittent dissipation of 3.5 w per sq in. over the same area.

3:3 The construction of the blade-heating system shall provide for a heating intensity on the leading-edge one-third of the heated area which is double that on the rear two-thirds.

3:4 The propeller-blade heating installation or its operation shall not cause a reduction of the normal propeller efficiency.

3:5 The construction of electrically heated blade shoes shall allow for trimming of the tip end when this region has become abraded by wear.

3:6 The passage of heated air through a propeller blade shall not cause an apparent increase in the propeller noise level.

3:7 The operation of the propeller ice-prevention system during reverse pitch braking is not required.

Miscellaneous Parts. Specifications for the provision of protection on regions and parts, the formation of ice on which does not create at once a direct hazard, are recommended as follows:

4:1 The formation of ice on the front of the fuselage, engine nacelles, propellers, spinners, or hubs shall be prevented if ice formations on these parts, individually or collectively, cause a significant reduction in the performance of the airplane, or if the formation causes danger to, or malfunctioning of, the affected part or any other part of the airplane.

4:2 The formation of ice shall be prevented by thermal means on the fuselage, and other places not otherwise specified, from which dislodged ice formations may cause damage to other parts of the airplane.

4:3 Radio antennas and masts should be located so as to minimize the formation of ice thereon, and the strength of these parts should provide for carrying maximum ice formations without structural failure.

4:4 Provision shall be made for the intermittent removal of ice from all protuberances, antenna wires, masts, and extending mechanisms when such formations reduce the specified performance of the airplane or adversely alter the operational usefulness of the airplane.

Specifications for the protection of minor functional parts are recommended as follows:

4:5 Provision shall be made for the prevention of ice formations by thermal means on air speed total- and stati-pressure orifices, on the mast supporting such instruments, and on the surface of the airplane where flush-type static orifices are employed.

4:6 Wherever possible, air-intake scoops should be designed so as to eliminate the vulnerability of the scoop to ice formations, otherwise provision shall be made for the prevention of ice by thermal means from air-inlet scoop and guide vanes within air scoops.

4:7 Provision shall be made for shielding all exposed mechanisms not otherwise protected from the formation of ice, the formation on which would cause damage or malfunctioning to the mechanism.

Engine Air-Induction System. The protection against ice in the engine air-induction system is considered to be of first importance by pilots and operators. No other phase of the icing problem can affect the performance and safety as suddenly and dangerously as does ice in the carburetor and other induction parts. The provision of satisfactory protection has been handicapped because of the circuitous channels of procurement and divided or questioned responsibility. Protection for the induction system involves considerations of engine, carburetor, airplane design, and airplane operations. In the past, the engine and carburetor have frequently been designed without consideration of the ice problem. In other instances, false claims have been made which have misled the pilots until authentic operating data were available.

The only satisfactory solution to the induction icing problem is one in which no ice is allowed to form during all operating condition. The operation of the system should not adversely alter the performance of the airplane and should not limit the operation of the engine when ice is being prevented. Whereas these requirements are important in consideration of reciprocating engines, they are even more important when turbine type engines are employed.

Recommended specifications for the protection of the engine air-induction system are as follows:

5:1 Provision shall be made for preventing the accumulation of ice in the engine air-induction system through the use of thermal means.

5:11 The thermal system of ice prevention shall provide for the heating of the walls, exposed parts, and protuberances in the induction system,to, or above, the freezing temperature of water; or

5:12 The thermal system of ice prevention shall provide for the heating of the engine air to a temperature above the freezing point of water at all points along the path of air flow.

5:2 The use of the thermal system shall not limit the power rating or manifold pressure at which the engine may be operated when the system is in use.

5:3 The use of the thermal system shall not reduce the power of the eingine (because of a reduced ram pressure in the engine manifold) to an extent which will reduce the operational efficiency of the airplane.

5:4 The operation of the thermal system shall not require adjustment by the pilot of the airplane nor shall any attention from the crew be required by the equipment while it is in use.

5:41 Required thermal modulation, where not inherent in the system, shall be provided by automatic devices.

Miscellaneous Mechanical Equipment. Good mechanical design of aircraft is a production of good engineering administration, a willingness on the part of the manufacturers to allow adequate time for design and tests of new developments, and an accurate statement by the operator who buys the airplane of the anticipated requirements. Some detail mechanical specifications are desirable, however, several items of which follow:

6:1 A source of heat or power for each component of the thermal system shall be provided which will have adequate capacity for all normal and emergency operating conditions and for all meteorological conditions to be encountered.

6:11 Operating conditions in which the thermal system shall be required to function are engine warm-up, taxiing, take-off, climb, climb with one engine inoperative, cruise at all loading and power conditions, cruise with one engine inoperative, 400 fpm let-down with 45 per cent or more engine power, 400 fpm let-down with one engine inoperative, and landing.

6:2 Provision shall be made to protect the airplane structure and equipment, which will be in contact with the circulated heating medium, against corrosion from active ingredients contained therein.

6:3 In so far as the output of the heating source is not inherently modulating, provision shall be made to limit the maximum temperature of the circulating medium to 350 F.

6:4 Provision shall be made, in systems employing exhaust gas-air heat exchanger or exhaust gas-air mixing equipment, to close the hot-air duct if a fire occurs in the engine nacelle.

6:41 In event of fire in the engine nacelle, the hot-air duct shall be closed with a stainless-steel valve by automatic means.

6:5 Provision shall be made for easy access to the equipment of the thermal system, for easy inspection, and for the repair of the wing and empennage leading edges, ducting, and valves by normal aircraft sheet-metal shop practices and without excessive cost.

6:6 An indication of good duct design shall be when the pressure losses in the duct do not exceed those occuring in the heat exchanger, combustion heater, or wing leading-edge internal heat-transfer system.

6:7 Provision shall be made to prevent the absorption of liquids such as hydraulic fluid or oil into the thermal insulation of hot-air ducts.

6:8 Only such insulating materials may be employed on the ducts which are fireproof, contain no volatile oils, and which do not deteriorate when subject to aircraft vibration.

6:9 Flexible fabric connectors may not be used in the air duct system.

Acceptance Tests. The approval and acceptance tests of the equipment should be given careful consideration in the specifications. Although the only permanent proof of acceptability will be satisfactory protection in ice over a long period of service, preliminary tests on one airplane can serve to show approximately the thermal qualities and therefore the ice protection to be afforded. It should be noted, however, that the only practical time to change the thermal ice-prevention system is when it is still on the drawing board.

Recommended specifications for the acceptance tests and instrumentation of the thermal system are as follows:

7:1 The capacity of the thermal system to produce and distribute the required quantities of heat to the protected components shall be demonstrated prior to flight tests and preferably prior to the assembly and fabrication of the components into the airplane.

7:11 The capacity of the thermal system shall be determined from airflow rates and air-temperature measurements.

7:12 The flow rate to each component of the thermal system shall be within 5 per cent of the designed flow rate when the rate through the air inlet is in accordance with the design value.

7:13 The quantity of heat delivered to each component of the system shall be within 10 per cent of the design value.

7:2 The capacity of the thermal system to modulate the air temperature within specified limits shall be demonstrated in accordance with the performance demonstration as specified in 7:1.

7:3 The measurement of temperatures may be by thermocouples and manual or automatic recording potentiometers.

7:4 Installations employing exhaust-gas exchangers or gas-air mixing devices shall demonstrate that the back pressure on the engine is within allowable limits, that specified temperature modulation is achieved, and that the capacity of the heat source is adequate for all conditions as specified in 6:11.

7:50 A demonstration of the control system shall be made prior to flight wherein all normal and emergency contingencies which may be encountered will be simulated.

7:51 The control system shall cope with all operational contingencies with the safety of the airplane and personnel maintained.

7:60 The performance of the thermal system shall be demonstrated in flight in dry air and in stratus-type clouds.

7:61 Flight-performance tests shall demonstrate the normal and emergency operation of all controls, burners, heaters, valves, safety devices, and equipment of the thermal system.

7:62 Flight-performance tests shall demonstrate that the heat is properly distributed to the various components of the heated system.

7:621 The demonstration of heat distribution shall be made in dry air, and stratus clouds at kinetic temperature above 32 F, and in cloud conditions as obtainable at kinetic temperatures between 0 and 32 F.

7:70 Provision shall be made and procedures outlined in printed form whereby all components of the thermal ice-prevention system may be observed in operation and inspected when the airplane is at rest on the ground.

7:80 The thermal system should be equipped with a means of indicating in flight that heat is or is not being supplied to the wings, empennage, and propellers. The indicator shall be within the full view of the pilot's, copilot's, or flight engineer's station.

Conclusion

The use of the thermal ice-prevention system involves many aspects of heat transfer. The progress which has been made in establishing a solution to the problem has, in large part, been due to the interest which has been given to the application of the thermal system by engineers who have given special study to this branch of engineering.

The use of the thermal system, however, has not been different from most other engineering applications of heat in that the problem involves many considerations which require a knowledge of other branches of engineering. In our present case, the aerodynamics of the wings, the propulsion of the propeller, the metallurgy of the structure materials, the economics of operational aeronautics, and many other branches of knowledge, which are important fields of specialization, must be considered.

The specifications and comments enumerated above cannot be expected to be complete in all detail. They do call attention, however, to many features of the thermal system that might otherwise not have been considered by engineers who have not had the opportunity to follow closely the research and development work on this problem. Giving to the design engineer in the factory and the operations engineer in the air line the most complete statement of the experiences of the research work should enable us to obtain the best equipment, at the least cost, and in the shortest time.

Acknowledgment

In the use of all information in this paper, acknowledgment is given to the N.A.C.A., by which the data were established, to the Army Air Forces and the Bureau of Aeronautics which sponsored many of the projects, and to the air lines and manufacturers who have faithfully encouraged and supported the work on the ice problem.

BIBLIOGRAPHY

1 "Recent Flight Research on Ice Prevention," by L. A. Rodert, L. A. Clousing, and W. H. McAvoy, A.R.R. N.A.C.A., January, 1942.

2 "Flight Tests of Thermal Ice-Prevention Equipment on a Lockheed 12A Airplane," by Richard Scherrer, A.R.R. N.A.C.A., November, 1943.

3 "Flight Tests of the Thermal Ice-Prevention Equipment on the B-17F Airplane," by B. C. Look, A.R.R. N.A.C.A., February, 1944.

4 "An Aircraft Double Windshield—Its Development and Use," by R. L. McBrien, *S.A.E. Journal*, vol. 51, 1943, Trans. Section, pp. 350–355.

5 "An Investigation of a Thermal Ice-Prevention System for a C-46 Cargo Airplane. IV—Results of Flight Tests in Dry-Air and Natural-Icing Conditions," by James Selna, C. B. Neel, Jr., and E. L. Zeiller, A.R.R. N.A.C.A., February, 1945.

6 "Tests of Thermal De-Icing Equipment for Propellers," by Richard Scherrer and L. A. Rodert, A.R.R. N.A.C.A., January, 1944.

7 "De-Icing of an Aircraft-Engine Induction System," by H. A. Essex, A.R.R. N.A.C.A., August, 1943.

8 "A Description of the Ju 88 Airplane Anti-Icing Equipment," by L. A. Rodert and Richard Jackson, R.B. N.A.C.A., September, 1942.

9 "A Report on the German Commercial Airline, the Deutsche Luft-Hansa," by O. E. Kirchner, S.A.E. Preprint, annual meeting, January, 1946.

10 "The Airplane Icing Problem and Its Alleviation Through Research," by A. R. Jones, S.A.E. Preprint, November 1, 1945.

11 "An Investigation of a Thermal Ice-Prevention System for a C-46 Cargo Airplane. VI—Dry-Air Performance of Thermal System at Several Twin- and Single-Engine Operating Conditions at Various Altitudes," by James Selna and H. L. Kees, A.R.R. N.A.C.A., May, 1945.

12 "An Investigation of a Thermal Ice-Prevention System for a C-46 Cargo Airplane. V—Effect of Thermal System on Airplane Cruise Performance," by James Selna, A.R.R. N.A.C.A., May, 1945.

13 "An Investigation of a Thermal Ice-Prevention System for a C-46 Cargo Airplane. VII—Effect of the Thermal System on the Wing-Structure Stresses as Established in Flight," by A. Jones and B. A. Schlaff, A.R.R. N.A.C.A., September, 1945.

14 "Kinetic Temperature of Wet Surfaces, A Method of Calculating the Amount of Alcohol Required to Prevent Ice, and the Derivation of the Psychrometric Equation," by J. K. Hardy, A.R.R. N.A.C.A., September, 1945.

15 "Report on the Development and Application of Heated Wings, Addendum I Army Air Forces Technical Report 4972, January 9, 1946," by Myron Tribus and J. R. Tessman.

16 "An Analytical Investigation of Thermal-Electric Means of Preventing Ice Formations on a Propeller Blade," by Richard Scherrer, A.R.R. N.A.C.A., August, 1944.

The Escher Wyss-AK Closed-Cycle Turbine, Its Actual Development and Future Prospects

By CURT KELLER,[1] ZURICH, SWITZERLAND

This paper is the first comprehensive presentation in this country of details of the gas-turbine process employing a closed cycle. In spite of grave handicaps entailed by the war, the development of this turbine proceeded from the first experimental installation in 1939, to the advanced designs which are now available for industrial application.

Introduction

UNLIKE combustion turbines little has so far been reported in the United States about the gas-turbine process employing a closed cycle. The first plant of this kind was completed in Switzerland during the summer of 1939, just before the outbreak of war, namely, an experimental installation of 2000-kw useful output, Fig. 1. The enforced seclusion of Switzerland during the last 6 years, and more especially the interruption of communications with America made it impossible to discuss this new AK-plant, developed by the Escher Wyss Engineering Works in Zurich according to proposals made by Ackeret[2] and Keller.

However, in spite of the many difficulties arising from the war, it nevertheless proved possible to try out the experimental plant until normal industrial operation was reached and to investigate fully all its components.

About a year ago Prof. H. Quiby (the successor of Professor Stodola at the Swiss Federal Institute of Technology in Zurich) carried out exhaustive official performance trials on the new plant. A report (8)[3] on these trials was published in June, 1945. These official trials represent the termination of the first phase of internal scientific development, and the results obtained have justified in every respect both the theoretical and practical expectations. Projects embodying such a closed-circuit plant for power generation or ship propulsion can now be realized, on the basis of the preliminary studies extending over a number of years, without unwarrantable technical risks being involved. The questions that arise in this connection and the constructional solutions which we consider suitable from the technical point of view will now be mainly dealt with.

Since 1939 a number of original publications have been made regarding the theoretical and physical basis of the AK-process, which are now also accessible to American engineers (several of these articles have already been printed in English). The Bibliography of the chief papers regarding this field, together with the short index at the end of this paper, are quite comprehensive.

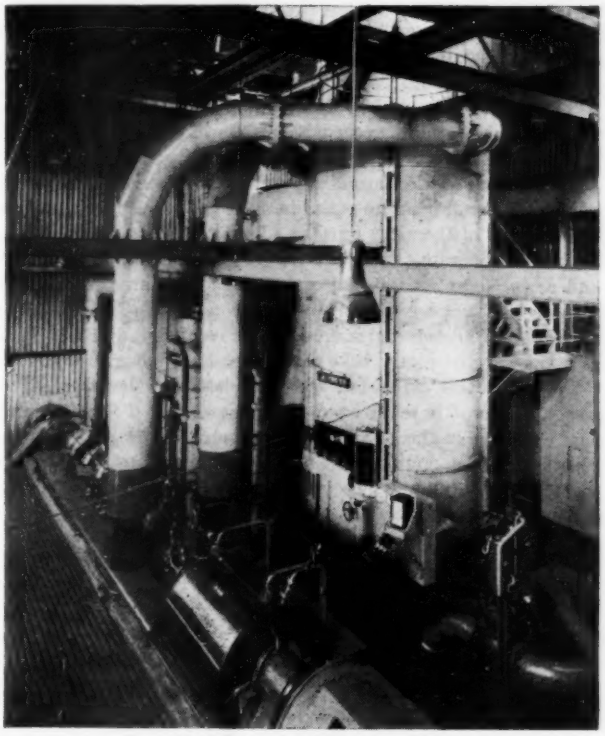


Fig. 1 General View of the First 2000-Kw Experimental Plant at Escher Wyss Works in Zurich, Switzerland

It will suffice therefore to give a brief summary of the chief characteristics of the new process as an introduction. Some information, but not all the data, was provided in a preliminary report which was read by R. T. Sawyer and discussed by S. A. Tucker during the June, 1945, meeting of the Society.

In recent months we have been favored by a number of visits from American engineers who came to the Escher Wyss Works, where information concerning the development work in connection with these AK-plants was given, and the trial installation itself was explained. As a consequence, our work in this field has become known among a wider circle of specialists.

The publications hitherto made with regard to the basis and development of the AK-process will be supplemented for the first time in the present paper by referring in greater detail to studies and designs, so far not published, for closed-circuit units which from the technical point of view are now practicable, and by remarks concerning the later uses and further possibilities of development. Since the research work and the whole field for such installations are very extensive, it is possible within the framework of the present paper to discuss only the principal ideas on the basis of examples.

[1] Director of Research, Escher Wyss Engineering Works.

[2] Professor of Aerodynamics and Flow Mechanics, Swiss Federal Institute of Technology, Zurich, Switzerland.

[3] Numbers in parentheses refer to the Bibliography at the end of the paper.

Contributed by the Oil and Gas Power Division and presented at the Annual Meeting, New York, N. Y., November 26–29, 1945, of The American Society of Mechanical Engineers.

Note: Statements and opinions advanced in papers are to be understood as individual expressions of their authors and not those of the Society.

Summary of Theoretical and Physical Bases of Closed Circuit and its Particular Features

As in the case of all other gas-turbine processes, it is our endeavor to approach as closely as possible the thermal efficiency of the ideal process for thermal prime movers, namely, the Carnot process, and furthermore with means which are simple in practice and at the same time economical. The closed gas cycle offers favorable possibilities for realizing this aim.

In the case of air or other technical gases the Carnot process proper, Fig. 2, is accompanied by numerous practical drawbacks, because for attaining the high initial temperatures T_1, which modern steels are capable of withstanding, very high pressure ratios P_1/P_2 from 200 to 300 have to be dealt with, especially during the adiabatic compression, which is difficult to realize in turbomachines.

The AK-process endeavors to bring about a cycle, the so-called double-isotherm cycle, which is thermodynamically equivalent to the Carnot cycle for gases. Fig. 3 illustrates this cycle in comparison with the Carnot cycle proper. The AK-process employs only small pressure ratios between A and B for isothermal compression of the air. Further adiabatic compression between B and C; according to Carnot, is intentionally dispensed with and replaced by an internal exchange of heat at constant final pressure of the preceding isothermal compression. The supply of heat from an external source by the combustion of fuel shall, as in the Carnot process, take place exclusively along the isotherm C-D. After this expansion with simultaneous development of power, the heat is reimparted to the gas along B-C by internal heat exchange in the circuit itself, whereby the pressure remains constant. This double-isotherm circuit has exactly the same theoretical efficiency as the Carnot cycle and is, consequently, dependent only upon the temperatures

$$\eta = \frac{T_1 - T_2}{T_1} \text{ (absolute temperatures)}$$

But the high pressure ratio, which is such a drawback, is entirely avoided; it can be reduced to a small fraction of the foregoing value, and one is not bound to a given relationship $P_{max} : P_{min}$ for attaining the maximum temperature T_1.

The hatched surfaces $ABCD$ in the entropy diagrams, Figs. 2 and 3, illustrate the work obtained for each unit weight of gas (air) for the Carnot circuit and for the double-isotherm circuit. This work is the difference between the turbine output $D'C'CD$ (= heat supplied from external source Q_{in}) and the compression work $A'B'BA$ (= heat carried away in cooling water Q_{out}). The relatively large proportion of compression work in the case of gas processes is clearly shown by the entropy diagram.

Complete isothermal compression and expansion can, of course, be only approximately realized in the machines that are available in practice. However, compression and expansion by stages, with intermediate cooling or heating (indicated by dotted lines on the AK-diagram) permit of this aim being put into practice to a considerable degree with only a few stages. The average temperatures T_1' for the supply and extraction of heat T_2' do not then deviate very considerably from the highest and lowest temperature of the ideal circuit. At the same time, the chief requirement of the thermal law is still largely fulfilled, namely, that the whole heat shall be imparted to the working medium at high temperature, and the remaining heat, after the development of power, be extracted at as low a temperature as possible.

An important new feature of the AK-process lies in the fact that the working medium is not taken from the atmosphere and afterward returned to the ambient air, as occurs in the case of all old reciprocating machines employing hot air, as well as in open-circuit gas turbines. Furthermore, since the AK-circuit is closed, it works with higher pressure of which the lowest pressure at the compressor inlet already lies considerably above atmospheric pressure. The chief characteristics, namely, a double-isotherm circuit with high-speed turbomachines and heat exchange, heat supply from an external source and raising of the

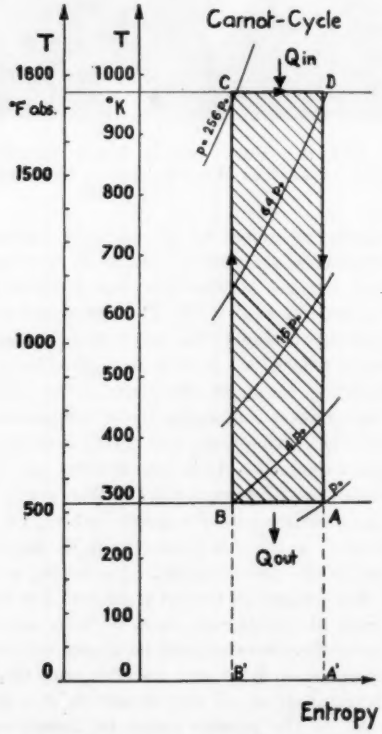


Fig. 2 Entropy Diagram of Carnot Process for Gases

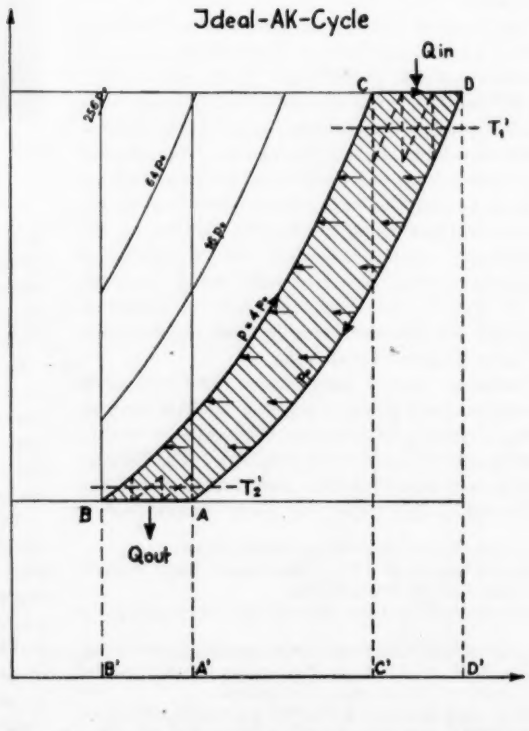


Fig. 3 Entropy Diagram of AK-Process With Complete Regeneration, Which Is Equivalent to Fig. 2

pressure level, have decisive consequences for the realization in practice, to which reference will now be made.

To illustrate the fundamental difference between the method of operation of the ordinary combustion turbine and the closed circuit of the AK-plant, simplified layouts for these different installations are compared with one another in Figs. 4 and 5. In

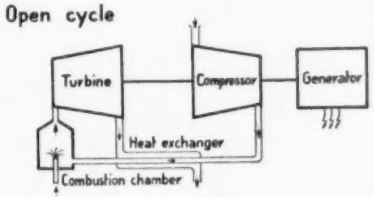


FIG. 4 SCHEMATIC DIAGRAM OF OPEN CIRCUIT OF COMBUSTION TURBINE WITH HEAT EXCHANGER

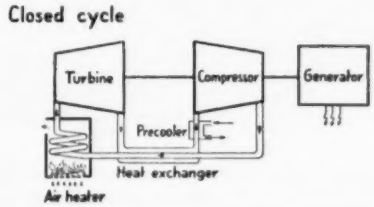


FIG. 5 SCHEMATIC DIAGRAM OF CLOSED CIRCUIT OF AK-PLANT

place of the combustion chamber, the closed-circuit system has an air heater which is heated from an external source, corresponding to the boiler of a steam-turbine plant. In comparison with the open-combustion turbine which discharges its waste air to the open, the only additional component of the AK-plant is a precooler which cools the working medium after it has passed through the turbine and heat exchanger, to as low a temperature as possible before being reinhaled by the compressor. The principal features of our process and the characteristics resulting therefrom may be summarized as follows:

The Closed Pressure Circuit. Soiling of runner or impeller blading as well as of heat-exchanger surfaces by combustion residue or other foreign matter is completely eliminated, which provides a guarantee that the efficiency of the machines and the heat-transmission coefficients will remain unchanged. The working medium, which is always clean, permits the adoption of small cross sections for the elements of the heat exchangers.

The system is so supercharged that the pressure at the suction branch of the compressor already lies considerably above atmospheric pressure. As a consequence of this supercharging the dimensions of all parts of the plant, both machines and heat exchangers, are considerably reduced, on the one hand owing to the smaller specific volume of the working medium, and on the other hand because of the considerably increased heat-transmission coefficients at a higher pressure. Such supercharged operation permits of the unit outputs being increased almost without limit.

External Heating. By separating the circuit of the working medium from that of the combustion air it becomes possible to employ any kind of solid, liquid, or gaseous fuel, such as bituminous coal, lignite, oil, or gas.

Output Regulation. The output of the plant can be varied by changing the pressure level without altering thet emperatures and while maintaining the efficiency practically unaltered at all loads. By raising or lowering the pressure level (brought about by temporarily supplying or extracting working medium to or from the circuit), the plant can be suited to any desired part load, simply by changing the density of its working medium. In doing this the flow conditions in the machines, the pressure ratios, the velocities, and the angles of attack to the blades remain practically unchanged, the same being true of the internal efficiency. Hence the machines always operate at exactly the same point of their pressure-volume characteristic. Consequently, the efficiency of the plant is almost equally high at part loads as at full load, only the constant losses arising from bearing friction and heat radiation being proportionately more pronounced at part loads.

The fact that the temperatures remain unchanged at all loads is a particular advantage for the practical operation of such plant at high temperatures. No regulating valves, etc., are provided in the circuit proper, i.e., either on the machines or auxiliaries. The means for controlling the supply and withdrawal of air, which is stored in cold compressed-air accumulators, are united in a regulating set outside the circuit of the working medium and are traversed only by cold air.

The Use of Other Gases. Other working media than air can be adopted only in the case of a closed circuit with an external supply of heat. The employment of suitable light gases, such as helium, for example, opens up the possibility of increasing the output of the plant for the same dimensions, or of further raising its efficiency, as a consequence of the particular physical characteristics of such gases for special purposes (drive of transport means or aircraft).

OPERATING CYCLES OF THE AK-PROCESS

The simplest air turbines operate with direct expansion in the turbine itself and with two intermediate coolers in the compressor, as may be seen in Fig. 6. The most favorable pressure ratio

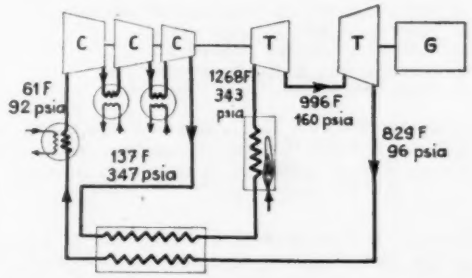


FIG. 6 DIAGRAM OF ONE-STAGE GAS TURBINE WITH MEASURED DATA OF CIRCUIT FOR FULL-LOAD OPERATION
(This was the first plant.)

for such a plant, with consideration of the efficiency and constructional requirements, is about 3 to 4 as for open-combustion turbines, with maximum pressures of 400 to 500 psi, depending upon the output. Since the efficiency is independent of the absolute pressure in all air circuits, these pressures are chosen only with regard to the constructional requirements. Even for the largest outputs no very high pressures are necessary, i.e., such as are encountered in steam turbines. For initial temperatures from 1200 to 1400 F, the discharge temperatures from the turbine are not higher than 750 to 950 F, so that no special alloyed steels are necessary for the heat exchangers. The example provided by the experimental plant proves that noteworthy thermal efficiencies can even now be attained with single-stage designs.

Fig. 7 shows the thermal efficiency which was measured during the official performance trials on the first experimental plant. In this connection it should be borne in mind that when this experimental plant was projected the chief intention was to try out the principle itself and test the co-ordination between the various components of the circuit. As a consequence of the in-

tended experimental work, the plant was laid out to insure easy accessibility to all parts thereof, so that measurements could be carried out without difficulty. Consequently, neither the arrangement nor the space requirements of the experimental plant may be taken as a criterion for later industrial installations which can be made much more compact.

The Sankey diagram, Fig. 8, shows the course of the heat quantities flowing through the various parts of the plant. Such a diagram applies in a similar manner to all single-stage installations. For each 1000 kw the AK-plant requires about 20 lb per sec working air in the circuit. In installations of larger output or to meet demands for higher efficiencies, we employ two-

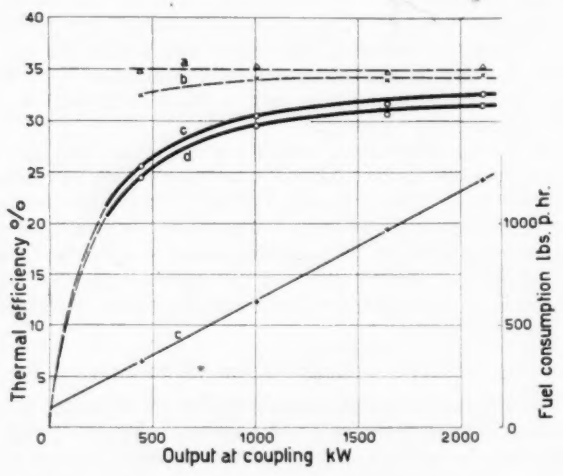


FIG. 7 OVER-ALL THERMAL EFFICIENCY OF PLANT, AS DETERMINED BY OFFICIAL TESTS CARRIED OUT IN DECEMBER, 1944
(Curves indicate effect of relatively large bearing and insulation losses as well as power needed for auxiliaries)

stage expansion with intermediate heating which can be easily put into effect, as the following examples demonstrate:

This two-stage expansion represents a further and sufficient approach to the double-isotherm process which it has been endeavored to realize from the beginning with the AK-process (see Fig. 3). Intermediate heating, or double heating, as we refer to it in the case of the AK-plant, brings about a saving in fuel of 10 to 15 per cent. Considerations of a theoretical and practical nature lead, in the case of double heating, to the increased pressure ratio of about 10.

As a result of the greater pressure ratio and consequently the larger heat drop in the case of double heating, with due consideration of the losses in the circuit, not only a considerable increase in the thermal efficiency is realized, but at the same time a further reduction is accomplished in the dimensions of the machines and auxiliaries. This applies, in particular, to the heat exchanger because the weight of the circulating working air per unit of output is considerably smaller (approximately 12 lb per sec per 1000 kw), and because the greater pressure ratio allows of larger pressure losses without reducing the efficiency.

Fig. 10 shows the conditions in the case of direct expansion (A) and double heating (B), with due consideration of the losses. The circuit with double heating (B), can be thought of as realized in practice by placing two single circuits (A) next to one another. If in both instances one takes the same values for the limit temperatures T_1, T_2, with the same machine efficiencies η_T, η_K but with twice the pressure losses $\epsilon_B = 2\,\epsilon_A$ and temperature differences $\Delta t_B = 2\,\Delta t_A$ in the recuperator for the case (B), then the course of the efficiencies applies for (A) and (B) equally, if only the pressure ratio is taken as abscissa for (A) and for (B) the square of this ratio. The definition of ϵ is $\epsilon = \frac{\Delta p}{p_1}$, $\epsilon_2 = \frac{\Delta p}{p_2}$

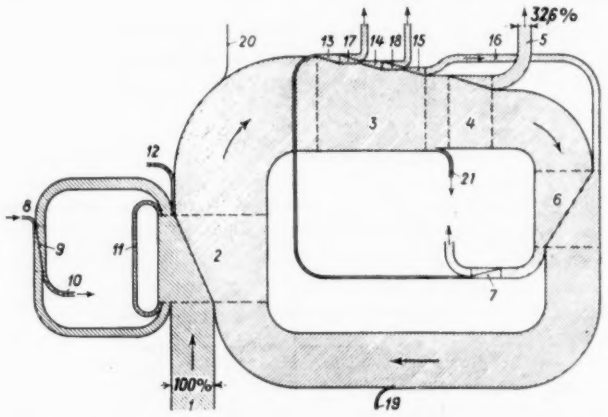


FIG. 8 SANKEY DIAGRAM FOR SINGLE-STAGE TEST UNIT, SHOWING QUANTITIES OF HEAT IN ACTION THROUGHOUT PLANT
(This is also typical for other installations of this kind.)

1	Calorific heat value of fuel	11	Circulating flue gases
2	Air heater	12	Heat losses of air heater
3	High-pressure turbine	13	Low-pressure compressor
4	Low-pressure turbine	14	Medium-pressure compressor
5	Output at turbine coupling	15	High-pressure compressor
6	Heat exchanger	16	High-pressure circuit air
7	Precooler	17	Low-pressure intercooler
8	Combustion air	18	High-pressure intercooler
9	Combustion-air preheater	19	Heat losses on high-pressure side
10	Chimney	20	Heat losses on low-pressure side
		21	Mechanical losses

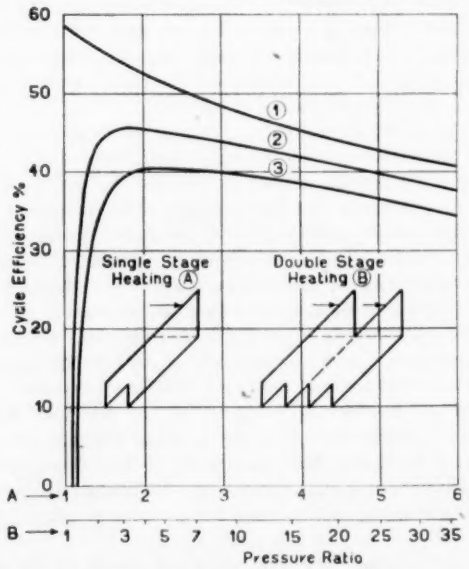


FIG. 9 CYCLE-EFFICIENCIES FOR SINGLE-STAGE AND TWO-STAGE INSTALLATIONS

Assumptions: $T_1 = 1200$ F, $T_2 = 80$ F $\eta_T = 91$ per cent, $\eta_c = 86$ per cent

Curve 2 valid for $\Delta t_A = 18$ F $\epsilon_A = 5$ per cent
or $\Delta t_B = 36$ F $\epsilon_B = 10$ per cent
Curve 3 valid for $\Delta t_A = 36$ F $\epsilon_A = 10$ per cent
or $\Delta t_B = 72$ F $\epsilon_B = 20$ per cent
Curve 1 valid for $\Delta t = 0$ $\epsilon = 0$
for both cases

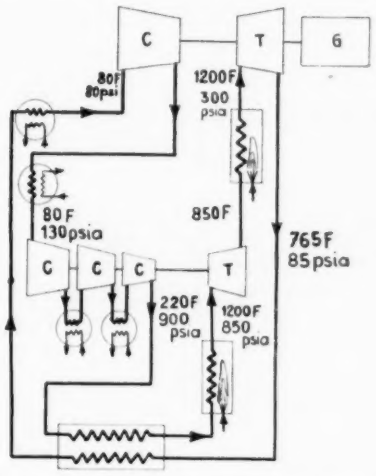


FIG. 10 DIAGRAM OF TWO-STAGE PLANT WITH INTERMEDIATE HEATING AND TYPICAL DATA OF CIRCUIT

Δp = pressure drop on high-pressure side with pressure p_1, or low-pressure side, p_2.

With reference to Fig. 9, curves 2 and 3 have been plotted for two different pairs of values Δt, ϵ. Assuming the same difference in temperature, for example $\Delta t = 36$ deg F, and the same pressure losses $\epsilon = 10$ per cent with direct expansion and double heating, the difference between curves 2 and 3 indicates the improvement by double heating. In the technically useful field of suitable pressure ratios, it amounts to 4 per cent absolute.

As already pointed out, the quantity of air in circulation becomes smaller owing to the greater pressure drop for double heating, so that the heat-exchanging surfaces are likewise reduced. If in the case of (*B*) one intentionally renounces to a certain extent an improvement in efficiency by allowing greater temperature and pressure losses as a consequence of increased velocities, the conditions will be those of the field between 2 and 3. However, in this way the surfaces of the heat exchangers as well as the other dimensions can be reduced considerably.

Installations with double heating operate according to the schematic diagram, Fig. 10. The corresponding Sankey diagram, Fig. 11, shows the reduced quantities of heat which are conveyed in comparison to Fig. 8. In actual installations, maximum pressures of 400 to 600 psia with back pressures of 40 to 60 psia will be adopted for small outputs, whereas for larger outputs above 10,000 kw, the pressure is raised to a maximum of 850 psia with about 85 psia back pressure. In this case also, the heat drops are so distributed that the heat exchanger can be built without requiring the use of special alloyed steels. The power stations and marine plants subsequently referred to operate according to this circuit.

EXAMPLES OF TYPICAL COMPONENTS OF CLOSED-CIRCUIT PLANTS

Although the duty of the various machines and apparatus remains fundamentally the same in all installations, various designs nevertheless result which are dependent upon the different outputs required, the uses to which the installations will be put, the efficiencies and the available fuels. The closed cycle, operating at a pressure above atmospheric, leads to conditions of construction which deviate considerably from other kinds of gas and steam turbines. The consistent application of knowledge gathered from the laws of flow, from up-to-date aerodynamics, and also concerning the improved properties of metals subjected to high temperatures, coupled with proper harmonizing of the various components, has in recent years led to ever-increasing simplicity for our designs. They deviate in many respects from the layouts usually encountered for turbomachines. An AK-plant is not simply an assembly of known components; the arrangement of the various parts in relation to one another and the course of the working medium through the whole installation are the subject of careful study, whereby due attention has been paid to heat expansion. Only in this way can the pressure losses in the pipings and the other secondary losses be reduced to an admissible measure.

In this connection it has proved advantageous that all parts of an AK-plant such as the turbines and compressors, as well as the heat exchangers and air heaters, form part of the actual manufacturing program of Escher Wyss, which specializes in the construction of turbomachines of all kinds. Thus all the components have been developed and built in the company's own works, the experience gathered in various fields being duly coordinated and proper use made of the latest research results obtained in the company's own hydraulic and caloric laboratories.

It should also be borne in mind that AK-installations are quite suitable for standardization. Thus for example, the whole range of stationary installations from 3000 to 50,000 kw can be dealt with by a few types of machines and auxiliaries. The component parts of the heat exchangers themselves as well as the regulating means can, for installations of these various sizes, be put together in suitable combinations. This standardization which has been attempted but never realized in the case of steam turbines will have a favorable influence on the price calculations.

Turbines and Compressors. Since the specific volume is re-

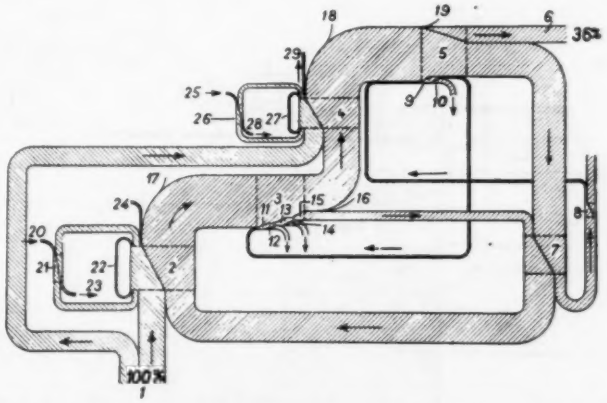


FIG. 11 SANKEY DIAGRAM FOR TWO-STAGE PLANT SIMILAR TO FIG. 8

1 Calorific heat value of fuel
2 High-pressure air heater
3 High-pressure turbine
4 Low-pressure air heater
5 Low-pressure turbine
6 Output at turbine coupling
7 Heat exchanger or recuperator
8 Precooler
9 Low-pressure compressor
10 Low-pressure intercooler
11 Medium-pressure compressor I
12 Medium-pressure intercooler
13 Medium-pressure compressor II
14 High-pressure intercooler
15 High-pressure compressor
16 Mechanical losses of high-pressure set
17 Heat losses on high-pressure side
18 Heat losses on medium-pressure side
19 Mechanical losses of low-pressure set
20 Combustion air of high-pressure air heater
21 Combustion-air preheater of high-pressure air heater
22 Circulating flue gases of high-pressure air heater
23 Chimney of high-pressure air heater
24 Heat losses of high-pressure air heater
25 Combustion air of low-pressure air heater
26 Combustion-air preheater of low-pressure air heater
27 Circulating flue gases of low-pressure air heater
28 Chimney of low-pressure heater
29 Heat losses of low-pressure air heater

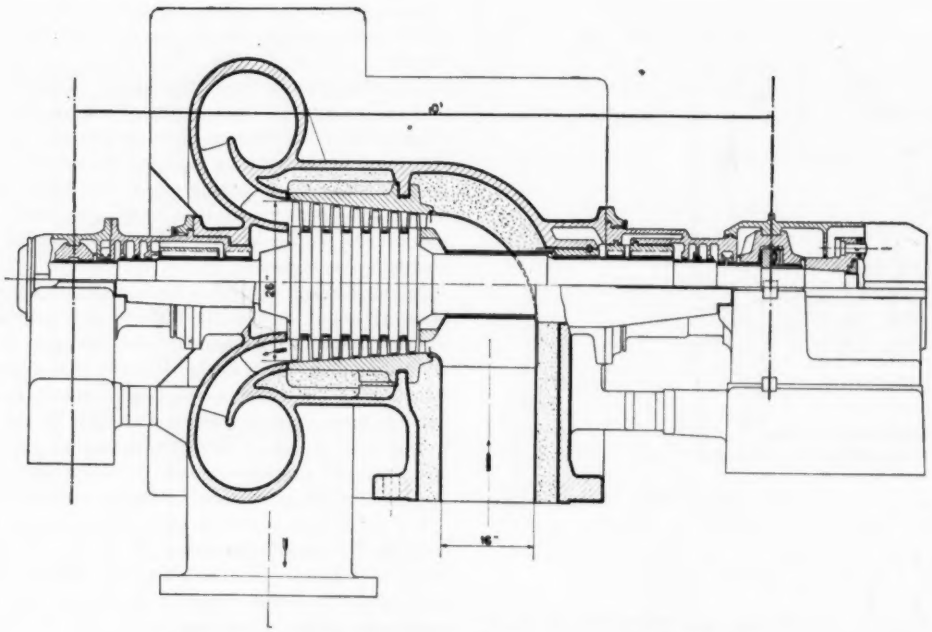


FIG. 12 CROSS SECTION THROUGH HP-TURBINE OF 25,000-KW SET
(The effective output of this turbine is 28,000 kw.)

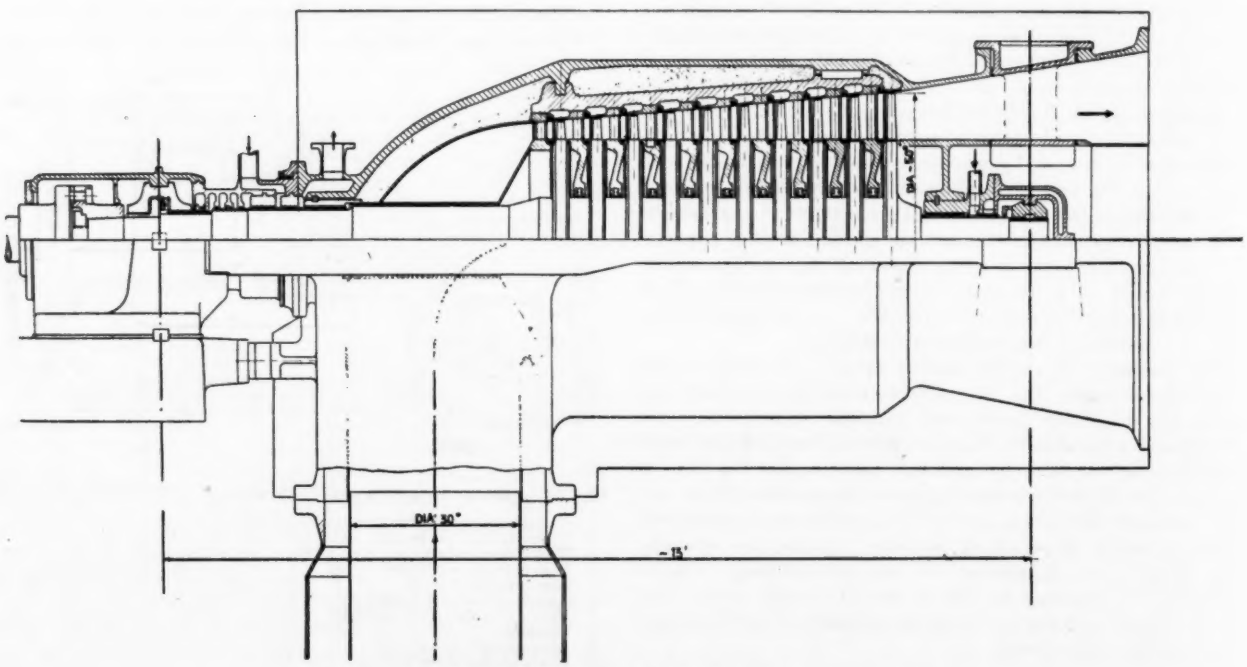


FIG. 13 CROSS SECTION THROUGH LP-TURBINE OF 25,000-KW SET
(The effective output of this turbine is 34,000 kw.)

duced owing to the raised working pressure of the closed circuit, the machines are astonishingly small when compared to open-circuit combustion turbines. In addition, the heat drop that has to be dealt with is much less than in the case of steam-turbine plants, so that the closed-circuit turbine has not many stages.

For informatory purposes the main dimensions of the rotors for standard AK-plants of various outputs have been indicated in Table 1. These dimensions may vary slightly according to the speed and blading (action or reaction) of the turbine, whether an axial or radial compressor and of course also in accordance with the pressure that is employed. For the greater part, however, the sizes of the machines will not prove very different from the figures indicated in Table 1. The fact that no regulating valves or stop valves are fitted to the machines leads to favorable conditions for the construction of such hot-air turbines.

This permits the adoption of constructional forms for the turbines which differ considerably from those usually employed for

TABLE 1 APPROXIMATE FIGURES FOR MACHINE OF CLOSED-CYCLE POWER PLANTS OF DIFFERENT OUTPUTS (60 CYCLES PER SEC)

Net output, kw	6000	12000	25000	50000	100000
Maximum pressure, psi	600	600	850	850	850
Maximum diameter of:					
High-pressure turbine, in	17	19	26	35	47
Low-pressure turbine, in	31	39	50	70	87
Maximum diameter of axial high-pressure compressor, in	10	12	16	20	27
Maximum diameter of axial low-pressure compressor, in	21	30	33	53	65

steam turbines, Figs. 12 and 13. Special attention has to be paid to the inlet and outlet losses which, as a result of the small pressure and temperature drops that are utilized, play a relatively important part. The absence of regulating devices permits of the turbine being situated, literally speaking, immediately in the piping which conducts the working medium, an arrangement with which one is familiar in the construction of hydraulic machines.

It is possible, for example, to pass the working medium through an inlet branch supply pipe to the first runner wheel without employing annular channels. The outlet can be made symmetrical and a considerable part of the kinetic energy can be recovered, for instance in spiral outlet casings as in hydraulic turbines or pumps. Such forms are also used for the axial-flow compressors. The small turbines also permit the adoption of double casings which are designed according to the same principle as the hot-air piping previously referred to. Between the thin internal shell and the external casing there is a layer of insulating material; the internal casing serves only for conducting the hot current, while the cold external casing takes up the pressure. The whole guide apparatus is fixed to the casing at a point where temperatures are low. In this manner the external casing is, even for high inlet temperatures, subject at the most only to the discharge temperature of the last stage (approximately 925 F). Thus although the turbine-inlet temperature is much higher, heat-resisting steel need not be adopted for the casing but only for the small internal parts.

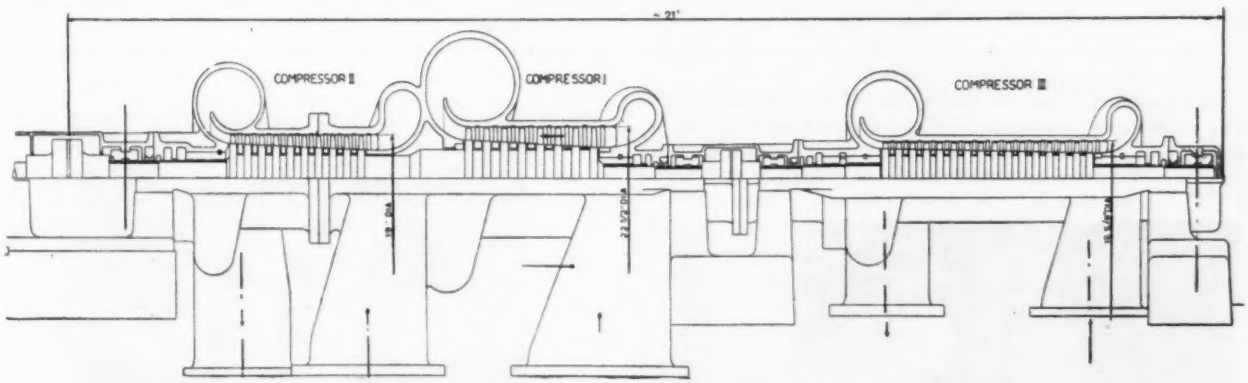


FIG. 14 CROSS SECTION THROUGH AXIAL-FLOW COMPRESSOR FOR 25,000-KW SET
(n = 6000 rpm.)

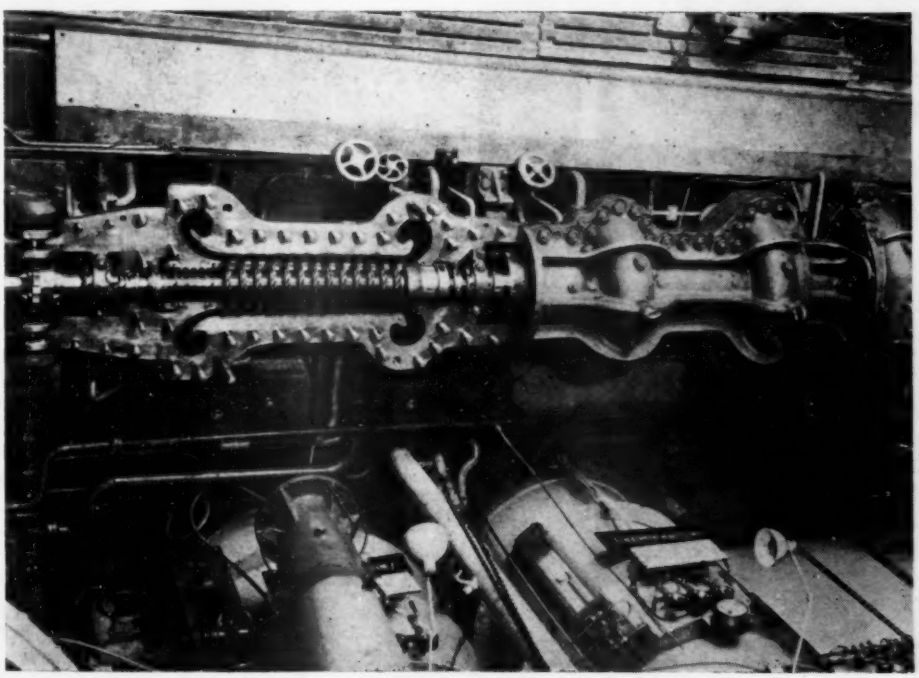


FIG. 15 VIEW OF AXIAL-FLOW COMPRESSOR WITH STREAMLINED INLET AND OUTLET CASING
(AK-Test Plant.)

Similar constructional principles, dictated by the latest knowledge in the field of flow techniques, apply also for the compressor and for the intermediate coolers forming part of the latter, Fig. 14.

Since relatively large quantities of air but small increases in pressure have to be dealt with, up-to-date axial-flow turbocompressors of the multistage type are particularly suitable for such duty. The high speeds needed for this type of compressor lie within limits which offer good constructional conditions also for the driving turbine. As a result of these high speeds the compressor set is of small dimensions even when dealing with the largest volumes. It has been possible to raise the efficiency of the bladings above the values attainable with radial compressors. This is again the outcome of systematic research in this particular field, Fig. 15.

As turbine and compressor always and at all loads work at the same operating point, high-quality blading need only be developed for this one point without compromises. For these conditions the course of the pressure-volume characteristic for part loads need not be considered. For the same reasons, for instance, in the case of small outputs of other gases, radial compressors can also be adopted thus leading to fewer stages.

Figs. 16 and 17 illustrate typical blading for AK-turbines and AK-compressors having stage efficiencies of more than 90 per cent. As a consequence of the raised pressure the Reynolds numbers of the machine bladings are of a considerably higher order, so that the percentage of friction losses becomes smaller. This holds good only for smooth and clean surfaces. Tests in our laboratories on a full-sized axial compressor inhaling ambient air, containing only usual workshop impurities, have proved that the blade efficiency dropped from 86 to 83 per cent during 12 hours continuous operation.

The rotating shafts of the machines are sealed from the ambient air by means of labyrinth glands or a combined system of labyrinth glands with liquid sealing, depending upon the size of the plant and the kind of gas employed. Good sealing is necessary in consideration of the losses, especially at smaller outputs or when employing special gases.

The glands illustrated in Fig. 18 have proved their merits in the case of the experimental plant. Sealing air extracted from the circuit is passed through a pipe to the labyrinth chambers. The pressure of this sealing air is at all loads always somewhat higher than the pressure inside the glands, corresponding to the point where it is bled from the circuit. In this way it becomes impossible for hot air to escape. From the point where sealing air is introduced another part branches off toward the exterior of the gland and flows into a collecting space which is connected to a point in the circuit where a somewhat lower pressure pre-



Fig. 16 Runner Wheel of HP-Turbine 12,000-Kw Set
(Diameter 32 in. approximately.)

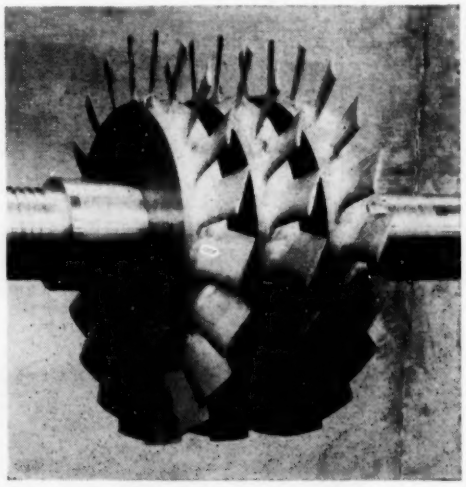


Fig. 17 Impeller of Modern Escher Wyss Axial-Flow Compressor

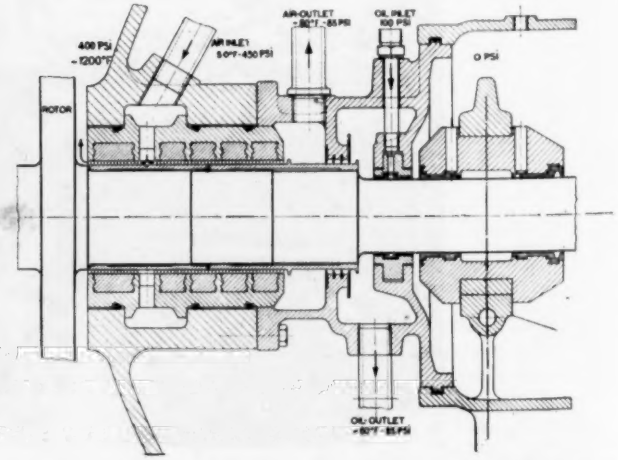


Fig. 18 Combined Labyrinth-Liquid Sealing for High-Temperature Turbines

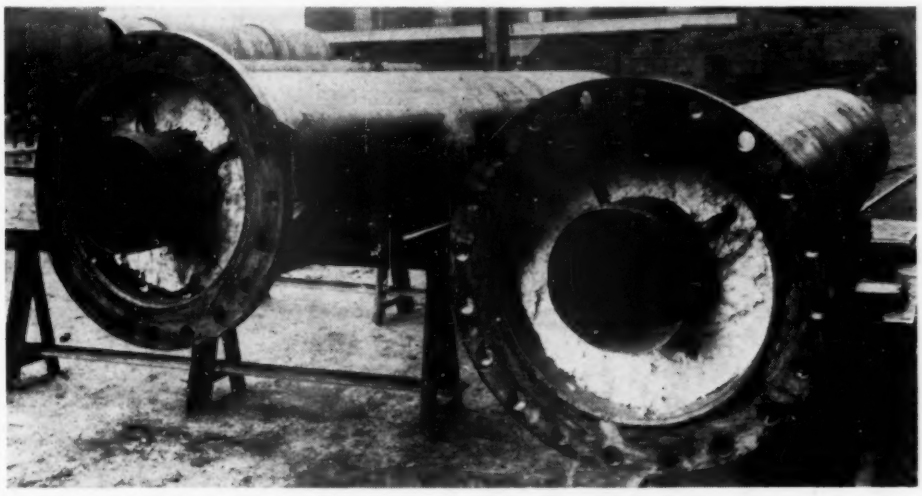


FIG. 19 DOUBLE-SHELL PIPING FOR HIGH-PRESSURE HOT AIR

vails. Outside these air-sealed labyrinth glands there is a ring through which oil under pressure is supplied to the shaft. This pressure oil prevents the escape of any air from the circuit. On either side of the pressure oil ring means are provided for leading the oil to a reservoir, which is under a suitable pressure above atmospheric, since it is connected to the interior of the circuit. The oil-sealing ring can also be combined with the bearing itself. By suitable connections of the sealing air pipes to the circuit it is possible to insure that at all loads, i.e., at all pressure levels, the sealing pressures will likewise rise and fall automatically, and that the direction of the current will remain the same; this without regulating valves of any kind having to be interconnected.

In practice the foregoing is very important for insuring the safety of the plant. The measures described have proved fully satisfactory in trial operation under the most exacting conditions. The sealing air, introduced to the end sections of the hot turbine shafts, is simultaneously utilized in an advantageous manner for cooling these parts, so that the bearing sections remain quite cold.

Hot-Air Piping. In order to reduce in so far as possible the quantity of metal capable of withstanding high temperatures, the hot-air piping has been made with double walls according to the same principle as for the turbines, Fig. 19. The design comprises a thin-walled internal tube of a heat-resisting material serving only for conducting the stream of gas. By means of openings this tube is relieved from the pressure in the heat-insulating space which surrounds it. The heat-insulating space in its turn is enclosed by a thicker-walled pipe of standard material which can easily take up the pressure of the working medium, since it is protected by the insulating material and therefore it is not under high temperature. The necessary measures are, of course, taken to prevent insulating material from gaining access to the tube. With this design much high-quality and expensive steel can be saved.

Air Heater. In the aerodynamic circuit the air heater plays a similar part to that of the steam boiler in a steam-turbine plant. The heat of the fuel is imparted indirectly to the working medium by heat-transmission surfaces, the combustion gases being kept away entirely from the machines.

Since no feedwater is employed, the air heater can, in principle and in contradistinction to a steam boiler, be installed in the open air without any building, all danger of freezing being nonexistent.

The design of the air heater is dependent upon the fuel that has to be dealt with. Coal-fired air heaters resemble in their design up-to-date steam boilers, as may be seen from the examples, Fig. 20 and Fig. 21. According to the present stage of development, the space requirements of coal-fired air heaters are not greater than those of up-to-date high-pressure boilers.

Fig. 20 shows a section through a coal-fired air heater with granulating chamber. This project for a 12,000-kw plant is conservative as regards the combustion chamber, as well as the stresses and temperatures for the tube walls, since care in this connection appears necessary for the first installation. It may, however, be definitely expected that subsequent developments will lead to the heating surfaces and the dimensions being considerably reduced. The inlet temperature of the tube nest in the convection section amounts to only about 1850 F. By returning the flue gases in the combustion chamber, its temperature is regulated and reduced. The tubes have diameters of approximately $1^1/_2$ to $^3/_4$ in. and have wall thicknesses of 0.15 to 0.1 in.

Fig. 21 shows a project for a plant of the same output with liquid-ash extraction and increased temperature in the combustion chamber for utilizing the radiation. The walls of the combustion chamber are lined with short tubes of small diameter. The air passes through them at high velocities so that the wall temperatures nevertheless remain sufficiently low, to permit of their being subjected to the radiation without further protection. In view of the fact that the waste gases from the air heater have relatively high temperatures as a result of the highly preheated circuit air, their waste heat is employed for preheating the combustion air. The use of preheated combustion air leads to an increase in the furnace temperature, particularly in cases where pulverized coal is used. For example, in plants burning pulverized coal such preheating of the secondary air is desirable since it permits a reduction in the size of the combustion chamber.

It is not purposed to deal further herein with the details of coal-fired air heaters, since our studies and investigations in this connection have not been completed in all respects. Experimental equipment for air heaters with pulverized-coal firing is being subjected to experimental work in Zurich. The behavior of ash and slag on hot tubes is being particularly studied. The results so far obtained justify the opinion that pulverized-coal firing will not present any fundamental difficulties for the AK-air heater.

Oil- or gas-fired heaters can be made more compact. In the case of the latter the possibility exists, especially where space is restricted as in marine installations, of supercharging the com-

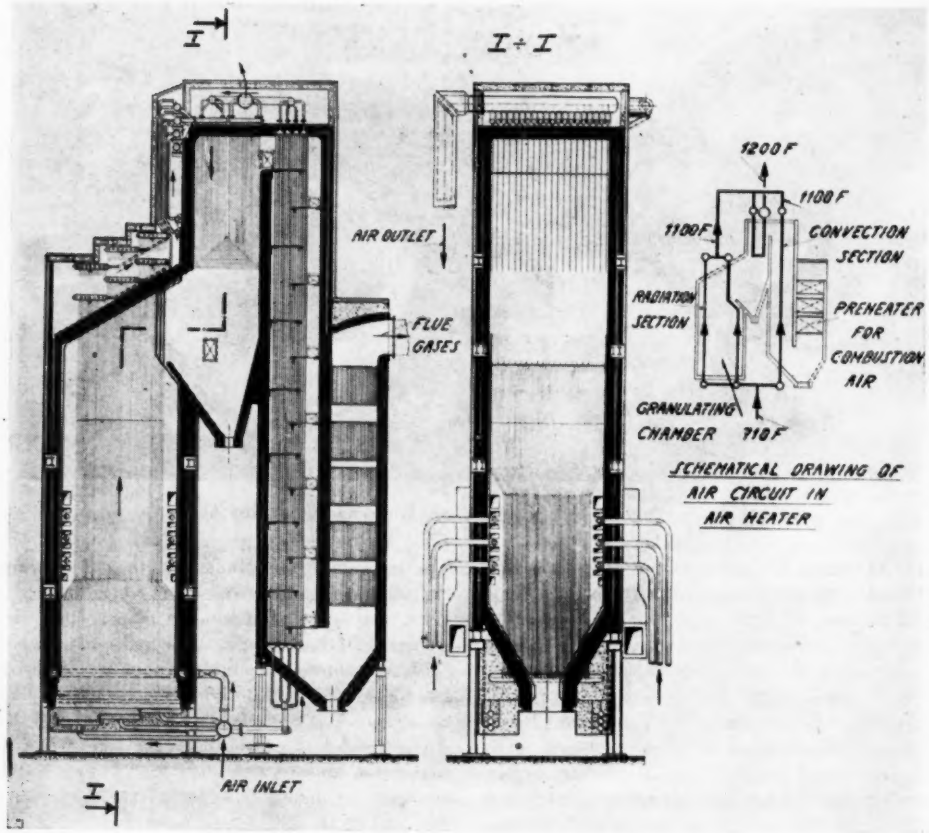


FIG. 20 AIR-HEATER FOR COAL-FIRING WITH GRANULATING CHAMBER

bustion chamber by which means the dimensions and weights can again be considerably reduced (down to one half the surface) compared to ordinary firing.

Fig. 22 shows an example of an oil-fired air heater for a 6000-kw plant with 600 psia and double heating. The tubes are arranged around a supercharged combustion chamber. The tube walls for heating the air in the first stage and in the second stage, 600 psia and 200 psia, respectively, are united in a common heater. In the case of this project the combustion chamber is lined with refractory material, and the heat is given up to the tubes mainly by convection. By raising the pressure of the combustion gas to about 45 to 70 psia, and with velocities of combustion gases from 100 to 160 fps, and air velocities inside the tubes from 65 to 130 fps, the heating surface can be kept small. For such projects it amounts to only 0.5 sq ft per kw net output of the plant.

The total weight of iron in such an air heater is less than 9 lb per kw. Of this figure the proportion of alloy steel is about 50 per cent. The tubes, which may expand in operation by about $2^1/_2$ in., can move freely in the upward direction. In order to keep the hot-air piping as short as possible the heated air for the high-pressure turbine and low-pressure turbine is discharged below. The shell of the heater is of ordinary steel and made airtight. It can be dismantled in a number of sections so that the tubes are easily accessible from the side and can be removed without difficulty. The shell serves at the same time as a support for the tubes.

Since the waste gases are still of high temperature (approximately 1000 F), they are expanded in an exhaust turbine and simultaneously cooled. The exhaust turbine drives the compressor for the combustion air. In this way a preheater for the combustion air can be entirely eliminated. The supercharging set need not be particularly efficient because most of the losses are recovered in the firing. As there is no regenerator there is little danger of detrimental soiling. The design of an air heater employing blast-furnace gas or natural gas is, for the greater part, the same as for oil-firing. The heating surfaces are likewise quite similar.

The design of the air heater according to Fig. 22 corresponds in principle to the one which has proved its merits in the experimental plant from the beginning, only with the difference that in the latter case firing under pressure was not adopted, for the sake of simplicity.

The working medium which has passed through the heat exchanger is supplied to the air heater always in a highly preheated state (600 to 750 F). However, the supply of heat does not bring about any change in condition (evaporation) as is the case in the steam boiler. Evaporating elements, large collectors, and the drums of steam boilers can therefore be dispensed with. Since the air is under pressure, the employment of tubes as heating elements is found to be the most satisfactory means. According to the fuel adopted and the temperature in the furnace, the heating surface is subdivided into a radiation section and a convection section.

In view of the fact that a gaseous medium has to be heated by means of combustion gas, higher tube-wall temperatures have at first to be considered than in the case of steam, where, as a result of the high heat-transmission coefficients on the water and steam side, the tube-wall temperatures are not much higher than the steam temperatures. The working pressures at which the

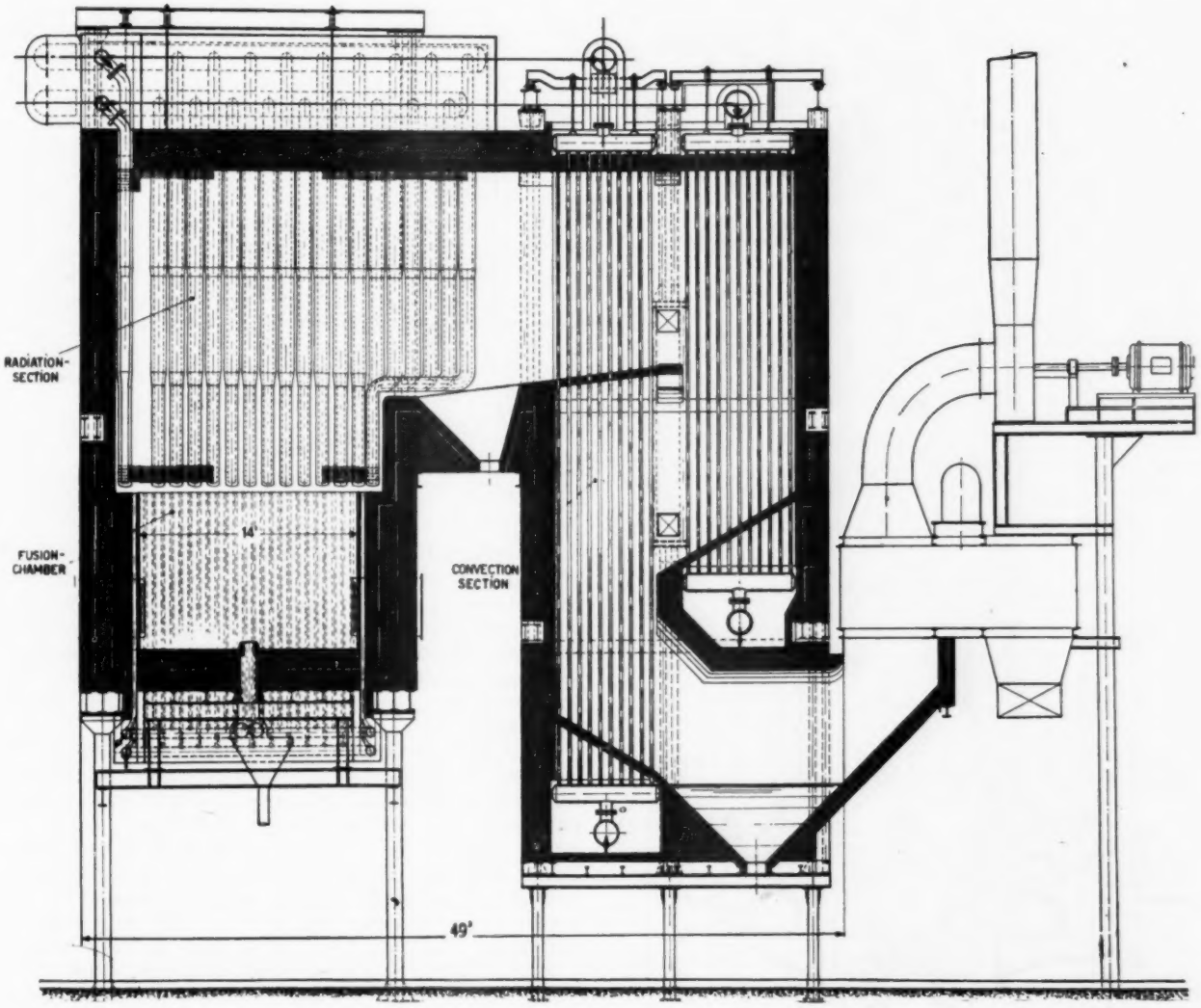


FIG. 21 AIR-HEATER WITH FUSING CHAMBER FOR PULVERIZED COAL

closed cycle operates have the same effect. The heat-transmission coefficient in the interior of the tubes can be so great that the tube-wall temperature is displaced to a considerable extent toward the cold side and comes within ranges to which alloyed steels nowadays obtainable on the market can be subjected without hesitation. The maxi mum temperature of the hottest tube wall can be forced down to 70 to 100 deg F of the final temperature of the air. The heat-transmission coefficient for the interior of the tube is

$$\alpha = c\,(w \cdot p)^{0.75}$$

where

c = constant factor
w = velocity
p = pressure

and accordingly proportional to the product $w \cdot p$.

Thus for the same velocities the heat-transmission coefficient, compared to conditions at atmospheric pressure, increases many times, for example, at 400 psi to 12 times, at 850 psi to 22 times. For practical cases heat-transmission coefficients of 100 to 200 Btu per sq ft per deg F per hr for the interior of the tubes can be reckoned with. Fig. 23 shows, by way of example, how for the same-percentage pressure drop $\epsilon = \Delta\, p/p$ per unit length, the tube-wall temperatures automatically fall as a consequence of increased pressure in the interior without velocity increase, so that the air-heater tubes can be subjected to the duty in the combustion chamber without special cooling measures being necessary.

A simple means for compensating for excessive combustion-chamber temperatures is a return circuit of the flue gases to the combustion chamber, whereby practically any desired temperature can be adhered to. This has been effected also in the oil-fired air heater of the test unit of 2000 kw.

It is often assumed that a very high velocity and a considerable detrimental pressure drop are necessary in the heater tubes for carrying away the quantity of heat. However, as a consequence of the pressure action and with suitable layouts this is by no means the case. For the air heater of a 400-psi plant the pressure drop is only about 10 to 15 psia; at 850 psi for two-stage heaters it totals 20 to 30 psi.

If the flow velocities in the interior of the tubes could be increased at will, any desired reduction of the tube-wall temperature down to the temperature of the air current inside the tubes could theoretically be envisaged. But this can be attained only with a loss of over-all efficiency.

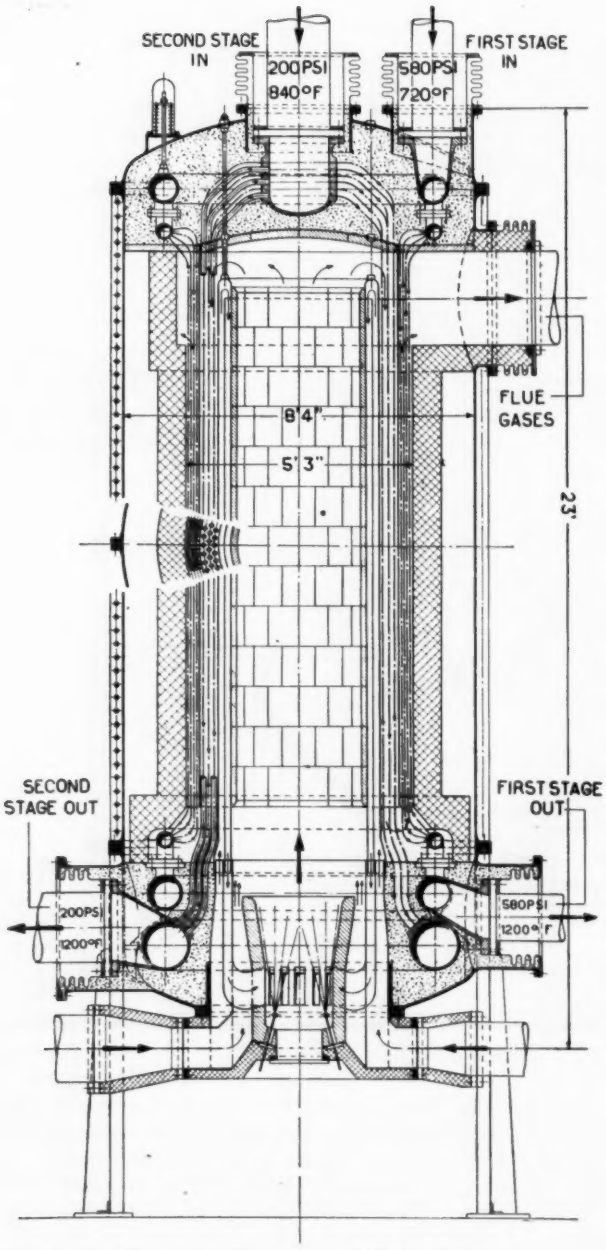


FIG. 22 OIL-FIRED AIR HEATER FOR 6000-KW SET SUPERCHARGED

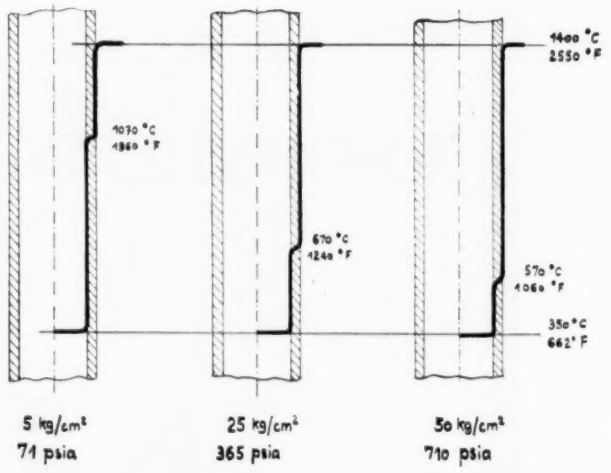


FIG. 23 INFLUENCE OF INSIDE PRESSURE OF AIR-HEATER TUBES ON WALL TEMPERATURE

An increase in the velocity involves the need for minimum pressure losses. Thus the velocity in the various heater sections will be increased only to such an extent as is necessary for attaining the admissible tube-wall temperature. This knowledge leads to the adoption of tubes having different diameters which are suited to the various ranges of temperature.

Careful calculations of all these problems have led to a series of fundamental circulation layouts for the working medium to be heated and for heating combustion gases. The wall temperature can be further reduced by suitable layouts employing countercurrents, parallel currents and transverse currents in the various heater sections.

Fig. 20 illustrates one of the many solutions that can be adopted in this connection. The countercurrent to be heated is subdivided at the inlet into two parallel currents, one of which, mainly subjected to radiation, flows as a direct current and the other, the temperature of which is raised by contact with heated parts, flows as a countercurrent to the flue gases. This brings about a reduction of temperature in the hottest sections. At the same time the subdivision into two or more parallel currents permits a considerable reduction in the total pressure losses. The two partial currents pass into a common final heater and collector pipe.

If it is desired to avoid excessively high temperatures in the radiation section, the pipes can be arranged in such a manner that final heating takes place in the section heated by contact, where the tubes are protected from the effects of radiation.

Only a part of the air heater must be made of special high-quality materials. In this connection the fact should not be lost sight of that for the working pressures concerned the wall stresses are astonishingly small (2500 to 4000 psi), even with thin tubes. Those figures still lie far below the creep limits of good alloy steels for the corresponding temperature ranges.

Heat Exchanger (*Recuperator*). Unless a heat exchanger is employed it is hardly possible to increase the thermal efficiency of any kind of gas turbine plant above about 20 per cent. The quantity of heat that has to be given up by the current of gas issuing from the turbine to the current of gas after the compressor at full regeneration is of the same magnitude as the quantity of heat which in the air heater is introduced from an external source.

The heat-transmission coefficients on both sides of the heat-exchanger surfaces are raised considerably in the case of the supercharged closed cycle. In combination with the small specific volume this offers possibilities of reducing considerably both dimensions and weights. A further point is that one can in principle adopt very small cross sections for the tubes, or other fine exchanger elements, because any danger of soiling is entirely eliminated.

The conditions for constructing a good heat exchanger of small dimensions are doubtless more favorable for a closed circuit than for gas turbines with which the flue gases pass through the heat exchangers. Apart from the high blading efficiency of the machines, the easy realization of a very high heat exchange is one of the chief reasons for the high over-all efficiency of closed-circuit installations, even when employing moderate temperatures.

In practice heat-transfer coefficients of 30 to 50 Btu per sq ft per deg F per hr, depending on the admissible pressure loss, may be taken as a basis. These figures are multiples of the heat-transfer coefficient characteristic of the heat exchangers for com-

bustion-gas turbines. For economical reasons one is compelled not to go too far with the recuperation in the case of the last-mentioned plants, since space and weight for the construction would become too great. According to available figures, such new two-stage installations require about 3 times or more heating surface. With the closed cycle we find surfaces of 1.5 to 3 sq ft per kw sufficient, depending upon the pressure, and furthermore for an over-all efficiency of the plant exceeding 33 per cent; the degree of recuperation being about 90 per cent. It is possible to bring the weight of the heating surfaces down to even less than 2 lb per kw. The following illustrations likewise indicate clearly that the heat exchangers of closed-circuit installations are relatively small.

In principle, any kind of heat-exchanging surface (flat or tubular), and any means for conducting the current can be adopted. However, since the plant operates under pressure, the use of simple steel tubes which can be manufactured at relatively low cost represents the given means for effecting this transmission.

Fig. 24 illustrates the design of a tubular exchanger operating according to the countercurrent principle and transmitting a maximum amount of heat with a minimum loss of pressure. The high-pressure air flows through the interior of the tubes and the external shell has to withstand only the lower back pressure. The apparatus can be arranged as desired, according to the available space or subdivided into two or more parts. The use of normal tubes of small diameter permits standardization of all heat-exchanger elements for the various outputs and thus to a large degree manufacture in series.

We employ tubes of only 0.15 to 0.25 in. diam. They are separated by special spacers which offer little resistance to the current of air. A large number of these thin tubes is assembled in a tube nest. In their turn the latter are connected by a small number of collector pipes. Separate removal of each tube nest is easily possible. In the case of stationary plants this can be effected, for example, by drawing the various tube sections out of the heat exchanger in an axial direction. For marine installations the shell of the heat exchanger is split and can be easily lifted, thus giving access to the tube nests from above. The tightness of each nest can be checked separately. However, since a perfectly clean medium flows on either side of the tube walls, there is no reason to fear interruptions in the operation.

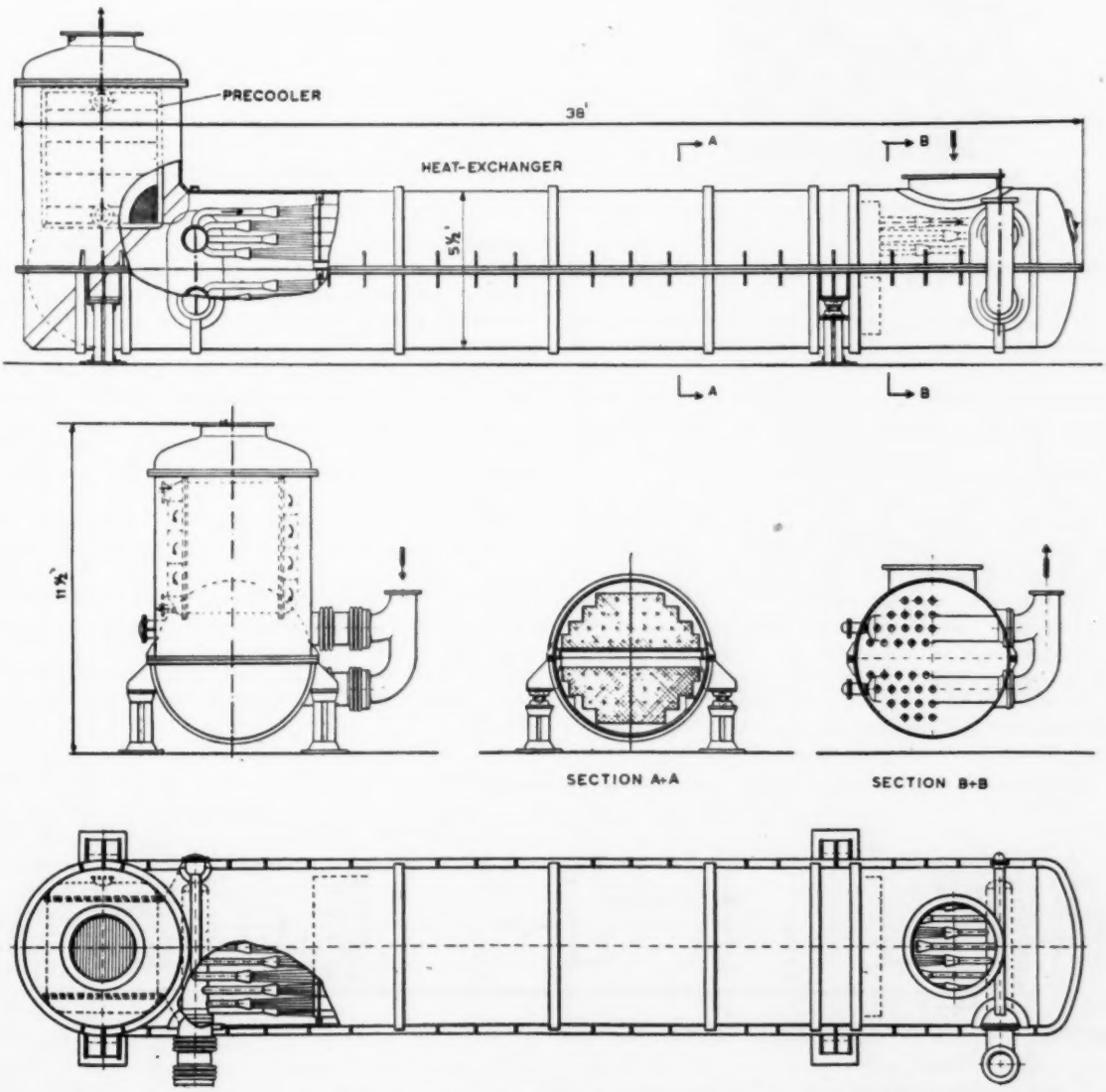


FIG. 24 HEAT EXCHANGER OR RECUPERATOR FOR CLOSED-CYCLE UNIT, BUILT UP OF SMALL-DIAMETER TUBES

Furthermore, the highest temperature in the heat exchanger amounts only to about 850 F, so that it is unnecessary to employ special-quality metals for the tubes. Fig. 25 shows a view in the part of the apparatus where the spacers are arranged; as may be noted, the external bright part where the low-pressure air flows is hardly obstructed by these distance pieces.

The temperature of the low-pressure air on issuing from the heat exchanger is about 200 to 250 F, after which it passes to a precooler, through which water circulates, for cooling in so far as possible down to the inlet temperature of the compressor, the object being to reduce the compression work. Since, as a result of the raised pressure the heat-transmission coefficients on the air side are also favorable in the precooler and in the intermediate coolers of the compressor, the surfaces and dimensions of these units are not large, in contradistinction to water-cooled air coolers when operating with small working pressures. Incidentally, the precoolers and intermediate coolers are of

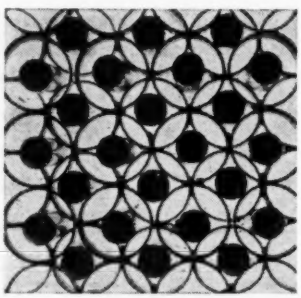


FIG. 25 VIEW OF SPACE ARRANGEMENT IN REGENERATOR

standard ribbed-tube design with water circulation through the tubes.

In many cases it is advantageous to combine the low-pressure turbine arranged in the circuit before the heat exchanger in the manner illustrated in Fig. 26. In this way additional pressure losses are avoided and the stream of air passes directly to the tube nests. As may be seen in Fig. 26, the heat exchanger, whether arranged in this or some similar manner, is an exceptionally simple apparatus that operates very reliably.

Governing. For raising the output, air is introduced to the circuit from a high-pressure accumulator of cold air, while for reducing the output, air is withdrawn from the circuit and passed to a low-pressure accumulator. Automatic governing for an installation with rigid couplings between the machines takes place fundamentally as follows: When load is thrown off the consequent rise in speed influences the centrifugal governor (pendulum) which causes the discharge side of the combined inlet-outlet valve to open, Fig. 27, so that air from the high-pressure branch of the circuit issues into the low-pressure accumulator LP. On the other hand, when load is thrown on the plant the resulting drop in speed causes the inlet side of the valve to open, as a consequence of which air from the high-pressure accumulator HP is admitted to the circuit at the same point.

For small reductions in load, and consequently only slight increases in speed, the main valve operates only within a small range without opening either the inlet or outlet. On the other hand, the by-pass valve opens and by-passes air from the high-pressure side of the circuit to the low-pressure side without developing output, so that the useful output of the plant is reduced.

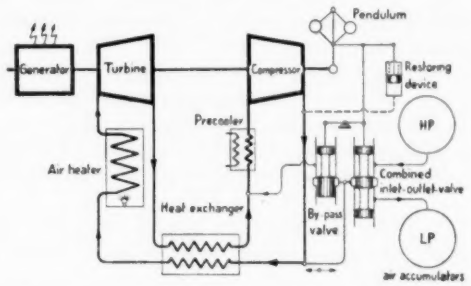


FIG. 27 SCHEME OF REGULATING DEVICE FOR ONE-SHAFT MACHINE SET

(Combination of inlet and outlet valve with by-pass valve.)

By regulating small and frequently recurring load fluctuations with the by-pass valve the air consumption from accumulator HP, for purposes of regulation, is reduced and charging work thus saved.

Regulation by supplying or withdrawing working medium to or from the high-pressure side of the circuit has the advantage of immediate efficacy, since the pressure ratio $p_H : p_L$ is immediately raised on air being admitted, thus causing the plant to give up additional output. Inversely, when air is withdrawn from the high-pressure side, the pressure ratio immediately drops, so that for example, when suddenly withdrawing less than 20 per cent of the air content of the circuit, it has dropped to such an extent that the transition from full load to no load has already taken place. On the other hand this "momentary effect" would be unsuitable for the supply or withdrawal of working medium on the low-pressure side.

When admitting or withdrawing air on the high-pressure side of the circuit the consumption of air for such regulating purposes is, in the case of quickly recurring small periodical load fluctuations, no longer proportional to the number of actual load fluctuations and instead increases relatively less, since insufficient time remains between the separate fluctuations for re-establishing the stationary pressure ratio, and the control consequently takes place chiefly under the influence of the "momentary effect," Fig. 28.

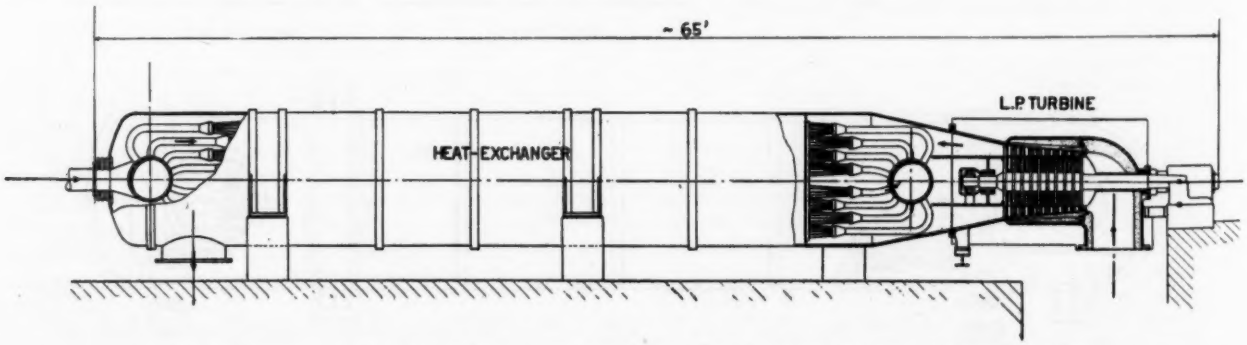


FIG. 26 COMBINATION OF HEAT EXCHANGER AND TURBINE TO CONSERVE SPACE AND PRESSURE LOSS

The influence of the momentary effect on the governing, which for known machine characteristics can also be calculated theoretically, has been checked by experiments. The pressure course, Fig. 29, plotted for a load-reducing action, shows that during the first moment the equilibrium in output is brought about by reducing the pressure ratio $p_H : p_L$; and that the pressure level only gradually drops to the final condition.

The regulation of the furnace, not indicated on the schematic drawing, Fig. 27, need not take place very quickly, thanks to the accumulation of heat in the heaters and apparatus. Changes in the power output of the turbine due to smaller deviations of the final heating temperature of the working air from its stationary value are compensated by automatic and temporary raising or lowering of the pressure level by a small amount.

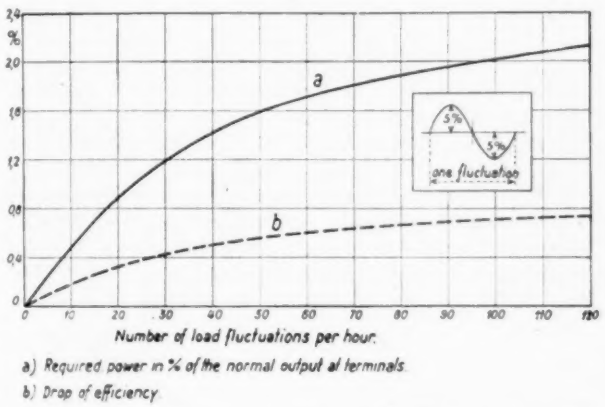


FIG. 28 POWER NEEDED IN PER CENT OF NET OUTPUT FOR PRODUCTION OF ACCUMULATED AIR AT LOAD FLUCTUATIONS OF ±5 PER CENT

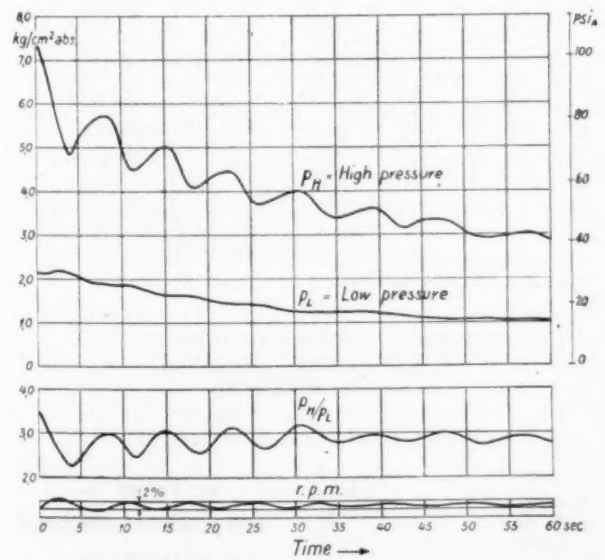


FIG. 29 PRESSURE VARIATION AT SUDDEN LOAD REDUCTIONS REVEALS "MOMENTARY EFFECT"

The method of regulation herein described has the advantage that the regulating means can be accommodated in a block outside the circuit proper, Fig. 30, that they are traversed only by cold air, and that under normal working conditions the air of the circuit does not pass through them, so that no additional throttling losses result.

For installations in which the turbine developing useful output is separated mechanically from the compressor set, which is particularly the case where useful output has to be given up at different speeds (for example, compressor drive, ship propulsion), the compressor set operates in the normal operating condition, thus remaining stable and without any special regulation. When the equilibrium is disturbed, i.e., during the supply and withdrawal of working medium for changing the useful output, deviations from a given speed range, either above or below, for the free-running compressor set, are prevented by partly by-passing the turbine developing useful output or the compressor-driving turbine by a special valve actuated from a speed-limiting governor of the compressor set, Fig. 31.

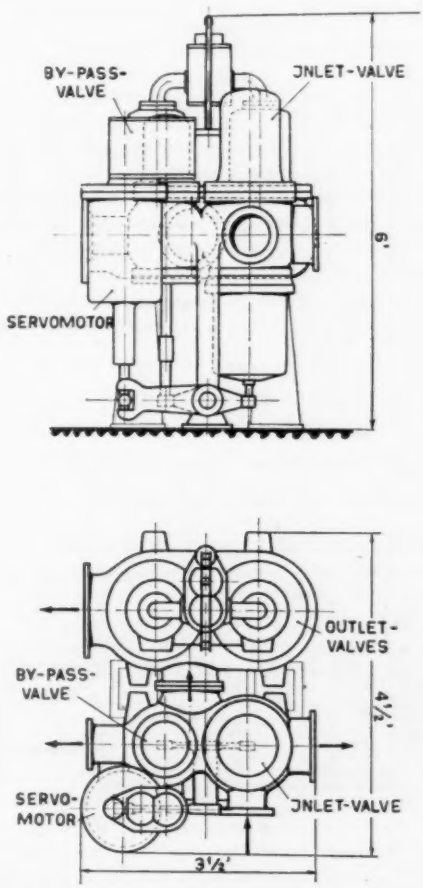


FIG. 30 REGULATING BLOCK FOR 12,000-KW SET

The test plant has worked for long periods entirely separated from the municipal network and supplying the whole works of Escher Wyss. On these occasions the regulating governing, already in its simplest form, proved to be very satisfactory.

PROJECTS FOR POWER STATIONS AND MARINE PLANTS

The disposition of the various machines and apparatus of an AK-plant within the available space does not involve special requirements. Air is not subject to the force of gravity like steam condensate, so that differences in level, such as are required for insuring passage of the condensate and feedwater, need not be provided for. Thus attention can be paid to a combination of the machines and apparatus in a small closed set with short connecting pipes in order to reduce losses of pressure and temperature to a minimum, of the utmost importance in such plants.

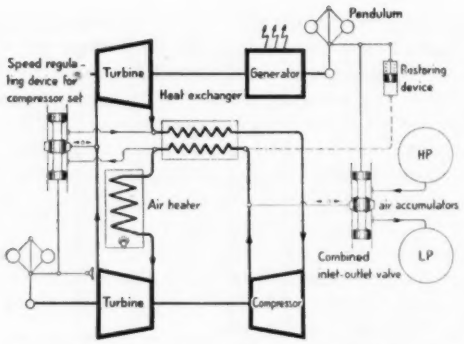


FIG. 31 SCHEMATIC DIAGRAM OF REGULATING DEVICE FOR TWO-SHAFT MACHINE SET
(Marine installations, for example.)

The limited number of auxiliary machines and other accessories greatly simplifies the operation of the plant, whereas in the case of high-pressure steam power stations for high thermal efficiencies, these auxiliaries have become rather cumbersome. The chief factors which bring about a considerable improvement, compared to a steam plant, are the elimination of feedwater, the necessary pumps and apparatus for its preparation, the small cooling-water consumption which amounts to only a fraction ($^1/_5$ to $^1/_{10}$) of that required in steam installations, the elimination of the condensing process with its condensate pumps and air pumps, and the absence of all fittings for very high pressures.

Closed-cycle installations may be operated entirely without water, in that intermediate cooling of the air in the compressor can be effected by employing ambient air as cooling means in place of water. For the large available temperature drops of the intermediate cooling, this arrangement with which cooling water is entirely eliminated, can be realized in an economical manner in contradistinction to steam plants where the condensing process at constant low temperature makes it necessary to endeavor to attain minimum temperature differences when giving up waste heat to the ambient air.

If one takes into account:

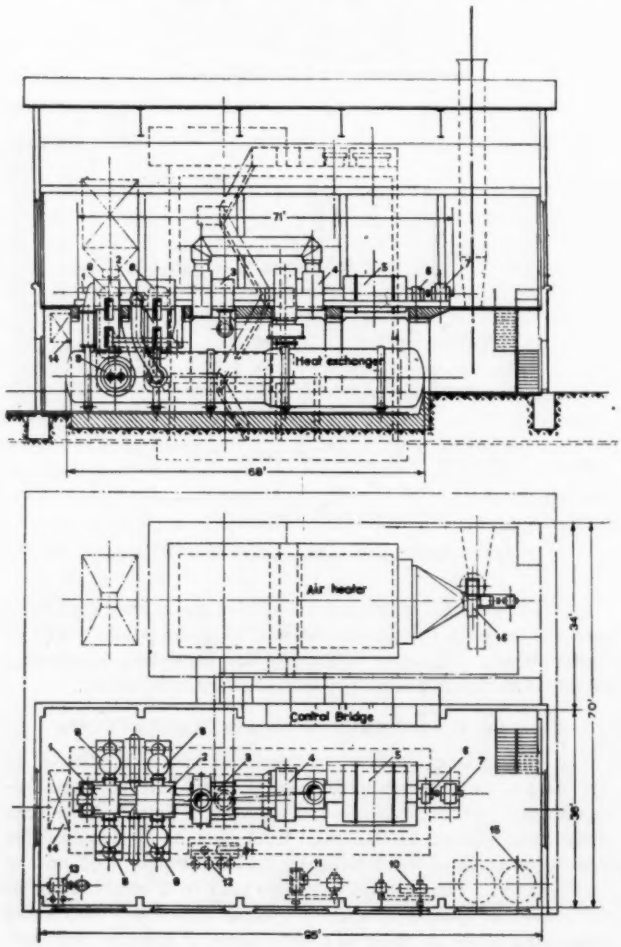
1 The relatively small expense involved for special materials capable of withstanding the high temperatures (as a consequence of the small dimensions resulting from supercharged operation);

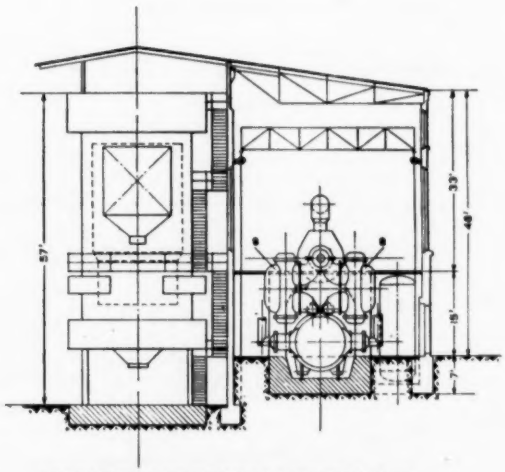
2 The simple layout of the plant (absence of extensive foundations);

3 The reduced number of accessories;

then it is evident that in spite of the higher thermal efficiency, compared with those of steam plants of the same output, the total costs of the two installations will not greatly differ from one another.

Fig. 31 illustrates, by way of example, a number of AK-installations such as are ready for construction. They are all characterized by high efficiencies, well above 30 per cent. These installations employ pure air as working medium. Fig. 32 illustrates a 12,000-kw plant with pulverized-coal firing for industrial





12000 KW AERODYNAMIC TURBINE WITH CLOSED CIRCUIT.

Legend
1 LP compressor
2 HP compressor
3 HP turbine
4 LP turbine
5 Turbo-alternator
6 Exciter
7 Starting motor
8 Intercooler
9 Precooler
10 Loading compressor for air accumulator
11 Loading compressor for circuit
12 Regulating station
13 Cooling-water-pump
14 Oil-tank
15 Air accumulators
16 Exhaust-gas blower

Air heater with pulverised-coal burner all in the open air.

FIG. 32 12,000-KW AK-SET FOR SINGLE-STAGE POWER PLANT WITH COAL-FIRING

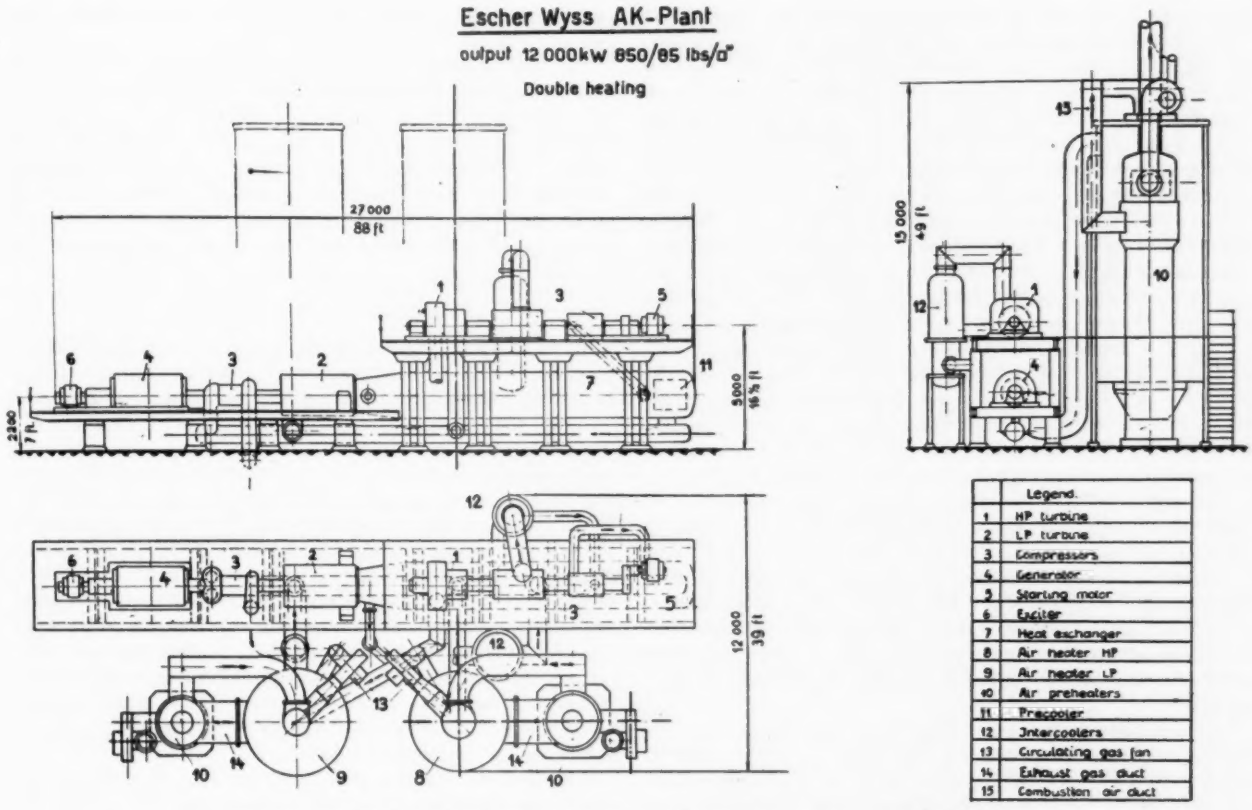


FIG. 33 12,000-KW AK-SET WITH OIL- OR GAS-FIRING, AND INTERMEDIATE HEATING

purposes. The air heater is installed in the open next to the powerhouse, thus considerably reducing the cost of the building. This is a plant with single-stage expansion. The working pressure at full load amounts to 400 F at the turbine inlet, the maximum temperature to 1200 F, and the back pressure to 115 psia. The machines are arranged all in one row. The high-pressure turbine drives the compressor serving the circuit while the low-pressure turbine drives the generator. The heat exchanger is installed underneath the machine set but can of course also be arranged elsewhere, for example, in the open, depending upon the available space. The weight of the circulating air is about 250 lb per sec. All the chief auxiliary drives that are required may be seen in the illustration. Their small number in comparison to the auxiliaries of up-to-date steam power plants is characteristic. The over-all thermal efficiency of such an installation amounts to at least 32 to 33 per cent at full load, still attaining 31 per cent at half load and 28 per cent at quarter load. Naturally these figures vary somewhat according to the quality of the coal.

Fig. 33 illustrates a project for a plant of the same output but arranged for oil- or gas-firing and double heating, the initial pressure being 850 psi and the back pressure 85 psi. The machine plant is subdivided into two independent sets. The high-pressure turbine 1 is fed from the first air heater 8 and drives a part of the compressor rotors. This compressor set is arranged above the heat exchanger 7. The low-pressure turbine 2 drives the generator 4 and the low-pressure part of the compressor 3. The low-pressure turbine and heat exchanger are built together, Fig. 26. The low-pressure turbine receives the reheated air at a pressure of 300 psi from the second air heater 9.

In these stationary installations where the space requirement is not of decisive importance, ordinary furnace-chamber pressures can be adopted for oil- and gas-fired air heaters. This means that the required heating surface becomes larger than for firing under pressure, but on the other hand the charging set is eliminated. In place of the latter an air preheater for the combustion air is adopted. In this case the air preheaters are built as tubular units. The air heaters are arranged immediately next to the machine set proper which leads to favorably short interconnecting pipe work. The fact that no excavation is required for the set and that it rests on a light foundation framework is worthy of note. All parts are easily accessible.

The starting motor 6 has an output of approximately 300 to 400 kw. On the basis of the present state of development, a thermal efficiency, including auxiliaries of 34 to 37 per cent, is attainable at full load and 30 to 33 per cent at one-fifth load. The efficiency is, of course, dependent upon the size of the heat-exchanger and air-heater surfaces as well as upon the cooling-water temperature. For an inlet temperature of 60 F and 160 F exit approximately 40 gal per sec are required. A steam plant of the same output needs about 5 times more. The circulating-air weight is approximately 150 lb per sec.

Fig. 34 illustrates the machine designed for a plant of 25,000 kw output. It remains the same for oil-, gas-, or pulverized-coal firing. Details of the corresponding machines are illustrated in Figs. 12, 13, and 14. The machinery plant can of course be arranged in two sets parallel to one another instead of in a single row, if the available space makes this preferable. When comparing with Fig. 33 it is apparent that the larger output calls for hardly any additional length, since it is primarily the diameter of the machines and auxiliaries which is increased.

An arrangement of the sets in parallel is preferable for marine installations. Fig. 35 shows a marine plant with oil firing for 8000 shp. This plant can be used for turboelectric drive or

for propulsion in conjunction with a variable-pitch propeller. It operates with 600 psi, 1200 F at the turbine inlet, with double heating and supercharged firing of the air heater. The combustion circuit is entirely separate from the working circuit proper, so that they do not influence one another during regulating actions. The reduced strain for the tubes in the case of supercharged firing permits of the wall thicknesses being reduced. The back pressure amounts to 60 psi. The air heater is arranged in front of the machine set. The heat exchanger lies amidships. On the one side is the compressor set for the circuit. It is driven by the high-pressure turbine. On the same side is the charging set for the combustion chamber which receives its drive from an exhaust turbine. The low-pressure turbine is the prime mover proper.

With this arrangement all parts are easily accessible and can be dismantled without difficulty since they all lie in the same plane. When the propeller speed is changed under varying loads, only the speed of the low-pressure turbine is correspondingly altered. The independent regulation of the two machine sets takes place according to the schematic drawing, Fig. 31.

The thermal efficiency of such a marine plant including auxiliaries amounts, at full load and 1200 to 1300 F, to about 32 to 34 per cent, and still attains at one-fifth load an efficiency of 27 to 30 per cent. The weight of the installation in relation to output is approximately 40 lb per shp. The weights, space requirements, and efficiencies are primarily dependent upon the surfaces that have to be adopted for the heat exchangers. The space requirements of a plant, according to Fig. 35, are approximately 2.4 cu ft per hp.

In accordance with present progress in metallurgy it is intended to operate AK-plants at temperatures of 1200 to 1300 F. Every future increase that can be made in the temperatures will, for each 10 deg F, lead to a saving in fuel of 0.75 per cent, i.e., for 40 deg F increase in temperature an improvement in the over-all thermal efficiency of about 1 per cent may be expected.

When making a comparison with open-cycle gas turbines, the pipes passing through the deck which are necessary for supplying the combustion air and for discharging the combustion gases should be borne in mind. Whereas a closed-cycle turbine requires practically the same quantity of fresh air and discharges about the same volumes of waste gas through the funnels as in the case of Diesel engines or steam plants, these volumes are many times greater for an open-cycle combustion-gas turbine because of the large surplus air volume of its working cycle for the purpose of reducing the temperature. Needless to say, the closed-cycle turbine is very suitable for turboelectric drive.

One cannot discuss new gas-turbine developments for marine propulsion without mentioning the future development of the propelling means.

The most suitable solution for reverse operation which, at the same time gives ideal operating conditions for the whole plant, is the adoption of variable-pitch propellers, thus obviating the necessity of installing a separate turbine for propelling the vessel astern. From wide experience in the building of Kaplan-type water turbines, in 1934 we developed such a new marine propeller based upon the same principles. No failures or defects have been reported from the 35 marine propellers already delivered.

Other Fields of Application

Remote Heating. In contrast to the condensing plant of steam turbines, where heating of the cooling water may amount to only a few degrees owing to the necessity of maintaining a good vacuum, the required elimination of heat from a closed circuit during the compression can involve a considerable increase in the temperature of the cooling water without any drawbacks resulting. In this way the quantity of cooling water is reduced from 10 to 20 per cent compared to steam plants. Furthermore, heating of the cooling water can be raised from 160 to 180 F, without alteration of the temperatures within the circuit. Thus the waste heat is given up at high temperature and can be utilized for heating purposes. It is particularly worthy of note that the entire quantity of waste heat can be made use of for heating purposes, without any modifications having to be made, as compared to operation without utilization of the waste heat. The final temperature of the cooling water can be raised to any desired level, for instance, by restricting the recuperation.

AK-Plant in Connection With Blast Furnace. In blast furnaces, coke ovens, oil fields, and refineries as well as in various branches of the chemical industry, large quantities of waste gas result from the processes employed.

Utilization of such surplus gases in open-cycle combustion turbines calls for compression of the gases to a pressure amounting to a few atmospheres, so that they can be burned in the combustion chamber which is under pressure. For this purpose the gases must be precooled and in the majority of cases also cleaned, i.e., all processes which involve considerable additional apparatus. In the case of a closed-cycle turbine the hot gases can be utilized just as they are, without preparation and compression of the fuel for the air heater, i.e., a possibility which increases the thermal over-all efficiency.

A closed-cycle turbine operated with blast-furnace gas can also be employed for direct drive of blast-furnace blowers. The

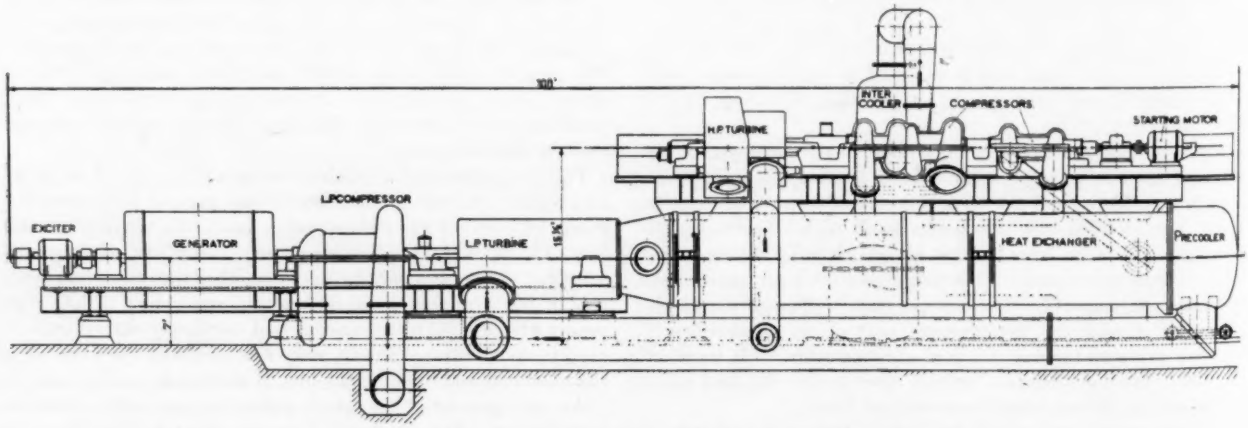


Fig. 34 Machine Set of 25,000-Kw AK-Plant 850 to 85 Psi

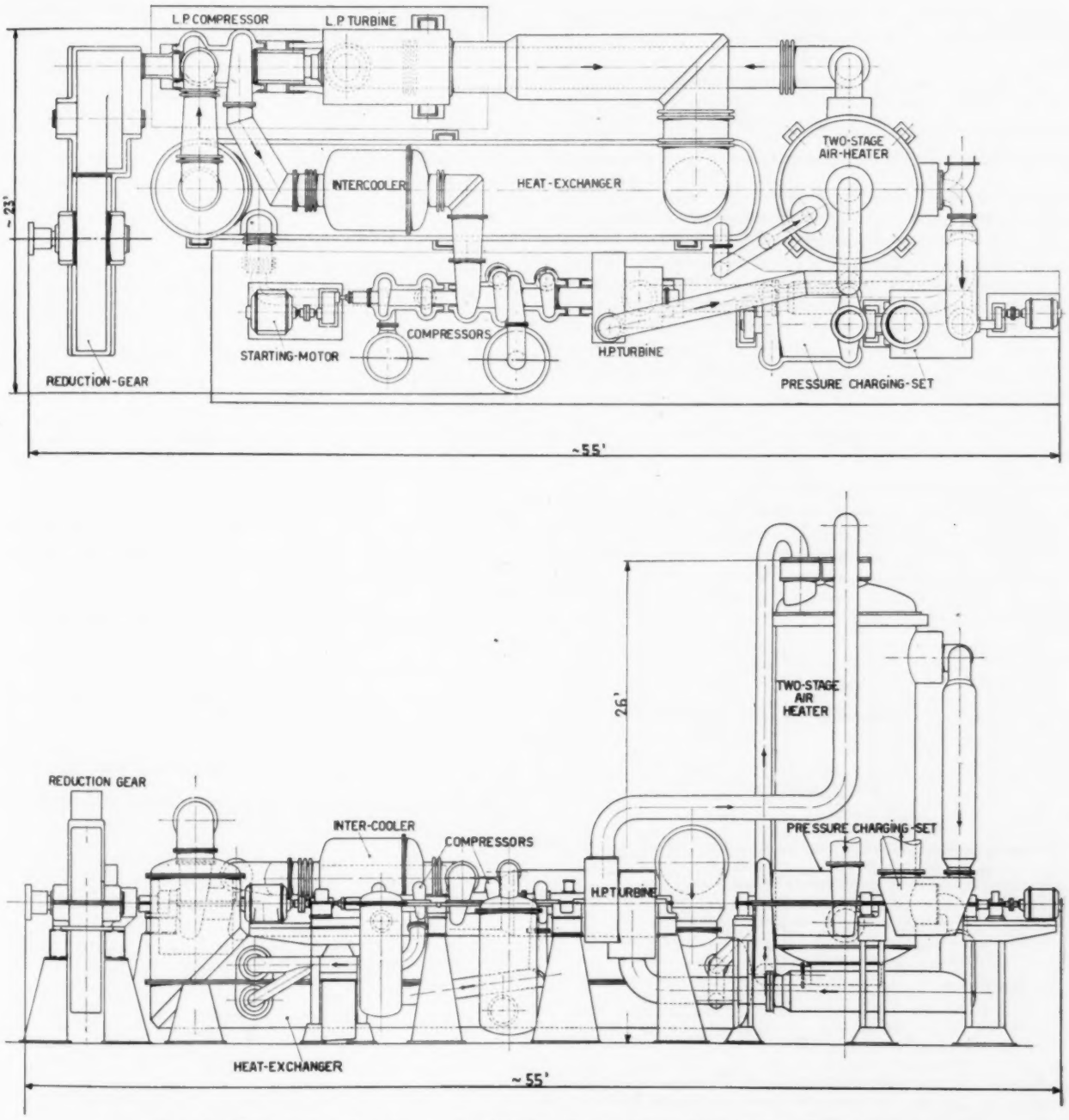


FIG. 35 LAYOUT OF A HIGH-EFFICIENCY 8000-SHP CLOSED-CYCLE UNIT FOR SHIP PROPULSION

arrangement of the turbine stages in conjunction with the compressor required for the circuit and the blast-furnace blowers, which must operate under widely differing speeds and loads, can be effected on similar lines to those already described in the preceding section concerning marine turbines. In this case also, the provision of two sets operating independently of one another may prove advantageous, since in this way a possibility is offered of attaining favorable thermal efficiencies over a large operating range, with regulation of the circuit density at different loads.

Another point to which brief reference may be made herein is that favorable combinations of blast furnaces, blast heaters, and air heaters for the power process can be realized for AK-plants. Particulars concerning such projects are to be found in a previous article (5).

Gas Generator and Fuel Producer. When coal is employed as fuel it may, according to its nature and quality, prove convenient to adopt gas generators in place of furnaces for producing the combustion gases for the air heater. In this connection, cleaning, cooling down, or compression are not necessary, such as are called for when an open cycle is adopted. The produced gas can be directly fired in an air heater.

REMARKS CONCERNING USE OF LIGHT GASES IN CLOSED CIRCUITS

The following remarks concerning the advantages of employing other gases are the result of theoretical studies that have been

carried out by Professor Ackeret. He has compiled his calculations in the following form especially for the purposes of this paper:

For congruent entropy diagrams the efficiency of the closed-circuit process is independent of the nature of the gas. When assuming congruency, it is taken for granted that the relative pressure losses $\frac{\Delta T}{T}$ and temperature losses $\frac{\Delta p}{p}$ are the same on all heat-transmission surfaces. However, in spite of this, the adoption of other gases can prove advantageous because the output of the plant can be considerably increased at the same efficiency and with only slightly changed dimensions. To prove this more decisively let us assume that gases of the same atomic number, for example, only biatomic or only monoatomic gases be employed, the molecular weight m of which can be continually changed. For example, by a mixture of helium and argon, m could be continually increased from 4 to 40. For gases of the same atomic number the magnitudes

$$k = C_p/C_v \text{ and } \sigma = \frac{\eta \cdot g \cdot C_p}{\lambda}$$

are as is known independent from m.

We may observe the heat transmission at a given point of a tube having the diameter D which is traversed at said point by gases with velocity u, density ρ, pressure p, temperature T and viscosity η. Between the wall and the gas a difference in temperature $\Delta T = \theta$ shall prevail. The following equation then applies for the shear stress

$$\tau = C_f \frac{\rho}{2} u^2$$

and for the heat transmission per unit of surface according to Reynolds and Prandtl

$$g = \frac{C_f}{2P} \rho g C_p \cdot u \cdot \theta$$

in which for Reynolds numbers of medium size $\mathbf{R} = \frac{\rho u D}{\eta}$ the following may according to Blasius be inserted

$$C_f = \frac{0.0791}{\sqrt[4]{\mathbf{R}}}$$

The expression

$$P = 1 + \frac{1.7^4}{\mathbf{R}^{1/4}} (\sigma - 1)$$

is in small measure dependent only on $\mathbf{R}$ and is about 1. According to Eucken, σ is connected with k and may be expressed with considerable accuracy by

$$\sigma = \frac{4k}{gk - 5}$$

For a short tube section the following can immediately be ascertained

$$dp = -4C_f \frac{\rho}{2} u^2 \frac{dx}{D}$$

Congruence of the entropy diagrams, i.e., the same efficiencies, is realized when $\frac{dp}{p}$ and $\frac{dT}{T}$ are of equal magnitude for the different gases. Hereby, however, dx must be somewhat changed. In order to utilize the material equally well in all cases, let us further assume that at full load the pressures are also equally large. For gases the following equation generally applies

$$R = \frac{R}{m} \qquad \rho = \frac{p}{gRT} = \frac{pm}{gRT}$$

and in addition for gases of the same atomic number

$$C_p = \frac{p}{m}$$

Thus if we require for the same $\frac{dp}{p}$, it follows that

$$\frac{dp}{p} = -2C_f \frac{\rho}{p} u^2 \frac{dx}{D} = -2C_f \frac{u^2}{gRT} \frac{dx}{D} = -2C_f k M^2 \frac{dx}{D}$$

in which M is the Mach number $= M = \frac{u}{a}$ (a = velocity of sound). The same $\frac{dT}{T}$ leads to

$$\frac{dT}{T} = \frac{2c_f}{PT} \theta \frac{dx}{D} = \text{const}$$

in other words, $\frac{c_f \cdot dx}{P}$ or, since we can look upon P as being practically constant, $c_f \cdot dx = \text{const}$ for all m; but from the foregoing it follows that $M = \text{const}$.

Thus we have as a condition $\frac{u}{a} = \text{const}$. But the velocity of sound

$$a = \sqrt{gkRT} = \sqrt{gk \frac{R}{m} \cdot T}$$

Consequently the flow velocity must increase with $\sqrt{\frac{1}{m}}$ if the same conditions of pressure and temperature are to be obtained.

For the element of length the following is obtained

$$\frac{dx}{D} = \frac{\frac{dp}{p}}{2c_f} \cdot \frac{1}{kM^2}$$

$\frac{dx}{D}$ is thus porportional to

$$\frac{1}{c_f} = \frac{\sqrt[4]{\frac{\rho u D}{\eta}}}{0.0791}$$

$$\frac{dx}{D} \sim \sqrt[4]{\frac{\rho u}{\eta}}$$

For the same temperatures the viscosity of gases having the same atomic number, with the one exception of hydrogen, differs only slightly (for the He-A mixture the viscosity varies between $m = 4$ and $m = 40$ only by about 10 per cent). Thus one can insert with sufficient accuracy $\frac{dx}{D}$ proportional to $\sqrt[4]{\rho \cdot u}$

From the foregoing we have

$$\frac{dx}{D} \sim \sqrt[4]{m \frac{1}{\sqrt{m}}} = \sqrt[8]{m}$$

i.e., only a rather small variation in the sense that for lighter gases the tubes become somewhat shorter. One sees immediately

where the advantage of light gases is to be found. The useful output of the machine is, namely, for the same tube diameter, proportional to $\rho u c_p$. It is also proportional to

$$m \frac{1}{\sqrt{m}} \cdot \frac{1}{m} = \frac{1}{\sqrt{m}}$$

Thus for lighter gases it will be considerably greater. Let us compare, for example, two gases, the molecular weights of which are as 1:9, then the velocity of flow adopted for the lighter gas must be 3 times greater; the output for the same efficiency becomes 3 times greater and the tube lengths for the heat exchanger are reduced by about 25 per cent. The weight of the charge of gas in the machine will increase somewhat more than m, becoming for this example less than $^1/_9$.

In physics the variation in the output can also be made clear in the following manner: According to Avogadro, the unit of volume for the same pressure and same temperature contains the same number of molecules, i.e., also just as many molecule degrees of freedom. Each molecule transports the same energy. However, since we are delivering 3 times the volume, it follows that 3 times the output will also be converted.

It is, however, known that in general light gases call for a larger number of stages (in the compressors and turbines). This is a drawback of light gases. In the case of the compressor, for example, the following equation obtains for the number of stages

$$n_k = \frac{2}{k-1} \frac{\ln \delta}{\psi M^2}, \quad \ln = \text{natural logarithm}$$

in which δ represents the adiabatic temperature ratio of the compressor, ψ the pressure coefficient. Thus in our case the law applies for the compressor (and also for the turbine) that n is proportional to $\frac{1}{M^2}$ in which M = peripheral velocity/sound velocity. Since $M \sim \sqrt{m}$ for the same peripheral speed, the number of stages would follow $1/m$, becoming, in the case of the example, 9 times greater. For the turbine there is little hope of deviating therefrom, but this does not apply to the compressor. Since the peripheral velocity of the axial impellers of the compressor does not reach the limit of their tensile strength, the peripheral velocity could, without impairing the efficiency by the Mach effect, be increased and the number of stages thus reduced.

As the weight of the machinery is relatively small in the case of a highly supercharged AK-plant, the increase in the number of stages could be accepted relatively easily, especially if it proves possible to employ radial impellers which can be operated up to the highest circumferential velocities without detrimental Mach effect.

For the heater tube the same heat-transmission coefficients as for water tubing are possible.

Comparative figures are given in Table 2 to facilitate understanding of the conditions. The comparisons relate to various gases and mixtures of gas with air.

As may be noted from the foregoing there are good prospects that further development work, especially in the case of installations for special purposes, will lead to higher efficiencies and reductions in the size of the plant. These remarks of Professor Ackeret confirm the author's opinion that the present development of the closed-cycle process by no means represents the ultimate attainable.

TABLE 2 COMPARISON OF DIFFERENT GASES FOR THE AK-PROCESS[a]

Gas	Air	He + CO_2	He + CO_2	He	H_2	
Mean molecular weight	29	8	6	4	2	
Specific heat, Btu/(lb)(deg F)	0.26	0.755	0.90	1.25	3.5	
Ratio of viscosity (T = const)	1	1	1	1	0.5	
Ratio of sound velocity	1	2.1	2.4	3	3.9	
Adiabatic pressure ratio for temperature ratio	4	2.92	2.71	2.52	3.65	
Volume, per cent CO_2 (1.45)	...	10	5	..	...	
Number of stages (ratio)	1	2.8	3.5	4.8	13.5	Constant circumferential velocity
Circumferential velocity	1	1.75	1.9	2.2	3.7	Constant number of stages
Diameter (ratio)	1	0.76	0.73	0.68	0.52	
Revolutions per min	1	2.30	2.6	3.3	7.1	
Heat exchanger						
Coefficient of heat transmission	1	1.86	2.12	2.56	4.35	
Number of tubes	1	0.66	0.62	0.56	0.27	(Ratio)
Length of tubes	1	0.82	0.76	0.70	0.85	
Surface area of tubes (weight)	1	0.54	0.47	0.30	0.23	
Heater						
Coefficient of heat transmission	1	1.6	1.7	2.0	4.0	(On one side)
Number of tubes	1	0.78	0.75	0.68	0.30	
Length of tubes	1	0.82	0.79	0.74	0.85	
Surface area of tubes (weight)	1	0.64	0.59	0.50	0.25	(Ratio)

[a] Machines assumed for equal output, maximum pressure, temperature and triangles of velocity; (ϵ) = const, T = const, p = const.

BIBLIOGRAPHY

1 "An Aerodynamic Thermal Power Plant," by J. Ackeret and C. Keller (in German), *Revue Polytechnique Suisse*, 1939, p. 229.

A short description is given of the working principle and its advantages, the efficiencies of the ideal process, the regulating possibilities of the plant and some data concerning the experimental plant.

2 "Hot Air Power Plant," by J. Ackeret and C. Keller, *The Engineer*, vol. 169, 1940, p. 373. Same contents as reference (1).

3 "Aerodynamic Thermal Power Plant With Closed-Circuit," by J. Ackeret and C. Keller (in German), *Zeitschrift des Vereines deutscher Ingenieure*, vol. 85, 1941, p. 491.

Primarily theoretical calculations. Carnot-cycle, double-isotherm cycle, limit outputs, influence of pressure level on dimensions of machines and apparatus as also on the efficiency, circuit efficiencies with consideration of the losses and of deviations from the double-isotherm circuit. Efficiencies to be expected in practice from further development work. Some constructional data about the Escher-Wyss experimental plant.

4 "The Aerodynamic Turbine Compared With Steam and Gas Turbines," by C. Keller, *Escher-Wyss News*, 1942–1943, p. 20.

A comparison of the ideal process with AK-plant, steam turbine, and combustion-gas turbine. Size of machines and heat exchangers of AK-plant and of combustion-turbine plant. The regulation, nozzle or throttle regulation for steam turbines, temperature regulation for combustion turbines, pressure-level regulation for AK-plant. A comparison of attainable thermal efficiencies and fuel costs. Various uses of the AK-plant.

5 "The Aerodynamic Turbine for Steel Works," by C. Keller and R. Ruegg (in German), *Revue Polytechnique Suisse*, vol. 122, 1943, no. 1, p. 1.

Various layouts for producing the blast in steel works in conjunction with AK-installations. Combined blast and air heater. Calculations for various cases with particulars about the heat consumption. Comparison of the space requirements of blast installations with AK-drive and other drives.

6 "Particulars as to the Present State of Development of the Aerodynamic Thermal Prime Mover," by J. Ackeret and C. Keller

(in German), *Revue Polytechnique Suisse*, vol. 123, 1944, no. 4, p. 37.

A preliminary report as to the results obtained up to the end of 1943, with the 2000-kw AK-experimental plant of Escher Wyss. Regulating tests and measurements of the thermal efficiency.

7 "The Aerodynamic Turbine 'Escher Wyss AK-Plant,'" (in German); "The Theoretical and Practical Foundations of the AK-Process," by J. Ackeret; "Realization of the New Thermal Power Plant," by C. Keller, and "Chief Results of the Official Performance Tests," by H. Quiby, *Neue Zürcher Zeitung*, no. 140, January 24, 1945.

A short historic review concerning the development of thermal prime movers and their theoretical bases. Description of the AK-process. The realization of the process in the 2000-kw experimental plant of Escher Wyss. General description of this plant and some projects for large installations. Preliminary information concerning the results obtained from the official tests carried out by Professor Quiby in December, 1944. Published on the occasion of the demonstration of the plant in January, 1945, to officials, the press, and other interested parties.

8 "Compte-Rendu des Essais de la Turbine Aérodynamique Escher Wyss AK," by H. Quiby, (in French), *Revue Polytechnique Suisse*, vol. 125, 1945, p. 269, and no. 24, p. 279.

A detailed description of the test results obtained by Professor Quiby in December, 1944, with the 2000-kw Escher Wyss AK-plant. Description of the plant and of its regulating equipment. Measuring results in the form of detailed tables, i.e., for four different loads on the machine. Course of the thermal efficiency in relation to the load. Behavior of the governing gear in practical operation. Diagrams relative to the speed and course of pressure in the plant under sudden load fluctuations, and when throwing load off.

9 "The Aerodynamic Turbine Escher Wyss 'AK-Plant,'" by C. Keller (in German), *Elektrizitaetsverwertung—Electrical Service*, vol. 20, 1945–1946, nos. 1–3, April–June, 1945, p. 81.

Reprint of a lecture given by Dr. C. Keller before a meeting called by the Swiss Hydraulic Association in March, 1945, in Zurich for discussing questions relating to hydraulic power and coal.

Description of the AK-process and of the experimental plant. Comparison with other machines. Projects for large installations, efficiency and Sankey diagrams according to the official measurements made on the experimental plant.

10 "The Aerodynamic Thermal Prime Mover, 'Escher Wyss AK-Plant,'" by F. Salzmann (in German), *Schweizerische Technische Zeitschrift*, 1945, no. 32, p. 413, and no. 33, p. 425.

The thermodynamic phenomena in the circuit and the basis for calculations. Pressure-volume diagrams. Thermal efficiencies of the ideal machine with consideration of losses, with and without intermediate heating. The Escher Wyss experimental plant and particulars about the test results. The uses of the plant.

11 "Some Remarks Concerning the Basis and Construction of the Thermal Power Plant Employing a Closed Air Circuit, 'Escher Wyss AK-Plant,'" by C. Keller (in German), *Schweizer Archiv. Fuer Angewandte Wissenschaft und Technik*, vol. 11, 1945, p. 225.

The theoretical basis and test results. Attainable efficiencies. Some general projects for large installations with single and double heating.

12 "The Theory and Performance of Axial-Flow Fans," by C. Keller and L. S. Marks, McGraw-Hill Book Company, Inc., New York, N. Y., 1937.

Theory and performance for use of fan designers.

13 "Performance Tests of 2000-Kw Closed-Cycle Unit. First Summary of Official Tests in the United States," by S. A. Tucker *Power*, August, 1945, p. 80.

Discussion

J. H. ANDERSON.[4] The author has made an excellent presentation of an outstanding achievement in engineering. Although time and further development will be required to determine whether the AK-system is to become an economic success, the author and his associates deserve only the highest praise for the ingenuity and perseverance required to turn this development into an engineering accomplishment of such obvious importance.

While this power plant could be compared to any prime mover, it seems most logical to compare it to a modern steam plant, for the simple reasons that both are externally fired and both can be built in large capacities. By the same logic, the open-cycle gas turbine most nearly compares with the Diesel power plant in its application and place in the economic structure.

It is, as the author has already pointed out, almost impossible to make an economic comparison between the AK-plant and a steam plant at the present stage of progress, but at the same time anyone will admit that this must be done eventually. With this in mind, it may be worth while to set down a few simple comparisons between the two types of plant.

Starting at the power unit, we have an air turbine in the AK-plant as compared with the steam turbine in the steam plant. Basically, the air turbine should be more efficient and cheaper for two reasons, i.e., there is no problem of handling liquids with attendant corrosion, and the volume ratio of expansion is far lower in the air turbine. Both of these considerations help to make a simpler and cheaper design possible, which should at least balance the problem of handling higher temperatures in the air turbine.

The air cooler and intercoolers in the AK-plant correspond to the steam condenser in the steam plant. Here the steam condenser is obviously much more expensive because more heat must be discharged at a much lower temperature difference. Also, the air-removal equipment and condensate pump are additional accessories required over and above those needed for the air coolers.

The compressor in the AK-plant corresponds to the boiler feed pump in the steam plant. Here the difference would appear to be in favor of the steam plant, although this must be subjected to thorough analysis.

The boiler, economizer, feedwater heaters, and superheater in the steam plant correspond to the air heater and recuperator in the AK-system. This is probably the largest question mark in a comparison of the two systems. In the air heater we have conditions roughly equivalent to those in the steam superheater. For this reason we have a higher average temperature difference to work with in the boiler. On the other hand, we have a lower heat input in the air heater. The recuperator is undoubtedly larger and more costly than the corresponding feedwater heaters. All in all, it is probable that the heaters in the AK-plant cost more than the corresponding heaters in the steam plant. Comments on this point by boiler manufacturers should be of great interest.

In the matter of auxiliaries, there would seem to be no question that the AK-plant is simpler and has less of them than the steam plant. This would be the case simply because in one case we have a liquid-gas plant, and in the other we have a pure gas plant.

Regardless of the present state of development, there can be no question but that the AK-plant is basically simpler to control than is the steam plant. Here again we have the simple reason that a gas is used throughout the system, instead of both a liquid and a gas.

It is difficult to make predictions on maintenance costs. However, it is probably safe to say that more machinery trouble is encountered from corrosion, wear, and solid deposits in any system where both liquid and gas are present than in a system where gas alone is present, and this is especially true in any system where variable temperatures are present. The problem of deposits on steam-turbine blades is a serious one which cannot be overlooked. While it is granted that the AK-system must operate with some higher metal temperatures than the steam system, it is probable that this will not cost as much in maintenance as other troubles in the steam plant.

It is perhaps foolish to pass judgment on the basis of the simple comparison here given, but even such a comparison should be enough to show that the AK-system deserves most

[4] Research Engineer, Ingersoll Rand Company, Phillipsburg, N. J. Mem. A.S.M.E.

careful consideration as an immediate competitor of the steam power plant.

The author has quite properly pointed out that the shaft seals are a critical component of this plant. This is obvious when one considers that there are probably 10 seals under high pressure. The ingenious method of using an oil seal at the lowest pressure in the system should make the seal losses roughly equivalent to those of an open-gas-turbine system. It would be interesting to learn what percentage of the losses was ascribed to the seals, and what clearances had to be maintained in the labyrinth packing to obtain this value of the losses.

The author has mentioned that the efficiency of an axial compressor dropped from 86 to 83 per cent during only 12 hr of operation in their shops. This does not seem to correspond fully with the experience of some others. For this reason it would be of value to have a further explanation as to how this drop in efficiency could be accounted for.

F. T. Hague.[5] The author's and Mr. Gygi's[6] visit to this country is both welcome and significant, in that it promises to focus increased attention on the study of gas-turbine power plants. The presentation of the paper, disclosing test results on a 2000-kw closed-type-cycle gas-turbine power plant, is evidence that the gas turbine for primary power generation is rapidly developing toward maturity.

It is becoming increasingly apparent that the complete gas-turbine power plant, which was a newcomer in this country 3 years ago, is making giant strides in being reduced to practice in several important lines of endeavor. Military releases have identified it as the fighting aircraft power plant of the future. Commercial interests view the prototype tests of propeller-drive gas turbines as a further boon to commercial aviation. In the locomotive field, powerful, compact gas-turbine power plants are currently being built. A high-efficiency open-cycle type of gas-turbine power plant has been demonstrated within the year, giving promise of application in fields of industrial power generation, and ship propulsion. The gas-turbine plant of which Escher Wyss has built a prototype, is the first reduction to practice of a design from which coal-burning central-station-type units of from 10 to 50,000-kw capacity may ultimately become a reality.

The author and his colleagues deserve high commendation for their engineering foresight in taking steps to reduce this type of gas-turbine power plant to practice several years before it was being given serious consideration elsewhere. It is only fitting to acknowledge that this foresight has given these engineers several years' time in which to study the theoretical and practical problems connected with this development. Their viewpoint on its ultimate accomplishment may well be more realistic than those who have been considering it for a shorter length of time. The fact that 98 per cent of Switzerland's power generation is water power presumably limited their combustion research with pulverized coal.

The proposed closed-cycle gas-turbine power plant is simple for engineers to understand who are already familiar with the open-cycle type of system. This closed-cycle system differs from open-cycle systems in one major respect; the physical size of the rotating and heat-exchange machinery is decreased as the system pressure is elevated. It is this characteristic of the closed cycle which makes it possible to build turbines and compressors for a 50,000-kw unit of smaller physical size than for a 5000-kw open-cycle unit. The closed-cycle type of system has its efficiency level affected in exactly the same manner as the open cycle with respect to any changes in maximum temperatures, compression ratio, intercooling, reheating or regeneration Like all good things, it is basically simple. This in no way detracts from the brilliance of the initial conception.

There are metallurgical limitations in the building of any high-temperature gas turbine. These are definitely less serious when the physical size of the parts is reduced. It may not be too much of an estimate to say that the metallurgical problems of a 25,000-kw closed-cycle plant will be comparable to those of a 5000-kw open-cycle plant. This is a favorable characteristic.

The practicability of the closed-cycle system may ultimately be determined by the problems associated with getting the heat from the fuel into the system. The author has elected to introduce the heat through an externally fired air heater, thus offering the possibility of using the cheapest grades of liquid fuels or pulverized coal. Such an air heater requires extensive use of high-priced stainless steel for temperatures above 1000 F. The precautions which must be taken to protect the tubes of such a gas-to-air heater from overheating, pose a difficult set of problems to the air-heater builder in designing an air heater comparable in both size and cost to a steam generator of equal plant capacity. Engineers interested in the development of a gas-turbine power plant will wait with interest to see how our air-heater manufacturers can meet these requirements at an economic cost when burning pulverized coal. Much, if not all, of the ultimate part that will be played by this cycle in primary power generation may well rest in the satisfactory solution of this air-heater problem when burning pulverized coal.

It is not to be expected that this and possibly other problems associated with this new form of gas-turbine power plant can be solved overnight. The problems involved in developing the steam cycle to its present level of performance and reliability required a long time for solution. We should, with equal consideration, concede that problems in connection with this new system which, at first glance, look to be formidable, may after further study actually yield to research and development. The engineering profession is learning to be optimistic regarding the possibilities of development of the gas turbine, and that optimism should be extended to studies of this new type of system.

M. L. Ireland, Jr.[7] The closed-cycle process at present appears to be the most practicable means to obtain single plant outputs in excess of about 6000 hp, and the author's company has shown unusual foresight in concentrating its efforts on this design.

For central-station applications this cycle offers the prospect of thermal efficiencies exceeding those now attainable with the most modern steam plants and this may well warrant the high development costs which must be incurred.

The prospect for closed-cycle marine gas-turbine power plants in excess of about 6000 hp appear to be less favorable for strictly commercial applications. Some idea of the initial cost and the operating and maintenance problems of such a plant can be gained from a comparison of the major components with the corresponding items of a steam-turbine plant for superheater conditions of 700 lb 850 F, as follows:

1 From the author's Fig. 35 we find that two air turbines are required which, though smaller in size, are probably more costly than the cross-compound steam-turbine unit because of the higher-temperature materials required.

2 Four air-circuit compressors and three intercoolers are required which correspond in function to the condensing and feedwater heating and pumping units of the steam plant. The cost of

[5] Assistant to Vice-President, Westinghouse Electric Corporation. Mem. A.S.M.E.

[6] Managing Director, Escher Wyss Engineering, Zurich, Switzerland.

[7] Engineering Technical Division, Newport News Shipbuilding and Dry Dock Co., Newport News, Va. Mem. A.S.M.E.

the compressors will probably more than offset the reduction in heat-exchange equipment, even when the increased circulating-water requirements of the steam plant are taken into account.

3 Even when pressure charging is employed, the air heater and regenerator when taken together appear to about equal the total heating surface, including air heaters of about 2 sq ft per hp, which is required for a steam plant of this size. Judging from the percentage of high-temperature materials required for the air heater, the cost will compare quite unfavorably.

4 The pressure-charging set for the air heater is understood to be necessary to reduce the dimensions of this unit, but this is felt to introduce undesirable complications for a marine unit which already contains so many novel features. In particular, it is believed that the pressure-fired boiler will be more sensitive to pressure and flow changes in the air circuit with consequent increased risk of damage to tubes subject to high thermal loading on the fuel-gas side.

5 There remain the high- and low-pressure accumulators, the control unit and the starting motor, which may be compared with the throttle and combustion-control elements of the steam plant.

When itemized in this way it is difficult to believe that the initial cost of the closed-cycle marine unit will compare at all favorably with a steam-turbine plant for, say, 700 psi 850 F at the superheater. The operating requirements appear to be quite similar, as in both cases primary control is applied to the weight flow of the working medium and the fuel control follows with a certain inevitable time lag. Considering the relative number of major rotating elements and the fact that combustion gases must pass over heat-exchanger tubes in both cases, there does not appear to be any evident advantage as regards maintenance.

The advantage in thermal efficiency over the conditions outlined for a steam plant is large, being approximately 15 per cent, but there remains a question, in this writer's mind at least, whether this will not be absorbed by increased capital charges and maintenance expense.

A substantial saving in weight is indicated which will be of importance for vessels carrying heavy cargoes. However, the fore-and-aft length of the closed-cycle unit in Figs. 35 and 36 is about 5 ft longer than the machinery compartment for a standard C-3 steam-turbine-driven cargo ship with 8500 shp. A considerable portion of the wing spaces abreast of the main plant will be required for generators, pumps, compressors and other ship's machinery and would be of little value for cargo space in any case. Therefore, in a cubic-capacity trade, the closed-cycle plant would probably be at a slight disadvantage.

In general it would appear that these factors can be considered only when a specific vessel and trade are under consideration and therefore should not be cited as intrinsic advantages or disadvantages of the closed-cycle plant as compared to a steam-turbine unit.

It is encouraging that the development of the controllable-pitch propeller has also been undertaken by the author's company and it is hoped that he will shed some light on one feature of this equipment which has given much cause for concern. During the process of reversing the propeller pitch it is necessary to move the blades back through the angle of zero lift, while the ship is still making headway. For a brief interval, while the blades are not fully reversed, they would appear to be receiving energy to drive the shaft which would result in an acceleration of the shaft speed. If the pitch control should become jammed in this position it would appear that dangerous overspeeding of the unit might occur. This situation would appear to be more critical for a gas-turbine plant than with Diesel engines which are believed to be the type of power plant to which the controllable-pitch propeller has so far been mainly applied.

JOSEPH KAYE.[8] This paper presenting a statement of the status of the closed-cycle gas-turbine power plant, brings to mind some interesting questions which it does not answer directly. (*a*) Does the closed-cycle gas-turbine plant possess any marked improvement in efficiency in comparison with other power plants of a similar nature, such as a steam power plant? (*b*) Is the size of the closed-cycle gas-turbine plant smaller than that of a comparable steam plant?

The closed-cycle gas turbine might also be compared with the more widely known combustion-gas turbine in regard to fuel consumption and size. However, such a comparison would be inconclusive at best, since different fuels are used at present for the two plants, and since the primary functions of the two plants are not similar. It should be noted that the closed-cycle gas turbine and the steam plant utilize the same fuels, perform the same primary functions, and possess parallel component parts.

For purposes of comparison, the following two power plants may be selected:

(*a*) The proposed closed-cycle gas turbine, shown in Fig. 10 of the paper, involves four compressors with three intercoolers, two turbines with two heaters, and a regenerator with an assumed effectiveness of 90 per cent. In addition a precooler is necessary at the entrance to the first compressor. The inlet temperature of each turbine is 1200 F, and from the data given in Fig. 10 the turbine efficiency is about 93 per cent and the compressor efficiency is about 90 per cent.

(*b*) The second power unit is the customary condensing steam power plant with one reheater present. For the purpose of this comparison the temperatures and pressures at each turbine inlet are taken as those in Fig. 10 of the paper. The condenser is assumed to operate at 1 in. Hg, and the feedwater pump to have an efficiency of 90 per cent. Regenerative feedwater heaters are omitted for simplicity; their effect on efficiency can be easily estimated from known data. The pressure drops in the boiler, superheater, and reheater are equal to the corresponding pressure drops in the high-pressure side of the regenerator, first heater, and second heater, respectively, as given in Fig. 10.

The efficiency of the proposed closed-cycle gas turbine in (*a*) is about 39 per cent allowing for external losses.

The efficiency of the steam power plant in (*b*) is about 38 per cent for turbine efficiencies of 93 per cent, and is about 35 per cent for turbine efficiencies of 85 per cent, allowing in each case for external losses. These efficiencies could be increased by 10 per cent through the introduction of several regenerative feedwater heaters. The efficiency could also be increased somewhat by the readjustment of the pressure ratios for the two turbines to yield the maximum steam cycle efficiency for the same temperatures.

On the basis of efficiency, the proposed closed-cycle gas turbine in (*a*) represents no marked improvement over the comparable steam plant in (*b*).

The power units in (*a*) and (*b*) may be compared on the basis of size. Consider first the turbines and compressors of (*a*) and the turbines and feed pump of (*b*). The turbines of (*a*) must deliver several times the power of the turbines in (*b*) for the same net power of the complete unit, since the power consumption of the feed pump in the steam unit in (*b*) is negligible compared to the power required to drive the compressors of the gas-turbine unit in (*a*). In other words, for a net power of 2000 hp, the turbines in the steam plant in (*b*) will deliver slightly more than 2000 hp, whereas the turbines of the unit in (*a*) must deliver about 4000 hp, and the compressors will absorb about 2000 hp. Even if the specific weight of the turbines in (*a*) is less than that for the turbines in the steam unit in (*b*), it is apparent that the steam

[8] Assistant Professor of Mechanical Engineering, Massachusetts Institute of Technology, Cambridge, Mass. Jun. A.S.M.E.

plant has a decided advantage with respect to size of its prime movers.

Consider next the size of the heat-transfer units of the closed-cycle gas turbine in (*a*) and of the steam plant in (*b*). Both units have a heater in which heat is transferred to the working fluid at high temperatures. Both units have a cooler for rejecting heat from the working fluid; in the case of unit (*a*), this cooler comprises the precooler and intercoolers, while for unit (*b*), it is the condenser. Moreover, the gas turbine in (*a*) has an additional piece of heat-transfer equipment, the regenerator.

For equal heat flows and similar constructional details, the size of the heaters and of the coolers will be determined mainly by the major resistances to heat transfer. Under these conditions the size of the heater of the gas turbine in (*a*) will be larger than that of the steam plant in (*b*) for several reasons: The thermal resistance of the high-pressure gas of the heater in (*a*) will be larger than the resistance of the high-pressure vaporizing fluid in the steam plant in (*b*). Then, the use of high-pressure combustion to reduce the thermal resistance on the flue-gas side of the heater is applicable to the steam power unit in (*b*) as well as to the gas turbine in (*a*). For equal heat flows and similar constructional details the combined size of the precooler and intercoolers of the gas turbine in (*a*) will be larger than the size of the condenser of the steam unit in (*b*). These heat-transfer units use water as the cooling agent, and they will have about the same thermal resistance on the cooling-water side. However, the thermal resistance of the low-pressure gas in (*a*) will be considerably greater than the resistance of the condensing steam in (*b*).

In conclusion, if the large size of the regenerator of the closed-cycle gas turbine in (*a*) is considered, it is apparent that the overall size of the equipment for the closed-cycle gas turbine in (*a*) will be greater than the size of the steam plant in (*b*) without a compensating gain in efficiency.

Alf Lysholm.[9] In the writer's opinion the high thermal efficiency is to a great extent due to the perfect aerodynamic design, especially of turbine and compressors, as well as to the high-efficiency 90 per cent regenerator, which has counterbalanced the inherent unavoidable losses of the closed cycle. These losses are as follows:

1 Losses in the externally fired air heater.

2 Aftercooler losses, including the loss caused by a higher inlet-air temperature of the first compressor, as compared to the open cycle. In cases where the cooling-water temperature is lower than the air temperature a precooler could be used with advantage for the open cycle.

3 "Feed"-pump losses.

The author states that the inlet volume for the open cycle is many times higher than that of the steam-turbine cycle. That is correct for an open simple gas-turbine cycle, but not for the reheat intercool cycle using the same or somewhat lower maximum pressure than that of the closed cycle.

In Table 3 of this discussion a comparison is given of the inlet volume of different gas-turbine cycles, as well as steam cycles, taking the author's data for the 8000-shp unit as a basis.

The table shows that the inlet volume of the open cycle, using the same maximum pressure as the AK-cycle, is only about 20 per cent higher than the combustion air volume of a steam-turbine plant operating at maximum load. As higher velocities in the ducts may be used for a gas turbine, the ducts will be of about the same dimensions as those of the steam plant.

Compared with the closed cycle the efficiency of the multiple-reheat-intercool cycle will be considerably higher, amounting to 10 to 15 per cent for the example just given. On account of the low air rate this combination is ideal for very large gas turbines.

As regards coal-firing, it should be noted that the open cycle also may be fitted with an external air heater if that should be required. In this case the additional heat losses due to combustion air amount to only a few per cent, as hot air from the gas-turbine exhaust may be used as combustion air in a "tail-end" boiler.

TABLE 3 COMPARISON OF VARIOUS GAS-TURBINE CYCLES[a]

Cycle	Air pressure, psi	Pressure ratio	Air rate, lb per hphr	Compressor-air-inlet volume, cfm	Combustion-air-inlet volume, cfm	Thermal efficiency, per cent
AK-double heat.....	600/60	10	33	15000	14000	33
Reheat intercool, 4-3-0.85.....	600/14.7	41	18	31000	.....	38
Reheat intercool, 3-2-0.85.....	250/14.7	17	24	41000	.....	37
Steam maximum load	14.7	..	..	.....	26000	17
Steam, normal load..	14.7	..	..	.....	19000	23

[a] The data in this table have been computed with a turbine efficiency of 88 per cent, and a compressor efficiency of 83 per cent.

Frederick Nettel.[10] The author mentions that the double-isotherm cycle (in which we recognize the Ericsson cycle) is in its theoretical form equivalent to the Carnot cycle, and seems to claim on this basis some sort of superiority for it. It must be kept in mind that the approach to the Carnot cycle is realized by assuming not only ideal compression and expansion, but also 100 per cent recuperation.

Under the same assumption, however, even the simple Brayton cycle approaches Carnot efficiency as the pressure ratio decreases. For thermodynamical purposes Fig. 3 can be interpreted as agglomeration of three Brayton cycles.

Any basic superiority of the double-isotherm cycle appears doubtful from this viewpoint, apart from quite fundamental additional considerations which enter the question as soon as even slight deviations from 100 per cent efficiencies are contemplated for compression, expansion and recuperation.

On the basis of fundamental thermodynamic research (the results of which are not yet released) it must be said that it is even doubtful whether any of the two cycles is particularly suited to approach Carnot efficiency with a minimum of heat-transfer surfaces, and in particular it must be doubted whether the intentional complete omission of any adiabatic compression is always helpful. Let us consider only the last stage of an isothermal compression. There we carry away compression heat by cooling, only to replace it immediately thereafter by heating. This is all right as long as the heating is obtained, so to speak, free of charge by 100 per cent recuperation, but if we have only 90 or 80, or 70 per cent recuperation it is sheer waste of heat. This is only one of the reasons why the Ericsson cycle is not the ideal to

[9] Consulting Engineer, Stockholm, Sweden.

[10] Consulting Engineer, Manhasset, Long Island, N. Y.

strive for in practical plants. Approaching a cycle which is best under ideal conditions does not give the plant that is best under conditions prevailing in practice, namely, with finite efficiencies of the components.

The interrelations between the method of intercooling, reheating, and recuperation, if applied simultaneously, are much more complex than it would appear from the presentation of the AK cycle, and that is the reason why the writer arrives at appreciably different results in setting up optimum conditions for open as well as closed cycles.

The author speaks of the supercharged closed cycle as "an important new feature" and mentions as its "chief characteristic" the changing of the density of the working fluid in accordance with the load to be furnished. Without wishing in the least to detract from the fact that Ackeret and Keller have introduced this principle for air "turbines," we must face history by mentioning that the closed cycle and density regulation were actually anticipated for air "engines" decades ago. However, this is not the place to go into details, and that does not change the fact that the application of this principle in a properly modified form has outstanding promise for high-power air turbines. In commenting on the merits of the AK cycle, its demerits and limitations need also to be given due consideration.

The utilization of coal as fuel is imperative if the gas or air turbine is ever to play an important role as a prime mover. The author points to the radical decrease in the size of heat exchangers and the favorable heat transfer to highly compressed air. He touches on the necessity to preheat the combustion air in the air heater furnace.[11] Since the stack gases from the furnace and the combustion air have to exchange heat near atmospheric pressure, this air heater does not profit in any way from the supercharging of the power cycle, and the necessary heat-transfer surface will be of the same magnitude as that of air heaters used in steam boilers. We know that those air heaters have surfaces which often are multiples of the boiler heating surfaces proper, and we know too that they determine the furnace efficiency, not only in steam power plants, but equally in air-turbine power plants of the AK-type. However, this is not necessarily the case in other closed or semi-closed plants of a modified layout and hook-up.

With reference to the section of the paper on operating cycles of the AK process: Two intermediate coolers and a pressure ratio of about 3 to 4 are mentioned as the most favorable for the simplest air-turbine plants. The author does not give any basis for this statement. Actually the best pressure ratio varies widely with recuperator effectiveness, top temperature at turbine inlet, turbine and compressor efficiencies, etc.

In practice an "oversize" heat exchanger can be made to cover up nearly any deviation from optimum layout, and this is what appears to have been done in the 2000-kw experimental AK plant, where a recuperator of close to 90 per cent effectiveness is being used. While a recuperator of 75 per cent effectiveness is already pretty large, one of almost 90 per cent is definitely oversize.

Now the author may reply that his recuperator is as such much smaller than those required in open gas-turbine plants due to the much better heat transfer resulting from supercharging. However, this would be beside the point if it can be shown that an equal or better efficiency can be reached in a similar plant of modified layout with smaller transfer surfaces; and that can be shown.

Actually, in a similar manner as indicated by Soderberg-Smith for open cycles, the optimum pressure ratios increase with increasing refinements (intercooling and reheating) but fall with rising effectiveness of the recuperator, and there is no short cut to fixing a ratio at 3 to 4 as "most favorable."

All Sankey diagrams show high furnace efficiencies obtained by air preheaters for the combustion air, but the text gives no indication of their size and the degree of air preheat.

In view of the foregoing, it is difficult to understand Fig. 9 fully. In the "Index of Figures" (referring to Fig. 9) a minor error (due probably to translation) has crept in. Only a small Δt_A = 18 deg F in combination with a large ϵ_B = 10 per cent can lead to the same curve 2 as a larger Δt_B = 36 deg F in combination with a smaller ϵ_A = 5 per cent. The same holds good for curve 3.

With reference to air heaters: Under this section the influence of preheated combustion air is stated "to lead to an increase in the furnace temperature," and that in plants burning pulverized coal "such preheating of the secondary air is desirable," since it permits a reduction in the size of the combustion chamber.

Every reason for favoring air preheating given is sound, but the most important fact, namely, that the AK plant would badly disappoint in efficiency without such a very large air preheater, may escape notice as the author proposes "not to deal further herein with the details of coal-fired air heaters."

There can be little doubt that supercharging of the air heater on the gas side has great merits for marine plants. However, the problem of regulation of the supercharging set and the problem of very low loads, for example in naval plants, is one of the most complicated that awaits solution. Probably the author did not go into these details as outside the scope of a general paper. It is in any case necessary for us to realize that supercharging of air heaters in closed or semiclosed air-turbine plants deserves closest attention in the future.

Do the figures 1.5 to 3 sq ft of heat-transfer surface per kw include the air preheaters for the combustion air?

Governing: The size of the air accumulators for a 50,000-kw plant would be interesting to know if we consider the possible tripping of the generator circuit breaker twice or three times within, say, $^1/_2$ hr.

The writer will conclude with some remarks regarding the efficiency curves in Fig. 7. According to the author, without altering the temperatures the efficiency of the plant should be almost equally high at part loads as at full load.

The curves, while comparing very well indeed with those of other prime movers, will necessarily show a steady drop with the load. The reason is simple enough; if at full load the tube material in the air heater is thermally fully utilized, a certain safe limiting wall temperature is reached. At lower loads the air density drops and with it the heat transfer from wall to air, and if we try now to maintain the top heating temperature the wall temperature would rise beyond a safe limit. Since that is inadmissible, a lowering of the top temperature becomes imperative, resulting in a somewhat lower efficiency.

While curve (*a*) is shown as a horizontal, this would seem attainable only if at full load the tube material would not be thermally fully utilized, thus admitting higher wall temperatures at partial loads. Whether or not a plant should be designed in this way will depend primarily on the load diversity factor of the plant during operation.

J. K. Salisbury.[12] After one has mastered the prerequisite elements of engineering, the problem of design of power-generating equipment becomes primarily one of economics. It is well recognized that any power plant consists primarily of a means for supplying heat to a system, and an accompanying means for rejecting less heat than is supplied. The difference between the

[11] Without, however, mentioning the conditions under which this must be done.

[12] Turbine Generator Engineering Division, General Electric Company, Schenectady, N. Y. Mem. A.S.M.E.

heat supplied and the heat rejected is equal to the power generated, according to the fundamental laws of thermodynamics. In many cases the supplying of heat to a system and the rejection of heat from a system requires the use of indirect heat-transfer surfaces. Both the weight and the quality, as well as the degree of fabrication of the materials which go into these heat-transfer surfaces determine to a large extent the cost of the power-generating system.

Typical exceptions to the generalization that power plants require heat-transfer surfaces are the open-cycle gas turbine and the Diesel engine. In these plants heat-transfer surface is not required because the heat generated within the working fluid is transferred by direct contact, thus eliminating an expensive type of surface, which must be suitable for operation at high temperatures, for high efficiency. Both of these power plants reject heat to the atmosphere through the medium of the exhaust gases. In the case of the Diesel engine, an appreciable portion is also rejected to the cooling water. Obviously, both of these plants thus eliminate a large item of expense.

Consider the general proposition of the transfer of heat through an indirect heating surface in the type of power plant which requires it. According to the well-known equation of heat transfer, the heat transferred Q, is given by the expression

$$Q = UA\,\Delta T$$

The last two factors in this equation represent material for interesting speculation. By increasing the value of A we can decrease the value of ΔT, with constant heat input Q. When we increase the surface area A, we increase the cost of the power plant; at the same time we reduce the value of the temperature difference ΔT; according to the second law of thermodynamics this improves the efficiency of the power plant. It is readily apparent that we may exchange cost of the power plant for efficiency of the power plant; when the cost increases the efficiency improves, when the cost decreases the efficiency becomes poorer. This principle is particularly apparent to any student of gas-turbine cycles, although it is also applicable to steam power plants.

The first factor in the heat-transfer equation, the heat-transfer coefficient U, is ordinarily not considered to be susceptible of much improvement. However, the author has, in the design of the plant described in the paper, indicated a method whereby U may be increased without appreciable direct cost. By increase of the pressure level in the system the heat-transfer coefficient is increased almost in direct proportion, thus reducing the value of A required for a given rating and efficiency. In other words, the use of the pressure cycle in which heat-transfer surfaces in regenerators are reduced by the use of high pressure on both sides of the surface, is considered to be of importance in the gas-turbine field. This principle permits realization of high efficiency without the usual accompanying high cost of the regenerator.

The engineering of the plant described in the paper indicates an acute awareness of the factors which are effective in yielding a high-efficiency power plant. The engineering of this plant cannot be questioned because in the first place the power plant has successfully performed, and in the second place the plant has produced a high efficiency. The author and the Escher Wyss Company are to be sincerely congratulated on their achievement. The advantages of this plant, in order of importance, seem to the writer to be as follows:

1 Control of output by variation of density, thus maintaining constant internal efficiency. (It is obvious that there is no inherent advantage in efficiency at a given load due to the use of the pressure cycle.)

2 The probable ability of the plant to burn coal.

3 The reduction in heating-surface cost per kilowatt.

4 The use of clean air in the circuit, avoiding decrease of compressor and turbine efficiency with use, and justifying the use of a larger regenerator.

5 The possibility of building units in larger ratings.

Although the engineering of this plant cannot be questioned, the economic situation does appear to be open to question, especially in the United States. It is recognized that any gas-turbine plant is handicapped by the requirement of a compressor rated at about $^2/_3$ of the total gross power output of the turbine. Thus the sum of the ratings of the compressor and turbine in nearly any gas-turbine plant is equal to about 4 or 5 times the net output. Intrinsically therefore the gas-turbine power plant uses machinery which, on the basis of its rating, should cost several times that of the turbine in a steam plant of the same rating. In the open-cycle gas-turbine plant this higher cost is partially offset by the elimination of expensive heat-transfer surface such as the boiler.

The closed-cycle plant suffers the same disadvantage, with respect to the cost of the rotating machinery, as the open-cycle plant and, in addition, requires the use of expensive indirect heat-transfer surface in the air heater. In the writer's opinion it is highly questionable whether this air heater, or one of similar capabilities, could be built in the United States for less than $75 per kw of plant rating. This price, when added to the higher price of the rotating machinery and regenerating equipment, would seem to make the total cost of a power plant of this type considerably higher than the usual price for steam power plants in the United States. The apparently higher fixed charges on such a plant would mitigate against its economic application in either industrial or central station plants, particularly the former, where the fixed charges are usually taken to be a higher percentage than in the central-station industry.

Even with the higher fixed charges, which in our judgment would obtain, such a plant might be acceptable, especially where the fuel cost is high, if it were impossible to build a plant with this efficiency in any other manner. Our studies, however, indicate that with equal ease a 2000-kw steam plant can be designed having an efficiency equal to that of the Escher Wyss closed-cycle plant. Such a steam plant would be designed for a somewhat higher pressure than the experimental plant operated in Switzerland, but for a lower temperature, to compensate for the higher pressure; the material requirements would be no more stringent than in the author's plant. The inlet steam conditions would be 600 psig 1200 F, and the exhaust pressure 0.66 in. Hg.

This exhaust pressure, according to our estimate, could be obtained with the temperature of the cooling water used in the Escher Wyss test plant. Using a turbine efficiency which includes some margin, a good feedwater-heating cycle, 5 per cent auxiliary power, and 92 per cent dry-boiler efficiency (equivalent to about 86 per cent on the usual basis), the thermal efficiency of the steam plant was found to be 30.4 per cent. While on first thought the superheating of steam to 1200 F seems to be difficult of accomplishment, it must be realized that in this country steam superheaters have already been built with an outlet temperature of 1400 F, for special applications. Furthermore, the quantity of heat which must be put into the superheated steam at high temperature, for a unit of energy output at the generator terminals, is considerably less, as will be shown.

The degree of severity of the metallurgical problems in the respective plants is described quite clearly by a statement of the relative quantity of heat put into the working fluid between given temperature limits, per unit of net energy output. One interesting way in which this may be done is to express the energy in-

put in units of kilowatt-hours, in order to make this energy directly comparable with the output of the generator. Since modern metallurgy does not recognize temperatures below 900 F as a problem, these temperatures will not be considered. In Table 4 of this discussion is included a mercury-steam plant, in which a mercury-vapor cycle is superposed on the 600-psig 1200 F steam cycle. While the writer's company is not prepared to build such a plant today, it is of academic interest in that it indicates the considerably smaller quantity of heat supplied at high temperatures in this cycle, despite the very high thermal efficiency of the plant.

TABLE 4 COMPARISON OF QUANTITY OF HEAT SUPPLIED AT VARIOUS TEMPERATURES PER UNIT ENERGY OUTPUT

(Kwhr of heat supplied per kwhr at generator terminals)

Temperature range, deg F	Escher-Wyss aerodynamic turbine plant	600 psig — 1200 F steam plant	500 psig — 1200 F mercury superposed on 600 psig — 1200 F steam plant
900–1000	0.578	0.131	0.119
1000–1100	0.584	0.132	0.119
1100–1200	0.590	0.131	1.464
1200–1268	0.405	0	0
Total, above 900	2.16	0.394	1.70
Plant thermal efficiency, per cent	30.5	30.4	37.8

This table is of great interest because it indicates that in a steam plant, designed for the stated steam conditions, only about $^1/_5$ as much heat per net kilowatt of output is required to be transferred at temperatures above 900 F. Even in the mercury-steam plant, which has a thermal efficiency considerably better than that of the closed-cycle plant, the heat transferred at temperatures above 900 F is considerably less, although admittedly a large proportion of the heat is transferred at 1200 F. This heat transfer, however, occurs from gas to boiling liquid, so that the metal temperatures approximate the boiling-liquid temperatures.

The writer would like to ask the author several detailed questions. In view of the fact that the average steam plant has a total heating surface in the boiler and the condenser of about 2 to 2.5 sq ft per kw of plant rating, what is the corresponding figure for the Escher Wyss plant, including regenerator, air heater, combustion-air heater, intercoolers, and precooler? Since, according to previously published information, the combined pressure drop on the high-pressure side of both the regenerator and air heater of the test plant was only 3.5 psi, how is this reconciled with the 10 to 15 psi pressure drop mentioned by the author for the air heater only? Published figures indicate that the recirculating-fan power in the test plant was only 2 kw, or 0.1 per cent of the net plant output. American experience in this connection has indicated that recirculating-fan powers are usually very much higher than this percentage. Will the author undertake an explanation of how such low fan power was achieved? Calculations by the writer indicate that the mechanical efficiency of the rotating machinery, based on the net generator output, is approximately 86 per cent. Even when all of the mechanical losses in the turbines are charged against the sum of the powers of both the turbines and compressors, the mechanical efficiency is only 97.4 per cent, a rather low value. Will the author state whether this low value is due to the oil seal used on the shaft ends or whether there is some other reason for the high losses?

Author's Closure

General. It is not an easy matter for the author to answer the many questions posed in the long discussions of this paper in as exhaustive a manner as he would like to do. The principal reason for this is the fact that this new system of gas turbines is actually still at the beginning of its practical development. Therefore, not all of the elements have found their final form. The field of application is very large and, always considering the principle of the high-density circuit, many solutions are possible. It is impossible to give definite and general answers, for example, for the best layout or for prices. They may vary widely with given conditions, such as cooling-water temperature or supply, air temperature, efficiencies asked for, necessary weight, etc.

A crew of engineers has worked for more than 10 years and not under favorable conditions, on this project to bring it to its present state, namely, actual installations in industrial plants. The deeper we went into details in our studies, the more we found, not only from the technical and physical but also from the economical point of view, that the closed-cycle power unit offers many operating advantages as well as higher efficiency, as compared with steam turbines and open-cycle combustion gas turbines in many applications, especially for ship propulsion and stationary plants.

It is an honor and a pleasure for us to see what great interest has been created by our visit to America, and in the discussion with many famous scientists and engineers. These discussions developed many new and helpful ideas for us and we derived some very useful data, especially from the metallurgists. All this encourages us to an optimistic outlook regarding broader realization of our objectives. We are much impressed and thankful for the open-minded criticism.

Before answering the several items of discussion in detail, the author would like to make a few general remarks which hold for many questions and allusions common to different discussers. It will be recalled that this conference was meant to give a general survey of what has been accomplished by the author's company during the war and to explain the physical base of the cycle. Naturally, we have constantly kept in mind the matter of economics for future plants. We know much more about costs now than we knew a year ago, as a consequence of relief in prices for different materials involved. Even at the present time, a closed-cycle plant of, say, 12,000 or 25,000 kw output with oil and gas firing does not cost much more than a modern steam plant, if one takes into account all the saving in space for the building, the foundations, the lack of feedwater preparation, etc.

In contradistinction to steam-turbine practice, the whole range of output from, say, 6000 to 50,000 kw can be covered by a few types of machines and apparatus only. Many elements, such as blades, tube bundles of heat-exchangers, headers, or air heaters, then auxiliaries as leakage compressors, regulating gear, etc., can more easily be simplified, classified, and normalized. This will help considerably in achieving low-cost fabrication methods, and therefore in lowering further the cost of a plant.

An oil-fired plant of about 17,000 hp net output is under construction now at the Escher Wyss Works in Zurich. It is hoped that, in the near future, much more can be said about prices, operating experience, and maintenance, based on facts. The overall efficiency, including all auxiliaries, of about 37 per cent at full load must also be considered when comparing prices and economy with other systems.

The author would like to point out that the construction of the test plant of 2000 kw at our works, which is dealt with extensively in the paper was started more than 10 years ago. This was really meant for development and research work and not as representative of later plants. All direct comparisons with other caloric plants concerning results achieved are therefore misleading. It may be of interest that in the same space which we used for the test plant, at the present state of technical development, we can install a 15,000 to 20,0000-hp plant. This shows that many simplifications and savings in construction based on the long experience and studies have been achieved.

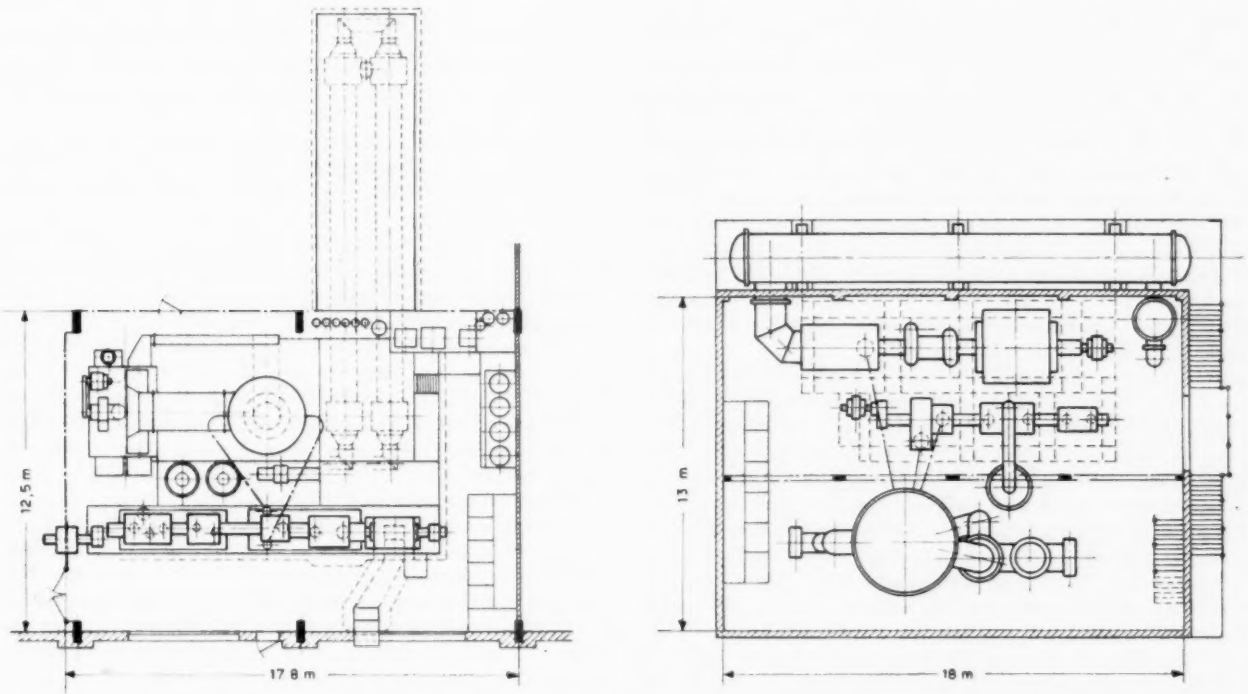


FIG. 36 SHOWS AREA COVERED BY TEST PLANT (LEFT) AND THE FIRST INDUSTRIAL APPLICATION (RIGHT) NOW UNDER WAY
(Test plant, 2000 kw; plant under construction, 12,500 kw.)

Fig. 36 of this closure shows the area covered by the test plant with which many American engineers are familiar, as well as the first industrial application now under way.[13] The saving is due mainly to the large output, and the choice of the higher pressure of 50 atm abs with a pressure ratio of about 10 between the low- and high-pressure sides because two-stage expansion is used.

All necessary details of this plant will be divulged to the engineering profession when it is finished. Therefore, the author begs the reader's indulgence for not going into detail here. However, it may be said that we are not only optimistic about the technical progress achieved but also concerning prices, as a result of the reasons given herein. In this respect, it must not be forgotten that the amount of special and expensive materials for the machines is small because the dimensions are small, as compared with other gas turbines.

On our last visit to America and England, it was gratifying to learn that the necessary tubes for the air heater can be produced on a normal commercial basis. They are similar to the type widely used for modern cracking plants under more severe conditions than occur in the AK heater. The total weight of heat-resisting material, compared with the total iron weight of the whole installation, amounts to only about 12 to 15 per cent. To give an idea; the cost of the air-heater tubes for a big plant amounts only to about 7 per cent of the total cost. These figures show that the supercharged cycle, because of its smaller machine dimensions and heat-exchanger surfaces, offers advantages generally not anticipated.

Reply to J. H. Anderson. The principal points concerning matters of cost have been dealt with in the foregoing general statement. In comparison with corresponding steam plants the better possibilities to normalize elements and to build standard plants will play a big role in the future and affect costs. As the air heater from the construction point of view is a simpler apparatus than a steam boiler, especially when supercharged-firing is used, there is no reason why this apparatus should cost more than a modern high-grade boiler.

The control and regulating system of the plant by varying the density only leads to valveless machines and apparatus in the cycle itself. The whole regulating block is a separate unit outside the cycle in cold atmosphere. This arrangement gives favorable operating conditions and much lower costs than the regulating device of modern high-pressure high-temperature steam turbines.

We have tried different shaft-seal constructions in the test plant. We now use the same liquid-seal method which has been widely used in our compressors for poisonous and dangerous chemical gases where shafts must be absolutely tight. As a consequence of the different alterations we have made in the test plant, the leakage loss has been relatively high. As the official report by Professor Quiby[14] on the trials shows, the compensation for air leakage amounts to about 30 kw at full load (2000 kw). The percentage loss in a new plant will be less.

The drop in efficiency of 3 per cent at a certain test compressor in a rather short time has been measured in different instances. It is believed that such losses depend naturally upon the individual form of guide vanes and runner blades. The difference in these friction losses in different airfoil-bladed machines may be due to the different Reynolds number involved. If a test is made with low velocities, the effect is naturally not so obvious as at high Reynolds number, where, as modern research on friction on plain and curved surfaces shows, the relative roughness plays a much bigger role.

Reply to F. T. Hague. It was very encouraging for us to have the opinion of an engineer who has dealt with many pioneer

[13] A brief description of the entire project is given under the title, "New Developments in Gas Turbine and Boiler-Plant Practice," *Power*, vol. 90, Aug., 1946; details of the Escher Wyss installations are given on pp. 88–90, of this article.

[14] Reprinted in *Oil Engine*, November, 1945.

efforts in the fields of steam and gas turbines and who has successfully carried new ideas on to realization. We can assure him that what seems to have occurred to him, when first studying our project, occurred to us also in the course of its development. Many details appeared to be formidable at first glance but our team of engineers has always found technical solutions. Construction of all elements has been based upon intensive research work in our laboratories. As we cannot accomplish all our objectives at the same time, we first have concentrated on the construction of oil- and gas-fired installations. For this purpose, we have arrived at simple arrangements for the air heater. The coal-fired air heater will be the next step to be achieved, based on actual studies and experiments. We are quite optimistic about this field too.

The principal problem in the case of pulverized-coal firing is the necessity for keeping slag and ash particles as far as possible away from the innermost rows of tubes near the combustion center. This can be effected by blowing in the recirculated flue gases, which serve for reducing the temperature of the furnace, along the whole inner tube wall between the tubes themselves. Tests which have been carried out in this connection show that this is already possible even in the case of small circulating volumes.

Since circulating gases at approximately 1000 F are relatively cold, the blown-in current has the additional action of bringing about quick cooling and granulation of the slag particles.

As Mr. Hague looks favorably and optimistically to the possibilities of the closed cycle, the author also would like to tell him that we think this system may also have a future application in connection with atomic power.

Reference has already been made to the advantages of employing light gases as the working medium for special purposes. For instance, helium or helium mixtures permit of heat-transmission values being attained which are of the same magnitude as for water. Thus, for otherwise similar conditions, the heating surfaces in a helium heater could again be considerably reduced compared to the air heater.

In so far as conditions can be foreseen, the closed helium circuit would prove suitable in a thermal power plant employing atomic energy. Since helium is neutral to the material of the pile and in addition has advantageous characteristics from the viewpoint of nuclear-physics in that, like graphite, it acts as a neutron moderator, the pile could be brought in direct contact with the gas. The pile might, in fact, possibly be arranged in a pressure vessel. The helium issuing from the compressor of the circuit could be supplied to the pile under a high pressure of 700 to 1400 psi, for increasing the heat-transmission figures and reducing the dimensions, and would afterward flow in direct contact as a cooling medium around the uranium rods, as also through bores in the graphite itself. In this way the pile would give up the heat which it produces by direct convection to the helium. It may be foreseen that under the assumptions mentioned (increased pressures) the large quantities of heat produced in the pile will, on account of the good heat transmission, be capable of being usefully taken up. In this manner no tubes would be required at all for the helium heater. Calculations show that if we assume a pile temperature of 1500 F as admissible, only a very small surface is needed to heat up the circulating helium to 1300 F.

For 1000 kw net output of the plant, about 15 to 20 sq ft in direct contact with the gas are sufficient without a greater total pressure loss than 3 to 4 per cent in the "pile heater." Therefore, a 50,000-kw plant would need only a heat-transfer surface of less than 1000 sq ft. Whether such dimensions are possible from the physical aspects is not yet known.

The adoption of a uranium pile in place of a combustion chamber would in the case of an open-circuit turbine be detrimentally affected by the fact that only small heat-transmission values are attainable with air. Furthermore, the nitrogen would absorb neutrons and the open air current continually deliver radioactive products to the atmosphere. Moreover, there would be the danger of the graphite in the pile being burned by the oxygen in the air.

The use of steam as working medium likewise has the drawback of a considerable absorption of neutrons and of a small heat transmission in the superheated condition, also requiring complicated installations.

It is also possible to combine a normal closed cycle working with air or another suitable gas with a "pile"-heater through an intermediate circuit bringing the heat from the pile to a heat exchanger (air heater with tubes). This intermediate circuit is closed too and would contain compressed helium in order to get high heat-transfer coefficients both in the pile and in the air heater. By this arrangement the working circuit with the machines is entirely separated and safe from radioactive particles. Calculations show that the necessary surface for the helium air heater amount only to about 200 plus 300 sq ft per 1000 kw when working with pressures of 60 to 80 ata.

We appreciate that the problems of utilizing the plant in conjunction with atomic energy are as yet unsolved and cannot yet be foreseen fully, particularly with regard to the construction. Nevertheless, the foregoing remarks show that the closed circuit has by no means reached the end of its development. On the contrary, this new principle opens up wide possibilities for the improved conversion of heat into mechanical energy.

Reply to M. L. Ireland, Jun. The method of estimating costs of future plants and the author's point of view upon that subject are discussed in the introduction to this closure. In connection with point 4, it may be said that all our recent studies show that pressurizing is very suitable for marine applications with oil-firing and also for gas-fired heaters in stationary plants. The control of the small charging set is not complicated.

The author agrees fully with the discusser's advice that only in specific cases can the different systems be reasonably compared.

We have made some studies for ship propulsion in the meantime and especially on the regulating problems in connection with variable-pitch propellers. Some of these problems were discussed by Dr. Salzmann, Chief Engineer of Research Laboratories of Escher Wyss, at the Detroit meeting of the A.S.M.E. in June, 1946. As a result of these studies, it may be said that we do not foresee any particular difficulties in regulating and stabilizing in connection with turboelectric drive or in combination with variable-pitch propellers.

For ships the closed air cycle offers an important advantage over the steam plant because of its ability to fit into given spaces as no gravity is acting on the working medium. All apparatus and machines can be arranged in a great variety of ways. The fact that the amount of air to be taken in for the closed-cycle air heater is the same as that of a Diesel engine or steam plant gives the same dimensions of inlet openings and outlet openings for the combustion gases. The combustion gas turbine needs many times more surface for these purposes.

Reply to Joseph Kaye. Our projects show that a closed-cycle power plant needs less total room than a corresponding steam plant of the same output. To give an idea; a 25,000-kw stationary plant can be built in a space of $90 \times 52 \times 40$ ft for oil or gasfiring. In this space all the auxiliaries, all the accumulators, and all the heaters and regenerators of the machines are situated. The weight will be about 35 to 40 lb per kw. Under favorable conditions, we can guarantee an efficiency at the coupling of the output turbine of 37 per cent at full load, 35 per cent at half load, and even 27 per cent at 20 per cent load, all auxiliaries included; this with a working temperature of about 1200 F. Higher temperatures of 1300 F or more, we believe, can be real-

ized in the very near future, after having gathered experience with the first plant. The figures cited can be attained by modern steam plants only for large outputs and with rather complicated installations.

Reply to Alf Lysholm. It is true that we use high-efficiency regenerators in the closed-cycle system and that we need, like all other turbine systems, highly efficient compressors and turbines. But just to realize high figures constantly the absolutely pure medium offers ideal possibilities in the supercharged cycle. The Reynolds numbers are very high and heat transfer is good. The simple open-cycle combustion gas turbine uses a great excess of air to cool down the combustion gases to allowable temperatures for the turbines. This cannot be changed. The closed cycle needs about the same amount of intake air as a Diesel or steam plant.

Concerning the reheat-intercool cycle mentioned for open gas turbines but with high pressures, the author is not familiar with the possibility of its practical realization. The high pressure ratio of about 40, involved in this system, will require other constructions in machines. It is also thought that the different reheat stages would lead to constructional complications. More reheat stages or intercooler stages could also be introduced in the closed cycle as already pointed out in the paper. Yet the theoretical gain of efficiency would, in our opinion, be balanced by additional mechanical pressure and temperature losses.

Reply to Frederick Nettel. We try to follow the theoretical double isothermal cycle as closely as possible because we think this is a suitable way for gas processes to approach the maximum possible efficiency between given temperature limits with simple technical means which, from the engineering, constructional, and metallurgical point of view, are available today and in the near future. Mr. Nettel mentions another approach to the best thermal output, but as he does not give further explanation, the author cannot very well discuss the possibilities. It may be that there are other schemes for gas turbines but we shall stick to the one idea explained. All the deductions concerning best pressure ratios, reheat factor in heat exchangers, etc., should be regarded only in connection with the double isothermal cycle. For other cycles there are naturally, as Mr. Nettel points out, other most favorable relations. We arrived at these relations, for example, of 3–4 for the best pressure ratio with direct expansion and 10–12 for double expansion, not only from the theoretical calculations of the cycle but also taking in account all the losses of pressure and temperature involved in practical plants. Also, the quantity of circulating gases for a given output plays an important role.

The supercharging of the air-heater furnace not only lowers the surface of its tubes but also the surface of the combustion-air preheaters, because a part of the heat of the combustion gases is used in the expansion turbine which drives the supercharging set.

Concerning the size of the heat exchanger, it may be said that 75 per cent effectiveness is too low to get high efficiencies with normal circuit temperatures of about 1200 to 1300 F; 90 per cent effectiveness is really the figure upon which our actual construction is based. This corresponds to temperature differences of 45 to 65 deg F in this apparatus between the two air streams. It is an important item of the closed cycle that this high effectiveness can be realized with comparatively small surface and in small space; the heat-transfer in coefficients is many times higher than in an open-cycle installation, and we have to deal with an absolutely pure medium, so that we can really choose small diameters of tubes without any danger of scaling. As Mr. Nettel does not explain how he will attain better efficiencies and with what means, the author can only explain here the reasons which led us to our design.

All indications of air preheat are given in Table 2 of Quiby's official report.[15] As Mr. Nettel explains, an error crept in the explanation of Fig. 9 of the paper. It should be read as explained in his discussion.

Our studies on supercharged air heaters led us to the opinion that the charging set is not so complicated an arrangement as perhaps it seems at first glance. All the regulating is established automatically to a great extent.

The figure of 1.5 sq ft of heat-transfer surface per kilowatt relates to the air-heater surface plus preheater for a supercharged heater set. The air-preheater surface is dictated by the point of view of economy and is different in ships from that in stationary plants.

The size of the accumulators depends upon the chosen pressure of the cold-storage air, and upon the "time-table" of the plant. The load variation, Mr. Nettel admits, is communically severe. To give an idea we would need about 100,000 cu ft.

Reply to J. K. Salisbury. We were much interested to have Mr. Salisbury's opinion of our work. As we know, he is in every respect an expert in the gas-turbine field. We would like to thank him again for the compliments he paid to the engineering work of our team. The author was gratified to have had several conversations with him on this subject, and the principal advantages of the plants he mentions in his discussion are just those which convinced us since the start of our work to stick to it through all development difficulties. In connection with Mr. Salisbury's survey of the economics of the situation, for the reasons explained in the introduction to this closure, the author can only agree with him that it is an open question. Naturally, the author is not too familiar with conditions in the United States. For the markets he knows better, he is not at all doubtful about cost development.

The air heater with pressure firing is much less expensive than Mr. Salisbury estimates. The costs for the whole plant are even less than 75 dollars per kw.

The comparison of a 2000-kw modern steam plant which can be built according to Mr. Salisbury's proposition, with the first 2000-kw closed-cycle test plant is not too favorable for the closed-cycle system. As explained in the introduction, one must not forget that the test plant was meant for other purposes than for industrial service and that it is a 10-year-old design. An up-to-date new design would naturally give much better values. Apart from that, at the present time we do not intend to build plants with such small outputs, because in this respect the author agrees fully with Mr. Salisbury: We think it would not pay. The advantages of the closed cycle are much more pronounced for plant ratings, say, above 5000 kw.

The last detailed questions of Mr. Salisbury can be answered as follows:

Surfaces. Our actual design is based on a total surface, including heater, regenerator, combustion-air heater preheater of about 4 to 5 sq ft per kw. These figures may change in the future with other designs. About 20 per cent relates to the air heater, 20 per cent to the preheater and coolers, and 60 per cent to the regenerator. Naturally, this changes the whole aspect.

Pressure Drop. The absolute pressure drop depends upon the pressure level used; 10 to 15 psi result with a maximum pressure of ~800 psi in modern design. The smaller value belongs to the air heater of the test plant.

Circulating Fan. In operation of the test heater, we only needed a very small amount of recirculated gas to cool and protect the tubes, and the furnace, as a consequence of the layout. The secondary air of combustion, led in a suitable way along the lower end of the temperature. In new air heaters the construction will be somewhat different and a bigger fan will be used.

Mechanical Losses. As Prof. Quiby pointed out in his report,[15] these losses were higher than usual because of the special arrange-

ment of the machine group and bearings. At least 1.5 per cent total efficiency could have been won with other design. The oil seals play only a minor role in the mechanical losses. But one must not forget that the mechanical losses, as derived from the tests also include the internal leakage losses of working air. Therefore, an exact figure for the mechanical losses cannot be calculated. Naturally, the rather high value is not inherent in the closed-cycle system and can be kept normal in other plants.

The Influence of Viscosity on Centrifugal-Pump Performance

By ARTHUR T. IPPEN,[1] CAMBRIDGE, MASS.

The wide use of centrifugal pumps in the oil industry demands that their performance characteristics for oil be predicted with reasonable assurance. A systematic study of performance changes with increasing viscosities had not been undertaken so far under controlled laboratory conditions. For the purpose of undertaking such a study theoretically and experimentally, the Hydraulic Laboratory of Lehigh University and the Cameron Pump Division of the Ingersoll-Rand Company co-operated in following through a comprehensive program of research at Lehigh University during 1944 and 1945. Over 200 performance tests for viscosities up to 10,000 SSU were completed on four variants of centrifugal pumps, employing a special test stand designed and built under war conditions.

The influence of viscosity changes on the head, discharge, and input-power characteristics of the pumps is demonstrated graphically and systematically for a wide range of viscosities and speeds. The usefulness of a special Reynolds number for pumps is demonstrated and test results are correlated on that basis. General conclusions are possible as to the influence of various features of design, since several pumps of different specific speeds were tested. A theoretical analysis establishes definitely the variables to be considered and places the discussion for the problem on a sound scientific basis, especially with regard to disk and ring losses.

Introduction

THE influence of viscosity on the performance of centrifugal pumps has not received, up to the present, the systematic attention of the pump engineers which this problem deserves in view of the ever-increasing use of the centrifugal pump for the transport of viscous liquids. A first pioneer effort, and so far the most extensive one, was made by Professor Daugherty (1)[2] about 20 years ago. Various papers (2, 3) have appeared since then, but they were never based on more than a relatively small number of field tests carried out by various investigators with greatly differing pumps. These tests were used to derive correction curves for efficiency by extensive extrapolation of the test information on hand and must clearly be recognized as a temporary means of considering the viscosity influence.

In recognition of the need of a systematic approach to this problem under controlled conditions, the Hydraulic Laboratory of Lehigh University and the Ingersoll-Rand Company of Phillipsburg, New Jersey, entered into a co-operative agreement to explore the behavior of centrifugal pumps when pumping oils. A special test stand was designed and constructed under wartime restrictions and over two hundred performance runs were made during 1944–1945 on four variants of centrifugal pumps with viscosities ranging up to 10,000 SSU. The influence of viscosity changes on the head, capacity, and input-power characteristics was systematically explored for each variant of pump and for several speeds. The usefulness of the Reynolds number for the presentation of these characteristics was demonstrated convincingly and all results are correlated on that basis. The data presented in the diagrams are those obtained in the present investigation only. No attempt was made to include information from other sources, since it was almost always found lacking in completeness. This situation is analogous to that existing for many years in the field of pipe friction, until finally the pertinent variables were definitely established and a final solution found.

It is to be hoped that the experiments reported here will bring forth many detailed experimental results in complete form from the files of various investigators, so that the conclusions drawn from this work may be either confirmed or be modified to fit into a more general picture. However, it is felt that the paper represents the first attempt to analyze the test results on the basis of all pertinent variables so that individual influences can be isolated more easily. Thus their share in the over-all effect of the viscosity on the performance of centrifugal pumps is to be recognized in relatively true proportions.

It may be mentioned that the paper had to be severely limited in presenting the information on hand. The descriptive part on the experiments had to be cut more than may be desirable from the viewpoint of clarity in order to include the fundamental results of greatest value to the engineer concerned with this problem. The same limitations had to be imposed on the theoretical part which covers only those aspects which are most useful and characteristic in explaining the results of the experiments as stated in graphical form.

EXPERIMENTAL PART

General Outline of Test Program

The stated purpose of the experimental study was to find, if possible, a specific relationship between viscosity on one hand and efficiency, head, capacity, and power input on the other hand. The results for four different variants of pumps were to be correlated. The choice of pumps was naturally restricted by the power supply of the hydraulic laboratory, by the range of the torsion-dynamometer, and by the available storage space for the oils used in the tests.

(*a*) *Specifications of Pumps Tested.* Under the circumstances the four pumps listed in Table 1 were chosen as most suitable and as of widest possible use in the pumping of highly viscous oils. All vital dimensions and normal-performance data for water are listed in Tables 1 and 2. Pump No. 1 was a single-stage, single-suction pump which could be fitted with hydraulically identical impellers of the closed and open type. This pump was relatively small and of low specific speed. The pump No. 2 was a single-stage double-suction pump which could be run with impellers of different diameter. Thus the specific speed was varied to a value of almost 3000 with a small impeller, however, not without some sacrifice in efficiency. The experiments covered, consequently, a range of specific speeds between 1000 and 3000 which is the range of most efficient operation for radial-flow pumps.

[1] Associate Professor of Hydraulics, Department of Civil and Sanitary Engineering, Massachusetts Institute of Technology.

[2] Numbers in parentheses refer to the Bibliography at the end of the paper.

Contributed by the Hydraulic Division and presented at the Annual Meeting, New York, N. Y., Nov. 26–29, 1945, of The American Society of Mechanical Engineers.

Note: Statements and opinions advanced in papers are to be understood as individual expressions of their authors and not those of the Society.

(*b*) *Properties of Liquids Employed.* The program of testing contemplated originally the use of water and of two oils as experimental liquids. For the latter the range of viscosities was defined by the range of temperatures seasonably obtainable, i.e., from almost normal outside temperature upward to a maximum produced by dissipating the power input. No special heating or cooling equipment was provided. The variation in the volume circulated was sufficient to obtain the desired range of temperatures and viscosities. Two black oils, giving a medium slope in the viscosity-temperature chart, were selected and are referred to subsequently as heavy oil (HO) and light oil (LO). A third oil was added, however, after the LO-runs were taken, since it appeared desirable to bridge the gap between the viscosity of water and that of the light oil.

This so-called thin oil (TO) was produced by mixing the light oil with a certain amount of fuel oil. The light oil proved to be extremely stable and its viscosity remained constant for almost half a year of intermittent testing. The thin oil and the heavy oil were affected somewhat by the pump testing and frequent analyses were made to adjust results for changes in viscosity whenever they exceeded the limits of permissible errors. Fig. 1 presents the essential data on viscosities and specific gravities for these oils.

(*c*) *Schedule of Testing Program.* The experiments started by determining the performance of each impeller of the two pumps for water. All impellers were tested as summarized in Table 2 for three different speeds with the exception of the largest impeller, which was run only for the two lower speeds, since the torque for the high speed exceeded the dynamometer capacity. The water tests checked very closely the performance of the pumps reported from the Ingersoll-Rand laboratory and served in addition the purpose of establishing working procedures and of finding out about the general performance of the test stand. After some minor alterations were completed, the four sets of runs

TABLE 1 PUMP DIMENSIONS

Pump No.	Imp. No.	File No.	Type	D_s	D_d	No. of Vanes	D_1	D_2	D_{sh}	B_2	D_R	B_R	$2 \cdot S_{R\,Av.}$
1	1 Closed	IL 11	Single Suction	4"	2"	7	2-1/2	7-1/4	15/16	1/2	3	7/8	.014
1	2 Open	IL 12	"	4"	2"	7	2-1/2	7-1/4	15/16	1/2	3	7/8	.014
2	1	IL 21	Double Suction	8"	6"	7	5-3/16	8-5/8	2-1/2	1-15/16	7	1-7/16	.016
	1B	IL 21	Double Clearance	8"	6"	7	5-3/16	8-5/8	2-1/2	1-15/16	7	1-7/16	.032
	1C	IL 21	Half Width Rings	8"	6"	7	5-3/16	8-5/8	2-1/2	1-15/16	7	23/32	.014
2	2	IL 22	Double Suction	8"	6"	7	5-3/16	11-5/8	2-1/2	1-7/16	7	1-7/16	.018

A

TABLE 2 PUMP PERFORMANCE DATA

Pump No.	Specific Speed for Water	Maximum Efficiency for Water	Liquids Tested	Approximate Speeds in RPM
IL 11	1163	75.0	W LO TO HO	2330 2875 3460
IL 12	1163	74.0	W LO TO HO	2350 2875 3460
IL 21	2622	80.0	W LO TO HO	1230 1890 2320
IL 22	1991	85.5	W LO TO HO	1240 1880
Graphic Notations			● ● ○ ○	○● ◔●◔●

were repeated for the light oil, covering usually the possible range of viscosities on the same day for any one speed. It was preferred to change the pumps and impellers rather than the liquids, thus avoiding contamination of one oil by the other, which would have become appreciable during the course of the testing program. The light oil was then cut by the addition of fuel oil to a lower viscosity and the four sets of runs were again repeated for this so-called thin oil. Finally the heavy oil was turned into the lines and the process was repeated a fourth time.

Thus two pumps with two impellers, as described in Table 1, were tested for four different liquids and for three different speeds. Six performance runs were taken for each oil in the average, so that the total number of tests exceeded 220.

Experimental Equipment

The experimental equipment was largely assembled under the restrictions of the wartime economy and therefore contains whatever could be made to serve on the test stand, from the material resources of the two co-operating agencies. The result of the planning on this basis, however, was adequate in every respect for the proper execution of the testing program.

(*a*) The general arrangement of the circulating system is shown in Fig. 2. Six 750-gallon tanks formed the basic storage units for two different oils. A triangular arrangement of three tanks each in two stories was decided to be the most compact and practical one with respect to piping and housing. When the pipes were filled with one oil, two additional tanks contained the same oil on two levels with the upper tank in the rear always empty and ready to be used as a volumetric-measuring tank. The upper tanks could be drained very fast by gravity into the lower tanks. The entire system of pipes and tanks may easily be analyzed from the isometric views in Fig. 2. The meter calibration circuit and the pump testing circuit are shown separately and are outlined by heavy lines. All tanks were open, however, all pipe ends were submerged considerably below the oil level, so that entrained air never posed any problem.

All the circulating was done by the test pumps driven by means of a torsion dynamometer, as illustrated in Figs. 3 and 4. The driving arrangement of the dynamometer was a system of pulleys and a 65-horsepower induction motor, which was powered from a special transformer set with 3-phase, 60-cycle, 220-volt alternating current. Automatic voltage regulation was provided in the 4400-volt main feeder line of the University, so that serious speed variations were never encountered during tests.

(*b*) *Measuring Equipment.* Pump discharges had to be metered over a wide range and three liquid meters shown in Fig. 5 were installed, therefore, in separate lines of 8 in., 6 in. and 4 in. diameter. Orifice meters were used for the 8 in. and 6 in. lines and a 4 × 2 in. Venturi happened to be available for the 4 in. line. The meter approaches were at least twenty-two diameters in length and the valves in the approach lines were only used in wide-open or completely closed position. The operation of the meters therefore was satisfactory at all times. All discharge regulation was done by means of valves at the end of the circuit, so that the entire system was normally under positive pressure. The orifice meter of 4.92 in. orifice diameter in the 8-in. line was used almost exclusively for the large pump and the 4 × 2-in. Venturi meter was adequate for the small pump, so that the 6 × 3.60-in. orifice was rarely used. The orifice plates were made of $^3/_8$-in. brass plates with a square edge of $^1/_{16}$ in. and a downstream bevel of 45 deg. The pressure connections were located one pipe diameter upstream and one-half pipe diameter downstream.

The temperatures of the liquids were checked at three points by means of standard thermowells and dial-type indicating thermometers. The latter were mercury-actuated and furnished

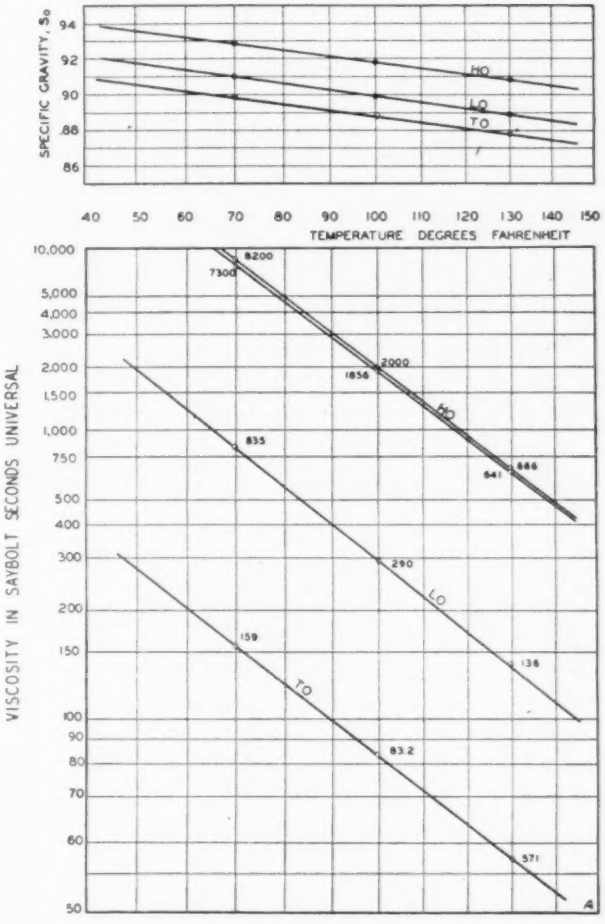


Fig. 1 Properties of Oils

with temperature-compensated capillary tubes. Readings to the nearest half degree Fahrenheit were deemed sufficient. The first well was located in the suction line of the pump about 4 ft upstream, the second was in the manifold immediately below the discharge line connection, and the third recorded the temperature of the liquid below the meters.

For visual checks, on the discharge and suction pressures, two Bourdon-type gages were included on the instrument board shown in Fig. 6; however, all discharge and suction heads used in the analysis were obtained from mercury-water manometers. The mercury manometer connected to the discharge side consisted of two differential gages connected in series, each of 6 ft length. A range of 50 psi could thus be covered without a balancing pressure. If the low pressure end of the manometer was placed under a 25 or 50-psi counterpressure, the range was extended to 100 psi. In the end the mercury gages arranged so as to require a minimum of corrections, saved considerable time since calibrations were unnecessary. The oil in the connecting lines was prevented from entering the water-mercury gages by means of large pots filled with oil in the upper half and water in the lower. The oil-water level in the pots was observed by means of glass gages and was checked and adjusted before every run. The same arrangement was used for the differential manometer connected to the liquid meters. Due to the relatively small differences in specific gravity of the oil and water, small changes of the oil-water level in the separating pots will not

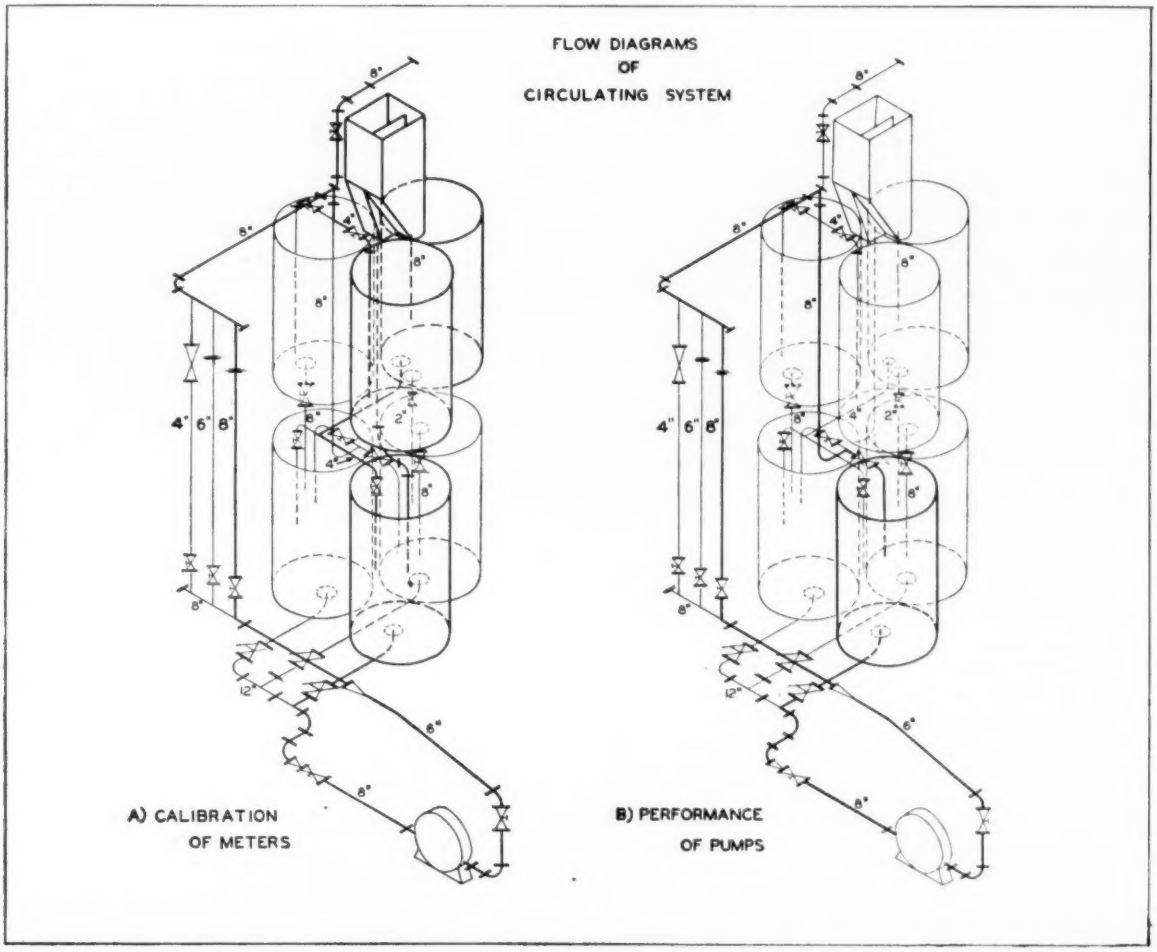


FIG. 2 LINE DIAGRAM OF CIRCULATING SYSTEM

affect the readings. The speed was measured with a Chrono-Tachometer and with a revolution counter electrically operated for $^1/_{10}$-minute intervals. It was read for every test point and comparisons were made with a Hassler Tachometer with results well within the precision of either instrument. The tachometer and revolution counter are connected to a synchronous motor powered from a generator mounted on the pump shaft.

EXPERIMENTAL PROCEDURES

(*a*) *Calibrations of Measuring Equipment.* All the instruments used were subjected to several calibrations during the experimental period. The mercury gages of course do not need special calibration, except that the Bourdon gage tester was checked against the mercury columns. All connecting lines were freed of air and particularly the discharge gage was checked before and after each run for air, by the use of a special water-air manometer, the latter indicating easily any errors of 0.01 ft of water column. Balance was always required within this limit and was always obtained.

The dynamometer bars were calibrated by careful static load tests and showed a constant torque per unit deflection over the entire range. Naturally the percentage of error of the reading for any run was dependent upon the torque range covered for any particular pump and speed.

The speed measurements were checked against simultaneous measurements taken with other tachometers and were found to be consistent within one fifth of one per cent, which was within the required limits.

The temperatures indicated by the dial thermometers were verified by the use of a mercury thermometer certified by the Bureau of Standards. The readings were also checked during runs by mercury thermometers in adjacent thermowells, which had been compared to the standard thermometers. Sticking of the dial hands was prevented by lightly tapping the glass cover.

The main problem in ascertaining the fundamental quantities for the performance of the pumps was encountered with the liquid meters. While the circulating system for calibrating purposes is indicated in Fig. 2, some of the phases of the calibrating runs merit mentioning. Noticeable temperature differences in the oil circulated had to be avoided. Therefore the oil was normally discharged from the line into the upper storage tank and from here by gravity back into the lower tank. The flow was then gradually switched over to the swing spout, thus taking the oil in the upper storage tank out of circulation. As soon as steady-flow conditions were established again through the meter, the flow was deflected into the measuring tank, while a constant level was maintained in the lower storage tank by admitting oil from the upper storage tank. This procedure naturally required considerable practice but worked out very satisfactorily. The results of the meter calibrations are given in Fig. 7 and are stated in a form which deviates somewhat from the orthodox way. The discharge coefficient C_D for the 4 × 2-in. Venturi meter is

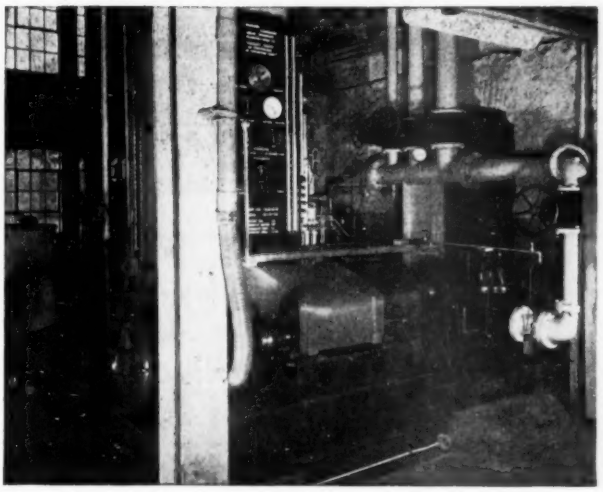


FIG. 3 GENERAL VIEW OF TEST SETUP

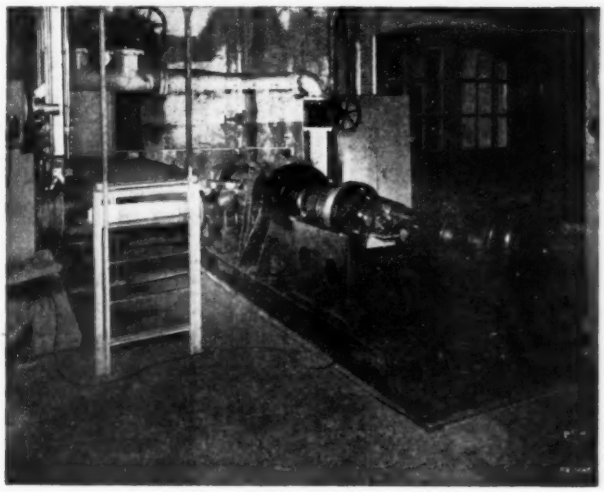


FIG. 4 PULLEY SYSTEM AND DYNAMOMETER

plotted against the Reynolds number for the 4-in-diameter pipe divided by the discharge coefficient C_D. Similarly the results for the 8 × 4.92-in. orifice meter are given in terms of a correction coefficient for viscosity K_m plotted against the pipe Reynolds number for the 8-in. pipe divided by the discharge coefficient. This latter quantity can be calculated directly from the differential-manometer readings and the correction coefficient K_m is thus obtained without trial and error. The discharge coefficient for water C_D, as introduced, is equal to 0.6185. The Venturi meter curve is compared to the curve given in the Fluid Meter Report of the A.S.M.E. and is seen to lie considerably below this curve. It is shown extending down to an experimental value of $C_D = 0.50$. The orifice curve is compared to Johanson's curve for a similar orifice in a 1-in-diameter glass tube and shows remarkable agreement. It may even be argued that the discrepancy is due to the slight difference in the orifice - pipe diameter ratio, which was 0.615 here, while Johanson's curve holds for 0.595.

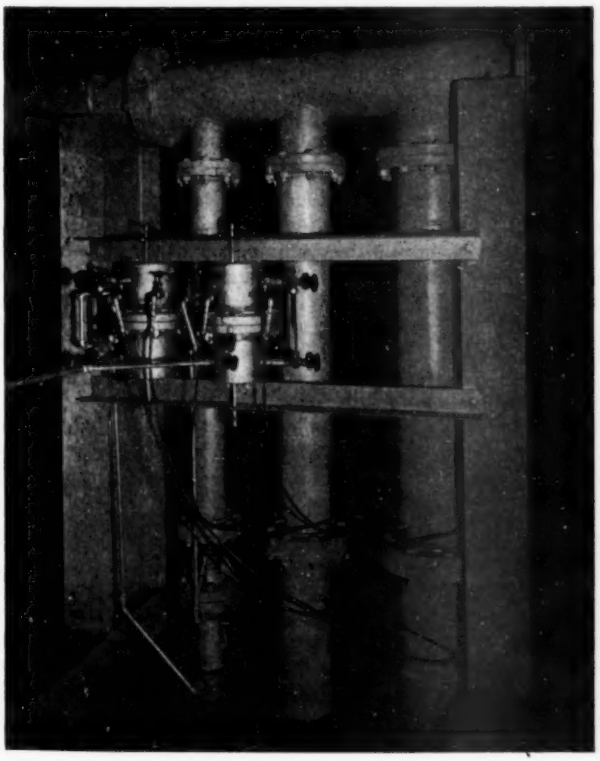


FIG. 5 VENTURI AND ORIFICE METERS

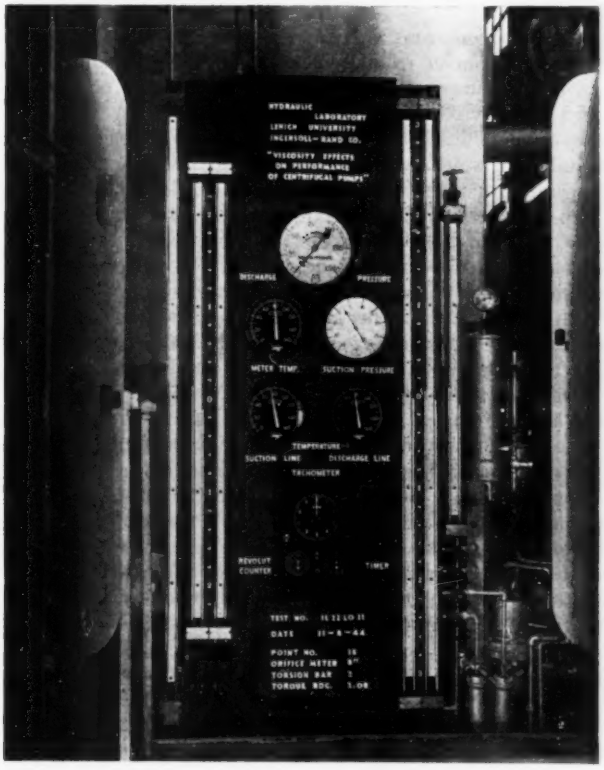


FIG. 6 MAIN INSTRUMENT PANEL

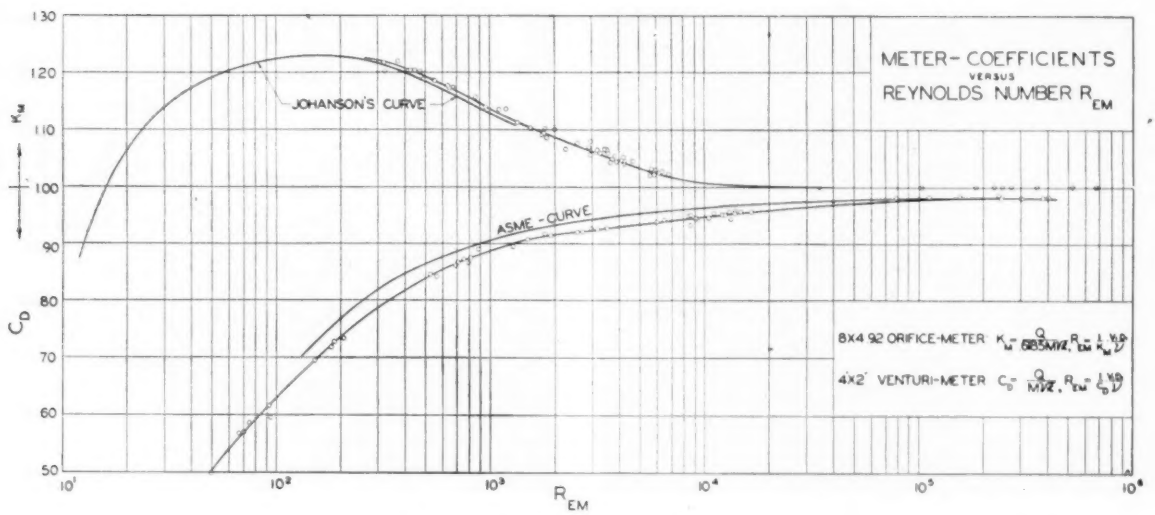


FIG. 7 FLUID-METER CALIBRATIONS

(*b*) *Typical Performance Tests.* Most operational difficulties were discovered and ironed out by running first a full series of experiments with water. Only minor improvements, however, were necessary, and definite procedures for the oil runs were formulated. The dimensionless performance curves shown in Fig. 8 are those obtained for the medium-specific-speed impeller IL 22 and they are typical of the range covered by individual tests. The almost complete absence of viscous effects for the normal range of operation with water was indicated by all water runs, proving, if it be necessary indeed, that the Reynolds numbers normally encountered with water are in the so-called "rough-flow" zone.

All performance runs with oil were carried out by recording all pertinent instrument readings photographically by means of a 35-mm Kodak camera. Thus readings for individual points were taken speedily and simultaneously for permanent reference. Runs of ten to fifteen test points were normally completed within ten minutes, which fact considerably diminished the increase in temperature during any run. Upon termination of one run the pump was operated near normal discharge and was run continuously, until the dissipation of power had resulted in bringing the temperature to the desired higher value. The experimental procedure was then repeated. The temperature of the oil could be varied for any of the higher speeds from about 70 to 125 deg by continuous running within one day. Thus five to eight performance runs were obtained within a four- to eight-hour period. Shutoff conditions were usually tested by closing down fairly fast from a large discharge, thus retaining a fairly normal temperature of the oil churned in the pump. At best, however, the shutoff points are only approximate, especially for the higher viscosities.

The temperature changes in the oil could be controlled by adjusting the volume of oil in circulation. If the temperature rise was too fast the entire volume of oil could be utilized by circulating through upper and lower storage tanks. A differential temperature between upper and lower tank also permitted to arrest the rise in temperature during any run after some practice. Small increases in temperature were permitted, say 2 to 3 deg F, and their influence was determined by taking additional points immediately after each run over the same range. Corrections to a constant temperature and hence to a constant viscosity could be made therefore in the analysis. However, usually such corrections were too small to influence the maximum efficiency in location and magnitude.

ANALYSIS OF TEST RESULTS

(*a*) *Computation Procedures.* As pointed out before, all data necessary for the performance calculations are contained on a 35-mm film strip which could be projected, point by point, on a screen made of tracing cloth. The readings were taken down by an observer behind the screen. The gages showed throughout the experiments very steady readings; fluctuations were largely eliminated by the viscous action of the oil in the connecting lines and by symmetrical constrictions in the mercury-manometer blocks. Two exposures were taken for every point, in order to discover changes in readings and to insure that all the information could be read clearly. If poor test points were discovered later in plotting the results, they were invariably traced to faulty readings from the film and were easily corrected by checking. The value of preserving thus on film the original measurements cannot be overemphasized, especially when insufficiently trained personnel must be entrusted with a major portion of the computing work.

The entire calculation procedure involving a great many steps was carefully worked out, so that a standard routine could be followed throughout and the evaluation of data from the film to the final performance graph could largely be left to personnel without technical training. Viscosities and specific gravities, velocity-head corrections, and discharge coefficients were read from graphs plotted to simple linear scales.

Since the discharge manometer in many runs indicated very small differences due to the exclusive use of the 8 × 4.92-in. orifice meter, these readings were also read directly, which upon comparison with the readings obtained from the film showed very good agreement. It was found practical then to take down also the speed and the torque readings during the run so that some calculations could be started immediately after the runs were taken, before the films were developed.

Pressure readings were not corrected for pipe friction losses between pump flange and piezometer connections. This refinement would have introduced additional computing work to an extent unjustified by its merits, the pressure connections in each case being located only one pipe diameter from the flanges. It is natural also that the percentage error in the over-all efficiency becomes greater for higher viscosities, so that the foregoing correction stays usually within the permissible margin. It may be stated that the accuracy of the results is referred to the efficiency loss

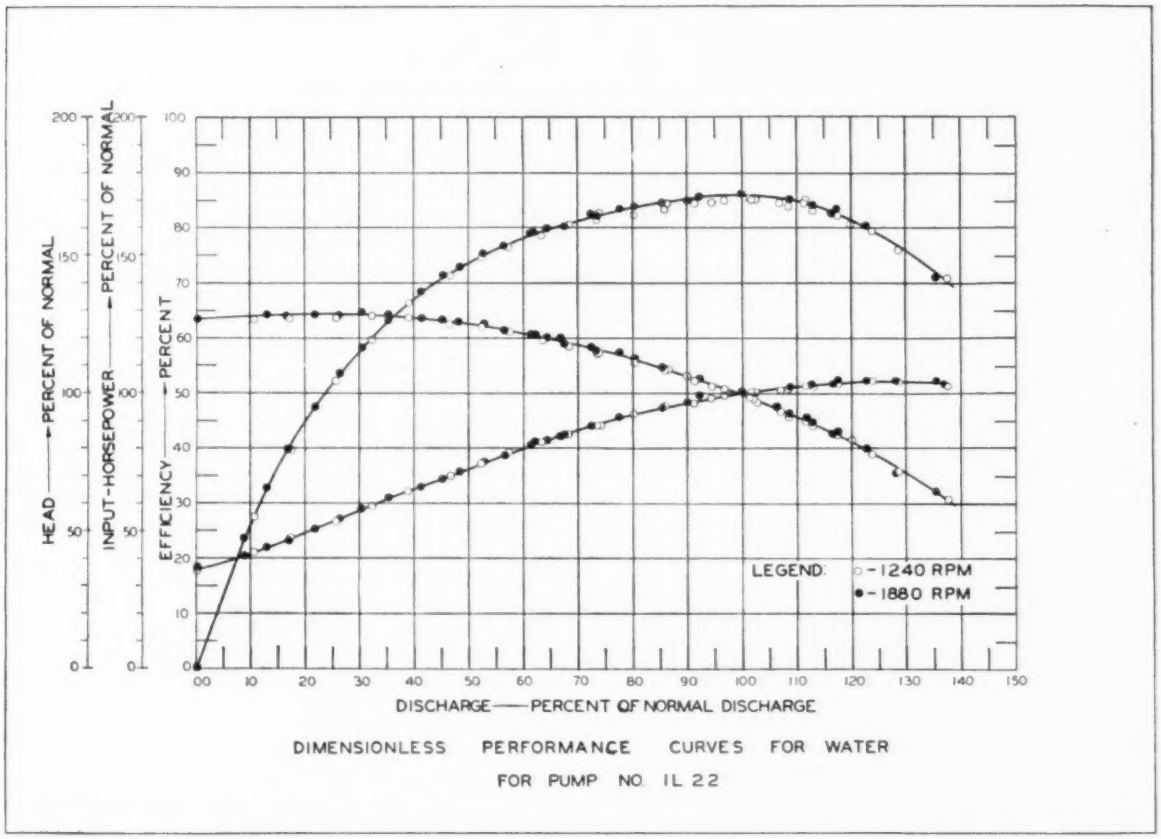


FIG. 8 EXAMPLE OF DIMENSIONLESS PERFORMANCE CHARACTERISTICS FOR WATER

$(100 - e)$ rather than to the efficiency (e) itself and that it is kept to ± 1 per cent in the average for $(100 - e)$.

(*b*) *Performance Characteristics.* Complete performance characteristics were plotted for all runs taken and discrepancies were therefore easily discovered. The influence of accidental errors is thereby minimized. Curves for successive runs were compared according to the order of their viscosities. These performance curves available for every run should yield upon further analysis additional experimental information concerning relative distribution of disk and ring losses, and on the operation near shutoff as well as at capacities larger and smaller than normal. The results presented in the following pages therefore touch only upon one phase of the problem under discussion, since maximum efficiency and normal capacities, head, and inputs are the only quantities considered at present in order to limit the scope of this paper.

ANALYTICAL PART

THEORY OF VISCOUS LOSSES IN CENTRIFUGAL PUMPS

(*a*) *Hydraulic Losses.* The so-called "hydraulic losses" in centrifugal pumps have been rather loosely defined in the past, since the thinking was predominantly influenced by the performance of pumps with thin fluids. With more viscous fluids the term "hydraulic losses" is here more definitely applied to the so-called "through-flow" losses, which are directly the result of skin friction and eddy systems along the primary path of the fluid passing through the pump. It is of course not possible to analyze these losses separately, since they depend on a considerable number of geometric variables, which may be briefly stated as follows:

1 Suction-pipe dimensions and shape of inlet which determine the state of flow at the entrance.

2 Design of pump inlet, eye diameter or its equivalent.

3 Shape, length, curvatures of impeller passages, contraction or expansion of cross sections.

4 Dimensions of volute, design of spiral, and diffuser.

It follows that in general the flow is nonuniform and that therefore pipe friction factors are not very useful here except in a very general way. In addition the curvatures encountered make any approach on the basis of boundary-layer theory impossible. A few general statements may be in order, however, in view of the conditions stated.

1 Every pump follows its own law of hydraulic resistance. Only the total losses can be determined experimentally, since they are interdependent.

2 Theories of individual losses will at best give only a very approximate quantitative explanation of the pump behavior. This may be extremely valuable, however, for the designer.

3 The relative weight of the losses will shift as a function of the specific speed and of Reynolds number. While skin-friction losses similar to pipe flow may predominate at low specific speeds, "body-resistance" losses will come to the fore with a change from radial to mixed and more or less axial flow for higher specific speed. In other words, since losses depend to a considerable extent on approach conditions, the character of the flow through the pump is more and more determined by the state of flow in the approach to the pump when higher specific speeds are reached. The relative length of the pump passages decreases with increasing specific speeds.

On the basis of these remarks, experimental results are indeed

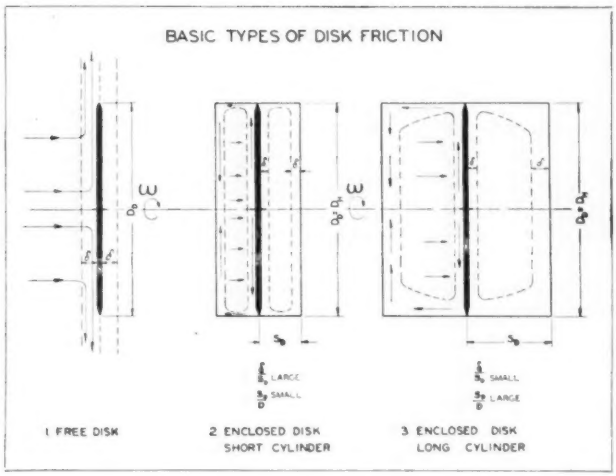


FIG. 9 BASIC TYPES OF DISK FRICTION

approached with hesitation. In retrospect it seems remarkable that the multitude of possible losses and geometric dissimilarities nevertheless produces statistical averages with a relatively narrow zone of deviations, as long as ring and disk friction losses remain comparable for the various pumps.

Energy losses for flows of a complex nature are customarily expressed in terms of velocity head of the mean flow. Choosing relative velocity at impeller exit as a suitable one, the difference between the head produced for water and the head for oil can be written as

$$H_l = (H_w - H_0) = C_R \cdot \frac{v_2^2}{2g} = C_R \cdot \frac{Q'^2_0}{a_2^2 \cdot 2g}$$

or dividing both sides by H_0

$$\frac{H_l}{H_0} = \left(\frac{H_w}{H_0} - 1\right) = C_R \cdot \left(\frac{Q'^2_0}{H_0}\right) \cdot \frac{1}{2g \cdot a_2^2} \quad \ldots\ldots [1]$$

wherein C_R is a function of Reynolds number, pump-design, and of roughness. Since $Q_0'^2/H_0$ was found practically constant for a wide range of Reynolds numbers, C_R can be obtained, if the water performance is known, from the plot of H_0/H_w against Reynolds number.

The question of a suitable Reynolds number was naturally the subject of considerable analytic experimentation. Eventually no particular advantage was found in any one as compared to another. However, the four fundamental forms stated below were calculated for all test points.

$$R_D = \frac{\omega \cdot r_2^2}{\nu} = \frac{u_2 \cdot d_2}{2 \cdot \nu} = \frac{\phi \sqrt{2gH_0} \cdot d_2}{2 \cdot \nu} = 2620 \frac{N d_2^2}{\nu \cdot 10^5} \quad \ldots\ldots [2a]$$

$$R_H = \frac{\sqrt{H_0} \cdot d_2}{\nu} \quad \ldots\ldots [2b]$$

$$R_S = \frac{v_i \cdot d_{ie}}{\nu} = \frac{283.7 \cdot Q_0}{d_{ie} \cdot \nu \cdot 10^5} \quad \ldots\ldots [2c]$$

$$R_P = R_S \cdot \frac{d_{ie}}{d_2} = \frac{283.7 \cdot Q_0}{d_2 \cdot \nu \cdot 10^5} = \frac{283.7 \cdot Q_0 \cdot b_2}{b_2 \cdot d_2 \cdot \nu \cdot 10^5} \quad \ldots\ldots [2d]$$

R_D and R_H differ essentially by the factor $\phi = u_2/\sqrt{2gH_0}$. Since ϕ very seldom differs greatly from unity, the reason for the small differences found in plotting the results against both is readily apparent. A small change in Reynolds number has little effect on the efficiency loss, while the differences due to pump design are more pronounced. The relatively best agreement between results for various pumps, especially for low Reynolds numbers, was obtained by using R_S, in which the equivalent or actual eye diameter of the impeller d_{ie} was introduced as the characteristic length. For practical reasons R_D was chosen, since it is most readily calculated from known quantities. In addition disk and ring friction losses are most easily expressed as a function of R_D. It offers, therefore, the most systematic approach toward separation of the afore-mentioned losses from the so-called "through-flow" losses.

(*b*) *Disk Friction.* The problem of friction losses due to the rotation of a circular disk in a fluid has received the attention of investigators in theory and by experiments. A comprehensive view of this problem, however, has been lacking and thus the fact remained obscured that the theoretical and experimental findings of the various investigators show considerable agreement, if the various phases of the problem are systematically related. Fig. 9 illustrates the basis on which the subsequent treatment rests. Two papers (6, 7) attack the following problems.

1 The disk rotating in an infinite space, filled with fluid.

2 The disk rotating in a housing of approximately equal diameter and with small clearances between disk and housing.

Case 1. Von Kármán (6) dealt with problem 1 and established that the resistance mechanism depends entirely on the formation of a boundary layer adjacent to the surfaces of the disk, within which the tangential velocity of the fluid increases from zero to $\omega \cdot r$. The theoretical velocity distribution within this boundary-layer is given by Fig. 10 for the laminar case. This layer functions like the impeller of a pump. Since the pressure on the periphery of the disk is atmospheric, a radial flow q_D results into the surrounding fluid at rest with an angular momentum $u_2 \cdot r_2$ per unit of mass. On this basis von Kármán established the basic equations summarized below for laminar and turbulent flow. It is to be noted at this point that all kinetic energy imparted to the fluid by disk action is dissipated in the surrounding space. In general the torque to be applied is defined for one side of the disk by

$$T_D = C_D \cdot \gamma \cdot r^3 \cdot \frac{u_2^2}{2g} \quad \ldots\ldots [3]$$

(*a*) In the case of laminar flow, which is of particular interest here, the boundary-layer thickness is given by

$$\frac{\delta}{r} = \frac{2.58}{\sqrt{R_D}} \quad \ldots\ldots [4]$$

and the discharge of the disk by

$$q_D = 0.137 \cdot (2\pi \cdot r \cdot \delta) \cdot u$$

The so-called coefficient of friction becomes

$$C_D = \frac{1.84}{\sqrt{R_D}} \quad \ldots\ldots [5]$$

(*b*) For turbulent flow and a "smooth" disk, one for which all roughness irregularities remain submerged in the laminar sub-layer, the boundary-layer thickness is

$$\frac{\delta}{r} = \frac{0.462}{R_D^{1/5}} \quad \ldots\ldots [6]$$

on the basis of the seventh-root law for the velocity distribution.

The so-called friction coefficient becomes

$$C_D = \frac{0.0728}{R_D^{1/5}} \quad \ldots\ldots [7]$$

Equations [5] and [7] are plotted as lines A and B in Fig. 11. The application to "rough" disks has not been carried through, but it is obvious that the treatment is analogous to the friction problem for flat plates and will give an expression involving the ratio ϵ/δ, wherein ϵ stands for absolute roughness. The scattering of experimental results obtained by different experimenters for large Reynolds numbers R_D is probably due to variations in ϵ/δ. This case, however, is of little importance for the problem here.

Case 2. The second case defined before was treated experimentally and theoretically by Schultz-Grunow (7) and was essentially confirmed by the excellent experiments of Zumbusch as quoted in the same paper, the results of which are represented by line E in Fig. 11. The basic assumptions for this case should be clearly kept in mind for the later discussion of the differences in von Kármán's and Schultz-Grunow's results. The cylindrical wall surrounding the disk is assumed nearly equal in diameter to the disk and is short enough axially so that friction losses on the periphery may be disregarded. Thus the fluid is confined to the space between disk and housing and the angular momentum imparted by the disk is no longer lost to the surrounding fluid. Since the circular housing plates must exert a torque equal and opposite to the torque applied to the disk, it follows that the fluid confined to the space between them must revolve with one half of the angular velocity of the disk, so that equal frictional shears may be developed on disk and circular housing plate. This fact also is confirmed by experiments and is a common assumption.

Schultz-Grunow obtained for the one-sided disk for

(*a*) Laminar flow

$$\frac{\delta}{r} = 2.17\,\frac{1}{\sqrt{R_D}} \qquad [8]$$

$$C_D = \frac{1.334}{\sqrt{R_D}} \qquad [9]$$

(*b*) Turbulent flow

$$C_D = \frac{0.0311}{R_D^{1/6}} \qquad [10]$$

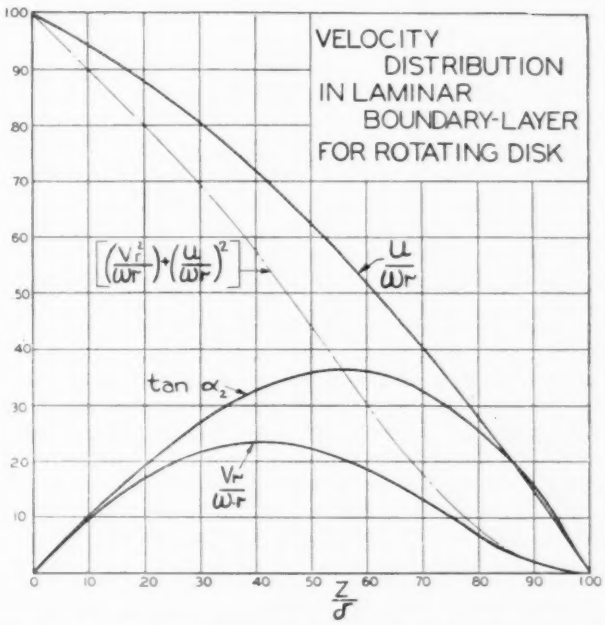


FIG. 10 VELOCITY DISTRIBUTION IN LAMINAR BOUNDARY LAYER NEAR ROTATING DISK

These results are given as lines C and D_1 in Fig. 11.

Case 3. A more general approach to the disk-friction problem becomes now possible as a result of the work discussed as Cases 1 and 2. Using von Kármán's expressions, a general equation can be written for the frictional torque for a differential angular velocity $(\omega_D - \omega)$. ω now denotes the angular velocity of the confined fluid, while ω_D represents the angular velocity of the disk. The results of this analysis may be reserved for a future paper, since space is lacking at this time. However, it is interesting to see the results of this analysis for the special case of $\omega/\omega_D = 1/2$. Introducing the latter ratio, the corresponding values of C_D are for

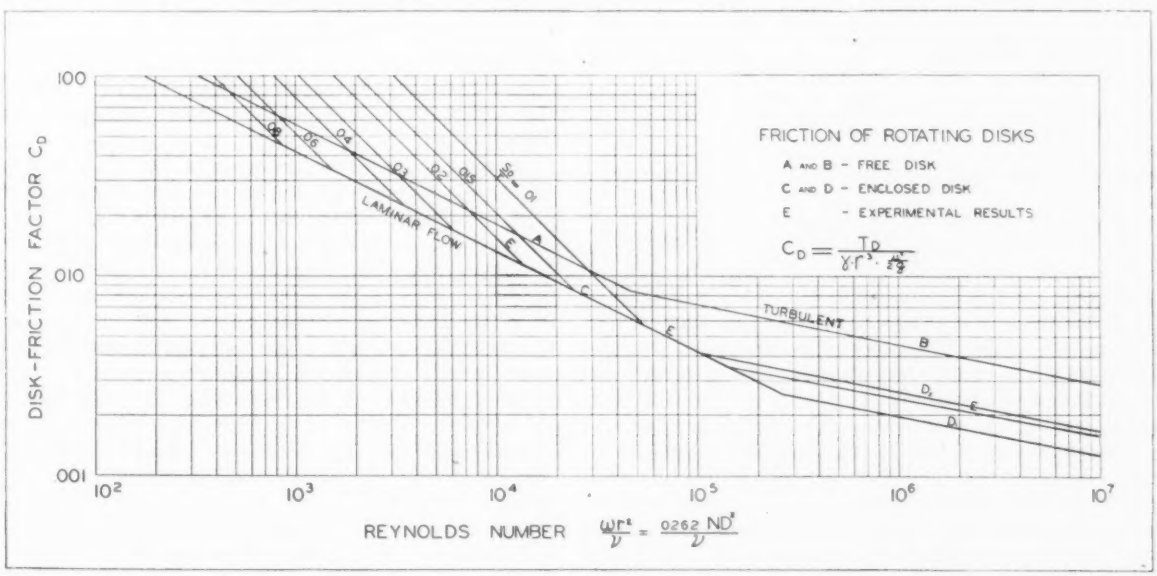


FIG. 11 GENERAL REYNOLDS NUMBER PLOT OF DISK-FRICTION COEFFICIENTS

(*a*) Laminar flow

$$C_D = \frac{1.300}{\sqrt{R_D}} \quad [11]$$

(*b*) Turbulent flow

$$C_D = \frac{0.0418}{R_D^{1/4}} \quad [12]$$

with corresponding lines C and D_2 in Fig. 11. It is seen that von Kármán's equations applied properly check Schultz-Grunow's results extremely well for laminar flow. For turbulent flow the agreement is not as good, but Equation [12] checks the experimental evidence better than Equation [10], since values for the numerical constant obtained experimentally increase from 0.037 to 0.040 with higher Reynolds numbers. The experimental result permits another interesting conclusion, namely, the influence of friction on the cylindrical housing is increasing relative to the circular wall friction, since the boundary-layer thickness δ decreases with increasing Reynolds numbers, while the clearance between disk and housing, S_D, is constant. In other words, ω decreases in terms of ω_D.

The general conclusions for the influence of disk friction on pump performance especially for viscous fluids are therefore as follows. Theoretically the case discussed by von Kármán (see Case 1) represents the maximum disk friction which requires $\omega = 0$ or $\omega = \omega_D$. Neither condition exists normally in pumps. The conditions generally met in pumps are discussed as Case 3, with $\omega \gtrless {}^1/_2\,\omega_D$. The special case $\frac{\omega}{\omega_D} = {}^1/_2$ gives a theoretical minimum disk friction. A further more extensive discussion must be delayed at present.

Case 4. Special Case of Small Clearances S_D. A clearance is said to be small here, if radial velocities become zero and if the tangential-velocity gradient becomes constant across the axial clearance S_D. An elementary analysis gives

$$C_D = \frac{\pi}{R_D} \cdot \frac{r}{S_D} \quad [13]$$

Comparing this expression with Equations [11] and [4] as modified for the case of $\frac{\omega}{\omega_D} = {}^1/_2$ so that

$$\frac{\delta}{r} = \frac{3.65}{\sqrt{R_D}} \quad [14]$$

the following relation between S_D and δ is derived

$$\frac{\delta}{r} = 1.51\,\frac{S_D}{2r} \quad [15]$$

This equation represents the intersections of the C_D vs. R_D lines in Fig. 11, where the laws of resistance change from Equation [11] to Equation [13]. The influence of the boundary layer disappears therefore as soon as the total boundary-layer thickness (2δ) is of the order of magnitude of the clearance S_D. The transition is naturally a gradual one. The factor 1.50 instead of unity is explained by the velocity distribution in the boundary layer and by the fact that the law for small clearances takes full effect only after the gradient of the velocity has become uniform throughout the width S_D. Necessary minimum clearances for pumps lifting viscous liquids can be calculated from [14] and [15] to avoid excessive disk friction. Of course the length δ need not enter at all, once its physical significance is recognized and one may write directly the expression for the minimum clearance S_D in terms of a limiting Reynolds number R_{Dl}

$$R_{Dl} = 5.83\left(\frac{d_2}{S_D}\right)^2 \quad [16]$$

below which the disk friction would be unnecessarily large. While [15] and [16] have been obtained on the basis of $\omega/\omega_D = {}^1/_2$, they do not necessarily depend seriously on this exact value, since the total thickness of the boundary layers remains fairly constant for $\omega/\omega_D = {}^1/_2$. A decrease of δ near the rotating disk will be compensated by an increase of δ' near the circular housing plate and *vice versa*.

(*c*) *Ring Losses.* Considering losses due to the wearing rings it is clear that the discussion must be concerned with two different types of losses:

1 Leakage of fluid through the annular space due to the pressure difference between entrance and exit section.

2 Torque losses due to the tangential shear developed by the rotation of the pump ring within the stationary housing ring.

The attention of the pump designer has been focused mainly on the leakage losses, since thin liquids will readily pass in quantity even through small clearances and since the torque losses for such liquids remain small. It is clear that the general thinking must be revised as soon as the pumps are used to lift viscous fluids, which are 10 to 2000 times more viscous than water.

After a careful scrutiny of all information on hand (9, 10, 11, 12), considerable analytical work, which cannot be included here, established the following points:

(*a*) Leakage is not affected by rotation, as long as turbulent flow in the clearance space persists.

(*b*) Leakage will be affected by rotation whenever rotation changes the state of flow from laminar to turbulent in the ring-space.

(*c*) In pumping oils the leakage flow is usually laminar and is reduced very fast to an insignificant quantity. Temperature gradients along its path, however, prevent ready calculation of its magnitude. Volumetric efficiency is approaching unity.

(*d*) The torque losses due to the tangential shear developed are increasing considerably in magnitude and greatly affect the over-all efficiency.

(*e*) Reduction in leakage and increasing torque losses influence the running temperature of the pump and therefore the over-all efficiency.

Points (*c*) to (*e*) deserve further discussion. It is clear that reduction in leakage concentrates the dissipation of increasing torque losses within a smaller and smaller volume of liquid. Considerable heating must therefore be expected, which is fortunate indeed, since otherwise the viscous torque would very soon become excessive. As it is, the oil entering the ring space is absorbing the torque losses and is heated up with consequent reduction in viscosity, which in turn reduces the viscous shear and increases somewhat the leakage. A considerable temperature-gradient exists along the axial length of the ring. Naturally the problem is a rather difficult one, since the increase in temperature depends on the flow of heat from the ring surfaces, the exchange of heat from the rings to the oil leaking through, and on the temperature-viscosity function of the oil itself. However, some analytical solution is possible on the basis of adiabatic flow, which furnishes at least a rather useful qualitative explanation of the phenomena encountered in the analysis of the pump test results. The results of this solution show that differences in efficiency must be ob-

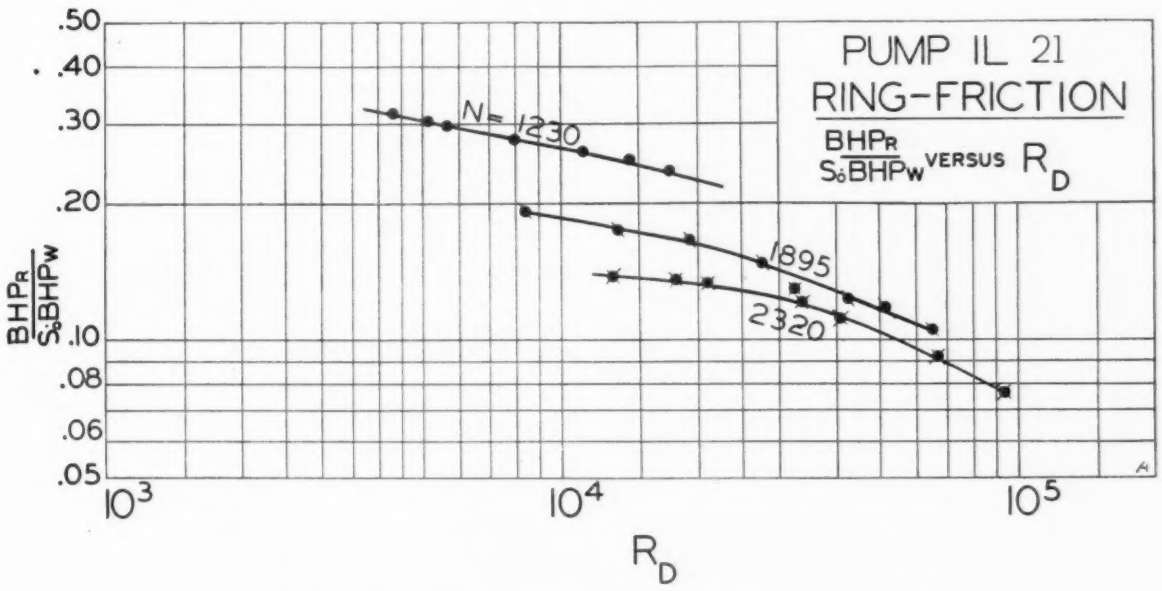


FIG. 12 EXAMPLE OF RING FRICTION AS A FUNCTION OF SPEED AND OF R_D

tained for the same Reynolds number R_D, if the speed of rotation is changed.

The horsepower loss BHP_R due to the tangential shear for one ring is given by the equation

$$BHP_R = \frac{3200 \cdot S_0}{\xi \cdot R_D} \cdot \frac{b_R}{S_R} \cdot \left(\frac{d_R}{d_2}\right)^3 \cdot \left(\frac{N}{1000}\right)^3 \cdot d_2^5 \quad \ldots\ldots [17]$$

This equation is easily derived by assuming a constant viscosity except for the dimensionless factor ξ. The latter is a function of the temperature gradient along the ring length b_R, of the temperature-viscosity relation for the oil and of the ring dimensions. This factor ξ is therefore responsible for the breakdown of hydraulic similarity, in so far as the ring flow is concerned, since obviously a constant ξ would result in a continuous curve for BHP_R as a function of R_D. Using the analytical and numerical results obtained for ξ, the ratios $BHP_R/S_0 \cdot BHP_w$ have been plotted for three speeds against R_D for pump IL 21. The latter shows the effect of ring friction most clearly. It may be stated again that these analytical results should be judged as qualitative rather than quantitative, until more evidence becomes available. The plot, however, brings out clearly that the shift in power and efficiency-loss curves found in Figs. 14 to 16 for the various speeds is at least partly due to ring losses.

It can further be shown that increasing the ring clearance or shortening of the axial length of the rings does not have a corresponding effect on the power losses. This has also been proved by a few experiments, which, however, are not sufficiently complete to allow general conclusions at this time. The reasons for this behavior are probably that both measures produce increased leakage, thereby increased cooling and correspondingly higher tangential shear.

(*d*) *Miscellaneous Losses.* The only losses not discussed so far are stuffing-box losses and bearing losses. The latter are not affected by the type of liquid pumped and little need be said about them here. The stuffing-box losses are of the same type as the ring losses; their variation with the Reynolds number for any given pump will accentuate the tendency toward dissimilarity of hydraulic behavior, produced by the influence of the ring losses.

SUMMARY OF EXPERIMENTAL RESULTS

(*a*) *General Discussion and Methods of Presentation.* All experimental data were plotted in the customary way, i.e., performance curves showing input horsepower, head, and efficiency were plotted against discharge from complete shutoff to the maximum flow, which was always larger than the normal flow. All analysis work started from these basic curves, of which there are more than 220 covering a range of viscosities from that for water to 10,000 SSU. The analysis as carried out in the following is only concerned with the effect of viscosity on the so-called "normal performance points" of the pump, i.e., on the maximum efficiency. The influence of the viscosity on the shape of the performance curves may give considerable insight into the relative distribution of the various losses. Time at present did not permit, however, any further exploitation of these results, which must be reserved for a future date. In the following are given the methods which were followed to obtain systematically the variation of maximum efficiency, head, and input-horsepower with increasing viscosities:

1 The first approach considered the normal discharge for water as a constant also for the oil runs. Corresponding efficiencies and heads were obtained from the oil-performance curves and dimensionless correction curves were plotted as a function of Reynolds number. This was feasible only for lower viscosities and seemed to provide a good basis for comparison with water runs since all average velocities remain the same for water and oil runs. Thus the influence of viscosity is shown immediately and clearly. Increasing viscosity causes changes in the velocity distributions everywhere in the pump, which tend to become more and more nonuniform. Thus the kinetic-energy content of the flow must increase at the expense of the potential energy and, in addition, friction losses also grow rapidly for lower Reynolds numbers. The conversion of the kinetic energy to potential energy is naturally accompanied by higher losses. The size of the volute may not favor the same efficiency of conversion as for water. Furthermore, the velocity-head corrections are calculated on the basis of average velocities rather than on the basis of true kinetic-energy contents. A large decrease in head is therefore noted together with the lowering of the efficiency. Since

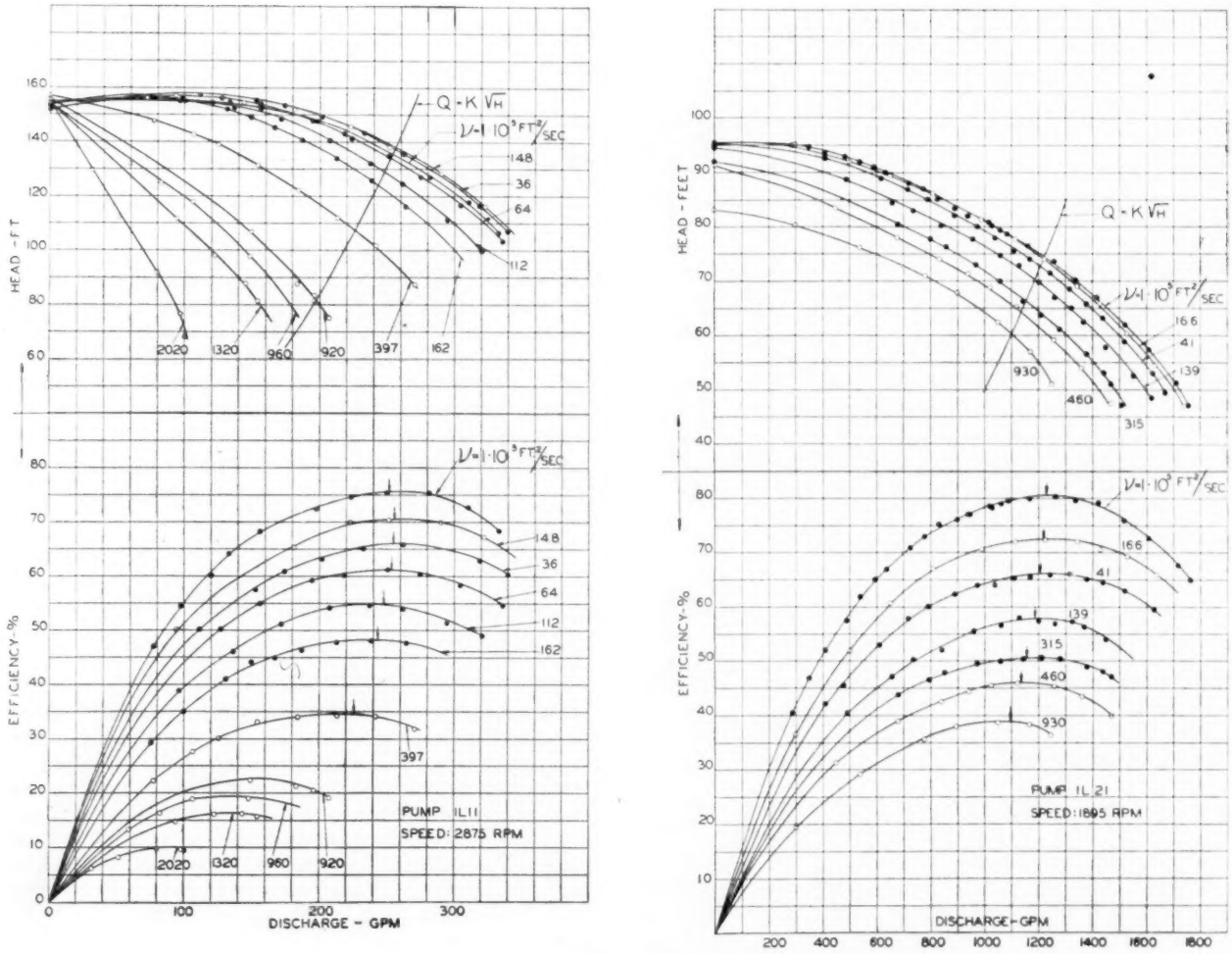


FIG. 13 EXAMPLES OF HEAD-CAPACITY AND EFFICIENCY-CAPACITY CURVES FOR VARIOUS PUMPS AND VISCOSITIES

the efficiency on the basis of constant Q_0 departs markedly from the maximum or peak efficiency for higher viscosities, the method proved very soon impractical, as can be seen from Fig. 13, and was therefore given up.

2 At times it has been suggested to assume a constant head, regardless of viscosity. This gives normal capacities which are very soon much lower than the one corresponding to maximum efficiency as can easily be verified on Fig. 13. However, for viscosities up to 100 SSU either method may be used without introducing large errors.

3 It was found that if the ratio $(Q_0/\sqrt{H_0})$ was assumed to remain constant as calculated from the water performance, a parabola could be plotted, which would intersect the head-discharge curves at the point of maximum efficiency, as shown in Fig. 13. This proved to be especially helpful in view of the fact that for lower viscosities it is impossible to decide by inspection only on a point of maximum efficiency and corresponding normal discharge, head, and power. This method was used therefore in plotting the information presented in the following graphs, which represent the essential results of the study for easy reference. These graphs give the complete Reynolds number characteristics for the practical range of operation for all four pump variants.

(b) Influence of Viscosity on Performance.

1 Normal Head and Capacity. A few general remarks are in order to explain Figs. 14 and 15. All heads and horsepower inputs are given in terms of their corresponding water equivalents and are plotted against R_D. The efficiency loss $(100 - e)/100$ was plotted in preference to the efficiency, since logarithmic scales are used, so that accidental errors are shown in correct proportion. All curves show the water performance points on the right-hand side in black with special marks to identify the different speeds. The points for thin oil are white, followed by light oil points in black, and finally the points for heavy oil are white again. This identification by liquids proved desirable, since differences in performance were discovered as the liquid was changed, even though the Reynolds numbers remained of the same order of magnitude. The explanation for these differences is given later with the reasoning relative to the shift of curves with speed. The general trend of the curves is self-explanatory with decreasing heads and with increasing power input and efficiency losses as the Reynolds number decreases. The striking influence of the disk-friction losses becomes apparent by comparing Fig. 11 with Figs. 14 and 15. The steep rise in efficiency losses is directly traceable to the change from turbulent to laminar disk-friction losses. A special curve for reduction in capacity was found unnecessary

since the discharge Q_0 can be obtained from H_0 on the basis of $Q_0 = K\sqrt{H_0}$ wherein $K = Q_w/\sqrt{H_w}$. The latter relationship was found to hold true for Reynolds numbers R_D as low as 3000 to 4000. Below these values of R_D the capacity decreased more rapidly, the head-capacity curves became very steep and the points of maximum efficiency had to be picked by inspection. This, of course, results in greater scattering of the points, since at the same time the general accuracy becomes lower. A slight shift in the capacity may produce an extremely large change in the head. However, it is felt that the lower limit of $R_D = 4000$ will terminate almost any range that might come up in actual practice.

2 Input Power. The input power curves represent a correction factor by which the water horsepower input (BHP_w), as corrected for specific gravity, is to be multiplied to get the horsepower input for oil (BHP_0). These curves indicate a rather large increase in the latter for Reynolds numbers, for which the head and capacity corrections are almost insignificant. This would be further proof of the contention that the decrease in efficiency and the increase in power input for Reynolds numbers near the 100,000 mark is mainly due to the disk and ring friction. It should also be noted that pumps IL 11 and IL 22 show the largest increase here, while IL 21 with a small impeller but relatively large rings and IL 12 with an open impeller show smaller values. The rise in input horsepower for lower values of R_D is more or less linear in a log-log plot, corresponding to the change with Reynolds number of all hydraulic losses including disk and ring friction. For all pumps, differences in power input are found for constant Reynolds numbers as a function of speed. This may be explained in part by the effect of ring and stuffing-box friction as outlined in a previous section. The running temperature for higher speeds increases, this in turn causes a reduction of the shearing stresses, and thereby a reduction also in the percentage of ring losses in terms of total power input. The larger the power output for a given pump, the smaller will be the ring losses in per cent of input power for the same Reynolds number.

It is obvious then that these differences should be most conspicuous for pump IL 21 where the output was very small and that the difference between low and medium speed for pump IL 22 is much less, since the impeller of the latter was 35 per cent larger in diameter for the same inlet and ring dimensions. It is clear, furthermore, that the results for pump IL 11 will show the influence under discussion even less, since the rings here are very small in proportion to the impeller and therefore have but little effect on the total losses. The stuffing-box losses will accentuate the phenomenon, since IL 21 and IL 22 are double-suction pumps, while IL 11 is of the single-suction type. The disk-friction losses in contrast to the ring-friction losses will in general be larger for low-specific-speed pumps. They will therefore affect the performance of IL 11 most of all and will have a minimum effect on the behavior of IL 21. This, of course, was one of the reasons for selecting these pumps. It should also be mentioned that the curves for power input correction and efficiency loss for the low speed are probably not of practical value, since such speeds are seldom employed. They were included in these tests mainly to bring out the effect of speed and in order to increase the range of Reynolds number for each oil.

3 Maximum Over-All Efficiency. The tendencies of the head and input-power correction curves are essentially reflected in the plot of the ratios $(100 - e)/100$ against Reynolds number. These curves will show all the discontinuities encountered with each of the other types to a somewhat larger scale. The question may be asked, why the efficiency loss was not given as a fraction of the efficiency loss for water. The argument against the latter method would be that the efficiency loss itself represents already, to a certain extent, a dimensionless factor of resistance for a given type of pump, similar to the pipe friction factor (f) for a given pipe with relative roughness (ϵ/d)[5]. Just as it would be unwise to divide all pipe-friction factors by the special values of (f) obtained for various values of ϵ/d, so nothing could be gained by dividing all efficiency losses by the water efficiency. Since all efficiency losses remain constant with respect to Reynolds number in the range of water or air performance, while Reynolds number determines the behavior for more viscous liquids, the analogy to pipe-friction phenomena is close. The relative roughness of the pipe would find its counterpart in a specific speed modified to include a relative-roughness parameter. However, such an undertaking must be postponed until such time when more experimental material, systematically sifted and co-ordinated, is available. The efficiency-loss curves for low Reynolds numbers show a reversal of the trend at which the losses increase. It was pointed out before that below Reynolds numbers of $R_D = 3000$ to 4000 the capacity decreases at a much faster rate than above those values. A special capacity correction curve should have been added, which, however, was not believed necessary in view of its negligible practical significance and of the somewhat uncertain evidence which permits a wide interpretation, as can easily be seen in Fig. 13. If wanted, it can of course be calculated from the other curves.

There is, however, an interesting explanation for the lower rate of increase of the efficiency losses, which takes into account the heat exchange in the pumps. If no heat were developed by ring, stuffing-box, and disk friction, the efficiency would reach insignificant values very fast. As it is, the heat developed when heavy oils are pumped, will slow down this development considerably. As the capacity decreases the cooling of the pump body decreases, so that the efficiency-loss curve will approach a value of unity only for very small Reynolds numbers. The ultimate performance will be such that oil can be pumped only as it is warmed up by the dissipation of almost the entire power input into heat. The fact that this tendency became apparent in the curves also points to the limits of the practical use to which centrifugal pumps may be gainfully employed in pumping viscous liquids.

Because it was desired to show the application of a different Reynolds number, the results for pumps IL 11 and IL 22 have been plotted against $R_S = (283.7 \cdot Q_0/d_{i_s} \cdot \nu \cdot 10^5)$. This, as is shown in Fig. 16, results in changing the order of magnitude of the Reynolds number by a factor of ten and since Q_0 will decrease somewhat with Reynolds number, the curves will be stretched over a wider range. But essentially nothing new is gained from this plot and the difficulty of having an unknown quantity Q_0 in the expression for R_S makes its usefulness quite doubtful.

GENERAL CONCLUSIONS

General Reynolds Number Characteristics

The results of the experimental and analytical work described so far show clearly that resistance of a centrifugal pump can be represented by distinct curves plotted against Reynolds number $R_D = 2620(Nd_2^2/\nu \cdot 10^5)$. Three curves are normally required to describe the behavior as a function of Reynolds number R_D:

1 Ratio of normal head for oil H_0 to the normal head for water: H_0/H_w

2 Ratio of normal power input for oil BHP_0 to the normal power input for water corrected for specific gravity: $BHP_0/(s_0 \cdot BHP_w)$.

3 The efficiency e or better the efficiency loss $(100 - e)$.

The capacity correction for the practical range of operation Q_0/Q_w is equal to the square root of the head correction: $\sqrt{H_0/H_w}$.

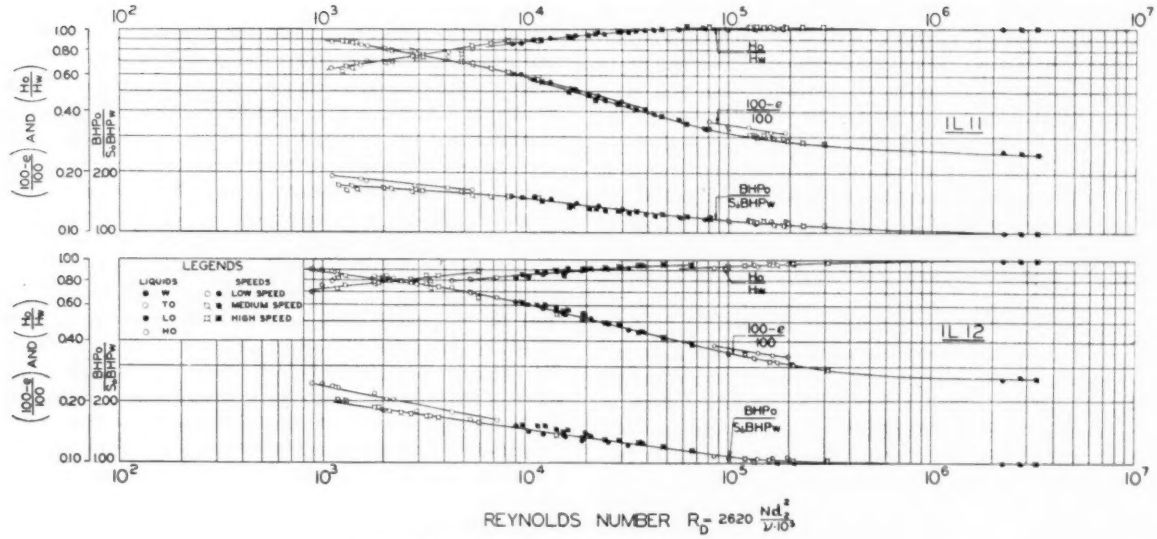


FIG. 14 RESULTS PLOTTED AGAINST R_D FOR PUMP IL 1

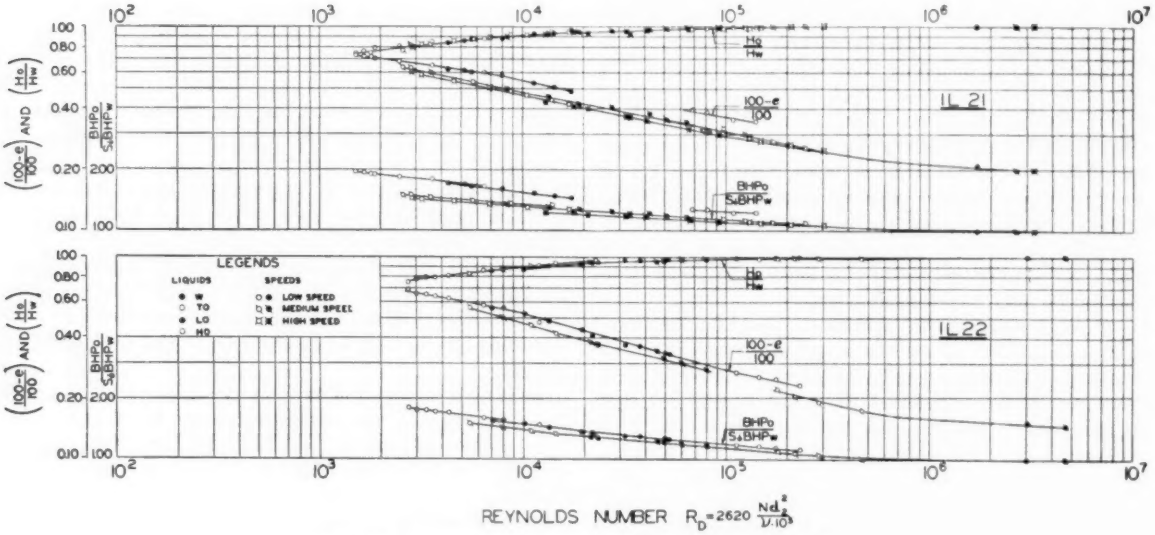


FIG. 15 RESULTS PLOTTED AGAINST R_D FOR PUMP IL 2

In order to facilitate the conversion from the conventional SSU units for the viscosity to $\nu \cdot 10^5$ in square feet per second as used for the computing of Reynolds number, the equations of conversion may be stated here

$$\text{for SSU} > 100, \quad \nu \cdot 10^5 = \left(0.237\ \text{SSU} - \frac{140}{\text{SSU}}\right) \ldots\ldots [18]$$

$$\text{for SSU} < 100, \quad \nu \cdot 10^5 = \left(0.244\ \text{SSU} - \frac{210}{\text{SSU}}\right) \ldots\ldots [19]$$

In Fig. 17 the Reynolds number characteristics for the "normal" pumps IL 11 and IL 22 have been summarized for the purpose of practical application. It is proposed to use these curves for making general corrections for a range of specific speeds from 800 to 2200 approximately. Values for pumps of different water efficiency may be interpolated.

It is of importance that the experimental material basic to the eventual adoption of correction curves be greatly increased by further analysis and co-ordination of available information and possibly by additional testing. It is naturally desirable to translate eventually all the calculations necessary at present in using these curves into graphical and tabular form for easy application in practice. It was felt, however, that it would be valuable to have first the benefit of an extensive discussion by all those interested in this problem, before too much time is spent in adapting the present results to practical use.

INFLUENCE OF DESIGN FEATURES ON THE REYNOLDS NUMBER CHARACTERISTICS

The general trend of the Reynolds number characteristics indicates three different zones within which the influence of the major losses is changing in weight.

1 For the range of water and air performance above $R_D \approx 10^6$ the efficiency losses are essentially due to the hydraulic

"through-flow" losses, followed in importance by disk friction and by leakage.

2 For Reynolds numbers $R_D \approx 10^6$ down to $R_D \approx 10^4$ the increase in power input is caused mainly by rapidly growing disk and ring friction losses, while through-flow losses increase at a comparatively low rate. The latter fact is indicated by the relatively small decrease in head and capacity, which proves that turbulent flow persists essentially throughout the pump. Leakage losses have assumed a negligible part.

3 For Reynolds numbers lower than $R_D \approx 10^4$ the through-flow losses increase more rapidly as indicated by a marked downward trend in head and capacity. Laminar-flow conditions are gradually established for the main flow. Disk and ring losses become less dominant and due to the large dissipation of power into heat on account of the latter the general rise in the efficiency losses is retarded.

Due to the complex nature of the flow through a pump it is naturally impossible to fix any Reynolds number R_D for the beginning of laminar-flow conditions for any one pump. It is even less possible to determine such a critical Reynolds number as a general criterion for all pumps. However, it is quite obvious that such a value of R_D would have little critical significance and is in no way analogous in this respect to the critical Reynolds number for pipe flow. The complexity of the losses and the non-uniform character of the flow preclude a sharp break in the line of resistance and point toward a very gradual and smooth transition between the two states of flow. This is indeed the conclusion to be drawn from the curves of Figs. 14–17.

A few additional conclusions may be drawn with respect to design characteristics: The head correction curves show that for low viscosities and low specific speed (pump IL 11) the head may increase at first above that produced for water. This is

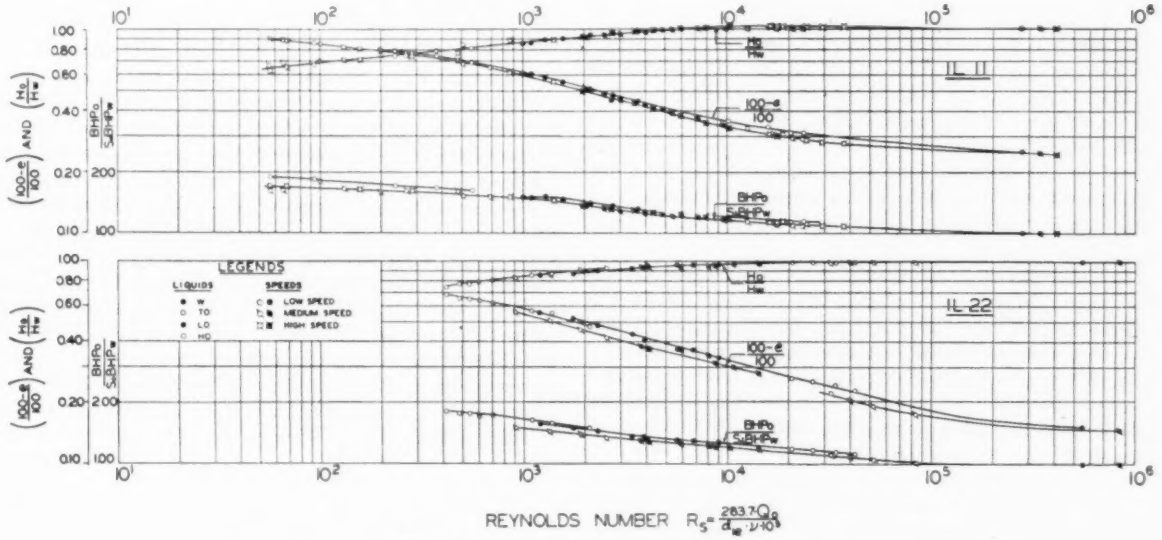


FIG. 16 RESULTS PLOTTED AGAINST R_S

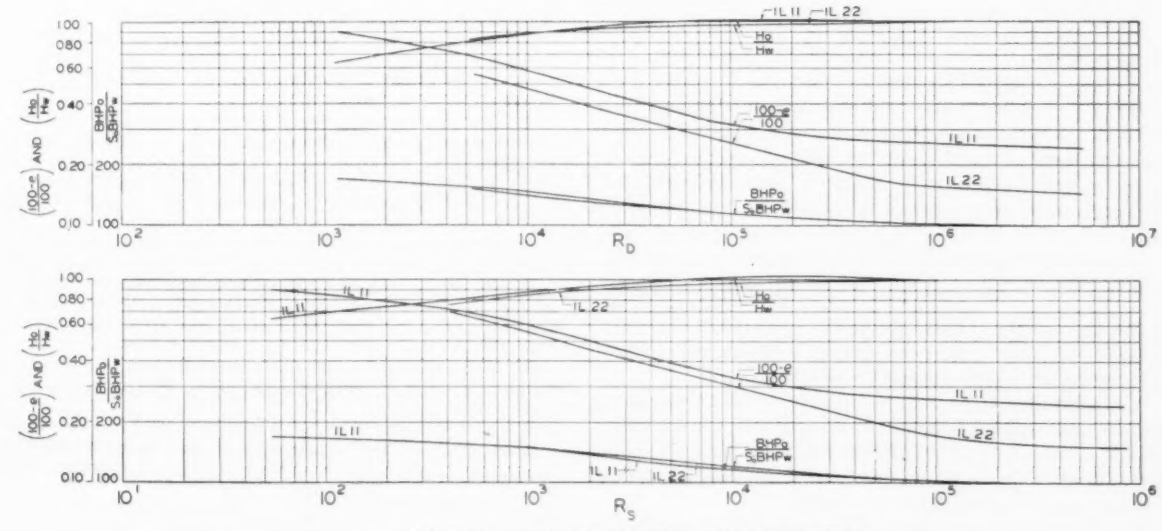


FIG. 17 GENERAL REYNOLDS NUMBER RELATIONS FOR SPECIFIC SPEEDS OF 1000 TO 2000

believed mainly due to the large effect of disk action for such pumps, since the pumping by disk action here becomes a considerable percentage of the total capacity. Further proof for this contention is supplied by the curves for the open impeller of the same pump, which show a lower head and lower power in the same range of Reynolds number.

If ring losses are to form a small part of the total losses, abnormally low speeds should be avoided. The useful output of a given pump is increased considerably for viscous conditions of flow by increasing the speed, since the influence of ring losses is diminished. This tendency is exemplified by the curves for the higher-specific-speed pump IL 21, which shows the greatest improvement with higher speeds, since ring and stuffing-box losses form a large percentage of the total losses for the lower speeds.

Individual losses, which are due to "hydraulic friction," to disk action, to ring and stuffing-box friction, are not easily separated at present but will vary apparently within reason in a proportional manner for pumps of conventional design. It may be assumed that a decrease in disk friction for a higher specific speed is compensated for in part by the relative increase in ring friction for this type of pump. However, there is still a net gain in efficiency when compared on the basis of constant Reynolds number and considering only the curves of Fig. 17. Compared on a percentage basis the efficiency losses differ less for low Reynolds numbers than for the water performance runs, since the curves converge rather rapidly for a certain range of R_D values.

A considerable increase in the running temperature for a given pump is caused by ring and stuffing-box friction. While the evidence on hand does not permit more than a qualitative estimate of the influence of the pump temperature on the performance, it may be stated that for a given Reynolds number and a given speed the efficiency is somewhat higher and the head produced is increased, if the running temperature is high. In the range of R_D, where Heavy Oil (HO) and Light Oil (LO) points overlap, the curves show a distinctly higher head for the former, since its temperature is high here while the Light Oil is cold. These remarks are made at this time with the intent of calling attention to the influence of the running temperature rather than with the idea of suggesting definite answers.

Attempts have been made during the evaluation of the data to analyze the individual losses separately and to deduct from the power input the influence of disk and ring friction. While expressions for disk friction give probably the order of magnitude of these losses correctly, the ring friction is not as easily calculated, since it is influenced to a decisive degree by large temperature changes in the ring space. For the time being, therefore, the attempt at isolation of the hydraulic losses from the input power was discontinued. But it is clear that eventually this phase of the problem will have to be solved, if further insight into the relative distribution of these losses is to be gained. This will be a very fruitful subject for further experimental studies.

Recommendations

On the basis of the information made available in this paper it is possible to propose some very definite future steps toward a final solution of the problem under discussion.

1 A considerable amount of detailed information, which up to date seemed irrelevant, should be disclosed by the profession as a result of the material published here. This material should be critically sifted and co-ordinated by a central agency on the basis of all the pertinent variables involved.

2 The information embodied in the performance curves and data, of which the results presented form an important but relatively small part, deserves further analysis. The influence of viscosity on part-load and overload operation should be cleared to a certain extent. Since disk and ring friction losses remain more or less fixed regardless of discharge, the detailed analysis of input and output curves should yield valuable information toward separation of these losses from the hydraulic losses.

3 The problem of ring friction should be studied further, analytically and experimentally. Applications toward improved stuffing-box design and use of mechanical seals may be included here.

4 Analytical studies should be undertaken to determine the influence of relative roughness and of specific speed as variables influencing the efficiency, so that eventually a set of universal performance curves may be plotted including these quantities in addition to Reynolds number.

5 Additional performance tests should be made with pumps of different design, especially with pumps of higher specific speeds. Such tests could be made on a much more economical basis now, since the pertinent variables and trends are established. Effects of changes in design should be systematically studied.

Acknowledgment

The study reported here represents an example of academic-industrial co-operation, which was sustained by the active interest of the administrative officers of Lehigh University and of the Ingersoll-Rand Company in this work. In this connection the author is especially indebted to Mr. W. M. Stanton of Ingersoll-Rand and to Prof. H. Sutherland of Lehigh University. Intimately connected with the technical phases of the work were Messrs. A. P. Brocklebank and H. Hornschuch, to whom the author wishes to express his particular appreciation. Mr. Ming Lung Pei was responsible for a great deal of analytical work. Thanks are due to a considerable number of other associates connected at various periods with this work and to the loyal co-operation of the staff members of the Hydraulic Laboratory of Lehigh University.

BIBLIOGRAPHY

1 R. L. Daugherty, "A Further Investigation of the Performance of Centrifugal Pumps When Pumping Oils." Bulletin 130, Goulds Pumps, Inc., 1926.

2 A. J. Stepanoff, "Pumping Viscous Oils With Centrifugal Pumps." *Oil and Gas Journal*, May, 1940.

3 N. Tetlow, "A Survey of Modern Centrifugal Pump Practice for Oilfield and Oil Refinery Services." The Institution of Mechanical Engineers, 1942, pp. 121–134.

4 A. H. Church, "Centrifugal Pumps and Blowers." John Wiley & Sons, Inc., New York, N. Y., 1944.

5 L. F. Moody, "Friction Factors for Pipe Flow." Trans. A.S.M.E., vol. 66, 1944, p. 671.

6 Th. von Kármán, "Laminar and Turbulent Friction." *Zeitschrift für Angewandte Mathematik und Mechanik*, vol. 1, no. 4, 1921, pp. 244–249.

7 F. Schultz-Grunow, "Frictional Resistance of Disks Rotating in Housings." *Zeitschrift für Angewandte Mathematik und Mechanik*, vol. 15, no. 4, 1935, pp. 191–204.

8 A. H. Gibson, "Hydraulics and Its Applications," fourth edition, 1930, The Macmillan Company, New York, N. Y., pp. 186–191.

9 E. Schneckenberg, "Durchfluss von Wasser durch konzentrische und exzentrische Drosselspalte mit und ohne Ringnuten." *Zeitschrift für Angewandte Mathematik und Mechanik*, vol. 11, no. 1, 1931, pp. 27–40.

10 S. Suzuki, "On the Leakage of Water Through Clearance Space." *Journal of Fac. of Eng.*, Univ. of Tokyo, vol. 18, no. 2, 1929, p. 71.

11 R. J. Cornish, "Flow of Water Through Fine Clearances With Relative Motion of the Boundaries." *Proceedings of the Royal Society*, London, Eng., 140 A, 1933, pp. 227–240. (Note: misprint p. 237, Fig. 7, $\frac{m^3}{\mu^2\rho} \cdot \frac{dp}{dx}$ should read $\frac{m^3 \cdot \rho}{\mu^2} \cdot \frac{dp}{dx}$.)

12 S. Goldstein, "The Stability of Viscous Fluid Flow Between Rotating Cylinders." *Proceedings of the Cambridge Philosophical Society*, vol. 23, Jan., 1937.

Discussion

N. TETLOW.[3] The writer would like to congratulate the author on his paper, which provides an outstanding contribution to our knowledge of the viscous-flow characteristics of the centrifugal pump. He would like to endorse the author's statement that previous investigations have provided only temporary methods of approach; they have, however, served a very useful purpose indeed pending the accumulation of knowledge which permits a more scientific study.

Past contributions to engineering societies, and in published works, have always given rise to a good deal of discussion in which the theoretical principles associated with the Reynolds number of a pump have been ventilated at considerable length. All previous treatment of this subject, however, has been purely academic and has not been supported by practical evidence.

The researches now recorded by the author have done much to fill in this missing information and permit us to make a more accurate assessment of the influence of Reynolds number on performance. The writer would go so far as to say that this paper provides the first convincing evidence that he has seen in which the influence of running speed is demonstrated.

It is encouraging to learn from the paper that the author proposes, at a later date, to reproduce the results of his observations in a form which will lend itself more easily to the solution of practical problems. It is hoped, therefore, that some suggestions regarding the method of approach will prove helpful.

The method adopted by the author to correlate an almost bewildering series of observations is to plot, in the Reynolds curves, only the pump performances corresponding to maximum efficiency. To do this he has suggested that the locus of the maximum-efficiency point on the head-capacity curves, follows the law $Q/\sqrt{H}$ = constant.

It will be seen from the paper that this is a reasonable method of approach, and it has induced the writer to examine, from this viewpoint, the information in his own possession. This examination suggests that the path of the maximum-efficiency point on the head-capacity curves corresponds more nearly to constant specific speed than to constant $Q/\sqrt{H}$.

As an example, the curve in Fig. 18, taken from a paper[4] by the writer, and plotted on the basis of imperial gallons per minute, shows the characteristics of an 8-in. single-stage volute pump when handling oils of different viscosities. On these curves has been superimposed the constant-specific-speed line $\frac{G_1}{G_2} = \left(\frac{H_1}{H_2}\right)^{3/4}$ which, it will be noted, corresponds with a fair degree of accuracy to the points of maximum efficiency. A study of the examples in Fig. 13 of the author's paper, shows a similar trend. It is suggested, therefore, that the use of constant specific speed not only corresponds more nearly to observed results but, for reasons which are given later in this discussion, may also have other advantages when the available information is applied to practical problems.

The writer has also analyzed the results of a number of viscous-flow tests in a series of curves in which head and efficiency performances are plotted against N_d in the manner suggested in the paper, but now on the basis of constant specific speed. The available number of tests is limited, but they do suggest that a reasonable measure of agreement may become possible, as indeed it should, if pumps of similar specific speeds are compared. There is a fair amount of "scatter" but not more than one might

[3] Consulting Mechanical and Electrical Engineer, Manchester, England.

[4] "A Survey of Modern Centrifugal Pump Practice for Oil Field and Oil Refinery Services," by N. Tetlow, Proceedings of The Institution of Mechanical Engineers, vol. 150, 1943, pp. 121–134.

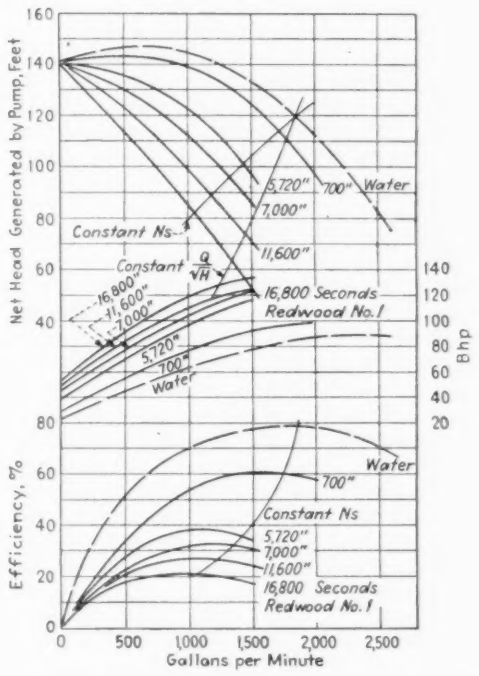


FIG. 18 TEST CHARACTERISTICS OF 8-IN VOLUTE PUMP HANDLING VISCOUS OIL PRODUCTS

expect, bearing in mind the large number of variables and the ever-present possibility of experimental errors. It is suggested, therefore, that a more complete investigation on this basis may prove illuminating.

If the writer's preliminary observations on this subject are supported by further investigation, then it should be possible to prepare a complete family of Reynolds curves to cover all variations in speed, size of pump, viscosity, etc., each curve corresponding to a particular specific speed. In this event, the advantage of using the constant-specific-speed line instead of the constant $Q/\sqrt{H}$ line proposed by the author will become evident. Given any duty to be performed, once the running speed is determined, it will then be possible to calculate the specific speed, a figure which will establish immediately the appropriate correction curve to be used.

Such a series of Reynolds curves to cover the usual range of specific speeds would provide a concise means of applying the results of the author's tests to practical problems. By their use the size of pump most suitable for the duty required could be established, the problem being simplified by our knowledge that the specific speed will be constant whether handling a viscous fluid or water.

It would be possible also to superimpose on the Reynolds curves the maximum-efficiency duties, when handling water, for any range of pumps available. Not the least advantage of this method of approach is the fact that maximum possible efficiency when handling the viscous fluid could be assured automatically.

The writer would like to have studied this method of approach more carefully, but the combination of postal delays and closing date for communications does not permit this. It does appear possible that there may be a reason, based on fundamental principles, why the constant-specific-speed line should correspond so nearly to maximum-efficiency performance. He would like the author to approach the problem from this angle and would be grateful for any observations he is able to contribute.

The writer has only one criticism to make regarding this

admirable contribution to engineering science. The value of the paper would have been increased enormously if the author had found it possible to append a list of the symbols and the units of measurement used throughout the paper. When dealing with such measurements as viscosity and Reynolds number, it is so easy to introduce an element of confusion that it is hoped he will find it possible to include this additional information in his closure to the paper.

A. HOLLANDER.[5] The author has made an important contribution to a subject which is badly neglected by the manufacturers of centrifugal pumps. It is regrettable that owing to the severe limitation of the length of the paper, some pertinent data were obviously omitted, thus preventing the examination of some aspects of the problem which are different from those of the author or held for future papers.

For example, the writer posed the question some years ago whether the affinity law broadened to include viscous liquids but narrowed down to head and capacity so as to exclude brake horsepower and efficiency and with these the external losses, is valid or not for the same Reynolds number. According to this law, taking a single impeller and having available the complete head-capacity (QH) curve for a given constant speed (N) and viscosity (ν) from shutoff to zero head, for another speed (KN), another complete head-capacity curve could be figured point by point for a viscosity ($K\nu$); the corresponding points of capacities would be KQ and of heads K^2H. Comparing the through-flow at any point of the impeller, the velocity diagrams should be similar for the two speeds of operation. The Reynolds numbers at different points of the impeller or case will vary for a single test point, but for the second test at a different speed and the same viscosity-speed ratio, they should vary the same way, because at any given point of the impeller or case the Reynolds numbers are identical for the two tests at corresponding capacities. For instance, if we have the test of pump IL11 at 2330 rpm and 10,000 SSU, we could figure the head-capacity curve for 1750 rpm, that is, $^3/_4$ speed for 7500 SSU, using as corresponding points $^3/_4$ capacities and $^9/_{16}$ heads. This is the only viscosity for which the foregoing test could be used at 1750 rpm. Going up in speed to 3500, the same test would give a performance for 15,000 SSU viscosity.

This prediction of the complete head-capacity characteristics from a test at a single speed for other speeds and viscosities, which have the same N/ν ratio (that is, the same Reynolds number) would be very desirable even if the best efficiency points were not at corresponding points due to a different change in the external losses. Unfortunately, the published data of the author (Figs. 14 to 17) show only one point of the performance curves at which $\frac{Q_0}{\sqrt{H_0}}$ is the same as the $\frac{Q_w}{\sqrt{H_w}}$ for the best efficiency point for water. Now the affinity law is valid for water (see Fig. 8, where the points coincide), so that

$$Q_{w1} = K_q N_1 \text{ and } \sqrt{H_{w1}} = K_h N_1$$

For any other speed

$$Q_{w2} = K_q N_2 \text{ and } \sqrt{H_{w2}} = K_h N_2$$

so that

$$\frac{Q_1}{\sqrt{H_1}} = \frac{Q_2}{\sqrt{H_2}} = \frac{K_q}{K_h} \text{ const}$$

means that corresponding points are plotted. What the author's modified affinity law tells us is, that for a given Reynolds number the H_0/H_w points should coincide. This is true for pump IL21, Fig. 15, showing a single line for this curve, and except for a short section for IL22, which shows about a 3 per cent deviation between $R_D = 10^4$ to 2.5×10^4.

The smaller pump IL11 shows a similar, and IL12 a somewhat greater deviation. Of course it would be instructive to see whether or not these deviations remain so small at other $\frac{Q}{\sqrt{H}}$ values for the whole performance curve. This would eliminate any doubt whether the deviations, amounting to something like ± 4 per cent, are due to experimental difficulties in a small region, which might arise if the flow at some point would be going through a Reynolds range between laminar and turbulent, where the repetition of a test point even in plain pipe flow is difficult. Also, it would be desirable to make tests with a much greater speed range, which would permit a similarly greater viscosity range for verification.

If, because of secondary effects, the affinity law were not fully valid, the second question that is posed is whether it would not be valid for geometrically similar pumps operating at speeds and viscosities giving the same Reynolds number against the same heads. In this case the speeds would be inversely proportional with the sizes and the viscosities proportional with the speeds. The velocities (peripheral, relative, and absolute) for corresponding points would be identical at the same heads, so that the corresponding flow rates would be proportional with the areas (square of the size ratio). Having made a set of tests at different speeds and viscosities with a single pump, we could predict the performance of a similar pump of size ratio (K_D) for speeds and viscosities ($1/K_D$) times the test figures.

A confirmation of these laws, which follow from a dimensional analysis, would leave as the only criterion for the prediction of the performance of similar pumps for viscous liquids the equation

$$\frac{K^2_D K_N}{K_\nu} = \text{const}$$

where K_D is the size ratio, K_N the rpm ratio, and K_ν the viscosity ratio.

It should be noted that, strictly speaking, the foregoing considerations are only valid if the leakage through the wearing rings is neglected; otherwise the zero point of the abscissa should be shifted by the amount of leakage, which differs for every head, even for a single Q-H curve at constant speed and viscosity. However, it seems that disregarding this leakage is permissible, because it is a relatively small percentage of the total flow (except near the shutoff point) and particularly for higher viscosities.

Lacking a reasonable theory, the reduction of Q and H at a constant speed and increasing viscosities can be determined only by experiments as the author conducted them. Even with a consistent design of a line, these should be repeated for different types, that is, pumps of different specific speeds over a wider range. Different hydraulic designs, such as single- and double-suction pumps, should come under different headings as primarily they should be compared between themselves, and only secondarily should the comparison be made between the two lines (a) for the same duty (Q, H, N) as the author did, and (b) for the same flow lines in the impeller, that is, taking one half of the capacity of the double-suction impeller, because it consists of two single-suction impellers pasted together with the central bridge omitted well below the outside diameter. For a given duty and particularly for low-specific-speed pumps, the single-suction pump should give better performance, and this even more pronouncedly for small sizes (lowest Reynolds numbers).

Going to the next step, that is, predicting at least one important point of the performance at different viscosities, the writer

[5] Associate Professor of Mechanical Engineering, California Institute of Technology, Pasadena, Calif. Mem. A.S.M.E.

would suggest for this, instead of the point of best efficiency, the point of maximum water or oil horsepower. This is a reasonably definite point, undisturbed by external friction losses, such as disk or ring friction, but dependent substantially upon the flow through the impeller and case only.

This approach would be in line with the author's laudible start of trying to separate the external losses, which could therefore be deducted from the brake horsepower. This figure, compared with the water or oil horsepower, would show the effect of viscosity on the flow or on the hydraulic efficiency of the pump.

The hesitation of the writer to use water or oil horsepower is due to the lack of an acceptable term, which should rightly be "output horsepower." After all, the pump is lifting in unit time a certain weight of liquid to a given height, and the product of these, times a constant, while regularly called "water horsepower," because water is the pumped liquid, is really output horsepower for any liquid.

It seems that for the two complete tests shown, the points of maximum output horsepower are on a line of

$$\frac{Q}{\sqrt[3.3]{H}} = \text{const}$$

Other tests indicate a different exponent of H, as one would expect from greatly varying designs.

These points of maximum output horsepower are for water not far from the best efficiency point, and if they separate further at greater viscosities it is a sign of a different change in the hydraulic and external losses. Any effort to obscure the condition with a single curve for the best efficiency point, as was always done, seems to give a finality to the results which is not warranted and would retard the more fundamental examination that is called for. The omission of the output-horsepower curve from the standard pump-performance curves which show head, efficiency, and brake horsepower as a function of flow rate at constant speed, is even for water objectionable, because it does not show some important characteristics of the pump which would lead to a more intelligent appraisal of its worth.

The value of the different maximum output horsepowers as a function of viscosity is really the function that the designer or user wants, after the QH function for maximum output horsepower is known. With the latter it gives the relative change of Q and H with viscosity. With the external losses determined for different viscosities, the hydraulic efficiency could be figured besides the over-all efficiency as was previously done to give a complete picture. Following this through for different types from zero to shutoff head would possibly shed some light on the very irregular flow at partial and overcapacities, not only on the maximum-output points hitherto compared. With this knowledge then, it might be possible to design better pumps for high-viscosity liquids, which oddly enough was successfully attempted in Professor Daugherty's first and still classical tests (1).

It might be argued and correctly so, that these notes are merely suggestions for a further program rather than criticism of the present paper. It is only fair to add that the author did make a valuable contribution and in more than one direction struck new paths, particularly in calling attention, to the writer's knowledge for the first time, that the wearing ring friction is a major external loss, which cannot be lumped together with the disk friction as a small additional loss.

L. F. Moody.[6] The effect of the viscosity of the fluid on pump performance has remained a problem without a satisfactory answer, and it has not been possible for pump designers to predict with any assurance the modification of water performance to be expected when pumping oils or other fluids. The existing data have been limited to more or less isolated tests and few comparisons under controlled conditions have been available. When looking for the effect of the change of a single variable, reliable conclusions can hardly be deduced from tests on separate pumps, for example, or from any tests where other variables do not remain identical. It is believed that the author's research is the first systematic study of the problem under carefully controlled conditions covering a wide enough range to establish definite conclusions.

The paper provides a wealth of data although, as mentioned by the author, further analysis is still needed to reduce the experimental results to readily usable form. The test data are now at hand, but the complex nature of the problem does not make it easy to apply the results to any specific case. It would be a valuable addition to the material included if sectional views of the pumps tested could be appended to the paper, as this information is necessary for complete analysis.

The method of analysis adopted in the paper is logical and sound, namely, the plotting of the performance with respect to a Reynolds number, which reduces the results to dimensionless form. Several useful forms of Reynolds number are used, one of which, R_D, depends upon the impeller speed and reflects directly the effects of disk friction and clearance friction, while other forms such as R_S and R_P reflect more directly the flow velocities. The plotting of the proportional-energy loss $\frac{100 - e}{100}$, or as the writer would prefer to express it, $1 - e$, (using e as a fraction rather than a percentage) is also a reasonable procedure.

With these data available, it would seem possible to arrive at some simple empirical rule which would permit us to modify the efficiency and head given by water performance to apply to oil, at least for light oils, over a moderate range of viscosities. The writer has found it difficult to read the small-scale logarithmic plottings, in the effort to find a satisfactory functional relation. Perhaps a function of some such form as the following may serve the purpose

$$e_W - e_0 = K(1 - e_W)\left(\log \frac{R_{DW}}{R_D}\right)^2$$

in which e_W = efficiency for water (as a fraction, not a percentage); $R_{DW} = R_D$ for water; and K is a coefficient, depending upon specific speed and perhaps other characteristics of the pump.

It is hoped that the author will be able to continue his own study of the problem, and to give us an easily applied rule which would serve at least as an approximation close enough for practical use.

The fact that the curves flatten out in the region of water performance, so that the behavior then practically ceases to be a function of Reynolds number, confirms the point of view expressed by the writer in the past, namely, that when handling water, the flow in usual sizes of pumps of normal specific speeds, and still more clearly in hydraulic turbines, falls in the zone of practically complete turbulence. Accordingly, the efficiency for water operation should be practically independent of the head, and be a function merely of the relative roughness of the surfaces exposed to the flow.

The research represented by this paper is an example of systematic hydraulic experimentation at its best, and care and thoroughness are evident throughout the undertaking. The results are valuable contributions to our knowledge.

R. L. Daugherty.[7] The author has investigated centrifugal-

[6] Professor of Hydraulic Engineering, Princeton University; Consulting Engineer, Worthington Pump and Machinery Corporation, Harrison, N. J. Fellow A.S.M.E.

[7] Professor of Mechanical Engineering, California Institute of Technology, Pasadena, Calif. Fellow A.S.M.E.

pump performance with oil viscosity as high as 10,000 Saybolt seconds, which is a viscosity of 2200 times that of water. This is probably about as high as there is any practical need for going.

The writer carried on extensive investigations in this field and under the same range of viscosity in 1924 and 1926, and the results were published in two bulletins.[8] Those investigations showed very clearly that capacity, head, and efficiency all diminish with increasing viscosity and that the effects were more noticeable with small pumps than with large ones.

Another factor which must certainly have an influence upon the variation of pump performance with viscosity is the specific speed. The author has made a start in presenting this phase of the subject. However, neither size nor specific speed will tell all the story. Thus in Fig. 19, which the writer has replotted from his earlier data, may be seen the difference in the performances of two pumps of the same size and of substantially the same specific speed when operated with fluids of different viscosities. It is seen that the design, which is more efficient for a fluid of low viscosity, is less efficient for a fluid of high viscosity.

The author has correlated his data on the basis of Reynolds number, but with a separate set of curves for each individual pump. If the rpm were also constant the only variable would be kinematic viscosity such as the writer has used in Fig. 19. Thus in Fig. 19, herewith, two viscosity scales have been added,

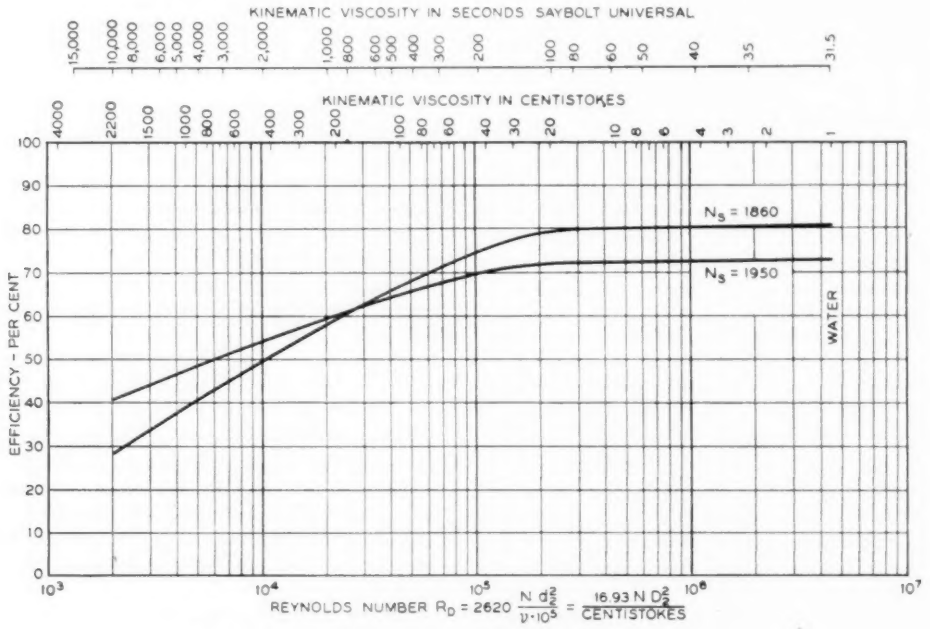


FIG. 19 PERFORMANCE CURVES FOR TWO 8-IN. PUMPS
(Impeller diameter = 13.5 in.; 1450 rpm.)

since viscosity is there the only variable entering into the Reynolds number. One of these viscosity scales is that for Saybolt seconds and the other is kinematic viscosity in centistokes. The former is used here because of its extensive employment in industry, but the latter is a scientific unit with more physical meaning. Thus since at 68.4 F the absolute viscosity of water is 1 centipoise, and its kinematic viscosity is 1 centistoke, the viscosity given in either centipoises or centistokes is at the same time an indication of the viscosity relative to water at that temperature.

The Reynolds number is computed by a formula in which N is revolutions per minute and d_2 is the impeller diameter in feet, while the kinematic viscosity is expressed in square feet per second. This viscosity is equal to the viscosity in centistokes multiplied by 0.00001076. The writer has adhered to this combination because it is the same used by the author, but in the writer's opinion it would be more convenient to compute this by $\frac{16.93\ ND_2^2}{\text{centistokes}}$ where D_2 is the diameter of the impeller in inches.

The specific speed has been computed as

$$N_s = \frac{\text{rpm} \times \sqrt{\text{gpm}}}{H^{3/4}}$$

This is obviously the same expression which the author has used for his values, but it is well to state this specifically since cubic feet per second or other units are often used instead of gallons per minute. In the case of a double-suction pump, it seems preferable to use one half of the total pump capacity in such a calculation, but the author does not indicate whether he has followed that practice or not in the values which he gives.

In Table 1 of the paper it would be desirable to define the meaning of the symbols there used since they are not obvious. In connection with Equations [2*a*, *b*, *c*, *d*], it should be stated that N is revolutions per minute, that d_2 is the diameter of the impeller in feet, although in Fig. 11, D is used for the same value.

It is to be hoped that the author or others may continue to obtain data on centrifugal-pump performances with different viscosities and with a range of sizes, specific speeds, and other design features so that eventually a comprehensive chart may be drawn up which would be a reliable guide for any combination of conditions. However, it is difficult to generalize with only a limited amount of data.

O. H. DORER.[9] The author's contribution toward the solution of the problem of viscosity effects in centrifugal pumps indicates

[8] Refer to Author's Bibliography (1); an earlier bulletin was published in 1924.

[9] Consulting Engineer, Worthington Pump and Machinery Corporation, Harrison, N. J. Mem. A.S.M.E.

a method of attack attempted by the writer some time ago and since abandoned. By this is meant the head corrections based upon percentage of water performance, and some classification numbering system similar to Reynolds number by using impeller diameter and finally unit speed (n), which is a function of impeller diameter.

Subsequently, a formula for

$$R_N = \frac{14{,}100 G^{1/2}}{\gamma} H_v^{1/4}$$

was adopted in which G = gpm, H_v = velocity head, γ = viscosity in centistokes. It is seen that the troublesome size factor has disappeared, and this is possible through substitutions in

$$Q = 0.785\ D^2 \sqrt{2gH_v}$$

the usual pipe formula, where H_v is the head creating the velocity.

In the centrifugal pump the velocity creates the head, so we can use a similar value for over-all Reynolds number. However, since the conception of H_v is from an original velocity determined not by the developed head, but by an internal head which overcame all head losses in the pump, the internal rather than the developed head is used. The internal head corresponds to input horsepower with a deduction for disk friction, bearing and stuffing-box loss. At zero capacity the recirculation capacity is considered in calculating internal head from the input power.

Of the input power, that part overcoming disk friction, bearing and stuffing-box loss is not a direct hydraulic-flow loss. A determination of this loss was made by placing solid dummy impellers in the pump casing having all details like the real impeller, except that the outer band normally used as discharge passage gives extra disk loss. Corrections were determined by extending the

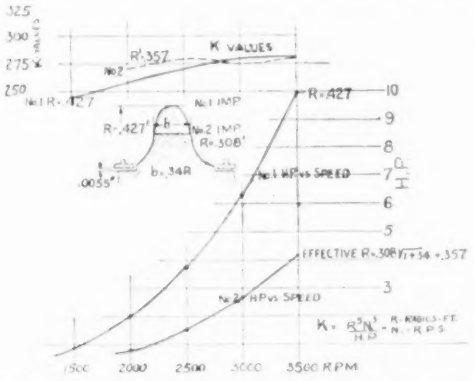


FIG. 20 WATER DISK HORSEPOWER OF DUMMY IMPELLERS
(10-hp dynamometer used; tests include bearings, stuffing boxes, and sealing rings.)

dummy to a rounded-nose affair, as illustrated in Fig. 20 of this discussion. (Water) disk horsepower follows the form of

$$\text{Hp} = \frac{R^5}{K} N_1^3$$

where R = radius, ft; N = rps; K averages 280.

Zur Nedden[10] found with simple disk tests

$$\text{Hp} = \frac{N_1^{2.9} R^{4.9}}{420} \text{ (average value)}$$

However, Gibson and Ryan tests are reported at

$$\text{Hp} = \frac{N_1^{2.9} R^{4.9}}{330}$$

Both of these are simple disks, polished, and in rough cast-iron surroundings; and neither of them can be considered as reflecting all the conditions surrounding impeller surfaces, ring, joints, etc. Hence their low values of horsepower are not considered to be applicable to centrifugal pumps.

In order to arrive at proper wall pressures, the dummy impellers were tested under pressures at mid-radius, as recorded by the actual impeller during its operation.

Disk horsepower bears a relationship to specific speed, a low specific speed having relatively more of this loss than higher-specific-speed pumps. The build-up of disk horsepower with viscosity may be very high on a low-specific-speed pump.

While ring-leakage loss is reflected in the net output, it is proper to allow for it in obtaining H_v. Practically, for water performance, H_v may be determined from H_a (actual head) by dividing it by the hydraulic efficiency, here defined as efficiency, not including disk horsepower. In any reasonable size pump ring leakage[11] is a small percentage; it may be neglected.

However, with viscous oils this ring leakage decreases to some extent, and in small pumps its decreasing rate could improve the oil head obtained, above water performance.

The basis for considering effects of viscosity states: (*a*) The increase in power input, corrected to unity specific gravity, is due to increased disk friction, see Fig. 23 of this discussion; (*b*) the decrease in head is due to several features, i. e., the frictions in the passages, the lag in attaining velocity imparted by the blades of the wheel, and finally, the poorer efficiency of velocity-head conversion within the pump.

While equal-size pumps are built with various spiral velocities, some relatively high, others relatively low, for similar specific speeds, it is clear the friction in the large-area spiral will not build up as fast with increase in viscosity as is the case in smaller-area spirals.

A similar situation applies to impeller passages; fewer vanes infer larger hydraulic mean radius and lesser frictions.

With both elements designed for low velocities to reduce frictions, there is an adverse effect in the hydraulic efficiency, and of velocity-head conversion. The problem in viscosity then boils down to which element is most destructive. It will be shown that frictions are more detrimental than the destruction of velocity-head efficiency in some designs of pumps.

Manifestly, each of these elements has a Reynolds number, and various rates of friction loss or head destruction; and while we apparently have a Reynolds number for the particular pump, there does not appear to be an over-all Reynolds-number system applicable to the range of pumps that may be used for viscous-oil applications in a manner similar to the pipe problem.

In this connection, the theory of action in a centrifugal impeller poses another problem. If all head is developed entirely through velocity, H_v is directly determined. However, some of the head is composed of centrifugal force which is at a maximum at the shutoff and at a minimum, at large flows. In fact, when centrifugal force is absent, cavitation begins. Principal formulas for centrifugal force are given as follow

$$H = \frac{YU_2}{g}(YU_2 - W) = \frac{\text{input hp} - \text{disk hp}}{0.1135\ (Q + \text{ring leak } Q)} \quad [20]$$

$$\text{Per cent centrifugal force} = 100 \times \left(\frac{H}{1.22\ N_1^2 R^2} - 0.5Y^2\right) \quad [21]$$

[10] "Influence of Disk Friction on Turbine-Pump Design," by F. Zur Nedden, Trans. A.S.M.E., vol. 37, 1915, pp. 83–107.

[11] Ring leakage was 2½ per cent for the 4-in. pump in which the dummy impeller was tested, and is independent of speed, for a given impeller.

where

U_2 = peripheral velocity, fps
W = horizontal backward component in usual velocity diagram, neglecting contraction
Q = volume delivered, cfs
R = radius impeller, ft
N_1 = revolutions per sec
H = impending head, ft

With the centrifugal-force element deducted, H_v is of a lower value and the viscosity would not affect centrifugal force except through additional lag of vane action on the fluid. In all following comparisons it has been assumed that no lag occurs.

The 8-in. Mather and Platt pump-head results have been investigated for viscosity at three rates of flow, Fig. 21 of this discussion. The sudden bump in the curve may be caused by change of oil, even though the viscosity scale is continuous. It is suspected that the type of oil has some influence. Here the hydraulic efficiencies have been calculated on the assumption that all generated head comes from velocity conversion. At the top of the sheet a series of n exponentials indicates variation with constant apparent Reynolds number.

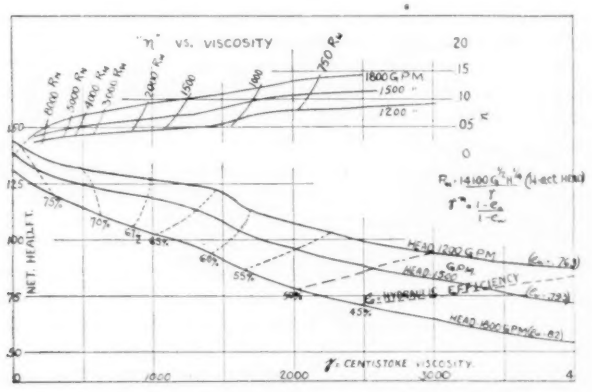


FIG. 21 PUMP-HEAD RESULTS ON MATHER & PLATT 8-IN. PUMP

Pipe frictions may be compared where viscosity is the only variable by an exponential n of viscosity; it is nearly 0.20. For head conversion in the centrifugal pump, this same exponent of viscosity is seen to be variable and considerably below 0.20.

The low n values of head, compared to frictional n values, infers that the head conversion which is the major part of H, does not decrease as fast with increase of viscosity as frictions increase. With the very heavy viscosities, the increase in n infers greater destruction in conversion of velocity to head than at low viscosities.

In order to substantiate these facts, the frictional slopes for impeller and spiral were calculated and allowed for, as well as the centrifugal force, and the remaining values represent hydraulic efficiency of velocity-head conversion.

$$\text{Friction slope} = \frac{2.7\, f H_v^{3/4}}{G^{1/2}}$$

through substitutions for size indicated in an earlier part of this discussion.

Considering the centrifugal-force element we can write

$$1 - \frac{2.7 f H_v^{3/4}}{G^{1/2}} = e_v = \frac{H_a - \text{CF} + F_r}{H - \text{CF}}$$

H_a = actual developed head
CF = centrifugal-force head

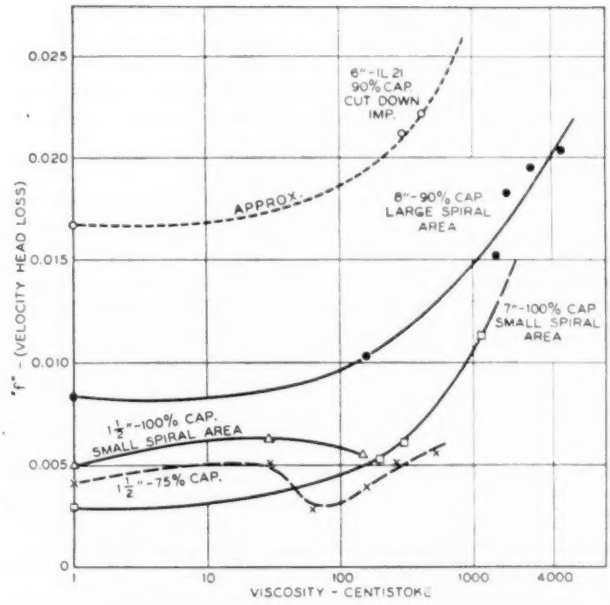


FIG. 22 FRICTIONAL SLOPES FOR PUMP IMPELLER AND SPIRAL

F_r = friction loss in spiral and impeller
H = impending head
C_v = velocity-to-head conversion efficiency factor

Here f is similar to the friction factor of pipe calculations, but refers specifically to a friction factor of velocity-head conversion.

Fig. 22 of this discussion gives the results of such an analysis and confirms that velocity-head conversion is not destroyed as rapidly in some designs as friction builds up. The small-spiral-area pumps are more efficient as water pumps having low f values.

The small 1½-in. pump seems to have better f values at 75 per cent capacity; however, this illustrates the ring-leakage effects which have been neglected, and which bear a larger percentage to output than is the case in large pumps. The decrease in leakage with increase of viscosity in the small pump is responsible for the apparent improvement in f values.

Confirming that friction and velocity-head destruction of head on viscous oils do not proceed at equal rates, the 8-in. and 7-in. pumps are compared (Table 3 of this discussion) on a common flow, and viscosity, viz. 1500 gpm at 1000 centistokes viscosity. The velocity through the spiral of the 7-in. pump is about 2¼ times that of the 8-in. pump. (The IL-21 pump is shown at 1050 gpm as 930 centistokes).

TABLE 3 COMPARISON OF 7-IN. AND 8-IN. CENTRIFUGAL WITH 6-IN. IL21 PUMP

	7-in. pump	8-in. pump	6-in. IL21 pump
H water	165	135	80
H oil	108.5	133	62½
Per cent head loss	34.2	16.2	21.9
Hydraulic efficiency, water, per cent	91.3	77.3	81.0
Net efficiency, water, per cent	85.0	73	80
Velocity efficiency, water	90	68	73.3
Velocity efficiency, oil	63.5	59	57.0
Friction, water	1.75	1.0	1.0 (estimated)
Friction, oil	23.8	13.2	9.8
f_w	0.00323	0.0119	0.0168
f_o	0.0118	0.0152	0.271
m exponential	0.302	0.303	0.46
Centrifugal force, ft	49.0	57.0	32.0 (w estimated at 10)

While the friction losses increased by an amount equal to 13.4 per cent of the developed water head, the loss in converted

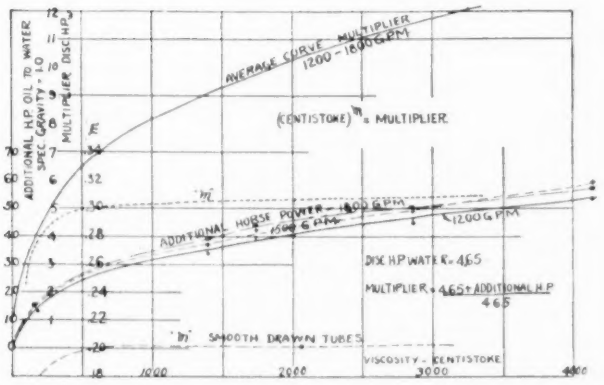


FIG. 23 EFFECTS OF INCREASING VISCOSITY ON PUMP PERFORMANCE

velocity head increased 21 per cent for the 7-in. pump. On the other hand, the 8-in. pump increases are 9.05 per cent and 6.6 per cent, respectively, for these items. The high f_w value of the IL21 pump is undoubtedly due to the large cutdown of impeller, resulting in a relatively long space between impeller and spiral. This space does not appear to affect results as badly on viscosity as in the case of the 7-in. pump, but more so than the 8-in. pump.

The changes in rates by which each element behaves in the different types of designs appear to nullify a universal application of over-all Reynolds numbering system with head and efficiency correction factors applied to the water performance.

The m exponentials affecting power are likewise variable; some high-head per stage pumps showing as low as 0.18. This suggests that rapidly moving disk surfaces create a film of apparently low viscosity or heating at the surfaces.

In conclusion, it appears necessary that more test results be provided to develop acceptable designs for best oil performances; and specific methods of calculation then are a matter of choice.

AUTHOR'S CLOSURE

The discussions submitted have contributed greatly to the further clarification of the complex problems involved in analyzing the influence of viscosity on the behavior of centrifugal pumps. The discussers have raised relatively few controversial points and have contributed instead from their own experiences valuable observations and suggestions for future work which need little additional comment. The author indicated at various times in the paper that the exploitation of the test data was only partly completed. Considerable information should be gained from further critical analysis of the individual performance curves with respect to separation of "external" from so-called "internal" losses, by comparisons with results of other experimenters, and by investigating the influence of such findings on established design procedures. The present paper was intended primarily to establish a common basis of discussion on the strength of extensive experimental evidence, to clarify the basic nature of the various losses, and to estimate their relative influence. The author feels greatly reassured since his line of attack was not seriously questioned. The work may now be continued toward eventual correction curves of more general validity.

A few remarks are in order to answer some specific problems raised by the various contributors. Mr. Tetlow brings up the question whether or not the specific speed N_S should remain constant regardless of viscosity: Curves drawn on the basis of $N_S = \text{const}$ (i.e., $\frac{Q}{H^{3/4}} = \text{const}$ for a given pump and a given speed) in the head-discharge curves give maximum efficiency points for high viscosities better than the author's method of keeping $\frac{Q}{\sqrt{H}}$ constant. Naturally various methods of defining normal capacity and normal head were discussed and tried during the analysis of the data and the present method was adopted essentially for practical reasons. Up to relatively high viscosities the efficiency corrections obtained by either method are practically identical. Applications where the efficiencies drop below 30 per cent or 25 per cent are not expected to be numerous. The efficiencies can be kept above these values by changing the type or the design of the pumps (see Professor Daugherty's example).

It seems contrary to experience with fluid friction that a single law should be valid from the range of "complete turbulence" through the turbulent transition zone into the completely laminar state of the "through flow." While reduced capacity and head result in a corresponding shift of the peak horsepower output, the higher rate of increase in the so-called external losses, especially disk and ring friction, will tend to produce a slower corresponding shift of the peak efficiency. The author agrees with the discussers who have pointed here to the need of further analysis so that the influence of the internal losses may eventually be separated from that caused by external losses.

For the present the method adopted seems the most useful one, since the assumed proportionality of Q and $\sqrt{H}$ enables the engineer to calculate these values for small changes in speed N and impeller diameter d_2, in accordance with established procedures derived from the affinity laws. It may also be called to mind that the usual concept of specific speed is associated with similar flow conditions in a given pump regardless of speed, resulting in the proportionality of speed to Q and $\sqrt{H}$ with constant proportionality factors. This precludes any influence of the viscosity on the flow conditions. If with increasing viscosities such influences result in a marked change in these proportionality factors, the geometric similarity of the through flow is disturbed though the boundaries and the speed may remain fixed.

For all practical purposes then, the pumping process is changed and it is hard to conceive of specific speed remaining constant under these conditions. The pump type may still be classified, however, by its water-specific-speed, and correction curves may be drawn on that basis. Since the change in the specific speed on the basis of $Q = K\sqrt{H}$ is inversely proportional to the discharge correction factor, the resulting increase in the specific speed remains relatively small. Finally, it may be added that the increasing external losses also have a certain effect on the specific speed, since they affect the location of the maximum efficiency point.

The exact significance of specific speed therefore is not too clear in connection with the problem of viscous influences on pump performance. It represents a classification number for normal water performance, where it remains constant for a given type of pump, since flow conditions remain geometrically similar regardless of speed and diameter. This similarity is due to the almost complete absence of variations in the viscous influences and to the minor variations of the external losses. This similarity will break down if the viscosity increases greatly and it seems reasonable to acknowledge this fact by a change in the specific speed.

The preparation of correction curves is not greatly affected by the definitions and correlations of normal discharge and normal head. The author agrees, however, with Mr. Tetlow in the desirability of further analysis and of theoretical investigations on the foregoing question.

Professor Hollander and Professor Daugherty have inquired into the definition of specific speed concerning single-suction and double-suction pumps. The author calculated the values of N_S

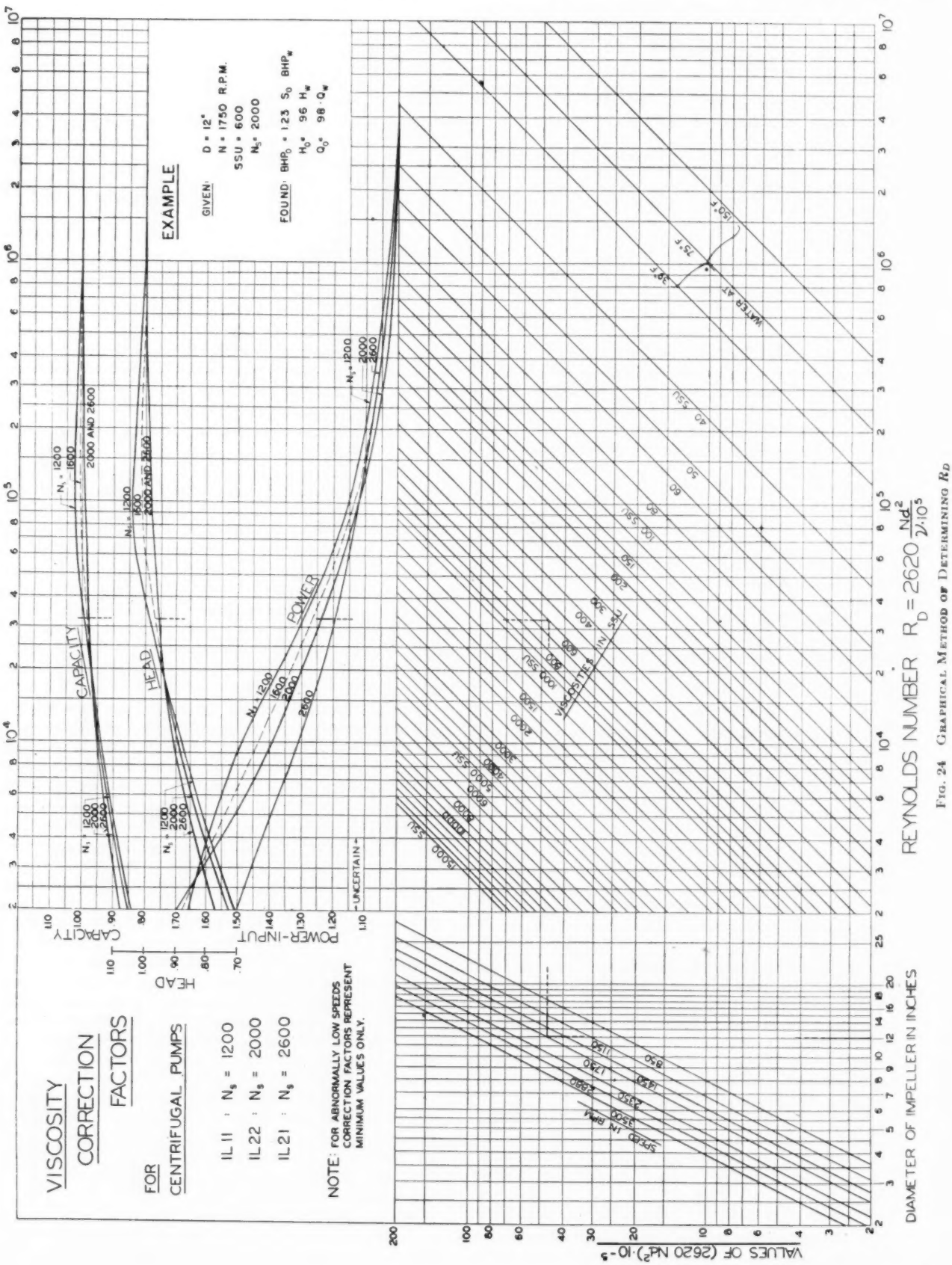


FIG. 24 GRAPHICAL METHOD OF DETERMINING R_D

using total discharge Q in gpm, H in ft, and N in rpm. It is believed that the distinction between single- and double-suction pumps need not be insisted upon in connection with the problem in question. Using only one half the capacity for a double-suction pump to obtain the characteristic specific speed is in order whenever problems concerning entrance conditions and especially cavitation phenomena are investigated. For the problem under discussion it is doubtful whether a better comparison to single-suction pumps would be obtained except for very high specific speeds. If a double-suction impeller were to be replaced by two single-suction impellers, the hydraulic losses would probably be changed very little; however, the horsepower input for each impeller would have to be corrected for greatly increased external losses, since disk- and ring-friction losses would be doubled. The corresponding decrease in the efficiency would offset the correction of the specific speed. Such corrections for external losses for these equivalent impellers could not be made in the present state of knowledge.

For water performance disk- and ring-friction losses form usually only a small part of the total losses, which are essentially hydraulic or internal losses there, so that such corrections would be of negligible order of magnitude. For these reasons it seemed preferable to state the specific speeds for the double-suction pumps (IL21 and IL22) on the basis of their full capacity. Further light on this question must come again from a possible separation of so-called external and internal losses.

Professor Hollander has given an admirable statement and summary of the consequences of the viscous changes on the affinity relations and points out the direction toward the considerable work ahead in this field. It is clear that the conventional thinking on these affinity questions will have to be revised considerably, whenever viscosity plays a major part in pump performance.

Professor Daugherty has plotted his test results against the Reynolds number R_D and since both sets of tests were run at the same speed, this plot is identical with that against the viscosity as the only variable in R_D. It should be noted carefully that the author's curves in Figs. 14 to 16 represent data for three different speeds and therefore correlate the test material for each pump on the basis of corresponding N/ν values, with the diameter being the only constant quantity in R_D. Professor Daugherty's pump of higher efficiency for high viscosities represents the first successful attempt at a special design for viscous influences and is therefore not directly comparable to the normal pump built for highest efficiency with water.

To facilitate further comparisons with tests of other experimenters, a graphical way of determining R_D is given in Fig. 24 of this closure, with corresponding results from the author's tests integrated into three sets of correction curves for head, capacity, and power. The efficiency corrections are not shown, but can be easily obtained for any Reynolds-number value by multiplying the head and capacity corrections and dividing the product by the power-input correction factor. The use of the chart is as follows: From a known value of the impeller diameter in inches on the left scale proceed vertically upward to the intersection with the proper speed line in rpm. From here continue horizontally across to the right to the intersection with the line marked with the given viscosity in SSU (Saybolt seconds Universal). The value of R_D may now be read on the bottom scale. A vertical line extended up will locate immediately the correction factors for capacity, head, and input power.

These correction curves represent the average values from the author's tests obtained for the higher speeds which are normally employed. The individual curves are identified by the corresponding approximate specific speeds. The diagram may thus serve as a more easily applied method for practical approximations, for which Professor Moody and Mr. Tetlow have asked. The user may be reminded, however, that no claim is made as to the general validity of the correction factors, since these are based only upon the tests and the methods of analysis reported in the paper. Material from other sources may be easily compared with these findings.

Professor Moody has offered the form of an efficiency correction function which seems basically sound. The author is especially in favor of his use of $(e_w - e_0)$ therein, which represents the absolute decrease of the efficiency due to the influence of viscosity. From some preliminary graphical studies of tests on many different pumps, it seems that $(e_w - e_0)$ produces the relatively best correlation of the results, again pointing to the predominant increase of external losses especially for lower viscosities.

The author gladly complies with Professor Moody's suggestion of showing the pumps tested in sectional views by courtesy of the Ingersoll-Rand Company. Fig. 25 presents the pump labeled IL11, which indicates the closed impeller, and Fig. 26 shows the pump IL22. It is to be recalled that pump IL21 differed from the latter only by having an impeller of smaller diameter.

Little can be added to Mr. Dorer's remarks which are concerned extensively with the analysis of individual internal and external losses. The author prefers the method of determining disk friction indicated in Fig. 11 of the paper, which is based upon sound analytical and experimental evidence and would like to call attention to the considerable influence of wearing-ring friction. Mr. Dorer's Reynolds number R_N is identical with the author's R_P, as can easily be verified by substituting for $(H_r)^{1/4}$

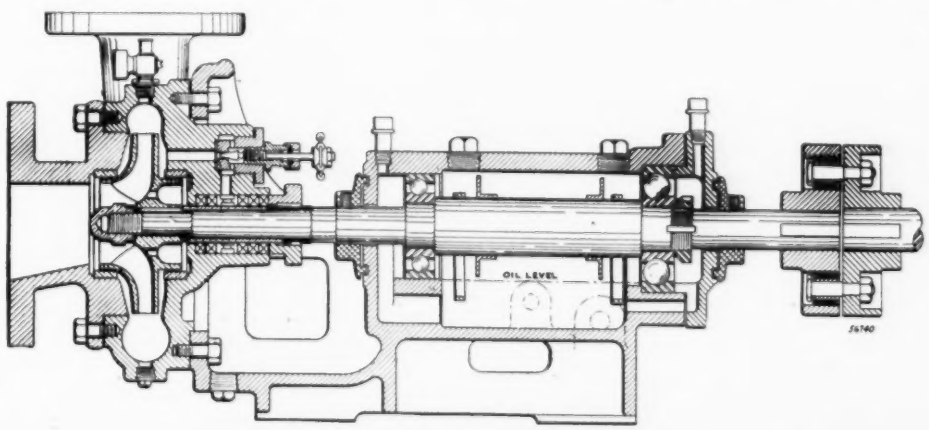


FIG. 25 CLOSED-IMPELLER-TYPE PUMP IL11

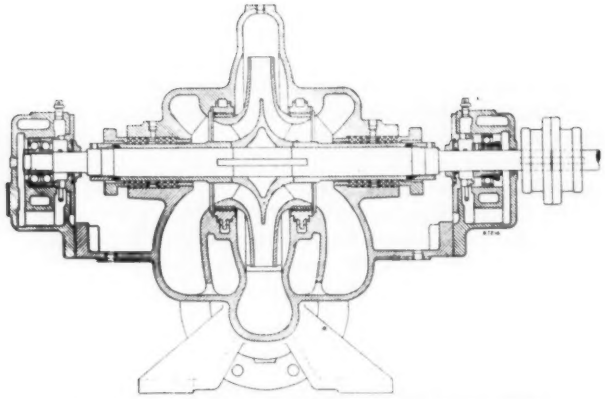


FIG. 26 DOUBLE-SUCTION CENTRIFUGAL PUMP, IL22

in terms of $\left(\frac{Q_0}{D^2}\right)^{1/2}$ and by changing the constants corresponding to units employed. This Reynolds number differs from R_D only by the proportionality factor relating Q_o to ND^3. Since these proportionality factors are dependent upon the viscosity and Reynolds number, their use in defining a Reynolds number is impractical, because trial-and-error methods have to be employed in solving for the correction factors. Reynolds number R_D is determined by diameter, speed, and viscosity and immediately locates the proper correction. Aside from this practical advantage, R_D is of particular significance for disk and ring friction as pointed out before.

In conclusion the author wishes to express his appreciation for the interesting contributions made in the discussion. They have helped greatly to stimulate and to clarify further thought on the complexities inherent in this problem of viscous effects on centrifugal-pump performance.

APPENDIX

AUXILIARY TABLE OF NOTATIONS

Tables 1 and 2 (all dimensions in inches):

D_s = diameter of suction pipe
D_d = diameter of discharge pipe
D_1 = diameter of entrance section of impeller
D_2 = diameter of exit section of impeller
D_{sh} = diameter of shaft
B_2 = width of exit section of impeller
D_R = diameter of wearing rings
B_R = width of wearing rings
$2\,S_R$ = diametral clearance of wearing rings

Fig. 7:

$$M = \frac{a_2\sqrt{2g}}{\sqrt{1-\frac{(d_2)^4}{(d_1)}}}$$

h = differential head of liquid, ft

Subscript (2) refers to orifice and Venturi-throat diameter; subscript (1) to diameter of line of approach. For water flowing through orifice $C_D = 0.6185$, and $K_M = 1.00$

Equations [1 to 17]:

H_w = head produced by pump for water, ft
H_0 = head produced by pump for oil, ft
Q_0' = discharge, cfs
Q_0 = discharge, gpm
d_{1_e} = equivalent eye diameter of impeller, ft
v_1 = velocity in equivalent eye section, fps
d_2 = impeller diameter, ft
b_2 = impeller width, ft
ω = angular velocity in radians per sec
N = rpm of disk or impeller
u_2 = tangential velocity at impeller exit, fps
v_2 = relative velocity at impeller exit, fps
r = radius of disk or impeller
δ = thickness of boundary layer near disk
S_D = clearance between disk and housing wall
d_R = diameter of rings, ft
b_R = width of wearing rings, ft
S_R = clearance between rings
γ = specific weight of fluid, lb per cu ft
S_0 = specific gravity of oil

Fig. 10:

$\omega \cdot r$ = tangential velocity of disk
u = tangential velocity of liquid in boundary layer
v_r = radial velocity of liquid in boundary layer

$$\tan \alpha_2 = \frac{v_r}{u}$$

z = distance from disk surface within boundary layer ($z_{max} = \delta$)

Fig. 11

D = diameter of disk in ft.

The Theory of Moving Sources of Heat and Its Application to Metal Treatments

By D. ROSENTHAL,[1] CAMBRIDGE, MASS.

The theory of moving sources of heat has been instrumental in providing the welding engineer with a scientific criterion of weldability of steels. The author outlines briefly the fundamentals of this theory and derives appropriate solutions for linear, two- and three-dimensional flow of heat in solids of infinite size or bounded by planes. Point, linear, and plane sources of heat are examined. The solutions obtained are then applied to welding problems. It is shown that these solutions are in good agreement with the experimental results, and that they afford a close analysis of the factors governing the heat flow in welding. The most interesting result of the theory, however, is the derivation of a single formula capable of predicting the time and rate of cooling with a fairly good accuracy for a wide variety of thicknesses of steel, ranges of temperature, and welding conditions. An attempt has been made also to show how this theory could be applied to other problems of metal treatment, such as rate of extrusion in continuous casting, or control of flame-hardening and continuous quenching operations.

Introduction

THE theory of heat flow due to a moving source so far has retained little attention in the general treatment of heat flow in metals. Yet the moving source of heat plays an important part in many metallurgical processes, notably in welding. In this latter case the theory of heat flow due to a moving source has been instrumental in establishing a scientific criterion of weldability (1).[2] Similar applications of the theory are feasible in other metallurgical processes, for example, in surface-hardening or continuous casting; but the somewhat involved mathematical analysis makes it rather hard for the industrial engineer to grasp the practical implications of the theory. The purpose of this paper is to overcome this shortcoming by putting more emphasis on applications. The first part deals briefly with the mathematical aspect of the theory; the second part describes the experimental work which has been carried out in connection with the applications to welding; and the third part outlines some of the feasible applications in other metallurgical branches.

Previous Work

Apparently the theory of heat flow due to a moving source originated in connection with arc welding. Many attempts, both experimental and theoretical, had been made to describe the temperature situation created by the arc welding. Most of these early attempts have been reviewed previously (2). Because of their approximate nature, there is little point in discussing them in the present paper.

The exact theory of heat flow due to a moving point source was first applied to arc welding by the author (3) in 1935, using the experimentally established principle of a "quasi-stationary" state (4). A particular case of the general solution was treated independently by Boulton and Lance Martin (5) in 1936. More recently, Bruce (6) applied the method of instantaneous sources to another particular case of welding and, in 1941, Mahla (7) extended this method to a three-dimensional case. The solution derived by Mahla does not differ materially from that obtained previously on the assumption of the quasi-stationary state, but the method is applicable also to nonquasi-stationary states, as shown in a later section. Unfortunately, in most cases the solution becomes too unwieldy for a direct practical application.

1 Theory of Heat Flow due to a Moving Source

The Differential Equation of the Quasi-Stationary State

Nomenclature. The following nomenclature will be used throughout the paper:

q = rate of heat, for ex., cal/sec
q' = rate of heat per unit length
q'' = rate of heat per unit section
v = speed of source
T = temperature
t = time
k = heat conductivity of metal. When expressed in C.G.S. units the dimensions of k are cal/sec cm deg C
$1/2\lambda$ = thermal diffusivity of the metal.[3] The dimensions of diffusivity are $\frac{\text{sq cm}}{\text{sec}}$ in C.G.S. units. On the other hand, if c is specific heat and ρ density, $2\lambda = \frac{c\rho}{k}$

Assumptions. Assumptions will be made as follows:

(*a*) The physical characteristics of the metal, i.e., k and λ are independent of the temperature.

(*b*) The speed v and the rate of heat input q are constant.

The Quasi-Stationary State. The differential equation of heat flow expressed in rectangular co-ordinates (x, y, z) which are referred to a fixed origin in the solid, has the well-known form

$$\frac{\partial^2 T}{\partial x^2} + \frac{\partial^2 T}{\partial y^2} + \frac{\partial^2 T}{\partial z^2} = 2\lambda \frac{\partial T}{\partial t} \quad \ldots\ldots\ldots\ldots [1]$$

Assume now that the heat is supplied by a point source of strength q moving with a constant speed v along the x-axis, and determine the temperature distribution around the heat source. This amounts to writing the differential Equation [1] with the point source as origin. To this end, replace in Equation [1] x by $\xi = x\text{-}vt$, where ξ is the distance of the point considered from the point source, and differentiate with respect to ξ. There follows

$$\frac{\partial^2 T}{\partial \xi^2} + \frac{\partial^2 T}{\partial y^2} + \frac{\partial^2 T}{\partial z^2} = -2\lambda v \frac{\partial T}{\partial \xi} + 2\lambda \frac{\partial T}{\partial t} \quad \ldots\ldots\ldots [2]$$

Experiment shows (4) that if the solid is long enough as com-

---

[1] Massachusetts Institute of Technology.

[2] Numbers in parentheses refer to the Bibliography at the end of the paper.

Contributed by the Heat Transfer Division and presented at the Semi-Annual Meeting, Detroit, Mich., June 17-20, 1946, of The American Society of Mechanical Engineers.

Note: Statements and opinions advanced in papers are to be understood as individual expressions of their authors and not those of the Society.

[3] The notation by means of a converse symbol multiplied by 2 is used here for the sake of convenience as will appear later.

pared to the extent of heat, the temperature distribution around the heat source soon becomes constant. In other words, an observer stationed at the point source fails to notice any change in the temperature around him as the source moves on. This state of heat flow is called quasi-stationary, and is defined by Equation [2] in which $\frac{\partial T}{\partial t} = 0$, i.e.

$$\frac{\partial^2 T}{\partial \xi^2} + \frac{\partial^2 T}{\partial y^2} + \frac{\partial^2 T}{\partial z^2} = -2\lambda v \frac{\partial T}{\partial \xi} \quad \ldots\ldots [3]$$

Equation [3] can be simplified by putting

$$T = T_0 + e^{-\lambda v \xi} \varphi(\xi, y, z) \quad \ldots\ldots [4]$$

where T_0 is the initial temperature of the solid and φ is a function to be determined. After substitution of Equation [4] in [3] and reduction of terms, the following equation is obtained

$$\frac{\partial^2 \varphi}{\partial \xi^2} + \frac{\partial^2 \varphi}{\partial y^2} + \frac{\partial^2 \varphi}{\partial z^2} - (\lambda v)^2 \varphi = 0 \quad \ldots\ldots [5]$$

or in the usual symbolic form

$$\nabla^2 \varphi - (\lambda v)^2 \varphi = 0 \quad \ldots\ldots [6]$$

Thus Equation [1] is reduced to a relatively simple form, which provides ready solutions for an infinite and semi-infinite solid, as will be shown presently.

Infinite and Semi-Infinite Solid

Linear Flow of Heat. In this case $\frac{\partial T}{\partial y} = \frac{\partial T}{\partial z} = 0$, and Equation [5] is reduced to

$$\frac{d^2 \varphi}{d\xi^2} - (\lambda v)^2 \varphi = 0 \quad \ldots\ldots [7]$$

The boundary conditions are

$$\frac{dT}{d\xi} \to 0 \quad \text{for} \quad \xi \to \pm\infty \quad \ldots\ldots [8]$$

Furthermore, considering a plane source with a rate of heat q'' per unit area

$$-\frac{dT}{d\xi} \times k \to q'' \quad \text{as} \quad \xi \to 0 \quad \ldots\ldots [9]$$

A general solution of Equation [7] can be written as follows

$$\varphi = C_1 e^{-\lambda v \xi} + C_2 e^{\lambda v \xi} \quad \ldots\ldots [10]$$

hence

$$T - T_0 = C_1 e^{-2\lambda v \xi} + C_2 \quad \ldots\ldots [11]$$

With reference to Equations [8] and [9] it is easy to see that $C_1 = 0$ when $\xi < 0$, hence for $\xi < 0$

$$T - T_0 = C_2 \quad \ldots\ldots [12]$$

Likewise $C_2 = 0$, when[4] $\xi > 0$, hence for $\xi > 0$

$$T - T_0 = C_1 e^{-2\lambda v \xi} \quad \ldots\ldots [13]$$

Also, since $T - T_0$ must have the same value for $\xi = 0$

$$C_1 = C_2$$

On the other hand, with reference to Equation [9]

$$C_1 2\lambda v k = q''$$

or, since

$$2\lambda k = c\rho$$

$$C_1 = C_2 = q''/c\rho v \quad \ldots\ldots [14]$$

hence for $\xi < 0$

$$T - T_0 = \frac{q''}{c\rho v} \quad \ldots\ldots [15]$$

and for $\xi > 0$

$$T - T_0 = \frac{q''}{c\rho v} e^{-2\lambda v \xi} \quad \ldots\ldots [16]$$

From Equation [16] it follows that $q''/c\rho v$ is the rise of temperature at the location of the source, i.e., for $\xi = 0$, and corresponds to the maximum value of temperature reached in the solid. Equation [15] shows that once this temperature has been reached, it remains even after the source has moved further. This, of course, is the result of lack of surface losses. Calling T_1 the maximum temperature in the solid, Equations [15] and [16] become finally
for $\xi < 0$

$$T = T_1 \quad \ldots\ldots [17]$$

for $\xi > 0$

$$T = T_0 + (T_1 - T_0) e^{-2\lambda v \xi} \quad \ldots\ldots [18]$$

Heat Dissipation; Infinite Rod. If temperature gradients in the cross section of the rod are neglected, Equations [17] and [18] can be made to include heat losses through the surface. Assuming Newton's law of radiation, the rate of heat losses through unit surface area is given by the following formula

$$h(T - T_0) \quad \ldots\ldots [19]$$

Here T is the temperature of the surface and T_0 is the temperature of the surrounding medium which we shall assume to be the same as the initial temperature of the rod; h is the heat dissipation. In problems of heat flow in metals it is customary (8) to use the ratio of heat dissipation to heat conductivity

$$H = \frac{h}{k} \quad \ldots\ldots [20]$$

H will be called the dissipation ratio.

With this in mind, the differential equation of linear heat flow with surface losses has the following form (9)

$$\frac{\partial^2 T}{\partial x^2} = 2\lambda \frac{\partial T}{\partial t} + \frac{PH}{A}(T - T_0) \quad \ldots\ldots [21]$$

Here P is the perimeter and A the area of the cross section of the rod. For the case of the quasi-stationary state this equation can be reduced, as easily seen from Equation [6], to

$$\frac{d^2 \varphi}{d\xi^2} - \left[(\lambda v)^2 + \frac{PH}{A}\right] \varphi = 0 \quad \ldots\ldots [22]$$

and the solution corresponding to Equations [17] and [18] can be rewritten to read
for $\xi < 0$

$$T = T_0 + (T - T_0) e^{(\sqrt{(\lambda v)^2 + PH/A} - \lambda v)\xi} \quad \ldots\ldots [23]$$

and for $\xi > 0$

$$T = T_0 + (T - T_0) e^{-(\sqrt{(\lambda v)^2 + PH/A} + \lambda v)\xi} \quad \ldots\ldots [24]$$

The rate of heat per unit area delivered to the rod is correspondingly
for $\xi < 0$

[4] This because $T = T_0$ for $\xi = \infty$.

$$q_1'' = k(T_1 - T_0)[\sqrt{(\lambda v)^2 + PH/A} - \lambda v] \quad [25]$$

for $\xi > 0$

$$q_2'' = k(T_1 - T_0)[\sqrt{(\lambda v)^2 + PH/A} + \lambda v] \quad [26]$$

Various applications of the foregoing equations will be found in Parts 2 and 3 of this paper.

Two-Dimensional Flow of Heat. In this case the heat flows in two directions, one of which is the x- or ξ-direction. The other direction will be taken along the y-axis, and there will be no flow in the z-direction. Thus $\partial T/\partial z = 0$, and Equation [5] becomes

$$\frac{\partial^2\varphi}{\partial\xi^2} + \frac{\partial^2\varphi}{\partial y^2} = (\lambda v)^2\varphi \quad [27]$$

The boundary conditions are

$$\left.\begin{aligned} \partial T/\partial\xi &\to 0 \quad \text{as } \xi \to \pm\infty \\ \partial T/\partial y &\to 0 \quad \text{as } y \to \pm\infty \end{aligned}\right\} \quad [28]$$

and, by considering a circle $2\pi r$ drawn around the heat source with $r = \sqrt{\xi^2 + y^2}$

$$-\frac{\partial T}{\partial r} 2\pi r k \to q' \quad \text{for } r \to 0 \quad [29]$$

where q' is the rate of heat of a linear source.

Because of the nature of the boundary conditions and the symmetrical form of Equation [27] with respect to ξ and y, φ depends only upon the distance r from the heat source, hence Equation [27] becomes in cylindrical co-ordinates[5]

$$\frac{d^2\varphi}{dr^2} + \frac{1}{r}\frac{d\varphi}{dr} - (\lambda v)^2\varphi = 0 \quad [30]$$

The solution of Equation [30] satisfying the boundary Condition [29] is known; it is the so-called modified Bessel function of the second kind and zero order, and is represented by the symbol $K_0(\lambda v r)$ (10).

It can be shown that this function tends to $\ln r$ as r tends to zero, hence $\frac{dK_0}{dr} \times r$ tends to a constant value. Thus $K_0(\lambda v r)$ fulfills the Condition [29]. On the other hand, this function tends to $\sqrt{\frac{\pi}{2\lambda v r}}\, e^{-\lambda v r}$ as r tends to infinity, whereby the boundary Condition [28] also is satisfied. The solution of the two-dimensional case therefore is

$$T - T_0 = \frac{q'}{2\pi k} e^{-\lambda v\xi} K_0(\lambda v r) \quad [31]$$

This solution will be discussed in Part 2 in connection with the welding of thin plates.

Thin Plates; Surface Losses. If the thickness g of the plate is small enough to neglect the temperature gradient in the z-direction, Equation [31] can be made to include heat losses through the surface. Calling H and H' the dissipation ratios at top and bottom face of the plate, respectively, and noting that PH/A appearing in Equation [22] becomes simply $\frac{H + H'}{g}$, there follows

$$\frac{d^2\varphi}{dr^2} + \frac{1}{r}\frac{d\varphi}{dr} - \left[(\lambda v)^2 + \frac{H + H'}{g}\right]\varphi = 0 \quad [32]$$

hence the solution

$$T - T_0 = \frac{q}{2\pi k g} e^{-\lambda v\xi} K_0\left[\sqrt{\lambda v^2 + \frac{H + H'}{g}}\, r\right] \quad [33]$$

where q/g, which appears instead of q', is the rate of heat per unit thickness, and q is the total rate of heat of the linear source.

Linear Source of Variable Strength; No Surface Losses. In previous discussion it has been assumed that the rate of heat q' per unit thickness was a constant. If this rate varies along the thickness, an appropriate solution similar to Equation [31] can be obtained by means of cosine series. To this end develop function $q'(z)$ in Fourier series, between $z = 0$ and $z = g$. Suppose this function reads as follows

$$q'(z) = q'(0)\sum_0^n A_n \cos\frac{\pi n z}{g} \quad [34]$$

Since $q'(z)$ is a cosine function of z, the same must be true for φ by virtue of Condition [29]. Thus the differential Equation [30] must be completed by adding the second derivative with respect to z, to read as follows

$$\frac{\partial^2\varphi}{\partial z^2} + \frac{\partial^2\varphi}{\partial r^2} + \frac{1}{r}\frac{\partial\varphi}{\partial r} - (\lambda v)^2\varphi = 0 \quad [35]$$

It is easy to see that this equation is satisfied by a function of the form

$$\cos\frac{\pi n z}{g} K_0\left(\sqrt{\lambda v^2 + \left(\frac{\pi n}{g}\right)^2}\, r\right) \quad [36]$$

Hence with reference to Equation [34]

$$T - T_0 = \frac{q_0'}{2\pi k} e^{-\lambda v\xi} \sum_0^n A_n \cos\frac{\pi n z}{g} K_0\left(\sqrt{\lambda v^2 + \left(\frac{\pi n}{g}\right)^2}\, r\right) \quad [37]$$

Solution [37] has been applied to the problem of flame-cutting, and the reader is referred to a previous publication for further developments (11).

Three-Dimensional Flow. In this case the boundary conditions are

$$\left.\begin{aligned} \partial T/\partial\xi &\to 0 \quad \text{for } \xi \to \pm\infty \\ \partial T/\partial y &\to 0 \quad \text{for } y \to \pm\infty \\ \partial T/\partial z &\to 0 \quad \text{for } z \to \pm\infty \end{aligned}\right\} \quad [38]$$

and by considering a spherical surface $4\pi R^2$ drawn around the heat source with radius $R = \sqrt{\xi^2 + y^2 + z^2}$

$$-\frac{\partial T}{\partial R} 4\pi R^2 k \to q \quad \text{for } R \to 0 \quad [39]$$

where q is the rate of heat of a point source.

Because of Conditions [38] and [39], and the symmetrical form of the differential Equation [5], φ depends only upon the distance R, hence using polar co-ordinates Equation [5] can be rewritten as follows[5]

$$\frac{d^2\varphi}{dR^2} + \frac{2}{R}\frac{d\varphi}{dR} - (\lambda v)^2\varphi = 0 \quad [40]$$

It is easy to see that

$$\frac{d^2\varphi}{dR^2} + \frac{2}{R}\frac{d\varphi}{dR} = \frac{1}{R}\frac{d^2(R\varphi)}{dR^2}$$

hence Equation [40] becomes

$$\frac{d^2(R\varphi)}{dR^2} - (\lambda v)^2 R\varphi = 0 \quad [41]$$

[5] Refer to (9), p. 12.

A solution of Equation [41] satisfying the boundary Conditions [38] obviously is

$$R\varphi = Ce^{-\lambda v R} \quad [42]$$

or

$$\varphi = \frac{Ce^{-\lambda v R}}{R}$$

This solution also satisfies Conditions [39] since $\frac{d\varphi}{dR} \times R^2$ tends to a constant value as $R \to 0$. Hence the corresponding temperature distribution

$$T - T_0 = \frac{q}{4\pi k} e^{-\lambda v \xi} \frac{e^{-\lambda v R}}{R} \quad [43]$$

This solution will be discussed in detail in connection with welding in Part 2.

Solid Bounded by Planes

The Method of Images. If the quasi-stationary state is to be preserved, the solid cannot be bounded by planes perpendicular to the direction of motion. However, the state can still remain quasi-stationary if the bounded planes are parallel to the direction of motion. This circumstance leaves out the linear flow, but retains the two- and three-dimensional flows. Assuming there is no heat loss through the bounding planes, the method of images can be used conveniently to obtain the required solutions.[6] It will be recalled that in this method fictitious sources are associated with the real source of heat in such a way that the bounding planes become planes of symmetry. Such an arrangement fulfills the condition of no radiation, and it is accomplished by locating the fictitious sources at the mirror reflections of the real source, the bounding planes acting as the corresponding plane mirrors.

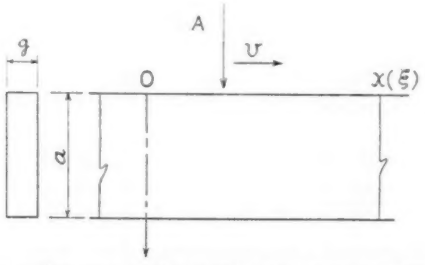


Fig. 1 Solid Bounded by Planes Paralleled to Direction of Motion

Two-Dimensional Flow. With reference to Fig. 1, the problem consists of determining the temperature distribution in a plate of width a and thickness g, heated by a linear source traveling along one of its edges. In accordance with the method of images just explained, imagine the plate extended to the size of a semi-infinite plate. Then the temperature due to the source q distributed over the thickness g would read, with reference to Equation [31]

$$T - T_0 = \frac{q}{\pi k g} e^{-\lambda v \xi} K_0(\lambda v r)$$

To this value now add the contributions of the mirror reflections of the source with respect to mirrors placed at $y = 0$ and $y = a$. These contributions are of the form

$$\frac{q}{\pi k g} e^{-\lambda v \xi} K_0(\lambda v r_n) \quad [44]$$

where

$$r_n = \sqrt{\xi^2 + (y \pm 2na)^2}$$

Hence the solution becomes

$$T - T_0 = \frac{q}{\pi k g} e^{-\lambda v \xi} \sum_{n=-\infty}^{n=+\infty} K_0(\lambda v r_n) \quad [45]$$

From the way this solution has been built it is obvious that

$$\frac{\partial T}{\partial y} = 0 \quad [46]$$

for $y = a$ and $y = 0$, which fulfills the boundary conditions along the two edges. Condition [29] also is fulfilled, for of all the terms $K_0(\lambda v r_n)$ which compose the solution, Equation [45], only the term $K_0(\lambda v r)$ contributes to the value of $q' = q/g$, the derivatives of the other vanishing as r when being multiplied by $2\pi r$. It remains to prove that

$$\frac{\partial T}{\partial \xi} \to 0 \quad \text{as} \quad \xi \to \pm\infty \quad [47]$$

This can be done best by transforming Equation [45] into a Fourier series. By proceeding as explained in Appendix 2, the following expression is obtained

For $\xi > 0$

$$T - T_0 = \frac{q}{c\rho a g v}\left[e^{-2\lambda v \xi} + \sum_1^\infty \frac{2}{\mu_n} e^{-(\mu_n + 1)\lambda v \xi} \cos\frac{\pi n y}{a}\right] \quad [48]$$

and for $\xi < 0$

$$T - T_0 = \frac{q}{c\rho a g v}\left[1 + \sum_1^\infty \frac{2}{\mu_n} e^{(\mu_n - 1)\lambda v \xi} \cos\frac{\pi n y}{a}\right] \quad [49]$$

where

$$\mu_n = \sqrt{1 + \left(\frac{\pi n}{\lambda v a}\right)^2} \quad [50]$$

and $c\rho$ is the volume specific heat.

By differentiating Equations [48] and [49] with respect to ξ, it is seen that the derived expression tends to zero for ξ tending to both + and — infinity as required by Conditions [47].

The characteristic feature of solution, Equation [49], is that it tends to a constant temperature, which is different from the initial temperature T_0, after the source has moved away from the section considered. Calling T_2 the new temperature, there follows from Equation [49] that, if $\xi \to -\infty$

$$T_2 - T_0 = \frac{q}{c\rho a g v} \quad [51]$$

The meaning of Equation [51] is very simple. It represents a uniform rise of temperature produced by the heat q in a volume of plate covered in unit time and can be explained as follows: Because of the quasi-stationary state the temperature situation around the heat source remains unchanged, and since there are no surface losses the amount of heat delivered in unit time must be employed to raise the temperature of an additional volume of plate $= agv$ far behind the source.

Putting Equation [51] in Equations [48] and [49], there follows

For $\xi > 0$

$$T - T_0 = (T_2 - T_0)\left[e^{-2\lambda v \xi} + \sum_1^\infty \frac{2}{\mu_n} e^{-(\mu_n + 1)\lambda v \xi} \cos\frac{\pi n y}{a}\right] \quad [52]$$

[6] Reference (9) p. 158.

and for $\xi < 0$

$$T - T_0 = (T_2 - T_0)\left[1 + \sum_1^\infty \frac{2}{\mu_n} e^{(\mu_n - 1)\lambda v \xi} \cos \frac{\pi n y}{a}\right] \quad [53]$$

By comparing Equations [52] and [53] with Equations [17] and [18], it is seen that the two-dimensional flow in a solid of a limited cross section tends to become linear at some distance from the source, and from Equation [50] it is apparent that this distance is so much shorter as the value of $\lambda v a$ is smaller; for example, as the plate is narrower. This trend is represented in Fig. 2 by

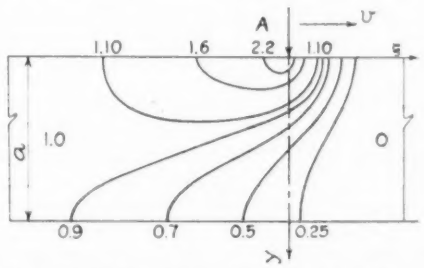


FIG. 2 TEMPERATURE DISTRIBUTION IN THIN AND NARROW PLATE DUE TO HEAT SOURCE MOVING ALONG ONE OF ITS EDGES
(Initial temperature taken as zero and final temperature as 1.)

means of isotherms, which for convenience have been marked in terms of the relative temperature $U = (T - T_0)/(T_2 - T_0)$. The value of $\lambda v a$ has been taken arbitrarily as 2. It is seen that in the upper half of the plate the relative temperature rises from a value = 0 in front of the source to a maximum which is greater than 1 in the vicinity of the source and then drops progressively down to 1 behind the source. The maximum temperature is so much more in excess of 1 as the layer under consideration is closer to the edge passed by the heat source. On the other hand, layers of metals which are close to the opposite edge never exceed 1. They approach this value asymptotically as the flow becomes more linear. This last situation is virtually reached in Fig. 2 at a distance which is smaller than twice the width of the plate.

For many practical applications, especially flame-hardening and quenching, solutions, Equations [52] and [53], have the disadvantage of becoming infinite at the location of the source. This, of course, is a direct consequence of the assumption that the heat source is reduced to a line. A more practical solution may be obtained by removing this restriction as will be shown later.

Two-Dimensional Flow; Plane Source. The inconvenience of having an infinite value of temperature at the location of the source disappears if the latter instead of being a single line is spread over a certain area, i.e., if it becomes a plane source. To demonstrate this proposition, suppose a source with a rate of heat = q'' per unit area covers the edge of the plate, Fig. 1, from point $\xi' = 0$ to point $\xi' = l$. This source can be represented as being composed of an infinite number of infinitely small linear sources $q'' d\xi$ set side by side from $\xi' = 0$ to $\xi' = l$. If q'' is constant, then $q'' = \frac{q}{gl}$ where q is the rate of heat of the plane source, hence $q'' d\xi' = \frac{q d\xi'}{lg}$. On the other hand, according to Equations [48] and [49], a linear source of strength $\frac{q d\xi'}{lg}$ placed at a distance ξ' from the origin contributes to the temperature of a point ξ, y in amount of

$$\frac{q d\xi'}{c\rho a g v l}\left[e^{-2\lambda v(\xi - \xi')} + \sum \frac{2}{\mu_n} e^{-(\mu_n + 1)\lambda v(\xi - \xi)'} \cos \frac{\pi n y}{a}\right] \quad [54]$$

for $\xi > \xi'$, and in amount of

$$\frac{q d\xi'}{c\rho a g v l}\left[1 + \sum \frac{2}{\mu_n} e^{(\mu_n - 1)\lambda v(\xi - \xi')} \cos \frac{\pi n y}{a}\right] \quad [55]$$

for $\xi < \xi'$. Three cases may be distinguished, according to whether the point ξ, y is located outside or inside the portion of plate covered by the plane source.

Case 1. If $\xi > l$, Equation [54] applies to all elementary sources from $\xi' = 0$ to $\xi' = l$, and by integrating Equation [54] from $\xi' = 0$ to $\xi' = l$, there follows

$$T - T_0 = \frac{q}{c\rho a g v}\left[\frac{(e^{-2\lambda v l} - 1)}{\lambda v l} e^{-2\lambda v \xi} + \sum \frac{2}{\mu_n(\mu_n + 1)} \frac{(e^{\lambda v l(\mu_n + 1)} - 1)}{\lambda v l} \times e^{-(\mu_n + 1)\lambda v \xi} \cos \frac{\pi n y}{a}\right] \quad [56]$$

Case 2. If $\xi < 0$, it is Equation [55] which applies to all elementary sources; hence by integrating Equation [55] from $\xi' = 0$ to $\xi' = l$, there follows

$$T - T_0 = \frac{q}{c\rho a g v}\left[1 + \sum \frac{2}{\mu_n(\mu_n - 1)} \times \frac{1 - e^{-\lambda v l(\mu_n - 1)}}{\lambda v l} \times e^{(\mu_n - 1)\lambda v \xi} \cos \frac{\pi n y}{a}\right] \quad [57]$$

Case 3. Finally, if $l > \xi > 0$, Equation [54] applies to all elementary sources for which $0 < \xi' < \xi$, and Equation [55] applies to all sources for which $\xi < \xi' < l$. By integrating each of these expressions within the limits of its applicability, we have

$$T - T_0 = \frac{q}{c\rho a g v}\left[\frac{1 - e^{-2\lambda v \xi}}{\lambda v l} + \left(1 - \frac{\xi}{l}\right) + \sum \frac{2}{\mu_n(\mu_n + 1)} \frac{1 - e^{-(\mu_n + 1)\lambda v \xi}}{\lambda v l} \cos \frac{\pi n y}{a} + \sum \frac{2}{\mu_n(\mu_n - 1)} \frac{1 - e^{-(\mu_n - 1)\lambda v(l - \xi)}}{\lambda v l} \cos \frac{\pi n y}{a}\right] \quad [58]$$

It is easy to see that the maximum value of temperature occurs at $\xi = 0$, $y = 0$. For this point

$$T_1 - T_0 = \frac{q}{c\rho a g v}\left[1 + \sum \frac{2}{\mu_n(\mu_n - 1)} \frac{1 - e^{-(\mu_n - 1)\lambda v l}}{\lambda v l}\right] \quad [59]$$

On the other hand, it follows from Equations [57] and [51] that for $\xi \to -\infty$, the temperature tends to the same constant value T_2 as in the case of a linear source. Therefore Equation [59] can be rewritten to read

$$T_1 - T_0 = (T_2 - T_0)\left[1 + \sum \frac{2}{\mu_n(\mu_n - 1)} \frac{1 - e^{-(\mu_n - 1)\lambda v l}}{\lambda v l}\right] \quad [60]$$

If the heat instead of being delivered is absorbed by the source, i.e., if the latter is replaced by a sink, then $T_0 > T_2 > T_1$, and Equation [60] becomes

$$T_0 - T_1 = (T_0 - T_2)\left[1 + \sum \frac{2}{\mu_n(\mu_n - 1)} \frac{1 - e^{-(\mu_n - 1)\lambda v l}}{\lambda v l}\right] \quad [61]$$

Both expressions, Equation [60] as well as [61], can find suitable applications in metal treatments, the former in flame-hardening, the latter in continuous quenching, as will be shown later in Part 3.

Remark. By comparing Equation [61] with Equation [53] it is seen that the former is represented by a series of the form

$1/n(n-1)$, while the latter is of the form $1/n$. But the series $1/n(n-1)$ is known to be absolutely convergent, whereas the series $1/n$ is divergent, if all terms are positives, and this is what happens at the location of the source, for which $\xi = 0$ and $y = 0$.

Three-Dimensional Flow. Solid bounded by planes $z = 0$ and $z = g$; no surface losses.

Following the pattern developed in the preceding section, imagine first the solid extended in the z-direction from $z = 0$ to $z = \infty$, covering one half of the space. Then the temperature due to the source of strength q located at $\xi = 0$, $y = 0$, $z = 0$ would read with reference to Equation [43]

$$T - T_0 = \frac{q}{2\pi k} e^{-\lambda v \xi} \frac{e^{-\lambda v R}}{R} \quad [43a]$$

The factor 2 in Equation [43a], as compared to 4 in Equation [43] accounts for one half of the space.

To Equation [43a] add now the contributions of the mirror reflections of the source with respect to planes $z = 0$ and $z = g$. These contributions are of the form

$$\frac{q}{2\pi k} e^{-\lambda v \xi} \frac{e^{-\lambda v R_n}}{R_n} \quad [62]$$

where

$$R_n = \sqrt{\xi^2 + y^2 + (z \pm 2ng)^2}$$

Hence the solution reads

$$T - T_0 = \frac{q}{2\pi k} e^{-\lambda v \xi} \sum_{-\infty}^{\infty} \frac{e^{-\lambda v R_n}}{R_n} \quad [63]$$

From the way this solution has been built it is obvious that

$$\frac{\partial T}{\partial z} = 0 \quad [64]$$

for $z = 0$ and $z = g$, which fulfills the condition of no radiation. Condition [39] also is fulfilled, since the derivative of all terms of Equation [63] tends to zero as R, when being multiplied by R^2, except the derivative of the term $n = 0$, which becomes a constant when being multipled by R^2.

Finally it is easy to see that

$$\left.\begin{aligned} \partial T/\partial \xi &\to 0 \quad \text{as } \xi \to \pm\infty \\ \partial T/\partial y &\to 0 \quad \text{as } y \to \pm\infty \end{aligned}\right\} \quad [65]$$

which fulfills the first two Conditions [38].

By a procedure similar to that explained in Appendix 2, solution of Equation [63] can be transformed into a Fourier series to read

$$T - T_0 = \frac{q}{2\pi k g} e^{-\lambda v \xi} \left\{ K_0(\lambda v r) + 2 \sum_1^{\infty} K_0 \left[r \sqrt{\lambda v^2 + \left(\frac{\pi n}{g}\right)^2} \right] \cos \frac{\pi n z}{g} \right\} \quad [66]$$

The similarity between Equations [66] and [31] is obvious. In fact, both solutions become practically identical for large values of r. This means that the solid behaves more and more like a thin plate as the distance from the heat source increases. Conversely, for values of r which are small as compared to the thickness g, Equation [63] differs little from Equation [43] which has been derived for an infinitely thick plate. This twofold aspect of solution [63] or [66] is well evidenced in the behavior of butt-welded plates, as will be demonstrated in Part 2.

Solid Bounded by a Cylinder

Because of the condition of the quasi-stationary state, the axis of the cylinder must be parallel to the direction of motion, and in most cases of practical interest it will coincide with the path of the moving source. Even so, it does not appear possible to obtain a simple solution of this problem. Recently, R. H. Cameron and the author have worked out a solution which, although far from being simple, is believed to be practically usable. However, because of the somewhat involved mathematical treatment of the solution, the presentation of their work is reserved for a separate publication.

2 APPLICATION TO ARC WELDING

Rate of Fusion of Electrode

In the process of welding, the heat generated by the arc causes the electrode to melt, thus providing the metal necessary for joining the parts to be welded. Assuming the electrode is long enough with respect to its diameter and neglecting the heat generated by the Joule effect, the process of melting for the first few inches of the electrode can be looked upon as being of a quasi-stationary nature, in so far as the temperature distribution around the welding arc is concerned. The rate of melting of the electrode is then the speed with which the arc moves along the electrode, and the temperature T at a point located at a distance ξ from the arc is equal, according to Equation [18], Part 1

$$T = T_0 + (T_1 - T_0) e^{-2\lambda v \xi} \quad [67]$$

Here, T_0 is the initial temperature, T_1 is the temperature at the location of the arc, i.e., the temperature of fusion, 2λ is the converse of thermal diffusivity, and v is the rate of fusion.

Equation [67] assumes that there are no surface losses, in other words, that the electrode is perfectly insulated. This assumption is an approximation but it offsets to a great extent the error introduced by neglecting the Joule effect in the electrode. That this is so is proved by the fact that the relation between the rate of fusion v and current density i, derived from the foregoing assumptions, is in good agreement with the experiment. This relation is obtained as follows:

It has been shown in Part 1 that in the absence of surface losses the rate of heat q'' absorbed in the electrode per unit area is

$$q'' = (T_1 - T_0) c\rho v \quad [68]$$

$c\rho$ is the specific volume heat content (c specific heat, ρ density), and T_1, T_0, and v, as previously, the temperature of fusion, the initial temperature, and the rate of fusion, respectively. On the other hand, q'' is a fraction of the heat generated by the arc, which is proportional to the product VI, where V is the voltage drop across the arc, and I is the current intensity. Experiment shows that for a given type of electrode the voltage drop V is fairly constant within a large range of current densities, and that for various types of coated-steel electrodes it varies between 25 and 35 volts. Thus for a given type of electrode of a diameter d, it is possible to write

$$q'' \frac{\pi d^2}{4} = fI \quad [69]$$

where f is a constant (13).

Substituting in Equation [68], there follows

$$\frac{fI}{\pi d^2/4} = (T_1 - T_0) c\rho v$$

hence

$$v = f_0 i \quad [70]$$

where

$$f_0 = \frac{f}{(T_1 - T_0)c\rho}$$

Relation, Equation [70] has been checked experimentally and has been found to hold within a reasonable degree of accuracy for moderate current densities and for the first 3 to 4 in. of the electrode. The values of f_0 reported in the literature for a mild-steel electrode lie between 1.24×10^{-3} and 1.56×10^{-3} cu in. per amp per min.

Substituting Equation [70] in [67] there follows

$$T = T_0 + (T_1 - T_0)e^{-2\lambda f_0 i\xi}$$

or putting

$$i = I \Big/ \frac{\pi d^2}{4}$$

$$T = T_0 + (T_1 - T_0)e^{-f'I\xi} \quad \ldots\ldots\ldots [71]$$

where

$$f' = \frac{2\lambda f_0}{\pi d^2/4} = \frac{8\lambda f_0}{\pi d^2} \quad \ldots\ldots\ldots\ldots\ldots [72]$$

In Fig. 3 the ratios of $(T - T_0)/(T_1 - T_0)$ have been plotted against the distance ξ from the location of the arc in inches, for four different values of current density, namely, 145, 165, 185, and 240 amp. These values may be considered as being within workable range of current intensities for a $^5/_{32}$-in. mild-steel electrode. The following values were used to calculate the factor f' appearing in Equation [71]

$2\lambda = 1.00$ sq in. per min

$f_0 = 1.25 \times 10^{-3}$ cu in. per amp per min

$d = {}^5/_{32}$ in.

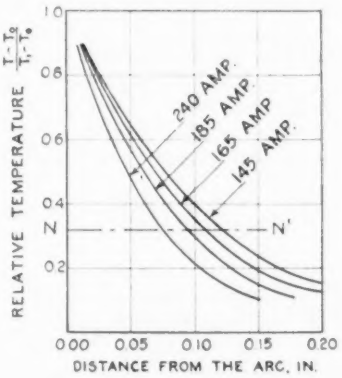


FIG. 3 TEMPERATURE DISTRIBUTION IN MILD-STEEL ELECTRODE FOR VARIOUS CURRENT INTENSITIES

It appears from Fig. 3 that the higher the current intensity the shorter is the range over which the electrode is affected by the heat of the arc. This condition is well illustrated in Fig. 4, which shows macroetched sections made through the axis of a $^5/_{32}$-in. electrode submitted to the current intensities mentioned. Because of the recrystallization process the part of the electrode which has been heated beyond some 950 F responds more readily to the etching (10 per cent solution of nitric acid) than the rest of the electrode. It is seen that in accordance with diagrams, Fig. 3, the extent of the recrystallized zone is greater for the low current intensity than it is for high current intensity, see also

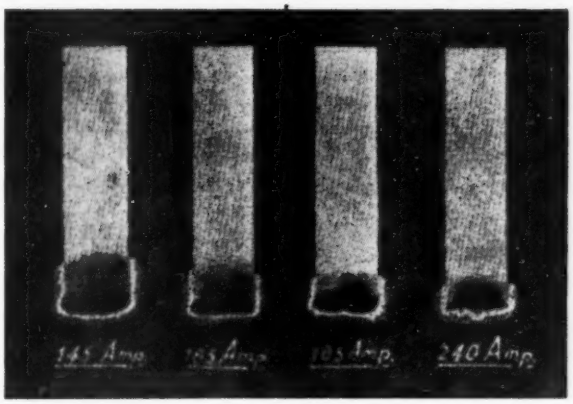


FIG. 4 HEAT-AFFECTED AREAS IN MILD-STEEL ELECTRODE FOR VARIOUS CURRENT INTENSITIES
(Courtesy *The Welding Journal.*)

line NN', Fig. 3, corresponding to the temperature of recrystallization of mild steel $(T_1 - T_0/T_1 - T_0 \approx 0.32)$.

ARC-WELDING OF THIN PLATES

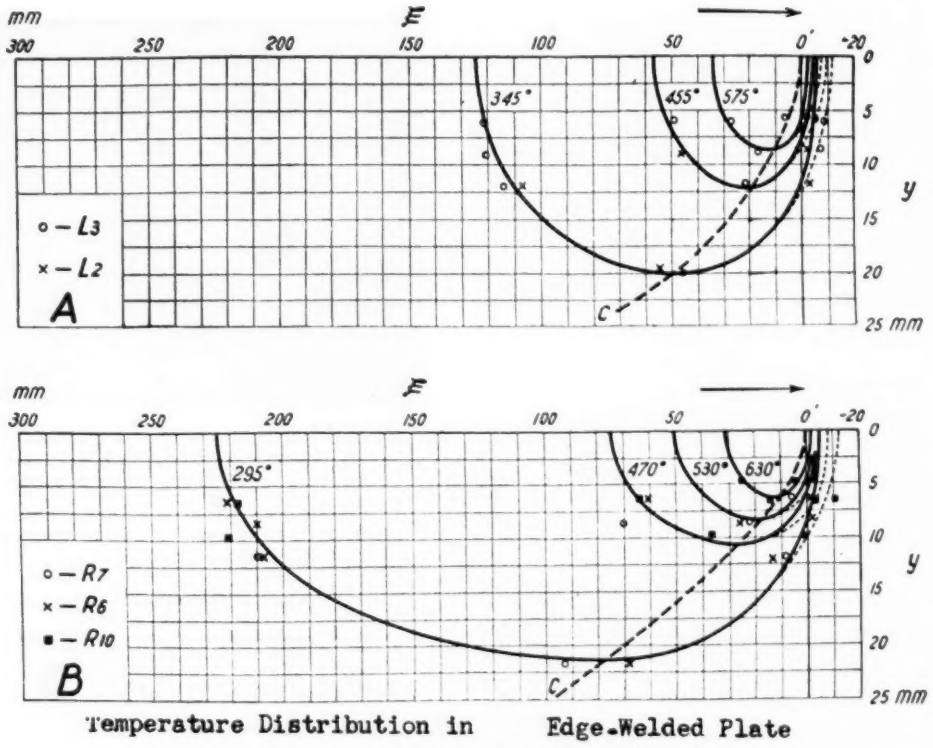
Temperature Distribution in an Edge-Welded Plate. The validity of Equation [31], Part 1, in the case of arc welding was tested experimentally by Schmerber and the author (12). They deposited a weld layer at a constant rate along one of the edges of a flat bar, 5.5 in. wide, and measured the variation of temperature in the bar produced by this operation. Assuming no losses of heat through the surface, the temperature can be taken as being uniform through the thickness. Hence the heat flow is of a two-dimensional nature, and Equation [31], Part 1, is applicable. For the purpose of computation, a constant value of heat conductivity k was adopted = 0.1 cal per deg C per cm per sec, but the diffusivity coefficient $1/2\lambda$ was made to vary according to a linear law with the temperature. Under these circumstances, the agreement between the measurement and computation was quite satisfactory, except at the immediate neighborhood of the arc, Fig. 5. There, the computed isotherms were closer to the origin than the measured values. This discrepancy could be explained by the fact that the theory considered the source of heat as a line, whereas in practice the source of heat had a finite size.

Rate of Cooling in Thin Butt-Welded Plates. On the basis of the foregoing experiment it can be expected that Equation [31] will be applicable also to the case of thin butt-welded plates. Hess and his co-workers (14) determined experimentally the rates of cooling produced very near to the weld in plates of various thicknesses. If the temperature is assumed constant through the thickness, these rates of cooling can also be derived from Equation [31] by differentiating the latter with respect to time. In so doing, attention is called to the fact that in the present application the rates of cooling are measured at some distance from the location of the heat source. Hence, according to the theory of Bessel functions (10), Equation [31] can be reduced to a more simple expression to read

$$T - T_0 = \frac{q}{2\pi kg}\sqrt{\frac{\pi}{2\lambda vr}}\, e^{-\lambda v\xi - \lambda vr}$$

$$= \frac{q}{2\pi kg}\,\frac{e^{-\lambda v(\xi + r)}}{\sqrt{vr}}\,\sqrt{\frac{\pi}{2\lambda}} \quad \ldots\ldots\ldots [73]$$

where T is the temperature measured at a distance $r = \sqrt{\xi^2 + y^2}$ from the source, T_0 the initial temperature, q the rate of heat input, v the speed of the source, and k, $c\rho$, and $1/2\lambda = k/c\rho$ as



Temperature Distribution in Edge-Welded Plate

FIG. 5 TEMPERATURE DISTRIBUTION IN EDGE-WELDED PLATE

(Continuous lines, calculated; broken lines, experimental. *A*, Current, 93 amp; welding speed, 0.21 cm per sec or 4.95 ipm. *B*, Current, 141 amp; welding speed, 0.43 cm per sec or 10.1 ipm. L2, L3, R7, R6, R10 are different specimens. Courtesy *The Welding Journal*.)

previously, the heat conductivity, volume specific heat, and heat diffusivity, respectively.

Along the weld, $y = 0$, hence $r = /\xi/$; also $\xi = -vt$, hence Equation [73] can be further simplified as follows

$$T - T_0 = \frac{1}{2\sqrt{\pi kc\rho}} \times \frac{q}{gv} \times \frac{1}{\sqrt{t}} \quad \ldots\ldots [74]$$

Expression q/gv represents, as it is easy to see, the amount of heat per unit section of plate, measured in the direction of welding. In practice, the welding conditions are defined by another value more readily determined, namely, the total amount of energy J/gv per unit section of plate supplied by the arc, expressed in joules per sq in. This value is related to the former by a coefficient which defines the heat efficiency of the arc, and which Hess and co-workers represented by the symbol (I.F.) input factor. Thus

$$T - T_0 = \frac{(\text{I.F.})}{2\sqrt{kc\rho\pi}} \times \frac{J}{gv} \times \frac{1}{\sqrt{t}} \quad \ldots\ldots [75]$$

or

$$(T - T_0)\sqrt{t} = C \text{ (independent of time)} \quad \ldots\ldots [76]$$

By differentiating with respect to time there follows

$$\frac{dT}{dt}\sqrt{t} + \frac{1}{2}\frac{T - T_0}{\sqrt{t}} = 0$$

or

$$\frac{dT}{dt} = -\frac{1}{2}\frac{T - T_0}{t} \quad \ldots\ldots [77]$$

Equation [77], due to Hess and co-workers (14), states that the rate of cooling at a given temperature T is proportional not only to this temperature but also to the converse of time t that it has taken for the point considered to cool down to the temperature T after the welding arc has passed through this point. In this respect the rate of cooling in welding is quite different from the rate of cooling in quenching, for which no dependence on time is assumed (15). As will appear later, the factor 1/2 at the right-hand side of Equation [77] is characteristic for the two-dimensional problem of welding.

If time t is eliminated from Equations [77] and [75], the following expression is obtained

$$\frac{dT}{dt} = -\frac{2\pi kc\rho}{(\text{I.F.})^2} \times \left(\frac{gv}{J}\right)^2 \times (T - T_0)^3 \quad \ldots\ldots [78]$$

or

$$\left(\frac{dT}{dt}\right)^{1/3} \times \frac{J}{vg} = \frac{\sqrt[3]{2\pi kc\rho}}{(\text{I.F.})} \times (T - T_0)^{2/3} \quad \ldots\ldots [79]$$

Since the right-hand side of Equation [79] is a constant for a given type of steel, electrode, and temperature T, the product on the left-hand side also must be constant, no matter what are the individual values of rates of cooling, energy inputs, and thickness. This condition has been tested for the case of 1/4-in. and 1/2-in. butt-welded plates using experimental results of Hess and co-workers (14), obtained very near to the weld.[7] When the products figuring on the left-hand side of Equation [79] are plotted as a function of rates of cooling at 1300 F, the diagram, Fig. 6, is obtained. From this diagram it appears that the 1/4-in. butt-welded plate behaves like a thin plate for all rates of cooling at 1300 F, while the 1/2-in. plate behaves like a thin plate only for rates of

[7] It can be shown that the rate of cooling very near to the weld is not appreciably different from that in the weld itself.

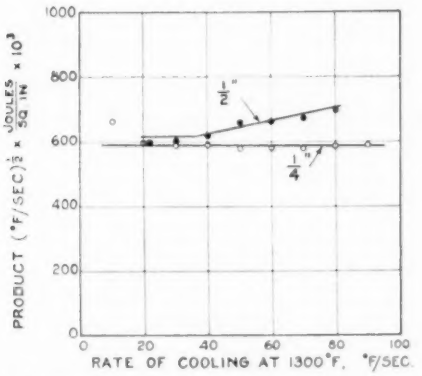


FIG. 6 TWO-DIMENSIONAL HEAT FLOW IN ¼- AND ½-IN. BUTT-WELDED PLATES AS EVIDENCED BY CONSTANT VALUE OF PRODUCT INDICATED

cooling at 1300 F which are smaller than 50 deg F per sec. The reason for this discrepancy will be discussed later.

ARC WELDING OF THICK PLATES

Rate of Cooling in Butt-Welded Plates. Following the ideas developed in the section on the arc welding of thin plates, it may be anticipated that since Equation [31] has approximated fairly well the conditions of heat flow in butt-welded plates, Equation [43] may approximate likewise the conditions of heat flow in thick butt-welded plates. If the observation is limited to the surface of the weld, the distance R, figuring in Equation [43], is simply the distance $/\xi/$ covered by the arc in a given period of time t; thus

$$T - T_0 = \frac{q}{2\pi k} \times \frac{1}{\xi} \quad \ldots\ldots [80]$$

Equation [80] does not contain explicitly the speed v, and it does not depend upon the diffusivity of the material. In fact the same expression is obtained, if the point source instead of being in motion remains stationary, except that in this case ξ represents not only the distance behind the source, but the distance from the source measured in any direction.[8] On the other hand, if ξ is expressed in terms of the distance covered by the arc in time t, then $\xi = vt$, and Equation [80] becomes

$$T - T_0 = \frac{1}{2\pi k} \times \frac{q}{v} \times \frac{1}{t} \quad \ldots\ldots [81]$$

The quantity (q/v) represents the heat input per unit length and is to be compared with a similar quantity (q/vg) used in the study of thin plates. As in the latter case, we shall write

$$q/v = (\text{I.F.})J/v \quad \ldots\ldots [82]$$

where J/v represents the total energy input of the arc per unit length and (I.F.) the heat efficiency of the arc. With reference to Equation [82], Equation [81] may be rewritten as follows

$$(T - T_0) \times t = C \text{ (independent of time)} \quad \ldots\ldots [83]$$

Hence by differentiating

$$\frac{dT}{dt} = -\frac{T - T_0}{t} \quad \ldots\ldots [84]$$

This expression, also due to Hess and co-workers (14), differs from Equation [77], derived previously for the rate of cooling in a thin plate, only by the absence of the factor 1/2. Thus if conditions of welding are such that the same temperature T is reached at the same time t in both the thin and thick plates, the rate of cooling still will be twice as great in the thick plate as in the thin one.

If time t is eliminated from Equations [84] and [81], then with reference to Equation [82] the following formula is obtained

$$\frac{dT}{dt} = -\frac{2\pi k}{(\text{I.F.})} \times \frac{v}{J} \times (T - T_0)^2 \quad \ldots\ldots [85]$$

or

$$\frac{dT}{dt} \times \frac{J}{v} = -\frac{2\pi k}{(\text{I.F.})} \times (T - T_0)^2 \quad \ldots\ldots [86]$$

The right-hand side of Equation [86] is a constant for a given temperature and a given material, hence the product on the left-hand side also must be constant for any particular value of rate of cooling, energy input, and speed.

Although, strictly speaking, this condition holds only for the points of weld deposit for which $R = \xi$, points of the base metal very close to the weld may be expected to satisfy the condition mentioned with a reasonable degree of accuracy. With this in mind, experimental results of Hess and co-workers (14) on 1 and 1½-in. steel plates have been used to compute the products figuring on the left-hand side of Equation [86] for various rates of cooling at 1300 F. When plotted as a function of these rates, they gave a fairly constant value, Fig. 7. The values for the 1½-in. plate are in general more consistent than those for the 1-in. plate. Thus the 1½-in. plate and to some extent also the 1-in. plate behave under the particular condition of cooling like plates of infinite thickness.

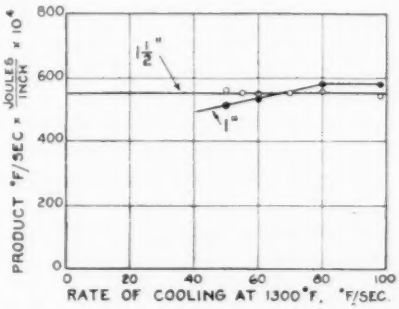


FIG. 7 THREE-DIMENSIONAL HEAT FLOW IN 1- AND 1½-IN. BUTT-WELDED PLATES AS EVIDENCED BY CONSTANT VALUE OF PRODUCT INDICATED

Determination of Heat Diffusivity From Rates of Cooling in Thin and Thick Butt-Welded Plates. If rates of cooling have been determined for a particular temperature T and known conditions of welding in a thin and thick butt-welded plate, then assuming the same heat efficiency (I.F.) in both cases, there follows when Equation [75] is divided by Equation [85]

$$\frac{\left[\left(\frac{dT}{dt}\right)^{1/2}\left(\frac{J}{vg}\right)\right]}{\left[\frac{dT}{dt} \times \frac{J}{v}\right]} = \sqrt{\frac{c\rho}{2k}} \times \frac{1}{\sqrt{\pi}} (T - T_0)^{-1/2} \quad \ldots [87]$$

but

$$\frac{c\rho}{2k} = \lambda$$

hence the diffusivity

$$\frac{1}{2\lambda} = \frac{1}{2\pi(T - T_0)} \times \frac{\left[\frac{dT}{dt} \times \frac{J}{v}\right]^2 \text{ thick plate}}{\left[\left(\frac{dT}{dt}\right)^{1/2} \times \frac{J}{vg}\right]^2 \text{ thin plate}} \quad \ldots [88]$$

[8] Reference (9) p. 151.

Substituting in Equation [88] the values taken from Figs. 6 and 7, for the $^1/_4$-in. and $1^1/_2$-in. plates, respectively, the value of the diffusivity becomes

$$\frac{1}{2\lambda} = \frac{1}{2\pi(1300 - 68)} \times \frac{(550 \times 10^4)^2}{(590 \times 10^3)^2} = 0.0112 \frac{\text{in.}^2}{\text{sec}}$$

$$= 0.072 \frac{\text{cm}^2}{\text{sec}}$$

as against the value of 0.0685, computed for pure iron from the data of the International Tables for 1300 F (16).

Considering the uncertainty attached to the determination of the heat conductivity k, and the probable error of measurements, this agreement appears quite satisfactory. However, it must be borne in mind that the assumption on which Equation [88] is based precludes any variation of the diffusivity with temperature, hence the value of 0.072 sq cm per sec must be regarded as an average rather than as a particular value of the diffusivity.

Temperature Distribution in Thick (and Thin) Arc-Welded Plates. On the basis of the foregoing results it can be assumed that the application of Equation [43] will yield a satisfactory picture of the temperature distribution during welding in thick butt-welded plates. More specifically, the conception will apply to a situation created by a top weld layer when the plates have been allowed to cool down to the room temperature. This situation is represented in Fig. 8 for various conditions of welding by means of a family of isotherms drawn around the instantaneous position of the electrode (11). Because of the quasi-stationary state of heat flow, the same figure may be used to depict the variation of temperature at a given section of plate and at various instances of welding.

For the purpose of computation, the following values were substituted in Equation [43], using C.G.S. units

q = 0.239 (I.F.) × V × I where 0.239 is the thermal equivalent of watts
(I.F.) = heat efficiency of arc assumed = 0.65 (12)
V = voltage drop in arc assumed = 25 volts (12)
I = current intensity in amp, variable
k = heat conductivity—0.1 cal per cm per deg C per sec, for steel and 0.485 cal per cm per deg C per sec for aluminum
λ = one half of the converse value of diffusivity, assumed = 5 sec per sq cm for steel and 1.2 sec per sq cm for aluminum

The main characteristics of the temperature distribution obtained under these conditions, Fig. 8, are as follows:

1 The rise of temperature in front of the heat source is much steeper than the fall of temperature behind the heat source.

2 Because of the fact that the heat does not propagate instantly in metals, the temperature does not pass through the maximum at the same time at various points of the same cross section. There is a lag at points which are farther away from the weld, as shown by curve n-n connecting the points of maximum temperature. This lag is a function of the speed of welding and diffusivity of metal (compare Fig. 8, A, B, and D).

3 Considering an instantaneous position of the electrode, curve n-n separates points in the solid with rising temperature from points in the solid with falling temperature.

As for the influence of the welding conditions, it is seen that:

1 An increase in the speed of welding, Fig. 8, A and B, produces a greater lag in the temperature distribution at a given cross section, hence the heat is more concentrated around the heat source. However, the temperature distribution along the line of welding, behind the electrode, remains unchanged, in accordance with Equation [80].

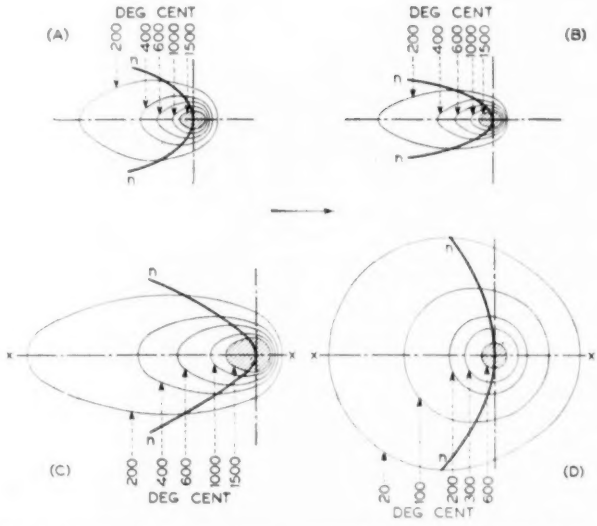


FIG. 8 TEMPERATURE DISTRIBUTION IN THICK BUTT-WELDED PLATE
(For details see the text. Courtesy of *The Welding Journal*.)

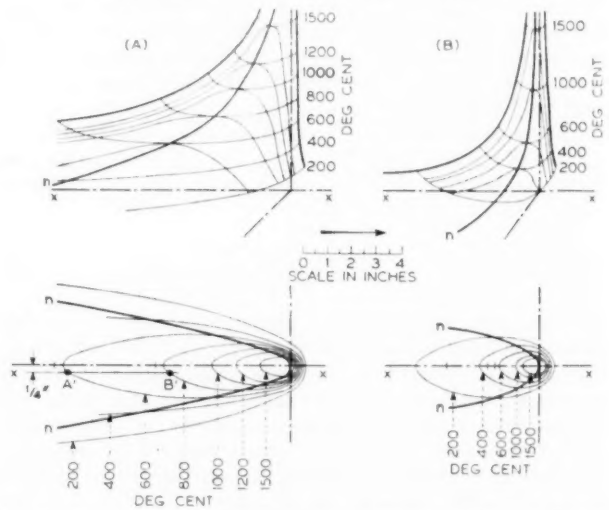


FIG. 9 TEMPERATURE DISTRIBUTION IN THIN AND THICK BUTT-WELDED PLATE
(*Left*, thin plate, 0.2 in. thick; *right*, thick plate. Same material, i. e., mild steel, and same welding technique in both cases, i.e., 200 amp, 8.3 ipm. Top view isometric projection; bottom view topographic projection. Courtesy of *The Welding Journal*.)

2 An increase in the current intensity, Fig. 8, A and C, extends the range of heat in the solid, but does not affect the shape of isotherms.

3 An increase in the heat conductivity and diffusivity of metal, Fig. 8, C and D, affects both the shape and the size of isotherms. The increase of the range of heating in front of the electrode is especially noteworthy.

4 An increase in the initial temperature, i.e., the preheating, causes a corresponding increase in the numerical value of each isotherm, but does not change its shape or size. However, the preheating has a marked effect upon the rate of cooling, as shown by Equation [85]. This effect is discussed in more detail in the experimental work on weldability (14) and (17).

Basically the same conclusions apply to thin welded plates, as can be easily demonstrated by means of Equation [73]. However, there is a fundamental difference in the conditions of welding of a thin and thick plate, due to the different nature of heat

flow. This difference is well apparent in the shape and size of isotherms drawn in Fig. 9.

Application to Actual Welding Practice

Determination of Cooling Time. In so far as welding practice is concerned, neither of the solutions already discussed is quite satisfactory. Because of the finite thickness of plates, the conditions of welding seldom correspond to that of a very thin or very thick plate. At a short distance from the arc there is a considerable temperature gradient through the thickness, but as the arc moves away from the section considered, the temperature becomes more uniform across the thickness. Thus the heat flow changes from a three-dimensional state to a two-dimensional one, as the distance from the arc increases. This condition has been discussed in Part 1, and an appropriate solution for this case has been obtained in the form of Equation [63].

In actual welding practice it is important to determine the time required for the weld to cool down to a given temperature, rather than to obtain a complete pattern of the temperature distribution around the electrode. Under these circumstances Equation [63] can be simplified by writing for a given spot of the weld bead, t seconds after it has been deposited on a plate of thickness, g

$$\xi = -vt;\ y = 0;\ z = 0$$

$$R_0 = |vt|;\ R_n = \sqrt{(vt)^2 + (2ng)^2},\ n = 1, 2, 3 \ldots . [89]$$

Substituting in Equation [63], there follows

$$T - T_0 = \frac{1}{2\pi k} \times \frac{q}{v} \times \frac{\mu}{t} \ldots\ldots\ldots\ldots [90]$$

where

$$\mu = 1 + 2 \sum \frac{e^{-\lambda v^2 t(s_n - 1)}}{s_n} \ldots\ldots\ldots\ldots [91]$$

and

$$s_n = R_n/vt$$

As previously, the rate of heat delivered to the plate will be replaced by the rate of energy input of thewelding arc, J multiplied by the heat efficiency of the arc (I.F.), thus

$$T - T_0 = \frac{(\text{I.F.})}{2\pi k} \times \frac{J}{v} \times \frac{\mu}{t} \ldots\ldots\ldots\ldots [92]$$

Equation [92] can be made to correspond "formally" to Equation [81] derived for a very thick plate, by introducing a "fictitious" time of cooling $t^* = t/\mu$, which for convenience we shall call the "reduced" time of cooling. With this in mind Equation [92] can be rewritten as follows

$$T - T_0 = \frac{(\text{I.F.})}{2\pi k} \times \frac{J}{v} \times \frac{1}{t^*} \ldots\ldots\ldots\ldots [93]$$

As seen from Equation [91], the reduced time of cooling depends upon the thickness of the plate g, on the speed of welding v, and the diffusivity of metal $1/2\lambda$. Actually, however, the thickness is the major factor, and for the usual range of welding speeds, from 6 to 12 ipm, the influence of speed can be neglected.

Fig. 10 shows the relation between the true and reduced time of cooling for various thicknesses of steel, assuming a diffusivity of 1 sq in. per min and a welding speed of 7 ipm. It is seen that as the time of cooling increases, the value of the reduced time of cooling, t^* differs more and more from that of the true time of cooling t, and so more so as the thickness is smaller. Since Equation [93] formally represents the conditions of a very thick plate and of a three-dimensional state of heat flow, the discrepancy between t and t^* is a measure of the departure from a three-dimensional heat flow. On the basis of Fig. 10 it may be predicted that in the vast majority of cases the $^1/_4$-in. plate will behave like a very thin plate, and the $1^1/_2$-in. plate like a very thick plate, and this prediction is in accordance with the findings of this and the preceding section. Also, it may be safely stated that plates over $1^1/_2$ in. thick will always behave like a very thick plate. Thus for plates thicker than $1^1/_2$ in. the reduced and the true cooling times are the same.

How well Equation [93] fits the actual conditions of welding is best determined by comparing the time of cooling computed from this formula using the chart, Fig. 10, with the time of cooling

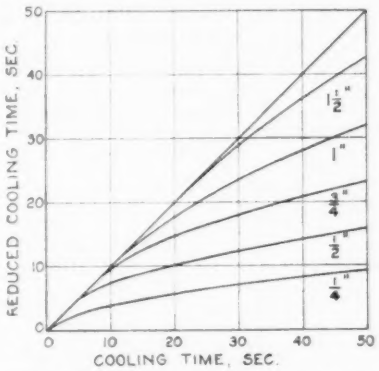


Fig. 10 Relation Between Cooling Time and Reduced Cooling Time for Plates of Various Thickness

measured in the experimental work of Hess and co-workers (14) on steel plates. In doing so, it must be remembered that the actual measurements of temperature were made not in the weld bead itself, but at a small distance from the bead. However, it can be shown that the error due to this factor is small after the first 5 to 10 sec of cooling. Another important factor is the proper choice of the heat efficiency (I.F.), and the heat conductivity k. From previous work (12), the I.F. was assumed to be 0.65. As for the heat conductivity k, a few trials showed that the value of $k = 0.080$ cal per deg C per sec fits best the experimental results at 1300 F. This value is commensurate with that determined previously, Equation [88].

Using the values given and expressing the temperature T in deg F, the energy input J/v in joules per in., and the reduced time t^* in seconds, Equation [93] reads for the case of butt-welded steel plates as follows

$$T - T_0 = 0.22 \left(\frac{J}{v}\right) \frac{1}{t^*}$$

hence the reduced time of cooling

$$t^* = \frac{0.22}{T - T_0} \frac{J}{v} \ldots\ldots\ldots\ldots [94]$$

Figs. 11 to 15, inclusive, show the agreement between computed and measured times of cooling for various thicknesses using three or four different energy inputs. The agreement in the important range of temperatures from 1300 to 575 F, is in general better than 5 per cent if no preheat is employed. The agreement is not as good with preheated plates, probably because the preheating operation was not maintained during welding (14). Notwithstanding this discrepancy, the general validity of Equation [93] in the range of temperatures from 1300 to 575 F may be considered as sufficiently established for practical purposes.

Determination of Rates of Cooling. By differentiating Equation [92] with respect to time there follows that (18)

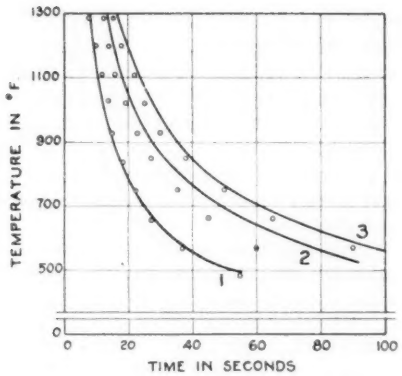


FIG. 11 WELD-COOLING CURVES IN 1/4-IN. PLATE AT ROOM TEMPERATURE

(Continuous lines computed; isolated circles measured by Hess and coworkers. 1, 17,000 joules per in.; 2, 22,800 joules per in.; 3, 28,000 joules per in.)

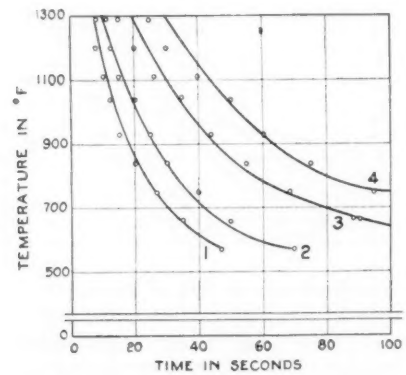


FIG. 12 WELD-COOLING CURVES IN 1/2-IN. PLATE AT ROOM TEMPERATURE

(Continuous lines computed; isolated circles measured by Hess and coworkers. 1, 34,900 joules per in.; 2, 41,000 joules per in.; 3, 56,100 joules per in.; 4, 68,700 joules per in.)

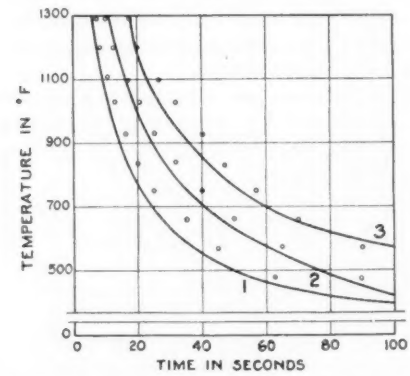


FIG. 13 WELD-COOLING CURVES IN 3/4-IN. PLATE AT ROOM TEMPERATURE

(Continuous lines computed; isolated circles measured by Hess and coworkers. 1, 46,000 joules per in.; 2, 65,000 joules per in.; 3, 72,000 joules per in.)

$$\frac{dT}{dt} = -\frac{(\text{I.F.})}{2\pi k}\frac{J}{v}\frac{\mu'}{t^2} \quad \ldots\ldots\ldots\ldots\ldots [95]$$

where

$$\mu' = 1 - 2\sum \frac{e^{-\lambda v^2 t(s_n-1)}}{s_n^2}[\lambda v^2 t(s_n-1)s_n - 1] \ldots [96]$$

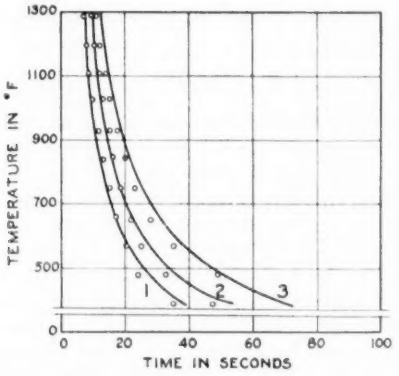


FIG. 14 WELD-COOLING CURVES IN 1-IN. PLATE; TEMPERATURE 37.4 F

(Continuous lines computed; isolated circles measured by Hess and coworkers. 1, 42,400 joules per in.; 2, 52,700 joules per in.; 3, 67,000 joules per in.)

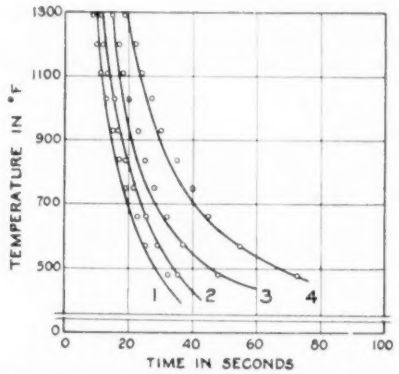


FIG. 15 WELD-COOLING CURVES IN 1 1/2-IN. PLATES AT ROOM TEMPERATURE

(Continuous lines computed; isolated circles measured by Hess and coworkers. 1, 53,000 joules per in.; 2, 63,500 joules per in.; 3, 76,400 joules per in.; 4, 100,500 joules per in.)

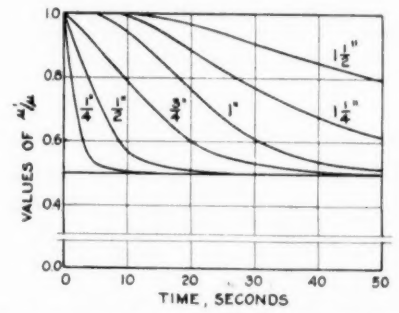


FIG. 16 RELATION BETWEEN WELD-COOLING TIME t AND COEFFICIENT $\left(\frac{\mu'}{\mu}\right)$ FOR VARIOUS THICKNESSES OF STEEL

hence by comparing Equation [96] with Equation [92]

$$\frac{dT}{dt} = -\frac{T - T_0}{t}\frac{\mu'}{\mu} \quad \ldots\ldots\ldots\ldots\ldots [97]$$

Equation [97] is of the same type as Equations [77] and [84] for the thin and thick plates, respectively; the only difference is that the coefficient (μ'/μ) instead of being a constant is a function of time and thickness, and to a much lesser degree of speed of welding and diffusivity. Assuming as previously, the value of 1 sq in. per min for the diffusivity and 7 ipm for the speed of welding, Fig. 16 shows the dependence of (μ'/μ) on time for various

thicknesses of plate. As expected, the values of (μ'/μ) vary between $^1/_2$ and 1, the line $^1/_2$ denoting conditions identical to that of a very thin plate and the value 1, conditions identical to that of a very thick plate. In accordance with previous results it is seen that the $^1/_4$-in. plate behaves like a thin plate less than 5 sec after the cooling process has started, whereas the $1^1/_2$-in. plate remains practically under the conditions of a very thick plate up to 30 sec of cooling.

Equations [93] and [97] along with charts, Figs. 10 and 16, may be used conveniently for a speedy determination of rates of cooling.

Suppose, for example, it is desired to determine the rates of cooling in a $^3/_4$-in. plate when using an energy input of 50,000 joules per in. The three following temperatures of preheat will be examined: 72 deg, 200 deg, and 400 deg F.

From Equation [93] the corresponding reduced times of cooling are 11.8, 13.7, and 18.4 sec.

Referring to the chart, Fig. 10, we find for a $^3/_4$-in. plate the true cooling times, namely, 13.5, 18.0, and 30.5 sec, respectively, and from the chart, Fig. 16, the corresponding values of (μ'/μ) = 0.72, 0.64, and 0.54, respectively.

Substituting in Equation [97], the following rates of cooling are obtained: 49.5 deg F per sec, 27.2 deg F per sec, and 10.5 deg F per sec, as compared to the values determined by Hess and coworkers, namely, 51 deg F per sec, 32 deg F per sec, and 15 deg F per sec. As expected, the computed rates of cooling are lower than those actually measured for higher temperatures of preheat.

3 MISCELLANEOUS APPLICATIONS OF THEORY OF MOVING SOURCES

Introduction

Because of lack of experimental data, the applications described in this part are of a more or less tentative character. The purpose of this discussion is not so much to arrive at numerical results as it is to find a scientific approach to the solution of the problems presented. In view of the success which such an approach has had in the problems of welding, it is believed that the considerations which follow will be of more than academic interest.

Rate of Extrusion in Continuous Casting. Continuous casting is a metallurgical process in which liquid metal is fed into a die and extruded in the form of a solid rod at a constant rate by means of a pair of rollers placed behind the die (19). To make the extrusion operation possible the rod must leave the die at a temperature at which the metal can be hot-worked and which consequently represents a given fraction of the temperature of fusion. In other words, the die must be capable of removing the heat from the cast metal to bring about the required drop of temperature. If radial temperature gradients in the rod are neglected, this drop of temperature may be regarded as being produced by a linear flow of heat with surface losses. On the other hand, by the process of extrusion each section of the rod is moved gradually from the inlet of the die where it is at the temperature of fusion T_1 to the outlet of the die, where it has been cooled down to the temperature of extrusion T_2. Thus the heat flow is of a quasi-stationary nature and Equation [23] is applicable. If the die is kept at a constant temperature T_0 and if the length of the die from the inlet to the outlet is L, then Equation [23] may be rewritten as follows

$$T_2 - T_0 = (T_1 - T_0)e^{-(\sqrt{\lambda^2 v^2 + PH/A} - \lambda v)L} \quad [98]$$

The remaining symbols in Equation [98] have the following meaning

λ = one half of the converse value of diffusivity
v = rate of extrusion
P = perimeter of rod
A = cross section of rod
H = dissipation ratio, see Equation [20]

For a circular rod of diameter D, the fraction $P/A = 4/D$. Putting further

$$\ln \frac{T_2 - T_0}{T_1 - T_0} = -m \quad [99]$$

Equation [98] becomes

$$m = \left[\sqrt{(\lambda v)^2 + \frac{4H}{D}} - \lambda v\right] L \quad [100]$$

or

$$m^2 = -2m\lambda vL + \frac{4HL^2}{D}$$

or

$$2\lambda vD = \frac{4HD}{m} \times \frac{L}{D} - m \Big/ \frac{L}{D} \quad [101]$$

Assuming a constant value of m, Equation [101] gives the relation between the rate of extrusion v and the mechanical and thermal characteristics of the extrusion. The former is represented by the ratio L/D which is a function of the friction between the die and the cast.

Since the load-carrying capacity of the rod at the outlet of the die has a limiting value, the higher the friction coefficient, the smaller the ratio L/D. On the other hand, the thermal characteristics of the extrusion process are determined (*a*) by the coefficient 2λ, which is the ratio of the volume heat capacity of the rod to its heat conductivity k, i.e., $\frac{c\rho}{k}$ (c = specific heat and ρ = density); and (*b*) by the coefficient H, which is the ratio of the heat dissipation h, and the heat conductivity of the rod, k. Thus both 2λ and H contain k in the denominator. This fact will be brought out later in the discussion.

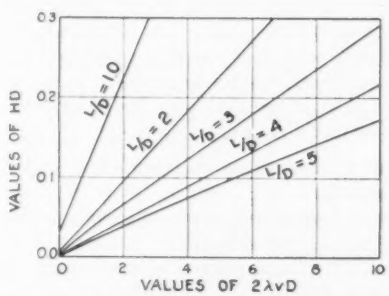


Fig. 17 Relation Between Rate of Extrusion and Heat-Dissipation Ratio in Continuous Casting

Fig. 17 shows the relation between the rate of extrusion and the surface transfer coefficient of the interface between the die and the rod for various values of L/D, computed according to Equation [101]. For the purpose of computation, the fraction $T_2 - T_0/T_1 - T_0$ has been taken as 0.7; thus ln 0.7 = —0.36. Likewise, dimensionless numbers rather than specific values of speed and dissipation ratio have been plotted in order to make the discussion more general. Because of the fact that for values of $L/D > 2$ the second term on the right-hand side of Equation [101] becomes very small as compared to the first one, the speed of extrusion increases almost proportionally to the coefficient H and the relative length of the die L/D. It also increases with the ratio $H/2\lambda$, which as pointed out previously, is nothing else but the ratio of the heat dissipation h to the volume heat capacity

of the metal. The fact that the heat conductivity of the cast metal does not appear in these relations is noteworthy. It shows, for example, that other conditions being equal, the rate of extrusion of copper wire will not be substantially greater than that of iron wire, in spite of the much higher heat conductivity, as the volume heat capacity is not very much different for these metals.

To obtain an approximate idea of the order of magnitude of the rate of extrusion which can be expected, assume the following values for an iron wire 1 cm diam ($\sim$ $^3/_8$-in.) when cast in a metallic die

h = 0.012 cal per sq cm per deg C per sec (20)
k = 0.08 cal per cm per deg C per sec (16)
$c\rho$ = 1.2 cal per cu cm (16)[9]

hence

$$HD = 0.15 \text{ and } 2\lambda D = 15 \text{ sec per cm}$$

Assuming further L/D = 2, 3, and 4, respectively, the following values of $2\lambda vD$ are obtained from Fig. 17: 3.15, 4.8, and 6.6, hence

v = 0.2 cm per sec, 0.33 cm per sec, and 0.44 cm per sec

Actually, these values may be substantially increased by improving both the heat dissipation h and the lubrication condition between the mold and cast, i.e., the ratio L/D, when using graphite instead of metal for the dies (19). At present, none of these coefficients is very accurately known to permit more than a qualitative statement. However, a method of obtaining a value of some of these coefficients is proposed in the following section.

Method of Determining Value of Diffusivity and Heat-Dissipation Ratio. Equations [23] and [24] provide a convenient method of obtaining, in a single experiment, the coefficients λ and H, the former being one half of the converse value of diffusivity, the latter the dissipation ratio. To this end the metal to be tested is formed into a thin-walled cylinder and surrounded by the medium whose value of H with respect to the metal in question is to be determined. A source of heat in the form of a coil is then moved inside the tube at a rate which will practically produce a uniform temperature distribution in the thickness of the tube, and of sufficient intensity to bring the temperature of the tube to the desired maximum value. The temperature of the surrounding medium is kept at a constant temperature T_0.

By means of thermocouples spot-welded to the tube, the temperature at a given cross section of the latter is taken for three positions of the heat source as follows:

1 Position x_1, for which the temperature has reached the maximum value T_1.

2 Position x_2, preceding the position x_1 and for which the temperature had a given value $T_2 < T_1$.

3 Position x_2' following the position x_1, and for which the temperature has dropped back to the value T_2.

Calling g the thickness of the tube, the ratio of the perimeter P to the cross section A, entering Equations [23] and [24] is simply $1/g$ thus

$$\frac{T_2 - T_0}{T_1 - T_0} = e^{-\left[\sqrt{(\lambda v)^2 + H/g} - \lambda v\right](x_1 - x_2)} \quad [102]$$

and

$$\frac{T_2 - T_0}{T_1 - T_0} = e^{-\left[\sqrt{(\lambda v)^2 + H/g} + \lambda v\right](x_2' - x_1)} \quad [103]$$

These two equations can be rewritten in a more simple form by putting

$$\ln \frac{T_2 - T_0}{T_1 - T_0} = -m \quad [104]$$

[9] Strictly speaking, coefficient 1.2 must also include the latent heat of fusion.

$$\frac{x_1 - x_2}{g} = u; \qquad \frac{x_2' - x_1}{g} = u' \quad [105]$$

hence

$$\frac{m}{u} = \sqrt{(\lambda v g)^2 + Hg} - \lambda v g \quad [106]$$

and

$$\frac{m}{u'} = \sqrt{(\lambda v g)^2 + Hg} + \lambda v g \quad [107]$$

Solving for λvg and Hg there follows

$$\lambda v g = \frac{m}{2}\left(\frac{1}{u'} - \frac{1}{u}\right) \quad [108]$$

and

$$Hg = \frac{m^2}{uu'} \quad [109]$$

hence finally the average diffusivity between the temperatures T_1 and T_2

$$\frac{1}{2\lambda} = \frac{4v}{m}\frac{(x_2' - x_1)(x_1 - x_2)}{(x_2 + x_2' - 2x_1)} \quad [110]$$

and the average dissipation ratio between $(T_1 - T_0)$ and $(T_2 - T_0)$

$$H = \frac{m^2 \times g^2}{(x_2' - x_1)(x_1 - x_2)} \quad [111]$$

Characteristically, the expression for diffusivity does not depend on the thickness of the tube and the expression of H does not depend on speed.

Control of Factors Governing Flame-Hardening and Continuous-Quenching of Steel Products. The purpose of flame-hardening is to produce a hardened case in steels of proper carbon and alloy content by raising the temperature of the case above the upper transformation point of steel Ac_3, and by quenching it as rapidly as possible in water. When dealing with parts of some length, such as gear rims or rails, the rise of temperature is accomplished by means of an oxyacetylene torch moving at a constant speed v, and the quenching, by a water sprinkler which moves closely behind the torch.

In what follows it will be assumed that the part has a rectangular section and that the flame of the oxyacetylene torch covers uniformly the surface over its whole width g, but that it extends over only a small portion l of its length. Thus the heat flow may be considered as being produced by a narrow plane source of heat moving at a constant speed, v. This case has been examined in Part 1, and Equations [51] and [60] have been derived to describe the temperature distribution around the heat source. Of these, Equation [51] represents an almost uniform rise of temperature which will result in the heated part throughout its thickness, at some distance behind the source, if there are no losses to the surrounding. This rise of temperature is then merely the consequence of the storing up of the heat, and if the latter is delivered at a rate of q thermal units per unit time, the rise of the temperature T_2 behind the source over the initial temperature T_0 is in accordance with Equation [51]

$$T_2 - T_0 = \frac{q}{c\rho agv} \quad [112]$$

As previously $c\rho$ (c=specific heat, ρ=density) represents the volume specific heat, and v the speed at which the source moves. As for the symbols a and g, their previous meanings must be inverted in order to keep up with the present description of things.

They are accordingly; a = the thickness, and g = the width of the heated part.

As has been shown in Fig. 2, for the case of a very narrow plane source, T_2 also represents the temperature at some depth below the location of the heat source. This temperature is quickly approached by the bulk of the metal as the heat source moves away from the section considered. For convenience, temperature T_2 will be called the "bulk" temperature. With this in mind, Equation [60] represents the relative rise of the maximum surface temperature T_1, as compared to the rise of the bulk temperature of the piece. Fig. 18 shows the same relation graphically. Here for convenience the converse of the relative rise of temperature, namely $(T_2 - T_0)/(T_1 - T_0)$, has been plotted as a function of a dimensionless number $\lambda v a$, whose significance will be explained shortly, and for various lengths l of the source referred to the thickness a of the piece l/a. Assuming that in flame-hardening the surface temperature is required to reach a constant value T_1 and that T_0 is the practically constant room temperature, Fig. 18 shows that the higher the number $\lambda v a$ the smaller will be the rise of the bulk temperature T_2. The same result is obtained by decreasing the relative length of the source l/a.

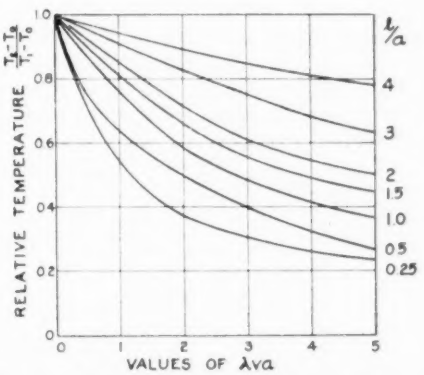


FIG. 18 RELATION BETWEEN RISE OF SURFACE TEMPERATURE T_1, AND THE RISE OF TEMPERATURE OF BULK OF MATERIAL T_2, FOR VARIOUS CONDITIONS OF FLAME-HARDENING

In order to interpret the number $\lambda v a$, attention is called to Equation [112]. If k is the heat conductivity of the material, it will be recalled that by definition

$$\frac{c\rho}{k} = 2\lambda \quad \ldots\ldots\ldots\ldots\ldots\ldots [113]$$

hence Equation [112] can be rewritten as follows

$$\lambda v a = \frac{q}{g} \times \frac{1}{2k(T_2 - T_0)} \quad \ldots\ldots\ldots\ldots [114]$$

In this relation q/g is the rate of heat per unit width and it may be considered as a characteristic of the heat source employed. When comparing Equation [114] with the chart, Fig. 18, it is found that $\lambda v a$ is a parameter which allows expression of the maximum surface temperature T_1, or the bulk temperature T_2, whichever is made variable, as a function of the heat characteristic (q/g) of the torch, and also another characteristic of the torch represented by the relative length l/a. Neither of these characteristics can be measured directly, but indirectly both can be determined by using Equation [114] and chart, Fig. 18, in reverse.

To this end, a trial experiment can be set up using a sample of the material to be treated in the form of a rectangular bar and measuring the temperature at a certain point of the surface and below the surface, while the latter is being heated, by passing over it the torch whose characteristics are to be determined. The following measurements are made:

1 Initial temperature, T_0.
2 Maximum temperature T_1 at the surface.
3 Temperature T_2, for which the surface temperature is almost the same as the depth temperature.
4 Speed of motion, v of the torch.
5 Width g, and thickness a of the bar.

Assuming an average constant value for λ and k, the value of q is thus determined from Equation [112] and the value of l from the chart, Fig. 18. For example, if $T_1 - T_0$ has been measured to be 800 C (1440 F) and $T_2 - T_0 = 400$ C (720 F), and if, furthermore, the speed at which the torch moved was 0.85 cm per sec, (0.336 ips), and the section of the bar 5 cm wide and 1 cm thick (about $2 \times {}^3/_8$ sq in.), then assuming, according to previous discussion, $k = 0.08$ cal per cm per deg C per sec, and $\lambda = 6$ sec per sq cm for steel, the value of q is found from Equation [114] as

$$q = 6 \times 0.85 \times 1 \times 5 \times 2 \times 0.08 \times 400 = 1640 \text{ cal per sec}$$

and l/a from the chart, Fig. 18, with $(T_2 - T_0)/(T_1 - T_0) = 0.5$ and $\lambda v a = 5.1$, as 2; hence $l = 2$ cm (= 0.79 in.).

If each torch thus has been rated for a given value of q and l, it then becomes possible to determine for what thickness of steel it is best fitted. As a usual practice, it may be attempted to keep the maximum surface temperature slightly above Ac_3 and the bulk temperature slightly below Ac_1, thus the ratio $(T_2 - T_0)/(T_1 - T_0)$ will be around 0.66, and the value of $\lambda v a$, according to Equation [114] around 0.01 (q/g), if q/g is expressed in cal per cm per sec. Assume, for example, a torch is used for which $q/g = 400$ cal per cm per sec, and $l = 2$ cm. It is required to find the thickness a for which it is fitted and the speed of motion v.

From Equation [114] $\lambda v a = 0.01 \times 400 = 4.00$ and from the chart, Fig. 18, the intersection of $(T_2 - T_0)/(T_1 - T_0) = 0.66$, and $\lambda v a = 4$, gives $l/a = 3$. Thus $a = {}^2/_3$ cm = 0.26 in. and since $\lambda v a = 4$, the speed $v = 1$ cm per sec, or about 23 ipm. If the bulk of the material is to be kept much below Ac_1, for example around 600 F, then $(T_2 - T_1)/(T_1 - T_0)$ is around 0.33 and $\lambda v a = 0.005$ (q/g). Hence with the same type of torch as before, $\lambda v a = 2$, and $l/a = 0.2$; $a = 2/0.2 = 10$ cm (4 in.). The speed, however, is reduced as much as the thickness has been increased, becoming only 1.5 ipm.

Continuous Quenching. If the heat, instead of being delivered to the piece, is being withdrawn at a rate of q thermal units per unit time, under conditions similar to that of flame-hardening, then Equation [114] and the chart, Fig. 18, can be used to control the final temperature T_2 to which the surface of a piece previously heated to a temperature T_0 will be automatically reheated after having been quenched down to the temperature T_1. This problem can be solved in a manner similar to that outlined for the flame-hardening. To make the conditions more specific, suppose it is desired to improve the hardness of the top surface of a rail by means of water-quenching, followed by tempering at 500 C (950 F). Using the theory of a moving-plane source, this treatment can be attempted in one continuous and single operation as follows: After the rail has left the rolling mill at some 980 C (1800 F), it is quenched by means of a water sprinkler moving at a constant speed v. The problem is then reduced to the determination of the characteristics of the water sprinkler in such a way that the surface of the rail after being quenched to the temperature of 20 C (86 F) is reheated to a bulk temperature of 500 C (950 F). To this end, suppose that the head of the rail is 2 in. wide and $1^1/_2$ in. thick, or approximately 5×4 sq cm, and that the heat content of the web can be neglected. Then by assuming that the water spray covers a surface of 5×5 sq cm, the value

of l/a is $5/4 = 1.25$. On the other hand, $(T_2 - T_0)/(T_1 - T_0) = \frac{500 - 980}{20 - 980} = 0.5$; hence from the chart, Fig. 18, $\lambda va = 3.2$. If this value is substituted in Equation [114], then by putting as previously $k = 0.08$ cal per cm per deg C per sec, and $\lambda = 6$ sec per sq cm, the value of q becomes

$$q = -3.2 \times 5 \times 0.16 \times 480 = -1240 \text{ cal per sec}$$

Since $\lambda va = 3.2$, the speed of motion is

$$v = 3.2/6 \times 4 = 0.132 \text{ cm per sec} = 3.15 \text{ ipm}$$

A similar computation will show that if it is desired to obtain a tempered martensite at 100 C (= 212 F) at the surface, the heat must be removed from the surface at a rate of 2280 cal per sec with the same speed of motion.

Before closing, emphasis again is put on the tentative character of the foregoing computation. There is obviously need for some preliminary experimentation before the theory expounded can be used as a practical tool much in the same way as this has been done for welding.

BIBLIOGRAPHY

1 "Guide to Weldability of Steels," edit., American Welding Society, New York, N. Y., 1942.

2 "Temperature Distribution During Welding—A Review of the Literature to January, 1937," by W. Spraragen and G. E. Claussen, *The Welding Journal*, vol. 16, September, 1937, p. 4.

3 "Theoretical Study of the Heat Cycle During Arc Welding" (in French), by D. Rosenthal, 2-eme Congres National des Sciences, Brussels, 1935, pp. 1277–1292.

4 "Temperature Measurements in Fusion Welding" (in German), by H. Bornefeld, Technische Zentralblatt für Praktische Metalbearbeitung, vol. 43, 1933, pp. 14–18.

5 "Residual Stresses in Arc-Welded Plates," by N. S. Boulton and H. E. Lance Martin, Proceedings of The Institution of Mechanical Engineers, vol. 133, 1936, p. 336.

6 "The Thermal Distribution and Temperature Gradient in the Arc Welding of Oil Casing," by W. A. Bruce, *Journal of Applied Physics*, vol. 10, 1939, pp. 578–585.

7 "Heat Flow in Arc Welding," by E. M. Mahla, M. C. Rowland, C. A. Shook, and G. E. Doan, *The Welding Journal*, vol. 20, no. 10, October, 1941, res. suppl., p. 459.

8 "Flow of Heat in Metals," by J. B. Austin, edit., American Society for Metals, Cleveland, Ohio, 1942, p. 103.

9 "Introduction to the Mathematical Theory of the Conduction of Heat in Solids," by H. S. Carslaw, Dover Publications, New York, N. Y., 1945, p. 38.

10 "Treatise on Bessel Functions and Their Applications to Physics," by A. Gray, G. B. Mathews, and T. M. Macrobert, The Macmillan Company, New York, N. Y., 1922.

11 "The Mathematical Theory of Welding and Cutting," by D. Rosenthal, *The Welding Journal*, vol. 20, May, 1941, res. suppl., p. 220.

12 "Thermal Study of Arc Welding. Experimental Verification of Theoretical Formulas," by D. Rosenthal and R. Schmerber, *The Welding Journal*, vol. 17, April, 1938, pp. 2–8.

13 "Three Lectures on Welding" (in Dutch), by D. Rosenthal, edit., the Dutch Welding Society, Amsterdam, 1936.

14 "The Measurement of Cooling Rates Associated With Arc Welding and Their Application to the Selection of Optimum Welding Conditions," by W. F. Hess, L. L. Merrill, E. F. Nippes, Jr., and A. P. Bunk, *The Welding Journal*, vol. 22, September, 1943, res. suppl., p. 377.

15 "Quenching and Hardenability of Hollow Cylinders," by J. H. Hollomon and C. Zener, Trans. American Society for Metals, vol. 33, 1944, pp. 1–17.

16 "Metals Handbook," American Society for Metals, Cleveland, Ohio, 1939, p. 424.

17 "A Tentative System for Preserving Ductility in Weldments," by G. E. Doan and R. D. Stout, *The Welding Journal*, vol. 22, July, 1943, res. suppl., p. 278.

18 "An Important Contribution to the Science of Welding," by D. Rosenthal, *The Welding Journal*, vol. 23, February, 1944, res. suppl., pp. 92–96.

19 "The Continuous Casting of Molten Metals—History, Requirements, Metallurgy, and Economics," by N. P. Goss, Trans. American Institute of Mining and Metallurgical Engineers, Institute of Metals Division, vol. 161, 1945, p. 487.

20 "On the Cooling of Steel in Ingot and Other Forms," by J. E. Fletcher, *The Journal of the Iron and Steel Institute*, vol. 98, no. 11 1918, p. 231.

Appendix 1

Use of Instantaneous Sources for Solution of Heat Flow Due to Moving Sources

The solution of heat flow in an infinite solid due to a source moving in a given direction may be obtained by adding the contributions of an infinite number of small instantaneous sources placed one behind the other at infinitely small intervals of time, along the direction of motion. If the direction of motion is taken as the x-axis, then the contribution of an infinitesimal instantaneous point source dQ placed at a distance x' from the origin at a time t', may be represented as follows in so far as the increase of temperature dT of a point (x, y, z) at any moment $t \geq t'$ is concerned[10]

$$dT = \frac{\sqrt{2\lambda}\, dQ}{8\pi^{3/2}k} \times \frac{1}{(t-t')^{3/2}} \times e^{-\frac{\lambda}{2(t-t')}[(x-x')^2+y^2+z^2]}$$

where dQ is the quantity of heat of the point source, k is the heat conductivity, and 2λ is the converse of heat diffusivity. However, if the law of motion is given, x' is a known function of t'; and the same is true for the amount of heat delivered by the moving source; thus

$$Q = \phi(t') \text{ or } dQ = \phi'(t')dt'$$

and

$$x' = f(t')$$

hence

$$T - T_0 = \frac{\sqrt{2\lambda}}{8\pi^{3/2}k} \int_0^t \frac{\phi(t')}{(t-t')^{3/2}} e^{-\frac{\lambda}{2(t-t')}\left\{[x-f(t')]^2+y^2+z^2\right\}} dt' \qquad \ldots\ldots [A]$$

This is the most general equation of heat flow in an infinite solid due to a moving-point source. Similar expressions can be derived for moving line and plane sources.

As a particular case, put

$$Q = qt'$$

and

$$x' = vt'$$

where q and v are constants.
Then Equation (A) becomes

$$T - T_0 = \frac{\sqrt{2\lambda}}{8\pi^{3/2}} \frac{q}{k} \int_0^t \frac{dt'}{(t-t')^{3/2}} e^{-\frac{\lambda}{2(t-t')}[(x-vt')^2+y^2+z^2]} \qquad \ldots\ldots [B]$$

Put

$$t - t' = \tau^2;\ x - vt = \xi;\ \xi^2 + y^2 + z^2 = R^2$$

There follows

$$T - T_0 = -\frac{\sqrt{2\lambda}}{8\pi^{3/2}} \frac{q}{k} \int_0^t \frac{2\tau d\tau}{\tau^3} e^{-\frac{\lambda}{2\tau^2}[R^2+2v\xi\tau^2+v^2\tau^4]}$$

$$= \frac{\sqrt{2\lambda}}{4\pi^{3/2}} \frac{q}{k} e^{-\lambda v\xi} \int_0^t \frac{d\tau}{\tau^2} e^{-\frac{\lambda R^2}{2\tau^2}-\frac{\lambda\tau^2}{2}}$$

[10] Reference (9), p. 150.

or letting $t \rightarrow \infty$

$$T - T_0 = \frac{\sqrt{2\lambda}}{4\pi^{3/2}} \frac{q}{k} e^{-\lambda v \xi} \int_0^\infty \frac{d\tau}{\tau^2} e^{-\frac{\lambda R^2}{2\tau^2} - \frac{\lambda \tau^2}{2}} \quad \ldots\ldots [C]$$

The infinite integral appearing in Equation [C] can be solved by means of the Bessel function $K_{1/2}(x)$. To this end put a new variable α, such that

$$\tau = \alpha R \sqrt{2\lambda} \quad \ldots\ldots [D]$$

The substitution of Equation [D] in Equation [C] gives

$$T - T_0 = \frac{q\sqrt{2\lambda}}{4\pi^{3/2} k} e^{-\lambda v \xi} \times \frac{1}{R\sqrt{2\lambda}} \int_0^\infty e^{-(\lambda v R)^2 \alpha^2 - 1/4\alpha^2} \alpha^{-2} d\alpha$$

But according to the theory of Bessel functions (10)

$$\int_0^\infty e^{-(\lambda v R)^2 \alpha^2 - 1/4\alpha^2} \alpha^{-2} d\alpha = \sqrt{2\lambda R}\ K_{1/2}(\lambda v R)$$

and furthermore

$$K_{1/2}(\lambda v R) = \frac{\sqrt{\pi}}{\sqrt{2\lambda v R}} e^{-\lambda v R},$$

hence finally

$$T - T_0 = \frac{q}{4\pi k} e^{-\lambda v \xi} \frac{e^{-\lambda v R}}{R}$$

This expression has been derived previously in Part 1 in a more simple way for a three-dimensional case.

Using similar procedures for the line and plane instantaneous sources, Expressions [31] and [18] can be derived for the two-dimensional and linear heat flow, respectively.

Appendix 2

Expansion of Solution [45] in a Fourier Series

As shown by Carslaw,[11] if $f(y)$ is an even function of y which can be expanded, as also $f(y \pm 2na)$, in a Fourier series of cosines of multiples $\pi y/a$, then

$$\sum_{-\infty}^{\infty} f(y \pm 2na) = \frac{1}{a} \int_0^\infty f(y) dy + \frac{2}{a} \sum_1^\infty \cos \frac{\pi n y}{a} \int_0^\infty f(y') \cos \frac{\pi n y'}{a} dy$$

Let $f(y) = K_0(\lambda v \sqrt{\xi^2 + y^2})$, then

$$\sum_{-\infty}^{\infty} K_0\left(\lambda v \sqrt{\xi^2 + (y \pm 2na)^2}\right) = \frac{1}{a} \int_0^\infty K_0\left(\lambda v \sqrt{\xi^2 + y^2}\right) dy + \frac{2}{a} \sum_1^\infty \cos \frac{\pi n y}{a} \times \int_0^\infty K_0\left(\lambda v \sqrt{\xi^2 + y'^2}\right) \cos \frac{\pi n y'}{a} dy'$$

But, by virtue of the integral representation of Bessel function (10)

$$\int_0^\infty K_0\left(\lambda v \sqrt{\xi^2 + y^2}\right) dy = \frac{1}{\lambda v} \int_0^\infty e^{-(\lambda v \xi)^2 t^2 - 1/4t^2} t^{-1} dt \times \int_0^\infty e^{-(\lambda v y)^2 t^2} d(\lambda v y) = \frac{1}{\lambda v} \frac{\sqrt{\pi}}{2} \int_0^\infty e^{-(\lambda v \xi)^2 t^2 - 1/4t^2} t^{-2} dt = \frac{\pi}{2\lambda v} e^{-\lambda v |\xi|}$$

[11] Reference (9), p. 159.

Likewise

$$\int_0^\infty K_0\left(\lambda v \sqrt{\xi^2 + y'^2}\right) \cos \frac{\pi n y'}{a} dy' = \frac{1}{\lambda v} \int_0^\infty e^{-(\lambda v \xi)^2 t^2 - 1/4t^2} t^{-1} dt \times \int_0^\infty e^{-(\lambda v y')^2 t^2} \cos\left(\frac{\pi n}{\lambda v a} \lambda v y'\right) d(\lambda v y')$$

$$= \frac{\sqrt{\pi}}{2\lambda v} \int_0^\infty e^{-(\lambda v \xi)^2 - \mu_n^2/4t^2} t^{-2} dt = \frac{\pi}{2\lambda v \mu_n} e^{-\lambda v \mu_n |\xi|}$$

where $$\mu_n = \sqrt{1 + \left(\frac{\pi n}{\lambda v a}\right)^2}$$

hence recalling that

$$2\lambda = \frac{c\rho}{k}$$

we obtain expression, Equation [48] or [49], according to whether ξ is positive or negative.

Discussion

R. H. Cameron.[12] This paper is of considerable interest to the writer as a mathematician, because it shows that data of important practical significance can be calculated by the use of higher mathematics and higher mathematical techniques. While undoubtedly many of the author's conclusions have been or will be checked directly by experiment, his methods make it possible quickly to calculate data and plot curves which could be obtained directly only by a very large number of time-consuming and costly experiments. His theory of quasi-stationary states simplifies many practical problems to the point where calculation is possible and provides a method of attack on other problems which have not yet been put on a mathematical basis.

The author's technique changes a problem involving moving heat sources into one involving only fixed sources or singularities, and thus extends the classical methods of treating fixed sources to the more difficult problems of moving sources. These methods apply to such apparently diverse problems as arc welding, the rate of extrusion of a continuous casting, continuous quenching, and the heating effects of the passage of a bullet in a gun barrel.

Finally, his methods can be used in connection with experimental work to suggest the design of experiments, the direction they should take, and the interpretation of the results. His method for determining the values of diffusivity and heat-dissipation ratio is an example in point.

M. W. Rubesin[13] and R. C. Martinelli.[14] The author has presented an extremly interesting and useful contribution to the field of heat conduction. It is interesting to note that, due to the quasi-stationary state existing about the moving source, the method of relaxation can be readily applied to the problem.

A heat balance is made on a lattice of sides δ and depth $\delta/2$ situated directly below the moving source and moving with the source at a velocity v. Consideration is taken of the heat generated by the source, the heat conducted into the lattice by conduction, and the heat carried into the lattice by the movement of material through the lattice. Heat balances are made on other lattices surrounding the one about the source and a set of relaxation patterns established. Calculations show that the results of this numerical method check reasonably with the analytical results of the author.

[12] Professor of Mathematics, University of Minnesota, Minneapolis, Minn.

[13] University of California, Berkeley, Calif.

[14] Assistant Professor of Mechanical Engineering, University of California. Mem. A.S.M.E.

Heat losses from the surface can also be accounted for by the method of relaxation.

Author's Closure

Professor Cameron's comments coming from a mathematician are very much appreciated. The technical man neither ignores nor belittles the value of the mathematics, but the thing he is primarily interested in is the final numerical value of the solution and not the way in which the latter has been obtained. Unfortunately, many a mathematician does not appreciate this point of view as fully as Professor Cameron does. They are inclined to consider the ultimate step of the analysis which consists of putting the solution in a form suitable for numerical computation as some sort of "puka" mathematics to be left to the computing machines. While the latter certainly are tremendous time savers, they hardly afford as complete a view of the problem as a mathematical analysis does, especially when it comes to the consideration of singularities. Some of the problems of heat flow require the use of the highest mathematical techniques, and it is only through the co-operation of mathematicians who are skilled in those techniques that a substantial progress in the theory of heat flow can be made.

The emphasis on the mathematical analysis does not preclude the use of numerical methods for particular applications. From this point of view the remarks made by Mr. Rubesin and Professor Martinelli are most welcome. The author is not enough familiar with the relaxation method to see the advantages that it offers in the treatment of a general problem of heat flow, like the one developed in the present paper, but he is aware of the possibilities which it affords in solving particular problems with specific boundary conditions. For example, he would be very much interested to see the discussers treat the following two problems which are of importance in arc welding:

1 Heat flow due to a moving plane source of a circular shape, and

2 Heat flow in a plate heated by a moving point source on one face and cooled by liquid medium on the other face.

The solution of the first problem may give a better insight into the phenomena of temperature distribution in the molten pool, and the second is of especial interest in ship-repair welding.

In closing the author wishes to thank all discussers for their kind interest in his paper.

Cutting Action of Reamers

By T. F. GITHENS,[1] CLEVELAND, OHIO

The cutting action of reamers resembles in many ways the cutting action of boring tools or twist drills. There is a common misconception that a reamer somehow gets into a hole and then scrapes the hole to size by means of its longitudinal cutting teeth. What really happens is that a reamer, a small amount larger than the hole to be finished, must cut its way into the hole by its entering teeth; and then produce a smoothly finished hole, round, straight, in proper alignment, and as near to the standard reamer size as possible. Reamers are provided with three kinds of clearance, point, peripheral, and longitudinal. Reamers can be made with combinations of positive, negative, and zero radial and axial rakes. The angle of the point and the feed per revolution affect the true rake angle of the cutting edge. Reamers must be kept sharp. The standard reamer made accurately to size and carefully used to produce a standard hole has been the most important factor in interchangeable manufacture. All classes of fit can be made by proper allowance on the shaft and the maintenance of the dependable standard hole produced by the standard reamers. These and other facts concerning reamers are explained in this paper.

Machine and Hand Reamers

A MACHINE reamer is a tool used for enlarging a hole, previously formed, and for freely cutting this hole as round, smooth, straight, in proper alignment, and as close to the standard or exact size as possible (1).[2]

A reamer is accomplishing its purpose when it cuts freely a round, smooth, straight hole its own size.

The principal parts of a machine reamer are shown in Fig. 1. These definitions and those for hand reamers are explained in the American Standard for Reamers (2).

The principal parts of a hand reamer are shown in Fig. 2.

Reamer Clearances

A reamer without clearance cannot cut because its cutting edges cannot get under the surface of the metal to lift or sever the chip from the metal. If forced into a hole it merely rubs or burnishes the surface of the hole and either heats the tool sufficiently to draw the temper, or tears the hole, or does both. A reamer having proper clearance cuts freely and smoothly (1).

There are three kinds of clearance on reamers, as follows:

1 Clearance on the entering ends of the teeth. This clearance is illustrated in Fig. 3 and is sometimes called "point" clearance.

2 Clearance along the lands or peripheral part of the reamer. This is sometimes called "radial relief" or clearance. This is illustrated in Fig. 5.

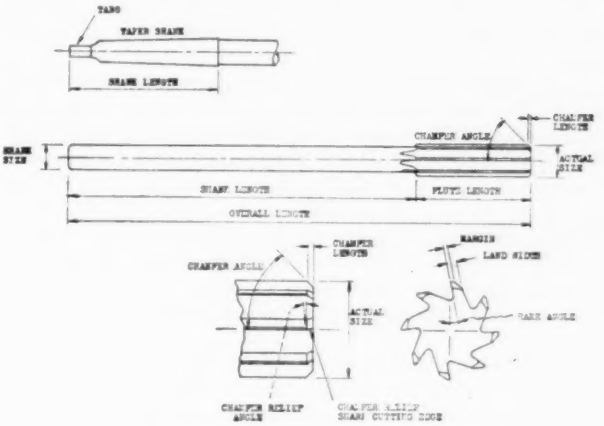


FIG. 1 MACHINE REAMER

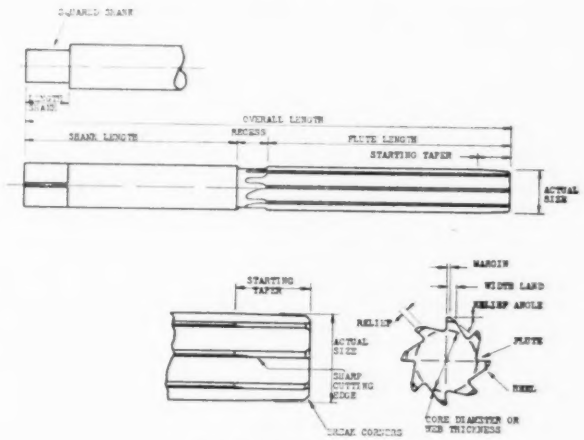


FIG. 2 HAND REAMER

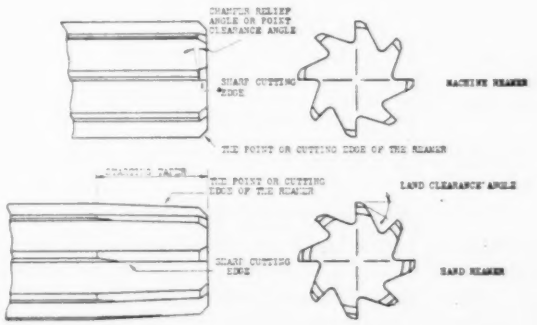


FIG. 3 CUTTING ENDS OR POINTS, SHOWING CUTTING EDGES AND CLEARANCES

3 "Longitudinal relief" or "back taper," which is a very slight taper of about 0.0001 in., which makes the reamer smaller toward the shank in order to prevent the back end from enlarging the hole or dragging and thereby roughing up the finish of the hole, Fig. 7.

---

[1] Mechanical Engineer, Cleveland Twist Drill Company. Mem. A.S.M.E.

[2] Numbers in parentheses refer to the Bibliography at the end of the paper.

Contributed by the Research Committee on Cutting Data and Bibliography and presented at the Semi-Annual Meeting, Detroit, Mich., June 17–20, 1946, of THE AMERICAN SOCIETY OF MECHANICAL ENGINEERS.

NOTE: Statements and opinions advanced in papers are to be understood as individual expressions of their authors and not those of the Society.

Point Clearance

The entering cutting edges on chucking reamers are usually beveled at an angle of from 40 to 50 deg for the purpose of keeping the extreme cutting corner as obtuse as possible, which helps to keep it sharp for a longer time. This cone shape also aids the reamer in centering itself in the work. These cone-shaped edges must be ground to a sharp edge with clearance for end-cutting, Fig. 3.

Hand reamers have a much longer taper, about 0.015 in. per in., and they are used for finishing purposes only. These reamers are but slightly smaller at the entering end, as it is necessary to remove only a small amount of metal in the finishing process. This long taper allows a scraping cut to be taken in such a manner that very accurate and smooth holes are produced. The taper edges must be ground to a sharp edge with clearance. A bevel of about 45 deg is also put at the long end of the tapering point to aid the hand reamer in entering the hole, but there should be so little stock left in the hole that this bevel should do no cutting, Fig. 3.

Fluted chucking reamers which are sometimes required for very accurate and smooth holes often have a slight second bevel in addition to that already mentioned, which acts like the taper on a hand reamer, thus making a smoother hole than would otherwise be the case. This is shown in Fig. 4; the length of this second taper need be only $^1/_{16}$ in. and must be ground to a sharp edge with proper clearance (1).

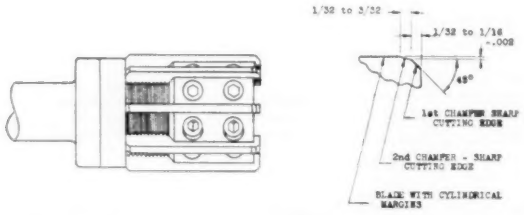


Fig. 4 Second Bevel on Point or Cutting Edges of Adjustable-Blade Reamers

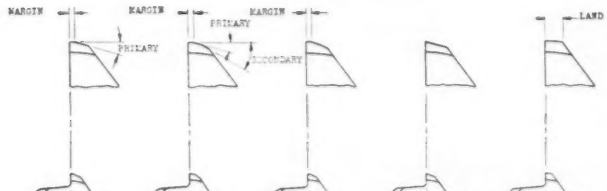


Fig. 5 Types of Side Clearance or Radial Relief

Side Clearance or Relief

Side clearance is illustrated in Fig. 5 and is formed by grinding away a portion of the land, usually leaving a slight cylindrical margin. The action of a reamer without side clearance is best understood by comparing a single tooth of the reamer with a boring tool having no clearance behind the cutting edge, as shown in Fig. 6, in which H is the hole to be bored, D the cutting edge, A is the side of the tool or peripheral land, with small sector B exactly concentric with the hole. Clearance is shown on the end of the boring tool at C.

It will be seen that great pressure would have to be exerted in the direction indicated by arrow X to hold the tool against the work, because the tool can cut the metal only at edge D, which enters the metal in the direction of the length of the hole, and

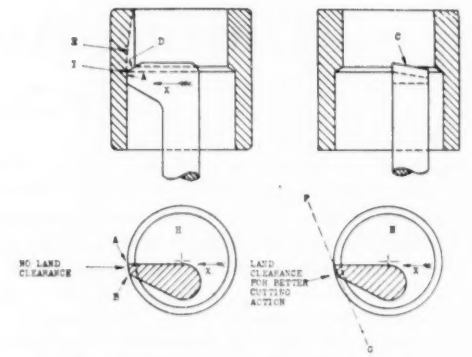


Fig. 6 Cutting Action of Boring Tool
(Land clearance improves performance.)

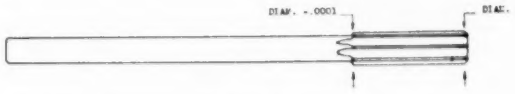


Fig. 7 Longitudinal Clearance or Back Taper

therefore there is no cutting action accomplished by the part shown at B. This part only rubs and as there is some spring to the tool it does not cleanly sever the chip produced by cutting edge D. Therefore part B is forced outward at each succeeding revolution as the tool is advanced, which results in producing a tapering hole as shown on dotted line E. This could be overcome only by exerting enough pressure in the direction of arrow X to hold sector B absolutely to its line of travel and by having the surface so hard and smooth that it could not tear the wall of the hole (1).

Another factor that also tends to produce a tapered hole and that requires additional pressure in the direction of the arrow is the dulling or rounding over of the extreme corner of the tool at 1. This dulling action is very severe at this point. The easiest and surest way to overcome these difficulties is to relieve the surface B along a line represented by FG. This reduces the required pressure in the direction shown by arrow X, and also lessens the trouble due to the dulling of the extreme cutting corner, and makes it possible to bore a hole the sides of which are practically parallel. The hole will also be smoother, as the side of the tool will scrape out the roughness left by the dulled corner as it follows after it. It must therefore be evident that a reamer without radial or side clearance is working under great difficulties and the chances for accurate work are small. It is also evident that as the surfaces of the reamer, which correspond to B, advance into the metal they should be lubricated and this can be done by lubricating the cutting edges as well.

Side relief is necessary for accurate reaming, yet a slight margin or cylindrical portion of the land must be left on the reamer to aid it to maintain correct size of the hole and allow the reamer to be sharpened many times without losing its original size. If the margin can be prevented from abrading or wearing away, the reamer can be sharpened back indefinitely. Of course some abrading and wear cannot be prevented, and commercial reamers are usually made a few ten-thousandths oversize so as to allow longer tool life and still produce accurate holes.

Rake Angles

The "rake angle" of a tool is the angle between the top cutting surface of a tool and a plane which is perpendicular to the surface of the work and to the direction of motion of the tool with respect to the work.

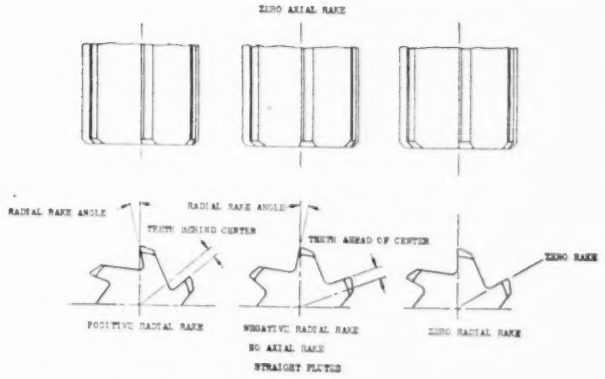


FIG. 8 TYPES OF RADIAL AND AXIAL RAKE

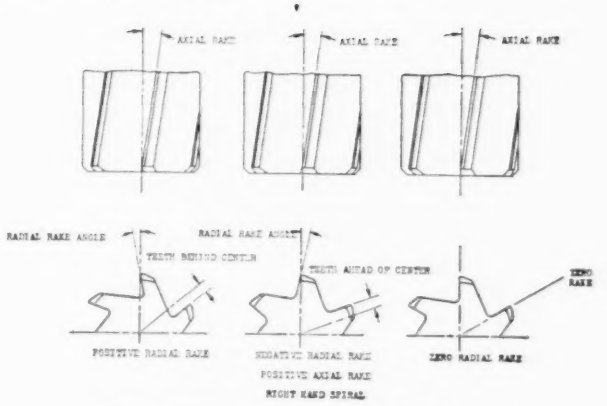


FIG. 9 TYPES OF RADIAL AND AXIAL RAKE

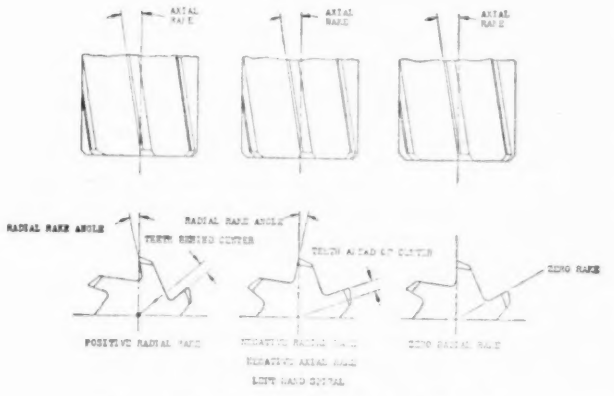


FIG. 10 TYPES OF RADIAL AND AXIAL RAKE

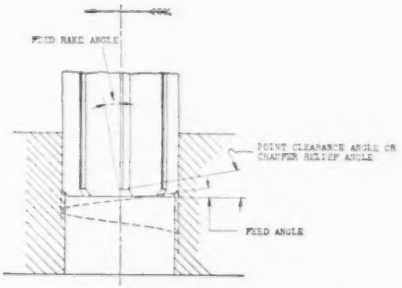


FIG. 11 RAKE ANGLE DUE TO FEED

(The angle that the reamer makes with the work as it feeds into the hole. Point clearance angle or chamfer relief angle should be greater than the feed angle shown. The action of the feed increases the rake angle of the reamer by the amount shown by the "feed-rake angle.")

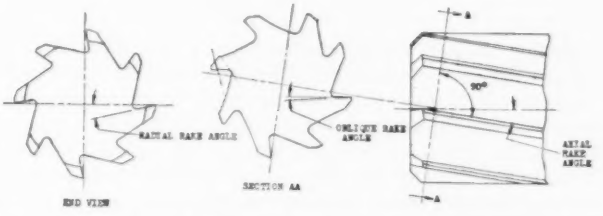


FIG. 12 RAKE ANGLE NORMAL TO HELIX ANGLE OR OBLIQUE RAKE ANGLE

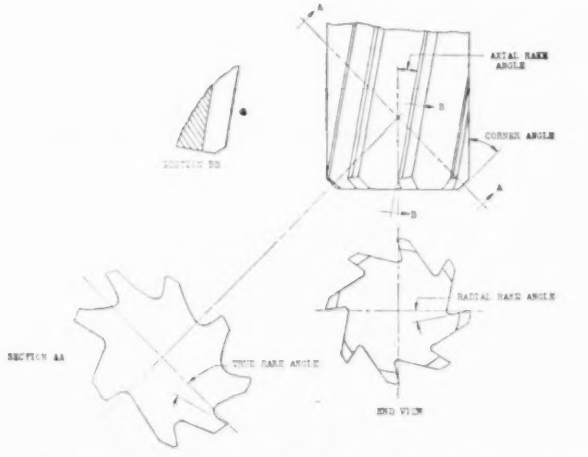


FIG. 13 TRUE RAKE ANGLE, NORMAL TO CUTTING EDGE OF CHAMFER, RESULTING FROM A GIVEN COMBINATION OF RADIAL-RAKE ANGLE, AXIAL-RAKE ANGLE, AND CORNER ANGLE OR POINT CHAMFER

The "axial-rake" angle is the same as the "helix angle." The "radial-rake" angle is the angle between the face of the flute and a radial line drawn to edge of the margin.

The best rake angle for each material, speed, feed, and machine-operating condition is a matter of trial and experiment.

Figs. 8, 9, and 10 show some possible combinations of axial and radial rakes with which reamers can be made.

Fig. 11 shows that the manner in which the reamer approaches

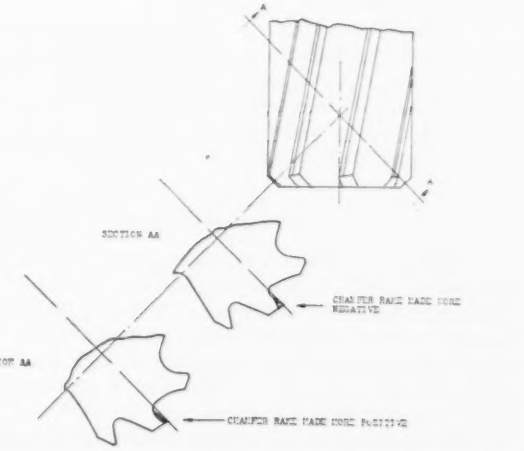


FIG. 14 POSITIVE OR NEGATIVE RAKE MAY BE VARIED ON CUTTING EDGES OF CHAMFER

the work affects the rake angle. The larger the feed per revolution the larger is the rake angle due to the feed.

Fig. 12 shows how the axial- and radial-rake angles combine to affect the oblique rake angle shown (3).

Fig. 13 shows a section at right angles to the point cutting edge at the actual and cutting edge of the reamer. This true rake angle depends upon the combined values of the radial rake, the axial rake, and the point angle or bevel.

Fig. 14 shows how in special cases with great care in grinding, the cutting rake of the point cutting edges may be varied for different materials and cutting conditions.

Form of Flutes

The style of flute is of the greatest importance, as its shape and area determine the relative strength of the tooth and the ability to carry away the chips. Large chip space and strength are desirable in all reamers but they are of greater importance in reamers designed for taper-reaming and for use in machines. The cutting face of a reamer tooth should have a fillet, see Fig. 15,

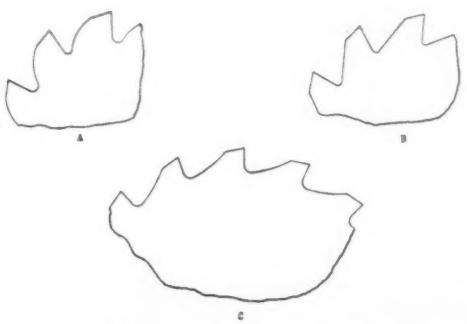


Fig. 15 Different Forms of Flutes Used for Various Types of Reamers

beginning about midway between the top and bottom of the tooth where great strength is desired, as in machine reamers, and nearer the bottom where the strength is of less importance, as in hand reamers. This fillet does not reduce the chip area materially because the chips tend to curl in most metals and this curl conforms to the shape of the fillet. Theoretically, the shape of the back of the tooth should be a convex parabola from the cutting edge to the base or junction of the fillet to obtain maximum strength. For manufacturing reasons a straight line or a concave curve which is tangent to the fillet and which lies outside the parabola is standard practice.

At *A* in Fig. 15 is shown a tooth with convex parabolic flank which is rarely used except on heavy chucking reamers where the cuts are heavy; at *B* is shown the straight flank; while at *C* is shown the concave-curve flank largely used by most manufacturers. Shape *C* provides a large chip area, and where uneven spacing is practiced the lands are most easily kept at uniform width (1).

Prevention of Chatter

Another desirable feature in a reamer, and especially a taper or hand reamer, is that it be able to cut a round smooth hole without chattering. There is an erroneous opinion prevalent that an even number of flutes chatter more than an odd number. This is a fallacy and our experience shows that an odd number of flutes will chatter as readily as an even number, especially when the reamer has more than four flutes.

Chatter may sometimes be eliminated by reducing the amount of clearance. To make reamers suitable for reaming most kinds of material met with in ordinary practice a considerable amount of clearance must be given, and this would produce chatter by biting in unless it is offset by some other features.

Chatter may sometimes be reduced by making the setup as rigid and strong as possible and by using pilots and guide bushings.

Chatter may also be reduced by cutting down the speed of the reamer. Speeds must not be so high as to permit chatter (5). Too low a feed may in some cases cause chatter due to glazing of the hole. Too much positive rake angle or too much negative rake angle may also cause chatter.

Reamers as commercially made usually have the cutting teeth unequally spaced. Fig. 16 shows a reamer with even spacing and a reamer with one type of uneven spacing. The reason for providing this uneven spacing is to reduce the possibility of chatter.

Fig. 17 shows a chucking reamer about to enter a hole. If the axis of rotation *A-A* of the reamer is exactly in line with the axis of the hole *B-B*, and all cutting conditions correct, such as speed not too high, feed not too low, amount of stock sufficient for a chip, rake not too hooked or too negative, the work and reamer rigidly held and guided if possible, there should be no chatter and a round, smooth, accurately sized hole should be produced.

However, if the axis of the reamer is out of line with the axis of the hole, or if a hard spot in the steel is cut, or if the reamer teeth are not sharpened accurately so that they are all at the same angle and length; one tooth of the reamer may cut a little deeper than the others, and in addition to the motion of rotation about its axis, the reamer will also acquire a secondary form of rotation as shown in Fig. 18.

This shows the situation greatly exaggerated. Tooth 1 has cut deeply into the metal and for an instant the reamer will rotate about the instantaneous center 1, until tooth 2 bites into the metal. Tooth 2 now becomes the instantaneous center of rota-

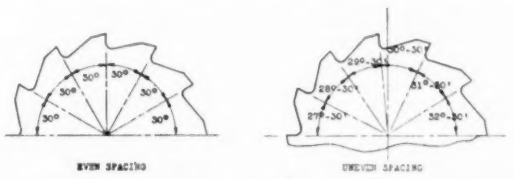


Fig. 16 Unequal Spacing of Flutes to Avoid Chatter

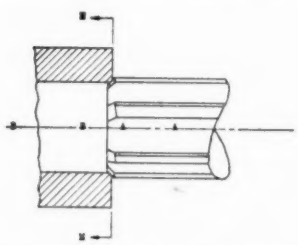


Fig. 17 Unequal Spacing of Flutes to Avoid Chatter



Fig. 18 (*left*) Unequal Spacing of Flutes to Avoid Chatter
(Section *M-M* of Fig. 17 greatly exaggerated. Reamer while rotating about its axis rotates also about center 1, a small amount, until tooth 2 cuts.)

Fig. 19 (*right*) Unequal Spacing of Flutes to Avoid Chatter
(Section *M-M* of Fig. 17 greatly exaggerated. Reamer while rotating about its axis rotates also about center 2, a small amount, until tooth 3 cuts.)

tion (see Fig. 19) and the reamer rotates until tooth 3 bites in, and so on all around the reamer. This continues while the reamer is rotating about its axis. A very bad condition such as described would result in chatter. If the teeth are unevenly spaced so that the distances between 1 and 2, 2 and 3, etc., are not the same, the jump or biting-in of the teeth will be unevenly distributed, and the cut gradually may become smooth and chatterless.

Cutting Action

The cutting action of a reamer has been shown in Fig. 6 to be similar in many respects to that of a boring tool. In Fig. 20 is shown a boring tool about to enlarge or finish-cut a rough hole. It must cut it sway into the hole by its sharp, cleared, end cutting edge *D*. Similarly the reamer must cut its way into the small rough hole by its sharp, cleared, end cutting beveled teeth or point.

The cutting action of a reamer is in some respects similar to that of a drill. Fig. 21 shows a drill about to cut through and enlarge a rough hole. The drill is larger than the rough hole and in order to enter, the drill must cut its way in. Similarly, in the same figure the reamer must be larger than the rough hole and must cut its way into the hole by its end cutting or beveled teeth. The cutting action of the longitudinal margins or lands is explained in connection with Fig. 6.

Fig. 22 shows the similarity of the cutting action of a drill and a hand reamer. The cutting action of a reamer is in some respects similar to that of an end mill as shown in Fig. 23, assuming that the direction of feed for both tools is helically axial.

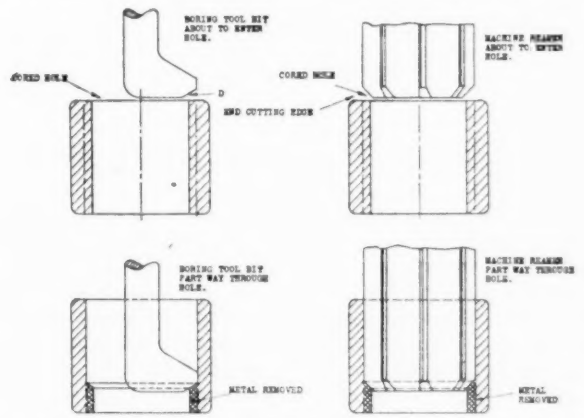


Fig. 20 Similarity of Cutting Action of a Boring-Tool Bit and a Reamer

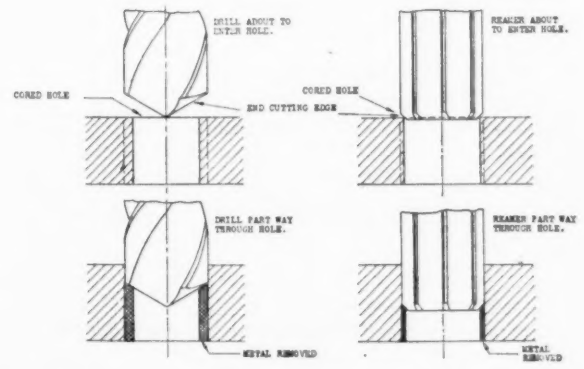


Fig. 21 Similarity of Cutting Action of a Twist Drill and a Machine Reamer

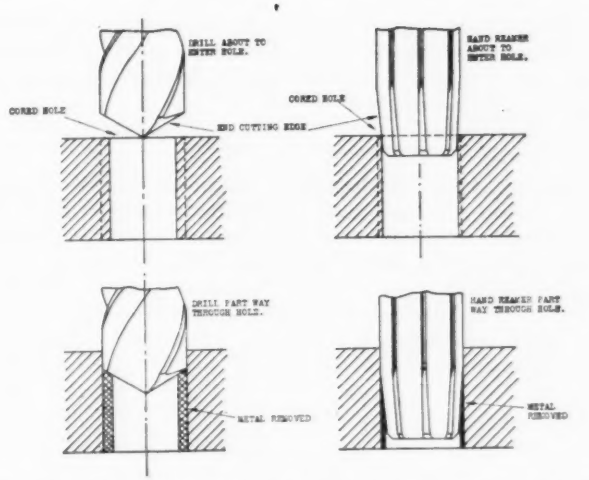


Fig. 22 Similarity of Cutting Action of a Twist Drill and a Hand Reamer

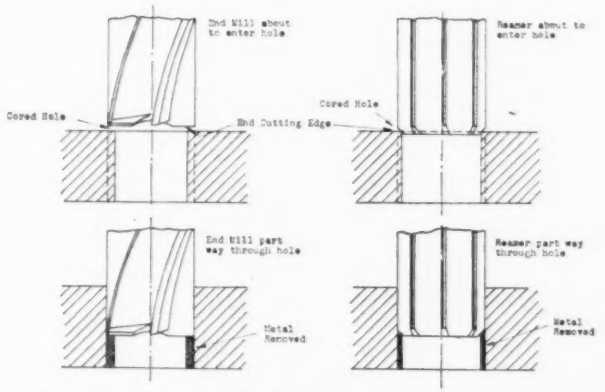


Fig. 23 Similarity of Cutting Action of an End Mill and a Machine Reamer

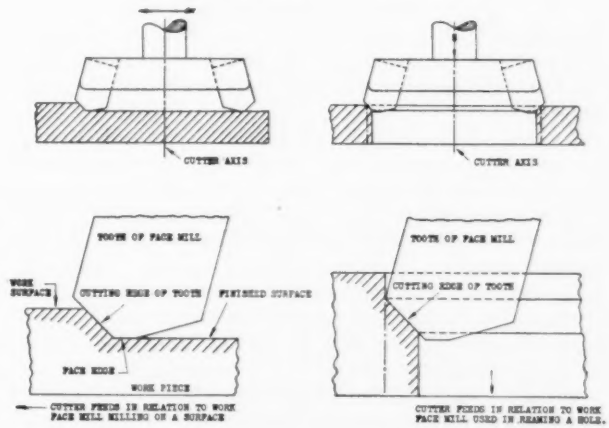


Fig. 24 Similarity of Cutting Action of a Face Mill and a Machine Reamer

The bodies of both tools fit in the holes they cut. Of course, in an end mill the direction of feed is usually perpendicular to the axis of the tool, not along the axis. Also an end mill will not usually produce as accurate a hole as a reamer because its longitudinal teeth are backed off sharp with no margins or lands.

Fig. 24 shows how a face mill, usually used for cutting along the surface of a piece of work, might be used to enlarge a hole.

This shows that the cutting action of face-milling teeth is essentially similar to that of reamer end cutting teeth. The lands or margins on a reamer serve the same purpose of smoothing the cut that the faces do on a face mill.

Reamer Sharpening

After a reamer has been used for a number of holes it will show signs of wear. These signs should be carefully watched and studied and at the proper time the reamer should be resharpened. In general, higher speeds will cause the reamer to dull faster, but higher speeds also give higher production. The finish required also determines the speed possible.

It will be noticed that the reamer will become dull along its once sharp edges *A-B*, Figs. 25 and 27, with the greatest wear at

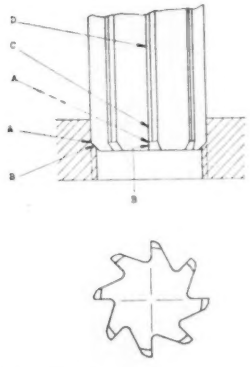


Fig. 25 Wear of Reamer Cutting Edges

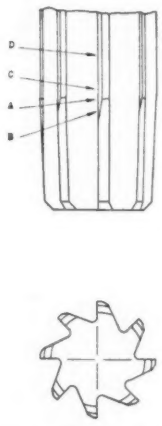


Fig. 27 Wear of Hand-Reamer Cutting Edges

the corners *A*. After a number of holes have been reamed the corner *A* will become completely rounded off. If the reamer is continued in use after this corner has become worn, the sharp edge along the margin *A-C* will also become worn and abraded starting at *A* and working back along the margin or land *A-C*. If the reamer is kept in use in this dull condition it will be completely ruined, the margins all the way back to *D* will become abraded, and the reamer cannot ream a smooth hole to the correct size.

The first result of using a dull reamer will probably be undersize holes, the reamer will be actually forced through the hole without cutting its true size. This of course, causes unnecessary wear on the reamer lands. If at the first sign of holes coming smaller in size the reamer is sharpened, holes up to size will be again produced.

To sharpen the reamer it is necessary to grind only the point or cutting edges back as shown at *A-D*, Figs. 26 and 28, with the proper clearance. The edges are ground back until the corner and marginal dullness between *A* and *C* is removed.

The importance of frequent reamer point sharpening for accurate and smooth holes cannot be overemphasized, especially as it is as simple an operation as drill point sharpening, and a very similar one. Frequent sharpening prolongs the life of the accurately sized reamer margins and lands, and guards against their abrading or wearing undersize and producing undersize holes.

Just how often a reamer should be sharpened or what tool life a reamer should have in minutes of use per grind or number of inches of holes reamed per grind must be determined by trial for each particular application.

In general, the higher the cutting speed the shorter will be the

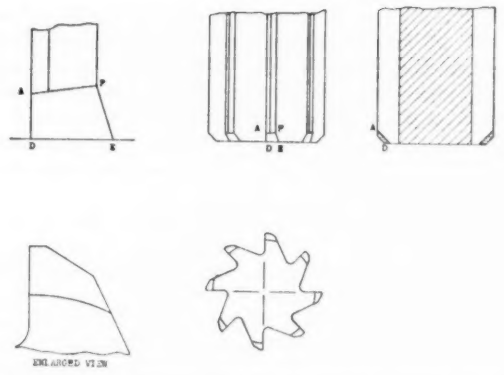


Fig. 26 Sharpening of Reamer-Point Cutting Edge

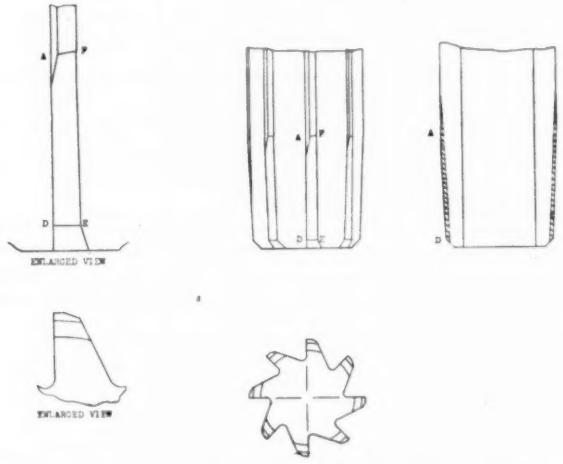


Fig. 28 Sharpening of Hand-Reamer Point Cutting Edge

tool life, but of course the high cutting speed has the advantage of high production, if the finish and accuracy of the holes produced are satisfactory.

On single-operation machines where it is a simple matter to take out a tool and resharpen it, low tool life and high production are desirable. On a multispindle automatic it might be uneconomical to change tools more than once a shift, and here slower speeds and longer tool life on a particular operation may be better.

In any case, the use of a dull tool is very poor economy. It is destructive of the reamer and productive of poor and unaccepta-

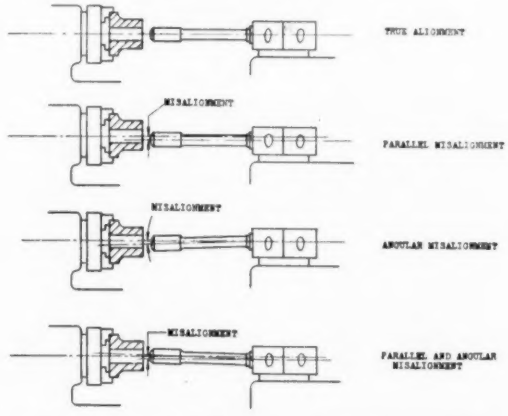


Fig. 29 Floating Toolholders and Alignment

ble work. Some methods for sharpening reamers are shown in Fig. 28.

Floating Toolholders

It should always be borne in mind that a reamer produces its best work when taking light cuts. If the holes are being finish-reamed in a machine, good work has been done by holding the reamer in a chuck, collet, or holder that will float smoothly without jumping. Some good work is done with holders that allow the reamer to float perpendicular to its axis as well as at an angle (1). This floating action is necessary because it is almost impossible to hold the reamer so that it is exactly concentric with the hole, and at the same time have the line of travel of the axis of the reamer coincide or line up with the axis of the hole. A reamer must align itself with the hole it is cutting for extreme precision. The lands or margins of the reamer must be a snug fit in the hole that the reamer is finishing. The axis of the rotating reamer must coincide within a very small amount with the axis of the tool.

This floating alignment and rigidity of cut are both difficult to attain but are necessary for good work.

Speeds, Feeds, and Lubricants

No definite rules can be given to cover the speeds and feeds that should be used in reaming. Several factors govern the correct feed and speed. The material to be reamed and the material of the reamer are perhaps the most important governing factors. The finish desired in the hole and whether hand feed or machine feed is used, govern the selection of the proper feed. The type of lubricant used, or whether the reamer is piloted or guided in any way, also influence the decision.

In general, reamers should be run at about one half to two thirds the speed of the corresponding drill. It is always best to start the reamer somewhat slower than this, and gradually increase the speed until the best condition is found. If the reamer is run at too slow a speed the production will suffer, while if run too fast, the wear on the reamer will dull it too soon. Somewhere between these two extremes is the proper speed which gives a high productivity with a long reamer life.

Feeds should be from 2 to 3 times the feed of the corresponding drill. The higher feed causes increased production and reduced tool wear. If too fine a feed is used, the reamer will be subjected to unnecessary wear. Too coarse a feed will produce feed marks in the hole. The desired finish must be balanced against the production per hour.

Feeds are governed by the size of the reamer and the material reamed. A general rule is first to try a feed of 0.002 to 0.004 in. per revolution for reamers smaller than $^1/_8$ in.; 0.004 to 0.008 for reamers $^1/_8$ to $^1/_4$ in.; 0.008 to 0.014 for reamers $^1/_4$ to $^1/_2$ in.; 0.014 to 0.030 for reamers $^1/_2$ to 1 in.; and 0.030 to 0.050 for reamers larger than 1 in. Alloy and hard steels should generally be reamed with the lighter feeds, while cast iron, brass, and aluminum are sometimes reamed with the heavier feeds. Suggested speeds for reamers are given in Table 1.

TABLE 1 SUGGESTED SPEEDS FOR HIGH-SPEED REAMERS

Material reamed	Speed, fpm
Aluminum and its alloys	130–200
Bakelite	70–100
Brass and bronze, ordinary	130–200
Bronze, high-tensile	50–70
Cast iron, soft	70–100
Cast iron, hard	50–70
Cast iron, chilled	20–30
Malleable iron	50–60
Magnesium and its alloys	170–300
Monel metal	20–30
Steel, machinery (0.2 to 0.3C)	50–70
Steel, annealed (0.4 to 0.5C)	40–50
Steel, tool (1.2C)	30–40
Steel, forgings	30–40
Steel, alloy	30–50
Steel, stainless, free-machining	40–50
Steel, stainless, hard	20–30

Lubricants

Lubricants have many functions, several of which are as follows:

1 To cool both the cutting edges of the tool and the work being machined. This can best be done by directing as large a volume of the coolant as possible on the cutting edges. On thin-walled work it often helps to allow a large volume of flow onto and around the piece.

2 To lubricate the chips; this aids in chip clearance.

3 To improve the finish of the work. The selection and proper application of the lubricant will materially influence the machined finish.

It is suggested that lubrication problems be referred to a reputable manufacturer of cutting oils. The following list of lubricants should be used as suggestions only:

1 Aluminum and its alloys: Soluble oil, kerosene, and lard-oil compounds, light nonviscous neutral oil, kerosene, and soluble-oil mixtures.

2 Brass: Dry, soluble oil, kerosene, and lard-oil compounds, light nonviscous neutral oil.

3 Copper: Soluble oil, winter-strained lard oil, oleic-acid compounds.

4 Cast iron: Dry or with a jet of compressed air for a cooling medium.

5 Malleable iron: Soluble oil, nonviscous neutral oil.

6 Monel metal: Soluble oil, sulphurized mineral oil.

7 Steel, ordinary: Soluble oil, sulphurized oil, high E.P. value mineral oil.

8 Steel, very hard and refractory: Soluble oil, sulphurized oil, turpentine.

9 Steel, stainless: Soluble oil, sulphurized mineral oil.

10 Wrought iron: Soluble oil, sulphurized oil, high animal-oil-content mineral-oil compound.

Regular Reamers and Basic Standard-Hole System of Tolerances

Varying degrees of accuracy result from the use of different tools employed in the drilling, boring, and reaming of holes. The cost of obtaining the accuracy required by some kinds of work would be prohibitive for others. Therefore the proper tools for producing holes in any class of work are those best adapted to produce the required accuracy from the standpoint of an over-all economy. By an over-all economy is meant the greatest number of suitably finished holes that can be produced for each dollar paid out for tools, labor, and machine expense.

Drilled holes are neither round, straight, nor of uniform diameter when compared with the accurate holes required by most industries, although they may be sufficiently accurate to meet the requirements of holes for rough bolts, rivets, and similar classes of work. When a close fit is required holes are usually finished by reaming. When holes of extreme accuracy are required it is necessary to use two reamers in order to obtain the desired results. For all such work as holes for pins, rods, or finished bolts, one reaming operation is sufficient, and even in many grades of machines the holes for journals are finished with a single machine-reaming operation. Before selecting a type of reamer for any class of work, it is advisable to study the cutting action of different reamers in order to select the one best adapted to each class.

In some shops the practice is to produce round, smooth, straight holes, as close to the standard or exact size as possible. All the tolerance or allowable error is above the basic or exact size. In other words, the hole must be slightly oversize, not

undersize. This enables holes to be produced in large numbers, which are sure to make the proper fits. Many shops insist that all holes in parts belonging to good work must be hand-reamed, and in such a manner that the work is subjected to no distortion due to holding or clamping. This is sometimes done by holding the hand reamer in a vise and passing the work over the reamer with a screwlike motion, the reamer scraping only a few thousandths out of the hole. Other shops insist that the holes be finished on the chucking machine, and in this case the chucking reamers must be accurate and the work not distorted by the chuck if good results are to be expected.

The standard reamer and the standard basic plug-and-ring gage have been the foundation of interchangeable manufacturing.

A standard basic 1-in. hole may be defined as one which will just receive a 1-in. plug gage which measures exactly 1 in. diam as measured on a measuring machine. The hole which receives this plug gage will also receive an accurately finished shaft of the same size (4).

In practical manufacturing the "go" gage is not usually exactly 1 in. diam but has a plus wear allowance and a plus manufacturing tolerance, which means that the basic hole in practical manufacturing is slightly large.

Commercial reamers are made slightly oversize because the hole made by the reamer must be large enough to receive the "go" working gage. Reamers as made commercially have also a slight plus wear allowance and a slight plus manufacturing tolerance (2). This assures that all holes carefully reamed as near to the exact size of the reamer as possible will all accept standard commercial "go" plug gages and will all receive finished shafts made to the correct sizes, with proper allowances between hole and shaft depending upon the class of fit wanted.

Many parts made by interchangeable mass-production methods depend upon the precision and uniformity of the reamer sizes to maintain hole sizes which will be basic, with a very small tolerance oversize. The holes are sure to be large enough and yet not too large to produce undesirable results.

American Standard for Allowances, Tolerances, and Gages for Metal Fits

Since 1926 the foregoing standard has been in use as a guide for the correct dimensions of holes made for interchangeable manufacturing.

This standard is based upon the same principles as the successful American Standard for Screw Threads ASA B1.1-1935. These are the same dimensions as published in Handbook H-28 Screw Thread Standards for Federal Services.

In both of these standards the minimum hole is taken as the basic or standard size. This means that the interference point or place where metal-to-metal fit occurs between hole and shaft will be at this basic dimension no matter what class of fit is specified. This is illustrated in Figs. 30 and 31.

The advantage of the standard-hole system is that it enables standard basic plug gages to be carried in stock and establishes definite minimum hole sizes, below which the holes cannot go, and maintains universal interchangeability.

If it is necessary to change tolerances or allowances on a given fit, this can be done in the basic-hole system without changing the "zero," "base," or "interference line," as the minimum hole is left constant, and the maximum hole, or minimum or maximum shaft sizes are changed. The standard plug gage always rejects any hole below basic size which might destroy interchangeability.

It is easier to produce plug gages, blocks, and measuring rods to high grades of precision, for use in measuring hole members than it is to produce gages for measuring shaft members. Hole members are best measured with fixed-size gages and also are best produced with fixed-size or solid reamers, or broaches. Shaft

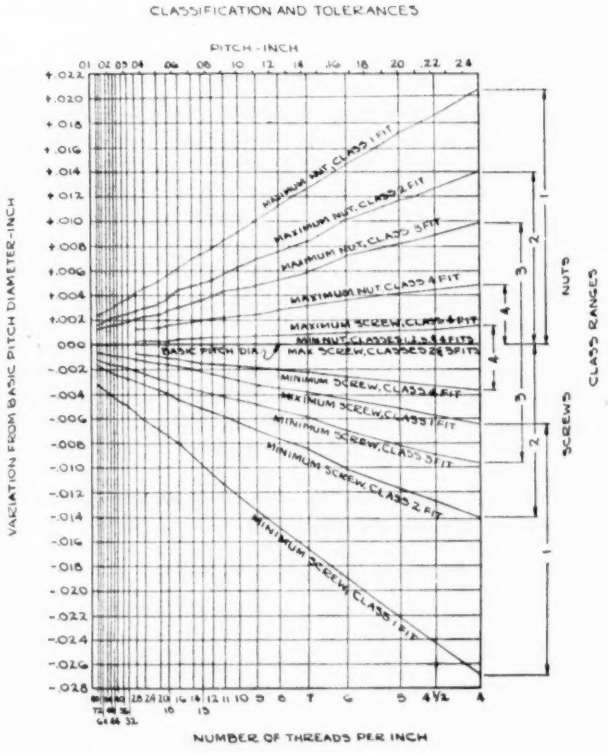


Fig. 30 Relation of Maximum and Minimum Pitch Diameters of Classes 1, 2, 3, and 4 Fits to Basic Pitch Diameters

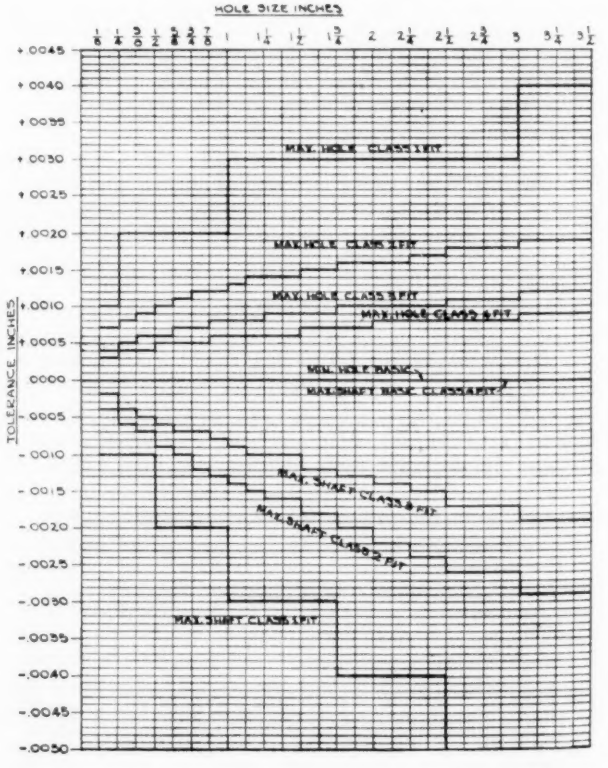


Fig. 31 Basic Minimum Hole for All Classes of Fits
(American Standards Association.)

members are more easily measured with adjustable gages and also more easily produced with adjustable tools such as lathe tools or grinding wheels. Changes in allowances or tolerances for various fits can thus be more readily made on the shaft member than on the hole member.

Fig. 32 shows how a standard commercial reamer would produce holes of any class of fit desired, if the reamer were carefully used so as to cut close to its exact size. Also, if properly sharpened and cared for, a long life of the reamer may be obtained before its lands are worn so undersize that the reamer will produce holes below the minimum size.

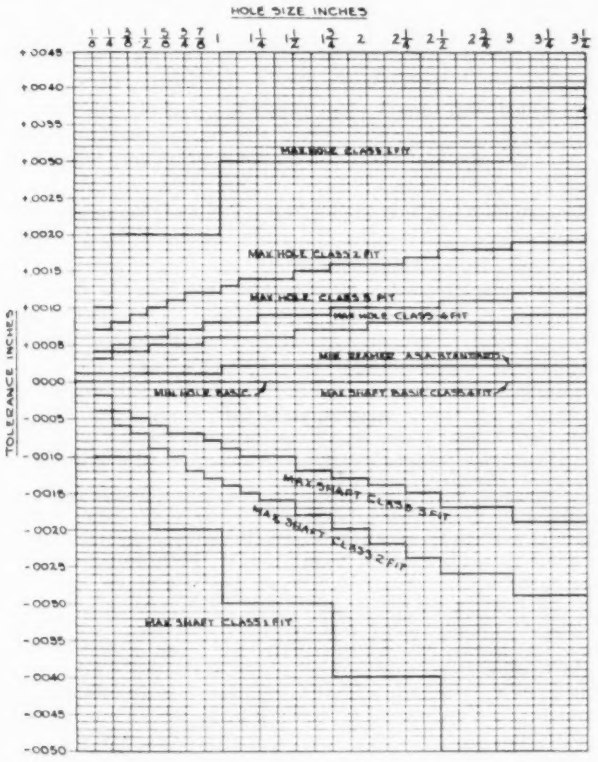


FIG. 32 STANDARD REAMER TO PRODUCE STANDARD HOLES OF ALL CLASSES OF FITS

Another advantage of the basic-hole system of fits is that it allows one standard-size reamer with definite tolerances to be carried in stock throughout industry for the convenience of the customer and user. These reamers will produce universal interchangeable work for any of the classes of fit.

The fact that the reamer is accurately sharpened to size is no guarantee that the hole made will be as accurate as the reamer. The accuracy of the hole depends upon many factors, such as hand- or machine-reaming, machinery and fixture in good condition or badly worn, the kind of material reamed, the kind of lubricant, and the skill and carefulness of the mechanic.

It was to take care of this great variety of working conditions that different tolerances were put on the various classes of standard holes in the report of Allowances and Tolerances of the American Standards Association, ASA B4a-1925.

It was realized by the committee which wrote this report that the one standard-size reamer will produce holes of varying tolerances depending upon the conditions of its use. Extreme accuracy and precision are usually expensive, and it is uneconomical to make a hole perfect when one not so good will serve the purpose just as well. Therefore the various classes of holes and fits were provided as a measure of economy. It was intended all along, however, that but one standard size of reamer would be necessary; careful use of this reamer would produce a Class 3 or 4 hole; rough, rapid, or worn machine use would produce a Class 1 hole.

It has sometimes been thought that large tolerances were put on rough holes to allow for wear on the reamer, whereas the large tolerances are really there to indicate that costly tooling and hand-finishing are not necessary when an inexpensive rapid job is sufficient for the purpose.

Long wear life of the reamer will be obtained by keeping the point sharp and the lands in good condition rather than by using an oversize reamer which will produce holes that are too large.

It has sometimes been suggested that the American Standard for Tolerances, Allowances, and Gages for Metal Fits should contain a basic-shaft standard as well as the present basic-hole standard. It is believed that it would be better not to do this because it would imply the standardizing and carrying in stock of a different minimum or basic plug gage for each class of fit for each nominal size of hole, Fig. 33. Also it would imply the use of a different-size reamer for each class of fit. These solid tools are difficult to produce and expensive to maintain. It is more eco-

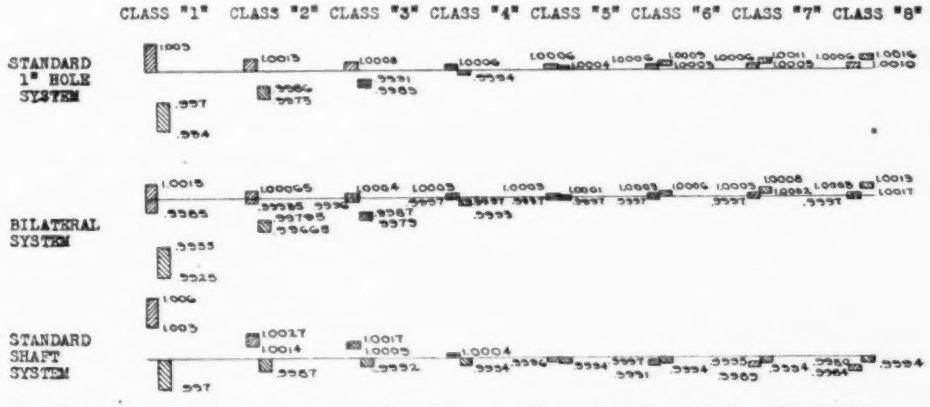


FIG. 33 STANDARD-HOLE SYSTEM USES ONE STANDARD BASIC-SIZE PLUG GAGE TO CHECK MINIMUM HOLE SIZE FOR ALL CLASSES OF FITS

(Sketch made to show that standard-hole system uses the one standard basic-size plug gage to check minimum hole size for all classes of fits. This means that interchangeability is positively maintained for any allowance between hole and shaft and any tolerance on shaft. The "zero line," "interference line," or "metal-to-metal fit contact line" is always at the basic dimension, always at the standard minimum hole. Standard stock reamers, if carefully used and maintained sharp, will produce these standard holes for a long period of reamer-wear life.)

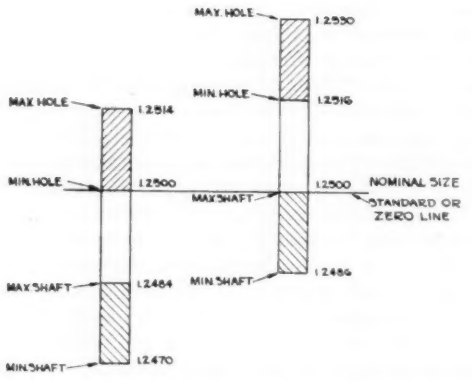


FIG. 34 HOLE SIZES FOR STANDARD-HOLE AND STANDARD-SHAFT SYSTEMS

nomical to obtain various classes of fit by maintaining standard holes and varying the shaft dimensions.

If for some particular reason it is found better to use the maximum size of the shaft as standard, as shown in Fig. 34, the size of hole becomes special and special drills and reamers must be obtained. Special tools are always more costly than the regular and also require longer waits for deliveries. As there is less use for a special tool, it lies in the toolroom for a longer time unused, and the overhead of manufacturing is increased.

For example, in Fig. 31 a standard shaft system of fit calls for 1.2500 as the maximum shaft size and 1.2516 as the minimum hole size. This can be considered the same as a basic-hole system of fits using a "special size" 1.2516 as the basic hole. This (as all standard shaft fits do) requires special-size reamers. From the tables of allowances and tolerances the maximum and minimum shafts and holes are easily found for special as well as standard sizes. In other words, the holes of the "standard-shaft" system, are nothing but "special" holes of the standard-hole system. The standard shaft system is really a special, nonstandard use of the standard-hole system.

In this connection E. C. Peck (1) states: "I see no need whatever for a basic shaft standard. The only example I have ever heard given is the one where two free fits are required on the ends of the shaft and a force or tight fit wanted in the center, and this has been done economically and satisfactorily for years by the 'basic-hole system.' All during World War I, I saw the drawings for millions of interchangeable parts, and I never saw any that were not made to the 'basic-hole' system."

Thus the publishing of special tables for the standard shaft system is unnecessary, as all the values for tolerances and allowances may be taken from the Standard Hole System of tables, merely by basing all the fits on the minimum-size hole.

CONCLUSIONS

A reamer is a cutting tool and like other cutting tools it must be provided with correct clearances, rakes, and other features of good tool design. Its cutting edges must be sharpened frequently to prolong the useful life of the tool and to produce accurately smoothly finished holes.

The standard reamer made with standard manufacturers' tolerance is one of the most important tools used by the interchangeable production manufacturers.

The standard reamer is an important feature of the standard-hole system of allowances and tolerances for metal fits and provides the most economical method of securing precision fits and universal interchangeability.

BIBLIOGRAPHY

1 "Types of Reamers and Their Use," by E. C. Peck, *Machinery*, vol. 25, December, 1918, pp. 335–337.

2 "Reamers," American Standards Association, American Standard B5.14-1941.

3 "Milling Cutters and How to Use Them: Special Rake Angles Used for Sintered Carbide Tools," by M. Martellotti, *American Machinist*, vol. 89, February 15, 1945, pp. 122–125.

4 "Tolerances, Allowances, and Gages for Metal Fits," American Standards Association, American Standard B4a-1925.

5 "Carbide-Tipped Tools," Cleveland Twist Drill Company booklet, 1945.

Utilization of Producer Gas in Industrial Furnaces

By D. B. HENDRYX,[1] PITTSBURGH, PA.

Producer gas is the cheapest artificial fuel per Btu that can be made from solid fuel. This paper discusses the economics, the equipment, and methods of generating producer gas for industrial uses.

MOST gas-producer projects look good on paper. The basic idea of a low-cost gaseous fuel, made from coal at a central point and distributed in pipes to the furnaces, is excellent and attractive.

Producer gas for industrial uses only is discussed in this paper, as contrasted to gas manufactured for public-service distribution. It is made from coal or coke, and the solid fuel is completely transformed into gas in the process. Producer gas is the cheapest artificial fuel per Btu that can be made from solid fuel.

Comparative Cost of Fuels

The economics of the fuel situation must be considered first. The cost of fuels can be compared on a Btu basis, but this must be the total cost of heat delivered to the furnace, including fuel and ash handling, power, steam, depreciation, etc. In most industrial districts, coal is the cheapest fuel, but for various reasons it frequently cannot be used in furnaces in its crude form, either on grates or as pulverized fuel. Such considerations as furnace temperature and atmosphere, reversing and regeneration, control, delayed combustion, radiant flame, localized heating, freedom from ash, handling of coal and ashes, and many others may rule out the use of coal.

Under such conditions, if natural gas or fuel oil is available at a reasonable price, or if a by-product fuel such as coke-oven or blast-furnace gas can be used, one would hesitate before building an expensive gas-producer plant, with its attendant dirt, heat, and operating difficulties. If the fuel requirements do not amount to more than 1500 lb of coal per hr, a gas producer would seldom be justified; but if coal is cheap compared to other fuels, and if a gaseous fuel is needed, the use of producer gas will be worth investigation.

Table 1 may be used for a quick comparison between the costs of several fuels. It shows the price that can be paid for fuel oil or natural gas as compared to cost of coal delivered to the gas-producer plant, taking into account the cost of making the producer gas, including depreciation, and the cost of heating and atomizing the oil. The cost of gasifying 1 ton of coal or coke was estimated at $1.75; but this figure might be higher or lower, depending upon the size of the plant, wage rates, number of men required for operation, and similar factors (see Table 2). This table does not agree at all with the comparisons made in the advertising matter of many manufacturers, for the reason that they use a much lower charge for producer operation.

The choice of fuels cannot always be made strictly on a cost basis. The supply of natural gas or oil may be restricted or cut off suddenly in the coldest winter weather, while coal will probably always be available, in spite of numerous recent threats against the life of one of our greatest industries. The relative prices of fuels do not remain constant. Since 1939, the price of natural gas has stayed the same in most districts, while coal has advanced 30 to 45 per cent, and fuel oil 50 to 100 per cent. Any of these conditions may make the construction of a gas-producer plant imperative.

As can be seen from the cost of gasifying coal shown in Table 2, the item of depreciation is a very appreciable part of the cost. But once the money for a producer plant has been spent, due to emergency conditions or for other reasons, the matter of depreciation can be neglected, and natural gas or oil would have to be about 10 per cent cheaper than indicated in Table 1, in order to compete with producer gas.

TABLE 1 COMPARISON OF FUEL COSTS

Hot raw producer gas			Fuel oil	Natural gas
Price of coal per ton delv'd. 27,000,000 Btu	Cost of producer gas per ton coal 19,200,000 Btu	Cost of producer gas per 1,000,000 Btu	Equivalent price per gal, or 145,000 Btu	Equivalent price per 1000 cu ft or 1,000,000 Btu
$2.00	$3.75	$0.195	$0.0253	$0.195
2.50	4.25	0.221	0.0291	0.221
3.00	4.75	0.247	0.0328	0.247
3.50	5.25	0.273	0.0366	0.273
4.00	5.75	0.299	0.0404	0.299
4.50	6.25	0.325	0.0442	0.325
5.00	6.75	0.351	0.0480	0.351
5.50	7.25	0.377	0.0517	0.377
6.00	7.75	0.403	0.0555	0.403
6.50	8.25	0.430	0.0594	0.430
7.00	8.75	0.456	0.0632	0.456

Cost of gasifying coal per net ton is assumed to be $1.75 (see Table 2).

Cost of producer gas per million Btu is based on:	Per lb coal
60 cu ft of gas at 60 F per lb coal, and 140 Btu per cu ft	8400 Btu
Sensible heat with gas delivered to furnace at 700 F, 60 cu ft of gas at 11 Btu per cu ft	660 Btu
Tar, 60 cu ft of gas at 0.0006 lb tar per cu ft and 15,000 Btu per lb tar	540 Btu
Total	9600

Heat in producer gas at 700 F per ton coal, 2000 × 9600 or 19,200,000 Btu.

Price of fuel oil allows for charge of $0.003 per gal for steam, power, and depreciation but no charge for depreciation. If depreciation charge on gas-producer plant is neglected, deduct $0.0046 per gal from price of oil shown.

Price of natural gas covers fuel cost only. If depreciation charge on gas-producer plant is neglected, deduct $0.032 per 1000 cu ft from price of gas shown.

Selection of Producer-Gas Fuel

If the foregoing considerations seem to warrant the construction of a producer plant, the next step is to decide what fuel will be used to make the gas. There are two distinct types of producer gas—that made from bituminous coal, and that made from anthracite or coke. Since bituminous coal in most parts of the country is cheaper than anthracite or coke, it follows that gas manufactured from it will be the cheapest gas that can be made. Cost alone, however, may not be the deciding factor.

If the heat requirements of the furnaces are large, if the gas can be burned in the furnaces through a few ports instead of a

[1] Chief Engineer, Harbison-Walker Refractories Company.

Presented at a joint meeting of the American Institute of Mining and Metallurgical Engineers and The American Society of Mechanical Engineers, Pittsburgh, Pa., Oct. 28–29, 1943.

Note: Statements and opinions advanced in papers are to be understood as individual expressions of their authors and not those of the Society.

TABLE 2 GAS-PRODUCER OPERATING COSTS

Fuel:	Small plant, 1 8-ft producer Per week	Per ton	Larger plant, 2 10-ft producers Per week	Per ton
Tons of coal gasified	120	...	400	...
Tons of coal used to generate steam for blowing producers	8	...	25	...
Operating cost:				
Labor				
Gas producer and boiler operator 1 man 168 hr at $.80	$134.40	...	$134.40	...
Dust removal from dust legs				
Small plant 16 hr at $.65	10.40	...	...	...
Larger plant 32 hr at $.65	...	...	20.80	...
Coal and ash handling at $.10 per ton coal	12.00	...	40.00	...
Burning out flues, once every 6 weeks, averaging 1 man per week 8 hrs at $.65	5.20	...	5.20	...
Repair labor				
Small plant, 1 man 4 hr at $.90	3.60	...	...	...
Larger plant, 1 man 8 hr at $.90	...	...	7.20	...
Total labor	$165.60	$1.28	$207.60	$0.52
Power				
Small plant 1100 kwhr at $.012	13.20	0.11	...	...
Larger plant 2400 kwhr at $.012	...	...	28.80	.07
Repair materials, including coal machinery, producers, auxiliaries, boilers, painting, etc., estimated average during life of plant	30.00	0.25	60.00	0.15
Boiler feedwater and producer cooling water, based on recirculation of cooling water, 190 gal per ton coal at $.10 per M gal	2.28	0.02	7.60	0.02
Oil, grease, waste, supplies	3.00	0.03	6.00	0.02
Coal for steam, at $3.50 per ton	28.00	0.23	87.50	0.22
Total cost of gasifying coal, no depreciation charge		$1.92		$1.00
Depreciation, on basis of 10 per cent per year on investment of the following:				
Small plant, and gas mains $60,000	115.00	0.96	...	...
Larger plant, and gas mains 100,000	...	...	192.00	.48
Total, including depreciation		$2.88		$1.48

large number of individual burners, and if the producers can be located near the furnaces, the selection would favor hot raw gas made from bituminous coal. If less fuel is needed, or if gas must be distributed to a number of furnaces or individual burners located at some distance from the producer plant, the greater expense of using anthracite or coke might be warranted. Wherever practical, both kinds of gases are used in their hot raw state.

It seems to be a current belief that a "gas coal," with a volatile content above 35 per cent, is the best fuel for bituminous producers. It does make a rich gas, and it is usually a free-burning coal which does not cake badly in the producer. On the other hand, the gas may contain more vaporized tar which will be objectionable unless the gas can be kept hot until it reaches the furnaces. The ideal producer fuel would be a 2 or 3-in. lump coal, with fines below $^3/_4$ in. screened out, having an ash-fusion point above 2500 F, and free-burning characteristics which prevent the top of the fuel bed from becoming a sticky mass and caking. In actual practice, mine-run or slack coals are often used at some reduction in capacity, although more dust is carried over into the mains when using fine coal. A gummy condition at the top of the fuel bed can be overcome by keeping it at a higher temperature. The amount of ash in the coal does not make as much difference as its fusion point does, and even coal with low-fusion ash can be used by applying more steam in the blast.

Mine-run or slack bituminous coal can be used in producers because the coking action at the top of the fuel bed will provide passages for the gas. When anthracite or coke fuel is used, the only openings for the flow of gas through the upper part of the charge will be the spaces between the particles of fuel. Therefore most of the dust finer than $^1/_4$ or $^3/_8$ in. must be screened out. The term "coke breeze" can cover a multitude of sins and, before deciding upon this as a source of gas, it must be positively ascertained that the quoted price covers a fuel sufficiently free of fines to make it usable in a producer. Much of the finer coke is now used at the plants where it is made, in producers for underfiring the by-product ovens, and in steam boilers.

The Gas-Producer Plant

To take its rightful place among other fuels, producer gas must be made at the lowest possible cost, with the minimum amount of labor and operating difficulties. The gas producer is an important item, but it is only one part of the gas-making plant. The best producer cannot make gas without the proper operation and control, and it cannot deliver gas to the furnaces without a proper distribution system. There are few places where proper planning and anticipation of difficulties will have a greater effect on the success of the project than in the design of a producer-gas system. This is particularly true when using bituminous coal.

It is possible to lay out a plant so that one man per shift can take care of either one or two producers, a boiler, and the handling of coal and ashes. He might have to have occasional help in cleaning out dust legs, or in dumping a car of coal, but on the other hand, if the producer is located close enough to the furnace, he may also serve as the furnace operator.

Coal can be discharged from trucks or cars through a hopper, feeder, and bucket elevator to the coalbins. A double-roll crusher should be provided so that mine-run coal can be used even if it is planned to use sized coal. Bins above the producers can be large enough to carry a 2-day supply of coal, which is the preferable arrangement, or the feed bins can be smaller with an auxiliary storage silo. The equipment should be designed so that no hand labor is necessary except in occasional emergencies when coal must be reclaimed from an outdoor stock pile. Segregation of coarse and fine coal in the bins must be minimized. It should never be necessary for an operator to enter a coal-feed bin, as there is always a slight danger that gas may leak up into the bin and the man might be overcome.

The operating floor of a producer plant is really the second floor of the building, level with the top of the producers. All control instruments, motor starters, steam gages, water columns, valves, and air blowers for the producers should be located on this operating floor. The boiler stack can sometimes be combined with the burnout stack for the gas lines. Ashes from producers and boilers should be discharged to a skip hoist or conveyer which delivers them to an overhead ash bin so that no hand labor is necessary.

The lower floor of the building should be enclosed, as the producers do not supply enough heat to prevent freezing around the wet ashes, floors, and conveyers. Floors and pits should be drained so that a hose can be used for cleaning. The operating floor must be well ventilated and should have large doors which can be left open in summer and closed in cold weather. Louvers are usually used in the side walls just underneath the coalbins so that no gas can accumulate in the building. Oxygen apparatus should be available in case a man is overcome with gas, although this would never happen under normal operating conditions. Water-cooled poker tips have to be built up by welding every few weeks, and chain-hoist equipment must be provided for handling them.

Approximately 100 gal of water per ton of coal must be converted into steam for the producer blast, in addition to any heating or power load on the boilers, and 200 gal per hr is needed for cooling the poker, top, and coal feeder of each producer, regardless of capacity. If water is scarce or expensive, the cooling water can be recirculated to a tank on the upper floor of the building. Water-cooled valves in the gas mains have been experimented with but have not proved very dependable.

Bituminous-Type Gas Producer

Gas has been made for years with little improvement in the producing and control equipment, auxiliaries, and operating procedure. Stationary and revolving hand-poked producers gave way to mechanical types, but even today possibly 75 per cent of the producer systems in service have gas-making equipment which requires sledging of clinkers and much hard labor, delivering a gas which varies in heat value and temperature. The old distribution mains are even worse, requiring much labor and weekly burnouts. These things have given producer gas made from bituminous coal a poor reputation in industry, even though the facilities are now available for dependable operation.

The modern bituminous gas producer is a revolving vertical steel cylinder lined with refractory brick, with a stationary water-cooled top through which coal is fed, gas is removed, and pokers are operated. The bottom is sealed by a revolving water-sealed ash pan, which encloses the air-blast hood and plows for continuously removing the ashes. The air blast is usually furnished by a steam-driven turboblower, at a pressure of about 10 in. of water, and gas leaves the producer at a temperature of 1250 to 1500 F, and a pressure up to 1 in. of water.

The producer manufacturers have done a fine job in developing machines which will make good gas with almost no interruptions when operated in a proper manner. They claim, however, with a great deal of justification, that it is almost impossible to get the users to spend the money for the correct flue system and control equipment needed to make the operation clean, dependable, and free from hard labor. The manufacturers have developed a simple rugged machine requiring almost no repairs. They have designed a center blast hood to give proper distribution of air without the use of tuyères in the outer walls. They have removed the arms which formerly obstructed the flow of ashes, and have provided for continuous ash removal, both of which help to maintain an even fuel bed and to prevent the loss of carbon in the ash. They have equalized the flow of air through the bed of hot coke by providing a means for stopping the rotation of the ash pan automatically for a few seconds at a time, while the upper part of the producer continues to revolve. This causes a grinding action in the fuel bed which reduces blowholes and unequal flow of gas. Coal feeders now give excellent distribution and control of feeding rate without leakage of gas. The motion of the water-cooled pokers has been changed to give more frequent and thorough agitation of the upper part of the fuel bed without plastering the hot sticky ash against the walls of the producer. Both the poking and grinding actions are necessary to break up the caking of the coal in the fuel bed, and to prevent channels and blowholes which cause hot spots in the fuel bed and to permit the gas to burn to CO_2 in the producer.

Auxiliary and Control Equipment

The operation of a producer must be kept constant, in the face of continually changing demands for gas, and many variations in fuel and fire bed. This is almost impossible under strictly manual operation.

Gas is made by blowing a mixture of steam and air through a deep bed of incandescent carbon. If air alone were used, the fuel bed would become very hot, resulting in clinker trouble in the producer and a very lean gas.

The fire bed of the producer contains four zones as follows:

1 The ash bed at the bottom, which protects the blast hood from the heat and aids in distributing air from the hood to the fuel bed.

2 The oxidation zone, where the only reaction is the almost complete combustion of carbon to CO_2, with the liberation of 14,550 Btu per lb of carbon. This zone is only about 6 in. thick and is the hottest zone in the producer.

3 The reduction zone above the oxidation zone, where the CO_2 is reduced to CO by the hot carbon, with a corresponding endothermic reaction of 5850 Btu per pound of carbon, and the steam reacts with the carbon to form hydrogen, CO and CO_2, further reducing the temperature of the fuel bed.

4 The distillation zone at the top where the volatile matter in the coal is distilled off and moisture is evaporated.

The fuel requires 2 hr or more to pass through these reactions, but the air, steam, and gas are in contact with the fuel for little more than 1 sec in a bituminous producer, and for possibly 3 sec in the coke type. It is therefore exceedingly important that the various zones are held constant in thickness, "porosity," and temperature, and it is evident that this can only be done with equipment that has been carefully developed for the purpose, with controls made as automatic as possible, and with intelligent operation. When the load varies, these factors become increasingly important. Variations in fineness or caking qualities of the coal, and in the fusion point of the ash, affect the operation.

Air must be delivered to the blast hood in a manner which can be automatically controlled by the demand for gas, in spite of variations in the resistance of the fuel bed. Older producers usually were equipped with steam-jet blowers, but the need for fan-type blowers is now almost universally recognized, and many old producers have been equipped with modern blast equipment. When used on bituminous producers, the blowers are directly connected to small variable-speed steam turbines, and the exhaust steam is connected into the air blast. On coke and anthracite producers, the steam pressure from the water-jacketed shell is not high enough to operate a turbine, and the blower is therefore driven by electric power.

In most plants, particularly where the gas demand is not constant, the volume of the air blast is controlled by a pressure regulator connected to the gas main. The pressure in the main is usually between 0.2 and 1 in. of water. If the furnace operator turns on more gas, the pressure in the main immediately drops and the regulator feeds more steam to the turbine. The small pipe between the gas main and the regulator is kept free from tar and dust by blowing a very small amount of air through it into the main. Variations in resistance of the fuel bed will not affect the accuracy of the control, and the operator can adjust his regulator to allow for the pressure needed in the gas mains. When used with a motor-driven blower, the regulator adjusts a damper in the air line.

The volume of gas leaving a producer cannot be measured, due to the tar and dust, but the amount of air blown to the producer can be indicated and this is a measure of the gas delivered. All producers should be equipped with an orifice plate in the air-blast line, with an indicating or recording differential gage on the instrument panel to show the operator how much air is being fed to each producer. The operator will then know when the furnaces are using more gas, and he can regulate his coal feed and make other adjustments accordingly. He will also know whether each producer is carrying its share of the load. This indication of air volume is used on very few producers, but all operators who have tried it report that it is one of the most valuable instruments in the plant.

Where a producer plant is operating in connection with a single furnace, and both the producer and the furnace are under the control of one man, automatic regulation can be obtained by means of volume instead of pressure. The furnace operator will adjust the volume-control instrument to give enough gas for the furnace, and this instrument will then automatically control the speed of the turbine so that a constant volume of air is fed to the producer, regardless of the resistance against which this air must be delivered. This method has the advantage that the producer

will deliver the required amount of gas, regardless of obstructions in the line between the producer and the furnace.

The amount of steam in the air blast is one of the most important factors in producer operation. In the reduction zone in the producer, the CO_2 is reduced to CO by contact with hot carbon, with a consequent absorption of heat amounting to 5850 Btu per lb of carbon. The hotter the fuel bed, the more rapid and complete will be this reaction, resulting in less CO_2 and more CO in the gas produced. The high temperature also results in more active action between the carbon and the steam. However, the temperature which can be maintained is limited by the fusing temperature of the ash, so enough steam must be introduced to lower the temperature of the reduction zone to a safe point, by combining with the hot carbon to form H_2, CO, and some CO_2.

When the old steam-jet blowers were used, the proportion of steam to air could not be accurately controlled and too much steam was usually put into the producers. When a turbine- or motor-driven blower is used, the amount of steam is adjusted by observing the temperature of the mixture of air and steam. This is usually at some point between 130 and 150 F. When the correct figure has once been determined for a certain coal, it is not difficult for a producer operator to maintain this so-called "saturation temperature." The exhaust steam from the turbine is discharged into the air blast, and some live steam is usually added. When more air is needed the turbine is speeded up, automatically adding more steam to the blast. Automatic temperature control of the blast is often furnished but is not absolutely needed when turbines are used. It is necessary when blowers are motor-driven.

Fig. 1 shows the blast temperatures corresponding to various inlet-air temperatures and pounds of steam per pound of coal. Fig. 2 shows results of tests reported by W. P. Chandler of Carnegie-Illinois Steel Corporation indicating the increase in the quality of the gas when the proportion of steam in the blast was decreased. In practice, however, it is usually dollar efficiency rather than thermal efficiency which counts, and as coals with high ash-fusion temperatures are rarely available, we choose more steam and a poorer gas rather than a job of sledging clinkers out of the producers.

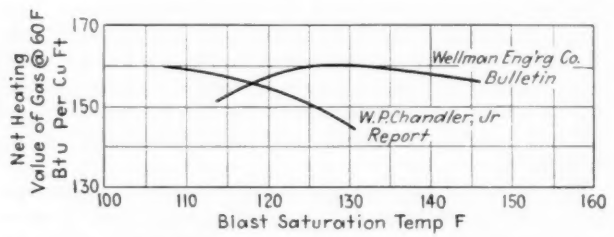


FIG. 1 RELATION BETWEEN STEAM USED PER POUND OF COAL AND BLAST SATURATION TEMPERATURE

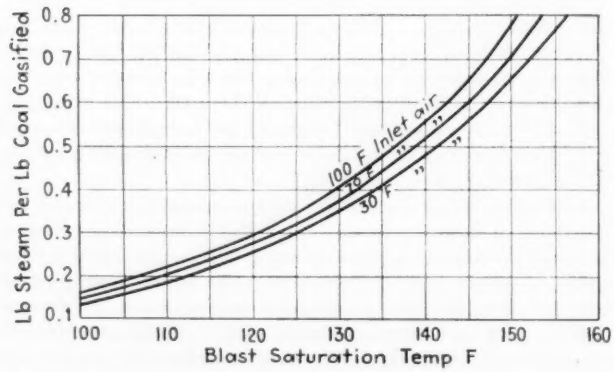


FIG. 2 RELATION BETWEEN HEATING VALUE OF GAS AND BLAST SATURATION TEMPERATURE

Producer gas is a very "lean" gas, due to the high percentage of inert nitrogen introduced with the oxygen in the blast. The use of steam as a reducing agent to lower the temperature of the fuel bed and prevent the formation of clinkers, actually enriches the gas because it adds hydrogen without increasing the amount of inert gases. However, fuel must be burned to generate the steam, and this fuel amounts to about 5 per cent of the coal gasified. Therefore, CO_2 is sometimes used in the blast, to lower the fuel-bed temperature, but this is only profitable where the CO_2 content of the gases is very high, as in the exhaust gases from lime kilns. Proper control of the percentage of CO_2 added to the blast is quite difficult.

High fuel-bed temperatures do not necessarily mean high gas temperatures leaving the producers. Gas temperatures usually run between 1250 and 1500 F, but may be as high as 1800 to 1900 F when used in kilns for burning limestone, where producers are usually located very close to the kilns.

All automatic producers have an adjustable mechanical coal feed. Practically all of these are adjusted by hand. There is a recording thermocouple in the gas stream leaving the producer, and the operator adjusts the coal feed to maintain a reasonably constant gas temperature. If more air is blown through the producer, the top of the fuel bed soon increases in temperature, and the operator feeds more coal to prevent the gas from getting too hot. If the operator is provided with an orifice meter on the air blast, he knows when more gas is being generated without waiting for the temperature to increase, and he can regulate his coal feed accordingly. Automatic regulation of coal feed is now being applied, using the temperature of the gas leaving the producer to regulate the rate of feed. This is very successful, as it re-

TABLE 3 PRODUCER-GAS DATA

Fuel used in producer	Bituminous coal	Anthracite coal	Coke breeze
Fuel gasified, lb per sq ft per hr	30–70	15–30	15–30
Volume of gas at 60 F, cu ft per lb coal	60	65	68
Temperature of gas leaving producer, deg F	1250–1500	550–650	550–650
Lower or net heating values, Btu:			
Coal or coke used, per lb	13500	12500	12000
Steam 0.4 lb per lb fuel (Anthracite and coke producers make own steam)	450	(450)	(450)
Heat input to producer, per lb fuel, Btu	13950	12500	12000
Raw producer gas, per cu ft at 60 F	140	130	120
Sensible heat of gas leaving producer per cu ft	23	10	10
Tar in hot gas leaving producer, 0.0006 lb tar per cu ft gas at 15,000 Btu	9	..	..
Heat output from producer, per cu ft, Btu	172	140	130
Heat output from producer, per lb fuel, Btu	10320	9100	8840
Efficiency of producer, not including losses in boiler or gas lines	73.9	72.7	73.6
Typical analysis of gas, per cent:			
CO	22.5	24.8	26.0
H_2	12.5	15.0	11.0
Hydrocarbons	3.1	0.9	0.7
CO_2	7.4	9.0	7.6
N_2	54.5	50.3	54.7
	100.0	100.0	100.0
Air for perfect combustion, cu ft per cu ft gas	1.17	1.04	0.95
Additional air for combustion of 0.0006 lb tar per cu ft of bituminous gas	0.11	...	...
	1.28		
Products of perfect combustion, cu ft per cu ft gas	2.14	1.83	1.76
Weight of producer gas, lb per cu ft	0.069	0.066	0.069
Weight of air for perfect combustion, lb per cu ft of gas	0.098	0.080	0.073
Weight of products of perfect combustion lb per cu ft of producer gas	0.167	0.146	0.142
Theoretical flame temperature, based upon gas at 60 F, deg F	3170	3150	3000

duces the work of the operator and improves the quality of the gas.

Table 3 gives general information on the different types of producer gas and is useful in the design of distribution systems, burners, and furnaces, and in the comparison of this gas with other fuel.

Distribution System for Bituminous Producer Gas

Raw gas made from bituminous coal is a hot dirty fuel to handle. It contains dust from the fine coal falling into the producer and soot from the cracking of the hydrocarbons. When using slack coal, the dust carried over into the mains may amount to 5 per cent of the weight of the coal. This will fill up a round pipe so rapidly that the flue would have to be cleaned or "burned out" once a week, shutting down the furnaces and producers during the operation.

This gas also contains tar vapors which will condense as the gas cools, gumming up valves and burners, seeping out of cleanout doors, and mixing with the dust to form a cokelike substance. It has a temperature of 1250 to 1500 F, when it leaves the producer, and therefore has nearly twice the volume of gas made from coke or anthracite and 18 times the volume of natural gas for the same Btu value. Consequently, mains and valves are large and costly. As a result, bituminous gas has been most frequently applied to large furnaces located near the producer plant and more rarely used where the gas must be distributed for greater distances and to a large number of burners.

Having outlined the causes of the difficulties encountered in the distribution of hot raw bituminous gas, the next step is to see what can be done to overcome them. In the case of old gas mains already in use, only a little improvement is possible without extensive alterations. Where a new distribution system is to be installed, it is entirely possible to increase the length of time between "burnouts" to 2 months, or even to a year, at the same time conserving the sensible heat of the gas and smoothing out the furnace operation.

Gas mains can be built without any horizontal bottom surfaces on which dust can accumulate. They can be constructed with a saw-tooth bottom, with provision for removing the dust at all of the low points. Dust will sometimes accumulate on the slopes but small openings can be provided for steam lances in the top of the pipe, so that the dust can be blown down into the pockets at the bottom. However, this is a hot and dirty job, and a better scheme is to install soot blowers at every point in the mains where dust can settle, with legs or pockets having double seals through which the dust can be removed while gas is flowing. These blowers can be standard boiler soot blowers, which will withstand the gas temperatures quite well, but are not entirely resistant to the higher burnout temperatures. On the other hand, if burnouts can be greatly reduced or eliminated by the soot blowers, the soot blowers will not be damaged by the burnouts.

The removal of the dust from the pockets is also a disagreeable job, particularly if it must be handled in wheelbarrows. This dust could be sluiced into a stream of water, but this is rarely available. A steam-ejector vacuum system is being used to remove the dust and deliver it in a dampened condition into the ash bin. This dust contains about 75 per cent carbon and 25 per cent ash and is "red hot" when removed from the mains.

To prevent trouble with the tar, the gas temperature must be kept high enough so that the vapors will not condense, or else the gas must be cooled and washed. Insulation of new gas lines is now relatively simple since insulating refractory brick can be used for the complete lining of the mains, and gas can be delivered 100 ft from the producer plant with a temperature loss of not more than 300 deg F, including dust catchers and mains. Washing of bituminous gas has been tried on numerous installations in the past, and there is at least one successful plant in operation today. However, it involves the use of expensive equipment and the loss of sensible heat amounting to 6 to 12 per cent of the total Btu content of the hot gas as well as the loss of the tar. Either the tar must be wasted, or costly recovery and handling equipment must be installed.

Producers and Distribution Systems for Anthracite and Coke Gas

Gas made from coke or anthracite, while higher in first cost, is cooler, cleaner, and easier to handle, and may be washed if necessary with less difficulty and loss of heat. It is comparatively free from dust as it leaves the producer because anthracite producers gasify only one half as much fuel as do the bituminous type, and because the fuel used contains less fines and almost no hydrocarbons, and flows directly from distributing pipes onto the top of the fuel bed instead of dropping through a stream of moving gases. It is entirely free from tar and has a temperature of about 600 F, making it possible to deliver it through steel pipe lines of smaller size, with insulation on the outside of the pipe. No time need be lost in burning out the mains. Higher pressures and velocities can be used and a booster blower can even be connected to increase the pressure of the gas after it leaves the producers. In the past this gas has usually been washed, but in recent installations the velocity has been increased by the use of bowers to the point where dust will not settle out, and gases are distributed in the hot raw condition. Standard valves, fittings, and burners can be used, and the burners require much less attention from the furnace operators.

The producers used for coke and anthracite are quite different from bituminous producers, mainly because these fuels do not contain tar and hydrocarbons. Therefore the fuel bed does not cake to any great extent and no mechanical poker is needed. The bed can be 5 ft deep instead of about 2.5 ft, resulting in cooler gas. The construction is very much simpler than in the bituminous machine, since the shell is stationary, while only the bottom revolves. The blast hood is large and is usually eccentric in shape, so that it grinds the ashes and agitates the fuel bed as it revolves. In some producers it is attached to the revolving ash pan in which case a deep water seal is used and the blast pressure is limited to approximately 20 in. of water. In others, the revolving blast hood supports the fuel bed, and ashes are discharged through the hood into a stationary hopper below. These producers can be operated with a blast pressure of several pounds, since no water seal is used. Coal feeders are either stationary or revolving. The producer shell is water-jacketed instead of being lined with brick and generates enough steam to mix with the air blast.

Refractories

The refractory-brick lining of a bituminous producer is subjected to continuous abrasion from the passage of fuel and ashes, and to occasional destruction from the formation of clinkers and the necessity of breaking them loose from the walls with heavy bars. The temperature of the lining usually is not excessive, but hot spots sometimes develop, due to channeling of the fires. A dense, strong, high-heat-duty brick is required to resist these conditions. The lining can be either $4\frac{1}{2}$ in. or 6 in. thick, backed up with $2\frac{1}{2}$ in. of strong insulation next to the shell. A high-temperature cold-setting refractory mortar should be used, and all joints should be kept as tight as possible. When using coal having a very low ash-fusion temperature a few courses of silicon-carbide brick are sometimes used at the clinker line.

Mains for carrying hot raw bituminous gas do not exceed 1400 F except during burnouts. Steam jets and lances must be used to stir up the dust. Formerly, mains were lined with $4\frac{1}{2}$ in. of

fireclay brick, sometimes surrounded with insulation. The development of lightweight refractory brick which will withstand these conditions has greatly simplified the construction of these mains. The entire 9-in. lining can be built of 2600-deg insulating refractories, or lower-temperature insulating brick can be used in the outer $4^1/_2$-in. portion. This brick is somewhat lower in cost and higher in insulating value. Flue linings usually involve a great deal of complicated brickwork and the use of insulating refractories which can be easily cut, sawed, ground, or rubbed into any desired shape greatly reduces the bricklaying labor cost. A cold-setting mortar should be used, with expansion joints about every 20 ft. No fireclay brick need be used except in the connection from the producer to the dust catcher, and for construction of the valve seats. Cast-iron seats are now seldom used.

Furnaces and Burners

Producer gas is not only a cheap fuel, but is admirably adapted to many heating operations, particularly where a soft luminous flame is desired. As can be seen from Table 3, it has a theoretical flame temperature of about 3100 F, as compared to 3700 F, for natural gas and 3800 F for oil. This makes it especially suited to steel reheating, where the entire furnace must be filled with a hazy slightly reducing flame and "hot spots" must be avoided. The same characteristics, at slightly higher temperatures, make it suitable for burning refractory brick. A glass tank can be completely filled with a luminous flame having the high radiation characteristics so desirable for heating this transparent molten bath. With producer gas, it is easy to get delayed combustion, even when using highly preheated air, an operation that is very difficult when using natural gas or oil.

Bituminous producer gas is used for firing vertical-shaft lime kilns and also rotary kilns for lime and other products where freedom from ash deposits is necessary. Freedom from ash makes it suitable for firing many ceramic products, where both bituminous and coke or anthracite gas are being used.

In many of these furnaces, the fuel requirements are large, and the gas and air are merely admitted through ports in the furnace walls. The air is usually preheated by regeneration or other means, and this preheating becomes very necessary when high temperatures must be reached. It is sometimes claimed that there is no object in keeping the gas hot between the producers and the furnaces, as this may reduce the furnace efficiency because the exhaust gases will not be cooled in the gas regenerators. Intermittent steam jets can be used if necessary in order to keep soot from building up on the reversing valves and burner ports.

Where a number of smaller burners have to be used, bituminous gas is usually fired through a cast-iron burner with a fireclay burner block. The gas flow is controlled by a slide or inverted-cone valve, which has to be opened and closed about once an hour to keep it clean. The air, preferably preheated, often acts as an injector to draw the gas into the burner block. A very short oxidizing flame can be obtained by using enough air and moving the air pipe away from the block. A reducing or delayed combustion flame is produced by using less air and moving the pipe closer to the throat of the burner. These burners must be thoroughly cleaned about once every 24 hr and large cleanout doors must be provided. Since the gas going to each burner cannot be measured, it is advisable to have an orifice and an indicating differential gage in each air line. The air can then be set for any desired quantity, and the gas adjusted to give the required temperature and flame quality.

Producer gas made from anthracite or coke, either washed or in the hot raw condition, can be burned in standard gas burners large enough to allow for the low Btu value of the gas, or it can be regenerated and burned in ports. It is particularly suited to plants where the burners are widely scattered, as in smaller heating furnaces, and in the underfiring of coke ovens.

Everything considered, producer gas made from bituminous coal, anthracite, or coke can be a very desirable fuel if proper consideration is given to the economic, engineering, and operating factors which so materially affect the success of the project.

Pulsation and Its Effect on Flowmeters[1]

By E. J. LINDAHL,[2] COLUMBUS, OHIO

Flowmeter readings are apt to be seriously in error if the fluid flowing through the meter is subjected to rapid recurring variations in velocity or pressure or both. Flow having these variations is thought of as being "pulsating flow." Much thought has been given to pulsating flow or pulsation and much has been written about it. It is the intention of this paper to bring together some of the results which have been published.

Causes and Effects of Pulsation

STEADY flow of a medium exists when the mass rate of flow through a device is constant, when the velocity, pressure, and temperature at any point remain constant, and when thermal equilibrium has been reached by the device through which the medium is flowing. In the case of unsteady flow, one or more of the conditions mentioned does not exist. Pulsating flow can exist when rapid velocity or pressure variations occur and is seen to be a special case of unsteady flow.

The causes of pulsation are numerous. One of the chief sources of pulsation in gas pipe lines is the reciprocating compressor. Another source is water surging back and forth in a low portion of a pipe line. Air enters the intake manifold of an internal-combustion engine having pulsation due to the pumping action of the engine pistons. Clattering check valves and undamped diaphragm regulators in a line are also offenders. Steam flowing to a reciprocating engine has pulsating flow. Any device that causes intermittent flows or pressures is a source of pulsation, since pulsations take place as a result of recurring rapid variations in either velocity or pressure.

One device which is greatly affected by pulsation and which concerns engineers is the inferential meter. While it is true that there are some pulsations which have no effect on the meter reading, there are other pulsations which render the meter reading invalid. Since the measurements which involve large quantities are made with flowmeters, it is extremely important from a dollars and cents standpoint that these meters read accurately. As a result, a great deal of time and money have been spent by concerns in the gas industry to determine means for reducing the errors in meter readings resulting from pulsation. This paper will deal chiefly with the effect of pulsation on meters. In passing, it might be said that at the present time very little study has been made to determine errors in the measurement of liquids having pulsating flow.

It is now generally accepted that any inferential-head meter will measure correctly if the secondary device will measure accurately the differential pressure across the primary element, and if the average of the square roots of the instantaneous readings can be determined. In the case of steady flow these operations are comparatively simple, but when the flow is at all unsteady this is not true.

If the differential is irregular as a result of rapid variations in velocity or pressure the meter is inaccurate because of the fact that most secondary devices are too sluggish to follow the actual changes in differential pressure caused by rapidly changing flow. Furthermore, the differential pressure, indicated by the secondary device, is an approximate average of the maximum and minimum differential pressures. When the square root of this average is taken, the resulting value is higher than the average of the square roots of the instantaneous differentials, and the flow as determined from the meter will be too high.

This can be illustrated by assuming that the flow through a meter varies in a manner such that the differential is, for example, 49 in. during one second and 25 in. the next second. The average rate of flow over this period is proportional to $\frac{(49)^{1/2} + (25)^{1/2}}{2}$ or 6; if the average meter differential is 37, the rate of flow as registered by the meter is proportional to $(37)^{1/2}$ or 6.083. The error due to pulsation is (6.083 — 6.000) /6.000 or 1.4 per cent.

According to most investigators the error is always positive, but cases of negative error have been found which have been attributed by some engineers to pulsation. The magnitude of the error may be up in the hundreds of per cent.

Mathematical Analysis of Pulsation Error

In order to show how pulsation acts to give erroneous meter readings a mathematical analysis of three types of waves will be made. It must be kept in mind that the method of calculating the error due to pulsation is only theoretical and no attempt should be made to apply it in a practical case. It will, however, indicate why pulsation error exists.

Three wave forms, i.e., the rectangular, the sine, and the triangular, will be analyzed. Two assumptions in regard to meter behavior are made in these analyses: (*a*) it is assumed that the pulsations occur with such rapidity that the portion of the meter upon which the differential is impressed cannot follow the rapidly fluctuating differential pressures; and (*b*) it is assumed that the wave is symmetrical and that the meter gives a reading which is the mean between the upper and lower limits of the pulsation wave.

The sine wave would result if a single-cylinder compressor had the connecting rod replaced by a Scotch yoke, as shown in Fig. 1(*a*), since the piston would have simple harmonic motion and the wave displacement assumed to follow the motion of the piston. The wave would then be as shown in Fig. 1(*b*), with p as the maximum displacement of the pulsation wave and with the angular displacement of the crankpin through one revolution plotted as the abscissa.

The rectangular wave form will be first discussed in detail, since its analysis presents less of a problem than the other two.

The differentials encountered are illustrated in Fig. 2(*a*) and apply to one revolution of the crank of a compressor. The phase angle of the crank is plotted as the abscissa and the instantaneous differential as the ordinate. The meter reading (indicated by h) is taken halfway between the maximum differential ($h + p$) due to the pulsation and ($h - p$) the minimum differential, p being the distance between the instantaneous differential and the meter reading. The instantaneous value of the true differential is indicated by H. If K is used to designate all of the constants, such as $(2g)^{1/2}$, velocity of approach factor, etc., then Q_m, the flow as indicated by the meter, is equal to $Kh^{1/2}$. If, instead of

[1] Thesis submitted to the Department of Mechanical Engineering and the Committee on Graduate Study and Research at the University of Wyoming in partial fulfillment of the requirements for the degree of Mechanical Engineer. Laramie, Wyoming, 1946.

[2] Assistant Professor of Mechanical Engineering, The Ohio State University. Mem. A.S.M.E

Contributed by the Research Committee on Fluid Meters and presented at the Semi-Annual Meeting, Detroit, Mich., June 17-20, 1946, of The American Society of Mechanical Engineers.

Note: Statements and opinions advanced in papers are to be understood as individual expressions of their authors and not those of the Society.

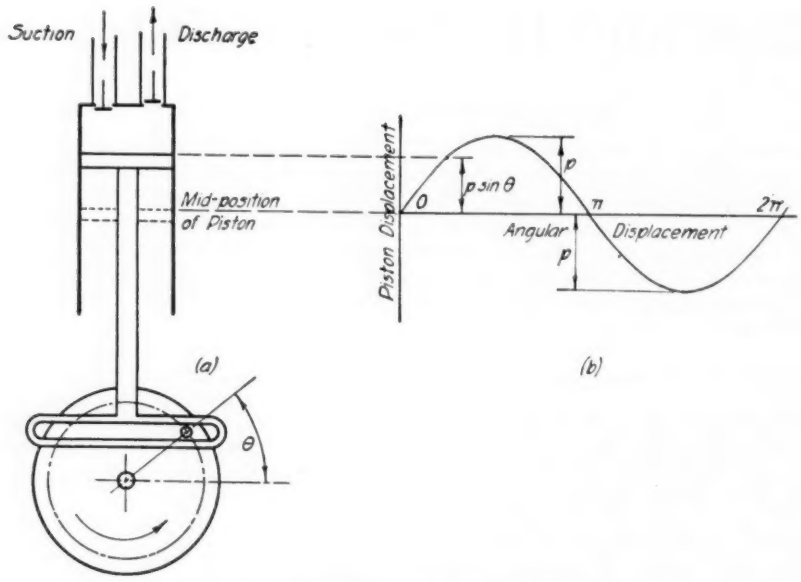


FIG. 1 GENERATION OF PULSATION WAVE

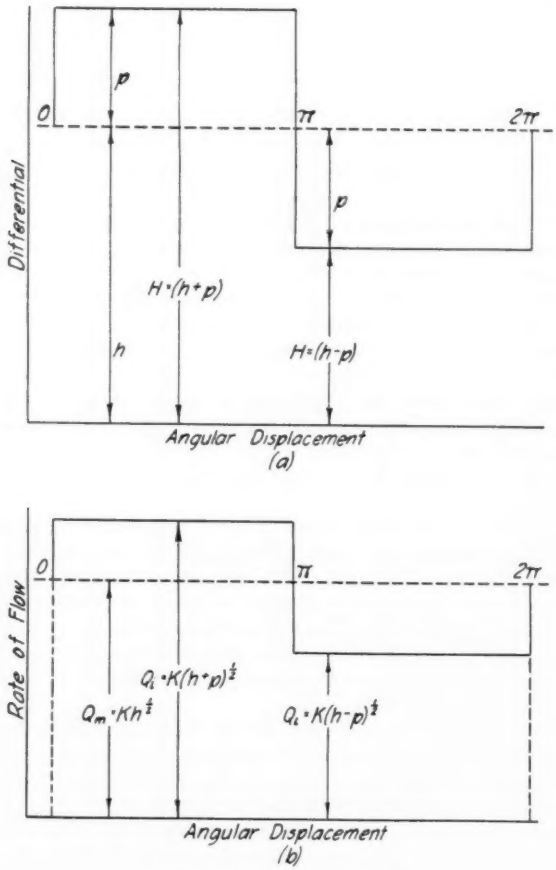


FIG. 2 RECTANGULAR WAVE

plotting the instantaneous differential, the instantaneous flow is plotted, the result is as shown in Fig. 2(*b*). If the area under the curve is taken for one cycle (angular displacement 0 to 2π), and the area is divided by the length of the cycle, there results the average ordinate which is the average rate of flow and

$$Q_a = \frac{K\,(h+p)^{1/2}\,\pi + K\,(h-p)^{1/2}\,\pi}{2\pi}$$

or

$$Q_a = \frac{K}{2}\,[(h+p)^{1/2} + (h-p)^{1/2}]$$

Then the ratio of the flow as determined by the meter to the actual rate of flow is

$$\frac{Q_m}{Q_a} = \frac{Kh^{1/2}}{\frac{K}{2}\,[(h+p)^{1/2} + (h-p)^{1/2}]}$$

or

$$\frac{Q_m}{Q_a} = \frac{2h^{1/2}}{(h+p)^{1/2} + (h-p)^{1/2}}$$

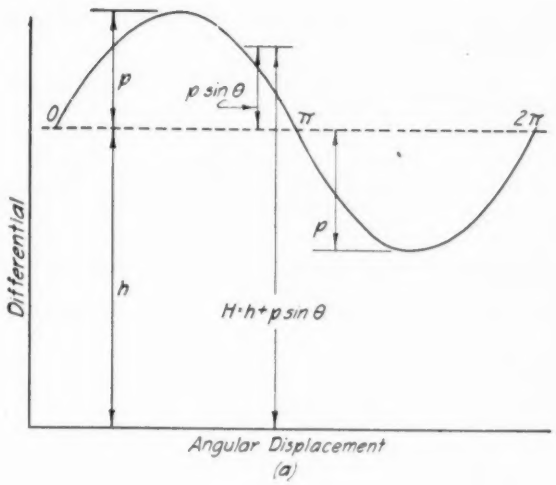
Sine Wave. As has been pointed out, a sine wave as shown in Fig. 3(*a*) will result theoretically if the connecting rod of a single-cylinder compressor is replaced by a Scotch yoke. Any distance H from the datum to the wave represents an instantaneous value of the true differential which for this particular wave form is $(h + p \sin \theta)$, while the distance h to the horizontal dashed line represents the differential as indicated by the meter. If K is again assumed to be the meter constant, the rate of flow as indicated by the meter is again $Q_m = Kh^{1/2}$, and the instantaneous true rate of flow is

$$Q_i = K(H)^{1/2} \text{ or } Q_i = K\,(h + p \sin \theta)^{1/2}$$

If the instantaneous true rates of flow are plotted the result is Fig. 3(*b*). In order to obtain the true average rate of flow it will again be necessary to determine the area under one cycle of the curve and divide this area by the length of one cycle. The flow which takes place while the crank turns through the angle $d\theta$ is

$$K\,(h + p \sin \theta)^{1/2}\,d\theta$$

and the total flow from one revolution of the crank is



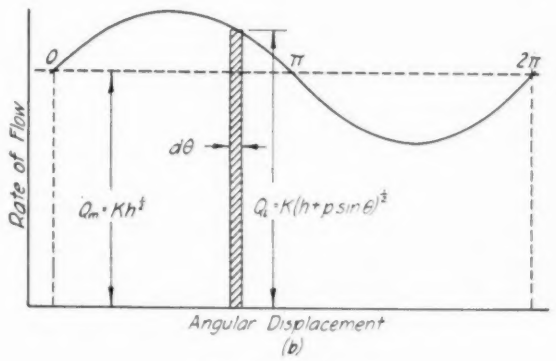


FIG. 3 SINE WAVE

$$K\int_0^{2\pi} (h + p \sin \theta)^{1/2}\, d\theta$$

The average flow over this cycle then is

$$Q_a = \frac{K}{2\pi}\int_0^{2\pi} (h + p \sin \theta)^{1/2}\, d\theta$$

If it is desired to find the actual discharge for pulsating flow from the foregoing equation, the equation must, of course, be integrated. This is done after the portion $(h + p \sin \theta)^{1/2}$ has been expanded by the binomial theorem. The binomial theorem in terms of symbols for five terms is

$$(a + b)^n = a^n + na^{n-1}b + \frac{n(n-1)}{2!}a^{n-2}b^2 + \frac{n(n-1)(n-2)}{3!}a^{n-3}b^3 + \frac{n(n-1)(n-2)(n-3)}{4!}a^{n-4}b^4$$

Then

$$(h + p \sin \theta)^{1/2} = h^{1/2} + \frac{p \sin \theta}{2h^{1/2}} - \frac{1}{8h^{3/2}}p^2 \sin^2 \theta + \frac{3}{48h^{5/2}}p^3 \sin^3 \theta - \frac{15}{384h^{7/2}}p^4 \sin^4 \theta = h^{1/2}\left[1 + \frac{p \sin \theta}{2h} - \frac{p^2 \sin^2 \theta}{8h^2} + \frac{p^3 \sin^3 \theta}{16h^3} - \frac{15\, p^4 \sin^4 \theta}{384h^4}\right]$$

and

$$Q_a = \frac{Kh^{1/2}}{2\pi}\int_0^{2\pi}\left[1 + \frac{p \sin \theta}{2h} - \frac{p^2 \sin^2 \theta}{8h^2} + \frac{p^3 \sin^3 \theta}{16h^3} - \frac{15\, p^4 \sin^4 \theta}{384h^4}\right] d\theta$$

or

$$Q_a = \frac{Kh^{1/2}}{2\pi}\left[\int_0^{2\pi} d\theta + \frac{p}{2h}\int_0^{2\pi} \sin \theta d\theta - \frac{p^2}{8h^2}\int_0^{2\pi} \sin^2 \theta d\theta + \frac{p^3}{16h^3}\int_0^{2\pi} \sin^3 \theta d\theta - \frac{15}{384}\frac{p^4}{h^4}\int_0^{2\pi} \sin^4 \theta d\theta\right]$$

Since

$$\int d\theta = \theta + c$$

$$\int \sin \theta\, d\theta = -\cos \theta + c$$

$$\int \sin^2 \theta\, d\theta = -\frac{1}{2}\cos \theta \sin \theta + \frac{1}{2}\theta + c$$

$$\int \sin^3 \theta\, d\theta = -\frac{1}{3}\cos \theta \sin^2 \theta - \frac{2}{3}\cos \theta + c$$

and

$$\int \sin^4 \theta d\theta = \frac{-\sin^3 \theta \cos \theta}{4} + \frac{3}{4}\left(-\frac{1}{2}\cos \theta \sin \theta + \frac{1}{2}\theta\right) + c$$

then the expression for discharge, when integrated is

$$Q_a = \frac{Kh^{1/2}}{2\pi}\left\{\theta - \frac{p}{2h}\cos \theta - \frac{p^2}{8h^2}\left[-\frac{1}{2}\cos \theta \sin \theta + \frac{1}{2}\theta\right] + \frac{p^3}{16h^3}\left[\frac{1}{3}\cos \theta \sin^2 \theta - \frac{2}{3}\cos \theta\right] - \frac{15}{384}\frac{p^4}{h^4}\left[-\frac{\sin^3 \theta \cos \theta}{4} + \frac{3}{4}\left(-\frac{1}{2}\cos \theta \sin \theta + \frac{1}{2}\right)\right]\right\}_0^{2\pi}$$

Since $\sin 2\pi = 0$, $\sin 0 = 0$, $\cos 2\pi = 1$, and $\cos 0 = 1$ when the limits have been substituted in the foregoing equation, the result is

$$Q_a = \frac{Kh^{1/2}}{2\pi}\left\{\left[2\pi\right] - \left[\frac{p}{2h}\right] - \left[\frac{p^2}{8h^2}\pi\right] + \left[\frac{p^3}{16h^3} \times \frac{-2}{3}\right] - \left[\frac{15}{384}\frac{p^4}{h^4} \times \frac{3}{4}\pi\right] - \left[\left(\frac{-p}{2h}\right) - \left(\frac{p^3}{16h^3} \times \frac{2}{3}\right)\right]\right\}$$

and

$$Q_a = \frac{Kh^{1/2}}{2\pi}\left[1 - \frac{p^2\pi}{8h^2} - \frac{15p^4\pi}{512h^4}\right]$$

or

$$Q_a = Kh^{1/2}\left[1 - \frac{p^2}{16h^2} - \frac{15}{1024}\frac{p^4}{h^4}\right]$$

Then the ratio of the rate of flow as indicated by the meter to the actual rate of flow when the pulsation is in the form of a sine wave, is

$$\frac{Q_m}{Q_a} = \frac{Kh^{1/2}}{Kh^{1/2}\left[1 - \frac{p^2}{16h^2} - \frac{15}{1024}\frac{p^4}{h^4}\right]}$$

or

$$\frac{Q_m}{Q_a} = \frac{1}{1 - \frac{p^2}{16h^2} - \frac{15}{1024}\frac{p^4}{h^4}}$$

It will be observed that if the amplitude of the pulsation p is zero, the flow as indicated by the meter is equal to the true rate of flow. If the meter differential and the amplitude of the pulsation are known the ratio of the two can be found and the percentage of error in the meter reading determined from the expression $\frac{Q_m - Q_a}{Q_a}$ which is equal to $\frac{Q_m}{Q_a} - 1$.

Triangular Wave Form. To take another hypothetical case, assume the wave form to be triangular as shown in Fig. 4(*a*). The reading of the meter is, as before, $K(h)^{1/2}$. The value of the instantaneous differential H in each case is as follows

$$\text{From 0 to } \frac{\pi}{2}: \quad H = h + \frac{2p\theta}{\pi}$$

$$\frac{\pi}{2} \text{ to } \frac{3}{2}\pi: \quad H = h + 2p\left(1 - \frac{\theta}{\pi}\right)$$

$$\frac{3}{2}\pi \text{ to } 2\pi: \quad H = h - 2p\left(2 - \frac{\theta}{\pi}\right)$$

When the instantaneous rate of flow is plotted the curve takes the form as indicated in Fig. 4(*b*) and the rate of flow is as noted in the figure.

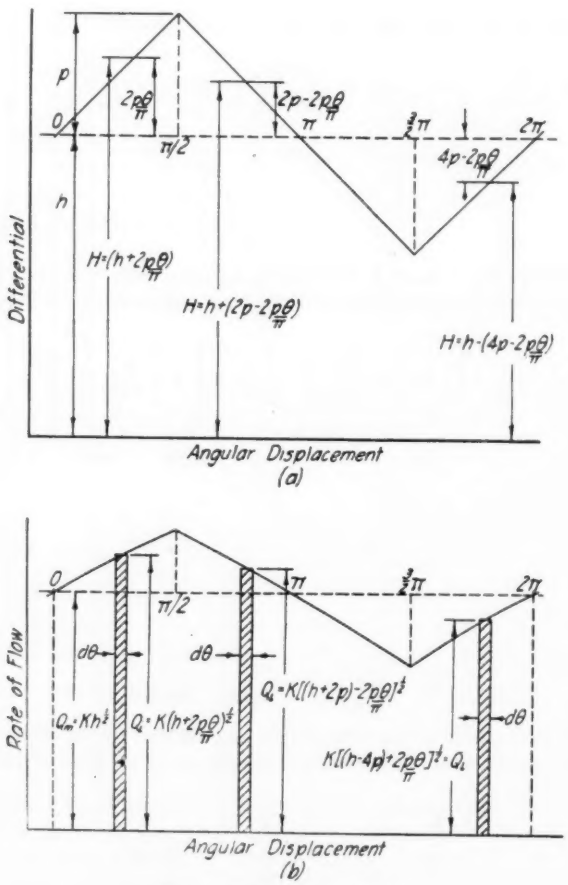


FIG. 4 TRIANGULAR WAVE

The flow during the period that the crank turns through a complete revolution is

$$Q_a = \frac{K}{2\pi}\left\{\int_0^{\frac{\pi}{2}}\left[h + \frac{2p\theta}{\pi}\right]^{1/2} d\theta + \int_{\frac{\pi}{2}}^{\frac{3\pi}{2}}\left[(h + 2p) - \frac{2p\theta}{\pi}\right]^{1/2} d\theta + \int_{\frac{3\pi}{2}}^{2\pi}\left[(h - 4p) + \frac{2p\theta}{\pi}\right]^{1/2} d\theta\right\}$$

This equation is of the form $(a + bu)^n du$ which when integrated is $\frac{(a + bu)^{n+1}}{b(n + 1)}$. Since in this case $n = 1/2$ the form when integrated is $\frac{(a + bu)^{3/2}}{3/2\ b}$.

Then

$$Q_a = \frac{K}{2\pi}\left\{\left[\frac{\left(h + \frac{2p\theta}{\pi}\right)^{3/2}}{3/2 \times \frac{2p}{\pi}}\right]_0^{\frac{\pi}{2}} + \left[\frac{\left(h + 2p - \frac{2p\theta}{\pi}\right)^{3/2}}{-3/2 \times \frac{2p}{\pi}}\right]_{\frac{\pi}{2}}^{\frac{3}{2}\pi} + \left[\frac{\left(h - 4p + \frac{2p\theta}{\pi}\right)^{3/2}}{3/2 \times \frac{2p}{\pi}}\right]_{\frac{3}{2}\pi}^{2\pi}\right\}$$

and

$$Q_a = \frac{K}{2\pi}\left\{\left[\frac{(h + p)^{3/2} - h^{3/2}}{\frac{3p}{\pi}}\right] - \left[\frac{(h - p)^{3/2} - (h + p)^{3/2}}{\frac{3p}{\pi}}\right] + \left[\frac{h^{3/2} - (h - p)^{3/2}}{\frac{3p}{\pi}}\right]\right\}$$

and finally

$$Q_a = \frac{K}{3p}\left[(h + p)^{3/2} - (h - p)^{3/2}\right]$$

Then

$$\frac{Q_m}{Q_a} = \frac{Kh^{1/2}}{\frac{K}{3p}\left[(h + p)^{3/2} - (h - p)^{3/2}\right]}$$

or

$$\frac{Q_m}{Q_a} = \frac{3ph^{1/2}}{(h + p)^{3/2} - (h - p)^{3/2}}$$

THE THEORY OF PULSATION

Numerous articles dealing with pulsation and the effects of pulsating flow have appeared in technical literature from time to time. Most of them deal with the inaccuracy of meters handling fluids subject to pulsation.

Among the first references is one by William Mayo Venable (1)[3] in 1905, which stated that piezometer tubes used in measuring the static head on centrifugal pumps gave values that were abnormally high. He attributed the error to pulsation caused by the limited number of vanes or blades in the pump runner.

[3] Numbers in parentheses refer to the Bibliography at the end of the paper.

In the 1914–1915 Proceedings of The Institution of Civil Engineers Prof. A. H. Gibson (2) pointed out that "most devices for measuring fluid motion do not record the true mean of a pulsating flow and that the error increases," and that "fluctuations in velocity (are) accompanied by fluctuations in pressure."

In 1916 three interesting and significant articles appeared pointing out the inaccuracy of meters when measuring fluids having pulsating flow. One by Allen Hazen (3) indicated that wide and sudden variations in flow cause errors in the head produced by a Venturi meter and that elastic pipe and too-small air chambers when used with reciprocating pumps cause these errors. Another by E. G. Bailey (4) stated that steam flowing to a reciprocating engine is erroneously measured by a flowmeter because of velocity and pressure variations. F. P. Fisher (5) attributed to pulsation the discrepancy in meter readings when the meters were placed some distance apart in a pipe line from a compressor.

In 1922 the results of an investigation by Judd and Pheley (6) appeared in a bulletin published by The Ohio State University Experiment Station. This was the first real attempt to determine the nature of pulsation and to study methods of eliminating pulsation itself and the detrimental effects of pulsation. The conclusions drawn by Judd and Pheley are still considered sound; in fact, most of the later theorizing and investigating has been based upon the ideas originally brought out by them. Subsequent investigations have served to substantiate their conclusions.

Their studies were made with air on Venturi meters, orifices, nozzles, and Pitot tubes. Among the pertinent conclusions which these two men drew up are the following:

(*a*) Pulsations in pipe lines consist of sudden changes in velocity and pressure of the fluid.

(*b*) Pressure changes cause the largest pulsations.

(*c*) The pressure change is in the form of a wave front resembling a traveling sound wave of low velocity.

(*d*) The pressure wave travels with the velocity of sound.

(*e*) Velocity of pulsation is independent of the velocity of fluid flowing.

(*f*) The effect of pulsation on a flowmeter is to increase the reading. The magnitude of the error is a function of frequency and pulsation, static pressure of the fluid, type of meter, and adjacent fixture in the pipe line.

(*g*) Pulsation must be eliminated or reduced greatly to have the meter read without appreciable error.

It was also pointed out by them and now generally believed that no correction factors can be applied to a meter reading to correct for the error caused by pulsation. In most of the correction equations several things, such as frequency of pulsation, the shape of the wave, the amplitude of the wave, etc., must be taken into account. It is also felt that errors due to rapid pressure change are far more severe than changes in velocity. The fact is that there can be errors caused by rapid pressure changes without the presence of changes in the rate of flow of the mass in the pipe line. This has been illustrated by placing a positive-displacement meter on a dead-ended line. The meter valves will clatter and the meter will register a flow if pulsation is present. Likewise, a reading will be indicated on a manometer across an inferential meter, such as an orifice, when placed in a dead-ended line if pulsation exists.

Studies which have been made indicate that in addition to the primary pressure waves in the fluid between the disturbance and the primary element, there are also pressure waves of different amplitude existing in the primary element on the side opposite from the disturbance; and suggest that these waves might be slightly out of time with the waves on the other side, so that the effect of pressure variation is multiplied at times. Then, in addition to the primary waves, there are harmonics which are affected by the size and shape of the conduit on both sides of the primary element. The differential across the primary element where pulsation exists is thus a complicated varying pressure made up of many elements. This was shown by an electrical instrument developed by S. R. Beitler (7) in connection with the pulsation research sponsored by the American Gas Association and The American Society of Mechanical Engineers.

With the equipment as originally used it was possible to obtain a record of the pressure variations on either side of the primary element. However, a study of these records (along the line of reasoning mentioned) indicated that a knowledge of the differential pressure was desirable, and a special mixing switch was designed which made it possible to secure a record not only of the inlet or outlet pulsation waves but the differential pulsation waves as well. Fig. 5 shows some of the records taken with this instrument under various conditions of pulsation.

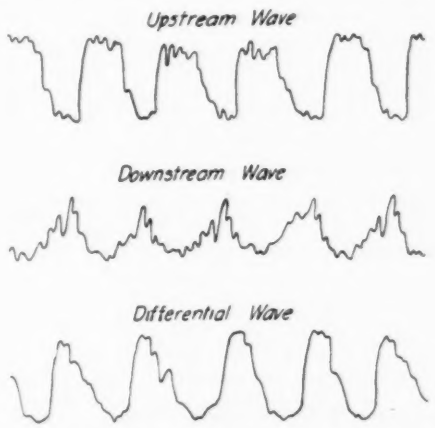


FIG. 5 ACTUAL PULSATION WAVES

A study of these records will show that there is no regularity of pulsation waves, and no apparent relation between the shape and amplitude of the waves on the two sides of the primary element, and that the differential wave bears no similarity to the other waves. These records were made at a gas-compressor station where the pulsation was produced by one compressor running at almost constant speed. The meter was placed directly on the outlet of the aftercooler so that the pulsations would be as nearly constant as possible. Because of the fact that the waves were so irregular it is practically impossible to include the effect of wave form in an equation for correcting the rate of flow.

If the pressure differential could be measured instantaneously, and if the square roots of these two pressures could be averaged, it is possible that a meter would indicate the rate of flow accurately. This would be true, because while the velocity through the primary element does not vary directly with changes in pressure waves, the energy present due to these waves will be used either in accelerating or decelerating the fluid passing through the primary element, so that the decelerations should balance the accelerations. The average flow will be indicated by the average of the square roots of the instantaneous differential pressures across the primary element.

While it is true that each meter installation presents its own problems and that each disturbance creates pulsations which cannot be analyzed, certain general conclusions in regard to pulsation can be drawn. In a paper by S. R. Beitler (8) which reports the results of research conducted at several stations, it is pointed out (*a*) that for a single diameter ratio the error becomes larger for decreasing values of the differential; (*b*) that

with a constant differential the error becomes larger with smaller diameter ratios; and (c) that at any one rate of flow the suction pulsation causes a smaller error than the discharge pulsation;

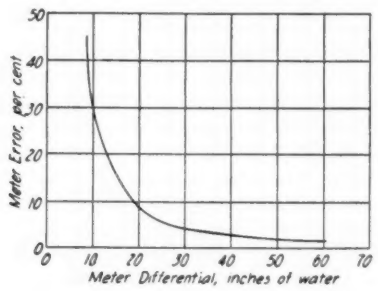


FIG. 6 DIFFERENTIAL VS. ERROR FOR ONE DIAMETER RATIO

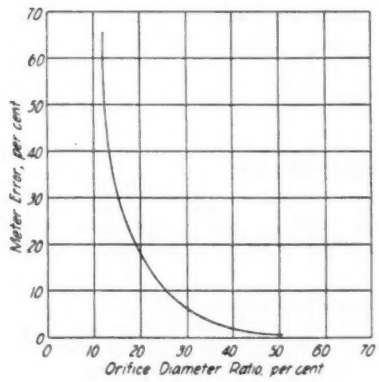


FIG. 7 DIAMETER RATIO VS. ERROR FOR A GIVEN DIFFERENTIAL

In other words, it might indicate severe pulsations while the pulsations might be so slight that the meter error would be negligible. A sketch of Mr. Bean's detector is shown in Fig. 8. The by-pass valve is left open until the pressure in the tank reaches main pressure. The by-pass is then closed, and if the drop of water moves back and forth pulsation is present. Any slight change in static pressure or a pulsation of appreciable magnitude causes the water to be withdrawn into either the gas main or the pressure tank. If the drop of water does not move the flow is certain to be pulsationless.

A device designed by S. R. Beitler (7) and J. E. Overbeck is similar to the one just described and is shown in Fig. 9. In this device the gas-pressure tank is connected to the meter-run line through a $^1/_2$-in. line in which is placed an orifice plate, the diameter of the orifice being $^1/_8$ in. The manometer shown in the figure is then piped up to measure the pressure drop across the

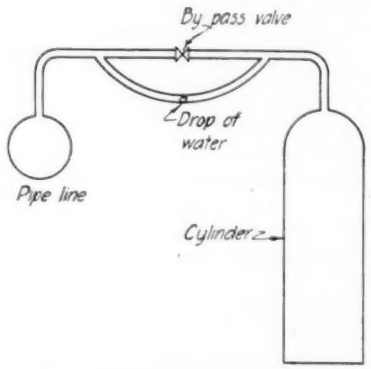


FIG. 8 PULSATION DETECTOR (BEAN)

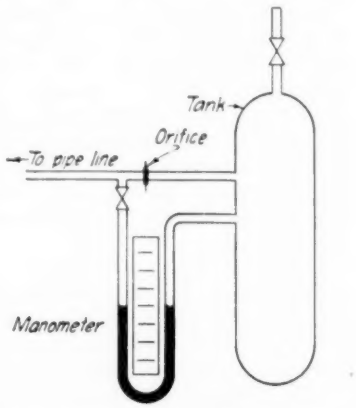


FIG. 9 PULSATION DETECTOR (BEITLER AND OVERBECK)

but suction pulsation is just as serious as discharge pulsation if the amplitude of the pulsation is the same in both cases. These conclusions have been substantiated by other tests. Figs. 6 and 7 show the results of tests reported in this paper.

The magnitude of the error depends upon the quantity of fluid being measured, the resistance and capacity between the disturbance and the meter, and the viscosity and density of the fluid being measured.

According to H. F. Hagen (15) tests on centrifugal- and propeller-type fans are apt to be in error because of erroneous velocity and pressure readings caused by pulsating flow.

Tests (10) that have been conducted reveal that the meters made by several manufacturers gave the same amount of error when tested simultaneously.

METHODS OF DETECTING PULSATION

If two meters are placed in series in a given line at some considerable distance apart and if the one nearer the potential source of pulsation gives a reading which differs from the reading given by the other by an amount greater than the usual discrepancy between meters, then it is certain pulsation has been created.

If a meter is subjected to constant quantity of flow and if the indicator on the meter produces a line which indicates a variable rate of flow by a wavy line, then the presence of pulsation can be suspected. This does not mean, however, that pulsation must exist if the meter charts have wavy lines nor does it mean that every case of pulsating flow will produce a wavy line.

One pulsation detector was devised by H. S. Bean (9) which had only the defect that it was too sensitive for most installations. $^1/_8$-in. orifice. As has been pointed out previously, an orifice subject to pulsations will show a differential pressure even when there is no flow. This device takes advantage of this fact, and a differential reading on the manometer is an indication of the presence of pulsations. This device partially overcomes the defect of Mr. Bean's pulsation detector in that the liquid does not escape so readily but large rapid changes in static pressure will force the liquid out of the manometer. Slight changes of static pressure will cause differentials on the manometer which are not caused by pulsations. As in the case of Mr. Bean's detector, if no differential is shown on the manometer then it is certain that no pulsation exists.

Another instrument, which was electrical and also devised by Professor Beitler, consisted of two diaphragms of stainless steel about 1 in. diam and $^1/_{32}$ in. thick which were connected to each side of the primary metering element by very short connections and so constituted that a pressure variation would be indicated by a very slight movement of the diaphragms. Piezoelectric crystals were used to indicate the motion of the diaphragms, and the voltage produced was amplified and recorded on a recording voltmeter. The whole apparatus gave a record of the wave form at both the inlet and outlet pressure taps. The recorder was capable of responding to very rapid fluctuations of the pressure, and the complete record of the form and amplitude of the pressure variations was made on a high-speed chart. The wave forms shown in Fig. 5 were recorded by this instrument. If no pulsation is present a straight line is drawn. The entire apparatus was constructed of standard types of instruments manufactured by Brush Development Corporation, Cleveland, O.

Another instrument described by T. K. M. Smith and R. E. Morter (10), which was used for detecting pulsation, was made up of a sylphon bellows to which a pen was attached. When pulsation causes the bellows to move the pen makes a mark on a strip chart driven by a spring motor. The record of the variations of pressure is thus made on the chart.

Elimination of Pulsation

Although it is now generally felt that no equation can be written for the error caused by pulsation and no meter can be built that will measure correctly if pulsation exists, many such equations and meters have been devised.

It was pointed out by Judd and Pheley (6) and since found true by others that: (*a*) it is not feasible to apply a correction factor to a meter since the correction factor would probably change with every installation and every condition of flow; (*b*) the laws of pulsating flow are not well enough known to set up an equation for a correction factor; and (*c*) each installation presents different problems. Most of the writers who have developed equations for correction factors have failed to take into account the complexity of the pulsation wave and have treated it as a simple one. Some of those who have devised meters which correct for pulsation have failed to take into account one very important fundamental, namely, that pulsation is the result of pressure variations as well as velocity variations.

Literature which deals with many of these equations and meters will be referred to.

J. L. Hodgson (11) presents the description of a device for metering air with pulsating flow. A vane which oscillates with the pulsations carries a pointer through a hairspring. The pointer indicates the mean of pulsations. The rapid motion of the pointer is damped by vanes in an oil bath. He gives an equation for calculating a coefficient to be used with the reading obtained with the damped reading to obtain the true rate of flow. Mr. Hodgson also has another paper dealing with the subject (12).

Prof. N. P. Bailey (13) discusses a patented device which he indicates will give true-flow air under pulsating conditions. The flow of water through a calibrated orifice is claimed to be proportional to the square root of the air velocity head. Professor Bailey also has discussed similar meters in other papers (14). C. A. Dawley has patented two meters which are claimed to read correctly even if the flow is pulsating; one was patented in 1927 and the other in 1928.

H. F. Hagen (15) describes an instrument he has developed for determining the shape of the pulsation wave created by a high-speed fan.

Equations for determining the error due to pulsation or for the calculation of correction factors to be applied to the flow equation for pulsationless flow have been prepared by N. P. Bailey (14), J. L. Hodgson (12), D. Gilmour (16), and A. H. Gibson (2).

It was thought for a time that the effect of pulsation could be eliminated in a meter by placing obstructions or throttles in the gage lines. In 1922 it was pointed out by H. P. Westcott (17) that this would have no beneficial effect. Tests conducted by Eagle and Daberko (18) at The Ohio State University in 1937 showed that such devices increased the error rather than reduced it.

As far as is known now, the only way to remove every trace of error due to pulsation is to eliminate the pulsation itself. There can, however, be a slight amount of pulsation present which will not seriously affect the meter readings.

Judd and Pheley (6), as a result of their work, set down some conclusions in regard to the practical elimination of pulsation which have since been substantiated. Among them are the following:

(*a*) Because of high velocity of pulsation an excessive length of pipe line would be necessary to destroy pulsation.

(*b*) Throttling is effective, but a great deal of throttling is required to reduce pulsation error.

(*c*) Abrupt volume enlargements in the pipe line will eliminate the error if of sufficient capacity.

(*d*) For the same capacity a volume with a large diameter is better than one of equal volume and smaller diameter.

(*e*) Combination of throttling with a volume forming a muffler device is probably best for mechanically removing pulsations.

(*f*) Revolving baffles are partially successful in removing pulsation.

(*g*) The effectiveness of any quieting device depends upon its ability to dissipate or change the energy of pulsation.

One sure way to reduce pulsation to a negligible quantity is to have sufficient pressure drop between the disturbance and the meter. This can be accomplished by an orifice or a partially closed valve. In tests that have been conducted the pulsation error on the downstream side was insignificant when the pressure drop through the restriction equaled or approached the critical. This, however, in the case of a compressor, is a costly method since the purpose of the compressor will partially be defeated.

A meter placed at a considerable distance from a disturbance will not be subjected to the same degree of error as a meter placed near the disturbance. Edward Sackett (19) points out that in one instance a meter placed 6 miles from a compressor had no error. E. P. Fischer (5) noted that a meter 17 miles from a compressor had no error while one near the compressor gave considerable error. Just how far pulsation will be carried in a transmission line depends upon a number of factors and will probably be different for every installation.

Volumes placed in a line have proved quite effective in reducing pulsation to the point where meter error is no longer appreciable. The fluid having pulsation is discharged into a tank having considerable volume from whence it flows on into the line again. Several modifications of this principle have been used with success. Smith and Morter (10) discuss the use of volume tanks. They also suggest that a tank have a volume of 100 cu ft per million cu ft of gas per 24 hr reduced to actual volume under the existing pressure and that the length of the cylindrical portion of the tank be 1.75 times its diameter. One tank of their design is shown diagrammatically in Fig. 10. The pressure drop through these tanks is very low.

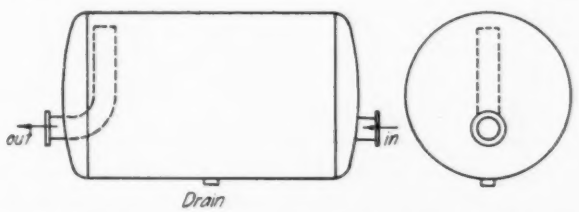


Fig. 10 Pulsation Eliminator Tank (From Smith and Morter)

Tests of volumes were conducted by Eagle and Daberko (18) in which they used the volumes in two different ways. The arrangement of the piping to the tank is shown diagrammatically in Fig. 11. The pulsation was produced by a two-stage compressor having a capacity of 350 cfm. In one series of tests they passed the air from the compressor directly through the tank by closing valve *A* and opening valve *B* (Fig. 11), valve *C* also being open; and in another series of tests they arranged the tank for "breathing" in the manner of a surge tank by opening valve *A* and closing valve *B* with the valve *C* being again open. It was found that the former method (passing the pulsating air directly through the tank) was far more effective in removing the pulsa-

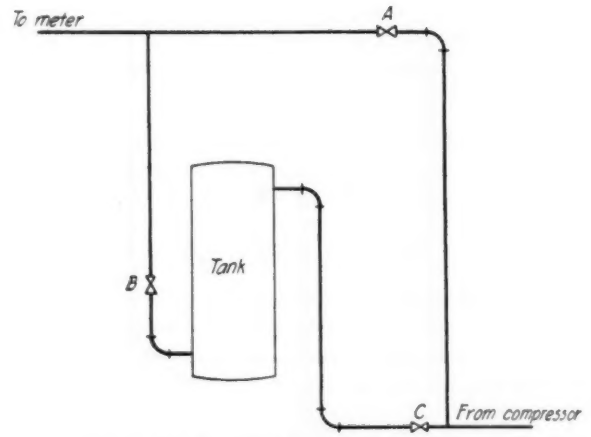


FIG. 11 OHIO STATE TEST TANK ARRANGEMENT

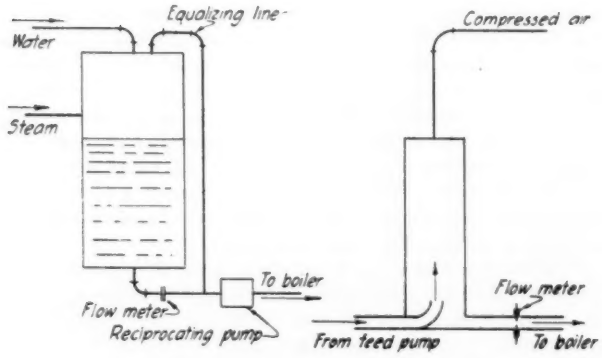


FIG. 12 PULSATION REDUCERS (MELAS)

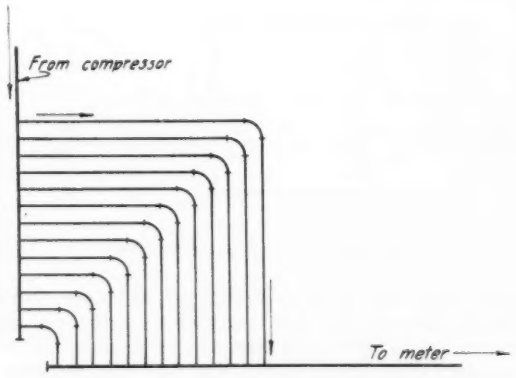


FIG. 13 PIPING FOR PULSATION REDUCTION (FISCHER)

tion than the latter. The tank used in these tests had a volume of 54 cu ft.

They also conducted tests when the air was passed directly through a tank having a volume of only 3 cu ft. They found that the smaller volume was about as effective in removing pulsation as the larger one. They then used the small volume lined with sound-absorbing material and placed baffles of the same material across the path of the air flow. They found that the acoustic material aided in removing pulsation to a small extent but that the acoustic material was destroyed under the action of the pulsation. They also found that the pressure drop through

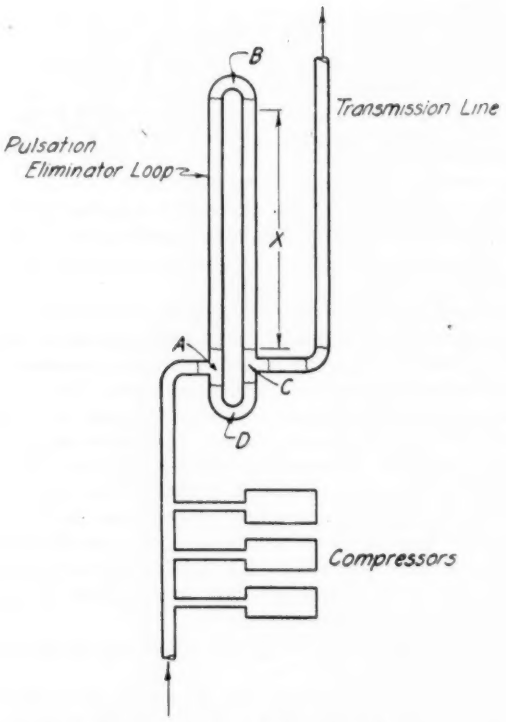


FIG. 14 PULSATION ELIMINATOR LOOP

the acoustical device was slight and concluded that the benefit was due to the sound-absorbing qualities of the device.

Two devices using the surge-tank principle are described by William Melas (20, 21, 22, 23) and shown in Fig. 12. It should be pointed out that these four articles are practically the same. Mr. Melas has used these devices in connection with a meter measuring the flow to a boiler feed pump.

F. P. Fischer (5) constructed a device (Fig. 13) which consisted of piping so arranged that various portions of the fluid under pulsating flow would have paths of different length so that the pulsation waves would interfere with one another as they joined the main pipe. Theory indicated that the waves would be broken up by this method. Elimination of the pulsation proved to be only partially accomplished.

In a report written by William Mosteller to J. T. Cortelyou, both of the Southern California Gas Company, Mr. Mosteller includes a discussion of the pulsation eliminator shown in Fig. 14. He points out that for maximum effectiveness in pulsation elimination, the length of the path *ABC* should equal the path *ADC* plus one half the length of the pulsation wave. Mr. Mosteller also gives an equation for calculating the wave length and the length X in the loop.

Tests made on a pipe line from a compressor before and after the installation of this type of loop indicated that the pulsation downstream from the eliminator was less severe after the eliminator had been installed. The pulsation in the line between the eliminator and the compressor was more severe in some sections of the line and reduced in other sections.

Another device which might be used as an eliminator is mentioned by Mr. Mosteller and is shown in Fig. 15.

After having studied a good many reports of test work, including some of the reports just discussed, L. K. Spink (24) has concluded that meter measurement accuracy may be improved by the following:

(*a*) Operating at a higher differential, i.e., in a multiple-

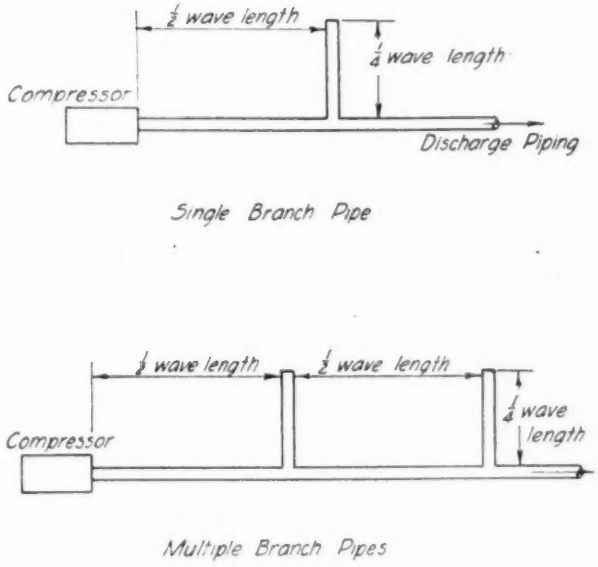


FIG. 15 ELIMINATORS CONSISTING OF BRANCH PIPES

meter run, shutting off one or more runs; or installing a smaller orifice in an existing meter run.

(*b*) Installing a higher range differential gage and changing operating conditions in order to use the increased range.

(*c*) Reducing the pipe-run diameter so as to use a higher orifice-to-pipe diameter ratio, still operating at differentials as high as practicable. Increasing the ratio of the orifice diameter to pipe-run diameter will reduce the pulsation error if the differential remains constant.

(*d*) Installing mufflers, headers, restrictions, or combinations of capacity and pressure drop between primary device and source of pulsation to reduce pulsation amplitude.

(*e*) Locating the primary device at a point where the pulsation amplitude is lower (as on the suction side of compressors).

MEASUREMENT OF PULSATION

Because of the fact that so many variables enter into an equation for pulsating error and because each installation has peculiarities of its own, computation of the error due to pulsation is out of the question. It is therefore necessary to have some instrument to determine the presence and extent of the pulsation error.

A second electrical instrument suggested by S. R. Beitler using piezoelectric crystals was developed in which the amplitude of the pulsation wave was measured by an indicating voltmeter mounted on top of a small box containing the diaphragm holders, the amplifier, and the mixing switch, so that the entire apparatus was self-contained. The power for amplification was supplied by dry cells so that the apparatus was portable. This instrument was also developed and manufactured by the Brush Development Corporation. Operating experience indicated that there was some question about the calibration of the electrical apparatus and, because of its sensitivity to pressure variations, it was extremely difficult to obtain a representative reading. A mechanical device which gives the amplitude of the differential-pulsation waves has been developed by S. R. Beitler (25) and J. E. Overbeck. This device, shown diagrammatically in Fig. 16, is a variation of the indicator and has proved very satisfactory in operation.

In its present form the mechanical pulsometer consists of two cylindrical volumes, *A* and *B*, Fig. 16, separated by a sylphon

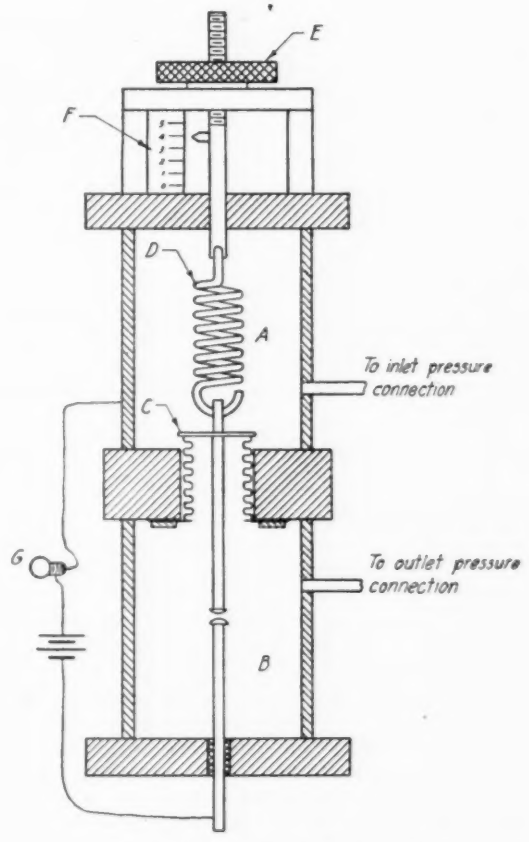


FIG. 16 MECHANICAL PULSOMETER

bellows *C* so that there will be no leakage between the two volumes which are connected to the inlet and outlet pressure connections of the meter, and as close to the primary element as possible. A coil spring *D* is mounted in volume *A*, which volume is connected to the high-pressure tap. The tension on this spring can be changed by turning the handwheel *E* which is outside the instrument. The scale *F* (each division represents $^1/_{16}$ in.) indicates the elongation of the spring. Electrical connections are arranged in volume *B*, which is connected to the low-pressure tap, so that any motion of the bellows caused by differential pressure will be indicated by a light *G* located on the outside of the instrument. During operation the tension of the spring is gradually increased until the light goes out. This indicates that the differential pressure has been equalized by the spring tension. When this occurs the tension of the spring should represent the differential pressure due to the flow plus the maximum amplitude of the differential pressures.

The instrument spring can be calibrated by comparing its scale readings with any differential gage when connected to a setup where there are no pulsations present. When measuring pulsation amplitude the instrument is almost totally unaffected by inertia, since the moving parts are practically at rest when the determination is made.

To determine the correlation between pulsometer reading, meter differential, and meter error a research project was sponsored by the American Gas Association and The American Society of Mechanical Engineers. A special test station, shown diagrammatically in Fig. 17, was constructed near Sugar Grove, Ohio, at the Crawford No. 2 Station of the Ohio Fuel Gas Company. (It was the good fortune of the author to be a member of the research working committee during the period that many of

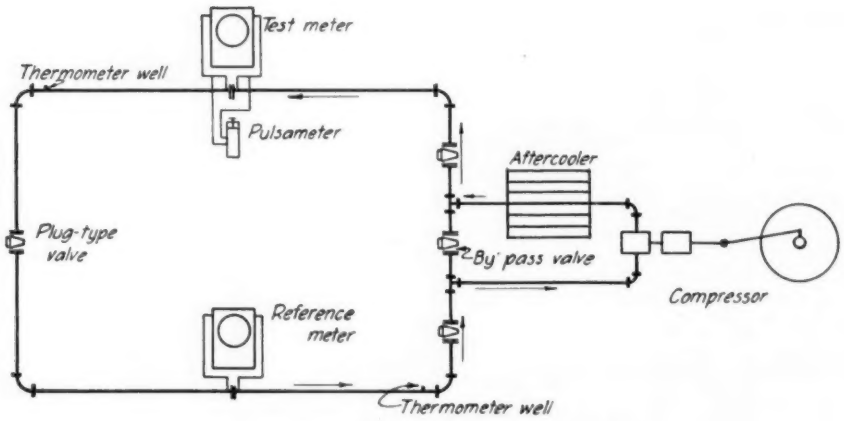


FIG. 17 ARRANGEMENT OF PULSATION TEST PIPING
(Crawford No. 2, Sugar Grove, Ohio.)

the tests were conducted.) This test station was built with two orifice meters in series, one on the discharge and the other on the suction line of a large gas compressor. Gas was supplied to the first orifice directly from the outlet of the aftercooler of one compressor, and after passing through the second orifice meter, was discharged back into the suction of the same compressor.

With this arrangement pulsation could be maintained as nearly constant as possible and the other measured conditions could be easily changed to give the pressures and rates of flow desired. Throttle valves (plug-type valves) were placed in the line between the two meters and also between the compressor and the inlet and outlet of the test setting. By means of these valves it was possible to regulate the pressure on either one of the meters so that it would not be subjected either to suction or discharge pulsations from the compressor.

This meter was then used as a standard or reference meter and the measurement error due to pulsation was determined by comparing the quantity indicated by the meter subjected to pulsation (or test meter) against that indicated by the reference meter. The test meter was equipped with both "flange" and "pipe" taps, and readings were taken on both simultaneously in order to determine what effect the location of pressure taps might have on the test results.

In order to eliminate the effect of small variations in orifice plates and runway construction, so-called "unity tests" were run for each arrangement of orifice plates. In making these tests the flow into and out of the setting was throttled to the extent that there was no pulsation on either meter. By comparing the quantities as measured by the two meters under these conditions, an indication was obtained of how close the meters would check each other when no pulsation was present.

As shown in Fig. 17, the setup is as it was arranged for the determination of discharge pulsation. When the study was made on the effect of suction pulsation the function of the meters was interchanged and the pulsometer was moved to the other meter.

Since changing the speed of the compressor would change the type of pulsation, a by-pass was built into the setting between the inlet and outlet so that it was not necessary to change the speed of the compressor in order to change the rate of flow through the setting. The compressor used was a two-cylinder double-acting Ingersoll-Rand machine having $18^1/_2$-in. × 48-in. cylinders and operating at approximately 70 rpm.

The curve shown in Fig. 18 was determined from the tests at this station. In preparing this curve the results of about 500 tests on orifices with diameter ratios of from 20 per cent to 80 per cent in 2-in., 4-in., and 6-in. lines were studied. It was decided not to attempt to determine any correction factors but to concentrate on the determination of the conditions under which meters would measure accurately. Taking many facts into consideration, it was decided that a meter, subject to pulsation, would be normally within the limits of commercial accuracy when the error was less than 1 per cent. Taking into account spot tests made with commercial setups and recording gages, it was felt that the probable accuracy of any individual test not subject to pulsation was within the range of ±0.5 per cent.

All of the test points were plotted on a large sheet, and the percentage of error was marked on the points. The line was then drawn through the points where the error was approximately 1.5 per cent. Because of the inherent limitations on the accuracy of the tests there were three or four points with an error greater than 1.5 per cent below the curve and ten or twelve points with less than 1 per cent error above the curve. It will be

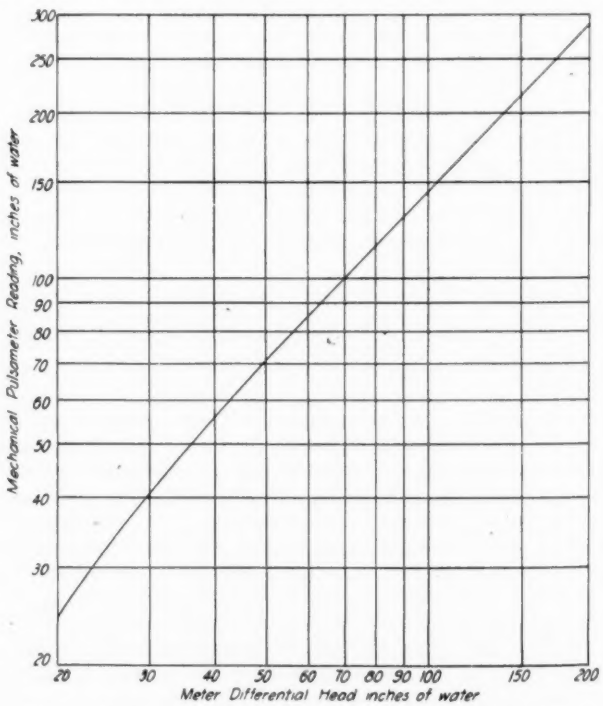


FIG. 18 RELATIONSHIP BETWEEN METER DIFFERENTIAL AND PULSOMETER READING FOR ONE PER CENT ERROR

noted that the same curve applies to both flange and pipe taps.

This curve can then be used to determine whether or not a meter measuring pulsation flow is accurate. It is necessary only to attach the pulsometer to the pressure taps and take a reading on it at the same time that the differential pressure is determined. The calibration curve is then consulted to find the pulsometer reading in inches of water. If the point, when plotted in Fig. 18, falls below the curve, then the pulsation error is less than 1 per cent and the meter is probably within the range of ordinary commercial accuracy. If the point falls above the curve, then the pulsation error is greater than 1 per cent, and the measurement with the meter will not be accurate.

For differential pressures less than 32 in. of water the experimental curve was intentionally curved downward at the lower readings, since operating experience has shown that measurements made at low differentials when the flow is pulsating, are very sensitive to changes in pulsation, and it was felt that the line should be lower than normal to allow the effect of these accidental variations. Because of erratic results the empirical curve was not drawn for differentials below 20 in. of water and if pulsations are present, it is believed better not to attempt to meter the flow where the differentials are as low as that. These curves were plotted on logarithmic paper so that points with the same percentage of error would be approximately the same distance from the curve for any value of the differential head.

In order to make use of the available test results all pulsometers must have the same general dimensions as the one used to determine the effect of pulsation, since the shape and dimensions will undoubtedly have some effect on the instrument reading. This pulsometer is patented and is now being built by the Refinery Supply Company, Tulsa, Okla.

As previously mentioned, the location of the curve drawn in Fig. 18 was determined by experiment, and it was thought that the results might be better understood if there was a rational explanation for drawing it in this manner. In order to see the relationship of the empirical curve to some theoretical curves, Fig. 19 was plotted.

Equations developed in the second section, "Mathematical Analysis," were used in obtaining these curves. Values of the error were found for several values of p/h. Then p/h was plotted against the meter error for each wave form, and the value of p/h for 1 per cent error for each of the three wave forms was determined from the curves. Then a relationship was set up between the pulsometer reading $(p + h)$ and the meter differential (h).

In comparing the theoretical curves with the empirical curve it has been assumed that the pulsometer reading is the sum of the differential plus the amplitude of the pulsation. These curves are all drawn for 1 per cent error. It will be seen that there is a reasonable degree of relationship between the empirical and theoretical curves.

Research to Be Done

Although pulsation has received considerable thought and attention for a number of years and although devices have been built which indicate the presence and others which to a degree indicate the magnitude of the pulsation, considerable work remains to be done.

No use of the pulsometer shown in Fig. 14 has been made in connection with a vapor having pulsating flow. Just how the instrument would behave if the volumes on both sides of the bellows or if the lines leading to the instrument were filled with a liquid remains to be learned through an investigation. At the present time it also seems quite necessary that an instrument be developed for use with meters having low differentials, say, 30 in.

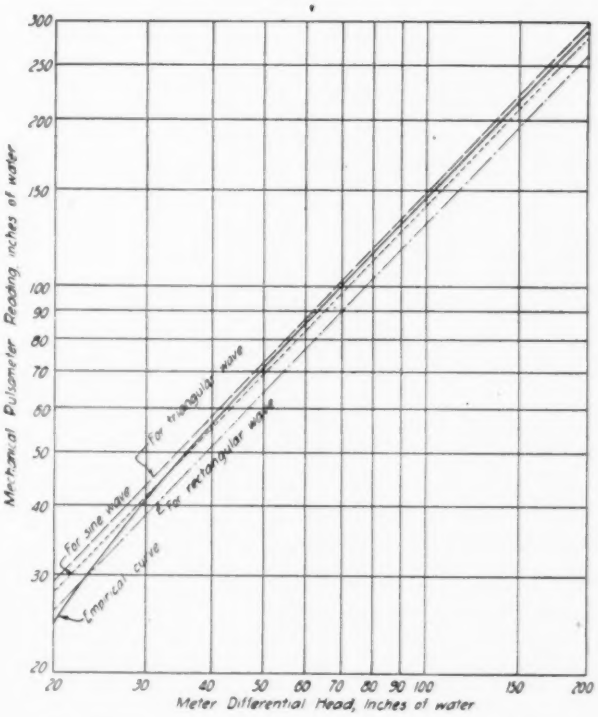


Fig. 19 Theoretical and Empirical Curves for One Per Cent Error

and less. The curve now used, Fig. 18, cannot be used with such low differentials with any degree of confidence.

It is also felt that more of a study of the pulsation theory should be made. Heretofore, pulsation produced by a commercial machine has usually been studied. It would seem to be logical to make a laboratory study of pulsations which could be carefully controlled and varied. In this way the degree of error produced by different devices and with different wave forms could be determined.

The studies mentioned are only a few which need to be made. There are, in fact, many others of equal importance.

BIBLIOGRAPHY

1 "Methods of Measuring Discharge and Head," by W. M. Venable, Trans. A.S.C.E., vol. 54, 1905, part D, pp. 502–504.

2 "Abnormal Coefficients of the Venturi Meter," by A. H. Gibson, Proceedings of The Institution of Civil Engineers, London, England, vol. 196, 1914–1915, pp. 391–408.

3 "Venturi Meters Inaccurate on Lively Lines," by Allen Hazen, *Power*, vol. 44, 1916, p. 354.

4 "Measurement of Steam Flow," by E. G. Bailey, *Power*, vol. 43, 1916, pp. 854–858.

5 "Establishing a Standard of Measurement for Natural Gas in Large Quantities," by F. P. Fisher, Trans. A.S.M.E., vol. 38, 1916, pp. 241–284.

6 "Effect of Pulsations on Flow of Gases," by Horace Judd and D. B. Pheley, The Ohio State University, Engineering Experiment Station, Bulletin No. 24, March 14, 1923.

7 "The Effect of Pulsating Flow on Gas Measurement," by S. R. Beitler, West Virginia University, Engineering Experiment Station, Technical Bulletin No. 16, February, 1940, pp. 201–217.

8 "The Effect of Pulsations on Orifice Meters," by S. R. Beitler, Trans. A.S.M.E., vol. 61, 1939, pp. 309–314.

9 "Survey of Metering of Pulsating Flows of Gas," by H. S. Bean, *Western Gas* (now called *Gas*), vol. 11, October, 1935, pp. 46–48 and 50.

10 "The Detection and Mitigation of Pulsation in Orifice Meters," by T. K. M. Smith and R. E. Morter, *Gas*, vol. 14, September, 1938, pp. 55–68.

11 "Commercial Metering of Air, Gas, and Steam," by J. L. Hodgson, Proceedings of the Institution of Civil Engineers, vol. 204, 1916–1917, part 2, pp. 108–193.
12 "The Laws of Similarity for Orifice and Nozzle Flows," by J. L. Hodgson, Trans. A.S.M.E., vol. 51, 1929, part 1, FSP-51-42, pp. 303–332.
13 "Pulsating Air Flow," by N. P. Bailey, Trans. A.S.M.E., vol. 56, 1934, pp. 781–786.
14 "Pulsating Air Velocity Measurement," by N. P. Bailey, Trans. A.S.M.E., vol. 61, 1939, pp. 301–308.
15 "Pulsation of Air Flow from Fans and Its Effect on Test Procedure," by H. F. Hagen, Trans. A.S.M.E., vol. 55, 1933, FSP-55-7, pp. 105–115.
16 "Integration and Pulsation Errors in Measurement of Quantities of Gas Flowing Through an Orifice," by D. Gilmour, *Journal of the Institution of Petroleum Technologists*, vol. 19, 1933, pp. 25–68.
17 "Measurement of Gas and Liquid by Orifice Meter," by H. P. Westcott, Metric Metal Works, Erie, Pa., 1922, pp. 143–152.
18 "An Investigation of Pulsating Flow and Pulsation Eliminators by Orifice Meters," by J. H. Eagle and W. A. Daberko, Thesis, Ohio State University, 1937.
19 "Compressor Pulsations—Their Effect on Orifice Meter Accuracy," by Edward Sackett, *Gas*, vol. 16, August, 1940, pp. 20–22.
20 "Measuring Pulsating Flow Accurately," by William Melas, *Water Works and Sewerage*, vol. 88, 1941, p. 289.
21 "Metering Pulsating Flow," by William Melas, *Power Plant Engineering*, vol. 45, July, 1941, p. 64.
22 "Minimizing Errors in Metering Pulsating Flows," by William Melas, *Instruments*, vol. 14, 1941, p. 206.
23 "How to Secure Accurate Readings in Measuring Pulsating Flow," by William Melas, *Steel*, vol. 109, November 10, 1941, pp. 82 and 115.
24 "Principles and Practice of Flow Meter Engineering," by L. K. Spink, The Foxboro Company, Foxboro, Mass., 1943, p. 174.
25 "Developments in the Measuring of Pulsating Flows With Inferential-Head Meters," by S. R. Beitler, E. J. Lindahl, and H. B. McNichols, Trans. A.S.M.E., vol. 65, 1943, pp. 353–356.
26 "Fluid Meters Report," published by A.S.M.E., 1937, p. 26.
27 "Operational Factors in Orifice Flow," by H. W. Swift, *London, Edinburgh, and Dublin Philosophical Magazine and Journal of Science*, seventh series, vol. 5, 1928, pp. 1–18.
28 "Eliminating Pulsating Errors in Orifice Meter Measurement," by T. K. M. Smith, *Western Gas*, vol. 8, January, 1932, pp. 38–42.
29 "Notes on Wave Motion," by C. W. Frick, for General Electric Company's Electrical Course, eighth semester, December, 1930.
30 "Pulsation as Encountered in Flowing Gases," by L. F. Scheel, *Western Gas*, vol. 6, October, 1930, pp. 46–48.

Discussion

J. E. Overbeck.[4] The writer has had the good fortune of working on some of the research studies explained, as well as of using some of these research data in practical applications.

If the operating gas-measurement engineers will take full advantage of the information now available, which is set forth in this paper, there is certainly much to be gained. In putting these data to practical application, the first step should be to make a study of all measuring stations to determine which are liable to be affected by pulsation. This can be done by reviewing all stations and determining which ones are located adjacent to compressor stations. The term "adjacent" may mean that the meters are located on the compressor-station lot, or it may mean that they may be up to 20 miles away from the compressor station where there is very little pressure drop or resistance between the measuring station and the compressor station.

Each station suspected should be checked with a mechanical-type pulsometer of the type shown in the author's Fig. 16, to determine whether or not the effect of pulsation is sufficient to cause an error in measurement. Such tests should be made under all of the operating conditions encountered, including rates of flow, number of compressors being operated, lines and connections being used, whether or not the gas is passing through scrubbers, coolers, dehydrators, etc. Generally, the pulsation effect will be the greatest with the least number of compressors being operated and with the least number of connections, etc. It is probable that these tests will eliminate a high percentage of the stations suspected, that is, the effect of pulsation will be within the limits as shown by the author's graph, Fig. 18.

Where the effect of pulsation exceeds these limits and is to be reduced, local conditions surrounding the meter stations are big factors, and which method to use, of course, will depend upon these local conditions. In many instances it may only be necessary to change operating conditions or make only slight changes in the equipment, such as changing orifice size, operating at higher differentials, etc.

From the operating standpoint, the charts shown in Fig. 6 and Fig. 7 of the paper, are helpful in determining whether or not to change the meter differential or change the orifice-to-pipe diameter ratio to obtain the most efficient results. For example, where it is not necessary or practical to change the pipe-run size, it will be found that it is more effective to operate at the highest differential, even though flow conditions require a slightly lower orifice-to-pipe diameter ratio.

For those stations where the pulsation effect is beyond the limits, as shown in Fig. 18, the suggested remedies pointed out by the author will certainly be helpful in reducing the error. Many other types of pulsation dampers have been used. Generally, any change in piping that will, through interference, break up the pulsation waves at the point of measurement will increase the frequency, lower the amplitude, and thus reduce the meter error.

It may be found necessary at some stations to make more than one change, that is, increase the orifice-to-pipe diameter, increase the operating differential range and install some pulsation dampers, or change the arrangement of piping between the source of pulsation and meter.

Author's Closure

The comments by Mr. Overbeck relative to checking and correcting meter installations for pulsation are a valuable addition to the paper.

The author feels certain that there are many others who have something to offer which will shed more light on pulsation. There should be several who have tried eliminators besides the ones shown. There should also be additional references. No doubt the theory of pulsation as given in the paper can be expanded.

The author will appreciate receiving any information on pulsation that any reader may have.

[4] Columbia Engineering Corporation, Columbus, Ohio.

Boiler Design for Extreme Load Variations

By M. H. KUHNER,[1] WORCESTER, MASS.

A summation of required design provisions for boilers adapted to operate under quick demand changes. Reference is made to the quick-pickup boiler in the Harbor Steam Plant of the City of Los Angeles and the steel-mill boiler at the Homestead Works of the Carnegie-Illinois Steel Corporation. The importance of water storage, unrestricted path for water and steam in circulation, steam release with minimum disturbance of water body in drum, steam-temperature control during unbalanced firing, and the effect of each item on the others, is discussed. Recommendations are made for determining required capacity of fuel-burning equipment and fans in reference to the extent and rapidity of steam-load changes.

MOST boilers in public-utility and industrial plants are called upon to carry reasonably steady steam loads. Changes in steam demand are gradual and are often predicted in sufficient time to permit required preparations for load increases or decreases. Boilers of what can be termed standard design usually give a good account of themselves under this type of service.

There are, however, other steam power plants, both public-utility and industrial, in which standard boilers would be quite unsuited. These are the plants where steam demand is unpredictable and where load changes are instantaneous and extreme. Steam-electric plants which stand by hydroelectric stations come under this category.

An outstanding example in the utility field is the Harbor Steam Plant of the City of Los Angeles, where a single boiler and turbine-generator unit must be prepared to pick up loads at the rate of 50,000 to 60,000 kw within seconds and without previous warning, Fig. 1.[2]

In the industrial field the steam power station of the Homestead Works of the Carnegie-Illinois Steel should be mentioned, Fig. 2. A single boiler and turbine-generator unit feeds steam and power into the lines of the entire system of "Big Steel's" Pittsburgh district. Whenever a deficiency in steam or power develops in any one of the steel-mill units, it must be made up by the Homestead Works Power Station. Instantaneous load-rate changes as great as 250,000 lb of steam per hr and 20,000 kw are quite frequent.

In the design of boilers suitable to serve safely and reliably in a power plant with sudden and extreme load variations, the following major points must be given careful consideration:

1 That portion of heat stored in the boiler which will become available at once for steam formation with reduction in pressure.

2 Path of water and steam through circulatory system.

3 Release of steam formed by flashing in the water body.

4 Control of steam temperature while steam output and firing rate are out of balance.

5 Effect of rapid thermal changes in steam, feedwater, and combustion gas on boiler pressure parts.

6 Methods of firing and capacity of fuel-burning equipment.

7 Selection of mechanical-draft equipment and drives as to type, capacity, and control.

8 Construction of setting enclosure for momentary high internal setting pressures.

9 Automatic equipment for control of firing and flow of fuel, air, gas, and feedwater.

Heat Storage

When the steam-output rate of a boiler increases elevenfold in a matter of 4 or 5 sec, as is the case with the Harbor Steam Plant boiler, it cannot be expected that the firing rate can be made to increase proportionately and at the same time. Response of the automatic control naturally lags because the control receives its primary impulse from steam pressure or steam flow. It takes time for the fans to speed up, for dampers to arrive at the new setting and for increased fuel and air quantities to reach the furnace. During this time lag the boiler is required to perform somewhat like a steam accumulator. Steam delivered over and above that quantity generated by the existing furnace heat input must be produced by flashing, using heat stored in the boiler water. Part of this heat is made available with reduction in boiler pressure. Steam is formed in the body of water contained in drums, tubes, and headers. The greater the weight of water below the working level, the more heat is available for flashing of steam and the smaller will be the pressure loss for a given steam output. To have the highest possible pressure and heat head available at the moment of load pickup, it is advisable to control the drum pressure of the boiler rather than the pressure at the superheater outlet or at the turbine throttle. The difference between the drum pressure existing at the moment of the beginning of the load pickup and the lowest drum pressure permissible for the work to be done determines the steaming rate during accumulator operation, and the maximum permissible time lag between start of high steam output and correspondingly increased furnace heat release.

The example of the Harbor Steam Plant boiler is probably best suited to illustrate the importance of heat storage. A standard boiler unit of 650,000 lb capacity at 1000 psig, 900 F usually contains approximately 2500 cu ft of internal cubical space below the working water level in drums, tubes, and headers. The Harbor boiler has 3500 cu ft. Its hourly steaming rate is between 60,000 and 100,000 lb, while it is under stand-by load. The drum pressure is maintained at 1040 psig. It can be assumed that during the low steaming rate of stand-by operation the space below the water line is occupied by substantially solid water, that is, water almost free of steam bubbles. The turbine is constructed so that the peak generating capacity can be maintained with 840 psig throttle pressure. Maximum pressure drop through the superheater, steam-temperature control system, and steam line from boiler to turbine, is approximately 100 psi. The boiler-drum pressure may therefore be permitted to drop 100 psi during accumulator operation before capacity power output of the plant is impaired.

Saturated water totaling 3500 cu ft at 1048 psig, which is the mean pressure between water level and lowest point of the system, equals 160,000 lb. It contains 551.9 Btu per lb, or a total of

[1] Chief Mechanical Engineer, Riley Stoker Corporation. Mem. A.S.M.E.

[2] "The Harbor Steam Plant Boiler," by Max H. Kuhner, *Power Plant Engineering*, vol. 49, June, 1945, pp. 86–89.

Contributed by the Power Division and presented at the Semi-Annual Meeting, Detroit, Mich., June 17–20, 1946, of The American Society of Mechanical Engineers.

Note: Statements and opinions advanced in papers are to be understood as individual expressions of their authors and not those of the Society.

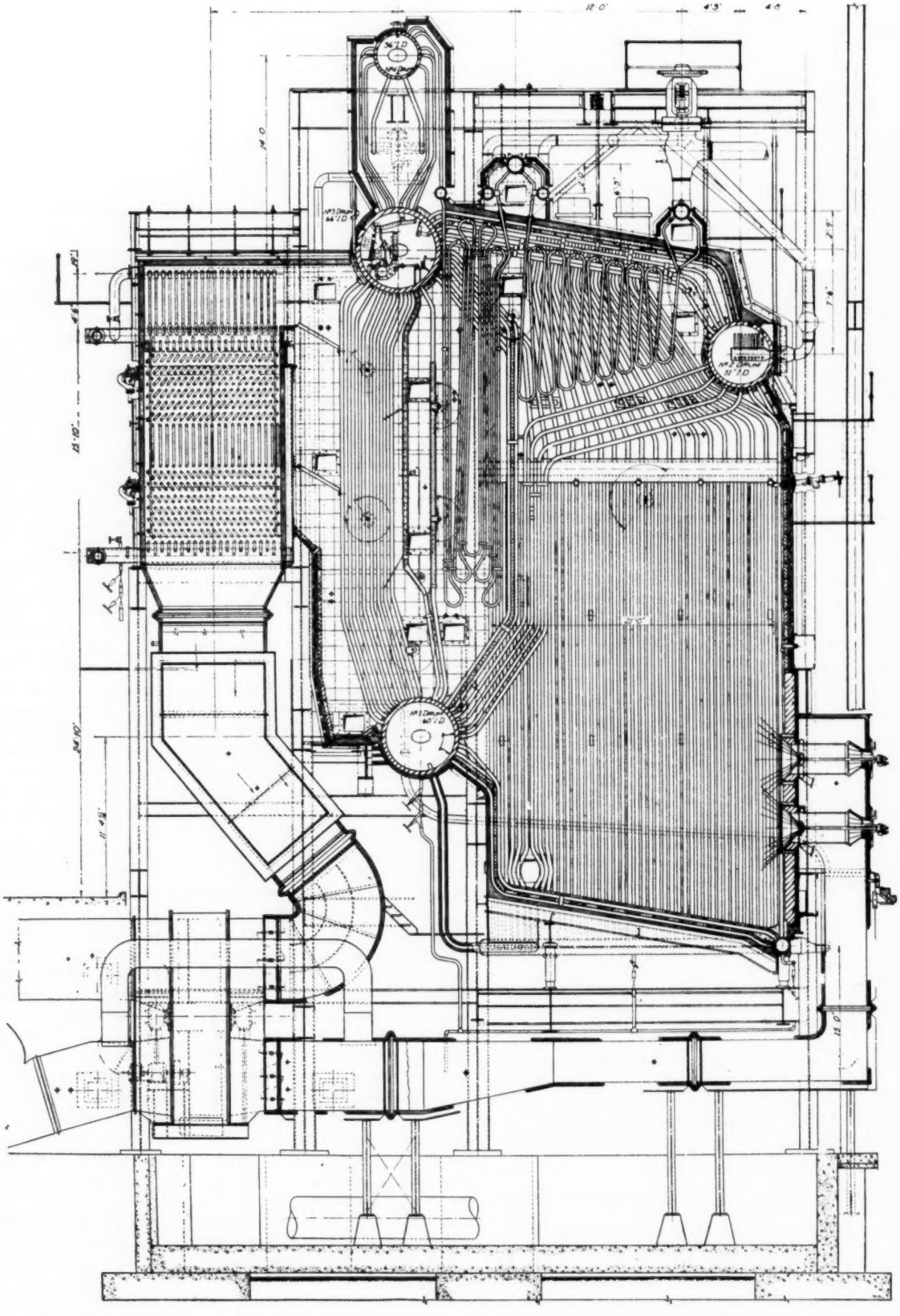


FIG. 1 THE HARBOR STEAM PLANT BOILER NO. 1

(650,000 lb per hr, 1040 psig drum pressure, 915 F steam temperature. Boiler and 65,000 kw turbine generator operate as "spinning reserve" for hydropower. Boiler automatically picks up steam-load rates of 600,000 lb per hr within a few seconds.)

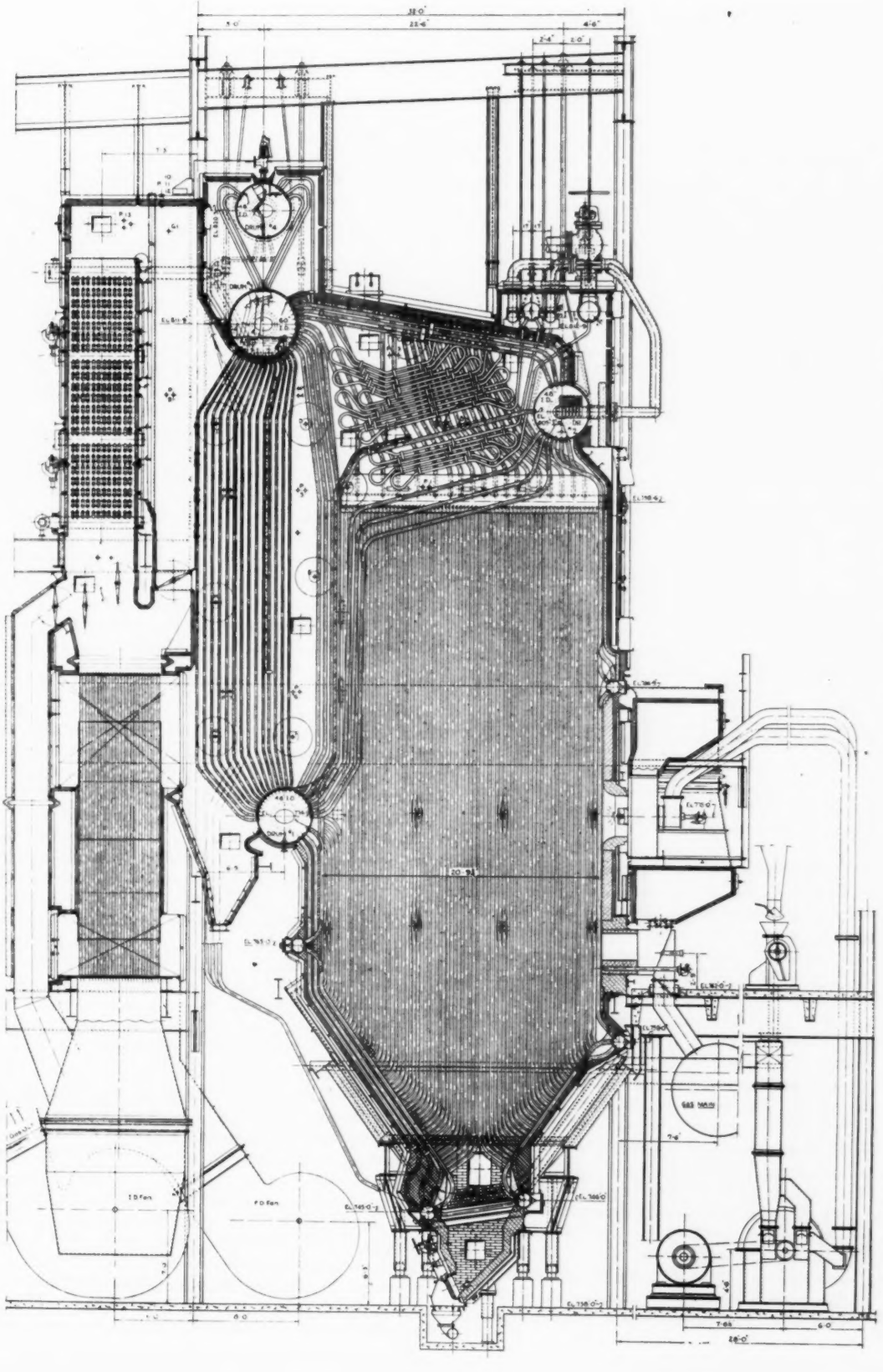


FIG. 2 450,000 LB PER HR BOILER UNIT OF CARRIE FURNACES PLANT, CARNEGIE ILLINOIS STEEL CORPORATION
(Steam-output rates change rapidly between 200,000 and 450,000 lb. Fuel is blast-furnace gas and pulverized coal. Steam temperature automatically controlled by heat-exchanger-type control.)

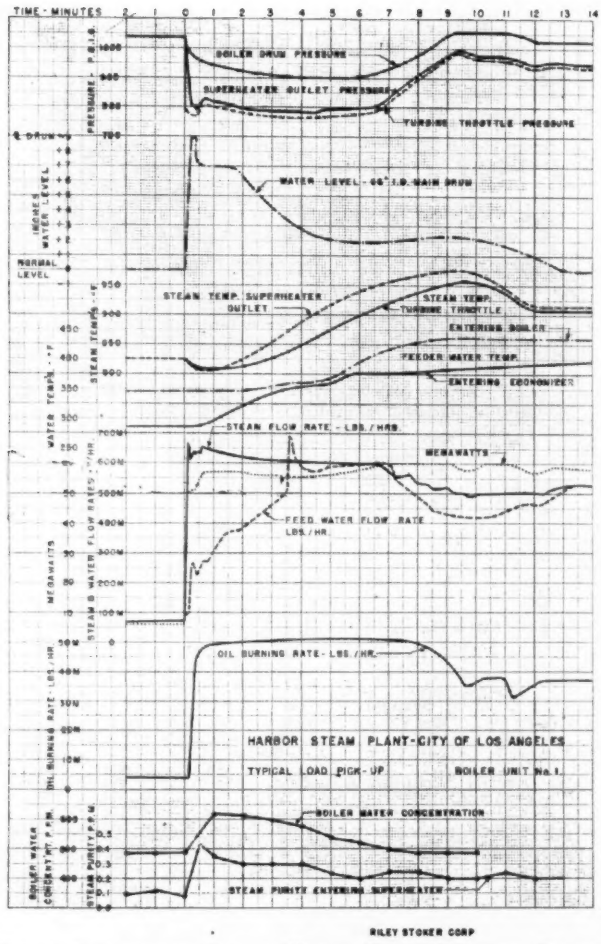


FIG. 3 PERFORMANCE DATA OF HARBOR BOILER RECORDED DURING TYPICAL STEAM-LOAD PICKUP FROM 70,000 LB STAND-BY RATE, TO APPROXIMATELY 650,000 LB PER HR

88,200,000 Btu. If the mean pressure is 100 psi lower, or 948 psig, each pound of water contains 537 Btu and the total heat in 160,000 lb of water is 85,900,000 Btu. The difference, 2,300,000, is available as heat to be flashed into steam.

The heat of evaporation at the mean pressure between the initial drum pressure (1040 psig) and the pressure at the end of the accumulator cycle (940 psig) is 648.5 Btu per lb; 2,300,000 divided by 648.5 = 3550 lb of steam can thus be flashed from boiler water.

The Harbor boiler must deliver steam at the rate of approximately 650,000 lb per hr to develop 55,000 kw output under rapid pickup conditions. The firing rate is established to produce only approximately 60,000 lb per hr prior to the moment the load rise begins. The difference at the rate of 590,000 lb per hr must be made up by flashed steam. A steaming rate of 590,000 lb per hr is 164 lb per sec; 3550 divided by 164 is 22; therefore the heat stored in the boiler water permits the maintenance of 650,000 lb per hr steam-output rate for only 22 sec duration if the firing rate corresponding to 60,000 lb steaming rate is maintained. The boiler-drum pressure will drop from 1040 psig to 940 psig during this period. The 22-sec time lag is usually sufficient for the fuel-burning rate to increase and to meet the new steam-output rate, Fig. 3.

CIRCULATORY SYSTEM

While the design for unidirectional circulation of water and steam is a basic requirement for all water-tube boilers, it becomes much more important where boilers are subjected to rapid load variations. Not only must the design of the system insure that there can be no stoppage or reversal of flow in any of the steaming tubes during a quick load change, but the path of water and steam must be easy and direct. Abrupt changes in internal cross-sectional area within the circulatory system must be avoided.

A sudden change in steam-output rate results in a momentary disturbance of the flow of water and steam in circulation. If the load suddenly rises with a resulting drop in drum pressure, steam is formed in the entire body of water contained in steaming tubes as well as in downflow and feeder tubes, wherever the water temperature corresponds with steaming temperature. The buoyancy of the steam globules formed in the downflow column opposes the downflow of solid water. The rate of circulation is naturally low during low rates of evaporation. If there are restrictions and obstructions placed in the path of natural circulation, a quick load rise will certainly produce stoppage and reversal of flow in some steaming tubes. This may lead to tube failures. If, on the other hand, the circulatory system is designed so that water and steam can find no serious obstruction in their path, full use can be made of the flywheel effect of the mass of water in motion.

It is calculated that the average circulating velocity of water in the Harbor boiler is approximately 2 fps during 60,000 lb per hr evaporation. The momentum of 80 tons of water traveling at this velocity is an effective force opposing the buoyancy of steam flashed in the water during a load pickup. It assures that unidirectional flow is maintained in all tubes. This boiler has been subjected to a number of rapid load pickups during the past 3 years. The performance recorded by curves, Fig. 3, is typical for such surges. No circulation difficulties were detected.

STEAM RELEASE

Releasing the steam generated in the open drum space of the main boiler drum above the water level prevents geysering and turbulence of the water body in the drum and seesawing of the water level. In general, this method effects rapid separation of steam from water. A design incorporating this provision is an advantage for all boilers regardless of type and service.[3]

Rapid steam-load changes are accompanied by water-level variations because the steam formed in the body of water during a sudden load rise, not paralleled by corresponding increase in heat input, tends to lift the water level. The volume of the fluid below the water level increases in direct proportion to the volume of steam formed in the water body. Conversely, a sudden reduction in load, accompanied by a slight rise in boiler pressure, causes steam globules already formed, to collapse, resulting in a shrinkage of the volume below the water line and a drop in water level.

It is important therefore that the drum in which steam is released and in which the working water level is to be maintained, be unusually large. The maximum rise in water level must not reduce steam-release space to the point where there is danger of water carry-over, and the drop in water level must not be such that the entrance to the downflow system becomes exposed and steam, in place of solid water, is permitted to enter the downflow column.

When the drum is equipped with a steam-cleaning and drying device the efficiency of this apparatus is usually dependent upon the height of the water level in the drum. If the level is too high the steam-purifying system may become flooded; if too low, dirty steam and boiler water may by-pass the purifier with disastrous results for superheater and turbine. Because large changes in water-level elevation cannot be prevented during

[3] "How Steam Is Released in Water-Tube Boiler Drums," by Max H. Kuhner, *Power Plant Engineering*, vol. 48, September, 1944, pp. 92–94.

sudden large changes in steam-output rates, it becomes necessary to study carefully the placement of steam-purifying equipment and a larger than normal drum diameter, or a separate steam-purifier drum is indicated.

The Harbor Steam Plant boiler is equipped with a 66-in-ID steam-release drum plus a 36-in-ID steam drum placed above at 14 ft vertical center distance. The volume of water contained in the 66-in-ID drum with the water line at normal elevation is 350 cu ft while the steam space above the water line is 1110 cu ft, Fig. 4. The normal water level is established at 9 in. below the horizontal center line of the 66 in. drum. The water level may rise 11 in. from normal during a load pickup or may drop 6 in. below normal with a sudden steam-load reduction before steam release, steam purification, and water supply to downflow column are affected. The effectiveness of this arrangement is indicated by the steam purity recorded during load pickups. The solids carried away in the steam usually increase momentarily from approximately 0.1 ppm to 0.5 ppm, Fig. 3.

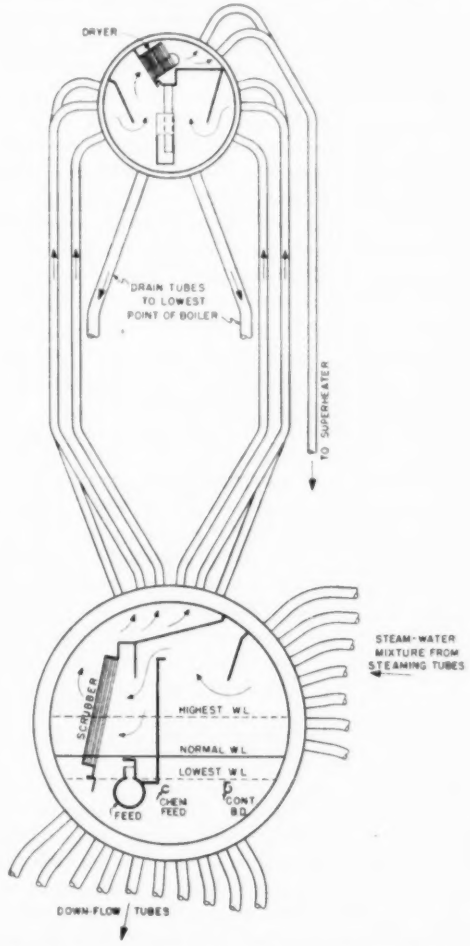


FIG. 4 STEAM-PURIFYING SYSTEM HARBOR STEAM PLANT BOILER NO. 1

STEAM-TEMPERATURE CONTROL

During normal operation of a central station or industrial boiler final temperature of steam delivered by the superheater is influenced by moisture content of the steam entering the superheater, steaming rate, length of flame, excess air used for combustion, type and kind of fuel, cleanliness of furnace wall and water heating surfaces placed ahead of the superheater, and cleanliness of the superheater surface. These are all factors which can change the steam temperature of an installation. A relatively simple system of steam-temperature control is usually sufficient to produce a workable steam-temperature characteristic in spite of the factors of normal operation mentioned. A system based on control of gas flow over superheater surface or on partial desuperheating is often sufficient to prevent a rise in steam temperature to the point where superheater and turbine are endangered, because each individual factor, or a combination of those mentioned, will not so seriously influence the final steam temperature that the range of a correctly designed control is exceeded.

With a quick-load-pickup boiler additional factors must be considered as affecting steam temperature. During a sudden load rise, and while the firing rate lags 20 to 30 sec behind the increased steam output, very little heat is applied to the superheater surface and a drop in steam temperature must be expected. On the other hand, steam temperature will rise sharply with a sudden drop in steam demand because the firing rate, corresponding with the higher load, continues several seconds after the load decrease has taken place. More heat is therefore applied to the superheater surface than can normally be carried away with the steam. Conditions are aggravated for a purely convection superheater because its normal characteristics produces a steeply rising temperature gradient with increasing steaming rate. A superheater designed so that part of the heat is received by radiation and the remainder by convection, produces a more uniform steam temperature over a wide range in load. Obviously therefore a superheater of this design insures a higher steam temperature at the beginning of the load-pickup cycle, and the effect on steam temperature by the unbalance of steam flow and firing rate at the moment of a sudden load drop is not as pronounced as with the purely convection superheater.

In addition to the points mentioned as affecting superheater performance there is one factor identified with quick-load-pickup boilers only which has a severe effect on steam temperature. Heat removed from boiler water by flashed steam, with the reduction in pressure, must be restored after the high steaming rate is established and while pressure is raised to normal. The fuel-burning rate is therefore not only that required to generate the steam delivered by the boiler, but in addition, that necessary to restore the heat to the boiler water and thus re-establish the normal operating pressure. The heat input to the superheater is considerably greater during the time pressure is being restored

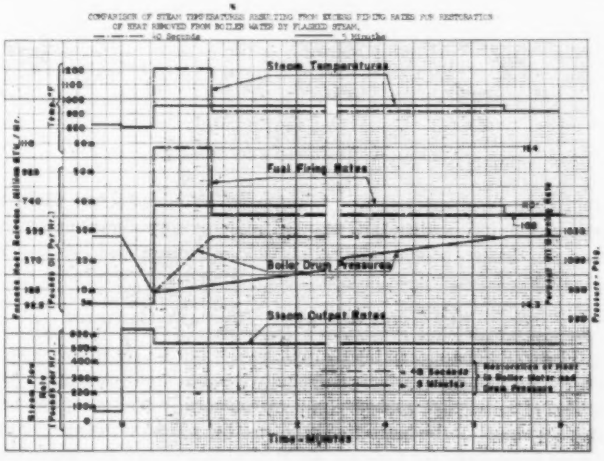


FIG. 5 COMPARISON OF STEAM TEMPERATURES RESULTING FROM EXCESS FIRING RATES FOR RESTORATION OF HEAT REMOVED FROM BOILER WATER BY FLASHED STEAM

than required for normal steam temperature at the existing steam flow. During this period steam-output rate and firing rate are out of balance with the firing rate a considerable percentage greater than needed for the steam output. The result is high steam temperature. The excess rate of firing is, of course, in inverse proportion to the time permitted to restore the heat in the boiler water and to establish normal drum pressure, Fig. 5. The maximum permissible steam temperature usually limits the excess rate of firing and thus controls the time required for restoring normal drum pressure.

Gas by-pass dampers for controlling steam temperature are too sluggish to be effective at the moment of a rapid load increase. The heat-exchanger type of control, or one employing direct-contact water sprays, is more suitable because its action is almost instantaneous if it receives its impulse automatically from the steam temperature, and especially so if the control anticipates a steam-temperature rise by receiving its primary impulse from steam flow.

Thermal Changes

It is apparent that rapid load changes produce rapid temperature changes in feedwater, steam, and combustion gas. Fig. 3 shows that during an instantaneous load pickup by the Harbor Steam Plant unit from 70,000 to approximately 630,000 lb steaming rate, the feedwater temperature rose from 270 to 380 F in less than 6 min, while the steam temperature dropped from 825 F to approximately 800 F in 45 sec, then rose to 975 F in 8 min. The increase in firing rate, from approximately 4000 lb of oil per hr to over 50,000 lb in less than 1 min, naturally produced a rapid rise in the temperature of combustion gas passing over the heating surfaces.

Rolled tube joints and welded pressure connections must be insulated against direct impact of combustion gas to prevent damage from temperature shocks. Feedwater entrance connections must be designed to prevent water of rapidly varying temperature from contacting the drum steel, Fig. 6. The entire pressure system must be suspended in a manner which permits free thermal expansion and contraction without placing unpredictable strains and stresses on pressure parts, setting enclosure, and supporting members.

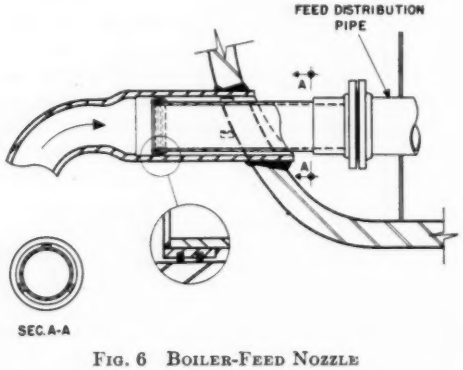


Fig. 6 Boiler-Feed Nozzle

Fuel-Burning Equipment, Type and Capacity

The rapid changes in heat-input rates required by widely varying steam demands call for extremely flexible fuel-burning equipment. Liquid and gaseous fuels are naturally well adapted for this service but burners must be of the wide-load-range type. There is no time for lighting additional burners or for changing burner tips or guns at the moment of load pickup. Neither will the available time permit taking burners out of service or making manual adjustments during a sudden drop in load.

In the case of the Harbor Steam Plant, where oil is the principal fuel, all ten burners are in service at all times. The combined burning rate is only approximately 4000 lb of oil per hr during stand-by operation, but in case of a load pickup the burning rate will have increased to more than 50,000 lb of oil per hr in less than 1 min, Fig. 3. A maximum burning rate of 60,000 lb per hr can be maintained.

Where coal must be burned stokers are usually not suitable because their operating characteristics prevent the required flexibility of heat liberation for quick steam-load changes. Pulverized-coal-firing is better adapted. Although response to load changes is rapid with correctly designed pulverized-coal equipment, the wide range of burner performance easily obtainable with oil and gas is usually not secured. A supplementary fuel, such as gas or oil, may have to assist the maintenance of stable ignition where the load swings to extremely low points.

An outstanding example of this method of operation is the steam-generating unit of the Rankin steam-electric station of the Carnegie-Illinois Steel Corporation, Fig. 2. This unit, of 450,000 lb per hr design capacity, is fired by blast-furnace gas as the main fuel, with pulverized coal to make up any deficiency. Sudden changes in steam demand at the rate of 250,000 lb per hr take place, and because the supply of the blast-furnace-gas fuel cannot be changed as rapidly as necessary to parallel steam demands (whatever quantity of blast-furnace gas remains from other operations in the steel mill must be burned under the boiler), the load swings must be handled by pulverized coal.

The typical steel-mill load of this plant differs from the spinning-reserve service of the Harbor Station. While Harbor receives its high load demands without warning as, for example, in case of a break in the transmission lines coming from the Boulder Dam hydroelectric station, the Rankin plant is usually informed of a major load change a few minutes in advance. If a load pickup is announced, pulverizers are started and remain spinning without coal. As soon as the steam demand exceeds the available supply of blast-furnace gas, raw-coal feeders start delivering coal to the mills, and within a few seconds a pulverized-coal flame is established in the furnace. The pulverized-coal burners contain oil pilots permanently maintaining an oil flame sufficient for instantaneous ignition of the pulverized coal and for support of the flame at extremely low burning rates.[4]

The capacity of fuel-burning equipment for boiler units subjected to extreme steam-load variation must be greater than for a standard boiler installation, because the heat to be released in the furnace immediately following a sudden load increase is not only that necessary to produce the steam actually generated in the boiler, but in addition, that necessary to restore boiler pressure and to replace the heat taken from boiler water while the boiler operated as a steam accumulator. This excess fuel-burning capacity must be determined by the time permissible, or available, starting with the moment of load pickup until full boiler pressure is restored. Fig. 5 shows that in the case of the Harbor Steam Plant unit an excess fuel-burning rate of 64 per cent would be required if it were necessary to restore full boiler pressure in 40 sec, whereas if 5 min were permissible, only approximately 10 per cent excess burning capacity would be necessary. This boiler is actually equipped with 28.5 per cent greater fuel-burning capacity than that required for the continuous steaming rate of 675,000 lb per hr

Mechanical-Draft Equipment

The selection of type, capacity, and driving method of fans is governed to a large extent by the required or desired rapidity and magnitude of steam-load changes for which the installation is designed. The construction of forced- and induced-draft fans must,

[4] "Modern Boilers for Steel Mill Plants," by M. H. Kuhner, *Power*, vol. 87, 1943, pp. 650–657.

in any event, be such that mechanical failures caused by the high stresses produced by the torque required for acceleration are prevented. The drive best suited for the requirements should be selected on the basis of the following considerations:

1 Direct-connected constant-speed alternating-current motors. Gas and air flow controlled by dampers or fan-inlet vanes. Quickest response to load change. High power consumption. High rate of wear and tear of fans and dampers. Operating units for dampers must be extra powerful.

2 Direct-connected variable-speed wound-rotor induction motors. Speed range only 50 per cent of maximum. Dampers required for accurate flow control. Power consumption relatively high, but lower than (1). Slower response to load changes.

3 Constant-speed alternating-current motors with hydraulic or electromagnetic couplings. Power consumption less than (1) and (2). Considerable time required for response to load changes. Dampers required for flow control in low load range.

(4) Direct-connected adjustable-speed direct-current motors, variable-voltage control (or electronic control when available for large motors). Economical power consumption. Quick response to load changes. Speed range corresponding to entire steam-load range. No dampers necessary for flow control. Motor generator set required. High investment cost. (Used with Harbor Steam Plant boiler).

The determination of capacity of mechanical-draft equipment must, of course, be governed by the capacity of the fuel-burning equipment. (Refer to section "Fuel-Burning Equipment, Type and Capacity.")

Boiler Settings

It cannot be expected that ten to twelvefold acceleration of burning rates, often taking place in less than 20 sec, will in every case occur without some disturbance of furnace conditions. In spite of the most carefully adjusted combustion control there is always the possibility that the increased fuel flow reaches the burners a fraction of a second in advance of the corresponding air supply. This may result in a furnace puff or, under severe conditions, in a light furnace explosion. One of the fans may speed up faster than the other, creating momentary high positive or negative pressures in furnace and gas passages.

It is evident that greater than ordinary care must be taken in the design and construction of the setting enclosure and gas and air passages. The setting must be strong enough to withstand minor gas and fuel explosions. It must remain tight under this severe service but it must also be sufficiently flexible to absorb internal shocks and damp them so that they are not transmitted to the supporting structure of the boiler and building. This calls for an entire steel shell enclosing the complete unit, reinforced and supported by a system of steel buckstays and girders which is independent of the main supporting structure. Permanent tightness of the joints of casing panels must be insured by flanges with closely spaced bolts, or by complete welding.[5]

The steel casing of the Harbor boiler is constructed to resist internal pressures up to 100 psf (approximately 19 in. water gage) without noticeable deflection. Air and gas passages are arranged for the most direct flow between furnace and fans.

Control Equipment

A reliable system for automatically controlling firing rate, air and gas flow, steam temperature, and feedwater flow must be in use with boilers operating under extreme load variations. It is impossible to attempt manual control of fuel, air, draft, steam, and water because all adjustments are required simultaneously and in step with the variation in steam demand.

It is not within the scope of this paper to recommend the type of control equipment to be used, but in selecting the equipment it must be kept in mind that the time lag of the control mechanism has a very important effect on the performance of the boiler equipment. The time consumed from the moment the control receives its first impulse of a load change, until the control has repositioned the equipment governing flow of fuel, air, gas, steam, and water, must be as short as mechanical limitations permit. If the response is fast the period during which the boiler must perform as a steam accumulator is short and the reduction in drum pressure is small. In this connection it is desirable to study the design of the equipment to be controlled because speedier response may be obtained by having the apparatus to be controlled designed for the least inertia. For example, multiple-leaf and louver dampers in air and gas passages have less inertia than large single-leaf dampers.

The combustion control receives its primary impulse either from steam pressure or steam flow. Because the time element of response to sudden steam-flow changes should be measured in fractions of a second, an arrangement whereby the primary impulse is received from power demand at the output side of the generator rather than from steam demand at the turbine throttle, might be worthy of consideration. Obviously the control mechanism must be self-compensating to avoid vicious hunting cycles.

It is demonstrated that the water level of a boiler rises sharply during a sudden load increase and drops as fast if the steam-output rate is suddenly reduced. The accumulator performance of a boiler and utilization of heat stored in the boiler water, are discussed in the section "Heat Storage." Keeping these facts in mind, it is readily apparent that it would be quite undesirable to have large quantities of relatively cold feedwater enter the boiler at the moment of a load surge. Cold feedwater would not only reduce the heat available in the boiler water for flashing steam, but would tend to raise the water level still further. On the other hand, the entrance of large quantities of colder feedwater is desirable when it immediately follows a sudden drop in steam demand. The water level is then below normal. Excessive heat in the boiler raises the pressure. Safety valves may start to pop. If there is heavy feedwater flow during this critical time the water level will be promptly restored to normal, and part of the excess heat in the boiler water will be dissipated in the fresh feedwater. It is indicated therefore that feedwater flow should be controlled solely by the working water level if the boiler is subjected to rapid load changes. With feedwater flow so controlled, the entrance of fresh water into the boiler is almost entirely interrupted during a sudden load rise and, conversely, large quantities of fresh feedwater will enter the boiler immediately after a sudden load drop. This action effectively stabilizes the water level and reduces the required distance between highest and lowest working levels.

Conclusion

A thorough analysis of the change taking place in a boiler during sudden and extreme steam-load variations must precede the design of the equipment. Expected magnitude of load swings and time permitted for restoring normal conditions in the boiler must be considered in determining the required volume below normal working level and the necessary capacity of fuel-burning equipment and fans. More time is available for response of control equipment when heat storage in boiler water is liberal, but large-diameter costly water drums and headers are required. A study will show whether large accumulator capacity of the boiler can be justified, or if the use of a more conventional boiler equipped with unusually large firing and fan equipment, and controls of extreme speed of response, is more economical.

[5] "Steel Encased Settings for Modern Steam Generating Units," by Max H. Kuhner, A.S.M.E., unpublished paper No. 716, 1940.

In conclusion it can be mentioned that a large number of the design points discussed as being important for boilers handling extreme load changes are equally desirable for boilers operating under more conventional central-station and industrial loads. Other points become of greater or lesser importance, proportionate to the range and rapidity of load changes. The problem thus narrows down to an intimate study of the plant load cycle, a clear understanding of what happens in a boiler during the expected changes in steam demand, and the solution of each problem thus developed by common-sense design.

Discussion

A. G. Ericson.[6] In this paper the author has capably analyzed and co-ordinated the major design factors to be considered in building a boiler for operation under extreme load variations. The importance of a large heat-storage capacity, made available by substantially increasing the size of the main boiler drum and by increasing the weight of water carried below the working level, is readily appreciated. This feature perhaps marks the essential difference from boilers of standard design and is a fundamental requirement for stable operating conditions. The quantity of heat available for flashing of steam within the allowable pressure drop sets the maximum permissible time lag between start of higher steam output and corresponding increased furnace heat release following rapid load rises. As discussed in the paper, the larger quantity of water circulating also assures that unidirectional flow will be maintained during rapid load pickups, and the larger drum size allows the necessary leeway to offset variations in water level accompanying load swings, preventing water carryover during load rises and entrance of steam to the downflow columns during load reductions.

Installation of rapid and reliable control equipment is particularly important as the time required for adjusting the burners, damper settings, feedwater flow, and fan speeds results in a heat deficiency that must be supplied by flashing, and extended lags result in proportionately greater steam-boiler temperature and pressure losses.

The author refers to the 450,000-lb per hr boiler in the No. 3 powerhouse at Carrie Furnaces, Rankin, Pa., as an example of a quick-pickup boiler in the industrial field. Although the boiler was designed for this service, the extreme load variations originally contemplated have not developed in actual operation. This powerhouse is the most efficient in the "Monongahela Valley Power System" of the Carnegie-Illinois Steel Corporation and functions as the major generating unit with an average load rating of 85 per cent of rated capacity. Flexibility of operation is essential, for although the operators are informed in advance of general power requirements, there are inevitably some load swings that cannot be foreseen.

Operation of this boiler, described by the author, through load swings of 100,000 lb per hr has been quite satisfactory. Depending upon boiler-operating conditions at the time, the steam pressure will vary up to 50 psi and the steam temperature rarely varies more than 15 deg F. The steam quality remains good and excessive variation in the water-level, geysering, or turbulence of the water body does not occur. Following a decrease in steam load, the temperature of the superheated steam is effectively regulated by a heat-exchanger type of control. This type of control has a slight disadvantage in imposing additional resistance to the flow of steam through the superheater, therefore causing a greater differential between boiler drums and line pressure. However, it is rapid and accurate and the high-temperature element of the superheater is protected against overheating.

In this respect, it may be added that superheat is one of the most important items requiring control in the modern power plant. Excessive steam temperature is likely to cause damage through creep stresses or loss in tensile strength in both the piping and turbine parts. In addition, fluctuation in steam temperature causes opening up of the joints in the high-pressure unit and steam chest of the turbine, resulting ultimately in leaks.

The benefits to be realized from careful and efficient application of the design features discussed in this paper are dependent principally upon the degree of accuracy with which future load cycles are analyzed and power requirements foreseen.

Dan Gutleben.[7] It is refreshing for an operator of a small sugar-refinery steam plant to learn that a condition can arise which requires a public-service plant to give thought to sudden large load fluctuations. Fortunately, the problem submits to logic and arithmetic in the hands of an experienced engineer. The sudden swings were once considered an unavoidable evil visited only upon the sugar-house engineer whose plant was beset with sugar boilers endowed with untold stupidity. The public-service plants, which set the pattern for steam-plant design, accomplished an amazing job and made empirical design facts available to industrial plants long before the bondholders were repaid for the cost of their full-size research. In 1931 when the Pennsylvania Sugar Company in Philadelphia installed two boilers of 250,000-lb per hr capacity and 400 psi pressure, there was a limit to the size of forged drums, besides their cost; and welding had not become available. Accordingly, the boiler designer's talents for meeting the specification of large and sudden swings did not include accumulator operation. That existed only in the good old Scotch marine boiler of revered memory. The design staff (to which the author was attached) answered our clamor for a steam flywheel by providing a six-drum design, two of the drums being on the economizer. The steam-separating drum was forged 51 in. in diam to suit an available mandrel.

Under a premeditated test, with one boiler on base load at 400 psi pressure, the second one was increased in output by 105,000 lb per hr in 2 min with no pressure drop discernible on the gage, and with a rise of 6 in. in the water level. With the thoughtlessness of the sugar-boiler operators this was improved. Early on a Sunday morning, as the demand tapered off, one boiler was shut down and then the boys phoned that the week-end job was complete. Suddenly a large quantity of thin sweet water was found that required to be concentrated and the hour for adjournment was at hand. Without notice, the flowmeter skyrocketed. The steaming rate jumped from 75,000 lb per hr to 225,000 lb. in two minutes, accompanied by a 15-inch spear in the water-level chart. In a public-service plant such a jump in water level would wreck some turbine blades, but in a sugar refinery allowance is made for stupidity, which is a "gift from heaven." Our plant is equipped with a steam accumulator which can provide an instantaneous supply of 40,000 lb of steam for the pans, but this "dinosaur egg" happened to be empty.

H. J. Klotz.[8] The subject of this paper is most timely, as indicated by the recent increase in the number of proposed power-station installations required to operate under wide load variations. The author is to be commended for his logical analysis of the problem and his clear-cut treatment of the various factors which have important influence on the successful operation of equipment under the severe conditions described. In fact, the success achieved in developments such as he has described has en-

[6] Chief Engineer, Homestead Steel Works, Carnegie-Illinois Steel Corporation, Munhall, Pa.

[7] Parkmerced, San Francisco, Calif.

[8] Chief Power Engineer, Stone & Webster Engineering Corporation, Boston, Mass. Mem. A.S.M.E.

couraged operators, never noted for their backwardness in asking for the impossible, to demand even greater load changes in smaller time intervals. Whereas the Harbor Steam Plant is required to handle a load increase at the rate of about 10 to 1 in a matter of seconds, operating conditions on some utility systems make it desirable to increase the ratio to 20 to 1. The resourcefulness of boiler and other equipment manufacturers, as typified by the work behind this excellent paper, leads the operators to expect that the increased severity of their requirements will be met.

Of the various factors involved, it would seem that all of the features described by the author, with the exception of the fuel-burning facilities, could be expected to be adapted without too great difficulty for the higher ratio of load increase. As pointed out in the paper, only gas and fuel oil are suitable for the minimum rates of firing required by installations of the type under consideration, and where pulverized coal is the basic fuel, supplemental use of the former fuels would be a necessity. A range in firing rates of 20 to 1 is a severe requirement which imposes serious problems in the achievement of a satisfactory design for burning even such flexible fuels as gas and fuel oil. Also, in this connection, a furnace arrangement suitable for stable combustion at the minimum firing rates is of great importance, especially in cases where pulverized coal is to be the basic fuel. Maintenance of stable combustion of course is the factor which prevents pulverized-coal firing from having the required maximum load range without use of supplemental fuel.

C. C. McKee.[9] The author has selected a subject that well deserves considerable attention; especially for those utilities which depend upon hydropower for the major portion or all of their electric supply. Usually in these systems, after installations are complete, the cost of hydropower generation, particularly secondary or dump power, is lower in the hydroplant. For this reason the power produced from steam plants is held at a minimum to reduce fuel cost. Under such circumstances steam plants are required to operate at minimum loads or about enough power to supply all auxiliary drives.

Then when a major disturbance occurs, such as loss of a transmission line, it is necessary for the steam plant to assume full load, without any previous warning, and with automatic controls to bring the steam generator into action, not only to meet all turbine requirements, but also to replace energy lost from the unit by the accumulator action while the automatic controls were bringing combustion and combustion equipment from low load to maximum capacity.

There are points of interest shown in Fig. 3 which are not indicated in the text of the paper. A study of the pressure-drop curves shows there was a slight indication for a return to normal between 30 and 40 sec. This indication was shown to much better advantage when these curves were plotted to a larger scale. The further drop following this point was caused by the feedheating system going into action at that time. This early increase of feedwater flow has been corrected and a recent test for quick pickup indicates that increased flow of feedwater was delayed for about 1½ min after application of load. There was little, if any, secondary pressure drop; however, the load picked up was less than that shown in Fig. 3 by about 5000 kw.

There is no rebuttal to the question that the boiler for such service must be designed to meet the severe demands; but automatic controls must also come in for their share of praise in their ability to be adjusted, timed, and synchronized to bring all steam-generating equipment to overload capacity in less than 25 sec.

Another interesting item which was checked in particular in our recent quick-pickup test is that the temperature of the feedwater entering the economizer was higher than that leaving, by some 10 deg. In the test data obtained for the curves in Fig. 3 the temperature readings for economizer feedwater in and out were read and indicated this condition, but they were considered unreliable. There was a reluctance to show this condition before checking it thoroughly. During the recent test this particular item was checked carefully, with the result that there is no hesitancy in saying that for a period of 2 to 2½ min, the temperature of the incoming feedwater is actually higher than the outgoing feedwater from the economizer. Our estimate of the reason for this condition is that it takes about that long to move the cold water through the economizer.

W. C. Rowse.[10] The writer, who is in charge of the Steam Design Section of the Los Angeles Department of Water and Power, set forth the fundamental requirements for a steam plant which must operate in parallel with hydroelectric plants in an article which appeared[11] before the first unit of the Harbor Steam Plant went into operation. In that article it was stated that the plant should have the ability to operate over a wide range of load factors with reasonably good economy and in addition, the ability to pick up full load instantly when floating on the line at a light load, which latter requirement affected the design of the boiler.

In his paper the author clearly sets forth the boiler-design problems and how they were solved, together with the results of the first quick-pickup test with special fast-recording instruments made on October 12, 1944. The writer's discussion of the paper will consist of a brief statement of actual experience in operation.

Following the usual ups and downs incidental to placing a new unit in operation, particularly the first unit of a new plant, by March 1, 1944, the plant settled down to regular operation, except for the 4000-kw house turbine-generator unit which was appropriated by the Federal Government and shipped to Russia. Since that date the plant has been subjected to all kinds of loads from a minimum output of 64,000 lb of steam per hr continuously to a maximum output of 723,000 lb of steam per hr for 1 hr, all under full-automatic control with all burners on and including quite a few cases of quick pickup of load in emergencies. The most publicized of these was the occasion on March 18, 1946, when two airplanes collided, cutting conductors on two circuits from Boulder Dam, thus cutting off 300,000 kw of generating capacity furnishing energy for the total load of 533,000 kw being carried at that time. Although the frequency at the Harbor Steam Plant dropped momentarily to 40 cycles and continued for 10 min at 50 cycles, which shut down the fans three times, the plant picked up 55,000 kw immediately and 75,000 kw within a few minutes and carried this 75,000 kw for 1 hr. The value of the accumulator effect of the boiler was abundantly demonstrated by the ability of the boiler to supply steam even during the fan outages. These fan outages were due partly to the low frequency of energy for auxiliaries which will not occur again because the turbine-driven house generator is now installed, and partly to the setting of the protective thermorelays on the fan drives, which latter has been corrected. Since March 1, 1944, the only unscheduled outages of the steam-generating unit were for three leaks in economizer welds which were repaired over week ends.

An exhaustive test was made of this boiler during the first part of 1944, under the supervision of Mr. Sheppard T. Powell, primarily to check circulation and to recommend boiler-feedwater

[9] Mechanical Engineer, Department of Water and Power, City of Los Angeles, Calif.

[10] Engineer of Steam Design, Department of Water and Power, City of Los Angeles, Calif. Mem. A.S.M.E.

[11] "Some Features of the Harbor Steam Plant of the Los Angeles Bureau of Power and Light," by W. C. Rowse, *Mechanical Engineering*, vol. 64, 1942, pp. 773–776.

treatment and control procedures. At first a total of over 100 readings and analyses were made on each shift. As knowledge of the circulatory and other characteristics of the boiler increased, some of these readings and analyses were discontinued until, after about 6 months, a normal feedwater-control procedure was evolved. One important result of these tests was to demonstrate clearly that the boiler had been properly designed especially as to positive circulation and delivery to the superheater of steam of the required purity.

On April 24, 1946, the installation of the 4000-kw house turbine was completed, and on May 8, 1946, a quick-pickup test was made, with adjustments to the automatic controls which resulted in holding back boiler feedwater longer, and in faster opening of the fuel-oil valve. The method of increasing the load instantly is interesting. One unit at Boulder Dam was loaded with the exact load which the Harbor Steam Plant was to pick up. The 4000-kw turbine-generator unit at the Harbor Steam Plant was carrying the auxiliaries, the main turbine-generator unit was carrying 10,000 kw on the low governor block, the high governor block was set for the load to be picked up and the governor was set for a slightly higher speed than 3600 rpm. When the circuit-breakers at the Boulder unit were opened, the momentary drop in system frequency tripped the low block on the Harbor unit which picked up the load instantly with only a momentary change in system frequency. Although the load picked up (48,000 kw) was not as large as the engineers desired, the results showed a great improvement in every way over the previous test of October 12, 1944. The time required for return to normal conditions was shorter, and the maximum steam temperature lower (only 925 F at turbine throttle) than the previous test. It should be noted that both tests were made under full automatic control.

The over-all efficiency of the plant has been better than the expected efficiency. A Willan's line, in which barrels of oil per month are plotted against kilowatt-hours net output per month, results in a formula of 5250 bbl of oil (6,250,000 Btu per bbl) per month for zero net output plus incremental oil at the rate of 595 kwhr net output per barrel of oil. This results in an over-all efficiency of 11,250 Btu per kwhr net output at rated capacity (62,000 kw net output), as compared with an expected value of 11,400 Btu.

Author's Closure

It is very gratifying to have the correctness of the conclusions reached with this paper verified by the actual performance experiences with quick load pickup boilers reported by Mr. Rowse, Mr. McKee, and Mr. Ericson. These discussers' comments are of specific interest because they point the way to further improvements in steam plants required to operate under unusual load conditions.

Progress in any field is gradual and if the steps forward are not too large the result of the future step can be predicted with reasonable accuracy by the experience with the present. A boiler load increase of 1 to 10 taking place in a few seconds and without trouble was considered quite hazardous only a relatively short time ago. Mr. Klotz mentions the future requirement for load pickups in the ratio of 1 to 20. A safe boiler design for this condition is today entirely feasible if the Harbor Steam Plant experiences are made the basis for this next step.

Mr. Gutleben's reference to the human element in steam plants points to the importance of the correctly designed complete automatic-control system mentioned by Mr. McKee, but the steam-plant operator is well advised not to take the designation "automatic" too literally. Automatic control cannot replace human thought. It is especially important in plants subjected to extreme load variations that the men in charge know intimately the sequence of the various operations normally performed by the controls. The operators must be trained to take over and operate manually in case of failure of the automatic controls. Several of the pickup tests referred to by Mr. Rowse were performed to acquaint the Harbor Plant operators with all that can happen during a bona fide pickup and to instill confidence in the equipment.

The valuable supplementary data and information supplied by the discussers are gratefully acknowledged.

Acid-Cleaning of Boilers and Auxiliary Equipment

By S. T. POWELL,[1] BALTIMORE, MD.

Acid-cleaning of equipment has been demonstrated over a long period as a useful and economical means for removing encrustations from boilers and many other types of power-plant equipment. This paper explains the use of various cleaning reagents and inhibitors, the procedure which should be followed, and the precautions to be taken to safeguard both personnel and equipment from the hazards inherent in the process.

THE use of acid to remove deposits from metallic surfaces has been practiced for many years and in widely divergent industries. Such processes have been and still are extensively employed for the removal of mill scale from sheets, plates, tubes, and other products in mills making steel and copper alloys, and enormous quantities of acid are used for such services. The economy and speed gained in removing deposits in this manner have directed attention to many applications, and the treatment has been extended to the cleaning of oil wells, water mains, heat-exchange equipment, boilers, and other equipment. The extensive acidizing of oil wells to improve yields, by removing deposits and opening the formations, did much to attract interest and suggest other applications.

One of the most interesting acidizing projects,[2] which was performed more than 25 years ago, was the cleaning of the entire piping system in The Bankers Trust Building in New York City, a 35-story office building. After 12 years of service the pipe lines throughout the structure were seriously clogged with corrosion products. It was estimated that repiping would cost from $100,000 to $300,000 and could be done only at serious inconvenience to the tenants. Sections of the piping system were cleaned by means of inhibited muriatic acid in about 8 hours, after the offices were closed on Saturdays. It is surprising that this novel method of cleaning pipe lines did not receive more widespread interest at that time since the basic principle of the procedure has much merit. It is obvious that removal of deposits is merely a temporary expedient and must be followed by other forms of corrective treatment to avoid their recurrence.

The removal of scale from boiler surfaces was a logical development after the practical application of acidizing for other uses was demonstrated. The most rapid expansion of this method of boiler cleaning, however, has occurred within the past 4 or 5 years because of the need for reducing boiler outages to a minimum, and because of the shortage of labor during the war period. The effectiveness of acid cleaning is demonstrated in Fig. 1 which shows the heavily encrusted tubes of a chemical evaporator. Fig. 2[3] shows the same evaporator after being cleaned.

Thousands of boilers and miscellaneous equipment units have been cleaned by acid during the last few years and a majority of these treatments have been successful. It is a recognized fact, however, that even though inhibitors may be used, these compounds do not completely prevent corrosion, but merely reduce the rate and extent of the attack. Under ordinary conditions the corrosion of the surfaces is relatively minor if an effective inhibitor is used, if the temperature is satisfactorily controlled, the contact time limited, and subsequent washing out and neutralization of remaining acid properly performed.

Considering the large number of boilers which have been acid-cleaned, there have been only a relatively few cases where noticeable corrosion has taken place; however, there is no accurate record of the extent to which all acid-treated equipment has been corroded. From our personal experience we are inclined to believe that where the temperatures have been properly maintained and if the acid was thoroughly removed from the surfaces after cleaning, the extent of attack has been minor, and repeated acidizing may be undertaken without seriously damaging equipment. The primary object of this paper is to direct attention to the potential possibility of serious damage if the work is performed carelessly and without proper regard to precautionary measures required to insure satisfactory results.

Although acidizing of boilers is most widely practiced in power plants, still there are many other applications in this field. These may be broadly classified as follows:

1 Boilers, economizers, superheaters.
2 Deaerators, vent condensers, and stage heaters.
3 Surface condensers and heat exchangers.
4 Feedwater-treating equipment.
5 Valves and miscellaneous equipment.

Each of these applications requires special study and the treatment must be selected and applied to meet the conditions encountered.

Mechanism of Effect of Inhibitors on Acid Corrosion

There are two general concepts regarding the mechanism by which inhibitors protect steel or other metals when in contact with acid solutions. One group of investigators[4] suggests the following mechanism: Iron goes into solution at the anodic regions, forming ions, while hydrogen is discharged in equivalent amount at the cathodic areas. The cathodic areas occur principally in the narrow spaces of grain boundaries in steel or between the slag and metal in wrought iron. Most inhibitors are bases or positively charged colloids which, when present, travel to the cathodic areas and are deposited and adsorbed on the surface. The electrochemical process is stopped when the reaction at either pole is stifled, and the inhibitor thus retards corrosion. It has also been stated that the presence of the inhibitor raises the hydrogen overvoltage above any potential which can exist in the acid-metal system.

A second explanation is that the inhibiting compounds serve to blanket the entire metal surface by a protective layer of the

---

[1] Consulting Chemical Engineer. Mem. A.S.M.E.

[2] "Removal of Rust From Pipe Systems by an Acid Solvent," by F. N. Speller, E. L. Chappell, and R. P. Russell, Trans. A.I.Ch.E., vol. 19, 1927, pp. 165–171.

[3] Reproduced by permission of The Dow Chemical Company, Midland, Mich.

Contributed by the Power Division and presented at the Semi-Annual Meeting, Detroit, Mich., June 17–20, 1946, of The American Society of Mechanical Engineers.

Note: Statements and opinions advanced in papers are to be understood as individual expressions of their authors and not those of the Society.

[4] "The Electrochemical Action of Inhibitors in the Acid Solution of Steel and Iron," by E. L. Chappell, R. E. Roetheli, and B. Y. McCarthy, *Industrial and Engineering Chemistry*, vol. 20, 1928, pp. 582–587.

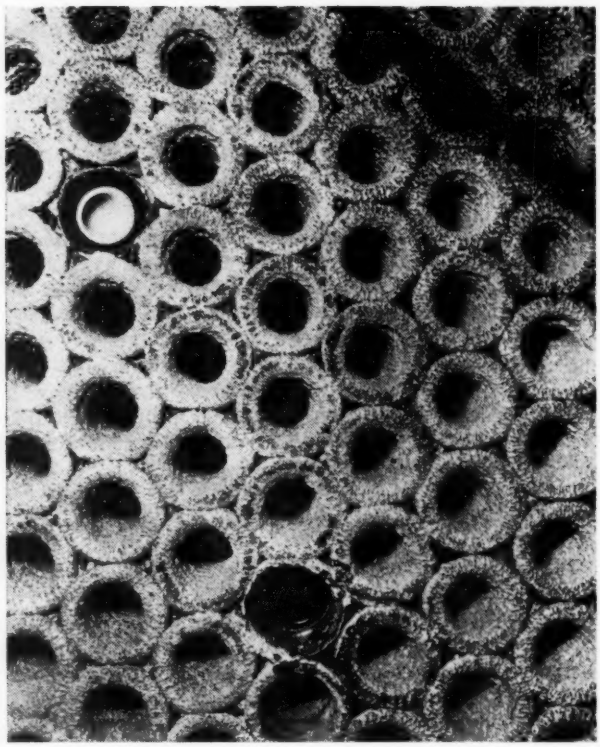


FIG. 1 SCALE ON EVAPORATOR TUBES, BEFORE ACID-CLEANING

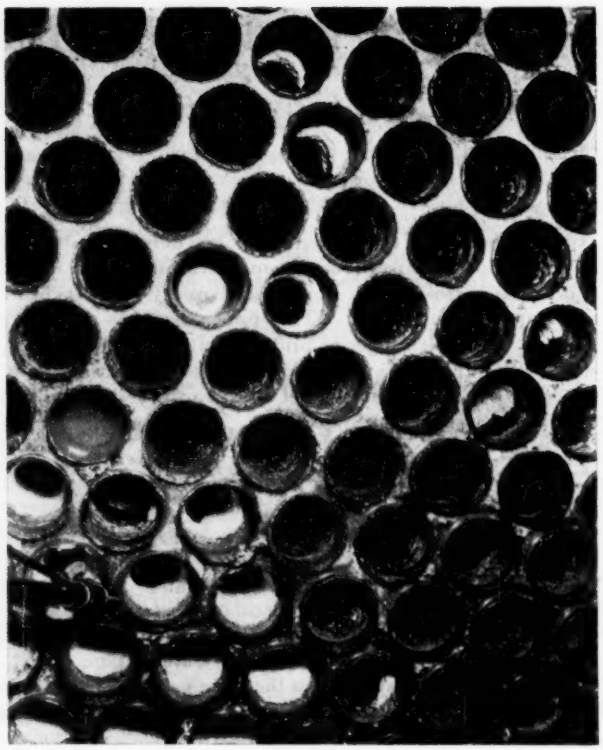


FIG. 2 CONDITION OF EVAPORATOR TUBES, SHOWN IN FIG. 1, AFTER ACIDIZING

organic compound used. This occurs as simple adsorption of the inhibitor ions on the metal surface, through the nitrogen atom which is a component in most organic inhibitors. The stereochemical structure of the inhibitor determines its effectiveness because the structure controls the degree of concentration that will occur.

Others have gone further and contend that inhibiting substances form a nonpermeable blanket through which the hydrogen cannot diffuse and which is limited to the metal surface, as contrasted to the oxide surface.

One investigator has submitted data to show that the action of inhibitors cannot be explained by the electrochemical or overvoltage theory nor by the formation of an impervious pore-free film on the oxide-free metal surface. Test results have been submitted to indicate that inhibitors are adsorbed simultaneously on both metal and oxide surfaces; however, the concentration is heavier on the clean metal surface. The film which forms increases the electrical resistance from liquid to metal, but the film is porous, being built up of molecule aggregates or micelles spaced closely together, similar to a pincushion filled with pins. The theory developed from these studies is that the long-chain molecules thus form long narrow channels similar to capillaries or gel structures. This condition is reflected in reduced diffusion velocity and migration velocity of the hydrogen and sulphate ions which are active in the corrosion of iron in sulphuric acid. The net result is a reduction in the corrosion of the metal, and inasmuch as a more concentrated film is present at the clean metal surface, the oxide is attacked relatively faster than the metal. This results practically in removal of the oxide and preservation of the metal surface.

It has been contended that the corrosion of some boilers during cleaning with inhibited hydrochloric acid is due largely to the formation of ferric chloride which, in itself, is a highly aggressive salt and against which the common inhibitors are not effective. According to this theory the inhibitors will retard the electrochemical reaction involving the displacement of the hydrogen of HCl by iron, but they will not prevent the oxidation-reduction reactions by which ferric chloride oxidizes metallic iron and copper to the ionic form. If metallic copper is in the sludge, ferric chloride attacks it as it does iron, producing cupric chloride which is also an oxidizing agent and a second source of trouble. It is held that the plating out of copper, or its solution to form a chloride, depends upon concentrations of the various ions present.

To limit the concentration of ferric chloride it has been suggested that the solution be constantly circulated and thereby avoid raising the ferric chloride to a level where active attack is possible. There is no assurance that circulation will bring about this desirable condition. If ferric chloride pockets or otherwise concentrates at surfaces and remains in a quiescent or semiquiescent state, it may react more slowly if only diffusion is available to carry away and remove the products of the reactions.

To support the foregoing theory, corrosion has been produced experimentally with dilute solutions of ferric chloride containing no hydrochloric acid except that resulting from hydrolysis.

It should be pointed out that if inhibitors retard corrosion by covering the entire surface and preventing contact with the acid, they should be equally effective against solutions of ferric or cupric chloride. If the impervious-film theory of inhibitor mechanism is correct, any specific vulnerability of the film to certain solutions would seem doubtful, but if the film leaves certain areas exposed, they could be attacked by oxidizing agents in the absence of an opposite electrode reaction. It is a known fact that inhibitors do not give complete protection, and the actual over-all attack which occurs may no doubt be aggravated by oxidizing agents. Whatever the role of ferric chloride and copper may be, it remains true that with proper care equipment can be acidized repeatedly without hazard.

Practical Effect of Acid-Cleaning on Boiler Steel

Studies of metal which has been repeatedly acid-cleaned show that some corrosion occurs each time, but the rate of attack is not sufficiently rapid, generally, even after many cleaning cycles, to cause serious concern. In some instances acidizing has been blamed for active attack on the metal when this treatment has not actually been responsible but has merely revealed the presence of corrosion which occurred previously and passed unnoticed because the pits and surface etching were filled and coated over with iron oxide or encrustations which the acid removed.

The effect of acidizing may be best evaluated by meticulously cleaning the surfaces before the acidizing, either by wire-brushing or local application of weak acid, and inspecting the metal for pitting, under low magnification and with tangential illumination. The same surface should be similarly cleaned and inspected after the entire unit has been acidized. The pitting shows up on stressed metal, hence for these inspections it is best to select the rolled ends of boiler tubes, the heads or nuts of highly strained bolts, the bends of angle irons, welded zones, etc. In most cases such scrupulous before-and-after inspections have not been made owing to the need for returning the equipment to service as quickly as possible after the cleaning has been completed, or because the operators were unaware of what to look for.

It is a well-known fact that the rate of attack on metals by acid or any other electrolyte is greatly affected by the internal stresses in the material. Examination of boilers which showed corrosion after acid-cleaning demonstrated that the most severe attack was on metal which had been greatly stressed. This condition was particularly pronounced on the flared end of tubes where stresses of large magnitude occurred as the result of cold-rolling. This is illustrated in Fig. 3 which shows the "honeycomb" type of attack that is characteristic in units where corrosion developed during acid-cleaning. A photomicrograph of a section of tube which has been attacked by acid is shown in Fig. 4. The honeycomb or lace form of deep pitting is more clearly demonstrated by the photomicrograph. Inspection of numerous boilers has further demonstrated that cold working of the metals used in the fabrication of internal appliances within the drum are also readily attacked by inhibited acid, even when the unstressed metal has shown no corrosion.



Fig. 3 Corrosion Resulting From Acid Attack on Stressed Metal at Flared End of Cold-Rolled Tube
(*A*, This shows honeycomb type of attack.)

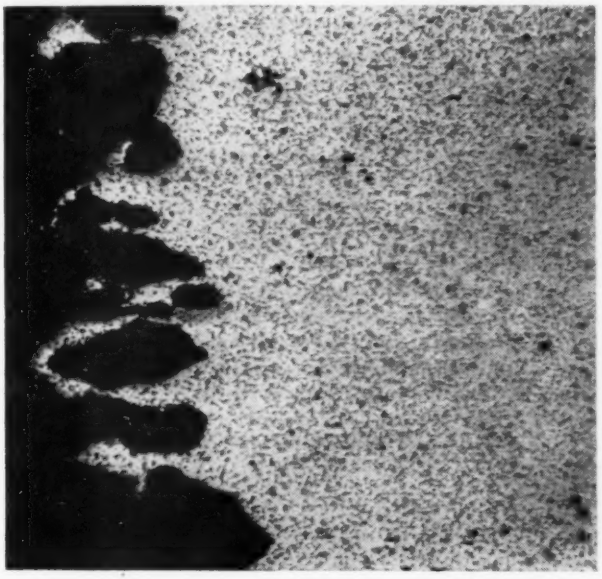


Fig. 4 Photomicrograph of Section of Boiler Tube Taken From Rolled End, Showing Honeycomb Attack During Acid-Cleaning

This type of attack has been observed by the author in a number of installations. Some of the boilers referred to had been acid-cleaned and the temperature of the acid solution was relatively high. In one case the attack was probably due to the effect of an acid contaminant in the feedwater and not to acid-cleaning. The pattern of the corrosion, however, was identical to the type and pattern of attack which was noted in acid-cleaned boilers. This occurrence tends to demonstrate that all corrosion of tube ends may not be the result of acid-cleaning, but may have resulted from some contaminant present in the feedwater. This observation suggests the need for an intensive investigation to determine all conditions which may be responsible for corrosive attack, and the avoidance of unwarranted criticism of acid-cleaning, which in the final analysis may not be responsible.

Some concern has been expressed as to the possible intercrystalline attack on steel due to the penetration of hydrogen into the steel during or subsequent to acid-cleaning. Although relatively large amounts of hydrogen may be generated during the cleaning period, investigations have shown no attack on the intercrystalline structure or any evidence of embrittlement attendant with such form of corrosion. Such investigations have not been extensive, still it seems reasonably safe to predict that embrittlement will not occur if temperature and strength of acid used is within the safe limits, and if the acidized units are thoroughly washed and acid adhering to the surfaces is completely neutralized.

Factors Influencing Effectiveness and Safety of Acidizing Equipment

There are numerous conditions which require control during

acidizing of any equipment in order to insure effective removal of encrustations from the surfaces and a minimum of corrosive attack on the metal. It is not possible to list specifically all of the many conditions which may be encountered, since there are a multitude of variables which may alter the effectiveness of the acidizing process. In general, however, the items which should be considered, and controlled if possible, are as follows:

1 Composition and concentration of acid.
2 Nature and composition of inhibitor.
3 Additional chemicals employed for their wetting, catalytic, or special solvent properties.
4 Temperature of the metal and of the solutions.
5 Circulation, mechanically induced or by diffusion.
6 Composition of the metal.
7 Physical and chemical composition of the scale to be removed.
8 Procedure followed, from taking equipment out of service through removal of acid and washing down and neutralization of acid remaining on the surfaces after treatment.

Time does not permit complete discussion of all the foregoing items, nor would it be appropriate to elaborate on all of them here, since many of them involve complex chemical reactions which are outside the scope of this paper. However, there are certain items in the list which may be profitably discussed as they are of interest to mechanical engineers and others responsible for acidizing of power-plant equipment.

Type and Concentration of Acidizing Solution. It is a common misconception that the cleaning of equipment requires merely the addition of a mineral acid, to which has been added a chemical inhibitor for the purpose of slowing down the rate of attack on metal surfaces. In some cases such treatment may effect the desired results provided temperature control and other conditions are adequately maintained. There are, however, certain types of encrustations occurring in boilers, condensers, and heat exchangers which completely resist solution by muriatic, sulphuric, or other common mineral acids. For instance, the silicate, sulphate and other scales, either alone or combined with other types of encrustations, are not appreciably soluble in muriatic acid. Where such compounds are encountered, hydrofluoric acid or other sources of the fluoride ion must be used to insure their removal.[5] Certain metallic deposits also resist solution, and where such are present, specific solvents must be employed. If oils or greases are encountered, special solvents are necessary for their removal, and effective acidizing results cannot be secured without first removing such materials.[6]

Experience has demonstrated, also, that in addition to the inhibiting chemicals, other compounds improve the effectiveness of the acidizing process. Most of these treatments involve trade secrets, and their use and application are the result and outgrowth of research and development, coupled with practical experience over a wide range of conditions encountered.

The strength of acid to be used should be governed by the time available for cleaning the equipment and the chemical composition of the acidizing solution. In the past the strength of the acid employed has been as high as 15 per cent. Recently, however, there has been a marked trend to the use of acid of lower strength, even though the cleaning takes more time. Concentrations now generally used are from 4 to 7 per cent.

Composition of Inhibitor. The technical literature on the subject of acid-cleaning and pickling of metal contains a long list of organic and inorganic substances which have been used as inhibiting agents to repress the attack on the metal, but which will permit the solution or removal of oxides or other deposits on the surface. A partial list of some of the materials which have been used is shown in Table 1. This list includes only a very small percentage of compounds which are available or have been employed. Actually, there are thousands of organic and inorganic substances which are known to have inhibiting properties. The relative effectiveness of these products varies widely, and they have specific adaptabilities for different services. Most inhibitors are harmless, but others are hazardous and should not be used. In this group are compounds of arsenic, cyanide, and some of the coal-tar by-products. At least one fatality has occurred from the use of an arsenic inhibitor. Operators should be warned against such materials and be informed of their potential danger.

TABLE 1 PARTIAL LIST OF MATERIALS USED OR INVESTIGATED FOR INHIBITING CORROSION OF METALS BY ACIDS

Niter cake	Aniline
Sumac leaves	Pyridine
Formaldehyde	Coal-tar extracts
Glue	Slaughterhouse wastes
Flour	Ethyl iodide
Starch	Paramethylaminophenyl sulphate
Gelatine	Carbozole
Glucose	Cyanide
Thiourea	Quinoline ethiodide
Arsenious oxide	Barium salts

NOTE: The inhibiting effect of the compounds listed, and many other substances, varies greatly as does their cost and availability. Some of these materials possess slight inhibiting value and some are dangerous to use. No inhibitor should be employed without specific information as to its effectiveness and the potential hazard involved in its use.

Practically, the selection of the inhibitor should be left to experts in this field, who should be advised in complete detail about the design of the equipment and the physical and chemical nature of the deposit to be removed. Organic inhibitors are marketed for cleaning operations (such as pickling) which can safely be handled by plant operators. For complex jobs involving major equipment units of the magnitude of boilers and heat exchangers, it is best to rely on the experienced contractor performing the work to select and prepare the acid solution, if the operating personnel in charge of the plant are not informed on the subject.

Temperature. Possibly the most controversial factor with regard to acidizing is the temperature at which the process is carried out, and there is fairly definite evidence that corrosion has occurred in a number of instances where temperatures have been high during cleaning. Many boilers have been cleaned at temperatures ranging from 170 to 180 F, and in one case the temperature was well above the boiling point of the solution and much damage was done. It is a known fact that the inhibiting effect of all chemicals used for retarding corrosion in acid solutions is rapidly reduced as the temperature is elevated. As the result of corrosion of equipment by acidizing at too high temperatures, there is now a trend toward maintaining the temperature of solution during the cleaning period between 140 and 160 F. If sufficient time is allowed for the cleaning, proper removal of the encrustations can ordinarily be effected at the lower temperatures.

In Fig. 5 is shown the extent of corrosion which occurred on the face and edge of caps in waterwall headers. It is probable that the relatively high temperature was responsible for the condition.

Circulation. Various schemes have been used requiring special equipment for applying the cleaning solution to the boiler. In some instances the operators merely inject the chemical into the top drum, while others prepare the solution in a tank and pump it into the boiler and recirculate from the tank back into the boiler. In the final analysis there is not now available sufficient evidence to prove that either circulation of acid by means of a pump, or circulation induced merely by diffusion current is a preferable scheme to use. Both procedures have been followed, in

[5] "Chemical Removal of Scale From Heat-Exchange Equipment," by F. N. Alquist, C. H. Groom, and G. F. Williams, Trans. A.S.M.E., vol. 65, 1943, p. 719.

[6] "Scale Removal by Chemical Means," by M. E. Brines, *Power Plant Engineering*, vol. 44, May, 1940, p. 47.



FIG. 5 CORROSION ON FACE AND SIDE OF CAP SHOWING HONEYCOMB TYPE OF ATTACK

large groups of boilers cleaned, without active corrosion occurring in either case.

Composition of Metal. The composition and the cleanliness of the metal are important factors in resisting or accelerating corrosion during acidizing of equipment. It has been observed repeatedly that low-grade steel containing slag inclusions or other impurities has been readily attacked during acid-cleaning, while the drum and tubes were not affected. In one installation the tops of practically all the acorn nuts used in the fabrication of the internal baffles were destroyed, and a similar condition was noted in a number of other units. To what extent the acid was responsible has not been fully determined, but it undoubtedly accelerated the rate at which the metal was attacked. It is a well-known fact that the material from which such nuts are constructed is low-grade metal, as might be expected, especially during the war years.

Ordinarily, black iron pipe, especially if cold-worked, is readily

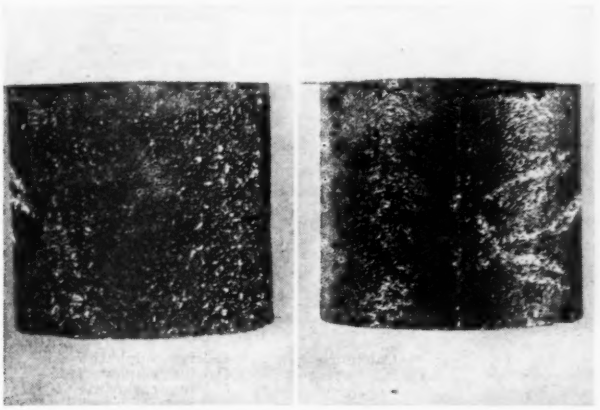


FIG. 6 NIPPLE CORRODED DURING ACIDIZING, ILLUSTRATING EFFECT OF ACID ON LOW-GRADE STEEL CONTAINING SLAG AND OTHER IMPURITIES

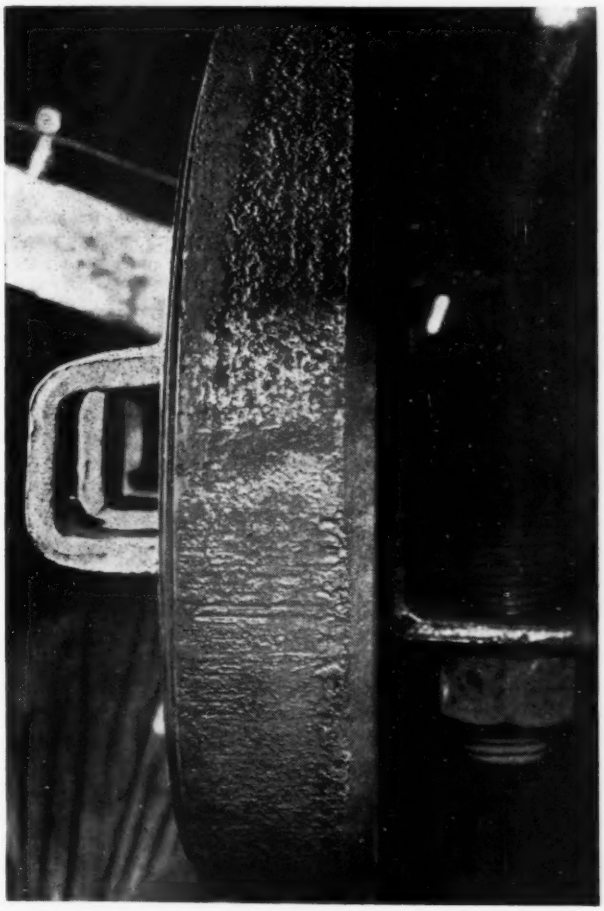


FIG. 7 CORROSION OF MANHOLE COVER SHOWING DEEP SURFACE CORROSION BY ACID ATTACK

(Exact cause for selective corrosion not accurately determined but probably presence of slag inclusions or change in metal structure due to flame-cutting. Note wasting and honeycomb type of attack.)

TABLE 2 TYPES OF DEPOSITS WHICH HAVE BEEN FOUND IN BOILERS, AUXILIARIES, AND MISCELLANEOUS POWER-PLANT EQUIPMENT

Principal ion	Common name	Mineralogical name	Formula determined by x-ray analysis
Group A Boiler and Superheater			
Barium	Barium carbonate	Witherite	$BaCO_3$
	Barium sulphate	Barite	$BaSO_4$
Calcium	Calcium carbonate	Calcite	$\beta CaCO_3$
	Calcium sulphate	Anhydrite	$CaSO_4$
	Calcium sulphate	Hemihydrate	$CaSO_4.0.5H_2O$
	Calcium hydroxide		$Ca(OH)_2$
	Calcium phosphate	Hydroxyapatite	$Ca_{10}(OH)_2(PO_4)_6$
	Calcium phosphate	Whitlockite	$\beta Ca_3P_2O_8$
Magnesium	Magnesium hydroxide	Brucite	$Mg(OH)_2$
Sodium	Sodium sulphate	Thenardite	$Na_2SO_4(V)$
Silicates	Silicon oxide	Quartz	SiO_2
	Sodium-iron-silicate	Acmite	$Na_2O.Fe_2O_3.4SiO_2$
	Sodium-alumina-silicate	Analcite	$Na_2O.Al_2O_3.4SiO_2.2H_2O$
	Sodium-alumina-silicate	Natrolite	$Na_2Al_2Si_3O_{10}.2H_2O$
	Sodium-alumina-silicate	Noselite	$Na_8Al_6Si_6O_{24}.SO_4$
	Sodium-calcium-silicate	Pectolite	$Na_2O.4CaO.6SiO_2.H_2O$
	Calcium silicate	Wollastonite	$\beta CaSiO_3$
	Calcium silicate	Xonotlite	$5CaO.5SiO_2.H_2O$
	Calcium-alumina-silicate	Cancrinite	$4Na_2O.CaO.4Al_2O_3.2CO_2.9SiO_2.3H_2O$
	Magnesium silicate	Serpentine	$3MgO.2SiO_2.2H_2O$
Iron	Iron oxide	Ferrous oxide	FeO
	Iron oxide	Hematite	Fe_2O_3
	Iron sulphide	Triolite	FeS
Group B Condenser, Evaporator, and Heat Exchanger			
Calcium	Calcium sulphate	Anhydrite	$CaSO_4$
	Calcium sulphate	Gypsum	$CaSO_4.2H_2O$
	Calcium carbonate	Aragonite	$CaCO_3$
	Calcium-sodium-silicate	Pectolite	$4CaO.Na_2O.6SiO_2.H_2O$
	Calcium-magnesium-carbonate	Dolomite	$CaCO_3.MgCO_3$
	Calcium fluoride	Fluorite	CaF_2
Copper	Copper sulphide		CuS
	Copper carbonate	Malachite	$CuCO_3.Cu(OH)_2$
	Copper iron sulphide		$CuFeS$
	Copper oxide	Cuprite	Cu_2O
Magnesium	Magnesium silicate	Forsterite	Mg_2SiO_4
	Magnesium hydroxide		$Mg(OH)_2$
	Magnesium silicate	Serpentine	$3MgO.2SiO_2.2H_2O$
Iron	Iron oxide	Magnetite	Fe_3O_4
	Iron oxide	Goethite	$Fe_2O_3.H_2O$
Sodium	Sodium-aluminum-silicate	Noselite	$Na_8Al_6Si_6O_{24}.SO_4$
Group C Steam and Condensate Line			
Ammonia	Ammonium bicarbonate	Teschemacherite	NH_4HCO_3
Iron	Iron carbonate	Siderite	$FeCO_3$
Sodium	Sodium sulphate		$Na_2SO_4(III)$
Group D Miscellaneous Power Plant Equipment			
Calcium	Calcium carbonate	Calcite	$\beta CaCO_3$
	Calcium carbonate	Aragonite	$\lambda CaCO_3$
	Calcium aluminate		$3CaO.Al_2O_3.6H_2O$
	Calcium phosphate	Phosphate	$Ca_2P_2O_8.H_2O$
Magnesium	Magnesium hydroxide	Brucite	$Mg(OH)_2$
Group E Turbine			
Copper	Copper sulphite	Chalcocite	Cu_2S
Nickel	Nickel oxide	Bunsenite	NiO
Silicates	Silicon oxide	Quartz	SiO_2
	Silicon oxide	Cristobalite	SiO_2
	Silicon oxide	Opal	SiO_2
Sodium	Sodium sulphate	Thenardite	$Na_2SO_4(V)$
	Sodium-carbonate-sulphate	Burkeite	$Na_2CO_3.2Na_2SO_4$
	Sodium chloride	Halite	$NaCl$

attacked by acid even though better grades of metal show no visible attack. The type and extent of the attack are illustrated in Fig. 6. This shows a nipple used as a spacer in the construction of internal baffles in a boiler which had been acid-cleaned. An identical type of corrosion was observed in a number of other units employing the same grade of material.

Corrosion of such parts in boilers or in other equipment is not of major importance and is presented here merely to illustrate the susceptibility to corrosion by acid when the metal in contact with the solution is not metallurgically clean.

Active corrosion occurred on manhole covers in two boilers operating under different conditions. The pattern of the attack is shown in Fig. 7. In one instance it was indicated that the metal may have been fairly hot when the boiler was acidized. In the second case the unit was relatively cold, but the feedwater had been contaminated with an acid compound prior to acidizing. It is believed that the condition of the surface of the metal may have made it more susceptible than other portions of the boiler. These conditions were noted on boilers supplied by different manufacturers.

Composition of Deposits. Table 2[7] shows a number of scales which have deposited in boilers and appurtenant power-plant equipment. Frequently such scale will be composed of several formations, each having specific solution characteristics. Furthermore, the composition and extent of the deposit will vary widely in different positions of the same equipment. This condition is demonstrated by the analysis of the encrustations removed from tubes in two sections of the same unit.

Procedure for Acid-Cleaning Boilers. There is no standardized procedure for acid-cleaning of equipment and no standard solution may be employed. It is obvious that the treatment must be guided and adjusted to meet the many variables encountered. Where the work is performed by a commercial company, the job is taken by contract and the contractor furnishes all the necessary appliances and the material for the complete acidizing, including washing down and neutralizing the residual acid when the cleaning of the equipment has been completed. Generally, it is preferable to have the work done by a trained and experienced contractor rather than to attempt the work by local operators, unless

[7] Acknowledgment is made to Dr. F. N. Alquist, of The Dow Chemical Company, who supplied much of the data included in Table 2.

the necessary trained personnel have been developed who can employ the proper technique for effective cleaning and prevention of the industrial hazard involved in such work.

The program of operation which is usually followed when cleaning boilers consists of the following steps, in the order given:

1 Drain the unit, cool, and inspect.

2 Adjust the temperature of the metal to the desired level by the addition of feedwater.

3 Drain.

4 Fill with inhibited acid.

5 Soak for a predetermined period.

6 Continue tests to determine reduction in strength of acid If concentrations drop rapidly and continue to fall, draining and refilling with the solution may be required.

7 When soaking period is completed, drain the unit.

8 Flush two or three times by pumping feedwater into unit and draining as the pH of the test samples indicates the necessity.

9 When flushing is completed, drain boiler and refill with 1 to 2 per cent solution of alkali (soda ash or caustic soda).

10 Drain, then fill with feedwater above the level in the top drum which was reached by the acid, and then drain to the normal water level.

11 Heat with a slow fire and steam at 10 to 25 psi for 2 hr or more.

12 Empty boiler completely if unit is to be inspected, otherwise lower concentration to desired point by blowing down, furnishing feedwater as required.

Whenever possible, boilers should be drained and inspected after acidizing, and a record kept of the condition of the surfaces for future reference and comparison with conditions observed at subsequent inspections.

There may be many deviations from the foregoing operation, but the general plan is indicative of the steps which should be followed to lessen the danger of corrosion.

Hazards

Since all mineral acids are highly corrosive, especially when concentrated, it is obvious that much care should be exercised to protect both the personnel performing the work and the equipment which is being cleaned. If the treatment is carried out by experienced operators who are cognizant of the dangers involved and take the necessary precautionary measures, the resulting hazards should be negligible Aside from the danger of the corrosive characteristics of the acid, the treatment involves a very definite hazard of fire and explosion if the hydrogen generated is not effectively removed and steps taken to prevent its discharge into the atmosphere. Extreme care should be used, also, to prevent hydrogen from pocketing in any equipment which is being acidized.

How many accidents have occurred from explosions from hydrogen during or subsequent to acidizing is not known but during the past 2 years three accidents of this kind have been reported. In one instance two workmen were killed and extensive damaged resulted from an explosion of a boiler. The accident was caused by failure to vent the gas from the boiler drum, the pocketed hydrogen being ignited by a spark from a flashlight used after the boiler was opened for inspection.

This accident demonstrated the extreme danger of acidizing equipment by persons not thoroughly informed of the reactions which occur when the acid is in contact with steel. The two other accidents reported were also explosions resulting from ignition of accumulated hydrogen gas. These accidents were not fatal to personnel, but resulted in appreciable damage to the equipment.

A number of injuries to personnel, resulting from burning or gassing, have come to the attention of the author. There is one case on record during the past year where an operator cleaning a boiler by inhibited acid was killed by arsenious oxide released by the inhibitor which contained an arsenic compound. This type should never be used, although such inhibitors are quite effective for retarding corrosion.

Conclusions

Experience clearly demonstrates that acid-cleaning of equipment is a useful and economical means for removing encrustations from boilers and many other types of power-plant equipment. However, it should never be undertaken or practiced by inexperienced persons who are not fully aware of the dangers involved. Furthermore, acidizing should be practiced only if and when such treatment is necessary. It is a very questionable procedure for any plant repeatedly to acid-clean equipment as a routine maintenance schedule. Such a program is unwarranted both from the standpoint of cost and over-all depreciation of equipment.

No equipment should be treated with acid unless there is assurance that the acid used can be completely removed after the cleaning process has been completed. Most powerhouse equipment is susceptible to cleaning by flushing and flooding with neutralizing alkaline solutions. However, there are certain appliances that are so constructed that adequate removal of acid cannot be effected, or can be done only with great inconvenience and at appreciable cost. In this group the nondraining superheater is an example of apparatus which does not lend itself to acid-cleaning. In some cases where the superheaters may become badly fouled with deposits which are not water-soluble, acid-cleaning may be practiced. If such work is undertaken it should be attempted only when there is assurance that adequate provision has been made for flushing and neutralization when the work is completed and before the unit is returned to service.

Discussion

F. N. Alquist.[8] The acid-cleaning of boilers and auxiliary equipment has been called to the notice of the Society several times in the past few years. Briefly, attention is directed to a discussion by C. H. Groom, G. Williams, and the writer,[9] on scale removal from heat-exchange equipment. Before this publication and since, we have been working in close contact with the power industry and many others on cleaning problems. The present paper is a valuable contribution to the literature on the subject. Data are also given in a paper by J. L. Wasco and the writer.[10]

Acid-cleaning is an economical method of cleaning power-plant equipment. However, the hazards of the acid-cleaning process should be fully recognized so that only experienced persons will be entrusted with cleaning. All engineers recognize that acidizing should be done only when necessary.

The author's statement, "It is a very questionable procedure for any plant to acid-clean equipment as a routine maintenance schedule," requires further discussion. For example, when should a high-pressure boiler be cleaned? The proper answer is to turbine selected tubes to find the extent of fouling. If the fouling rate thus determined is such that annual cleaning is re-

[8] Organic Research Laboratory, The Dow Chemical Company, Midland, Mich.

[9] "Chemical Removal of Scale From Heat-Exchange Equipment," discussion by C. H. Groom, G. Williams, and F. N. Alquist, Trans. A.S.M.E., vol. 65, 1943, pp. 719–722.

[10] "Chemical Removal of Calcium Sulfate Scale," by J. L. Wasco and F. N. Alquist, *Industrial and Engineering Chemistry*, vol. 38, April, 1946, pp. 394–397.

quired, then the plant is acid-cleaned annually on a routine maintenance schedule. These decisions are made by the plant engineers on the basis of cost and over-all depreciation values. The practice of the writer's company on its boilers shows variable times for extent of fouling depending upon water treatments and loads.

It is well that the power industry be made aware of the distinction between corrosion due to operation and corrosion due to improper cleaning procedures. A proper conclusion to be drawn is to maintain treating temperatures as low as possible during cleaning and as stated, preferably between 140 and 160 F.

The author has ably discussed the theories of inhibition. Fifteen years of research by the writer's company on acid inhibitors indicates that both the inhibitor and the acid concentration must be selected so as to give a low corrosion rate under cleaning conditions.

Experience gained on thousands of installations where forced circulation has been compared to circulation by convection, shows that forced circulation is only occasionally necessary.

That the effect of inhibited acid varies as the metals differ in composition has been known in the art for a long time. Power-industry engineers have found that operation corrosion as well as corrosion in cleaning depends upon the composition of the metals involved. Considering Figs. 3, 4, 5, 6, and 7 in the paper, no statement can be made as to how much corrosion is due to operation and how much is due to cleaning.

The steps outlined under procedure for acid-cleaning boilers are good but, under the war-emergency conditions, these steps were not always used because of lack of time; however the engineers of the power industry now follow them more closely.

Finally, the hazards of handling acids and venting the hydrogen that may be produced during the cleaning operation are well known both to the chemical and power industries. With proper safety precautions and helpful papers such as this one, the power industry can take economic advantage of acid-cleaning methods

R. E. Hall[11] and C. E. Kaufman.[12] We are in agreement with the general facts on acid-cleaning of boilers as developed by the author. More incisive analysis of some of the factors involved brings to light some significant considerations that require emphasis.

Acid used for the process is supplied with an inhibitor, that is, a substance whose purpose is to minimize or prevent attack of the acid on the boiler steel, while not interfering with its dissolving effect on other substances such as the calcium carbonate and phosphate, the iron oxide, etc., comprising the boiler sludge and scale. Concentration of the inhibitor in the acid-cleaning solution is a function of the type of inhibitor used, concentration of acid employed, and temperature at which the job of acid-cleaning is done. Thus one can depend upon the inhibitor to protect against direct attack of the metal by the acid within rather generous temperature limitations, if the concentration of inhibitor required in relation to the acid is consistently maintained, and if the products of reaction of the acid with the boiler sludge or scale are not of themselves potent in their attack on the metal, regardless of the inhibitor.

As a matter of fact, these products of reaction divide into two classes, one of which is innocuous as regards the boiler metal; the other of which is highly aggressive in attack on the metal, even with any usual inhibitor present in the acid solution. Materials which give rise to the first class comprise the calcium and magnesium salts of the boiler sludges and scales; those giving rise to the second class are the iron oxides, either magnetite or hematite. Whether formed in the feed line by the action of dissolved oxygen and thence entering the boiler, or whether formed in the boiler itself by reaction of boiler metal with the bonded oxygen of the boiler water, these oxides represent high oxidizing capacity. Concentrated bit by bit as the boiler is operated and held harmless by the insolubility of the oxides in the boiler water, they await only the trigger action of the acid solution which dissolves them to bring this concentrated oxidizing capacity into play against the boiler metal. Metallic copper, so frequently associated with the iron oxides, may enter into but cannot initiate the oxidation reactions, nor can it contribute thereto. In fact, by plating out on the metal it may even be protective in some measure.

Let us explore conditions in a thin layer of the acid-cleaning solution adjacent to the metal when the sludge or scale consists primarily of insoluble calcium and magnesium salts, and the normally quite low percentage of iron oxide. The acid dissolves the deposit, forming calcium and magnesium chloride, both of which are stable salts devoid of oxidizing capacity. Because of this, they originate no attack on the metal, and the protection provided by the inhibitor in the acid remains intact, unless undue temperature elevation has adversely affected protective conditions. Barring undue temperature, whether flow of the acid-cleaning material over the surfaces is provided for by means of circulating the solution or whether there is or is not considerable agitation of the solution by dissolving such material as carbonate, a protective concentration of the inhibitor in relation to the acid content of the solution prevails at the surfaces.

Let us now explore conditions in the thin film of acid-cleaning solution adjacent to the boiler metal, when the sludge in the boiler is mainly magnetic oxide Fe_3O_4, which dissolves forming ferric and ferrous ions. It is readily demonstrated that the ferric ion is the most important factor in promoting attack.

Fundamentally the aggressiveness of solutions containing ferric ion can be explained on the basis of the following reaction

$$2Fe^{+++} + Fe \longrightarrow 3Fe^{++} \quad \ldots\ldots\ldots\ldots [1]$$

It will be noted that this process does not intrinsically involve the disappearance or formation of an acid or a base. Therefore it might be presumed that the inhibitors customarily employed to stifle acid attack on steel would not be well adapted to minimize the reaction of ferric ion with metal. Laboratory tests have confirmed this point.

In the laboratory we have run a number of agitated-solution tests at 150 F, for 6 hr, in which the reality of ferric-ion attack is clearly apparent. For example, when 1 per cent Fe_3O_4 was added to an inhibited acid solution, attack on an inserted steel strip was increased nearly threefold as measured by weight loss. The loss, representing about one third of the potential attack as just defined in Equation [1] was undoubtedly limited by the incomplete solubility of the added iron oxide, behavior which of course may be found in full-scale cleaning operations. When the ferric material was present in considerably greater concentrations and as completely soluble chloride, without acid but with a standard inhibitor present, attack actually considerably exceeded that predicted from reaction [1].

In the removal of deposits from boilers by acid-cleaning, when magnetic iron oxide, for example, goes into the circulating acid, what quantitative potential has it for producing damage? If it is assumed that 1000 gal of cleaning acid builds up to contain homogeneously distributed in solution 1 per cent or 83.3 lb of material originally Fe_3O_4, 20 lb of iron can be dissolved if Reaction [1] goes to completion. If, for example, the dissolution of iron is assumed to take place evenly within 3-in. tubing, the general loss of metal will amount to less than 0.001 in. If, however, the ferric ion is not homogeneously distributed in the acid solution, but rather is selectively concentrated in localized areas

[11] Hall Laboratories, Inc., Pittsburgh, Pa. Mem. A.S.M.E.
[12] Hall Laboratories, Inc.

rich in magnetic oxide, then serious pitting or wastage in such areas may be expected.

Avoidance of such corrosion we believe is best effected by steadily maintained circulation of the acid-cleaning fluid so that localized high concentrations of ferric chloride cannot occur, and by limiting concentration of ferric chloride in the acid-washing solution through adequate blowdown and replenishment of acid solution, thus protecting against too much loss of metal in general corrosion of the surfaces by even the homogeneously distributed ferric chloride which develops mainly at the surfaces or in particular spots in the boiler. Satisfactory control of ferric-ion concentration can be established by analysis.

For the boilers that develop magnetic oxide by the bonded-oxygen process in regions where high heat release renders intolerable any decrease in circulation, acid-cleaning does a specially significant job, in that by cleansing the surfaces of iron oxide, and thus bringing back the original designed circulation in the tubes, the conditions for reaction of the bonded oxygen of the boiler water with the tube metal are minimized. Thus periodic acid-cleaning as required can keep circulation at these points maintained at a level where any formation of iron oxide will be slight, and the boiler will be dependable.

Naturally, acid-cleaning should not be looked upon as something to supplant normal careful procedure in taking care of the boiler. Nevertheless, especially in cases such as those comprised in the circumstances just discussed, it can play a very effective part. Likewise, alkaline-cleaning processes in some instances, dependent upon the composition of material to be removed, are more feasible than acid-cleaning.

No mention has been made of acid-cleaning operations involving nonferrous metals. It would be interesting to know if such cleaning has been conducted and the general types of inhibitors, if any, which proved useful.

L. E. Hankison.[13] This paper is especially valuable because it tells of the dangers that may be encountered, not only to the equipment being cleaned, but also to the personnel engaged in doing the cleaning. The definite warning given by the author that acid-cleaning should never be undertaken or practiced by inexperienced persons who are not fully aware of the dangers involved, should not be ignored. It is evident that this work should be done either by someone commercially in the acid-cleaning field, or by someone who is professionally able to prescribe the proper acid to be used, its strength, the inhibitor to be used, the proper temperature and the length of time for its contact, and then the best way to dispose of the partially spent acid, as well as the proper material and method of neutralizing or removing the residual acid from the equipment. This service presumably can be had only at a cost which must be charged against the benefits that may be obtained by acid-cleaning.

There is another, and probably a much greater cost that must be borne by those who indulge in this means of keeping their equipment in service. It is the loss in efficiency and capacity of the equipment from the time the surface begins to foul until the deposit is of sufficient magnitude to justify removing the equipment from service for acid-cleaning. By using the average between the clean condition and the fully fouled condition as the approximate continuous loss, it can readily be appreciated that this cost is quite considerable and should be avoided if at all possible.

It is our belief that it is much cheaper and very much more satisfactory to secure the services of competent water-conditioning consultants whose aim is to avoid the necessity of any cleaning rather than to acid-clean and bear the costs that have just been outlined. We believe that with this consulting service and properly trained operating personnel to carry out their recommendations, acid-cleaning, or any other type of cleaning that requires equipment outages is unnecessary. Of course, this implies properly designed equipment operated at ratings so that steam pockets, hideout, or reverse circulation is not experienced.

Acid-cleaning has a very important place in power-station operation when the equipment is run at ratings beyond the normal ability of the heat-transfer surface to function. In this case the surface may oxidize or change to form an insulation to a point where overheating and failure will follow. Acid-cleaning may remove the deposit that has been formed and prevent the equipment from failing.

There is another situation where acid-cleaning is beneficial and, in fact, is the only practical means of restoring equipment to serviceable operating condition. During the war, when materials such as condenser tubes and the personnel for their installation were very hard or impossible to obtain, condenser leakage allowed silica to build up in some of our boilers to a point where it was deposited as an incrustation that caused tube failures. Acid-washing restored the boilers to good operating condition, where they have continued to function with the aid of the proper water-conditioning previously mentioned.

One other acid-cleaning experience should be mentioned. Due to water leakage through the packing of the boiler feed pumps into the bearing cavities, it was found difficult to keep oil in the bearing reservoirs. An oil-company representative recommended that the straight mineral oil which had always been used be replaced with a compounded oil that would not float out so easily. This was done and the bearing situation was remedied, but this oil was emulsifiable and such oil as did leave the bearing reservoirs would not separate out in the drip collectors but was carried through into the boilers. There it mixed with the boiler sludge forming a tarry mass containing a small percentage of oil that adhered to the surfaces and caused burnouts. It was thought that increased alkalinity would dissolve this mass but it was not cleared up by this means, so we decided to acid-clean to dissolve the embedded sludge. Acid-cleaning partially dissolved this mass. It also removed much of the protective coating of iron oxide and probably other iron compounds that had been formed on the water surface of the tubes by some reaction of the treating chemical, and which are considered beneficial and desirable.

The presence of this iron compound can be well illustrated by our boiler-gasket experience. Due to scarred or cut hand-hole-seat surfaces, it was considered necessary to use solid copper gaskets to make these parts tight. It was recognized that copper gaskets between the iron or steel surfaces and in the presence of the alkaline boiler water as the electrolyte were not conducive to long gasket life, yet we were never able to find even the slightest attack on these gaskets and they were considered entirely satisfactory. After the boilers were acid-cleaned new gaskets would not last 3 months and we have records of heavy new gaskets practically entirely disappearing in 2 months of operation. This caused us temporarily to abandon copper gaskets. We now believe that the protective coating has been restored by the continued use of treatment, and are trying a few copper gaskets which we hope will again give satisfactory service.

As a further indication that acid-cleaning is detrimental in removing the beneficial iron-compound coating, our experience with corrosive barnacles should be related. After the boilers were acid-cleaned, large quantities of iron-oxide scale were found lodged in the tube headers and also in the tubes that had sluggish circulation. Frequent boiler outages were necessary until all this scale was removed from the system. These outages allowed the internal boiler surfaces to be exposed to atmospheric air, and

[13] Superintendent, Efficiency Department, West Penn Power Company, Pittsburgh, Pa. Mem. A.S.M.E.

small rust spots were formed. These rust spots may have provided the insulation that promoted barnacle growth and boiler-tube failures resulted. This is being given further study. It is now believed that the protective surfaces previously described have been fully restored, as failures of this type have not been experienced during the last 1½ years.

While it is agreed that cleaning with acid is beneficial under certain extraordinary conditions, we wish to emphasize the part of the author's conclusion which says, "It is a very questionable procedure for any plant repeatedly to acid-clean equipment as a routine maintenance schedule." We believe that good housekeeping, coupled with intelligent water-conditioning to eliminate the need for acid-cleaning, is the preferred method of operating power-station equipment.

W. R. LaMotte.[14] The writer's company has been particularly interested in the cleaning of boilers by this method. It was first tried in 1939 to clean one of the 350-psi boilers at Kearny generating station. The results were so gratifying, both from the standpoint of low cost and degree of cleanliness obtained, that acid-cleaning has been standard practice at that station ever since. In 1940 the practice was extended to the 1250-psi boilers in the Public Service system. These high-pressure boilers were first acid-cleaned at half yearly intervals, but more recently they have been cleaned annually. As a result, some of them have been cleaned ten and eleven times.

This experience tends to confirm what the author has written concerning the precautionary measures which are advisable in the use of acid for boiler cleaning. The best inhibitor procurable should be used and solution and metal temperature should be kept well below the temperature at which the manufacturer states the inhibitor will break down, the time of contact should be limited, and the various hazards should be recognized and adequate protection provided.

In fact, we differ only with the following statement of the author: "It is a very questionable procedure for any plant repeatedly to acid-clean equipment as a routine maintenance schedule. Such a program is unwarranted both from the standpoint of cost and over-all depreciation of equipment." We look upon acid-cleaning as the normal and best way to clean periodically the internal surfaces of high-pressure boilers. Nothing so far discovered has indicated that measurable harm has been done during the past 5 years.

Perhaps one reason for the foregoing has been the practice of using low acid concentrations, in the range ½ to 1 per cent HCl, as contrasted with the range of 4 to 15 per cent discussed by the author. These satisfactory results have been achieved using presently available inhibitors, and certainly improvement in inhibitors can be expected in the future. High-pressure boilers now on order are so designed that the tubes cannot be cleaned by conventional methods; only by the use of liquids can the internal surfaces be reached. It has been our experience that the art of treating the boiler water has not progressed sufficiently to dispense entirely with internal cleaning.

E. L. McDonald.[15] Our company was one of the early users of inhibited acid for cleaning power-plant equipment. For years we have acid-cleaned various heaters, feed lines, pumps, economizers, etc., all under the guidance of the station chemist.

Much was learned from our early experience. For example, do not try to clean old equipment too fast or too well with any scale-removing compound. Scale removed from the tube sheet of a steam-crane boiler by trisodium phosphate exposed loosely rolled tubes and caused a great number of leaks that did not exist when scale covered them. Scale removed from the cast-iron junction boxes of an economizer by acid-cleaning exposed porous spots in the box that did not leak before the removal of scale.

When the shortage of labor during the war first prompted us to employ a commercial acid-cleaning company, we had the idea we could pump the acid to the boiler through the blowoff line which emptied into a sewer at a convenient location for tying-in the acid truck, thus saving the cost of an acid feed line. After a short period of time the acid pumped through the line removed the scale and a great number of leaks developed, which again were not evident when the scale protected them.

All of this is in keeping with the author's statement to the effect that acid is frequently blamed for corrosion which actually existed before the acid was applied and was not evident until the acid removed the scale. The writer has observed corroded surfaces, similar to the type shown in the paper, in boilers and turbine casings that had not been acid-cleaned.

While we have made substantial savings by acid-cleaning with our own crew and equipment, we have not found acid-cleaning of large steam-generating units, as performed by a commercial cleaning company, to be very cheap. The average on five boilers with about 20,000 sq ft of surface each was $84 per 1000 sq ft of surface. This was about 40 per cent higher than the previous mechanical cleaning cost. On these five boilers a 5 per cent acid solution was used. On three boilers cleaned at a later date, using 3½ per cent solution, the cost dropped to $52 per 1000 sq ft of surface. This was still about 15 per cent higher than the previous mechanical cleaning cost. However, two items definitely favored acid-cleaning, i.e., a shorter boiler outage, and a better job of cleaning. The fact is that it is practically impossible to clean the modern steam-generating unit mechanically.

Mention has been made that the control of acid temperature is important. A thermometer in the acid line can tell a false story. High "spot" temperatures can exist in a boiler if heat is transmitted from brickwork not previously cooled before acid treatment is applied.

The author comments on the possible metal loss due to acid-cleaning; however, it should be remembered the old rotary tube cleaner also removed metal and, before water treatment reached its present stage, more than one boiler tube had to be replaced due to this metal loss. Also, in our own case, we believe the loss of metal, due to corrosion and erosion on the outside of the tube, would exceed any loss of metal on the inside. During acid-cleaning, metal test strips have been hung in boilers, carefully weighed before and after the acid-cleaning, and have given us an idea of the possible metal loss.

Mention is also made of the hazard of generating hydrogen gas when acid-cleaning, and the author comments on a particular boiler explosion. A very serious explosion also occurred last year when acid-cleaning a condenser at the Wichita Station of the Kansas Gas & Electric Company. Details of this are covered in an article by E. D. St. John,[16] which should certainly be read by anybody contemplating acid-cleaning of such equipment.

While acid-cleaning of any equipment has merit, it should not be undertaken except under the guidance of a competent chemist or other competent help.

F. U. Neat.[17] In connection with acid-cleaning, the writer believes that considerably more importance should be attached

[14] General Superintendent of Generation, Public Service Electric and Gas Company, Newark, N. J. Mem. A.S.M.E.

[15] Kansas City Power & Light Company, Kansas City, Mo. Mem. A.S.M.E.

[16] "Repairs to Steam Turbine Unit Following Hydrogen Explosion," by E. D. St. John, *Power Plant Engineering*, vol. 50, no. 3, March, 1946, pp. 64–68.

[17] Assistant to Superintendent of Power Production Stations, Consolidated Gas Electric Light & Power Company, Baltimore, Md.

to the possibility of hydrogen embrittlement. Pickling embrittlement is too well known in the steel world to lead us to do anything but go well on the safe side with regard to removing hydrogen. Particularly in the case of boilers, it is quite possible that we may open up crevices in seams and around tubes and these crevices must be stopped. However, if we should permit the rerolling of tubes or calking of joints without making certain the removal of occluded hydrogen, then we are guilty of negligence. The writer's practice is to rinse the boiler thoroughly, after which a solution of 2 to 5 per cent soda ash is boiled in the boiler for 8 to 12 hr at from atmospheric pressure to 50 psi under open vents before the boiler is opened for inspection and certainly before any cold-working of the boiler metal is permitted. This boiling procedure accomplishes reasonable removal of hydrogen gas from the boiler and occluded hydrogen from the metal, largely prevents after-rust, and partially re-establishes the protective coating of magnetic oxide. It may also assist in the loosening of remaining scales which are incompletely soluble in acid.

Attention is also called to a remark by the author which may be misconstrued. In his discussion of the hazards involved he states that the discharge of hydrogen to the atmosphere must be prevented. The writer feels certain that the author really meant that the vents must be piped to the outside in such a manner as to make reasonably sure that discharged hydrogen may not re-enter the building and that these vents be taken from as near the top of the equipment as is possible. If vents are left open during the fill and drain-rinsing operations and then during the boiling-out procedure, we are assured nearly complete removal of hydrogen in the equipment.

H. B. Oatley.[18] Deposits on the heat-transfer surfaces of several types of vessels are very generally recognized by designers as well as users. This is particularly true for vessels or pipe lines conveying liquids at increasingly higher temperatures and pressures.

Attention has been given to the use of purification systems for the removal of these undesirable elements which cause failure of the apparatus. Acid-cleaning has been used with beneficial results by those who, like the author, realize the dangers of such use. The reverse is also true.

The paper has called attention to the outstanding features of this acid treatment and the dangers of such cleaning are clearly and emphatically stated in the author's conclusions.

The increasing severity of operation has brought the designer to the doorstep of the metallurgists for better material, which is to be more highly resistant to deteriorating effects resulting from impeded heat transfer. It may also be said that the chemical industry is looked to by those who require more effective and less dangerous scale-removing methods, entailing the use of chemical inhibitors.

W. F. Ryan.[19] The development of inhibited acids for the cleaning of metal surfaces is just another example of the fact that many of us were born 30 years too soon. When the writer recalls his filthy and laborious efforts to clean boilers and oil coolers in the old 74th Street Station, he wishes that the Dow development engineers had not been so dilatory in the development of acid-cleaning. His successors in the operating field can have these jobs performed with less labor and worry than he experiences when he sends his shirt to the laundry.

In saying less worry, he is not relying entirely on the fact that it may be easier to replace a boiler than to get a new shirt. The author's precautionary remarks are timely and well taken but, on the other hand, the hazards are very slight if one is willing to pay somebody else to worry about them. Most of the adverse experience with which the writer is familiar, has arisen from misguided efforts to save a few dollars by doing the job without experienced supervision or adequate equipment.

In addition to the routine cleaning of boilers, there are special conditions under which the use of acid-cleaning may pay tremendous dividends; for example, in a paper mill it was discovered that the two high-pressure boilers had accumulated an unusual amount of sludge due to changes in the raw-water supply. One tube was blistered and concern was felt for the rest of the heating surfaces. One would not ordinarily think of using acid to remove sludge, but based upon previous experience it was anticipated that a production loss equivalent to one half of the mill's output for at least 7 days would be involved in shutting down the boilers, allowing them to cool sufficiently, cleaning them thoroughly, and getting them back on the line. This was at a time when the mill output was heavily oversold and such a loss of production would be a major catastrophe. Dowell Incorporated was consulted regarding the practicability of using acid in this situation and found that both boilers could be cleaned in a single day. The two boilers were satisfactorily cleaned by circulation of inhibited acid and the entire operation consumed less than 19 hr. The cost of the acid-cleaning was of the order of $500, while the production hours that were gained were worth many thousands.

Another instance of high return on a small investment was experienced in the cleaning of cooling coils in large process tanks. For years these coils which are used with raw hard water, were installed with 3 times the calculated surface in order to compensate for the gradual accumulation of scale. At the end of 2 or 3 years the coils were removed and replaced. The coil itself was not extremely expensive, but the replacement required draining and cleaning the tank with attendant loss of valuable materials. By the use of acid the coil can be cleaned in place with no loss of production or of materials. Life of the coil will be at least equal to that of the tank, and when new tanks are installed the cooling coils can be designed in correct proportion to the demand for heat transfer.

The use of acid-cleaning in power plants and process industries is still in its infancy, with new time-saving and money-saving applications arising every day. Every operating or maintenance engineer who is confronted with the periodic cleaning of metal surfaces should investigate thoroughly what can be accomplished by this method.

H. G. Thielscher.[20] We have acid-cleaned eleven boilers in our plants with satisfactory results. The work has been performed by a commercial chemical company. The strength of the acid solutions used was 5 per cent, the length of time contained in the boilers varied from 5 to 14 hr, and the temperature of the boiler metal and acid solution ranged from 150 F to 190 F. Forced circulation of the solution was not used. We do not know the nature or composition of the inhibitors used as this is considered secret information by the commercial companies. Subsequent examination of these boilers has not revealed any definite evidence of acid corrosion.

Included in the boilers, which were acid-cleaned, was a new 525,000-lb per hr 675-psig 900 F total steam temperature 3-drum boiler, which was acid-cleaned immediately after the conventional boiling and drying-out period. The results obtained were excellent, and an appreciable saving was effected in the time

[18] Vice-President and Consulting Engineer, The Superheater Company, New York, N. Y. Mem. A.S.M.E.

[19] Stone & Webster Engineering Corporation, Boston, Mass. Fellow A.S.M.E.

[20] Mechanical Engineer, Potomac Electric Power Company, Washington, D. C. Mem. A.S.M.E.

and labor ordinarily required to prepare the drums for Apexiorizing. In addition, we believe a more permanent Apexior job was obtained because of the cleanliness of the metal surfaces after acid-cleaning. We expect to continue this practice of acid-cleaning new boilers before they are placed in service. The superheater in this boiler was the vertical nondraining type and was filled with clean warm water before admitting the acid solution to the boiler. In some of our older boilers we had deposits of analcite. The acid-cleaning did not remove these deposits but did soften them up so they were readily removed by turbining.

We agree with the author that there are corrosion and explosion hazards attached to the acid-cleaning of equipment, but, like him, we believe these hazards are negligible when proper procedures and precautions are observed.

G. F. Williams.[21] This paper gives an exceptionally clear picture of chemically removing scales and sludges with acid-base solvents. The author is to be congratulated on this excellent paper which so ably relates the history of acid-cleaning and points out that its effective application involves a careful consideration of all pertinent factors. When one considers the complexity of the questions involved, which deal not only with chemical engineering but also with metallurgy, electrochemistry and other sciences, it is even more apparent that all factors must be carefully weighed by one thoroughly trained and experienced in this line of work in order that the accumulated scale may be removed safely.

It is interesting to note that over 25 years ago the entire piping system of a large building was successfully cleaned of scale by the use of acid-base solvent but, as the author points out, "It is surprising that this novel method of cleaning pipe lines did not receive more widespread interest at that time since the basic principle of the procedure has much merit." Possibly the difficulties experienced on this job were sufficiently serious to deter this type of work in the immediate future and the present commercial use of acid-cleaning may be due in no small degree to the experience gained in using millions of gallons of inhibited acid-base solvents during the last few years for increasing the flow of oil wells.

In only a few cases has any corrosion been noted in boilers following acid-cleaning, and in most of these there was considerable evidence that the corrosion could have taken place during operation of the equipment rather than during the cleaning job. Our company, during the last 10 years, has made over 50,000 separate treatments using inhibited acid-base solvents on oil wells and industrial equipment, and in less than 0.1 per cent of these jobs has any question been raised concerning the possibility of corrosion due to the use of inhibited solvent. In fact, it is the opinion of many operators of large steam-generating equipment that the metal loss from cleaning with acid-base solvents is less than that which results from mechanical cleaning methods.

The manhole cover, shown in Fig. 7 of the paper, showed definite corrosion upon inspection following an acid-cleaning job, but as this unit was not inspected immediately prior to cleaning, there is room for considerable uncertainty as to the cause of the corrosion. Representatives of the writer's company were present with the author and others at the time this inspection was made. Other places on the edges of the manhole covers in this boiler showed occasional large corrosion "pits" much deeper and much larger than anything shown in Fig. 7. It seems practically impossible that such a large amount of metal could have been removed from such a small area in the few hours' time in which acid was in contact with the metal. Probably factors other than cleaning with inhibited acid-base solvent contributed to this corrosion.

One of the conclusions to this paper, viz., "It is a very questionable procedure for any plant repeatedly to acid-clean equipment as a routine maintenance schedule," might be clarified. Certainly any preconceived schedule for periodical cleaning without any knowledge of the rate at which scale is formed would be questionable, but whenever there is sufficient scale accumulation to warrant its removal, acid-cleaning is the best and sometimes the only feasible way of removing it. After the deposition rate of scale in a boiler is known and therefore the frequency with which it must be removed, it seems entirely reasonable that acid-cleaning could be done on a routine maintenance basis.

[21] Development Engineer, Dowell Incorporated, Tulsa, Okla. Mem. A.S.M.E.

Author's Closure

The comments presented on the author's paper by the several discussers are constructive and justify much consideration by those interested in the subject.

The theory on the mechanism of corrosion, as brought out by Messrs. Hall and Kaufman, requires consideration and indicates the need for further research along these lines. Although there is much disagreement among engineers as to the relative merits of circulation to avoid concentration cells, as suggested by Dr. Hall, this is a desirable procedure under some circumstances and, where it can be carried out in a practical manner, circulating the solution may conceivably overcome the tendency to cause spotty corrosion of the metal. Regardless of the advantages offered by circulation during cleaning of apparatus there are many cases, especially those involving cleaning of large boilers designed with complex circuits, where circulating the solution can not be readily affected. It is obvious that uniform circulation through a large unit is difficult and it is doubtful if pumping the solution through units will insure much better movement of the solution over the metal than may be obtained by normal thermal circulation which occurs during the cleaning process.

Regardless of these apparent operating difficulties to carry out the procedures for avoiding corrosion as suggested by Dr. Hall, the problem warrants further study. It is hoped that the Hall Laboratories, Inc., and other interested groups will continue to study and develop means for overcoming many of the troublesome problems encountered in the acid-cleaning technique.

Dr. Alquist's statement that "The effect of inhibited acid varies as the metals differ in composition" has been known in the art for a long time. Power-industry engineers have found that corrosion during operation as well as corrosion in cleaning depends upon the composition of the metals involved. This has not been fully appreciated by many operators. Why some metal corrodes during acid cleaning to a greater extent than others, when the cleaning procedures are practically identical, is not clearly understood but no doubt is related to the composition of the metal and other metallurgical characteristics.

The instructive and informative research now being carried out by The Dow Chemical Company under the guidance of Dr. Alquist and his associates should reveal much valuable information and place acidizing of equipment on a much more exact basis than is now possible with our limited knowledge. It is hoped that this and other organizations carrying on research in this field will release their findings from time to time. Such dissemination of data should serve as an invaluable guide to the profession.

The author is in agreement with many of the comments made by Mr. Hankison, since our experiences have paralleled his regarding a number of difficulties described. The acid attack on copper gaskets during cleaning of boilers has been encountered

many times with varying degrees of severity. These difficulties and other precautionary remarks mentioned by Messrs. Hankison, LaMotte, and MacDonald and the other discussers, demonstrate the need for intelligent planning and control for safe and effective treatment of any equipment by inhibited acid solutions.

With regard to Mr. Neat's comments, namely, "Attention is also called to a remark by the author which may be misconstrued," the author's precautionary remark, of course, related to adequate venting to the outside atmosphere. We regret if our statement in the text has been misconstrued by others. It is presumed to be obvious that the avoidance of a fire or explosion hazard would require complete and adequate venting outside the building by suitable facilities.

The aim and purpose motivating the preparation and presentation of the author's paper was to direct attention to the economic and practical value of acidizing boilers and other auxiliary equipment. The very favorable comments by so many engineers and chemists indicate that designers and operators agree with our viewpoint, differing only in details of application of the process. There are a number of unsolved factors which are not well understood and therefore may not be adequately evaluated. It is hoped that our effort has focused attention on these matters and will stimulate further study of the problem.

The Theory of Plasticity— An Outline of Work Done in Russia[1]

By W. W. SOKOLOVSKY,[2] MOSCOW, U.S.S.R.

The theory of plasticity as an important part of the mechanics of continuous materials has occupied the attention of many Russian workers in recent years. In the first paper in this field[3] published in 1935, by S. Sobolev (17)[4] the propagation in time of a plastic zone was investigated around a circular hole in an infinite plate. The plastic zone was assumed to have a polar symmetric shape. Based on the works of L. Prandtl, Th. von Kármán, R. von Mises, H. Hencky, A. Nadai, and others, more recently, a group of young Russian engineers have investigated further the theory of plasticity and added many new developments to it. While the investigations abroad and in Europe, outside of Russia, were being aimed at establishing the validity of the theory of plasticity, most of the papers appearing in the literature in Russia were devoted to the solutions of concrete problems. This review does not attempt to discuss broadly the work done in the theory of plasticity. The author confines himself to certain parts of the theory which have been developed in Russia. Naturally those closest to his own scientific interests have been selected for treatment.

Plastic Stress-Strain Relations—Theory of Viscous Bodies—Stability Questions

THE equations expressing the state of strain beyond the limits of elasticity have been the subject of investigation by a number of scientists, among them, N. Belayev (1), L. Kachanov, A. Ilyushin, and A. Ishlinsky. These studies constitute a development of the Mises-Hencky theory of plasticity, which has won general recognition.

Hencky gave the equations for the components of deformation expressed through the components of stress; of considerable interest are the inverse expressions. The latter were obtained by L. Kachanov (14) both for the case of ideal plasticity according to the Mises conditions, and for the more general case of a strain-hardening material according to the Schmidt conditions. L. Kachanov strengthened the validity of the Mises-Hencky theory and investigated in detail the equations of equilibrium and of motion of a plastic body by basing them on a number of interesting energy theorems derived from the principles of the calculus of variation (13, 15).

A. Ilyushin (5) contributed new equations, valid for the process of unloading, to the Mises-Hencky theory of plasticity. He assumes that the intensity of the shearing stresses is proportional to the unit shears. This makes it possible to consider problems dealing with the active process of "loading," as well as the passive process of "unloading." The results obtained are particularly important in their application to stability beyond the limit of elasticity, of which examples will be given later.

The theory of viscous materials was evolved in Russia by A. Ilyushin (4). In addition to the well-known hypothesis of Saint Venant of the coincidence of the maximum rate of shear with the greatest vector of the shearing stress, this theory is based on the assumption that the maximum shearing stress in flow is always larger than a constant σ_s and is a linear function of the maximum rate of shear. For example, in the case of a circular bar, Fig. 1, the normal stress σ_z is assumed equal to

$$\sigma_z = \sigma_s + \mu\dot{\epsilon}_z \quad \text{(see footnote[5])}$$

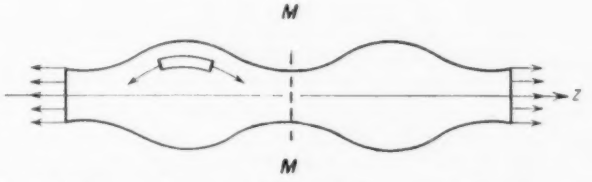


Fig. 1 Assumed Shape of Bar for Discussing Stability of Deformation in Tension

where μ is the coefficient of viscosity and $\dot{\epsilon}_z$ the rate of strain.

The most interesting problems in the theory of deformation of such viscous bodies, which were raised by A. Ilyushin and solved by him and other authors, are those dealing with the stability of stretching or compression of strips, bars, and plates.

The problem was solved by A. Ishlinsky (8) for the case of a cylindrical bar of circular cross section with the radius a. He reduced the problem to an equation which he integrated by means of Bessel's functions.

He found, for example, for a bar having the small deviation

[1] This is a brief summary of an address which was made by Dr. Sokolovsky on June 21, 1945, at a meeting of the Institute of Theoretical Mechanics in Moscow during the Science Congress of the Allied Nations which was held in Moscow and in Leningrad in commemoration of the 220th anniversary of the founding of the Academy of Sciences of the U.S.S.R. The writer of this introductory note has been privileged to present an English translation of the original manuscript to the Journal of Applied Mechanics. This translation which was received in Moscow by the writer on June 29, 1945, was prepared by N. Talickish, editor of the *Journal of Applied Mathematics and Mechanics*. American readers will be grateful to Dr. Sokolovsky and to Mr. Talickish for acquainting them with a number of recent remarkable investigations by Russian engineers into the theory of plasticity which otherwise would have remained unknown in this country owing to the difficulties of the language.—A. Nadai.

[2] Professor, Institute of Theoretical Mechanics of the Academy of Sciences in the U.S.S.R.

[3] Papers on the application of the theory of plasticity to bars in building mechanics appeared somewhat earlier. Reference to these will be omitted in this review.

[4] Numbers in parentheses refer to the Bibliography at the end of the paper.

Discussion of this paper should be addressed to the Secretary, A.S.M.E., 29 West 39th Street, New York, N. Y., and will be accepted until April 10, 1946, for publication at a later date. Discussion received after the closing date will be returned.

Note: Statements and opinions advanced in papers are to be understood as individual expressions of their authors and not those of the Society.

[5] A viscous substance having a definite yield stress deforming when the stress is larger than a certain stress σ_s, "yield value," was postulated long ago in the United States in "Fluidity and Plasticity," by Eugene C. Bingham, McGraw Hill Book Company, New York, N. Y., 1922, p. 440 (p. 217; fig. 78, p. 219), and his assumption was used to explain the behavior of many actual substances in applications; also, "Ten Lectures on Theoretical Rheology," by M. Reiner, published by Rubin Mass, Jerusalem, Palestine, 1943, p. 133. (This note added by A. Nadai.)

$\delta \cdot \sin nz$ from the form of a circular cylinder which is subjected to stretching, that the ratio of this deviation to the radius of an undisturbed cylindrical surface tends either to increase (unstable deformation) or to decrease (stable deformation). This depends on the velocity of deformation. An analogous phenomenon takes place when strips or plates are deformed. The causes of this phenomenon may easily be ascertained, Fig. 1. The rates of strain in the narrower cross sections $M-M$ of a bar must be larger than in other sections, since the true stresses in them are larger, and hence these cross sections will decrease the more quickly. On the other hand, the curvatures of the trajectories of the main stresses level out the deformations. These factors taken together determine the process of deformation as a whole.

Stability of deformation depends on whether the expression

$$J_1(\gamma h)\, J_0(\bar{\gamma} h) + J_1(\bar{\gamma} h) J_0(\gamma h)$$

is positive or negative. In this expression $h = na$ and γ and $\bar{\gamma}$ are a complex number and its conjugate value, which depend on the velocity of deformation and on the constants σ_s and μ. It is interesting to note that conditions may be set up in which the relative deviation of the form of the bar from that of a cylinder may be increased owing to compression. A. Ilyushin has proved this phenomenon experimentally.

Elastico-Plastic Bending of Plates and Shells

An interesting section of the theory of plasticity, which has been considerably developed in Russia, is the theory of the elastico-plastic bending of plates and shells. This theory is based on the Kirchoff-Love hypothesis of the "rectilinear element" and is a generalization of the theory of the bending of beams.

The starting point in this problem is the condition of ideal plasticity of Mises

$$\sigma_\alpha^2 + \sigma_\beta^2 - \sigma_\alpha \sigma_\beta + 3\,\tau_{\alpha\beta}^2 = \sigma_s^2$$

where σ_α, σ_β are the normal components of stress, $\tau_{\alpha\beta}$ the shearing stress, and σ_s the yield stress.

Or the condition of the more general form may be postulated

$$\left| \sqrt{\sigma_\alpha^2 + \sigma_\beta^2 - \sigma_\alpha \sigma_\beta + 3\tau_{\alpha\beta}^2} \right| = F\left(\left| \sqrt{\epsilon_\alpha^2 + \epsilon_\beta^2 + \epsilon_\alpha \epsilon_\beta + \frac{1}{4}\gamma_{\alpha\beta}^2} \right| \right)$$

($\epsilon_\alpha, \epsilon_\beta$, and $\gamma_{\alpha\beta}$ are the components of strain) where the z-axis is normal to the middle surface of the shell, β = const and α = const are curvilinear co-ordinates on the middle surface, and F is a power function. This latter condition takes the strain-hardening of the material into consideration.

Both of the conditions mentioned are somewhat simplified by neglecting the shearing-stress components $\tau_{\alpha z}$, $\tau_{\beta z}$ and the unit shears $\gamma_{\alpha z}$, $\gamma_{\beta z}$ in comparison with σ_α, σ_β, and ϵ_α, ϵ_β.

A. Ilyushin (5) considered the rotationally symmetric plastic state set up in circular cylindrical shells loaded by normal pressures uniformly distributed along a range of the generatrix.

Fig. 2 shows the distribution of the plastic zones over the meridional cross section of a cylindrical shell. A completely plastic state throughout the thickness of the shell may be set up along a range of the generatrix. This is an important feature distinguishing this problem from that of the bending of beams; for in the bending of beams a completely plastic state may arise only at points on the axis of the beam and not throughout a range.

The author (21) has investigated the elastico-plastic state in a

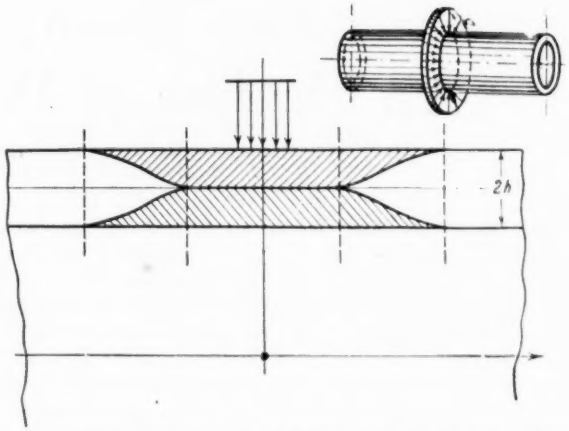


Fig. 2 Distribution of Plastic Zones in Wall of Cylindrical Shell

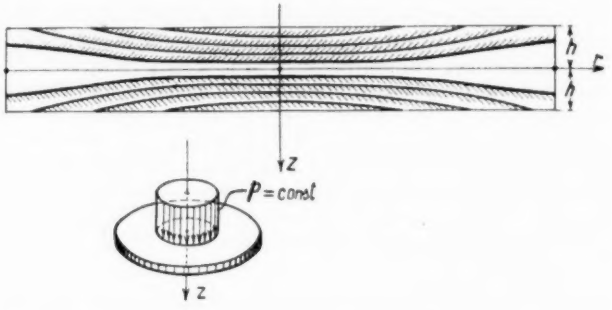


Fig. 3 Successive Expansion of Plastic Zones in Circular Plate

circular plate of radius a, subjected to the action of a rotationally symmetric distribution of an arbitrary load.

Fig. 3 shows the successive growth and expansion of the plastic zones through the thickness of the plate in a meridional cross section due to an increase of a uniformly distributed load over the surface of the plate p = constant.

When

$$p = 6.58\, \sigma_s \frac{h^2}{a^2}$$

($2h$ = plate thickness, a = radius of plate, σ_s = yield stress in tension) a pure plastic state (a completely plastic state throughout the thickness of the plate) arises at the center, and simultaneously the entire plate passes into a pure plastic state. The same phenomenon takes place when the load is distributed over any one of the concentric circles of the plate. This is an interesting feature distinguishing this problem from that of the bending of beams, for the rise of a pure plastic state at one point of the beam does not induce a pure plastic state throughout the beam.

Fig. 4 represents the relationship between the value of the deflection f in the center of the plate and the value of the increasing load p.

A. Ilyushin obtained the finite relationship between the stress resultants T_α, T_β, S and moments M_α, M_β, H for a completely plastic state of a shell. This condition arises out of the Mises condition of plasticity and may be expressed in terms of two parameters.

This finite relationship between resultants of stress and moments may be applied to the solution of problems of the com-

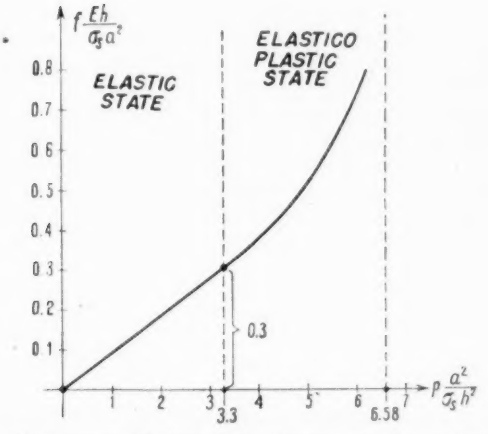


FIG. 4 DEFLECTION VERSUS LOAD CURVE FOR PLATE SHOWN IN FIG. 3

pletely plastic state by means of the methods of the calculus of variations.

In the particular case of rotationally symmetric deformations without axial stretching, the resulting formulas take the form

$$T_\alpha = \pm \frac{\sqrt{\xi}}{2} \ln \frac{\sqrt{1+\xi}+1}{\sqrt{1+\xi}-1}$$

$$M_\alpha = \pm \frac{2}{\sqrt{3}} \left(\sqrt{1+\xi} - \frac{\xi}{2} \ln \frac{\sqrt{1+\xi}+1}{\sqrt{1+\xi}-1} \right)$$

where ξ is a parameter.

These formulas give the relationship between the values of the longitudinal stress resultant T_α and the bending moment M_α in case of a pure plastic state of a shell.

Stability of compressed bars beyond the limit of elasticity was investigated by Th. von Kármán in 1909. Von Kármán's formula for plasticity with linear strain-hardening gives the following value for the critical length l_{cr} of the bar (beyond which the bar loses its stability) beyond the limit of elasticity

$$l_{cr} = i\pi \sqrt{\frac{K}{\sigma}}, \qquad K = \frac{4EE_1}{(\sqrt{E}+\sqrt{E_1})^2}$$

where K is the so-called von Kármán or reduced modulus of buckling, E is the modulus of elasticity, and E_1 is the modulus of linear strain-hardening (i is an integer).

For the case of ideal plasticity, $E_1 = 0$, the critical length of the bar is equal to zero

$$l_{cr} = 0$$

A. Ilyushin (6) investigated the stability of plates and shells beyond the limits of plasticity; his starting point was the Mises-Hencky theory of plasticity and the law of unloading. For the sake of simplicity the material was assumed as incompressible in both the elastic and plastic zones (Poisson's ratio $\nu = 1/2$).

Loss of stability lies in the fact that for certain magnitudes of the external forces, besides the initial state of equilibrium, another state of stress

$$\sigma_\alpha + \delta\sigma_\alpha, \sigma_\beta + \delta\sigma_\beta, \tau_{\alpha\beta} + \delta\tau_{\alpha\beta}, \epsilon_\alpha + \delta\epsilon_\alpha, \epsilon_\beta + \delta\epsilon_\beta, \gamma_{\alpha\beta} + \delta\gamma_{\alpha\beta}$$

becomes possible and that (excluding eccentrically applied loads) the transition from the first state into the second occurs with no change of forces.

If the plate is in a pure plastic state prior to loss of stability, then after loss of stability, generally speaking, two zones form throughout the thickness of the plate; in one of them loading will continue and it will remain plastic, and in the other unloading will begin and it will become elastic. On the boundary between these two zones the intensity of the shearing deformation is constant.

A. Ilyushin expresses the increments of the moments and forces in terms of the deflection of the middle surface of the plate and derives the basic differential equation of stability, which is a generalization of Bryan's equation for elastic cases. He investigated a number of interesting particular cases of stability, among them the case of instability of a rectangular plate with two free edges compressed by a load uniformly distributed along the two other edges.

It is interesting to note that if a material with ideal plasticity is assumed, the calculation proves the existance of a plastic zone only in the plate after loss of stability (the elastic zone vanishes). It was found that the critical length of the plate is not zero but, when $2h$ is the thickness of the plate, is equal to

$$l_{cr} = \frac{\pi}{3} h \sqrt{\frac{E(1-\psi)}{\sigma_s}}$$

where σ_s is the yield stress, and ψ is a variable, increasing in the process of flow from 0 to 1. At the beginning of flow $\psi = 0$, and the critical length will be one half of the corresponding critical length in the elastic state.

The application of this theory to shells made it possible to investigate the rotationally symmetric case of the stability of a circular cylindrical shell compressed by external pressure and an axial force.

Mention must also be made of simpler elastico-plastic problems. Among these are the cases of plastic equilibrium of a hollow sphere, of a hollow cylinder, and the torsion and simultaneous stretching of a circular bar. These problems, which have wide practical application, were studied by Smirnov-Alayev (16), N. Belayev (2), and the author (20).

In solving these problems, the Mises-Hencky theory was employed, under the assumption of the incompressibility of the plastic material. This assumption has a strong influence upon the value of the displacements and does not permit satisfying completely the conditions of the continuity of all the components of stress and displacements on the boundary between the elastic and the plastic zones.

An objective of recent work is to avoid these defects of the theory. This requires employing the exact theory of Mises-Hencky by taking into consideration the compressibility of the material in both the elastic and the plastic zones.

The method evolved for the solution of this problem may be applied to the condition of ideal plasticity of Mises-Hencky or to the Schmidt condition of strain-hardening of the material. The solutions of these problems are given either in closed form or reduced to one of the usual nonlinear equations of the first order.

PLASTIC STATE OF PLANE STRAIN AND PLANE LIMITING STATE OF EQUILIBRIUM OF A SOIL

The starting point for the theory of the plastic state of plane strain (strain $\epsilon_z = 0$) may be the Saint Venant theory of plasticity or the Mises-Hencky theory; while the starting point for the theory of the limiting cases of equilibrium in loose materials may be Koetter's equation.

The condition of plasticity, according to the Saint Venant and the Mises-Hencky theories, has the form

$$(\sigma_x - \sigma_y)^2 + 4\tau_{xy}^2 = 4k^2 \quad \ldots\ldots\ldots\ldots [1]$$

where for the Saint Venant theory $k = \sigma_s/2$ and for the Mises-Hencky theory $k = \sigma_s/\sqrt{3}$ where σ_s = yield stress for tension.

The condition of limiting equilibrium, according to the Koetter theory, is

$$(\sigma_x - \sigma_y)^2 + 4\,\tau_{xy}^2 = \sin^2\rho(\sigma_x + \sigma_y + 2\,k\,\operatorname{ctg}\rho)^2 \ldots [2]^6$$

where ρ is the angle of internal friction and k is the coefficient of cohesion.

The two equations of equilibrium

$$\frac{\partial\sigma_x}{\partial x} + \frac{\partial\tau_{xy}}{\partial y} = X, \quad \frac{\partial\tau_{xy}}{\partial x} + \frac{\partial\sigma_y}{\partial y} = Y \ldots\ldots\ldots [3]$$

together with conditions of Equation [1] or [2], comprise a system of three equations for determining the three unknowns σ_x, σ_y, and τ_{xy}.

The system of Equations [1] and [2] has been investigated by a number of scientists, among them M. Levy, H. Hencky, L. Prandtl, H. Reissner, H. Geiringer, W. Prager, A. Nadai, and S. Christianovich. These equations belong to the hyperbolic type and hence possess two families of characteristics (lines of slip) which are orthogonal curves in the x, y-plane. Equations [1] and [3] may be reduced to two linear canonic equations (if both families of characteristics are curvilinear), or, as was shown by S. Christianovich, have integrals with an arbitrary function (if one of the families of the characteristics consists of straight lines).

Continuing the interesting work of Geiringer and Prager, Christianovich (24) solved the boundary-value problem for the distribution of stresses in the plastic zones outside and within a closed contour, assuming that the stresses are given along this contour. The problem can be reduced to the Cauchy boundary-value problem for the canonic equations mentioned, for given values along a segment of a curve in certain auxiliary planes represented by means of the characteristic curves.

For obtaining numerical solutions to these boundary problems of Christianovich and of the theory of loose materials, the Massot method was employed in which the solution of the corresponding equations is reduced to defining the magnitude of the functions sought in a finite number of the points of intersection of the characteristics. In addition a number of important theorems on the properties of these solutions were derived.

The system for Equations [2] and [4] was set up by Koetter and investigated by Nadai, H. Reissner, and the author (19). It belongs to the hyperbolic type of equation and possesses two families of characteristics (curves of slip) intersecting each other in the x, y-plane at constant angles. The equations mentioned may also be reduced to the so-called canonic form.

The problem of the pressure of a loose soil on a retaining wall was investigated by Th. von Kármán for the case of a vertical retaining wall. The angle of friction between the wall and the soil is equal to the angle of internal friction of the soil. The author (19) has developed a general method of solving the basic problems of limiting equilibria in soils.

The particular feature of these problems is the presence of angular points on the contour and the discontinuity of the boundary stresses at certain points, which prevents the direct application of the Christianovich method.

This obstacle may be avoided by introducing solutions having particular points, each of which has a corresponding range of characteristics in the plane of the characteristics. The problem of limiting equilibrium of a soil may now be reduced to various combinations of boundary-value problems (the Cauchy, the Riemann, and the so-called mixed boundary-value problem) for a canonic system of equations, to which Koetter's equation may be reduced. A number of problems of the theory of a soil[7] will be examined, including the retaining wall, the stability of slopes and grounds under foundations, and the pressure of the ground between parallel walls.

As an illustration let us consider the Prandtl-Reissner generalized problem of a soil with a horizontal boundary which is taken as the x-axis. Determine the minimum normal stresses q along the negative x-axis so that the soil is in a limiting equilibrium under the action of the stresses $\sigma_y = p(x)$ and $\tau_{xy} = t(x)$, which are given along the positive x-axis. Fig. 5 represents the distribution of the characteristics (lines of slip) and the distribution of stresses along the negative x-axis. The determination of the net of characteristics and of the state of stress in the domains OAB, OBC, and OBD raises the Cauchy, Riemann, and mixed problems, respectively, for the canonic system of equations in the auxiliary plane of the characteristics. The solution in the domain OBC has the singular point O. The sought load q_0 at the point O can be expressed in closed form (for $k = 0$)

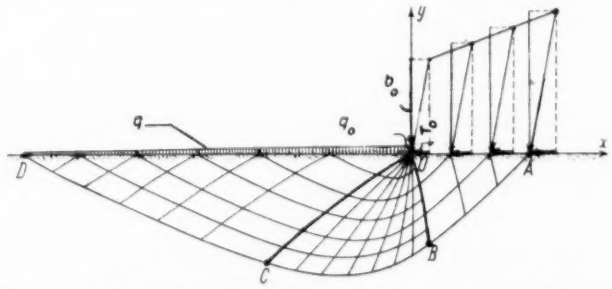


FIG. 5 SLIP PLANES AND STRESSES IN A SOIL SUBJECTED TO NORMAL AND SHEARING LOADS

$$q_0 = p_0 \frac{1 - \sin\rho}{\cos^2\mu[1 + \cos\rho \cdot \sqrt{\operatorname{tg}^2\rho - \operatorname{tg}^2\mu}]} e^{\left\{-\left[\pi+\mu+\arcsin\frac{\sin\mu}{\sin\rho}\right]\operatorname{tg}\rho\right\}}$$

where

$$\operatorname{tg}\mu = t_0/p_0, \quad p_0 = p(0), \quad t_0 = t(0)$$

The problem of the stability of the slope may be taken as another illustration of the foregoing. Let the normal pressure along the positive x-axis be given; find the form of the surface slope for a state of limiting equilibrium of a soil.

Fig. 6 shows the distribution of the characteristics and the form of the curve[8] bounding the slope. The state of stress in the domain OAB is given in closed form; where the characteristics (lines of slip) are two families of parallel straight lines. The determination of the net of characteristics and of the state of stress in the domains OBC and OBD raises the Riemann and mixed problems, respectively, for the canonic system of equations in the auxiliary plane of the characteristics. The solution in the domain OBC has the singular point O. Incidentally, the slope of the curve at the point O may be given in finite form.

For the case of a soil with ideal cohesion $\rho = 0$, the foregoing problem may be solved in finite form. The slope profile is given by the formula

$$x = \frac{2k}{\gamma} \ln \frac{\cos\left(\frac{p}{2k} - 1 - \frac{\gamma}{2k}\,y\right)}{\cos\left(\frac{p}{2k} - 1\right)} \ldots\ldots\ldots [4]$$

[6] In Equation [2], the European notation "ctg" ρ is used which is equivalent to "ctn" ρ in American usage. In succeeding equations, "tg" is equivalent to "tan;" arcsin $\{-\}$ is the same as $\sin^{-1}\{-\}$, etc.

[7] Of course it is supposed that the volume forces (weight of soil) are taken into consideration.

[8] For this problem, the line of repose appears to be similar to a straight line, but usually it has sufficiently large curvature.

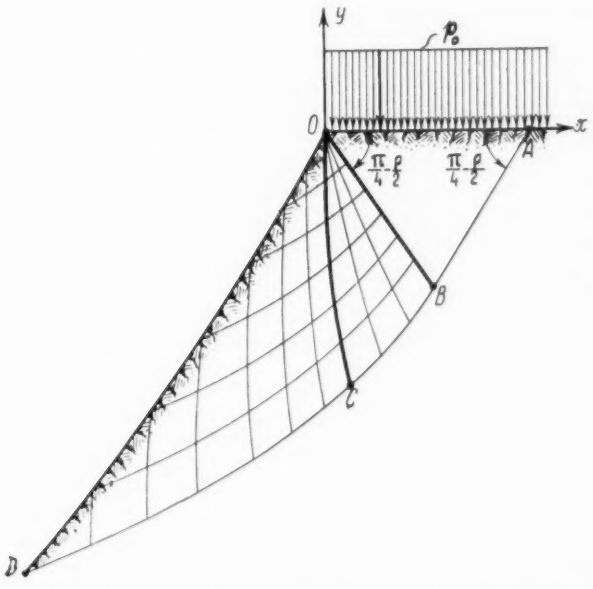


FIG. 6 SLIP PLANES IN A SLOPING SOIL SUBJECTED TO NORMAL LOADS ON PLATEAU

where γ is the weight per unit of volume.

A new problem (19) has been submitted for a limiting equilibrium of an anisotropic stratified medium, whose angle of internal friction $\bar{\rho}$ and coefficient of cohesion $\bar{k}$ over the horizontal planes $y = \text{const}$ are less than the angle of internal friction ρ and the coefficient of cohesion k over other planes

$$\bar{\rho} < \rho, \quad \bar{k} < k$$

The conditions of limiting equilibrium of a stratified soil may be expressed by the following equations

$$(\sigma_x - \sigma_y)^2 + 4\,\tau_{xy}^2 = \sin^2\rho\,(\sigma_x + \sigma_y + 2\,k\,\operatorname{ctg}\rho)^2 \ldots [5]$$

when

$$|\tau_{xy}| \leqq \sigma_y \operatorname{tg}\bar{\rho} + \bar{k}$$

and

$$|\tau_{xy}| = \sigma_y \operatorname{tg}\bar{\rho} + \bar{k} \ldots\ldots\ldots\ldots\ldots [6]$$

when

$$(\sigma_x - \sigma_y)^2 + 4\,\tau_{xy}^2 \leqq \sin^2\rho\,(\sigma_x + \sigma_y + 2k\,\operatorname{ctg}\rho)^2$$

Equation [5] coincides with the condition of the limiting equilibrium for an isotropic medium, while Equation [6] is valid for an isotropic stratified medium.

Employing these equations, various problems of the limiting equilibrium of a stratified medium may be solved.

In considering, for example, the Prandtl generalized problem, three zones must be distinguished in the soil. In these zones the limiting equilibrium is described by Equations [5] and [6]. The boundary between these zones is sought and must be determined in the process of the solution of the problem. For the sake of brevity, we shall limit ourselves to presenting the finite formula for the value q_0 at the point

$$0 \text{ (when } k = \bar{k} = 0,\ t = 0)$$

$$q_0 = p_0 \frac{(1 - \sin\rho)\,[\cos\bar{\rho} - \sqrt{\sin^2\rho - \sin^2\bar{\rho}}]}{(1 + \sin\rho)\,[\cos\bar{\rho} + \sqrt{\sin^2\rho - \sin^2\bar{\rho}}]}\, e^{\left\{-2\operatorname{tg}\rho\,\arcsin\frac{\sin\bar{\rho}}{\sin\rho}\right\}}$$

$p_0 - q_0$ is the value of the discontinuous drop of the normal boundary stresses at the point 0.

The comparison of this formula with the corresponding formula for the isotropic medium $\bar{\rho} = \rho$ shows that the magnitude q_0 for the stratified medium is larger than the corresponding magnitude for the isotropic medium, which is also obvious from physical considerations.

Further applications of methods developed in the theory of soils to plastic states of plane strain make it possible to consider a number of problems raised by H. Hencky and L. Prandtl.

As an illustration, we shall give a simple finite formula which occurs in the problem of driving a rough-surfaced circular punch of radius a into a plastic body (the maximum force of friction being constant and equal to τ). The value of the force P is related to the angle γ by the formulas, Fig. 7

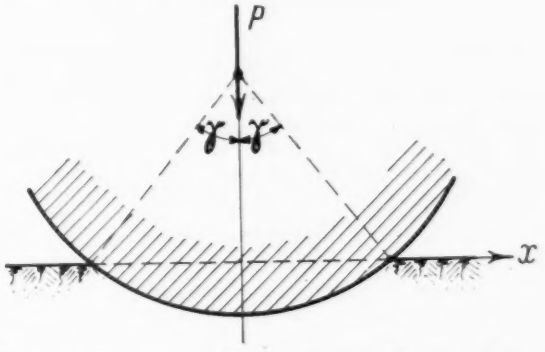


FIG. 7 INDENTATION OF PLASTIC BODY BY CIRCULAR PUNCH

for $2\gamma \leq \arcsin t$

$$\frac{P}{ka} = 2\,(\pi + 2)\sin\gamma$$

for $2\gamma \geq \arcsin t$

$$\frac{P}{ka} = 2\,(\pi + 2)\sin\gamma_* + 2\,(\sin\gamma - \sin\gamma_*)\,(\pi + 1 + \arcsin t + \sqrt{1 - t^2}) - 4\,(\gamma\sin\gamma - \gamma_*\sin\gamma_* + \cos\gamma - \cos\gamma_*) + 2t\,(\cos\gamma_* - \cos\gamma)$$

where

$$2\,\gamma_* = \arcsin t, \quad t = \frac{\tau}{k}$$

More complex problems may also be solved, for example, compression of a plastic strip of finite length between two rough-surfaced parallel plates.[9]

The important problem of the rolling of metals was raised by Th. von Kármán and further investigated by A. Nadai. The problem was further developed in Russia by C. Shevchenko, who considered this problem as a plane problem of the theory of plasticity. He found the distribution of the stresses throughout the thickness of the strip.

A few words may be said in conclusion concerning the axially symmetric problem investigated by A. Ishlinsky. It is known that the axially symmetric problem becomes statically determinable after assuming that not a condition of plasticity is considered according to Saint Venant or Mises, but a "completely plastic" body is postulated, according to Haar and von Kármán, in which the two principal shearing stresses in every point are equal to the constant of plasticity.

[9] Prandtl solved the same problem for strips of infinite length.

This problem was first considered by Hencky. A detailed investigation of the equations was carried out by A. Ishlinsky (10), who solved the problem of driving a ball into a plastic body (Brinell hardness test). The ratio between σ_s and H_B has the order

$$\frac{\sigma_s}{H_B} \approx 0.38$$

(σ_s = yield stress for compression, H_B = Brinell hardness.)

Experimental results obtained in driving steel balls into zinc and lead gave

$$\frac{\sigma_s}{H_B} \approx 0.34 - 0.36$$

Plastic States of Plane Stress

The starting point for the theory of the plastic states of plane stress may be either the Saint Venant or the Mises theory of plasticity. We shall consider both of these theories, investigated by the author (22, 23).

The Saint Venant condition of plasticity assumes that the maximum shearing stress is constant

$$|\tau|_{max} = \frac{1}{2}\sigma_s$$

For a state of plane stress ($\sigma_3 = 0$) this condition is presented in two forms, depending on the signs of the two principal stresses σ_1, σ_2 which are not equal to zero.

If σ_1 and σ_2 have different signs, i.e., $\sigma_1\sigma_2 \leqq 0$, the maximum shearing stress acts in planes parallel to the z-axis, and

$$|\tau|_{max} = \frac{1}{2}|\sigma_1 - \sigma_2|$$

If σ_1 and σ_2 have the same signs, i.e., $\sigma_1\sigma_2 > 0$, the maximum shearing stress acts in planes inclined to the z-axis at angles $\pi/4$ and

$$|\tau|_{max} = \frac{1}{2}|\sigma_1|, \quad (|\sigma_1| > |\sigma_2|)$$

In terms of the components of stress σ_x, σ_y, τ_{xy}, these conditions of plasticity may be presented in the form of the following equations

$$(\sigma_x - \sigma_y)^2 + 4\tau_{xy}^2 = 4k^2 \quad \ldots\ldots [7]$$

for

$$\sigma_x\sigma_y \leq \tau_{xy}^2$$

and

$$\sigma_x\sigma_y - \tau_{xy}^2 = \sigma_s(|\sigma_x + \sigma_y| - \sigma_s) \quad \ldots\ldots [8]$$

for

$$\sigma_x\sigma_y \geq \tau_{xy}^2$$

where

$$k = \sigma_s/2$$

The first of these equations coincides with the condition of plasticity for the state of plane strain (strain $\epsilon_z = 0$), while the second occurs only for a state of plane stress ($\sigma_3 = 0$).

The Huber-Mises condition of plasticity substitutes for the two conditions Equations [7] and [8], one equation

$$\sigma_x^2 + \sigma_y^2 - \sigma_x\sigma_y + 3\tau_{xy}^2 = \sigma_s^2 \quad \ldots\ldots [9]$$

The equations of equilibrium

$$\frac{\partial\sigma_x}{\partial x} + \frac{\partial\tau_{xy}}{\partial y} = 0, \qquad \frac{\partial\tau_{xy}}{\partial x} + \frac{\partial\sigma_y}{\partial y} = 0 \quad \ldots\ldots [10]$$

must also be satisfied.

We note that the system of Equations [7] and [10], if the constant is taken equal to $k = \sigma_s/\sqrt{3}$, coincides with the system of equations describing the plastic state of plane strain, according to the Mises theory. Consequently, a case of plane stress of Saint Venant is identical with a case of plane strain of Mises, provided that

$$\sigma_x\sigma_y < \tau_{xy}^2 \text{ and } k = \sigma_s/\sqrt{3}$$

The system of Equations [8] and [10] may be integrated in finite form. The integrals contain two arbitrary functions. The characteristics are a family of straight lines in the x, y-plane.

The system of Equations [9] and [10] may belong either to the hyperbolic or to the elliptic type, depending upon the character of the state of stress.[10]

When these equations are of the hyperbolic type, they have two families of characteristics intersecting at variable angles. Equations [9] and [10], in the domain where they are hyperbolic, may be reduced to a system of two linear equations, canonic equations (if both families of characteristics are curvilinear), or permit of integrals with an arbitrary function (if one of the families of characteristics consists of straight lines).

Our first illustration (23) is the problem of a plate with an aperture, along whose contour distributed stresses are applied, the plate being stretched by distributed forces at infinity. This problem may be solved either according to the Saint Venant or the Mises theory of plasticity.

In the particular case of a circular hole of radius a with an axially symmetric distribution of stresses, the solution of the problem can be obtained in finite form.

As an illustration, Fig. 8 shows the pattern of the characteristic curves, constructed according to the theory of Saint Venant for an inner pressure ($\sigma_r < 0$). The plastic ring domains $a \leq r < c$ and $c < r < \infty$ are zones in which the systems of Equations [7],

[10] Roughly speaking, Equations [9] and [10], in the domain where they are hyperbolic, correspond to Equations [7] and [10], and in the domain where they are elliptic to Equations [8] and [10].

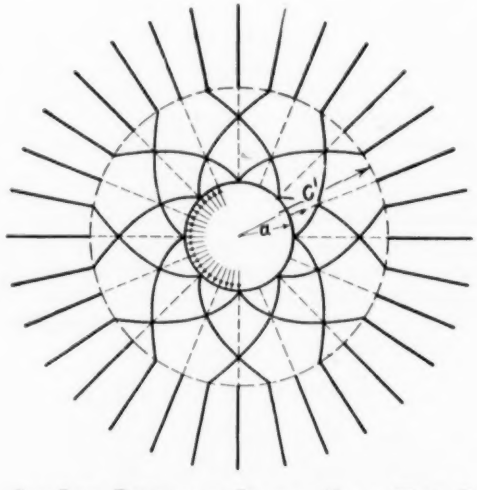


Fig. 8 Slip-Line Pattern in Infinite Plate With Circular Hole
(Saint Venant theory of plasticity.)

[10], and [8], [10] hold, respectively. The boundary between these zones is a circle of radius c.

Fig. 9 shows the form of the characteristic curves constructed according to the Mises theory,[11] also for the same value of the

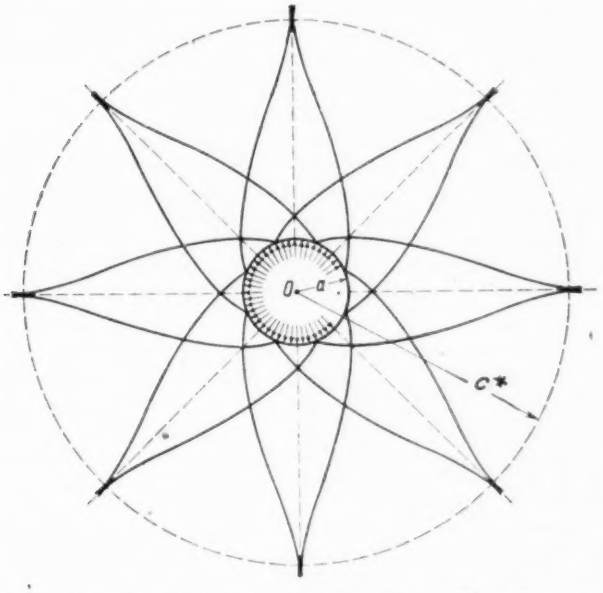


FIG. 9 SLIP-LINE PATTERN IN INFINITE PLATE WITH CIRCULAR HOLE
(Mises theory of plasticity.)

pressure, $\sigma_r < 0$. The plastic ring domains $a \leq r < c^*$ and $c^* < r < \infty$ are hyperbolic and elliptic zones for the system, Equations [8] and [10], respectively. The boundary between these zones is a circle of radius c^*.

Fig. 10 shows the case where internal pressure is absent $\sigma_r = 0$. The solid lines show the distribution of stresses according to the

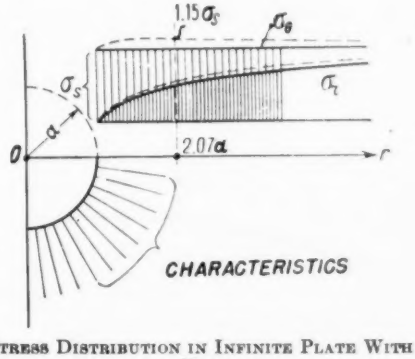


FIG. 10 STRESS DISTRIBUTION IN INFINITE PLATE WITH CIRCULAR HOLE

theory of Saint Venant, while the broken lines show the distribution of stresses according to the theory of Mises.

The states mentioned require uniformly distributed stresses of equal intensity in all directions

$$\sigma_r = \sigma_\theta = \sigma_s$$

at infinity.

In the general case of an arbitrary noncircular aperture, the problem may also be solved.

[11] The solution of this problem according to the Mises theory of plasticity belongs to A. Nadai.

Fig. 11 illustrates two regions of the characteristics outside an elliptic aperture, along the contour of which a uniformly distributed normal pressure is applied $\sigma_n < 0$, $\tau_{ln} = 0$, the calculation being made according to the theory of plasticity of Saint Venant.

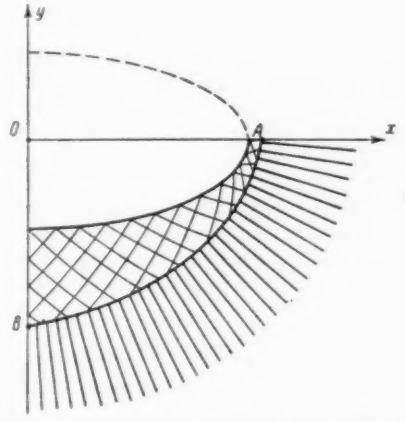


FIG. 11 SLIP-LINE PATTERN IN INFINITE PLATE WITH ELLIPTICAL HOLE
(Saint Venant theory of plasticity.)

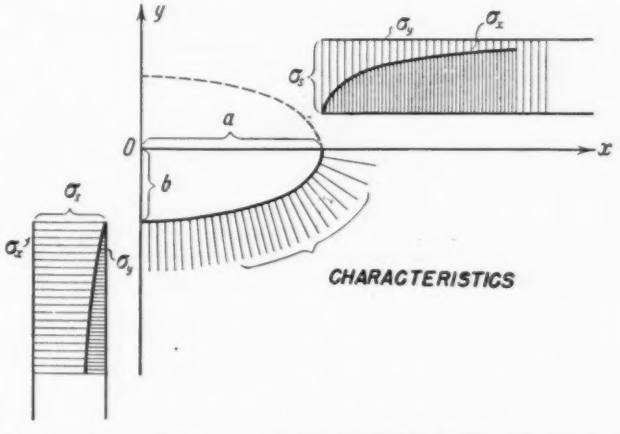


FIG. 12 STRESS DISTRIBUTION IN INFINITE PLATE WITH ELLIPTICAL HOLE

It will readily be seen that near the elliptic aperture the state of stress is described by Equations [7] and [10]; while at a distance from it, it is defined by Equations [8] and [10]. The net of the characteristics and the stress components near the aperture, where the characteristics are two families of curves, were determined by the Christianovich method. The net of the characteristics and the stress components at a distance from the aperture, where the former ones consist of straight lines, may be determined by defining the arbitrary function of the corresponding integrals (the solution may be given in finite form). The conditions of continuity of all the components of stress make it possible to determine the boundary curve between the two zones.

Fig. 12 illustrates the case of absence of internal pressure $\sigma_n = \tau_{ln} = 0$. The characteristics are normal to the contour, and the problem may be solved in finite form. The following formulas for the stresses along the x-axis and y-axis are given as illustrations:

Along the x-axis

$$\sigma_x = \sigma_s\left(1 + \frac{b^2}{a^2 - b^2 - a\,|x|}\right), \quad \sigma_y = \sigma_s, \quad \tau_{xy} = 0$$

and along the y-axis

$$\sigma_x = \sigma_s, \quad \sigma_y = \sigma_s\left(1 - \frac{a^2}{a^2 - b^2 + b\,|y|}\right), \quad \tau_{xy} = 0$$

where a and b are the semiaxes of the elliptical contour.

The foregoing distribution of stress requires the uniform stresses

$$\sigma_x = \sigma_y = \sigma_s, \quad \tau_{xy} = 0$$

at infinity.

As a second illustration (23), we may mention the problem of the distribution of stresses in a strip of material drawn through a fixed rigid die; the angle between the inclined sides of the die is equal to 2γ. The maximum force of friction between the die and the plastic strip is assumed to be constant and equal to τ. It is assumed that at the narrow end of the die cross section, $x = 0$

$$\sigma_x = p = \text{const}, \quad \tau_{xy} = 0, \quad \sigma_y < \sigma_x$$

Incidentally, any other assumption might have been made as to the distribution of stresses σ_x over the cross section $x = 0$. This would have significance only at the narrow butt end of the die. Therefore, in solving the problem according to the Saint Venant theory, the interesting closed solution for a wedge suggested by A. Nadai may also be employed.

Figs. 13 and 14 show the pattern of the characteristics in the plastic strip and the distribution of the pressures along the contact line, which are determined according to the theories of Saint Venant and Mises. The net of characteristics and stress components in the domains ABC, $CDEF$, ... where one of the families of characteristics is composed of straight lines, may be determined by defining the arbitrary functions of the corre-

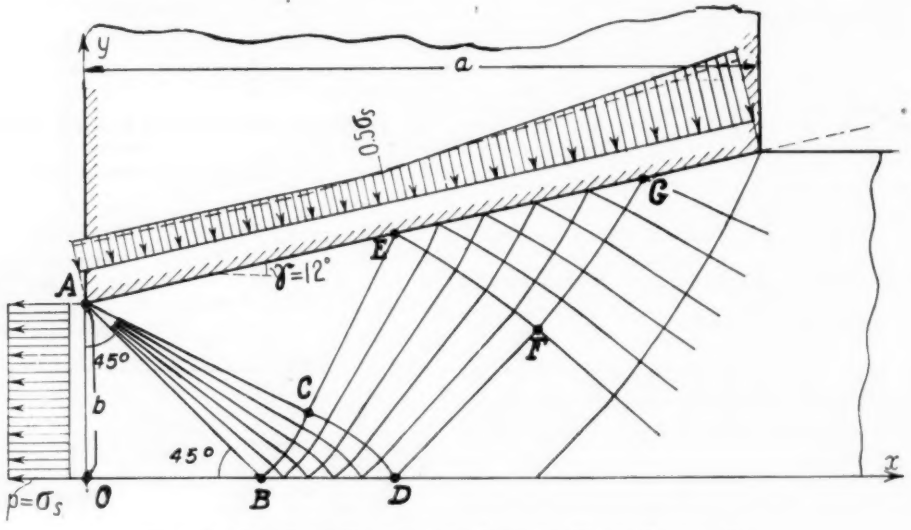


FIG. 13 SLIP-LINE PATTERN FOR STRIP IN WEDGE-SHAPED DIE
(Saint Venant theory of plasticity.)

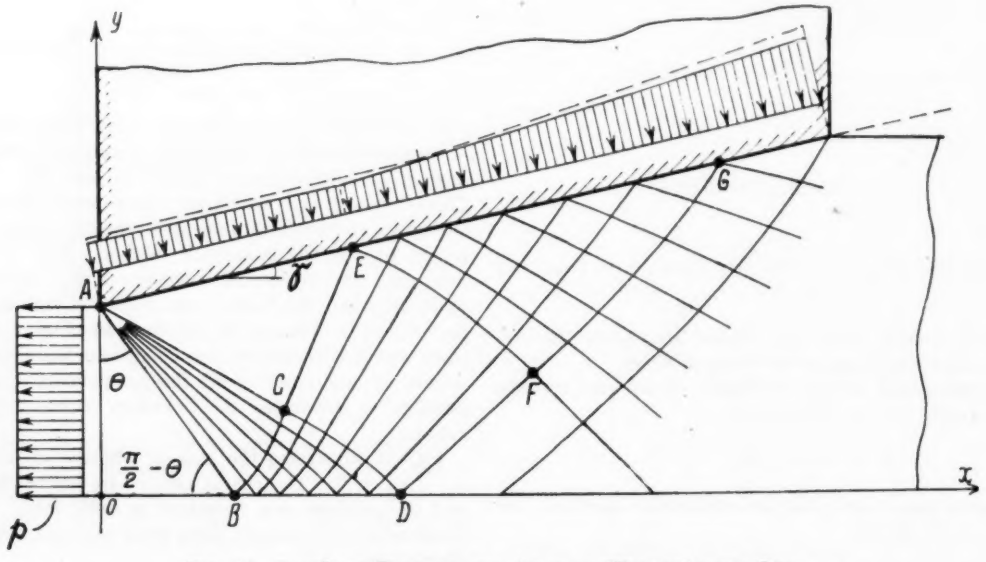


FIG. 14 SLIP-LINE PATTERN FOR STRIP IN WEDGE-SHAPED DIE
(Mises theory of plasticity.)

sponding integrals for the equations of plasticity (the solution is obtained in closed form). The net of characteristics and stress components in the domains *BCD*, *EFG*, ... where both families of the characteristics are curvilinear may be determined by solving the mixed boundary problems for the corresponding canonic equations (the calculation being made according to the approximate method of Massot). The drawing stresses p over the cross section O–A may be found from the conditions of equilibrium

$$pb = -\text{tg}\ \gamma \int_0^a \sigma_n\, dx + \tau a$$

where a is the length of the die, $2b$ is the thickness of the strip after drawing, γ the angle of inclination of the die, σ_n the normal stress, and τ = const the friction along the contact surface.

It is interesting to note that the net of the characteristic curves in the Saint Venant theory does not depend on the parameter p, while the net of the characteristics according to the Mises theory does depend on p.

The problem of drawing, according to the Saint Venant theory for a state of plane stress (if we will take $k = \sigma_s/\sqrt{3}$), may be treated as the same problem, according to the Mises theory for a state of plane strain. Therefore, comparison of the results may offer a conception of the differences resulting in the investigation of an infinitely wide and of a very thin strip.

The difference between the pressures along the contact lines can be seen from a comparison of the solid and the broken pressure lines in Figs. 13 and 14.

The solution of the problem of the elastico-plastic torsion of a cylindrical bar of an oval cross section, bounded by the contour

$$x = [a + b\,(\cos 2\alpha + 2)]\sin\alpha, \quad y = -[a + b\,(\cos 2\alpha - 2)]\cos\alpha, \qquad \text{for } b/a \leq 1/3$$

(where α is the slope of the contour toward the x-axis; this contour approaches an ellipse with semiaxes $a + b$ and $a - b$) was the subject of a previous investigation by the author (18).

The state of stress in the bar is described by the equation of equilibrium

$$\frac{\partial \tau_{xz}}{\partial x} + \frac{\partial \tau_{yz}}{\partial y} = 0$$

and by the equation

$$\frac{\partial \tau_{yz}}{\partial x} - \frac{\partial \tau_{xz}}{\partial y} = 2G\theta$$

in the elastic zone, where θ is the angle of twist per unit of length; and by the condition of plasticity

$$\tau_{xz}^2 + \tau_{yz}^2 = k^2$$

in the plastic zone. The components of stress and displacement are continuous on the boundary between the elastic and plastic zones.

The solution of this problem was obtained in finite form. The formula for the torque M, depending on the angle of twisting, is

$$|M| = \frac{2\pi}{3} ka^3 \left[1 - \frac{1}{8\Theta^3} - \frac{9}{2}\beta^2 - \frac{1}{2\Theta}\left(\frac{1}{4\Theta^2} - 2\beta^2\right)\sqrt{1 + 16\,\beta^2\Theta^2}\right]$$

The formula holds for

$$\Theta \geq \frac{1 - \beta}{(1 + \beta)(1 - 3\beta)}$$

where

$$\Theta = \frac{Ga}{k}|\theta|, \quad \beta = b/a$$

The well-known formula for a circular cylindrical bar follows from this formula as a particular case, if $\beta = 0$.

Fig. 15 shows one quarter of the oval cross section. The contour of this oval, shown by the solid line, differs but little from the ellipse, shown by the broken line. The distorted surface of the initially plane cross section after twisting is represented in the figure by means of contour lines. The co-ordinates of these curves may be calculated from finite formulas for given axial displacements.

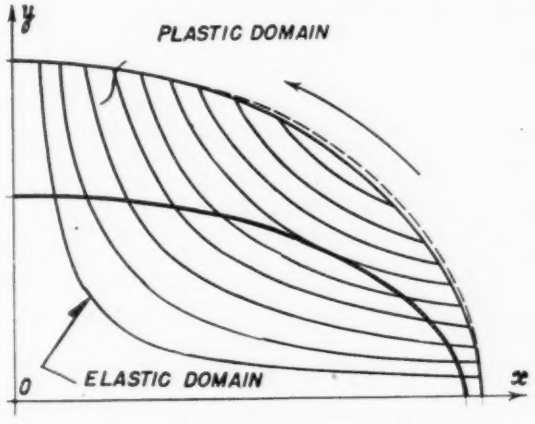


FIG. 15 TORSION OF ELLIPTICAL BAR

Using complex variables, I. Galin has solved the problem of the elastico-plastic torsion of a cylindrical bar having a polygonal cross section. As an example, the calculation was carried out in detail for a bar of square cross section.

The shapes of the plastic zones which were obtained by this calculation were closely similar to those which were observed by the sand-heap torsion analogy of A. Nadai.

BIBLIOGRAPHY

1 "Theory of Plastic Deformation," by N. M. Belayev, Bulletin of the Academy of Sciences of U.S.S.R. (to be abbreviated as follows: "Bulletin A.S."), OTN, 1937, no. 1, pp. 49–70.

2 "The Stresses and Deformations in Thick Walled Cylinders in the Elastic and Plastic Condition of the Material," by N. M. Belayev and A. K. Sinitsky, Bulletin A.S., OTN, 1938, no. 2, pp. 3–54, and no. 4, pp. 21–49.

3 "Elastico-Plastic Torsion of Prismatic Bars Having Polygonal Cross Sections," by L. A. Galin, *Journal of Applied Mathematics and Mechanics* (to be abbreviated as follows: J.o.A.M.a.M.), Moscow, vol. 8, no. 4, 1944.

4 "Deformation of Plastico-Viscous Materials," by A. A. Ilyushin, Scientific Notes of the State University in Moscow, U.S.S.R. issue 39, 1940.

5 "Some Problems of the Theory of Plasticity," by A. A. Ilyushin, J.o.A.M.a.M., vol. 7, no. 4, 1944.

6 "Stability of Plates and Shells Beyond the Limit of Elasticity," by A. A. Ilyushin, J.o.A.M.a.M., vol. 8, no. 5, 1944.

7 "Finite Relations Between the Forces and Moments and Their Relation to the Deformation in the Theory of Shells," by A. A. Ilyushin, J.o.A.M.a.M., vol. 9, 1945, no. 1, pp. 101–110.

8 "Stability of the Plastico-Viscous Flow of a Round Bar," by A. Ishlinsky, J.o.A.M.a.M., vol. 7, 1943, no. 2, pp. 109–130.

9 "Stability of the Plastico-Viscous Flow of a Circular Plate," by A. Ishlinsky, J.o.A.M.a.M., vol. 7, 1943, no. 6, pp. 405–412.

10 "The Axially Symmetric Problem of Plasticity and the Brinell Hardness Test," by A. Ishlinsky, J.o.A.M.a.M., vol. 8, 1944, no. 3, pp. 201–224.

11 "Equations of Deformation of Nonelastic and Plastico-Viscous Bodies," by A. Ishlinsky, Bulletin A.S., OTN, nos. 1 and 2, 1945.

12 "Deformations in Space of Nonelastic and of Plastico-Viscous Bodies," by A. Ishlinsky, Bulletin A.S., OTN, no. 3, 1945.

13 "Concerning the Mechanics of Plastic Solids," by L. M. Kachanov, Bulletin J.o.A.M.a.M., vol. 4, 1940, no. 3, pp. 37–42.

14 "Elastico-Plastic Conditions of Hard Bodies," by L. M. Kachanov, J.o.A.M.a.M., vol. 5, 1941, no. 3, pp. 431–438.

15 "Principles of Variation for Elastico-Plastic Solids," by L. M. Kachanov, J.o.A.M.a.M., vol. 6, 1942, nos. 2–3, pp. 187–196.

16 "Theory of the Distribution of Stresses Produced by the Flash Welding of Cylinders," by G. Smirnov and G. A. Alayev (Book), 1940.

17 "Problem of the Propagation of Plastic States," by I. L. Sobolev; papers of the Seismologic Institute of the Academy of Sciences of U.S.S.R., no. 49, 1935.

18 "On One Problem of the Elastic-Plastic Torsion," by W. W. Sokolovsky, J.o.A.M.a.M., vol. 6, 1942, nos. 2–3, pp. 241–246.

19 "Statics of Loose Materials," by W. W. Sokolovsky (Book,) published by the Academy of Sciences of U.S.S.R., Moscow, 1942.

20 "Elastic-Plastic Equilibrium of a Cylindrical Tube in the Presence of Strain Hardening," by W. W. Sokolovsky, J.o.A.M.a.M., vol. 7, no. 4, 1943.

21 "Elastic-Plastic Bending of a Circular and a Ring-Shaped Plate," by W. W. Sokolovsky, J.o.A.M.a.M., vol. 8, 1944, no. 2, pp. 141–166.

22 "Equations of the Plastic Equilibrium Under Plane Stress Conditions," by W. W. Sokolovsky, J.o.A.M.a.M., vol. 9, 1945, no. 1, pp. 111–128.

23 "Some Problems Concerning the Plane Plastic State of Stress," by W. W. Sokolovsky, vol. 9, no. 3, 1945.

24 "The Plane Problem of the Mathematical Theory of Plasticity for the Case in Which the External Forces Are Given for a Closed Boundary Curve," by C. A. Christianovich, *Mathematical Journal*, vol. 1, 43, no. 4, 1938.

A Velocity-Modified Temperature for the Plastic Flow of Metals

By C. W. MACGREGOR[1] and J. C. FISHER,[2] CAMBRIDGE, MASS.

Based on the work of Eyring and others relating to the creep problem, a velocity-modified temperature is developed for representing by means of a single variable the combined effects of strain rate and temperature on the stress reaction in a tension specimen. Available data are analyzed, indicating that the velocity-modified temperature is equally applicable to the tension test conducted at both slow and rapid rates and to the creep test. The data also indicate that the stress reaction, corresponding to tests at very slow and very rapid rates of deformation, may be found from tension tests at moderate strain rates and appropriately raised or lowered temperatures.

THE effects of different testing temperatures and true strain rates on the stress-strain properties of various metals tested in tension have been reported in an earlier paper (1).[3] Most of the previous investigations referred to therein were devoted to a study of the influence of temperature and speed of testing on the ordinary stress-strain properties as contrasted to the true stress-strain values. In addition an over-all rate of strain between the heads of the testing machine or over a standard gage length was usually employed where rates of strain were measured. Since the gage length changes as the specimen deforms and the rate of strain varies widely along the axis of the test bar when necking occurs, the more commonly used definition of strain rate obtained by dividing the rate of head motion by the initial gage length of the specimen entails certain errors.

This difficulty is overcome by using the true stress-strain approach (1, 2) in which the true strain is $\epsilon = q' = \log_e (A_0/A)$, where A_0 is the original area and A the instantaneous area of the cross section of the specimen. The value of ϵ is the actual strain at the smallest diameter of the specimen where it is deforming most rapidly. The time derivative of the true strain, $\frac{d\epsilon}{dt}$, then defines the true strain rate. This value can be maintained constant during any one test by varying the rate of head motion.

The experiments referred to (1) showed that in the temperature range $-70\ \text{C} \leq T \leq 665\ \text{C}$ and for true strain rates $5 \times 10^{-5}\ \text{sec}^{-1} \leq \dot{\epsilon} \leq 500 \times 10^{-5}\ \text{sec}^{-1}$, the true stress in a tension specimen of S.A.E. 1020 steel depends only on the true strain ϵ and a velocity-modified temperature $T_m = T\left(1 - k \log_e \frac{\dot{\epsilon}}{\dot{\epsilon}_0}\right)$, where T is the absolute testing temperature, $\dot{\epsilon}$ is the constant true strain rate of the test, $\dot{\epsilon}_0$ is taken as $100 \times 10^{-5}\ \text{sec}^{-1}$, and k is a constant. The same was found to be true for S.A.E. 1045 steel and brass over smaller temperature ranges. Expressed symbolically then $S = f(\epsilon, T_m)$. In this manner the stress becomes a function of only two variables instead of a function of the three variables ϵ, $\dot{\epsilon}$, and T.

The principal objects of the present paper are to discuss the velocity-modified-temperature concept in greater detail and to show further evidence of its possible utility over a much wider range of strain rates extending from those found in slow creep tests to those present in rapid tension tests. In order to accomplish this, pertinent creep and rapid tension-test data available in the literature have been analyzed from the velocity-modified-temperature point of view.

The Velocity-Modified Temperature

Based on an absolute reaction-rate approach similar to that used in the problem of viscosity, Eyring (3) has developed a theory for the velocity of plastic flow as a function of temperature and stress. From the same standpoint, an expression for the velocity of secondary creep has been developed by Kauzmann (4) and has been discussed by Dushman, Dunbar, and Huthsteiner (5). At moderate stresses this expression is of the form

$$\frac{\dot{\epsilon}}{\dot{\epsilon}_0} = A \frac{T}{T_0} e^{-\frac{f^*(S)}{T}} \quad \text{.....[1]}$$

where $\dot{\epsilon}$ is the secondary creep rate, T is the absolute temperature, $f^*(S)$ is a function of the applied stress, and $\dot{\epsilon}_0$, A, and T_0 are constants.

Taking natural logarithms of both sides of Equation [1] and rearranging, the equation may be written as

$$T\left(1 - k \log_e \frac{\dot{\epsilon}}{\dot{\epsilon}_0} \frac{T_0}{T}\right) = f_0(S) \quad \text{.....[2]}$$

where $k = 1/\log_e A$ and $f_0(S) = f^*(S)/\log_e A$. Equation [2] indicates that the quantity $T\left(1 - k \log_e \frac{\dot{\epsilon}}{\dot{\epsilon}_0} \frac{T_0}{T}\right)$ is a function of the applied stress. Conversely, the stress is a function of

$$T\left(1 - k \log_e \frac{\dot{\epsilon}}{\dot{\epsilon}_0} \frac{T_0}{T}\right)$$

or

$$S = f\left[T\left(1 - k \log_e \frac{\dot{\epsilon}}{\dot{\epsilon}_0} \frac{T_0}{T}\right)\right] \quad \text{.....[3]}$$

The range of temperatures encountered in investigations of secondary creep is usually small, and the ratio T_{max}/T_{min} is often less than 1.3. In contrast to this, the range of creep rates is large, and the ratio $\dot{\epsilon}_{max}/\dot{\epsilon}_{min}$ is generally between 100 and 1000. When the range of temperatures is small, T_0 can be chosen so that $T_0/T \cong 1$. Making this approximation, Equation [3] reduces to

$$S = f\left[T\left(1 - k \log_e \frac{\dot{\epsilon}}{\dot{\epsilon}_0}\right)\right] \quad \text{.....[4]}$$

---

[1] Professor of Applied Mechanics, Department of Mechanical Engineering, Massachusetts Institute of Technology. Mem. A.S.M.E.

[2] Instructor, Department of Mechanical Engineering, Massachusetts Institute of Technology.

[3] Numbers in parentheses refer to the Bibliography at the end of the paper.

Contributed by the Applied Mechanics Division and presented at the Annual Meeting, New York, N. Y., Nov. 26–29, 1945, of The American Society of Mechanical Engineers.

Discussion of this paper should be addressed to the Secretary, A.S.M.E., 29 West 39th Street New York, N. Y., and will be accepted until April 10, 1946, for publication at a later date. Discussion received after the closing date will be returned.

Note: Statements and opinions advanced in papers are to be understood as individual expressions of their authors and not those of the Society.

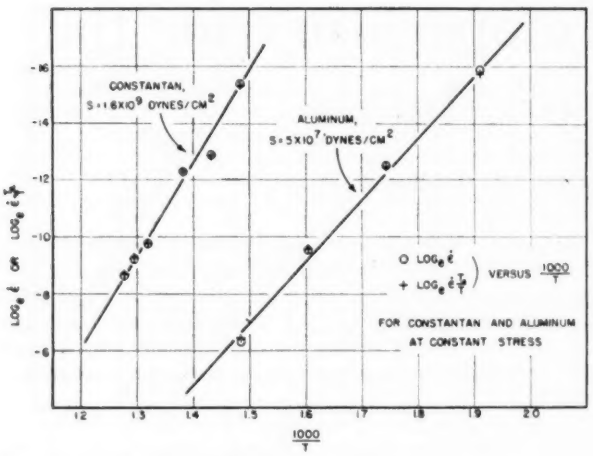


FIG. 1 $\text{LOG}_e\ \dot{\epsilon}$ AND $\text{LOG}_e\ \frac{\dot{\epsilon}T_0}{T}$ VERSUS $1000/T$ FOR THE SECONDARY CREEP OF CONSTANTAN AND ALUMINUM AT CONSTANT STRESS
(Data from Dushman, Dunbar, and Huthsteiner, ref. 5.)

Equation [4] can be derived also from the relationship

$$\frac{\dot{\epsilon}}{\dot{\epsilon}_0} = Ae^{-\frac{f^*(S)}{T}} \quad \ldots\ldots\ldots\ldots\ldots\ldots [5]$$

which is an approximation to Equation [1], in a manner similar to the derivation of Equation [3] from Equation [1].

Fig. 1 shows $\log_e\left(\frac{\dot{\epsilon}T_0}{T}\right)$ plotted versus $1000/T$ for the secondary creep of aluminum and constantan at constant stress from the data of Dushman, Dunbar, and Huthsteiner (5). Here T_0 has the value $\sqrt{T_{max}T_{min}}$. Fig. 1 also includes a plot of $\log_e \dot{\epsilon}$ versus $1000/T$ for the same experimental data. These curves are representative of those which may be obtained from the results of other carefully controlled measurements of the secondary creep rate. Since all of the curves in Fig. 1 are linear within the experimental error, and since both methods of plotting give points which are very nearly coincident, it may be concluded that Equations [1] and [5] are both satisfactory for a discussion of the creep data available at the present time. For this reason the simpler functional relationships contained in Equations [4] and [5] will be employed henceforth in this analysis, although it must be kept in mind that for an analysis of future work of a high degree of precision it may be desirable to use the relationships given in Equations [1] and [3], and for very low stresses an expression still more general than Equation [1] may be required (4).

The form of the relationship in Equation [4] can be found by considering a series of tests made at the constant strain rate $\dot{\epsilon}_0$. Equation [4] then reduces to

$$S = f(T) \quad \ldots\ldots\ldots\ldots\ldots\ldots [6]$$

and a plot of S versus testing temperature gives the functional form of f for the value of $\dot{\epsilon}_0$ chosen. Equation [4] states that the stress corresponding to a test at an arbitrary strain rate $\dot{\epsilon}$ and an arbitrary temperature T will be the same as for a test at the strain rate $\dot{\epsilon}_0$ and temperature $T\left(1 - k\log_e\frac{\dot{\epsilon}}{\dot{\epsilon}_0}\right)$. The quantity $T\left(1 - k\log_e\frac{\dot{\epsilon}}{\dot{\epsilon}_0}\right)$ is then the value of the temperature abscissa at which the stress value corresponding to a test at the strain rate $\dot{\epsilon}$ and temperature T must be plotted in order to coincide with the stress versus temperature curve for tests at the constant rate $\dot{\epsilon}_0$.

In practice a series of tests is conducted at a number of values of $\dot{\epsilon}$. The curve of S versus T_m for these tests should be identical with the curve of S versus T for tests at the particular rate $\dot{\epsilon}_0$, although it may have happened that none of the tests actually proceeded at the rate $\dot{\epsilon}_0$.

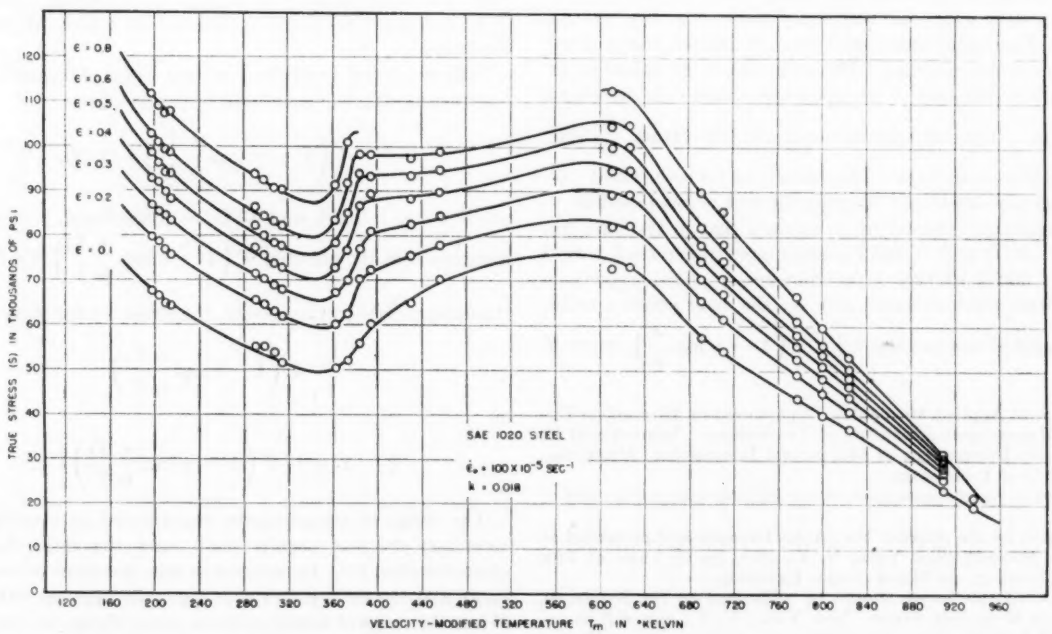


FIG. 2 STRESS VERSUS VELOCITY-MODIFIED TEMPERATURE AT CONSTANT STRAIN VALUES FOR CONSTANT TRUE-STRAIN-RATE TENSION TESTS OF S.A.E. 1020 STEEL

(Temperature and velocity values follow: At —70 C, 25 C, and 100 C, $\dot{\epsilon} = 5\times, 20\times, 100\times$, and 500×10^{-4} sec^{-1}; at 170 C, $\dot{\epsilon} = 20\times$ and 500×10^{-4} sec^{-1}; at 320 C, $\dot{\epsilon} = 5\times$ and 20×10^{-4} sec^{-1}; at 440 C and 665 C, $\dot{\epsilon} = 100 \times$ and 500×10^{-4} sec^{-1}; at 525 C, $\dot{\epsilon} = 20\times, 100\times$, and 500×10^{-4} sec^{-1}. After MacGregor and Fisher, ref. 1.)

The quantity $T\left(1 - k \log_e \frac{\dot{\epsilon}}{\dot{\epsilon}_0}\right)$ has been called the velocity-modified temperature and has been designated (1) by the symbol T_m. With this notation, Equation [4] takes the form

$$S = f(T_m) \quad [7]$$

According to Equation [7], it should be possible for a given choice of $\dot{\epsilon}_0$ to select a value of k so that when stress is plotted versus T_m, a smooth curve will result.

It was suggested (1) that the functional relationship between stress and velocity-modified temperature might hold for tension tests at arbitrary temperatures and true strain rates as well as for secondary creep. Tension tests conducted at constant true strain rates showed that at a given strain the stress reaction in the specimen depended on the velocity-modified temperature, or in general

$$S = f(T_m, \epsilon) \quad [8]$$

From a series of true stress-strain tension tests conducted at constant true strain rates over a considerable range of temperatures, the stress reactions corresponding to a number of strain values were determined for several materials (1). Figs. 2 and 3 show the stress reactions for S.A.E. 1020 steel and for S.A.E. 1045 steel plotted as functions of the velocity-modified temperature for different strain values. Smooth curves were obtained for S as a function of T_m at constant strain as predicted by Equation [8]. Each closely grouped set of points in these figures corresponds to tests conducted at a given temperature.

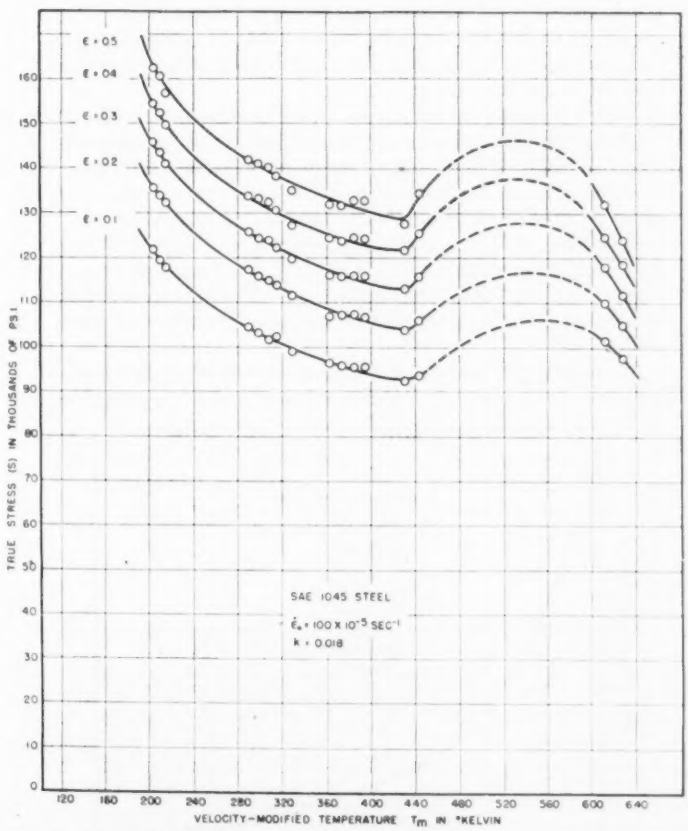


FIG. 3 STRESS VERSUS VELOCITY-MODIFIED TEMPERATURE AT CONSTANT STRAIN VALUES FOR CONSTANT TRUE-STRAIN-RATE TENSION TESTS OF S.A.E. 1045 STEEL

(Temperature and velocity values follow: At —70 C, $\dot{\epsilon}$ = 5×, 20 ×, and 100 × 10^{-5} sec^{-1}; at 25 C and 100 C, $\dot{\epsilon}$ = 5×, 20×, 100×, and 500 × 10^{-5} sec^{-1}; at 65 C, $\dot{\epsilon}$ = 500 × 10^{-5} sec^{-1}; at 170 C, $\dot{\epsilon}$ = 100× and 500 × 10^{-5} sec^{-1}; at 320 C, $\dot{\epsilon}$ = 5× and 20 × 10^{-5} sec^{-1}. After MacGregor and Fisher, ref. 1.)

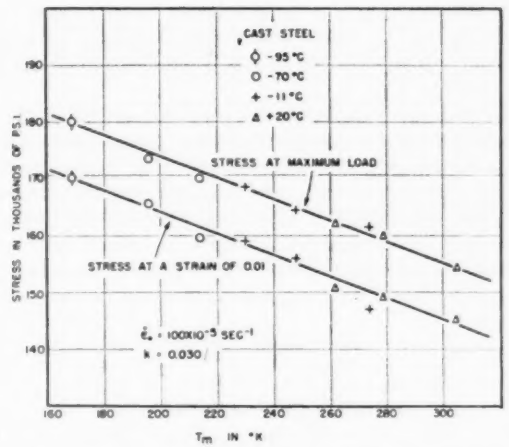


FIG. 4 STRESS AT MAXIMUM LOAD AND STRESS AT A STRAIN OF 0.01 VERSUS VELOCITY-MODIFIED TEMPERATURE FOR TENSION TESTS OF A CAST STEEL

(Temperature and velocity ranges follow: —95 C ≤ T ≤ 20 C and 1.7 × 10^{-4} sec^{-1} ≤ $\dot{\epsilon}$ ≤ 6.0 × 10^{-2} sec^{-1}. Data from Zener and Hollomon, ref. 6.)

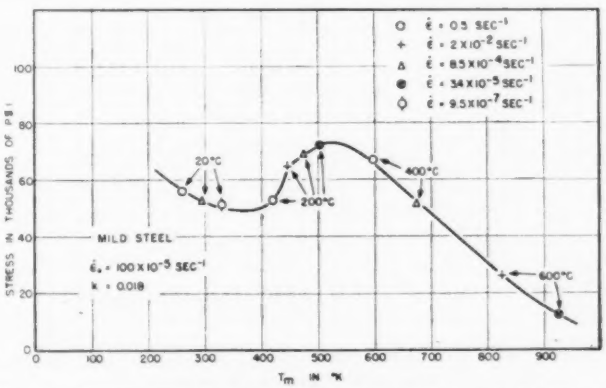


FIG. 5 STRESS AT A STRAIN OF 0.1 VERSUS VELOCITY-MODIFIED TEMPERATURE FOR TENSION TESTS OF MILD STEEL

(Temperature and velocity ranges follow: 20 C ≤ T ≤ 600 C and 9.5 × 10^{-7} sec^{-1} ≤ $\dot{\epsilon}$ ≤ 0.5 sec^{-1}. Data from Manjoine, ref. 7.)

For increasing temperatures, the stress reaction in the specimen is found farther to the right along the curve. In each group of points corresponding to tests at a given temperature the stress reaction is found farther to the right along the curve for decreasing strain rates.

As an illustration, for the group of points in Fig. 2 for the S.A.E. 1020 steel plotted near 300 K, the point lying to the left corresponds to a true strain rate of 500 × 10^{-5} sec^{-1} and the point lying to the right in this group corresponds to 5 × 10^{-5} sec^{-1}, while all the points in the group were for the testing temperature of 25 C.

Further examples of the application of the velocity-modified temperature T_m to tension-test data are given in Figs. 4 and 5. Fig. 4 shows the stress at the maximum load and at a strain of 0.01 plotted as a function of T_m from data given by Zener and Hollomon (6) for a cast steel. In Fig. 4 the over-all strain rates over a fixed gage length were of about the same order of magnitude as the true strain rates of Figs. 2 and 3, while the temperature range —95 C ≤ T ≤ 20 C was smaller. The stress at a strain of 0.1 for a mild steel is plotted versus the velocity-modified temperature T_m in Fig. 5, from data reported by Manjoine (7). The temperature range was slightly smaller than for Figs. 2 and

3, but the strain rates covered a larger range from 9.5×10^{-7} sec^{-1} to 0.5 sec^{-1}. Figs. 4 and 5 show essentially the same general utility of the velocity-modified temperature as do Figs. 2 and 3.

The qualitative similarity between the effects of increasing temperature and decreasing velocity has previously been pointed out by Carpenter and Robertson (8). The present results indicate that the use of the velocity-modified-temperature concept makes this relationship a quantitative one for the tension test. Points may be obtained on the curve of stress versus velocity-modified temperature to the left of a given point either by increasing the speed or by decreasing the temperature; and points may be obtained to the right of a given point by decreasing the speed or increasing the temperature.

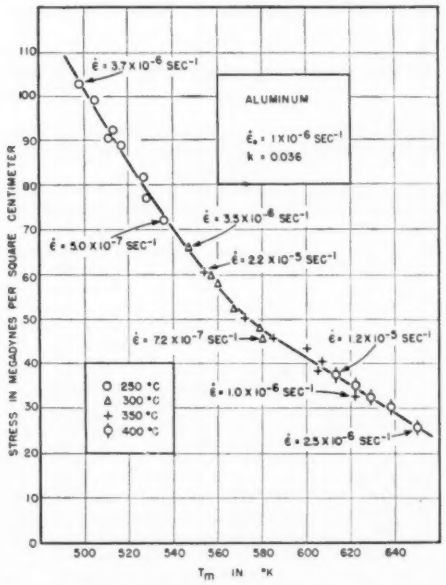


FIG. 6 STRESS VERSUS VELOCITY-MODIFIED TEMPERATURE FOR SECONDARY CREEP OF ALUMINUM

(Temperature and velocity ranges follow: 250 C $\leq T \leq$ 400 C and 5.0×10^{-7} $sec^{-1} \leq \dot{\epsilon} \leq 2.2 \times 10^{-5}$ sec^{-1}. Data from Dushman, Dunbar, and Huthsteiner, ref. 5.)

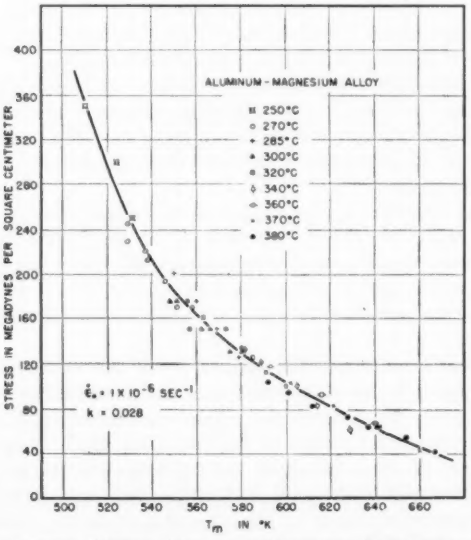


FIG. 7 STRESS VERSUS VELOCITY-MODIFIED TEMPERATURE FOR SECONDARY CREEP OF AN ALUMINUM-MAGNESIUM ALLOY

(Temperature and velocity ranges follow: 250 C $\leq T \leq$ 380 C and 2.7×10^{-7} $sec^{-1} \leq \dot{\epsilon} \leq 2.9 \times 10^{-5}$ sec^{-1}. Data from Dushman, Dunbar, and Huthsteiner, ref. 5.)

APPLICATION OF VELOCITY-MODIFIED TEMPERATURE TO CREEP TESTS

Since the velocity-modified temperature T_m appeared to be quite useful in connection with slow and rapid tension tests, its application to the creep problem was investigated.

Figs. 6 and 7 are based on creep data reported by Dushman, Dunbar, and Huthsteiner (5) for aluminum and an aluminum-magnesium alloy. In Fig 6 the stress is plotted as a function of the velocity-modified temperature T_m for the secondary creep of aluminum in the temperature range 250 C $\leq T \leq$ 400 C and for strain rates 5.0×10^{-7} $sec^{-1} \leq \dot{\epsilon} \leq 2.2 \times 10^{-5}$ sec^{-1}. Fig. 7 shows the stress reaction versus T_m for the secondary creep of an aluminum-magnesium alloy in the temperature range 250 C $\leq T \leq$ 380 C and for strain rates 2.7×10^{-7} $sec^{-1} \leq \dot{\epsilon} \leq 2.9 \times 10^{-5}$ sec^{-1}. It will be noted that groups of points representing tests at different temperatures frequently overlap in these figures.

Referring to Fig. 6, it can be seen that an increase in strain rate causes the same effect on the stress reaction as does a decrease in temperature. For example, the point corresponding to a test at $\dot{\epsilon} = 3.7 \times 10^{-6}$ sec^{-1}, $T = 250$ C lies to the left of the point corresponding to $\dot{\epsilon} = 3.5 \times 10^{-6}$ sec^{-1}, $T = 300$ C. The latter point, in turn, lies to the left of the one corresponding to $\dot{\epsilon} = 2.5 \times 10^{-6}$ sec^{-1}, $T = 400$ C. In general, points corresponding to equal values of $\dot{\epsilon}$ are ordered with temperatures increasing to the right. Similarly, the point corresponding to a test at $\dot{\epsilon} = 3.7 \times 10^{-6}$ sec^{-1}, $T = 250$ C lies to the left of the point corresponding to $\dot{\epsilon} = 5.0 \times 10^{-7}$ sec^{-1}, $T = 250$ C. In general, points corresponding to equal values of T are ordered with velocity increasing to the left.

More specifically, consider the point at the stress value 61 megadynes/cm² obtained by a test carried out at the temperature $T = 623$ K = 350 C and the strain rate $\dot{\epsilon} = 2.2 \times 10^{-5}$ sec^{-1}. It is evident from Fig. 6 that this same stress value could have been obtained with various combinations of strain rate and temperature, such as a test at a strain rate $\dot{\epsilon} = \dot{\epsilon}_0 = 1 \times 10^{-6}$ sec^{-1} and a temperature $T = 554$ K = 281 C, or a test at a strain rate of 2.5×10^{-6} sec^{-1} and a temperature $T = 573$ K = 300 C, since all of these temperature-velocity pairs give the same value of T_m.

Although Fig. 6 has been discussed in greater detail, essentially the same conclusions may be drawn from Fig. 7 for the creep of

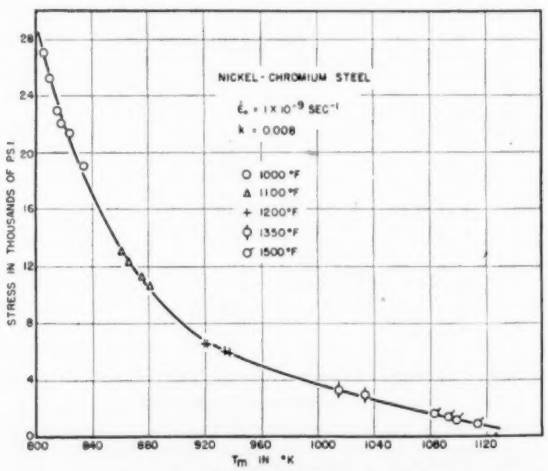


FIG. 8 STRESS VERSUS VELOCITY-MODIFIED TEMPERATURE FOR SECONDARY CREEP OF A NICKEL-CHROMIUM STEEL—STEEL B

(Temperature and velocity ranges follow: 538 C $\leq T \leq$ 816 C and 2.8×10^{-11} $sec^{-1} \leq \dot{\epsilon} \leq 2.1 \times 10^{-9}$ sec^{-1}. Data from Norton, ref. 9.)

an aluminum-magnesium alloy, and from Fig. 8, for a nickel-chromium steel. The latter was plotted from creep data reported by Norton (9).

In many creep tests the secondary creep rate is not determined and the test is not conducted at a constant true strain rate. The most common tests are those conducted at constant load (10). These usually do not extend beyond the region of primary creep, an initial period of relatively rapid and decreasing strain rate. Although such data are not as useful in checking the velocity-modified-temperature concept; in order to apply Equation [7], formulated for tests at constant true strain rates, to tests of this sort it is assumed that the value of $\dot{\epsilon}$ may be taken as the average strain rate, $\frac{\epsilon}{t}$, where ϵ is the strain value in question and t is the time required to reach that strain. Determining $\dot{\epsilon}$ in this way, Equation [7] should be *approximately* satisfied by the results of primary creep tests.

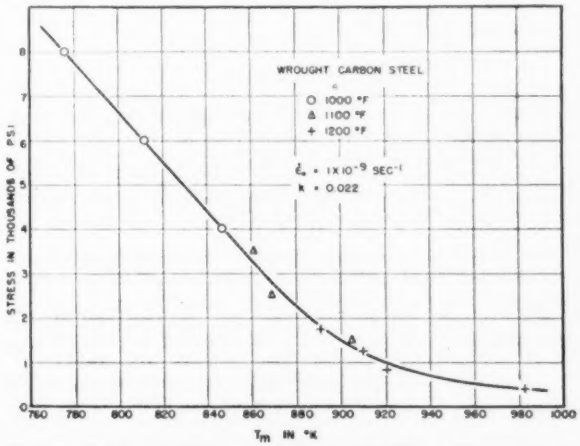


FIG. 9 STRESS AT PLASTIC STRAIN OF 0.001 AS FUNCTION OF VELOCITY-MODIFIED TEMPERATURE FOR PRIMARY CREEP OF A WROUGHT CARBON STEEL

(Temperature and velocity ranges follow: 538 C $\leq T \leq$ 649 C and 5.0×10^{-11} sec^{-1} $\leq \dot{\epsilon} \leq 6.9 \times 10^{-9}$ sec^{-1}. Data from "Creep Data" book, ref. 10.4)

Fig. 9 shows stress plotted as a function of T_m for the primary creep of low-carbon steel at a plastic strain of 0.001, according to data given in reference (10).[4] The temperature range was 538 C $\leq T \leq$ 649 C, and the strain rates were 5.0×10^{-11} sec^{-1} $\leq \dot{\epsilon} \leq 6.5 \times 10^{-9}$ sec^{-1}.

[4] Reference 10, pp. 20–21.

The velocity-modified-temperature concept can also be applied *approximately* to data such as that given by Tapsell and Johnson (11) for tests extending into the tertiary creep range, where the strain rate begins to increase with strain. Defining again $\dot{\epsilon}$ as the average value $\frac{\epsilon}{t}$, stress may be plotted versus T_m for a given strain. Such a curve is shown in Fig. 10 for a forged steel at a strain of 0.05. The temperature range here was 472 C

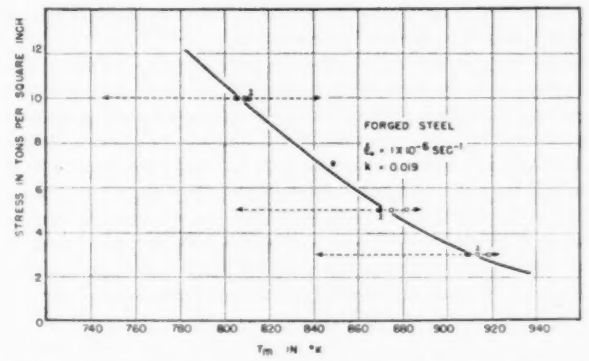


FIG. 10 STRESS AT A STRAIN OF 0.05 VERSUS VELOCITY-MODIFIED TEMPERATURE FOR TERTIARY CREEP OF A FORGED STEEL

(Temperature and velocity ranges follow: 472 C $\leq T \leq$ 650 C and 1.0×10^{-8} sec^{-1} $\leq \dot{\epsilon} \leq 7.7 \times 10^{-6}$ sec^{-1}. Dotted lines indicate temperature spread for points at each stress. Data from Tapsell and Johnson, ref. 11.)

$\leq T \leq$ 650 C, and the range of strain rates was 1.0×10^{-8} sec^{-1} $\leq \dot{\epsilon} \leq 7.7 \times 10^{-6}$ sec^{-1}. The dotted lines in Fig. 10 indicate the spread of testing temperatures for points at each stress.

A tension test of a low-carbon steel made at a constant true strain rate of $\dot{\epsilon} = 100 \times 10^{-5}$ sec^{-1} lasts approximately 20 min. If the stress reaction in creep tests or in high-speed tension tests for a given strain is plotted versus T_m for a value of $\dot{\epsilon}_0 = 100 \times 10^{-5}$ sec^{-1} the resulting curve may be used to determine the temperatures for which tension tests conducted at the constant true strain rate $\dot{\epsilon} = \dot{\epsilon}_0$ will give the same stress reactions as observed in the creep or high-speed tests.

In Fig. 11 the data of Manjoine (7), Tapsell and Johnson (11), MacGregor and Fisher (1) and the "Creep Data" book (10) are plotted with stress as a function of T_m for $\dot{\epsilon}_0 = 100 \times 10^{-5}$ sec^{-1}. The data from these various sources are for different low-carbon steels and at different values of strain, as listed in Fig. 11. In spite of this, Fig. 11 indicates that tension tests conducted at the constant true strain rate $\dot{\epsilon} = 100 \times 10^{-5}$ sec^{-1} may be used to ob-

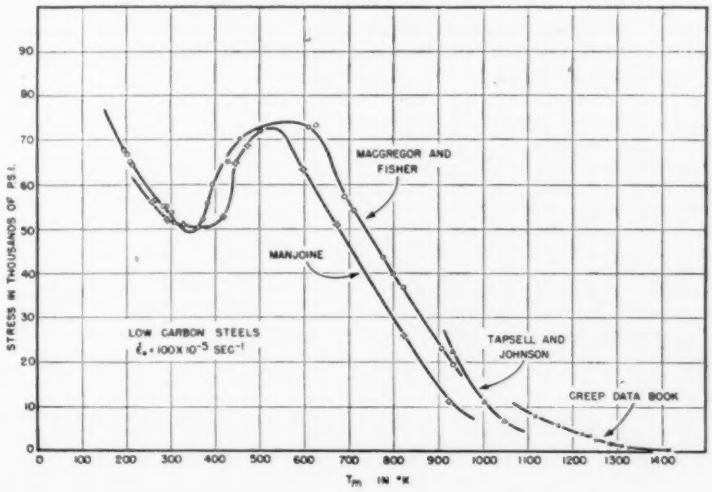


FIG. 11 STRESS VERSUS VELOCITY-MODIFIED TEMPERATURE FOR SEVERAL LOW-CARBON STEELS

(Strains, and temperature and velocity ranges follow:

1 Data from MacGregor and Fisher, ref. 1
Strain = 0.1, —70 C $\leq T \leq$ 665 C, 5×10^{-8} sec^{-1} $\leq \dot{\epsilon} \leq 500 \times 10^{-5}$ sec^{-1}

2 Data from Manjoine, ref. 7
Strain = 0.1, 20 C $\leq T \leq$ 600 C, 9.5×10^{-7} sec^{-1} $\leq \dot{\epsilon} \leq 0.5$ sec^{-1}

3 Data from Tapsell and Johnson, ref. 11
Strain = 0.05, 472 C $\leq T \leq$ 650 C, 1.0×10^{-8} sec^{-1} $\leq \dot{\epsilon} \leq 7.7 \times 10^{-6}$ sec^{-1}

4 Data from "Creep Data" book, ref. 10
Plastic strain = 0.001, 538 C $\leq T \leq$ 649 C, 5.0×10^{-11} sec^{-1} $\leq \dot{\epsilon} \leq 6.9 \times 10^{-9}$ sec^{-1})

tain essentially the same stress reactions as were obtained in the creep tests reported in the "Creep Data" book (10),[4] if the tests are made at temperatures from 1120 K (847 C) to 1420 K (1147 C), assuming of course that the velocity-modified-temperature concept holds for the range of velocities in question. Similarly, to obtain the same stress reactions as were reported in the creep tests of Tapsell and Johnson, tension tests at temperatures from 935 K (662 C) to 1050 K (777 C) and at a strain rate of $\dot{\epsilon} = 100 \times 10^{-6}$ sec^{-1} may be used. In order for this to be true the stress reaction must of course be measured at the proper strain for all cases where it depends on strain as well as on T_m.

An obvious inference from the foregoing discussion is that the true stress-strain tension test, conducted at constant true strain rates, may have some application in the development of a rational short-time creep test, when use is made of the velocity-modified-temperature concept. Although there are definite indications of the possibility of developing a short-time creep test in this manner, no final conclusions regarding such an application can be reached at this time owing to the fact that so few experimental data of the necessary type are available. An experimental program now being undertaken by the authors may serve to throw further light on the problem.

Conclusions

The following conclusions may be drawn:

1 The expression for the velocity of secondary creep at moderate stresses derived from Eyring's theory for the velocity of plastic flow,

$$\frac{\dot{\epsilon}}{\dot{\epsilon}_0} = A \frac{T}{T_0} e^{-\frac{f^*(S)}{T}}$$

and its approximation

$$\frac{\dot{\epsilon}}{\dot{\epsilon}_0} = A e^{-\frac{f^*(S)}{T}}$$

are consistent with the results of secondary-creep measurements, within the experimental error of the data reviewed.

2 The stress reaction in a specimen undergoing secondary creep is a function of the velocity-modified temperature

$$T_m = T \left(1 - k \log_e \frac{\dot{\epsilon}}{\dot{\epsilon}_0}\right)$$

where T is the absolute testing temperature, $\dot{\epsilon}$ is the true strain rate, and $\dot{\epsilon}_0$ and k are constants.

3 For large ranges of temperatures and velocities with extreme limits of $-95\ \text{C} \leq T \leq 665\ \text{C}$ and $9.5 \times 10^{-7}\ \text{sec}^{-1} \leq \dot{\epsilon} \leq 0.5\ \text{sec}^{-1}$ the stress reaction in a tension specimen being tested at a constant true strain rate has been shown to depend on the velocity-modified temperature and the strain.

4 The stress reaction in a specimen undergoing primary or tertiary creep is an *approximate* function of the velocity-modified temperature and the strain when the value of $\dot{\epsilon}$ is taken to be $\frac{\epsilon}{t}$.

5 By use of the velocity-modified temperature, there are definite indications that the stress reaction corresponding to tests at very slow and very rapid rates of deformation may be found from tension tests at moderate strain rates and appropriately raised or lowered temperatures.

6 Further experimentation employing constant true-strain-rate tests is necessary in order to determine the full range of applicability of the concept of velocity-modified temperature, and to discover any refinements in the relationship

$$\frac{\dot{\epsilon}}{\dot{\epsilon}_0} = A e^{-\frac{f^*(S)}{T}}$$

that may prove to be required.

Bibliography

1 "Tension Tests at Constant True Strain Rates," by C. W. MacGregor and J. C. Fisher, Journal of Applied Mechanics, Trans. A.S.M.E., vol. 67, 1945, p. A-217.

2 "The True Stress-Strain Tension Test—Its Role in Modern Materials Testing," by C. W. MacGregor, *Journal of The Franklin Institute*, August, 1944, pp. 111–135, and September, 1944, pp. 159–176.

3 "Viscosity, Plasticity, and Diffusion as Examples of Absolute Reaction Rates," by H. Eyring, *Journal of Chemical Physics*, vol. 4, 1936, p. 283.

4 "Flow of Solid Metals From the Standpoint of the Chemical-Rate Theory," by W. Kauzmann, Trans. A.I.M.E., vol. 143, 1941, pp. 57–81.

5 "Creep of Metals," by S. Dushman, L. W. Dunbar, and H. Huthsteiner, *Journal of Applied Physics*, vol. 15, 1944, p. 108.

6 "Effect of Strain Rate Upon Plastic Flow in Steel," by C. Zener and J. H. Hollomon, *Journal of Applied Physics*, vol. 15, 1944, p. 22.

7 "Influence of Rate of Strain and Temperature on Yield Stresses of Mild Steel," by M. J. Manjoine, Journal of Applied Mechanics, Trans. A.S.M.E., vol. 66, 1944, p. A-211.

8 "Metals," by H. Carpenter and J. M. Robertson, Oxford University Press, New York, N. Y., 2 vols., 1939.

9 "The Creep of Steel at High Temperatures," by F. H. Norton, McGraw-Hill Book Company, Inc., New York, N. Y., 1929.

10 "Compilation of Available High-Temperature Creep Characteristics of Metals and Alloys," compiled by Creep Data Section of Joint Research Committee on Effect of Temperature on the Properties of Metals, published jointly by A.S.T.M. and A.S.M.E., March, 1938.

11 "The Strength at High Temperatures of a Cast and a Forged Steel as Used for Turbine Construction," by H. J. Tapsell and A. E. Johnson, Department of Scientific and Industrial Research, Engineering Research, Special Report No. 17, published by His Majesty's Stationery Office, London, Eng., 1931.

Design of Crankpins for Locomotives

By O. J. HORGER[1] and W. I. CANTLEY[2]

This progress report presents the results of a fatigue investigation made on full-size 9½-in-diam crankpins by the Association of American Railroads. The primary object of this study was to develop an improved crankpin-and-wheel assembly which will alleviate crankpin fatigue failures occurring in the wheel-fit portion in service. A total of 50 full-size crankpin-and-wheel assemblies were tested, using four different types of pins. All pins were of plain-carbon steel, normalized and tempered, having a carbon content of 0.52 per cent and manganese of 0.80 per cent. Large double-ended cantilever-type fatigue machines subjected the crankpin-and-wheel assemblies to rotating-bending stresses. The fatigue resistance of the conventional assembly, against the crankpin breaking off in the wheel fit, may be expressed as 100 per cent. The other three types of pins gave values of 136, 146, and over 200 per cent (Table 7). Even with this greatly improved breaking-off strength, shallow fatigue cracks were found to initiate in the wheel-fit portion of all four types of pins at bending stresses much below what was required to propagate the cracks to complete fracture.

Introduction

THE Association of American Railroads (A.A.R.) has been conducting a program of research covering the fatigue-testing of full-size 9½-in-diam crankpins since July, 1942. Two progress reports[3] have been issued to members of A.A.R. presenting the results of this investigation up to April, 1944. The present paper advances these findings and also notes that this investigation is still in progress.

It is well known that a press fit is a source of extremely high stress concentration. Crankpins either in laboratory test or in service operation may completely break off inside the wheel fit at bending stresses which are only a fraction of the fatigue strength of the same material without a press fit.[4,5,6] For this reason mileage limits are usually established as a means of preventing service failures of crankpins.

While crankpins seldom actually break off inside of the wheel fit within the service mileage established, it is not uncommon to find fatigue cracks in the wheel-fit portion of the pin in various stages of crack propagation. Such service failures have been the subject of earlier study and two reports have been issued by A.A.R.[7] The initiation and development of these fatigue cracks have been found from laboratory tests to occur at very much lower bending stresses than that required to break off the pin. This condition is generally too little understood and appreciated.[8] These laboratory tests permit a study of this fatigue-crack initiation and propagation so that means of improving conditions may be determined.

It is realized that laboratory-test conditions cannot parallel service operation. The fatigue-strength values given in this report, however, permit a relative rating of various types of crankpins as to their fatigue resistance or life expectancy. It would be expected that this same order of rating would be reflected from service operation, but the percentage difference between the various types obtained in service would not necessarily be the same as that obtained in laboratory tests.

Crankpins in service may also develop fatigue failure at one of the journal fillets, but the present investigation was confined to a study of failures in the wheel-fit portion.

Crankpin Forgings

The steel in the crankpin forgings was made by the acid-open-hearth process. It was poured into big-end-up hot-top ingots of the round corrugated type. The ingot weight was about 8000 lb and had a mean diameter of approximately 23 in., while the ingot proper was 59 in. long. The hot top was approximately 16 in. diam × 19 in. long. A pipe-eliminator compound was used on the top of the steel in the hot top when pouring was completed to aid in reduction of the depth of pipe.

The ingots were heated to a forging temperature of approximately 2050 F, and forged under a steam-hydraulic press to blooms approximately 12 in. sq. The final blooming temperature was generally between 1600 and 1700 F. The blooms were allowed to cool to atmospheric temperature and surface defects were removed by chipping or scarfing. The blooms were then reheated to a forging temperature of 2050 F for approximately 1 hr per in. of thickness, and the pin forgings were made under a steam-hydraulic press with the finishing temperature approximately 1600 F. About ⅝ in. stock on each diameter was allowed in the rough forging over the rough-machined diameters. The forgings

---

[1] Chief Engineer, Railway Division, The Timken Roller Bearing Company, Canton, Ohio. Mem. A.S.M.E.

[2] Mechanical Engineer, Association of American Railroads, Chicago, Ill. Mem. A.S.M.E.

[3] "Locomotive Crankpin Tests—9½-In. Diameter," First Progress Report, March 11, 1943; Second Progress Report, April 4, 1944; Office of Mechanical Engineer, Association of American Railroads, Chicago, Ill.

[4] "Achsbrüche bei Eisenbahnfahrzeugen und ihre Ursachen," by R. Kühnel, *Stahl und Eisen*, vol. 40, 1932, p. 965.

[5] "Fatigue of Shafts at Fitted Members With a Related Photoelastic Analysis," by R. E. Peterson and A. M. Wahl, JOURNAL OF APPLIED MECHANICS, Trans. A.S.M.E., vol. 57, 1935, p. A-1.

[6] "Locomotive Axle and Wheel Research," by T. V. Buckwalter and P. C. Paterson, The Timken Roller Bearing Company, Canton, Ohio, 1935.

Contributed by the Railroad and Applied Mechanics Divisions and presented at the Annual Meeting, New York, N. Y., Nov. 26–29, 1945, of THE AMERICAN SOCIETY OF MECHANICAL ENGINEERS.

Discussion of this paper should be addressed to the Secretary, A.S.M.E., 29 West 39th Street, New York, N. Y., and will be accepted until April 10, 1946, for publication at a later date. Discussion received after the closing date will be returned.

NOTE: Statements and opinions advanced in papers are to be understood as individual expressions of their authors and not those of the Society.

[7] "Failures and Performance of Main Crank Pins on Steam Locomotives," first progress report, May, 1938; final report, May, 1940, Office of Mechanical Engineer, Association of American Railroads, Chicago, Ill. This latter report presented service data on 43,468 steam locomotives for a period of 9 months during which time 1695 main crankpins were removed and 151 or 9 per cent were found defective. Of these defective pins, 83 were removed from freight locomotives of which 41 per cent showed failure inside the wheel fit, and 32 per cent failed flush with the wheel-hub face (which is interpreted as also being in the wheel fit, but failure occurred at the end of the fit, rather than in the journal fillet). The remaining 68 pins were found defective from passenger locomotives, of which 54 per cent showed failure inside the wheel fit, and 18 per cent failed flush with the hub face.

[8] Various phases of fatigue failure discussed in "Locomotive Axle Testing," by T. V. Buckwalter, O. J. Horger, and W. C. Sanders, Trans. A.S.M.E., vol. 60, 1938, p. 335.

TABLE 1 CHEMICAL AND PHYSICAL PROPERT ES FOR CRANKPINS AND WHEEL CENTERS

HEAT NO.	SERIAL NO.	PHYSICAL PROPERTIES Y.P.	U.S.	Elong.	R. of A.	B.H.N.	Izod	CHEMICAL PROPERTIES C.	Mn.	P.	Sul.	Sil.	Chr.	Ni.	Mo.
CRANK PIN FORGINGS (REPORTED BY FORGE SHOP) * Maximum values															
E-8746	1-10	50,500	92,000	26.0	46.5			.50	.77	.030	.031	.27			
"	11-16	51,000	92,000	27.0	48.0										
"	17-20	51,000	92,000	27.0	48.0										
"	27-30	50,500	88,500	28.0	48.0										
E-8841	21-26	51,000	96,500	25.0	42.0			.50	.81	.033	.033	.29			
M-104-37, Class A		48,000	86,000	24	38	Min. unless shown		.40/.55	.60/.90	.045*	.05*	.15	.15*	.25*	
PROPERTIES OF REPRESENTATIVE HEATS FROM WHICH WHEEL CENTER CASTINGS WERE POURED * Maximum values															
4830		42,500	85,000		25.0			.32	.70	.019	.022	.44			
4834		42,500	85,500		25.0			.28	.72	.017	.025	.39			
4844		41,000	87,500		26.0			.28	.76	.020	.023	.41			
4861		40,000	82,000		27.5			.30	.79	.020	.023	.41			
4890		42,500	87,000		25.0			.27	.72	.023	.023	.40			
4906		42,500	89,000		25.0			.30	.72	.016	.023	.40			
4911		39,500	82,000		26.0			.31	.72	.015	.023	.39			
M-201-36, Grade B		38,000	70,000	24	36	Min. unless shown			.85*	.05*	.06*				
LOCATION ACTUAL CHEMICAL AND PHYSICAL PROPERTIES DETERMINED ON FAILED WHEEL CENTER CASTING NO. C-3															
Longitudinal; ℄ of Specimen 3/8" from bore		41,000 44,500	66,500 74,250	5.5 17.0	8.5 23.0	149 149	17-17-18								
Longitudinal; ℄ of Specimen 1-1/2 from bore		44,000 41,700 44,000	73,000 73,000 71,500	10.0 13.5 11.0	21.4 26.6 16.0	143 143 143	20-19-19								
Transverse; ℄ of Specimen 3/8" from bore		48,800 39,000 41,600	77,500 70,000 74,800	25.5 9.8 14.0	42.0 13.4 18.3	149 149 149	20-23-21	.39	.68	.039	.022	.030	.13	.15	.04
Transverse; ℄ of Specimen 1-1/2" from bore		42,000 42,500 46,400	74,500 71,200 77,100	15.0 12.0 23.5	27.6 20.4 38.1	143 143 143	22-20-22								

were normalized and tempered in accordance with A.A.R. Specification M-104-37, Class A.[9]

The crankpins tested were taken from two different heats of steel as indicated in Table 3, there being 38 pins from one heat and 12 from another heat. Ladle analysis and physical properties[10] are given in Table 1. Additional chemical analysis was made from turnings taken from the outer diameter of the wheel seat of each crankpin at the time it was prepared for fatigue-testing. The values obtained were in substantial agreement with the ladle analysis given in Table 1, but residual alloys present were found to be 0.03 to 0.10 per cent Cr, 0.16 to 0.21 per cent Ni, and nil to 0.03 per cent Mo. Also additional physical properties, given in Table 2, were determined from the wheel seat of most of the crankpins following the fatigue test.[11]

Design and Properties of Wheel Centers

The crankpins were mounted and tested in the two following different types of wheel centers or disk[12] both of which were purchased to A.A.R. Specification M-201-36, Grade B, for steel castings:[9] (1) Double-plate type of disk, Fig. 1; (2) spoke type of disk, Fig. 2.

To simulate the influence of the large mass of metal on the axle side of a wheel center, as the pin is applied on a locomotive, a solid counterweight was cast on the test disks as shown in Fig. 1.[13]

TABLE 2 SUMMARY OF PHYSICAL PROPERTIES OF CRANK PINS

Heat No.		E-8747		E-8841	
No. Crank Pin Seats Investigated		10		2	
Location of Specimens		Surface	Midway	Surface	Midway
Ultimate Strength, psi	Max.	100,600	99,200	96,900	97,200
	Av.	91,300	91,200	95,900	95,900
	Min.	84,000	84,500	95,000	94,500
Yield Point Strength, psi	Max.	56,400	53,400	53,000	48,000
	Av.	49,600	47,600	50,200	46,700
	Min.	41,300	39,500	47,500	45,000
Elongation in 2", %	Max.	29.0	28.0	24.0	24.5
	Av.	26.9	25.8	24.0	23.2
	Min.	22.0	23.0	24.0	23.0
Reduction of Area, %	Max.	56.2	54.8	47.9	43.9
	Av.	49.8	47.9	46.2	42.5
	Min.	43.2	41.6	44.6	41.4
Izod, Ft. Lbs.	Max.	26.0	25.0	21.5	19.0
	Av.	20.0	18.0	19.2	17.1
	Min.	14.0	9.0	18.0	15.0
Tensile Brinell	Max.	197	197	187	187
	Av.	179	178	185	186
	Min.	163	163	183	183
Cross Section Brinell	Max.	205	192	187	187
	Av.	188	183	187	187
	Min.	179	170	187	187

[9] Manual of Standard and Recommended Practice Association of American Railroads, Mechanical Division, Chicago, Ill.

[10] These properties were determined on longitudinal 0.505-in-diam specimens taken at midway radius from prolongations on the end of a forging from each furnace charge.

[11] These properties determined on Izod impact specimens of the three-notch type and 0.505-in-diam tensile specimens were machined from both longitudinal surface layers and at midway radius

[12] It was originally intended to use only the first type of disk, but a number of fatigue failures developed in these disks when the crankpins mounted in them were tested at 16,000 psi and above. For this reason, the spoke-type disk was generally used when testing pins at 16,000 psi and above, but not below 16,000 psi, with the exception of pin No. 6R tested at 10,500 psi. These spoke wheels were ones which were already cast for other test purposes and so were immediately available. The use of the two types of disks is not believed to influence the comparative value of the fatigue results on the four types of pins investigated.

[13] This counterweight was balanced by filling the diametrically opposite pockets of the disk with lead. This balancing was done before the disk was mounted on the crankpin and required accurate balancing in order to rotate at 1500 rpm in the test machine without vibration.

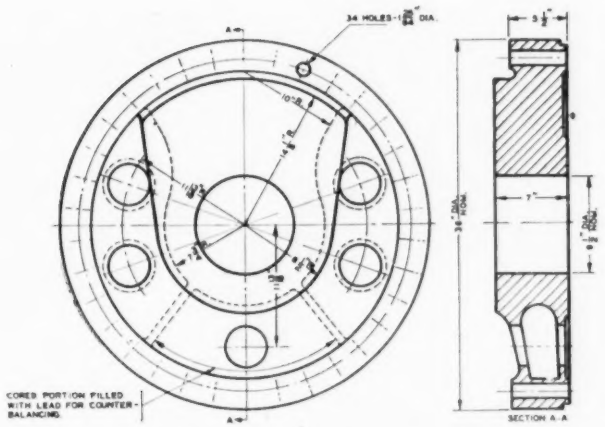


FIG. 1 DOUBLE-PLATE DISK REPRESENTING WHEEL CENTER

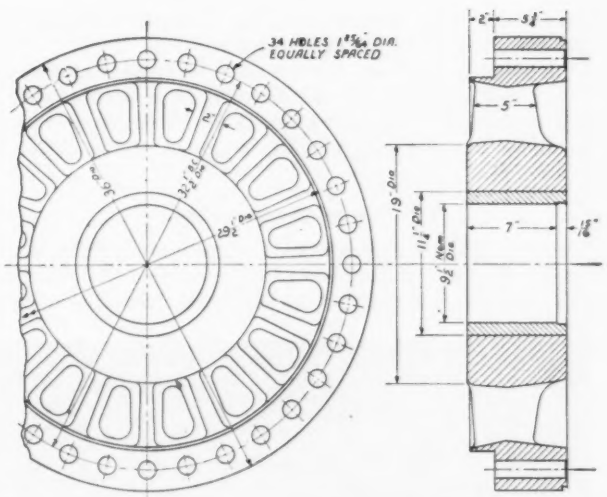


FIG. 2 SPOKE-TYPE WHEEL USED TO TEST CRANKPINS AT 16,000 PSI AND ABOVE

Chemical and physical properties of the double-plate-type disk are given in Table 1, as furnished by the foundry. Brinell-impact-meter readings made on the hub face of these wheels ranged between 149 and 164 Bhn, and these hardness readings agreed closely with those obtained on some of the same castings using the regular Brinell hardness tester. Table 1 also shows comparable data obtained from tensile and impact tests and chemical analysis on specimens from one of these disks which developed fatigue failure. The ductility characteristics found are much lower than those required by the specification. It is not unusual to find that specimens cut from actual castings give lower values than required by the specification, which is based on specimens taken from prolongations attached to the casting.

The spoke wheels available happened to have a nominal bore of $11^1/_4$ in.; therefore a cast-steel bushing to the same specification as the cast disks was press-fitted about 0.015 in. tight into the bore of these wheels. The bushing was then bored out to receive the crankpin, leaving a nominal $^7/_8$-in-thick wall section. Brinell-impact-meter readings made on these bushings usually gave 149 Bhn, although a few values of 137 Bhn were obtained.

CRANKPIN-AND-WHEEL ASSEMBLIES INVESTIGATED

Four different crankpin conditions were investigated,[14] consisting of two crankpin designs and two surface treatments, as indicated in Fig. 12. These may be described as follows:

Type 1 A straight cylindrical pin pressed into a wheel center having a straight cylindrical bore.

Type 2 Identical to type 1, except outer end of crankpin wheel seat was tapered 0.008 in. on diameter for a distance inside the wheel fit of $1^1/_4$ in.

Type 3 Identical to type 1, except wheel-fit portion of crankpin was cold-rolled.

Type 4 Identical to type 1 except wheel-seat portion of crankpin was flame-hardened.

All types of crankpins were prepared for test from 10 to $10^1/_8$-in-diam rough-turned forgings which were approximately $^1/_2$ in. to $^3/_4$ in. larger in diameter than the finished diameter at which they were tested. The pins were rough-turned in one cut to about $9^5/_8$ in. diam, and a second cut was taken about $^1/_{16}$ in. deep. Then finish cuts were taken about $^1/_{64}$ in. deep with the lathe operating at 45 rpm and a feed of $^1/_{64}$ in. per revolution. The finish cut was made with a broad-nosed tool having a contour radius of approximately 3 in. and produced a very good quality of turned finish.

Wheel bores for all designs of crankpins were bored with a straight cylindrical hole having a $^1/_{32}$-in. radius at each end of the bore. The finish cut in the wheel bore was made with a broad-nosed tool similar to that used on the crankpin, and the depth of

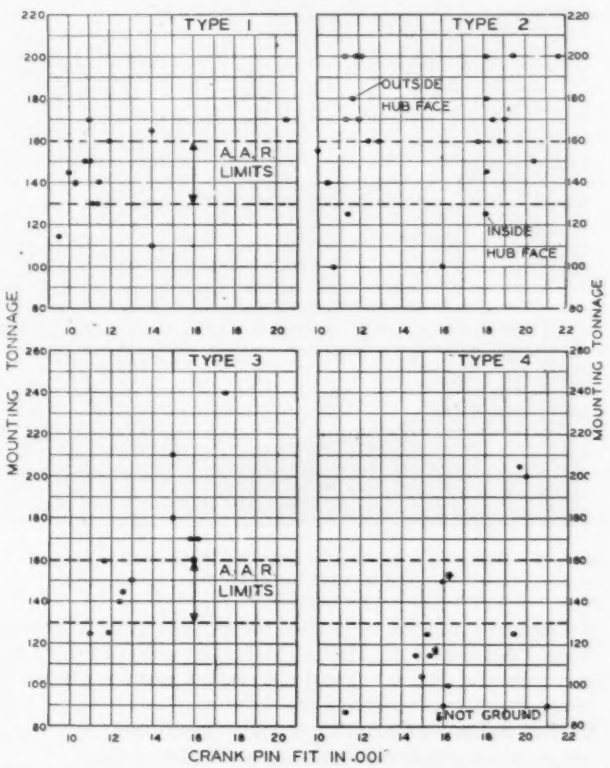


FIG. 3 COMPARISON CHART SHOWING MOUNTING TONNAGE VERSUS TOTAL FIT ON DIAMETER

[14] In all cases the design of pin was such that the wheel-seat diameter was the same as the diameter of the main side-rod journal. This shape was used because (*a*) this design already exists on some locomotives where the factors of cylinder stroke, wheel-hub sections, and journal-bearing pressure present certain design limitations, and (*b*) it would have less fatigue resistance than a pin in which the wheel seat was connected by an ample transition radius to a smaller diameter at the main side-rod journal portion. For these reasons, the least favorable design condition at the wheel seat was first investigated.

the cut was about 0.003 in. with the boring mill operating 15 rpm and a feed of $^1/_{32}$ in. per revolution.

All wheel centers were pressed onto the crankpins using the A.A.R. recommended lubricant[9] mixed in the proportions of 12 lb of white lead to 1 gal of boiled linseed oil. A summary of the fit allowance and mounting tonnage is plotted in Fig. 3, for all types of pins.

Type 3 Pins—Surface-Rolled

Type 3 pins were given a good smooth-turned finish at the fitted portion as just described and then surface-cold-rolled in a lathe, as shown in Fig. 4. The rolling device, illustrated in Fig. 5,

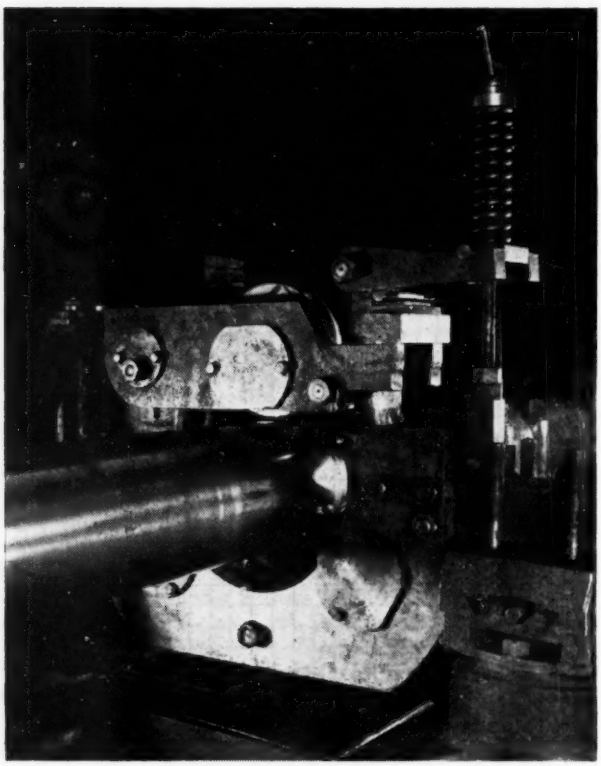


Fig. 4 Method of Surface-Rolling Wheel-Fit Portion of Crankpin in a Lathe

is equipped with three 10-in-diam rollers, the top roller having a contour radius of 5 in., and the two bottom rollers having a contour radius of $1^1/_2$ in. The $1^1/_2$-in-radius contour rollers give some penetration or thickness of cold-worked layer of metal, while the 5-in-radius contour roller tends to give the surface a good smooth finish suitable for mounting a press-fitted wheel.

The rolling procedure was to rotate the pin on lathe centers at 28 rpm and move the rolling device along the crankpin length with a feed of $^1/_{32}$ in. per revolution of the pin. The roller pressure was applied along the length of the crankpin wheel-seat surface, as shown in Fig. 6, where the inner and last 4-in. length of the crankpin fit was left about $^1/_{32}$ in. oversize. After the rolling operation was completed, this 4-in. length was remachined[15] to the

[15] This procedure permits the removal of any irregularities of surface finish which may be caused at the time the rolling pressure is being decreased. It also provides a pin length of 4 in. which has been turned and 3 in. of rolled surface for engagement in the wheel fit. As an alternative method, the pin is ground after rolling, removing not over 0.010 in. on the diameter, but this method was not tested in fatigue and it is not known if the fatigue resistance is decreased by removal of this rolled surface skin.

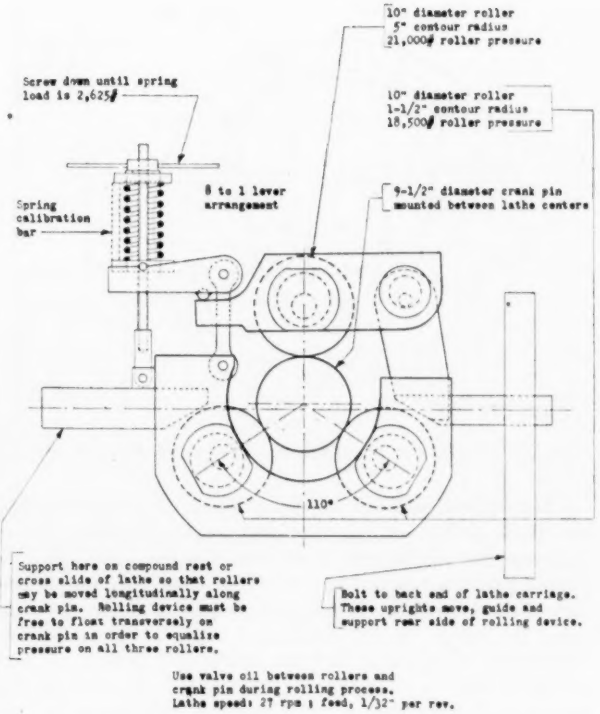


Fig. 5 Rolling Device for Preparing Wheel Seats of Type 3 Crankpins

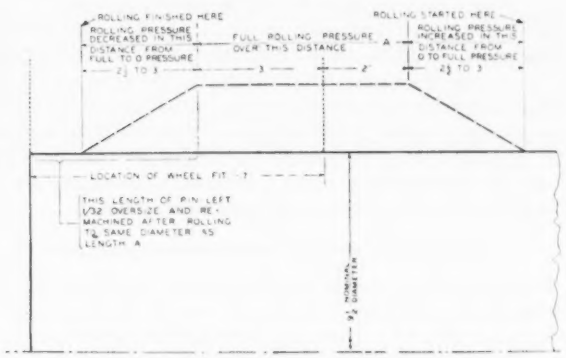


Fig. 6 Rolling Diagram for Crankpin Wheel Seats, Type 3

same diameter as the pin at the section where it was rolled at full pressure.

The reduction in pin diameter due to rolling varied between 0.0013 in. on some wheel seats to 0.0028 in. on others. A highly polished finish was obtained from rolling. Following the rolling and machining operation, the wheel was mounted on the crankpin, using the A.A.R. white lead and linseed oil mixture.

Type 4 Pins—Flame-Hardened

Crankpins were flame-hardened in a vertical position[16] while rotating at 260 rpm, as shown in Fig. 7. Before preparing fatigue specimens, four different case depths were investigated by flame-hardening $9^1/_2$-in. rounds. The speed of the lead screw was

[16] A circular gas head and water quench ring assembly surrounded the pin, which moved vertically along the axis of the pin by means of a motor-driven lead screw. A series of twenty flame heads, with seven tips (No. 56 drill size) per head, constituted the heating ring. A special water-quenching ring $10^1/_2$ in. diam was mounted directly below the heating head.



FIG. 7 METHOD OF FLAME-HARDENING WHEEL-FIT PORTION OF CRANKPINS

changed to give four different flame speeds which resulted in the hardness gradients shown in Fig. 8. Some softening may take place at the surface, but this soft layer is ground off before the wheel is mounted.

Two separate groups of crankpins were flame-hardened for fatigue tests. In the first group, eight crankpin wheel seats were flame-hardened so as to obtain a case depth of approximately 1/4 in., using a flame speed of 2 3/4 in. per min. The wheel seats of all pins were magnafluxed after flame-hardening and before grinding to determine if thermal cracks had developed on the surface during flame treatment. All wheel seats were found to be cracked. Considerable difficulty was encountered in grinding the wheel seats as these thermal cracks progressed deeper with the grinding. It was necessary to remove 0.071 to 0.108 in. stock from the diameter of each wheel seat to eliminate all traces of the thermal cracks.

It was believed that the thermal cracks found on the first group of pins could be eliminated by using a modified flame-hardening procedure,[17] so six additional crankpin wheel seats were flame-hardened. The flame speed was increased from 2 3/4 ipm used on the first group to 3 1/8 ipm on the second group of crankpins. The gas consumption was 0.25 cu ft per sq in. of pin surface which compares with 0.35 obtained on the first group. Both groups of pins were stress-relieved after hardening for 8 hr in an oil bath heated to 400 F. The surface hardness on the wheel fit ranged from 66 to 70 scleroscope on the first group of eight, as compared with 72 on the second group of six wheel seats. This hardness generally increased appreciably after the soft skin had been removed in the grinding operation.

This second group of pins were magnafluxed after flame-hardening, and all wheel seats were found to be cracked, but not as severely as those of the first group of flame-hardened pins. Four of these wheel seats were ground before fitting to wheels and the other two were not ground before mounting the wheels.[18] On this second group, it was necessary to remove only 0.038 to 0.040

[17] The thermal cracks which developed in the first group of crankpins were tentatively attributed to the cold quenching water used, so that the quench water was heated to approximately 85 F, for the second group. It was also believed that a case of less depth would require less surface heating and reduce the tendency to develop thermal cracks.

[18] The wheel seats on both ends of crankpin No. 4 were not cracked in the region of the outside hub face, but only in the region of the inside hub face. Crankpin No. 4 was therefore selected to be used for test where the wheel seat was not ground.

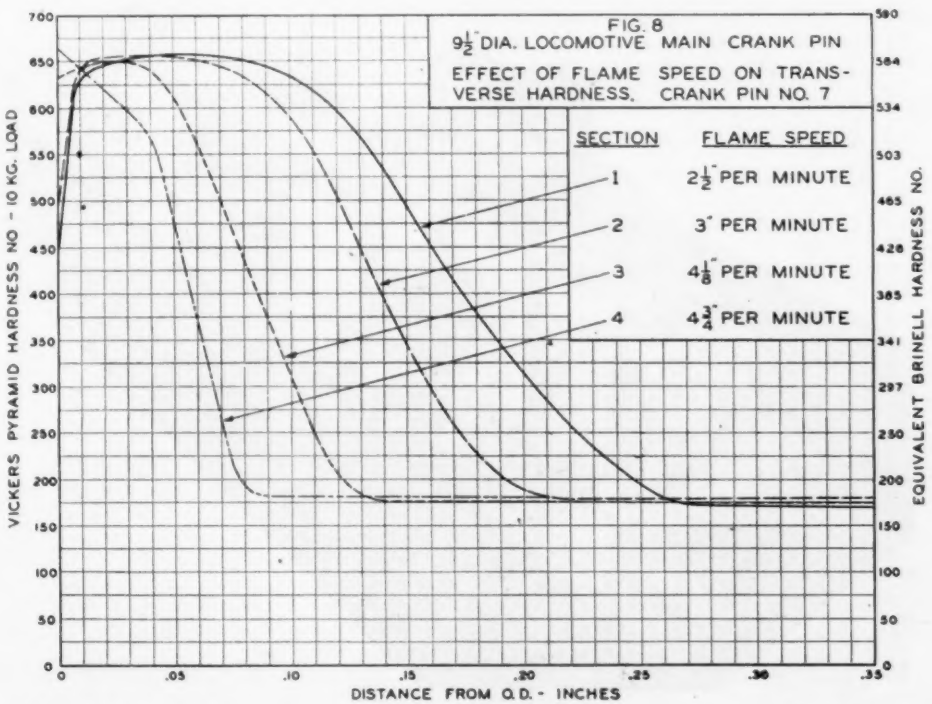


FIG. 8 EFFECT OF FLAME SPEED ON TRANSVERSE HARDNESS OF 9 1/2-IN-DIAM LOCOMOTIVE MAIN CRANKPIN, NO. 7

in. stock on the diameter. Magnaflux examination after grinding indicated that all quench cracks had been removed from the critical section of the four wheel seats.[19]

Method of Testing

A typical wheel-and-crankpin assembly ready for fatigue test is shown in Fig. 9. The machine in which these pins were tested is illustrated in Fig. 10. The crankpin is tested as a rotating cantilever beam,[20] as shown diagrammatically in Fig. 11. The wheel mounted on the crankpin is bolted at the rim to a flanged head located on either end of the main spindle of the testing machine. A constant spring load is applied on the end of the crankpin opposite the end on which the wheel is mounted. After one wheel seat is tested on the long crankpin[21] the pin is

[19] There was still some indication of thermal cracks at the inside and unstressed end of the wheel fit, but inasmuch as they were well away from the test section they were allowed to remain. A thermal crack found in the region of the test section of wheel seat No. 8R was outside the wheel fit and on this account was not removed. After the completion of the fatigue test on this pin, the depth of the crack had not increased, as determined from a micrographic study.

[20] See reference 3, First Progress Report, p. 26. The A.A.R. recommended design practice is 16,000 psi allowable stress for main crankpins but crankpins on locomotives are not subjected to a complete stress reversal. It is recognized that these laboratory tests impose a complete stress reversal and give a much lower endurance limit than would be obtained if the pins were subjected to the stress range of actual service operation which varies from about zero to a maximum stress value. Abnormal stresses from locomotive operation are also discussed. This divergence between road operation and laboratory testing should not influence the value of comparative data presented here. Also see "The Design of Railway Axles and Crankpins," by R. Eksergian, Trans. A.S.M.E., vol. 60, 1938, p. 153.

[21] See reference 3, First Progress Report, p. 5, for reasons that crankpins for test purposes were longer than those used in service. This length influences direct shearing stresses but they do not usually exceed 2000 psi. Such stresses are small compared with the bending and press-fit stresses in the pin and should have little or no influence of practical importance on the value of these comparative tests.

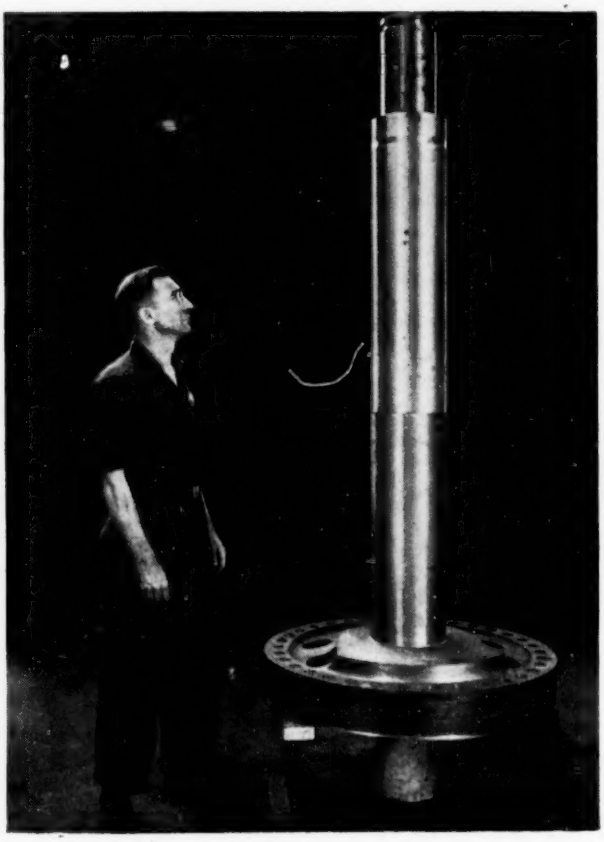


Fig. 9 Crankpin Assembly Ready for Fatigue Test

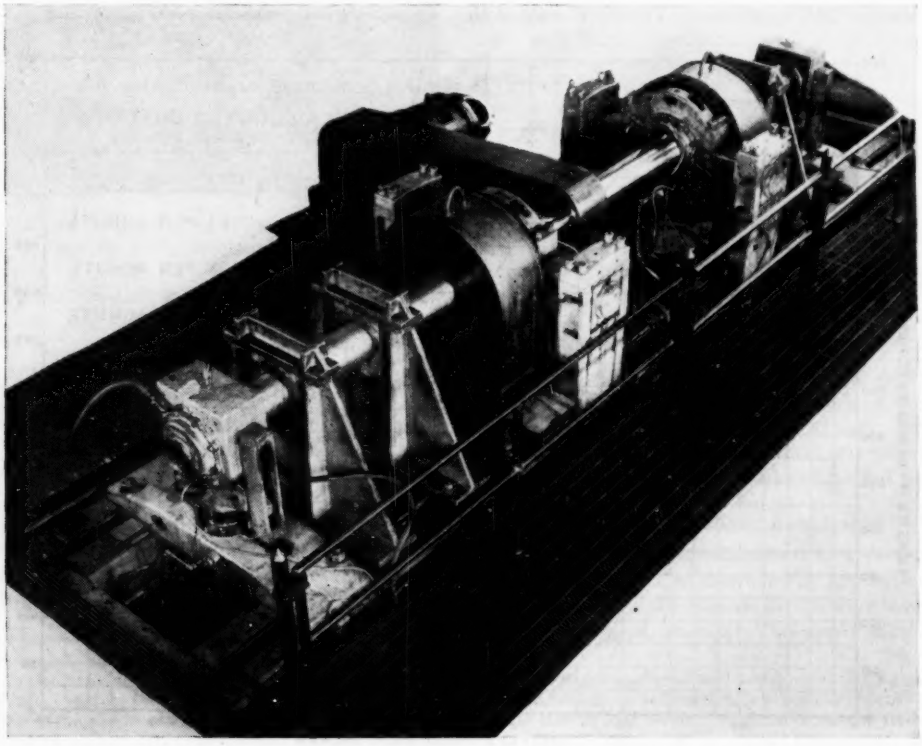


Fig. 10 Double-Ended Cantilever Beam Fatigue Machine With 9 1/2-In-Diam Crankpins in Test

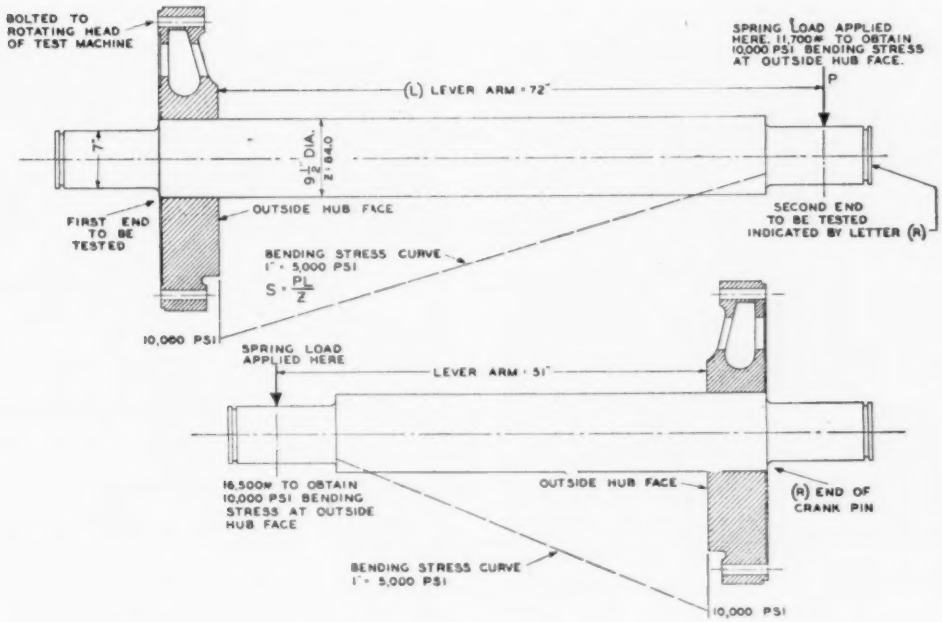


FIG. 11 CRANKPIN TEST ASSEMBLY

reversed, and a wheel is mounted on the opposite end for a second fatigue test in accordance with Fig. 11. Crankpin bending-stress values given in this report are nominal stresses in the pin at the outside hub face of the wheel, calculated on the basis of the elementary beam formulas, given in Fig. 11.

All crankpins were tested at 1500 rpm for a duration of about 85,000,000 revolutions, which is equivalent to 300,000 miles (not necessarily locomotive miles) on 72-in. wheels, unless the pin failed before that time. The wheels were then pressed off and the wheel fit magnafluxed, and photomicrographs made through any fatigue cracks which were detected.

RESULTS OF FATIGUE TEST

Type 1 Crankpins. Fatigue tests were completed on fifteen type 1 crankpins at stress levels from 5000 through 22,000 psi, and the test results are given in the comparison Table 3, and S-N diagram, Fig. 12. It will be noted that nine of these crankpins broke off in the wheel fit, and the lowest stress at which breaking-off occurred was 12,000 psi, after running an equivalent of 160,500 miles (45,000,000 revolutions). Tests made at the lowest stress level of 5000 psi developed fatigue cracks 0.0045 in. deep in the wheel fit after an equivalent of 309,000 miles (86,700,000 revolutions).

A typical fatigue fracture for any type of pin is illustrated in Fig. 13, showing how the crankpin breaks off a short distance inside the wheel fit.

On the basis of these tests, the safe allowable bending stress to prevent breaking off of type 1 pin inside the wheel fit is 11,000 psi and to prevent fatigue cracks initiating is some value less than 5000 psi.

Type 2 Crankpins. Fatigue tests were completed on twelve type 2 crankpins at stress levels from 5000 through 19,000 psi. The results are given in Table 3 and shown in S-N curves, Fig. 12, in comparison with tests made on the other types. Only two type 2 crankpins broke off in the wheel fit; these occurred at 16,000 and 19,000 psi bending stress after 20,800 and 14,850 equivalent miles (5,840,000 and 4,160,000 revolutions), respectively. Tests made at the lowest stress level of 5000 psi developed fatigue cracks 0.003 in. deep in the wheel fit after an equivalent 321,000 miles (90,000,000 revolutions).

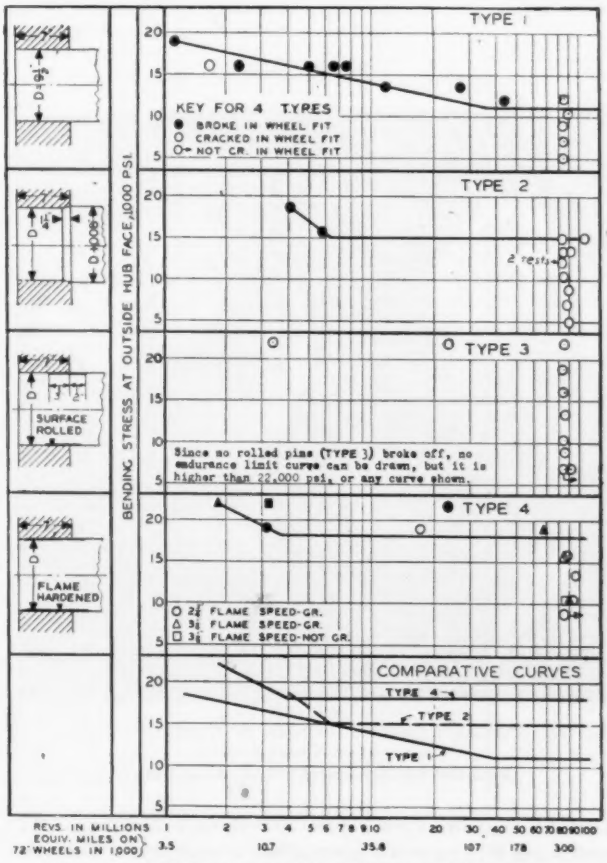


FIG. 12 S-N CURVES FOR FOUR TYPES OF CRANKPINS

Type 3 Crankpins. Fatigue tests were completed on ten type

TABLE 3 A.A.R. FATIGUE TESTS ON VARIOUS TYPES OF 9½-IN-DIAM LOCOMOTIVE MAIN CRANKPINS[a]

BENDING STRESS AT OUTSIDE HUB FACE psi	TYPE 1 Straight Fit				TYPE 2 Str.5-3/4"; .008" Taper 1-1/4				TYPE 3 Rolled Fit				TYPE 4 Flame Hardened Fit			
	PIN NO.	REVS. IN MILLIONS	EQUIV. MILES 72" WHEELS	CONDITION OF WHEEL FIT AFTER TEST	PIN NO.	REVS. IN MILLIONS	EQUIV. MILES 72" WHEELS	CONDITION OF WHEEL FIT AFTER TEST	PIN NO.	REVS. IN MILLIONS	EQUIV. MILES 72" WHEELS	CONDITION OF WHEEL FIT AFTER TEST	PIN NO.	REVS. IN MILLIONS	EQUIV. MILES 72" WHEELS	CONDITION OF WHEEL FIT AFTER TEST
22,000	25R2	0.783	1,393	Broken					29	87.3	311,000	Cr. 0.205"†	24	23.4	83,700	Broken †
									17	3.47	12,400	Cr. .052"*	6	1.84	6,560	Broken †
									9	22.9	81,600	Cr. .143"*	4	3.23	11,500	Broken †
19,000	13R	1.14	3,920	Broken	3R	4.16	14,850	Broken	20R	86.2	307,000	Cr. .087" †	8	68.7	245,000	Broken †
													22R	3.16	11,150	Broken †
													24R	17.45	62,200	Cr. .129"* †
16,000	13RR	1.66	5,920	Cr.0.560"	28	5.84	20,800	Broken	30	86.8	310,000	Cr. .029"	23	89.0	317,500	Cr. .016"
	28R	2.36	8,420	Broken									8R	88.6	316,000	Cr. .062" †
	7	5.00	17,820	Broken												
	7R	7.74	27,600	Broken												
	21	6.67	23,800	Broken												
15,000					16	84.7	302,000	Cr. .144"								
					16R	106.2	379,000	Cr. .087"								
13,500	1	27.13	96,750	Broken	1R	85.4	304,500	Cr. .068"	17R	88.7	316,000	Cr. .0095	22	96.4	343,500	Cr. .037"
	11R	11.68	41,600	Broken	11	91.4	325,800	Cr. .125"								
12,000	19	87.6	312,500	Cr. .1065	19R	84.3	300,000	Cr. .064"								
	10	45.0	160,500	Broken	10R	84.4	301,000	Cr. .059"								
10,500	26	89.0	317,500	Cr. .0295	26R	86.1	307,000	Cr. .059"	27	84.4	301,000	Cr. .004"	25R	94.1	335,500	Cr. .0053"
													4R	84.3	300,000	Cr. .090"
													6R	88.5	315,000	Cr. .014" †
9,000	5	85.8	306,000	Cr. .028"	5R	90.0	321,000	Cr. .038"	27R	84.3	300,000	Cr. .0018	23R	84.5	301,500	Not Cr.
7,000	21R	85.5	305,000	Cr. .0075	13	86.8	310,000	Cr. .009"	30R	84.8	302,000	Not Cr.	Wheel fit of crank pins 4 & 4R not ground. All other flame hardened wheel fits ground.			
									20	91.7	327,000	Cr. .005"				
5,000	3	86.7	309,000	Cr. .0045"	9R	90.0	321,000	Cr. .003"	Pin 11R tested with high press fit same as Type 2							

Pins nos. 1 through 20 and 27 through 30 from one heat and pins nos. 21 through 26 from another heat.
† Indicates spoke wheel - all others double plate
* Wheel Failed

[a] Material: Crankpins—A.A.R. Spec. M-104-37, Class A.N.& T.; wheel centers—M-201-36, Grade B.

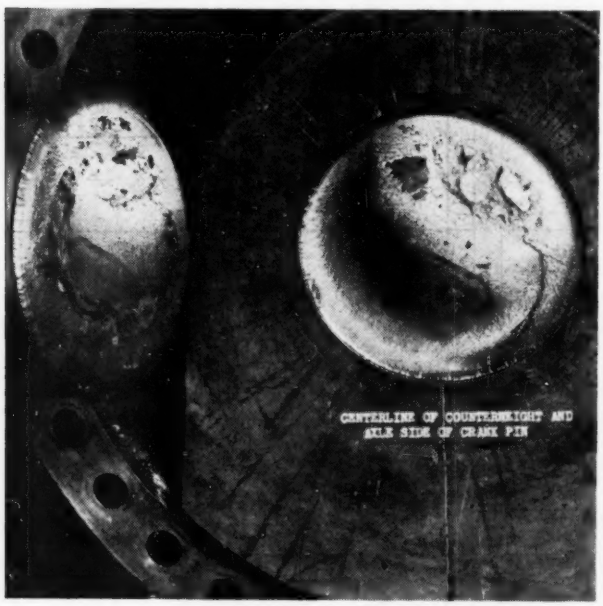


FIG. 13 TYPICAL FATIGUE FRACTURE IN WHEEL-FIT PORTION OF CRANKPIN, TYPES 1 AND 2
(Note that failure initiated toward axle side of pin.)

3 crankpins at stress levels from 7000 through 22,000 psi. The results and S-N curve are summarized in comparison with other types of crankpins in Table 3 and Fig. 12. None of these crankpins broke off during the entire test so that the endurance limit is greater than 22,000 psi. Eight of these pins completed their test run of 300,000 equivalent miles (85,000,000 revolutions), and two pin tests were discontinued at 12,400 and 81,600 equivalent miles (3,470,000 and 22,900,000 revolutions), because the wheels in which they were mounted developed fatigue failure. While no pins broke off even at stresses as high as 22,000 psi, nine of these ten pins exhibited fatigue cracks in the wheel-fit portion, as determined by magnaflux and micrographic examination made after the fatigue test. A typical failure of this kind is illustrated in Fig. 14, indicating a band of numerous fatigue cracks having a maximum depth of 0.085 in. after 307,000 equivalent miles (86,200,000 revolutions) at 19,000 psi.

Type 4 Crankpins. Results obtained from fatigue tests on thirteen flame-hardened pins are shown in Table 4, as well as in Table 3 and S-N curve in Fig. 12, where the results are compared with those from the other three types of crankpins. A fatigue fracture, illustrated in Fig. 15, developed late in life after 245,000 equivalent miles (68,700,000 revolutions). After opening up the crack, it was found to be 5½ in. deep. On the basis of these data, type 4 pin, ground after flame-hardening, has an allowable fatigue strength of 16,000 to 18,000 psi against breaking off in the wheel fit.

DISCUSSION OF FATIGUE TESTS

Propagation of Fatigue Cracks. Even after running any of the four types of crankpins at bending stresses below the endurance-limit value, at which they broke off in the wheel fit, it was found that fatigue cracks were present. These cracks were found in the pin, just inside the wheel fit, after a fatigue test of 300,000 equivalent miles (85,000,000 revolutions). In each case the maximum depth of the fatigue cracks in every pin was measured as given in Table 3. A straight-line relationship appears to exist between this crack depth and the bending stress when these values are plotted logarithmically as was done in Fig. 16.

In the case of type 1 pin, for example, the slope portion of the curve, Fig. 16, shows a linear relationship up to a stress of 12,000 psi, at which stress the pin breaks off. The upper portion of the curve being a horizontal line indicates that at 12,000 psi the

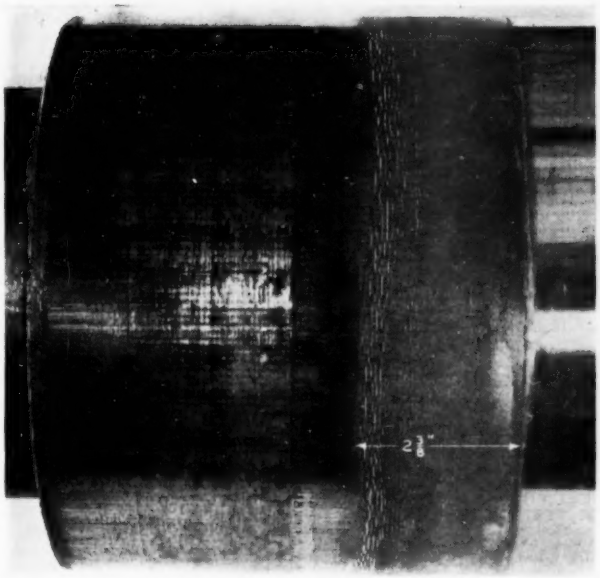


FIG. 14 TYPICAL FATIGUE FAILURE IN WHEEL-FIT PORTION OF SURFACE-ROLLED PIN, TYPE 3
(Dimension indicates distance that fatigue cracks extend inside wheel fit from the hub face of the wheel.)

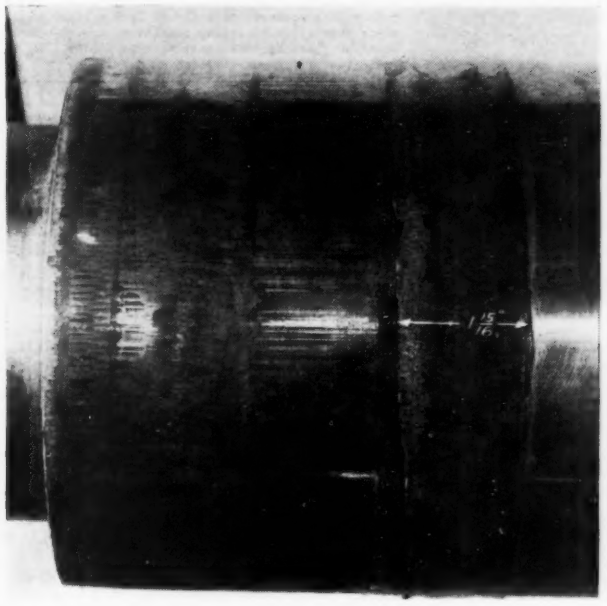


FIG. 15 TYPICAL FATIGUE FAILURE IN WHEEL-FIT PORTION OF FLAME-HARDENED PIN, TYPE 4
(Dimension indicates distance that fatigue cranks extend inside wheel fit from the hub face of the wheel.)

TABLE 4 COMPARISON OF FATIGUE TESTS ON FLAME-HARDENED CRANKPINS

	FLAME SPEED: 2-3/4" per min.						FLAME SPEED: 3-1/8" per min.											
	WHEEL FIT GROUND						WHEEL FIT GROUND						WHEEL FIT NOT GROUND					
					WHEEL DATA						WHEEL DATA						WHEEL DATA	
Bending Stress at Outside Hub Face psi	Pin No.	Revs. in Mill-ions	Remarks Regarding Condition of Wheel Fit After Test	Case Depth, Ins & R_c Surface Hardness	Fit on Dia., in.	Mount-ing Tons	Pin No.	Revs. in Mill-ions	Remarks Regarding Condition of Wheel Fit After Test	Case Depth, Ins & R_c Surface Hardness	Fit on Dia., in.	Mount-ing Tons	Pin No.	Revs. in Mill-ions	Remarks Regarding Condition of Wheel Fit After Test	Case Depth, Ins & R_c Surface Hardness	Fit on Dia., in.	Mount-ing Tons
22,000	24	23.4	Broken ‡	.200" 53.5/54	.0200	210	6	1.84	Broken ‡	.145" 53.5/54.5	.0198	205	4	3.23	Broken ‡	.130" 54/55	.0160	150
19,000	22R	3.16	Broken ‡	.165" 50/55	.0210	90	8	68.7	Broken ‡	.155" 54/55	.0195	125						
	24R	17.45	Cr..129"	.210" 53.5/54.5	.0200													
16,000	23	89.0	Cr..016"	.200" 54.5/55	.0113	87	8R	88.6	Cr..062"‡	.175" 53/53.5	.0195	105						
13,500	22	96.4	Cr..037"	.205" 54.5	.0163	100												
10,500	25R	94.1	Cr..0053"	.170 55/55.5	.0150	105	6R	88.5	Cr. .014"‡	.125" 54.5/55	.0153	125	4R	84.3	Cr..090"	.125"	.0155	115
9,000	23R	84.5	Not Cr.		.0155	90												

Pins nos. 1 through 20 and 27 through 30 were from one heat and pins nos. 21 through 26 from another heat.

"Wheel Failed

‡ Indicates Spoke Wheel-all others double plate

Case depth of flame hardened layer was obtained by measurement on Macroetch.

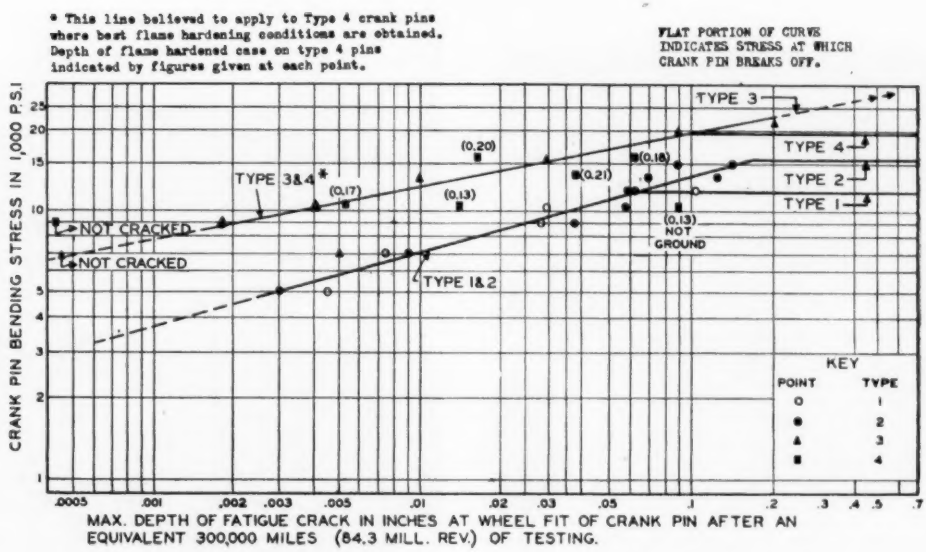


FIG. 16 COMPARATIVE PROPAGATION OF FATIGUE CRACKS IN CRANKPIN WHEEL SEATS

fatigue crack becomes infinitely deep, meaning that the pin will break off as found in these tests.

The slope portion of a similar curve drawn for type 2 pins, Fig. 16, coincides with that drawn for type 1 crankpins, except that the upper end of the slope extends toward a higher stress of 16,000 psi before the pin breaks off, whereas type 1 pin breaks off at 12,000 psi. This graphical analysis indicates that the fatigue cracks tend to initiate and propagate in both types 1 and 2 crankpins in the same manner up to 12,000 psi.[22]

All points showing crack depth for rolled pins, Fig. 16, fall close to the line drawn except for one point at 7000 psi. Two crankpins were tested at a stress of 7000 for 300,000 equivalent miles (85,000,000 revolutions); one pin was found not cracked, while the other had a maximum crack depth of 0.005 in. Even at 22,000 psi, the fatigue crack was only 0.205 in. deep after an equivalent 300,000 miles. At 16,000 psi both types 1 and 2 pins broke off after 17,820 to 27,600 equivalent miles, whereas type 3 pin at the same stress was only cracked 0.016 in. deep after over 10 times the mileage, or 300,000 equivalent miles.

The graphic relationship between crack depth and bending stress, Fig. 16, indicates considerable scatter for type 4 flame-hardened pins. It is believed, however, that the curves for types 3 and 4 pins would be about the same up to 19,000 psi, assuming best flame-hardening conditions.

A further graphical comparison may be drawn between the ratio of the crack depth of types 1 and 2 pins with type 3, as shown in Fig. 17. Here the full-line ratio curves are calculated from the curves in Fig. 16, and these ratios are shown on the lower horizontal scale; the broken line and the upper horizontal-crack-depth scale in Fig. 17 are merely repeated from Fig. 16. These studies, Figs. 16, 17, indicate that the fatigue-crack depth and its propagation for the rolled pin (type 3) were only a fraction of what was found on the unrolled pins (types 1 and 2). Therefore type 3 pin offers a means of increasing greatly the factor of safety over types 1 and 2 against breaking off in service and/or

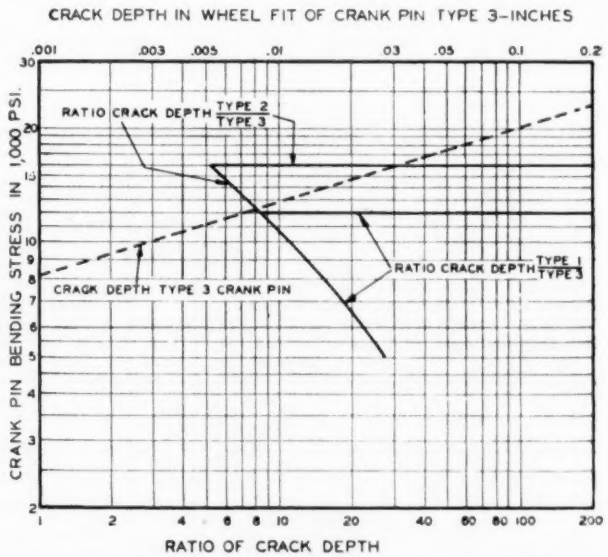


FIG. 17 RATIO OF FATIGUE-CRACK DEPTH IN TYPES 1 AND 2 CRANKPINS TO THAT IN TYPE 3

(Flat horizontal portion of ratio curves indicates infinite crack depth at bending stress at which crankpin breaks off in the wheel fit.)

increasing present safe mileage limits already established on types 1 and 2 pins.

The question often arises as to how deep below the surface the rolling penetrates, and this was investigated on a typical rolled pin No. 27. Photomicrographs were made to detect changes in structure in the longitudinal plane of the rolled portion of the wheel fit, as shown in Fig. 18. It is apparent that the structure at the surface is little, if any, changed from that $^{5}/_{8}$ in. below the surface. This does not mean that changes have not taken place, as X-ray examinations made on similar cold-worked pieces have indicated structural displacements in the cold-worked layer. A hardness survey in Fig. 19 was also made in a longitudinal plane through the surface and core layers. The Vickers hardness is increased from 180 at the surface before rolling to about 230 after rolling and drops off in a linear manner to a penetration of about

[22] An interesting speculation may be made by extrapolating the lower portion of the sloped line as shown by the dotted lines. It indicates that at even 3000 psi fatigue cracks 0.0005 in. deep would develop. Conclusions based on such extrapolation are dangerous, but the curve does help explain the practical findings in service, in that fatigue cracks initiate at very low bending stresses.

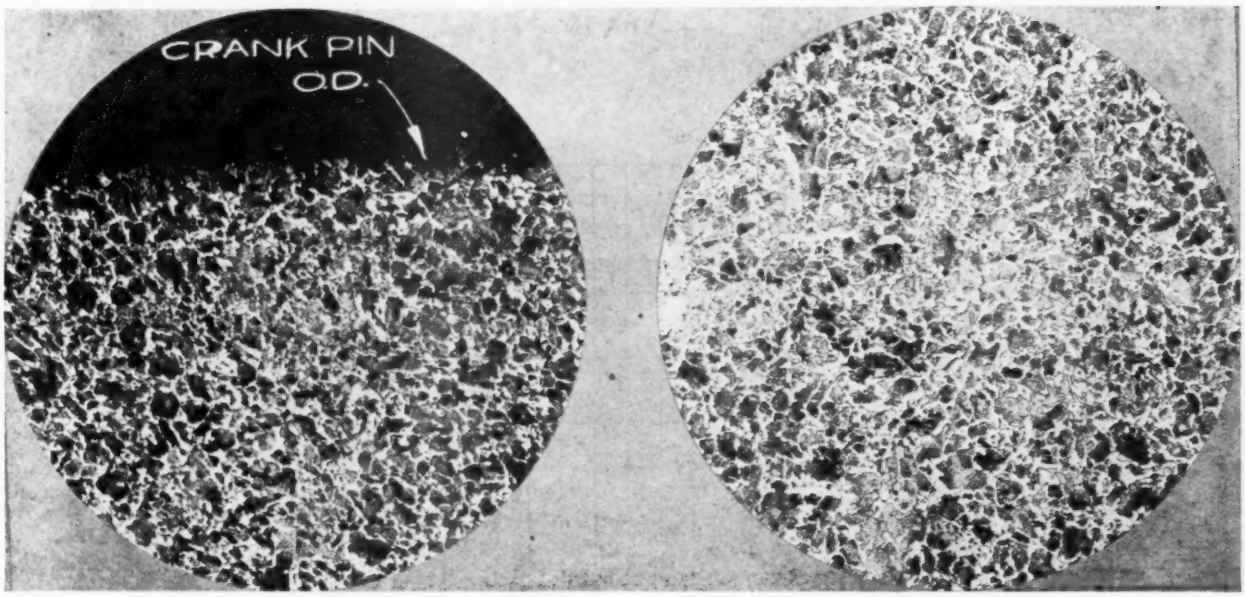


FIG. 18 PHOTOMICROGRAPH OF SURFACE AND CORE LAYERS OF CRANKPIN AFTER SURFACE-ROLLING; ×90

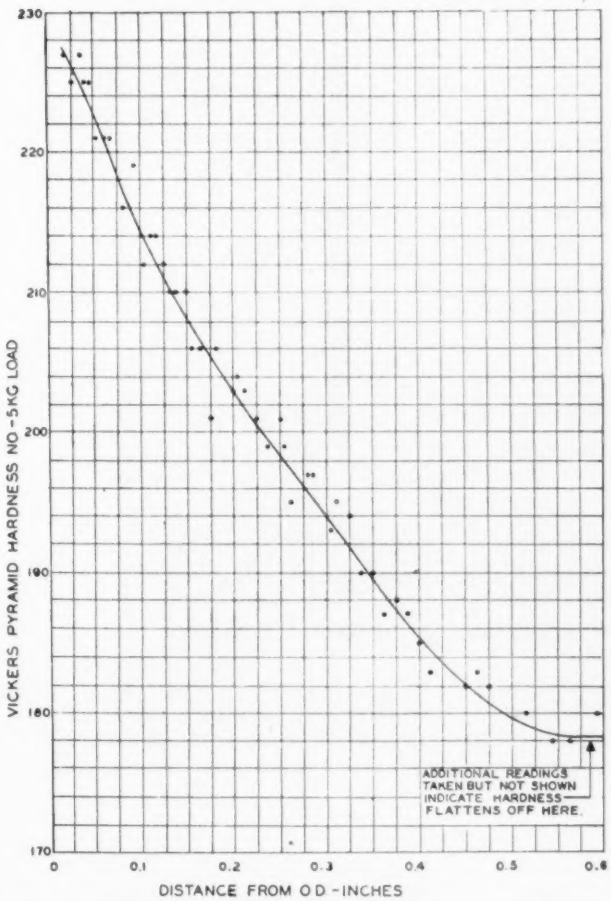


FIG. 19 HARDNESS GRADIENT OF SURFACE LAYER OF ROLLED CRANKPIN

$^{9}/_{16}$ in. below the surface to the original hardness of about 180.[23]

It is interesting to note from Table 4 and Fig. 16, that the crack depths on the rolled pins (type 3) ranged from 0.005 in. deep at 7000-psi stress to 0.205 in. deep at 22,000 psi. This cold-worked layer $^{1}/_{2}$ in. deep certainly offers much increased resistance to the fatigue crack propagating through this layer than the pins with the unrolled surface.

Flame-Hardened Pins of Type 4. There are not sufficient data in Tables 3 and 4 from tests on flame-hardened pins to draw general conclusions as to the influence on fatigue strength of the factors of case depth and whether the pins should or should not be ground after flame-hardening. The trend of the results, however, does show that the deeper case depths lead to a higher endurance-limit value as well as less depth of fatigue crack after 300,000 equivalent miles (85,000,000 revolutions) than the shallow case. If the pin is not ground after flame-hardening and before mounting the wheel, then the fatigue resistance seems to be lower than if the wheel seat is ground.

Photomicrographs and hardness surveys made on pins after the fatigue test are shown in Fig. 20, for a flame speed of $3^{1}/_{8}$ ipm, and in Fig. 21, of $2^{3}/_{4}$ ipm.

A number of pins were found to have thermal cracks after fatigue-testing which were not detected by magnaflux[24] before testing. None of the thermal cracks found showed any evidence of having propagated during the fatigue test.[25] Fig. 22 shows a photomicrograph through a thermal crack found in a highly stressed region of pin No. 23 after test. Some of the pins which broke off in the fatigue test (Table 4) may have fractured through

[23] Similar micrographic and hardness studies were made on rolled sections cut transverse to the axis of the pin but the findings were in close agreement with those just given made on the horizontal planes.

[24] Both wet and dry methods were used as discussed in reference (3), first report, p. 20, and second report p. 28. High surface residual compressive stresses from flame-hardening may press sides of crack together and make detection difficult with 3000-ampere a-c unit used here.

[25] Such thermal cracks are opened up during the fatigue testing and were detected by magnaflux and also by etch examinations of longitudinal slices through wheel fit of pin. Thermal cracks follow the grain boundaries while fatigue cracks pass through the grains.

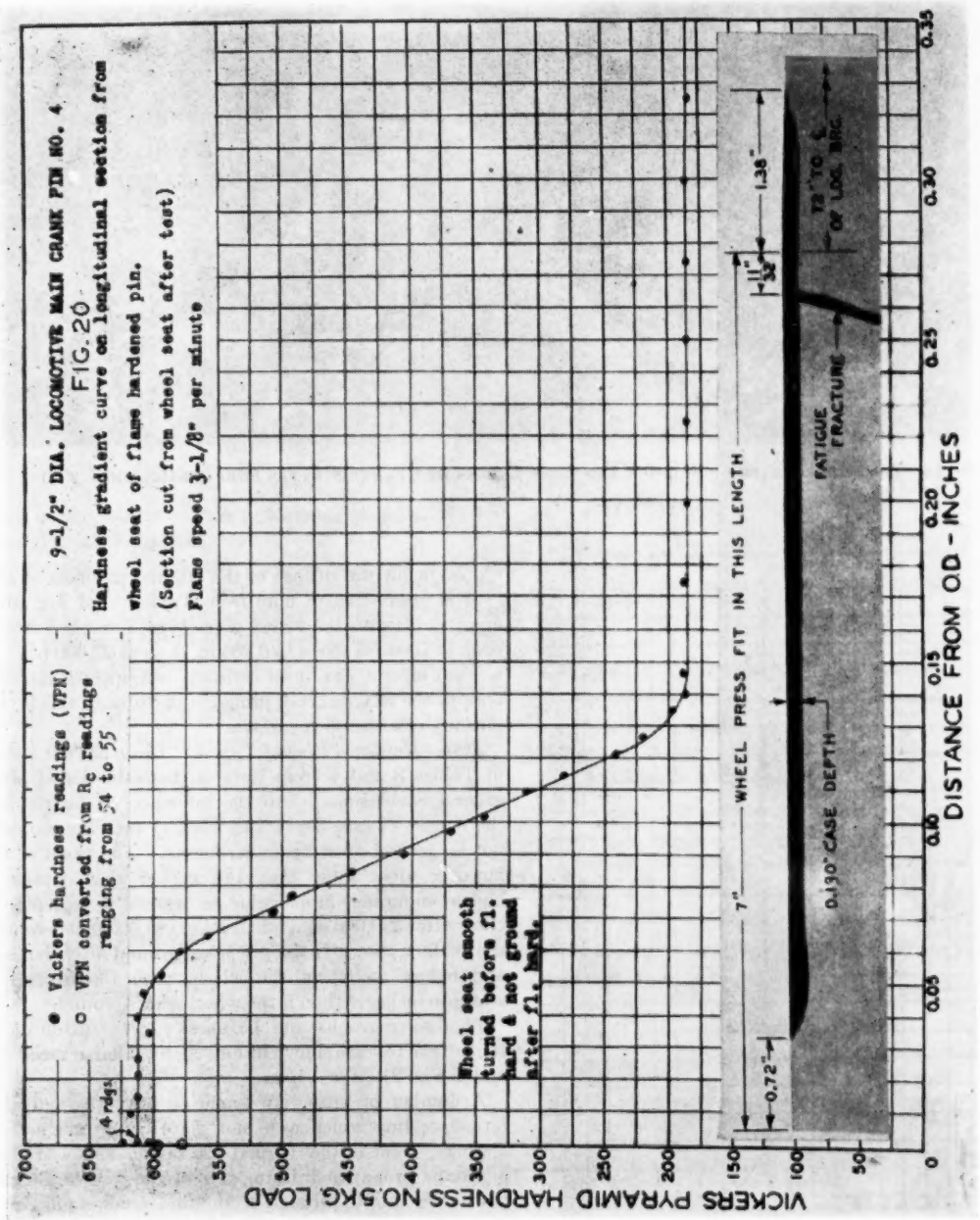


FIG. 20 HARDNESS GRADIENT CURVE ON LONGITUDINAL SECTION FROM WHEEL SEAT OF FLAME-HARDENED PIN OF 9½-IN-DIAM LOCOMOTIVE MAIN CRANKPIN NO. 4
(Section cut from wheel seat after test. Flame speed 3⅛ ipm.)

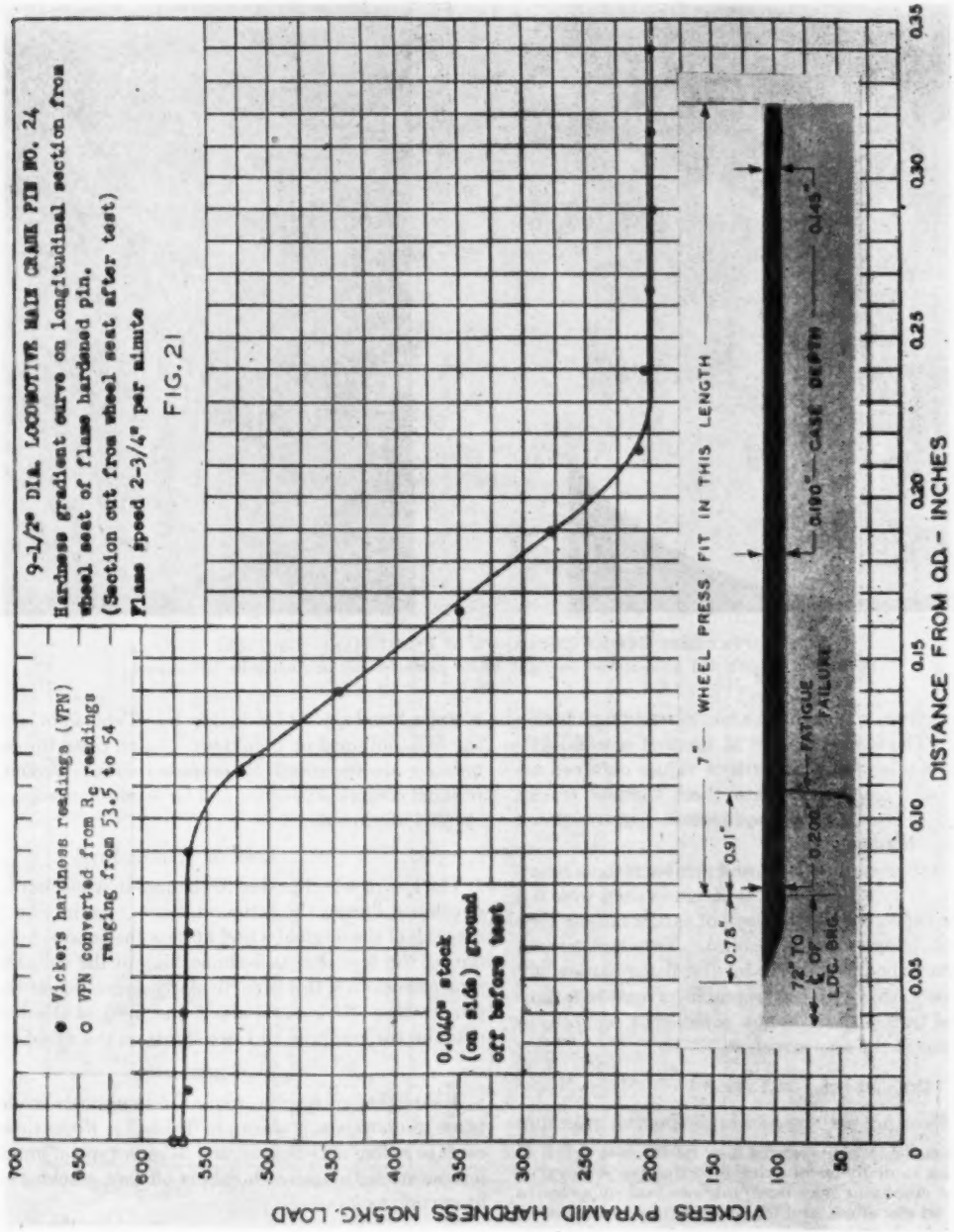


FIG. 21 HARDNESS GRADIENT CURVE ON LONGITUDINAL SECTION FROM WHEEL SEAT OF FLAME-HARDENED PIN OF 9½-IN-DIAM LOCOMOTIVE MAIN CRANKPIN NO. 24
(Section cut from wheel seat after test. Flame speed 2¾ ipm.)

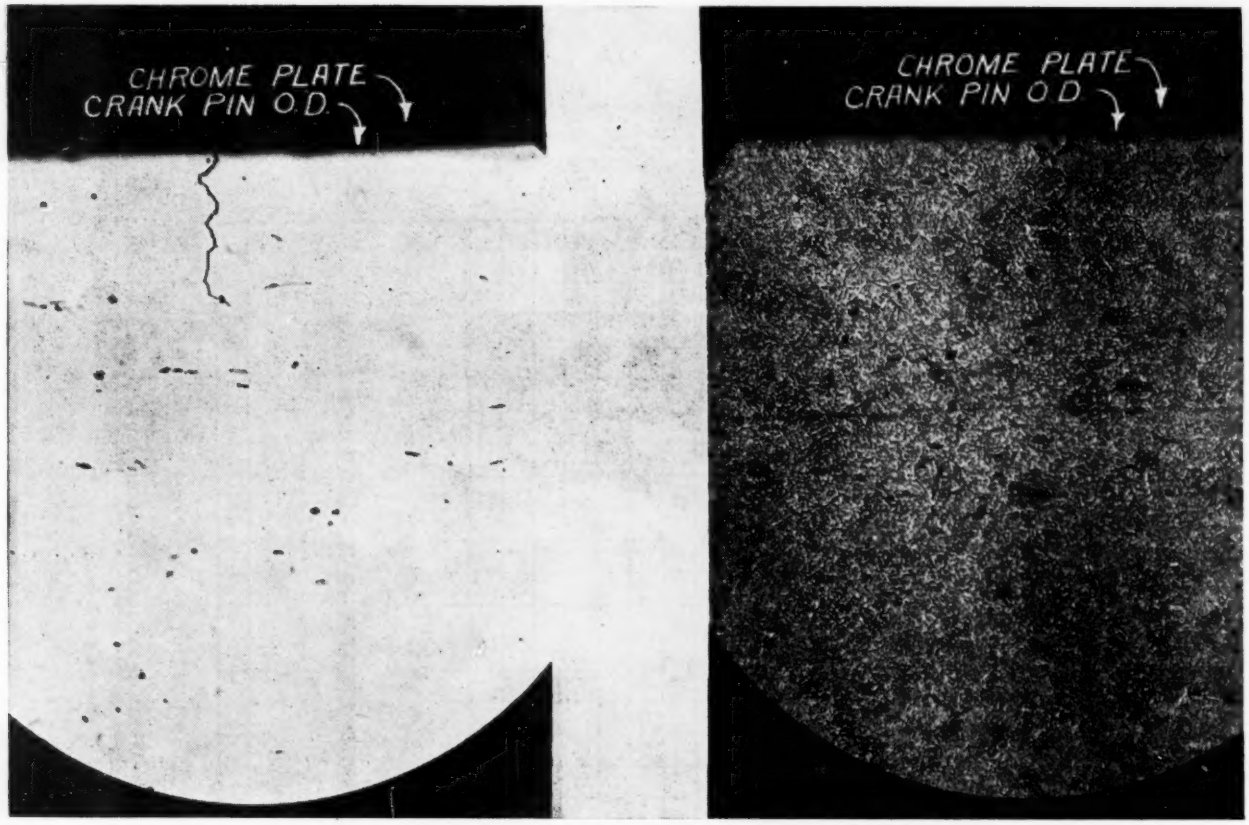


FIG. 22 THERMAL CRACKS ON SURFACE OF FLAME-HARDENED PINS; ×75
(Unetched on left and nital-etched on right where crack follows original grain boundaries.)

a thermal crack, but there was no means for determining whether this was the case. The mere presence of thermal cracks introduces some doubt as to whether the fatigue values obtained are influenced by thermal cracks. Despite these thermal cracks, the flame-hardened pins still gave improved fatigue resistance over type 1 not flame-hardened.

While the flame-hardened pins indicated greater fatigue resistance than exhibited by types 1 and 2, the fatigue values were not as high as would be expected[26] on the basis of earlier fatigue tests of press-fitted members presented in Table 5. Very high surface residual stresses established in the surface after flame-hardening[27] are believed to be associated with the favorable increase in fatigue resistance indicated, although it is not possible to separate or appraise the influence of the case structure.

ROLLED PINS OF TYPE 3

A review of the literature with respect to the fatigue resistance of press-fitted assemblies is shown in Table 6, in comparison with the data obtained on crankpins. In all cases the fatigue characteristics are improved by surface rolling. Presence of surface residual compressive stress and/or strain-hardening is responsible for this improvement.

LOSS OF WHEEL FIT

The loss of wheel fit due to changes in wheel bore and crankpin developed during the fatigue test is given in Fig. 23. In some cases all of the original wheel fit near the outside hub face was lost during the test due to bellmouthing of the wheel bore and rubbing corrosion;[28] this is particularly noticeable at the high crankpin stresses. In general about one third of this loss of fit takes place on the crankpin and two thirds on the wheel center.

CONCLUSIONS

A summary of results from all fatigue tests made on the four types of crankpins is shown in Table 7. From these data a percentage rating may be assigned to each type of crankpin as to its fatigue strength against breaking off (not cracking) in the wheel-fit portion as follows:

	Per cent
Type 1	100
Type 2	136
Type 3	Over 200
Type 4	146 to 164

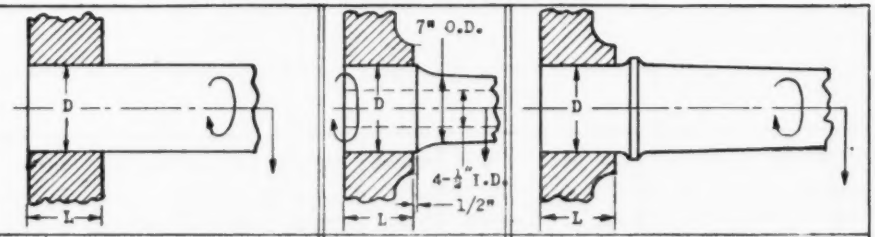
[26] Some explanation for this divergence may be (*a*) case depth or relative depth of case to diameter of axle; (*b*) excessive removal of stock ground off the crankpins may leave low residual compressive stresses on surface; (*c*) size effect, and (*d*) presence of thermal cracks on crankpins. All members in Table 5 except $9^1/_2$-in. pins were flame-hardened by spinning method when entire length of hardened area was heated and quenched at one time and no thermal cracks were detected. Disadvantages of this method are large gas demand and quenching large areas. Crankpins were done by progressive spinning method so that a relatively short length of wheel fit was heated and quenched at one time. This latter method was used on axle wheel seats 8 in. diam without thermal cracking, but axles were preheated to 200 F before hardening.

[27] "Correlation of Residual Stresses in the Fatigue Strength of Axles," by O. J. Horger and H. R. Neifert, JOURNAL OF APPLIED MECHANICS, Trans. A.S.M.E., vol. 64, 1942, p. A-85.

[28] The presence of rubbing corrosion found on all 50 pins tested was accompanied by fatigue cracks with exception of one pin (Type 3, No. 30R, at 7000 psi). Some fundamental work was reported on such corrosion, "Investigation of the Fretting Corrosion of Closely Fitted Surfaces," by G. A. Tomlinson, P. L. Thorpe, and H. J. Gough, Journal and Proceedings of The Institution of Mechanical Engineers, vol. 141, 1939, pp. 223–249.

TABLE 5 COMPARISON OF FATIGUE RESISTANCE OF VARIOUS FLAME-HARDENED WHEEL FITS

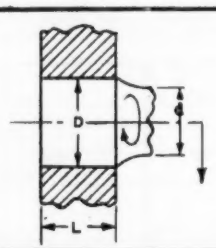
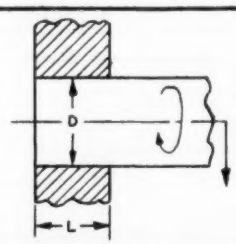
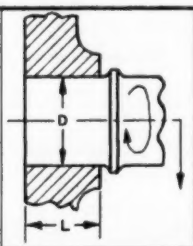
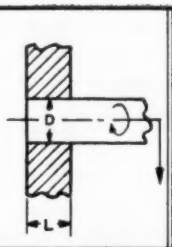
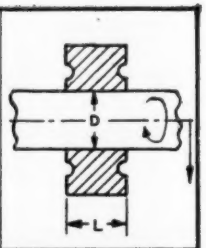
Hub Material Kind Steel	BHN
(a)0.27-0.32% C Cstg.	143-149
(b)0.67-0.82% C St.Forg.	237-249
(c)0.67-0.82% C Forgings	285-321



D, in. (References in brackets)		(3) 9 1/2"		(30) 2"		(27,29) 7 9/16"		(27,29) 1 3/4"		(31) 7"	(29)
L, in.		7"		1 3/8"		7"		1 3/4"		7"	
Ratio, D/L; Hub Material		1.35 (a)		1.45 (b)		1.08 (b)		1 (c)		1 (b)	
No. of Specimens tested		15	13	48	12	4	3	24	8	27	2
FH = Flame Hard.; NFH = Not Flame Hard.		NFH	FH	NFH	FH	NFH	FH	NFH	FH	NFH	FH
Flame Hardened Area	Case Depth, In.	-	1/8 to 1/4"	-	5/16"	-	3/4"	-	13/32"	-	1/2"
	Surface Hard. Equiv. BHN	178	495 to 560	215	530	240	550	182	580	187	560
Phys.Prop. at Surface before Flame Hardening - for Axle	Tensile Strength,psi.	92,000		88,800		103,500 - 106,000		91,000		93,800	
	Yield Point,psi.	50,200		47,800		61,000 - 63,500		53,000		51,500	
	Elong, % in 2"	25.7		32		22.0 - 23.0		25.0		22.7	
	Red. of Area, %	49.2		48.5		41.9 - 42.2		45.4		36.8	
	Izod, ft.lbs.	20.2		-		13 - 16		-		10.3	
Chemistry from O.D. Axle Turnings	C %	0.51		0.45-0.49		0.50		0.46		0.48	
	Mn %	0.79		0.67-0.77		0.73		0.58		0.57	
	Si %	0.30		0.20-0.26		0.27		0.22		0.24	
Allowable Max. Bending Stress in Crank Pin or Axle to prevent	Initiation of Fatigue Cracks,psi.	<5,000	<10,500	8,000	25,000	12,500	19,000*	9,000	25,000	9,000	-
	Breaking off of Crank Pin or Axle, psi.	11,000	16,000 to 18,000	13,000	>45,000	12,000	>22,000	11,000	>35,000	11,000	>21,200

[29] "Passenger Car Axle Tests," Fifth Progress Report, May 27, 1941, Official Mechanical Engineer, Association of American Railroads, Chicago, Ill.
[30] "Fatigue Strength of 2-In. Axles With Surfaces Metal-Coated and Flame-Hardened," by O. J. Horger and T. V. Buckwalter, Proceedings of the A.S.T.M., vol. 40, 1940, pp. 733-743.
[31] Same as (29) but Third Progress Report, June 1, 1939.
* Two axles tested at 19,000 psi; one was not cracked in wheel fit after 159,000 equivalent miles while the second was cracked 0.005 in. deep after an equivalent 175,000 miles.

TABLE 6 COMPARISON OF FATIGUE RESISTANCE OF VARIOUS COLD-ROLLED WHEEL FITS

Hub Material Kind Steel BHN (a)0.27-0.32% C Catg. 143-149 (b)0.67-0.82% C St.Forg. 237-249 (c)0.67-0.82% C Forgings 285-321 (e)0.06-0.13% C;Ult.54,000 psi;El.22% (f)0.42% C; Ult.73,800 psi El. 34% R.A. 51%															
D and d, in. (Ref. in brackets) L, in. Ratio, D/L; Hub Material		(8) 11½"-10-5/8" 8" 1.44 (a)		(32)7-9/16"- 6-3/4" 7" 1.08 (b)		(3) 9-1/2" 7" 1.35 (a)		2" 1-3/8" 1.45 (b)		(29) 1-3/4" 1-3/4" 1 (c)		(33) 0.55" - - (e)		(5) 1-5/8" 1-1/2" 1.08 (f)	
N.R.= not rolled; R.= rolled		N.R.	R.	N.R.	R.	N.R.	R.	N.R.(30)	(8) R.	N.R.	R	N.R.	R.	N.R.	R.
No. of assemblies tested		7	4	14	6	15	10	48	31	24	25	-	-	-	-
Cold Rolled Surface	Depth of rolled surface	-	-	-	-	-	9/16"	-	-	-	-	-	-	-	-
	Surface Hardness Equivalent BHN	192	-	187	-	178	230	215	-	182	-	-	-	-	-
Phys.Prop. at Surface before Cold Rolling - for axle	Tensile Strength,psi.	93,000		93,800		92,000		88,800		91,000		95,000		73,800	
	Yield Point,psi.	65,000		51,500		50,200		47,800		53,000		54,000		37,200	
	Elong.% in 2"	27.5		22.7		25.7		32		25.0		22.0		34.0	
	Red.of Area, %	69.0		36.8		49.2		48.5		45.4		-		51.0	
	Izod, Ft.Lbs.	-		10.3		20.2		-		-		-		-	
Chemistry from O.D.Axle Turnings	C, %	0.27		0.49		0.51		0.45-0.49		0.46		0.57		0.42	
	Mn, %	(Ni 3.1%) 0.9		0.57		0.79		0.67-0.77		0.58		0.55		0.62	
	Si, %	0.29		0.24		0.30		0.20-0.26		0.22		0.29		0.15	
Allowable Max. Bending Stress in Crank Pin or Axle to prevent:	Initiation of Fatigue Cracks,psi.	<10,500	<10,500	12,000	-	<5,000	<7,000	8,000	9,000	9,000	10,500	-	-	-	-
	Breaking off of Crank Pin or Axle, psi.	15,000 to 18,000	>19,000	14,000	>17,000	11,000	>22,000	13,000	34,000	11,000	>38,000	22,000	38,000	18,700	23,800

[8] Additional unpublished data from reference (8).
[22] Same as (29) but Sixth Progress Report, Sept. 17, 1942.
[33] "Der Einfluss von Einspann—und Kraftangriffsstellen auf die Dauerhaltbarkeit," by A. Thum and F. Wunderlich, *Zeitschrift des Vereines deutscher Ingenieure*, vol. 77, 1933.

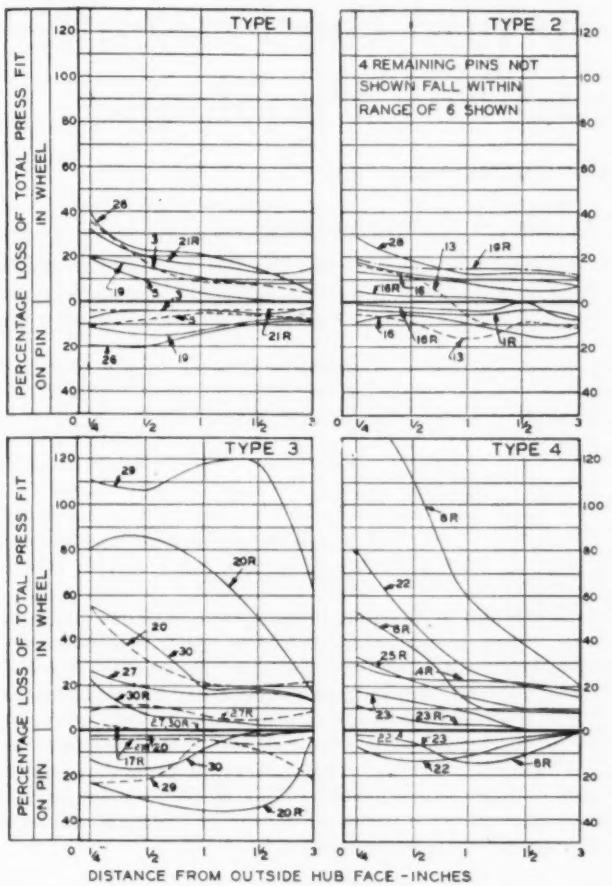
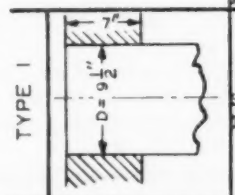
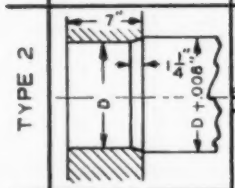
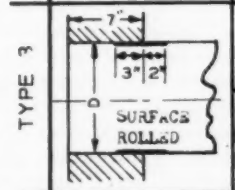
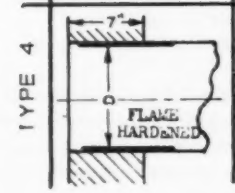


FIG. 23 COMPARISON CURVES SHOWING LOSS OF WHEEL FIT, ALL TYPES
(Basis of 30,000 equivalent miles.)

TABLE 7 SUMMARY OF FATIGUE TESTS

	No. of Crank Pin Fits Tested & Surface Finish	Allowable Max. Bending Stress in Wheel Seat to Prevent Breaking off of Crank Pin. P.S.I.	%
TYPE 1 	15 Smooth Turned	11,000	100
TYPE 2 	12 Smooth Turned	15,000	136
TYPE 3 	10 Smooth Turned Then Rolled	Greater than 22,000	Greater than 200
TYPE 4 	11 Ground After Flame Hardening	16,000 to 18,000	146 to 164

ACKNOWLEDGMENTS

Appreciation is extended to the railroad members of the Association of American Railroads, Crankpin Committee, who guided this research; K. Cartwright, Chief Mechanical Engineer, New York, New Haven & Hartford Railroad; E. L. Bachman, General Superintendent Motive Power, Pennsylvania Railroad; J. B. Blackburn, Mechanical Engineer, Chesapeake & Ohio Railroad; G. W. Bohannon, Assistant Chief Mechanical Officer, Chicago & North Western Railroad; also H. R. Neifert, Supervisory Research Engineer, and F. M. Dieringer, Engineer, both of The Timken Roller Bearing Company, who carried out the actual testing.

No difficulty was experienced with the preparation of types 1, 2, and 3 crankpins. Some difficulty was experienced with thermal cracks developing in the flame-hardening of type 4 pins. Caution should be exercised in the application of flame-hardening as the procedure followed here was too critical, and fatigue values much lower than those given here could be obtained, depending on the degree to which thermal cracks are produced in flame-hardening and removed by grinding.

This project is being continued and fatigue tests are now being made on quenched and tempered crankpins as well as on pins of various designs.

On Dimensional Analysis and the Presentation of Data in Fluid-Flow Problems

By E. R. VAN DRIEST,[1] CAMBRIDGE, MASS.

The method and application of dimensional analysis are discussed, making use of the fundamental concept of function. The π theorem is restated and proved in general form.

Pipe friction, drag of spheres, and flow through Venturi meters are examples used to illustrate the rearrangement of dimensionless products of a relationship to obtain the most convenient form for presentation of data.

Introduction

THROUGH a comprehensive paper published in 1914, E. Buckingham[2] formally introduced dimensional analysis to the scientific world. It was in this paper that the famous theorem, commonly known as the Buckingham π theorem, was first explicitly stated. Although a concise form of proof of the theorem was given, it has not been readily understandable to the student of fluid mechanics. Furthermore, the young scientist has difficulty in understanding the process of rearrangement of the dimensionless products of a relationship to obtain the most convenient form for presentation of the data. In an attempt to clarify this situation, the present paper was written.

Purpose of Dimensional Analysis

The principal purpose of dimensional analysis from the engineering point of view is the arrangement of the variables of a physical relation so that, without destroying the generality of the relationship, it may be more easily determined experimentally. The method is particularly valuable when the number of variables is so great (usually four or more) that the data cannot be plotted conveniently using a co-ordinate axis for each variable. By dimensional analysis it is possible to arrange the variables into a lesser number of dimensionless groups which can be represented on co-ordinate axes.

Two or three variables can be plotted as (*a*) and (*b*) of Fig. 1, while four variables would require repetitions of (*b*), five would require repetitions of graphs for four, etc. The advantage of reducing the number of quantities to be plotted is obvious, not only because of the simplicity of presentation of the data, but also because of the possibility of determining an analytical formula for the general function.

Function Concept and Grouping of Variables

The variable Q_1 is said to be a function of the variables $Q_2, Q_3, Q_4, \ldots Q_n$, if for some values of $Q_2, Q_3, Q_4, \ldots Q_n$ there correspond values of Q_1. This idea is written symbolically as

$$Q_1 = f(Q_2, Q_3, Q_4, \ldots Q_n) \quad [1]$$

It is absolutely essential to note that this concept is written in symbolic form because it does not have to be expressible by an analytical formula; indeed a graph is sufficient to indicate the relationship.

Once such a function is established or assumed, then a function will still exist even after the variables are intermultiplied in any manner whatsoever. For example, taking

$$z = f(x, y)$$

the following functions will exist

$$z = f_1(xy, y), \quad xz = f_2(x, x^2y)$$

or

$$x^a y^b z = f_3(xy^c z^d, x^e y z^g), \text{ etc.}$$

The principle of dimensional homogeneity will now be introduced. The principle states that each and every term of a correct physical equation must have the same dimensions. Hence if Equation [1] is a correct physical relation, and the left-hand side is made dimensionless in any manner, the right-hand side must also become dimensionless, which means that each variable of the right-hand side is combinable with other variables of the equation to form a dimensionless product. Thus by the foregoing process of intermultiplication, Equation [1] can be written in the nondimensional form as symbolized by

$$\pi_1 = \phi(\pi_2, \pi_3, \pi_4, \ldots \pi_n) \quad [2]$$

If in any assumed physical relation any Q is not combinable with any other Q's to form a dimensioness product, then that Q cannot appear in the original function. In such cases the corresponding π in Equation [2] would be zero. This dimensionless grouping is therefore a method of eliminating, early, those variables which cannot appear in an assumed function. Further, if any π's of Equation [2] are necessarily the same to satisfy the condition of dimensional homogeneity, then that is the way in which the Q's forming those π's must appear in the function. An example of this latter case occurs when two length variables appear in a function along with other variables that do not contain the length dimension; to satisfy the condition of dimensional homogeneity, the two length variables would have to appear as a ratio. Such early grouping of the variables is another advantage of the use of the principle of dimensional homogeneity.

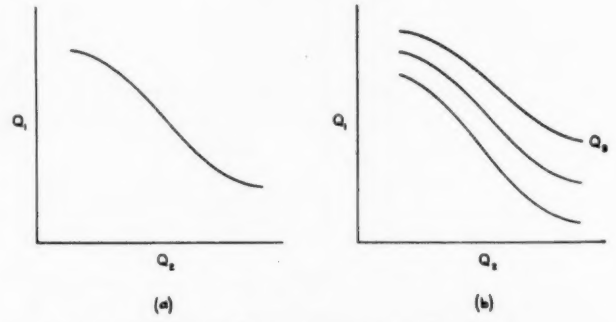


FIG. 1 GRAPHICAL REPRESENTATION OF FUNCTIONS

---

[1] Assistant Professor of Mechanical Engineering, Massachusetts Institute of Technology. Mem. A.S.M.E.

[2] "On Physically Similar Systems: Illustrations of the Use of Dimensional Equations," by E. Buckingham, *Physical Review*, second series, vol. 4, 1914, pp. 345–377.

Contributed by the Applied Mechanics Division and presented at the Annual Meeting, New York, N. Y., Nov. 26–29, 1945, of THE AMERICAN SOCIETY OF MECHANICAL ENGINEERS.

Discussion of this paper should be addressed to the Secretary, A.S.M.E., 29 West 39th Street, New York, N. Y., and will be accepted until April 10, 1946, for publication at a later date. Discussion received after the closing date will be returned.

NOTE: Statements and opinions advanced in papers are to be understood as individual expressions of authors and not of the Society.

While the two cases of the preceding paragraph show some results of the use of dimensional analysis, yet the greatest advantage of the method lies in the fact that through its use it is not necessary to write out n π's, one for each variable of the original function, but only i π's, where $i < n$, unless the Q's are all dimensionless, whereupon $i = n$. Equation [2] then becomes

$$\pi_1 = \phi(\pi_2, \pi_3, \pi_4, \ldots \pi_i) \ldots\ldots\ldots\ldots\ldots\ldots [3]$$

Such a result has obviously great value since by reducing the number of π's in Equation [2], the function may be plotted on a reduced number of co-ordinates.

The π Theorem

The number of dimensionless groups that are necessary to represent Equation [2] completely is of course the number of independent π's that can form, by proper combination, any other possible π's. It will be seen that this number depends upon the number of variables involved and the greatest number of variables which will not form a dimensionless product.

Theorem. The number of independent dimensionless products is $i = n - k$, where k is the greatest number of Q's that will not combine to form a dimensionless product, or, in other words, where k is the number of Q's whose units can be used to measure all the variables. The number k cannot exceed m, the number of fundamental dimensions used to measure the variables in the mass, length, time, etc., system.

The number k cannot exceed m because any greater number of Q's than m always will form a dimensionless product. To prove this, first write an expression for any π using more than m Q's, say, $(m + 1)$ Q's; thus

$$Q_1^{x_1} Q_2^{x_2} \ldots Q_m^{x_m} Q_{m+1}^{x_{m+1}} = \pi \ldots\ldots\ldots\ldots [4]$$

If the dimensions of Q are given by, say

$$p_1^{a_1} p_2^{a_2} \ldots p_m^{a_m} = [Q]$$

where $p_1, p_2, \ldots p_m$ are the fundamental dimensions measuring Q, then the dimensional equation for Equation [4] will be

$$(p_1^{a_1} p_2^{a_2} \ldots p_m^{a_m})^{x_1} (p_1^{b_1} p_2^{b_2} \ldots p_m^{b_m})^{x_2} \ldots (p_1^{\alpha_1} p_2^{\alpha_2} \ldots p_m^{\alpha_m})^{x_m} (p_1^{\beta_1} p_2^{\beta_2} \ldots p_m^{\beta_m})^{x_{m+1}} = [\pi] = 1 \ldots [5]$$

Equating the exponents to zero in order to eliminate each p results in m equations as follows

$$\left.\begin{array}{ll} p_1: & a_1x_1 + b_1x_2 + \ldots + \alpha_1x_m + \beta_1x_{m+1} = 0 \\ p_2: & a_2x_1 + b_2x_2 + \ldots + \alpha_2x_m + \beta_2x_{m+1} = 0 \\ \ldots\ldots & \ldots\ldots\ldots\ldots\ldots\ldots\ldots\ldots\ldots \\ p_m: & a_mx_1 + b_mx_2 + \ldots + \alpha_mx_m + \beta_mx_{m+1} = 0 \end{array}\right\} \ldots [6]$$

Since the set of m homogeneous Equations [6] has $(m + 1)$ unknowns, it will yield solutions of x other than zero; it follows that any greater number of Q's than m will always form a dimensionless product.

Proceeding with the proof of the theorem, assume that the number k has been determined. Then, in order to form a π containing $(k + 1)$ Q's, there must exist a sufficient number of independent π's to eliminate, upon combination, the $n - (k + 1) = n - k - 1$ remaining Q's; furthermore, to form a π containing less than $(k + 1)$ Q's, it will still be necessary to eliminate only $(n - k - 1)$ Q's because the extra Q's to be eliminated can be chosen to be noncombinable with the Q's forming the particular π and hence will automatically disappear. The elimination process is shown as follows: The grouping of i independent π's to form a certain π will appear algebraically thus

$$\pi_1^{x_1} \pi_2^{x_2} \ldots \pi_i^{x_i} = \pi$$

whence

$$(Q_1^{a_1} Q_2^{a_2} \ldots Q_{n-k-1}^{a_{n-k-1}} \ldots Q_n^{a_n})^{x_1} (Q_1^{b_1} Q_2^{b_2} \ldots Q_{n-k-1}^{b_{n-k-1}} \ldots Q_n^{b_n})^{x_2} \ldots (Q_1^{\alpha_1} Q_2^{\alpha_2} \ldots Q_{n-k-1}^{\alpha_{n-k-1}} \ldots Q_n^{\alpha_n})^{x_i} = \pi \ldots [7]$$

where the exponents are, of course, different from those of Equation [5]. In order to eliminate a Q, the exponents of that Q must be made to vanish. Hence when $(n - k - 1)$ Q's are to disappear, there will result $(n - k - 1)$ equations as follows, if, say, the first $(n - k - 1)$ Q's are to be eliminated

$$\left.\begin{array}{ll} Q_1: & a_1x_1 + b_1x_2 + \ldots + \alpha_1x_i = 0 \\ Q_2: & a_2x_1 + b_2x_2 + \ldots + \alpha_2x_i = 0 \\ \ldots\ldots & \ldots\ldots\ldots\ldots\ldots\ldots\ldots\ldots\ldots \\ Q_{n-k-1}: & a_{n-k-1}x_1 + b_{n-k-1}x_2 + \ldots + \alpha_{n-k-1}x_i = 0 \end{array}\right\} \ldots [8]$$

Now, since Equations [8] are homogeneous in the variables x_1, x_2, $\ldots x_i$, solutions other than $x_1 = x_2 = \ldots = x_i = 0$ will exist provided there are more unknowns than equations. Hence a sufficient condition that any π can be formed by i independent π's is that $i = n - k$. It is to be noted that this elimination process is precisely the same as that by which fundamental dimensions were caused to vanish in the formation of a π from a set of Q's.

In order to complete the proof of the theorem it must also be shown that $i = n - k$ is a necessary condition that any π can be formed, or in other words, that s independent π's, where $s < n - k$, can never represent all the possible π's. To demonstrate this, observe that $n - k$ independent π's can always be found by merely taking any set of k Q's, noncombinable among themselves, and combining them with each of the remaining Q's in turn. Since this set of $n - k$ independent π's can represent all the other possible π's by the foregoing reasoning, it can of course form one of the s π's. This new one of the s π's can then be substituted for one of the $(n - k)$ π's that definitely contributed to the formation of the new π, thus creating a new set of $n - k$ independent π's. Using this new set of $(n - k)$ π's, another of the s π's, other than that one already obtained belonging to the s set, can be formed and substituted for one of the new set. After all of the s π's are constructed and substituted in succession, it is seen that there are still $n - k$ independent π's, including the s π's. Hence, since the remaining $(n - k - s)$ π's are independent of the s π's, a lesser number of independent π's than $n - k$ can never represent all possible dimensionless products.

Although it is seen that any $i = n - k$ independent π's will represent all possible dimensionless groups that can be formed by the variables of a function, the simplest procedure to follow in selecting $n - k$ independent π's is to take a certain set of k Q's that will not form a dimensionless product and combine them with each of the remaining Q's in turn.

The π theorem is therefore proved in general without any assumption as to the form of the original function or the use of any complex mathematics. It is to be noted that in the foregoing statement of the theorem, $n - m$ is not necessarily the number of independent π's required to specify a function, since more may be needed depending upon the problem at hand. The procedure, however, is to see if any m Q's can be found which will not form a dimensionless product, and if all sets of m Q's will form such a product, then to continue down until the greatest number is found.

As an example, consider the propeller problem where the thrust T is assumed to be a function of the axial velocity V, the diameter D, the rotational speed N, the density of the fluid ρ, and the viscosity of the fluid μ. In symbolic form

$$T = f(V, D, N, \rho, \mu) \ldots\ldots\ldots\ldots\ldots [9]$$

The number of fundamental dimensions m involved is three, viz.,

mass, length, and time, and three variables can be found which will not form a dimensionless quantity; hence $n - k = n - m = 6 - 3 = 3$ independent π's will be necessary to represent the function. They may be chosen at random as

$$\frac{T}{\rho V^2 D^2}, \quad \frac{\rho V^2}{N\mu}, \text{ and } \frac{T}{\rho N^2 D^4}$$

to represent Equation [9] by

$$\frac{T}{\rho V^2 D^2} = \phi\left(\frac{\rho V^2}{N\mu}, \frac{T}{\rho N^2 D^4}\right)$$

or, systematically, by taking three of the variables, say, ρ, D, V, that will not form a π, and combining them with each of the remaining variables giving

$$\frac{T}{\rho V^2 D^2}, \quad \frac{VD\rho}{\mu}, \text{ and } \frac{V}{ND}$$

to represent Equation [9] by

$$\frac{T}{\rho V^2 D^2} = \psi\left(\frac{VD\rho}{\mu}, \frac{V}{ND}\right)$$

It will be of interest to note the number of possible dimensionless groups that can be formed by the n variables. The combinations of n variables taken $k + 1$ at a time are given by

$$\frac{n!}{(k+1)!(n-k-1)!}$$

which gives for the propeller example, $\frac{6!}{4!.2!} = 15$. Written out, these are

$$\frac{T}{\rho V^2 D^2}, \frac{T\rho}{\mu^2}, \frac{T}{\rho N^2 D^4}, \frac{T\rho}{\mu^2}, \frac{TN^2}{\rho V^4}, \frac{T\rho}{\mu^2}, \frac{T}{VD\mu}, \frac{V}{ND}, \frac{T}{\mu N D^2}, \frac{TN}{\mu V^2},$$
$$\frac{VD\rho}{\mu}, \frac{V}{ND}, \frac{ND^2\rho}{\mu}, \frac{\rho V^2}{N\mu}, \frac{V}{ND}$$

The products $\frac{T\rho}{\mu^2}$ and $\frac{V}{ND}$ appear more than once so that there are eleven different π's available from the six variables. This example shows clearly how the problem of almost hopeless plotting of one variable in terms of five variables can be readily reduced to that of the plotting of one variable quantity against but two.

As another illustration, consider the case of a fluid flowing through an orifice, and assume that the velocity V depends only on the difference in pressure Δp, and the density of the fluid ρ, or

$$V = f(\Delta p, \rho) \quad \ldots\ldots\ldots\ldots\ldots\ldots [10]$$

Now, although the number of fundamental dimensions is three, viz., mass, length, and time, the greatest number of variables which will not form a dimensionless product is 2. Therefore, there will be $3 - 2 = 1$ independent π to yield

$$\phi\left(\frac{\rho V^2}{\Delta p}\right) = 0.$$

and $\frac{\rho V^2}{\Delta p}$ will be a constant. This is a very simple case where k is less than m; it shows the generality of the π theorem as stated.

Another example of where k is less than m can be found by adding a compressibility term to the variables of Equation [10]. Accordingly

$$V = f_1(\Delta p, \rho, E)$$

where E is the modulus of compressibility of the fluid. Since $k = 2$, there will appear 2 independent π's thus

$$\frac{V}{\sqrt{\frac{\Delta p}{\rho}}} = \phi_1\left(\frac{V}{\sqrt{\frac{E}{\rho}}}\right)$$

The Physical Interpretation of Dimensionless Products

Sometimes it is helpful to attach a physical interpretation[3] to the dimensionless products of a function. The heat-transfer problem lends itself readily to such a treatment and therefore will be used as an example.

Considering the transfer of heat q to or from a liquid of mean cross-sectional temperature θ_m flowing in a smooth pipe with wall at temperature θ_w, the film coefficient $h = \frac{q}{\theta_w - \theta_m}$ is found to be a function of the diameter D, the mean velocity V the density ρ, the viscosity μ, the specific heat c, and the thermal conductivity k, or

$$h = f(D, V, \rho, \mu, c, k)$$

There are four fundamental dimensions which describe these quantities, viz., mass, length, time, and temperature, and four quantities are available which will not form a dimensionless product. Hence, $7 - 4 = 3$ independent π's exist and a set can be found easily by choosing D, μ, ρ, and k as basic. There follows

$$\frac{hD}{k} = \phi\left(\frac{VD\rho}{\mu}, \frac{c\mu}{k}\right)$$

In this equation, $\frac{hD}{k}$ is called the Nusselt number, $\frac{VD\rho}{\mu}$ the Reynolds number, and $\frac{c\mu}{k}$ the Prandtl number.

Now the rate of heat transfer by molecular action is given by

$$q_m = k\frac{d\theta}{dy} \quad \ldots\ldots\ldots\ldots\ldots\ldots [11]$$

where θ is the mean temperature at a point. Furthermore, the heat transfer by turbulent action can be written similarly

$$q_t = k'\frac{d\theta}{dy} \quad \ldots\ldots\ldots\ldots\ldots\ldots [12]$$

where k' can be called the turbulence coefficient of thermal conductivity. Division of Equation [12] by Equation [11] gives

$$\frac{q_t}{q_m} = \frac{k'}{k} \quad \ldots\ldots\ldots\ldots\ldots\ldots [13]$$

But q_t can be placed equal to the product of a local heat-transfer coefficient h_L and the differential temperature $d\theta$, thus

$$q_t = h_L d\theta$$

so that

$$k' = h_L dy$$

and Equation [13] becomes

$$\frac{q_t}{q_m} = \frac{h_L dy}{k}$$

a local Nusselt number which is a function of the over-all Nusselt number $\frac{hD}{k}$. It is therefore seen that the Nusselt number is a

[3] "The Analogy Between Fluid Friction and Heat Transfer," by Th. von Kármán, Trans. A.S.M.E., vol. 61, 1939, pp. 705–710.

dimensionless quantity which can be thought of as the ratio of turbulent heat transfer to molecular heat transfer.

The Reynolds number can be interpreted in a similar way by first writing for the turbulent shear stress

$$\tau_t = \rho\epsilon \frac{dv}{dy} = \rho \sqrt{\overline{v_y'^2}}\, l \frac{dv}{dy} = \sqrt{\overline{v_y'^2}}\, l \frac{d(\rho v)}{dy} \quad \ldots\ldots [14]$$

where v is the mean velocity, v_y' the transverse-velocity fluctuation, l the mixing length at a point, and ϵ the turbulence-exchange coefficient. For molecular shear

$$\tau_m = \mu \frac{dv}{dy} = \frac{\mu}{\rho} \frac{d(\rho v)}{dy} \quad \ldots\ldots\ldots\ldots [15]$$

The ratio of Equations [14] and [15] is

$$\frac{\tau_t}{\tau_m} = \frac{\sqrt{\overline{v_y'^2}}\, l\rho}{\mu} = \frac{\epsilon}{\nu}$$

a local Reynolds number which is a function of the over-all Reynolds number $\frac{VD\rho}{\mu}$. The Reynolds number can therefore be thought of as a measure of the ratio of the turbulent momentum exchange and an effective molecular momentum exchange.

The Prandtl number can now be interpreted as connecting the momentum and heat transfer due to molecular action. For, again

$$\tau_m = \mu \frac{dv}{dy} = \frac{\mu}{\rho} \frac{d(\rho v)}{dy}$$

and

$$q_m = k \frac{d\theta}{dy} = \frac{k}{\rho c} \frac{d(\rho c\theta)}{dy}$$

from which, for the same gradient

$$\frac{\tau_m}{q_m} = \frac{c\mu}{k}$$

The Peclet number is the product of the Reynolds and Prandtl numbers, and hence can be thought of as connecting the turbulent momentum with the molecular heat exchange, thus

$$\text{Peclet number} = \frac{VD\rho}{\mu} \cdot \frac{c\mu}{k} = \frac{\rho c VD}{k}$$

$$= \frac{\tau_t}{\tau_m} \cdot \frac{\tau_m}{q_m} = \frac{\tau_t}{q_m}$$

The foregoing physical interpretations of the various dimensionless numbers involved in the heat-transfer problem may be represented diagrammatically by Fig. 2.

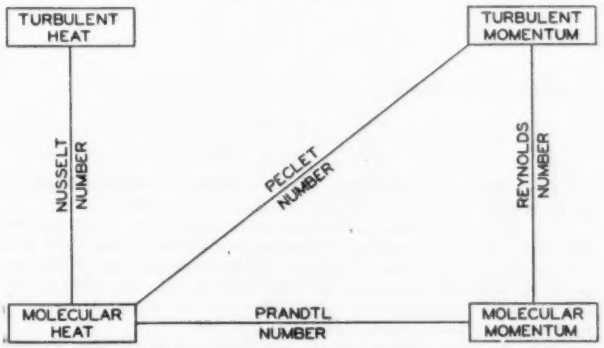


FIG. 2 PHYSICAL INTERPRETATION OF DIMENSIONLESS NUMBERS INVOLVED IN THE HEAT-TRANSFER PROBLEM

Since the heat-transfer problem is reducible from seven variables to three groups of variables, the type of graph shown by (*b*) in Fig. 1 is all that is necessary for presentation of the data.

Another interesting engineering problem is that of sediment transportation by a liquid flowing in an open channel. The solution of this problem has not met with as much success as the heat-transfer problem, probably because of the great number of variables involved. If the sediment grains are spherical and uniform in size, the channel bed saturated with sediment, and the channel wide relative to its depth, a concentration coefficient $h = \dfrac{\text{Mean concentration of sediment flowing}}{\text{Concentration of sediment at the bed}} = \dfrac{N_m}{N_b}$ may be assumed dependent upon the diameter of the sediment D, the fall velocity of the sediment η, the mean velocity of flow V, the depth of flow d, the density of the fluid ρ, and the viscosity of the fluid μ. Hence

$$h = f(D, \eta, V, d, \rho, \mu)$$

There are three fundamental dimensions, viz., mass, length, and time, and three variables can be found which will not form a dimensionless product; hence $7 - 3 = 4$ independent π's exist. Choosing d, V, and ρ as the common variables

$$\frac{N_m}{N_b} = \phi\left(\frac{\eta}{V}, \frac{Vd\rho}{\mu}, \frac{D}{d}\right) \quad \ldots\ldots\ldots\ldots [16]$$

To plot this function, a set of graphs such as (*b*) in Fig. 1, should be anticipated unless one of the terms of Equation [16] is found to have no effect upon the relation.

Introducing the shear at the bed τ_0, which is a function of D, V, d, ρ, and μ, there results furthermore

$$\frac{\tau_0}{\rho V^2} = f_1\left(\frac{\sqrt{\frac{\tau_0}{\rho}}\, d\rho}{\mu}, \frac{D}{d}\right)$$

and Equation [16] may be written in the form

$$\frac{N_m}{N_b} = \phi_1\left(\frac{\eta}{\sqrt{\frac{\tau_0}{\rho}}}, \frac{\sqrt{\frac{\tau_0}{\rho}}\, d\rho}{\mu}, \frac{D}{d}\right)$$

or, by combination of the last two terms

$$\frac{N_m}{N_b} = \phi_2\left(\frac{\eta}{\sqrt{\frac{\tau_0}{\rho}}}, \frac{\sqrt{\frac{\tau_0}{\rho}}\, D\rho}{\mu}, \frac{D}{d}\right) \quad \ldots\ldots\ldots [16a]$$

Interpreting physically the dimensionless products involved in Equation [16*a*], the term $\eta/\sqrt{\frac{\tau_0}{\rho}}$ is a measure of the suspension ability of the turbulent fluid since

$$\tau = \rho \overline{v_x' v_y'} \sim \rho \sqrt{\overline{v_x'^2}}\, \sqrt{\overline{v_y'^2}} \sim \rho \overline{v_y'^2}$$

so that

$$\frac{\eta}{\sqrt{\frac{\tau_0}{\rho}}} \sim \frac{\eta}{\sqrt{\overline{v_y'^2}}}$$

where v_x' and v_y' are the instantaneous velocity fluctuations at a point parallel and vertically perpendicular to the mean flow, respectively. The third term is a Reynolds number and may be interpreted as the ratio of the diameter of a particle of sediment

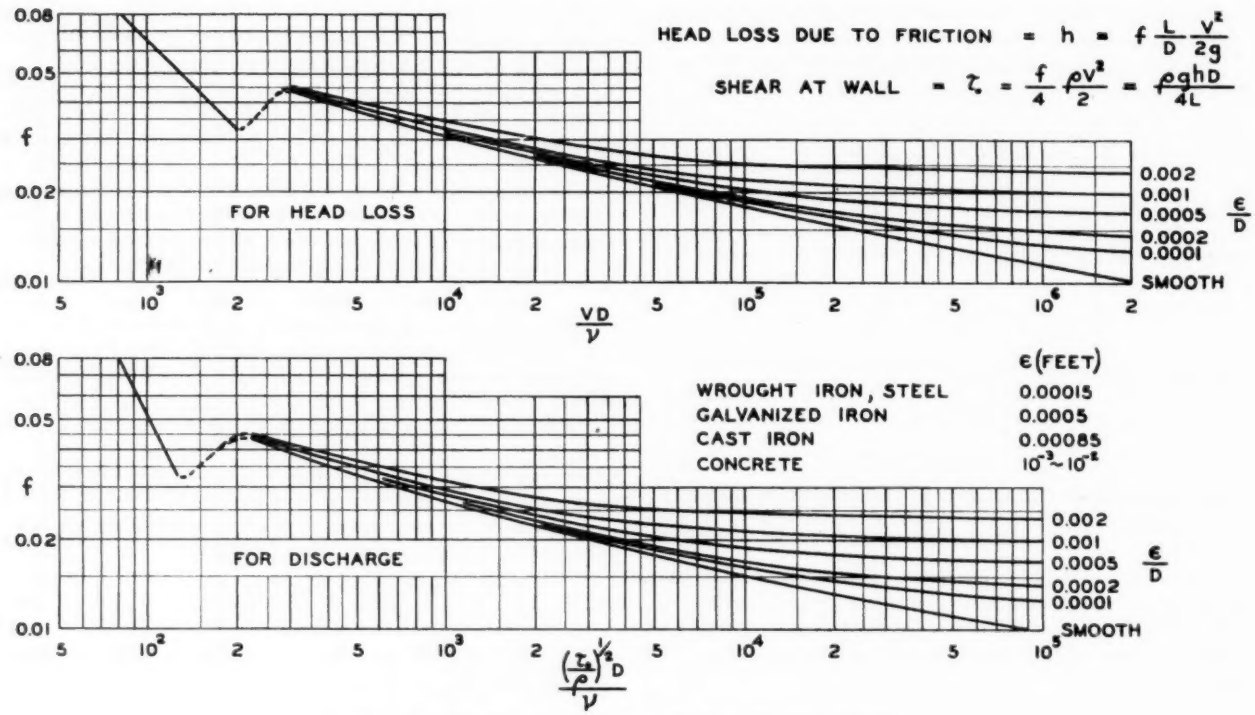


FIG. 3 FRICTION COEFFICIENTS FOR COMMERCIAL PIPES[4]

to the thickness of the laminar layer δ since $\delta \sim \frac{\nu}{\sqrt{\frac{\tau_0}{\rho}}}$; therefore this term may be thought of further as an indication of the exposure of the sand grains in the bed to the turbulent fluid outside the laminar boundary layer. At low flows, the Reynolds number will be influential, while at high flows, it will probably disappear from the function. The term D/d may be called the relative grain-size factor. Indeed, the corresponding terms of Equation [16] are expressions for the same physical pictures.

The element of arbitrariness in the procedures outlined is obvious, since other interpretations can often be given to the same dimensionless quantities.

PHYSICAL SIMILARITY

Another advantage of the method of dimensional analysis is that the method allows model studies to be made of physical problems so that information may be obtained without knowledge of the exact relationship of the variables involved.

With reference to Equation [3], viz.

$$\pi_1 = \phi(\pi_2, \pi_3, \pi_4, \ldots \pi_i)$$

it is seen that if ϕ is held constant, then π_1 will be constant and

$$(\pi_1)_m = (\pi_1)_p$$

where m and p refer to the model and prototype, respectively. Now the simplest way to fix the function ϕ is to fix the π's within ϕ; therefore, if certain information is desired before the construction of a large expensive structure, that information may be obtained by building a model and attempting to hold constant all the π's affecting the π in which one is interested. The word "attempting" is used because in most engineering problems such complete success is practically impossible.

When two systems are performing in such a manner that all the corresponding dimensionless products are equal, those systems are said to be physically similar. Such similarity may include thermal, dynamic, and geometric similarity as in the case of the heat-transfer problem previously cited.

PRESENTATION OF DATA

Once a relationship between several variables has been determined by the plotting of any set of independent dimensionless quantities involving the variables, the idea of function allows one to plot graphs corresponding to any other set of independent dimensionless products. As a result of such manipulation of functions, the solution of many problems by the method of successive approximations can be eliminated.[5,6,7,8] The first example to be considered will be that of pipe friction.

It has been found by experiment that in the flow of incompressible fluids through pipes, the shear τ_0 at the wall is a function of the mean cross-sectional velocity V, the diameter of the pipe D, the density of the fluid ρ, the viscosity of the fluid μ, and the absolute roughness ϵ, or

$$\tau_0 = \phi(V, D, \rho, \mu, \epsilon)$$

whence

$$\frac{\tau_0}{\rho V^2} = \psi\left(\frac{VD\rho}{\mu}, \frac{\epsilon}{D}\right)$$

In terms of the Darcy f

$$\frac{8\tau_0}{\rho V^2} = f\left(\frac{VD\rho}{\mu}, \frac{\epsilon}{D}\right) \quad \ldots\ldots\ldots\ldots\ldots\ldots [17]$$

---

[4] Basic data adapted from "Friction Factors for Pipe Flow," by L. F. Moody, Trans. A.S.M.E., vol. 66, 1944, p. 671.

[5] "A Survey of Flow Calculation Methods," by S. P. Johnson, A.S.M.E. Summer Meeting, Miscellaneous Papers, June, 1934, p. 98.

[6] "Solving Pipe Flow Problems With Dimensionless Numbers," by A. A. Kalinske, *Engineering News-Record*, vol. 123, 1939, p. 23.

[7] "Direct Determination of Coefficients for Flow Meters," by R. C. Binder, *Instruments*, June, 1942, p. 196.

[8] "Evaluation of Boundary Roughness," by H. Rouse, Proceedings Second Hydraulics Conference, University of Iowa Bulletin No 27, 1943, p. 105.

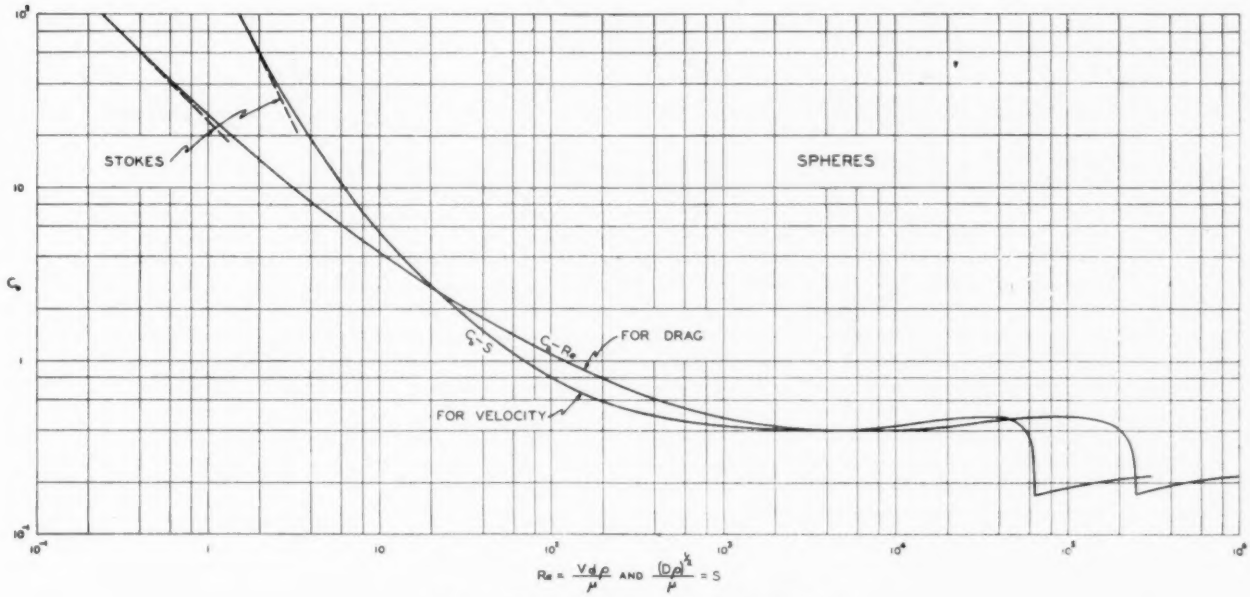


FIG. 4 DRAG COEFFICIENTS FOR SPHERES[9]

which is plotted[4] in Fig. 3 for a range of $\frac{\epsilon}{D}$, called the relative roughness.

The functional representation of Equation [17] by the graph allows direct determination of the wall friction or head loss, upon a knowledge of the discharge, diameter, and wall material of the pipe, but requires a solution by successive approximation when the discharge is desired. In order to obviate the latter rather laborious method, it is only necessary to rewrite Equation [17] thus

$$\frac{8\tau_0}{\rho V^2} = f\left(Re, \frac{\epsilon}{D}\right) = f_1\left(Re \cdot f^{1/2}, \frac{\epsilon}{D}\right)$$

$$= f_1\left[\frac{VD}{\nu} \cdot \frac{\left(\frac{\tau_0}{\rho}\right)^{1/2}(8)^{1/2}}{V}, \frac{\epsilon}{D}\right]$$

$$= f_2\left[\frac{\left(\frac{\tau_0}{\rho}\right)^{1/2} D}{\nu}, \frac{\epsilon}{D}\right]$$

which can readily be plotted (see Fig. 3) from the f — Re diagram by the relation

$$\frac{\left(\frac{\tau_0}{\rho}\right)^{1/2} D}{\nu} = Re \cdot \left(\frac{f}{8}\right)^{1/2}$$

Therefore, knowing the wall friction, diameter, and roughness of a pipe, the discharge can be determined directly.

A second example which illustrates the application of the concept of function is the problem of drag of a sphere moving in an incompressible fluid. Here it is found that the total drag D is related to the speed V, the diameter d, and the density and viscosity of the fluid. Hence

$$D = \phi(V, d, \rho, \mu)$$

or

$$\frac{D}{\rho/2AV^2} = C_D\left(\frac{Vd\rho}{\mu}\right) = C_D\,(Re) \ldots\ldots\ldots [18]$$

where C_D is called the drag coefficient and A is the projected area This equation is plotted[9] in Fig. 4.

The relationship given by Equation [18] and its graph is in the best form for the direct determination of the drag, knowing the speed of the sphere, but it is not in the best form for the calculation of the speed given the drag. Hence it is necessary to change the independent π's as follows

$$\frac{D}{\frac{\rho}{2}AV^2} = C_D(Re) = C_{D_1}(Re \cdot C_D^{1/2})$$

$$= C_{D_1}\left[\frac{Vd\rho}{\mu} \cdot \frac{D^{1/2}}{\left(\frac{\rho}{2}\right)^{1/2}\left(\frac{\pi}{4}\right)^{1/2} dV}\right]$$

$$= C_{D_1}\left[\frac{(D\rho)^{1/2}}{\mu} \cdot \left(\frac{8}{\pi}\right)^{1/2}\right]$$

$$= C_{D_2}\left[\frac{(D\rho)^{1/2}}{\mu}\right] \ldots\ldots\ldots\ldots\ldots\ldots [19]$$

where

$$\frac{(D\rho)^{1/2}}{\mu} = \left(\frac{\pi}{8}\right)^{1/2} \cdot Re \cdot C_D^{1/2}$$

Equation [19] which is plotted also in Fig. 4, is now in the proper form for direct determination of the speed once the drag is given.

A third illustration is that of the Venturi meter in which the velocity V_2 at the throat of diameter D_2 is given by

$$V_2 = C\left(\frac{V_2 D_2}{\nu}, \frac{D_2}{D_1}\right)\sqrt{\frac{2gh}{1 - (D_2/D_1)^4}} = CM\sqrt{2gh}$$

or

$$\frac{V_2}{M\sqrt{2gh}} = C\left(\frac{V_2 D_2}{\nu}, \frac{D_2}{D_1}\right) \ldots\ldots\ldots\ldots [20]$$

[9] Basic data adapted from "Das Widerstandsproblem," by F. Eisner, Proceedings Third International Congress Applied Mechanics, Stockholm, Sweden, 1931.

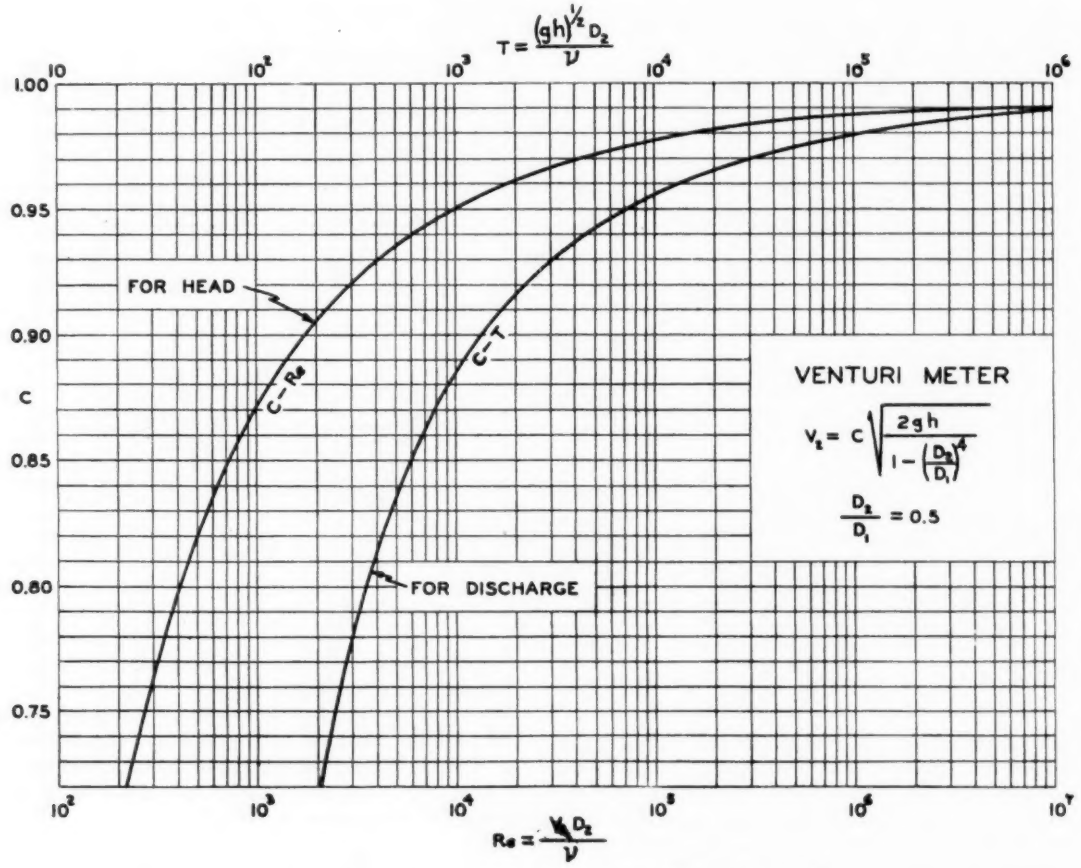


FIG. 5 VELOCITY COEFFICIENTS FOR A VENTURI METER[10]

where

$$M = \frac{1}{\sqrt{1 - (D_2/D_1)^4}}$$

and h is the difference in the static heads at the throat (2) and base (1).

Again, while Equation [20] is most useful for calculation of the head given the discharge, yet its graph requires the use of successive approximation to determine the discharge given the head. A simple manipulation can take care of this situation; thus

$$\frac{V_2}{M\sqrt{2gh}} = C\left(\frac{V_2 D_2}{\nu}, \frac{D_2}{D_1}\right) = C\left(Re, \frac{D_2}{D_1}\right)$$

$$= C_1\left(\frac{Re}{C}, \frac{D_2}{D_1}\right) = C_1\left(\frac{V_2 D_2}{\nu} \cdot \frac{\sqrt{2gh}M}{V_2}, \frac{D_2}{D_1}\right)$$

$$= C_1\left(\frac{\sqrt{2gh}\, D_2}{\nu} \cdot M, \frac{D_2}{D_1}\right)$$

$$= C_2\left[\frac{(gh)^{1/2} D_2}{\nu}, \frac{D_2}{D_1}\right] \quad \text{.....[21]}$$

where

$$\frac{(gh)^{1/2} D_2}{\nu} = \frac{Re}{C} \cdot \frac{1}{\sqrt{2}M}$$

Fig. 5 shows both Equations [20][10] and [21]. The discharge can now be found directly through the graph and Equation [21].

The rearrangement of the dimensionless products of a function may be useful also in finding the best mode of presentation of the data for a particular problem. For example, in the pipe-friction problem where

$$\frac{8\tau_0}{\rho V^2} = f\left(Re, \frac{\epsilon}{D}\right) \quad \text{.....[22]}$$

another function may have been found, viz.

$$\frac{8\tau_0}{\rho V^2} \cdot \frac{VD\rho}{\mu} = f_b\left(Re, \frac{\epsilon}{D}\right)$$

or

$$\frac{8\tau_0 D}{V\mu} = f_b\left(Re, \frac{\epsilon}{D}\right) \quad \text{.....[23]}$$

but Equation [23] involves a much larger variation than Equation [22] in the more common turbulent range of flow and therefore is not so well suited for presentation as Equation [22].

[10] Data adapted from "Fluid Meters, Their Theory and Application," Part 1, A.S.M.E., 1937, pp. 56 and 100.

A Uniform Method for Determining Angular Accelerations in Mechanisms

By L. R. KOENIG,[1] ST. LOUIS, MO.

The purpose of this paper is to disclose a more reliable and uniform method, applicable to mechanisms in general, for determining directly the angular accelerations of the constituent links. The method completely suffices where the determination of angular accelerations is the end in view. Although it is independent of normal, tangential, and total accelerations of points on the links, reliable determinations of such accelerations are considerably facilitated with the aid of the acquired angular accelerations. Angular-acceleration problems may be solved with increased assurance because; (*a*) only velocity-vector considerations are required in the necessary kinematic layouts; (*b*) full advantage may be taken of the process of inversion in simplifying velocity-vector layouts, which is not possible when acceleration vectors are employed; and (*c*) the method gives considerable insight into the effects of the various factors controlling the angular accelerations.

Nomenclature

The following nomenclature is used in this paper:

- ω = angular velocity, radians per sec
- α = angular acceleration, radians per sec per sec
- V = linear velocity of a point, superscripts being used to distinguish different vectors
- k = instantaneous line of three rotopoles[2] of three rigid systems moving relatively
- V^k = velocity along line k of a moving point on line k
- r = radial distance between the two rotopoles in a given rigid system and located on line k
- ϕ = tangent rolling circles respectively attached at a given instant to relatively moving rigid systems and reproducing their angular movements, as will be elucidated below.
- —— line segment; thus (a——a), or (ab——af)
- //////// reference system, body or link, generally fixed with respect to the earth, such as a machine frame, to be indexed F

Capital English letters from the first part of the alphabet symbolize rigid point systems, thus, A, B, C, F . . . etc. Such systems include as particular cases the rigid links, either moving or stationary, of mechanisms.

Pairs of lower-case English letters designate the rotopoles of the corresponding capital-lettered, rigid, point systems; thus a pair of coincident points a and b on links A and B, respectively, when they are at the rotopole for these links, are indexed ab.

It should be noted more carefully than is the ordinary practice that where two rotopoles are associated with one rigid system (for example, rotopoles ab and bf with system B) each rotopole is constituted by two coincident points, making four in all, of which only the two points having the common letter b are in the system B and determine a unique line segment b——b therein. Thus line segment b——b between rotopoles ab and bf is on system B. According to the notation adopted, points a and f in the foregoing case belong to relatively moving systems A and F on which are other line segments a——a and f——f, respectively. In the case of three relatively moving systems A, B, and F, rotopoles ab, bf, and af are collinear according to Aronhold's theorem,[3] and line segments a——a, b——b, and f——f are therefore necessarily coincident.

Subscripts used in connection with any symbol designate the entity to which the symbol applies, thus V_{ab} is the velocity of the rotopole ab; $V_{fc}{}^{k}$ is the velocity along line k of rotopole fc, etc.

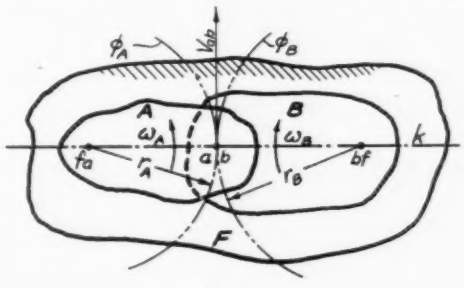


Fig. 1

Basic Considerations

Assume, Fig. 1, three rigid point systems (in a more limited sense bodies, or links) A, B, F, moving relatively, which have rotopoles fa, ab, and bf. These rotopoles necessarily lie upon a straight line k (Aronhold's theorem).[3] Let body F be stationary and without acceleration relative to the desired frame of reference, generally the earth. It follows that at any given instant a line k passing through points f——f is stationary and without acceleration relative to the frame of reference. To this line k are to be referred angular motions of the moving systems A and B.[4] Point ab is the common rotopole of the two relatively moving systems A and B, being coincident points a and b on bodies A and B, respectively, and has in each, relative to F, the same tangential velocity, thus

$$V_{ab} = \omega_A\,(a——a) = \omega_B\,(b——b) \quad \ldots\ldots\ldots\ldots [1]$$

[1] Assistant Professor of Mechanical Engineering, Washington University. Member, firm Haynes and Koenig, St. Louis, Mo. Mem. A.S.M.E.

[2] The term "rotopole" is considered to be preferable to the variety of formerly used equivalent English terms, such as instantaneous center, instant center, and centro. The term "rotopole" has been suggested and its advantages discussed by A. E. R. de Jonge in "A Brief Account of Modern Kinematics," Trans. A.S.M.E., vol. 65, 1943, pp. 663–675. It is employed throughout this paper.

Contributed by the Applied Mechanics Division and presented at the Annual Meeting, New York, N. Y., Nov. 26–29, 1945, of The American Society of Mechanical Engineers.

Discussion of this paper should be addressed to the Secretary, A.S.M.E., 29 West 39th Street, New York, N. Y., and will be accepted until April 10, 1946, for publication at a later date. Discussion received after the closing date will be returned.

Note: Statements and opinions advanced in papers are to be understood as individual expressions of authors and not of the Society.

[3] Ascribed to Aronhold by A. E. R. de Jonge,[2] but heretofore often called Kennedy's theorem.

[4] It may be observed that successive lines k drawn through successive positions assumed by rotopoles fa and bf may, in time, be angularly related, but each is simply a new line upon which attention is being fixed at the instant and has no angular velocity or acceleration, the line k being determined always by a set of motionless points f——f in the motionless reference system F.

Circles ϕ_A and ϕ_B drawn in the systems A and B, respectively, centered at rotopoles fa and bf, respectively, and rolling tangentially at ab will, at the instant under consideration, reproduce the angular motions of systems A and B relative to the fixed line k in the fixed system F. These angular motions are the same as those that originally determined the rotopoles fa, ab, and bf.[5] Thus from Equation [1] and Fig. 1

$$\frac{\omega_A}{\omega_B} = \frac{(b\text{——}b)}{(a\text{——}a)} = \frac{r_B}{r_A} \quad [2]$$

Now, r_A and r_B are the radii of instantaneous circles ϕ_A and ϕ_B but, since rotopoles fa, ab, and bf may advance toward or away from one another on line k as successive positions of line k are assumed, these radii r_A and r_B, in many linkages, may change throughout finite time intervals, although this is not universally the case.[6] Thus at any given instant the following relations in Fig. 1 hold relatively to system F

$$\omega_A r_A = V_{ab} = \omega_B r_B \quad [3]$$

Differentiating Equation [3] with respect to time yields

$$\frac{d(\omega_A r_A)}{dt} = \frac{d(\omega_B r_B)}{dt} \quad [4]$$

Then

$$\omega_A \frac{dr_A}{dt} + r_A \frac{d\omega_A}{dt} = \omega_B \frac{dr_B}{dt} + r_B \frac{d\omega_B}{dt} \quad [5]$$

But since

$$\frac{d\omega_A}{dt} = \alpha_A \quad [6]$$

and

$$\frac{d\omega_B}{dt} = \alpha_B \quad [7]$$

Substituting Equations [6] and [7] in Equation [5] will yield

$$\omega_A \frac{dr_A}{dt} + r_A \alpha_A = \omega_B \frac{dr_B}{dt} + r_B \alpha_B \quad [8]$$

Hence

$$r_B \alpha_B = \omega_A \frac{dr_A}{dt} + r_A \alpha_A - \omega_B \frac{dr_B}{dt} \quad [9]$$

Transposing and simplifying

$$\alpha_B = \frac{1}{r_B}\left(\omega_A \frac{dr_A}{dt} - \omega_B \frac{dr_B}{dt} + \alpha_A r_A\right) \quad [10]$$

Also, since from Fig. 1 and Equation [2]

$$\frac{\omega_A}{\omega_B} = \frac{r_B}{r_A} \quad [11]$$

then

$$\omega_B = \frac{\omega_A r_A}{r_B} \quad [12]$$

and substituting Equation [12] in Equation [10] yields

$$\alpha_B = \frac{1}{r_B}\left(\omega_A \frac{dr_A}{dt} - \frac{\omega_A r_A}{r_B}\frac{dr_B}{dt} + \alpha_A r_A\right) \quad [13]$$

Equation [13] provides for the uniform procedure without acceleration vectors. It is general for any three relatively moving rigid systems, and thus also for any three rigid links in any mechanism. The left-hand term α_B of Equation [13] is the desired angular acceleration of a rigid point system B, which may be any link in any mechanism.

The factor ω_A in the bracket is the assigned or known angular velocity with respect to the frame of reference F of some link A, and α_A is its assigned or known angular acceleration. The frame of reference F is the fixed link or frame of the mechanism, if results relative to the earth are desired.

The first and second terms in the bracket, respectively, include the factors $\frac{dr_A}{dt}$ and $\frac{dr_B}{dt}$ which are the rates of change in time of the radii of circles ϕ_A and ϕ_B. Thus $\frac{dr_A}{dt}$ may be evaluated by determining the instantaneous velocity difference along line k of rotopoles ab and fa; and likewise $\frac{dr_B}{dt}$ may be evaluated by determining the instantaneous velocity difference along line k of rotopoles ab and bf. These velocity differences are obtainable from well-known rotopole and velocity-vector layouts, as will be exemplified later. The lengths r_A and r_B may be obtained from the mechanism layout, wherein the determined positions of the rotopoles fa, ab, and bf determine these radii.

The ordinary rotopole and velocity-vector layout supplies all of the substitutions required in Equation [13] and provides all of the engineering accuracy required. Nevertheless, it will be clear that the layout may be treated algebraically in order to increase the accuracy of the substitution values to any extent worth while. In practice, the latter is very seldom necessary. The process of kinematic inversion may be used at will for simplifying velocity-vector solutions, because "relative" velocities between links are unaffected thereby; hence the correctness of values for $\frac{dr_A}{dt}$ and $\frac{dr_B}{dt}$ is unaffected by inversion. This is an important advantage of the method over the prior use of "acceleration" vectors wherewith inversions may never be employed.

As to signs in Equation [13], any assumed independent angular velocity ω_A is indicated plus, whether clockwise or anticlockwise. Then α_A is positive for increase in angular velocity in that direction and negative for a decrease. A positive result for the dependent acceleration α_B indicates an acceleration which is in the direction of rotation of link B, in whatever direction that may be; and a negative result indicates a deceleration with respect to that same direction. The factor $\frac{dr_A}{dt}$ is evaluated positive when r_A is increasing, and $\frac{dr_B}{dt}$ is evaluated positive when r_B is increasing. Decreasing values make these factors negative and they must then be so indicated. Due care should be exercised to retain the negative sign between the first and second terms in addition to the proper signs to be applied to $\frac{dr_A}{dt}$ and

[5] It may be noted that in the case of free bodies, external forces determine the motions and hence the rotopoles; but in a closed, kinematically constrained chain of rigid links, it is only the characters of the pairs connecting the links that determine the relative motions, and which determine the rotopoles. All rotopoles in a kinematically constrained chain of links may always be located at any position assumed at a given instant.

[6] In some linkages these radii r_A and r_B do not change as, for example, in an ordinary gearset wherein ab is the fixed pitch point, fa and bf are the fixed gear centers, and the circles ϕ_A and ϕ_B centered on fa and bf, and tangent at ab, are the pitch circles. Such special cases, as will appear, also respond to the present treatment, and although trivial among the problems in hand, they help to illustrate the universality of the method.

$\frac{dr_B}{dt}$, operating algebraically with these signs in arriving at a solution.

Application of Method to Mechanisms

In any closed kinematically constrained linkage all of the rotopoles are determinable. This includes the three rotopoles of any selected three links. In application the method herein described amounts to determining from a scaled layout of the mechanism in the position desired the numerical substitutions required on the right-hand side of Equation [13]. In any linkage, no matter how complex, the process is only one of choosing as the three links for primary consideration a link A having a known independent angular velocity ω_A and independent angular acceleration α_A (for brevity to be called the independent link); F the reference link, generally the frame of the mechanism; and the link B of which the dependent angular acceleration α_B is desired (for brevity to be called the dependent link). Designate these three links accordingly and find their three rotopoles, thus also determining the instantaneously fixed line k. This is the same procedure often followed in linkage-velocity problems.

From this layout the relative velocities of the three rotopoles along line k will produce $\frac{dr_A}{dt}$ and $\frac{dr_B}{dt}$. Substitute these along with the values of ω_A, α_A, r_A, and r_B and solve for the desired α_B in Equation [13]. Any additional rotopoles which will facilitate finding the velocities represented by $\frac{dr_A}{dt}$ and $\frac{dr_B}{dt}$, or which will facilitate velocity determinations, may readily be found and employed in the usual way.

An example will now be worked out, showing how the entire problem of substituting in Equation [13] reduces to an ordinary linkage velocity and dimensional problem. The particular example has been selected to bring out several points of interest in the method.

Example. Consider the quadric link mechanism A, B, C, F, in the position shown in Fig. 2, wherein the independent driving link A in the actual machine is 1.65 in. long and the remaining links are in proportion, link F being the frame of reference with $\alpha_F = 0$. Let the independent angular velocity $\omega_A = 10$ radians per sec, and the independent angular acceleration $\alpha_A = 6$ radians per sec per sec. Required is the dependent angular acceleration of all links in radians per sec per sec. The solution for the link B will first be given.

Lay out the linkage to any scale in the desired position, Fig. 2, and determine in the usual manner the six rotopoles *ab*, *af*, *bf*, *ac*, *bc*, and *fc*.[7] It will be seen at once that factors $\frac{dr_A}{dt}$ and $\frac{dr_B}{dt}$ (rates of change of r_A and r_B) are in this case the same, both being the velocity along line k of the intersection at rotopole *ab*, rotopoles *af* and *bf* being fixed. Rotopole *ab* is always at the intersection between the fixed line k, and the line (*ab*——*bc*) moving with link C. The velocity of this intersection may readily be found, since line (*ab*——*bc*) is at the instant rotating about rotopole *fc*. Thus to a convenient velocity scale let V_{ac}^1 be the tangential velocity of point $ac = 10 \times 1.65 = 16.5$ ips. Rotate V_{ac}^1 into the radius (*ab*——*fc*), thus obtaining V_{ac}^2. Draw the direct proportioning line ϑ, determining V_{ab}^1 which for the purpose is drawn parallel to V_{ac}^2. Vector V_{ab}^1 represents the instantaneous velocity of *ab*, considered as being on line (*ab*——*bc*) in link C, the velocity being relative to the fixed link F. Draw the vector V_{ab}^2 parallel to line (*ab*——*bc*), which represents the relative movement along line (*ab*——*bc*) of the intersection at *ab*. Thus V_{ab}^k, which equals $V_{ab}^1 + V_{ab}^2$, is the desired velocity of rotopole *ab* on line k, and evaluates $\frac{dr_A}{dt}$ and $\frac{dr_B}{dt}$. To the same scale that V_{ac}^1 represents 16.5 ips, as just found, V_{ab}^k represents 54.30 ips $= \frac{dr_A}{dt} = \frac{dr_B}{dt}$. To full scale $r_A = 2.87$ in. and $r_B = 7.12$ in. Substituting in Equation [13] the values given for $\frac{dr_A}{dt}$, $\frac{dr_B}{dt}$, r_A, r_B and the assumed values of ω_A and α_A, we obtain

$$\alpha_B = \frac{1}{7.12}\left[(10 \times 54.30) - \left(\frac{10 \times 2.87}{7.12} \times 54.30\right) + (6 \times 2.87)\right]$$

$$= 47.90 \text{ radians per sec per sec}$$

angular acceleration of link B.

This first part of the example illustrates a case wherein both radii r_A and r_B change at the same rate. It also illustrates a ase wherein the line k, as well as being instantaneously fixed,

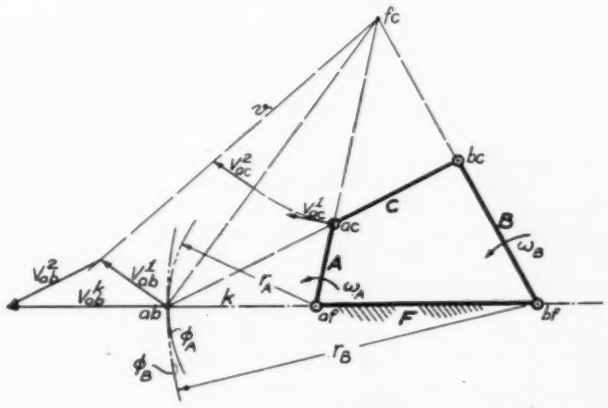


Fig. 2

is also permanent in all possible positions of the mechanism, no inversion being called for.

Next the angular acceleration of the connecting link will be obtained. In Fig. 3, for clarity of explanation, the identical mechanism in Fig. 2 has been redrawn and relettered. The scale has also been changed. If desired, Fig. 2 could have been used except that for the purpose of this paper it is preferred that the symbols of the drawing be changed to accord with those of Equation [13]. It is the object to find α_B, the angular acceleration of the connecting link now lettered B. The angular velocity and acceleration of crank A are the same as in Fig. 2. The rotopoles also are located the same as in Fig. 2, except that they have different symbols in view of the change of link symbols B and C. The rotopoles *af*, *ab*, and *bf* associated with the fixed link F, independent link A, and dependent link B produce a new instantaneously fixed line k between fixed points *f*——*f*.

Radius $r_A = 1.65$ in., full scale, and constant. Therefore in this case $\frac{dr_A}{dt} = 0$. Radius $r_B = 4.12$ in. The factor $\frac{dr_B}{dt}$ is determined by the velocity along moving line (*af*——*ab*) extended, of its intersection at *bf* with moving line (*cf*——*bc*) extended. Vector V_{ab}^1 is the same as was V_{ac}^1 in Fig. 2, namely, $10 \times 1.65 = 16.5$ ips. If the mechanism is inverted, releasing F and holding A, the problem of the movement on line k of the intersection at *bf* is simplified.

Thus the velocity V_p of point p on link F at radius r_A is set up inversely as shown, equal in length to V_{ab}^1. By the proportion line ϑ^1 vector V_{af} is determined on link C. Link C in the inver-

[7] Not all of the rotopoles are always required but all have been shown to facilitate discussion. The method of finding these is not discussed, being well known.

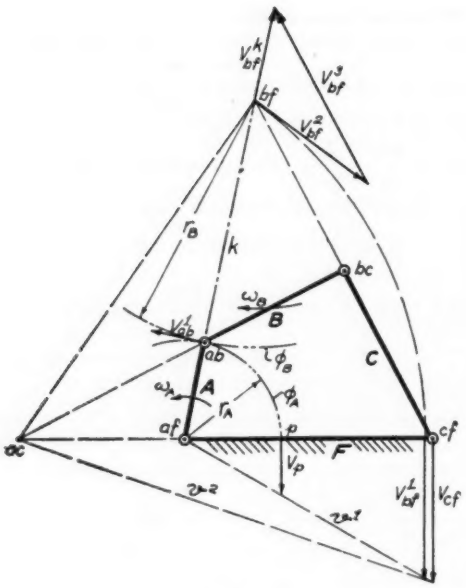


FIG. 3

sion swings about rotopole *ac*. Now *bf* is a point always on line (*cf*——*bc*), extended, and moves with *C*. Its motion with (*cf*——*bc*), extended, may be found by drawing the porportion line ϑ^2 from rotopole *ac* to the end of V_{cf}. Then vector V_{bf}^1 is determined at the radius of point *bf* from point *ac*. Hence, rotate V_{bf}^1, back to point *bf* to determine V_{bf}^2, which is located at 90 deg to (*ac*——*bf*). This vector V_{bf}^2 is, in the inversion, the velocity relative to the frame of a point on link *C* at the intersection *bf*. Vector V_{bf}^3, drawn parallel to line (*cf*——*bc*) represents the relative velocity of the intersection along line (*cf*——*bc*), extended. Remembering that line (*af*——*ab*), extended, is fixed in the inversion V_{bf}^2, + V_{bf}^3, = V_{bf}^k, = $\frac{dr_B}{dt}$. To the same scale that V_{ab}^1 = 16.5 ips, V_{bf}^k, = 28.25 ips = $\frac{dr_B}{dt}$.

Substituting in Equation [13] we obtain

$$\alpha_B = \frac{1}{4.12}\left[0 - \left(\frac{10 \times 1.65}{4.12} \times 28.25\right) + (6 \times 1.65)\right]$$

$$= -25.29 \text{ radians per sec per sec}$$

the negative sign denoting a deceleration.

This second part of the example illustrates a case wherein one radius r_A does not change; and also one wherein the inversion method may be used, although it is to be emphasized that the problem could have been solved without inversion, if preferred.

The advantages of the method increase when applied to more complex mechanisms but lack of space precludes further examples.

CONCLUSION

In regard to the insight into problems afforded by the method, the following points are of interest:

The first and second terms in the brackets in Equation [13] disappear when the independent variable ω_A becomes 0. The independent variable α_A in the third term is then exclusively the independent controlling acceleration factor in a given mechanism at a given position. Under such conditions, the mechanism is starting from rest from the position assumed. The third term disappears when α_A also becomes 0. The mechanism then has no motion and no acceleration in the assumed position.

On the other hand, the first and second terms in the bracket, if not zero, depend on the angular velocity ω_A of link *A*, whatever that may be at the instant. But even with $\omega_A > 0$ either or both of these two terms will disappear when, respectively, either or both factors $\frac{dr_A}{dt}$ or $\frac{dr_B}{dt}$ becomes 0, that is, when r_A or r_B remains constant. This constancy (or lack of it) is determined only by the character of the linkage. A gearset, referred to elsewhere in the paper,[6] is an obvious case in point. In that case these first and second terms both become 0 because r_A and r_B are constant, while the third term may or may not become 0, depending upon whether or not the driving gear is accelerating (note α_A in this third term within the brackets).

The foregoing and other deductions that may be drawn from Equation [13] provide a penetrating attack on all angular-acceleration problems in linkages.

It is interesting to note that if at a given position of a given mechanism operating at a certain instantaneous angular velocity of a link *A*, it would be desired to have zero angular acceleration of a certain link *B*, this could be solved simply by setting the right side of Equation [13] equal to 0 and solving for α_A, all other factors being known. Also, the equating could be done against values $\neq 0$ where the desired angular acceleration α_B of link *B* is to be $\neq 0$. Many other avenues of procedure are opened by the method.

It may be remarked that the angular accelerations obtained are useful in many investigations, for example, in determining turning moments necessary to accelerate the links. Also, once the angular acceleration of a link is known, in addition to its angular velocity and its center of acceleration, the normal, tangential, and total linear acceleration of any point on it is readily available. Thus the tangential acceleration of the point is simply the product of its angular acceleration and its radius from the acceleration center; its normal acceleration is the product of the square of its angular velocity and the same radius; and the total acceleration is the square root of the sum of the squares of the tangential and normal accelerations. Regarding the required factors of angular velocity and center of acceleration, the former is usually quite easy to find, and the latter, although not always easy to locate, is often obvious, for example, in cases of links pinned to the frame (see links *A* and *B* in Fig. 2).

Stresses in Rotating Disks at High Temperatures

By A. STANLEY THOMPSON,[1] LESTER, PA.

A general method was found by which the problem of the rotating disk with any arbitrary profile could be solved, including the effect of plastic flow and of variable temperature, and including the change with temperature of modulus of elasticity, coefficient of thermal expansion, and allowable stress. The solution requires for its application to a specific disk only the elementary arithmetic involved in completion of a tabular form sheet. Two applications of the method are made. For an arbitrary disk profile, an integral equation was found which converges rapidly to the radial stress distribution in a series of successive substitutions. For an arbitrary choice of radial stress, the necessary disk profile can be found in one calculation. Appendix 1 gives an example of the use of the method for the design of a partially plastic disk with a central hole.

Nomenclature

The following nomenclature is used in the paper:

- r, R = independent variables expressing radial distance, in.
- a = radius of bore in disk, in.
- b = radius to rim of disk, in.
- c = radius to junction of elastic and plastic portions of disk, in.
- h, h_R = thickness of disk at radius r, R, in.
- ω = angular speed of rotation, radians per sec
- ρ = mass density of disk material, lb sec^2 per in.^{4}
- σ_r, σ_R = radial stress at radius r, R, psi
- σ_t = tangential stress at radius r, psi
- σ_y = yield strength of disk material at radius r, psi
- E = modulus of elasticity, psi
- T = temperature at radius r, deg F
- α = coefficient of thermal expansion, in. per in. per deg F
- μ = Poisson's ratio
- u = radial deformation, in.
- ϵ_r = radial strain, in. per in.
- ϵ_t = tangential strain, in. per in.

$$S_r = (1 - \mu)\sigma_r + E\alpha T$$

$$f(r) = \int_a^r \frac{hE}{r^{2+\mu}}\,dr \qquad f(R) = \int_a^R \frac{hE}{r^{2+\mu}}\,dr$$

$$g(r, R) = \frac{h}{r} + (1 + \mu)\frac{r^\mu}{E}\{f(r) - f(R)\}$$

$$H_a = \frac{a^{1+\mu}}{E_a}\{\sigma_{t,a} - \sigma_{ra} + S_{ra}\}$$

$$k(r) = \int_a^r \frac{E}{r^{2+\mu}\sigma_r}\,dr \qquad k(R) = \int_a^R \frac{E}{r^{2+\mu}\sigma_r}\,dr$$

$$p(r) = \frac{1}{\sigma_r}\left(\frac{d\sigma_r}{dr} + \rho\omega^2 r\right)$$

$$q(r, R) = \frac{1}{r\sigma_r} + (1 + \mu)\frac{r^\mu}{E}\{k(r) - k(R)\}$$

General

It has been verified that the method described in this paper gives the usual solutions for the parallel-sided rotating plastic disk (1),[2] the parallel-sided rotating elastic disk, with or without a central hole (2), the parallel-sided stationary elastic disk with variable temperature (2), and the uniform-strength rotating elastic disk (3).

The limits to the accuracy attainable are lack of knowledge of material properties, the amount of tabular work done, and inaccuracies in assumptions stated.

Partial or total plasticity of the disk can be calculated. Allowance can be made for stress concentrations and concentrated masses. The equations written apply equally well to solid disks or to disks with holes.

Assumptions. In all calculations for the elastic state, Poisson's ratio has been assumed constant. The actual variation for five different steels is given by Everett and Miklowitz (4). The author of this paper knows of no data for high-temperature materials.

The disks involved are considered thin in the sense that stresses in the axial direction are neglected. Temperature is assumed to vary only linearly with axial distance, and the radial temperature distribution used is that at the axial middle plane of the disk.

For the plastic state, the maximum-shear theory was taken as the criterion for yielding. This is a matter of convenience since the more accurate octahedral-stress theory (5) becomes burdensome in this case. The maximum-shear theory is thought to give a sufficiently good approximation.

All variables involved are considered to be symmetrical about the axis of rotation of the disk.

The stress-strain curve assumed is that shown in Fig. 1 (6). It is assumed that there is no strain-hardening, which should be nearly true for high temperatures.

Mathematical Development

The development of the equations for the rotating disk is divided into three parts, as follows:

1 The equilibrium condition is expressed in a form in which it can be handled numerically.

2 The compatibility condition is written in terms of stresses, instead of strains as is usual, this expression being integrated to give a relationship for tangential stress in terms of radial stress.

3 The compatibility and equilibrium conditions are combined to eliminate σ_t, giving an expression for σ_r in terms of thickness. For the plastic condition, the maximum-shear theory is

---

[1] Design Engineer, Aviation Gas Turbine Division, Westinghouse Electric Corporation.

Contributed by the Applied Mechanics Division and presented at the Annual Meeting, New York, N. Y., Nov. 26–29, 1945, of The American Society of Mechanical Engineers.

Discussion of this paper should be addressed to the Secretary, A.S.M.E., 29 West 39th Street, New York, N. Y., and will be accepted until April 10, 1946, for publication at a later date. Discussion received after the closing date will be returned.

Note: Statements and opinions advanced in papers are to be understood as individual expressions of their authors and not those of the Society.

[2] Numbers in parentheses refer to the Bibliography at the end of the paper.

used instead of the compatibility condition to determine tangential stress.

The Equilibrium Condition

The equilibrium equation for a thin rotating disk of variable thickness is (2)

$$\frac{1}{h}\frac{d(rh\sigma_r)}{dr} - \sigma_t + \rho\omega^2 r^2 = 0 \quad [1]$$

This equation can be expanded by differentiating the product

$$\frac{r}{dr}\sigma_r\frac{dh}{h} - (\sigma_t - \sigma_r) + \left(r\frac{d\sigma_r}{dr} + \rho\omega^2 r^2\right) = 0$$

Solving for thickness

$$\frac{dh}{h} = \left[-\frac{1}{\sigma_r}\left(\frac{d\sigma_r}{dr} + \rho\omega^2 r\right) + \frac{1}{r\sigma_r}(\sigma_t - \sigma_r)\right]dr \quad [2]$$

On integration between the limits $r = a$ and $r = R$, the expression for thickness of the disk becomes

$$\frac{h_R}{h_a} = e^{\varphi(R)} \quad [3]$$

where

$$\varphi(R) = \int_a^R \left[-p(r) + \frac{1}{r\sigma_r}(\sigma_t - \sigma_r)\right]dr$$

$$p(r) = \frac{1}{\sigma_r}\left(\frac{d\sigma_r}{dr} + \rho\omega^2 r\right)$$

For both the solid disk and for the disk with a central hole and no press fit, the denominator of the integrand of $\varphi(R)$ becomes zero where $r = a$. For a usable equation in the vicinity of $r = a$, $\varphi(R)$ must have a finite integrand at $r = a$. By use of Equation [1]

$$\lim_{r\to a}\left[-\frac{1}{\sigma_r}\left(\frac{d\sigma_r}{dr} + \rho\omega^2 r\right) + \frac{1}{r\sigma_r}(\sigma_t - \sigma_r)\right] = \lim_{r\to a}\frac{1}{h}\frac{dh}{dr}$$

This limit is finite for any reasonable disk shape, and Equation [3] is usable for either a solid disk or for a disk with a central hole.

Equation [1] may be solved for tangential stress

$$\sigma_t = \frac{1}{h}\frac{d(rh\sigma_r)}{dr} + \rho\omega^2 r^2 \quad [4a]$$

$$= \frac{r}{h}\frac{d(h\sigma_r)}{dr} + \sigma_r + \rho\omega^2 r^2 \quad [4b]$$

$$= r\frac{d\sigma_r}{dr} + \left(\frac{r}{h}\frac{dh}{dr} + 1\right)\sigma_r + \rho\omega^2 r^2 \quad [4c]$$

Equation [4] may be solved for radial stress

$$\sigma_R = \frac{1}{h_R R}\left[\int_a^R h(\sigma_t - \rho\omega^2 r^2)dr + ah_a\sigma_{ra}\right] \quad [5a]$$

$$= \frac{1}{h_R}\left[\int_a^R \left\{\frac{h}{r}(\sigma_t - \sigma_r) - \rho\omega^2 rh\right\}dr + h_a\sigma_{ra}\right] \quad [5b]$$

$$= \int_a^R \frac{1}{r}\left\{\sigma_t - \sigma_r\left(1 + \frac{r}{h}\frac{dh}{dr}\right)\right\}dr - \left[\frac{\rho\omega^2 r^2}{2}\right]_a^R + \sigma_{ra} \quad [5c]$$

As will be seen later, the form of Equation [5a] is useful for the plastic case, since σ_r does not appear on the right side. Equation [5b] is the most useful for finding the stress distribution in an arbitrary elastic disk, since the form of Equation [5a] causes it to converge very slowly for small values of R, and since Equation [5c] has a more complicated form, and a derivative under the integral sign.

Compatibility Condition for Elastic Disk

For a two-dimensional stress distribution symmetrical about an axis, the radial and tangential strains are related to the radial deformation by the expressions

$$\epsilon_r = \frac{du}{dr} \quad [6]$$

$$\epsilon_t = \frac{u}{r} \quad [7]$$

Eliminating u from Equations [6] and [7] gives the compatibility equation in terms of strains

$$\epsilon_r - \frac{d}{dr}(r\epsilon_t) = 0 \quad [8]$$

From Hooke's law for the elastic case

$$\epsilon_r = \frac{1}{E}(\sigma_r - \mu\sigma_t) + \alpha T \quad [9]$$

$$\epsilon_t = \frac{1}{E}(\sigma_t - \mu\sigma_r) + \alpha T \quad [10]$$

Combining Equations [8], [9], and [10] gives the compatibility equation in terms of stresses

$$\frac{\sigma_r - \mu\sigma_t + E\alpha T}{E} - \frac{d}{dr}\left\{\frac{r(\sigma_t - \mu\sigma_r + E\alpha T)}{E}\right\} = 0 \quad [11]$$

Equation [11] can be rewritten

$$-\mu\left\{\frac{\sigma_t - \sigma_r + S_r}{E}\right\} - \frac{d}{dr}\left\{\frac{r(\sigma_t - \sigma_r + S_r)}{E}\right\} + (1 + \mu)\frac{S_r}{E} = 0 \quad [12]$$

where

$$S_r = (1 - \mu)\sigma_r + E\alpha T$$

Multiplying through by r^μ

$$\frac{d}{dr}\left\{\frac{r^{1+\mu}(\sigma_t - \sigma_r + S_r)}{E}\right\} - \frac{(1 + \mu)r^\mu S_r}{E} = 0 \quad [13]$$

Integrating this expression from $r = a$ to $r = r$, and solving for σ_t

$$\sigma_t = \sigma_r - S_r + \frac{E}{r^{1+\mu}}\left[(1 + \mu)\int_a^r \frac{r^\mu S_r}{E}dr + H_a\right] \quad [14]$$

where

$$H_a = \frac{a^{1+\mu}}{E_a}\{\sigma_{ta} - \sigma_{ra} + S_{ra}\}$$

For the solid disk, $a = 0$, and it becomes necessary to evaluate the indeterminate quantity

$$\lim_{r\to 0}\frac{E}{r^{1+\mu}}\left[(1 + \mu)\int_0^r \frac{r^\mu S_r}{E}dr + H_a\right]$$

$$= \lim_{r\to 0}\frac{E}{r^\mu}\left[\frac{r^\mu}{E}S_r\right] = S_{r0}$$

This evaluation of the indeterminate quantity gives $\sigma_{r0} = \sigma_{t0}$ for the solid disk as would be expected.

Equations for Elastic Disk

Equations [3], [4], and [5] are expressions of the equilibrium condition for the rotating thin disk. Equation [14] is an expression of the compatibility condition in terms of stress. These equations can be combined to find the stress in an arbitrary disk profile, or to find the profile necessary for a required stress distribution.

Substitution of Equation [14] into Equation [5b] gives an integral equation for radial stress in terms of thickness.

$$\sigma_R = \frac{1}{h_R}\left[\int_a^R \left\{\frac{h}{r}\left(-S_r + \frac{E}{r^{1+\mu}}\left[(1+\mu)\int_a^r \frac{r^\mu S_r}{E}dr + H_a\right]\right) - \rho\omega^2 rh\right\} dr + h_a\sigma_{ra}\right] \quad [15]$$

Partial integration of the repeated integral in Equation [15] gives (Appendix 2)

$$(1+\mu)\int_a^R \frac{hEdr}{r^{2+\mu}}\int_a^r \frac{r^\mu S_r dr}{E} \quad [16]$$

$$= -(1+\mu)\int_a^R \left\{f(r) - f(R)\right\}\frac{r^\mu S_r}{E}dr$$

where

$$f(r) = \int_a^r \frac{hE}{r^{2+\mu}}dr \qquad f(R) = \int_a^R \frac{hE}{r^{2+\mu}}dr$$

Substitution of Equation [16] into Equation [15] gives

$$\sigma_R = \frac{1}{h_R}\left[-\int_a^R g(r,R)S_r dr - \int_a^R \rho\omega^2 rh dr + H_a f(R) + h_a\sigma_{ra}\right] \quad [17]$$

where

$$g(r,R) = \frac{h}{r} + (1+\mu)\frac{r^\mu}{E}\left\{f(r) - f(R)\right\}$$

Equation [17] is an integral equation for the radial stress in terms of an assumed thickness and known variables of temperature, modulus of elasticity, and thermal coefficient of expansion.

Substitution of Equation [14] into Equation [3] gives an expression for thickness in terms of radial stress in the disk.

$$\varphi(R) = \int_a^R\left[-p(r) + \frac{1}{r\sigma_r}\left(-S_r + \frac{E}{r^{1+\mu}}\left[(1+\mu)\int_a^r \frac{r^\mu S_r}{E}dr + H_a\right]\right)\right]dr \quad [18]$$

On performance of partial integration of the repeated integral (Appendix 2)

$$\varphi(R) = -\int_a^R\left[p(r) + \frac{S_r}{r\sigma_r} + (1+\mu)\left\{\int_a^r \frac{Edr}{r^{2+\mu}\sigma_r} - \int_a^R \frac{Edr}{r^{2+\mu}\sigma_r}\right\}\frac{r^\mu S_r}{E} - \frac{H_a E}{r^{2+\mu}\sigma_r}\right]dr \quad [19]$$

$$= -\int_a^R [p(r) + q(r,R)S_r]dr + H_a k(R) \quad [20]$$

where

$$k(r) = \int_a^r \frac{Edr}{r^{2+\mu}\sigma_r} \qquad k(R) = \int_a^R \frac{Edr}{r^{2+\mu}\sigma_r}$$

$$q(r,R) = \frac{1}{r\sigma_r} + (1+\mu)\frac{r^\mu}{E}\left\{k(r) - k(R)\right\}$$

Substitution of Equation [20] into Equation [3] gives for thickness

$$\frac{h_R}{h_a} = e^{-\int_a^R [p(r) + q(r,R)S_r]dr + H_a k(R)} \quad [21]$$

Evaluation for the solid disk of the terms in Equations [17] and [21] can be done by taking limits as the radius approaches zero. However, since the curves for both radial and tangential stress have stationary values at the center of the disk, the numerical work can be simplified by assuming that the disk has a region, $0 < r < a$ (where a is a small dimension compared with the radius to the rim of the disk), in which $\sigma_R = \sigma_r = \sigma_t = \sigma_{ra} = \sigma_{ta}$. The procedure for the solid disk, aside from the assumption of constant stress for $r < a$, is identical with that for the disk with a hole of radius a.

By solving Equation [17] for the tangential stress at the edge of a small hole of radius a, and at radius a on a solid disk, it can be found that the ratio of these stresses as $a \to 0$ is

$$\lim_{a\to 0}\frac{\sigma_{ta}}{\sigma_{ra}} = (1-\mu) + h_a E_a \lim_{a\to 0}\frac{a^{-(1+\mu)}}{\int_a^b \frac{hE}{r^{2+\mu}}dr} = (1-\mu) + \frac{(1+\mu)a^{-(2+\mu)}h_a E_a}{h_a E_a a^{-(2+\mu)}} = 2$$

This ratio is in agreement with theory.

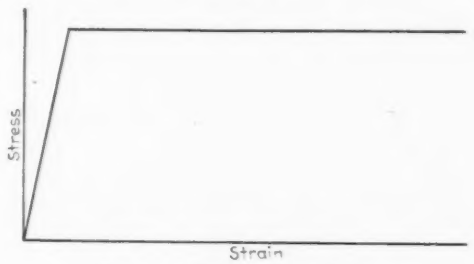


Fig. 1 Stress-Strain Curve

Equation for Plastic Disk

Over any portion of a disk in which the stresses are elastic, it is necessary to find a solution for the distribution of radial and tangential stresses satisfying both the equilibrium and compatibility conditions. It is reasonable to expect that this is true for the plastic case also. However, on the assumption of a stress-strain curve such as is shown in Fig. 1, where the modulus of elasticity is zero in the plastic range, the compatibility condition is satisfied automatically. This assumes that there is no strain-hardening, which seems reasonable for disks operating at high temperatures. Only the equilibrium condition need be fulfilled by the stress solution in the plastic region.

According to the maximum-shear theory, plastic flow occurs when the maximum shearing stress, determined as one half the difference in the maximum and minimum principal stresses, passes a certain value. In our case σ_t, σ_r, and σ_s are principal stresses, of which $\sigma_s = 0$ and σ_t is generally the maximum. We can write for the maximum shearing stress

$$\tau = \frac{\sigma_t - \sigma_s}{2} = \frac{\sigma_t}{2}$$

We can write for the tangential stress in the plastic portion of the

disk, assuming the yielding will occur when the maximum shearing stress is one half the tensile yield strength of the material

$$\sigma_t = \sigma_y \quad \ldots\ldots [22]$$

where σ_y is the yield stress of the disk material in tension.

From Equations [22] and [5a], the radial stress in the plastic range is

$$\sigma_R = \frac{1}{h_R R}\left[\int_a^R h(\sigma_y - \rho\omega^2 r^3)dr + a h_a \sigma_{ra}\right] \quad \ldots\ldots [23]$$

From Equations [22] and [23] it can be seen that, for a disk which is plastic in the center, σ_t will generally be larger than σ_r in the plastic region, and hence will be the largest principal stress. The only effect of variable temperature on the stress in the plastic region will be to change the yield point. At the outside of the disk where $\sigma_t < 0$, the criterion for yielding becomes

$$\tau = \frac{\sigma_r - \sigma_t}{2}$$

Substitution of Equation [22] into Equation [3] gives an expression for the thickness form necessary to maintain a given radial stress in a disk operating under conditions of plastic flow

$$\left.\begin{aligned} \varphi(R) &= \int_a^R \left[-p(r) + \frac{1}{r\sigma_r}(\sigma_y - \sigma_r)\right] dr \\ \frac{h_R}{h_a} &= e^{\varphi(R)} \end{aligned}\right\} \quad \ldots\ldots [24]$$

Equations for Partially Plastic Disk

In order to use the same tabular work for the elastic and the partially plastic disk, Equation [17] can be written

$$\sigma_R = \frac{1}{h_R}\left[-\int_a^R g^*(r, R)S_r dr + \int_a^c g^*(r, R)S_r dr - \int_a^R \rho\omega^2 r h dr + \int_a^c \rho\omega^2 r h dr + H_c f^*(R) + h_c\sigma_{rc}\right] \quad \ldots\ldots [25]$$

where

$$f^*(R) = \int_c^R \frac{hE dr}{r^{2+\mu}} = f(R) - f(c)$$

$$f^*(r) = \int_c^r \frac{hE dr}{r^{2+\mu}} = f(r) - f(c)$$

$$g^*(r, R) = \frac{h}{r} + (1+\mu)\frac{r^\mu}{E}\{f^*(r) - f^*(R)\} = g(r, R)$$

The radial stress in the elastic portion of the disk is then

$$\sigma_R = \frac{1}{h_R}\left[-\int_a^R g(r, R)S_r dr + \int_a^c g(r, R)S_r dr - \int_a^R \rho\omega^2 r h dr + H_c\{f(R) - f(c)\} + h_c\sigma_{rc}\right] \quad \ldots\ldots [26]$$

The tangential stress in the elastic portion of the disk is then

$$\sigma_t = \sigma_r - S_r + \frac{E}{r^{1+\mu}}\left[(1+\mu)\left\{\int_a^r \frac{r^\mu S_r}{E} dr - \int_a^c \frac{r^\mu S_r}{E} dr\right\} + H_c\right] \quad \ldots\ldots [27]$$

Acknowledgment

The author wishes to express his appreciation to Dr. A. Nadai, Research Laboratory, Westinghouse Electric Corporation, for criticisms and suggestions, and to Mr. J. A. Perna of the Aviation Gas Turbine Division of Westinghouse Electric Corporation, for testing the adequacy of the method.

Bibliography

1 "Plasticity," by A. Nadai, McGraw-Hill Book Company, Inc., New York, N. Y., 1931, p. 212.
2 "Theory of Elasticity," by S. Timoshenko, McGraw-Hill Book Company, Inc., New York, N. Y., 1934, pp. 66–69 and 364–376.
3 "Steam and Gas Turbines," by A. Stodola, McGraw-Hill Book Company, Inc., New York, N. Y., 1927, p. 376.
4 "Poisson's Ratio at High Temperatures," by F. L. Everett and Julius Miklowitz, *Journal of Applied Physics*, vol. 15, 1944, pp. 592–598.
5 "Plastic Behavior of Metals in the Strain Hardening Range. Part I," by A. Nadai, *Journal of Applied Physics*, vol. 8, 1937, pp. 205–213.
6 "Stress Distribution in Rotating Disks of Ductile Material After the Yield Point Has Been Reached," by A. Nadai and L. H. Donnell, Trans. A.S.M.E., vol. 51, 1929, paper APM-51-16.

Appendix 1

Example. This example presents the design of a disk to operate under the following conditions:

N = 12,000 rpm
σ_{rb} = 13,000 psi
a = 0.75 in.
b = 6.00 in.
h_b = 1.314 in.

The temperature, modulus of elasticity, coefficient of thermal expansion, and thickness are tabulated against radial distance in Table 1, which shows the complete tabular form for those calculations which are independent of the assumption for radial stress. Table 2 shows the tabular form for those calculations, for the elastic and the partially plastic disk, which are dependent on the assumption for radial stress. Table 3 shows the calculations for the totally plastic disk. Fig. 2 shows the disk shape and the radial and tangential stresses that resulted for the elastic, partially plastic, and plastic conditions. Residual tangential stresses are shown also (difference between elastic and partially plastic stresses).

The following figures for the partially plastic disk illustrate the evaluation of boundary constants. From Equation [26]

$$\sigma_{Rb} = \frac{1}{h_b}\left[-\int_a^b g(r, R)S_r dr + \int_a^c g(r, R)S_r dr - \int_a^b \rho\omega^2 r h dr + \int_a^c \rho\omega^2 r h dr + H_c\{f(b) - f(c)\} + h_c\sigma_{rc}\right]$$

From the table for the partially plastic disk

$$13{,}000 = -235{,}000 - 22{,}000 + 0 + 10^6 H\left\{\frac{43.80 - 13.29}{1.314}\right\} + \frac{1.5 \times \sigma_{rc}}{1.314}$$

$$23.2 \times 10^6 H + 1.141\sigma_{rc} = 270{,}000$$

$$23.2 \times 10^6 H = \frac{23.2 \times 10^6}{E_c}(\sigma_{tc} - \sigma_{rc} + S_c) = 0.957\sigma_{tc} - 0.290\sigma_{rc} + 184{,}300$$

$$0.957\sigma_{tc} + 0.851\,\sigma_{rc} = 270{,}000 - 184{,}000 = 86{,}000 \ldots [a]$$

TABLE 1 DISK STRESS CALCULATIONS

Disk Properties

0	1	2	3	4	5	6	7	8	9
r	r^{μ}	h	E	T	αT	$E\alpha T$	$\rho\omega^2 rh$	$\frac{1}{hR}\int_a^R \rho\omega^2 rh\,dr$	$\frac{hE}{r^{2+\mu}}$
Multiplier			(x10^6)		(x10^{-6})				(x10^6)
.750	.918	1.500	24.20	800	7,700	186,300	1,300	0	70.30
1.000	1.000	1.500	24.00	810	7,950	190,800	1,800	0	36.00
1.250	1.069	1.500	23.80	830	8,200	195,200	2,200	1,000	21.38
1.500	1.129	1.500	23.60	840	8,450	199,400	2,700	1,000	13.93
1.750	1.183	3.000	23.40	880	8,700	203,600	6,200	1,000	19.38
2.250	1.276	3.000	23.00	920	9,200	211,600	8,000	2,000	10.68
2.500	1.316	1.900	22.80	960	9,450	215,500	5,600	4,000	5.27
3.000	1.390	1.700	22.40	1000	9,950	222,900	6,000	6,000	3.05
3.500	1.456	1.500	22.00	1040	10,450	229,900	6,200	9,000	1.85
4.000	1.516	1.300	21.60	1080	10,950	236,500	6,200	13,000	1.16
4.500	1.570	1.100	21.20	1100	11,450	242,700	5,900	18,000	.73
5.000	1.621	.900	20.80	1140	11,950	248,600	5,300	26,000	.46
5.500	1.668	.700	20.40	1160	12,450	254,000	4,600	35,000	.28
5.625	1.679	.700	20.30	1180	12,575	255,300	4,700	38,000	.27
5.875	1.701	1.314	20.10	1200	12,825	257,800	9,200	21,000	.45
6.000	1.712	1.314	20.00	1220	12,950	259,000	9,300	22,000	.43

TABLE 1 (*Continued*)

Disk Properties

10	11	12	13	14		15		16
$f(r)$	$(1+\mu)\frac{r^{\mu}}{E}$	$(1+\mu)\frac{r^{\mu}}{E}f(r)$	$\frac{h}{r}$	$g(r,R)$		$g(r,R)dr$		$E\alpha T$
(x10^6)	(x10^{-6})			(x10^{-6}f(R)		(x10^{-6}f(R)		
0	.0493	0	2.000	2.000-	.0493			
						.528-	.0130	188,600
13.29	.0542	.720	1.500	2.220-	.0542			
						.577-	.0141	193,000
20.46	.0583	1.193	1.300	2.393-	.0583			
						.618-	.0151	197,300
24.88	.0622	1.548	1.000	2.548-	.0622			
						.772-	.0160	201,500
29.05	.0657	1.909	1.714	3.623-	.0657			
						1.898-	.0345	207,800
36.57	.0720	2.633	1.333	3.966-	.0720			
						.952-	.0184	213,600
38.57	.0750	2.893	.760	3.650-	.0750			
						1.874-	.0389	219,200
40.65	.0806	3.276	.567	3.843-	.0806			
						1.969-	.0417	226,400
41.88	.0860	3.602	.429	4.031-	.0860			
						2.061-	.0443	233,300
42.64	.0911	3.885	.325	4.201-	.0911			
						2.152-	.0469	239,600
43.12	.0963	4.152	.244	4.396-	.0963			
						2.244-	.0494	245,700
43.42	.1013	4.398	.180	4,578-	.1013			
						2.334-	.0519	251,300
43.61	.1062	4.631	.127	4,758-	.1062			
						.598-	.0134	254,700
43.65	.1075	4.693	.114	4.816-	.1075			
						1.232-	.0272	256,600
43.74	.1100	4.811	.224	5.035-	.1100			
						.633-	.0138	258,400
43.80	.1113	4.875	.219	5.094-	.1113			

TABLE 2 DISK STRESS CALCULATIONS

ELASTIC DISK

17	18	19		20	21	22	23	
r	S_r	$\int_a^R g(r,R) S_r dr$		$\frac{1}{h_R}\int_a^R g(r,R) S_r dr$	σ_r	S_r	$\int_a^R g(r,R) S_r dr$	
Multiplier		($\times 10^{-6} f(R)$)					($\times 10^{-6} f(R)$)	
.750		0	- 0	0	0		0	- 0
	189,600	100,100	- 2,470			196,000	103,500	- 2,550
1.000		100,100	- 2,470	45,000	21,000		103,500	- 2,550
	193,000	111,400	- 2,720			210,800	121,600	- 2,970
1.250		211,500	- 5,190	70,000	30,000		225,100	- 5,520
	197,300	121,900	- 2,980			220,000	136,000	- 3,320
1.500		333,400	- 8,170	87,000	35,000		361,100	- 8,840
	201,500	155,600	- 3,220			220,000	169,800	- 3,520
1.750		489,000	- 11,390	53,000	18,000		530,900	- 12,360
	207,600	394,000	- 7,160			220,900	419,300	- 7,620
2.250		883,000	- 18,550	68,000	20,000		950,200	- 19,980
	213,600	203,400	- 3,930			231,400	220,300	- 4,260
2.500		1,086,400	- 22,480	115,000	31,000		1,170,500	- 24,240
	219,200	410,800	- 8,530			241,200	450,000	- 9,380
3.000		1,497,200	- 31,010	139,000	32,000		1,622,000	- 33,620
	226,400	445,800	- 9,440			248,800	489,900	- 10,380
3.500		1,943,000	- 40,450	166,000	32,000		2,111,900	- 44,000
	233,200	480,600	- 10,330			255,300	526,200	- 11,310
4.000		2,423,600	- 50,780	199,000	31,000		2,638,100	- 55,310
	239,600	515,600	- 11,240			261,300	562,300	- 12,250
4.500		2,939,200	- 62,020	241,000	31,000		3,200,400	- 67,560
	245,700	551,400	- 12,140			267,100	599,400	- 13,200
5.000		3,490,600	- 74,160	301,000	30,000		3,799,800	- 80,760
	251,300	586,500	- 13,040			272,700	636,500	- 14,150
5.500		4,077,100	- 87,200	396,000	31,000		4,436,300	- 94,910
	254,700	152,300	- 3,410			276,800	165,500	- 3,710
5.625		4,229,400	- 90,610	392,000	32,000		4,601,800	- 98,620
	256,600	316,100	- 6,980			272,700	336,000	- 7,420
5.875		4,545,500	- 97,590	211,000	14,000		4,937,800	- 106,040
	258,400	163,600	- 3,570			267,800	169,500	- 3,700
6.000		4,709,100	- 101,160	212,000	13,000		5,107,300	- 109,740

$10^6 H = 7,410$

	24	25	26	27	28	29
	$\frac{1}{h_R}\int_a^R g(r,R) S_r dr$	σ_r	$\int_a^R \frac{(1+\mu)}{E} S_r dr$	Col 26 + H_a	$\frac{E}{r(1+\mu)}$ (Col 27)	σ_t
Multiplier			($\times 10^{-6}$)	($\times 10^{-6}$)		
	0	0	0	7,960	280,000	94,000
	47,000	23,000	2,500	10,510	253,000	69,000
	75,000	32,000	5,520	13,480	241,000	56,000
	94,000	36,000	8,840	16,800	234,000	46,000
	57,000	19,000	12,360	20,320	229,000	31,000
	73,000	21,000	19,980	27,940	224,000	18,000
	124,000	32,000	24,240	32,200	223,000	17,000
	150,000	33,000	33,620	41,580	223,000	10,000
	179,000	33,000	44,000	51,960	224,000	4,000
	215,000	32,000	55,310	63,270	225,000	-2,000
	261,000	31,000	67,560	75,520	227,000	-7,000
	326,000	30,000	80,760	88,720	228,000	-12,000
	425,000	33,000	94,910	102,870	229,000	-15,000
	425,000	32,000	98,620	106,580	229,000	-16,000
	228,000	14,000	106,040	114,000	229,000	-25,000
	229,000	13,000	109,740	117,700	229,000	-26,000

TABLE 2 (*Continued*)
ELASTIC DISK

From Col. 23 $10^6 H = 7,960$

TABLE 2 (*Continued*)
PARTIALLY ELASTIC DISK

	30 $\frac{1}{h_R}\int_c^R g(r,R)S_r dr$	31 σ_r	32 $\int_c^R (1+\mu)\frac{r^\mu}{E}S_r dr$	33 Col 32 $+H_c$	34 $\frac{E}{r^{1+\mu}}$(Col 23)	35 σ_t
Multiplier			(x10^{-6})	(x10^{-6})		
		0				75,000
	0	18,000	0	10,800	259,000	74,000
	41,000	28,000	2,970	13,790	246,000	61,000
	67,000	33,000	6,290	17,090	238,000	50,000
	47,000	18,000	9,810	20,610	233,000	35,000
	70,000	21,000	17,430	28,230	226,000	20,000
	121,000	33,000	21,690	32,490	225,000	19,000
	150,000	34,000	31,070	41,870	225,000	12,000
	182,000	32,000	41,450	52,250	225,000	5,000
	219,000	33,000	52,760	63,560	226,000	-1,000
	267,000	33,000	65,020	75,820	227,000	-7,000
	333,000	33,000	78,220	89,020	228,000	-12,000
	435,000	36,000	92,370	103,170	230,000	-14,000
	435,000	34,000	96,080	106,880	230,000	-15,000
	235,000	14,000	103,500	114,300	231,000	-23,000
	236,000	13,000	107,200	119,000	232,000	-23,000

From Col. 23 — From Col. 23 — 10^6H = 10,790

TABLE 3 DISK STRESS CALCULATIONS
PLASTIC DISK

36 r	37 $\rho\omega^2r^2h$	38 $\frac{1}{h_R}\int_a^R \rho\omega^2r^2h\,dr$	39 σ_t	40 $h\frac{\sigma_t}{\sigma_{t0}}$	41 $\frac{1}{h_R}\int_a^R h\frac{\sigma_t}{\sigma_{ta}}dr$	42 σ_r	43 σ_t
.750	1,000	0	75,000	1.500	0	0	28,000
1.000	1,800	0	74,000	1.480	.249	7,000	28,000
1.250	2,800	1,000	73,000	1.459	.395	10,000	27,000
1.500	4,100	1,000	72,000	1.448	.491	13,000	27,000
1.750	10,400	1,000	71,000	2.830	.312	8,000	26,000
2.250	18,000	2,000	69,000	2.745	.449	11,000	26,000
2.500	14,000	3,000	68,000	1.712	.755	18,000	25,000
3.000	18,000	5,000	66,000	1.484	.861	19,000	24,000
3.500	21,700	6,000	63,000	1.286	.967	21,000	24,000
4.000	24,800	9,000	61,000	1.062	1.091	21,000	23,000
4.500	26,500	12,000	59,000	.868	1.244	23,000	22,000
5.000	26,500	18,000	57,000	.684	1.452	23,000	21,000
5.500	25,300	24,000	55,000	.512	1.776	25,000	21,000
5.625	26,400	25,000	54,000	.508	1.800	25,000	20,000
5.875	54,000	12,000	53,000	.935	.965	15,000	20,000
6.000	55,800	15,000	53,000	.943	1.004	13,000	20,000

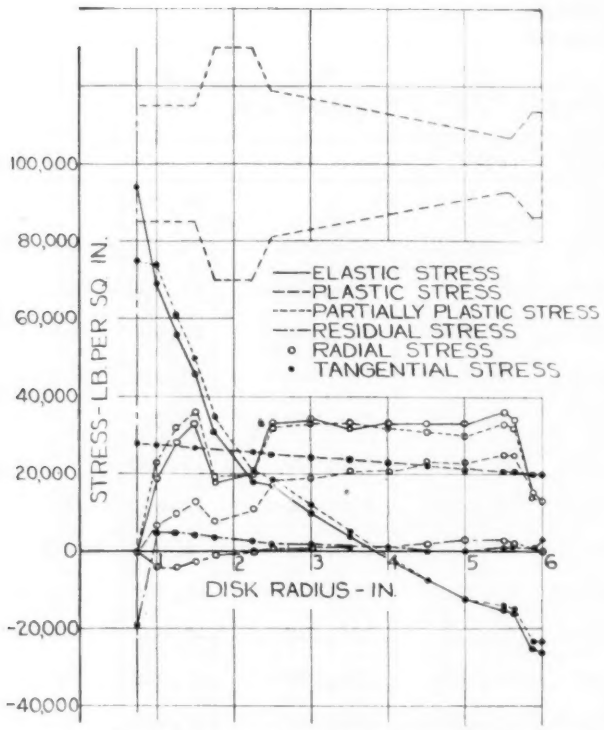


FIG. 2 DISK SHAPE AND RADIAL AND TANGENTIAL STRESSES

From the solution for the plastic disk

$$\sigma_{re} = 0.249\,\sigma_{ta} = 0.249 \times \frac{75}{74}\,\sigma_{t_c} = 0.253\sigma_{te} \ldots\ldots [b]$$

Combining Equations [a] and [b]

$$\sigma_{te} = \frac{86{,}000}{1.169} = 73{,}600$$

$$\sigma_{re} = 18{,}400$$

$$10^6 H = 10{,}800$$

In the numerical work for this example, the increment for integration of a function $F(r)$ was taken as

$$\frac{F(r) + F(r + \Delta r)}{2}\,\Delta r$$

This causes an appreciable error in $f(r)$ (column 10, Table 1), since column 9 has considerable curvature and slope for small values of r. For a closer evaluation of $f(r)$ and of σ_r, smaller increments of r or a more accurate averaging process should be used for small values of r.

Appendix 2

PARTIAL INTEGRATION OF REPEATED INTEGRAL

In the repeated integral

$$\int_a^R F(r)dr \int_a^r G(r)dr$$

let

$$F(r)dr = dv \qquad v = \int_a^r F(r)dr$$

$$\int_a^r G(r)dr = u \qquad du = G(r)dr$$

then

$$\int_a^R udv = \Big[uv\Big]_a^R - \int_a^R vdu$$

and substituting values for u, v, du, dv

$$\int_a^R F(r)dr \int_a^r G(r)dr$$

$$= \left[\int^r G(r)dr \int_a^r F(r)dr\right]_a^R - \int_a^R \left(\int_a^r F(r)dr\right) G(r)dr$$

$$= \int_a^R \left(\int_a^R F(r)dr - \int_a^r F(r)dr\right) G(r)dr$$

Nonlinear Theory of Elasticity With Small Deformations

By E. STERNBERG,[1] CHICAGO, ILL.

Previous investigations of nonlinear theory of elasticity have been concerned largely with the problem of finite deformations. In this paper the assumption of "infinitesimal" deformations is retained whereas Hooke's law is replaced by a general second-order approximation of nonlinear stress-strain laws. Applications to uniaxial tension and compression as well as torsion of right circular cylinders are considered in detail. The results obtained indicate second-order effects which were previously unnoticed because of the early linearization of the extended stress-strain relations.

Nomenclature

The following nomenclature is used in the paper:

W = strain-energy density (strain-energy function, elastic potential)
G = modulus of rigidity of classical theory
ν = Poisson's ratio of classical theory
E = modulus of elasticity of classical theory
$A' = G\frac{1-\nu}{1-2\nu}$, $B' = -2G$ = elastic parameters of classical theory
A, B, C, and $a = \frac{A}{G}$, $b = \frac{B}{G}$, $c = \frac{C}{G}$ = additional elastic parameters of nonlinear theory
$\epsilon_x, \epsilon_y, \epsilon_z; \gamma_{xy}, \gamma_{yz}, \gamma_{zx}$ = components of strain in Cartesian co-ordinates
r, θ, z = cylindrical co-ordinates
u, v, w = radial, transverse, and axial components of displacement in cylindrical co-ordinates
$\epsilon_r, \epsilon_\theta, \epsilon_z; \gamma_{r\theta}, \gamma_{\theta z}, \gamma_{zr}$ = components of strain in cylindrical co-ordinates
$\sigma_r, \sigma_\theta, \sigma_z; \tau_{r\theta}, \tau_{\theta z}, \tau_{zr}$ = components of stress in cylindrical co-ordinates
$\epsilon_1, \epsilon_2, \epsilon_3$ and $\sigma_1, \sigma_2, \sigma_3$ = principal strains and principal stresses
J_1, J_2, J_3 = invariants of strain tensor
ϵ, ρ = axial and transverse components of strain, respectively, in the uniaxial state of stress
$\sigma, s = \frac{\sigma}{G}$ = axial normal stress in the uniaxial state of stress
R, l = radius and length, respectively, of right circular cylinder
$I_0 = \frac{\pi R^4}{4}$ = polar moment of inertia of cross section
K = unit angle of twist
KR = characteristic angle of twist
M = resultant torque in torsion problem
P = resultant axial force in torsion problem

Introduction

The classical theory of elasticity involves two major approximations, i.e., the assumption of "infinitesimal deformations," and the linearization of the stress-strain relations. According to the first assumption, the space derivatives of the components of the displacement vector are considered small throughout the continuum so that the squares and products of these quantities may be neglected. The second assumption is pronounced in the form of Hooke's law. As a consequence of the foregoing approximations, the homogeneous system of basic equations of the classical theory is linear and thus admits the superposition of solutions.

Both hypotheses have been found useful for a wide variety of problems and elastic media. However, throughout the development of the theory of elasticity, problems have been encountered to which the linearization of the strain-displacement relations is not applicable. Hooke's law, in turn, though adequately representative of the behavior of most elastic materials under small strains, is subject to similar limitations. As is well known, there are solids which obey the linear stress-strain law only for a very limited range of strain, or which fail to do so altogether; for example, cast iron, numerous minerals, cement, and concrete. For the reasons mentioned, various generalizations of the classical theory have long been suggested. Among the more recent contributions, those of F. D. Murnaghan and M. A. Biot must be mentioned especially.

Most of the literature on nonlinear elasticity is primarily concerned with the treatment of finite deformations. In the present discussion the assumption of infinitesimal deformations is retained, whereas Hooke's law is extended to a general second-order approximation of nonlinear stress-strain relations for the homogeneous, isotropic medium. This extension is based on a generalization of the elastic potential, first introduced by W. Voigt.[2] There results a five-parameter theory of elasticity which contains the classical theory as a limiting case. This paper includes applications to uniaxial tension and compression of cylinders, and to torsion of right circular cylinders. Particular emphasis is placed on the interpretation of the solutions given. The approach used here differs from that of Voigt as the partial linearization of the newly gained law of elasticity is abandoned. In this way there appear important second-order effects previously unnoticed.

Extension of Elastic Potential and Generalization of Hooke's Law

The mathematical formulation of the concept of elasticity is based on the principle of conservation of energy. From the viewpoint of the energy-conservation laws of thermodynamics the ideal elastic behavior of a medium in the isothermal or adia-

[1] Assistant Professor, Department of Applied Mechanics, Illinois Institute of Technology.

Contributed by the Applied Mechanics Division and presented at the Annual Meeting, New York, N. Y., Nov. 26–29, 1945, of The American Society of Mechanical Engineers.

Discussion of this paper should be addressed to the Secretary, A.S.M.E., 29 West 39th Street, New York, N. Y., and will be accepted until April 10, 1946, for publication at a later date. Discussion received after the closing date will be returned.

Note: Statements and opinions advanced in papers are to be understood as individual expressions of their authors and not those of the Society.

[2] "Über eine anscheinend nothwendige Erweiterung der Theorie der Elasticität," by W. Voigt, *Annalen der Physik und Chemie*, vol. 52, 1894, pp. 536–555; see also, "Finite Deformations of an Elastic Solid," by F. D. Murnaghan, *American Journal of Mathematics*, vol. 59, 1937, pp. 235–260.

batic state, under the influence of surface and body forces, necessitates the existence of a strain-energy function.[3] This strain-energy function, here denoted by W, in the case of a homogeneous medium is independent of the position vector and is assumed to depend exclusively on the components of the strain tensor and the temperature. Since the following discussion will be confined to isothermal conditions, any reference to the temperature may be omitted and $W = W(\epsilon_x, \ldots \gamma_{xy}, \ldots)$.

The principle of virtual displacements, under the supposition of infinitesimal deformations, yields the components of stress as partial derivatives of W with respect to the corresponding components of strain

$$\sigma_x = \frac{\partial W}{\partial \epsilon_x}, \ldots \tau_{xy} = \frac{\partial W}{\partial \gamma_{xy}} \ldots\ldots\ldots\ldots\ldots [1]$$

If the medium is isotropic, the elastic potential W must be invariant under orthogonal transformations of the co-ordinate system therefore depending solely on the invariants of the strain tensor; thus

$$W = W(J_1, J_2, J_3)$$

where

$$J_1 = \epsilon_x + \epsilon_y + \epsilon_z$$

$$J_2 = \epsilon_x\epsilon_y + \epsilon_y\epsilon_z + \epsilon_z\epsilon_x - {}^1/_4(\gamma^2_{xy} + \gamma^2_{yz} + \gamma^2_{zx}) \ldots [2]$$

$$J_3 = \begin{vmatrix} \epsilon_x & {}^1/_2\gamma_{xy} & {}^1/_2\gamma_{xz} \\ {}^1/_2\gamma_{yx} & \epsilon_y & {}^1/_2\gamma_{yz} \\ {}^1/_2\gamma_{zx} & {}^1/_2\gamma_{zy} & \epsilon_z \end{vmatrix}$$

Once $W = W(J_1, J_2, J_3)$ is known, the stress-strain relations are generated by Equation [1]. Hypotheses as to the specific form of the strain-energy function must derive their ultimate justification from experiment. Assuming W to be an analytic function of the invariants of strain, the elastic potential is represented by the power series

$$W = A'J_1^2 + B'J_2 + AJ_1^3 + BJ_1J_2 + CJ_3 + \ldots\ldots [3]$$

where the coefficients A', B', A, B, C, etc., are parameters depending on the elastic properties of the medium. The omission of the constant term from the series [3] merely indicates the choice of the arbitrary zero level of W at the origin. The absence of the term linear in the components of strain, that is, involving J_1 alone, conforms to the conventional agreement that all components of stress vanish in the unstrained state.

In the classical theory, where Hooke's law is valid, the linear stress-strain relations are obtained as a first-order approximation by neglecting in the expansion for W, all terms of degree higher than two in ϵ_x, ϵ_y, etc. The elastic potential then appears as the homogeneous, quadratic form in the components of strain, $W = A'J_1^2 + B'J_2$. Thus the third-degree invariant J_3 does not enter W at all. The coefficients A' and B' are usually expressed in terms of Poisson's ratio ν, and the modulus of rigidity G

$$A' = G\frac{1-\nu}{1-2\nu}, \quad B' = -2G \ldots\ldots\ldots\ldots [4]$$

If terms of higher degree are retained in the expansion for W, Equation [1] leads to a multiple constant nonlinear law of elasticity. Such an extension of the elastic potential is compatible with the assumption of infinitesimal deformations because of the influence of the new elastic constants. Moreover, it is warranted only if the experimentally determined coefficients of the higher powers of ϵ_x, ϵ_y, ... in the stress-strain relations, that is, the new elastic constants, are large compared to the geometric coefficients of the nonlinear terms in the exact strain-displacement relations.

In the present treatment, as in Voigt's paper,[2] all terms of W up to the third degree in ϵ_x, ϵ_y, ... are taken into account. The number of independent elastic parameters is thus extended to five. The corresponding stress-strain relations represent the most general second-order law of elasticity consistent with the assumptions made. According to Equations [1], [2], [3], and [4], these stress-strain relations are

$$\left.\begin{aligned} \sigma_x &= 2G\left[\epsilon_x + \frac{\nu}{1-2\nu}(\epsilon_x + \epsilon_y + \epsilon_z)\right] + 3A(\epsilon_x + \epsilon_y \\ &\quad + \epsilon_z)^2 + B[\epsilon_y^2 + \epsilon_z^2 + 2\epsilon_x\epsilon_y + 3\epsilon_y\epsilon_z + 2\epsilon_z\epsilon_x - \frac{1}{4}(\gamma_{xy}^2 \\ &\quad + \gamma_{yz}^2 + \gamma_{zx}^2)] + C\left(\epsilon_y\epsilon_z - \frac{1}{4}\gamma_{yz}^2\right) \\ \sigma_y &= \ldots, \sigma_z = \ldots \\ \tau_{xy} &= G\gamma_{xy} - \frac{1}{2}B(\epsilon_x + \epsilon_y + \epsilon_z)\gamma_{xy} - \frac{1}{4}C(2\epsilon_z\gamma_{xy} \\ &\quad - \gamma_{yz}\gamma_{zx}) \\ \tau_{yz} &= \ldots, \tau_{zx} = \ldots \end{aligned}\right\} \ldots [5]$$

The requirement of stable equilibrium of the medium in the unstrained state, in the classical theory, imposes the inequalities

$$G > 0, \quad -1 < \nu < \frac{1}{2} \ldots\ldots\ldots\ldots [6]$$

which are necessary and sufficient for the positive definite character of the quadratic form which represents the elastic potential in that case. Clearly, the foregoing inequalities remain necessary and sufficient for the positive definite character of the generalized W in a neighborhood of the origin. The new parameters A, B, and C, however, are not subject to any deductive limitations and in the absence of adequate experimental information, the discussion must proceed on the basis that these constants may assume any set of real values.

Both the equations of equilibrium in terms of stresses, and the equations of compatibility in terms of strains, are unaffected by the generalization of Hooke's law just given. An attempt to write these two systems of equations in terms of displacements and stresses, respectively, necessitates the solution of the stress-strain relations for the components of strain. This leads to highly inconvenient forms.

Because of this difficulty, the semi-inverse approach, i.e., starting with displacements, will in general be advantageous. The procedure may be outlined as follows: Guided by the corresponding classical solution, an appropriate system of displacements is assumed and the components of strain are computed. The components of stress then follow from Equations [5]. These are introduced into the equations of equilibrium which are subject to the boundary conditions of the problem. One thus arrives, generally, at three nonlinear differential equations, the solution of which may require methods of approximation. Such approximations will be based on the known classical solution in whose neighborhood the desired solution is bound to remain.

Uniform Tension and Compression of Cylinders

The object of studying the uniaxial state of stress is to examine the nature of the deviations from Hooke's law to which the present generalization is adaptable. This application should, furthermore, indicate the physical significance of the elastic constants.

[3] See, for example, "A Treatise on the Mathematical Theory of Elasticity," by A. E. H. Love, fourth edition, Cambridge, 1934, chapt. 3.

Referring the state of stress to its principal axes, let

$$\frac{\sigma_1}{G} = s, \sigma_2 = \sigma_3 = 0, \epsilon_1 = \epsilon, \epsilon_2 = \epsilon_3 = \rho$$

where s is the dimensionless axial normal stress, ϵ the corresponding component of strain, and ρ the transverse component of strain. With

$$a = \frac{A}{G}, \quad b = \frac{B}{G}, \quad c = \frac{C}{G}$$

Equations [5] now yield

$$(3a + b)\epsilon^2 + (12a + 5b + c)\epsilon\rho + (12a + 3b)\rho^2 + \frac{2\nu}{1 - 2\nu}\epsilon + \frac{2}{1 - 2\nu}\rho = 0 \ldots [7]$$

$$s = 2\epsilon + \frac{2\nu}{1 - 2\nu}(\epsilon + 2\rho) + 3a(\epsilon + 2\rho)^2 + b(4\epsilon\rho + 5\rho^2) + c\rho^2 \ldots [8]$$

Equation [7] relates the axial and the transverse components of stress and will be called Poisson's equation. The relation $\rho = \rho(\epsilon;\ \nu, a, b, c)$ represents a four-parameter family of conics, each member of which passes through the origin. For $a = b = c = 0$, Poisson's equation reduces to the classical straight line $\rho = -\nu\epsilon$, which is tangential to the family at $(\epsilon = 0, \rho = 0)$. The meaning of ν is now given by $\nu = \left.\frac{d\rho}{d\epsilon}\right|_{\epsilon=0}$. The Poisson curve is a hyperbola, parabola, or ellipse, according as the discriminant

$$13b^2 + c^2 + 36ab + 10bc + 24ac \gtrless 0$$

Elimination of ρ between Equations [7] and [8] leads to the stress-strain relation for the case of uniaxial tension or compression. In general, $s = s(\epsilon)$ is irrational. The family of stress-strain curves $s = s(\epsilon;\ \nu, a, b, c)$ passes through $(\epsilon = 0, s = 0)$, and at that point is tangential to the classical member $s = \frac{E}{G}\epsilon$. Here E is the modulus of elasticity of the linear theory, so that $E = 2G(1 + \nu)$. The new meaning of E is apparent from $E = \left.\frac{d\sigma}{\epsilon d}\right|_{\epsilon=0}$. Both $\rho = \rho(\epsilon)$ and $s = s(\epsilon)$ are, in general, double-valued. However, but one of the branches of the corresponding curves conforms to $\rho_{(\epsilon=0)} = 0$ and $s_{(\epsilon=0)} = 0$ and is thus physically significant. Furthermore

$$\rho(\epsilon;\ \nu, a, b, c) = -\rho(-\epsilon;\ \nu, -a, -b, -c)$$

$$s(\epsilon;\ \nu, a, b, c) = -s(-\epsilon;\ \nu, -a, -b, -c)$$

Hence, a reversal in sign of the new elastic constants gives rise to a reflection with respect to both co-ordinate axes of the Poisson curve as well as of the stress-strain curve.

An exhaustive treatment of the two four-parameter families of curves under consideration is cumbersome and serves no particular advantage from the viewpoint of the present discussion. Figs. 1 to 6, inclusive, show examples of Poisson curves and stress-strain curves for the hyperbolic, the parabolic, and the elliptic case referred to. It should be kept in mind that the values of ν, a, b, and c used in these and subsequent examples are purely arbitrary and were chosen with a view to illustration only.

The nature and magnitudes of the deviations from the classical straight lines depend on the new parameters a, b, and c which largely determine the slopes and curvatures of the curves in question. The corresponding influence of ν is of a higher order, since the variation of ν is known to be relatively insignificant. The dependence of the ratio of lateral and axial strains on ϵ is in agreement with results of tests performed on materials which do

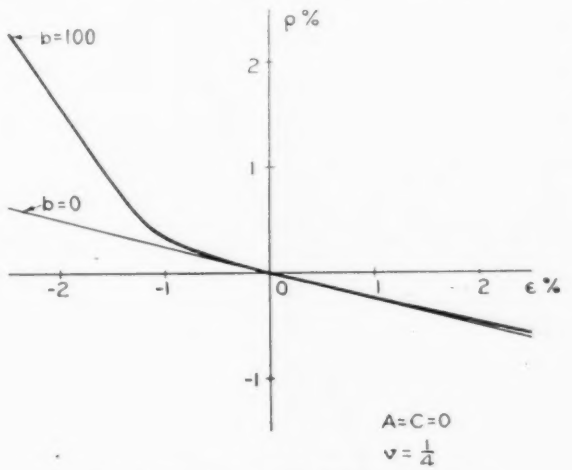


FIG. 1 POISSON CURVE, HYPERBOLIC CASE

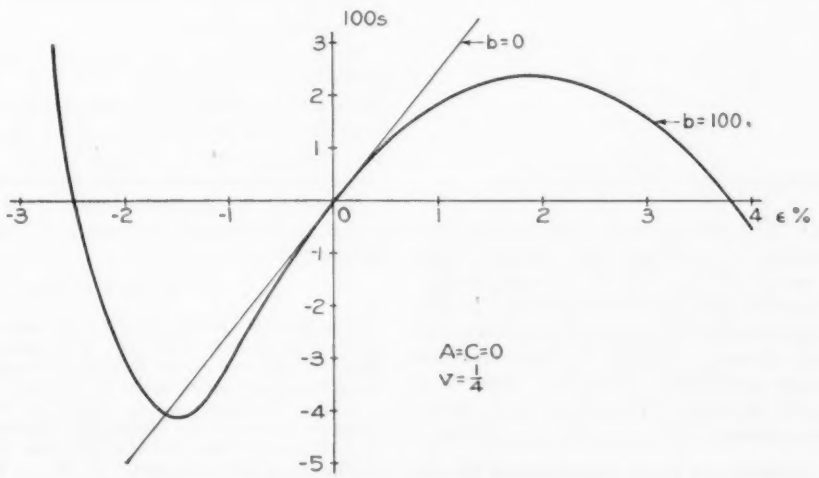


FIG. 2 STRESS-STRAIN CURVE, HYPERBOLIC CASE

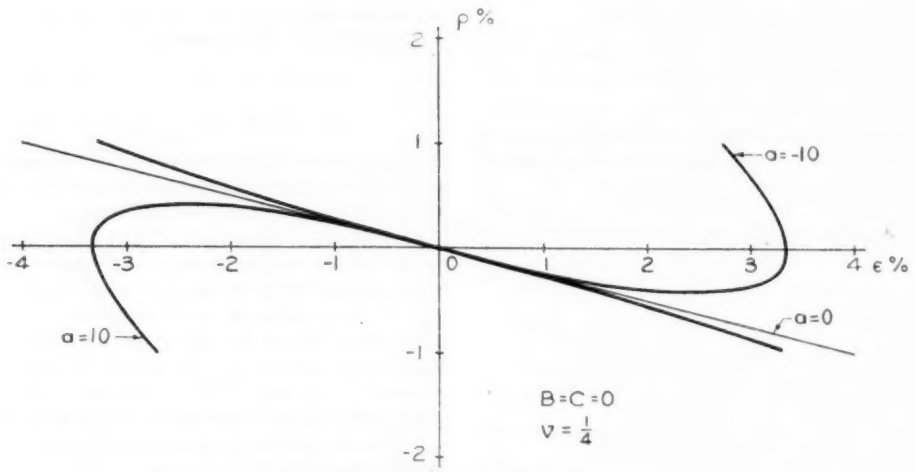


FIG. 3 POISSON CURVES, PARABOLIC CASE

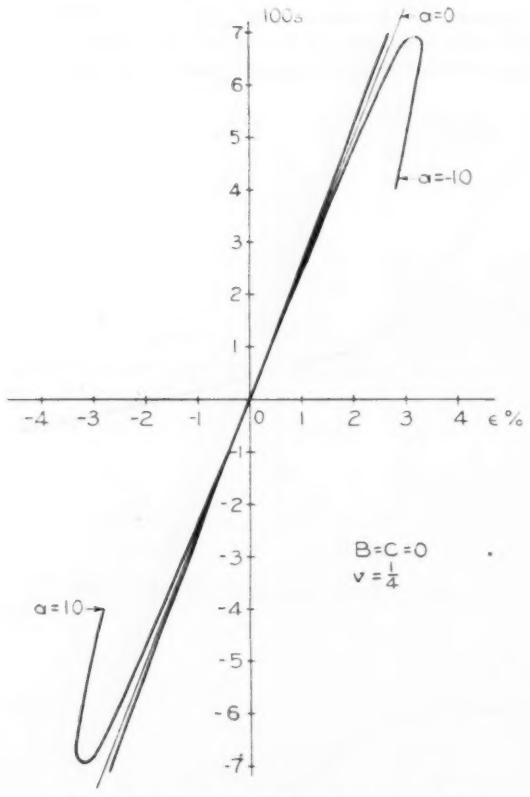


FIG. 4 STRESS-STRAIN CURVES, PARABOLIC CASE

not obey Hooke's law.[4] As a consequence of the second-order law of elasticity, $\rho(\epsilon)$ and $s(\epsilon)$ are no longer odd functions, which implies a behavior in tension different from that in compression.

It seems important that the extended elastic potential, in contrast to the classical approach, leads to a natural breakdown of the theory beyond a critical range of strain. In this connection Figs. 3 to 6, inclusive, are particularly instructive. Here both $\rho(\epsilon)$ and $s(\epsilon)$ are real only for a finite interval of ϵ, and stresses maintained at the levels corresponding to ϵ_{max} or ϵ_{min} would have to be interpreted as conditions of failure. For the homogeneous, uniaxial state of stress, $\sigma_{(\epsilon)} = \dfrac{dW_{(\epsilon)}}{d\epsilon}$. Hence the relative extrema and the zeros of $s(\epsilon)$ correspond to inflection points and relative extrema of $W(\epsilon)$, respectively. Clearly, values of ϵ which imply $W < 0$ are again physically insignificant, and the equilibrium consistent with $W = W_{max}$ is unstable (see, for example, Fig. 2).

It is seen that the generalized elastic potential affords a characterization of the phenomenon of yielding and lends itself to a representation of the transition to the plastic range.[5] This characterization is, however, purely descriptive in nature; an explanation of the phenomenon mentioned cannot be sought in the approach presented here.

TORSION OF CIRCULAR CYLINDERS

(a) *Differential Equations and Boundary Conditions of Problem.* Saint Venant torsion of circular cylinders has been treated in various ways under hypothesis of finite deformations.[6] Seth[5] furthermore draws attention to the added importance of determining higher-order effects arising in this problem because of their influence on the thermal and electrical conductivity of twisted wires. The treatment given by Voigt, on the basis of infinitesimal deformations and of the partially linearized second-order stress-strain law, leads to results which deviate essentially from those arrived at here.

Let R and l denote the radius and the length, respectively, of the right circular cylinder. Let (r, θ, z) be cylindrical co-ordinates with the origin at the center of the base circle and the z-axis coincident with the geometric axis of the cylinder. Let (u, v, w), $(\epsilon_r, \ldots \gamma_{r\theta}, \ldots)$, and $(\sigma_r, \ldots \tau_{r\theta}, \ldots)$ denote the corresponding components of displacement, strain, and stress, respectively.

Guided by the classical solution of the torsion problem as well as by considerations of symmetry, the displacement field is assumed as

$$u = u_{(r)},\ v = g_{(r)}z,\ w = \alpha z \ldots\ldots\ldots\ldots\ldots [9]$$

[4] Über das elastische Verhalten von Beton mit besondered Berücksichtigung der Querdehnungszahl, by H. Yoshida, J. Springer, Berlin, Germany, 1930.

[5] Qualitatively similar results have been obtained on the basis of finite deformations; see F. D. Murnaghan,[2] and "Finite Strain in Elastic Problems," by B. R. Seth, *Philosophical Transactions of the Royal Society of London*, series A, vol. 234, 1934–1935, pp. 231–264.

[6] "Zur Elastizitätstheorie endlicher Verschiebungen," by R. Kappus, *Zeitschrift fur angewandte Mathematik und Mechanik*, vol. 19, 1939, pp. 271–285, and 344–361; also, "Elastizitätstheorie zweiter Ordnung mit Anwendungen," by M. A. Biot, *Zeitschrift fur angewandte Mathematik und Mechanik*, vol. 20, 1940, pp. 89–99; B. R. Seth, loc. cit.[5]

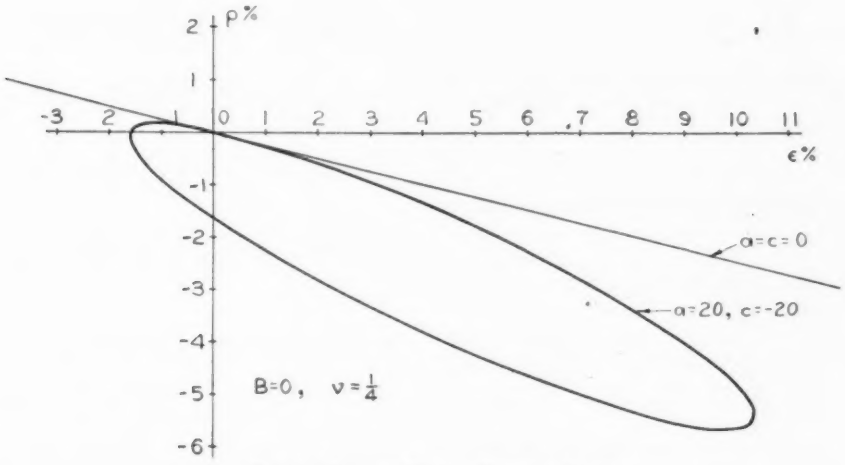


FIG. 5 POISSON CURVE, ELLIPTIC CASE

where the functions $u_{(r)}$, $v_{(r)}$, and the constant α are to be determined consistent with the equations of equilibrium and the boundary conditions. The strain-displacement relations for infinitesimal deformations now lead to the components of strain

$$\epsilon_r = \frac{du}{dr},\ \epsilon_\theta = \frac{u}{r},\ \epsilon_z = \alpha;\ \gamma_{r\theta} = \left(\frac{dg}{dr} - \frac{g}{r}\right) z, \gamma_{\theta z} = g,\ \gamma_{zr} = 0 \quad \ldots [10]$$

In accordance with Equations [10], the stress-strain relations Equations [5] take the form

$$\left.\begin{aligned}
\sigma_r &= 2G\left[\frac{du}{dr} + \frac{\nu}{1-2\nu}\left(\frac{du}{dr} + \frac{u}{r} + \alpha\right)\right] + 3A\left(\frac{du}{dr} + \frac{u}{r} + \alpha\right)^2 \\
&\quad + B\left\{\frac{u^2}{r^2} + \alpha^2 + 2\frac{u}{r}\frac{du}{dr} + 3\alpha\frac{u}{r} + 2\alpha\frac{du}{dr} - \frac{1}{4}\left[\left(\frac{dg}{dr} - \frac{g}{r}\right)^2 z^2 + g^2\right]\right\} + C\left[\alpha\frac{u}{r} - \frac{1}{4}g^2\right] \\
\sigma_\theta &= \ldots, \quad \sigma_z = \ldots \\
\tau_{r\theta} &= G\left(\frac{dg}{dr} - \frac{g}{r}\right) z - \frac{1}{2}B\left(\frac{du}{dr} + \frac{u}{r} + \alpha\right)\left(\frac{dg}{dr} - \frac{g}{r}\right) z \\
&\quad - \frac{1}{2}C\alpha\left(\frac{dg}{dr} - \frac{g}{r}\right) z \\
\tau_{\theta z} &= G\,g - \frac{1}{2}B\left(\frac{du}{dr} + \frac{u}{r} + \alpha\right) g - \frac{1}{2}C\frac{du}{dr}\,g \\
\tau_{zr} &= \frac{1}{4}C\left(\frac{dg}{dr} - \frac{g}{r}\right) gz
\end{aligned}\right\} \quad \ldots [11]$$

In the absence of body forces, the equations of equilibrium are

$$\left.\begin{aligned}
\frac{\partial\sigma_r}{\partial r} + \frac{1}{r}\frac{\partial\tau_{r\theta}}{\partial\theta} + \frac{\partial\tau_{rz}}{\partial z} + \frac{\sigma_r - \sigma_\theta}{r} &= 0 \\
\frac{\partial\tau_{rz}}{\partial r} + \frac{1}{r}\frac{\partial\tau_{\theta z}}{\partial\theta} + \frac{\partial\sigma_z}{\partial z} + \frac{\tau_{rz}}{r} &= 0 \\
\frac{\partial\tau_{r\theta}}{\partial r} + \frac{1}{r}\frac{\partial\sigma_\theta}{\partial\theta} + \frac{\partial\tau_{\theta z}}{\partial z} + \frac{2\tau_{r\theta}}{r} &= 0
\end{aligned}\right\} \quad \ldots\ldots [12]$$

The assumed system of displacements Equations [9] by aid of Saint Venant's principle is adaptable to the following loading casse:

Case 1: Pure torsion of a circular cylinder constrained against axial displacements of the end-sections.

Case 2: Pure torsion of an unconstrained cylinder.

The boundary conditions for Case 1 become

$$u_{(r=0)} = 0 \quad \ldots [13a]$$

$$\sigma_{r\,(r=R)} = 0 \quad \ldots [13b]$$

$$\tau_{r\theta\,(r=R)} = 0 \quad \ldots [13c]$$

$$\tau_{zr\,(r=R)} = \tau_{zr\,(z=0)} = \tau_{zr(z=l)} = 0 \quad \ldots [13d]$$

$$\iint \tau_{\theta z} r\,dS = M \quad \ldots [13e]$$

$$w_{(z=0)} = w_{(z=l)} = 0 \quad \ldots [13f]$$

where S denotes the region of the cross section, and M the magnitude of each of the couples applied to the end sections. In Case 2, the boundary conditions are identical with Equations [13], except for the condition of constraint Equation [13f] which is to be replaced by

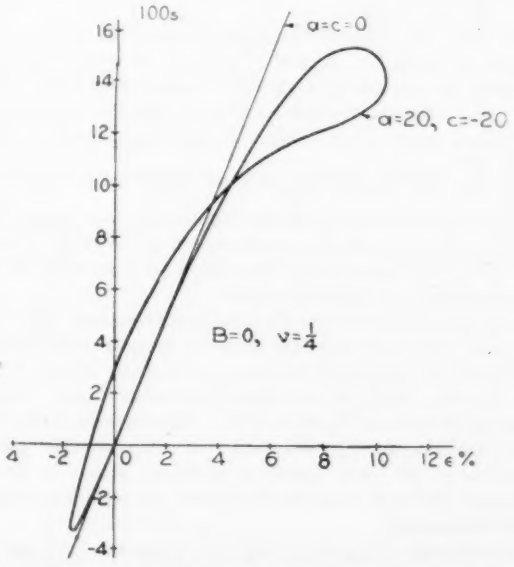


FIG. 6 STRESS-STRAIN CURVE, ELLIPTIC CASE

$$\iint_s \sigma_z dS = 0$$

(*b*) *Linearization.* Upon substitution of Equations [11] into Equations [12], the last two of the equations of equilibrium are seen to be satisfied identically by

$$g_{(r)} = Kr \quad \text{[14]}$$

With this determination of g, the first of Equations [12] becomes

$$\frac{d}{dr}\left(\frac{du}{dr}+\frac{u}{r}\right)+\frac{3}{2}\frac{(1-2\nu)}{(1-\nu)}a\frac{d}{dr}\left(\frac{du}{dr}+\frac{u}{r}+\alpha\right)^2 + \frac{(1-2\nu)b}{2(1-\nu)}\left\{2\alpha\frac{d}{dr}\left(\frac{du}{dr}+\frac{u}{r}\right)+\frac{1}{r}\left[2u\frac{d^2u}{dr^2}+\left(\frac{du}{dr}\right)^2-\frac{u^2}{r^2}\right]\right\} = 8Fr \quad \text{[15]}$$

where

$$F = \frac{(1-2\nu)(2b+3c)K^2}{64(1-\nu)} \quad \text{[16]}$$

Boundary conditions, Equations [13*c*] and [13*d*], are automatically satisfied for $v = Krz$. Conditions Equations [13*a*, *b*, and *f*] are disposed of by means of α and the two arbitrary constants appearing in the general solution of Equation [15]. Once $u_{(r)}$ is known, condition Equation [13*e*] is reached by determination of K.

From the foregoing observations, it is clear that the present problem hinges upon the solution of Equation [15]. Equation [15] is an ordinary differential equation of the second order and degree. A solution conforming to $u_{(r=0)} = 0$ may be obtained by means of a power series expansion, or through Piccard's method. In either case, the boundary conditions lead to transcendental equations in the constants of integration.

There are, however, two special instances for which closed, exact solutions are readily established. If $B = C = 0$, the desired integral of Equation [15] is $u_{(r)} = K_1 r$, K_1 being an arbitrary constant. Here, the solution both for Case 1 and Case 2 reduces to the well-known solution of the linear theory. Thus the presence of A alone in the generalized elastic potential does not give rise to any deviation from the classical results. If, in turn, $A = B = 0$, Equation [15] becomes linear. The exact solution for this case is given later.

In view of the difficulties inherent in the exact treatment of the general problem (A, B, and C present), it seems expedient to linearize the system of equations consisting of Equations [11] and [15]. The radial displacement $u_{(r)}$ and the axial component of strain α vanish identically in the classical solution. Hence u, α, $\frac{du}{dr}$, $\frac{d^2u}{dr^2}$, and any products of these quantities with powers of r, may be regarded as small of the first order in the present solution which must remain in the neighborhood of the classical solution. One is thus led to neglect in Equations [11] and [15] all second-degree terms of the type described.

It would be conceivable that the approximation suggested defeats the very purpose of the problem under consideration, and leads back to the trivial solution of the linear theory. Such is not the case, since the new elastic constants B and C enter the linear right term of Equation [15]. The essential difference between the linearized system and the corresponding system of equations of the linear theory of elasticity is that in the latter, Equation [15] is homogeneous whereas in the former it remains nonhomogeneous.

Substitution of Equation [14] into Equation [11] and subsequent linearization leads to

$$\left.\begin{aligned}
\sigma_r &= 2G\left[\frac{du}{dr}+\frac{\nu}{1-2\nu}\left(\frac{du}{dr}+\frac{u}{r}+\alpha\right)\right]-\frac{1}{4}(B+C)K^2r^2\\
\sigma_\theta &= 2G\left[\frac{u}{r}+\frac{\nu}{1-2\nu}\left(\frac{du}{dr}+\frac{u}{r}+\alpha\right)\right]-\frac{1}{4}BK^2r^2\\
\sigma_z &= 2G\left[\alpha+\frac{\nu}{1-2\nu}\left(\frac{du}{dr}+\frac{u}{r}+\alpha\right)\right]-\frac{1}{4}BK^2r^2\\
\tau_{\theta z} &= GKr-\frac{1}{2}B\left(\frac{du}{dr}+\frac{u}{r}+\alpha\right)Kr-\frac{1}{2}C\frac{du}{dr}Kr\\
\tau_{r\theta} &= \tau_{zr} = 0
\end{aligned}\right\} \quad \text{[17]}$$

Similarly, Equation [15] becomes

$$\frac{d}{dr}\left(\frac{du}{dr}+\frac{u}{r}\right) = 8Fr \quad \text{[18]}$$

The general solution of Equation [18] is

$$u_{(r)} = K_1 r + \frac{K_2}{r} + Fr^3$$

where K_1, K_2 are arbitrary constants, and Equation [13*a*] requires $K_2 = 0$. The constants K_1 and α are determined by Equations [13*b*] and [13*f*]; the components of stress are then computed from Equation [17], and $M = M_{(K)}$ follows from Equation [13*e*]. The complete solutions for Case 1 and Case 2 will be summarized.

(*c*) *Solutions.*

Case 1:

$$\alpha = 0,\ K_1 = \frac{(1-2\nu)K^2R^2}{64(1-\nu)}[(2b-c)-2\nu(2b+c)]. \quad \text{[19]}$$

$$\sigma_r = \frac{G[2(1-2\nu)b-(1+2\nu)c]K^2}{32(1-\nu)}(R^2-r^2) \quad \text{[20]}$$

$$\sigma_\theta = \frac{G[2(1-2\nu)b-(1+2\nu)c]K^2}{32(1-\nu)}(R^2-3r^2) \quad \text{[21]}$$

$$\sigma_z = \frac{GK^2}{16(1-\nu)}\{[4(2\nu-1)b+6\nu c]r^2+\nu[2(1-2\nu)b-(1+2\nu)c]R^2\} \quad \text{[22]}$$

$$\tau_{r\theta} = \tau_{zr} = 0$$

$$\tau_{\theta z} = GK[(1-\mu_1\mu_3K^2R^2)r-\mu_1\mu_3K^2r^3] \quad \text{[23]}$$

where

$$\left.\begin{aligned}
\mu_1 &= \frac{1-2\nu}{128(1-\nu)}\\
\mu_2 &= (2b+3c)(4b+3c)\\
\mu_3 &= [2b-c-2\nu(2b+c)](2b+c)
\end{aligned}\right\} \quad \text{[24]}$$

The resultant axial reaction $P = \iint_s \sigma_z dS$, so that

$$P = \frac{\pi GK^2R^2}{8}[(2\nu-1)b+\nu c] \quad \text{[25]}$$

$$M = \frac{\pi GR^4}{6}K[3-\mu_1(2\mu_2+3\mu_3)K^2R^2] \quad \text{[26]}$$

$$u = K_1 r + Fr^3,\ v = Kr,\ w = 0 \quad \text{[27]}$$

where K_1 and F are given by Equations [19] and [16], respectively.

For $A = B = 0$, the foregoing solution is exact if Equation [22] is replaced by, and P is computed consistent with,

$$\sigma_z = \frac{\nu GcK^2}{16(1-\nu)}[6r^2 - (1+2\nu)R^2] + \frac{(1-2\nu)^2Gc^2K^4}{4096(1-\nu)^2}[3r^2-(1+2\nu)R^2][9r^2-(1+2\nu)R^2] \quad [28]$$

Case 2:

$$\alpha = \frac{(1-2\nu)b - \nu c}{16(1+\nu)}K^2R^2 \quad [29]$$

$$K_1 = \frac{K^2R^2}{64(1-\nu^2)}\{4\nu(\nu-1)[(1-2\nu)b-\nu c] + (1-2\nu)(1+\nu)[2(1-2\nu)b-(1+2\nu)c]\} \quad [30]$$

σ_r and σ_θ as in Equations [20] and [21].

$$\sigma_z = \frac{G}{16(1-\nu)}[2(1-2\nu)b - 3\nu c]K^2(R^2-2r^2)$$

$\tau_{r\theta}$, τ_{zr}, $\tau_{\theta z}$, and M as in Case 1, provided μ_3 is replaced by

$$\mu_3' = \mu_3 + \frac{4(1-\nu)}{(1+\nu)(1-2\nu)}[(1-2\nu)b - \nu c]^2.$$

$$u = K_1 r + Fr^3, \; v = Kr, \; w = \alpha z$$

with K_1, F, and α as in Equations [30], [16], and [29], respectively.

(*d*) *Discussion of Results.* If $A = B = 0$, the foregoing results for Case 1 and Case 2 reduce to the classical solution. The new elastic constant A does not appear in the approximate solution given, and thus the influence of A in the problem under consideration is of a higher order than that of B or C. The nonlinear characteristics of the material give rise to a modification of $\tau_{\theta z(r)}$ and $M_{(K)}$, which now follow a parabolic law. In addition, there appear the "secondary" stresses σ_r, σ_θ, and σ_z which vanish identically in the classical solution.

The tangential displacement component $v = Kr$ coincides with that of the linear problem; hence the unit angle of twist is again constant. The radial displacement $u_{(r)}$, and the axial displacement $w_{(z)}$ of Case 2, are secondary in the foregoing sense. The cross sections remain circular but undergo a radial dilatation which, in Case 2, is accompanied by a uniform axial dilatation. The signs of the secondary components of stress and displacement, that is, whether they represent tension or compression, expansion or contraction, are governed by the relative values of the elastic constants ν, A, B, and C. The magnitudes of the deviations from the classical solution depend on these elastic constants and are proportional to the square or cube of the unit angle of twist in the approximation here considered.

The formulas for the torque $M = M_{(K)}$, Equation [26], and for the shear stress $\tau_{\theta z} = \tau_{\theta z(r)}$, Equation [23], require further and more detailed discussion.

According to Equation [26], $M = M_{(KR;\, R,\, G,\, \mu_1,\, \mu_2,\, \mu_3)}$ represents a family of cubical parabolas, each member of which passes through the origin, and is tangential at this point to the classical straight line $M = GKI_0$. By Equation [6], $G > 0$ and $-1 < \nu < \frac{1}{2}$. Furthermore, $R > 0$ and without loss of generality, $K \geq 0$. Since $2\mu_2 + 3\mu_3 \leq 0$ is incompatible with $\nu < \frac{1}{2}$ unless $b = c = 0$, and excluding the classical case, one has

$$\mu_1 > 0, \; 2\mu_2 + 3\mu_3 > 0 \quad [31]$$

Hence by Equation [26]

$M_{(KR)} = 0$ for $KR = 0$ and for $KR = K_0$, $M > 0$ for $0 < KR < K_0$ and $M < 0$ for $K_0 < KR$. $M = M_{max}$ for $KR = \frac{K_0}{\sqrt{3}}$ where $K_0 = \sqrt{\frac{3}{\mu_1(2\mu_2+3\mu_3)}}$ and K_0 is always real because of Equation [31]. Finally, $M < GKI_0$ for $0 < K$.

Thus, regardless of the values of R, ν, G, B, and C, the torque required to produce a prescribed angle of twist is less than that consistent with the linear solution. A typical $M_{(KR)}$ diagram is shown in Fig. 7. The question as to the physically significant range of KR must be decided by experiment. However, as in the case of uniform tension or compression an upper bound for this range is evident.

$$\int_0^{KR} M_{(KR)} d(KR)$$

is proportional to the total strain-energy, and clearly, values of KR which imply negative values of this integral must be excluded. Furthermore, a torque maintained at the level of M_{max} is to be interpreted as a condition of elastic failure, provided the corresponding angle of twist still belongs to the elastic range. In this way the breakdown of the theory, for strains beyond a critical range, is again seen to be inherent in the solution itself.

For the reason just mentioned, the discussion of $\tau_{\theta z} = \tau_{\theta z(r)}$ may be limited to

$$KR < \frac{K_0}{\sqrt{3}} = \frac{1}{\sqrt{\mu_1(2\mu_2+3\mu_3)}} \quad [32]$$

According to Equation [23],

$$\tau_{\theta z} = \tau_{\theta z(r;\, K,\, R,\, G,\, \mu_1,\, \mu_2,\, \mu_3)}$$

represents a family of parabolas passing through the origin. The parabolas degenerate into straight lines if and only if $\mu_2 = 0$, that is, if either $b = c = 0$ (classical case) or $b = \frac{-3c}{2}$ or $b = \frac{-3c}{4}$.

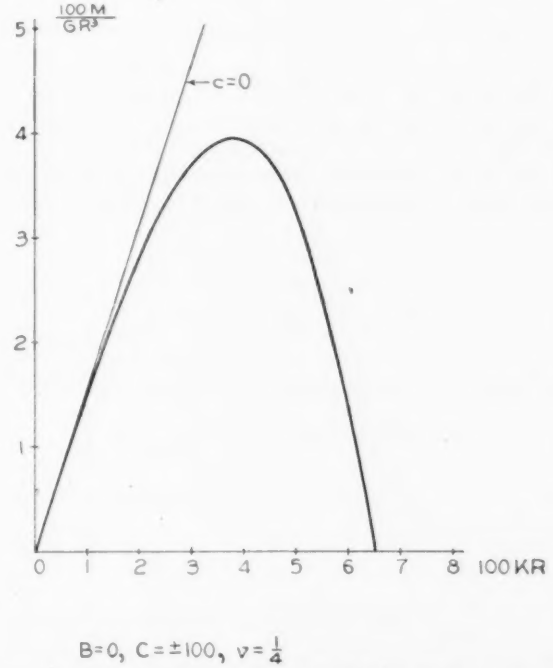


FIG. 7 TORSION, DIMENSIONLESS TORQUE VERSUS CHARACTERISTIC ANGLE OF TWIST; CASE 1

Again excluding the degenerated cases, let $\mu_3 \neq 0$. It follows from Equation [6] that

$$\mu_2 + \mu_3 > 0,\ \mu_2 + 2\mu_3 > 0 \quad \ldots\ldots\ldots\ldots [33]$$

The inequalities [31], [32], and [33] imply

$$1 - (KR)^2\mu_1\mu_3 > 0 \quad \ldots\ldots\ldots\ldots\ldots [34]$$

Observing Equation [23], now classify as follows:

(*A*) $\mu_3 > 0$:

$\tau_{\theta z} = 0$ for $r = 0$ and $r = r_0$, $\tau_{\theta z} > 0$ for $0 < r < r_0$, $\tau_{\theta z} < 0$ for $r > r_0$, $\tau_{\theta z} = \tau_{\theta z\,\max}$ for $r = \dfrac{r_0}{\sqrt{3}}$, where

$$r_0 = \sqrt{\frac{1 - \mu_1\mu_3(KR)^2}{\mu_1\mu_2K^2}}\ \text{(real)} \quad \ldots\ldots\ldots\ldots [35]$$

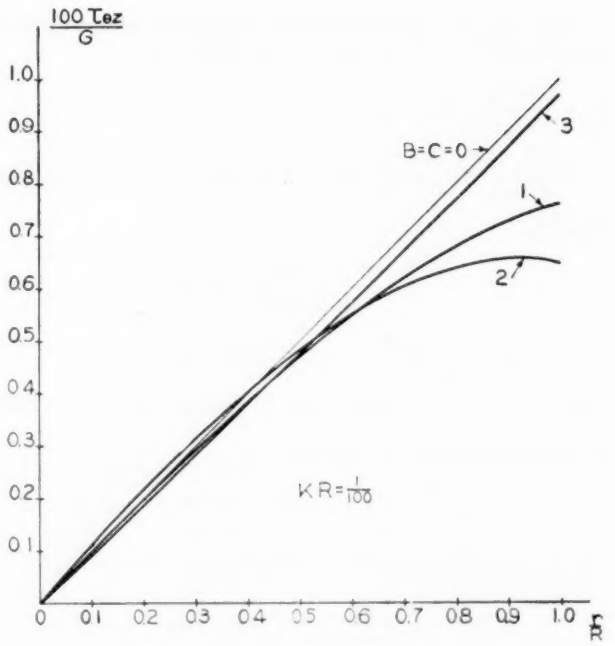
Inequalities [32] and [33] imply $r_0 > R$, and thus a reversal of $\tau_{\theta z}$ is impossible. If the characteristic angle of twist $KR > \dfrac{1}{\sqrt{\mu_1(3\mu_2 + \mu_3)}}$, then $\dfrac{r_0}{\sqrt{3}} > R$ and in this instance $\tau_{\theta z}$ is increasing for $0 \leq r \leq R$. For larger values of KR, $\tau_{\theta z\,\max}$ is reached inside the boundary. In either case, however, it is readily seen that $\tau_{\theta z\max} < GKR$, regardless of the value of μ_3.

(*B*) $\mu_3 < 0$, $\mu_2 > 0$:

$\tau_{\theta z}$ is increasing for $0 \leq r \leq R$ and $\tau_{\theta z} < GKr$ for $0 < r \leq R$.

Since $\mu_3 < 0$, $\mu_3 \leq 0$ is excluded by [33], the foregoing classification is exhaustive. Thus, regardless of the values of R, ν, G, B, C, and for all physically significant values of K, the maximum shear stress $\tau_{\theta z\max}$ is less than that consistent with the linear theory. Since the foregoing discussion of $M_{(K)}$ and $\tau_{\theta z(r)}$ remains valid if μ_3 is replaced by μ_3', the conclusions apply equally to Case 2. Fig. 8 shows typical $\tau_{\theta z(r)}$ curves.

Although the error depends on the value of C, it is of some interest to compare the exact solution for $A = B = 0$, Case 1, with the approximate solution based on the linearization: for $C = 100G$, $KR = \dfrac{1}{100}$, $\nu = \dfrac{1}{4}$, the discrepancy in the values of $\sigma_{z\max}$ is approximately 1.3 per cent. In connection with Case 2, it should further be observed that a measurement of the radial dilatation $u_{(R)}$ and the axial dilatation $w_{(l)}$ would suffice for the determination of the new elastic constants B and C. However, in general, these secondary displacements may be expected to be so small as to render accurate measurements impracticable.



1 . . . $\nu = \frac{1}{8}$, $b = c = 100$; $\mu_2 > 0$, $\mu_3 > 0$.

2 . $\nu = \frac{1}{4}$, $b = 0$, $c = \pm 300$; $\mu_2 > 0$, $\mu_3 < 0$.

3 . . . $\nu = \frac{1}{4}$, $b = -100$, $c = 100$; $\mu_2 < 0$, $\mu_3 > 0$.

FIG. 8 TORSION, DISTRIBUTION OF SHEAR STRESS $\tau_{\theta z}$; CASE 1

In the solution given by Voigt,[2] $M_{(K)}$ and $\tau_{\theta z(r)}$ are identical with the classical solution because of the particular, and apparently too strong, linearization employed there. In view of the present results, Voigt's general assertion that the angle of twist remains a linear function of the torque, even upon application of the extended elastic potential, must be considered erroneous.

ACKNOWLEDGMENTS

The author wishes to express his appreciation to Dr. M. A. Sadowsky, Associate Professor of Mathematics at Illinois Institute of Technology, and to Dr. Max Dehn, Visiting Professor of Mathematics at Black Mountain College, for most valuable suggestions and criticisms.

Compressible Flows Obtainable From Two-Dimensional Flows Through the Addition of a Constant Normal Velocity

By H. PORITSKY,[1] SCHENECTADY, N. Y.

This paper demonstrates that exact solutions of the flow of compressible fluids can be obtained by starting with two-dimensional steady-state flows and superposing upon them a velocity of constant magnitude and direction at right angles to the planes of the two-dimensional flows, while at the same time, the pressure, density, and temperature of the fluid at each point are unchanged. The procedure is demonstrated by several examples, one of which is of interest in connection with the discharge of exhaust gases from a gas engine through the tail cone and tail pipe in cases where the circulation has not been completely removed from the flow. Another example is the flow around a "sweepback" or "arrow" wing. This example is illustrated for supersonic flows on plane oblique shocks and on the Meyer-Prandtl expansion around an edge.

Introduction

SINCE comparatively few solutions of the problem of flow of compressible fluids at velocities comparable with sonic velocities are available, it is of interest to work out whatever simple examples can be furnished by theory to illustrate such flows. In the following it is shown that exact solutions of the flow of compressible fluids can be obtained by starting with two-dimensional steady-state flows and superposing upon them a velocity of constant magnitude and direction at right angles to the planes of the two-dimensional flow, while at the same time the pressure, density, and temperature of the fluid at each point are unchanged.

This procedure is illustrated by several examples. The first one is the two-dimensional compressible fluid flow furnished by a "vortex-source" or "vortex-sink;" the velocity distribution for this has been worked out by Binnie and Hooker, (1),[2] while the aspect of the flow lines is given by Ringleb, (2). The resulting three-dimensional flow, obtained by adding a constant axial velocity, is a flow which spirals about an axis and converges or diverges; it is of interest in connection with the discharge of exhaust gases from a gas engine through the tail cone and tail pipe in cases where the circulation has not been completely removed from the flow.

Another example of nontrivial flows, obtained from two-dimensional flows by the superposition of a constant normal velocity, is the flow around a "sweepback" or "arrow" wing. It is shown that by starting with the normal flow around a wing and superposing a constant velocity parallel to the span of the wing, one obtains the flow around a wing whose span is oblique to the flow vector, provided that the viscosity phenomena within the boundary layer be neglected. A sweepback wing is known to possess much higher stalling speeds at high Mach numbers and is of great interest in connection with high-speed aircraft.

The foregoing example is illustrated for supersonic flows on plane oblique shocks and on the Meyer-Prandtl expansion around an edge. It is shown that by superposing a normal velocity component on these well-known solutions, one obtains a compression shock and an expansion flow such as would occur to each side of a thin plate bounded by a straight edge placed so that its edge is oblique to the velocity vector of a supersonic stream.

Addition of Constant Normal Velocity Component to Two-Dimensional Flows

A constant velocity component

$$v_z = V = \text{const (in time and space)} \quad \ldots\ldots [1]$$

if added to a two-dimensional fluid flow of a compressible fluid, will result in a possible flow of that fluid. By a two-dimensional flow is meant a flow for which $v_z = 0$, and for which the velocity components v_x, v_y, and the pressure p, density ρ, and temperature T depend on x and y only. At the same time, we assume that p, ρ, T are not affected by the addition of the constant velocity component [1].

To prove the foregoing statement, we proceed to show that the equations of the fluid motion are still satisfied. We thus compare two cases, one of a two-dimensional flow F of a fluid in adiabatic compression, the other, a similar flow F', but with the constant axial velocity V added. For the flow F', the components of velocity v_x and v_y, and the pressure p, density ρ, temperature T are exactly the same functions of x and y as for F, and they are thus independent of z just as in the latter case. However, the aspect of the field of flow is different because of the addition of V in the z-direction.

The fluid-flow equations comprise the equation of continuity

$$\frac{\partial \rho}{\partial t} + \frac{\partial}{\partial x}(\rho v_x) + \frac{\partial}{\partial y}(\rho v_y) + \frac{\partial}{\partial z}(\rho v_z) = 0 \quad \ldots\ldots [2]$$

the dynamical equations

$$\left.\begin{aligned} a_x &= \frac{\partial v_x}{\partial t} + v_x\frac{\partial v_x}{\partial x} + v_y\frac{\partial v_x}{\partial y} + v_z\frac{\partial v_x}{\partial z} = -\frac{1}{\rho}\frac{\partial p}{\partial x} \\ a_y &= \frac{\partial v_y}{\partial t} + v_x\frac{\partial v_y}{\partial x} + v_y\frac{\partial v_y}{\partial y} + v_z\frac{\partial v_y}{\partial z} = -\frac{1}{\rho}\frac{\partial p}{\partial y} \\ a_z &= \frac{\partial v_z}{\partial t} + v_x\frac{\partial v_z}{\partial x} + v_y\frac{\partial v_z}{\partial y} + v_z\frac{\partial v_z}{\partial z} = -\frac{1}{\rho}\frac{\partial p}{\partial z} \end{aligned}\right\} \quad \ldots [3]$$

[1] Engineering General Division, General Electric Company. Mem. A.S.M.E.

[2] Numbers in parentheses refer to the Bibliography at the end of the paper.

Contributed by the Applied Mechanics Division and presented at the Annual Meeting, New York, N. Y., Nov. 26–29, 1945, of The American Society of Mechanical Engineers.

Discussion of this paper should be addressed to the Secretary, A.S.M.E., 29 West 39th Street, New York, N. Y., and will be accepted until April 10, 1946, for publication at a later date. Discussion received after the closing date will be returned.

Note: Statements and opinions advanced in papers are to be understood as individual expressions of their authors and not those of the Society.

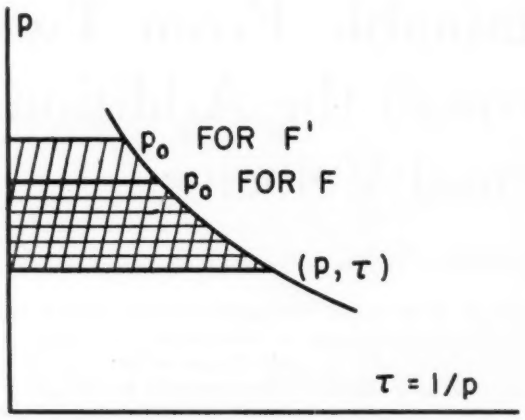


FIG. 1

and the assumption of an isentropic relation

$$p = p(\rho) = \frac{p_0}{\rho_0^k}\rho^k \quad \ldots\ldots [4]$$

between the pressure and density. For the two-dimensional flow F the last term on the left side of Equation [2] vanishes due to v_z being zero; for the modified flow F' it becomes

$$\frac{\partial(\rho v_z)}{\partial z} = V\frac{\partial \rho}{\partial z}$$

and vanishes due to the fact that ρ is independent of z. Hence Equation [2] is still satisfied. Similarly the terms $v_z\,\partial v_x/\partial z$, $v_z\,\partial v_y/\partial z$ in the first two Equations [3] vanish both for F and F', and every term in the first two Equations [3] retains its value in passing from F to F'. As regards the third Equation [3], its terms still vanish due to the constancy of v_z in time and space and to the vanishing of $\partial p/\partial z$.

An alternative proof is offered by referring the two-dimensional flow F to a set of axes, which are translated uniformly in the direction of the z-axis with velocity $-V$. Such a change of axes leads from one Newtonian system to another and does not affect the accelerations of the fluid particles; on the other hand the quantities, p, T, being static (that is, relative to a system moving with the local gas velocity) are not affected by the change of axes.

While in the foregoing we have neglected the effects of viscous (as well as of turbulent) shears, no assumption has been made in regard to whether the flow F possesses a scalar potential or not, that is, whether it is irrotational or not. If the two-dimensional flow is irrotational so that it possesses a velocity potential ϕ such that

$$(v_x, v_y) = \left(\frac{\partial \phi}{\partial x}, \frac{\partial \phi}{\partial y}\right) \quad \ldots\ldots [5]$$

then the addition of a constant v_z still leads to an irrotational field with

$$\phi + Vz \quad \ldots\ldots [6]$$

as its velocity potential. On the other hand, if the flow possesses vorticity so that no scalar velocity potential ϕ exists, then the addition of a constant v_z does not affect the vorticity either in magnitude or direction.

Under the assumptions of irrotationality, the Bernoulli equation

$$\left.\begin{aligned} \frac{\partial \phi}{\partial t} + \frac{v^2}{2} + P(\rho) &= \text{const} \\ P(\rho) &= \int \frac{dp}{\rho} \end{aligned}\right\} \quad \ldots\ldots [7]$$

follows from Equations [3], [4]. For steady flow this can be written as

$$\frac{v^2}{2} + P(\rho) = 0, \quad P(\rho) = \int_{p_0}^{p} \frac{dp}{\rho} = \int_{p_0}^{p} \tau\, dp \quad \ldots [8]$$

where $\tau = 1/\rho$ is the specific volume and p_0 the "stagnation pressure," that is, the pressure from which a gas at rest can be expanded isentropically to acquire a velocity v. While the same (p, ρ) curve obtains for the original motion and for the modified motion, the pressure p_0 is different for F, F' since $v^2/2$ differs by the constant amount $V^2/2$. The shaded areas in Fig. 1 represent the values of $v^2/2$ for the two-dimensional and the modified flows.

It may be shown that the inclusion of viscosity terms in the equations of motion does not affect the main conclusion reached in the foregoing. However, the boundary condition of zero slip has to be examined independently for F and F'

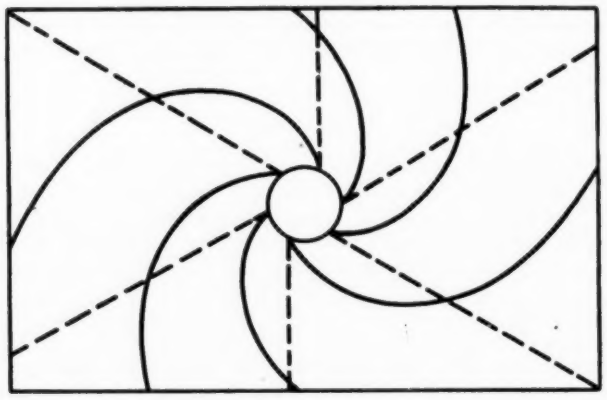


FIG. 2

APPLICATION TO A COMPRESSIBLE VORTEX SOURCE AND SINK

The flow lines of a compressible vortex source or sink may be found in Ringleb (2) and are reproduced here as Fig. 2. Two sets of flow lines are shown, one drawn as solid lines, the other as broken lines: they correspond to the two possible flows, one in which the velocity vanishes at infinity, the other one where it is everywhere supersonic, and the flow, if outward, is ever expanding. They are referred to as "converging" and "diverging" flows, respectively. Both flows are characterized by a natural boundary, a cylindrical surface at which the radial velocity component is equal to the local sound velocity (and the flow lines in the hodograph plane become tangent to the characteristics).

Addition of a constant velocity $v_z = V$ results in spiraling streamlines whose projection on the (x, y) plane have the same general aspect as in Fig. 2. The flow lines lie on proper surfaces of rotation any two of which may be regarded as possible boundaries. We proceed to plot the section of these surfaces made by an axial plane; these sections are obtained by neglecting the vortex component of velocity v_θ and plotting a curve by means of the relation

$$\frac{dr}{dz} = \frac{v_r}{v_z} = \frac{v_r}{V} \quad \ldots\ldots [9]$$

Binnie and Hooker tabulate and plot the velocity of the two-dimensional vortex source by utilizing the ratios

$$\left.\begin{aligned} R &= r/r^* \\ \theta &= v/a^* \end{aligned}\right\} \quad \ldots\ldots\ldots\ldots\ldots\ldots [10]$$

where r^* is the radius at which the fluid velocity for the converging flow is equal to the local velocity of sound a^*. They consider the special case of convergent flow for which the streamlines make an angle of 45 deg with the circle $R = 1$ so that at $r = r^*$, $v_r = v_\theta = a^*/\sqrt{2}$. The limit circle (cylinder) is given by $R = 0.946$. We shall consider the same case.

Utilizing the Binnie-Hooker equations and introducing V_s, V_r as a ratio of v_s, v_r to a^* (even though r^* is no longer the radius at which the fluid velocity is equal to the local sound velocity), and Z as the ratio z/r, the following cases

$$V_s = V/a^* = 0.05, 0.1, 0.5$$

were examined for the convergent flow and are plotted in Fig. 3. The procedure followed in obtaining these consisted in subtracting from the two-dimensional resultant velocity θ the tangential component $V_\theta = \sqrt{2}/R$ leading to

$$V_R = \sqrt{\theta^2 - \frac{2}{R^2}} \quad \ldots\ldots\ldots\ldots\ldots\ldots [11]$$

then dividing by the proper V_s to obtain the ratio dR/dZ and plotting a curve with the slope dZ/dR.

Writing Equation [9] in the form

$$\frac{dZ}{dR} = \frac{V}{V_R}, \quad Z = V \int \frac{dR}{V_R} \quad \ldots\ldots\ldots\ldots\ldots [12]$$

it will be seen that the curves in Fig. 3 can be obtained from each other by proper "stretching" or "compression" in the z-direction of any one curve.

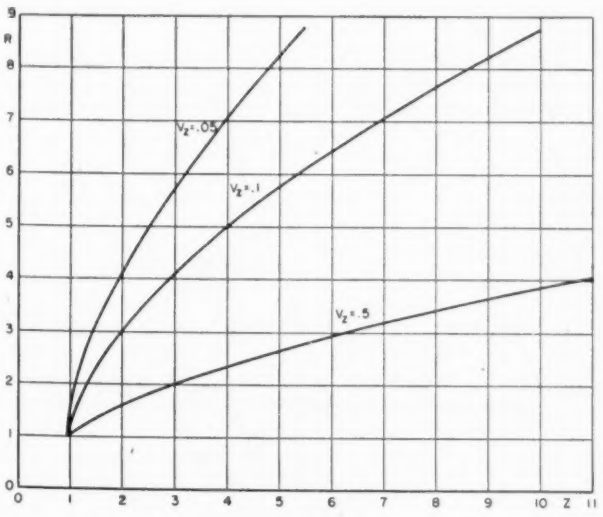


FIG. 3

For large R, the flow resembles incompressible flow so that

$$V_R = \text{const}/R \quad \ldots\ldots\ldots\ldots\ldots\ldots [13]$$

thus reducing Equations [12] to

$$Z = \text{const} \times R^2 \quad \ldots\ldots\ldots\ldots\ldots\ldots [14]$$

that is, to parabolic shape. Only a two-parameter family of shapes can be obtained by the present method (by varying V_R/V_θ and V_R/V_s at $R = 1$). The outer and inner boundaries of the flow field are of the same shape. These restrictions are due to an inherent limitation of the method which does not allow variation of V_s with r.

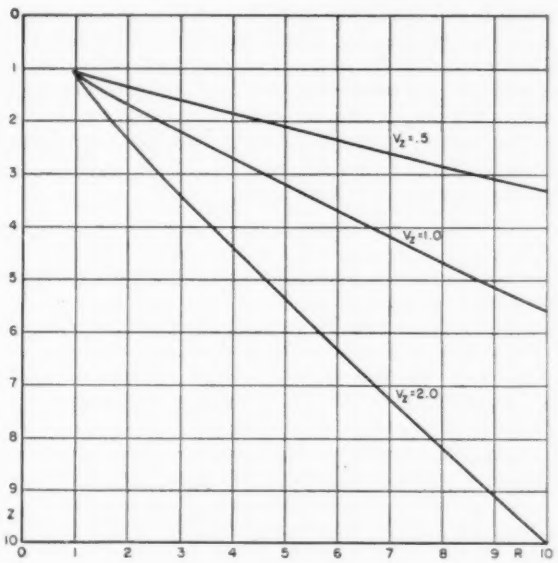


FIG. 4

Fig. 4 shows a similar (r, z) curve for the Binnie-Hooker example for the expanding flow and for

$$V_s = V/a^* = 0.5, 1, 2$$

These curves show very little curvature and now a conical surface is obtained at $R = \infty$.

SWEEPBACK OR ARROW WINGS

As a second application of the procedure for obtaining flows described in the first two sections, we consider the flow around "sweepback" or "arrow" wings, that is, around a pair of wings whose spans are inclined at an angle $\pm \sigma$ toward the main flow. It is known that with such wings higher Mach numbers may be attained before the onset of the "compressibility burble" with its resulting loss of lift and increase in drag.

Let σ be the angle of sweepback of a wing, and suppose that it is of infinite span, and that it is placed in a stream of velocity U. Resolve U into components $U \cos \sigma$, $U \sin \sigma$ normal to the wing span and parallel to it. Consider first the flow F corresponding to the velocity

$$U \cos \sigma \quad \ldots\ldots\ldots\ldots\ldots\ldots [15]$$

normal to the wing span, and let F' be the flow obtained from F by the addition of the component

$$U \sin \sigma \quad \ldots\ldots\ldots\ldots\ldots\ldots [16]$$

tangential to that span; then F' will represent the flow relative to the sweepback type of wing, provided the boundary-layer phenomena are negligible. As shown in the second section, the pressures for F and F' at corresponding points are equal. We thus arrive at the conclusion that the lift and drag experienced by a long wing of sweepback angle σ in a stream of velocity U is the same as that of the same wing in a stream of velocity $U \cos \sigma$ flowing normally to the wing span, the vectors correspond-

ing to U, $U \cos \sigma$, and the wing span being coplanar. In equation form

$$\left.\begin{aligned} \bar{L}(U) &= L(U \cos \sigma), \\ \bar{D}(U) &= \cos \sigma \, D(U \cos \sigma) \end{aligned}\right\} \quad \ldots\ldots\ldots\ldots [17]$$

where L is the lift, D the drag, as functions of the speed, and bars indicate sweepback. The factor $\cos \sigma$ in the last term is due to the fact that the drag of the normal wing is normal to the wing and only the component of D in the direction of the main flow U is the drag proper, the other component tending to collapse the wing. Assuming similarly that the loss of lift and increased drag of F are not affected by the addition of the tangential velocity, it follows that

$$\bar{U}_{cr} = \sec \sigma \, U_{cr} \ldots\ldots\ldots\ldots\ldots\ldots [18]$$

where $\bar{U}_{cr}$, U_{cr} refer to the critical velocities of the inclined and of the normal wing, respectively.

Equations [17] are valid particularly at supersonic speeds where the drag is due primarily to wave resistance and not to boundary-layer phenomena. At subsonic speeds this is not the case. Assuming that the boundary-layer phenomena are determined by the pressure and velocities of the flow of a perfect compressible flow outside a thin boundary layer, we see that in comparing the normal and sweepback wings with their flows F, F', it will be found that the pressures at corresponding points are the same, but the velocities for the flow F' are larger than for the flow F. No simple relation between the boundary layers of the flows F, F' can be established, even if the sidewise acceleration of F' be neglected. While the pressure gradients inside the F boundary layer are smaller, this is made up for by added length of flow lines and (if the boundary-layer thickness is assumed to be the same) by increased viscous drag. It is therefore not surprising that while experimentally higher stalling speeds are observed with sweepback wings, the critical speeds do not increase as predicted by Equation [18]. Of course, further discrepancies between the theory outlined and actual tests are to be expected due to the finite span of an actual wing with the resulting interference at the fuselage or between the two wings at their intersection in case there is no fuselage, and at the wing tips.[3]

Oblique Plane Shock

As an application of the theory, we will consider in this section and the following the flow taking place at the leading edge of a thin flat plate (or flat wing) placed in a supersonic stream so that it is inclined to the direction of flow and so that its leading edge is oblique to the flow. On the compression side an oblique plane shock takes place which will now be discussed; the expansion on the other side will be treated in the next section.

Rankine and Hugoniot developed the equations for a normal plane shock,[4] based on continuity of mass, momentum, and energy considerations, and Meyer developed the corresponding relations for an oblique plane shock.[5] The resulting relations are represented in (3) as curves of constant pressure ratios $x = p_2/p_0$, $y = p_1/p_0$ in an $(\alpha, \beta\text{-}\alpha)$ plane, where as shown in Fig. 5, α, β are the angles between the velocity vectors before and after the shock, and the normal to the plane of the shock; p_1, p_2 the pressures before and after the shock; p_0 the stagnation pressure prior to the shock. In passing through the shock the gas suffers an increase in entropy through the conversion of some of the kinetic energy of the normal velocity into heat energy. As a result, the gas acquires a different stagnation pressure p_3. The ratio $z = p_3/p_0$ may be found from (3), where curves of constant y are plotted in an (x, z) plane.

We consider now a shock produced by a thin plate whose straight-edge boundary is placed obliquely to the stream flow. As shown in Fig. 6, we choose the x-axis in the direction of flow, and let the (x, y) plane $ABCD$ contain EF, the edge of the plate $EFGH$. Let σ be the angle of sweepback between EF and the y-axis, and let ω be the angle between the plate $EFGH$ and the (x, y) plane.

Let U, p, be the velocity and pressure of the gas stream under consideration. We introduce the flow F as the flow of velocity

$$U_1 = U \cos \sigma \ldots\ldots\ldots\ldots\ldots\ldots [19]$$

normal to the z-axis and to the edge EF and pressure p_1 impinging on the plate $EFGH$ at an angle of attack ω. From the Meyer relations and the curves in (3), the plane of shock $EIFJ$, the pressure p_2, and velocity U_2 are determined. The flow F' is now obtained by leaving the planes $EFGH$, $EFJI$ unchanged, superposing the velocity component

$$U \sin \sigma \ldots\ldots\ldots\ldots\ldots\ldots [20]$$

parallel to the edge EF on the flow to each side of the plane of shock $EFGH$, and leaving p_1, p_2 (and the densities ρ_1, ρ_2 and temperatures T_1, T_2) unchanged. To justify this procedure one cannot apply the arguments of the second section, since the flow is actually discontinuous and no longer isentropic. The justification follows directly by noting that the equations of conservation of mass, of momentum, and energy across the plane of shock in the flow F are still satisfied after the addition of the component $U \sin \sigma$ leading to F'.

It will be noted that the static pressure p_0, (as well as the stagnation pressure p_3 for F beyond the plane of shock) are no longer true stagnation pressures for the flow F'. A direct expression of these quantities in terms of the two geometric angles ω, σ might be of interest.

It is of interest to point out that the Meyer equations for oblique shock (for $\sigma = 0$) may be derived from the normal shock by the similar procedure of addition of the tangential velocity

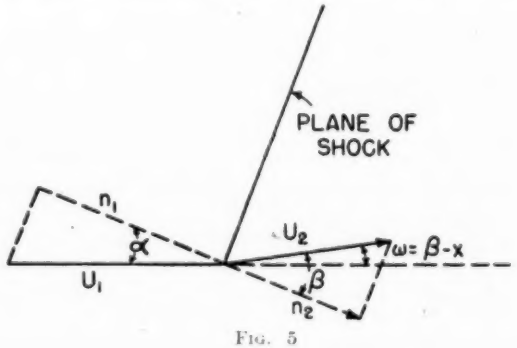


Fig. 5

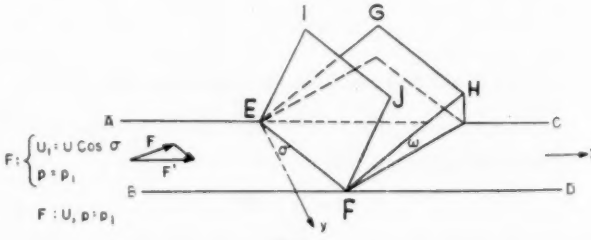


Fig. 6

[3] Since this was written, it has been pointed out to the author that the present theory of an oblique wing has been anticipated by Betz and others in Germany.

[4] See, for instance, reference (3), p. 217; reference (4), p. 325.

[5] Reference (3), p. 237; reference (4), p. 330.

component t to the discontinuous normal components n_1, n_2 to each side of the plane of shock.

It will be recalled that if ω is large and U_1, though supersonic, is close to sonic velocity, the shock equations of Meyer yield no solution. Under these conditions, the shock produced by a wedge of angle 2ω placed symmetrically in a supersonic flow U_1 differs considerably from the Meyer type; it is detached from the wedge; it has a curved shock locus with variable entropy increase along different stream lines; along the flow line through the corner (edge) of the wedge it is normal to flow. To the author's knowledge this flow has not been derived analytically, though many excellent schlieren figures of it are available in the literature. It may happen that U_1 in Equation [19] and ω fall in this range; the flow F' can still be derived from F by the addition of $U \sin \sigma$, but until more knowledge of the flow of the subsonic region of F becomes available, the foregoing is but an empty statement. However, even in the present state of the art, the range of velocities and angles within which this happens can be determined, though by the rather awkward procedure of looking for a solution of a different type (Meyer shock for $U_1 = U \cos \sigma$) and finding that it does not exist.

Oblique Prandtl-Meyer Expansion Around an Edge

A complete treatment of the two-dimensional expansion flow around a corner is given in (3)[6] and (4). The velocity as well as the pressure is constant along each of a family of straight lines through the origin (that is, planes through the edge); in the hodograph plane the velocity vector describes a characteristic curve, i.e., an epicycloid.

Addition of a constant velocity component parallel to the edge to the flow F permits one to handle flows F' which constitute an expansion around an edge of a dihedral angle of an oblique supersonic stream. The velocity and pressure are still constant over planes through the edge. In the hodograph space the velocity vector describes a plane curve (epicycloid) lying in a plane normal to the edge.

The oblique shocks of the preceding section and the oblique expansion around an edge can be utilized to obtain many features of the flow around a polyhedron placed in a supersonic stream, since this theory may be applied even when the successive edges encountered by the (bent) stream lines are not parallel to each other. However, at the vertices of the polyhedral angles, features not covered by this analysis arise at the juncture of the various regimes F'.

[6] Reference (3), p. 243; reference (4), p. 312.

BIBLIOGRAPHY

1 "The Radial and Spiral Flow of a Compressible Fluid," by A. M. Binnie and S. G. Hooker, *Philosophical Magazine*, vol. 23, Jan.-June, 1937, pp. 597–606.

2 "Exakte Lösungen der Differentialgleichungen einer adiabatischen Strömung," by F. Ringleb, *Zeitschrift für Angewandte Mathematik und Mechanik*, vol. 20, Aug., 1940, pp. 185–198.

3 Taylor and Maccoll in Aerodynamic Theory, edited by W. F. Durand, vol. 3, pp. 209–252.

4 "Handbuch der Physik," by J. Ackeret; edited by Geiger and Scheel, J. Springer, Berlin, Germany, vol. 7, 1927.

Discussion

Bending of Thin Curved Tubes[1]

ARTHUR MCCUTCHAN.[2] The author has rederived expressions to account for the greater flexibility of curved tubes subjected to bending both in the plane of the bend and perpendicular to the plane of the bend. Similar derivations by Wahl (1),[3] Hovgaard (2), and Vigness (3) have been published. Experimental verification of the greater flexibility of curved pipe has been presented by Wahl, Hovgaard, Vigness, and by Cope and Wert (4).

The range of curved tubes or pipes encountered in usual piping practice embraces values of the author's K expression above 0.075. The deflections in the plane of the bend found by tests described in the references cited verify the von Kármán formulas hence support the author's results as given in curves 1 and 7, Fig. 3 of the paper, for values of K above 0.075. (Note that K in this paper corresponds approximately to $h/3.3$ in Wahl's and Hovgaard's papers and that D corresponds to K or $1/K$ of those papers.)

For values of the author's K from 0.01 to 0.075, it would seem that some test substantiation that the author's curve 1 is preferable to the von Kármán's curve 2 is required. A difference of 5 to 1 in the flexibility factor D at the lower extremity of the K values is too great to accept without such proof.

The author's conclusion that the coefficient of deflection D also applies to bending perpendicular to the plane of the bend is not supported by the tests reported by Vigness (3). Curved tubes loaded by sidewise forces, torsion, or bending deflect more than solid sections due to flattening of the cross section at 45 deg to the plane of the bend, but the ratio is not the same as obtains in the case of bending in the plane of the bend.

If the author has some experimental evidence which can be given in support of his theoretical derivations, it would seem desirable to include it in the closure to his paper.

BIBLIOGRAPHY

1 "Stresses and Reactions in Expansion Pipe Bends," by A. M. Wahl, Trans. A.S.M.E., vol. 50, 1928, paper FSP-50-49.

2 "The Elastic Deformation of Pipe Bends," by Wm. Hovgaard, *Journal of Mathematical Physics*, M.I.T., vol. 5, 1926, pp. 69–108; vol. 7, 1928, pp. 193–297; vol. 8, 1929, pp. 293–344.

3 "Elastic Properties of Curved Tubes," by Irwin Vigness, Trans. A.S.M.E., vol. 65, 1943, pp. 105–120.

4 "Load-Deflection Relations for Large Plain, Corrugated, and Creased Pipe Bends," by E. T. Cope and E. A. Wert, Trans. A.S.M.E., vol. 54, 1932, paper FSP-54-12, pp. 115–159.

P. S. SYMONDS[4] AND IRWIN VIGNESS.[4] This paper presents a new solution to what is by now an old problem. The flexibility and stress-intensification factors which occur in curved tubes bent in the plane of curvature have been determined by von Kármán[5] and Hovgaard.[6] Their results are routinely used by engineers in the design of high-temperature high-pressure piping systems.[7] A recent paper[8] by one of the writers has extended the theory to bending out of the plane of curvature, to the same degree of approximation as that of von Kármán and Hovgaard.

Most of these solutions are expressed in terms of trigonometric series which converge rapidly. For tubes of commonly used wall thicknesses and bend radii, sufficient accuracy is usually obtained by neglecting all but the first term of the trigonometric series. Experimental results[6,8] show that the assumption that the bend radius is very large compared to the tube radius (made in all these solutions), as well as other simplifying approximations, are valid for bends of radii greater than 4 or 5 pipe diam.

When the quantity $\lambda \equiv tR/a^2$ (where t = wall thickness, R = bend radius, a = tube radius) is less than about 0.5, it is necessary to keep more than one term of the trigonometric series used in the solution. This was done by von Kármán in his original paper, in which results are given corresponding to 2- and 3-term solutions, and valid for $\lambda \geqslant$ about 0.1. Jenks[9] later presented values obtained by the use of sufficient terms to make them applicable to $\lambda \geqslant 0.05$. No derivation or experimental verification was given by Jenks, but his values were apparently obtained under the same assumption as von Kármán's, namely, that the bend radius is very large compared to the tube radius. When this condition is not satisfied, as, for example, in pipes having ratios R/a equal to 3 or 2, then these results may not be correct even though λ is sufficiently large. Calculations have been made by one of the writers, in which von Kármán's analysis was followed, but without neglecting a/R. The values of flexibility and stress factors for $R/a = 3$ and 2 were found to differ only slightly from each other and from those obtained by von Kármán and Jenks. These results are plotted in Fig. 1 of this discussion, together with the curve given by Beskin, using the more familiar notation λ rather than Beskin's K.

Unfortunately, while it is convenient to use these theoretical

[1] By Leon Beskin, published in the March, 1945, issue of the JOURNAL OF APPLIED MECHANICS, Trans. A.S.M.E., vol. 67, p. A-1.

[2] Engineer, Engineering Division, The Detroit Edison Company, Detroit, Mich. Jun. A.S.M.E.

[3] Numbers in parentheses refer to the Bibliography at the end of this discussion.

[4] Mechanics and Electricity Division, Naval Research Laboratory, Anacostia Station, Washington, D. C.

[5] "Über die Formänderung dünnwandiger Röhre," by Th. von Kármán, *Zeitschrift des Vereines deutscher Ingenieure*, vol. 55, 1911, p. 1889.

[6] See McCutchan's bibliography reference (2).

[7] "Piping Handbook," by J. H. Walker and Sabin Crocker, McGraw-Hill Book Company, Inc., New York, N. Y., 1939, chapt. 7.

[8] "Elastic Properties of Curved Tubes," by Irwin Vigness, Trans. A.S.M.E., vol. 65, 1943, p. 105.

[9] Discussion by H. E. Jenks of paper, "Design of Steam Piping to Care for Expansion," by W. H. Shipman, Trans. A.S.M.E., vol. 51, 1929, paper FSP-51-52.

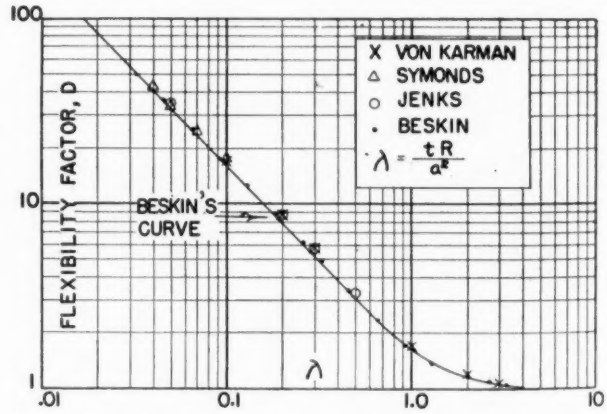


FIG. 1 COMPARISON OF CALCULATED FLEXIBILITY FACTORS FOR BENDING IN THE PLANE OF THE BEND

values, it must be recognized when working with short-radius bends that the actual flexibility factor depends greatly upon the type of restraints at the ends of the bends, which have been neglected in all of the theories. As an example, the experimental values of the flexibility factors (for pure bending in the plane of the bend) are given in the following table for tube bends having $R/a = 3, \lambda = 0.043$:

Bend	Flexibility factor
180° Bend with long tangents	37
90° Bend with tangents	32
90° Bend with flange at one end	18
90° Bend with flange at both ends	8

In the case of bending transverse to the plane of the bend, the measured flexibility factors are found to depend to an important extent upon how the loading is applied, and which deflection is measured (of the two major rotations and the displacement), as well as upon the end restraints. Considerable work has been done recently at the writers' laboratory on these problems, complete results of which will be published as soon as possible.

In examining the author's analysis, the following additional comments have occurred to us:

1 The "exactness" of the author's solutions should be qualified more explicitly than the author has done in his "Introduction." It is evident that fundamental approximations have been made in writing the strain-energy Equations [5] and [36] (applying to bending in the plane of the bend and transverse to this plane, respectively). In the in-plane bending case, for example, the assumptions are made, but not stated, that strain-energy terms, due to a transverse normal stress flow, due to any shear stresses, and due to axial local bending moments, are negligible in comparison with those arising from the longitudinal normal stress and the transverse local bending moments. In the transverse bending case, these assumptions, together with others, are also tacitly made. Most of these assumptions are plausible and probably justified, although some of those applying to transverse bending seem to be erroneous, according to experimental work that has been done at this laboratory. Solutions of this type can be shown to be sufficiently exact for any given purpose only by either (*a*) showing that, as more complete energy expressions are used, negligible changes in the final results are obtained, or (*b*) comparing results with those obtained experimentally. In this case probably only the latter test is practicable; such comparisons are cited by previous investigators (von Kármán, Hovgaard, Vigness, and others.) Mr. Beskin's analysis (particularly that for bending out of the plane of the bend) would have been more convincing if he had applied either of these tests.

2 We would appreciate having some additional information as to the meaning of the author's Equations [21], [22], [23], and [26], which are given as the equilibrium equations for an element of the tube wall in the transverse-bending case. The first three equations are readily derived for an element of sides $ad\theta$ and $(R - a\cos\theta)d\phi$ acted upon by the normal stress flows $\bar{n}_\phi$, $\bar{n}_\theta$, by the shear stress flow $\bar{q}$ ("along meridians and parallels"), by a local transverse bending moment $\bar{m}$, and by the fictitious normal pressure $\bar{W}$. However, the fourth equation of equilibrium for this stress system is

$$\frac{\partial}{\partial\theta}\left[\bar{m}\,(R - a\cos\theta)\right] = 0$$

Instead of this, the author quotes "the well-known relation for a circle," Equation [25], which he then modifies to take account of the variation of the element length around the circumference of the tube, obtaining Equation [26]. But Equations [25] and [26] pertain to a quite different set of stress flows, namely, that consisting of $\bar{n}_\theta$, $\bar{m}$, $\bar{W}$ and a radial shear flow V_θ on the sides $(R - a\cos\theta)d\phi$. By combining the four equilibrium equations of the element acted on by this system one obtains readily Equation [26]. This new system, however, does not yield Equations [21], [23] nor does the first system lead to Equation [26], in any way we have been able to discover. Further explanation of these equations would be helpful, in addition to the author's statement that "torsion and bending between adjacent sections are neglected."

3 As mentioned, experimental work done at the writers' laboratory indicates that some of the assumptions made in the analysis for the transverse-bending case are of questionable validity. In pure transverse bending, as the author says, all stresses are functions of both ϕ and θ. He then eliminates ϕ by assuming that "all flows and moments are of the same type as M_B and M_T." Thus for the case $M_B = M\cos\phi$, $M_T = M\sin\phi$, he writes $\bar{q}\,(\theta, \phi) = q(\theta)\sin\phi$, while $\bar{n}_\theta$, $\bar{n}_\phi$, $\bar{m}$, and $\bar{W}$ are all taken as proportional to $\cos\phi$.

This assumption, that stresses and displacements are proportional only to the corresponding moment, is a natural one, and one which we have made in our work. However, we have made many measurements of the diameter changes of 90-deg and 180-deg tube turns loaded so that the bending moment vanishes at either the one end or at both ends. All of these measurements show that the diameter change, as one goes around the bend, is not simply proportional to the bending moment. At the end of the bend where the bending moment is zero, the diameter change may be as much as $^1/_3$ or $^1/_2$ of the maximum value in the bend. This has a large effect on the deflection of the bend. These and many other tests we have made indicate that the simple concept of flexibility factor, as used by pipe-stress analysts, and as defined again by the author, is no longer applicable when a short-radius tube turn is loaded transversely. It is hoped that descriptions of these tests and analytical work will be published soon.

4 We are not clear what the third section of the paper, entitled, "Validity of Assumption That Ratio R/a Is Great—Corrections for Small Values of R/a," proves in regard to the bending of thin-walled curved tubes. It is, we believe, well known that in a solid curved bar, of thin rectangular section, the hyperbolic theory agrees well with the exact solution, both as to the maximum stresses and the bar deflection, even when R/a is as small as 2, while the linear-stress theory disagrees considerably in maximum stress values (about 35 per cent in error for $R/a = 2$), but is not so far off in the deflection values (about 5 per cent in error for $R/a = 2$).

We question whether these facts are a demonstration that a theory of thin-walled tubes which neglects "difference of length along the inner and outer circumferences" will be satisfactory with respect to deflections, but unsatisfactory with respect to stresses. While the errors could hardly be less than these, they might be much greater. The significant mechanism causing the increased flexibility of a thin-walled curved tube is the deformation of the cross section, and the resultant complete redistribution of stresses over the circumference. The effect of this redistribution is quite different from that of the redistribution of stresses which takes place in a solid curved bar. Hence it is difficult to see the application of the author's comparison with solid-bar results. As pointed out previously, the only convincing argument is either a more complete theoretical analysis of the actual problem, or experimental verification.

Author's Closure

It is extremely regrettable that Mr. McCutchan has not examined thoroughly the difference between the methods con-

sidered in the present paper and the preceding literature. A comparison is made herein.

1 The von Kármán theory has been derived from the same hypotheses as the author's theory, the only difference residing in the accuracy of the mathematical derivation. As pointed out in the author's paper, von Kármán has assumed that a 2- or 3-term expression may be used to represent the stress distribution. The author has used a series development, which enabled him to limit the error to any predetermined value. This method has shown that von Kármán's expression is valid in all the useful range of tube proportions, assuming that the physical hypotheses introduced either by von Kármán or by the author are justified. This justification is given by tests made in a fairly wide range, which validate both methods. Since von Kármán's results represent a first approximation of the author's results, the latter should be used in all the cases where there is a discrepancy between the two theories. However, the author's results may become incorrect if the physical and mathematical assumptions made by both von Kármán and the author are not satisfied. The author has already pointed out that the radius of curvature must be at least double that of the tube radius. In addition, the wall thickness must be sufficient to avoid local instability, a condition which defines an upper limit of the ratio a/t.

These considerations show why Mr. McCutchan is misled when he requires test to decide which, of von Kármán's results or the author's, must be considered as correct.

2 Mr. McCutchan makes a still greater error when he opposes the tests reported by Vigness[10] with the author's theoretical results. In the summary of his paper, Vigness[11] clearly indicates "A flexibility factor is obtained which is identical with that found for the bending of pipe in the plane of its bend." Further, Vigness[12] reproduces (Equations [3] and [35]) von Kármán's formula and states: "The rigidity factor is identical to that derived by von Kármán and Hovgaard for bending in the plane of the bend. It may now be applied generally to the flexural rigidity of tubes." The tests presented by Vigness confirm these conclusions, as it results directly from his Tables 3 and 4. This confirms the author's results, since the latter are nearly identical to Vigness-von Kármán expressions for the tube proportions used in the tests. At the same time, Mr. McCutchan's statement that the Vigness paper does not confirm the author's results is entirely invalidated.

In respect to tests presented in Table 1 of Vigness' paper, which Mr. McCutchan probably mistook as showing a difference between in-plane and out-of-plane bending, it must be noted that the values corresponding to $P = 1$ have been calculated by Vigness, using the hypothesis that the tube curvature has no influence on the out-of-plane bending. The discrepancy with test results is used as an argument by Vigness to prove that conventional methods must be revised, which is the object of his paper. The author, using the coefficient $D = 1.97$, resulting from the tube dimensions, finds by a strain-energy calculation that the end deflection (including bending and torsion) is $\Delta x = 0.064$ instead of the measured value 0.060, and the value 0.037 calculated by the Karelitz and Marchand (conventional) method.

These results show a difference of 7 per cent between the author's theory and the tests; difference easily explained by the fact that around each reversal of curvature, the sections are more rigid than found by the theoretical formula developed for constant curvature. The difference of 7 per cent indicates that 19 per cent of the tube length is not affected by the curvature effect (figure obtained when the torsional deflection is eliminated). In other terms, it can be assumed that the rigidity constant varies linearly between the value $1/EI$ and D/EI, the first value corresponding to the point of inflection, the second at some distance from it, chosen in such manner that the affected lengths represent 38 per cent of the tube development. This length represents 0.9 in. on either side of a point of inflection, a result which seems reasonable when compared with the average diameter of the tube, which is 0.72 in.

In conclusion, it can be stated that, in contradiction with Mr. McCutchan's assertion, his references confirm the validity of the author's theory, instead of disproving it.

A complete discussion of the points raised by Messrs. Symonds and Vigness would require a completely new paper and is beyond the scope of a closure. For this reason, only succinct indications are given hereinafter.

1 (*a*) It was felt that it is useless to insist on the simplifications made in the analysis of in-plane bending, which are conventional in stress analysis of thin tubes and of frames. It has been shown time and again that the moment of inertia of a thin tube can be calculated considering that all the material is concentrated along the mean circumference, and that axial loads and shears produce negligible deflections in thin frames, such as constituted by a slice of a tube. When the limit case of very thick tubes (solid sections, $t/a = 2$) is considered, the analysis developed in the third section of the paper shows that, in this case also, deformations due to transversal stresses (which are the limit of normal stresses and shears) are negligible, since the conventional formulas for straight beams can be used to calculate deflections (see Table 2). This, incidentally, explains one of the purposes of the third section (see comment 4). More specifically, the secondary effects are the following:

(*a*) *Axial Local Bending.* The total moment of inertia of a straight tube is

$$I_0 = \pi a^3 t + \frac{\pi a t^3}{4}$$

For a curved tube, the corrected value to be used in deflection computations is

$$\frac{\pi a^3 t}{D} + \frac{\pi a t^3}{4} = \frac{\pi a^3 t}{D}\left(1 + \frac{\lambda D}{4}\frac{t}{R}\right)$$

In this equation $\lambda = tR/a^2$. The factor $\lambda Dt/4R$ represents the correction due to axial local bending. Since $\lambda D = 1.6$ for a wide range of values of λ, the correction factor has the value $t/2.5R$ and is generally negligible. For the tube examined by Symonds and Vigness ($\lambda = 0.043$, $R/a = 3$; $t/a = 0.014$), the correction is 0.2 per cent. For this tube, the deflection coefficient has the theoretical value $D = 38$ (Fig. 3 of paper), against $D = 37$ measured for a 180-deg bend, without end restraint, which shows the degree of reliability of the formula developed in the paper.

(*b*) *Shears and Normal Stresses.* Shear flows V_θ and normal stress flows n_θ can be determined as functions of the basic quantities z and y

$$V_\theta = \frac{dm}{ad\theta} = \frac{dz}{d\theta}\frac{M}{2\pi R}; \quad n_\theta = V_\theta \cot\theta$$

in which

$$\frac{dz}{d\theta} = \Sigma \sin 2n\theta \,[b_{2n-1} - b_{2n+1}]$$

$$\frac{dz}{d\theta}\cot\theta = 1 + \Sigma \cos 2n\theta \,[b_{2n-1} + b_{2n+1}]$$

Thus the initial Equation [8] must be completed by the terms

$$pH^2\int_0^{2\pi}\left(\frac{dz}{d\theta}\right)^2 d\theta + H^2\int_0^{2\pi}\left(\frac{dz}{d\theta}\cot\theta\right)^2 d\theta$$

[10] See McCutchan's bibliography reference (3).
[11] Ibid., p. 105.
[12] Ibid., pp. 107 and 115.

with

$$H^2 = \left(\frac{t}{a}\right)^2 \frac{1}{12(1-\nu^2)}; \quad p = \frac{6E}{5G}$$

To expressions, Equations [13] and [14], must be added

$$pH^2\pi[(1-b_3)^2 + (b_3-b_5)^2 + \ldots.] + H^2\pi[2 + (1+b_3)^2 + (b_3+b_5)^2 + \ldots..]$$

Equations [15] must be completed by terms such as

$$pH^2[2b_{2n+1} - b_{2n-1} - b_{2n+3}] + H^2[2b_{2n+1} + b_{2n-1} + b_{2n+3}]$$

These modified equations lead to more accurate coefficients b. If the uncorrected coefficients b are used, a value of D can be obtained by simple addition of the terms corresponding to the deflections neglected heretofore. As these terms are relatively small, the corrections to the coefficients b are small and the correct value of D is very close to the value thus calculated, which is too high. The correction to expression, Equation [20], for D is

$$\frac{a^2}{4R^2}[2 + \Sigma(b_{2n-1} + b_{2n+1})^2 + p\Sigma(b_{2n-1} - b_{2n+1})^2] = \frac{a^2}{R^2}\omega$$

For $p = 3.25$, it is found

K	0.01	0.1	1
ω	2.5	1.43	1.54

Thus the corrected value of D, designated by D_c, is

$$D < D_c \leq D + \frac{a^2\omega}{R^2}$$

For a thick tube with a great curvature (say, $K = 0.1$ or $t = a/10$; $R = 3a$), the factor $a^2\omega/R^2$ is smaller than 0.1, which represents a relative error for D smaller than 2 per cent. For a thin tube the error is smaller. For the tube just examined

$$D_c = D + 25; \quad D = 38$$

and the error is smaller than 1 per cent.

For a solid rectangular section, the quantity $D_c - D$ is represented by column 5 of Table 2, which confirms the results established here. These results show that it is fairly simple to determine what terms can be neglected in an analysis of the type examined here; this contradicts Symonds' and Vigness' opinion, who feel that such an analysis is not practicable.

1 (*b*) The same simplifications have been used for the analysis of transverse bending. It has been specifically indicated in the paper that only the bending of each segment of the tube has been considered, while perpendicular local bending moments as well as torsion between segments have been neglected, which is the meaning of the sentence: "Torsion and bending between adjacent sections are neglected." An analysis similar to the one indicated under 1*a*—(*a*) would justify these simplifications, and an analysis similar to the one indicated under 1*a*—(*b*) would justify the fact that secondary normal stresses and shears have been neglected.

The equations for transverse bending are conventional equations of equilibrium of surfaces with a double curvature and can be found in any textbook on shell analysis. For instance, Love (5)[13] derives the following equations, in which the notations α and β correspond to θ and ϕ of the paper, respectively: Equation [45-1] corresponding to Equation [22] of the paper; Equation [45-2] to Equation [23]; Equation [45-3] to Equation [21]. The only difference resides in the fact that the fictitious load $\overline{W}$ is replaced by derivatives of shears such as

$$\frac{\partial[V_\theta(R - a\cos\theta)]}{\partial\theta}\frac{1}{a(R - a\cos\theta)}$$

which represent the actual value of the fictitious right-hand member of Equation [21]. Equation [25] or [26] is derived by combining equations such as Equations [21], [22], and the equations of equilibrium between moments and shears, which replace the obviously incorrect equation written by Symonds and Vigness

$$\frac{\partial}{\partial\theta}[\overline{m}(R - a\cos\theta)]$$

which should be (see Love's Equation [46–2])

$$\frac{\partial}{\partial\theta}[\overline{m}(R - a\cos\theta)] - \overline{V}_\theta(R - a\cos\theta)a = 0$$

Symonds and Vigness did not realize that there is only one system of stress flows and unit moments; this system is $\overline{n}_\theta$, $\overline{n}_\phi$, $\overline{V}_\theta$, $m = \overline{m}_\theta$ ($\overline{m}_\phi$, $\overline{V}_\phi$ and the torsion are neglected). For simplicity of presentation, this system has been divided into $\overline{n}_\theta$, $\overline{W}$, $\overline{n}_\theta$ and $-\overline{W}$, $\overline{V}_\theta$, $\overline{m}$, $\overline{n}_\theta$. The second system is a conventional loading of a ring and corresponds to the equations

$$\frac{\partial\overline{m}}{\partial\theta} = a\overline{V}_\theta; \quad \frac{\partial\overline{V}_\theta}{\partial\theta} = -a\overline{W} + \overline{n}_\theta; \quad \frac{\partial\overline{n}_\theta}{\partial\theta} = -\overline{V}_\theta$$

In these equations the length factor $1 - a\cos\theta/R$ has been omitted. Combination of these equations leads to Equation [25] or to the correct Equation [26] of the paper, if the length factor is introduced.

3 It is a classical result (6) for shells in form of surface of revolution that if a loading is a periodical function of the type $M_B = M_1\cos n\phi$; $M_T = M_2\sin n\phi$, all the internal stresses and strains are of the same form, provided the edge loads and displacements correspond to the corresponding boundary values defined by this solution. Thus there is no assumption made in this analysis, at least for a given system of edge conditions, which shows the error of Symonds' and Vigness' statement, "the assumptions . . . . are of questionable validity."

This analysis is as exact as the corresponding analysis for in-plane bending, in which it is considered that the stresses are the same in all sections, which is obvious for reason of symmetry. The same concept of symmetry, generalized to include the concept of orthogonality, explains why periodical solutions of different periods are independent on a shell in form of a surface of revolution. These facts have been applied for many years in the theory of shells of revolution, especially in the case of reinforced-concrete construction (7, 8).

With regard to the edge conditions, it can be indicated that the solution developed in this paper strictly follows the semi-inverse method invented by Saint Venant (9), which consists in finding an arbitrary solution of the equations of equilibrium and of deformation, in which edge conditions are disregarded. It is known that a change in edge conditions affects but slightly the general deflections of solid bodies. In recent years, especially in connection with aircraft structures, it has been realized that when thin structures are considered, edge conditions may have much greater importance. This is especially true for open shells in the form of beams, in which case edge conditions are the main factor in the determination of stresses, a fact which has led the author to suggest an extension of the Saint Venant principle for this case (10). In the case of closed beams the influence of the edge conditions is less important, but may not be negligible, as proved by the tests indicated by Symonds and Vigness for in-plane bending.

[13] Numbers in parentheses refer to the Bibliography at the end of this closure and follow numerically from the bibliography at the end of the McCutchan discussion.

As regards the transverse bending test indicated by Symonds and Vigness, the following can be noted: If the tests had been repeated by applying end moments on a 180-deg bend, the middle section would have been submitted to torque only and for pure reason of symmetry, its dimensions would not have changed. The argument against the mathematical derivation which has been put forward in this case is an example of incorrect conclusions drawn from test which do not correspond to the conditions chosen for a theoretical analysis.

If a refined theory of bending of curved tubes is to be developed, it must follow the conventional pattern established by Saint Venant: (*a*) Find a solution by a semi-inverse method, which has been the aim of the present paper; (*b*) find the variations to this solution which are due to changes of the end conditions. From the experience he has gathered in the problem of straight beams (11), the author feels that the solution of the problem of end effects is a fairly simple one, at least with regard to the theoretical analysis. The actual computation, however, may be somewhat lengthy. Basically, the method is as follows:

For a bend of angle α, it is necessary to add terms of the form $\cos \pi n\phi/\alpha$, $\sin \pi n\phi/\alpha$ to the existing terms, in order to obtain double infinite series in θ and ϕ. Then various edge conditions can be satisfied without great difficulty.

4 The fact that the ratio R/a has but a small influence on the rigidity is confirmed by the analysis that Symonds and Vigness have made on pipes having this ratio equal to 3 or 2. Thus their questioning on the validity of this fact seems superfluous.

As regards the third section of the paper, they believe, "It is well known that in a solid curved bar . . . . the hyperbolic theory agrees well with the exact solution . . . . as to . . . . the bar deflection." However, the purpose of Table 2 of the paper is not to confirm this belief, but on the contrary to show that it is erroneous. The hyperbolic theory is less correct than the straight beam theory with regard to deflections, although it is acceptable as regards stress distribution. The results for a rectangular section are obviously valid for very thick tubes. It is thus necessary to prove the point for thin tubes, a calculation which has precisely been made by Symonds and Vigness.

The true reason for which stresses are affected by the value of the ratio a/R while total deflections are practically unaffected resides in the fact that stresses are modified in an approximately linear manner by R/a, while the total deflection, which is obtained by adding strains on both sides of the neutral line, is affected by a factor proportional to $(a/R)^2$. In addition, the transversal stresses omitted in the hyperbolic distribution compensate to a great extent the previous effect, which causes the final coefficient of $(a/R)^2$ in the formula for deflection to be extremely small. If a complete analysis, introducing the factor (a/R) in an explicit manner, is required, the following method can be applied:

The general equations of equilibrium of shells of revolution under symmetric loading are conventional. The equations written by Timoshenko (12) can be applied. Combining the three equations of equilibrium, and omitting the longitudinal local bending (see 1*a*), the following equation can be established

$$\frac{1}{a^2}\left(\frac{d^3}{d\theta^3}+\frac{d}{d\theta}\right)[m(R+a\sin\theta)]+n\cos\theta+\frac{d}{d\theta}(n\sin\theta)=0$$

It can be shown that this equation can be replaced by

$$a^2 n=\frac{d}{d\theta}\left[\frac{1}{\sin\theta}\,\frac{d}{d\theta}\{m(R+a\sin\theta)\}\right]$$

If the unknown m is replaced by

$$m'=m(R+a\sin\theta)/R$$

this equation becomes identical to Equation [4] of the paper. However, the problem is modified because the strain-energy expression becomes

$$\frac{1}{2}\left[\int_0^{2\pi}\frac{n^2 d\theta}{Et}\left(1+\frac{a}{R}\sin\theta\right)+\int_0^{2\pi}\frac{m'^2 d\theta}{EI\left(1+\frac{a}{R}\sin\theta\right)}\right]$$

Thus with the same relation, Equation [9], between the two unknowns y and z, the quantity to be minimum is (instead of Equation [8])

$$K^2\int_0^{2\pi}y^2\left(1+\frac{a}{R}\sin\theta\right)d\theta+\int_0^{2\pi}\frac{Z^2 d\theta}{1+\frac{a}{R}\sin\theta}$$

Because of the existence of antisymmetric terms $\frac{a}{R}\sin\theta$ in this equation, the series Equations [11], [12] defining y and z must be completed by terms with opposite symmetry

$$y=2\Sigma(2n+1)b_{2n+1}\sin(2n+1)\theta+2\Sigma n g_n\cos n\theta$$

$$z=\Sigma(b_{2n-1}-b_{2n+1})\frac{\cos 2n\theta}{2n}+\Sigma(g_{n+1}-g_{n-1})\frac{\sin n\theta}{n}$$

After $1\Big/\left(1+\frac{a}{R}\sin\theta\right)$ is replaced by its series expansion and y and z are replaced by the foregoing developments, the equation for minimum strain energy can be replaced by simultaneous equations in which the coefficients b_{2n+1} and g_n are the unknowns. These equations are of more complicated form than Equations [15] and are functions of the two parameters K and a/R. A method of successive approximations can be applied since, for small values of a/R, the solution developed in the paper represents a first approximation. Thus for increasing values of a/R, each solution found for a given value of a/R is a first approximation for a somewhat greater value of this quantity, and the solutions for the whole range of useful values of a/R can be found.

It is presumed that these indications may prove useful for further developments of the theory of curved thin tubes.

BIBLIOGRAPHY

5 "A Treatise on the Mathematical Theory of Elasticity," by A. E. H. Love, fourth edition, Cambridge University Press, 1927, p. 534 and ss.

6 Reference (5), par. 337.

7 Fr. Dischinger, Schalen und Rippenkuppeln, in "Handbuch für Eisenbeton," fourth edition, Wilhelm Ernst and Son, Berlin, Germany, vol, 6, 1928, chap. 2, p. 194 and ss.

8 "Statik und Dynamic der Schalen," by W. Flügge, Julius Springer, Berlin, Germany, 1934.

9 Reference (5), p. 19.

10 "Stress Analysis of Open Cylindrical Membranes," by L. Beskin, *Journal of the Aeronautical Sciences*, Oct., 1944, p. 343 and ss.

11 "Determination of the Effective Width of the Compression Flanges of T-Beams," by L. Beskin (Beschkine), International Association for Bridge and Structural Engineering Publications, Zurich, Switzerland, vol. V, 1938, p. 65 and ss.

12 "Theory of Plates and Shells," by S. Timoshenko, McGraw-Hill Book Company, Inc., New York, N. Y., 1940, par. 92, p. 450 and ss, Equations [258].

Yielding and Fracture of Medium-Carbon Steel Under Combined Stress[1]

C. W. MacGregor[2] and L. F. Coffin, Jr.[3] A program quite

[1] By E. A. Davis, published in the March, 1945, issue of the Journal of Applied Mechanics, Trans. A.S.M.E., vol. 67, 1945, p. A-13.

[2] Professor of Applied Mechanics, Massachusetts Institute of Technology, Cambridge, Mass. Mem. A.S.M.E.

[3] Instructor, Massachusetts Institute of Technology, Cambridge, Mass. Jun. A.S.M.E.

similar to that reported by the author was carried out in the Research Laboratories for Mechanics of Materials at M.I.T. during the winter of 1940–1941. Although an initial phase of this program was completed by that time, the more extended study planned had to be postponed due to the writers' activities on other war research. In view of the similarity of the initial program with the present study reported by Mr. Davis, a summary of this work is included herein.

Tubular test specimens were machined from 2-in-diam bars of S.A.E. 1020 steel, cut from a 20-ft length of stock. The chemical analysis for this material was as follows:

C	Mn	P	S
0.20	0.55	0.009	0.027

Prior to machining, the bars were carefully annealed at 1650 F and furnace-cooled. All tubular specimens were drilled, reamed, and lapped to an internal diameter of 1.00 in. and were turned and polished giving a wall thickness of 0.1 in. Those tubes subjected to internal pressure and axial tension had a gage length of 4 in., while those tested under internal pressure and axial compression were machined to a 2-in. length. Torsion specimens were 12 in. long and $^1/_2$ in. diam over the test region. Details of the grips and equipment used may be found in a previously published paper.[4]

Prior to testing, all tubes were carefully scribed with a network of fine scratches such that the grid spacing was approximately 0.1 in. in both the axial and circumferential directions. These networks were scribed with a commercial diamond set in a jig. The tubes were mounted in a lathe with the scriber attached to the cross-feed, in such a manner that the cross-feed micrometer screw could be used for indexing. The grids then were measured carefully by means of a cathetometer, to the nearest 0.0001 in. All tubes were traversed with a dial-gage device,[4] so that the wall thickness at any point in the gridwork area was known to 0.0001 in. Finally, the outside diameters were measured throughout the test area.

The tubes were then subjected to internal pressure and axial load. The ratio of the internal pressure to axial load was maintained at a constant predetermined value throughout each test. No measurements were taken during the test, although the maximum and fracture loads were recorded. After rupture, the networks, wall thicknesses, and outside diameters of all tubes were again measured, following the same procedure as in the initial measurements.

Octahedral shearing strains were computed for all elements of the network in the region of fracture and the strains corresponding to the largest octahedral shearing strain were recorded as the fracture strains of the tube in question. In this connection it should be mentioned that the values determined were true strains.

The fracture stresses were admittedly more approximate. For cases where tubes ruptured with a circumferential crack, the minimum wall thickness and the average diameter around the circumference were measured and the stresses evaluated from expressions similar to Equations [14], [15], and [16] in the paper. Where axial fractures occurred, the minimum wall thickness was used, together with the diameter 90 deg from the point of fracture, assuming the tube was axially symmetrical before rupture and Equations [14], [15], and [16] again applied. The stresses so evaluated were average true stresses.

The results of this investigation are given in Table 1 of this discussion. The octahedral shearing strains $\bar{\gamma}_n$ at fracture vary from 0.980 in. per in. for pure tension to 0.592 for a ratio of $\bar{\sigma}_t/\bar{\sigma}_a$ of 2.465. The octahedral shearing stress, $\bar{\tau}_n$, remains reasonably constant over the range of stress ratios tested. Of particular interest is the constancy of the maximum principal shearing stress at fracture, varying from 44,500 to 48,600 psi. Each of the fracture principal strains was measured separately, thus their sum serves as a reasonable check on the measurements. It will be noted from Table 1 that the sum of the principal strains is quite small, although varying in sign, depending upon the stress ratio.

It will be seen that the variation of $\bar{\gamma}_n$ with stress ratio is not as severe in the M.I.T. tests as in those reported by the author. It is felt that the difference in the method of fracture-strain measurements is largely responsible for this. In cases where the rupture occurs circumferentially, fracture strains are accurately found from the wall thickness at the neck, and the average diameter at this point, since the tube remains essentially symmetrical with respect to the axis. Indeed the octahedral shearing strains for the two series of tests compare quite favorably for this type of fracture. However, when longitudinal rupture occurs, axial symmetry no longer exists, and diameter measurements are not a very reliable criterion for fracture strains. Use of an externally scribed network overcomes this difficulty, since tangential and axial elements at the point of fracture can be measured readily.

In the tests reported by the author, it was shown that fracture occurred when the principal shearing stress reached a critical value, but that this critical value was not the same in all directions. For example, the average shearing stress at fracture for those specimens which failed by a circumferential rupture was approximately 55,000 psi and for those which failed by a longitudinal crack the average shearing stress was about 40,000 psi.

In the M.I.T. tests reported herein, fracture occurred when the principal shearing stress reached a critical value, as reported by the author, but the critical value was very nearly the same in all directions. For example, the average principal shearing stress at fracture for those specimens which failed by a circumferential crack was 47,800 psi, while for those failing by a longitudinal crack, the average shearing stress was 47,000 psi.

It would appear that both the tests reported in the paper and

[4] "Combined Stress Experiments on a Nickel-Chrome-Molybdenum Steel," by J. M. Lessells and C. W. MacGregor, *Journal of The Franklin Institute*, vol. 230, August, 1940, pp. 163–182.

TABLE 1 RUPTURE DATA—M.I.T. TESTS; ANNEALED S.A.E. 1020 STEEL[a]

Ratio $\bar{\sigma}_t/\bar{\sigma}_a$	—1.00[b]	0	+0.534	+1.039	+2.115	+2.465	+3.195
$\bar{\sigma}_a$	48200	97200	90000	89600	39900	36300	27580
$\bar{\sigma}_t$	—48200	0	48100	93100	84300	89500	88000
$\bar{\sigma}_r$	0	0	—4165	—5525	—4690	—5140	—4800
$\bar{\epsilon}_a$	0.506	0.696	0.501	0.487	0.005	—0.011	—0.068
$\bar{\epsilon}_t$	—0.506	—0.315	—0.056	0.114	0.417	0.378	0.445
$\bar{\epsilon}_r$	0	—0.372	—0.452	—0.654	—0.450	—0.346	—0.367
$\epsilon_a + \bar{\epsilon}_t + \bar{\epsilon}_r$	0	0.009	—0.007	—0.053	—0.028	0.022	0.010
$\bar{\tau}_{rt}$	24100	0	26130	49310	44500	47320	46400
$\bar{\tau}_{ra}$	24100	48600	47080	47560	22300	20720	16190
$\bar{\tau}_{at}$	48200	48600	20950	1750	22200	26600	30210
$\bar{\gamma}_{rt}$	—0.506	0.057	0.396	0.768	0.867	0.724	0.812
$\bar{\gamma}_{ra}$	—0.506	1.068	0.953	1.141	0.500	0.335	0.299
$\bar{\gamma}_{at}$	1.012	1.011	0.557	0.373	0.412	0.389	0.513
$\bar{\tau}_n$	39300	45800	38450	45700	36300	36700	36700
$\bar{\gamma}_n$	0.827	0.980	0.782	0.950	0.722	0.592	0.672

[a] True stresses and true strains used throughout; stresses in psi units.
[b] The a and t directions here do not mean axial and tangential as in the other cases.

those included herein seem to favor the maximum-shearing-stress criterion for fracture for these materials. However, further work is needed to establish this fact definitely.

W. R. Osgood.[5] An investigation of combined stress could not be in better hands than those of the author, a careful experimenter; Dr. Nadai, a pioneer in the field of plasticity; and Captain Roop, a friend of research with a rare appreciation of the double role of theory and test. It is a constant source of pride also that our Navy Department fosters the highest type of engineering research, as exemplified by the co-operation of the David Taylor Model Basin in the author's investigation.

A few questions and remarks occur to the writer in reading the paper under discussion. It is not clear just how the notches of the impact specimens were oriented in relation to the bar. Was the notch in the transverse specimen parallel to the axis of the bar and that of the longitudinal specimen perpendicular to the radius normal to the specimen?

It seems that the machining operations after annealing may have introduced sufficient anisotropy to account for some of the difference in behavior of the specimens in the tangential and axial directions. There is some evidence for this possibility in Figs. 5, 6, 8, 9, and 22. If conditions were the same in the tangential and axial directions, the $\bar{\sigma}_a$-curves in Figs. 5, and 6 should coincide with the $\bar{\sigma}_t$-curves in Figs. 8 and 9, respectively. Actually, the curves in Figs. 8 and 9 lie below those in Figs. 5 and 6, respectively. On the other hand, the machining conditions for the two subsize specimens, Fig. 3, were identical, and the two curves for these specimens, Fig. 22, are practically identical, probably within the unavoidable limits of error of the tests.

Except for the specimen for which $\sigma_t/\sigma_a = 2$, the scatter in the points in Fig. 21 may well lie within the experimental error to be expected. If the scatter is greater than can be accounted for by the experimental error, it may be that anisotropy of the material accounts for it. The anomalous behavior of specimen "$\sigma_t/\sigma_a = 2$" may be due to mechanical properties different from those of the other specimens. Was it perhaps taken from the end of the original 18-ft bar?

Since isotropic engineering materials are a rarity, means of taking anisotropy into account are worth considering. For example, in analyzing tests of orthotropic materials, probably the commonest engineering type, it may be well to seek to make use of one or more significant properties associated with each of the three planes of symmetry. By way of illustration only, one might consider plots of

$$\bar{l}_n = \frac{2}{3}\sqrt{\bar{l}_{at}^2 + \bar{l}_{tr}^2 + \bar{l}_{ra}^2}$$

against

$$\bar{g}_n = \frac{2}{3}\sqrt{\bar{g}_{at}^2 + \bar{g}_{tr}^2 + \bar{g}_{ra}^2}$$

where

$$\bar{l}_{at} = \frac{1}{2}\left(\frac{\bar{\sigma}_a}{S_a} - \frac{\bar{\sigma}_t}{S_t}\right), \quad \bar{l}_{tr} = \frac{1}{2}\left(\frac{\bar{\sigma}_t}{S_t} - \frac{\sigma_r}{S_r}\right), \quad \bar{l}_{ra} = \frac{1}{2}\left(\frac{\bar{\sigma}_r}{S_r} - \frac{\bar{\sigma}_a}{S_a}\right)$$

and

$$\bar{g}_{at} = \frac{E_a}{S_a}\bar{\epsilon}_a - \frac{E_t}{S_t}\bar{\epsilon}_t, \quad \bar{g}_{tr} = \frac{E_t}{S_t}\bar{\epsilon}_t - \frac{E_r}{S_r}\bar{\epsilon}_r, \quad \bar{g}_{ra} = \frac{E_r}{S_r}\epsilon_r - \frac{E_a}{S_a}\bar{\epsilon}_a$$

S_a, S_r, S_t, E_a, E_r, E_t being parameters associated with the a, r, and t directions. It might be that such plots would show less scatter than plots of the octahedral shearing stress against the octahedral shearing strain. The S's might be secant yield strengths or tensile strengths, and the E's might be moduli of elasticity.

Were the stresses $\bar{\sigma}_t$ at rupture for specimens for which $\sigma_t/\sigma_a = 0.775$, 0.800, and 0.875 based upon the maximum internal diameter through the bulge? Presumably they were. If the mean internal diameter of the cross section through the bulge was used, the computed stresses would be too low.

The picture presented by the energy data, Table 2 of the paper, is a disturbing one. Unless the material were anisotropic, one would expect the same values of energy for $\sigma_t/\sigma_a = 0$ as for $\sigma_t/\sigma_a = \infty$ and for $\sigma_t/\sigma_a = 0.500$ as for $\sigma_t/\sigma_a = 2$. Actually these energies differ by factors of 7 and 8, respectively. It is hard to believe that the material was sufficiently anisotropic to account for any such great difference. The energies were presumably computed from "the areas under the curves of true stress versus natural strain which are shown in Figs. 5 to 14." As soon as necking or local bulging begins, as the author states, it is no longer possible to measure reductions of area and elongations locally in the neck or the bulge. Nor is it possible to measure stresses accurately.

When necking occurs, as for $\sigma_t/\sigma_a = 0$, positive stresses $\bar{\sigma}_t$ and negative strains $\bar{\epsilon}_t$ are undoubtedly set up, although the author gives $\bar{\sigma}_t = 0$ in Table 1. The same would apply for small values of $\sigma_t/\sigma_a > 0$. On the other hand, when unsymmetrical longitudinal bulging occurs, as for $\sigma_t/\sigma_a = \infty$, positive stresses $\bar{\sigma}_a$ and positive strains $\bar{\epsilon}_a$ are set up which are larger in the bulge because of the bulge than in the rest of the tube. At failure the stresses $\bar{\sigma}_a$ may be expected to be much larger in the bulge than the average stress $\bar{\sigma}_a$ for the entire cross section. The same would hold true for large values of $\sigma_t/\sigma_a < \infty$. Consequently, in Figs. 5 to 14 a $\bar{\sigma}_t$-curve for $\sigma_t/\sigma_a = 0$ is not negligible, and for values of $\sigma_t/\sigma_a > 0.762$ the last points of the $\bar{\sigma}_a$-curves are probably considerably low. If this is the case, $\int \bar{\sigma}_t\, d\bar{\epsilon}_t$ would be negative for $\sigma_t/\sigma_a = 0$, and $\int \bar{\sigma}_a\, d\bar{\epsilon}_a$ would be greater for $\sigma_t/\sigma_a > 0.762$ than given in Table 2; and the W values would be more nearly in line. If the picture in Table 2 cannot be explained in some such way as this, then the whole technique of making combined-stress tests by means of tubes is open to serious question, and we are left in a fine pickle.

The agreement of the various test results in Fig. 21 is so good, except at rupture, that one would like to believe it should be at rupture too, that is, one would like to believe that the octahedral shearing stress should be the same at rupture for all combinations of stress. And it may in fact be, for the reasons suggested in the preceding paragraph. In Fig. 21 the last point for each test may be just as inaccurate as the last points referred to in Figs. 5 to 14. The alternative is that the octahedral shearing stress-octahedral shearing strain law holds approximately up to rupture and then suddenly some other law dominates. This would be an unpleasant pill to swallow.

In the last paragraph of the section "Tests on Solid Specimens," the author states, "the mean diameter of the tube corresponds to the width." It seems to the writer that the mean circumference of the tube should correspond to the width, giving $M = 0.024$. This value of M fits as well as or better than $M = 0.074$ in the last line of Table 3.

Author's Closure

The author is pleased to have the test data of Drs. MacGregor and Coffin added to the discussion of his paper. It is encouraging to learn that they have been able to obtain such data without being troubled by what so obviously seems to be anisotropy in the material used by the author. The discussers believe that the method of measuring the strains at fracture may account for some

[5] Materials Engineer, National Bureau of Standards, Washington, D. C.

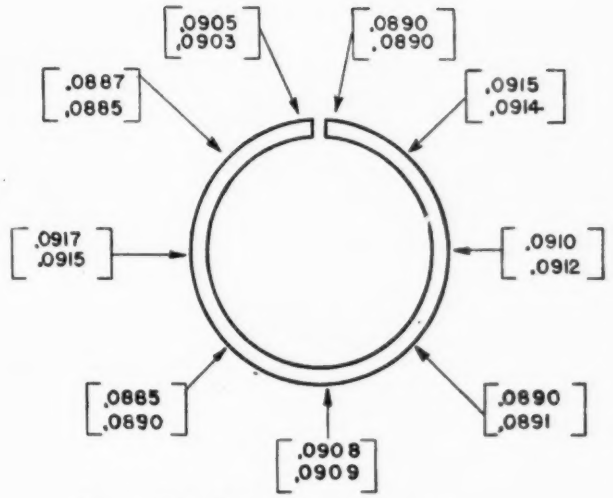


FIG. 1 WALL THICKNESS AT RUPTURE $\sigma_t/\sigma_a = \infty$

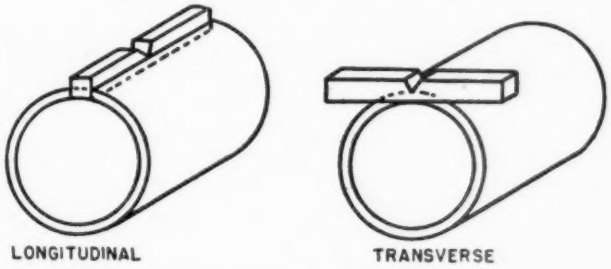


FIG. 2 ORIENTATION OF IMPACT SPECIMEN

of the apparent anisotropy. These methods of measuring strains at rupture may warrant some further discussion.

The scribed-network method will certainly yield the tangential and axial strains in the vicinity of the fracture. The only drawbacks involved are the tediousness of the process and the fact that the accuracy of any strain measurement decreases as the gage length is made shorter. For tubes where a local bulge might appear just before a longitudinal fracture occurs, this scribed network is undoubtedly the best of all known methods of determining the strains at fracture. In the tests reported in the paper there was no evidence of a localized bulge. Although, for safety reasons, the tubes had to be enclosed while they were under pressure, some of the tubes were measured shortly before fracture occurred. For example, in Fig. 9 of the paper it can be seen that the next to the last test point is quite close to the rupture point. Yet at that point the specimen was only 0.003 in. out of round. Furthermore, it cannot be said that the wall of the tube necked down in thickness at the point where fracture occurred.

Fig. 1 of this closure shows the wall thickness around the tube at the section where fracture started. These measurements which were made with ball-point micrometers show some irregularities in the wall thickness, but to the author they indicate that up to rupture the tube was loaded symmetrically and that the increase in mean circumference or mean diameter was a good measure of the tangential strain at fracture. If a scribed network had been used it is very probable that the results would have been unchanged.

An attempt will now be made to reply to Dr. Osgood's remarks. The sketch in Fig. 2 of this closure will answer the question concerning the orientation of the notches. About the anisotropy due to machining, the author can only admit the possibility of such a condition. However, such machining detriments as scratches and toolmarks would tend to lessen the strength of the specimen in the axial rather than in the tangential direction. The location, in the original bar, of a particular specimen is not known. The stresses at rupture in all specimens were based upon the dimensions of the tube at the location of the rupture and at the time the rupture occurred. For the specimens where $\sigma_t/\sigma_a = 0.775$, 0.800, and 0.875, respectively, there was no evidence of a bulge existing before the tubes ruptured. The author agrees with Dr. Osgood's statement in his last paragraph. It would have been more logical to have used the mean circumference as a measure of the effective width of the tubular specimen.

In regard to the energy data, the author is aware that many questions still remain to be answered. The energy represented by the stresses set up in the necked or bulged regions should be taken into account. This, unfortunately, is not easy to do. An attempt was made to calculate the tangential stress in the necked region of the pure-tension test. These calculations were based on assumptions that all bending stresses could be neglected and that the shape and thickness of the specimen could be represented by simple mathematical expressions. For energy determination it would be necessary to have, in addition to the stress, a history of the tangential strain, and since no record of the profile of the neck was obtained as the neck developed it would have required further assumptions to calculate the energy due to this component of the stress. For these reasons Table 2 of the paper does not contain the energies resulting from the stresses set up in the necked regions.

The Structural Efficiency of Wing Covers[1]

H. L. COX,[2] H. E. SMITH,[2] AND F. T. BARWELL.[2] The conception of "continued cellularization" introduced by the authors represents an interesting method of approach to the general problem and one which leads naturally to the conception of a continuous expanded filling in a sandwich structure. On the other hand, we suggest that the authors have been overhasty in applying this conception, and cannot accept their conclusion that "the ideal web has a vanishingly small area." It appears to us that the authors' Equation [4] is in error, because the cellular web has not the same effective flexural rigidity laterally as longitudinally. Lateral deformation can occur merely by flexure of the thin vertical faces in Fig. 2, the cells of the web being thus deformed in shear. When this effect is taken into account the buckling stress for the cellular web is reduced very considerably.

Moreover, even in relation to flexure longitudinally, the possibility of shear deformation of the webs must not be overlooked. In general the web of a beam fulfills two functions, (*a*) to hold the flanges at a fixed distance apart, and (*b*) to prevent relative lateral movement of the flanges. The effect of shear deformation in reducing the buckling stress of a beam is well known, and as the web is more and more highly "cellularized," the shear stiffness of the web will be progressively reduced. The conditions for the optimum structure when this effect is taken into account become very complex.

Nor is it safe to ignore the function (*a*) of the web. In ordinary structural engineering the thinnest practical webs fulfill this function virtually completely; but a highly cellularized structure must be much less adequate in this respect and the possibility of local wrinkling of the flanges of the beam occurring partly as

[1] By A. F. Donovan, Martin Goland, and J. N. Goodier, published in the March, 1945, issue of the JOURNAL OF APPLIED MECHANICS, Trans. A.S.M.E., vol. 67, 1945, p. A-8.

[2] Department of Scientific and Industrial Research, Engineering Division, National Physical Laboratory, Teddington, Middlesex, England.

a result of extension or compression of the web through the thickness of the beam must be considered. The conditions governing this type of instability are not yet fully established; the problem presents special difficulties on account of the anisotropic characteristics of cellular webs. In addition there are indications that failure of the web to fulfill function (*a*) may very seldom represent a limiting design condition, because inadequacy to fulfill function (*b*) may usually be exclusively important. However, the possible unimportance of this "Brazier effect" in practical cases must not be presumed *ab initio*.

Expanded materials of the solid foam type represent a class of highly cellularized materials, and the development of sandwich structures follows the principles laid down by the authors. It is interesting therefore to notice that as the degree of expansion of a solid foam is increased, the mechanical properties are reduced more rapidly than the density; in particular for several materials there appears to be a critical density below which the materials become definitely spongelike. It is one of the aims of research at present in progress in this country to examine this correlation quantitatively and to attempt to establish a theoretical basis for the mechanical properties of foams in relation to the properties of the solid base material.

Finally we would refer to the work of two of the writers in relation to the problem of least weight of structures of more normal types.[3]

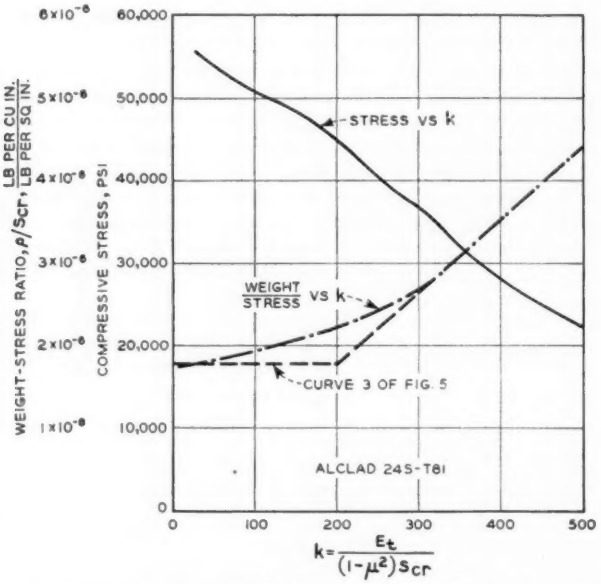


FIG. 1 TYPICAL COMPRESSIVE STRESS-STRAIN AND STRESS-TANGENT MODULUS CURVES

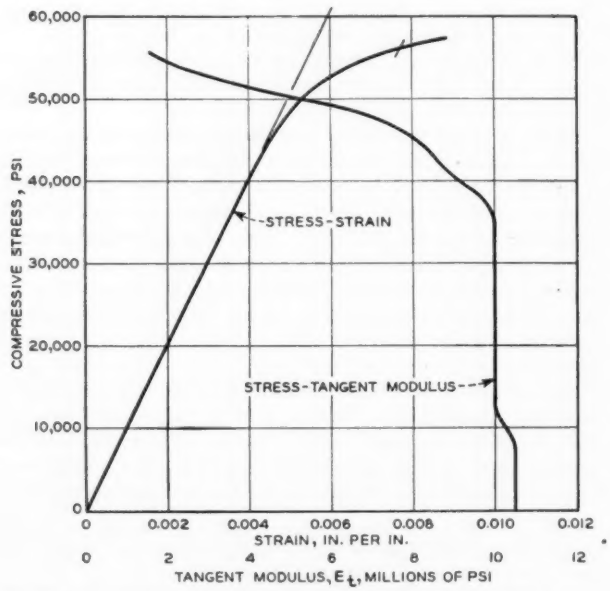


FIG. 2 RELATIONS BETWEEN *k* AND STRESS, AND BETWEEN *k* AND WEIGHT-STRESS RATIO

MARSHALL HOLT.[4] The suggestion made by the authors that the sharp bends in the curves of Fig. 5 of the paper might be relieved is a good one. As the curves are now drawn, it is tacitly assumed that the stress-strain curves are simply straight lines with a maximum value of stress equal to the compressive yield strength. Actually of course the stress-strain curves are not as simple as this since the curves depart gradually from the initial modulus line, and the yield strengths are merely arbitrarily chosen points on the curves. Any method used for rounding the curves in Fig. 5 should take into account the variable slope of the stress-strain curve and consequent variable effective modulus. Such a procedure for Alclad 24S-T81 is indicated in Figs. 1 and 2 of this discussion, in which the tangent modulus or slope of the stress-strain curve has been taken as the effective modulus.

A typical compressive stress-strain curve for Alclad 24S-T81, having a value of compressive yield strength equal to the minimum specified tensile yield strength, is shown in Fig. 1 herewith. Also shown is the relation between stress and tangent modulus. Fig. 2 shows the relation between stress and k as determined from Equation [14] of the paper, and the assumption that Poisson's ratio is constant for stresses above as well as in the elastic stress range. In this case

$$k = \frac{E_t}{(1 - \nu^2)S} \quad \ldots\ldots\ldots\ldots\ldots\ldots [1]$$

The curve for comparing weights of panels was obtained by plotting the foregoing values of k against the factor ρ/S. This curve for Alclad 24S-T81 is also shown in Fig. 2 of this discussion. When compared with curve 3 in Fig. 5 of the paper, also shown in Fig. 2 herewith, it appears to give a reasonable rounding. The other curves in Fig. 5 might be rounded in a similar manner. It would not be surprising if the relative positions of the curves change for restricted ranges of the value of k.

In the determination of the distribution efficiency of an actual panel by comparison of its weight with that of an ideal panel, it would seem more reasonable to make the comparison on the basis of the ultimate load developed by the actual panel. In the numerical example, the panel is unduly penalized since it was built sturdy enough to support 192,500 lb, but given credit for supporting only 146,500 lb. Perhaps the trouble lies in the definition of effective area and our inability to determine it exactly

AUTHORS' CLOSURE

The problem the authors originally set themselves was to formulate an ideal compression cover to belong to and serve as a standard for the whole class of stiffened sheet constructions which buckle in simple two-way flexure. It was realized, too late to affect the present paper, that preoccupation with the simple flexural type of deformation had led to an "ideal" construction which escapes this classification and that the problem must be

[3] Two papers in process of publication by the British Aeronautical Research Committee, in the R. and M. series, Nos. 1922 and 1923.

[4] Research Engineer, Aluminum Company of America, Aluminum Research Laboratories, New Kensington, Pa.

reconsidered, admitting shearing flexibility and extensibility of the core or webs in the direction of the thickness.

Apart from this, Equation [4] is not actually in error because the cellular web has not the same rigidity laterally and longitudinally. For since the limiting case is an evanescent web or core, there is no objection to making it cellular both ways like a building divided into small rooms. Moreover, so little core material is required to prevent premature buckling of the sheets on the core as an elastic foundation that the evanescent web could still reasonably be retained as the ideal. But when the requirement of shear rigidity is considered, it appears that an appreciable amount of material must be assigned to the core. When the shearing deformation of the core is important, the extensibility in the thickness, and variation of curvature through the thickness also become important, and the analysis becomes much more difficult, as Messrs. Cox, Smith, and Barwell have indicated.

It has been found possible, however, to arrive at the critical load of a sandwich plate (continuous isotropic core) taking all these things into account, and this solution is now at a stage where numerical evaluation for any given case is feasible. It is not obvious, however, that the continuous core represents the best use of the material. The method of weight comparison developed by Messrs. Cox, Smith, and Barwell is clearly of great value in determining the relative merits of various possible constructions. For the setting of a standard by which to measure structural efficiency, the question of what is the ideal construction remains open.

As Mr. Holt suggests it may, except where buckling is definitely not wanted, be preferable to make comparisons on the basis of ultimate loads. The load to be used must of course be calculated for the ideal standard. In beginning this study the authors chose first to regard buckling as failure, the difficulties of reliable calculation being then least.

A New Design Criterion for Wire Rope[1]

Shortridge Hardesty.[2] The design criterion developed by the authors, $B = 2T/UdD$, contains the *total* tension in the rope in the numerator, and the *unit* tensile strength of the wire in the denominator. It is interesting to note the form which the criterion takes when the unit tensile strength of the wire is replaced by the ultimate strength of the rope, which results in putting *total* values in both numerator and denominator.

Since the ultimate strength of the rope is approximately 85 per cent of the sum of the strengths of the individual wires, and since the metallic area of a wire rope is approximately $0.4d^2$ for a 6 × 19 construction, and not much different for other hemp-center constructions, the ultimate strength of the rope is approximately

$$U = 0.85\,Au = 0.85 \times 0.4d^2u = 0.34ud^2$$

in which U is the ultimate strength of the rope in pounds, and u is the ultimate strength of the wire in pounds per square inch. From this we find

$$u = \frac{3U}{d^2}$$

Substituting the foregoing value for the unit strength of the wire in the authors' criterion, there results

$$B = \frac{2Td}{3UD}$$

It will be noted that T/U is the safety factor of the rope, and that d/D is the ratio of the diameter of the rope to the diameter of the sheave. It is therefore evident that the criterion is merely the product of the safety factor by the rope-sheave diameter ratio, which factors have usually been considered the determining ones in wire-rope design.

The writer's principal experience with wire ropes has been in connection with vertical-lift bridges, for which purpose unusually long rope life is desired. The movable-bridge specifications of the American Railway Engineering Association require a safety factor of $^1/_{10}$ for counterweight ropes and $^1/_6$ for operating ropes, as the latter ropes can be replaced more readily. The rope-sheave ratio is required to be $^1/_{75}$ for counterweight ropes and $^1/_{45}$ for operating ropes. Substituting these values in the criterion given, there results

$$\text{Counterweight ropes } {}^2/_3 \times {}^1/_{10} \times {}^1/_{75} = 0.0009$$
$$\text{Operating ropes } {}^2/_3 \times {}^1/_6 \times {}^1/_{45} = 0.0025$$

The writer has considered the A.R.E.A. requirements for counterweight ropes unnecessarily conservative, and has generally used safety factors ranging from $^1/_8$ to $^1/_{7.5}$ and rope-sheave ratios ranging from $^1/_{80}$ to $^1/_{70}$. This means that in our practice the criterion has ranged between the two values

$${}^2/_3 \times {}^1/_8 \times {}^1/_{80} = 0.0011$$
$${}^2/_3 \times {}^1/_{7.5} \times {}^1/_{70} = 0.0013$$

Fig. 3 of the authors' paper indicates that the 0.0013 value is low enough to give long life for the rope, and that the 0.0011 value is well on the safe side.

B. L. Lonngren.[3] In making comparisons of wire ropes, running over sheaves, the writer has used for some time past a design criterion

$$C = \frac{\text{Breaking strength of rope}}{\text{Load on rope}} \times \frac{\text{Drum diameter}}{\text{Rope diameter}} = \frac{U_{\text{rope}}}{T} \times \frac{D}{d}$$

with the breaking strength of rope U_{rope} obtained directly from the rope manufacturers' catalogues. The quotient

$$\frac{U_{\text{rope}}}{T}$$

is the factor of safety in tension.

The breaking strength of a rope in tension is

$$U_{\text{rope}} = k_1 \times \frac{\pi d^2}{4} \times U$$

where U is the ultimate tensile strength of a wire in pounds per square inch, and k_1 is a constant, depending upon the rope cross section, which multiplied with the rope area gives the net wire area in square inches. If $k_1 \times \frac{\pi}{2}$ is marked k, criterion C can be written

$$C = k \times \frac{d^2U}{2T} \times \frac{D}{d} = k \times \frac{UdD}{2T}$$

assuming that $k = 1$, it is interesting to note that

[1] By D. C. Drucker and H. Tachau, published in the March, 1945, issue of the Journal of Applied Mechanics, Trans. A.S.M.E., vol. 67, 1945, p. A-33.

[2] Hardesty & Hanover, Consulting Engineers, New York, N. Y.

[3] Engineer, Bucyrus Erie Company, South Milwaukee, Wis. Mem. A.S.M.E.

$$C = \frac{UdD}{2T}$$

or the inverted expression for

$$B = \frac{2T}{UdD}$$

as proposed by the authors.

Authors' Closure

The authors were pleased to learn that the values of T/U' and d/D chosen by Mr. Hardesty on the basis of his extensive experience led to the figure for B, suggested by their interpretation of the published experimental data. They feel, however, that this fact emphasizes all the more a trouble with present design.

The usual design procedure, as given by Mr. Hardesty and stated in wire-rope handbooks, catalogues, and articles, is to choose the rope to carry the tensile force and then fix the sheave diameter in ratio to the rope diameter. Obviously this procedure leads to a safe and useful wire-rope-and-sheave combination. One of the main points of the paper was that such a design is only one of many having as long a life. Some other rope, possibly a much larger one on a considerably smaller sheave, might be better suited to the job.

The transformation of $B = 2T/UdD$ to const$(T/U')(d/D)$ was given and analyzed in our complete report to the Whiting Corporation. However, rather than being a preferred form, it should be avoided, because it will lead the designer to continue to think in terms of tension and bending separately and so unduly restrict his choice of rope and sheave. Furthermore, the multiplication of two stresses is not physically in line with our usual concepts of design. The authors believe that the dimensionless number B in its proposed form is most convenient for practical use. It has the decided advantage of indicating substitution of a fatigue limit for the ultimate strength when the action of wire rope is more clearly understood and the controlling stress definitely known.

The criterion C, apparently used successfully by Mr. Lonngren, serves as a welcome additional check. It also, however, is split into two terms and so may restrict desirable freedom of choice.

Book Reviews

Thermodynamic Properties of Air

Thermodynamic Properties of Air. By Joseph H. Keenan and Joseph Kaye. John Wiley & Sons, Inc., New York, N. Y., 1945. Cloth $7^1/_2 \times 10$ in., iii and 73 pp., $2.25.

Reviewed by John G. Lee[1] and Newman A. Hall[2]

In his earlier volume on the "Thermodynamic Properties of Steam," Professor Keenan established basic data which has become authoritative for analytical work on steam power. The presentation and basis for the present companion volume on the "Thermodynamic Properties of Air" is of such excellent caliber that it will be accepted as equally authoritative.

Recent spectroscopic research has provided a physical basis for accurate thermodynamic data on gases that wholly supersedes earlier calorimetric measurements. The properties of nitrogen and oxygen as established by Johnston and interpolated by Heck[3] form the basis for the tables.

A comparison with a recent recalculation of the basic thermodynamic data[4] indicates a maximum difference in constant pressure specific heat of less than $^2/_{10}$ of 1 per cent. It is very probable, accordingly, that future refinements will have a negligible effect on the acceptance of these tables as standard.

The data is arranged in a manner similar to that of the earlier abbreviated presentation under the same title.[5] The arrangement of tabular data is very convenient for the solution of practical problems.

The small effect of molecular interaction forces in air at low pressures permits the assumption of the perfect equation of state. Accordingly, the primary energy functions may be expressed as functions of temperature alone. Table 1 presents enthalpy, internal energy, and constant-pressure entropy with reference to a base temperature of 400 F abs. In the same table are given isentropic pressure and volume ratios relative to the state at 400 F abs. The tabular intervals are 1 F from 300 F abs to 3000 F abs, and 10 F from 3000 F abs to 6500 F abs.

Table 2 lists the isothermal entropy change, $R \log_e N$, for pressure ratios N at tabular intervals of 0.01 from 1 to 10.

Table 3 lists constant volume and constant pressure specific heat, specific heat ratio, velocity of sound, and critical mass flow for the temperature range 200 F abs to 6400 F abs; and viscosity, thermal conductivity, and Prandtl number for the range 400 F abs to 2400 F abs.

A series of functions of pressure ratio and polytropic exponent are listed in Tables 4 through 9. Four-place logarithmic tables to the base 10 and base e are included as well as Fahrenheit and Centigrade conversion tables. A convenient listing of conversion factors completes the volume.

A full discussion of the source material for Tables 1 and 3 is given. Also included are a series of examples amply illustrating the use of all the tables.

[1] Assistant Director of Research, United Aircraft Corporation, East Hartford, Conn.

[2] Research Division, United Aircraft Corporation, East Hartford, Conn.

[3] "The New Specific Heats," Addenda to and Discussion of paper by R. C. H. Heck, *Mechanical Engineering*, vol. 63, 1941, pp. 126–135.

[4] Bureau of Standards, Research Paper 1634, February, 1945.

[5] "A Table of Thermodynamic Properties of Air," by Joseph H. Keenan and Joseph Kaye, Journal of Applied Mechanics, Trans. A.S.M.E., vol. 65, 1943, pp. A-123 to A-130.

Theoretical Analysis of Perforated Shear Webs

By CHU-KIA WANG,[1] DENVER, COLO.

This paper presents theoretical studies on perforated shear webs. The procedures provide for the analysis of the plane-stress condition in an infinitely long plate of finite width with a plain circular hole and in a rectangular or square plate with a circular hole, which may be plain, or reinforced with rim, or ring, or both. Numerical results are obtained for infinitely long and square plates with plain holes of different sizes, and in the case of square plates, also with various ways of reinforcing.

Nomenclature

The following nomenclature is used in the paper:

- F = stress function
- F_a = approximate stress function
- F_t = true stress function
- n = an integer
- m = particular value of n
- i = number of terms in series considered
- x, y = rectangular co-ordinates
- ρ, θ = polar co-ordinates
- $\widehat{xx}, \widehat{yy}, \widehat{xy}$ = stress components in rectangular co-ordinates
- $\widehat{\rho\rho}, \widehat{\theta\theta}, \widehat{\rho\theta}$ = stress components in polar co-ordinates
- q = uniform shearing stress along edges of shear web
- N, S = normal and tangential co-ordinates
- $2a, 2b$ = dimensions of rectangular panel
- f, g, p, q = arbitrary coefficients in stress function
- h = radius of circular hole
- k = outer radius of ring
- t = thickness of plate
- H, K = indexes referring to region H (ring) and region K (outside of ring)
- μ = Poisson's ratio
- A = sectional area of rim
- σ = direct normal stress in rim
- u, v = radial and tangential displacements

Introduction

A flat rectangular plate under the action of pure uniform shearing stress along its edges is a common structural member. Such a plate may be called a shear web. For purposes of weight saving or access, one or more circular holes may be made in the middle of the shear web. The holes may be plain or reinforced around the rim in various ways. Shear webs with plain or reinforced circular holes in them are called perforated shear webs.

The determination of the stress components at any point of a perforated shear web presents itself as a problem of theoretical analysis. Howland and Stevenson[2] had a rigorous mathematical solution for the analysis of the stresses in a perforated strip, when the boundary conditions at the parallel edges and those around the hole were known. Hengst[3] obtained an approximate solution of the tangential stresses at the rim of a plain circular hole in the center of a square plate under the action of equal tensile stresses on the four sides, or the action of equal tensile and compressive stresses on the two pairs of opposite sides. Timoshenko[4] used the theory of bending of curved bars in obtaining an approximate solution of the stress condition around a circular hole reinforced with a bead. Gurney[5] had an exact solution for plane-stress distribution of the problem of an infinite plate with a circular hole reinforced by a rectangular bead. Beskin[6] determined the stress distribution around strengthened circular holes in plates subjected to edge loads at infinity. The present paper deals with the stress analysis of an infinitely long plate of finite width with a plain circular hole and of a finite rectangular plate with a circular hole, either plain or reinforced in various ways.

Infinitely Long Plate of Finite Width With a Plain Circular Hole

Let F be the Airy's stress function. Then the stress components are:

In rectangular co-ordinates

$$\widehat{xx} = \frac{\partial^2 F}{\partial y^2} \quad \widehat{yy} = \frac{\partial^2 F}{\partial x^2} \quad \widehat{xy} = -\frac{\partial^2 F}{\partial x \partial y} \qquad [1]$$

In polar co-ordinates

$$\widehat{\rho\rho} = \frac{1}{\rho^2}\frac{\partial^2 F}{\partial \theta^2} + \frac{1}{\rho}\frac{\partial F}{\partial \rho} \quad \widehat{\theta\theta} = \frac{\partial^2 F}{\partial \rho^2} \quad \widehat{\rho\theta} = -\frac{\partial}{\partial \rho}\left(\frac{1}{\rho}\frac{\partial F}{\partial \theta}\right) \qquad [2]$$

The solution of a two-dimensional stress problem is to find F such that $\widehat{xx}$, $\widehat{yy}$, $\widehat{xy}$, as expressed by Equation [1], or $\widehat{\rho\rho}$, $\widehat{\theta\theta}$, $\widehat{\rho\theta}$, as expressed by Equation [2] satisfies prescribed values at the specified boundaries with the further requirement that $\nabla^4 F = 0$.

In the present case, following the procedure of Howland and Stevenson,[2] let

$$F = F_0 + F_1 + F_2 + F_3 + F_4 + \ldots$$

F_0 is the stress function for an infinite plate under action of pure shear; F_1 cancels the shearing and normal stresses at the rim of the hole, but introduces undesirable stresses at the straight boundaries $x = \pm a$, Fig. 1. Also, F_2 cancels such stresses at

---

[1] Engineer, National Resources Commission of China.

Presented at the Meeting of the Cincinnati Section, Cincinnati, Ohio, Oct. 2–3, 1945, of The American Society of Mechanical Engineers.

Discussion of this paper should be addressed to the Secretary A.S.M.E., 29 West 39th Street, New York, N. Y., and will be accepted until July 10, 1946, for publication at a later date. Discussion received after the closing date will be returned.

Note: Statements and opinions advanced in papers are to be understood as individual expressions of their authors and not those of the Society.

[2] "Bi-Harmonic Analysis in a Perforated Strip," by R. C. J. Howland and A. C. Stevenson, Philosophical Transactions of the Royal Society of London, series A, vol. 232, 1933–1934, pp. 155–222.

[3] "Beitrag zur Beurteilung des Spannungszustandes einer gelochten Scheibe," by H. Hengst, *Zeitschrift für Angewandte Mathematik und Mechanik*, vol. 18, Feb., 1938, pp. 44–48.

[4] "On Stresses in a Plate With a Circular Hole," by S. Timoshenko, *Journal of The Franklin Institute*, vol. 197, 1924, pp. 505–516.

[5] "An Analysis of the Stresses in a Flat Plate With a Reinforced Circular Hole Under Edge Forces," by C. Gurney, Aeronautical Research Committee, R. and M. No. 1834, Feb., 1938.

[6] "Strengthening of Circular Holes in Plates Under Edge Forces," by Leon Beskin, Journal of Applied Mechanics, Trans. A.S.M.E., 1944, p. A-140.

the straight boundaries but introduces new stresses around the hole. Again, F_1 cancels such stresses around the hole, and so on.

For an infinite plate under action of pure shearing stress q

$$F_0 = -qxy = -\frac{1}{2} q\rho^2 \sin 2\theta \quad \ldots\ldots\ldots\ldots [3]$$

from which

$$\widehat{\rho\rho} = +q \sin 2\theta \quad \widehat{\theta\theta} = -q \sin 2\theta \quad \widehat{\rho\theta} = +q \cos 2\theta$$

The next stress function F_1 must be constructed to cancel these values of $\widehat{\rho\rho}$ and $\widehat{\rho\theta}$ on the circle $\rho = h$. If we assume

$$F_1 = \left(\frac{F_2^{(0)}}{\rho^2} + G_2^{(0)}\right) \sin 2\theta$$

the relevant stress components are

$$\widehat{\rho\rho} = -2\left[\frac{3F_2^{(0)}}{\rho^4} + \frac{2G_2^{(0)}}{\rho^2}\right] \sin 2\theta \quad \widehat{\theta\theta} = +\frac{6F_2^{(0)}}{\rho^4} \sin 2\theta$$

$$\widehat{\rho\theta} = +2\left[\frac{3F_2^{(0)}}{\rho^4} + \frac{G_2^{(0)}}{\rho^2}\right] \cos 2\theta$$

and these will be found to cancel the tractions on the circle $\rho = h$ if

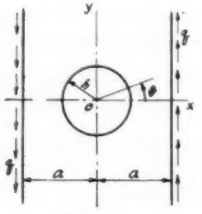


FIG. 1

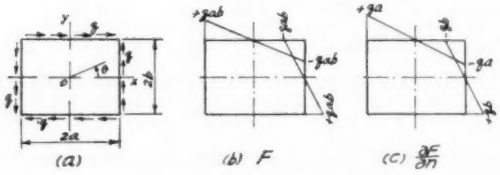


FIG. 2

$$F_2^{(0)} = q\left(-\frac{1}{2} h^4\right) \qquad G_2^{(0)} = q\,(+h^2)$$

Thus

$$F_1 = q\left[h^2 - \frac{1}{2}\frac{h^4}{\rho^2}\right] \sin 2\theta \quad \ldots\ldots\ldots\ldots [4]$$

It is to be noted that $F_0 + F_1$ gives the stress function for an infinitely large plate with a circular hole under action of pure shear

$$F_0 + F_1 = q\left[-\frac{\rho^2}{2} + h^2 - \frac{1}{2}\frac{h^4}{\rho^2}\right] \sin 2\theta \quad \ldots\ldots [5]$$

The general form[7] of the solution of the type considered can be expressed by

$$\sum_1^\infty F_n = \sum_1^\infty \left\{\frac{f_{2n}}{\rho^{2n}} + \frac{g_{2n}}{\rho^{2n-2}} + p_{2n}\rho^{2n} + q_{2n}\rho^{2n+2}\right\} \sin 2n\theta. \quad [6]$$

According to Howland and Stevenson,[2] the coefficients in Equation [6] can be evaluated as follows

$$\left.\begin{aligned} f_{2n} &= \sum_{(r)} F_{2n^{(r)}} \qquad p_{2n} = \sum_{(r)} P_{2n^{(r)}} \\ &= \sum_{p=1}^{\infty} \left\{{}^{2n}\kappa_{2p} f_{2p} + {}^{2n}\mu_{2p} g_{2p}\right\} \\ g_{2n} &= \sum_{(r)} G_{2n^{(r)}} \qquad q_{2n} = \sum_{(r)} Q_{2n^{(r)}} \\ &= \sum_{p=1}^{\infty} \left\{{}^{2n}\nu_{2p} f_{2p} + {}^{2n}\omega_{2p} g_{2p}\right\} \end{aligned}\right\} \ldots [7]$$

where

$$\left.\begin{aligned} F_{2n^{(r+1)}} &= \sum_{p=1}^{\infty} \left\{{}^{2n}s_{2p} F_{2p^{(r)}} + {}^{2n}t_{2p} G_{2p^{(r)}}\right\} \\ G_{2n^{(r+1)}} &= \sum_{p=1}^{\infty} \left\{{}^{2n}u_{2p} F_{2p^{(r)}} + {}^{2n}v_{2p} G_{2p^{(r)}}\right\} \\ {}^{n}s_p &= h^{2n}\left\{(n-1)\,{}^{n}\kappa_p + n h^2\,{}^{n}\nu_p\right\} \\ {}^{n}u_p &= -h^{2n-2}\left\{n\,{}^{n}\kappa_p + (n+1)h^2\,{}^{n}\nu_p\right\} \\ {}^{n}t_p &= h^{2n}\left\{(n-1)\,{}^{n}\mu_p + n h^2\,{}^{n}\omega_p\right\} \\ {}^{n}v_p &= -h^{2n-2}\left\{n\,{}^{n}\mu_p + (n+1)h^2\,{}^{n}\omega_p\right\} \end{aligned}\right\} \ldots [8]$$

Values of ${}^{n}\kappa_p$, ${}^{n}\mu_p$, ${}^{n}\nu_p$, and ${}^{n}\omega_p$ for even values of p and n are given by Howland and Stevenson.[2]

The numerical procedure is as follows, for a particular value of h:

1 Compute ${}^{n}s_p$, ${}^{n}t_p$, ${}^{n}u_p$, and ${}^{n}v_p$ for various even values of p and n.

2 With known values of $F_2^{(0)}$ and $G_2^{(0)}$ as base, compute $F_{2n}^{(r+1)}$ and $G_{2n}^{(r+1)}$ for increasing values of n and r.

3 Compute f_{2n}, g_{2n}, p_{2n}, and q_{2n} for increasing values of n. After the arbitrary constants in the stress function $F = F_0 + \sum_1^\infty F_n$ have been thus determined, the stress components follow directly by the application of Equation [2].

Rectangular Plate With a Plain or Reinforced Circular Hole

The stress function F, for the case of a rectangular plate with a circular hole, either plain or reinforced with rim only, can be expressed as the sum of an infinite series in sin $2n\theta$ with four arbitrary coefficients in each term. If only i terms are considered, then $2i$ of the conditions required for the determination of the $4i$ coefficients are supplied by the boundary conditions at the rim of the hole. The assumption that the area integral of the square of the difference between the true $\nabla^2 F$ and that as approximated by the sine series shall be a minimum, an assumption which was introduced by Hengst,[3] furnishes the other $2i$ conditions. An application of Green's theorem in the plane reduces this area integral to a line integral around the boundary. The compatibility condition $\nabla^4 F = 0$, by nature of the assumed expression for the stress function, is always satisfied. With a finite number of terms in the series, the boundary conditions at the straight edges are only approximately satisfied; the degree of approximation depends on the number of terms used in the series.

Let the stress function approximated by the first i terms of the series be

[7] "Theory of Elasticity," by S. Timoshenko, McGraw-Hill Book Co., New York, N. Y., 1934, p. 114.

$$F = \sum_1^i \left(\frac{f_{2n}}{\rho^{2n}} + \frac{g_{2n}}{\rho^{2n-2}} + p_{2n}\rho^{2n} + q_{2n}\rho^{2n+2} \right) \sin 2n\theta \ldots [9]$$

from which

$$\frac{\partial F}{\partial \rho} = \sum_1^i \left(\frac{-2nf_{2n}}{\rho^{2n+1}} - \frac{2(n-1)g_{2n}}{\rho^{2n-1}} + 2np_{2n}\rho^{2n-1} + 2(n+1)q_{2n}\rho^{2n+1} \right) \sin 2n\theta \ldots [10]$$

$$\widehat{\rho\rho} = \sum_1^i \left(\frac{-2n(2n+1)f_{2n}}{\rho^{2n+2}} - \frac{2(n+1)(2n-1)g_{2n}}{\rho^{2n}} - 2n(2n-1)p_{2n}\rho^{2n-2} - 2(n-1)(2n+1)q_{2n}\rho^{2n} \right) \sin 2n\theta \ldots [11]$$

$$\widehat{\theta\theta} = \sum_1^i \left(+ \frac{2n(2n+1)f_{2n}}{\rho^{2n+2}} + \frac{2(n-1)(2n-1)g_{2n}}{\rho^{2n}} + 2n(2n-1)p_{2n}\rho^{2n-2} + 2(n+1)(2n+1)q_{2n}\rho^{2n} \right) \sin 2n\theta \ldots [12]$$

$$\widehat{\rho\theta} = \sum_1^i \left(+ \frac{2n(2n+1)f_{2n}}{\rho^{2n+2}} + \frac{2n(2n-1)g_{2n}}{\rho^{2n}} - 2n(2n-1)p_{2n}\rho^{2n-2} - 2n(2n+1)q_{2n}\rho^{2n} \right) \cos 2n\theta \ldots [13]$$

$$\nabla^2 F = \widehat{\rho\rho} + \widehat{\theta\theta} = \sum_1^i \left(-\frac{4(2n-1)g_{2n}}{\rho^{2n}} + 4(2n+1)q_{2n}\rho^{2n} \right) \sin 2n\theta$$

Let

$$-\frac{4(2n-1)}{\rho^{2n}} \sin 2n\theta = \phi_{2n}{}^g \qquad 4(2n+1)\rho^{2n} \sin 2n\theta = \phi_{2n}{}^q$$

Then

$$\nabla^2 F = \sum_1^i (g_{2n}\phi_{2n}{}^g + q_{2n}\phi_{2n}{}^q) \ldots [14]$$

Let Q be the area integral of the square of the error in $\nabla^2 F$

$$Q = \int\int \left[\nabla^2 F - \sum_1^i (g_{2n}\phi_{2n}{}^g + q_{2n}\phi_{2n}{}^q) \right]^2 dxdy = \min$$

In order that Q be a minimum, the following conditions must be satisfied for each value of m

$$\frac{\partial Q}{\partial g_{2m}} = 0 \qquad \frac{\partial Q}{\partial q_{2m}} = 0$$

Then

$$\frac{\partial Q}{\partial g_{2m}} = \int\int \frac{\partial}{\partial g_{2m}} \left[\Delta^2 F - \sum_1^i (g_{2n}\phi_{2n}{}^g + q_{2n}\phi^q{}_{2n}) \right]^2 dxdy = 0$$

or

$$\int\int \left[\nabla^2 F - \sum_1 (g_{2n}\phi_{2n}{}^g + q_{2n}\phi_{2n}{}^q) \right] \frac{\partial}{\partial g_{2m}} \left[\nabla^2 F - \sum_1^i (g_{2n}\phi_{2n}{}^g + q_{2n}\phi_{2n}{}^q) \right] dxdy = 0$$

or

$$\sum_1^i \int\int (g_{2n}\phi_{2n}{}^g + q_{2n}\phi_{2n}{}^q)\phi_{2m}{}^g dxdy = \int\int \nabla^2 F \phi_{2m}{}^g dxdy \ldots [15]$$

The right side of Equation [15] can be written as

$$\int\int \nabla^2 F \phi_{2m}{}^g dxdy = \int\int (\phi_{2m}{}^g \nabla^2 F - F\nabla^2 \phi_{2m}{}^g) dxdy = \int_c \left(\phi_{2m}{}^g \frac{\partial F}{\partial N} - F \frac{\partial \phi_{2m}{}^g}{\partial N} \right) dS \ldots [16]$$

because $\nabla^2 \phi_{2m}{}^g = 0$ and by use of Green's theorem in the plane.[8] Substitution of Equation [16] into Equation [15] gives

$$\sum_1^i \int\int (g_{2n}\phi_{2n}{}^g + q_{2n}\phi_{2n}{}^q)\, \phi_{2m}{}^g dxdy = \int_c \left(\phi_{2m}{}^g \frac{\partial F}{\partial N} - F \frac{\partial \phi_{2m}{}^g}{\partial N} \right) dS \ldots [17]$$

In the same way, from $\dfrac{\partial Q}{\partial q_{2m}} = 0$

$$\sum_1^i \int\int (g_{2n}\phi_{2n}{}^q + q_{2n}\phi_{2n}{}^q)\phi_{2m}{}^q dxdy = \int_c \left(\phi_{2m}{}^q \frac{\partial F}{\partial N} - F \frac{\partial \phi_{2m}{}^q}{\partial N} \right) dS \ldots [18]$$

There are i equations each from Equations [17] and [18]. Thus $2i$ conditions are obtained for the determination of the constants in the stress function Equation [9].

The right side of Equation [17], or Equation [18] is the line integral around both the external and the internal boundaries. F_t and $\dfrac{\partial F_t}{\partial N}$ around the external boundary depend only on the external loading and can be readily determined.[9] F_i and $\dfrac{\partial F_i}{\partial N}$ around the internal boundary are both equal to zero for a plain hole, but are not yet known when the hole is reinforced with a rim. Nevertheless, we can substitute the approximate values of F_a and $\dfrac{\partial F_a}{\partial N}$, found by substituting h for ρ in Equations [9] and [10], into the right side of Equation [17] or Equation [18] for the internal boundary. Then we can transpose these terms involving f_{2n}, g_{2n}, p_{2n}, and q_{2n} to the left side. It should be noted that if the line integral goes counterclockwise at the external boundary, it must go clockwise at the internal boundary.

Expressions for the boundary conditions at the edge of the hole will now be considered. For a plain circular hole, $\widehat{\rho\rho}_h = 0$ and $\widehat{\rho\theta}_h = 0$ at $\rho = h$. Thus

$$\widehat{\rho\rho}_h = \sum_1^i \left\{ -\frac{2n(2n+1)f_{2n}}{h^{2n+2}} - \frac{2(n+1)(2n-1)g_{2n}}{h^{2n}} - 2n(2n-1)p_{2n}h^{2n-2} - 2(n-1)(2n+1)q_{2n}h^{2n} \right\} \sin 2n\theta = 0 \ldots [19]$$

[8] "Advanced Calculus," by William F. Osgood, The Macmillan Co., New York, N. Y., 1935, p. 224.

[9] "Graphostatics of Stress Functions," by H. M. Westergaard, Trans. A.S.M.E., vol. 56, 1934, pp. 141–150.

$$\widehat{\rho\theta}_h = \sum_1^i \left\{ + \frac{2n(2n+1)f_{2n}}{h^{2n+2}} + \frac{2n(2n-1)g_{2n}}{h^{2n}} - 2n(2n-1)p_{2n}h^{2n-2} - 2n(2n+1)q_{2n}h^{2n} \right\} \cos 2n\theta = 0 \quad [20]$$

In order to insure that the middle member of Equation [19] vanishes, the coefficients of $\sin 2\theta$, $\sin 4\theta \ldots \sin 2i\theta$ must each be zero. The same is true for Equation [20]. Thus $2i$ conditions are derived. When the hole is reinforced with a rim of area A, the equations of equilibrium of a segment of rim in the radial and tangential directions, Fig. 3, give



FIG. 3

$$\sigma A = \widehat{\rho\rho}_h ht \quad [21]$$

$$A\frac{\partial\sigma}{\partial\theta} + \widehat{\rho\theta}_h ht = 0 \quad [22]$$

Also, at $\rho = h$, the circumferential strain in the rim must be equal to that of the plate, or

$$\sigma = \widehat{\theta\theta}_h - \mu\,\widehat{\rho\rho}_h \quad [23]$$

Eliminating σ by the use of Equation [23], we have Equations [21] and [22] in the form

$$A\widehat{\theta\theta}_h - (\mu A + ht)\widehat{\rho\rho}_h = 0 \quad [24]$$

$$A\frac{\partial\widehat{\theta\theta}_h}{\partial\theta} - \mu A\frac{\partial\widehat{\rho\rho}_h}{\partial\theta} + \widehat{\rho\theta}_h ht = 0 \quad [25]$$

Making coefficients of $\sin 2\theta$, $\sin 4\theta \ldots \sin 2i\theta$ in Equations [24] and [25] each equal to zero, we derive $2i$ conditions.

For the case of a rectangular plate with a circular hole reinforced with a ring only or with both rim and ring, two different stress functions will have to be assumed, one for the ring (region H), and the other for the region outside of the ring (region K). Thus $8i$ conditions are required for the determination of the $8i$ arbitrary coefficients in the two assumed stress functions F_H and F_K: $2i$ from the boundary conditions at the rim (region H); $2i$ from the fundamental assumption by applying Equations [17] and [18] to region K; $4i$ from the continuity conditions at the outer circumference of the ring. These continuity conditions are as follows:

For equilibrium of forces at the common circular boundary $\rho = k$

$$\widehat{\rho\rho_k}^H t_H = \widehat{\rho\rho_k}^K t_K \quad [26]$$

$$\widehat{\rho\theta_k}^H t_H = \widehat{\rho\theta_k}^K t_K \quad [27]$$

For compatibility of displacements u in the radial direction and v in the tangential direction

$$u_k^H = u_k^K \quad [28]$$

$$v_k^H = v_k^K \quad [29]$$

Expressions for u and v are as follows:

$$u = \sum_1^i \left\{ + \frac{2n(1+\mu)f_{2n}}{\rho^{2n+1}} + \frac{2[(n+1)+\mu(n-1)]g_{2n}}{\rho^{2n-1}} - 2n(1+\mu)\rho^{2n-1}p_{2n} - 2[(n-1)+\mu(n+1)]\rho^{2n+1}q_{2n} \right\} \sin 2n\theta \quad [30]$$

$$v = \sum_1^i \left\{ - \frac{2n(1+\mu)f_{2n}}{\rho^{2n+1}} - \frac{2[(n-2)+\mu n]g_{2n}}{\rho^{2n-1}} - 2n(1+\mu)\rho^{2n-1}p_{2n} - 2[(n+2)+\mu n]\rho^{2n+1}q_{2n} \right\} \cos 2n\theta \quad [31]$$

NUMERICAL APPLICATIONS

For the infinitely long plate of finite width with a plain circular hole, numerical work is done for five cases with $h = 0.1a$, $0.2a$, $0.3a$, $0.4a$, and $0.5a$ (see Table 1).

TABLE 1(a) INFINITELY LONG PLATE OF FINITE WIDTH WITH PLAIN CIRCULAR HOLE

$\widehat{\theta\theta}$=Aqsin2θ+Bqsin4θ+Cqsin6θ+Dqsin8θ+Eqsin10θ

$\widehat{\theta\theta}$ at ρ=h	A	B	C	D	E
h=0.1a	-4.1078	-0.0012			
h=0.2a	-4.4453	-0.0191	-0.0004		
h=0.3a	-5.0577	-0.0996	-0.0053	-0.0003	
h=0.4a	-6.0367	-0.3292	-0.0301	-0.0021	-0.0001
h=0.5a	-7.5563	-0.8700	-0.1193	-0.0105	-0.0011

TABLE 1(b) INFINITELY LONG PLATE OF FINITE WIDTH WITH PLAIN CIRCULAR HOLE

Distance from Center of Hole	$\widehat{\theta\theta}$ at θ=0° in terms of q					
	No Hole	h=0.1a	h=0.2a	h=0.3a	h=0.4a	h=0.5a
0	1.000					
0.1a	1.000	0.000				
0.2a	1.000	1.348	0.000			
0.3a	1.000	1.217	1.448	0.000		
0.4a	1.000	1.143	1.464	1.527	0.000	
0.5a	1.000	1.103	1.383	1.712	1.716	0.000
0.6a	1.000	1.079	1.311	1.666	2.051	2.114
0.7a	1.000	1.062	1.251	1.570	2.023	2.577
0.8a	1.000	1.046	1.190	1.447	1.847	2.459
0.9a	1.000	1.028	1.115	1.275	1.533	1.973
1.0a	1.000	1.000	1.001	1.003	1.006	1.028

TABLE 2(a) SQUARE PLATE WITH PLAIN CIRCULAR HOLE

$\widehat{\theta\theta}$=Aqsin2θ+Bqsin6θ+Cqsin10θ

$\widehat{\theta\theta}$ at ρ=h	A	B	C
h=0.1a	-4.127	0.000	
h=0.2a	-4.531	-0.001	
h=0.3a	-5.283	-0.009	
h=0.4a	-6.53	-0.06	
h=0.5a	-8.58	-0.23	
h=0.5a (3 terms)	-8.637	-0.322	-0.001

TABLE 2(b) SQUARE PLATE WITH PLAIN CIRCULAR HOLE

Distance from Center of Hole	$\widehat{\theta\theta}$ at θ=0° in terms of q					
	h=0.1a	h=0.2a	h=0.3a	h=0.4a	h=0.5a (2 terms)	h=0.5a (3 terms)
0.1a	0.00					
0.2a	1.35	0.00				
0.3a	1.22	1.46	0.00			
0.4a	1.14	1.47	1.54	0.00		
0.5a	1.10	1.38	1.72	1.71	0.00	0.00
0.6a	1.08	1.30	1.65	2.03	2.05	2.10
0.7a	1.06	1.24	1.55	1.99	2.50	2.56
0.8a	1.04	1.18	1.42	1.82	2.40	2.45
0.9a	1.03	1.11	1.28	1.55	2.01	1.97
1.0a	1.01	1.03	1.09	1.18	1.34	1.05

TABLE 3(*a*) SQUARE PLATE WITH CIRCULAR HOLE REINFORCED WITH RIM ONLY

σ, $\overline{\rho\rho}$, $\overline{\theta\theta}$ = Aqsin2θ+Bqsin6θ
$\overline{\rho\theta}$ = Cqcos2θ+Dqcos6θ

At ρ = h		σ		$\overline{\rho\rho}$		$\overline{\theta\theta}$		$\overline{\rho\theta}$	
		A	B	A	B	A	B	C	D
40% Reinf. (A=0.2ht)	h=0.1a	-2.468	0.000	-0.494	0.000	-2.616	0.000	+0.987	0.000
	h=0.2a	-2.647	0.000	-0.529	0.000	-2.806	0.000	+1.059	0.000
	h=0.3a	-2.966	-0.002	-0.593	0.000	-3.144	-0.002	+1.186	+0.003
	h=0.4a	-3.460	-0.012	-0.692	-0.002	-3.667	-0.013	+1.384	+0.014
	h=0.5a	-4.19	-0.05	+0.84	-0.01	-4.44	-0.05	+1.68	+0.06
100% Reinf. (A=0.5ht)	h=0.1a	-1.538	0.000	-0.770	0.000	-1.770	0.000	+1.539	0.000
	h=0.2a	-1.630	0.000	-0.815	0.000	-1.875	0.000	+1.630	0.000
	h=0.3a	-1.788	-0.001	-0.894	0.000	-2.057	-0.001	+1.788	+0.003
	h=0.4a	-2.028	-0.005	-1.014	-0.002	-2.333	-0.005	+2.028	+0.014
	h=0.5a	-2.37	-0.02	-1.19	-0.01	-2.73	-0.02	+2.37	+0.06
200% Reinf. (A=ht)	h=0.1a	-0.946	0.000	-0.946	0.000	-1.230	0.000	+1.892	0.000
	h=0.2a	-0.994	0.000	-0.994	0.000	-1.292	0.000	+1.988	0.000
	h=0.3a	-1.077	0.000	-1.077	0.000	-1.400	-0.001	+2.154	+0.002
	h=0.4a	-1.201	-0.002	-1.201	-0.002	-1.561	-0.003	+2.401	+0.013
	h=0.5a	-1.38	-0.01	-1.38	-0.01	-1.79	-0.01	+2.75	+0.05

TABLE 3(*b*) SQUARE PLATE WITH CIRCULAR HOLE REINFORCED WITH RIM ONLY

	Distance from Center of Hole	$\overline{\rho\theta}$ at θ=0° in terms of q				
		h=0.1a	h=0.2a	h=0.3a	h=0.4a	h=0.5a
40% Reinf. (A=0.2ht)	0.1a	0.99				
	0.2a	1.31	1.06			
	0.3a	1.18	1.50	1.19		
	0.4a	1.11	1.40	1.67	1.40	
	0.5a	1.08	1.30	1.62	1.91	1.74
	0.6a	1.06	1.23	1.52	1.90	2.29
	0.7a	1.04	1.18	1.42	1.78	2.27
	0.8a	1.03	1.13	1.32	1.61	2.06
	0.9a	1.02	1.09	1.21	1.41	1.86
	1.0a	1.01	1.03	1.07	1.13	1.24
100% Reinf. (A=0.5ht)	0.1a	1.54				
	0.2a	1.29	1.63			
	0.3a	1.15	1.52	1.79		
	0.4a	1.09	1.36	1.73	2.04	
	0.5a	1.06	1.26	1.58	2.00	2.43
	0.6a	1.05	1.19	1.45	1.84	2.39
	0.7a	1.04	1.15	1.35	1.68	2.18
	0.8a	1.03	1.11	1.26	1.52	1.92
	0.9a	1.02	1.07	1.17	1.34	1.61
	1.0a	1.01	1.02	1.06	1.11	1.20
200% Reinf. (A=ht)	0.1a	1.89				
	0.2a	1.28	1.99			
	0.3a	1.13	1.53	2.16		
	0.4a	1.08	1.33	1.77	2.41	
	0.5a	1.06	1.23	1.55	2.06	2.81
	0.6a	1.04	1.17	1.41	1.81	2.44
	0.7a	1.03	1.13	1.31	1.62	2.13
	0.8a	1.02	1.10	1.23	1.46	1.85
	0.9a	1.01	1.06	1.15	1.30	1.55
	1.0a	1.00	1.02	1.05	1.10	1.18

TABLE 4 SQUARE PLATE WITH CIRCULAR HOLE REINFORCED WITH RING ONLY

$\overline{\rho\rho}$, $\overline{\theta\theta}$ = Aqsin2θ+Bqsin6θ
$\overline{\rho\theta}$ = Cqcos2θ+Dqcos6θ

h=0.5a

Reinforcing k		$t_H=3t_K$ 40% 0.5477a	$t_H=3t_K$ 100% 0.6124a	$t_H=3t_K$ 200% 0.7071a	$t_H=2t_K$ 40% 0.5916a	$t_H=2t_K$ 100% 0.7071a	$t_H=2t_K$ 200% 0.8660a
$\overline{\theta\theta}^H$ at ρ=h	A	-5.21	-4.39	-3.93	-5.84	-5.24	-4.75
	B	-0.10	-0.08	-0.06	-0.13	-0.10	-0.10
$\overline{\rho\rho}^H$ at ρ=k	A	-0.30	-0.28	-0.12	-0.42	-0.20	+0.15
	B	+0.01	+0.02	+0.04	+0.02	+0.07	+0.11
$\overline{\theta\theta}^H$ at ρ=k	A	-3.40	-1.37	-0.29	-2.79	-0.88	+0.05
	B	-0.03	0.00	0.00	-0.03	-0.01	+0.09
$\overline{\rho\theta}^H$ at ρ=k	C	+0.71	+0.88	+0.84	+1.17	+1.25	+0.99
	D	+0.03	+0.03	+0.03	+0.05	+0.06	+0.02
$\overline{\rho\rho}^K$ at ρ=k	A	-0.90	-0.84	-0.35	-0.84	-0.40	+0.70
	B	+0.01	+0.07	+0.12	+0.05	+0.14	+0.22
$\overline{\theta\theta}^K$ at ρ=k	A	-3.58	-1.54	-0.36	-2.92	-0.94	+0.09
	B	-0.03	+0.01	+0.03	-0.02	+0.01	+0.12
$\overline{\rho\theta}^K$ at ρ=k	C	+2.12	+2.65	+2.52	+2.35	+2.50	+1.98
	D	+0.09	+0.10	+0.09	+0.11	+0.11	+0.04
		$\overline{\rho\theta}$ at θ=0° in terms of q					
$\overline{\rho\theta}$ at ρ=0.5a		0.00	0.00	0.00	0.00	0.00	0.00
$\overline{\rho\theta}$ at ρ=k		2.21			2.46		
$\overline{\rho\theta}$ at ρ=0.6a		2.38	0.89	0.84	2.47	1.17	1.09
$\overline{\rho\theta}$ at ρ=k			2.75				
$\overline{\rho\theta}$ at ρ=0.7a		2.36	2.43	0.38	2.43	1.32	1.29
$\overline{\rho\theta}$ at ρ=k				2.60		2.61	
$\overline{\rho\theta}$ at ρ=0.8a		2.14	2.08	2.10	2.19	2.20	1.18
$\overline{\rho\theta}$ at ρ=k							2.01
$\overline{\rho\theta}$ at ρ=0.9a		1.76	1.70	1.67	1.81	1.77	1.82
$\overline{\rho\theta}$ at ρ=1.0a		1.46	1.23	1.21	1.27	1.25	1.25

For the plate with finite dimensions, numerical computation is done only for a square shear panel, which is antisymmetrical with respect to the x- and y-axes and symmetrical with respect to the lines $\theta = \pm \frac{\pi}{4}$. Therefore, in the expression for the stress function, n can only be odd. Only two terms, $n = 1$ and $n = 3$, are used in all examples. The variables considered in the different cases are as follows:

(*a*) Square shear panel with a plain circular hole:

5 examples; $h = 0.1a$, $0.2a$, $0.3a$, $0.4a$, or $0.5a$ (see Table 2).

(*b*) Square shear panel with a circular hole reinforced with rim only:

15 examples; $h = 0.1a$, $0.2a$, $0.3a$, $0.4a$, or $0.5a$.

Amount of reinforcing = 40 per cent, 100 per cent, or 200 per cent of original hole material (see Table 3).

(*c*) Square shear panel with a circular hole reinforced with ring only:

6 examples; $h = 0.5a$ $\quad t_H = 3t_K$ or $2t_K$

Amount of reinforcing = 40 per cent, 100 per cent, or 200 per cent of original hole material (see Table 4).

(*d*) Square shear panel with a circular hole reinforced with both rim and ring:

6 examples; $h = 0.5a$ $\quad t_H = 3t_K$ or $2t_K$

Amount of reinforcing = 40 per cent, 100 per cent, or 200 per cent of original hole material (see Table 5).

Curves for selected cases are presented as Figs. 4 to 6.

Check on Boundary Conditions

As previously stated, the solution of a two-dimensional stress problem is to find a stress function F, such that the resulting stresses satisfy prescribed values at the specified boundaries with the further requirement that $\nabla^4 F = 0$. In the present problem, no matter how many terms are used in the sine series for the

TABLE 5 SQUARE PLATE WITH CIRCULAR HOLE REINFORCED WITH BOTH RIM AND RING

σ, $\widehat{\rho\rho}$, $\widehat{\theta\theta}$ = Aqsin2θ+Bqsin6θ
$\widehat{\rho\theta}$ = Cqcos2θ+Dqcos6θ

h=0.5a						
Reinforcing Equally Divided between Rim and Ring						
	$t_H=3t_K$			$t_H=2t_K$		
Reinforcing	40%	100%	200%	40%	100%	200%
A	$0.1ht_K$	$0.25ht_K$	$0.5ht_K$	$0.1ht_K$	$0.25ht_K$	$0.5ht_K$
k	0.5244a	0.5590a	0.6124a	0.5477a	0.6124a	0.7071a
σ^H at ρ=h A	-4.52	-2.98	-2.07	-4.73	-3.21	-2.13
σ^H at ρ=h B	-0.06	-0.03	-0.02	-0.07	-0.03	-0.02
$\widehat{\rho\rho}^H$ at ρ=h A	-0.15	-0.25	-0.35	-0.24	-0.40	-0.53
$\widehat{\rho\rho}^H$ at ρ=h B	0.00	0.00	0.00	0.00	0.00	0.00
$\widehat{\theta\theta}^H$ at ρ=h A	-4.57	-3.07	-2.18	-4.80	-3.33	-2.29
$\widehat{\theta\theta}^H$ at ρ=h B	-0.06	-0.03	-0.02	-0.07	-0.03	-0.02
$\widehat{\rho\theta}^H$ at ρ=h C	+0.30	+0.50	+0.69	+0.47	+0.80	+1.07
$\widehat{\rho\theta}^H$ at ρ=h D	+0.01	+0.02	+0.02	+0.02	+0.03	+0.02
$\widehat{\rho\rho}^H$ at ρ=k A	-0.29	-0.31	-0.20	-0.42	-0.32	-0.03
$\widehat{\rho\rho}^H$ at ρ=k B	0.00	+0.01	+0.02	+0.01	+0.03	+0.04
$\widehat{\theta\theta}^H$ at ρ=k A	-3.67	-1.59	-0.45	-3.26	-1.24	-0.38
$\widehat{\theta\theta}^H$ at ρ=k B	-0.03	0.00	0.00	-0.03	-0.01	-0.01
$\widehat{\rho\theta}^H$ at ρ=k C	+0.65	+0.85	+0.86	+1.06	+1.24	+1.10
$\widehat{\rho\theta}^H$ at ρ=k D	+0.02	+0.02	+0.02	+0.04	+0.04	+0.03
$\widehat{\rho\rho}^K$ at ρ=k A	-0.87	-0.94	-0.60	-0.85	-0.63	-0.05
$\widehat{\rho\rho}^K$ at ρ=k B	0.00	+0.03	-0.05	+0.02	+0.06	+0.09
$\widehat{\theta\theta}^K$ at ρ=k A	-3.85	-1.78	-0.57	-3.38	-1.33	-0.39
$\widehat{\theta\theta}^K$ at ρ=k B	-0.03	0.00	+0.01	-0.02	0.00	+0.01
$\widehat{\rho\theta}^K$ at ρ=k C	+1.94	+2.56	+2.58	+2.11	+2.49	+2.20
$\widehat{\rho\theta}^K$ at ρ=k D	+0.07	+0.07	+0.06	+0.08	+0.07	+0.06
	$\widehat{\rho\theta}$ at θ=0° in terms of q					
$\widehat{\rho\theta}$ at ρ=0.5a	0.31	0.52	0.71	0.49	0.83	1.09
$\widehat{\rho\theta}$ at ρ=k	2.02	2.63		2.19		
$\widehat{\rho\theta}$ at ρ=0.6a	2.31	2.51	0.90	2.34	1.28	1.27
$\widehat{\rho\theta}$ at ρ=k			2.64		2.56	
$\widehat{\rho\theta}$ at ρ=0.7a	2.29	2.21	2.17	2.30	2.25	1.14
$\widehat{\rho\theta}$ at ρ=k						2.26
$\widehat{\rho\theta}$ at ρ=0.8a	2.07	1.93	1.81	2.08	1.94	1.85
$\widehat{\rho\theta}$ at ρ=0.9a	1.73	1.61	1.50	1.74	1.61	1.51
$\widehat{\rho\theta}$ at ρ=1.0a	1.25	1.20	1.16	1.24	1.20	1.16

ary by Green's theorem in the plane. Thus, let F_t and F_a be the true and approximate stress functions. Then

$$Q = \int\int (\nabla^2 F_t - \nabla^2 F_a)^2 dxdy = \min$$

$$Q = \int\int (\nabla^2 F_t - \nabla^2 F_a)^2 dxdy = \int\int [(\nabla^2 F_t - \nabla^2 F_a)(\nabla^2 F_t - \nabla^2 F_a) - (F_t - F_a)(\nabla^4 F_t - \nabla^4 F_a)]dxdy$$

$$= \int_c \left[\nabla^2(F_t - F_a)\frac{\partial}{\partial N}(F_t - F_a) - (F_t - F_a)\nabla^2\frac{\partial}{\partial N}(F_t - F_a)\right] dS = \min$$

At the internal boundary: When the hole is plain, F_t, $\frac{\partial F_t}{\partial N}$, F_a, and $\frac{\partial F_a}{\partial N}$ are all zero; when there is a rim, F and $\frac{\partial F}{\partial N}$ at the circular boundary are treated as unknowns. So the error minimized, or the quantity Q, is due to incomplete satisfaction of the boundary conditions around the external boundary only.

The stresses $\widehat{xx}$ and $\widehat{xy}$ at the straight edges of the square shear panel are computed for five cases. At the right edge, $\widehat{xx}$ should be zero and $\widehat{xy}$ should be $+q$. The errors in $\widehat{xx}$ and $\widehat{xy}$ at the right edge from the mid-point to the upper right corner for the five cases are plotted in Fig. 7. The errors at the corners are quite large, especially for large holes. However, the disturbance across the upper right corner, which amounts to a force very nearly perpendicular to the diagonal, is compression when two

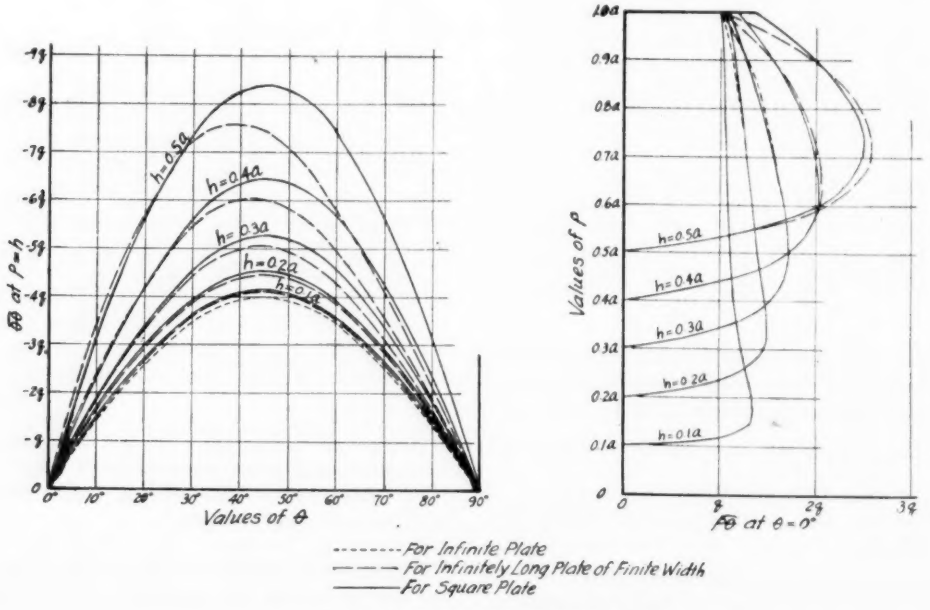


FIG. 4 PLAIN PERFORATIONS IN SHEAR WEBS

stress function, the compatibility condition $\nabla^4 F = 0$ and the internal boundary conditions are always satisfied. It is then logical to conclude that the fundamental assumption, that the area integral of the square of error in $\nabla^2 F$ shall be a minimum, must have something to do with the external boundary. This area integral can be reduced to a line integral around the boundterms are used and is tension when three terms are used. Thus the computed stress concentrations at the rim of the hole tend to be too large for two terms and too small for three terms. The closeness between the maximum $\widehat{\theta\theta}$ values 8.35q and 8.316q for the plain circular hole $h = 0.5a$ shows that the effect of corner disturbance is small.

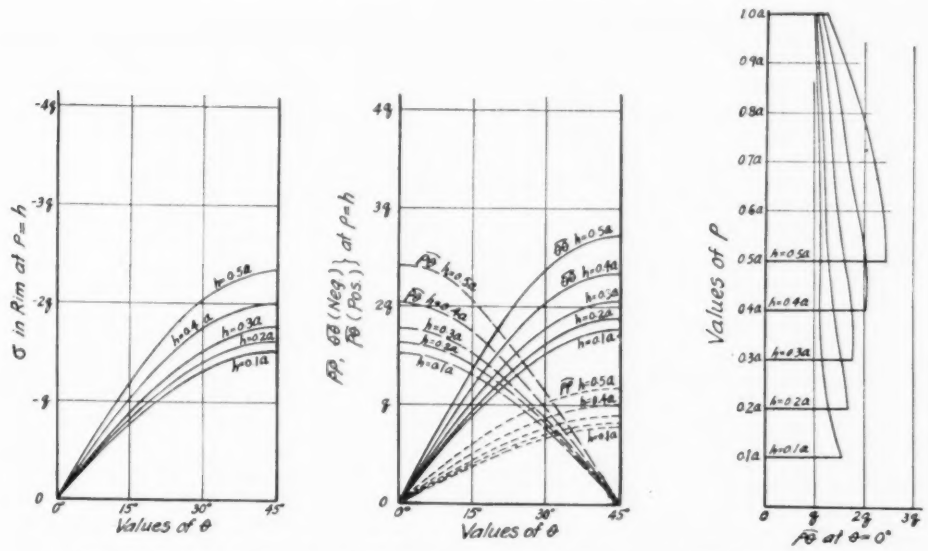


FIG. 5 SQUARE SHEAR PANEL WITH CIRCULAR HOLE REINFORCED WITH RIM ONLY
(Amount of reinforcing = 100 per cent hole material.)

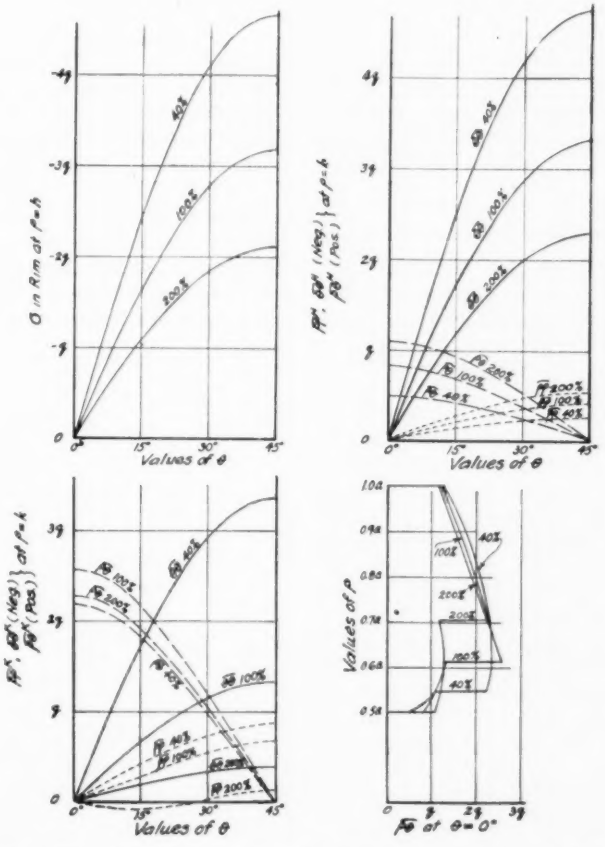


FIG 6 SQUARE SHEAR PANEL WITH CIRCULAR HOLE; EQUAL REINFORCEMENT IN RIM AND RING, $t_H = 2t_K$

DISCUSSION

The theoretical results, though giving some indication of the effects of such variables as hole diameter, amount and ways of reinforcement, etc., must await experimental data for justification. The chief uncertain factors are (1) the abrupt change of thickness at the outer radius of the ring where in the theoretical analysis the stresses are assumed to be uniformly transmitted from the thin plate to the thick ring, and (2) the nonuniform transmission of stress through the riveted or welded connection, while in the analysis the whole piece is considered monolithic.

The uncertainty involved in applying the theoretical results to flanged holes for the purpose of web-lightening in aeronautical

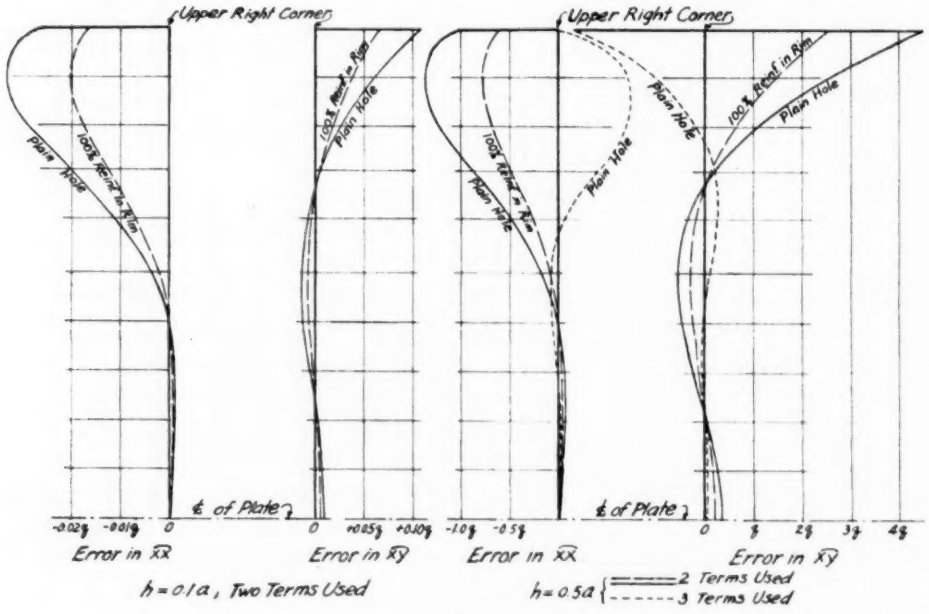


FIG. 7 CHECK ON BOUNDARY STRESSES

structures is even much greater. The flange is usually turned in one way at an angle. The action of this eccentric rim is unknown. When experimental data become available, the theoretical results may help the interpretation in regard to such variables as the hole diameter-panel length ratio, and the flange size.

ACKNOWLEDGMENT

The portion of the paper dealing with plain perforations was done while the author was a member of the Structures Department of the Research Laboratory, Curtiss-Wright Corporation, Airplane Division. The author wishes to thank Mr. Martin Goland, of the laboratory, for his suggestion of the problem. The balance of the paper is based on a thesis submitted in partial fulfillment of the requirements for the degree of Doctor of Philosophy in Engineering in the Graduate School of the University of Illinois. The thesis is written under the joint adviserships of Profs. T. C. Shedd, N. M. Newmark, and H. S. Stillwell; to all three the author is much indebted. Special appreciation is due to Professor Newmark for his numerous suggestions in the theoretical justification of the method and in the arrangement and wording of this paper.

On the Velocity Distribution of Turbulent Flow in Pipes and Channels of Constant Cross Section

By CHI-TEH WANG,[1] PROVIDENCE, R. I.

This paper follows the Prandtl conception of momentum transport and gives a critical examination of the so-called Prandtl-Nikuradse formula and the von Kármán formula for the velocity distribution of the turbulent flow in tubes or channels at large Reynolds number. It shows that both formulas would not give a good picture of the turbulent flow near the center of the conduit, and indeed they actually do not. A new formula for the velocity distribution is developed from a study of the mixing-length distribution across the section. This new formula checks quite well with the experiments and yields the same skin-friction formula as derived by von Kármán and Prandtl, which itself is in very good agreement with experiments.

Nomenclature

The following nomenclature is used in the paper:

u, v, w = mean velocities at any point in direction of and perpendicular to axis of pipe, respectively
u', v' = velocity fluctuation in x- and y-directions, respectively
$\overline{u'v'}$ = time mean value of $u'v'$
y = distance from wall
r = radius of circular pipe or half the distance between walls of a channel
u_{max} = u at $y = r$
$\xi = y/r$
$\eta = 1 - \frac{y}{r}$
τ = shearing stress at any point
τ_0 = shearing stress at wall
ρ = mass density of fluid
$v_* = \sqrt{\tau_0/\rho}$ = "friction velocity"
μ = coefficient of viscosity
ν = kinematic viscosity
ln = natural logarithm
κ = von Kármán's universal constant
k = linear parameter defining wall roughness
l = Prandtl's mixing length
R = $u_{max} r/\nu$ = Reynolds number
u = average velocity in pipe or channel
$c_f = \tau_0/\frac{1}{2}\rho(u_{max})^2$ = coefficient of friction
δ_l = thickness of laminar sublayer

[1] Assistant Professor of Aeronautical Engineering, Daniel Guggenheim Airship Institute, Akron, Ohio (now on leave of absence); Research Associate, Brown University.

Presented at a meeting of the Applied Mechanics Division, Cincinnati, Ohio, October 3, 1945, of The American Society of Mechanical Engineers.

Discussion of this paper should be addressed to the Secretary, A.S.M.E., 29 West 39th Street, New York, N. Y., and will be accepted until July 10, 1946, for publication at a later date. Discussion received after the closing date will be returned.

Note: Statements and opinions advanced in papers are to be understood as individual expressions of their authors and not those of the Society.

Introduction

The turbulent flow in tubes and channels of constant cross section has been successfully described by the so-called logarithmic laws bearing the names of Prandtl-Nikuradse and von Kármán. Both von Kármán's original derivations (1, 2)[2] and those given by Prandtl (3, 4) have been based primarily on von Kármán's conception of turbulent-flow-pattern similarity.

These logarithmic laws give a very good agreement between theory and experiments in connection with skin friction; but a rather poor agreement in connection with the velocity distribution across the tube or channel. This poor agreement in velocity distribution was first questioned by Gurjienko (5) in his study of the skin-friction problem for an airship. Goldstein (6) further cast doubts on the exactness of the similarity theory. The problem was subsequently discussed by Millikan (7) and von Mises (8). In fact, von Kármán (9) himself has pointed out that the strict similarity of the actual motion is too severe a restriction and can hardly be expected to exist in regions of finite extent.

Von Kármán (9) has further pointed out that the development of turbulence depends on the balance between the transfer of energy from the mean motion into the fluctuations and the dissipation due to fluctuations, and the equations based on this conception would be expected to give a satisfactory theory of turbulence. Although the author shares this view with von Kármán, until such a theory can be developed to a practical form, the classical mixing-length theory, nevertheless, is still the only theory so far which furnishes a reasonable physical picture of the turbulent flow.

This paper follows the Prandtl conception of momentum transport and gives a critical examination of the so-called Prandtl-Nikuradse formula and the von Kármán formula for the velocity distribution of the turbulent flow in tubes or channels at large Reynolds number. It shows that both formulas would not give a good picture of the turbulent flow near the center of the conduit, and indeed they actually do not. A new formula for the velocity distribution is developed from a study of the mixing-length distribution across the section. This new formula checks quite well with the experiments and yields the same skin-friction formula as derived by von Kármán and Prandtl, which itself is in very good agreement with experiments.

Review of Fundamental Concepts

The first detailed theoretical investigations of turbulence are due to Reynolds (10). By considering the time mean of the equations of motion of an incompressible turbulent fluid, Reynolds has shown that the spatial and temporal oscillations of the velocity occurring in the mixing movement affect the average motion like an internal friction. Taking a simple two-dimensional flow in which

[2] Numbers in parentheses refer to the Bibliography at the end of the paper.

$$u = u(y), \qquad v = w = 0$$

the Reynolds expression for the total frictional stress in turbulent flow is

$$\tau = \mu \frac{du}{dy} - \overline{\rho u'v'} \quad \ldots\ldots [1]$$

The first part is the viscous or laminar friction. The second part is contributed by turbulence and is the apparent or turbulent friction. This turbulent friction can be interpreted as due to the momentum transfer from layer to layer because of the velocity fluctuations. As in the case of the flow just mentioned, the excess of momentum in the direction of the mean flow carried by the fluid per unit volume is $\rho u'$, and the fluid volume passing through a unit area perpendicular to the y-direction is equal to v'.

Experiments have shown that in the turbulent flow along a wall, there exist roughly three regions. Near the wall there is a thin layer called the laminar sublayer in which the rate of shear is very great while the turbulent velocity component perpendicular to the wall is very small, so that the turbulent stress is insignificant compared with the laminar stress. Farther from the wall there is another region in which the turbulent stresses and the laminar stresses are of the same order of magnitude. Finally, further out there is a region in which the laminar stresses may be neglected in comparison with the turbulent stresses.

For flows in pipes and channels in the important range of high Reynolds number, experiments indicate that the laminar sublayer is very thin, and the laminar friction is a negligible part of the total friction except in the immediate neighborhood of the wall. Equation [1] can then be written as

$$\tau = -\overline{\rho u'v'} \quad \ldots\ldots [2]$$

Prandtl then proposed the hypothesis that in the turbulent exchange lumps of fluid are supposed to transfer momentum from one layer to another just as molecular agitation transfers properties like heat and momentum in a nonturbulent fluid. The transfer of momentum is supposed to be affected by the motion of lumps of fluid which leave a layer in which their momentums are those of the mean flow in the neighborhood, and move in a direction transverse to the mean flow through a distance l. At this point they are supposed to mix with the surrounding fluid, so that their momentums become identical with the average momentum of the fluid in that region.

Let us pass now to a continuous flow exemplified in Fig. 1 by a velocity curve $u = u(y)$, o-o being a plane parallel to the axis of the main motion. Assume that there is a turbulent mixing process present, with cross-current pulsating velocities $\pm v'$. Let l be the distance from o-o to some other layer b-b where a particle, animated by the pulsating vertical velocity v', could reach a layer adjacent to o-o and be embedded there. Following a simple reasoning, one may put

$$\overline{|u'|} = \text{const} \cdot l \cdot \frac{du}{dy} \quad \ldots\ldots [3]$$

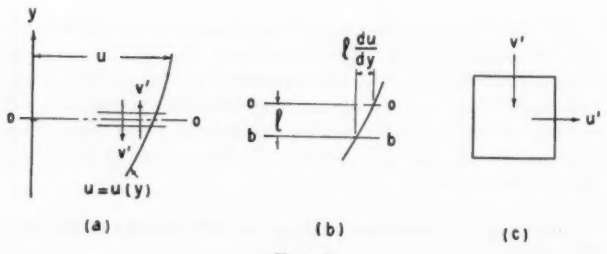


FIG. 1

where $\frac{du}{dy}$ is the local velocity gradient at o. From the continuity condition, to maintain constancy of mass, the velocity fluctuations in the axis and in the cross-current directions must compensate each other (see Fig. 1c), and therefore on the average the components u' and v' must be of the same order. One may then write

$$\overline{u'v'} = \text{const} \cdot \overline{|u'|} \cdot \overline{|v'|} = \text{const} \cdot l^2 \cdot \left(\frac{du}{dy}\right)^2 \quad \ldots\ldots [4]$$

where $\overline{|u'|}$ and $\overline{|v'|}$ are the time mean values of the absolute values of u' and v', respectively. Since l is a relative measure of the flow pattern, one may define l by writing

$$\tau = \rho l^2 \left(\frac{du}{dy}\right)^2 \quad \ldots\ldots [5]$$

where l is the Prandtl mixing length of momentum transport.

In circular pipes or in channels, it is known that

$$\tau = \tau_0 \left(1 - \frac{y}{r}\right) \quad \ldots\ldots [6]$$

where τ_0 is the shearing stress at the wall. By combining Equations [5] and [6], we have

$$\tau_0 \left(1 - \frac{y}{r}\right) = \rho l^2 \left(\frac{du}{dy}\right)^2 \quad \ldots\ldots [7]$$

or

$$\frac{l}{r} = \frac{v_* \sqrt{1-\xi}}{\frac{du}{d\xi}} = \frac{v_* \sqrt{\eta}}{-\frac{du}{d\eta}} \quad \ldots\ldots [8]$$

where $\xi = y/r$, and $\eta = 1 - \xi$, and $v_* = \sqrt{\frac{\tau_0}{\rho}}$.

Distribution of Mixing Length Across Conduit

Equation [8] gives the relationship at a point between the mixing length, the friction velocity v_*, the velocity gradient, and the position of the point. It seems important to investigate the existence of any law which might govern the distribution of the mixing length.

Following the experimental results by Fritsch (11), von Kármán obtains the "velocity-defect law" at large Reynolds number as

$$\frac{u_{\max} - u}{v_*} = f(\xi) \quad \ldots\ldots [9]$$

This law is assumed to hold throughout the flow, except in the immediate neighborhood of the wall, and the function f is a function of the position of the cross section of the conduit only. Differentiating Equation [9], we have

$$-\frac{1}{v_*}\frac{du}{d\xi} = f'(\xi)$$

and combining it with Equation [8], we have

$$\frac{l}{r} = -\frac{\sqrt{1-\xi}}{f'(\xi)} = g(\xi) \quad \ldots\ldots [10]$$

where g is another function of the position of the cross section of the conduit only. Therefore, we have proved that the mixing

length at high Reynolds number is independent of the Reynolds number, the friction velocity, and the wall roughness, but depends only on the position of the cross section. A review of Nikuradse's experiments (12, 13) indicates the correct relationship of Equation [10]. Experimental mixing-length distributions have been calculated by Nikuradse, and he shows that, for Reynolds numbers greater than 6×10^4, the mixing-length distribution, both in the smooth and rough pipes, can be represented by a single curve when $\frac{l}{r}$ is plotted against $\frac{y}{r}$.

From the consideration of symmetry, the $\frac{l}{r}$ versus $\frac{y}{r}$ curve must be symmetrical with respect to the axis of the conduit. Since this curve must have a continuously turning tangent at the axis, the slope of the curve there must be zero. These considerations lead to the assumption that this curve can be represented by the following series

$$\frac{l}{r} = a + b\eta^2 + c\eta^4 + \ldots \quad [11a]$$

$$= (a + b + c + \ldots) + (-2b - 4c + \ldots)\xi + (b + 6c + \ldots)\xi^2 + \ldots \quad [11b]$$

Now consider a region near the wall. The paths of the particles perpendicular to the flow are bounded by the wall; and they tend to be zero in the neighborhood of a smooth wall, and of the order of magnitude of the depths of the irregularities in a rough wall. Therefore, l must tend to zero as we approach the smooth wall, but toward a relatively small finite value if the wall is somewhat rough.

Furthermore, let us limit ourselves to a narrow strip near the wall, in which the change of shearing stress can be neglected. If we suppose that l is determined by the configuration of the boundaries and by the physical constants, then l and y are the only lengths which enter directly into the problem. The other quantities which enter are μ, ρ, and the constant value τ_0 of the shearing stress. Only two independent dimensionless combinations can then be formed, namely, l/y and yv_*/ν. When the influence of viscosity is neglected, we have

$$\frac{l}{y} = \kappa$$

where κ is von Kármán's universal constant and has been determined to be equal to 0.4.

Therefore, in the region near the wall but outside the laminar sublayer, the mixing-length distribution curve must be of the form

$$\frac{l}{r} = \kappa\xi + \text{higher-order terms in } \xi \quad [12]$$

Equation [11] applies to a region $\epsilon_1 \leq \xi \leq 1$, where ϵ_1 is a small positive quantity, and Equation [12] applies to a region $0 < \xi \leq \epsilon_2$, where ϵ_2 is another small positive quantity. Assume there is a region $\epsilon_1 \leq \xi \leq \epsilon_2$ in which Equation [11], and Equation [12] can be applied. If we take the first three terms in Equation [11a], the foregoing discussion would give us the following two relations

$$\left.\begin{aligned} a + b + c &= 0 \\ -2b - 4c &= 0.4 \end{aligned}\right\} \quad [13]$$

Another relation must be furnished in order to determine these constants uniquely, and this relation can be obtained from Nikuradse's mixing-length distribution curve. We must note here that since a numerical differentiation is necessary to compute l, the process is usually inaccurate, especially toward the axis of the conduit where l is determined by two small quantities. A point on the curve at $\frac{y}{r} = 0.5$ is therefore arbitrarily chosen; since it is as good as any, it gives $\frac{l}{r} = 0.116$. Substituting into Equations [11], we have

$$a + 0.25b + 0.0625c = 0.116 \quad [14]$$

Solving Equations [13] and [14] simultaneously, we obtain

$$a = 0.14, \quad b = -0.08, \quad c = -0.06$$

It is very interesting to see that these constants have exactly the same values given by Prandtl to approximate Nikuradse's experimental curve.

Equation [11] can now be written as

$$\frac{l}{r} = 0.14 - 0.08\,\eta^2 - 0.06\,\eta^4 \quad [15]$$

and checks very well with Nikuradse's curve, Fig. 4. This is the mixing-length equation applied to both smooth and rough pipes or channels at large Reynolds number except in the immediate neighborhood of the wall.

Examination of Prandtl-Nikuradse and von Kármán Formulas for Velocity Distribution

It has been shown in the foregoing section that in a region near the wall, τ can be regarded as equal as constant τ_0 and $\frac{l}{y} = \kappa$. Substituting these relationships into Equation [5] and integrating, Prandtl gives the following wall velocity formula for velocity distribution near the wall

$$\frac{u}{v_*} = \frac{1}{\kappa} \ln \frac{yv_*}{\nu} + c \quad [16]$$

where c is a constant. Applying this formula to his experimental data, Nikuradse found that it can be applied with a good approximation even up to the middle of the tube. By substituting the boundary condition that at $y = r$, $u = u_{max}$, Nikuradse obtains

$$\frac{u_{max} - u}{v_*} = -\frac{1}{\kappa} \ln \xi \quad [17]$$

This is the so-called Prandtl-Nikuradse formula.

Von Kármán assumes a similar pattern of the turbulent flow and has put forth his assumption of the mixing length as

$$l = \frac{du}{dy} \Big/ \frac{d^2u}{dy^2} \quad [18]$$

Substituting Equation [18] into Equation [7] and integrating, von Kármán's formula for velocity distribution is as follows

$$\frac{u_{max} - u}{v_*} = -\frac{1}{\kappa} [\ln (1 - \sqrt{\eta}) + \sqrt{\eta}] \quad [19]$$

Plots of Equation [17] with $\frac{u_{max} - u}{v_*}$ against $\ln \xi$ and Equation [19] with $\frac{u_{max} - u}{v_*}$ against $[\ln(1 - \sqrt{\eta}) + \sqrt{\eta}]$ are shown in Figs. 2 and 3. It is seen that the experimental points do not lie on the respective straight lines. Gurjienko (5) suggests the use of two κ's for approximating the experimental values, but there does not seem any theoretical justification. It may be

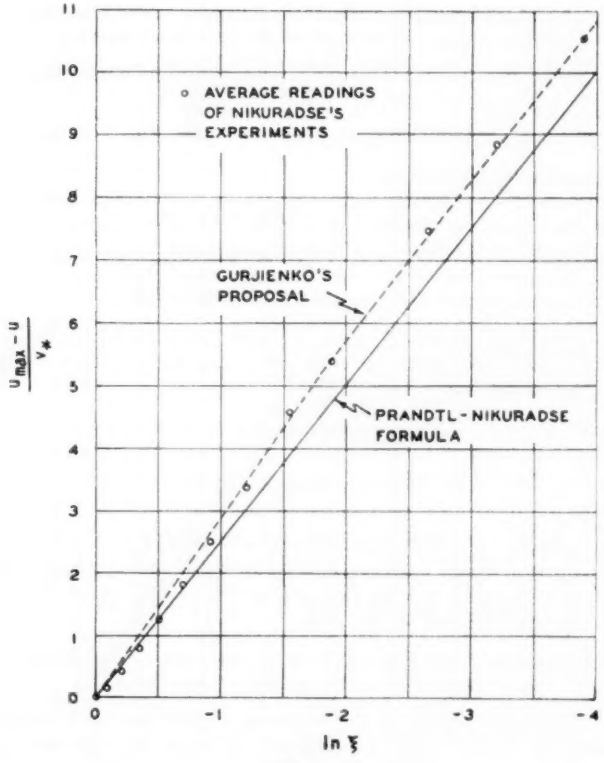


FIG. 2

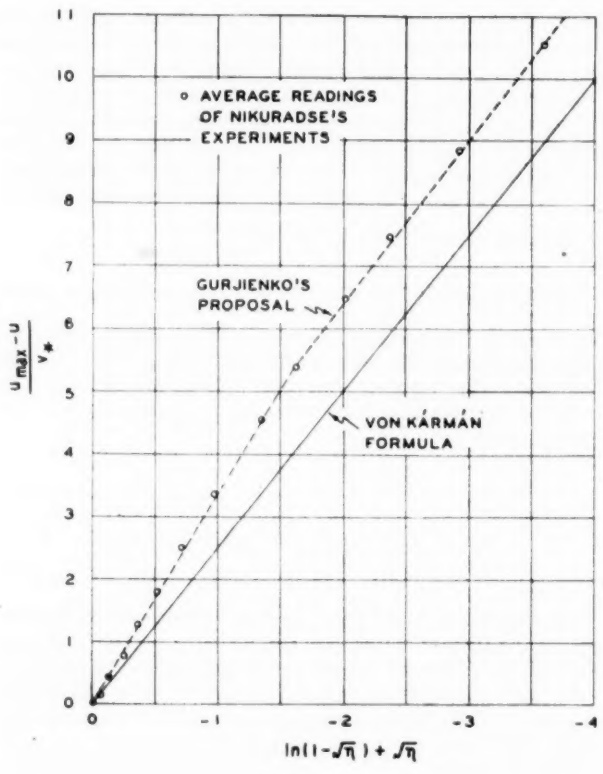


FIG. 3

pointed out here that Equation [16] fits the experimental results (4, 12) much better than Equation [17]. This difference is due to the fact that the boundary condition at the middle of the pipe is used in deriving Equation [17], whereas it is not used in Equation [16]. Equation [16] gives a good over-all fit to the experimental data except near the middle of the tube.

It is worth while to mention another inconsistency in the two formulas mentioned. The velocity gradients in the Prandtl-Nikuradse and von Kármán formulas are, respectively

$$\left.\begin{aligned}\left(\frac{du}{d\xi}\right)_P &= \frac{v_*}{\kappa}\frac{1}{\xi}\\ \left(\frac{du}{d\xi}\right)_K &= \frac{v_*}{2\kappa}\frac{1}{1-\sqrt{1-\xi}}\end{aligned}\right\} \quad \ldots\ldots\ldots\ldots [20]$$

at the center of the pipe. Both expressions give finite values of the velocity gradient. The result appears to be inconsistent, as naturally the velocity curve must pass through the maximum with zero velocity gradient there.

Substituting $\frac{du}{d\xi}$ from Equation [20] into Equation [8], the mixing lengths of the Prandtl-Nikuradse and von Kármán formula are, respectively

$$\left.\begin{aligned}\left(\frac{l}{r}\right)_P &= \kappa\,\xi\sqrt{1-\xi}\\ \left(\frac{l}{r}\right)_K &= 2\kappa\sqrt{1-\xi}\,(1-\sqrt{1-\xi})\end{aligned}\right\} \quad \ldots\ldots [21]$$

Equations [21] are plotted in Fig. 4. The inconsistencies of mixing lengths of both formulas with the Nikuradse curve may furnish a good explanation why these formulas do not check with experiments near the center of the pipe.

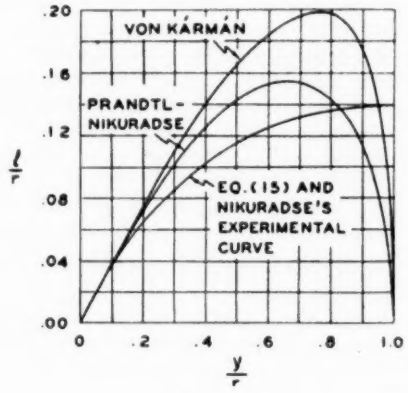


FIG. 4

Comparing Figs. 2 and 3, we find that the Prandtl-Nikuradse formula gives a better approximation to the experimental results than the von Kármán formula. This is again clearly seen in Fig. 4; but it must be noted that this better agreement with the experiments is purely accidental because $\frac{l}{r}$ was assumed to be equal to $\kappa\,\xi$ in the original derivation; therefore, the entirely different form of $\frac{l}{r}$ obtained in Equations [21] can be explained in no other way than as an accident.

NEW FORMULA FOR VELOCITY DISTRIBUTION

A formula for the velocity distribution can be derived from the expression for the mixing length as given by Equation [15]. Equation [15] can be written as

$$\frac{l}{r} = 0.06\,(1-\eta^2)(2.33+\eta^2)$$

Expanding in partial fractions

$$\frac{1}{\left(\frac{l}{r}\right)} = \frac{1}{0.2}\left(\frac{1}{1-\eta^2}+\frac{1}{2.33+\eta^2}\right) \quad [22]$$

Substituting Equation [22] into Equation [8] and rearranging, we obtain

$$-\frac{1}{v_*}\frac{du}{d\eta} = \frac{\sqrt{\eta}}{0.2}\left(\frac{1}{1-\eta^2}+\frac{1}{2.33+\eta^2}\right) \quad [23]$$

or

$$-\frac{1}{v_*}\int du = \frac{1}{0.2}\left(\int \frac{\sqrt{\eta}\,d\eta}{1-\eta^2}+\int \frac{\sqrt{\eta}\,d\eta}{2.33+\eta^2}\right)$$

Letting $x = \sqrt{\eta}$, there results

$$-\frac{1}{v_*}\int du = \frac{1}{0.2}\left(\int \frac{2x^2\,dx}{1-x^4}+\int \frac{2x^2\,dx}{2.33+x^4}\right) \quad [24]$$

Equation [24] can easily be integrated.[3] After substituting the boundary condition that $u = u_{max}$ at $\eta = 0$ into the resulting expression, the equation becomes

$$\frac{u_{max}-u}{v_*} = \frac{1}{\kappa}\left\{\ln\frac{1+\sqrt{\eta}}{1-\sqrt{\eta}} - 2\tan^{-1}\sqrt{\eta} - \frac{1}{\sqrt{2a}}\ln\frac{\eta+\sqrt{2a\eta}+a}{\eta-\sqrt{2a\eta}+a} + \sqrt{\frac{2}{a}}\tan^{-1}\frac{\sqrt{2a\eta}}{a-\eta}\right\} \quad [25]$$

where $\kappa = 0.4$ and $a = \sqrt{2.33} = 1.53$. Equation [25] is applied to both smooth and rough pipes or channels at large Reynolds number, except in the immediate neighborhood of the wall. The limit of "large" Reynolds number from Nikuradse's experiments is $R > 6 \times 10^4$.

The formula is plotted in Fig. 5 and checks very well the experimental results. The velocity gradient is given by Equation [23] and is zero at the center of the pipe. Thus this formula does not have the inconsistency of the other formulas.

The skin-friction, or wall velocity, formulas can be derived from Equation [25] when it is applied to the region near the wall ($\epsilon_1 < \xi < \epsilon_2$). Note that $\eta = 1-\xi$. For the region near the wall, $\xi << 1$, and $\sqrt{1-\xi} \cong (1-{}^1/_2\,\xi)$. Equation [25] can then be written as

$$\frac{u_{max}-u}{v_*} \cong \frac{1}{\kappa}\left\{\ln\frac{1+1-\frac{\xi}{2}}{1-1+\frac{\xi}{2}} - 2\tan^{-1}\left(1-\frac{\xi}{2}\right) - \frac{1}{\sqrt{2a}}\ln\frac{1-\xi+\sqrt{2a}\left(1-\frac{\xi}{2}\right)+a}{1-\xi-\sqrt{2a}\left(1-\frac{\xi}{2}\right)+a} + \sqrt{\frac{2}{a}}\tan^{-1}\frac{\sqrt{2a}\left(1-\frac{\xi}{2}\right)}{a-1+\xi}\right\}$$

$$\cong -\frac{1}{\kappa}\ln\xi + c \quad [26]$$

[3] By using from Dwight's "Integration Table" (14) formulas 170.2 and 171.2.

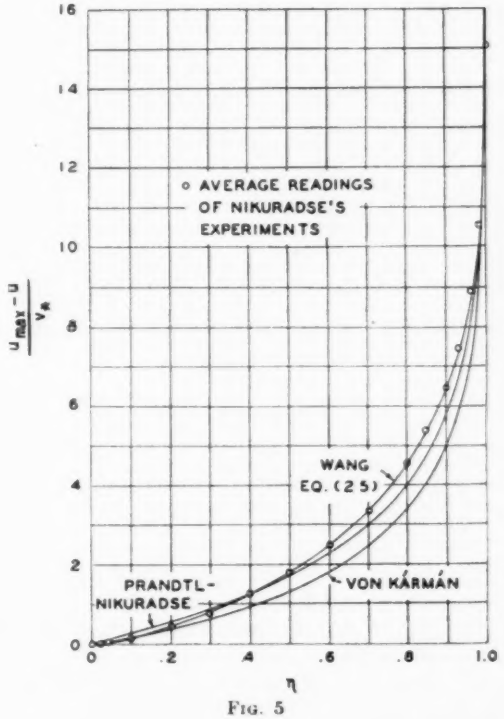


FIG. 5

Equation [26] can be easily transformed into Prandtl's wall velocity formula, which is applied to the outside of the laminar sublayer. Thus we see that for small ξ, our formula is exactly the same as Prandtl's wall velocity formula, and it is applied to a much larger region than we have expected. It can be actually applied to a region from the laminar sublayer to the axis of the conduit.

Here we shall divide the turbulent flows into three categories or regimes, as follows:

(*a*) One in which the roughness is so small as to have no effect, conditions being the same as if the wall were ideally smooth. We shall refer to this as "smooth-wall flow."

(*b*) One in which viscosity or rather Reynolds number has no effect and the roughness is the controlling factor. We shall refer to this as "rough-wall flow."

(*c*) An intermediate or transition regime between (*a*) and (*b*) in which both viscosity and roughness are important.

In the case of "smooth-wall flow," the thickness of the laminar sublayer and the velocity outside the sublayer can only depend on the friction at the wall, the viscosity, and the fluid density. On the basis of dimensional considerations, the velocity $u_{\delta lam}$ just outside the laminar sublayer may be expressed as

$$u_{\delta lam} = Av_* \quad [27]$$

and the thickness of the layer as

$$\delta_{lam} = B\frac{\nu}{v_*} \quad [28]$$

By applying Equation [26] to the outside of laminar sublayer and combining with Equations [27] and [28], we have

$$u_{max} = \frac{v_*}{\kappa}\left(\ln\frac{v_* r}{\nu} + C'\right) \quad [29]$$

where C' includes the constants A, B, C, etc. Introducing the coefficient of friction

$$C_f = \frac{\tau_0}{\frac{1}{2}\rho u_{max}^2}$$

and Reynolds number

$$\mathbf{R} = \frac{u_{max} r}{\nu}$$

we have

$$\frac{\kappa\sqrt{2}}{\sqrt{C_f}} = \ln\left(\mathbf{R}\sqrt{C_f}\right) + C'' \quad [30]$$

where $C'' = C' - \ln\sqrt{2}$. With the constant determined by Nikuradse, the skin-friction formula is

$$\frac{1}{\sqrt{C_f}} = 1.77 \ln\left(\mathbf{R}\sqrt{C_f}\right) + 3.54 \quad [31]$$

In the case of "rough-wall flow," we may start with Equation [26] and follow Prandtl's reasoning to obtain the formula

$$\frac{u}{v_*} - 2.5 \ln\frac{y}{k} = 2.5 \ln\frac{v_* k}{\nu} + 5.5 \quad [32]$$

as given by Prandtl (4), where k is a linear parameter defining the wall roughness introduced by von Mises (15).

It is seen that Equation [25] leads to the same skin-friction formulas as derived by von Kármán and Prandtl.

Conclusion

The turbulent flow in a tube is not isotropic in nature. The description of the state of turbulence by the statistical theory therefore becomes quite complicated. Although von Kármán has presented a detailed discussion of the Couette problem or the two-dimensional flow with constant shearing stress from the point of view of energy transport and dissipation, and vorticity dissipation, the extension of his theory to the case of pressure flow in pipes or channels seems to be difficult to carry out.

At present, it seems that one has to be satisfied with the semi-empirical mixing-length theory and to use the more accurate formula for velocity distribution as derived in this paper. Obviously, this new formula is much more complicated than the original logarithmic laws. When an approximate velocity profile is needed, the Prandtl-Nikuradse formula is recommended, because not only is it simpler in form, but it also gives a better agreement with the experimental results than the von Kármán formula. The different formulas are plotted to compare with Nikuradse's experimental results in Fig. 5.

TABLE 1

η	$\frac{u_{max} - u}{v_*}$ Nikuradse's experiment[a]	$\frac{u_{max} - u}{v_*}$ Theoretical Eq. [25]
0.00	0.00	0.00
0.02	0.02	0.01
0.04	0.04	0.04
0.10	0.15	0.15
0.20	0.42	0.43
0.30	0.77	0.80
0.40	1.26	1.26
0.50	1.80	1.81
0.60	2.50	2.49
0.70	3.37	3.34
0.80	4.56	4.49
0.85	5.39	5.28
0.90	6.48	6.37
0.93	7.47	7.31
0.96	8.85	8.75
0.98	10.55	10.50
1.00	15.09	

[a] Average of Nikuradse's test results at $\mathbf{R} > 6 \times 10^4$ (reference 12).

Bibliography

1 "Mechanische Aehnlichkeit und Turbulenz," by Theodore von Kármán, Gesellschaft wissenshaftlich zu Göttingen, Germany, 1930, pp. 58–76.

2 "Mechanische Aehnlichkeit und Turbulenz," by Theodore von Kármán, Proceedings of the Third International Congress for Applied Mechanics, Stockholm, Sweden, vol. 1, 1930, pp. 85–93.

3 "Zur turbulenten Strömung in Rohren und längs Platten, by L. Prandtl, Ergebnisse den Aerodynamischen Versuch. zu Göttingen, Germany, part 4, 1932, pp. 18–29.

4 "Aerodynamic Theory," by W. F. Durand, Julius Springer, Berlin, Germany, vol. 3, 1935, p. 127.

5 "Universal Logarithmic Law of Velocity Distribution as Applied to the Investigation of Boundary Layer and Drag of Streamline Bodies at Large Reynolds Number," by G. Gurjienko, Trudi, Central Aero Hydrodynamical Institute, Moscow, Russia, Rep. 257, 1936; U. S. N.A.C.A. Tech. Memo. No. 842, Washington, D. C., 1937.

6 "The Similarity Theory of Turbulence, and Flow Between Parallel Planes and Through Pipes," by S. Goldstein, Proceedings of the Royal Society of London, England, series A, vol. 159, 1937, pp. 473–496.

7 "A Critical Discussion of Turbulent Flows in Channels and Circular Tubes," by C. B. Millikan, Proceedings of the Fifth International Congress for Applied Mechanics, Cambridge, Mass., 1938, pp. 386–392.

8 "Some Remarks on the Laws of Turbulent Motion in Tubes," by R. von Mises, Theodore von Kármán Anniversary Volume Contributions to Applied Mechanics, California Institute of Technology, Pasadena, Calif., 1941, p. 317.

9 "The Fundamentals of the Statistical Theory of Turbulence," by Theodore von Kármán, *Journal of the Aeronautical Sciences*, vol. 4, 1937, pp. 131–138.

10 "On the Dynamical Theory of Incompressible Viscous Fluids and the Determination of the Criterion," by O. Reynolds, Trans. of the Royal Society of London, England, series A, vol. 186, 1896, pp. 123–164; also, "Hydrodynamics," by H. Lamb, sixth edition, Cambridge University Press, London, England, 1932, p. 674.

11 "Der Einfluss der Wandrauhigkeit auf die turbulente Geschwindigkeitsverteilung in Rinnen," by W. Fritsch, Abhandlungen aus den Aero. Inst. an der Technischen Hochschule Aachen, Germany, Heft 8, 1928, pp. 45–62.

12 "Gesetzmässigkeiten der turbulenten Strömmung in glatten Rohren," by J. Nikuradse, Forschungsheft 356, Berlin, Germany, V.D.I. Verlag, 1932.

13 "Strömungsgesetze in rauhen Rohren," by J. Nikuradse, Forschungsheft 361, Berlin, Germany, V.D.I. Verlag, 1933.

14 "Tables of Integrals and other Mathematical Data," by H. B. Dwight, The Macmillan Company, New York, N. Y., 1934, p. 35.

15 "Elemente der technischen Hydromechanik," by R. von Mises, Leipzig, Germany, 1914.

Measurements of Friction in a Pipe for Subsonic and Supersonic Flow of Air

By J. H. KEENAN[1] and E. P. NEUMANN,[2] CAMBRIDGE, MASS.

The apparent friction coefficient was determined experimentally for the flow of air through smooth pipes at subsonic and supersonic velocities. Values of the Mach number ranged from 0.27 to 3.87, and of Reynolds number from 1×10^5 to 8.7×10^6. In supersonic flow the results were found to be strongly influenced by the presence of oblique shocks formed at the junction of nozzle and pipe. The effect of these shocks on the coefficient of friction was determined. Nozzle forms were devised which eliminated the shocks and their effects. It was found that at distances from the pipe inlet greater than 50 diam the apparent coefficient of friction for compressible flow at Mach numbers greater or less than 1 is approximately equal, for equal Reynolds numbers, to the coefficient of friction for incompressible flow with completely developed boundary layer. Mach numbers greater than 1 are rarely maintained for lengths greater than 50 diam. For attainable lengths, the coefficient of friction is a function of the ratio of length to diameter and the Reynolds number, with the Mach number at entrance determining the maximum attainable length.

Nomenclature

The following nomenclature is used in the paper:

a = cross-sectional area of test pipe, sq ft
D = diameter of test section, ft
d = throat diameter of nozzle, in.
F = wall friction force, lb
G = mass rate of flow per unit area, lb per sq ft per sec
g = acceleration given to unit mass by unit force, ft per sec per sec
h = enthalpy, ft-lb per lb
k = ratio of specific heats
L = length of test section, ft
$\mathbf{M}$ = Mach number $= V/\sqrt{gc_p(k-1)T_m J}$
p = pressure, psfa
$\mathbf{R}$ = Reynolds number, GD/μ
T = temperature, deg F abs
T_m = mean stream temperature at a given cross section of test pipe, deg F abs
T_i = mean stream temperature at the initial state of fluid stream, i.e., where $V = 0$ (deg F abs)
V = mean velocity of fluid stream at given cross section of test pipe, ft/sec
v = specific volume, cu ft per lb
w = mass rate of flow, lb per sec
x = distance along test section, ft

λ = friction coefficient $= \dfrac{\tau}{\frac{1}{2}\rho V^2}$

$\lambda = \left(\int_{x=0}^{x=L} \lambda dx\right) \Big/ L$

λ_c = friction coefficient calculated from

$$\frac{1}{\sqrt{4\lambda_c}} = -0.8 + 2 \log \mathbf{R}\sqrt{4\lambda_c}$$

with $\mathbf{R}$ based on T_m

λ_i = friction coefficient calculated from preceding equation with $\mathbf{R}$ based on T_i

μ = mean stream viscosity $= 1.147 \times 10^{-5} \dfrac{491.6 + 205.2}{T_m + 205.2} \left(\dfrac{T_m}{491.6}\right)^{3/2}$ lb/(ft sec)

ρ = mass density $\left(\dfrac{1}{vg}\right)$

τ = friction force per unit of wall surface, psf
θ = angle between walls of entrance nozzle

Subscripts:

i refers to initial state of fluid stream where velocity is zero
1 and 2 refer to arbitrary datum sections along test pipe

Constants used in calculations:

k = ratio of specific heats, 1.4
c_p = specific heat at constant pressure, 0.240 Btu/F lb
J = number of ft-lb in 1 Btu = 778.3

Introduction

The effect of friction on the flow of compressible fluids in pipes of uniform cross-sectional area was investigated analytically by Grashof (1)[3] and Zeuner (2), who arrived at a relationship between velocity and friction coefficient for perfect gases. Stodola (3) showed that the curves of Fanno permit a general graphical treatment for any law of friction. Frössel (4) presented the first extensive measurements of friction coefficients for the flow of air through a smooth tube with velocities above and below the velocity of sound. His measured coefficients for both subsonic and supersonic compressible flow appear to be in excellent agreement at corresponding Reynolds numbers with coefficients measured for incompressible flow. Keenan (5) presented experimental data on commercial pipe for the flow of water and for the flow of steam at subsonic velocities. These indicated that the friction coefficient is the same for the same Reynolds number for an incompressible fluid and for subsonic flow of a compressible fluid.

In the subsonic region the measurements of Frössel and of

[1] Professor of Mechanical Engineering, Massachusetts Institute of Technology. Mem. A.S.M.E.
[2] Assistant Professor of Mechanical Engineering, Massachusetts Institute of Technology.

Contributed by the Applied Mechanics Division and presented at the Annual Meeting, New York, N. Y., Nov. 26–29, 1945, of The American Society of Mechanical Engineers.
Discussion of this paper should be addressed to the Secretary, A.S.M.E., 29 West 39th Street, New York, N. Y., and will be accepted until July 10, 1946, for publication at a later date. Discussion received after the closing date will be returned.

Note: Statements and opinions advanced in papers are to be understood as individual expressions of their authors and not those of the Society.

[3] Numbers in parentheses refer to the Bibliography at the end of the paper

Keenan were in accord in that they revealed no variation of the friction coefficient which was peculiar to compressible fluids. In the supersonic region the measurements of Frössel pointed to a similar conclusion. Frössel's data for this region were published as a chart[4] which, despite its small scale, seemed to reveal great irregularities in the data. The friction coefficients, which were computed from the derivatives of the curves through the experimental points, must have been subject to great uncertainty.

Object of Investigation

Some preliminary investigations (6) into supersonic flow of air which were made in the laboratory of mechanical engineering at the Massachusetts Institute of Technology indicated friction coefficients appreciably different from those reported by Frössel. The present investigation was undertaken in an attempt to resolve this disagreement and to obtain some dependable experimental data on supersonic flow with friction. In order to tie the investigation into previous studies of the flow of incompressible fluids, some measurements of subsonic flow were included.

Test Apparatus

The arrangement of the test apparatus is shown in Fig. 1. Air is supplied by either a two-stage steam-driven compressor or a rotary electric-driven compressor. At the discharge from the compressor is a receiver to smooth out fluctuations in flow. For some tests a dehumidifying system was used to remove moisture from the air leaving the compressor. This dehumidifying system consists of a cooling coil followed by a heating coil. It is connected into the system as shown in Fig. 1.

The air stream is introduced into the test pipe through a rounded-entrance nozzle of circular cross section. Details of the nozzles used in different tests are shown in Figs. 2 to 5, inclusive.

[4] Reference (4), Fig. 7.

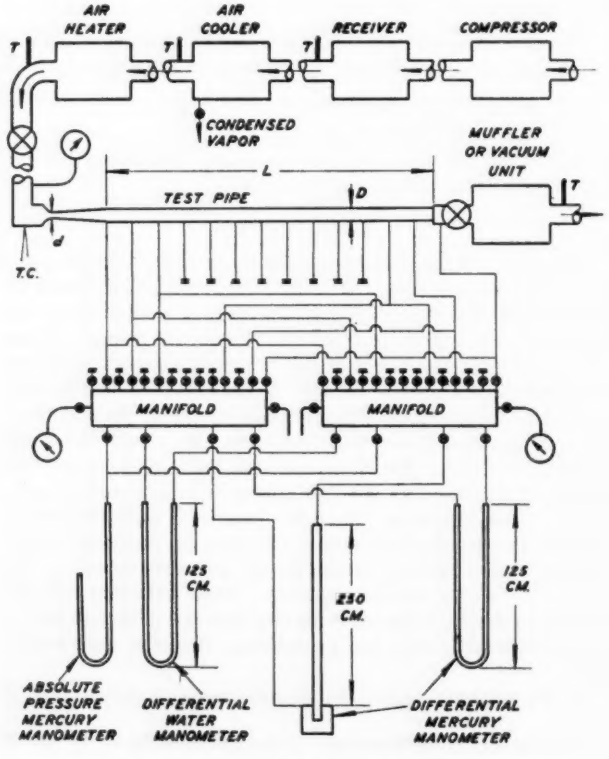


Fig. 1 Diagram of Test Apparatus

The test pipe is in each instance a piece of standard drawn-brass tubing. For the subsonic tests the inside diameter of the tube was 0.375 in. For the supersonic tests three tubes were used having inside diameters of 0.4375, 0.498, and 0.945 in., respectively.

The air stream leaving the test pipe is discharged either to the atmosphere or to an ejector which uses steam as the primary fluid.

The pressure measurements, from which the friction coefficients are calculated, were made at holes of 0.020 in. diam drilled in the tube wall. To avoid a burr at the inside edges of the pressure holes, the inside of the test pipe was carefully polished with fine emery cloth. Connections between the pressure holes, manifolds, and manometers are made with $^1/_4$-in. copper tubing.

All pressure differences were measured with simple U-tube manometers. In the supersonic test the pressures in the test pipe were generally small fractions of an atmosphere. They were measured with an absolute mercury manometer. With the aid of a sliding marker on the manometer scales, pressure differences could be read to 0.01 cm. Pressures higher than 50 psig before the inlet nozzle were measured with a calibrated Bourdon gage; lower pressures were measured with a mercury column.

The temperature of the air stream in front of the nozzle could be measured by either a copper-constantan thermocouple or a mercury-in-glass thermometer. Readings were usually made with the thermometer.

The discharge coefficient for the 0.375-in-diam subsonic nozzle was determined by means of a gasometer. The discharge coefficients for each supersonic nozzle were obtained from the A.S.M.E. data on nozzle coefficients (7).

Method of Testing

The air compressor was started and sufficient time allowed to elapse to obtain steady-state conditions before any readings were taken. Temperature readings were taken at definite intervals of time. Pressure differences between a given pair of taps were measured on either a mercury manometer or a water manometer, depending on the magnitude of the difference to be measured. In order to establish a continual check against possible leakage from either of the two manifolds, pressure differences were recorded for each pair of taps, with the higher pressure first in one manifold and then in the other. To check against possible leakage from the connections between the pressure taps and the manifold, a soap-and-water solution was applied at each connection. For the supersonic runs, where the pressures measured were below atmospheric pressure, the manometer system was tested by subjecting it to a pressure higher than atmospheric before starting a test.

Results of Tests

Apparent Friction Coefficient. The results of these tests are shown principally in terms of the apparent friction coefficient λ. This term is intended to represent for any cross section of the stream the quantity

$$\frac{2\tau}{\rho V^2}$$

where τ denotes the shear stress at the pipe wall, ρ the mean density, and V the mean velocity. In reality the apparent friction coefficient is defined in terms of the measured quantities, flow per unit area and pressure, through the equations

$$h_i = \frac{G^2 v^2}{2g} + \frac{k}{k-1} pv \quad \ldots\ldots\ldots\ldots\ldots [1]$$

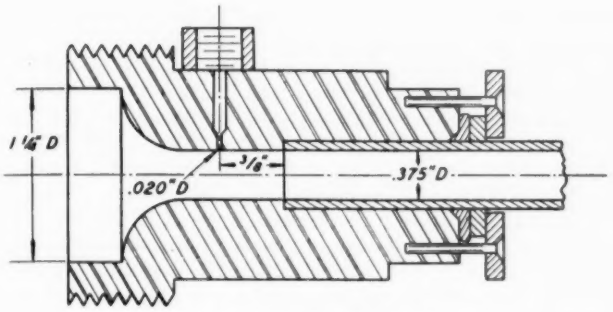


FIG. 2 ENTRANCE NOZZLE *A*

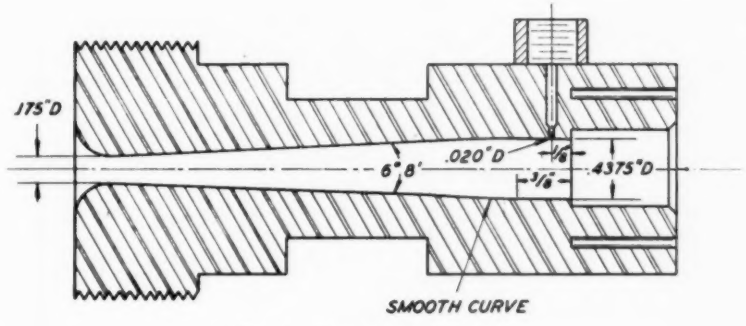


FIG. 3 ENTRANCE NOZZLE *B*

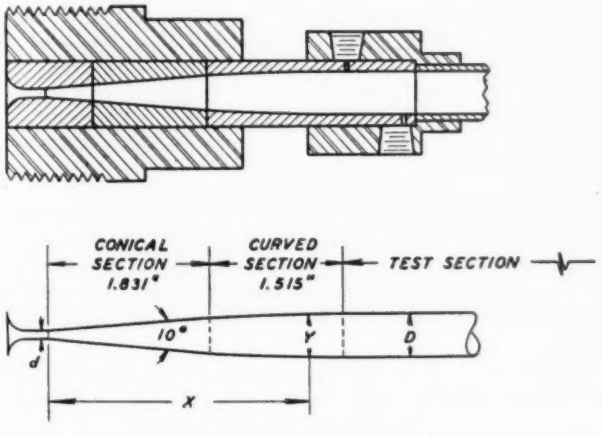


FIG. 4 ENTRANCE NOZZLE *C*

DIMENSIONS FOR NOZZLE CONTOUR

d = 0.107 in. diam D = 0.495 in. diam

x in.	y in.
0	0.107
1.831	0.427
1.855	0.431
1.887	0.436
1.914	0.440
1.943	0.444
1.977	0.448
2.022	0.453
2.062	0.457
2.107	0.461
2.158	0.465
2.231	0.470
2.301	0.474
2.379	0.478
2.511	0.483
2.661	0.487
2.876	0.491
3.036	0.493
3.143	0.494
3.346	0.495

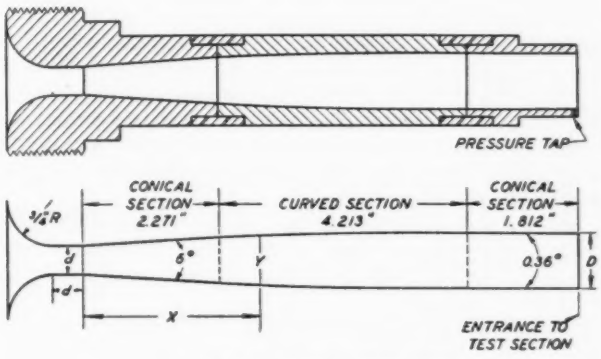


FIG. 5 ENTRANCE NOZZLE *E*

DIMENSIONS FOR NOZZLE CONTOUR

d = 0.562 in. diam D = 0.945 in. diam

x in.	y in.
0	0.562
2.271	0.800
2.308	0.804
2.365	0.809
2.423	0.815
2.487	0.821
2.552	0.826
2.625	0.832
2.700	0.837
2.783	0.843
2.869	0.849
2.959	0.854
3.056	0.860
3.161	0.865
3.281	0.871
3.412	0.877
3.550	0.882
3.704	0.888
3.884	0.894
4.075	0.899
4.300	0.905
4.558	0.910
4.862	0.916
5.259	0.922
5.795	0.927
6.484	0.933
8.296	0.945

$$\lambda = \frac{gD}{2G^2(x_2 - x_1)}\left[\frac{c_p T_i J(k-1)}{2k}\left(\frac{1}{v_1^2} - \frac{1}{v_2^2}\right) - \frac{G^2}{g}\frac{(k+1)}{2k}\ln\frac{v_2}{v_1}\right] \quad [2]$$

which were derived in reference (5).

In terms of L/D, k, and $\mathbf{M}$ for a perfect gas Equation [2] becomes

$$\lambda = \frac{D}{4L}\left\{\frac{1}{2k}\left[\frac{2 + \mathbf{M}_1^2(k-1)}{\mathbf{M}_1^2} - \frac{2 + \mathbf{M}_2^2(k-1)}{\mathbf{M}_2^2}\right] - \left(\frac{k+1}{k}\right)\ln\sqrt{\frac{[2 + \mathbf{M}_1^2(k-1)]\mathbf{M}_2^2}{[2 + \mathbf{M}_2^2(k-1)]\mathbf{M}_1^2}}\right\} \quad [3]$$

Equation [2] is identical with the statement

$$\lambda = \frac{2\tau}{\rho V^2}$$

if the velocity across each section is so nearly uniform that the mean velocity found from the flux of kinetic energy is identical with that found from the flux of momentum, or if the flux of momentum and the flux of kinetic energy do not change from section to section.

The flow of an incompressible fluid in a pipe at a great distance downstream from the entrance satisfies the latter condition. The flow of a compressible fluid satisfies neither condition. It is probable, however, that the former is nearly satisfied in compressible flow at a great distance downstream from the entrance,

provided that the longitudinal pressure gradient is not inordinately large.

The magnitude of the true friction coefficient ($2\tau/\rho V^2$) can be found only from a determination of the magnitude of the shear stress at the pipe wall. If the shear stress is to be measured directly, the experimental difficulties are formidable; if it is to be deduced from pressure measurements, either the analytical difficulties or the uncertainties introduced by supposition are likely to prove discouraging.

The apparent friction coefficient, on the other hand, may be rather simply deduced from common types of measurement. Moreover, when its value is known it may be readily applied to the design of passages.

The adoption of the apparent friction coefficient for reporting the results of measurements of the type presented here will facilitate comparison between data from different sources. The calculation of the apparent friction coefficient involves the simplest calculation and the minimum extraneous hypothesis consistent with reducing the measurements to a basis of comparison. The test of Frössel (4) and Keenan (5) have been so presented.

In all subsequent paragraphs the term "friction coefficient" is to be interpreted to mean "apparent friction coefficient," as defined by Equation [2].

The variation in pressure along the length of the test pipe is shown in Fig. 6. For test 1 the pressure in the exhaust space after the end of the pipe was below the sound pressure, that is, the pressure at the state of maximum entropy; consequently, the flow through the pipe was the maximum flow corresponding to the initial condition of the air stream. For test 2 the air stream was throttled behind the pipe, and for tests 3 and 4 in front of the pipe, to produce pressures at the pipe exit in excess of the sound pressure, which resulted in turn in a flow less than the maximum flow for the existing initial conditions.

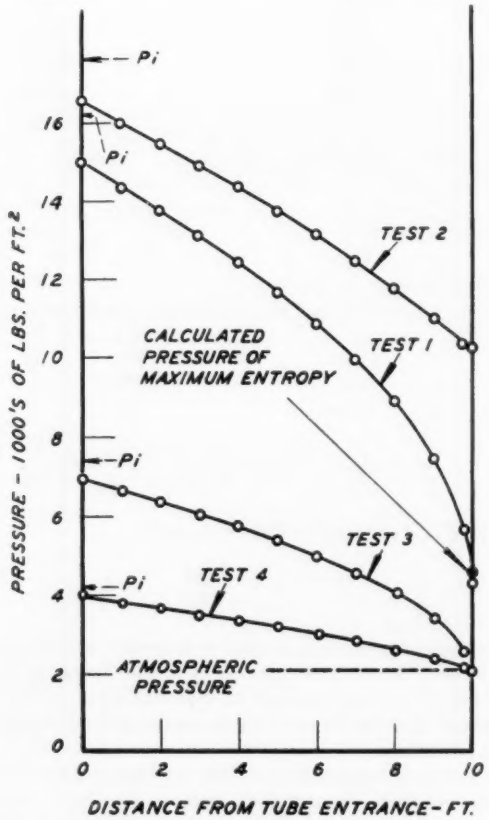


FIG. 6 PRESSURE DISTRIBUTION ALONG TEST PIPE FOR SUBSONIC FLOW

In Fig. 7 the arithmetic mean of the friction coefficients, corresponding to the intervals of pipe length between pressure taps for each test, is plotted against the arithmetic mean of the Reynolds number. The length interval from 0 to 1 ft was omitted from the calculation of the mean because the velocity profile was doubtless changing greatly in this interval. The last 3 inches of length were also omitted because of the effect on velocity and pressure distribution of the abrupt discharge into the exhaust space. Thus the data in Fig. 7 correspond to a well-developed boundary layer, and as stable a velocity profile as the conditions of compressible flow permit.

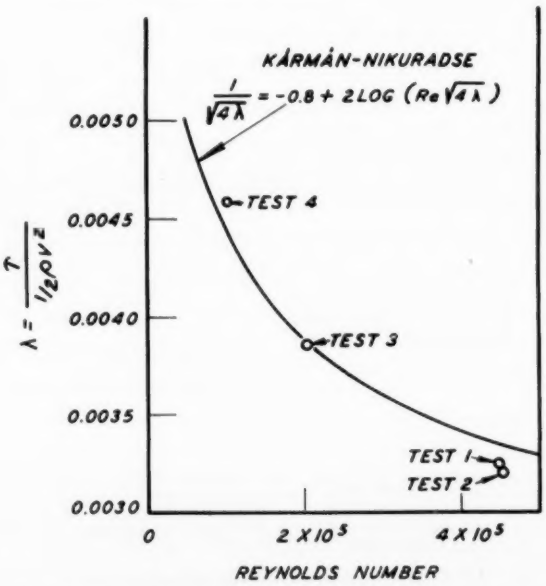


FIG. 7 FRICTION COEFFICIENTS FOR SUBSONIC FLOW COMPARED WITH THOSE FOR INCOMPRESSIBLE FLOW

The von Kármán-Nikuradse relation between friction coefficient and Reynolds number for incompressible flow is shown by the curve in Fig. 7. The greatest discrepancy between the present results and this curve is of the order of 3 per cent, which is approximately the degree of uncertainty in the present measurements.

Figs. 8 and 9 show the variation along the length of the tube of friction coefficient, mean temperature, and Mach number for tests 1 and 2. The values of friction coefficient for incompressible flow, corresponding to the Reynolds number at each point along the length of the pipe, are shown by the dash curve in Fig. 8. In test 1 the Mach number ranges from 0.32 to 1 and in test 2 from 0.3 to 0.47. In both tests, however, the agreement between the measured friction coefficients and those for incompressible flow is consistently good. This agreement confirms the conclusion reached by Keenan and by Frössel that for subsonic velocities the friction coefficient is a function of the Reynolds number and is not appreciably affected by change in the Mach number.

SUPERSONIC FLOW

Length of Test Pipe. The length of the test pipe for supersonic tests is limited by the divergence ratio of the nozzle that feeds the pipe. In supersonic flow in a pipe the pressure increases and the velocity decreases in the direction of flow. For a sufficiently

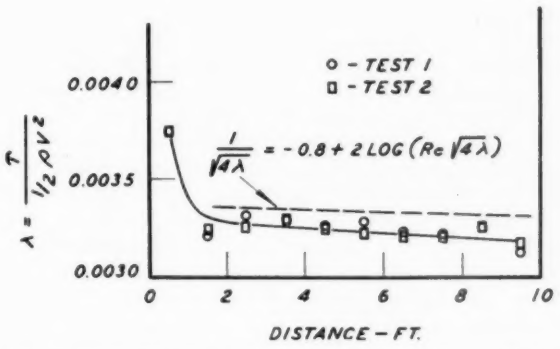


FIG. 8 FRICTION COEFFICIENT AGAINST DISTANCE ALONG PIPE FOR SUBSONIC FLOW

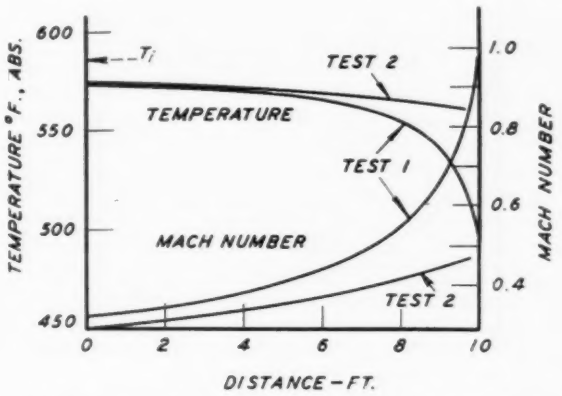


FIG. 9 TEMPERATURE AND MACH NUMBER AGAINST DISTANCE ALONG PIPE FOR SUBSONIC FLOW

low pressure in the exhaust space, the length of supersonic flow may be increased by lengthening the pipe until the velocity at the exit of the pipe has been reduced to the velocity of sound. Any further increase in the length of the pipe will decrease the length of supersonic flow, because a transverse shock will be established upstream from the previous exit section and velocities downstream from the shock will be subsonic. The maximum length of supersonic flow attained in the present tests is 50 diam.

The Nozzle. If the junction between the divergent nozzle passage and the test pipe is not properly designed, an oblique shock wave will form at or near the junction. This wave will extend down and across the stream until it encounters the opposite wall and then will reflect back and forth along the length of the pipe. Fig. 10, from the thesis of Huron and Nelson (8), shows such oblique waves in a two-dimensional nozzle. Since in crossing the oblique shock the pressure rise in the stream is almost discontinuous, measurements of pressure variation along the test pipe become difficult to interpret. Moreover, it appears probable that the existence of the shock stimulates thickening of the boundary layer and so influences strongly the magnitude of the friction coefficient. Under extreme conditions the oblique shock may initiate separation of the stream from the wall.

With the aid of the method of Shapiro (9), nozzles were designed so as to introduce the stream into the test pipe without the formation of an oblique shock of sufficient intensity to affect the measured pressures. Fig. 11 (from reference 8) shows the flow



FIG. 10 SCHLIEREN PHOTOGRAPH OF OBLIQUE SHOCK FRONTS FORMED AT ENTRANCE TO TUBE OF RECTANGULAR CROSS SECTION
(Divergence ratio = 3.50, θ = 30 deg, depth of passage perpendicular to plane of photograph = 0.400 in., cross-sectional area of parallel passage = 0.280 sq in. Exposure time 1/10 sec. Photograph from reference 8.)



FIG. 11 SCHLIEREN PHOTOGRAPH OF NOZZLE WITH TRANSITION LENGTH FROM DIVERGENT PASSAGE TO PARALLEL PASSAGE DESIGNED TO AVOID OBLIQUE SHOCK FRONTS
(Divergence ratio = 3.50, depth of passage perpendicular to plane of photograph = 0.400 in., cross-sectional area of parallel passage = 0.280 sq in. Exposure time 1/10 sec. Photograph from reference 8.)

from a two-dimensional nozzle which is comparable to the test nozzles and which was designed by the same method. The first photographs taken, by the Schlieren method, of flow through this nozzle showed a clear field in both nozzle and tube. In order to make visible the pattern of flow and to demonstrate that shock waves if present would be discernible, the walls of the nozzle and the parallel passage were knurled. Each rib of the knurling set up a disturbance of small magnitude which extended across the stream in the manner of an oblique shock. Since the presence of these small disturbances could be detected, the presence of an oblique shock would also be detected. The walls at the junction of the nozzle and tube and for a short interval in the passage a little distance downstream from the junction were left unknurled to permit a shock to be more readily distinguished, but none appeared.

Effect of Angle of Divergence. To determine the effect on the apparent friction coefficient of oblique shocks in the test pipe, a series of tests were made using entrance nozzles with conical divergent sections of different angles of divergence θ. The junction of the nozzle and pipe were in each case a sharp corner.

The variation in pressure along the test pipe for various values of the angle of divergence is shown in Fig. 12. For an angle of 24 deg the pressure decreases along the first 10 diam of pipe length. This decrease appears to be an extension of the expansion from the nozzle into the test pipe. It is doubtless caused by separation of the stream from the walls of the nozzle.

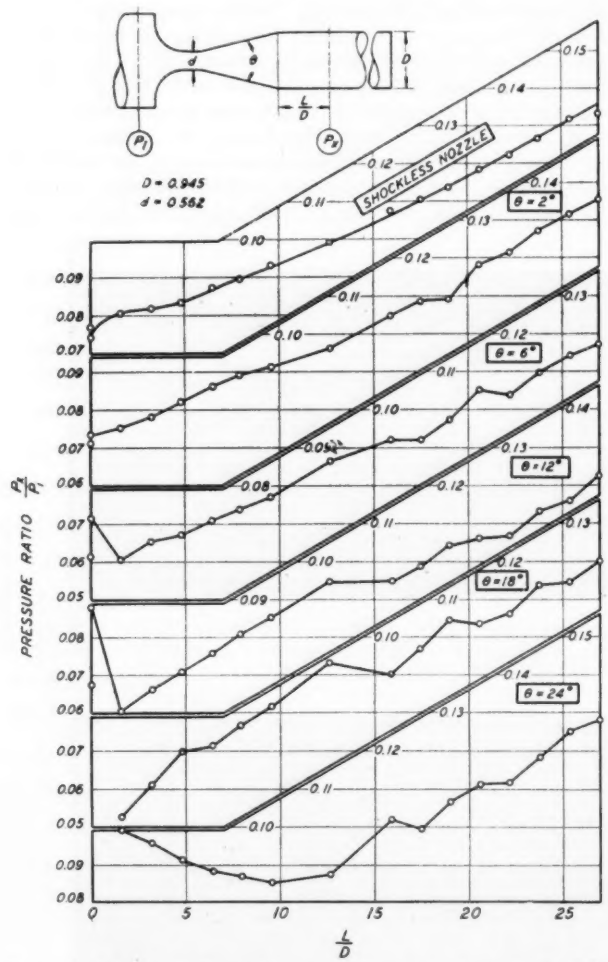


Fig. 12 Pressure Ratio Against Distance Along the Pipe Using Entrance Nozzles With Different Angles of Divergence (θ)

θ deg	Mach number at nozzle exit
2	2.08
6	2.29
12	2.16

For angles of 12 deg or less, the rise in pressure across the corner at the junction was measured by means of pressure taps located immediately before and after the corner. The measured pressure rise is shown in each instance by the interval between the two points at zero value of L/D. The ratio of pressures across the joint varies from 1.30 for an angle of 12 deg to 1.03 for an angle of 2 deg. The departure from 1 in the latter figure is hardly in excess of the uncertainty in the pressure measurements. For an angle of 6 deg, the ratio is 1.16. The analysis of Meyer (10) indicates a pressure ratio of 1.22 across the oblique shock arising from a change of direction of 3 deg at a Mach number of 2.29. This analysis is applicable only to two-dimensional flow which the flow near the tube wall should approximate. The experimental and analytical values appear to be of the same order of magnitude.

It may be seen in Fig. 12 that as the angle of divergence decreases, the pressure rise at the junction decreases, and the curve of pressure against distance becomes smoother. With a nozzle designed for shock-free conditions the curve becomes smooth and the rise in pressure at the junction becomes zero within the precision of the pressure measurements.

Although measurements made under other than shock-free conditions are not considered valid, a study was made of the effect on the apparent friction factor of nozzles of the ordinary type. Such nozzles were used, presumably, by Frössel who gave no indication that he had developed a special nozzle for the purposes of his tests. The friction coefficients, computed from the curves in Fig. 12, are plotted in Fig. 13 against the angle of divergence of the nozzle. These friction coefficients are the mean coefficients for the interval of length between values of L/D of 1.59 and 27—approximately the same as that used by Frössel.

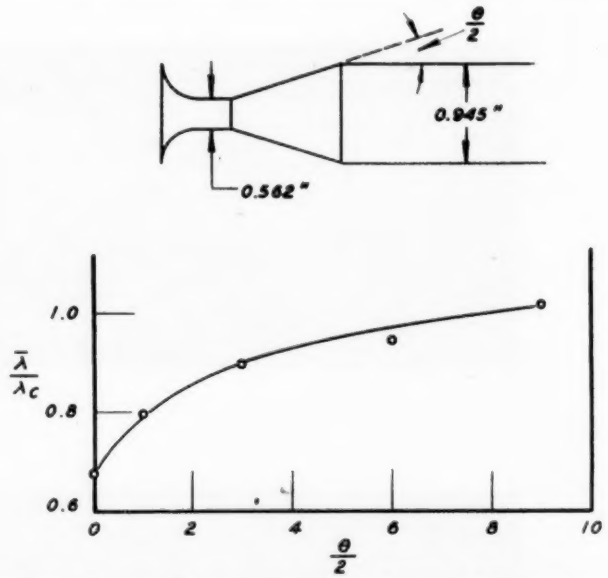


Fig. 13 Ratio of Measured Apparent Friction Coefficient to Friction Coefficient for Incompressible Flow Against Angle of Divergence θ

(The friction coefficient is the mean value of the apparent friction coefficient for the interval of test section from $L/D = 1.59$ to $L/D = 26.98$. The value of λ_c was computed from the von Kármán-Nikuradse relation between Reynolds number and friction coefficient.)

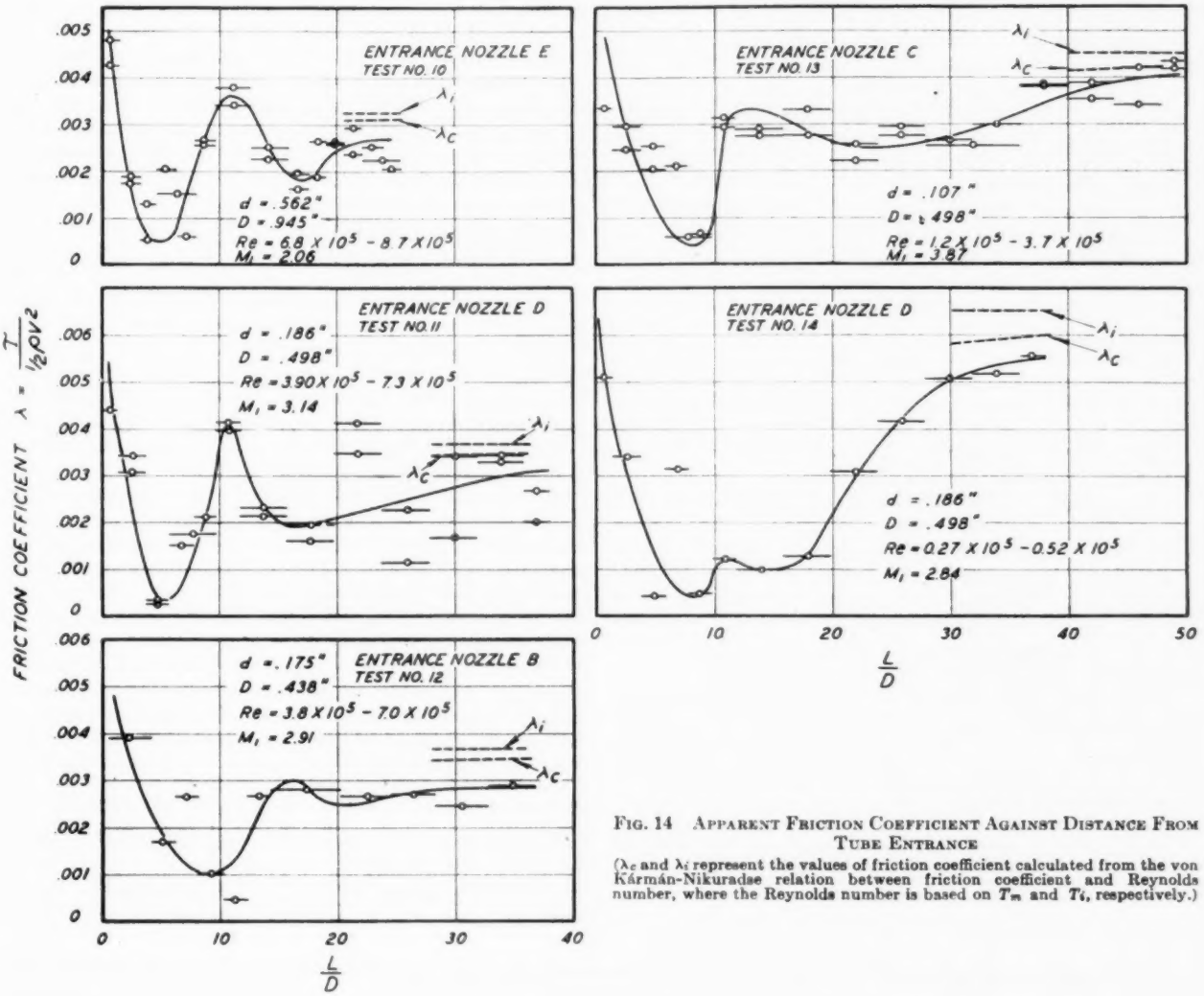


FIG. 14 APPARENT FRICTION COEFFICIENT AGAINST DISTANCE FROM TUBE ENTRANCE

(λ_c and λ_i represent the values of friction coefficient calculated from the von Kármán-Nikuradse relation between friction coefficient and Reynolds number, where the Reynolds number is based on T_m and T_i, respectively.)

According to the data in Fig. 13 the friction coefficient for a given Reynolds number approaches the von Kármán-Nikuradse value for incompressible flow as the angle of divergence increases. Perhaps this is evidence of the increase in thickness of the boundary layer caused by the oblique shock. The von Kármán-Nikuradse value is obtained from flow at large values of L/D where the boundary layer fills the cross section, and turbulence is fully developed. In supersonic flow the presence of an oblique shock may have an effect on the boundary layer similar to the effect of length in incompressible flow.

Apparent Friction Coefficient. The apparent friction coefficient is plotted against distance from the entrance to the test pipe in Fig. 14. The two extremities of the horizontal line which passes through each test point in Fig. 14 show, respectively, the positions at which the two pressures used in calculating the value of the friction coefficient were measured. Thus each point represents a mean value of the apparent friction coefficient over a short interval of length. The pressure difference across this interval was in each instance very small, and any irregularity in the pressure distribution or any error in a pressure measurement had therefore an exaggerated effect on the calculated friction coefficient. For this reason the points in Fig. 14 scatter over a band of considerable width. Nevertheless, a definite pattern is discernible which is common to all five sets of data. Near the entrance to the test pipe the coefficient decreases sharply with increasing distance along the pipe. At a distance of 5 to 10 diam the coefficient passes through a minimum. At greater distances there is evidence of a maximum followed by another minimum.

The data in Fig. 14 are not sufficiently precise to establish the number of maxima and minima or the amplitude of the fluctuations in the value of the coefficient, but an attempt to approximate these is represented by the solid lines in the figure. A somewhat similar variation in friction coefficient near the entrance to a pipe has been shown for flow of an incompressible fluid by Kirsten (11) and by Brooks, Craft, and Montrello (12). It is doubtless a phenomenon relating to the transition from laminar to turbulent flow in the boundary layer. No exact correspondence between pairs of curves in Fig. 14 should be expected because the degree of development of the boundary layer at pipe entrance varied from test to test with the length and other dimensions of the nozzle. The one exception is the pair of curves in the middle of the figure which were obtained with the same nozzle and test pipe.

On each of the charts in Fig. 14 are shown, by dash lines, values of the friction coefficients λ_i and λ_c calculated from the von Kármán-Nikuradse relation for incompressible fluids. The coefficients λ_i and λ_c are calculated using, respectively, the Reynolds numbers corresponding to the viscosity at the temperature before

the inlet nozzle where the velocity is zero and that at the mean stream temperature. In view of the "recovery" of temperature in the boundary layer, some value intermediate between these two would seem to be most appropriate.

For distances from the entrance greater than 20 diam, the trend of the coefficient is definitely upward. The limit of this trend appears to be a horizontal line or a curve with ordinates approximately equal to λ_i or λ_c.

The five charts in Fig. 14 may be roughly grouped into those of high Reynolds number, the left-hand three, and those of low Reynolds number, the right-hand two. The left-hand curves show a distinct similarity in pattern and position, whereas the right-hand group shows in comparison lower values at the minimum point and higher values at large values of L/D.

No analogous trend with Mach number can be discerned. Although the top and middle charts in the left-hand group have Mach numbers at entrance of 2.06 and 3.09, respectively, they differ less than the two middle charts which have Mach numbers of 3.09 and 2.84, respectively. Differences appear to depend on Reynolds number rather than Mach number.

To test whether the changes in characteristics were the result merely of accidental differences between test pipes and entrance nozzles, two tests were run with the same test pipe and nozzle at approximately the same Mach number but with different Reynolds numbers. These are shown by the two middle charts in Fig. 14. The differences between these two charts are consistent with the differences between any other pair of charts for two different Reynolds numbers.

The conclusion seems tenable, therefore, that for values of L/D greater than 50 the apparent coefficient of friction for compressible flow at Mach numbers greater or less than 1 is approximately equal, for equal Reynolds numbers, to the coefficient of friction for incompressible flow.

For Mach numbers greater than 1, however, values of L/D greater than 50 are rarely encountered; and for values less than 50, the apparent coefficient of friction is generally less than that given by the von Kármán-Nikuradse formula for the same Reynolds number. Since the present tests do not exceed a Reynolds number of 8.7×10^5, this last conclusion is open to question if the Reynolds number exceeds 1,000,000.

Because of a slight irregularity at the junction of the nozzle and the test pipe, the data of test 12 at small values of x/D were considered to be less reliable than those of the other tests. The data of test 12 are, nevertheless, in substantial accord with those of the other tests. If they were shown in Fig. 15 they would not alter in any way the conclusions drawn below. The figure is somewhat simplified by omitting them.

Mean Apparent Friction Coefficient. In Fig. 15 the mean apparent friction coefficient between the entrance to the test pipe and any value of L/D is plotted against that value of L/D. This method of plotting has two advantages: (*a*) This mean friction coefficient is more readily applied to design calculations than the more nearly point values in Fig. 14; (*b*) Since it is computed in general from a larger measured pressure difference, the values of the ordinate in Fig. 15 are less affected by small experimental errors and irregularities and therefore yield a smoother curve.

The curves in Fig. 15 consistently with those in Fig. 14 show certain trends with increasing Reynolds number: The point of minimum mean friction coefficient moves to lower values of L/D, and the rate of increase of friction coefficient with L/D at the higher values of L/D decreases. On each curve is given the Reynolds number corresponding to the viscosity at zero velocity (the "complete-recovery" value), and at the right-hand margin is shown the corresponding value of the coefficient of friction for an incompressible fluid at large values of L/D.

The experimental curves are extrapolated in Fig. 15 as they would go if the values for incompressible flow were the asymptotes. The extrapolations cannot, however, extend to the asymptotes. It can be shown from Equation [3] that for a fixed value of the Mach number at entrance, there is a corresponding maximum value of $\lambda \frac{L}{D}$ which will occur when $\mathbf{M}_2 = 1$. That maximum value represents an equilateral hyperbola cutting across Fig. 15. Segments of such hyperbolas are shown for entrance Mach numbers of 1.5, 2, 3, 4, and infinity. For an entrance Mach number of 1 the corresponding hyperbola is

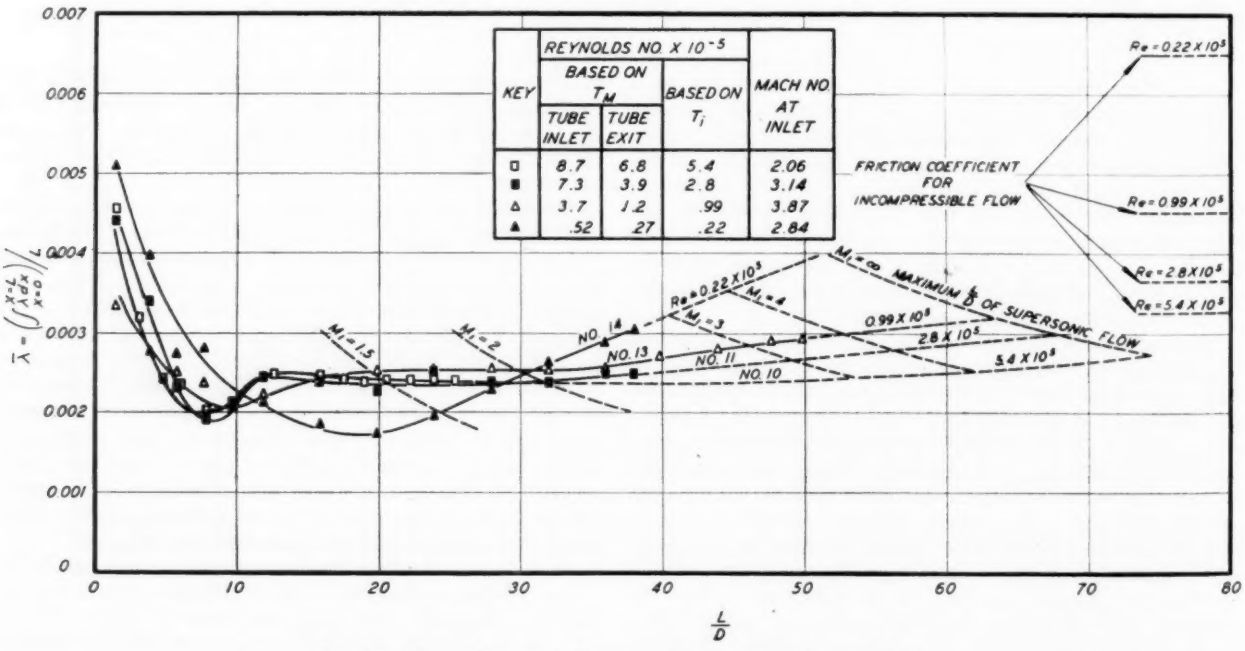


FIG. 15 MEAN APPARENT FRICTION COEFFICIENT AGAINST L/D

formed by the two axes of co-ordinates, and the maximum value of L/D is zero for any finite value of λ.

At the lower values of L/D some variation from the curves in Fig. 15 may be expected if the nozzle design is not identical with the corresponding one employed here. Large departures from these values will result, as indicated in Fig. 13, if oblique shocks are formed at the junction of nozzle and test pipe. But with a carefully designed nozzle and a smooth test pipe the mean apparent friction coefficient should be in close accord with the curves in Fig. 15.

Comparisons

In subsonic flow two previous experimental investigations by Keenan (5) and Frössel (4) indicated that for large values of L/D the apparent friction coefficient is essentially independent of Mach number and is, within experimental error, the same function of Reynolds number as the friction coefficient for incompressible fluids. The present investigation, as shown in Fig. 7, confirms these conclusions.

In supersonic flow the only previous experimental investigation is that of Frössel (4). His conclusion is the same as for subsonic flow, namely, that the apparent friction coefficient at the attainable values of L/D is the same function of Reynolds number as the friction coefficient for incompressible fluids at large values of L/D. The present investigation does not confirm this conclusion. It indicates that the apparent friction coefficient is a function of L/D as well as Reynolds number over the attainable range of L/D, and that the effect of Mach number is to limit the range of values of L/D.

Frössel concludes that his measured friction coefficients are represented within the precision of measurement by the von Kármán-Nikuradse relation. Thus the comparisons of this relation with the present data, as given in Figs. 14 and 15, are in effect comparisons of Frössel's data with the present data. It should be remembered, however, that Frössel's data for supersonic velocities spread over a band with a width of about 20 per cent, and that the method of computing them seems to leave much room for uncertainty.

Frössel offers no discussion of the development of nozzles suitable to his purpose, and the only published illustrations of his nozzles are to such a small scale that little dependable information can be obtained from them. These illustrations, however, are not inconsistent with the assumption that his nozzles were of the conical type with an angle of divergence in the order of 15 deg. The data in Fig. 13 indicate that for angles of this magnitude Frössel's conclusions have been confirmed. For supersonic flow without oblique shocks, however, the conclusions of Frössel have not been confirmed.

For subsonic conditions the minimum exit pressure for a given length of pipe is obtained by lowering the pressure in the exhaust space until the pressure in the exit plane ceases to fall. Then the entrance Mach number corresponding to the exit-plane pressure may be determined by measurements at the inlet. In Fig. 6 the measured pressure from the tap nearest the exit-plane is compared with the calculated minimum pressure (the pressure of maximum entropy). The measured pressure falls slightly below the calculated minimum. This is in accord with similar observations made by Frössel.

In supersonic flow an experimental determination of the maximum pressure is more difficult. The divergence ratio of the nozzle fixes the Mach number at entrance. The maximum pressure will be attained at the exit only if the pipe attached to the nozzle is the longest pipe which will not cause a transverse pressure shock. The maximum pressure cannot be attained, therefore, although it may be approximated closely by a tedious method of trial and error. Where it has been nearly attained in these tests it has always been slightly less than the calculated maximum.

Conclusions

For values of L/D greater than 50 the apparent coefficient of friction for compressible flow at Mach numbers greater or less than 1 is approximately equal, for equal Reynolds numbers, to the coefficient of friction for incompressible flow with completely developed boundary layer.

For Mach numbers greater than 1, however, values of L/D greater than 50 are rarely encountered. For values of L/D less than 50, the coefficient of friction is a function of L/D and Reynolds number. It is generally less than that given by the von Kármán-Nikuradse formula if the Reynolds number is less than 10^6. The effect of Mach number is to limit the range of values of L/D.

For Mach numbers greater than 1, the mean apparent coefficient of friction decreases rapidly from a relatively high value at entrance to a minimum value which it attains within a distance of 20 diam from the entrance. Beyond this minimum point the mean coefficient rises with increasing distance along the tube and appears to approach as a limit the value given by the von Kármán-Nikuradse formula. The point values of the apparent coefficient appear to attain the formula value at a distance of approximately 50 diam from the tube entrance; the mean values of the coefficient would attain the limit at perhaps twice this distance from the entrance.

The variation in coefficient of friction with L/D for supersonic flow is similar to that observed in the flow of incompressible fluids. An adequate comparison cannot be made, however, until more extensive information is available as to the effect of L/D in the flow of incompressible fluids.

The minimum observed pressure in subsonic pipe flow and the maximum observed pressure in supersonic pipe flow are each slightly less than the value calculated on the basis of the assumption that the velocity is uniform across any section.

The apparent coefficient of friction is strongly influenced by the presence of oblique shock waves in the tube.

The junction of the tube with an ordinary conical nozzle causes oblique shock waves, the amplitude of which increases with increasing angle of the cone. The apparent coefficient of friction also increases with increasing angle of the nozzle cone, and appears to attain approximately the von Kármán-Nikuradse value when the angle of the cone is 15 deg or more.

Acknowledgment

This investigation, conducted at the Massachusetts Institute of Technology prior to April, 1944, was sponsored by and conducted with the financial assistance of the National Advisory Committee for Aeronautics. Experimental data appear in tabular form in Technical Note Number 963 of the N.A.C.A.

BIBLIOGRAPHY

1 "Theoretische Maschinenlehre," by F. Grashof, L. Voss, Leipzig, Germany, 1875, pp. 593–597.

2 "Technical Thermodynamics," by G. Zeuner, Leipzig, Germany, 1900, pp. 264–273.

3 "Steam and Gas Turbines," by A. Stodola, McGraw-Hill Book Company, Inc., New York, N. Y., vol. 1, 1927, p.61.

4 "Flow in Smooth Straight Pipes at Velocities Above and Below Sound Velocity," by W. Frössel, N.A.C.A. TM, No. 844, 1938.

5 "Friction Coefficients for the Compressible Flow of Steam," by Joseph H. Keenan, Journal of Applied Mechanics, Trans. A.S.M.E., vol. 61, 1939, p. A-11.

6 "Friction Factors for Air Flowing in Straight Pipes at Supersonic Velocities," by C. Mueller and R. O'Connell, B.S. Thesis, Mechanical Engineering Department, Massachusetts Institute of Technology, Cambridge, Mass., 1941.

7 Instruments and Apparatus Special Subcommittee on the

Measurement of Fluid Flow: Flow Measurement, 1940. Information on Instruments and Apparatus, part 5. Measurement of Quantity of Materials, chapt. 4. Flow Measurement by Means of Standardized Nozzles and Orifice Plates. A.S.M.E. Power Test Codes, The American Society of Mechanical Engineers, New York, N. Y., 1940.

8 "Investigation of Supersonic Flow in Nozzles and Tubes," by F. Huron and N. Nelson, M.S. Thesis, Naval Architecture Department, Massachusetts Institute of Technology, Cambridge, Mass., 1944.

9 "Nozzles for Supersonic Flow Without Shock Fronts," by A. H. Shapiro, JOURNAL OF APPLIED MECHANICS, Trans. A.S.M.E., vol. 66, 1944, p. A-93.

10 "Über zweidimensionale Bewegungsvorgänge in einem Gas, das mit Überschallgeschwindigkeit strömt," by Th. Meyer, *Mitteilungen über Forschungsarbeiten ouf dem Gebiete des Ingenieurwesens*, vol. 62, 1908, pp. 31–67.

11 "Experimentelle Untersuchung der Entwicklung der Geschwindigkeitsverteilung bei der turbulenten Rohrströmung," by H. Kirsten, Dissertation, University of Leipzig, Leipzig, Germany, 1927.

12 "Friction Factor for Turbulent Flow in Transition Region for Straight Pipe," by W. B. Brooks, J. P. Craft, and J. Montrello, M. S. Thesis, Naval Architecture Department, Massachusetts Institute of Technology, Cambridge, Mass. 1943.

A Study of Flow of Plastics Through Pipes

By R. C. BINDER[1] AND J. E. BUSHER[2]

The pipe friction coefficient for true fluids is usually expressed as a function of Reynolds number. This method of organizing data has been extended to tests on the flow of different suspensions which behaved as ideal plastics in the laminar-flow range and as true fluids in the turbulent-flow range. In the laminar-flow range, Reynolds number below about 2100, the denominator in Reynolds number is taken as the apparent viscosity. The apparent viscosity can be determined from the yield value and the coefficient of rigidity. In the turbulent-flow range, the denominator in Reynolds number is an equivalent or turbulent viscosity equal to the dynamic viscosity of a true fluid having the same friction coefficient, velocity, diameter, and density as that of the plastic. The various experimental data on plastics correlate well with this extension of the method for true fluids.

Nomenclature

The following nomenclature is used in the paper:

- D = internal diameter of pipe
- f = pipe friction factor
- g = gravitational acceleration
- h = head loss, unit length of flowing substance
- L = length of pipe
- S = shear stress, force per unit area
- S_0 = yield value or stress of an ideal plastic, force per unit area
- V = average velocity of flowing substance
- ΔP = drop in pressure in the length L
- ρ = density, mass per unit volume, as slugs per cubic foot
- η = coefficient of rigidity
- μ = dynamic viscosity
- μ_a = apparent viscosity of an ideal plastic
- μ_T = turbulent viscosity of an ideal plastic

Introduction

Much experimental data are available on the steady flow of various fluids, as oil, water, and air, through circular pipes. From the point of view of flow characteristics, such fluids may be classified as true or homogeneous fluids. The pipe-flow data for true fluids has been well organized and established in forms convenient for general use. On the other hand, there is a definite lack of organized data on the flow of heterogeneous fluids, suspensions, and plastics through pipes. Different investigators have provided some data on the flow of suspensions through pipes; these suspensions had plastic properties. This paper presents an organization and correlation of the test data of these various investigators and expresses the results in a form which extends the latest organization established for true fluids.

In practice can be found many examples of heterogeneous fluids, in which fine particles, as sand, dust, clay, paper pulp, industrial solids, or sewage sludge, are suspended in water. The problem of the flow of a suspension or plastic is much more complicated than that of a true fluid. Among the problems involved in the transportation of suspensions is that of predicting friction losses, and that of providing suitable pumps and motors for moving the material. The pipe friction loss of a suspension may be considerably higher than that of the fluid carrier alone at the same velocity.

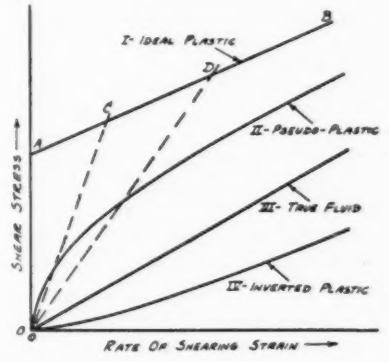


Fig. 1 Stress - Rate of Strain Relations for Different Substances

Fig. 1 shows diagrammatically the relation between shear stress and rate of shearing strain for different substances. Curve III, for a true fluid, shows a linear relation passing through the origin. The slope of curve III, the absolute or dynamic viscosity, is constant. The dynamic viscosity of a true fluid is uniquely determined by the temperature and pressure. It is not generally appreciated that this fact represents a great simplification of many flow problems.

Curve I, for what will be called an "ideal plastic," indicates a relative motion between layers, or deformation, only at a shear stress exceeding a certain minimum, the yield value. The curve AB is linear. The ratio of shear stress to rate of shearing strain or the "apparent viscosity" for a plastic is not constant. The dotted lines CO and DO have different slopes at different velocities; the same substance at different velocities has different apparent viscosities. This variation accounts for one of the main complications found in the flow of plastics.

Consider the flow between two parallel plates a distance x apart. Let S represent the shear stress on each plate, S_0 the yield value of the plastic, and v the velocity of one plate with respect to the other. The coefficient of rigidity η is defined as the ratio

$$\eta = \frac{(S - S_0)x}{v} \quad \ldots\ldots\ldots\ldots\ldots\ldots [1]$$

An ideal plastic can be specified by the yield value and the coefficient of rigidity. The coefficient of rigidity has the same dimensions as dynamic viscosity.

Curves II and IV in Fig. 1 indicate other possible relations between shear stress and rate of shear. Curve II might be termed a

[1] Professor of Mechanical Engineering, Schools of Mechanical Engineering and Aeronautics, Purdue University, W. Lafayette, Ind. Mem. A.S.M.E.

[2] Research and Development Department, Tube Turns, Inc., Louisville, Ky.

Contributed by the Applied Mechanics Division and presented at the Annual Meeting, New York, N. Y., Nov. 26–29, 1945, of The American Society of Mechanical Engineers.

Discussion of this paper should be addressed to the Secretary, A.S.M.E., 29 West 39th Street, New York, N. Y., and will be accepted until July 10, 1946, for publication at a later date. Discussion received after the closing date will be returned.

Note: Statements and opinions advanced in papers are to be understood as individual expressions of their authors and not those of the Society

"pseudoplastic," and curve IV might be called an "inverted plastic."

Laminar Flow of an Ideal Plastic

The well-known Hagen-Poiseuille law for the laminar flow of a true fluid in a pipe can be expressed in the form

$$\frac{\Delta PD}{4L} = \frac{8V}{D}\mu \quad [2]$$

where ΔP represents the pressure loss in the length L, V the average velocity, D the internal pipe diameter, and μ the absolute or dynamic viscosity of the fluid. It is common practice to express the head loss h in the form

$$h = \frac{fLV^2}{D\,2g} \quad [3]$$

where the dimensionless friction factor f is a function of the dimensionless Reynolds number $N = \rho VD/\mu$. For the laminar flow of a true fluid, the friction factor is given by the simple relation

$$f = \frac{64}{N} \quad [4]$$

Consider next the laminar flow of an ideal plastic through a circular pipe. Imagine a central cylindrical mass of length L and radius y. The velocity at radius y is u. For steady motion there are two resultant forces, a pressure force, and a shear force. The pressure force is $\Delta P\pi y^2$. The shear stress S at y is

$$S = -\eta\frac{du}{dy} + S_0 \quad [5]$$

The first term in Equation [5] is negative because the velocity decreases as the radius increases. The shear force equals the stress S times the area $2\pi yL$. For equilibrium, a balance of forces gives

$$\Delta P\pi y^2 = 2\pi yL\left[-\eta\frac{du}{dy} + S_0\right]$$

$$\eta\frac{du}{dy} = S_0 - \frac{\Delta P}{2L}y \quad [6]$$

Equation [6] is the basic differential equation for the flow of an ideal plastic. The velocity gradient is zero in a central region in which the shear stress is equal to or less than the yield value; that is, there is a central core which moves as a solid plug. After integrating Equation [6] and evaluating the constants from the boundary conditions, the final result can be arranged in the form

$$\frac{\Delta PD}{4L} = \frac{8V}{D}\eta + \frac{4}{3}S_0 \quad [7]$$

A complete discussion of the intermediate steps in deriving Equation [7] can be found in Bingham's book (1),[3] or in a paper by Babbitt and Caldwell (5). A comparison of Equations [2] and [7] is of interest. If the yield value S_0 were zero, then Equation [7] would reduce to Equation [2], and the coefficient of rigidity would approach the dynamic viscosity. Equation [7] can be written as

$$\frac{\Delta PD}{4L} = \frac{8V}{D}\left[\eta + \frac{DS_0}{6V}\right]$$

$$\frac{\Delta PD}{4L} = \frac{8V}{D}\mu_a \quad [8]$$

[3] Numbers in parentheses refer to the Bibliography at the end of the paper.

where

$$\mu_a = \eta + \frac{DS_0}{6V} \quad [9]$$

The factor μ_a is an apparent viscosity. Equation [8] is similar in form to the Hagen-Poiseuille law. Thus the friction factor for the laminar flow of an ideal plastic can be expressed as

$$f = \frac{64}{N} \quad [10]$$

if the Reynolds number for the plastic is expressed with the apparent viscosity. Thus for the laminar flow of an ideal plastic, $N = \rho VD/\mu_a$.

The next step is to consider the available experimental data, and their agreement with the analytical relations. Busher (2) made some measurements on the flow of suspensions through copper pipe at various temperatures, velocities, and concentrations. The flowing substance was a heated mixture of grain suspended in water. Fig. 2 shows the head loss as a function of velocity. Note that the head loss for the suspension in some cases is much higher than that for water at the same velocity.

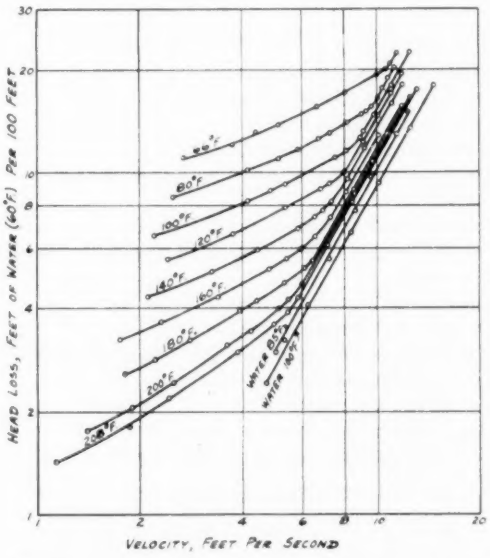


Fig. 2 Friction Loss for Grain Suspensions in 3-In. Copper Pipe

An inspection of Equation [7] shows that if the factor $\Delta PD/4L$ is plotted as a function of $8V/D$, then for an ideal plastic the vertical intercept is $4S_0/3$, and the slope of the curve is the coefficient of rigidity. Busher's data are plotted with these particular co-ordinates in Fig. 3. Many of the experimental points fall on straight lines. In some cases at the high velocities the curve deviates from the straight line as turbulent flow is reached. On the other hand, at velocities lower than those measured, the curves may deviate like a pseudoplastic. But in the laminar-flow range covered by the experimental points, the grain suspensions behaved much as an ideal plastic.

For each temperature, the yield point and the coefficient of rigidity, as determined from Fig. 3, were used to calculate the apparent viscosity and the Reynolds number. Fig. 4 shows the unified correlation of the data at the different temperatures. There is very close agreement between the experimental points and the line $f = 64/N$ in the laminar-flow region through a Reynolds number of 2130.

Gregory (3) made some tests on the flow of clay slurry through a

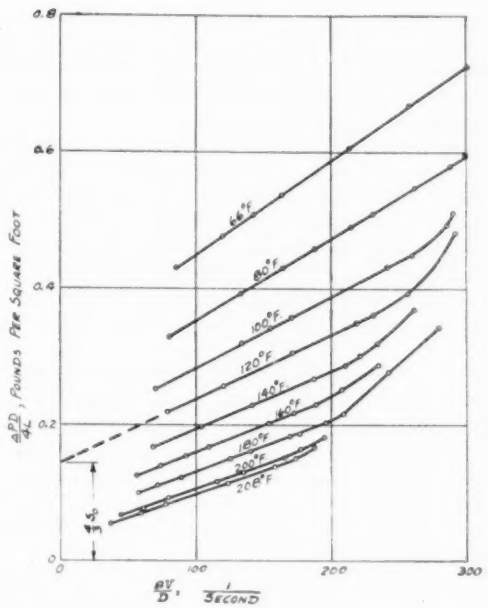


FIG. 3 PRESSURE-VELOCITY RELATIONS FOR GRAIN SUSPENSIONS IN 3-IN. COPPER PIPE

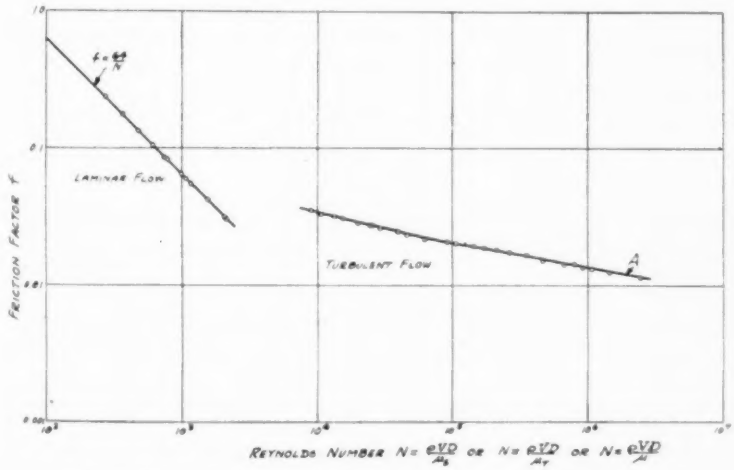


FIG. 4 FRICTION FACTOR VERSUS REYNOLDS NUMBER FOR GRAIN SUSPENSIONS IN 3-IN. COPPER PIPE

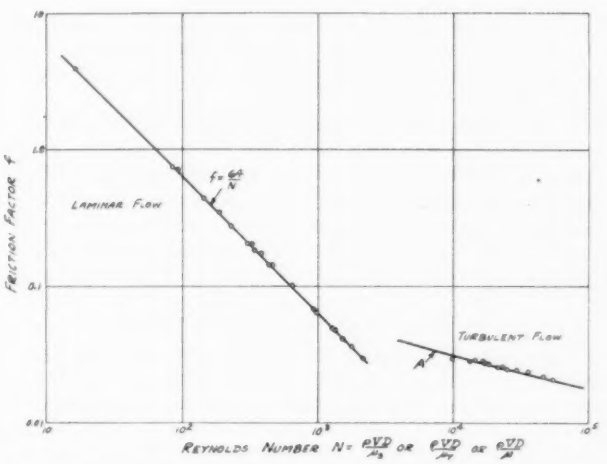


FIG. 6 FRICTION FACTOR VERSUS REYNOLDS NUMBER FOR CEMENT-ROCK SUSPENSIONS IN 3/4-IN. BRASS, 1 1/2-IN. BRASS, AND 3-IN. PIPE

4-in. cast-iron pipe. Some results are given in Fig. 5 and show good agreement with the ideal-plastic relation. Laminar flow was found at a Reynolds number as high as 2070.

Wilhelm, Wroughton, and Loeffel (4) presented the results of an extensive series of tests on suspensions of cement rock in water. Tests were made at different velocities, at different concentrations, and with 3/4-in. brass, 1 1/2-in. brass, and 3-in. wrought-steel pipe. The results are shown in Fig. 6. For laminar flow there is close agreement between the experimental results and the simple analytical relation for an ideal plastic. Laminar flow was realized with a Reynolds number as high as 2150.

Babbitt and Caldwell (5) made a series of tests on the flow of sewage sludge in 1-in., 2-in., and 3-in. pipes. The results for laminar flow are shown in Fig. 7, with the highest Reynolds number at 1850. There is close agreement between the experimental results and the simple analytical relation for an ideal plastic.

Most lubricating oils at ordinary pressures and temperatures act as true fluids. At high pressures, however, some oils exhibit plastic properties. Fig. 8 shows the results of two tests on sperm oil through a capillary tube (internal diameter 0.0456 cm) made by Norton, Knott, and Muenger (6). One test was

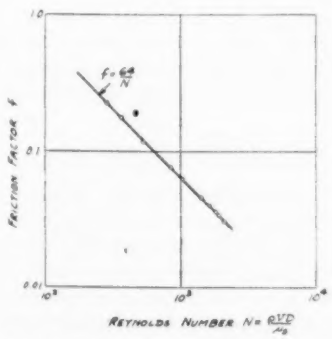


FIG. 5 FRICTION FACTOR VERSUS REYNOLDS NUMBER FOR CLAY SLURRY IN 4-IN. CAST-IRON PIPE

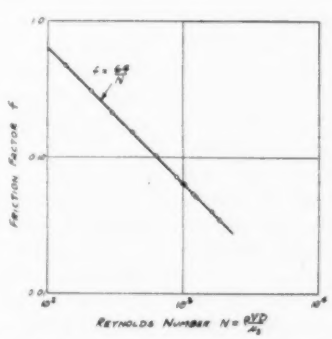


FIG. 7 FRICTION FACTOR VERSUS REYNOLDS NUMBER FOR SEWAGE SLUDGE IN 1-IN., 2-IN., AND 3-IN. PIPES

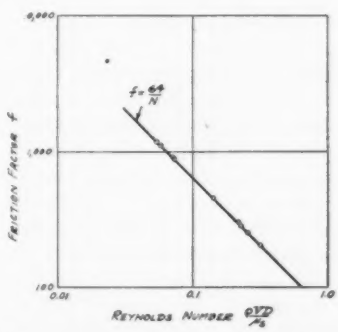


FIG. 8 FRICTION FACTOR VERSUS REYNOLDS NUMBER FOR SPERM OIL THROUGH CAPILLARY
(Oil acted as a plastic because of high pressure.)

at an average pressure of 31,500 psi, and the other at 35,000 psi. At these high pressures the test results fell close to the curve for an ideal plastic. The friction factors are rather high and the Reynolds numbers are rather low.

It is somewhat generally established that the flow of a true fluid is laminar if the Reynolds number is under about 2100. Laminar flow may exist at higher Reynolds numbers, but the flow may be unstable. The data of different investigators indicate that it seems safe to formulate a similar rule for an ideal plastic. The flow of an ideal plastic is laminar if the Reynolds number, based on the apparent viscosity, is under about 2100.

Determination of Apparent Viscosity

The foregoing study of the pertinent data of different investigators yields a simple correlation. There is a practical important question as to the determination of the apparent viscosity or the yield value and the coefficient of rigidity. Babbitt and Caldwell (5) conclude that the yield value and the coefficient of rigidity each is independent of the size and roughness of the pipe. If this conclusion is accepted as satisfactory, then a test with a model pipe could be used to determine the yield value and the coefficient of rigidity for a particular plastic, and predictions could be made for the flow of the same plastic through a prototype pipe. This procedure appears to be good technique, in the same way that the use of a capillary-tube viscometer is considered good technique in measuring the dynamic viscosity of a true fluid. There is some scatter in the data of Babbitt and Caldwell; the yield value from a test on one pipe size may differ from the yield value from a test on another pipe size by as much as 20 per cent. About the same scatter is found in the data on cement-rock suspensions. This scatter may not be too unreasonable if it is noted that the pipe flow data for true fluids may scatter 5 to 10 per cent above and below mean values.

Turbulent Flow

A plastic may behave as a true fluid when the flow is turbulent. Fig. 2 shows some features which are typical of the results of different investigators. The two lines marked "water" are results obtained from actual tests with water in the pipe; the points shown are for turbulent flow. Consider a test of a suspension at a certain temperature. As the velocity increases, the curve changes in slope and approaches a straight line practically parallel to the water curves. These features suggest the possibility of correlating the data on suspensions in a manner similar to that used for water or any other true fluid.

For the turbulent flow of true fluids the friction factor is commonly expressed as a function of Reynolds number at constant roughness values. The main problem for plastic flow is the formulation of a suitable factor to replace the dynamic viscosity in the Reynolds number. Different trials showed that the use of an "equivalent" or "turbulent" viscosity provided a suitable method for organizing results. From one test of a grain suspension is determined a value of the friction factor. This friction factor for the suspension corresponds to a certain Reynolds number for a true fluid flowing through a pipe of the same roughness. For this Reynolds number, and a given density, velocity, and diameter for the suspension, there is thus determined an equivalent or "turbulent" viscosity μ_T for the suspension. The available data show that the turbulent viscosity is practically constant for all rates of shear; it is analogous to a dynamic viscosity.

A complete discussion of Fig. 4 can now be given. In the laminar-flow range only, Reynolds numbers below about 2100, the denominator in the Reynolds number is the apparent viscosity μ_S and can be determined from the yield value and the coefficient of rigidity. Curve A represents the tests with water flowing through the pipe; the denominator in Reynolds number is the dynamic viscosity μ of the true fluid. The experimental points in the turbulent range are for the suspension; the denominator in the Reynolds number is the turbulent viscosity μ_T. The experimental points in the turbulent range follow closely the curve for a true fluid.

A similar discussion applies to the results on cement-rock suspensions shown in Fig. 6. In the laminar-flow range only, the denominator in the Reynolds number is the apparent viscosity μ_s. Curve A is adapted from the data of Stanton and Pannell (7) for smooth drawn pipe; the denominator in the Reynolds number is the dynamic viscosity μ. The experimental points in the turbulent range match fairly well with curve A; the denominator in the Reynolds number for the experimental points is the turbulent viscosity μ_T.

Babbitt and Caldwell (8) made a large series of tests on the turbulent flow of sludges. A number of different clay suspensions and sewage sludge were used, together with different pipe sizes, $^1/_2$ in., 1 in., 2 in., and 3 in. They found that the water suspensions behaved as true fluids in the turbulent range. They concluded that the data correlated well if the denominator in the Reynolds number was taken as the dynamic viscosity of the dispersion medium of the sludge.

In the experiments of Babbitt and Caldwell, apparently the turbulent viscosity did not differ from the dynamic viscosity of the dispersion medium. In other cases, however, there may be a considerable difference between the two viscosities. Fig. 9

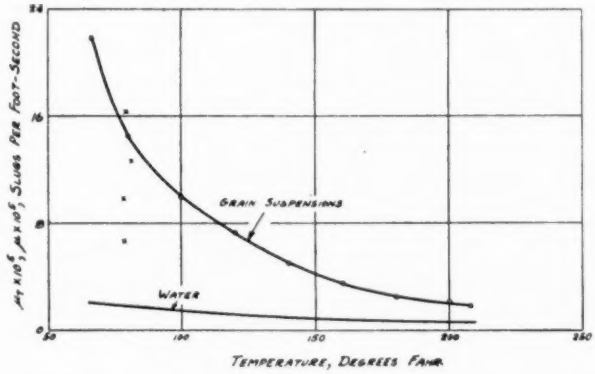


Fig. 9 Turbulent Viscosity and Dynamic Viscosity Versus Temperature

(Crosses refer to cement-rock suspensions.)

shows a plot of turbulent viscosity of the grain suspension and the dynamic viscosity of the dispersion medium water each as a function of temperature. The difference between the two viscosities is large at the low temperatures and decreases as the temperature is increased. The crosses in Fig. 9 are for the different cement-rock suspensions. The turbulent viscosity in each case was greater than the dynamic viscosity of water at the same temperature.

Flow of Pseudoplastics and Inverted Plastics

The foregoing discussion deals with ideal plastics. It would be desirable to have a similar simple organization of data for plastics other than ideal. At the present time there are not sufficient complete published data to draw any reliable general conclusions. For one thing, if the substance is not a true fluid or an ideal plastic, the stress vs. rate-of-strain relation may become very complicated.

One set of test data, however, shows an interesting special case. Wilhelm, Wroughton, and Loeffel made some tests on filter-cel suspensions (4). The results of one test of this suspension in a

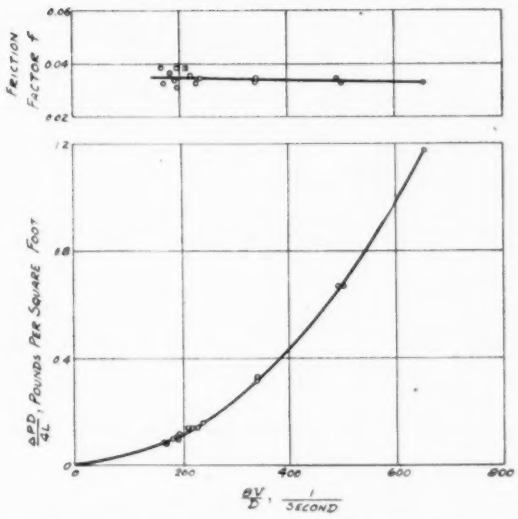


FIG. 10 PRESSURE-VELOCITY RELATION FOR FILTER-CEL SUSPENSION IN 1¼-IN. PIPE

1¼-in. pipe are given in Fig. 10, using the same co-ordinates as in Fig. 3. Fig. 10 shows that the apparent viscosity increases with rate of shear. The relation in a large range of velocities closely approximates a parabola. If the relation is parabolic, then the equation for pressure drop can be written as

$$\frac{\Delta PD}{4L} = C\left(\frac{8V}{D}\right)^2$$

$$\Delta P = \frac{C256LV^2}{D^3} \quad \ldots\ldots\ldots\ldots\ldots\ldots [11]$$

where C is a constant. For a given suspension, pipe diameter, and length, the pressure drop is solely a function of the square of the velocity. In other words, the friction factor f is constant. The test data show an almost constant friction factor over a wide variation of velocity. A constant friction factor means a constant Reynolds number. For a given diameter and density, a constant Reynolds number means a constant ratio between the velocity V and the apparent viscosity μ_a.

CONCLUSION

A number of different investigators have provided data on the flow of suspensions. Different substances were tested, different pipe sizes were used, and different ranges of flow were covered. These substances behaved as ideal plastics in the laminar-flow range and as true fluids in the turbulent-flow range. These test data have been organized in a form which extends the conventional plot of friction factor versus Reynolds number for true fluids. In the laminar-flow range, Reynolds numbers below about 2100, the denominator in Reynolds number is taken as the apparent viscosity of the plastic. This apparent viscosity can be determined from the yield value and coefficient of rigidity. In the turbulent-flow range, the denominator in the Reynolds number is taken as an equivalent or "turbulent" viscosity. This turbulent viscosity is the viscosity a true fluid would have for the same friction factor as the plastic. The turbulent viscosity of a suspension may be much higher than the dynamic viscosity of the dispersion medium of the suspension.

BIBLIOGRAPHY

1 "Fluidity and Plasticity," by E. C. Bingham, McGraw-Hill Book Co. Inc., New York, N. Y., 1922, p. 222.

2 "A Qualitative and Quantitative Study of Pumping Grain Suspensions in Water," by J. E. Busher, M.S. thesis, Purdue University, 1943.

3 "Pumping Clay Slurry Through a Four-Inch Pipe," by W. B. Gregory, *Mechanical Engineering*, vol. 49, 1927, p. 609.

4 "Flow of Suspensions Through Pipes," by R. H. Wilhelm, D M. Wroughton, and W. L. Loeffel, *Industrial and Engineering Chemistry*, vol. 31, 1939, p. 622.

5 "Laminar Flow of Sludges in Pipes With Special Reference to Sewage Sludge," by H. E. Babbitt and D. H. Caldwell, University of Illinois Engineering Experiment Station, Bulletin No. 12, Nov., 1939.

6 "Flow Properties of Lubricants Under High Pressure," by A. E. Norton, M. J. Knott, and J. R. Muenger, Trans. A.S.M.E., vol. 63, 1941, p. 631.

7 "Similarity of Motion in Relation to the Surface Friction of Fluids," by T. E. Stanton and J. R. Pannell, Philosophical Transactions of the Royal Society of London, vol. 214, 1914, p. 199.

8 "Turbulent Flow of Sludges in Pipes," by H. E. Babbitt and D H. Caldwell, University of Illinois Engineering Experiment Station Urbana, Ill., Bulletin No. 323, Nov., 1940.

Action of Forces and Moments Symmetrically Distributed Along a Generatrix of a Thin Cylindrical Shell

By F. K. G. ODQVIST,[1] STOCKHOLM, SWEDEN

Applications of the present subject theory have been made to monolithic structures by certain Scandinavian engineers who have treated the subject and related problems in a series of papers. The author has confined his studies to more slender structures, such as welded and riveted plate containers, ship hulls, and similar applications, to which a simplified form of the theory may be applied. For an isotropic shell with no stiffeners, explicit formulas are developed in important cases, where the external load is applied to a cylindrical shell, distributed along a generatrix.

THE present subject and related problems have been treated in a series of papers by Scandinavian engineers (1–5).[2] Having in mind applications to monolithic concrete structures, reinforced by stiffeners, for roofs, container walls, and the like, some of these writers have taken the more complete equations of cylindrical shells as a point of departure for their investigations. For the application to more slender structures such as welded and riveted plate containers, steam boilers, ship hulls, or even monocoque structures, the author (3) has confined his work to the simplified form of the theory, laid down by H. Schorer (6). Thus for an isotropic shell with no

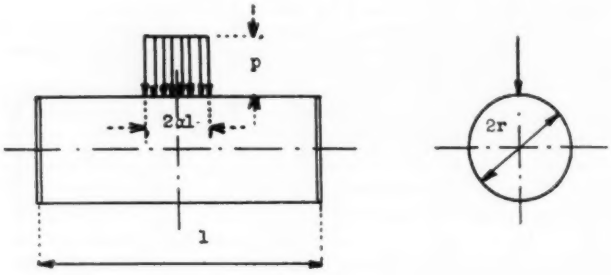


FIG. 1

stiffeners, it has been possible to develop explicit formulas in a series of important cases, where the external load is applied to a cylindrical shell, distributed along a generatrix, Figs. 1 to 3, inclusive.

The treatment has therefore been confined to forces and moments, symmetrically distributed and constant along the part $2\alpha l$ around the middle of a generatrix of a cylinder of length l with its ends linked to stiff circular plates. With the notations

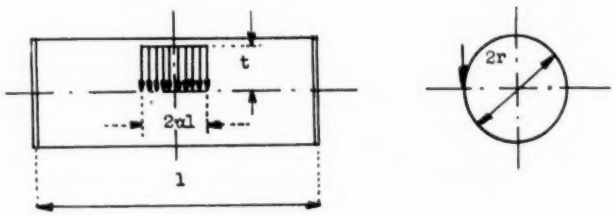


FIG. 2

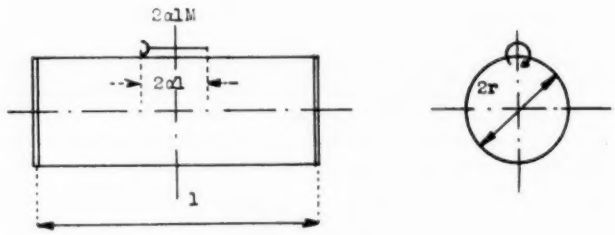


FIG. 3

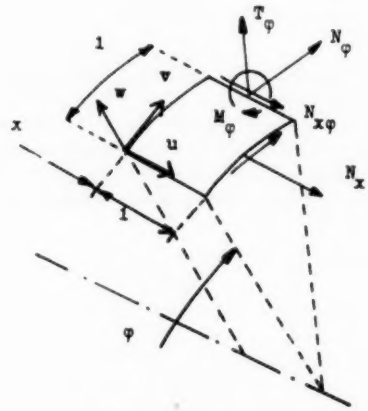


FIG. 4

in Fig. 4, Schorer's theory may be presented in the following form:

$$\frac{\delta^8 M_\varphi}{\delta\varphi^8} + \frac{12(1-\beta^2)r^8}{h^2}\frac{\delta^4 M_\varphi}{\delta x^4} = 0 \quad \ldots\ldots\ldots\ldots [1]$$

$$M_\varphi = \sum_n \Big[e^{-m_1\sqrt{n}\varphi}\,(C_{1n}\sin m_2\sqrt{n}\varphi + C_{2n}\cos m_2\sqrt{n}\varphi) + e^{-m_2\sqrt{n}\varphi}\,(D_{1n}\sin m_1\sqrt{n}\varphi + D_{2n}\cos m_1\sqrt{n}\varphi)\Big]\cos n\pi x/l \quad [2]$$

where $C_{1n} \ldots D_{2n}$ are constants to be determined by the conditions at the loaded generatrix. The thickness of the shell is h; x is counted positive from the middle of the generatrix. With the notation (β = Poisson ratio)

$$m = [12(1-\beta^2)]^{1/8}\,(r/h)^{1/4}\,(\pi r/l)^{1/2} \cong 2.39(r/h)^{1/4}\,(r/l)^{1/2} \quad [3]$$

---

[1] Professor of Strength of Materials, Royal Institute of Technology.

[2] Numbers in parentheses refer to the Bibliography at the end of the paper.

Discussion of this paper should be addressed to the Secretary, A.S.M.E., 29 West 39th Street, New York, N. Y., and will be accepted until July 10, 1946, for publication at a later date. Discussion received after the closing date will be returned.

NOTE: Statements and opinions advanced in papers are to be understood as individual expressions of their authors and not those of the Society.

we have

$$\left.\begin{aligned} m_1 &= m\cos\pi/8 = 0.92388\,m \\ m_2 &= m\sin\pi/8 = 0.38268\,m \end{aligned}\right\} \quad \ldots\ldots [4]$$

The sums are to be extended over all positive odd integers n.

Essential for the validity of the theory is that m shall be comparatively large, say, greater than 5. With $M\varphi$ being known, the following quantities may be obtained by recurrence, using new series of constants

rT_φ	$C_{1n}^{(1)}$	$C_{2n}^{(1)}$	$D_{1n}^{(1)}$	$D_{2n}^{(1)}$	..... [5]
rN_φ	$C_{1n}^{(2)}$	*	*	*	..... [6]
$-\pi r^2 N_{x\varphi}/l$	$C_{1n}^{(3)}/n$	*	*	*	..... [7]
$-\pi^2 r^3 N_x/l^2$	$C_{1n}^{(4)}/n^2$	*	*	*	..... [8]
$-\pi^3 r^3 Ehu/l^3$	$C_{1n}^{(4)}/n^3$	*	*	*	..... [9]
$-\pi^4 r^4 Ehv/l^4$	$C_{1n}^{(5)}/n^4$	*	*	*	..... [10]
$\pi^4 r^4 Ehw/l^4$	$C_{1n}^{(6)}/n^4$	*	*	*	..... [11]
$\pi^4 r^4 Eh\dfrac{\delta w}{\delta\varphi}/l^4$	$C_{1n}^{(7)}/n^4$	*	*	*	..... [12]

derived successively by means of the formulas

$$\left.\begin{aligned} C_{1n}^{(i+1)} &= \sqrt{n}\,[-m_1 C_{1n}^{(i)} - m_2 C_{2n}^{(i)}] \\ C_{2n}^{(i+1)} &= \sqrt{n}\,[m_2 C_{1n}^{(i)} - m_1 C_{2n}^{(i)}] \\ D_{1n}^{(i+1)} &= \sqrt{n}\,[-m_2 D_{1n}^{(i)} - m_1 D_{2n}^{(i)}] \\ D_{2n}^{(i+1)} &= \sqrt{n}\,[m_1 D_{1n}^{(i)} - m_2 D_{2n}^{(i)}] \end{aligned}\right\} \quad [i = 0 \ldots 6] \ldots\ldots [13]$$

where $C_{1n}^{(0)} \ldots D_{2n}^{(0)}$ are the same as $C_{1n} \ldots D_{2n}$. To obtain a quantity of the left column in expressions [5] to [12], one has to introduce the corresponding set of constants in Equation [2], but for the quantities $N_{x\varphi}$ and u, where $\sin n\pi x/l$ is to be substituted for $\cos n\pi x/l$.

The external loads per unit of length of the generatrix should be developed in Fourier's series, that is, according to Figs. 1 to 3.

$$\left.\begin{matrix} p(x) \\ t(x) \\ M(x) \end{matrix}\right\} = \sum_n \left\{ \begin{matrix} p_n \\ t_n \\ M_n \end{matrix} \right\} \cos n\pi x/l, \quad \begin{matrix} p_n \\ t_n \\ M_n \end{matrix} = \frac{4}{\pi n} \sin n\pi\alpha \begin{Bmatrix} p \\ t \\ M \end{Bmatrix} \quad \ldots\ldots [14]$$

The conditions at the loaded generatrix are for $\varphi = 0$:

(*a*) the case of Fig. 1

$$2T_x = p(x), \quad N_{x\varphi} = 0, \quad v = 0, \quad \frac{\delta w}{\delta\varphi} = 0 \ldots\ldots [15]$$

(*b*) the case of Fig. 2

$$2N_\varphi = t(x), \quad M_\varphi = 0, \quad u = 0, \quad w = 0 \ldots\ldots [16]$$

(*c*) the case of Fig. 3

$$2M_\varphi = M(x), \quad N_\varphi = 0, u = 0 \quad w = 0 \ldots\ldots [17]$$

Using the foregoing expressions, we obtain

$$\left.\begin{aligned} &(a)\ C_{1n} = -(\sqrt{2}-1)C_{2n} = (\sqrt{2}-1)D_{1n} = -D_{2n} = \frac{pr\sqrt{2-\sqrt{2}}}{2\pi mn\sqrt{n}} \sin n\pi\alpha \\ &(b)\ C_{1n} = -C_{2n} = D_{1n} = D_{2n} = -\frac{tr}{\pi\sqrt{2}m^2n^2} \sin n\pi\alpha \\ &(c)\ C_{1n} = D_{1n} = 0, \quad C_{2n} = D_{2n} = \frac{M}{\pi n} \sin n\pi\alpha \ldots\ldots \end{aligned}\right\} \ldots [18]$$

Equations [18] together with [5] to [13] contain the solution of our three problems. For the deflections $w(x, 0)$ and $v(x, 0)$ in radial and circumferential direction, respectively, we get, along the loaded generatrix, the following

Case (*a*)

$$w(x, 0) = -\frac{\sqrt{2-\sqrt{2}}\,[12(1-\beta^2)]^{5/8} l^{3/2} r^{3/4}\, p}{\sqrt{2}\,\pi^{5/2} E h^{5/4}} \sum_n \frac{\sin n\pi\alpha \cos n\pi x/l}{n^2\sqrt{n}} \ldots\ldots [19]$$

Case (*b*)

$$v(x, 0) = -\frac{\sqrt{2-\sqrt{2}}\,[12(1-\beta^2)]^{3/8} l^{5/2}\, t}{\sqrt{2}\,\pi^{7/2} r^{3/4} h^{7/4} E} \sum_n \frac{\sin n\pi\alpha \cos n\pi x/l}{n^3\sqrt{n}} \ldots [20]$$

$$\frac{\delta w}{r\delta\varphi}(x, 0) = -\frac{\sqrt{2-\sqrt{2}}\,[12(1-\beta^2)]^{5/8} l^{3/2}\, t}{\sqrt{2}\,\pi^{5/2} r^{1/4} h^{9/4} E} \sum_n \frac{\sin n\pi\alpha \cos n\pi x/l}{n^2\sqrt{n}} \ldots\ldots [21]$$

Case (*c*)

$$\frac{\delta w}{r\delta\varphi}(x, 0) = \frac{[12(1-\beta^2)]^{7/8} r^{1/4} l^{1/2} M}{\pi^{3/2}\sqrt{2-\sqrt{2}}\, h^{11/4} E} \sum_n \frac{\sin n\pi\alpha \cos n\pi x/l}{n\sqrt{n}} \ldots\ldots [22]$$

Equations [19] to [22] may be combined to solve statically indeterminate problems in connection with the supports of cylindrical containers such as marine steam boilers.

To investigate the action of a single concentrated radial force P in the middle of a generatrix, we may put $2\alpha lp = P$ and let α tend to zero. The passage to the limit may be carried out in Equation [19], term by term. The result is

$$\lim_{\alpha = 0} = \frac{1}{\pi\alpha} \sum_n \frac{\sin n\pi\alpha}{n^2\sqrt{n}} = \sum_n \frac{1}{n\sqrt{n}} = 1.689$$

In such case we get for the deflection

$$w(0, 0) = -1.689 \frac{\sqrt{2-\sqrt{2}}\,[12(1-\beta^2)]^{3/8} r^{3/4} l^{1/2}\, P}{\sqrt{2\pi}\, 2\pi h^{5/4} E} \ldots [23]$$

In this case the quantity N_φ will become infinite at the origin. The effect of a concentrated transverse force $T = 2\alpha lt$ may be similarly investigated.

In case (*c*) the sum in Equations [22], though convergent, does not permit of a passage to the limit $\alpha = 0$, in which case it becomes divergent. Moreover some of the series corresponding to expressions [5] to [12] will show extremely slow convergence in all cases (*a*) to (*c*), a thing already noticed by Aas-Jakobsen in attacking the equations of the general theory, where in some cases he has been compelled to use up to 49 terms of his expansions in order to obtain acceptable numerical results. As a means of improving the convergence of such series, the author suggests using Kummers' transformation, which in this case may be utilized in the following form, valid for α less than $1/2$

$$\left.\begin{aligned} \sum_n \frac{\sin n\pi\alpha}{\sqrt{n}} &= \frac{1}{2\sqrt{2\alpha}} + \frac{\alpha}{2} + \sum_n s_n \sin n\pi\alpha \ldots\ldots \\ \sum_n \frac{\sin n\pi\alpha}{n\sqrt{n}} &= \pi\sqrt{\alpha/2} - \pi\alpha/2 + \sum_n c_n \sin n\pi\alpha \end{aligned}\right\} \ldots [24]$$

where

$$\left.\begin{aligned} s_n &= 1/\sqrt{n} - 2S(n\pi/2)/\sqrt{n} - 2\sin n\pi/2/\pi^2 n^2 \\ c_n &= 1/n\sqrt{n} - 2C(n\pi/2)/n\sqrt{n} + 2\sin n\pi/2/\pi n^2 \end{aligned}\right\} \quad \ldots [25]$$

and $S(z)$, $C(z)$ are Fresnel's integrals of the argument $z = n\pi/2$, tabulated for instance in (7). The sums to the right in Equation [24] converge much more rapidly than those to the left and may be used for the calculation of the stresses in the neighborhood of the points of application of the load.

Experiments in support of the foregoing theory have been carried out with a carefully produced steel cylinder at the Royal Technical Institute, Stockholm. Equation [23] was found to fit experimental data for a cylinder with $m = 5.09$ within experimental errors, which were of the order of 1 per cent. The order of magnitude of the stresses also fitted the corresponding formulas.

The theory permits of generalization, e.g., to the case of longitudinal stiffeners (3). In the case of transverse stiffeners it is generally more convenient to use a simple approximate theory, considering the stiffener as a curved beam supported on the shell as an elastic foundation with a spring constant determined from conditions of axial symmetry. Also this simple theory has been confirmed by experiments. A somewhat more elaborate theory taking account of the general theory of cylindrical shells (nonsymmetrically loaded) has been worked out by Lundgren (4), and Aas-Jakobsen (5).

BIBLIOGRAPHY

1 "Über das Randstörungsproblem an Kreiszylinderschalen," by A. Aas-Jakobsen, Oslo, Norway, *Bauingenieur*, vol. 20, 1939, pp. 394–405.

2 "Einzellasten auf Kreiszylinderschalen," by A. Aas-Jakobsen, *Bauingenieur*, vol. 22, 1941, pp. 343–346.

3 "The Load Carrying Action of Thin Cylindrical Shells," by F. K. G. Odqvist, IVA-handl, Stockholm, Sweden, no. 164, 1942, pp. 1–53; published in Swedish with English summary.

4 "Einzellasten auf Zylinderschalen mit Ringversteifungen," by H. Lundgren, Bygningsstatiske meddelelser, Copenhagen, Denmark, vol. 13, 1942, pp. 1–24.

5 "Enkeltlaster på sylinderskall," by A. Aas-Jakobsen, 1943, pp. 1–32; manuscript, written in Norwegian, mentioned by courtesy of the author.

6 "Line Load Action on Thin Cylindrical Shells," by H. Schorer, American Society of Civil Engineers, vol. 61, 1935, pp. 281–316.

7 "Tables of Functions," by E. J. Jahnke and F. Emde, second edition, Leipsig, Germany, 1933, p. 108; for asymptotic expansions, see first edition, Berlin, Germany, 1909, p. 24.

Equivalent Circuits for the Numerical Solution of the Critical Speeds of Flexible Shafts

By GABRIEL KRON,[1] SCHENECTADY, N. Y.

A special type of equivalent circuit is developed that is particularly suited for the numerical calculation of the critical speeds of uniformly rotating shafts. The shaft may consist of several spans rotating in flexible bearings supported by a flexible foundation. Either the various spans may be asymmetrical along two principal axes or the bearings may have asymmetrical flexibilities. The same circuits are, of course, valid also for the study of the natural frequency of vibration of a skewed asymmetrical beam held by flexible supports at several points, such as a turbine bucket. The circuits may be solved by slide rule, by punch-card methods, or by a "network analyzer." The procedure is self-checking as the correctness of the numbers may be checked at any stage of the calculations. For the symmetrical case, the results are identical with those found by the method of Prohl (1)[2] or Myklestad (2), even though the circuit method requires fewer calculations. In general, the equivalent circuits for the various spans, bearings, overhung loads, and foundations are independent and are interchangeable for different combinations of shaft structure. Also, any variation in a component part leaves the circuits of the other parts unchanged. A punch-card study of a turbine generator shaft with fixed bearings carrying a high-pressure turbine, a low-pressure turbine, and a generator is given in a companion paper by A. W. Rankin (3).

Introduction

DURING the last few years many papers have appeared, both in this country and abroad, calling renewed attention to the analogy existing between simple mechanical structures and electrical circuits, a relation well known but little used for over a century. In this analogy, mass and inductance, spring and capacitance, play identical roles; similarly current takes the place of force, and voltage that of displacement. (The dual analogy, with an interchange of mass and spring, force and displacement, is also frequently employed.) Apparently both electrical and mechanical engineers find this interplay of concepts useful and of benefit in their respective fields. The arrival of the a-c network analyzer, on which the electrical circuits may be quickly solved, accelerated the diffusion of these parallel ideas.

In all such studies each component unit of the mechanical system has one degree of freedom. For instance, each mass and spring have a linear displacement in the x direction only, or each mass and spring rotate around the x-axis only. However, for the greatest number of cases, each mechanical unit has two or more degrees of freedom and, in the most general case, it has six; in particular, three translations along the x-, y-, z-axes and three rotations around them.

Electrical analogs of planar and spatial elastic structures built up from units with two to six degrees of freedom are developed in references (4, 6), and network-analyzer results are shown in references (5, 7). In problems of the critical speeds of large flexible shafts, such as those of turbogenerator sets, it has been found that no presently available network analyzer is equipped with units sufficiently flexible to cover the very large range of values required by the shaft constants. Hence the need arose to solve the electrical networks numerically either by hand or by punch-card machines.

During the calculations it was discovered that the electrical network could be transformed into a new form that required far fewer numerical steps. These transformations are intimately connected with the properties of electrical networks, and apparently no mechanical analog of them exists. These new equations and networks are developed in Appendix 1 while the body of the paper limits itself to the description and development of a routine procedure of calculation.

It is felt that the use of the electrical network has facilitated the introduction of the following features:

1 The number of additions and multiplications required for the calculation of a single beam section is less than the number of operations used in similar problems employing purely mechanical concepts (references 1 and 2).

2 The electric circuit has enabled the development of a method of check that can be used at any particular stage during the calculation. It is believed that one not already acquainted with general circuit parameters in a matrix form, concepts known to (some) electrical engineers, would have had difficulty in discovering these formulas.

3 The fact that each degree of freedom has an identical electrical network (see Fig. 3) greatly reduces the number of operations necessary to route the punched cards through the machines.

Because of the employment of an electrical network in preference to a mechanical network or to a set of algebraic equations, certain simplifications have become almost obvious. For instance, in Appendix 1 of this paper a complicated set of beam equations is reduced to a simplified set by first establishing an equivalent circuit for the former, simplifying the electrical network, then writing the resultant simple equations by an inspection of the network. The same procedure is performed by algebraic manipulations in Appendix 1 of the companion paper by Rankin. There seems to be no mechanical analog of the procedure, and the algebraic manipulations must follow willy-nilly the electric-circuit manipulations.

---

[1] Consulting Engineer, General Electric Company.

[2] Numbers in parentheses refer to the Bibliography at the end of the paper.

Contributed by the Applied Mechanics Division and presented at the Annual Meeting, New York, N. Y., Nov. 26–29, 1945, of The American Society of Mechanical Engineers.

Discussion of this paper should be addressed to the Secretary, A.S.M.E., 29 West 39th Street, New York, N. Y., and will be accepted until July 10, 1946, for publication at a later date. Discussion received after the closing date will be returned.

Note: Statements and opinions advanced in papers are to be understood as individual expressions of their authors and not those of the Society.

SYMMETRICAL SHAFT AND BEARING

Equivalent Circuit of a Section

The equivalent circuit of a constant-diameter section of a symmetrical rotating shaft—to be used in numerical calculations—is given in Fig. 1. The voltages D to ground at both ends

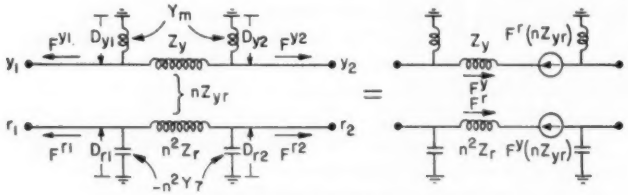


FIG. 1 EQUIVALENT CIRCUIT OF A SECTION

of the section represent:

1 Linear displacement along y.
2 Angular displacement along r.

The currents F at both ends represent:

1 Shear along y.
2 Moment along r.

The values of the constants taken from reference (4) are given in Table 1. The Z's represent impedances, the Y's admittances. The transformation ratio n in Fig. 1 may be selected for any convenient scale. The mass of the section is divided into two equal parts placed at the two ends of the section. The moment of inertia and gyroscopic force of the section are only cursorily treated. Their consideration only changes the value of the ground capacitors as shown in Figs. 14–16, inclusive.

TABLE 1 CALCULATIONS OF CONSTANTS

Section inertia, in.^{4} $= I$
Section length, in. $= L$
Section weight, lb $= W$
N = number of 1000 rpm
$B = EI$

$$M = \frac{W/2}{386.4} \quad \omega^2 = \left(\frac{1000 \times 2\pi}{60}\right)^2 = 10{,}965$$

The admittances are

$$Y_2 = \frac{12B}{L^3} \quad Y_6 = \frac{6B}{L^2} \quad Y_7 = \frac{2B}{L} \quad Y_m = (M\omega^2)\,N^2$$

The circuit constants are

$$Z_y = \frac{2}{Y_2} \quad Z_r = \frac{2}{Y_7} \quad Z_{yr} = \frac{3}{Y_6}$$

$$Y_y = Y_{mi} + Y_{mj} \quad | \quad Y_r = -Y_{7i} - Y_{7j}$$

where i and j indicate adjacent sections

Equivalent Circuit of a Span

When several sections form a span between two bearings, the resultant circuit is shown in Fig. 2. It should be noted:

1 That the mutual inductance of every other section is reversed. (This is shown in Appendix 1.)

2 That the two admittances in parallel existing at the interconnections may be combined into one, giving the final circuit in Fig. 3.

When several spans exist, the alteration in the signs of Z_{yr} should be continued without interruption so that some spans may start with a negative Z_{yr}. (The alternation in the sign of Z_{yr} is not due to any assumed sign convention. It was introduced to simplify the electric circuit of each span.

Schedule of Calculations

Let a single section on the resultant span network in Fig. 3 be considered. (This network section is not identical with a beam section as the ground coils of two neighboring beam sections in Fig. 2 have been combined.) By an inspection of Fig. 3 the following set of equations may be written expressing the unknown right-hand quantities (primed) in terms of known left-hand quantities (unprimed) as

$$\left.\begin{aligned} D_y' &= D_y - Z_y F^y - Z_{ry} F^r \\ D_r' &= D_r - Z_r F^r - Z_{ry} F^y \\ F^{y\prime} &= F^y - Y_y D_y' \\ F^{r\prime} &= F^r - Y_r D_r' \end{aligned}\right\} \quad \ldots\ldots\ldots\ldots [1]$$

Here D and D' are identical with D_1 and D_2 of a beam section, but F and F' are not the same as F^1 and F^2, that is, F and F' do not represent actual shears and moments in the beam. They have a physical meaning only in the electrical network and have no mechanical equivalent.

Calculations of Spans Between Flexible Bearings

When the bearings are flexible at both ends of a span, the basic calculation consists of impressing a unit voltage D_1 or current F^1 at the left (the other three quantities remaining zero) and calculating by the previous equations the four voltages and currents appearing at the other end. The following two cases are possible:

1 The whole shaft is calculated through without dividing the shaft into spans.

In that case only any two of the four possible unit quantities are impressed on the left end of the shaft. However, every time a bearing flexibility is changed the whole calculation has to be repeated for all spans and for all speeds.

2 Each span is calculated separately, irrespective of the presence of bearings.

In that case all four of the possible unit quantities are impressed at the left end of each span in succession. Once the span has been calculated at a particular speed, the same calculations are used for all variations in bearing flexibilities.

Impressing two unit voltages and two unit currents, the four separate calculations give sixteen different constants in the form of four equations, shown schematically in Table 2.

TABLE 2 RESULTS OF NUMERICAL CALCULATIONS ON A SPAN

		Impressed unit quantities at left end of span			
		D_{y1}	D_{r1}	F^{y1}	F^{r1}
Calculated quantities at right end of span	$D_{y2} =$	a	b	i	j
	$D_{r2} =$	c	d	k	l
	$F^{y2} =$	e	f	m	n
	$F^{r2} =$	g	h	o	p

Also for every given speed N, a new set of sixteen numbers has to be calculated.

Instead of assuming a single unit D or F at a time, it is possible to assume four unknowns simultaneously, namely, D_{y1}, D_{r1}, F^{y1}, and F^{r1}, so that at each step four constants are calculated instead of one. The number of resultant operations does not

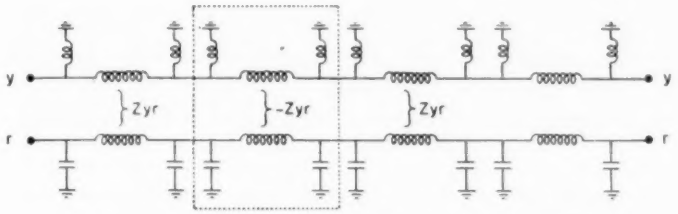


FIG. 2 INTERCONNECTION OF SECTIONS INTO A SPAN

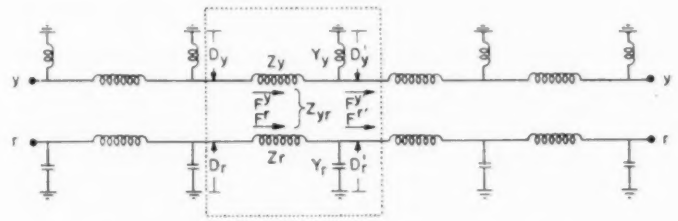


FIG. 3 RESULTANT EQUIVALENT CIRCUIT OF A SPAN

change; on the other hand, the circuit constants Z_y, Z_r, etc., have to be looked up only once instead of four times.

CHECK ON CALCULATION

In order to check the correctness of the four numbers derived at any part of the span, say one third or halfway along the span, it is necessary that two columns be calculated simultaneously, in particular either F^{y1} and F^{r1} or D_{y1} and D_{r1}. The two sets of calculations may be done by two separate calculators proceeding with a different column and checking their results at any part of the circuit. If at some point of the circuit one of the calculators has column F^{r1} (namely, j, l, n, and p), the other has column F^{y1} (namely, i, k, m, and o), then their numbers are correct if (using Equation [29] of Appendix 2)

$$ol + mj = in + kp \quad \ldots\ldots [2]$$

For the two other columns D_{y1} and D_{r1}, the numbers are correct if

$$ch + af = eb + dg \quad \ldots\ldots [3]$$

CALCULATION OF SPAN EQUIVALENT CIRCUIT

If the circuits are solved on a network analyzer, it is necessary to set up an equivalent circuit representing the results of Table 2. Those not interested in such a solution may leave this section out and may represent the span network by a blank rectangle, as in Fig. 5.

The sixteen numbers found for a particular speed do not yet represent the self and mutual admittances of the equivalent circuit. The latter are also sixteen in number, forming a symmetrical set as shown in Equation [4]. They are found by the formulas shown in Table 3. There are also two checks (Y_e and Y_f) on the correctness of calculations

$$\begin{array}{c|c|c|c|c} & D_{y1} & D_{r1} & D_{y2} & D_{r2} \\ \hline F^{y1} = & Y_a & Y_e & Y_f & Y_g \\ \hline F^{r1} = & Y_e & Y_b & Y_h & Y_i \\ \hline F^{y2} = & Y_f & Y_h & Y_e & Y_j \\ \hline F^{r2} = & Y_g & Y_i & Y_j & Y_d \end{array} \qquad \bar{I} = \bar{Y}\,\bar{E} \quad \ldots\ldots [4]$$

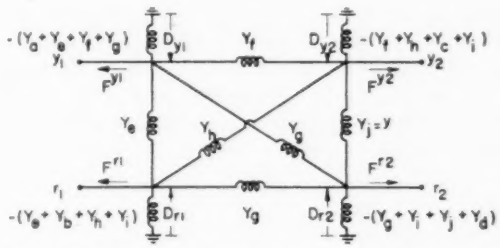


FIG. 4 EQUIVALENT CIRCUIT OF A SPAN BETWEEN TWO BEARINGS

TABLE 3 CALCULATION OF SELF AND MUTUAL ADMITTANCES

Find $D = il - kj$

$$Y_f = \frac{l}{D} \quad Y_g = -\frac{j}{D} \quad Y_h = -\frac{k}{D} \quad Y_i = \frac{i}{D}$$

$$Y_a = -(Y_g c + Y_f a) \quad Y_b = -(Y_h b + Y_i d)$$

$$Y_e = -(Y_g d + Y_f b) = -(Y_h a + Y_i c)$$

$$Y_c = Y_f m + Y_h n \quad Y_d = Y_i p + Y_g o$$

$$Y_j = Y_i n + Y_g m = Y_f o + Y_h p$$

The equivalent circuit in Fig. 4 is formed as follows:

1 The mutual admittances of Equation [4] also represent the mutual coils between corresponding junctions. For instance, Y_h in row r_1 and column y_2 is the coil lying between junctions r_1 and y_2.

2 The coils to ground are found by adding up the four admittances in the respective columns and changing the sign. For instance, the admittance of the coil from junction y_1 to ground is

$$Y_{ga} = -(Y_a + Y_e + Y_f + Y_g) \quad \ldots\ldots [5]$$

INTERCONNECTION OF SPANS, BEARINGS, AND FOUNDATIONS

The spans are interconnected in series as shown in Fig. 5, while the bearing flexibilities along y are shown as shunts to grounds between spans. (Of course coils in parallel may be replaced by a single coil.)

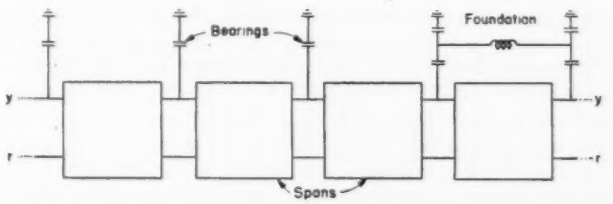


FIG. 5 INTERCONNECTED SPANS, BEARINGS, AND FOUNDATIONS

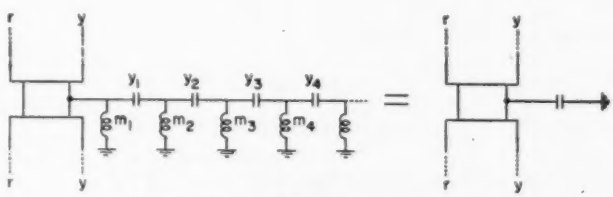


FIG. 6 BEARING EQUIVALENT CIRCUIT

Each bearing admittance may itself be the resultant of a more complex circuit. For instance, in Fig. 6 is shown a generator bearing circuit in detail. The bearing circuits themselves may be interconnected by circuit elements representing the nature of the foundation.

When the bearing and foundation motions are all assumed to exist only along a single linear direction y, their equivalent circuit is the conventional circuit of masses and springs connected in shunt or series. However, the bearing may have a tilting motion along the axis r, to be taken care of by an appropriate shunt admittance along r.

Reduction of Overhung Sections

If, beyond the last bearing, an overhung section exists as shown in Fig. 7(a), the axes y_2 and r_2 may be eliminated and the circuit replaced by three coils as shown in Fig. 7(b). These coils may be combined with parallel coils already existing to the left of the bearing so that the representation of the overhung section requires no extra coils.

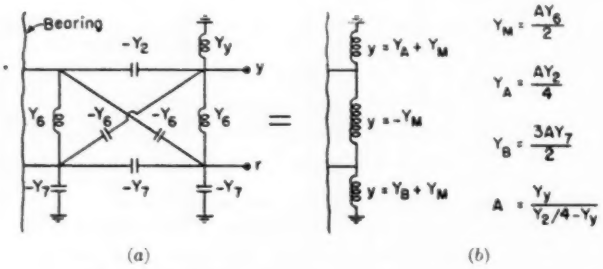


Fig. 7 Reduced Equivalent Circuit of Overhung Section

When the overhung section exists ahead of the first bearing, then the axes Y_1 and r_1 are eliminated, resulting again in the foregoing circuit but with the sign of Y_6 reversed.

The two cases cited assumed that the overhung section had a positive Y_6. With a negative Y_6, the signs change correspondingly.

The resultant equivalent circuit of several spans with bearing flexibilities, overhung sections, and foundations is shown in Fig. 8.

Numerical Calculation of Critical Speeds

The natural frequencies are calculated in two steps, as follows:

1 Assume unit voltage D_{y1} impressed on the left-hand side of the shaft, Fig. 8, with the other voltage D_{r1}, and the two currents F^{y1} and F^{r1} being zero. Calculate the two voltages and two currents D_{y2}', $F^{y2}{}'$, D_{r2}', and $F^{r2}{}'$ appearing on the right-hand side of the shaft, as shown in Fig. 8.

2 Assume unit voltage E_{r1} impressed on the left-hand side, with the other three quantities zero, and calculate the four right-hand quantities D_{y2}'', $F^{y2}{}''$, D_{r2}'', and $F^{r2}{}''$.

Both currents on the left-hand side of the shaft are zero. One of the resultant currents on the right-hand side, say, $F^{y2} = F^{y2}{}' + F^{y2}{}''$, may also be made equal to zero by changing the unit voltage D_{r1} to xD_{r1} so that

$$F^{y2} = F^{y2}{}' + xF^{y2}{}'' = 0$$

from which $x = -F^{y2}{}'/F^{y2}{}''$. With xD_{r1} impressed, the other right-hand current F^{r2} becomes

$$F^{r2} = F^{r2}{}' - \left(\frac{F^{y2}{}'}{F^{y2}{}''}\right) F^{r2}{}'' \quad \ldots\ldots\ldots\ldots\ldots [6]$$

representing the "excess moment." Now at those speeds N at which the excess moment F^{r2} becomes zero, all four currents are zero and the speed is a critical speed. By assuming a variable speed N, the values of F^{r2} may be plotted against N. The calculations may be checked again at any desired point by Equation [2].

When the presence of the foundation is considered under one or more spans, Fig. 8, an unknown potential D is introduced at junction A. If the unknown D is carried along to junction B, it is possible to solve for it, since the outgoing horizontal current at junction B is zero. More complicated mesh circuits may also be solved in an analogous manner by carrying along two or more unknown voltages simultaneously with the unit voltage until they can be determined.

Instead of assuming first a unit voltage D_{y1} impressed, then another unit voltage D_{r1}, it is possible to impress two voltages simultaneously, namely, 1 along D_{y1} and x along D_{r1}, and carry through the network two sets of currents and voltages. The number of numerical operations to be performed is the same in either case.

Calculation of Spans Between Rigid Bearings

When all bearings are rigid, the deflections D_y at the bearings are zero. In that case it is sufficient to impress two unit quantities on each span instead of four. Several possibilities of calculations are open. In one method F^{r1} and xF^{y1} are assumed (F^{r1} and F^{y1} are both unity, while x is unknown.) The two sets of calculations are now performed simultaneously. The resultant four equations of Table 2 become

		$x F^{y1}$	F^{r1}
$D_{y2} = i\,x F^{y1} + j F^{r1}$	=	i	j
$D_{r2} = k\,x F^{y1} + l F^{r1}$	=	k	l
$F^{y2} = m\,x F^{y1} + m F^{r1}$	=	m	n
$F^{r2} = o x F^{y1} + p F^{r1}$	=	o	p

$\ldots\ldots [7]$

At the end of each span D_{y2} is equated to zero, thereby allowing the determination of the unknown x.

ASYMMETRICAL SHAFT OR BEARINGS

Asymmetrical Shaft

One or more of the spans may have different elastic constants

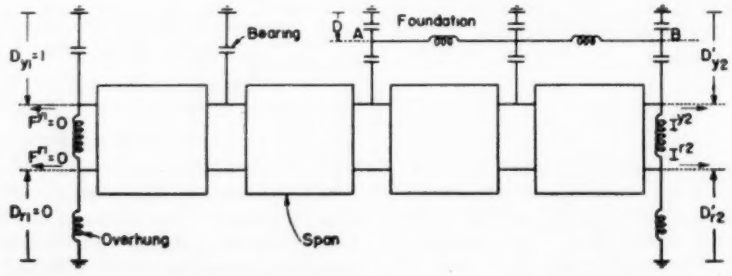


Fig. 8 Resultant Equivalent Circuit of a Shaft

along two principal axes at right angles. For instance, in a turbine shaft the generator span is asymmetrical due to the presence of slots. In such cases it will be assumed that the bearings and foundations are symmetrical.

When the principal axes in each of the asymmetrical spans are parallel, then each principal axis is treated independently of the other with the method of the previous section of the paper. Two sets of critical speeds have to be calculated for the two axes independently.

When the principal axes in each of the asymmetrical sections are not parallel but are at a constant angle (different between different sections), then, at least for one section, the two circuits along the two sets of axes y, r and z, q are not independent but are interconnected. The detailed equivalent circuit of a section to be put on the analyzer is given in Fig. 10 and Table 5 of reference (4). For numerical calculations the circuit may be simplified by multiplying the rows and columns of r_2 and q_2 by -1. Then four mutual admittances appear, as shown in Fig. 9, in a manner analogous to Fig. 1. The four ground admittances are

$$\left.\begin{array}{l|l} Y_{r1} = -(Y_5+Y_{12}+Y_{23}+Y_{27}) & Y_{q1} = -(Y_6+Y_{12}+Y_{24}+Y_{27}) \\ Y_{r2} = -(Y_5-Y_{12}+Y_{23}+Y_{27}) & Y_{q2} = -(Y_6-Y_{12}+Y_{24}+Y_{27}) \end{array}\right\} \quad \ldots [8]$$

$$\bar{Y} = \begin{array}{c|cccc} & \bar{y} & \bar{r} & \bar{z} & \bar{q} \\ \hline \bar{y} & -Y_{12} & Y_{15} & Y_9 & Y_{20} \\ \bar{r} & Y_{15} & Y_{24} & Y_{21} & -Y_{27} \\ \bar{z} & Y_9 & Y_{21} & -Y_3 & Y_{18} \\ \bar{q} & Y_{20} & -Y_{27} & Y_{18} & Y_{23} \end{array} \quad \ldots [9]$$

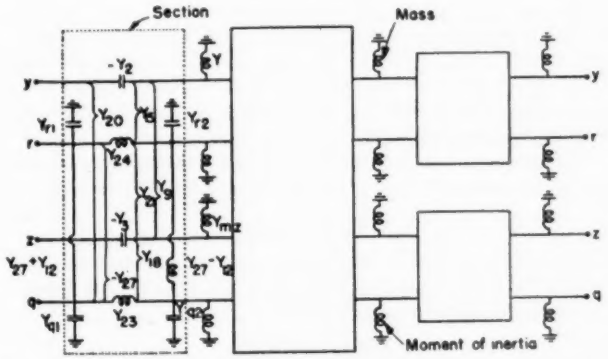


FIG. 9 EQUIVALENT CIRCUIT OF SHAFT WITH ASYMMETRICAL, TWISTED SECTION

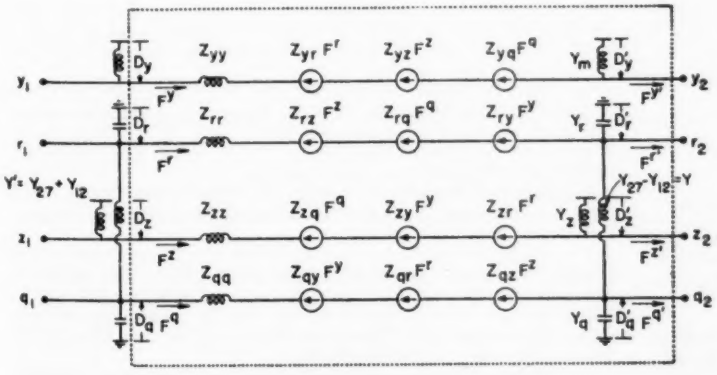


FIG. 10 EQUIVALENT CIRCUIT OF ASYMMETRICAL, TWISTED SECTION

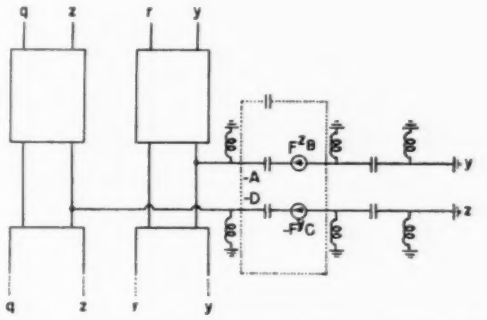


FIG. 11 EQUIVALENT CIRCUIT OF ASYMMETRICAL BEARING

Its inverse has to be calculated to find the self and mutual impedances $\bar{Z}$ needed for the numerical calculations, Fig. 11.

$$\bar{Z} = \begin{array}{c|cccc} & \bar{y} & \bar{r} & \bar{z} & \bar{q} \\ \hline \bar{y} & Z_{yy} & Z_{yr} & Z_{yz} & Z_{yq} \\ \bar{r} & Z_{ry} & Z_{rr} & Z_{rz} & Z_{rq} \\ \bar{z} & Z_{zy} & Z_{zr} & Z_{zz} & Z_{zq} \\ \bar{q} & Z_{qy} & Z_{qr} & Z_{qz} & Z_{qq} \end{array} \quad \ldots [10]$$

The equivalent circuit to be used for this numerical procedure is shown in Fig. 10 in which the induced voltages due to mutual inductances are shown by generators. By inspection of Fig. 10 the following set of eight equations may be written for the asymmetrical shaft in analogy to the set of Equations [1]

$$\left.\begin{array}{l} D_y' = D_y - Z_{yy}F^y - Z_{yr}F^r - Z_{yz}F^z - Z_{yq}F^q \\ D_r' = D_r - Z_{rr}F^r - Z_{rz}F^z - Z_{rq}F^q - Z_{ry}F^y \\ D_z' = D_z - Z_{zz}F^z - Z_{zq}F^q - Z_{zy}F^y - Z_{zr}F^r \\ D_q' = D_q - Z_{qq}F^q - Z_{qy}F^y - Z_{qr}F^r - Z_{qz}F^z \\ F^{y\prime} = F^y - Y_y D_y' \\ F^{r\prime} = F^r - Y_r D_r' - Y(D_r' - D_q') \\ F^{z\prime} = F^z - Y_z D_z' \\ F^{q\prime} = F^q - Y_q D_q' - Y(D_q' - D_r') \end{array}\right\} \quad \ldots [11]$$

Here again the equations do not represent a beam section. They correspond to a section of the electrical network on.

ASYMMETRICAL BEARING

If an asymmetrical coupling between the bearing flexibilities along the y and z directions is assumed, the form of this coupling is

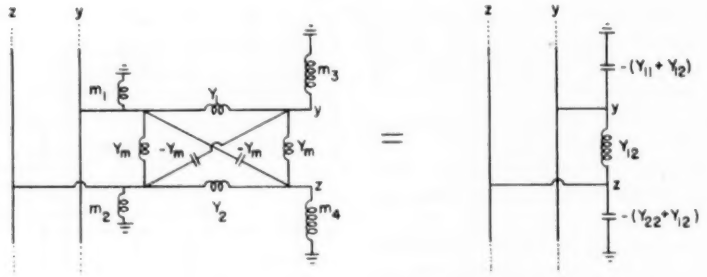
$$\bar{Y} = \begin{array}{c|cc} & \bar{y} & \bar{z} \\ \hline \bar{y} & -A & B \\ \bar{z} & -C & -D \end{array} \quad \ldots [12]$$

where C is different from B (say, $B = KC$) and has usually opposite sign.

For numerical calculations, such an asymmetrical coupling may be represented by generators, as shown in Fig. 11.

REDUCTION OF BEARING CIRCUIT

Each of the bearing circuits may be replaced by an equivalent delta (employing only three coils) by the following steps:



(a) (b)

FIG. 12 STEPS IN THE REDUCTION OF AN ASYMMETRICAL BEARING CIRCUIT

1 The simple series-shunt circuits along y and z may be replaced by an equivalent coil m so that the bearing circuit becomes that in Fig. 12(a).

2 The latter circuit is reduced to three coils, Fig. 12(b), by the following formulas

$$Y_{11} = -m_1 + \frac{m_3[Y_m^2 - Y_1(Y_2 + m_4)]}{(Y_1 + m_3)(Y_2 + m_4) - Y_m^2} \quad \ldots\ldots [13]$$

$$Y_{22} = -m_2 + \frac{m_4[Y_m^2 - Y_2(Y_1 + m_3)]}{(Y_1 + m_3)(Y_2 + m_4) - Y_m^2} \quad \ldots\ldots [14]$$

$$Y_{12} = \frac{m_3 m_4 Y_m}{(Y_1 + m_3)(Y_2 + m_4) - Y_m^2} \quad \ldots\ldots [15]$$

The resultant simplified circuit of the shaft system to be put on the network analyzer or to be solved numerically is shown in Fig. 13.

NUMERICAL CALCULATION OF CRITICAL SPEEDS

The critical speeds are calculated in a manner analogous to that shown under the same heading of the first section of the paper. However, now four different unit voltages and currents are impressed on the left-hand side in succession, instead of two, and eight different quantities are calculated on the right-hand side instead of four.

To determine the "excess moment" along, say, r, three of the resultant right-hand currents are to be made equal to zero instead of one. Changing three of the impressed voltages by x, y, and z, respectively, the "excess moment" is

$$\left.\begin{aligned} F^{r2} = F^{r2'} &+ \left[\frac{a(kh - gl) + e(fl - jh) + i(jg - fk)}{Det}\right] F^{r2''} \\ &+ \left[\frac{a(cl - kd) + e(jd - bl) + i(bk - jc)}{Det}\right] F^{r2'''} \\ &+ \left[\frac{a(gd - ch) + e(bh - fd) + i(fc - bg)}{Det}\right] F^{r2''''} \end{aligned}\right\} \quad \ldots\ldots [16]$$

where the right-hand currents are denoted by letters according to the scheme

$$\begin{vmatrix} F^{x2'} & F^{x2''} & F^{x2'''} & F^{x2''''} \\ F^{y2'} & F^{y2''} & F^{y2'''} & F^{y2''''} \\ F^{q2'} & F^{q2''} & F^{q2'''} & F^{q2''''} \end{vmatrix} = \begin{vmatrix} a & b & c & d \\ e & f & g & h \\ i & j & k & l \end{vmatrix} \quad [17]$$

When the presence of a foundation introduces extra meshes, they are again taken care of by extra variables as in the first section with the same heading.

Instead of assuming one impressed unit voltage at a time, it is possible to introduce two impressed voltages, say, 1 along axis y_1 and x along r_1, and carry two sets of numbers. Afterward a unit voltage may be impressed along axis z_1 and x along q_1. Or it is even possible to introduce four voltages simultaneously, say, 1 along axis y_1, x along r_1, y along z_1, and z along q_1, and carry four sets of numbers simultaneously throughout the network. Again the number of operations is not decreased with either method, but the procedure may be speeded up.

It is possible to check the correctness of the numbers at any particular bearing by the use of Equation [29], Appendix 2.

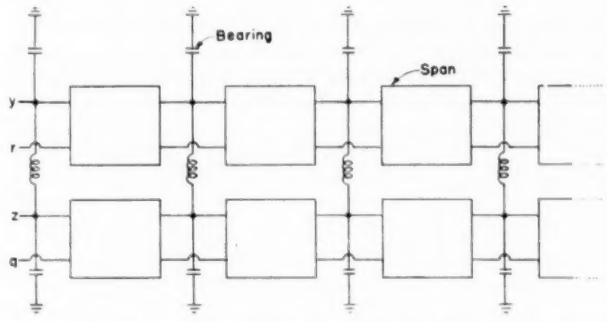


FIG. 13 SIMPLIFIED EQUIVALENT CIRCUIT OF SHAFT WITH ASYMMETRICAL BEARINGS

ACKNOWLEDGMENT

The author wishes to acknowledge his indebtedness to G. K. Carter, C. Concordia, and H. S. Shott of the General Electric Company for numerous discussions.

BIBLIOGRAPHY

1 "A General Method for Calculating Critical Speeds of Flexible Rotors," by M. A. Prohl, JOURNAL OF APPLIED MECHANICS, Trans. A.S.M.E., vol. 67, 1945, pp. A-142.

2 "A New Method of Calculating Natural Modes of Uncoupled Bending Vibration of Airplane Wings and Other Types of Beams," by N. O. Myklestad, *Journal of the Aeronautical Sciences*, vol. 2, no. 2, April, 1944, pp. 153–162.

3 "The Calculation of Flexible-Shaft Critical Speeds by Means of Punched-Card Machines," by A. W. Rankin, companion paper, presented at the Annual Meeting, New York, N. Y., Nov. 26–29, 1945, of THE AMERICAN SOCIETY OF MECHANICAL ENGINEERS and published in this issue, pp. A-117–A-126.

4 "Tensorial Analysis and Equivalent Circuits of Elastic Structures," by G. Kron, *Journal of The Franklin Institute*, vol. 238, no. 6, December, 1944, pp. 400–442.

5 "Network Analyzer Solution of the Equivalent Circuits for Elastic Structures," by G. K. Carter and G. Kron, *Journal of The Franklin Institute*, vol. 238, no. 6, December, 1944, pp. 443–452.

6 "Electric Circuit Models for the Vibration Spectrum of Polyatomic Molecules," by G. Kron, the *Journal of Chemical Physics*, vol. 14, no. 1, January, 1946, pp. 19–31.

7 "Network Analyzer Tests of Equivalent Circuits of Vibrating Polyatomic Molecules," by G. K. Carter and G. Kron, the *Journal of Chemical Physics*, vol. 14, no. 1, January, 1946, pp. 32–34.

Appendix 1

Simplified Equivalent Circuits of a Beam

The admittance matrix and equivalent circuit of a beam with mass Y_m and moment of inertia Y_I are given in Equation [18] and in Fig. 14, reproduced from reference (4).

$$\bar{Y} = \begin{array}{c|cccc} & \bar{y}_1 & \bar{r}_1 & \bar{y}_2 & \bar{r}_2 \\ \hline \bar{y}_1 & Y_2 - Y_m & Y_6 & -Y_2 & Y_6 \\ \bar{r}_1 & Y_6 & 2Y_7 - Y_I & -Y_6 & Y_7 \\ \bar{y}_2 & -Y_2 & -Y_6 & Y_2 - Y_m & -Y_6 \\ \bar{r}_2 & Y_6 & Y_7 & -Y_6 & 2Y_7 - Y_I \end{array} \qquad \left.\begin{array}{l} \bar{I} = \bar{Y}\,\bar{E} \\ \bar{F} = \bar{Y}\,\bar{D} \end{array}\right\} \quad \ldots\ldots\ldots [18]$$

The constants are shown in Table 1. With this sign convention, the equivalent circuits of beams may be interconnected in shunt and in series in arbitrary manner, the same way as the beams are.

This circuit is not in a form to be used for numerical calculations, hence let the directions of D_{r2} and F^{r2} on the beam be changed by multiplying the row and column of r_2 by —1.

$$\bar{Y} = \begin{array}{c|cccc} & \bar{y}_1 & \bar{r}_1 & \bar{y}_2 & \bar{r}_2 \\ \hline \bar{y}_1 & Y_2 - Y_m & Y_6 & -Y_2 & -Y_6 \\ \bar{r}_1 & Y_6 & 2Y_7 - Y_I & -Y_6 & -Y_7 \\ \bar{y}_2 & -Y_2 & -Y_6 & Y_2 - Y_m & Y_6 \\ \bar{r}_2 & -Y_6 & -Y_7 & Y_6 & 2Y_7 - Y_I \end{array} \quad \ldots [19]$$

Then, provided the signs on the circuit remain unchanged, all mutual admittances at junction r_2 also change signs, while all ground coils assume different values as shown in Equation [19] and Fig. 15. In particular, there is no coil in parallel with the mass.

With this new sign convention, the circuits cannot be interconnected in arbitrary manner, only in series and then even with certain precautions only, as will be presently shown.

The four Equations [19] $\bar{F} = \bar{Y}\,\bar{D}$ may be rewritten as

$$\left.\begin{array}{rl} F^{y1} + Y_m D_{y1} &= Y_2 (D_{y1} - D_{y2}) + Y_6 (D_{r1} - D_{r2}) \\ F^{r1} + (Y_1 - Y_7)\, D_{r1} &= Y_6 (D_{y1} - D_{y2}) + Y_7 (D_{r1} - D_{r2}) \\ F^{y2} + Y_m\, D_{y2} &= -(F^{y1} + Y_m\, D_{y1}) \\ F^{r2} + (Y_I - Y_7)\, D_{r2} &= -[F^{r1} + (Y_I - Y_7)\, D_{r1}] \end{array}\right\} \quad \ldots [20]$$

These equations may be simplified by a simplification of its electrical equivalent circuit shown in Fig. 15. It may be noted in the latter that part of the circuit without the grounds represents a transformer shown in Fig. 16 (because of the presence of four identical cross-coils Y_6, two of them plus, the other two minus). The admittance matrix of the transformer is

$$\bar{Y} = \begin{array}{c|cc} & & \\ \hline & -Y_2 & Y_6 \\ & Y_6 & -Y_7 \end{array} \quad \ldots\ldots\ldots [21]$$

Its impedance matrix is

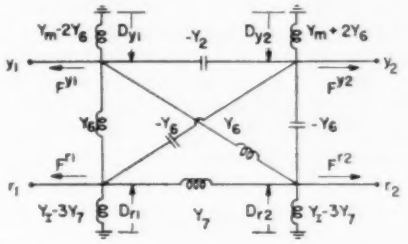


Fig. 14 Original Equivalent Circuit of a Beam Section

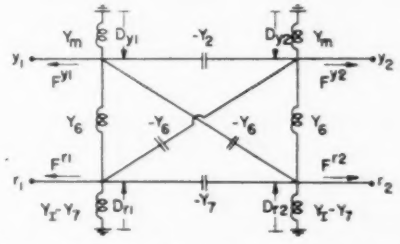


Fig. 15 Simplified Equivalent Circuit of a Section

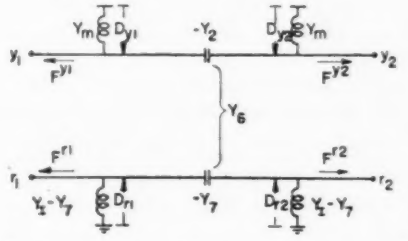


Fig. 16 Transformer Representation of a Section

$$\bar{Z} = \begin{array}{|c|c|} \hline Z_y & Z_{yr} \\ \hline Z_{yr} & Z_r \\ \hline \end{array} = \begin{array}{|c|c|} \hline \dfrac{2}{Y_2} & \dfrac{3}{Y_6} \\ \hline \dfrac{3}{Y_6} & \dfrac{2}{Y_7} \\ \hline \end{array} = \begin{array}{|c|c|} \hline \dfrac{L^3}{6B} & \dfrac{L^2}{2B} \\ \hline \dfrac{L^2}{2B} & \dfrac{L}{B} \\ \hline \end{array} \quad \ldots [22]$$

so that the final equivalent circuit is that shown in Fig. 1.

When the equivalent circuits of two neighboring sections are placed side by side as in Fig. 2, it can be noted that the two shunt impedances along each axis may be combined into one coil, as shown in Fig. 3. The equations of one repetitive section in Fig. 3 may now be written down by simple inspection as

$$\left.\begin{array}{rl} D_y' &= D_y - Z_y F^y - Z_{ry} F^r \\ D_r' &= D_r - Z_r F^r - Z_{ry} F^y \\ F^{y\prime} &= F^y - Y_y\, D_y' \\ F^{r\prime} &= F^r - Y_r\, D_r' \end{array}\right\} \quad \ldots\ldots\ldots [23]$$

The step from Equation [19] (or [18]) to Equation [23] used in the numerical work has been accomplished by purely electrical considerations. The same steps are retraced algebraically in Appendix 1 of the companion paper by Rankin (3) by following closely the electrical manipulations.

Because of the change in sign of the axis r_2 the beam sections can now be interconnected in series only with the precaution that the second beam section has opposite signs along r_1 instead of along r_2. This is equivalent to changing the signs of Y_6 in the

matrix of Equation [19] and in the circuit, Fig. 2; leaving the signs of currents and voltages unchanged.

Because of the alternation of Y_6, the absolute potentials on the lower lines, namely, the angles, also alternate in sign, forming a zigzag curve. In the original network in Fig. 14 the angles form a smooth curve; on the other hand, the coils representing masses contain another coil in parallel.

Appendix 2

General Circuit Parameters

The numerical method of starting with known D's and F's at one end and finding the D's and F's at the other end is equivalent to calculating the general circuit parameters $\bar{A}$, $\bar{B}$, $\bar{C}$, and $\bar{D}$ of the system

$$\begin{array}{|c|c|c|c|}\hline D_{y1} & D_{x1} & F^{y1} & F^{x1} \\ \hline \end{array}$$

$$\begin{array}{|c|c|}\hline D_{y2} \\ \hline D_{x2} \\ \hline F^{y2} \\ \hline F^{x2} \\ \hline \end{array} = \begin{array}{|c|c|c|c|}\hline a & b & i & j \\ \hline c & d & k & l \\ \hline e & f & m & n \\ \hline g & h & o & p \\ \hline \end{array} = \begin{array}{|c|c|}\hline \bar{A} & \bar{B} \\ \hline \bar{C} & \bar{D} \\ \hline \end{array} \quad \ldots [24]$$

However, each parameter now consists of a matrix instead of a number. The self and mutual admittances may be found as follows

$$\left.\begin{aligned} \bar{D}_2 &= \bar{A}\,\bar{D}_1 + \bar{B}\,\bar{F}_1 \\ \bar{F}_2 &= \bar{C}\,\bar{D}_1 + \bar{D}\,\bar{F} \end{aligned}\right\} \ldots\ldots\ldots\ldots [25]$$

From the first equation of Equation [25]

$$\bar{F}_1 = \bar{B}^{-1}\,\bar{D}_2 - \bar{B}^{-1}\,\bar{A}\,\bar{D}_1 \ldots\ldots\ldots\ldots [26]$$

Substituting into the second equations

$$\left.\begin{aligned} \bar{F}_1 &= (-\bar{B}^{-1}\,\bar{A})\,\bar{D}_1 + (\bar{B}^{-1})\,\bar{D}_2 = \bar{Y}^{11}\,\bar{D}_1 + \bar{Y}^{12}\,\bar{D}_2 \\ \bar{F}_2 &= (\bar{C} - \bar{D}\,\bar{B}^{-1}\,\bar{A})\,\bar{D}_1 + (\bar{D}\,\bar{B}^{-1})\,\bar{D}_2 = \bar{Y}^{21}\,\bar{D}_1 + \bar{Y}^{22}\,\bar{D}_2 \end{aligned}\right\} [27]$$

Or, from the second equation

$$\bar{D}_1 = \bar{C}^{-1}\,\bar{F}_2 - \bar{C}^{-1}\,\bar{D}\,\bar{F}_1$$

Substituting into the first equations

$$\left.\begin{aligned} \bar{D}_1 &= (-\bar{C}^{-1}\,\bar{D})\,\bar{F}_1 + (\bar{C}^{-1})\,\bar{F}_2 = \bar{Z}_{11}\,\bar{F}_1 + \bar{Z}_{12}\,\bar{F}_2 \\ \bar{D}_2 &= (\bar{B} - \bar{A}\,\bar{C}^{-1}\,\bar{D})\,\bar{F}_1 + (\bar{A}\,\bar{C}^{-1})\,\bar{F}_2 = \bar{Z}_{21}\,\bar{F}_1 + \bar{Z}_{22}\,\bar{F}_2 \end{aligned}\right\} \ldots [28]$$

Because of the symmetry of $\bar{Y}^{11}$, $\bar{Y}^{22}$ and $\bar{Z}_{11}$, $\bar{Z}_{22}$, four relations follow

$$\left.\begin{aligned} 1 \quad -\bar{B}^{-1}\,\bar{A} &= (-\bar{B}^{-1}\,\bar{A})_t \\ 2 \quad \bar{D}\,\bar{B}^{-1} &= (\bar{D}\,\bar{B}^{-1})_t \end{aligned}\right| \left.\begin{aligned} 3 \quad -\bar{C}^{-1}\,\bar{D} &= (-\bar{C}^{-1}\,\bar{D})_t \\ 4 \quad \bar{A}\,\bar{C}^{-1} &= (\bar{A}\,\bar{C}^{-1})_t \end{aligned}\right\} [29]$$

The second and fourth relations give the two checks used in the numerical calculations. An additional set of checks follows from the symmetry of $\bar{Y}^{12}$ with $\bar{Y}^{21}$ and $\bar{Z}_{12}$ with $\bar{Z}_{21}$

$$\bar{B}\,\bar{C}_t - \bar{A}\,\bar{D}_t = \bar{1} \quad \text{or} \quad \bar{C}\,\bar{B}_t - \bar{D}\,\bar{A}_t = \bar{1} \ldots\ldots [30]$$

$$\left.\begin{aligned} (ie + jf) - (am + bn) &= 1 \\ (kg + lh) - (co + dp) &= 1 \end{aligned}\right| \left.\begin{aligned} (ig + jh) - (ao + bp) &= 0 \\ (ke + lf) - (cm + dn) &= 0 \end{aligned}\right\} [31]$$

The self and mutual admittances of the equivalent circuit are from Equations [27]

$$\bar{Y}^{12} = \bar{B}^{-1} \mid \bar{Y}^{11} = -\bar{B}^{-1}\,\bar{A} \mid \bar{Y}^{22} = \bar{D}\,\bar{B}^{-1} \ldots\ldots [32]$$

and are given in detail in Table 3.

Calculation of the Multiple-Span Critical Speeds of Flexible Shafts by Means of Punched-Card Machines

By A. W. RANKIN,[1] SCHENECTADY, N. Y.

In turbine design, the critical speeds must be adequately spaced from the normal running speed to assure a smoothly operating unit. It is essential therefore that these critical speeds be predicted early in the design. To overcome general methods of calculating multiple-span critical speeds of irregular shafts, the author has devised a method employing standard punched-card business machines to avoid the prohibitive manual calculations hitherto involved in such work.

Nomenclature

THE following nomenclature is used in the paper:

In addition to the specific subscripts of the quantities given below, the auxiliary subscripts 0, 1, 2 are used to indicate initial values on the left overhang and first and second bearings, respectively.

Unprimed letters refer to the left-hand quantities on any incremental mesh circuit in Fig. 4, or incremental shaft section in Figs. 14 and 15; primed letters refer to the corresponding right-hand quantities.

A, B, C, D = general factors used only for description of multiplier operations [5]

d_{y11}, d_{y2} = calculated values of D_y, based upon assumed initial conditions, Equations [2a, b], respectively

d_r, d_{r2} = calculated values of D_r, based upon assumed initial conditions Equations [2a, b], respectively

D_y, D_r = shaft deflection and slope, respectively

E = Young's modulus

f_{y1}, f_{y2} = calculated values of F_y, based upon assumed initial conditions, Equations [2a, b], respectively

f_{r1}, f_{r2} = calculated values of F_r, based upon assumed initial conditions, Equations [2a, b], respectively

F_y, F_r = shaft shear and moment, respectively (see discussion at close of Appendix 1)

g = gravity acceleration = 386

i, j = adjacent shaft sections; Appendix 1

I = effective inertia of each incremental shaft length

l = length of each incremental shaft length

M = moment on end of each incremental shaft length; Appendix 1

N = Speed in thousands of rpm

P = acceleration forces = $\frac{1}{2}\frac{W}{g}\omega^2 y$

s = shear force on end of incremental shaft length Appendix 1

$S = s + P$

W = weight of each incremental shaft length

y = shaft deflection; Appendix 1

Y_7, Y_m = admittances to ground in Fig. 2; defined in Table 1

Y_r = sum of adjacent Y_7 values

Y_y = sum of adjacent Y_m values

Z_r, Z_{ry}, Z_y = line impedances as shown in Figs. 2, 3, and 4; defined in Table 1. (Note that Z_{ry} alternates in sign in progressing through successive sections as shown in Figs. 2 and 3.)

α, β = co-ordinate systems; defined in Fig. 2(a)

θ = shaft slope; Appendix 1

ω = speed, radians per sec

General

THE important role in turbine design played by the critical speeds of multiple-span flexible shafts is too well known to require more than a superficial introduction. It is sufficient to note that to guarantee a smooth-running unit the critical speeds must be adequately spaced from the normal running speed. It is therefore essential that these disturbing critical speeds be accurately predicted during the design stage. A practicable, quick method of calculating multiple-span critical speeds accurately would accordingly be of not inconsiderable benefit in practical design.

Several accurate and general methods of calculating multiple-span critical speeds of irregular shafts are available in the technical literature, but in the author's experience these methods, while completely competent in a technical sense, are not satisfactory for routine design or development because of the discouraging number of calculations which must be made. This criticism becomes more specific when one realizes that it is not possible to calculate critical speeds directly; it is necessary to start at a speed less than the first important critical speed and repeat the calculation for successively higher speeds until the practical range is covered. The critical speeds are then those speeds for which all the boundary conditions are satisfied; for speeds other than the critical speeds it will be found that one boundary condition remains unsatisfied. The number of assumed speeds for a typical four-bearing shaft, for instance, can be realized by noting that the lowest critical speed may be down to 1000 rpm while the highest of practical interest may be around 5000 rpm. In order to determine accurately all the critical speeds and modes of vibration, it is necessary to use 200-rpm increments or smaller.

In addition to the large number of assumed speeds, it is necessary to divide an irregular shaft into a number of incremental lengths. For a typical four-bearing turbine-generator set, about thirty such incremental lengths are necessary. The calculation sequence must be repeated for each incremental length for each assumed speed. It is accordingly evident why numerical investigations of critical speeds of multiple-bearing sets have heretofore been limited strictly to the most important cases.

[1] Turbine Generator Engineering Division, General Electric Company. Mem. A.S.M.E.

Contributed by the Applied Mechanics Division and presented at the Annual Meeting, New York, N. Y., Nov. 26–29, 1945, of The American Society of Mechanical Engineers.

Discussion of this paper should be addressed to the Secretary, A.S.M.E., 29 West 39th Street, New York, N. Y., and will be accepted until July 10, 1946, for publication at a later date. Discussion received after the closing date will be returned.

Note: Statements and opinions advanced in papers are to be understood as individual expressions of their authors and not those of the Society.

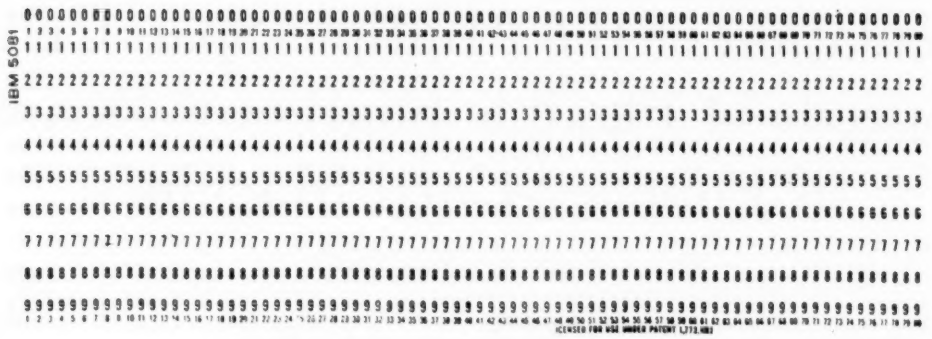


FIG. 1 STANDARD I.B.M. CARD; TYPE 5081

It is the purpose of this paper to show how standard punched-card machines[2] can be employed to eliminate the prohibitive manual calculations just discussed.

Punched-card machines are standard machines now in relatively wide use in machine accounting. The data under study are fed into these machines by means of cards of the type shown in Fig. 1. These cards are punched in accordance with the known data, and the machines are actuated by contacts through the punched holes. The results of the operations performed by the machines are punched automatically on cards in a similar fashion. Such machines have already been discussed to some extent in the technical literature. Eckert (1)[3] has described their application to astronomical calculations; McPherson (2) has described the various machines, and the mathematical operations which they can perform; Kormes (3, 4) has discussed the solution of both differential equations and field problems; Critchlow (5) has already pointed out that these machines can be "successfully and economically" used in aircraft flutter studies; and there are several other publications on their application to technical problems.

Although punched-card machines could undoubtedly be applied to the methods of calculating critical speeds already available in the technical literature, for instance, the methods of Myklestad (6) or of Prohl (7), the studies of the author have been confined principally to the equivalent-circuit analogies of Kron (8), and his relations and equations will be used in this paper. It will be necessary, therefore, to digress somewhat and summarize Kron's equations for calculating critical speeds. This summary is given in the following section. The reader is referred to the companion paper by Kron[4] for the original derivation of these equations, although a derivation without the use of the equivalent-circuit analogue is given in Appendix 1 of this paper. Kron's relations appear to be particularly well suited to punched-card methods of solution because of their highly repetitive nature.

It should be noted that although the method of calculation as presented in this paper is based upon the equivalent electric circuit, yet the a-c network analyzers (9) now in fairly wide use on various technical problems do not have sufficient range for this application. It has been found by trial that the number of digits needed in the calculation of multiple-span critical speeds is too great for the network analyzers now available. Satisfactory results have been obtained for many mechanical vibration problems by means of network analyzers but for long shafts on several bearings, it is necessary to resort to calculating machines using a large number of digits.

Basic Analytical Relations

In the equivalent-circuit analogy, the shaft deflection and slope, D_y and D_r, respectively, are represented by voltages to ground, while the shear and moment, F_y and F_r, respectively, are represented by line currents. The shaft is first divided into an adequate number of incremental lengths, and the basic equivalent circuit in Fig. 2 is constructed. Note that Z_{ry} is a mutual impedance between the upper and lower circuits. The impedances Z and admittances Y are given in Table 1. Note that the coordinate systems alternate at the extremities of each beam increment, as indicated by the α and β designations.

TABLE 1 IMPEDANCES Z AND ADMITTANCES Y

$$Y_{ri} = -\frac{2EI_i}{l_i} \qquad Y_r = Y_{ri} + Y_{rj}$$

$$Y_{mi} = .5\,\frac{W_i}{g}\,\omega^2 \qquad Y_y = Y_{mi} + Y_{mj}$$

$$Z_r = \frac{l}{EI} \qquad Z_{ry} = \pm\frac{l^2}{2EI} \qquad Z_y = \frac{l^3}{6EI}$$

The circuit in Fig. 2 is known as the basic equivalent circuit because each circuit section is a complete representation of the corresponding beam section. The shear and moment acting on each section are obtained by direct measurement of the current in the upper and lower horizontal branches, respectively, *at the circuit sectioning points marked by the dashed lines.* This basic circuit can be reduced to the less complex circuit in Fig. 3, the condensed basic equivalent circuit, by adding the adjacent Y_r and Y_m values. This condensed circuit has fewer meshes and is accordingly easier to handle in numerical calculations, but it should be noted that the terminal points of each section (the dashed lines in Fig. 2) are no longer directly available since they were submerged when the adjacent Y_r and Y_m values were added.

The condensed circuit in Fig. 3 is used for the calculation of all parts of the shaft except the boundary points, such as shaft ends or rigid[5] bearings, at which points auxiliary stations are set up by means of which the true terminal points are obtained without disturbing the symmetry of the basic equations given in the following paragraph.

A representative mesh circuit for an incremental length of the condensed circuit in Fig. 3 is shown in Fig. 4. From this circuit

[2] The machines used for the study presented in this paper were manufactured by the International Business Machines Corporation, The experience of the author is limited to these machines.

[3] Numbers in parentheses refer to Bibliography at end of paper.

[4] "The Equivalent Circuits for the Numerical Solution of the Critical Speeds of Flexible Shafts," by Gabriel Kron, also presented at the 1945 Annual Meeting of THE AMERICAN SOCIETY OF MECHANICAL ENGINEERS.

[5] In this paper, the term "rigid bearings" signifies bearings with no flexibility in the vertical or horizontal directions. All bearings are assumed of a ball-seat type equivalent to a pin through a beam, and the term "rigid" refers only to flexibility in the journal supports.

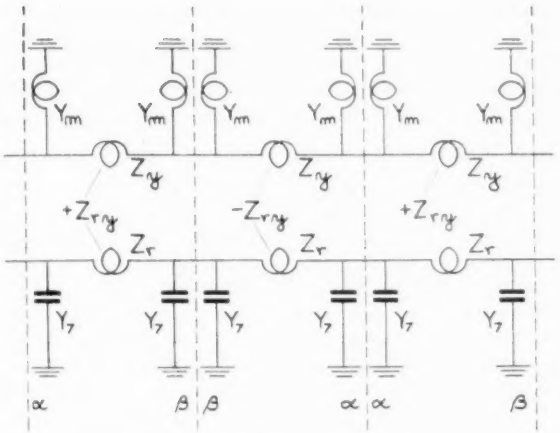


FIG. 2 BASIC EQUIVALENT CIRCUIT

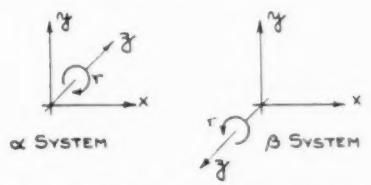


FIG. 2(a) CO-ORDINATE SYSTEMS FOR FIG. 2

it is evident that the right-hand currents and voltages are related to the corresponding left-hand quantities by the Equations [1a, b, c, d]

$$D_y' = D_y - F_y Z_y - F_r Z_{ry} \quad [1a]$$

$$D_r' = D_r - F_r Z_r - F_y Z_{ry} \quad [1b]$$

$$F_y' = F_y - D_y' Y_y \quad [1c]$$

$$F_r' = F_r - D_r' Y_r \quad [1d]$$

The foregoing are the basic analytical equations for the calculation of critical speeds. The method of obtaining a numerical solution of these equations is essentially as described by Prohl. Beginning at the free end of the shaft, the initial conditions, defined by Equations [2a] and [2b], are separately employed, and two independent solutions are thereby obtained.

$$D_{y0} = 1,\ D_{r0} = F_{y0} = F_{r0} = 0 \quad [2a]$$

$$D_{r0} = 1,\ D_{y0} = F_{r0} = F_{y0} = 0 \quad [2b]$$

If the shaft ends are in bearings rather than free as assumed in this paper, the initial conditions are as already discussed by Myklestad or by Prohl. The method of calculating past a rigid bearing has been previously described by Prohl, but for completeness this method is also given in Appendix 2 of this paper. In either case, the numerical solution will continue as described in the following paragraph.

Beginning with the initial conditions Equations [2a, b], and applying Equations [1a, b, c, d] as often as is necessary, the deflection, slope, shear, and moment at any point along the shaft can be written as in Equations [3a, b, c, d], respectively.

$$D_y = d_{y1} D_{y0} + d_{y2} D_{r0} \quad [3a]$$

$$D_r = d_{r1} D_{y0} + d_{r2} D_{r0} \quad [3b]$$

$$F_y = f_{y1} D_{y0} + f_{y2} D_{r0} \quad [3c]$$

$$F_r = f_{r1} D_{y0} + f_{r2} D_{r0} \quad [3d]$$

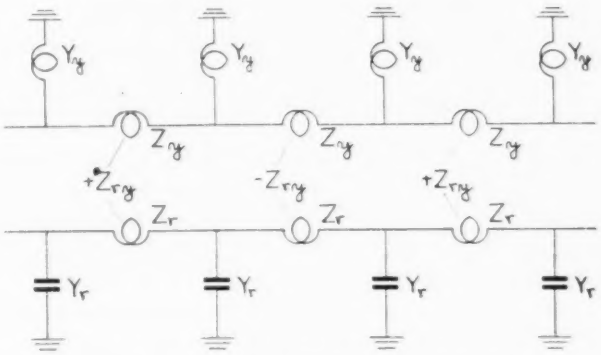


FIG. 3 CONDENSED BASIC EQUIVALENT CIRCUIT

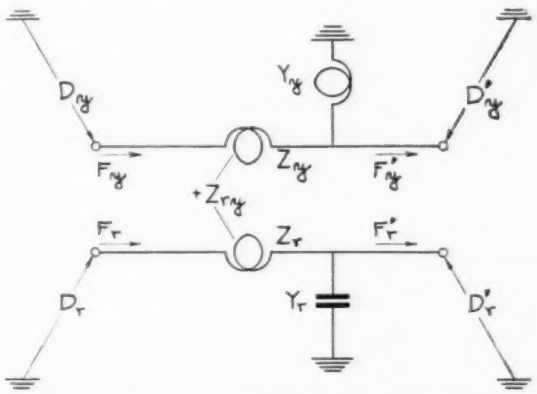


FIG. 4 REPRESENTATIVE MESH SECTION FROM CONDENSED BASIC EQUIVALENT CIRCUIT

By means of Equations [3a, b, c, d], one of the two remaining known boundary conditions is applied. The critical speeds are then those speeds for which the remaining boundary condition is automatically fulfilled; for speeds other than critical speeds it will be found that the last boundary condition cannot be fulfilled. For instance, if the shaft ends on a free overhang, there must be zero shear and zero moment at the end. Setting Equation [3c] equal to zero and substituting into Equation [3d] gives Equation [4a] for the moment at the end of the shaft

$$F_r = \left(f_{r2} - \frac{f_{r1} f_{y2}}{f_{y1}} \right) D_{r0} \quad [4a]$$

The critical speeds are those speeds for which Equation [4a] equals zero. These critical speeds can best be determined by plotting F_r, the "excess moment," against the assumed speed.

As a second example, if the shaft ends at a rigid bearing, there must be zero deflection and zero moment. Making Equation [3a] equal to zero and substituting into Equation [3d] gives Equation [4b] for the moment at the end of the shaft. As in the foregoing, the critical speeds are then those speeds for which the excess moment, Equation [4b], is equal to zero

$$F_r = \left(f_{r2} - \frac{f_{r1} d_{y2}}{d_{y1}} \right) D_{r0} \quad [4b]$$

The foregoing completes the summary of Kron's equations for the determination of critical speeds. The solution of these equations by means of punched-card machines is described in the next section.

Application of Punched-Card Machines

The machines used in the study presented in this paper are as follows:

1 A key-punch machine for punching the original data manually.

2 An interpreter for typing automatically the identifying data on each card.

3 A multiplier for performing the necessary multiplications.

4 A reproducer for transcribing automatically selected data from a given position on one set of cards to the same or a different position on another set of cards.

5 A duplicator for duplicating cards automatically when necessary.

6 A numeric listing machine for reading selected data from a set of cards and listing them as directed.

7 A sorting machine for necessary card sorting.

With the exception of the multiplier, all are standard machines available in accounting departments geared to general machine accounting. The multiplier is itself a standard multiplying punch with the addition of a standard device called an "algebraic sign control." By means of the latter, the multiplier can be plugged to perform either of the following operations, with due regard for the algebraic signs of all components

$$A \pm (B \times C) = D \quad \ldots\ldots\ldots\ldots\ldots\ldots [5]$$

A, B, and C are automatically read from a card, the selected operation [5] is performed, and the result D with its algebraic sign is automatically punched into a designated position on the same card.

To obtain a solution of the critical-speed problem, standard I.B.M. cards, type 5081, Fig. 1, were divided into fields[6] and the two types of cards shown in Fig. 5 were printed. Type 1 cards are used for calculating D_y' and F_y', and type 2 cards are used for calculating D_r' and F_r'. Two cards are needed of each type for each incremental shaft length for each assumed speed; one card is used for the application of the initial conditions, Equations [2a], and the second for the initial conditions, Equations [2b]. Four cards are thus needed for each station for each assumed speed as follows:

Type 11: Initial conditions [2a]; calculation of D_y' and F_y'
12: Initial conditions [2a]; calculation of D_r' and F_r'
21: Initial conditions [2b]; calculation of D_y' and F_y'
22: Initial conditions [2b]; calculation of D_r' and F_r'

The shaft weight and stiffness values Z_y, Z_r, Z_{ry}, Y_y, and Y_r are punched into fields, 7, 8, and 9, and the type, station, and assumed speeds are simultaneously punched into fields 1, 2, and 3. Note that Z_y, Z_r, Z_{ry}, Y_r, and the type and station need be hand-punched into only one card for each station; as these data do not change with speed, the remaining cards for each station can be punched automatically on the reproducer. Only Y_y and the assumed speed need be hand-punched on each card, and even the assumed speed can be punched automatically on the reproducer by first making master cards to cover the desired speed range. In addition, note that types 21 and 22 can be completely punched automatically from types 11 and 12, respectively.

The assumed initial conditions, Equations [2a, b], are hand-punched into fields 4, 5, and 6 of the cards for the first station, and all the necessary preliminary punching is then completed.

The calculations of Equations [1a, b] must be performed in two steps since, as shown in operations [5], the multiplier can perform only $A \pm (B \times C) = D$. The cards with the initial conditions are placed in the multiplier with the latter plugged to read fields 4, 5, and 7, calculate $4 - (5 \times 7)$, and punch the result into field 10. With this operation, the quantity [6a] has been calculated and punched into the cards of types 11 and 21, and the quantity [6b] has been calculated and punched into the cards of types 12 and 22.

$$D_y - F_y Z_y \quad \ldots\ldots\ldots\ldots\ldots\ldots [6a]$$

$$D_r - F_r Z_r \quad \ldots\ldots\ldots\ldots\ldots\ldots [6b]$$

Upon completion of this operation for all cards, the multiplier is replugged to read fields 10, 6, and 8, calculate $10 - (6 \times 8)$, and punch the result into field 11, and the cards are sent through the multiplier again. Upon completion of this second operation, and the punching of the result into field 11, the last product on the right-hand side of Equations [1a, b] have been calculated and subtracted from the quantities defined in [6a, b]. D_y' has thus been calculated and punched in cards of types 11 and 21, and D_r' has been calculated and punched in cards of types 12 and 22.

The replugging of the multiplier, as mentioned in the foregoing paragraph, takes practically no time as the plugging is done on detachable plugboards, and the necessary number of these are plugged for the required operations before the first run is made. Replugging the multiplier accordingly requires only the removal of one plugboard and the insertion of another, and this is a matter of a few seconds. A new "skip" bar, which positions the field in which the punching is to be done, must also be changed with each plugging change, but this is also a matter of seconds.

By means of a third plugboard, the multiplier is now plugged to read fields 5, 9, and 11, calculate $5 - (9 \times 11)$, and punch the result in field 12, and the cards are run through a third time. With the completion of this operation, F_y' has been calculated and punched on cards of types 11 and 21, and F_r' has been calculated and punched on cards of types 12 and 22, in accordance with Equations [1c, d]. The calculations are thus completed for the first incremental shaft length.

The primed quantities, calculated and punched on the first set of cards in accordance with Equations [1a, b, c, d], now become the unprimed quantities for the next incremental shaft length, and accordingly must be transferred to the cards for the next incremental shaft length. The cards for the first incremental shaft length are accordingly fed into a reproducer plugged to read fields 11 and 12, as calculated in the foregoing paragraphs, and these calculated data are punched into fields 4 and 5 of the cards for the second incremental shaft length.

With the foregoing operation, D_y and F_y have been punched into cards of types 11 and 21, and D_r and F_r into cards of types 12 and 22. To punch F_r and F_y into field 6, the cards for this second incremental shaft length are divided into two groups; types 11 and 21 in one group and 12 and 22 in the second group. These two groups are sent through the reproducer with the latter plugged to read field 5 in one group of cards and punched into field 6 of the other group of cards. Two runs are needed to punch field 6 in both groups of cards. By these two runs, F_r has been punched into the cards of types 11 and 21 for the second incremental shaft length, and F_y into the cards of types 12 and 22. As with the multiplier, the replugging of the reproducer for these transcribing operations takes little time as detachable plugboards are preplugged for the necessary operations.

The foregoing completes the punching of the cards for the second incremental shaft length. These are then placed in the multiplier, and the operations described in the foregoing paragraphs are repeated until the end of the shaft is reached. At this point, the final cards are placed in a numeric listing machine plugged to read and list fields 11 and 12 (D_y' and F_y', and D_r' and F_r'), and the excess moment is obtained from the listed data by manual calculations.

[6] A field is merely a group of columns in which data of a particular nature will always appear. The cards of Fig. 5 have twelve such fields each.

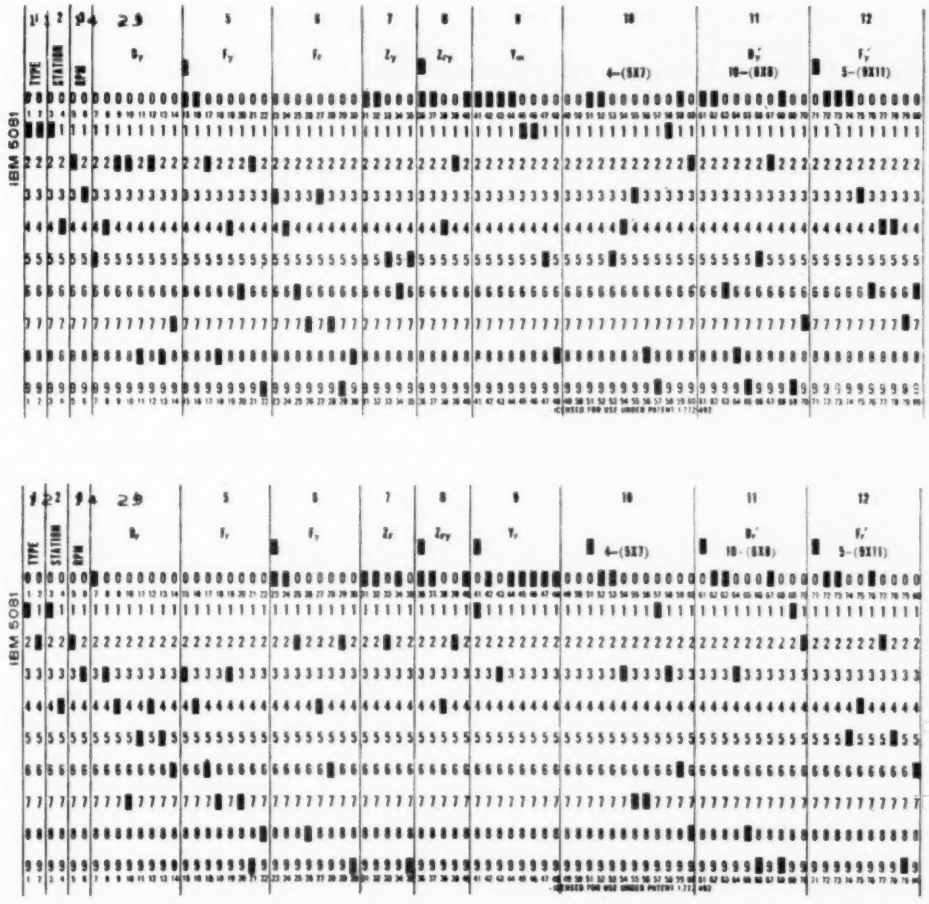


FIG. 5 TWO TYPES OF CARDS USED FOR CALCULATION OF CRITICAL SPEEDS BY MEANS OF PUNCHED-CARD MACHINES
(Upper type 1; lower type 2. The Y_m on the type 1 cards should be Y_y.)

Another method of obtaining the excess-moment curve is to place the final cards in a reproducer plugged to transfer fields 11 and 12 into new cards, and the excess moment can then be obtained by the multiplying machine. The cards containing the calculation of the excess moment are then placed in the numeric listing machine plugged to read and list the calculated excess moment, and the critical speeds are then obtained by plotting the listed data.

The modes of vibration are obtained by means of Equation [3*a*]. The final boundary conditions will give D_{r0} in terms of D_{y0} and will give the critical speeds. The type 11 and 21 cards are placed in a sorter, and all the speeds closest to the calculated critical speeds are picked out. The d_{y1} values from the type 11 cards are punched automatically by means of the reproducer into field 5 of a new set of cards. The d_{y2} values from the type 21 cards are similarly punched into field 11 of the new set of cards, and D_{r0} in terms of D_{y0}, as obtained from the calculation of the excess moment, is gang-punched into field 9. These new cards are then placed in the multiplier, and with the plugboard plugged to calculate $5 + (9 \times 11)$, the result is punched in field 12, the quantity thus punched in field 12 being the amplitude of vibration. These cards are then placed in the listing machine plugged to read and list field 12. A plot of the listed data will then give the mode of vibration.

NUMBER OF DIGITS

It is recognized that in any calculation of critical speeds, a relatively large number of digits is required as the excess moment is normally the difference between two large numbers. The multiplying machine used in the study presented in this paper can handle eight digits in the multiplier and eight digits in the multiplicand and can punch ten digits in the operation given by [5]. These two extra digits are used in permitting the growth of the calculated data, and in determining when to shift decimals in the various plugboards. Of the ten digits in field 12, for instance, the first (column 71) is used to record the sign, while the second (column 72) is punched zero so long as there are only eight digits in the calculated quantities, these eight digits being punched in columns 73 to 80, inclusive. By passing a needle through the zero of column 72, it is a simple matter to determine when the calculated quantity has increased from eight to nine digits since the (ninth) digit punched in column 72 will no longer be zero. It is then necessary to shift the decimal on the plugboard. In this way the requisite accuracy can be easily maintained throughout the entire calculation. The growth of fields 10 and 11 is handled in the same way.

NUMERICAL EXAMPLE

As an example of the methods described in the foregoing paragraphs, numerical calculations were made on the four-bearing stationary turbine-generator model shown in Fig. 6. Considerable test data were available on this model, and calculations for the case of rigid bearings were accordingly made to test both the

correctness of Kron's equivalent-circuit analogies as well as the efficacy of the punched-card method of solution.

The model was divided into twenty-six incremental lengths which when added to the auxiliary stations at the rigid bearings gave a total of thirty stations. The speed range under study was from 1500 rpm to 4500 rpm in 200-rpm increments, thereby giving a total of $30 \times 16 \times 4 = 1920$ cards.

One day was required for the calculation of the shaft stiffness and weight constants, and another day was required to punch these data into the cards. Complete calculations for three stations could be made in 1 hr, thus requiring 10 hr for the shaft calculations, exclusive of the auxiliary calculations at the rigid bearings. The latter calculations required about 6 hr total, so about 4 days were required for the entire study. It should be noted, however, that a complete set of punched cards is now available for this model, and if any design changes are suggested, only the cards applying to the particular part of the shaft which is changed will require any appreciable time for repunching, since all the other cards can be quickly punched automatically on the reproducer.

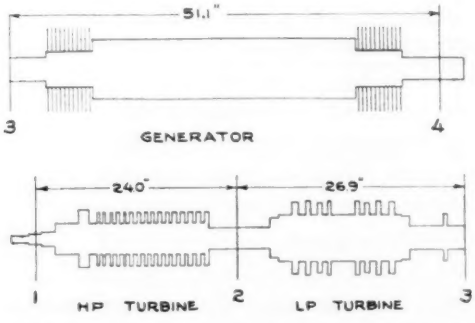


FIG. 6 STATIONARY TURBINE-GENERATOR MODEL USED FOR NUMERICAL EXAMPLE, SHOWING LOCATION OF BEARINGS 1, 2, 3, AND 4 (Vertical scale on this drawing is 5 times the horizontal scale. In order to conserve space, this drawing shows the model parted at the No. 3 bearing; actually, the turbines are rigidly connected to the generator and form a single-shaft unit on four bearings.)

Calculations were first made to determine the single-span critical speeds of the three elements. The results of these calculations together with corresponding values determined by test are given in Table 2.

TABLE 2 SINGLE-SPAN CRITICAL SPEEDS

	Calculated, rpm	Test, rpm
High-pressure turbine and turbine overhang	3900	3900
Low-pressure turbine	4095	4165
Generator and generator overhang	1865	1840

The calculations for the complete four-bearing set, in Fig. 6, were begun at the free end of the high-pressure turbine overhang. The curve of excess moment obtained at bearing No. 2 is shown in Fig. 7. The calculated first critical of the high-pressure turbine and its overhang is 3900 rpm, and the test value was likewise 3900 rpm.

The curve of excess moment obtained at bearing No. 3 is shown in Fig. 8. The calculated first critical speed of the assembly of high-pressure and low-pressure turbine and turbine overhang is 3995 rpm, while the test value was 3980 rpm.

The curve of excess moment obtained at the free end of the generator-shaft overhang is shown in Fig. 9. The calculated first-critical speed of the complete four-bearing model was 2025 rpm, while the results of two tests were 2120 rpm and 2050 rpm. The calculated second critical of the complete four-bearing model was 4180 rpm, while the results of two tests were 4165 rpm and 4205 rpm.

The foregoing checks between calculated and test values are remarkably close, especially in view of the difficulty of determining the correct effective inertias, as well as the known variations in Young's modulus.

The modes of vibration for the first and second critical speeds are shown in Fig. 10. These modes actually were plotted for 1900 rpm and 4100 rpm, respectively, rather than for the exact critical speeds, but they are in good agreement with the known modes of the first and second criticals.

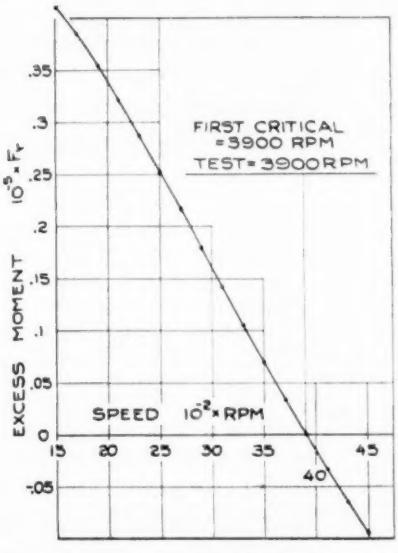


FIG. 7 EXCESS-MOMENT CURVE FOR HIGH-PRESSURE TURBINE AND TURBINE OVERHANG OF FIG. 6

In a preceding paragraph it was pointed out that to investigate any proposed design change, only the cards applying to the particular part of the shaft being changed need be repunched manually. As an example of the time required to determine the effect of any design change, the low-pressure element of the model shown in Fig. 6 was stiffened in order to increase its single-span first critical speed. The total time required to make this change and determine the new four-bearing critical speeds was less than 1 day. The excess-moment curve for this modified set, employing the low-pressure element with the high single-span critical speed, is shown in Fig. 11. Note that the four-bearing criticals have been changed only to a minor degree. Fig. 11 illustrates one of the most important advantages of the punched-card method of solution, i.e., the rapidity with which the effect of changes can be obtained means that contemplated design changes can be thoroughly studied during the preliminary layout stages.

Fig. 12 illustrates the manner in which data are obtained from the numeric listing machine. This specific illustration shows the listed deflections from which was plotted the mode of vibration for the second critical speed shown in Fig. 10. Similar listings were obtained to plot all the curves in Figs. 7, 8, 9, 10, and 11, as well as those curves from which Table 2 was obtained. It is important to note that it is unnecessary ever to read any data, calculated or otherwise, directly from the punched cards. These data are either automatically transcribed to new cards for further calculations, or they are listed in the manner shown in Fig. 12.

ACKNOWLEDGMENT

The author takes great pleasure in acknowledging the cooperation of his associates in the General Electric Company in the study presented in this paper. Thanks are extended to L. H.

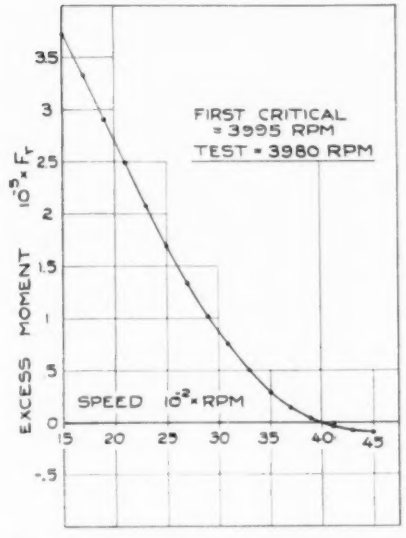


FIG. 8 EXCESS-MOMENT CURVE FOR ASSEMBLY OF TURBINE OVERHANG, HIGH-PRESSURE TURBINE, AND LOW-PRESSURE TURBINE OF FIG. 6

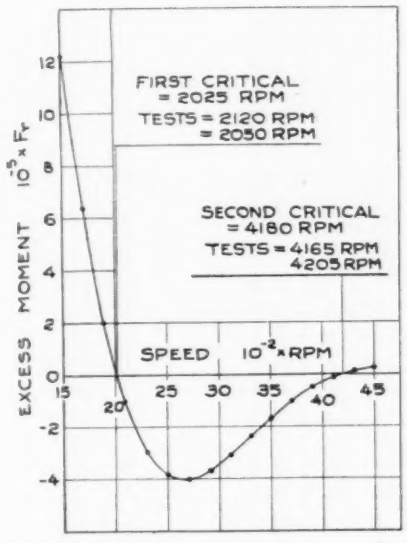


FIG. 9 EXCESS-MOMENT CURVE FOR COMPLETE FOUR-BEARING MODEL OF FIG. 6

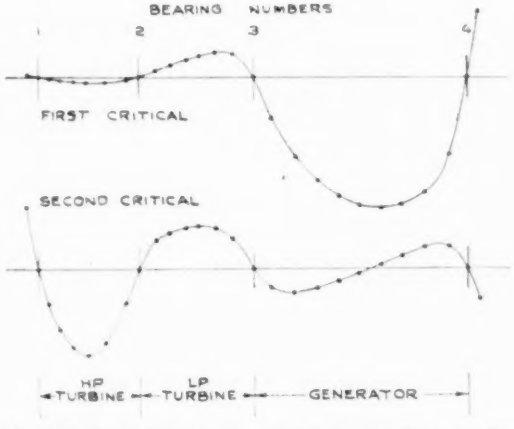


FIG. 10 MODES OF VIBRATION FOR FIRST AND SECOND CRITICAL SPEEDS OF COMPLETE FOUR-BEARING MODEL OF FIG. 6

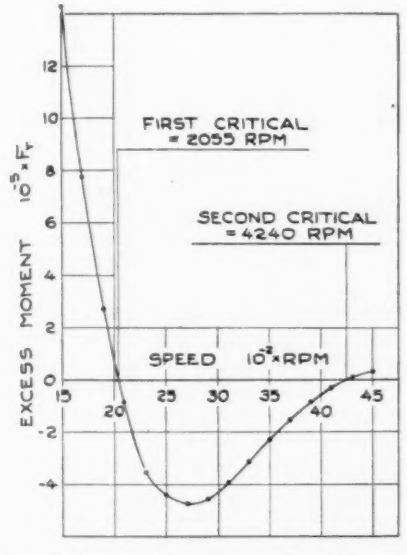


FIG. 11 EXCESS-MOMENT CURVE FOR FOUR-BEARING MODIFIED MODEL USING HIGH-CRITICAL LOW-PRESSURE TURBINE

Auchmoody for his continued encouragement; to G. Kron for permission to publish the foregoing summary of his critical-speed equations; and to O. A. Thorne of the Works Accounting Division on whose I.B.M. machines this study was made. Particular thanks are extended to T. H. Cowie of the Works Accounting Division without whose patient instruction in machine operation the author would have had very little success; and to F. S. Tebbutt of the International Business Machines Corporation for his willing and competent co-operation.

BIBLIOGRAPHY

1 "Punched-Card Methods in Scientific Computations," by W. J. Eckert; published by The Thomas J. Watson Astronomical Computing Bureau, Columbia University, New York, N. Y., 1941.

2 "Mathematical Operations With Punched Cards," by J. C. McPherson, *Journal of the American Statistical Association*, vol. 37, 1942, pp. 275–281.

3 "Integration of Linear Second-Order Differential Equations by Means of Punched Cards," by M. Kormes, *Review of Scientific Instruments*, vol. 14, 1943, p. 118.

4 "Numerical Solution of Initial Value Problems by Means of Punched-Card Machines," by J. P. Kormes and M. Kormes, *Review of Scientific Instruments*, vol. 16, 1945, pp. 7–9.

5 "Measurement and Prediction of Aircraft Vibration," by E. F. Critchlow, *S.A.E. Journal*, vol. 52, 1944, pp. 368–379.

6 "A New Method of Calculating Natural Modes of Uncoupled Bending Vibration of Airplane Wings and Other Types of Beams," by N. O. Myklestad, *Journal of the Aeronautical Sciences*, April, 1944, pp. 153–162.

7 "A General Method for Calculating Critical Speeds of Flexible Rotors," by M. A. Prohl, JOURNAL OF APPLIED MECHANICS, Trans. A.S.M.E., vol. 67, 1945, p. A-142.

8 "Tensorial Analysis and Equivalent Circuits of Elastic Structures," by Gabriel Kron, *Journal of The Franklin Institute*, vol. 238, 1944, pp. 399–442.

9 "A New A-C Network Analyzer," by H. P. Kuehni and R. G. Lorraine, Trans. A.I.E.E., vol. 57, 1938, p. 67.

Appendix 1

DERIVATION OF SHAFT EQUATIONS

The fundamental shaft equations given by Equations [1*a*, *b*, *c*, *d*] will be derived in this appendix without recourse to the elec-

| | | |

With the chosen co-ordinate systems, the relations, Equations [11*a*, *b*] are physically self-evident.

$$y_j = y_i' \quad [11a]$$

$$\theta_j = \theta_i' \quad [11b]$$

Equating the shear forces, as in Equation [12*a*], gives S_j in terms of S_i, as in Equation [12*c*].

$$s_i' + s_j = 0 \quad [12a]$$

$$s_j = s_i + \frac{1}{2}\frac{W_i}{g}\omega^2 y_i + \frac{1}{2}\frac{W_i}{g}\omega^2 y_i' + \frac{1}{2}\frac{W_j}{g}\omega^2 y_j - \frac{1}{2}\frac{W_j}{g}\omega^2 y_j \quad [12b]$$

$$S_j = S_i + \left(\frac{1}{2}\frac{W_i}{g}\omega^2 + \frac{1}{2}\frac{W_j}{g}\omega^2\right) y_j \quad [12c]$$

Equating the moments, as in Equation [13*a*], gives M_j in terms of M_i, as in Equation [13*c*].

$$M_i' + M_j = 0 \quad [13a]$$

$$M_j = M_i - \frac{2EI_i}{l_i}\theta_i - \frac{2EI_i}{l_i}\theta_i' - \frac{2EI_j}{l_j}\theta_j + \frac{2EI_j}{l_j}\theta_j \quad [13b]$$

$$\left(M_j - \frac{2EI_j}{l_j}\theta_j\right) = \left(M_i - \frac{2EI_i}{l_i}\theta_i\right) - \left(\frac{2EI_i}{l_i} + \frac{2EI_j}{l_j}\right)\theta_j \quad [13c]$$

The shaft Equations [1*a*, *b*, *c*, *d*] of the electrical analogue can be obtained from the foregoing by means of the following substitutions

$$\left.\begin{aligned} Y_{\gamma i} &= -\frac{2EI_i}{l_i} & Y_r &= Y_{\gamma i} + Y_{\gamma j} \\ Y_{mi} &= \frac{1}{2}\frac{W_i}{g}\omega^2 & Y_y &= Y_{mi} + Y_{mj} \end{aligned}\right\} \quad [14]$$

$$Z_r = \frac{l}{EI} \qquad Z_{ry} = \frac{l^2}{2EI} \qquad Z_y = \frac{l^3}{6EI}$$

$$\left.\begin{aligned} y_i &= D_y & y_i' &= y_j = D_y' \\ \theta_i &= D_r & \theta_i' &= \theta_j = D_r' \\ S_i &= -F_y & S_j &= -F_y' \\ M_i - \frac{2EI_i}{l_i}\theta_i &= M_i + Y_{\gamma i}\theta_i = -F_r \\ M_j - \frac{2EI_j}{l_j}\theta_j &= M_j + Y_{\gamma j}\theta_j = -F_r' \end{aligned}\right\} \quad [15]$$

Substituting Equations [14] and [15] into Equations [9*a*], [9*b*], [12*c*], and [13*c*], gives the basic shaft Equations [16*a*, *b*, *c*, *d*]. Note that these equations are identical with Equations [1*a*, *b*, *c*, *d*], which were obtained by the electrical analogue.

$$D_y' = D_y - Z_y F_y - Z_{ry} F_r \quad [16a]$$

$$D_r' = D_r - Z_r F_r - Z_{ry} F_y \quad [16b]$$

$$F_y' = F_y - Y_y D_y' \quad [16c]$$

$$F_r' = F_r - Y_r D_r' \quad [16d]$$

Note that Z_{ry} alternates in sign in progressing through the successive shaft sections.

It is evident from the last two expressions in Equations [15], that in general F_r and F_r' are not true moments because of the presence of the $\frac{2EI}{l}\theta$ factors. They are called moments in this paper, and used as such, because their numerical values are of importance only at boundary points, such as rigid bearings or shaft ends, at which points they do become true moments. At these boundary points, the $\frac{2EI_j}{l_j}\theta_j$ term becomes zero, either because the shaft ends at the ith section, or because the rigid bearing appears between the ith and jth sections. In either case, F_r' becomes numerically equal to $-M_j$ and is a true moment. In a similar manner, the $\frac{2EI_i}{l_i}\theta_i$ term is dropped at the initial boundaries, and F_r is then a true moment.

It is also evident that in general F_y and F_y' are not true shear forces but differ from the latter by the terms $\frac{1}{2}\frac{W}{g}\omega^2 y$. Like the foregoing F_r and F_r', however, the numerical values of F_y and F_y' are of importance only at boundary points, and at these points they become true shear forces by simply dropping the offending $\frac{1}{2}\frac{W}{g}\omega^2 y$ terms.

It is emphasized that F_r, F_r', F_y, and F_y', which in general are not true moments or shears, are merely convenient variables which greatly simplify and shorten the numerical solutions of critical-speed problems. At boundary points these variables must be properly handled in order to force them to reduce to true moments and shears. In the electrical circuit, the boundary values are applied at the shaft-sectioning points, marked by the dashed lines in Fig. 2. This was mentioned in the discussion of the equivalent electrical circuits, at which it was pointed out that the adjacent Y_m and Y_γ values should not be added together at the boundary points. The method of modifying the corresponding mechanical equations at the boundary points, as was described in the foregoing paragraphs, can be most easily visualized by a study of the equivalent electrical circuit.

Appendix 2

Rigid Bearings

The method of carrying the calculations past a rigid bearing will be given in this appendix. Consider the simple two-bearing

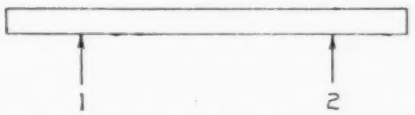


Fig. 15 Two-Bearing Shaft for Appendix 2

shaft of Fig. 15. Let the initial conditions at the left end be as given in Equations [2*a*, *b*]. The variables F_r, F_y, etc., must be modified at the known boundary points, as described in Appendix 1, so that at these points true moments and shears will be obtained.

Using Equations [3*a*, *b*, *c*, *d*], let the calculated values at the first bearing be

$$D_{y1} = d_{y11}D_{y0} + d_{y21}D_{r0} \quad [17a]$$

$$D_{r1} = d_{r11}D_{y0} + d_{r21}D_{r0} \quad [17b]$$

$$F_{y1} = f_{y11}D_{y0} + f_{y21}D_{r0} \quad [17c]$$

$$F_{r1} = f_{r11}D_{y0} + f_{r21}D_{r0} \quad [17d]$$

Setting D_{y1} equal to zero eliminates D_{y0}. Substituting into Equations [17*b*, *d*] gives D_{r1} and F_{r1}

$$D_{r1} = \left(- \frac{d_{y21} d_{r11}}{d_{y11}} + d_{r21} \right) D_{r0} \quad [18a]$$

$$F_{r1} = \left(- \frac{d_{y21} f_{r11}}{d_{y11}} + f_{r21} \right) D_{r0} \quad [18b]$$

Setting D_{y1} equal to zero fixes the deflection at zero corresponding to a rigid bearing, and also eliminates one variable, D_{y0}. The bearing reaction at the first bearing is unknown, however, and it is accordingly necessary to introduce a new shear variable corresponding to the unknown bearing reaction. The calculations immediately to the right of the first bearing are accordingly started with the two initial conditions defined by

$$D_{r1} = D_{r1},\ F_{r1} = F_{r1},\ D_{y1} = F_{y1} = 0 \quad [19a]$$

$$F_{y1} = 1,\ D_{y1} = D_{r1} = F_{r1} = 0 \quad [19b]$$

At the second bearing, equations analogous to Equations [17*a*, *b*, *c*, *d*] are obtained, except that D_{y0} is replaced by F_{y1}. The unknown D_{r0} is still present since the quantities defined by conditions [19*a*] are directly proportional to D_{r0}. Specifying zero deflection ($D_{y2} = 0$), corresponding to a rigid bearing, will give the unknown shear F_{y1} in terms of D_{r0}, and eliminates one unknown. A second unknown shear must be introduced, however, corresponding to the unknown bearing reaction at No. 2 bearing, and the calculations immediately to the right of No. 2 bearing are started with the two initial conditions defined by

$$D_{r2} = D_{r2},\ F_{r2} = F_{r2},\ D_{y2} = F_{y2} = 0 \quad [20a]$$

$$F_{y2} = 1,\ D_{y2} = D_{r2} = F_{r2} = 0 \quad [20b]$$

At the free end to the right in Fig. 15, equations for the shear and moment are obtained analogous to Equations [17*c*, *d*], except that D_{y0} is now replaced by F_{y2}. The known boundary condition of zero shear at the free end will give F_{y2} in terms of D_{r0}. Substituting into the moment equation will give the expression for "excess moment" in terms of D_{r0}. Those speeds for which the excess moment is zero, independent of the value of D_{r0}, are then the critical speeds.

Design and Application of Rail-Transportation Gearing

By D. R. MEIER[1] and J. C. RHOADS,[2] ERIE, PA.

The special requirements of rail-transportation gears are described in this paper together with a description of various types of gear failures. The major design considerations are discussed and methods given for the calculation of gear-tooth stresses. Several charts used in making design calculations are included.

Nomenclature

The following nomenclature is used in the paper:

A, B, A', B' = constants
DP = diametral pitch
F = face width
H_B = Brinell hardness
M = pinion torque
P_1 = load per inch of face per inch of pinion pitch diameter
N = number of teeth in pinion
N_A = number of teeth in action
W = tangential tooth load
d_p = pinion pitch diameter
p = circular pitch
S_b = bending stress
S_c = compressive stress
S_f = endurance-limit value of compressive stress
ϕ = pressure angle
y = Lewis tooth form factor
R = gear ratio

Introduction

Gears have greatly influenced the development of electric drive for rail-transportation vehicles. A summary of various aspects of the design and application of such gearing is presented in this paper, in a form suitable for direct application in design work.

Historical Review

Although some of the early electric motors were gearless with the motor armature directly on the axle, the industry did not progress rapidly until motors were geared to the axle. The early gears were cast and relatively soft, but their quality steadily improved and greater loads were carried as design knowledge was acquired. Gear development has kept pace with motor development, so that as motor constants permitted higher armature speeds, gears were available to utilize these speeds. The progress in traction-motor design in the last 35 years is shown in Fig. 1,

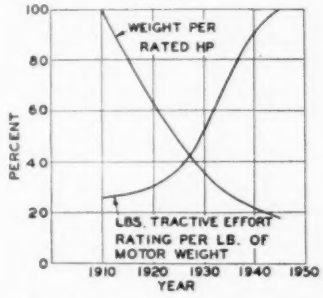


Fig. 1 Progress in Motor Design; Single-Reduction Gearing

prepared from data on motors in service. All of these motors are geared to the axle through single-reduction gearing. The gearing has had a greater effect on the increase in tractive effort per pound weight than on the decrease in weight per horsepower. Tractive effort is a torque function and is therefore directly dependent on gear ratio, whereas increased horsepower per unit weight must be accompanied by fundamental motor-design changes in addition to speed increase.

Application

General Requirements

The requirements for railway gearing are quite different from those of other types of gearing.

Life. The life should be many times that of automotive gearing. Fig. 2 is a view of a pinion taken after 1,500,000 miles

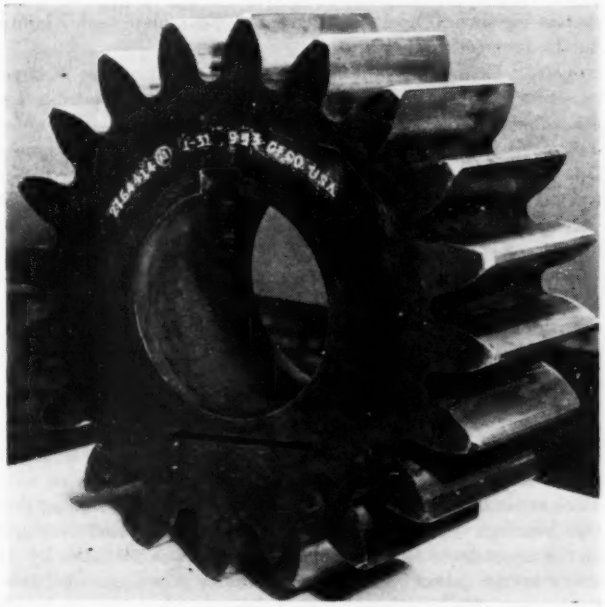


Fig. 2 Condition of Railway Motor Pinion After 1,500,000 Miles of Locomotive Operation

[1] Design Engineer, Mechanical Design Section, Transportation Motor Division, General Electric Co.

[2] Head of Mechanical Design Section, Transportation Motor Division, General Electric Co.

Contributed by the Railroad and Applied Mechanics Divisions and presented at the Annual Meeting, New York, N. Y., Nov. 26–29, 1945, of The American Society of Mechanical Engineers.

Discussion of this paper should be addressed to the Secretary, A.S.M.E., 29 West 39th Street, New York, N. Y., and will be accepted until July 10, 1946, for publication at a later date. Discussion received after the closing date will be returned.

Note: Statements and opinions advanced in papers are to be understood as individual expressions of their authors and not those of the Society.

service, showing negligible wear. The amount of wear depends to a great extent on the maintenance and the type of service. The life of switching-locomotive gears should be measured in hours rather than in miles because of the large amount of low-speed high-torque operation. In most cases automotive gearing can be designed for a finite number of load cycles, below the endurance limit. Railway gearing on the other hand must usually be designed for 10,000,000 or more cycles of load application, which is practically equivalent to designing for the endurance limit.

Loading. The load on railway gears varies from extremely high load at low speeds to a relatively light load at high speeds. There are two general types of duty curves which the motor follows. Fig. 3 shows a comparison of the characteristic curves

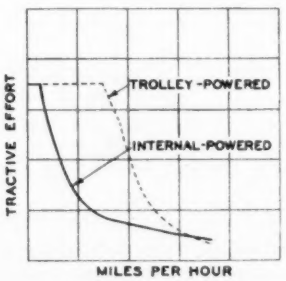


FIG. 3 CHARACTERISTIC CURVES FOR INTERNAL-POWERED AND TROLLEY-POWERED LOCOMOTIVES

for internal-powered locomotives, and trolley locomotives. Because of limited power the internal-powered locomotive develops maximum tractive effort only to a relatively low speed, and as the speed increases the tractive effort decreases, following a constant horsepower curve. The trolley locomotive, with much less of a power limitation, can for a short period develop maximum tractive effort up to several times the speed of the internal-powered locomotive.

Capacity. The gears must have enough capacity to run under adverse conditions of wear and lubrication without complete failure. A gear failure on a locomotive may tie up the whole system for several hours or may cause a complete motor failure due to overspeeding.

Noise. Gear noise is relatively unimportant except in street cars or subways, since the noise of the wheels on the rails and other background noise tends to subordinate the gear noise. This situation will change as reductions are made in other noises. But with operators and passengers relatively far removed from the gears, noise will always be of less consequence on vehicles of this type than on applications where the operating personnel must be very close to the gears.

Backlash. Railway gears are made to operate with backlash that may be considered excessive for some types of gears. It has been found from experience that far less trouble is encountered with excessive backlash than with insufficient backlash, since involute-gear action is independent of backlash.

TYPICAL APPLICATION

Fig. 4 shows a typical axle-hung railway motor. Fig. 5 is a sketch showing the load reactions of such a motor on an axle. The gear-center distance is held by the armature and axle suspension bearings. The motor-armature pinion is carried overhung on the armature shaft. The gear-load reactions are taken by the axle suspension bearings and by the motor nose suspended from the truck. The locating thrust of the motor is taken by flanges on the axle suspension bearings. At maximum gear loads for the direction of rotation of the motor shown in Fig. 5, the reaction

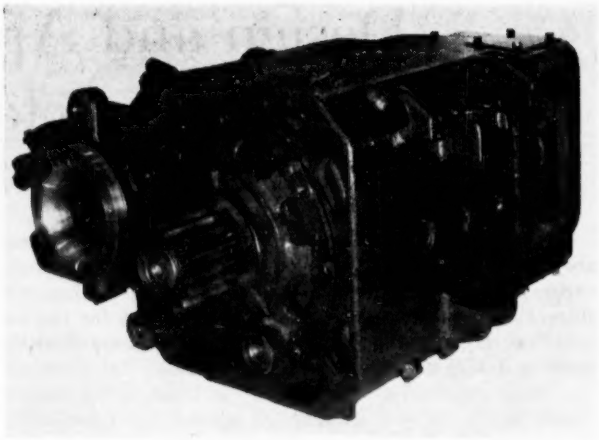


FIG. 4 TYPICAL AXLE-HUNG RAILWAY MOTOR

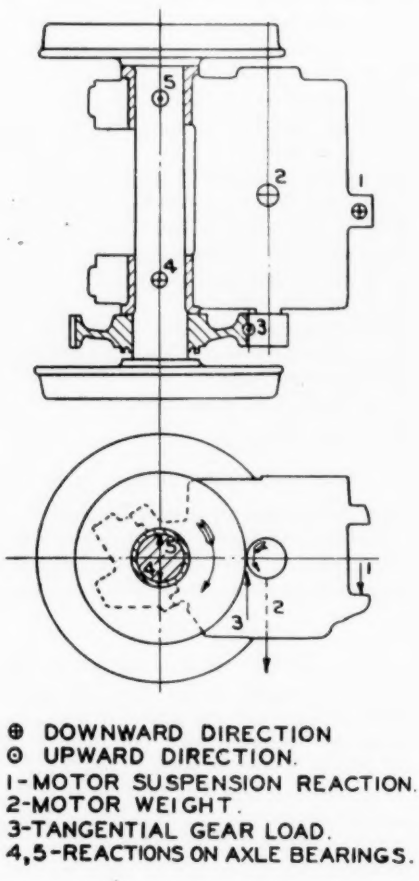


FIG. 5 SKETCH OF RAILWAY MOTOR SHOWING LOAD REACTIONS ON MOTOR PARTS

on the axle bearing adjacent to the gear is down, whereas the reaction on the opposite bearing is up. This results in a misalignment of the gear mesh equal to the bearing clearance divided by the length between bearings.

Gear cases are usually made in two halves with the split on a horizontal plane through the gear centers, to provide easy removal for maintenance and inspection. Considerable clearance is provided in the gear-case fit around the axle to take care of axle-lining wear. Gaskets are not used at the joints. For these rea-

sons lubricants of very high viscosity must be used to keep leakage to a minimum.

In general it is necessary to have motors interchange on axles, although experience is dictating the need for keeping gears and pinions together. Some railroads are removing pinions when a motor is removed. The pinion is then wired to the axle until such time as a new motor is applied, when the proper pinion is mounted on the new motor shaft. Gears that are worn together maintain conjugate tooth action, but a pinion worn with one gear and mated with another will generally have excessively rough tooth action, which may cause loose armature punchings, insulation failures, broken shafts, failed bearings, and actual gear failures.

Typical Failures

There are five general types of failures encountered on railway-type gearing.

Tooth Breakage. Tooth breakage is usually caused by fatigue and occurs rather infrequently in railway applications. Fig. 6

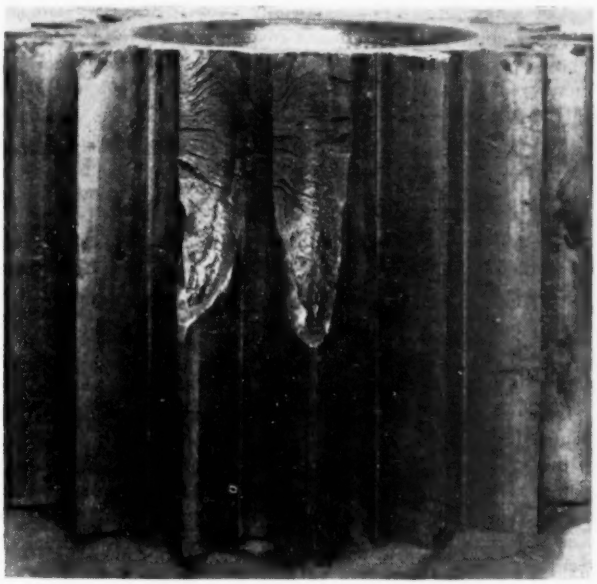


Fig. 6 Fatigue Failure on Railway-Motor Pinion

shows a typical breakage failure. It should be noted that the start of the fatigue crack is usually located some distance in from the more heavily loaded end of the tooth. This may be due to a tendency to shift the load inboard because of local deflections at the end of the tooth. Such a failure necessitates replacement of the broken element, and generally also of the mating member since it is common for a tooth to get caught in the mesh when it breaks out. It is also possible for the armature shaft to be bent when such a failure occurs.

Pitting. Pitting of gearing is a rather common failure caused by too high a compressive stress for the material used (1, 3, 4).[3] It is thought that pitting failures are caused by high subsurface shear stresses, which cause fatigue cracks to form and progress to the tooth surface. It is also thought that the lubricant enters these cracks under high pressure as the tooth undergoes load and causes the crack to progress still further. Finally a small piece of the material breaks out, leaving a craterlike cavity. Quite generally these pits occur near or slightly below the pitch line. In many cases pitting shows up early in the life of a set of gears. Fig. 7 shows pitting on a railway pinion of about 450 Bhn, which has been operated on test at a load exceeding its design limit. A certain amount of pitting does not necessarily mean that gearing must be removed from service, as it is not uncommon for very heavily loaded gears to pit when new, and for the pitting to stop as the gears wear to more nearly full-face contact.

Spalling. Spalling is a type of failure (sometimes termed shelling or flaking) wherein large pieces of the tooth surface may come out almost anywhere on the profile from the root to the tip of the tooth. Fig. 8 shows a spalled motor pinion. This type of failure is generally attributed to improper material, heat-treatment, or processing. Such a failure is far more serious than pitting, because a considerably higher percentage of the surface is removed.

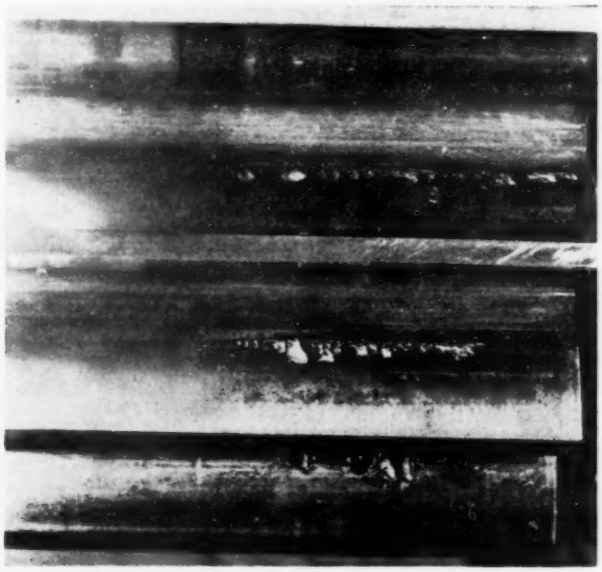


Fig. 7 Pitting of Tooth Surface Due to Excessive Load

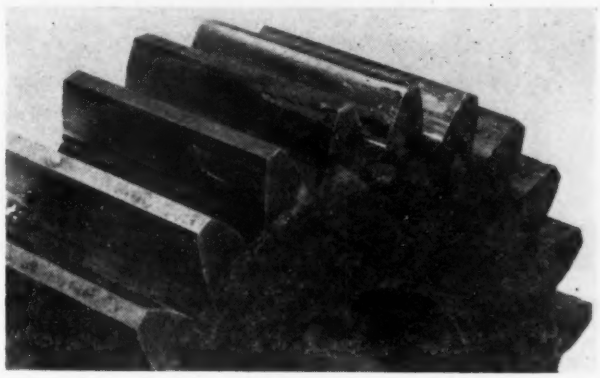


Fig. 8 Spalling of Tooth Surface

Scuffing. Scuffing is caused by metal-to-metal contact between a mating gear and pinion, due either to improper lubricant or to improper lubrication. This phenomenon has been well described in the literature (5). In most railway-gear applications, scuffing is due to lack of lubrication and not to excessive loads or speeds. In some instances, gears that are very heavily loaded at high speeds will scuff even with the proper amount of

[3] Numbers in parentheses refer to the Bibliography at the end of the paper.

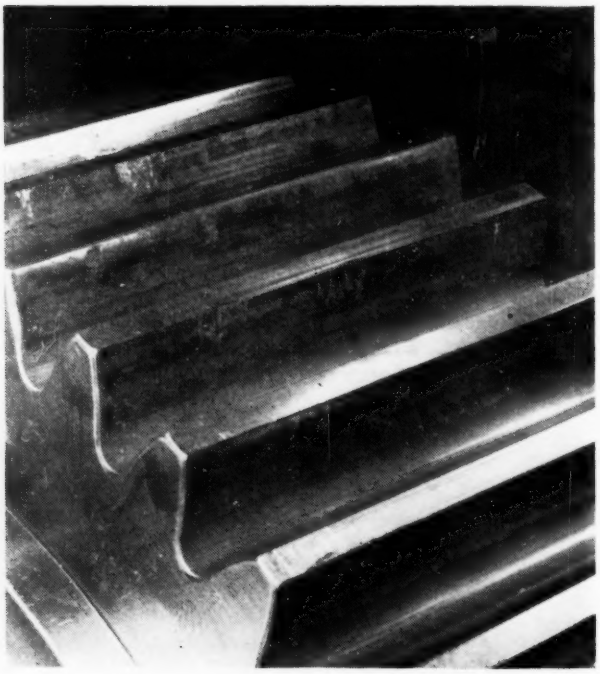


FIG. 9 SCUFFING CAUSED BY IMPROPER LUBRICATION

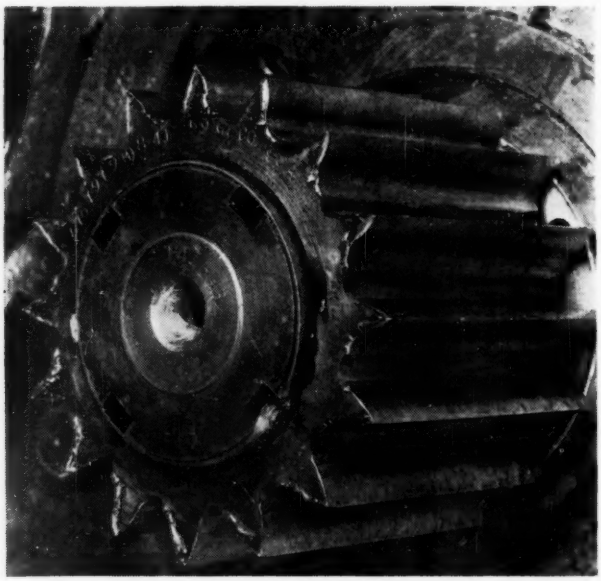


FIG. 10 EXCESSIVE WEAR CAUSED BY INSUFFICIENT LUBRICATION

lubricant, and in such cases extreme-pressure lubricants are indicated. Fig. 9 shows a gear in the early stages of scuffing. It should be noted that the scuffing takes place only where sliding occurs. There is no evidence of scuffing near the pitch line, since in this region little or no sliding takes place. This view also shows fine pitting of a different nature from that shown in Fig. 7. This difference is thought to be due to difference in materials.

Wear. Excessive wear may be caused by insufficient or improper lubrication. Fig. 10 shows what may happen when gears are run without lubricant. Another cause for excessive wear is abrasive material in the lubricant, which acts as a lapping compound and can cause a great amount of wear. Such wear is characterized by a lapped appearance varying from a highly polished to a deeply scratched surface, depending on the size of foreign particles in the lubricant. The scratches are radial from root to tip on the profile.

Experience has shown that where it is possible to provide oil-tight gear cases which will retain lubricants of reasonable viscosity, and which will keep foreign material out of the lubricant, gear wear is negligible.

TYPE OF GEARING USED

Spur gears are used in the majority of railway applications because (*a*) they create no end thrust; (*b*) they are simple in design and easy to manufacture; (*c*) they are interchangeable; (*d*) they are not critical with respect to center distances; (*e*) they have good efficiency.

Other types of gearing such as helical, spiral-bevel, and hypoid are used on special applications where noise, geometry, or other considerations dictate their use.

Axle-hung railway motors usually have antifriction armature bearings, but sleeve-type axle suspension bearings. The axle bearings may operate with relatively large diametral clearance, therefore it is important that the gears used be able to accommodate themselves to the spread in centers which occurs with wear.

DESIGN

MAJOR CONSIDERATIONS

The major considerations in the design of railway gears are as follows:

1 Tooth strength in bending.
2 Tooth surface durability.
3 Tooth proportions.
4 Number of teeth in action.

By far the most important of these is tooth strength. A failure due to tooth breakage may seriously damage the motor or break the mating gear member. Even if no damage results, expensive equipment must be taken out of service to make repairs. Adequate strength for wear must be provided, but excessive wear is not as serious as tooth breakage because replacements can usually be made before complete failure occurs.

Since the traction-motor size and weight are so closely dependent on gear ratio, there is always the incentive to get as much gear reduction as possible on new designs. This applies especially to high-tractive-effort, slow-speed, switching locomotives. The gear diameter is determined by the wheel diameter and the clearance to be provided between the gear case and the rail; therefore the pinion must be reduced in size if higher reductions are to be obtained.

It has been shown, Fig. 3, that the maximum load on the gearing occurs at the lowest speed on the characteristic curve. The pitch-line velocity at this point may be from 200 fpm on internal-powered switching locomotives to 2000 fpm on trolley locomotives. In the case of internal-powered locomotives, on maximum reduction the pitch-line speed is so low as to make dynamic loading negligible; therefore static-stress calculations are used directly. In the case of locomotives where greater pitch-line speeds are used, the calculations are also made on a static-stress basis, but the values of allowable stress are decreased, based on service and test data to allow for increased dynamic loading.

For all stress calculations it will be assumed that the load is uniformly distributed along the face of the tooth. It is realized that this condition cannot be obtained in practice, because of

slight misalignment due to machining errors, bearing wear, and deflection of loaded parts, including the shaft, bearings, pinion, and gear teeth. Therefore, in using the equations of elasticity to calculate stresses, it will be recognized that the assumption of uniform distribution of load is not valid. However, this need not detract seriously from the value of the calculations as long as conventional design proportions, for which service data are available, are used.

Bending Stress

It has been found satisfactory to use the Lewis formula (Appendix 2) for the calculation of bending stress. This is more conservative than methods which involve the number of teeth in action, or methods which are based on applying the load at the highest point on the tooth at which one tooth carries all of the load. However, in a field of service where interchanging of gears and pinions is freely practiced, with the probable result that worn (nonconjugate) profiles will be run together and where operation under adverse conditions occurs frequently, conservatism must be practiced.

It is usually desirable to provide 10 to 15 per cent greater strength in the pinion tooth than in the gear tooth, because of the greater number of revolutions of the pinion with attendant greater wear.

The problem of obtaining sufficient strength in the pinion tooth tends to limit the design, because strengthening the tooth requires coarsening the pitch, which works to the detriment of good tooth action. Stubbing the teeth has the same effect, though in some cases it may be preferable to using a coarser pitch.

In using the Lewis equation for bending, it has been found convenient to express the tooth form factor y, in the form

$$y = \frac{N}{A'N + B'} \quad [1]$$

where A' and B' are arbitrary constants. As is shown in Appendix 2, this equation may be combined with the Lewis equation

$$S_b = \frac{W}{pFy} \quad [2]$$

to give the equation

$$S_b = P_1(AN + B) \quad [3]$$

where P_1 is the pounds per inch of face per inch of pinion pitch diameter.[4]

For three systems of gearing examined by this method, it developed that the constants A and B could be made integral numbers and still have the expression accurate within a few per cent for numbers of teeth between 15 and 35. This satisfactorily covers the range of pinion-tooth numbers normally used. It is not necessary that this expression apply to the gear, since the gear-tooth strength is not limiting.

Equation [3] is convenient for calculating bending stresses because it eliminates the necessity for consulting a table of y factors. Also it utilizes the independent variable P_1 as it is used later in the compressive-stress equation. If the value of P_1 is substituted in Equation [3], together with the value of permissible bending stress, the minimum number of teeth for satisfactory strength may be calculated. If this number turns out to be prohibitively low, an increase in pinion volume will be required, as will be evident from reference to Equation [6].

It will be noted that the foregoing relations do not take stress concentration due to tooth-fillet radii into account. Since practically all of the gearing used on railway motors has continuous-radius fillets, in which the ratio of fillet size to tooth size is approximately a constant, it is assumed that the stress-concentration factor is the same for all teeth.

It is recognized that any method of calculation of tooth bending stress is approximate unless sufficient test data are available to permit the development of empirical relations for correlating bending stress with fatigue life. Such data are obtained from testing machines and actual service.

Compressive Stress

The load is transmitted from pinion to gear through a relatively narrow contact band formed by the elastic deformation of the contacting surfaces. The compressive stress at the contacting surfaces depends on the unit load, the radii of curvature of the surfaces, and the modulus of elasticity. It has been shown that the compressive stress is the criterion for pitting of gear teeth and rollers. The compressive stress also influences the rate of wear of gear teeth when they are loaded below the pitting limit. The equations for calculating the compressive stress between curved surfaces are well known (2). The equation for cylindrical surfaces in contact is easily modified to give the following equation for surface-contact stress at the pitch line of steel gears and pinions[5]

$$S_c = 3240 \sqrt{\frac{P_1(1 + 1/R)}{\sin \phi \cos \phi}} \quad [4]$$

For 20-deg pressure-angle gearing, this reduces to

$$S_c = 5710 \sqrt{P_1(1 + 1/R)} \quad [5]$$

Equation [4] shows that the effect of increasing the pressure angle is to lower the compressive stress. It also shows that the compressive stress is independent of the number of teeth for a given diameter and ratio. The criterion for severity of loading is the variable P_1, the pounds per inch of face, per inch of pinion-pitch diameter. It has already been shown that this variable can conveniently be used to calculate bending stress.

To facilitate the calculation of compressive stress, the curves shown in Fig. 11 are used. These curves show the compressive stress as a function of the unit loading P_1, for the various gear ratios and pressure angles. They serve equally well for calculating the stress on existing gear sets or for designing new gear sets.

By combining the tangential-load equation $W = 2M/d_p$ with $P_1 = W/d_pF$, the relationship

$$d_p^2F = \frac{2M}{P_1} \quad [6]$$

is obtained. This equation shows that the pinion volume is proportional to the torque and inversely proportional to P_1. The value of P_1 may be established by choosing the value of compressive stress and referring to the curves of Fig. 11. The same result may be obtained by combining Equations [4] and [6] to give

$$d_p^2F = \frac{2M\ (1 + 1/R)}{\left(\frac{S_c}{3240}\right)^2 \sin \phi \cos \phi} \quad [7]$$

This relationship shows that the volume of the pinion-pitch cylinder is inversely proportional to the square of the compressive stress. Where weight and space are important the use of high compressive stresses is therefore necessary.

[4] This method applied to the 20-deg full-depth system, for which y factors are given in reference (1), leads to the equation $S_b = P_1(2N + 22)$. This equation has an error of less than 2 per cent between 15 and 35 teeth.

[5] For internal gears the $1/R$ term has a minus sign.

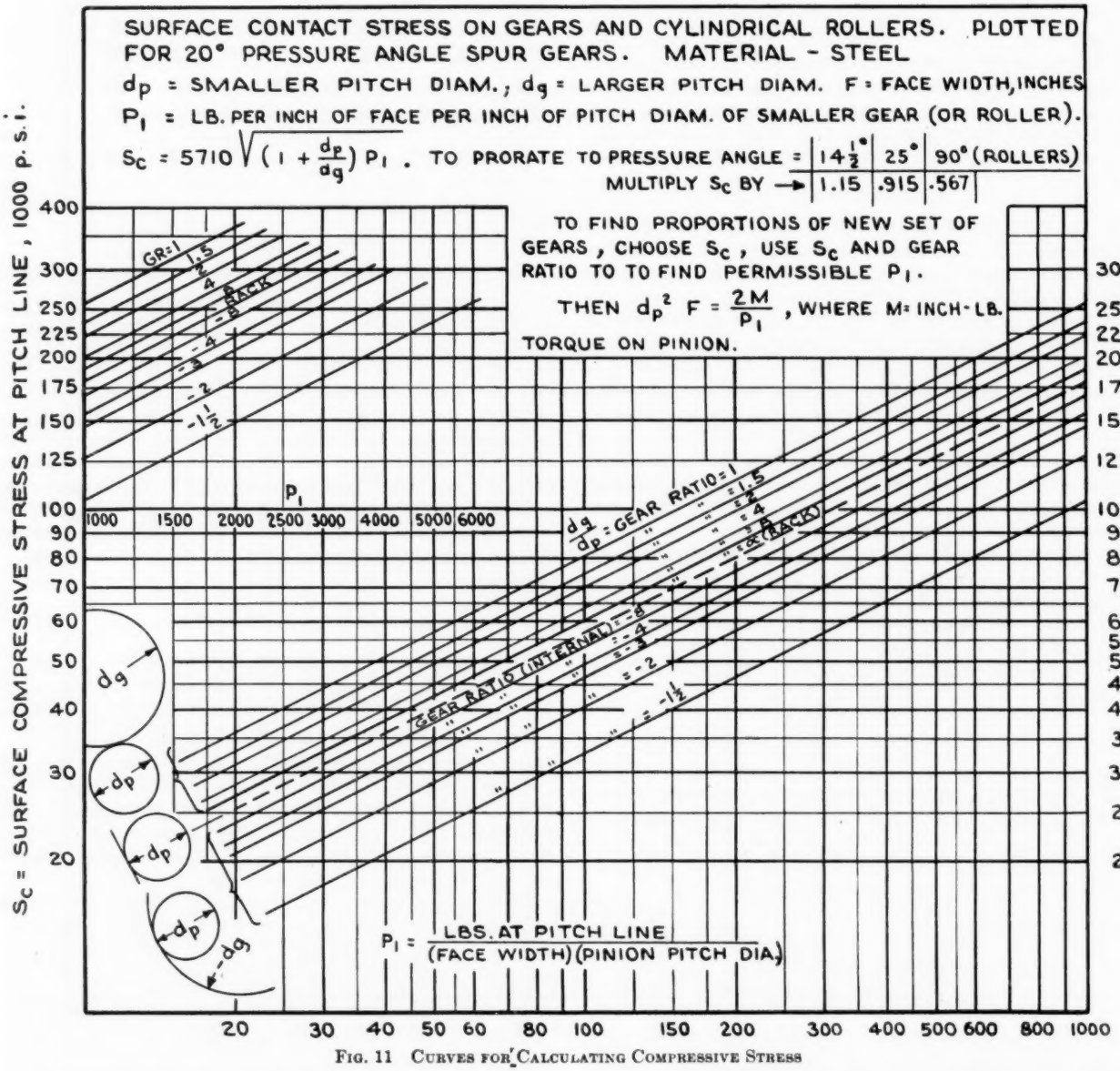


FIG. 11 CURVES FOR CALCULATING COMPRESSIVE STRESS

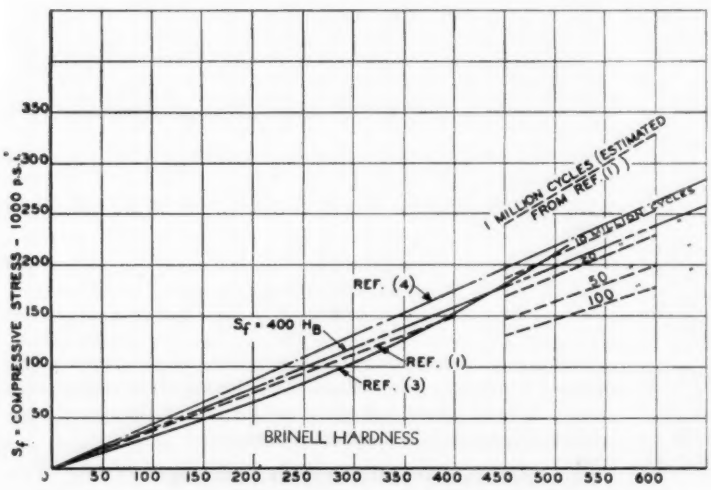


FIG. 12 SURFACE ENDURANCE LIMIT FOR STEEL

The magnitude of the compressive stress which will give satisfactory life may be judged by the designer from experience. Data from various tests are also available. Data from the tests of Way (3), and Niemann (4) and also the data given by Buckingham (1) are plotted in Fig. 12. These curves show that the endurance limit of steel in surface compression is approximately

$$S_f = 400(H_B) \quad [8]$$

Since the tensile strength is about 500 times the Brinell hardness number, the endurance limit for surface compression is roughly 80 per cent of the tensile strength.

The applicability of roll-test data to gear design may be questioned but it has been the authors' experience that gears will operate successfully at stresses approaching the value of 400 times the Brinell hardness. This experience covers quite a wide variety of designs, including different types of materials, heat-treatments, and

manufacturing methods, together with various designs of gear elements and mountings. Just how close to this value the gears may be stressed depends on (*a*) how much dynamic load will be superimposed on the static load (a function of the pitch-line speed, the mass and stiffness of the connected parts, and the errors in various parts, particularly the gears); (*b*) how well the load will be distributed over the tooth length; (*c*) the life expected in the gearing, (*d*) other factors such as surface finish, etc.

Fig. 13 has been plotted from Equations [7] and [8] to show the relationship between pinion-torque capacity per unit volume and material hardness.

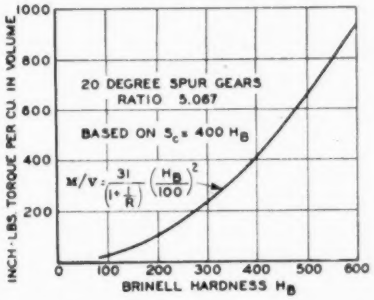


FIG. 13 RELATION OF PINION-TORQUE CAPACITY TO MATERIAL HARDNESS

The ratio of bending stress to tensile strength tends to be higher for hard materials than for soft materials, assuming that in each case the material is loaded to its compressive-stress endurance limit. This is illustrated in Table 1. This table shows that as advantage is taken of harder materials for carrying higher loads, bending failures are more likely to occur than pitting failures.

TABLE 1 15-TOOTH, 2½ DIAMETRAL-PITCH PINION, 76/15 RATIO, 20-DEG-PRESSURE-ANGLE FULL-DEPTH INVOLUTE

Brinell hardness, Bhn	300	600
Approximate tensile strength, psi	150000	300000
$S_c = 400\ (H_B)$	120000	240000
P_l = lb per in. per in.	441	1764
$S_b = P_l\ (2N + 22)$	22900	91600
Ratio (S_b/ultimate strength)	0.153	0.306

PROPORTIONS

There are many different systems of spur gearing in use, involving different pressure angles and tooth proportions. Fig. 14 shows a comparison between four different designs of the same ratio. The 14½-deg and 20-deg-pressure-angle designs with standard proportions are well known. The 20-deg and 25-deg long- and short-addendum designs are growing in popularity.

Gearing of higher pressure angles operates at lower compressive stress for the same unit loading. The relative magnitudes of compressive stress at the pitch line on 14½-deg, 20-deg, and 25-deg pressure-angle gearing are 100 per cent, 87 per cent, and 79.5 per cent, respectively. Also the higher-pressure-angle systems have teeth of superior strength in bending.

When the number of teeth in the pinion is small it may be necessary to undercut the tooth to provide clearance for the tip of the gear tooth as it goes through action. For full-depth involute systems, this occurs when the number of teeth is 32 or less on 14½-deg pressure angle, and 18 or less on 20-deg pressure angle.

Fig. 14 shows the amount of undercut present in each design. There is no undercut present in the 20-deg and 25-deg long- and short-addendum designs. Undercutting weakens the tooth and decreases the number of teeth in action. It will be noted that the 14½-deg design is so badly undercut as to make it undesirable for use on power-transmission systems, because there are only 1.049 teeth in action. This does not provide sufficient overlap in

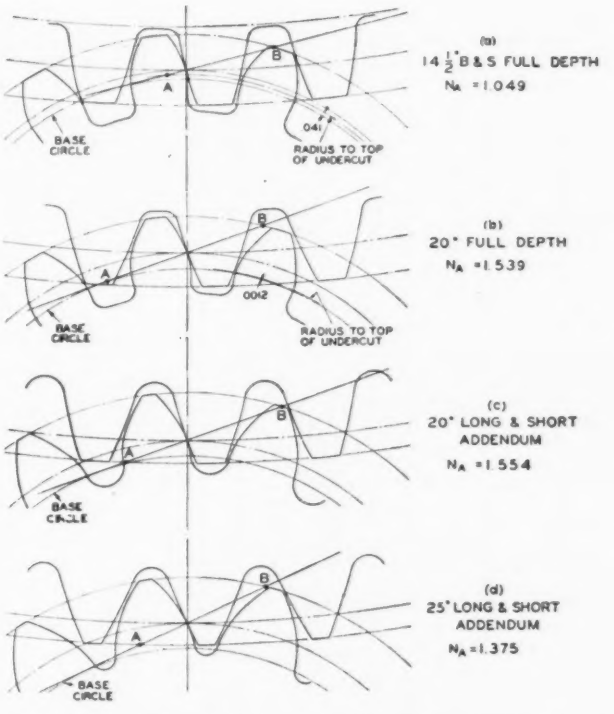


FIG. 14 GEAR-TOOTH ACTION; COMPARISON OF INVOLUTE-TOOTH FORMS

(Ratio 76/15. Duration of contact points *A* to *B*.)

tooth action between adjacent teeth to transmit the load smoothly.

Since there is frequent use of pinions of as few as 15 teeth in railway-motor design, it is not desirable to use a design of gearing in which the pinion must be undercut. It has been found advantageous to use 20-deg-pressure-angle long- and short-addendum gearing. The combination most often used is one in which the pinion addendum is approximately 35 per cent longer, and the addendum of the gear 35 per cent shorter than the standard proportions of $1/DP$. When these addenda are used, the pinion tooth is made thicker than standard to balance the strength between the gear and the pinion.

Fig. 15 shows a 20-deg-pressure-angle tooth laid out to these proportions, together with some other tooth designs for comparison. The heavy lines on the tooth surfaces show the portions of

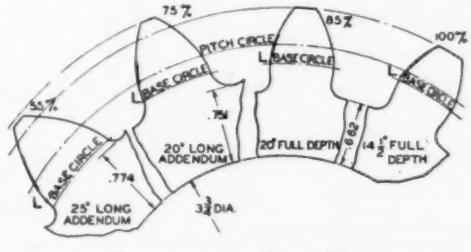


FIG. 15 COMPARISON OF TOOTH PROPORTIONS

the profiles on which full load is taken by one tooth. The percentage figures represent comparative bending stresses for equal loading. The dots on the tooth surfaces marked "L" are located at the lowest points of contact. The 25-deg tooth has the same width of top land as the 20-deg long-addendum tooth. Both are proportioned so that the pinions and their mating gears may be

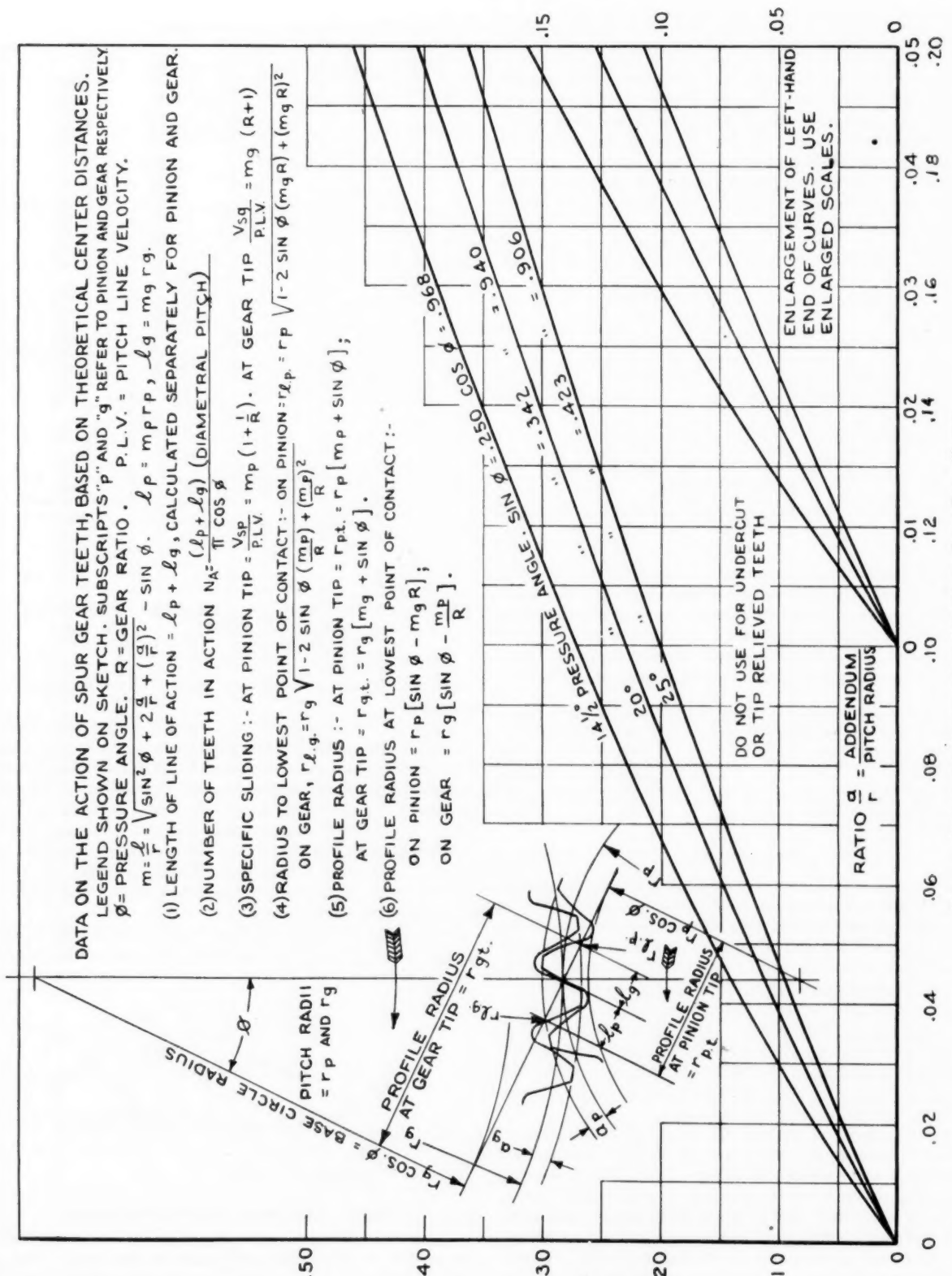


FIG. 16 CHART FOR CALCULATING ACTION OF SPUR-GEAR TEETH

cut with the same hob. This results in slightly less addendum on the 25-deg tooth design.

The principal advantages of the 20-deg and 25-deg long-addendum designs are as follows:

1 There is no undercutting of the tooth, even on a 15-tooth pinion.

2 Greater tooth strength is provided.

3 The root diameter is larger. This permits the use of a larger shaft for the same metal section between tooth root and bore, or a thicker metal section for the same shaft size. The 25-deg tooth has the disadvantage that the number of teeth in action is relatively low, Fig. 14.

The design of the root fillet radius was never given serious attention until it was discovered that the fatigue life in bending was greatly influenced by the stress concentration at the fillet. The development of the continuous-radius fillet began about 1930. It is now widely used for all heavily loaded gearing where tooth breakage is a problem. The continuous-radius fillet is formed by a cutting tool having a round-nosed tip. When the tool is used to cut the particular number of teeth for which it was designed, the fillet radius will be a portion of the arc of a circle, tangent to the tooth profile at a point just below the lowest point of contact. When a different number of teeth is cut, the fillet radius is a compound radius still tangent to the profile. In the case of form-ground teeth the fillet radius may always be an arc of a single radius.

The continuous-radius-fillet design reduces the stress-concentration factor in bending to a minimum, because it gives the maximum fillet radius possible for a given design.

Number of Teeth in Action

The tooth proportions normally used result in a number of teeth in action between 1 and 2. There is usually no attempt to obtain a minimum of two teeth in action.

During the first phase of contact on a particular tooth, two teeth work together to carry the load. In the next phase, one tooth carries the load alone, and in the final phase two teeth share the load. The average number of teeth in contact varies from 1.5 to 1.7 for most designs. This number may be permitted to go considerably lower, possibly to 1.35, without disturbing seriously the smoothness of action. However, the calculation of compressive stress at the pitch line only may not be adequate for such a case, because, at the beginning of the period when the total load is carried by one tooth, contact will take place considerably below the pitch line where the radius of curvature of the pinion-tooth profile is appreciably less than at the pitch line, with correspondingly higher compressive stress. This is illustrated in Fig. 15. A comparison of the 20-deg long- and short-addendum design with the 20-deg full-depth design shows that the former has an advantage in this respect.

Figs. 14 (*c*) and (*d*) show that contact between the pinion and the gear begins at point A, where the outside diameter of the gear intersects the line of action (pinion driving). Contact ends at point B, where the outside diameter of the pinion cuts the line of action. At any instant the number of teeth in action is an integral number, usually 1 or 2. The average number of teeth in action is found by dividing the length of the line of action AB by the base pitch. The base pitch is the distance between adjacent teeth measured along the line of action and is equal to $\frac{\pi}{DP}\cos\phi$.

It will be noted that contact does not begin as described in the preceding paragraph for the designs in Fig. 14 (*a*) and (*b*), because the pinion teeth are undercut to obtain clearance for the tip of the gear tooth. Contact begins at the intersection of the line of action with the circle formed by the radius to the top of the undercut. It will be noted in Fig. 14 (*b*), that even a very slight undercut shortens the line of action considerably.

The calculation of the number of teeth in action is facilitated by the use of the chart, Fig. 16.

This chart also shows a method for calculating some other items of interest in design. While this chart is marked for use only when the gears being studied are to be operated on theoretical centers, it may be used for nonstandard centers provided that the operating addenda, pitch radii, and pressure angles are used.

BIBLIOGRAPHY

1 "Manual of Gear Design, Section Two," by Earle Buckingham, *Machinery*, vol. 43, 1935, pp. 143–145.

2 "Strength of Materials, Part 2," by S. Timoshenko, second edition, D. Van Nostrand Co., Inc., New York, N. Y., 1941, p. 358.

3 "Westinghouse Roller and Gear Pitting Tests," by Stewart Way, paper presented at 24th Annual Meeting of the American Gear Manufacturers Association, May, 1940.

4 "Walzenfestigkeit und Grübchenbildung von Zahnrad- und Wälzlager-Werkstoffen," by G. Niemann, *Zeitschrift des Vereines deutscher Ingenieure*, vol. 87, 1943, pp. 521, 522, 523.

5 "Dimensional Value of Lubricants in Gear Design," by J. O. Almen, *S.A.E. Journal*, vol. 50, 1942, pp. 373–380.

Appendix 1

Gear-Tooth Action

The transfer of power from one involute gear to another may be compared to the action of a crossed belt, Fig. 17. Since the base circles bear the same relation in diameter to each other as do the pitch circles, there will be rolling contact at the pitch point (provided there is no belt slippage) just as in mating involute gears. The "line of action" will be represented by the tight or driving side of the belt.

The tooth profile is generated in a manner geometrically equivalent to tracing a line with a pencil attached to a string as it is unwound from the base circle, as shown in Fig. 18. The string is analogous to the line of action of Fig. 17. It is evident that the involute curve is everywhere normal to the string used for its construction. Likewise, in involute gears the tooth profiles are always normal to the line of action.

Rolling contact exists in involute gears only at the pitch point. On either side of this point the tooth surfaces slide relative to

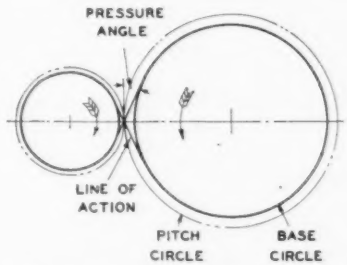


Fig. 17 Crossed-Belt Analogy

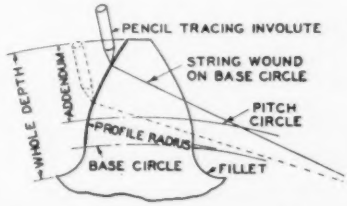


Fig. 18 Tooth Cross Section, Showing Method of Tracing Involute

each other, the sliding increasing in magnitude with increasing distance from the pitch point. For the 20-deg long- and short-addendum design, maximum sliding velocity occurs at the tip of the pinion tooth. Specific sliding is defined as the ratio of the sliding velocity to the pitch-line velocity. Fig. 16 shows a method of calculating the specific sliding at the tooth tips.

Appendix 2

The value of the tooth form factor y may be expressed as

$$y = \frac{N}{A'N + B'} \quad [9]$$

where A' and B' are arbitrary constants.

This expression for y is substituted in the Lewis equation

$$S_b = \frac{W}{pFy} \text{ to give } S_b = \frac{W(A'N + B')}{pFN} \quad [10]$$

Since the circular pitch

$$p = \frac{\pi}{DP} \quad [11]$$

then

$$pN = \frac{\pi}{DP}(N) = \pi d_p \quad [12]$$

Substituting this in Equation [10]

$$S_b = \frac{W}{\pi d_p F}(A'N + B') = \left(\frac{W}{d_p F}\right)(AN + B) \quad [13]$$

By definition

$$P_1 = \frac{W}{d_p F} \quad [14]$$

therefore

$$S_b = P_1(AN + B) \quad [15]$$

Local Stress Distribution in Cylindrical Shells

By LEON BESKIN,[1] DOWNEY, CALIF.

The stress distribution in cylindrical shells with light frames is very different from the conventional beam distribution in the neighborhood of the applied loads. The problem is examined hereafter for circular cylinders with circular frames of constant section. The case of an indefinite shell with one loaded frame is examined in detail, and diagrams are given for the following unit conditions: Concentrated radial force, tangential force, couple.

Nomenclature

The following nomenclature is used in the paper:

A, a = total frame-section area and equivalent area for shear

B, b_k = applied local couple and coefficient of trigonometric development (in a frame)

C = structure constant (Equations [34])

D = rigidity factor (Equation [30]): $\frac{1}{D_{k,j}} = \frac{1-\eta_j}{R^2}\left[\frac{\mu_{k,j}^2}{I_j} + \frac{\varphi_k^2}{A_j} + \frac{E}{G}\frac{\sigma_k^2}{a_j}\right]$

e = eccentricity

E, G = moduli of the material

F = axial force in frame

h = effective thickness of skin (stringers included)

H = load constant (Equations [35])

I = moment of inertia of frame

j = reference number of frame

k = reference number of harmonic

K = constants (Table 3)

L = distance between frames

M = moment in frame

M_x, M_y, M_z = external moments on structure

m, n = constants (Equation [39])

N = normal flow in beam

P, p_k = applied radial load and coefficient (in frame)

Q, q_k = applied shear flow (in frame)

R = radius of shell

S = shearing force in frame

t = effective thickness in shear

T = shear flow in beam

V = load constant (Equations [31])

W = strain energy

X, Y, Z = external loads on structure

x, y, z = axes of reference (z along the axis of beam)

α, β = constants (Table 1)

γ, δ, δ' = constants (Equations [38]): $\delta_k = \frac{ED_kL}{Gtk^2}$; $\delta'_k = \frac{D_kL^3}{hR^2}$

Γ_0 = concentrated load (Equation [62])

Δ = constants (Equations [66])

ϵ' = constant (Equation [40])

λ = constant (Equation [41])

μ = constant (Equation [26])

$$\mu_{k,j} = \frac{R^2}{k^2}\left(\frac{1}{k_2 - 1} - \eta_j\right); \quad \bar{\mu}_{k,j} = -\mu_{k,j}$$

$\eta = e/R$

ξ = constant (Equation [38])

φ = constant (Equation [26])

$$\varphi_k = -\frac{R^2}{k^2 - 1}; \quad \bar{\varphi}_k = -\varphi_k$$

ψ = constant (Equation [37])

σ = constant (Equation [26])

$$\sigma_k = -\frac{R^2}{k(k^2 - 1)}; \quad \bar{\sigma}_k = \sigma_k$$

ρ = constant (Equation [47])

θ = angle (Fig. 2)

Ω = constant (Equation [19])

$$\Omega_{k,j} = \frac{N_{k,j+1} - N_{k,j}}{L_{j+1}} + \frac{N_{k,j-1} - N_{k,j}}{L_j}$$

Introduction

It is well known that the actual stress distribution in beams constituted by a thin skin with light frames is very different from the distribution given by the conventional beam theory. Especially, when one frame only is loaded, the conventional methods lead to excessive bending moments in the loaded frame, and zero bending in the adjacent frames. Actually, the total moment calculated by conventional methods is distributed between the loaded frame and the adjacent frames, and the shear distribution in the beam near the loaded frame does not coincide with the conventional distribution. However, the conventional distribution is reached at some distance from the loaded frame, and this distance defines the region in which all the frames are subjected to bending.

The object of this paper is the analysis of the stress in the neighborhood of a load acting on a thin circular beam with light frames. The analysis applies to circular beams with a skin of uniform thickness and equally spaced equal stiffeners, and with frames of constant section.

The method of analysis applied in this paper has been used under restrictive conditions by N. J. Hoff,[2] this author having neglected the influence of the eccentricity of the frames and of the axial and shearing deformations. In the case of light frames and concentrated loads, the two first factors given cannot be neglected, and the diagrams which follow show that their con-

[1] Design Specialist, Vultee Field Division, Consolidated-Vultee Aircraft Corporation.

Contributed by the Applied Mechanics Division and presented at the Annual Meeting, New York, N. Y., November 26–29, 1945, of The American Society of Mechanical Engineers.

Discussion of this paper should be addressed to the Secretary, A.S.M.E., 29 West 39th Street, New York, N. Y., and will be accepted until July 10, 1946, for publication at a later date. Discussion received after the closing date will be returned.

Note: Statements and opinions advanced in papers are to be understood as individual expressions of their authors and not those of the Society.

[2] "Stresses in a Reinforced Monocoque Cylinder Under Concentrated Symmetric Transverse Loads," by N. J. Hoff, Journal of Applied Mechanics, Trans. A.S.M.E., vol. 66, 1944, p. A-235.

sideration may lead to double the moments obtained by the approximate theory.

These results apply only for light frames, because cylindrical shells with a circular section and a skin of constant thickness do not warp under the action of a shear distributed according to the beam theory. Thus, if the frames do not deflect under the applied loads, the deflected sections of the beam remain plane under the action of the shear strain, and the conventional beam distribution can be applied. The lateral extension due to Poisson's ratio effect is neglected hereafter, because the corresponding skin deformations are incompatible with the frame deformation. This effect is negligible in the case of a thin skin, a narrow strip of which follows the frame deformations without appreciably modifying the general equilibrium. This strip must be included in the frame section properties. It is assumed that only the frames have a bending rigidity, and that the stiffeners are submitted to axial loads only.

The general method is developed in part 1. Trigonometric developments are used to represent stresses, loads, and deflections. Each harmonic corresponds to a problem which is the mathematical analogue of the problem of a beam with elastic supports which coincide with the frames of the actual beam. In part 2, the general method is applied to the determination of the stress distribution in a loaded frame of an indefinite shell, in the two cases, intermediate frame, end frame. Diagrams are given for three unit loadings of an intermediate frame (concentrated loads): (1) Radial force; (2) tangential force; (3) couple (axis parallel to the center line).

PART 1 GENERAL METHOD OF ANALYSIS

Equilibrium of Shell

All the applied loads are concentrated at the frames, so that there is no hoop tension, and the state of stress is defined by the following:

N = normal stress flow in skin in direction of generators
T = shear flow in skin in direction of generators and perpendicular direction

Because there are no surface loads, the shear flow T is constant along a generator between two consecutive frames.

The relation of equilibrium between N and T is

$$\frac{\partial N}{\partial z} + \frac{1}{R}\frac{\partial T}{\partial \theta} = 0 \qquad [1]$$

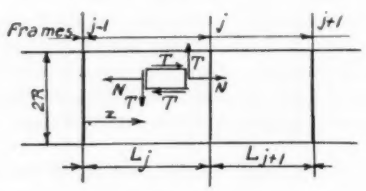


Fig. 1

in which (Fig. 1)

z = distance along center line of shell
θ, R = angle defining point of circumference and radius of shell

Since T is a function of θ only, N is a linear function of the abscissa x between two consecutive frames.

Let

L_j = distance between consecutive frames numbered $j-1, j$
$N_j(\theta)$ = value of N along frame j
$T_j(\theta)$ = value of T in span j

In a span j, by application of Equation [1], it is found

$$T = T_j(\theta) = -\int \frac{\partial N}{\partial z} R d\theta = -\int \frac{R}{L_j} [N_j(\theta) - N_{j-1}(\theta)] d\theta. \qquad [2]$$

$N_j(\theta)$ can be represented by a trigonometric series

$$N_j(\theta) = N_{0,j} + N_{1,j}\cos\theta + \overline{N}_{1,j}\sin\theta + \ldots\ldots + N_{k,j}\cos k\theta + \overline{N}_{k,j}\sin k\theta + \ldots \qquad [3]$$

By substitution of Expression [3] in Equation [2], it is found

$$T_j(\theta) = T_{0,j} + \frac{R}{L_j}\sum_{K=1}^{\infty}\frac{1}{k}[(\overline{N}_{k,j} - \overline{N}_{k,j-1})\cos k\theta - (N_{k,j} - N_{k,j-1})\sin k\theta] \ldots\ldots [4]$$

The terms $N_{0,j}$ disappear from Equation [4] because they have the same value at both ends of each span, since they correspond to a constant axial load.

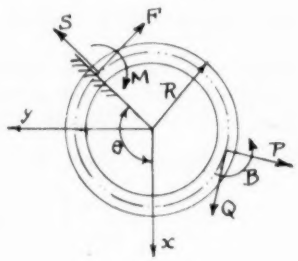


Fig. 2

Equilibrium of Frames

Let (Fig. 2)

$M_j(\theta)$; $S_j(\theta)$; $F_j(\theta)$ = bending moment, shearing force, axial force, respectively, in a frame numbered j
$P_j(\theta)$; $Q_j(\theta)$; $B_j(\theta)$ = radial loads, tangential loads, distributed couples, respectively, acting on a frame on a unit length of circumference

These loads are composed of external forces which are designated by P^*, Q^*, B^*, respectively, and of differences between shear flows T acting on the two sides of a frame, which give tangential loads Q and couples B in the frames, due to the frame eccentricity.

Term e_j being the distance between the shell and the neutral line of the frame (eccentricity of the frame), the couples B due to the shears are equal to $Q\eta_j R$, in which $\eta_j = e_j/R$.

The resulting loads on a frame due to the external loads and the differences of shear flows from the shell are developed in trigonometric series, in which, for simplicity, index j is omitted.

Normal loads

$$P = p_0 + \sum_k p_k \cos k\theta + \sum_k \bar{p}_k \sin k\theta \ldots\ldots [5]$$

Tangential loads

$$Q = q_0 + \sum_k \bar{q}_k \cos k\theta + \sum_k q_k \sin k\theta \ldots\ldots [6]$$

Couples

$$B = R\left[b_0 + \sum_k \bar{b}_k \cos k\theta + \sum_k b_k \sin k\theta\right] \ldots\ldots [7]$$

The external loads are represented by expressions similar to Equations [5], [6], [7], in which all quantities are starred (P^*, ... b_k^*). Their resultants are

$$\left.\begin{array}{ll} X = \pi R(p_1^* - q_1^*); & M_x = \pi R N_1; \\ Y = \pi R(\bar{p}_1^* + \bar{q}_1^*); & M_y = -\pi R N_1; \\ Z = 2\pi R N_0 & M_z = 2\pi R(b_0^* - q_0^*) \end{array}\right\} \quad [8]$$

The constant term p_0^* represents a uniform pressure on a frame and is disregarded, since it produces a simple hoop load in the frame. The coefficients p, q, b, N, which do not appear in Equations [8], can be considered as "perturbations," while the terms which appear in Equations [8] represent the conventional beam distributions.

Terms q_0^*, b_0^* correspond to an applied torque, and the condition of equilibrium is

$$q_0^* - b_0^* = 0 \quad [9]$$

These terms do not cause any bending or axial load in the frame, and the shearing force in the frame is constant

$$S = s_0 = -Rq_0 \quad [10]$$

Terms N_0, N_1, $\bar{N}_1$ are distributed according to the beam theory and do not produce any stress in the frames.

Terms p_1^*, q_1^*, $\bar{p}_1^*$, $\bar{q}_1^*$, correspond to a transversal resultant passing through the center of the frame. The corresponding conditions of equilibrium are

$$p_1 - q_1 = 0; \quad \bar{p}_1 + \bar{q}_1 = 0 \quad [11]$$

Replacing p_1 by q_1 and $\bar{p}_1$ by $-\bar{q}_1$, the quantities M, S, F, can be represented by the expressions

$$\frac{M}{R^2} = (b_1 \cos\theta - \bar{b}_1 \sin\theta) + \sum_{K=2}^{\infty} \left\{ \left[\frac{kp_k - q_k}{k^2 - 1} + b_k \right] \frac{\cos k\theta}{k} + \left[\frac{k\bar{p}_k + \bar{q}_k}{k^2 - 1} - b_k \right] \frac{\sin k\theta}{k} \right\} \quad [12]$$

$$\frac{S}{R} = -q_0 - \sum_{K=2}^{\infty} \left[\frac{kp_k - q_k}{k^2 - 1} \sin k\theta - \frac{k\bar{p}_k + \bar{q}_k}{k^2 - 1} \cos k\theta \right] \quad [13]$$

$$\frac{F}{R} = (q_1 \cos k\theta - \bar{q}_1 \sin k\theta) - \sum_{k=2}^{\infty} \left[\frac{p_k - kq_k}{k^2 - 1} \cos k\theta + \frac{\bar{p}_k + k\bar{q}_k}{k^2 - 1} \sin k\theta \right] \quad [14]$$

These expressions satisfy the equations of equilibrium of the frame

$$\frac{dM}{d\theta} + RB - RS = 0; \quad \frac{dS}{d\theta} + RP - F = 0; \quad \frac{dF}{d\theta} + RQ + S = 0 \quad [15]$$

They also satisfy the conditions of compatibility of deformation; this can be verified in a straightforward manner by application of methods of strain energy to the terms corresponding to k greater than 1 and to the terms b_1, $\bar{b}_1$, q_0. The application of strain-energy methods to the terms q_1, $\bar{q}_1$ leads to a modification of Equations [12], [13], [14], but this conclusion is incorrect, because of an inconsistency of the conventional formulas for rings, which can be shown as follows:

The radius of a segment of a ring does not change under the action of an axial force, but the angle of the segment is modified. Under the action of forces of the type $q_1 \cos\theta$, the total angle for the ring does not change, which shows that no bending is required to close the ring and that the foregoing solution is correct. The coefficients q_1, $\bar{q}_1$ being defined by Equations [11] are disregarded hereafter.

Condition of Deformation

Deformations are examined hereafter by strain-energy methods. The strain energy of the structure is decomposed as follows, (even terms only are written, which correspond to cos $k\theta$ for normal stresses, normal forces and couples, and to sin $k\theta$ for shears):

(*a*) *Axial Stresses in Shell Between Two Frames, $j-1$, j.* Integration of $[N(\theta)]^2 d\theta$, with

$$N(\theta) = \frac{z}{L_j} \sum N_{k,j} \cos k\theta + \frac{L_j - z}{L_j} \sum N_{k,j-1} \cos k\theta \quad [16]$$

leads to an expression of the strain energy in the form of a sum of factors $W_{N,k,j}$

$$2W_{N,k,j} = \frac{\pi R L_j}{3Eh_j} (N_{k,j}^2 + N_{k,j-1}^2 + N_{k,j} N_{k,j-1}) \quad [17]$$

h is the effective skin thickness, which includes the correction for buckling and for the stringers (which are replaced by an equivalent skin).

(*b*) *Shearing Stresses in Shell Between Two Frames, $j-1$, j.* Integration of $[T(\theta)]^2 d\theta$ leads to an expression of the strain energy in the form of a sum of factors $W_{T,k,j}$

$$2W_{T,k,j} = \frac{\pi R^3}{G t_j L_j k^2} (N_{k,j} - N_{k,j-1})^2 \quad [18]$$

in which t_j is the skin gage to be used for shear.

(*c*) *Stresses in a Frame j.* The forces applied to a loaded frame are the external loads, defined by p_k^*, q_k^*, b_k^*, and the eccentric shear flows in the shell. A term $q_{k,j}$ due to shear flow is

$$q_{k,j} = \frac{R\Omega_{k,j}}{k}; \quad \text{with } \Omega_{k,j} = \frac{N_{k,j+1} - N_{k,j}}{L_{j+1}} + \frac{N_{k,j-1} - N_{k,j}}{L_j} \quad [19]$$

$\Omega_{k,j}$ represents the change of slope of the $N_{k,j}$ diagram at the frame j. The couple corresponding to $q_{k,j}$ is

$$q_{k,j} e_j = R\eta_j q_{k,j}$$

Thus, the quantities p, q, b are defined as follows:

Frame submitted to external loads

$$p_{k,j} = p_{k,j}^*; \quad q_{k,j} = q_{k,j}^* + \frac{R}{k}\Omega_{k,j}; \quad b_{k,j} = b_{k,j}^* + \frac{R\eta_j}{k}\Omega_{k,j} \quad [20]$$

Redistributing frame

$$p_{k,j} = 0; \quad q_{k,j} = \frac{R}{k}\Omega_{k,j}; \quad b_{k,j} = \frac{R\eta_j}{k}\Omega_{k,j} \quad [21]$$

The quantities which appear in the expressions of M, S, F (Equations [12], [13], [14]) can be grouped as follows (because of difference of signs, both odd and even terms are written)

$$\left.\begin{array}{l} M = \sum M_{k,j} \cos k\theta + \sum \bar{M}_{k,j} \sin k\theta \\ S = \sum S_{k,j} \sin k\theta + \sum \bar{S}_{k,j} \cos k\theta \\ F = \sum F_{k,j} \cos k\theta + \sum \bar{F}_{k,j} \sin k\theta \end{array}\right\} \quad [22]$$

with the relations

$$\left.\begin{array}{l} M_{k,j} = \dfrac{R^2}{K}\left[\dfrac{kp_{k,j} - q_{k,j}}{k^2 - 1} + b_{k,j}\right] = M_{k,j}^* - \Omega_{k,j}\mu_{k,j} \\ \bar{M}_{k,j} = \dfrac{R^2}{K}\left[\dfrac{k\bar{p}_{k,j} + \bar{q}_{k,j}}{k^2 - 1} - \bar{b}_{k,j}\right] = \bar{M}_{k,j}^* - \bar{\Omega}_{k,j}\bar{\mu}_{k,j} \end{array}\right\} \quad [23]$$

$$\left.\begin{aligned} S_{k,j} &= -R\,\frac{kp_{k,j} - q_{k,j}}{k^2-1} = S_{k,j}{}^{*} - \Omega_{k,j}\sigma_k \\ \bar{S}_{k,j} &= R\,\frac{k\bar{p}_{k,j} + \bar{q}_{k,j}}{k^2-1} = \bar{S}_{k,j}{}^{*} - \bar{\Omega}_{k,j}\bar{\sigma}_k \end{aligned}\right\} \quad \ldots [24]$$

$$\left.\begin{aligned} F_{k,j} &= -R\,\frac{p_{k,j} - kq_{k,j}}{k^2-1} = F_{k,j}{}^{*} - \Omega_{k,j}\varphi_k \\ \bar{F}_{k,j} &= -R\,\frac{\bar{p}_{k,j} + k\bar{q}_{k,j}}{k^2-1} = \bar{F}_{k,j}{}^{*} - \bar{\Omega}_{k,j}\bar{\varphi}_k \end{aligned}\right\} \quad \ldots [25]$$

In these expressions, the following notations are used

$$\left.\begin{aligned} &\mu_{k,j} = \frac{R^3}{k^2}\left(\frac{1}{k^2-1} - \eta_j\right);\quad \varphi_k = -\frac{R^2}{k^2-1}; \\ &\qquad\qquad \sigma_k = -\frac{R^2}{k(k^2-1} \\ &\bar{\mu}_{k,j} = -\mu_{k,j};\quad \bar{\varphi}_k = -\varphi_k;\quad \bar{\sigma}_k = \sigma_k \end{aligned}\right\} \quad \ldots [26]$$

$$\left.\begin{aligned} M_{k,j}{}^{*} &= \frac{R^2}{k}\left[\frac{kp_{k,j}{}^{*} - q_{k,j}{}^{*}}{k^2-1} + b_{k,j}{}^{*}\right]; \\ \bar{M}_{k,j}{}^{*} &= \frac{R^2}{k}\left[\frac{k\bar{p}_{k,j}{}^{*} + q_{k,j}}{k^2-1} - \bar{b}_{k,j}{}^{*}\right] \\ S_{k,j}{}^{*} &= -R\,\frac{k\bar{p}_{k,j}{}^{*} - q_{k,j}{}^{*}}{k^2-1}; \\ \bar{S}_{k,j}{}^{*} &= R\,\frac{k\bar{p}_{k,j}{}^{*} + \bar{q}_{k,j}{}^{*}}{k^2-1} \\ F_{k,j}{}^{*} &= -R\,\frac{p_{k,j}{}^{*} - kq_{k,j}{}^{*}}{k^2-1}; \\ \bar{F}_{k,j}{}^{*} &= -R\,\frac{\bar{p}_{k,j}{}^{*} + k\bar{q}_{k,j}{}^{*}}{k^2-1} \end{aligned}\right\} \quad \ldots [27]$$

Quantities $M_{k,j}{}^{*}$ ..... $F_{k,j}{}^{*}$ are the coefficients of moment, shear, axial force of the developments of conventional solutions in trigonometric series.

Integration of M^2, S^2, F^2 along a circle of radius $(1-\eta)R$ and division by the corresponding section constants gives the strain energy in a frame. The section constants are

I_j = moment of inertia of frame
A_j = section area of frame
a_j = section area of frame resisting to shear

The strain energy on a frame is thus expressed as a sum of terms $W_{R,k,j}$ (only even terms are indicated)

$$2W_{R,k,j} = \pi R(1-\eta_j)\left\{\frac{1}{EI_j}[M_{k,j}{}^{*} - \mu_{k,j}\Omega_{k,j}]^2 + \frac{1}{EA_j}[F_{k,j}{}^{*} - \varphi_k\Omega_{k,j}]^2 + \frac{1}{Ga_j}[S_{k,j}{}^{*} - \sigma_k\Omega_{k,j}]^2\right\} \quad \ldots [28]$$

Omitting terms which do not contain the redundant unknowns $N_{k,j}$, Equation [28] can be written as follows

$$2W_{R,k,j} = \frac{\pi R^3}{ED_{k,j}}[(\Omega_{k,j})^2 - 2V_{k,j}\Omega_{k,j}] \quad \ldots [29]$$

In these expressions

$$\frac{1}{D_{k,j}} = \frac{1-\eta_j}{R^2}\left[\frac{\mu_{k,j}{}^2}{I_j} + \frac{\varphi_k{}^2}{a_j} + \frac{E}{G}\frac{\sigma_k{}^2}{a_j}\right] \quad \ldots [30]$$

$$\left.\begin{aligned} V_{k,j} &= \frac{(1-\eta_j)D_{k,j}}{R^2}\left[\frac{\mu_{k,j}M_{k,j}{}^{*}}{I_j} + \frac{\varphi_k F_{k,j}{}^{*}}{A_j} + \frac{E\sigma_k S_{k,j}{}^{*}}{Ga_j}\right] \\ \bar{V}_{k,j} &= \frac{(1-\eta_k)D_{k,j}}{R^2}\left[\frac{\bar{\mu}_{k,j}\bar{M}_{k,j}{}^{*}}{I_j} + \frac{\bar{\varphi}_k\bar{F}_{k,j}{}^{*}}{A_j} + \frac{E\bar{\sigma}_k\bar{S}_{k,j}{}^{*}}{Ga_j}\right] \end{aligned}\right\} \quad \ldots [31]$$

Adding all the terms corresponding to a given value of the coefficient k, an even term W_k of the strain energy of the total structure is

$$\left.\begin{aligned} \frac{2W_k}{\pi R} &= \sum_j \frac{L_j}{3Eh_j}(N_{k,j}{}^2 + N_{k,j-1}{}^2 + N_{k,j}N_{k,j-1}) \\ &\quad + \sum_j \frac{R^2}{Gb_jL_jk^2}(N_{k,j} - N_{k,j-1})^2 \\ &\quad + \sum_j \frac{R^2}{ED_{k,j}}\left[\frac{N_{k,j+1} - N_{k,j}}{L_{j+1}} + \frac{N_{k,j-1} - N_{k,j}}{L_j}\right]^2 \\ &\quad - 2\sum_j \frac{V_{k,j}R^2}{ED_{k,j}}\left[\frac{N_{k,j+1} - N_{k,j}}{L_{j+1}} + \frac{N_{k,j-1} - N_{k,j}}{L_j}\right] \end{aligned}\right\} \quad \ldots [32]$$

The problem is thus reduced to the determination of groups of coefficients $N_{k,j}$ (or $\bar{N}_{k,j}$) corresponding to a given value of k.

Solution of Statically Indeterminate Problem

Differentiation of Equation [32] in respect to each unknown $N_{k,j}$ (or $\bar{N}_{k,j}$) leads to equations of the type

$$C_{k,j,j-2}N_{k,j-2} + C_{k,j,j-1}N_{k,j-1} + C_{k,j}N_{k,j} + C_{k,j,j+1}N_{k,j+1} + C_{k,j,j+2}N_{k,j+2} = H_{k,j} \quad \ldots [33]$$

in which

$$\left.\begin{aligned} C_{k,j,j-2} &= \frac{R^2}{D_{k,j-1}L_jL_{j-1}};\quad C_{k,j,j+2} = \frac{R^2}{D_{k,j+1}L_{j+1}L_{j+2}} \\ C_{k,j,j-1} &= \frac{L_j}{6h_j} - \frac{ER^2}{Gt_jK^2L_j} - \frac{R^2}{D_{k,j}L_j}\left(\frac{1}{L_j} + \frac{1}{L_{j+1}}\right) \\ &\quad - \frac{R^2}{D_{k,j-1}L_j}\left(\frac{1}{L_{j-1}} + \frac{1}{L_j}\right) \\ C_{k,j,j+1} &= \frac{L_{j+1}}{6h_{j+1}} - \frac{ER^2}{Gt_{j+1}K^2L_{j+1}} - \frac{R^2}{D_{k,j}L_{j+1}} \\ &\quad \left(\frac{1}{L_j} + \frac{1}{L_{j+1}}\right) - \frac{R^2}{D_{k,j+1}L_{j+1}}\left(\frac{1}{L_{j+1}} + \frac{1}{L_{j+2}}\right) \\ C_{k,j} &= \frac{L_j}{3h_j} + \frac{L_{j+1}}{3h_{j+1}} + \frac{ER^2}{GK^2}\left(\frac{1}{t_jL_j} + \frac{1}{t_{j+1}L_{j+1}}\right) \\ &\quad + \frac{R^2}{D_{k,j}}\left(\frac{1}{L_j} + \frac{1}{L_{j+1}}\right)^2 + \frac{R^2}{D_{k,j-1}L_j{}^2} + \frac{R^2}{D_{k,j+1}L_{j+1}{}^2} \end{aligned}\right\} \quad \ldots [34]$$

and

$$H_{k,j} = \left\{-V_{k,j}\left(\frac{1}{L_j} + \frac{1}{L_{j+1}}\right) + \frac{V_{k,j+1}}{L_{j+1}} + \frac{V_{k,j-1}}{L_j}\right\}\frac{R^2}{D_{k,j}} \quad \ldots [35]$$

When, in Equation [33], $N_{k,j}$ is replaced by $\bar{N}_{k,j}$, coefficients $C_{k,j}$ remain unchanged, while $H_{k,j}$ is replaced by

$$\bar{H}_{k,j} = \left\{-\bar{V}_{k,j}\left(\frac{1}{L_j} + \frac{1}{L_{j+1}}\right) + \frac{\bar{V}_{k,j+1}}{L_{j+1}} + \frac{\bar{V}_{k,j-1}}{L_j}\right\}\frac{R^2}{D_{k,j}} \quad \ldots [36]$$

Equation [33] can be applied to all the intermediate frames of a shell. It must be modified for the frames next to an end frame. The end frame corresponding to $j = 0$, the terms containing L_0

must be omitted. If the frame $j = 0$ corresponds to a free end, Equation [33] does not apply to it, and the constants $N_{k,0}$ are defined in terms of the applied longitudinal end loads.

In the special case of constant section properties (equal distances between frames, constant cross section, equal frames), Equations [33] can be written in the simplified form

$$N_{k,j-2} + N_{k,j+2} - (2\xi_k + 4)(N_{k,j-1} + N_{k,j+1}) + (\gamma_k + 2)N_{k,j} = L\{V_{k,j+1} + V_{k,j-1} - 2V_{k,j}\} = \psi_{k,j} \quad \ldots\ldots [37]$$

in which

$$\left.\begin{aligned} \xi_k &= \frac{1}{2}(\delta_k - \delta_k'/6); \quad \gamma_k = 4 + 2\delta_k + 2\delta_k'/3 \\ \delta_k &= \frac{ED_kL}{Gtk^2}; \quad \delta_k' = \frac{D_kL^2}{hR^2} \end{aligned}\right\} \quad \ldots [38]$$

(quantities $V_{k,j}$ and $D_{k,j}$ are defined by Equations [31]).

Equations [37] are equations of finite differences and can be solved by conventional methods.[3] For instance, when a series of consecutive frames is not loaded, quantities $V_{k,j}$ and $\psi_{k,j}$ are equal to zero for a series of frames, and solutions of Equations [37] can be written in the form

$$N_{k,j} = n_k'(\epsilon_k')^{-j} + n_k''(\epsilon_k'')^{-j} + m_k'(\epsilon_k')^{j} + m_k''(\epsilon_k'')^{j} \quad \ldots [39]$$

in which n_k', n_k'', m_k', m_k'' are defined by end conditions while $\pm\epsilon_k'$ and $\pm\epsilon_k''$ are the four roots of the equation

$$(\epsilon_k)^2 + (\epsilon_k)^{-2} - (2\xi_k + 4)(\epsilon_k + \epsilon_k^{-1}) + \gamma_k + 2 = 0 \quad \ldots [40]$$

This equation is solved in two steps by introducing the unknown λ_k defined by

$$\lambda_k^2 - 2\xi_k\lambda_k + \delta_k' = 0 \qquad [41]$$

so that the equation in ϵ_k becomes

$$\epsilon_k + \frac{1}{\epsilon_k} = \lambda_k + 2 \quad \ldots\ldots [42]$$

When quantities ϵ_k', ϵ_k'' are defined, substitution of Equations [39] for $N_{k,j}$ into the Equations [37] for which the second member is different from zero, or into the conditions of equilibrium at the end of the shell, leads to linear equations defining the constants n_k', n_k'', m_k', m_k''. In the case of a small number of frames, it is advantageous to use Equations [37] directly; this corresponds to the method used by Hoff.[2]

The solutions of Equations [37] can be of the types given in Table 1.

For an indefinite shell, the solutions must tend toward zero toward the infinite end and are

$$\left.\begin{aligned} &\text{Case 1} \quad N_{k,j} = (\alpha_k)^{-j}(n_k' \sin \beta_k j + n_k'' \cos \beta_k j) \\ &\text{Cases 2, 3} \quad N_{k,j} = n_k'(\epsilon_k')^{-j} + n_k''(\epsilon_k')^{-j} \end{aligned}\right\} \quad \ldots\ldots [43]$$

The limit cases 4, 5 are not examined hereafter.

The ratio δ_k/δ_k', equal to $(EhR^2)/(GtL^2K^2)$, defines the law of distribution of the quantities $N_{k,j}$. For large values of this ratio, the curve representing $N_{k,j}$ is aperiodic (case 3) or has a very long period (case 1). For small values of this ratio, the curve representing $N_{k,j}$ has a short period. Some curves $N_{k,j}$ are represented in Fig. 3.

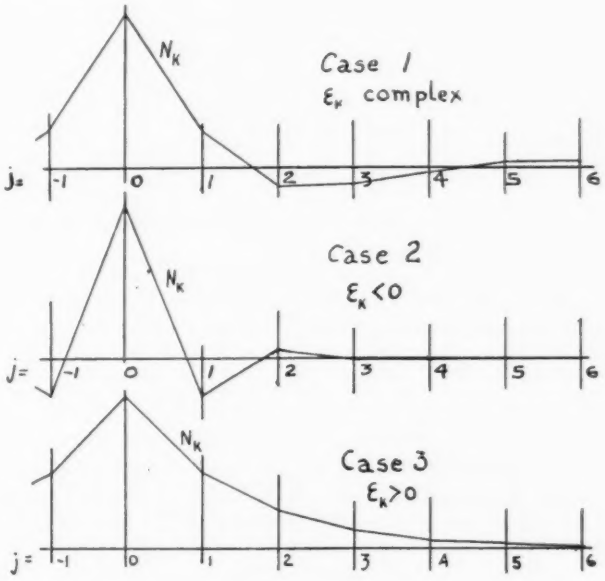


FIG. 3

Writing Equations [37] for the loaded frame and the adjacent frame, the end conditions which define N_k', N_k'' are defined as follows: Intermediate frame loaded in its plane

$$\left.\begin{aligned} N_{k,0}(\gamma_k + 2) - (4\xi_k + 8)N_{k,1} + 2N_{k,2} &= -2V_{k,0}/L \\ N_{k,1}(\gamma_k + 3) - (2\xi_k + 4)(N_{k,0} + N_{k,2}) + N_{k,3} &= +V_{k,3}/L \end{aligned}\right\} \quad \ldots [44]$$

End frame loaded (in its plane and by end forces N_k^*)

$$\left.\begin{aligned} N_{k,0} &= N_k^* \\ N_{k,1}(\gamma_k + 2) - (2\xi_k + 4)N_{k,2} + N_{k,3} &= +V_{k,0}/L \end{aligned}\right\} \quad \ldots [45]$$

These formulas are applied in part 2 for various loading conditions.

Load Reduction in Frame, Due to Shell Rigidity

Equations [23], [24], [25] can be rewritten in the form

$$\left.\begin{aligned} \Delta_{k,0}^m &= 1 - \frac{M_{k,0}}{M_{k,0}^*} = \mu_{k,0}\frac{\Omega_{k,0}}{M_{k,0}^*} = (1 - \rho_{k,0})\frac{\mu_{k,0}V_{k,0}}{M_{k,0}^*} \\ \Delta_{k,0}^f &= 1 - \frac{F_{k,0}}{F_{k,0}^*} = \varphi_k\frac{\Omega_{k,0}}{F_{k,0}^*} = (1 - \rho_{k,0})\frac{\varphi_kV_{k,0}}{F_{k,0}^*} \\ \Delta_{k,0}^s &= 1 - \frac{S_{k,0}}{S_{k,0}^*} = \sigma_k\frac{\Omega_{k,0}}{S_{k,0}^*} = (1 - \rho_{k,0})\frac{\sigma_kV_{k,0}}{S_{k,0}^*} \end{aligned}\right\} \quad \ldots [46]$$

[3] "Mathematical Methods in Engineering," by Th. von Kármán and M. A. Biot, McGraw-Hill Book Company, Inc., New York, N. Y., 1940, chapt. 11, sec. 2, and chapt. 10, sec. 2.

TABLE 1 SOLUTIONS FOR EQUATION [37]

Case	ξ_k^2/δ_k'	$6\delta_k/\delta_k'$	ϵ_k	Solutions
1	>1	$\gtrless 1$	Complex $\epsilon_k = \alpha_k(\cos\beta_k \pm i \sin\beta_k)$	$(\alpha_k)^{\pm j} \sin j\beta_k$; $(\alpha_k)^{\pm j} \cos j\beta_k$
2	>1	<1	Negative	$(\epsilon_k')^{\pm j}$; $(\epsilon_k'')^{\pm j}$
3	>1	>1	Positive	
4	=1	<1	Double negative	$(\epsilon_k)^{\pm j}$; $(\epsilon_k)^{\pm j}$
5	=1	>1	Double positive	

In these equations

$$\rho_{k,0} = 1 - \frac{\Omega_{k,0}}{V_{k,0}} \quad [47]$$

or

$$\left.\begin{aligned} \rho_{k,0} &= 1 - \frac{2(N_{k,0} - N_{k,1})L}{V_{k,0}} \quad \text{(intermediate frame)} \\ &= 1 - \frac{(N_{k,0} - N_{k,1})L}{V_{k,0}} \quad \text{(end frame)} \end{aligned}\right\} \quad [48]$$

Since terms such as $M_{k,0}$ and $M_{k,0}{}^*$ represent the bending moment due to the harmonic k, with and without skin effect, the coefficients $\rho_{k,0}$ represent the relative "decrease" of the load due to the continuity of the skin.

In redistributing frames, coefficients of the same type may be used to determine the relative "load" introduced in these frames by the continuity of the skin

$$\Delta_{k,j}{}^m = \frac{M_{k,j}}{M_{k,0}{}^*} = -\mu_k \frac{\Omega_{k,j}}{M_{k,0}}; \quad \rho_{k,j} = -\frac{\Omega_{k,j}}{V_{k,0}} \quad [49]$$

From Equations [44], it appears that ratios such as $N_{k,0}\,L/V_{k,0}$ are independent of the loading and can be expressed as functions of the structure constants γ_k, ξ_k or δ_k, δ_k'. This result applies to the quantities ρ, but not to the quantities Δ. Quantities NL/V and ρ are determined in part 2 for various values of δ_k, δ_k'.

When the frame deformations due to shear and axial load are neglected, $\Delta_{k,0}{}^m = 1 - \rho_{k,0}$, and the frame load in the loaded frame is thus reduced in the ratio $\rho_{k,0}/1$, as compared with the conventional solution. The factors $\rho_{k,0}$ and $\rho_{k,j}$ show how the moments in the frames along a definite section defined by the value of θ are distributed between the frames. When $\rho_{k,0} = 1$; $\rho_{k,j} = 0$, there is no redistribution, and the conventional methods can be applied. The sum of all the factors $\rho_{k,0}$, $\rho_{k,j}$ for all the frames is equal to 1, and the relative values of the factors ρ shows the trend of the distribution of bending between the frames. If exact values are required, it is necessary to use the coefficients Δ.

PART 2 FORMULAS FOR VARIOUS LOADING CONDITIONS

General Loading of Intermediate Frame of Infinite Beam

In the cases (1), (2), (3) of Table 1, Equations [44] are as follows:

Case (1)

$$\left.\begin{aligned} &2n_k'\left[-(2\xi_k+4)\frac{1}{\alpha_k}\sin\beta_k + \frac{1}{\alpha_k{}^2}\sin 2\beta_k\right] \\ &+ n_k''\left[\gamma_k + 2 - (2\xi_k+4)\frac{1}{\alpha_k}\cos\beta_k + \frac{2}{\alpha_k{}^2}\cos 2\beta_k\right] \\ &\qquad = -\frac{2V_k}{L} \\ &n_k'\left[(\gamma_k+3)\frac{1}{\alpha_k}\sin\beta_k - (2\xi_k+4)\frac{1}{\alpha_k{}^2}\sin 2\beta_k \right. \\ &\qquad \left. + \frac{1}{\alpha_k{}^3}\sin 3\beta_k\right] \\ &+ n_k''\left[(\gamma_k+3)\frac{1}{\alpha_k}\cos\beta_k - (2\xi_k+4)\right. \\ &\qquad \left.\left(1 + \frac{1}{\alpha_k{}^2}\cos 2\beta_k\right) + \frac{1}{\alpha_k{}^3}\cos 3\beta_k\right] = \frac{V_k}{L} \end{aligned}\right\} \quad [50]$$

Cases (2), (3)

$$\left.\begin{aligned} &n_k'[\gamma_k + 2 - (4\xi_k+8)\epsilon_k' + 2(\epsilon_k')^2] \\ &\quad + n_k''[\gamma_k + 2 - (4\xi_k+8)\epsilon_k'' + 2(\epsilon_k'')^2] = -\frac{2V_k}{L} \\ &n_k'[(\gamma_k+3)\epsilon_k' - (2\xi_k+4)\{1 + (\epsilon_k')^2\} + (\epsilon_k')^3] \\ &\quad + n_k''[(\gamma_k+3)\epsilon_k'' - (2\xi_k+4)\{1 + (\epsilon_k'')^2\} \\ &\qquad + (\epsilon_k'')^3] = \frac{V_k}{L} \end{aligned}\right\} \quad [51]$$

The values of $\Omega_{k,0}$ are as follows:

Case (1)

$$\Omega_{k,0} = -\frac{2}{L}\left[n_k'\frac{\sin\beta_k}{\alpha_k} + n_k''\left(\frac{\cos\beta_k}{\alpha_k} - 1\right)\right] \quad [52]$$

Cases (2), (3)

$$\Omega_{k,0} = \frac{2}{L}[n_k'(1-\epsilon_k') + n_k''(1-\epsilon_k'')] \quad [53]$$

The values of $\Omega_{k,j}$ are as follows:

Case (1)

$$\Omega_{k,j} = -\frac{2}{L(\alpha_k)^j}\left[\left\{1 - \frac{1}{2}\left(\alpha_k + \frac{1}{\alpha_k}\right)\cos\beta_k\right\}(n_k'\sin\beta_k j + n_k''\cos\beta_k j) + \frac{1}{2}\left(\alpha_k - \frac{1}{\alpha_k}\right)\sin\beta_k(n_k'\cos\beta_k j - n_k''\sin\beta_k j)\right] \quad [54]$$

Cases (2), (3)

$$\Omega_{j,k} = \frac{1}{L}[\lambda_k' n_k'(\epsilon_k')^j + \lambda_k'' n_k''(\epsilon_k'')^j] \quad [55]$$

When ϵ is nearly equal to 1, the previous equations do not give very accurate results and can be replaced by developments in series of powers, which are hereafter limited to the first terms

Case (1)

$$\left.\begin{aligned} &\beta_k \log\alpha_k = \frac{1}{2}\sqrt{\delta_k' - \xi_k{}^2}; \quad (\log\alpha_k)^2 - \beta_k{}^2 = \xi_k \\ &\log\alpha_k = \sqrt{\frac{1}{2}\left(\xi_k + \sqrt{\delta'}\right)}; \\ &\beta_k = \sqrt{\frac{1}{2}\left(-\xi_k + \sqrt{\delta_k'}\right)} \\ &n_k' = -\frac{V_k}{4\beta_k L}; \quad n_k'' = \frac{V_k}{4L\log\alpha_k} \end{aligned}\right\} \quad [56]$$

$$-\frac{\Omega_{k,0}}{V_k} = 1 - \frac{3(\log\alpha_k)^2 - \beta_k{}^2}{4\log\alpha_k} = 1 - \frac{2\xi_k + \sqrt{\delta_k'}}{\sqrt{8\left(\xi_k + \sqrt{\delta_k'}\right)}} \quad [57]$$

Cases (2), (3) [— for Case (2), + for Case (3)]

$$\left.\begin{aligned} &\log\epsilon_k' = \sqrt{\mp\,\xi_k + \xi_k'}; \quad \log\epsilon_k'' = \sqrt{\mp\,\xi_k - \xi_k'} \\ &\xi_k' = \sqrt{\xi_k{}^2 - \delta_k'} \end{aligned}\right\} \quad [58]$$

$$-\frac{\Omega_{k,0}}{V_k} = 1 - \frac{(\log\epsilon_k')^3 - (\log\epsilon_k'')^3}{4\xi_k'} \quad [59]$$

General Loading of End Frame of Infinite Beam

Equations [44] can be applied to this case

Case (1)

$$\left.\begin{aligned} & n_k'' = N_k^* \\ & n_k'\left[(\gamma_k+2)\frac{\sin\beta_k}{\alpha_k} - (2\xi_k+4)\frac{\sin 2\beta_k}{(\alpha_k)^2} + \frac{\sin 3\beta_k}{(\alpha_k)^3}\right] \\ & + n_k''\left[-(2\xi_k+3) + (\gamma_k+2)\frac{\cos\beta_k}{\alpha_k} - (2\xi_k+4)\right. \\ & \left.\frac{\cos 2\beta_k}{(\alpha_k)^2} + \frac{\cos 3\beta_k}{(\alpha_k)^3}\right] = \frac{V_k}{L} \end{aligned}\right\} \quad [60]$$

Cases (2), (3)

$$\left.\begin{aligned} & n_k' + n_k'' = N_k^* \\ & n_k'[-(2\xi_k+3) + (\gamma_k+2)\epsilon_k' - (2\xi_k+4)(\epsilon_k')^2 \\ & + (\epsilon_k')^3] + n_k''[-(2\xi_k+3) + (\gamma_k+2)\epsilon_k'' \\ & - (2\xi_k+4)(\epsilon_k'')^2 + (\epsilon_k'')^3] = \frac{V_k}{L} \end{aligned}\right\} \quad [61]$$

Numerical Tables

Two independent dimensionless variables (δ_k and δ_k') define the properties of a circular shell with frames for a given harmonic k. These quantities are designated by δ, δ'. The other coefficients are given in Table 2 as functions of δ and of δ/δ'.

Terms λ', λ'', ϵ', ϵ'' are given in the case of real roots, and log α, β, $\frac{1}{\alpha}$, β deg are given in the case of complex roots. Ratios such as ρ, Ln/V, LN/V are also calculated for the cases of load on an intermediate and an end frame.

Diagram, Fig. 4, gives ρ_0 for the case of an intermediate frame

Influence of Frame Eccentricity, and of Axial and Shearing Deflection of Frames

The quantity δ_k is proportional to D_k; in D_k, the term containing A is predominant for large values of k when there is no eccentricity. If there is an eccentricity, the terms containing η and A are predominant, which shows that great errors can be committed when the eccentricity is neglected. This explains the importance of the eccentricity, noted in the introduction: Terms of bending (without eccentricity) and shear are of sixth degree in k, while terms of flexure (due to eccentricity) and axial load are of fourth degree. Thus, when the eccentricity and the axial deformation are neglected in a frame, the influence of the high harmonics is underestimated, which leads to erroneous results, especially in the case of concentrated loads. On the contrary, no important error is made when the shear term is neglected, since it is of sixth order and normally of small importance for the first harmonics, at least for flexible frames. The relative influence of the eccentricity and of the axial deformation can be easily determined in a frame constituted by two flanges

$$I = Ae_0^2 = AR^2\eta^2$$

$$\frac{1}{D_k} = \frac{R^2(1-\eta)}{A(k^2-1)^2}\left\{1 + \left[1 - \frac{1}{k^2}\left(1 + \frac{1}{\eta}\right)\right]^2\right\}$$

If $1/\eta k^2$ is negligible (k large), D_k is equal to Ak^4/R^2. In this case bending and axial deformations equally contribute to the flexibility of the frame, while for a frame without eccentricity, the axial deformation only is important.

Distribution of Loads in Frame Under Action of Concentrated External Forces and Couples.

A unit impulse function[4] can be used to represent the load. Because of the periodicity of the solution, the integrals used in conventional representations of step functions are replaced by sums. Calling Γ_0 the applied concentrated load and $\Gamma(\theta)$ the equivalent step function, it is known that

$$\Gamma(\theta) = \frac{\Gamma_0}{\pi R}\left(\frac{1}{2} + \sum_{K=1}^{\infty}\cos k\theta\right) \quad [62]$$

By application of Equation [62] to various loading conditions, the following coefficients are obtained

$$\left.\begin{aligned} & \text{Radial force} \quad p_k^* = \frac{P_0}{\pi R};\ q_k^* = 0\ ;\ b_k^* = 0 \\ & \text{Tangential force} \quad \bar{p}_k^* = 0\ ;\ \bar{q}_k^* = \frac{Q_0}{\pi R}\ ;\ \bar{b}_k^* = \frac{Q_k\eta}{\pi R} \\ & \text{Couple} \quad \bar{p}_k^* = 0\ ;\ \bar{q}_k^* = 0\ ;\ \bar{b}_k^* = \frac{B_0}{\pi R^2} \end{aligned}\right\} \quad [63]$$

The load coefficients M, S, F are as follows:

$$\left.\begin{aligned} & \text{Radial} \quad M_{k,0}^* = \frac{RP_0}{\pi(k^2-1)};\ F_{k,0}^* = \frac{P_0}{\pi(k^2-1)}; \\ & \qquad S_{k,0}^* = \frac{KP_0}{\pi(k^2-1)} \\ & \text{Tangential} \quad \bar{M}_{k,0}^* = \frac{RQ_0}{\pi k}\left[\frac{1}{k^2-1} - \eta\right]; \\ & \qquad \bar{F}_{k,0}^* = \frac{Q_0 k}{\pi(k^2-1)};\ \bar{S}_{k,0}^* = \frac{Q_0}{\pi(k^2-1)} \\ & \text{Couple} \quad \bar{M}_{k,0}^* = -\frac{B_0}{\pi k};\ \bar{F}_{k,0}^* = 0;\ S_{k,0}^* = 0 \end{aligned}\right\} \quad [64]$$

The values of V_k are as follows:

$$\left.\begin{aligned} & \text{Radial} \quad V_k = \frac{R^2P_0}{\pi(k^2-1)^2} \\ & \left[\frac{R^2}{Ik^2}\left\{(1-\eta(k^2-1)\right\} + \frac{1}{A} + \frac{E}{Ga}\right](1-\eta) \\ & \text{Tangential} \quad \bar{V}_k = \frac{R^2Q_0}{\pi(k^2-1)^2} \\ & \left[\frac{R^2}{Ik^2}\left\{1-\eta(k^2-1)\right\}^2 + \frac{k}{A} + \frac{E}{Gak}\right](1-\eta) \\ & \text{Couple} \quad \bar{V}_k = -\frac{R^3B_0}{\pi k^3 I}\left[\frac{1}{k^2-1} - \eta\right](1-\eta) \end{aligned}\right\} \quad [65]$$

The values of $\Delta_{k,0}^m$ can be written in the following form:

$$\left.\begin{aligned} & \text{Radial load} \quad \Delta_{k,0}^m = (1-\rho_{k,0})\frac{f_k''(f_k''+f_k''')}{(f_k'')^2+f_k'} \\ & \text{Tangential load} \quad \Delta_{k,0}^m = (1-\rho_{k,0}) \\ & \text{Couple} \quad \Delta_{k,0}^m = (1-\rho_{k,0})\frac{(f_k'')^2}{(f_k'')^2+f_k'} \end{aligned}\right\} \quad [66]$$

In these expressions, constants f_k are as follows

$$f' = \frac{k^2I}{R^2}\left(\frac{k^2}{A} + \frac{E}{Ga}\right);\ f_k'' = 1-\eta(k^2-1);$$

$$f_k''' = \frac{k^2I}{R^2}\left(\frac{1}{A} + \frac{E}{Ga}\right) \quad [67]$$

The corrections to the conventional solutions are thus

[4] Footnote reference (3), p. 395.

TABLE 2 COEFFICIENTS AS FUNCTIONS OF δ AND δ/δ'

					Real and Complex Constants*				Intermediate Frame					End Frame					
	δ	ξ	τ	$\sqrt{\xi^2-\delta}$	$\left\{\frac{\chi'}{\text{Log }\alpha}\right\}$	χ'' β	$\frac{\varepsilon'}{1/\alpha}$	ε'' β deg.	$-\frac{Ln'}{V}$	$-\frac{Ln''}{V}$	ρ_0	ρ_1	$-\frac{LN_0}{V}$	$-\frac{LN_1}{V}$	$-\frac{Ln'}{V}$	$-\frac{Ln''}{V}$	ρ_0	ρ_1	$-\frac{LN_1}{V}$	$-\frac{LN_2}{V}$
(1)	(2)	(3)	(4)	(5)	(6)	(7)	(8)	(9)	(10)	(11)	(12)	(13)	(14)	(15)	(16)	(17)	(18)	(19)	(20)	(21)
$\delta/\delta'=100$	.0001	.00005	4.00020	.00100	.02293	.02177	.97735	1°11'50"	-11.484	10.903	.012	.012	10.903	10.409	-11.647	0	.0460	.0437	-.9610	-1.0070
	.001	.00050	4.00201	.00320	.04268	.03648	.95812	2°05'25"	- 6.853	5.857	.024	.023	5.857	5.369	-26.285	0	.0821	.0781	-.9179	-1.7578
	.01	.00499	4.02007	.00870	.08658	.05004	.91707	2°51'53"	- 5.162	2.785	.0592	.0536	2.785	2.3143	-18.360	0	.1585	.1415	-.8415	-1.5415
	.1	.04992	4.20067	.03861	.08853	.01131	.74346	.89917	1.90588	-.68854	.16096	.11843	1.21735	.79783	4.2930	-4.2930	.3315	.2389	-.6685	-1.0981
	.3	.14975	4.60200	.13937	.28912	.01038	.58777	.90319	.93142	-.18248	.26740	.15657	.74895	.38265	1.6830	-1.6830	.4691	.2702	-.6309	- .7915
	1.	.49917	6.00667	.48905	.98821	.01012	.38399	.90433	.45506	-.05136	.44918	.17221	.40370	.12829	.66736	- .66736	.6327	.2471	-.3473	- .4474
	3.	1.49750	10.02000	1.48745	2.98495	.01005	.20940	.90465	.21974	-.01683	.65575	.13720	.20291	.03079	.27247	- .27247	.8106	.1678	-.1894	- .2110
	10.	4.99167	24.06667	4.98164	9.97331	.01003	.08411	.90475	.08480	-.00502	.84563	.07109	.07978	.00259	.09273	- .092731	.9239	.0769	-.0761	- .0753
	100.	49.91667	204.66667	49.90665	99.82332	.01002	.00982	.90479	.00982	-.00050	.98064	.00963	.00932	.00036	.009930	- .009930	.9911	.0096	-.0089	- .0051
$\delta/\delta'=10$	.0001	.00005	4.00021	.00316	.04007	.03914	.96072	2°15'35"	-6.339	6.239	.020	.020	6.239	5.749	-24.350	0	.0770	.0739	-.9230	-1.7720
	.001	.00049	4.00207	.00999	.07243	.06895	.93013	3°56'55"	-3.6300	3.4469	.0379	.0373	3.4469	2.9659	-13.506	0	.1349	.1247	-.8651	-1.6005
	.01	.00492	4.02067	.03124	.13516	.11556	.87357	6°36'34"	-2.2022	1.8128	.0774	.0719	1.8128	1.3515	-7.577	0	.2382	.2016	-.7618	-1.3220
	.1	.04917	4.20667	.08709	.27310	.15813	.76102	9°03'40"	-1.56853	.89261	.18048	.13570	.89261	.48285	-4.833	0	.4208	.2878	-.5792	- .8705
	.3	.14750	4.62000	.09080	.39841	.11120	.67139	6°22'20"	-2.17241	.58920	.28413	.16969	.58920	.28113	- 6.050	0	.5492	.3000	-.4508	- .6016
	1.	.49167	6.06667	.37618	.86814	.11519	.40618	.71335	.56085	-.22220	.46130	.17951	.33865	.06930	.96328	- .96328	.7103	.2551	-.2897	- .3244
	3.	1.47500	10.20000	1.36954	2.84453	.10547	.21605	.72372	.23536	-.05852	.66332	.14018	.17684	.00850	.30800	- .30800	.8436	.1698	-.1564	- .1869
	10.	4.91667	24.66667	4.81390	9.73056	.10277	.08588	.72672	.08714	-.01614	.84913	.07184	.07100	-.00414	.09738	- .097384	.9376	.0741	-.0624	- .0607
	100.	49.16667	204.66667	49.06487	98.23153	.10180	.00998	.72780	.00999	-.00160	.98110	.00967	.00838	-.00107	.010166	- .010166	.9927	.0092	-.0073	- .0054
$\delta/\delta'=1$	.0001	.00004	4.00027	.01000	.07089	.07053	.93157	4°02'29"	-3.5472	3.5237	.0356	.0354	3.5237	3.0415	-13.218	0	.1322	.1228	-.8678	-1.6128
	.001	.00042	4.00267	.03162	.12741	.12476	.88039	7°08'50"	-2.0061	1.9644	.0657	.0629	1.9644	1.4972	-7.061	0	.2261	.1948	-.7739	-1.3530
	.01	.00417	4.02667	.09992	.22908	.21791	.79526	12°29'10"	-1.15508	1.08015	.11989	.11083	1.08015	.64010	-3.678	0	.3675	.2828	-.6325	- .9832
	.1	.04167	4.26667	.31347	.42688	.36425	.65255	20°52'10"	-.69251	.56066	.24043	.18074	.56066	.18087	-1.832	0	.5742	.3324	-.4258	- .6192
	.3	.12500	4.80000	.53327	.58614	.44433	.55618	25°27'30"	-.55935	.38759	.31672	.20692	.38759	.06094	-1.295	0	.6903	.3082	-.3097	- .3112
	1.	.41667	6.66667	.90906	.84345	.50057	.43022	28°40'50"	-.46153	.23430	.51769	.19958	.23430	-.00686	- .8951	0	.8152	.2304	-.1848	- .1349
	3.	1.25000	12.00000	1.19896	1.17896	.41954	.30760	24° 2'20"	-.45588	.12618	.70430	.14541	.12618	-.02167	- .7551	0	.9054	.1361	-.0946	- .0832
	10.	4.16667	30.66667	2.71314	6.87980	1.45353	.11408	.31903	.11655	-.09514	.86992	.07089	.05140	-.01364	.17758	-.17758	.9636	.0570	-.0364	- .0158
	100.	41.66667	270.66667	40.41882	82.11554	1.21780	.01189	.31852	.01207	-.00597	.98393	.00925	.00610	-.00194	.012310	-.012310	.9958	.0069	-.0042	- .0015
$\delta/\delta'=0.1$	.0001	-.00003	4.00087	.03162	.12584	.12564	.88175	7°11'56"	-1.9951	1.9812	.0630	.0621	1.9812	1.5127	-7.036	0	.2225	.1947	-.7775	-1.3603
	.001	-.00033	4.00867	.10000	.22116	.22304	.79919	12°46'46"	-1.1357	1.1058	.1106	.1078	1.1058	.6611	-3.613	0	.3613	.2818	-.6387	- .9966
	.01	-.00333	4.08667	.31621	.40067	.39439	.66987	22°35'50"	-.64916	.60618	.20325	.17559	.60618	.20780	-1.713	0	.5513	.3124	-.4487	- .5550
	.1	-.03333	4.86667	.99944	.72262	.68778	.48548	39°21'20"	-.38509	.31055	.37152	.21010	.31055	-.00219	- .7647	0	.7643	.2946	-.2357	- .1768
	.3	-.10000	6.60000	1.72916	.96201	.88171	.38212	50°41'20"	-.30296	.20977	.50288	.23794	.20977	-.03879	- .939	0	.8540	.2713	-.1460	- .0707
	1.	-.33333	12.66667	3.44466	1.31590	1.14061	.26824	65°21'10"	-.22777	.11967	.67638	.18691	.11967	-.02114	- .2951	0	.9281	.1278	-.0719	- .0161
	3.	-1.00000	30.00000	5.38517	1.73052	1.39817	.17719	80°06'30"	-.16167	.05935	.82742	.10972	.05935	-.02694	- .1799	0	.9686	.0699	-.0314	- .0019
	10.	-3.33333	90.66667	9.42809	2.26403	1.43328	.10393	82°07'10"	-.11279	.02626	.93292	.01427	.02225	-.01130	- .1047	0	.9892	.0213	-.0108	- .0003
	100.	-33.33333	870.66667	10.54093	-22.79241	45.87126	-.01821	-.02389	.05227	-.01976	.99238	.00523	.00214	-.00133	.01738	-.01738	.9969	.0031	-.0031	- .0001

* Corresponding to real or complex values of col. (5)

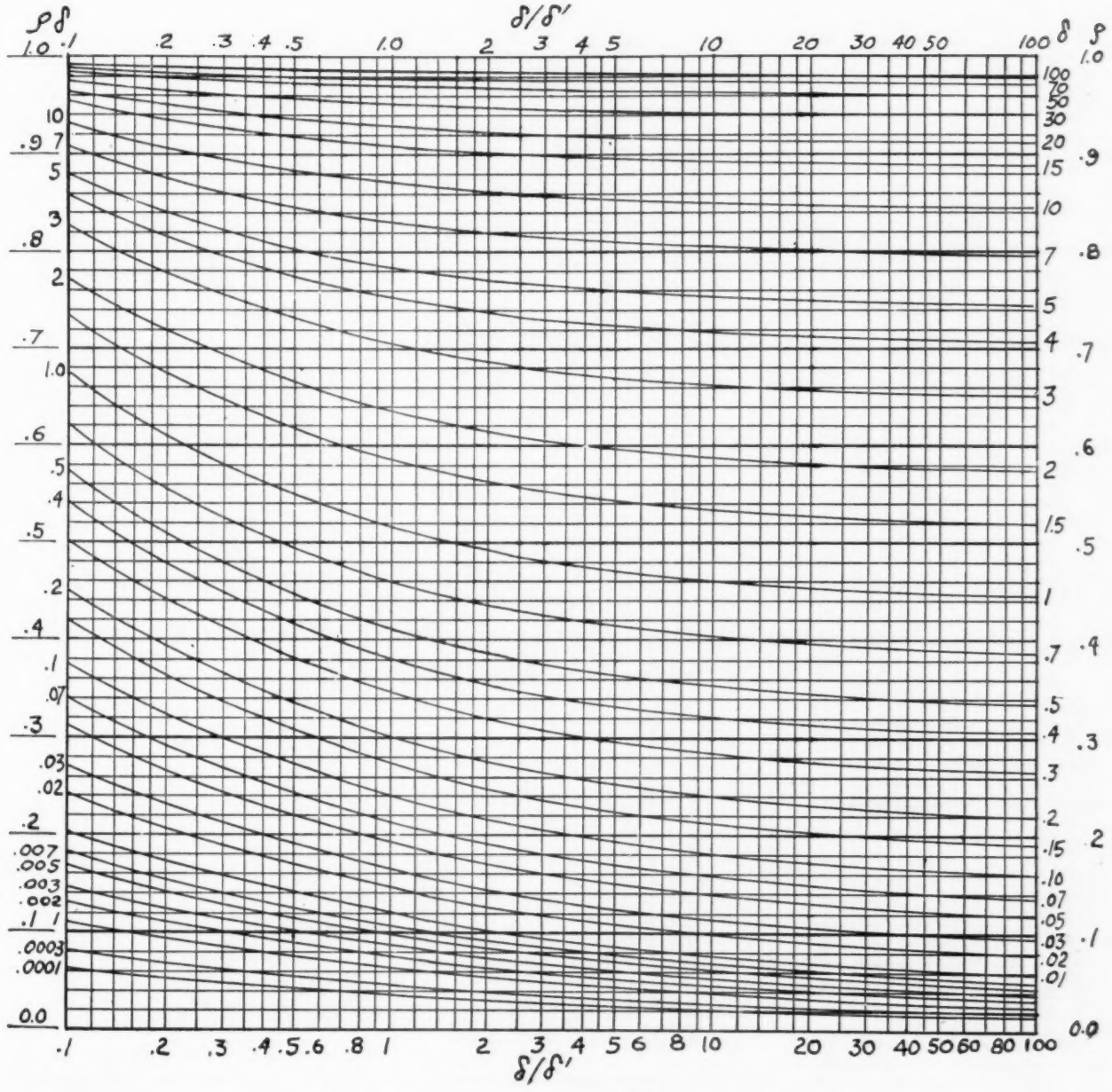


FIG. 4 VALUES FOR ρ AS A FUNCTION OF δ AND OF δ/δ'

NOTATIONS

$$\delta = \frac{EDL}{Gtk^2};\quad \delta' = \frac{DL^2}{hR^2};\quad 1-\delta = \frac{1-M/M^*}{\mu V/M^*} = \frac{1-F/F^*}{\varphi V/F^*} = \frac{1-S/S^*}{\sigma V/S^*}$$

$$\frac{1}{D} = \frac{1-\eta}{R^2}\left[\frac{\mu^2}{I} + \frac{\varphi^2}{A} + \frac{E}{G}\frac{\sigma^2}{a}\right];\quad V = \frac{(1-\eta)D}{R^2}\left[\frac{\mu M^*}{I} + \frac{\varphi F^*}{A} + \frac{E\sigma S^*}{Ga}\right]$$

$$\mu = \pm\frac{R^2}{k^2}\left(\frac{1}{k^2-1} - \eta\right);\quad \varphi = \pm\frac{R^2}{k^2-1};\quad \sigma = -\frac{R^2}{k(k^2-1}};\quad \eta = \frac{e}{R}$$

Upper sign for symmetric load, lower for antisymmetric load) M, S, F, and M^*, S^*, F^* = maximum moment, shear, axial load in a ring with a shell and without a shell, loaded periodically by the harmonic of rank K.)

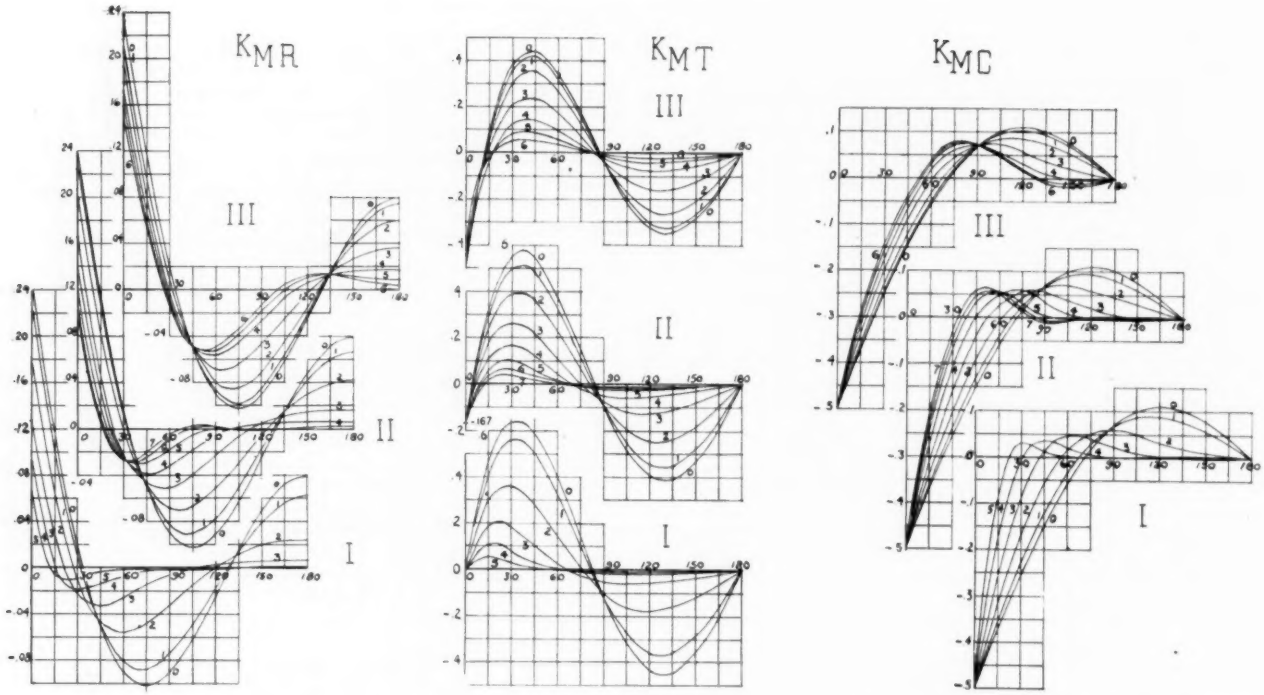


FIG. 5 DIAGRAMS OF BENDING MOMENTS IN FRAMES AS FUNCTIONS OF ECCENTRICITY, $\eta = e/R$ OF THE FRAMES AND OF TWO VARIABLES AL/tR^2 AND R^2h/L^3t

(See Tables 3 and 4 for the definitions of the symbols.)

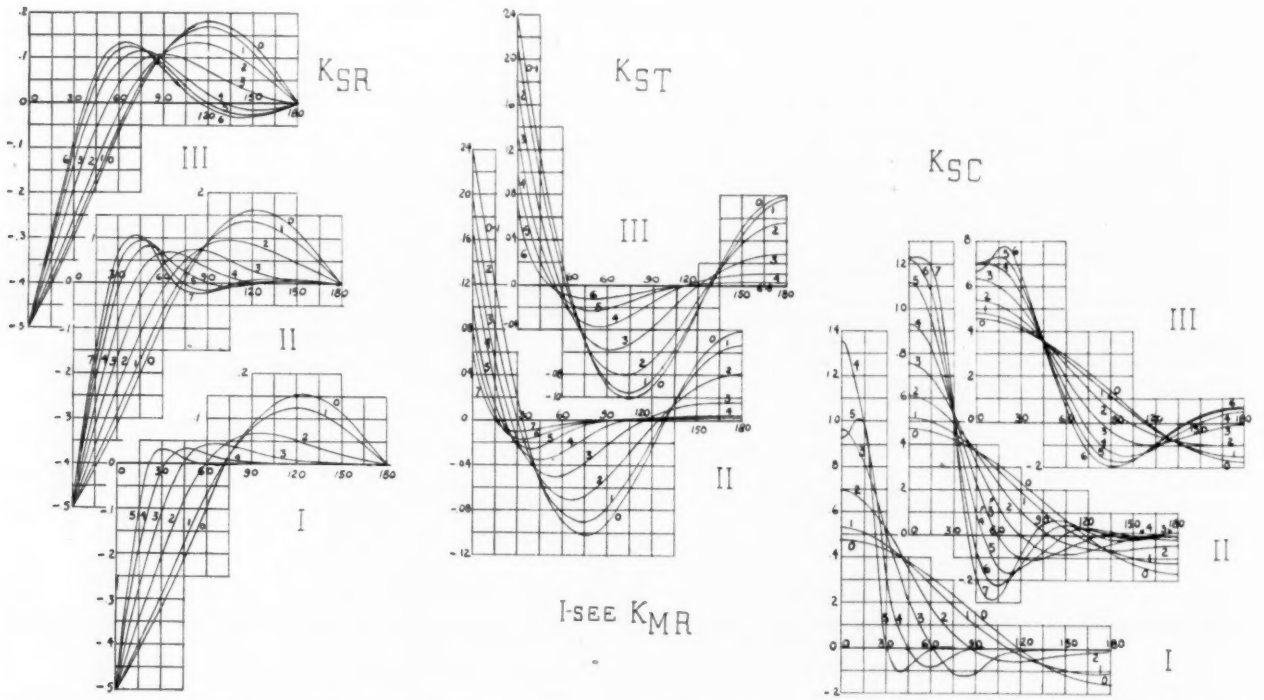


FIG. 6 DIAGRAMS OF SHEARING FORCES IN FRAMES AS FUNCTIONS OF ECCENTRICITY $\eta = e/R$ OF THE FRAMES AND OF TWO VARIABLES AL/tR^2 AND R^2h/L^3t

(See Tables 3 and 4 for the definitions of the symbols.)

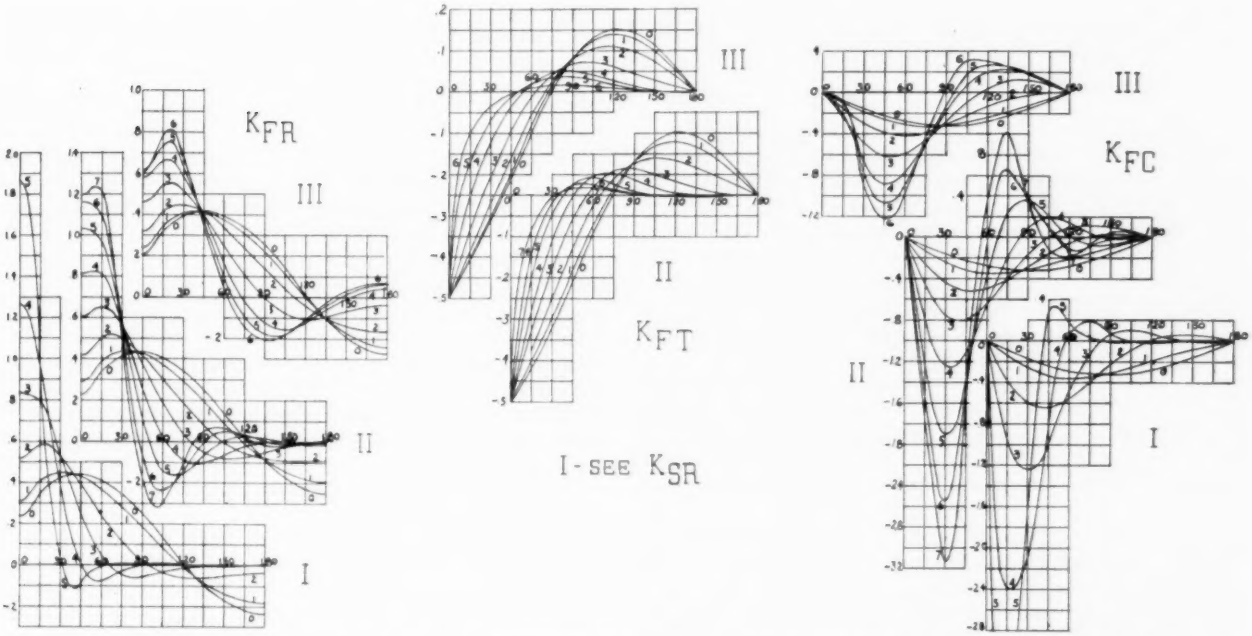


FIG. 7 DIAGRAMS OF AXIAL FORCES IN FRAMES AS FUNCTIONS OF ECCENTRICITY $\eta = e/R$ OF THE FRAMES AND OF TWO VARIABLES AL/tR^2 AND R^2h/L^2t

(See Tables 3 and 4 for the definitions of the symbols.)

$$\left.\begin{aligned} M_{k.0}^* - M_{k.0} &= \Delta_{k.0}^m M_{k.0}^*; \\ S_{k.0}^* - S_{k.0} &= \Delta_{k.0}^m S_{k.0}^* \frac{\sigma_k}{\mu_k} \\ F_{k.0}^* - F_{k.0} &= \Delta_{k.0}^m F_{k.0} \frac{\varphi_k}{\mu_k} \end{aligned}\right\} \quad \ldots\ldots [68]$$

TABLE 3 COEFFICIENTS FOR LOADED INTERMEDIATE RING IN AN INDEFINITE SHELL ($E/G = 2.6$)

Internal load	Applied concentrated load: Radial P_0	Tangential Q_0	Couple B_0/R
Moment M/R	K_{MR}	K_{MT} (—)	K_{MC} (—)
Shear S	K_{SR} (—)	K_{ST}	K_{SC}
Axial F	K_{FR}	K_{FT} (—)	K_{FC} (—)

TABLE 4 VALUES OF PARAMETERS IN FIGS. 5, 6, 7

Curve group	η	Parameter	Curve no. 1	2	3	4	5	6	7
I	0	IL/R^4t	0.1	0.01	0.001	0.0001	0.00001	..	..
II	1/30	$AL/(1-\eta)tR^2$	100	20	4	0.8	0.16	0.04	0.01
III	1/10	$AL/(1-\eta)tR^2$	20	4	0.8	0.16	0.04	0.01	..

NOTE: Curves nos. 0 correspond to conventional solution (infinitely rigid frame).

The quantities $M_{k.0}^*$ are defined by Equations [64] and, from the values of μ_k, σ_k, φ_k it results that

$$\frac{\sigma_k}{\mu_k} = \frac{k}{[1-\eta(k^2-1)]R}; \quad \frac{\varphi_k}{\sigma_k} = -k \ldots\ldots [69]$$

In the diagrams, Fig. 5, deflections in shear are neglected, and I is replaced by $Ae_0^2 = AR^2\eta^2$, so that

$$f_k' = k^4\eta^2; \quad f_k''' = k^2\eta^2 \ldots\ldots [70]$$

Thus, the resulting moment at any point of the frame is the difference between the conventional solution (equal to $\Sigma M_{k.0}^* \cos k\theta$) and the correction $\Sigma M_{k.0}^* \Delta_{k.0}^m \cos k\theta$ which is a rapidly converging series.

For an indefinite shell, the problem is defined in terms of three dimensionless quantities which, for each harmonic, can be δ_k, δ_k', η. In turn, δ_k and δ_k' can be expressed as functions of k and two other dimensionless quantities. This leads to the following three independent variables:

1 Ratio $\eta = e/R$ (eccentricity)

2 Ratio ALE/R^2tG; this ratio defines

$$\delta_k = \frac{ALE}{R^2tG} \frac{1}{\frac{1}{k^2}\left[\frac{1}{\eta(k^2-1)} - 1\right]^2 + \left[\frac{k}{k^2-1}\right]^2}$$

3 Ratio $\delta_1/\delta_1' = R^2hE/L^2tG$; this ratio defines $\delta_k/\delta_k' = (\delta_1/\delta_1')(1/k^2)$

DIAGRAMS FOR BENDING MOMENTS, AXIAL FORCES, AND SHEARING FORCES IN FRAMES

The diagrams, Figs. 5, 6, 7, represent bending moments, axial forces, and shearing forces, respectively, in the frames as functions of the eccentricity $\eta = e/R$ of the frame and of the two variables AL/tR^2 and R^2h/L^2t. It has been found that this last ratio has but a small influence on the results; generally, this influence, for R^2h/L^2t varying between 10 and 100, is less than 5 per cent. An average value of 31.25 has been chosen for this parameter.

In the case of a frame without eccentricity, the axial deformation has been neglected, and the variable replacing AL/tR^2 is IL/tR^4.

The coefficients for a loaded intermediate ring in an indefinite shell ($E/G = 2.6$) are given in Table 3.

The coefficients K are ratios such as

$$K_{MR} = \frac{M/R}{P_0}$$

so that

$$M = K_{MR}RP_0$$

They have been computed for angles θ varying by increments of 15 deg from 0 to 180°. The antisymmetric functions are marked (—).

Sliding Friction Under Extreme Pressures—1

By S. J. DOKOS,[1] EAST PITTSBURGH, PA.

The program of this investigation on sliding friction is concerned with the evaluation of the frictional forces which occur under very high contact pressures and under varying conditions of speed, temperature, and lubrication. The work presented herein covers the experiments which have been made on sliding friction at normal temperatures. Further experiments on boundary lubrication at normal temperatures and sliding friction at elevated temperatures will be reported in a second paper.

This report indicates the behavior of sliding friction when large normal loads react between surfaces in contact over a wide range of sliding velocities. At velocities less than one inch per second magnified photographs of the ruptured surfaces indicate clearly this phenomenon of stick-slip. From the experimental records obtained it was possible to show that a functional relation exists between the following variables: (1) The sliding velocity, (2) the normal load, and, (3) the frequency of stick-slip. New experimental evidence is presented indicating that the natural frequency of the apparatus involved influences the phenomenon of stick-slip.

Introduction

VERY little is known concerning the nature of sliding friction which accompanies plastic forming of metals at normal and at elevated temperatures. It is well known, however, that during the rolling of steel, the forging of shells, the extrusion of tubes, the drawing of wire, or the piercing of billets, very high frictional forces oppose the flow of metal. Numerous theoretical papers presented by Siebel (1),[2] Trinks (2, 3), Nadai (4, 5), Sachs (6) and others have investigated these plastic-flow problems.

Particular attention was paid in these investigations to the influence of friction on the surface of the metal undergoing plastic deformation and to the power requirements. The insufficient data which existed concerning both the effect of friction and the values of the coefficients of friction has retarded the complete solution of these problems. Recently, the wire-drawing process has been investigated, in connection with the present report, by E. A. Davis and the writer (7), as a possible means for an experimental determination of the coefficient of sliding friction under large contact pressures.

The machine used in this investigation for determining the frictional forces between metallic surfaces consists in general of a horizontal disk rotating around a vertical axis and a pin sliding on the surface of the disk. On the upper surface of the disk, at the suggestion of Dr. A. Nadai, a number of concentric ridges and grooves were machined. A cylindrical contact rests under a known load on one of the ridges while the disk rotates with a constant velocity. The frictional forces are automatically recorded by means of a special measuring device. The disk can be surrounded by an electric-resistance furnace and preheated to a given temperature. Although several investigators, among whom F. P. Bowden (8) and M. Muskat (9) should be quoted, have used this method, it is believed that several important improvements have been added to the apparatus for measuring the frictional forces and to study the behavior of sliding materials under very heavy pressures.

[1] Research Engineer, Westinghouse Research Laboratories.

[2] Numbers in parentheses refer to the Bibliography at the end of the paper.

Discussion of this paper should be addressed to the Secretary, A.S.M.E., 29 West 39th Street, New York, N. Y., and will be accepted until July 10, 1946, for publication at a later date. Discussion received after the closing date will be returned.

Note: Statements and opinions advanced in papers are to be understood as individual expressions of their authors and not those of the Society.

Previous Investigations

A considerable amount of experimental research on friction has been done in the past both in England and in this country on special questions related to friction at normal temperatures. It cannot be the purpose of this report to offer a complete review of the vast amount of available literature on related questions. However, a few investigations which seem to have a relation to the present work will be quoted.

Various proposals have been made concerning the nature of sliding friction. The early investigations of Amontons (10) attributed it to resistance due to the mechanical interlocking of the irregularities of the surfaces in contact. This, in turn, has been superseded by the view that the resistance to motion is due to intermolecular forces at the point of contact. Tomlinson (11) has presented a molecular theory, according to which sliding friction is due to the attractive and repulsive forces between molecules at the surfaces in contact, so that friction is a surface phenomenon. More recently, from the work done by Bowden and his associates, it has been indicated that neither of these assumptions is entirely correct and that the frictional effects are not confined to the surfaces alone. The sliding which occurs causes a localized plastic deformation of the solid, which extends to a great depth beneath the surface; consequently, friction must also be dependent on the bulk properties of the solids. This interpretation has also been suggested by Merchant and Ernst (12).

Bowden and Ridler (13), while performing experiments on the friction between unlubricated surfaces, observed fluctuations in friction and concluded that kinetic friction may not be constant. In order to investigate this phenomenon Bowden and Leben (14) constructed a special apparatus for measuring these fluctuations. The measuring device incorporates two vibratory systems. One measures the tangential reaction between the surfaces, and its frequency is controlled by a bifilar suspension. The other applies the normal force and is controlled by a circular spring. Both systems have a high natural frequency of approximately 1000 cycles per sec. An apparatus of this type was assumed to be capable of recording any changes in friction provided the natural frequency of the measuring device is higher than the frequency of the variations in friction.

The measuring apparatus was used to apply the normal load to a flat plate which can be driven by a water piston. When the plate was set in motion the slider was observed to move along with the surface plate as though the two had stuck together until the friction force became sufficient to jerk the slider loose and bring it back into position to repeat the process. The investigators concluded that this phenomenon was a result of high pressures and of high temperatures (13) at the points of contact causing local welding and plastic flow, and that the observed "stick-slips" were the manifestations of these welds and the subsequent rupture of the contacts. Bowden and Leben believe that this phenomenon is inherent to the sliding of metals, and that these fluctuations are characteristic of the mechanism of friction.

In a later investigation Bowden, Leben, and Tabor (15) indi-

cated that the intermittent motion produced is influenced by the natural frequency, the moment of inertia, and the damping of the moving parts along with the sliding velocity of the metals in contact. However, it was also clearly shown that the nature of sliding was decidedly influenced by the properties of the metals in contact. In several subsequent experimental investigations the thought was expressed by Blok (16) and Morgan, Muskat, and Reed (9) that the periodic variations of the frictional forces observed by Bowden and Leben may have been influenced or even entirely caused by the elasticity of the apparatus.

Friction Machine

The machine used in the work described in this paper, Figs. 1 to 3, consists essentially of a disk holder approximately 12 in. in diameter, revolving around a vertical axis upon which exchangeable disks *a*, can be fastened. On one of the ridges of the machined disk the rubbing contact *b* rests under a known normal load. The vertical holder carrying the small contact cylinder, which

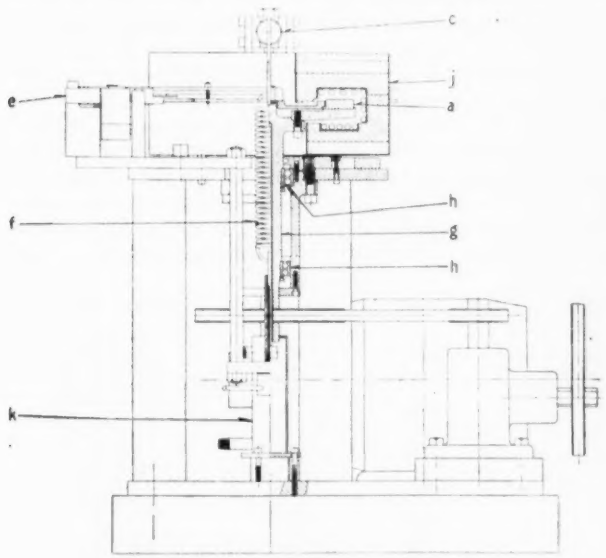


Fig. 1 Friction Apparatus, Front View

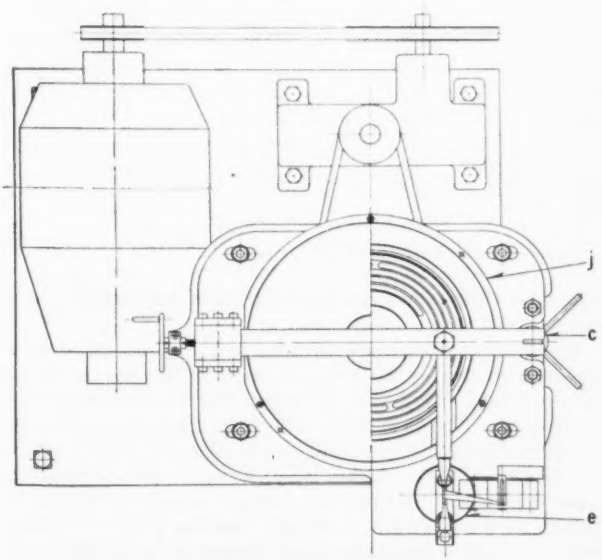


Fig. 2 Friction Apparatus, Top View

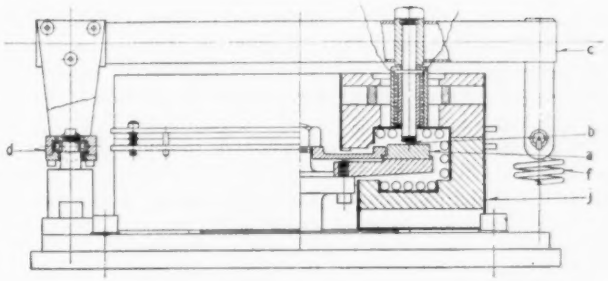


Fig. 3 Friction Apparatus, Deflecting Arm View

slides on the disk along one of its generatrixes, is attached to a rigid arm *c* pivoted on a universal-joint *d*, so that it can move freely up or down or to either side. The dynamometer for measuring the frictional force consists of a thin flexible steel ring *e*. The elastic deflection of the ring is a measure of the frictional force and is magnified by means of a pointer deflected by leaf springs.

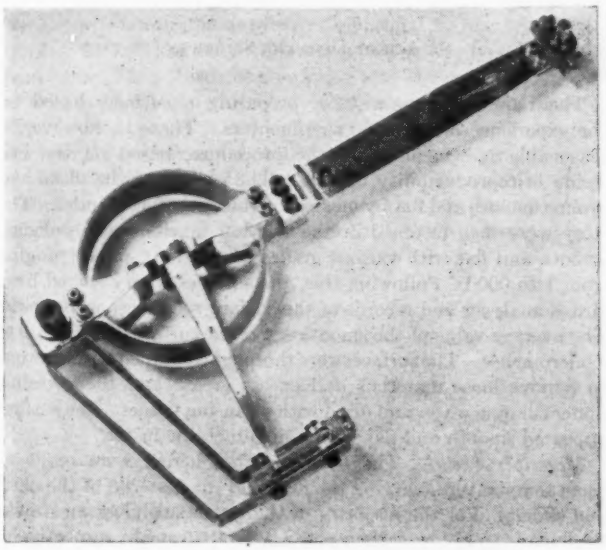


Fig. 4 System for Measuring Friction Force

Fig. 4 shows this device. The pointer scribes a fine scratch on waxed paper which is slowly moved by a clock device. The desired normal load is applied to the deflecting arm by a spring *f*. The rotating table which carries the metal disks is mounted on ball bearings and can, by suitable gearing, be driven at velocities varying from 1.6×10^{-4} to 300 ips. In the slowest test approximately 60 hr were required to make a complete revolution of the disk. An electric-resistance furnace *j* covers the ring, and the temperature can be varied from room temperature to 1200 C. The entire machine is rigidly constructed and well mounted to prevent any vibrations. The vertical shaft can be cooled by a water jacket.

Unlike the high-frequency measuring devices used by several investigators (9, 14), in which the phenomenon of stick-slip prevailed, it was thought advisable to design the normal load device and the dynamometer so that an average frictional force was obtained at sliding velocities larger than 1 ips. The normal loading system has a natural frequency in the vertical direction of 200 cycles per sec, and the measured frequency of the dynamometer for a motion in the horizontal direction is approximately 150 cycles per sec. Since stick-slip is influenced by the elasticity

of the measuring devices, the mechanical properties of the rotating mechanism, and the velocity of rotation, it is not present in the recorded diagrams at comparatively high speeds because of the low natural frequency of the system and the amount of damping in the moving parts.

Preparation of Surfaces. The width of the ridges, machined in the disk, is slightly less than the width of the contact cylinder. Thus the cylindrical contact covers the entire width of the ridge during the test, as shown in Fig. 5.

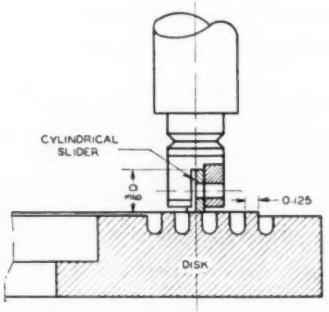


FIG. 5 SKETCH OF DISK AND SLIDER IN CONTACT

There are numerous ways of preparing a surface, based on the experience of various experimenters. There is, however, a reasonable agreement as to the procedure, based on the criterion of reproducibility of data. The surface of the disks was ground smooth and flat by means of a rotary surface grinder. The rings were then fastened in the friction machine and polished smooth and flat with various grades of polishing paper ranging from 1 to 0000. Following this, the surfaces were checked by a Brush analyzer and records of the surface roughness were made. The average value of the smoothness of the surfaces was from 2 to 7 microinches. The surfaces were thoroughly cleaned with acetone to remove loose materials and excess grease and then washed under running water and dried with cleansing tissue. The surface appeared smooth and flat with a high metallic luster.

Materials Tested. The tests reported herein were made at room temperature, varying the load and the material of the disks and sliders. For the majority of the tests the sliders and disks were made from low-carbon and S.A.E. 1045 steels, respectively. Three types of metals were used, as follows:

1 No. 1 steel; a low-carbon steel with 0.2 per cent carbon.
2 No. 2 steel; medium-carbon steel (S.A.E. 1045).
3 No. 3 steel; tool steel with 0.7 per cent carbon.

TESTS ON SLIDING FRICTION AT VARIOUS PRESSURES AND SLIDING VELOCITIES

This investigation deals with observations on the friction between sliding surfaces which are free from any lubricating agent. Although, as mentioned, numerous investigators have dealt with the theoretical and experimental aspects of dry friction, in most of these tests comparatively low normal loads were applied. It is hoped that the information presented herein will offer new observations on the mechanism of friction particularly under heavy normal forces. Consideration is given to the influence (*a*) of velocity, (*b*) of load, and (*c*) of various metals on friction. The sliding velocity was varied over a wide range in order to obtain, at relatively high pressures, a relation between the sliding velocity, the coefficient of friction, and the normal load.

Conflicting evidence on the effect of velocity on sliding friction has been presented by a number of the early investigators. In 1781, Coulomb (18) concluded that velocity has very little effect on dry friction between metals. On the other hand, the experiments of Galton and George Westinghouse (17) in which the braking action of a cast-iron block on a hard steel tire was measured indicated that friction decreased greatly with increased speed. Recently, numerous investigators have shown that a variation does exist and that sliding friction decreases with speed.

Papenhuyzen (18) has shown this velocity-friction relation as the velocity was varied over a wide range, while investigating the fundamentals of the skidding of automobile tires on road materials. From these experiments Papenhuyzen indicated three velocity ranges in which the frictional characteristics were of a different nature, namely, (*a*) that at low sliding velocities only uniform sliding was observed, (*b*) that at a sharply defined first critical velocity, frictional vibrations occurred of the stick-slip type, and (*c*) that at sliding velocities greater than the second critical velocity, frictional vibrations of the simple harmonic type occurred. In the first range, friction increased slightly with speed. At higher sliding velocities an average coefficient of friction was deduced which is considerably lower than the static friction.

The speed of the rotating disk was varied over a range of 2.6×10^{-4} to 500 rpm, corresponding to a relative sliding velocity of 1.6×10^{-4} to 300 ips. The observed coefficients of friction are plotted in Fig. 6, as the ordinate, and the sliding velocities are represented on a logarithmic scale for various values of the normal force. Materials in contact are various steels. In these tests the sliding cylinder was made of mild steel and the disk of an S.A.E. 1045 steel. The normal load was varied from 50 to 200 lb at the various velocities and as indicated by the curves has a decided influence on their shape. The results obtained from these tests are given in Table 1. The coefficient of friction at the slower velocities is measured at the point of maximum frictional force.

TABLE 1 EFFECT OF VELOCITY AND NORMAL LOAD ON FRICTION

Velocity of disk, ips	Normal load, lb	Coefficient of friction	Stick-slip frequency, cycles per sec
1.6×10^{-4}	50	0.56	7.6×10^{-3}
	100	0.55	5.0×10^{-2}
	150	0.49	3.3×10^{-2}
	200	0.515	1.2×10^{-2}
1.44×10^{-3}	50	0.43	9.0×10^{-2}
	100	0.47; 0.43	4.5×10^{-2}; 5.8×10^{-2}
	150	0.49	2.8×10^{-2}
	200	0.465	1.9×10^{-2}
	250	0.62	5.5×10^{-2}
1.18×10^{-2}	50	0.34	1.65
	100	0.30	9.0×10^{-1}
	150	0.43	4.2×10^{-1}
	200	0.45	1.92×10^{-1}
	250	0.66	5.0×10^{-2}
9.6×10^{-2}	50	0.26	....
	100	0.32	....
	150	0.28; 0.31	8
	200	0.375	5
5.76×10^{-1}	50	0.24	50
	150	0.27	43
2.31	50	0.22	....
	150	0.20	....
20.4	50	0.20	....
	100	0.185	....
	150	0.175	....
	200	0.17	....
54.0	50	0.20	....
	200	0.15	....
300	50	....[a]	....
	200	....[a]	....

[a] Values of friction could not be determined.

Two types of friction are indicated in Fig. 6, one called stick-slip friction following the term introduced by Bowden and Leben, and the other a smooth sliding friction. Further analysis of stick-slip friction will be given later. It is sufficient at present to state that in general two distinct ranges of friction exist. At velocities less than 1 ips stick-slip takes place; at speeds greater than this value, which will be called the critical velocity of friction, a smooth friction record is obtained. Another point of interest, shown in Fig. 6, is that three velocity ranges can be distinguished, namely, (*a*) velocities less than 4×10^{-4} ips, in which the coeffi-

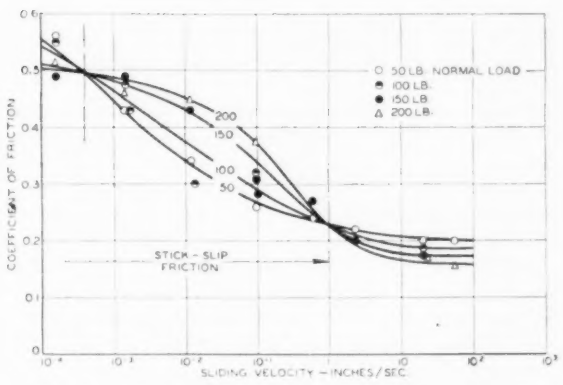


FIG. 6 VELOCITY-FRICTION CURVES AT VARIOUS LOADS

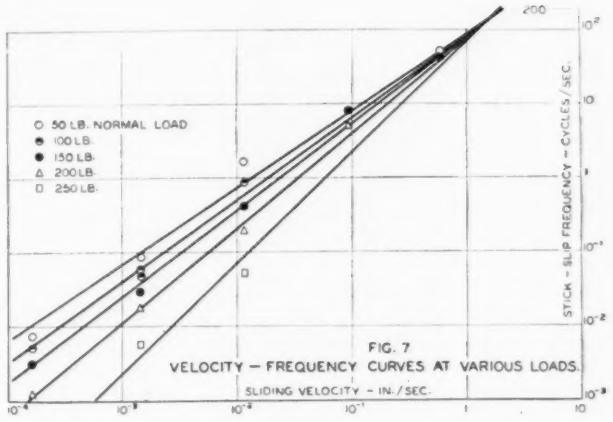


FIG. 7 VELOCITY-FREQUENCY CURVES AT VARIOUS LOADS

cient of friction decreases with increased normal load, (*b*) velocities greater than 4×10^{-4} ips and less than the critical velocity, in which the coefficient of friction increases with increased normal load, and (*c*) velocities greater than the critical velocity, in which the coefficient of friction decreases with increased load.

The following steel combinations in sliding contact were investigated: (*a*) Mild steel on Nos. 1, 2, and 3 steel disks, and (*b*) 18-8 stainless steel on Nos. 1, 2, and 3 steel disks. Along with these some friction tests using copper and aluminum rubbing on the various steel disks were made. In Table 2 are the friction

TABLE 2 COEFFICIENT OF FRICTION FOR VARIOUS METALS IN CONTACT

Disk material	Contact slider material	Coefficient of friction
No. 1 steel	No. 1 steel	0.18–0.23
	18-8 Stainless steel	0.18–0.22
No. 2 steel[a]	No. 1 steel	0.17–0.20
	18-8 Stainless steel	0.16–0.20
	Copper (V.H., 98)	0.23–0.32
No. 3 steel	No. 1 steel	0.18–0.22
	18-8 Stainless steel	0.16–0.19
	Commercial hard copper (V.H., 98)	0.18–0.28
	Aluminum	0.16–0.20

[a] The applied load and speed were constant throughout all tests. The applied load was 50 lb. The disk revolved at a velocity of 20 ips.
V.H. designates Vickers hardness.

values corresponding to these metal combinations. In each case more than one test was made with the exception of those in which copper and aluminum sliders on steel were used. The applied normal load and the velocity were constant throughout each test. The normal load was 50 lb, and the disk revolved at a velocity of approximately 20 ips. The maximum pressures observed as calculated from the measured area of contacts were of the order of 60,000 psi. Unit pressures in pounds per square inch were continuously decreasing during each test, since, due to wear, the apparent contact areas continuously increased.

An examination of the coefficient-of-friction values reveals that no noticeable variation exists between the various steel combinations. Therefore within reasonable experimental accuracy, we may conclude that at the same velocity, normal load, and surface finish, the coefficient of friction is the same for all steels which were investigated.

THE MECHANISM OF STICK-SLIP

As stated in the investigations of Bowden and Leben (14), and Bowden, Leben, and Tabor (15), it has been shown that stick-slip is a general characteristic of the mechanism of friction and of the experimental apparatus. With the present apparatus the critical velocity is 1 ips, due to the natural frequency of the tangential measuring device and the damping in the system. Since the natural frequency of the apparatus and stick-slip seem to be related in some manner, the frequency of stick-slip and the sliding velocity were plotted on log-log paper, as shown in Fig. 7. An examination of the curves reveals that their point of intersection is at the velocity at which the fluctuations recorded cease and the stick-slip frequency is approximately equal to the natural frequency of both the tangential measuring device and the normal load arm. Thus it can be concluded that the natural frequency of the apparatus has a decided effect on the frequency of stick-slip.

From the experimental results shown in Fig. 7, a definite relation exists between the frequency of stick-slip and the sliding velocity. Thus the stick-slip frequency f_s can be expressed as a function of the sliding velocity v, in the following form

$$f_s = kv^n \quad [1]$$

The physical constants k and n are functions of the normal load. Thus for the various loads plotted, the equations of the curves are

$$\left.\begin{array}{ll} (50\text{ lb}) & f_s = 87.4\, v^{1.04} \\ (100\text{ lb}) & f_s = 84.5\, v^{1.11} \\ (150\text{ lb}) & f_s = 82.2\, v^{1.17} \\ (200\text{ lb}) & f_s = 77.2\, v^{1.27} \\ (250\text{ lb}) & f_s = 63.0\, v^{1.48} \end{array}\right\} \quad [2]$$

(The units of f_s and v are cycles per second and inches per second, respectively.)

Since the velocity is constant throughout a test, an expression can be obtained for determining the distance of slip. The distance s traversed per cycle is proportional to the sliding velocity and inversely proportional to the frequency of stick-slip. Thus

$$s = \frac{v}{f_s} = \frac{1}{kv^{n-1}} \quad [3]$$

From the preceding equation the distance of slip can be calculated at any normal load and at any sliding velocity.

In addition to the velocity-frequency curves which are analyzed, some consideration is given to the effect of the normal load on the stick-slip frequency at a constant velocity. This effect is shown by two curves at different velocities in Fig. 8. For the particular velocities chosen the stick-slip frequency can be expressed as a function of the normal load L, in the following manner

$$f_s = C_1 e^{C_2 L} \quad [4]$$

where C_1, C_2 are constants.

This equation will hold for normal loads greater than 35 lb and less than 200 lb. From a test run by Bowden and Leben at a velocity of 0.006 cm per sec and a reaction of 400 g between the

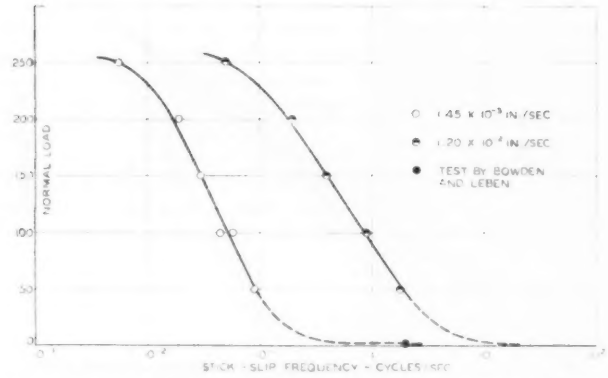


FIG. 8 FREQUENCY - NORMAL LOAD CURVES AT VARIOUS VELOCITIES

surface, the nature of the curve at the higher loads can be deduced. When the normal load is increased in magnitude to greater than 200 lb, the curves taper off in the form of an inverted *S*. This seems reasonable, since eventually pressures are reached in which the contact slider plastically deforms very rapidly. Similarly, at lighter loads, the frequency of stick-slip would increase at an accelerated rate. Thus it can be concluded that the curves become asymptotic to the abscissa and to a maximum normal load line.

Photographs of both the surfaces of the disks and the friction records were taken. Fig. 9 shows a magnification of the surface of the disk and a typical record of the test taken with the lower surface moving at a velocity of 1.6×10^{-4} ips and with a reaction of 50 lb between the two surfaces. The passage of time is from left to right. The upper trace of the record is used as a zero position in determining the coefficient of friction. The pointer, as shown in Fig. 4, deflects upward as the tangential force is increased. The distance between the maximum friction and the zero trace can be measured and the load determined. The measured frictional force divided by the normal load is the value of the coefficient of friction. Increments of the coefficients of friction are indicated in the figure. The recorded trace represents the variation of the tangential force with time. As indicated by the records, the force opposing motion is not constant but varies in definite cycles during sliding. These fluctuations follow a definite pattern in which the tangential force increases steadily up to a maximum force and instantly drops to a lower value. The dis-

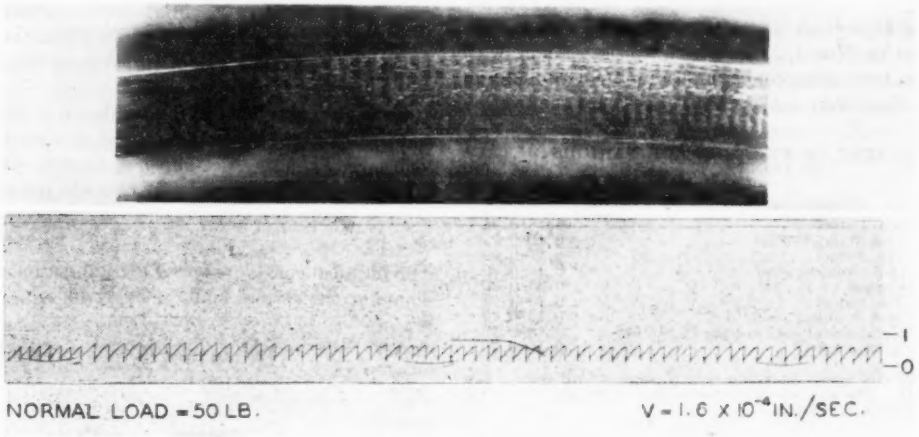


FIG. 9 MAGNIFIED SURFACE OF DISK AND RECORD OF TEST

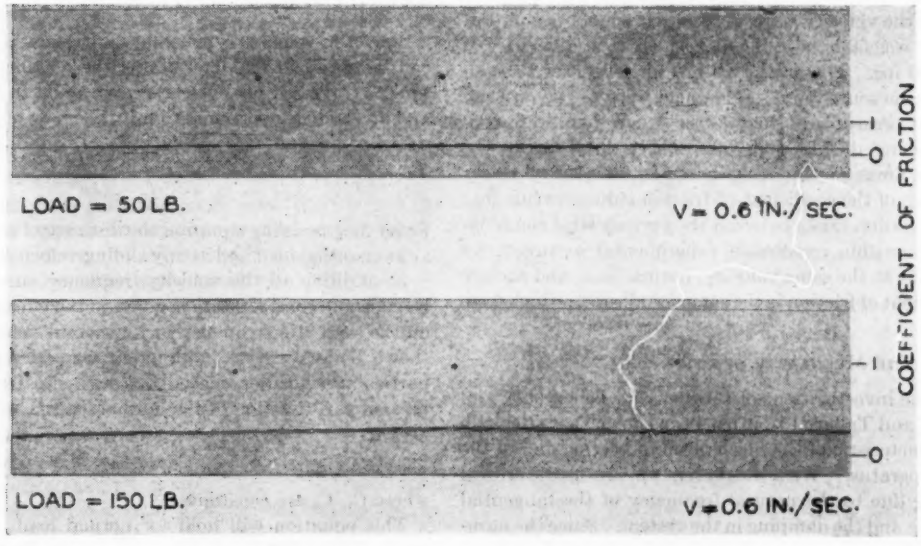


FIG. 10 STICK-SLIP FRICTION NEAR THE CRITICAL VELOCITY

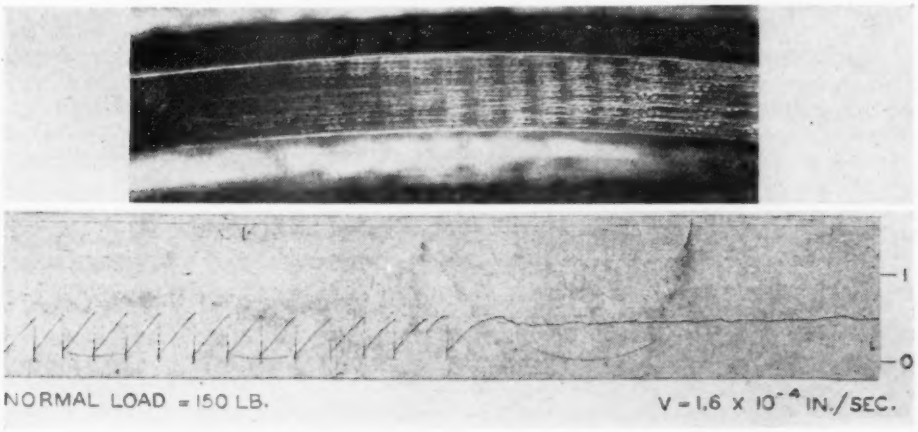


FIG. 11 MAGNIFIED SURFACE OF DISK AND RECORD OF TEST

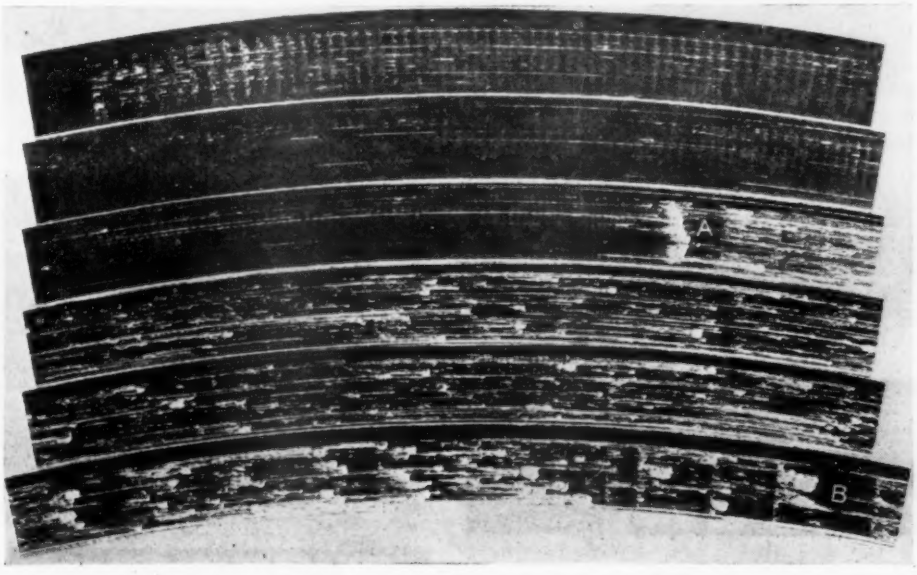


FIG. 12 CONDITION OF COMPLETE SURFACE AFTER TEST
(Record of test shown in Fig. 13.)

tance through which the slider slips is a function of the velocity. The vibrations are of the stick-slip type at the slower speeds; as the speed of the disk is increased and approaches the critical velocity of the apparatus, the fluctuations take the form of simple harmonic vibrations, as shown in Fig. 10. At the higher loads stick-slip continues until the surface of the metal is ruptured, after which plastic smearing of the metal occurs. The friction varies in a radical manner and is, with exceptions, void of the stick-slip phenomenon. An examination of Figs. 11 and 13 indicates what may occur after the surface is severely ruptured.

Fig. 11 shows the effect of increased load when compared with Fig. 9, the velocity remaining the same. At the higher loads the surface of the disk is more susceptible to rupture. This is shown to illustrate that the identical number of stick-slips was recorded, as there are stick-slip markings on the surface of the disk. The time required for the tangential force to reach its maximum value, as determined from the record, is 300 sec. The distance through which the slider slips can be measured directly from the photograph of the magnified surface, or it can be calculated from Equation [3]. The average value of one cycle measured from the disk is 0.051 in., which is in close agreement with that calculated by Equation [3] (0.053 in.).

In order to illustrate what happens to the entire surface of the disk throughout a complete test, a magnified photograph of the complete surface was made as shown in Fig. 12. As the disk rotates in a counterclockwise direction, the cylindrical contact moves in a relative direction from left to right. The complete record of the test is shown in Fig. 13. The amplitude of the frictional force decreased, and the frequency of stick-slip increased as the test progressed. The surface of the disk was ruptured at point *A* where large portions of the metal were torn from the slider and adhered to the surface of the disk. After rupture occurred, the surface became rougher as the test proceeded. As the contact slider passed over the ruptured surface, stick-slip occurred in a radical manner, as shown at *B*, on the surface.

The wear produced by high pressures on the surface of the disk and on the contact slider is shown in Figs. 14 and 15. The worn surfaces (*a*) and (*c*) mark the beginning, and the surfaces (*b*) and (*d*) the ends of the tests. The contact (*a*) had a normal reaction between the surfaces of 50 lb and contact (*b*) had a reaction of

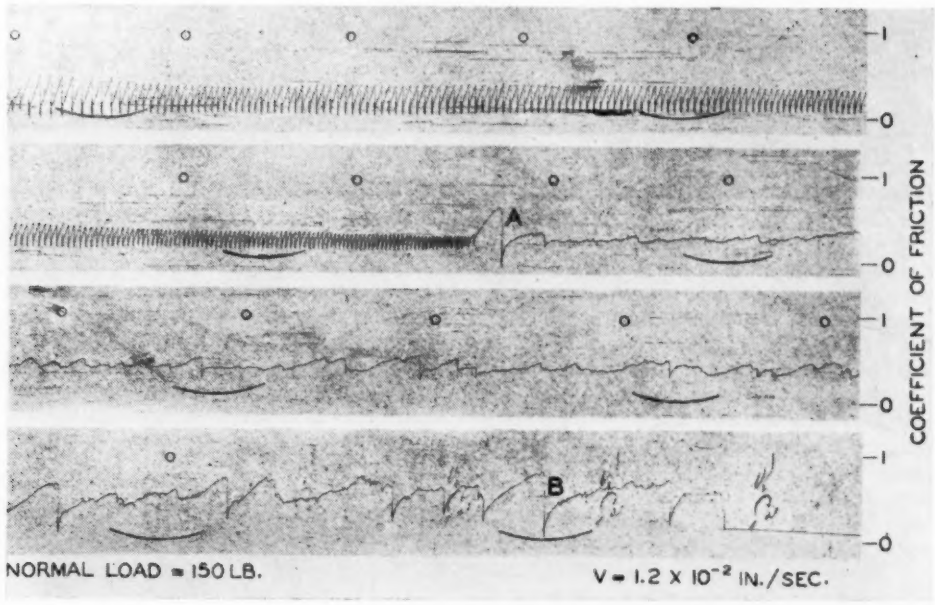


FIG. 13 COMPLETE RECORD OF TEST REPRODUCED IN FIG. 12

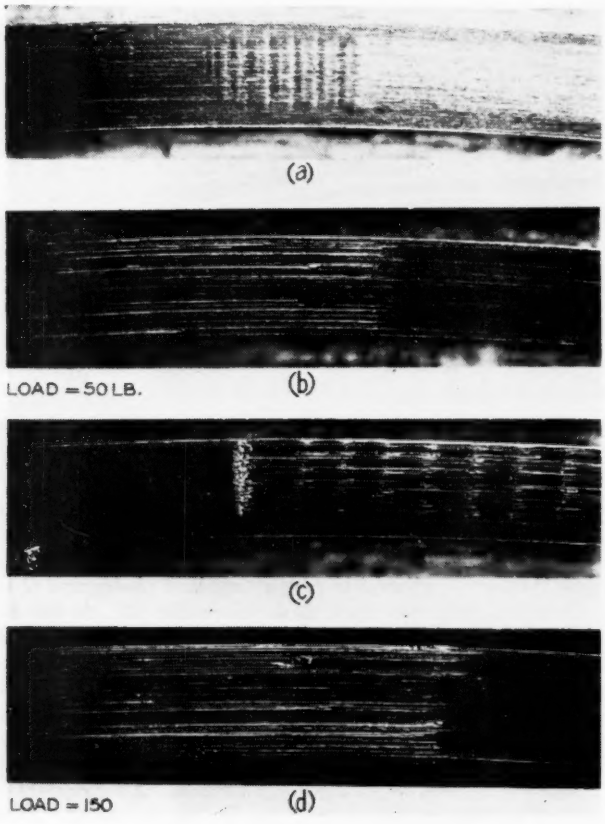


FIG. 14 EFFECT OF STICK-SLIP ON SURFACE OF DISK
(Velocity = 1.44 × 10⁻³ ips.)

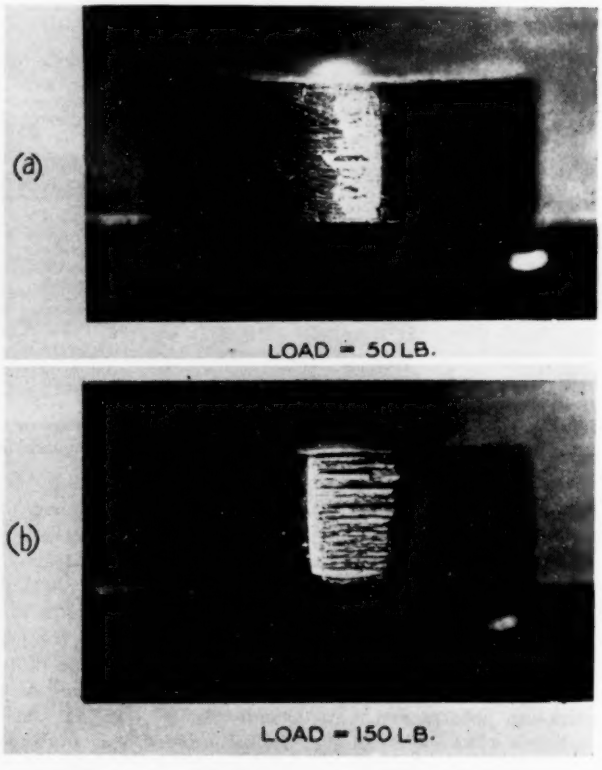


FIG. 15 SLIDING SURFACE OF CYLINDRICAL SLIDERS
Velocity = 1.44 × 10⁻³ ips.)

150 lb. The leading edge of the contact sliders is smooth in comparison to the rest of the sliding surface. This should be the case since the leading edge was continually in contact with the highly polished surface of the disk. However, as the disk continued to rotate, portions of metal were torn from the slider. These particles of metal adhered to the surface of the disk.

In order to illustrate more clearly what occurs when high pressures are applied to sliding metals, two tests were made at different velocities. Fig. 16 shows magnified reproductions of the surface of the disk. The normal reaction between the surfaces

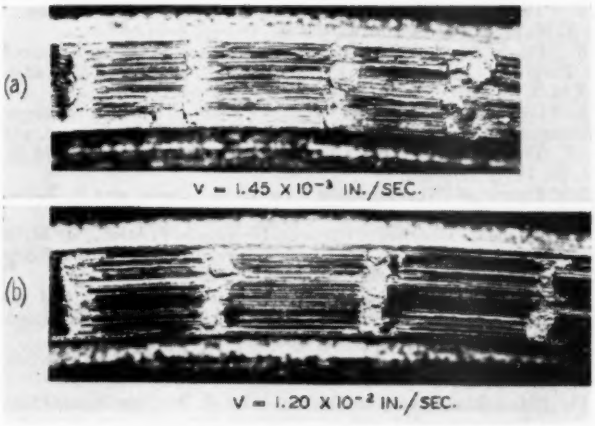


FIG. 16 SURFACES OF DISK UNDER EXTREME PRESSURES
(Normal load = 250 lb.)

was 250 lb in both tests. The distance of slip measured from the photograph of Fig. 15 (*a*) is 0.205 in., and at the faster speed the distance of slip is 0.160 in. At the load applied in these tests the particles torn from the cylindrical sliders are clearly outlined in both photographs. At these velocities enough time prevailed for plastic deformation to occur between the two surfaces. The irregularities of the polished surfaces in contact are points of highly concentrated pressures which caused the elevated portions of the surface to flow plastically and to interlock. As the tangential force increases, a point is reached where the actual area of the metal being sheared, multiplied by the ultimate shearing stress of the metal, is approximately equal to the maximum frictional force before slip occurs. This is graphically illustrated by the reproduced photographs of the surfaces. In these tests the projected areas of shear were measured; although this is not the actual area of shear, it illustrates what does occur in all cases where these effects are not clearly seen. The average projected area as measured with a planimeter is 3×10^{-3} sq in. The frictional force as measured from the record is approximately 150 lb. The ultimate shearing strength of the mild steel is assumed to be 35,000 psi. Therefore the calculated force necessary to shear the steel is approximately 105 lb. However, the actual area of shear cannot be measured and is greater than the projected area which should increase the calculated value. Another consideration is that the slider may have sheared some metallic junctions from the disk. In most cases this would not occur, since the disk has a higher hardness than the slider, as is illustrated by the slider reproductions in Fig. 15.

DISCUSSION

When metal surfaces slide on one another, penetration and distortion of the metals occur to some depth beneath the surface. The frictional force and the nature of sliding are influenced by the bulk properties of the metals, and the mechanism of friction cannot be regarded as only a surface effect. The early investigations of Amontons (10) attributed the nature of sliding friction to the resistance to motion due to the mechanical interlocking of the irregularities of the surface. Recently, Bowden and Leben (14) have suggested that the frictional resistance of metals is primarily due to the shearing of metallic junctions formed by adhesion and welding at these points of contact, and to the work of ploughing surface irregularities of the harder metal through the softer one.

From the work presented herein, in which extreme pressures are employed, the nature of the surfaces previously in contact indicate on a rather quantitative basis the amount of plastic deformation which has occurred. Thus the interlocking of the surface irregularities, brought about by the plastic deformation of the surfaces of the disk and slider, cause the shearing of these metallic junctions. This is particularly significant, when an examination is given to the magnified reproduction of these surfaces. Bowden, Moore, and Tabor (19), in the investigation of the ploughing and adhesion of sliding metals, show by microexamination the nature and extent of the welding and ploughing which occurred at smaller pressures. A reasonable explanation can be given for the shearing of metal. Although the surfaces in contact may be carefully polished, ridges and valleys will still be present in the surfaces.

In a recent publication by Bowden and Tabor (20), the actual area of contact between stationary and moving surfaces was determined by measuring the electrical conductance between the metals. The results showed the real area of contact was very small and was almost independent of the apparent area of contact. These tests have also shown that the deformation of the surfaces was mainly plastic, although elastic deformation has also a decided effect on the surfaces.

The early work of Coulomb and Amontons (21) concluded that the frictional force was (*a*) independent of the area of contact, and (*b*) proportional to the applied load. These relations between the frictional force, the area of contact, and the load, in the light of recent work, are not very apparent. As has been shown in this report, the frictional force is decidedly influenced by both the velocity of sliding metals and by the applied load. This is clearly shown in Fig. 6 of this paper.

The effect of this type of apparatus on the nature of motion has been of particular interest to various investigators. Bowden, Leben, and Tabor (15) have indicated that the intermittent motion produced is influenced by the natural frequency, the moment of inertia, and the damping of the moving parts. Along with the mechanical properties of the system, the type of motion will be decidedly influenced by the velocity. This has been clearly shown by the reproduced records of the stick-slips at various velocities, and at the same applied load. Beyond question, however, the nature of sliding is decidedly influenced by the properties of the metals in contact.

From the experimental curves in Fig. 7 the range of stick-slip, for steel on steel has been defined. At velocities greater than the critical velocity, stick-slip has not been recorded due to the frequency of stick-slip. At the slower velocities the surfaces remain in contact for a relatively long time during the "stick" period. While the surfaces are at rest relative to each other, plastic deformation occurs which allows the macroscopic irregularities of the surfaces to flow and interlock. This welding and adhesion produces larger coefficients of friction than would be obtained under the same conditions of load and surface smoothness at higher velocities.

CONCLUSIONS

1 For clean contact surfaces the coefficient of slidng friction greatly increases with decreasing velocity.

2 Two distinct types of sliding friction are recorded by the dynamometer at the various velocities. At velocities less than the critical velocity stick-slip friction is present and at sliding velocities greater than the critical velocity, a uniform friction record is obtained.

3 Three velocity ranges were obtained in which the coefficient of friction is decidedly influenced by the normal load. In the slowest and fastest velocity range the coefficient of friction decreases with increasing load. In the intermediate range of velocity the opposite occurs.

4 The sliding velocity - stick-slip frequency curves indicate that the nature of sliding friction is influenced by the mechanical properties of the apparatus.

5 The point of intersection of the various velocity-frequency curves occurs at a certain critical velocity, beyond which stick-slip is no longer recorded. The frequency at this point is approximately equal to the natural frequency of the dynamometer and the normal load arm.

6 The stick-slip frequency f, can be expressed as a simple function of the normal load L, and the sliding velocity v. This relation holds for the range of the normal load investigated.

7 The validity of the laws of Amontons and Coulomb are not apparent from the results of this investigation.

8 When high pressures exist between the surfaces, great distortion occurs beneath the surface of the metals in contact. Thus friction is not merely a surface effect but is dependent on the bulk properties of the metals in contact.

9 At high pressures large particles of the softer metal are sheared off and adhere to the plastically deformed surface of the harder metal.

Acknowledgments

Acknowledgments are due to The American Society of Mechanical Engineers for supporting the plans of this investigation; to the Engineering Foundation in New York; to the Atlantic Refining Company, Philadelphia, Pa.; Esso Laboratories, Standard Oil Development Company, Elizabeth, N. J.; Shell Development Company, San Francisco, Calif.; Standard Oil Company of Indiana, Whiting, Ind.; The Texas Company, New York, N. Y., for funds made available for this investigation; and to the Westinghouse Research Laboratories in East Pittsburgh, Pa., for the experimental facilities offered. Further thanks are particularly due to Dr. A. Nadai for supervising the project, and for many valuable suggestions offered during the course of the investigation, and to Dr. L. W. Chubb, Director of the Westinghouse Research Laboratories for support received from the Laboratories.

BIBLIOGRAPHY

1 "Die Formgebung im bildsamen Zustande," by Erick Siebel, Düsseldorf, Verlag Stahleisen, 1932.

2 "Roll Pass Design," by W. Trinks, The Penton Publishing Company, Cleveland, Ohio, vols. 1 and 2, second edition, 1933.

3 "Forces Acting in the Piercing of Cylinders," by W. Trinks, A.S.M.E. Forging of Steel Shells, 1944, pp. 11–14.

4 "The Forces Required for Rolling Steel Strip Under Tension," by A. Nadai, Trans. A.S.M.E., vol. 61, 1939 p. A-54.

5 "Plastic State of Stress in Curved Shells: The Forces Required for Forging of the Nose of High-Explosive Shells," by A. Nadai, A.S.M.E. Forging of Steel Shells, 1944, pp. 31–44.

6 "Drawing Thin-Walled Tubing With a Moving Mandrel Through a Single Stationary Die," by G. Sachs, J. D. Lubahn, and D. P. Tracy, JOURNAL OF APPLIED MECHANICS, Trans. A.S.M.E., vol. 66, 1944, p. A-199.

7 "Theory of Wire-Drawing," by E. A. Davis and S. J. Dokos, Trans. A.S.M.E., vol. 66, 1944, p. A-193.

8 "Physical Properties of Surfaces, I—Kinetic Friction," by W. G. Beare and F. P. Bowden, Philosophical Transactions of the Royla Society of London, Eng., vol. 234, 1935, pp. 329–354.

9 "Studies in Lubrication. X. Friction Phenomena and the Stick-Slip Process," by F. Morgan, M. Muskat, and D. W. Reed, *Journal of Applied Physics*, vol. 12, 1941, pp. 743–752.

10 "Mémoires de Mathematique et de Physique," by Amontons, 1699, pp. 259–286.

11 "Molecular Theory of Friction," by G. A. Tomlinson, *Philosophical Magazine*, vol. 7, series 7, 1929, pp. 905–939.

12 "Surface Friction of Clean Metals—A Basic Factor in the Metal Cutting Process," by H. Ernst and M. E. Merchant, Proceedings on Friction and Surface Finish, Massachusetts Institute of Technology, June, 1940, pp. 76–101.

13 "Physical Properties of Surfaces. III. The Surface Temperature of Sliding Metals," by F. P. Bowden and K. E. Ridler, Proceedings of the Royal Society of London, Eng., vol. 154, 1936, pp. 640–656.

14 "The Nature of Sliding and the Analysis of Friction," by F. P. Bowden and L. Leben, Proceedings of the Royal Society of London, Eng., vol. 169, 1938–1939, pp. 371–391.

15 "The Sliding of Metals, Frictional. Fluctuations and Vibrations of Moving Parts," by F. P. Bowden, L. Leben, and D. Tabor, *The Engineer*, vol. 168, 1939, pp. 214–217.

16 "Fundamental Mechanical Aspects of Boundary Lubrication," by H. Blok. *S.A.E. Journal*, vol. 46–47, 1940, pp. 54–68.

17 "Railway Brakes. On the Coefficient of Friction From Experiments on Railway Brakes," by Douglas Galton, *Engineering*, vol. 26, 1878, pp. 153–154.

18 "Wryvingsproeven in Verband met het Slippen van Autobanden," by P. J. Papenhuyzen, *De Ingenieur*, vol. 53, 1938, pp. 75–81.

19 "The Ploughing and Adhesion of Sliding Metals," by F. P. Bowden, A. J. W. Moore, and D. Tabor, *Journal of Applied Physics*, vol. 14, 1943, pp. 80–91.

20 "The Area of Contact Between Stationary and Moving Surfaces," by F. P. Bowden and D. Tabor, Proceedings of the Royal Society of London, Eng., vol. 169, 1938–1939, pp. 391–413.

21 "Collected Works," by W. D. Hardy, Cambridge University Press, London, Eng., 1936.

A Photoelectric Method of Measuring Damping in Metal Forks at Elevated Temperatures

By T. E. POCHAPSKY[1] AND W. J. MASE,[1] COLUMBUS, OHIO

Engineering measurements of internal friction in metals have been obtained from the decay characteristics of tuning forks of metals of interest. A damping program at Battelle Memorial Institute, conducted for the Office of Scientific Research and Development, called for such measurements at temperatures up to 1500 F, and it was necessary to develop suitable apparatus for obtaining accurate results at those elevated temperatures. A photoelectric method of measuring tine amplitude decay, using shutters on a vibrating fork to modulate light directed at a photocell, was developed. It proved to give very satisfactory results and had none of the mechanical difficulties in operation and uncertainties in results that were encountered at high temperatures when platinum-wire Sauereisen-cemented strain gages were used. It was necessary to reduce energy losses from the fork to its support by using a compliant coupling. This suspension worked so well that the lower limit of decrement measurements was probably determined by acoustic losses. It is believed that such losses added less than 0.00004 to the decrements of steel forks. This report includes details of construction of the equipment and reviews tests performed to establish its accuracy.

Introduction

INFORMATION on the damping capacities of metals has become important in designing high-speed machinery which utilizes the natural internal friction of metals to suppress resonant vibrations. A method of obtaining such data from the free-vibration decay characteristics of tuning forks made of metals of interest was recently described by Carl Schabtach and R. O. Fehr.[2] A similar approach was used at Battelle to obtain measurements at temperatures up to 1500 F.

Strain gages, used by Schabtach and Fehr, did not prove to be an accurate means of measuring tine vibration amplitudes at the desired elevated temperatures. Experience with the ceramic-body gages showed that they failed mechanically at high temperatures and that they absorbed energy from vibrating forks. Consequently, results were uncertain. This prompted an investigation of a photoelectric method of measurement which was developed and found to give almost trouble-free operation and satisfactory results. In addition, it was necessary to take steps to reduce energy losses to the fork support, so extending the useful range of measurements. The following sections describe the photoelectric equipment, methods of reducing extraneous losses, and tests carried out to establish the accuracy of the apparatus. Comments on experience with the strain-gage method are also included.

Photoelectric Method of Measuring Damping in Tuning Forks

After a tuning fork is excited, it continues to vibrate until the energy of excitation is dissipated, partly as heat in the fork and partly as sound in the air and the fork support. If external losses are sufficiently small, the logarithmic decrement of the amplitude of tine vibration can be used as a measure of the internal dissipation or damping of the fork metal.

The percentage of strain energy lost during a cycle generally varies with the stress and is not constant throughout the fork. The decrement obtained from the tine displacement, however, is a reliable value of the average which would be obtained in the usual types of bending. Following Schabtach and Fehr, decrements in the present work were determined at various nominal peak bending stresses at the base of a tine during vibration decay.

Records of fork amplitude decay were obtained with the electro-optical system illustrated in Figs. 1 and 2. To obtain a measurement, shutters were fastened rigidly to each tine, as illustrated, and the fork was supported so that the shutters interrupted a beam of light on its way to a photocell. The shutter separation varied directly with the tine amplitude and vibration of the tines caused a corresponding modulation of the light flux. This variation at the cell generated an alternating voltage which was amplified and passed through a recording galvanometer. From the photographic record it was possible to determine both the frequency and the logarithmic decrement of the amplitude of the fork at any stress maximum during decay. A typical record is shown in Fig. 3.

A diagram of the associated electrical equipment is shown in Fig. 4. The amplifier circuit was conventional and any good commercial unit could be modified for the purpose. Microphonics and hum were reduced sufficiently by using inverse feedback, careful filtering, and shockproof mountings.

Fidelity of Measuring System

The following tests were made to guarantee the proportionality between record and fork amplitudes:

1 The uniformity of illumination in the shutter plane was checked by passing 1000-cycle modulated light through a small opening in a screen in that plane, and noting that there was no variation in the signal when the opening was moved about the plane. Further confirmation was obtained when no signal resulted from vibrating a slit screen in the shutter plane.

2 The photocell was checked by determining that its output was proportional to the light flux directed at it. One especially

[1] Battelle Memorial Institute.

[2] "Measurement of the Damping of Engineering Materials During Flexural Vibration at Elevated Temperatures," by Carl Schabtach and R. O. Fehr, JOURNAL OF APPLIED MECHANICS, Trans. A.S.M.E., vol. 66, 1944, p. A-86.

For presentation at a meeting of the Applied Mechanics Division, Buffalo, N. Y., June 21–22, 1946, of THE AMERICAN SOCIETY OF MECHANICAL ENGINEERS.

Discussion of this paper should be addressed to the Secretary, A.S.M.E., 29 West 39th Street, New York, N. Y., and will be accepted until July 10, 1946, for publication at a later date. Discussion received after the closing date will be returned.

NOTE: Statements and opinions advanced in papers are to be understood as individual expressions of their authors and not those of the Society.

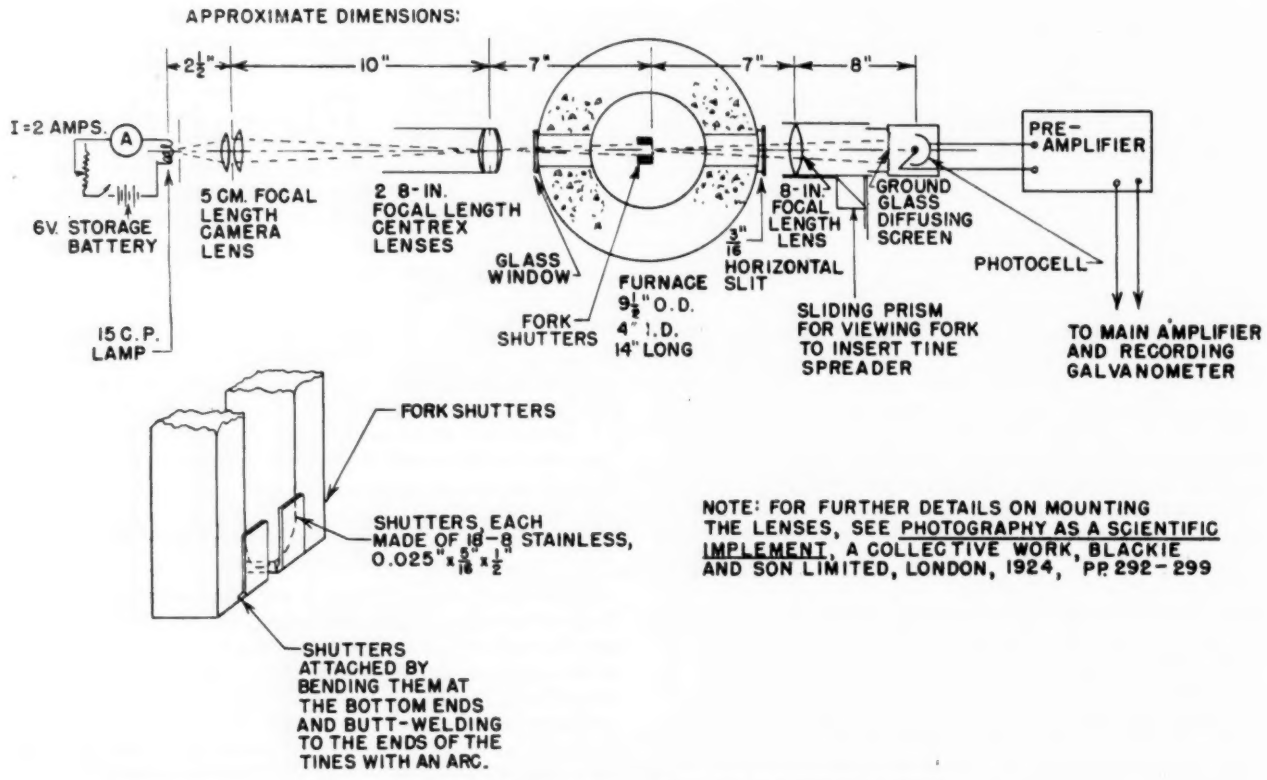


FIG. 1 DIAGRAM OF OPTICAL SYSTEM USED FOR MEASURING DAMPING

revealing test was run in which the cell was exposed to light from an unobstructed filament, 60-cycle a c heated, as well as to the steady light passing between the shutters of an excited fork.

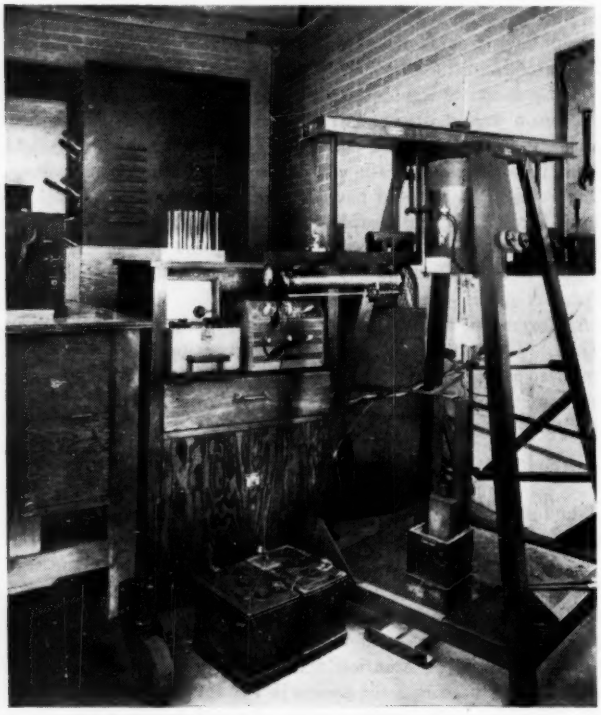


FIG. 2 EQUIPMENT USED TO MEASURE DAMPING

Analysis of the amplified and recorded output showed that the gain of the system remained constant and that electrical transients following excitation were dissipated within a few hundredths of a second. Cross-modulation was of the order of 1 per cent.

3 The over-all linearity of the system was confirmed by measuring initial record amplitudes and finding them to be proportional to the corresponding initial time displacements. Damping measurements with the system also agreed with similar measurements on the same fork obtained with SR-4 paper strain gages at low temperatures.

ENERGY LOSSES FROM VIBRATING FORKS TO THE EXTERIOR

To make certain that most of the fork vibratory energy was dissipated in internal friction, measurements were made to determine whether any significant losses took place through the support or at the shutters.

Losses to the Support. Energy flow through the support was apparent in tests on a normally machined low-damping fork when a decrement of 0.00055 was obtained with a rigid connection to the support bar, while a value of 0.00033 was obtained with a cushioned connection. Further investigation showed that the drainage of energy through the rigid support was serious when the tines were unbalanced, as shown in Fig. 5. A compliant coupling between the fork and the support bar practically prevented such losses, so that reliable results, Fig. 5, could be obtained even for a badly unbalanced low-damping fork.

The construction of the coupling was such that it kept the fork positioned in the light field even after a spreader was jerked abruptly from between the tines. The design is illustrated in Fig. 6. As can be seen, the fork was suspended from two crossed horizontal springs fastened to a ring which, in turn, was suspended by four vertical wires. This bird-cage-type construction minimized mass motion of the fork, but at the same time did not



FIG. 3 TYPICAL RECORD OF AMPLITUDE DECAY FOR A FORK EXCITED AT 1500 F
(Timing lines occur every 0.01 sec.)

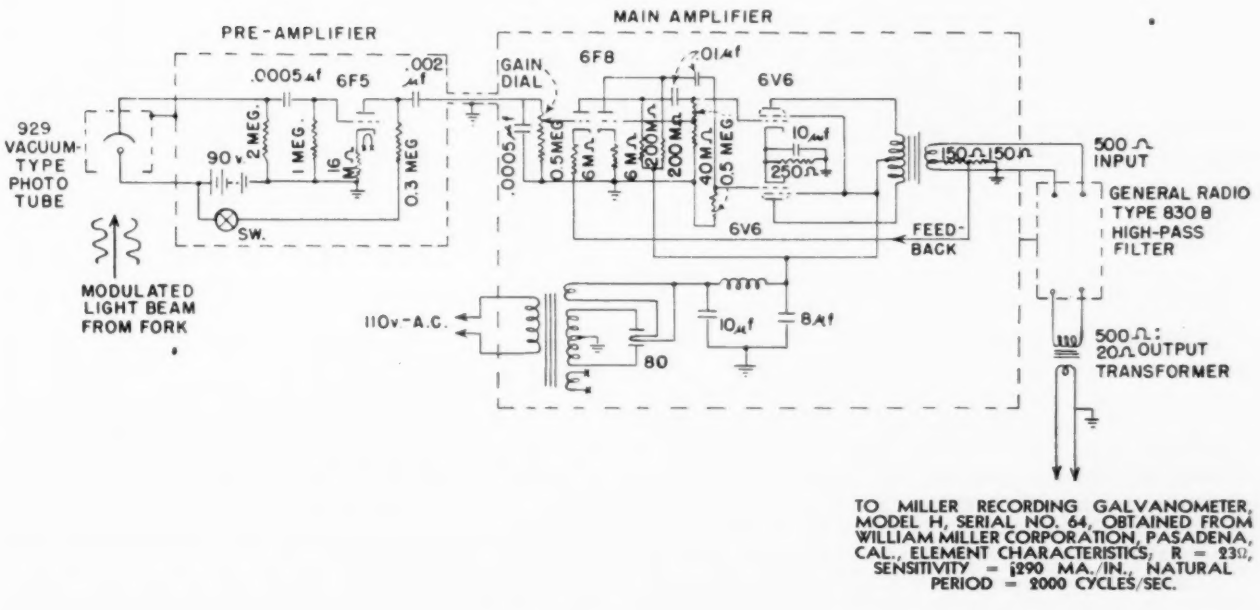


FIG. 4 AMPLIFIER CIRCUITS USED TO RECORD FORK VIBRATION

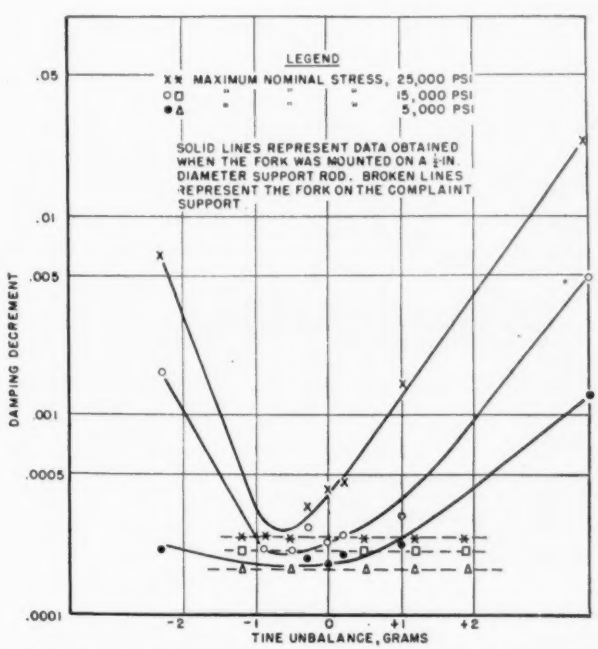


FIG. 5 EFFECT OF TINE UNBALANCE ON DAMPING OF A FORK AT ROOM TEMPERATURE

offer much loading to high-frequency vibratory motion at the base of the fork. A washer supported by four solid posts, so as to form a table just under the springs, prevented damage to the delicate springs when the spreader was jerked out.

The coupling was made of a low-damping high-temperature alloy and measurements showed that it reduced losses as effectively at a temperature of 1200 F as it did at room temperature. It was strong enough to take the punishment of repeated tests at 1500 F. Significant dimensions are noted in the illustration.

Shutter Losses. The stainless-steel shutters on the forks received a slight amount of vibratory strain energy when they followed the motion of the tines. Dissipation, however, was negligible, and shutter weights could be increased from ½ g up to 3.3 g without definitely influencing results at 1200 F. The decrement of the test fork was 0.00035 at that temperature.

Energy Radiated as Sound. No measurements were made of acoustic-energy losses inasmuch as they were considered small enough to ignore in the test program for which the equipment was built. Rough computation suggested that decrements determined for steel forks had an addition of the order of 10^{-5} because of air loading. A decrement of 0.0002 was obtained for a Dowmetal fork, indicating that air loading added less than 0.00004 to decrements for steel. Lacking definite data, it is suggested that the latter figure be used as the error of measurement in the low-decrement range. This is sufficiently accurate for most

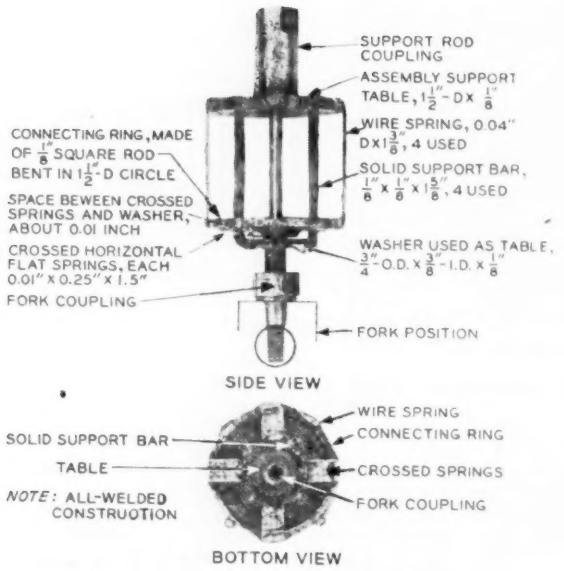


FIG. 6 ILLUSTRATION OF COMPLIANT SUPPORT

engineering work; a fork with a decrement of 0.0001 can normally be heard for over a minute after striking.

COMMENTS ON PHOTOELECTRIC AND STRAIN-GAGE MEASUREMENTS

Operation of the apparatus was practically trouble-free, especially when compared to the trials of earlier measurements with strain gages. Details of these gages are shown in Fig. 7. Most of the difficulties with gages resulted because it was necessary to use platinum-wire elements to withstand corrosion by the ceramic gage body at the higher temperatures and such elements were relatively insensitive to strain. Consequently, weak and noisy signals were obtained. Tests were frequently interrupted because of element failure at the time of excitation during the measurements at the 900 F test temperature. At higher temperatures the ceramic tended to blister from the fork. These factors led to an uncertainty in results which could not always be checked because the properties of the metals changed markedly with the history of the forks. It was also found that a ceramic gage, advanced 1/4 in. up the base of a tine, absorbed enough energy to add about 0.0002 to the decrements of steel forks near room temperature.

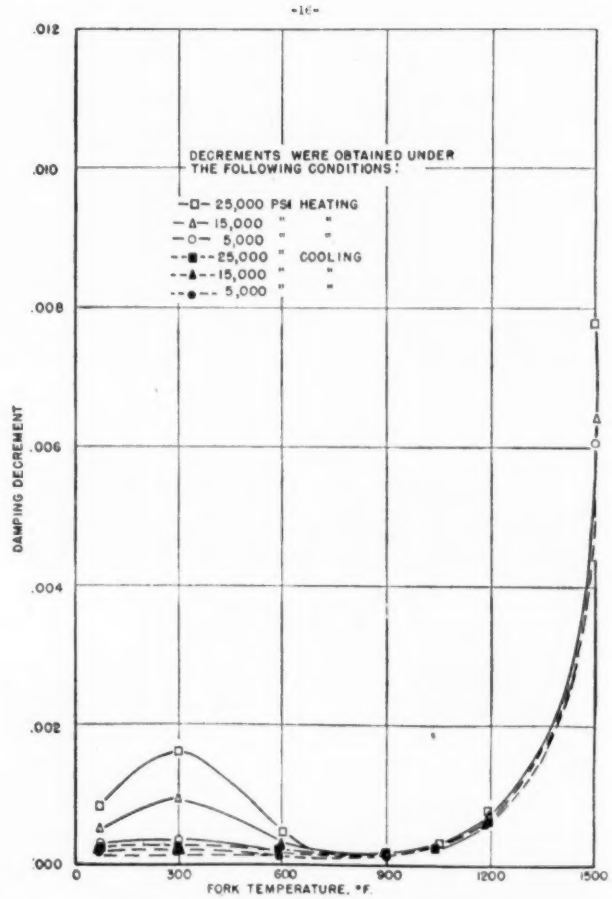
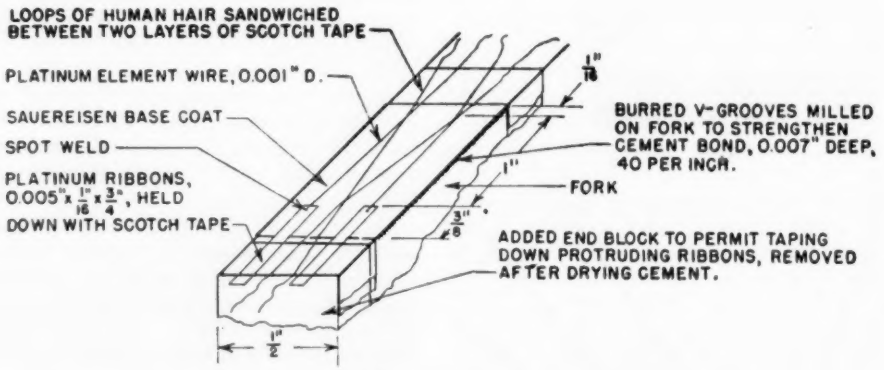


FIG. 8 TYPICAL DAMPING RESULTS FOR A HEAT-RESISTING ALLOY

Failure of the gages in this work was a consequence of steps



NOTE: THE SCOTCH TAPE WAS REMOVED AFTER COATING THE ASSEMBLY WITH A THIN LAYER OF SAUEREISEN CEMENT AND BAKING AT 400° F. THIS CONSTRUCTION WAS PATTERNED AFTER THAT USED BY SCHABTACH AND FEHR, EXCEPT THAT A PLATINUM WIRE, RATHER THAN NICHROME, GAGE ELEMENT WAS USED. NICHROME WIRE COULD NOT WITHSTAND CHEMICAL ATTACK BY THE CEMENT AT HIGH TEMPERATURES.

FIG. 7 CONSTRUCTION OF A HIGH-TEMPERATURE STRAIN GAGE ON SIDE OF A TUNING FORK

taken to obtain results at high temperatures. At lower temperatures, sensitive and carefully placed gages could be used successfully, and might be preferred instead of the optical arrangement because of the simpler associated equipment. On the other hand, the new procedure may have advantages in a long series of tests because it is easier to install shutters than to build gages on forks. The relatively high sensitivity of the photocell is also desirable.

Accuracy of Equipment

The over-all accuracy of measurements with the photoelectric apparatus could not be established definitely for lack of forks to be used as standards. Based on the favorable characteristics of the equipment, in most cases a ± 10 per cent accuracy should include the slight errors caused by distortion in the circuits, as well as by inaccuracies in measuring the slopes of traces. Repeat tests on stable forks gave results which were consistent within less than these limitations. A fixed decrement error of less than $+0.00004$ for steel would include acoustic losses. Techniques of measurement could probably be elaborated to give a much better certified accuracy, but damping was found to be so dependent on fork history that the present accuracy was more than sufficient for the measurements of interest. This accuracy should hold at temperatures up to at least 1500 F. Measurements could probably be made at substantially higher temperatures with small loss in precision.

Some of the vibration records showed a spurious low-frequency transient modulation 5 to 10 per cent in magnitude following excitation. The source of this was not satisfactorily determined although rotation of the compliantly suspended fork may have contributed in producing it. There is also a possibility that it was caused, at least in part, by energy interchanges in the fork, inasmuch as similar modulation was found on some of the records obtained with strain gages. Most of the effect of these transients was averaged out by using a graphical method of analyzing records, but they would probably cause important errors at very high decrements, say, above 0.1.

The present equipment has been used in measurements on a series of alloys. Typical results are shown in Fig. 8.

Acknowledgment

The authors are indebted to the Office of Scientific Research and Development for permission to publish these results.

The authors also wish to thank Carl Schabtach and R. O. Fehr of the General Electric Company, for volunteering information on their strain-gage method of measuring damping with tuning forks, prior to publishing the results of their work.

Discussion

A New Device for the Solution of Transient-Vibration Problems by the Method of Electrical-Mechanical Analogy[1]

E. N. KEMLER[2] AND C. R. FREBERG.[3] The method of using analogies which the authors outline has, as they point out, been well known for some time. Many of the earlier articles have been concerned with use of the analogue as a qualitative tool rather than as a quantitative one. Actually the methods which have been proposed along these lines permit the design of electrical models of mechanical, acoustical, or fluid systems. Several references are available which show other applications than those mentioned by the authors of the paper. These give a more detailed approach to the general problems than is given in the paper (1, 2, 3, 4, 5, 6).[4]

The significance of the mass-inductance and mass-capacitance circuits can best be illustrated by the fundamental difference between many common electrical and mechanical systems. The ordinary electrical system has a known signal or voltage applied to it. In the normal or mass-inductance analogue, this corresponds to putting a known force on the mechanical. Many mechanical systems, however, have a known motion rather than a known force applied to them. This would correspond to impressing a known velocity on the electrical analogue. Since voltage generators are more common than current generators, it is desirable to be able to have an analogue on which the equivalent of the velocity could be readily imposed. The mass-capacitance circuit is such a one. This is also known as the inverted system because some measurements have no immediate meaning in the mechanical system. Measurements that are desired may therefore become extremely difficult. The type of analogue to be used will therefore depend on the type of problem to be solved, as well as on the information desired.

In the solution of transient problems, a time scale is often needed. One means of introducing a time scale is to use an oscillograph with a Z-axis gain. An oscillator connected to this terminal can be used for putting timing marks on the diagram (2).

The simplest type of problem to which the electrical model can be put is that of finding the natural frequencies in multimass systems (1, 4). Here an oscillator can be applied to the system, and its response over a wide range of frequencies can be determined. The determination of such frequencies is usually not too critically influenced by the amount of damping if high-quality inductances are used. When amplitudes, velocities, or accelerations are to be measured, however, the effect of damping becomes critical. The problem usually is one of determining the amount of equivalent velocity damping in the mechanical system.

The terms connecting the mechanical and electrical systems can be obtained by reducing the differential equations to dimensionless form, dimensional analysis, or by the procedure developed in the paper (1, 4, 5). Once these relations have been worked out, the setting up of the equivalent electric circuit is simple. This general method of solving multimass problems certainly deserves more use than it has been given.

BIBLIOGRAPHY

1 "Elements of Mechanical Vibrations," by C. R. Freberg and E. N. Kemler, John Wiley & Sons, Inc., New York, N. Y., 1944, chapt. 8.

2 "Models and Analogues for Solving Design Problems," by E. N. Kemler, *Product Engineering*, vol. 13, 1942, pp. 660–661.

3 "An Experimental Method of Determining Sucker Rod Loads," by E. N. Kemler, Trans. A.I.M.E., vol. 118, 1936, pp. 89–98.

4 "The Solution of Vibration Problems by Use of Electrical Models," by C. R. Freberg, Purdue University Engineering Experiment Station Bulletin, Research Series No. 92, 1944.

5 "Electrical Models in the Teaching and Application of Vibration Theory," by E. N. Kemler and C. R. Freberg, *The Journal of Engineering Education*, vol. 34, 1943, pp. 274–281.

6 "Mathematical and Physical Principles of Engineering Analysis," by W. C. Johnson, McGraw-Hill Book Company, Inc., New York, N. Y., 1944.

[1] By H. E. Criner, G. D. McCann, and C. E. Warren, published in the September, 1945, issue of the JOURNAL OF APPLIED MECHANICS, Trans. A.S.M.E., vol. 67, p. A-135.

[2] Head, Engineering Research Division, Southern Research Institute, Birmingham, Ala.

[3] Assistant Professor of Mechanical and Aeronautical Engineering, Purdue University, Lafayette, Ind.

[4] Numbers in parentheses refer to the Bibliography at the end of this discussion.

The Theory of Ejectors[1]

G. M. DUSINBERRE.[2] The writer has been accustomed to think of the air ejector, in steam-condenser service, as having approximately a constant volume characteristic, that is, it behaves like a reciprocating compressor at constant speed and volumetric efficiency. It tends to handle at a constant volume rate whatever mixture of steam and air may enter its suction, whatever the partial and total pressures may be, within the normal operating range. Will the author comment on how this empirical relation checks with his theory?

The "efficiency" or criterion of performance proposed by the author is novel, simple, and has obvious merit in setting a standard for this type of apparatus. It deserves further study and one hopes that the author will continue his experimental and analytical work in this direction.

It may be pointed out that this criterion offers a direct basis of comparison only as between ejectors and not with other systems of compression. This is not objectionable from a practical viewpoint because the ejector wins a place on the basis of first cost, compactness, and maintenance rather than on economy of actuating fluid. However, it is of theoretical interest to compare the author's standard with that of an engine-compressor system in which the actuating fluid expands to the discharge pressure in a reversible adiabatic engine, and the induced fluid is handled in a reversible adiabatic compressor driven by the engine.

For simplicity, assume both fluids the same pure substance so the conventional h-s diagram may be used, Fig. 1 of this discussion. Let A represent the state of the actuating fluid, B the state of the induced fluid, and solid line CD the discharge pressure. Then E will represent the result of reversible mixing as outlined in the author's Appendix 1. The flow ratio will be AE/EB.

[1] By H. G. Elrod, Jr., published in the September, 1945, issue of the JOURNAL OF APPLIED MECHANICS, Trans. A.S.M.E., vol. 67, p. A-170.

[2] Assistant Professor of Mechanical Engineering, Virginia Polytechnic Institute, Blacksburg, Va. Now on duty at U. S. Naval Academy, Annapolis, Md. Mem. A.S.M.E.

For the engine-compressor system, AC will be the engine work and BD the compressor work, per pound. In this system the flow ratio will have to be inversely as the work per pound, or as AC/BD.

Now if we deal with a part of the wet-vapor region where the discharge-pressure line is straight at all points involved, the broken line FED represents this situation. The engine work is

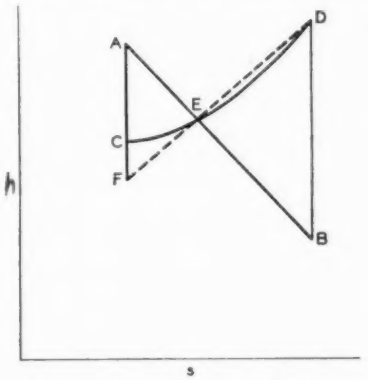


FIG. 1 CONVENTIONAL h-s DIAGRAM

now AF, per pound, and the flow ratio is AF/BD. Inspection shows that this is equal to the ratio AE/EB for the reversible mixing system and greater than the ratio AC/BD for the more general case of the engine-compressor system.

This is to say that the author's criterion sets a higher standard than is attainable in general by an engine-compressor system operating adiabatically.

R. B. ENGDAHL.[3] This paper presents for the first time for dissimilar fluids a comparison between theoretically and experimentally determined performance curves of ejectors. The agreement is good and indicates that the analysis with its assumptions can be used with confidence to explore areas uncharted either analytically or experimentally.

One such area is entered when the boiler operator applies steam-actuated secondary-air jets to a furnace operating under a strong induced draft. The performance of the jets under this condition has never been measured. In Fig. 7 of the paper all points above the curve $P_{30} = 1.0$ are in this region. The theoretical curves show that for an area ratio of 13.5 and for low actuating pressure ratios, the entrainment is increased by the reduced outlet pressure so long as the outlet velocity is below the velocity of sound. This was to be expected, but the author's equations now permit calculation of the amount of this increase for the area ratios commonly used for overfire jets.

The conclusion that neglect of wall friction has little effect on the calculated performance bears out the experimental finding that considerable additional length of mixing tube beyond the optimum 7.5 diam reduces the performance only very little. That wall friction is such a minor item emphasizes the well-known profligacy of jets as consumers of energy. Many well-conceived ideas for jet-actuated thermal equipment will remain economically unfeasible until the mechanical efficiency of the jet can be improved. The author has contributed distinctly toward an understanding of jet action which may bring about that improvement.

R. E. HANSEN.[4] The author's proof (Appendix 1 of the paper) that a reversible mixing apparatus gives the best possible flow ratio is predicated on the conditions

$$p_i > p_3 > p_a \quad \ldots\ldots\ldots\ldots\ldots\ldots [1]$$

The conditions necessary for the operation of a reversible ejector are

$$p_i > p_a \quad \ldots\ldots\ldots\ldots\ldots\ldots [2]$$

$$p_3 > p_a \quad \ldots\ldots\ldots\ldots\ldots\ldots [3]$$

$$(h_i - h_a) > (h_2 - h_b) \quad \ldots\ldots\ldots\ldots\ldots\ldots [4]$$

where h_a is enthalpy of the actuating fluid after adiabatic expansion to pressure p_a, and h_b that of the final mixture if expanded adiabatically to pressure p_a. Condition [3] is not strictly necessary to operation of an ejector, but it is necessary to justification of one, because if it does not hold, the induced fluid will proceed to pressure p_3 unaided. For an actual irreversible ejector condition [4] would become

$$e_1(h_i - h_a) > \frac{1}{e_2}(h_3' - h_b') \quad \ldots\ldots\ldots\ldots\ldots\ldots [5]$$

where e_1 is efficiency of the actuating nozzle and e_2 that of the diffuser. Conditions [2], [3], [4], and [5] do not exclude the boiler injector operated by exhaust steam at low pressure ($p_3 > p_i$) as does condition [1].

Condition [4] follows from the kinetic-energy equation of the ejector

$$w_i(h_i - h_a) = (w_i + w_a)(h_3 - h_b) \quad \ldots\ldots\ldots\ldots\ldots\ldots [4a]$$

For the case of interest, $(w_i + w_a) > w_i$; moreover, $(h_i - h_a)$ and $(h_3 - h_b)$ must always be positive. Condition [4] follows therefore from [4a]. It may be possible to state the conditions of operation without direct reference to conditions [2] and [4], but it is believed that these conditions will be implicit in any such statement.

Analysis presented in Appendix 1 of the paper cannot be extended to cover the case where $p_3 > p_i$, because if W and Q become negative, that is, if work is converted into heat instead of vice versa, there is no exception to the second law.

J. H. KEENAN.[5] This paper will bear careful scrutiny by those interested in ejectors. It is based on the well-established one-dimensional analysis which has proved so effective in predicting the performance of ejectors of large area ratio with small pressure ratio. The significance of the restrictions employed here and of the differentiation for maximum flow ratio is not immediately evident. Unfortunately, the accord with experiment is not expressly indicated.

The second-law analysis for limiting flow ratios is apparently new. The efficiency defined in terms of this analysis is more rational than any previously proposed. To be serviceable, however, an efficiency must be so defined that it does not vary too widely with ordinary variations in the conditions for which ejectors are designed. The present paper offers no information on this point.

AUTHOR'S CLOSURE

The author acknowledges with appreciation the interesting contributions of the discussers.

The empirical relation suggested by Commander Dusinberre might be restated as follows:

"If the temperature and pressure of the actuating fluid, the temperature of the induced fluid, and the exhaust pressure are

[3] Research Engineer, Battelle Memorial Institute, Columbus, Ohio. Jun. A.S.M.E.

[4] Mechanical Engineer, Ebasco Services Incorporated, New York, N. Y.

[5] Professor of Mechanical Engineering, Massachusetts Institute of Technology, Cambridge, Mass. Mem. A.S.M.E.

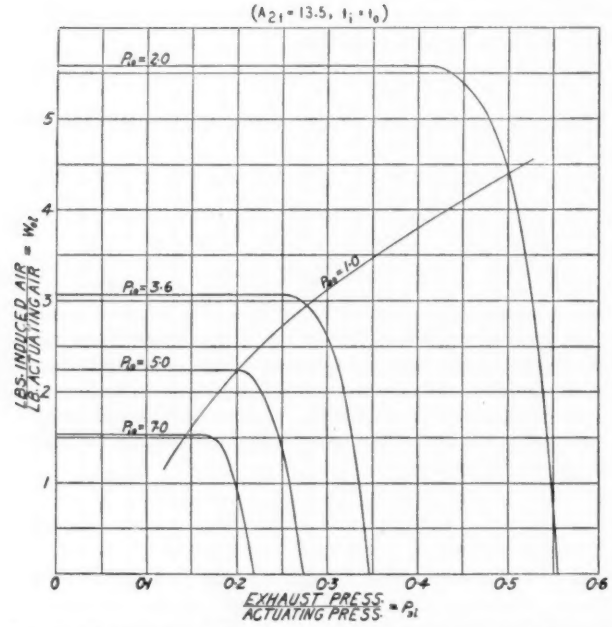


FIG. 2 THEORETICAL PERFORMANCE OF COMPLETE AIR EJECTOR

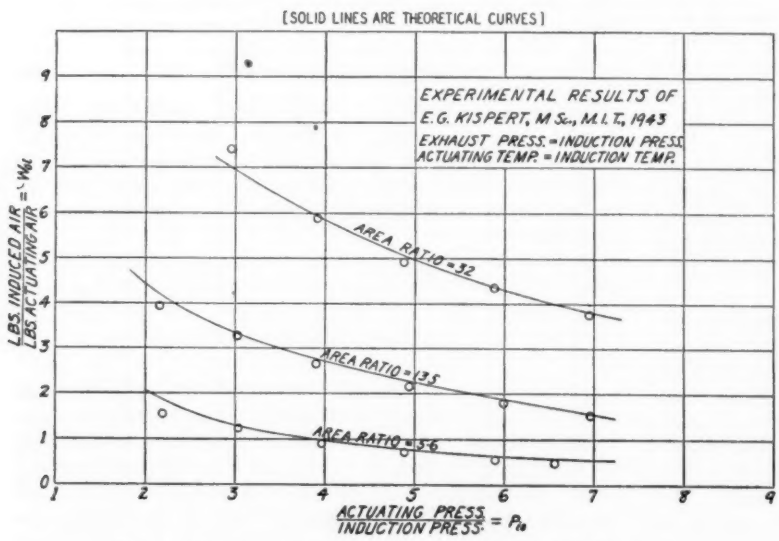


FIG. 3 PERFORMANCE CURVES OF COMPLETE AIR EJECTOR

specified, V' the induced volume flow rate (cu ft per sec) will remain constant."

This statement is interpreted to apply only to high-vacuum ejectors. At a high vacuum and at a fixed temperature all vapors behave as perfect gases. Hence we write

$$w_0 = \left(\frac{V'}{RT_0}\right) p_0$$

According to this equation, the induced flow does not cease until the induction pressure reaches zero. However, it is a consequence of Equations [4] to [9], inclusive, of the paper, that the induced flow ceases at a finite pressure. This pressure corresponds to a blocked-off suction, when the ejector is, in reality, a sudden enlargement. Therefore the rule suggested by Commander Dusinberre is inconsistent with the ejector theory, although this inconsistency may not invalidate the rule as a useful approximation over the normal operating range of high-vacuum ejectors.

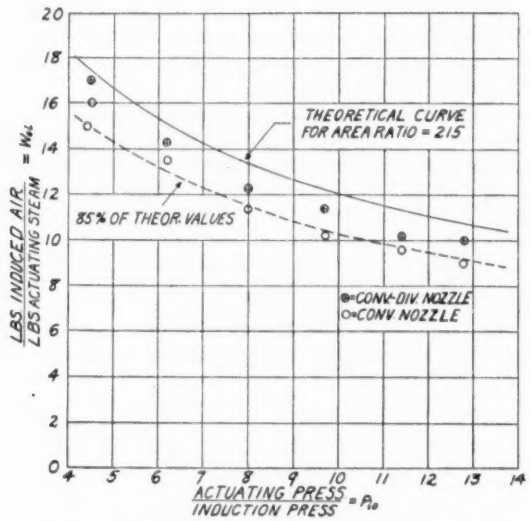


FIG. 4 PERFORMANCE OF SIMPLE STEAM-AIR EJECTOR
(This illustration appears as Fig. 10, in reference 5 of the paper.)

Commander Dusinberre has provided an apt and interesting comparison between the ejector efficiency proposed by the author and that commonly used. The author's criterion sets a higher standard because it allows for utilization of the difference in temperature between the actuating and induced fluids. Although the effect of this temperature difference upon actual ejector performance is rather uncertain, it is logical and necessary that an allowance be made for it. For example, using the engine-compressor standard, we should find the efficiency of a boiler-water injector to be infinite.

For the special case where the isobar FD (Commander Dusinberre's Fig. 1), lies in the wet-vapor region, the temperature difference does not exist, and the two efficiencies are identical.

Mr. Engdahl's discussion pertains to an unabridged, unpublished paper on ejectors. The illustrations to which he refers are included in this closure as Figs. 2, 3, and 4. Their terminology is the same as that of the present paper, except that capital letters are used to denote ratios. In the computation of the theoretical curves the following assumptions were made: Actuating-nozzle exit in mixing-tube throat, nozzle efficiencies 100 per cent, diffuser efficiency for complete ejector, 75 per cent. The refinements mentioned in the sixth section of the paper were employed, although the friction and velocity-distribution allowances affected the results but slightly.

If (1) the inlet conditions and outlet pressure of the working fluids are prescribed, and if (2) $p_i > p_3 > p_0$, Appendix 1 of the paper proves that a reversible ejector yields the maximum, or limiting, flow ratio. Since certain types of ejectors, such as the boiler-water injector, can operate in exception to the second condition (that is, with $p_3 > p_i$), Appendix 1 does not, in such instances, guarantee the reversible flow ratio as a proper standard for comparison. Mr. Hansen writes with this thought in mind.

The general condition necessary to the operation of a reversible

ejector is that there exist a state on the exhaust isobar, p_3, such that

$$w_i h_i + w_o h_0 = (w_i + w_o) h_3$$

$$w_i s_i + w_o s_0 = (w_i + w_o) s_3$$

where, by convention, w_i and w_o are understood to be positive. The additional condition, $p_i > p_3 > p_o$, is sufficient, but unnecessary, to insure the more general condition given.

Mr. Hansen's Equation [2] is not a condition, but a definition of p_i and p_o. His Equation [3] follows from the general condition just mentioned. Equation [4] follows from Equation [4*a*], but Equation [4*a*] does not follow from the conservation of energy, and the author does not believe it can be substantiated. But despite these limitations, the conditions postulated by Mr. Hansen are fulfilled in many practical situations.

The graphical proof for the limiting flow ratio as given in the second section of the paper is valid for the case of the boiler-water injector. This proof depends only upon the following general properties of a Mollier chart:

1 Isobars have finite, positive slope

$$\left(\frac{dh}{ds}\right)_p = T$$

2 Their slope either increases or remains constant

$$\left(\frac{d^2h}{ds^2}\right)_p = \left(\frac{dT}{ds}\right)_p = \frac{T}{C_p} \geq 0 \text{ because } C_p \geq 0$$

3 A given isobar lies continuously above all isobars of lower pressure

$$\left(\frac{dh}{dp}\right)_s = v$$

No proof has yet been given for the case of dissimilar fluids when $p_3 > p_i$.

Professor Keenan correctly states that Flugel's one-dimensional analysis has proved effective in predicting ejector performance. However, a paper by Professor Keenan and E. P. Neumann[6] constituted the only comparison with experiment published in the English literature at the time of preparation of the present paper. This comparison was for ejectors without diffusers. Personally, the author did not consider the theory as "well established" until he made many numerical comparisons with published data. Figs. 3 and 4 of this closure are two such comparisons.

The significance of the differentiation for maximum flow ratio is that it provides an expression for the optimum area ratio explicitly in terms of the specified operating conditions. Optimum area ratios for many different vapors and conditions can be speedily obtained. The accord with experiment can be judged by comparison with Fig. 5 of this closure. This figure shows the purely experimental results of A. D. Third.[7] For the example illustrated in his figure, the method of "A Design Problem" in the paper yields

$$\frac{\text{Diffuser diam}}{\text{Nozzle diam}} = 2.68$$

$$\text{Air suction (per } {}^1/_{10} \text{ sq in. nozzle area)} = 0.0674$$

$$\text{Efficiency} = 17.1 \text{ per cent}$$

In the author's opinion, an efficiency, to be serviceable, must be so defined that it provides a desired answer, whether or not it simultaneously becomes a good "G" factor. Ejector efficiencies, as computed from the definition of the present paper, vary

[6] Refer to Bibliography (2) of the paper.

[7] Refer to Bibliography (4) of the paper.

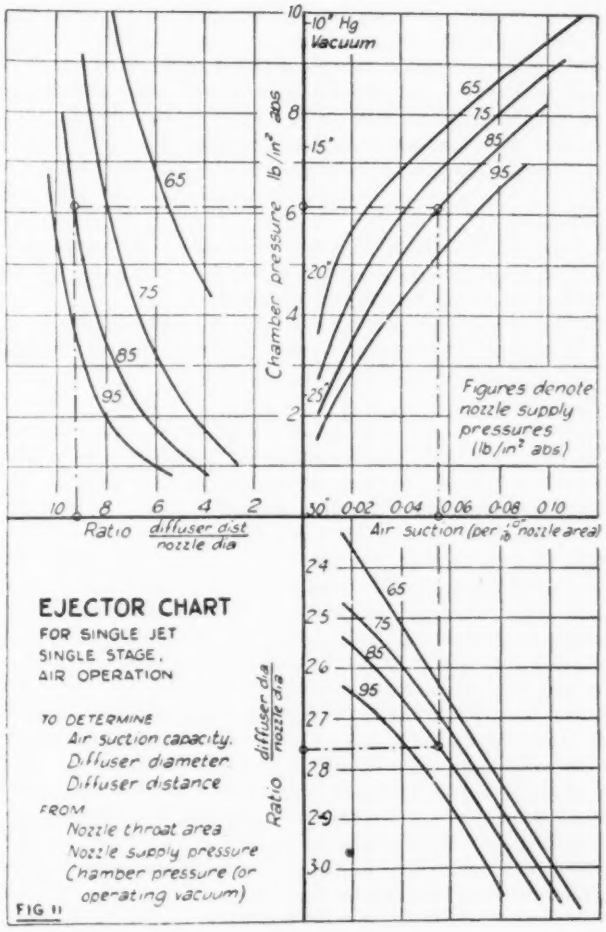


FIG. 5

widely with operating conditions. This variation is significant, since it emphasizes the inflexibility of the average ejector.

Since publication of the paper the author has proved that Table 1 is exact for any substance of which the enthalpy may be expressed by

$$h = A + Bpv$$

between states (2) and (3). Thus the validity of Table 1 is greatly extended.

Fatigue Strength of $5^1/_4$-In-Diam Shafts as Related to Design of Large Parts[1]

R. E. PETERSON.[2] The results of the most recent Timken tests are of considerable interest. Referring to footnote 7 of the paper, the values of k_t' turn out to be 1.36 for the $^{27}/_{32}$-in-radius fillet and 1.86 for the $^9/_{32}$-in-radius fillet. The corresponding q values are 0.50 and 0.72, respectively.

The statement is made that an endurance limit of 36,000 psi was obtained, and it is estimated that a similar plain polished

[1] "Fatigue Strength of $5^1/_4$-In-Diam Shafts as Related to Design of Large Parts," by O. J. Horger, T. V. Buckwalter, and H. R. Neifert, published in the September, 1945, issue of the JOURNAL OF APPLIED MECHANICS, Trans. A.S.M.E., vol. 67, p. A-149.

[2] Manager, Mechanics Department, Westinghouse Research Laboratories, East Pittsburgh, Pa. Mem. A.S.M.E.

specimen of about 5 in. diam would give 30,000 psi. In calculating q values where low factors are used, much depends upon the basic endurance-limit value used. If a value of 34,500 psi is used for the q calculations, it is interesting to note that full sensitivity is obtained for both cases. From a research standpoint, tests of 5-in-diam polished specimens without stress concentration would represent a valuable contribution, and it is hoped that such tests will be made by Timken since no other laboratory can do so.

The results of fillet-rolling show again the large improvement obtainable in this manner. It is our understanding that this method is in considerable use in Germany.

Tests with large specimens are difficult and expensive; the Timken Laboratory deserves a great deal of credit from the engineering profession in general for its work.

E. L. Robinson.[3] This paper contributes some valuable and much-needed data on the fatigue strength of shafts with variable diameter. This is a subject about which there is much too little reliable information and great uncertainty. There are innumerable applications, all of which stand to benefit from the accumulation of the type of information given. Not only is information needed on the effect of fillet radii of different sizes but also on the size effect. Furthermore, data accumulated on one composition of alloy may not be applicable to others. Indeed there are results to show that this is the case. Thus the tests need repetition on other materials and with various finishes.

One detail of the discussion seems to require comment, and that is the wording used to describe the characteristic coefficients which represent and evaluate the results. Table 4 of the paper gives the test values for k_f, k_t, and q each of which has a separate and distinct value which should be given attention in analyzing the results. This type of analysis follows a theory of behavior which, in so far as the writer knows, was first attributed to Ernst Lehr and Richard Mailänder.[4]

The reasoning is simple: Each geometric shape has a definite characteristic stress concentration as long as the deformation is elastic, which Lehr called the "shape factor." The words "elastic stress concentration" describe this factor k_t. With simple sections, k_t may be calculated mathematically. With more complicated sections it may be found by photoelastic analysis. Sometimes it can only be guessed at and then analysis can be no better than the guess.

Only with materials which are 100 per cent "sensitive" is the strength reduced correspondingly with the increase in stress at the point of concentration. The tests give the ratio of strength of a plain shaft to a filleted shaft k_f which Lehr called the "notch factor," or "fillet factor." It is confusing when the authors speak of k_f as the "stress-concentration factor." If it were, there would be no point in computing the stress concentration k_t or the degree of sensitivity q.

The "sensitivity" is the ratio of the actual weakening of the shaft due to the fillet to the theoretical weakening, assuming failure to be due to elastic stress concentration. Some materials approach 100 per cent sensitivity, which is an undesirable characteristic. Other materials have very little sensitivity, and such materials do not suffer much due to stress concentration. This is desirable, provided the base endurance strength is not also low.

In offering these comments the writer would not like to appear unappreciative of the work done. Rather it appears to him to be so important that a plea for a little more meticulous use of terminology in presenting results seems appropriate.

[3] Turbine Engineering Department, General Electric Company, Schenectady, N. Y. Mem. A.S.M.E.

[4] "Einfluss von Hohlkehlen an abgesetzten Wellen auf die Biegewechselfestigkeit," by E. Lehr and R. Mailänder, *Zeitschrift des Vereines deutscher Ingenieure*, vol. 79, No. 33, August 17, 1935, pp. 1005–1011.

A Simplified Method of Determining Hoop Stresses in Fan Rotors[1]

S. H. Christensen.[2] If we find the true mean value of tangential (hoop) stress by integrating Equation [6] of the paper, and also use this equation for the true boundary stresses f_1 and f_4, we find that the true ratio of boundary to mean stress differs from the author's approximation, Equations [5] and [7], according to the curves given in Fig. 1 herewith.

Another relation of interest is f_1/f_4, the ratio of inner to outer boundary tangential stress when given by Equation [6] of the paper. Its deviation from the ratio r_4/r_1 is shown in Fig. 2.

These second-order differences are primarily due to the effect of lateral fiber contraction as given by Poisson's ratio (our curves were based on $\sigma = 0.3$ for steel). These relations also occur, but in a more complicated form, in disks having varying thickness.

Large errors in the computed boundary stresses will occur if any of the methods reviewed in the author's paper (including Haerle's method[3]) is applied to "side-wheel-plate rotors" or disks

[1] By G. F. Lake, published in the June, 1945, issue of the Journal of Applied Mechanics, Trans. A.S.M.E., vol. 67, p. A-65.

[2] Carrier Corporation, Syracuse, N. Y. Jun. A.S.M.E.

[3] "Strength of Rotating Discs," by H. Haerle, *Engineering*, Aug. 9, 1913, pp. 131–133.

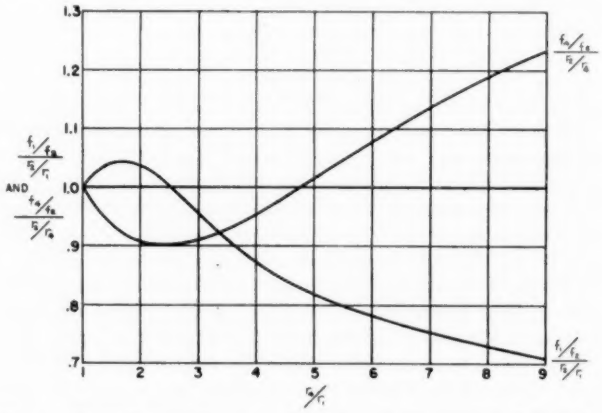


Fig. 1 True Stress Ratio of Tangential Boundary Stress to Tangential Mean Stress, From Equation [6] of Paper, Divided by Author's Approximate Stress Ratio, From Equations [5] and [7]

(For constant-thickness disk. Poisson's ratio, $\sigma = 0.3$.)

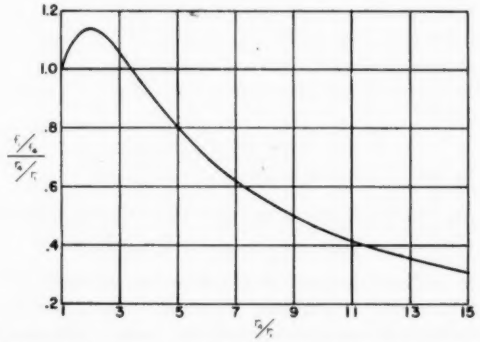


Fig. 2 True Ratio of Inner-Boundary Stress f_1 to Outer-Boundary Tangential Stress f_4, From Equation [6], Divided by Radius Ratio, r_4/r_1

(For constant-thickness disk. Poisson's ratio, $\sigma = 0.3$.)

whose meridian plane is (even slightly) inclined from the perpendicular to the axis of rotation. This is due to an additional degree of freedom being imposed upon the deflection by this inclination. At small angles of inclination (only 5 deg in some cases), the hoop-stress distribution in thin disks is already reversed, being greatest at the outer radius and least at the inner radius. The tangential stress distribution in inclined disks (conical shells) nearly follows, with radius, that of a thin ring (proportional to the radius squared).

Since the practical construction of high-efficiency side-wheel-plate rotors demands a conical or inclined section and not a surface whose meridian plane is perpendicular to the axis of rotation, as idealized in this paper, the method proposed is therefore not applicable to the computation of stresses in side-wheel-plate rotors of the type usually met with in practice.

A. M. G. Moody.[4] Although the author's method is approximate, it should give satisfactory results and be very helpful in problems where the radial extent of the rotor is small relative to the outside radius, and where the radial load to be carried is small. In presenting this method, however, the author makes a comparison which to the writer seems most unfair. In estimating the saving in time and effort made by using this method, the standard of reference is a so-called exact method. The impression one gets is that the author has read some textbook and has set out from there to produce a shorter method. In practice, one does not use the method which the author assumes to be the standard.

The field of disk and rotor stresses happens to be one of the most richly treated in all the literature of stress analysis. Not only do we have fundamental treatments by Stodola, Holzer, Grammel, Martin, and others, but we also have a wealth of short-cut methods based on the use of families of curves. These include the methods of Donath, Keller, Malkin, Martin, and others. These differ primarily in the nature of the profile chosen as standard. Among the profiles which have been treated are parallel-sided, conical, hyperbolic, and exponential. Each of these has something to recommend it and the relative merits will not be discussed here. They have been well treated in a paper by S. Tumarkin.[5]

Now the method of Donath, for instance, is quite easily applied to such a case as that treated by the author. Offhand, it would be hard to say whether or not it is quicker than the author's, although there is surely no great difference in the time and effort involved. But Donath's method is general, and enormously flexible, while the author's method is special and sharply restricted in applicability. Thus even if the new method made possible a slight saving, there would be a strong argument for using the more general one, except in the unlikely event that many rotors of this type and none of any other were to be figured.

Stanley Thompson.[6] Since radial stresses are neglected, no account can be made of the effect of abrupt changes in section. If we consider a portion of a disk for which a step occurs in the central portion of the disk (say, at a bolt circle) as shown in Fig. 3 of this discussion, the tangential strain will be the same on each side of the step for a short distance (neglecting stress concentrations). Using the author's nomenclature, we can write

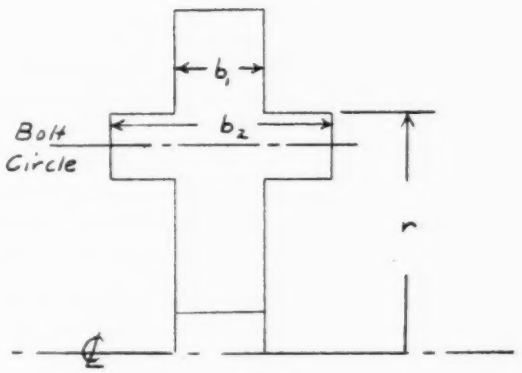


Fig. 3

$$\epsilon_t = \frac{1}{E}(f_1 - \sigma q_1) = \frac{1}{E}(f_2 - \sigma q_2)$$

From this

$$f_1 - f_2 = \sigma(q_1 - q_2) \quad \ldots\ldots\ldots\ldots\ldots\ldots [1]$$

Considering the equilibrium equation

$$\frac{1}{b}\frac{d(rbq)}{dr} - f + \rho\omega^2 r^2 = 0$$

this can be rewritten

$$\frac{db}{b} + \frac{dq}{q} + \frac{dr}{r}\left(1 - \frac{f - \rho\omega^2 r^2}{q}\right) = 0$$

This can be written in difference form

$$\frac{\Delta b}{b} + \frac{\Delta q}{q} + \frac{\Delta r}{r}\left(\frac{1 - f - \rho\omega^2 r^2}{q}\right) = 0$$

Since for the step

$$\Delta r = 0, \quad \frac{\Delta b}{b} = \frac{b_1 - b_2}{b_1}, \quad \frac{\Delta q}{q} = \frac{q_1 - q_2}{q_1}$$

then

$$q_1 - q_2 = q_1\frac{(b_2 - b_1)}{b_1} \quad \ldots\ldots\ldots\ldots\ldots [2]$$

Combining Equations [1] and [2]

$$\frac{f_1 - f_2}{f_1} = \frac{\sigma q_1}{f_1}\frac{(b_2 - b_1)}{b_1} = \frac{\sigma q_1}{f_1}\left(\frac{b_2}{b_1} - 1\right) \quad \ldots\ldots [3]$$

If we assume a step for which

$$\frac{b_2}{b_1} - 1 = 1$$

$$\sigma = 0.3 \qquad \frac{q_1}{f_1} = \frac{1}{2}$$

then

$$\frac{f_1 - f_2}{f_1} = \frac{0.3}{2} = 0.15, \text{ or } 15 \text{ per cent}$$

The error in this step by the approximate method would be 15 per cent. This error would always be on the conservative side for a step outward from the disk.

Using the parallel-sided disk checked by the author, the maximum radial stress divided by the tangential stress at the same point is

[4] Blower Division, Elliott Company; formerly, Chief Research Engineer, De Laval Steam Turbine Company. Mem. A.S.M.E.

[5] "Methods of Stress Calculation in Rotating Disks," by S. Tumarkin, Report No. 262 of the Central Aero-Hydrodynamical Institute, Moscow, Russia, 1932; now issued in translation as N.A.C.A. Technical Memorandum No. 1064, Sept., 1944.

[6] Development Engineer, Westinghouse Electric Corporation, Lester, Pa.

$$\frac{q_1}{f_1} = \frac{\left(1 - \frac{1}{3}\right)}{1 + \frac{2 \times 0.7}{3.3 \times 3} + \frac{1}{9}} = \frac{4}{9(1.267)} = 0.35$$

The error for a 2-1 step here would be $(0.3 \times 0.35 = 0.105)$ $10^1/_2$ per cent. For a disk with high radial loading (blades on periphery) this error would become greater in direct proportion to the increase in radial stress. If radial and tangential stresses were equal the error would be 30 per cent for a 2-1 step.

Hence the method does not enable one readily to allow for stress concentration due to holes in the disk, etc.

In the example used by the author, the assumption that one half the blade load is carried by each rotor should be tentative. Since the structure is redundant, a close approximation to the stress picture would require revising this estimate to correlate the deformations in the two wheels. In the present case, the less heavily loaded main wheel would tend to carry part of the load assumed to be carried by the side-wheel-plate rotor.

Where it is not necessary to determine stresses too accurately (by sum and difference curves), this method seems to offer a rapid means of finding the approximate stress picture. Formulas [4] and [5] of the paper show at a glance the advantage of keeping the mass of the disk concentrated as near the center as possible (assuming density of blades and rotor have the same radial distribution), but it is important to realize that the stress distriubtion can be changed without changing the position of r_2.

Author's Closure

The curves in Figs. 1 and 2 prepared by Mr. Christensen, are useful in showing the limiting ratio of boundary radii of fan rotors to which the simplified method could be applied. As the author suggested, these curves show that the approximation involved becomes too coarse beyond an $\frac{r_4}{r_1}$ ratio of about 3.

With regard to the effect of the inclination of rotating-disk sections, the author agrees that it would be necessary to take account of this in the case of single disks. However, in the case of side-wheel-plate rotors, the author is of the opinion that the freedom allowed by the inclination is largely prevented by the restraint imposed as a result of attachment through the blades to the main rotor.

The author would like to refute Mr. Moody's charge of unfairness in presenting the simplified method, as he has no wish to detract from the work of recognized authorities in the field of disk and rotor stresses. The exact methods were chosen as a basis of reference in order to make the comparison as concise as possible. The short-cut methods of the authorities cited do not appear to be so well known in England as in America. It seems to the author that graphical methods such as Donath's can only be used with ease after acquiring a certain degree of familiarity with them, which can only be gained by fairly frequent practice. Where this is so the author has no doubt that results can be quickly obtained and readily applied to design problems. The author has, however, approached the problem from the point of view of the fan user rather than that of the fan designer. He is consulted occasionally on the effect on fans in service of such factors as corrosion, increase in speed, and increase in operating temperature, and has felt the need for a method of assessing quickly the stresses involved.

The author is indebted to Mr. Thompson for his method of analysis whereby the error at a step can be deduced but is inclined to think that a value of $^1/_2$ for $\frac{q_1}{f_1}$ will in most cases overestimate the radial stress. He is not clear how the value of $\frac{q_1}{f_1} = 0.35$ is derived for the example chosen in the paper. The value deduced by the author is as follows

$$\text{Mean hoop stress in hub (radius 9 in.)} = f_m \times \frac{r_2}{9} = \frac{18.6 \times 10.2}{9} = 21.1 \text{ tons per sq in.}$$

The hoop stress in the hub, considered as a ring detached from the side wheel plate, would be

$$31.1 \times \left(\frac{9}{15}\right)^2 = 11.2 \text{ tons per sq in.}$$

The radial stress at the step must be sufficient to account for the difference of 9.9 tons per sq in. between these two values. This is obtained as

$$9.9 \times \frac{\text{Cross-sectional area of hub}}{\text{Radius to step} \times \text{width of disk at step}} = \frac{9.9 \times 1.92}{9.5 \times 1.125}$$

$$= 1.78 \text{ tons per sq in.}$$

The hoop stress at the step (radius 9.5 in.) = 20 tons per sq in. so that

$$\frac{q_1}{f_1} = \frac{1.78}{20} = 0.089 \text{ only}$$

With regard to the blade loading, it is agreed that the less heavily loaded main wheel would tend to carry a greater share of this loading than the side-wheel-plate rotor, but the author is of the opinion that the departure from equal sharing of the loading would not be great, because it is thought that the action of the blades in resisting the centrifugal loading would approach more nearly to that of beams than cantilevers fixed to the main wheel.

Parallel Columns With Common Lateral Supports[1]

K. R. Jackman[2] and C. Conaway.[3] Since the theory developed in this paper conforms with what theoricians might call "exact methods" in elastic-stability theory, it may be expected that it furnishes an accurate description of the behavior of the idealized structure which the author has investigated. However, the semimonocoque structures which have suggested the problem may differ in their behavior from the hypothetical structure. In fact, three reasons for conservatism of the theory in design applications are apparent:

1 A semimonocoque beam such as an airplane wing may sometimes be loaded considerably in excess of the point where buckling of the compression panels occurs before total failure results. The theory is designed to give only the buckling stress.

2 Bulkheads in a semimonocoque beam are often supported by the tension surface. The theory does not take account of such support.

3 Restraints that arise from membrane action of the skin are significant in a cambered wing. The author has not considered these restraints in the present theory.

The writers' company has recently performed several tests which serve to indicate how important these factors may be. These will be discussed as follows:

[1] By H. L. Langhaar, published in the Dec., 1945, issue of the Journal of Applied Mechanics, Trans. A.S.M.E., vol. 67, p. A-253.

[2] Chief Test Engineer, Engineering Test Laboratories, Consolidated Vultee Aircraft Corporation, San Diego, Calif.

[3] Research Engineer, Engineering Test Laboratories, Consolidated Vultee Aircraft Corporation, San Diego, Calif.

Beam No. 18. This was a flat-topped box beam with four simple-beam-type bulkheads with simply supported ends. It is therefore the type of beam for which the theory should determine the buckling load quite accurately. The following constants are given:

I = 0.028 in.[4] bulkhead
L = 8 in., w = 29 in., r = 0.0895 in.
t_e = average thickness of plate-stringer combination = 0.168 in.

By Equation [7] of the paper, the bulkhead spring coefficient is

$$C = \frac{\pi^4 EI \text{ (bulkhead)}}{w^4} = \frac{\pi^4 \times 10.5 \times 10^6 \times 0.028}{29^4} = 40.3 \text{ psi}$$

Hence

$$\frac{CL^3}{EI} = \frac{CL^3}{Et_e} = \frac{40.3 \times 8^3}{10.5 \times 10^6 \times 0.168 \times 0.0895^2} = 1.46$$

The theory of Shou-Ngo Tu[4] then yields

$$S_{cr} = 3500 \text{ psi}$$

r = radius of gyration
S_{cr} = buckling stress

Actually, the compression surface of this beam did not buckle in the Euler sense. Rather, the behavior of the compression panels was an accelerated bending which eventually became so severe that the beam would carry no additional load. Fig. 1 of this discussion is an experimental curve which shows the buckling deflection ("humping" with respect to the spars) versus axial stress. It is questionable whether the predicted buckling stress indicated on this curve coincides with actual buckling. However, it is clear that the beam carried considerable load in excess of buckling. This is undoubtedly due to the fact that buckling occurred early, and that the spar flanges were capable of picking up the load when the compression panels buckled.

Beam No. 17. Beam No. 17 was like beam No. 18, but it had full-depth bulkheads with three vertical struts. No diagonal trussing was provided and therefore the bulkheads had very little shear stiffness. The bulkhead coefficient, based upon the combined stiffness of the upper and lower bulkhead chord members, has been calculated by the theory of Equation [7] of the paper to be 59.6 psi. Hence, by the theory of Shou-Ngo Tu,[4] the buckling stress should have been 4100 psi.

An experimental deflection curve for the panels of this beam is shown in Fig. 1. Here, again, the theoretical buckling stress was greatly exceeded, partly because of the capacity of the spar flanges to pick up load, and partly because the bulkheads were supported by the tension surface.

Beam No. 11. This beam was similar to beam No. 18, but the compression surface was cambered. The ratio of beam width to radius of camber was 0.41. Since the theory takes no account of camber the same computation procedures apply as in the example of beam No. 18. These calculations yield S_{cr} = 3200 psi.

Fig. 1 shows an experimental deflection curve for this beam. It is seen that the beam carried a much higher stress than the predicted buckling stress (3200 psi). A comparison of the curves for beam No. 11 and beam No. 18 shows that camber has a decidedly beneficial effect.

The general conclusion to be drawn from the three tests cited is that the theory establishes a conservative procedure for calculating the requisite stiffness of wing bulkheads.

[4] "Column With Equal-Spaced Elastic Supports," by Shou-Ngo Tu, *Journal of the Aeronautical Sciences*, vol. 11, no. 1, Jan., 1944, p. 67.

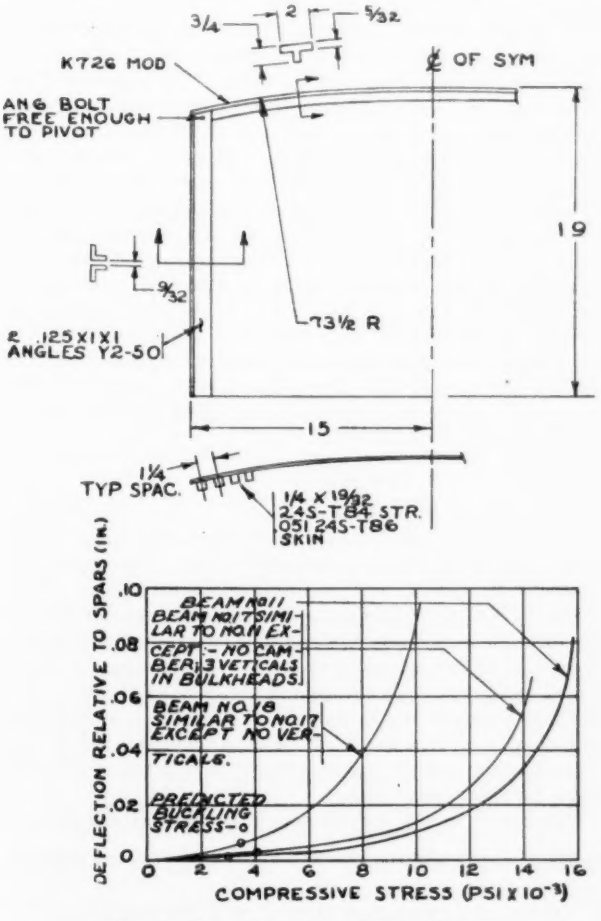


FIG. 1 BEAM DEFLECTION VERSUS STRESS

AUTHOR'S CLOSURE

The author believes that the comments of Messrs. K. R. Jackman and C. Conaway on his paper Parallel Columns With Common Lateral Supports are correct. The tests which they discuss had not been performed at the time the original paper was written, and therefore a discussion of the test data could not be included in it.

Cumulative Damage In Fatigue[1]

R. B. BLAND[2] AND A. A. PUTNAM.[3] Of the four assumptions upon which the author bases his development of the damage concept, the first two should be put in more general form. In regard to the first assumption, rather than specify a sinusoidal loading cycle, it only appears necessary to specify a "simple" cycle, i.e., one in which $d\sigma/dt$ changes sign only twice during a cycle. No work can be recalled by the writers in which it has been shown that the shape of a simple cycle is important. Furthermore, if the shape is an important factor, rate of loading and creep effects would be significant and thus the cycle frequency would also be an important variable.

In regard to the second assumption, the derivation of $\sum \frac{n}{N} = 1$

[1] By M. A. Miner, published in the September, 1945, issue of the JOURNAL OF APPLIED MECHANICS, Trans. A.S.M.E., vol. 67, p. A-159.
[2] Structural Engineer, National Advisory Committee for Aeronautics, Washington, D. C.
[3] Mechanical Engineer, National Advisory Committee for Aeronautics, Washington, D. C. Jun. A.S.M.E.

presented implies that the work per cycle is constant for each magnitude of cycle. This assumption is not necessary for the derivation. All that is required is that (*a*) the rate of work input as a function of the fraction of total cycles to failure at any one magnitude of cycle be independent of the cycle size, and (*b*) that the material does not care how the work is put in. This results in an equation for the rate of work input of the form

$$\frac{dw}{d\left(\frac{n}{N}\right)} = f\left(\frac{n}{N}\right)$$

rather than the special case

$$\frac{dw}{d\left(\frac{n}{N}\right)} = W$$

and would allow the rate of work input and the damage to remain small until just before failure, thus explaining the absence of significant effects of fatigue-stressing on other properties such as tensile strength and impact resistance.

The third assumption is not pertinent to the concept of damage and is apparently only to be used to justify an approximate method of relating various stress ratios. It so happens that one of the writers was formerly associated with a major airplane manufacturer in this same field of work and had occasion to develop methods of fatigue analysis that could be applied to parts still on the drawing board. Due to the lack of adequate material data, it was necessary to attempt to predict fatigue strength at various range ratios and cycle numbers from fatigue-strength data for completely reversed stress. It was subsequently found that the results obtained from the use of the Goodman diagram for this purpose were so seriously in error that the entire project had to be discarded.

As an example of the error involved in this approximation, it is possible to compare the extreme range of test values given in Fig. 1(*b*) of the author's paper, with the derived value. At $\frac{S}{S_u} = 0.5$ the possible R values range from 0.65 to 0.2 and the corresponding minimum stress values range from 0.32 S_u to 0.1 S_u; at $\frac{S}{S_u} = 0.3$ the possible R values range from 0.2 to —1 and the minimum stress values range from 0.06 S_u to —0.3 S_u (compression). The writers would not consider this range of values to be a good approximation, and still wider deviations are to be found when applying the Goodman diagram at lower cycle numbers. The writers believe that due to the inherent inaccuracies of the "approximation" the Goodman diagram is not usable at all for this type of work, where margins greater than 10 to 15 per cent, on stress, are considered excessive. In fact, if data are available to define the actual shape of the Goodman diagram so that the straight-line approximation need not be used, then those data can define the entire fatigue surface and the Goodman diagram is superfluous. Parenthetically, the writers would like to know if the derived curve in Fig. 1(*b*), likewise represents the other extreme range of test values.

The confirmation of the concept of cumulative damage is based upon 22 tests in which a large number of variables were present. For this reason it is difficult to determine if any trends are present due to the magnitude of cycles, sequence of cycles, or range ratio. However, statistical tests were applied to the data in which only two magnitudes of cycles were used, with the result that a correlation was found between the difference in ranges of stress and the absolute value of $\sum \frac{n}{N} - 1$. Such a correlation is to be expected if the concept of cumulative damage is not exactly correct.

Again, if it is assumed that a stabilization of the work input associated with a certain magnitude of cycle takes place in about 100 cycles, it would be expected that the concept of cumulative damage would not be seriously in error for tests such as these where one magnitude of cycle is run for about 10^4 times before a different magnitude of cycle is run. However, it does not follow that this law should hold when the number of the same magnitude of cycles in sequence is only of the order of 10^2, 10^1, or even 10^0. The data presented, plus the data of Stickley which is mentioned (6 different magnitudes of cycles), show an increased deviation of the results from those predicted on the basis of cumulative damage with increasing number of different magnitudes of cycles.

If failure is the result of strain hardening as outlined by the theory of Orowan,[4] a family of curves, on a plot of per cent damage at the second stress to the per cent cycle ratio at the first stress, would result, one curve for each combination of stress and cycle ratio. These curves would be centered about the curve determined by $\sum \frac{n}{N} = 1$. However, a small number of tests which give only one or two points on a curve would give a pattern of points which would not reveal the curves (especially with the scatter inherent in fatigue tests) but which would appear random about the curve for $\sum \frac{n}{N} = 1$. In other words, the number of variables in these tests is so large and the number of tests is so small that from them no conclusions can be drawn as to the correctness of any theory.

The concept of cumulative damage does give a method of making an estimate of life of structures with discrete types of loading, and what may be more important at the present state of knowledge, it gives a basis for comparing various structures under the same loading. However, caution must be used in extending the theory to many of the problems common to industry. For example, the loads on an airplane wing, caused by atmospheric turbulence, occur in a more or less random manner about a fairly constant mean load. If the fatigue life of a structural member in the wing is to be determined by using this concept, should the deviations from the mean load be paired in pairs of equal absolute but opposite numerical magnitude to form cycles about the mean load, or considered each separately, or grouped statistically to form cycles of various amplitudes and mean stresses similar to actual sequence of loads? Large factors will separate the lives so obtained and there is no reason to believe that any one of these methods is least in error.

Author's Closure

Messrs. Bland and Putnam's comments regarding the more general nature of both the cycle of loading and the broader form of the expression for damage are appreciated. The remarks are justified by experimental information available at present. Their comments concerning the lack of accuracy of the modified Goodman diagram are correct; however, it should be pointed out that no use of this method was made in the development or experimental confirmation of the cumulative-damage concept. The Goodman diagram was introduced to provide an approximate method in cases where suitable SN-curves are not available. The author heartily concurs that this approach is at best a poor substitute for experimental data.

With regard to any possible correlation between difference in ranges of stress and the absolute value of $\sum \frac{n}{N}$, the following

[4] "Theory of the Fatigue of Metals," by E. Orowan, Proceedings of the Royal Society of London, series A, vol. 171, 1939, p. 79.

additional tests have been completed using steel specimens, and they do not show a significant trend.

Seven rotating-beam specimens (flash-welded 4130 steel tubes) were tested at various numbers of stress magnitudes ranging from two to ten. The average value for $\sum \frac{n}{N}$ was 1.11; for a specimen run at ten different stress values, $\sum \frac{n}{N} = 1.06$; for nine levels, 0.86; and for five levels, 1.20.

Nine flat sheet specimens of S.A.E. 4130 steel were tested at from two to four different stress levels and at various stress-ratio values. The average value was $\sum \frac{n}{N} = 0.94$, the maximum 1.43 (at two levels), and the minimum 0.69 (also at two levels).

It is noted that the over-all average for the original 22 aluminum-alloy specimens plus these 16 steel specimens results in $\sum \frac{n}{N}$ deviating by only 1.5 per cent from the theoretical value of 1.

To establish the effects of a number of different magnitudes of stress, another experimenter has tested an aluminum-alloy specimen for 28 excursions of a repeating stress pattern which contained four different magnitudes of stress, all at a constant value of mean stress.

The failure occurred at a $\sum \frac{n}{N}$ only 1 per cent different from the theoretical value. No significant correlation with the number of magnitudes of stress is apparent for the data presented on either aluminum or steel specimens.

The suggestion that stabilization of work input occurs at some relatively small number of cycles, say, 100, offers interesting possibilities for modification if the cumulative-damage concept does not accurately represent this region of loading. However, the author has conducted experiments at very high loads (95 to 100 per cent of the ultimate strength for 24S-T alclad sheet specimens), obtaining results that are not subject to rational analysis owing to scatter. However, since the structural aluminum alloys normally fail at from 1000 to 10,000 cycles of loading (varying with stress ratio and normal scatter) at 95 per cent of the ultimate tensile strength, there is only this narrow region at very high stresses within which the cumulative damage is not adequate for present analysis purposes. Of course for a practical case, material with various stress concentrations must be considered, but here again the usual margin of safety found in a structure will normally obviate stresses of such a magnitude as to result in fatigue failures in less than 1000 cycles.

The use of the cumulative-damage concept provides considerably greater accuracy in the analysis of the effects of gust loads on aircraft structures than is warranted by presently available information on the frequency of occurrence of atmospheric disturbances. Also, it is the task of the analyst and the experimenter to determine the proper method for handling gust loadings, a problem independent from that of the damage question.

The general comments regarding conclusions drawn from a small number of tests with a large number of variables are valid to the extent that a precise analysis is not possible at present by use of the cumulative-damage concept nor is that the intent. The present status of all fatigue-analysis methods, and experiments, is such that any significant trend which may be shown to exist is very useful in spite of limited accuracy. The need is great for further experimentation on general fatigue problems and the damage question in particular.

The author wishes to acknowledge an original theoretical approach to the problem of repeated loadings of aircraft structures in which a damage criterion was previously proposed by P. H. Denke, of the Douglas Aircraft Company, Santa Monica, Calif.

Book Reviews

Theory of Structures

THEORY OF STRUCTURES. By S. Timoshenko and D. H. Young. McGraw Hill Book Company, Inc., New York, N. Y., 1945. Cloth, $5^3/_4 \times 8^3/_4$ in., xiv and 488 pp., 477 illus., $5.

REVIEWED BY J. N. GOODIER[1]

THIS is a theory of structures in the orthodox sense of civil engineering, reflecting the authors' lifelong interest, both scholarly and practical, in the subject. The text, as will be expected by readers of other works from the same pens, is extremely clear. It makes minimum demands on the reader—a reviewable knowledge of elementary mechanics and strength of materials—and at the same time maintains a scrupulous regard for logical completeness and continuity.

The required elements of plane statics are given in the first chapter, in the form of a review extended to the funicular polygon and the method of virtual displacements, which is subsequently used to very good advantage in many places. The required space statics is given under "statically determinate space structures" in the fourth chapter. The reader thus needs only a first course in mechanics, and for the second part of the book also strength of materials, to be able to proceed. He will be led through the simple truss problems normally encountered in statics to Maxwell diagrams, compound and complex trusses, and the application of virtual displacements. Influence lines are developed for beams, three-hinged arch ribs, simple trusses, compound trusses, and three-hinge arch trusses. Statically determinate problems end with a chapter on space trusses completing rather less than half the book.

The second half begins with strain energy, the principle of virtual displacements, Castigliano's theorem (and its offshoots such as least work), and the reciprocal theorem. These theorems then find application to the deflection of pin-jointed trusses. Graphical determination of deflections, like all the methods developed, is well illustrated, even if one of the diagrams seems to be there as a warning to the student that sometimes a formidable tangle will result in spite of the best of intentions! The fictitious load methods of Mohr and Müller-Breslau follow. The chapter on statically indeterminate pin-jointed trusses includes a discussion of influence lines when there are several redundant members and a brief section on space trusses. The chapter on beams and

[1] Professor in Charge, Department of Mechanics of Engineering, Cornell University, Ithaca, New York, N. Y. Mem. A.S.M.E.

frames proceeds through the slope-deflection equations, continuous beams, simple bents and frames, to continuous frames and solutions by successive approximation culminating in the Hardy Cross method. Data are given for haunched beams. In the last chapter, the thorough discussion of arch analysis is supplemented by several tables useful in calculating thrust, and there is a critical discussion of the "thin bar" formulas, based on the thick-curved-bar theory which is developed as a preliminary.

The book is a valuable treatise on methods for the engineer and is well arranged for the use of students. It has 269 problems covering all parts except the more advanced questions of frames and arches.

The Meaning of Relativity

THE MEANING OF RELATIVITY. By Albert Einstein. Second Edition. Princeton University Press, Princeton, New Jersey, 1945. Cloth, 5 × 7¾ in., 135 pp., 6 figs., $2.

REVIEWED BY J. ORMONDROYD[1]

THE first edition of this book, published in 1922, covered a series of lectures given by Mr. Einstein in May, 1921, at Princeton University. The text of this edition differs from that of the first edition only by the inclusion of an Appendix on the "Cosmologic Problem." The dust cover states that the book is "intended for the general reader who has some understanding of modern physics and advanced mathematics." It is probably fair to remark at the outset that the understanding of modern physics and advanced mathematics of most engineers will not suffice for the intelligent reading of this book. The physical knowledge required by the putative reader is a thorough understanding of Newtonian mechanics and Maxwell's electrodynamical theories. On the mathematical side Riemannian geometry and tensor analysis must be known. One further prerequisite would be that the reader had already attempted some serious study of the theory of relativity from some other source. For anyone having the complete background as outlined above, Mr. Einstein's four lectures would be considered a magnificent summary by the master to his disciples.

In the first chapter of the book Einstein gives a brief introduction to prerelativistic physics and the notation, concepts, and operations of tensor analysis. Here again if the reader knows this subject in advance he will probably recognize a masterful summarization, but if he does not he will gain nothing but confusion and a sense of futility.

[1] Captain, U.S.N.R., David Taylor Model Basin, Navy Department, Washington, D. C. Mem. A.S.M.E.

The second chapter deals with the theory of special relativity. The engineering reader would probably find it easier to get the ideas of special relativity from some other book. A great many expositions of the theory of special relativity have been published, some of them treated in language suitable to the background which most engineers actually possess.

The third chapter gives the underlying physical ideas of the general theory of relativity. These are followed by an extensive consideration of the tensor analysis and the tensor equations which form the mathematical foundation of the theory. If the engineering reader pays close attention to the physical reasoning he will gain a clear insight into the meaning of General Relativity. The tensor analysis and tensor equations will probably leave him bewildered as in chapter one.

The fourth chapter contains a discussion of the three widely known triumphs of the general theory of relativity. Pages 92 to 97 of this chapter show the quantitative deductions which predicted the shift of spectral lines toward the red in radiations which emanate from the sun and other heavy stellar bodies, the bending of light rays in the neighborhood of the sun or any concentration of mass, and the motion of the perihelion of the planet Mercury. All of these are small effects totally outside the possibility of prediction by Newtonian mechanics; but all capable of observational confirmation.

The theory of relativity has enjoyed widespread interest because the principles and experiments which form its foundation, and the few outstanding results which it has predicted, are understandable to a public reasonably well versed in physics and mathematics. For this reason the Appendix which treats the "Cosmologic Problem" is probably the most understandable and enjoyable chapter in the whole book. Here the relationship between the Hubble expansion and the average curvature of the space of the universe, the age of the universe, and the conflict between the relativistic age and the age deduced from the consequences of nuclear physics are discussed. These are all questions which would interest any reader who possesses even mediocre physical and mathematical knowledge.

The reviewer of this book has decided that in order to understand Mr. Einstein's summary of the theory of relativity he would have to make a serious study of some such books as "The Elementary Theory of Tensors," by T. Y. Thomas, "Applications of the Absolute Differential Calculus," by A. J. McConnell or "Riemannian Geometry," by L. P. Eisenhart (named in order of sophistication), and at least the chapters on relativity in some general work on mathematical physics such as "Foundations of Physics," by Lindsay and Margenau. There is no easy road to the understanding of the meaning of relativity.

Internal Friction in Engineering Materials

By J. M. ROBERTSON[1] AND A. J. YORGIADIS[2]

This paper is a report on some experiments conducted on the subject of internal friction or damping in solid engineering materials, with apparatus and technique comparatively new to the field. The use of this equipment and technique enabled the measurement of internal friction in a more direct way than most if not all of the methods used by previous investigators. In the light of the results reported, empirical relations are presented for the variation of internal friction with stress amplitude in the range of engineering stresses. These relations are compared with the findings of others.

Internal Friction—Damping Capacity

INTERNAL friction or damping capacity is that property of a solid material which results in energy absorption when the material is stressed cyclically.

Concept of Internal Friction. The original conception of internal friction or damping in solids was that this phenomenon is associated with a viscous force proportional to the strain velocity. This reasoning was through analogy with viscous friction in fluids. Kelvin (1),[3] one of the early researchers in this field, presented internal friction as a viscous phenomenon; but his experiments made in 1865 on wires in torsion did not verify this hypothesis. As early as 1912 internal friction was presented by Hopkinson and Williams (2) as a hysteresis phenomenon in which the loss was due to the noncoincidence of the upward and downward portions of the stress-strain diagram of a material under cyclic loading. The stress-strain diagram for a complete stress cycle thus corresponded to a closed loop. Through analogy with the phenomenon of magnetic hysteresis, Hopkinson and Williams suggested the appelation "elastic hysteresis." This term was somewhat of a misnomer for, as noted by Föppl (3) it is due to the lack rather than the presence of an elastic quality of the material.

In analyzing internal friction, Föppl (3) assumed that any strain may be considered to be composed of an elastic and plastic portion, the latter being the cause of the hysteresis and energy loss. The energy stored in a strained body is only partly recoverable in release of the stress and strain; that associated with the plastic component of the total strain is not recoverable and is dissipated into heat. Föppl and his co-workers (3, 4) preferred to call this the "damping" or the "damping capacity," as it represented the amount of energy a vibrating system would dissipate through internal friction in one cycle of vibration.

Methods of Expression. Internal friction has been expressed in various ways by different investigators, depending partly on the method of measurement and analysis involved. Although incorrect and decidedly misleading, internal friction is still sometimes expressed in terms of a viscosity coefficient, due to the convenience of analytical treatment. A large number of observers have presented data on internal friction in terms of the logarithmic decrement or rate-of-vibration-decay factor δ, which in many cases was the quantity determined experimentally. This representation lacks considerably in physical significance when applied to the steady vibrations of structural members. Although his test involved the measurement of vibration decay, Föppl presented his data in terms of the "specific" damping capacity, as von Hydekampf (4) termed it. This is the ratio of the energy loss per cycle ΔW, to the vibrational energy in the member W

$$\psi = \frac{\Delta W}{W} \quad \ldots\ldots\ldots\ldots\ldots\ldots\ldots\ldots [1]$$

On the basis of certain assumptions it can be shown that ψ is approximately equal to 2δ, see Lazan (5).

Since the time of Hopkinson and Williams (2) and Rowett (6), many experimenters have expressed internal friction in terms of the energy loss per cycle of vibration, ΔW, which is termed the damping capacity in this paper. Other methods of expressing internal friction are in terms of the bluntness of the resonance curve, in terms of a "frictional stress" related to the width of the hysteresis loop (Canfield 7), and in terms of the resonance amplification factor A_r, a reciprocal function of the damping. Some of the foregoing methods are open to serious objections especially when used quantitatively for engineering materials.

Significance of Internal Friction. The function of internal friction in aiding the other sources of damping in keeping down the amplitude of vibratory motion, and hence the stress amplitude by absorbing energy is of prime significance, as is well known. As Föppl pointed out in connection with the vibration of long transmission wires, airplane structures, airplane propellers, turbine blades, and engine crankshafts, the presence of internal friction in large amounts is a desirable property of materials. He noted that a material of high damping capacity and comparatively low fatigue strength may be superior to one of high fatigue strength and lower damping. In this country the extreme importance of damping in connection with the vibrations of turbine blades has been pointed out by Hague (8).

Internal friction is not always a desirable property of engineering materials. It is the presence of internal friction which is responsible for the phenomenon of shaft "whirl," see Kimball, (9, 10, 11). Also materials of high internal friction heat up when subjected to repeated vibratory stresses, resulting in a decrease in the strength of the material, as at higher temperatures the strength of materials, especially plastics, is lower than at normal temperatures. Besides this, internal friction is of some interest in connection with the fatigue properties of materials. Dorey (12) concluded that the fatigue strength of a material could be ascertained from a plot of the damping capacity as a function of stress. Föppl (3) disagreed with this idea but felt that the notch sensitivity of the material is dependent upon its damping capacity. However, not all materials show this dependency. A good summary of the significance of internal friction in relation to

---

[1] Assistant Professor of Engineering Mechanics, Pennsylvania State College, State College, Pa. Jun. A.S.M.E.

[2] Research Engineer, Sonntag Scientific Corp., Greenwich, Conn.; formerly Research Assistant, Engineering Experiment Station, Pennsylvania State College.

[3] Numbers in parentheses refer to Bibliography at end of the paper.

Presented at the National Meeting of the Applied Mechanics Division, Buffalo, N. Y., June 21–22, 1946, of The American Society of Mechanical Engineers.

Discussion of this paper should be addressed to the Secretary, A.S.M.E., 29 West 39th Street, New York, N. Y., and will be accepted until October 10, 1946, for publication at a later date. Discussion received after the closing date will be returned.

Note: Statements and opinions advanced in papers are to be understood as individual expressions of their authors and not those of the Society.

fatigue strength was presented in the Battelle Memorial Institute book (13).

Measurement of Internal Friction. The most common method used for the measurement of internal friction is the rate-of-vibration-decay method, using the torsional-pendulum form of apparatus, or vibrating bars or beams. More data have been taken by this method than all the other methods combined. The drawbacks of the freely decaying vibrations method, due to the apparatus and method of evaluating test data, are such as to mask the fundamental nature of the variation of damping capacity with stress. At high rates of decay the decrement cannot be associated with any specific stress or strain amplitude; transforming values of the decrement into the damping capacity involves assumptions concerning the elastic modulus; and the tests are performed in a transient state when stress surges exist, resulting in variations in the stress distribution.

Föppl (3) listed several methods of measuring damping which were used under his direction at the Wöhler Institute in Germany: namely, (*a*) Static measurement, as first used by Rowett (6); (*b*) starting-up tests, involving measurement of the rate of temperature rise; (*c*) a steady-state thermal-equilibrium method, first used by Hopkinson and Williams (2); (*d*) a resonant-vibration method, involving measurement of energy input; and (*e*) the torsional-vibrations-decay method. The last was the basic method used by Föppl and his co-workers. Although he claimed to have obtained good agreement between the methods listed, they are open to various objections. The static method, also used by Dorey (12), involves the measurement of the width of the hysteresis loop for a complete stress cycle (generally in torsion), cannot be used for materials subject to creep, and requires high-precision measurements. Data obtained by thermal means have little significance as internal friction varies with temperature. The resonance-vibrations method can be successfully used if the measured losses are only those which are due to damping in the specimen. This is possible with the equipment developed by Lazan (5).

Kimball and Lovell (11) used a novel method in which the lateral deflection (whip) of a loaded cantilever rotating beam was measured. Another method which has been used involved the measurement of the width of the resonance curve of a vibrating bar or beam, such vibration being caused by a magnetic or crystal oscillator. The data obtained by this last method are generally at such low stresses as to be lacking in engineering significance. Furthermore, such measurements cannot be identified with any particular stress amplitude as different parts of the test are carried on at different stresses.

Principal Factors Affecting Internal Friction

In spite of a large amount of theoretical and experimental work on the nature of internal friction in solids, there is available no physical theory for this phenomenon, except at the very lowest strains which are out of the range of engineering interest. A good summary of these theories is presented in a book by Seitz (14), where the effects due to thermoelastic causes, ferromagnetism, and internal dislocations in the structures of the crystal lattice are discussed theoretically and in the light of experiment. In the realm of engineering stresses internal friction is probably the result of irreversible plastic actions.

The factors of importance in regard to internal friction of engineering materials in the engineering range of stresses appear to be as follows: Stress or strain amplitude, nature of the stress or strain (i.e., normal, shearing, or combined), frequency, temperature, and the nature or kind of material.

Frequency Effect. A conclusive proof of the lack of frequency effect on internal friction in the range of engineering stresses was obtained by Kimball and Lovell (11) in their experimental study of metals, glass, celluloid, rubber, and wood (a total of 18 different materials). They found the logarithmic decrement to be entirely independent of frequency (i.e., stress or strain velocity) for frequencies between 2 and 200 cps. According to Föppl (3), there is no frequency effect except at very low frequencies for materials subject to creep when the frequency is so low that the strain velocity is of the same order of magnitude as the creep velocity. The occurrence of creep as a separate phenomenon not of concern in damping was also noted by Leaderman (15). Ockleston (16), in a study of a vibrating steel beam, found practically no frequency effect between 23 and 45 cps. Gemant (17) measured the damping in a steel tube at frequencies between 300 and 4600 cps and noted no significant variation, although his data showed some scatter.

Prior to this the complete lack of frequency dependence of damping was indicated by Hopkinson and Williams (2) and Rowett (6). In the first of these investigations measurements were made dynamically (under resonant vibrations) at 136 cps by thermal methods and statically for a steel under normal (tension-compression) stresses. Continuing this work but with thin-walled tubes in torsion (thus making the static tests susceptible to greater sensitivity), Rowett studied a similar steel statically and at 67 cps by means of the torsional-pendulum-decay method. The static torsion methods allowed the measurement of the width of the loop over the complete stress cycle for several stress ranges. In Fig. 1 is shown one of his measured loops and in Fig. 2 plots are given of his data on damping capacity as a function of stress amplitude. From this figure the agreement he noted between static and dynamic data is apparent. Rowett was able to re-evaluate the static data of Hopkinson and Williams and to show that it agreed with their dynamic data within the experimental accuracy.

A few experimenters have noted a frequency variation, but their results were obtained at much higher frequencies and at much lower stresses in the material. It does not appear certain that their measurements at the different frequencies were necessarily at the same stress amplitude, with which variable the internal friction varies greatly.

Stress Amplitude. The most important variable affecting internal friction in solids is the stress or strain amplitude of the cyclic action. Some attention has been paid to this fact by certain investigators but many have ignored it or tried to minimize its importance. Hopkinson and Williams (2) and Rowett (6) were among the first to indicate this stress dependency. The first of these investigators found the energy loss per cycle (damping capacity) to vary about as the fourth power of the stress amplitude. Their data were probably influenced by temperature variations due to the method of measurement. Rowett's measurements both static and dynamic, indicated that the damping capacity ΔW varied as the third power of the stress. In the presentation of his data in Fig. 2 the straight lines, representing the trend of the points, are drawn to the third power. The line for the hard-drawn material represents the equation he derived from his dynamic tests. In a study of the hysteresis loss in five crankshaft steels by static tests, such as used by Rowett (except that they were on solid specimens), Dorey (12) found that up to a certain stress (6000 to 12,000 psi), the damping capacity increased with the third power of the stress amplitude.

If the third-power stress variation of damping capacity, noted by Rowett and Dorey, is expressed in terms of the specific damping capacity ψ (see Equation [1]), it is found that ψ should vary about as the first power of the stress amplitude. This assumes, among other things, that the dynamic modulus of elasticity of the material is constant. Föppl (3), von Hydekampf (4), Hatfield, Stanfield, and Rotherham (18, 19), and Contractor and Thompson (20) presented data on internal friction in the form of graphs

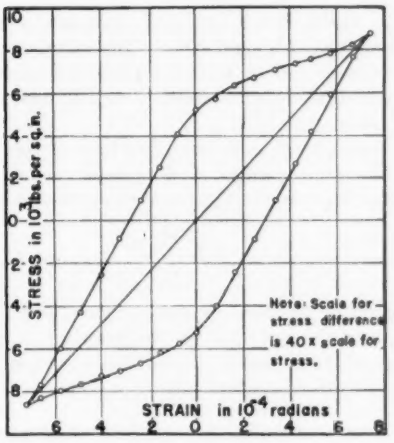


FIG. 1 HYSTERESIS LOOP FOR STEEL (ANNEALED) UNDER TORSION AS OBTAINED BY ROWETT

(This is the static stress-strain curve obtained by measuring the stress width of the loop for different strains. Note that the stress width is shown greatly exaggerated.)

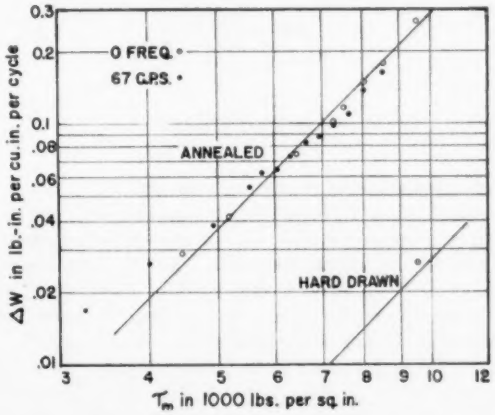


FIG. 2 ROWETT'S DATA ON DAMPING CAPACITY OF STEEL IN TORSION PLOTTED VERSUS MAXIMUM SHEARING UNIT STRESS AMPLITUDE

(For the annealed steel the open symbols represent the data obtained statically; the solid symbols represent that obtained at 67 cps. In the case of the hard-drawn steel, the solid line represents data obtained at 67 cps; the single point shown, open symbol, was obtained statically.)

of ψ or δ versus stress or strain amplitude. Due to the effect of other factors, perhaps, the first-power variation was not too apparent.

Kimball and Lovell (11) found the energy loss per cycle per unit volume (damping capacity, ΔW) to vary as the second power of the stress amplitude, from which it followed that the rate of vibration decay was logarithmic, i.e., the logarithmic decrement δ was constant for any material. However, Ockleston (16), who attempted to compare this relation with data obtained from a vibrating steel beam, found the decay of vibration was not logarithmic and δ, therefore, to be a function of amplitude. Interpreting his data in terms of the damping capacity, it appears that ΔW varied about as the third power for a considerable range. The correct interpretation of such tests as these is quite difficult if not impossible, as in both cases the stresses varied considerably throughout the specimens.

Other Factors. Temperature, nature of the stress involved, and the nature or kind of material are other factors upon which the internal friction depends. Measurements by Hatfield, Stanfield, and Rotherham (18, 19) showed that the specific damping capacity increased rapidly with increase in temperature above normal for a considerable range of temperature. Other papers presenting data on the influence of temperature are those of Contractor and Thompson (20) and Schabtach and Fehr (21).

As to the effect of the nature of stress involved, there are few data available since most of the experiments have only been performed in torsion. There is evidence that the internal friction under shearing stress is different from that under normal stress (3, 5). The effect of previous stress history of the specimen was noted by Kelvin (1), Föppl (3), Dorey (12), Lazan (5), Kutsay and Yorgiadis (22), and Hempel (23). Briefly, their results indicate that if a material is undergoing repeated cyclic straining at essentially constant amplitude, its internal friction is changed with the number of stress cycles, ultimately reaching a constant value for any specific stress. Kutsay and Yorgiadis (22) noted a change of as much as 10 times in the damping capacity of magnesium alloys due to cyclic straining. It has also been noted that the damping capacity of mild steels decreases due to cyclic stressing at low amplitudes and increases at high stress amplitudes see Lazan, (5).

Hempel (24) in a study of the damping and fatigue properties of cast irons, found that the value of ψ, corresponding to a certain stress amplitude, was lower the higher the tensile strength of the cast iron. For plastics it has been noted that the damping capacities of different materials were an inverse function of their elastic moduli (25). This type of relation cannot be expected to apply to metals such as steels, for which there is no variation in modulus but a large variation in damping.

APPARATUS AND METHODS USED

The method of test used in obtaining the data presented in this paper corresponds to method 4 listed by Föppl. The particular equipment used was developed by Lazan (5) and used by him and Kutsay and Yorgiadis (22). Briefly, the vibratory system consists of a centrifugal-force mechanical oscillator, maintaining resonant vibration in a specimen which is the flexible member of the vibrating system. The energy input to the system is obtained from measurement of the amplitude of the motion and the force amplitude of the oscillator.

Torsional Tests. The arrangement used to measure the damping under torsional vibration is shown in Fig. 3. The upper end of the specimen is rigidly attached to a heavy frame by means of collet and chuck. From the lower end of the specimen are suspended the mechanical oscillator and its synchronous driving motor. The oscillator was driven at different multiples and submultiples of synchronous speed by means of interchangeable gears. As shown, the oscillator is adjusted to produce a sinusoidal torque by means of eccentric masses at the ends of two counterrotating shafts. In Fig. 3 only one pair of the eccentric masses is visible; the other pair is on the rear face of the oscillator, rotating 180 deg out of phase with those shown. The result is a sinusoidally varying torque about the axis of the specimen. The magnitude of this torque at any particular speed is adjusted by varying the size of the masses and their eccentricities. The movable poises shown on oscillator-motor assembly in Fig. 3 are used to adjust the moment of inertia of the assembly. Such adjustment enables the tuning of the system to resonance. This is a single-degree-of-freedom system under forced torsional oscillation, the specimen acting as the spring, and the oscillator-motor unit acting as an adjustable inertia. The exact condition of resonance is determined by a 90-deg phase lag between the oscillator torque and the angular displacement of the unit; this lag is measured under stroboscopic light by means of the phase indicator shown on the oscillator. The amplitude of the torsional oscillations is measured with a micrometer microscope.

On the basis of the assumption of sinusoidal torque and sinusoidal motion, the following analytical equations may be ob-

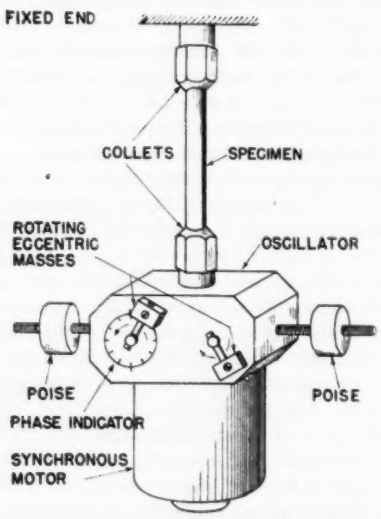


FIG. 3 EXPERIMENTAL ARRANGEMENT USED TO OBTAIN TORSIONAL OSCILLATIONS IN SPECIMEN WITH MECHANICAL OSCILLATOR FOR DAMPING-CAPACITY DETERMINATIONS

tained for resonance conditions of vibration. The maximum shear stress at the surface of the cylindrical specimen is

$$\tau_m = \frac{D\omega^2 I\theta}{2Jg} \quad [2]$$

where

D = outside diameter of specimen
J = polar moment of inertia of specimen
ω = circular frequency = $2\pi f$
g = acceleration of gravity
I = moment of inertia of oscillator-motor unit
θ = amplitude of torsional oscillation (radians)

The damping capacity, the energy absorbed by internal friction per unit volume of material per cycle, is determined from the relation

$$\Delta W = \frac{\pi T\theta}{AL} \quad [3]$$

where

T = amplitude of applied torque
A = cross-sectional area of specimen
L = length of specimen

The dynamic modulus of rigidity (shear modulus) of the material is

$$G = \frac{L\omega^2 I}{Jg} \quad [4]$$

Direct-Stress Tests. The experimental setup used to test materials under direct stress (tension-compression) consists of the two-mass single-degree-of-freedom system shown in Fig. 4. The same oscillator is used, with the rotating eccentric masses adjusted to produce a sinusoidal axial force in the specimen (masses on same shaft now rotating in phase). The specimen acts as the spring between the two weights, W_1 and W_2, vibrating in opposite phase. These two weights are supported on rollers, which gives them freedom of horizontal movement with negligible frictional losses (as noted from the experimental results). The magnitude of the oscillator force at any particular speed is adjusted by varying the size of the rotating masses and their eccentricity. The system is tuned to resonance by changing W_1 and W_2 with weights ΔW_1 and ΔW_2. The exact condition of the resonance is determined by a 90-deg phase lag between the oscillator force and the displacement of W_2, as measured with a micrometer microscope.

The relationships for resonant vibrations of this system are based upon the same assumptions as those for the torsional case. The maximum direct stress (tension or compression) is

$$\sigma = \frac{\omega^2 W_2 a}{Ag} \quad [5]$$

W_2 is the weight of the block, oscillator, motor, and other attachments shown on the right side of the specimen in Fig. 4; a is the amplitude of the motion W_2; and, the other symbols are the same as for the torsional case. The damping capacity is determined from

$$\Delta W = \frac{\pi F a}{AL} \quad [6]$$

where F is the amplitude of the oscillator force. The dynamic modulus of elasticity of the material is

$$E = \frac{L\omega^2 W}{Ag} \quad [7]$$

Here

$$W = \frac{W_1 W_2}{W_1 + W_2}$$

is the effective weight of the two-mass system.

Equations [2] to [7], inclusive, were used to obtain the damping capacity and dynamic modulus of materials under resonant vibrations with the apparatus described. All the data presented in this paper were obtained within 10 deg of resonance, most of them being obtained within about 5 deg. A more complete description of the apparatus and its uses can be found in papers by Lazan (5) and Kutsay and Yorgiadis (22). In connection with the question of the external losses due to the supporting structure for the apparatus, it might be mentioned that considerable difficulty was experienced in finding a sufficiently rigid support from which to suspend the torsional setup. In fact, for the lower stresses the data given for the torsional damping capacity probably include some energy which was lost through the supports. No such difficulty was noted in the case of the horizontal direct-stress apparatus as the vibratory load in the specimen is not transmitted to the foundation and the losses in the rollers are apparently negligible.

DATA ON DAMPING CAPACITY

Measurements were made of the damping capacity of six metallic alloys under both torsional and longitudinal vibrations. Three

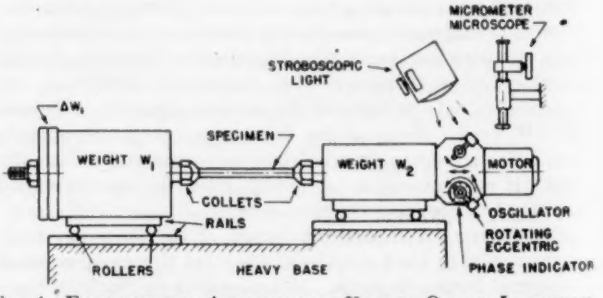


FIG. 4 EXPERIMENTAL ARRANGEMENT USED TO OBTAIN LONGITUDINAL VIBRATIONS IN SPECIMEN WITH MECHANICAL OSCILLATOR FOR DAMPING-CAPACITY DETERMINATIONS

TABLE 1 SUMMARY OF EXPERIMENTAL RESULTS

Material				Experimental Data				
Description	Approximate[a] rockwell hardness	Yield strength, 1000 psi Direct	Shear	$\Delta W/\sigma^3$ 10^{-12}	Stresses, 1000 psi	$\Delta W/\tau_m^3$ 10^{-12}	Stresses, 1000 psi	K
Lucite, methyl - methacrylate resin		6[b]		390	0.4–1.8			
Bakelite, grade X laminated-phenolic (paper base)		6[c]		65	0.3–3			
Plywood (1/4 in. birch, resin - bonded under 1000 psi); specific gravity, 1.05		5[d]		16	0.5–5			
Magnesium alloy M (1.5 per cent Mn) extruded tubing	F 17	9 C[e] (21 T)		1.0	1.8–4.5	9.2	1.0–4.0	0.48
Magnesium alloy J-1 (6.5 per cent, Al 1 per cent Zn, 0.2 per cent Mn) extruded tubing.	B 25 (F 77)	12 C[e] (21 T)		0.55	2.2–9.0	3.9	1.4–5.0	0.51
Monel metal (67 per cent Ni, 30 per cent Cu, 1.4 per cent Fe, 1 per cent Mn) seamless tubing:								
3/4 in. diam.	B 89	68[f]	48[b]	0.05	8.0–34	0.27	3.0–30	0.57
1/2 in. diam.	B 93	74[f]	54[b]	0.03	10–60	0.19	9.0–18	0.54
S.A.E. 1025 steel, seam-welded tubing, "as welded"	B 64	64[b]	22[b] (17[g])	0.05	9–34	0.4	4.0–20	0.51
S.A.E. X4130 steel, seam-welded tubing, "normalized"	B 96	80[b]	52[b]	0.043	9–45	0.2	5.0–37	0.60
Steel tubing—Rowett (0.17 per cent C, 0.24 per cent Mn):								
Annealed			12.5			0.29	4.5–10	
Hard drawn			31			0.027	up to 11	

[a] As measured by authors. [b] Approximate yield point or yield strength estimated from producer's data book. [c] Estimated from 12,500 psi tensile strength given by producer's data book. [d] Compression test by authors. [e] From producer's data book, C is in compression, T in tension. [f] From producer's book, proportional limits are 48 and 54. [g] Rough torsion test by authors.

NOTE: All data in inch-pound-second units.

plastic materials were tested under longitudinal vibrations only. The particular materials studied are listed in Table 1; their static yield strengths being given in columns 3 and 4. All tests were conducted under completely reversed stress cycles in which the variation was from a maximum positive value to a numerically equal maximum negative value, the range of stress being twice the stress amplitude, i.e., the mean stress was zero. In all cases the stress to which the data are referred is the maximum amplitude measured from zero. The inch-pound-second dimensional system is used throughout and the data are presented in such units.

For the three plastic materials, lucite (methyl-methacrylate resin), bakelite (paper-base laminated phenolic, grade X), and a plywood (resin-bonded plywood molded under high pressure), the relationship between damping capacity and stress (tension-compression) is shown in Fig. 6. It will be noted that the data are presented on logarithmic co-ordinates. The straight lines, drawn with a slope of 3, indicate that the damping capacity of these materials is proportional to the third power of the stress amplitude, as noted by Rowett; thus

$$\Delta W = C_1\sigma^3 \quad [8]$$

In column 6 of the table are given the minimum and maximum stresses for which experimental verification of Equation [8] was obtained. The value of C_1 in this equation is recorded in column 5 of the table, for these three materials; ΔW is in inch-pounds per cubic inch per cycle and σ is in pounds per square inch.

Each of these materials was run at two speeds, 48 and 68 cps, without any noticeable speed effect appearing in the data, as may be seen in Fig. 6. The plywood was also tested in two diameters 1/2 and 3/4 in. at both speeds and showed no size effect. For each speed, size, and material, tests were run with specimens of at least two lengths to enable the evaluation of end-condition effects, which were sometimes significant. The sharp discontinuity in the bakelite data at about 3000 psi could not be checked due to a lack of material.

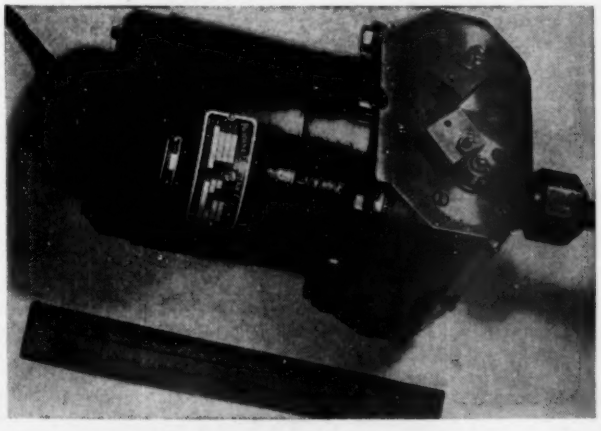


FIG. 5 MECHANICAL OSCILLATOR

In Fig. 7 data are presented for four of the metals, namely, the extruded magnesium-alloy tubing (Dowmetal J-1), S.A.E. 1025 seam-welded steel tubing "as welded," S.A.E. X 4130 seam-welded alloy-steel tubing normalized, and a cast iron. All materials were tested in the as-received condition. The duration of each particular measurement was kept as short as possible to prevent the introduction of work-hardening effects. The results are again plotted on logarithmic co-ordinates and include data obtained under both longitudinal and torsional vibration. In some cases more than one specimen was studied to eliminate any accidental factors. The results obtained under longitudinal vibration (tension-compression stresses) have been brought into

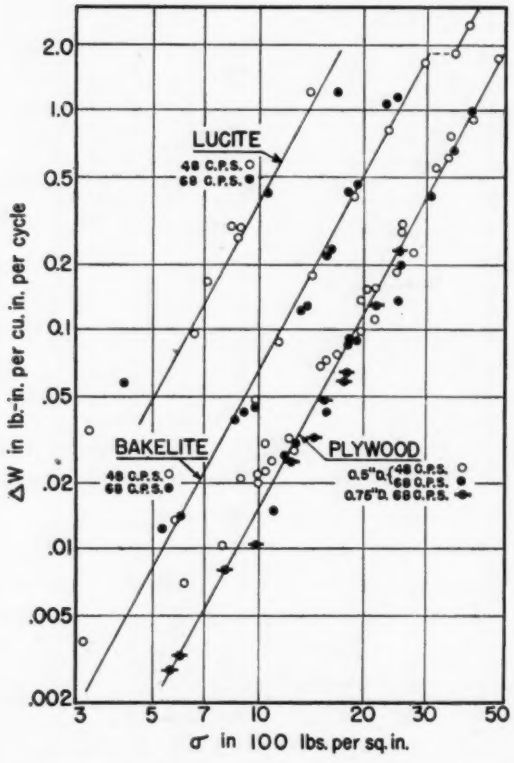


FIG. 6 DAMPING CAPACITY ΔW VERSUS σ, AMPLITUDE OF DIRECT STRESS, I.E., TENSION-COMPRESSION FOR PLASTIC MATERIALS

agreement with those obtained under torsional vibration (shearing stresses) by multiplying the longitudinal-stress amplitudes by a factor K, whose value for each material (except the cast iron which was tested only in torsion) is shown on the figure and is listed in Table 1. Again the data lie very close to the straight lines representing the relations

$$\Delta W = C_1\sigma^3 \quad [8]$$

$$\Delta W = C_2\tau_m^3 \quad [9]$$

The limits of stress for which these were found to apply, and the values of the constants C_1 and C_2 are given in Table 1. The torsional tests for the steels include data taken at two frequencies 9 and 19 cps, while the cast-iron data were taken at 19 and 30, cps, again indicating no frequency effect.

It will be noted that beyond a certain value of the stress, the data deviate from the straight line of slope 3, the damping then increasing at a much higher rate. Such a phenomenon was noted especially by Dorey (12), at comparatively lower stresses. There is some variation among the different specimens of the materials as to the exact stress at which this change occurs. It appears to occur at a stress corresponding approximately to the yield strength of the material. For example, in the case of the 1025 steel a rough static test indicated that the shearing yield point was about 17,000 psi, which is about the transition point in Fig. 7.

Ideally, to evaluate correctly the effect of stress on the damping or internal friction, all fibers of the specimen should be stressed the same amount. This condition was achieved in the longitudinal-vibration tests but could not be ideally attained in the torsional tests. All torsional data are plotted against the shear stress in the outermost fiber of the specimen, this being the maximum stress. Both grades of steel specimens were $^3/_4$-in-diam tubes of 0.035-in. wall, in which the stress variation throughout the specimen was less than 10 per cent of the maximum. In the case of the steel, therefore, the conditions were not far from the ideal. In the case of the magnesium data, however, the specimens were $^3/_4$-in. tubes of $^1/_8$-in. walls; the variation between maximum and minimum stress then being approximately one third the maximum. Nevertheless, the damping capacity varies as the third power of the stress amplitude, and the actual error due to this factor is considerably less than that indicated by the stress variation.

Experiments have also been run on monel-metal drawn seamless tubing under both torsional and longitudinal vibration, as indicated in Table 1. Two sizes were studied, $^3/_4$-in. and $^1/_2$-in. diam of 0.028 in. wall thickness. Due to slight differences in treatment, as was verified by hardness measurements, the properties of these two were slightly different. Also given in the table are similar data obtained for extruded magnesium alloy M, which was tested under the same conditions as alloy J-1. Finally the table contains data obtained by Rowett (6) on $^5/_8$-in-diam 0.05-in. wall tubing in torsion. These data are presented graphically in Fig. 2 and are included for comparative purposes.

It is common practice to present data on internal friction as the dimensionless ratio ψ, which is called the "specific damping capacity" or "relative damping." As indicated by Equation [1], this is the ratio of the damping capacity to the elastic energy stored in a unit volume of material at the maximum stress. In the direct-stress case this elastic energy is taken as $W = \frac{\sigma^2}{2E}$. Values of ψ thus determined from the experimental data are plotted in Fig. 8 for the bakelite, X4130 steel, and magnesium

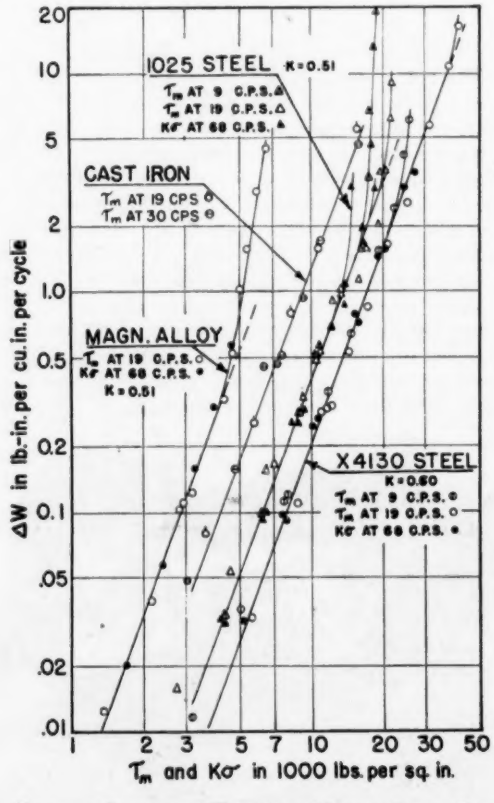


FIG. 7 DAMPING CAPACITY ΔW OF FOUR METALS UNDER TORSIONAL VIBRATIONS, OPEN SYMBOLS, AND LONGITUDINAL VIBRATIONS, SOLID SYMBOLS

(The torsional data are plotted versus the maximum shear stress amplitude. The longitudinal data are plotted versus the direct stress amplitude times the factor K.)

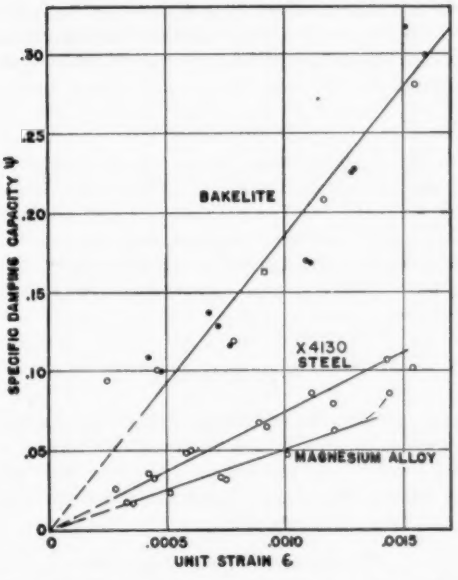


FIG. 8 SPECIFIC DAMPING CAPACITY ψ VERSUS UNIT STRAIN ϵ IN DIRECT STRESS FOR LAMINATED BAKELITE AT 48 CPS, OPEN SYMBOLS AND 68 CPS, SOLID SYMBOLS; AND S.A.E. X4130 STEEL AND MAGNESIUM ALLOY J-1 AT 68 CPS

alloy J-1. The variable ϵ is used as the abscissa in this plot, as it is more fundamental to plot one dimensionless quantity as a function of another rather than as a function of a dimensional one, i.e., the unit stress σ. This plot indicates that the specific damping capacity is roughly a linear function of the unit strain.

DYNAMIC MODULUS

In the course of the experiments, data were obtained on the variation in the dynamic modulus of elasticity of the materials with stress amplitude. Such data are of interest in the interpretation of internal-friction data as it is often necessary to make certain assumptions concerning the nature of the dynamic modulus. For instance, it is generally assumed that the dynamic modulus has a constant value identical with that of the static modulus.

The dynamic moduli of rigidity (shearing moduli) for the S.A.E. X4130 steel and magnesium alloy J-1 are presented in Fig. 9 as functions of the maximum shear stress. These moduli were calculated from the experimental data with Equation [4] and are seen to decrease with increasing stress.

The dynamic moduli of elasticity (tension-compression moduli) of the S.A.E. X4130 steel, magnesium alloy J-1, and the bakelite are shown in Fig. 10. These were calculated by means of Equation [7], and as in the case of the moduli of rigidity, are seen to

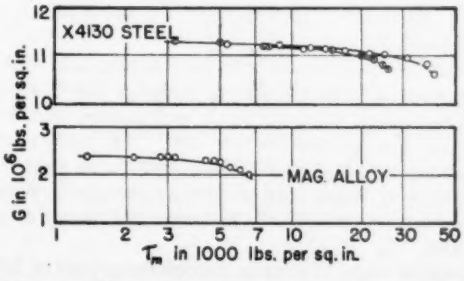


FIG. 9 DYNAMIC MODULUS OF RIGIDITY, I.E., SHEAR MODULUS AS A FUNCTION OF MAXIMUM SHEAR STRESS-AMPLITUDE FOR S.A.E. X4130 STEEL AND MAGNESIUM ALLOY J-1

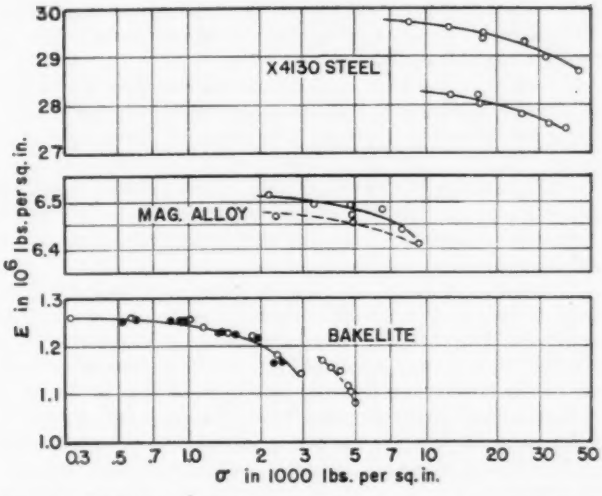


FIG. 10 DYNAMIC MODULUS OF ELASTICITY AS A FUNCTION OF DIRECT, I.E., TENSION-COMPRESSION, STRESS AMPLITUDE FOR S.A.E. X4130 STEEL, MAGNESIUM ALLOY J-1, AND LAMINATED BAKELITE

decrease with increasing stress amplitude. In the case of the steel the 5 per cent discrepancy between the two curves, obtained on supposedly identical specimens from the same piece of tubing, is of the same order of magnitude as the effect of variations noted in the wall thickness of the specimens. In the case of the magnesium the lower dotted curve was obtained after the material had been worked slightly in testing at the higher stresses. The discontinuity previously noted in the bakelite data at about 3000 psi is again apparent in the modulus.

DISCUSSION OF RESULTS

The behavior of materials under static or dynamic forces is governed by complex laws not expressible by simple exact relationships. However, in nearly every case this behavior can be represented approximately by simple, empirical relationships which have been found to possess sufficient accuracy for engineering purposes. Hooke's law and Poisson's ratio are good examples of approximate relationships which have been universally accepted for use in engineering calculations. While most mechanical properties of materials have been interrelated by such simple expressions, internal friction has not been so related to other properties due to the conflicting experimental results.

It is believed that the drawbacks of the experimental techniques commonly used in damping-capacity determinations have masked the existence of the general relationships such as were revealed by the tests in this paper. These tests were by no means exhaustive enough to warrant generalization for all materials under all possible conditions. The kinds of materials (ferrous and nonferrous metals, wood, and plastics) and ranges of stress amplitudes covered are felt to be complete enough to indicate a few of the general relationships applicable to internal friction. Under a great number of widely varying conditions, internal friction as measured by the damping capacity is subject to variations expressible by simple approximate rules to be discussed.

Stress Amplitude. For the engineering range of stresses, the damping capacity of a material (energy loss per unit volume per cycle) for completely reversed stress cycles is directly proportional to the third power of the stress amplitude. This third-power variation noted by Rowett and Dorey for steel in shear, applies equally well to other engineering materials under both shearing and normal stresses as long as the stress amplitude is below the yield strength. Whether or not a lower limit exists,

below which this variation does not hold, is beyond the scope of this paper for if such a limit exists it appears to be below the range of engineering interest.

If a material has been subjected to working effects at a particular stress amplitude, then the third-power variation may not apply for stresses in the immediate vicinity. Kutsay and Yorgiadis (22), as a result of tests on the effect of cold-work on the damping capacity of magnesium alloys, reported very significant discontinuities in the damping capacity versus stress relationships in the vicinity of the stress at which cold-working was done.

Frequency. Although the range of frequencies studied was too small to be used as the basis of definite conclusions, the data reported indicate that the damping capacity of materials is independent of frequency of stressing. This is in agreement with the results of the majority of investigators, at least in the range of engineering stresses, as noted in an earlier part of this paper.

Nature of Stress. For the two types of stress systems covered in these tests, the damping capacity of a material was found to be the same under shear stress as under normal (tension-compression) stress, provided the shear-stress amplitude was K times the normal-stress amplitude. Experimental values of the constant K obtained for six of the materials tested are presented in the last column of Table 1, and are seen to vary between 0.48 and 0.60. These are nearly equal to the value 0.577 which is the ratio of shear to normal stress to produce the same distortion energy.

The concept of the action of materials being related to the distortion energy as distinct from the energy associated with change of volume is well known in connection with the theories of failure. The theoretical derivation of the ratio between shear and normal stresses on this basis is given by Timoshenko (28). The value 0.577 is independent of Poisson's ratio or any other special property of the material and holds good for all isotropic materials obeying Hooke's law.

The agreement between the experimental stress ratios for equal damping capacity and the stress ratio for equal distortion energy is relatively good, since damping is a sensitive property that cannot be measured with great accuracy. It is therefore deduced that the damping capacity in isotropic materials is associated only with the distortion of the material and not with any change of volume under stress.

A few other experimenters have noted a correlation between damping under shear and normal stresses but have tried to correlate the damping capacity with shear stress and not distortion energy. Under this assumption the ratio K should be 0.500 and not 0.577. Föppl (3) presents data on a steel for which K is 0.570 and states that for other steels it varies between 0.53 and 0.60. These values were arrived at indirectly and are not felt to be conclusive.

The theory that distortion is the cause of inelastic behavior of materials (damping being one phase of inelasticity) is further evidenced by findings in the field of high pressures. Bridgeman (26) see also Nadai (27), has reported little or no yielding or permanent set (an inelastic action) in materials which have been subjected to exceedingly high hydrostatic pressures which cause no distortion energy, even though the acting pressures were many times the intensity of the yield strength observed under unidirectional stressing. If these materials had possessed internal friction of any magnitude under such a stress system, it would have manifested itself in the occurrence of a permanent set.

Conclusions

In the light of the experimental results presented, and the discussion of the results of others, the following conclusions appear to be justified:

Internal friction in materials, as represented by the damping capacity, is independent of the frequency, is proportional to the third power of the stress amplitude, and is due only to the distortion of the material.

Acknowledgment

The various metallic alloys studied were obtained through the co-operation of the following: The International Nickel Company, Inc., the Steel and Tubes Division of the Republic Steel Corporation; and the Dow Chemical Company. The tests were conducted in the Materials Testing Laboratory of the Pennsylvania State College, with equipment developed there by Dr. B. J. Lazan.

Appendix

Equations [3] and [6] by means of which the values of ΔW presented were determined from the experimental measurements are special cases of the relation for the work done by a harmonically varying force upon a harmonic motion of the same frequency. This relation is (29)

$$\text{Work per cycle} = \pi F a \sin \phi \quad [10]$$

where ϕ is the phase angle between the force and displacement.

In the experimental setups used in obtaining the data presented in this paper, mechanical energy was transmitted from the mechanical oscillator to the test specimen which absorbed all or nearly all of it. For the direct-stress-vibration case, the end away from the oscillator (W_1 end) had no energy-feeding device, and hence could only absorb energy. At the oscillator end the displacement was accurately measured and the forces acting were determined as to magnitude and phase relation. It was thus possible to determine accurately the energy supplied to the specimen. The major part of this energy was absorbed by the specimen as damping and the rest passed through the specimen to the support or to W_1.

At the oscillator end of the specimen two forces were acting; an inertia force A, due to the motion of mass W_2 (which included the oscillator and motor), and a force B, due to the rotating eccentrics on the oscillator. Force A was sinusoidal or very nearly so and in phase with the harmonic displacement. The phase angle in Equation [10] for this force was therefore zero, indicating that it did no work on the specimen. Force B was known from the weights and eccentricities of the rotating eccentrics and the oscillator speed. The phase angle between this force and the displacement a was obtained by direct observation, and the dynamics of the system adjusted until the angle was 90 deg. From Equation [10] the work done by this force on the specimen or the energy supplied to the specimen was

$$\text{Work per cycle} = \pi F a \sin 90 \text{ deg} = \pi F a \quad [11]$$

If Equation [11] is divided by the volume of the test specimen Equation [6] results. Equation [3] for the torsional tests is obtained in similar fashion.

It should be noted that in both the torsional- and direct-stress tests the electrical and mechanical losses in the electric motor and the mechanical oscillator in no way entered into the determination of the internal friction ΔW. The total energy absorbed by the system, i.e., the watts input to the electric motor, was considerably larger than the energy loss due to damping in the specimen but in none of the tests was this energy determined or measured.

One possible cause of error in the determinations of ΔW could be in the assumption that all of the energy supplied to the specimen was actually absorbed by damping. Some energy was

transmitted to the foundation of the apparatus. In the case of the tests in the horizontal-direct-stress apparatus there was little loss of energy to the foundation. The vibrating system in this case was free-floating, with the main vibratory forces of the masses not being transmitted to the supporting structure at all. This was because the masses were supported on the lightly loaded, highly polished, hardened rollers and rails. The coefficient of rolling friction for this roller-rails system was very small.

The torsional tests were performed on a system in which one end of the specimen was fixed to a relatively rigid structure. As noted under "Apparatus and Methods," difficulty was experienced in finding a rigid and heavy enough structure to which to attach the equipment. Some vibration was transmitted to this support, and it is believed that an error of significant magnitude could be introduced as a result of this loss, particularly in tests of specimens of low damping capacity.

The method used in measuring damping capacity is relatively new and untried. In order to obtain some idea of its reliability measurements were made on one material using the time-honored method of vibration decay. The tests were made on the $^3/_4$-in. monel tubing as it had one of the lowest damping characteristics of the materials studied and any extraneous losses as just discussed would be relatively more serious for it. The specimen used in the decay tests was cut from the same length of tubing as the specimens used with the oscillator. One end of the specimen was attached to a heavy rigid support with a collet chuck and the other end attached with a collet chuck to a rectangular metal bar having a moment of inertia about the specimen axis of 1340 lb-in.^{2} The specimen was vertical with the bar hanging from it. With a specimen length of 10 in., the natural frequency of the system was 7.6 cps.

The metal bar was first rotated through a certain small angle, so as to subject the specimen to a torsional load. The bar was then released, allowing it to oscillate angularly, subjecting the specimen to torsional oscillations which decayed because of damping in the specimen. The decay in amplitude of this torsional oscillation was measured as a function of the number of cycles. The amplitude a, at various numbers of cycles after the start of the oscillation, was plotted as a function of the number of cycles and the slope of this curve was taken for various values of a. The specific damping capacity was then obtained from the relation

$$\psi = \frac{2}{a}\frac{da}{dn} \qquad [12]$$

The unit shearing strain γ was obtained from the known values of length and diameter of the specimen, and the angular deformation of the bar at the end of the specimen.

The data thus obtained are presented in Fig. 11 together with similar data obtained with the mechanical-oscillator test apparatus at frequencies of 9 and 19 cps. The results seem to agree to a certain extent, although both sets of data show considerable scatter in the range of strains in which the decay data were taken It is probable that if a more refined apparatus had been used for the vibrations-decay method, the two sets of data would have been in closer agreement. This comparison of the data obtained by the two methods indicates that the oscillator method is at least as reliable as the commonly accepted method, and furthermore, that no serious energy losses were ignored in determining the damping capacity from the experimental data taken with the oscillator.

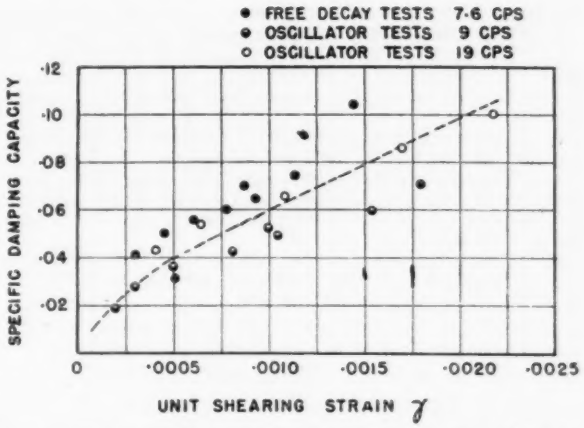


FIG. 11 SPECIFIC DAMPING CAPACITY VERSUS UNIT SHEARING STRAIN FOR TUBULAR MONEL METAL, TAKEN BOTH WITH MECHANICAL-OSCILLATOR METHOD AND WITH FREE-VIBRATION-DECAY METHOD

BIBLIOGRAPHY

1 "On the Elasticity and Viscosity of Metals," by Sir William Thompson, Lord Kelvin, Proceedings of the Royal Society of London, May 18, 1865; Mathematical and Physical Papers, vol. 3, Cambridge University Press, London, England, 1890, pp. 22 et seq.

2 "The Elastic Hysteresis of Steel," by B. Hopkinson and G. T. Williams, Proceedings of the Royal Society (A), vol. 87, 1912, pp. 502–511; Scientific Papers of Bertram Hopkinson, Cambridge University Press, London, England, 1921, pp. 99–107.

3 "The Practical Importance of the Damping Capacity of Metals, Especially Steels," by O. Föppl, *Journal of the Iron and Steel Industries*, vol. 134, 1936, pp. 393–455.

4 "Damping Capacity of Materials," by G. S. von Hydekampf, Proceedings of the American Society for Testing Materials, vol. 31, part 1, 1931, pp. 157–175.

5 "Some Mechanical Properties of Plastics and Metals Under Sustained Vibrations," by B. J. Lazan, Trans. A.S.M.E., vol. 65, 1943, pp. 87–104.

6 "Elastic Hysteresis in Steel," by F. E. Rowett, Proceedings of the Royal Society, London, England (A), vol. 89, 1914, pp. 528–543.

7 "Internal Friction as a Physical Test of Materials," by R. H. Canfield, Proceedings of the Third International Congress for Applied Mechanics, Stockholm, 1931, vol. II, pp. 311–322; also "Internal Friction in Metals," by R. H. Canfield, *Physical Review*, vol. 32, 1928, pp. 520–530.

8 "Superposed Turbine Blade Research," by F. T. Hague, *Mechanical Engineering*, vol. 62, 1940, pp. 275–277.

9 "Vibration Prevention in Engineering," by A. L. Kimball, John Wiley and Sons, Inc., New York, N. Y., 1932, p. 133.

10 "Internal Friction Theory of Shaft Whirling," by A. L. Kimball, *Physical Review*, second series, vol. 21, 1923, p. 703.

11 "Internal Friction in Solids," by A. L. Kimball and D. E. Lovell, *Physical Review*, second series, vol. 30, 1927, pp. 948–959.

12 "Elastic Hysteresis in Crank-Shaft Steels," by S. F. Dorey, Proceedings of The Institution of Mechanical Engineers, vol. 123, 1932, pp. 479–535.

13 "Prevention of Failure of Metals Under Repeated Stress," by the Battelle Memorial Institute, John Wiley & Sons, Inc., New York, N. Y., 1941, p. 210.

14 "The Physics of Metals," by F. Seitz, McGraw-Hill Book Co., Inc., New York, N. Y., 1943, pp. 152–163 and 301–302.

15 "Creep, Elastic Hysteresis, and Damping in Bakelite Under Torsion," by H. Leaderman, Trans. A.S.M.E., vol. 61, 1939, p. A-79.

16 "The Damping of the Lateral Vibration of a Mild Steel Bar," by A. J. Ockleston, *Philosophical Magazine*, seventh series, vol. 26, 1938, pp. 705–712.

17 "The Measurement of Solid Friction of Plastics," by A. Gemant, *Journal of Applied Physics*, vol. 11, 1940, pp. 647–653.

18 "The Damping Capacity of Engineering Materials," by W. H. Hatfield, G. Stanfield, and L. Rotherham, Trans. N. E. Coast Institution of Engineers and Shipbuilders, vol. 63, 1942, pp. 273–332.

19 "The Damping Capacity of Engineering Materials," by W. H. Hatfield, G. Stanfield, and L. Rotherham, *Engineering* (London), vol. 153, 1942, pp. 478–480, 498–500, and 519–520.

20 "The Damping Capacity of Steel and Its Measurement," by G. P. Contractor and F. C. Thompson, *Journal of the Iron and Steel Institute*, vol. 138, 1940, pp. 157–218.

21 "Measurement of the Damping of Engineering Materials

During Flexural Vibration at Elevated Temperatures," by C. Schabtach and R. O. Fehr, Trans. A.S.M.E., vol. 66, 1944, p. A-86.

22 "On the Torsional Damping Capacity of Solid Magnesium-Alloy Rods as Affected by Cold-Working," by A. U. Kutsay and A. J. Yorgiadis, *Journal of the Aeronautical Sciences*, vol. 10, 1943, pp. 303–310.

23 Discussion of reference (3), by M. Hempel, *Journal of the Iron and Steel Institute*, vol. 134, 1936, pp. 427–437.

24 "Fatigue Characteristics of Ordinary and Malleable Cast Iron," by M. Hempel, *Zeitschrift des Vereines deutscher Ingenieure*, vol. 85, 1941, pp. 290–292; (British Min. Aircraft Prod., R.T.P. Trans. no. 1214).

25 "Plywood Characteristics Disclosed by Vibration Tests," by A. J. Yorgiadis and J. M. Robertson, *Aero Digest*, April 1, 1944, pp. 76, 77, 80, 81, 196, 198, 201, 202, 204.

26 "The Compressibility of Thirty Metals," by P. W. Bridgeman, Proceedings of The American Academy of Arts and Sciences, vol. 58, 1923, p. 166; "Compressibility of 46 Substances to 50,000 Kg/cm,²" by P. W. Bridgeman, Proceedings of The American Academy of Arts and Sciences, vol. 74, 1940, p. 21; "Pressure Volume Relations for Seventeen Elements to 100,000 Kg/cm,²" by P. W. Bridgeman, Proceedings of The American Academy of Arts and Sciences, vol. 74, 1941, p. 425.

27 "Plasticity," by A. Nadai, McGraw-Hill Book Co., Inc., New York, N. Y., 1931, p. 10.

28 "Theory of Elasticity," by S. Timoshenko, McGraw-Hill Book Co., Inc., New York, N. Y., 1934, p. 137.

29 "Mechanical Vibrations," by J. P. Den Hartog, McGraw-Hill Book Co., Inc., New York, N. Y., 1940, p. 14.

Concentrated-Force Problems in Plane Strain, Plane Stress, and Transverse Bending of Plates[1]

By P. S. SYMONDS,[2] WASHINGTON, D. C.

A general method is described for the solution of problems of transverse bending of thin plates acted on by concentrated normal forces, and of problems of plane stress or plane strain, in which concentrated forces are applied to the boundaries. The solution is taken in two parts: (*a*) The special functions which give the stresses or deflections in the neighborhood of the concentrated forces. (*b*) A complementary function, satisfying the appropriate biharmonic equation, such that the complete solution satisfies the boundary conditions of the problem. For certain types of boundaries, this complementary function can be determined by expanding the concentrated-force functions as infinite trigonometric series. Then by addition of general solutions of the appropriate biharmonic equation, the required boundary conditions may be satisfied. The method is first illustrated by solving the plate-bending problem, for which the solution is known, of a clamped circular disk loaded by a transverse force at any point. It is then applied to the problem of an infinite plate fixed at an inner circular boundary, with outer edge free, and loaded by a transverse force at any point. This solution is obtained in finite form, and typical curves of deflection, bending moments, and shear forces are given in Figs. 3 to 8, inclusive. Using this result, solutions are next obtained for ring-shaped plates of finite outer radius, with the force applied either at the outer edge or at any point between the inner clamped edge and the outer free edge. The former case was previously solved by H. Reissner. Curves comparing the maximum moments and shears in the infinite plate with those of the annular plate with force either at the outer edge, or inside the ring are given in Figs. 9 to 12, inclusive. Finally, a solution is given of the problem in plane stress of a large plate containing an elliptical hole, which is loaded by line forces at the ends of the minor axes of the ellipse. Curves showing results of this solution are given in Figs. 14 and 15.

Introduction

THE subject of this paper is the determination of stresses and displacements due to concentrated forces. The term "concentrated force" is used here in the sense of the mathematical abstraction, in which infinite force intensities acting over infinitesimal areas define finite point or line forces. The stresses and displacements calculated are therefore valid only at sufficiently great distances from the load points, according to Saint Venant's principle. Problems of transverse bending of thin plates loaded by normal point forces, and problems of plane stress or plane strain in which line forces are applied to boundaries may be treated by the method used here, which is of general application when the boundaries consist of concentric or nonconcentric circles, hyperbolas, or ellipses. The method makes use of the known functions which express the required singularities at the load points, appropriate to each of the two classes of problems considered. These functions are discussed briefly as follows:

In the Poisson-Kirchhoff theory of bending of thin plates (1, 2),[3] the stress couples and shears per unit length of arc are obtained in terms of the deflection w of the middle surface of the plate, w being a solution of the equation

$$D\nabla^4 w = p \qquad [1]$$

where $\nabla^4 = \partial^4/\partial x^4 + 2\partial^4/\partial x^2\partial y^2 + \partial^4/\partial y^4$, p is the transverse-load intensity, and $D = Eh^3/12(1 - \nu^2)$ is the plate "flexural rigidity." The following function gives the deflection in the neighborhood of a concentrated transverse force

$$w = \frac{F}{8\pi D} r^2 \log r \qquad [2]$$

This function is the singular part of the Green's function for a thin plate. It represents the deflection due to a transverse force F at the origin of co-ordinates r, θ, since the resultant of the vertical shear forces over any curve enclosing the origin is $-F$. Moments and shears per unit length of arc corresponding to Equation [2] are infinitely large at the origin. When plates of any shape and type of edge support are acted upon by concentrated transverse forces, the solution w consists of the foregoing function together with other functions, which are solutions of $\nabla^4 w = 0$ and are so chosen that the edge conditions of the particular problem are satisfied.

In the case of problems of plane stress or strain, the following stress functions specify the stress in the neighborhood of concentrated forces

$$\chi = -\frac{F}{\pi} r\theta \sin\theta \qquad [3]$$

$$\chi = -\frac{F}{2\pi} r\theta \sin\theta + F\frac{1-\nu}{4\pi} r \log r \cos\theta \qquad [4]$$

Both of these expressions represent the stresses due to a line force F per unit thickness placed at the origin of the polar co-ordinates r, θ, and acting in the positive direction of the initial line, $\theta = 0$. Equation [3] gives Michell's "simple radial distribution" (3) in which

---

[1] Taken from Ph.D. thesis presented to Cornell University, Ithaca, N. Y.

[2] Instructor in Mechanics of Engineering, Cornell University, Ithaca, N. Y.; now at U. S. Naval Research Laboratory.

Contributed by the Applied Mechanics Division and presented at the Annual Meeting, New York, Nov. 27–Dec. 1, 1944, of THE AMERICAN SOCIETY OF MECHANICAL ENGINEERS.

Discussion of this paper should be addressed to the Secretary, A.S.M.E., 29 West 39th Street, New York, N. Y., and will be accepted until October 10, 1946, for publication at a later date. Discussion received after the closing date will be returned.

NOTE: Statements and opinions advanced in papers are to be understood as individual expressions of their authors and not those of the Society.

[3] Numbers in parentheses refer to the Bibliography at the end of the paper.

$$\sigma_r = -\frac{2F}{\pi}\frac{\cos\theta}{r}$$

$$\sigma_\theta = \tau_{r\theta} = 0$$

All lines passing through the origin are free from stress, while the force resultant of the stresses on any semicircle with its center at the origin is equal to $-F$, in the direction of the initial line. However, the expressions for the displacements contain terms proportional to $\theta \sin\theta$, $\theta\cos\theta$, so that, if the displacements are not to be many-valued, the value of θ must be restricted to an interval, $\alpha \leq \theta \leq 2\pi - \alpha$. Equation [4] defines a stress system such that the force resultant of the stresses on any circle with center at the origin is equal to $-F$ in the direction of the initial line. However, the displacements corresponding to this function are single-valued for any range of θ. Both Equations [3] and [4] lead to infinite values of stress and displacement at the origin. Solutions of plane-strain or plane-stress problems in which concentrated forces act normal to boundaries of any shape must consist of either function, Equation [3] or Equation [4], to give the required singularities at each load point, plus other stress functions chosen so that the particular boundary conditions are satisfied.

One method which has been employed in problems of plane strain or stress, when concentrated forces are applied to boundaries, is that of expressing the stress distribution on the boundaries corresponding to the concentrated force as a Fourier series, in an angular co-ordinate appropriate to the problem. The required stress distributions on all boundaries can then be obtained by applying the known trigonometric series expressing the most general form of stress function in the co-ordinate system used. General stress functions have been developed in polar (4), elliptic (5), and bipolar co-ordinates (6), so that this method could be applied to problems in which boundaries are conveniently expressed by one of these co-ordinate systems.

An example of the application of this method is the solution by Filon (7) of the problem of a thin circular ring with isolated forces applied to the inner and outer edges in several ways. A general difficulty of this method, however, is the slow convergence of the series in the neighborhood of the forces, which makes numerical evaluation tedious if not impossible. This difficulty may be overcome, as was done by Filon in the case of the circular-ring problem, by summation of the slowly convergent part of the solution, but in other than polar co-ordinates this is generally not possible.

The method here presented avoids the difficulties of slow convergence by the use, in finite form, of the concentrated force functions appropriate to either plane problems or plate problems. It is shown how these functions may be readily expanded in the form of trigonometric series in a suitable co-ordinate system. Then by the addition of an auxiliary function, expressed as a trigonometric series in the same co-ordinates, the required values of stress or of displacement on the boundaries may be obtained.

This method is suitable for problems in which the boundary curves are expressed by the constancy of a co-ordinate of one of the three co-ordinate systems: polar, bipolar, or elliptic co-ordinates. The types of boundary curves conveniently expressed by these co-ordinate systems: are, respectively, concentric circles; nonconcentric circles (or a circle near an infinite straight line, or two circles of any radii and center distance); and hyperbolas or ellipses. The reason for the limitation of the method to problems in which one of these systems is employed is that, in each of these systems, the typical potential functions have the form

$$\phi = e^{\pm n\alpha}\cos n\beta$$

$$\phi = e^{\pm n\alpha}\sin n\beta$$

while the rectangular co-ordinates are given by functions of the type

$$x = f_1(\alpha)\cos\beta$$

$$y = f_2(\alpha)\sin\beta$$

Therefore, the typical biharmonic functions in these co-ordinate systems have the form

$$x = x\phi = g_1(\alpha)\cos\beta\begin{matrix}\cos n\beta\\ \sin n\beta\end{matrix}$$

$$X = y\phi = g_2(\alpha)\sin\beta\begin{matrix}\cos n\beta\\ \sin n\beta\end{matrix}$$

Thus, the typical harmonic and biharmonic functions may be easily written as trigonometric series in the curvilinear co-ordinate β.

1—APPLICATION TO TRANSVERSE BENDING OF PLATES

Clamped Circular Plate With Noncentral Force

A plate problem whose solution is known will be solved first as an illustration of the present method. This is the problem of a clamped circular disk loaded by a transverse force at an arbitrary point. The solution was first obtained in series form by Clebsch, and is quoted by Timoshenko (8). The solution was also obtained in finite form by Michell (9).

We write as the general form of solution

$$\frac{8\pi D}{F}w = r_1^2\log r_1 + w'(r,\theta) \qquad [5]$$

Here the term $r_1^2\log r_1$ gives the necessary singularity at the point of application of the force F (see Fig. 1), where r_1 is distance from the load point, while r, θ are polar co-ordinates with origin at the center of the plate. The term $w'(r,\theta)$ is an auxiliary function, satisfying $\nabla^4 w' = 0$, which enables us to obtain the boundary conditions.

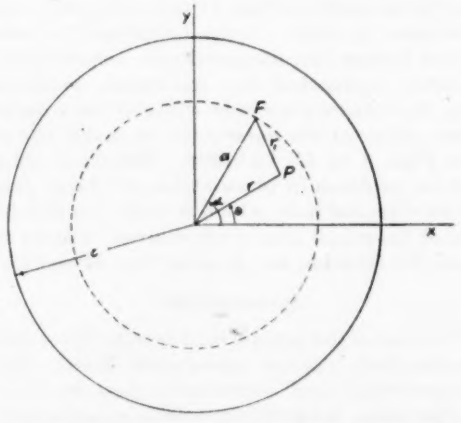


Fig. 1 Clamped Plate Loaded by Noncentral Force

We now write the term $r_1^2\log r_1$ in terms of r, θ, and express our result as an infinite trigonometric series. Two series are required, one valid for $r < a$ and the other for $r > a$. The point $P(a, \alpha)$ denotes the load point, while $P(r, \theta)$ is any point of the plate. We use the relation

$$r_1^2 = r^2 + a^2 - 2ar\cos(\theta - \alpha)$$

Regarding $\overline{OP}$, $\overline{PF}$, $\overline{OF}$ as vectors specified by the complex variable $z = x + iy = re^{i\theta}$

$$\overline{OP} = z = re^{i\theta}$$
$$\overline{OF} = z_0 = ae^{i\alpha}$$
$$\overline{PF} = z_0 - z = r_1 e^{i\phi}$$

It follows that

$$\log r_1 = Re[\log \overline{PF}] = Re[\log (z_0 - z)]$$

where Re denotes the real part of the expression in brackets. To obtain the series for $r < a$, we write

$$\log r_1 = Re\left[\log z_0 \left(1 - \frac{z}{z_0}\right)\right] = Re\left\{\log z_0 - \sum_{1,2..}^{\infty} \frac{1}{n}\left(\frac{z}{z_0}\right)^n\right\}$$

$$= \log a - \sum_{1,2..}^{\infty} \frac{1}{n}\left(\frac{r}{a}\right)^n \cos n\,(\theta - \alpha)$$

$$r_1^2 \log r_1 = [r^2 + a^2 - 2ar\cos(\theta - \alpha)]\left\{\log a - \sum_{1,2..}^{\infty} \frac{1}{n}\left(\frac{r}{a}\right)^n \cos n\,(\theta - \alpha)\right\}$$

We obtain, after reduction, the series
$(r < a)$

$$r_1^2 \log r_1 = (a^2 + r^2)\log a + r^2 + \left[-2ar\log a - \frac{1}{2}\frac{r^3}{a} - ar\right]\cos(\theta - \alpha)$$
$$+ a^2 \sum_{n=2,3..}^{\infty}\left\{\frac{1}{n(n-1)}\left(\frac{r}{a}\right)^n - \frac{1}{n(n+1)}\left(\frac{r}{a}\right)^{n+2}\right\} \cos n\,(\theta - \alpha) \ldots\ldots [6a]$$

The corresponding series for $r > a$ is obtained by writing $z_0 + \overline{FP} = z$, where $\overline{FP} = r_1 e^{i\phi'}$

$$\log r_1 = Re[\log \overline{FP}] = Re\left[\log z\left(1 - \frac{z_0}{z}\right)\right]$$

The following series is obtained
$(r > a)$

$$r_1^2 \log r_1 = a^2 + (a^2 + r^2)\log r + \left[-ar - \frac{1}{2}\frac{a^3}{r} - 2ar\log r\right]\cos(\theta - \alpha) + a^2 \sum_{n=2,3..}^{\infty}\left\{\frac{1}{n(n-1)}\left(\frac{a}{r}\right)^{n-2} - \frac{1}{n(n+1)}\left(\frac{a}{r}\right)^n\right\} \cos n\,(\theta - \alpha) \ldots [6b]$$

We now have to determine the auxiliary function $w'(r, \theta)$. This must be biharmonic, in the form of a trigonometric series in r, θ, which together with the series, Equations [6a] and [6b], satisfies the boundary conditions. These are that at the clamped edge $r = c$, $w = \dfrac{\partial w}{\partial r} = 0$; while at $r = 0$, w and its derivatives must be regular. A suitable function, satisfying $\nabla^4 w' = 0$, is

$$w'(r, \theta) = R_0 + \sum_{n=1,2..}^{\infty} R_n(r) \cos n\,(\theta - \alpha) \ldots\ldots [7]$$

where

$$R_0 = A_0 + B_0 r^2 + C_0 \log r + D_0 r^2 \log r$$
$$R_1 = A_1 r + B_1 r^3 + C_1 r^{-1} + D_1 r \log r$$

For $n \geq 2$

$$R_n = A_n r^n + B_n r^{-n} + C_n r^{n+2} + D_n r^{-n+2}$$

The constants A_n, B_n, etc., are to be determined by the boundary conditions.

To satisfy the conditions at $r = 0$, we must have

$$C_0 = D_0 = C_1 = D_1 = B_n = D_n = 0$$

The conditions at $r = c$ require

$$A_0 = \frac{c^2 - a^2}{2} - a^2 \log c$$

$$B_0 = -\frac{a^2}{2c^2} - \frac{1}{2} - \log c$$

$$A_1 = \frac{a^3}{c^2} + 2a \log c$$

$$B_1 = \frac{a}{c^2} - \frac{a^3}{2c^4}$$

$$A_n = \frac{a^2}{c^n}\left[\frac{1}{n}\left(\frac{a}{c}\right)^n - \frac{1}{n-1}\left(\frac{a}{c}\right)^{n-2}\right]$$

$$C_n = \frac{a^2}{c^{n+2}}\left[\frac{1}{n}\left(\frac{a}{c}\right)^{n-2} - \frac{1}{n+1}\left(\frac{a}{c}\right)^n\right]$$

The complete solution is therefore
$(r < a)$

$$\frac{8\pi D}{F} w = (a^2 + r^2)\log\frac{a}{c} + \frac{(c^2 + r^2)(c^2 - a^2)}{2c^2} - \frac{a^2}{2}\left[\frac{2r(c^2 - a^2)}{a^2 c^2} + \frac{r^3(a^2 - c^2)^2}{a^4 c^4} - \frac{4r}{a^2}\log\frac{c}{a}\right]\cos(\theta - \alpha)$$
$$+ \sum_{n=2,3..}^{\infty} \frac{a^n}{n(n-1)}\left\{\frac{r^n}{c^{2n}}\left[(n-1)a^2 - nc^2 + \frac{c^{2n}}{a^{2n-2}}\right] + (n-1)\frac{r^{n+2}}{c^{2n}}\left[1 - \frac{n}{n+1}\frac{a^2}{c^2} - \frac{1}{n+1}\frac{c^{2n}}{a^{2n}}\right]\right\}\cos n\,(\theta - \alpha) \ldots [8a]$$

$(r > a)$

$$\frac{8\pi D}{F} w = (a^2 + r^2)\log\frac{r}{c} + \frac{(a^2 + c^2)(c^2 - r^2)}{2c^2} - \frac{a^2}{2}\left[\frac{1}{r} - \frac{4}{a^2} r\log\frac{c}{r} + \frac{2r(c^2 - a^2)}{a^2 c^2} - \frac{r^3(2c^2 - a^2)}{a^2 c^4}\right]\cos(\theta - \alpha)$$
$$+ \sum_{n=2,3..}^{\infty} \frac{a^n}{n(n-1)}\left\{\frac{r^n}{c^{2n}}\left[(n-1)a^2 - nc^2 + (n-1)r^2 - \frac{n(n-1)}{n+1}\frac{a^2 r^2}{c^2}\right] + \frac{1}{r^n}\left[r^2 - \frac{n-1}{n+1}a^2\right]\right\}\cos n\,(\theta - \alpha) \ldots [8b]$$

This result is the same as that of Clebsch quoted by Timoshenko (8).[4]

[4] There is a discrepancy which is obviously due to a typographical error. Timoshenko gives $\frac{4r}{a^2}\log\frac{c}{r}\cos(\theta - \alpha)$ in the series for $r < a$ instead of $\frac{4r}{a^2}\log\frac{c}{a}\cos(\theta - \alpha)$. The former would lead to a singularity in $\frac{\partial w}{\partial r}$ at $r = 0$, which is inadmissible.

Large Plate Clamped at Inner Circular Boundary

The solution of the problem of an infinitely large plate clamped at an inner circular edge, with outer edge free, and loaded by a concentrated force at an arbitrary point, will now be obtained. From this result the solutions are found for finite ring-shaped plates, with the concentrated force applied either at the outer edge or at any point between the edges.

Taking first the case of the infinite plate, we write, as in the problem just solved

$$\frac{8\pi D}{F} w = r_1^2 \log r_1 + w'(r, \theta) \quad \ldots\ldots\ldots\ldots [5]$$

where, as before, r_1 is the distance from the load point F, r, θ are polar co-ordinates with origin at the center of the inner circle (see Fig. 2), and w' is a biharmonic function such that the required

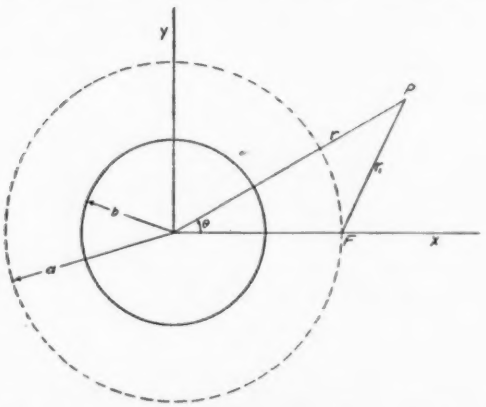


Fig. 2 Infinite Plate Clamped at Circular Edge

edge conditions are obtained. The term $r_1^2 \log r_1$ is taken in the form of Equations [6a], [6b], and the auxiliary function w' as given by Equation [7]. The boundary conditions at the clamped edge ($r = b$) are $w = \dfrac{\partial w}{\partial r} = 0$. At the outer edge ($r \to \infty$) the conditions are

$$V_n = Q_n - \frac{\partial M_{nt}}{\partial s} = 0$$

$$M_n = 0$$

where M_n, M_{nt} are bending and twisting moments, respectively, and Q_n is the shear force, all taken per unit length of arc; the co-ordinate axes n, t being normal and tangential, respectively, to the edge. These conditions are easily obtained in the case of an infinitely large plate, the solution being independent of the particular boundary curve of the outer edge. To satisfy the conditions at the outer edge, we must have $B_0 = B_1 = A_n = C_n = 0$, $D_0 = -1$, $D_1 = 2a$. To satisfy the conditions at the clamped edge we require

$$A_0 = 2b^2 \log b \left(1 + \log \frac{a}{b}\right) - (a^2 + b^2) \log a - b^2$$

$$C_0 = -b^2 \left[1 + 2 \log \frac{a}{b}\right]$$

$$A_1 = \frac{b^2}{a} + 2a \log \frac{a}{b}$$

$$C_1 = ab^2 - \frac{b^4}{2a}$$

$$B_n = b^{n+2} \left[\frac{1}{n}\left(\frac{\ }{a}\right)^{n} - \frac{1}{n+1}\left(\frac{b}{a}\right)^{n}\right]$$

$$D_n = b^n \left[\frac{1}{n}\left(\frac{b}{a}\right)^{n} - \frac{1}{n-1}\left(\frac{b}{a}\right)^{2}\right]$$

Substituting these values in the general solution, and introducing the dimensionless variables

$$\rho = \frac{r}{b}, \qquad q = \frac{a}{b}$$

the following solution is obtained

$(r < a, \rho < q)$

$$\left.\begin{aligned}\frac{8\pi D}{Fb^2} w = {} & (\log q + 1)(\rho^2 - 1) - [\rho^2 + 1 + 2 \log q] \log \rho \\ & + \left[(q^{-1} - q)\rho - \frac{1}{2} q^{-1}\rho^3 + \left(q - \frac{1}{2} q^{-1}\right)\rho^{-1} \right. \\ & \left. + 2q\rho \log \rho \right] \cos\theta + \sum_{n=2,3..}^{\infty} \left\{ \frac{q^{-n+2}}{n(n-1)} \rho^n \right. \\ & - \frac{q^{-n}}{n(n+1)} \rho^{n+2} + \left(\frac{q^{-n+2}}{n} - \frac{q^{-n}}{n+1}\right)\rho^{-n} \\ & \left. + \left(\frac{q^{-n}}{n} - \frac{q^{-n+2}}{n-1}\right)\rho^{-n+2} \right\} \cos n\theta\end{aligned}\right\} \quad \ldots [9a]$$

$(r > a, \rho > q)$

$$\left.\begin{aligned}\frac{8\pi D}{Fb^2} w = {} & q^2 - 1 - (q^2 + 1) \log q + (q^2 - 1 \\ & - 2 \log q) \log \rho + \left[(q^{-1} - q + 2q \log q)\rho \right. \\ & \left. + \left(q - \frac{1}{2} q^3 - \frac{1}{2} q^{-1}\right)\rho^{-1} \right] \cos\theta \\ & + \sum_{n=2,3..}^{\infty} \left\{ \left(\frac{q^n}{n(n-1)} + \frac{q^{-n}}{n} - \frac{q^{-n+2}}{n-1}\right)\rho^{-n+2} \right. \\ & \left. + \left(\frac{q^{-n+2}}{n} - \frac{q^{n+2}}{n(n+1)} - \frac{q^{-n}}{n+1}\right)\rho^{-n} \right\} \cos n\theta\end{aligned}\right\} \quad \ldots [9b]$$

It may be verified that the foregoing result satisfies the boundary conditions and that the two solutions Equations [9a] and [9b] have proper values at the load circle $r = a$. At this circle the functions w, $\dfrac{\partial w}{\partial r}$, M_r are continuous, but the shear resultant

$$V_r = Q_r - \frac{1}{r} \frac{\partial M_{r\theta}}{\partial \theta}$$

is discontinuous due to the presence of the force. It may be checked that the solutions, Equations [9a], [9b] give, in the limit as r approaches a

$$\lim_{r \to a} \left[(V_r)_{r>a} - (V_r)_{r<a} \right] = -\frac{F}{\pi a} \left[\frac{1}{2} + \sum_{1,2..}^{\infty} \cos n\theta \right]$$

This is the Fourier series representing the concentrated force F as a line loading on the circle $r = a$.

The series appearing in Equations [9] may be summed, the series terms all being similar to the following

$$S_1 = \sum_{2,3..}^{\infty} \frac{q^n}{n(n-1)} \frac{\cos n\theta}{\rho^{n-2}} = \rho^2 \sum_{2,3..}^{\infty} \frac{x^n}{n(n-1)} \cos n\theta$$

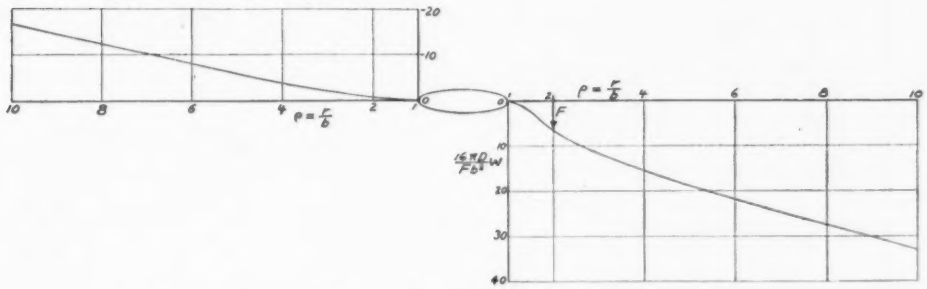


FIG. 3 INFINITE PLATE: DEFLECTION ALONG LINE, $y = 0$; $q = 2$

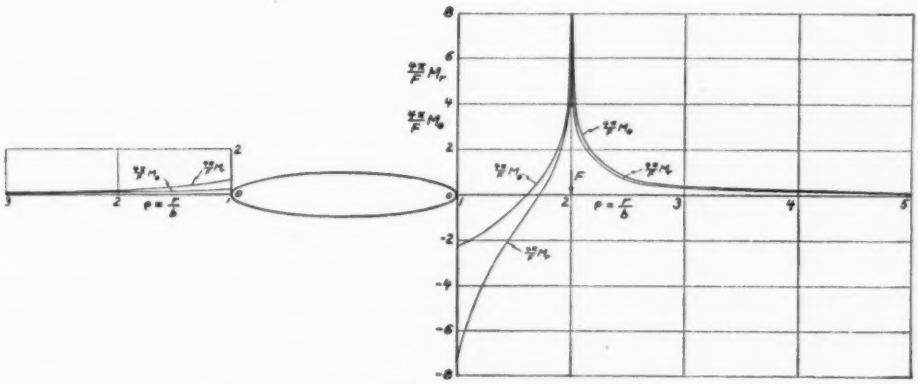


FIG. 4 INFINITE PLATE: BENDING MOMENTS ALONG LINE, $y = 0$; $q = 2$

where $x = \dfrac{a}{r} < 1$. Writing $z = xe^{i\theta}$ this is given by

$$S_1 = \rho^2 Re[(1-z)\log(1-z) + z]$$

where Re denotes "real part of." After summing, by methods similar to this, all the series terms in Equations [9], the following expression is obtained for both Equations [9a] and [9b]

$$\frac{8\pi D}{Fb^2} w = \frac{1}{2}(q^2 + \rho^2 - 2q\rho\cos\theta)\log\frac{q^2+\rho^2-2q\rho\cos\theta}{1+q^2\rho^2-2q\rho\cos\theta} + (q^2-1)\log\rho + (\rho^2-1)\log q - 2\log q\log\rho \quad [10]$$

Curves showing the deflection w along the central line ($\theta = 0$, π) are given in Fig. 3, for $q = \dfrac{a}{b} = 2$. The deflection under the load is given by

$$w(a, 0) = \frac{Fb^2}{4\pi D}\log q(q^2 - 1 - \log q)$$

The slopes at great distances from the clamped edge (neglecting terms in q/ρ compared to unity) are

$$\frac{\partial w}{\partial x} = \frac{Fb}{8\pi D} \times q\left(\log q^2 - 1 + \frac{1}{q^2}\right), \qquad \frac{\partial w}{\partial y} = 0$$

These show that the deflection surface of the plate, far from the clamped circle, is a plane inclined to the undeflected surface. The strain energy of the plate is concentrated in a relatively small region including the clamped edge and the load point.

Curves[5] showing the bending moments M_r, M_θ, on the central line ($\theta = 0, \pi$) are given in Fig. 4, for $q = 2$. Plots of Q_r, V_r on the same line are given in Figs. 5, 6. The variation of M_r, Q_r along the clamped edge ($r = b$) is shown in Figs. 7, 8. The curves of Figs. 9, 10 show the maximum values of the bending moment M_r and shear Q_r (at $r = b$, $\theta = 0$) as functions of $q = a/b$; these are given by the following expressions

$$(M_r)_{max} = (M_r)_{\substack{r=b\\ \theta=0}} = -\frac{F}{2\pi}(1 + q + \log q)$$

$$(Q_r)_{max} = (Q_r)_{\substack{r=b\\ \theta=0}} = \frac{F}{2\pi b}\frac{(1+q)^2}{q-1}$$

The finite form of the solution of this problem suggested that it might be obtainable directly, rather than by the series method. This was found to be the case. In Appendix 1 is outlined a solution of the problem by means of an inversion transformation, making use of the solution of Michell for the problem of a clamped circular plate loaded by a noncentral transverse force.

SOLUTIONS FOR PLATES WITH FINITE OUTER RADIUS

The solution for an infinite plate, Equation [10] can be used to obtain solutions for ring-shaped plates of finite outer radius, with the force applied either at the outer edge or at any point between the inner clamped edge and the outer edge. The first case, in which the force is applied at the outer boundary, was solved by H. Reissner (10). The method used by Reissner was that of applying directly the general series solution, Equation [7], and determining the constants A_n, etc., so as to obtain the required conditions at the inner and outer radii, which are as follows

[5] In all calculations Poisson's ratio ν has been taken as 0.3. Expressions for bending moments and shears are given in reference (2), p. 259.

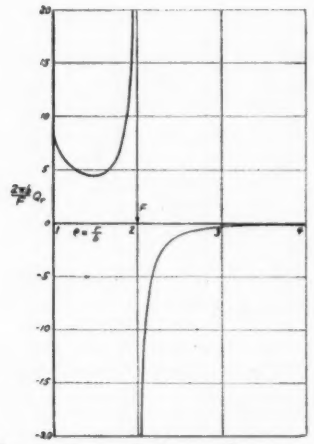


FIG. 5 SHEAR Q_r ALONG LINE $y = 0$
(Infinite plate, $q = 2$.)

$$\left.\begin{aligned} (w)_{r=b} &= \left(\frac{\partial w}{\partial r}\right)_{r=b} = 0 \\ (M_r)_{r=a} &= 0 \\ (V_r)_{r=a} &= \left(Q_r - \frac{1}{r}\frac{\partial M_{r\theta}}{\partial \theta}\right)_{r=a} = \frac{F}{\pi a}\left[\frac{1}{2} + \sum_{n=1,2..}^{\infty} \cos n\theta\right] \end{aligned}\right\} \quad ..[11]$$

where b, a are inner and outer radii, respectively. However, the same results can be obtained by making use of the solution just found for the infinite plate, in closed form (Equation [10]), to express the singularity in V_r at the outer edge. This solution, when evaluated at $r = a$, $(\rho = q)$, leads to shears V_r in addition to those corresponding to the force F, and to a distribution of bending moments M_r. These additional shears and moments

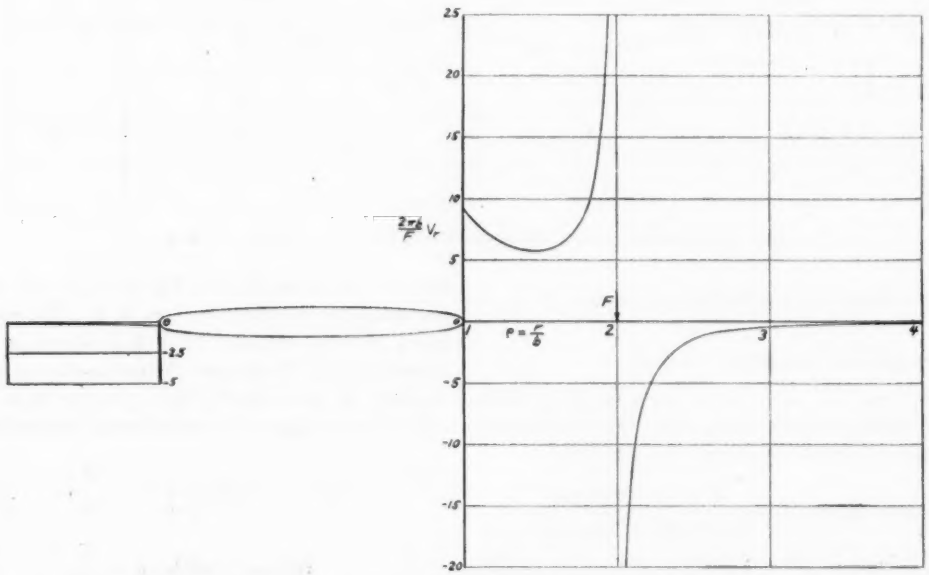


FIG. 6 INFINITE PLATE: RESULTANT SHEAR V_r ALONG LINE $y = 0$; $q = 2$

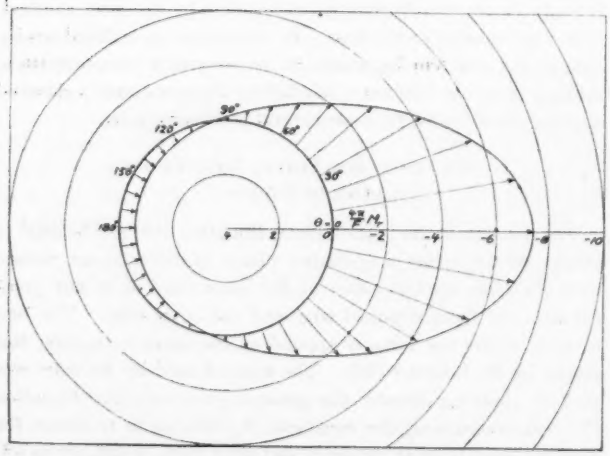


FIG. 7 BENDING MOMENT AT CLAMPED EDGE, $r = b$
(Infinite plate, $q = 2$.)

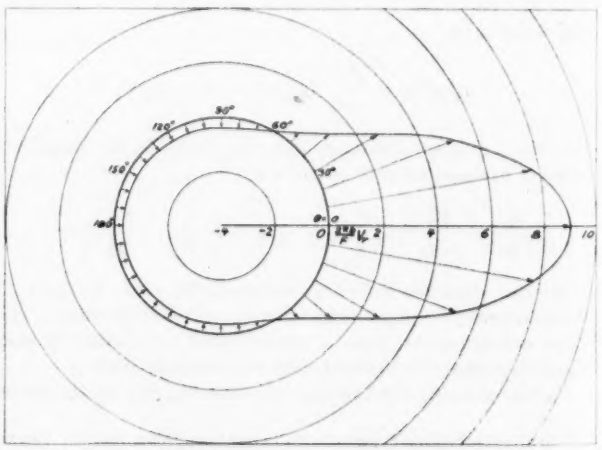


FIG. 8 SHEAR AT CLAMPED EDGE, $r = b$
(Infinite plate, $q = 2$.)

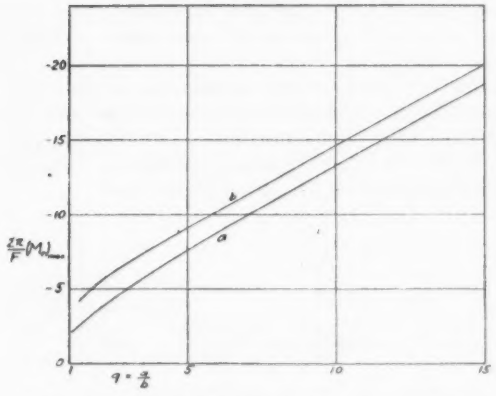


FIG. 9 MAXIMUM BENDING MOMENT (M_r AT $r = b$, $\theta = 0$) AS FUNCTION OF q = Ratio $\frac{\text{Distance of Force From Center of Clamped Circle}}{\text{Radius of Clamped Circle}}$
(Curve *a*, infinite plate; Curve *b*, force applied at edge of plate.)

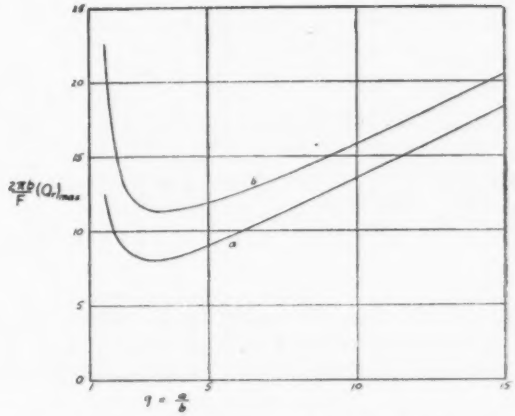


FIG. 10 MAXIMUM SHEAR (Q_r AT $r = b$, $\theta = 0$) AS FUNCTION OF q = Ratio $\frac{\text{Distance of Force From Center of Clamped Circle}}{\text{Radius of Clamped Circle}}$
Curve *a*, infinite plate; Curve *b*, force applied at edge of plate.)

may be expressed as trigonometric series by evaluating the series form of solution of the infinite-plate problem, (obtained for $r < a$), Equation [9a], at $r = a$. They may then be annulled by applying the general series solution in polar co-ordinates, and determining the coefficients A_n, etc., so as to give conditions, Equations [11]. In this method, the shear and moment distributions which must be annulled by the general series solution are small and are rapidly convergent, and the contribution to the moments and shears in the plate of the auxiliary solution is small compared to that of the infinite-plate solution, which is easily calculated since it is given in finite form. Hence the labor of the calculation is probably considerably less than that required in Reissner's method, in which the general series solution is itself employed to obtain the singularity at the outer boundary.

The solution of Reissner's problem, using the present method, is obtained as follows: We take the solution in the form

$$w = 2w_1 + w_2 \quad \ldots\ldots\ldots\ldots\ldots\ldots [12]$$

where w_1 is the solution previously obtained for an infinite plate, given by either Equation [9a] or Equation [10], and w_2 is the general biharmonic solution, Equation [7]. The function $2w_1$ leads to the following expressions for M_r and

$$V_r = Q_r - \frac{1}{r}\frac{\partial M_{r\theta}}{\partial \theta}$$

on the circle $r = a(\rho = q)$

$$(M_{r1})_a = \frac{F}{\pi}\frac{1-\nu}{4}\left\{1 - (1 + 2\log q)q^{-2} + (1 - q^{-2})^2\cos\theta + \sum_{2,3..}^{\infty}\left(2\frac{1+\nu}{1-\nu}\left[\frac{1}{n} + \left(1 - q^2 - \frac{1}{n}\right)q^{-2n}\right] + n(q - q^{-1})^2 q^{-2n}\right)\cos n\theta\right\} \quad [13a]$$

$$(V_{r1})_a = \frac{F}{\pi a}\left\{\frac{1}{2} + \sum_{1,2..}^{\infty}\cos n\theta + \frac{1}{2} + \sum_{1,2..}^{\infty}\left[nq^2 - n + 1 + \frac{1-\nu}{4}n^2(q - q^{-1})^2\right]q^{-2n}\cos n\theta\right\} \quad [13b]$$

The arbitrary constants of the auxiliary solution w_2 are now determined so as to annul the foregoing expression for $(M_{r1})_a$ and to annul all but the first two terms in the expression for $(V_{r1})_a$ which express the required singularity due to the applied force at the outer boundary. In addition, the conditions $(w_2)_{r=b} = \left(\frac{\partial w_2}{\partial r}\right)_{r=b} = 0$ must be satisfied. After solving for the constants A_n, B_n, etc., and substituting in Equation [12], the following complete solution is obtained

$$\left.\begin{aligned}\frac{8\pi D}{Fb^2}w = {} & (q^2 + \rho^2 - 2q\rho\cos\theta)\log\frac{q^2 + \rho^2 - 2q\rho\cos\theta}{1 + q^2\rho^2 - 2q\rho\cos\theta} \\ & + 2(\rho^2 - 1)\log q + 2(q^2 - 1)\log\rho - 4\log q\log\rho \\ & + (\rho^2 - 1)\log\rho + \frac{1}{2} \\ & \times\left\{\frac{1 + 3\nu + 3(1-\nu)q^{-2} + 2\log q[1 + \nu + 2(1-\nu)q^{-2}]}{1 + \nu + (1-\nu)q^{-2}}\right\} \\ & \times(1 - \rho^2 + 2\log\rho) + \left\{\left[\frac{2q^{-1} - (1-\nu)(1-q^{-2})q^{-3}}{3 + \nu + (1-\nu)q^{-4}}\right]\right. \\ & \times(\rho^3 - 2\rho + \rho^{-1}) + q(\rho - \rho^{-1} \\ & \left. - 2\rho\log\rho)\right\}\cos\theta + 8\sum_{n=2,3..}^{\infty}\left\{K_n\left[\frac{\rho^{n+2}}{n+1} - \frac{\rho^n}{n}\right.\right. \\ & \left.\left. + \frac{\rho^{-n}}{n(n+1)}\right] - L_n\left[\frac{\rho^n}{n(n-1)} - \frac{\rho^{-n+2}}{n-1} + \frac{\rho^{-n}}{n}\right]\right\}\cos n\theta\end{aligned}\right\} \quad \ldots\ldots\ldots [14]$$

Here the constants K_n, L_n ($n \geqslant 2$) in the series expression are the solutions of the pairs of simultaneous equations

$$\left.\begin{aligned}f_nK_n + g_nL_n &= \alpha_n \\ h_nK_n + k_nL_n &= \beta_n\end{aligned}\right\} \quad \ldots\ldots\ldots\ldots [15]$$

where

$$f_n(q) = -2\frac{1+\nu}{1-\nu} - q^{-2} - n - q^{-2n-2} + nq^{-2}$$

$$g_n(q) = q^{-2} + (n+1)q^{-2n-2} + 2\frac{1+\nu}{1-\nu}q^{-2n} - nq^{-2n}$$

$$h_n(q) = -2\frac{1+\nu}{1-\nu} - 2 + q^{-2} - nq^{-2} - q^{-2n-2} + n$$

$$k_n(q) = -q^{-2} - 2 - n - 2\frac{1+\nu}{1-\nu}q^{-2n} + (n+1)q^{-2n-2}$$

$$\alpha_n(q) = -\frac{1}{2}\frac{1+\nu}{1-\nu}\frac{q^{-n}}{n} + \frac{1}{2}\frac{1+\nu}{1-\nu}\left(q^2 - 1 + \frac{1}{n}\right)q^{-2n} - \left(\frac{q-q^{-1}}{2}\right)^2 nq^{-2n}$$

$$\beta_n(q) = -q^{-1}\left[\frac{1}{1-\nu}\left(q^2 - 1 + \frac{1}{n}\right)nq^{-2n} + \left(\frac{q-q^{-1}}{2}\right)^2 n^2q^{-2n}\right]$$

The maximum values of M_r and Q_r for this problem (occurring at $r = b$, $\theta = 0$) are shown in Figs. 9, 10, as functions of $q = a/b$. These maximum values are given by the following expressions

$$(M_r)_{max} = \frac{F}{\pi}\left\{-(1 + q + \log q) - \frac{1}{2} + \frac{1}{4}\frac{1 + 3\nu + 3(1-\nu)q^{-2} + 2[1 + \nu + 2(1-\nu)q^{-2}]\log q}{1 + \nu + (1-\nu)q^{-2}} + \frac{1}{2}q - \frac{2q^{-1} - (1-\nu)(1-q^{-2})q^{-2}}{3 + \nu + (1-\nu)q^{-4}} - 4\sum_{2,3\ldots}^{\infty}(K_n - L_n)\right\} \quad \ldots\ldots [16]$$

$$(Q_r)_{max} = \frac{F}{\pi b}\left\{\frac{(1+q)^2}{q-1} - \frac{1}{2} - \frac{1}{2}q - \frac{2q^{-1} - (1-\nu)(1-q^{-2})q^{-2}}{3 + \nu + (1-\nu)q^{-4}} - 4\sum_{2,3\ldots}^{\infty} n(K_n + L_n)\right\} \quad \ldots\ldots [17]$$

where the constants K_n, L_n, etc., are determined by Equations [15]. As an example of the relative magnitudes of the contributions from the infinite-plate solution $2w_1$ and from the auxiliary function w_2, the calculation of $(M_r)_{max}$ for the case $q = a/b = 1.5$ gives the following results

$$(M_{r1})_{max} = \frac{F}{2\pi}(-5.8110)$$

$$(M_{r2})_{max} = \frac{F}{2\pi}(0.3629 + 0.7915 + 0.1342) = \frac{F}{2\pi}(1.2887)$$

$$(M_r)_{max} = -4.522\frac{F}{2\pi}$$

(This is the case calculated by Reissner, who gives the value $[M_r]_{max} = -4.45F/2\pi$). The contribution of all the series terms for $n \geq 2$ (0.1342) is less than 3 per cent of the value of $(M_r)_{max}$. It is interesting to note that the maximum bending moment found for the case when the force is applied at the outer edge is considerably greater than that found for the case when the force acts at the same distance from the clamped edge, but the plate extends a large distance beyond the load point (for example, for $a/b = 1.5$, these values are $\frac{2\pi}{F}(M_r)_{max} = -4.522, -2.905$, respectively).

The intermediate cases, when the outer circular edge is at a finite distance from the load point, will be considered below.

The solution of the problem of a ring-shaped plate, clamped at its inner edge $r = b$ and free at the outer edge $r = c$, and loaded by a concentrated force at any point $r = a$, where $b < a < c$, may also be obtained by modifying the solution for the infinite plate previously found. The required solution is the sum of the infinite-plate solution, Equation [10], and the general series solution, Equation [7], where the arbitrary constants of Equation [7], are now determined so as to give the conditions

$$\left.\begin{aligned}(w)_{r=b} &= \left(\frac{\partial w}{\partial r}\right)_{r=b} = 0\\ (M_r)_{r=c} &= 0\\ (V_r)_{r=b} &= \left(Q_r - \frac{1}{r}\frac{\partial M_{r\theta}}{\partial \theta}\right)_{r=b} = 0\end{aligned}\right\} \quad \ldots\ldots [18]$$

The typical curves for M_r, V_r (Figs. 4, 6) from the infinite-plate solution show that these both decrease rapidly to zero beyond the load point. Hence, in the solution for plates with finite outer radius, the contribution from the auxiliary solution, required to annul M_r, V_r on $r = c$, will be small compared to that of the infinite-plate solution, unless the outer edge is very close to the load point.

The complete solution is

$$w = w_1 + w'$$

where w_1 is the infinite-plate solution, given by Equation [10] and w' is taken in the form of Equation [7].

The distributions of M_r, V_r which must be annulled are obtained from the series form of the infinite-plate solution, valid, for $r > a$ ($\rho > q$), Equation [9b]. These are evaluated at $r = c$ ($\rho = c/b = s$), and annulled by means of w'. After calculating the constants A_n, B_n, etc. and simplifying, the complete solution is found to be

$$\left.\begin{aligned}\frac{8\pi D}{Fb^2}w = {} & \frac{1}{2}(q^2 + \rho^2 - 2q\rho\cos\theta)\log\frac{q^2 + \rho^2 - 2q\rho\cos\theta}{1 + q^2\rho^2 - 2q\rho\cos\theta} + (q^2 - 1)\log\rho\\ & + (\rho^2 - 1)\log q - 2\log q\log\rho\\ & + \frac{(q^2 - 1 - 2\log q)(\rho^2 - 1 - 2\log\rho)}{2\frac{1+\nu}{1-\nu}s^2 + 2} + \frac{(q^3 - 2q + q^{-1})(\rho^3 - 2\rho + \rho^{-1})}{2\frac{3+\nu}{1-\nu}s^4 + 2}\cos\theta\\ & + \sum_{n=2,3\ldots}^{\infty}\left\{P_n\left[\frac{\rho^{n+2}}{n+1} - \frac{\rho^n}{n} + \frac{\rho^{-n}}{n(n+1)}\right] - Q_n\left[\frac{\rho^n}{n(n-1)} - \frac{\rho^{-n+2}}{n-1} + \frac{\rho^{-n}}{n}\right]\right\}\cos n\theta\end{aligned}\right\} \quad \ldots [19]$$

where $\rho = r/b$, $q = a/b$, $s = c/b$, and the quantities P_n, Q_n are determined from the simultaneous equations

$$\left.\begin{aligned}f_nP_n + g_nQ_n &= \phi_n\\ h_nP_n + k_nQ_n &= \psi_n\end{aligned}\right\} \quad \ldots\ldots [20]$$

where

$$f_n(s) = -2\frac{1+\nu}{1-\nu} - s^{-2} - n - s^{-2n-2} + ns^{-2}$$

$$g_n(s) = s^{-2} + (n+1)s^{-2n-2} + 2\frac{1+\nu}{1-\nu}s^{-2n} - ns^{-2n}$$

$$h_n(s) = -2\frac{1+\nu}{1-\nu} - 2 + s^{-2} - ns^{-2} - s^{-2n-2} + n$$

$$k_n(s) = -s^{-2} - 2 - n - 2\frac{1+\nu}{1-\nu}s^{-2n} + (n+1)s^{-2n-2}$$

$$\phi_n = s^{-2n}\left\{\left(1 - \frac{2}{n}\frac{1+\nu}{1-\nu}\right)[q^n + (n-1)q^{-n} - nq^{-n+2}] + [(n+1)q^{-n+2} - q^{n+2} - nq^{-n}]\,s^{-2}\right\}$$

$$\psi_n = s^{-2n}\left\{\left(1 + \frac{4}{n(1-\nu)}\right)[q^n + (n-1)q^{-n} - nq^{-n+2}] + [(n+1)q^{-n+2} - q^{n+2} - nq^{-n}]\,s^{-2}\right\}$$

The maximum values of M_r, Q_r (at $r = b$, $\theta = 0$) are given by the following expressions

$$(M_r)_{max} = \frac{F}{2\pi}\left\{-(1 + q + \log q) - \frac{q^3 - 1 - 2\log q}{2\dfrac{1+\nu}{1-\nu}s^2 + 2} - \frac{q^3 - 2q + q^{-1}}{\dfrac{3+\nu}{1-\nu}s^4 + 1} - \sum_{2,3..}^{\infty}(P_n - Q_n)\right\} \quad [21]$$

$$(Q_r)_{max} = \frac{F}{2\pi b}\left\{\frac{(1+q)^2}{q-1} - \frac{q^3 - 2q + q^{-1}}{\dfrac{3+\nu}{1-\nu}s^4 + 1} - \sum_{2,3...}^{\infty} n(P_n + Q_n)\right. \quad [22]$$

The interesting feature of the curves of Figs. 11, 12, which show these maximum values as functions of $s/q = c/a$ for the cases $q = 1.5, 2.0$, is the rapid decrease of $(M_r)_{max}$ and $(Q_r)_{max}$ when the plate extends only slightly beyond the load point. For example, the calculation for $q = a/b = 1.50$, $s = c/b = 1.55$, gives

$$\frac{c}{a} = \frac{1.55}{1.50} = 1.034; \quad \frac{2\pi}{F}(M_r)_{max} = -2.905 - .391 = -3.296$$

so that the maximum bending moment already differs by less than 15 per cent from the value which it would have if the plate extended indefinitely beyond the load point (—2.905); the value of $\frac{2\pi}{F}(M_r)_{max}$ found for the case when the force was applied directly to the outer edge was —4.522.

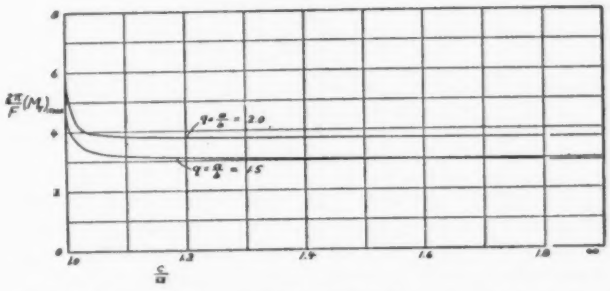


FIG. 11 MAXIMUM BENDING MOMENT (M_r AT $r = b$, $\theta = 0$) AS FUNCTION OF c/a =

Ratio $\frac{\text{Radius of Outer Free Edge}}{\text{Distance of Force From Center of Clamped Circle}}$

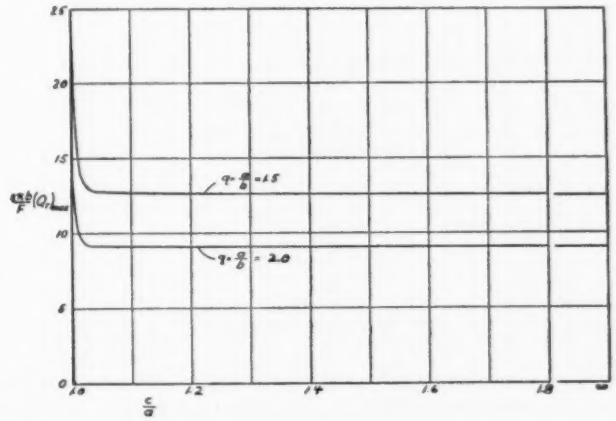


FIG. 12 MAXIMUM SHEAR (Q_r AT $r = b$, $\theta = 0$) AS FUNCTION OF c/a = RATIO $\frac{\text{RADIUS OF OUTER FREE EDGE}}{\text{DISTANCE OF FORCE FROM CENTER OF CLAMPED CIRCLE}}$

2 APPLICATION TO PLANE STRESS AND PLANE STRAIN

The solution will now be given for the problem of determining the stress in an infinite plate containing an elliptical hole, loaded by a pair of concentrated forces acting at the ends of the minor axes of the ellipse.

We require a stress function X which satisfies the equation of plane stress (or plane strain), $\nabla^4 X = 0$, and which leaves the ellipse free from stress everywhere except at the load points, where the normal stress is infinite in such a way that the resultant force over an arc including each load point is equal to $-F$. We write the solution in the form (see Fig. 13)

$$X = -\frac{F}{\pi}x\theta_1 - \frac{F}{\pi}x\theta_2 + X'(x, y) \quad [23]$$

The stress functions $-\frac{F}{\pi}x\theta_1$, $-\frac{F}{\pi}x\theta_2$ are those for concentrated normal forces at $z_1 = ib$, $z_2 = -ib$, while $X'(x, y)$ is an auxiliary biharmonic function, chosen so that the required stress conditions on the ellipse are satisfied. Although the stress function $\frac{F}{\pi}x\theta$ leads to many-valued displacements, it was shown by Michell (3), as a result of a general theory of dislocations, that when these functions are written for several forces acting at a hole in a plate the resultant dislocations vanish, provided the forces are in equilibrium among themselves. In the present case the forces are self-equilibrating, so that the simple radial stress functions are suitable.

In order to determine the function X' the concentrated-force functions are expanded in trigonometric series in elliptic co-ordinates ξ, η, such that η is an angular co-ordinate, while the distribution of stresses over any elliptical contour will be obtained by assigning to the other co-ordinate a constant value, $\xi = \xi_1$. In particular, the stresses on an ellipse $\xi = \xi_0$ passing through the load points $z = \pm ib$ are obtainable. Since the general solution of the biharmonic equation, $\nabla^4 X = 0$, leads to stresses expressible in the same form

$$\sigma_\xi = f(\xi)\begin{Bmatrix}\cos n\eta \\ \sin n\eta\end{Bmatrix}, \quad \tau_{\xi\eta} = g(\xi)\begin{Bmatrix}\cos n\eta \\ \sin n\eta\end{Bmatrix}$$

suitable functions of this type may now be added in order to annul all stresses on the ellipse ξ_0 except those corresponding to concentrated forces normal to the elliptical boundary, at the load points.

In expanding the radial stress functions, we use the conformal transformation

$$z = c\cosh\zeta$$

where

$$z = x + iy = re^{i\theta};\ \zeta = \xi + i\eta$$

Equating real and imaginary parts, we obtain the relations

$$x = c \cosh \xi \cos \eta$$
$$y = c \sinh \xi \sin \eta$$

It is seen that the curves ($\xi = \xi_1 = $ const) transform to ellipses in the x,y-plane with foci at $x = \pm c$, and having major and minor semiaxes a_1, b_1 equal to $c \cosh \xi_1$, $c \sinh \xi_1$, respectively. Angle η is the eccentric angle of any ellipse $\xi = \xi_1$. The curves ($\eta = \eta_1 = $ const) transform to hyperbolas with foci at $x = \pm c$. We arbitrarily restrict η to the range $0 \leqslant \eta < 2\pi$.

Letting X_1 denote the concentrated normal force function, this is (referring to Fig. 13)

$$X_1 = -\frac{F}{\pi} x\ (\theta_1 + \theta_2) = -\frac{F}{\pi} x\ (\phi_2 - \phi_1)$$

dropping the term proportional to x. Now the vector

$$\overline{OP} = z = z_1 + r_1 e^{i\phi_1} = z_2 + r_2 e^{i\phi_2}$$
$$\phi_1 = Im[\log (z - z_1)]$$
$$\phi_2 = Im[\log (z - z_2)]$$

where Im denotes "imaginary part of." Hence

$$X_1 = \frac{F}{\pi} x\, Im[\log (z - z_1) - \log (z - z_2)]$$

$$= \frac{Fc}{\pi} \cosh \xi \cos \eta\, Im[\log c\ (\cosh \zeta - \cosh \zeta_1) - \log c\ (\cosh \zeta - \cosh \zeta_2)]$$

But we can write

$$\cosh \zeta - \cosh \zeta_1 = \frac{1}{2} e^{\zeta}(1 - e^{\zeta_1 - \zeta})(1 - e^{-\zeta_1 - \zeta})$$

$$\log (1 - e^{\zeta_1 - \zeta}) = -\sum_{n=1,\,2\ldots}^{\infty} \frac{1}{n} e^{n(\zeta_1 - \zeta)}, \text{ etc.}$$

Substituting, we obtain

$$X_1 = \frac{Fc}{\pi} \cosh \xi \cos \eta \sum_{n=1,\,2\ldots}^{\infty} \left\{ -\frac{1}{n} e^{n(\xi_1 - \xi)} \sin n(\eta_1 - \eta) + \frac{1}{n} e^{-n(\xi_1 + \xi)} \sin n(\eta_1 + \eta) + \frac{1}{n} e^{n(\xi_2 - \xi)} \sin n(\eta_2 - \eta) - \frac{1}{n} e^{-n(\xi_2 + \xi)} \sin n(\eta_2 + \eta) \right\}$$

After introducing the values

$$\zeta_1 = \xi_0 + i\frac{\pi}{2}$$

$$\zeta_2 = \xi_0 + i\frac{3\pi}{2}$$

the foregoing reduces finally to

$$X_1 = -\frac{2Fc}{\pi} \left\{ \sinh \xi_0 \cosh \xi e^{-\xi} - \cosh \xi \sum_{n=2,\,4\ldots}^{\infty} (-1)^{n/2} \left[\frac{\sinh (n-1)\xi_0 e^{-(n-1)\xi}}{n-1} - \frac{\sinh (n+1)\xi_0 e^{-(n+1)\xi}}{n+1} \right] \cos n\eta \right\} \quad [24]$$

The stresses σ_ξ, $\tau_{\xi\eta}$ are now derived from X_1 and evaluated on the ellipse $\xi = \xi_0$. General expressions for stresses in terms of orthogonal curvilinear co-ordinates are as follows (11)

$$\sigma_\xi = \frac{1}{J^2} \frac{\partial^2 X}{\partial \eta^2} + \frac{1}{J^3} \left(\frac{\partial X}{\partial \xi} \frac{\partial J}{\partial \xi} - \frac{\partial X}{\partial \eta} \frac{\partial J}{\partial \eta} \right)$$

$$\sigma_\eta = \frac{1}{J^2} \frac{\partial^2 X}{\partial \xi^2} + \frac{1}{J^3} \left(\frac{\partial X}{\partial \eta} \frac{\partial J}{\partial \eta} - \frac{\partial X}{\partial \xi} \frac{\partial J}{\partial \xi} \right)$$

$$\tau_{\xi\eta} = -\frac{1}{J^2} \frac{\partial^2 X}{\partial \xi \partial \eta} + \frac{1}{J^3} \left(\frac{\partial X}{\partial \xi} \frac{\partial J}{\partial \eta} + \frac{\partial X}{\partial \eta} \frac{\partial J}{\partial \xi} \right)$$

The quantities J, ϕ are the so-called stretch and rotation factors, defined by the relation

$$dz = \left(\frac{dz}{d\zeta} \right) d\zeta = (Je^{i\phi}) d\zeta$$

In the case of elliptic co-ordinates

$$\frac{dz}{d\zeta} = c \sinh \zeta = c \sinh (\xi + i\eta)$$

$$J^2 = \frac{c^2}{2} (\cosh 2\xi - \cos 2\eta)$$

$$\tan \phi = \tan \eta \cot \xi$$

In elliptic co-ordinates, the stresses are given by

$$\left.\begin{aligned} \frac{2}{c^2} J^4 \sigma_\xi &= (\cosh 2\xi - \cos 2\eta) \frac{\partial^2 X}{\partial \eta^2} + \sinh 2\xi \frac{\partial X}{\partial \xi} - \sin 2\eta \frac{\partial X}{\partial \eta} \\ \frac{2}{c^2} J^4 \sigma_\eta &= (\cosh 2\xi - \cos 2\eta) \frac{\partial^2 X}{\partial \xi^2} - \sinh 2\xi \frac{\partial X}{\partial \xi} + \sin 2\eta \frac{\partial X}{\partial \eta} \\ \frac{2}{c^2} J^4 \tau_{\xi\eta} &= -(\cosh 2\xi - \cos 2\eta) \frac{\partial^2 X}{\partial \xi \partial \eta} + \sinh 2\xi \frac{\partial X}{\partial \eta} + \sin 2\eta \frac{\partial X}{\partial \xi} \end{aligned}\right\} \quad [25]$$

The stresses on the ellipse ξ_0, derived from the concentrated force functions are as follows

$$\frac{2\pi}{Fc^2} J^4 (\sigma_\xi)_{\xi_0} = -\frac{1}{2} (e^{\xi_0} - 2e^{-3\xi_0} + e^{-7\xi_0}) - 4 \cosh^3 \xi_0 \sum_{n=2,\,4\ldots}^{\infty} (-1)^{n/2} \cos n\eta + \sum_{n=2,\,4\ldots}^{\infty} (-1)^{n/2} e^{-2n\xi_0} \left\{ 2 \cosh \xi_0 + 3 \cosh 3\xi_0 - \cosh 7\xi_0 + n \left[-\frac{1}{2} \sinh \xi_0 + \sinh 5\xi_0 + \frac{1}{2} \sinh 7\xi_0 \right] \right\} \cos n\eta \quad [26a]$$

$$\frac{2\pi}{Fc^2} J^4 (\tau_{\xi\eta})_{\xi_0} = -2 \sinh \xi_0 \sinh 2\xi_0 \sin 2\eta$$

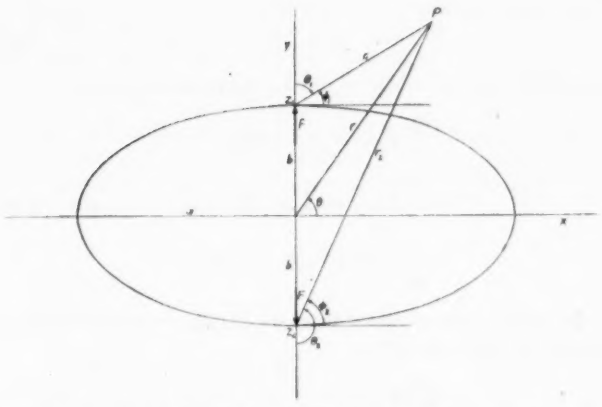


FIG. 13 INFINITE PLATE WITH ELLIPTICAL HOLE, FORCES APPLIED ALONG MINOR AXES OF ELLIPSE

$$+\sum_{n=2,4..}^{\infty}(-1)^{n/2}e^{-2n\xi_0}\left\{3\cosh 3\xi_0-\cosh 5\xi_0-2\cosh 7\xi_0 +n\left[-\frac{1}{2}\sinh\xi_0+\sinh 5\xi_0+\frac{1}{2}\sinh 7\xi_0\right]\right\}\sin n\eta \quad [26b]$$

As a check on these results, we note that in the limit as $\xi_0 \to \infty$, $c \to 0$ so that $a = b = \frac{1}{2}ce^{\xi_0}$, the ellipse reduces to a circle of radius r_0, and the stresses $(\sigma_\xi)_{\xi_0}$, $(\tau_{\xi\eta})_{\xi_0}$ should reduce to those on a circle of radius r_0 produced by a pair of forces at the ends of a diameter. For all points on the circle, except the load points, where the stresses are not defined, these stresses are as follows

$$(\sigma_r)_{r_0} = \frac{F}{\pi}\frac{1}{r_0}$$

$$(\tau_{r\theta})_{r_0} = 0$$

In Equations [26], in the limit as $\xi_0 \to \infty$, $c \to 0$, while $\left(\frac{1}{2}ce^{\xi_0} = r_0 = \text{const.}\right)$, we have first

$$\frac{\pi}{F}r_0^4(\sigma_\xi)_{\xi_0} = \frac{c^3e^{3\xi_0}}{4}\sum_{n=2,4..}^{\infty}(-1)^{n/2}\cos n\eta$$

$$\frac{\pi}{F}r_0^4(\tau_{\xi\eta})_{\xi_0} = 0$$

But it may be shown that for $\eta \neq \pi/2 \neq 3\pi/2$

$$\sum_{n=2,4..}^{\infty}(-1)^{n/2}\cos n\eta = -\frac{1}{2}$$

Hence the stresses on the ellipse ξ_0 reduce to the correct limiting values when the ellipse becomes a circle.

The boundary conditions which must be satisfied are as follows: (*a*) All stresses vanish at infinitely large distances from the hole; (*b*) at the elliptical edge $(\tau_{\xi\eta})_{\xi_0} = 0$ everywhere, while $(\sigma_\xi)_{\xi_0} = 0$ everywhere except at the load points $(\xi_0, \pi/2)$ and $(\xi_0, 3\pi/2)$; here $-(\sigma_\xi)_{\xi_0}$ is infinite in such a way that the resultant normal force on an arc passing through either of the load points is equal to $-F$. The required stress $(\sigma_\xi)_{\xi_0}$ may be expressed as a Fourier series. We obtain the series in the form

$$J^4\sigma_\xi = A_0 + \sum_{n=2,4..}^{\infty}A_n\cos n\eta$$

Using the conditions that $\sigma_\xi = 0$ everywhere except at $\eta = \pi/2$, $3\pi/2$, and that at these points

$$\int_{\pi/2-\epsilon}^{\pi/2+\epsilon}\sigma_\xi ds_\eta = -F, \qquad \int_{3\pi/2-\epsilon}^{3\pi/2+\epsilon}\sigma_\xi ds_\eta = -F$$

where ϵ is an arbitrary small positive number, and ds_η is an element of arc of the ellipse $\xi = \xi_0$

$$ds_\eta = cd\eta\sqrt{\cosh^2\xi_0\sin^2\eta+\sinh^2\xi_0\cos^2\eta}$$

We obtain, finally, for the required stresses on the ellipse ξ_0

$$\frac{2\pi}{Fc^3}J^4\sigma_\xi = -4\cosh^3\xi_0\left[\frac{1}{2}+\sum_{n=2,4..}^{\infty}(-1)^{n/2}\cos n\eta\right] \quad [27a]$$

$$\tau_{\xi\eta} = 0 \quad [27b]$$

These may be checked by evaluating the limiting case $\xi \to \infty$ $c \to 0$ so that $\frac{ce^{\xi_0}}{2} = r_0$. The foregoing reduces to

$$\sigma_\xi \to (\sigma_r)_{r_0} = -\frac{2F}{\pi r_0}\left[\frac{1}{2}+\sum_{2,4..}^{\infty}(-1)^{n/2}\cos n\eta\right]$$

This result, for the normal stresses on a circle of radius r_0 due to concentrated forces F at the ends of a diameter, agrees with that given by Filon (7).

We now have to determine the auxiliary stress function X' so that the complete solution yields the stresses of Equations [27]. Subtracting Equations [27] from [26], the following stresses must be annulled by the stress function X':

$$\left.\begin{aligned}\frac{2\pi}{Fc^3}J^4\sigma_\xi' = &-\frac{1}{2}(e^{\xi_0}-2e^{-3\xi_0}+e^{-7\xi_0})+2\cosh^3\xi_0\\ &+\sum_{n=2,4..}^{\infty}(-1)^{n/2}e^{-2n\xi_0}\left\{2\cosh\xi_0\right.\\ &+3\cosh 3\xi_0-\cosh 7\xi_0+n\left[-\frac{1}{2}\sinh\xi_0+\sinh 5\xi_0\right.\\ &\left.\left.\left.+\frac{1}{2}\sinh 7\xi_0\right]\right\}\cos n\eta\end{aligned}\right\} \quad [28a]$$

$$\left.\begin{aligned}\frac{2\pi}{Fc^3}J^4\tau_{\xi\eta}' = &-2\sinh\xi_0\sinh 2\xi_0\sin 2\eta\\ &+\sum_{n=2,4..}^{\infty}(-1)^{n/2}e^{-2n\xi_0}\left\{3\cosh 3\xi_0-2\cosh 7\xi_0\right.\\ &-\cosh 5\xi_0+n\left[-\frac{1}{2}\sinh\xi_0+\sinh 5\xi_0\right.\\ &\left.\left.\left.+\frac{1}{2}\sinh 7\xi_0\right]\right\}\sin n\eta\end{aligned}\right\} \quad [28b]$$

The typical harmonic solutions, i.e., solutions of

$$\nabla^2\phi = \frac{\partial^2\phi}{\partial\xi^2}+\frac{\partial^2\phi}{\partial\eta^2} = 0$$

are $\phi = e^{\pm a\xi} \cos a\eta$, $e^{\pm a\xi} \sin a\eta$ where a is a constant. The general biharmonic solution is made up of harmonic functions, together with biharmonic functions $x\phi$, $y\phi$. The typical biharmonic solutions in elliptic co-ordinates are easily obtained by substituting the appropriate expressions for x and y (11).

Of the eight characteristic harmonic and biharmonic solutions, only the following yield stresses of proper symmetry in the present problem

$$\phi = Ae^{-n\xi} \cos n\eta \quad \ldots\ldots\ldots\ldots\ldots [29a]$$

$$X = B[e^{-(n+2)\xi} \cos n\eta + e^{-n\xi} \cos (n+2)\eta] \quad \ldots\ldots [29b]$$

where A, B are arbitrary constants, and n is an even integer.

Using Equations [25], these functions yield stresses as follows

$$\left.\begin{aligned}\frac{2}{c^2} J^4 e^{n\xi} \sigma_\xi = &\left[A\frac{n(n-1)}{2} + B\frac{n(n+1)}{2} e^{-2\xi}\right] \cos (n-2)\eta + \left\{-A(n^2 \cosh 2\xi + n \sinh 2\xi)\right. \\ &+ B\left[\frac{(n+2)(n+3)}{2} - e^{-2\xi}(n^2 \cosh 2\xi \right. \\ &\left.\left. + (n+2) \sinh 2\xi)\right]\right\} \cos n\eta + \left\{A\frac{n(n-1)}{2}\right. \\ &+ B\left[\frac{n(n-1)}{2} e^{-2\xi} - (n+2)^2 \cosh 2\xi \right. \\ &\left.\left. - n \sinh 2\xi\right]\right\} \cos (n+2)\eta + B\frac{(n+2)(n+4)}{2} \\ &\cos (n+4)\eta\end{aligned}\right\} [30a]$$

$$\left.\begin{aligned}\frac{2}{c^2} J^4 e^{n\xi} \tau_{\xi\eta} = &\left[A\frac{n(n+1)}{2} + B\frac{(n+2)(n+1)}{2}\right. \\ &\left. e^{-2\xi}\right] \sin (n-2)\eta + \left\{-A(n^2 \cosh 2\xi + n \sinh 2\xi)\right. \\ &+ B\left[\frac{n(n+3)}{2} - e^{-2\xi} n(n+2) \cosh 2\xi \right. \\ &\left.\left. - e^{-2\xi} n \sinh 2\xi\right]\right\} \sin n\eta + \left\{A\frac{n(n-1)}{2}\right. \\ &+ B\left[\frac{(n+2)(n-1)}{2} e^{-2\xi} - n(n+2) \cosh 2\xi \right. \\ &\left.\left. - (n+2) \sinh 2\xi\right]\right\} \sin (n+2)\eta + B\frac{n(n+1)}{2} \\ &\sin (n+4)\eta\end{aligned}\right\} [30b]$$

$$\left.\begin{aligned}\frac{2}{c^2} J^4 e^{n\xi} \sigma_\eta = &\left[-A\frac{n(n+1)}{2} - B\frac{(n+4)(n+1)}{2}\right. \\ &\left. e^{-2\xi}\right] \cos (n-2)\eta + \left\{A(n^2 \cosh 2\xi + n \sinh 2\xi)\right. \\ &+ B\left[-\frac{n^2+n+2}{2} + e^{-2\xi}(n+2) \sinh 2\xi \right. \\ &\left.\left. + e^{-2\xi}(n+2)^2 \cosh 2\xi\right]\right\} \cos n\eta \\ &+ \left\{-A\frac{n(n-1)}{2} + B\left[-\frac{n^2+3n+4}{2} e^{-2\xi}\right.\right. \\ &\left.\left. + n^2 \cosh 2\xi + n \sinh 2\xi\right]\right\} \cos (n+2)\eta \\ &- B\frac{(n-2)(n+1)}{2} \cos (n+4)\eta\end{aligned}\right\} [30c]$$

The special solution

$$X = A_0\xi \quad \ldots\ldots\ldots\ldots\ldots [31]$$

also yields stresses of the required symmetry as follows

$$\left.\begin{aligned}\frac{2}{c^2} J^4 \sigma_\xi &= A_0 \sinh 2\xi \\ \frac{2}{c^2} J^4 \tau_{\xi\eta} &= A_0 \sin 2\eta \\ \frac{2}{c^2} J^4 \sigma_\eta &= -A_0 \sinh 2\xi\end{aligned}\right\} \quad \ldots\ldots\ldots\ldots [32]$$

In order to annul the stresses on the ellipse ξ_0 expressed by Equations [28], we take

$$\frac{\pi}{Fc} X' = A_0\xi + \sum_{n=2,4,\ldots}^{\infty} \left\{A_n e^{-n\xi} \cos n\eta + B_n[e^{-n\xi} \cos (n-2)\eta + e^{-(n-2)\xi} \cos n\eta]\right\} [33]$$

The constants A_0, A_n, B_n are determined by solving simultaneously the infinite number of equations which express the conditions that the stresses of Equations [28] are annulled, term by term. These equations are of the type

$$a_n A_{n-2} + b_n A_n + c_n A_{n+2} + d_n B_{n-4} + e_n B_{n-2} + f_n B_n + g_n B_{n+2} = -q_n$$

$$a_n A_{n-2} + b_n A_n + c_n A_{n+2} + d_n' B_{n-4} + e_n' B_{n-2} + f_n' B_n + g_n' B_{n+2} = -q_n'$$

where $a_n \ldots$, $b_n \ldots$, etc., are constants for a given ellipse, i.e. for a given value of ξ_0, while q_n, q_n' are the coefficients of the nth terms in the series for σ_ξ'', $\tau_{\xi\eta}''$ given by Equations [28].

In the numerical evaluation of the constants, the following method of successive approximations has been found successful: The terms for $n = 0, 2$ of Equation [33] are first used as a partial stress function X_1', and evaluated so that the terms in $n = 0, 2$ of Equations [28] are removed. The stress function X_1', containing three constants A_0', A_2', B_2' determined in this way, contributes new stresses proportional to $\cos 4\eta$, $\sin 4\eta$. Next, a partial stress function X_2' is used, consisting of the terms for $n = 4$ of Equation [33], and constants A_4', B_4' evaluated so as to cancel the total stresses proportional to $\cos 4\eta$, $\sin 4\eta$ due both to the original system of stresses to be annulled, and to the partial stress function X_1'. The second stress function X_2', however, contributes new stresses of order $n = 0, 2, 6$. Further partial stress functions X_3', $X_4' \ldots$ are next evaluated so as to cancel, successively, the terms in 6η, 8η, ... The system of functions X_1', $X_2' \ldots$ replaces the original stresses which were to be annulled with a new set of stresses which, because of the numerical relationships of the terms of the general solutions, Equations [30] and [32], are smaller than the original values. By repeating this process, the "residual" stresses may be reduced to any desired values. The required auxiliary stress function is the sum of all the partial stress functions evaluated in this manner.

Calculations have been made for two ellipses, having $\xi_0 = 0.5$, 0.25, respectively (corresponding to minor and major axes in the ratios $b/a = \tanh \xi_0 = 0.462$, 0.245, respectively). The important stresses, (aside from those at the load points, which are not defined in the present analysis), are the tensile stresses σ_η, on the line $y = 0$ (coinciding with the major axis of the ellipse). These stresses are shown in Fig. 14, together with the corresponding stresses for a circle of radius a equal to the semimajor axis of the ellipses.

The complete solution for the case of a circular hole in an infinite plate, loaded by two forces at the ends of a diameter, (or by any number of concentrated forces placed symmetrically around the circle), is given in Appendix 2. It has been verified that the areas under the curves in Fig. 14, converted to proper units, have the value $F/2$, within the accuracy of the plots. The curves indicate that these tensile stresses are sharply localized near the ends of the major axis of the ellipse, and that their maximum value increases rapidly as the ellipse becomes flatter.

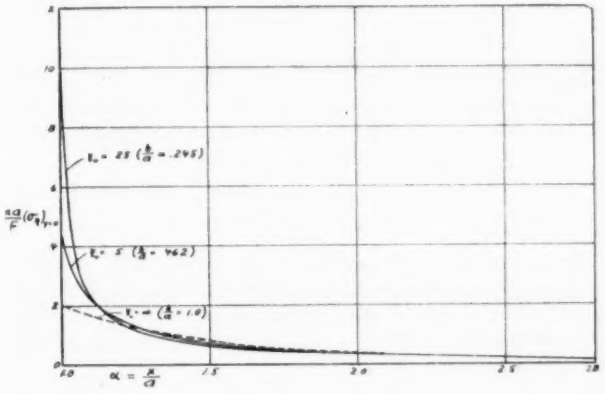


FIG. 14 TENSILE STRESSES $\frac{\pi a}{F}(\sigma_\eta)_{\eta=0}$ ALONG LINE OF MAJOR AXIS OF ELLIPSE
(a = semimajor axis of ellipse.)

Fig. 15 is a plot of the maximum tensile stress as a function of the ratio b/a of the ellipse. However, the present method cannot be applied easily when the ellipse is very flat, corresponding to ξ_0 much less than about 0.25, since the series (Equations [28]), expressing the stresses to be annulled, then decrease very slowly, and the numerical solution becomes extremely laborious. The solution in its present form is therefore not suitable for investigating the limiting case when the ellipse is narrowed to a line or "crack."

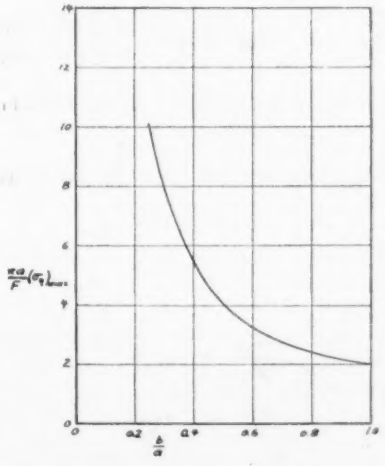


FIG. 15 VARIATION OF MAXIMUM TENSILE STRESS WITH b/a = RATIO OF MAJOR TO MINOR AXIS OF ELLIPSE

In conclusion, it may be noted that problems of concentrated moments could be treated in the same general manner as those of concentrated forces. It may be readily verified that the functions expressing the singularities are

$$\text{(Transverse bending)} \quad w = \frac{M}{4\pi D} r \log r \cos\theta$$

$$\text{(Plane stress or strain)} \quad X = \frac{M}{2\pi}\theta$$

These are analogous to Equations [2] and [3], respectively. Moreover, the solutions obtained for concentrated forces yield those for concentrated moments by differentiation. For example, the solution of the infinite-plate problem, Equation [10], may be written as

$$w = F\phi(a)$$

where a is the radial co-ordinate of the load point. Then the corresponding solution for a moment M is

$$w = \lim_{\substack{\epsilon \to 0 \\ F\epsilon \to M}} \left\{ F\phi(a+\epsilon) - F\phi(a) \right\} = M \frac{\partial \phi}{\partial a}$$

ACKNOWLEDGMENT

The author wishes to express his appreciation to Prof. J. N. Goodier of Cornell University for suggesting these problems and for invaluable aid in their solution.

BIBLIOGRAPHY

1 "A Treatise on the Mathematical Theory of Elasticity," by A. E. H. Love, Cambridge University Press, London, England, Fourth edition, 1927, chapt. 22.
2 "Theory of Plates and Shells," by S. P. Timoshenko, McGraw-Hill Book Company, Inc., New York, N. Y., 1941, chapt. 4.
3 "Elementary Distributions of Plane Stress," by J. H. Michell, Proceedings of the London Mathematical Society, vol. 32, 1900, p. 35.
4 "On the Direct Determination of Stress in an Elastic Solid, With Application to the Theory of Plates," by J. H. Michell, Proceedings of the London Mathematical Society, vol. 31, 1899, p. 100.
5 "Stresses in a Plate Due to the Presence of Cracks and Sharp Corners," by C. E. Inglis, Trans. Institution of Naval Architects, London, 1913, part 1.
6 "Two-Dimensional Elasticity in Bipolar Co-Ordinates," by G. B. Jeffery, *Philosophical Transactions* of the Royal Society, vol. 221A, 1921, p. 265.
7 "The Stresses in a Circular Ring," by L. N. G. Filon, The Institution of Civil Engineers, England, selected papers, 1924, No. 12.
8 Reference (2), p. 266.
9 "The Flexure of a Circular Plate," by J. H. Michell, Proceedings of the London Mathematical Society, vol. 34, 1902, p. 223.
10 "Über die Unsymmetrische Biegung dünner Kreisringplatten," by H. Reissner, *Ingenieur Archiv*, vol. 1, 1929, p. 72.
11 "A Treatise on Photoelasticity," by E. G. Coker and L. N. G. Filon, Cambridge University Press, London, England, 1931, p. 538.

Appendix 1

The following is a solution, based on the transformation of inversion, of the problem of a large plate clamped at a circular edge and acted on by a concentrated transverse force at any point. The inversion transformation is a conformal transformation defined by the equation

$$z' = \frac{a^2}{z}$$

where

$$z' = x' + iy' = r'e^{i\theta'}, \; z = x + iy = re^{i\theta}$$

and a (the "radius of inversion") is a real number. It is seen that the transformation consists of an "inversion" of the modulus, $r' = a^2/r$, plus a reflection about the real axis.

The properties of this transformation which are useful in the present problem are the following: If X is a biharmonic function in the r,θ-plane, then r'^2X is biharmonic in the r', θ' plane. Thus

w is a deflection function in the r,θ-plane, r'^2w is a deflection function in the r',θ'-plane. The slopes in the r',θ'-plane are equal to

$$\frac{\partial}{\partial r'}(r'^2w) = \frac{2a^2}{r}w - \frac{a^4}{r^4}\frac{\partial w}{\partial r}$$

$$\frac{1}{r'}\frac{\partial}{\partial \theta'}(r'^2w) = \frac{a^2}{r}\frac{\partial w}{\partial \theta}$$

Hence a boundary along which $w = \dfrac{\partial w}{\partial r} = \dfrac{1}{r}\dfrac{\partial w}{\partial \theta} = 0$ (i.e., a clamped edge), in the r,θ-plane, transforms into a clamped edge in the r',θ'-plane.

Another useful property of the transformation is the fact that circles transform into circles. In particular, a circle in the z-plane with center on the real axis, distance c from the origin and having a radius b, transforms into a circle in the z'-plane whose corresponding values are

$$c' = [a^2/(c^2 - b^2)]c,\ b' = [a^2/(c^2 - b^2)]b$$

For example, when the circle passes through the origin ($c = b$), it transforms into a straight line. Again, if $a^2 = c^2 - b^2$, the circle inverts into itself. Michell (9) obtained in this way the solution for the deflection of a clamped circular plate loaded by a concentrated normal force at an arbitrary point. A second inversion leads to the solution of the present problem.

Michell's solution utilizes the following result for the deflection of a clamped circular plate loaded by a central force

$$w = \frac{F}{8\pi D}\left[r^2 \log \frac{r}{b} + \frac{1}{2}(b^2 - r^2)\right]$$

The inversion is performed with respect to a point 0 outside the plate, so that $R' = a^2/R$, where R, R' are distances from 0 to points P, P', respectively (see Fig. 16). Taking $a^2 = b^4/e^2 - b^2$, $c = b^2/e$, the following result is obtained for the deflection of a clamped circular plate loaded by a force F at a distance e from the center of the circle

$$w = \frac{F}{8\pi D}\left[p^2 \log \frac{pb}{R'e} + \frac{1}{2}\left(\frac{R'^2e^2}{b^2} - p^2\right)\right]$$

where the co-ordinates p, R' are as shown in Fig. 16.

If we now perform a second inversion, this time taking the center of the circle 0 as the center of inversion (see Fig. 17), and the radius of inversion equal to the radius b of the circle, then the area within the circle transforms to the infinite area outside the circle. The load point F transforms to F' at distance a from 0, while P transforms to P' at distance r from 0, where $a = b^2/e$, $r = b^2/r'$. Since in the previous transformation c was equal to b^2/e, we have now $a = c$, so that $F'P = R'$. Thus we now have the case of an infinite plate clamped at a circle of radius b and loaded at distance a from the center. Using the relations

$$p^2 = \frac{b^4}{r^2} + \frac{b^4}{a^2} - \frac{2b^4}{ra}\cos\theta$$

$$R'^2 = \frac{b^4}{r^2} + a^2 - \frac{2b^2a}{r}\cos\theta$$

and changing to the dimensionless variables $\rho = r/b$, $q = a/b$

$$w = \frac{Fb^2}{16\pi D}\left[(q^2 + \rho^2 - 2q\rho\cos\theta)\log\frac{q^2 + \rho^2 - 2q\rho\cos\theta}{1 + q^2\rho^2 - 2q\rho\cos\theta} + (q^2 - 1)(\rho^2 - 1)\right]$$

This result satisfies the conditions at the clamped edge, and gives the necessary singularity at the load point. However, the conditions required at the outer free edge are not satisfied, since the foregoing solution leads to a uniform bending moment at large values of ρ, equal to

$$M_r = M_\theta = \frac{F}{8\pi D}(1 + \nu)(q^2 - 1 - 2\log q)$$

This bending moment can be removed by adding a function w' such that

$$\frac{\partial w'}{\partial \rho} = \frac{Fb^2}{16\pi D}\left[-2\rho(q^2 - 1 - 2\log q)\right] + \frac{c_1}{\rho}$$

$$w' = \frac{Fb^2}{16\pi D}\left[-\rho^2(q^2 - 1 - 2\log q) + c_1\log\rho + c_2\right]$$

Evaluating the constants C_1, C_2 so that the conditions at the clamped edge are satisfied, we obtain, finally

$$w = \frac{Fb^2}{8\pi D}\left\{\frac{1}{2}(q^2 + \rho^2 - 2q\rho\cos\theta)\log\frac{q^2 + \rho^2 - 2q\rho\cos\theta}{1 + q^2\rho^2 - 2q\rho\cos\theta} + (q^2 - 1)\log\rho + (\rho^2 - 1)\log q - 2\log q\log\rho\right\}$$

This is the result, Equation [10], found by the series-expansion method.

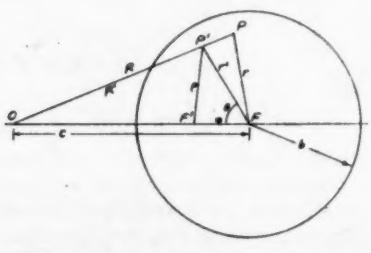


FIG. 16 CIRCULAR PLATE CLAMPED AT $r = b$: INVERSION TO OBTAIN DEFLECTION DUE TO NONCENTRAL FORCE

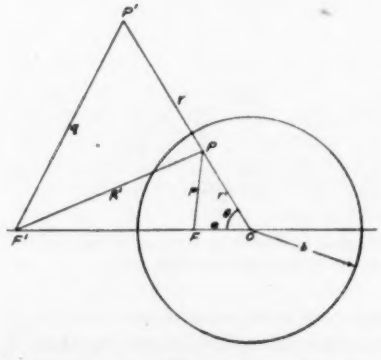


FIG. 17 INFINITE PLATE CLAMPED AT $r = b$: INVERSION TO OBTAIN DEFLECTION DUE TO FORCE AT ARBITRARY POINT OF PLATE

Appendix 2

Problems in which any number of equal concentrated forces are placed symmetrically around the edge of a circular hole in an infinite plate (the forces lying in the plane of the plate and acting normal to the edge) have simple solutions in finite form. If the stress functions for the simple radial stress distribution are added, for the given arrangement of forces, the shear stress on the load circle is found to be zero, owing to the symmetry of loading. The normal stress on the load circle due to the combination of simple radial distributions is easily shown to be given by $\sigma_0 = nF/\pi d$ where n is the number of symmetrically disposed forces each equal to F, and d is the diameter of the hole.

This uniform tensile stress may be annulled by adding the stress distribution corresponding to the stress function $X' = A \log r$, namely

$$\sigma_r' = Ar^{-2} \qquad \tau_{r'\theta} = 0 \qquad \sigma_\theta' = -Ar^{-2}$$

where r is distance measured from the center of the hole. In the case of two forces at the ends of a diameter (a limiting case of the elliptical-hole problem previously solved), we have $\sigma_0 = 2F/\pi d = F/\pi r_0$ (where r_0 is the radius of the hole), and $A = -Fr_0/\pi$. In terms of x, y co-ordinates, taken as shown in Fig. 13 of the paper, the stresses on the line $y = 0$ are given by

$$(\sigma_y)_{y=0} = \frac{4F}{\pi} \frac{r_0^3}{(x^2 + r_0^2)^2} + \frac{Fr_0}{\pi} \frac{1}{x^2}$$

$$(\sigma_x)_{y=0} = \frac{4F}{\pi} \frac{r_0 x^2}{(x^2 + r_0^2)^2} - \frac{Fr_0}{\pi} \frac{1}{x^2}$$

The maximum tensile stress (at $x = r_0$) is $(\sigma_y)_{r_0} = 2F/\pi r_0$. Similar results are easily obtained for any other number of symmetrical forces.

Buckling Under Locally Hydrostatic Pressure

By G. H. HANDELMAN,[1] PROVIDENCE, R. I.

The instability of a simple pin-supported beam when subject to a locally hydrostatic pressure distribution, the intensity of which is a function of distance along the beam only, is discussed in this paper. In particular, the pressure is assumed to follow a polynomial law given by Equation [1]. The problem, basic assumptions, and precise definition of locally hydrostatic pressure are stated in the first section of the paper. The second section contains a discussion of the equations of equilibrium from which the basic differential equation is derived. The solutions of this differential equation satisfy the boundary conditions only for certain discrete values of the parameters involved, and these values in turn define the buckling loads. In the third section the buckling loads are tabulated for several cases in comparison with the buckling loads for the same beam subject only to an end thrust. The appendix contains a mathematical discussion of the solution of the basic differential equation and a derivation of the formula for the buckling loads.

Introduction

AMONG the various types of loading of a simple beam with pin ends which might produce instability, the case of loading by locally hydrostatic pressure does not appear to have been discussed. By a locally hydrostatic pressure distribution is meant one in which the intensity of the pressure is a function of the distance along the center line of the beam only. Such a distribution is a generalization of the linear pressure distribution which arises when a prismatic bar is placed vertically in a heavy liquid. This paper is concerned, then, with the buckling of a thin, uniform, prismatic beam with pin supports under such a loading.

Let the origin of co-ordinates be taken at one of the pin supports, the x-axis directed along the undeformed center line of the beam, and the y-axis vertically upward as shown in Fig. 1. The length of the beam is denoted by l and the area of the cross section is A. The pressure distribution $p(x)$ is assumed to be given by the following law

$$p(x) = p_0\left[1 - k\left(\frac{x}{l}\right)^m\right] \quad \ldots\ldots\ldots\ldots [1]$$

where p_0 is the head pressure, the pressure at $x = 0$, m is non-negative, and k is a constant with values in the range 0 to 1. When $m = 1$, Equation [1] reduces to the linear case mentioned.

As indicated by the choice of co-ordinate axes in Fig. 1, the slider is assumed to be at the high-pressure end of the beam ($x = 0$). It will be shown in a later section that if the role of slider and simple pin support are reversed buckling cannot occur.

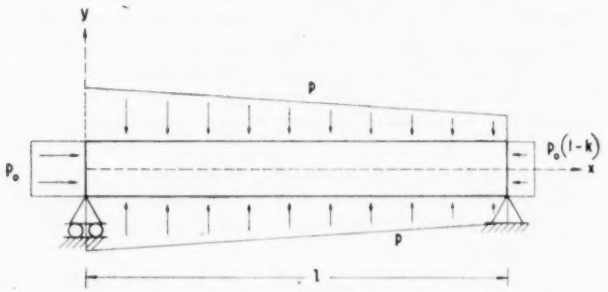


FIG. 1 PRESSURE DISTRIBUTION FOR $m = 1$, $k = \frac{1}{2}$

Equations of Equilibrium

Consider a small element in the deformed state subject only to a pressure distribution of the locally hydrostatic type, Fig. 2. Since the element is small, the variation of the pressure along the portion of the center line considered, ds, can be neglected. The element would be in equilibrium if additional uniform pressure distributions p were added to the faces as shown in Fig. 2. Since these additional pressures are not present, the resultant

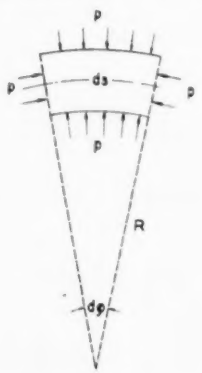


FIG. 2

force produced by the pressure which does occur must be equal in magnitude and opposite in direction to that produced by the added pressure. The face pressures are equivalent to a force pA, acting normal to each of the two cross sections which bound the element; and these forces have a resultant $pAd\varphi = pAds/R$ acting along the normal to the center line in the direction of the convex side (R is the radius of curvature of the center line). Consequently, the pressure distribution which does act on the wedge has a resultant of magnitude $pA\ ds/R$ directed along the normal to the center line pointing toward the concave side.

The equilibrium conditions for an element of the beam under the complete system of forces acting can now be set up under the assumption that the deflection, $y = y(x)$, is small. On the basis of the result just obtained the element is subject to a restoring force $pA\ ds/R = -pA\ d^2y/dx^2$, for small deflections, acting in the negative y-direction as well as internal shear forces, S, pulls P, and bending moments M, as shown in Fig. 3. The equilibrium condition for components in the horizontal direction is

$$dP = 0 \quad \text{or} \quad P = \text{const} \ldots\ldots\ldots\ldots [2]$$

---

[1] Research Associate in Applied Mathematics, Brown University.

Presented at the National Meeting of the Applied Mechanics Division, Buffalo, N. Y., June 21–22, 1946, of THE AMERICAN SOCIETY OF MECHANICAL ENGINEERS.

Discussion of this paper should be addressed to the Secretary, A.S.M.E., 29 West 39th Street, New York, N. Y., and will be accepted until October 10, 1946, for publication at a later date. Discussion received after the closing date will be returned.

NOTE: Statements and opinions advanced in papers are to be understood as individual expressions of their authors and not those of the Society.

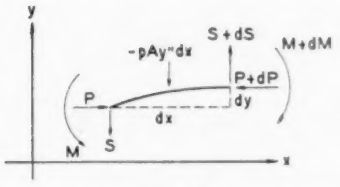


FIG. 3

The components in the vertical direction must satisfy the equation

$$S - pAy''dx = S + dS$$

or

$$S' = -pAy'' \quad \ldots\ldots [3]$$

where $S' = dS/dx$. Finally, the moment equation reduces to

$$Pdy + Sdx = dM$$

provided that terms of higher order are neglected. This last equation may be rewritten as

$$Py' + S = M' \quad \ldots\ldots [4]$$

Equation [4] can be simplified by differentiating with respect to the independent variable x and taking into account Equations [2] and [3], that is

$$M'' - (P - pA)y'' = 0 \quad \ldots\ldots [5]$$

Now the bending moment M and the deflection y are connected by the usual Euler-Bernoulli law for small deflections

$$\frac{M}{EI} = -y''$$

where E is Young's modulus and I is the polar moment of inertia of the cross section taken about an axis passing through the centroid and perpendicular to the plane of bending. Thus Equation [5] can be written in such a way that the bending moment M is the only dependent variable

$$M'' + (P - pA)\frac{M}{EI} = 0 \quad \ldots\ldots [6]$$

In addition, the boundary conditions for pin supports (namely, the vanishing of the bending moment at both ends) must be added, that is

$$M(0) = M(l) = 0 \quad \ldots\ldots [7]$$

The pressure p has been assumed to follow the law given in Equation [1], and this must be inserted in Equation [6]. For the slider at $x = 0$, $P = p_0A$, therefore

$$P - pA = kp_0A\left(\frac{x}{l}\right)^m = kP\left(\frac{x}{l}\right)^m$$

and Equation [6] becomes

$$M'' + \frac{kP}{EI}\left(\frac{x}{l}\right)^m M = 0 \quad \ldots\ldots [8]$$

CALCULATION OF CRITICAL PRESSURE

The differential equation for the bending moment, Equation [8], can be integrated in terms of Bessel functions. Since the equation is homogeneous, solutions cannot be determined which will satisfy the boundary conditions, Equation [7], for all values of the parameter P. The smallest nonvanishing value P for which solutions of the boundary-value problem do exist defines the critical pressure. The general solution of Equation [8] together with a discussion of the boundary conditions is given in the Appendix. It will be shown there that the critical end force P_{cr} is given by the formula

$$P_{cr} = \frac{(m+2)^2\,\xi_m^2}{4k} \cdot \frac{EI}{l^2} \quad \ldots\ldots [9]$$

where ξ_m is the first nonvanishing zero of the Bessel function of first kind of order $1/(m+2)$, $J_{1/(m+2)}(\xi)$.

The critical head pressure, p_{0cr}, can be found by noting that $p_{0cr} = P_{cr}/A$; thus

$$p_{0cr} = \frac{(m+2)^2\xi_m^2}{4k} \cdot \frac{E}{(l/\kappa)^2}$$

where κ is the radius of gyration of the cross section.

In the case of a simply supported beam subject to an end force $\bar{P}$, the first buckling load is known to be given by $\bar{P}_{cr} = \pi^2EI/l^2$. Buckling under locally hydrostatic pressure can be compared with this simple case by means of an equivalence factor e defined as

$$e = \frac{\bar{P}_{cr}}{P_{cr}} = \frac{4k\pi^2}{(m+2)^2\xi_m^2}$$

This factor is plotted in Fig. 4 as a function of m for various values of the parameter k. Since the coefficient of pressure decrease k enters linearly, e can be found for values of k other than those given by multiplying the results for $k = 1$ by the desired value of k. Since $\xi_0 = \pi$, the equivalence factor for $k = 1$

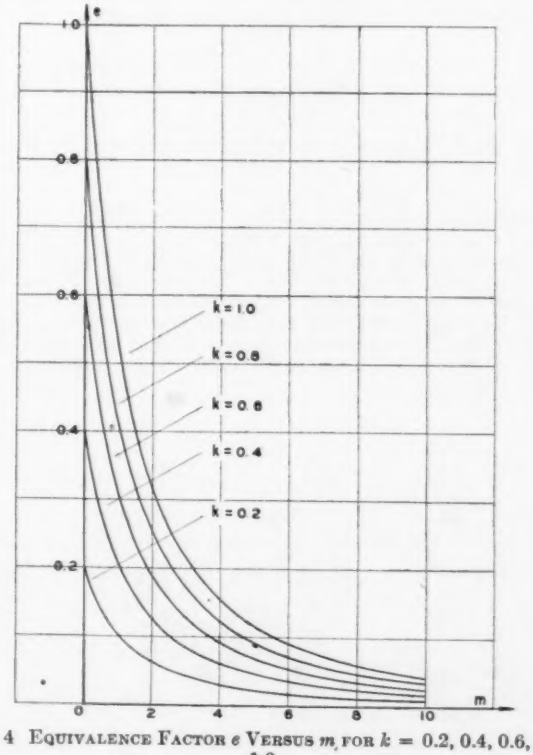


FIG. 4 EQUIVALENCE FACTOR e VERSUS m FOR $k = 0.2, 0.4, 0.6, 0.8, 1.0$

$m = 0$, reduces[2] to 1, that is, for this limiting case the critical end load is simply the classical Euler load as one would expect.

It should be noted that in the case of a constant pressure dis-

[2] "Tables of Functions With Formulas and Curves," by E. Jahnke and F. Emde, Dover Publications, New York, N. Y., 1943, p. 167.

tribution, $k = 0$, the bar cannot buckle. This result may be read from Equation [9] or found directly by considering the differential equation and boundary conditions.

In case the slider is at the low-pressure end of the beam, $x = l$, the condition $P = p_0A$ must be replaced by $P = p_0A(1 - k)$. Then

$$P - pA = p_0Ak\left[\left(\frac{x}{l}\right)^m - 1\right]$$

and the differential Equation [8] must be replaced by

$$M'' + \frac{kAp_0}{EI}\left[\left(\frac{x}{l}\right)^m - 1\right]M = 0 \quad \ldots\ldots\ldots [10]$$

Now the function

$$\frac{kAp_0}{EI}\left[\left(\frac{x}{l}\right)^m - 1\right] \leqq 0$$

for $0 \leqq x \leqq l$. Equation [10] is a special case of the general Sturm-Liouville differential equation, the solutions of which have been studied extensively. In particular, it is known that if the coefficient of M is nonpositive in the interval $0 \leqq x \leqq l$, the solution can have but one zero in that interval.[3] Thus it is impossible to fulfill the boundary conditions $M(0) = M(l) = 0$ and buckling cannot take place.

ACKNOWLEDGMENT

The author wishes to express his appreciation to Prof. W. Prager of Brown University and to Prof. I. S. Sokolnikoff of the University of Wisconsin for many helpful suggestions.

Appendix

The general solution of the differential Equation [8] is of the form[4]

$$M = A\sqrt{x}\,J_{1/(m+2)}\left[\frac{2}{m+2}\sqrt{\frac{kP}{EIl^m}}\,x^{(m+2)/2}\right] + B\sqrt{x}\,J_{-1/(m+2)}\left[\frac{2}{m+2}\sqrt{\frac{kP}{EIl^m}}\,x^{(m+2)/2}\right]. \quad [11]$$

where $J_{1/(m+2)}(\xi)$ is the Bessel function of first kind of order $1/(m+2)$, $J_{-1/(m+2)}(\xi)$ is the Bessel function of first kind of order $-1/(m+2)$, and A and B are constants to be determined from the boundary conditions. Since $J_p(\xi)$ vanishes at $\xi = 0$ for $p > 0$, the first term of Equation [11] automatically fulfills the boundary condition $M(0) = 0$. The Bessel function of negative order $J_{-p}(\xi)$, $p > 0$, has a singularity at $\xi = 0$; it will be necessary to investigate this more closely. The following approximate formula[5] can be used to study the behavior of the Bessel function of negative order for $|\xi| \ll 1$

$$J_{-1/(m+2)}(\xi) = \frac{(1/2\xi)^{-1/(m+2)}}{\Gamma[1 + 1/(m+2)]}$$

where $\Gamma[1 + 1/(m+2)]$ is the gamma function evaluated for the argument $1 + 1/(m+2)$. Since this function does not vanish for $m \geqq 0$, $J_{-1/(m+2)}(\xi)$ behaves like $(2/\xi)^{1/(m+2)}$ near the origin. This result can be applied to the second term of Equation [11] to yield

$$\lim_{x\to 0}\sqrt{x}\,J_{-1/(m+2)}\left[\frac{2}{m+2}\sqrt{\frac{kP}{EIl^m}}\,x^{(m+2)/2}\right] = C\sqrt{x}\left[\frac{2}{x^{(m+2)/2}}\right]^{1/(m+2)} = \text{const} \neq 0$$

where C is a nonvanishing constant. Thus B must vanish if the first boundary condition is to be satisfied.

The second boundary condition $M(l) = 0$, will yield the desired critical value, for it requires that

$$J_{1/(m+2)}\left(\frac{2}{m+2}\,l\sqrt{\frac{kP}{EI}}\right) = 0$$

Let ξ_m be the first nonvanishing zero of $J_{1/(m+2)}(\xi)$, then the critical end force, P_{cr}, will be given by

$$\frac{2}{m+2}\cdot l\cdot\left(\frac{kP_{cr}}{EI}\right)^{1/2} = \xi_m \quad \text{or} \quad P_{cr} = \frac{(m+2)^2\,\xi_m^2}{4k}\cdot\frac{EI}{l^2}$$

[3] "Ordinary Differential Equations," by E. L. Ince, Dover Publications, New York, N. Y., 1944, p. 226.

[4] "Bessel Functions for Engineers," by N. W. McLachlan, Oxford University Press, 1934, ex. 47, p. 39. The solution given in the reference cited is written in terms of Bessel functions of first and second kind. This may be rewritten with Bessel functions of first kind of positive and negative order since $1/(m+2)$ is not an integer (ibid., p. 23). The succeeding argument is somewhat simplified by this substitution.

[5] Ibid., p. 158.

An Empirical Approach to the Fatigue-Strength Analysis of Structures

By HENRY W. FOSTER[1] and VICTOR SELIGER[1]

A method of fatigue-strength analysis for fabricated structures, based on laboratory fatigue-test data, is proposed in this paper. To this end the nature of structural fatigue strength is discussed with the view of defining the necessary correlating assumptions and the type of experimental data needed.

An example of this method is presented for structures fabricated from Alclad 24S-T aluminum alloy and analysis results are compared with actual test results.

Nomenclature

N = number of cycles of loading required to produce failure.
F_{tu} = ultimate tensile strength of material.
F_{tf} = fatigue strength of material in terms of maximum stress attained during a cycle.
F_{vf} = fatigue strength of material in terms of varying stress attained during a cycle.
f_{tf} = maximum stress in part, based on net area without regard to stress concentrations = average maximum stress.
f_{vf} = varying stress in part, based on net area without regard to stress concentrations = average varying stress.
R = ratio of minimum stress to maximum stress in a loading cycle.
K_t = elastic-stress-concentration factor.
K_f = effective stress-concentration factor in fatigue = F_{tf}/f_{tf}, for constant R on applied external loading.
K_m = ratio of effective maximum stress at stress raiser to average maximum stress across section.
K_v = ratio of effective varying stress at stress raiser to average varying stress across section.
f_t = $K_m f_{tf}$ = effective maximum stress developed at stress raiser.
f_v = $K_v f_{vf}$ = effective varying stress developed at stress raiser.
(g) = all stress values are calculated on the basis of net area except when subscript g is used denoting stress calculation of the basis of gross area.

Introduction

THE analysis of a structure for life expectancy may be divided into three practically independent problems: 1, The determination of the spectrum of external loading to which the structure will be subjected; 2, the determination of the fatigue strength of the structure under any given loading condition; and 3, the correlation of the expected loading with the fatigue strength of the structure. This paper deals with the second problem only, and presents a method for determining the fatigue strength of a fabricated structure from basic data which may be determined experimentally.

The fatigue strength of a structure is often regarded as if it were a quantity entirely separate from the static strength of the same structure. Actually, the strength of a structure is a function of the same variables whether it is defined for static failure in tension, i.e., one-half cycle at a range ratio of 0, or for any other one of the infinite number of ways in which it may be loaded. The importance of each of the variables of course does depend on which one of the ways of loading determines failure, but it should be emphasized that the strength of a structure is just as much an engineering quantity for one type of loading as for any other, and is just as susceptible to rational analysis. The fact that we do not know what causes fatigue failure need worry us no more than the fact that we do not know the mechanism by which static failure operates. We customarily use empirically determined constants as a basis for the design of structures for static strength, and there is no reason why experimentally determined constants cannot be used as the basis for a rational method of design for fatigue strength.

It is the purpose of this paper to discuss structural fatigue strength with the view to defining the nature of the experimental data and of the correlating assumptions which would permit the fatigue analysis of fabricated structures to be based on material properties obtainable in the laboratory.

The Definition of Fatigue Strength

Any fluctuating load possesses both maximum and minimum values, and two loading parameters must be used in combination with a number of cycles to define fatigue strength. These loading parameters must be chosen from among the following: maximum load, minimum load, mean load, or varying load, or any one of these may be combined with the dimensionless ratio of any two. For convenience, R, the ratio of minimum to maximum load in a loading cycle, has been used in combination with

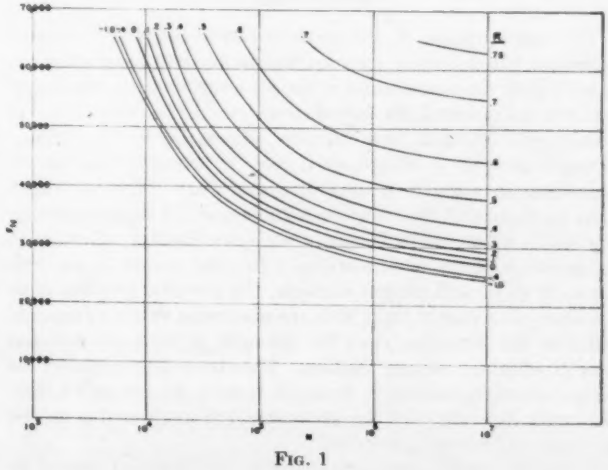


Fig. 1

[1] Research Engineers, Lockheed Aircraft Corporation, Burbank, Calif.

Contributed by the Applied Mechanics Division and presented at the Annual Meeting, New York, N. Y., Nov. 26–29, 1945, of The American Society of Mechanical Engineers.

Discussion of this paper should be addressed to the Secretary, A.S.M.E., 29 West 39th Street, New York, N. Y., and will be accepted until October 10, 1946, for publication at a later date. Discussion received after the closing date will be returned.

Note: Statements and opinions advanced in papers are to be understood as individual expressions of their authors and not those of the Society.

the maximum load in presenting a great deal of experimental fatigue-strength data, and must be brought into any review of data. A family of R curves defining the fatigue strength of Alclad 24S-T sheet is shown as Fig. 1. There is, however, an inherent disadvantage in this method of presentation in that it precludes explicit definition of the varying load, the only load which can repeatedly perform work on the material. It tends, upon cursory inspection of data, to lay undue emphasis on the value of the maximum load as it would indicate an increase in allowable maximum load with increasing R even if the fatigue strength of the material were independent of the maximum load. This fact is important since, as will be seen later, it affects certain other parameters which have been defined in terms of R.

A much more direct and descriptive set of parameters for the definition of a repeated loading condition is the combination of varying with maximum load in a loading cycle. In such a way a true physical picture of the loading cycle is presented, for the varying load defines the magnitude of the variation of load in a cycle, and the maximum load defines the level at which the variation of loading takes place. In Fig. 2 the curves of Fig. 1 are replotted to show the fatigue strength of Alclad 24S-T sheet on

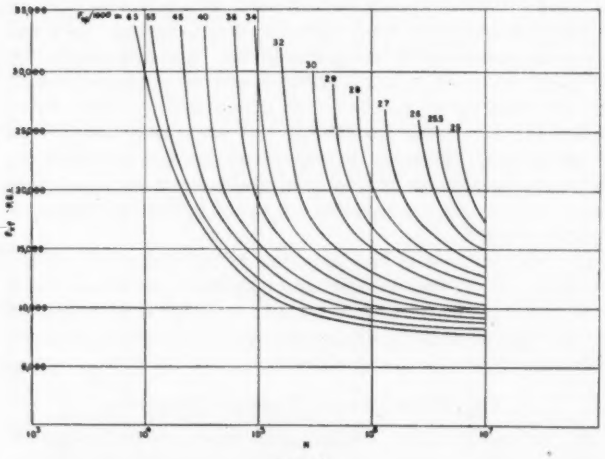


FIG. 2

this basis. This latter method of defining fatigue strength will be used in the subsequent discussion, except where resort must be made to data which are available only in the form of R curves.

VARIABLES INVOLVED IN DEFINING THE FATIGUE STRENGTH OF STRUCTURES

For the purposes of the static-strength analysis of tension structure, it is generally assumed that failure will occur when the most highly stressed portion of the structure reaches the failure stress of the material, the failure stress having been determined in static tests of small test coupons. Similarly, in the fatigue-strength analysis of structures it may be assumed that failure will occur in a given number of cycles when the most highly stressed portion of the structure is subjected to a repeated stressing which would cause failure in the same number of cycles in fatigue tests of the basic material. In other words, in analyses for both static and fatigue strength, the essential problem is to correlate the external loads with the maximum values of internal stress in the structure, since the strength of the basic material may be obtained for any loading. The stress determination for fatigue-strength analysis is, however, usually more complex than the stress determination for static-strength analysis due to the action of the following factors:

1 In the fatigue-strength analysis, two different values of external load must be correlated with internal stress: The peak values of internal stress must be determined from maximum values of external load; and the magnitude of the stress variation in a loading cycle must be determined from the magnitude of the external-load variation.

2 Since the magnitude of the average stress in a structure is usually much lower in fatigue-strength analyses than in static-strength analyses, the usual static-strength assumption that yielding of the material will practically level out the local stress concentrations cannot be made. This means that in correlating external loads with internal stresses the very local stress peaks, which are generally considered to be of minor importance in a static-strength analysis, are usually of considerable importance in a fatigue-strength analysis.

The first of these factors is of course inherent in the definition of fatigue strength; in the second factor lies almost the entire difference between a fatigue-strength analysis and a static-strength analysis, even though its importance is entirely a function of the magnitude of the applied load rather than any peculiar property associated with the fatigue strength of materials. Hence the only new methods needed in the fatigue analysis are those which will define the very local stress values in terms of average stress values, and the remainder of this paper will be concerned with that problem only.

STRESS-CONCENTRATION FACTORS

Any discontinuity in a loaded part will cause a local concentration of stress at the changed section, and the ratio of the peak stress at the discontinuity to the average stress across the section is called the stress-concentration factor. As long as the material is completely elastic, the value of this stress-concentration factor will depend entirely on the geometry of the structure, and is defined as the elastic-stress-concentration factor, K_t. Its value may be determined mathematically by elastic theory, or experimentally by photoelastic measurements, and will vary in practical structure from slightly greater than unity for a very gradual change in section to as high as 10 or 12 for a shear joint which transmits all the load from one sheet to another. This factor is generally considered to be a constant for any particular discontinuity, but in certain cases the geometry of the structure changes sufficiently under load to alter its value. An instance of this which may be important (it has never been evaluated) is a countersunk rivet in single shear, where local bearing pressure varies with load due to rivet rotation.

Fortunately, the true value of this elastic-stress-concentration factor is very rarely realized as a determining factor in the strength of structures, because when the material becomes inelastic at the point of maximum stress, the stress and strain distribution change at that point in a manner which reduces the ratio of peak stress to average stress, i.e., reduces the value of the actual stress-concentration factor. The amount of this alleviation apparently depends almost entirely on the stress-strain characteristics of the material and on the magnitude of the elastic-stress-concentration factor, and thus it appears likely that the alleviation may be evaluated as a basic material property which may be used in determining fatigue strength where discontinuities exist.

Effective Stress-Concentration Factor, K_f: An effective stress-concentration factor, K_f, has been defined (1)[2] as the ratio of the fatigue strength of the basic material to the fatigue strength of a structure at a constant number of cycles to failure and a constant range ratio of applied load. This concentration factor, so defined, is the reciprocal of the structural efficiency factor under repeated loading, since it defines the ratio of structural cross-

[2] Numbers in parentheses refer to table of references at the end of the paper.

sectional area to unnotched-material cross-sectional area necessary to carry a given applied load for a given number of cycles. However, it will relate to the actual stress condition in the structure only when the applied loading is completely reversed, that is, when $R = -1.0$, as will be shown later.

Assumptions for Fatigue Analysis

Since, as we have shown in Fig. 2, fatigue strength is a function of the magnitudes of both the maximum and varying stresses, it is readily apparent that the effect of a discontinuity on both of these stresses must be evaluated for the proper correlation of the fatigue strength of the basic material with the fatigue strength of a structure. In other words, we must be able to define both the true stress level and the true varying stress at a stress raiser in terms of average stresses, before basic-material strength data may be used to determine the fatigue strength of composite structures.

This analysis is founded on the principle of referring to certain constants determined from fatigue tests. The following assumptions are those which will allow us to relate these constants with the alleviation of stress at a stress raiser to provide a general relationship between applied average stress values and the fatigue strength of a structure.

The first assumption is that fatigue life is a function of stress magnitude only, i.e., that failure will occur in a given number of cycles in any part when the highest existing local values of varying stress and maximum stress correspond to the combination necessary to produce failure in the same number of cycles in tests of the basic material.

The second assumption is that for any one material the value of the peak stress at a stress raiser is a function only of the average value of the maximum stress across the pertinent section and the value of the elastic-stress-concentration factor. This seems reasonable since we know that the product of the average maximum stress and the elastic-stress-concentration factor $f_{tf}\ K_t$ is equal to the peak stress f_t in the elastic range for all values of K_t. When the material is locally plastic, however, the amount of alleviation might well be different for different values of K_t, since the stress gradient is increased with increasing values of K_t and hence the restraint offered the most highly stressed locality by the surrounding material would be expected to vary with the value of K_t. This is the reason for assuming that K_t is an independent variable. It will be seen that since $K_t\ f_{tf}$ is linearly related to strain, being the stress value for purely elastic conditions, the curves resulting from a plot of f_t vs. $K_t\ f_{tf}$ must be quite similar in shape to a stress-strain curve for the basic material. It should be particularly noted, however, that the resulting curve or curves obtained from fatigue-test results could not be expected to be identical with a stress-strain curve for the material determined at the same rate of loading, for two reasons: 1 The strain distribution cannot be expected to be the same as under elastic conditions after the material has become plastic locally, due to the support of the surrounding elastic material; and 2 the curves determined from fatigue-test results must include the effect of repeated loading in locally changing the properties of the material through work-hardening. In other words, the peak-stress value found from fatigue-test results must be an effective value only, since it probably would not be actually reached or approximated until the loading had been continued for a number of cycles.

The third assumption is that the value of the varying stress at a stress raiser is a function only of the average value of the varying stress across the pertinent section and the value of K_t. This is similar to assumption 2 for the maximum stress and it should be noted that the value of the local varying stress is assumed to be independent of the value of the local maximum stress, that is, the stress level at which the repeated stressing occurs is *not* assumed to have any effect on the magnitude of the varying stress. We might picture this physically by plotting $f_{vf}\ K_t$ against f_v. Since $f_{vf}\ K_t$ is linearly related to strain (similar to $f_{tf}\ K_t$), a repeated loading would plot as a hysteresis loop whenever the magnitude of the local varying stress was large enough for inelastic action to occur, and under this assumption, the shape of the hysteresis loop is independent of the stress level at which the repeated loading occurs. Fig. 3 illustrates the second and third assumptions, showing plots of f_t and f_v vs. $K_t\ f_{tf}$ and $K_t\ f_{vf}$ for several different loading conditions: Case A shows a loading at which alleviation of maximum stress occurs, but no alleviation of varying stress; Case B shows a loading at which alleviation occurs on both the maximum stress and the varying stress; Case C shows the same value of varying stress as Case B, but occurring at a different stress level; and Case D shows the conditions for completely reversed loading where the stress magnitude is large enough so that inelastic action occurs.

Case D furnishes the correlation between the amount of alleviation of varying stress and the amount of alleviation of maximum stress. Since by definition, the varying stress and the maximum stress are identical when the loading is completely reversed about 0 stress (i.e., when $R = -1.0$), the same function

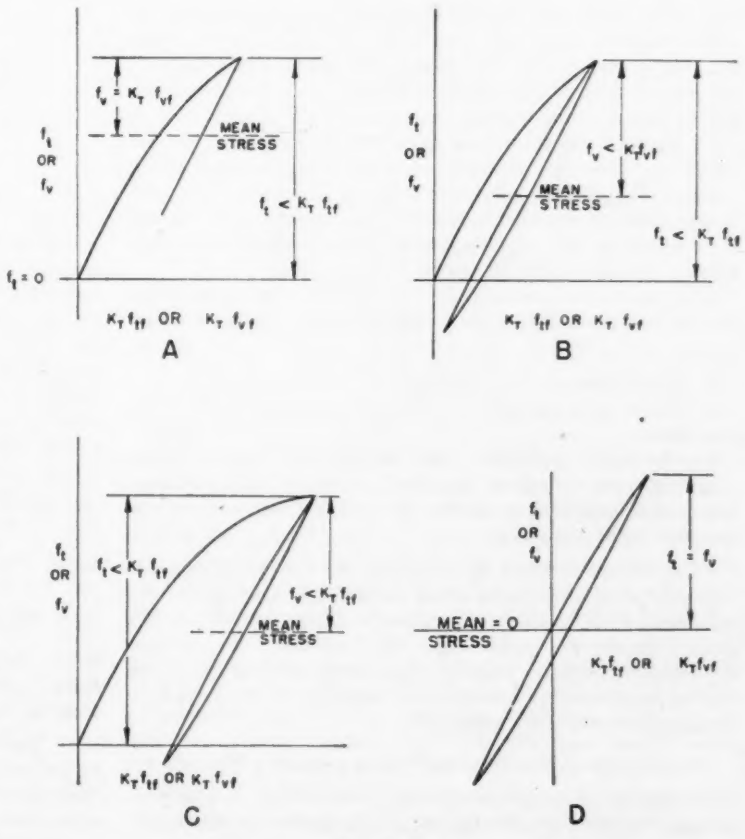


Fig. 3

must necessarily describe the alleviation of both maximum and varying stresses each with respect to its own magnitude.

It will be noted that under these assumptions the true ratio of minimum to maximum stress (the range ratio) may be quite different from the range ratio of applied external loading: The maximum stress is always greater than the varying stress unless the loading is completely reversed; hence the alleviation of maximum stress must always be greater than the alleviation of varying stress unless the external loading is completely reversed. The consequence of this is that the true loading at a stress raiser will always tend toward a completely reversed condition, and the true range ratio will always be less than the nominal range ratio when any alleviation of stress is present at a discontinuity, except when the external loading is completely reversed.

It will also be noted that K_f, the effective stress-concentration factor in fatigue, being defined to represent the over-all change in fatigue strength, does not describe the alleviation due to plastic flow of either the maximum or the varying stress unless the external loading is completely reversed. Instead, it is a measure of the net effect of the magnitude of the elastic-stress-concentration factor, the alleviation of maximum stress by inelastic action, the alleviation of varying stress by inelastic action, and the change in apparent material strength due to change in range ratio. Since K_f is defined on the basis of maximum stress at constant range ratio of external loading, and since, as previously mentioned, constant-range-ratio curves have a defined spacing which is not related to the strength of the material, it may be readily seen that when the true range ratio of a notched part is lower than the nominal range ratio, it is quite possible for K_f to be numerically larger than K_t without the true ratio of peak stress to average stress exceeding K_t.

Therefore in order to evaluate separately the effect of alleviation on the maximum and the varying stress, two other effective stress-concentration factors may be defined; K_m, the ratio of the true maximum stress to the average maximum stress, and K_v, the ratio of the true varying stress to the average varying stress. Under the stated assumptions, these factors will be equal to each other and to K_f when the loading is completely reversed, but not under any other loading condition in which any inelastic action occurs. The essential point here is that K_f is defined in terms of fatigue strength and may be determined experimentally; hence if we determine the fatigue strength of specimens at $R = -1.0$, we may also determine the values of K_m and K_v.

With these assumptions it is now possible to enumerate the information necessary to the fatigue-strength analysis of structures:

1 The geometry of the structure.

2 The fatigue strengths of the basic materials used in the structure.

3 The fatigue strengths under completely reversed loading of several types of idealized "notched" specimens having different values of K_t and fabricated from the same basic materials as the structure to be analyzed.

From the geometry of the structure the correlation between "average" stress or nominal stress and external load may be determined by the usual static analysis methods, and the elastic-stress-concentration factor may be evaluated; the fatigue strengths of the basic materials and of the notched specimens may be determined by test and used to determine the stress alleviation properties of the material.

Hypothetical Example of Fatigue-Analysis Method

An example of the proposed analysis method will now be presented. We shall assume that we have available the completely reversed axial fatigue strength characteristics of several notched specimens made from Alclad 24S-T. These specimens may have included thin strips with circular or elliptical holes, hyperbolic notches, or other types of stress raisers inducing definitely known elastic-stress-concentration factors. Fig. 4 shows such hypothetical data. The upper curve of the same figure represents the completely reversed fatigue-strength characteristics of Alclad 24S-T material, and thus corresponds to a notch possessing an elastic-stress-concentration factor of 1.0.

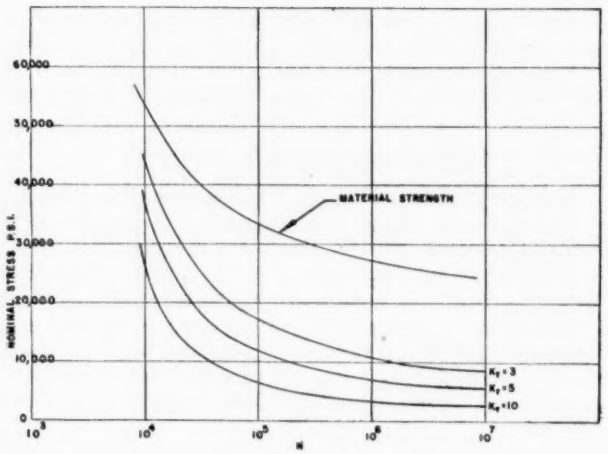


Fig. 4

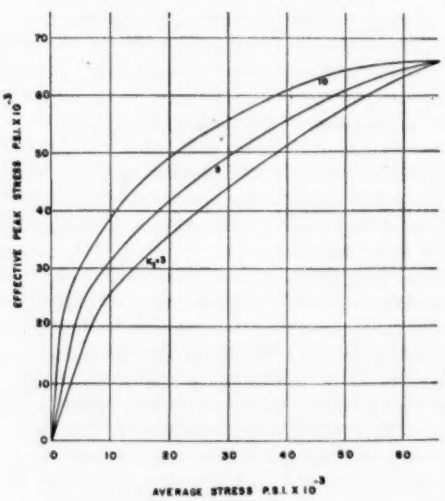


Fig. 5

Since these curves are all representative of the completely reversed stress condition, it follows from the previous discussion that for any particular N and K_t, K_f, K_m, and K_v are equal to the ratio of material strength to notched-specimen strength. Thus for $K_t = 3$ and $N = 10^6$, $K_f = K_m = K_v = \dfrac{27{,}300}{10{,}500} = 2.6$; for $K_t = 10$ and $N = 10^5$, $K_f = K_m = K_v = \dfrac{33{,}500}{6500} = 5.15$, and so forth. In order to obtain from these idealized notched-specimen data the relation between the nominal and the effective or peak stresses, one of two procedures may be followed:

1 Directly from Fig. 4 the notched-specimen strength may be plotted against the material strength for a series of N values. This procedure would, on the basis of our hypothetical data, result in three curves corresponding to K_t's of 3, 5, and 10. These curves, shown in Fig. 5, define the notch sensitivity of a material

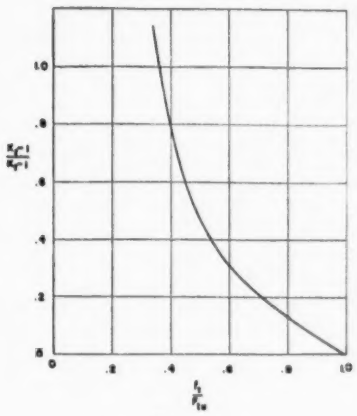


FIG. 6

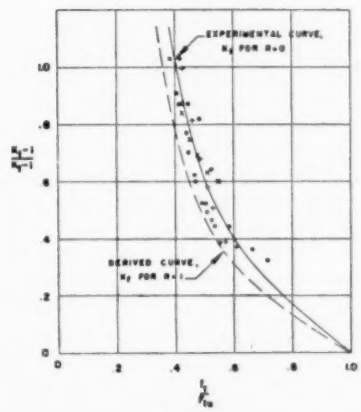


FIG. 7

under any condition of loading, including static, for those three values of K_t, for which Fig. 5 may be used to predict the fatigue strength of a structure fabricated from that material, since the effective values of maximum and varying stress may be determined and used in conjunction with the basic material data, Fig. 2, to determine the life.

2 In order to use the available data to obtain the relationship of Fig. 5 for other values of K_t, an intermediate curve, for the purpose of interpolation and extrapolation, may be plotted from the available data. Such a curve, shown in Fig. 6, relates K_t, K_f, and the peak stress implicit in the form of nondimensional parameters, bringing all the available data together into one curve, which may then be used to plot the relations of Fig. 5 for as many additional values of K_t as may appear necessary. Such a full set of curves is shown in Fig. 8.

With the information of Fig. 8 on hand, an Alclad 24S-T structure may be analyzed for fatigue. Let us suppose, for example, that the structure has at its critical section a notch inducing an elastic-stress-concentration factor of 4, i.e., $K_t = 4$, and that the structure is loaded axially under an alternating nominal stress varying between 20,000 and 30,000 psi. Hence the average maximum stress is 30,000 psi and the average varying stress is ±5000 psi. Going into the $K_t = 4$ curve of Fig. 8 it is found that these stresses correspond to an actual maximum stress of 47,500 psi and an actual varying stress of 20,000 psi. Fig. 2 shows that this combination of stresses corresponds to a life of 32,000 cycles, and the analysis of the structure is complete for that particular loading condition.

In a similar way we may determine the fatigue strength of any structure having a known K_t.

Demonstration of Analysis Method for Alclad 24S-T Structures

The following demonstration of the proposed method does not adhere strictly to the previously outlined procedure, because data on notched specimens under completely reversed loading were not available. By resorting to a tested empirical relationship (2) a large amount of data on various kinds of notched specimens were reduced to the range ratio of 0 (load varying between 0 and maximum.) These data were then plotted as shown in Fig. 7 to show the form of the relationship between K_t, K_f, and the apparent peak stress obtained by multiplying the nominal maximum stress by K_f. Then by trial and error, a law of variation for completely reversed stress ($R = -1$) was determined that would give the experimentally found values of K_f at $R = 0$. This curve is also plotted on Fig. 7 and corresponds to that of Fig. 6 obtained from hypothetical data. This curve was then used to obtain the relation between the average varying and maximum stresses and the effective or peak varying and maximum stresses for constant values of K_t. Fig. 8 is such a plot for several values of K_t. It should be noted that this plot indicates the alleviation of peak stresses at a discontinuity initiates at peak stresses as low as 20,000 psi for 24S-T. This explains why the actual magnitude of the elastic-stress-concentration factor is rarely effective in practice.

Fig. 8 may be used to predict the fatigue strength of a structure fabricated from Alclad 24S-T material.

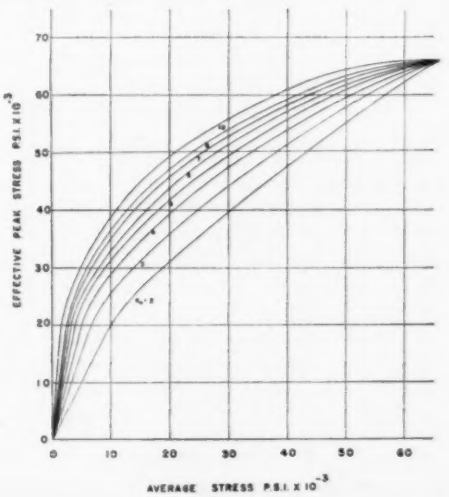


FIG. 8

Figs. 9, 10, and 11 show S-N curves at $R = 0.2$, $R = 0.4$, and $R = 0.6$, respectively for Alclad 24S-T perforated sheet predicted by this method and plotted against the test points. The value of K_t in this case was 2.6. Fig. 12 shows a similar plot for a 24S-T Alclad single-row riveted lap joint having a K_t of 6.1. K_t was determined in this latter case from the values determined photoelastically by Frocht and Hill (3) for pin-loaded double shear joints. Fig. 13 is a similar plot for a 24S-T Alclad double-row riveted joint compared with points obtained from tests of a geometrically identical specimen manufactured from Alclad 24S-T86 material. In the latter case the K_t of 5.0 was obtained by interpolation between the photoelastically determined value for pin-loaded double shear joints (complete shear transfer) and the value for perforated sheet (no shear transfer).

Some of the disparagement between the predicted and actual curves may be attributed to the fact that lack of adequate data led to rather arbitrary methods for the evaluation of constants The accuracy of this evaluation was further detracted from by

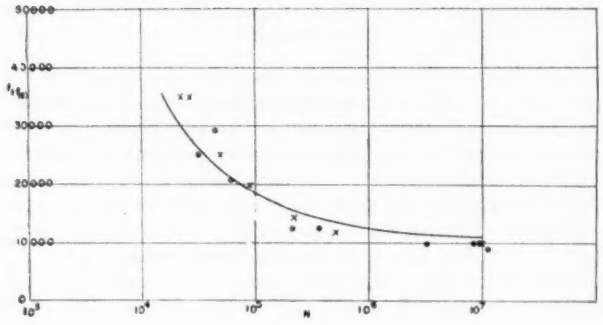


FIG. 9

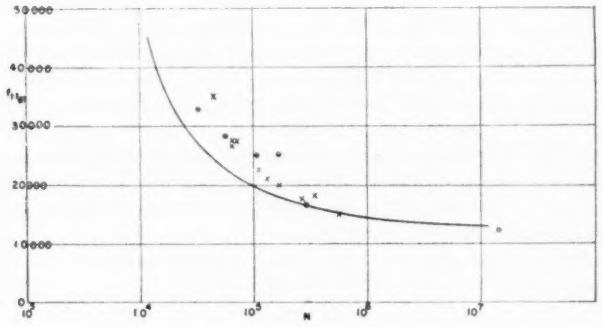


FIG. 10

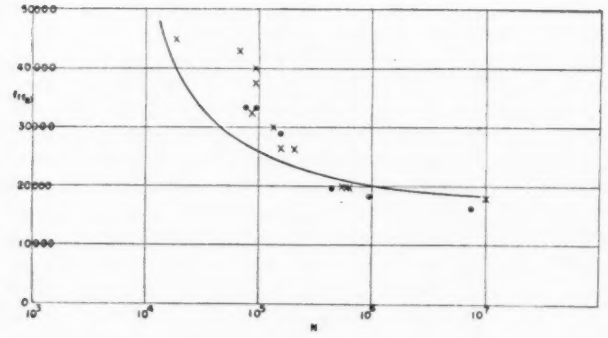


FIG. 11

the fact that specimens made from both the QQA-362 specification material and the ANA-13 specification material were used in conjunction with the known fatigue-strength characteristics only of the former; whereas some recent check tests have shown that the fatigue properties of the two materials diverge considerably, particularly in the low-cycle high stress range.

CONCLUSIONS

This paper has brought out the principal distinction between the problems involved in the development of fatigue and static-strength-analyses methods. This distinction has been shown to lie in the need for evaluating the strictly local stress conditions at stress raisers, whenever the problem of fatigue strength arises, and emphasis has been placed on the nature of the experimental data which would be adequate to determine these conditions.

The lack of complete basic data necessary for the development of the proposed analysis forbids a rigorous proof of the validity of

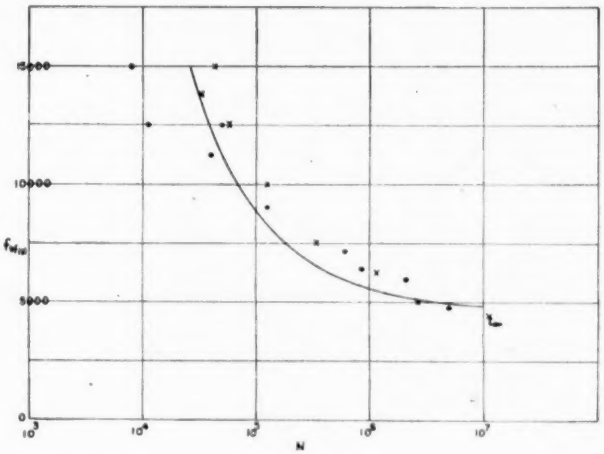


FIG. 12

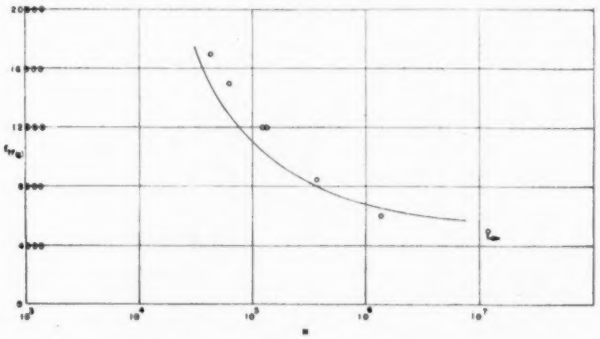


FIG. 13

the assumptions upon which it is based. The real proof must await the time the basic data become available, and the proposed method can be used directly. We feel that in view of the importance to the airframe engineer of a good fatigue-analysis method, the procurement of these data should be placed high on the list of the research laboratories' agenda.

ACKNOWLEDGMENT

The authors wish to express their appreciation to Mr. D. W. Drake for his valuable suggestions.

REFERENCES

1 "Effect of Rivet Pitch on the Fatigue Strength of 0.025–0.025 Alclad 24S-T Riveted Joints," by Victor Seliger, N.A.C.A. Technical Note No. 900, July, 1943.

2 "A Suggested New Parameter for Fatigue Strength Analysis," by Victor Seliger, American Society for Testing Materials, Bulletin No. 132, January, 1945.

3 "Stress-Concentration Factors Around a Central Hole in a Plate Loaded Through a Pin in the Hole," by M. M. Frocht and H. N. Hill, JOURNAL OF APPLIED MECHANICS, Trans. A.S.M.E., vol. 62, 1940, p. A-5.

GENERAL REFERENCES

"Fatigue-Test Results, Their Use in Design Calculations," by E. C. Hartman, Product Engineering, February, 1941.

"Stress-Concentration Phenomena in Fatigue of Metals," by R. E. Peterson, JOURNAL OF APPLIED MECHANICS, Trans. A.S.M.E., vol. 55, paper APM-55-19, 1933.

"Effect of Material, Loading, and Stress-Concentration Factors on Design," by George H. Neugebauer, Cooper Union Bulletin, March, 1943.

An Elementary Theory of the Bourdon Gage

By ALFRED WOLF,[1] TULSA, OKLA.

A theory of the Bourdon gage is presented based upon two elements of strain, namely, the bending of the walls in a transverse section through the gage tubing, and a longitudinal extension parallel to the axis of the tubing. Practical formulas are derived for the calculation of the sensitivity and the torque of the Bourdon gage. An estimate is made of the maximum stress. The sensitivity of a very thin-walled gage is shown to be proportional to the inverse first power of the wall thickness. Results of a few measurements show agreement with the theory.

Introduction

A SIMPLE qualitative explanation of the behavior of a Bourdon-gage element was given by Lord Rayleigh (1)[2] on the basis of a theorem of Gauss on the bending of surfaces. Pressure applied internally to a tube of oval section results in a change of shape of the section; the action of the gage then follows from the invariance of the product of the two principal curvatures of the middle surface of the tubing.

Other contributions to the theory of the Bourdon pressure gage were made by E. Hill (2), A. M. Worthington (3), A. G. Greenhill (4), and L. Maurer (5). The only paper in which a definite formula is derived for the sensitivity of the Bourdon gage is that of Chido Sunatani (6).

In the present paper an attempt is made to base the theory on two elements of strain, the bending of the walls in a transverse section through the tubing and a longitudinal extension and contraction parallel to the axis of the tubing; both elements are of equal importance. The procedure may be regarded as an application of the direct methods of the calculus of variations. As expected, maximum stress calculated in this manner is not as close an approximation as the sensitivity and the torque.

The pressure element of a Bourdon gage is made of tubing of oval section, the axis of the tubing being bent into an arc of a circle which lies in a plane of symmetry of the gage element, and has the radius R; the long axis of the oval section of the tubing is perpendicular to the plane of the circle. When pressure is applied the radius of curvature increases by δR: The quantity $\delta R/R$ for unit pressure will be referred to as the sensitivity of the gage. It is postulated in the following that the pressure element is mounted in such manner that only bending moments are applied to its ends; consequently, that δR is always constant along the pressure element.

The torque of the gage is defined in the following manner: Let one end of the gage element be attached to a rigid support and let pressure be applied; the other end of the element will then move a certain distance because of the change in curvature of the axis of the tubing; the external bending moment which must be applied to the free end of the element to restore the deflection to zero will be defined as the torque of the Bourdon gage for any given pressure, and will be denoted T.

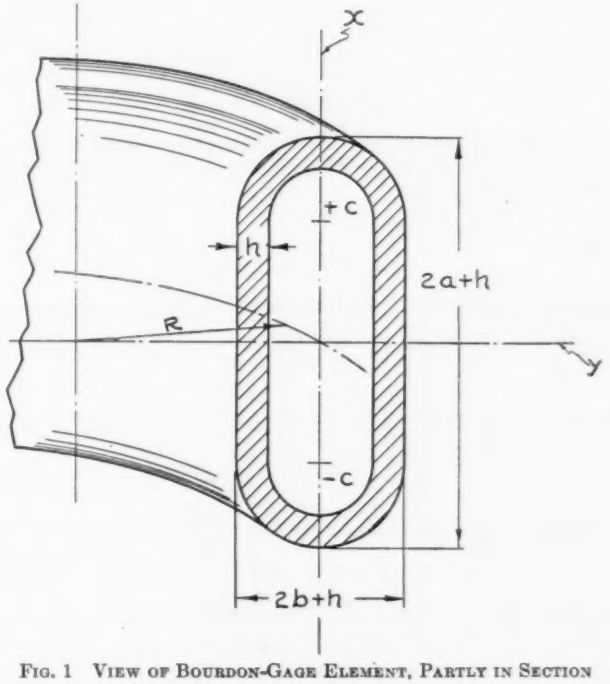


Fig. 1 View of Bourdon-Gage Element, Partly in Section

In the next section an expression will be derived for the potential energy of the gage element under pressure, and from it will be deduced a differential equation for the elastic displacement of the middle surface of the tubing. All subsequent calculations are based upon these two equations. Some of the formulas may, by a slight modification, be applied to tubing of arbitrary cross section but more often the formulas are valid only for sections with two axes of symmetry. In the third section the direct method of the calculus of variations is discussed which constitutes the practical means for the solution of the problem; the same section contains formulas for the sensitivity and the torque in the limiting case $R \rightarrow \infty$.

In the fourth section practical formulas are given for the calculation of torque and sensitivity for a specific shape of cross section of tubing which approaches closely that supplied by manufacturers. In the fifth section the maximum stress in gage elements is dealt with; only approximate results are obtained. In the concluding section a few examples are given of the accuracy to be expected from the formulas.

Potential Energy of the Bourdon Gage

Consider a transverse section through the Bourdon-gage-element tubing, and refer it to a set of rectangular co-ordinate axes x, y; their origin is to be at the center of the oval section, the x-axis is perpendicular to the plane of the circle into which the axis of the tubing is bent, the y-axis points away from the center of the same circle. When pressure is applied, the components of the infinitesimal elastic displacement of the middle line of a transverse section through the walls, relative to the center of the oval, parallel to the x- and y-axes, respectively, will be denoted ξ, η.

---

[1] Geophysical Research Corporation.

[2] Numbers in parentheses refer to the References at the end of the paper.

For presentation at the National Meeting of the Applied Mechanics Division, Buffalo, N. Y., June 21–22, 1946, of The American Society of Mechanical Engineers.

Discussion of this paper should be addressed to the Secretary, A.S.M.E., 29 West 39th Street, New York, N. Y., and will be accepted until October 10, 1946, for publication at a later date. Discussion received after the closing date will be returned.

Note: Statements and opinions advanced in papers are to be understood as individual expressions of their authors and not those of the Society.

All these variables are regarded as functions of the length of arc s along the middle line of a transverse section of the walls of the tubing. One of the simplifying assumptions introduced is the neglect of any change of length along that line. From this assumption and from

$$x'^2 + y'^2 = 1$$

it follows

$$x'\xi' + y'\eta' = 0 \quad \text{[A1]}$$

in which the primes denote differentiation with respect to s.

Writing ρ for the radius of curvature of the middle line of a transverse wall section,

$$\frac{1}{\rho} = x'y'' - y'x''$$

and the change of curvature resulting from elastic displacement

$$\delta\left(\frac{1}{\rho}\right) = y''\xi' + x'\eta'' - y'\xi'' - x''\eta'$$

which may be transformed with the aid of Equation [A1] into

$$\delta\left(\frac{1}{\rho}\right) = \frac{d}{ds}\left(\frac{\eta'}{x'}\right) \quad \text{[A2]}$$

The change of internal volume per unit length of tubing is

$$\delta V = \delta \int y\,dx = \int ds(y\xi' + x'\eta)$$

Making use of Equation [A1] and employing integration by parts

$$\delta V = \int ds\,\eta\left[x' + \frac{d}{ds}\left(\frac{yy'}{x'}\right)\right] \quad \text{[A3]}$$

The potential energy per unit length of tubing due to the bending of the walls and to the increase in volume is

$$\frac{E_1h^3}{24}\int ds\left[\delta\left(\frac{1}{\rho}\right)\right]^2 - p\,\delta V$$

where

$$E_1 = \frac{E}{1-\sigma^2}$$

E = Young's modulus
σ = Poisson's ratio
h = wall thickness
p = pressure

Besides the potential energy of transverse bending of the walls, the extension of elements parallel to the axis of the tubing will be considered; this is regarded as a function of s only. A simple geometrical consideration of the effect of simultaneous change of the radius of curvature of the axis of the tubing, the length of which remains constant, and of the elastic displacement of the walls, leads to the expression

$$\frac{R + \delta R + y + \eta}{R + \delta R} - \frac{R + y}{R}$$

for the extension of filaments parallel to the axis of the tubing, which, to a sufficient approximation, may be written

$$\frac{\eta}{R} - \frac{y}{R}\frac{\delta R}{R}$$

The total potential energy W per unit length of tubing will be assumed to be the sum of the energies of transverse bending of the walls and of the longitudinal extension parallel to the axis of the tubing; thus

$$W = \int ds\left\{\frac{E_1h^3}{24}\left[\frac{d}{ds}\left(\frac{\eta'}{x'}\right)\right]^2 + \frac{Eh}{2R^2}\left[\eta - y\frac{\delta R}{R}\right]^2 - p\eta\left[x' + \frac{d}{ds}\left(\frac{yy'}{x'}\right)\right]\right\} \quad \text{[1]}$$

There is no rigorous foundation for adding the energies of bending and of longitudinal extension; this step is justified mainly by its success. However, the foregoing procedure can be shown to be correct in the special case of an infinitely long plane strip of moderate thickness, subjected simultaneously to pressure on one side and to uniform longitudinal strain.

Since W is a minimum, it follows by well-known methods

$$\frac{d}{ds}\left[\frac{1}{x'}\frac{d^2}{ds^2}\left(\frac{\eta'}{x'}\right)\right] + \frac{12E}{R^2h^2E_1}\left[\eta - y\frac{\delta R}{R}\right] = \frac{12p}{E_1h^3}\left[x' + \frac{d}{ds}\frac{yy'}{x'}\right] \quad \text{[2]}$$

When $R \to \infty$ Equation [2] reduces to

$$\frac{d}{ds}\left[\frac{1}{x'}\frac{d^2}{ds^2}\left(\frac{\eta'}{x'}\right)\right] = \frac{12p}{E_1h^3}\left[x' + \frac{d}{ds}\left(\frac{yy'}{x'}\right)\right] \quad \text{[2a]}$$

which is clearly solvable by quadratures. Equation [2] can be solved by quadratures in the special case of rectangular cross section, a fact which may be used for an extension of the present theory.

To determine the sensitivity of the Bourdon gage, Equation [2] should be solved with $\delta R/R$ regarded as a parameter; the solution must be substituted in Equation [1] and the value of $\delta R/R$ must be found which makes W a minimum.

The torque of the gage is determined by a similar procedure. Assume $\delta R/R = 0$ in Equation [2] and substitute the solution in Equation [1]. The resulting value W_1 is the potential energy of the gage under pressure when constrained from changing its curvature. The torque of the gage is given by

$$T = \frac{2R(W_1 - W)}{\delta R/R} \quad \text{[3]}$$

which may be verified by considering the work done by external bending moments in reducing the radius of curvature of the gage element from $R + \delta R$ to R, which is $W_1 - W$, and which also is equal to $\frac{1}{2}T$ times the angular deflection of the gage element per unit of its length $\frac{1}{R}\frac{\delta R}{R}$.

Application of Direct Method of Calculus of Variations

The practical method of attack on the Bourdon-gage problem makes use of the minimum property of the energy W. A solution of Equation [2a] or a function proportional to it, is obtained first; it will be denoted $\eta_0(s)$. It is then postulated

$$\eta(s) = B\eta_0(s)$$

where B is an undetermined constant, and this expression is substituted in Equation [1], leading to

$$W = a_{11}B^2 + a_{12}B\frac{\delta R}{R} + a_{22}\left(\frac{\delta R}{R}\right)^2 + a_{23}B \quad \text{[4]}$$

in which the coefficients $a_{11} \ldots a_{23}$ are now known functions of the dimensions of the gage, elastic constants, and pressure. Since W must be a minimum for variations with respect to B and $\delta R/R$, the following results are obtained

$$B = \frac{-2a_{12}a_{33}}{4a_{11}a_{22} - a_{12}^2} \quad [5]$$

$$\frac{\delta R}{R} = \frac{a_{12}a_{33}}{4a_{11}a_{22} - a_{12}^2} \quad [6]$$

The value of W_1 is derived by substituting $\delta R/R = 0$ in Equation [4] and then determining the minimum value of the resulting expression. This procedure leads to

$$T = \frac{Ra_{12}a_{33}}{2a_{11}} \quad [7]$$

It may be of interest at this point to derive some simple formulas applicable to the case $R \to \infty$.

Since Equation [2a] is exact in this case, $B \to 1$; further

$$a_{12}^2/a_{11}a_{22} \to 0$$

It follows

$$\left(\frac{\delta R}{R}\right)_\infty = \frac{\int \eta y \cdot ds}{\int y^2 \cdot ds} \quad [8][3]$$

$$(T)_\infty = \frac{Eh}{R} \int \eta y \cdot ds \quad [9]$$

Explicit formulas for the function η can be deduced easily from Equation [2a]. First, from Equations [A2] and [2a]

$$\delta\left(\frac{1}{\rho}\right) = \frac{6p}{E_1 h^3}(r^2 - \bar{r}^2) \quad [10]$$

where $r^2 = x^2 + y^2$, and $\bar{r}^2$ is the mean value of r^2 on the middle surface of the tubing. Equation [10] will be used in connection with the problem of maximum stress. If the length of arc s is measured from a point at which $x = 0$, the solution of Equation [10] satisfying appropriate periodicity conditions is

$$\eta = \frac{6p}{E_1 h^3}\left\{x\int_0^s r^2 \cdot ds - \int_0^s xr^2 \cdot ds - \frac{sx}{s_0}\int_0^{s_0} r^2 \cdot ds + \bar{r}^2 \int_0^s x \cdot ds\right\} + \text{const.} \quad [11]$$

where s_0 is the total length of the middle line of a transverse section through the gage-element walls. The constant of integration is determined from

$$\int_0^{s_0} \eta \cdot ds = 0$$

It is clear that explicit formulas for sensitivity and torque can be derived from Equations [8], [9], and [11] but the subject will not be pursued any further since it is not important for applications.

Practical Formulas for Sensitivity and Torque of a Bourdon Pressure Gage

A specific shape of cross section of the gage-element tubing will be postulated in what follows. The oval formed by the middle line of the transverse cross section of the walls will be assumed to be made up of two parallel straight-line portions of length $2c$ each, a distance $2b$ apart, and terminated by two half circles of radius b. The straight-line portions of the oval are parallel to the x-axis, and hence perpendicular to the plane of the circle into which the axis of the tubing is bent. The long axis of the oval has the length $2a = 2b + 2c$, the short axis has the length $2b$. The outside dimensions of the tubing are $2a + h \times 2b + h$, h being the wall thickness.

The function $\eta(s)$ which is to be substituted in Equation [1] is chosen as a solution of Equation [2a] multiplied by an indeterminate constant. On the straight-line portions of the oval contour

$$\eta(s) = \alpha + \frac{1}{2}\beta s^2 + \frac{1}{12}\gamma s^4 \quad [12]$$

where s is measured from the respective centers of the straight-line portions, and varies between $-c$ and $+c$. On the half circles terminating the oval contour, it is assumed

$$\frac{d}{d\phi}\left(\frac{1}{x'}\frac{d\eta}{d\phi}\right) = A + B\cos\phi \quad [13]$$

which is a consequence of Equation [2a], and in which the angle ϕ is taken to vary from $-\frac{\pi}{2}$ to $+\frac{\pi}{2}$. The condition of continuity of $\eta, \eta', \eta'', \eta'''$ at the points at which the straight-line portions of the contour meet the half circles $\left(\phi = \pm\frac{\pi}{2},\ s = \pm c\right)$ determines the constants α, β, γ, A in terms of B (refer to Appendix).

The substitution of Equations [12] and [13] in Equation [1] leads to explicit expressions for the coefficients $a_{11} \ldots a_{33}$ which are given in the Appendix. The algebra is very tedious but presents no difficulty, and leads to

$$\frac{\delta R}{R} = \frac{4}{15}\frac{p}{E_1}\frac{a^4}{bh^3}\frac{F}{1 + \frac{4}{35}\frac{E}{E_1}\frac{a^4}{R^2h^2}F_1} \quad [14]$$

$$T = \frac{16}{15}\frac{pE}{E_1}\frac{ba^4\left[a + \left(\frac{\pi}{4} - 1\right)b\right]}{Rh^3}\frac{F}{1 + \frac{8}{21}\frac{E}{E_1}\frac{a^4}{R^2h^2}F_2} \quad [15]$$

The factors F, F_1, F_2, as well as the factor G introduced in the next section, are rational functions of b/a which approach unity as $b/a \to 0$. Their values are derived from the expressions for the coefficients $a_{11} \ldots a_{33}$ and are given in Table 1.

TABLE 1 VALUES OF F AND G FACTORS

b/a	F	F_1	F_2	G
0.0	1.000	1.000	1.000	1.000
0.1	1.273	1.040	1.207	0.934
0.2	1.469	1.059	1.373	0.852
0.3	1.574	1.057	1.498	0.757
0.4	1.574	1.024	1.572	0.652

A consideration of Equations [14] and [15] makes evident the fact that the theory of pure bending of thin shells cannot correctly represent the behavior of the Bourdon pressure gage when the ratio a^4/R^2h^2 is much greater than unity. For sufficiently small values of h the sensitivity of the gage becomes inversely proportional to the first power of the wall thickness; longitudinal extensions parallel to the axis of the tubing are then the predominant factor.

Maximum Stress in a Bourdon Gage

The distribution of stress in a gage element under pressure cannot be derived with any precision from the preceding theory. Approximate results may, however, be attained by postulating the maximum stress to be due to the transverse bending of the walls of the tubing. According to Equation [10] the curvature of the middle line, and hence the stress in this type of deformation is proportional to $r^2 - \bar{r}^2$. Maximum stress is found on one

[3] A similar formula is given by E. Hill (2) who, however, does not attempt to evaluate η. Hill's formula was employed by Sunatani (6) in the special case of elliptic cross section.

of the axes of the oval section of the tubing where r is a maximum or a minimum. In most practical applications, when $b/a < 0.48$, the point of maximum stress is at the intersection of the long axis of the oval and the inner surface of the walls of the tubing. It may be noted that in dealing with a tube which is only slightly elliptical, the maximum stress is on the short axis of the ellipse.

The value of the maximum stress S will be assumed to be given by the simple relation

$$S = \frac{E_1 h}{2} \delta \left(\frac{1}{\rho}\right)$$

The calculations of the preceding section then lead immediately to the formula

$$S = \frac{E_1 h}{2} \frac{A + B}{b^2} = 2p \frac{a^2}{h^2} \frac{G}{1 + \frac{4}{35} \frac{E}{E_1} \frac{a^4}{R^2 h^2} F_1} \quad \ldots\ldots [16]$$

The values of G as a function of b/a are shown in Table 1.

Conclusion

A reasonably good confirmation of Equations [14] and [15] was obtained from some measurements on the Amerada bottom-hole pressure gage, carried out at the laboratory of the Geophysical Research Corporation. No satisfactory method was developed for the measurement of maximum stress, but it is reasonably certain that values of stress furnished by Equation [16] are too great, especially for thick-walled tubing. For illustration of experimental data the examples given in Table 2 may suffice.

TABLE 2 EXPERIMENTAL DATA

R	a	b	h	p	$\delta R/R$ obs	$\delta R/R$ calc.	T obs	T calc.
0.39	0.099	0.027	0.006	275	0.0183	0.0193	0.71	0.71[a]
0.39	0.109	0.035	0.0157	2000	0.0220	0.0186	5.65	5.35[b]
0.39	0.107	0.037	0.016	3000	0.0275	0.0243	6.9	7.9
0.38	0.109	0.037	0.0205	4360	0.0190	0.0197	9.5	9.9
0.38	0.111	0.042	0.0265	9250	0.0190	0.0198	18.6	19.1[c]

[a] Yield point observed at 800 psi; calculated S = 150,000 psi.
[b] Yield point observed at 3200 psi; calculated S = 160,000 psi.
[c] Calculated S = 190,000 psi at 9250 psi.
NOTE: The dimensions are given in inches, pressures in psi, torques in pi; the pressure element was made of steel (E = 30,000,000 psi, σ = 0.3).

Appendix

Referring to Equations [12] and [13], and writing $b/c = \zeta$

$$A = \left(\frac{1}{3\zeta} - \zeta\right)\left(1 + \frac{\pi}{2}\zeta\right)^{-1} B$$

$$\alpha = \left[\frac{1}{24} + \frac{5\pi}{48}\zeta + \frac{5}{6}\zeta^2 + \frac{\pi}{4}\zeta^3 + \left(\frac{\pi^2}{8} - 1\right)\zeta^4\right]\zeta^{-3} \left(1 + \frac{\pi}{2}\zeta\right)^{-1} B$$

$$\beta = -\left(\frac{1}{6} + \frac{\pi}{4}\zeta + \zeta^2\right)\zeta^{-3}\left(1 + \frac{\pi}{2}\zeta\right)^{-1} B$$

$$\gamma = \frac{1}{2\zeta^3} B$$

The expressions for $a_{11} \ldots a_{33}$ are

$$a_{11} = \frac{h^3 E_1}{6b^3}\left[\frac{1}{45} + \frac{\pi}{15}\zeta + \frac{2}{3}\zeta^2 + \frac{\pi}{4}\zeta^3 + \left(\frac{\pi^2}{8} - 1\right)\zeta^4\right]\zeta^{-3} \left(1 + \frac{\pi}{2}\zeta\right)^{-1} + \frac{2Ehb}{R^2}\left\{\frac{\pi}{8}\left(\frac{\pi^2}{6} - 1\right)\frac{A^2}{B^2} + \left(\frac{26}{9} - \frac{\pi^2}{4}\right)\frac{A}{B} + \frac{\pi}{32}\left(\frac{\pi^2}{3} - \frac{3}{2}\right) + \frac{1}{\zeta B^2}\left[\alpha^2 + \frac{1}{20}\beta^2 + \frac{1}{1296}\gamma^2 + \frac{1}{3}\alpha\beta + \frac{1}{30}\alpha\gamma + \frac{1}{84}\beta\gamma\right]\right\}$$

$$a_{12} = -\frac{4Echb^2}{R^2}\left[\frac{1}{45} + \frac{\pi}{15}\zeta + \frac{2}{3}\zeta^2 + \frac{7\pi}{24}\zeta^3 + \left(\frac{\pi^2}{8} - \frac{2}{3}\right)\zeta^4 + \frac{\pi}{24}\zeta^5\right]\zeta^{-3}\left(1 + \frac{\pi}{2}\zeta\right)^{-1}$$

$$a_{22} = \frac{2Echb^2}{R^2}\left(1 + \frac{\pi}{4}\zeta\right)$$

$$a_{33} = -4pc\left[\frac{1}{45} + \frac{\pi}{15}\zeta + \frac{2}{3}\zeta^2 + \frac{\pi}{4}\zeta^3 + \left(\frac{\pi^2}{8} - 1\right)\zeta^4\right]\zeta^{-3} \left(1 + \frac{\pi}{2}\zeta\right)^{-1}$$

REFERENCES

1 "On the Bending and Vibration of Thin Elastic Shells," by Lord Rayleigh, Proceedings of the Royal Society of London, England, vol. 45, 1889, p. 105.
2 E. Hill, Messenger of Mathematics, 1, 1872.
3 "Bourdon's Pressure Gauge," by A. M. Worthington, *Nature*, 41, January 30, 1890, p. 216.
4 "Bourdon's Pressure Gauge," by A. G. Greenhill, *Nature*, 41, April 3, 1890, p. 517.
5 "Ueber die Deformation gekruemmter elastischer Platten," by L. Maurer, *Archiv der Mathematik und Physik*, 6, 1904, pp. 1 and 260.
6 Chido Sunatani, published in Japan, journal and date unknown

The Influence of Oil-Film Journal Bearings on the Stability of Rotating Machines

By A. C. HAGG,[1] EAST PITTSBURGH, PA.

The self-excited vibration caused by the lubricating films of journal bearings and commonly called oil-film whirl or oil whip is discussed. The upper limit of whirling frequency has been found to be one-half rotational frequency in the general case; actually the phenomenon will manifest itself at a frequency which is invariably below this limit. Stability criteria have been developed for certain common systems in terms of bearing and rotor parameters. The tilting-pad bearing of Michell has been established as a so-called "stable" or "nonwhirling" bearing. This bearing and related types are probably the only oil-film journal bearings which are incapable of exciting oil whip, regardless of the system to which they are applied. Qualitatively the results of the paper appear to be in agreement with observations. In certain cases, results have been substantiated experimentally.

Nomenclature

The following nomenclature is used in the paper:

Symbol		Dimensions
a	= radius of journal	L
η	= radial clearance of journal in bearing	L
ϵ	= eccentricity of journal	L
b	$= \frac{\epsilon}{\eta}$	Dimensionless
l	= circumferential length of bearing surface	L
w	= width of bearing surface	L
A	= projected area of journal	L^2
Ω	= angular velocity of journal	T^{-1}
ω	$= \frac{d\theta}{dt}$ = angular velocity of journal center about bearing center	T^{-1}
μ	= viscosity of lubricant	$ML^{-1}T^{-1}$
N	= rpm of journal	T^{-1}
p	= load per unit projected journal area	$ML^{-1}T^{-2}$
B	= bearing-force constant	MT^{-1}
c, D	= bearing-damping constants	MT^{-1}
m	= mass, usually rotor mass	M
ω_n	= natural frequency of rotor in bending or on "spring" of lubricating film	T^{-1}
T	= bearing torque constant	ML^2T^{-1}
I_1	= rotor inertia about rotating axis	ML^2
I_2	= rotor inertia through CG and normal to I_1	ML^2

Introduction

A self-excited vibration known as oil-film whirl or oil whip sometimes occurs in rotating machines employing oil-film journal bearings. Usually the rotor is the major vibrating element, although in some machines the instability may be manifest to the same or greater degree in nonrotating parts; in either case the forces doing work in support of the vibration come from oil-film pressures of the bearings. Oil-film whirl is characterized by relative motion of journal and bearing in an area-enclosing path usually circular or elliptical, and in the direction of machine rotation. The motion of the rotor proper or of the nonrotating elements may or may not be magnified, depending upon the masses and flexibilities of the system. In many cases the vibration frequency may be nearly one-half rotational frequency; however, the frequency of oil-film excited vibration is invariably less than one-half rotational frequency.

It may be mentioned in passing that unbalance vibration, alone or in combination with oil-film excitation, may cause instability at a frequency which is exactly one-half or one-third rotational frequency. This phenomenon has been fully explained by Baker,[2] and can be corrected or reduced to oil-film whirl by sufficiently good rotor balancing.

Instability caused by oil-film journal bearings has been investigated from time to time,[3,4,5] and the phenomenon has been controlled in many cases with success. However, oil-film whirl remains a troublesome vibration problem, especially in the higher-speed machines and in those with vertical shafts.

The present discussion covers some of the rational aspects of this stability problem, and draws attention to certain types of journal bearings which are useful in securing machine stability.

Upper Limit of Whirling Frequency

The upper limit of whirling frequency is determined by the bearing. Robertson[4] has shown by means of hydrodynamical theory that, neglecting friction forces, the resultant film force due to journal rotation in an ideal bearing is at right angles to the eccentricity, and is just balanced by resultant force due to whirling when the whirling frequency is one-half rotational frequency. This result represents the upper limit of whirling frequency for an unloaded ideal bearing. The same result can be deduced more directly by considering the continuity condition that the volume of lubricant passing through the film at some point A, Fig. 1, must equal the volume passing point B plus the volume required to fill the void of the receding journal. In the limiting condition no pressure can exist in the film, hence side leakage is zero, and it follows that

$$\frac{a\Omega}{2}(\eta + \epsilon) = \frac{a\Omega}{2}(\eta - \epsilon) + 2a\omega\epsilon \quad \ldots\ldots\ldots [1]$$

and

---

[1] Research Engineer, Research Laboratories, Westinghouse Electric Corporation.

Contributed by the Applied Mechanics Division and presented at the Annual Meeting, New York, N. Y., November 26–29, 1945, of The American Society of Mechanical Engineers.

Discussion of this paper should be addressed to the Secretary, A.S.M.E., 29 West 39th Street, New York, N. Y., and will be accepted until October 10, 1946, for publication at a later date. Discussion received after the closing date will be returned

Note: Statements and opinions advanced in papers are to be understood as individual expressions of their authors and not those of the Society.

[2] "Self-Induced Vibrations," by J. G. Baker, Trans. A.S.M.E., vol. 55, 1933, paper APM-55-2, sect. 13.

[3] "Shaft Whipping Due to Oil Action in Journal Bearings," by B. L. Newkirk and H. D. Taylor, *General Electric Review*, August, 1925, vol. 28, 1925, p. 559.

[4] "Whirling of a Journal in a Sleeve Bearing," by D. Robertson, *Philosophical Magazine*, series 7, vol. 15, 1933, p. 113.

[5] "Oil-Film Whirl—A Nonwhirling Bearing," by B. L. Newkirk and L. P. Grobel, Trans. A.S.M.E., vol. 56, 1934, p. 607.

$$\omega = \frac{\Omega}{2} \quad \ldots\ldots [2]$$

The same result is obtained regardless of where points A and B are taken.

The same continuity condition may be applied to the general case given in Fig. 2. Assuming that the pressures due to a steady

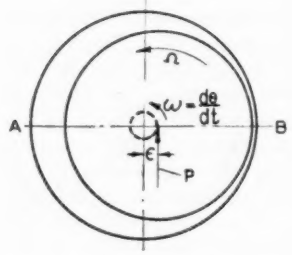


FIG. 1 IDEAL JOURNAL BEARING

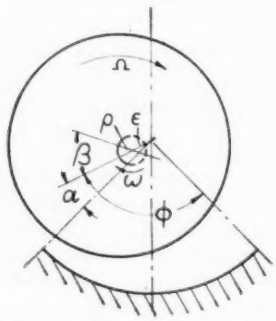


FIG. 2 PARTIAL JOURNAL BEARING

load do not influence the circulation caused by whirling

$$\frac{a\Omega\rho}{2}\cos(\phi+\beta) = -\frac{a\Omega\rho}{2}\cos(\alpha+\beta) + a\omega\rho\cos(\alpha+\beta) - a\omega\rho\cos(\phi+\beta) \quad \ldots\ldots [3]$$

and

$$\omega = \frac{\Omega}{2} \quad \ldots\ldots [2]$$

In reality the upper limit of whirling frequency is reduced more or less from $\frac{\Omega}{2}$ because of fluid friction and bearing leakage.

The actual oil-whirl frequency of a given system is dependent upon other factors besides the bearing; however, it is important to note that whatever its value, it must be less than one half the running frequency of the journals.

IDEAL CASE OF OIL-FILM WHIRL

Referring to Fig. 1, the equations of motion for small oscillations of a journal mass in a fixed ideal bearing are, in polar coordinates

$$\left.\begin{aligned} m\frac{d^2\epsilon}{dt^2} - m\epsilon\left(\frac{d\theta}{dt}\right)^2 &= 0 \\ m\epsilon\frac{d^2\theta}{dt^2} + 2m\frac{d\epsilon}{dt}\frac{d\theta}{dt} &= P \end{aligned}\right\} \quad \ldots\ldots [4]$$

where P can be surmised to be of the form

$$P = B\left(\Omega - 2\frac{d\theta}{dt}\right)\epsilon$$

where B is the bearing characteristic. Its value has been determined by Robertson,[4] and a simplified approximate expression is

$$B = \frac{6\pi\mu w a^2}{\eta^2}$$

Substituting the value of P in Equation [4], assuming a solution of the form $\epsilon = \epsilon_0 e^{\lambda t}$, and remembering that $\frac{d\theta}{dt}$ is a constant for linear systems

$$\lambda^2 + \frac{B}{m}\lambda \pm \frac{B\Omega}{2m} = 0 \quad \ldots\ldots [5]$$

solving for λ

$$\lambda = -\frac{B}{2m} \pm \sqrt{\left(\frac{B}{2m}\right)^2 \mp \frac{B\Omega}{2m}} \quad \ldots\ldots [6]$$

It is evident that a value of λ exists which is real and positive for all values of Ω greater than zero, hence ϵ increases with time and the motion is unstable. From Equation [4]

$$\lambda^2 = \left(\frac{d\theta}{dt}\right)^2$$

and the whirling velocity is

$$\frac{d\theta}{dt} = \omega = -\frac{B}{2m} + \sqrt{\left(\frac{B}{2m}\right)^2 + \frac{B\Omega}{2m}} \quad \ldots\ldots [7]$$

which can be rewritten

$$\omega = -\frac{B}{2m}\left[1 - \sqrt{1 + \frac{2m\Omega}{B}}\right] \quad \ldots\ldots [8]$$

In many cases $\frac{2m\Omega}{B}$ is small compared to unity, and expanding the radical of Equation [8] in a power series and neglecting higher-order terms this equation reduces to

$$\omega \backsimeq \frac{\Omega}{2} \quad \ldots\ldots [9]$$

Hence even though the natural frequency of the system is zero, the driving force is sufficiently strong to give whirling near the upper limit of frequency.

In practical cases with unloaded bearings the amplitude of whirl is limited by the bearing clearance, yet for rigid rotors the conditions with respect to the vibration still correspond closely to the ideal case. Any contact of the journal and bearing effects a tuning of the system so that the frequency may be higher than that indicated in Equation [8].

A vertical pump motor rotor with a self-aligning ball bearing at the top and an 8 × 8-in. full journal bearing at the bottom was observed to whirl in the manner of a pendulum, and from a few revolutions to 1200 rpm the whirling frequency held to slightly less than one-half rotational frequency in accord with calculations based upon the ideal case. Vertical turboblowers and high-speed motors have been observed to exhibit the same characteristics with respect to frequency. The model, Fig. 12, whirled at a frequency slightly less than one-half running frequency when fitted with a full journal bearing as can be noted from records of the vibration Fig. 13 (*a*) and (*b*).

In the lower-speed machines, bearing clearances of about 0.001 in. per in. diam of bearing usually reduces the vibration of rigid rotors to permissible limits. It appears that eccentric running of the journals caused by rotor unbalance may in some cases eliminate whirling of rigid rotors in bearings of small clearance.

DISCUSSION OF THE PROBLEM OF MACHINE STABILITY

The previous example of whirling of a journal mass in a fixed ideal bearing is useful in visualizing the action of the lubricating film in exciting a vibration, and actual cases do occur which can be explained in this simple manner. However, the situation in general is very much more complicated. Formal mathematical consideration of the general case becomes hopelessly complex; however, a qualitative examination can be useful in showing the possible extent of the stability problem and in appraising the

applicability of stability criteria for special cases. For this purpose a dynamical idealization consisting of three spring-damper-mass systems in series, as shown in Fig. 3, is probably sufficiently representative. The parameters k_1, c_1, and m_1 represent the nonrotating parts; k_2 and c_2 represent the lubricating film where c_2 may be positive or negative; and m_2, k_3, c_3, and m_3 represent the rotating element. Of these parameters k_1, c_1, m_1, m_2, and m_3 can be considered as constants and the remaining ones are functions of speed and load, especially k_2 and c_2.

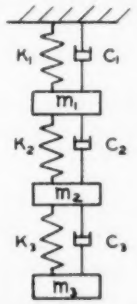


FIG. 3 DYNAMICAL SYSTEM

When the parameters c_1, c_2, and c_3 are positive, i.e., damping elements, it is clear without any analysis that the system is stable for all modes of vibration. In actual cases c_1 is always positive and c_3 can usually be considered negligibly small so that the possibility of self-excited vibration of some natural mode rests with the oil-film parameter c_2. If c_2 is positive the system is stable; if it is negative the system may or may not be unstable. The final answer in this latter case must of course depend upon all parameters of the system. On an energy basis the system is stable when the total damping energy of the system exceeds the total exciting energy for any mode of vibration. This permits the possibility of a negative value of c_2 in a stable system.

Relative motion between the masses m_1 and m_2 is required for the oil film to do work on the system, hence the mode of self-excited oil whirl involves relative motion of journal and bearing. Cases have been observed where the self-excited mode involved considerable motion of both rotating and nonrotating parts; however, the massiveness and the damping of nonrotating parts usually results in small motions of m_1 compared to motions of m_2, and for analysis the bearing may be considered as fixed and the case simplified to a two-mass system. The same situation would occur when the natural frequency of the nonrotating element is high compared to the natural frequency of the rotor.

When the natural frequency of the rotor is somewhat greater than the upper limit of whirling frequency, that is, about one half the running frequency, the rotor behaves as a rigid body so that with fixed bearings the case is a one-mass system, corresponding to the system assumed in the example of the preceding section.

Assumption of fixed bearings is usually essential for a stability analysis, and this assumption is a fairly reasonable one in most cases, and leads to useful results. However, the possibly more complex nature of the stability problem should be kept in mind, in spite of simplifying assumptions for analytical purposes, especially in the diagnosis of a particular case at hand where the mode of vibration can usually be determined. The elimination of oil whip in a particular turbine by a prop under a steam supply pipe becomes less mysterious with the broader view of the problem. It should also become clear that the experimenter must understand his test system if rational results are to be obtained.

SYSTEMS WITH PARTIAL BEARINGS UNDER STEADY LOAD

Partial bearings with clearance are extensively used in the support of horizontal rotors; therefore it is of especial interest to consider systems employing this type of bearing.

The characteristics of the partial bearing can be noted in Fig. 4 which shows the position of the journal center, i.e., the parameters ϵ and γ, as a function of the operating variable $\left(\frac{a}{\eta}\right)^2 \frac{\mu N}{p}$. Naturally the journal locus varies with arc length and width of

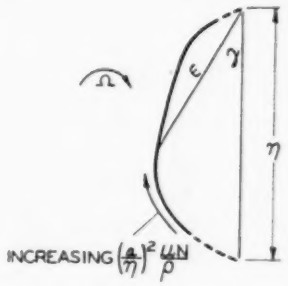


FIG. 4 JOURNAL LOCUS

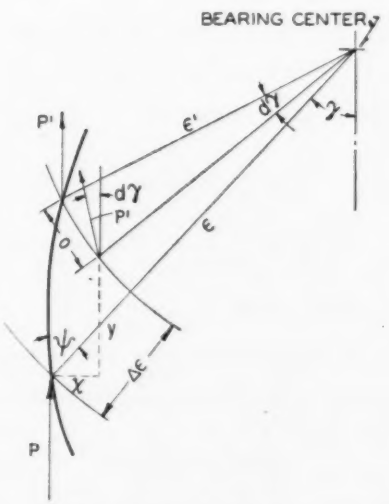


FIG. 5 JOURNAL LOCUS

bearing; however, the loci are similar for the various partial bearings with clearance.

Considering a small angular displacement of a journal $d\gamma$ from some position of equilibrium ϵ and γ, from geometry of the lubricating film, it will be assumed that the resultant film force acting on the journal will not change appreciably in magnitude, but will change its direction by the angle of the displacement. Referring to an enlarged section of the journal locus, Fig. 5, the forces F_x and F_y on the journal for the small displacement (x, y) are

$$\left.\begin{aligned} F_x = P'\frac{o}{\epsilon} &= \frac{P}{\epsilon}\Big[x(\sin\gamma\tan\psi + \cos\gamma) \\ &\qquad - y(\sin\gamma - \cos\gamma\tan\psi)\Big] \\ F_y = \frac{\partial P}{\partial \epsilon}\Delta\epsilon &= \frac{\partial P}{\partial \epsilon}(x\sin\gamma + y\cos\gamma) \end{aligned}\right\} \quad [10]$$

(a) *Rigid Rotor in Fixed Bearings.* If we let

$$\left.\begin{aligned} k_1 &= \frac{P}{\epsilon}(\sin\gamma\tan\psi + \cos\gamma) \\ D_1 &= \frac{P}{\epsilon}(\sin\gamma - \cos\gamma\tan\psi) \\ k_2 &= \frac{\partial P}{\partial\epsilon}\cos\gamma \\ D_2 &= \frac{\partial P}{\partial\epsilon}\sin\gamma \end{aligned}\right\} \quad \ldots\ldots\ldots [11]$$

and assume for the moment that the rotor mass is supported by a single bearing, the equations of motion of the rotor which partakes of the same motion as the journal are[6]

$$\left.\begin{aligned} m\frac{d^2x}{dt^2} + c\frac{dx}{dt} + k_1x - D_1y &= 0 \\ m\frac{d^2y}{dt^2} + c\frac{dy}{dt} + k_2y + D_2x &= 0 \end{aligned}\right\} \quad \ldots\ldots\ldots [12]$$

where m is the mass of the rotor and c is the bearing damping constant taken to be approximately the same in the x- and y-directions.

Assuming a solution of Equation [12] of the form

$$x = A_1e^{\lambda t}, \quad y = A_2e^{\lambda t}$$

the characteristic equation is obtained

$$\lambda^4 + 2\left(\frac{c}{m}\right)\lambda^3 + \left(\frac{k_1}{m} + \frac{k_2}{m} + \frac{c^2}{m^2}\right)\lambda^2 + \left(\frac{k_1c}{m^2} + \frac{k_2c}{m^2}\right)\lambda + \frac{k_1k_2}{m^2} + \frac{D_1D_2}{m^2} = 0 \ldots\ldots [13]$$

This equation is of the form

$$\lambda^4 + a_3\lambda^3 + a_2\lambda^2 + a_1\lambda + a_0 = 0$$

and for stability, by Routh's criteria, the coefficients $a_3 \ldots . a_0$ must be positive, and

$$a_1a_2a_3 > a_1^2 + a_3^2a_0$$

The first requirement is always satisfied and the second requirement yields the condition for stability

$$(k_1 - k_2)^2 + 2c^2\left(\frac{k_1}{m} + \frac{k_2}{m}\right) > 4D_1D_2 \ldots\ldots [14]$$

Solution of Equations [12], assuming zero damping, gives the stability criterion

$$(k_1 - k_2)^2 > 4D_1D_2 \ldots\ldots\ldots\ldots [15]$$

which is, as expected, simply condition [14] without the damping term. This result corresponds to Stodola's criterion, and it may be quite pessimistic because the damping term

$$2c^2\left(\frac{k_1}{m} + \frac{k_2}{m}\right)$$

in the condition, Equation [14], is seldom negligibly small, and in many cases it may be larger than

$$(k_1 - k_2)^2$$

Criterion [14] is applicable to the usual approximately symmetrical system in which the rotor mass is contained between the bearings, and the average film pressure is about the same in each bearing, because in this case the mode of vibration yielding the lower frequency will correspond to the conditions for which Equations [12] are written, namely, that the journals and rotor partake of the same motion. Naturally the various bearing constants in criterion [14] will be the sums of the individual bearing constants.

The constants in criterion [14] can be evaluated for systems employing the 120-deg bearing from the curves, Figs. 6 and 7, and with the following formulas[7]

$$\frac{\partial P}{\partial\epsilon} = \left(\frac{a}{\eta}\right)^2\frac{\mu N}{\eta(b_1 - b_2)}\left(\frac{1}{G_1} - \frac{1}{G_2}\right)A \ldots\ldots [16]$$

where G_1 and G_2 are two values of the operating variable corresponding to b_1 and b_2 taken from the curve Fig. 6(b), in the immediate vicinity of the operating point

$$\tan\psi = \frac{b'(\gamma' - \gamma)}{b - b'} \ldots\ldots\ldots\ldots [17]$$

where b and γ specify the journal position under operating conditions, and b' and γ' define a point at slightly increased value of the operating variable, that is to the left of the operating journal position in Fig. 7.

The damping constant c can be extracted from a later development Equation [43] and is

$$c = \frac{\mu}{2\eta^3}\left(\frac{l^2w^2}{l^2 + w^2}\right) \ldots\ldots\ldots\ldots [18]$$

where the quantities are as defined in the nomenclature.

Criterion [14] indicates, not quite directly, that decreasing values of $\left(\frac{a}{\eta}\right)^2\frac{\mu}{p}$ gives increasing stable speed limits; however, the damping term permits the possibility of a stable system even though the journals are running nearly concentrically. These indications have not as yet been substantiated by systematic tests, but qualitatively the criterion appears to follow field observations.

By considering possible modes of rotor vibration, equivalent systems can be constructed for overhung rotors and for special bearing loadings so that criterion [14] may be applied in these cases.

(b) *Flexible Rotor in Fixed Bearings.* A system in which the lowest natural frequency of the rotor in bending is less than the upper limit of whirling frequency is usually unstable. With lightly loaded bearings this upper limit is a maximum of $\frac{\Omega}{2}$, as established in the section, "Upper Limit of Whirling Frequency," and the stability criterion may be expressed as

$$\omega_n > \frac{\Omega}{2} \ldots\ldots\ldots\ldots [19]$$

which may also be interpreted as the condition for which criterion

[6] "Kritische Wellenstörung Infolge der Nachgiebigheit des Oelpolsters im Lager," by A. Stodola, *Schweizerische Bauzietung*, vol. 85, 1925, p. 265; also "Kritische Drehzahlen als Folge der Nachgiebigheit des Schmiermittels im Lager," by C. Hummel, *Forschungsarbeiten*, V. D. I., Heft 287, 1926. Stodola's equations written specifically for the half-bearings are similar to Equation [12] except the damping term is omitted.

[7] Curves are plotted for real bearings from data in "Effects of Side-Leakage in 120-Degree Centrally Supported Journal Bearings," by S. J. Needs, Trans. A.S.M.E., vol. 56, 1934, table 2, p. 726. Data on other bearings are contained in the paper, "Characteristics of Centrally Supported Journal Bearings," by E. O. Waters, Trans. A.S.M.E., vol. 64, 1942, pp. 711–719.

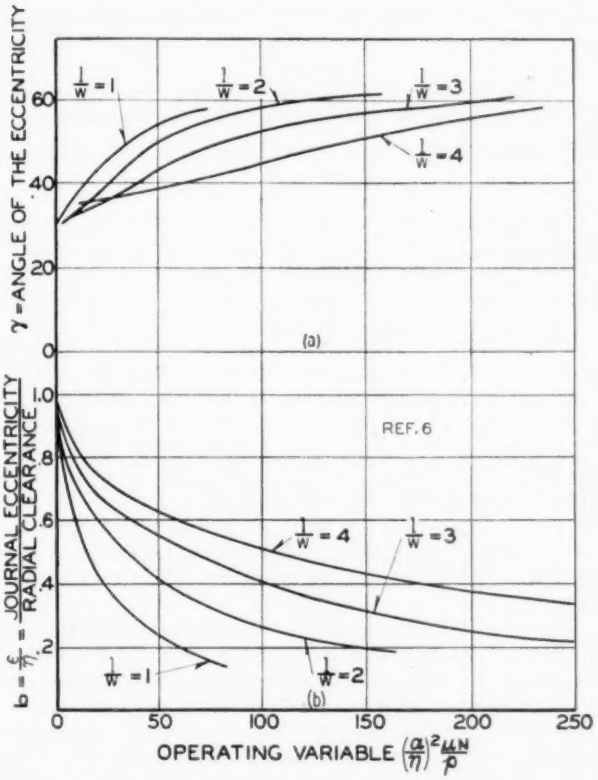


FIG. 6 CHARACTERISTICS OF 120-DEG-CLEARANCE BEARINGS

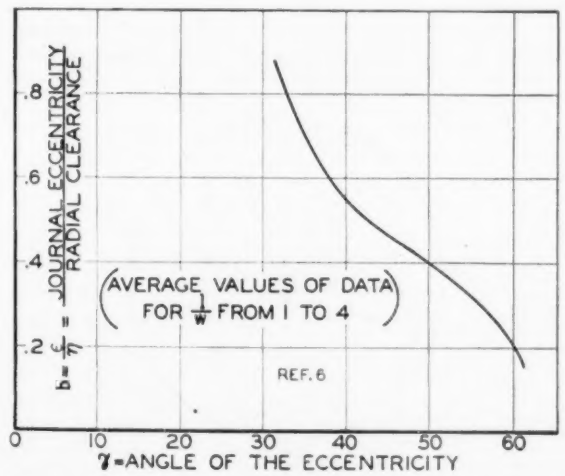


FIG. 7 CHARACTERISTICS OF 120-DEG-CLEARANCE BEARINGS

[14] applies. With heavily loaded bearings the factor $1/2$ in criterion [19] may be replaced by a smaller one, perhaps $1/3$, because the upper limit of whirling frequency is reduced by the increased side leakage which accompanies high film pressures.

Sometimes the mode of vibration may involve small relative motion of journal and bearing so that the energy input to the system is not sufficient to overcome whatever damping exists, and the speed at which instability occurs may be appreciably higher than that indicated by criterion [19]. Heavy and asymmetrical loading of the bearings and possibly imperfect lubrication may occur with bending vibration of the rotor, and doubtless these effects influence the stability characteristics of a system. On these bases it seems plausible that rotors whose mass is contained between bearings may have a higher stable speed than overhung rotors, even though the lowest natural frequencies are the same.

It is desirable to keep the lowest natural frequency of the rotor greater than one-half rotational speed of the machine; however, observance of this rule alone does not preclude the possibility of oil whirl of the rotor as a rigid body, and hence criterion [14] should also be satisfied.

In some designs observance of one or both of the stability criteria for partial bearings may be very difficult or even impossible, and in these cases it may be necessary to employ special damping devices or to substitute other type bearings which are discussed later.

FIXED-PAD BEARINGS

A fixed-pad bearing is a multiple-film type (see Fig. 8) consisting of a series of tapered pads over the bearing surface, each pad being separated by a longitudinal groove. These bearings are especially useful from a stability standpoint for rigid rotors in which the bearing load might be in any direction or for vertical guide purposes.

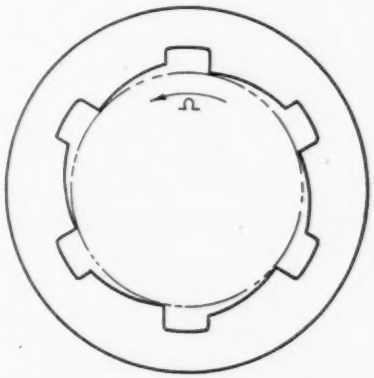


FIG. 8 FIXED-PAD BEARING

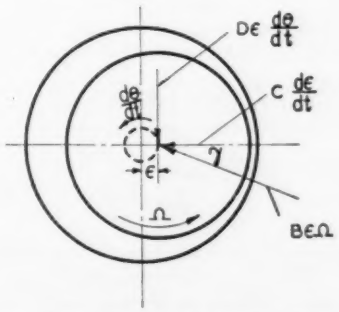


FIG. 9 FORCE SYSTEM, FIXED-PAD BEARING

The characteristics of this bearing are similar to a full sleeve bearing except the resultant film force acting on the journal for eccentricities up to about one half the radial clearance is at some smaller angle to the line connecting journal and bearing centers, as indicated in Fig. 9.

Considering a symmetrical system in which the bearings are lightly loaded, as, for example, a vertical rotor, the equations of motion for the rotor mass which executes the same motion as the journals are

$$\left.\begin{aligned} m\frac{d^2\epsilon}{dt^2} - m\epsilon\left(\frac{d\theta}{dt}\right)^2 + B\Omega\epsilon\cos\gamma + c\frac{d\epsilon}{dt} = 0 \\ m\epsilon\frac{d^2\theta}{dt^2} + 2m\frac{d\epsilon}{dt}\frac{d\theta}{dt} + D\epsilon\frac{d\theta}{dt} - B\Omega\epsilon\sin\gamma = 0 \end{aligned}\right\} \quad \ldots [20]$$

assuming $\epsilon = \epsilon_0 e^{\lambda t}$ in Equation [20] and remembering that $\frac{d\theta}{dt}$ is a constant for oscillations of linear systems, the characteristic equation is

$$\lambda^4 + \left(\frac{D}{m} + \frac{c}{m}\right)\lambda^3 + \left(\frac{D^2}{4m^2} + \frac{B\Omega\cos\gamma}{m} + \frac{cD}{m^2}\right)\lambda^2 + \left(\frac{DB\Omega\cos\gamma}{m^2} + \frac{cD^2}{4m^3}\right) + \left(\frac{D^2B\Omega\cos\gamma}{4m^3} - \frac{B^2\Omega^2\sin^2\gamma}{4m^2}\right) = 0 \quad [21]$$

and the criterion for stability becomes

$$\frac{D^2B\Omega\cos\gamma}{4m^3} > \frac{B^2\Omega^2\sin^2\gamma}{4m^2} \quad [22]$$

which if $B\Omega > 0$ simplifies to

$$\frac{D^2\cos\gamma}{mB\sin^2\gamma} > \Omega \quad [23]$$

Referring again to Fig. 9, at the threshold condition the forces at right angles to the displacement ϵ yield

$$D = \frac{\Omega}{\left(\frac{d\theta}{dt}\right)} B\sin\gamma \quad [24]$$

Substituting Equation [24] into criterion [23] and taking the upper limit of frequency

$$\omega = \frac{d\theta}{dt} = \frac{\Omega}{2}$$

a further simplification of criterion [23] is obtained

$$\frac{4B\cos\gamma}{m} > \Omega \quad [25]$$

This condition for stability is equivalent to criterion [14] where $k_1 = k_2$.

The corresponding criterion for the angular mode in which gyroscopic effect must be taken into account is

$$\frac{4T\cos\gamma}{I_2 - 2I_1} > \Omega \quad [26]$$

where the quantities are as defined in the nomenclature.

Criteria [25] and [26] as previously mentioned apply to the symmetrical case, i.e., where the resultant of bearing forces, for a given rotor translation is directed approximately through the center of gravity of the rotor. Criterion [26] can also be applied to any known angular mode by taking the bearing moments and rotor inertia about the nodal point.

If we multiply criterion [25] by Ω we get a familiar looking form

$$\omega_n > \frac{\Omega}{2} \quad [25a]$$

since $B\Omega\cos\gamma$ is the "spring constant" of the bearing. This suggests that asymmetrical systems can be considered by calculating the natural frequency of the rotor on the "springs" of the lubricating films and then testing for stability using Criterion [25a].

A series of experiments, the details of which cannot be revealed at this time, were carried out to test the validity of criteria [25] and [26] and the results were in good agreement with predictions, utilizing measured load-deflection characteristics of the test bearings.

A recent article[8] in the German literature gives some characteristics of the multiple-pad bearing which may prove useful in stability studies.

Tilting-Pad Bearings

The stability aspects of the tilting-pad journal bearing seem to have been neglected in the literature. This is quite unusual because it has most interesting and useful characteristics; indeed the tilting-pad bearing can be rightly classified as a so-called "stable" or "nonwhirling" bearing.[9]

The stability of dynamical systems considered in previous sections was indicated from the character of the solution of the equations of motion. For the case of the tilting-pad bearing, an energy consideration appears attractive because it leads to a more complete result. Evidently if the exciting energy or work done per cycle of displacement, by the oil-film pressures generated by journal rotation, is less than the damping energy or work done per cycle on the oil film as a result of machine vibration, the system is stable. Conversely, an excess of exciting energy for some mode of vibration indicates the possibility of self-induced vibration.

In the development which follows it is assumed that the bearing-pad arrangement satisfies conditions for the static stability of the rotor; that the flow of lubricant is laminar in character; that each pad is mounted at a point which can be called the pad pivot point, and that this point is fixed relative to the bearing assembly; that the pad-pivot-point friction is small compared to other forces and can properly be neglected, and that thus a pad adjusts its position about the pivot point under the action of the oil-film pressures alone.

(a) *Exciting Energy.* Considering a single pad of the bearing assembly, the lubricating-film forces caused by journal rotation are, Fig. 10, the resultant P of the film pressures acting on the journal through its center, a reaction of the film pressures P' equal to P and acting along a line through the center of pad curvature, a fluid friction force F acting on the journal and a reaction F' acting on the pad. If d is the moment arm of P' about the pad

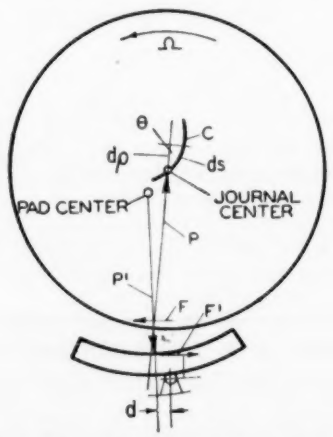


Fig. 10 Force System of Tilting-Pad Journal Bearing

[8] "Reibungswiderstand und Tragkraft eines Gleitschuhes endlicher Breite," by W. Frossel, *Forschung auf dem Gebiete des Ingenieurwesens*, vol. 13, No. 2, March and April, 1942.

[9] The Nomy-pad bearing is also a "stable" type although it may not be particularly applicable to the higher-speed machines where stability becomes a problem.

pivot point, and g is the moment arm of F' about the same point, by equilibrium of the pad

$$d = \frac{F'}{P'} g$$

The moment arm g is small (possibly zero) compared to other pad dimensions, and since the quantity $\frac{F'}{P'}$ the coefficient of friction is very small compared to unity, the moment arm d becomes so extremely small that P' can be considered as always acting through the pad pivot point. Further, the center of pad curvature and the journal center are separated by a small distance compared to the bearing radius, and it follows that the lubricating force P acting on the journal through its center is directed through the pad pivot point.

Because the bearing pad is pivoted and free to rotate, not only is the direction of P from pivot point to journal center, but the magnitude of P is a single-valued function of the distance ρ separating the pivot point and journal center.

$$P = f(\rho) \ldots\ldots\ldots\ldots\ldots\ldots [27]$$

where $f(\rho)$ is a single-valued function of the magnitude of ρ only. The work done on the journal and its counterparts by P for a displacement of the journal center along any curve c is expressed by the line integral

$$\text{Work} = \int_c f(\rho) \cos\theta ds \ldots\ldots\ldots\ldots [28]$$

where θ is the angle between the direction of the force P, that is the direction of ρ, and the direction of the displacement ds on the curve c.

But $\cos\theta = \frac{\partial\rho}{\partial s}$, so that Equation [28] becomes

$$\text{Work} = \int_c f(\rho) d\rho \ldots\ldots\ldots\ldots\ldots [29]$$

If c is a closed curve, the important result is obtained that the work W_P done by the principal force P during one complete cycle is

$$W_P = \oint_c f(\rho) d\rho = 0 \ldots\ldots\ldots\ldots [30]$$

because the integration is carried out over a range of ρ first in one sense and then in the opposite sense. It follows that zero work is done on the rotor by the film pressures of a plurality of pads making up the bearing without stipulation as to number or arrangement, and that this result is not altered by the effect of a steady bearing load or by machine characteristics as for example critical speeds.[10]

The result Equation [30] does not hold true for the plain journal bearing or a fixed-pad bearing previously considered because in these cases the direction of P is not always through a fixed point in the bearing, so that for these we do not have $\cos\theta = \frac{\partial\rho}{\partial s}$, and hence we may not pass from Equation [28] to Equations [29] and [30].

The friction force F acting on the journal does positive work on the rotor if the journal center moves along some area-enclosing path in a direction opposite to the journal rotation. However, it can be judged that this effect is negligibly small, and rightly so because calculations indicate that the rotational frequency would have to be several hundred times the lowest natural frequency of the system before the friction energy could overcome damping in the bearing which will now be considered.

[10] It is obvious that similar conclusions apply to any motion of the bearing and associated parts considering the journal as fixed.

(*b*) *Damping Energy.* In the previous part of this section the forces considered were generated by rotation of the journal about its center; in this part the forces considered are generated by motion of the journal center along some curve as may be effected by machine vibration. It is assumed that the force functions are approximately linear for eccentricities of the journal center up to about one half the radial clearance η, and so for the purpose at hand the effect of journal rotation on the force component caused by journal center motion can be neglected.

A given displacement of the journal toward a particular pad results in a decrease in the film thickness h, and during the displacement lubricant is "squeezed" out of the decreasing clearance volume; conversely, if the displacement is away from the pad the lubricant is "drawn" into the increasing clearance volume.

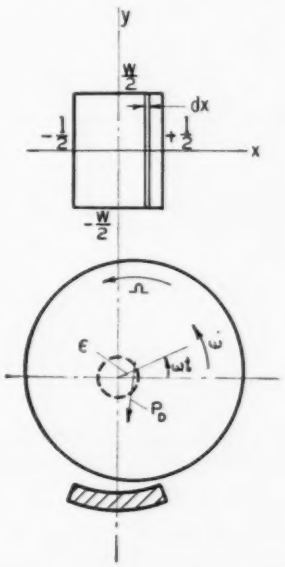


FIG. 11 DAMPING FORCE-ENERGY SYSTEM

In either case the resulting force is in opposition to the journal center velocity during the displacement and thus the motion is damped.

Neglecting inertia forces, the equation of laminar flow of fluid between two planes is

$$\frac{dp}{dx} + \frac{12 Q_x \mu}{h^3} = 0 \ldots\ldots\ldots\ldots [31]$$

where $\frac{dp}{dx}$ is the pressure gradient, Q_x is the flow in the x-direction, μ is the viscosity of the fluid, and h is the distance separating the planes. For the present case, Fig. 11, where the journal center is executing a circular motion about the bearing center, that is a harmonic vibration, and assuming flow in the x-direction only

$$\left.\begin{aligned} Q_x &= \epsilon\omega x \cos\omega t \\ h_0 &= \eta + \epsilon \sin\omega t \end{aligned}\right\} \ldots\ldots\ldots\ldots [32]$$

where h_0 is the film thickness at the pivot point and is taken to represent the average h over the pad; the pivot is assumed to be approximately in the center of the pad. Letting

$$\Phi = \frac{\epsilon\omega \cos\omega t}{(\eta + \epsilon \sin\omega t)^3}$$

Equation [31] becomes

$$\frac{dp}{dx} + 12\mu\Phi x = 0 \quad \ldots\ldots [33]$$

Integrating Equation [33] and using the boundary conditions at $x = \pm \frac{l}{2}$, $p = 0$, the pressure p is

$$p = 6\mu\Phi\left[\left(\frac{l}{2}\right)^2 - x^2\right] \quad \ldots\ldots [34]$$

The total force P_x over the area of the pad of width w for flow in the x-direction is

$$P_x = 6\mu\Phi w \int_{-l/2}^{+l/2}\left[\left(\frac{l}{2}\right)^2 - x^2\right] dx$$

or

$$P_x = \mu\Phi w l^3 \quad \ldots\ldots [35]$$

Similarly if flow occurs in the y-direction only

$$P_y = \mu\Phi l w^3 \quad \ldots\ldots [36]$$

Actually flow occurs in both x- and y-directions, i.e., the flow is in parallel, and the resisting or damping force P_D is

$$P_D = \frac{P_x P_y}{P_x + P_y} \quad \ldots\ldots [37]$$

or

$$P_D = \mu\Phi\left(\frac{l^3 w^3}{l^2 + w^2}\right) \quad \ldots\ldots [38]$$

The work done per cycle W by the rotor on the oil film (period = T) for a circular oscillation of the journal center about the bearing center is

$$W = \int_0^T P_D v dt \quad \ldots\ldots [39]$$

The force P_D is given by Equation [38], v is $\epsilon\omega \cos \omega t$, substituting $d(\omega t)$ for dt, and changing the upper limit to 2π

$$W = \mu\omega\epsilon^2\left(\frac{l^3 w^3}{l^2 + w^2}\right)\int_0^{2\pi} \frac{\cos^2 \omega t d(\omega t)}{(\eta + \epsilon \sin \omega t)^3} \quad \ldots\ldots [40]$$

The definite integral in Equation [40] can be evaluated to a good approximation by substituting η^3 for the denominator of the function under the integral sign, and W for n pads becomes

$$W = \frac{n\pi\mu\omega\epsilon^2 l^3 w^3}{\eta^3(l^2 + w^2)} \quad \ldots\ldots [41]$$

For square pads of side s Equation [41] becomes

$$W = \frac{n\pi\mu\omega\epsilon^2 s^4}{2\eta^3} \quad \ldots\ldots [42]$$

Equation [41] is damping energy per cycle of journal oscillation, whether the oscillation is forward or backward with respect to journal rotation, because the forces in either case oppose journal center motion.

The damping constant c for a tilting-pad bearing can be readily determined from Equation [41] by dividing by $2\pi\epsilon^2\omega$

$$c = \frac{n\mu}{2\eta^3}\left(\frac{l^3 w^3}{l^2 + w^2}\right) \quad \ldots\ldots [43]$$

The damping of the tilting-pad bearing, as indicated by the foregoing formulas, is of the same order of magnitude as the damping in other types of journal bearings; however, in contradistinction to the more conventional types, the tilting-pad bearing is incapable of doing work on the journal regardless of the mode of machine vibration. Hence not only is the bearing incapable of exciting or sustaining a vibration, but the bearing damping is effective in overcoming rotor frictional effects which sometimes lead to instability.[11,12,13]

(*c*) *Experiments.* A simple experimental model, shown in cross section in Fig. 12, was improvised to check qualitatively the

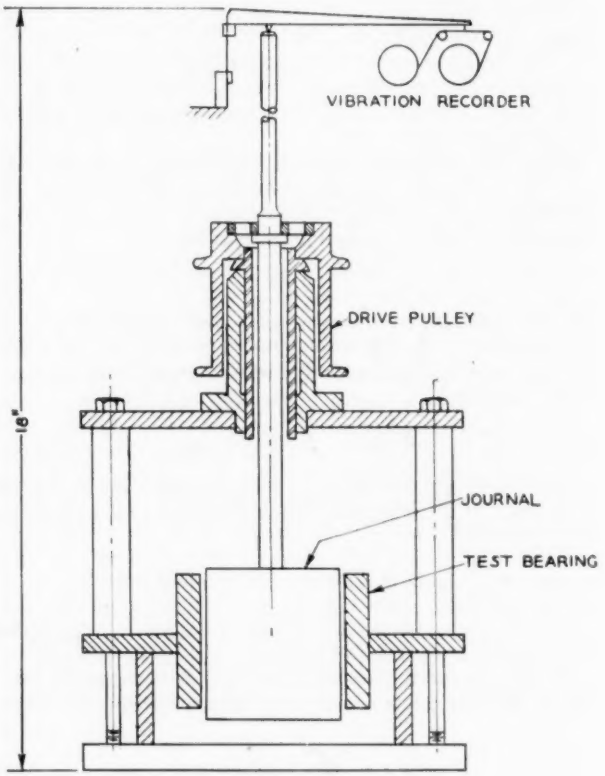


FIG. 12 TEST MODEL

results of the analysis. The journal consisted of a brass plug about 2.7 in. diam and 3 in. long, and was supported through a spindle by means of a metal disk attached to a drive pulley. The drive pulley in turn was supported by close-fitting guide bearings and a thrust surface. The metal disk acted as a spring hinge and the rotor vibration was about this hinge in the manner of a pendulum. The natural frequency of this system was very low; about 3 cycles per sec. The upper extension of the spindle was utilized with a stylus and recorder to secure records of a lateral component of the journal center motion.

A plain guide bearing was installed in the model initially to check whether damping in the model other than that in the test bearing could obscure the results, and also to secure oil-whirl records for comparative purposes. Two tests were carried out with a plain bearing using light mineral oil for the lubricant; the viscosity of the oil was 18 centipoises at the operating temperature. The first test was made with a bearing clearance of 0.005

[11] "Shaft Whipping," by B. L. Newkirk, *General Electric Review*, vol. 27, March, 1924, pp. 169–178.

[12] "Internal Friction Theory of Shaft Whirling," by A. L. Kimball, *General Electric Review*, vol. 27, April, 1924, pp. 244–251.

[13] "Influence of Friction Forces on the Stability of High-Speed Rotors," by P. Kapitza, *Journal of Physics*, Institute for Physical Problems, Moscow, U.S.S.R., vol. 1, 1939, no. 1, pp. 29–50.

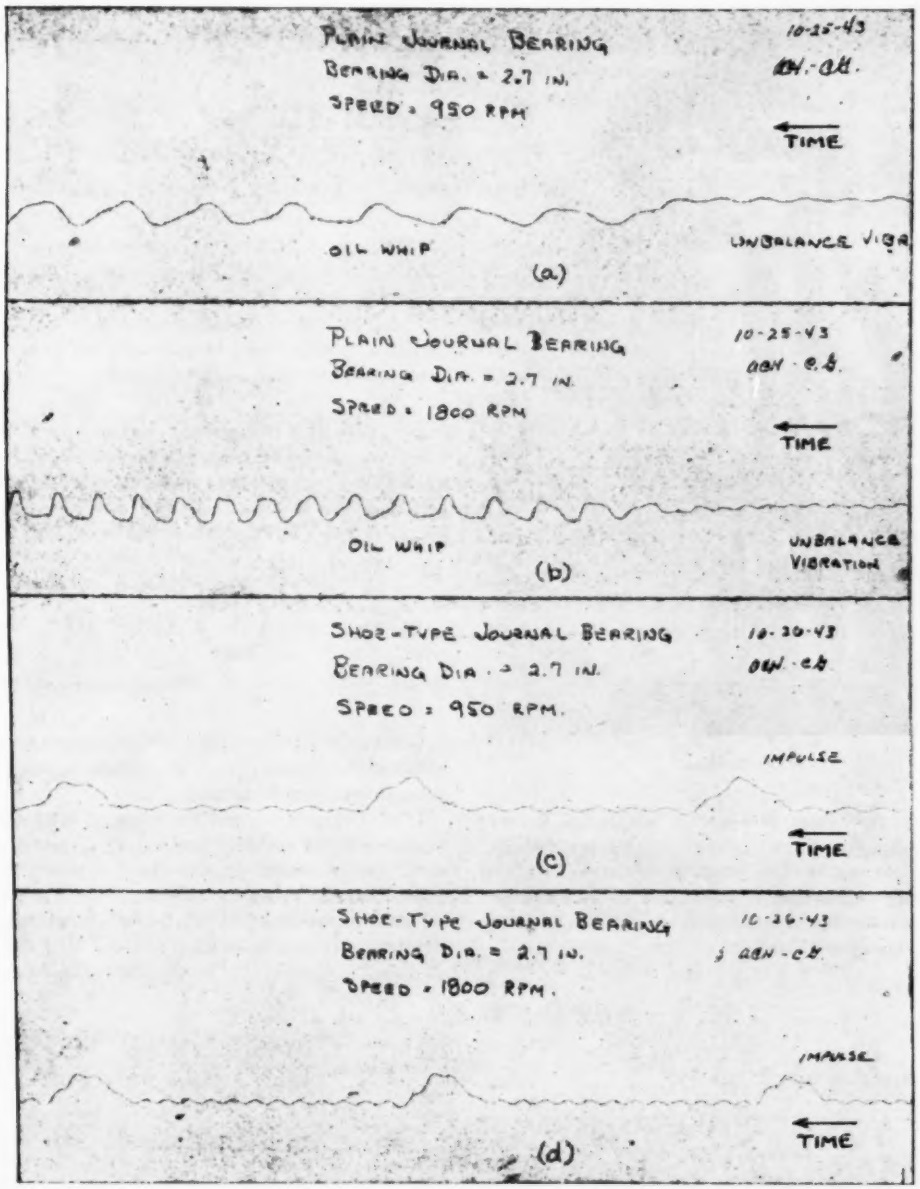


FIG. 13 VIBRATION RECORDS

in. on the diameter, and in the second test the clearance was increased to 0.030 in. on the diameter. In both cases violent whirling occurred at a frequency of slightly less than one-half rotational frequency; the amplitude of vibration was, of course, considerably greater in the second test. Records of this vibration at 950 rpm and 1800 rpm are shown in Fig. 13(*a*) and (*b*). The right-hand part of the record in which only unbalance vibration is shown was obtained by damping the rotor by hand; it can be noticed that upon release the whipping starts within 1 revolution of the journal.

The tilting-pad bearing tested consisted of six segmental pads which were supported radially through pivot buttons by a steel ring, and were held in position by flat steel strips. The flat strips, besides providing axial and tangential support for the pads, also provide a slight spring action which holds the pads against the steel ring. One or more pads could be readily removed from the bearing assembly and thus the effect of number and arrangements of pads on stability could be checked. The model with the pad bearing installed is shown in Fig. 14.

Two sets of tests were carried out with various numbers and arrangements of the bearing pads as identified in Fig. 15. The lubricant was the same as previously used. As indicated in the table, the model was stable in all cases. Records of the journal vibration operating with a six-pad arrangement and 0.030 in. diametral clearance are shown in Fig. 13(*c*) and (*d*). The jumps in the records were caused by load impulses applied to the journal by hand in an effort to excite vibration. It can be noted that the journal motion caused by the impulse is damped out within about 2 revolutions of the journal, and all that remains is the forced vibration caused by unbalance.

SUMMARY AND CONCLUSION

The self-excited vibration commonly called oil-film whirl or oil whip has been discussed and methods of approaching this in-

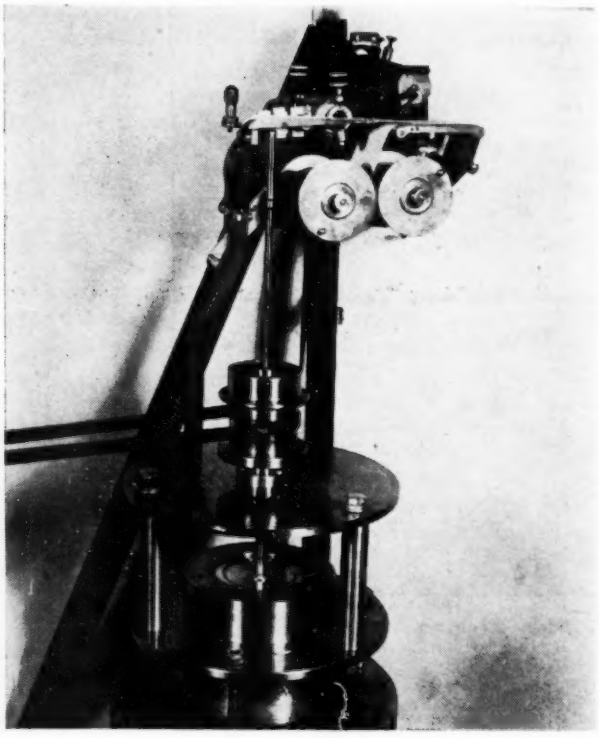


FIG. 14 TEST MODEL

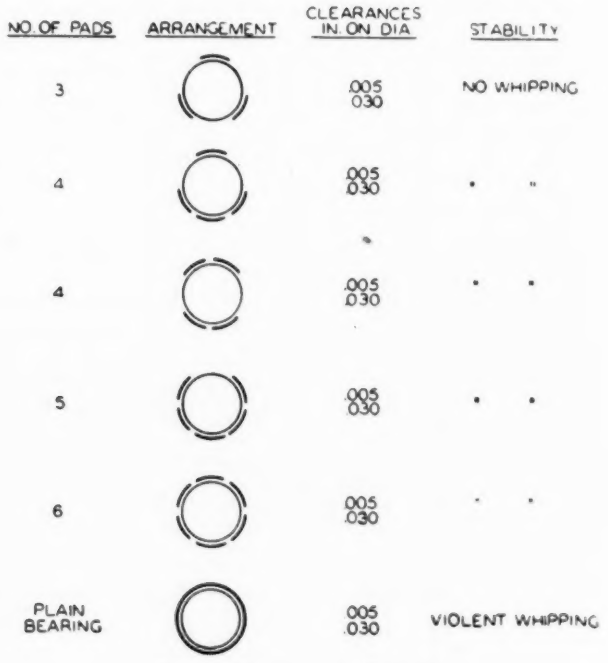


FIG. 15 STABILITY OF BEARINGS

creasingly important vibration problem in a rational manner have been indicated. For certain common systems stability criteria have been developed. The tilting-pad bearing has been found to be incapable of exciting or sustaining a vibration and hence appears very promising in application to high-speed rotors where stability is sometimes difficult to achieve.

Qualitatively, the results of this paper appear to be in agreement with observations. In certain cases criteria have been substantiated experimentally.

It is obviously beyond the scope of this paper to classify and pigeon-hole the stability problem in terms of the many possible variations in conditions and types of machines; however, it is hoped that the methods and results are a step toward the establishment of rational and practicable design criteria for achieving stability of rotating machinery.

Analytical Expressions for Principal Strains

By W. T. THOMSON,[1] MADISON. WIS.

Recent methods by G. Murphy (1)[2] and N. J. Hoff (2) enable the graphical evaluation of principal strains from strains measured along any three intersecting lines. When the two angles between gage lines are equal, the principal strains may be determined from simple analytical expressions without reference to the graphical solution.

STRAIN rosettes are generally constructed with equal angles between gages, the common rosettes having gages oriented at 45 or 60 deg with each other. When gage 1 and 3 are symmetrically oriented with respect to gage 2, as shown in Fig. 1, the principal strains may be evaluated from the following equations

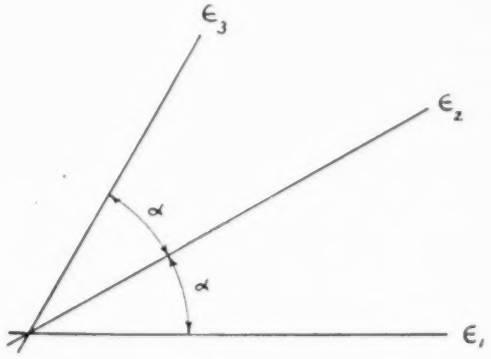


FIG. 1

$$\tan[2(\alpha + \theta) - 90] = \frac{(\epsilon_1 - 2\epsilon_2 + \epsilon_3)}{(\epsilon_1 - \epsilon_3)\tan\alpha} \quad \ldots\ldots [1]$$

$$\epsilon_{\substack{\max \\ \min}} = \epsilon_2 + \frac{(\epsilon_1 - 2\epsilon_2 + \epsilon_3)}{2\sin 2\alpha \tan\alpha} \pm \frac{(\epsilon_1 - \epsilon_3)}{2\sin 2\alpha \cos[2(\alpha + \theta) - 90]} \quad \ldots\ldots [2]$$

$$\lambda_{\max} = \frac{(\epsilon_1 - \epsilon_3)}{\sin 2\alpha \cos[2(\alpha + \theta) - 90]} \quad \ldots\ldots [3]$$

where

θ = angle measured from principal strain to ϵ_1 (positive counterclockwise)

α = angle between gages

Proof. Construct Mohr's circle, Fig. 2, as outlined by G. Murphy (1). The construction is started by scaling ϵ_1, ϵ_2, ϵ_3, horizontally from an arbitrary vertical axis. Lines, each making the angle α with the vertical, are then drawn through an arbitrary point D on the vertical through ϵ_2. The intersection of these lines with verticals through ϵ_1 and ϵ_3 determines the circle ACD. The center of the circle O is now determined and the line OA then makes an angle 2θ and the graphical solution is complete.

To develop the analytical expressions for the principal strains, continue with the following construction. Draw a perpendicular bisector to line AC. It will pass through the center of the circle and point B, and the triangle ABC will be isosceles with the two equal angles equal to α. Triangles ABO, ABD, and ABC all subtend the same arc, and hence angle $BCA = \alpha$ and angle $BOA = 2\alpha$. The other angles are then obvious from the diagram.

The angle θ between the principal strain and ϵ_1 is determined from the right triangle ACE, from which the following equation is obtained

$$\tan[2(\alpha + \theta) - 90] = \frac{(\epsilon_1 - 2\epsilon_2 + \epsilon_3)}{(\epsilon_1 - \epsilon_3)\tan\alpha} \quad \ldots\ldots [1]$$

For the magnitudes of the principal strains, the co-ordinate of the center of the circle is determined and the radius R of the circle is added or subtracted. The co-ordinate of the center of the circle is

$$O'O = \epsilon_2 + R\sin[2(\alpha + \theta) - 90] \quad \ldots\ldots [a]$$

From triangle ACE

$$AC = \frac{(\epsilon_1 - \epsilon_3)}{\cos[2(\alpha + \theta) - 90]} \quad \ldots\ldots [b]$$

From triangle AFO

$$R = \frac{AC}{2\sin 2\alpha} = \frac{(\epsilon_1 - \epsilon_3)}{2\sin 2\alpha \cos[2(\alpha + \theta) - 90]} \quad \ldots\ldots [c]$$

Substituting for R in [a]

$$O'O = \epsilon_2 + \frac{(\epsilon_1 - \epsilon_3)}{2\sin 2\alpha} \cdot \tan[2(\alpha + \theta) - 90]$$

$$= \epsilon_2 + \frac{(\epsilon_1 - 2\epsilon_2 + \epsilon_3)}{2\sin 2\alpha \tan\alpha} \quad \ldots\ldots [d]$$

Adding or subtracting R, the principal strains become

$$\epsilon_{\substack{\max \\ \min}} = \epsilon_2 + \frac{(\epsilon_1 - 2\epsilon_2 + \epsilon_3)}{2\sin 2\alpha \tan\alpha} \pm \frac{(\epsilon_1 - \epsilon_3)}{2\sin 2\alpha \cos[2(\alpha + \theta) - 90]} \quad \ldots\ldots [2]$$

The maximum shear strain is the difference of the principal strains, which from Equation [2] becomes

$$\lambda_{\max} = \epsilon_{\max} - \epsilon_{\min} = \frac{(\epsilon_1 - \epsilon_3)}{\sin 2\alpha \cos[2(\alpha + \theta) - 90]} \quad \ldots [3]$$

---

[1] Associate Professor of Mechanics, University of Wisconsin.

[2] Numbers in parentheses refer to the Bibliography at the end of the paper.

Presented at the National Meeting of the Applied Mechanics Division, Buffalo, N. Y., June 21–22, 1946, of THE AMERICAN SOCIETY OF MECHANICAL ENGINEERS.

Discussion of this paper should be addressed to the Secretary, A.S.M.E., 29 West 39th Street, New York, N. Y., and will be accepted until October 10, 1946, for publication at a later date. Discussion received after the closing date will be returned.

NOTE: Statements and opinions advanced in papers are to be understood as individual expressions of their authors and not those of the Society.

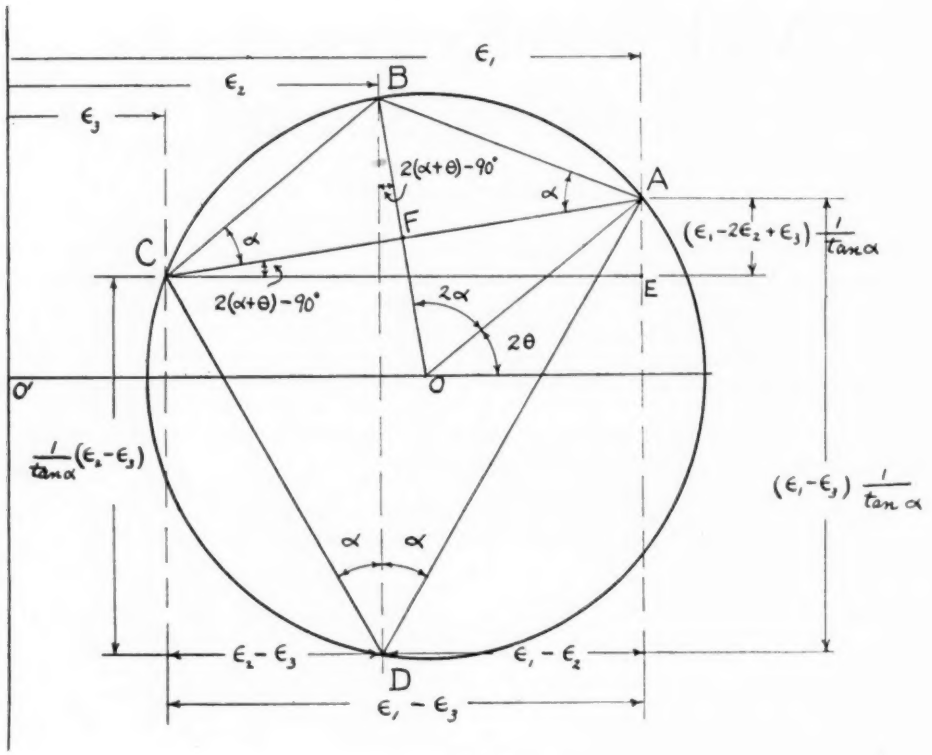


FIG. 2

Special Case for $\alpha = 45$ Deg. When $\alpha = 45$ deg, the line AC becomes the diameter of the circle. The substitution of $\alpha = 45$ deg into the general equations results in the following special equations

$$\tan 2\theta = \frac{(\epsilon_1 - 2\epsilon_2 + \epsilon_3)}{(\epsilon_1 - \epsilon_3)}$$

$$\epsilon_{\substack{\max \\ \min}} = \frac{\epsilon_1 + \epsilon_3}{2} \pm \frac{(\epsilon_1 - \epsilon_3)}{2 \cos 2\theta}$$

$$\lambda_{\max} = \frac{\epsilon_1 - \epsilon_3}{\cos 2\theta}$$

Special Case for $\alpha = 60$ Deg. Substituting $\alpha = 60$ deg, the special equations for the 60-deg rosettes become

$$\tan (30 + 2\theta) = \frac{(\epsilon_1 - 2\epsilon_2 + \epsilon_3)}{\sqrt{3}(\epsilon_1 - \epsilon_3)}$$

$$\epsilon_{\substack{\max \\ \min}} = \frac{1}{3}(\epsilon_1 + \epsilon_2 + \epsilon_3) \pm \frac{(\epsilon_1 - \epsilon_3)}{\sqrt{3} \cos (30 + 2\theta)}$$

$$\lambda_{\max} = \frac{2(\epsilon_1 - \epsilon_3)}{\sqrt{3} \cos (30 + 2\theta)}$$

BIBLIOGRAPHY

1 "A Graphical Method for the Evaluation of Principal Strains From Normal Strains," by G. Murphy, JOURNAL OF APPLIED MECHANICS, Trans. A.S.M.E., vol. 67, 1945, p. A-209.

2 "A Graphic Resolution of Strain," by N. J. Hoff, JOURNAL OF APPLIED MECHANICS, Trans. A.S.M.E., vol. 67, 1945, p. A-211.

3 "A Graphical Solution for Strains and Stresses From Strain Rosette Data," by R. Contini, *Journal of the Aeronautical Sciences*, vol. 12, 1945, pp. 47–50.

4 "Circles of Strain," by J. A. Wise, *Journal of the Aeronautical Sciences*, vol. 7, 1940, pp. 438–440.

5 "A Semi-Graphical Method for Analyzing Strains Measured on Three or Four Gage Lines Intersecting at 45°," by H. N. Hill, National Advisory Committee for Aeronautics, Technical Note 709, 1939.

Flat Spring With Large Deflections

By F. HYMANS,[1] NEW YORK, N. Y.

This paper gives an analysis of a flat spring initially curved and inserted in the apparatus of which it is an element in a buckled condition. The unstressed spring is shaped in the arc of a circle, and it is shown that then, and only then, the problem may be reduced to that of an initially straight bar by adding to the actually impressed force a couple which, if acting alone, produces the initial curved shape. On this basis the paper ascertains the various possible shapes of the buckled spring and the forces associated with them. It is shown that these must have at least one point of inflection of the elastic line. More particularly, there are two shapes, each with a single point of inflection, yet differing widely in their properties. In one of them there is a range of instability while the other is stable throughout. Finally, it is shown how by a suitable variation of parameter shapes two or more points of inflection may be obtained.

THIS paper is concerned with a rather unusual case of a flat spring which has been proposed as an element in one of the designs of the author's company. In its initial and unstressed shape, as shown in dotted lines in Fig. 1, it is formed in the arc of a circle of radius R. The spring is then buckled inward by hand, its ends fitted between two supports B and B_1, whereupon the spring when freed of constraint assumes some shape as BAB_1 shown in full lines in Fig. 1. In this shape the spring is equilibrated by two equal and opposite forces Q, and the problem is to determine shape and properties of the buckled spring under the action of various forces Q.

One of these properties is that the curvature at B and B_1 remains unaltered at the initial value $1/R$ inasmuch as at the said points the forces Q have no bending moment. On account of symmetry it is also clear that only one half of the spring, say, the half AB, need be considered with the end A appearing as clamped or fixed, as shown in Fig. 2(*a*).

The initial curvature at any point of the spring as for example at C is $1/R$. If then ρ is the radius of curvature at C in the stressed configuration, the change in curvature in the present case will be expressed by

$$1/\rho + 1/R$$

The + sign here is used because of the fact that in the stressed condition the curvature of the element under consideration is the reverse of the initial curvature.

According to the theory of flexure, the change in curvature must equal the bending moment divided by the flexural rigidity EI, and with spring referred to axes AX and AY in Fig. 2*a*, this leads to the equation

$$1/\rho + 1/R = Q(y_B - y)/EI \quad \ldots\ldots\ldots\ldots [1]$$

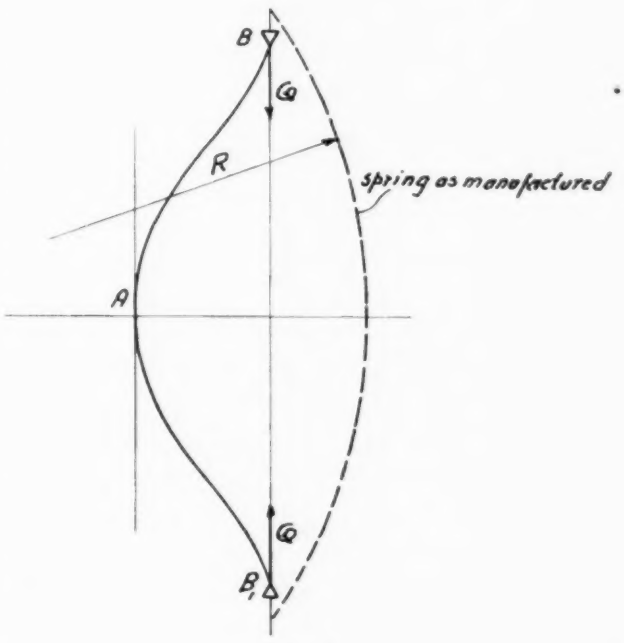


FIG. 1

Placing

$$1/R = M/EI \quad \ldots\ldots\ldots\ldots\ldots\ldots [1a]$$

M has the meaning that it is the couple which if acting at the free end of an initially straight spring will bend it into the arc of a circle of radius R and so will produce its initial curved shape.

Substituting for R in Equation [1] gives

$$1/\rho = \{-M + Q(y_B - y)\}/EI$$

This, however, is the equation of a bar, initially straight, subject at its free end B to a force Q and a couple M, as shown in Fig. 2(*b*). Thus the problem can be reduced to that of an initially straight spring by adding to the force Q a couple M, a simplification possible only when the initial shape is the arc of a circle.

We proceed then on the basis of a straight spring clamped at A and subject at B to a force Q and couple M, both shown dotted in Fig. 2(*c*). These, as is known, may be replaced by a single force Q shown in full lines and acting at a distance h from A, given by

$$h = M/Q \quad \ldots\ldots\ldots\ldots\ldots\ldots [2]$$

Thus the problem can further be conceived as that of an initially straight spring fixed at A, provided at B with a rigid arm h, subject at its free end to a force Q. As the actually applied force Q (dotted vector in Fig. 2*c*) remains vertical in all configurations of the spring, the equivalent force Q at the free end of lever h also remains vertical and the arm h in each configuration of the spring must be conceived as so attached as to remain horizontal.

While dealing with the present problem in this manner it must be understood that M as related to the initial curvature by (*1a*) is a constant. Varying the loading of the spring requires then the simultaneous varying of both the magnitude of Q at the end of

---

[1] Otis Elevator Company. Mem. A.S.M.E.

Presented at the National Meeting of the Applied Mechanics Division, Buffalo, N. Y., June 21–22, 1946, of THE AMERICAN SOCIETY OF MECHANICAL ENGINEERS.

Discussion of this paper should be addressed to the Secretary, A.S.M.E., 29 West 39th Street, New York, N. Y., and will be accepted until October 10, 1946, for publication at a later date. Discussion received after the closing date will be returned.

NOTE: Statements and opinions advanced in papers are to be understood as individual expressions of their authors and not those of the Society.

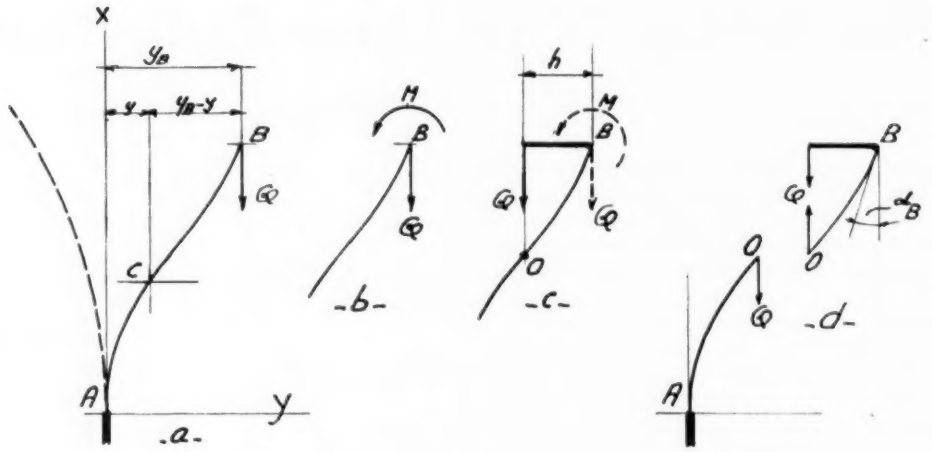


FIG. 2

lever h and the length of h, so as to satisfy the relation of Equation [2] in every instance. An increase in Q is then associated with a decrease of h and vice versa. In view of the sense of rotation of M in connection with the permanently downward direction of the actually applied force Q at B, it is clear that the free end of lever h always lies to the left of B. Therefore h remains a positive quantity under all conditions of loading.

In replacing the dotted vectors Q and M in Fig. 2(*c*) by a single force Q, it is immediately apparent that a point O in the line of action of Q is a point of inflection of the elastic line inasmuch as the bending moment at that point is zero. Shapes with more than one point of inflection, if they exist, must have all such points on the line of action of Q. Shapes with points of inflection outside this line cannot occur. Furthermore, if the spring be cut at its point of inflection O, as in Fig. 2(*d*), the mutual action of one portion on the other at O can only be a force. Therefore branch OA presents the well-known case of a column[1] fixed at A and subject to a force Q at O. The upper branch OB is also a column loaded at O by a force Q but fixed at B under an angle α_B with the vertical.

Since in the loaded spring the curvature at B remains the initial curvature, as there must be at least one point of inflection somewhere between A and B, and inasmuch as the elastic line at A must be tangent to the vertical, it is easy to draw some plausible characteristic shape for the spring. One such shape is shown in Fig. 3 on the basis of which the analysis proceeds.

The origin of axes is most conveniently taken at the point of inflection O, and branch OB of the elastic line is referred to vertical and horizontal axes OX and OY drawn in full lines, while for branch OA the axes are reversed as shown by the dotted lines OX' and OY'. In this arrangement of axes, general equations developed for one branch also apply to the other.

Taking a point E on branch OB or E' on OA the bending moment with due respect to their respective system of axes is

$$M_b = +Qy$$

and hence the rigorous equation of the elastic line is

$$d\alpha/ds = -Qy/EI \quad \ldots\ldots\ldots\ldots\ldots\ldots [3]$$

where $d\alpha/ds$ is the curvature at E, respectively E', α the slope of the elastic line at these points, and (ds) is an element of the arc.

Substituting

$$ds = dy/\sin \alpha$$

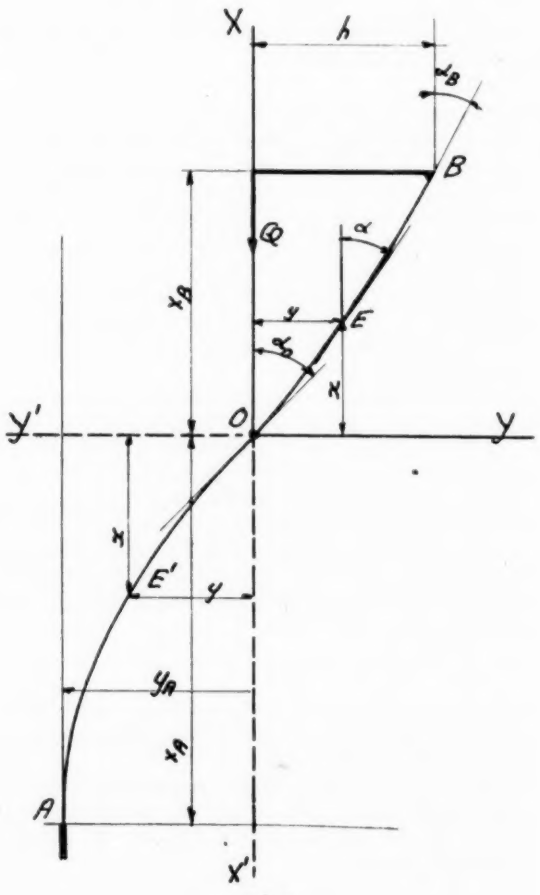


FIG. 3

we obtain

$$\sin \alpha d\alpha = -Qydy/EI$$

Noting that at O the slope of the elastic line is α_0 and $y = 0$, we have by integration

$$\left[\cos \alpha\right]_{\alpha_0}^{\alpha} = \frac{Q}{2EI}\left[y^2\right]_0^y$$

whence

$$y\sqrt{Q/2EI} = \pm\sqrt{\cos \alpha - \cos \alpha_0} \quad \ldots\ldots\ldots [4]$$

[1] "Der belastete stab", by L. Saalschuetz. Published by B. G. Teubner, Leipzig, Germany, 1880.

Leaving it for the present undecided whether the + or — sign must be used in the foregoing, one requirement is that y must be real and the term under the radical on the right must therefore be positive. Now α_0 is the slope of the elastic line at O, and in the present problem the only slopes possible at that point may be expressed as $0 \leqq \alpha_0 \leqq \pi$. While thus the slope at O with respect to the system of axes is limited to a positive angle not greater than π, we may without loss of generality specify slopes at other points as either positive or negative angles limited to $0 \leqq \alpha \leqq +\pi$ in the first case and to $0 \geqq \alpha \geqq -\pi$ in the second.

With slopes so limited the expression under the radical in Equation [4] is positive only when α, whether positive or negative, is numerically smaller or at most numerically equal to α_0.

Should the elastic line have more than one point of inflection, all such points as already stated must lie on the line of action of Q. With the system of axes as in Fig. 3, y for all such points is zero, and thus we derive from Equation [4]

$$\cos \alpha = \cos \alpha_0$$

$$\alpha = \pm \alpha_0$$

Hence it is one property of the elastic line in the present problem that at points of inflection the slopes are numerically equal and greater than at other points.

Writing Equation [4] in the form

$$y = \pm 2 \sqrt{EI/Q} \sin \frac{\alpha_0}{2} \sqrt{1 - \frac{\sin^2 \alpha/2}{\sin^2 \alpha_0/2}} \quad \ldots\ldots [4a]$$

we introduce at this point a new variable φ, expressed by

$$\frac{\sin \alpha/2}{\sin \alpha_0/2} = \sin \varphi \quad \ldots\ldots [5]$$

Therein φ is a parameter of the elastic line specifying its slope in function of the slope at O. All quantities related to the configuration of the elastic line will be expressed in function of φ which so becomes the independent variable.

From Equation [5] we derive for future use by differentiation

$$d\alpha = \frac{2 \sin \frac{\alpha_0}{2} \cos \varphi d\varphi}{\sqrt{1 - \sin^2 \frac{\alpha_0}{2} \sin^2 \varphi}} \quad \ldots\ldots [5a]$$

With the new variable according to Equation [5], Equation [4a] becomes

$$y = \pm 2 \sqrt{EI/Q} \sin \frac{\alpha_0}{2} \cos \varphi \quad \ldots\ldots [6]$$

In this equation $\sin \alpha_0/2$ is always positive in view of an earlier conclusion that α_0 is a positive angle not greater than π. To φ, however, we can always assign such values that make $\cos \varphi$ either positive or negative as may suit the problem. It appears therefore to be only a matter of convenience to use the + or — sign in Equation [6]. Deciding to use the former, we write

$$y = 2 \sqrt{EI/Q} \sin \frac{\alpha_0}{2} \cos \varphi \quad \ldots\ldots [6a]$$

According to Equation [6a], shapes as in Fig. 3 with positive ordinates only with respect to the chosen system of axes will be obtained where $\cos \varphi$ is positive for all points of the elastic line. For such shapes, then, φ must be an angle in the first or fourth quadrants, and without loss of generality we may limit φ in the case first named to angles expressed by $0 \leqq \varphi \leqq +\pi/2$ and in the latter case to angles $0 \geqq \varphi \geqq -\pi/2$. The next step is to determine for immediate and future use the value of the parameter φ at the terminals of branches OA and OB, Fig. 3.

These are obtained from Equation [5], and with the object of developing the equations for shapes with positive ordinates, as in Fig. 3, the values to be assigned to φ must comply with the conclusions previously reached. Thus we have

$$\left.\begin{array}{l} \text{At } A;\ \alpha = 0; \text{ whence according to Equation [5] } \sin \varphi = 0; \\ \qquad\qquad \text{and } \varphi = 0 \\ \text{At } O;\ \alpha = \alpha_0; \text{ whence according to Equation [5] } \sin \varphi = \\ \qquad\qquad +1; \text{ and } \varphi = \pi/2 \end{array}\right\} \quad [7]$$

At B, Fig. 3, the slope $\alpha = \alpha_B$ and denoting by φ_B the corresponding value of φ, we further obtain from Equation [5]

$$\sin \frac{\alpha_B}{2} = \sin \frac{\alpha_0}{2} \sin \varphi_B \quad \ldots\ldots [7a]$$

with the understanding that the value to be assigned to φ_B is not greater than $\pi/2$ nor smaller than $-\pi/2$.

The ordinates at B and A are obtained from Equation [6a]. For the former, substitute $y = h$ and $\varphi = \varphi_B$ and for the latter $y = y_A$ and $\varphi = 0$ to obtain

$$h = 2 \sqrt{EI/Q} \sin \frac{\alpha_0}{2} \cos \varphi_B \quad \ldots\ldots [8]$$

$$y_A = 2 \sqrt{EI/Q} \sin \frac{\alpha_0}{2} \quad \ldots\ldots [8a]$$

whence

$$y_A = h/\cos \varphi_B \quad \ldots\ldots [8b]$$

For the purpose of numerical calculations we modify Equation [8] by eliminating Q from it by means of the relation $Qh = M$, which results in

$$\sqrt{h} = 2 \sqrt{EI/M} \sin \frac{\alpha_0}{2} \cos \varphi_B$$

Herein EI/M is the initial radius of curvature R of the spring, whence

$$h = 4R \sin^2 \frac{\alpha_0}{2} \cos^2 \varphi_B \quad \ldots\ldots [9]$$

Another and necessary relation between the variables is obtained by determining the length of branches OB and OA. Denoting the first by S_{OB}, the latter by S_{OA} and by l, the length of the spring from A to B we have

$$l = S_{OB} + S_{OA}$$

For the determination of S_{OB} and S_{OA} we return to general Equation [3]

$$d\alpha/ds = -Qy/EI$$

and substitute therein for $d\alpha$ from Equation [5a] and y from Equation [6a]. This gives

$$\sqrt{Q/EI}\, ds = -\frac{d\varphi}{\sqrt{1 - \sin^2 \frac{\alpha_0}{2} \sin^2 \varphi}} \quad \ldots\ldots [10]$$

Its integration from O to B where according to Equations [7] and [7a], the corresponding values of φ are $\pi/2$ at O and φ_B at B gives S_{OB}. Similarly S_{OA} is obtained by integration from O to A with $\varphi = 0$ at A and $\varphi = \pi/2$ at O. Hence

$$\left.\begin{aligned}\sqrt{Q/EI}\,S_{OB} &= -\int_{\varphi=\pi/2}^{\varphi=\varphi_B}\frac{d\varphi}{\sqrt{1-\sin^2\frac{\alpha_0}{2}\sin^2\varphi}}\\ &= \int_0^{\pi/2}\frac{d\varphi}{\sqrt{1-\sin^2\frac{\alpha_0}{2}\sin^2\varphi}} - \int_0^{\varphi_B}\frac{d\varphi}{\sqrt{1-\sin^2\frac{\alpha_0}{2}\sin^2\varphi}}\end{aligned}\right\}\quad[11]$$

and

$$\left.\begin{aligned}\sqrt{Q/EI}\,S_{OA} &= -\int_{\varphi=\pi/2}^{\varphi=0}\frac{d\varphi}{\sqrt{1-\sin^2\frac{\alpha_0}{2}\sin^2\varphi}}\\ &= \int_0^{\pi/2}\frac{d\varphi}{\sqrt{1-\sin^2\frac{\alpha_0}{2}\sin^2\varphi}}\end{aligned}\right\}$$

or, in the usual notation of elliptic integrals

$$\sqrt{Q/EI}\,S_{OB} = K - F\left(\frac{\alpha_0}{2}\cdot\varphi_B\right)\quad[12a]$$

$$\sqrt{Q/EI}\,S_{OA} = K\quad[12b]$$

Adding these we obtain

$$l\sqrt{Q/EI} = 2K - F\left(\frac{\alpha_0}{2}\cdot\varphi_B\right)$$

or with $Q = M/h$ and $M/EI = 1/R$

$$l\sqrt{1/R} = \left\{2K - F\left(\frac{\alpha_0}{2}\cdot\varphi_B\right)\right\}\sqrt{h}$$

and eliminating h between this equation and Equation [9]

$$\frac{l}{2R} = \sin\frac{\alpha_0}{2}\cos\varphi_B\left\{2K - F\left(\frac{\alpha_0}{2}\cdot\varphi_B\right)\right\}\quad[13]$$

There remains now the determination of the abscissas of the elastic line. For an arbitrary point E on OB or E' on OA we have

$$ds = \frac{dx}{\cos\alpha} = \frac{dx}{1-2\sin^2\frac{\alpha}{2}}$$

or according to Equation [5]

$$ds = \frac{dx}{1-2\sin^2\frac{\alpha_0}{2}\sin^2\varphi}$$

Substituting for ds in Equation [10] we obtain

$$\sqrt{Q/EI}\,dx = -\frac{\left(1-2\sin^2\frac{\alpha_0}{2}\sin^2\varphi\right)d\varphi}{\sqrt{1-\sin^2\frac{\alpha_0}{2}\sin^2\varphi}}$$

$$= -2\sqrt{1-\sin^2\frac{\alpha_0}{2}\sin^2\varphi}\,d\varphi + \frac{d\varphi}{\sqrt{1-\sin^2\frac{\alpha_0}{2}\sin^2\varphi}}$$

Noting that $x = 0$ at O where, according to Equations [7], the corresponding value of φ is $\pi/2$ we obtain by integration

$$\sqrt{Q/EI}\left[x\right]_0^x = -2\int_{\pi/2}^{\varphi}\sqrt{1-\sin^2\frac{\alpha_0}{2}\sin^2\varphi}\,d\varphi + \int_{\pi/2}^{\varphi}\frac{d\varphi}{\sqrt{1-\sin^2\frac{\alpha_0}{2}\sin^2\varphi}}\quad[14]$$

or

$$x\sqrt{Q/EI} = 2\int_0^{\pi/2}\sqrt{1-\sin^2\frac{\alpha_0}{2}\sin^2\varphi}\,d\varphi - 2\int_0^{\varphi}\sqrt{1-\sin^2\frac{\alpha_0}{2}\sin^2\varphi}\,d\varphi - \int_0^{\pi/2}\frac{d\varphi}{\sqrt{1-\sin^2\frac{\alpha_0}{2}\sin^2\varphi}} + \int_0^{\varphi}\frac{d\varphi}{\sqrt{1-\sin^2\frac{\alpha_0}{2}\sin^2\varphi}}$$

which in the usual notations for elliptic integrals assumes the form

$$x\sqrt{Q/EI} = 2\left\{E - E\left(\frac{\alpha_0}{2}\cdot\varphi\right)\right\} - K + F\left(\frac{\alpha_0}{2}\cdot\varphi\right)\quad[14a]$$

The abscissas x_B and x_A of the end points of the elastic line, Fig. 3, are obtained from Equation [14a] by substituting x_B and x_A for x and $\varphi = \varphi_B$, respectively, $\varphi = 0$, the latter according to Equations [7] and [7a] being the values of φ for the points B and A. Hence

$$x_B\sqrt{Q/EI} = 2\left\{E - E\left(\frac{\alpha_0}{2}\cdot\varphi_B\right)\right\} - K + F\left(\frac{\alpha_0}{2}\cdot\varphi_B\right)\quad[14b]$$

and

$$x_A\sqrt{Q/EI} = 2E - K\quad[14c]$$

In view of Equations [12a] and [12b] these can be written

$$x_B = 2\sqrt{EI/Q}\left\{E - E\left(\frac{\alpha_0}{2}\cdot\varphi_B\right)\right\} - S_{OB}\quad[15a]$$

and

$$x_A = 2\sqrt{EI/Q}\,E - S_{OA}\quad[15b]$$

As stated in connection with the derivation of Equation [7a], φ_B in the foregoing equations must either be a positive or negative angle numerically smaller than $\pi/2$ for shapes as in Fig. 3, with positive ordinates only. However, for a negative φ_B, numerical calculations require some modification of these equations and for that reason that case will be considered later.

An example is here worked out for a spring according to the following data

Initial radius of curvature $R = 11.25$ in.; length of spring A to B, $l = 6.75$ in.; $EI = 540$ lb $\times$ in.^{2}; $M = EI/R = 540/11.25 = 48$ in. $\times$ lb; $EI/M = R = 11.25$ in.

$$l/2R = \frac{6.75}{2\times 11.25} = 0.3$$

The limiting case where equilibrium is possible occurs for $\alpha_B = 0$ and in that case the tangent at B, Fig. 3, becomes parallel to the tangent to the elastic line at A. In the absence of an ex-

ternal force between A and B it can be concluded without mathematics that the point of inflection then lies midway between A and B, that the two branches of the elastic line must be identical in shape, of equal lengths and so positioned as to be diametrically symmetrical with respect to O.

With $\alpha_B = 0$ in Equation [7a], $\varphi_B = 0$ and therewith we obtain from Equation [13]

$$l/2R = 2K \sin \alpha_0/2$$

or numerically

$$K \sin \alpha_0/2 = 0.15$$

for the calculation of α_0. By the use of a table of elliptical integrals it will be found that $\alpha_0/2 = 5° -28'$, $K = 1.5744$ and $K \sin \alpha_0/2 = 1.499$ which is close enough to the desired value of 0.15. Similarly with $\varphi_B = 0$, we obtain as expected from Equations [8b] and [9]

$$y_A = h = 4R \sin^2 \alpha_0/2 = 45 \sin^2 5° - 28' = 0.410 \text{ in.}$$

and thence from Equation [2]

$$Q = M/h = 48/0.410 = 116.96 \text{ lb}$$

Also as expected $\varphi_B = 0$ in Equations [12a] and [12b] results in $S_{OB} = S_{OA}$ so that

$$S_{OB} = S_{OA} = l/2 = 6.75/2 = 3.375 \text{ in.}$$

With $S_{OB} = S_{OA}$ and $\varphi_B = 0$ in Equations [15a] and [15b], we obtain

$$x_B = x_A = 2\sqrt{EI/Q}\, E - l/2$$

E for a modulus of $5° -28'$ is 1.5672 and thus

$$x_B = x_A = 2 \times 1.5672 \sqrt{540/116.96} - 3.375 = 3.360 \text{ in.}$$

In Fig. 5 the shape of the spring for $\alpha_B = 0$ is given by curve 1. By assuming various values for α_B, other shapes of the same general type may be obtained in the manner just followed for $\alpha_B = 0$. It is, however, simpler to assume various values of α_0 and to obtain from Equation [13] the corresponding values of φ_B for each of them. To facilitate these calculations we have plotted in Fig. 4 the values of

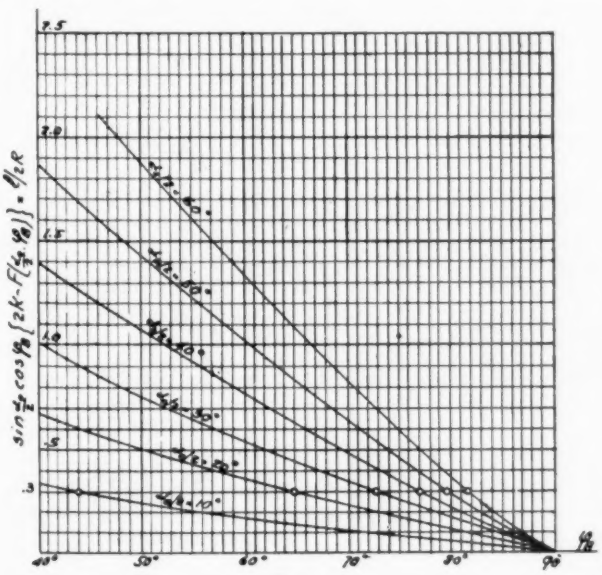


FIG. 4

$$\sin \frac{\alpha_0}{2} \cos \varphi_B \left\{2K - F\left(\frac{\alpha_0}{2} \cdot \varphi_B\right)\right\},$$

as ordinates against φ_B as abscissas for an assumed $\alpha_0/2 = 10°$, 20°, 30°, 40°, etc. According to Equation [13] the ordinates of these curves represent the corresponding values of $l/2R$ which in this example is 0.3. Thus, drawing a horizontal at 0.3 from the axis of φ_B, the intersections with the curves for $\alpha_0/2 = 10°$, 20°, etc., give the values of φ_B which are solutions of Equation [13] for the selected values of $\alpha_0/2$, subject to the accuracy obtainable in the preparation of such curves. Each of these determines a shape of the elastic line of the general type of Fig. 3, as well as of the load Q associated with it.

For example for $\alpha_0/2 = 10°$, the graph gives a value of $\varphi_B = 44°$ which, according to accurate calculations happens to be true within a few seconds. From tables of elliptic integrals we then obtain for $\alpha_0/2 = 10°$ and $\varphi_B = 44°$: $K = 1.5828$; $F(10°, 44°) = 0.7700$; $E = 1.5589$; $E(10°, 44°) = 0.7659$, and the calculations proceed as follows

From Equation [7a]

$$\alpha_B/2 = 6° - 56'$$
$$\alpha_B = 13° - 52'$$

From Equation [9]

$$h = 0.702 \text{ in.}$$

From Equation [2]

$$Q = M/h = 48/0.702 = 68.36 \text{ lb}$$

From Equation [8b]

$$y_A = 0.971 \text{ in.}$$

From Equations [12a] and [12b]

$$S_{OB} = 2.301 \text{ in.}; \quad S_{OA} = 4.459 \text{ in.}$$

From Equations [15a] and [15b]

$$x_B = 2.151 \text{ in.}; \quad x_A = 4.314 \text{ in.}$$

A check on the accuracy of these results may be obtained by adding S_{OB} and S_{OA} which should give $l = 6.75$ in.

Results of these and similar calculations are given in Table 1 and the corresponding shapes of the spring are shown in Fig. 5.

With reference to Fig. 5, the properties of the spring for a positive φ_B are the following:

1 The loads Q to produce increasing deformations first diminish and then increase, whereby the point of inflection O steadily moves upward.

2 For the same load Q there are two different shapes with different deformations as, for example, shapes 3 and 5. For shapes between these the load Q is less and if, after having the spring in equilibrium in shape 3, it is given a slight displacement to the right it will not return to 3 but will assume shape 5. In fact shapes 1, 2, 3, 4 are unstable. Stable shapes are 5 and 6 where Q increases with increasing deformation.

3 Assuming that the spring is in equilibrium in shape 5 with $Q = 51.02$ lb, if then Q be suddenly reduced to, say, 48 lb, slightly below the apparent minimum of 49.2 lb in shape 4, the spring will snap back over center toward its initial unstressed shape. In this manner vigorous snap action can be obtained by slight reduction of the load.

A second set of shapes, also with all ordinates positive with respect to the chosen system of axes, is associated with a negative φ_B, provided that φ_B according to what was said in connection with the derivation of Equation [7a] is an angle not smaller than $-\pi/2$. As the sine of such an angle is negative it follows from Equation [7a] that the slope of the elastic line at B is also a negative angle. For a general discussion, one such shape is shown in

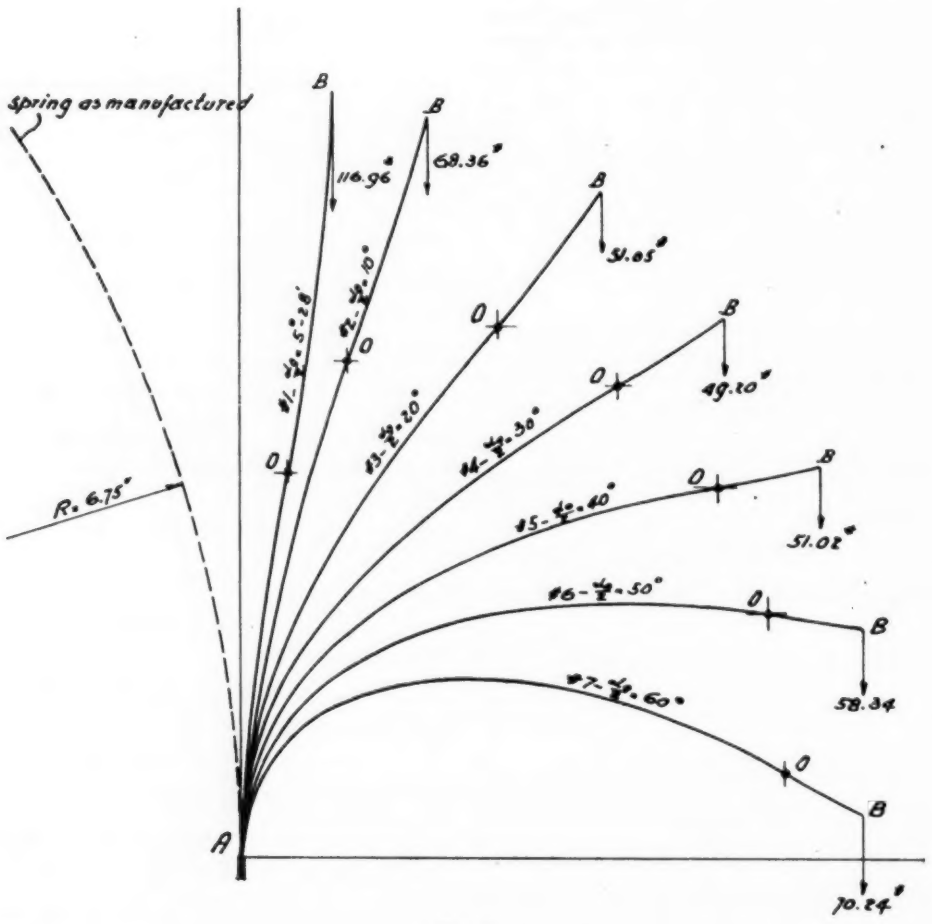


FIG. 5

Fig. 6, referred to the same system of axes adopted before, and various facts become evident without recourse to mathematics.

If we produce BB_1 parallel to OX and CD normal to and bisecting BB_1 it will be seen that the bending moment is the same for all points of arc BCB_1 located symmetrically with respect to CD. In the absence of an external force between B and B_1 it follows that arc BC is the same as B_1C and that both are positioned symmetrically with CD. At C then the ordinate is a maximum and the slope zero. Furthermore, at B as at B_1 the bending moment is $Qh = M$, and the curvature at these points is the initial curvature. Because of symmetry with respect to CD the slopes at the said points are equal in magnitude, negative at B and positive at B_1. Thus at B in Fig. 3 and B_1 in Fig. 6 the curvatures are the initial curvature and the slopes are both positive, from which follows that arc AOB_1 in Fig. 6 and AOB in Fig. 3 are similar as to shape.

Next, at A and C the tangents to the elastic line are parallel, from which we conclude that arcs OA and OC are identical as to shape, of equal lengths and positioned diagonally symmetrical with respect to O. From this follows that $y_C = y_A$ and $x_C = x_A$. With reference to a negative φ_B, the complete elliptic integrals K and E being independent of φ_B remain unchanged. For the incomplete elliptic integrals, however, we have

$$F\left(\frac{\alpha_0}{2} \cdot -\varphi_B\right) = -F\left(\frac{\alpha_0}{2} \cdot \varphi_B\right)$$

and

$$E\left(\frac{\alpha_0}{2} \cdot -\varphi_B\right) = -E\left(\frac{\alpha_0}{2} \cdot \varphi_B\right)$$

Thus of the previous equations only Equation [7a] and those comprising incomplete elliptic integrals experience changes in sign and in sign only. However, for the sake of completeness the equations which follow comprise all of the equations used in the present numerical computations, including those not affected by a negative φ_B

$$\left.\begin{aligned}
&\sin(-\alpha_B/2) = \sin\frac{\alpha_0}{2}\sin\varphi_B \text{ changed from Equation [7}a\text{]}\\
&\sqrt{Q/EI}\,S_{OB} = K + F\left(\frac{\alpha_0}{2}\cdot\varphi_B\right) \text{ changed from Equation [12}a\text{]}\\
&\sqrt{Q/EI}\,S_{OA} = K \quad \text{unchanged Equation [12}b\text{]}\\
&l/2R = \sin\frac{\alpha_0}{2}\cos\varphi_B\left\{2K + F\left(\frac{\alpha_0}{2}\cdot\varphi_B\right)\right\} \text{ changed from Equation [13]}\\
&x_B = 2\sqrt{EI/Q}\left\{E + E\left(\frac{\alpha_0}{2}\cdot\varphi_B\right)\right\} - S_{OB} \text{ changed from [15}a\text{]}\\
&x_A = 2\sqrt{EI/Q}\,E - S_{OA} \quad \text{unchanged [15}b\text{]}
\end{aligned}\right\} \ldots [16]$$

The limiting case of equilibrium occurs as before for $\varphi_B = 0$ and

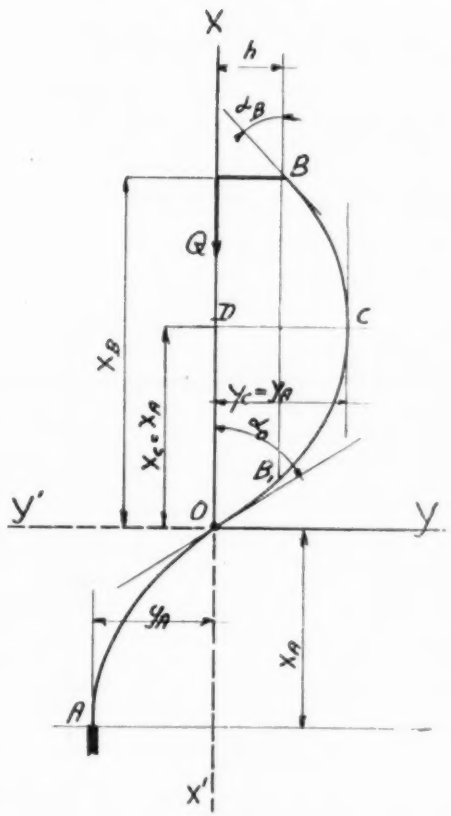


FIG. 6

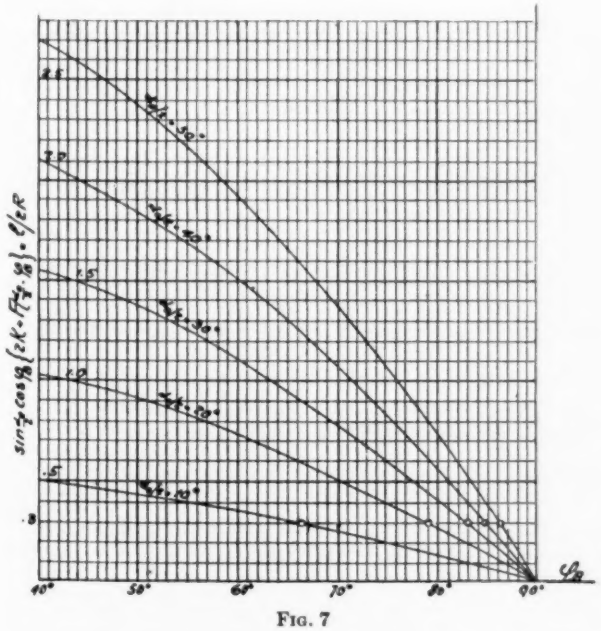


FIG. 7

the corresponding shape is obviously the same as No. 1 in Fig. 5. Again, as an aid in calculations Fig. 7 is the plot of

$$\sin\frac{\alpha_0}{2}\cos\varphi_B\left\{2K + F\left(\frac{\alpha_0}{2}\cdot\varphi_B\right)\right\}$$

TABLE 1 RESULTS OF ANALYTICAL CALCULATIONS

$\alpha_0/2$ deg-min	α_0 deg-min	α_B deg-min	h in.	y_A in.	X_A in.	X_B in.	Q, lb	Shape Fig. 5
5–28	10–56	0	0.410	0.410	3.360	3.360	116.96	No. 1
10	20	13–52	0.702	0.971	4.314	2.151	68.36	No. 2
20	40	36–7	0.940	2.225	4.643	1.200	51.05	No. 3
30	60	57–4	0.976	3.305	4.138	0.590	49.20	No. 4
[40	80	77–34	0.941	4.183	3.251	0.179	51.02	No. 5
50	100	97–53	0.823	4.660	2.055	—0.157	58.34	No. 6
[60	120	118–1	0.683	4.802	0.747	—0.384	70.24	No. 7

which is the function on the right of the fourth of Equations [16] against φ_B as abscissas for several values of $\alpha_0/2$. Drawing as before a line parallel to the axis of φ_B at a distance 0.3 from it, the intersections with the curves for $\alpha_0/2 = 10°, 20°, 30°$, etc., disclose the corresponding values of φ_B that satisfy the fourth of Equation [16]. The process of calculation is otherwise the same as employed earlier and the results are given in Table 2.

TABLE 2 RESULTS OF CALCULATIONS

$\alpha_0/2$ deg-min	α_0 deg-min	α_B deg-min	h in.	$y_A = y_C$ in.	$X_A = X_C$ in.	X_B in.	Q lb	Shape Fig. 8
5–28	10–56	0	0.410	0.410	3.36	3.36	116.96	..
10	20	—18–20	0.216	0.542	2.392	4.171	222.48	No. 1
20	40	—39–15	0.187	0.991	2.068	3.909	257.34	No. 2
30	60	—59–30	0.167	1.371	1.713	3.323	287.28	No. 3
40	80	—79–37	0.147	1.653	1.285	2.545	326.70	No. 4
50	100	—99–40	0.125	1.814	0.800	1.620	385.22	No. 5

The corresponding shapes are drawn in Fig. 8 and it will be seen that the properties of shapes associated with a negative φ_B are radically different. All of the present shapes are stable and by increasing or decreasing the load the spring can be brought from one shape into another.

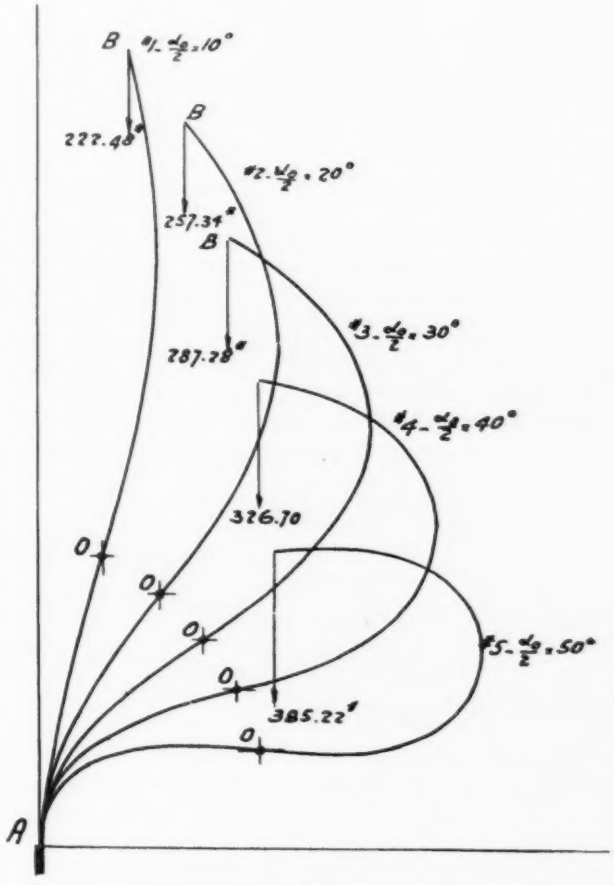


FIG. 8

It will have been noted in the foregoing that shapes according to Fig. 3 and Fig. 6 are associated with the particular values assigned to the parameter φ at the ends of branches OA and OB. With these assigned the values of φ at other points become intermediate between the terminal values.

As there is no restriction in the values that may suitably be assigned to φ at the terminals so long as they satisfy Equation [5], there are, in addition to the shapes discussed before, an infinity of others although none of them is of practical value. To be noted is that in the shapes of Fig. 3 and Fig. 6 the value of φ at A and B are smaller than at O and this rule must be observed to obtain other shapes. One example may suffice.

With reference to Fig. 9 which shows one of the shapes referred to with two points of inflection, let us assign to φ the same values at O and B as in Equations [7] and [7a] so that branch OB will be the same as to shape as in Fig. 3. At A, Fig. 9, $\alpha = 0$ and according to Equation [5] $\sin \varphi = 0$. However, instead of taking $\varphi = 0$ as in Equations [7], we shall now take $\varphi = -\pi$ with the result, as explained later, that we obtain arc $OCO'A$ of Fig. 9 instead of OA of Fig. 3.

While the first of Equations [11] remains undisturbed, the limit $\varphi = 0$ in the second must be replaced by $\varphi = -\pi$, whence

$$\sqrt{Q/EI}\, S_{OA} = \int_{-\pi}^{\pi/2} \frac{d\varphi}{\sqrt{1 - \sin^2 \frac{\alpha_0}{2} \sin^2 \varphi}} = 3K$$

Instead of Equation [13] we then have

$$l/2R = \sin \frac{\alpha_0}{2} \cos \varphi_B \left\{ 4K - F\left(\frac{\alpha_0}{2} \cdot \varphi_B \right) \right\}$$

For slopes and ordinates Equations [5] and [6] remain valid. As to the abscissas, Equation [14b] for x_B remains unaltered, and Equation [14a] applies to that portion of branch OA where φ is positive. Where φ is negative we have to replace φ in Equation [14a] by $-\varphi$ which results in

$$x \sqrt{Q/EI} = 2 \left\{ E + E\left(\frac{\alpha_0}{2} \cdot \varphi \right) \right\} - K - F\left(\frac{\alpha_0}{2} \cdot \varphi \right)$$

Now the general character of the curve is sufficiently disclosed by considering the terminal values $\varphi = \pi/2$ at O and $\varphi = -\pi$ at A, together with the more significant intermediate values $\varphi = 0$ and $\varphi = -\pi/2$. The corresponding slopes are obtained from (5), the ordinates will be given by Equation [6a], and the abscissas determined for positive values of φ by means of Equation [14a] or the foregoing equation for negative values.

In this manner we obtain the following

For $\varphi = \pi/2$; $\alpha = \alpha_0$; $y = 0$; $x = 0$. . . . point O in Fig. 9

For $\varphi = 0$; $\alpha = 0$; $y = 2\sqrt{EI/Q} \sin \alpha_0/2$; $x = \dfrac{2E - K}{\sqrt{Q/EI}}$

. . . . . point C in Fig. 9

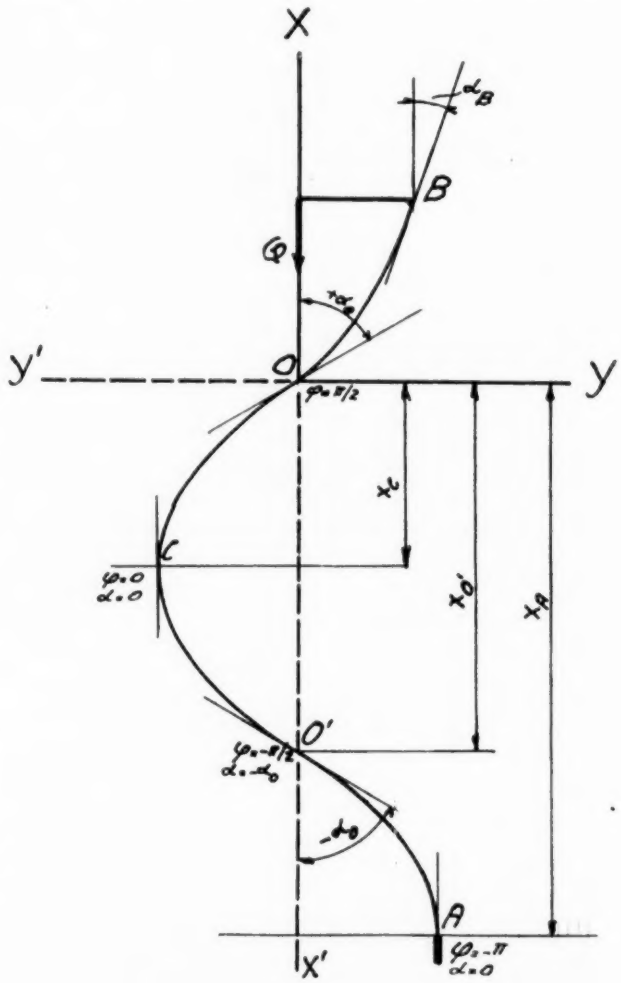


FIG. 9

For $\varphi = -\pi/2$; $\alpha = -\alpha_0$; $y = 0$; $x = \dfrac{4E - 2K}{\sqrt{Q/EI}}$

. . . . . point O' in Fig. 9

For $\varphi = -\pi$; $\alpha = 0$; $y = -2\sqrt{EI/Q} \sin \alpha_0/2$;

$x = \dfrac{6E - 3K}{\sqrt{Q/EI}}$ . . . . . point A in Fig. 9

To be noted is that $x_{O'} = 2x_C$, $x_A = 3x_C$, that arcs OC, CO', $O'A$ are of equal lengths and identical as to shape.

Steady Turbulent-Flow Equations of Continuity, Momentum, and Energy for Finite Systems

By E. R. VAN DRIEST,[1] CAMBRIDGE, MASS.

The steady turbulent-flow equations for continuity, momentum, and energy were derived for certain finite systems. It was found that for an incompressible fluid the continuity relation contained neither nonuniform velocity-distribution correction terms nor turbulence terms, that the momentum equation involved velocity-distribution corrections and mean-square velocity fluctuations, and that the energy relation contained not only velocity-distribution corrections and mean-square terms but in addition mean-cube and double- and triple-correlation terms. The correction factors for nonuniform velocity distribution were evaluated for fully developed open channel and pipe flow. Through the momentum law the effect of turbulence was shown quantitatively in the case of the hydraulic jump in open channels and the sudden expansion in closed conduits.

Introduction

ALTHOUGH the conventional steady-flow momentum and energy equations as used by civil and mechanical engineers have proved to be sufficiently accurate in most cases of application, it will be of interest to derive the more complete equations involving the turbulence terms and the nonuniformity of velocity distribution, and to point out the effect of such factors in some problems.

The steady turbulent-flow equations for continuity, momentum, and energy are derived by first writing the fundamental equations for conservation of mass, the second law of motion, and the first law of thermodynamics, respectively, and then averaging these over time according to the method of Osborne Reynolds. The relations derived are not differential equations[2] but are instead equations that apply to finite systems of matter. Moreover, the equations are by their very nature macroscopic in that they do not involve the inner mechanism of the turbulence but pertain only to mean values at the statistical boundaries of the system.

Continuity

A definite system to be considered will be that of an expanding conduit, as shown in Fig. 1. A more general system could be chosen, but the resulting equations would not be any more instructive.

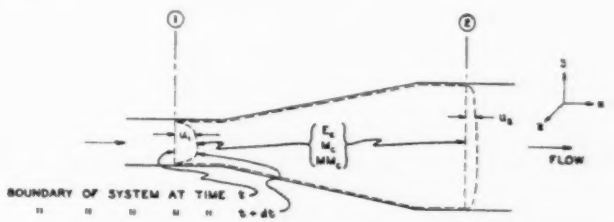


FIG. 1 FLOW THROUGH AN EXPANDING CONDUIT

The law of conservation of matter states that for any system of mass M, $\frac{dM}{dt} = 0$. Then for the system of Fig. 1 there follows

$$\int^{A_1} \rho_1 u_1 dA dt + M_{c/t} = M_{c/t+dt} + \int^{A_2} \rho_2 u_2 dA dt \quad [1]$$

in which ρ and u are the density and instantaneous axial velocity at a point of a section, respectively, and M_c is the matter in the volume common to the initial and final boundaries as indicated in the figure.

Averaging Equation [1] over the time T yields

$$\frac{1}{T}\int_{t-T/2}^{t+T/2}\int^{A_1} \rho_1 u_1 dA dt dt + \frac{1}{T}\int_{t-T/2}^{t+T/2} M_{c/t}\,dt = \frac{1}{T}\int_{t-T/2}^{t+T/2} M_{c/t+dt}\,dt + \frac{1}{T}\int_{-T/2}^{t+T/2}\int^{A_2} \rho_2 u_2\,dA\,dt\,dt$$

or

$$\int^{A_1} \overline{\rho_1 u_1}\,dA = \int^{A_2} \overline{\rho_2 u_2}\,dA \quad [2]$$

where

$$\overline{\rho u} = \frac{1}{T}\int_{t-T/2}^{t+T/2} \rho u dt$$

and

$$\frac{1}{T}\int_{t-T/2}^{t+T/2} M_{c/t}\,dt = \frac{1}{T}\int_{t-T/2}^{t+T/2} M_{c/t+dt}\,dt$$

in the steady state. If the fluid is incompressible and $u_1 = \overline{u_1} + u_1'$, $u_2 = \overline{u_2} + u_2'$ where the bar denotes the mean at a point and the prime the turbulent fluctuation, Equation [2] becomes

$$\int^{A_1} \overline{\overline{u_1} + u_1'}\,dA = \int^{A_2} \overline{\overline{u_2} + u_2'}\,dA$$

or

---

[1] Assistant Professor of Mechanical Engineering, Massachusetts Institute of Technology. Mem. A.S.M.E.

[2] For a study of the differential equations of turbulent flow the reader is referred to the following:

"On an Extension of Reynolds Method of Finding Apparent Stress and the Nature of Turbulence," by P. Y. Chou, *Chinese Journal of Physics*, vol. 4, 1940, pp. 1–33.

"On Velocity Correlations and the Solutions of the Equations of Turbulent Fluctuation," by P. Y. Chou, *Quarterly of Applied Mathematics*, vol. 3, 1945, pp. 38–54.

"Pressure Flow of a Turbulent Fluid Between Two Infinite Parallel Planes," by P. Y. Chou, *Quarterly of Applied Mathematics*, vol. 3, 1945, pp. 198–209.

Presented at the National Meeting of the Applied Mechanics Division, Buffalo, N. Y., June 21–22, 1946, of THE AMERICAN SOCIETY OF MECHANICAL ENGINEERS.

Discussion of this paper should be addressed to the Secretary, A.S.M.E., 29 West 39th Street, New York, N. Y., and will be accepted until October 10, 1946, for publication at a later date. Discussion received after the closing date will be returned.

NOTE: Statements and opinions advanced in papers are to be understood as individual expressions of their authors and not those of the Society.

$$\int^{A_1} \bar{u}_1 dA = \int^{A_2} \bar{u}_2 \, dA \quad \ldots\ldots\ldots\ldots [3]$$

since $\int^{A} \overline{u'} dA = 0$. Equation [3] can now be written in terms of the mean for the section, thus

$$U_1 A_1 = U_2 A_2 \quad \ldots\ldots\ldots\ldots [4]$$

where $U = \dfrac{1}{A} \int^{A} \bar{u} \, dA$

It is seen that Equation [4], the familiar equation of continuity, is unaffected by turbulence terms for the flow of an incompressible fluid.

Momentum

Application of Newton's second law of motion to a system, such as in Fig. 1, yields

$$F_x = \frac{d}{dt} \int^{M} u dM =$$

$$\frac{\left(\int^{A_2} \rho_2 u_2^2 dA dt + MM_{c/t+dt}\right) - \left(\int^{A_1} \rho_1 u_1^2 dA dt + MM_{c/t}\right)}{dt}$$

$$= \int^{A_2} \rho_2 u_2^2 \, dA - \int^{A_1} \rho_1 u_1^2 dA + \frac{d(MM_c)}{dt}$$

where MM_c is now the momentum in the volume common to the two positions of the boundaries, and F_x is the resultant of the forces acting on the boundaries in the x-direction. When this equation is averaged over the time T there results in the steady state

$$\bar{F}_x = \int^{A_2} \overline{\rho_2 u_2^2} \, dA - \int^{A_1} \overline{\rho_1 u_1^2} \, dA \quad \ldots\ldots\ldots [5]$$

since $\dfrac{\overline{d(MM_c)}}{dt} = \dfrac{d(\overline{MM_c})}{dt} = 0$

If the fluid is incompressible, Equation [5] becomes

$$\bar{F}_x = \rho \int^{A_2} \overline{u_2^2} \, dA - \rho \int^{A_1} \overline{u_1^2} \, dA$$

$$= \rho \int^{A_2} \overline{(\bar{u}_2 + u_2')^2} \, dA - \rho \int^{A_1} \overline{(\bar{u}_1 + u_1')^2} \, dA$$

$$= \rho \left(\int^{A_2} \bar{u}_2^2 \, dA - \int^{A_1} \bar{u}_1^2 \, dA + \int^{A_2} \overline{u_2'^2} \, dA - \int^{A_1} \overline{u_1'^2} \, dA \right)$$

$$\ldots\ldots\ldots\ldots [6]$$

The last two terms on the right-hand side of Equation [6] are the turbulence terms which must be taken into account in any exact treatment of a flow problem using the momentum law.

The Hydraulic Jump. The hydraulic jump, which is a gravity shock wave in an open channel, will now be considered in detail. The profile of such a shock is shown in Fig. 2.

For the system bounded by sections 1 and 2, Equation [6] becomes

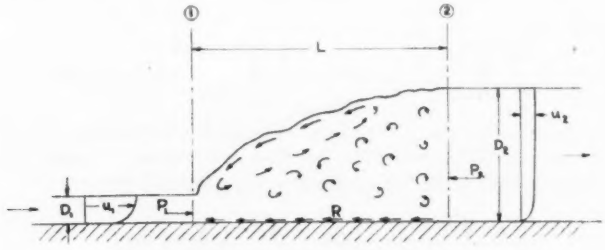


Fig. 2 The Hydraulic Jump

$$P_1 - P_2 - R = \frac{\gamma b D_1^2}{2} - \frac{\gamma b D_2^2}{2} - R =$$

$$\frac{\gamma}{g} \left(\int^{A_2} \bar{u}_2^2 \, dA - \int^{A_1} \bar{u}_1^2 \, dA + \int^{A_2} \overline{u_2'^2} \, dA - \int^{A_1} \overline{u_1'^2} \, dA \right) \quad [7]$$

in which P_1 and P_2 are the hydrostatic forces before and after the jump, D_1 and D_2 are the corresponding depths, R is the skin friction between 1 and 2, γ is the unit weight of the fluid, and b is the width of the channel.

Introducing the coefficients

$$\alpha_1 = \frac{\int^{A_1} \bar{u}_1^2 \, dA}{U_1^2 A_1} = \frac{\int^{A_1} \bar{u}_1^2 \, dA}{U_1^2 b D_1}$$

$$\alpha_2 = \frac{\int^{A_2} \bar{u}_2^2 \, dA}{U_2^2 A_2} = \frac{\int^{A_2} \bar{u}_2^2 \, dA}{U_2^2 b D_2}$$

$$I_1 = \frac{\int^{A_1} \overline{u_1'^2} \, dA}{U_1^2 A_1} = \frac{\int^{A_1} \overline{u_1'^2} \, dA}{U_1^2 b D_1}$$

$$I_2 = \frac{\int^{A_2} \overline{u_2'^2} \, dA}{U_2^2 A_2} = \frac{\int^{A_2} \overline{u_2'^2} \, dA}{U_2^2 b D_2}$$

it follows that

$$D_1^2 - D_2^2 - \frac{2R}{b\gamma} = \frac{2}{g} [(\alpha_2 + I_2) U_2^2 D_2 - (\alpha_1 + I_1) U_1^2 D_1] \quad [8]$$

It is seen that α_1 and α_2 are the correction factors for nonuniform velocity distribution and I_1 and I_2 are the turbulence-correction terms.

Since by Equation [4] $U_1 D_1 = U_2 D_2$, Equation [8] may be written

$$D_1^2 - D_2^2 - \frac{2R}{b\gamma} = \frac{2U_1^2 D_1}{g} [(\alpha_2 + I_2) D_1/D_2 - (\alpha_1 + I_1)]$$

whence upon rearrangement

$$\frac{D_2}{D_1} \left[\left(1 + \frac{D_2}{D_1}\right) \left(1 - \frac{D_2}{D_1}\right) - \frac{2R}{\gamma b D_1^2} \right] = \frac{2U_1^2}{gD_1} \left[(\alpha_2 + I_2) - (\alpha_1 + I_1) \frac{D_2}{D_1} \right]$$

or

$$J \left[(J + 1)(J - 1) + \frac{R}{P_1} \right] = 2\mathbf{F}^2 [(\alpha_1 + I_1) J - (\alpha_2 + I_2)] \quad \ldots\ldots [9]$$

where $J = \dfrac{D_2}{D_1}$, $P_1 = \dfrac{\gamma}{2} b D_1^2$, $\mathbf{F} = \dfrac{U_1}{\sqrt{gD_1}}$

$\mathbf{F}$ being called the Froude number.

Equation [9], or rather,

$$\mathbf{F}^2 = \frac{J \left[(J + 1)(J - 1) + \dfrac{R}{P_1} \right]}{2[(\alpha_1 + I_1) J - (\alpha_2 + I_2)]} \quad \ldots\ldots [10]$$

will now be used to study the effects of the velocity profile, skin friction, and turbulence upon calculations ignoring these factors.

In the case of a uniform velocity profile, and in the absence of skin friction and turbulence, Equation [10] reduces to

$$\mathbf{F}^2 = \frac{1}{2} J(J + 1) \quad \ldots\ldots [11]$$

which is plotted as the heavy line in Fig. 3.

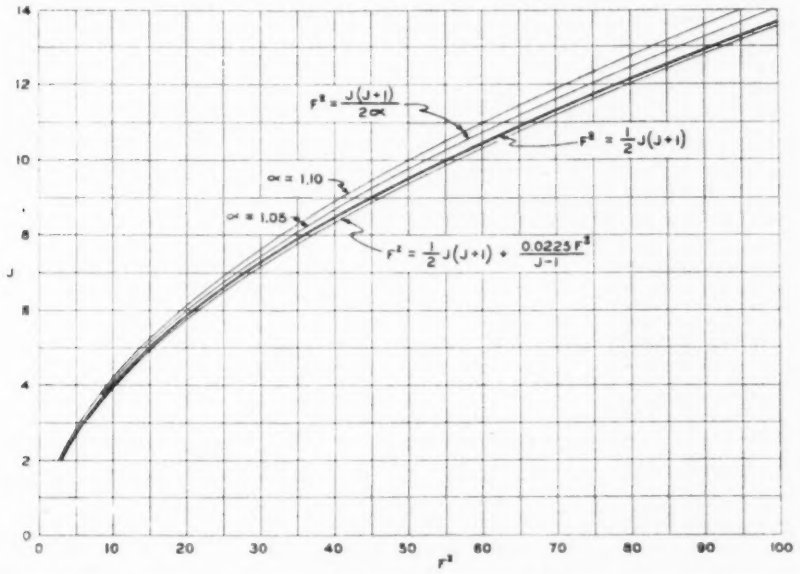


FIG. 3 EFFECT OF VELOCITY DISTRIBUTION AND SKIN FRICTION ON DEPTH AFTER THE HYDRAULIC JUMP

(*a*) *Effect of Velocity Distribution.* Considering only the velocity-distribution factors, Equation [10] becomes

$$F^2 = \frac{J(J+1)(J-1)}{2(\alpha_1 J - \alpha_2)} \quad [12]$$

It is seen at once that if $\alpha_2 = 1$ and $\alpha_1 > 1$, the effect is to shift the curve in Fig. 3 to the left, whereas if $\alpha_1 = 1$ and $\alpha_2 > 1$, the effect is to shift the curve to the right. Since the effect of α_1 compared to α_2 is magnified by the value J, the net tendency is toward the left. For the case when $\alpha_1 = \alpha_2$, a set of curves is plotted in Fig. 3.

It will now be of interest to determine values of α for infinitely wide open channels with known velocity-distribution functions. In the case of laminar flow,

$$u = \frac{3}{2} U \left(2\frac{y}{D} - \frac{y^2}{D^2} \right) \quad [13]$$

where y is measured from the bottom of the channel, so that

$$\alpha = \frac{\int_0^D u^2 dy}{U^2 D} = \frac{6}{5} = 1.20$$

In the case of fully developed turbulent flow, the von Kármán velocity-defect law is used, namely

$$\bar{u} = \bar{u}_{max} + \frac{1}{\kappa}\sqrt{\frac{\bar{\tau}_0}{\rho}} \ln \frac{y}{D} \quad [14]$$

from which is readily obtained[2]

$$U = \bar{u}_{max} - \frac{1}{\kappa}\sqrt{\frac{\bar{\tau}_0}{\rho}} \quad [15]$$

where τ_0 is the shear at the bottom and κ is the universal constant.

Subtraction of Equation [15] from Equation [14] gives

$$\bar{u} = U + \frac{1}{\kappa}\sqrt{\frac{\bar{\tau}_0}{\rho}}\left(1 + \ln \frac{y}{D}\right) \quad [16]$$

whence

$$\alpha = \frac{\int_0^D \bar{u}^2 dy}{U^2 D} = 1 + \left(\frac{\sqrt{\frac{\bar{\tau}_0}{\rho}}}{\kappa U}\right)^2 \quad [17]$$

$$= 1 + \left(\frac{\bar{u}_{max}}{U} - 1\right)^2 \quad [18]$$

Data on clear water flowing in an open channel were obtained from experiments on rough channels[2] and these data together with the results of computation of α (computed from Equation [17]) are presented in Table 1. The results are plotted in Fig. 4, and an average line is extended through the points to indicate the general trend. Term ϵ is the size of the roughness grains glued to the channel bottom.

(*b*) *Effect of Skin Friction.* Skin friction tends to shift the basic curve, Equation [11], in Fig. 3 to the right, and an estimate of this effect can be obtained as follows:

The term $\frac{R}{P_1}$ of Equation [10] can be written for wide channels

$$\frac{R}{P_1} = \frac{2\int_L \tau_0 dL}{\gamma D_1^2} \quad [19]$$

Since

$$\tau_0 = c_f \frac{\rho}{2} U^2 = c_f \frac{\rho}{2} \frac{(U_1 D_1)^2}{D^2}$$

it follows that

$$\int_0^L \tau_0 dL = c_f \frac{\rho}{2} (U_1 D_1)^2 \int_L \frac{dL}{D^2} \quad [20]$$

where D is the depth at any point along the jump and c_f is assumed constant. It is further assumed that the shock expands linearly whence

$$dL = \frac{L}{D_2 - D_1} dD$$

[2] "Transportation of Suspended Sediment by Water," by Vito A. Vanoni, Proceedings of the A.S.C.E., vol. 70, 1944, p. 793.

TABLE 1 DATA ON CLEAR WATER FLOWING IN OPEN CHANNEL

$\sqrt{\frac{\tau_0}{\rho}}$ fps	U fps	D ft	$\frac{\epsilon}{D}$	$\frac{b}{D}$	$\frac{UD}{\nu}$	α	β	$\frac{U}{U_{max}}$
0.197	3.62	0.481	0.003	5.76	171000	1.018	1.050	0.880
0.200	3.60	0.496	0.003	5.58	175000	1.019	1.053	0.877
0.197	3.45	0.481	0.003	5.76	162000	1.020	1.055	0.873
0.211	3.38	0.554	0.005	5.00	183000	1.024	1.065	0.863
0.193	3.21	0.462	0.006	6.00	146000	1.023	1.061	0.868
0.138	1.99	0.234	0.012	11.83	45600	1.030	1.079	0.851

NOTE: κ is taken as 0.40. Term ν is kinematic viscosity.

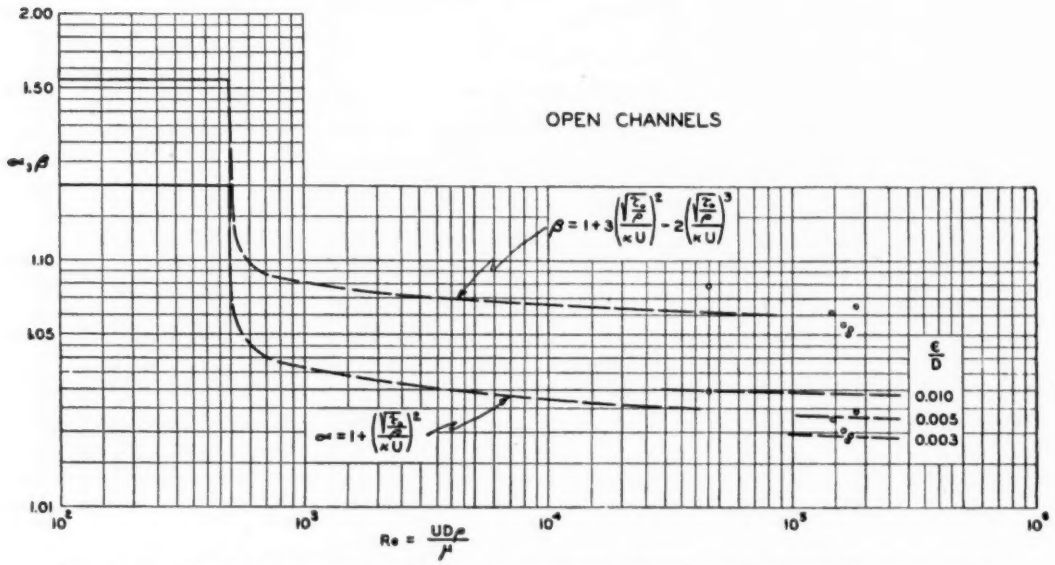


FIG. 4 MOMENTUM- AND ENERGY-CORRECTION FACTORS FOR NONUNIFORM VELOCITY DISTRIBUTION IN INFINITELY WIDE-OPEN CHANNELS

and Equation [20] becomes

$$\int_0^L \tau_0 dL = c_f \frac{\rho}{2} U^2 \frac{D_1}{D_2} L$$

which results in

$$\frac{R}{P_1} = c_f \frac{\mathbf{F}^2}{J} \cdot \frac{L}{D_1} \quad \ldots\ldots [21]$$

Now data obtained by Bakhmeteff and Matzke[4] show that the length of the jump is represented fairly well by

$$\frac{L}{D_1} = 6\mathbf{F}$$

so that

$$\frac{R}{P_1} = 6 \frac{c_f}{J} \mathbf{F}^2 \quad \ldots\ldots [22]$$

When Equation [10] contains only the effect of skin friction, it becomes by Equation [22]

$$\mathbf{F}^2 = \frac{J(J+1)(J-1) + 6c_f \mathbf{F}^2}{2(J-1)}$$

$$= \frac{1}{2} J(J+1) + \frac{3c_f \mathbf{F}^2}{J-1} \quad \ldots\ldots [23]$$

For purposes of computation a reasonably high value of c_f can be obtained by first placing $c_f = \frac{f}{4}$, where f is the friction factor for pipe flow, and then choosing a value $f = 0.03$, giving $c_f = 0.0075$. Equation [23] then is written

$$\mathbf{F}^2 = \frac{1}{2} J(J+1) + \frac{0.0225 \mathbf{F}^2}{J-1} \quad \ldots\ldots [24]$$

This equation is plotted in Fig. 3 and indicates an extreme effect of skin friction.

(c) *Effect of Turbulence.* Equation [10], including only the turbulence terms, is

$$\mathbf{F}^2 = \frac{J(J+1)(J-1)}{2[(J-1) + (I_1 J - I_2)]} \quad \ldots\ldots [25]$$

In such cases where the fluid enters the shock turbulent-free, $I_1 = 0$ and

$$\mathbf{F}^2 = \frac{J(J+1)(J-1)}{2(J-1-I_2)} \quad \ldots\ldots [26]$$

The Bakhmeteff-Matzke data were obtained in just such a case, and hence the effect of turbulence should make itself felt according to Equation [26]. That this is true can be seen from Fig. 5 which shows the basic Equation [11], Equation [26] for various values of I_2, and the data.

Since the shock wave is known to be a generator of intense turbulence, the fall of the data to the right of the basic curve is undoubtedly due principally to the turbulence effect. It should be noted that the average intensity of turbulence as defined by I_2 is upward of 100 per cent for the higher values of relative depth J.

[4] "The Hydraulic Jump in Terms of Dynamic Similarity," by B. A. Bakhmeteff and A. E. Matzke, Trans. A.S.C.E., vol. 101, 1936, p. 631.

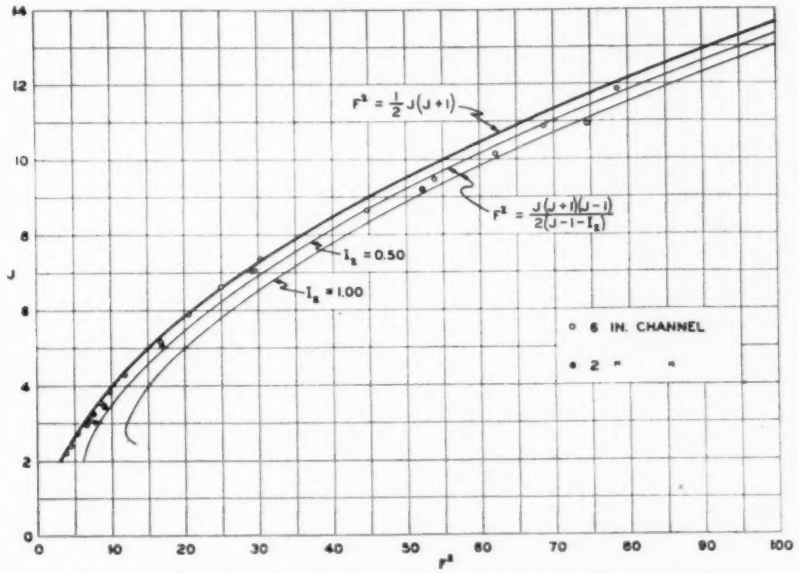


FIG. 5 THE EFFECT OF TURBULENCE ON DEPTH AFTER THE HYDRAULIC JUMP

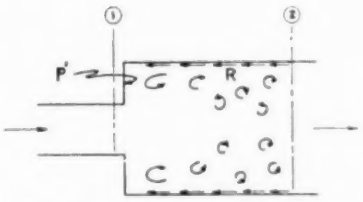


FIG. 6 THE SUDDEN ENLARGEMENT

The Sudden Enlargement. When Equation [6] is applied to the sudden enlargement of Fig. 6 there results

$$p_1A_1 + p'(A_2 - A_1) - p_2A_2 - R = \rho\left(\int^{A_2}\bar{u}_2^2\,dA - \int^{A_1}\bar{u}_1^2\,dA + \int^{A_2}\overline{u_2'^2}\,dA - \int^{A_1}\overline{u_1'^2}\,dA\right) = \rho U_2A_2[(\alpha_2 + I_2)U_2 - (\alpha_1 + I_1)U_1]$$

whence

$$\frac{(p_1 - p')\frac{A_1}{A_2} + p' - p_2 - \frac{R}{A_2}}{\rho U_1^2} = \frac{A_1}{A_2}\left[(\alpha_2 + I_2)\frac{A_1}{A_2} - (\alpha_1 + I_1)\right] \quad [27]$$

where p' is the average pressure over the annular plate, and p_1 and p_2 are the average pressures over sections 1 and 2, respectively.

If it is assumed that $p_1 = p'$, $R = 0$, $\alpha_1 = \alpha_2 = 1$ and $I_1 = I_2 = 0$, Equation [27] reduces to

$$\frac{p_1 - p_2}{\rho U_1^2} = \frac{A_1}{A_2}\left(\frac{A_1}{A_2} - 1\right) \quad [28]$$

or, introducing $E = \frac{p_2 - p_1}{\rho U_1^2/2}$ and $m = \frac{A_2}{A_1}$

$$E = \frac{2}{m}\left(1 - \frac{1}{m}\right) \quad [29]$$

With regard to the velocity-distribution correction for flow in pipes, the value of α can be determined analytically if the equation of velocity distribution is known.

For laminar flow through a long pipe of inner radius r_0

$$u = 2U\left(1 - \frac{r^2}{r_0^2}\right) \quad [30]$$

whereupon

$$\alpha = \frac{\int^A u^2dA}{U^2A} = \frac{\int_0^{r_0} u^2 2\pi r dr}{U^2\pi r_0^2} = \frac{4}{3} = 1.33$$

For fully developed turbulent flow, the von Kármán velocity-defect law, viz.

$$\bar{u} = \bar{u}_{max} + \frac{1}{\kappa}\sqrt{\frac{\tau_0}{\rho}}\ln\frac{y}{r_0} \quad [31]$$

leads to the expression[5]

$$U = \bar{u}_{max} - \frac{3}{2}\frac{1}{\kappa}\sqrt{\frac{\tau_0}{\rho}} \quad [32]$$

subtraction of which from Equation [31] yields

$$\bar{u} = U + \frac{1}{\kappa}\sqrt{\frac{\tau_0}{\rho}}\left(\frac{3}{2} + \ln\frac{y}{r_0}\right) \quad [33]$$

whence

$$\alpha = \frac{\int^A \bar{u}^2\,dA}{U^2A} = 1 + \frac{5}{4}\left(\frac{\sqrt{\frac{\tau_0}{\rho}}}{\kappa U}\right)^2 \quad [34]$$

$$= 1 + \frac{5}{9}\left(\frac{\bar{u}_{max}}{U} - 1\right)^2 \quad [35]$$

Equation [34] can be written in terms of the friction factor f by first noting that

[5] "Strömungsgesetze in rauhen Rohren," by J. Nikuradse, *Forschungsheft*, 361, V.D.I., 4, 1933, pp. 1–22.

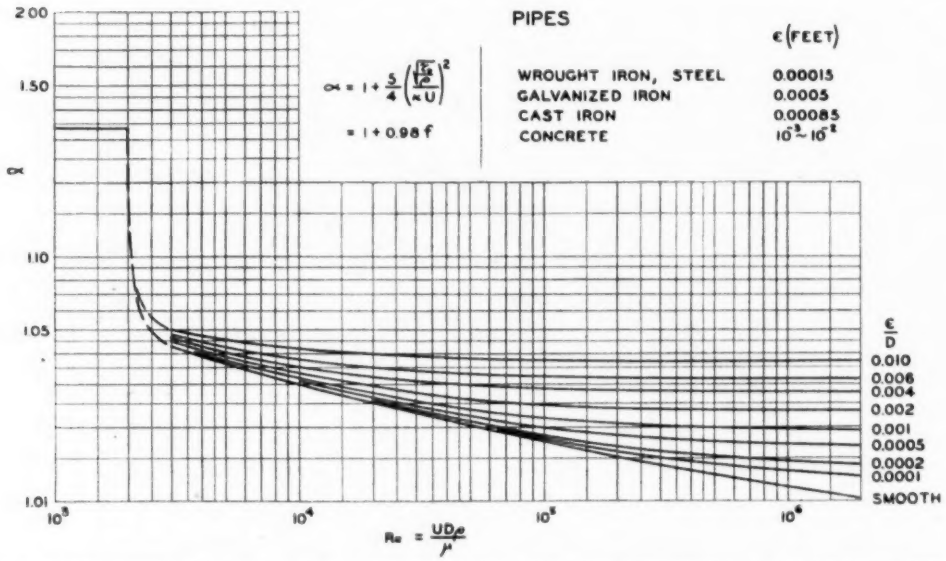


FIG. 7 MOMENTUM-CORRECTION FACTOR FOR NONUNIFORM VELOCITY DISTRIBUTION IN COMMERCIAL PIPES

$$\sqrt{\frac{\tau_0}{\rho}}\Big/U = \sqrt{\frac{f}{8}}$$

so that for a value of $\kappa = 0.40$

$$\alpha = 1 + \frac{5}{4}\frac{1}{\kappa^2}\cdot\frac{f}{8} = 1 + 0.98f \quad \ldots\ldots\ldots\ldots [36]$$

$$= 1 + f \text{ (approx.)}$$

Fig. 7 shows a plot of Equation [36], using factors[6] for commercial pipes.

The sudden enlargement is another seat of turbulence generation[7] and therefore it is to be expected that the intensity of turbulence at section 2 will have considerable effect upon the data. Assuming that $p_1 = p'$ and including only the turbulence terms, Equation [27] becomes

$$E = \frac{2}{m}\left[\left(1 - \frac{1}{m}\right) + \left(I_1 - I_2\frac{1}{m}\right)\right] \quad \ldots\ldots\ldots [37]$$

and if I_1 is negligible compared to $\frac{I_2}{m}$, then there follows

$$E = \frac{2}{m}\left(1 - \frac{1}{m} - \frac{I_2}{m}\right) \quad \ldots\ldots\ldots\ldots [38]$$

Fig. 8 shows the base Equation [29] along with Equation [38] for various values of I_2. Also in this figure are plotted data given by Gibson.[8] Of course, the presence of skin friction and the fact that p' is somewhat less[7] than p_1 will tend to shift the data in Fig. 8 to smaller values of E. Nevertheless, an appreciable part of the total shift must be due to the turbulence, particularly at greater values of m, as is evident from the plot. An observed value of 150 per cent for the average intensity of turbulence defined by I_2 should be noted.

[6] "Friction Factors for Pipe Flow," by L. F. Moody, Trans. A.S.M.E., vol. 66, 1944, p. 671.

[7] "Conversion of Kinetic to Potential Energy in Flow Expansions," by A. A. Kalinske, Proceedings of the A.S.C.E., vol. 70, 1944, pp. 1545–1564.

[8] "Hydraulics and Its Applications," by A. H. Gibson, fourth edition, Constable and Company, London, England, p. 92.

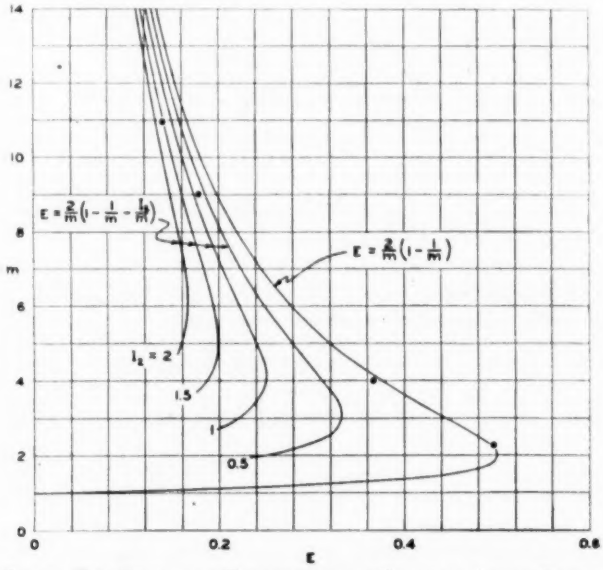


FIG. 8 THE EFFECT OF TURBULENCE ON PRESSURE AFTER SUDDEN ENLARGEMENT

ENERGY

The steady turbulent-flow-energy equation for finite systems is derived from the first law of thermodynamics which reads

$$dE = dQ - dW \quad \ldots\ldots\ldots\ldots [39]$$

in which dE is the change in internal energy of a system, dQ is the heat transferred to the system and dW is the work done by the system during an infinitesimal change of state. Assuming no heat transfer or shaft work, application of Equation [39] to the system in Fig. 1 for the change in state over the time interval dt yields

$$\int^{A_2} i_2\gamma_2 u_2\, dA\, dt - \int^{A_1} i_1\gamma_1 u_1\, dA\, dt + \frac{1}{2g}\int^{A_2} q_2{}^2\gamma_2 u_2\, dA\, dt$$

$$- \frac{1}{2g}\int^{A_1} q_1{}^2\gamma_1 u_1\, dA\, dt + E_{c/t+dt} - E_{c/t} = -\int^{A_2} p_2 u_2\, dA\, dt$$

$$+ \int^{A_1} p_1 u_1 \, dA \, dt - \int^{A_2} \tau_{xy_2} v_2 \, dA \, dt - \int^{A_2} \tau_{xz_2} w_2 \, dA \, dt + \int^{A_1} \tau_{xy_1} v_1 \, dA \, dt + \int^{A_1} \tau_{xz_1} w_1 \, dA \, dt \quad \ldots\ldots [40]$$

where i_1 and i_2 are the molecular internal energies per unit weight, v_1 and v_2 the transverse velocities in the y-direction, w_1 and w_2 the transverse velocities in the z-direction, and τ_1 and τ_2 the transverse shear stresses at sections 1 and 2, respectively, all of which are instantaneous; furthermore, $q^2 = u^2 + v^2 + w^2$, and E_c is the energy in the volume common to the initial and final positions of the boundary of the system. Following the previous procedure, the average of Equation [40] is

$$\int^{A_2} \overline{i_2 \gamma_2 u_2} \, dA - \int^{A_1} \overline{i_1 \gamma_1 u_1} \, dA + \frac{1}{2g} \int^{A_2} \overline{q_2^2 \gamma_2 u_2} \, dA - \frac{1}{2g} \int^{A_1} \overline{q_1^2 \gamma_1 u_1} dA = - \int^{A_2} \overline{p_2 u_2} \, dA + \int^{A_1} \overline{p_1 u_1} \, dA - \int^{A_2} \overline{\tau_{xy_2} v_2} \, dA - \int^{A_2} \overline{\tau_{xz_2} w_2} \, dA + \int^{A_1} \overline{\tau_{xy_1} v_1} \, dA + \int^{A_1} \overline{\tau_{xz_1} w_1} \, dA \quad \ldots\ldots [41]$$

Assuming incompressibility and dividing through by the mean weight rate of flow, viz.

$$\gamma \int^{A_1} \bar{u}_1 \, dA = \gamma \int^{A_2} \bar{u}_2 \, dA$$

there results per unit weight of fluid flowing

$$\frac{\int^{A_1} \overline{i_1 u_1} dA}{\int^{A_1} \bar{u}_1 \, dA} + \frac{\frac{1}{2g} \int^{A_1} \overline{q_1^2 u_1} \, dA}{\int^{A_1} \bar{u}_1 \, dA} + \frac{\int^{A_1} \overline{p_1 u_1} \, dA}{\gamma \int^{A_1} \bar{u}_1 \, dA} + \frac{\int^{A_1} \overline{\tau_{xy_1} v_1} \, dA}{\gamma \int^{A_1} \bar{u}_1 dA} + \frac{\int^{A_1} \overline{\tau_{xz_1} w_1} \, dA}{\gamma \int^{A_1} \bar{u}_1 \, dA} = \frac{\int^{A_2} \overline{i_2 u_2} \, dA}{\int^{A_2} \bar{u}_2 \, dA} + \frac{\frac{1}{2g} \int^{A_2} \overline{q_2^2 u_2} \, dA}{\int^{A_2} \bar{u}_2 \, dA} + \frac{\int^{A_2} \overline{p_2 u_2} \, dA}{\gamma \int^{A_2} \bar{u}_2 \, dA} + \frac{\int^{A_2} \overline{\tau_{xy_2} v_2} \, dA}{\gamma \int^{A_2} \bar{u}_2 \, dA} + \frac{\int^{A_2} \overline{\tau_{xz_2} w_2} \, dA}{\gamma \int^{A_2} \bar{u}_2 \, dA} \quad \ldots\ldots [42]$$

The next step is to substitute $i = \bar{i} + i'$, $p = \bar{p} + p'$, $u = \bar{u} + u'$, $v = \bar{v} + v'$, and $w = \bar{w} + w'$. Equation [42] then expands to

$$\frac{\int^{A_1} \bar{i}_1 \bar{u}_1 \, dA}{\int^{A_1} \bar{u}_1 \, dA} + \frac{\int^{A_1} \overline{i_1' u_1'} \, dA}{\int^{A_1} \bar{u}_1 \, dA} + \frac{\frac{1}{2g} \int^{A_1} (\bar{u}_1^2 + \bar{v}_1^2 + \bar{w}_1^2) \bar{u}_1 \, dA}{\int^{A_1} \bar{u}_1 \, dA} + \frac{\frac{1}{2g} \int^{A_1} (\overline{u_1'^2} + \overline{v_1'^2} + \overline{w_1'^2}) \bar{u}_1 \, dA}{\int^{A_1} \bar{u}_1 \, dA} + \frac{\frac{2}{2g} \int^{A_1} (\bar{u}_1 \overline{u_1'^2} + \bar{v}_1 \overline{u_1' v_1'} + \bar{w}_1 \overline{u_1' w_1'}) \, dA}{\int^{A_1} \bar{u}_1 \, dA} + \frac{\frac{1}{2g} \int^{A_1} (\overline{u_1'^3} + \overline{u_1' v_1'^2} + \overline{u_1' w_1'^2}) \, dA}{\int^{A_1} \bar{u}_1 \, dA} + \frac{\int^{A_1} \bar{p}_1 \bar{u}_1 \, dA}{\gamma \int^{A_1} \bar{u}_1 \, dA} + \frac{\int^{A_1} \overline{p_1' u_1'} \, dA}{\gamma \int^{A_1} \bar{u}_1 \, dA} + \frac{\int^{A_1} \overline{\tau_{xy_1} v_1} \, dA}{\gamma \int^{A_1} \bar{u}_1 \, dA} + \frac{\int^{A_1} \overline{\tau_{xy_1}' v_1'} \, dA}{\gamma \int^{A_1} \bar{u}_1 \, dA} + \frac{\int^{A_1} \overline{\tau_{xz_1} w_1} \, dA}{\gamma \int^{A_1} \bar{u}_1 \, dA} + \frac{\int^{A_1} \overline{\tau_{xz_1}' w_1'} \, dA}{\gamma \int^{A_1} \bar{u}_1 \, dA} = \frac{\int^{A_2} \bar{i}_2 \bar{u}_2 \, dA}{\int^{A_2} \bar{u}_2 \, dA} + \frac{\int^{A_2} \overline{i_2' u_2'} \, dA}{\int^{A_2} \bar{u}_2 \, dA} + \frac{\frac{1}{2g} \int^{A_2} \bar{u}_2^3 \, dA}{\int^{A_2} \bar{u}_2 \, dA} + \frac{\frac{1}{2g} \int^{A_2} (\overline{u_2'^2} + \overline{v_2'^2} + \overline{w_2'^2}) \bar{u}_2 \, dA}{\int^{A_2} \bar{u}_2 \, dA} + \frac{\frac{2}{2g} \int^{A_2} \bar{u}_2 \overline{u_2'^2} \, dA}{\int^{A_2} \bar{u}_2 \, dA} + \frac{\frac{1}{2g} \int^{A_2} (\bar{u}_2 \overline{u_2'^2} + \bar{v}_2 \overline{u_2' v_2'} + \bar{w}_2 \overline{u_2' w_2'}) \, dA}{\int^{A_2} \bar{u}_2 \, dA} + \frac{\frac{1}{2g} \int^{A_2} (\overline{u_2'^3} + \overline{u_2' v_2'^2} + \overline{u_2' w_2'^2}) \, dA}{\int^{A_2} \bar{u}_2 \, dA} + \frac{\int^{A_2} \bar{p}_2 \bar{u}_2 \, dA}{\gamma \int^{A_2} \bar{u}_2 \, dA} + \frac{\int^{A_2} \overline{p_2' u_2'} \, dA}{\gamma \int^{A_2} \bar{u}_2 \, dA} + \frac{\int^{A_2} \overline{\tau_{xy_2} v_2} \, dA}{\gamma \int^{A_2} \bar{u}_2 \, dA} + \frac{\int^{A_2} \overline{\tau_{xy_2}' v_2'} \, dA}{\gamma \int^{A_2} \bar{u}_2 \, dA} + \frac{\int^{A_2} \overline{\tau_{xz_2} w_2} \, dA}{\gamma \int^{A_2} \bar{u}_2 \, dA} + \frac{\int^{A_2} \overline{\tau_{xz_2}' w_2'} \, dA}{\gamma \int^{A_2} \bar{u}_2 \, dA} \quad \ldots\ldots [43]$$

If the sections 1 and 2 are taken such that $\bar{v} = \bar{w} = 0$, Equation [43] reduces to

$$\frac{\int^{A_1} \bar{i}_1 \bar{u}_1 dA}{\int^{A_1} \bar{u}_1 \, dA} + \frac{\int^{A_1} \overline{i_1' u_1'} \, dA}{\int^{A_1} \bar{u}_1 \, dA} + \frac{\frac{1}{2g} \int^{A_1} \bar{u}_1^3 \, dA}{\int^{A_1} \bar{u}_1 \, dA} + \frac{\frac{1}{2g} \int^{A_1} (\overline{u_1'^2} + \overline{v_1'^2} + \overline{w_1'^2}) \bar{u}_1 \, dA}{\int^{A_1} \bar{u}_1 \, dA} + \frac{\frac{2}{2g} \int^{A_1} \bar{u}_1 \overline{u_1'^2} \, dA}{\int^{A_1} \bar{u}_1 \, dA} + \frac{\frac{1}{2g} \int^{A_1} (\overline{u_1'^3} + \overline{u_1' v_1'^2} + \overline{u_1' w_1'^2}) \, dA}{\int^{A_1} \bar{u}_1 \, dA} + \frac{\int^{A_1} \bar{p}_1 \bar{u}_1 \, dA}{\gamma \int^{A_1} \bar{u}_1 \, dA} + \frac{\int^{A_1} \overline{p_1' u_1'} \, dA}{\gamma \int^{A_1} \bar{u}_1 \, dA} + \frac{\int^{A_1} \overline{\tau_{xy_1}' v_1'} \, dA}{\gamma \int^{A_1} \bar{u}_1 \, dA} + \frac{\int^{A_1} \overline{\tau_{xz_1}' w_1'} \, dA}{\gamma \int^{A_1} \bar{u}_1 \, dA} = \frac{\int^{A_2} \bar{i}_2 \bar{u}_2 \, dA}{\int^{A_2} \bar{u}_2 \, dA} + \frac{\int^{A_2} \overline{i_2' u_2'} \, dA}{\int^{A_2} \bar{u}_2 \, dA} + \frac{\frac{1}{2g} \int^{A_2} \bar{u}_2^3 \, dA}{\int^{A_2} \bar{u}_2 \, dA} + \frac{\frac{1}{2g} \int^{A_2} (\overline{u_2'^2} + \overline{v_2'^2} + \overline{w_2'^2}) \bar{u}_2 \, dA}{\int^{A_2} \bar{u}_2 \, dA} + \frac{\frac{2}{2g} \int^{A_2} \bar{u}_2 \overline{u_2'^2} \, dA}{\int^{A_2} \bar{u}_2 \, dA} + \frac{\frac{1}{2g} \int^{A_2} (\bar{u}_2 \overline{u_2'^2} + \bar{v}_2 \overline{u_2' v_2'} + \bar{w}_2 \overline{u_2' w_2'}) \, dA}{\int^{A_2} \bar{u}_2 \, dA} + \frac{\int^{A_2} \bar{p}_2 \bar{u}_2 \, dA}{\gamma \int^{A_2} \bar{u}_2 \, dA} + \frac{\int^{A_2} \overline{p_2' u_2'} \, dA}{\gamma \int^{A_2} \bar{u}_2 \, dA} + \frac{\int^{A_2} \overline{\tau_{xy_2}' v_2'} \, dA}{\gamma \int^{A_2} \bar{u}_2 \, dA} + \frac{\int^{A_2} \overline{\tau_{xz_2}' w_2'} \, dA}{\gamma \int^{A_2} \bar{u}_2 \, dA} \quad \ldots [44]$$

The extreme complexity of the energy Equation [44] compared to the simplicity of the momentum Equation [6] is immediately apparent. Whereas the momentum equation involves only mean-square terms, the energy equation contains mean squares, mean cubes, and double and triple correlations. Some measurements[7,9,10,11] of the mean-square terms have been made so that some information is available as to their variation, but no information is available concerning the double and triple correlations involved in the energy equation.

The energy of mean motion can be computed provided the ve-

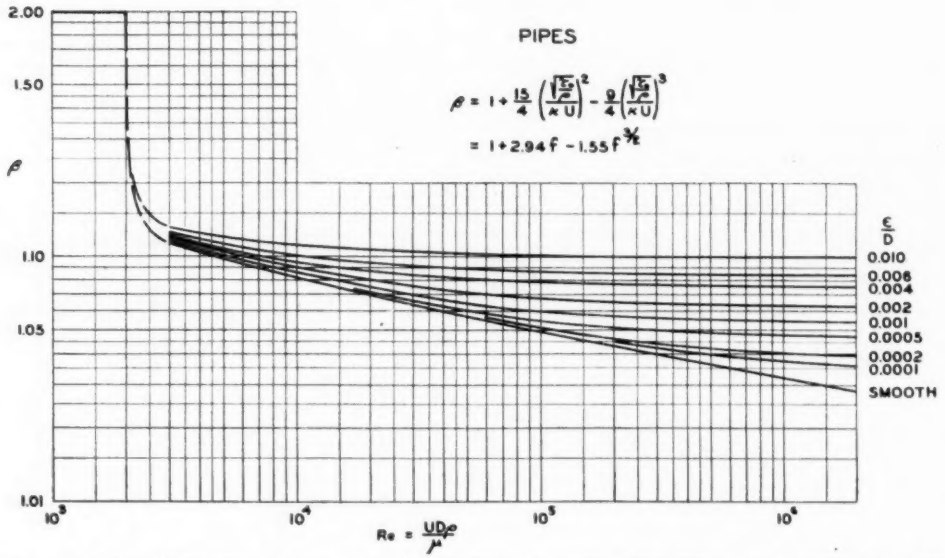


FIG. 9 ENERGY-CORRECTION FACTOR FOR NONUNIFORM VELOCITY DISTRIBUTION IN COMMERCIAL PIPES

locity distribution is known. The correction factor for nonuniform distribution, viz.

$$\beta = \frac{\int \bar{u}^3 dA}{U^3 A} \quad \text{.....[45]}$$

can be obtained for certain distributions as follows:

(*a*) Open channels (laminar): Use of Equation [13] gives

$$\beta = \frac{54}{35} = 1.54$$

(*b*) Open channels (turbulent): Use of Equation [16] leads to

$$\left.\begin{aligned} \beta &= 1 + 3\left(\frac{\sqrt{\tau_0/\rho}}{\kappa U}\right)^2 - 2\left(\frac{\sqrt{\tau_0/\rho}}{\kappa U}\right)^3 \\ &= 1 + 3\left(\frac{\bar{u}_{max}}{U} - 1\right)^2 - 2\left(\frac{\bar{u}_{max}}{U} - 1\right)^3 \end{aligned}\right\} \quad [46]$$

Values of β were computed from the Vanoni data[9] and Equation [46], and these results are also entered in Table 1. Furthermore, the results are plotted in Fig. 4, and an average line is extended through the points to indicate the general trend.

(*c*) Pipes (laminar): By use of Equation [30] it follows that

$$\beta = 2.00$$

(*d*) Pipes (turbulent): The turbulent velocity-distribution Equation [33] yields

$$\left.\begin{aligned} \beta &= 1 + \frac{15}{4}\left(\frac{\sqrt{\tau_0/\rho}}{\kappa U}\right)^2 - \frac{9}{4}\left(\frac{\sqrt{\tau_0/\rho}}{\kappa U}\right)^3 \\ &= 1 + \frac{5}{3}\left(\frac{\bar{u}_{max}}{U} - 1\right)^2 - \frac{2}{3}\left(\frac{\bar{u}_{max}}{U} - 1\right)^3 \end{aligned}\right\} \quad [47]$$

Again noting that $\sqrt{\tau_0/\rho}\,\Big/ U = \sqrt{f/8}$ and using $\kappa = 0.40$, Equation [47] may be written

$$\begin{aligned} \beta &= 1 + \frac{15}{4}\frac{1}{\kappa^2}\frac{f}{8} - \frac{9}{4}\frac{1}{\kappa^3}\left(\frac{f}{8}\right)^{3/2} \\ &= 1 + 2.94f - 1.55f^{3/2} \quad \text{.....[48]} \\ &= 1 + 3f \text{ (roughly)} \end{aligned}$$

Equation [48] is plotted in Fig. 9, again making use of the friction factors[6] for commercial pipes.

It should be noted that for wide-open channels or for pipes, if $\alpha = 1 + \eta$, then $\beta = 1 + 3\eta$ (approx.).

SUMMARY AND CONCLUSION

The steady turbulent-flow equations for continuity, momentum, and energy have been derived for certain finite systems. It was found for a liquid that the continuity relation contained neither nonuniform velocity-distribution correction terms nor turbulence terms, that the momentum equation involved velocity-distribution corrections and mean-square velocity fluctuations, and that the energy relation contained not only velocity-distribution corrections and mean-square terms but in addition mean-cube and double- and triple-correlation terms. The correction factors for nonuniform velocity distribution were evaluated for fully developed open-channel and pipe flow. The effect of turbulence was shown quantitatively in the case of open and closed sudden expansions making use of the momentum law.

In any exact analysis of turbulent-flow problems the turbulence terms must of course be taken into account. Indeed, before such foregoing momentum and energy equations can be used, knowledge of the variation of the turbulence terms including the double and triple correlations must be available.

---

[9] "Investigations of Turbulent Flow by Means of the Hot-Wire Anemometer," by F. L. Wattendorf and A. M. Kuethe, *Physics*, vol. 5, 1934, pp. 153–164.

[10] "Investigations of Velocity Fluctuations in a Turbulent Flow," by F. L. Wattendorf, *Journal of the Aeronautical Sciences*, vol. 3, 1936, pp. 200–202.

[11] "On the Static Pressure in Fully Developed Turbulent Flow," by A. Fage, Proceedings of the Royal Society of London, series A, vol. 155, 1936, pp. 576–596.

Design Data

It is important that the data contained in technical papers be made readily available to designing engineers. In order to satisfy these needs of industry, this section of the Journal includes a concise presentation of data and information drawn chiefly from papers previously published by the Applied Mechanics Division of The American Society of Mechanical Engineers.

The data have been prepared by a subcommittee of the Applied Mechanics Division—S. Timoshenko, R. E. Peterson, J. Ormondroyd, J. N. Goodier, and J. M. Lessells.

Calculation of Stress in Crane Hooks

By A. M. WAHL[1]

Two methods for calculating stress in crane hooks which have given good results in practice are described. One method, based on a numerical integration of the curved-bar equations, involves only slide-rule accuracy and may be used for irregular shapes of cross section. The second or analytical method is based on an analysis of an equivalent trapezoidal section, and is applicable to hooks having sections which do not deviate too much from the trapezoidal form. Comparison of the results of the two methods when applied to actual crane hooks indicates that the more rapid analytical method is sufficiently accurate for most practical purposes.

THE usual method of calculation of stress in crane hooks having an irregular cross section is based on curved-bar theory, the equations being integrated using numerical or graphical means (1).[2] However, these methods in general involve small differences between two quantities nearly equal, and for this reason the numerical work must be carried out with considerable precision in order to obtain reasonably accurate final values. To avoid this and to utilize slide-rule methods of calculation, the equations developed by Perkins (2) have been applied. In conjunction with Simpson's rule for numerical integration, this procedure has been found to yield good results in practical work; the method will be described in Part 1 of this paper.

In addition, a more rapid analytical method for calculating crane hooks where the critical section approximates a trapezoid is also described (Part 2). Results obtained by this method have been checked for several practical hooks against the numerical integration method of Part I and found to yield good agreement; also the method has been utilized in practical computation with good results.

The methods described here are limited to the usual case where the resultant load P on the hook passes through the center of curvature O, Fig. 1. It is also assumed that the critical section AA' is at right angles to the resultant load, as is true of the majority of practical hooks.[3]

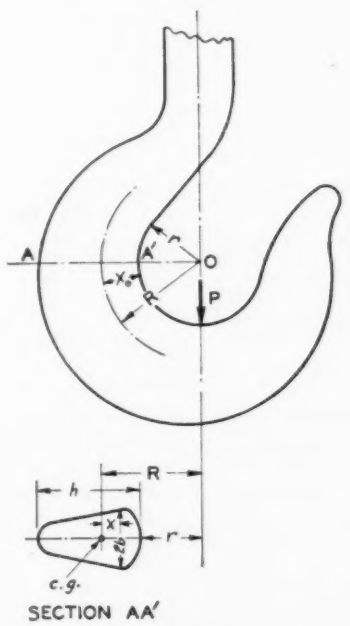


FIG. 1 CRANE HOOK WITH IRREGULAR SECTION

PART 1 NUMERICAL INTEGRATION METHOD FOR HOOK WITH IRREGULAR CROSS SECTION

(*a*) *Theory.* The equation for maximum tensile stress S_{max} (including the direct stress due to the load P) at point A', Fig. 1, may be expressed as

$$S_{max} = \frac{P(R-r)}{Fr} \quad \ldots\ldots\ldots\ldots\ldots [1]$$

where the function F is

$$F = \frac{2}{R}\int \frac{x^2 b\,dx}{R-x} \quad \ldots\ldots\ldots\ldots\ldots [2]$$

This integral is taken over the whole cross section.

P = load on hook, Fig. 1
x = distance from center of gravity to any point of section
r = inside radius of curvature
R = distance from center of curvature O to center of gravity of critical section AA'
$2b$ = width of section at distance x from c.g.

---

[1] Research Engineer, Westinghouse Electric Corporation, East Pittsburgh, Pa. Mem. A.S.M.E.

[2] Numbers in parentheses refer to the References at the end of paper.

[3] If these conditions are not fulfilled, methods described in references (1) and (2 may be used.

Discussion of this paper should be addressed to the Secretary, A.S.M.E., 29 W. 39th St., New York, N. Y., and will be accepted until October 10, 1946, for publication at a later date. Discussion received after the closing date will be returned.

To calculate the stress using Equation [1], it is necessary to evaluate the integral of Equation [2] which may be done numerically using Simpson's rule (3). In the following method or procedure, the depth h of the hook cross section has been divided into 30 equal parts (which has given good results in practice).[5] On this basis the detailed procedure for calculating stress in the hook is as follows.

(*b*) *Procedure for Evaluating Stress.* Lay out half of critical section of hook to scale as shown in Fig. 2.

Divide cross section of hook into 30 equal parts as shown. Spacing Δ between each line is equal to $h/30$ where h = depth of critical section. Measure the half widths $b_1, b_2, b_3 \ldots\ldots\ldots b_{29}$ at each point, Fig. 2.

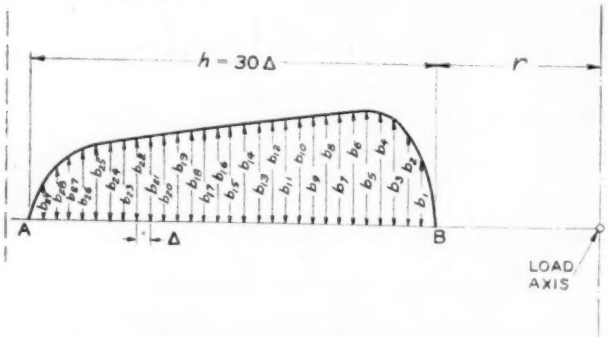


FIG. 2 DIVISION OF HALF SECTION OF CRANE HOOK INTO 30 EQUAL SPACES

Make up a table similar to Table 1 as follows:

In column 1 tabulate $b_1, b_2, b_3 \ldots\ldots\ldots b_{29}$

In column 2 tabulate $2b_1, b_2, 2b_3, b_4 \ldots\ldots\ldots 2b_{29}$ as shown.

The sum of the figures in column 2 is equal to A_2.

In column 3 tabulate $\Delta, 2\Delta, 3\Delta, \ldots\ldots 29\Delta$.

The elements of column 4 are taken equal to the corresponding ones of column 2 multiplied by column 3. Thus the first element of column 4 is equal to $2b_1\Delta$, the second element is b_2 times $2\Delta = 2b_2\Delta$, the third $2b_3$ times $3\Delta = 6b_3\Delta$, etc.

The sum of the elements of column 4 is taken equal to A_4.

Divide A_4 by A_2. The result will be equal to x_0, the distance from point A' of Fig. 1 to the center of gravity of the cross section. The radius R then becomes (from Fig. 1)

$$R = r + x_0$$

Next, in column 5 tabulate the quantities $c_1 = r + \Delta$, $c_2 = r + 2\Delta$, $c_3 = r + 3\Delta$, etc.

In column 6 tabulate $a_1 = (x_0 - \Delta)$, $a_2 = (x_0 - 2\Delta)$, $a_3 = (x_0 - 3\Delta)$, etc., and in column 7, a_1^3, a_2^3, a_3^3, etc.

In column 8 tabulate the quantities $2b_1a_1^3/c_1$, $b_2a_2^3/c_2$, $2b_3a_3^3/c_3$, etc. Each element of column 8 is equal to the corresponding element of column 2 multiplied by that of column 7 and divided by that of column 5.

The sum of the elements of column 8 is taken equal to A_8.

Applying Simpson's rule and using Equations [1] and [2] the maximum tensile stress at the critical section A', Fig. 1, then becomes

$$S_{max} = \frac{3Px_0R}{4r\,\Delta\,A_8} \ldots\ldots\ldots\ldots\ldots [3]$$

(*c*) *Numerical Example.*[4] As an example of the application of this numerical integration method, a hook having the following dimensions was calculated. The load P is taken as 100,000 lb.

$r = 4.5$ in.
$h = 9.59$ in.
$\Delta = h/30 = 0.32$ in.

Values of b_1, b_2, etc., representing the half width of the cross section, Fig. 2, are listed in column 1 of Table 2.

$A_2 = 129.3$ = sum of figures of column 2
$A_4 = 603.0$ = sum of figures of column 4

$$x_0 = \frac{A_4}{A_2} = \frac{603.0}{129.3} = 4.66 \text{ in.} = \text{distance of c.g. from } A' \text{ (Fig. 1)}$$

$R = r + x_0 = 4.5 + 4.66 = 9.16$ in.

With the value of x_0 known, the values of columns 6, 7, and 8 are computed. $A_8 = 100.3$ = sum of figures of column 8.

[4] The author is indebted to G. G. Setterlund of the Westinghouse Electric Corporation for carrying out in these calculations as well as those of Part 2.

TABLE 1

1	2	3	4[a]	5	6[b]	7	8[c]
b_1	$2b_1$	Δ	$2b_1\Delta$	$c_1 = r + \Delta$	$a_1 = x_0 - \Delta$	a_1^3	$2b_1a_1^3 + c_1$
b_2	b_2	2Δ	$2b_2\Delta$	$c_2 = r + 2\Delta$	$a_2 = x_0 - 2\Delta$	a_2^3	$b_2a_2^3 + c_2$
b_3	$2b_3$	3Δ	$6b_3\Delta$	$c_3 = r + 3\Delta$	$a_3 = x_0 - 3\Delta$	a_3^3	$2b_3a_3^3 + c_3$
b_4	b_4	4Δ	$4b_4\Delta$	$c_4 = r + 4\Delta$	$a_4 = x_0 - 4\Delta$	a_4^3	$b_4a_4^3 + c_4$
b_5	$2b_5$	5Δ	$10b_5\Delta$	$c_5 = r + 5\Delta$	$a_5 = x_0 - 5\Delta$	a_5^3	$2b_5a_5^3 + c_5$
b_6	b_6	6Δ	$6b_6\Delta$	$c_6 = r + 6\Delta$	$a_6 = x_0 - 6\Delta$		
b_7	$2b_7$	7Δ	$14b_7\Delta$	$c_7 = r + 7\Delta$			
b_8	b_8	8Δ	$8b_8\Delta$	$c_8 = r + 8\Delta$			
b_9	$2b_9$	9Δ	$18b_9\Delta$	$c_9 = r + 9\Delta$			
b_{10}	b_{10}	10Δ	$10b_{10}\Delta$				
b_{11}	$2b_{11}$	11Δ	$22b_{11}\Delta$			etc.	etc.
b_{12}	b_{12}	12Δ	$12b_{12}\Delta$				
b_{13}	$2b_{13}$	13Δ	$26b_{13}\Delta$				
b_{14}	b_{14}	14Δ	$14b_{14}\Delta$				
b_{15}	$2b_{15}$	15Δ	$30b_{15}\Delta$	etc.	etc.		
b_{16}	b_{16}	16Δ	$16b_{16}\Delta$				
b_{17}	$2b_{17}$	17Δ	$34b_{17}\Delta$				
b_{18}	b_{18}	18Δ	$18b_{18}\Delta$				
b_{19}	$2b_{19}$	19Δ	$38b_{19}\Delta$				
b_{20}	b_{20}	20Δ	$20b_{20}\Delta$				
b_{21}	$2b_{21}$	21Δ	$42b_{21}\Delta$				
b_{22}	b_{22}	22Δ	$22b_{22}\Delta$				
b_{23}	$2b_{23}$	23Δ	$46b_{23}\Delta$				
b_{24}	b_{24}	24Δ	$24b_{24}\Delta$				
b_{25}	$2b_{25}$	25Δ	$50b_{25}\Delta$				
b_{26}	b_{26}	26Δ	$26b_{26}\Delta$				
b_{27}	$2b_{27}$	27Δ	$54b_{27}\Delta$				
b_{28}	b_{28}	28Δ	$28b_{28}\Delta$				
b_{29}	$2b_{29}$	29Δ	$58b_{29}\Delta$				

A_2 = sum of figures in column 2
A_4 = sum of figures in column 4
A_8 = sum of figures in column 8
$\Delta = h/30$
[a] Column 4 = column 2 times column 3
[b] Value of $x_0 = A_4/A_2$
[c] Column 8 = column 2 times column 7 divided by column 5.

TABLE 2 NUMERICAL EXAMPLE

Location no.	1 (b, in.)	2	3	4	5	6	7	8
1	1.70	3.40	.32	1.09	4.82	4.34	18.81	13.30
2	2.38	2.38	.64	1.52	5.14	4.02	16.11	7.48
3	2.79	5.58	.96	5.36	5.46	3.70	13.70	14.00
4	3.02	3.02	1.28	3.86	5.78	3.38	11.41	5.96
5	3.23	6.46	1.60	10.32	6.10	3.06	9.38	9.95
6	3.32	3.32	1.92	6.36	6.42	2.74	7.51	3.88
7	3.38	6.76	2.24	15.14	6.74	2.42	5.86	5.90
8	3.40	3.40	2.56	8.71	7.06	2.10	4.41	2.12
9	3.39	6.79	2.88	19.55	7.38	1.76	3.17	2.91
10	3.38	3.38	3.20	10.81	7.70	1.46	2.13	0.94
11	3.37	6.74	3.52	23.75	8.02	1.14	1.30	1.09
12	3.34	3.34	3.84	12.82	8.34	0.82	0.672	0.27
13	3.32	6.64	4.16	27.60	8.66	0.50	0.250	0.19
14	3.30	3.30	4.48	14.79	8.98	0.18	0.032	0.01
15	3.29	6.58	4.80	31.60	9.30	—0.14	0.019	0.01
16	3.24	3.24	5.12	18.60	9.62	—0.46	0.212	0.07
17	3.21	6.42	5.44	34.85	9.94	—0.78	0.607	0.39
18	3.20	3.20	5.76	18.45	10.28	—1.10	1.21	0.38
19	3.18	6.36	6.08	38.65	10.58	—1.42	2.02	1.21
20	3.13	3.13	6.40	20.05	10.90	—1.74	3.03	0.87
21	3.10	6.20	6.72	41.60	11.22	—2.06	4.24	2.34
22	3.06	3.06	7.04	21.53	11.54	—2.38	5.66	1.50
23	2.98	5.96	7.36	43.80	11.86	—2.70	7.3	3.68
24	2.88	2.88	7.68	22.15	12.18	—3.02	9.13	2.15
25	2.72	5.44	8.00	43.50	12.50	—3.34	11.15	4.86
26	2.58	2.58	8.32	21.42	12.82	—3.66	13.40	2.70
27	2.38	4.76	8.64	41.20	13.14	—3.98	15.84	5.74
28	2.00	2.00	8.96	17.91	13.46	—4.30	18.50	2.75
29	1.50	3.00	9.28	28.00	13.78	—4.62	21.25	4.63
30	0	0	9.60	0	14.10	—4.94	24.40	0
$\Delta = 0.32$		$\Sigma = 129.3$ $= A_2$		$\Sigma = 603.0$ $= A_4$				$\Sigma = 100.3$ $= A_8$

From Equation [3] the maximum tensile stress at A' (Fig. 1) then becomes

$$S_{max} = \frac{3Px_0R}{4r\ \Delta\ A_3} = \frac{3\ (100{,}000)\ (4.66)(9.16)}{4\ (4.5)\ (0.32)\ (100.3)} = 22{,}200 \text{ psi}$$

Results obtained by using this method have been checked against those using the graphical method described by Timoshenko[5] for several practical hooks. Agreement was obtained in all cases within a few per cent which may be considered satisfactory in view of the possible error inherent in the use of the graphical method. In addition, as mentioned later, the numerical integration method has also been checked against the analytical method of Part 2.

PART 2 ANALYTICAL METHOD FOR HOOK OF APPROXIMATE TRAPEZOIDAL SHAPE

(*a*) *Method of Analysis.* The analytical method given in this part is intended to apply to hooks with cross sections having a shape such as shown by the full lines of Fig. 3, and which do not deviate too much from a trapezoidal form. This includes a large number of practical crane-hook sections. This method, while approximate, is much faster than the numerical integration method of Part 1, and in the cases to which it has been applied, it has given close agreement with the latter method.

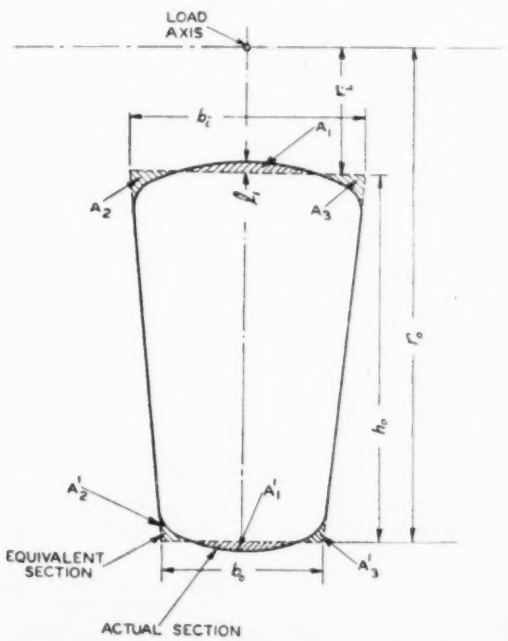


FIG. 3 CRANE-HOOK SECTION OF APPROXIMATE TRAPEZOIDAL FORM

Essentially the analytical method is based on the assumption of an equivalent trapezoidal section having an area equal to that of the actual section. The stress computed in this way is then corrected for the stress increase in the actual section resulting from the fact that the fibers nearest the center of curvature are farther from the neutral axis than in the case of the equivalent trapezoidal section. It is again assumed that the resultant load on the hook passes through the center of curvature of the curved part and that the critical section is at 90 deg to the resultant load.

Referring to Fig. 3, the full lines represent the actual hook section and the dashed lines the equivalent trapezoidal section. The equivalent section is so chosen that the shaded area A_1 is equal to the areas $A_2 + A_3$. Likewise $A_1' = A_2' + A_3'$. Referring to Fig. 3 let

b_i, b_0 = inside and outside widths of equivalent trapezoid, respectively

r_i, r_0 = inside and outside radii of equivalent trapezoid, respectively

$\alpha = b_0/b_i$; $\beta = r_0/r_i$

With these notations, the formulas for bending stress S_b at point A, Fig. 4, at the inside of the trapezoidal section as derived from curved-bar theory become[6]

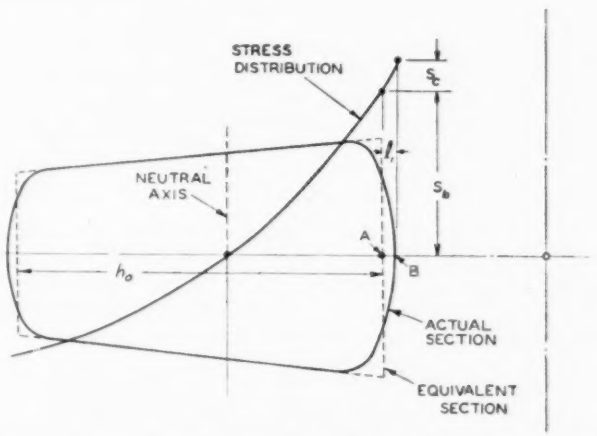


FIG. 4 STRESS DISTRIBUTION OVER CROSS SECTION OF CRANE HOOK

$$S_b = \frac{2PK_1\left(K_2 - \dfrac{1}{\beta - 1}\right)}{b_i r_i (1 + \alpha)(K_1 - K_2)} \quad [4]$$

where

$$K_1 = \frac{1}{\beta - 1} + \frac{2\alpha + 1}{3(\alpha + 1)} \quad [5]$$

$$K_2 = \frac{\dfrac{1}{2}(1 + \alpha)}{\dfrac{(\beta - \alpha)}{(\beta - 1)}\log_e \beta - (1 - \alpha)} \quad [6]$$

In general the factors K_1 and K_2 should be calculated to four significant figures. To do this the use of log tables or a computing machine is advisable.

In Fig. 4 the distribution of stress over the section due to bending alone is indicated. It should be noted that the stress S_b calculated from Equation [4] yields the bending stress at point A at the inside of the equivalent trapezoid. Because of greater distance from the neutral axis the bending stress at B in the actual hook will be appreciably larger than that at point A by an amount S_e as shown. If l_1 is the distance between points B and A then the stress augment S_e will be given approximately by

$$S_e = l_1\left(\frac{dS}{dy}\right)_0 \quad [7]$$

where $(dS/dy)_0$ is the value (at point A, Fig. 4) of the derivative of the stress S with respect to distance y from the neutral axis. From the equations of curved-bar theory, the derivative $(dS/dy)_0$ may be obtained, and by substitution in Equation [7], using the previous notations, the stress augment S_e becomes

[5] Reference (1) page 75.

[6] See reference (1), page 68, for method of derivation.

$$S_e = \frac{S_b K_2 l_1}{r_i[K_2 - 1/(\beta - 1)]} \quad [8]$$

where K_2 is given by Equation [6].

The stress due to direct tension is

$$S_t = \frac{P}{A} \quad [9]$$

where A is the area of the cross section.

$$A = \frac{h_0(b_0 + b_i)}{2} \quad [10]$$

where h_0 = depth of equivalent trapezoid, Fig. 3.

The maximum stress S_{max} in the hook at the critical section will be the sum of the bending stress S_b Equation [4], the stress augment S_e, Equation [8], and the direct tension stress S_t Equation [9]. This gives

$$S_{max} = S_b + S_e + S_t \quad [11]$$

(*b*) *Numerical Example.* These equations have been applied to the hook section having a depth of 8 inches and a maximum width of 5 inches, and the approximate shape shown in Fig. 3. By choosing the area $A_1 = A_2 + A_3$ and $A_1' = A_2' + A_3'$ the following values for the equivalent trapezoid were obtained

$$b_i = 5.1,\ b_0 = 3.9,\ r_i = 4.5,\ r_0 = 12.07,\ l_1 = 0.25 \text{ in.}$$

$$\alpha = b_0/b_i = 0.765,\ \beta = r_0/r_i = 2.68,\ A = 34 \text{ sq in.}$$

Using these values in Equations [5] and [6]

$$K_1 = 1.073$$
$$K_2 = 0.9930$$
$$K_1 - K_2 = 0.080$$

Taking the load P equal to 50,000 lb and using these values in Equations [4], [8], and [9], we find

$$S_b = 13{,}200 \text{ psi};\ S_e = 1830 \text{ psi};\ S_t = 1470 \text{ psi}$$

Adding these the maximum stress becomes

$$S_{max} = 16{,}500 \text{ psi}$$

Computation on this section using the numerical integration method of Part 1 showed a stress value of 16,200 psi which is quite close to the figure obtained by the analytical method.

Similar calculations on a hook section of 9½ in. depth and 6 in. maximum width with the same inside radius showed a figure of 11,000 psi for the analytical method and 10,900 psi for the numerical integration method. This would seem to indicate that the former is sufficiently accurate for most purposes for sections approximating the shape shown in Fig. 3.

Conclusions

The results of calculations on actual crane-hook sections, indicate that for sections such as shown in Fig. 4, which do not deviate too much from a trapezoidal form, the relatively rapid analytical method of Part 2 is sufficiently accurate for practical use.

For irregular sections or for an independent check on the results obtained by the analytical method of Part 2, the numerical integration method of Part 1 has also been found useful.

REFERENCES

1 "Strength of Materials," by S. Timoshenko, second edition, part 2, D. Van Nostrand Company, New York, N. Y., 1941, p. 65.

2 "Stresses in Curved Bars," by H. C. Perkins, Trans. A.S.M.E., vol. 53, 1931, p. 201.

3 "Mathematical Methods in Engineering" by Th. von Kármán and M. A. Biot, McGraw-Hill Book Company, 1940, p. 5.

Discussion

Tension Tests at Constant True Strain Rates[1]

LAWFORD H. FRY.[2] The authors discuss the effect of temperature and strain velocity on the stress-strain properties of various materials. In describing testing methods, the authors say, "The value of the true strain rate was controlled by adjusting the head motion of the testing machine." This reads as though the assumption were made that the travel of the crosshead of the testing machine is the same as the strain of the specimen. This is certainly not the case.

The writer has shown:[3] "Only a small fraction of the crosshead travel appears as strain in the specimen. The proportion of strain to crosshead travel varies during a test as the load is increased, but is unaffected by the rate of crosshead travel." Methods are given in the paper[3] just quoted for comparing the travel of the crosshead with the rate of strain. It would be interesting to have information as to this relationship in the case of the machine used by the authors and the various specimens tested.

Incidentally as a minor point, attention is called to the authors' statement, "The standard 0.505-in-diam tension specimen was employed throughout the testing program." Presumably the authors refer to the standard 2-in-gage-length specimen of the American Society for Testing Materials. Reference to A.S.T.M. Specification E 8-42, Fig. 3, will show that the diameter of the 2-in. specimen is $^1/_2$ in. plus or minus 0.01 in.

S. TIMOSHENKO.[4] The writer would like to bring to the attention of American engineers some recent investigations made in Russia by N. N. Davidenkov. This investigation deals with calculation of true stresses and true strains at the minimum diameter of tension test bars of Armco iron stretched to various degrees of reduction of the cross-sectional area. Eight 1-in-diam bars were stretched up to reduction of area from 41 per cent to 69.2 per cent, after which they were cut at the minimum diameter. The minimum cross sections were polished and microscopically investigated. Numerous measurements of average changes of dimensions of grains showed that radial and tangential strains ϵ_r and ϵ_t are equal and are constant over the entire cross section. Their values obtained from these measurements were in very good agreement with the average values obtained from measurements of the minimum diameter of the test pieces. This indicates that the strains calculated from the measurements of the reduction of area represent true strains.

To obtain the true stress distribution, Davidenkov makes the usually accepted assumption

$$\frac{\sigma_l - \sigma_t}{\epsilon_l - \epsilon_t} = \frac{\sigma_l - \sigma_r}{\epsilon_l - \epsilon_r} \qquad [1]$$

from which he concludes that for $\epsilon_l = \epsilon_r$ we must also have $\sigma_r = \sigma_t$. To calculate these stresses and also the stresses σ_l in the axial direction, the curvature $1/R$ of the longitudinal fibers of the stretched bars at the surface was measured and it was assumed that for any inside fiber at the distance x from the axis of the bar the curvature is

$$\frac{1}{\rho} = \frac{1}{R}\frac{x}{a} \qquad [2]$$

where a is the minimum radius of the stretched bar. This expression for curvature was substituted into the equation of equilibrium of an infinitesimal element and in this way was obtained

$$d\sigma_r = \frac{1}{\rho}(\sigma_l - \sigma_r)\,dx = \frac{x}{Ra}(\sigma_l - \sigma_r)\,dx$$

By integration, we find

$$\sigma_r = (\sigma_l - \sigma_r)\frac{a^2 - x^2}{2Ra} \qquad [3]$$

It is seen that the radial stress σ_r increases as we proceed from the surface of the specimen to its axis. It vanishes at the surface and becomes a maximum at the axis.

From Equation [1] of this discussion we conclude that for $\epsilon_r = \epsilon_t$ the difference $\sigma_l - \sigma_r$ must be constant for the entire cross section. Denoting that constant value by σ_0, we obtain

$$\sigma_l = \sigma_0 + \sigma_r \qquad [4]$$

The summation of stresses σ_l must give us the tensile force S stretching the bar. Hence, using Equations [3], and [4], we find

$$\int_A \sigma_l\,dA = \sigma_0 \int_0^a \left(1 + \frac{a^2 - x^2}{2Ra}\right) 2\pi x\,dx$$

$$= \sigma_0 \pi a^2 \left(1 + \frac{a}{4R}\right) = S$$

$$\sigma_\theta = (\sigma_l)_{\min} = \frac{S}{\pi a^2\left(1 + \frac{a}{4R}\right)} \qquad [5]$$

$$(\sigma_l)_{\max} = \sigma_0\left(1 + \frac{a}{2R}\right) \qquad [6]$$

It is seen that the longitudinal stress is not uniformly distributed over the minimum cross section of the stretched bar and that its maximum value at the axis of the bar depends upon the magnitude of the ratio $a/2R$.

This represents the principal result of Davidenkov's work. We see that the simple tensile test brings us to a complicated stress distribution at the reduced cross section. Thus it seems desirable, in studying the effect of speed on the stress-strain relation, to use the experiments in which stress distribution is not affected by plastic deformation. Such conditions can be approached in torsion of tubular specimens. Several experiments of this kind with tubes of lead were made some time ago by James Jamieson at the University of Michigan.

[1] By C. W. MacGregor and J. C. Fisher, published in the Dec., 1945, issue of the JOURNAL OF APPLIED MECHANICS, Trans. A.S.M.E., vol. 67, p. A-217.

[2] Director of Research, The Locomotive Institute, New York, N. Y. Fellow A.S.M.E.

[3] "Speed in Tension Testing and Its Influence on Yield Point Values," by L. H. Fry, Proceedings of the A.S.T.M., vol. 40, 1940, p. 625.

[4] Professor of Theoretical and Applied Mechanics, Department of Mechanical Engineering, Stanford University, Stanford University, Calif. Fellow A.S.M.E.

Authors' Closure

The question of the control of the strain rates was brought up by Mr. Fry.

No assumption was either made or used in our experiments to the effect that the travel of the crosshead of the testing machine is the same as the strain of the specimen as mentioned by Mr. Fry. In fact the paper emphasizes that one of the reasons for developing the true-strain-rate approach was just to avoid such an inequality between rate of head motion and the rate of straining of the specimen. Mr. Fry is referred to the first paragraph under the heading "Testing Procedure" which brings this out clearly. The last sentence of this paragraph states "If the rate of head motion is constant it is not true that the strain rate is also constant."

In the authors' tests, the *true strain rate of the specimen* was maintained *constant* by *varying* the rate of head motion of the testing machine throughout each test so that the proper minimum diameter was attained at the appropriate time. Since the true strain $\epsilon = 2 \log_e \frac{d_0}{d}$, the absolute value of the true strain rate is

$$\dot{\epsilon} = 2 \frac{\dot{d}}{d} \qquad [1]$$

where $\dot{\epsilon}$, d, and $\dot{d}$ are the true strain rate, the instantaneous diameter, and the time rate of change of the instantaneous diameter, respectively. To maintain a constant true strain rate it is only necessary then to force the diameter of the specimen to follow a certain predetermined schedule of values with respect to time by varying the rate of head motion of the testing machine through adjustments of the control valve. Hence it is the true strain rate of the specimen which is maintained constant and *not* the rate of head motion.

In addition to the difference between the rate of head motion and the strain rate of the specimen to which Mr. Fry refers, it is also true that due to the increase in gage length of a specimen under tension, the true strain rate is not obtained by dividing the change in gage length per unit of time by the original gage length. While this procedure does not make any appreciable error at the yield point, the error increases with the amount of strain. In Fig. 2 of Mr. Fry's paper,[5] for example, the effect of strain rate on the tensile strength is shown. Unless a correction was made for increase of gage length these values do not represent true strain rates.

Likewise, during necking, even if a correction is made for increased gage length which originally was, say, 2.0 in., the definition of strain rate customarily used has little physical significance due to the great variation in strain rate along the test bar. These various disadvantages are overcome through the use of the true-strain-rate definition employed in the paper and given by Equation [1] of this closure.

Professor Timoshenko has very kindly called the authors' attention to a recent interesting paper by N. N. Davidenkov and N. I. Spiridonova in which a discussion is given of the true stress and true strain conditions in a necked tension specimen. Previous contributions on this same subject have been made by E. Siebel[6] and P. W. Bridgman.[7] The Davidenkov formula is the same as the one given earlier by Siebel.

The formula developed in the paper referred to by Professor Timoshenko is based in part on the assumed validity of Equation [1] of his discussion, namely, the equality of the stress difference and strain difference ratios. Davidenkov points out that this has not yet been proved experimentally as fully accurate, but that it is used as a first approximation.

Davidenkov attempts to prove experimentally that the axial strain is constant across the necked specimen by measuring grain sizes after the specimen has necked down. The scatter of his observations and the absence of control measurements on undeformed specimens reduces the significance of his results.

Tests conducted by the authors two years ago on large 2-in-diam. round steel specimens showed that at the minimum section the average true axial strain $\epsilon = \log_e \frac{A_0}{A}$ determined from diameter measurements was substantially greater than the true axial strain at the surface of the specimen $\epsilon_s = \log_e \frac{l}{l_0}$ as determined by the separation of closely spaced scribed circumferential lines at the minimum section. The possible effect of the curvature of the surfaces at the neck was investigated, and found to be negligible for scribed lines spaced as closely as in these tests. For two such tests carried to strains of about 0.6 to 0.65 the value of $\epsilon = \log_e \frac{A_0}{A}$ was in fact greater than the value of $\epsilon_s = \log_e \left(\frac{l}{l_0}\right)_{\text{at surface}}$ by 8 per cent in the first test and 10 per cent in the second at the minimum section. The second test was carried to a slightly greater true strain than the first. This variation is difficult to reconcile with a constant axial strain value across the minimum section.

Since there is some question as to the validity of the assumptions used by Davidenkov and Spiridonova in their analysis, as well as some question as to the validity of their experimental results as indicated in particular by the existence of experimental contradiction to their observations, the authors have felt that any "correction" of the average true stress would not be justified at this time, as the determination of the correction factor depends on uncertain and controversial premises. Further, if a "correction" of the average true stress is made, then the results of the authors' tests on round bars indicate that a similar correction of the average true strain should be made. Until the question of the strain and stress distribution in the neck of a tension specimen is more satisfactorily determined and conflicting observations have been reconciled, the authors prefer to deal directly with the average true stress (P/A at the minimum section) and the average true strain ($\epsilon = \log_e \frac{A_0}{A}$ at the minimum section).

Professor Timoshenko mentions the use of hollow torsion bars as a more suitable form of test. Our experience has been that if sufficiently thin-walled torsion-test specimens are used to provide a uniform state of stress, considerable difficulty is encountered due to plastic buckling. If the uniform gage length is made small to overcome this, the effect of an unknown restraint is introduced. On the other hand, if the wall is thick enough to prevent buckling, an appreciable error is introduced in the calculation of the stress. The use of solid torsion bars is thus preferable for these reasons and also because of the greater amount of machining necessary for hollow specimens.

The authors would like to take this opportunity to thank Mr. Fry and Professor Timoshenko, and also those who contributed oral discussion to this paper, for bringing to their attention several problems of interest in connection with the constant-true-strain-rate tension test.

---

[5] "Speed in Tension Testing and Its Influence on Yield Point Values," by L. H. Fry, Proceedings of the A.S.T.M., vol. 40, 1940, p. 625.

[6] "Effect of Lateral Contraction in Tensile Test on Strain Hardness of Metals," by E. Siebel, *Berichte der Fachausschusse des Vereines deutscher Eisenhuttenleute*, vol. 71, no. 5, 1925, pp. 1 and 2.

[7] "Stress Distribution at Neck of Tension Specimen," by P. W. Bridgman, Transactions, American Society for Metals, vol. 32, 1944, p. 553.

The Axial Vibration of Turbine Disks[1]

E. L. Robinson.[2] This paper emphasizes the importance of knowing the natural frequencies of axial vibration of turbine disk wheels and presents a method for calculating these frequencies. The author has followed the formulation of energies given by Stodola[3] but has worked out and tabulated coefficients applicable to a somewhat different type of deflection curve. It would be interesting to check through the mathematics from the beginning, but this would divert discussion from matters of more consequence. Suffice it to say that it is advantageous to perform the circular integration around a complete circumference rather than over one half the angular distance between nodal radii as done by Stodola. This detail, however, does not affect the validity of the result.

It is unfortunate that the wheels whose frequencies are of least importance are the ones whose frequencies are most easily computed. On the other hand, the exhaust-stage wheels, having long buckets and the lowest frequencies, are the ones whose frequencies it is most important to know and, at the same time, the ones for which it is most difficult to make a reliable calculation.

For more than 20 years the writer's company has made it a point to determine the critical frequencies of such wheels by actual test, using the methods described by Campbell.[4] Throughout this period it has been the opinion of the writer that it was possible by calculation to predict the frequencies of a wheel with sufficient accuracy to assure that it could be tuned satisfactorily for use, and thus preclude any possibility of having to scrap a wheel after its manufacture had been completed. On the other hand, when it is necessary to work to reasonably close margins from resonance, it has never appeared proper to dispense with the test determination of the actual frequencies. There are certain rather fundamental reasons why this is so.

With wheels having short buckets some one of the "high-node" types of vibration will occur in proximity to running speed, and such wheels must be sufficiently rugged to withstand the vicissitudes of service even if operating on a high-node resonance. The margins between one resonance and another are too small to assure avoidance.

With such wheels the potential energy of bending is very largely in the wheel and but little in the buckets. Even though a considerable fraction of the kinetic energy of vibration is in the buckets, this may be estimated with reasonable accuracy.

On the other hand, with long exhaust-stage buckets it is often the case that almost all of the energy of bending as well as practically all of the kinetic energy of vibration is in the buckets. In this case what goes on in the web of the wheel is of minor consequence, but what goes on in the attachment of the buckets to the rotor, whether a wheel or a drum, is of controlling importance. It is necessary to consider whether the attachment is such as to bend the rim of the wheel or the outermost continous ring of material in the rotor both in the radial and tangential directions or only in a tangential direction. There may be a very sharp curvature in the radial direction, but much of this may be provided by hinging so that it may or may not result in bending the outer ring of the disk or rotor in a radial direction. How to represent this portion of the structure in any scheme of calculation is almost certain to be vital with long buckets. When the true frequency has been determined by test it is always possible to sketch in an equivalent rim or to say what proportion of a heavy wheel or drum participates in bending. However, the real problem is not to explain in a satisfactory manner what has been found by test but to determine it without a test.

The shape of deflection curve is most important, but the writer has never found it possible to use a standard curve for more than a limited type of wheel design. Admitting that the assumed deflection curve may differ from the true curve and still yield a reasonably good answer, it must also be admitted that if the curve is not of a reasonably correct shape, the resulting calculated frequency can be so much off as to be of no value.

When confronted with the double set of uncertainties as to how to describe a rim or ring of attachment while at the same time having to choose a reasonable deflection curve, either choice having a wide and important effect on the answer, it becomes almost impossible to proceed without reference to the analyses of the behavior of many similar designs whose frequencies have been determined by test.

The writer realizes that this is not a very comforting situation. Without wishing to appear unappreciative of an excellent attack upon the problem of the frequencies of a wheel with short buckets, it does seem necessary to point out some of the very real limitations when the problem involves long buckets.

W. E. Trumpler, Jr.[5] In assuming a simplified analytical form for the vibratory deflection curve of a radial element, it is evident that the effect of complications such as a heavy rim and blades attached to it, cannot be adequately accounted for. The author has provided certain empirical correction factors to take care of a range of these effects. However, it is possible in the range of practical design, that the rim and the blades become the controlling influence on the disk frequency.

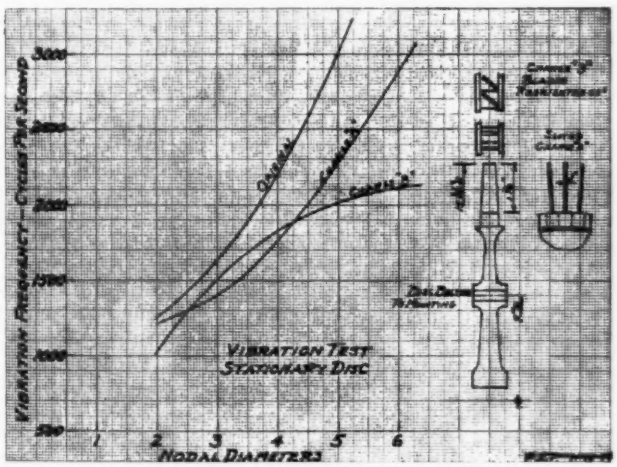


Fig. 1 Vibration Test Results Showing Effect of Several Changes in Rim and Blades

To demonstrate that this possibility exists, reference is made to some recent tests run in the laboratory of the Westinghouse Steam Division at South Philadelphia. Fig. 1 of this discussion shows the data for the small disk as drawn approximately to scale. Although this disk is mounted by bolting rather than a shrink or

[1] By A. M. G. Moody, published in the March, 1945, issue of the Journal of Applied Mechanics, Trans. A.S.M.E., vol. 67, p. A-48.

[2] Turbine Engineering Department, General Electric Company, Schenectady, N. Y. Mem. A.S.M.E.

[3] "Steam and Gas Turbines," by A. Stodola, translated by L. C. Loewenstein, McGraw-Hill Book Company, Inc., New York, N. Y., 2 volumes, 1927.

[4] "The Protection of Steam-Turbine Disk Wheels From Axial Vibration," by W. Campbell, Trans. A.S.M.E., vol. 46, 1924, pp. 31–160.

[5] Turbine Engineering Department, Steam Division, Westinghouse Electric Corporation, Philadelphia 13, Pa. Jun. A.S.M.E.

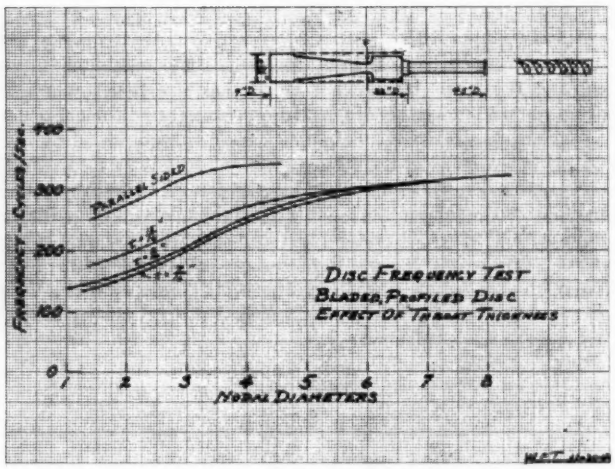


FIG. 2 RESULTS OF STATIONARY TEST ON DISK WITH VARIOUS PROFILES

drive fit at the bore, it acts in the common modes of vibration just like any other disk, assuming the hub at the bolt circle. In the original test the simulated blades were machined from the solid rotor. In the second test, indicated as change "A," slots were cut between blades through part of the rim. In the last one, marked change "B," the blades were sawed off and soldered back at an orientation of 45 deg. Here is a demonstration of the important effect which several apparently minor changes have on the frequency. The mass was not substantially affected. In the case of the reoriented blades, the curve seems to become asymptotic to a line which is approximately equal to the lowest mode blade frequency, that about its minimum axis. A high-frequency low-mass magnetic vibrator was used to excite these vibrations.

The results of another series of tests on a disk are shown in Fig. 2. These blades are shrouded in small groups. Having run the first test with the unprofiled wheel, it was possible then to recut the disk with profiles of successively smaller neck thickness. Here it is seen that all the frequency curves approach the same line, which again is found to be the lowest mode blade-group frequency.

These tests indicate that in the system of wheel, rim, and blades, all three elements have importance of the same order over a wide range of practical interest. Of course there are some situations where only the blade frequency is of interest, and some where the blades are so small that only disk vibration is involved (with corrections), but there is an important range where a satisfactory analysis cannot ignore a combined consideration. This has been pointed out previously by I. Malkin.[6]

The restrictions imposed by the Rayleigh-Ritz method are such that in order to take into account adequately the effect of blades and rim, we have resorted to a different approach which has given highly satisfactory results at least for those systems for which we have experimental data.

It would be of considerable interest and help to those applying his method if the author would report the correlation of calculated and test frequencies so that limits for rim and blade proportions may be indicated for satisfactory results.

AUTHOR'S CLOSURE

Mr. E. L. Robinson's contributions to the field of mechanical problems in turbine design and particularly to the subject of disk vibration have been so considerable that it is a source of great satisfaction to the author to have his comments on the subject paper. All his points are well taken, and while some of them were touched upon in the paper, they should perhaps have been given more emphasis. The method described is simply of no value for wheels having extremely long blades. In the paper it was suggested that a blade length equal to 40 per cent of the radius of the disk proper be adopted as an upper limit. Excellent results have been obtained with blades close to this length.

To be sure, Mr. Robinson's point that the longer blades are precisely those which it is important to know accurately is perfectly valid. Nevertheless, the author feels that it is of real value to the designer to have a relatively simple and quick method for making sure of wheels with short blades which, as pointed out in the paper, do constitute the large majority of all turbine wheels.

More emphasis might well have been given to testing, though this has been well treated in the literature, as will be seen by reference to the papers listed in the bibliography given by the author. No program of vibration calculation should be contemplated which is not closely tied in with experimental checks. The method presented would not have been developed if previously described methods had not failed to check closely with experimental observations.

Mr. Trumpler's discussion presents some interesting information and, like Mr. Robinson's, emphasizes the importance of the blades. The difference in frequency caused by reorienting the blades is large, and indicates that in practice if a blade design radically different from the conventional were to be tried, too much faith should not be placed in calculations. This would, however, be an unusual situation. Furthermore, it applies only to relatively long blades. One thought which it gives rise to is that blade length alone is not the determining criterion, since a disk whose hub diameter is a large percentage of its rim diameter, such as that indicated in Fig. 1 of the discussion, would naturally be more susceptible to changes in blade shape than one supported nearer the center.

Unfortunately, the author has no clear information on the range in which blades and disk both have a major effect on the frequency, and can only repeat that the method is not to be used there. With blades having a length of nearly 40 per cent of the radius, calculations have come consistently within 5 per cent of the test values and this is considered satisfactory.

The author wishes to express his appreciation to Messrs. Robinson and Trumpler for valuable and interesting discussions.

Distribution of Tooth Load Along a Pinion[1]

D. W. DUDLEY.[2] The authors of this paper have obtained a precise mathematical solution to one of the gear-designer's most complicated problems. Considering the complexity of the results, it is not surprising that approximate and rule-of-thumb methods have been used in the past to govern the relation of pinion face width to pinion diameter.

In spite of the complexity of the direct mathematical solution of the load-distribution problem, the solution obtained may be checked by simple deflection formulas. It is only necessary to take the distribution of load curve, w_f versus l, and replace this loading by a series of concentrated loads spaced at regular intervals; these concentrated loads having individual amounts proportional to the w_f value for each of their locations, and a total

[6] "On a Generalization of Kirchhoff's Theory of Transversal Plate Vibrations in the Vibration Problem of Steam Turbine Disks," by I. Malkin, *Journal of The Franklin Institute*, vol. 234, Oct., 1942, pp. 355–370; and vol. 234, Nov., 1942, pp. 431–452.

[1] By H. Poritsky, A. D. Sutton, and A. Pernick, published in the June, 1945, issue of the JOURNAL OF APPLIED MECHANICS, Trans. A.S.M.E., vol. 67, 1945, p. A-78.

[2] Gear Engineering Division, General Electric Company, River Works, Lynn, Mass.

value equal to the total applied load. By superpositioning the deflections of these concentrated loads, total deflections can be obtained. If a sufficiently large number of concentrated loads are used, the total deflections obtained by this method should closely check with those obtained by the equations in the paper. The writer has used this method to check numerical answers to the illustrative problems given.

The solution of the distribution-of-load problem can probably be best put into a proper perspective by considering it as step 2 of a problem of 3 steps. Step 1 is the determination of the various stiffness constants. This in itself is no small problem, since the geometry of the gear teeth and the pinion cross section tend to place them in a boundary region where the usual textbook formulas for bending, torsion, and shear do not apply exactly. The bending of a helical gear tooth is particularly difficult, since such a tooth in different transverse sections is loaded simultaneously from the base to the tip. Formulas for the stiffness constants can best be obtained by making a careful study of the pinion-and-gear geometry and then "calibrating" tentative formulas by actual laboratory check.

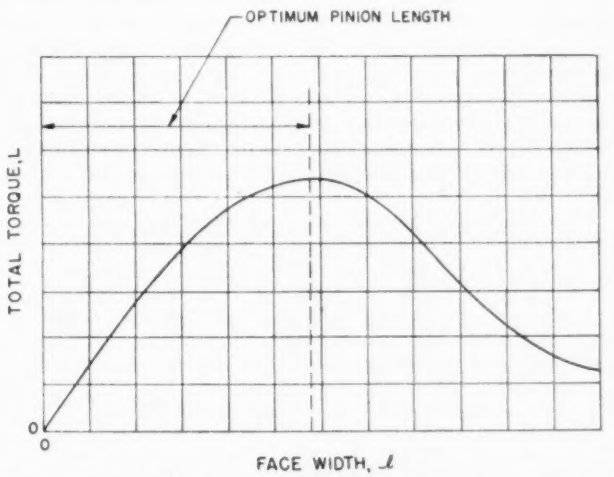


FIG. 1 TORQUE CAPACITY OF A PINION WHEN CONTACT PRESSURE IS HELD CONSTANT

The second part of the general problem is, of course, the solution for the load distribution using the given stiffness constants. The third part of the problem is the actual application of the results to solve a design problem. Here it is necessary to consider the expected range of cutting inaccuracies, the effect of lubrication, the effect of dynamic load, possible corrective wear, and changes in alignment which can be made in the casing. From a consideration of all these, the designer should be able to decide what constitutes the optimum design.

A few words should be said to define the optimum design from the standpoint of load distribution since neither in this paper nor in the parallel paper by Lewis[3] was there a clear statement of the ultimate objective in load-distribution studies. A designer limited by a certain maximum intensity of contact pressure and given a pinion of certain diameter, a certain size and shape of pinion teeth, and a certain specified pinion cross section must decide what face width will carry the maximum torque. Fig. 1 of this discussion shows schematically how the torque carrying capacity of a pinion might be plotted as a function of its face width. Locating the high point of this torque curve is of course the final solution to the load-distribution problem.

[3] "Load Distribution of Reduction Gears," by F. M. Lewis, published in the June, 1945, issue of the JOURNAL OF APPLIED MECHANICS, Trans. A.S.M.E., vol. 67, 1945, p. A-87.

In summary, the writer feels that the paper presented by Messrs. Poritsky, Sutton, and Pernick, while not a complete work in itself on the subject of gear deflection, is still a big step forward in the direction of more scientific handling of the deflection problem.

ALEXANDER HAMMER.[4] The mathematical solution of such a complex problem on load distribution along the pinion, as presented itself after the authors took so many deciding factors into consideration, is clear and comprehensive to the gear designer. The authors emphasize that the examples chosen do not correspond to actual design practice but were selected for the purpose of bringing out, in an exaggerated manner, the effect of some of the factors involved. But if the method is applied to problems which do correspond to actual and good design practice, the difference in the results when the actual load distribution is taken into consideration, or when uniformly distributed load is assumed, is not so pronounced.

Messrs. C. R. Waller and A. Peterson,[5] of the writer's company, assuming uniformly distributed load along the pinion, established load-carrying capacities based on certain designing factors, which in turn did not allow an increase in the sum of torsional and lateral deflection above 0.001 in. These factors have guided our design for many years. More recently, we have conducted an elaborate investigation in which helix angle, pressure angle in plane of rotation, contact ratios in the axial and radial planes, i.e., the number of teeth in contact in the same planes, the total length of contact and especially tip relief, were taken into consideration. Although we increased our load-carrying capacities, we did not exceed the allowable 0.001 in. for the total, i.e., the sum of torsional and lateral deflection.

It is noted that the load-concentration curve established for a double-helical pinion, which the authors selected as a practical example, shows a maximum load-concentration factor at the torque end of the pinion as high as 1.9, but elimination of the negative portion of the load will lead to a decrease of this value. Making the tooth more flexible, using tip relief, we reduce the stiffness, causing considerable reduction in the maximum load-concentration factor.

Taking the effect of the oil film between mating teeth into consideration, we have been able, by using E. K. Gatcombe's method,[6] to determine the minimum thickness and the width of the oil wedge which separates the tooth surfaces. It was found that the width of the supporting wedge was considerably larger than the Hertz contact area and after determining the supporting effect of this wedge along the line of contact for the different mating phases, it was safe to assume that the oil film will induce a more evenly distributed load concentration.

The increased load carrying capacities applied to unchanged transmitted horsepower do indicate an allowable decrease in the width of face of pinion, which in turn leads to a considerable reduction in the maximum value of the load-concentration factor. In one of the examples given by the authors, a 25 per cent reduction in the face width produces a 31.5 per cent reduction in the maximum value of w_f.

There are many other factors, mostly taken into consideration by the authors, which have a tendency to equalize the load distribution along the face width of the pinion. Of course, one knows that a very small misalignment gap may affect the load

[4] Research Engineer, De Laval Steam Turbine Company, Trenton, N. J.

[5] "Reduction Gears," by C. R. Waller and A. Peterson, chapt. 8 in *Marine Engineering*, vol. 1, edited by H. L. Seward, published by The Society of Naval Architects and Marine Engineers, New York, N. Y., 1942.

[6] "Lubrication Characteristics of Involute Spur Gears," by E. K. Gatcombe, Trans. A.S.M.E., vol 67, 1945, pp. 177–188.

distribution profoundly, but on the other hand, with tooth relief we could achieve absolutely uniform load distribution for a particular applied torque. The authors state that this relief did not exceed 0.00019 in. for the example considered, but for practical consideration such small differences could be expected to be relieved by the wear on the teeth under high load.

Practical experience gained from actual performance and measurements taken in our gear department verify the deflection results which were calculated, assuming uniform load distribution along the face of the pinion, and taking the previously mentioned corrective factors into consideration. But for special gear-reduction problems where the designing factors are predetermined to such an extent that one cannot keep the ratio of face width to pitch diameter under 2.5, the method given by the authors will find a most welcome application.

Authors' Closure

The authors are grateful to Messrs. D. W. Dudley and Alexander Hammer for their interesting discussions of the paper and have read with interest F. M. Lewis's paper.[3] It is quite true as Mr. Dudley points out, that the calculation of the stiffness constants is the first step the gear designer is faced with in solving the problem of distribution of load. Except in section 3, very little was said about this step, since—due to space limitation—the attempt was made to concentrate on the effect of these constants, after they had been determined, upon the load distribution. While approximate methods of calculating these constants are known,[7] it is clear that their precise evaluation is not a simple matter and involves complex analysis, good engineering judgment, as well as measurements, to substantiate the approximate theoretical formulas which can be worked out.

It is of interest to point out that the Hertz compressibility effect near the contact region yields a compression which is not linear with the load thus resulting in a variable and a nonlinear substitute for Equation [11] or [13]. Furthermore, owing to the variable curvatures and the variable bending stiffness, there is a slight variation in tooth deflection as contact proceeds from the pitch line in either direction; this effect and the variation of the number of teeth in the arc of action lead to a variation in stiffness constant as contact moves along a tooth, and may produce a pulsation of half tooth frequency.

[7] "The Strength of Gear Teeth," by S. Timoshenko and R. V. Baud, *Mechanical Engineering*, vol. 48, 1926, p. 1108.

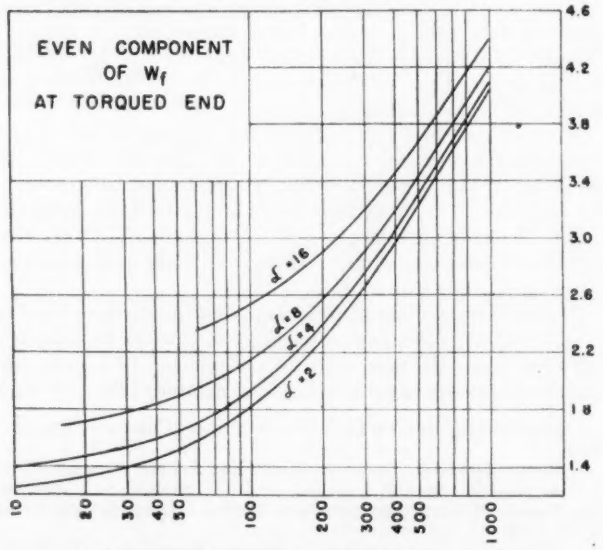


Fig. 2 Even Component of w_f at Torqued End

The effect of the oil film in increasing the equivalent tooth flexibility reported by Mr. Hammer is interesting and is worth reporting in the literature.

The successive-approximation method described by Mr. Lewis in his paper is a welcome alternative to the analytical method of the authors' paper. For almost any problem, it is well to have several alternative ways of solution and be able to choose the proper one for the particular occasion. As a matter of fact, the authors, too, had tried a graphical successive approximation method on the rather flexible pinion of Example 1, but after carrying out several steps and finding no signs of convergence, gave up the attempt, being pressed for time.

In defense of the analytical method the authors wish to state that it is not really as complex as might appear at first sight. The "complex" appearance of the solution ("complex" in the sense of complex numbers) can, of course, be completely eliminated by adding conjugate imaginary terms. By breaking the solution into an even component and odd one, it was possible to minimize the algebraic work involved in the determination of the constants; in examining the effect of misalignment, it then turned out that only the odd solution was changed while the even one remained unchanged. Thus a physical meaning was obtained for the simplification which first was suggested by analytical expediency.

By further algebraic reduction, the effect of the two pertinent design constants α and β on the stress factor in the middle of the pinion and at its end was computed for the even component of the load. For these calculations the authors are indebted to

TABLE 1 VALUES OF w_f AT TORQUED END

β	α = 2	α = 4	α = 8	α = 16
9	1.230	1.378	...	...
36	1.424	1.560	1.812	...
100	1.820	1.934	2.150	2.537
225	2.408	2.496	2.668	2.985
441	3.089	3.153	3.290	3.545
784	3.754	3.809	3.916	4.126
1296	4.349	4.395	4.494	4.680

TABLE 2 VALUES OF w_f AT MID-POINT

β	α = 2	α = 4	α = 8	α = 16
9	0.8835	0.8163	....	....
36	0.7777	0.7191	0.6187	....
100	0.5650	0.5225	0.4488	0.3365
225	0.2589	0.2371	0.1975	0.1374
441	—0.0717	—0.0765	—0.0844	—0.0950
784	—0.3519	—0.3454	—0.3330	—0.3099
1296	—0.5421	—0.5304	—0.5083	—0.4680

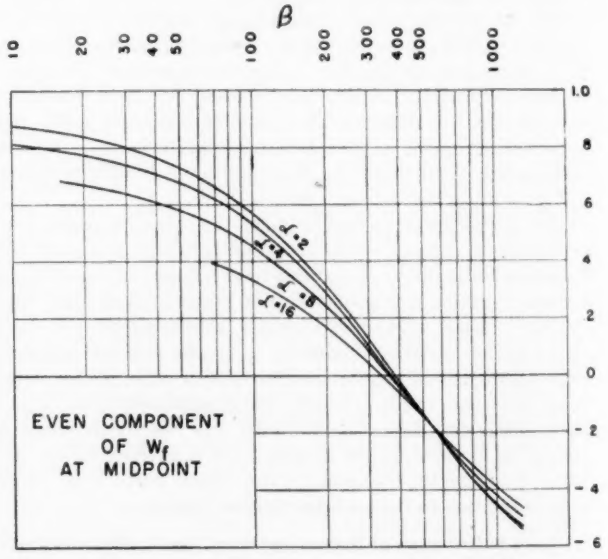


Fig. 3 Even Component of w_f at Mid-Point

W. B. Jordan. Tables 1 and 2 and Figs. 2 and 3 show the resulting values of w_f as a function of β for various α's. A glance at these curves will show whether any proposed design, that is, any value of α and β, will lead to a very flexible pinion or not. Clearly high flexibility relative to the tooth stiffness is obtained when the maximum stress-concentration factor in Fig. 2, departs appreciably from unity, while in Fig. 3 there is a tendency for low or even negative value of w_f at the middle.

Quite a few years ago there was evidence of difficulty at the ends of a pinion of rather extreme proportions. This difficulty was remedied by a change of design which served to increase the diameter slightly and alter the tooth form. Recent review of the case in accordance with the methods set forth in the paper reveals that the design change resulted in a decrease in β from 438 to 257 and α from 9.8 to 7.0. The concentration factor at the torqued end was thus reduced from 3.3 to 2.7 and at the middle the change was from —0.08 to +0.15.

The ratio of length to diameter is often used as a measure of pinion flexibility and for the case just cited, the change in this ratio was from 3.74 to 3.38. That this ratio is not the complete criterion for determining allowable pinion flexibility can be inferred from a consideration of a third pinion having a ratio of 3.9. This pinion has operated satisfactorily for the past decade; however, in this case, the tooth stiffness is greatly reduced so that the values of α and β are 7.36 and 359. Comparison of the first and third pinions on the basis of amount of wear relief to uniformize the load indicates that a maximum of 0.0008 in. would be required in the latter as against 0.003 in. in the former.

The Effect of Transverse Shear Deformation on the Bending of Elastic Plates[1]

L. H. Donnell.[2] It may be of interest in connection with this excellent paper to present another method of considering transverse shear strains in plates, which the writer developed at Chance Vought Aircraft to solve certain problems involving sandwich-type plates. The method seems to approach the problem from a somewhat different and perhaps simpler viewpoint than the author's, but the solution is doubtless much more approximate than his.

It will be helpful to review first the case of shear deformation
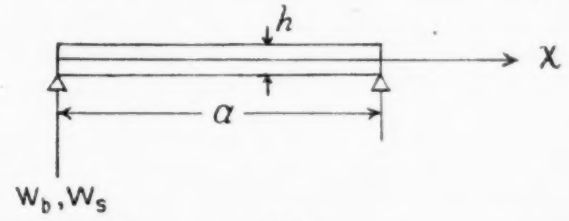


Fig. 1

in rectangular beams.[3] The lateral deflection due to shear, designated by w_s, can be considered to be superposed on the usual deflection due to bending, which will be designated by w_b. The bending moment per unit width of section is, Fig. 1

$$m \approx -\frac{Eh^3}{12}\frac{d^2w_b}{dx^2} \quad \ldots\ldots [1]$$

and the transverse shear force per unit width of section is

$$f_s = \frac{dm}{dx} \approx -\frac{Eh^3}{12}\frac{d^3w_b}{dx^3} \quad \ldots\ldots [2]$$

The additional slope of the deflection curve due to transverse shear is, for the symmetrical case

$$\frac{dw_s}{dx} = \frac{n f_s}{h G} \approx -\frac{n(1+\mu)h^2}{6}\frac{d^3w_b}{dx^3} \quad \ldots\ldots [3]$$

where n is a numerical factor having a value between 1.5 (which it would have if there were no restraint against warping of cross sections) and 1.0 (if there were complete restraint against warping of all cross sections.) Actually there is always some restraint against warping due to symmetry or end fixity, and a value of $n = 1.2$ can be used for most practical cases.

$$w_s = -\frac{1}{2}\beta a^2\frac{d^2w_b}{dx^2} + C \quad \ldots\ldots [4]$$

where a is the length of the beam, C is an integration constant which can be determined from the condition that $w_s = 0$ at reactions, and

$$\beta = \frac{n(1+\mu)}{3}\left(\frac{h}{a}\right)^2 \quad \ldots\ldots [5]$$

For the general case another constant C' should be added to the right-hand side of Equation [3]. $C'x$ to the right-hand side of Equation [4], and C and C' determined from the two end conditions for w_s.

As an example of the application of the fundamental Equation [4] consider the case of a beam supported at the ends and with a uniformly distributed load q per unit length. From elementary beam theory the deflection due to bending is

$$w_b = \frac{q}{24\,EI}(a^3x - 2ax^3 + x^4) \quad \ldots\ldots [6]$$

Using Equation [4] and the end condition $x = 0 : w_s = 0$ to determine C, we find

$$w_s = \frac{\beta q a^2}{4\,EI}(ax - x^2)$$

The maximum deflection is therefore increased by the factor

$$\left[1 + \left(\frac{w_s}{w_b}\right)_{x=\frac{a}{2}}\right] = (1 + 4.8\,\beta) \quad \ldots\ldots [7]$$

Similarly, the factor for increase of the maximum deflection due to shear is found to be $(1 + 24\,\beta)$ for the case of a uniform load and fixed ends. For the case of a concentrated load in the middle, this factor is found to be $(1 + 6\,\beta)$ for supported ends and $(1 + 24\,\beta)$ for fixed ends.

In the case of buckling of struts the buckling load is reduced due to shear by a factor similar to Equation [7], since the bending moments are proportional to $w_b + w_s$, while the internal resisting moments are the same as if w_b alone were the deflection. For a hinged-end strut, if we assume that

$$w_b = W_b \sin\frac{\pi x}{a} \quad \ldots\ldots [8]$$

we find from Equation [4] and the condition $x = 0 : w_s = 0$

$$w_s = \frac{\pi^2}{2}\beta W_b \sin\frac{\pi x}{a} = \frac{\pi^2}{2}\beta w_b \quad \ldots\ldots [9]$$

[1] By Eric Reissner, published in the Journal of Applied Mechanics, Trans. A.S.M.E., vol. 67, 1945, p. A-69.

[2] Research Professor of Mechanics and Director of Mechanics and Aeronautics Research Laboratory, Illinois Institute of Technology, Chicago, Ill. Mem. A.S.M.E.

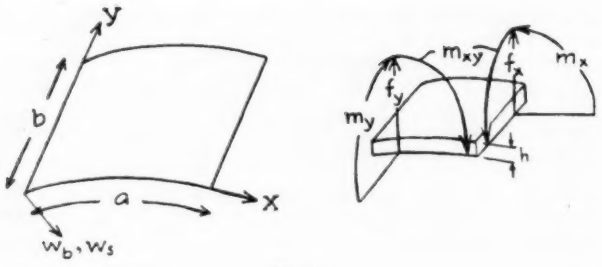


FIG. 2

Since w_s has the same shape as w_b, the usual equilibrium conditions will be satisfied if the critical load is reduced by the factor

$$\left(1 + \frac{w_s}{w_b}\right) = \left(1 + \frac{\pi^2}{2}\beta\right) \approx (1 + 5\beta) \quad \ldots\ldots [10]$$

which checks with a solution obtained in a somewhat different manner.[3] Similarly, the buckling load of a fixed-end strut is decreased by a factor

$$(1 + 2\pi^2\beta) \approx (1 + 20\beta)$$

This method will now be extended to the case of a plate or shell, such as is shown in Fig. 2 of this discussion. The bending and twisting moments per unit length of section are

$$\left.\begin{aligned} m_x &= -D\left(\frac{\partial^2 w_b}{\partial x^2} + \mu\frac{\partial^2 w_b}{\partial y^2}\right) \\ m_y &= -D\left(\frac{\partial^2 w_b}{\partial y^2} + \mu\frac{\partial^2 w_b}{\partial x^2}\right) \\ m_{xy} &= -D(1-\mu)\frac{\partial^2 w_b}{\partial x \partial y} \end{aligned}\right\} \quad \ldots\ldots [11]$$

From the moment equilibrium of an element, and using Equation [11], we obtain

$$\left.\begin{aligned} f_x &= \frac{\partial m_y}{\partial x} + \frac{\partial m_{xy}}{\partial y} = -D\frac{\partial}{\partial x}(\nabla^2 w_b) \\ f_y &= \frac{\partial m_y}{\partial y} + \frac{\partial m_{xy}}{\partial x} = -D\frac{\partial}{\partial y}(\nabla^2 w_b) \end{aligned}\right\} \quad \ldots\ldots [12]$$

Using Equation [5] as in the derivation of Equation [8] and taking $\mu = 0.3$, for the symmetrical case

$$\left.\begin{aligned} \frac{\partial w_s}{\partial x} &= \frac{nf_x}{Gh} = -0.55\,\beta a^2\frac{\partial}{\partial x}(\nabla^2 w_b) \\ \frac{\partial w_s}{\partial y} &= \frac{nf_y}{Gh} = -0.55\,\beta a^2\frac{\partial}{\partial y}(\nabla^2 w_b) \end{aligned}\right\} \quad \ldots\ldots [13]$$

where β is the same as defined by Equation [5]. Integrating, we obtain

$$w_s = -0.55\,\beta a^2\nabla^2 w_b + C \quad \ldots\ldots [14]$$

where C is a constant of integration, as before, which can be determined from edge conditions. There are no variables of integration, as usual in the integration of partial derivatives, because both Equations [13] would not be satisfied if they were present.

As an example of the application of the basic Equation [14], consider the case of a flat or curved panel with hinged edges, whose deflection, neglecting shear, can always be expressed in the form

$$w_b = \sum_{\substack{m=\\1,3,\ldots.}}\sum_{\substack{n=\\1,3,\ldots.}} W_{mn}\sin\frac{m\pi x}{a}\sin\frac{n\pi y}{b} \quad \ldots\ldots [15]$$

Substituting this expression in Equation [14] and using the condition $x = y = 0 : w_s = 0$, we find

$$w_s = 5.4\,\beta\sum_m\sum_n\left(m^2 + n^2\frac{a^2}{b^2}\right)W_{mn}\sin\frac{m\pi x}{a}\sin\frac{n\pi y}{b} \quad [16]$$

Values of the coefficients W_{mn} can be obtained by strain-energy methods, which have been worked out in general form for the case of a flat panel. For example, for a flat panel under uniformly distributed pressure p, it is found that

$$W_{mn} = \left(\frac{192\,(1-\mu^2)pa^4}{\pi^6 Eh^3}\right)\frac{1}{mn\left(m^2 + n^2\frac{a^2}{b^2}\right)^2} \quad \ldots\ldots [17]$$

The deflection in the middle is therefore increased due to shear by the factor

$$\left[1 + \left(\frac{w_s}{w_b}\right)_{x=\frac{a}{2},\,y=\frac{b}{2}}\right] = 1 + 5.4\beta\left[\frac{\sum\sum\dfrac{\sin\frac{m\pi}{2}\sin\frac{n\pi}{2}}{mn\left(m^2 + n^2\frac{a^2}{b^2}\right)}}{\sum\sum\dfrac{\sin\frac{m\pi}{2}\sin\frac{n\pi}{2}}{mn\left(m^2 + n^2\frac{a^2}{b^2}\right)^2}}\right] \quad \ldots\ldots [18]$$

The final fraction converges rapidly and it is sufficient to calculate it for the first few terms, say, for m, n (1, 1) (1, 3) (3, 1) (3, 3) in this manner the factor is found to be

$$(1 + 9.7\,\beta) \text{ for } \frac{a}{b} = 1; \quad (1 + 6.0\,\beta) \text{ for } \frac{a}{b} = \frac{1}{2} \quad \ldots\ldots [19]$$

For the buckling of a flat panel under a uniform compressive stress in the b direction, the theory, neglecting shear, indicates that the deflection consists of one term only of Equation [15], and for this term $m = n = 1$ when $a > b$, and $m = 1$, $n \approx b/a$ when $a < b$. Using these values in Equations [15] and [16], we find that the factor by which the deflection is increased and hence the buckling stress is decreased by shear is

$$\left.\begin{aligned} &\left[1 + 5.4\left(1 + \frac{a^2}{b^2}\right)\beta\right] \quad \text{when } a > b \\ &(1 + 10.8\,\beta) \quad \text{when } a < b \end{aligned}\right\} \quad \ldots\ldots [20]$$

These methods apply equally well to "large-deflection" or "second-order" plate and shell theories, but in this case the additional deflections due to shear should be calculated from the deflections given by ordinary small-deflection theory, and then added to the deflections given by the large-deflection theory.

D. C. DRUCKER.[4] The remarkable extension of the theory of plates presented in this paper is of great interest both to the elastician and to the practical engineer. Therefore it would seem to be worth noting that experimental results published by

[3] "Theory of Elastic Stability," by S. Timoshenko, McGraw-Hill Book Co., Inc., New York, N. Y., 1936, p. 139.

[4] Supervisor, Mechanics of Solids, Armour Research Foundation, Illinois Institute of Technology, Chicago, Ill. Jun. A.S.M.E.

Goodier and Lee,[5] and by the writer[6] substantiate the theory for the circular hole in a bent plate when the diameter of the hole and the thickness of the plate are comparable. Their data, which were obtained by photoelastic means, are given in Table 1 of this discussion. Term K is the stress-concentration factor based on the stress in the gross section.

TABLE 1 EXPERIMENTAL RESULTS FOR A CIRCULAR HOLE IN A BENT PLATE

K	Hole diam. / Plate thick.	Hole diam. / Plate width	Plane stress correction factor[a]	Corrected K
		Drucker		
2.50	0.50	0.091	3/3.03	2.48
2.40	1.00	0.182	3/3.10	2.32
2.30	1.50	0.273	3/3.26	2.11
		Goodier and Lee		
1.92	2.04	0.129	3/3.05	1.89
2.00	3.06	0.194	3/3.13	1.92
2.09	4.08	0.258	3/3.24	1.94
2.33	6.12	0.388	3/3.64	1.92

[a] "Mechanical Springs," by A. M. Wahl, Penton Publishing Co., Cleveland, Ohio, 1944, p. 300.

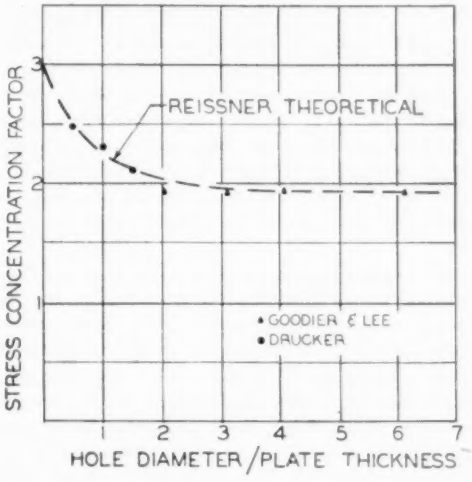


FIG. 3

The dots and triangles plotted in Fig. 3 of this discussion, represent the data arbitrarily corrected for the finite width of plate by the factors which hold for the case of pure tension (see footnote to Table 1 of this discussion). Many of the points are thus subject to question, but the most important value of 2.5 for a $^1/_8$-in. hole in a $^1/_4$-in. plate is not affected.

Although the agreement between theory and experiment is very good, some caution must still be exercised in the application of the results. Of necessity the experimenters also assumed that the distribution of the stress through the thickness was linear, or more precisely, they interpreted their experimental results on this basis. Nonlinear distributions, especially local disturbances at or near the surfaces of the plate, would thus be averaged out and could not easily be detected.

Another point of interest is that the large value found by the author for the magnitude of the transverse shearing stress when the plate is thin is very close to the residual shearing stress at the boundary of the hole appearing in the theory of moderately thick plates.

[5] "An Extension of the Photoelastic Method of Stress Measurement to Plates in Transverse Bending," by J. N. Goodier and G. H. Lee, JOURNAL OF APPLIED MECHANICS, Trans. A.S.M.E., vol. 63, 1941, p. A-27.

[6] "The Photoelastic Analysis of Transverse Bending of Plates in the Standard Transmission Polariscope," by D. C. Drucker, JOURNAL OF APPLIED MECHANICS, Trans. A.S.M.E., vol. 64, 1942, p. A-161.

J. N. GOODIER.[7] The paper is an interesting attempt to free the small-deflection theory of plates from one of its most serious defects, i.e., its inability to meet the conditions of prescribed bending moment, twisting moment, and transverse shear force at an edge, except by replacing the horizontal (in the plane) shear stress of the twisting moment by statically equivalent vertical stress. The error so introduced is local to the edge, but, as in stress concentration at a hole, this is often objectionable.

The author's theory makes two principal assumptions, (1) that the stress components σ_x, σ_y, τ_{xy} are linear through the thickness; (2) that at an edge the displacements u_n, u_s vary linearly, and w does not vary, through the thickness. The second raises some questions because the essence of the theory is to take into account deformation due to shear (τ_{xz}, τ_{yz}) and transverse stress (σ_z) as well as bending stress (σ_x, σ_y, τ_{xy}). The shear deformation will cause departure from linearity of u_n, u_s, and the effects of σ_z will cause w to vary through the thickness.

Terms such as, but slightly different from, those introduced by the author can be derived by somewhat more elementary considerations without making the assumption (2). But also the well-known equations of the old theory can equally well be derived without neglecting any part of the deformation, that is, by making assumption (1) alone. The analysis follows:

Making assumption (1), that is, starting from Equations [1*a*], [1*b*], [1*c*] of the paper, Equations [2*a*], [2*b*], [4] for τ_{xz}, τ_{yz} and σ_z follow from the differential equations of equilibrium. The strain components can then be evaluated, and from these the curvatures and twist of the plate, of the middle surface, or the faces, or of intermediate surfaces, can be found by means of the identities

$$\frac{\partial^2 w}{\partial x^2} = \frac{\partial e_{xz}}{\partial x} - \frac{\partial e_{-z}}{\partial z}, \quad \frac{\partial^2 w}{\partial y^2} = \frac{\partial e_{yz}}{\partial y} - \frac{\partial e_{yy}}{\partial z}, \quad 2\,\frac{\partial^2 w}{\partial x \partial y} = \frac{\partial e_{yz}}{\partial x} + \frac{\partial e_{xz}}{\partial y} - \frac{\partial e_{xy}}{\partial z}$$

For instance, the first of these gives for the curvature of the middle surface

$$\left(\frac{\partial^2 w}{\partial x^2}\right)_{z=0} = -\frac{12}{Eh^3}(M_x - \nu M_y) + \frac{3(1+\nu)}{Eh}\frac{\partial V_x}{\partial x} + \frac{3\nu}{2Eh}p$$

Comparing this with the expression multiplying δM_x in Equation [13] of the paper, it will be observed that the terms involving V_x and p are of the same nature as the author's, but the numerical coefficient in the $\partial V_x/\partial n$ term is here 3, instead of the author's 12/5, and in the p-term it is here 3/2 instead of the author's 12/10.

The twist of the middle surface is found from the third identity as

$$2\left(\frac{\partial^2 w}{\partial x \partial y}\right)_{z=0} = -\frac{24(1+\nu)}{Eh^3}H_{xy} + \frac{3(1+\nu)}{Eh}\left(\frac{\partial V_y}{\partial x} + \frac{\partial V_x}{\partial y}\right)$$

Again 3 appears instead of the author's 12/5.

If instead of considering the curvatures and twist of the middle surface we evaluate them for the upper or lower face of the plate, the terms in V_x, V_y, p disappear, and the results are of exactly the same form as in the unmodified plate theory. This shows that the "correction terms" express (granted assumption 1) the difference in curvature and twist between the middle surface and the upper or lower surface. It is therefore not en-

[7] Professor of Mechanics, Cornell University, Ithaca, N. Y. Mem. A.S.M.E.

tirely consistent to disregard the variation of w through the thickness, as in the author's assumption (2).

The expressions for the curvatures and twist of the upper (or lower) face can be used just as well as those of the middle surface. In conjunction with the equations of equilibrium, they will yield the usual equation $D\nabla^4 w = p$ for the deflection. The boundary conditions must now of course be put in terms of the upper (or lower) face deflection. This theory would thus consist of all the usual equations, but nevertheless takes into account all kinds of deformation.

In a problem where the boundary conditions are in terms of the edge deflection, it would differ from the theory incorporating "correction terms" only in employing the face deflection at the edge instead of the middle-surface deflection. In a problem specifying bending moment, twisting moment, and transverse shearing force at an edge, as at a free edge, it would proceed exactly as does the old theory—and be equally unable to satisfy three conditions exactly, instead of two. We are thus confronted with this question: Why should a theory involving precisely the same assumptions, but using the deflection of the middle surface instead of that of the face, lead to the possibility of satisfying all three edge conditions?

Author's Closure

The author appreciates Professor Donnell's comments and the communication of his earlier unpublished results on the effect of transverse-shear deformation on the bending deflection and buckling loads of elastic plates. He would like to say that for the problems considered by Professor Donnell and restricting attention to isotropic homogeneous plates, these earlier results are substantially confirmed by results which can be obtained from the author's formulas. It may be permitted to say, however, that as far as the author can see, Professor Donnell's approach to the subject does not include the possibility of satisfying three edge conditions instead of the two conditions which are used in the theory without transverse-shear deformation, and also in the theory of moderately thick plates. The author thinks that as a consequence of this it is not possible to apply Professor Donnell's formulas to the two problems to which the author's results were applied, namely, (1) the problem of Saint Venant torsion of a rod with rectangular cross section; (2) the problem of the stress concentration at the edge of a circular hole in transversely bent plates.

In these and other problems, but not in the problems considered by Professor Donnell, it is essential that provision be made to take account of the fact that the stresses may change substantially within edge zones, the width of which is of the order of magnitude of the plate thickness itself. The possibility of providing for this necessity is given not by including extra terms in the relations between couples and curvatures[8] (as in Equations [II] to [IV] of the paper under discussion), but rather by replacing the relations

$$(V_x, V_y) = -D\left(\frac{\partial}{\partial x}, \frac{\partial}{\partial y}\right)\nabla^2 w \qquad [21]$$

which are used in the theory of thin as well as of moderately thick plates, by the relations

$$\left(1 - \frac{h^2}{10}\nabla^2\right)(V_x, V_y) = -D\left(\frac{\partial}{\partial x}, \frac{\partial}{\partial y}\right)\nabla^2 w \qquad [22]$$

which were obtained in the author's paper.

The author is grateful to Dr. Drucker for the two additional references to experimental results and in particular for his kindness in supplying a comparison between the results of the photoelastic tests and the calculated data of the present paper.

Dr. Drucker brings up an important point by mentioning that in interpreting the results of the photoelastic experiments as well as of the calculations, one is led to what might be called "stress couple concentration factors" rather than to stress-concentration factors. To calculate the difference between these two kinds of factors it would be necessary to extend the theory in such a way that in addition to components of the bending stresses which vary linearly across the thickness, there are taken into account additional terms which vary across the thickness like, say, cubic parabolas. The author believes that such an extension, while analytically quite heavy, could be made and numerical results be obtained.

It is the author's feeling that the differences between stress-couple-concentration factors and stress-concentration factors should, in order of magnitude, not go beyond 10 per cent of the values of the couple-concentration factors obtained in the paper and possibly be appreciably smaller than this.

Professor Goodier raises some interesting questions concerning the meaning of the author's results by contrasting them with formulas which he obtains without the use of a minimum-energy principle. He finds that in so doing two different kinds of results are obtained, depending upon whether attention is focused on the middle surface of the plate or on the face surfaces of the plate. Perhaps one should say that the variational method used in the paper strikes in a natural way a balance between the two possibilities indicated by Professor Goodier and leads then also automatically to the appropriate three boundary conditions of the problem.

Professor Goodier further questions the compatibility of the author's assumptions regarding the distribution of stress across the thickness and of the distribution of the displacements at the edge across the thickness. The author is indebted to Professor Goodier for bringing up this point. It has led the author to reconsider the question of the displacements in the interior as well as at the edge, and he finds that his analysis, while not needing reinterpretation in so far as the two applications which were made in the paper are concerned, does stand in need of such reinterpretation in so far as the meaning of the Lagrangian multiplier w is concerned. It is found that the quantity w which occurs in Equations [I] to [VI] of the paper, does not represent an approximation to the transverse deflection of the middle surface (or of the face surfaces) but rather represents an approximation to a weighted average across the thickness of the deflections W of all surfaces contained in between the two faces of the plates. This average w is, for the assumed stress distribution

$$w = \frac{\int_{-h/2}^{h/2}\left[1 - \left(\frac{z}{h/2}\right)^2\right] W dz}{\int_{-h/2}^{h/2}\left[1 - \left(\frac{z}{h/2}\right)^2\right] dz} \qquad [23]$$

Likewise one should not define the quantities $\bar{u}_n'$ and $\bar{u}_s'$ which occur in Equations [15a] and [15b] by means of Equations [9a] and [9b], but rather in the following way

$$\bar{u}_n' = \frac{\int_{-h/2}^{h/2} \bar{u}_n \frac{z}{h/2} dz}{\int_{-h/2}^{h/2} z \frac{z}{h/2} dz}, \qquad \bar{u}_s' = \frac{\int_{-h/2}^{h/2} \bar{u}_s \frac{z}{h/2} dz}{\int_{-h/2}^{h/2} z \frac{z}{h/2} dz} \qquad [24]$$

Only these averaged components of direction change of the normal to the undeformed middle surface are of importance in the present theory. Distributions of $\bar{u}_n$ and $\bar{u}_s$ across the thickness which lead to the same values of $\bar{u}_n'$ and $\bar{u}_s'$ are equivalent within the framework of the present developments.

[8] For the inclusion of such extra terms see also "Theory of Plates and Shells," by S. Timoshenko, McGraw-Hill Book Company, Inc., New York, N. Y., 1940, p. 111.

Cylindrical Buckling of Sandwich Plates

By J. N. GOODIER,[1] ITHACA, N. Y.

In the buckling of "sandwich plates" with a relatively easily deformed interior, or core, material, the core is not stiff enough to keep plane sections plane when the bending occurs. The core must then be analyzed according to the equations of plane strain, but the fact that the bending takes place in the presence of thrust means that terms representing the destabilizing tendency of the thrust must be included. The resulting problem is solved in the present paper for a sandwich plate in "cylindrical buckling"—that is in a mode analogous to that of the hinged column.

Nomenclature

The following nomenclature is used in the paper: Subscript 1 designates faces; subscript 2 the core

E_1, E_2 = Young's moduli

ν_1, ν_2 = Poisson's ratios

P = thrust per unit width on sandwich plate

t = thickness of each face

h = thickness of core

$r = t/h$

$\rho = E_1/E_2$

$D_1 = E_1t^3/12(1-\nu_1^2)$

$\lambda = \dfrac{\nu_2 E_2}{(1-2\nu_2)(1+\nu_2)}$, $G = \dfrac{E_2}{2(1+\nu_2)}$ ..... Lamé constants of core

α = 2π/wave length of sinusoidal deformation

$\epsilon = \alpha h/2$

$\gamma = 2 + \dfrac{\lambda}{G} = \dfrac{2(1-\nu_2)}{1-2\nu_2}$

σ_{z2} = critical stress in core

$\sigma = -\sigma_{z2}$

$s = \sigma/2G$

$$c_1 = \frac{2E_1}{3(1-\nu_1^2)G} = \frac{4}{3}\,\frac{1+\nu_2}{1-\nu_1^2}\,\rho$$

$$c_2 = 2\alpha t \cdot \frac{1-\nu_1\nu_2+2r\rho(1-\nu_2^2)}{2r(1-\nu_1\nu_2)+(1/\rho)(1-\nu_1^2)} = c_2' r\epsilon$$

$$c_2' = 4\rho \cdot \frac{1-\nu_1\nu_2+2r\rho(1-\nu_2^2)}{1-\nu_1^2+2r\rho(1-\nu_1\nu_2)}$$

Introduction

By "sandwich plate," Fig. 1, is meant a nonhomogeneous flat thin plate made by bonding two like cover sheets (the faces) to a plate of another material (the core). The combination is required to withstand as much compression (e.g., vertically in Fig. 1) as possible without buckling. Several types of buckling are conceivable. The whole plate being simply, or otherwise, supported, it may buckle as a whole as a homogeneous plate would, Fig. 2(*a*); or the faces, stiffened by the action of the core as an elastic support, may buckle to a rather small wave length. A symmetrical mode of this kind is indicated in Fig. 2(*b*). Such modes have been investigated by Gough, Elam, and de Bruyne

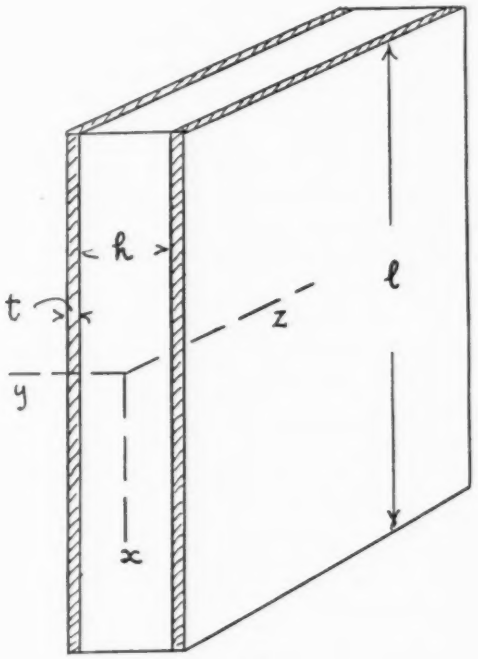


Fig. 1

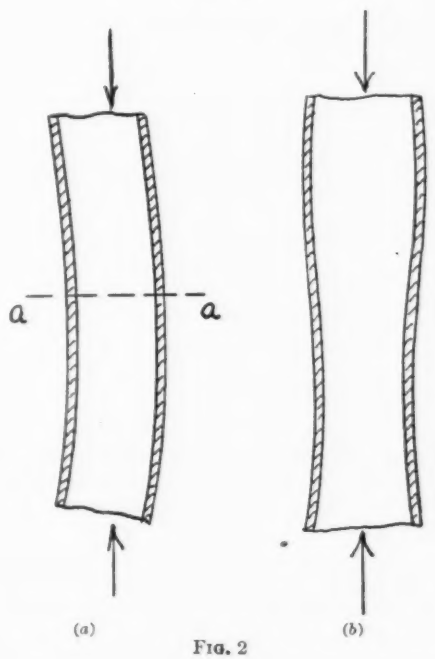


Fig. 2

[1] Professor of Mechanics, Cornell University. Mem. A.S.M.E.

Presented at the National Meeting of the Applied Mechanics Division, Buffalo, N. Y., June 21–22, 1946, of The American Society of Mechanical Engineers.

Discussion of this paper should be addressed to the Secretary, A.S.M.E., 29 West 39th Street, New York, N. Y., and will be accepted until January 10, 1947, for publication at a later date. Discussion received after the closing date will be returned.

Note: Statements and opinions advanced in papers are to be understood as individual expressions of their authors and not those of the Society.

(1),[2] and by Hoff and Mautner (2), who have observed in tests and made calculations for, a "skew" mode different from Fig. 2(*a*) or (*b*). The stresses occurring at the bond when the buckling deformation occurs constitute distributed loads on the faces, which at the same time are under compression. They also constitute distributed loads on the core. In these investigations, the displacements of faces and core at the interface are equated. In calculating the displacements of the core the fact that the core is also under compression has been disregarded. When the Young's modulus of the core is relatively small, a case of practical interest, the compressive stress in the core is also relatively small. But the question of whether or not the pre-existing compressive stress in the core can be ignored in computing the displacements due to the stresses appearing at the interface will depend upon whether the core is far from instability or not under its own compression; and its critical compressive stress will be small if its Young's modulus is small. Evidently the smallness of the compressive stress in the core relative to that in the faces is not conclusive.

The usual object of the sandwich construction is to stabilize the plates, which are essentially the (compressive) load-bearing elements, by holding them at a suitable distance apart by means of a light core. The greatest stabilization would be achieved by a core stiff enough to cause the sandwich to deform as a homogeneous plate does, i.e., with plane sections remaining plane in bending. Then, taking a unit width of plate normal to the paper in Fig. 2, the section by a plane such as *aa* would have a moment of inertia $^1/_2\ th^2$. Ignoring the bending stresses in the core, the critical thrust for buckling to cylindrical form is given by the Euler formula as

$$N_1 = \pi^2 E_1' \cdot \frac{1}{2}\, th^2/l^2 \qquad [1]$$

where $E'\ (1 - \nu_1^2)$ is the Young's modulus of the face material. The corresponding critical compressive strain in the faces is $N_1/2tE_1$ or

$$\pi^2 h^2/(1 - \nu_1^2)4l^2 \qquad [2]$$

The same strain will, of course, exist in the core.

If now the core without the faces is considered in the same way, its critical load per unit width is

$$N_2 = \pi^2 E_2' \left(\frac{1}{12}\, h^3\right) \Big/ l^2$$

and the critical strain is

$$N_2/hE_2$$

or

$$\pi^2 h^2/(1 - \nu_2^2)12l^2 \qquad [3]$$

This is only about one third of the critical strain just calculated for the two plates constrained to simple bending as a single section. Such behavior of the plates clearly requires the core to be at a stress some 3 times its own critical stress and therefore it cannot be realized.

Instead of considering the behavior of the faces as a section themselves, we may examine how they behave when part of a homogeneous plate of thickness h. The critical strain of such a plate is

$$\pi^2 h^2/12(1 - \nu_1^2)l^2 \qquad [4]$$

This is less than the value given by Equation [2] by a factor $^1/_3$, for when the faces are part of a homogeneous section they are subject to forces at their attachment to the rest of the section. The critical strain of the core by itself is the same as Equation [4] except for the Poisson's ratio. Thus if the core is to cause the faces to act as they would when part of a solid section, it must work at its own critical strain.

The actual state at buckling of a sandwich plate with a core of light material will of course be different. In the present investigation of it the compressive stress in the core is taken into account, the results being applicable to sandwich plates of any face-core thickness ratio and any homogeneous isotropic materials.

Initial State Under Compression

By "initial state" is meant the compressed state of the sandwich just before buckling. The sandwich is under thrust P per unit width (in the x-direction, axes as in Fig. 1) and is taken to be in a state of plane strain in the x, y plane, as it will be except locally at the vertical edges, in accordance with Saint Venant's principle. With subscripts 1 and 2 designating faces and core, respectively, continuity of the strain components ϵ_x, ϵ_z, at an interface requires

$$\left.\begin{aligned} \frac{1}{E_1}(\sigma_{x1} - \nu_1\sigma_{z1}) &= \frac{1}{E_2}(\sigma_{x2} - \nu_2\sigma_{z2}) \\ \frac{1}{E_1}(\sigma_{z1} - \nu_1\sigma_{x1}) &= \frac{1}{E_2}(\sigma_{z2} - \nu_2\sigma_{x2}) \end{aligned}\right\} \qquad [5]$$

Since the stress components σ_{x1} and σ_{x2} constitute the thrust P

$$2t\sigma_{x1} + h\sigma_{x2} = -P \qquad [6]$$

and, since the components σ_{z1} and σ_{z2} form a zero resultant on sections parallel to the x, y plane

$$2t\sigma_{z1} + h\sigma_{z2} = 0 \qquad [7]$$

These four equations yield

$$\sigma_{x1} = -\frac{P}{h} \cdot \frac{1 - \nu_1\nu_2 + 2r\rho(1 - \nu_2^2)}{4r(1 - \nu_1\nu_2) + \frac{1}{\rho}(1 - \nu_1^2) + 4r^2\rho(1 - \nu_2^2)} \qquad [8]$$

$$\sigma_{x2} = -\frac{P}{h} \cdot \frac{2r(1 - \nu_1\nu_2) + \frac{1}{\rho}(1 - \nu_1^2)}{4r(1 - \nu_1\nu_2) + \frac{1}{\rho}(1 - \nu_1^2) + 4r^2\rho(1 - \nu_2^2)} \qquad [9]$$

Equations of Faces

Fig. 3 represents an element (of unit width) of the left-hand face of Fig. 1 after buckling has occurred. It is cut out by planes parallel to the y, z plane at x and $x + dx$ in the initial state. These sections are regarded as remaining plane and normal to the middle surface. The forces exerted by the core are, to the first order, $p'dx$, $q'dx$, p' and q' being interface stress components. The thrust in the face is no longer the initial thrust P_1 (corresponding to σ_{x1}) and is now designated as $P_1 - p_1't$.

The equations of equilibrium are

$$\frac{dM}{dx} + Q - q'\frac{t}{2} = 0 \qquad [10]$$

$$\frac{dQ}{dx} - P_1\frac{d^2v_1}{dx^2} - p' = 0 \qquad [11]$$

$$q' - t\frac{dp_1'}{dx} = 0 \qquad [12]$$

where v_1 is the deflection of the face in the y direction.

[2] Numbers in parentheses refer to the Bibliography at the end of the paper.

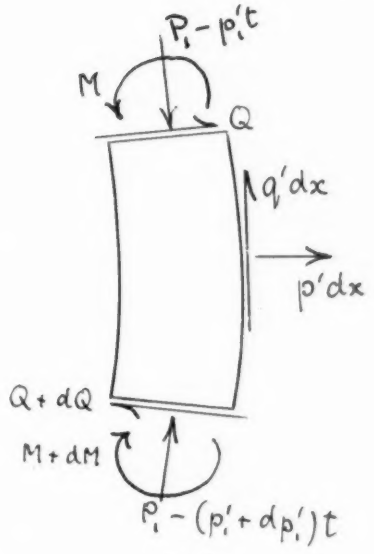


FIG. 3

In Equation [11] the product $p_1't\,\frac{d^2v_1}{dx^2}$ has been dropped. The buckling under investigation is infinitesimal, that is, the stresses and displacements appearing on buckling may be as small as we please. We have also

$$M = D_1\frac{d^2v_1}{dx^2} \quad \ldots\ldots\ldots\ldots\ldots\ldots [13]$$

These equations yield

$$D_1\frac{d^4v_1}{dx^4} + P_1\frac{d^2v_1}{dx^2} + p' - \frac{t}{2}\frac{dq'}{dx} = 0 \quad \ldots\ldots\ldots [14]$$

Since the modes of deformation to be considered are either symmetrical or antisymmetrical with respect to the middle plane (x, z) of the sandwich, it is not necessary to consider the other face separately. Since they are also to be sinusoidal in x, we write $v_1 = V \sin \alpha x$, $p' = p \sin \alpha x$, $q' = q \cos \alpha x$, $p_1' = p_1 \sin \alpha x$, giving Equations [12] and [14] the forms

$$q - \alpha t p_1 = 0 \quad \ldots\ldots\ldots\ldots\ldots\ldots [12a]$$

$$(D_1\alpha^4 - P_1\alpha^2)V + p + \frac{\alpha t}{2}\cdot q = 0 \quad \ldots\ldots\ldots [14a]$$

EQUATIONS OF CORE, ANTISYMMETRICAL DEFORMATION

The mode of buckling deformation is now taken to be antisymmetrical with respect to the x, z plane, that is, the displacement component v is even in y, the component u odd in y. The normal stress components are then odd in y, and the shearing component of the type τ_{xy} is even in y. This is the case in the simple flexural buckling of a homogeneous section. Here, however, it is not appropriate to assume that the deformation of the core is like that of simple bending. For instance, if the core is very light and flexible it exerts very little restraint on the faces, and they buckle virtually as two independent sheets, Fig. 5. Then the core is stretched on the left and contracted on the right to conform to the faces. These are exactly the opposites of the strains produced by simple bending of the core in a similar state of over-all deformation.

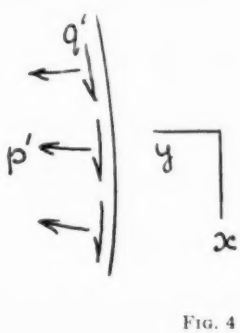


FIG. 4

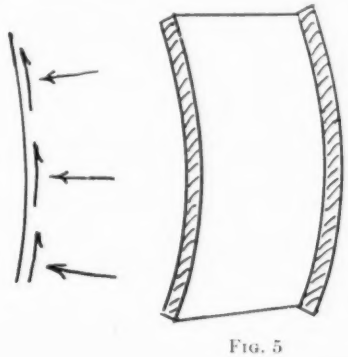


FIG. 5

In the "cylindrical" bending of a sandwich, as in a homogeneous plate, the displacement w is zero except in the local zone at the free vertical edges, and u, v are independent of z. The deformation is thus one of plane strain. General equations of equilibrium for a solid slightly deformed from a state of initial stress have been derived in a form suitable for the present purpose by Biezeno and Hencky (3) and by Biot (4). The initial stress in the core has uniform components σ_{x2}, σ_{y2}, the other components being zero. In the buckled state the stress and strain are referred to axes which have rotated with the material, as defined by the authors quoted. The stress components are written $S_{xx} + s_{11}$, etc., $S_{xy} + s_{12}$, etc., where $S_{xx}\ldots$, $S_{xy}\ldots$, are the components of initial stress. For uniform initial stress and no body force the equations (Biot)[3] are three of the type

$$\frac{\partial s_{11}}{\partial x} + \frac{\partial s_{12}}{\partial y} + \frac{\partial s_{13}}{\partial z} + (S_{xx} - S_{yy})\frac{\partial \omega_z}{\partial y} - 2S_{xy}\frac{\partial \omega_z}{\partial x} + S_{xy}\frac{\partial \omega_x}{\partial z}$$

$$- (S_{xx} - S_{zz})\frac{\partial \omega_y}{\partial z} - 2S_{xz}\frac{\partial \omega_y}{\partial x} - S_{xz}\frac{\partial \omega_z}{\partial y} + S_{yz}\left(\frac{\partial \omega_y}{\partial y} - \frac{\partial \omega_z}{\partial z}\right)$$

$$\ldots\ldots = 0 \quad [15]$$

where ω_x, ω_y, ω_z are the components of the rotation, $\frac{1}{2}$ curl (u, v, w).

In the present problem

$$S_{xx} = \sigma_{x2},\ S_{yy} = 0,\ S_{zz} = \sigma_{z2},\ S_{xy} = S_{yz} = S_{zx} = 0$$

Also, since the displacement u, v, w is plane strain $\omega_x = \omega_y = 0$, and ω_z is independent of z. The three equations of the type of Equation [15] reduce to

$$\frac{\partial s_{11}}{\partial x} + \frac{\partial s_{12}}{\partial y} + \frac{\partial s_{13}}{\partial z} + \sigma_{x2}\frac{\partial \omega_z}{\partial y} = 0 \quad \ldots\ldots\ldots [16]$$

$$\frac{\partial s_{22}}{\partial y} + \frac{\partial s_{23}}{\partial z} + \frac{\partial s_{12}}{\partial x} + \sigma_{x2}\frac{\partial \omega_z}{\partial x} = 0 \quad \ldots\ldots\ldots [17]$$

$$\frac{\partial s_{33}}{\partial z} + \frac{\partial s_{13}}{\partial x} + \frac{\partial s_{23}}{\partial y} = 0 \quad \ldots\ldots\ldots\ldots [18]$$

The stress components s_{ij} are related to the displacement by Hooke's law, that is, by three equations of the type

$$s_{11} = \lambda(e_{11} + e_{22}) + 2Ge_{11} \quad \ldots\ldots\ldots\ldots [19]$$

and three of the type

$$s_{12} = 2Ge_{12} \quad \ldots\ldots\ldots\ldots\ldots\ldots [20]$$

where e_{11}, etc., are $\partial u/\partial x$, etc., e_{12} is $\frac{1}{2}(\partial v/\partial x + \partial u/\partial y)$, to the first order, and λ, G are the Lamé constants of the core. Substitution of Equations [19] and [20] in [16] and [17] yields

$$G\left(\frac{\partial^2 u}{\partial x^2} + \frac{\partial^2 u}{\partial y^2}\right) + (G + \lambda)\frac{\partial e}{\partial x} - \sigma\frac{\partial \omega}{\partial y} = 0 \quad \ldots\ldots [21]$$

[3] Reference (4a), Equation 4.7, p. 484.

$$G\left(\frac{\partial^2 v}{\partial x^2}+\frac{\partial^2 v}{\partial y^2}\right)+(G+\lambda)\frac{\partial e}{\partial y}-\sigma\frac{\partial \omega_z}{\partial x}=0 \quad [22]$$

where

$$e=\partial u/\partial x+\partial v/\partial y, \quad \omega_z=\tfrac{1}{2}(\partial v/\partial x-\partial u/\partial y)$$

and σ is written for $-\sigma_{x2}$. Equation [18] is satisfied identically on account of the plane strain.

The boundary conditions associated with the equations of the type of Equation [15] are three of the type

$$\begin{aligned}\Delta f_x &= s_{11}\alpha+s_{12}\beta+s_{13}\gamma+(S_{xx}\omega_y-S_{xy}\omega_x)\alpha\\&+(S_{yx}\omega_y-S_{yy}\omega_x)\beta+(S_{zx}\omega_y-S_{yx}\omega_z)\gamma\\&+S_{xx}(e_{yy}+e_{zz})\alpha+S_{xy}(e_{xx}+e_{zz})\beta\\&+S_{xz}(e_{xz}+e_{yy})\gamma-(S_{xy}e_{xy}+S_{xz}e_{xz})\alpha\\&-(S_{xx}e_{xy}+S_{xx}e_{yz})\beta-(S_{xx}e_{xz}+S_{xy}e_{yz})\gamma\end{aligned}$$

where Δf_x is the x-component of boundary force, accompanying the displacement u, v, w, per unit area (before deformation), and α, β, γ are the direction cosines of the normal to the boundary element; e_{xx}, etc., are $\partial u/\partial x$, etc., and e_{xy}, etc., are $\tfrac{1}{2}(\partial v/\partial x+\partial u/\partial y)$, etc., being identical with $e_{11}\ldots$, $e_{12}\ldots$, to the first order. For the core face $y=h/2$, $\alpha=\gamma=0$, $\beta=1$, and the first boundary condition reduces to

$$\Delta f_x = s_{12}+\sigma e_{xy}$$

or

$$\Delta f_x=\left(1+\frac{\sigma}{2G}\right)s_{12} \quad [23]$$

The second boundary condition reduces to

$$\Delta f_y = s_{22} \quad [24]$$

and the third to

$$\Delta f_z = s_{23}$$

The values of Δf_x, Δf_y and Δf_z required at the interface are q', p', and 0. The third boundary condition is identically satisfied, and the first two become

$$q'=s_{12}, \quad p'=s_{22} \quad [25]$$

neglecting $\sigma/2G$ in comparison with unity.

The problem of the core is thus to obtain a solution of Equations [21] and [22], satisfying conditions [25]. It must also satisfy the conditions of continuity of displacement at the interface. The displacement v must be the deflection v_1 of the face. The displacement w is already taken as zero in both core and face. The remaining condition is continuity of strain in the x-direction between core and face. In the investigations of Gough, Elam, and de Bruyne (1) and of Hoff and Mautner (2), the displacement u is taken as zero at the interface, on the ground that the deformation of the face is preponderantly the deflection v_1. This assumption is of doubtful value here for several reasons. It does not simplify the calculations much and it is not correct in the limiting case, useful as a check, when the thickness of face, or the Young's modulus of the face, goes to zero, and only the core is left. For then the core buckles in the Euler manner. The displacement u at the face is then small, it is true, but the implied imposition of a constraint to make it zero is not unimportant. In fact, in the work of Gough, Elam, and de Bruyne it leads to the conclusion that the critical stress for infinite wave length is not zero and invalidates their results for long wave lengths. It may easily be seen that if plane sections remain plane, as of course they do to an adequate approximation in the buckling of the core alone when the wave length is several times the thickness, such a constraint introduces complete stabilization.

Sinusoidal Deformation

The Equations [21] and [22] are satisfied by

$$u=\cos\alpha x[A\sinh\alpha y+Ck(1-\beta)\sinh k\alpha y] \quad [26]$$

$$v=\sin\alpha x[A\cosh\alpha y+C(1-k^2\beta)\cosh k\alpha y] \quad [27]$$

where α, A, C are as yet arbitrary, and $k^2=\dfrac{1-s}{1+s}$, $\beta=\dfrac{1}{\gamma}(1+s)$, $s=\dfrac{\sigma}{2G}$, $\gamma=2+\dfrac{\lambda}{G}=\dfrac{2(1-\nu_2)}{1-2\nu_2}$. The wave length of the deformation, $2\pi/\alpha$, will be kept arbitrary, and a critical value of s determined to correspond to it. Simple sinusoidal modes of buckling are to be expected, as counterparts of the modes of the homogeneous plate, but the existence of other modes for the sandwich plate remains an open question.

The solution in Equations [26] and [27] can be used directly in conjunction with Equations [19], [20], [25], [14], and the conditions of continuity of displacement at the interface to establish the condition for the critical load as a transcendental equation. This equation is very intractable and a different procedure is followed which results in an explicit formula for the critical load.

Limit of Sinusoidal Core Displacements for $s \to 0$

When $s=0$ (i.e., $\sigma=0$) Equations [21] and [22] reduce to those of ordinary plane strain in the elastic solid free from initial stress. The sinusoidal solution is

$$u=\cos\alpha x(A'\sinh\alpha y+C'\alpha y\cosh\alpha y) \quad [28]$$

$$v=\sin\alpha x\left[\left(A'-C'\frac{\gamma+1}{\gamma-1}\right)\cosh\alpha y+C'\alpha y\sinh\alpha y\right] \quad [29]$$

with A' and C' arbitrary.

But taking the solution Equations [26] and [27] in the limit $s\to 0$, we have $k\to 1$, $\beta\to 1/\gamma$ and, in the limit

$$u=\cos\alpha x\left[A\sinh\alpha y+C\left(1-\frac{1}{\gamma}\right)\sinh\alpha y\right] \quad [30]$$

$$v=\sin\alpha x\left[A\cosh\alpha y+C\left(1-\frac{1}{\gamma}\right)\cosh\alpha y\right] \quad [31]$$

These agree with Equations [28] and [29] only for the special case $C'=0$. The discrepancy arises from the fact that in a completely defined problem A and C in Equations [26] and [27] would be determined from boundary conditions and would emerge as functions of k and β. It is to be expected therefore that A and C must be involved in the limiting process. Write

$$k=1+\eta=1-s+\frac{1}{2}s^2-\frac{1}{2}s^3\ldots$$

Then Equation [26] may be expanded as

$$u=\cos\alpha x\left\{[A+Ck(1-\beta)]\sinh\alpha y+Ck(1-\beta)\left(\frac{\eta^2\alpha^2y^2}{2!}+\frac{\eta^4\alpha^4y^4}{4!}+\ldots\right)\sinh\alpha y+Ck(1-\beta)\left(\eta\alpha y+\frac{\eta^3\alpha^3y^3}{3!}+\ldots\right)\cosh\alpha y\right\}$$

Let

$$Ck(1-\beta)\eta = C' \quad \text{and} \quad A + Ck(1-\beta) = A' \ldots\ldots [32]$$

Then

$$u = \cos \alpha x \left\{ A' \sinh \alpha y + C' \alpha y \cosh \alpha y + C' \left[\eta \cdot \frac{\alpha^2 y^2}{2!} + \eta^3 \cdot \frac{\alpha^4 y^4}{4!} + \ldots \right] \sinh \alpha y + C' \left[\eta^2 \cdot \frac{\alpha^3 y^3}{3!} + \ldots \right] \cosh \alpha y \right\} \ldots\ldots [33]$$

If the limiting process is carried out with $C \to \infty$, $A \to \infty$ in such a way that C', A' remain finite, the limiting form of Equation [33] is [28], and the limiting form of Equation [27] will be shown later to be [29].

Now the conditions under which Equations [26] and [27] are to be used involve small values of s and therefore the appropriate values of A and C are likely to be very large. It becomes advantageous to employ the constants A' and C' which do not tend to infinity in the limiting case.

Sinusoidal Deformation for Small s

In the application of the present theory the quantity s will be of the order of the allowable strains, say, 5×10^{-3}. We retain terms up to and including s^2, and it will be seen in the result that this is adequate.

Replacing η by its expansion in terms of s, we have from Equation [33]

$$u = \cos \alpha x \left\{ A' \sinh \alpha y + C' \left[\alpha y \cosh \alpha y + \frac{1}{2} \left(-s + \frac{1}{2} s^2 \right) \alpha^2 y^2 \sinh \alpha y + \frac{1}{6} s^2 \alpha^3 y^3 \cosh \alpha y \right] \right\} \ldots. [34]$$

The expansion of Equation [27] in powers of η is

$$v = \sin \alpha x \left\{ \left[A + C(1-k^2\beta) \left(1 + \eta^2 \cdot \frac{\alpha^2 y^2}{2!} + \ldots \right) \right] \cosh \alpha y + C(1-k^2\beta) \left(\eta \alpha y + \eta^3 \frac{\alpha^3 y^3}{3!} \ldots \right) \sinh \alpha y \right\} \ldots [35]$$

Now, in accordance with Equation [32]

$$C(1-k^2\beta)\eta = C' \frac{1-k^2\beta}{k(1-\beta)}$$

This can be expanded in powers of s, with the result

$$C' \left\{ 1 + \frac{\gamma+1}{\gamma-1} s + \frac{(\gamma+1)^2}{2(\gamma-1)^2} s^2 + \frac{3\gamma^3 - 7\gamma^2 + 7\gamma + 1}{2(\gamma-1)^3} s^3 \right\} \ldots\ldots [36]$$

The combination $A + C(1-k^2\beta)$ has the value

$$A + \frac{C'}{\eta} \left\{ 1 + \frac{\gamma+1}{\gamma-1} s + \frac{(\gamma+1)^2}{2(\gamma-1)^2} s^2 + \frac{3\gamma^3 - 7\gamma^2 + 7\gamma + 1}{2(\gamma-1)^3} s^3 \ldots \right\}$$

and on expansion of $1/\eta$ in powers of s this becomes

$$A' - C' \left\{ \frac{\gamma+1}{\gamma-1} + \frac{\gamma(\gamma+1)}{(\gamma-1)^2} s + \frac{\gamma(3\gamma^2-6\gamma+7)}{2(\gamma-1)^3} s^2 \ldots \right\}$$

On substitution of these developments in Equation [35], and expansion of η, Equation [35] becomes

$$v = \sin \alpha x \left\{ \left[A' - C' \left(\frac{\gamma+1}{\gamma-1} + \frac{\gamma \cdot (\gamma+1)}{(\gamma-1)^2} s + \frac{\gamma(3\gamma^2-6\gamma+7)}{2(\gamma-1)^3} s^2 + \ldots \right) \right] \cosh \alpha y + C' \left[\left(1 + \frac{\gamma+1}{\gamma-1} s + \frac{(\gamma+1)^2}{2(\gamma-1)^2} s^2 \right) \alpha y \sinh \alpha y - \frac{1}{2} \left(s + \frac{\gamma+3}{2(\gamma-1)} s^2 \right) \alpha^2 y^2 \cosh \alpha y + \frac{1}{6} s^2 \alpha^3 y^3 \sinh \alpha y \right] \right\} \ldots. [37]$$

The limiting forms of Equations [34] and [37] as $S \to 0$ agree with Equations [28] and [29]. The results, Equations [34] and [37], can also be obtained directly from the differential Equations [21] and [22], dividing them through by $2G$, replacing $\sigma/2G$ by s, taking $u = \Sigma u_n s^n$, $v = \Sigma v_n s^n$ and equating the coefficients of each s^n to zero.

Critical Condition From Small s Solution

Writing

$$\left. \begin{aligned} s_1 &= -\frac{1}{2} s + \frac{1}{4} s^2, \; s_2 = \frac{1}{6} s^2, \; s_3 = \frac{\gamma+1}{\gamma-1} + \frac{\gamma(\gamma+1)}{(\gamma-1)^2} s + \frac{\gamma(3\gamma^2-6\gamma+7)}{2(\gamma-1)^3} s^2 \\ s_4 &= -\frac{1}{2} s - \frac{\gamma+3}{4(\gamma-1)} s^2, \; s_5 = 1 + \frac{\gamma+1}{\gamma-1} s + \frac{(\gamma+1)^2}{2(\gamma-1)^2} s^2 \end{aligned} \right\} \ldots [38]$$

the values of $s_{22} = p \sin \alpha x$ and $s_{12} = q \cos \alpha x$ are computed, by formulas of the types of Equations [19] and [20], from Equations [34] and [37] and yield

$$p = A' \cdot 2G\alpha \sinh \epsilon + C'\alpha \{ \lambda [(s_5 - s_3) \sinh \epsilon + (s_5 + 2s_4 - 1)\epsilon \cosh \epsilon + (s_4 + 3s_2 - s_1)\epsilon^2 \sinh \epsilon] + 2G[(s_5 - s_3) \sinh \epsilon + (2s_4 + s_5)\epsilon \cosh \epsilon + (s_4 + 3s_2)\epsilon^2 \sinh \epsilon + s_2\epsilon^3 \cosh \epsilon] \} \ldots [39]$$

$$q = G\alpha \{ 2A' \cosh \epsilon + C'[(1 - s_3) \cosh \epsilon + (1 + 2s_1 + s_5)\epsilon \sinh \epsilon + (s_1 + 3s_2 + s_4)\epsilon^2 \cosh \epsilon + 2s_2\epsilon^3 \sinh \epsilon] \} \ldots\ldots [40]$$

The value of V (defined by $v_{y=\frac{h}{2}} = V \sin \alpha x$) is from Equation [37]

$$V = A' \cosh \epsilon + C'(-s_3 \cosh \epsilon + s_3\epsilon \sinh \epsilon + s_4\epsilon^2 \cosh \epsilon + s_2\epsilon^3 \sinh \epsilon) \ldots\ldots [41]$$

On substitution from these in Equation [14a] (with $v_1 = v_{y=\frac{h}{2}}$)

$$(D_1\alpha^4 - P_1\alpha^2) \{ A' \cosh \epsilon + C'(-s_3 \cosh \epsilon + s_3\epsilon \sinh \epsilon + s_4\epsilon^2 \cosh \epsilon + s_2\epsilon^3 \sinh \epsilon) \} + A'(2G\alpha \sinh \epsilon + G\alpha^2 t \cosh \epsilon) + C'\alpha \{ \lambda [(s_5 - s_3) \sinh \epsilon + (s_5 + 2s_4 - 1)\epsilon \cosh \epsilon + (s_4 + 3s_2 - s_1)\epsilon^2 \sinh \epsilon] + 2G[(s_5 - s_3) \sinh \epsilon + (2s_4 + s_5)\epsilon \cosh \epsilon + (s_4 + 3s_2)\epsilon^2 \sinh \epsilon + s_2\epsilon^3 \cosh \epsilon] + G \cdot \frac{\alpha t}{2} [(1 - s_4) \cosh \epsilon + (1 + 2s_1 + s_5)\epsilon \sinh \epsilon + (s_1 + 3s_2 + s_4)\epsilon^2 \cosh \epsilon + 2s_2\epsilon^3 \sinh \epsilon] \} = 0$$

Dividing by αG, writing

$$\frac{D_1\alpha^3}{G} = \frac{E_1 t^3 \alpha^3}{12(1-\nu_1^2)G} = c_1 r^3 \epsilon^2$$

and

$$\frac{P_1\alpha}{G} = -\frac{\sigma_{x1} t \alpha}{G} = c_2 s$$

where

$$c_2 = 2\alpha t \frac{\sigma_{x1}}{\sigma_{x2}} = 2\alpha t \cdot \frac{1 - \nu_1\nu_2 + 2r\rho(1 - \nu_2^2)}{2r(1 - \nu_1\nu_2) + \frac{1}{\rho}(1 - \nu_1^2)}$$

we have

$$A'\{(c_1r^3\epsilon^3 - c_2s)\cosh\epsilon + 2\sinh\epsilon + 2r\epsilon\cosh\epsilon\} + C'\{(c_1r^3\epsilon^3 - c_2s)(-s_3\cosh\epsilon + s_5\epsilon\sinh\epsilon + s_4\epsilon^2\cosh\epsilon + s_2\epsilon^3\sinh\epsilon) + \gamma(s_5 - s_3)\sinh\epsilon + [\gamma(s_5 + 2s_4) - \gamma + 2 + r(1 - s_3)]\epsilon\cosh\epsilon + [\gamma(s_4 + 3s_2) - (\gamma - 2)s_1 + r(1 + 2s_1 + s_5)]\epsilon^2\sinh\epsilon + [2s_2 + r(s_1 + 3s_2 + s_4)]\epsilon^3\cosh\epsilon + 2rs_2\epsilon^4\sinh\epsilon\} = 0 \ldots [42]$$

Continuity of stress and of the displacement v is assured by Equation [42]. In addition, the displacement u is to be continuous at the interface. This condition may equally well be taken as continuity of the strain e_x. In the face there is strain $\frac{1}{2}t\,d^2v_1/dx^2$ at the interface due to bending. This is, however, not an adequate representation of the strain if the analysis is to be valid for all values of face and core moduli. For when the face and core are of the same material the plate will buckle in the Euler fashion, plane sections remaining plane. The state of the face (a thin surface skin) is then predominantly one of tension or compression, rather than bending with a neutral surface at mid-thickness (of the face). The strain in the face is therefore taken as due to both bending and direct stress (p_1'), and the continuity of e_x at the interface is expressed by

$$\frac{t}{2}\frac{d^2v_1}{dx^2} + \frac{1 - \nu_1^2}{E_1}\frac{q'}{\alpha t} = \left(\frac{\partial u}{\partial x}\right)_{y = h/2} \ldots\ldots\ldots [43]$$

where Equation [12a] has been employed, and the term on the right refers to the core. By means of Equations [41], [40], and [34], Equation [43] becomes after some rearrangement

$$A'(2\cosh\epsilon + 3c_1r\epsilon\sinh\epsilon - 3c_1r^2\epsilon^2\cosh\epsilon) + C'\{(1 - s_2)\cosh\epsilon + (1 + 2s_1 + s_5)\epsilon\sinh\epsilon + (s_1 + 3s_2 + s_4 + 3c_1r + 3c_1r^2s_3)\epsilon^2\cosh\epsilon + (2s_2 + 3c_1rs_1 - 3c_1r^2s_5)\epsilon^3\sinh\epsilon + (3c_1rs_2 - 3c_1r^2s_4)\epsilon^4\cosh\epsilon - 3c_1r^2s_2\epsilon^5\sinh\epsilon\} = 0 \ldots\ldots [44]$$

Equations [44] and [42] are rewritten in the form

$$A'\chi_1 + C'(\chi_2 + \chi_3 s + \chi_4 s^2) = 0 \ldots\ldots\ldots\ldots [44a]$$

$$A'(\chi_5 - c_2\chi_6 s) + C'[(\chi_7 - c_2 s)(\chi_8 + \chi_9 s + \chi_{10}s^2) + \chi_{11} + \chi_{12}s + \chi_{13}s^2] = 0 \ldots\ldots\ldots\ldots [42a]$$

and the χ's, which can be computed from Equation [38], are

$$\chi_n = \psi_n + c_1r\epsilon^2\psi_n', \quad n = 1, 2, 3, 4$$

$$\chi_5 = \psi_5\epsilon + c_1r^3\epsilon^3\psi_5'$$

$$\chi_6 = \psi_6$$

$$\chi_7 = c_1r^3\epsilon^3$$

$$\chi_8, \chi_9, \chi_{10} = \psi_8, \psi_9, \psi_{10}$$

$$\chi_{11}, \chi_{12}, \chi_{13} = \psi_{11}\epsilon, \psi_{12}\epsilon, \psi_{13}\epsilon$$

where

$$\psi_1 = 2\cosh\epsilon, \qquad \psi_1' = \frac{3}{\epsilon}(\sinh\epsilon - r\epsilon\cosh\epsilon)$$

$$\psi_2 = -\frac{2}{\gamma - 1}\cosh\epsilon + 2\epsilon\sinh\epsilon$$

$$\psi_2' = 3\left[\left(1 + r\frac{\gamma + 1}{\gamma - 1}\right)\cosh\epsilon - r\epsilon\sinh\epsilon\right]$$

$$\psi_3 = -\frac{\gamma(\gamma + 1)}{(\gamma - 1)^2}\cosh\epsilon + \frac{2}{\gamma - 1}\epsilon\sinh\epsilon - \epsilon^2\cosh\epsilon$$

$$\psi_3' = 3\left\{r\frac{\gamma(\gamma + 1)}{(\gamma - 1)^2}\cosh\epsilon - \left(\frac{1}{2} + r\frac{\gamma + 1}{\gamma - 1}\right)\epsilon\sinh\epsilon + \frac{1}{2}r\epsilon^2\cosh\epsilon\right\}$$

$$\psi_4 = -\frac{\gamma(3\gamma^2 - 6\gamma + 7)}{2(\gamma - 1)^3}\cosh\epsilon + \left(\frac{1}{2} + \frac{(\gamma + 1)^2}{2(\gamma - 1)^2}\right)\epsilon\sinh\epsilon + \left(\frac{3}{4} - \frac{\gamma + 3}{4(\gamma - 1)}\right)\epsilon^2\cosh\epsilon + \frac{1}{3}\epsilon^3\sinh\epsilon$$

$$\psi_4' = 3r\frac{\gamma(3\gamma^2 - 6\gamma + 7)}{2(\gamma - 1)^3}\cosh\epsilon + \left(\frac{3}{4} - 3r\frac{(\gamma + 1)^2}{2(\gamma - 1)^2}\right)\epsilon\sinh\epsilon + \left(\frac{1}{2} + 3r\frac{\gamma + 1}{4(\gamma - 1)}\right)\epsilon^2\cosh\epsilon - \frac{1}{2}r\epsilon^3\sinh\epsilon$$

$$\psi_5 = \frac{2}{\epsilon}(\sinh\epsilon + r\epsilon\cosh\epsilon) \qquad \psi_5' = \psi_6 = \cosh\epsilon$$

$$\psi_8 = -\frac{\gamma + 1}{\gamma - 1}\cosh\epsilon + \epsilon\sinh\epsilon$$

$$\psi_9 = -\frac{\gamma(\gamma + 1)}{(\gamma - 1)^2}\cosh\epsilon + \frac{\gamma + 1}{\gamma - 1}\epsilon\sinh\epsilon - \frac{1}{2}\epsilon^2\cosh\epsilon$$

$$\psi_{10} = -\frac{\gamma(3\gamma^2 - 6\gamma + 7)}{2(\gamma - 1)^3}\cosh\epsilon + \frac{(\gamma + 1)^2}{2(\gamma - 1)^2}\epsilon\sinh\epsilon - \frac{\gamma + 3}{4(\gamma - 1)}\epsilon^2\cosh\epsilon + \frac{1}{6}\epsilon^3\sinh\epsilon$$

$$\psi_{11} = -\frac{2\gamma}{\gamma - 1}\frac{\sinh\epsilon}{\epsilon} + \left(2 - \frac{2r}{\gamma - 1}\right)\cosh\epsilon + 2r\epsilon\sinh\epsilon$$

$$\psi_{12} = -\gamma\frac{\gamma + 1}{(\gamma - 1)^2}\frac{\sinh\epsilon}{\epsilon} + \frac{\gamma}{\gamma - 1}\left(2 - r\frac{\gamma + 1}{\gamma - 1}\right)\cosh\epsilon - \left(1 - \frac{2r}{\gamma - 1}\right)\epsilon\sinh\epsilon - r\epsilon^2\cosh\epsilon$$

$$\psi_{13} = \gamma\left(\frac{(\gamma + 1)^2}{2(\gamma - 1)^2} - \frac{\gamma(3\gamma^2 - 6\gamma + 7)}{2(\gamma - 1)^3}\right)\frac{\sinh\epsilon}{\epsilon} + \left[\gamma\left(\frac{(\gamma + 1)^2}{2(\gamma - 1)^2} - \frac{\gamma + 3}{2(\gamma - 1)}\right) - r\frac{\gamma(3\gamma^2 - 6\gamma + 7)}{2(\gamma - 1)^3}\right]\cdot\cosh\epsilon + \left[\gamma\left(\frac{1}{2} - \frac{\gamma + 3}{4(\gamma - 1)}\right) - \frac{1}{4}(\gamma - 2) + r\left(\frac{1}{2} + \frac{(\gamma + 1)^2}{2(\gamma - 1)^2}\right)\right]\epsilon\sinh\epsilon + \left[\frac{1}{3} + r\left(\frac{3}{4} - \frac{\gamma + 3}{4(\gamma - 1)}\right)\right]\cdot\epsilon^2\cosh\epsilon + \frac{r}{3}\epsilon^3\sinh\epsilon$$

Functions θ and ϕ being defined by

$$\theta = -\frac{2}{\epsilon^3}(\sinh 2\epsilon - 2\epsilon)$$

$$\phi = \frac{4}{\gamma - 1}(\sinh^2 \epsilon - \gamma \cosh^2 \epsilon)$$

the following useful relations may be established

$$\psi_1\psi_{11} - \psi_5\psi_2 = \theta\epsilon^2, \ \psi_5\psi_3 - \psi_1\psi_{12} = \phi$$

The ψ's, θ, and ϕ are all chosen so that their expansions as power series in ϵ begin with terms of order 1.

The condition that Equations [44a] and [42a] should permit nonzero values of A' and C'' yields an equation for the critical value of s

$$\left[\chi_7\chi_{10} + \chi_{13} - \frac{\chi_5\chi_4}{\chi_1} - c_2\left(\chi_9 - \frac{\chi_6\chi_3}{\chi_1}\right)\right]s^2 + \left[\chi_7\chi_9 + \chi_{13} - \frac{\chi_5\chi_3}{\chi_1} - c_2\left(\chi_8 - \frac{\chi_6\chi_2}{\chi_1}\right)\right]s + \chi_7\chi_8 + \chi_{11} - \frac{\chi_5\chi_2}{\chi_1} = 0 \quad \ldots [45]$$

The term in s^3 is disregarded, being incomplete because powers of s beyond s^2 were not retained in Equations [34] and [37]. The values of ϵ to be expected in practical problems are such that the coefficients of s^2 and s in Equation [45] are of the same order of magnitude. On the other hand s, being the critical stress in the core divided by twice the shear modulus of the core, is necessarily small, of the order of the compressive strain in core and faces at the critical load. A reasonable upper limit for this is 5×10^{-3}. Consequently, an adequate approximation to the critical value of s may be obtained from Equation [45] by discarding the term in s^2. On introducing the functions ψ, θ, ϕ, the solution is found as

$$s = \frac{\theta\epsilon^2 + c_1 r\epsilon^2[\psi_1'\psi_{11} - \psi_5\psi_2' + r^2(\psi_1\psi_3 - \psi_5'\psi_2) + c_1 r^3\epsilon^2(\psi_1'\psi_3 - \psi_5'\psi_2')]}{\phi + c_2' r(\psi_{11}\psi_8 - \psi_6\psi_2) + c_1 r\epsilon^2[c_2' r(\psi_1'\psi_3 - \psi_6\psi_2') + \psi_5\psi_3' - \psi_1'\psi_{12} + r^2(\psi_5'\psi_3 - \psi_1\psi_9) - c_1 r^3\epsilon^2(\psi_1'\psi_9 - \psi_5'\psi_2')]} \quad \ldots [46]$$

Limiting Cases

If $E_1 \to 0$ we have in the limit a core with faces of vanishing stiffness which have ceased to exert any constraint on the core. The corresponding limiting value of Equation [46] ($c_1 \to 0$, $c_2' \to 0$) should lead to the Euler value for cylindrical buckling of the core alone. The limiting value obtained is

$$s = \frac{\gamma - 1}{2} \cdot \frac{\sinh 2\epsilon - 2\epsilon}{\epsilon(\gamma \cosh^2 \epsilon - \sinh^2 \epsilon)}$$

This can be small only if ϵ is small, that is, if the wave length of the buckling deformation is many times the thickness. On expansion in powers of ϵ^2 the leading term is $\epsilon^2/[3(1 - \nu)]$ which is the Euler value.

If $r \to 0$, but E_1 is left unrestricted, we should again expect the same result and it is in fact obtained from Equation [46].

The limit of Equation [46] for long wave lengths ($\epsilon \to 0$) may be obtained by expanding the θ, ϕ, ψ functions in powers of ϵ^2 and so reducing Equation [46] is a power series in ϵ^2. The leading term of this expansion is

$$s = \frac{\dfrac{1}{3(1 - \nu_2)} + \dfrac{rE_1}{3(1 - \nu_1^2)G}(3 + 6r + 4r^2)}{1 + 2r\rho\dfrac{1 - \nu_1\nu_2 + 2r\rho(1 - \nu_2^2)}{1 - \nu_1^2 + 2r\rho(1 - \nu_1\nu_2)}} \cdot \epsilon^2$$

This, however, is exactly the result obtained by a simple direct calculation based upon the assumption that plane sections remain plane, using the straightforward flexural rigidity of the composite section in the Euler formula. We have therefore established that the sandwich plate, no matter how deformable the core is, will always buckle in the "plane sections remain plane" manner for a sufficiently long wave length. In fact, however, the wave length for a very deformable core will be that of short corrugation and will not be determined by the distance between supports. The present result contrasts with the conclusion by Gough, Elam, and de Bruyne that the critical stress for long wave lengths ($\epsilon \to 0$) approaches a nonzero limit.[4]

The Equations [34] and [37] for the displacements in the core take into account the destabilizing effect of the compressive stress in the core. If this effect is disregarded,[5] we put $s = 0$ in s_1, s_2, s_3, s_4, and s_5, and the resulting expressions are simply those of plane strain in the core. The effect of this in Equations [44a] and [42a] is the disappearance of the terms in χ_3, χ_4, χ_9, χ_{10}, χ_{12}, χ_{13}. The effect on Equation [46] is to leave the numerator unchanged, and to change the denominator to

$$c_2' r(\psi_1\psi_8 - \psi_6\psi_2) + c_1 r\epsilon^2 c_2' r(\psi_1'\psi_8 - \psi_6\psi_2') \quad \ldots [47]$$

The question arises as to whether the change is important or not. This depends upon the magnitude of [47], relative to that of the other terms in the denominator of Equation [46], which are

$$\phi + c_1 r\epsilon^2[\psi_5\psi_3' - \psi_1'\psi_{12} + r^2(\psi_5'\psi_3 - \psi_{11}\psi_8) - c_1 r^3\epsilon^2(\psi_1'\psi_9 - \psi_5'\psi_2')] \quad \ldots [48]$$

Now c_1 and c_2' are of the same order of magnitude as ρ, the ratio of the Young's moduli of face and core. Taking the ψ, θ, ϕ functions as of the same order of magnitude, it is clear that [48] will be small compared with [47] only if $r^2\epsilon^2$ is small compared with 1. If the faces are thin, r is small, but the buckling is then likely to take the form of corrugations of short wave length and so rather large ϵ. When the wave length is equal to the core thickness, the value of ϵ is π. Numerical evaluation of Equation [46] will show the range of validity of the method adopted by Gough, Elam, and de Bruyne and Hoff and Mautner for very deformable cores. At the other extreme it will show what range of core stiffnesses will cause the sandwich to buckle in a "plane sections remain plane" fashion to a given approximation.

Acknowledgment

The investigation was carried out as part of the research program of the structures department of the Curtiss-Wright Corporation Research Laboratory,[6] Buffalo, N. Y., under the direction of Mr. A. F. Donovan, head of the department, and Dr. C. C. Furnas, director of the laboratory.

BIBLIOGRAPHY

1 "The Stabilization of a Thin Sheet by a Continuous Supporting Medium," by G. S. Gough, C. F. Elam, and N. A. de Bruyne, *Journal of the Royal Aeronautical Society*, vol. 44, no. 349, 1940, p. 12.

2 "The Buckling of Sandwich Type Panels," by N. J. Hoff and S. E. Mautner, *Journal of the Aeronautical Sciences*, vol. 12, no. 3, 1945, p. 285.

3 "On the General Theory of Elastic Stability," by C. B. Biezeno and H. Hencky, Koninklijke Akademie van Wetenschappen te Amsterdam, Proceedings, vol. 31, 1928, no. 6.

4 (*a*) "Non-Linear Theory of Elasticity and the Linearized Case for a Body Under Initial Stress," by M. A. Biot, *Philosophical Magazine*, vol. 27, sect. 7, 1939, p. 468.

(*b*) "Theory of Elasticity With Large Displacements and Rotations," Proceedings of the Fifth International Congress for Applied Mechanics, 1938, p. 117.

---

[4] Reference (1), p. 26.

[5] As in references (1) and (2).

[6] Now the Cornell Aeronautical Laboratory.

Addendum

In deriving the boundary conditions [25] for the core the quantity $\sigma/2G$ ($= s$) was neglected in comparison with unity. From the physical point of view it appears unlikely that the stability criterion can be significantly affected by so small a change in the boundary forces of the core—or the faces. From the mathematical point of view the change is open to objection, since it does affect the coefficients of s and s^2 derived subsequently, and the final formula [46] obtained for the critical value of s. The required changes in the calculations follow.

The boundary conditions [25] become

$$q' = (1 + s)s_{12}, \quad p' = s_{22} \ldots\ldots\ldots\ldots [25c]$$

Thus Equation [39] remains unchanged but the right hand side of Equation [40] must be multiplied by $1 + s$.

Equation [42] now becomes

$$A'\{(c_1r^3\epsilon^3 - c_2s)\cosh\epsilon + 2\sinh\epsilon + (1 + s)\,2r\epsilon\cosh\epsilon\}$$
$$+ C'\{(c_1r^3\epsilon^3 - c_2s)(-s_3\cosh\epsilon + s_5\epsilon\sinh\epsilon + s_4\epsilon^2\cosh\epsilon$$
$$+ s_2\epsilon^3\sinh\epsilon) + \gamma(s_5 - s_3)\sinh\epsilon + [\gamma(s_5 + 2s_4) - \gamma + 2$$
$$+ r(1 + s)(1 - s_3)]\,\epsilon\cosh\epsilon + [\gamma(s_4 + 3s_2) - (\gamma - 2)s_1$$
$$+ r(1 + s)(1 + 2s_1 + s_5)]\epsilon^2\sinh\epsilon + [2s_2 + r(1 + s)$$
$$(s_1 + 3s_2 + s_4)]\epsilon^3\cosh\epsilon + 2r(1 + s)s_2\epsilon^4\sinh\epsilon\} = 0 \ldots [42c]$$

and Equation [44] becomes

$$A'\{2(1 + s)\cosh\epsilon + 3c_1r\,\epsilon\sinh\epsilon - 3c_1r^2\epsilon^2\cosh\epsilon\}$$
$$+ C'\{(1 + s)(1 - s_3)\cosh\epsilon + (1 + s)(1 + 2s_1 + s_5)\,\epsilon\sinh\epsilon$$
$$+ [(1 + s)(s_1 + 3s_2 + s_4) + 3c_1r + 3c_1r^2s_3]\epsilon^2\cosh\epsilon$$
$$+ [2(1 + s)s_2 + 3c_1rs_1 - 3c_1r^2s_5]\epsilon^3\sinh\epsilon + [3c_1rs_2 - 3c_1r^2s_4]\epsilon^4\cosh$$
$$\epsilon - 3c_1r^2s_2\epsilon^5\sinh\epsilon\} = 0 \ldots\ldots\ldots\ldots\ldots\ldots [44c]$$

These equations can be written in the form (replacing Equations [44a] and [42a])

$$A'(\chi_1 + 2\chi_6 s) + C'(\chi_2 + \chi_3 s + \chi_4 s^2) = 0 \ldots\ldots [44ac]$$
$$A'[\chi_5 + \chi_6(2r\epsilon - c_2)s] + C'[(\chi_7 - c_2 s)(\chi_8 + \chi_9 s + \chi_{10}s^2) + \chi_{11}$$
$$+ \chi_{12}s + \chi_{13}s^2] = 0 \ldots\ldots [42ac]$$

The definitions of the functions χ in terms of the functions ψ, ψ' are unchanged. The definitions of the functions ψ' are unchanged. The definitions of the functions ψ are unchanged except as follows:

$$\psi_3 : \text{Add } -\frac{2}{\gamma - 1}\cosh\epsilon + 2\epsilon\sinh\epsilon$$

$$\psi_4 : \text{Add } -\frac{\gamma(\gamma + 1)}{(\gamma - 1)^2}\cosh\epsilon + \frac{2}{\gamma - 1}\epsilon\sinh\epsilon - \epsilon^2\cosh\epsilon$$

$$\psi_{12} : \text{Add } r\left\{-\frac{2}{\gamma - 1}\cosh\epsilon + 2\epsilon\sinh\epsilon\right\}$$

$$\psi_{13} : \text{Add } r\left\{-\frac{\gamma(\gamma + 1)}{(\gamma - 1)^2}\cosh\epsilon + \frac{2}{\gamma - 1}\epsilon\sinh\epsilon - \epsilon^2\cosh\epsilon\right\}$$

Equation [45] for the critical value of s is now replaced by one derived from Equations [44ac] and [42ac]. The coefficient of s^2 is changed by the addition of

$$2\frac{\chi_6}{\chi_1}(\chi_7\chi_9 + \chi_{12} - c_2\chi_8) - 2r\epsilon\frac{\chi_3\chi_6}{\chi_1}$$

The term independent of s remains the same, both in form and in the definitions of the χ-functions. The changes in the coefficient of s may be seen from the final equation for s obtained by discarding the term in s^2. This is

$$\{\chi_1(\chi_7\chi_9 + \chi_{12} - c_2\chi_8) + 2\chi_6(\chi_7\chi_8 + \chi_{11}) - \chi_2\chi_6(2r\epsilon - c_2) -$$
$$\chi_3\chi_5\}s = \chi_2\chi_5 - \chi_1(\chi_7\chi_8 + \chi_{11}) \ldots\ldots\ldots\ldots [46c]$$

This result has been checked for the limiting cases considered in the paper. It satisfies them all. In the first result given under "Limiting Cases", to the term $\epsilon(\gamma\cosh^2\epsilon - \sinh^2\epsilon)$ appearing in the denominator, the term $-(1/2)(\gamma - 1)(\sinh 2\epsilon - 2\epsilon)$ must be added. Since this term is of order ϵ^3 it does not alter the conclusion.

Two further checks are possible, and are met by Equation [46c]. One is the limiting case $h \to 0$, so that the sandwich reduces to a plate of the face material of thickness $2t$. The limiting form of Equation [46c] yields the required Euler result for long wave lengths. The other is the limiting case $E_2 \to 0$, so that the sandwich reduces to two independent plates (the faces) of thickness t. The limiting form of Equation [46c] again yields the required Euler result for long wave lengths. Here the expansion in powers of ϵ^2 is made (to obtain the leading term) *after* passing to the limit as $E_2 \to 0$.

General Stress-Strain Laws of Elasticity and Plasticity

By A. GLEYZAL,[1] WASHINGTON, D. C.

The stress-strain laws discussed in this paper apply to problems where the material is elastic in some regions and plastic in others, for example, in a plastic-torsion problem or in a plastic-bending problem. These laws have experimental verification for metals in cases where strains are small and stresses and strains are either monotonically increasing or monotonically decreasing at any one point.

Introduction

THE laws to be considered are of the same form as the laws of elasticity. It is sometimes possible in a given plasticity problem to write down immediately the equations for the problem by merely referring to already known equations for the problem in the elastic case. Of course, account must be taken of the fact that the elastic constants are replaced by quantities which are functions of the strains.

The laws may be written in tensor form and apply to finite strains if the strain components of finite strain are defined in such a way that they form a tensor. For infinitesimal or finite strains the axes of principal stress coincide with the axes of principal strain. The stresses according to these laws depend upon the final strains alone and not upon the "strain path."

These laws for finite strains are therefore of simple nature. The extent of their validity would, however, require experimental determination for any given material.

The General Stress-Strain Law

The general laws we shall consider for elasticity and plasticity are

$$\left.\begin{aligned} &\frac{\sigma_1-\sigma_2}{\epsilon_1-\epsilon_2}=\frac{\sigma_2-\sigma_3}{\epsilon_2-\epsilon_3}=\frac{\sigma_3-\sigma_1}{\epsilon_3-\epsilon_1} \quad [1a]\\ &\tau=\tau(\gamma) \quad [1b]\\ &\sigma=\sigma(\delta) \quad [1c]\end{aligned}\right\} \quad [1]$$

where, by definition

$$\left.\begin{aligned} &\tau=\frac{1}{3}\sqrt{(\sigma_1-\sigma_2)^2+(\sigma_2-\sigma_3)^2+(\sigma_3-\sigma_1)^2} \quad [2a]\\ &\gamma=\frac{1}{3}\sqrt{(\epsilon_1-\epsilon_2)^2+(\epsilon_2-\epsilon_3)^2+(\epsilon_3-\epsilon_1)^2} \quad [2b][2]\\ &\sigma=\frac{1}{3}(\sigma_1+\sigma_2+\sigma_3) \quad [2c]\\ &\delta=\frac{1}{3}(\epsilon_1+\epsilon_2+\epsilon_3) \quad [2d]\end{aligned}\right\} \quad [2]$$

$\sigma_1, \sigma_2, \sigma_3$, and $\epsilon_1, \epsilon_2, \epsilon_3$ are principal stresses and strains, respectively, whose axes are assumed to coincide at each point of the material. Later these equations will be expressed in general tensor form and this requirement on the principal axes will be a consequence of the tensor equations. The terms $\tau(\gamma)$ and $\sigma(\delta)$ are functions associated with the material, the same for all types of deformation, provided that all strains are either monotonically increasing or monotonically decreasing.

Nadai (1)[3] has shown that for small strains, τ and γ as just given are, respectively, the shear stress and shear strain in an octahedral plane, i.e., a plane making equal angles with each of the three principal directions of stress.

The first and second of Equations [1] have been considered by Nadai (2) and subjected to experimental verification by Schmidt (3) and Davis (4). The third law is a new plasticity law which we consider in conjunction with the other two plasticity laws in this paper. It may be stated as follows: The average stress σ at a point is an invariant function of the average strain δ at the point for a given material.

Implications and Development

Equations [1] are three equations in the three principal stresses and three principal strains. They may be solved for the principal stresses in terms of the principal strains as follows: Let λ be the ratio

$$\lambda=\frac{\sigma_1-\sigma_2}{\epsilon_1-\epsilon_2}=\frac{\sigma_2-\sigma_3}{\epsilon_2-\epsilon_3}=\frac{\sigma_3-\sigma_1}{\epsilon_3-\epsilon_1}$$

Multiplying both members of Equation [2b] by λ there is found, using Equation [2a]

$$\lambda=\tau/\gamma$$

Equation [1a] may then be rewritten

$$\left.\begin{aligned} &\sigma_1-\sigma_2=\frac{\tau}{\gamma}(\epsilon_1-\epsilon_2)\\ &\sigma_2-\sigma_3=\frac{\tau}{\gamma}(\epsilon_2-\epsilon_3)\\ &\sigma_3-\sigma_1=\frac{\tau}{\gamma}(\epsilon_3-\epsilon_1)\end{aligned}\right\} \quad [3]$$

Using the first two of Equations [3], we get by subtraction

$$\sigma_1+\sigma_3-2\sigma_2=\frac{\tau}{\gamma}(\epsilon_1+\epsilon_3-2\epsilon_2)$$

or

$$\sigma_1+\sigma_2+\sigma_3-3\sigma_2=\frac{\tau}{\gamma}(\epsilon_1+\epsilon_2+\epsilon_3-3\epsilon_2)$$

Therefore

---

[1] David Taylor Model Basin, Navy Department.

[2] Employment of $1/3$ or $2/3$ as coefficient in the expression for γ depends on the choice of definition of shear strain. For this report we have used $1/3$.

Presented at the National Meeting of the Applied Mechanics Division, Buffalo, N. Y., June 21–22, 1946, of The American Society of Mechanical Engineers.

[3] Numbers in parentheses refer to the Bibliography at the end of the paper.

Discussion of this paper should be addressed to the Secretary, A.S.M.E., 29 West 39th Street, New York, N. Y., and will be accepted until January 10, 1947, for publication at a later date. Discussion received after the closing date will be returned.

Note: Statements and opinions advanced in papers are to be understood as individual expressions of their authors and not those of the Society.

$$\sigma_2 = \frac{\tau}{\gamma}(\epsilon_2 - \delta) + \sigma$$

This equation may also be written

$$\sigma_2 = \frac{\tau}{\gamma}\epsilon_2 + \left(\frac{\sigma}{\delta} - \frac{\tau}{\gamma}\right)\delta$$

Two similar equations exist for σ_1 and σ_3. Thus when the two invariant functions $\sigma = \sigma(\delta)$ and $\tau = \tau(\gamma)$ are known, the following equations give the principal stresses in terms of principal strains only

$$\left.\begin{aligned}\sigma_1 &= \frac{\tau}{\gamma}\epsilon_1 + \left(\frac{\sigma}{\delta} - \frac{\tau}{\gamma}\right)\delta \\ \sigma_2 &= \frac{\tau}{\gamma}\epsilon_2 + \left(\frac{\sigma}{\delta} - \frac{\tau}{\gamma}\right)\delta \\ \sigma_3 &= \frac{\tau}{\gamma}\epsilon_3 + \left(\frac{\sigma}{\delta} - \frac{\tau}{\gamma}\right)\delta\end{aligned}\right\} \quad \ldots\ldots\ldots\ldots [4]$$

We now write these laws in tensor form in order to facilitate their use in non-Cartesian co-ordinate systems and to remove the possibility of ambiguity of their meaning. After the laws have been so written we shall return again to the Cartesian notation.

It follows from Equations [2] and [4] and the requirement that the principal axes of stress coincide with those of principal strain that the general tensor equation is referred to an arbitrarily chosen curvilinear system of co-ordinates x^i, $i = 1, 2, 3$, is

$$\sigma_{ij} = \frac{\tau}{\gamma}\epsilon_{ij} + \delta\left(\frac{\sigma}{\delta} - \frac{\tau}{\gamma}\right)g_{ij}, \quad (i, j = 1, 2, 3) \ldots\ldots [5]$$

where σ_{ij} is the stress tensor, and the quantities ϵ_{ij}, g_{ij}, σ, δ, τ and γ are defined as follows:

A definition of a strain tensor ϵ_{ij} which has a clear meaning for finite strains as well as infinitesimal strains is obtained by setting $\epsilon_{ij} = (1/2)(g_{ij} - h_{ij})$, where the co-ordinate system x^i, $i = 1, 2, 3$, is considered to remain embedded in the material as it deforms and the two tensors h_{ij} and g_{ij} are the coefficients of the fundamental tensor in the x^i co-ordinate system before and after deformation, respectively. That is, the square of the differential of arc length before deformation is

$$ds^2 = \sum_j \sum_i h_{ij}dx^i dx^j, \quad (i, j = 1, 2, 3)$$

and after deformation is

$$ds^2 = \sum_j \sum_i g_{ij}\, dx^i\, dx^j, \quad (i, j = 1, 2, 3)$$

The invariant quantities σ, δ, τ, and γ for the general co-ordinate system x^i are

$$\sigma = \frac{1}{3}\sum_j \sum_i g^{ij}\sigma_{ij}, \quad (i, j = 1, 2, 3)$$

$$\delta = \frac{1}{3}\sum_j \sum_i g^{ij}\epsilon_{ij}, \quad (i, j = 1, 2, 3)$$

$$\tau = \frac{1}{3}\left[3\left(\sum_l \sum_k \sum_j \sum_i g^{ij}g^{kl}\sigma_{ik}\sigma_{jl}\right) - \left(\sum_j \sum_i g^{ij}\sigma_{ij}\right)^2\right]^{1/2}, \quad (i, j, k, l = 1, 2, 3)$$

$$\gamma = \frac{1}{3}\left[3\left(\sum_l \sum_k \sum_j \sum_i g^{ij}g^{kl}\epsilon_{ik}\epsilon_{jl}\right) - \left(\sum_j \sum_i g^{ij}\epsilon_{ij}\right)^2\right]^{1/2}, \quad (i, j, k, l = 1, 2, 3)$$

where the contravariant tensor g^{ij} is computed from the values of g_{ij} by solving the following system of nine linear equations.

$$\sum_j g^{ij}g_{jk} = \delta^i{}_k, \quad (i, j, k = 1, 2, 3)$$

$\delta^i{}_k$ in this equation is the "*Kronecker delta*," that is, $\delta^i{}_k = 0$ if $i \neq k$ and $\delta^i{}_k = 1$ if $i = k$.

Equation [5] implies that at all times the principal axes of stress coincide with those of finite strain.

These equations are similar to the elasticity equations and suggest the following equations to be satisfied by generalized quantities E and ν, where E is Young's modulus and ν is Poisson's ratio

$$\left.\begin{aligned}\frac{E}{1+\nu} &= \frac{\tau}{\gamma} \\ \frac{E}{1+\nu}\frac{\nu}{1-2\nu} &= \frac{1}{3}\left(\frac{\sigma}{\delta} - \frac{\tau}{\gamma}\right)\end{aligned}\right\} \quad \ldots\ldots\ldots [6]$$

In the elastic range, when E and ν are constant, the expression $\frac{1}{3}\cdot\frac{E}{(1-2\nu)}$ is the bulk modulus of elasticity as would be expected; the quantity $E/(1+\nu)$ may be termed the octahedral-shear modulus.

We may solve Equations [6] for E and ν in terms of τ, γ, σ, and δ; there results

$$\left.\begin{aligned}E &= \frac{3\frac{\tau}{\gamma}}{2 + \frac{\delta}{\sigma}\frac{\tau}{\gamma}}; \qquad \nu = \frac{1 - \frac{\delta}{\sigma}\frac{\tau}{\gamma}}{2 + \frac{\delta}{\sigma}\frac{\tau}{\gamma}}\end{aligned}\right\} \quad \ldots\ldots\ldots [7]$$

Consequently the general stress-strain relations are given either by Equations [4] or by the following equation of familiar form

$$\left.\begin{aligned}\sigma_1 &= \frac{E}{1+\nu}\left(\epsilon_1 + \frac{\nu}{1-2\nu}\Delta\right) \\ \sigma_2 &= \frac{E}{1+\nu}\left(\epsilon_2 + \frac{\nu}{1-2\nu}\Delta\right) \\ \sigma_3 &= \frac{E}{1+\nu}\left(\epsilon_3 + \frac{\nu}{1-2\nu}\Delta\right)\end{aligned}\right\} \quad \ldots\ldots\ldots [8]$$

where $\Delta = 3\delta$, E and ν are defined by Equations [7], and $\tau(\gamma)$ and $\sigma(\delta)$ are considered to be known functions which for our purposes define the material.

Since τ and σ are functions of γ and δ, respectively, E and ν may each be regarded as functions of the three principal strains ϵ_1, ϵ_2, and ϵ_3 only. E and ν then may also be considered to be the fundamental functions which describe the material, in place of $\tau(\gamma)$ and $\sigma(\delta)$.

A step in the direction of generalization would be to assume at the start of a theory that the two functions

$$\tau = \tau(\gamma, \delta)$$

and

$$\sigma = \sigma(\gamma, \delta)$$

are functions of γ and δ, instead of γ alone or of δ alone. In view of experimental evidence one may go, rather, in the direction of particularization and consider that $\sigma(\delta)$ is the linear function $3k\delta$, where the constant k is the bulk modulus of elasticity for the material. That the same value of k is also reasonably valid in the plastic range has been verified experimentally for a number of materials in the case of compression (5, 6). Equations [7] show that if $\sigma = 3k\delta$, then E and ν do not depend on δ but only on γ.

Equionsat [8] may be solved for the strains giving

$$\left.\begin{aligned} \epsilon_1 &= \frac{1}{E}\left[\sigma_1 - \nu\,(\sigma_2 + \sigma_3)\right] \\ \epsilon_2 &= \frac{1}{E}\left[\sigma_2 - \nu\,(\sigma_3 + \sigma_1)\right] \\ \epsilon_3 &= \frac{1}{E}\left[\sigma_3 - \nu(\sigma_1 + \sigma_2)\right] \end{aligned}\right\} \quad \ldots\ldots\ldots [9]$$

If ν is taken to be $^1/_2$ in these equations it is seen that the mean strain $\delta = {}^1/_3\,(\epsilon_1 + \epsilon_2 + \epsilon_3)$ is identically zero.

If it is assumed that $\delta = 0$, Equations [1] reduce to certain well-known laws of plasticity (1, 2). Thus Equations [4] or [9] include simultaneously both these plasticity laws and the ordinary elasticity equations.[4]

It is interesting to note that Equations [1] imply, when $\sigma = 3k\delta$, that different hydrostatic pressures p applied to a solid do not change the relationship of the increments of stress, $\sigma_1 - p$, $\sigma_2 - p$, $\sigma_3 - p$ and strain, $\epsilon_1 - p/3k$, $\epsilon_2 - p/3k$, $\epsilon_3 - p/3k$. In other words, suppose stress-strain measurements in the elastic or plastic range are made upon a solid under ordinary atmospheric pressure. Then imagine the entire test laboratory to be put under high atmospheric pressure and the test repeated. The observed stresses and strains will have, according to Equations [1], the same relation in the second test as in the first test. To prove this statement we need merely note that if $\sigma_1, \sigma_2, \sigma_3; \epsilon_1, \epsilon_2, \epsilon_3$, satisfy Equations [1] with $\sigma = 3k\delta$, then the quantities

$$\bar{\sigma_1} = \sigma_1 + p, \quad \bar{\sigma_2} = \sigma_2 + p, \quad \bar{\sigma_3} = \sigma_3 + p$$
$$\bar{\epsilon_1} = \epsilon_1 + p/3k, \quad \bar{\epsilon_2} = \epsilon_2 + p/3k, \quad \bar{\epsilon_3} = \epsilon_3 + p/3k$$

also satisfy Equations [1], with $\bar{\sigma} = 3k\bar{\delta}$, for all values of p. After compression of the entire test laboratory the stresses and strains are $\sigma_1 = p$, $\sigma_2 = p$, $\sigma_3 = p$, $\epsilon_1 = p/3k$, $\epsilon_2 = p/3k$, $\epsilon_3 = p/3k$. Hence the observed quantities in the repeated test after compression are $\sigma_1 = \bar{\sigma_1} - p$, $\sigma_2 = \bar{\sigma_2} - p$, $\sigma_3 = \bar{\sigma_3} - p$, $\epsilon_1 = \bar{\epsilon_1} - p/3k$, $\epsilon_2 = \bar{\epsilon_2} - p/3k$, $\epsilon_3 = \bar{\epsilon_3} - p/3k$. These stresses and strains are identical with those of the original test.

When the shear strains are small Equations [1], [8], or [9] are the laws of elasticity even though the principal strains may be large, as when a high hydrostatic pressure is applied. When the

[4] It is not possible to solve for stresses in terms of strain if δ is taken to be zero, since the stresses are then determined only up to an additive quantity which may be taken to be the hydrostatic stress.

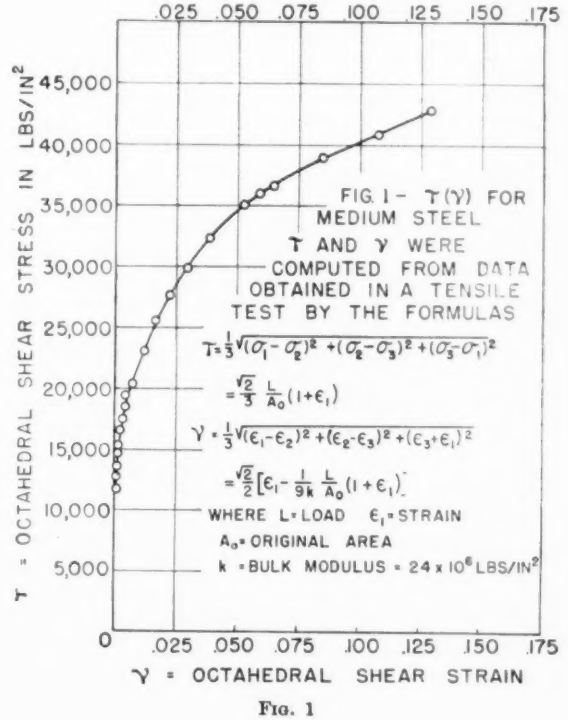


Fig. 1

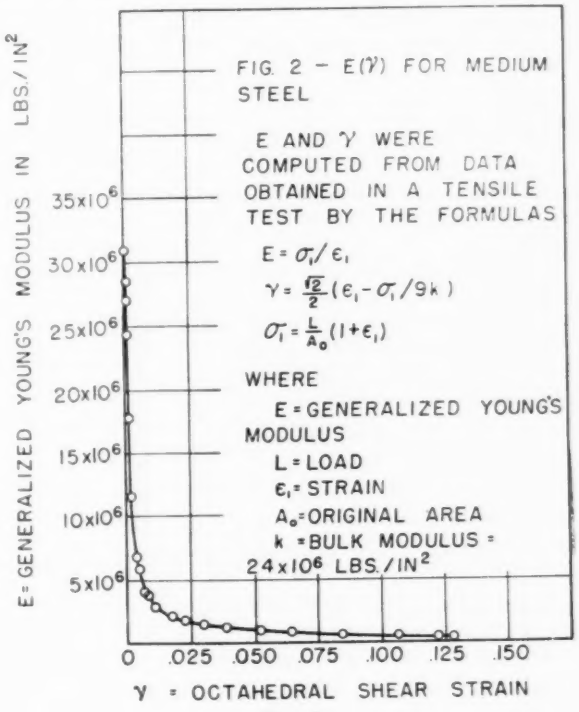


Fig. 2

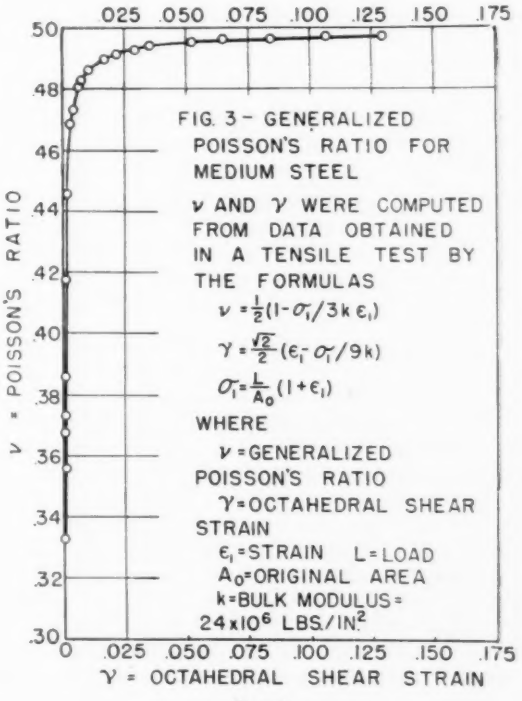


Fig. 3

shear strains are large these equations are very nearly the plasticity equations written in the foregoing. These facts correspond to the known properties of a material such as steel in its elastic and plastic behavior under ordinary or under high pressures.

$\tau(\gamma)$ and $\sigma(\delta)$ in Terms of Quantities Measured in a Tensile Test

To complete the theory of this paper we write equations for the two invariant functions $\tau(\gamma)$ and $\sigma(\delta)$ in terms of quantities measured in a tensile test. Let σ_1, $\sigma_2 = 0$, $\sigma_3 = 0$, be the stresses and ϵ_1, $\epsilon_2 = \epsilon_3$, be the strains in a tensile test. In elasticity theory it is known that

$$E = \sigma_1/\epsilon_1$$

and

$$\nu = -\epsilon_2/\epsilon_1$$

But these equations apply equally well in the present theory since they may be derived from the general stress-strain relations, Equations [8].

Thus E is the slope of the line joining a point on the uniaxial stress-strain curve to the origin. The quantity ν is Poisson's ratio (5) and should be expected to vary between its value of approximately 0.3 in the elastic range and its approximate value 0.5 in the plastic range.

If the function $\sigma(\delta)$ is taken to be $3k\delta$ the parametric equations for E and ν in terms of σ_1 and ϵ_1 may be found as follows: The equation $\sigma = 3k\delta$ implies for the tensile specimen

$$\sigma_1 = 3k\,(\epsilon_1 + 2\epsilon_2)$$

therefore

$$\epsilon_2 = -\frac{1}{2}\,\epsilon_1 + \frac{1}{6}\,\sigma_1/k \qquad [10]$$

Consequently the parametric equations for E and ν are

$$E = \sigma_1/\epsilon_1$$

$$\nu = \frac{1}{2}\left(1 - \frac{1}{3}\,\frac{\sigma_1}{\epsilon_1}\,\frac{1}{k}\right)$$

As ϵ_1 increases, σ_1/ϵ_1 becomes small in comparison with k and as a consequence ν approaches 1/2 as expected. Equations [2] for τ and γ imply for the tensile test

$$\tau = \frac{\sqrt{2}}{3}\,\sigma_1 \qquad \gamma = \frac{\sqrt{2}}{3}\,(\epsilon_1 - \epsilon_2)$$

Making use of Equations [8], the parametric equations for τ and γ are found to be

$$\tau = \frac{\sqrt{2}}{3}\,\sigma_1 \qquad \gamma = \frac{\sqrt{2}}{2}\,(\epsilon_1 - 1/9\,\sigma_1/k)$$

The term $\frac{1}{9}\,\sigma_1/k$ becomes negligible in comparison with ϵ_1 as ϵ_1 increases, but is appreciable for ϵ_1 in the elastic range. Inclusion of this term in the equation for γ is therefore of some importance in a tensile-test determination of $\tau(\gamma)$ for ranges which include the elastic range.

Fig. 1 shows a graph of $\tau(\gamma)$ for medium steel computed from results of a tensile test where we have assumed $k = 24 \times 10^4$ psi. Figs. 2 and 3 show E and ν corresponding to this $\tau(\gamma)$ for the case where $\sigma = 3k\delta$.

BIBLIOGRAPHY

1 "Theories of Strength," by A. Nadai, Trans. A.S.M.E., vol. 55, 1933, paper APM-55-15.

2 "Plastic Behavior of Metals in the Strain-Hardening Range," by A. Nadai, *Journal of Applied Physics*, vol. 8, March, 1937, p. 205.

3 "Über den Zusammenhang von Spannungen und Formänderungen im Verfestigungsgebeit," by R. Schmidt, *Ingenieur-Archiv*, vol. 111, 1932, p. 215.

4 "Yielding and Fracture of Medium-Carbon Steel Under Combined Stress," by E. A. Davis, JOURNAL OF APPLIED MECHANICS, Trans. A.S.M.E., vol. 67, 1945, p. A-13.

5 "The Compression of 46 Substances to 50,000 Kg/Cm^2," by P. W. Bridgman, Proceedings of the American Academy of Arts and Sciences, vol. 74, 1940, p. 21.

6 "The Compressibility of Solids Under Extreme Pressures," by F. D. Murnaghan, Theodore von Kármán Anniversary Volume, California Institute of Technology, Pasadena, Calif., 1941, p. 121.

Supersonic Nozzle Design

By A. E. PUCKETT,[1] PASADENA, CALIF.

A two-dimensional flow field in which the velocity is everywhere supersonic can always be represented approximately by a number of small adjacent quadrilateral flow fields in each of which the velocity and pressure are constant. These quadrilaterals must be separated by lines representing waves in the flow; changes in velocity and pressure through any wave can be computed. By increasing the number of small areas into which the complete flow field is divided, the accuracy of this approximate solutions may be increased without limit. This constitutes the "method of characteristics" solution, which has been known for many years. This method may be applied to the graphical computation of flow in a supersonic nozzle, with the particular aim of producing uniform supersonic flow at the end of the nozzle. It is pointed out that such a computation is essentially simple and rapid, and its essential features are presented in a form which, it is hoped, may be easily applied to engineering problems.

Nomenclature

The following nomenclature will be used in the paper:

- w = velocity of flow
- a = velocity of sound
- $\mathbf{M}$ = Mach number = w/a
- a^* = critical speed of sound
- θ = Prandtl-Meyer angle
- θ_a = flow inclination
- N = speed index = 2θ
- γ = ratio of specific heats, C_p/C_v
- A_e = nozzle exit area
- A^* = nozzle throat area

Introduction

The computation of exact or nearly exact flows of a frictionless incompressible fluid around general two-dimensional boundaries offers problems of some mathematical difficulty. The additional condition that the density of the fluid may vary will complicate the problem under certain conditions; however, in those cases where the velocities in the flow field are everywhere greater than the local speed of sound, a fundamental simplication occurs. The equations of motion assume such a form that they may be solved graphically, in a step-by-step process. This process is known to mathematicians as the "method of characteristics." It was first applied to supersonic flows by Prandtl and Busemann (1)[2] in 1929 and has been much used since. Although the discussion in the present paper is limited to two-dimensional flows, a similar but more complicated method has been developed for three-dimensional flows, with axial symmetry (2).

The "method of characteristics" provides a means of computing the flow through a given two-dimensional supersonic nozzle. It also provides a means of determining the shape of the walls of a supersonic nozzle in such a way that the velocity at the end of the nozzle is uniform and parallel across the entire section. The use of the method of characteristics for this purpose was also described by Prandtl and Busemann, and has been familiar to aerodynamists for some years; it is primarily for the purpose of making the technique more accessible to engineers that it is described in the present paper.

A rigorous mathematical derivation of the method of characteristics can be given; it can be shown in this way that by taking sufficiently small steps in the process, the result may be brought arbitrarily close to the exact continuous solution. It is only in this sense that the solution is approximate; its error can be made as small as desired. It is also possible to deduce the method from much more simple physical reasoning; this course will be pursued in the present paper and, it is hoped, will compensate in clarity for any lack of mathematical rigor.

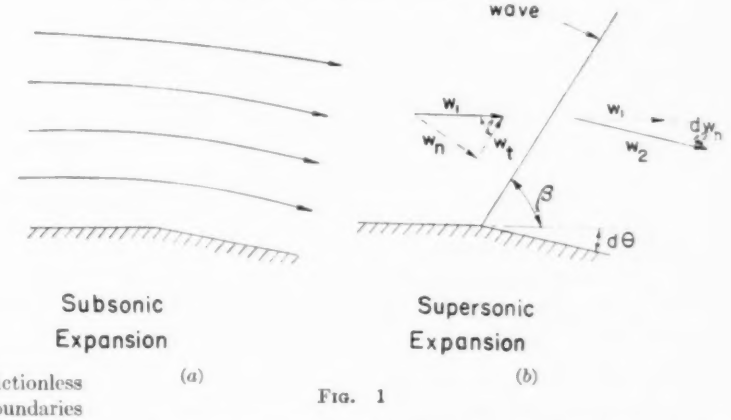


Fig. 1

The basic feature of a supersonic flow which distinguishes it from subsonic flow is the fact that a disturbance in the boundary of the flow makes its presence known only in roughly one half of the total flow field, that is, a disturbance produces a standing wave in the flow and the effect of the disturbance is felt only downstream of the wave. In Fig. 1(*a*) is shown the effect of a sudden expansion in the wall bounding a subsonic flow; it is seen that the effect is propagated symmetrically through the whole field.

The same disturbance in a supersonic flow will produce a standing wave, propagating in a downstream direction. In Fig. 1(*b*) is shown the resulting supersonic flow field. The initial velocity w_1, is undisturbed upstream from the wave and is changed to w_2 on the downstream side. If we thus construct a flow field by adding in the effect of one disturbance after another, proceeding in a downstream direction, the solution upstream will not be disturbed. It can be shown that a general supersonic flow field can be imagined to consist of an infinite number of such disturbance waves. The fundamental idea of the method of characteristics is to replace the infinite number of waves by a finite number which can then be treated separately. In the areas between waves, the velocity magnitude and direction are considered constant. Therefore it is necessary to replace the actual boundaries of the flow by approximate boundaries with a finite number

---

[1] California Institute of Technology.

[2] Numbers in parentheses refer to the Bibliography at the end of the paper.

Presented at the National Meeting of the Applied Mechanics Division, Buffalo, N. Y., June 21–22, 1946, of The American Society of Mechanical Engineers.

Discussion of this paper should be addressed to the Secretary, A.S.M.E., 29 West 39th Street, New York, N. Y., and will be accepted until January 10, 1947, for publication at a later date. Discussion received after the closing date will be returned.

Note: Statements and opinions advanced in papers are to be understood as individual expressions of their authors and not those of the Society.

of disturbances. In other words, a curved boundary is replaced by a number of straight-line segments, with a definite angle between each.

Changes Through a Single Wave

The only mathematical treatment necessary is the computation of the flow changes produced by a single disturbance wave. The effect of the wave produced by the wall bend in Fig. 1(*b*) is to deflect the flow through an angle $d\theta$. It also produces a change in the speed and pressure of the flow, which are determined only by $d\theta$. These changes may be computed from the simple equations of motion for the fluid in differential form. If w_n is the component of w_1 normal to the wave, then conservation of mass for the flow across the wave requires that

$$\rho w_n = (\rho + d\rho)(w_n + dw_n) \quad [1]$$

or

$$w_n d\rho + \rho dw_n = 0$$

Let w_t be the component of w_1 parallel to the wave front; then conservation of momentum parallel to the wave requires that

$$\rho w_n w_t = (\rho + d\rho)(w_n + dw_n)(w_t + dw_t) \quad [2]$$

or

$$dw_t = 0$$

That is, the only velocity increment produced by the wave is normal to it. The momentum component normal to the wave is conserved if

$$\rho w_n dw_n + dp = 0 \quad [3]$$

Eliminating dw_n between Equations [1] and [3] gives

$$w_n^2 = \frac{dp}{d\rho} = a^2 \quad [4]$$

where a is the local speed of sound.

Thus the velocity component normal to the wave is the speed of sound. Use of the energy equation will show that the process across the wave is isentropic, and $dp/d\rho$ is computed using the isentropic law

$$p = \text{const}\ \rho^\gamma \quad [5]$$

Since $w_n = w \sin \beta$ where β is the wave angle, we have

$$\sin \beta = \frac{a}{w} = \frac{1}{\mathbf{M}} \quad [6]$$

where $\mathbf{M}$ is the local Mach number. The wave angle β is then called the "Mach angle." The increase in length of the velocity w_1 is given by

$$dw = dw_n \sin \beta \quad [7]$$

while the change in flow direction must be equal to

$$d\theta = \frac{dw_n \cos \beta}{w} \quad [8]$$

From Equations [7] and [8], the relation between increase in speed and change in flow direction is immediately found

$$\frac{dw}{w} = \tan \beta\, d\theta$$

or using Equation [6]

$$\frac{dw}{w} = \frac{d\theta}{\sqrt{\mathbf{M}^2 - 1}} \quad [9]$$

This equation is the only result necessary to perform the step-by-step computation through any number of waves. It must be observed, however, that $\mathbf{M}$ is a function of w which must include the variation in the speed of sound, a, with w. The Mach number and w are related by

$$\left(\frac{w}{a^*}\right)^2 = \frac{\gamma + 1}{\gamma - 1 + 2/\mathbf{M}^2} \quad [10]$$

where a^* is the "critical speed of sound," a constant for the entire flow. This may be deduced from the energy equation for the fluid (3). If this relation is used in Equation [9], with $\bar{w} = w/a^*$, then

$$d\theta = \sqrt{\frac{\bar{w}^2 - 1}{1 - \frac{\gamma - 1}{\gamma + 1}\bar{w}^2}} \cdot \frac{d\bar{w}}{\bar{w}} \quad [11]$$

With Equation [11] the successive flow changes through a series of bends in a wall, such as in Fig. 2, may be computed. If

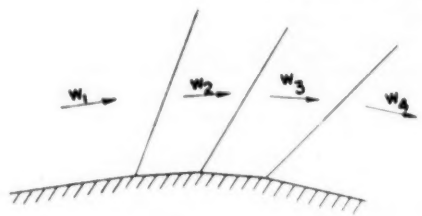


Fig. 2

$\bar{w}_1$ is given, the increments producing $\bar{w}_2$ and $\bar{w}_3$ are obtained from Equation [11]; it is necessary to compute only the Mach numbers corresponding to $\bar{w}_1$, $\bar{w}_2$, and $\bar{w}_3$ in order to draw the Mach wave at the proper angles, as given by Equation [6]. It should be pointed out that the waves described so far are "expansion waves," since the $d\theta$ shown will, according to Equations [9] and [3], produce a drop in pressure.

The evaluation of Equation [11] for every wave in the flow becomes a tedious computation, but may be avoided by noticing that Equation [11] may be integrated, resulting in a function $\theta = \theta(\bar{w})$. Since $\bar{w}$ is also a function of $\mathbf{M}$, we may finally express θ as a function of $\mathbf{M}$; the explicit relation becomes

$$\theta = \sqrt{\frac{\gamma + 1}{\gamma - 1}} \tan^{-1}\left[\sqrt{\frac{\gamma - 1}{\gamma + 1}}\sqrt{\mathbf{M}^2 - 1}\right] - \tan^{-1}\sqrt{\mathbf{M}^2 - 1} \quad [12]$$

The constant of integration has been chosen so that $\theta = 0$ at $\mathbf{M} = 1$. This is, of course, the relation obtained by Prandtl and Meyer (4), in computing the flow around a single sharp corner. The θ so defined is sometimes called the Prandtl-Meyer expansion angle. The function may be tabulated for small integral increments in θ, such as 1 deg. This is done in Table 1. It is now convenient to subdivide the boundaries of the flow in such a way that the angles between adjacent segments are integral multiples of 1 deg. It will also be convenient to let the Mach number in the initial flow region correspond exactly to one of the entries in Table 1. Then the Mach number resulting from the disturbance of any further waves in the flow can be read directly from the table. For instance, if, in Fig. 1(*b*), the initial velocity w_1, represents a Mach number of $\mathbf{M} = 2.022$, and $d\theta = 2$ deg, the Mach number following the wave will be $\mathbf{M} = 2.096$.

The foregoing computations will apply equally well to a wave originating at a disturbance on the upper boundary of the flow, as in Fig. 3. The only difference is that in this case the expansion

wave produces an upward deflection of the flow. It is seen that all disturbance waves will belong in one of two classes or families; those produced by disturbances on the lower wall, which we call the "lower family," and those produced by disturbances on the upper wall, which we may call the "upper family."

Intersection of Two Waves

The only fundamental problem now remaining in the computation of a supersonic flow field is the investigation of the flow following the intersection of two waves of opposite families. Such an intersection is indicated in Fig. 4. If $\mathbf{M}_1$ is given, then $\mathbf{M}_2$ and $\mathbf{M}_3$ are determined by $d\theta_1$ and $d\theta_2$, respectively. The important remaining physical fact is that the wave W_1 which produced an initial deflection of $d\theta_1$ in the flow will continue to produce the same deflection after it has intersected W_2, that is, W_1' produces also a deflection

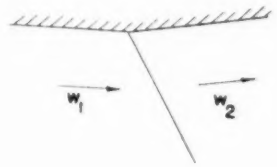


Fig. 3

$$\left.\begin{aligned} a + b &= N \\ (a - b)/2 &= \theta_a \end{aligned}\right\} \qquad [13]$$

It is now apparent that a wave of the upper family of strength $d\theta$ increases a by $2d\theta$, while a wave of the lower family increases b by $2d\theta$. The co-ordinate a records only changes due to the upper family and b records only changes due to the lower family. This is illustrated in Fig. 5 where both waves are assumed to be of strength $d\theta$.

The process of computing the flow change from one region to another, as in Fig. 4, is thus reduced to the purely mechanical process of making appropriate changes in a (or b) for each passage through a wave of the upper (or lower) family. The local speed and flow direction may be determined immediately from Equations [13]. The disturbance waves are drawn at the Mach angles determined by the local Mach number, as listed in Table 1. The accuracy of the construction will be improved by using the average of the wave angles corresponding to the Mach numbers before and after a wave. The angle must then be measured relative to the average flow direction. This average wave angle can

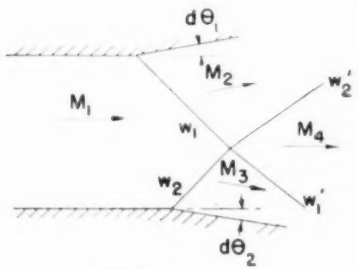


Fig. 4

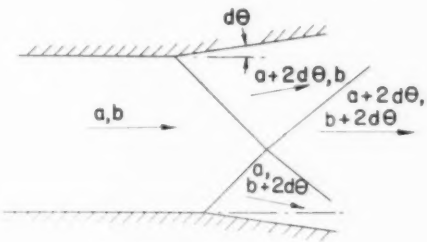


Fig. 5

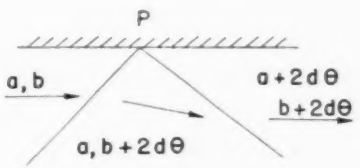


Fig. 6

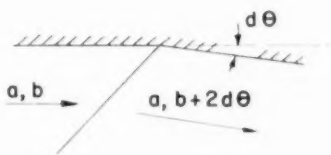


Fig. 7

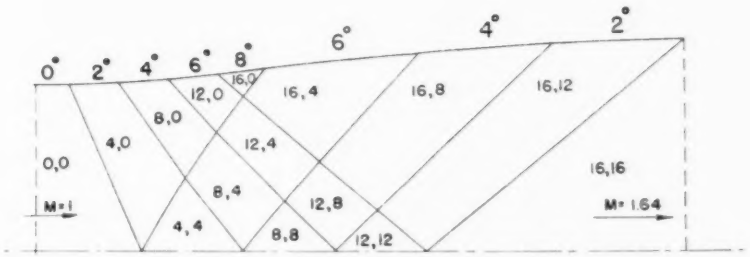


Fig. 8

$d\theta_1$. The same is true of W_2. The Mach number $\mathbf{M}_4$ is obtained from $\mathbf{M}_1$ by finding the θ corresponding to $\mathbf{M}_1$ in Table 1, and adding increments $d\theta_1$ and $d\theta_2$. It is seen that the flow which passes through W_2 and W_1' will experience the same Mach number change as that passing through W_1 and W_2'. The direction of the flow in region 4 will be determined by the fact that the flow has been deflected through an angle $(d\theta_1 - d\theta_2)$ upward, in going through either W_1 and W_2' or W_2 and W_1'. The only "graphical construction" of this elementary flow field lies in drawing the waves W_2' and W_1' at the Mach angles determined by $\mathbf{M}_2$ and $\mathbf{M}_3$, measured relative to the flow direction in regions 2 and 3.

It is desirable to have some notation for recording conveniently the Mach numbers and flow directions in each successive elementary flow field. Let the direction of the velocity vector in any flow region, referred to any initial datum direction, be denoted by θ_a. The speed or Mach number in any region may be described by the θ defined in Equation [12] and tabulated in Table 1; for reasons connected with the more rigorous mathematical development of the method it is actually convenient to adopt the speed index N, where $N = 2\theta$. Thus N is a function only of $\mathbf{M}$. We may now define the flow direction and Mach number in each region by a pair of numbers (a, b) having the following properties

be obtained directly by interpolation in Table 1.

Intersection of Wave and Wall

One more basic elementary wave pattern must be mentioned before proceeding with the design of a supersonic nozzle. If a wave from one wall strikes a straight segment of the opposite wall, it is reflected, but in a manner which must be computed. In Fig. 6 an expansion wave W_1 strikes the upper wall at P. It must be reflected in such a way that the flow is deflected again parallel to the wall; therefore the strength of W_1' (as measured by the deflection it produces) is the same as W_1. The reflected wave now belongs to the upper family, but is still an expansion wave. The angle of the reflected wave is not, of course, equal to the angle of the incident wave.

Had the wall to the right of P in Fig. 6 been inclined downward at angle $d\theta$, as in Fig. 7, that is, parallel to the flow in region 2, no reflected wave would be required to satisfy the boundary condition. This might be described as "canceling" the incoming wave since W_1 simply ends on the wall. It will be seen later that this is one of the fundamental principles required in the design of a supersonic nozzle.

The tools are now at hand to compute the flow through or to

TABLE 1 FUNCTIONS OF EXPANDING FLOW

$\theta°$	M	β	N	$\theta°$	M	β	N	$\theta°$	M	β	N
0.0	1.0000	90.00	0	30.5	2.1530	27.68	61	61.0	3.6610	15.86	122
0.5	1.0508	72.10	1	31.0	2.1723	27.41	62	61.5	2.6948	15.71	123
1.0	1.0808	67.70	2	31.5	2.1913	27.16	63	62.0	3.7288	15.56	124
1.5	1.1078	64.50	3	32.0	2.2105	26.90	64	62.5	3.7632	15.41	125
2.0	1.1328	61.96	4	32.5	2.2298	26.65	65	63.0	3.7980	15.26	126
2.5	1.1559	59.89	5	33.0	2.2492	26.40	66	63.5	3.8332	15.12	127
3.0	1.1770	58.17	6	33.5	2.2688	26.15	67	64.0	3.8690	14.98	128
3.5	1.1973	56.68	7	34.0	2.2885	25.91	68	64.5	3.9052	14.84	129
4.0	1.2170	55.29	8	34.5	2.3090	25.66	69	65.0	3.9417	14.70	130
4.5	1.2362	53.99	9	35.0	2.3288	25.43	70	65.5	3.9788	14.56	131
5.0	1.2554	52.77	10	35.5	2.3485	25.21	71	66.0	4.0164	14.42	132
5.5	1.2745	51.66	11	36.0	2.3688	24.99	72	66.5	4.0548	14.28	133
6.0	1.2935	50.63	12	36.5	2.3895	24.77	73	67.0	4.0940	14.14	134
6.5	1.3120	49.66	13	37.0	2.4108	24.53	74	67.5	4.1338	14.00	135
7.0	1.3300	48.75	14	37.5	2.4316	24.29	75	68.0	4.1738	13.86	136
7.5	1.3478	47.90	15	38.0	2.4525	24.07	76	68.5	4.2135	13.73	137
8.0	1.3649	47.11	16	38.5	2.4730	23.86	77	69.0	4.2543	13.60	138
8.5	1.3825	46.33	17	39.0	2.4942	23.64	78	69.5	4.2960	13.46	139
9.0	1.4005	45.57	18	39.5	2.5156	23.43	79	70.0	4.3385	13.33	140
9.5	1.4178	44.58	19	40.0	2.5372	23.22	80	70.5	4.3820	13.19	141
10.0	1.4350	44.18	20	40.5	2.5590	23.01	81	71.0	4.4257	13.06	142
10.5	1.4522	43.52	21	41.0	2.5810	22.80	82	71.5	4.4704	12.92	143
11.0	1.4688	42.92	22	41.5	2.6028	22.59	83	72.0	4.5158	12.79	144
11.5	1.4858	42.30	23	42.0	2.6254	22.38	84	72.5	4.5620	12.66	145
12.0	1.5028	41.72	24	42.5	2.6484	22.19	85	73.0	4.6086	12.53	146
12.5	1.5195	41.15	25	43.0	2.6716	21.98	86	73.5	4.6558	12.40	147
13.0	1.5365	40.60	26	43.5	2.6948	21.79	87	74.0	4.7031	12.28	148
13.5	1.5540	40.05	27	44.0	2.7179	21.59	88	74.5	4.7505	12.15	149
14.0	1.5710	39.53	28	44.5	2.7412	21.39	89	75.0	4.7979	12.02	150
14.5	1.5878	39.04	29	45.0	2.7643	21.21	90	75.5	4.8504	11.89	151
15.0	1.6045	38.54	30	45.5	2.7879	21.02	91	76.0	4.9032	11.76	152
15.5	1.6213	38.08	31	46.0	2.8120	20.83	92	76.5	4.9557	11.64	153
16.0	1.6380	37.63	32	46.5	2.8361	20.65	93	77	5.009	11.52	154
16.5	1.6550	37.17	33	47.0	2.8610	20.46	94	78	5.119	11.27	156
17.0	1.6723	36.73	34	47.5	2.8855	20.28	95	79	5.232	11.02	158
17.5	1.6892	36.30	35	48.0	2.9105	20.09	96	80	5.349	10.78	160
18.0	1.7061	35.88	36	48.5	2.9360	19.91	97	81	5.470	10.53	162
18.5	1.7230	35.48	37	49.0	2.9616	19.73	98	82	5.595	10.29	164
19.0	1.7401	35.08	38	49.5	2.9873	19.56	99	83	5.724	10.07	166
19.5	1.7572	34.69	39	50.0	3.0131	19.38	100	84	5.867	9.81	168
20.0	1.7743	34.31	40	50.5	3.0393	19.21	101	85	6.008	9.58	170
20.5	1.7915	33.93	41	51.0	3.0660	19.06	102	86	6.155	9.35	172
21.0	1.8090	33.54	42	51.5	3.0925	18.87	103	87	6.311	9.12	174
21.5	1.8268	33.19	43	52.0	3.1193	18.70	104	88	6.472	8.88	176
22.0	1.8445	32.83	44	52.5	3.1463	18.53	105	89	6.643	8.66	178
22.5	1.8622	32.48	45	53.0	3.1737	18.38	106	90	6.820	8.43	180
23.0	1.8795	32.15	46	53.5	3.2015	18.21	107	91	7.008	8.21	182
23.5	1.8973	31.82	47	54.0	3.2293	18.04	108	92	7.202	7.98	184
24.0	1.9150	31.49	48	54.5	3.2576	17.87	109	93	7.407	7.77	186
24.5	1.9325	31.16	49	55.0	3.2865	17.72	110	94	7.623	7.54	188
25.0	1.9502	30.85	50	55.5	3.3158	17.55	111	95	7.852	7.32	190
25.5	1.9680	30.54	51	56.0	3.3451	17.40	112	96	8.093	7.10	192
26.0	1.9861	30.23	52	56.5	3.3747	17.24	113	97	8.350	6.88	194
26.5	2.0041	29.93	53	57.0	3.4055	17.08	114	98	8.622	6.67	196
27.0	2.0222	29.64	54	57.5	3.4365	16.92	115	99	8.907	6.45	198
27.5	2.0402	29.35	55	58.0	3.4675	16.76	116	100	9.210	6.23	200
28.0	2.0585	29.06	56	58.5	3.4985	16.61	117	101	9.539	6.02	202
28.5	2.0770	28.78	57	59.0	3.5295	16.46	118	102	9.887	5.80	204
29.0	2.0957	28.49	58	59.5	3.5612	16.31	119	103	10.260	5.60	206
29.5	2.1145	28.23	59	60.0	3.5937	16.16	120	104	10.658	5.38	208
30.0	2.1336	27.97	60	60.5	3.6270	16.01	121	105	11.081	5.18	210

design a supersonic nozzle. The principal elements of such a nozzle are shown in Fig. 8. The nozzle is considered to commence at the throat, across which it is assumed that the Mach number is uniformly 1; the validity of this assumption will depend on the shape of the subsonic contraction section which must precede the throat. An expanding section follows and then a return to a parallel section at the end of the nozzle. It is generally the object of the nozzle design to produce a uniform parallel flow in this exit section, which in our computational system means simply a flow with no disturbance waves present.

Nozzle Design

(*a*) *Maximum Expansion.* The simplest type of nozzle design is illustrated in Fig. 8. The shape of the initial expansion is arbitrary up to the point where the maximum expansion angle is reached, being governed generally by considerations of continuity with the curvature of the subsonic contraction. In Fig. 8 the diverging wall is represented by segments at angles of 2 deg to each other, and expanding up to a maximum angle of 8 deg. Four expansion waves are produced and their graphical construction follows the procedure previously outlined. The nozzle may be drawn symmetrically about the center line, or, as is done here, the center line is replaced by a solid wall; the flow solution must be the same in either case. The four initial expansion waves are reflected from the center line and return to the outer wall.

It is now that the fundamental idea of the nozzle design is applied; in order to achieve an ultimately wave-free supersonic flow, each of these expansion waves must be canceled at some time, using the principle illustrated in Fig. 7. At the point where the first returning expansion wave strikes the wall, the wall is deflected inward by an amount equal to the strength of the wave, in this case 2 deg. This is done with each of the other waves. When the last wave has been canceled, the walls have automatically become parallel again, and a uniform wave-free flow is produced. In this case the final Mach number will be **M** = 1.638. The wall shape following the point where the last expansion wave was produced is completely determined by the graphical construction.

It will be noticed that 8 deg is the largest expansion angle which could have been used to produce this Mach number without the introduction of compression waves and hence an actual recontraction in the nozzle. Thus the maximum permissible expansion angle for any nozzle design is exactly one half of the "Prandtl-Meyer" angle θ, corresponding to the final Mach number, or

$$\theta_{max} = N/4 \quad [14]$$

(*b*) *Less Than Maximum Expansion.* A design utilizing this maximum permissible expansion angle to produce a certain Mach number, will produce the shortest possible nozzle for a given initial rate of divergence (curvature). However, the same Mach number can be produced in a nozzle having any expansion angle

less than 8 deg by allowing the initial expansion waves to reflect a proper number of times from the wall. For instance, in Fig. 9 is shown a nozzle design for the same Mach number, using a maximum expansion angle of 4 deg. The elimination of 4 deg of expansion on the wall from the previous design requires the

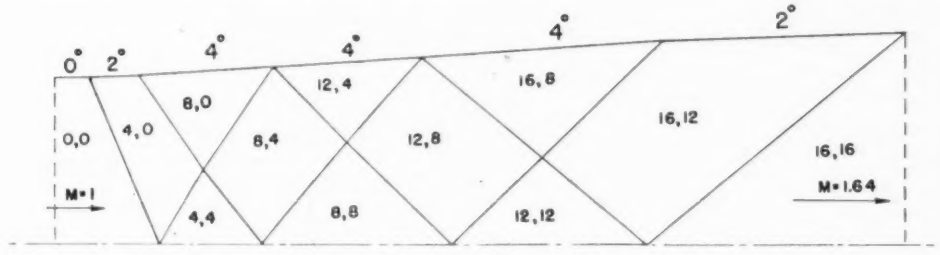


FIG. 9

reflection of two 2-deg waves, to supply the additional required expansion in the flow. Thus if the maximum permissible expansion angle is θ_{max}, and the expansion angle actually used is θ_0, the number n of reflected waves of strength $d\theta$ is given by

$$n = \frac{\theta_{max} - \theta_0}{d\theta} \quad \ldots\ldots\ldots\ldots\ldots\ldots [15]$$

In general, it cannot be said that either the design using θ_{max} or the design using a smaller expansion angle, is superior. If boundary-layer growth and friction losses are likely to be objectionable, it is obviously advantageous to use the shortest possible nozzle design. This point of view was apparently predominant in the German supersonic wind-tunnel designs. On the other hand, the longer a nozzle, the less critical is its design in so far as producing a uniform final velocity is concerned. If the expansion angle is small enough, almost any smooth curve connecting the throat to exit section will produce a reasonably uniform final velocity. Therefore it may be conservative design practice to use an expansion angle less than θ_{max}, say, one half to two thirds as large.

(*c*) *Steps in Nozzle Design.* The steps in nozzle design may be listed briefly as follows:

1 Determine from Table 1 the speed index N most closely corresponding to the desired design Mach number.

2 Determine the maximum permissible expansion angle θ_{max}, using Equation [14]. Choose a nozzle expansion angle θ_0, equal to or less than this.

3 Choose an expansion curve from the throat to θ_0 and divide this into suitable straight segments. The disturbance wave strength used might be 1 or 2 deg, depending upon the accuracy desired.

4 Construct the expansion waves produced by this section and their intersections and reflections from the center line. If θ_0 is less than θ_{max}, determine the necessary number of reflections from the wall using Equation [15].

5 Construct the section canceling all expansion waves, and producing a parallel flow.

The final nozzle shape should actually consist of a smooth curve faired through all the points of intersection of waves with the wall. This can be accomplished best on a plot with exaggerated vertical ordinates. It is important to note that a check on the over-all graphical construction may be obtained by computing the ratio of the exit area, A_e, produced by the construction to the throat area A^*, and comparing this with the theoretical area ratio deduced for one-dimensional flow, which is given by

$$\frac{A_e}{A^*} = \frac{1}{\mathbf{M}} \left\{ \frac{1 + \frac{\gamma - 1}{2} \mathbf{M}^2}{\frac{\gamma + 1}{2}} \right\}^{\frac{\gamma + 1}{2(\gamma - 1)}} \quad \ldots\ldots\ldots [16]$$

Since the flow in both throat and exit section is one-dimensional, these two area ratios should agree within the error of the graphical construction. It should be pointed out that the entire graphical construction is a very rapid and mechanically simple process, which can be carried out in a matter of only a few hours. The mechanical processes can be performed by a draftsman with no particular reference to their physical meaning.

(*d*) *Approximate Method.* One further approximation in the construction is sometimes possible, which will shorten the labor involved still more. It will be noted in both Fig. 8 and Fig. 9, that the flow pattern at a section through the point of maximum expansion consists of nearly uniformly spaced fields with constant Mach number. Thus the flow is almost uniformly radial at that section. Therefore it appears feasible to design a nozzle by starting at the section of maximum expansion, and assuming a uniform radial flow. This amounts to assuming the existence of uniformly spaced wave quadrilaterals with constant Mach number and flow direction varying uniformly. The number of waves which must be present is, of course, determined by the expansion angle used, and is given by

$$m = \frac{\theta_0}{d\theta} \quad \ldots\ldots\ldots\ldots\ldots\ldots [17]$$

The design for the nozzle in Fig. 8, starting at the section of maximum expansion, and assuming uniform radial flow at that section, is shown in Fig. 10. Using this design procedure, it is necessary to connect the maximum expansion point with a throat of the correct size by a smooth curve representing the expansion

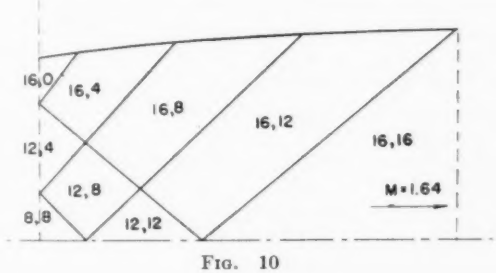


FIG. 10

section. It is clear that the accuracy of the assumption of uniform radial flow will depend to some extent upon the uniformity of the curvature of this section. The correct throat size must be computed in this case from Equation [16].

BOUNDARY-LAYER EFFECTS

The discussion so far has pertained to the approximate solution of the flow of a nonviscous fluid. In a real fluid some viscous effects must be present, but it can be shown that they are, for the most part, confined in a thin layer next to the walls of the flow, called the boundary layer. The real flow then consists essentially of a core of nonviscous flow, and thin layers of retarded

flow along the walls. It can be shown that the perfect fluid core behaves as though it were flowing between walls which lie somewhere in the boundary layer, inside the physical walls. These "effective walls" are displaced inside the true walls by a certain fraction of the boundary-layer thickness, called the "displacement thickness." The displacement thickness is also an important parameter in general boundary-layer theory (5); it is defined as the distance through which the wall of a channel carrying a perfect fluid would have to be displaced in order to produce the same reduction in mass flow that is caused by the actual boundary layer.

The nozzle computations made previously may now be considered to apply to a perfect fluid flowing between certain effective walls. The physical walls of a real flow which would

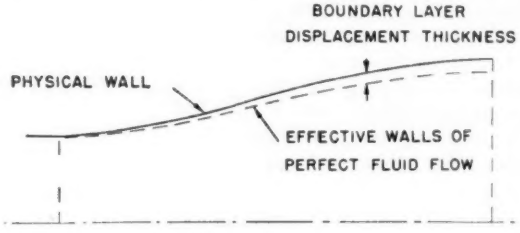


FIG. 11

have the same internal characteristics as the computed flow will lie exactly one displacement thickness outside of the effective walls (see Fig. 11). The displacement thickness increases from nearly zero at the throat to a value depending upon the Reynolds number, length, and Mach number in the nozzle. It continues to increase through the test section (following the exit section of the nozzle), which means that the actual nozzle walls must diverge slightly through the test section in order to maintain a constant velocity.

It should be noted that the boundary layer forms on all four walls of the nozzle; however, it is generally convenient to make boundary-layer corrections only to the top and bottom walls of a two-dimensional channel. As a first crude approximation, the total correction for all four walls might be divided between the top and bottom walls only. The detailed computation of the boundary-layer displacement thickness is outside the scope of the present paper, but some order of magnitude figures may be given for design purposes. Some theoretical estimates of the rate of boundary-layer growth have been made for the 2.5-in. supersonic wind tunnel at the Guggenheim Aeronautical Laboratory, California Institute of Technology, and comparisons made with boundary-layer profiles measured in the wind tunnel. The following rough figures will give an indication of the size of the effects obtained.

The rate of increase through a square test section is such that an expansion of the top and bottom walls by 0.007 to 0.010 in. per in. of length on each wall, will roughly provide the necessary compensation for all four walls. This figure has been found to be useful for a wide range of Reynolds numbers, from $\mathbf{R} = 5 \times 10^5$ to $\mathbf{R} = 5 \times 10^6$ based upon test section height, and for Mach numbers of the order of 1.5 to 2.5. The thickness of the boundary layer in a 2.5-in. wind-tunnel nozzle at a Mach number of 1.5 and Reynolds number of 5×10^5 is roughly 0.15 in.; of this, the displacement thickness is about 0.040 in. If the friction coefficient is assumed independent of Reynolds number, the displacement thickness would increase approximately linearly with the nozzle size. Increasing Mach number increases boundary-layer thickness, due essentially to the additional heating in it. In the 2.5-in. nozzle, the total boundary-layer thickness at $\mathbf{M} = 4$ is roughly 0.25 in.

TABLE 2 TYPICAL NOZZLE ORDINATES, MAXIMUM EXPANSION TO EXIT SECTION

M = 1.99		M = 2.42		M = 2.82		M = 3.24		M = 3.62		M = 4.04	
x	y	x	y	x	y	x	y	x	y	x	y
0	7.50	0	7.50	0	7.50	0	7.50	0	7.50	0	7.50
4.38	7.42	4.52	7.42	5.62	7.40	4.94	7.41	5.52	7.40	5.94	7.40
8.36	7.28	8.69	7.28	9.70	7.26	9.43	7.26	10.39	7.23	11.20	7.21
11.97	7.09	12.47	7.08	13.38	7.07	13.47	7.05	14.89	7.00	16.10	6.96
15.19	6.88	15.91	6.84	16.64	6.84	17.15	6.79	18.75	6.73	20.22	6.67
18.06	6.62	19.04	6.56	19.67	6.57	20.41	6.50	22.24	6.42	23.94	6.34
20.65	6.35	21.80	6.27	22.35	6.29	23.41	6.19	25.39	6.09	27.17	6.00
21.84	6.20	24.34	5.96	24.80	5.99	26.03	5.87	28.08	5.76	30.11	5.64
		26.57	5.65	26.95	5.69	28.42	5.53	30.56	5.41	32.69	5.28
		27.58	5.49	28.90	5.37	30.46	5.21	32.73	5.07	34.95	4.92
				30.70	5.07	32.35	4.87	34.66	4.73	36.96	4.57
				32.20	4.77	33.99	4.56	36.35	4.40	38.69	4.23
				32.90	4.62	35.44	4.25	37.87	4.08	40.26	3.90
						36.13	4.09	39.20	3.77	41.62	3.58
								39.80	3.62	42.79	3.29
										43.32	3.15
$\theta_0 = 7°$		9°		12°		13°		14°		15°	

It is also clear that the method in general may be applied to a wide variety of two-dimensional supersonic-flow problems, and that it forms a very powerful tool for investigation in this field.

CONCLUSIONS

Using the methods outlined in the paper, the graphical construction of a two-dimensional supersonic nozzle to produce uniform parallel flow at any desired Mach number is a relatively rapid and simple process. As an example of the application of the method, several nozzle shapes have been designed using the approximate method described, in which uniform radial flow is assumed at the maximum expansion section. These are given in Table 2; the abscissas x are measured from the nozzle exit section, and the ordinates y are measured from the nozzle center line. Only that part of the nozzle between exit section and maximum expansion angle is given. This section must be connected to a throat of the proper size (computed from Equation [16]) by a smooth curve of reasonably low curvature. The scale may be revised by changing x and y in the same ratio. It will be noticed that the expansion angles used, θ_0, correspond roughly to one half of the maximum permissible θ_{max}, so that the shape of the curve from throat to maximum expansion section should not be too critical. No correction for boundary layer has been made.

BIBLIOGRAPHY

1 "Nährungsverfahren zur zeichnerische Ermittlung von ebenen Strömungen mit Überschall geschwindigkeit," by L. Prandtl and A. Busemann, *Stodola Festschrift*, Zurich, 1929, p. 499.

2 "Einführung in die Gasdynamik," Sauer, Edwards, Ann Arbor, Mich., 1945, p. 137.

3 "Introduction to Aerodynamics of a Compressible Fluid," by H. W. Liepmann and A. E. Puckett, John Wiley & Sons, Inc., New York, N. Y., 1946, chapt. 3.

4 "Über zweidimensional Bewegungsvorgange in einem Gas," by Th. Meyer, *Mitteilungen über Forschungsarbeiten*, vol. 62, 1908, pp. 31–67.

5 "Aerodynamic Theory," by W. F. Durand, Julius Springer, Berlin, 1935, vol. 3, p. 89.

6 "Application of the Methods of Gas Dynamics to Water Flows With Free Surface," by Ernst Preiswerk; part 1, "Flow With No Energy Dissipation," U.S. N.A.C.A. TM No. 934, 1940; part 2, "Flows With Momentum Discontinuities (Hydraulic Jumps)," U.S. N.A.C.A. TM No. 935, 1940.

7 "The Mechanics of Compressible Fluids," by G. I. Taylor and J. W. Maccoll, reference (5).

8 "Steam and Gas Turbines," by Aurel Stodola, McGraw-Hill Book Company, Inc., New York, N. Y., 1927, pp. 43 and 129.

Analytical Design of Centrifugal Air Compressors

By C. CONCORDIA[1] and M. F. DOWELL[2]

The object of this paper is to describe a general method of design and analysis which has been developed for, and applied primarily to, the design of supercharger centrifugal impellers. The method has also been used as a systematic means for the analysis of such impellers as well as for the design of the corresponding diffusers and of gas-turbine compressors and turbines. The development was undertaken with the idea of obtaining, as nearly as possible, a self-sufficient and self-contained rational design method which would be influenced as little as possible by preconceived notions of what the impeller blades should look like. The method is also complete in the sense that it is not used merely as a guide to the character of the blade shape, e.g., to determine limiting curvatures. Instead, one starts from and uses the basic laws of the fluid motion to determine the required flow path and thus the complete blade shape. On the other hand, the fullest use has been made of available experience and test results as checks of the theory.

Nomenclature

The following nomenclature is used in the paper:

- ρ = mass density of fluid, lb-sec^2/ft^4
- t = time, sec
- r = radial distance to air particle, ft
- θ = angular position of air particle, radians
- $\omega = d\theta/dt$ = angular velocity of air, radians per sec
- ω_w = angular velocity of impeller, radians per sec
- $\alpha = d\omega/dt = d^2\theta/dt^2$ = angular acceleration of air, radians per sec^2
- p = pressure, psf
- B = angular position of blade element $= \theta - \omega_w t$, radians
- z = axial distance, ft
- $v_r = dr/dt$ = radial component of air velocity, fps
- $v_z = dz/dt$ = axial component of air velocity, fps
- v_{s+r} = resultant of axial and radial velocities, fps
- ω_1, ω_2 = initial (entrance) and final (exit) angular velocities, respectively, of air, radians/sec
- $\omega_{rel} = \omega - \omega_w$ = angular velocity of air relative to the wheel, radians/sec
- r_1, r_2 = initial and final radii respectively of flow line, ft

Subscripts b, m, and o refer to back wall, median flow line, and open face as defined in Fig. 1

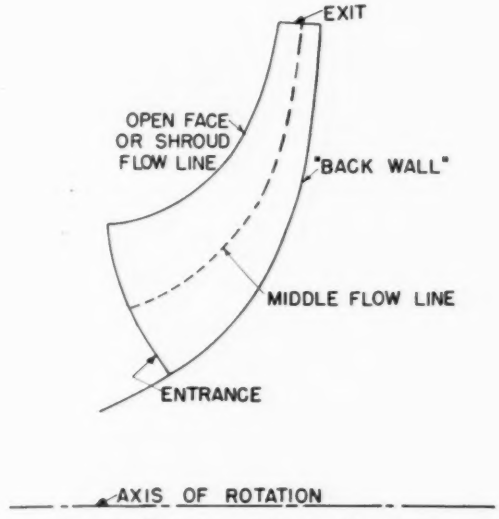


Fig. 1 Tangential View of Impeller
(Section in axial-radial plane.)

- μ = fluid viscosity
- δ = boundary layer thickness
- $p' = p - p''$ (see Equation [13])

Description of Method

The procedure has been to set up first the equations of equilibrium of an air particle in terms of a system of cylindrical co-ordinates suited to the form of the centrifugal compressor to be studied. The three equations of equilibrium for an element of a compressible perfect fluid of density ρ and pressure p, in cylindrical co-ordinates r, θ, and z, are

Tangential acceleration

$$\rho\left(r\frac{d^2}{dt^2}\theta + 2\frac{dr}{dt}\frac{d\theta}{dt}\right) = \rho\,(r\alpha + 2v_r\omega) = -\frac{\partial p}{r\partial\theta} \quad [1]$$

Radial acceleration

$$\rho\left(\frac{d^2}{dt^2}r - r\left(\frac{d\theta}{dt}\right)^2\right) = \rho\left(\frac{d}{dt}v_r - r\omega^2\right) = -\frac{\partial p}{\partial r} \quad [2]$$

Axial acceleration

$$\rho\frac{d^2}{dt^2}z = \rho\frac{d}{dt}v_z = -\frac{\partial p}{\partial z} \quad [3]$$

These equations are simply an expression of Newton's second law and are assumed to hold along any streamline within the fluid. In order to solve these equations without further approximation it would be necessary to integrate them over the whole space within any one impeller passage and consider proper boundary conditions along the passage walls. This has been avoided by the distribution of the boundary forces within the fluid,[3] as for

[1] Central Station Engineering Divisions, General Electric Company, Schenectady, N. Y. Mem. A.S.M.E.

[2] Aircraft Gas Turbine Engineering Division, General Electric Company, Lynn River Works, Lynn, Mass.

Presented at the National Meeting of the Applied Mechanics Division, Buffalo, N. Y., June 21–22, 1946, of The American Society of Mechanical Engineers.

Discussion of this paper should be addressed to the Secretary, A.S.M.E., 29 West 39th Street, New York, N. Y., and will be accepted until January 10, 1947, for publication at a later date. Discussion received after the closing date will be returned.

Note: Statements and opinions advanced in papers are to be understood as individual expressions of their authors and not those of the Society.

[3] "Investigation of Single-Stage Axial Fans," by P. Ruden, *Luftfahrtforschung*, vol. 14, July 20, 1937, pp. 325–346; also September 20, 1937, pp. 458–473.

an infinite number of blades. The condition of the fluid is then in the first approximation independent of angle and the various streamlines may be separately considered.

The determination of blade shapes and passages by means of these equations is as follows:

The equation of tangential force, Equation [1], is regarded as the most significant since it exhibits the primary effect of the impeller on the air in imparting a rotary motion by means of the tangential pressure gradient between the blades. In this equation, $\partial p/\partial\theta$ is replaced by $\Delta p/\Delta\theta$ where Δp is the pressure difference across each blade at any point along the path (the blade loading), and $\Delta\theta$ is the angular distance between adjacent blades. Thus Equation [1] becomes

$$\rho\,(r\alpha + 2\,v_r\omega) = -\frac{\Delta p}{r\,\Delta\theta} \qquad [4]$$

This equation is used to calculate step by step the angular acceleration α, the angular velocity ω, and finally the relative angular position B of an air particle as it travels through the impeller, for a given blade loading Δp, density distribution ρ, and radial component of velocity v_r. The basic premise of this procedure is that blade loading is the most significant factor, so that a given blade loading is desirable as compared with some other kind of loading.

For preliminary calculations the desirable distribution of pressure across the blade as a function of radius was chosen on a common-sense basis by following the rule that the air should be accelerated gradually, with the force starting at zero and increasing to a more or less uniform maximum value over the middle portion of the blade and then decreasing to a small (but not necessarily exactly zero) value at the exit. Thus shocks at entrance and exit, as well as pulsations of pressure at the entrance to the diffuser, are minimized, and on the other hand no portion of the blade escapes its proper share of the work.

It will be shown later how other criteria of good blade loading have also been applied. In the foregoing discussion the whole passage is regarded as lumped into a single flow line with a force proportional to $\Delta p/\Delta\theta$ acting on the air. From the mathematical point of view, the original partial differential equation has been reduced to an ordinary differential equation solvable by a step-by-step process or by means of the differential analyzer.

In Equation [1] it is evident that ρ and v_r must also be specified. The procedure has been to estimate ρ first from available test results and finally from pressure-rise curves calculated from the radial- and axial-force equations. From another point of view, the ratio of blade loading to density ($\Delta p/\rho$) may be regarded as the quantity specified so that it is not necessary for the present to know ρ. The velocity v_r does not have to be guessed but may be independently assigned, since when ρ is known the passage contour in the axial-radial plane, that is, in the tangential view as shown in Fig. 1, may be determined by means of the equation of continuity to produce any desired axial-radial component v_{z+r} of velocity. In this sense the flow line is regarded as a middle or median line, and the velocity as an average velocity, since we know that in actuality there is a variation of velocity across the passage. The v_r for any particular shape of median flow line and assigned v_{z+r} may be found by measuring the slope of the flow line in the $z + r$ plane directly from a sketch such as that in Fig. 1.

Calculations have shown that the blade shape so determined is rather insensitive to variations in the density distribution, but on the other hand the radial component of velocity is very important. The practical result is that the axial-radial passage contour may be and has been used as a control of the blade shape for any specified loading, and conversely one must remember that if the axial-radial contour is changed the blade shape should be changed correspondingly. There may evidently be an infinite number of properly co-ordinated axial-radial passage contours and blade shapes, all presumably having reasonably good performance.

Application of Formulas to Impeller Design

One of the first applications of these equations was to an impeller having a nearly uniform radial velocity. The resulting blade shape, in its axial view, Fig. 2, has a backward curvature at the entrance and the exit (because of the light blade loading at entrance and exit) and a forward curvature in its middle portion. As such reversals of curvature are undesirable from the standpoint of construction, a general study of blade shape as affected by the radial component of velocity as well as by other factors was undertaken.

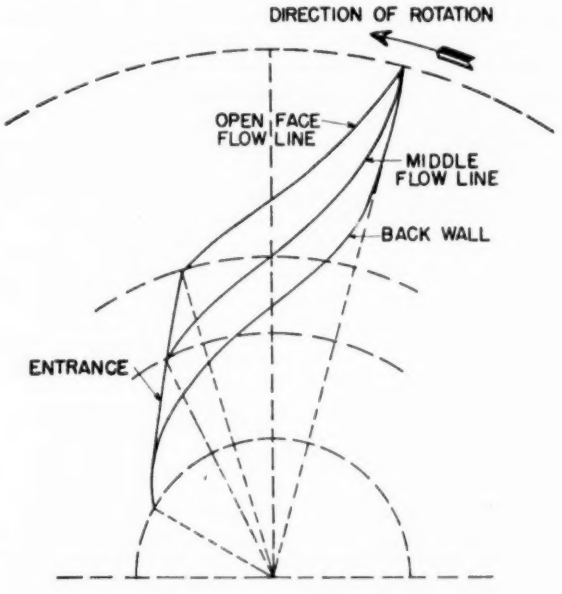


Fig. 2 Axial View of Radial-Flow Impeller

Some preliminary work was done by hand step-by-step integration of Equation [4] and this indicated almost at once that a proper reduction of the radial component of velocity at the inlet could eliminate the initial backward curvature. The entrance velocity thus should be principally axial and should turn around more or less gradually to a nearly radial exit, so that the impeller changes gradually from axial to radial.

A continuation of the work by a study of several hundred specific cases on the differential analyzer has shown that a proper axial-radial velocity distribution can result in a simple blade shape as far as the median flow line is concerned, but has brought out the fact that the passage contour (in the tangential view) necessary to produce the simplest median flow line (in the axial view) may have certain undesirable features, and moreover may not correspond to the simplest flow lines along these contours.

As just implied, following the determination of the middle flow line, we must calculate the two extreme flow lines, i.e., along the back wall (see Fig. 1) and along the open face (or shroud, if any). To do this we must estimate a velocity component v_r along these lines. This is done, as in the case of the median ρ, first by experience and finally from a consideration of the fact that zero circulation should exist within the fluid up the streamline along the open face or back wall and back down the middle line. This calculation of circulation cannot be made until a blade shape and the corresponding angular velocities have been calculated, as until

then we know neither the relative velocities nor the length of the path.

It is also necessary to have in some sense an equality of over-all effect on the fluid among the various flow lines. In the designs made so far, this has been accomplished by making the work done on the fluid equal for all flow lines, which simply means that the tangential components of exit velocity must be inversely proportional to the exit radii,[4] or that the angular velocities at the exit must be inversely proportional to the square of the radii

$$\left.\begin{aligned} v_{\theta 2b}\, r_{2b} &= v_{\theta 2m}\, r_{2m} = v_{\theta 2o}\, r_{2o} \\ \text{or} \qquad \omega_{2b}\, r_{2b}^2 &= \omega_{2m}\, r_{2m}^2 = \omega_{2o}\, r_{2o}^2 \end{aligned}\right\} \quad \ldots\ldots\ldots\ldots [5]$$

As a final check the circulation around the blade along the three flow lines is calculated to see if it varies by any significant amount.

It was stated previously that the variation of density ρ through the impeller is computed from the axial- and radial-force equations. Actually, these Equations [2] and [3] require some modification in order to put them into the best form for computation.

According to the original assumption, there is everywhere within the fluid a pressure gradient ($\partial p/\partial\theta$), or ($\Delta p/\Delta\theta$). This corresponds physically to the assumption of an infinite number of blades, and as shown in Fig. 3, the effect of the gradient is

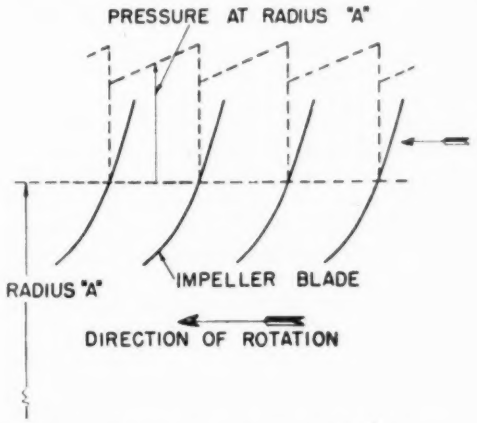


FIG. 3 VARIATION OF PRESSURE WITH ANGLE

canceled each time one passes through a blade, so that there is no net pressure variation in the tangential (θ) direction. This shows that if one is to integrate the pressure gradient from entrance to exit, one must take care to avoid passing through a blade if the proper pressure rise is to be obtained. The differential pressure rise may be written as

$$dp = \frac{\partial p}{\partial r}\, dr + \frac{\partial p}{\partial z}\, dz + \frac{\partial p}{\partial \theta}\, d\theta \ldots\ldots\ldots\ldots [6]$$

Substituting for $\partial p/\partial r$ and $\partial p/\partial z$ from Equations [2] and [3]

$$dp = \rho \left[r\omega^2 dr - \frac{dv_r}{dt}\, dr - \frac{dv_z}{dt}\, dz \right] + \frac{\partial p}{\partial \theta}\, d\theta \ldots\ldots [7a]$$

In this expression $dr/dt = v_r$ and $dz/dt = v_z$, thus

$$dp = \rho\, [r\omega^2 dr - v_r\, dv_r - v_z dv_z] + \frac{\partial p}{\partial \theta}\, d\theta \ldots\ldots [7b]$$

or, since

$$v_r^2 + v_z^2 = v_{z+r}^2 \ldots\ldots\ldots\ldots\ldots\ldots\ldots\ldots [7c]$$

$$dp = \rho\, (r\omega^2 dr - v_{z+r}\, dv_{z+r}) + \frac{\partial p}{\partial \theta}\, d\theta \ldots\ldots\ldots [7d]$$

Finally, in order to avoid passing through an impeller blade $d\theta$ must be taken equal to dB, the change in blade angle, while $\partial p/\partial\theta$ is replaced by $\Delta p/\Delta\theta$, so that one obtains

$$dp = \rho\, [r\omega^2 dr - v_{z+r}\, dv_{z+r}] + \frac{\Delta p}{\Delta \theta}\, dB \ldots\ldots\ldots [8]$$

This equation may be evaluated for each interval along the flow path, as all the quantities are now known, that is, ρ, v_{z+r}, and $\Delta p/\Delta\theta$ were previously assigned in order to solve Equation [4], ω is found from the step-by-step solution of Equation [4], and B is found by numerically integrating ($\omega - \omega_w$), the angular velocity relative to the impeller, with respect to time.

Having found p by summation of the dp of Equation [8], one may find a new ρ curve from a suitable relation $(\rho/\rho_0)^\gamma = (p/p_0)$. Experience has shown that the values of (dp) found from Equation [8] must be multiplied by a factor of from 70 to 80 per cent to check test values. This is presumably because of the fact that losses have been neglected. Although more complete expressions including the effect of surface friction have been developed, we have preferred to depend directly on estimates based upon tests for the magnitude of the pressure rise, using Equation [8] only to determine the shape of the curve. The calculated pressures are also useful in a relative sense to compare the performance of different impellers.

In the same way Equation [4] has not been modified, since the effect of friction is merely to increase the required blade loading without significantly changing its shape. These two simplifications are legitimate because of the fact that we are not trying to determine the performance, i.e., the efficiency and pressure ratio, of a given impeller, but rather are trying to determine directly the optimum design having maximum efficiency for any assigned pressure ratio.

It might have been supposed that the pressure rise could be computed more simply by the relation

$$dp = -\rho v\, dv \ldots\ldots\ldots\ldots\ldots\ldots [9]$$

where v is the total velocity of the air relative to the impeller. However, the form, Equation [8], is believed to have the advantages of convenience and of showing clearly the fundamental design components which contribute to the pressure rise. For example, the first term $\rho\, r\omega^2 dr$ represents the centrifugal pressure rise and may be compared to a similar term $\rho\, r\omega_w^2 dr$ which represents the corresponding pressure rise in a straight radial-blade impeller. The second term $-\rho\, v_{z+r}\, dv_{z+r}$ is the pressure rise due to the fluid flow through the impeller neglecting the effects of the blades (that is, it represents the impeller as an annular diffusing passage), and thus shows directly the effect of changes in the shape of the axial-radial cross section. The third term shows the direct action of the blades in pushing on the air and is the only term which would exist in a purely axial-flow fan with constant axial velocity.

In evaluating the total circulation within the fluid passage a path, Figs. 1 and 2, is chosen up the back wall, across the impeller exit (this portion is not necessarily negligible, since the exit velocity is not necessarily normal to the exit cross section), down the open face, and down the entrance. The integral of the component of relative velocity (in line with this path) with respect to path length is taken and evaluated numerically. This integral is the circulation in co-ordinates moving with the impeller, so to it must be added $+ 2A\omega_w$ in order to obtain the circulation with respect to co-ordinates fixed in space, where A is the net

[4] "Energy Transfer Between a Fluid and a Rotor for Pump and Turbine Machinery," by S. A. Moss, C. W. Smith, and W. R. Foote. Trans. A.S.M.E., vol. 64, 1942, pp. 567–597.

projected area of the blade in the axial view as shown in Fig. 2. To obtain this projected area we must consider negative as well as positive areas if the projections of the back wall and open face lines overlap. With the conventions chosen in Fig. 2, a positive area is obtained if the enclosed portion is on the left as one proceeds along the path (see Fig. 2).

In evaluating the total circulation about the blade along each of the three flow lines, the pressure loading Δp has been used to compute the corresponding difference of velocity, and this has been numerically integrated along each path.

Differential Analyzer Simplifies Computing Process

It is evident from the foregoing description that this design method is straightforward and simple in theory but entails a considerable amount of numerical work. In principle, a sort of successive approximation solution of the force equations in the three dimensions for each flow line and a successive consideration of the three flow lines must be made. In practice, however, the relative unimportance of the density distribution allows some separation of the equations so that the blade shape may be found for many cases without checking each flow line to see if the pressure rise has exactly the assumed shape. This fact has permitted the saving of a great deal of time by use of the differential analyzer[5] for some of the calculations.

Determination of Optimum Blade Loading

Since the basis of most of the work is the shape of the curve of pressure difference across the blade, the question of what is the best pressure loading is of prime importance. This question has been approached in three ways: (1) As just noted, by the common-sense consideration that the pressure should be small at entrance and exit and should not have any reversals of curvature; (2) by comparisons of calculated pressure loadings for several impellers which have already been tested; and (3) by a consideration of the possibility of boundary-layer separation.

The application of method (1) needs no further discussion.

For method (2) an instrument, Fig. 4, was built and has been

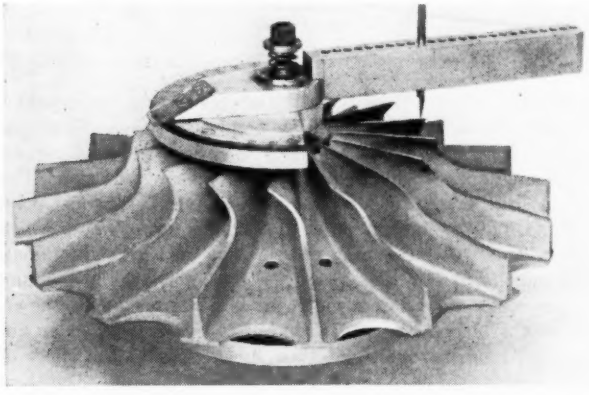


Fig. 4 Device for Measurement of Impeller-Blade Contours

used for the detailed measurement of the blade contours. From these measurements and for given impeller speeds and flow conditions, the blade loadings are computed by Equation [4]. Calculations have been made for operating conditions of both good and poor performance so that a correlation of performance and blade loading could be made.

Method (3) is the assignment of the blade loading in such a way that separation is avoided. This can be done only indirectly. The procedure has been to plot the curves of pressure for both surfaces of the blade, taking as a first approximation

$$p_s = p \pm (\Delta p/2) \quad [10]$$

where the two values of p_s are the surface pressures and p is the pressure calculated as described in connection with Equation [8]. The criterion of separation involves the boundary-layer thickness, density, relative velocity, pressure gradient along the flow path, and the impeller rotational speed. One may, as an approximation, write that in order to avoid separation we must have[6]

$$\frac{\delta\,(dp'/ds)}{\rho\, v^2} < \frac{K}{R_\delta} \quad [11]$$

where s is the distance along the flow path, v is the relative velocity, K is a constant, R_δ $(= v\delta\rho/\mu)$ is Reynolds number for the boundary layer, and μ is the fluid viscosity.

Equation [11] may also be written in the form

$$\frac{dp'}{ds} < \frac{K\,\mu\, v}{\delta^2} \quad [12]$$

In the present case the "pressure gradient" (dp'/ds) is not the actual pressure gradient but a corrected gradient found by subtracting from the actual gradient a centrifugal-pressure gradient to which we are entitled by virtue of the impeller rotation; or, from the actual pressure we subtract a centrifugal pressure p''

$$(p'' = \omega_w^2 \int_{r_0}^{r} \rho\, r\, dr) \quad [13]$$

before computing the gradient. This pressure p'' may be regarded as representing that developed in a rotating impeller having no flow, and for which there will of course be no separation regardless of the magnitude of the pressure gradient.

For the centrifugal impellers considered this centrifugal-pressure gradient has been extremely important, being in most cases 4 or 5 times as great as the residual-pressure gradient (dp'/ds) which tends to produce separation. Thus a proper estimate of the separation condition depends much more upon a proper calculation of the pressure-rise distribution than upon an exact knowledge of the boundary-layer thickness or of the quantity K. Moreover, it is evident that the best shape of loading curve will bear little resemblance to the best shape for an airfoil in a free stream, and will also vary widely depending upon other features of the design.

Discussion of Results and Conclusions

The studies made by the methods outlined have led to an improved understanding of the proper and necessary correlation between the over-all passage contour (as projected in the axial-radial plane) and the blade shape. The inherent relations among the three principal flow lines considered, and the necessity for a proper consideration of all three, are brought out. In addition, the effect of various factors such as density, shape, and magnitude, Fig. 5, of blade loading, initial spin, and design speed have been determined, as well as the best blade shapes for certain specific designs.

One might loosely classify the method as an attempt to solve the complete aerodynamic-design problem roughly, rather than any one part of it exactly. The partial differential equations of equilibrium have been reduced to a series of one-dimensional equations and solved in succession. The equations of continuity and of circulation have been applied to the whole passage as a unit (or at most in two parts). The merits of these assumptions must be judged by the results obtained, and on this basis they have

[5] "A New Differential Analyzer," by H. P. Kaehni and H. A. Peterson, Trans. A.I.E.E., vol. 63, May, 1944, pp. 221–227.

[6] "Modern Developments in Fluid Dynamics—Vol. II," by S. Goldstein, Oxford University Press, London, England, 1938, p. 533.

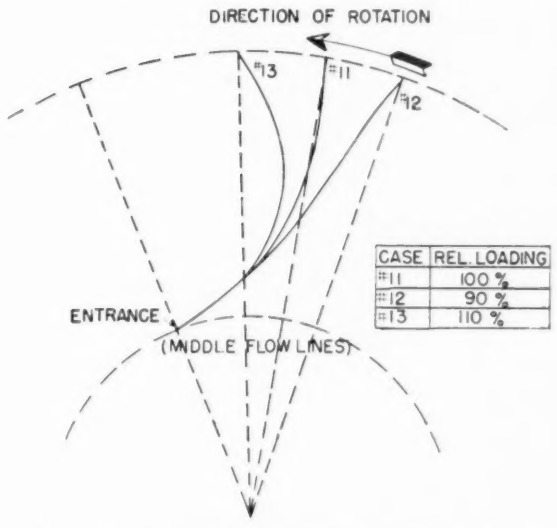


FIG. 5(a) AXIAL VIEW OF CENTRIFUGAL IMPELLERS; EFFECT OF MAGNITUDE OF BLADE PRESSURE LOADING ON BLADE SHAPE

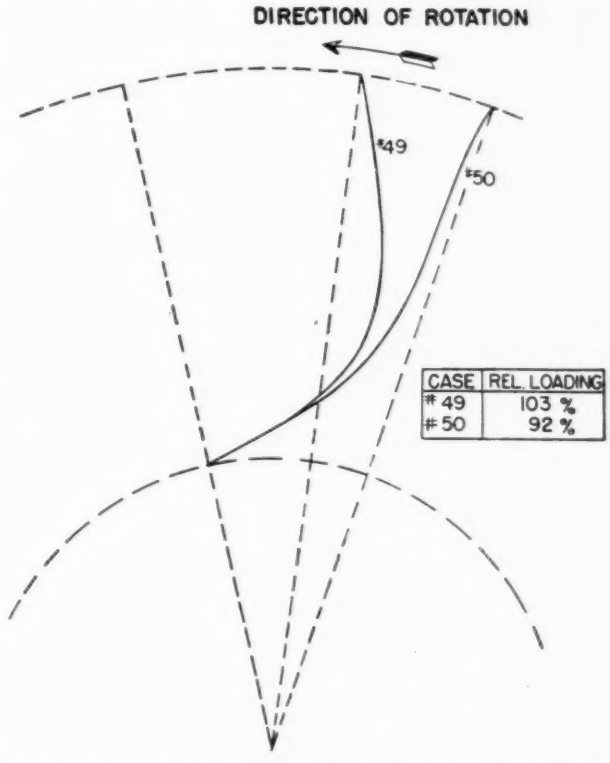


FIG. 5(b) AXIAL VIEW OF MIDDLE FLOW LINES OF CENTRIFUGAL IMPELLERS; EFFECT OF MAGNITUDE OF BLADE PRESSURE LOADING ON BLADE SHAPE

been amply justified. Tests on several impellers have shown considerable increases in efficiency, flow capacity, and maximum attainable pressure ratio.

Not the least of the benefits has come from the systematic analysis of all types of impellers. It has been possible on more than one occasion to explain differences in performance among various experimental impellers which seemed practically alike on even a careful qualitative inspection, since the analysis provides a means of looking at the fundamental physical effects of design changes rather than merely at the geometrical dimensions themselves. This form of analysis may be compared to the methods of smoke and dust precipitation, since a more or less even precipitation is taken as a criterion of good performance. However, in the analytical method one may take on paper any speed, however high, as the design speed, as opposed to the test method which may be used only at moderate speeds, and also one may obtain a quantitative idea of the magnitude and detailed distribution of the loading over the blade surface, so that the optimum loading from the aerodynamic standpoint may be approached.

ACKNOWLEDGMENT

The authors are indebted to Miss Helen Poulos for innumerable calculations, to Dr. J. R. Weske for referring them to the work of Ruden, to Dr. H. Poritsky for several discussions of separation and boundary-layer phenomena, and to the staff of the General Electric Company who operate the differential analyzer.

Forced Torsional Vibrations With Damping: An Extension of Holzer's Method

By J. P. DEN HARTOG[1] AND J. P. LI[2]

An extension of Holzer's method is given for the case of damped systems of discreet as well as of uniformly distributed inertias and flexibilities. For discreet systems the modification in the Holzer table consists of replacing I by $I - jc_0/\omega$, and of replacing k by $k + j\omega c_i$, whereby most numbers in the tables become complex. The meaning of the real part of any complex number is that quantity which is in time-phase with the motion at the free end, while the imaginary part is 90 deg out of time-phase with that motion. For distributed systems the results are given by Equations [12] and [12a] for a free forward end; by Equations [13] and [13a] for a damped forward end, while the letters a and b appearing in these results are defined by Equations [8] and [8a].

1 Nomenclature

The following nomenclature is used in the paper:

a, b . . . . numbers depending on system constants, defined by Equations [8] and [8a] or by [9]

A, B, C, D
C_1, C_2, C_3, C_4 } . . . . integration constants

c . . . . torsional damping constant

I . . . . moment of inertia

j . . . . imaginary unit

k . . . . torsional spring constant

l . . . . length of shaft

p . . . . roots, defined by Equation [8]

P, Q . . . . angular displacement functions of x, being the in-phase (real) and the quadrature (imaginary) components of that angle

x . . . . distance along shaft, between 0 and l

φ . . . . angle of torsional displacement

ω . . . . frequency

Subscripts:

1 . . . . per unit length (in a distributed system)

i . . . . inner or internal (damping)

o . . . . outer or external (damping to ground)

$n, (n-1)$ . . . . running number of disk

2 Scope and Object of This Paper

In the calculation of the free and forced vibrations of torsional systems with small damping, the method of Holzer is widely used. It consists of determining the shapes and frequencies of the free vibrations, disregarding damping. The damping is subsequently taken into consideration by equating its energy dissipation during one cycle to the work done by the exciting forces during that cycle Obviously this method is satisfactory and reliable only when the natural frequency and particularly the vibrating shape of the system are practically independent of damping. In most practical systems this is true enough, justifying the widespread use of this simple method of calculation. Exceptions occur in cases where two flywheels in the middle of the system are coupled to each other by a dashpot only, or by a dashpot transmitting a torque which is considerable compared to the spring torque transmitted between these two flywheels.

An old practical example of this condition is the Lanchester damper or the sprung "damped dynamic vibration absorber." Other cases are hydraulic or inductive electric couplings tying two parts of the system together, as they occur in ship drives. In all such cases the energy dissipation in the device obviously is zero for zero damping. But the energy dissipation is also zero for large (infinite)damping, because then the two halves of the coupling are rigidly tied together by the dashpot, which changes the shape of the vibration altogether. These devices are used in practice with a damping between zero and infinity so that the damping torque as well as the relative motion are considerable, resulting in a maximum energy dissipation. The shape of the vibration then is somewhere between that for zero damping and solid coupling and differs considerably from either. For such cases the simple Holzer method breaks down and it is necessary to consider the damping directly with all its complications of changing phase angles.

In his original publication,[3] Holzer gave the method of Section 3 of this paper in great detail. It is here repeated in a simplified manner. For engine systems with a large number (six or more) of identical cylinders, it is advantageous to consider the engine as a uniformly distributed elasticity and inertia. For zero damping this leads to the Lewis method,[4] which in principle is also given in Holzer's book.[3] The calculations for a system with uniformly distributed elasticity, inertia, and damping are given by Holzer[3] only for the case of free vibration and in a very complicated manner. In this paper, the forced vibrations of such systems are investigated, which is believed to be a new contribution.

3 The Holzer Table for Damped Systems

The discussion is based on the usual engine idealization where the moving parts of each crank are replaced by an equivalent flywheel and an equivalent torsional stiffness. The damping is assumed to be linear and can consist of two parts represented by (a) a dashpot between each flywheel and ground and (b) dashpots between each flywheel and the one or two neighbor flywheels. The damping constants corresponding to these two types are designated as c_o, for "outer" or external damping and c_i for "inner" or internal damping.

The Newton equation of motion for the nth disk (Fig. 1) is

$$I_n\ddot{\varphi}_n + k_n(\varphi_n - \varphi_{n+1}) + k_{n-1}(\varphi_n - \varphi_{n-1}) + c_{no}\dot{\varphi}_n + c_{ni}(\dot{\varphi}_n - \dot{\varphi}_{n+1}) + c_{n-1,i}(\dot{\varphi}_n - \dot{\varphi}_{n-1}) = 0 \ldots . [1]$$

---

[1] Professor of Mechanical Engineering, Massachusetts Institute of Technology. Mem. A.S.M.E.

[2] Assistant in Mechanical Engineering, Massachusetts Institute of Technology.

Contributed by the Applied Mechanics Division for presentation at the Annual Meeting, New York, N. Y., December 2–6, 1946, of The American Society of Mechanical Engineers.

Discussion of this paper should be addressed to the Secretary, A.S.M.E., 29 West 39th Street, New York, N. Y., and will be accepted until January 10, 1947, for publication at a later date. Discussion received after the closing date will be returned.

Note: Statements and opinions advanced in papers are to be understood as individual expressions of their authors and not those of the Society.

[3] "Die Berechnung der Drehschwingungen," by H. Holzer, J. Springer, Berlin, 1922.

[4] "Torsional Vibration in the Diesel Engine," by F. M. Lewis, Trans. Society of Naval Architects and Marine Engineers, vol. 33, 1925, pp. 109–145.

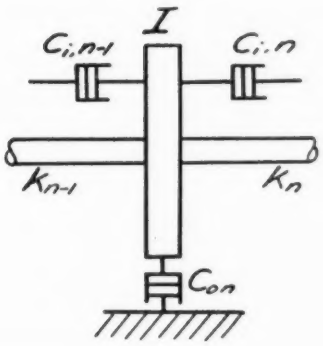


FIG. 1

The method used by Holzer consists of finding the end torque necessary to cause a steady-state *forced* vibration of an assumed frequency ω at unit amplitude at the other end. With damping the steady-state motions at the various disks are still harmonic motions at frequency ω, but they no longer have the same phase from disk to disk, or

$$\varphi_n = A_n \sin \omega t + B_n \cos \omega t \quad \ldots\ldots [2]$$

for which we can use the shorthand notation $\varphi_n = A_n + jB_n$. Differentiation of Equation [2] amounts to multiplication by $j\omega$ of the shorthand notation and two differentiations amount to multiplication by $-\omega^2$ of the shorthand notation. Substituting Equation [2] into [1] gives

$$(-I_n\omega^2 + j\omega c_{no})\varphi_n + (k_n + j\omega c_{ni})(\varphi_n - \varphi_{n+1}) + (k_{n-1} + j\omega c_{n-1,i})(\varphi_n - \varphi_{n-1}) = 0 \quad \ldots [3]$$

This equation differs from the undamped one only in that $I_n\omega^2$ is replaced by $I_n\omega^2 - j\omega c_{no}$, and in that k_n is replaced by $k_n + j\omega c_{ni}$.[5] The computations of the Holzer table are identical with those of the undamped case, except that, as a result of the two foregoing replacements, most numerical figures in the table are complex.

In the undamped case the end torque or "remainder torque" is a real number, which means that the torque is in phase with the motion at the opposite end. Here the remainder torque is a complex quantity, containing components in phase with and in quadrature to the motion at the other end. In the undamped case, there are certain frequencies ω for which the remainder torque becomes zero, which means that the system can have a steady-state vibration without any external excitation. With the presence of damping, this obviously can no longer be the case. The remainder torque never becomes zero, but, for certain values of ω, it becomes a minimum, and we may define these frequencies as the "damped natural frequencies," which for small damping differ but slightly from the undamped, true, natural frequencies.

This modified form of the Holzer table appears in a few examples later in the paper.

4 Systems With Uniformly Distributed Inertia, Elasticity, and Damping

The differential equation of torsional vibration for a shaft with uniformly distributed inertia, elasticity, internal and external damping is

$$I_1\ddot{\varphi} + c_{1o}\dot{\varphi} = k_1\varphi'' + c_{1i}\dot{\varphi}'' \quad \ldots\ldots [4]$$

where dots mean $\partial/\partial t$ and dashes mean $\partial/\partial x$, as usual. The angle will not have the same time phase along the length of the shaft so that we assume the solution in the form

$$\varphi = P(x) \sin \omega t + Q(x) \cos \omega t \quad \ldots\ldots [5]$$

where P and Q are real functions of x only. This represents a forced vibration of frequency ω, the forcing torque to be applied at the end of the shaft. Note that Equations [5] and [4] are generalizations of [2] and [1], respectively.

Substitute the assumption, [5] into [4], and set the terms proportional to sin ωt and cos ωt independently equal to zero

$$\left.\begin{aligned} I_1\omega^2 P + k_1 P'' + c_{1o}\omega Q - c_{1i}\omega Q'' &= 0 \\ I_1\omega^2 Q + k_1 Q'' - c_{1o}\omega P + c_{1i}\omega P'' &= 0 \end{aligned}\right\} \quad \ldots\ldots [6]$$

Since these are linear differential equations in $P(x)$ and $Q(x)$, we set, as usual

$$P = P_0 e^{px} \qquad Q = Q_0 e^{px}$$

and substitute

$$\left.\begin{aligned} (I_1\omega^2 + k_1 p^2)P_0 + (c_{1o}\omega - c_{1i}\omega p^2)Q_0 &= 0 \\ (-c_{1o}\omega + c_{1i}\omega p^2)P_0 + (I_1\omega^2 + k_1 p^2)Q_0 &= 0. \end{aligned}\right\} \quad \ldots\ldots [7]$$

In this homogeneous set of algebraic equations in P_0 and Q_0, the determinant must be zero or

$$(I_1\omega^2 + k_1 p^2)^2 = -(c_{1o}\omega - c_{1i}\omega p^2)^2$$

which is an equation of the fourth degree in p, having the four roots

$$p_{1,2,3,4} = \pm \sqrt{\frac{-I_1\omega^2 \pm j\omega c_{1o}}{k_1 \pm j\omega c_{1i}}} \quad \ldots\ldots [8]$$

for which we can write

$$p_{1,2,3,4} = \pm a \pm jb \quad \ldots\ldots [8a]$$

where a and b in each case can be found numerically from I_1, k_1, c_{1o}, c_{1i}, and ω in the simplest manner semigraphically in the complex plane diagram, but for the sake of completeness they are given explicitly

$$\left.\begin{aligned} b^2 &= \frac{\sqrt{(-k_1 I_1\omega^2 + c_{1i}c_{1o}\omega^2)^2 + (k_1 c_{1o}\omega + I_1 c_{1i}\omega^3)^2} + {}^1/_2(k_1 I_1\omega^2 - c_{1i}c_{1o}\omega^2)}{k_1^2 + c_{1i}^2\omega^2} \\ a^2 &= \frac{1}{2b} \cdot \frac{k_1 c_{1o}\omega + I_1 c_{1i}\omega^3}{k_1^2 + c_{1i}^2\omega^2} \end{aligned}\right\} \quad \ldots [9]$$

Also from Equation [7] it follows that the ratio P_0/Q_0 must be

$$\frac{P_0}{Q_0} = -\frac{c_{1i}\omega p^2 - c_{1o}\omega}{I_1\omega^2 + k_1 p^2}$$

and upon substitution of the values Equation [8a] for p this is found to be

$$\frac{P_0}{Q_0} = +j \quad \text{for the roots } p = a + jb \text{ and } p = -a - jb$$

$$\frac{P_0}{Q_0} = -j \quad \text{for the roots } p = a - jb \text{ and } p = -a + jb$$

Thus the P and Q functions become

$$\left.\begin{aligned} P &= C_1 e^{(a+jb)x} + C_2 e^{(-a-jb)x} + C_3 e^{(a-jb)x} + C_4 e^{(-a+jb)x} \\ Q &= -jC_1 e^{(a+jb)x} - jC_2 e^{(-a-jb)x} + jC_3 e^{(a-jb)x} + jC_4 e^{(-a+jb)x} \end{aligned}\right\} . [10]$$

Since from the physics of the situation the functions P and Q

[5] A similar result is shown in Equation [24] of the paper, "Torsional Vibration in Geared-Turbine Propulsion Equipment," by H. Poritsky and C. S. L. Robinson, *Journal of Applied Mechanics*, Trans. A.S.M.E., vol. 62, 1940, p. A-117.

must be real functions of x, it is useful to rewrite these expressions, splitting them into real and imaginary parts. After a little algebra Equations [10] can thus be written as

$$P = \cos bx[A \cosh ax + B \sinh ax] + j \sin bx[C \cosh ax + D \sinh ax]$$

$$Q = \sin bx[B \cosh ax + A \sinh ax] - j \cos bx[D \cosh ax + C \sinh ax]$$

The integration constants A to D may be real, imaginary, or complex, but P and Q must be real. This can be accomplished either by making $C = D = 0$ and A and B real, or also by making $A = B = 0$, with C and D purely imaginary. Either supposition leads essentially to the same solution, which is

$$\varphi = [A \cosh ax + B \sinh ax] \cos bx \sin \omega t + [A \sinh ax + B \cosh ax] \sin bx \cos \omega t \quad \ldots\ldots [11]$$

in which A and B are arbitrary (real) constants, while a and b are formally defined by Equations [9], although numerically they can be computed more easily from Equations [8] and [8a].

The constants A and B are determined by the condition of the end $x = 0$. For the usual case of a free end $\varphi' = 0$ and $\varphi = 1.000$, we have

$$\varphi = 1.000[\cosh ax \cos bx \sin \omega t + \sinh ax \sin bx \cos \omega t] \quad [12]$$

For the less frequent case of a built-in end or for an infinite flywheel at the end, the boundary conditions are $\varphi = 0$ and $\varphi' = 1.000$, so that

$$\varphi = \frac{1.000}{\sqrt{a^2 + b^2}} \cdot [\sinh ax \cos bx \sin \omega t + \cosh ax \sin bx \cos \omega t] \quad [13]$$

The torque $M(x)$ along the shaft in general is

$$M(x) = k_1\varphi'(x) + c_{1i}\dot{\varphi}'(x) \quad \ldots\ldots [14]$$

and in particular for the case of a free end at $x = 0$

$$M(x) = \sin \omega t[(k_1a - \omega c_{1i}b) \sinh ax \cos bx - (k_1b + \omega c_{1i}a) \cosh ax \sin bx] + \cos \omega t[(k_1b + \omega c_{1i}a) \sinh ax \cos bx - (k_1a - \omega c_{1i}b) \cosh ax \sin bx] \quad \ldots\ldots [12a]$$

For the case of a damped end at $x = 0$, we have

$$M(x) = \frac{\sin \omega t}{\sqrt{a^2 + b^2}}[(k_1a - \omega c_{1i}b) \cosh ax \cos bx - (k_1b + \omega c_{1i}a) \sinh ax \sin bx] + \frac{\cos \omega t}{\sqrt{a^2 + b^2}}[(k_1b + \omega c_{1i}a) \cosh ax \cos lx + (k_1a - \omega c_{1i}b) \sinh ax \sin bx] \ldots. [13a]$$

To find the remainder torque or the amplitude at the end l of the shaft, the quantity x has to be replaced by l in Equations [12], [12a], [13], or [13a] as the case may be.

It is important that the results of Equations [12], [13], [12a], and [13a] are all in terms of real quantities, immediately fit for numerical computations. The only complex quantities used are in Equations [8] and [8a] for the determination of a and b. The results so given are not in the form we are accustomed to for the nondamped case. It is possible to write the solution of the differential Equation [4] in a form directly comparable to the undamped case, but at the expense of being full of complex quantities not directly fit for numerical computation. This form is written below for the case of a free end

$$\varphi(x) = \cos \Phi \frac{x}{l} \qquad \varphi(l) = \cos \Phi$$

$$M(l) = [K + j\omega C_i]\Phi \sin \Phi$$

where

$$\Phi = \sqrt{\frac{I\omega^2 - j\omega C_0}{K + j\omega C_i}}$$

and

$$\left.\begin{aligned} I &= lI_1 \\ K &= k_1/l \\ C_0 &= lc_{10} \\ C_i &= c_{1i}/l \end{aligned}\right\} \text{are the system constants for the entire system of length } l.$$

This result for zero damping reduces immediately to Lewis' solution.

5 Example With Discreet Masses

As a first example, consider the system in Fig. 2, consisting of four equal inertias of 10^4 lb-in-sec,^{2} coupled by two stiffnesses of 10^6 in-lb/radian, a stiffness of 0.5×10^6 in-lb/radian, and by a central dashpot of constant c_i, which we propose to give several numerical values. For $c_i = 0$, the system falls into separate parts with the one natural frequency $\omega^2 = 200$. For $c_i = \infty$, the two central masses are united, and the same motion at $\omega^2 = 200$ is possible, but in addition there is a natural motion with a node in the center at $\omega^2 = 100$. Table 1 is a sample Holzer table.

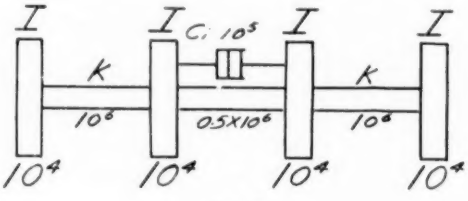


Fig. 2

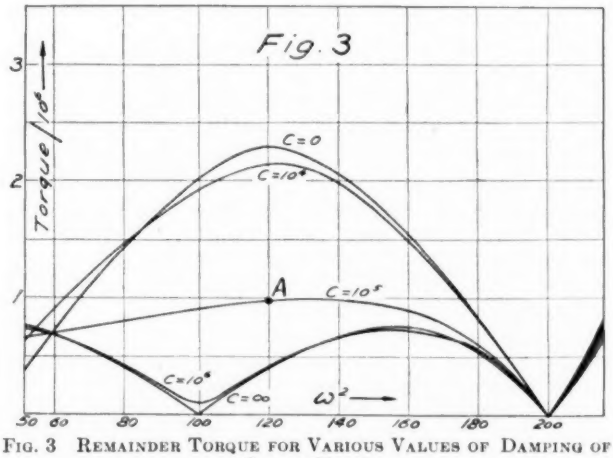


Fig. 3 Remainder Torque for Various Values of Damping of System Fig. 2

TABLE 1 SAMPLE HOLZER TABLE FOR EXAMPLE WITH DISCREET MASSES[a]

No.	$\frac{I\omega^2 - j\omega c_0}{10^6}$	φ	$\frac{(I\omega^2 - j\omega c_0)\varphi}{10^6}$	$\Sigma/10^6$	$\frac{k + j\omega c_i}{10^6}$	$\frac{\Sigma}{k + j\omega c_i}$
1	$1.200 + 0.000j$	$1.000 + 0.000j$	$1.200 + 0.000j$	$1.200 + 0.000j$	$1.000 + 0.000j$	$1.200 + 0.000j$
2	$1.200 + 0.000j$	$-0.200 + 0.000j$	$-0.240 + 0.000j$	$0.960 + 0.000j$	$0.500 + 1.095j$	$0.331 - 0.725j$
3	$1.200 + 0.000j$	$-0.531 + 0.725j$	$-0.637 + 0.870j$	$0.323 + 0.870j$	$1.000 + 0.000j$	$0.323 + 0.870j$
4	$1.200 + 0.000j$	$-0.854 - 0.145j$	$-1.025 - 0.174j$	$-0.702 + 0.696j$	.....	.....

[a] In this table $c_i = 10^6$; $\omega^2 = 120$; $\omega = 10.95$.

The absolute value of the remainder torque is

$$| -0.702 + 0.696j | 10^6 = 0.988 \times 10^6$$

plotted as point A in Fig. 3.

The results of a large number of similar calculations are shown likewise in that figure, from which it can be seen that $c = 10^4$ is a "small" damping; $c = 10^6$ is a "large" damping, while $c = 10^5$ is an intermediate value.

6 Example With Uniformly Distributed Characteristics

Consider a system of six equal inertias, each $I = 10^3$ lb-in-sec^2, coupled by five shafts each of $k = 10^7$, having dashpots c_0 from each inertia to ground and dashpots c_i between inertias. Table 2 is a sample Holzer table for this problem.

TABLE 2 SAMPLE HOLZER TABLE FOR EXAMPLE WITH UNIFORMLY DISTRIBUTED CHARACTERISTICS[a]

No.	$\frac{I\omega^2 - j\omega c_0}{10^6}$	φ	$\frac{I\omega^2 - j\omega c_0}{10^6}$	$\Sigma/10^6$	$\frac{k + j\,\omega c_i}{10^6}$	$\frac{\Sigma}{k + j\omega c_i}$
1	$1.000 - 0.316j$	1.000	$1.000 - 0.316j$	$1.000 - 0.316j$	$10.000 + 0.632j$	$0.098 - 0.038j$
2	$1.000 - 0.316j$	$0.902 + 0.038j$	$0.914 - 0.247j$	$1.914 - 0.563j$	$10.000 + 0.632j$	$0.187 - 0.068j$
3	$1.000 - 0.316j$	$0.715 + 0.106j$	$0.749 - 0.120j$	$2.663 - 0.683j$	$10.000 + 0.632j$	$0.261 - 0.085j$
4	$1.000 - 0.316j$	$0.454 + 0.191j$	$0.515 + 0.047j$	$3.178 - 0.636j$	$10.000 + 0.632j$	$0.312 - 0.083j$
5	$1.000 - 0.316j$	$0.142 + 0.274j$	$0.228 + 0.229j$	$3.406 - 0.407j$	$10.000 + 0.632j$	$0.336 - 0.062j$
6	$1.000 - 0.316j$	$-0.194 + 0.336j$	$-0.089 + 0.398j$	$3.317 - 0.009j$	.....	.....

[a] In this table, $I = 10^3$; $k = 10^7$; $c_0 = 10^4$; $c_i = 2 \times 10^4$; $\omega^2 = 1000$.

The engine can also be considered as a uniformly distributed beam and treated by means of Equations [12], [12a], [8], and [8a] in which, by taking the length of one crank throw as the unit of length, we have

$$I_1 = 10^3 \qquad k_1 = 10^7 \qquad c_{i1} = 10^4 \qquad c_{i1} = 2 \times 10^4 \qquad l = 6$$

Assuming the same frequency $\omega^2 = 1000$ as in the previous Holzer table, we find by graphical construction and computation in the complex plane from Equations [8]and [8a]

$$al = 1.914 \qquad bl = 0.355$$

Substituting these values into Equation [12] and using tables for the hyperbolic and trigonometric functions, we can plot the shape $\varphi(x)$ of the vibration and compare it with the result φ in the third column of the Holzer table. In Fig. 4, the real (in phase) and imaginary (in quadrature) parts of the two solutions are plotted, and it is seen that very good agreement is obtained if each discreet inertia is placed in the middle of the corresponding distributed length so that the distributed shaft protrudes half a crank throw beyond the first and last inertias. Also, by substituting into Equation [12a], the shaft torque distribution is found as a complex quantity, which should be compared to the fifth column in the Holzer table, and again Fig. 5 shows good agreement.

The remainder torque of the system was calculated for a range of frequencies by means of Equations [12a], [8], and [8a], and the result is shown in Fig. 6. The damping in this case is so large that the second critical frequency is hardly recognizable.

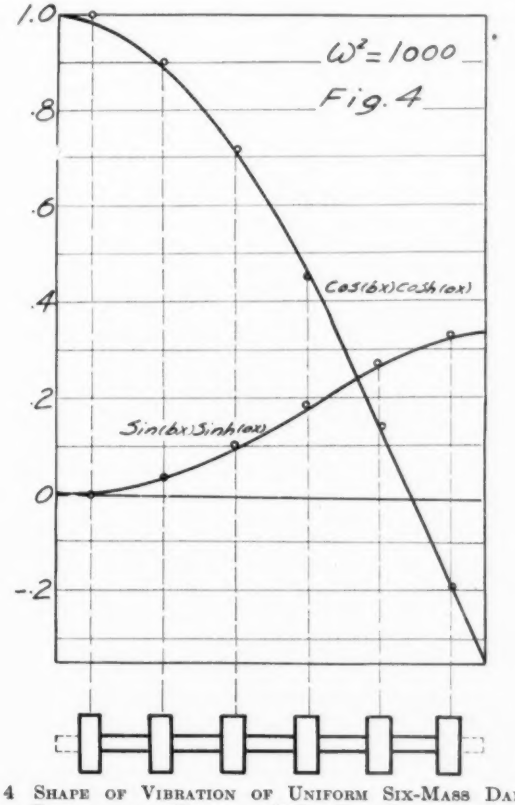


Fig. 4 Shape of Vibration of Uniform Six-Mass Damped System, Calculated by Equation [12] in Full Lines, and by the Holzer Table in Circled Points

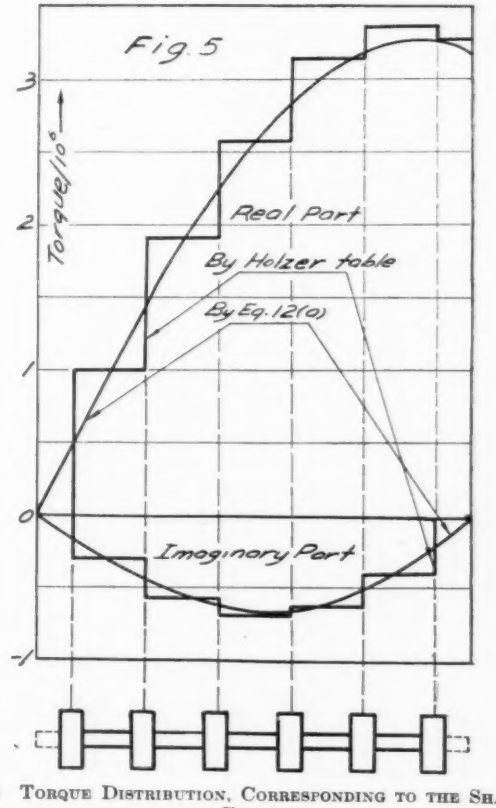


Fig. 5 Torque Distribution, Corresponding to the Shape in Fig. 4

(Curved line is Equation [12a], and stepped line is the Holzer table.)

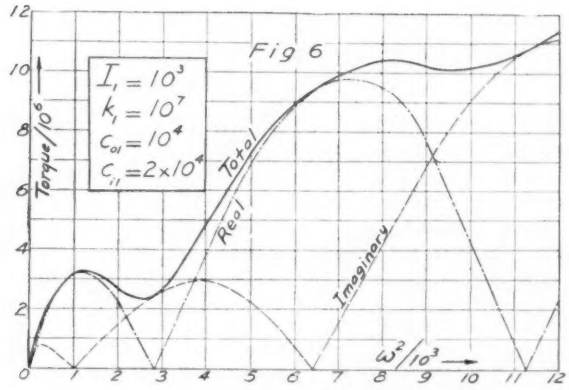


FIG. 6 REMAINDER TORQUE PLOTTED VERSUS SQUARED FREQUENCY FOR A UNIFORMLY DISTRIBUTED SYSTEM

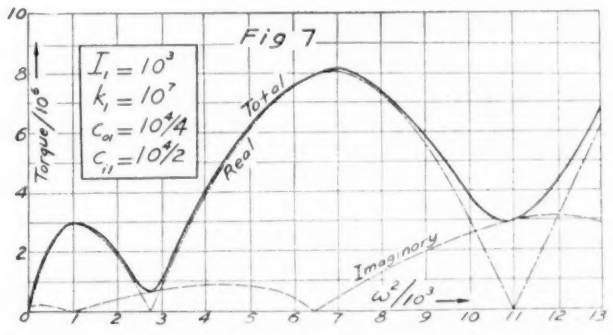


FIG. 7 SAME AS FIG. 6, EXCEPT THAT DAMPING IS 4 TIMES SMALLER

The system was again calculated for a damping 4 times as small internally as well as externally, and the remainder torque is shown in Fig. 7. In this case the shape of the vibration is not seriously affected by the damping, and it has been verified that the remainder torques at the two natural frequencies $\omega^2 = 2730$ and $\omega^2 = 10{,}920$ can be calculated with reasonable accuracy by the familiar method of dissipation-energy input-balance. However, this is not so for Fig. 6, and it is for such cases of large damping that the method just described becomes useful.

Orthogonal Functions Used in the Solution of Linear Difference Problems

By S. U. BENSCOTER,[1] HAMPTON, VA.

A method of solution of linear difference equations is presented in which the solution is assumed in terms of a finite set of orthogonal functions which satisfy the boundary conditions. A formula for the latent roots of the matrix of the system of equations is obtained. A simple formula is then derived for the reciprocal matrix in terms of the latent roots and latent vectors. A simple numerical example is presented.

Nomenclature

The following nomenclature is used in the paper:

m = bending moment
n = an integer
x = number of support
ϕ = primary flexibility
γ = secondary flexibility
δ = angular dislocation
λ = latent root

Introduction

The possibility of expressing the reciprocal of a matrix in terms of its latent roots and vectors is well known. The use of this procedure in solving a system of nonhomogeneous linear algebraic equations has found little practical application. This is due to the fact that there are many methods of solving such a system of equations, and of computing the reciprocal matrix, which require less time. However, in the case of linear difference problems, the use of the latent roots and vectors may provide a more rapid method of determining the reciprocal matrix than any other available procedure. This is due to the fact that a simple formula for the latent roots can be developed for a certain class of problems. The use of orthogonal functions, which are the latent vectors of a matrix, in the solution of general indeterminate structures has been developed by Prof. J. B. Wilbur.[2] The method of solution to be presented will be given in application to a specific problem in structural analysis rather than using generalized mathematical form.

Difference Equation and Boundary Condition

In the analysis of a continuous beam resting on a series of simple supports, which are fixed against translation, an equation of three moments may be associated with each support, except the first and last supports. A difference problem arises when every beam span is of identical physical construction. The individual spans need not be prismatic or symmetrical about their own center lines. Consider the two spans adjacent to the support numbered x of a beam of many spans as shown in Fig. 1(*a*). The flexibility matrix for each of the spans is shown. The flexibility matrix is symmetrical in accord with Maxwell's law of reciprocal displacements. The equation associated with the support numbered x is

$$\gamma m_{x-1} + (\phi_a + \phi_b) m_x + \gamma m_{x+1} = -\delta_x \quad [1]$$

The quantity δ_x is the angular dislocation which would occur at the x th support if the beam were cut at this support, and the two adjacent supports, to give simple beam action in the two adjacent spans. This angular dislocation is illustrated in Fig. 1(*b*).

The boundary conditions may be explained by reference to the three-span beam shown in Fig. 2. The loading is arbitrary. The determinate, indeterminate, and resultant moment diagrams are shown. It is apparent that the boundary conditions on the set of joint moments, which are governed by the equations of three moments, are that the value at the first and last support shall be zero. If x is the number of the support, the boundary conditions are that $m_x = 0$ when $x = 0$ and $x = 3$. The functions $\sin \frac{n\pi x}{3}$ satisfy these conditions for all integral values of n.

Method of Solution

The method of solution will be explained by reference to a four-span beam as shown in Fig. 3(*a*). The solution may be assumed in the form

$$m_x = \sum_{n=1}^{3} a_n \sin \frac{n\pi x}{4} \quad [2]$$

The number of terms in the series to be used is equal to the number of unknowns to be determined. Equation [2] corresponds to three linear algebraic equations which may be written in the following matrix form

$$\begin{bmatrix} m_1 \\ m_2 \\ m_3 \end{bmatrix} = \sin \begin{bmatrix} \pi/4 & 2\pi/4 & 3\pi/4 \\ 2\pi/4 & 4\pi/4 & 6\pi/4 \\ 3\pi/4 & 6\pi/4 & 9\pi/4 \end{bmatrix} \begin{bmatrix} a_1 \\ a_2 \\ a_3 \end{bmatrix} \quad [3]$$

$$= \begin{bmatrix} \sqrt{2}/2 & 1 & \sqrt{2}/2 \\ 1 & 0 & -1 \\ \sqrt{2}/2 & -1 & \sqrt{2}/2 \end{bmatrix} \begin{bmatrix} a_1 \\ a_2 \\ a_3 \end{bmatrix} \quad [4]$$

The m_x values are hereby expressed as linear functions of the a_n values. It will be necessary to have the a_n values expressed as linear functions of the m_x values at a later step in the analysis. Solving for the a_n values in terms of the m_x values is greatly simplified by the fact that the columns of the square matrix of coefficients are orthogonal column vectors. This is true because the solution has been assumed in terms of orthogonal functions which have been evaluated only at equally spaced values of the angle variable.

Equation [4] may be written in contracted matrix form as

$$[m] = [S][a] \quad [5]$$

where $[m]$ is the column vector of m_x values, $[a]$ is the column vector of a_n values, and $[S]$ is the square matrix of coefficients. It should be noted that the matrix $[S]$ is symmetrical and that all of its column vectors have the same norm, and hence the same

---

[1] Structural Engineer, N.A.C.A., Langley Memorial Aeronautical Laboratory, Langley Field, Va.

[2] "Characteristic Redundants Used for Analyzing Statically Indeterminate Structures," by J. B. Wilbur, Proceedings of the A.S.C.E., vol. 70, 1944, pp. 829–851.

Contributed by the Applied Mechanics Division and presented at the Annual Meeting, New York, N. Y., December 2–6, 1946, of The American Society of Mechanical Engineers.

Discussion of this paper should be addressed to the Secretary, A.S.M.E., 29 West 39th Street, New York, N. Y., and will be accepted until January 10, 1947, for publication at a later date. Discussion received after the closing date will be returned.

Note: Statements and opinions advanced in papers are to be understood as individual expressions of their authors and not those of the Society.

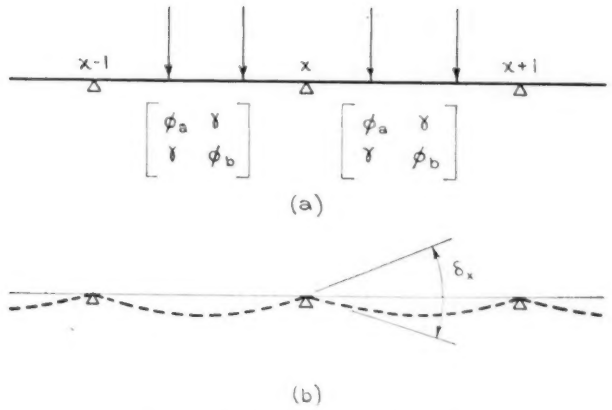


FIG. 1 SPANS ADJACENT TO THE xTH SUPPORT

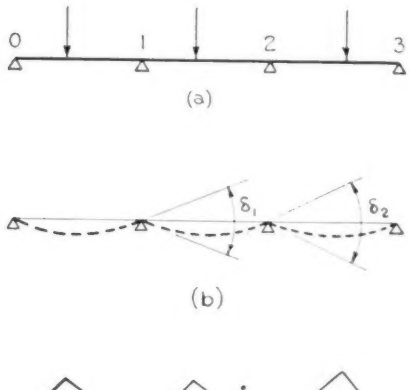


FIG. 2 CONTINUOUS-BEAM MOMENT DIAGRAMS

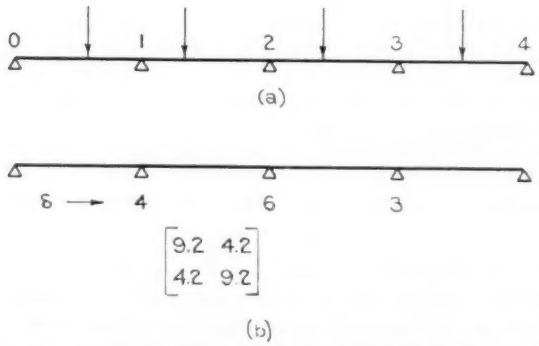


FIG. 3 FOUR-SPAN CONTINUOUS BEAM

normalizing factor. Because of these facts the product of $[S]$ by itself gives a scalar matrix which may be written as a scalar factor times the identity matrix

$$[S][S] = 2[I] \quad [6]$$

This equation is easily checked by using the "row by column" rule for matrix multiplication. Multiplying Equation [5] through by $[S]$ gives

$$[S][m] = 2[I][a] = 2[a] \quad [7]$$

or

$$[a] = {}^1/_2[S][m] \quad [8]$$

Thus it is seen that the a_n values are expressed as linear functions of the m_x values by a set of coefficients which are just one half of the values of the elements of $[S]$.

In order to substitute the assumed solution into the difference equation, it is necessary to compute m_{x-1} and m_{x+1}. This is done by substituting $x - 1$ and $x + 1$ into Equation [2] for x

$$m_{x-1} = \Sigma a_n \left[\sin \frac{n\pi x}{4} \cos \frac{n\pi}{4} - \cos \frac{n\pi x}{4} \sin \frac{n\pi}{4} \right] \quad [9]$$

$$m_{x+1} = \Sigma a_n \left[\sin \frac{n\pi x}{4} \cos \frac{n\pi}{4} + \cos \frac{n\pi x}{4} \sin \frac{n\pi}{4} \right] \quad [10]$$

Substitution of Equations [2], [9], and [10] into Equation [1] gives

$$(\phi_a + \phi_b) \Sigma a_n \sin \frac{n\pi x}{4} + 2\gamma \Sigma a_n \cos \frac{n\pi}{4} \sin \frac{n\pi x}{4} = -\delta_x \quad [11]$$

Combining terms gives

$$\Sigma a_n \left(\phi_a + \phi_b + 2\gamma \cos \frac{n\pi}{4} \right) \sin \frac{n\pi x}{4} = -\delta_x \quad [12]$$

Let

$$\lambda_n = \phi_a + \phi_b + 2\gamma \cos \frac{n\pi}{4} \quad [13]$$

Then

$$\Sigma a_n \lambda_n \sin \frac{n\pi x}{4} = -\delta_x \quad [14]$$

This equation corresponds to three linear equations expressing the δ_x values as linear functions of the quantities $a_n\lambda_n$. The coefficients of these linear equations again form the matrix $[S]$. In expanded matrix form the equations may be written

$$\begin{bmatrix} \sqrt{2}/2 & 1 & \sqrt{2}/2 \\ 1 & 0 & -1 \\ \sqrt{2}/2 & -1 & \sqrt{2}/2 \end{bmatrix} \begin{bmatrix} a_1\lambda_1 \\ a_2\lambda_2 \\ a_3\lambda_3 \end{bmatrix} = \begin{bmatrix} \delta_1 \\ \delta_2 \\ \delta_3 \end{bmatrix} \quad [15]$$

In contracted matrix form this equation becomes

$$[S][a\lambda] = -[\delta] \quad [16]$$

The column vector $[a\lambda]$ must be separated in the following manner

$$[a\lambda] = \begin{bmatrix} a_1\lambda_1 \\ a_2\lambda_2 \\ a_3\lambda_3 \end{bmatrix} = \begin{bmatrix} \lambda_1 & 0 & 0 \\ 0 & \lambda_2 & 0 \\ 0 & 0 & \lambda_3 \end{bmatrix} \begin{bmatrix} a_1 \\ a_2 \\ a_3 \end{bmatrix} = [\Lambda][a] \quad [17]$$

The matrix $[\Lambda]$ is a diagonal matrix of λ_n values. Equation [16] becomes

$$[S][\Lambda][a] = -[\delta] \quad [18]$$

The column vector $[a]$ may be eliminated by substituting Equation [8]

$${}^1/_2[S][\Lambda][S][m] = -[\delta] \quad [19]$$

Inspection of the columns of $[S]$ shows that the normalizing

factor is $\sqrt{2}$. It is convenient to introduce the matrix $[T]$ defined by

$$[T] = \frac{1}{\sqrt{2}}[S] \quad [20]$$

The matrix $[T]$ is its own reciprocal as may be seen from Equation [6]

$$[T][T] = [I] \quad [21]$$

The columns of $[T]$ are orthonormal (normalized orthogonal) column vectors. The matrix $[T]$ is called an orthogonal matrix, although it would seem more reasonable to call it an orthonormal matrix in agreement with the type of column vectors which it contains.

Equation [19] may now be written

$$[T][\Lambda][T][m] = -[\delta] \quad [22]$$

It is now necessary to return to the original system of equations which is to be solved. Referring to Equation [1], it may be seen that the system of equations may be written in the following matrix form

$$\begin{bmatrix} \Sigma\phi & \gamma & 0 \\ \gamma & \Sigma\phi & \gamma \\ 0 & \gamma & \Sigma\phi \end{bmatrix} \begin{bmatrix} m_1 \\ m_2 \\ m_3 \end{bmatrix} = - \begin{bmatrix} \delta_1 \\ \delta_2 \\ \delta_3 \end{bmatrix} \quad [23]$$

where

$$\Sigma\phi = \phi_a + \phi_b \quad [24]$$

This matrix equation may be written in the following contracted form

$$[\Phi][m] = -[\delta] \quad [25]$$

In this equation $[\Phi]$ is the square matrix of coefficients. Comparing Equation [25] with Equation [22], it is seen that the matrix $[\Phi]$ has been replaced by a product of matrixes

$$[\Phi] = [T][\Lambda][T] \quad [26]$$

From this transformation it is seen that the matrixes $[\Phi]$ and $[\Lambda]$ are similar. Hence the diagonal elements of $[\Lambda]$ are the latent roots of $[\Phi]$, and the columns of $[T]$ are the latent vectors of $[\Phi]$. In characteristic value problems, which are governed by homogeneous equations, the latent roots of the matrix are very useful in obtaining the solution and are given by the simple formula of Equation [13]. In the present problem, the elements of $[\delta]$ are considered to be a set of unrelated constants which are not a function of the independent variable. A solution for $[m]$ in terms of $[\delta]$ involves the use of the reciprocal of the coefficient matrix $[\Phi]$.

Multiplying through Equation [25] by $[\Phi]^{-1}$ gives

$$[m] = -[\Phi]^{-1}[\delta] \quad [27]$$

A convenient formula for the rapid calculation of $[\Phi]^{-1}$ is obtained from Equation [26]. A law of matrix algebra states that the reciprocal of a product of matrixes is equal to the product of their reciprocals in reverse order. Since $[T]$ is its own reciprocal the formula becomes

$$[\Phi]^{-1} = [T][\Lambda]^{-1}[T] \quad [28]$$

The reciprocal of a diagonal matrix is obtained by replacing each diagonal element by its own reciprocal. Hence $[\Lambda]^{-1}$ is given in expanded form as follows

$$[\Lambda]^{-1} = \begin{bmatrix} 1/\lambda_1 & 0 & 0 \\ 0 & 1/\lambda_2 & 0 \\ 0 & 0 & 1/\lambda_3 \end{bmatrix} \quad [29]$$

Thus it is seen that a simple and rapid method of computing the reciprocal matrix becomes available through the use of orthogonal functions. The practical benefit of the method shows up more effectively with higher-order difference equations. The final formula for $[m]$ is obtained by substituting Equation [28] in Equation [27]

$$[m] = -[T][\Lambda]^{-1}[T][\delta] \quad [30]$$

It is of interest to note that the matrix $[T]$ is a standard universal matrix applicable to all beams. The effect of the physical properties of the beam is contained entirely in $[\Lambda]^{-1}$ which may be quickly computed for any given beam.

Numerical Example

Consider the four-span beam shown in Fig. 3(*b*). A set of δ values is shown directly beneath the intermediate supports. It is assumed that these values have been computed from the loading and beam properties. The flexibility values for a span are assumed to be as shown in the matrix beneath the beam. The individual beam spans are assumed to be nonprismatic but symmetrical about their own center line. This means that $\phi_a = \phi_b$.

The system of equations to be solved is as follows

$$\begin{bmatrix} 18.4 & 4.2 & 0 \\ 4.2 & 18.4 & 4.2 \\ 0 & 4.2 & 18.4 \end{bmatrix} \begin{bmatrix} m_1 \\ m_2 \\ m_3 \end{bmatrix} = - \begin{bmatrix} 4 \\ 6 \\ 3 \end{bmatrix} \quad [31]$$

The matrix $[T]$ may be determined as

$$[T] = \begin{bmatrix} 0.5 & 0.707 & 0.5 \\ 0.707 & 0 & -0.707 \\ 0.5 & -0.707 & 0.5 \end{bmatrix} \quad [32]$$

The latent roots are computed as

$$\lambda_1 = 18.4 + 8.4 \cos \frac{\pi}{4} = 24.34$$

$$\lambda_2 = 18.4 + 8.4 \cos \frac{\pi}{2} = 18.4$$

$$\lambda_3 = 18.4 + 8.4 \cos \frac{3\pi}{4} = 12.46$$

Calculating the reciprocals of these numbers gives the matrix $[\Lambda]^{-1}$

$$[\Lambda]^{-1} = \begin{bmatrix} 0.0411 & 0 & 0 \\ 0 & 0.0543 & 0 \\ 0 & 0 & 0.0803 \end{bmatrix} \quad [33]$$

The reciprocal matrix is computed in two steps

$$[\Lambda]^{-1}[T] = \begin{bmatrix} 0.205 & 0.290 & 0.0205 \\ 0.0384 & 0 & -0.0384 \\ 0.0401 & -0.0567 & 0.0401 \end{bmatrix} \quad [34]$$

$$[\Phi]^{-1} = [T][\Lambda]^{-1}[T] = \begin{bmatrix} 0.0574 & -0.0139 & 0.0032 \\ -0.0139 & 0.0606 & -0.0139 \\ 0.0032 & -0.0139 & 0.0574 \end{bmatrix} \quad [35]$$

The bending moments are given by

$$\begin{bmatrix} m_1 \\ m_2 \\ m_3 \end{bmatrix} = - [\Phi]^{-1} \begin{bmatrix} 4 \\ 6 \\ 3 \end{bmatrix} = - \begin{bmatrix} 0.1558 \\ 0.2663 \\ 0.1016 \end{bmatrix} \quad [36]$$

For any other loading condition a new set of $[\delta]$ values can be determined and multiplied by $[\Phi]^{-1}$ to obtain an immediate solution.

Conclusion

By assuming the solution of a linear difference problem in terms of appropriate orthogonal functions, which satisfy the boundary conditions, a simple method becomes available for computing the latent roots and vectors of the matrix of the system of equations. The transformation matrix of latent vectors is a universal matrix of elements which are not dependent upon the properties of the structure. The reciprocal matrix may be computed rapidly from the latent roots and vectors.

A Note on the Damped Vibration Absorber

By JOHN E. BROCK,[1] ST. LOUIS, MO.

IN THE following, formulas for optimum damping for three cases of the dynamic vibration absorber with damping are presented and the method of derivation is indicated. The writer is prejudiced against notes and papers which are not self-contained and self-explanatory; in the present instance, however, it would require twenty paragraphs of material readily available elsewhere to introduce three paragraphs of new results. Accordingly, reference is made to the book, "Mechanical Vibrations," by J. P. Den Hartog.[2] Using the notation employed by Den Hartog, and referring to the figures accompanying his text, the following remarks apply:

1 *Case of Optimum Tuning.* In this case, $f = 1/(1 + \mu)$, and the abcissas of points P and Q of the $(g, x_1/x_{st})$ diagram are, respectively

$$g_1 = \sqrt{\frac{1 - \sqrt{\mu/(2 + \mu)}}{1 + \mu}}\ ; \quad g_2 = \sqrt{\frac{1 + \sqrt{\mu/(2 + \mu)}}{1 + \mu}} \ldots [1]$$

while the common ordinate is

$$\left(\frac{x_1}{x_{st}}\right)_{g = g_1} = \left(\frac{x_1}{x_{st}}\right)_{g = g_2} = \sqrt{1 + \frac{2}{\mu}} \ldots [2]$$

In order to cause the curve of (x_1/x_{st}) vs. g to pass horizontally through point P, we first require that it pass through a point P' of abscissa $g = \sqrt{\frac{1 - \sqrt{\mu/(2 + \mu)} + \delta}{1 + \mu}}$ and ordinate $(x_1/x_{st}) = \sqrt{1 + \frac{2}{\mu}}$, and then let δ approach zero as a limit. Solving Den Hartog's equation [57] for $(c/c_c)^2$, we get

$$\left(\frac{c}{c_0}\right)^2 = \frac{(f^2 - g^2) - (x_1/x_{st})^2\left\{\mu f^2 g^2 - (1 - g^2)(f^2 - g^2)\right\}^2}{4g^2\left\{(x_1/x_{st})^2\left[1 - (1 + \mu)g^2\right]^2 - 1\right\}} \ldots [3]$$

If $g = \sqrt{\frac{1 - \sqrt{\mu/(2 + \mu)} + \delta}{1 + \mu}}$, $(x_1/x_{st}) = \sqrt{1 + \frac{2}{\mu}}$ is substituted in Equation [3], we obtain a result of the form

$$\left(\frac{c}{c_0}\right)^2 = \frac{A_0 + A_1\delta + A_2\delta^2 + A_3\delta^3 + \ldots}{B_0 + B_1\delta + B_2\delta^2 + B_3\delta^3 + \ldots} \ldots [4]$$

Since Equation [3] assumes the indeterminate form 0/0 if $\delta = 0$, it is clear that $A_0 = B_0 = 0$ and that our desired result is given by

$$(c/c_0)^2 = A_1/B_1 \ldots [5]$$

Performing the indicated operations and rationalizing the result, we obtain

$$(c/c_0)^2 = \frac{\mu\left[3 - \sqrt{\mu/(2 + \mu)}\right]}{8(1 + \mu)^3} \ldots [6]$$

By a similar process, we obtain

$$(c/c_0)^2 = \frac{\mu\left[3 + \sqrt{\mu/(2 + \mu)}\right]}{8(1 + \mu)^3} \ldots [7]$$

for a horizontal tangent at point Q. Clearly, a convenient average value is

$$(c/c_0)^2 = \frac{3\mu}{8(1 + \mu)^3} \ldots [8]$$

2 *Case of Constant Tuning.* In this case, $f = 1$, and the abscissas of points P and Q are, respectively

$$g_1 = \sqrt{1 - \sqrt{\mu/(2 + \mu)}}\ ; \quad g_2 = \sqrt{1 + \sqrt{\mu/(2 + \mu)}} \ldots [9]$$

while the ordinates are, respectively

$$\left(\frac{x_1}{x_{st}}\right)_{g = g_1} = \frac{1}{(1 + \mu)\sqrt{\mu/(2 + \mu)} - \mu}\ ;$$

$$\left(\frac{x_1}{x_{st}}\right)_{g = g_2} = \frac{1}{(1 + \mu)\sqrt{\mu/(2 + \mu)} + \mu} \ldots [10]$$

It is seen that the ordinate of point P is greater than that of point Q. Accordingly, it is desired that the $(g, x_1/x_{st})$ curve pass horizontally through point P for optimum damping. Employing the process used previously, we obtain

$$(c/c_0)^2 = \frac{\mu(3 + \mu)\left[1 + \sqrt{\mu/(2 + \mu)}\right]}{8(1 + \mu)} \ldots [11]$$

3 *Case of Lanchester Type Damper (Viscous Damping).* In this case, $f = 0$, and the abscissas of points P and Q are, respectively

$$g_1 = 0; \quad g_2 = \sqrt{2/(2 + \mu)} \ldots [12]$$

while the ordinates are

$$\left(\frac{x_1}{x_{st}}\right)_{g = g_1} = 1; \quad \left(\frac{x_1}{x_{st}}\right)_{g = g_2} = 1 + 2/\mu \ldots [13]$$

Employing the process used previously in order the make the curve pass horizontally through point Q, we obtain

$$(c/c_0)^2 = \frac{1}{2(1 + \mu)(2 + \mu)} \ldots [14]$$

for optimum damping.

---

[1] Instructor in Applied Mathematics, Washington University.

[2] "Mechanical Vibrations," by J. P. Den Hartog, McGraw-Hill Book Company, Inc., New York, N. Y., 1940, pp. 115–129.

Contributed by the Applied Mechanics Division for presentation at the Annual Meeting, New York, N. Y., December 2–6, 1946, of The American Society of Mechanical Engineers.

Discussion of this paper should be addressed to the Secretary, A.S.M.E., 29 West 39th Street, New York, N. Y., and will be accepted until January 10, 1947, for publication at a later date. Discussion received after the closing date will be returned.

Note: Statements and opinions advanced in papers are to be understood as individual expressions of their authors and not those of the Society.

An Improved Fuse Escapement for the Mark 18 and Other U. S. Navy Mechanical Time Fuses

By F. G. KELLY and J. L. ZAR,[1] WEST ORANGE, N. J.

Theoretical shortcomings of previous Army and Navy fuse escapements are pointed out. The development of a new escape wheel and lever is described, in which spurious torques due to the fall of escape-wheel teeth against the pallets are eliminated; and a tooth shape is derived which delivers accelerating impulses symmetrically about the neutral position of the lever. Fuses with the new escapement have a timing rate which is independent of driving torque over the range of torques encountered; they can be assembled with one size of wheel and lever and with no hand-matching, function at low driving torques, and have given improved firing-test performance.

THIS paper describes a revision of the conventional wheel and oscillating-lever type of time-fuse escapement. A typical mechanical time fuse is shown in Fig. 1 and its mechanism is illustrated by the schematic diagram, Fig. 2.[2] Fig. 3 shows the revised escapement, approximately 4 times full size, illustrating the working engagement.

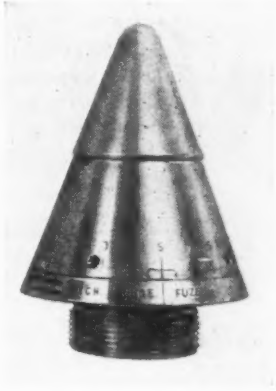


FIG. 1 TYPICAL MECHANICAL TIME FUSE

Development of this escapement was undertaken for the following reasons:

(*a*) *To Produce a Better Timekeeper.* The rate of the original Mark 18 escapement is relatively sensitive to driving torque. Since the driving torque diminishes as the fuse runs out, there is a timing error which increases rapidly with the time of flight. Fig. 4 shows the timing error in seconds versus running time for an average Mark 18 fuse, operating at constant spin. The timing of this escapement varies between the curves "fast limit" and "slow limit" in Fig. 4.[3] Since this characteristic is not the same for each fuse, there results a scattering of the firing time from this cause which may amount to ±0.10 sec after 45 sec of flight.[4] The new escapement was designed with a view toward minimizing the torque sensitivity or flattening the curve in Fig. 4.

(*b*) *To Reduce the Cost and Time of Manufacture.* The Mark 18 fuse design required very exact escapement dimensions. In its manufacture, hand-matching of escape levers and wheels was required because, with the closest tolerances that could be maintained in production, the parts could not be made accurately enough. Ten sizes of wheels were necessary, varying in steps of 0.001 in. in diam. Selection of the proper size of wheel for each individual fuse was left to the judgment of a skilled operator. In those cases where a poorly matched escapement was selected, the error was not detected until the fuse was completely assembled and tested. Consequently, there was a small percentage of rejects due to faulty escapements which had to be reworked. The second object of this development was to obtain an escapement in which a single size of wheel would serve for all fuses.

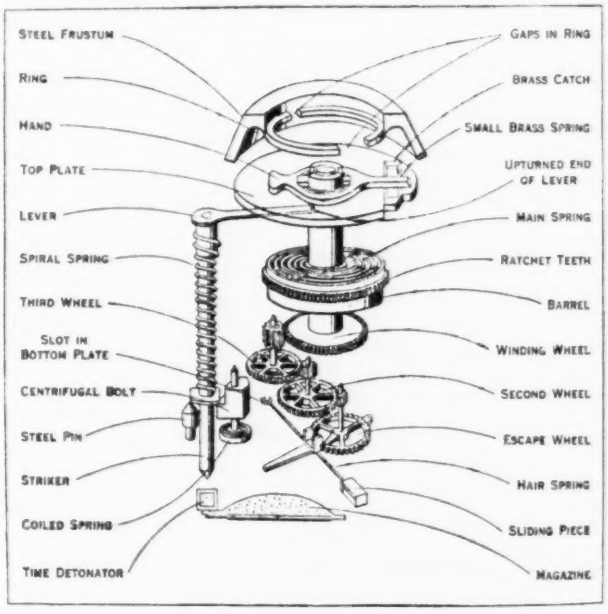


FIG. 2 SCHEMATIC DIAGRAM OF TYPICAL MECHANICAL TIME-FUSE MECHANISM

[1] Thomas A. Edison, Incorporated.

[2] Acknowledgment is made to the Encyclopedia Britannica for permission to reproduce Fig. 2, which was taken from the Encyclopedia, fourteenth edition, vol. 1, p. 826.

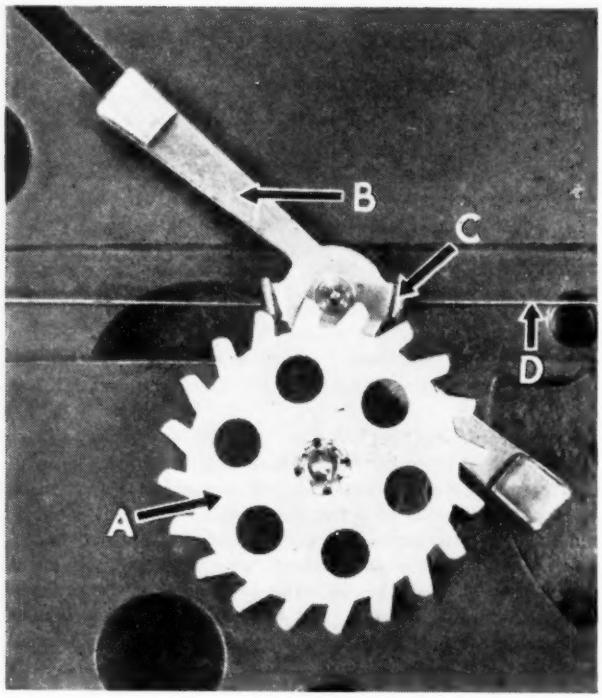
[3] The curve marked "fast limit" is the Navy's fast tolerance limit at the time of this development. The other two curves are taken from dynamic test data on actual fuses. In these, the initial rate was purposely made fast to compensate for the normal slowing of the escapement toward the end of its run.

. Contributed by the Applied Mechanics Division and presented at the Annual Meeting, New York, N. Y., December 2–6, 1946, of THE AMERICAN SOCIETY OF MECHANICAL ENGINEERS.

Discussion of this paper should be addressed to the Secretary, A.S.M.E., 29 West 39th Street, New York, N. Y., and will be accepted until January 10, 1947, for publication at a later date. Discussion received after the closing date will be returned.

NOTE: Statements and opinions advanced in papers are to be understood as individual expressions of their authors and not those of the Society.

[4] In actual firing, the dispersion in timing is more than this due to the effects of centrifugal force, which diminish during fuse flight. These effects are important but are not discussed in this report because those parts which are sensitive to spin were not changed. The new escapement has approximately the same spin dependence as the Mark 18.



A escape wheel
B escape lever
C escape-lever pallet
D escapement spring

Top plate is removed to show parts

FIG. 3 NEW ESCAPEMENT IN OPERATING ENGAGEMENT, APPROXIMATELY 4 TIMES FULL SIZE

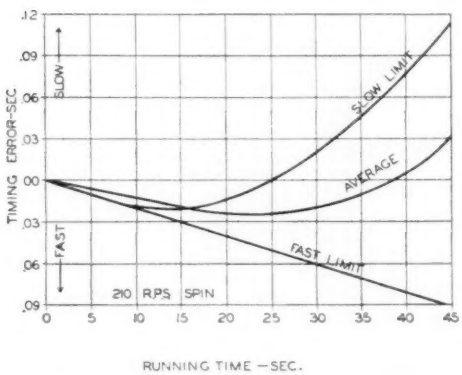


FIG. 4 TIMING ERROR OF MARK 18 FUSE AT CONSTANT SPIN

DEVELOPMENT

This work has been limited to revisions of the standard fuse escapement because it was necessary to incorporate the results into large quantity fuse production with a minimum of changes.

The first considerations were toward developing the best possible time-keeping properties. Later considerations were toward producing the broadest and deepest tooth which the pallet amplitude would permit, and the least critical tooth form. These last objectives were to minimize the effects of manufacturing variations on the operation of the escapement, and to obtain the maximum possible depth of engagement for maximum safety of operation.

In a fuse, the escape lever and hairspring approximate a simple harmonic oscillator maintained in continuous oscillation by impulses supplied through contact of the escape wheel with the pallets. It is well known (1, 2, 3)[5] that if the frequency of a mechanical oscillating system is to be made independent of variations in driving force, the driving impulses should arrive, on the average, when the mass is passing through its neutral position. This is the position of greatest velocity when the lever is moving. It is also the rest position when the lever is stationary. If this condition is met the frequency of oscillation is independent of the driving force and the escapement is a good timekeeper.

Analyses of the Navy and Army escapements have been made to determine how the driving impulses act and any other causes for their relatively high sesnsitivity to variation in driving torque.

MARK 18 OR NAVY ESCAPEMENT

A limited analysis of the Mark 18 escapement for causes contributing to its torque sensitivity is given here. Reference is made to Fig. 5 in which the escape pallets are shown in their neutral positions. The escape-wheel teeth are shown in a position where the trajectory of the tips of the pallets can touch the base circle.[6] Left and right sides are both shown in this same phase of escapement for convenience, but are actually $^1/_2$ cycle apart in time.

In the Mark 18 escapement there are several impulses of momentum delivered to the lever during each oscillation cycle. What may be thought of as the normal driving impulse is the

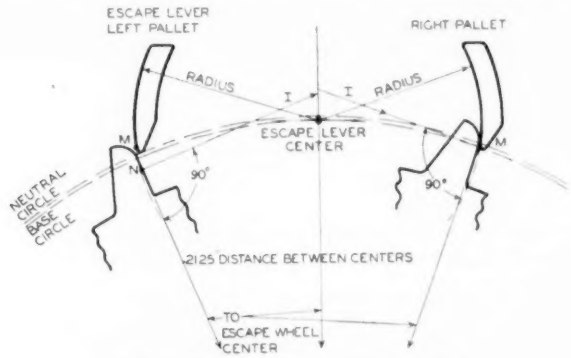


FIG. 5 MARK 18 ESCAPEMENT ACTION
(The fall impulses *I*, act above the escape-lever center.)

force of the escape-wheel tooth against the pallet as the curved portion of the tooth moves under it. Torque on the lever results from the slope of the tooth contour. Referring to Fig. 5, it will be seen that the curved or working portion of the tooth occurs almost entirely above the neutral circle. This means that the working impulses do not occur at the neutral circle but above it. Therefore, if these were the only impulses acting, the escapement would be highly torque-sensitive. As will be seen later there are other types of impulses present and the over-all torque sensitivity of the escapement depends upon the general effect of all.

Another and large impulse of momentum results from the fall impact of a tooth against a pallet. This follows the escape of another tooth from the opposite pallet. Unless the line of action of this fall impact passes through the center of rotation of the escape lever, it will affect the oscillation frequency. An analysis was made to determine the direction of action of the fall-impact force. This involved factors such as the coefficient of friction, the direction of motion of the lever, and the relative velocity of the teeth and pallets. Some of these factors are uncer-

[5] Numbers in parentheses refer to the Bibliography at the end of the paper.

[6] The phrase "base circle" is used here in the same sense as in gear-tooth design. It is the circle at which the generated tooth contour starts. In this case it intersects the points beyond which the tooth begins to escape beneath the pallet.

tain and the conclusions are only approximate, but it appeared that the most probable direction of the impact force is the vector I in Fig. 5. This is in the direction of motion of the escape-wheel tooth, at right angles to the radius of the wheel at the point of impact.

Fall impact on the left pallet occurs at a variable point, N, anywhere along the straight portion of the tooth depending upon the operating torque on the wheel. At the right pallet the fall occurs always at the same point, M, on the base circle, because the tooth is sufficiently undercut for the right-hand angular position. Fall impacts contain a great deal of momentum due to the large angular distance through which the escape wheel has accelerated before being stopped. They occur at a time when the escape lever is about farthest from its neutral position, and in the Mark 18 fuse exert a large and variable clockwise moment about the escape-lever center, hence are a major factor contributing to the torque sensitivity of the escapement.[7]

To summarize, the major impulses which drive the escape lever of the Mark 18 fuse are as follows:

1 The normal driving impulses, which are clockwise for the left pallet and counterclockwise for the right, supply momentum to the lever. These occur outside the neutral circle.

2 The fall impulses partly cancel each other because the one on the left side drives the lever while the right one retards it. They occur within the neutral circle. The left impulse originates from a variable point on the tooth, but the right one originates from a fixed point.

3 The absence of a true "dead-beat" action on the left pallet due to the forward slope of the straight portion of the tooth contributes two additional clockwise impulses to the left pallet There is no counterpart for the right pallet.

The torque sensitivity of this escapement is attributable to the fact that the net resultant of these several impulses varies in amount and direction with the driving torque, and does not in general average about the neutral position of the lever.

Mark 22 or U. S. Army Escapement

Fig. 6 is a layout of the Army escapement similar to Fig. 5. The normal driving impulses very nearly straddle the points of maximum velocity of the pallets. This is shown in Fig. 6 by the neutral circle intersecting the working face of the tooth near its mid-point. However, as in the Mark 18, there are the same off-neutral fall impulses, I. This escapement is an improvement over the Mark 18 in that both fall impulses occur on the base circle. There are no impulses due to imperfect dead-beat action. For this reason, it is probably a less erratic escapement. This fuse is also relatively torque-sensitive.

New Escapement

After the foregoing analysis to determine the possibility for improvement in existing escapements, a new design was undertaken. An analysis of the new escapement, similar to those in Figs. 5 and 6, is shown in Fig. 7 and the component parts are illustrated in detail in Figs. 10 and 11. The new escapement was designed according to the following principles:

1 Location of the wheel and level centers in the fuse plates and the center distance were not changed so that the remainder of the fuse would be unaffected by changes in the escapement.

2 The leading edge of the escape tooth was undercut sufficiently to cause the fall impact to occur at the point P on the base circle under all conditions.

[7] This explains the tendency of the Mark 18 escapement to lock on its right pallet under excess operating torque. The strong counterclockwise fall impulses throw the lever into deep engagement on its right side where a small amount of friction stops the motion completely.

3 The base circle of the wheel was located with respect to the centers of the wheel and lever so that the line of action of the fall impact I, taken in the direction of motion of the tooth, passes through the center of rotation of the lever. This prevents the fall impacts from producing driving torques and disturbing the frequency of oscillation.

4 An escape tooth form was derived as outlined in the next section. It delivers an efficient impulse over the major part of the curved portion of the tooth. It was made as broad as possible, consistent with the amount of space available, so as to obtain a maximum depth of engagement for reasons of safety.

5 The tips of the pallets were located so that the normal accelerating impulses occur symmetrically about each side of the neutral circle, that is, the neutral circle was made to intersect the curved portion of the tooth at the mid-point of the angle subtended by the radii OP and OR from the center of the lever to the ends of the curved portion of the tooth.

6 In designing the escape wheel, it was desirable to have as many teeth as possible and still allow free pallet action with adequate tolerances. These considerations permitted up to 24 teeth, but the number chosen was 20 to allow an easy change-over in the dynamic test equipment used with the former 30-tooth escapement.

7 In order for the new fuse with two thirds as many teeth to run as long as the Mark 18 (45 sec), it was necessary to reduce the oscillation frequency of the escapement proportionately. This was done by adding weights to the ends of the lever and keeping the same hairspring.

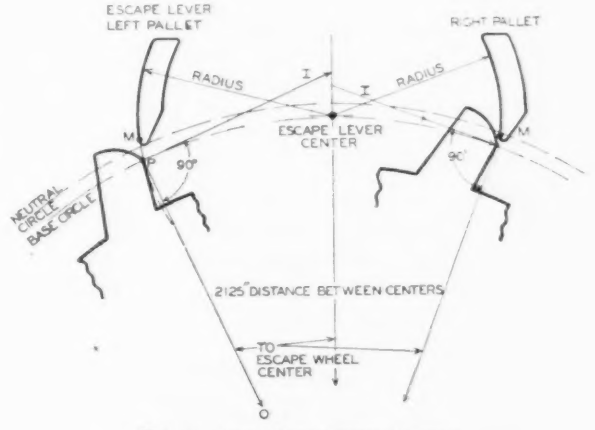


Fig. 6 Army Escapement Action
(The fall impulses I act above escape-lever center.)

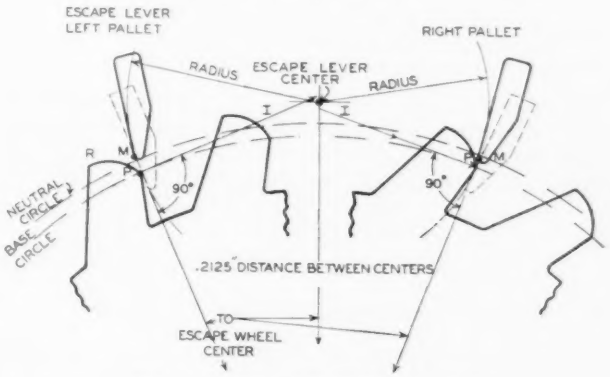


Fig. 7 Action of New Escapement
(The escapement is designed so that the fall impulses I come, on the average, at the escape-lever center.)

8 The manufacture of the new lever was simplified by making the pallets straight-sided instead of cylindrical and by swaging rather than grinding the angle of their back surfaces. (These are the surfaces which operate against the angles of the back sides of the escapement teeth during reverse running of the fuse when it is being wound.)

9 In adapting the new escapement to the Mark 18, a small amount of routing was necessitated in the No. 2 plate to clear the weights added to the lever.

10 Since the new escapement operates at 108.8 cycles per sec instead of 163.2, the dynamic test equipment was changed to accommodate the lower oscillation frequency. The same fuse standards and test tables were used, but the signal amplifier and the first stage of multivibrators driving the printer bar were tuned to 215 cycles per sec. Thus the dynamic test tapes obtained with the new fuse were identical in appearance and interpretation with those obtained for the Mark 18.

Derivation of Escape-Wheel Tooth Form

The tooth form was designed to transfer energy from the wheel to the lever efficiently and to produce the driving impulses, on the average, when the lever was passing through its neutral position. To transfer energy efficiently, the time of contact of the pallet with the tooth during the escape phase was made as long as possible by providing a broad tooth. To place the impulses properly it was not sufficient to use the geometrical layout as explained in item 5 previously. It was also desired to have a tooth form which would apply approximately a constant force to the escape lever during the entire time that the pallet and tooth are in contact.

The form for the escape surface is derived by assuming a wheel accelerating from rest under a uniform torque, a pallet traveling with uniform angular velocity, and by tracing the curve described by the pallet contact point M on the wheel. Assumption of a uniform angular velocity for the pallet is not strictly correct, but the approximation has not led to serious error as can be judged from the test results.

In order to simplify the discussion, losses in the oscillating lever will first be neglected. Following this treatment the derived tooth form will be corrected for these losses in a manner to be described.

In the derivation, reference is made to Fig. 8 and the following nomenclature is used:

- r = mean wheel radius at curved portion of tooth
- θ = angle turned by wheel from position where pallet tip M leaves point P on tooth, radians
- α = angular acceleration of wheel
- t = time, sec
- I = moment of inertia of escape wheel and driving gears
- v = maximum velocity of pallet
- T = driving torque accelerating wheel

Co-ordinates of the points M, x, and y are not rectangular. They are measured along arcs about C and O, centers of the wheel and lever, respectively. The constant acceleration of the escape wheel leads to an equation for the x-co-ordinate of the tooth

$$\alpha = T/I \quad [1]$$

$$x = r\theta = {}^1/_2\ \alpha t^2 r = {}^1/_2 T t^2 r/I \quad [2]$$

From the approximation of constant velocity of the pallet

$$y = vt \quad [3]$$

hence

$$x = {}^1/_2\ (rT/v^2 I) y^2 \quad [4]$$

The last equation shows the tooth form to be approximately parabolic (approximate because the co-ordinates are not exactly rectangular).

The tooth form is evaluated from Equation [4]. The displacement of the pallet is

$$y = A \sin 2\pi ft \quad [5]$$

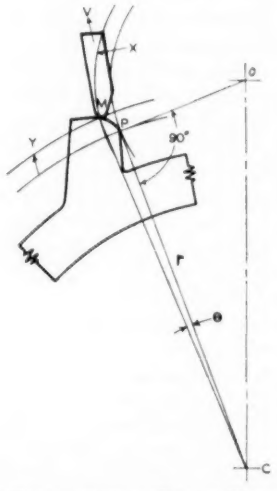


Fig. 8 Generation of Escape Tooth Form
(C is the center of the escape wheel; o is the center of the escape lever.)

where A is the amplitude of the pallet oscillation and f is its frequency, 108.8 cycles per sec. The average value of lever amplitude ϕ for the Mark 18 fuse, as manufactured, was ± 8 deg. The least value which would fully uncover the light exit slot used for dynamic regulation, was ±7 deg. The maximum amplitude allowed by stops was ±18 deg. Because higher amplitudes enhance the safety of a fuse, the minimum amplitude of oscillation of the new escapement was chosen as ± 8.5 deg. Using $R = 0.08$ in. for the radius of the point M on the pallet tip

$$A = R\phi \quad [6]$$

$$v = 2\pi fA = 8.1 \text{ in. per sec} \quad [7]$$

The moment of inertia of the Mark 18 escape wheel and pinion plus the inertias of the next two gears of the train multiplied by the squares of their speed ratios to that of the escape wheel was calculated very carefully. This value, 90 per cent of which was in the escape wheel and pinion, was

$$I = 7.2 \times 10^{-6} \text{ lb sq in} = 0.021 \text{ g sq cm} \quad [8]$$

The inertia of the remainder of the gear train was negligible. The foregoing value of inertia is that which must be accelerated by the fuse torque in the operation of the escapement. The same value of inertia in the new escapement wheel was obtained by making it 0.012 in. thick instead of 0.010 in. thick, it being slightly smaller in diameter than the original wheel.

The driving torque at the center shaft of the Mark 18 fuse, produced by the centrifugal sectors and starting springs, is 3000 gram-cm at the start of flight and 1100 gram-cm after 47 sec of flight.

Calculation of the torque efficiency of the gear train under actual flight conditions was made and was found to be 28 per cent. Multiplying the central-shaft torque values by this factor and by the gear-train ratio (1/275), the actual torques applied to the escapement shaft are 3.1 gram-cm maximum, and 1.1 gram-cm minimum. The minimum of these torques, together with other numerical constants previously given, were substituted in

Equation [4] and numerical values of x and y obtained. These are plotted in Fig. 9, curve A, on curved co-ordinates having radii of curvature originating at the wheel center C and lever center O.

The tooth form just calculated is based on the assumption of no frictional losses in the escapement. Actually, various losses cause the lever to lose momentum between impulses. In order to maintain the oscillation it is therefore necessary for the tooth to exert torque on the pallets during each driving impulse. This consumes part of the driving torque. The net torque accelerating the wheel equals the difference between the gear-train torque and that absorbed by the lever.

In order to maintain the same 8.5-deg minimum lever amplitude, it is necessary to correct the tooth form for frictional losses.

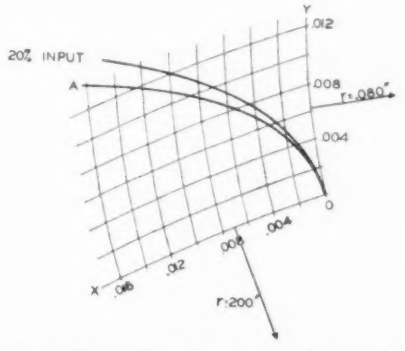


FIG. 9 CALCULATED TOOTH FORM PLOTTED ON CURVED CO-ORDINATES

Referring to Equation [4], if v is to remain unchanged, y must be varied inversely as the square root of T, since r and I are fixed.

Losses in the lever have been arbitrarily estimated to consume 20 per cent of the driving torque. All ordinates of the tooth form must therefore be increased by $1/\sqrt{0.8} = 1.1$. In Fig. 9 a corrected tooth-form curve marked "20 per cent input" has been drawn with all ordinates increased 10 per cent over their no-loss values.

In applying the 20 per cent input curve to the wheel, as shown in Fig. 10, the tooth form was approximated by a single circular arc of radius 0.020 in., terminating in a tangential line at 80 deg to the wheel radius. Due to manufacturing tolerances on so small a tooth, this approximation is adequate.

TEST RESULTS

Three pilot lots totaling about 400 escapements were produced with parts as shown in Figs. 10 and 11 and put into Mark 18 clock assemblies. These assemblies were given exhaustive laboratory and firing tests. While the laboratory results were excellent, the firing tests were at first disappointing as there were a number of duds and short-time firings. Trouble was traced to cap slippage and a mechanical interference with the W-74 safety-lever plate. Later, when this was corrected, the firing tests confirmed the engineering conclusions as to the timekeeping ability and reliability of the new escapement.

Characteristics, as revealed by tests on the pilot lots and by subsequent experience in production and use, are summarized as follows:

(*a*) *Timekeeping Ability.* The effect of driving torque on the rate of the escapement is less than one tenth that of the original Mark 18 escapement. When plotted on the graph, Fig. 4, the average production fuse with the new escapement gives a straight line for the timing-error versus running-time curve. If the initial timing rate is adjusted correctly, there is no appreciable accumulated timing error. Even when the engagement was purposely mismatched to test the effect of tolerance extremes on performance, the variation in rate after 45 sec of running, as determined by dynamic test, was never more than 0.08 per cent. The accumulated timing error was never more than 0.03 sec.

(*b*) *Reduction in Cost and Time of Manufacture.* In the pilot lots of escapements, one size of wheel and lever was manufactured and assembled without selection. Likewise, in production, only one size of wheel and lever was manufactured. No hand-matching was used or required. Skilled operators were eliminated in escapement assembly with consequent speed-up of the operation and reduction of cost.

In the final dynamic testing there were considerable savings due to increased rapidity of test and fewer retests. With the new escapement, the rate is inherently stable. The test operator was reasonably certain that if the initial rate were set correctly, the fuse would run well within tolerances. With the old escapement the rate was highly variable, and it was necessary for the operator to start the clock on the fast tolerance in order to fall within limits at the end of the run. There were 10 to 20 per cent of fuses which would not fall within the tolerance limits due to excessive change in rate. The borderline cases caused hesitancy and uncertainty and required retesting. The rejects had to be reassembled with other escapements.

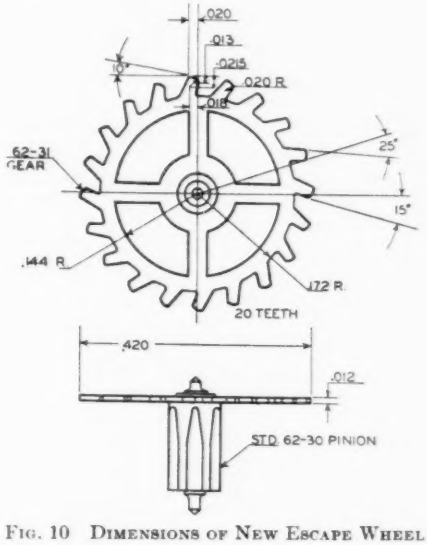


FIG. 10 DIMENSIONS OF NEW ESCAPE WHEEL

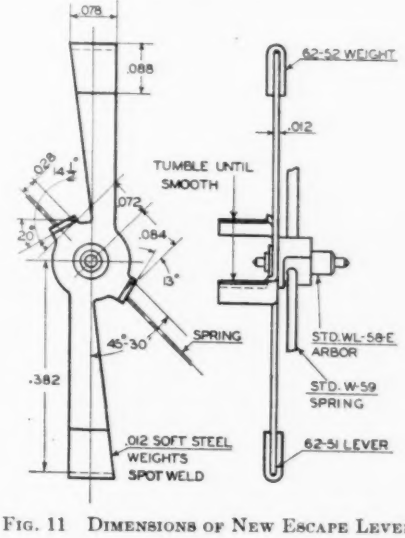


FIG. 11 DIMENSIONS OF NEW ESCAPE LEVER

The manufacture of the lever was simplified and expedited by swaging the back angles of the pallets, which formerly had been ground, reducing the number of grinding operations and amount of handling. The manufacture and stocking of the wheel was simplified by a reduction from ten sizes and ten part numbers to one size and one part number.

(*c*) *Tolerance in Engagement.* The following engineering test was made on the new design: In the escapement plates, saw cuts were made around the pivot holes for the escape wheel so that the center distance between wheel and lever could be adjusted by bending the resulting ribs. A series of tests were made with center distances varying from 0.2090 in. to 0.2160 in. (the correct center distance being 0.2125 in.). Over the entire range, the escapement would run and could be regulated to give good timing. This represented a range of engagement which would have required fourteen sizes of escape wheels had the experiment been attempted with the old escapement.

(*d*) *Low Operating Torque.* It was found that fuses with the new escapement would run full time with less than one half the normal operating torque. In the Mark 18 fuse, the available operating torque approaches the minimum running torque for the old escapement. If under actual service conditions, the gear-train friction becomes excessive, there is the likelihood that the old escapement would fail to run full time. With the new escapement this danger is lessened.

(*e*) *Self-Starting Characteristic.* The escapement was found to be self-starting for separations of the lever and wheel pivots ranging from 0.211 in. to the maximum that could be used. As soon as the normal torque is applied to the gear train, the majority of fuses with the new escapement would start to run. However, because of the wide range of escapement engagements encountered in production, the centrifugal starting device found in the Mark 18 is still necessary for that fraction of the fuses which requires a flick for starting. The easier starting of the new escapement contributes to the reliability of the fuse.

(*f*) *Firing Performance.* After several months of production experience with fuses using the new escapement, a comparison of firing results with figures for the old fuse showed a dispersion in firing time at long settings of about one half the value of the older escapement. Out of 35 lots of fuses tested at the proving grounds, there was not a single dud. Several factors other than the timing of the escapement contribute to the dispersion in firing time.

Acknowledgments

The development of this escapement was undertaken at the suggestion of Mr. K. G. Berggren, vice-president and manager of the Special Products Division of the authors' company. Certain theoretical work was contributed by Dr. J. Hornbostel. Trouble-shooting, assistance in firing-testing, and compilation of firing-test data were done by W. J. Meyers, Lieutenant U.S. N.R. Thanks are also due members of the Special Products Division, too numerous for individual mention, who aided in production and testing of the pilot lots of fuses.

BIBLIOGRAPHY

1 "The Science of Clocks and Watches," by A. L. Rawlings, Pitman Publishing Corporation, New York, N. Y., 1945, pp. 107–111.

2 "Constant Frequency Oscillators," by F. B. Llewellyn, *Bell System Technical Journal*, vol. 11, 1932, p. 67.

3 "A Dictionary of Applied Physics," by Sir Richard Glazebrook, Macmillan & Company, London, vol. 3, 1923, pp. 210–212.

Control and Prediction of Pulsation Frequency in a Duct System

By W. R. HEATH[1] and W. R. ELLIOT,[2] BUFFALO, N. Y.

The authors present the results of studies on compressor-duct systems which are characterized by unstable operation over some portion of the performance curves. The principles of the Helmholtz resonator are explained, and the prediction of pulsations in a duct system may be developed by considering that the system acts as a simple Helmholtz resonator. For certain cases electrical analogy is used to explain acoustical conditions in the duct. Methods of preventing pulsations are described.

CERTAIN compressor-duct systems exhibit unstable operating characteristics over a portion of the performance curve. Compressors are usually selected for such a capacity that stable operation will be maintained; however, it is sometimes necessary to reduce the volume delivered beyond the critical point on the performance curve, with the result that operation is unstable.

A typical performance curve for a single-stage centrifugal compressor is shown in Fig. 1. That this compressor may be unstable in operation at any point to the left of the peak pressure and stable at any point to the right may be demonstrated as follows (1).[3]

Consider the compressor to be operating at any point to the left of P, where an increase in static pressure is accompanied by an increase in capacity. If for any reason there is a slight rise in the static pressure against which the compressor is operating, the volume of air delivered will be increased. This increase in capacity results in a still further increase in static pressure creating even greater unbalance. Therefore the static pressure in the system is temporarily higher than that for the corresponding capacity on the compressor performance curve as, for example, at the point A. Conversely, if the static pressure is momentarily decreased, the resulting decrease in capacity causes a still further drop in static pressure, which is now less than the pressure corresponding to the capacity on the performance curve, as at B.

The actual operation of the compressor may be conceived to be not on the performance curve but around a loop close to the performance curve of the compressor. The minimum pressure which occurs during a cycle may be as low as the shutoff pressure, so that air flow through the compressor momentarily ceases. However, the pulsation, which occurs as the static pressure varies, may be of such high frequency or of such small magnitude that it is not detectable by the human ear.

If the compressor is operating at any point to the right of the peak pressure, operation may be shown to be stable by a similar method of reasoning, and pulsation does not occur.

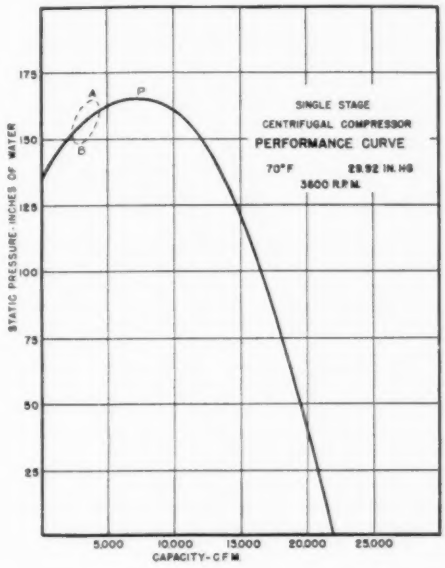


FIG. 1

HELMHOLTZ RESONATOR

When a compressor is operating on the unstable portion of its performance curve, the duct system to which it is connected acts as a Helmholtz resonator, and the frequency of the pulsation which occurs depends on the size and distribution of this system.

A simple Helmholtz resonator (2, 3) is shown in Fig. 2. This consists essentially of a relatively large volume V_0, connected to the outside through a neck of area S and length L. Such a resonator has practically uniform compressions and rarefactions in the main body, which is alternately compressed and expanded by movement of the air in the neck. The ratio of the area S to the length L of the neck is called the "conductivity" of the resonator. In the case of a circular orifice in the thin-walled chamber, the conductivity is equal to the diameter of the opening.

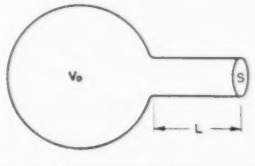


FIG. 2 HELMHOLTZ RESONATOR

The frequency of pulsation of a simple resonator with dry air at 70 F is

$$f = \frac{c}{2\pi}\sqrt{\frac{S}{LV_0}} = 178\sqrt{\frac{S}{LV_0}}$$

---

[1] Assistant Chief Engineer, Buffalo Forge Co.

[2] Research Engineer, Buffalo Forge Co. Mem. A.S.M.E.

[3] Numbers in parentheses refer to the Bibliography at the end of the paper.

Contributed by the Applied Mechanics Division and presented at the Annual Meeting, New York, N. Y., December 2–6, 1946, of THE AMERICAN SOCIETY OF MECHANICAL ENGINEERS.

Discussion of this paper should be addressed to the Secretary, A.S.M.E., 29 West 39th Street, New York, N. Y., and will be accepted until January 10, 1947, for publication at a later date. Discussion received after the closing date will be returned.

NOTE: Statements and opinions advanced in papers are to be understood as individual expressions of their authors and not those of the Society.

where

f = frequency of pulsation, cycles per sec
S = area of neck of resonator, sq ft
L = length of neck, ft
V_0 = volume of resonator, cu ft
c = velocity of sound in air, fps

From the form of the Helmholtz equation, it is apparent that the frequency of pulsation depends only on the three variables included in the equation and is independent of other quantities which may be variables in a duct system. It has been determined by both Lieberg (4) and Pochettino (5) that the shape of the orifice or neck has no effect except that a mouth with a large aspect ratio reduces the damping effect.

Prediction of Pulsation Frequency

The results of a series of tests conducted in the laboratory are given in Table 1. From this experimental work it has been found that the frequency of pulsation, if it occurs in a duct system, can be very closely approximated by considering that the system acts as a simple Helmholtz resonator. The following quantities may be substituted in the original Helmholz equation:

TABLE 1 LABORATORY PULSATION TEST RESULTS

TEST NO	VOLUME OF SYSTEM V_0	LENGTH OF NECK L	DIAMETER OF SMALL DUCT	CALCULATED FREQUENCY PULSATIONS PER MINUTE	OBSERVED FREQUENCY PULSATIONS PER MINUTE	DIAGRAM OF DUCT SYSTEMS
1	144	28 0	14"	174	173	
2	144	22 1	14"	196	186	
3	102 5	28 0	14"	206	210	
4	102 5	22 1	14"	234	229	
5	61	28 0	14"	267	285	
6	61	22 1	14"	302	296	
7	90	16 2	14"	290	270	
8	49	16 2	14"	392	400	
9	62 9	28 5	10"	225	240	
10	38 7	28 5	10"	255	280	

S = area of small duct, sq ft
D = impeller diameter, ft
L = $2\pi D$ plus length of transformation piece plus length of small duct, ft
V_0 = volume of ductwork plus transformation piece plus compressor, cu ft

The validity of the simple relationship established was subsequently verified in several wind tunnels. The computed and actual frequencies of same are tabulated in Table 2. It should be noted that it made no difference whether the volume V_0 was on the inlet or discharge side of the compressor or whether situated partly on both sides.

TABLE 2 WIND-TUNNEL TESTS

No.	Installation	S	L	V	—Frequency— Calculated	Observed
1	Blower	25	66	7250	77.4	77–80
2	Blower and exhauster (same unit as no. 1)	25	43	80500	28.7	27–28
3	Two compressors operating in parallel both exhausting from one chamber and blowing into another	27	100	99000	23	21–26

One interesting observation was that no pulsation was detectable until the static pressure was 8.9 in. of water or higher. At and close to this pressure point, pulsations could be started by causing a slightly higher static pressure temporarily, but they quickly died away. It is probable that below this static pressure any incipient pulsations are damped out and this may explain why pulsation is not a problem in most ventilating systems.

The one case for which the established relationship has not proved valid is when the compressor discharges into a long narrow duct with no "concentrated" volume. In this case, the frequency is invariably much higher than that predicted by the established empirical relationship. An explanation may be found in the analogous cases of electrical and acoustical phenomena. According to Weinbach (6), "the natural or resonant frequency of an electrical circuit with distributed capacitance, as they occur, for example, in a line, is 57 per cent greater than the resonant frequency of a circuit having an equal capacitance as the line but in a 'lumped' form."

Based on this electrical analogy, the constant in the Helmholtz equation should, for a long pipe of small diameter, be increased to 280 instead of 178.

Borderline cases in both electrical and acoustical phenomena cannot be predicted with too great accuracy. By a borderline case is meant one in which the volume of the duct is partly distributed and partly concentrated. For this case, the frequency will lie between that for a concentrated volume and that for an equal distributed volume.

Of some interest is the fact that in the electrical system, those factors which have no effect on the frequency of pulsation have no effect in the analogous acoustical system. These may be listed briefly as follows:

1 Variation in compressor speed or in the volume of air handled has no effect on the frequency.

2 Variation in static pressure has no effect on f, except in that the pressure developed may be low enough that damping prevents audible pulsation.

3 Introduction of a high resistance in either an electrical or a mechanical system is a method of preventing pulsation.

The pulsations produced by a compressor-duct system are of particular importance when the frequency of the pulsations is low. At low frequencies, high-amplitude beats result in increased noise level and in considerable pressure variations within the duct system. These pulsations may be detected as individual beats by the human ear up to a frequency of about 450 per min. Above 600 per min individual pulsations cannot be detected and are objectionable only in that the noise level possibly may be increased.

By predetermining whether or not pulsation is to be a problem, precautions may be taken to insure stable operation over the entire working range.

Prevention of Pulsation

When required operating conditions are such that the static pressure must be maintained but at a volume below the critical volume, pulsation may be prevented by by-passing a portion of the air delivered by the compressor (7).

For example, it may be necessary for the compressor to deliver a volume of air at the static pressure indicated by the point R, Fig. 3. In this case the volume at the point S may be delivered by the compressor at the required static pressure, the required volume admitted to the duct system and the excess volume, volume S minus volume R, by-passed to atmosphere. This allows the compressor to handle a volume greater than the critical volume and to operate on the stable portion of the performance curve. This system of bleeding the excess air delivered by the compressor is more wasteful of power than the other methods of control, as the power required remains constant for all volumes below the critical volume. It can, however, be applied to any

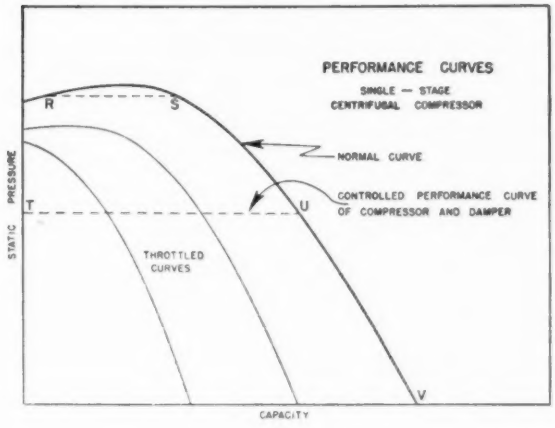


FIG. 3

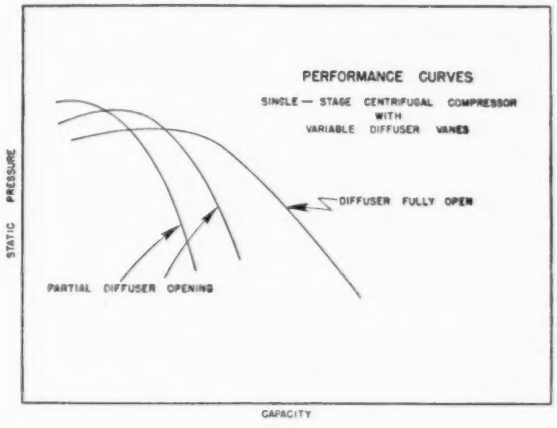


FIG. 4

centrifugal compressor and has the advantage that it allows a high static pressure to be maintained. The amount of air bled can be controlled by controlling the minimum velocity pressure at the inlet or discharge, or by controlling the horsepower input to the compressor.

A second method of pulsation control is to throttle close to the compressor and obtain a multiplicity of performance curves as indicated in Fig. 3. If control is to be obtained by throttling, the static pressure may be maintained constant over the major portion of the operating range, with the result that the controlled performance curve of the fan plus the damper can be represented by the line *TUV*, Fig. 3. Use of a throttle either before or after the compressor results in increased resistance in the system with consequent reduction in efficiency. However, as throttling reduces the horsepower required for a given volume, this method of control is less wasteful than bleeding. In the case of multistage compressors satisfactory control possibly may not be achieved solely by throttling because of the inherently large volume of the compressor, which itself may act as a resonator with a frequency low enough to be objectionable.

Prevention of pulsation by the use of variable diffuser vanes after the compressor is an efficient control method. This consists of providing movable vanes which may be adjusted automatically or manually. By use of diffuser vanes, the static pressure is maintained and regulation may be obtained nearly down to zero volume. Regulation by diffuser vanes results in a series of operating curves for various diffuser settings, as shown in Fig. 4. The envelope of these curves indicates the limit of stable operation for various settings of the diffuser. Diffuser vanes are applicable to both single-stage and multistage compressors. They require additional space and also have the disadvantage that they add to the initial cost of the compressor. They should be used only when conditions justify this additional cost.

Other methods of control are by varying the speed by use of turbine drive or variable-speed motor, and by use of a substage compressor ahead of the regular first stage (8). By this latter method when the volume required drops below the critical volume the excess air required to prevent pulsation is by-passed to the inlet of the substage fan. Part of the energy in the otherwise blowoff waste air is put back on the shaft through this substage fan acting as an air turbine.

BIBLIOGRAPHY

1 "Mechanical Vibrations," by J. P. Den Hartog, second edition, McGraw-Hill Book Company, Inc., New York, N. Y., 1940, p. 332.

2 "Sound," by E. G. Richardson, third edition, E. Arnold & Company, London, England, 1940, p. 213.

3 "A Textbook of Sound," by A. B. Wood, second edition, The Macmillan Company, New York, N. Y., 1941, p. 197.

4 "Experimental Investigations of the Damping of Sound Resonators," by Pavel Lieberg, *Journal of the Russian Physico-Chemical Society*, vol. 28, 1896, pp. 93–120.

5 "Sullo smorzamento delle dibrazioni in un resonatore Acustico," by Alfredo Pochettino, Atti R. Delle R. Accademia dei Lincei, Rendiconti, vol. 8, 1899 (Sem. 1), pp. 260–264.

6 "Principles of Transmission in Telephony," by M. P. Weinbach, The Macmillan Company, New York, N. Y., 1924, p. 55.

7 "Compresseurs et Soufflantes Centrifuges," Brown Boveri Review, Jan.-Feb.-March, 1920 (Feb., 1920), p. 37.

8 "Joint Intelligence Objectives Agency," Final Fiat Report No. 489, R. D. Madison, Nov. 13, 1945.

The Theory of Curved Beams

BY G. C. BEST,[1] SAN DIEGO, CALIF.

In this paper, the theory of curved beams is developed by a somewhat different procedure from that customarily employed. Deflections at the centroid are first assumed and then loads and stresses resulting from these deflections are estimated. This process works out in a somewhat more orderly fashion than the conventional development. Throughout, all measurements are to the centroidal axis rather than to the neutral axis. Final results are presented in such a form that satisfactory accuracy may be obtained from slide-rule computations and approximate integration. Hence the procedure is applicable to any section, it being unnecessary first to develop a special formula for each different section. An illustrative example is given. The theory is extended to cover the case of unsymmetrical bending of curved beams. The effects of torsion, which will probably also occur in the generalized case, are not treated. These can be superimposed upon stresses due to bending.

Nomenclature

The following nomenclature is used in the paper:

A = area of cross section
R = distance from center of curvature to center of gravity (CG) of section
z = radial co-ordinate; positive outward, measured from CG of section
P = axial load at centroid, positive when producing tension at centroid
M_x = moment about x-axis (i.e., having x-arm), positive when producing tension on positive side of x-axis
M_z = moment about z-axis (i.e., having z-arm), positive when producing tension on positive side of z-axis.
M_{xx} = moment about x-axis = M_z
M_{zz} = moment about z-axis = M_x
ϵ = strain at centroidal axis, positive for extension
φ = rotation about x-axis (through CG of section), positive when producing extension for positive z
ψ = rotation about z-axis (through CG of section), positive when producing extension for positive x
E = Young's modulus
$\epsilon' = E\epsilon$
$\varphi' = E\varphi$
$\psi' = E\psi$

$$A' = \int \frac{dA}{1 + \frac{z}{R}}$$

$$Q_x' = \int \frac{zdA}{1 + \frac{z}{R}}$$

$$Q_z' = \int \frac{xdA}{1 + \frac{z}{R}}$$

$$I_x' = \int \frac{x^2dA}{1 + \frac{z}{R}} = I_{zz}' \text{ (i.e., subscripts are similar to moment subscripts)}$$

$$I_z' = \int \frac{z^2dA}{1 + \frac{z}{R}} = I_{xx}'$$

$$I_{xz}' = \int \frac{xzdA}{1 + \frac{z}{R}}$$

$a = A'$
$b = Q_x'$
$c = Q_z'$
$d = I_x'$
$e = I_z'$
$f = I_{xz}'$
D = determinant of system (refer to Equations [5])

$$J' = \frac{e}{1 + e/AR^2}$$

δ = distance from neutral axis to centroid of section, always positive

Introduction

In the following work the same assumptions are made as in the conventional development. In particular, radial plane sections remain plane, and stresses do not exceed the proportional limit. The centroidal axis of the beam considered lies in the (x, y) plane and the radius of curvature of this centroidal axis is R. Radial sections are all identical, i.e., the section is constant, though not

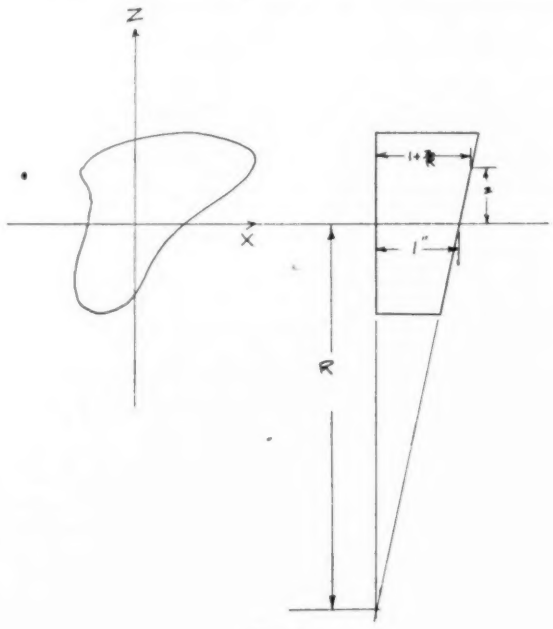


Fig. 1

[1] Stress Analyst.

Contributed by the Applied Mechanics Division and presented at the Annual Meeting, New York, N. Y., December 2–6, 1946, of The American Society of Mechanical Engineers.

Discussion of this paper should be addressed to the Secretary, A.S.M.E., 29 West 39th Street, New York, N. Y., and will be accepted until January 10, 1947, for publication at a later date. Discussion received after the closing date will be returned.

Note: Statements and opinions advanced in papers are to be understood as individual expressions of their authors and not those of the Society.

necessarily symmetrical about the z-axis. Radial planes are passed through the beam at two adjoining points 1 in. apart on the centroidal axis, isolating a portion of the beam as shown in Fig. 1. Inner and outer edges have been altered into straight lines for simplicity since the effect of this change is negligible; i.e., involves only second-degree infinitesimals.

Rotation About X-Axis. One face is then rotated relative to the other about the x-axis through an angle of φ radians. The stress at a point located a distance z from the x-axis is

$$\sigma = \frac{Ez\varphi}{1 + \frac{z}{R}}$$

The resulting loads at the center of gravity (CG) of the section are

$$\left.\begin{aligned} P_\varphi &= \int \sigma dA = \int E\frac{z\varphi}{1+\frac{z}{R}}dA = E\varphi\int\frac{zdA}{1+\frac{z}{R}} = E\varphi Q_x' \\ M_{x\varphi} &= \int \sigma x dA = \int \frac{Ez\varphi x}{1+\frac{z}{R}}dA = E\varphi\int\frac{zxdA}{1+\frac{z}{R}} = E\varphi I_{xz}' \\ M_{z\varphi} &= \int \sigma z dA = \int \frac{Ez^2\varphi}{1+\frac{z}{R}}dA = E\varphi\int\frac{z^2dA}{1+\frac{z}{R}} = E\varphi I_z' \end{aligned}\right\} \ldots [1]$$

Rotation About Z-Axis. Similarly, if one face rotates relative to the other about the z-axis through the angle of ψ radians, the stress σ at a point a distance x from the z-axis and z from the x-axis is

$$\sigma = \frac{E\psi x}{1 + \frac{z}{R}}$$

The resulting loads at the CG are

$$P_\psi = E\psi Q_z' \qquad M_{x\psi} = E\psi I_z' \qquad M_{z\psi} = E\psi I_{xz}' \ldots [2]$$

Uniform Extension. If one face is moved away from the other a distance ϵ without rotation, the stress at a point z from the x-axis is

$$\sigma = \frac{E\epsilon}{1 + \frac{z}{R}}$$

and resulting loads at the CG are

$$P_\epsilon = E\epsilon A' \qquad M_{x\epsilon} = E\epsilon Q_x' \qquad M_{z\epsilon} = E\epsilon Q_z' \ldots [3]$$

Relations Between Section Moments and Areas. It is possible to write

$$I_z' = \int\frac{z^2dA}{1+\frac{z}{R}} = R\int\frac{z^2dA}{R+z}$$
$$= R\int\frac{z(z+R-R)dA}{R+z} = R\int zdA - R^2\int\frac{zdA}{R+z}$$

The first integral = 0 since z is measured from the centroid; hence

$$I_z' = -R^2\int\frac{zdA}{R+z} = -R\int\frac{zdA}{1+\frac{z}{R}} = -RQ_x'$$

or in the simpler notation

$$e = -Rc$$

By similar manipulations all told there are the following relations

$$e = -Rc \qquad a = \frac{e}{R^2} + A \qquad f = -Rb \ldots [4]$$

General Formulas

Adding the loads at the centroid produced by deformations ϵ, ψ, φ gives

$$\left.\begin{aligned} P &= P_\epsilon + P_\psi + P_\varphi = a\epsilon' + b\psi' + c\varphi' \\ M_x &= M_{x\epsilon} + M_{x\psi} + M_{x\varphi} = b\epsilon' + d\psi' + f\varphi' \\ M_z &= M_{z\epsilon} + M_{z\psi} + M_{z\varphi} = c\epsilon' + f\psi' + e\varphi' \end{aligned}\right\} \ldots [5]$$

The determinant D of this system is symmetrical and reduces, in view of Relations [4], to

$$D = A(de - f^2) \ldots [6]$$

Adding stresses due to all three displacements gives

$$\sigma = \frac{1}{1+\frac{z}{R}}(\epsilon' + x\psi' + z\varphi') \ldots [7]$$

Solving Equations [5] for ϵ', ψ', φ' and making use of Relations [4] gives

$$\left.\begin{aligned} \epsilon' &= \frac{P}{A} + \frac{M_z}{AR} \\ \psi' &= \frac{Ae}{D}M_x - \frac{Af}{D}M_z \\ \varphi' &= \frac{P}{AR} - \frac{Af}{D}M_x + \left(\frac{1}{AR^2} + \frac{Ad}{D}\right)M_z \end{aligned}\right\} \ldots [8]$$

Inserting these values in Equation [7] and rearranging gives

$$\sigma = \frac{P}{A} + \frac{(ex-fz)}{(ed-f^2)} \times \frac{M_x}{1+\frac{z}{R}} + \left[\frac{1}{AR} - \frac{1}{\left(1+\frac{z}{R}\right)} \times \frac{(xf-dz)}{(de-f^2)}\right]M_z \ldots [9]$$

It can be seen that for an axial load alone the stress is constant, i.e., $\sigma = P/A$. For the case $R = \infty$ (i.e., a straight beam), Equation [9] simplifies into Swain's formula (1),[2] consideration being given to the difference in definitions in terms and sign conventions.

Symmetrical Sections

If the section is symmetrical about the z-axis and $M_z = 0$, Equation [9] simplifies considerably since $b = f = 0$. In this case, neglecting the term involving P, Equation [9] becomes

$$\sigma = M_x\left[\frac{1}{AR} + \frac{z}{\left(1+\frac{z}{R}\right)e}\right] \ldots [10]$$

[2] Numbers in parentheses refer to the Bibliography at the end of the paper.

This corresponds to the form in which this formula appears in reference (2).

Or the stress may be expressed in the following form, corresponding to reference (3)

$$\sigma = \frac{M_z(z + \delta)}{J'\left(1 + \frac{z}{R}\right)} \quad \ldots\ldots\ldots\ldots\ldots\ldots [11]$$

where

$$J' = \frac{e}{1 + e/AR^2} = \frac{I_z'}{1 + I_z'/AR^2} \quad \ldots\ldots\ldots [11a]$$

and δ = distance from centroid to neutral axis; always considered positive

$$\delta = J'/AR \quad \ldots\ldots\ldots\ldots\ldots\ldots [11b]$$

The curved-beam factor K of reference (2) becomes

$$K = \frac{I(1 + \delta/z)}{J'(1 + z/R)} \quad \ldots\ldots\ldots\ldots\ldots [11c]$$

These relationships may be obtained by setting $\sigma = 0$ (neutral axis) in Equation [10], recalling that δ is always positive and making use of Relations [4].

Computation of Section Properties

In reference (2) the term Z is defined as "changing symbols to correspond with the notation used in this article"

$$Z = -\frac{1}{A}\int \frac{z}{R + z}\, dA$$

For large R this term will be very small, the co-ordinate z being measured to the CG of the section. Hence, if a slide rule is used and the integral evaluated by approximate methods, differences between slide-rule-computed values of nearly the same amount will occur and considerable loss in accuracy will result. To reduce this effect Z can be written

$$Z = e/AR^2$$

where

$$e = R\int \frac{z^2 dA}{R + z}$$

Here the only differences which occur are in the denominator in adding R to z when z is negative, since the numerators are always positive, being squares. The error in z will be the error in estimating the position of the centroid and $R + z$ will contain a larger percentage of error than z if $R + z < |z|$.

This effect, however, is much less serious than that encountered in the first-mentioned integral since, in the computation of e, the denominator term $R + z$ never approximately equals zero, and only a few terms of the sum are appreciably affected. It should be noted that, for sharp curvature, it is necessary to divide the area into more divisions near the center of curvature where $R + z$ will change rapidly than further from it.

Example Problem

In the following problem, the stress at the extreme inner fiber of the section, shown in Fig. 2, will be computed. The distance R

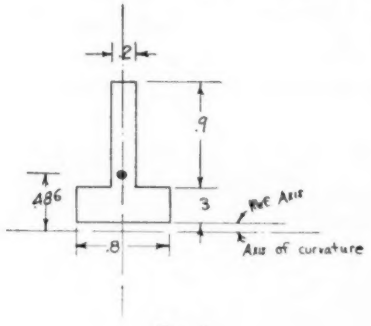


Fig. 2

from the centroidal axis to the axis of curvature is 0.486 in. The applied moment $M_z + = 3300$ in-lb. Since the section is one of those for which a curved-beam factor K has already been computed, see reference (2), this stress can be obtained from the formula

$$\sigma = \frac{MzK}{I}$$

In this case $K = 3.63$ since $R/c = \frac{0.486}{0.406} = 1.20$. From the following computations $z = -0.406$ and $I = 0.05069$; hence

$$\sigma = \frac{+3300(-0.406)(3.63)}{0.05069} = -96{,}000 \text{ psi}$$

All computations given in Table I are made upon the slide rule.

BIBLIOGRAPHY

1 "Airplane Structures," by A. S. Niles and J. S. Newell, second edition, John Wiley & Sons, Inc., New York, N. Y., 1938.

2 "Advanced Mechanics of Materials," by F. B. Seely, John Wiley & Sons, Inc., New York, N. Y., 1932.

3 "Strength of Materials," by S. Timoshenko, second edition, D. Van Nostrand Company, Inc., New York, N. Y., vol. 2, 1940–1941.

4 "Strength of Materials," by A. Morley, Longmans, Green & Company, Inc., New York, N. Y., 1940.

TABLE 1 COMPUTATION OF SECTION PROPERTIES. (SECTION SHOWN IN FIG. 2)

1 z'	2 dz = Int. const	3 z	4 xdz (2) × (3)	5 $xz'dz$ = (1) × (4)	6 z_{CG} (1) − z	7 z^2_{cg} = (6)^2	8 z^2dA = (4) × (7)	9 R + (6) = 0.486 + (6)	10 (8)/(9)
0	0.025	0.8	0.0200	0	−0.406	0.1660	0.00332	0.080	0.04150
0.075	0.100	0.8	0.0800	0.0060	−0.331	0.1090	0.00875	0.155	0.05650
0.150	0.050	0.8	0.0400	0.0060	−0.256	0.0652	0.00261	0.230	0.01135
0.225	0.100	0.8	0.0800	0.0180	−0.181	0.0326	0.00261	0.305	0.00855
0.30	0.025	0.8	0.0200	0.0060	−0.106	0.0112	0.00022	0.380	0.00058
0.30	0.075	0.2	0.0150	0.0045	−0.106	0.0112	0.00017	0.380	0.00045
0.525	0.300	0.2	0.0600	0.0316	+0.119	0.0142	0.00085	0.605	0.00140
0.750	0.150	0.2	0.0300	0.0226	+0.344	0.1180	0.00354	0.830	0.00427
0.975	0.300	0.2	0.0600	0.0582	+0.569	0.3205	0.01920	1.055	0.01820
1.200	0.075	0.2	0.0150	0.0180	+0.794	0.6300	0.00942	1.280	0.00737
Σ	1.200		0.4200 = A	0.1709 = Q			0.05069 = I		0.15017 = I_z'/R

$$\bar{z} = \frac{Q}{A} = \frac{0.1709}{0.4200} = 0.406$$

$$I_z' = 0.15017 \times 0.486 = 0.073$$

$$J' = 0.073/[1 + 0.073/0.42 \times 0.486^2] = 0.073/1.735 = 0.0422$$

$$\delta = \frac{J'}{AR} = 0.0422/0.420 \times 0.486 = 0.206$$

Equation [11] gives $\sigma = \dfrac{+3300[-0.406 + 0.206]}{0.0422[1 - 0.406/0.486]} = \dfrac{3300 \times (-0.200)}{0.0422 \times 0.163} = -96{,}200$ psi

Discussion

A General Method for Calculating Critical Speeds of Flexible Rotors[1]

A. H. Ehlinger.[2] The author is to be congratulated for the valuable contribution he has made in the field of critical-speed studies. In regard to the application of gyroscopic effect of rotating disks, the writer wishes to point out a few simple relationships which might be helpful. For example, if the disk were set up on rectangular co-ordinates, Fig. 1 of this discussion, with the

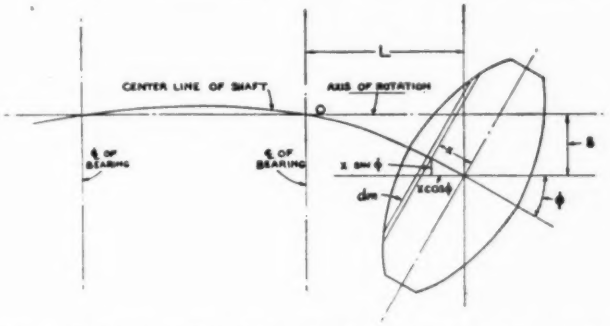


Fig. 1 Example of Disk Set Up on Rectangular Co-Ordinates

origin lying at the center of gravity of the disk and the X-axis coinciding with the center line of the shaft, then A and B may be defined as follows

$$A = \int Z^2dm + \int Y^2dm = 2\int Z^2dm$$
$$B = \int Z^2dm + \int X^2dm$$
$$A - B = \int Z^2dm - \int X^2dm$$

The last equation can also be derived by treating the disk as a series of thin disks. Den Hartog[3] shows that the moment exerted by the inertia forces on a thin rotating disk may be expressed as follows

$$M = \omega^2\phi \int Z^2dm$$

where

ω = speed of rotation, radians per sec
ϕ = angle of inclination between shaft center line and axis of rotation at location of disk, radians

The foregoing equation could also be used for a series of thin disks. However, one must not overlook the effect this would have on the bending moment due to transverse forces on the shaft. To illustrate, let us consider a disk of mass m overhung on a shaft at a distance L from point 0, the nearest support. Considering the disk as a point mass located at its center of gravity, the moment at point 0 due to transverse loading will be as follows

$$M_0 = m\omega^2\delta L$$

where

δ = deflection of center of gravity of disk

Now consider the disk divided into an infinite number of thin disks each having a mass dm. Assume all disks normal to the shaft and that angle ϕ remains constant. The increment of moment at point 0 due to any one of these elemental disks will be

$$dM_0 = \omega^2(\delta \pm X \sin\phi)(L \pm X\cos\phi)dm$$

Since ϕ is small, $\sin\phi = \phi$, and $\cos\phi = 1$.
Therefore

$$dM_0 = \omega^2(\delta \pm X\phi)(L \pm X)dm$$

The signs are positive when dm lies beyond the center of gravity of the whole mass and are negative when dm lies within the center of gravity.

Summing up moments within the center-of-gravity point

$$M_1 = \omega^2(\delta L\int dm - \phi L\int Xdm - \delta\int Xdm + \phi\int X^2dm)$$

Summing up moments beyond the center-of-gravity point

$$M_2 = \omega^2(\delta L\int dm + \phi L\int Xdm + \delta\int Xdm + \phi\int X^2dm)$$

By definition, $\int Xdm$ is of the same magnitude on either side of the center of gravity. Therefore in the addition of M_1 and M_2 the terms containing $\int xdm$ with opposite signs will cancel out, and the total moment at point 0 due to transverse loading is as follows

$$M_0 = M_1 + M_2 = m\omega^2\delta L + \omega^2\phi\int X^2dm$$

The total bending moment at point 0 due to the rotating disk becomes

$$M_B = M_0 - M$$
$$= m\omega^2\delta L + \omega^2\phi\int X^2dm - \omega^2\phi\int Z^2dm$$
$$= m\omega^2\delta L - \omega^2\phi(A - B)$$

The foregoing derivation is further proof that error is involved when the rotating disk is considered as a mass concentrated in a thin disk of thickness dX. It is also interesting to note that for a sphere $A = B$, and there would be no change in moment due to gyroscopic effect as applied to the rotating case.

A. M. G. Moody.[4] To be seen in perspective, the author's method should be compared with the many methods which have been developed in the past for calculating critical speeds. A work by Holba[5] presents more than a dozen methods, all about equally frightful to apply. To be sure, for lowest critical speeds of relatively simple shafts, present methods, as described in the standard works of Timoshenko and Den Hartog, are perfectly

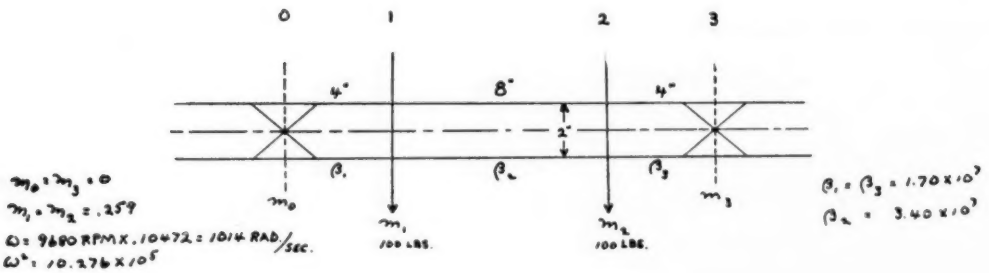
[1] By M. A. Prohl, published in the September, 1945, issue of the Journal of Applied Mechanics, Trans. A.S.M.E., vol. 67, p. A-142.

[2] Assistant Engineer, Blower and Compressor Department Allis-Chalmers Manufacturing Company, Milwaukee, Wis. Jun. A.S.M.E.

[3] "Mechanical Vibrations," by J. P. Den Hartog, McGraw-Hill Book Company, Inc., New York, N. Y., second edition, 1940, pp. 296–298.

[4] Chief Blower Engineer, Elliott Company, Jeannette, Pa., formerly Chief Research Engineer, De Laval Steam Turbine Company, Trenton, N. J. Mem. A.S.M.E.

[5] "Berechnungsverfahren zur Bestimmung der kritischen Drehzahlen von geraden Wellen," by J. J. Holba, J. Springer, Vienna, 1936.



m	ΔV	V	ΔX	ΔM	M	$\frac{M}{2}$	$\frac{M}{6}$	$\frac{M'}{M''}$	$\beta \times 10^7$	$\frac{\beta M'}{\beta M''}$ $\times 10^7$	$\frac{\Delta Y'}{\Delta X}$ $\times 10^7$	ΔX	$\Delta Y'$ $\times 10^7$	$\Delta Y''$	Y $\times 10^7$	$m\omega^2$	θ $\times 10^7$
0	0	1.000			0	0	0	.667	1.70	1.134	.134	4.00	4.536	0	0	0	0
		1.000	4.00	4.00	4.00	1.333	.667	1.333		2.267					4.536	.266 x 10^6	
1	.121	1.121	8.00	8.968	12.968	4.323	2.161	3.494	3.40	1.880	5.281	8.00	122.25	0	126.79	.266 x 10^6	
								4.990		16.966							
2	3.373	4.494	4.00	17.976	30.944	10.315	5.157	9.480	1.70	16.116	48.363	4.00	193.45	0	320.24	0	69.57
3	0							12.476		21.209							
										69.572							
0	0	0			0	0	0	0	1.70	0	0	4.00	0	4.00	0	0	1.00
		0	4.00	0	0	0	0	0		0					4.00	.266 x 10^6	
1	.106	.106	8.00	.848	.848	.283	.141	.141	3.40	.479	.479	8.00	3.832	8.00	15.83	.266 x 10^6	
								.283		.962							
2	.421	.527	4.00	2.108	2.956	.985	.493	.776	1.70	1.319	2.760	4.00	11.040	4.00	30.87	0	5.67
3	0							1.126		1.914							
										4.674							

FIG. 2 DEMONSTRATION OF AUTHOR'S METHOD OF CALCULATING CRITICAL SPEEDS

satisfactory. But the writer agrees with the author that no method based upon the Rayleigh approach that has to his knowledge been presented for higher critical speeds can compare with this as a practical working method.

A suggestion, however, is in order: The example given in the paper is very complicated. Admittedly, this is the type of problem which shows the new method to the best advantage. Nevertheless, it would be easier to master the procedure if a simple example, easily checked in the handbooks, were given. This would also tend to build confidence in the method since no one ever questions a handbook result.

The writer has therefore taken it upon himself to give a crude illustration of what he means. The example, Fig. 2 of this discussion, shows a two-bearing shaft, 2 in. diam, 16 in. between bearing centers, with two 100-lb loads each 4 in. from a bearing. The critical speed calculated from the formula given in Marks's handbook is 9680 rpm. Starting with this as an assumed speed and applying the author's method, we find, as would be expected, that we have no residual moment.

From Fig. 2

$$y_3 = (320.24 \times 10^{-7}V_0) + (30.87 \times 10^{-7}\theta_0) = 0$$

$$\theta_0 = -\frac{320.24}{30.87} \quad V_0 = -10.37V_0$$

$$M_3 = 30.94V_0 + 2.956\theta_0$$
$$= 30.94V_0 - 30.65V_0$$

H. PORITSKY.[6] We believe that the author's method is far superior to methods at present available and in common use This is particularly true when it comes to the calculation of the second and third critical speeds and also for rotors with multiple bearings and overhanging spans.

The methods commonly employed for critical-speed calculations are based upon Rayleigh's method and consist in assuming the shape of vibration, calculating the potential and kinetic energies, and computing the natural frequency from the ratio of these two. This procedure is justified by the fact that a first-order departure in the assumed shape of vibration from the true shape results only in a second-order error in the frequency. Moreover, the lowest critical is lower than any frequency which can be obtained by the foregoing method. In calculating the lowest frequency, it is customary to assume a deflection shape equal to the gravity deflection. This calculation may be improved by replacing the gravity weights by centrifugal loads derived from the gravity deflection and determining the resulting deflection; by similar further repetition the lowest critical can be accurately obtained.

When it comes to the higher critical, however or to rotors with several spans, it is clear that the gravity deflection is a very poor approximation, and various rather arbitrary schemes, all of them ill-founded, have been used for guessing the shape which will form the starting point of the calculations. With a poorly guessed shape the discrepancy between the computed vibration frequency and the true values of critical frequencies is likely to be considerable. Furthermore, for the second and higher critica s, an assumed shape may lead to a frequency which is either higher or lower than the true frequency, and it is impossible to tell which of two calculations is to be preferred.

Finally the foregoing method of iteration, which converges for the lowest critical, does not converge when applied to the higher critical speeds, unless the assumed shape satisfies a proper "orthogonality condition" relative to the shapes of the lower critical speeds. This condition is rather inconvenient to apply and only multiplies the uncertainties of the existing methods of computing critical speeds.

[6] Engineering General Division, General Electric Company, Schenectady, N. Y. Mem. A.S.M.E.

As compared with the uncertainties mentioned, the method developed by the author is clear-cut and straightforward. It consists essentially in numerical integration of the differential equation of beam deflections for an assumed frequency. Since proper boundary conditions apply at either end of each span, two solutions have to be obtained over each span before all of the boundary conditions can be satisfied. Two or more frequencies have to be tried before the true critical frequency is determined by the vanishing of a proper residual moment.

The interpretation in terms of a finite number of thin disks on a massless shaft is illuminating and makes the method similar to Holzer's method for torsional vibrations. It will be noted that in the latter domain, Holzer's method has been universally adopted even though the Rayleigh method of assuming shapes is available here, too. It is the writer's opinion that a similar situation will soon obtain in the field of critical speeds of rotors, and the enthusiasm of several people who have tried the method in cases where long involved calculations hitherto have yielded relatively uncertain information only serves to corroborate it.

It may be pointed out in conclusion that the integration of the deflection may be carried out by means of the differential analyzer, though as many distinct solutions would still have to be obtained before the boundary conditions can be satisfied as outlined herein.

ERNEST L. ROBINSON.[7] This paper makes a very definite contribution to the technique of computation of the transverse critical speeds of rotating shafts, especially a shaft with several spans; it is bad enough to get the transverse critical speed of a single span by equating kinetic energy of rotation to the internal energy of bending for a variety of assumed deflection curves. This much-used technique works when one has a fairly good notion of the true shape. It is not necessary to be too precise but it is necessary to be pretty good. It is easily possible to be pretty bad. The likelihood of being pretty bad increases greatly when the arrangement of loadings and shaft diameters becomes complex and it gets almost hopeless with several spans. There is no doubt that skillful estimates are possible by existing methods, especially when the approximate answer is known from long experience. But when that is not the case, a straightforward way to proceed is most welcome indeed.

The writer recently sent the author the loadings and diameters for a complex four-bearing tandem-compound turbine generator set which had been the basis of analysis for several months. It must be admitted that these were wartime months and help was limited. However, using less than a week's time of one expert comptometer operator, the author produced the first critical speed, including its actual deflection curve and handed it to the writer at the meeting when he presented his paper. The calculations agreed closely with tests which had just been made on a dynamically similar model, both as regards frequency and shape of the deflection curve.

The paper, of course, still leaves to experienced engineering judgment the questions as to whether shaft speed should be restricted to values below the first critical or whether it is preferable to run through one or more critical speeds and operate at or between higher critical speeds.

STANLEY THOMPSON.[8] In his abstract, the author states that the Stodola process for finding critical speeds lacks generality in that critical speeds other than the fundamental cannot be determined definitely.

[7] Turbine Engineering Department, General Electric Company, Schenectady, N. Y. Mem. A.S.M.E.

[8] Design Development Engineer, Westinghouse Electric Corporation, Aviation Gas Turbine Division, Lester, Pa.

Den Hartog[9] gives a formula

$$a_n = \frac{\int_0^l \mu_1(x) y(x) y_n(x) dx}{\int^l \mu_1(x) y_n^2(x) dx}$$

by use of which the Stodola process is generalized to higher modes. By evaluating a_n the amount of any known mode present in an arbitrary curve can be determined and the mode removed. By the reasoning used by Den Hartog,[10] if the first mode, for instance, is removed, the Stodola process converges to the second mode.

The amount of work involved in the Stodola process is quite comparable to that in the present paper, since essentially the same operations are performed, but in different order. For the calculation of a first-mode critical, approximately the same number of trials would be needed to find the frequency by either method.

With the author's method it is possible to calculate any desired mode without determining lower modes which is not possible with the Stodola process.

AUTHOR'S CLOSURE

The author wishes to thank Messrs. Ehlinger, Moody, Poritsky, Robinson, and Thompson for their constructive comments.

Mr. Ehlinger has presented an alternative derivation for the "gyroscopic effect" due to the disk moment of inertia. This confirms the momentum analysis used in the paper. He points out that for a sphere the two moments of inertia A and B are equal and therefore the gyroscopic effect disappears. This condition also exists for the case of a thick disk, as may be seen by examining Equations [51] and [52] of the paper

$$A = B, \text{ when } \frac{h}{D} = \sqrt{\frac{3}{4}} = 0.866$$

where: h = axial thickness
D = diameter

The author is indebted to Mr. Moody for a sample calculation dealing with a very simple rotor. This makes a valuable addition to the paper.

Dr. Portisky has presented an excellent comparison of various critical-speed calculation methods with which the author is in complete accord.

Mr. Robinson has indicated the difficulties which arise in applying Rayleigh's method. It should be pointed out that this method usually gives good results for the first critical speed of single-span rotors if the assumed deflection curve is taken equal to the static deflection curve. The first critical speed of two-span rotors and some three-span rotors can often be calculated with sufficient accuracy if a static deflection curve is used where the direction of the gravity loading is reversed in going from one span to the next. For the calculation of the first critical speed of complicated multispan rotors Rayleigh's method does not provide a satisfactory line of attack; and for the calculation of higher critical speeds the basic principle of the method is not applicable. Incidentally, the second as well as the first critical speed was calculated by the author for the four-bearing turbine generator set mentioned by Mr. Robinson.

Mr. Thompson has taken exception to the following statement in the abstract of the paper ". . . the methods for which the computations are comparatively simple, such as the familiar methods of Rayleigh and Stodola, lack generality in that critical speeds other than the fundamental cannot be definitely determined." The Stodola method to which reference is made is the simple itera-

[9] Reference 3 of Ehlinger discussion, "Mechanical Vibrations," p. 193.

[10] Ibid., pp. 194–196.

tion procedure described in detail by Den Hartog[11] which converges only for the fundamental mode of vibration. This method can be modified or generalized as pointed out by both Mr. Thompson and Dr. Poritsky, so that higher critical speeds can be evaluated, but when this method is thus generalized it does not appear to the author that the calculation procedure will be as practical or straightforward as that given in the author's paper.

Messrs. N. A. Boukidis and R. J. Ruggiero in a recently published paper[12] give a working procedure for calculating natural-frequencies which is based on this generalization of the Stodola process. One disadvantage of their procedure is the large number of significant figures which must be carried in the computations in order to get definite values for the higher criticals, and these authors make the following recommendation ". . . the safest procedure is to retain as many significant digits as the calculating machine to be used will handle."

The Effect of Triaxiality on the Technical Cohesive Strength of Steels[1]

L. R. Jackson.[2] Through the use of some exceptionally carefully obtained data on the strength of notched steel bars, the authors have made a distinct contribution to the difficult problem of fracture under combined stresses.

Their interpretation of their results depends to a large extent upon the premise that, after a small amount of plastic flow has relieved stress concentration, both the longitudinal and radial stresses are substantially uniformly distributed over the base of the notch.

This premise and its consequences deserve some further comment.

Assuming that the premise is true, one of the methods they have used to compute the radial and circumferential stresses is through the use of Equation [5], which involves the measurement of stress at maximum load for both notched and unnotched bars.

There is some recent information, not cited by Sachs and Lubahn, which provides further support for this method of computation.

As they point out, this computation depends upon three assumptions (in addition to the assumption of uniform stress distribution):

1 That the metal flow obeys either the "maximum shear condition" or the "energy of distortion condition."

2 That the maximum load is reached after the same amount of flow in both the notched and unnotched bars.

3 That a given amount of flow results in the same state (hardness) of the metal regardless of stress system under which that amount of flow was obtained.

The first of these assumptions has a rather extensive experimental background, and while the last two assumptions would appear in any case to be good approximations there is some additional evidence supporting them.

Regarding assumption 2, Gensamer[3] has shown that in a simple tension test the maximum load is reached when

$$\frac{dS_0}{d\delta} = S_0 \qquad [1]$$

where S_0 is the tensile stress and δ is the true strain.

Or that

$$\delta = \int_{S_{0y}}^{S_{0m}} \frac{dS_0}{S_0} = \ln \frac{S_{0m}}{S_{0y}} \qquad [2]$$

where S_{0m} is the stress when maximum load is reached and S_{0y} is the stress when plastic flow begins.

Assuming with the authors that enough plastic flow has occurred to eliminate stress concentration, and make Equation [5] of the paper

$$\frac{S_T}{S_L} = 1 - \frac{S_0}{S_L} = k \text{ (a constant)} \qquad [3]$$

The load L at any time during plastic flow as measured on a tensile machine is

$$L = S_L A \qquad [4]$$

where A is the instantaneous area and can be computed from the relation

$$\delta = \ln \frac{A_0}{A}$$

$$A = A_0 e^{-\delta} \qquad [5]$$

from Equation [3]

$$S_L = \frac{S_0}{1 - k}$$

and

$$L = \frac{S_0}{1 - k} A_0 e^{-\delta} \qquad [6]$$

At maximum load, $dL = 0$ or

$$dL = \frac{A_0}{1 - k} e^{-\delta} dS_0 - \frac{A_0}{1 - k} e^{-\delta} S_0 d\delta = 0 \qquad [7]$$

from which

$$\frac{dS_0}{d\delta} = S_0 \qquad [8]$$

This is identical with Equation [1] of this discussion, obtained for simple tension, and indicates that except for the small amount of flow required to eliminate stress concentrations and establish $\frac{S_T}{S_L} = k$, the true strain is the same at maximum load for both notched and unnotched bars.

With respect to the third assumption, Bridgman[4] has recently obtained some data indicating that if a steel is plastically deformed by a combination of hydrostatic pressure and tension and subsequently tested in simple tension, the true stress - true strain curve so obtained is a prolongation of the one obtained in simple tension, and starts at the point which would be predicted from the amount of strain it had previously received under combined stresses. That is, at least for combinations involving hydrostatic pressure and tension, it appears that strain-hardening does not depend to a large extent upon the stress system producing that hardening.

[11] "Mechanical Vibrations," by J. P. Den Hartog, McGraw-Hill Book Co., Inc., New York, N. Y., second edition, 1940, pp. 188–192.

[12] "An Iterative Method for Determining Dynamic Deflections and Frequencies," by N. A. Boukidis and R. J. Ruggiero, *Journal of he Aeronautical Sciences*, vol. 11, no. 4, October, 1944, pp. 319–328.

[1] By George Sachs and J. D. Lubahn, published in the Dec., 1945, issue of the Journal of Applied Mechanics, Trans. A.S.M.E., vol. 67, p. A-241.

[2] Research Supervisor, Battelle Memorial Institute, Columbus, Ohio. Mem. A.S.M.E.

[3] "Yield Point in Metals," by M. Gensamer, Trans. A.I.M.E, vol. 128, 1938, pp. 104-117.

[4] "Effects of High Hydrostatic Pressure on the Plastic Properties of Metals," by P. W. Bridgman, *Reviews of Modern Physics*, vol. 17, 1945, pp. 3–14.

While the foregoing arguments support the method used by the authors to compute the triaxiality of the stress system, the validity of the method still rests on the premise that the stress distribution is substantially uniform. The authors present indirect evidence that this is correct; however, it might be possible to produce an experimental proof which should be quite convincing along the following lines:

As the authors have pointed out, it is difficult experimentally to produce a known hydrostatic tension; however, it is relatively easy to produce known hydrostatic compression. If notched bars similar to those used by Sachs and Lubahn were pulled under hydrostatic pressure, it should be possible to use a value of pressure which would just cancel the hydrostatic tension as computed by their methods. If their initial premise is correct and the hydrostatic tension provided by the notch is substantially constant, then the bars should break as though the stress applied were simple tension.

D. J. McAdam, Jr.[5] The comment made in the paper concerning the investigation of technical cohesive strength by the writer and associates may give an incorrect impression to those who have not read our papers. The first of these comments is "...only a limited amount of information of a rather speculative nature is available regarding the effect of triaxiality on the cohesive strength (17, 18)."[6] The amount of information obtained in our investigation, however, is not limited to the two papers (17, 18), but has been presented in six papers. Three of these are more recent than the two papers mentioned and two of the three have been in print for $1^1/_4$ and $2^1/_4$ years, respectively. A list of six papers (*a* to *f*), together with three additional papers (*g*, *h*, *i*), which are now preprinted, appears at the end of this discussion. Far from being merely "speculative," these papers present the results of extensive experiments on a great variety of ferrous and nonferrous metals, in various conditions as regards heat-treatment and work hardening. The temperatures range between room temperature and —188 C. The notched tensile specimens used varied widely in notch depth, notch angle, and root radius.

The derived curves of variation of strength and ductility with notch angle and with notch depth made it possible to distinguish the influences of the transverse radial stress and the stress concentration, and to reveal the influence of the radial-stress ratio (ratio of mean transverse radial stress to mean longitudinal stress) on the breaking stress. Each of the papers (*a* to *i*) shows that the "technical cohesion limit" tends to increase with increase in the radial-stress ratio and does so increase unless the influence of the radial-stress ratio is masked by associated variations of the stress concentration and ductility. It was also stated that the "technical cohesive strength" (a property of the metal) of a brittle metal may be represented by a curved surface in a diagram with the three principal stresses as co-ordinates, and that the "initial" technical cohesive strength of a ductile metal may be pictured approximately by a similar surface outside the surface representing yield but inside the generally more complex surface representing fracture, after the varying plastic deformation due to the varying ductility. Any point on such a surface represents a technical cohesion limit.

It was also reported that plastic deformation increases the technical cohesive strength continuously, at a decreasing rate, and only slightly less rapidly than it increases the flow stress. It was shown in numerous diagrams that this small differential effect of plastic deformation accounts for the wide variations of ductility with the radial-stress ratio and with other factors that have even slight differential effect on flow stress and cohesion limit.

In a previous paper by the authors (9) is the following statement: "The cohesive strength of a heat-treated steel increases with increasing triaxiality, only slightly less rapidly than the flow stress (shear stress), confirming McAdam's conceptions. The closeness of these two relations accounts for the rapid changes from a ductile to a brittle condition, which may be caused by rather small changes in metal structure or type of load application." A less complete statement of the same ideas is given by the authors in the third conclusion of their present paper.

The evidence for the first conclusion stated at the end of the paper now under discussion does not appear convincing. Moreover, even if the ratio between the mean radial and longitudinal stresses does remain constant throughout the first 5 per cent of strain, there is much redistribution of both stresses, and the ratio between the radial and longitudinal stresses at the origin of fracture probably differs considerably from the initial ratio of mean values. The values for radial-stress ratio used in the writer's diagrams were obtained by an empirical method, and the diagrams represent qualitatively the variations of strength and ductility with the radial-stress ratio. The authors' implication that our empirical derivation is similar to theirs is incorrect (*c*, *d*).

Results of our experiments (*c*, *d*, *e*, *f*, *g*) indicate that the second conclusion presented by the authors is not generally correct. Many of our curves of variation of strength and ductility with the notch angle show clearly that plastic deformation of only 2 per cent leaves an objectionable amount of stress concentration, in some metals at least, when the initial stress concentration is high. The amount of plastic deformation required for satisfactory reduction of the stress concentration varies with the metal, with the notch characteristics, and with the temperature. This amount of plastic deformation sometimes is as high as 30 per cent, and stress concentration may affect the entire flow-stress curve to the point of fracture. The explanation for the slow relief of initially high stress concentration probably is that plastic deformation causes first a quick partial relief of the concentration but that the relief of stress concentration is associated with the development of a deformation gradient and a resultant hardness gradient. Because of this hardness gradient, further diminution of stress concentration is relatively slow. Moreover, the evidence presented by the authors for their second conclusion is not convincing, but may be interpreted in different ways which cannot now be discussed.

The linear variations of cohesion with plastic strain, represented in Fig. 19 of the paper, is not in accordance with the evidence obtained in our experiments with metals that had been cold-worked various amounts. Moreover, as the increase of cohesive strength with plastic deformation is the result of work-hardening, it would be expected that the increase would be at a decreasing rate, qualitatively similar to the increase of the flow stress. As the rate of work-hardening of heat-treated steels, such as those used by the authors, is relatively slow, the curvilinear variation of the cohesive strength would be less prominent than if they had used metals that harden rapidly with plastic deformation.

The fourth conclusion by the authors is of some value as an empirical criterion. In a paper (*i*) now preprinted, the writer discusses the complete three-dimensional diagram representing fracture, and concludes that fracture is determined by a limiting value of some shearing stress, either the maximum shearing stress or the octahedral shearing stress. This critical shearing stress, however, is not constant, but decreases with increase in the volume stress and becomes zero when the stress is polar-symmetric ($S_1 = S_2 = S_3$).

[5] Metallurgist, U. S. Department of Commerce, National Bureau of Standards, Washington, D. C.

[6] Numbers in parentheses refer to the Bibliography which was published at the end of the original paper.

REFERENCES

(*a*) "The Technical Cohesive Strength of Metals," by D. J. McAdam, Jr., JOURNAL OF APPLIED MECHANICS, Trans. A.S.M.E., vol. 63, 1941, p. A-155.

(*b*) "The Technical Cohesive Strength and Yield Strength of Metals," by D. J. McAdam, Jr., American Institute of Mining and Metallurgical Engineers, Tech. Pub. no. 1414, January, 1942; also Transactions, vol. 150, Iron and Steel Division, 1942, pp. 311–357.

(*c*) "An Investigation of the Technical Cohesive Strength of Metals," by D. J. McAdam, Jr., and R. W. Mebs, American Institute of Mining and Metallurgical Engineers, Tech. Pub. no. 1615; Metals Technology Division, vol. 10, 1943.

(*d*) "The Technical Cohesive Strength and Other Mechanical Properties of Metals at Low Temperatures," by D. J. McAdam, Jr., and R. W. Mebs, Proceedings of the A.S.T.M., vol. 43, 1943, p. 661.

(*e*) "The Variation of the Strength, Resistance to Oxidation, and Electrical Conductivity of Metals With Temperature," by D. J. McAdam, Jr., and G. W. Geil, Trans. A.S.M., vol. 33, 1944, pp. 514–534.

(*f*) "The Technical Cohesive Strength of Metals in Terms of the Principal Stresses," by D. J. McAdam, Jr., American Institute of Mining and Metallurgical Engineers, Tech. Pub. no. 1782; Metals Technology Division, vol. 11, 1944, p. 31.

(*g*) "The Effect of Combined Stresses on the Mechanical Properties of Steels Between Room Temperature and —188°C," by D. J. McAdam, Jr., G.W. Geil, and R. W. Mebs, Preprint No. 22, A.S.T.M., 1945.

(*h*) "The Effects of Combined Stresses and Low Temperatures on the Mechanical Properties of Some Non-Ferrous Metals," by D. J. McAdam, Jr., G. W. Geil, and R. W. Mebs, Preprint No. 18, A.S.T.M., 1945.

(*i*) "Fracture of Metals Under Combined Stresses," by D. J. McAdam, Jr., Preprint No. 29, A.S.T.M., 1945.

CLARENCE ZENER[7] AND J. H. HOLLOMON.[8] On their first reading of this paper the writers were skeptical of the conclusions contained therein that the technical cohesive strength increases with increasing triaxiality. They therefore examined the original data contained in the authors' previous paper (9) in an attempt to see if the influence of strain could be more completely eliminated. This paper contains the data for five tests of the S.A.E. steel heat-treated to the 220,000-psi strength level in which the strain at fracture lay within the narrow range from 0.026 to 0.028. These data are presented as Fig. 1 of this discussion. The conclusions reached by the authors are apparently incontrovertible.

[7] Institute for the Study of Metals, University of Chicago, Chicago, Ill.

[8] Captain, Ordnance Department, Watertown Arsenal, Watertown, N. Y.

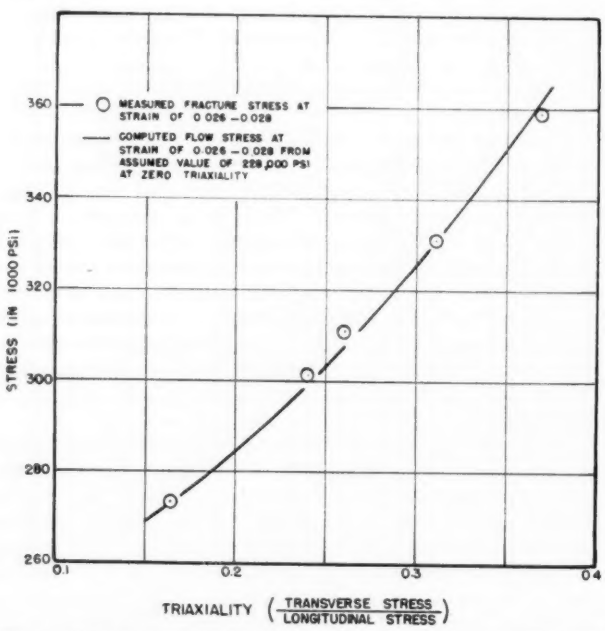


FIG. 1 DEPENDENCE OF FRACTURE STRESS UPON BIAXIAL TENSION

At fracture the flow stress intersects the virtual cohesive stress. The measured fracture stresses in the strain range 0.026 to 0.028 should therefore also be the flow stresses at the same value of the triaxiality. In order to test this viewpoint a flow stress curve was computed as a function of the triaxiality and this curve is also shown in Fig. 1. Complete agreement is obtained.

AUTHORS' CLOSURE

Mr. Jackson offers proof for the validity of our assumption that the ultimate strength values for notched and unnotched specimens, respectively, can be taken as the stresses the ratios of which depend primarily on the magnitude of the (average) transverse stress relative to the (average) longitudinal stress. It should be pointed out, however, that whereas the theoretical analysis of the maximum load strains referred to by Mr. Jackson should apply correctly for conditions where the stress and strain are uniformly distributed over the cross section, the stress and strain gradients present in notched specimens may be such that the necking strain for the notched specimen might be considerably different from that of the unnotched specimen. The stress-concentration factor is reduced practically to unity after a small plastic strain has occurred, i.e., it is reduced to a value which has a negligible amount of effect on the stress at fracture. However, the small stress-concentration factor which remains after a small plastic strain has occurred and the changes of this quantity with further plastic flow may be sufficiently large to affect the shape of the stress-strain curve, and thus also the maximum load strain, or "necking strain." Furthermore, the triaxiality may depend slightly on the amount of strain (because of changes in notch contour, for example) and this also would affect the shape of the stress-strain curve and the necking strain for the notched specimen. The magnitude of the effects which small changes in the triaxiality and stress-concentration factor may have on the necking strain is indicated by data on heat-treated steels presented in a previous publication.[9] According to these results, the necking strain may be higher for a notched specimen than for an unnotched specimen, and apparently increases with increasing notch depth. For other materials, however, particularly those possessing large strain-hardening rates, the necking strain of a notched specimen may be considerably less than that of an unnotched specimen of the same materials, as follows:

CONVENTIONAL LONGITUDINAL NECKING STRAIN

Type of specimen	Copper	Mild steel
Unnotched, per cent	53	31
Notched, per cent	43	22

Regarding Mr. McAdam's comments, we feel that the value of his work is generally recognized, particularly regarding the wide range of variables he has investigated, and we have expressed this in our paper. On the other hand, it appears that many others feel, with us, that a complete understanding of the notched tensile test cannot be reached without an extensive fundamental investigation under conditions which reduce the number of variables to a minimum. According to the most basic laws of research, definite and generally recognized conclusions can be drawn only from series of tests in each of which all the variables have been eliminated except one and which therefore require a long and tedious procedure if the validity of any general conception is to be proved conclusively. Our efforts have been primarily in this

[9] "Notched-Bar Tensile Tests on Heat-Treated Low-Alloy Steels," by G. Sachs and J. D. Lubahn, Trans. American Society for Metals, vol. 32, 1943, pp. 125–158, Fig. 7.

direction, and consequently the experimentation has been aimed at a study of the effect of one variable at a time. Certainly, the last word regarding the dependence of the conditions at fracture upon the state of stress has not yet been spoken. Many extensive additional investigations will be required to establish the basic function which has so far been found to be particularly elusive.

There is one factor regarding notched tensile tests which perhaps should be clarified at this time. This is the dependence of the triaxiality upon progressive plastic strain. It has been mentioned in the paper that nearly the same triaxiality value was obtained by measurements in the elastic region and after a rather small amount of plastic strain, say, five per cent. For very large plastic strains it is recognized that appreciable variations in triaxiality might occur, especially because of changes in the notch contour, and possibly also because of small changes in stress-concentration factor and deformation gradient.

VARIATIONS IN TRIAXIALITY WITH PLASTIC STRAIN

	Plastic strain per cent	Triaxiality
Copper	2	0.32
	50	0.17
Heat-treated low-alloy steel	2	0.33
	13	0.29

It should be observed that the larger the plastic strain involved, the larger is the variation in triaxiality. Certainly, over the range of strains investigated in the paper, it may be concluded that variations in triaxiality may be neglected.

We are particularly indebted to Messrs. Zener and Holloman, who obtained quantitative agreement with our analysis by a different approach, and who have thereby contributed significantly to a more basic understanding of the notched tensile test.

Stresses in a Cylindrical Shell Due to Nozzle or Pipe Connection[1]

WALTER SAMANS.[2] The work done in these tests confirms what has always been the supposed type of deformation in the shell of a drum subject to internal pressure at a point where piping was attached. As the authors point out, it is not complete and needs to be supplemented by a whole series of tests to become of use to the designer.

It is not possible to have codes for boilers or pressure vessels show methods of computation for all types of loadings on the vessel causing secondary stresses, although there is a tendency to keep adding that type of information in appendixes. The general acceptance of that practice would depend on whether or not it is agreed that codes shall become a handbook of engineering information. It would seem better that such data be collected and published separately, letting the codes be the guide on the selection of materials and working stresses as applied to the membranes of vessels.

The test was made on a type of shell having two different thicknesses and, as the authors acknowledge, too short to avoid the effect of the end restraint. There was no opportunity to apply internal pressure to the shell, and this would indicate that the outward deformation, where the maximum tensile stress existed axially in the attached pipe, would not be decreased or increased by internal pressure, while the compressive forces on the opposite side would be reduced.

For every combination of shell diameter and thickness, with diameter and thickness of attached pipe, there would be an internal pressure at which the deformation would be substantially the maximum. In the test, the pipe attached to the thin shell had better be reinforced as would be required by code rules, to get a true comparison with practice. As the pipe becomes larger it may be found that the reinforcement should continue around the connected pipe as a ring; although it is recognized that the authors have confined this particular paper to ordinary sizes of pipe connections on boiler drums.

In the particular assembly, there may have been some condition of restraint imposed by the half of the vessel of greater thickness on the thinner wall, and likewise proportionately less restraint by the half of the vessel having the thin wall on the deformation due to the loading of the pipe inserted in the thick wall.

For the application of this principle to large drums at high temperatures, as used in the oil-refining industry and in which sizes of connected piping may be as much as 30 in., the effort in design is to minimize the travel of the pipe near the drum by proper expansion joints and support independent of the vessel. Therefore, the amount of deflection in the pipe should be segregated between that due to the flexure in the pipe itself and that due to distortion in the vessel wall around the connection. For that segregation, it is necessary or at least seems desirable to reproduce the pressure in the vessel. In this connection there is no indication that the experiment reported in this paper could include the out-of-roundness in diameter produced by the loads on the piping. With two-way stresses existing in the shell, the deformations are not strictly a measure of stress, and in fact the stress may be higher than the deformation indicates due to Poisson's ratio.[3]

On the whole, however, this experiment indicates the need for further work of the same kind, but carried out more extensively. For instance, there might be two models each longer than used here, in which various sizes of pipe are attached in a row in sufficient distance from each other. These pipes could be of different lengths, the larger pipe being at the top and the longest, and so on down. This might permit simultaneous loadings or loadings applied on each pipe in turn without much effort in changing the attachment. In order to obtain the full value of such tests and retain the value of balanced loading, a symmetrical arrangement of piping on both sides similar to the original tests could be used. There should be two separate cylinders of different thicknesses and then the connection of the pipe to the cylinder could be made in a different manner on opposite sides, particularly as to the type of ring reinforcement around the pipe to maintain the circular shape. This should produce less distortion in the shell.

The tests could also be amplified to take care of torsional moments on the pipe.

Altogether the authors have opened up by direct action a new field of investigation in connection with the safe use of pressure vessels which has been too long deferred.

AUTHORS' CLOSURE

Mr. Samans' comments are well applied to this paper and are very much appreciated by the authors. He brings in the question of whether or not methods of computation for loadings causing secondary stresses should be included in codes for boilers or pressure vessels. The authors agree with him that the subject has not reached the stage where this could intelligently and simply be accomplished.

As pointed out by Mr. Samans, it is true that many other arrangements could be adapted, including adding of reinforcing pads around the connections to the shell which would provide additional data and which certainly should be given full considera-

[1] By G. J. Schoessow and L. F. Kooistra, published in the June, 1945, issue of the JOURNAL OF APPLIED MECHANICS, Trans. A.S.M.E., vol. 67, p. A-107.

[2] Administrative Engineer, Sun Oil Company, Philadelphia, Pa. Mem. A.S.M.E.

[3] Unless a correction was made to allow for this.

tion if additional tests are contemplated by any of our readers.

Regarding the question of deformations not strictly a measure of stress, it may be pointed out that the stresses reported in the paper were the results of two-dimensional strain-gage readings that were corrected for deformation due to Poisson's ratio and therefore in so far as the authors know are correct and true stresses. In points where the direction of the principal stresses was not known, strain-gage rosettes were used to determine both direction and magnitude. By Mr. Samans' footnote comment,[3] he appreciates that possibly this correction was made.

As pointed out in the paper, the authors realize that this is just the beginning of the accumulation of actual data on a construction that is commonly used today and in which the value of secondary stresses becomes more important as higher design membrane stresses are allowed and the vessel walls become correspondingly thinner and have less margin of working stress available to absorb these secondary bending stresses.

We hope that this paper will help to stimulate thinking along the proper lines and will lead to additional strain-gage investigations and mathematical analyses.

Experimental Investigation of Turbulence Diffusion—A Factor in Transportation of Sediment in Open-Channel Flow[1]

A. A. KALINSKE.[2] The writer has been carrying on experimental investigations on the subject of the author's paper for several years and he is gratified to note that the author's final conclusions are, in general, in agreement with his. Several years ago, in conversation with the writer, the author expressed the opinion that the curve relating the mean-square deviation of the globules to the downstream distance did not approach a straight line. The writer strongly disagreed, as his own data indicated otherwise, and also he stated that if a straight line were not approached this would indicate an infinite scale for the turbulence which, of course, is physically impossible in a finite channel. The writer is pleased to note that the author now comes to a similar conclusion.

The mere fact that a power law fits the experimental data does not indicate that such a law is physically correct. Power laws can be made to fit data; however, the derivatives or integrals obtained from such power laws may give results physically impossible. If such is the case, there is no particular significance in considering such a law.

The writer, in the past, has used the globule-injection and photographic method for obtaining eddy-diffusion data; however, the use of another method, described in a recent paper[3] by the writer, has given much better results and was much less laborious; this method consisted of injecting into the flowing water a mixture of hydrochloric acid and alcohol, the proportions adjusted to the density of the water, and then taking samples of the water at various points downstream. If samples are taken for 1 min or longer, the sample has a true average concentration of the injected mixture. The sample is then analyzed for chloride concentration, which is a fairly simple procedure.

Others, including the writer, have made investigations relating to turbulence diffusion and have published their results; however, the author appears to have overlooked these references.[4] The writer believes they should be included in author's bibliography.

H. W. LIEPMANN.[5] The author's method of measuring some characteristics of turbulent motior is a welcome addition to the experimental technique used in the study of turbulent flows.

The evaluation of these measurements using the exponential correlation law is very interesting. The exponential law has been found, in numerous investigations of isotropic turbulence in air, to approximate the actual correlation curve very closely except near the origin. Hence the writer agrees with the author that it is more reasonable to fit the measurements to the exponential curve than to a power law. The results obtained by the author for the magnitude of the fluctuation level $\frac{\sqrt{\overline{v^2}}}{U}$ can be compared roughly with measurement of the same quantity in the turbulent boundary layer near a flat plate carried out in a wind tunnel at the California Institute of Technology, with the use of hot-wire anemometers. Fig. 1 of this discussion gives a comparison between the author's results for $\frac{\sqrt{\overline{v^2}}}{U}$ as a function of the wall distance y (curve I) and the direct hot-wire measurements in the boundary layer (curve II).

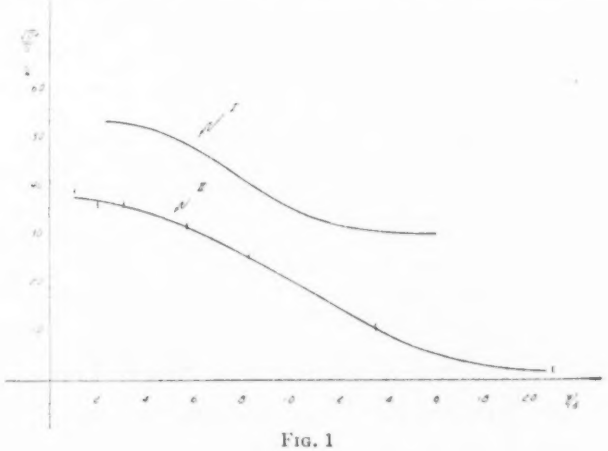


FIG. 1

The boundary-layer thickness δ for the water-channel measurements was taken as 4.8 in., corresponding roughly to the distance from the wall in which the mean velocity U varies. It is seen that for $\frac{y}{\delta} < 1$, the behavior of $\frac{\sqrt{\overline{v^2}}}{U}$ is quite similar in the two cases. The absolute magnitude of $\frac{\sqrt{\overline{v^2}}}{U}$ is somewhat larger in the water channel as compared with the boundary-layer measurements. For $\frac{y}{\delta} > 1$, curves I and II are evidently quite different. This latter fact is due to the difference in the turbulence levels of the uniform streams. The level is much lower in the wind tunnel than in the water channel.

[1] By E. R. Van Driest, published in the June, 1945, issue of the JOURNAL OF APPLIED MECHANICS, Trans. A.S.M.E., vol. 67, p. A-91.

[2] Associate Professor, University of Iowa, and Associate Director, Iowa Institute of Hydraulic Research, Iowa City, Iowa.

[3] "Eddy Diffusion," by A. A. Kalinske and C. L. Pien, *Industrial and Engineering Chemistry*, vol. 36, 1944, p. 220.

[4] "Eddy Diffusion," by W. L. Towle and T. K. Sherwood, *Industrial and Engineering Chemistry*, vol. 31, 1939, p. 457.

"Mass Transfer Between Phases," by T. K. Sherwood and B. B. Woertz, *Industrial and Engineering Chemistry*, vol. 31, 1939, p. 1034.

"Turbulence in Open Channel Flow," by A. A. Kalinske and J. M. Robertson, *Engineering News-Record*, vol. 126, 1941, pp. 539–541.

"Experiments in Eddy-Diffusion and Suspended-Material Transportation in Open Channels," by A. A. Kalinske and C. L. Pien. Trans., American Geophysical Union, vol. 24, 1943, pp. 530–536.

[5] Daniel Guggenheim Aeronautical Laboratory, California Institute of Technology, Pasadena, Calif.

It should also be mentioned that correlation curves which do not approach zero rapidly enough to insure a finite value of the scale integral are sometimes encountered in wind-tunnel measurements. This is often due to pulsations in the stream, i.e., velocity fluctuations other than true turbulent fluctuations.

The writer does not believe that the periodic wandering of the globules, as shown in Fig. 5 of the paper, indicates the existence of a "regular turbulence" pattern. In studying records of random fluctuations one may often tend to see pseudoperiodicities. If, however, periodicities of this type have been observed consistently, the writer would be inclined to attribute them to periodic pulsations in the stream rather than to a turbulence pattern. In this connection the wake of the injection tube should be considered. The Reynolds number based on the diameter of the tube used in the author's measurements is of the order of a few hundred. Hence a von Kármán vortex street will exist in the wake of the tube, and consequently a certain amount of regular fluctuation must be expected. The distance between the vortexes is of the order of 5 times the diameter of the cylinder or about 0.1 in. in the presented measurements; this is of the same order of magnitude as the length l_1 which was determined to be about 0.2 to 0.4 in. The influence of the vortex street will, of course, diminish rapidly downstream; however, the influence of these regular fluctuations, e.g., upon the initial motion of the globules, should not be overlooked.

It is to be hoped that the experiments will be continued. The investigations of true isotropic turbulence in water flow behind a grid using the method of the author appears to be of great interest.

J. M. Robertson.[6] Knowledge of the eddy diffusivity, its magnitude and manner of variation in the channel, allows prediction of the manner of distribution of suspended material in a flowing stream. Experimentally the diffusion coefficient can best be determined by direct measurement of the diffusion of some foreign material, of heat, of salinity, or other quality or content of the fluid. In air the diffusion of heat was used by Schubauer[7] to measure the magnitude of the turbulent velocity fluctuations; the diffusion of smoke from chimneys was used by Taylor[8] as an indication of the nature of the diffusion process; and the diffusion of carbon dioxide and hydrogen was used by Towle and Sherwood[9] to determine the diffusion coefficient. In a water stream, Richardson[10] used the diffusion of dye to measure the diffusivity.

At the University of Iowa the determination of the diffusion coefficient by means of the measurement of the spread of oil droplets has been accomplished with seemingly good results.[11,12,13,14] As this method is extremely tedious and cannot be used in the presence of appreciable amounts of suspended sediment, another method was developed by Kalinske and Pien.[14] In this method the diffusion of chlorides in the water at various distances from the point of injection was obtained chemically on samples taken at the desired locations; a relatively easy process. At present this seems to be the best method developed for measuring the diffusion.

As noted by the author, the diffusion coefficient D defined by Equation [9] of the paper, can be expressed either in terms of the correlation coefficient or the rate of spread of particles, thus

$$D = \sqrt{\overline{v^2}}\, l_1 = \overline{v^2} \int_0^{T_1} R_\xi d\xi = \frac{1}{2}\left(\frac{d\overline{Y^2}}{dt}\right)_{\max}$$

The correlation coefficient R_ξ is at present little more than a concept used in arriving at more useful relations; it is obviously difficult to follow a particle as it moves in a fluid stream and to measure its velocity from time to time. Therefore knowledge about diffusion must come from direct measurement, i.e., from a study of the variation in $\overline{Y^2}$. The fundamental relation for the variation of $\overline{Y^2}$ is presented in Equation [12] of the paper, which may be written

$$\frac{d\overline{Y^2}}{dx} = \frac{2\overline{v^2}}{U} \int_0^{\xi} R_\xi d\xi$$

using the relation $U = dx/dt$. As noted by the author for values of time greater than some time T_1

$$\int_0^{\xi \geq T_1} R_\xi d\xi = \text{const}$$

Thus, for such times, integration gives

$$\overline{Y^2} = \frac{2\overline{v^2} X_0}{U^2}(X - X_0) = \frac{2D}{U}(X - X_0)$$

where X_0 is a constant distance related to T_1 and the velocity U. The linear relation indicated by this relation for distances considerably larger than X_0 is quite apparent in the data previously presented.[12,13] Measurements made for distances up to 4 times X_0, indicated that the linear relation applied for values greater than 2 times X_0.[13] This constant was found to vary between 0.18 and 0.61 ft for different channels (0.94 ft and 2.5 ft widths, smooth and rough bottoms), depths (0.5 to 1.25 ft), velocities of flow (0.4 to 1.5 fps), and locations in the channel. For distances less than $2X_0$ the variation in $\overline{Y^2}$ was the same for the various cases when the data were presented in the dimensionless form

$$\frac{\overline{Y^2}U}{2DX_0} = \text{function}\left(\frac{X}{X_0}\right)$$

If a very accurate picture of the variation in the left side of this relation with values of X/X_0 between zero and 2 could be obtained, it would be possible to obtain R_ξ by differentiation. As it is quite difficult to obtain very accurate measurements of $\overline{Y^2}$ at small distances with the usual proportions of the measuring apparatus used, conclusions as to the nature of this correlation coefficient based upon such measurements appear to be quite uncertain.

In most discussions of the relation of turbulence diffusion to the transportation of suspended material it is assumed that the diffusion coefficient D is equal to the momentum transfer coefficient ϵ, defined by the well-known shear relation

$$\tau = \epsilon \frac{d\rho U}{dy}$$

As the density ρ of water, or water and sediment, varies but little, one need only know the vertical velocity distribution and the

---

[6] Assistant Professor of Engineering Mechanics, Pennsylvania State College, State College, Pa. Jun. A.S.M.E.

[7] "A Turbulence Indicator Utilizing the Diffusion of Heat," by G. B. Schubauer, N.A.C.A. Tech. Report 524, 1935.

[8] "Diffusion by Continuous Movements," by G. I. Taylor, Proceeding of the London Mathematical Society, vol. 20, 1921, p. 196.

[9] "Eddy Diffusion," by W. L. Towle and T. K. Sherwood, *Industrial and Engineering Chemistry*, vol. 31, 1939, p. 457.

[10] "An Experimental Study of Turbulence Diffusion," by E. G. Richardson, Proceeding of the Physical Society of London, vol. 49, 1937, p. 479.

[11] "Application of Statistical Theory of Turbulence to Hydraulic Problems," by A. A. Kalinske and E. R. Van Driest, Proceedings of the Fifth International Congress of Applied Mechanics, 1938, p. 416.

[12] "Experimental Studies of Liquid Turbulence," by A. A. Kalinske, Proceedings of the Hydraulics Conference, University of Iowa, 1940, p. 50.

[13] "Turbulence in Open Channel Flow," by A. A. Kalinske and J. M. Robertson, *Engineering News-Record*, 1941, p. 539.

[14] "Experiments in Eddy Diffusion and Suspended-Material Transportation in Open Channels," by A. A. Kalinske and C. L. Pien, Trans. American Geophysical Union, vol. 24, 1943, pp. 530–536.

shear to compute ϵ. This was done by Kalinske and the writer,[13] and the values of ϵ were found to agree reasonably well with the measured values of D both in magnitude and mode of variation, an indication that the assumed equivalence of these two factors is reasonably accurate. More important than this, however, was the close agreement found by Kalinske and Pien[14] between measured suspended sediment distributions and those computed on the basis of measured values of D. This is a check of the usual sediment-suspension theory and an indication of the reliability of the method used in obtaining the diffusion coefficient.

The measurements of D referred to[13,14] indicate that in the center of a channel it is probably zero at the bottom (as theory indicates), increases with distance from the bottom to a maximum value at about mid-depth, and then decreases as the free surface is approached, but does not necessarily become zero at the surface. Closed-channel studies by Towle and Sherwood,[9] and Sherwood and Woertz[15] indicate that in the turbulent range, D increases approximately linearly with increasing Reynolds numbers. For flows below the critical (laminar flow), the diffusion would be that predicted by the molecular theory such as presented by the author's Equation [5]. The order of magnitude of such diffusion may be 0.01 to 0.0001 that of turbulent diffusion.

Author's Closure

With regard to Professor Kalinske's discussion it is evident that he is under certain misconceptions. It should be appreciated by him that the data on diffusion were collected in 1940. As stated in the paper these data in spite of the large number of observations taken did not prove to be of sufficient accuracy to warrant definite conclusions as to the exact shape of the mean-square deviation and resulting correlation curves. In the author's conversation with Professor Kalinske the fact that the desired limiting straight line could not easily be located was indicated. This point was stressed rather than that the data did not approach a straight line. The use of the exponential correlation law was suggested by Dr. H. L. Dryden who reviewed the test data.

With reference to a bibliography, it was out of place to include one of an exhaustive nature and therefore the paper included only those references which would provide the reader with sufficient background to analyze the data. Since the paper was prepared for publication prior to Professor Kalinske's publications of 1943 and 1944, obviously these particular references could not be included. The author is, however, very happy to learn of the less laborious injection and sampling method recently used at the University of Iowa.

The author sincerely appreciates the encouraging comments by Dr. Liepmann. The data presented in Fig. 1 of his discussion are very interesting. The divergence of the two curves is undoubtedly due to the side-wall effect of the water channel. The disturbance of the flow by the insertion of the injection tube is certainly a major objection to the use of such instruments in making measurements near the origin. In addition to the generation of Kármán vortexes, there are two other sources of error, namely, the vibration of the tube and the inertial effect of the globules at the point of introduction. The vibration of the tube can be practically eliminated. Although the length l_1 was found to be of the same order of magnitude as the distance between the vortices of the Kármán vortex street, it should not be concluded that the magnitude of l_1 is due to the vortex street, which as Dr. Liepmann points out, will diminish rapidly downstream. The order of magnitude in this case is purely coincidental.

The remarks of Professor Robertson are appreciated.

[15] "Mass Transfer Between Phases—Rule of Eddy Diffusion," by T. K. Sherwood and B. B. Woertz, *Industrial and Engineering Chemistry*, vol. 31, 1939, p. 1034.

Dynamics of an Elastic Bar[1]

K. J. DeJuhasz.[2] The present paper is a valuable addition to the existing literature on the dynamics of elastic bars in general, and of long trains in particular, to which important field the author has previously made several basic contributions. The value of these papers resides not only in the solution of definite problems, but also in the precise definitions of characteristics and concepts peculiar to train dynamics, such as "speed of progressive force application," "propagation ratio," "passing point," and others. The results of the author's analysis appear to be transferable, with suitable adaptations to other elastic phenomena such as surges in springs, in hydraulic piping, behavior of chains, and others.

The paper is, however, somewhat difficult to read and understand which detracts somewhat from its general usefulness. This is due partly to its extreme conciseness, omission of derivations, and insufficient explanations, which was no doubt imposed on the author by limitation of space. But the difficulty of understanding is partly inherent in the method of treatment which is preponderantly mathematical and makes insufficient use of graphic illustrations.

In recent years increasing use has been made of the graphical method of analysis in treating problems involving elastic columns. For the explanation of this method reference is directed to previous literature.[3] The present discussion will be restricted only to the illustration of the graphical method on two of the cases treated by the author.

Case 1. A Constant Force Acts at the End of a Solid Elastic Bar. This phenomenon is illustrated in Fig. 1 of this discussion. Fig. 1(*a*) represents the t-x diagram, in which a point denotes a certain cross section x, and a certain instant of time t. In this diagram the progress of a disturbance along the bar is represented by straight lines having the slope

$$\tan(\pm\varphi) = \pm V = \Delta x/\Delta t = \sqrt{k/m}$$

Fig. 1*b* represents the V-P diagram in which a point denotes the velocity V and force P, existing in a certain cross section x of the bar, at a certain time t. Any change of force involves a proportional change of velocity and vice versa, for which $\Delta P/\Delta V = \tan(\pm\alpha) = \sqrt{mk}$.

It is assumed that the bar is initially at rest, $V = 0$, and there is no force, $P = 0$; this condition is represented in the V-P diagram by point 1. At $t = 0$ instant (t-x diagram) a force P_1 is applied at the end A. The problem is to find the velocity and force in all cross sections of the bar at subsequent instants of time.

The changing of the loading at the end A from zero to P_1 constitutes a disturbance, as a result of which the velocity is changed from zero to V_2, the new state of the end A being defined by point 2, situated on the tan α line drawn from point 1 at its intersection with the $P = P_1$ line. This disturbance travels toward the end B of the bar. On its arrival there, after the elapse of L/V time,

[1] By O. R. Wikander, published in the June, 1945, issue of the Journal of Applied Mechanics, Trans. A.S.M.E., vol. 67, p. A-101.

[2] Professor of Engineering Research, Engineering Experiment Station, The Pennsylvania State College, State College, Pa. Mem. A.S.M.E.

[3] Graphical Analysis of Surges in Mechanical Springs," by Kalman J. DeJuhasz, *Journal of The Franklin Institute*, vol. 226, 1938, pp. 505–526, and 631–644.

"Graphical Analysis of Impact of Elastic Bars," by K. J. DeJuhasz, Journal of Applied Mechanics, Trans. A.S.M.E., vol. 64, 1942, p. A-122.

Discussion by K. J. DeJuhasz of paper: "Calculation of Load and Stroke in Oil-Well Pump Rods," by B. F. Langer and F. H. Lamberger, Journal of Applied Mechanics, Trans. A.S.M.E., vol. 65, 1943, p. A-178.

the bar tension is relieved, $P = 0$, and the new state of the bar will be represented by point 3 in the V-P diagram, which is at the intersection of the tan $(-\alpha)$ line drawn from point 2 with the $P = 0$ line. This is a new disturbance which travels from end B to end A, as shown in the t-x diagram by the line tan $(-\varphi)$ drawn from the point 1, representing the $t = L/V$ instant of time. This procedure is continued in the manner shown; a t-x diagram is obtained showing the triangular zones 1,2,3,4,5,6, ... ; each of which zones is characterized by a V-P condition as given in the V-P diagram by similarly marked points 1,2,3, 4,5,6, ...

Erecting the V and P co-ordinates, as ordinates, over the plane t, x as a base, the stereogram of force, Fig. 1(*c*), and the stereogram of velocity, Fig. 1(*d*) are obtained. Any cross section of these at a given x value will give the history of force, respectively, of velocity at that point in the bar. Forming the integral $v\,dt = S$ and erecting these values over the t,x plane as a base gives the stereogram of travel, Fig. 1(*e*).

It is seen that the force and velocity existing at a given instant are different at the different cross sections X of the bar, except at the instants L/V, $2L/V$, $3L/V$, ... and so on.

Case 2. A Constant Force Acts on a Body Connected to a Solid Elastic Bar. This phenomenon is illustrated in Fig. 2 of this discussion, with the approximation that the "body" is treated as a short thick bar of L_1 length, having a wave resistance $\sqrt{m_1 k_1} = \tan \gamma$, and the bar itself as having a greater length $L_2 = 4\,L_1$ and a smaller wave resistance $\sqrt{m_2 k_2} = \tan \alpha$. The speed of propagation

$$\sqrt{k_1/m_1} = \sqrt{k_2/m_2} = \tan \varphi$$

is assumed to be the same for both bars.

The t-x diagram is shown in Fig. 2(*a*), and the V-P diagram in Fig. 2(*b*). This latter shows the points 2,4,6,8, ... characterizing the state of velocity and force for the point A, the points 3,5,7,9, ... for point B, and points 4′,6′,8′,10′ . . . . . for point C. From the t-x and v-p diagrams, stereograms of force, velocity, and travel could be obtained in a manner similar to that shown for Case 1. Instead of that, only the history diagrams of velocity and force are given in Fig. 2(*c*), for the three points A,B, and C in the bar.

Other cases dealt with in the paper could be treated by the method of graphical analysis, but even these two examples show the clarity, easy applicability, and flexibility of the graphical method, which is able to yield an insight into the fine details of the phenomena, which is not possible to attain by mathematical methods, or only at prohibitive labor and complication.

The mathematical and graphical methods complement each other; broadly it can be stated that the mathematical method has the advantage in the solution of steady states, while the graphical method has the advantage in the solution of transient phenomena.

Author's Closure

The method of graphical analysis, developed by Mr. DeJuhasz, and applied by him to two elastic-bar problems, is very interesting and should be useful in the solving of and the checking of the solution of other problems of that nature.

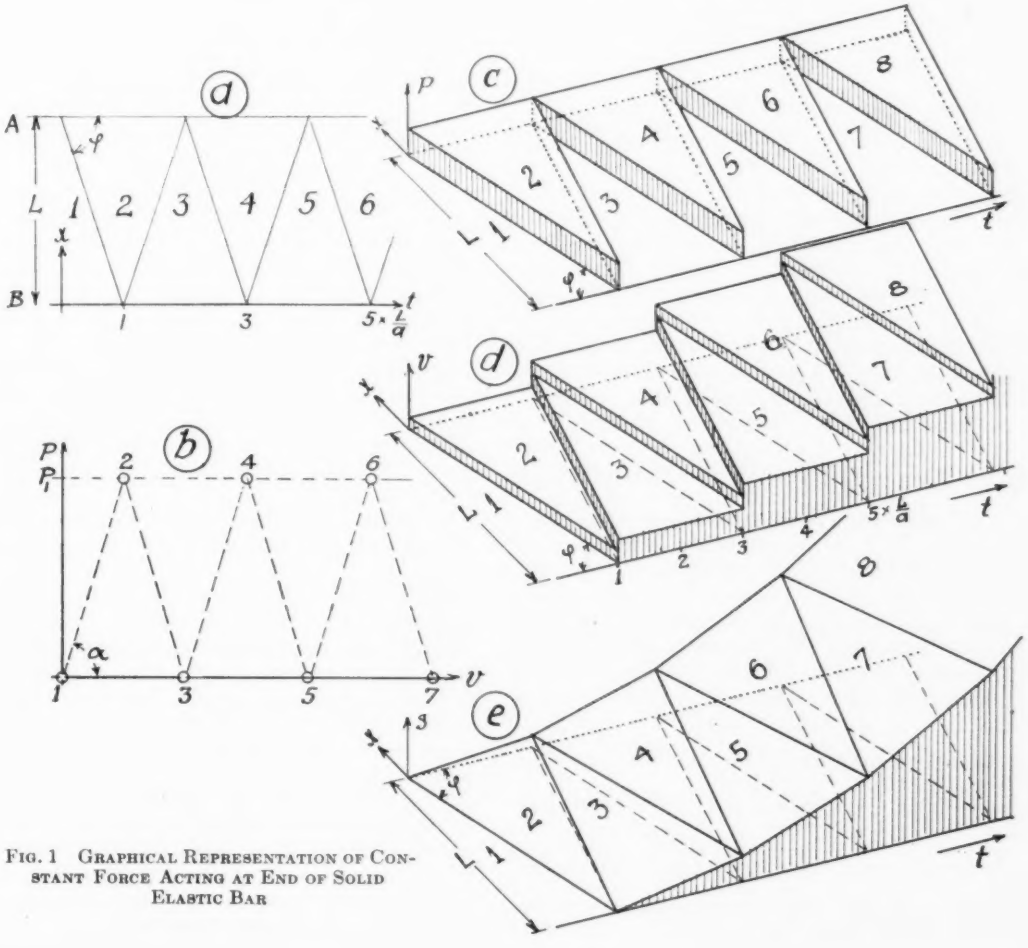


Fig. 1 Graphical Representation of Constant Force Acting at End of Solid Elastic Bar

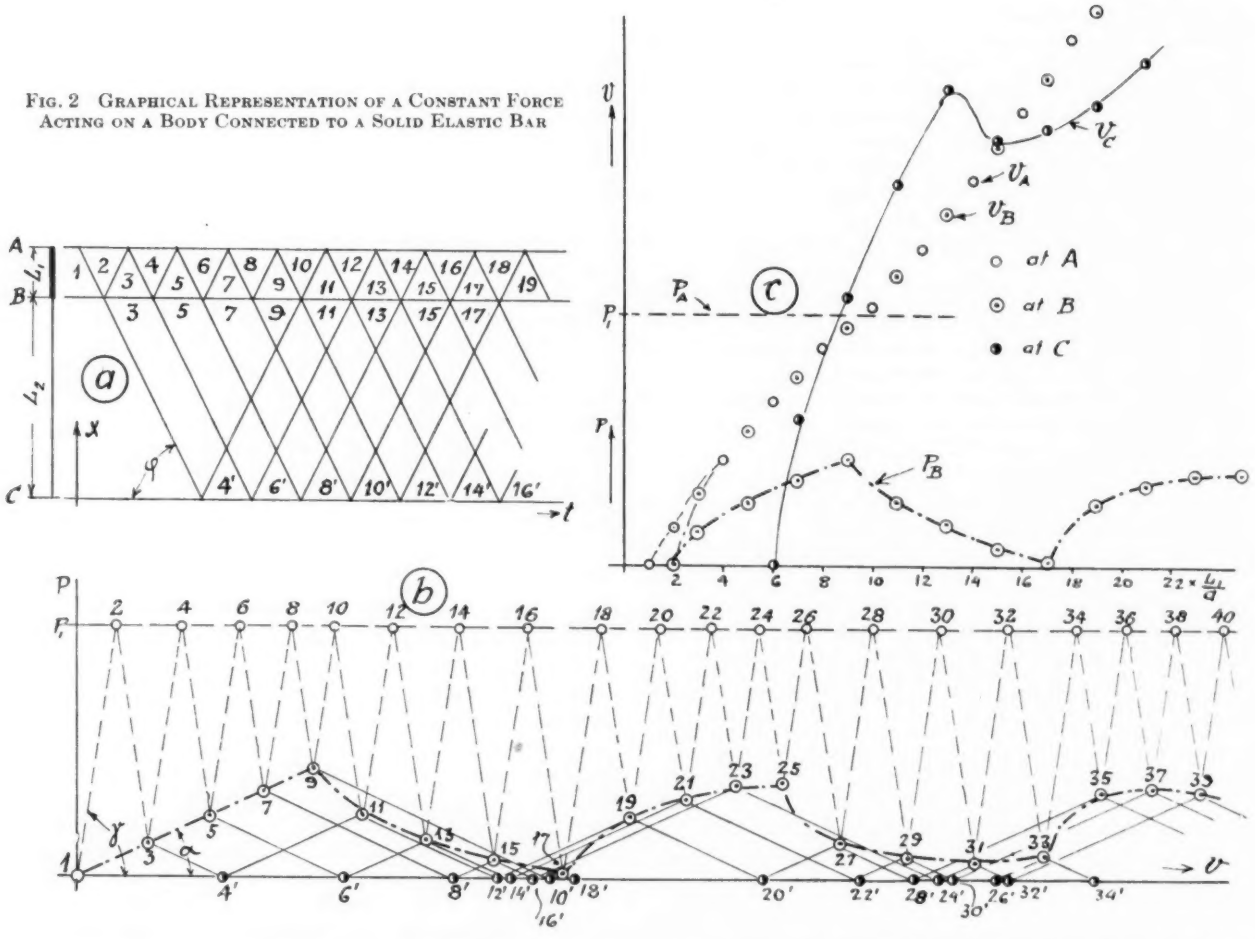


FIG. 2 GRAPHICAL REPRESENTATION OF A CONSTANT FORCE ACTING ON A BODY CONNECTED TO A SOLID ELASTIC BAR

The analytical method used in the paper is largely based on a graphical analysis of the mechanics of an elastic bar, published in an earlier paper.[4] For this reason as well as due to space limitation, derivations and explanations were kept to a minimum.

In a companion paper,[5] treating the application of elastic bar mechanics to railroad trains, a more generous use has been made of graphic illustrations so as to make up for the deficiency to which Mr. DeJuhasz refers.

Design of Crankpins for Locomotives[1]

KENNETH CARTWRIGHT.[2] The failure of a main crankpin on a modern high-speed locomotive usually results in serious consequences. For this reason, most roads limit the life of main crankpins to that which experience has shown to be acceptable without service failures, and the pins are arbitrarily renewed on this basis. This results in considerable recurring maintenance expense. An increase in the fatigue life of main crankpins will both minimize possibility of service failures and also reduce maintenance expense.

Unfortunately, on modern steam locomotives in so far as the actual design of the crankpin is concerned, there is not much that can be done. The diameter of the wheel-fit portion of the pin is limited by the diameter of the driving axle, the stroke, and the necessity of leaving a sufficient bridge of metal in the wheel center between the axle and crankpin fits. On modern locomotives with high piston thrust, the diameter of the wheel-fit portion of the crankpin under the foregoing limitations necessarily results in high unit stresses. The diameter of the side-rod journal of the pin is usually the same diameter as the wheel-fit portion of the pin, being necessitated by limitations of bearing pressure in the middle connection bushings, and this combination of equal diameters of the side-rod journal portion and wheel-fit portion of the pin results in the least favorable design from the standpoint of fatigue life.

Inasmuch as these limitations preclude designing the pin so as to reduce the unit stresses, it is necessary, in order to increase the fatigue life, to develop some means of increasing the resistance of the pin to breaking under high unit stresses. This might be done by changing the material. Results of a questionnaire sent to the locomotive voting members of the Association of American Railroads (A.A.R.), however, showed that the great majority of main crankpin failures occurred with pins made of plain-carbon steel, and also that the great majority of main crankpins removed by reason of having reached a mileage limitation, or having reached a wear limit, or found cracked on inspection were plain-carbon-steel pins. It was therefore decided that if some means could be found to increase the fatigue life of the plain-carbon-steel pin, immediate benefit would result.

[4] "Draft Gear Action in Long Trains," by O. R. Wikander, Trans. A.S.M.E., vol. 57, 1935, pp. 317–334.

[5] "Draft Gear Action in Train Service," by O. R. Wikander, Trans. A.S.M.E., vol. 66, 1944, pp. 691–696.

[1] By O. J. Horger and W. I. Cantley, published in the March, 1946, issue of the JOURNAL OF APPLIED MECHANICS, Trans. A.S.M.E., vol. 68, p. A-17.

[2] Chief Mechanical Engineer, New York, New Haven, and Hartford Railroad, New Haven, Conn. Mem. A.S.M.E.

The paper clearly outlines the work that has been done along these lines and shows that by various methods of treating the surface of the wheel fit of the crankpin, increases in fatigue life up to double that of the conventional plain-carbon-steel crankpin can be obtained. The work is by no means complete and additional tests now in progress and those contemplated will undoubtedly afford other and perhaps better means of accomplishing the desired results.

Results to date, however, do afford those railroads having difficulties with plain-carbon main crankpins with means of improving the performance. The various methods, as outlined in the paper, are simple and reliable and capable of being readily integrated with existing shop practice.

MORRIS P. TAYLOR.[3] As described, the method of fatigue-testing on parts of actual size is accurate and eliminates all possible scale effects, as well as the effect of size on strength of the forged steel used. However, as the paper is somewhat in the nature of a preliminary report, as stated by the authors, it may be pertinent to discuss several factors that should be investigated in the succeeding work, as follows:

1 Many locomotive crankpins do not have a uniform diameter of hub fit and side-rod journal portion, as did the parts tested. Probably, in a majority of cases the hub fit is from 1/4 to 3/8 in. larger than the side-rod journal when new; and as the side-rod journal is re-turned at general shoppings the difference may be as much as 3/4 in. before the pin is removed. The connecting radius is usually 1/4 or 3/8 in., the pin having about the form as shown in the left-hand illustration in Table 6 of the paper. It would be interesting to determine by test whether this enlargement of the hub fit is advantageous and to what extent. It is also important to know the best dimension for the connecting radius of fillet, within the limits as allowed by the side-rod bearing.

It is also evident that with rolled pins, type 3, the technique would have to be altered owing to the connecting fillet, and also the fillet would have to be rerolled when the pin is quartered and turned without removing it from the wheel. Possibly the best method would be to shot-blast the fillet.

2 In all the tests described, the pins were apparently pressed in from the outside of the wheel hub, and part of the loss of fit, as shown in Fig. 23 of the paper, may have been due to the scruffing effect as the pins were pressed in. There are several good arguments for reversing this process, and pressing the pins into the wheels from the inside,[4] so the surface of the bore next to the outer face (on a locomotive) is not scruffed by the entire length of the pin fit being pressed past it. Of course such a method could not be used with the type 2 fit, as the taper is at the wrong end; but it might be possible to bore the hub with a slight taper, smaller on the outside by 0.003 in. or so, and obtain an excellent fit with uniform distribution of pressure between hub and pin.

3 It is shown that flame-hardening is of advantage but is a questionable practice due to possible thermal cracks. Possibly the process of induction-hardening, because of the exact control, would give better results, especially as the hardness could be held to various limits as were indicated by test results.

4 It would be well to try the effect of prestressing the bore of the hub, by pressing through a slightly oversized tapered plug, or some such method, to get an autofrettage effect. This might eliminate the fretting corrosion.

5 Several designs of stress-relieving grooves may be worth trying. One possible method would be to put a rolled groove in the pin, next to the hub. It would also be possible to put an inverted fillet in the hub to relieve the stress concentration at the face of the wheel.

The research carried out thus far, as outlined in the paper, is of great value to locomotive designers. The foregoing discussion is not in any way meant as a criticism, but entirely as a series of suggested topics that are worth considering for future research, The only possible criticism is that the Association of American Railroads should have started work along these lines some years ago, as crankpin overstressing has been a serious problem on large locomotives for many years.

[3] Engineer, Joshua Hendy Iron Works, Sunnyvale, Calif. Mem. A.S.M.E.

[4] The terms "inside" and "outside" have been used as applying to an actual locomotive; thus in Fig. 11 of the paper, the outside would be the side of the wheel on which the force is applied.

AUTHORS' CLOSURE

The discussion of both Cartwright and Taylor indicates a keen realization of the many controversial factors involved in crankpin design practice. Many of the influences mentioned by Taylor have been under investigation. Application of some of these ideas indicate that much benefit will be derived but this will be the subject for a later progress report.

A Uniform Method for Determining Angular Accelerations in Mechanisms[1]

A. E. R. DE JONGE.[2] Before commenting on the author's paper proper, the writer deems it necessary to say first a few words about the science of mechanisms and particularly about its subsidiary science, kinematics, with which the paper is concerned.

During more than a decade previous to the publication of the writer's first paper on kinematics and mechanisms,[3] only a few papers had been published in this country on these subjects, and although they professed to present something new, they scarcely did so in reality. After the presentation before the A.S.M.E. in 1941 of his second paper,[4] by which the writer had tried to stir up a more active interest in the science of mechanisms and its subsidiary sciences,[5] he had the satisfaction of seeing that a few papers on mechanisms and particularly on accelerations in complex linkages appeared, among which there were of especial interest two by Messrs. Hall and Ault.[6,7] After the writer's third paper[8] had been presented before the A.S.M.E. in December, 1943, some further papers appeared, from which there may be selected for special mention one by L. Beskin.[9] All these papers, which are the most significant ones on plane kinematics published in this country, deal with but one particular phase of this science, namely, with accelerations. Now, a further paper on this same subject has been presented by Professor Koenig.[1]

One cannot escape the temptation of making some comparisons

[1] By L. R. Koenig, published in the March, 1946, issue of the JOURNAL OF APPLIED MECHANICS, Trans. A.S.M.E., vol. 68, p. A-41.

[2] Mem. A.S.M.E.

[3] "Kinematic Synthesis of Mechanisms," by A. E. R. de Jonge, *Mechanical Engineering*, vol. 62, 1940, pp. 537–542.

[4] "What is Wrong With 'Kinematics' and 'Mechanisms'?" by A. E. R. de Jonge, *Mechanical Engineering*, vol. 64, 1942, pp. 273–278.

[5] Author's closure to the discussion on (4), *Mechanical Engineering*, vol. 64, 1942, pp. 744–751, particularly p. 745.

[6] "How Acceleration Analysis Can Be Improved," by A. S. Hall, and E. S. Ault, *Machine Design*, vol. 15, part 1, 1943, pp. 100–102, 162, and 164; part 2, ibid., March, 1943, pp. 90–92, 168, and 170.

[7] "Auxiliary Points Aid Acceleration Analysis," by A. S. Hall and E. S. Ault, *Machine Design*, vol. 15, no. 11, November, 1943, pp. 120–123, and 234.

[8] "A Brief Account of Modern Kinematics," by A. E. R. de Jonge, Trans. A.S.M.E., vol. 65, 1943, pp. 663–675.

[9] "Simplified Method Shortens Acceleration Analysis," by L. Beskin, *Machine Design*, vol. 16, June, 1944, pp. 113–116.

between the papers cited. In the first paper by Messrs. Hall and Ault,[6] these authors considered it necessary to use complex quantities in order to attain their end. This was entirely unnecessary, as the result could have been obtained with quite elementary means. In their second paper[7] the same authors returned to simple vector equations, which, undoubtedly, is a most commendable step, although they still used an analytical approach. Mr. Beskin, on the other hand, showed[9] how the same result could have been obtained by means of the inflection circle and inflection "pole," to which the writer had drawn attention in his third paper.[8] Mr. Beskin, incidentally, caught an error by Messrs. Hall and Ault in the designation of a "floating link" in their second paper. Mr. Beskin's much simpler method led him to the same result which the two authors had obtained by more complex analytical methods. Mr. Beskin's approach is therefore a step in the right direction, keeping Lord Kelvin's well-known statement in mind, to which the writer has referred several times on previous occasions, namely, that a problem is never solved until it has been reduced to its simplest terms. The only fault that can be found with Mr. Beskin's paper is that he, too, has used algebraical formulas to determine simple vector quantities while using otherwise a geometrical method, but it is due to the latter that he arrived at a considerable simplification of the problem. Actually, he could have used the geometrical method all the way through with still greater simplification in obtaining his final result.

Let us now consider Professor Koenig's paper. He, too, deals with the limited subject of accelerations, indicating thereby that this subject is yet uppermost in the minds of American engineers. The writer still hopes that his third paper,[8] "A Brief Account of Modern Kinematics," may ultimately prove an incentive for American engineers to attack the far more difficult problems of kinematic synthesis of mechanisms. A slight attempt in this direction has been made by two young students of the City College of New York, who presented a paper entitled "A System of Kinematic Analysis" before the student branch of the A.S.M.E. at that college. Although they dealt with a system of "analysis" of mechanisms, this system has a distinct bearing on the kinematic synthesis of mechanisms. The system they presented is Assur's system of the composition of link mechanisms.[10]

Professor Koenig starts from the two different expressions for the pole velocity of two plane systems rotating about fixed centers in a third and fixed system, the "frame." By expressing this pole velocity by the respective angular velocities and the "radii of the instantaneous rolling circles," which, in fact, are nothing but the pole distances, he obtains a basic equation which he subjects to differentiation with respect to time. Then he substitutes in the various terms of this differential equation the meaning of the differential quotients as well as the original equation from which he started, and obtains thereby, in a straightforward manner, a relation which contains only the known angular velocities, the acceleration of a member of known motion, and the velocities of change of length of the pole distances as known quantities.

This is indeed a simple solution, and to the best of the writer's knowledge, this solution is new. For this reason he recommended the paper for presentation before the A.S.M.E. when requested for his opinion about it. As this is a completely new approach, Professor Koenig deserves commendation for having added this interesting solution to our knowledge of the theory of accelerations.

Although the writer has no fault to find with the method as such, there are a few pitfalls which he believes should be pointed out here. One of these Professor Koenig has mentioned himself, namely, the great importance of determining the proper signs for the various terms of his final equation. This is absolutely essential if correct results are to be obtained. A second pitfall is the scaling of the various quantities from the diagrams with the appropriate scales, before the terms can be calculated. In this process errors in scaling may easily be committed due to the different scales that have to be used. The third, and by far the most important pitfall, however, is that the "rotopoles" which are required to be found, do not always fall within the limits of the paper on which the diagrams are drawn. In that case a different approach will have to be used which Professor Koenig has neither explained nor even indicated.

It is a great pity that this method of solution does not lead to a completely graphical determination of the final result, that is, of the desired angular acceleration. Nevertheless, the calculations are simple, and once the various terms are calculated from the scaled quantities of the diagrams, the calculation of the angular acceleration consists only of additions and subtractions.

Professor Koenig then shows the application of this method to a crank-lever mechanism, that is, to a four-link chain, one link of which is fixed. He determines first the angular acceleration of the lever from the known velocity and angular acceleration (the latter assumed to be zero) of the crank. No fault can be found with this application, the most interesting part being the way in which he obtains graphically the velocities of change of the pole distances.

Secondly, he determines for the same mechanism the angular acceleration of the connecting rod, using the same method but applying the principle of inversion. Although this application of the new method is quite correct, in practice, where time is the most essential factor, he would not have had to go to all this trouble as he could have obtained it by applying some known theorems from the theory of accelerations. For this angular acceleration of the connecting rod can be obtained far more simply from the known total accelerations of its two end points. That of the crankpin can be determined geometrically with ease since only a normal acceleration is present (the angular acceleration of the crank, and thus the tangential acceleration of the crankpin, being assumed to be zero). The other for the lever-connecting pin can also be obtained easily once the angular acceleration of the lever has been found; for instance, by Professor Koenig's method as used in the first part of the example. This angular acceleration determines the tangential component of the lever-pin acceleration, and its normal acceleration is derived readily, in a graphical way, from its velocity and the length of the lever. By combining both, the total acceleration results, and consequently also the distribution of the total accelerations along the whole length of the connecting rod. The end points of the components of these accelerations normal to the connecting rod lie on a straight line which makes with the center line of the connecting rod an angle that measures the angular acceleration of the connecting rod. However, it was Professor Koenig's intention to illustrate, by this second part, the application of his method to the case of a generally moving link and at the same time, the usefulness of the principle of inversion.

The writer has to find one important fault with Professor Koenig's paper. This fault is not attributable to him, however, but rather to the Applied Mechanics Division who prepared it for publication. When the paper was first presented to the writer for his opinion of it, the paper contained a number of further examples of application, among which the last, which referred to a complex mechanism, was by far the most interesting. In that case the method proves particularly valuable because it still remains relatively simple while other methods become far more involved. That these examples were eliminated from the paper is definitely to its detriment, and must be regretted very much by the profession. It is the writer's considered opinion that the

[10] The paper exists only in manuscript form.

author should be permitted to publish the missing part of his paper, perhaps in his "author's closure" to the discussion, in which case, however, further opportunity should be made available to discuss this missing part.

A few remarks must be made, however, regarding some of the details and terminology of the paper, for there are a number of items which the writer appreciates, and others which he does not like. Among the former is the courage of the author to break away from the antiquated and cumbersome terminology, and to use instead some of the new terms proposed by the writer, especially the term "rotopole." However, the author did not follow through, for he speaks of "instantaneously fixed lines k" of rotopoles, instead of calling these simply "pole lines k." He also has the courage of calling the three-pole theorem the "Aronhold" theorem instead of "Kennedy's" theorem, as recommended by the writer. This is appreciated for the reason of historical truth. On the other hand, he has not followed the advice of the writer of using for the line connecting the end points of the velocities of a link the accepted term "theta line,"[8] but calls this line instead the "proportioning line" and has designated it by ϑ in the text and by v in the figures. This introduces only further confusion, and the writer hopes that the author will change his mind and use in the future the now firmly established terms "theta line" and "theta angle."[8]

The greatest fault to be found with the author's paper concerns his extremely cumbersome system of notations which unnecessarily complicates the reading of the paper. Had he adopted the European system of notations, the paper would be far simpler and more pleasant to read. Thus he speaks of "point systems," meaning, however, "plane systems" of points, lines, curves, angles, etc. Had he designated the systems by $S_1, S_2, S_3, \ldots$, or simply by 1, 2, 3, ..., points by capital Roman letters and line segments by lower-case Roman letters, he would not have found it necessary to use for a line segment such cumbersome combinations as (*ab*—*af*) for example. Had he even designated the rotopoles of systems 1 and 2 by P_{12}, of systems 2 and 3 by P_{23}, and of systems 1 and 3 by P_{13}, he could have written the line segments between rotopoles as $P_{12}P_{23}$, $P_{13}P_{23}$, $P_{12}P_{13}$, or simply by lower case Roman letters, as he finally has done, and so forth. Velocities are usually designated by a lower case v with subscript, while turned velocities in the velocity diagrams (that is, velocities turned by 90 deg in the direction of the acting angular velocity) are frequently designated by a capital V with subscript. Pole lines are usually designated by a lower case p with subscript, pole velocities by a lower case u, and, if necessary, with a suitable subscript, the circles of curvature of the polodes (not the "instantaneous rolling circles") by a π with appropriate subscripts, while ϕ is reserved for variable angles. There is no reason why the "frame" should be designated by a capital Roman **F**, as it is simply a link (or system) of a kinematic chain, which latter, by fixing this link to the surrounding space, becomes a definite mechanism. Use of superscripts is to be avoided and is generally unnecessary, as they may lead to errors in being taken for powers. Only primes are permissible.

In addition, the author speaks of "kinematic layouts" and "vector layouts" instead of using the accepted terms of "kinematic skeleton diagrams," or simply "skeleton diagrams," and "vector diagrams" or "vector polygons."[8] An almost unpardonable sin, however, is the changing of notations in examples relating to mechanisms obtained from the same kinematic chain, by fixing only a different link in the different examples. These are some of the more outstanding defects.

Nevertheless, these defects should not detract from the real value of the paper, for Professor Koenig has produced a very creditable piece of work on which he should be complimented highly and which, no doubt, will prove useful to the profession. As stated, it forms a valuable addition to our knowledge of the theory of accelerations.

Author's Closure

The author appreciates Mr. de Jonge's thorough understanding of the subject, his constructive criticism, and his efforts to encourage a more active interest in the sciences of mechanisms and kinematics.

He is in agreement with Mr. de Jonge's position that the subject of kinematic synthesis of mechanisms deserves more attention, and is of the opinion that an important key will be found in that field when there is discovered a thoroughly sound criterion for kinematic constraint in mechanisms. He hopes in the future to perfect one that in its present formative stage is too complex. Meanwhile, his paper was directed particularly toward the simplification of acceleration problems in mechanisms because in his experience, these, by the usual methods, became so involved in cases of complex machines as to invite the use of empirical methods.

Mr. de Jonge's analyses of the author's basic procedure and applications are correct. Regarding pitfalls, any prospective user of the new method has, between Mr. de Jonge and the author, been sufficiently warned. Fortunately, the requirements for maintaining proper signs and scales systematically are within expected engineering skill.

The matter of rotopoles falling off the paper constitutes a more serious problem. When it occurs it may be offset, to some extent, by such means as are used in velocity analyses requiring rotopoles; for example, (1) by reducing scale in positions involving remote rotopoles not at infinity, in so far as is possible before accuracy is unduly sacrificed; (2) by using the so-called connecting-link and orthogonal-component method of velocity transfers; and (3) trigonometrically calculating distances to inaccessible rotopoles. It may be pointed out that rotopoles at infinity often give less trouble than distant finite points, because the resulting constructions frequently become degenerate in such a way that answers become obvious. Thus for example, in Equation [13] of the paper, when r_B becomes infinite, α_B becomes 0. While, from the viewpoint of the labor involved, the three procedures mentioned are not ideal, many mechanisms occur wherein such procedures are not required. The following is an example to the point (Fig. 1 of this closure), in which the terminology of the author's original paper has been retained.

The author would at this point prefer to adopt a larger number of Mr. de Jonge's suggested system of notation (some have been adopted in the following), except that a substantial consistency between this communication and the author's original paper is believed to be imperative.

Fig. 1 shows a quick-return mechanism A, B, C, F in which the driving crank A is 2 in. long to full scale. The other dimensions are in proportion. Let $\omega_A = 3$ radians per sec, and $\alpha_A = 0$. Required is the angular acceleration α_B of the lever B in the position shown. The frame of reference is F.

Determine the rotopoles *bf*, *af*, and *ab*, establishing pole line k, as shown; also *ac* and *cb*. To full scale $r_A = 1.66$, and $r_B = 5.16$. To a convenient scale draw $V_{ac} = \omega_A(ac——af) = 3 \times 2 = 6$ in. per sec.

Vector V_{ac} has two components, V^1_{ac} representing the instantaneous translation of line (*ac*——*cb*) parallel to itself along line (*ac*——*bf*); and V^2_{ac} representing the tangential velocity of point *ac* on line (*ac*——*cb*). Note that the line (*ac*——*cb*) also has absolute rotation around center *bf* as it swings with (*ac*——*bf*), to which it remains perpendicular. Vector V^1_{ac} is transferred to point *ab* as V^1_{ab}. This represents the component of translating movement of line (*ac*——*cb*) parallel to itself. This movement affects the position of point *ab*.

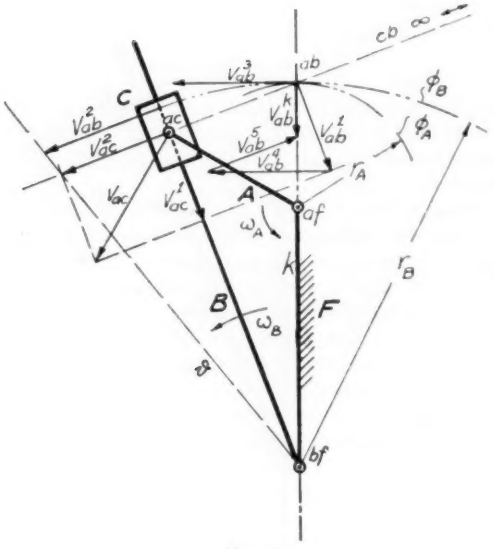


FIG. 1

Returning to V^2_{ac}, the theta line ϑ from point bf proportions V^2_{ab}, which is placed at r_B from bf. Swing V^2_{ab} into ab and draw V^3_{ab} which represents the velocity effect on point ab had by the rotary component of movement of line (ac——cb) around center bf. Add V^3_{ab} to V^1_{ab} by transferring V^3_{ab} to V^4_{ab}. Vector V^5_{ab} drawn from the end of V^4_{ab} and parallel to (ac——cb) and reaching to pole line k determines $V^k_{ab} = \frac{dr_A}{dt} = \frac{dr_B}{dt}$. Velocity V^k_{ab} represents (—2.19) in. per sec to the same scale that V_{ac} = 6 in. per sec. The negative sign indicates that r_A and r_B are decreasing, and hence that $\frac{dr_A}{dt}$ and $\frac{dr_B}{dt}$ are decreasing. Substituting in Equation [13] of the original paper, we obtain

$$\alpha_B = \frac{1}{5.16}\left[\left(3 \times (-2.19)\right) - \left(\frac{3 \times 1.66}{5.16} \times (-2.19)\right) + 0\right] = -0.863$$

radians per sec per sec, deceleration of B.

It will be noted that in at least the usual proportions of this mechanism, no required rotopole becomes inherently inaccessible, regardless of the position of the mechanism, and on the foregoing basis an entire history of its acceleration throughout a cycle can be conveniently determined. It should be noted that only the direction of cb is required.

This example is one of those which were in the author's original manuscript before condensation for publication. The remaining two examples, which Mr. de Jonge believes should also appear, are shown in Figs. 2 and 3 of this closure. The example of Fig. 2 shows how pole-velocity operations may be performed on the pole line k without an inversion and by vector subtraction. The example in Fig. 3, as mentioned by Mr. de Jonge, is of interest in showing the relative simplicity of the method when applied to a complex mechanism.

Fig. 2 shows a slider-crank mechanism A, B, C, F, in which the crank A is 2 in. long, actual size. The other links are in proportion. Let ω_A = 10 radians per sec, and α_A = 10 radians per sec per sec. The dependent angular acceleration of link B is required.

Lay out the linkage to scale in the proper position and determine the necessary rotopoles as shown, particularly af, ab, and bf, determining pole line k. Since the crank length (af——ab) is constant it may be seen that $\frac{dr_A}{dt} = 0$. However, r_B is changing in time, this being due to the change in time along moving pole line k of the intersection at bf. The movement of this intersection bf on the pole line is determined by the relative movements of the lines (bc——cf) and (af——ab) extended. Lay out V_{ab} perpendicular to line (af——ab) and by the theta line ϑ^1 find the parallel vector V^1_{bf}, which is the movement of a point coincident with bf but on line (af——ab) extended. Note that line (af——ab) swings on point af. Point bf may also be considered to have a coincident point on line (bc——cf) which is translating parallel to itself and with the slider C. This translation is found by swinging V_{ab} into (bc——cf) and drawing V^1_{ab}. Then drawing the theta line ϑ^2 determines V_{bc} which, reproduced as V^2_{bf}, is the motion of a point coincident with bf on line (bc——cf). Vectorially subtract V^1_{bf} from V^2_{bf} as indicated, thus obtaining vector ($V^2_{bf} - V^1_{bf}$) shown. This represents the translation at bf of line (bc——cf) relatively to line (af——bf). A component vector V^3_{bf} drawn through the end of this vector parallel to (bc——cf) represents the relative motion of bf along line (bc——cf) and determines $V^k_{bf} = \frac{dr_B}{dt}$.

Now $V_{ab} = \omega_A(af$——$ab) = 10 \times 2 = 20$ in. per sec, and to

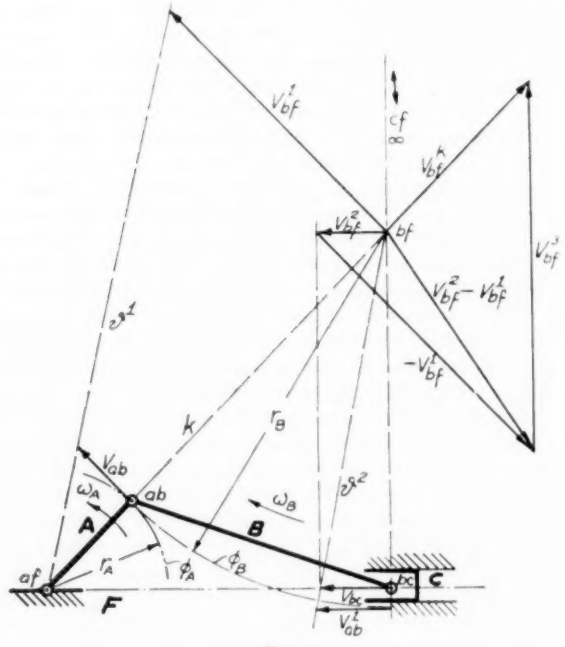


FIG. 2

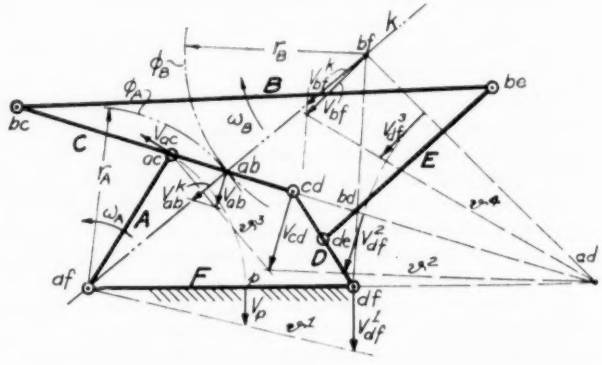


FIG. 3

the same scale that V_{ab} represents 20 in. per sec, V^k_{bf} represents 54.4 in. per sec $= \frac{dr_B}{dt}$. Also, by scale, $r_A = 2$ and $r_B = 6.06$. Substituting in Equation [13] of the original paper, we obtain

$$\alpha_B = \frac{1}{6.06}\left[0 - \left(\frac{10 \times 2}{6.06} \times 54.4\right) + (10 \times 2)\right] = -26.35$$

radians per sec per sec deceleration.

Note that when A is vertical, r_B becomes infinite and $\alpha_B = 0$, constituting one of the degenerate dimensional cases previously mentioned. Also, r_B may be calculated when bf falls off the paper, being a determinable part of the hypotenuse of the right triangle af, bf, bc, the base and angle of which (under the crank) are known, r_A being also known. V^1_{bf} may also be computed being in a simple right triangle. From this point on the graphical vector subtractions and additions may be brought into the area of the drawing board since they may be laid out independently of the mechanism skeleton.

In the complex mechanism which is of particular interest and shown in Fig. 3 of this closure, let link A be 2.13 in. long; $\omega_A = 2$ radians per sec counterclockwise; and $\alpha_A = -10$ radians per sec per sec deceleration. Required is the angular acceleration of link B. Note that link B has both of its connections through C, A and E, D twice removed from the reference frame F. By former methods this problem would be extremely troublesome.

Solution: Determine the rotopoles shown, including af, ab, and bf on pole line k. The other centers shown are of use in the solution, as will appear. $V_{ac} = \omega_A(af\text{——}ac) = 2 \times 2.13 = 4.26$ in. per sec. Let the velocity scale at full size be 0.50 in. = 4.26 in. per sec. Invert the mechanism, holding A and allowing F to move. Draw V_{ac} to the chosen scale and rotate it to p on F and, in view of the inversion, reverse it to produce V_p. By means of the theta line ϑ^1 determine V^1_{df}, noting that df is on link D which in the inversion rotates about ad. Rotate V^1_{df} into $(cd\text{——}ad)$, thus obtaining V^2_{df}. By means of the theta line ϑ^2 find V_{cd}. Now line $(ac\text{——}cd)$ determines the movement of ab considered to be on $(ac\text{——}cd)$. This line rotates on ac in the inversion. Therefore, by the theta line ϑ^3 find V_{ab}. A line drawn through the end of V_{ab} parallel to $(ac\text{——}cd)$ determines $V^k_{ab} = \frac{dr_A}{dt}$. Since V_{ac} to full scale is 0.61 in. long, $V^k_{ab} = \frac{4.26 \times 0.61}{0.50} = -5.18$ in. per sec $= \frac{dr_A}{dt}$. The negative sign arises from the fact that r_A is shortening.

As to $\frac{dr_B}{dt}$, or V^k_{bf}, it depends upon the motion of line $(bd\text{——}df)$ relative to the pole line k. This is because $(bd\text{——}df)$ extended determines bf. Since $(bd\text{——}df)$ contains line $(d\text{——}d)$ in link D which swings about point ad, swing V^1_{df} into the radius line $(ad\text{——}bf)$ obtaining V^3_{df} and by the theta line ϑ^4 find V_{bf}. A line drawn through the end of V_{bf} parallel to $(df\text{——}bf)$ determines $V^k_{bf} = 1.04$ in. (full scale). Now $V^k_{ab} - V^k_{bf}$ represents the rate at which r_B is decreasing $= 0.61 - 1.04 = -0.43$ in. Then $\frac{4.26 \times (-0.43)}{0.50} = -3.66$ in. per sec $= \frac{dr_B}{dt}$.

To full scale $r_A = 2.46$; $r_B = 2.46$. This equality is coincidental. Then substituting in Equation [13] of the original paper we obtain

$$\alpha_B = \frac{1}{2.46}\left\{\left[2 \times (-5.18)\right] - \left[\frac{2 \times 2.46}{2.46} \times (-3.66)\right] + \left[(-10) \times 2.46\right]\right\} = -9.56$$

radians per sec per sec decleration for link B.

This problem brings out the point that the rate at which r_B changes may depend upon the relative velocity of two rotopoles along the pole line k. However, the third pole on pole line k never moves, since it is always chosen on the frame. The examples given herein and in the original paper therefore exhaust all of the variations which will occur in respect to rotopole movements on the pole line.

Referring to the questions of notations which were raised, the author agrees that a lower-case p is a more appropriate index for the pole line; a lower-case u for pole velocity; and π for the circles of curvature of polodes (the author's instantaneous rolling circles). He is not convinced that the designation of a line segment as $P_{12}P_{23}$ is any simpler than, or as descriptive as $(a\text{——}a)$ or $(ab\text{——}af)$, for example. Superscripts were intended mostly to indicate sequences in the procedures. In any event, and fortunately, the controversial designations were used only in the proofs and examples, and do not appear in the working Equation [13]. Nevertheless, Mr. de Jonge's suggestions will be kept in mind on any future work on this subject. Some of the author's choices of designations grew out of his way of looking at the problem—"instantaneous rolling circles," for example.

In closing, the author wishes to thank Mr. de Jonge for his generous appraisal of the paper. It is sincerely hoped that his predictions as to the usefulness of the work to the profession will be fulfilled.

Book Reviews

Experimental Stress Analysis

EXPERIMENTAL STRESS ANALYSIS Proceedings of the Society for Experimental Stress Analysis, vol. 3, no. 1. Edited by C. Lipson and W. M. Murray. Published and distributed by Addison-Wesley Press, Inc., Cambridge, Mass., 1945. Cloth, 8½ × 11 in., xviii and 154, $5.

REVIEWED BY A. M. WAHL[1]

THE present volume, edited by C. Lipson and W. M. Murray, consists of a collection of twelve articles which treat a rather wide variety of problems having to do primarily with the determination of stress in structures and machine components and the evaluation of the effects of these stresses in terms of danger of failure. Many of the papers report very interesting observations of service failures and methods for reproducing these failures in the laboratory. However, it was the reviewer's impression that the value of several of these papers could be enhanced considerably for designers in general if more detailed theoretical stress analyses were given to supplement the experimental work. Perhaps the omission of such theoretical matter is justifiable, however, in a publication devoted primarily to experimental methods.

Coming now to individual articles, there are three papers devoted largely to applications and uses of wire resistance (SR-4) strain gages. The first of these by L. M. Ball on "Strain Gage Technique" contains much detailed technical information relat-

[1] Mechanics Department, Research Laboratories, Westinghouse Electric Corporation, East Pittsburgh, Pa. Mem. A.S.M.E.

ing to the use of SR-4 gages, which should be of direct value to engineers using these gages in practical work. Such subjects as thermoelectric potentials, kinds of adhesives, music-wire leads for locations subject to vibration, strain-gage circuits, gage adaptations for measuring deflections, and the like, are treated in this paper. The second paper by K. F. Sibila treats the use of wire resistance gages in wind-tunnel models and describes the associated electrical equipment. The third paper on SR-4 gage applications is by Thurston and Cushman on precision determination of weight. The primary element in this equipment, used for determining loaded weights of airplanes, consists of a small cell (weight $2^1/_2$ lb) containing steel columns to which are cemented SR-4 gages. Load on the columns is measured by the change in resistance of the gages. Although the capacity of each cell is 50,000 lb, the authors state that visible deflection of the cell may be obtained by pressing on it with the finger; this gives an indication of the sensitivity of the device.

The use of models in stress analysis is treated in four papers. The first of these by S. F. Tingley discusses models for structural problems such as are encountered in airship design. This paper brings out the difficulty of simulating, in a model girder, the various stiffnesses of the prototype. A model girder of the so-called "fishworm" type, which is used for stiffness simulation, is discussed in considerable detail. Another paper by Pearce and Modrovsky treats the use of a plastic model (made from a slab of lucite) of a double row aircraft engine crankshaft. This paper gives an interesting analysis of stresses around an oil hole in a crankshaft based on elastic theory for an infinitely wide plate. The peak stress thus obtained is reduced in the ratio of 2.2 to 3 on the basis of strain measurements on several crankshafts. In the reviewer's mind, there is some question as to the accuracy of the stress distribution obtained theoretically for an infinitely wide plate when applied to a shaft with a transverse hole, and it would seem desirable to check this using short-gage-length extensometers on a large model. However, as these authors point out, too great accuracy in the stress analysis is futile in this case because of the large unknown factor of stress increase due to resonant vibration in engine crankshafts.

Another paper treating of model methods is that by T. J. Higgins on "Stress Analysis of Shafting as Exemplified by Saint Venant's Torsion Problem." Among other things, this author discusses discrepancies in the published torsional stress-concentration factors for shafts having fillets or grooves as obtained from various sources. It is suggested that there is need for further tests on actual shafts in order to resolve the differences in the published results.

In a paper on "Photoelasticity as a Designer's Tool," R. E. Orton treats the use of photoelastic models in the design of a tool for a steel strapping band. This paper also gives considerable detail relative to the technique of annealing and polishing bakelite models.

The application of brittle coatings to the study of impact stresses is discussed by Ellis and Stern. Practical problems involved in the use of brittle coatings for analysis of impact problems are considered. Interesting patterns showing strains in the breech of a shotgun on firing and in an aircraft landing-gear strut are also presented.

Certain problems connected with aircraft-engine design are discussed by F. R. McFarland. This author shows that bolt tightness is an important factor in reducing the variable stress range at critical locations in connecting rods due to a given load range. As shown by other investigators, it is also brought out that, because of variations in friction coefficient, bolt torque is not a good indication of bolt tightness. Another pertinent conclusion reached in connection with torsional fatigue failures of highly stressed splines is that the index error of the spline is an extremely important factor in the fatigue strength.

The inadequacy of static tests as a measure of strength of airplane structural components is clearly indicated in a paper by Jewett and Gordon. These investigators reach the conclusion that for structural parts subject to repeated loading in service (even for relatively few cycles) a repeated-load test is necessary to duplicate service types of failure while a static test may be misleading. It is of interest to note that in many components of the aircraft structure failure may occur within about 5000 to 15,000 cycles or less at loads under $^3/_4$ the ultimate static strength. Another article dealing with airplane components is that by G. E. Holback which treats of shear tests on various types of riveted joints for aluminum sheets. An interesting correlation of a large amount of test data on different types of riveted joints by means of nondimensional methods of plotting is given in this paper.

A rather comprehensive investigation of the effect of mechanically induced residual stresses (due to shot-peening, surface-rolling, or cold-bending) in an aluminum alloy is reported in an article by D. G. Richards. In this investigation, residual stresses were measured by determining the change in curvature of a simple rectangular beam, as successive surface layers were machined off. This author reports that for specimens rolled crosswise of the longitudinal axis there was a residual compressive stress at the surface, while for specimens rolled parallel to the longitudinal axis there was a residual tension at the surface with the specimen in equilibrium after rolling. It would be of interest to have an explanation of why these residual tensions are produced in some cases by surface rolling. Another point brought out by this investigation was that by simple cold-bending of a V-notch specimen the fatigue strength may be increased up to 100 per cent in some cases. The beneficial effects of shot-peening on stress corrosion resistance are also emphasized.

It is the reviewer's opinion that this collection of articles will warrant considerable study by engineers, designers, and stress analysts.

Torsional Vibration

EVALUATION OF EFFECTS OF TORSIONAL VIBRATION. S.A.E. War Engineering Board, October, 1945. (Compiled by the Torsional Vibration Committee of the S.A.E. War Engineering Board for the use of the U. S. Navy at the Request of Capt. L. F. Small, Bureau of Ships.) Cloth, 8 × 11 in., 577 pp., illustrated, $5.

PREPARED BY BERNARD UCKO[2]

CONFRONTED with a rather disturbing variety of approach and treatment of the torsional vibration problem, the U. S. Navy requested the S.A.E. War Engineering Board to sponsor committee activities with the object to gather, from experienced and authoritative sources, a comprehensive survey of the state of the art.

This volume is the final report of the Torsional Vibration Committee. Owing to its origin it is presented as a series of independent company contributions rather than in the sequence determined by the subject matter. The ensuing danger of discontinuity has been largely overcome by a concise yet comprehensive summary.

Deviating from its actual arrangement the book may be divided into four parts: (1) Measuring techniques; (2) calculation methods; (3) evaluation of nominal stresses, including stress-concentration and fatigue considerations; (4) recommendations and plans for further activities.

The first section gives a broad survey of practically all instruments. The General Motors phase-shift torsiograph, described

[2] Mechanical Engineer, International-Plainfield Motor Co., Plainfield, New Jersey.

by L. F. Hope, is based on the measurement of the phase difference between two signals. The absence of contact brushes and of seismic elements should avoid some of the difficulties usually encountered in electrical instruments. The General Motors mechanical torsiograph is a development of the well-known Summers instrument. It proves that satisfactory results can be obtained with a reasonably simple apparatus. The absence of a continuous record remains, however, a definite disadvantage if accurate evaluation is intended. J. D. Swannack and F. P. Porter present a thorough investigation of continuously recording mechanical instruments of the seismic type.

Chrysler (L. M. Ball, S. T. Foresman, E. E. Zimmerman, and H. R. Smith reporting) uses mechanical and electrical instruments, both employing the seismic principle. The mechanical polar torsiograph utilizes a light beam as the indicating medium. This permits phase determination and should facilitate limiting the record to its proper duration, which is rather troublesome on the mechanically indicating polar type. The electrical methods are based on the velocity pick-up pioneered by Sperry—M.I.T., but employ integrating amplifying circuits of original design. The use of a recording frequency analyzer appears to be an innovation in vibration recording. The description of the circuits emphasizes the pains taken to obtain stability of calibration.

Caterpillar, as reported by A. Goloff, relies on the conventional velocity pick-up method for simple installations while using an interesting application of strain gages on more complicated systems. Direct strain measurements permit, of course, stress determination without recourse to computed normal elastic lines. The results are obviously satisfactory, although the preparatory work of wiring and bonding the numerous strain gages must necessarily be a time-consuming task.

The General Motors walking-beam calibrator, discussed by A. W. Zmuda, is apparently the first mechanical device which permits independent changes of rotational as well as of vibrational frequencies during operation. The Caterpillar rocking-arm calibrator is actuated by a cam rather than by the usual eccentric.

The chapters on calculations were contributed by L. F. Hope, C. Criswell, F. P. Porter, L. M. Ball, S. T. Foresman, and A. Goloff. Hope discusses various methods, noting the increasing use of mechanical aids. C. Criswell describes the design problems of the G.M. "harmonic balancer." F. P. Porter illustrates his unique reduction method with a number of numerical examples which prove conclusively the accuracy of this approach. A second article by Porter is an exhaustive treatise on pendulum dampers, including even the less frequently met forms of this device.

L. M. Ball calls attention to the usefulness of electrical analogies. The simplified calculation method by the same author uses the conception of a torsional standing wave. There is no doubt that much time can be saved by this and also by analogy methods. The question arises, however, whether the physical significance of every step remains as evident as by the use of more conventional means. S. T. Foresman relates the evolution of damper designs within the Chrysler Corporation, illustrating the use of rubber in shear. A subsequent section is devoted to pendulum dampers. The conclusions concerning the proper fields for rubber and pendulum dampers are most interesting. The following report by Ball deals with the procedure followed in applying rubber dampers to automotive engines. A. Goloff concludes the survey of dampers with an interesting study on the design and the application of pendulum dampers. Not everybody, however, will agree with his conclusions. There is little doubt that the rather expensive pendulum damper is out of place wherever a simpler and cheaper device will suffice.

Papers by C. W. Gadd, J. O. Almen, A. L. Boegehold, L. M. Ball, Dr. C. Lipson and H. W. Fall form the section on the evaluation of nominal stresses. Gadd, Ball, and Fall outline the object and technique of stress analysis and of fatigue testing of crankshafts. Significant differences in their approach are apparent. There is obviously no agreement whether torsional fatigue tests should be made on full crankshafts, on a complete throw, or on a single journal specimen. These divergent opinions may be caused by the widely different engine types investigated. Full shaft or full throw specimens appear to be best suited as they are likely to include the influence of the manufacturing processes. A closer agreement exists in respect to bending-fatigue tests, where a single throw can approximate the actual loading conditions. Gadd's views that cast aluminum and magnesium specimens are not suitable for static tests can not be shared without reservations. The inherent lack of complete homogeneity in cast elements should not affect tests which are usually made on two or more specimens. The low modulus of the light metals, on the other hand, facilitates the strain measurements. Fall's precise and clear discourse on the significance of nominal stresses is a particularly pleasant example of technical reporting. The importance of residual stresses is discussed by Almen. Boegehold surveys crankshaft steels and their heat-treatment, no mention being made of cast materials. Dr. Lipson contributes a brief report on fatigue tests of aircraft-engine journals. The effect of progressive understressing is of special interest.

The book concludes with reports and recommendations. Detailed suggestions cover the specifications of torsiographs. Instrument manufacturers would do well to be guided by these laboratory-tested recommendations. Torsional-vibration data summary forms, suggested by Prof. Den Hartog, call attention to the desirability of arriving at generally accepted agreements on this subject.

It is hoped that the proposed co-operative test program will be continued, although the war emergency has passed. The suggested revision of torsional stress specifications will be of interest to engine builders as well as to the underwriting companies.

The proposed investigation of calculation methods, aimed at simplification, is likely to prove difficult. It is somewhat puzzling why the first step in this direction, the use of a common terminology, has not been taken here. Beyond this, standardization in these matters can necessarily not go far without conjuring the danger of regimentation.

Although clearly and readably written this report is, of course, by no means a textbook for beginners. To the engineer who is familiar with the subject, however, it is certain to prove of great value. The vast experimental and analytical experience, so generously proffered by the numerous contributors, makes the book a unique addition to the library of every engineer interested in vibration problems.

Statistical Thermodynamics

STATISTICAL THERMODYNAMICS. By Erwin Schrödinger. Second edition. The Macmillan Company, Cambridge University Press Department, New York, N. Y., 1946. Cloth, 5 × 7½ in., 88 pp., $1.50.

REVIEWED BY JOSEPH KAYE[3]

IT is uncommon to find a masterly exposition of the basic principles of statistical thermodynamics in a mere booklet of 88 pages. Schrödinger's little book is just that. Perhaps one reason for the unusual nature of the book is that its author is one of the founders of quantum mechanics.

The book is composed from a series of seminar lectures delivered at the School of Theoretical Physics, Dublin Institute for

[3] Assistant Professor of Mechanical Engineering, Massachusetts Institute of Technology, Cambridge, Mass. Jun. A.S.M.E.

Advanced Studies. The method of attack consists of a critical analysis of the assumptions usually made in solving the basic problem in statistical thermodynamics, namely, how to determine the distribution of a given amount of energy over N identical systems. In the first few chapters the method of the most probable distribution and Gibbs's method of the mean distribution are carefully analyzed and it is shown that both methods lead to the same result.

In the last two chapters the author discusses some of the interesting results of statistical analysis. The third law, the Gibbs paradox, the comparison of "classical" and quantum mechanics, the Fermi-Dirac and the Bose-Einstein statistics, and the problem of radiation are discussed with clarity and understanding.

This book is not recommended for engineers who are not trained in the field of statistical thermodynamics or who are not well versed in the mathematical methods used in the treatment. For those who are and, in particular, for teachers of thermodynamics it will be an invaluable aid.

Mathematical Theory of Elasticity

MATHEMATICAL THEORY OF ELASTICITY. By I. S. Sokolnikoff and R. D. Specht. Cloth, 6 × 9 in., vii and 373 pp. and 57 figures. McGraw-Hill Book Co., Inc., New York, N. Y., 1946. $4.50.

Reviewed by C. B. Biezeno[4]

IN the preface to his book, after having made some introductory remarks, the author states that his treatise, having to deal with objects of the real world, is not concerned with the world of abstraction. Its prime concern is to reduce to calculations the stresses and strains in an elastic body subjected to the action of a system of prescribed external forces. On the other hand, it may be stated that neither does the book deal with the innumerable elementary questions which are encountered in elementary engineering practice, the solution of which can be given by all those who have followed the normal courses of applied mechanics at any of the universities in this country. It has been written for the rapidly increasing number of research engineers who have to deal with the more intricate problems in the field of applied mechanics and who therefore must be acquainted with the underlying mathematical principles of their science. From this point of view it can only be expected, that the author lays great stress on the formal side of his subject, and it is not surprising that, in departure from the practice commonly followed in books on applied mathematics, the tensor calculus is introduced to convince the reader of the use of this discipline in some special fields (as, for example, the theory of shells) and of its compactness and clarity. It must be appreciated however, that the insistence on tensor notation is not carried too far, and no better proof of the sense of reality of the author can be given than by this statement, that whenever the economy of thought achieved by tensor symbolism is in doubt, it is dropped in favor of the customary scalar notation. The first three chapters are dedicated to the analysis of strain, the analysis of stress, and to the stress-strain relations (100 pages).

The fourth chapter (180 pages) representing the bulk of the book is devoted to the extensive mathematical treatment of homogeneous beams under tension, torsion, and flexure. In this chapter a characteristic feature of the book comes into full development and when a special problem requires the elucidation of some mathematical expedient, mathematical excursions are made. In this way the reader gets conveniently acquainted with the complex form of Fourier series, with some results of the complex variable theory (the theorem of Harnack, the formulas of Schwarz and Poisson), conform mapping, curvilinear co-ordinates, etc. The mechanical treatment of the beam can be said to be a most exhaustive one.

The fifth and last chapter of the book is concerned with the variational methods which find their principal exponent in the theorem of minimum potential energy. Here again the reader is incidentally made acquainted with mathematical discipline: the variational problem and Euler's equation. The principal mechanical subjects treated here are: the theorems of work and reciprocity, the Rayleigh-Ritz method, Galerkin's method, the error function, the estimation of error in the minimal integral, and the stress function for torsion, relaxation of boundary conditions.

Whereas Love's unsurpassed treatise on elasticity and some other books in the same field will still be used by a relatively small number of specialists, it may be expected that this book will be used by a greater number of scientific workers in the field of applied mechanics. The authority of the author, showing itself in his broad knowledge of the foreign literature and in his clear style, will be recognized by everyone who reads the book with due attention.

[4] Professor of Applied Mechanics, University of Delft, Holland.

Hydraulics

A TREATISE ON APPLIED HYDRAULICS. By Herbert Addison. Third edition. John Wiley & Sons, Inc., New York, 1945. Cloth, 5¼ × 8¼ in., ix and 614 pp. $6.50. Illustrated.

REVIEWED BY A. T. GIFFORD[5]

THE change in title of this third edition from "textbook" to "treatise" is in keeping with the author's statement in his original preface that "The purpose of this book is to present a compact summary of the fundamental principles of hydraulics, and of the manner in which they are applied by the engineer." In the present volume the last part of the purpose definitely overshadows the first and thereby brings the book into the category of a reference work.

Part 1 is in the nature of a textbook, but the proofs are somewhat abbreviated and at times not too rigorous. The continuity of thought, however, is excellent and the field of hydraulic theory is well covered. The chapters on flow through closed conduits and dynamic pressure of liquids are extremely well written. There are many excellent graphs included in this portion of the book and several excellent tables. It is very interesting to note that all tabular values are given in both English and metric units.

Part 2, on practical applications of hydraulics, covers practical piping problems, control of water in open channels, hydraulic turbines, all types of pumps, hydraulic transmission of energy, and hydraulic measurements. The charts and tables in this section are very useful and should cover almost all situations met with in practice. Where necessary the author has introduced additional theory to cover the specific principles involved in the particular hydraulic machinery under discussion. He has made a special effort to include all methods of using and operating hydraulic machinery and also the best construction methods. The fact that he has used principally English machinery and methods in his descriptions and illustrations in no way detracts from the value of this portion of the book.

The almost 200 examples in the back of the book covering every chapter are very well chosen. Detailed solutions are given for approximately fifty per cent of them and the answers are given for the remainder. The large bibliography included in this book has been assembled from all parts of Europe and the United States and enhances the value of this book as a reference work.

[5] Associate Professor of Hydraulic Engineering, Massachusetts Institute of Technology, Cambridge, Mass.

Transactions

of the

A.S.M.E.

SOCIETY RECORDS—PART 1

D. Robert Yarnall, President of The American Society of Mechanical Engineers, 1945-1946 ..... *Portrait and Biography*

Council and Committee Personnel ..... RI-5—RI-38

Officers and Council 5
Standing Committees 6
Special Committees 7
Special Council Committees 8
A.S.M.E. Representatives on Other Activities 9
Professional Divisions 10
Sections 15
Student Branches 23
Research Committees 25
Standardization Committees 28
Power Test Codes Committees 34
Safety Committees 36
Boiler Code Committees 38

Woman's Auxiliary to the A.S.M.E. RI-39

Awards RI-40

Honorary Members RI-43

Past-Presidents, Treasurers, and Secretaries RI-44

Index RI-45

FEBRUARY, 1946

VOL. 68, NO. 2

Transactions

of The American Society of Mechanical Engineers

Published on the tenth of every month, except March, June, September, and December

---

OFFICERS OF THE SOCIETY

D. Robert Yarnall, *President*

K. W. Jappe, *Treasurer* C. E. Davies, *Secretary*

COMMITTEE ON PUBLICATIONS:

L. N. Rowley, Jr., *Chairman*

W. A. Carter J. M. Juran

H. L. Dryden Ronald B. Smith

George A. Stetson, *Editor* K. W. Clendinning, *Managing Editor*

ADVISORY MEMBERS OF THE COMMITTEE ON PUBLICATIONS:

N. C. Ebaugh, Gainesville, Fla. Hunter R. Hughes, Jr., Dallas, Texas O. B. Schier, 2nd., New York, N. Y.

Junior Member

Joseph M. Sexton, New York, N. Y.

Published monthly by The American Society of Mechanical Engineers. Publication office at 20th and Northampton Streets, Easton, Pa. The editorial department is located at the headquarters of the Society, 29 West Thirty-Ninth Street, New York 18, N. Y. Cable address, "Dynamic," New York. Price $1.50 a copy, $12.00 a year; to members and affiliates, $1.00 a copy, $7.50 a year Changes of address must be received at Society headquarters two weeks before they are to be effective on the mailing list. Please send old as well as new address.... By-Law: The Society shall not be responsible for statements or opinions advanced in papers or ... printed in its publications (B13, Par. 4).... Entered as second-class matter March 2, 1928, at the Post Office at Easton, Pa., under the act of August 24, 1912....

Copyrighted, 1946, by The American Society of Mechanical Engineers. Reprints from this publication may be made on condition that full credit be given the Transactions of the A.S.M.E. and the author, and that date of publication be stated.

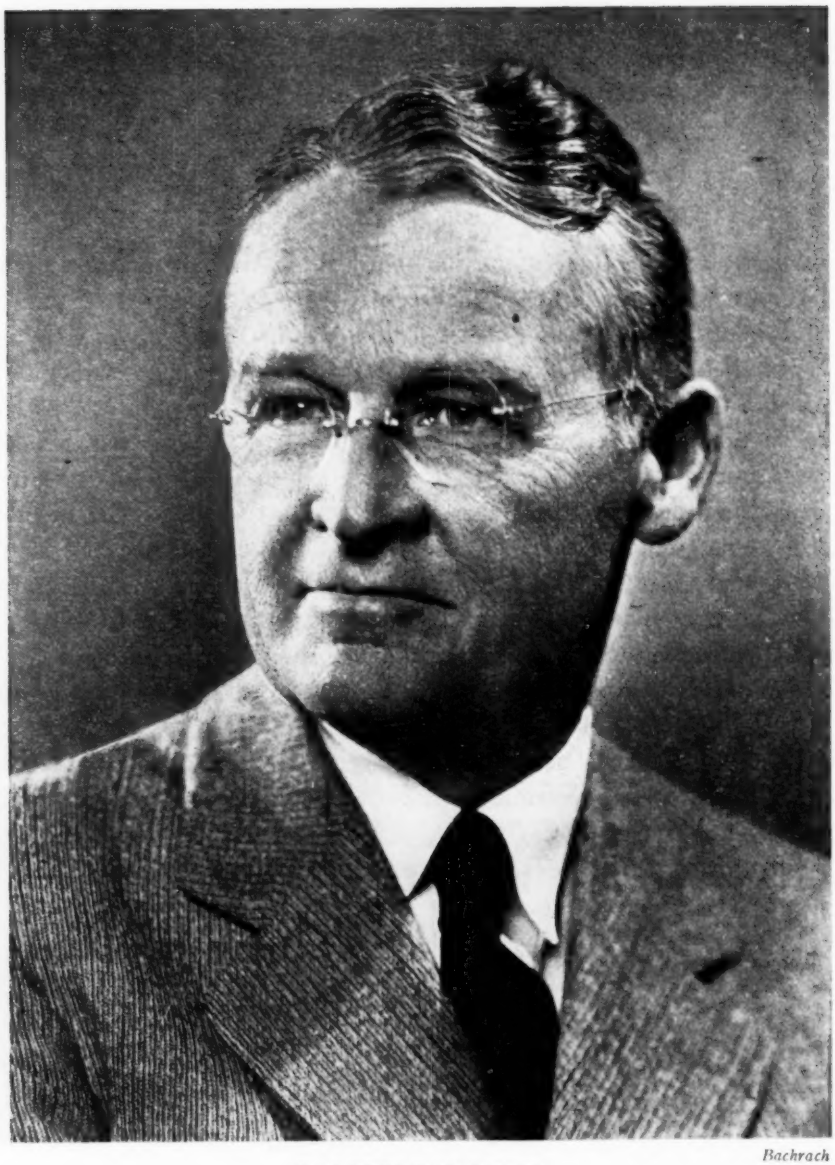
Foreword

THE Transactions of The American Society of Mechanical Engineers include selected technical papers and reports delivered at meetings of the Society, its Professional Divisions, and its Sections, the *Journal of Applied Mechanics* (contributions of the Applied Mechanics Division), certain records of the Society of permanent value, and indexes to its publications.

In order to secure the advantages of timeliness and greater usefulness in issuing these Society Records, the material comprising them is divided into a number of parts, each one of which is mailed as a supplement to one of the regular monthly issues of the Transactions. For 1946, the first of these, the present issue, contains the personnel of the Council and committees for the year. Another, to be issued sometime later in the year, will contain memorial notices of deceased members. The indexes to miscellaneous publications, *Mechanical Engineering*, and to the Transactions themselves, must, necessarily, be issued in 1947, and will probably be mailed as a supplement to the January issue of that year.

In binding the 1946 Transactions, all of these parts of the Society Records will be assembled at the back of the volume as has been customary for some years. To aid in locating references in the bound volumes, the page numbers of the sections containing the *Journal of Applied Mechanics* and the Society Records are preceded by the letters A and RI, respectively.

THE COMMITTEE ON PUBLICATIONS



Bachrach

D. ROBERT YARNALL

PRESIDENT OF THE AMERICAN SOCIETY OF MECHANICAL ENGINEERS
1945-1946

D. Robert Yarnall

D. Robert Yarnall, co-founder and president of the Yarnall-Waring Company of Chestnut Hill, Philadelphia, Pa., and for more than a quarter of a century prominently and actively identified in an engineering capacity, was born on June 28, 1878, in Delaware County, Pa., a son of Edward S. and Sidney S. (Garrett) Yarnall, both of American Quaker ancestry for generations.

D. Robert Yarnall attended Westtown School and the University of Pennsylvania, from which he was graduated in 1901 with the degree of bachelor of science in mechanical engineering. He received the further degree of mechanical engineer in 1905.

Shortly after his collegiate career he went to work for the Coatesville Boiler Works and allied companies as an engineer and remained with them for five years. His next position was with Stokes & Smith Co., Philadelphia, in a similar capacity, with whom he also remained for five years. In 1912 be became vice-president and general manager of the Nelson Valve Company of Philadelphia and held this position until 1918. In 1908, with B. G. Waring, he organized the firm of Yarnall-Waring Company and has been continuously identified with the company to the present time, today holding the office of president of the company, to which duties he devotes most of his time and attention. The company manufactures power-plant specialties. He is also a director and president of the James G. Biddle Company of Philadelphia, who are manufacturers of electrical instruments.

He became a junior member of the A.S.M.E. in 1903, a member in 1911, and a Fellow in 1936. He was a manager of the Society from 1917 to 1920. As the representative of the A.S.M.E. he served as director and chairman of the Committee on Public Affairs of the American Engineering Council. He has been a director and vice-president of The Engineering Foundation; trustee of The Franklin Institute; president of the Engineers' Club of Philadelphia for the term of 1929-1930; vice-president and director of the American Friends Service Committee; member of Sigma Xi fraternity. For eleven years he was presiding clerk of the Philadelphia Yearly Meeting of the Society of Friends; and he is chairman of the board of directors of Pendle Hill School and of the Committee of Westtown School. He is also a professional engineer of the State of Pennsylvania, and a member of the Engineers' Club of New York and the Philadelphia Cricket Club.

On November 1, 1937, Mr. Yarnall was elected president of the United Engineering Trustees—joint agency for the four founder societies of civil, mining and metallurgical, mechanical, and electrical engineers.

Mr. Yarnall's work at design and construction in conjunction with his business for more than forty years has resulted in many patents on valves and steam specialties. These devices, manufactured by his company, are in use in practically every government controlled steam-operated ship, as well as in all high-pressure steam-generating plants in the United States. He is the author of technical papers which have been published in *Mechanical Engineering* and A.S.M.E. Transactions.

He was awarded the Hoover Medal in 1941, and in the following year was made Doctor of Engineering by Lehigh University.

Mr. Yarnall served as a member of the Commission having charge of feeding German children in 1920, being stationed there for about nine months, and during the latter part of his stay in Berlin served as chairman of that Commission. In 1924 he was again sent to Germany under the auspices of the American Friends Service Committee and the General Allen Committee, having charge of the liquidation of the relief program. In June, 1938, he and Mrs. Yarnall were sent by American Friends Service Committee to Austria to assist in organization of relief of refugees. Subsequently, as a representative of this Committee, he went to Berlin to protest to the German government against atrocities of 1938-1939. In 1941, he was a member of the Commission to England to make a survey of relief needs due to the war and to consult the British Government about the shipment of more food through the blockade for the aid of children and mothers of France. He was appointed a member of the City Planning Commission, Philadelphia, Pa., in 1942, and was reappointed in 1944 for a full term of five years.

The American Society of Mechanical Engineers

HEADQUARTERS: 29 West 39th St., New York 18, N.Y.
MID-WEST OFFICE: Room 1920, 205 West Wacker Drive, Chicago 6, Ill.

The members of the Council and of its standing and special committees given on the following pages are those in office on January 1, 1946, serving for the official year 1945-1946. The terms of office of members of other committees are not fixed by the official calendar.

OFFICERS AND COUNCIL

PRESIDENT

D. Robert Yarnall

PAST-PRESIDENTS

Terms expire December

William A. Hanley (1946)
James W. Parker (1947)
Harold V. Coes (1948)
Robert M. Gates (1949)
Alex D. Bailey (1950)

VICE-PRESIDENTS

Term expires 1946

Alton C. Chick—I *
Rudolph F. Gagg—II
Edward E. Williams—IV
Thomas S. McEwan—VI
Linn Helander—VIII

Term expires 1947

A. R. Stevenson, Jr.—III
Samuel R. Beitler—V
J. Calvin Brown—VII

* Roman numerals indicate Region.

DIRECTORS AT LARGE

Term expires 1946

Samuel H. Graf
David Larkin
John E. Lovely
James M. Rorert

Term expires 1947

Daniel S. Ellis
Arthur J. Kerr

Term expires 1949

Edgar J. Kates
J. Noble Landis

TREASURER

K. W. Japppe

SECRETARY

C. E. Davies

CHAIRMEN OF STANDING COMMITTEES

Representatives on Council without vote

Finance, W. H. Sawyer
Meetings and Program, R. A. North
Publications, L. N. Rowley, Jr.
Admissions, T. H. Wickenden
Professional Divisions, J. A. Goff
Sections, O. B. Lyman
Constitution and By-Laws (To be appointed)
Honors and Awards, L. W. Wallace
Relations With Colleges, R. P. Reece
Education and Training for the Industries, L. J. Fletcher
Library, E. F. Church, Jr.
Research, J. F. Downie Smith
Standardization, J. Hall Taylor
Power Test Codes, A. G. Christie
Safety, H. W. Gabor
Professional Conduct, W. F. Ryan

EXECUTIVE COMMITTEE OF THE COUNCIL

D. Robert Yarnall, *Chairman*
D. S. Ellis
R. F. Gagg
J. N. Landis
A. R. Stevenson, Jr.

Advisory Members: Chairmen of the Finance, Sections, and Professional Divisions Committees

SECRETARIAL STAFF

Ernest Hartford, *Executive Assistant Secretary* (Sections, Divisions, Student Branches, Membership, Meetings, etc.)
C. B. LePage, *Assistant Secretary* (Technical Committees)
R. L. Sackett, *Assistant to the Secretary*
George A. Stetson, *Editor*
Frederick Lask, *Advertising Manager*
D. C. A. Bosworth, *Comptroller*

STANDING COMMITTEES

FINANCE

W. H. Sawyer, *Chairman* * (1947)
F. E. Lyford, *Vice-Chairman* (1949)
H. E. Whitaker (1946)
G. L. Knight (1948)
J. H. Lawrence (1950)

Council Representatives

David Larkin (1946)
A. J. Kerr (1947)

MEETINGS AND PROGRAM

R. A. North, *Chairman* * (1946)
D. S. Walker (1947)
P. W. Thompson (1948)
G. B. Warren (1949)
L. C. Morrow (1950)

Junior Advisers

C. H. Carman, Jr. (1946)
E. S. Rowell (1946)

PUBLICATIONS

L. N. Rowley, Jr., *Chairman* * (1946)
W. A. Carter (1947)
H. L. Dryden (1948)
J. M. Juran (1949)
R. B. Smith (1950)

Advisory Members (1946)

N. C. Ebaugh
H. R. Hughes, Jr.
O. B. Schier, II

Junior Adviser

J. M. Sexton (1946)

(Personnel of Biography Committee, p. RI-7)

ADMISSIONS

T. H. Wickenden, *Chairman* * (1946)
D. W. R. Morgan (1947)
G. E. Hulse (1948)
J. P. Kottcamp (1949)
E. H. Barlow (1950)

Advisory Member

S. D. Sprong (1946)

PROFESSIONAL DIVISIONS

J. A. Goff, *Chairman* * (1946)
J. M. Talbot (1947)
W. L. H. Doyle (1948)
B. S. Cain (1949)
T. R. Olive (1950)

Junior Advisers

J. J. Jacobs, Jr. (1946)
R. M. Titus (1947)

(Personnel of Professional Divisions Executive Committees, p. RI-10)

* Representative on the Council.

SECTIONS

Oliver B. Lyman, *Chairman* *
A. R. Mumford
S. D. Moxley
L. E. Jermy
J. A. Keeth

Junior Adviser

J. W. Simonson

(Personnel of Sections' Executive Committees, p. RI-15)

CONSTITUTION AND BY-LAWS

W. J. Cope (1946)
A. M. Gompf (1947)
F. W. Miller (1948)
H. H. Snelling (1949)
L. C. Smith (1950)

Junior Adviser

A. H. Gottesman (1947)

HONORS AND AWARDS

L. W. Wallace, *Chairman* * (1946)
R. C. Muir (1947)
E. W. O'Brien (1948)
C. M. Allen (1949)
To be appointed (1950)

(Personnel of Medals Committee, p. RI-7)

RELATIONS WITH COLLEGES

R. P. Reece, *Chairman* *
H. J. Brown
Herbert Kuenzel
H. R. Pearson
G. L. Sullivan

Advisory Members

E. Stanley Ault
N. P. Bailey
D. S. Clark
W. J. Cope
R. H. Porter

(Student Branches and Officers, p. RI-23)

EDUCATION AND TRAINING FOR THE INDUSTRIES

L. J. Fletcher, *Chairman* * (1947)
R. L. Goetzenberger (1946)
C. J. Freund (1948)
M. M. Boring (1949)
G. R. Cowing (1950)

Advisory Members (1946)

J. W. Barker
Lillian M. Gilbreth
H. R. Kutz
O. D. Montgomery

LIBRARY

E. F. Church, Jr., *Chairman* * (1947)
P. H. Hardie (1948)
G. F. Bateman (1949)
The Secretary, C. E. Davies, *Ex-Officio*

RESEARCH †

J. F. Downie Smith, *Chairman* * (1946)
Herman Weisberg (1947)
G. A. Hawkins (1948)
E. L. Robinson (1949)
To be appointed (1950)

STANDARDIZATION †

J. Hall Taylor, *Chairman* * (1946)
E. J. Bryant (1947)
D. S. Ellis (1948)
F. Hugh Morehead (1949)
F. K. Mitchell (1950)

POWER TEST CODES †

A. G. Christie, *Chairman* * (1946)
W. A. Carter, *Vice-Chairman* (1947)

Term expires 1946

A. G. Christie
Paul Diserens
N. R. Gibson
W. W. Johnson
E. B. Powell

Term expires 1947

W. A. Carter
W. L. H. Doyle
H. B. Oatley
R. B. Smith
W. J. Wohlenberg

Term expires 1948

Louis Elliott
G. A. Orrok, Jr.
Arvid Peterson
R. A. Sherman
P. W. Swain

Term expires 1949

S. N. Fiala
A. E. Grunert
L. F. Moody
T. E. Purcell
E. B. Ricketts

Term expires 1950

Theodore Baumeister
C. C. Franck
P. H. Hardie
B. V. E. Nordberg
M. C. Stuart

SAFETY †

H. W. Gabor, *Chairman* * (1947)
J. R. Connelly, *Vice-Chairman* (1948)
E. R. Granniss (1946)
R. B. Renner (1949)
J. J. Zeitner (1950)

PROFESSIONAL CONDUCT

W. F. Ryan, *Chairman* * (1948)
M. C. Maxwell (1947)
H. O. Croft (1949)

† Personnel of all Technical Committees, pp. RI-25-39.

SPECIAL COMMITTEES

BIOGRAPHY

(Special Committee of Publications Committee)

ROY V. WRIGHT, *Chairman*
R. E. FLANDERS
J. W. ROE

BOILER CODE

H. B. OATLEY, *Chairman*
H. E. ALDRICH, *Vice-Chairman*
D. S. JACOBUS, *Honorary Chairman*
C. A. ADAMS
T. B. ALLARDICE
H. C. BOARDMAN
P. R. CASSIDY
R. E. CECIL
A. J. ELY
V. M. FROST
W. P. GERHART
W. D. HALSEY
W. F. HESS
T. McL. JASPER
C. O. MYERS
C. W. OBERT
JAMES PARTINGTON
D. B. ROSSHEIM
D. L. ROYER
WALTER SAMANS
J. W. TURNER
S. K. VARNES
A. C. WEIGEL
F. S. G. WILLIAMS

J. W. SHIELDS, *Secretary*
M. JURIST, *Assistant Secretary*

Honorary Members

W. H. BOEHM
W. F. DURAND
E. R. FISH
C. E. GORTON
A. M. GREENE, JR.
W. G. HUMPTON
C. L. HUSTON
W. F. KIESEL, JR.
J. O. LEECH
M. F. MOORE
I. E. MOULTROP
H. LEROY WHITNEY

(Personnel of Boiler Code Committees, pp. RI-38-39)

DUES-EXEMPT MEMBERS' CONTRIBUTIONS

F. D. HERBERT, *Chairman*
C. F. DIETZ
L. H. FRY
S. M. MARSHALL
N. T. McKEE
C. W. OBERT
C. R. PLACE
E. B. RICKETTS
J. W. ROE
K. W. JAPPE, *Treasurer*

MEDALS

(Special Committee of Board of Honors and Awards)

Term expires 1946

L. W. WALLACE, *Chairman*
E. C. HUTCHINSON
W. H. KENERSON
ERIK OBERG

MEDALS
(Continued)

Term expires 1947

F. H. COLVIN
L. H. FRY
P. E. HOLDEN
R. C. MUIR

Term expires 1948

F. M. FEIKER
E. L. HOPPING
E. W. O'BRIEN
C. T. RIPLEY

Term expires 1949

C. M. ALLEN
N. E. FUNK
WARNER SEELY
B. R. VAN LEER

Term expires 1950

J. B. ENNIS
B. P. GRAVES
H. R. WESTCOTT
(To be appointed)

NOMINATING COMMITTEE FOR 1946

H. E. MARTIN, *Chairman*
W. W. BABCOCK, *Secretary*

Region

I J. W. ZELLER, Boston, Mass.
W. K. SIMPSON, Waterbury, Conn., *1st Alternate*
L. J. HOOPER, Holden, Mass., *2nd Alternate*

II H. E. MARTIN, New York, N.Y., *Chairman*
J. H. SENGSTAKEN, New York, N.Y., *1st Alternate*
ADOLF EHRBECHT, New York, N.Y., *2nd Alternate*

III A. R. SMITH, Schenectady, N.Y.
C. E. MILLER, Washington, D.C., *1st Alternate*
R. C. DANNETTEL, Baltimore, Md., *2nd Alternate*
W. H. CHAFFEE, Westfield, N.J., *3rd Alternate*

IV P. R. YOPP, Atlanta, Ga.
N. H. BROWN, Charlotte, N.C., *1st Alternate*
J. B. JONES, Blacksburg, Va., *2nd Alternate*
H. G. MOUAT, Birmingham, Ala., *3rd Alternate*

V E. J. MARTIN, Ivorydale, Ohio
F. H. VOSE, Cleveland, Ohio, *1st Alternate*
W. D. SHELDON, JR., Galt, Ont., Can., *2nd Alternate*

VI W. W. BABCOCK, Peoria, Ill., *Secretary*
H. O. CROFT, Iowa City, Iowa, *1st Alternate*
F. P. SHANNON, Louisville, Ky., *2nd Alternate*

VII R. L. DYER, Seattle, Wash.
F. B. LEE, Seattle, Wash., *Alternate*

VIII H. R. HUGHES, JR., Dallas, Texas
L. J. CUCULLU, New Orleans, La., *1st Alternate*
O. L. LEWIS, Tulsa, Okla., *2nd Alternate*

SECTIONS IN NOMINATING COMMITTEE REGIONS

REGION I

BOSTON
BRIDGEPORT
GREEN MOUNTAIN
HARTFORD
NEW HAVEN
NEW LONDON
PROVIDENCE
WATERBURY
WESTERN MASSACHUSETTS
WORCESTER

REGION II

METROPOLITAN (N.Y.) AND MEMBERS OUTSIDE THE UNITED STATES (EXCEPT ONTARIO SECTION MEMBERS)

REGION III

ANTHRACITE-LEHIGH VALLEY
BALTIMORE
BUFFALO
CENTRAL PENNSYLVANIA
ITHACA
PHILADELPHIA
PLAINFIELD
ROCHESTER
SCHENECTADY
SUSQUEHANNA
SYRACUSE
WASHINGTON, D.C.

REGION IV

ATLANTA
BIRMINGHAM
EAST TENNESSEE
FLORIDA
GREENVILLE
MEMPHIS
PIEDMONT-NORTH CAROLINA
RALEIGH
SAVANNAH
VIRGINIA

REGION V

AKRON-CANTON
CINCINNATI
CLEVELAND
COLUMBUS
DAYTON
DETROIT
ERIE
ONTARIO
PENINSULA
PITTSBURGH
TOLEDO
WEST VIRGINIA
YOUNGSTOWN

REGION VI

CENTRAL ILLINOIS
CENTRAL INDIANA
CHICAGO
FORT WAYNE
LOUISVILLE
MILWAUKEE
MINNESOTA
NEBRASKA
ROCK RIVER VALLEY
ST. JOSEPH VALLEY
ST. LOUIS
TRI-CITIES

REGION VII

INLAND EMPIRE
OREGON
SAN FRANCISCO
SOUTHERN CALIFORNIA
UTAH
WESTERN WASHINGTON

REGION VIII

COLORADO
KANSAS CITY
MID-CONTINENT
NEW ORLEANS
NORTH TEXAS
SOUTH TEXAS

SPECIAL COUNCIL COMMITTEES

(Dates in parentheses denote expiration of terms)

BOARD OF REVIEW

JOHN HAYDOCK, *Chairman* (1946)
T. M. KNOOP (1947)
A. D. BLAKE (1948)

BOARD ON CODES AND STANDARDS

HOWARD COONLEY, *Chairman*
JOHN E. LOVELY
Chairmen of Committees on Boiler Code, Power Test Codes, Safety, Standardization, A.S.M.E. Representative on American Standards Association, *Ex-Officio*

BOARD ON TECHNOLOGY

R. F. GAGG, *Chairman*
C. B. PECK, *Vice-Chairman*
(To be appointed)

Chairmen of Committees on Sections, Meetings and Program, Professional Divisions, Publications, Research, *Ex-Officio*

COMMITTEE ON NUCLEAR ENERGY APPLICATION

A. D. BAILEY, *Chairman*
A. L. BAKER
G. B. PEGRAM
A. R. STEVENSON, JR.
W. I. WESTERVELT

ENGINEERS' CIVIC RESPONSIBILITIES

ROY V. WRIGHT, *Chairman*
GANO DUNN
F. A. FAVILLE
M. H. FIES
LILLIAN M. GILBRETH
H. B. OATLEY
J. W. ROE
H. H. SNELLING
D. ROBERT YARNALL

Chairmen of Committees on Sections and Relations With Colleges, *Ex-Officio*

Junior Representative

W. WHITANEN

FREEMAN AWARD

CLARKE FREEMAN, *Chairman*
E. C. HUTCHINSON
W. H. MCBRYDE

INTERNATIONAL RELATIONS

R. M. GATES, *Chairman* (1946)
ERNEST PRAGST (1947)
JOSEPH POPE (1948)
R. S. DAMON (1949)
F. B. TURCK (1950)

Advisory Members

W. L. BATT
WALLACE CLARK
M. L. COOKE
HOWARD COONLEY
COL. P. R. FAYMONVILLE
A. M. GREENE, JR.
H. A. LARDNER
J. C. PARKER
E. A. PRATT
H. S. ROGERS
MAJ. GEN. C. M. WESSON

Secretary

G. H. KUECHLER

LECTURESHIPS

C. B. PECK, *Chairman*
A. G. CHRISTIE
H. N. DAVIS
W. F. DURAND
F. L. WILKINSON, JR.

MEMBERSHIP DEVELOPMENT

W. M. SHEEHAN, *Chairman*
J. CALVIN BROWN
H. C. R. CARLSON
W. L. H. DOYLE

(Continued)

MEMBERSHIP DEVELOPMENT

(Continued)

J. W. ESHELMAN
D. E. FIELDS
DAVID LARKIN
J. J. MCCARTHY
T. S. MCEWAN
ROSCOE W. MORTON
A. R. MUMFORD
E. W. O'BRIEN
W. L. RICHESON
P. T. SOWDEN
L. W. WALLACE
J. L. WALSH

ORGANIZATION

WALLACE CLARK, *Chairman*
H. V. COES
R. M. GATES
ALFRED IDDLES
E. J. KATES
G. L. KNIGHT
President-Elect, *Ex-Officio*

PENSION

G. L. KNIGHT, *Chairman*
K. W. JAPPE, *Treasurer*
W. H. SAWYER, *Chairman*, Finance Committee, *Ex-Officio*

REGISTRATION OF ENGINEERS

W. G. CHRISTY, *Chairman*
S. H. GRAF
J. A. MCPHERSON
F. H. PROUTY
DARROW SAGE
H. H. SNELLING

Junior Representatives

To be appointed

A.S.M.E. REPRESENTATIVES ON OTHER ACTIVITIES

See also A.S.M.E. Representatives on Other Research Committees, etc., pages RI-27, 32, 36, 37, 39
(Dates in parentheses denote expiration of terms)

AMERICAN ASSOCIATION FOR THE ADVANCEMENT OF SCIENCE

SECTION M, ENGINEERING

F. D. Carvin R. L. Sackett

AMERICAN DOCUMENTATION INSTITUTE

H. W. Craver

AMERICAN STANDARDS ASSOCIATION

Alfred Iddles (1946)
W. H. Hill (1948)

Alternates

C. B. LePage (1946)
W. C. Mueller (1946)

AMERICAN YEAR BOOK CORPORATION

C. E. Davies

CENTER FOR SAFETY EDUCATION

E. R. Granniss

THE ENGINEERING FOUNDATION

J. Schuyler Casey (1947)
A. A. Potter (1947)
W. Trinks (1948)

COLUMN RESEARCH COUNCIL

L. H. Donnell H. L. Whittemore
S. Timoshenko

RESEARCH PROCEDURE COMMITTEE

W. Trinks (1946)

E.I.C.-A.S.M.E. JOINT CONFERENCE

(The Engineering Institute of Canada)

A. G. Christie A. E. White
J. W. Parker

ENGINEERING SOCIETIES LIBRARY BOARD

E. F. Church, Jr. (1947)
P. H. Hardie (1948)
G. F. Bateman (1949)
Secretary, A.S.M.E., *Ex-Officio*

ENGINEERING SOCIETIES MONOGRAPHS COMMITTEE

J. A. Goff (Professional Divisions)
J. M. Juran (Publications)

ENGINEERING SOCIETIES PERSONNEL SERVICE, INC.

Ernest Hartford, *President of the Corporation* and A.S.M.E. representative, Metropolitan Advisory Committee

(Continued)

ENGINEERING SOCIETIES PERSONNEL SERVICE, INC.

(Continued)

R. N. Osterman, Chicago Advisory Committee
C. J. Freund, Detroit Advisory Committee
H. J. Berg, San Francisco Advisory Committee

ENGINEERS' COUNCIL FOR PROFESSIONAL DEVELOPMENT

R. L. Goetzenberger (1946)
J. W. Parker (1947)
J. E. Younger (1948)

COMMITTEE ON EMPLOYMENT CONDITIONS FOR ENGINEERS

Warner Seely

ENGINEERS JOINT COUNCIL

(Presidents and Secretaries of National Societies)

President, Junior Past-President, Secretary } *Ex-Officio*

Subcommittees

ECONOMIC STATUS OF THE ENGINEER

E. G. Bailey P. T. Onderdonk
L. J. Fletcher

ORGANIZATION OF ENGINEERING PROFESSION

H. V. Coes P. T. Onderdonk

ENGINEERS' NATIONAL RELIEF FUND

Ernest Hartford

JOHN FRITZ MEDAL BOARD OF AWARD

J. W. Parker (1946)
H. V. Coes (1947)
R. M. Gates (1948)
A. D. Bailey (1949)

GANTT MEDAL BOARD OF AWARD

E. H. Schell (1946)
J. M. Juran (1947)
D. B. Porter (1948)
J. A. Willard (1949)

DANIEL GUGGENHEIM MEDAL BOARD OF AWARD

J. M. Clark (1946)
C. B. Veal (1947)
A. R. Stevenson, Jr. (1948)

JOSEPH A. HOLMES SAFETY ASSOCIATION

J. F. Barkley

HOOVER MEDAL BOARD OF AWARD

W. H. Kenerson (1947)
S. F. Voorhees (1949)
H. N. Davis (1951)

INTER-AMERICAN DEVELOPMENT COMMISSION

A. M. Greene, Jr. C. M. Muchnic
W. H. McBryde

INTERNATIONAL ELECTROTECHNICAL COMMISSION

U.S. NATIONAL COMMITTEE

Paul Diserens Francis Hodgkinson

MARSTON AWARD

A. A. Potter (1949)

NATIONAL BUREAU OF ENGINEERING REGISTRATION

W. G. Christy

NATIONAL FIRE WASTE COUNCIL

J. A. Neale

NATIONAL MANAGEMENT COUNCIL

J. M. Talbot (1947)—Wallace Clark, *Alternate*
J. M. Juran (1948)—F. A. Turck, *Alternate*
W. R. Mullee (1949)—D. B. Porter, *Alternate*

NATIONAL RESEARCH COUNCIL

DIVISION OF ENGINEERING AND INDUSTRIAL RESEARCH

A. E. White (1948)

ALFRED NOBLE PRIZE

C. R. Soderberg (1949)

UNITED ENGINEERING TRUSTEES, INC.

H. A. Lardner (1946)
G. L. Knight (1947)
J. Schuyler Casey (1948)

VERMILYE MEDAL ADVISORY COMMITTEE

W. D. Fuller (1947)

WASHINGTON AWARD COMMISSION

H. S. Philbrick (1946)
J. R. Michel (1947)

WORLD POWER CONFERENCE

EXECUTIVE COMMITTEE, U.S. NATIONAL COMMITTEE

President, *Ex-Officio*

PROFESSIONAL DIVISIONS

ARTICLE B6A, PAR. 16: The Standing Committee on Professional Divisions shall, under the direction of the Council, have supervision of the Professional Divisions of the Society.

STANDING COMMITTEE

J. A. GOFF, *Chairman* (1946)
J. M. TALBOT (1947)
W. L. H. DOYLE (1948)
B. S. CAIN (1949)
T. R. OLIVE (1950)

Junior Advisers

J. J. JACOBS, JR. (1946)
R. M. TITUS (1947)

Liaison Representative, Sections

A. R. MUMFORD

Applied Mechanics

Organized, 1927

H. PORITSKY, *Chairman*

EXECUTIVE COMMITTEE

H. PORITSKY, *Chairman*
H. W. EMMONS, *Secretary*
MARTIN GOLAND
R. P. KROON
W. M. MURRAY

Associates

J. P. DEN HARTOG
RUPEN EKSERGIAN
J. N. GOODIER
J. C. HUNSAKER
J. H. KEENAN
G. B. PEGRAM
R. E. PETERSON
E. O. WATERS
B. M. WOODS

Research Secretary

JESSE ORMONDROYD

Liaison Representatives

Aviation Liaison Group, J. C. HUNSAKER
Co-ordination Committee of Heat Transfer Division, H. W. EMMONS
Railroad Division Group, W. I. CANTLEY
San Francisco Section, W. M. MOODY

JOURNAL OF APPLIED MECHANICS

J. M. LESSELLS, *Editor*

SPONSORS

Dynamics, F. M. LEWIS
Elasticity, STEPHEN TIMOSHENKO
Experimental Stress Analysis, W. M. MURRAY
Fluid Mechanics, H. W. EMMONS
Lubrication, L. M. TICHVINSKY
Plasticity, A. L. NÁDAI
Strength of Materials, C. R. SODERBERG
Thermodynamics, J. A. GOFF

Aviation

Organized, 1920

F. K. TEICHMANN, *Chairman*

EXECUTIVE COMMITTEE

F. K. TEICHMANN, *Chairman*
J. E. YOUNGER, *Executive Secretary*
HERMAN HOLLERITH, JR.
R. P. KROON
E. S. THOMPSON
F. W. WEICK

Junior Advisers

B. E. DEL MAR
F. H. FOWLER, JR.
MARTIN GOLAND

GENERAL COMMITTEE

West Coast Committee

T. E. COLVIN, *Chairman*
L. M. K. BOELTER
JOHN DELMONTE
W. E. MASON
WILLIAM SCHROEDER
F. R. SHANLEY

Southwest Committee

M. J. THOMPSON, *Chairman*
M. V. BARTON

Central and East Committee

N. P. BAILEY
LUIS DE FLOREZ
R. M. HEINTZ
R. B. LEA
D. C. PRINCE
J. T. RETTALIATA
R. G. STANDERWICK
J. E. SUTHERLAND
F. L. YERZLEY

Associates

E. E. ALDRIN
J. M. CLARK
C. H. DOLAN
R. F. GAGG
ALEXANDER KLEMIN
E. A. SPERRY, JR.
A. R. STEVENSON, JR.

Liaison Representatives, Professional Divisions

Applied Mechanics, M. V. BARTON, MARTIN GOLAND, J. N. GOODIER, R. E. PETERSON, J. E. YOUNGER
Heat Transfer, L. M. K. BOELTER, H. S. GORDON, R. H. NORRIS, W. W. REASER
Hydraulic, R. G. FOLSOM, THEODORE VON KARMAN
Industrial Instruments, ED S. SMITH
Management, R. E. GILLMOR
Metals Engineering, R. G. STURM, R. F. TEMPLIN
Oil and Gas Power (Gas Turbines), R. F. GAGG, C. W. GOOD
Production Engineering, R. F. GAGG.
Rubber and Plastics, JOHN DELMONTE, G. M. KLINE, J. F. DOWNIE SMITH
Wood Industries, ALEXANDER KLEMIN

Liaison Representatives, Other Activities

Daniel Guggenheim Medal Board of Award, J. M. CLARK, A. R. STEVENSON, JR., C. B. VEAL
Education and Training for the Industries, Standing Committee, A. R. STEVENSON, JR.
Institute of the Aeronautical Sciences, J. E. YOUNGER

BIOMECHANICS COMMITTEE

F. K. TEICHMANN, *Chairman*
L. D. CARSON
EUGENE DUBOIS
RUPEN EKSERGIAN
R. F. GAGG
C. M. GRATZ
L. E. GRIFFITH
P. E. HOVGARD

NOISE CONTROL

HERMAN HOLLERITH, JR., *Chairman*
MARTIN GOLAND
KENNETH JACKSON
F. K. TEICHMANN

Consulting Engineering Group

Organized, 1943

M. X. WILBERDING, *Chairman*

EXECUTIVE COMMITTEE

M. X. WILBERDING, *Chairman*
P. L. BATTEY
J. G. BERGER
S. LOGAN KERR
F. H. PROUTY

Fuels

Organized, 1920

J. E. TOBEY, *Chairman*

EXECUTIVE COMMITTEE

J. E. TOBEY, *Chairman*
D. C. WEEKS, *Secretary*
T. C. CHEASLEY
D. S. FRANK
E. R. KAISER

Associates

J. F. BARKLEY
R. J. BENDER
E. D. BENTON
O. F. CAMPBELL
A. H. CANNON
W. G. CHRISTY
B. J. CROSS
R. B. ENGDAHL
M. D. ENGLE
H. F. HEBLEY
J. H. KERRICK
W. J. KING
T. A. MARSH
M. A. MAYERS
J. R. MICHEL
C. E. MILLER
A. R. MUMFORD
A. L. NICOLAI
E. C. PAYNE
W. E. REASER
R. L. ROWAN
R. A. SHERMAN
A. W. THORSON
E. C. WEBB
J. I. YELLOTT

COAL TESTING CODE

Organized, 1939, Jointly With A.I.M.E.

R. L. Rowan, *Chairman*
J. E. Tobey, *Vice-Chairman*

A.S.M.E. Representatives

J. F. Barkley
H. C. Carroll
R. A. Foresman
R. M. Hardgrove
J. H. Kerrick
T. A. Marsh
A. R. Mumford
W. T. Reid
R. A. Sherman
L. A. Shipman
A. W. Thorson

DOMESTIC FUELS

T. C. Cheasley
T. A. Marsh
R. A. Sherman
J. E. Tobey

HONORS AND AWARDS

M. D. Engle

JOINT AWARDS

PERCY NICHOLLS' AWARD COMMITTEE
A.S.M.E. Representatives

O. F. Campbell (1948)
J. F. Barkley (1950)

MODEL SMOKE LAW

J. F. Barkley, *Chairman*
O. F. Campbell
A. G. Christie
W. G. Christy
C. F. Hardy
T. A. Marsh
T. E. Purcell
R. A. Sherman
R. R. Tucker

PROGRAM AND MEETINGS

E. R. Kaiser, *Chairman*
W. E. Reaser

REVIEW OF PAPERS

J. E. Tobey, *Chairman*
M. D. Engle
E. R. Kaiser
D. C. Weeks

Graphic Arts

Organized, 1922, as Printing Industries Division. Name changed, 1935.

Inactive

Heat Transfer

Organized, 1938, as Heat Transfer Professional Group. Reorganized, 1941.

(Committees to be appointed)

Hydraulic

Organized, 1926

L. J. Hooper, *Chairman*

EXECUTIVE COMMITTEE

L. J. Hooper, *Chairman*
G. R. Rich, *Secretary*
G. T. Abernathy
J. F. Roberts
R. E. B. Sharp

CAVITATION

R. E. B. Sharp, *Sponsor*
L. F. Moody, *Chairman*
R. T. Knapp
J. M. Mousson
W. J. Rheingans
G. F. Wislicenus

Representatives of Other Societies

American Society for Testing Materials, F. N. Speller
The Engineering Institute of Canada, Ernest Brown
The Institution of Mechanical Engineers, G. S. Baker

HYDRAULIC PRIME MOVERS

J. F. Roberts, *Sponsor* and *Chairman*
A. Aberli
E. H. Collins
J. P. Growdon
L. F. Harza
P. L. Heslop
G. Jessup
F. H. Rogers
F. Schmidt
S. O. Schomberger
S. H. Van Patter

PUMPING MACHINERY

G. T. Abernathy, *Sponsor*
R. L. Daugherty, *Chairman*
B. F. Tillson
Hans Ulmann

WATER HAMMER

G. R. Rich, *Sponsor*
S. Logan Kerr, *Chairman*
N. R. Gibson
Eugene Halmos
L. F. Moody
R. S. Quick
E. B. Strowger

Affiliated Societies and Their Representatives

American Society of Civil Engineers, N. R. Gibson, Ford Kurtz
American Water Works Association, F. M. Dawson, L. H. Kessler

Industrial Instruments and Regulators Division

Organized, 1936, as Committee on Industrial Instruments and Regulators, of Process Industries Division. Reorganized, 1943, as a Division

Ed S. Smith, *Chairman*

EXECUTIVE COMMITTEE

Ed S. Smith, *Chairman*
J. C. Peters, *Secretary*
J. J. Grebe
E. S. Lee
H. F. Moore

COMMITTEE CHAIRMEN

Application, R. D. Webb
Bibliography and Translations, H. L. Mason
By-Laws, E. D. Haigler
Design, W. G. Brombacher
Membership, C. F. Kayan
Papers, P. W. Keppler
Terminology, H. F. Moore
Theory, A. F. Sperry

Liaison Representatives

M. F. Behar, Instrument Society of America
C. O. Fairchild, American Institute of Physics
J. J. Grebe, American Institute of Chemical Engineers
K. H. Hubbard, Recorder-Controller Section, Scientific Apparatus Makers of America
A. Ivanoff, The Institution of Mechanical Engineers
Everett S. Lee, A.I.E.E. Committee on Instruments and Measurements
I. M. Stein, Gibson Island Conferences of American Association for the Advancement of Science

Machine Design Group

Organized, 1945

J. F. Downie Smith, *Chairman*

EXECUTIVE COMMITTEE

J. F. Downie Smith, *Chairman*
B. P. Graves, *Secretary*
Colin Carmichael
L. F. Nenninger
G. F. Nordenholt

GENERAL COMMITTEE

J. B. Armitage
Earle Buckingham
E. W. Clem
P. T. Eisele
T. F. Githens
K. M. Holt
W. F. Huck
P. W. Keppler
M. H. Kuhner
F. J. Oliver
R. E. Orton
D. V. Waters

Management

Organized, 1920

A. I. PETERSON, *Chairman*
G. M. VARGA, *Secretary*
CARLOS DEZAFRA, *Assistant Secretary*

EXECUTIVE COMMITTEE

A. I. PETERSON, *Chairman*
J. A. WILLARD, *Vice-Chairman*
A. S. KNOWLES
J. K. LOUDEN
W. R. MULLEE

Research Secretary

E. H. HEMPEL

Contact Secretary, Sections

W. R. MULLEE

GENERAL COMMITTEE

L. A. APPLEY
J. R. BANGS
R. M. BARNES
W. L. BATT
C. W. BEESE
WALLACE CLARK
H. V. COES
K. H. CONDIT
CARLOS DEZAFRA
N. E. ELSAS
S. P. FISHER
W. D. FULLER
L. M. GILBRETH
R. E. GILLMOR
G. E. HAGEMANN
E. H. HEMPEL
P. E. HOLDEN
W. F. HOSFORD
J. M. JURAN
W. A. KERR
D. S. KIMBALL
W. H. KUSHNICK
H. B. MAYNARD
T. S. MCEWAN
L. C. MORROW
P. T. NORTON, JR.
A. M. PERRIN
D. B. PORTER
G. A. RIETZ
I. H. SCHELL
E. L. SPRAY
A. R. STEVENSON, JR.
J. M. TALBOT
F. B. TURCK
L. W. WALLACE

Liaison Representatives, Sections

Atlanta, S. C. HALE
Birmingham, H. L. FREEMAN
Chicago, H. P. DUTTON
Cincinnati, R. J. SHORT
Cleveland, G. T. TRUNDLE, JR.
Columbus, P. N. LEHOCZKY
Detroit, K. R. HERMAN
Los Angeles, D. S. CLARK
Louisville, C. ELDRIDGE
Metropolitan, M. S. SYMON
Milwaukee, B. V. E. NORDBERG
New Orleans, E. L. COWAN
Philadelphia, C. S. GOTWALS
San Francisco, G. H. RAITT
Seattle, H. J. MCINTYRE
South Texas, V. M. FAIRES
Waterbury, R. S. STORRS

SUBCOMMITTEE CHAIRMEN

Administrative Organization, W. R. MULLEE
Depreciation Studies, P. T. NORTON, JR.
Distribution, F. B. TURCK
Industrial Conservation, A. M. PERRIN
Industrial Relations, W. H. KUSHNICK
Quality Control, A. I. PETERSON
Work Standardization, J. K. LOUDEN

Liaison Representatives, Other Activities

Co-ordination Committee on Gas Turbines, J. A. WILLARD
Co-ordination Committee of the Heat Transfer Division, J. M. TALBOT
Education and Training for the Industries Standing Committee, LILLIAN M. GILBRETH
Gantt Medal Board of Award: see page 9
National Management Council: see page 9
Plant Layout Standards Models Committee, G. E. HAGEMANN
Professional Divisions Standing Committee, J. M. TALBOT

Materials Handling

Organized, 1920

F. J. SHEPARD, JR., *Chairman*

EXECUTIVE COMMITTEE

F. J. SHEPARD, JR., *Chairman*
C. H. BARKER, JR., *Secretary*
C. F. DIETZ
R. W. MALLICK
J. B. WEBB

Associates

H. E. BLANK, JR.
W. C. CARL
N. W. ELMER
G. E. HAGEMANN
H. C. KELLER
BERNARD LESTER
M. C. MAXWELL
R. H. MCLAIN
F. E. MOORE
P. D. OESTERLE
A. M. PERRIN
M. W. POTTS
SIDNEY REIBEL
R. B. RENNER
E. D. SMITH
H. E. STOCKER
G. R. WADLEIGH

Junior Associates

A. J. BURKE
CORNELIUS CROWLEY
E. Z. GABRIEL
R. W. GRUNDMAN
D. D. JONES
W. G. PLENTY
JOHN SCHUETTINGER

MATERIALS HANDLING SAFETY COMMITTEE

R. B. RENNER, *Chairman*

SAFETY CODE FOR BULK MATERIALS CONVEYORS

C. S. HUNTINGTON, *Chairman*

SAFETY CODE FOR PACKAGE CONVEYORS

H. C. KELLER, *Chairman*

PLANT LAYOUT STANDARDS MODELS

R. W. MALLICK

STANDARD NOMENCLATURE

M. W. POTTS, *Chairman*

STANDARDIZATION OF SHIPMENTS ON SKIDS AND PALLETS

C. H. BARKER, JR., *Chairman*
H. E. STOCKER, *Vice-Chairman*
C. E .MOCHRIE
P. F. NYDEGGER
M. W. POTTS
F. J. SHEPARD, JR.

Metals Engineering

Organized, 1927, as Iron and Steel Division. Reorganized, 1940.

R. D. BRIZZOLARA, *Chairman*

EXECUTIVE COMMITTEE

R. D. BRIZZOLARA, *Chairman*
J. F. YOUNG, *Secretary*
E. O. DIXON
J. J. KANTER
J. M. LESSELLS
R. G. STURM

ADVISORY COMMITTEE

J. H. HITCHCOCK
J. H. ROMANN
M. D. STONE
W. TRINKS
T. H. WICKENDEN

GENERAL COMMITTEE

L. F. COFFIN
SABIN CROCKER
D. S. ELLIS
F. P. HUSTON
R. E. KENNEDY
NORMAN MOCHEL
S. D. MOXLEY
P. M. MUELLER
R. A. NORTH
E. S. PATCH
G. A. PUGH
W. M. SHEEHAN
T. R. WEBER
A. E. WHITE
A. W. WINSTON

Oil and Gas Power

Organized, 1921

E. J. KATES, *Chairman*

EXECUTIVE COMMITTEE

E. J. KATES, *Chairman*
L. N. ROWLEY, *Secretary*
C. F. FOELL, *Associate Secretary*
C. E. BECK
G. C. BOYER
R. T. SAWYER
LEE SCHNEITTER

Associates

HANS BOHUSLAV
H. G. BRYAN
G. J. DASHEFSKY
H. E. DEGLER
E. S. DENNISON
W. L. H. DOYLE
M. A. ELLIOTT
C. F. FOELL
C. W. GOOD
F. G. HECHLER
P. B. JACKSON
W. F. JOACHIM
H. C. LENFEST
B. V. E. NORDBERG
M. J. REED
R. B. RICE
T. M. ROBIE
J. A. WORTHINGTON

Research Secretary

LEE SCHNEITTER

Liaison Representatives

Aviation Liaison Group, R. T. SAWYER
Diesel Engine Manufacturers Association, R. B. RICE
Heat Transfer Division, F. G. HECHLER
Railroad Division, R. T. SAWYER
Society of Naval Architects and Marine Engineers, B. V. E. NORDBERG

HONORS AND AWARDS

LEE SCHNEITTER, *Chairman*
C. W. GOOD

OIL ENGINE POWER COST

H. C. MAJOR, *Chairman*
H. C. LENFEST, *Secretary*
H. G. BRYAN
E. HALE CODDING
MALCOLM DUNCAN
JOHN EARLE
R. G. ELY
J. H. GALLAWAY
E. J. KATES
A. B. MORGAN
M. J. REED
T. M. ROBIE
R. T. SAWYER
LEE SCHNEITTER
P. H. SCHWEITZER
J. B. SIMS
R. H. STIER
C. A. TRIMMER

OIL AND GAS POWER CONFERENCES

1947 Meeting Location Selection Committee

E. J. KATES, *Chairman*
L. N. ROWLEY
LEE SCHNEITTER

MEETINGS AND PAPERS

R. T. SAWYER, *Chairman*
HANS BOHUSLAV
G. C. BOYER
ROBERT CRAMER
P. B. JACKSON

PUBLICITY

C. F. FOELL, *Chairman*

Power Division

Organized, 1920

J. A. KEETH, *Chairman*

EXECUTIVE COMMITTEE

J. A. KEETH, *Chairman*
G. B. WARREN, *Secretary*
F. M. GIBSON
H. D. HARKINS
T. B. STILLMAN
J. I. YELLOTT

Process Industries

Organized, 1934

C. F. KAYAN, *Chairman*

EXECUTIVE COMMITTEE

C. F. KAYAN, *Chairman*
T. R. OLIVE, *Secretary*
E. J. DEVLIN
J. W. HUNTER
WILLIAM RAISCH
ARNOLD WEISSELBERG

Research Secretary

ARNOLD WEISSELBERG

Liaison Representatives

Heat Transfer Division, E. J. DEVLIN
Professional Divisions Standing Committee, T. R. OLIVE
San Francisco Section, HERMAN DISHINGTON

COMMITTEE CHAIRMEN

Agriculture, L. E. POTTER
Air Conditioning and Refrigeration, C. F. KAYAN
Distillation and Evaporation, D. F. OTHMER
Drying, ARNOLD WEISSELBERG
Fluids Handling, C. H. CARMAN, JR.
Manufactured and Natural Gas, E. J. DEVLIN
Mechanical Separation, RICHARD O'MARA
Paper Awards and Honors, VICTOR WICHUM
Petroleum, WILLIAM RAISCH
Program, J. W. HUNTER
Sanitation, WILLIAM RAISCH
Sugar, F. M. GIBSON
Sulphur, B. E. SHORT
Vegetable Oils, R. W. MORTON

Production Engineering

Organized, 1921, as Machine Shop Practice Division. Reorganized, 1941.

J. L. ALDEN, *Chairman*

EXECUTIVE COMMITTEE

J. L. ALDEN, *Chairman*
C. L. TUTT, JR., *Secretary*
F. O. HOAGLAND
H. B. LEWIS
A. F. MURRAY

Advisory Committee

SOL EINSTEIN
E. W. ERNST
ERIK OBERG
WARNER SEELY

GENERAL COMMITTEE

J. B. ARMITAGE
F. H. COLVIN
B. P. GRAVES
W. H. KASSEBOHM
J. E. LOVELY
FRED LUCHT
M. E. MARTELLOTTI
L. S. MARTZ
W. H. OLDACRE
A. A. SCHWARTZ

Railroad

Organized, 1920

K. F. NYSTROM, *Chairman*

EXECUTIVE COMMITTEE(RR1)

K. F. NYSTROM, *Chairman*
E. L. WOODWARD, *Secretary*
B. S. CAIN (1949)
P. W. KIEFER (1948)
J. M. NICHOLSON (1950)
W. C. SANDERS (1947)

GENERAL COMMITTEE (RR2)

K. F. NYSTROM, *Chairman*
E. R. BATTLEY (1948)
W. H. BASELT (1948)
C. H. BECK (1949)
K. A. BROWNE (1947)
W. I. CANTLEY (1950)
E. D. CAMPBELL (1947)
J. E. DAVENPORT (1946)
C. M. DARDEN (1947)
E. P. GANGEWERE (1949)
F. P. HUSTON (1950)
R. P. JOHNSON (1950)
E. S. PEARCE (1948)
C. E. POND (1949)
A. A. RAYMOND (1946)
H. H. URBACH (1946)

ADVISORY COMMITTEE (RR3)

Past-Chairmen

A. I. LIPETZ
D. S. ELLIS
J. R. JACKSON
J. G. ADAIR
W. M. SHEEHAN

Research Secretary

KENNETH CARTWRIGHT

Liaison Representatives

Admissions Standing Committee, F. E. LYFORD
Heat Transfer Division, Co-ordination Committee, L. H. FRY
Professional Divisions Standing Committee, B. S. CAIN
Co-ordination With Oil and Gas Power Division, R. T. SAWYER
Contact With American Association of Railroads, C. T. RIPLEY, *Chairman*, D. S. ELLIS, W. M. SHEEHAN
San Francisco Section, M. P. TAYLOR

Rubber and Plastics Division

Organized, 1937, as Committee on Rubber and Plastics of Process Industries Division and made a Subdivision in 1940. Reorganized as a Group in 1942, and as a Division in 1943.

J. H. BOOTH, *Chairman*

EXECUTIVE COMMITTEE

J. H. BOOTH, *Chairman*
H. M. RICHARDSON, *Secretary*
J. F. DOWNIE SMITH, *Senior Member*
D. H. CORNELL
F. W. WARNER

ADVISORY COMMITTEE

JOHN DELMONTE
G. M. KLINE
E. F. RIESING
R. G. SEAMAN
F. L. YERZLEY

GENERAL COMMITTEE

COLIN CARMICHAEL
E. N. CUNNINGHAM
F. HOUSEHOLDER
W. NEWLIN KEEN
J. W. LISKA
G. W. NEELY
PHILIP SMITH
A. V. TABOLSKY
J. H. TEEPLE
C. L. TUTT, JR.
F. W. WARNER
F. J. WEHMER

Textile

Organized, 1921

C. D. BROWN, *Chairman*

EXECUTIVE COMMITTEE

C. D. BROWN, *Chairman*
A. B. STUDLEY, *Northern Vice-Chairman*
To be appointed, *Southern Vice-Chairman*
W. A. SMITH, JR., *Secretary*
S. B. EARLE, *Southern Representative*
J. W. COX, *Inter-Society Representative*

Associates

F. L. BRADLEY
L. D. COBB
M. A. GOLRICK, JR.
W. O. JELLEME
J. O. LINDSAY
J. J. MCELROY
C. S. PARSONS
J. W. VAUGHAN, JR.

ACTIVITIES COMMITTEE

A. B. STUDLEY, *Co-Chairman*
To be appointed, *Co-Chairman*
R. D. BROUWER
O. W. CLARK
M. H. IRONS
W. O. JELLEME
W. R. KENT
N. M. MITCHELL
J. D. ROBERTSON
H. SEARLES
A. N. SHELDON
R. G. SHEPHERD
W. W. STARKE

ADVISORY COMMITTEE

A. D. ASBURY
A. L. BROWN
W. D. FALES
M. E. HEARD
W. B. HEINZ
R. J. MCCONNELL
ALBERT PALMER
BRACKETT PARSONS
J. D. ROBERTSON
A. N. SHELDON
E. WADSWORTH STONE
R. W. VOSE

ADVISORY COMMITTEE

D. R. GRAY
M. J. MACDONALD
R. H. MCCARTHY
C. B. NORRIS
T. D. PERRY

GENERAL COMMITTEE

C. L. BABCOCK
P. H. BILHUBER
A. W. DUNBAR
G. E. FRENCH
J. S. MATHEWSON
R. R. SMITH
H. M. SUTTON
F. F. WANGAARD
W. B. WILKINS

COMMITTEE CHAIRMEN

Dimensional Limits and Allowances, A. C. FEGEL
Forest Protection, H. S. JONES
Wood Finishing, M. J. MACDONALD

Wood Industries

Organized, 1921

A. C. FEGEL, *Chairman*

EXECUTIVE COMMITTEE

A. C. FEGEL, *Chairman*
To be appointed, *Secretary*
F. J. HANRAHAN
C. B. LUNDSTROM
E. D. MAY

SECTIONS

ARTICLE B6A, PAR. 17: The Standing Committee on Sections shall, under the direction of the Council, have supervision of the Sections of the Society.

STANDING COMMITTEE ON SECTIONS

OLIVER B. LYMAN, *Chairman*

A. R. MUMFORD
S. D. MOXLEY
L. E. JERMY
J. A. KEETH

Junior Adviser

J. W. SIMONSON

REGIONAL VICE-PRESIDENTS

REGION	
I	A. C. CHICK
II	R. F. GAGG
III	A. R. STEVENSON, JR.
IV	E. E. WILLIAMS
V	S. R. BEITLER
VI	T. S. McEWAN
VII	J. CALVIN BROWN
VIII	LINN HELANDER

REGIONAL SECRETARIES

REGION	
I	W. P. SAUNIER
II	HERMAN WEISBERG
III	J. C. REED
IV	E. S. THEISS
V	A. C. PASINI
VI	W. H. OLDACRE, O. E. E. ZAHN — *Co-Secretaries*
VII	M. B. HOGAN
VIII	R. P. HAHN

OFFICERS CHOSEN BY 1945 GROUP DELEGATES AT CHICAGO, JUNE, 1945

E. S. THEISS, *Speaker*
J. C. REED, *Vice-Speaker*
R. P. HAHN, *Secretary*
A. C. PASINI, *Chairman of Agenda*

AKRON-CANTON

Organized: 1920
Territory: Counties of Richland, Ashland, Medina, Summit, Portage, Wayne, Stark, Holmes, Tuscarawas, Carroll, and Coshocton in Ohio
Place of Meeting: As selected monthly
Numbers of Members: 203

EXECUTIVE COMMITTEE

R. W. HURSH, *Chairman*
M. C. PIERCE, *Vice-Chairman*
E. D. GEORGE, *Secretary-Treasurer*
E. W. ALLARDT
C. R. BECKWITH
M. R. BOWERMAN
D. H. CORNELL
Z. N. HARRIS
E. B. MANSFIELD
H. S. McCOOL
G. C. McMULLEN
R. G. MINNS
R. I. SUTTON
J. H. VANCE
A. G. WALKER

ANTHRACITE-LEHIGH VALLEY

Organized: 1920, as Lehigh Valley; reorganized, 1928, as Anthracite-Lehigh Valley
Territory: Counties of Bradford, Susquehanna, Wayne, Sullivan, Wyoming, Lackawanna, Columbia, Luzerne, Monroe, Pike, Schuylkill, Carbon, Berks, Lehigh, Northampton in Pennsylvania, and Warren in New Jersey
Place of Meeting: One meeting annually at Allentown, Bethlehem, Easton, Hazleton, Pottsville, Reading, Scranton, and Wilkes-Barre
Local Organization: The Engineers' Club of Lehigh Valley
Number of Members: 215

EXECUTIVE COMMITTEE

C. H. FOLMSBEE, *Chairman*
J. A. GISH, JR., J. A. LLOYD, WALTER TALLGREN — *Vice-Chairmen*
J. W. BLISS, *Secretary-Treasurer*
W. E. ANDERSON
C. W. BELL
K. W. BLOOM
E. A. GORNEY
L. D. GRABOSKI
S. I. HAMMOND
T. E. JACKSON
T. Y. MULLEN
L. E. MYLTING
R. L. RANSOM
C. T. REILLY
D. D. SCHULZ
H. C. SCHWEIKART

ATLANTA

Organized: 1913
Territory: Radius of sixty miles from Atlanta, Ga.
Place of Meeting: Atlanta Athletic Club
Luncheon meeting every Monday at 12:30 p.m. at Atlanta Athletic Club
Number of Members: 119

EXECUTIVE COMMITTEE

J. A. DODD, *Chairman*
C. L. HUEY, *Vice-Chairman*
R. L. ALLEN, *Secretary-Treasurer*
A. C. KEISER, JR.
R. S. KING
EARLE MAULDIN
M. J. McWHORTER
J. W. PARKER, JR.
B. D. SMITH
T. E. SMITH
V. F. WATERS

BALTIMORE

Organized: 1916
Territory: Radius of thirty miles from Baltimore, Md.
Place of Meeting: Engineers Club of Baltimore
Number of Members: 310

EXECUTIVE COMMITTEE

J. H. POTTER, *Chairman*
H. W. WOODWARD, *Vice-Chairman*
L. E. CARTER, *Secretary-Treasurer*
R. C. DANNETTEL
J. D. ELDER
R. J. GREEN
E. H. HANHART
H. H. HOLLERITH
S. F. ROBERTSON

BIRMINGHAM

Organized: 1915
Territory: Radius of sixty miles from Birmingham, Ala.
Place of Meeting: Tutwiler Hotel
Number of Members: 103

EXECUTIVE COMMITTEE

D. H. GULDBERG, *Chairman*
J. B. EMORY, *Vice-Chairman*
C. M. ELLIS, *Secretary-Treasurer*
J. E. HANNUM
H. G. MOUAT

BOSTON

Organized: 1909
Territory: Radius of thirty miles from Boston, Mass.
Place of Meeting: Mass. Inst. of Technology

(*Continued*)

BOSTON
(Continued)

Local Organization: Engineering Societies of New England
Number of Members: 790

EXECUTIVE COMMITTEE

W. P. SAUNIER, *Chairman*
R. D. STAUFFER, *Vice-Chairman*
A. J. FERRETTI, *Secretary-Treasurer*
E. K. BANCROFT
ALTON KIRKPATRICK
C. W. MACGREGOR

BRIDGEPORT

Organized: 1917, as a Branch of Connecticut Section; reorganized as a Section, 1923
Territory: Fairfield County, Conn.
Place of Meeting: Stratfield Hotel
Local Organizations: The Bridgeport Tool Engineers Association; The Bridgeport Engineers Club
Number of Members: 203

EXECUTIVE COMMITTEE

W. E. HOGAN, *Chairman*
J. F. BANTHIN, *Vice-Chairman*
J. P. HEUMANN, *Treasurer*
W. H. SNIFFEN, *Secretary*
H. E. ADAMS
RUDOLF BECK
J. L. CORCORAN
F. G. D'ARCY
J. K. HAMIL
P. A. IBOLD
J. H. POWERS

BUFFALO

Organized: 1915
Territory: Radius of thirty miles from Buffalo, N.Y.
Place of Meeting: Markeen Hotel, 1391 Main St.
Local Organization: Engineering Society of Buffalo
Number of Members: 223

EXECUTIVE COMMITTEE

A. W. ECKSTROM, *Chairman*
C. GALE KIPLINGER, *Vice-Chairman*
N. S. SNYDER, *Secretary*
C. E. HARRINGTON, *Treasurer*
C. A. ROSS
J. L. YATES

CENTRAL ILLINOIS

Organized: 1937
Territory: All the territory in Central Illinois between the following counties on the northern boundary: Bureau, LaSalle, Knox, Stark, Putnam, Marshall, Livingston, Peoria; counties on the southern boundary: Pike, Scott, Morgan, Sangamon, Macon, Piatt, Douglas, and Edgar
Place of Meeting: Hotel Pere Marquette or Caterpillar Show Room
Number of Members: 116

EXECUTIVE COMMITTEE

R. S. STAINTON, *Chairman*
W. F. BIGGS, C. W. HAM, R. E. MCCLAIN } *Vice-Chairmen*
B. R. MILLER, *Secretary-Treasurer*

CENTRAL INDIANA

Organized: 1916
Territory: Radius of eighty miles from Indianapolis, within Indiana
Place of Meeting: Indianapolis Athletic Club
Local Organization: Indiana Engineering Society
Number of Members: 191

EXECUTIVE COMMITTEE

FERDINAND JEHLE, *Chairman*
H. L. SOLBERG, *Vice-Chairman*
G. H. GOBLE, *Secretary-Treasurer*
M. E. BECHTOLD
H. A. BOLZ
J. K. LOMAN
CARL WISCHMEYER

CENTRAL PENNSYLVANIA

Organized: 1921
Territory: Radius of approximately sixty miles from State College, Pa.
Place of Meeting: State College and Altoona, Pa.
Number of Members: 76

EXECUTIVE COMMITTEE

J. C. REED, *Chairman*
R. Y. SIGWORTH, *Vice-Chairman*
E. E. AMBROSIUS, *Acting Secretary-Treasurer*
J. S. DOOLITTLE
R. L. HULSIZER
L. B. JONES

CHICAGO

Organized: 1913
Territory: Radius of fifty miles from Chicago, Ill.
Headquarters: Mid-West A.S.M.E. Office, Room 1920, 205 West Wacker Drive, Chicago 6, Ill.
Place of Meeting: Civic Opera Bldg., 20 North Wacker Drive
Meetings: Tuesday, 7:30 p.m.
Local Organization: Western Society of Engineers
Number of Members: 1,073

EXECUTIVE COMMITTEE

J. C. MARSHALL, *Chairman*
LT. COL. H. M. BLACK, B. H. JENNINGS, A. H. JENS, L. M. JOHNSON, R. M. KRAUSE } *Vice-Chairmen*
H. L. NACHMAN, *Secretary-Treasurer*
C. C. AUSTIN
R. H. BACON
R. C. CLOUGH
F. D. COTTERMAN
C. O. DOHRENWEND
L. M. ELLISON
F. S. HARTENBERG
F. H. LANE
J. P. MAGOS
T. S. MCEWAN
J. R. MICHEL
W. H. OLDACRE
F. S. ORR
R. M. OSTERMANN
C. W. PARSONS
D. I. PAYNE
J. D. PIERCE

JUNIOR CHAIRMEN

R. C. CLOUGH
J. D. PIERCE

CINCINNATI

Organized: 1912
Territory: Radius of thirty miles from Cincinnati, Ohio
Place of Meeting: Herman Schneider Foundation (Engineering Society Building)
Local Organization: Engineers' Club of Cincinnati
Number of Members: 222

EXECUTIVE COMMITTEE

M. E. MARTELLOTTI, *Chairman*
R. J. SHORT, *Vice-Chairman*
H. B. WELGE, *Secretary*
A. T. BLACKBURN
W. S. BOYNTON
HANS ERNST
H. W. GUDMENS
H. L. HAWORTH
J. H. HEIMBROCK
H. S. MALANY
C. A. MITCHELL
E. W. VINNEDGE
J. M. WALTER
G. K. WANAMAKER
B. J. YEAGER

CLEVELAND

Organized: 1918
Territory: Counties of Lorain, Cuyahoga, Lake, Geauga, and Ashtabula in Ohio
Place of Meeting: Cleveland Engineering Society Club
Local Organization: Cleveland Engineering Society
Number of Members: 383

EXECUTIVE COMMITTEE

H. S. COLBY, *Chairman*
E. B. CRANKSHAW, *Vice-Chairman*
E. R. MCCARTHY, *Secretary-Treasurer*
J. W. AVERY
COLIN CARMICHAEL
R. C. SESSIONS
H. L. SPENCE
W. G. STEPHAN
F. H. VOSE

COLORADO

Organized: 1919
Territory: Entire State of Colorado
Place of Meeting: Albany Hotel, Denver, Colo.
Local Organization: Colorado Engineering Council (Colorado Society of Engineers)
Number of Members: 97

EXECUTIVE COMMITTEE

D. R. COLLINS, *Chairman*
J. F. RANSOM, *Vice-Chairman*
A. A. WOODWARD, *Secretary-Treasurer*
H. L. HARTENBURG
J. Y. PARCE
W. M. RICHTMANN
G. H. WOEBLING

COLUMBUS

Organized: 1920
Territory: Counties of Union, Delaware, Licking, Madison, Franklin, Fayette, Pickaway, and Ross in Ohio

Place of Meeting: Battelle Memorial Institute and The Ohio State University
Number of Members: 108

EXECUTIVE COMMITTEE

R. B. ENGDAHL, *Chairman*
A. P. JOHNSON, *Vice-Chairman*
W. H. BROWNE, *Secretary-Treasurer*
W. L. Davis
T. H. KERR
E. J. LINDAHL
L. R. TANSLEY
S. H. YOST

DAYTON

Organized: 1926
Territory: Counties of Drake, Miami, Champaign, Preble, Montgomery, Greene, and northern part of Butler and Warren in Ohio
Place of Meeting: Engineers' Club of Dayton
Local Organization: Engineers' Club of Dayton
Number of Members: 182

EXECUTIVE COMMITTEE

COLLINS WIGHT, *Chairman*
BURSON TREADWELL, *Vice-Chairman*
R. G. OLT, *Secretary*
A. W. KIMMEL, *Treasurer*
B. F. DOWNEY
M. J. FOLEY
F. B. NORTHRUP
A. L. PASCHALL
F. W. STEIN

DETROIT

Organized: 1916
Territory: Radius of thirty miles from Detroit, Mich.
Place of Meeting: Horace H. Rackham Educational Memorial, 100 Farnsworth Avenue, Detroit, Mich.
Local Organization: Engineering Society of Detroit
Number of Members: 565

EXECUTIVE COMMITTEE

A. C. PASINI, *Chairman*
R. K. WELDY, *Secretary-Treasurer*
J. W. BRENNAN
W. L. EDEL
R. V. ELEY
H. K. GANDELOT
F. T. HARRINGTON
J. W. MACKENZIE
R. C. PORTER
O. A. SODERBERG
R. H. STELLWAGEN
J. J. UICKER

JUNIOR GROUP

D. E. JAHNCKE, *Chairman*
H. D. CHICOINE
V. E. SCHAEFER
R. W. WAYMAN

EAST TENNESSEE

Organized: 1922
Territory: All counties in Tennessee east of the west boundary of Scott, Morgan, Cumberland, White, Warren, Coffee, Moore, Franklin; Belle County in Kentucky; and Rossville, Dade, Walker, Cattasa, Whitfield, Murray, Gordon, Chattooga in Georgia
Place of Meeting: Places varies
Local Organization: Chattanooga Engineers Club and Knoxville Technical Club
Luncheon Meeting every Monday noon at Chattanooga Engineers Club
Number of Members: 168

EXECUTIVE COMMITTEE

L. G. HALLER, *Chairman*
A. W. HARRIS, *Vice-Chairman*
J. MACK TUCKER, *Secretary-Treasurer*
J. L. FRANKUM
P. J. FREEMAN
C. B. KERNS
F. A. SALMON
J. L. TARWATER
F. H. THOMAS
J. R. THOMAS

ERIE

Organized: 1917
Territory: Radius of thirty miles from Erie, Pa.
Place of Meeting: Erie County Court House
Number of Members: 92

EXECUTIVE COMMITTEE

A. J. SHOWLER, *Chairman*
G. H. KAEMMERLING, *Vice-Chairman*
J. M. PASICK, *Secretary-Treasurer*
G. W. BACH
F. G. BRINIG
H. E. GOETZ
C. I. RAINESALO
M. S. REED
H. B. JOYCE, *Ex-Officio*

FLORIDA

Organized: 1925
Territory: State of Florida
Place of Meeting: Various cities in state
Local Organization: Florida Engineering Society, Gainesville, Fla.
Number of Members: 117

EXECUTIVE COMMITTEE

S. L. STEWART, II, *Chairman*
JOHN HUNTER, *1st Vice-Chairman*
J. T. LEGGETT, *2nd Vice-Chairman*
G. E. REMP, *Secretary-Treasurer*
P. C. CAPPS
ROBERT MAJOR
R. Y. POOL

FORT WAYNE

Organized: 1939
Territory: Counties of LaGrange, Steuben, Noble, DeKalb, Whitley, Allen, Wabash, Huntington, Wells, Adams, Miami, Blackford and Jay in Indiana; Counties of Williams, Defiance, Paulding, Van Wert and Mercer in Ohio
Local Organization: Fort Wayne Engineers' Society
Number of Members: 36

EXECUTIVE COMMITTEE

F. C. MASON, *Chairman*
I. A. PLANCK, *Vice-Chairman*
R. E. GALLATIN, *Secretary*
C. F. HARROD, *Treasurer*
E. S. BUCK
K. K. COOPER

GREEN MOUNTAIN

Organized: 1923
Territory: Entire State of Vermont and neighboring and closely related communities of Claremont and Hanover, N.H.
Place of Meeting: Springfield, Windsor, Vt., and Claremont, N.H.
Local Organization: Vermont Engineering Society
Number of Members: 58

EXECUTIVE COMMITTEE

C. H. ADAMS, *Chairman*
F. T. GEAR, *Vice-Chairman*
F. A. JOHNSON, *Secretary-Treasurer*
E. D. CLARK
H. L. DAASCH
D. T. HAMILTON
J. B. JOHNSON

GREENVILLE

Organized: As a Branch, 1923; as a Section, 1927
Territory: Radius of sixty miles from Greenville, S.C.
Place of Meeting: Meetings held at Greenville, Clemson College, S.C., Canton, Asheville, and Enka, N.C.
Number of Members: 62

EXECUTIVE COMMITTEE

A. KEITH POOSER, *Chairman*
E. M. WILLIAMS, *Vice-Chairman*
J. W. VAUGHAN, JR., *Secretary-Treasurer*
R. H. CHAPMAN
S. B. EARLE
P. B. KRIEK
G. R. MORGAN
R. S. PRUITT

HARTFORD

Organized: 1917, as Branch of Conn. Section; reorganized, 1923; New Britain Section merged with Hartford Section, July 1, 1940
Territory: Hartford County except that portion served by New Britain Section
Place of Meeting: Hartford Electric Light Company
Number of Members: 203

EXECUTIVE COMMITTEE

T. F. CASSIDY, JR., *Chairman*
E. R. LEWIS, JR. } *Vice-Chairmen*
J. C. WALTERS }
A. E. ANDERSON
J. S. APPLEYARD
HERBERT BURDICK
SIDNEY CORNELL
WILLIAM FERGUSON
E. P. HERRICK
F. O. HOAGLAND
R. D. KELLER
L. B. LE BEL
W. S. PAINE
K. E. PEILER
H. F. RAMM
H. P. SMITH
L. C. SMITH
C. C. STEVENS
S. J. TELLER
ALBERT VUILLEUMIER
MISS HOPE M. WOHNUS

INLAND EMPIRE

Organized: 1921
Territory: East of Columbia River in State of Washington, and Counties of Okanogan and Benton, and part of Northern Idaho
Place of Meeting: Davenport Hotel, Spokane
Luncheons: Wednesdays at 12:00 noon, Davenport Hotel, Spokane
Local Organization: Associated Engineers of Spokane
Number of Members: 39

Executive Committee

I. A. Shirk, *Chairman*
D. R. Gray, *Vice-Chairman*
N. W. Humphrey, *Secretary-Treasurer*
F. W. Candee
H. F. Gauss
L. J. Pospisil

ITHACA

Organized: 1936
Territory: Radius of thirty miles from Ithaca plus following cities: Binghamton, Corning, Endicott, Geneva, Painted Post
Place of Meeting: Alternately in different cities of Section territory, as announced
Number of Members: 100

Executive Committee

F. S. Erdman, *Chairman*
C. W. Vail, *Vice-Chairman*
H. C. Perkins, *Secretary-Treasurer*
W. G. Baird
S. W. Fairman
J. C. Kennedy
M. P. Whitney

KANSAS CITY

Organized: 1921
Territory: Radius of sixty miles from Kansas City, Mo.
Place of Meeting: University Club
Local Organization: Engineers' Club of Kansas City
Number of Members: 170

Executive Committee

R. P. Hahn, *Chairman*
Chester Cotter, *Vice-Chairman*
C. C. Holt, *Secretary*
Weldon Mooney, *Treasurer*
H. B. Atherton
B. B. Brainard
E. S. Gray
H. E. Manuel
L. T. Mart
N. L. Miller

LOUISVILLE

Organized: 1922
Territory: Radius of thirty miles from Louisville, Ky. (includes Lexington, Ky.)
Place of Meeting: University of Louisville, Louisville, Ky.
Local Organization: Engineers and Architects Club
Number of Members: 75

Executive Committee

O. C. Krause, *Chairman*
E. J. Dreyer, *Vice-Chairman*
J. E. Glass, Secretary
W. V. Hambleton, *Treasurer*
J. H. Davis
A. G. Rosenbaum
F. P. Shannon, *Ex-Officio*

MEMPHIS

Organized: 1923
Territory: Radius of sixty miles from Memphis, Tenn., and eastern half of Arkansas including all the territory east of a line drawn north and south through the western boundary of the City of Little Rock
Number of Members: 33

Executive Committee

C. K. Sharp, *Chairman*
G. R. Schneider, *Vice-Chairman*
J. H. Tole, *Secretary-Treasurer*
E. H. Elam
R. M. King
W. H. Roberts
J. J. Thomason

METROPOLITAN

Organized: 1910
Territory: Metropolitan District, New York and New Jersey
Place of Meeting: Engineering Societies Building, 29 West 39th Street, New York, N.Y., and Newark, N.J.
Number of Members: 3,983

Executive Committee

R. W. Flynn, *Chairman*
W. L. Betts, *Secretary*
H. R. Kessler, *Treasurer*
A. D. Blake
F. P. Brand
E. V. David
E. D. Grimison
J. H. Sengstaken
Herman Weisberg
Adolf Ehbrecht, *Ex-Officio*

Junior Group

J. M. Sexton, *Chairman*
E. S. Rowell, *Vice-Chairman*
J. W. Simonson, *Secretary*
J. P. Pollak, *Treasurer*

MID-CONTINENT

Organized: 1919
Territory: Entire State of Oklahoma; territory in Arkansas not included in Memphis Section; part of Louisiana; and territory in Texas north of the southern boundaries of the counties of Gaines, Dawson, Bordon, Scurry, Fisher, Jones, and Shackelford
Place of Meeting: Usually Mayo Hotel, Tulsa, Okla.
Luncheon Meetings with Engineers Club of Tulsa, Mondays at 12:00 noon
Local Organization: Engineers Club of Tulsa
Number of Members: 191

Executive Committee

O. L. Lewis, *Chairman*
J. T. Carmichael, F. J. Daasch, L. Wood Jackson, Gwynne Raymond, V. J. Walker } *Vice-Chairmen*
W. F. Stewart, *Secretary*
C. A. Stevens, *Treasurer*
D. O. Barrett
R. A. Colgin
D. E. Fields
D. E. Foster
C. O. Glasgow
J. D. Jones
F. D. Ratcliffe
W. S. Sherman
H. G. Thuesen

MILWAUKEE

Organized: 1904
Territory: Radius of fifty miles from Milwaukee, Wis.
Place of Meeting: Wisconsin Club
Local Organization: Engineers' Society of Milwaukee
Luncheon Meetings once each month, 3rd Wednesday at Wisconsin Club
Number of Members: 286

Executive Committee

T. A. Wetzel, *Chairman*
H. L. Heywood, *Secretary*
M. E. Ruess, *Treasurer*
S. J. Gates
E. G. Huber
Sebastian Judd
E. H. Laabs
G. V. Minniberger
J. T. Rettaliata

MINNESOTA

Organized: Minneapolis, 1913; St. Paul, 1913; the two Sections merged, 1934
Territory: Entire State of Minnesota
Place of Meeting: Minnesota Union, Univ. of Minnesota
Local Organization: Minneapolis Engineers' Club, Minnesota Federation of Architectural and Engineering Societies
Number of Members: 132

Executive Committee

E. S. Howard, *Chairman*
F. M. Thuney, *Vice-Chairman*
A. O. Lee, *Secretary-Treasurer*
W. H. Erskine
D. M. Forfar
L. C. Sprague
L. S. Whitson
M. S. Wunderlich

NEBRASKA

Organized: 1922
Territory: State of Nebraska, and Council Bluffs, Iowa
Place of Meeting: Lincoln and Omaha
Local Organization: Engineers' Clubs of Lincoln and Omaha
Luncheon Meeting every Wednesday noon at the Omaha Engineers' Club—4th Monday Evening at Lincoln
Number of Members: 57

EXECUTIVE COMMITTEE

J. W. KURTZ, *Chairman*
J. K. LUDWICKSON, *Vice-Chairman*
CHAS. A. N. ARMSTRONG, *Secretary-Treasurer*
N. H. BARNARD
A. A. LUEBS
O. R. PRATT

NEW HAVEN

Organized: 1912; reorganized, 1923
Territory: Portions of New Haven and Middlesex Counties, Conn.
Place of Meeting: Mason Laboratory, Yale University
Number of Members: 101

EXECUTIVE COMMITTEE

A. S. REDWAY, *Chairman*
A. D. WILCOX, *Secretary-Treasurer*
E. E. CASPELL
H. D. FISHER
I. T. HOOK
C. A. HORST
B. R. ONUF

NEW LONDON

Organized: 1930, as the Norwich Section; name changed, 1943
Territory: Counties of Tolland, Windham, and New London in Connecticut, and Westerly District in Rhode Island
Place of Meeting: New London Junior College, Pequot Ave., New London, Conn.
Number of Members: 43

EXECUTIVE COMMITTEE

K. P. HANSON, *Chairman*
L. A. LACHMAN, *Secretary-Treasurer*
W. E. BEANEY
J. S. LEONARD
FRANK PERUTZ
E. R. STEPHAN

NEW ORLEANS

Organized: 1916
Territory: All of Louisiana except the northern part allotted to Mid-Continent Section
Place of Meeting: Room 422, St. Charles Hotel
Local Organization: Louisiana Engineering Society
Number of Members: 162

EXECUTIVE COMMITTEE

A. M. HILL, *Chairman*
E. A. MCLELLAN, *Vice-Chairman*
M. C. ABRAHM, *Secretary-Treasurer*
F. B. BLACKSTONE
E. L. DENNIS
F. R. MENDOW
R. L. NALL
R. M. SEAGO

NORTH TEXAS

Organized: 1922
Territory: All of Texas north of an approximately straight line through Del Rio, Fredericksburg, Georgetown, Cameron, Nacogdoches, and Center, including the cities mentioned, and south of north boundaries of the counties of Parmer, Castro, Swisher, Briscoe, Hall, and Childress. Also the City of Texarkana, Ark.
Place of Meeting: Dallas Power & Light Co. Bldg. Auditorium
Local Organization: Technical Club of Dallas
Number of Members: 158

EXECUTIVE COMMITTEE

E. J. WACKER, *Chairman*
O. A. ST. CLAIR, C. H. SHUMAKER } *Vice-Chairmen*
H. R. HUGHES, JR., *Secretary-Treasurer*
J. H. KEYES
G. E. KIDD
H. R. PEARSON
D. C. PFEIFFER

ONTARIO

Organized: 1917
Territory: Province of Ontario, Canada
Place of Meeting: Hart House, University of Toronto
Number of Members: 241

EXECUTIVE COMMITTEE

R. C. WIREN, *Chairman*
W. R. TRUSLER, *Secretary-Treasurer*
C. E. BEYNON
L. J. CLAYTON
J. W. GALLOWAY
J. S. HALL
S. J. LIDDINGTON
JAMES MCKENZIE
A. I. SCOTT
W. D. SHELDON
FREDERICK TRUMAN
H. H. ANGUS, S. G. CLARKE } *Ex-Officio*

JUNIOR GROUP

D. G. HUBER, *Chairman*
WILLIAM BRUCE, *Secretary-Treasurer*
G. J. JARRELL
D. J. PARRISH
E. J. W. SHEARE

OREGON

Organized: 1919
Territory: State of Oregon and that territory in Washington within a radius of thirty miles from Portland, Ore.
Place of Meeting: Usually Public Service Bldg., Portland, Ore.
Local Organization: Oregon Society of Engineers
Number of Members: 76

EXECUTIVE COMMITTEE

A. J. CHAPUT, *Chairman*
B. J. DICK, *Vice-Chairman*
J. C. OTHUS, *Secretary*
G. E. JOOST, *Treasurer*
M. M. CLAYTON
L. T. HAYS
K. W. KETCHUM

PENINSULA

Organized: 1923
Territory: West of the east boundaries of the following counties: Emmet, Charlevoix, Antrim, Kalkaska, Missaukee, Clare, Isabell, Gratiot, Clinton, Eaton, Calhoun, and Branch, Mich.
Place of Meeting: Grand Rapids, Mich.
Luncheon Meeting last Thursday noon each month
Local Organization: Engineers' Club of Grand Rapids
Number of Members: 78

EXECUTIVE COMMITTEE

J. M. GORRIE, *Chairman*
D. C. MCSORLEY, *1st Vice-Chairman*
K. E. CROWSER, *2nd Vice-Chairman*
C. J. KUENZEL, *Secretary-Treasurer*
C. P. BUCK
J. R. DEHAMMER
G. E. GEBBEN
C. G. LOHMANN
C. A. HAMILTON, *Ex-Officio*

PHILADELPHIA

Organized: 1912
Territory: Counties of Bucks, Montgomery, Chester, Philadelphia, Delaware, Pa., and the State of Delaware
Place of Meeting: Philadelphia Engineers' Club, 1317 Spruce Street, Philadelphia, Pa.
Local Organization: Philadelphia Engineers' Club
Luncheon Meeting every Thursday noon at 12:30 p.m. at Philadelphia Engineers' Club
Number of Members: 1,244

EXECUTIVE COMMITTEE

J. J. MCCARTHY, *Chairman*
S. T. MACKENZIE, *Vice-Chairman*
M. C. RANDALL, *Secretary-Treasurer*
C. B. CAMPBELL
J. P. CLARK
B. F. KEENE
W. J. KINDERMAN
STANLEY MOYER
G. M. MUSCHAMP
H. E. SCHOCH, JR.
G. B. THOM
A. W. THORSON
B. W. WEBB

JUNIOR GROUP

H. E. SCHOCH, JR., *Chairman*
E. N. ROBERTSON, *Vice-Chairman*
FRED HIRSCH, *Secretary-Treasurer*

PIEDMONT—NORTH CAROLINA

Organized: As a Branch, 1923; as a Section, 1927; name changed from Charlotte Section to Piedmont—North Carolina, July 1, 1940
Territory: Radius of seventy-five miles from Charlotte, N.C.
Luncheon Meeting every other Monday at 1:00 p.m. at Efirds Department Store Dining Room
Local Organization: Charlotte Engineers Club
Number of Members: 51

EXECUTIVE COMMITTEE

T. O. SILLS, *Chairman*
F. R. JACKSON, *Vice-Chairman*
N. H. BROWN, *Secretary-Treasurer*
E. H. BRANDT, JR.
J. H. DOUTHIT
J. T. POTTER
C. E. STINE
T. W. WILSON

PITTSBURGH

Organized: 1920
Territory: Counties bounded by and including Beaver, Butler, Venango, Forest, Jefferson, Indiana, Somerset, Fayette, Greene, and Washington, Pa.
Place of Meeting: Engineers' Society of Western Pennsylvania, William Penn Hotel
Local Organization: Engineers' Society of Western Pennsylvania
Number of Members: 525

Executive Committee

H. F. Hebley, *Chairman*
Tomlinson Fort, *Vice-Chairman*
T. O. Schrader, Jr., *Secretary*
K. F. Treschow, *Treasurer*
G. E. Dignan
J. N. Evans
J. F. Mattern
W. T. Reid
G. W. Smith

PLAINFIELD

Organized: 1921
Territory: Plainfield and territory included between Elizabeth, Bound Brook, Metuchen, and Watchung, N.J.
Place of Meeting: Elizabeth Carteret Hotel, Elizabeth, and Plainfield Masonic Temple, Plainfield
Local Organization: Plainfield, Engineers Club, Singer Engineering Society
Number of Members: 223

Executive Committee

J. D. Potter, *Chairman*
R. H. Chankalian, P. C. Osterman } *Vice-Chairmen*
G. N. Hodge, *Secretary*
P. N. Fimbel, *Treasurer*
W. L. Boswell
A. J. De Matteo
M. J. Grubelich
H. F. Skarbek

PROVIDENCE

Organized: 1920
Territory: Radius of thirty miles from Providence, R.I.
Place of Meeting: Providence Engineering Society Building, 195 Angell St., Providence, R.I.
Local Organization: Providence Engineering Society
Number of Members: 190

Executive Committee

E. W. Harrington, *Chairman*
F. C. Tanner, *Vice-Chairman*
Charles Haggerty, *Secretary-Treasurer*
J. B. Coleman
W. M. Davies, Jr.
E. M. Gordon
B. P. Graves
E. A. Johnson
A. H. MacGillivray
G. W. Kelsey, *Ex-Officio*

RALEIGH

Organized: As a Branch, 1923; as a Section, 1927
Territory: Radius of sixty miles from Raleigh, N.C.
Place of Meeting: North Carolina State College, Raleigh, N.C.; Duke University, Durham, N.C.
Local Organizations: North Carolina Society of Engineers, Raleigh Engineers Club
Number of Members: 40

Executive Committee

E. S. Theiss, *Chairman*
E. O. Gibbs, *Vice-Chairman*
W. A. Hinton, *Secretary-Treasurer*
G. W. Baity
F. J. Reed
R. B. Rice
F. B. Turner
H. I. West

ROCHESTER

Organized: 1919
Territory: Radius of thirty miles from Rochester, N.Y.
Place of Meeting: Rochester Engineering Society Rooms, Sagamore Hotel
Local Organization: Rochester Engineering Society, Sagamore Hotel
Luncheon Meeting every Tuesday at 12:15 p.m. at Sagamore Hotel
Number of Members: 148

Executive Committee

W. A. Schell, *Chairman*
A. E. Schell, *Secretary-Treasurer*
M. L. Baxter
E. R. Birkicht
A. S. Hamilton
C. E. Krause
J. T. Lindsey
H. L. Mason
C. B. McCathron
C. C. Ross

ROCK RIVER VALLEY

Organized: 1926
Territory: Thirty miles east and west of Madison, Wis., and extending southward through Rockford, Ill.
Place of Meeting: Madison, Wis., Beloit, Wis., and Rockford, Ill.
Local Organization: Rock River Valley Engineering Council
Number of Members: 82

Executive Committee

E. L. Dahlund, *Chairman*
L. A. Wilson, *Vice-Chairman*
R. S. Smith, *Secretary-Treasurer*
W. C. Fischer
B. R. Granberg
R. R. Smith
J. D. Swannack

ST. JOSEPH VALLEY

Organized: 1929
Territory: Counties of La Porte, Starke, Pulaski, St. Joseph, Marshall, Fulton, Elkhart, and Kosciusko in Indiana, and Cass and Berrien Counties in Michigan
Place of Meeting: South Bend, Ind.
Number of Members: 70

Executive Committee

C. Robert Egry, *Chairman*
G. R. McNeil, *Vice-Chairman*
R. C. Fitch, *Secretary-Treasurer*
O. K. Fay
P. T. Sprague
L. E. Waddington
C. C. Wilcox
O. E. Zahn

ST. LOUIS

Organized: 1909
Territory: Radius of thirty miles from St. Louis, Mo.
Place of Meeting: Place varies
Local Organization: Engineers' Club of St. Louis
Number of Members: 235

Executive Committee

P. H. Buxton, *Chairman*
J. C. Parmely, *Vice-Chairman*
G. R. Hughins, *Secretary-Treasurer*
R. M. Boyles
Herbert Kuenzel
R. P. Schlatter
R. C. Thumser

SAN FRANCISCO

Organized: 1910
Territory: All territory north of the northern boundaries of the counties of San Luis Obispo, Kern, and San Bernardino
Place of Meeting: Engineers' Club, 206 Sansome St.
Luncheon Meetings, Tuesdays, California Hotel, Oakland; Thursdays, Engineers' Club, San Francisco
Local Organization: San Francisco Engineers' Club
Number of Members: 792

Executive Committee

H. E. Prescott, *Chairman*
M. P. O'Brien, *Vice-Chairman*
F. W. Beichley, *Secretary-Treasurer*
Major W. A. Doble
W. S. Everett
E. G. Gothberg
V. A. Rumble
Alf Hansen, *Ex-Officio*

SAVANNAH

Organized: 1923
Territory: Radius of 125 miles from Savannah in Georgia
Place of Meeting: Savannah Hotel
Local Organization: Engineers' Council of Savannah Chamber of Commerce
Number of Members: 28

Executive Committee

D. E. Kehoe, *Chairman*
T. H. Gardner, *Vice-Chairman*
B. J. Sams, *Secretary-Treasurer*
W. H. Artley
A. M. Ormond
L. C. Roesell

SCHENECTADY

Organized: As a Branch, 1919; as a Section, 1927
Territory: Radius of thirty miles from Schenectady, N.Y.
Place of Meeting: Rice Hall
Number of Members: 255

EXECUTIVE COMMITTEE

A. O. WHITE, *Chairman*
J. B. NOLAN, *1st Vice-Chairman*
I. A. TERRY, *2nd Vice-Chairman*
N. P. BAILEY, *3rd Vice-Chairman*
F. R. FOWLER, *Secretary*
CHARLES CONCORDIA, *Treasurer*
J. S. APPERSON, III
C. M. GARDINER
C. J. WALKER

SOUTHERN CALIFORNIA

Organized: 1915 as Los Angeles Section; reorganized, 1941
Territory: South of southern boundaries of following counties: Monterey, Kings, Tulares, and Inyo, Calif.
Place of Meeting: Barker Bros. Store
Local Organization: Technical Societies of Los Angeles
Luncheon Meetings Thursdays at 12:00 noon at Engineers' Club
Number of Members: 734

EXECUTIVE COMMITTEE

R. G. ROSHONG, *Chairman*
J. S. EARHART, *Vice-Chairman*
V. A. PETERSON, *Secretary-Treasurer*
E. O. BERGMAN
J. W. DAILEY
L. V. HORNE
R. F. O'MARA
V. L. PEICKII
A. R. WEIGEL

JUNIOR GROUP

C. M. SANDLAND, *Chairman*
J. I. BREWSTER, *Secretary*
D. A. R. JONES, *Member at Large*

SOUTH TEXAS

Organized: 1919
Territory: South Texas and the northern part of the State not included in the North Texas Section territory
Place of Meeting: No fixed meeting place, but all meetings held in Houston
Number of Members: 197

EXECUTIVE COMMITTEE

C. J. ECKHARDT, JR., *Chairman*
J. G. H. THOMPSON, *Vice-Chairman*
J. B. T. DOWNS, *Secretary-Treasurer*
D. D. ALTON
M. L. BEGEMAN
P. E. DARLING
V. M. FAIRES
B. W. FARQUHAR
H. G. HIEBELER
COMDR. M. I. KEARNS
R. H. KNIPPING
G. W. LOWTHER
H. F. MOLLER
A. B. STEEN, JR.

SUSQUEHANNA

Organized: 1927
Territory: Counties of Cumberland, Dauphine, Lebanon, Adams, York, and Lancaster
Place of Meeting: Engineering Society of York, and at Lancaster twice a year
Local Organization: Engineering Society of York and Engineers' Society of Pennsylvania, Harrisburg, Pa.
Number of Members: 99

EXECUTIVE COMMITTEE

E. L. ROGERS, *Chairman*
C. H. NEIMAN, JR., *Vice-Chairman*
J. A. GALAZZI, *Secretary-Treasurer*
E. W. GALLENKAMP
G. DUGAN JOHNSON
L. S. MORSE, SR.
E. M. POWELL
E. O. REESE, III
G. I. SMITH

SYRACUSE

Organized: 1920
Territory: Radius of thirty miles from Syracuse, N.Y.
Place of Meeting: Ball Room of the Onondaga Hotel
Local Organization: The Technology Club of Syracuse
Number of Members: 105

EXECUTIVE COMMITTEE

G. I. VINCENT, *Chairman*
J. A. KING, *Vice-Chairman*
L. EDWARD POTTER, *Secretary-Treasurer*
H. T. AVERY
H. W. JEFFCOCK
W. E. JOHNSON
M. B. MOYER
D. V. SHETLAND
H. P. SONTAG
M. F. WILLIAMS

TOLEDO

Organized: 1920
Territory: Radius of thirty miles from Toledo, Ohio
Place of Meeting: University Club, Toledo, Ohio
Local Organization: Affiliated Technical Societies of Toledo
Number of Members: 66

EXECUTIVE COMMITTEE

PAUL GRAVELLE, *Chairman*
W. A. NELDEN, *Vice-Chairman*
*R. H. HUNTINGTON, *Secretary-Treasurer*
H. A. BENNETT
JOHN GILLETT
F. E. GRAVES
J. C. GREINER
WILLIAM MCCANDLESS
F. J. MEYER
L. S. PLATOU
O. C. SCHULTZ
ARTHUR VOTSBERGER

TRI-CITIES

Organized: 1920
Territory: Radius of thirty miles from Moline, Ill.
Place of Meeting: Rock Island, Ill., Moline, Ill., and Davenport, Iowa
Luncheon Meeting every Wednesday, Davenport Hotel, 12:00 noon
Number of Members: 86

EXECUTIVE COMMITTEE

C. A. CARLSON, *Chairman*
C. C. ANDERSON, *Vice-Chairman*
R. A. CROSS, *Secretary-Treasurer*
H. O. CROFT
J. M. HARTMAN
K. R. HODGES

* Resigned Oct. 13, 1945.

UTAH

Organized: 1923
Territory: State of Utah
Place of Meeting: University Club, Salt Lake City
Local Organization: Utah Society of Professional Engineers
Number of Members: 39

EXECUTIVE COMMITTEE

M. B. HOGAN, *Chairman*
D. A. ELKINS, *Vice-Chairman*
R. E. KUNKEL, *Secretary-Treasurer*
W. J. COPE
H. L. ZETTERMAN

VIRGINIA

Organized: 1919
Territory: State of Virginia
Place of Meeting: Richmond, Norfolk, Blacksburg, Charlottesville, Roanoke, University, Petersburg
Local Organization: Central Virginia Engineers Club of Hampton Roads
Number of Members: 231

EXECUTIVE COMMITTEE

ARTHUR ROBERTS, JR., *Chairman*
H. R. HOPKINS, F. Q. SAUNDERS } *Vice-Chairmen*
J. B. JONES, *Secretary*
W. J. BARBER, *Treasurer*
A. L. BELL
D. W. BENNETT
D. H. GRENOBLE
A. B. HETTRICK
M. L. IRELAND, JR.
A. F. MACCONOCHIE
F. Q. SAUNDERS

WASHINGTON, D.C.

Organized: 1919
Territory: District of Columbia
Place of Meeting: Auditorium, Potomac Electric Power Co., 10th & E Sts., Washington, D.C.
Number of Members: 530

EXECUTIVE COMMITTEE

RUDOLPH MICHEL, *Chairman*
B. C. CRUICKSHANKS, *Vice-Chairman*
C. E. BERBERICH, *Secretary-Treasurer*
L. R. BURDICK
R. S. DILL
MORTON GERLA
F. J. HANRAHAN
H. P. HARWOOD
F. EVERETT REED, JR.
M. A. MASON, *Ex-Officio*

WATERBURY

Organized: 1917, as a Branch; reorganized as a Section, 1923
Territory: Litchfield County and a portion of New Haven County
Place of Meeting: Elton Hotel
Number of Members: 75

EXECUTIVE COMMITTEE

J. H. RAUB, *Chairman*
T. M. RIANHARD, SR., *Vice-Chairman*
E. W. SODERBERG, *Secretary-Treasurer*
H. C. ASHLEY

(*Continued*)

WATERBURY
(Continued)

A. W. Miner
P. E. Peterson
R. W. Simpson
R. S. Storrs
C. M. Warner

WESTERN MASSACHUSETTS

Organized: 1922
Territory: Includes counties of Berkshire, Franklin, Hampden, and Hampshire
Place of Meeting: Highland Hotel, Springfield, Mass.
Local Organization: Engineering Society of Western Massachusetts
Number of Members: 94

Executive Committee

J. R. Connelly, *Chairman*
Sidney Low, *Vice-Chairman*
D. A. Bartlett, *Secretary-Treasurer*
Leo Kresser
W. S. Mabb

WESTERN WASHINGTON

Organized: 1919
Territory: State of Washington west of Columbia River with exception of territory included in 30-mile radius of Portland, Ore.
Place of Meeting: Engineers' Club, Seattle, Wash.
Local Organization: Seattle Engineers' Club
Luncheon Meetings daily at noon at Engineers' Club, Seattle
Number of Members: 224

Executive Committee

F. B. Lee, *Chairman*
O. F. Lamson, *Vice-Chairman*
R. W. Crain, *Secretary-Treasurer*
R. L. Dyer
R. L. Rockwell
F. R. Young

WEST VIRGINIA

Organized: 1925
Territory: State of West Virginia, South of Parallel 39
Place of Meeting: Charleston, W.Va.
Number of Members: 71

Executive Committee

J. L. Barker, Jr., *Chairman*
C. B. Cochran, *Vice-Chairman*
Donald Thompson, *Secretary-Treasurer*
J. C. Bond, *Assistant Secretary*
W. B. Bible, Jr.
M. C. Brooke
O. C. Lang
G. D. MacMillan
L. B. McQuaide
R. D. Webb

WORCESTER

Organized: 1915
Territory: Radius of thirty miles from Worcester, Mass.
Place of Meeting: Sanford Riley Hall, Worcester Poly. Inst.
Local Organization: Worcester Engineering Society
Number of Members: 131

Executive Committee

E. H. Smith, *Chairman*
F. E. Bailey, *Vice-Chairman*
C. C. Tucker, *Secretary-Treasurer*
F. W. Mierke
H. F. Ritterbusch
R. L. Rougemont
R. H. Tolman
R. H. Wood

YOUNGSTOWN

Organized: 1928
Territory: Counties of Trumbull, Mahoning, and Columbiana in Ohio, and Mercer and Lawrence in Pennsylvania
Place of Meeting: Republic Rubber Co. Club Rooms, Albert St., Youngstown, Ohio
Number of Members: 48

Executive Committee

H. W. Smith, *Chairman*
F. J. Bowers, *Secretary-Treasurer*
C. H. Legler
W. J. Longacher
H. E. Melin

STUDENT BRANCHES

ARTICLE B6A, PAR. 20: The Standing Committee on Relations With Colleges shall, under the direction of the Council, have supervision of the Student Branches of the Society and of such work of the Society as aims to further the education of engineers through the colleges and schools of accepted standing.

STANDING COMMITTEE, RELATIONS WITH COLLEGES

R. P. REECE, *Chairman*
H. J. BROWN
HERBERT KUENZEL
H. R. PEARSON
G. L. SULLIVAN

E. STANLEY AULT
N. P. BAILEY
D. S. CLARK
W. J. COPE
R. H. PORTER
Advisory Members

Communicate with Student Branch through Honorary Chairman

Name and Location	Year Authorized	Chairman	Secretary	Honorary Chairman
Akron, Univ. of, Akron, Ohio	1924	T. J. FISTER	D. W. HARE	F. S. GRIFFIN
Alabama Polytechnic Inst., Auburn, Ala.	1920	.....	.....	C. R. HIXON
Alabama, Univ. of, University, Ala.	1931	.....	.....	D. H. SHENK
Arizona, Univ. of, Tucson, Ariz.	1937	.....	.....	M. L. THORNBURG
Arkansas, Univ. of, Fayetteville, Ark.	1910	M. C. MEASEL	.....	R. G. PADDOCK
British Columbia, Univ. of, Vancouver, B.C., Can.	1938	T. F. SCOTT	D. R. STEVENS	F. W. VERNON
Brown Univ., Providence, R.I.	1923	.....	.....	P. N. KISTLER
Bucknell Univ., Lewisburg, Pa.	1916	WILLIAM ALLEN	E. S. BEREZ	G. M. KUNKLE
California Inst. of Tech., Pasadena, Calif.	1914	E. J. MILLER	L. V. SCHMIDT	R. L. DAUGHERTY
California, Univ. of, Berkeley, Calif.	1912	F. R. ROJESKI	BARBARA QUIMBY	H. A. JOHNSON
Carnegie Inst. of Tech., Pittsburgh, Pa.	1913	A. J. PEPPER	W. I. SCHERB	D. C. SAYLOR
Case School of Applied Science, Cleveland, Ohio	1913	D. W. JONES	L. C. HOPPER	F. H. VOSE
Catholic Univ. of America, Washington, D.C.	1922	E. F. KELLEY	R. L. CASLIN	M. E. WESCHLER
Cincinnati, Univ. of, Cincinnati, Ohio	1909	R. E. LIPPERT	W. H. FRIEDLANDER	C. A. JOERGER
Clarkson College of Tech., Potsdam, N.Y.	1930	JOHN KELSEY	E. J. BOROWIEC	EDWARD MCHUGH
Clemson A. & M. College, Clemson College, S.C.	1921	W. C. MCELREATH	H. R. RICHARDSON	B. E. FERNOW
Colorado A. & M. College, Ft. Collins, Colo.	1914	K. L. RIEKE	E. M. COLPITTS	J. H. SCOFIELD
Colorado, Univ. of, Boulder, Colo.	1914	D. G. MCPHERSON	L. M. KUH	W. S. BEATTIE
Colorado School of Mines Div., Golden	——	.....	.....	W. M. RICHTMANN
Columbia Univ., New York, N.Y.	1909	ALAN COOK	FREDERICK HOLTE	J. E. ENGLUND
Connecticut, Univ. of, Storrs, Conn.	1941	GREGORY BATTICK	CLARENCE KOSLOSKY	K. P. HANSON
Cooper Union Inst. of Tech., New York, N.Y.	1920	.....	.....	W. A. VOPAT
Cooper Union Night School of Engineering., New York, N.Y.	1920	IRVING CHAIT	G. N. RULLO	E. A. SALMA
Cornell Univ., Ithaca, N.Y.	1908	W. E. BARR	SID RUMBOLDT	L. D. CONTA
Delaware, Univ. of, Newark, Del.	1929	W. M. O'CONNELL	GORDON BREWER	LEO BLUMBERG
Detroit, Univ. of, Detroit, Mich.	1930	V. S. RYKWALDER	ROBERT KRAUSE	H. J. MCAULAY
Drexel Inst. of Tech., Philadelphia, Pa.	1920	.....	B. W. JAY	KENNETH RIDDLE
Duke Univ., Durham, N.C.	1935	N. M. LOVE	LEE WINISTSKY	T. C. COOKE
Florida, Univ. of, Gainesville, Fla.	1926	.....	.....	N. C. EBAUGH
George Washington Univ., Washington, D.C.	1924	R. E. KEMELHOR	MARY FREEMAN	A. F. JOHNSON
Georgia School of Tech., Atlanta, Ga.	1915	R. H. KERCE	C. R. SCHNEIDER	R. L. SWEIGERT
Idaho, Univ. of, Moscow, Idaho	1925	DONALD KAMP	J. C. POINTNER	H. F. GAUSS
Illinois Inst. of Tech., Chicago, Ill.	1940	M. N. SPECTOR	JOSEPH VICELI	R. A. BUDENHOLZER
Illinois, Univ. of, Urbana, Ill.	1909	S. R. SPRAGUE	ROBERT AHERN	K. J. TRIGGER
Iowa State College, Ames, Iowa	1919	ROGER BOWDEN	DONALD RAUSH	H. J. STOEVER
Iowa, State Univ. of, Iowa City, Iowa	1913	.....	.....	E. C. LUNDQUIST
Johns Hopkins Univ., Baltimore, Md.	1917	.....	.....	F. W. KOUWENHOVEN
Kansas State College, Manhattan, Kan.	1914	H. O. CRISS	M. H. ROOD	A. J. MACK
Kansas, Univ. of, Lawrence, Kan.	1909	J. F. MCGUCKIN	W. F. PRO	P. J. POTTER
Kentucky, Univ. of, Lexington, Ky.	1911	.....	.....	S. B. WALTON
Lafayette College, Easton, Pa.	1919	J. T. MCSHANE	D. J. BUSTRAAN	P. B. EATON
Lehigh Univ., Bethlehem, Pa.	1911	H. G. P. SNYDER	M. W. BROSSMAN, JR.	F. V. LARKIN
Louisiana State Univ., University, La.	1916	J. E. YERGER	BARBER BECKER	WILLIAM WHIPPLE
Louisville, Univ. of, Louisville, Ky.	1928	H. M. SCHMIDT	D. E. SMITH	J. H. DAVIS
Maine, Univ. of, Orono, Maine	1910	W. C. CHESEBROUGH	HELEN GORDON	I. H. PRAGEMAN
Marquette Univ., Milwaukee, Wis.	1923	RICHARD CRONIN	EARL SMITH	J. E. SCHOEN
Maryland, Univ. of, College Park, Md.	1937	BERNARD LUBARSKY	ROBERTA FLANAGAN	J. W. JACKSON
Massachusetts Inst. of Tech., Cambridge, Mass.	1909	ROBERT WHITE	RICHARD KROHE	W. M. MURRAY
Michigan College of Min. & Tech., Houghton, Mich.	1930	K. E. GATES	ROBERT MCINDOO	A. P. YOUNG
Michigan State College, East Lansing, Mich.	1917	.....	.....	L. C. PRICE
Michigan, Univ. of, Ann Arbor, Mich.	1914	JAY JOHNSON	NANCY ALEXANDER	F. L. SCHWARTZ
Minnesota, Univ. of, Minneapolis, Minn.	1913	R. T. MURPHY	E. J. CARR	A. W. ANDERSON
Mississippi State College, State College, Miss.	1926	.....	.....	.....
Missouri School of Mines & Metallurgy, Rolla, Mo.	1930	R. A. TAPPMEYER	ALBERTO OLIVARES	A. V. KILPATRICK
Missouri, Univ. of, Columbia, Mo.	1909	.....	.....	M. M. BOLSTAD
Montana State College, Bozeman, Mont.	1920	GEORGE SEEL	M. P. SULLIVAN	R. E. GIBBS
Nebraska, Univ. of, Lincoln, Neb.	1909	SHIGEO NAKANISHI	I. C. CONE	N. H. BARNARD
Nevada, Univ. of, Reno, Nev.	1928	J. M. GLYNN	J. H. THOMPSON	J. R. VANDYKE
Newark College of Engineering, Newark, N.J.	1924	W. H. SIMPSON	M. A. KEENAN	H. E. WALTER

Name and Location	Year Authorized	Chairman	Secretary	Honorary Chairman
New Hampshire, Univ. of, Durham, N.H.	1926	CHESTER CHATFIELD	J. A. HAWKE	TENKO KAUPPINEN
New Mexico State College of A. & M. Arts, State College, New Mex.	1938	P. F. TRIVIZ	EVA BLANCHARD	A. M. LUKENS
New Mexico, Univ. of, Albuquerque, New Mex.	1935	PAUL DUGAN	LOUIS PREVIATI	A. D. FORD
New York, College of the City of, New York, N.Y.	1922	JEROME FALK	BERNARD BREITMAN	S. J. TRACY
New York Univ. (Day School), New York, N.Y.	1909	.....	G. E. FORKAS	F. L. SINGER
New York Univ. Evening School, New York, N.Y.	1933	E. M. EDWIN	R. C. WOOD	F. L. SINGER
North Carolina State College, Raleigh, N.C.	1920	P. T. FUGATE	G. R. GREENE	WALTER LOWEN
North Dakota Agric. College, Fargo, N.D.	1929	.....	.....	R. M. DOLVE
North Dakota, Univ. of, Grand Forks, N.D.	1923	.....	.....	.....
Northeastern Univ., Boston, Mass.	1922	ROBERT SAUMSIEGLE	ROBERT WIENER	F. A. STEARNS
Northwestern Univ., Evanston, Ill.	1935	A. W. ELLER	W. A. NEELEY	JOEL BAILEY
Notre Dame, Univ. of, Notre Dame, Ind.	1929	G. H. MACKAY, JR.	A. C. SARTORE	C. R. EGRY
Ohio Northern Univ., Ada, Ohio	1922	R. J. SMYTH	JULES CROFT	A. R. WEBB
Ohio State Univ., Columbus, Ohio	1911	G. S. KEPLEY	MAX BRILL	F. W. MARQUIS
Oklahoma A. & M. College, Stillwater, Okla.	1921	.....	.....	C. M. LEONARD
Oklahoma, Univ. of, Norman, Okla.	1917	B. G. THACKER	J. G. JACKSON	E. M. SIMS
Oregon State College, Corvallis, Ore.	1909	A. T. WILLIS	WILLIAM HATALSKY	C. A. ARENTS
Pennsylvania State College, State College, Pa.	1909	JOHN ZOSZAK	ELISABETH GRIFFITH	J. S. DOOLITTLE
Pennsylvania, Univ. of, Philadelphia, Pa.	1925	ROBERT MOSTERTZ	ROBERT BREDIN	SERGE GRATCH
Pittsburgh, Univ. of, Pittsburgh, Pa.	1917	.....	.....	J. A. DENT
Polytechnic Inst. of Brooklyn, Brooklyn, N.Y.	1909	HARRY RICH	DOMINICK CASALE	E. F. CHURCH, JR.
Polytechnic Inst. of Brooklyn Evening School, Brooklyn, N.Y.	1909	IRVING HANDELMAN	J. P. DEROSA	E. F. CHURCH, JR.
Pratt Inst., Brooklyn, N.Y.	1923	.....	.....	K. E. QUIER
Princeton Univ., Princeton, N.J.	1926	.....	.....	A. E. SORENSON
Puerto Rico, Univ. of, Mayaguez, P.R.	1923	ARMANDO VIVONI	RAUL TORRES	I. W. TRUETTNER
Purdue Univ., West Lafayette, Ind.	1909	W. M. BYERLEY	C. W. KAY	D. S. CLARK
Queen's Univ., Kingston, Ont., Can.	1941	J. W. SODEN	A. B. HOPKINS	E. J. C. SCHMIDLIN
Rensselaer Polytechnic Inst., Troy, N.Y.	1910	R. S. WICK	ROBERT CONOVER	K. H. WHITE
Rhode Island State College, Kingston, R.I.	1930	N. D. ANDREWS	O. R. PANSA	E. L. CARPENTER
Rice Inst., Houston, Tex.	1926	C. M. SMITH	C. V. DRESSER	J. B. T. DOWNS
Rochester, Univ. of, Rochester, N.Y.	1945	J. W. KROSSE	K. F. SCHOCH	E. K. FALLS
Rose Polytechnic Inst., Terre Haute, Ind.	1926	.....	.....	EDWARD ECKERMAN
Rutgers Univ., New Brunswick, N.J.	1920	J. E. SALADINO	W. A. SAILLIARD	C. O. HEATH, JR.
Santa Clara, Univ. of, Santa Clara, Calif.	1925	JOHN BEVIS	JOSEPH SPILLANE	G. L. SULLIVAN
South Dakota State College, Brookings, S.D.	1935	ROBERT NELSON	J. C. MCWAYNE	L. L. AMIDON
Southern California, Univ. of, Los Angeles, Calif.	1929	JAMES COLACHIS	WILLIAM MIROFF	V. C. GEORGE
Southern Methodist Univ., Dallas, Tex.	1933	D. R. TURNER	C. R. FERGUSON	C. A. BESIO
Stanford Univ., Stanford University, Calif.	1909	.....	.....	W. A. MASON
Stevens Inst. of Tech., Hoboken, N.J.	1908	WILLIAM ROWLEY	J. E. KRANTZ	K. J. MOSER
Swarthmore College, Swarthmore, Pa.	1921	JOHN EASTER	ROBERT GAGE	M. B. MOORE
Syracuse Univ., Syracuse, N.Y.	1912	MARTIN HANNAH	JACK SILVERMAN	S. T. HART
Tennessee, Univ. of, Knoxville, Tenn.	1923	BOB GRASS	M. P. FAIN	F. H. THOMAS
Texas, A. & M. College of, College Station, Tex.	1921	B. W. LEVY	A. S. MIJALIS	C. W. FILES
Texas Technological College, Lubbock, Tex.	1930	ELBERT RANKIN	CARL JENSEN	L. J. POWERS
Texas, Univ. of, Austin, Tex.	1921	PAUL WOOLRICH	ROBERT BURNS	DANA YOUNG
Toronto, Univ. of, Toronto, Ont., Can.	1933	E. J. DURAND	N. L. BROWN	I. W. SMITH
Tufts College, Medford, Mass.	1917	E. R. WENTLING	LEROY FROEBERG	D. A. FISHER
Tulane Univ. of Louisiana, New Orleans, La.	1933	FELICIEN PERRIN	L. W. SALATHE	J. K. MAYER
U.S. Naval Academy, Postgraduate School, Annapolis, Md.	1925	.....	.....	P. J. KIEFER
Utah, Univ. of, Salt Lake City, Utah	1923	A. W. RAY, JR.	J. R. BUTLER	W. J. COPE
Vanderbilt Univ., Nashville, Tenn.	1928	W. R. GREEN	T. C. HARLIN	J. E. BOYNTON
Vermont, Univ. of, Burlington, Vt.	1922	.....	.....	R. G. CHAPMAN
Villanova College, Villanova, Pa.	1925	GEORGE BACSIK	H. N. BOMBICK	G. H. AUTH
Virginia Polytechnic Inst., Blacksburg, Va.	1915	F. F. FISHER, III	GLENN A. MAIN, JR.	J. L. JONES
Virginia, Univ. of, University, Va.	1923	ALLEN MARKS	W. F. JOHNSON, JR.	H. P. FULLERTON
Washington, State College of, Pullman, Wash.	1920	.....	.....	F. W. CANDEE
Washington Univ., St. Louis, Mo.	1911	MELVIN FRANZEL	WING LEONG	R. R. TUCKER
Washington, Univ. of, Seattle, Wash.	1917	J. L. HUMPHREY	E. J. SHARKEY	R. W. CRAIN
West Virginia Univ., Morgantown, W.Va.	1922	.....	.....	H. M. CATHER
Wisconsin, Univ. of, Madison, Wis.	1909	G. E. HLAVKA	MILDRED SMITH	P. S. MYERS
Worcester Polytechnic Inst., Worcester, Wis.	1914	H. L. SCHIMMACK	A. E. ROCKWOOD	L. J. HOOPER
Wyoming, Univ. of, Laramie, Wyo.	1925	.....	.....	C. E. ANDERSON
Yale Univ., New Haven, Conn.	1910	J. R. KISTLER	W. A. FEE	S. W. DUDLEY

RESEARCH COMMITTEES

ARTICLE B6A, PAR. 24: The Standing Committee on Research shall, under the direction of the Council, have supervision of the research activities of the Society.

The first Standing Committee on Research was organized in 1909.

STANDING COMMITTEE

J. F. DOWNIE SMITH, *Chairman* (1946)
HERMAN WEISBERG (1947)
G. A. HAWKINS (1948)
E. L. ROBINSON (1949)
To be appointed (1950)

LUBRICATION

Appointed October, 1915, to investigate the fundamental problems of lubrication, to formulate results of investigations previously made, and to keep in touch with contemporary research in this field

(Reorganized May, 1936)

B. L. NEWKIRK, *Chairman*
S. J. NEEDS, *Secretary*
A. L. BEALL
W. E. CAMPBELL
H. A. EVERETT
P. G. EXLINE
J. C. GENIESSE
M. D. HERSEY
C. M. LARSON
F. C. LINN
S. A. McKEE
E. S. PEARCE
W. A. ZISMAN

FLUID METERS

Appointed 1916 to develop the theory of fluid meters of all kinds and to report on the best methods for their installation and use

(Reorganized July, 1926)

R. J. S. PIGOTT, *Chairman*
J. R. CARLTON, *Secretary*
H. S. BEAN
S. R. BEITLER
R. K. BLANCHARD
B. O. BUCKLAND
LOUIS GESS
E. W. JACOBSON
A. J. KERR
T. H. KERR
I. O. MINER
M. P. O'BRIEN
W. S. PARDOE
L. K. SPINK
R. E. SPRENKLE
T. R. WEYMOUTH
M. J. ZUCROW

STRENGTH OF GEAR TEETH

Appointed in December, 1921, to investigate factors affecting the strength and life of gear teeth

R. E. FLANDERS, *Chairman*
C. H. LOGUE, *Secretary*
EARLE BUCKINGHAM
A. M. GREENE, JR.
C. W. HAM
F. E. McMULLEN
E. W. MILLER
ERNEST WILDHABER

METAL CUTTING DATA AND BIBLIOGRAPHY

Appointed in September, 1923, to study the problems of metal cutting, including tool materials, tool design, speeds and feeds

(Reorganized December, 1943)

M. E. MARTELLOTTI, *Chairman*
O. W. BOSTON
W. C. DE GRAFF
F. M. FISHER
W. W. GILBERT
T. F. GITHENS
W. L. KENNICOTT
F. W. LUCHT
F. J. OLIVER

CUTTING FLUIDS

Appointed in September, 1923, to study the problems of metal cutting, including lubrication and cooling

(Reorganized December, 1943)

O. W. BOSTON, *Chairman*
J. T. BEARD
JOSEPH GESCHELIN
F. W. LUCHT
M. E. MARTELLOTTI
W. H. OLDACRE
DON WANGELIN
G. P. WITTEMAN

MECHANICAL SPRINGS

Appointed May, 1924, to determine the status of the mechanical-spring art, to promote and conduct necessary and adequate research, and to develop the art to the point of standardization

J. R. TOWNSEND, *Chairman*
C. T. EDGERTON, *Secretary*
R. D. BRIZZOLARA, *Alternate*
R. W. COOK
W. T. DONKIN
RUPEN EKSERGIAN
G. E. HANSEN
A. C. KELLER
BENJAMIN LIEBOWITZ
DAVID LOFTS
D. J. McADAM, JR.
L. C. PESKIN
R. E. PETERSON
J. W. ROCKEFELLER, JR.
B. W. ST. CLAIR
M. F. SAYRE
T. R. WEBER
KEITH WILLIAMS
J. K. WOOD
F. P. ZIMMERLI

ELEVATORS

Appointed June, 1924, to study the function and operation of elevator safeties and buffers and their associated mechanisms and to develop methods of test for the approval of elevator safety devices

(Reorganized August, 1940)

D. J. PURINTON, *Chairman*
J. A. DICKINSON, *Secretary*
S. W. JONES, *Ex-Officio*
E. M. BOUTON
K. A. COLAHAN
G. P. KEOGH
J. J. MATSON
M. B. McLAUTHLIN
W. S. PAINE
C. A. PETERS

EFFECT OF TEMPERATURE ON THE PROPERTIES OF METALS

Appointed December, 1924, as a Joint Research Committee of the A.S.T.M. and the A.S.M.E. to encourage the investigation and accumulation of data on the properties of metals used in the mechanic arts at extremely high and low temperatures

N. L. MOCHEL, *Chairman*
H. J. KERR, *Vice-Chairman*
J. W. BOLTON, *Secretary*
W. H. ARMACOST
A. B. BAGSAR
A. D. BAILEY
F. E. BASH
C. L. CLARK
E. S. DIXON
F. B. FOLEY
J. R. FREEMAN, JR.
H. J. FRENCH
H. W. GILLETT
A. J. HERZIG
G. F. JENKS
J. J. KANTER
C. E. MACQUIGG
V. T. MALCOLM
R. F. MILLER
HENRY NORTH
E. L. ROBINSON
J. H. ROMANN
A. E. WHITE
J. S. WORTH
Director, National Bureau of Standards, U.S. Department of Commerce
Representative of Bureau of Ships, U.S. Navy Department

BOILER FEEDWATER STUDIES

Appointed March, 1925, as a Joint Research Committee of the American Boiler Manufacturers Association, American Railway Engineering Association, American Water Works Association, Edison Electric Institute, the American Society for Testing Materials, and the A.S.M.E. to study methods of analysis and treatment of boiler feedwater for stationary and railroad practice

EXECUTIVE COMMITTEE (Total personnel, 41)

C. H. FELLOWS, *Chairman*
R. C. BARDWELL, *Vice-Chairman*
J. B. ROMER, *Secretary*
A. G. CHRISTIE *
R. E. COUGHLAN
B. W. DE GEER
MAX HECHT
H. E. JORDAN

(*Continued*)

* Official A.S.M.E. representative serving on this committee.

BOILER FEEDWATER STUDIES
(Continued)

P. B. Place
S. T. Powell
F. N. Speller
M. F. Stack
G. E. Tate
E. H. Tenney
A. E. White *

CONDENSER TUBES

Appointed May, 1925, to investigate and report on the causes of failure of tubes used in steam condensers and similar heat interchange apparatus

A. E. White, *Chairman*
D. C. Weeks, *Vice-Chairman*
P. A. Bancell
H. Y. Bassett
R. A. Bowman
E. S. Bunn
D. K. Crampton
C. A. Crawford
R. E. Dillon
C. O. Evans
J. R. Freeman, Jr.
V. M. Frost
C. F. Harwood
G. C. Holder
W. C. Holmes
J. C. Phillips
W. B. Price
J. S. Rodgers
Director, Bureau of Ships, U.S. Navy Department

WORM GEARS

Appointed May, 1927, to investigate certain problems in connection with the action of worm gear drives and to recommend improvements in their design, manufacture, and use

Earle Buckingham, *Chairman*
G. H. Acker
L. R. Buckendale
A. A. Ross
B. F. Waterman
Representative of Bureau of Ships, U.S. Navy Department

STRENGTH OF VESSELS UNDER EXTERNAL PRESSURE

Appointed June, 1929, to develop reliable design data on the strength of cylindrical and spherical surfaces under external pressure, particularly with reference to jacketed vessels

F. V. Hartman, *Chairman*
M. B. Higgins
E. C. Korten
H. E. Saunders
E. E. Shanor
R. G. Sturm
D. B. Wesstrom
D. F. Windenburg
Dana Young

WIRE ROPE

Appointed April, 1930, to investigate existing rope so that it may be better understood and more effectively used

W. H. Fulweiler, *Chairman*
H. LeR. Brink
A. H. McDougall
B. V. E. Nordberg
W. S. Paine
W. J. Ryan
George Simpson
L. E. Young

CRITICAL PRESSURE STEAM BOILERS

Appointed June, 1931, to study the characteristics of high-pressure forced-circulation steam-generating units

H. L. Solberg, *Chairman*
W. H. Armacost
A. D. Bailey
C. L. Clark
F. S. Clark
C. H. Fellows
H. J. Kerr
E. C. Petrie
E. L. Robinson
W. H. Rowand
P. W. Thompson

PLASTIC FLOW OF METALS

Appointed October, 1938, to study plasticity in the particular field of rolling of steel

A. L. Nadai, *Chairman*
C. W. MacGregor, *Secretary*
E. C. Bain
C. L. Eksergian
LeVan Griffis
J. H. Hitchcock
W. P. Roop
M. D. Stone
W. Trinks

FURNACE PERFORMANCE FACTORS

Appointed in October, 1941, to collect and rationalize data on the performance of commercially important furnaces as an aid to design and operation

A. R. Mumford, *Chairman*
John Blizard
O. F. Campbell
W. A. Carter
B. J. Cross
T. B. Drew
F. G. Ely
A. C. Fieldner
J. H. Harlow
H. C. Hottel
E. L. Lindseth
W. H. McAdams
J. R. Michel
G. R. Milne
A. J. Nerad
E. B. Powell
A. A. Raymond
W. T. Reid
W. C. Schroeder, *Alternate*
L. B. Schueler, *Alternate*
R. A. Sherman
Philip Sporn
A. W. Thorson
Herman Weisberg
W. J. Wohlenberg

FORGING OF STEEL SHELLS

Appointed in October, 1941, to study methods of shell manufacture under modern conditions

M. D. Stone, *Chairman*
W. Trinks, *Projects Director*
John Dierbeck
M. S. Evans
D. W. Fletcher
W. M. Frame
W. N. Howley
A. F. Macconochie
W. P. Muir
A. L. Nadai
A. R. Nettenstrom
George Sachs
A. E. Van Cleve
U.S. Army, Ordnance Department
U.S. Navy, Bureau of Ordnance

DEMOLITION BOMB BODIES

Appointed in October, 1943, to study methods of demolition bomb body manufacture under modern conditions

M. D. Stone, *Chairman*
W. O. Clinedinst, *Secretary*
W. Trinks, *Projects Director*
G. M. Croft
F. C. Fantz
W. M. Frame
R. Furrer
J. M. Hopkins
H. B. Liggett
A. L. Nadai
George Sachs
U.S. Army, Ordnance Department
U.S. Navy, Bureau of Ordnance

INTERNAL-COMBUSTION ENGINES

Appointed in September, 1944, to prosecute, correlate, analyze, and report on research relating to efficiency, reliability, maintenance, and operating conditions of internal-combustion engines

Lee Schneitter, *Chairman*
W. L. H. Doyle
M. A. Elliott
C. W. Good
W. F. Joachim

FINISHING AND MACHINING OF H.E. STEEL SHELLS

Appointed in February, 1945, to study and critically compare the various methods of machining and finishing steel shells

D. W. Fletcher, *Chairman*
R. W. Biggs, *Secretary*
W. Trinks, *Projects Director*
O. W. Boston
W. C. De Graff
M. S. Evans
D. M. Galloway
C. G. Grazioso
W. N. Howley
M. L. Katke
M. D. Stone
U.S. Army, Ordnance Department

PROPERTIES OF GASES AND GAS MIXTURES

Appointed in June, 1945, to assemble and co-ordinate present available data on the properties of gases and gas mixtures

J. A. Goff, *Chairman*
H. W. Emmons
Serge Gratch
Gerhard Herzberg
H. L. Johnston
R. V. Kleinschmidt
E. L. Robinson
F. D. Rossini
R. B. Smith

AUTOMATIC REGULATION THEORY

Appointed in November, 1945, to supply basic data for correlating the apparent conflicts between the various approaches to the theory of automatic process control

C. E. Mason, *Chairman*
G. S. Brown
D. P. Campbell
C. O. Fairchild
Herbert Harris, Jr.
Nicholas Minorsky
George Philbrick
A. F. Sperry

A.S.M.E. Representatives on Other Research Committees

See also A.S.M.E. Representatives on Other Activities, page RI-9

AMERICAN CO-ORDINATING COMMITTEE ON CORROSION

American Society for Testing Materials

C. H. Fellows
S. L. Kerr

FATIGUE PHENOMENA OF METALS

American Society for Testing Materials

C. T. Edgerton

METALLURGICAL RESEARCH

Advisory Committee to the National Bureau of Standards

C. H. Bierbaum

PROPERTIES OF REFRACTORY MATERIALS

Advisory Committee to the National Bureau of Standards

E. B. Powell

WATER FOR INDUSTRIAL USES (D-19)

American Society for Testing Materials

B. J. Cross

STANDARDIZATION COMMITTEES

ARTICLE B6A, PAR. 23: The Standing Committee on Standardization shall advise the Council on the dimensional standardization work of the Society, including relations with the American Standards Association.

The first Standing Committee on Standardization was organized in April, 1911.

STANDING COMMITTEE

J. HALL TAYLOR, *Chairman* (1946)
E. J. BRYANT (1947)
D. S. ELLIS (1948)
F. HUGH MOREHEAD (1949)
F. K. MITCHELL (1950)

STANDARDIZATION AND UNIFICATION OF SCREW THREADS (B1)

* *Joint sponsorship with the Society of Automotive Engineers. Sectional Committee originally organized in June, 1921. Reorganized in May, 1929*

A.S.M.E. Members (Total personnel, 39)

E. J. BRYANT, *Chairman*
A. M. HOUSER, *Vice-Chairman* †
EARLE BUCKINGHAM
G. S. CASE
T. G. CRAWFORD
L. W. KATTELLE, *Alternate*
H. C. E. MEYER
P. V. MILLER †
W. C. MUELLER
R. H. PERRY
W. C. STEWART, *Alternate*
G. T. TRUNDLE, JR.

SUBCOMMITTEE CHAIRMAN

No. 7 on Screw Threads for High Temperature Bolting, W. H. GOURLIE

PIPE THREADS (B2)

* *Joint sponsorship with the American Gas Association. Sectional Committee originally organized in 1913. Reorganized December, 1927*

A.S.M.E. Members (Total personnel, 41)

A. S. MILLER, *Chairman*
C. B. LEPAGE, *Acting Secretary*
C. A. BADEAU
A. F. BREITENSTEIN †
E. J. BRYANT
E. S. CORNELL, JR.
J. J. CROTTY
A. M. HOUSER †
L. W. KATTELLE
P. V. MILLER †
F. HUGH MOREHEAD
L. N. SHANNON
O. M. TISHLARICH
FRANK THORNTON, JR.
ROWLAND TOMPKINS
B. B. WESCOTT
J. H. WILLIAMS

SUBCOMMITTEE CHAIRMAN

No. 1 on Editing and Gaging, A. M. HOUSER

* Note: All of these standards committees for which the Society is sponsor or joint sponsor, or on which it has representation, are organized under the procedure of the American Standards Association.

† Official A.S.M.E. representative serving on this committee.

BALL AND ROLLER BEARINGS (B3)

* *Joint sponsorship with the Society of Automotive Engineers. Sectional Committee organized December, 1920*

A.S.M.E. Members (Total personnel, 18)

W. P. KENNEDY, *Vice-Chairman* †
D. E. BATESOLE †
L. A. CUMMINGS
O. H. DORER
F. G. HUGHES
G. E. HULSE †
W. L. ILIFF †
L. F. NENNINGER
S. M. WECKSTEIN †
ERNEST WOOLER

ALLOWANCES AND TOLERANCES FOR CYLINDRICAL PARTS AND LIMIT GAGES (B4)

* *Sole sponsorship. Sectional Committee originally organized in June, 1920. Reorganized in December, 1930*

A.S.M.E. Members (Total personnel, 36)

J. E. LOVELY, *Chairman* †
F. E. BANFIELD, JR.
F. S. BLACKALL, JR.
E. J. BRYANT
EARLE BUCKINGHAM †
F. H. COLVIN †
T. G. CRAWFORD
R. E. W. HARRISON
F. O. HOAGLAND
E. N. JACOBI
H. C. E. MEYER
P. V. MILLER
W. C. MUELLER
E. C. PECK †
R. H. PERRY
W. C. SCHOENFELDT
C. C. STEVENS
G. T. TRUNDLE, JR.

SMALL TOOLS AND MACHINE TOOL ELEMENTS (B5)

* *Joint sponsorship with the National Machine Tool Builders' Association, and the Society of Automotive Engineers. Sectional Committee organized September, 1922*

A.S.M.E. Members (Total personnel, 32)

W. C. MUELLER, *Chairman* †
F. O. HOAGLAND, *Vice-Chairman*
J. B. ARMITAGE
O. W. BOSTON
E. J. BRYANT
EARLE BUCKINGHAM
F. H. COLVIN
S. A. EINSTEIN
J. P. GILL
L. N. HAMPTON, *Alternate*
H. E. HARRIS
JOHN HAYDOCK
J. P. LAUX †
J. E. LOVELY †
A. F. MURRAY †
ERIK OBERG †
FRANK THORNTON, JR.

TECHNICAL COMMITTEES

EXECUTIVE COMMITTEE

A.S.M.E. Members (Total personnel, 4)

W. C. MUELLER, *Chairman*
F. O. HOAGLAND, *Vice-Chairman*
H. E. HARRIS

No. 1 on T-SLOTS

A.S.M.E. Members (Total personnel, 7)

ERIK OBERG, *Chairman*
J. B. ARMITAGE
HARRY CADWALLADER, JR.
S. A. EINSTEIN
F. O. HOAGLAND

No. 2 on TOOL-POSTS AND TOOL SHANKS

A.S.M.E. Members (Total personnel, 8)

O. W. BOSTON, *Chairman*
F. S. BLACKALL, JR.
GRANGER DAVENPORT
M. E. LANGE

No. 3 on MACHINE TAPERS

A.S.M.E. Members (Total personnel, 20)

E. J. BRYANT, *Chairman*
J. B. ARMITAGE
F. S. BLACKALL, JR.
EARLE BUCKINGHAM
F. H. COLVIN
B. P. GRAVES
E. E. GRIFFITHS
H. E. HARRIS
F. O. HOAGLAND
J. H. HORIGAN
G. W. METZ, *Alternate*
L. F. NENNINGER

No. 4 on SPINDLE NOSES AND COLLETS FOR MACHINE TOOLS

A.S.M.E. Members (Total personnel, 5)

J. E. LOVELY, *Chairman*
H. W. FAHRLANDER
E. D. GANGWERE
F. O. HOAGLAND

No. 5 on MILLING CUTTERS

A.S.M.E. Members (Total personnel, 19)

J. B. ARMITAGE
A. N. GODDARD
E. E. GRIFFITHS
J. H. HORIGAN
G. W. METZ, *Alternate*
E. K. MORGAN
ERIK OBERG
E. DON VANCIL

No. 6 on DESIGNATIONS AND WORKING RANGES OF MACHINE TOOLS

A.S.M.E. Members (Total personnel, 19)

JOHN HAYDOCK, *Chairman*
T. H. DOAN
H. W. FAHRLANDER
H. W. FAUS
B. P. GRAVES
J. J. MCBRIDE
L. F. NENNINGER
E. R. SMITH

No. 7 on Twist Drill Sizes

A.S.M.E. Members (Total personnel, 6)

W. C. Mueller, *Chairman*
E. E. Griffiths
J. H. Horigan
G. W. Metz, *Alternate*

No. 8 on Jig Bushings

A.S.M.E. Members (Total personnel, 8)

E. E. Griffiths — G. W. Metz, *Alternate*
J. H. Horigan

No. 9 on Punch Press Tools

A.S.M.E. Members (Total personnel, 13)

D. H. Chason — H. E. Harris
E. W. Ernest — G. W. Metz, *Alternate*
E. E. Griffiths — D. M. Palmer

No. 10 on Forming Tools and Holders

A.S.M.E. Members (Total personnel, 10)

W. C. Mueller, *Chairman*
W. E. Blank
E. E. Griffiths
G. W. Metz, *Alternate*
L. D. Spence

No. 11 on Chucks and Chuck Jaws

A.S.M.E. Member (Total personnel, 9)

J. E. Lovely, *Chairman*

No. 12 on Cut and Ground Thread Taps

A.S.M.E. Member (Total personnel, 7)

J. E. Ennis

No. 13 on Splines and Splined Shafts

A.S.M.E. Members (Total personnel, 20)

J. B. Armitage — F. O. Hoagland
H. W. Fahrlander — J. E. Lovely
R. E. W. Harrison

No. 17 on Nomenclature for Small Tools and Machine Tool Elements

A.S.M.E. Members (Total personnel, 12)

O. W. Boston, *Chairman and Secretary*
F. S. Blackall, Jr.
F. H. Colvin
H. E. Harris
F. O. Hoagland

No. 19 on Single-Point Cutting Tools

A.S.M.E. Members (Total personnel, 2)

F. H. Colvin, *Chairman*
O. W. Boston, *Secretary*

No. 20 on Reamers

A.S.M.E. Members (Total personnel, 15)

F. H. Colvin — J. H. Horigan
T. F. Githens — O. E. Koehler
E. E. Griffiths — G. W. Metz, *Alternate*

No. 21 on Tool-Life Tests for Single-Point Tools

A.S.M.E. Members (Total personnel, 9)

O. W. Boston, *Chairman*
E. E. Griffiths
M. F. Judkins
F. W. Lucht
G. W. Metz, *Alternate*
H. L. Moir

No. 23 on Machine Pins

A.S.M.E. Members (Total personnel, 14)

G. W. Metz, *Secretary* — J. J. McBride
E. E. Griffiths — R. H. Smith

GEARS (B6)

** Joint sponsorship with the American Gear Manufacturers Association. Sectional Committee organized June, 1921*

A.S.M.E. Members (Total personnel, 23)

U. S. Eberhardt, *Chairman*
Earle Buckingham, *Vice-Chairman* †
G. H. Acker
A. H. Candee †
S. L. Crawshaw
L. H. Fry
C. B. Hamilton, Jr.
D. T. Hamilton
O. A. Leutwiler †

SUBCOMMITTEE CHAIRMEN

No. 3 on Nomenclature, D. T. Hamilton
No. 9 on Inspection, Granger Davenport

PIPE FLANGES AND FITTINGS (B16)

** Joint sponsorship with the Heating, Piping and Air Conditioning Contractors National Association, and the Manufacturers Standardization Society of the Valve and Fittings Industry. Sectional Committee organized November, 1921*

A.S.M.E. Members (Total personnel, 51)

C. P. Bliss, *Chairman* †
A. L. Baker
L. W. Benoit †
John Blizard, *Alternate*
A. L. Brown
Sabin Crocker
Ferdinand Fink
V. M. Frost
H. E. Haller
F. H. Hehemann
J. S. Hess
H. A. Hoffer †
A. M. Houser †
C. A. Kelting †
J. R. Kruse
M. B. MacNeille
F. Hugh Morehead
L. S. Morse, Sr.
A. W. Oakley
Fred Ophuls
Ludwig Skog
J. E. Stark
J. R. Tanner †
J. H. Taylor
Rowland Tompkins
G. W. Watts
J. H. Williams
J. H. Zink

SUBCOMMITTEE CHAIRMEN

No. 1 on Cast Iron Flanges and Flanged Fittings, A. M. Houser
No. 2 on Screwed Fittings, F. Hugh Morehead
No. 3 on Steel Flanges and Flanged Fittings, L. D. Burritt
No. 4 on Materials and Stresses, A. M. Houser
No. 5 on Face to Face Dimensions of Ferrous Flanged Valves, J. R. Tanner
No. 6 on Malleable Iron or Steel Brass Seat Unions (to be appointed)
No. 8 on Marking of Pipe Fittings, F. Hugh Morehead

SHAFTING (B17)

** Sole sponsorship. Organized October, 1918*

A.S.M.E. Members (Total personnel, 11)

C. B. LePage, *Secretary*
H. C. E. Meyer
L. C. Morrow
L. W. Williams †

BOLT, NUT, AND RIVET PROPORTIONS (B18)

** Joint sponsorship with the Society of Automotive Engineers. Sectional Committee organized March, 1922*

A.S.M.E. Members (Total personnel, 48)

W. R. Halliday, *Chairman* †
W. C. Stewart, *Alternate, Secretary*
H. E. Aldrich
F. C. Billings
B. G. Braine
G. S. Case
T. G. Crawford
H. P. Frear
A. R. Gatewood
A. M. Houser †
Herman Koester †
J. J. McBride, *Alternate*
W. C. Mueller
S. F. Newman
R. H. Perry
J. R. Tanner †
R. J. Whelan
E. M. Whiting
V. R. Willoughby

SUBCOMMITTEE CHAIRMEN

No. 3 on Slotted and Recessed Head Screws, F. P. Tisch
No. 9 on Socket Head Cap and Set Screws, Herman Koester

PLAIN AND LOCK WASHERS (B27)

** Joint sponsorship with the Society of Automotive Engineers. Sectional Committee organized March, 1926*

A.S.M.E. Members (Total personnel, 41)

W. R. Bryans — H. C. E. Meyer
T. G. Crawford — J. S. Morehouse
W. R. Halliday — W. C. Mueller †
C. H. Loutrel — E. M. Whiting †
J. J. McBride

SUBCOMMITTEE CHAIRMEN

No. 1 on Plain Washers, W. L. Barth
No. 2. on Spring Washers, E. D. Cowlin

TRANSMISSION CHAINS AND SPROCKETS (B29)

** Joint sponsorship with the Society of Automotive Engineers, and the American Gear Manufacturers Association. Sectional Committee originally organized September, 1917. Reorganized December, 1926*

A.S.M.E. Members (Total personnel, 13)

J. M. Bryant † — E. B. Nichols †
Joseph Joy — D. B. Perry
L. V. Ludy † — C. R. Weiss

CODE FOR PRESSURE PIPING (B31)

** Sole sponsorship. Sectional Committee originally organized November, 1926. Reorganized December, 1937*

A.S.M.E. Members (Total personnel, 82)

ALFRED IDDLES, *Chairman* †
L. W. BENOIT, *Alternate*
J. D. CAPRON, *Alternate*
L. H. CARR, *Alternate*
D. H. COREY
SABIN CROCKER
J. J. CROWE, *Alternate*
H. D. EDWARDS
V. M. FROST
T. W. GREENE, *Alternate*
H. E. HALLER
J. S. HAUG
H. A. HOFFER
G. G. HOLLINS
E. L. HOPPING
A. M. HOUSER †
D. S. JACOBUS
T. M. JASPER
H. E. KEELER
C. A. KELTING
E. H. KRIEG
G. SINDING-LARSEN
M. B. MACNEILLE
H. C. E. MEYER
J. W. MOORE
F. HUGH MOREHEAD
H. H. MORGAN
L. S. MORSE, SR.
H. H. MOSS, *Alternate*
R. M. NEE
E. W. NORRIS
C. W. OBERT
A. L. PENNIMAN, JR.
E. B. RICKETTS
C. S. ROBINSON †
J. H. ROMANN
D. B. ROSSHEIM
G. W. SAATHOFF
G. K. SAURWEIN
LUDWIG SKOG
H. S. SMITH
J. E. STARK
J. R. TANNER
J. H. TAYLOR
J. H. VANCE
H. L. WHITTEMORE
J. H. WILLIAMS
E. J. WISEMAN, *Alternate*
T. F. WOLFE
J. H. ZINK

SUBCOMMITTEE CHAIRMEN

Subcommittee on Scope and Intent, SABIN CROCKER
No. 1 on Plan, Scope, and Editing, SABIN CROCKER
No. 2 on Power Piping, ALFRED IDDLES
No. 4 on Gas and Air Piping, J. S. HAUG
No. 5 on Refrigeration Piping, A. B. STICKNEY
No. 6 on Oil Piping, L. D. BURRITT
No. 7 on Piping Materials and Identification, F. HUGH MOREHEAD
No. 8 on Fabrication Details, LUDWIG SKOG
No. 9 on District Heating Piping, G. K. SAURWEIN

WIRE AND SHEET METAL GAGES (B32)

** Joint sponsorship with the Society of Automotive Engineers. Sectional Committee originally organized November, 1928. Reorganized November, 1939*

A.S.M.E. Members (Total personnel, 32)

A. P. COTTLE
E. W. ERNEST
J. F. HOWE †
F. G. WILSON †

SCREW THREADS FOR HOSE COUPLINGS (B33)

** Sole sponsorship. Sectional Committee organized October, 1928*

A.S.M.E. Members (Total personnel, 21)

A. L. BROWN, *Secretary*
L. W. BENOIT
A. F. BREITENSTEIN †
J. J. CROTTY
W. E. DUNHAM †
F. C. ERNST, *Alternate*
H. C. E. MEYER
J. H. WILLIAMS

WROUGHT IRON AND WROUGHT STEEL PIPE AND TUBING (B36)

** Joint sponsorship with the American Society for Testing Materials. Sectional Committee organized May, 1928*

A.S.M.E. Members (Total personnel, 36)

H. H. MORGAN, *Chairman*
SABIN CROCKER, *Secretary*
J. S. ADELSON
H. E. ALDRICH
F. S. CLARK, *Alternate* †
A. R. GATEWOOD
NEWELL HAMILTON
D. S. JACOBUS †
J. J. KANTER
H. C. E. MEYER
F. HUGH MOREHEAD
H. B. OATLEY †
J. H. ROMANN
LUDWIG SKOG †
J. R. TANNER
A. E. WHITE

SUBCOMMITTEE CHAIRMEN

Pipe and Tubing for Low Temperature Service, J. J. SHUMAN
Pipe and Tubing for High Temperature Service, J. R. TANNER

PRESSURE AND VACUUM GAGES (B40)

** Sole sponsorship. Sectional Committee organized December, 1930*

A.S.M.E. Members (Total personnel, 40)

M. D. ENGLE, *Chairman*
A. W. LENDEROTH, *Secretary* †
E. J. BRYANT
J. P. CAVANAUGH †
J. J. CROWE
PAUL DISERENS
C. H. GRAESSER
W. F. JONES
R. J. KEHL
J. C. MCCUNE †
A. H. MORGAN
H. B. REYNOLDS
W. C. SCHOENFELDT

STOCK SIZES, SHAPES AND LENGTHS FOR HOT AND COLD FINISHED IRON AND STEEL BARS (B41)

** Sole sponsorship. Sectional Committee organized June, 1930*

A.S.M.E. Members (Total personnel, 24)

C. D. ALLEN
F. H. DECHANT
E. W. ERNEST
H. D. TANNER
L. W. WILLIAMS †

SUBCOMMITTEE CHAIRMEN

No. 1 on Hot Rolled Steel, HENRY WYSOR
No. 2 on Cold Finished Steels, L. E. CREIGHTON

SPECIFICATIONS FOR LEATHER BELTING (B42)

** Sole sponsorship. Sectional Committee organized May, 1931*

A.S.M.E. Members (Total personnel, 21)

H. T. COATES
R. W. DRAKE †
P. G. RHOADS

CLASSIFICATION AND DESIGNATION OF SURFACE QUALITIES (B46)

** Joint sponsorship with the Society of Automotive Engineers. Sectional Committee organized December, 1932*

A.S.M.E. Members (Total personnel, 64)

R. F. GAGG, *Chairman*
E. R. BOYNTON, *Secretary*
E. J. ABBOTT
L. W. BENOIT
E. J. BRYANT
T. G. CRAWFORD
R. C. DEALE †
U. S. EBERHARDT
S. A. EINSTEIN
W. W. GILBERT
R. E. W. HARRISON †
F. O. HOAGLAND
H. J. HOLTZCLAW
R. T. KENT
H. F. KURTZ
J. H. LANSING
JOSEPH MANUELE
C. C. STEVENS
W. C. STEWART
J. S. TAWRESEY
C. H. WHITAKER
ERNEST WOOLER

SUBCOMMITTEE CHAIRMEN

Special Subcommittee on Revision and Editing, R. F. GAGG

SHAFT COUPLINGS, INTEGRALLY FORGED FLANGE TYPE FOR HYDROELECTRIC UNITS (B49)

** Sole sponsorship. Sectional Committee organized October, 1943*

A.S.M.E. Members (Total personnel, 18)

R. E. B. SHARP, *Chairman* †
D. J. MCCORMACK, *Secretary* †
D. L. BARBOUR
L. F. MOODY
G. R. RICH
E. B. STROWGER
R. V. TERRY
W. F. UHL

COMBUSTION SPACE FOR SOLID FUELS (B50)

** Sole sponsorship. Sectional Committee organized June, 1933*

A.S.M.E. Members (Total personnel, 19)

C. E. Bronson, *Chairman*
W. G. Christy
John Hunter
A. J. Johnson
V. G. Leach †
J. P. Magos
J. F. McIntire
F. L. Meyer
C. A. Reed
John Van Brunt †

SUBCOMMITTEE CHAIRMEN

No. 1 on Purpose and Scope, C. E. Bronson
No. 2 on Combustion and Design, B. M. Guthrie
No. 3 on Warm Air Furnaces, J. H. Manny
No. 4 on Steel Heating Boilers, W. B. Russell
No. 5 on Cast Iron Boilers, J. F. McIntire

SCHEME FOR IDENTIFICATION OF PIPING SYSTEMS (A13)

** Joint sponsorship with the National Safety Council. Sectional Committee organized June, 1922*

A.S.M.E. Members (Total personnel, 30)

E. E. Ashley
W. L. Bunker
Crosby Field
H. L. Miner
F. L. Newcomb
H. S. Smith
Frank Thornton, Jr.
Rowland Tompkins
Frank Umbehocker †

MINIMUM REQUIREMENTS FOR PLUMBING AND STANDARDIZATION OF PLUMBING EQUIPMENT (A40)

** Joint sponsorship with The American Public Health Association. Sectional Committee organized November, 1928*

A.S.M.E. Members (Total personnel, 41)

C. B. LePage, *Secretary*
J. F. Carney, *Alternate*
J. J. Crotty
A. M. Houser †
W. K. McAfee
A. H. Morgan †
W. R. Webster †

SUBCOMMITTEE CHAIRMEN

Research Committee on Plumbing, F. M. Dawson
Temporary Editing Committee on Plumbing Code, G. N. Thompson
No. 1 on Minimum Requirements for Plumbing, Theodore Irving Coe
No. 2 on Staple Vitreous China Plumbing Fixtures, H. R. Van Sciver
No. 3 on Staple Porcelain (All Clay) Plumbing Equipment, H. R. Van Sciver
No. 4 on Enameled Sanitary Ware, A. H. Cline, Jr.
No. 5 on Traps (to be appointed)
No. 6 on Brass Plumbing Products (to be appointed)
No. 7 on Brass Fittings for Flared Copper Tubes, F. L. Riggin
No. 8 on Cast Iron Soil Pipe and Fittings (to be appointed)
No. 9 on Gasoline, Oil and Grease Separators (to be appointed)
No. 11 on Soldered Fittings for Tubing, A. M. Houser
No. 12 on Minimum Air Gaps in Plumbing Systems, W. K. McAfee
Subgroup on American Standard Plumbing Code, A. H. Morgan

ROLLED THREADS FOR SCREW SHELLS OF ELECTRIC SOCKETS AND LAMP BASES (C44)

** Joint sponsorship with the National Electrical Manufacturers Association. Sectional Committee organized June, 1929*

A.S.M.E. Members (Total personnel, 13)

E. J. Bryant †
Earle Buckingham †
A. B. Morgan, *Alternate*

LETTER SYMBOLS AND ABBREVIATIONS FOR SCIENCE AND ENGINEERING (Z10)

** Joint sponsorship with the American Association for the Advancement of Science, American Institute of Electrical Engineers, American Society of Civil Engineers, and the Society for the Promotion of Engineering Education. Sectional Committee originally organized January, 1926. Reorganized October, 1935*

A.S.M.E. Members (Total personnel, 41)

S. A. Moss, *Vice-Chairman* †
S. R. Beitler, *Alternate* †
K. H. Condit
L. C. Lichty
R. E. Peterson †
G. A. Stetson
Frank Thornton, Jr.

SUBCOMMITTEE CHAIRMEN

Executive Committee, H. M. Turner
Steering Committee, H. M. Turner
No. 1 on Letter Symbols and Signs for Mathematics, A. A. Bennett
No. 2 on Symbols for Hydraulics (to be appointed)
No. 3 on Symbols for Mechanics, R. E. Peterson
No. 4 on Symbols for Structural Analysis, Albert Haertlein
No. 5 on Symbols for Heat and Thermodynamics, S. A. Moss
No. 6 on Symbols for Illuminating Engineering, A. E. Parker
No. 7 on Aeronautical Symbols, G. W. Lewis
No. 8 on Symbols for Electrical Quantities, Edward Bennett
No. 9 on Symbols for Radio, H. M. Turner
No. 10 on Symbols for Physics, H. K. Hughes
No. 11 on Abbreviations for Scientific and Engineering Terms, G. A. Stetson
No. 12 on Symbols for Chemical Engineering, J. H. Perry

STANDARDS FOR DRAWINGS AND DRAFTING ROOM PRACTICE (Z14)

** Joint sponsorship with the Society for the Promotion of Engineering Education. Sectional Committee organized September, 1926*

A.S.M.E. Members (Total personnel, 42)

L. W. Benoit
H. P. Frear
A. C. Harper
E. R. Hill
Samuel Ketchum †
C. W. Keuffel
F. R. Laney
H. B. Langille
H. M. McCully
Rudolph Michel, *Alternate*
F. W. Ming
W. C. Mueller
E. B. Neil
J. W. Owens
F. C. Panuska
Ed S. Smith †
Rowland Tompkins

SUBCOMMITTEE CHAIRMEN

Subcommittee on Revision, F. G. Higbee
Subcommittee on Design and Dimensioning with Tolerances and Allowances for Interchangeable Manufacture, H. L. Keller

GRAPHIC PRESENTATION (Z15)

** Sole sponsorship. Sectional Committee organized December, 1926*

A.S.M.E. Members (Total personnel, 31)

G. E. Hagemann, *Secretary* †
C. M. Bigelow
Wallace Clark
H. M. McCully
D. B. Porter †

SUBCOMMITTEE CHAIRMEN

Preferred Practice for Time Series Charts, F. E. Croxton
Engineering and Scientific Graphs, W. A. Shewhart

GRAPHICAL SYMBOLS AND ABBREVIATIONS FOR USE ON DRAWINGS (Z32)

** Joint sponsorship with American Institute of Electrical Engineers. Sectional Committee organized June, 1936*

A.S.M.E. Members (Total personnel, 43)

E. E. Ashley
J. M. Barnes
L. W. Benoit
G. F. Habach
D. T. Hamilton
W. J. Kunz †
H. M. McCully
W. C. Mueller
L. L. Munier
F. C. Panuska †
W. C. Stewart
T. R. Thomas

SUBCOMMITTEE CHAIRMEN

No. 1 on Symbols for Use in Mechanical Engineering, W. J. Kunz
No. 2 on Symbols for Use in Electrical Engineering (to be appointed)
No. 3 on Abbreviations for Use on Drawings, W. J. Kunz

DEVELOPMENT OF STATISTICAL APPLICATIONS IN ENGINEERING AND MANUFACTURING

Joint sponsorship with the American Mathematical Society, American Society for Testing Materials, American Statistical Association, and Institute of Mathematical Statistics. Appointed in December, 1929

A.S.M.E. Members (Total personnel, 10)

A. G. Ashcroft
W. H. Fulweiler
L. K. Sillcox †
J. S. Tawresey †

SPECIAL STANDARDS COMMITTEE ON STEAM TURBINES

K. M. Irwin, *Chairman*
G. A. Gaffert, *Secretary*
R. C. Allen
C. B. Campbell
A. G. Christie
E. H. Krieg
A. L. Penniman, Jr.
W. F. Ryan
G. B. Warren

SPECIAL COMMITTEE ON STANDARDIZATION OF THERBLIGS, PROCESS CHARTS, AND THEIR SYMBOLS

D. B. Porter, *Chairman*
G. M. Varga, *Secretary*
R. W. Allen
R. M. Barnes
C. H. Cox
L. M. Gilbreth
J. O. P. Hummel
H. B. Maynard
J. A. Piacitelli

A.S.M.E. Representatives on Miscellaneous Standardization Committees

See also A.S.M.E. Representatives on Other Activities, page RI-9

ACOUSTICAL MEASUREMENTS AND TERMINOLOGY (Z24)

** Sponsor body: Acoustical Society of America*

(To be appointed)

AERONAUTICS (D9)

** Sponsor body: Society of Automotive Engineers*

E. A. Sperry, Jr.

BUILDING CODE REQUIREMENTS FOR LIGHT AND VENTILATION (A53)

** Sponsor bodies: Federal Housing Administration, and U.S. Public Health Service*

F. R. Scherer

CAST IRON AT ELEVATED TEMPERATURES

Subcommittee of American Society for Testing Materials Committee A-3 on Cast Iron

D. B. Rossheim

COAL AND COKE (D5)

Committee of American Society for Testing Materials

R. M. Hardgrove

DEFINITIONS OF ELECTRICAL TERMS (C42)

** Sponsor body: American Institute of Electrical Engineers*

F. O. Ellenwood

DRAINAGE OF COAL MINES (M6)

** Sponsor body: American Mining Congress*

O. M. Pruitt

ELECTRIC WELDING APPARATUS (C52)

** Sponsor body: American Welding Society*

R. E. Kinkead

SPECIFICATIONS FOR FIRE TESTS OF BUILDING CONSTRUCTION AND MATERIALS (A2)

** Sponsor bodies: ASA Fire Protection Group, National Bureau of Standards, and American Society for Testing Materials*

R. C. Parlett

FOREST FIRE PROTECTION

Committee of National Fire Protection Association

C. B. White

JOINT CONFERENCE COMMITTEE ON PIPING CODES AND STANDARDS

C. A. Kelting, *Chairman*
Sabin Crocker
V. M. Frost
A. M. Houser
Alfred Iddles
J. R. Kruse
F. Hugh Morehead
D. B. Rossheim
J. E. Stark
F. S. G. Williams
J. H. Zink

LOADING PLATFORMS AT FREIGHT TERMINALS AND WAREHOUSES (E12)

** Sponsor body: American Trucking Association, Inc.*

M. C. Maxwell

MANHOLE FRAMES AND COVERS A(35)

** Sponsor bodies: ASA Telephone Group, and American Society of Civil Engineers*

Anton Hansen

ASA MECHANICAL STANDARDS COMMITTEE

Alfred Iddles, *Chairman* †
A. L. Baker, *Alternate* †
Kenneth Cartwright, *Alternate*
S. L. Crawshaw
J. E. Ennis
E. W. Ernest
F. O. Hoagland
E. L. Hopping
M. E. Lange, *Alternate*
F. Hugh Morehead
H. H. Morgan
J. E. Stark, *Alternate*
Frank Thornton, Jr.
H. L. Whittemore, *Alternate*

Executive Committee,
Alfred Iddles, *Chairman*
F. Hugh Morehead, *Vice-Chairman*
J. E. Ennis
F. O. Hoagland
H. H. Morgan

METHODS OF TESTING WOOD (04)

** Sponsor bodies: U.S. Forest Service, and American Society for Testing Materials*

C. M. Bigelow

MISCELLANEOUS OUTSIDE COAL-HANDLING EQUIPMENT (M10)

** Sponsor body: American Mining Congress*

Ralph Sargent

PETROLEUM PRODUCTS AND LUBRICANTS (Z11)

** Sponsor body: American Society for Testing Materials*

R. G. N. Evans
S. J. Needs
(H. J. Masson, *Alternate*)

PREFERRED NUMBERS (Z17)

** Special Committee of ASA*

K. H. Condit

RATING OF RIVERS (A36)

** Sponsor body: U.S. Geological Survey*

D. W. Mead

ROTATING ELECTRICAL MACHINERY (C50)

** Sponsor body: ASA Electrical Standards Committee*

C. D. Wilson

SPECIFICATIONS FOR CAST IRON PIPE AND SPECIAL CASTINGS (A21)

** Sponsor bodies: American Gas Association, American Society for Testing Materials, American Water Works Association, and the New England Water Works Association*

J. E. Gibson
L. R. Howson

SPECIFICATIONS FOR CLEAN BITUMINOUS COAL (M26)

** Sponsor body: American Institute of Mining and Metallurgical Engineers*

R. A. SHERMAN
(E. L. LINDSETH, *Alternate*)

SPECIFICATIONS FOR SIEVES FOR TESTING PURPOSES (Z23)

** Sponsor bodies: American Society for Testing Materials, and National Bureau of Standards*

R. M. HARDGROVE

THERMAL INSULATING MATERIALS (C16)

Committee of American Society for Testing Materials

R. H. HEILMAN

U.S. INTERDEPARTMENTAL COMMITTEE ON SCREW THREADS

E. J. BRYANT A. M. HOUSER

VOLUME WATER HEATING

Committee of American Gas Association

MARC RESEK

WIRE ROPES FOR MINES (M11)

** Sponsor body: American Mining Congress*

E. S. WELLHOFER

ASA STANDARDS COUNCIL

ALFRED IDDLES †
W. H. HILL †
(C. B. LEPAGE, *Alternate* †)
(W. C. MUELLER, *Alternate* †)

POWER TEST CODES COMMITTEES

ARTICLE B6A, PAR. 27: The Standing Committee on Power Test Codes shall, under the direction of the Council, have supervision of all the activities of the Society in connection with the A.S.M.E. Power Test Codes, including the interpretation of such codes.

The first Standing Committee on Power Test Codes was organized in December, 1918, to revise and extend the Power Test Codes which had been formulated by various technical committees appointed to develop particular codes. This work began in 1884.

STANDING COMMITTEE

A. G. CHRISTIE, *Chairman* (1946)
W. A. CARTER, *Vice-Chairman* (1947)

Term expires 1946

A. G. CHRISTIE
PAUL DISERENS
N. R. GIBSON
W. W. JOHNSON
E. B. POWELL

Term expires 1947

W. A. CARTER
W. L. H. DOYLE
H. B. OATLEY
R. B. SMITH
W. J. WOHLENBERG

Term expires 1948

LOUIS ELLIOTT
G. A. ORROK, JR.
ARVID PETERSON
R. A. SHERMAN
P. W. SWAIN

Term expires 1949

S. N. FIALA
A. E. GRUNERT
L. F. MOODY
T. E. PURCELL
E. B. RICKETTS

Term expires 1950

THEODORE BAUMEISTER
C. C. FRANCK
P. H. HARDIE
B. V. E. NORDBERG
M. C. STUART

---

(1) GENERAL INSTRUCTIONS

Appointed December, 1918

Reorganized September, 1939

THEODORE BAUMEISTER, *Chairman*
PAUL DISERENS
HENRY KREISINGER
R. H. SNYDER
C. R. SODERBERG
M. C. STUART

(2) DEFINITIONS AND VALUES

Appointed December, 1918

Reorganized June, 1936, November, 1945

LOUIS ELLIOTT, *Chairman*
C. S. CRAGOE
A. E. GRUNERT
L. S. MARKS
R. A. SHERMAN
R. B. SMITH

(3) FUELS

Appointed December, 1918

Reorganized April, 1944

R. A. SHERMAN, *Chairman*
O. F. CAMPBELL
H. C. CARROLL
T. D. DELBRIDGE
F. G. ELY
S. B. FLAGG
F. W. KEATOR
M. A. MAYERS
W. NACOVSKY
E. X. SCHMIDT
W. A. SELVIG
L. SHNIDMAN

(4) STATIONARY STEAM-GENERATING UNITS

Appointed December, 1918

E. R. FISH, *Chairman*
A. D. BAILEY
M. W. BENJAMIN
B. J. CROSS
MARTIN FRISCH
F. X. GILG
P. H. HARDIE
R. M. HARDGROVE
E. L. LINDSETH
E. L. MCDONALD
E. B. POWELL
R. SHELLENBERGER

(5) RECIPROCATING STEAM ENGINES

Appointed December, 1918

Reorganized December, 1931

A. G. CHRISTIE, *Chairman*
K. S. M. DAVIDSON
HENRIK GREGER
J. A. HUNTER
H. G. MUELLER
B. V. E. NORDBERG
A. V. SAHAROFF
A. G. WITTING

(6) STEAM TURBINES

Appointed December, 1918

Reorganized November, 1945

W. E. CALDWELL, *Chairman*
PETER CHERDANTZEFF
A. G. CHRISTIE
C. C. FRANCK
V. M. FROST
A. E. GRUNERT
FRANCIS HODGKINSON
P. H. KNOWLTON
T. E. PURCELL
C. A. ROBERTSON

(7) RECIPROCATING STEAM-DRIVEN DISPLACEMENT PUMPS

Appointed December, 1918

R. D. HALL, *Chairman*
E. H. BROWN
J. E. GIBSON
G. L. KOLLBERG
M. B. MACNEILLE
D. W. MEAD
L. A. QUAYLE

(8) CENTRIFUGAL AND ROTARY PUMPS

Appointed December, 1918

Reorganized March, 1936, November, 1945

F. G. SWITZER, *Chairman*
K. W. BEATTIE
A. P. BROCKLEBANK
B. K. ERDOSS
ALADAR HOLLANDER
HARRY KNECHT
L. F. MOODY
WILLIAM PARDOE
ARVID PETERSON
H. L. ROSS
W. C. RUDD
FRANKLIN THOMAS
R. W. WATSON

(9) DISPLACEMENT COMPRESSORS AND BLOWERS

Appointed December, 1918

Reorganized October, 1935

PAUL DISERENS, *Chairman*
G. T. FELBECK
C. R. HOUGHTON
J. F. HUVANE
R. M. JOHNSON
J. F. DOWNIE SMITH

(10) CENTRIFUGAL AND TURBO-COMPRESSORS AND BLOWERS

Appointed December, 1918

Reorganized October, 1929

ARVID PETERSON, *Chairman*
THEODORE BAUMEISTER
C. A. BOOTH
W. H. CARRIER
THOMAS CHESTER
A. H. CHURCH
E. D. CURLEY
L. E. DAY
Z. G. DEUTSCH
S. H. DOWNS
B. K. ERDOSS
P. E. GOOD
J. J. GROB
H. F. HAGEN
F. H. JENKINS
R. M. JOHNSON
W. E. JOHNSON
H. D. KELSEY
W. W. LAWRENCE
R. D. MADISON
J. H. MARCHANT
L. S. MARKS
A. M. G. MOODY
R. B. SMITH
M. C. STUART

(11) FANS

Appointed December, 1944

M. C. Stuart, *Chairman*
Theodore Baumeister
C. A. Booth
W. H. Carrier
Thomas Chester
E. D. Curley
S. H. Downs
B. K. Erdoss
J. J. Grob
H. F. Hagen
F. H. Jenkins
W. W. Lawrence
R. D. Madison
L. S. Marks

(12) CONDENSERS, WATER HEATING, AND COOLING EQUIPMENT

Appointed December, 1918

P. H. Hardie, *Chairman*
C. H. Baker, Jr.
J. F. Grace
D. W. R. Morgan
H. B. Reynolds
P. E. Reynolds

(13) REFRIGERATING SYSTEMS

Appointed December, 1918

Reorganized May, 1939

B. H. Jennings, *Chairman* †
A. C. Buensod
J. C. Consley
R. G. Ewer †
W. F. Jones †
M. A. Nelson †
A. W. Oakley
C. L. Svenson
Frank Zumbro †

(14) EVAPORATING APPARATUS

Appointed December, 1918

B. N. Bump
E. A. Newhall
H. L. Parr
L. C. Rogers

(15) STEAM LOCOMOTIVES

Appointed December, 1918

W. F. Kiesel
H. B. Oatley
G. E. Rhoads
L. K. Sillcox

(16) GAS PRODUCERS

Appointed December, 1918

C. D. Smith

† Official A.S.M.E. representative serving on this committee.

(17) INTERNAL-COMBUSTION ENGINES

Appointed December, 1918

Reorganized May, 1928, March, 1939

Lee Schneitter, *Chairman*
W. L. H. Doyle, *Secretary*
J. C. Barnaby
G. C. Boyer
H. E. Degler
L. B. Jackson
E. J. Kates
E. C. Magdeburger
B. V. E. Nordberg
Russell Pyles
M. J. Reed
W. W. Schettler
O. D. Treiber

(18) HYDRAULIC PRIME MOVERS

Appointed December, 1918

Reorganized October, 1931

S. Logan Kerr, *Chairman*
G. T. Abernathy
C. M. Allen
K. W. Beattie
N. R. Gibson
J. P. Growdon
T. H. Hogg
L. J. Hooper
C. W. Hubbard
D. J. McCormack
L. F. Moody
W. J. Rheingans
G. R. Rich
J. F. Roberts
J. D. Scoville
E. B. Strowger
R. V. Terry
N. S. Van Patter

(19) INSTRUMENTS AND APPARATUS

Appointed December, 1918

W. A. Carter, *Chairman*
C. M. Allen
W. C. Andrae
E. G. Bailey
H. S. Bean
L. J. Briggs
J. D. Davis
K. J. DeJuhasz
R. E. Dillon
F. M. Farmer
J. B. Grumbein
W. W. Johnson
W. H. Kenerson
E. S. Lee
E. L. Lindseth
S. A. Moss
R. J. S. Pigott
E. B. Ricketts
W. A. Sloan
R. B. Smith
I. M. Stein

(20) SPEED, TEMPERATURE AND PRESSURE RESPONSIVE GOVERNORS

Appointed December, 1921

Reorganized February, 1940

Raymond Sheppard, *Chairman*
C. L. Avery
W. L. H. Doyle
Herbert Estrada
S. N. Fiala
W. C. Holmes
P. G. Ipsen
C. E. Kenney
S. Logan Kerr
A. F. Schwendner
H. Steen-Johnson
M. J. Steinberg
H. E. Stickle

(21) DUST SEPARATING APPARATUS

Appointed October, 1934

M. D. Engle, *Chairman*
Ollison Craig, *Secretary*
A. D. Bailey
H. H. Bubar
W. G. Christy
H. O. Croft
J. M. DallaValle
H. O. Danz
H. C. Dohrmann
J. W. Fehnel
H. F. Hagen
P. H. Hardie
C. W. Hedberg
J. H. Leech
H. E. Macomber
H. C. Murphy
B. F. Tillson

(22) GAS TURBINES

Organized October, 1945

J. J. Yellott, *Chairman*
Alan Howard
W. J. King
R. V. Kleinschmidt
T. J. Putz
J. T. Rettaliata
R. Tom Sawyer
R. B. Smith

SPECIAL SUBCOMMITTEE ON CO-ORDINATING CODES FOR PTC COMMITTEES NOS. 9, 10, AND 11

Appointed April, 1944

M. C. Stuart, *Chairman*
Theodore Baumeister
Paul Diserens
J. J. Grob
R. M. Johnson
R. D. Madison

A.S.M.E. Representatives on Other Technical Committees

See also A.S.M.E. Representatives on Other Activities, page RI-9

COMMITTEE ON REDEFINING SO-CALLED STANDARD TON OF REFRIGERATION

Sponsor body: American Society of Refrigerating Engineers

G. B. Bright

COMMITTEE ON GASEOUS FUELS (D-3)

Sponsor body: American Society for Testing Materials

E. X. Schmidt

COAL TESTING CODE COMMITTEE

Joint sponsorship with the American Institute of Mining and Metallurgical Engineers

A. R. Mumford

SPECIFICATIONS FOR PRIME MOVER SPEED GOVERNING

Joint sponsorship with the American Institute of Electrical Engineers

C. L. Avery
Herbert Estrada
C. E. Kenney
A. F. Schwendner
Raymond Sheppard
C. R. Soderberg

SAFETY COMMITTEES

Article B6A, Par. 25: The Standing Committee on Safety shall advise the Council on the activities of the Society having to do with engineering and industrial safety, except the activities of the Boiler Code Committee, for which special provision is made.

The first Standing Committee on Safety was appointed in October, 1921.

STANDING COMMITTEE

H. W. Gabor, *Chairman* (1947)
J. R. Connelly, *Vice-Chairman* (1948)
E. R. Granniss (1946)
R. B. Renner (1949)
J. J. Zeitner (1950)

SAFETY CODE FOR ELEVATORS (A17)

* *Joint sponsorship with The American Institute of Architects, and the National Bureau of Standards. Sectional Committee originally organized November, 1922*

Reorganized June, 1940

A.S.M.E. Members (Total personnel, 35)

O. P. Cummings
C. R. Callaway
J. W. Degen †
D. L. Holbrook †
Bassett Jones †
M. B. McLauthlin
W. S. Paine
W. H. Seaquist, *Alternate* †
S. F. Voorhees
H. L. Whittemore

SUBCOMMITTEE CHAIRMEN

Executive Committee, D. J. Purinton
Emergency Elevator Rules, D. J. Purinton
Existing Elevators, D. J. Purinton
Inspectors' Manual, K. A. Colahan
Wire Rope, D. J. Purinton
Working, G. H. Reppert

* Note: All of the safety committees for which the Society is sponsor or joint sponsor, or on which it has representation, are organized under the procedure of the American Standards Association.

† Official A.S.M.E. representative serving on this committee.

SAFETY CODE FOR MECHANICAL POWER TRANSMISSION APPARATUS (B15)

* *Joint sponsorship with the International Association of Industrial Accident Boards and Commissions, and the National Conservation Bureau. Sectional Committee organized February, 1921*

A.S.M.E. Members (Total personnel, 20)

G. M. Naylor, *Chairman* †
P. G. Rhoads, *Secretary*
D. C. Wright †

SAFETY CODE ON COMPRESSED AIR MACHINERY AND EQUIPMENT (B19)

* *Joint sponsorship with the American Society of Safety Engineers—Engineering Section of National Safety Council. Sectional Committee organized May, 1923*

A.S.M.E. Members (Total personnel, 21)

D. L. Royer, *Chairman*
H. D. Edwards
W. J. Graves
R. M. Johnson

SAFETY CODE FOR CONVEYORS AND CONVEYING MACHINERY (B20)

* *Joint sponsorship with the National Conservation Bureau. Sectional Committee originally organized November, 1925, reorganized April, 1937*

A.S.M.E. Members (Total personnel, 46)

D. L. Royer, *Chairman*
N. W. Elmer, *Alternate* †
W. J. Graves
W. G. Hudson
M. A. Kendall †
William Moeller
P. T. Onderdonk
C. G. Pfeiffer
R. B. Renner
F. J. Shepard, Jr.
J. G. Wheatley

SUBCOMMITTEE CHAIRMEN

No. 1 on All Types of Chain Conveyors, Belt Conveyors, Belt Elevators Including Steel Belt, and Screw, Track or Scraper Conveyors, C. G. Pfeiffer
No. 2 on Gravity Conveyors and Chutes, Live Roll Conveyors, H. G. Dalton
No. 3 on Cable-Operated and Cable Flight Conveyors and Cableways, R. McA. Keown
No. 4 on Air, Steam, or Liquid Conveyors, J. J. McNulta
No. 5 on Tiering, Piling, and Stacking Conveyors, J. G. Wheatley

SAFETY CODE FOR CRANES, DERRICKS AND HOISTS (B30)

* *Joint sponsorship with U.S. Navy Department, Bureau of Yards and Docks. Sectional Committee organized November, 1926*

A.S.M.E. Members (Total personnel, 45)

J. C. Wheat, *Chairman*
Lewis Price †
F. H. Schwerin
R. H. White †
H. L. Whittemore

SUBCOMMITTEE CHAIRMAN

Executive Committee, J. C. Wheat

A.S.M.E. Representatives on Other Safety Committees

See also A.S.M.E. Representatives on Other Activities, page RI-9

SAFETY CODE FOR ABRASIVE WHEELS (B7)

** Sponsor bodies: Grinding Wheel Manufacturers Association of United States and Canada, and International Association of Industrial Accident Boards and Commissions*

J. W. STREET

SAFETY CODE FOR CONSTRUCTION WORK (A10)

** Sponsor bodies: The American Institute of Architects, and National Safety Council*

(To be appointed)

CO-OPERATION WITH OTHER ENGINEERING SOCIETIES

Committee of American Society of Safety Engineers—Engineering Section of National Safety Council

H. L. MINER

ASA SAFETY CODE CORRELATING COMMITTEE

H. W. GABOR J. J. ZEITNER, *Alternate*

SAFETY CODE FOR EXHAUST SYSTEMS (Z9)

** Sponsor body: International Association of Industrial Accident Boards and Commissions*

(To be appointed)

SAFETY CODE FOR FLOOR AND WALL OPENINGS, RAILINGS AND TOE BOARDS (A12)

** Sponsor body: National Safety Council*

A. E. WINDLE

SAFETY CODE FOR FORGING AND HOT METAL STAMPING (B24)

** Sponsor bodies: American Drop Forging Institute, and National Safety Council*

(To be appointed)

SAFETY CODE FOR LADDERS (A14)

** Sponsor body: American Society of Safety Engineers—Engineering Section of National Safety Council*

H. C. HOUGHTON

SAFETY CODE FOR LAUNDRY MACHINERY AND OPERATION (Z8)

** Sponsor bodies: American Institute of Laundering, International Association of Governmental Labor Officials, and National Association of Mutual Casualty Companies*

E. J. CARROLL

SAFETY CODE FOR LIGHTING FACTORIES, MILLS, AND OTHER WORK PLACES (A11)

** Sponsor body: Illuminating Engineering Society*

A. W. LUCE

LOW VOLTAGE ELECTRICAL HAZARDS

Special Committee of the American Society of Safety Engineers—Engineering Section of National Safety Council

(To be appointed)

SAFETY CODE FOR MECHANICAL REFRIGERATION (B9)

** Sponsor body: American Society of Refrigerating Engineers*

O. A. ANDERSON
E. W. GALLENKAMP
W. F. JONES
A. W. OAKLEY, *Alternate*

PANEL OF CONSULTANTS TO ADVISE THE MERCHANT MARINE COUNCIL AT U.S. COAST GUARD HEADQUARTERS, WASHINGTON, D.C.

D. S. JACOBUS

SAFETY CODE FOR PAPER AND PULP MILLS (P1)

** Sponsor body: National Safety Council*

R. L. WELDON

SAFETY CODE FOR POWER PRESSES AND FOOT AND HAND PRESSES (B11)

** Sponsor body: National Safety Council*

(To be appointed)

SAFETY CODE FOR PREVENTION OF DUST EXPLOSIONS (Z12)

** Sponsor bodies: National Fire Protection Association, and U.S. Department of Agriculture*

R. M. FERRY
W. S. REARICK, *Alternate*

SAFETY CODE FOR PROTECTION OF HEADS, EYES, AND RESPIRATORY ORGANS OF INDUSTRIAL WORKERS (Z2)

** Sponsor body: National Bureau of Standards*

T. A. WALSH, JR.
T. F. HATCH, *Alternate*

SAFETY CODE FOR PROTECTION OF INDUSTRIAL WORKERS IN FOUNDRIES (B8)

H. M. LANE

SAFETY IN QUARRY OPERATIONS (M28)

** Sponsor body: National Safety Council*

REDFIELD PROCTOR

SAFETY CODE FOR RUBBER MACHINERY (B28)

** Sponsor bodies: International Association of Industrial Accident Boards and Commissions and National Safety Council*

E. S. AULT

SPECIFICATIONS AND METHOD OF TEST FOR SAFETY GLASS (Z26)

** Sponsor bodies: National Bureau of Standards and National Conservation Bureau*

T. A. WALSH, JR.

SAFETY CODE FOR TEXTILES (L1)

** Sponsor body: National Safety Council*

M. A. GOLRICK, JR.

SAFETY CODE FOR VENTILATION (Z5)

** Sponsor body: American Society of Heating and Ventilating Engineers*

(To be appointed)

SAFETY CODE FOR WALKWAY SURFACES (A22)

** Sponsor bodies: The American Institute of Architects, and American Society of Safety Engineers—Engineering Section of National Safety Council*

G. K. PALSGROVE

SAFETY CODE FOR WORK IN COMPRESSED AIR (Z28)

** Sponsor body: International Association of Industrial Accident Boards and Commissions*

L. J. EIBSEN

SPONSORING COMMITTEE FOR THE CENTER FOR SAFETY EDUCATION

(Joint activity of New York University and National Conservation Bureau)

Sponsor body: Association of Casualty and Surety Executives

E. R. GRANNISS

BOILER CODE COMMITTEES

ARTICLE B6A, PAR. 26: The Special Committee on Boiler Code shall, under the direction of the Council, have supervision of all the activities of the Society in connection with the A.S.M.E. Codes for Pressure Vessels, including the interpretations of these codes.

The first Special Committee on Boiler Code was organized in September, 1911.

MAIN COMMITTEE

H. B. OATLEY, *Chairman*
H. E. ALDRICH, *Vice-Chairman*
D. S. JACOBUS, *Honorary Chairman*
C. A. ADAMS
T. B. ALLARDICE
H. C. BOARDMAN
P. R. CASSIDY
R. E. CECIL
A. J. ELY
V. M. FROST
W. P. GERHART
W. D. HALSEY
W. F. HESS
T. McL. JASPER
C. O. MYERS
C. W. OBERT
JAMES PARTINGTON
D. B. ROSSHEIM
D. L. ROYER
WALTER SAMANS
J. W. TURNER
S. K. VARNES
A. C. WEIGEL
F. S. G. WILLIAMS

J. W. SHIELDS, *Secretary*
M. JURIST, *Assistant Secretary*

Honorary Members

W. H. BOEHM
W. F. DURAND
E. R. FISH
C. E. GORTON
A. M. GREENE, JR.
W. G. HUMPTON
C. L. HUSTON
W. F. KIESEL, JR.
J. O. LEECH
M. F. MOORE
I. E. MOULTROP
H. LEROY WHITNEY

CONFERENCE COMMITTEE

A. H. AGATON, California
T. R. ARCHER, Delaware
M. L. BLAIR, Arkansas
B. M. BOOK, Pennsylvania
A. C. BOZEMAN, Knoxville, Tenn.
J. N. BRIGGS, Toronto, Can.
C. M. BRITAIN, Seattle, Wash.
H. S. BRUNSON, Minnesota
L. CARLTON, Texas
A. J. CLAY, Memphis, Tenn.
D. J. CODY, Kansas City, Mo.
A. L. COLBY, Louisiana
CLIFF CUMMINGS, Tulsa, Okla.
R. H. DALRYMPLE, Utah
G. W. DEAN, Michigan
M. A. EDGAR, Wisconsin
W. H. FURMAN, New York
GERALD GEARON, Chicago, Ill.
MATTHEW GIBSON, Maryland
J. J. GRAY, Nova Scotia, Can.
C. W. HARNESS, Iowa
S. E. HEDGES, Canal Zone
R. C. JOUGHIN, Tampa, Fla.
D. H. KAHLOW, Washington
H. K. KUGEL, District of Columbia
J. E. LEDDY, New Orleans, La.
E. C. LUSTER, Miami, Fla.
C. E. MCGINNIS, Los Angeles, Calif.
C. O. MANN, Indiana
W. H. MAYHEW, Saskatchewan, Can.
D. P. MILLER, Nebraska
H. H. MILLS, Detroit, Mich.
J. A. MURDOCK, Massachusetts
R. M. MURRAY, Rhode Island
W. L. NEWTON, Oklahoma
L. C. PEAL, Nashville, Tenn.
A. C. RASMUSSEN, Omaha, Neb.
THEO. REYNOLDS, Quebec, Can.
CHARLES SATTLER, West Virginia
E. K. SAWYER, Maine
J. F. SCOTT, New Jersey
ROBT. SCOTT, Alberta, Can.
F. H. SHUFORD, North Carolina
F. W. SMITH, Oregon
WM. E. SMITH, Hawaiian Islands
R. A. STEWART, Manitoba, Can.
M. A. TRUE, St. Louis, Mo.
E. W. WAGNER, Ohio
T. McL. JASPER
J. J. KANTER
H. J. KERR
A. B. KINZEL
V. T. MALCOLM
R. F. MILLER
N. L. MOCHEL
M. S. NORTHUP
E. L. ROBINSON
D. B. ROSSHEIM
A. P. SPOONER
S. K. VARNES
A. E. WHITE

EXECUTIVE COMMITTEE

D. S. JACOBUS, *Chairman*
H. E. ALDRICH, *Vice-Chairman*
H. C. BOARDMAN
A. J. ELY
V. M. FROST
H. B. OATLEY
C. W. OBERT
JAMES PARTINGTON

SUBCOMMITTEES

BOILERS OF LOCOMOTIVES

JAMES PARTINGTON, *Chairman*
J. M. HALL
H. G. MILLER
H. B. OATLEY

CARE OF STEAM BOILERS AND OTHER PRESSURE VESSELS IN SERVICE

F. M. GIBSON, *Chairman*
D. C. CARMICHAEL
V. M. FROST
J. R. GILL
FRANK HENRY
J. A. HUNTER
H. J. KERR
P. B. PLACE
S. T. POWELL
C. W. RICE
J. B. ROMER
W. C. SCHROEDER
F. G. STRAUB

CODE SYMBOL STAMPS

C. O. MYERS, *Chairman*
H. E. ALDRICH
W. D. HALSEY

CO-ORDINATION

V. M. FROST, *Chairman*
W. D. HALSEY
H. B. OATLEY
C. W. OBERT

FERROUS MATERIALS

E. C. CHAPMAN, *Chairman*
J. G. ALTHOUSE
A. B. BAGSAR
L. D. BURRITT
C. L. CLARK
H. J. FRENCH
M. B. HIGGINS
A. HURTGEN

HEATING BOILERS

J. W. TURNER, *Chairman*
C. E. BRONSON
T. D. CASSERLY
J. A. DARTS
WM. FERGUSON
L. N. HUNTER

MATERIAL SPECIFICATIONS

P. R. CASSIDY, *Chairman*
E. H. DAVIDSON
W. P. GERHART
P. J. SMITH
T. G. STITT
A. C. WEIGEL

MINIATURE BOILERS

J. W. TURNER, *Chairman*
WM. FERGUSON
W. H. FURMAN
E. W. MEARS
J. G. WHEATLEY

NONFERROUS MATERIALS

H. B. OATLEY, *Chairman*
W. F. BURCHFIELD
H. L. BURGHOFF
F. W. DAVIS
J. R. FREEMAN, JR.
W. P. KLIMENT
N. L. MOCHEL
R. L. TEMPLIN

POWER BOILERS

H. E. ALDRICH, *Chairman*
T. B. ALLARDICE
P. R. CASSIDY
V. M. FROST
W. D. HALSEY
D. L. ROYER
A. C. WEIGEL
E. J. WISEMAN

RULES FOR INSPECTION

D. L. ROYER, *Chairman*
T. B. ALLARDICE
W. H. FURMAN
E. B. VAN SANT
GUSTAVE WELTER

SPECIAL DESIGN

D. B. WESSTROM, *Chairman*
H. C. BOARDMAN
R. E. CECIL
T. W. GREENE
E. C. KORTEN

F. L. PLUMMER
D. B. ROSSHEIM
E. O. WATERS
F. S. G. WILLIAMS

UNFIRED PRESSURE VESSELS

WALTER SAMANS, *Chairman*
H. C. BOARDMAN
R. E. CECIL
PAUL DISERENS
A. J. ELY
W. D. HALSEY
K. V. KING
D. B. ROSSHEIM
D. B. WESSTROM

WELDING

Members of A.S.M.E. Boiler Code Committee

JAMES PARTINGTON, *Chairman*
W. B. BUNN
O. R. CARPENTER
E. C. CHAPMAN
J. H. DEPPELER
W. D. HALSEY
J. T. PHILLIPS
K. L. WALKER

Members of Conference Committee of American Welding Society

C. W. OBERT, *Chairman*
C. A. ADAMS
H. C. BOARDMAN
WALTER SAMANS
A. C. WEIGEL

SPECIAL COMMITTEES

APPROVAL OF NEW MATERIALS

C. A. ADAMS, *Chairman*

BOLTED FLANGED CONNECTIONS

F. S. G. WILLIAMS, *Chairman*

CLAD VESSELS

S. K. VARNES, *Chairman*

DISHED HEADS

H. C. BOARDMAN, *Chairman*

FAILURE OF SPHERICAL HYDROGEN STORAGE TANK

F. L. NEWCOMB, *Chairman*

FEEDWATER

C. W. RICE, *Chairman*

JACKETED VESSELS

WALTER SAMANS, *Chairman*

LAYER VESSELS

H. C. BOARDMAN, *Chairman*

LOW TEMPERATURE VESSELS

C. W. OBERT, *Chairman*

OPENINGS AND REINFORCEMENTS

F. S. G. WILLIAMS, *Chairman*

PLATE SPECIFICATIONS FOR BOILERS AND UNFIRED PRESSURE VESSELS

P. R. CASSIDY, *Chairman*

PROCEDURE

H. E. ALDRICH, *Chairman*

RADIOGRAPHIC EXAMINATION OF WELDED JOINTS

C. A. ADAMS, *Chairman*

REVISION OF SECTION VIII OF THE A.S.M.E. BOILER CODE

E. R. FISH, *Chairman*

SAFETY VALVE REQUIREMENTS

H. B. OATLEY, *Chairman*

STEEL FLANGES FOR LOW PRESSURES AND LOW TEMPERATURES

(To be appointed)

API-ASME COMMITTEE ON UNFIRED PRESSURE VESSELS

WALTER SAMANS, *Chairman*

A.S.M.E. Representatives

H. C. BOARDMAN
R. E. CECIL
D. S. JACOBUS
T. McL. JASPER
JAMES PARTINGTON

A.P.I. Representatives

A. J. ELY
M. B. HIGGINS
K. V. KING
WALTER SAMANS
T. D. TIFFT

THE WOMAN'S AUXILIARY TO THE A.S.M.E.

The Woman's Auxiliary to the A.S.M.E. was organized on May 10, 1923, and its Constitution and By-Laws was approved by the Council of the A.S.M.E. on October 27, 1924. The objects of the Auxiliary are to render service to all that pertains to the interest of the profession of mechanical engineering; to co-operate with any committees of the A.S.M.E.; to assist the sons and daughters of the members of the Society or worthy students of mechanical engineering in obtaining scholarships; and to promote any other objects consistent with the aims or objects of the A.S.M.E.

NATIONAL OFFICERS

President, MRS. J. NOBLE LANDIS
First Vice-President, MRS. JUSTIN J. MCCARTHY
Second Vice-President, MRS. EARL B. SMITH
Third Vice-President, MRS. D. K. WRIGHT
Fourth Vice-President, MRS. P. M. KING
Fifth Vice-President, MRS. F. M. FARMER
Recording Secretary, MRS. RANDALL B. PURDY
Corresponding Secretary, MRS. L. W. BENNETT
Treasurer, MRS. CHARLES E. GUS

STANDING COMMITTEE CHAIRMEN

Courtesy, MRS. CROSBY FIELD
Student Loan, MRS. F. M. GIBSON
Membership, MRS. G. E. HAGEMANN
Publicity, MRS. C. H. KENT
Sections, MRS. G. W. FARNY
Custodian, MRS. WALDO M. MCKEE

COUNCIL REPRESENTATIVES

ROBERT M. GATES
ALEX D. BAILEY

OFFICERS OF LOCAL SECTIONS

CLEVELAND

Chairman, MRS. D. K. WRIGHT

LOS ANGELES

Chairman, MRS. RAYMOND G. ROSHONG

METROPOLITAN

Chairman, MRS. G. W. NIGH
First Vice-Chairman, MRS. G. J. NICASTRO
Second Vice-Chairman, MRS. C. HIGBIE YOUNG
Third Vice-Chairman, MRS. A. R. CULLIMORE
Recording Secretary, MRS. W. L. ILIFF
Corresponding Secretary, MRS. C. F. KAYAN
Treasurer, MRS. A. W. ANDERSON

PHILADELPHIA

Chairman, MRS. F. W. MILLER

AWARDS

The following paragraphs deal with the medals, awards, scholarships, and loan funds which come within the jurisdiction of the A.S.M.E. Other awards available to Student Members are listed in *Mechanical Engineering*, February, 1938, page 183. The Society also participates with other engineering societies in a number of joint awards. Further details concerning all the awards may be obtained from the headquarters of the Society.

Honorary Membership, to which persons of acknowledged professional eminence are elected by unanimous vote of the Council under the provisions of the By-Laws and Rules. A list of honorary members is given on page RI-43.

Life Membership, which may be conferred by the Council for distinguished service to the Society; or secured by a member by payment for an annuity in accordance with the provisions of the By-Laws.

A.S.M.E. Medal, established by the Society in 1920 to be presented, together with an engraved certificate, for distinguished service in engineering and science. May be awarded for general service in science having possible application in engineering.

Holley Medal, instituted and endowed in 1924 by George I. Rockwood, Past Vice-President of the Society, to be bestowed, together with an engraved certificate, for some great and unique act of genius of engineering nature that has accomplished a great and timely public benefit.

Worcester Reed Warner Medal, established in 1930, provision for which was made in the will of Worcester Reed Warner, Honorary Member of the Society, is a gold medal to be bestowed, together with an engraved certificate, for an outstanding contribution to permanent engineering literature.

Melville Prize Medal for Original Work, established in 1914 by the bequest of Rear-Admiral George W. Melville, Honorary Member and Past-President of the Society, to be presented, together with an engraved certificate, for an original paper or thesis of exceptional merit, presented to the Society by a member for discussion and publication during the calendar year previous to the year of award, to encourage excellence in papers. Only papers of single authorship are eligible. The medal may be presented annually.

Spirit of St. Louis Medal, established by an endowment fund created in 1929 by citizens of St. Louis, Mo., to be awarded for meritorious service in the advancement of aeronautics. This medal will be awarded at the discretion of the Council of the Society at approximately three-year periods upon the recommendation of its Board of Honors and Awards.

Spirit of St. Louis Junior Award, established in 1938 by an endowment fund created by the General Committee for the 1935 Aeronautic Meeting in St. Louis; a cash award of $50 and certificate made every three years, for the best paper on an aeronautic subject presented at any A.S.M.E. meeting during the three-year period either personally by the author (a Junior Member of the Society under thirty years of age) or by a Junior Member designated by him, and submitted to the Board of Honors and Awards within a reasonable period (to be determined by the Committee) after its initial presentation.

Pi Tau Sigma Medal Award, established in 1938, endowed by Pi Tau Sigma, the national honorary mechanical engineering fraternity, to be presented annually, together with an engraved certificate, to a young mechanical engineer for outstanding achievement in his profession within the ten years after graduation from a regular four-year mechanical engineering course of a recognized American college or university. Any mechanical engineering graduate, not more than thirty-five years of age, whose achievement has been all or in part in any field including industrial, educational, political, research, civic, etc., is eligible.

Junior Award, annual cash award of $50, established in 1914, from a fund created by Henry Hess, Past Vice-President of the Society, to be presented, together with an engraved certificate, for the best paper or thesis submitted during the calendar year previous to the year of award by a Junior Member not more than thirty years of age. Papers of joint authorship are eligible.

Charles T. Main Award, annual cash award of $150, established in 1919 from a fund created by Charles T. Main, Past-President of the Society, to be awarded, together with an engraved certificate, to a Student Member of the Society, for the best paper within the general subject of the influence of the profession upon public life. The exact subject is assigned by the Board of Honors and Awards, subject to the approval of the Council, and is announced each year through the Honorary Chairmen of the Student Branches.

Student Awards, two annual cash awards of $25 each, established in 1914, from a fund created by Henry Hess, Past Vice-President of the Society, to be presented, together with engraved certificates, for the best papers or theses submitted by Student Members. The awards for 1932 and subsequent years have been given, one for undergraduate and the other for postgraduate work.

SCHOLARSHIPS AND LOAN FUNDS

Max Toltz: Loan Fund of $15,000 established by Major Max Toltz, former member of the Council of the Society, the income to be used for assistance to Student Members.

John R. Freeman: Fund of $25,000 established in 1926 by John R. Freeman, Past-President of the Society, the income to be used for travel scholarships and research.

Woman's Auxiliary: Educational Loan Fund offered by the Woman's Auxiliary to the Society to assist sons and daughters of members or worthy students of mechanical engineering. Calvin W. Rice Memorial Scholarship Fund for students in mechanical engineering from South America.

RECIPIENTS OF AWARDS

The names of the recipients of the different awards to date are given in the following lists, together with the dates of presentation, and the services or papers for which the awards were made. There were no awards for the years not listed.

A.S.M.E. Medal

1921 Hjalmar Gotfried Carlson, in recognition of the services rendered the Government because of his invention and part in the production of 20,000,000 Mark III drawn steel booster casings used principally as a component of 75-mm high explosive shells, but also used extensively in gas shells and bombs

1922 Frederick Arthur Halsey, for his paper describing the premium system of wage payments presented before the Society at the Providence Meeting in 1891, as the adoption of the methods there proposed has had a profound effect toward harmonizing the relations of worker and employer

1923 John Ripley Freeman, for his eminent service in engineering and manufacturing by his meritorious work in fire prevention and the preservation of property

1926 R. A. Millikan, in recognition of his contributions to science and engineering

1927 Wilfred Lewis, for his contributions to the design and construction of gear teeth

1928 Julian Kennedy, for his services and contributions to the iron and steel industry

1929 William LeRoy Emmet, for his contributions in the development of the steam turbine, electric propulsion of ships, and other power-generating apparatus

1931 Albert Kingsbury, for his research and development work in the field of lubrication

1933 Ambrose Swasey, for his contributions to the advancement of the engineering profession and for his part in the development of the turret lathe and the astronomical telescope

1934 Willis H. Carrier, in recognition of his research and development work in air-conditioning

1935 Charles T. Main, for distinguished achievements in the textile and other industries, in engineering education, and for eminent service to the engineering profession

1936 Edward Bausch, for meritorious mechanical developments in the field of optics

1937 Edward P. Bullard, for outstanding leadership in the development of station-type machine tools

1938 Stephen J. Pigott, for outstanding leadership in marine propulsion and construction

1939 James E. Gleason, for service to the cause of safer and better transportation

1940 Charles F. Kettering, for outstanding inventions and research

1941 THEODOR VON KÁRMÁN, for his brilliance as a teacher, his researches in elasticity and many fields of physics and mechanics, and his distinguished leadership in the fields of aerodynamics and aircraft design
1942 E. G. BAILEY, for achievement and leadership in steam and combustion engineering
1943 LEWIS K. SILLCOX, pre-eminent learned technologist—lover of wisdom—inspirer of men
1944 EDWARD G. BUDD, for the development of stainless-steel railway passenger cars
1945 WILLIAM F. DURAND, world renowned authority in hydrodynamic and aerodynamic science and its practical application; great teacher with an inspiring character and a unique capacity for lucidity and simplicity in imparting highly technical material; trusted adviser to Government in the solution of many intricate scientific problems in peace and during two world wars

HOLLEY MEDAL

1924 HJALMAR GOTFRIED CARLSON, for his inventions and processes which made possible the timely production of drawn steel booster casings for artillery ammunition, thereby aiding victory in World War I (diploma in recognition of achievements presented in 1921)
1927 ELMER AMBROSE SPERRY, for achievements and inventions that have advanced the naval arts, including the gyroscope that has freed navigation from the dangers of the fluctuating magnetic compass
1929 BARON CHUZABURO SHIBA, for his contributions to knowledge through fundamental research, including the field of aerodynamics, by the development of ultra-rapid kinematographic methods
1934 IRVING LANGMUIR, for his contributions to science and engineering, including the development of gas-filled incandescent lamps, thoriated filament for thermionic emission, atomic hydrogen welding, phase control operation of the thyratron tube, and fundamental research in oil films
1936 HENRY FORD, for revolutionary influence through invention and practice on transportation and on mass production methods in manufacturing
1937 FREDERICK G. COTTRELL, for pre-eminent public service—the invention of electric precipitation—advancement of the science of gas liquefaction—gifts for engineering research
1938 FRANCIS HODGKINSON, for meritorious services in the development of the steam turbine
1939 CARL E. JOHANSSON, in recognition of his pioneer work in the development of basic measuring gages
1940 EDWIN HOWARD ARMSTRONG, for his leadership in the field of radio communication
1941 JOHN C. GARAND, for the invention and development of the semi-automatic rifle, which has been adopted by the U.S. Army as the U.S. Rifle, Caliber .30, M1, an outstanding contribution to our national defense
1942 ERNEST O. LAWRENCE, for originating the cyclotron, a unique invention for producing high-speed electrified particles, and for adapting it to research in physics, chemistry, medicine, and the properties of engineering materials
1943 VANNEVAR BUSH, for machines used in easing applied mathematics from computational barriers
1944 CARL L. NORDEN, for the invention and development of the Norden bombsight and other valuable devices which should hasten the peace
1945 SANFORD A. MOSS, for his many contributions over a long period of years to the development of centrifugal compressors, particularly as related to the highly successful application of turbosuperchargers to internal-combustion engines in the field of aeronautics

WORCESTER REED WARNER MEDAL

1933 DEXTER S. KIMBALL, for his contributions to efficiency in management as exemplified by his recently revised "Principles of Industrial Organization" and by his many articles, engineering society papers, and public addresses
1934 RALPH E. FLANDERS, for his contributions to a better understanding of the relationship of the engineer to economic problems and social trends as exemplified by the many papers which he has presented
1935 STEPHEN TIMOSHENKO, for his contributions to the theory of the design of elastic structures and the treatment of dynamics of moving machinery
1936 CHARLES M. ALLEN, for his early and continued hydraulic laboratory work and for the permanent value of the papers on his development of methods of testing large hydraulic turbine installations
1937 CLARENCE F. HIRSHFELD, for his research and contributions to the theory and practice of heat-power engineering as exemplified by books and papers
1938 LAWFORD H. FRY, for contributions relating to improved locomotive boiler design and utilization of better materials in railway equipment
1939 RUPEN EKSERGIAN, for influential papers of permanent value in A.S.M.E. Transactions
1940 WILLIAM BENJAMIN GREGORY, for distinguished work in hydraulic engineering, which has been the basis for many engineering papers
1941 RICHARD VYNNE SOUTHWELL, for his many distinguished services to engineering and science through papers and publications in many fields, including aeronautics, theory of structures, elasticity, and hydrodynamics
1942 FRED H. COLVIN, for his contributions to both technical advancement and improvement in management in the metal-working industries, as influenced by more than fifty years of articles and books—particularly American Machinists' Handbook
1943 IGOR I. SIKORSKY, for contributions inspiring creative engineering, especially in aeronautics
1944 EARLE BUCKINGHAM, for original contributions to engineering literature
1945 JOSEPH M. JURAN, for his outstanding contributions to the problem of quality control in mass production and his splendid records of such work as are contained in his books "Bureaucracy, A Challenge to Better Management" and "Management of Inspection and Quality Control"

MELVILLE PRIZE MEDAL FOR ORIGINAL WORK

1927 LEON P. ALFORD, "Laws of Manufacturing Management"
1929 JOSEPH W. ROE, "Principles of Jig and Fixture Practice"
1930 HERMAN DIEDERICHS and WILLIAM D. POMEROY, "The Occurrence and Elimination of Surge or Oscillating Pressure in Discharge Lines From Reciprocating Pumps"
1931 ARTHUR E. GRUNERT, "Comparative Performance of a Pulverized-Coal-Fired Boiler Using Bin System and Unit System of Firing"
1932 ALEXEY J. STEPANOFF, "Leakage Loss and Axial Thrust in Centrifugal Pumps"
1933 WILLIAM E. CALDWELL, "Characteristics of Large Hell Gate Direct-Fire Boiler Units"
1935 OSCAR R. WIKANDER, "Draft-Gear Action in Long Trains"
1936 H. A. STEVENS HOWARTH, "The Loading and Friction of Thrust and Journal Bearings With Perfect Lubrication"
1937 ALFRED J. BÜCHI, "Supercharging of Internal-Combustion Engines With Blowers Driven by Exhaust-Gas Turbines"
1938 ALPHONSE I. LIPETZ, "Air Resistance of Railrod Equipment"
1939 LESTER M. GOLDSMITH, "High-Pressure High-Temperature Turbine-Electric Steamship *J. W. Van Dyke*"
1940 CARL A. W. BRANDT, "The Locomotive Boiler"
1941 ROGER V. TERRY, "Development of the Automatic Adjustable-Blade-Type Propeller Turbine"
1942 J. KENNETH SALISBURY, "The Steam-Turbine Regenerative Cycle—An Analytical Approach"
1944 ERNEST L. ROBINSON, "Bursting Tests of Steam-Turbine Disk Wheels"
1945 WILLIAM J. KING, "The Unwritten Laws of Engineering"

SPIRIT OF SAINT LOUIS MEDAL

1929 DANIEL GUGGENHEIM, founder of the Guggenheim Fund for the Promotion of Aeronautics
1932 PAUL LITCHFIELD, for his work in encouraging and sponsoring airship design and construction in this country
1935 WILL ROGERS, for his splendid, constructive, and unselfish work in the achievement of aviation, and the building up of public confidence in aviation through his articles in the press, over the radio, and from the speaker's platform
1938 JAMES H. DOOLITTLE, for meritorious service in the advancement of aeronautics
1941 JOHN E. YOUNGER, for notable contributions to the science of airplane design, particularly in the conception, analysis, and supervision of the development of the fundamental design principles, requirements, and criteria which first assured the success of the pressure-cabin type of high-altitude airplane

1944 George W. Lewis, for leadership in direction and encouragement of aeronautical research, having an extensive influence on aeronautical engineering during the past quarter century

Spirit of Saint Louis Junior Award

1941 Wilbur W. Reaser, "Calculation of the Heat Loss From an Airplane Cabin"
1944 Martin Goland, "The Influence of the Shape and Rigidity of an Elastic Inclusion on the Transverse Flexure of Thin Plates"

Pi Tau Sigma Medal

1938 Wilfrid E. Johnson, for his development work in the field of refrigeration
1939 John I. Yellott, Jr., in recognition of significant achievements in steam-flow research and engineering education; also contributions on "Supersaturated Steam" and "Condensation of Flowing Steam in Diverging Nozzles"
1940 George A. Hawkins, for significant achievements in high-pressure steam research and engineering education
1941 R. Hosmer Norris, for outstanding achievement in mechanical engineering, particularly in the heat-transfer field
1942 John T. Rettaliata, for outstanding achievement in mechanical engineering

Junior Award

1915 Ernest O. Hickstein, "Flow of Air Through Thin Plate Orifices"
1916 L. M. McMillan, "The Heat Insulating Properties of Commercial Steam-Pipe Coverings"
1919 E. D. Whalen, "Properties of Airplane Fabrics"
1921 S. Logan Kerr, "Moody Ejector Turbine"
1922 R. H. Heilman, "Heat Losses From Bare and Covered Wrought-Iron Pipe at Temperatures up to 800 Degrees Fahrenheit"
F. L. Kallam, "Preliminary Report on the Investigation of the Thermal Conductivity of Liquids"
1923 S. S. Sanford and Sabin Crocker, "The Elasticity of Pipe Bends"
1924 R. H. Heilman, "Heat Losses Through Insulating Material"
1925 Gilbert S. Schaller, "An Investigation of Seattle as a Location for a Synthetic Foundry Industry"
1927 William M. Frame, "Stresses Occurring in the Walls of an Elliptical Tank Subjected to Low Internal Pressure"
1928 M. D. Aisenstein, "A New Method of Separating the Hydraulic Losses in a Centrifugal Pump"
1929 Arthur M. Wahl, "Stresses in Heavy, Closely Coiled Helical Springs"
1930 Ed Sinclair Smith, "Quantity-Rate Fluid Meters"
1931 M. K. Drewry, "Radiant-Superheater Developments"
1932 Edmond M. Wagner, "Frictional Resistance of a Cylinder Rotating in a Viscous Fluid Within a Coaxial Cylinder"
1933 Townsend Tinker, "Surface Condenser Design and Operating Characteristics"
1934 John I. Yellott, Jr., "Supersaturated Steam"
1935 Stanley J. Mikina, "Effect of Skewing and Pole Spacing on Magnetic Noise in Electrical Machinery"
1936 Harwood F. Mullikan, Jr., "Evaluation of Effective Radiant Heating Surface and Application of the Stefan-Boltzman Law to Heat Absorption in Boiler Furnaces"
1937 Leslie J. Hooper, "American Hydraulic-Laboratory Practice"
1938 Arthur C. Stern, "Separation and Emission of Cinders and Fly Ash"
1940 Robert E. Newton, "A Photoelastic Study of Stresses in Rotary Disks"
1941 John T. Rettaliata, "The Combustion Gas Turbine"
1942 Winston M. Dudley, "Analysis of Longitudinal Motions in Trains of Several Cars"
1943 Troels Warming, "Power Pulsation Between Synchronous Generators"
1945 Bruce E. Del Mar, "Presentation of Centrifugal-Compressor Performance in Terms of Nondimensional Relationships"

Charles T. Main Award

1925 Clement R. Brown, Catholic University of America. Subject: "The Influence of the Locomotive on the Unity of the United States"
1926 W. C. Saylor, Johns Hopkins University. Subject: "The Effect of the Cotton Gin Upon the History of the United States During Its First Seventy Years"
1927 No Award. Subject: "Scientific Management and Its Effect Upon the Industries"
1928 Robert M. Meyer, Newark College of Engineering. Subject: "Scientific Management and Its Effect Upon Manufacturing"
1929 No Award. Subject: "The Influence of Engineering on Farm Production"
1930 Jules Podnossoff, Polytechnic Institute of Brooklyn. Subject: "The Value of the Safety Movement in the Industries"
1931 Robert E. Klise, University of Michigan. Subject: "Interchangeability—Its Development and Significance in Industry"
1932 Marshall Anderson, University of Michigan. Subject: "Apprenticeship and Vocational Training"
1933 George D. Wilkinson, Jr., Newark College of Engineering. Subject: "Progress in the Prevention of Smoke and Atmospheric Pollution"
1934 Philip P. Self, Colorado State College. Subject: "Air Conditioning—Its Practicability and Relation to Public Welfare"
1935 G. Lowell Williams, Lafayette College. Subject: "Coordinated Transportation—An Economic Comparison of Railroad, Bus, Truck, Water, and Air Transportation for Long and Short Haul"
1936 No Award. Subject: "Developments in the Generation and Distribution of Power and Their Effect Upon the Consumer"
1937 Allan P. Stern, Case School of Applied Science. Subject: "The Influence of the Introduction of Labor Saving Machinery Upon Employment in the United States"
1938 Edward W. Connolly, University of Detroit. Subject: "Economic Limitations in Engineering Design, With Concrete Examples"
1939 James R. Bright, Lehigh University. Subject: "The Economics of Investment in New Manufacturing Equipment—With Concrete Cases"
1940 Frank De Pould, Case School of Applied Science. Subject: "What Has Been the Effect of Technological Advance on Employment?"
1941 John J. Balun, University of Detroit. Subject: "The Need and Possibilities of Participation by Engineers in Public Affairs"
1942 Bernard J. Isabella, Case School of Applied Science. Subject: "The Engineer and Preparation for the Coming Peace"
1943 Mitchell C. Kazen, University of Detroit. Subject: "Government as Affected by Engineering"
1944 Fred M. Piaskowski, University of Detroit, "A Case Study of Labor-Management Co-operation"
1945 Jack Drandell, Southern Methodist University, "Engineering in the New South"

Student Award

1916 Boynton M. Green, Stanford University, "Bearing Lubrication"
Howard E. Stevens, Rensselaer Polytechnic Institute, "An Investigation of the Dynamic Pressure on Submerged Flat Plates"
M. Adam, Louisiana State University, "The Adaptability of the Internal-Combustion Engine to Sugar Factories and Estates"
1917 H. R. Hammond and C. W. Holmberg, The Pennsylvania State College, "Study of Surface Resistance With Glass as the Transmission Medium"
1919 C. F. Leh and F. G. Hampton, Stanford University, "An Experimental Investigation of Steel Belting"
W. E. Helmick, Stanford University, "An Experimental Investigation of Steel Belting"
1920 Howard G. Allen, Cornell University, "Wire Stitching Through Paper"
1921 Karl H. White, University of Kansas, "Forces in Rotary Motors"
Richard H. Morris and Albert J. R. Houston, University of California, "A Report Upon an Investigation of the Herschel Type of Improved Weir"
1923 Charles F. Olmstead, University of Minnesota, "Oil Burning for Domestic Heating"
H. E. Doolittle, University of California, "The Integrating Gate: A. Device for Gaging in Open Channels"

1924 George Stuart Clark, Stanford University, "Two Methods Used for the Determination of the Gasoline Content of Absorption Oils in Absorption Plants"
L. J. Franklin and Charles H. Smith, Stanford University, "The Effect of Inaccuracy of Spacing on the Strength of Gear Teeth"

1925 Harry Pease Cox, Jr., Rensselaer Polytechnic Institute, "A Study of the Effect of End Shape on the Towing Resistance of a Barge Model"
W. S. Montgomery, Jr., and E. Ray Enders, Jr., The Pennsylvania State College, "Some Attempts to Measure the Drawing Properties of Metals"

1926 R. E. Peterson, University of Illinois, "An Investigation of Stress Concentration by Means of Plaster of Paris Specimens"
Cecil G. Heard, University of Toronto, "Pressure Distribution Over U.S.A. 27 Aerofoil With Square Wing Tips—Model Tests"

1927 Alfred H. Marshall, Princeton University, "Evaporative Cooling"
Roger Irwin Eby, University of Washington, "Measurement of the Angular Displacement of Flywheels"

1928 Clarence C. Franck, Johns Hopkins University, "Condition Curves and Reheat Factors for Steam Turbines"

1929 Frank Vernon Bistrom, University of Washington, "An Investigation of a Rotary Pump"
William Wallace White, University of Washington, "An Investigation of a Rotary Pump"

1930 Gerard Eden Claussen, Polytechnic Institute of Brooklyn, "High-Temperature Oxidation of Steel"
Harold L. Adams and Richard L. Stith, University of Washington, "A Wind Tunnel for Undergraduate Laboratory Experiments"

1931 Jules Podnossoff, Polytechnic Institute of Brooklyn, "Pressure and Energy Distribution in Multi-Stage Steam Turbines Operating Under Varying Conditions"

1932 H. E. Foster, Jr., University of Tennessee, "Factors Affecting Spray Pond Design" (Undergraduate Award)
William A. Mason, Stanford University, "An Experimental Investigation of the Flame Propagation in Internal-Combustion Engines" (Postgraduate Award)

1933 Hugo V. Cordiano, Polytechnic Institute of Brooklyn, "Thermal Analysis of Lithium-Magnesium System of Alloys" (Undergraduate Award)
James A. Ostrand, Jr., Princeton University, "Sudden Enlargement in the Open Channel" (Postgraduate Award)

1934 H. Reynolds Hudson, Georgia School of Technology, "Dynamic Balance and Functional Utility Applied to Automotive Design" (Undergraduate Award)

1935 Charles P. Bacha, Rutgers University, "The Behavior of Metals Subjected to Combined Stress" (Postgraduate Award)
Robert W. Beal, Oregon State College, "Do Lubricating Oils Wear Out?" (Undergraduate Award)

1936 Leon B. Stinson, Oklahoma Agricultural and Mechanical College, "Polymerized Motor Fuels; Their Economic Significance" (Undergraduate Award)
DeWitt D. Barlow, Jr., Princeton University, "The Critical Speeds of Lateral Vibrations of Shafts With Gyroscopic Effects" (Postgraduate Award)

1937 Gino J. Marinelli, Rensselaer Polytechnic Institute, "Investigation of the Towing Resistance of a Model Submarine Hull" (Undergraduate Award)

1938 Marshall C. Long, Princeton University, "An Investigation Into the Angular Characteristics of an Adjustable Blade Current Meter" (Postgraduate Award)
Donald C. McSorley, Michigan State College, "Humidity Insulation" (Undergraduate Award)

1939 David T. James, Michigan State College, "Bells—Concerning Their Tones" (Undergraduate Award)

1940 George W. Shepherd, Jr., Princeton University, "An Automatic Mechanical Control for Synchronizing Prime Movers" (Postgraduate Award)
Edward D. Rowan, Oregon State College, "Powder Metallurgy" (Undergraduate Award)

1941 G. Walker Gilmer, III, University of Florida, "Center of Pressure Characteristics of a Marconi Yacht Sail" (Undergraduate Award)

1942 Arthur W. McClure, Princeton University, "A Specific Speed Analysis of Turbosuperchargers for Aircraft" (Postgraduate Award)
J. Packard Laird, Princeton University, "An Analysis of Motorcycle Behavior" (Undergraduate Award)

1943 William L. Hutton, Princeton University, "The Aerodynamic Development of the Star Sail" (Undergraduate Award)

1944 Nelson B. Hammond, University of Pennsylvania, "An Investigation of Silver Solder Penetration in Brass Joints" (Undergraduate Award)

1945 John W. Erickson, Illinois Institute of Technology, "Increasing the Efficiency of Gas Turbine Cycles" (Undergraduate Award)

Freeman Travel Scholarship

1927	Herbert N. Eaton	1933	H. J. Casey
1928	Blake R. Van Leer	1934	H. J. Casey
1929	Robert T. Knapp	1935	Victor L. Streeter
1931	Reginald Whitaker	1936	Victor L. Streeter
1932	G. Ross Lord		

HONORARY MEMBERS

HONORARY MEMBERS IN PERPETUITY

Alexander Lyman Holley, Founder of the Society. Died 1882.

John Edson Sweet, Founder of the Society. Died 1916.

Henry Rossiter Worthington, Founder of the Society. Died 1880.

DECEASED HONORARY MEMBERS

	ELECTED	DIED
Leon Pratt Alford	1941	1942
Horatio Allen	1880	1889
Lorenzo Allievi	1937	1941
Sir William Arrol	1905	1913
Sir John Audley Frederick Aspinall	1911	1937
William Wallace Atterbury	1925	1935
Sir Benjamin Baker	1886	1907
Edmund Bruce Ball	1939	1944
Johann Bauschinger	1884	1893
Sir Henry Bessemer	1891	1898
Sir Frederick Joseph Bramwell	1884	1903
John Alfred Brashear	1908	1920
Gustave Canet	1900	1908
Andrew Carnegie	1907	1919
Daniel Kinnear Clark	1882	1896
Rudolph Julius Emmanuel Clausius	1882	1888
Hutchinson I. Cone	1936	1941
Sir John Coode	1889	1892
Mortimer Elwyn Cooley	1928	1944
Peter Cooper	1882	1883
Charles de Fréminville	1919	1936
Carl Gustaf Patrick de Laval	1912	1913
Rudolph Diesel	1912	1913
Alex Dow	1936	1942
James Dredge	1886	1906
Victor Dwelshauvers-Dery	1886	1913
Thomas Alva Edison	1904	1931
Alexandre Gustave Eiffel	1889	1923
Marshal Ferdinand Foch	1921	1929
Sir Charles Douglas Fox	1900	1921
John Ripley Freeman	1932	1932
John Fritz	1900	1913
Major General George Washington Goethals	1917	1928
Franz Grashof	1884	1893
Rear Admiral Robert Stanislau Griffin	1920	1933
Otto Hallauer	1882	1883
Charles Haynes Haswell	1905	1907
Nathanael Greene Herreshoff	1921	1938
Friedrich Gustav Herrmann	1884	1907
Gustav Adolph Hirn	1882	1890
Joseph Hirsch	1889	1901
Ira N. Hollis	1928	1930
Robert Woolston Hunt	1920	1923
Benjamin Franklin Isherwood	1894	1915
Albert Kingsbury	1940	1943
Henri Léauté	1891	1916
Erasmus Darwin Leavitt	1915	1916
Henri Le Chatelier	1927	1936
Charles Thomas Main	1939	1943
Anatole Mallet	1912	1919
Charles H. Manning	1913	1919
Rear Admiral George Wallace Melville	1910	1912
George A. Orrok	1936	1944
The Honorable Sir Charles Algernon Parsons	1920	1931

(*Continued*)

DECEASED HONORARY MEMBERS
(Continued)

	ELECTED	DIED
Charles Talbot Porter	1890	1910
Edwin Jay Prindle	1939	1942
Auguste C. E. Rateau	1919	1930
Sir Edward J. Reed	1882	1906
Franz Reuleaux	1882	1905
Calvin Winsor Rice	1931	1934
Palmer C. Ricketts	1931	1934
Henri Adolphe-Eugene Schneider	1882	1898
Charles M. Schwab	1918	1939
James A. Seymour	1940	1943
C. William Siemans	1882	1883
Viscount Ei-ichi Shibusawa	1929	1931
Aurel Stodola	1941	1942
Ambrose Swasey	1916	1937
Elihu Thomson	1930	1937
Henry Robinson Towne	1921	1924
Henri Tresca	1882	1885
Edward N. Trump	1943	1944
William Cawthorne Unwin	1898	1933
Samuel Matthews Vauclain	1920	1940
Henry Hague Vaughan	1939	1942
Oskar von Miller	1912	1934
Francis A. Walker	1886	1897
Worcester Reed Warner	1925	1929
George Westinghouse	1897	1914
Sir William Henry White	1900	1913
Sir Alfred Fernandez Yarrow	1914	1932

LIVING HONORARY MEMBERS

	ELECTED
William Lamont Abbott	1940
Charles M. Allen	1944
Robert W. Angus	1940
William L. Batt	1942
Francis Blossom	1943
Rear Admiral Harold Gardiner Bowen	1945
Ralph Budd	1943
Lieutenant General Levin H. Campbell, Jr.	1944
Willis H. Carrier	1942
Gano Dunn	1944
William Frederick Durand	1934
Charles E. Ferris	1942
Arthur M. Greene, Jr.	1940
Herbert Clark Hoover	1925
Clarence Decatur Howe	1941
Jerome C. Hunsaker	1942
Dugald Caleb Jackson	1945
David Schenck Jacobus	1934
Masawo Kamo	1929
Dexter Simpson Kimball	1939
Vice-Admiral Emory S. Land	1944
Lieutenant General Andrew G. L. McNaughton	1943
Sir (Standen) Leonard Pearce	1944
Grande Ufficiale Ing. Pio Perrone	1920
Andrey Abraham Potter	1945
Harry R. Ricardo	1942
Vice-Admiral Samuel Murray Robinson	1941
Sir William Arthur Stanier	1945
Major General William H. Tschappat	1938
Right Honorable Lord Weir	1920
Major General Charles Macon Wesson	1941
Wong Wen-hao	1945
Orville Wright	1918
Roy V. Wright	1943

PAST-PRESIDENTS

Dates in parentheses denote year of death.

Alexander Lyman Holley, *Chairman of the Preliminary Meeting for Organization of The American Society of Mechanical Engineers* (1882)

1880–1882	Robert Henry Thurston (1903)
1883	Erasmus Darwin Leavitt (1916)
1884	John Edson Sweet (1916)
1885	Josephus Flavius Holloway (1896)
1886	Coleman Sellers (1907)
1887	George H. Babcock (1893)
1888	Horace See (1909)
1889	Henry Robinson Towne (1924)
1890	Oberlin Smith (1926)
1891	Robert Woolston Hunt (1923)
1892	Charles Harding Loring (1907)
1893–1894	Eckley Brinton Coxe (1895)
1895	Edward F. C. Davis (1895)
1895	Charles Ethan Billings (1920)
1896	John Fritz (1913)
1897	Worcester Reed Warner (1929)
1898	Charles Wallace Hunt (1911)
1899	George Wallace Melville (1912)
1900	Charles Hill Morgan (1911)
1901	Samuel T. Wellman (1919)
1902	Edwin Reynolds (1909)
1903	James Mapes Dodge (1915)
1904	Ambrose Swasey (1937)
1905	John Ripley Freeman (1932)
1906	Frederick Winslow Taylor (1915)
1907	Frederick Remsen Hutton (1918)
1908	Minard Lafever Holman (1925)
1909	Jesse Merrick Smith (1927)
1910	George Westinghouse (1914)
1911	Edward Daniel Meier (1914)
1912	Alexander Crombie Humphreys (1927)
1913	William Freeman Myrick Goss (1928)
1914	James Hartness (1934)
1915	John Alfred Brashear (1920)
1916	David Schenck Jacobus
1917	Ira Nelson Hollis (1930)
1918	Charles Thomas Main (1943)
1919	Mortimer Elwyn Cooley (1944)
1920	Fred J. Miller (1939)
1921	Edwin S. Carman
1922	Dexter Simpson Kimball
1923	John Lyle Harrington (1942)
1924	Frederick Rollins Low (1936)
1925	William Frederick Durand
1926	William Lamont Abbott
1927	Charles M. Schwab (1939)
1928	Alex Dow (1942)
1929	Elmer Ambrose Sperry (1930)
1930	Charles Piez (1933)
1931	Roy V. Wright
1932	Conrad N. Lauer (1943)
1933	A. A. Potter
1934	Paul Doty (1938)
1935	Ralph E. Flanders
1936	William L. Batt
1937	James H. Herron
1938	Harvey N. Davis
1939	Alexander G. Christie
1940	Warren H. McBryde
1941	William A. Hanley
1942	James W. Parker
1943	Harold V. Coes
1944	Robert M. Gates
1945	Alex D. Bailey

TREASURERS

Apr. 1880—Dec. 1881	Lycurgus B. Moore *
Dec. 1881—Nov. 1884	Charles W. Copeland (1895)
1884—1925	William H. Wiley (1925)
1925—1935	Erik Oberg
1935—1944	William D. Ennis
1944—date	K. W. Jappe

SECRETARIES

Organization Meeting, 1880	Samuel S. Webber, Jr. (1921)
Acting Secretary, Apr.-Nov. 1880	Lycurgus B. Moore *
Nov. 1880—Mar. 1883	Thos. Whiteside Rae (1895)
1883—1906	Frederick R. Hutton (1918)
1906—1934	Calvin W. Rice (1934)
1934—date	Clarence E. Davies

* Deceased. Year not known.

Index to Society Records, Part 1

The page numbers in this section are preceded by the letters "RI," which are omitted in the following index.

Abbreviations and Symbols, Graphical, Comm.. 31
Abbreviations and Symbols, Letter, Comm.... 31
Abrasive Wheels, Rep. on Safety Comm..... 37
Acoustical Measurements, Rep. on Comm.... 32
Administrative Organization Comm..... 12
Admissions Comm. 6
Advertising Manager, A.S.M.E..... 5
Aeronautic Div. *See* Aviation Div.
Aeronautics, Rep. on Standardization Comm... 32
Agriculture Comm. 13
Air Conditioning Comm..... 13
Alfred Noble Prize, A.S.M.E. Rep..... 9
Allowances and Tolerances, Gages, Comm.... 28
American Association for the Advancement of Science, A.S.M.E. Reps..... 9
American Documentation Institute, A.S.M.E. Rep. 9
American Standards Association, A.S.M.E. Reps. 9
American Year Book Corporation, A.S.M.E. Rep. 9
Applied Mechanics Div. Comms..... 10
ASA Mechanical Standards Comm., Reps. on.. 32
ASA Safety Code Correlating Comm., Reps. on. 37
ASA Standards Council, Reps. on..... 33
A.S.M.E. Medal
  Recipients 40
  Statement about 40
Assistant Secretaries, A.S.M.E..... 5
Automatic Regulation Theory Comm..... 27
Aviation Div. Comms..... 10
Awards, A.S.M.E.
  Recipients 40
  Statements about 40
Awards Comm. *See* Honors and Awards
Ball and Roller Bearings Comm..... 28
Biography Comm. 7
Biomechanics Comm. 10
Board of Honors and Awards..... 6
Board of Review..... 8
Board on Standards and Codes..... 8
Board on Technology..... 8
Boiler Code
  Comm. 7, 38
  Conference Comm. 38
  Exec. Comm. 38
  Procedure Comm. 39
  Revision of Section VIII, Special Comm.. 39
  Subcomms. 38
Boiler Feedwater Studies Comm..... 25
Boilers, Material Specifications Comm..... 38
Boilers, Openings, Comm..... 39
Boilers, Power, Comm..... 38
Boilers, Rules for Inspection of, Comm..... 38
Boilers, Special Design of, Comm..... 38
Bolted Flanged Connections Comm..... 39
Bolt, Nut, and Rivet Proportions Comm..... 29
Building Code for Light and Ventilation, Rep. on Comm. 32
Bulk Materials Conveyors Comm..... 12
Calvin W. Rice Scholarship..... 40
Cast Iron at Elevated Temperatures, Rep. on Comm. 32
Cast Iron Pipe, Reps. on Comm..... 32
Cavitation Comm. 11
Center for Safety Education, A.S.M.E. Rep..9, 37
Charles T. Main Award
  Recipients 42
  Statement about 40
Chucks and Chuck Jaws Comm..... 29
Coal and Coke, Rep. on Comm..... 32
Coal, Clean Bituminous, Reps. on Comm..... 33
Coal-Handling Equipment, Rep. on Comm.... 32
Coal Mines, Drainage, Rep. on Comm..... 32
Coal Testing Code, Reps. on Comm.
  Fuels Division 11
  Power Test Codes..... 36
Code Symbol Stamps Comm..... 38
Colleges, Relations With, Comm.....6, 23
Column Research Comm., A.S.M.E. Reps.... 9
Compressed Air, Work in, Rep. on Safety Comm. 37
Compressed Air Machinery and Equipment, Safety Comm. 36
Compressors and Blowers
  Centrifugal and Turbo, Comm..... 34
  Displacement, Comm. 34
Comptroller, A.S.M.E. 5
Condensers, Water Heating, and Cooling Equipment Comm. 35
Condenser Tubes Comm..... 26
Constitution and By-Laws Comm..... 6
Construction Work, Rep. on Safety Comm.... 37
Consulting Engineering Group, Exec. Comm... 10
Conveyors and Conveying Machinery, Safety Comm. 36
Co-ordinating Comm. (Corrosion), Reps. on.. 27
Co-ordinating Comm. (Power Test Codes)... 35
Co-ordination Comm. (Boiler Code)..... 38
Correlating Comm., ASA Safety Code, Reps. on Comm. 37
Corrosion, Co-ordinating Comm., Reps. on.... 27
Council, A.S.M.E.
  Exec. Comm. 5
  Members of 5
  Special Comms. 8
Cranes, Derricks, and Hoists, Safety Comm... 36
Cut and Ground Thread Taps Comm..... 29
Cutting Fluids Comm..... 25
Cutting Tools, Single-Point, Comm..... 29
Daniel Guggenheim Medal Board of Award, A.S.M.E. Reps. 9, 10
Definitions and Values, Power Test Codes Comm. 34
Demolition Bomb Bodies Comm..... 26
Depreciation Studies Comm..... 12
Dimensional Limits and Allowances Comm.... 14
Directors at Large..... 5
Dished Heads Comm..... 39
Displacement Pumps, Reciprocating Steam-Driven, Comm. 34
Distillation and Evaporation Comm..... 13
Distribution Comm. 12
Domestic Fuels Comm..... 11
Drawings and Drafting Room Practice Comm. 31
Drying Comm. 13
Dues-Exempt Members' Contributions Comm.. 7
Dust Explosions, Reps. on Safety Comm..... 37
Dust Separating Apparatus Comm..... 35
Economic Status of the Engineer, A.S.M.E. Reps. 9
Editor, A.S.M.E. 5
Education and Training for the Industries Comm. 6
Education, Safety, Center for, A.S.M.E. Rep..9, 37
E.I.C.-A.S.M.E. Joint Conference, A.S.M.E. Reps. 9
Electrical Definitions, Rep. on Comm..... 32
Electric Sockets and Lamp Bases Comm..... 31
Electric Welding Apparatus, Rep. on Comm.. 32
Elevators Comm. 25
Elevators, Safety Code Comm..... 36
Employment Conditions for Engineers, AS.M.E. Rep. 9
Engineering Foundation, A.S.M.E. Reps..... 9
Engineering Profession Organization, A.S.M.E. Reps. 9
Engineering Registration, National Bur. of, A.S.M.E. Rep. 9
Engineering Societies, Co-operation in Safety Work, Rep. on Comm..... 37
Engineering Societies Library Board, A.S.M.E. Reps. 9
Engineering Societies Monographs Comm., A.S.M.E. Reps. 9
Engineering Societies Personnel Service, Inc., A.S.M.E. Reps. 9
Engineers' Civic Responsibilities Comm..... 8
Engineers' Council for Professional Development, A.S.M.E. Reps..... 9
Engineers Joint Council, A.S.M.E. Reps..... 9
Engineers' National Relief Fund, A.S.M.E. Rep. 9
Evaporating Apparatus Comm..... 35
Exhaust Systems, Rep. on Safety Comm..... 37
Fans Comm. 35
Feedwater, Boiler Code Comm..... 39
Feedwater Studies, Boiler, Comm..... 25
Ferrous Materials Comm..... 38
Finance Comm. 6
Fire Tests, Building Construction and Materials, Rep. on Comm..... 32
Flanges, Steel, Comm. (Boiler Code)..... 39
Floor and Wall Openings, Railings, and Toe Boards, Rep. on Safety Comm..... 37
Fluid Meters Comm..... 25
Fluids Handling Comm..... 13
Forest Fire Protection, Rep. on Comm..... 32
Forest Protection, Wood Industries Div. Comm. 14
Forging and Hot Metal Stamping, Rep. on Safety Comm. 37
Freeman Award Comm..... 8
Freeman Scholarship, *See* John R. Freeman Travel Scholarships
Fritz Medal Board of Award, A.S.M.E. Reps.. 9
Fuels, Domestic, Comm..... 11
Fuels, Power Test Code Comm..... 34
Fuels Div. Comms..... 10
Furnace Performance Factors Comm..... 26
Gages, Pressure and Vacuum, Comm..... 30
Gantt Medal Board of Award, A.S.M.E. Reps.. 9
Gas Producers Comm..... 35
Gas Turbines Comm..... 35
Gaseous Fuels, Rep. on Comm..... 30
Gases, Properties of, Comm..... 27
Gears Comm. 29
Gear Teeth, Strength of, Comm..... 25
George Westinghouse Bust Comm. *See* National Honors Comm.
Glass, Safety, Rep. on Comm..... 37
Graphic Arts Div..... 11
Graphic Presentation Comm..... 31
Group Delegates Officers..... 15
Guggenheim Medal Board of Award, AS.M.E. Reps. 9, 10
Heating Boilers Comm..... 38
Heat Transfer Div..... 11
Holley Medal
  Recipients 41
  Statement about 40
Holmes Safety Association, A.S.M.E. Rep..... 9
Honorary Members, List of..... 43
Honorary Membership, Statement about..... 40
Honors and Awards
  Board of 6
  Special Comm. on Medals..... 7
Hoover Medal Board of Award, A.S.M.E. Reps. 9
Hose Couplings, Screw Threads, Comm..... 30
Hydraulic Div. Comms..... 11
Hydraulic Prime Movers
  Hyd. Div. Comm..... 11
  Power Test Codes Comm..... 35
Hydrogen Storage Tank Comm..... 39
Industrial Conservation Comm..... 12
Industrial Instruments and Regulators Div. Comms. 11
Industrial Relations Comm..... 12
Industrial Workers, Foundries, Protection of, Rep. on Safety Comm..... 37
Industrial Workers, Protection of, Reps. on Safety Comm. 37
Industries, Education and Training for, Comm. 6
Instruments and Apparatus, Power Test Codes Comm. 35
Inter-American Development Commission, A.S.M.E. Reps. 9
Internal-Combustion Engines
  Power Test Codes Comm..... 35
  Research Comm. 26
International Electrotechnical Commission, A.S.M.E. Reps. 9
International Relations Comm..... 8
Iron and Steel Bars Comm..... 30
Iron and Steel Div. *See* Metals Engineering Div.
Jacketed Vessels Comm..... 39
Jig Bushings Comm..... 29
John Fritz Medal Board of Award, A.S.M.E. Reps. 9
John R. Freeman Travel Scholarships
  Recipients 43
  Statement about 40
Joseph A. Holmes Safety Association, A.S.M.E. Rep. 9
Journal of Applied Mechanics, Editor..... 10
Junior Award
  Recipients 42
  Statement about 40
Ladders, Rep. on Safety Comm..... 37
Laundry Machinery, Rep. on Safety Comm.... 37
Layer Vessels Comm..... 39
Leather Belting Comm..... 30
Lectureships Comm. 8
Library Comm. 6
Life Membership, Statement about..... 40
Lighting Factories, Mills, Rep. on Safety Comm. 37
Loading Platforms, Rep. on Comm..... 32
Locomotives, Boilers of, Comm..... 38
Low Voltage Electrical Hazards, Rep. on Safety Comm. 37
Lubrication Comm. 25
Machine Design Group, Comms..... 11
Machine Pins Comm..... 29
Machine Shop Practice Div. *See* Production Engineering Div.
Machine Tapers Comm..... 28
Machine Tool Elements Comm..... 28
Machine Tools, Designations and Working Ranges, Comm. 28
Main Award. *See* Charles T. Main Award
Management Div. Comms..... 12
Manhole Frames and Covers, Rep. on Comm... 32
Manufactured and Natural Gas Comm..... 13
Marston Award, A.S.M.E. Rep..... 9
Materials Handling Div. Comms..... 12
Materials, New, Boiler Code Comm..... 39
Max Toltz Loan Fund, Statement about..... 40
Mechanical Power-Transmission Apparatus, Safety Comm. 36
Mechanical Refrigeration, Reps. on Safety Comm. 37
Mechanical Separation Comm..... 13
Mechanical Springs Comm..... 25
Mechanical Standards, Reps. on Comm..... 32
Medals Comm. 7
Meetings and Program Comm..... 6
Melville Medal
  Recipients 41
  Statement about 40
Membership Comm., Standing. *See* Admissions Comm.
Membership Development Comm..... 8
Merchant Marine Council Consultants Panel, Rep. on 37
Metallurgical Research, Rep. on Comm..... 27

Metal Cutting Data and Bibliography Comm.. 25
Metals, Effect of Temperature on, Comm.... 25
Metals Engineering Div. Comms..... 12
Metals, Fatigue Phenomena of, Rep. on Comm. 27
Metals, Plastic Flow of, Comm..... 26
Mid-West Office, Location of..... 5
Milling Cutters Comm..... 28
Miniature Boilers Comm..... 38
Model Smoke Law Comm..... 11
Monographs Comm., A.S.M.E. Reps..... 9
National Bureau of Engineering Registration, A.S.M.E. Rep. 9
National Fire Waste Council, A.S.M.E. Rep.... 9
National Management Council, A.S.M.E. Reps. 9
National Research Council, A.S.M.E. Rep.... 9
Noble Prize, A.S.M.E. Rep..... 9
Noise Control Comm..... 10
Nomenclature, Machine Tools, Comm..... 29
Nomenclature, Standard, Comm..... 12
Nominating Comm. 7
Nonferrous Materials Comm..... 38
Officers 5
Oil and Gas Power Div. Comms..... 12
Oil Engine Power Cost Comm..... 13
Openings and Reinforcements Comm. (Boiler Code) 39
Organization Comm. 8
Package Conveyors Comm..... 12
Paper and Pulp Mills, Rep. on Safety Comm.. 37
Past-Presidents, List of..... 44
Pension Comm. 8
Petroleum Comm., Process Industries Div.... 13
Petroleum Products and Lubricants, Reps. on Comm. 32
Pipe and Tubing Comm..... 30
Pipe Flanges and Fittings Comm..... 29
Pipe Threads Comm..... 28
Piping Codes and Standards, Joint Conference Comm., Reps. on Comm..... 32
Piping Systems, Identification, Comm..... 31
Pi Tau Sigma Award
Recipients 42
Statement about 40
Plant Layout Standards Models Comm..... 12
Plastic Flow of Metals Comm..... 26
Plate Specifications Comm. (Boiler Code).... 39
Plumbing Equipment Comm..... 31
Power Boilers Comm..... 38
Power Div., Exec. Comm..... 13
Power Test Codes Comm., Standing.....6, 34
Power Test Codes Comms., Technical..... 34
Power Test Codes, General Instructions Comm. 34
Preferred Numbers, Rep. on Comm..... 32
President 5
Presses, Rep. on Safety Comm..... 37
Pressure Piping, Code for, Comm..... 30
Pressure Vessels in Service, Care of, Comm.. 38
Pressure Vessels, Unfired
A.P.I.-A.S.M.E. Comm. 39
A.S.M.E. Comm. 39
Prime Movers
Hyd. Div. Comm..... 11
Power Test Codes Comm..... 35
Speed Governing Specifications, Reps. on Comm. 36
Process Industries Div. Comms..... 13
Production Engineering Div. Comms..... 13
Professional Conduct Comm..... 6
Professional Divs. Comm., Standing.....6, 10
Professional Divs. Exec. Comms..... 10
Publications Comm.
Special 7
Standing 6
Pumping Machinery Comm..... 11
Pumps, Centrifugal and Rotary, Comm..... 34
Pumps, Reciprocating Steam-Driven Displacement, Comm. 34
Punch Press Tools Comm..... 29
Quality Control Comm..... 12
Quarry Operations, Rep. on Safety Comm.... 37
Railroad Div. Comms..... 13
Rating of Rivers, Rep. on Comm..... 32
Reamers Comm. 29
Refractory Materials, Properties of, Rep. on Comm. 27
Refrigerating Systems Comm..... 35
Registration of Engineers Comm..... 8
Relations With Colleges Comm.....6, 23
Representatives on Other Activities
A.S.M.E. 9
Boiler Code 39
Power Test Codes..... 36
Research 27
Safety 37
Standardization 32
Research Comm., Standing.....6, 25
Research Comms., Technical..... 25
Research Procedure Comm. of Engineering Foundation, A.S.M.E. Rep..... 9
Research Secretaries
Applied Mechanics 10
Management 12
Oil and Gas Power..... 12
Process Industries 13
Railroad 13
Review, Board of..... 8
Rice Scholarship. *See* Calvin W. Rice Scholarship
Rotating Electrical Machinery, Rep. on Comm. 32
Rubber and Plastics Div. Comms..... 13
Rubber Machinery, Rep. on Safety Comm.... 37
Safety Comm., Materials Handling..... 12
Safety Comm., Standing.....6, 36
Safety Comms., Technical..... 36
Safety Education, Center for, A.S.M.E. Rep..9, 37
Safety Valve Requirements Comm..... 39
Safety Work, Co-operation With Other Societies, A.S.M.E. Rep..... 37
St. Louis Junior Award. *See* Spirit of St. Louis Junior Award
St. Louis Medal. *See* Spirit of St. Louis Medal
Sanitation Comm. 13
Scholarships and Loan Funds, Statement about. 40
Screw Threads for Hose Couplings Comm.... 30
Screw Threads, Standardization, Comm..... 28
Screw Threads, U.S. Comm., Reps. on..... 33
Secretarial Staff, A.S.M.E..... 5
Secretaries, List of..... 44
Secretaries (Regional) 15
Sections
Exec. Comms. 15
Nominating Comm., Regions of..... 7
Standing Comm. 6, 15
Shaft Couplings Comm..... 30
Shafting Comm. 29
Shells, Steel, Comms..... 26
Shipments on Skids and Pallets Comm..... 12
Sieves for Testing Purposes, Rep. on Comm.. 33
Single-Point Cutting Tools Comm..... 29
Single-Point Tool-Life Tests Comm..... 29
Small Tools Comm..... 28
Solid Fuels, Combustion Space for, Comm.... 31
Speed, Temperature and Pressure Responsive Governors Comm. 35
Spindle Noses and Collets Comm..... 28
Spirit of St. Louis Medal
Recipients 41
Statement about 40
Spirit of St. Louis Junior Award
Recipients 42
Statement about 40
Splines and Splined Shafts Comm..... 29
Springs, Mechanical, Comm..... 25
Standardization Comm., Standing.....6, 28
Standardization Comms., Technical..... 28
Standards and Codes, Board on..... 8
Standards Council, Reps. on..... 33
Standard Ton of Refrigeration, Rep. on Comm. 36
Standing Comms. 6
Statistics in Engineering and Manufacturing Comm. 32
Steam Boilers, Critical Pressure, Comm..... 26
Steam Boilers in Service, Care of, Comm.... 38
Steam Engines, Reciprocating, Comm..... 34
Steam-Generating Units, Stationary, Comm... 34
Steam Locomotives Comm..... 35
Steam Turbines Comm..... 34
Steam Turbines, Special Standards Comm.... 32
Steel Shells, Forging of, Comm..... 26
Steel Shells, H. E., Finishing and Machining of, Comm. 26
Strength of Gear Teeth Comm..... 25
Strength of Vessels Comm..... 26
Student Awards
Recipients 42
Statement about 40
Student Branches, List of..... 23
Sugar Comm. 13
Sulphur Comm. 13
Surface Qualities Comm..... 30
Symbols and Abbreviations
Graphical, Comm. 31
Letter, Comm. 31
Symbol Stamps, Boiler Code, Comm..... 38
Technical Committees
Boiler Code 38
Power Test Codes..... 34
Research 25
Safety 36
Standardization 28
Technical Committees, Standing..... 6
Technology, Board on..... 8
Testing Wood, Rep. on Comm..... 32
Textile Div. Comms..... 14
Textiles, Rep. on Safety Comm..... 37
Therbligs, Process Charts, and Their Symbols, Special Comm. 32
Thermal Insulating Materials, Rep. on Comm. 33
Toltz Fund. *See* Max Toltz Loan Fund
Tool Holders Comm..... 29
Tool Posts and Shanks Comm..... 28
Transmission Chains and Sprockets Comm.... 29
Treasurers, List of..... 44
T-Slots Comm. 28
Twist Drill Sizes Comm..... 29
Unfired Pressure Vessels
A.P.I.-A.S.M.E. Comm. 39
A.S.M.E. Comm. 39
United Engineering Trustees, Inc., A.S.M.E. Reps. 9
Vegetable Oils Comm..... 13
Ventilation, Rep. on Safety Comm..... 37
Vermilye Medal Advisory Comm., A.S.M.E. Rep. 9
Vessels, Clad, Comm..... 39
Vessels, Jacketed, Comm..... 39
Vessels, Layer, Comm..... 39
Vessels, Low Temperature, Comm..... 39
Vessels, Strength Under External Pressure, Comm. 26
Vice-Presidents (Regional) 5, 15
Walkway Surfaces, Rep. on Safety Comm.... 37
Warner Medal. *See* Worcester Reed Warner Medal
War Manpower Commission. *See* Consultative Comm. on Engineering
Washers, Plain and Lock, Comm..... 29
Washington Award Commission, A.S.M.E. Reps. 9
Water for Industrial Uses, Rep. on Comm... 27
Water Hammer Comm..... 11
Water Heating, Volume, Rep. on Comm..... 33
Welded Joints, Radiographic Examination of, Comm. 39
Welding Comm. 39
Welding Apparatus, Electric, Rep. on Comm.. 32
Westinghouse Bust Comm. *See* National Honors Comm.
Wire and Sheet Metal Gages Comm..... 30
Wire Rope Comm..... 26
Wire Rope for Mines, Rep. on Comm..... 33
Woman's Auxiliary, Officers of..... 39
Woman's Auxiliary Scholarship..... 40
Wood Finishing Comm..... 14
Wood Industries Div. Comms..... 14
Worcester Reed Warner Medal
Recipients of 41
Statement about 40
Work Standardization Comm..... 12
World Power Conference, A.S.M.E. Rep..... 9
Worm Gears Comm..... 26

IN TWO SECTIONS—SECTION TWO

Transactions

of the

A.S.M.E.

SOCIETY RECORDS

(Including Indexes to Publications for 1946)

Depositories for A.S.M.E. Transactions in the United States RI-47

A.S.M.E. Transactions in Central and South America and Great Britain RI-50

Indexes to A.S.M.E. Papers and Publications RI-51

- Regular Society Publications, 1946 . . . . . RI-51
- Publications Issued in 1946 . . . . . RI-51
- How to Find Papers Presented at 1946 A.S.M.E. Meetings RI-51
- Publications Developed by the Technical Committees RI-51
- Biographies RI-52
- Books and Pamphlets on Special Subjects RI-53
- Regular Society Periodicals RI-53

Index to *Mechanical Engineering,* 1946 . . . . . RI-55

Index to Transactions of the A.S.M.E. for 1946 . . . . . RI-68

JANUARY, 1947

VOL. 69, NO. 1

Transactions

of The American Society of Mechanical Engineers

Published on the tenth of every month, except March, June, September, and December

---

OFFICERS OF THE SOCIETY:

EUGENE W. O'BRIEN, *President*

K. W. JAPPE, *Treasurer* C. E. DAVIES, *Secretary*

COMMITTEE ON PUBLICATIONS:

L. N. ROWLEY, JR., *Chairman*

H. L. DRYDEN RONALD B. SMITH

J. M. JURAN JOHN HAYDOCK

GEORGE A. STETSON, *Editor* K. W. CLENDINNING, *Managing Editor*

ADVISORY MEMBERS OF THE COMMITTEE ON PUBLICATIONS:

N. C. EBAUGH, GAINESVILLE, FLA. HUNTER R. HUGHES, JR., DALLAS, TEXAS

Published monthly by The American Society of Mechanical Engineers. Publication office at 20th and Northampton Streets, Easton, Pa. The editorial department is located at the headquarters of the Society, 29 West Thirty-Ninth Street, New York 18, N. Y. Cable address, "Dynamic," New York. Price $1.50 a copy, $12.00 a year; to members and affiliates, $1.00 a copy, $7.50 a year. Changes of address must be received at Society headquarters two weeks before they are to be effective on the mailing list. Please send old as well as new address. . . . By-Law: The Society shall not be responsible for statements or opinions advanced in papers or . . . printed in its publications (B13, Par. 4). . . . Entered as second-class matter March 2, 1928, at the Post Office at Easton, Pa., under the Act of August 24, 1912. . . .

Copyrighted, 1947, by The American Society of Mechanical Engineers. Reprints from this publication may be made on condition that full credit be given the Transactions of the A.S.M.E. and the author, and that date of publication be stated.

Depositories for A.S.M.E. Transactions in the United States, Including Territories and Dependencies

BOUND copies of the complete Transactions of The American Society of Mechanical Engineers will be found in the libraries in the United States and other countries which are listed on the following pages.

Alabama

Auburn.....Engineering Library, Alabama Poly. Inst.
Birmingham.....Public Library
University.....Library, University of Alabama

Arizona

Tucson.....Library, University of Arizona

Arkansas

Fayetteville.....Engineering Library, University of Arkansas

California

Berkeley.....Library, University of California
Long Beach.....Public Library
Los Angeles.....Public Library
University of Southern California
Oakland.....Oakland City Library
Teachers' Professional Library
Pasadena.....Library, California Institute of Technology
Santa Clara.....Library, University of Santa Clara
San Diego.....Public Library
San Francisco....Engineers Club of San Francisco
Mechanics Institute
Public Library (Civic Center)
Stanford Univ....Library, Stanford University

Colorado

Boulder.....Library, University of Colorado
Denver.....Public Library
Fort Collins.....Colorado State College of Agriculture and Mechanic Arts

Connecticut

Bridgeport.....Public Library
Hartford.....Public Library
New Haven.....Public Library and Yale University
Storrs.....University of Connecticut
Waterbury.....Silas Bronson Library

Delaware

Newark.....University of Delaware
Wilmington.....Wilmington Institute Free Library

District of Columbia

Washington.....George Washington and Catholic Universities; Library of Congress; National Bureau of Standards Library; Scientific Library, U. S. Patent Office

Florida

Gainesville.....University of Florida
Jacksonville.....Free Public Library
Miami.....Public Library
Tampa.....Public Library

Georgia

Atlanta.....Carnegie Public Library
Georgia School of Technology
Savannah.....Public Library

Hawaii

Honolulu.....University of Hawaii Library

Idaho

Moscow.....University of Idaho

Illinois

Chicago.....John Crerar Library; Library, Illinois Institute of Technology; Museum of Science and Industry; Public Library of Chicago; Western Society of Engineers
Evanston.....Northwestern University
Moline.....Public Library
Peoria.....Public Library
Urbana.....University of Illinois

Indiana

Evansville.....Public Library
Fort Wayne.....Public Library
Indianapolis.....Public Library and Indiana State Library
Notre Dame.....Library, University of Notre Dame
Terre Haute.....Rose Polytechnic Institute
West Lafayette...Library, Purdue University

Iowa

Ames.....Iowa State College
Des Moines.....Public Library
Iowa City.....State University of Iowa

Kansas

Kansas City.....Public Library, Huron Park
Lawrence.....Library, University of Kansas
Manhattan.....Kansas State College
Wichita.....Wichita City Library

Kentucky

Lexington.....University of Kentucky
Louisville.....Speed Scientific School
University of Louisville

Louisiana

Baton Rouge.....Louisiana State University
New Orleans.....The Howard-Tilton Memorial Library
Louisiana Engineering Society
Public Library
Tulane University

Maine

Orono.....University of Maine

Maryland

Annapolis.....United States Naval Academy
Baltimore.....Engineers Club of Baltimore
Johns Hopkins University
Public Library
College Park.....Library, University of Maryland

Massachusetts

Boston.....Boston Public Library
Engineering Societies of New England
Northeastern University
Cambridge.....Harvard University (Engineering Library)
Massachusetts Institute of Technology
Fall River.....Public Library
Lynn.....Free Public Library
New Bedford.....Free Public Library
Springfield.....Springfield City Library
Tufts College.....Tufts College
Worcester.....Free Public Library
Worcester Polytechnic Institute

Michigan

Ann Arbor.....University of Michigan
Detroit.....Cass Technical High School
Highland Park Public Library
Public Library
University of Detroit
East Lansing.....Michigan State College
Flint.....Public Library
Grand Rapids....Public Library
Houghton.....Michigan College of Mining & Technology
Jackson.....Public Library

Minnesota

Duluth.....Public Library
Minneapolis.....Minneapolis Public Library (Engineering and Circulating Libraries)
University of Minnesota
St. Paul.....James Jerome Hill Reference Library

Mississippi

State College.....Mississippi State College

Missouri

Columbia.....University of Missouri
Kansas City.....Public Library
Rolla.....Missouri School of Mines and Metallurgy
St. Louis.....Engineers Club of St. Louis; Public Library; Washington University; Mercantile Library

Montana

Bozeman.....Montana State College

Nebraska

Lincoln.....University of Nebraska
Omaha.....Public Library

Nevada

Reno.....University of Nevada Library

New Hampshire

Durham.....University of New Hampshire

New Jersey

Bayonne.....Free Public Library
Camden.....Free Public Library
Elizabeth.....Free Public Library
Hoboken.....Stevens Institute of Technology
Jersey City.....Free Public Library
Newark.....Free Public Library
Newark College of Engineering
New Brunswick..Rutgers University
Paterson.....Free Public Library
Princeton.....Princeton University
Trenton.....Free Public Library

New Mexico

Albuquerque.....University of New Mexico
State College.....New Mexico State College

New York

Albany.....New York State Library
Brooklyn.....Polytechnic Institute
Pratt Institute
Brooklyn Public Library
Buffalo.....The Grosvenor Library
Engineering Society of Buffalo
Buffalo Public Library
Ithaca.....Cornell University
Jamaica, L. I.....Queens Borough Public Library
New York.....College of the City of New York
Columbia University
Cooper Union
Engineering Societies Library
New York Museum of Science and Industry
New York University Library
Public Library
Potsdam.....Clarkson College of Technology
Rochester.....Rochester Engineering Society
Schenectady.....Union College
Syracuse.....Public Library
Syracuse University
Troy.....Rensselaer Polytechnic Institute
Utica.....Public Library

North Carolina

Chapel Hill.....University of North Carolina
Durham.....Duke University
Raleigh.....North Carolina State College

North Dakota

Fargo.....North Dakota State Agricultural College
Grand Forks.....University of North Dakota

Ohio

Ada.....Ohio Northern University
Akron.....Public Library
University of Akron
Canton.....Public Library
Cincinnati.....Engineers Club of Cincinnati
Public Library
University of Cincinnati
Cleveland.....Case School of Applied Science
Cleveland Engineering Society
Fenn College
Public Library
Columbus.....The Ohio State Library
Ohio State University
Public Library
Dayton.....Engineers Club of Dayton
Toledo.....Public Library
University of Toledo
Youngstown.....Public Library

Oklahoma

Norman.....Oklahoma University
Oklahoma City...Public Library
Stillwater.....Oklahoma A.&M. College
Tulsa.....Public Library

Oregon

Corvallis.....Oregon State College
Portland.....Portland Library Association

Pennsylvania

Allentown.....Free Library
Bethlehem.....Lehigh University
Easton.....Lafayette College
Public Library
Erie.....Public Library
Lewisburg.....Bucknell University
Philadelphia.....Drexel Institute
Engineers Club
Franklin Institute
The Free Library
University of Pennsylvania
Pittsburgh.....Carnegie Free Library of Allegheny
Carnegie Institute of Technology
Carnegie Library (Schenley Park)
Engineers' Society of Western Pennsylvania
University of Pittsburgh
Reading.....Public Library
Scranton.....Public Library
State College.....Pennsylvania State College
Swarthmore.....Swarthmore College
Villanova.....Villanova College
Wilkes-Barre.....Public Library

Puerto Rico

Mayaguez.....University of Puerto Rico

Rhode Island

Kingston.....Rhode Island State College
Providence.....Brown University
Providence Engineering Society
Public Library

South Carolina

Clemson College..Library, Clemson College

South Dakota

Brookings.....South Dakota State College

Tennessee

Kingsport.....Public Library
Knoxville.....University of Tennessee
Memphis.....Goodwin Institute
Nashville.....Vanderbilt University

Texas

Austin.....University of Texas
College Station...Texas Agricultural & Mechanical College
Dallas.....Public Library
Southern Methodist University
El Paso.....Public Library
Fort Worth.....Carnegie Public Library
Houston.....Public Library
Rice Institute
Lubbock.....Texas Technological College
San Antonio.....Carnegie Library

Utah

Salt Lake City...University of Utah
Public Library

Vermont

Burlington.....University of Vermont

Virginia

Blacksburg.....Virginia Polytechnic Institute
Charlottesville...University of Virginia

Lexington.....Virginia Military Institute
Norfolk.....Public Library
Richmond.....Virginia State Library

Washington
Pullman.....State College of Washington
Seattle.....Engineers Club
Public Library
University of Washington
Spokane.....Public Library
Tacoma.....Public Library

West Virginia
Morgantown.....West Virginia University

Wisconsin
Madison.....Library, University of Wisconsin
Milwaukee.....Marquette University
Public Library
Vocational School Library

Wyoming
Laramie.....Wyoming University

A.S.M.E. Transactions in Central and South America and Great Britain

Argentina

Buenos Aires.....Biblioteca de la Sociedad Cientifica

Australia

Adelaide.....Public Library of Adelaide
Melbourne.....Public Library of Victoria
Perth.....University of Western Australia Library
Sydney.....Public Library of Sydney

Brasil

Rio de Janeiro...Bibliotheca da Escola Polytechnica
Bibliotheca Nacional
São Paulo.....Bibliotheca da Escola Polytechnica

Canada

Kingston.....Queen's College
Montreal.....Ecolé Polytechnique
Engineering Institute of Canada
McGill University
Toronto.....University of Toronto, Library
Vancouver.....University of British Columbia

Chile

Santiago.....Universidad de Chile, Facultad de Ciencias Fisicas y Matematicas (Engg. School)

Cuba

Havana.....Cuban Society of Engineers

England

Birmingham.....Birmingham Public Libraries
Bristol.....University of Bristol
Cambridge.....University of Cambridge
Leeds.....University of Leeds
Liverpool.....Liverpool Engineering Society
Public Library of Liverpool
London.....City and Guild Engineering College
Institution of Automobile Engineers
London (*Continued*)
The British Coal Utilization Research Association
The Institution of Mechanical Engineers
Institution of Civil Engineers
Institution of Electrical Engineers
The Junior Institution of Engineers
The Royal Aeronautical Society
Manchester.....Manchester Public Libraries (Reference Library)
Oxford.....Oxford University
Newcastle-upon-Tyne.....The North-East Coast Institution of Engineers and Shipbuilders
Sheffield.....Sheffield Public Libraries

India

Bangalore.....Mysore Engineers Association
Calcutta.....Bengal Engineering College
Poona.....Poona College of Engineering
Rangoon.....University of Rangoon

Ireland

Belfast.....Queen's University of Belfast

Mexico

Mexico City.....Asociacion de Ingenieros y Arquitectos de Mexico
Library of the Escuela de Ingenieros Mecanicos y Electricistas

Scotland

Glasgow.....Royal Technical College
Mitchell Library

South Africa

Cape Town.....University of Cape Town
Johannesburg....South African Institute of Engineers

Wales

Cardiff.....Cardiff Public Library

Indexes to A.S.M.E. Papers and Publications

THIS and the following pages will serve as a guide to the current publications of the A.S.M.E.

Regular Society Publications, 1946

Mechanical Engineering, monthly (see index on page RI-55)
A.S.M.E. Transactions, monthly including the *Journal of Applied Mechanics* (see index on page RI-68)
A.S.M.E. Mechanical Catalog and Directory, 1947 edition.

Publications Issued in 1946

Metal Cutting Data (monthly publication)
Sources of Information on Instruments
1944 Oil-Engine Power Cost Report

American Standards

Drawings and Drafting-Room Practice
Inspection and Tolerance of Gears
Involute Splines
Tool Life Tests

Boiler Construction Code

1946 Addenda to:
- Locomotive Boiler Code
- Low-Pressure Heating Boiler Code
- Miniature Boiler Code
- Power Boiler Code
- Unfired Pressure Vessel Code
- Specifications for Materials
- Welding Qualifications

Power Test Codes

Stationary Steam Generating Units

How to Find Papers Presented at 1946 A.S.M.E. Meetings

THE technical programs of the meetings of the Society and of its Professional Divisions have been published in *Mechanical Engineering* and may be located by consulting the index on pages RI-55-RI-67. A majority of these papers were published, or will be published, in *Mechanical Engineering* or the Transactions (including the *Journal of Applied Mechanics*) and may be located by reference to the indexes of these publications.

Publications Developed by the Technical Committees

THE Society's technical committees, the first of which was organized many years ago and all of which have been continuously at work on codes, standards, research, and other special reports, have developed a series of publications of permanent value to the membership. The following list is presented here for record and for ready reference. This list covers the entire group of publications of these committees completed and published.

To assist members in securing copies of these publications the sale price is also given. A discount of 20 per cent is allowed to A.S.M.E. members on all publications except where otherwise noted.

A.S.M.E. AMERICAN STANDARDS

Bolt, Nut, and Rivet Proportions

Large Rivets (B18.4—1937), $0.80
Plow Bolts (B18f—1928), $0.45
Round Unslotted-Head Bolts (B18.5—1939), $0.60
Slotted-Head Proportions; Machine Screws, Cap Screws, and Wood Screws (B18c—1930), $0.55
Small Rivets (B18a—1927 with 1942 Addendum), $0.40
Tinners', Coopers', and Belt Rivets (B18g—1928, with 1942 Addendum), $0.45
Track Bolts and Nuts (B18d—1930), $0.50
Wrench-Head Bolts and Nuts and Wrench Openings (B18.2—1941), $0.80

Piping and Pipe Fittings

Air Gaps and Backflow Preventers in Plumbing Systems (A40.4—1942 and A40.6—1943), $0.55
Brass Fittings for Flared Copper Tubes (A40.2—1936), $0.45
Cast-Iron Pipe Flanges and Flanged Fittings for 25 Lb Maximum Saturated Steam Pressure (B16b2—1931), $0.50
Cast-Iron Pipe Flanges and Flanged Fittings Class 125 (B16a—1939), $0.60
Cast-Iron Pipe Flanges and Flanged Fittings Class 250 (B16b—1944), $0.55.
Cast-Iron Pipe Flanges and Flanged Fittings for 800 Lb Maximum Hydraulic Pressure (B16b1—1931), $0.45.
Cast-Iron Soil Pipe and Fittings (A40.1–1935), $0.80
Cast-Iron Long Turn Sprinkler Fittings for 150 and 250 Lb Maximum Saturated Steam Pressure (B16g—1929) and Addendum (B16g1—1937), $0.60
Cast-Iron Screwed Fittings for 125 and 250 Lb Maximum Saturated Steam Pressure (B16d—1941), $0.50
Cast-Iron Screwed Drainage Fittings (B16.12—1942), $0.55
Code for Pressure Piping (B31.1—1942), $2.50
Face-to-Face Dimensions of Ferrous Flanged and Welding End Valves (B16.10—1939), $0.65
Ferrous Plugs, Bushings, Lock Nuts, and Caps (B16.14—1943), $0.50
Malleable-Iron Screwed Fittings for 150 Lb Maximum Saturated Steam Pressure (B16c—1939), $0.60
Pipe Threads (B2.1—1945), $1.50
Scheme for the Identification of Piping Systems (A13—1928), $0.60
Steel Pipe Flanges and Flanged Fittings for 150 to 2500 Lb Maximum Steam Service Pressure (B16e—1939), $1.50
Soldered-Joint Fittings (A40.3—1941), $0.55
Steel Butt-Welding Fittings (B16.9—1940), $0.50
Threaded Cast-Iron Pipe for Drainage, Vent, and Waste Services (A40.5—1943), $0.30
Wrought-Iron and Wrought-Steel Pipe (B36.10—1939), $0.60

Letter and Graphical Symbols and Charts

Abbreviations for Scientific and Engineering Terms (Z10.1—1941), $0.45
Drawings and Drafting-Room Practice (Z14.1—1946), $1.50
Engineering and Scientific Charts for Lantern Slides (Z15.1—1932), $0.60
Engineering and Scientific Graphs for Publications (Z15.3—1943), $0.90
Graphical Symbols for Use on Drawings in Mechanical Engineering (Z32.2—1941), $0.60
Letter Symbols for Gear Engineering (B6.5—1943), $0.30
Letter Symbols for Hydraulics (Z10.2—1942), $0.45
Letter Symbols for Mechanics of Solid Bodies (Z10.3—1942), $0.30
Letter Symbols for Heat and Thermodynamics (Z10c—1943), $0.65
Time Series Charts (Z15.2—1938), $1.50

AMERICAN STANDARDS—MISCELLANY

Fire-Hose Coupling Screw Threads (B26—1925), $0.30
Hose Coupling Screw Threads (B33.1—1935), $0.30
Indicating Pressure and Vacuum Gages (B40—1939), $0.50
Preferred Thickness for Uncoated Thin Flat Metals (B32.1—1941), $0.30
Rolled Threads for Screw Shells of Electric Sockets and Lamp Bases (C44—1931, Reaffirmed in 1946), $0.45
Gear Tolerances and Inspection (B6—1946), $0.80
Preferred Standards for Large 3600-Rpm 3-Phase 60-Cycle Condensing Steam Turbine-Generators (published 1945), $0.30
Shaft Couplings (B49—1932), $0.45
Spring Lock Washers (B27.1—1944), $0.35
Spur Gear Tooth Form (B6.1—1932) $0.55

SMALL TOOLS AND MACHINE TOOL ELEMENTS

Machine Tapers (B5.10—1943), $0.75
Milling Cutters (B5c—1930), $0.90
Reamers (B5.14—1941), $0.90
Taps—Cut and Ground Threads (B5.4—1939), $1.50
Terminology and Definitions for Single-Point Cutting Tools (B5.13—1939), $0.50
Adjustable Adapters (B5.11—1937), $0.60
Chucks and Chuck Jaws (B5.8—1936), $0.55
Circular and Dovetailed Forming Tool Blanks and Holding Elements (B5.7—1943), $0.60
Shafting and Stock Keys (B17.1—1943), $0.55
Markings for Grinding Wheels (B5.17—1943), $0.30
Involute Splines, Side Bearings (B5.15—1946), $0.80
Jig Bushings (B5.6—1941), $0.45
Spindle Noses and Arbors (B5.18—1943), $0.30
Rotating Air Cylinders and Adapters (B5.5—1932), $0.45
Tool Shanks and Tool Posts (B5.2—1943), $0.45
Tool Life Tests (B5—1946), $0.55
T-Slots, Their Bolts, Nuts, Tongues, and Cutters (B5a—1941), $0.45
Twist Drills (B5.12—1940), $0.65
Code for Design of Transmission Shafting (B17c—1927), $0.90
Screw Threads for Bolts, Nuts, Machine Screws, and Threaded Parts (B1.1—1935), $0.75
Screw Threads for High-Strength Bolting (B1.4—1945), $0.30
Screw Thread Gages and Gaging (B1.2—1941), $0.75
Acme and Other Translating Threads (B1.3—1941), $0.55
Tolerances, Allowances, and Gages for Metal Fits (B4a—1925), $0.60
Woodruff Keys, Keyslots, and Cutters (B17f—1930), $0.45

BOILER CONSTRUCTION CODE

1946 Editions:
- Boilers of Locomotives, $1.00
- Low-Pressure Heating Boiler Code, $1.00
- Miniature Boiler Code, $0.75
- Power Boiler Code, $2.75
- Specifications for Materials, $3.50
- Suggested Rules for Power Boilers, $1.25
- Unfired Pressure Vessel Code, $2.00
- Welding Qualifications, $0.90

Boiler Code Interpretation Service, $5.00 annually
API-ASME Code for Unfired Pressure Vessels
1943 Edition, with 1944 Supplement, $2.00

POWER TEST CODES AND AUXILIARY SECTIONS

TEST CODES FOR

Atmospheric Water-Cooling Equipment (1930), $0.55
Coal Pulverizers (1944), $0.85
Displacement Compressors, Vacuum Pumps, and Blowers (1939), $0.90
Dust Separating Apparatus (1941), $0.90
Evaporating Apparatus (1941), $0.60
Feedwater Heaters (1927), $0.45
Fans (1945), $1.00
Gaseous Fuels (1944), $0.90
Gas Producers (1928), $0.65
Hydraulic Prime Movers (1938 with 1942 Addenda), $0.75
Reciprocating Steam-Driven Displacement Pumps (1927), $0.80
Reciprocating Steam Engines (1935), $0.80
Refrigerating Systems (1927), $0.65
Steam Condensing Apparatus (1938), $0.80
Steam Locomotives (1941), $0.65
Stationary Steam Generating Units (1946), $0.75

INSTRUMENTS AND APPARATUS

General Instructions (1945), $0.55
Definitions and Values (1945), $0.80
Part 1—General Considerations (1935), $0.45
Part 2—Pressure Measurement
- Chapter 1, Barometers; Chapter 6, Tables, Multipliers, and Standards (1941), $0.75
- Chapter 2, Static and Total Pressure, Static Holes and Tubes, and Impact Tubes, $0.75
- Chapter 3, Static Pressure Hole, Static Tube, or Impact Tube (1945), $0.75
- Chapter 4, Bourdon, Bellows, Diaphragm, and Deadweight Gages (1938), $0.75
- Chapter 5, Liquid Column Gages (1942), $0.75

Part 3—Temperature Measurement
- Chapter 1, General; Chapter 5, Pyrometric Cones; Chapter 6, Liquid-in-Glass Thermometers; and Chapter 7, Bourdon-Tube Thermometers (1931), $0.75
- Chapter 2, Radiation Pyrometers (1936), $0.65
- Chapter 3, Thermocouple Thermometers or Pyrometers (1940), $0.75
- Chapter 4, Resistance Thermometers (1945), $0.80
- Chapter 8, Optical Pyrometers (1940), $0.45

Part 4—Head Measuring Apparatus (1933), $0.45
Part 5—Chapter 4, Flow Measurement by Means of Standardized Nozzles and Orifice Plates (1940), $2.75
Part 6—Electrical Measurements (1934), $1.25
Part 8—Measurement of Indicated Horsepower (1941), $0.75
Part 9—Heat of Combustion (1943), $0.50
Part 11—Determination of Quality of Steam (1940), $0.55
Part 12—Measurement of Time (1942), $0.50
Part 13—Speed Measurements (1939), $0.55
Part 14—Linear Measurements (1936), $0.65
Part 15—Measurement of Surface Areas (1944), $0.75
Part 16—Density Determinations (1931), $0.40
Part 17—Determination of the Viscosity of Liquids (1931), $0.75
Part 18—Humidity Determinations (1932), $0.60
Part 20—Smoke-Density Determinations (1945), $0.75
Part 21—Leakage Measurements (1942), $0.75

RESEARCH

Fluid Meters:
- Part 1—Theory and Application (1937), $3.25
- Part 3—Selection and Installation (1933), $1.75

Report of the A.G.A.-A.S.M.E. Committee on Orifice Coefficients. (1935), $2.75
Tests on Electrical Equipment for Drilling Rotary Drilled Oil Wells (1932), $0.85
Tests on Steam Equipment for Drilling Rotary Drilled Oil Wells (1933), $0.85
Bibliography on Aircraft Plywood (1944), $1.00
Bibliography on Marketing Research (1935), $1.00
Bibliography on the Cutting of Metals (published 1945), $6.50
Riveted Joints—A Critical Review of the Literature Covering Their Development, with Bibliography and Abstracts of the Most Important Articles (Published 1945), $4.50
Sources of Information on Instruments (published 1945), $0.75

SAFETY CODES

Safety Code for Cranes, Derricks, and Hoists (B30.2—1943), $1.80
Safety Code for Elevators (A17.1—1937 with 1942 Supplement), $1.50
Elevator Inspectors' Manual (A17.2—1945), $1.50
Safety Code for Jacks (B30.1—1943), $0.40
Safety Code for Mechanical Power-Transmission Apparatus (B15—1927, Reaffirmed in 1935 without change), $0.45
Compressed-Air Machinery and Equipment (B19—1938), $0.40
Description and Schematic Layouts of Various Types of Undercar Safeties and Governors (published 1945), $0.40
Handling and Socketing of Wire Rope (published 1945), $0.25

Biographies

BIOGRAPHIES issued under the sponsorship of the A.S.M.E. Biography Committee are as follows:
Autobiography of an Engineer, by W. LeR. Emmet (1940), $3.50

Autobiography of John Fritz (1940), $3.25
Biography of Fred J. Miller (1941), $1.25
Life of Henry Laurence Gantt, by L. P. Alford (1934), $5.00

Books and Pamphlets on Special Subjects

Automatic Control Terms (1946) (no discount allowed), $0.25
Automotive-Diesel Engine Cost and Performance Data (1943), $0.25
Corrosion-Resistant Metals (1936), $1.25
Creative Engineering (1944), $0.75
Creative Thinking (1946) (no discount allowed), $0.25
Unwritten Laws of Engineering (1944) (no discount allowed), $0.25
Design Data on Strength of Materials, Book 1 (1944), $1.50
Design Data on Mechanics (1944), $1.50
Engineering's Part in the Development of Civilization (1939), $1.50
Flow of Water in Pipes and Pipe Fittings (1941), $8.00
Furnace-Performance Factors (1944), $1.00
General Discussion on Lubrication (1938) (no discount allowed), $6.50
Graphitization of Steel Piping (1943–1944 and 1945), $2.50
Hydraulic Structures (1937), $18.00
I.S.A. Tolerance System (1942), $2.50
Manual on Cutting of Metals (1939), $5.00
Manual of Consulting Practice (1939), $0.40
Oil Engine Power Cost Report (1944), $1.25
Reflections on the Motive Power of Heat (1943), $2.75
Theoretical Steam Rate Tables (1937), $1.25

Regular Society Periodicals

*Mechanical Engineering**—Annual subscription rate in United States $6.00; to Canada $6.75; elsewhere, $7.50
A.S.M.E. Transactions,* including *Journal of Applied Mechanics*, Annual subscription rate in United States, $12.00, elsewhere, $12.75
1946 A.S.M.E. Mechanical Catalog and Directory, $3.00 (sent gratis to members upon request)
Metal Cutting Data: Annual subscription rate in the United States $15.00; to Canada $15.75; elsewhere $16.50.

*Subscription price included in A.S.M.E. membership dues.

Index photographed at the
beginning for the convenience
of the microfilm user.